UNIVERSITY OF ILLINOIS AT
CHICAGO CIRCLE
801 SO. MORGAN
CHICAGO, IL. 60607

Digitized by the Internet Archive
in 2025

https://archive.org/details/physics-abstracts_1977-1980_80-83_cumulative-indexgeo-mas

Q
1
S3
V.80-83
1977-80
SUB.
INDEX
GEO-MAS
N/e
Sci

Physics Abstracts

Volumes 80-83 1977-1980

Cumulative Subject Index

Geo—Mas

29 July 1982

inspec
The Institution of Electrical Engineers

© 1981 The Institution of Electrical Engineers

CUMULATIVE SUBJECT INDEX 1977-80

Coverage

The present index provides a subject key to all papers abstracted in *Physics Abstracts* for the years 1977–80. It therefore comprises all relevant entries included in the six monthly subject indexes for the same period.

Subject Headings

In the course of the four years covered by this index the list of subject headings has been revised and new headings have been added. The present index uses the latest (i.e. 1980) version of the list. Entries for articles abstracted in the 1977, 1978 and 1979 volumes have been examined and, where appropriate, re-indexed under the new headings.

Arrangement

The subject headings are arranged in alphabetical order. The entries under each are prepared so that the most significant or 'key' words appear first and thus determine the position and grouping of entries in the alphabetical sequence under each heading.

Where the names of specific inorganic substances are significant under a given heading, the entries relating to them are found as a second alphabetical listing arranged by the chemical formulae of the particular elements or compounds.

Form of entry

The information contained in the subject index may be illustrated by an example.

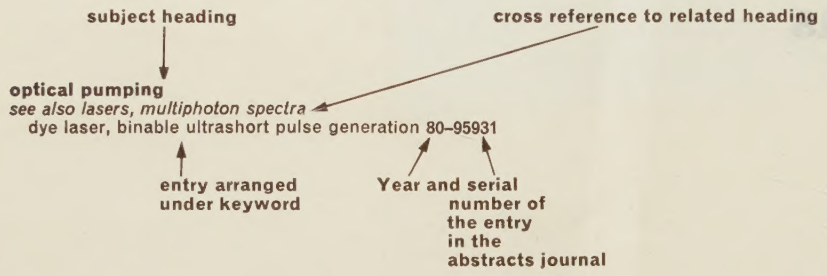
subject heading
cross reference to related heading
optical pumping
see also lasers, multiphoton spectra
dye laser, binable ultrashort pulse generation 80–95931
entry arranged under keyword
Year and serial number of the entry in the abstracts journal

How to use the index

The Subject index provides an alphabetical subject key to the articles included in the abstracts journal. Some general guidance on its use is given below:

1. Look in the index for the name of the specific subject in which you are interested. In most cases this name will be a heading in the index and you will find relevant articles listed under it. The majority of the subject headings fall into the following categories: property, phenomena, substance or named objects, instrument, device, theory, method, process, application, event.
2. Occasionally you will be directed from the subject heading chosen to a different heading under which the relevant or additional articles are listed.
3. If you do not find the subject heading you first chose, try a more general heading.
4. Each entry under the heading relates to an article appearing in the abstracts journal and gives the serial number of that article in the journal preceded by the last two digits of the current year, e.g. 78–12345; i.e. Abstract number 12345 in the abstracts journal for 1978.

   The language of the article, if it is not in English, is also indicated, e.g. optical fibre, three-wave stimulated Raman scattering (French) 0–78902.

   Each entry starts with a Keyword or Keyphrase considered to be most relevant to the heading. On sorting these Keywords, the qualifying prefixes are usually ignored (e.g. n-Ge is sorted under Ge).

   There are three main keyword lists; arabic numerals, alphabetical A–Z, and chemical symbols (organic substances are written and not given as chemical formula). More than one Keyword list may be present under each subject heading.

   For document on, say 'photoemission of silicon' at least two access points 'photoemission' and 'elemental semiconductors' are provided. Under the heading 'photoemission' the Keyword will be 'Si' and under 'elemental semiconductors' the Keyword will also be 'Si'.

   In a case like this, it is advisable and quicker to use the heading 'photoemission' and go straight to the chemical symbol list for 'Si' because there are few entries listed under 'photoemission'.

Printed by Unwin Brothers Limited, The Gresham Press, Old Woking, Surrey

Abbreviations and Acronyms

Abbreviations and acronyms are used in the modifiers in all INSPEC Cumulative Subject Indexes. Individual terms should be readily understood in the context of the subject headings. **Inorganic substances** are usually given by their chemical formulae. Iron and aluminium garnets appear in the formulae lists as MIG and MAG (where M is metal element, e.g. YIG and YAG); $(Pb,La)(Zr,Ti)O_3$ and $Ce_2Mg_3(NO_3)_{12}$ appear as PLZT and CMN respectively. **Organic substances** including **liquid crystals** are not given as formulae but common abbreviations are used.

ABS resin	acrylonitrile-butadiene-styrene
AC	alternating current
ACV	air cushion vehicle
A/D	analogue-to-digital
ADP	administrative data processing
AES	Auger electron spectra(oscopy)
AF	audio frequency
AFC	automatic frequency control
AFL	abstract family of languages
AGC	automatic gain control
AGR	advanced gas-cooled reactor
AM	amplitude modulation
ANS	Astronomical Netherlands Satellite
APACHE	accelerator for physics and chemistry of heavy elements
APR	acoustic paramagnetic resonance
APS	appearance potential spectra(oscopy)
APW	augmented plane wave
ATR	attenuated total reflection
ATS	applications technology satellite
ATWS	anticipated transients without scram
AVC	automatic volume control
BARITT	barrier injection transit time
BBEA	4-butoxybenzal-4'-ethylaniline
BCC	body centred cubic
BCD	binary-code decimal
BFO	beat-frequency oscillator
BWO	backward wave oscillator
BWR	boiling water reactor
BWT	backward wave tube
CAD	computer aided design
CAI	computer assisted instruction
CARS	coherent antiStokes Raman scattering (spectra)
CATV	community antenna TV
CB	citizen band
CBOOA	cyanobenzylidene octyloxyaniline
C-CD	charge-coupled device
CDI	collector diffusion isolation
CDM	code division multiplexing
CDW	charge-density wave
CEM	channel electron multiplier
CEPA	coupled electron pair approximation
CERN	Conseil Européen pour la Recherche Nucléaire
CESR	conduction electron spin resonance
CGTO	contracted Gaussian-type orbital
CHF	coupled Hartree-Fock
CI	configuration interaction
CIEH	charge iterated extended Huckel
CIHY	configuration interaction Hylleras
CNDO	complete neglect of differential overlap
COC	cholesteryl oleyl carbonate
COM	computer output to microform (fiche or film)
COOB	4,4'-cyano-octyloxy-biphenyl
CP	charge, parity
CPA	coherent potential approximation
CPSK	coherent phase shift keying
CPT	charge, parity, time
CRO	cathode ray oscilloscope
CRT	cathode ray tube
CS	coupled states
CSM	continuous slowing down models
CTR	controlled thermonuclear reactor
CVD	chemical vapour deposition
CW	continuous wave
D/A	digital-to-analogue
DBR	distributed Bragg reflector
DC	direct current
DDC	direct digital control
DDL	diode-diode logic
DECENT	distribution of exact classical energy transfer
DESY	Deutsches Electron Synchrotron
DF	Dirac-Fock
DFB	distributed feedback
DH	double heterostructure
DIL	dual-in-line
DITE	divertor in torus experiment
DLTS	deep level transient spectra(oscopy)
DM	delta modulation
DMSO	dimethyl sulphoxide
DMSS	Defence Meteorological Satellite System
DOBAMBC	p-decyloxybenzylidene p'-amino 2-methyl butyl cinnamate
DODS	different orbitals for different spins
DORIS	Dopple-ring-Speicher
DOVETT	double velocity transit time
DP	data processing
DPCM	differential pulse code modulation
DPPH	diphenylpicrylhydrazyl
DPSK	differential phase shift keying
DSC	differential scanning calorimetry
DTA	differential thermal analysis
DV-Xα	discrete variational Xα method
E1,E2	electric dipole, quadrupole
EAS	extensive air shower
EB	exponential Born
EBBA	4-ethoxybenzylidene-4'n-butylaniline
EBR	experimental breeder reactor
EBT	Elmo Bumpy Torus
ECC	emergency core cooling
ECELR	epithermal critical experiment laboratory reactor
ECG	electrocardiography (-gram)
EDA	ethylene diamine
EDP	electronic data processing
EDTA	ethylene diamine tetra-acetic acid
EEBAC	ethyl-4-(4'ethoxy-benzylidene-amino) cinnamate
EEG	electroencephalography (-gram)
EELS	electron energy loss spectra
EFM	extended Flygare method
EHD	electrohydrodynamics
EHF	extremely high frequency
EHP	electron-hole potential method
EHT	extended Huckel theory
EHV	extra high voltage
ELDOR	electron electron double resonance

ELF	extremely low frequency
EM	electromagnetic
EMC	electromagnetic compatibility
EMF	electromotive force
EMG	electromyography(-gram)
ENDOR	electron nuclear double resonance
EOS	earth observatory satellite
EPEN	empirical potential energy function based on interactions of electrons and nuclei
EPMA	electron probe microanalysis
EPR	electron paramagnetic resonance
ERG	electroretinography(-gram)
ERPS	extramolecular relaxation polarisation shift
ERTS	earth resources technology satellite
ESCA	electron spectroscopy for chemical analysis
ESCAR	experimental superconducting accelerating ring
ESFI	epitaxial silicon film on insulator
ESS	electronic switching system
EUV	extreme ultraviolet
EXAFS	extended X-ray absorption fine structure
FBR	fast breeder reactor
FCC	face centred cubic
FDM	frequency division multiplex(ing)
FDNC	frequency dependent negative conductance
FDNR	frequency dependent negative resistance
FEM	field emission microscopy
FET	field effect transistor
FFHR	fusion-fission hybrid reactor
FFT	fast Fourier transform
FFTF	fast flux test facilities
FIM	field ion microscopy
FM	frequency modulation
FPT	finite perturbation theory
FSK	frequency-shift keying
FSGO	floating spherical Gaussian orbitals
FTR	fast test reactor
GAMBIT	gate modulated bipolar transistor
GANIL	grand accelerateur national a ions Lourds
GARP	global atmospheric research programme
GATE	GARP Atlantic tropical experiment
GCFR	gas-cooled fast breeder reactor
GCM	generator coordinate method
GHF-NO-CI	generalised Hartree-Fock/natural orbital/ configuration interactions
GIAO	gauge-invariant atomic orbitals
GO	Gaussian orbitals
GOO	generalised Overhauser orbitals
GPM	ground potential model
GSO	general spin orbitals
GTO	Gaussian-type orbitals
GVB	generalised valence bond
HAM	hydrogenic atoms in molecules
HBAB	hexyloxybenzylidene-p' aminobenzonitrile
HBT	N-(p-hexyloxybenzylidene)-p-toluidene
HCDA	hypothetical core disruptive accident
HCP	hexagonal close packed
HEED	high energy electron diffraction
HF	high frequency or Hartree-Fock
HFB	Hartree-Fock-Bogoliubov
HFER	hot fuel examination facility
HFIR	high flux isotope reactor
HFO	Hartree-Fock-Overhauser
HFS	hyperfine structure
HLW	high level waste (radioactive)
HMO	Huckel molecular orbitals
HOAB	heptyloxyazoxybenzene
HOBHA	p-n-heptyloxy-benzylidene-p-n heptylaniline
HOMO	highest occupied molecular bitals
HORM	hybrid orbital rehybridisatic method
HTGR	high temperature gas-cooled actor
HV	high voltage
HVEM	high voltage electron microscopy
HWR	heavy water reactor
IAEA	International Atomic Energy Authority Agency
IBPBAC	isobutyl-4-(4'-phenylbenzylideneamino) cinnamate
IC	integrated circuit
ICDF	intermediate coupling Dirac-bck
IDT	interdigital transducer
IEPA	independent electron pair approximation
IF	intermediate frequency
IGFET	insulated gate field effect traristor
IKO	Institute v. Kernph Ouder Amterdam
I^2L	integrated injection logic
I^3L	isoplanar I^2L
ILS	instrument landing system
IMPATT	impact avalanche transit time
INDO	intermediate neglect of differential overlap
INDOR	internuclear double resonance
ING	intense neutron generator
INO	iterative natural orbital
INTELSAT	international telecommunications satellite consortium
I/O	input/output
IOC-ω	inclusion of the overlap charges in the omega
IR	infrared
IRDO	intermediate retention of differential overlap
ISABELLE	intersecting storage and acceleration
ISR	intersecting storage ring
ISX	impurity study experiment
ITEP	Institute of Theoretical and Experimental Physics
IU	Indiana University
IVO	improved virtual orbitals
JET	Joint European torus
JAERI	Japan Atomic Energy Research Institute
JINR	Joint Institute for Nuclear Research
KEK	Japan National Laboratory for High Energy Physics
KKR	Korringa-Kohn-Rostoker
LAMPF	Los Alamos meson physics facility
LC	inductance-capacitance
LCAO	linear combination of atomic orbitals
LCBO	linear combinations of (semi-localised) band orbitals
LCGO	linear combination of Gaussian orbitals
LCP	large coil program
LCRO	linear combination of Rydberg orbitals
LEC	liquid encapsulated Czochralski
LED	light emitting diode
LEED	low energy electron diffraction
LEP	large electron positron
LET	linear energy transfer
LF	low frequency
LMC	Large Magellanic Cloud
LMFBR	liquid metal fast breeder reactor
LMTO	linear combination of muffin tin orbitals
LOCA	loss of coolant accident
LOCE	loss of coolant experiment
LOFT	loss of flow test facility
LPE	liquid phase epitaxy
LSA	limited space charge accumulation

LSD	local spin density
LSI	large-scale integration
LTE	local thermodynamic equilibrium
LUMO	lowest unoccupied molecular orbitals
LV	low voltage
LWR	light water reactor
MADO	Mulliken approximation for differential overlap
M1,M2	magnetic dipole, quadrupole
MBBA	4-methoxybenzylidene-4'-n-butyl-aniline
MBE	molecular beam epitaxy
MBPT	many body perturbation theory
MCD	magnetic circular dichroism
MCPESCF	multiconfiguration paired excitation SCF
MCZDO	multi-centre zero differential overlap
MEDO	multipole expansion of diatomic overlap
MESFET	metal-semiconductor field effect transistor
MF	medium frequency
MFP	mean free path
MHD	magnetohydrodynamics
MIC	microwave integrated circuit
MIEHM	modified iterative extended Huckel method
MIM	metal-insulator-metal
MIS	metal-insulator-semiconductor or management information system
MIT	Massachusetts Institute of Technology
MMF	magnetomotive force
MNOS	metal-nitride-oxide-semiconductor
MO	molecular orbitals
MOCIC	molecular orbital constraint of interaction coordinates
MODPOT	model potential
MOS	metal-oxide-semiconductor
MOSFET	metal-oxide-semiconductor field effect transistor
MOST	metal-oxide-semiconductor transistor
MRD	multi-reference double excitation
MRINDO	modified Rydberg INDO
MSI	medium scale integration
MSR	molten salt reactor
MSU	Michigan State University
MTBF	mean-time between failures
MTF	modulation transfer function
MTXα	muffin-tin Xα
MUF	maximum usable frequency
MWH	Mulliken-Wolfsberg-Helmholz-semi-empirical method
NAL	National Accelerator Laboratory
NAND	not-and(logic)
NC	numerical control
NCMET	non-closed shell many electron theory
NDDO	neglect of diatomic differential overlap
NDT	nondestructive testing
NEMO	non-empirical molecular orbitals
NEVE	non-empirical valence electron
NIC	negative impedance convertor
NMR	nuclear magnetic resonance
NNDO	neglect of non-neighbour differential overlap
NOR	not-or(logic)
NPOST	non-perturbative open-shell theory
NPSO	non-paired spatial orbitals
NQR	nuclear quadrupole resonance
NRC	nuclear regulatory committee
NRM	natural remanent magnetisation
NTO	natural transition orbitals
OAO	orbiting astronomical observatory
OCR	optical character recognition
ODMR	optical detection of magnetic resonance
OER	oxygen enhancement ratio
OGO	orbiting geophysical observatory
OPHF	orbital polarised Hartree-Fock
OPW	orthogonal plane wave
OR	operations research
ORELA	Oak Ridge electron linear accelerator
ORNL	Oak Ridge National Laboratory
OSO	orbiting solar observatory
OTF	optical transfer function
PAA	paraazoxyanisole
PABX	private automatic branch exchange
PAC	perturbed angular correlation
PAHR	post accident heat removal
PAM	pulse amplitude modulation
PAMPUS	photons for atomic and molecular processes and universal studies
PAP	paraazoxyphenetole
PBF	power bursts facility
PBR	pebble bed reactor
PBX	private branch exchange
PC	printed circuit
PCAC	partially conserved axial currents
PCB	printed circuit board
PCGVB	pairwise correlated generalised valence bond
PCILOCC	perturbative configuration interaction using localised orbitals for crystal calculation
PCM	pulse code modulation
PCX	plasma confinement experiment
PDX	poloidal divertor experiment
PEP	positron electron proton
PETRA	positron electron tandem ringbeschleuniger anlage
PF	power factor
PFM	pulse frequency modulation
PHWR	pressurised heavy water reactor
PID(PI,PD)	proportional+integral+differential (derivative)
PLA	phase locked arrays
PLC	programmable logic control
PLL	phase locked loops
PLT	Princeton Large Torus
PM	pulse modulation
PMMA	polmethylmethacrylate
PMDR	phosphorescence microwave double resonance
PNDO	partial neglect of differential overlap
PNO-CI	pair natural orbital configuration interaction
POL	pair orthogonalised Lowdin
POPAE	protons on protons and electrons
POPOP	phenyl-oxazolyl-phenyl-oxazolyl-phenyl
POS	point of sale
PPDP/S	Pariser-Parr-Del Bene-Pople/Segal calculations
PPI	plan position indicator
PPM	pulse position modulation or parts per million
PPP	Pariser-Parr-Pople
PRDDO	partial retention of diatomic differential overlap
PRF	pulse recurrence (repetition) frequency
PROM	programmable read-only-memory or Pockels readout optical modulator
PS	proton synchrotron (CERN)
PSK	phase shift keying
PTFE	polytetrafluoroethylene
PTM	pulse time modulation
PVC	polyvinyl chloride
PWM	pulse width modulation
PWR	pressurised water reactor

QCD	quantum chromodynamics
QDMBPT	quasi-degenerate many-body perturbation theory
QED	quantum electrodynamics
QPSK	quaternary phase shift keying
RAM	random access memory
RBE	relative biological effectiveness
RC	resistance-capacitance
RCNDO	Rydberg CNDO
R & D	research and development
RF	radio frequency
RFI	radio frequency interference
RHEED	reflection high energy electron diffraction
RINDO	Rydberg INDO
RKKY	Rudermann-Kittel Kasuya-Yosida
RLC	resistance-inductance-capacitance
RMS	root-mean-square
ROM	read-only memory
RPA	random phase approximation
RPM	relaxation potential model
SAMO	simulated ab initio molecular orbitals
SAS	small astronomy satellite
SAW	surface acoustic waves
SCF	self consistent field
SCL	space charge limited
SCPT	self consistent perturbation theory
SCR	silicon controlled rectifier
SDM	space division multiplexing
SDO	shielded diatomic orbitals
SEHF	spin extended Hartree-Fock
SEM	scanning electron microscope
SFE	solar-flare effect
SGHWR	steam generating heavy water reactor
SHF	superhigh frequency
SHG	second harmonic generation
SIMS	secondary ion mass spectrometer
SIN	Swiss Institute of Nuclear Research
SINDO	scaled INDO
SISAM	spectrometer with interference selective amplitude modulation
SMC	Small Magellanic Cloud
SMS	synchronous meteorological satellite
S/N	signal-to-noise
SOG	strongly orthogonal geminal
SOS	silicon on sapphire
SPA	separated pair approximation
SPC	stored program control
SPEAR	Stanford positron electron asymmetric ring
SPHF	spin polarised Hartree-Fock
SPIN-CIPSI	spin symmetry adapted generalisation of CIPSI
SPS	super proton synchroton (CERN)
SQUID	superconducting quantum interference device
SRMCASE	symmetry-restricted-multiconfiguration annihiliation of single excitations
SSB	single sideband
SSC	sudden storm commencement
SSI	supersonic transport
STD	salinity-temperature-depth or subscriber trunk dialling
STEM	scanning transmission electron microscopy
STO	Slater-type orbitals
STOL	short take-off and landing
STP	Slater-transfer Preuss
SUHFC	spin unrestricted Hartree-Fock with local approximation for correlations
SW	short wave
SWR	standing wave ratio
SXAPS	soft X-ray appearance potential spectrum
TBBA	terephthal-butylaniline
TCNE	tetracyanoethylene
TCNQ	tetracyanoquinodimethane
TCR	temperature coefficient of resistance
TDHF	time dependent Hartree-Fock
TDM	time division multiplex(ing)
TDMA	time division multiple access
TDPAC	time differential perturbed angular correlation
TE	transverse electric
TEA	transversely excited atmospheric
TEM	transverse electromagnetic or transmission electron microscopy
TEXT	Texas Experimental Tokamak
TFTR	Tokamak fusion test reactor
TGFB	triglycine fluoroberyllate
TGS	triglycine sulphate
TGSe	triglycine selenate
TJS	transverse junction stripe
TLD	thermoluminescent dosimeter(-ry)
TM	transverse magnetic
TMMC	tetramethylammonium manganese chloride
TOP	transient overpower accident
TNS	The next step
TRAPATT	trapped plasma avalanche triggered transit
TREAT	transient reactor test facility
TRM	thermoremanent magnetisation
TSC	thermally stimulated currents
TSEE	thermally stimulated exo-electron emission
TTF	tetrathiofulvalinium
TTL	transistor transistor logic
TTT	tetrathiotetracene
TUCA	transient undercooling accident
TV	television
TW	travelling wave
TWT	travelling wave tube
UCHF	uncoupled Hartree-Fock
UHF	ultra high frequency unrestricted Hartree-Fock
UHV	ultra high voltage
UKAEA	United Kingdom Atomic Energy Authority
ULF	ultra low frequency
UMD	unitised microwave devices
UPS	ultraviolet photoelectron spectra
US	ultrasonic
UV	ultraviolet
VB	valence bond
VCR	video cassette recorder
VDM	vector dominance model
VDU	visual display unit
VHF	very high frequency
VLBI	very long base line interferometry
VLF	very low frequency
VLSI	very large scale integration
VOR	VHF omnidirectional range
VPE	vapour phase epitaxy
VRC	visual record computer
VRDDO	variable retention of diatomic differential
VSB	vestigial sideband
VSEPR	valence shell electron pair repulsion
VSWR	voltage standing wave ratio
VTOL	vertical take-off and landing
VTR	voltage transformation ratio or video tape recorder
VUV	vacuum ultraviolet
VVER	water moderated water cooled reactors
WWER	water moderated water cooled reactors
XPS	X-ray photoelectron spectra
ZEBRA	zero energy breeder reactor assembly
ZGS	zero gradient synchrotron
ZPPR	zero power plutonium reactor

geophysical prospecting continued
continental shelf, possibility of geoelec. mapping 78−57341
contour map aeromagnetic data computer processing 78−7819
contouring irregularly spaced data 77−64180
core drilling equipment for permafrost regions *(French)* 80−77140
critical mineral resources 79−5482
cross-borehole EM probing, location of high-contrast anomaly 80−72639
cross-borehole EM probing for tunnel location 77−78545
crustal resistivity, sounding data from South Africa, ridge regression inversion appl. 78−7561
crustal seismic reflection studies, Canadian Shield, weighted vertical stacking 77−87089
Curie depth determination from aeromag. spectra, W.USA 77−60349
data analysis, interpretive patterns, influence of meas. noise and meas. device accuracy 80−90235
data management and analysis systems for hydrogeochemical reconnaissance 78−20520
DC apparent resistivity method, topographic correction *(Chinese)* 78−24375
DC resistivity sounding method, appl. to evaluation of non-uniform water-bearing formation 78−40474
deep electrical soundings, southern Africa, using Cabora Bassa power line 77−86770
deep EM sounding and profiling 77−9326
deep magnetic-variation sounding, geoelectric and geothermal interpretation of results 78−44765
deep magnetotelluric and magnetovariational sounding results in Ciscaucasian area 77−78096
deep probing and refraction seismograms, computer processing *(Russian)* 79−84528
deep seismic data processing, digital techniques appl. *(Italian)* 78−40719
deep water surveying, new techniques 78−85730
delayed neutron probe characts. for uranium exploration, field meas. 79−53568
depositional facies interpretation from seismic date 80−4122
depth determ. from seismic refraction data, iterative method 78−96302
depth measuring apparatus for borehole logging 79−5643
description of methods used at Umex Thierry deposit, Canada 77−25783
dielectric permittivity determ., water saturation effects *(Russian)* 79−62626
differential geomagnetic sounding 77−53225
digital seismic prospecting, in oil and gas bearing provinces of Ukrainian SSR 79−96836
dip selective migration vel. determ. 77−41187
dipole electric sounding method and application to Tuscany geothermal area 80−97762
dipole electrical soundings, perpendicular, numerical procedure for direct interpretation 79−34732
dipole soundings data obtained along crooked line, transform. 79−44259
dipole-dipole deep geoelectric soundings over geological structures 80−101449
direct current regimes, theorem proof 78−96131
direct current resistivity method, elec. fields in random cond. layered Earth 80−77171
directional antenna, miniature, design, for geophys. probing from boreholes 79−12297
Dnieper-Donets depression, magnetotelluric sounding data rel. to deep struct. *(Russian)* 78−96170
Dnieper-Donets depression, sedimentary cover struct. along Jagotin-Baturin profile *(Russian)* 78−92806
Dong-Xing Oil Field, seismic survey, three-dimens. interpretation of complex fault struct. *(Chinese)* 79−100833
drill hole or sample area-of-influence determ., FORTRAN IV program 77−5327
drill-rod telemetry, calcs. for toroidal coil source 78−85710
dual wavelength thermal IR scanner as potential airborne geophysical exploration tool 77−41183
effectiveness of geophysical and geochemical methods, evaluation *(Spanish)* 77−9552
electric field intensity vertical component meas. 77−91209
electric near zone field development method testing in NW.Kola Peninsula *(Russian)* 80−85761
electric potential probing of underground struct. *(German)* 80−82089
electric sounding data analysis, use of reciprocal geoelec. section 80−90237
electrical conductivity, model for quantitative interpretation of towed-bird airborne EM system meas. 79−5447
electrical conductivity rel. to random networks and mixing laws 77−44971
electrical properties of layered medium, anisotropy resolution by joint inversion 78−16173
electrical prospecting, induced polarisation decay curve, dynamic characts. *(Hungarian)* 80−21842
electrical prospecting equipment with focusing effect, detect. of cavity in lower half-space *(Russian)* 78−28336
electrical prospecting problems soln. for inhomogeneous media 79−88487
electrical resistivities overlayered Earth, transformation using digital filters 78−96304
electrical sounding, peculiarities of section and zonation of Volyn-Podolian margin of E.European platform *(Russian)* 78−48964
electrical sounding, pots. of simple bodies in half-space *(Russian)* 79−34744
electrical sounding for dissemminated sulphide ores, electrochemical model of induced-polarisation phenomenon 79−92526
electrical sounding methods, applied EM depth sounding 77−45173
electrical sounding methods, statistical evaluation, expt. design 77−45172
electrode arrays comparison for induced polarization and apparent resistivity responses 79−58107
electromagnetic sounding transient pulse induction method, one-loop version 80−101448
electroprospecting, direct problem soln. for ideally conducting hemisphere in space with point source *(Russian)* 79−34745
electroprospecting, inductive methods, resolving capabilities 79−84498
elemental sensitivity data modeling for in situ neutron capture gamma-ray experiments 79−61928
elliptical borehole logging, resistivity tool response characts. 77−87103
EM airborne profiles, sphere model for interpretation 77−45171
EM coupling in electrical prospecting systems 77−64193
EM depth sounding expt. in Tunisia 77−64192
geophysical prospecting continued
EM depth sounding interpretation, master tables, book 80−86043
EM exploration, target near dipping contact, response modelling 79−8595
EM field build-up sounding method, resolution 78−16176
EM field properties reproduction, spherical, by real meas. devices *(Russian)* 78−85729
EM field sounding, appl. of composite obs. patterns in near field *(Russian)* 79−44270
EM fields in halfspace with ore body, local element transformation 79−66828
EM fields of dipole in metal cased borehole 77−46672
EM fields of horizontal electric dipole on polarisable half-space surface 78−69283
EM fields of vertical mag. dipole over thin conductive overburden 78−65183
EM frequency sounding, crustal struct. determ. 78−49167
EM frequency sounding in horizontal coils system, field test 77−49182
EM frequency soundings, exptl. study 79−58129
EM in-line dip-angle meas. of vertical tabular conductors, graphical interpretation method 77−41189
EM induction, freq. and transient responses of EM fields created by currents in confined conductors 79−29702
EM induction in conducting stratified medium, numerical analysis 79−34740
EM induction in thin sheet conductivity anomalies at Earth's surface 80−76907
EM induction in thin sheets, statistical theory 77−86769
EM inverse interpretation, trend influence 78−81103
EM lateral waves, Earth-sounding radar obs. 77−44909
EM logging in inhomogeneous media, axisymm. problem 79−39877
EM methods with distant source, terrain relief effects 79−79735
EM modelling of transmissions through in situ gasified coal seam 79−12298
EM probing, expt. curves features due to seismoelec. effects *(Russian)* 79−39643
EM prospecting, harmonic and transient fields behaviour on surface of two-layer medium 79−92478
EM prospecting, inverse problem 79−53583
EM prospecting, wave type and direction from EM field short-period vars. anal. *(Russian)* 78−85474
EM remote sensing, computerized geophysical tomography 80−77169
EM remote sensing, reconstruction algorithms for geophysical applications in noisy environments 80−77168
EM remote sensing of inhomogeneities in ground, numerical modelling 80−77165
EM response of conductive inhomogeneity in layered Earth 77−40976
EM response of dipping half plane embedded in conducting rock 80−90236
EM shielding of sources within metal-cased borehole 77−40979
EM sounding, analogue model meas. for horizontal mag. dipole embedded in conducting medium 79−12068
EM sounding, detectability of intermediate layers, time domain anal. 80−72641
EM sounding, diffr. of field of infinitely long cable over wedge-shaped conducting media *(Russian)* 78−40484
EM sounding, induced polarisation effect on near-field form. *(Russian)* 79−39641
EM sounding, interpretation of transients in Laplace space representation *(Russian)* 78−40483
EM sounding, multicoil II airborne system 80−51554
EM sounding, topographic effect in three-dimensional cond. model 77−25639
EM sounding methods, theoretical principles 78−49166
EM sounding of permafrost, appl. of resonating antenna method 77−64333
EM sounding over permafrost region, computer-assisted anal. 77−2086
EM sounding with mag. susceptibility in layered Earth model parameters 77−53226
EM subsurface profile from HF meas., reconstruction technique algorithms appl. 77−45199
EM time-domain sounding of multilayered Earth 79−57850
EM time-domain system, decay pattern of mag. field and voltage response of cond. bodies 79−58108
EM transient response of vertical elec. dipole in homogeneous anisotropic medium *(Polish)* 77−52970
EM wave excitation by dipole emitters buried in stratified media 78−48966
EM wave refl. and transmission coeffs., linear ramp model of crust 80−61759
EM wideband freq. response conversion to transient response using segmented transform. 78−77349
energy and mineral resources rel. to plate tectonic research 78−7606
energy propag. of EM field of dipole source on conducting halfspace 77−9330
SW.England heat flow anomaly 77−49041
English Peak District, geological mapping, EM prospecting method 80−3924
environmental samples anal. for U, Th, neutron activation anal. data resolution for high throughput system 79−11848
epithermal neutron fields in nuclear geophysics *(Russian)* 80−85658
equipment for Hungary, charact. 78−7787
exploration by Electromagnetic Transient Underground Radar 77−17262
exploration geophysics, 41st meeting of European Assoc. of Exploration Geophysicists, Hamburg, Germany (1979 May 29 to June 1) 80−51943
exploration geophysics, 48th Annual International SEG Meeting, San Francisco, CA (1978 October 29 to November 2) 80−8441
exploration seismology, wave refl., refr. and diffr. in media with elliptical vel. depend. 79−5454
exploratory drilling exhaustion sequence plot program 78−57334
faults prospecting via seismic refr. method, model expt. and features of seismograms *(Chinese)* 79−12286
finite difference schemes, instability due to boundary conditions in elastic media 77−21912
N.Finland, magneto-telluric expts. 79−44093
folded and crystalline basements of deep cavities, determ. from seismic data *(Russian)* 79−39692
Fourier analysis of gravimetric and magnetometric anomalies *(Rumanian)* 79−58123
fracture zones mag. features 77−78092

geophysical prospecting continued
frequency EM sounding, anomalous high cond. bands discovery in crystalline foundation *(Russian)* 78−96137
galvanic prospecting effects, calc. via method of sub-areas 80−56348
Gamburtsev graphical method for three-dimens. gravity anomaly calc. 77−41203
gamma-gamma logging problems with large probe length, Monte Carlo soln. 77−37437
gamma-gamma method, angular spectral selection of scattered gamma quanta 77−45185
gamma-ray logging K-factors, correction of error 79−84278
gamma-ray logging of boreholes, exact inverse filters 80−94609
gamma-ray spectrometric logging and surface exploration equipment calibration 78−85706
gamma-ray spectrometry, factor analysis appl. 78−7778
gamma-ray surveys, allowance for scattered gamma radiation *(Russian)* 80−105067
gamma-ray surveys, fields of view of airborne detectors 80−51555
gamma-rays from extended sources, energy distrib. calc., rel. to remote spectroscopy 78−61586
gas deposits, distribution related to Earth's rotation and local geological conditions *(Russian)* 79−83545
generalized reflection coefficients for a layered medium and asymmetrical source *(Chinese)* 79−100964
geochemical exploration using marine mineral suspensates 78−88936
geodesy and prospecting procedures *(German)* 77−70588
geoelectric deep crustal *(German)* 80−56626
geoelectric inhomogeneities, position determination by variable geomag. field method 80−89956
geoelectric sounding, controlled-source DC pot. problem by self-pot. Green's function 80−77136
geoelectrical method for thickness var. detection 79−2384
geoelectrical prospecting, resistivity method for geophydrological problems 77−9527
geoelectrical prospecting, thin-layer problem 79−44095
geoelectrical prospecting in marine areas, dipole and unipole resistivity methods 80−56641
geoelectrical prospecting in marine areas, resistivity methods 78−65417
GEOLOG computerised technique for field observation recording and interpretation 78−7774
geological and geophysical methods for evaluating shallow platform structures *(Russian)* 79−62623
geological data management, conf., 1975, Nov., Paris, France 77−53198
geological prospecting data processing system, Poland *(Polish)* 78−88929
geological section local inhomogeneities determ. by reflected-wave probing method *(Russian)* 79−39947
geological stratum sounding by UHF radar *(German)* 79−8702
geomagnetic depth sounding by means of oceanographic and aeromagnetic surveys 80−77166
geomagnetic sounding, exclusion method for local distortions *(Russian)* 77−45196
geophysical cybernetics *(Russian)* 79−48488
geothermal energy, high-temp. electronics development 80−11997
geothermal energy exploration using chemical geothermometers and mixing models 78−69503
geothermal energy investigations in Sweden 79−74488
geothermal energy prospecting by geophys. methods, review 78−7803
geothermal energy prospects in Brazil 79−74487
geothermal energy resources, low enthalpy, in Denmark 79−74489
geothermal energy resources in Oregon, USA, elec. and EM sounding obs. 80−97761
geothermal exploration techniques, improvement for resource assessment of United States 79−70428
geothermal prospecting, via field station GS-1 with thermoquartz resonators *(Russian)* 78−93000
geothermal reservoirs, downhole meas. of thermal conductivity 78−61618
geothermal reservoirs true temp. determ. by resistivity method 77−49043
geothermal resources, exploration via seismic noise sources mapping 77−81828
geothermal resources in USA, National Exploration Program 80−72011
geothermal well logging instrumentation, hybrid microcircuit design, performance 79−96845
geothermal well-logging, high temp. instrum., passive components fabrication 80−40266
N.Germany, magnetotelluric meas. of nearly circular salt dome 77−64201
Ghana, gravity mapping and interpretation 77−78080
Grass Valley, Nevada, USA, microseisms in geothermal exploration 80−21647
gravimagnetic anomalies, interpretation on basis of pots. classes with inverse problem finite form 80−21847
gravimetric prospecting problem appl. of nonsmooth function minimisation methods 77−41180
gravimetric sinusoid variation detect. near Moscow and Sukham *(Russian)* 77−86747
gravimetric sounding, vertical and horizontal gravity gradients relative precision 79−84500
gravimetry, direct and inverse problems soln. for hemispherical bodies *(Russian)* 79−35012
gravimetry inverse problem, assembling principle for constructing solns. *(Russian)* 77−44898
gravitational attraction of circular disc 77−52959
gravitational logging and role in combined geological and geophysical research *(Russian)* 77−70868
gravitational prospecting, inverse problem approximate soln. *(Russian)* 79−39927
gravity and magnetic anomalies of arbitrary bodies, FFT method for rapid computation 77−41186
gravity and magnetic sounding, separation of anomalies of comparable horizontal dimensions 80−94606
gravity and magnetic surveys, nonlinear analytical prolongation method, for inverse problem *(Russian)* 79−21037
gravity anomalies, automatic interpretation for 2-dimens. masses 77−41188
gravity anomalies due to finite inclined dykes, interpretation using Fourier transform. 77−53223
gravity anomalies extrapolation in structural gravity prospecting *(Russian)* 79−39951
gravity anomalies interpretation, computer modelling 79−34971

geophysical prospecting continued
gravity anomaly data processing system, involving interactive computer graphics *(French)* 80−94610
gravity anomaly interpretation, pot. fields linear anal. *(Russian)* 79−35011
gravity anomaly interpretation methods for Pripyat trough studies *(Russian)* 77−91293
gravity interp. data processing techniques, shortening operators 77−64179
gravity measurements, borehole data accuracy 79−5632
gravity profile interpretation, linear inverse problem 77−73875
gravity profile inversion by method 78−69476
gravity prospecting, accuracy, meas. spacings and contour intervals calc. techniques *(Russian)* 79−44272
gravity sounding, calc. of gravity field of three-dimensional masses 80−94451
ground exploration and geological evaluation using remote sensing from space platforms 78−40682
ground water, India, Wenner electrode obs., seasonal and salinity depends. 79−92551
groundwater, EM freq. sounding in Tunisia 77−9529
groundwater and bedrock topology, gravity exploration in glaciated areas 77−91289
groundwater exploration, geomorphological studies in Rajasthan desert 79−53375
groundwater exploration in hard rock terrain 77−41075
groundwater resources in Kalahari Basin, geoelec. survey 78−3830
Gulf of Oman, gas hydrate layers trapping free gas 79−29746
HF EM induction profiling, of boreholes in underground mines *(Polish)* 80−51547
HF EM logging in inhomogeneous media 77−81791
horizontal infinite trapezoidal prism, gravity effect, Fourier spectrum 77−87095
horizontally multilayered Earth models, recurrence formulae for layer eigenfunctions 80−90246
horizontally stratified medium as reference large scale system 77−87093
Hungary, petroleum deposits rel. to sandstone litho-stratigraphy 77−86884
Hungary Eocean brown coal basins, geophysical exploration by well logging methods *(Hungarian)* 80−104938
hydrocarbon bearing anticlines, pattern space of seismic anomalies, location tool and theory 80−17234
hydrocarbon exploration, seismic signatures of sedimentation models using synthetic seismograms 77−21913
hydrocarbon well logging, nuclear techniques 77−37443
hydrochemical, APDC coprecipitation and X-ray spectrometry for trace element determ. 77−37445
hydrothermal alteration minerals, near IR spectra for remote sensing use 80−81871
Iceland, magnetotelluric investigation of lower crust and upper mantle 79−66612
image analysis system for Earth resources surveys 79−5644
in situ capture gamma analysis of large mineral samples 80−61215
induced polarisation, book 77−41216
induced polarisation, multifrequency mineral discrimination and inductive coupling removal 79−5448
induced polarisation (IP) sounding, effects of EM coupling in electrode arrays over uniform half-space 80−101324
induced polarisation method, in situ soln. chemistry effects 78−3964
induced polarisation methods for ore body tracing *(German)* 80−82084
induced polarisation response of multilayered Earth with no resistivity contrast 77−64196
induced polarisation sounding, response of polarisable inhomogeneous sphere 79−44092
induced polarisation sounding method, freq. depend. of measured parameters *(Russian)* 79−74836
induced polarisation technique for prospecting 78−69473
induced polarisation theory, stochastic rock model appl. *(Russian)* 79−88250
induced polarisation vertical electric sounding curves, correl. analysis *(Russian)* 77−9565
induced polarization method, saturation effect *(Chinese)* 77−91280
induced polarization method, time domain and freq. domain comparative anal. 78−20351
induced polarization models, parametric study 78−7560
induced-polarization freq.-domain method, metallic mineral deposits *(Italian)* 79−16686
induction logging, longit. geometric factors *(Chinese)* 77−66998
induction logging, numerical soln. by transition process method 77−56751
induction-logging tools, sonde eccentricity effect on response 79−12300
inductive dipole profiling, screening effect of surface deposits 77−81792
inductive dipole sounding anomaly, low-impedance overburden screening *(Russian)* 78−81106
inductive logging near single and multiple conductive bodies, scale model results 79−16696
interpretation methods, conf. (Bratislava, Czechoslovakia, May 1974) *(German)* 79−35001
interpretation of time-domain airborne electromagnetic (INPUT) anomalies 79−2383
inverse filtering for seismic long period statics determ. 77−41192
inverse gravity problem, infinite polygonal cylinders 78−53607
inverse gravity problem, unified least-squares method 77−73872
inverse log.-potential problems, integral and functional eqn. analysis 77−40968
inverse problem for n layers, inversion method for reducing nonuniqueness 80−4128
inverse problem uniqueness and impulse response data 77−73678
inverse problems, max. entropy method, extreme models 78−65230
inverse problems, nonlinear eqn. soln., Tikhonov algorithm 77−41200
inverse problems, potential theory for interpretation 78−7557
inversion probes in γ-γ methods, laminar medium, nuclear geophysics 79−34992
Jharia Coalfield, India, coal seam mapping by elec. resist. methods 80−4133
kimberlite pipes, exploration geophysics appl. 80−51393
kinematic multiple wave analogues strongest families, parameter prediction algorithm *(Russian)* 79−39943
Kokchetav mountain massif, magnetotelluric soundings 77−40981
land seismic reflection exploration data acquisition systems 77−29444
land seismology, appl. of mini-SOSIE 77−21917

geophysical prospecting continued
lateral induction logging, calibration of apparatus *(Russian)* 79−39941
lateral logging three-electrode probe, effective field model *(Russian)* 78−53762
lateral resistivity logging, effectiveness increase *(Russian)* 78−53760
Laterolog 7 resistivity logging, field tests 78−61574
Laterolog borehole resist. logging device, function and applications 80−85755
layered media, relative intensity of total multiply refl. waves *(Russian)* 78−28176
layered system, spectral function, waveform determ. at depth 78−16172
lenticular low-vel. inclusion effect on seismic wave pattern, US modelling 77−41006
LF seabed sounding *(Russian)* 80−67431
line source DC apparent resistivity profiles, basement effect 77−78091
linearized inverse problems, mathematical methods 77−73871
low-amplitude structure with oil (gas) deposits, parameters from gravity test data *(Russian)* 79−44271
magnetic anomalies, interpretation by singular point method 77−53229
magnetic anomalies, three-dimensional potential fields conversion and pseudo-gravit. field computation 77−82026
magnetic anomalies interpretation, computer modelling 79−34971
magnetic anomaly, due to alkaline rocks petroleum prospecting *(Rumanian)* 80−12338
magnetic anomaly interpretation, pot. fields linear anal. *(Russian)* 79−35011
magnetic anomaly of thin dyke, curve fit by calculator program 80−98228
magnetic anomaly reduction to mag. pole *(Chinese)* 79−100963
magnetic anomaly sounding, estimation of cover thickness above magnetised mass *(Russian)* 80−105069
magnetic assessment technique for titanomagnetite in Waipipi ironsands, New Zealand 80−17254
magnetic deep sounding data interpretation, use of equivalent current systems 79−25190
magnetic field probing problems, approx. anal. *(Russian)* 79−84108
magnetic induced polarization method, theoretical problems *(Chinese)* 79−100962
magnetic profiling, separation of geomag. vars. into external and internal parts *(Russian)* 79−39991
magnetic profiling of geological contact, harmonci inversion method 80−77137
magnetic prospecting, 3-D anisotropic body mag. field calcs. and algorithm 80−4141
magnetic prospecting, inverse problem approximate soln. *(Russian)* 79−39927
magnetic prospecting, inverse problem soln., decomposition iteration method *(Russian)* 80−4134
magnetic prospecting, optical filtering of airborne and ground data 77−25797
magnetic prospecting inverse problem, linear programming *(Russian)* 78−15955
magnetic sounding, anomaly field vertical intensity autocovariance function *(German)* 79−34746
magnetic sounding, magnetostatic field problem, soln. in high susceptibility case via method of subsections 80−105065
magnetic variation sounding, anomalies above inhomogeneities of Earth spherical model 77−13056
magnetized buried object, depth determ. errors *(Russian)* 79−20750
magnetometric and electrometric methods for landslide dynamics investigation 77−87091
magnetometric resistivity anomalies, two-dimensional struct., mag. field determ. method 80−12334
magnetometric resistivity method field test on plateau 77−40977
magnetotelluric analysis for layered Earth, matrix relation 78−32008
magnetotelluric and geothermal surveys in NW Germany, comparisons 80−12336
magnetotelluric and magnetovariation methods, elec. cond. functions 77−32982
magnetotelluric and telluric parameters, cross-correlation estimates 79−92484
magnetotelluric anisotropic data, inversion technique 77−60475
magnetotelluric diagrams 77−2087
magnetotelluric field in homogeneous layer with cylindrical inclusion *(Russian)* 78−53617
magnetotelluric meas. using SQUID magnetometer, remote reference technique 79−29866
magnetotelluric method for investigation of media with monotonically changing cond. 77−78439
magnetotelluric probing, data interpretation, reliability estimate *(Russian)* 79−39949
magnetotelluric probing, input impedance determ. accuracy, noise effects *(Russian)* 79−39950
magnetotelluric probing in complex geoelec. conditions, data interpretation *(Russian)* 79−39932
magnetotelluric probing phase curves, horizontally inhomogeneous medium *(Russian)* 79−39931
magnetotelluric prospecting methods, exact surface impedance for spherically concentric Earth model 80−46129
magnetotelluric rapid profiling across Berici-Euganean ridge eastern edge 77−48998
magnetotelluric resistivity and phase soundings interpretation, graphical procedure 78−40473
magnetotelluric signals digitization equipment *(French)* 77−87092
magnetotelluric sounding, audio-frequency, case history at Cavendish geophysical test range 80−51324
magnetotelluric sounding, effect of primary field inhomogeneity *(Russian)* 77−86774
magnetotelluric sounding, expt. study of edge effect 77−78441
magnetotelluric sounding, fields of vertical mag. dipole over vertically inhomogeneous Earth 79−34736
magnetotelluric sounding, fundamental model 80−77167
magnetotelluric sounding, inverse problems soln. 78−49162
magnetotelluric sounding, multiple-reflection method appl. to inverse problem soln. 78−61581
magnetotelluric sounding, plane EM field over polarized section *(Russian)* 77−86775
magnetotelluric sounding localization and accuracy improvement *(Russian)* 78−53754
magnetotelluric sounding method development in USSR 78−49169
magnetotelluric sounding over models of continuously varying conductivity 78−32009
magnetotelluric soundings, effect of field vertical components on impedance determ. *(Russian)* 78−48963
magnetotelluric studies in Central Urals and Transurals 79−25194
magnetotelluric studies in USSR, review 78−49168
magnetotelluric study, S.Scotland, fieldwork, data anal. and results 79−29705
magnetotelluric study, S.Scotland, Monte-Carlo data inversion, geophys. and tectonic implications 79−29706
magnetovariational sounding curves, effect of relief of high-impedance basic horizon 78−85475
marine electrical prospecting, EM field buildup by immersed dipole 77−70595
marine gamma-spectrometric surveying problems 79−2390
marine heavy mineral deposits, extraction, X-ray spectrometric anal. *(German)* 78−20551
marine minerals exploration, Mobile Initial Condition Indicator approach 79−5687
marine oil and gas prospecting, new techniques appl. 79−53560
marine seismic exploration, coherent noise attenuation in very long arrays 79−74840
marine seismic exploration data acquisition systems 77−29445
marine seismic exploration ship 77−64449
marine seismic surveying, potential efficiency of shot grouping *(Russian)* 78−40702
marine seismology, attenuation of multiples by antiaveraging *(French)* 77−64215
marine survey instrumentation, requirements and appls. 79−84508
marine survey vessels, multiple use 79−53561
Martinique, aeromag. survey, conductivity anomaly existence *(French)* 77−86754
matched electromagnetic pulse transmission, for good conducting media 79−36823
measuring loop antenna characteristic improvement 78−49174
metallic mineral deposits of Australia mag. induced polarisation survey results 80−98223
microwave dielectric constant logging, EM wave propag. method 80−12558
mineral anal. by track etch method 78−20553
mineral deposit evaluation with Metalog gamma-ray anal. technique 77−64446
mineral discovery probability, quantitative fall-backs of naturalist classifications 77−53204
mineral exploration, computer uses, limitations and requirements 77−53207
mineral exploration, effect of tropical weathering on elec. and EM meas. 79−88246
mineral exploration, remote-sensing appls., book 77−37450
mineral exploration and plate tectonics 78−7607
mineral exploration techniques, changes 79−100979
mineral prospecting by airborne EM method *(Japanese)* 78−24392
mineral prospecting by tunable laser spectroscopy 77−60500
mineral resource data bases 77−53203
Mineral Resources Development Centre, developing countries computer aid 77−53215
mineral resources of Armenian territory foundation, evidence from struct. and age data *(Russian)* 79−74874
Mini-Sosie high resolution seismic reflection system, operational principles 78−85707
mining and prospecting research, examples of mineraology contrib. *(French)* 79−5475
Miocene sediments, Carpathian Foreland, statistical anal. of repeated borehole meas. 78−49146
N.Morocco, geomag. vars. recording, cond. anomaly existence *(French)* 77−86755
Mossbauer gravimeter 77−37444
multispectral aerial photography, Khomas Trough region gossaniferous outcrop identification 77−5346
multispectral aerial photography, rock type identification in NW Cape Province, S.Africa 77−5345
natural gas in permafrost and speed of longitudinal sound in clathrate hydrates 80−88275
natural radioactive series, secular equilib. investigation method 79−2381
natural resource determ. from weather satellite TV images 77−70876
near-borehole elastic wave linear velocimeter *(Russian)* 77−60492
Neumann problem for potential in toroidal coords. for axial symmetry 77−64182
neutron borehole measurements, rock density effects *(Russian)* 79−88500
Newfoundland, offshore oil and gas production, associated problems 79−87946
NMR logging, probe polarization field *(Russian)* 77−87120
normal moveout difference curve improvement 77−17225
nuclear and acoustic logger for cased well and open hole studies 77−87098
nuclear borehole logging system 79−25353
nuclear geophysical methods, geometric factor *(Russian)* 77−87121
nuclear oil well logging using 14 MeV neutron-excited gamma-ray spectrometry 79−48581
nuclear raw materials prospecting, isotopic dating methods *(Russian)* 79−30925
nuclear techniques in exploration for energy related minerals and metal ores 77−37438
ocean bottom, underwater towed EM source for geophysical exploration 79−74971
offshore seismic refraction surveying, nonexplosive energy sources *(Russian)* 78−53752
oil, exploration and exploitation instrumentation 79−34982
oil, new seismic reflection techniques 78−73541
oil and gas, geophysical exploration forecasting up to year 2000 *(Russian)* 77−87122
oil and gas exploration, information content of geochem. parameters *(Russian)* 79−39957
oil and gas formations, prediction prior to drilling *(Russian)* 79−39970
oil and gas in non-anticlinal traps, reflected wave seismic survey possibilities *(Russian)* 78−12013
oil and gas well profiles, appl. of combined well-logging techniques *(Russian)* 78−40705

geophysical prospecting continued
oil and gas-bearing sites, mathematical selection methods *(Russian)* 77−9560
oil deposits rel. to sea ice chemistry 79−12128
oil exploration, seismic appls. 78−96151
oil exploration seismic data processing, white noise estimators 78−3973
oil field data, fast processing *(Russian)* 79−84540
oil well productivity rel. to seismic reflection amplitude 78−69295
oil-gas province basement, gravity field studies *(Russian)* 80−85759
Oklo fossil nuclear reactors, ion analysis exam. of U grains and gangue *(French)* 80−21758
Oklo natural fission reactors, geophysical eval. of U distrib., topography, sedimentology and structure *(French)* 80−21755
Oklo natural fission reactors, U radiometric meas. and isotopic anal. *(French)* 80−21754
Oklo natural reactors, mining, geology and tectonics *(French)* 80−21743
ore analysis by selective gamma-gamma method, elimination of geometrical effects 78−44425
ore body, mag. survey of Itapicuru greenstone belt, Bahia, Brazil 80−81879
ore body distrib. in Baisoara mine, gravity anomaly data *(Rumanian)* 78−20347
ore body total mass and coords. determ. from gravimetric anomaly *(Russian)* 77−86746
ore reserve estimation, in three-dimensional deposite using FORTRAN IV Function Segment 77−87085
orebodies location in mineworkings, muon hodoscope appl. 79−84491
orogenic regions deep crustal probing by natural EM fields surface impedance vars. 77−13060
pegmatite ores in Tanco mine area, SE.Manitoba, in Canada, exploration methods 79−48577
penetration zone shaping, numerical soln. *(Russian)* 79−39958
permafrost discontinuity geometry and physical props. determ., Schefferville, Canada *(French)* 77−66990
permafrost fossil patterns, S.W. Ontario, resistivity mapping 77−66991
permafrost thickness determ. in wells in N. Canada 77−66989
petroleum, digital recording of ultrasonic signals [petroleum prospecting] 78−73552
petroleum deposits, screening effect on seismic exploration *(Russian)* 77−44939
petroleum deposits and gas wells, prospecting in W.Caspian Sea area *(Russian)* 77−64281
petroleum exploration, implementation guidelines for promotion of electronics in oil and gas sector 79−80039
petroleum exploration, marine seismic data for detrital sediments 78−96303
petroleum gravimetric prospecting, effect of isostatic anomalies *(Spanish)* 77−9319
petroleum traps, synthetic seismic sections 79−53311
phosphates, U content, α-ray autoradiography, fluorimetry, estimation 78−20414
polarisable half-space, current pulses, transient EM field 78−96130
potential field data, interpretation using information theory and cybernetics 77−73861
potential field data interpretation, generalized matrix inversion method 77−87087
potential fields due to vertical circular cylinder and dike, statistical anal. 79−34972
Precambrian Fe formations, Schefferville, Canada, vertical mag. contouring 77−64495
Preslav anticline, oil and gas prospecting data anlaysis *(Russian)* 78−32085
pseudobaseband pulse radar 78−24398
pulse excitation for EM freq. sounding 77−81793
pulse neutron logging, quantitative information analysis *(Russian)* 79−84541
pulsed gamma-ray method for rocks density determ. theory *(Russian)* 79−39956
pulsed-neutron U logging, probing distance determ. 77−64476
Quebec, heat flow data anal., borehole obs. in small area 77−81846
radar symposium, London (Oct. 1977) 78−24395
radiation and isotopes appl., development trends 78−55041
radioactive element conc. from γ-ray intensity meas., numerical method 79−18059
radioactive logging, inverse case, regularisation technique *(Russian)* 79−88501
radioactive minerals, thermoluminescence radiation dosimetry appl. 78−32244
radioactive ores, specific sensitivity of NaI(Tl) scintillator in γ-ray meas. 78−81449
radiometric exploration meas. standardisation advantages and methods 78−28325
radiometry diagrams, statistical standardisation check *(Russian)* 78−69483
radionuclide survey of USA, ERDA aerial radiometric and magnetic survey 78−12027
Raft River geothermal area, Idaho, seismic refr. study 80−3963
ray theoretical seismograms, construction methods 79−34761
redox logging for minerals, model studies 77−64466
reflected and transmitted filter functions for simple subsurface geometries 77−44924
reflection seismic exploration, data processing requirements 78−96325
reflection seismic method for Silurian reef detect. in N.Michigan 77−2265
reflection seismic recordings, minimum entropy deconvolution 78−81423
reflection seismology, tool for energy resource exploration, book 78−96162
reflection seismology, use of kepstrum in signal anal. 78−81425
reflection seismology, wavefront synthesis for vel. estimation and downward continuation 79−16392
regional resource appraisal, statistical methods 78−28326
regularization method and uniqueness problems in study of regional flat-layered structs. 78−49161
regularization method in mag. and gravity anomalies interpretation 78−49163
Reis crater, struct. from geoelec. Schlumberger soundings *(German)* 77−64207
remote sensing, appls. of technology 77−5349
remote sensing, principles and interpretation, book 79−12319
remote sensing by artificial satellites *(Japanese)* 78−16211

geophysical prospecting continued
remote sensing of Earth's resources using satellites, review of techniques 79−16714
remote sensing surveys in geologic exploration 77−56631
residual Bouguer anomalies, line masses depth estimation via Backus-Gilbert min. distance criterion 79−44257
resistance logging, continued fractions method appls. *(Russian)* 78−3971
resistance method, oil-gas field appl. *(Russian)* 79−20749
resistive/conductive beds, limiting detection depth in line electrode systems 78−44760
resistivity and induced polarization, modified pseudosection 78−7562
resistivity and induced polarization modelling using buried electrodes 78−11802
resistivity curves, finite difference evaluation method 80−89937
resistivity curves of horizontally multilayered models, calc. methods 80−46283
resistivity finite-difference modelling, practical approach 79−29878
resistivity interp., application of rules of composition 77−64194
resistivity logging, direct problem soln. using graphic display *(Russian)* 78−69481
resistivity logging tool response, sonde position effect 77−86759
resistivity logging using ring probes *(Russian)* 77−86778
resistivity mapping using airborne multicoil EM survey system 78−77348
resistivity modelling for arbitrarily shaped three-dimens. structs. 80−3920
resistivity probing of exponential Earth with homogeneous overburden 77−49180
resistivity profiles, electrode arrangement comparison 79−88486
resistivity prospecting, use of signal contrib. sections 80−21836
resistivity response of buried cables 79−92483
resistivity sounding, buried electrode data interpretation using layered Earth model 79−29701
resistivity sounding, computer program for related Hankel transforms numerical integration 79−92599
resistivity sounding, dipole to Schlumberger curve transformation by digital linear filters 78−45015
resistivity sounding, direct interpretation, developments 77−9530
resistivity sounding, interpretation, descending and ascending methods 79−66810
resistivity sounding, technique for obs. crustal dilatancy prior to earthquakes 79−92609
resistivity sounding by bipole-dipole method, theory 80−101450
resistivity sounding data, numerical anal., multi-vertical Earth model 77−70597
resistivity sounding interpretation, approx. method 77−41185
resistivity sounding interpretation without borehole control 77−9328
resistivity sounding master curves, rapid computation 80−51560
resistivity sounding on multi-layered Earth with transitional layers, theory 78−40475
resistivity sounding on multilayered Earth with transitional layers, examples 78−69282
resistivity sounding over transition layer model, comments 77−40978
resistivity soundings, detect. of underground cavities, rel. to hydrogeology *(Italian)* 77−86758
resistivity soundings over horizontal strata, man/computer interpretation system 78−45014
resistivity survey, noise elimination, fluctuating Earth currents 79−92480
resistivity surveying, apparatus, interpretation, undergrad. fieldwork 78−49623
resistivity surveys for study of coastal aquifers, Bahia, Brazil 79−57977
resource potential, geochemical surveys of large areas in USA and Alaska 79−30924
river bottom sediments, in situ neutron activation anal. appl. 77−87115
rock elastic wave absorption meas. and recording instrument *(Russian)* 79−29891
rotating current dipole method, field test 77−87094
Rumania, geothermal gradients rel. to hydrocarbon deposits *(Rumanian)* 77−29266
salt, seismic prospecting by well logging *(Rumanian)* 78−20566
salt mines, radar propag. in rock salt 78−96215
Salton Sea geothermal area, California, temp. gradients, onshore and offshore meas. 80−3962
seafloor petroliferous structures, results from surface geothermal survey *(Russian)* 78−40527
sedimentary rocks containing water and oil, dielectric constant and losses *(Russian)* 79−20747
seismic cross sounding, data interpretation via reflected wave method *(Russian)* 78−92796
seismic data, common depth point ray modelling for three dimensional isovelocity layers 77−21914
seismic data deconvolution 78−53736
seismic data processing, Karhunen-Loeve transform. appl. *(French)* 79−44258
seismic data processing, predictive deconvolution method appl. 79−8725
seismic data processing, predictive dynamic deconvolution *(Rumanian)* 80−8454
seismic data teleprocessing global network 77−29255
seismic depth section, algorithm for tracing horizons *(Russian)* 77−66891
seismic detonation of buried source, ground vibrations 77−73667
seismic digital processing techniques for petroleum and natural gas 77−29469
seismic exploration, deep refls. unravelling via seismic stripping 79−34970
seismic exploration, effect of multiple scatt. on wave field spectral comp. *(Russian)* 79−8607
seismic exploration, elastic wave source and receiver grouping *(Russian)* 77−9563
seismic exploration, iterative identification of non-invertible autoregressive moving-average systems 78−81422
seismic exploration, nature of arc-shaped line-ups common depth point seismic profiles *(Russian)* 79−44134
seismic exploration, peg-leg multiples and dipping reflectors 78−7580
seismic exploration, signal processing method for circular arrays 80−4123
seismic exploration, technique and processing, book 80−51975
seismic exploration, vibroseis signals with prescribed power spectrum 78−40495

geophysical prospecting continued
seismic exploration for oil and gas-bearing structures *(Russian)* 77−45195
seismic exploration problems of complicated basins, S.China appl. *(Chinese)* 79−100961
seismic holography, kinematic mutuality of reflected and refracted waves *(Russian)* 78−69298
seismic imaging by holography, techniques and appls. 79−66831
seismic profiling of Black and Azov Sea floor, methods 80−89970
seismic prospecting, common depth point vels. critical values for stratified homogeneous forms. *(Russian)* 79−39668
seismic prospecting, effect of spatial deflection during longit. obs. *(Russian)* 79−39945
seismic prospecting, far field waves definition criteria *(Russian)* 79−39965
seismic prospecting, inverse kinematic case soln. in layered Earth using reciprocal points *(Russian)* 79−44268
seismic prospecting, inversion of refl. data 77−21915
seismic prospecting, minimisation of distortion caused by geophone-ground coupling 79−44256
seismic prospecting, multiple reflected signal attenuation, least squares estimation procedure 80−85596
seismic prospecting, overlying sequence stratification effect on basement vel. determ. *(Russian)* 79−39961
seismic prospecting, signals detect. under conditions of limited information about signals and noise 77−9536
seismic prospecting problem soln. *(Russian)* 79−74859
seismic prospecting techniques for oil resources *(French, English)* 80−21362
seismic Rayleigh channel waves for reflection method, dipping coal seam discontinuity obs. 78−69471
seismic reflection data inversion 78−96307
seismic reflection method, using vertical array technique 78−36306
seismic reflection profiling on land with controlled source 77−64450
seismic refraction method, vel. determ. and error anal. 80−90229
seismic shallow refraction records, reflections from overburden-bedrock interface 77−78115
seismic signals, adaptive deconvolution 78−53737
seismic sounding, common-depth-point method, prestack migration method for deformed refl. layer 80−98251
seismic surveys, establishment of zero time 77−21916
seismic travel times in plane layered media, computation 77−41191
seismic V_p/V_s as a potential hydrocarbon indicator 77−17102
seismic velocities in geological strata with curvilinear boundaries, three-dimens. case *(Russian)* 79−39928
seismic velocity in unconsolidated sand reservoir, effect of brine-gas mixture 77−17030
seismic wave attenuation in nonresolvable cyclic stratification 78−7578
seismic wave field parameters optimal estimation *(Russian)* 78−28177
seismic waves interference effects in thin layers 78−92780
seismogram inversion and pseudo velocity logs, lithology identification 77−87088
seismogram synthesis in multilayered dissipative media 79−2382
seismograms and mutual conversion of longitudinal and surface waves 77−70610
seismology, correlation refraction method, appl. to granite terrain weathered zone 80−90230
self-potential anomalies near vertical contacts 80−3919
self-potential method in geothermal exploration 80−4125
sequential search for geophysical objects, expt. design *(German)* 77−29464
shallow-water mineral exploration by controlled-source audiomagnetotellurics and resistivity profiling 77−5356
shear wave generator in borehole, construction, expt. results 78−40692
W Sicily, mag. survey, site for geomag. observatory 77−86757
siesmic sounding, screening in media with inclined boundaries *(Russian)* 78−92794
Slatioarele-Arges salt dome, well logging evaluation *(Rumanian)* 78−20373
sounding techniques, fundamental functions for horizontally stratified Earth 77−21918
spectrometer, PbSe diode laser, for air pollution monitoring and mineral prospecting 77−82044
spectrometer for underwater gamma surveying, calibration 79−21066
spherical ore mass, interpretation of vertical anomalies 78−40476
static potential data inversion, generalized linear inverse 77−40967
stationary well quadrupole logging in layers of restricted thickness *(Polish)* 80−12556
submarine cable EM field rel. to geophysical prospecting at sea *(Russian)* 78−20557
subsoil exploration, role of electronics *(Spanish)* 78−20552
subsurface EM techniques for oil exploration 77−17263
subsurface radar for Earth's surface remote probing 79−8724
subsurface radar using video pulse for deep probing in Earth, pulse propag. in lossy media using LF window 80−74282
sulphide mineralisation in Rajasthan, and Gujarat, India, induced polarisation surveys results 79−39714
sulphide minerals, induced polarisation, decay curves theory *(German)* 79−29709
sulphide prospect in California copper belt, broadband EM study 80−72503
surface borehole and inter-borehole EM logging method *(Polish)* 77−53220
tectonic dislocations prospecting in complex media, appl. to seismic surface waves correl. method *(Russian)* 79−8605
telluric and magnetotelluric methods, comparison for sedimentary structures 78−3713
telluric anomalies caused by shallow structs., ellipsoidal approx. 77−56573
telluric current meas. in audio and subaudio freq. range, characts. 77−86760
telluric currents method for overhang bodies search *(Russian)* 79−88496
telluric profiling technique for apparent pseudo-resistivity mapping *(French)* 78−69285
temperature and pressure transducers with ground-level tape recorder, hydrodynamic logging in boreholes *(Russian)* 78−53761
temperature gradients continuous logging system 77−82052
three-frequency computational method for two-layer CFS data 79−16688
time-domain EM method, optimum pulse shape selection 77−45167
geophysical prospecting continued
transient EM fields, two-layer polarizable Earth 77−64199
transient EM prospecting using interactive minicomputer 79−62604
transient EM sounding in thin cond. layer with inhomogeneities *(Russian)* 79−84530
transient EM wave prospecting 80−76905
transient EM well-logging using vertical electric dipole *(Polish)* 80−41367
travel-time curves, theory 80−94473
truncated plate, gravity gradient determ. 77−44890
Turam method, normal values calc. *(Spanish)* 77−9551
two dimensional inhomogeneity modelling, resistivity and induced polarisation response 77−17023
two-fold resistivity mapping of lateral inhomogeneities 78−61573
underground quarries, EM detection *(French)* 78−96306
underwater towed EM source for geophys. exploration 79−5676
uraniferous materials prospecting, influence of disequilib. and ^{222}Rn amanation factor variability 79−62498
uranium exploration, photomultiplier tube, solid-state, for improved gamma counting techniques 79−54748
USSR, new oil and gas bearing regions *(Russian)* 78−32098
vector EM system, magnetic field measurements, field applications 79−84499
vertical electric sounding for salt-bearing structures *(Russian)* 78−3714
vertical electrical sounding dipole-dipole filter coeffs. 78−12006
vertical frequency effect sounding in induced polarization and galvanic resistivity methods 78−69284
vertical magnetic dipole on two-layer Earth, transient EM fields 80−76906
VLF scattering by perfectly conducting half plane below stratified overburden 78−57167
VLF surface mode propag., wave tilt meas. 80−77139
VLF-EM method, model study 77−49181
VLF-EM modelling of conductors 79−79736
water detection in volcanic region of Armenia, elec. profiling and sounding methods 80−85753
water exploration, geophysical methods, International School 1st course proc. (Erice, Italy, 1975 April 15-26) 77−9526
water resources in Africa, techniques 80−61818
wave tilt sounding of multilayered structures 80−61926
well logging, data transmission and processing *(Russian)* 79−62625
well logging, electric, geometrical factors determ. from electrostatic field successive approx. *(Chinese)* 80−105057
well logging, multiple measuring systems 79−26049
well logging data correction, shallow vel. struct. prediction *(Russian)* 77−86837
well logging with short-lived radioactive source 79−53563
well-logging for density, γ-γ log with computerised instrumentation *(Hungarian)* 80−21843
Wenner resistivity soundings, vertical contact effect 78−20541
wire loop laid on ground, radiation resistance calc., antenna for parametric depth sounding *(Chinese)* 78−61565
wire-line core barrels for exploratory drilling 80−98482
Yerington mine, Nevada, in situ induced polarisation and mag. susceptibility meas. 80−51323
Al in Fe ores and coal, nuclear activation logging 79−80042
Au deposit location in Canton Bousquet, Quebec *(French)* 77−53051
Au ores, neutron activation and mathematical programming *(Rumanian)* 78−20565
Au trace anal. with portable X-ray analyser 78−49160
Cu deposits, exploration using LANDSAT-1 imagery 79−2398
Fe ore, magnetic anomaly detect. *(Russian)* 78−16009
Fe ore deposits from gravity and magnetic anomalies, determ. accuracies *(Russian)* 79−84536
Fe ores, exploration with integrated aeroelectromagnetic and magnetic methods 79−16690
Fe ores, grade, bulk density, porosity determ. by nuclear geophysical methods 79−48570
Ge(Li) and intrinsic Ge detectors in borehole sondes for U and coal exploration 77−37442
Li, needs and resources, conf., Corning, USA (Oct. 1977) 79−48473
Mn nodule undersea mining data file, management and statistical anal. 77−53206
Rn and Th dosimetry, plastic solid state nuclear track detectors appl. 78−20556
Rn, isotope separation by barrier technique, U prospecting appl. 78−21770
Rn mapping in U exploration, exclusion of ^{220}Rn signal 80−61916
Rn, moisture insensitive monitoring using solid detectors 79−31228
^{222}Rn mapping in U exploration, use of mat to avoid hole drilling 80−82087
Th, analytical geochemical prospecting methods 80−72635
U abundance in Himalayan plants, fission track method 80−101305
U, analytical geochemical prospecting methods 80−72635
U and Th, resources and prospecting techniques and equipment development in India 79−30923
U assay in boreholes using Ge gamma spectrometers 79−53571
U borehole logging by prompt fission neutron technique, log interpretation 79−53567
U borehole logging system, delayed neutron activation anal. method using ^{252}Cf source 79−53569
U boreholes, in situ assay using prompt fission neutron technique 77−37441
U content determ. using liquid scintillation spectroms. *(Czech)* 78−69487
U deposit, Saima alkaline massif, NE China 79−16470
U deposits, Canadian Uranium Reconnaissance Program 77−37439
U deposits, in situ assay logging system using delayed fission neutrons 77−37440
U deposits in USA, genesis and exploration 79−84267
U deposits prospecting, use of ^{222}Rn content of air *(Spanish)* 77−78303
U exploration, airborne phoswich detector system 79−53576
U exploration, application of mineralisation models, British Isles 79−84273
U exploration, borehole probe with LED for γ-ray spectrum stabilisation 79−45552
U exploration, delayed fission neutron and prompt fission neutron logging, comparison of predicted signals 79−39879
U exploration, intrinsic Ge detector for use in borehole sonde 77−9547
U exploration, LANDSAT data merged with geol. and geophysics data 80−56651

geophysical prospecting continued
U exploration, meas. of ^{222}Rn concs. in Earth using nuclear track technique 79−53574
U exploration, pattern recognition appl. 77−66999
U exploration, prompt fission neutron logging technique, computer modelling 79−53566
U exploration, radiation transport anal. for borehole logging probes 79−53565
U exploration, via Rn long-distance migration in Earth, subterrestrial fluid convection hypothesis 77−37246
U exploration and assay, nuclear methods 77−41228
U, exploration and assessment technology survey 79−53564
U, exploration and evaluation techniques for ore bodies 79−26536
U exploration and international cooperation 78−86628
U, exploration and prospecting methods 80−85768
U, exploration in Australia, Alligator Rivers Uranium Province 79−30922
U, exploration in Australia 79−48471
U exploration in Egypt, exploration under arid conditions 79−26538
U exploration of the Oklo natural fission reactors, review *(French)* 80−21753
U exploration probes, meas. spatial depend. of delayed neutron signals 79−34989
U exploration with computer-processed LANDSAT data 78−7777
U exploration with electronic alpha cups 78−7781
U, geochemistry of inclosure radioactivity 80−85766
U in geological samples, rapid determ. using X-ray fluorescence anal. methods 79−88479
U in natural waters, field meas. technique 78−85705
U in rock samples, meas. by track registration in plastic detectors 78−73533
U, in situ mining, Wyoming State regulations and environmental monitoring 79−88510
U logging by prompt fission neutrons, effect of neutron-absorbing rock anal. 77−64477
U, modern prospecting techniques evaluation, Athabaska sandstone deposits 79−26537
U, nature and exploration in US sandstone deposits, educational module 80−36799
U ore assaying by delayed fission neutron process 79−53536
U ore bodies ground level radiometric surveys, overburden effects correction techniques 79−88485
U ore deposits, review of methods of prospecting *(German, English)* 77−21925
U ore deposits, sulphide-free, unusual mineral assocs. in oxidation zone 77−25682
U ore detection, Rn gas cencentration meas. using alpha sensitive plastic detectors 80−94617
U ore detection, using trace detection sensitive to ^{222}Rn α-particles *(Hungarian)* 78−77339
U ore detection using integrated meas. of long-distance transport of ^{220}Rn 80−98476
U ore exploration, Rn gas conc. meas. using alpha sensitive plastic films 80−94618
U ore grade direct determ. by photoneutron assay method 79−53570
U ore zone logging, corrections for prompt fission neutron data 79−88353
U ores, integrated Rn emanation mapping for gases long-distance migration detect. 78−85560
U prospecting, ^{222}Rn and ^{210}Pb meas. 79−53573
U prospecting, airborne radiometric meas., ground conc. estimation 79−53575
U, prospecting at exploratory borehole, spatial depend. of delayed-neutron signals 78−7817
U, prospecting by active neutron logging, evaluation models 80−98480
U prospecting by γ-ray logging of borehole, factors affecting resolution 80−98463
U prospecting using microdistrib. anal. of Siwalik vertebrate fossils by nuclear Track Etch tech. 80−98489
U pulsed neutron logging, minimisation of neutron absorber effects 77−37446
U, quantitative determs. from gamma-ray logs, digital time series analysis 79−48580
U redistribution and mobility during metamorphism of volcanogenic formations 77−64283
U reserves, technological status 77−34398
U resource evaluation by neutron activation anal. 78−85741
U, sandstone-type ores, charged particle track analysis 80−91405
U, solution mining, in situ leach method 79−87983
U, solution mining facilities, operational and environmental aspects 79−87984
U well logging, gamma-ray spectra calc. using discrete ordinates transport code 79−53572
U/Th prospecting, use of alpha sensitive plastic films 79−39980
U-bearing rocks, radioactive disequilib. determ., isotopes relative abundance meas. 78−57330
^{235}U/^{238}U ratio, non-destructive field meas. for geophysical prospecting 80−21862
^{235}U-fission track micromapping, exam. of U mobilisation processes in Precombrian sediments 80−98477
^{238}U concentration in ore, absolute determ. by gamma-ray spectroscopy 77−13133

geophysical techniques
see also atmospheric techniques; hydrological techniques; ionospheric techniques; oceanographic techniques
acoustic holography applied to seismic data processing 80−46268
acoustic log primary signals recording, synchronous orthogonal detect. appl. *(Russian)* 79−88498
acoustic logging, signals limited spectrum rel. to time interval and damping determ. accuracy *(Russian)* 79−39971
acoustic logging data, on-line computer interpretation techniques 80−90239
acoustic logging data averaging for seismic wave fields *(Russian)* 77−73673
acoustic logging in cased wells, effect of excited wave freq. on results *(Russian)* 78−40707
acoustic microscopy of sedimentary rock samples 79−12292
acoustic signal mean frequency meas. *(Russian)* 78−81441
actinide abundance determ. for rocks using NaI detectors 79−80043
active faults, aerial photographs interpretation *(Japanese)* 78−96124

geophysical techniques continued
active microwave sensing of Earth surface *(Japanese)* 78−16214
active remote sensing with radar, radiative transfer theory, half-space random media appl. 79−8721
adaptive deconvolution, processing technique for time-varying seismic data 77−91287
adaptive deconvolution of seismic signals 78−53737
adaptive predictive deconvolution of nonstationary seismic data 77−87096
aerial photography, high altitude, aspects and results 78−36309
aerial photography, multispectral, soil survey in New Zealand 78−85728
aerial photography for densification of urban geodetic nets 77−78462
aerial reconnaissance film interrogation by optical matched filtering 77−78484
aerial triangulation, bridging with independent horizontal control 79−25184
aeromagnetic anomaly from remanently magnetised Precambrian schist belt, Karnataka, India harmonic inversion 79−44094
aeromagnetic control network construction in USSR, metric principles 77−21676
aeromagnetic data, diurnal drift removal by least squares 79−53529
aeromagnetic data from different times with varying specifications, integration method 80−4127
aeromagnetic survey of sedimentary cover thickness, using 1-D spectral anal. 80−77138
aerotriangulation by Skylab Earth terrain camera photography 77−33209
aftershocks prediction, implications of dilatancy-fluid diffusion theory 80−85604
air pollution detection, X-ray fluorescence spectroscopy, proton induced 77−36831
air survey methods *(Dutch)* 78−3972
airborne EM mapping, aircraft altitude and displacement currents effects 77−52975
airborne gamma-ray spectrometry data processing using multivariable statistical analysis 79−35004
airborne gravimetry, topographic corrections for gradients 77−40966
airborne radiometric data inversion, radioactive elements conc. mapping 78−77347
airborne radiometry, statistical noise reduction 77−17220
airphoto interpretation, teaching using computer 79−48999
altimetric data file acquisition automatic digital correlation method 78−61633
American Society of Photogrammetry Annual Convention, Washington, USA (March 1978) 80−4149
ancient geomagnetic field intensity, early research 77−37131
ancient magnetic field intensity determ. by nonthermal method 77−52980
anisotropic seismic surface-wave dispersion, isotropic inversion significance 78−96156
anomalies of mag. and gravity field, anal. by unitary method 80−89932
anomaly detection, FORTRAN IV programs for statistical method appl. *(Rumanian)* 77−41214
anomaly source models, statistical parameters rel. to pot. fields obtained by superposition *(German)* 79−34783
Antarctic bedrock mapping, using radar *(German)* 77−56770
antenna two-element array, insulated, in relatively dense medium 77−25794
apparent resistivity of perfectly cond. sphere buried in half-space, calc. 77−2269
AR method for seismic moment calcs. WWSSN instrument appl. 80−21828
archaeomagnetic field magnitude meas., combined thermal and alternating field demagnetisation 79−74830
array algebra appls. 79−44702
array algebra for multilinear least squares prediction and filtering 78−69470
array algebra techniques in multilinear least squares problems 78−36296
artificial satellite systems for Earth gravity field meas. 79−53298
asbestos fibres identification, electron microscope techniques comparison 78−66012
astronomical latitude, azimuth and longitude, simultaneous determ. method 77−60339
asymmetric bilateral rupture process anal. method *(Chinese)* 80−76911
atmosphere and Earth's surface photometric charcts-observation and recording *(Russian)* 77−5412
atmosphere visibility trends, appl. of ridit anal. 80−82051
ATS-6 electron content data presentation 78−61593
Australian magnetic observatories 80−72632
automated shipboard acquisition and processing of offshore geophys. data *(Russian)* 78−53750
automatic contouring of faulted subsurfaces 77−45170
automatic contouring of geological data, review 78−7820
autoregression order selection 77−2270
autoregressive spectral estimates, geophysical applications 77−29471
autoregressive technique, appl. to astronomy and geodynamics *(Chinese)* 80−85869
basaltic bodies, flow and emplacement direction from mag. susceptibility anisotropy meas. 79−29766
basaltic magmas classification, use of Ti, Zr, Y, Sr, K, P and Nb distribs. 77−5150
basalts petrology, from crystallised silicate melt and other inclusions in olivine 77−2146
basement rock type determ. using magnetic anomalies 77−45166
bicubic spline interpolation for aeromagnetic surveys 80−17405
binary seismic holography, kinematic principle *(Russian)* 78−92795
Bingham distrib. function in palaeomagnetic studies 80−72649
biostratigraphic data quantification 79−62593
biostratigraphical logging methods 79−62594
biostratigraphy methods, comparison 79−62502
biotite+apatite geothermometer, re-examination 78−85704
Black Sea continental platform, seismic prospecting method appl. *(Rumanian)* 78−20564
blind zone problem with multiple refraction layer overburden, soln. 80−17241
block tectonics analysis in Mongolia, appl. of two-dimensional autocorrelation anal. 80−56469
body wave seismograms, simple computational method 79−84492
body-wave seismograms synthesis, modified first motion approximation 78−73315
borehole acoustic logging, calc. of transient acoustic waveform 80−72640

geophysical techniques continued
borehole acoustic velocity measurement system, within or between boreholes 80−51557
borehole EM wave exploration, digital holography technique appl. *(Chinese)* 80−82080
borehole logging, minicomputer appl. *(Russian)* 79−84538
Bouguer regional anomalies reduction, appl. to deep geological struct. study *(Russian)* 78−48958
Bremmer series decomposition of solns. to lossless wave eqn. in layered media 78−53738
Burg maximum entropy method, possible instability 79−80045
cadastral survey administration, Bavaria, centralised and decentralised data processing *(German)* 77−2288
calibration of remote sensors by time averaging *(Russian)* 77−78452
carbonate mineral identification by CO_2 evolution on heating 80−90248
cartography, point transfer error determ. 80−17227
cartography, use of electronically controlled drawing machines *(German)* 78−20348
cartography development of present 1:500000 map of Bavaria *(German)* 77−2081
cartography stereomapping processes 78−61631
catastrophic earthquakes prediction, development monitoring via seismic b-value time and space scanning *(Chinese)* 79−12072
cavity radius estimation for contained nuclear explosions 79−16712
cavity research with geoelectrical resistivity methods, theoretical and exptl. investigations 80−56625
chamber methods for soil gas fluxes determ., numerical evaluation 79−16700
charged particle track analysis of sandstone-type U ore 80−91405
chemical demagnetisation for red sandstones 80−26620
chemical microanalysis of geological samples by X-ray microscopy near absorption edge with synchrotron radiation 78−20527
classifier model for multi-observational anal. 77−78533
clay bed, slope form and bedding dip correl., computer calc. *(German)* 77−64282
clay layer, non-homogeneous, consolidation estimation method 79−58110
climatology, statistical methods *(French)* 78−32252
coal basin evaluation, appl. of gravity profile across Bonnet Plume Basin, Yukon Territory, Canada 80−76898
coal fields of India, seam thickness by elec. and γ-logging 80−51394
coal formations seismic tracing, interference waves appl. *(Russian)* 79−74858
coal layer thickness meas., EM technique 78−53740
coal prospecting by seismic profiling, new technique testing 80−17404
coal research, appl. of neutron activation anal. 78−85740
coal seam, gasified, burn front monitoring via EM refls. 77−41212
coal seam mapping using electrical resistivity methods 80−4133
coastal geomorphology from satellite imagery, appl. to Bermuda 79−5470
color map automatic digitisation, spectral classification scanner technique 80−17424
common depth point survey data, vel. characts. determ., refl. interfaces inclination angles *(Russian)* 78−53753
common depth point survey technique appl. in permafrost conditions *(Russian)* 78−53751
complex demodulation for nonstationary data anal. *(French)* 79−70922
complex materials, charged particle anal., range effect corrections, geological material appl. 77−48738
composite optential fields in three-dimensional space, singular points numerical characts. determ. *(Russian)* 79−96833
composite processing, appl. to reflected wave complex spectra *(Russian)* 79−84531
computation nets, significance in increasing efficiency of geologo-geophysical research 79−96835
computation of theoretical seismograms for arbitrary shaped fault 77−9373
computer 3-dimens. plotting, irregular to regular grid data conversion 77−5328
computer-aided seismic anal. and discrimination 77−81815
conductivity determ. using single superconducting coil 77−41184
conductivity model, three-dimens., perturb. and induction arrows calc. 77−73633
contact surface parameters determ., regularisation method *(Russian)* 78−53756
contacting surface depth and shape determ., random and sytematic errors *(Russian)* 79−39935
continental plates pre-Tertiary velocities from palaeomag. data 80−21848
continental shelf, possibility of geoelec. mapping 78−57341
convolution product, deconvolution problem *(French)* 79−44275
coring and squeezing technique for study of subsurface water chem. 78−57332
coring method for lake surface sediments 77−9520
corrective gradient projection method applied to seismic array processing 77−17222
correlation analysis of geophysical fields, input conditions *(German)* 79−35014
correlation analysis of global potential fields *(German)* 77−29466
correlation function anal. of geomag. field reversals 80−21622
correlation theory, use of quantiles 77−91291
counter-orbiting polar satellites, geodesy information in modified relativity mission 79−62426
coupled solid/fluid/surface wave dynamic interaction problem, improved fluid superelement 78−81108
coupled vector systems of nonlinear parabolic partial differential eqns., soln., geophys. appl. 77−41468
criterion matrices, appl. to design of homogeneous isotropic geodetic networks *(German)* 79−100983
crop classification from Landsat data, pattern recognition, temporal trend analysis 78−65440
cross-borehole EM probing, location of high-contrast anomaly 80−72639
crust and upper mantle global density determ. by terrestrial and satellite gravity obs. 79−62592
crust deep structure, determ. via nearby earthquakes converted seismic waves 80−30999
crustal deformation analysis, models for estimation of parameters *(German)* 80−101319
crustal motions detect. using spaceborne laser ranging systems 78−92995
crustal movements, recent, estimation, geodetic obs. goodness concept restatement 79−57840
geophysical techniques continued
crustal radiogenic heat production, depth depend. modelling by variational approach 80−72464
crustal rise meas., methods used since 1895 in Rumania *(Rumanian)* 80−8281
crustal stress meas. limits 79−48588
crustal struct. from seismic response of local earthquakes, appl. in Lipari, Eolian Islands 78−40494
crustal structure, investigation via seismic reverberation 79−66820
crustal structure determ. from Rayleigh wave signature, Nevada Test Site (NTS) explosions appl. 79−66632
crustal structure determ. method for San Andreas fault system 77−91284
crustal structure estimation from acoustic reflection meas., Cramer-Rao bound 77−5369
crustal structure modelling using teleseismic body-wave conversions 77−91283
crustal vertical movement detection, noise reduction in sea-level records 79−2395
cubic spline approximation method for inaccurate r.m.s. velocity data 80−17406
damped and constrained least squares method with application to gravity interpretation 79−66830
data acquisition, analysis and display from Geostationary Operational Environmental Satellite 80−17382
data analysis, freq. estimator of truncated real sinusoids 80−73161
data analysis, interpretive patterns, influence of meas. noise and meas. device accuracy 80−90235
data analysis, random values separation *(Russian)* 79−74983
data analysis by collocation method 80−77130
data analysis of multivariate data set, canonical anal. 80−73333
data interpretation of acoustic wave log *(Russian)* 79−84539
data inversion from diffraction-limited multiwavelength remote sensing 79−39976
data logger, portable, for ground surveys 80−26615
data processing, underground mapping reflection seismic method 78−96325
data processing optical system with randomly misaligned parameters, geophys. fields anal. *(Russian)* 79−84524
data reduction, detrending and smoothing of random data 80−67425
data upward and downward continuation as inverse problems 79−44262
dating, use of $CaSO_4$:Dy photostimulated thermolum. for high-exposure dosimetry 77−9262
dating methods using thermoluminescence *(German)* 80−105076
dating techniques, effects of thermal annealing on track etching rate of sphene, $CaTiSiO_5$ 78−65435
dating techniques from weathering, applied to Sierra Nevada, California, glacial deposits 80−8451
dating using ESR *(Japanese)* 79−48437
DC resistivity measurements, interpretation 79−5449
DC resistivity modelling for axially symmetric bodies, finite element method appl. 79−5445
DC resistivity sounding method, appl. to evaluation of non-uniform water-bearing formation 78−40474
deconvolution in freq. domain using self-matching filter 78−69477
deconvolution of borehole temp. gradient logs 77−91288
deconvolution of seismic data using homomorphic filtering 77−81823
deep magnetic-variation sounding, geoelectric and geothermal interpretation of results 78−44765
deep magnetotelluric sounding, model of geoelectric section 78−44768
deep magnetotelluric sounding, surface geoelectric section effects *(Russian)* 80−85588
deep magnetovariation sounding curves, resolution of elec. cond. model parameters 79−53300
deep sea cores sedimentation rates determ. by fission/alpha track counting 78−61392
deep seismic data processing, digital techniques appl. *(Italian)* 78−40719
deep seismic sounding and gramimetry, combined data interpretation 80−21845
deep seismic sounding for studying seismic anisotropy of crust and upper mantle 77−70855
deep-sea basalts groups, identification from clinopyroxenes statistical anal. 80−41437
deep-sea cores, ^{231}Pa dating via ^{227}Th counting 78−32238
deformation meas. of crustal movements *(German)* 77−33220
deformed rocks solid-body rot., determ. using natural indicators 79−79842
density logging, influence of standard material comp. on readings *(Russian)* 79−74989
depth determ. from seismic refraction data, iterative method 78−96302
depth sections from seismic time sections, regulated directional reception method *(Russian)* 77−45192
desert environment mapping and monitoring, worldwide 77−78489
deterministic signals spectral anal., comparison of max. entropy method and nonrecursive technique 79−58112
dielectric permittivity determ., water saturation effects *(Russian)* 79−62626
dielectric relaxation measurement of ice and rocks, blocking layer method 80−103914
differential geomagnetic sounding 77−53225
differential thermal analysis, appl. to irradiated materials 79−62484
differentiation, construction of accurate approximation to first derivative *(Russian)* 77−9873
digital, seismic recordings, dynamic range compression *(Russian)* 79−39930
digital correlation of complex exponentiated data *(German)* 79−44279
digital data compositon for satellite and radar imagery 80−67413
digital filters for long and short period seismic signal extraction from noise 77−81824
digital generation of accurate synthetic seismograms 80−85779
digital image anal. for natural resources inventories 78−96326
digital image processing for resources monitoring 78−96328
digital image processing techniques for planetary program and Earth resources information 78−96408
digital orthophoto production using scanning microdensitometers 80−41571
digital recording and anal. of broadband seismic data at Graefenberg array 79−25348
digital seismic data processing, struct. anal. of graphs *(Russian)* 78−53749

geophysical techniques continued
digital seismic prospecting, in oil and gas bearing provinces of Ukrainian SSR 79−96836
digital signal modelling and classification with the teleseismic data 78−73325
digital signal processing appls. to seismology 79−29915
digital stereo mapping, flexible algorithm 79−84543
digital thermal inertia image construction and interpetation 78−4001
digital thermal IR scanner data temporal correlatibility 77−78525
digital time-domain finite length filter, exact wave-shaping 77−2266
dike burial depth estimation by mag. palaeogeobarometric method 80−98220
dip selective migration vel. determ. 77−41187
dipole electric sounding method and application to Tuscany geothermal area 80−97762
dipole electrical soundings, perpendicular, numerical procedure for direct interpretation 79−34732
dipole soundings data obtained along crooked line, transform. 79−44259
directional data sets, axial asymmetry 80−21851
discrete design 80−200
dispersion staining method for refr. index meas. of a thin crystal section 80−8433
distance measurement, electro-optical nonperiodic errors rel. to use of plane mirrors *(German)* 77−9324
distance measurement, multi-wavelength instrument 77−29484
diving waves in multilayered medium, time-distance curve transformation 78−69472
Dnieper-Donets depression, sedimentary cover struct. determ. by seismic common depth point method *(Russian)* 78−92806
Duhamel's integral numerical evaluation, earthquakes response spectra calc. appl. 79−21035
dyke injection direction determination, new criterion based on wall minerals ang. relations 79−79843
dynamic fracture strength of oil shale, expt. determ. method 79−48584
dynamic spectra of non-stationary signals, operator calculus appl. 79−35002
Earth, planetary dynamics obs. by satellite geodesy 77−81785
Earth's resistivity determination, by surface meas. 78−24393
Earth conductivities, mapping via multifreq. airborne EM system 79−5446
Earth crust, dielectric const. determ. from rocks elec. parameters correl. at high temps. *(Russian)* 79−8628
Earth crust and upper mantle structure, experimental study by converted waves *(Chinese)* 79−12093
Earth crust in situ stress field, determ. via hydrofracturing, fracture mechanics approach 78−81435
Earth crust investigation, gravity and seismic methods combined appl. *(Russian)* 79−74987
Earth crust Recent vertical movements, four-dimensional modelling and appl. to S.California uplift 79−80055
Earth crust stress changes, in situ monitoring 79−29884
Earth crust stress measurement by overcoring, diagnostic stress-relief curves 79−29886
Earth crust vertical movements, computer-generated time-space domain presentation 79−80056
Earth electrical parameters, determination from horizontal antennas input impedance meas. 80−90259
Earth free oscillation data inversion, asymptotic approach 79−92624
Earth free oscillations, interpretation of unresolved split normal mode multiplets spectra 79−74845
Earth gravity field anomalies sources, depths determ. 79−16366
Earth interior density distrib., determ. from gravity logging data *(Russian)* 78−92999
Earth interior exploration, via seismic body waves focused at epicentre antipode 79−16399
Earth interior mass distributions, modelling by gravimagnetic fields 79−96750
Earth interior Q-structure, determ. from seismic pulse rise time 80−72438
Earth mantle, exploration via oceanic Sa seismic waves 77−73670
Earth resource thermal imaging by airborne system, possible LED use 78−93010
Earth resources rocket, enriched air propulsion system 77−2259
Earth resources satellite data information processing *(French)* 79−53526
Earth resources sensing, LANDSAT system features 78−96330
Earth strain measurement, He-Ne I_2 stabilised laser reliability as interferometer source 80−106545
Earth structure seismic investigation, new methods using common-point obs. *(Russian)* 79−74981
Earth surveying 79−100805
Earth tide information from counter-orbiting polar satellites 77−2083
Earth tide obs., meteorological wave separation method *(Russian)* 78−4014
Earth tide observations processing, individual monthly sets weightings *(Russian)* 78−88789
Earth tide recorder photoelec. compensation method to acquire data 80−77129
Earth tides measurement, cavity effect in tunnels of various cross-sections *(Russian)* 78−88784
Earth tides observations, monthly data set anal. *(Russian)* 78−88786
Earth tremors true velocities, determ. from seismograms 79−96743
earthquake acceleration hazard map, sensitivity to input seismic parameters 79−44111
earthquake accelerograms, spectrum compatible, generation method 80−3933
earthquake ages, determ. in central Asia via lichenometry 79−92505
earthquake coordinates determ. using Mir-1 computer of Urgent Reports Service 77−78440
earthquake detectability, estimates for 478 globally distributed seismograph stations 78−15976
earthquake epicentre determ. using P-wave arrival-time differences 80−101328
earthquake fault plane soln. optimum search procedure using wave-amplitude data 78−45011
earthquake focal depth determ. from long-period P-waves signal characts. 77−9355
earthquake focal depth determ. using Rayleigh surface waves, principal mode and harmonics obs. 78−61351
earthquake focal depth determination method 80−56389
geophysical techniques continued
earthquake foci motion, typification technique, seismotectonic problems soln. 78−61350
earthquake foreshocks, differentiation from earthquake swarms via seismic waveform variability *(Japanese)* 80−67342
earthquake frequencies, stochastic modelling *(Japanese)* 80−94480
earthquake hypocentres inverse problem soln. for local tridimensional network *(French)* 77−56738
earthquake information processing 77−73856
earthquake local magnitude determ. from strong-motion accelerograms 79−12290
earthquake magnitude calc. method for seismograph recordings during early 20th century *(Italian)* 79−84118
earthquake magnitude determ. using undamped seismographs, appl. to Japanese earthquakes (1901 to 1925) *(Japanese)* 80−94484
earthquake magnitude determination, body wave anal. 80−4139
earthquake magnitudes determ. from longit. core waves *(German)* 77−70603
earthquake maximum ground acceleration determ. using overturned gravestones *(Japanese)* 80−101453
earthquake observation techniques *(Japanese)* 78−28340
earthquake pair technique for surface waves to study Rekyjanes Ridge crest study 80−90021
earthquake parameter determ. computer technique *(Chinese)* 80−77126
earthquake precursory changes of He in soil, daily variation limitations 80−94469
earthquake prediction, biosystem behaviour as precursor 79−39673
earthquake prediction, bursts of aftershocks as strong earthquakes long-term precursors 80−41406
earthquake prediction, changes in short-period geomag., vars. before 1972 Sitka, Alaska, earthquake 80−76923
earthquake prediction, electrokinetic and magnetic anomalies associated with dilatant regions in a layered Earth 79−39658
earthquake prediction, fault-plane solns. for microearthquakes preceding Hollister, California earthquake 80−3936
earthquake prediction, foreshock activity of 1971 San Fernando earthquake, California 79−66626
earthquake prediction, foreshocks charact. rel. to premonitory slip on faults 80−3944
earthquake prediction, from micro-earthquake obs. near Wakayama city, Kii Peninsula, Central Japan 80−31001
earthquake prediction, geomag. investigations in Middle Asia seismoactive regions 80−26464
earthquake prediction, implications of energy release statistics in and near Japan (1915 to 1978) 80−94471
earthquake prediction, implications of tectonomagnetic studies in Tajikistan 80−26446
earthquake prediction, long-range forecasting via precursor swarm 78−15975
earthquake prediction, pattern recognition as a method of data analysis 80−4157
earthquake prediction, precursors classification 79−88264
earthquake prediction, search for seismomag. effect during Gazly earthquake (1976 May 17) 80−26463
earthquake prediction, search for time-depend. P-wave travel times from mining explosions 78−44788
earthquake prediction, seismic b-values vars. before large earthquakes *(Chinese)* 79−12073
earthquake prediction, time-predictable recurrence model for large Japanese earthquakes 80−85598
earthquake prediction, using He/Ar and N_2/Ar ratio vars. in fault zone groundwater air bubbles 78−88803
earthquake prediction, workshop, Strasbourg, France, (1980 January 31 to February 1) 80−62396
earthquake prediction and warning, theoretical review 79−5455
earthquake prediction for Haicheng, China, 1975 February 4, US report 77−78109
earthquake prediction from tectonomagnetism, implications of magnetite mag. susceptibility under press. 80−26504
earthquake prediction in Garm region, appl. of weak earthquakes space-time sequence 80−21653
earthquake prediction piezomag. response depth depend. rel. to tectonomagnetism as earthquake precursor 80−26465
earthquake prediction using scale invariant inclusion theory 77−49032
earthquake risk, assessment via focal mechanism consistency parameter of seismic activity *(Chinese)* 79−12074
earthquake seismic moment tensor elucidation from teleseismic data 80−104915
near-earthquake studies, importance of surface or interface P-wave 79−66628
earthquake swarms, differentiation from foreshocks via similarity of seismic waveform *(Japanese)* 80−67342
earthquake true ground motion reconstruction using Fourier transforms 77−86787
earthquake waves synthesis using prediction error filter 79−62630
earthquakes, automatic identification from microearthquake network data 78−81412
earthquakes, automatic recognition and timing from single traces 79−66822
earthquakes, centrifuge modelling 78−81429
earthquakes, fault plane soln. from relative amplitudes of P and pP 77−73669
earthquakes, intermediate and deep focus, body-wave magnitude scale and activity temporal var. 80−3943
earthquakes, max. magnitude determ. for Japan 77−9365
distant earthquakes focal depths, determ. from fundamental mode and harmonic Rayleigh surface waves 80−21654
earthquakes global location using minimum information *(German)* 80−56627
earthquakes maximum magnitude prediction, geotectonic method and appl. to N.Italy area 78−40493
earthquakes occurrence time forecasting results of expt. 79−53315
earthquakes source parameters, applicability of short-period surface waves 77−91040
earthquakes source spectrum determ. using code of seismic oscills. 79−48405
echo sounding and seismic profiling 77−70865
elastic wave fields, discrete wave number representation in three space dimensions 80−3945
electric currents, induced, via gradient fluxgate and SQUID magnetometers 80−98231

geophysical techniques continued
electric near zone field development method testing in NW.Kola Peninsula *(Russian)* 80−85761
electric potential probing of underground struct. *(German)* 80−82089
electric sounding data analysis, use of reciprocal geoelec. section 80−90237
electrical and EM measurements, tropical weathering effect 79−88246
electrical conductivity, model for quantitative interpretation of towed-bird airborne EM system meas. 79−5447
electrical conductivity anomalies, detect. from repeated high-accuracy geomag. field obs. *(Russian)* 79−96736
electrical conductivity determ. of core samples 79−67345
electrical conductivity estimation using gradient data from magnetometer arrays 77−73867
electrical logging of volcano's lava dykes, implications of flowing lava elec. cond. meas. 80−72498
electrical prop. meas. of Ukrainian shield rocks at high hydrostatic press. *(Russian)* 77−73721
electrical properties of layered medium, anisotropy resolution by joint inversion 78−16173
electrical prospecting, induced polarisation decay curve, dynamic charcts. *(Hungarian)* 80−21842
electrical resistivities overlayered Earth, transformation using digital filters 78−96304
electrical resistivity meas. for sandstone porosity determ. 77−9528
electrical resistivity sounding curves, numerical interpretation *(Chinese)* 80−89934
electrical sounding, elec. fields in random cond. layered Earth 80−77171
electrical sounding, peculiarities of section and zonation of Volyn-Podolian margin of E.European platform *(Russian)* 78−48964
electrical sounding, pot. field around subsurface electrically excited conductors 80−98230
electrical sounding, pots. of simple bodies in half-space *(Russian)* 79−34744
electrical sounding, theoretical apparent resistivity curves calc. *(Italian)* 78−40472
electrical sounding for dissemminated sulphide ores, electrochemical model of induced-polarisation phenomenon 79−92526
electrical sounding methods, applied EM depth sounding 77−45173
electrical sounding methods, statistical evaluation, expt. design 77−45172
electrically conducting fluid core location from external mag. obs. 78−32248
electromagnetic sounding, hybrid-ray approx. 80−72412
electromagnetic sounding transient pulse induction method, one-loop version 80−101448
electrometry inverse problems, soln. via variational method *(Russian)* 77−44915
electron microprobe, and ion microanalyser, appls. in mineralogy *(French)* 79−5628
electron microprobe, automated, evolution of quantitative elementary point anal. in geosciences *(French)* 78−78046
electron microscopy, high resolution, appl. to wollastonite individual silicate chains obs. 79−100829
electron microscopy, use in Earth sciences 80−105091
electron multiple scattering technique for intergrown polytypes identification appl. to chloritoid 80−70184
electronic communication methods in geology, review 77−17252
electroprospecting, direct problem soln. for ideally conducting hemisphere in space with point source *(Russian)* 79−34745
element analysis of geological and extraterrestrial samples, laser mass spectra 79−16717
elemental concentration of geological samples 78−85268
EM airborne profiles, sphere model for interpretation 77−45171
EM depth sounding interpretation, master tables, book 80−86043
EM distance measurement (EDM), single-wavelength, data ratios rel. to line length changes resolution 80−4143
EM field, conf., Hurbanovo, Czechoslovakia (Oct. 75) 79−39646
EM field properties reproduction, spherical, by real meas. devices *(Russian)* 78−85729
EM field sounding, appl. of composite obs. patterns in near field *(Russian)* 79−44270
EM fields in halfspace with ore body, local element transformation 79−66828
EM frequency sounding in horizontal coils system, field test 77−49182
EM frequency soundings, exptl. study 79−58129
EM in-line dip-angle meas. of vertical tabular conductors, graphical interpretation method 77−41189
EM induction, freq. and transient responses of EM fields created by currents in confined conductors 79−29702
EM induction in conducting stratified medium, numerical analysis 79−34740
EM induction in layered Earth by surface loop, transient response 80−72410
EM induction of laterally inhomogeneous anisotropic ground, VLF method 80−85754
EM induction surveying, transient time-domain EM method 80−98227
EM methods for determining dielec. const. and resistivity of ground, review 80−22382
EM probing of permafrost terrain, theory 78−28323
EM prospecting, harmonic and transient fields behaviour on surface of two-layer medium 79−92478
EM prospecting, wave type and direction from EM field short-period vars. anal. *(Russian)* 78−85474
EM remote sensing, computerized geophysical tomography 80−77169
EM remote sensing, reconstruction algorithms for geophysical applications in noisy environments 80−77168
EM remote sensing of inhomogeneities in ground 80−77165
EM response of Earth surface, aircraft remote sensing *(Chinese)* 80−104859
EM sounding, analogue model meas. for horizontal mag. dipole embedded in conducting medium 79−12068
EM sounding, boundary conditions for EM field above two-dimensional inhomogeneous struct. 80−85595
EM sounding, computation of multilayer response 79−92618
EM sounding, detectability of intermediate layers, time domain anal. 80−72641
EM sounding, diffr. of field of infinitely long cable over wedge-shaped conducting media *(Russian)* 78−40484
EM sounding, induced polarisation effect on near-field form. *(Russian)* 79−39641
geophysical techniques continued
EM sounding, interpretation of transients in Laplace space representation *(Russian)* 78−40483
EM sounding, iterative ray tracing between boreholes for underground image reconstruction 80−98466
EM sounding, numerical modelling of new multi-freq. system 80−56623
EM sounding, scatt. from buried wires 79−16369
EM sounding, subsurface propag. from horizontal elec. dipoles 80−98229
EM sounding, topographic effect in three-dimensional cond. model 77−25639
EM sounding, transients, from two horizontal thin conducting strata *(Russian)* 78−40485
EM sounding, VLF-EM profiles, topographic correction based on model studies 80−101452
EM sounding of buried axial conductor, time-domain response 80−105059
EM sounding of conductive circular cylinder, expt. and theoretical results 80−105058
EM sounding of dipping half plane embedded in conducting rock 80−90236
EM sounding of ice, visit to Arctic and Antarctic Research Institute, Leningrad 80−4504
EM sounding of permafrost, appl. of resonating antenna method 77−64333
EM sounding over horizontally layered media, total field resistivity mapping 79−16693
EM soundings, multifrequency, topographic and misorientation effects study 80−101451
energy balance maps from remotely sensed imagery 77−37433
environmental analysis, recent advances, book 80−41961
environmental science, trace analysis *(Japanese)* 77−87116
Eotvos effect variations allowance in gravimetric studies, data processing 79−74969
error analysis for remote reference magnetotellurics 80−12335
exploration geophysics, 41st meeting of European Assoc. of Exploration Geophysicists, Hamburg, Germany (1979 May 29 to June 1) 80−51943
exploration geophysics, 48th Annual International SEG Meeting, San Francisco, CA (1978 October 29 to November 2) 80−8441
exploration geophysics, appl. to kimberlite pipes 80−51393
exploration seismology, wave refl., refr. and diffr. in media with elliptical vel. depend. 79−5454
exploration with integrated aeroelectromagnetic and magnetic methods for Fe ores 79−16690
explosion seismology, appl. to continental Moho throws and dips sounding 80−85620
explosion seismology, appl. to seismic waves vel. change meas. in S.Kanto area from Tateyama explosions *(Japanese)* 80−67338
explosion seismology, geophones for recording shear waves 80−101447
explosion seismology, residual static correction problem, iterative soln. anal. 80−101334
explosion seismology data analysis *(Hungarian)* 80−21841
explosion seismology in Central Europe, book 77−25662
explosion seismology primary signal form., effect of partial multiple refl. *(Russian)* 78−85484
fault motion meas. by satellite laser ranging, San Andreas appl. 79−79786
fault stress direction determ. 80−8455
faults prospecting via seismic refr. method, model expt. and features of seismograms *(Chinese)* 79−12286
feature space mapping, linear transformation for improved colour image interpretability 77−78499
fibre optics appl., IR LED and optical cables improvements 78−59123
field configurations, analytical description in terms of differential geometry *(Russian)* 79−74986
filtration algorithms taking into account noise in input data, efficiency 79−25344
finite difference schemes, instability due to boundary conditions in elastic media 77−21912
fissile material assay, cyclic method of neutron activation and delayed-neutron counting 77−34395
fission track dating of zircon, improved etching techniques 77−29457
fission track dating technique 77−45203
fission track dating technique 80−36417
fission track dating using U glasses, error analysis 80−95503
fission track etching and annealing anal., muscovite, dating appl. 78−32036
fission Xe isotope dating technique 79−21043
focal depth and seismicity depth determ. in Iran and Turkey 80−61779
fold shape analysis, expansion of dip isogons use and preliminary investigations implications 79−39986
fold strain analysis using elliptical particles in deformed oolitic limestone 80−61787
forestland location in western Massachusetts, direct LANDSAT resource anal. 77−78529
Fourier analysis of gravimetric and magnetometric anomalies *(Rumanian)* 79−58123
Fourier expansions for anomalous geophysical fields *(Russian)* 79−62624
fracture creep, meas. using interference of light with equal optical paths *(Chinese)* 80−82113
fractured zone dip-angle and width, seismic determ. *(Japanese)* 77−17228
Frank's method for obtaining crustal shear strains from survey data 77−41177
frazil ice conc. meas. system using laser Doppler velocimeter 77−25796
frequency EM sounding, anomalous high cond. bands discovery in crystalline foundation *(Russian)* 78−96137
frequency-filter anal. of surface waves, fast method, west Pacific region appl. 79−48573
function, analytic continuation for Earth surface *(Russian)* 79−35008
galvanic prospecting effects, calc. via method of sub-areas 80−56348
Gamburtsev graphical method for three-dimens. gravity anomaly calc. 77−41203
gamma-gamma logging problems with large probe length, Monte Carlo soln. 77−37437
gamma-ray logging of boreholes, exact inverse filters 80−94609
gamma-ray spectrometry, factor analysis appl. 78−7778
gamma-spectrometric anal. of geochemical samples, data bank system 80−31120

geophysical techniques continued
garnets, triangle diagrams for physical determ. 77−70839
generalisation of Laplace expansion to Earth's surface 77−60337
generalized ray and reflectivity methods of waveform synthesis, comparison 79−84501
geobarometer for plagioclase and spinel lherzolite using enstatite Al_2O_3 content 77−2142
geobarometry and geothermometry, rel. to mineral comp. and partial melting in Josephine Peridotite 77−81880
geocentre position variation determ. using geostationary satellite obs. 80−82083
geochemical exploration using marine mineral suspensates 78−88936
geochemical haloes analysis using X-ray radiometric methods 77−53231
geochronology and cosmochronology, convention on use of decay consts. 78−28189
geodesic, small displacement meas., with three-mode laser 80−77748
geodesic interference distance meas. using semicond. lasers 80−77175
geodesic networks design for crustal movements study *(German)* 80−76897
geodesy, appl. of modern automatic drafting system *(German)* 78−15952
geodesy, base line estimation using single passes of laser data 80−3910
geodesy, base-free intersections method *(Russian)* 79−96731
geodesy, co-geoid appl. to interpolation of vertical deflection and to geoid determ. *(German)* 77−9323
geodesy, development and form. of calc. of trigonometric networks *(German)* 78−15947
geodesy, geodynamical evaluation of Doppler satellite obs. 80−76893
geodesy, geometrical and dynamic methods, development *(Polish)* 78−88780
geodesy, Helmert type variance-covariance-component estimator appl. 80−101318
geodesy, horizontal networks, height-controlled three-dimens. adjustment 80−101444
geodesy, interpolation method using multiquadratic eqns. *(German)* 78−15951
geodesy, measurement and instrumentation techniques *(German)* 77−33219
geodesy, parameter accuracy improvement by choice and quality of obs. 79−44078
geodesy, radio interferometric technique, 1.24 km base line vector determ. 78−40686
geodesy, satellite orbital elements and station coords. determ. by least-squares collocation *(Russian)* 78−49296
geodesy, statistical, mathematical struct. and appls. 79−29696
geodesy, systematic errors detect. by hypothesis tests using adjustment in sections *(German)* 79−44083
geodesy, techniques and appls., review *(German)* 77−60344
geodesy applied to crustal movement measurement, instrumentation trends and prospect 79−29738
geodetic applications of very long baseline interferometry 80−109274
geodetic data inversion, mathematical formulation for fault-plane solns. 78−12016
geodetic global coordinate systems geocentric origins, comparison from uniformly distributed data 79−57839
geodetic measurements using artificial satellites, refractive influence of ionosphere *(French)* 79−58133
geodetic network adjustment, sparse symmetric matrices profile improvement algorithm 77−48989
geodetic networks connection problems, stiffening problem, error anal. 80−81799
geodetic research, objectives, meas. techniques and data processing methods *(German)* 80−101317
geodetic solutions based on NAVSTAR Global Positioning System satellites Doppler meas., accuracy 79−100803
geodynamic research techniques using satellites 80−109282
geoelectric deep crustal *(German)* 80−56626
geoelectric dipolar techniques, archaeological appl. 79−16687
geoelectric inhomogeneities, position determination by variable geomag. field method 80−89956
geoelectric sounding, controlled-source DC pot. problem by self-pot. Green's function 80−77136
geoelectric soundings, direct interpretation using filtered Bessel functions 79−74965
geoelectrical method for thickness var. detection 79−2384
geoelectrical methods for detecting mineshafts 77−64451
geoelectrical prospecting, thin-layer problem 79−44095
geoelectrical prospecting in marine areas, dipole and unipole resistivity methods 80−56641
geoelectrical prospecting in marine areas, resistivity methods 78−65417
geographic information processing *(Japanese)* 79−74978
geoid anomalies, interpretation techniques 80−3897
geoid computation, effects of deviations of sea surface from geoid 77−64177
geoid figure determ., dynamic method 78−16175
geoid improvement in local areas, satellite to satellite tracking appl. 79−62423
geoid undulations and gravity anomalies, recovery from Geos 3 altimeter data 80−3896
geological and geophysical methods for evaluating shallow platform structures *(Russian)* 79−62623
geological contact magnetic profiling, inverting by harmonic method 80−77137
geological history computation from field survey and map data in FORTRAN 77−9522
geological lineament interpretation, multi-attribute method 79−2399
geological materials, spectrographic thermometry and manometry using DC arc 78−16796
geological materials mechanical behaviour, studies via stress relaxation testing method 78−96309
geological records, coding method based on data transmission theory *(Russian)* 80−17383
geological samples, f/α particle track anal. for U, Th and isotropic disequilibria 78−7799
geological samples, prep. for SEM 79−12785
geological section prediction, appl. of seismic waves integral spectrum parameters *(Russian)* 79−8705
geological stratum sounding by UHF radar *(German)* 79−8702
geological structure research, LANDSAT data anal. *(Italian)* 80−109281
geological surface breaks, filter and anal. methods *(French)* 78−9338
geophysical techniques continued
geological-geophysical zoning possibility 78−57342
geology, area and centre of mass rapid computation 77−9507
geology, discrimination using dual freq. and polarization imaging radar 79−12293
geology education, crystallography course 79−58459
geomag. variations separation into quiet and disturbed components by natural orthogonal components method 80−3922
geomagnetic and gravity anomaly data, curve-matching optimisation method *(Chinese)* 80−89935
geomagnetic anomalies, large scale, surveys, comparisons of geomag. field models with obs. 80−72425
geomagnetic D_{st} variations analyses, comparison using distortion free filter 80−17419
geomagnetic depth sounding, use of vertical component 77−91290
geomagnetic depth sounding below magnetometer arrays for atmos. research 80−98486
geomagnetic depth sounding by means of oceanographic and aeromagnetic surveys 80−77166
geomagnetic field, spectrum spatial analysis method *(Russian)* 77−91292
geomagnetic field changes determ., noise reduction techniques 80−26636
geomagnetic field computation, accuracy of construction of external Dirichlet problem boundary condition 78−44766
geomagnetic field computation, surface vertical component from aeromagnetic survey 80−105061
geomagnetic field horizontal component, absolute value determ. method 78−81420
geomagnetic field intensity vector, components determ. from absolute value 79−53534
geomagnetic field intensity vector components, determ. from magnitude, error estimate 78−73308
geomagnetic field long-period variations, spectra anal. methods *(Russian)* 79−34743
geomagnetic field meas. from near-Earth orbit, review of obs. 80−56347
geomagnetic field microstructure separation, digital filtering methods 78−69480
geomagnetic field total intensity anomalies, charts for quick determ. using horizontal plates *(Spanish)* 79−100982
geomagnetic fields space-time filtering 77−49178
geomagnetic fluctuations, spectral stacking and smoothing rel. to Earth global elec. cond. character 80−17231
geomagnetic K-index estimation by computer 78−36305
geomagnetic measurements and data processing, new methods 79−39988
geomagnetic monitoring system for International Magnetospheric Study 79−29882
geomagnetic noise reduction, appl. in field gradient meas. in Colorado 77−29249
geomagnetic palaeointensities determ. from submarine pillow basalts, effects of seafloor weathering 80−3927
geomagnetic pulsations, detect. using solenoid with ferrite core 78−24384
geomagnetic quietest days in year selection, AE and Dst indices levels occurrence 79−66877
geomagnetic regional and local fields, local function representations 80−98225
geomagnetic secular variations, space-time separation into fields of separate centres *(Russian)* 79−96738
geomagnetic sounding, exclusion method for local distortions *(Russian)* 77−45196
geomagnetic transfer functions at pulsation periods 80−72417
geomagnetic $V_{ZZ}(V_\Delta, Z_a)$ anomalies over stratified bodes, interpolation analytic method *(Russian)* 79−39968
geomagnetic virtual poles determination from seamounts, implications of Mount Shasta magnetisation 79−39637
geophone sensitivity in Chebyshev optimised arrays 80−21835
geopotential fields, filtering and transform. theory using information on input data noise 78−61584
geopotential fields interpretation, statistical algorithms *(German)* 77−29461
geopotential fields singularities localization in three dimens. space 79−74968
Georgian Bay, chlorophyll conc. from airborne spectral refl. meas. 78−16202
Geos 3 altimetry, geoid comparison with gravimetric geoid 80−3898
Geos 3 satellite altimetry, short-wavelength geoid resolution capability near Blake Escarpment 80−3902
geothermal areas in Iceland, H-water isotope thermometer appl. 78−69384
geothermal areas in Tuscany, location via geochemical and isotopic methods 77−49049
geothermal energy, heat extraction from hot dry rock masses 78−61378
geothermal exploration, appl. of ground Rn survey to Puna geothermal area, Hawaii 80−85657
geothermal exploration techniques, improvement for resource assessment of United States 79−70428
geothermal problems, digital and analogue simulation *(Rumanian)* 77−29510
geothermal prospecting, via field station GS-1 with thermoquartz resonators *(Russian)* 78−93000
geothermal research by IR scanning, image processing 77−64458
geothermal reservoirs, downhole meas. of thermal conductivity 78−61618
geothermal reservoirs true temp. determ. by resistivity method 77−49043
geothermal resources, nucl. techniques in geochemical studies 78−85746
geothermal surveying, with IR radiation thermometer and thermistor thermometer *(Japanese)* 77−70619
geothermal surveys, peculiarities rel. to search for fracture waters in Ukrainian Shield *(Russian)* 80−104935
geothermal systems, sulphate-water O isotope thermometry 78−69383
geothermal tracing with atmospheric and radiogenic noble gases 78−69502
geothermal well logging, temp. meas. utilising melting props. of materials 80−56659
geothermometer using Na/Li ratio in geothermal waters *(French)* 79−53369
geothermometry, appl. of plagioclase-garnet-Al_2SiO_5-quartz assemblage 77−2147
geothermometry, chemical and isotopic techniques 78−69501
geothermometry, electrochem. O_2 fugacity meas. appls. 77−2256
geothermometry and geobarometry for single pyroxene phase 77−2254
geothermometry using co-existing pyroxenes, model 77−2255

geophysical techniques continued
geotoxicity hazard index for radioactive waste storage 80−97822
glacier ice thickness meas., gravity profiling technique 78−32253
glacier thickness meas. using dielectric permeability characts. 78−89500
glaciology of Columbia Icefield, surveying techniques 78−61445
gradient magnetotelluric marine sounding method 79−62599
graphical methods for plane intersection line orientation determ. 79−58103
graphics computing system linked with signal enhancement seismograph, description and application 80−4131
gravimagnetic anomalies, interpretation on basis of pots. classes with inverse problem finite form 80−21847
gravimeter network adjustment, equiprobable interval method of sample classification 79−29889
gravimetric and deep seismic sounding, data interpretation *(Russian)* 79−39937
gravimetric and seismic methods combination for initial seismic data crustal vel. sections 80−105070
gravimetric anomalies, automatic deconvolution method 80−85574
gravimetric estimation technique using FFT, inertial navigation systems appls. 79−25376
gravimetric inverse problem, fast algorithm for calc. of filter operators *(German)* 77−70854
gravimetric meas., terrain relief effects, polyhedron approx. 80−3895
gravimetric prospecting problem appl. of nonsmooth function minimisation methods 77−41180
gravimetric sounding, vertical and horizontal gravity gradients relative precision 79−84500
gravimetry, direct and inverse problems soln. for hemispherical bodies *(Russian)* 79−35012
gravimetry inverse problem, assembling principle for constructing solns. *(Russian)* 77−44898
gravitational field, regularising algorithm for numerical model construction *(Russian)* 77−44899
gravitational harmonics, anal. from artificial satellites shallow reson. orbits 78−40805
gravitational logging and role in combined geological and geophysical research *(Russian)* 77−70868
gravitational prospecting, inverse problem approximate soln. *(Russian)* 79−39927
gravity, anomalies separation from background field, FON computer program *(Russian)* 78−53757
gravity, anomalous fields, stochastic harmonic analysis 79−35003
gravity, inverse problems, nonlinear eqn. soln., Tikhonov algorithm 77−41200
gravity, measurement from aeroplane via aerogravimetric apparatus *(Russian)* 78−40704
gravity 5° mean anomalies, recovery from ATS 6/Geos 3 satellite to satellite range-rate obs. 80−41366
gravity and magnetic, anomalies, linear anal. *(Russian)* 78−53755
gravity and magnetic anomalies, conformal deform. method for singular points determ. *(Russian)* 79−39934
gravity and magnetic anomalies, new interpretation theory 79−84509
gravity and magnetic anomalies, source depth estimation, spectral method 79−92631
gravity and magnetic anomalies due to rectangular prismatic bodies, spectral anal. 77−53222
gravity and magnetic anomalies of arbitrary bodies, FFT method for rapid computation 77−41186
gravity and magnetic anomalies of cylindrical bodies, separation procedure *(Russian)* 77−9325
gravity and magnetic anomaly computation algorithm 78−7779
gravity and magnetic anomaly direct computation 78−7780
gravity and magnetic field interpretation, optimal computing scheme construction 77−33201
gravity and magnetic sounding, separation of anomalies of comparable horizontal dimensions 80−94606
gravity anomalies, automatic interpretation for 2-dimens. masses 77−41188
gravity anomalies, derivative harmonic function restoration *(Russian)* 80−85577
gravity anomalies, regional background separation *(Russian)* 78−40703
gravity anomalies, second derivative method formulae evaluation by Fourier transform 79−100987
gravity anomalies, singular points interpretation 79−92622
gravity anomalies, stratified bodies, separation technique *(Russian)* 79−39933
gravity anomalies at Earth topographic gravity anomalies at Earth topographic surface, determ. by cosmic methods 80−56337
gravity anomalies due to finite inclined dykes, interpretation using Fourier transform. 77−53223
gravity anomalies interpretation, algorithm for calc. gravit. attraction of models of structural features *(Russian)* 78−53758
gravity anomalies interpretation, computer modelling 79−34971
gravity anomalies interpretation, graticule spacing and depth discrimination 77−53224
gravity anomalies measured in Krivoj Rog basin (Krivbas) underground workings, interpretation *(Russian)* 78−85466
gravity anomalies prediction using collocation and known density information 80−26626
gravity anomalies with periodical struct., data interpretation 77−78433
gravity anomaly calculation, geological substructs. *(Hungarian)* 80−21605
gravity anomaly data processing system, involving interactive computer graphics *(French)* 80−94610
gravity anomaly due to geologic contact, Fourier transform method for horiz. profile 80−94447
gravity anomaly from masses distributed over infinite regions, interpretation theory 80−82103
gravity anomaly interpretation methods for Pripyat trough studies *(Russian)* 77−91293
gravity anomaly inverse problem, least-squares soln. 80−98214
gravity anomaly probing by satellite-to-satellite tracking 77−56768
gravity base at Newcastle upon Tyne University, England 79−29693
gravity complex fields interpretation via minimisation method, automated system appl. *(Russian)* 79−35006
gravity data handling using collocation and least squares methods 79−29870
gravity data processing techniques, generalised method 77−53247
gravity data reduction for geological interpretation *(Russian)* 79−84537
geophysical techniques continued
gravity disturbance covariance functions, upward continuation integrals 78−85468
gravity field analysis, approximation of Stokes and Vening-Meinesz eqns. allowing for initial data errors 80−101459
gravity field extension to oil-gas province basement studies *(Russian)* 80−85759
gravity field of three-dimensional masses, calc. algorithms 80−94451
gravity field vertical gradient calc. methods 79−16689
gravity intensity variations, use of AChF-3 pendulum clock 80−104856
gravity interpretation, simple gradient method for geological contact 78−28332
gravity measurement, effects of atmospheric processes *(Russian)* 78−48957
gravity measurement, logarithmic pot. from anomalous masses of variable density 77−52961
gravity measurements, borehole data accuracy 79−5632
gravity observations in boreholes, terrain effects, theory 80−98462
gravity perturbing potential, calc. by Stokes eqn. 79−62428
gravity potential on mobile base, second derivatives determ. *(Russian)* 79 39954
gravity profile interpretation, linear inverse problem 77−73875
gravity profile inversion by method 78−69476
gravity prospecting, accuracy, meas. spacings and contour intervals calc. techniques *(Russian)* 79−44272
gravity prospecting, determ. of parameters of low-amplitude struct. with oil (gas) deposits *(Russian)* 79−44271
gravity regional anomalies, interpretation via mechanical modelling of crustal structs. form. *(Russian)* 78−49154
gravity surveys in glacier-covered regions, glacier sounder appl. 79−16697
gravity two-dimensional potential fields, singular points determ. *(Russian)* 79−39925
gravity $V_{zz}(V_{\Delta}, Z_a)$ anomalies over stratified bodies, interpretation analytic method *(Russian)* 79−39968
gravity vector and geodetic position survey, inertial navigation system appl. 79−29914
gravity vertical gradient meas. for detection of small geological and anthropogenic forms 77−17223
gravity vertical gradients, charts for quick determ. using horizontal plates *(Spanish)* 79−100982
Greenland ice sheet topography from satellite radar altimetry 78−81233
gridding of geophysical data, in FORTRAN 79−62596
ground conditions classification of LANDSAT data by anal. of variance procedures 77−78532
ground cover remotely sensed by radar, backscatter cross-section 80−46279
ground mapping resolution accuracy of scanning radiometer from geostationary satellite 77−73858
ground movement reconstruction from earthquake recording 78−49165
ground resistivity, airborne survey using VLF plane waves, resolution studies 80−12333
groundwater chemical geothermometer, Na-K-Ca temp. with Mg correction 80−51357
Hankel inversion of gravity profiles, numerical procedure 80−56619
Heat Capacity Mapping Mission, methods and appls. 79−5640
heat flow determ. method in oil fields 77−82021
heat flow determination, Bournac, Haute-Loire, geotherm proposal 80−8259
heat flow meas. by temp. wave reduction method, appl. to Crimea *(Russian)* 79−20774
heat flow measurement, vertical groundwater movement correction 80−3969
height and geoid determ. in Western Harz 3-dimens. test net *(German)* 77−70592
height meas. from satellite images using zoom height finder 78−36308
HF EM induction profiling, of boreholes in underground mines *(Polish)* 80−51547
high altitude low contrast imaging, sensor requirements 80−4152
high-pressure calibration scale based on Au, Ag and Cu melting curves, revision 80−39260
holographic interferometry for study of wave propagation in rock 78−20536
holographic terrain displays in 3D 78−78979
homomorphic deconvolution by log spectral averaging 78−28329
horizontal ground motion, two-dimensional, evaluation for structs. design 79−48419
horizontally multilayered Earth models, recurrence formulae for layer eigenfunctions 80−90246
hot dry rock geothermal reservoir fracture mapping techniques 80−81419
Hurst range of independent normal summands, distribution 78−16081
hydraulic fractures mapping using elec. potential technique 78−69543
hydraulic fracturing for stress meas. in hard and soft earthen material 77−9577
hydraulically induced crack, mapping by point source signals diffr. meas. 79−48572
hydrocarbon exploration, seismic signatures of sedimentation models using synthetic seismograms 77−21913
hydrochemical prospecting, APDC coprecipitation and X-ray spectrometry for trace element determ. 77−37445
hydrofracturing stress meas. technique, American field results 77−9576
hydrology, method of characts. with fixed net for slowly varying nonstationary flows *(German)* 79−5515
hydrometer particle size analysis calc. method 79−62590
hydrothermal alteration mapping, airborne spectroradiometric data anal. and LANDSAT data appl. 79−34973
hydrothermal system, temp. measurement scale based on chem. comp. of gas fraction 80−98277
IBIS, geographic information system based on digital processing and image raster data type 77−56747
ice sheets in polar regions, radio obs. appls. 78−81419
image registration, similarity measures and preprocessing techniques 78−32240
image scanner technology for digital mapping systems 80−85773
imagery interpretation and geological lineament reproducibility 77−53250
imaging radar measurement of surface roughness, appl. to Askja Caldera, Iceland 79−16426
impedance frequency sounding for multilayer geoelectric profile *(Russian)* 77−29517

geophysical techniques continued
in-situ seismic methods for crack anisotropy in NW.England Carboniferous Limestone 80−17240
induced polarisation, multifrequency mineral discrimination and inductive coupling removal 79−5448
induced polarisation (IP) sounding, effects of EM coupling in electrode arrays over uniform half-space 80−101324
induced polarisation meas. using discharge transient recorder 78−65398
in situ induced polarisation sounding, meas. at Yerington mine, Nevada 80−51323
induced polarisation sounding, response of polarisable inhomogeneous sphere 79−44092
induced polarisation sounding for sulphide mineralisation in Rajasthan and Gujarat, India 79−39714
induced polarisation sounding method, freq. depend. of measured parameters *(Russian)* 79−74836
induced polarisation soundings interpretation, freq.-effect transform function definition and appl. 80−56624
induced polarisation technique for prospecting 78−69473
induced-polarization freq.-domain method, metallic mineral deposits *(Italian)* 79−16686
induction logging, longit. geometric factors *(Chinese)* 77−66998
induction logging, numerical soln. by transition process method 77−56751
induction sounding of stratified media using vertically displaced sensors *(Russian)* 79−58119
inductive logging near single and multiple conductive bodies, scale model results 79−16696
inductive magnetisation sounding, inverse mag. problem numerical soln. *(Russian)* 79−34747
inorganic gas chromatography for determ. of H_2O and CO_2 in rocks and minerals 80−85767
instrumental neutron activation, analysis for silicate rocks and minerals 78−20548
instrumental neutron activation technique for sample anal. 79−53550
interactive computerised data acquisition system for geotechnical meas. *(Italian)* 78−7771
interference fields separation, statistical algorithms *(German)* 77−29462
interferometric methods for distance meas., recent crustal movements appl. 79−80057
interpolation error operator, digital time series error detect. and correction 78−3963
interpolation of digitized curves for seismograms 77−40999
interpretation methods, conf. (Bratislava, Czechoslovakia, May 1974) *(German)* 79−35001
interpretation of time-domain airborne electromagnetic (INPUT) anomalies 79−2383
interpretation problems, soln., correl. theory of homogeneous random fields appl. 79−100986
inverse filter with optimum error distribution 77−81825
inverse filtering for seismic long period statics determ. 77−41192
inverse geophysical problems, statistical soln. methods *(German)* 77−29460
inverse gravimetric problem, appl. of simplex method 77−56740
inverse gravimetric problem, direct soln., trap method 79−58101
inverse gravimetry problem, three-dimens., trial and error method of soln. 79−62607
inverse gravity problem, unified least-squares method 77−73872
inverse gravity/mag. problem, appl. of linear programming, basic numerical techniques 79−53581
inverse isostatic problem, global soln. for Pratt and Airy hypotheses 80−3893
inverse logarithmic-potential problem for contact surface, solvability in finite form 77−82025
inverse methods applied to continuation problems in geophysics 79−53579
inverse normal mode problem, ideal soln. with finite spectral data 79−34974
inverse problem for n layers, inversion method for reducing nonuniqueness 80−4128
inverse problem for seismic wave eqns. in one dimens. *(French)* 79−44138
inverse problem soln., complex interpretation *(German)* 77−29463
inverse problem stability, one-dimens. wave eqn., seismic profiles appl. 79−84490
inverse problems, resolution anal. for discrete systems 78−49153
inverse problems, soln. via component ranking method using information on region with possible solns. *(Russian)* 77−13131
inverse problems soln. by method of dynamic models *(Russian)* 78−85714
inverse seismometry problem soln., limits of appl. 79−62606
inversion method for seismic kinematic data 80−90240
inversion of long range seismic profiles 77−73878
inversion of microseismic array cross spectra 80−98243
inversion of satellite magnetic anomaly data 80−12563
inversion of two-dimensional resistivity and induced-polarisation data 79−16695
inversion procedure for anisotropic magnetotelluric data 77−60475
invisible information imaging techniques 77−5819
ion microprobe analysis technique, appl. to zone plagioclase of different magmatic environments 79−34815
ion of U grains and gangue, Oklo study *(French)* 80−21758
i.r. remote sensing, Earth surface imaging *(German)* 77−9567
IR remote sensing, relative importance of reflected and emitted flux density in 3 to 14 μm range 79−92542
IR remote sensing measurements, conceptual considerations and surface temp. estimation, review 79−34984
IR technology, conf. II (San Diego, California, 1976, August 26-7) 77−45891
IR technology utilisation, symposium, San Diego, CA, USA (Aug. 79) 80−86037
ISO FORTRAN IV program for generating isopleth maps on small computers 78−57157
isotope abundance ratios, determ. with Si whisker field desorption ion source 80−11975
isotope geothermometry in the Larderello geothermal field 78−69312
isotope techniques, appls. to geothermal systems in New Zealand 78−69313
isotropic reconstruction of track-type airborne geophysical surveys, 2D filler design 79−66844

geophysical techniques continued
Kolmogorov-Wiener least-squares filters appl. to geophys. anomalies separation 78−61580
L-S fabric scheme appl. to structural mapping and palaeostrain anal. 77−78176
Lageos, laser satellite tracking, meas. of Earth's rotation and Earth's crust movement 77−41206
lake identification by closed planar curve analysis using LANDSAT *(Japanese)* 80−26635
lake sediment thermal diffusivity estimation from field obs. 77−2253
lake sedimentation rates from ^{137}Cs measurements 80−4048
land seismology, appl. of mini-SOSIE 77−21917
land system classification of Jordan, appl. of Landsat imagery 79−2388
land use mapping by radar imagery 80−8449
land-use map, remote sensing derived, accuracy test method 78−7805
land-use mapping by machine processing of LANDSAT-1 data 77−78467
land-use photo classification using optical spectrum anal. 78−12023
land-use/soil survey data processing for resource planning 78−7804
Landsat data, line detection algorithm 80−77150
LANDSAT data clustering, four-dimensional histogram approach 77−78524
LANDSAT data correction for haze, Sun angle and background reflectance effects 77−78491
LANDSAT data for geological studies in India, digital anal. 77−78511
LANDSAT data for metropolitan land cover inventory 77−78536
LANDSAT data high-level computer processing 78−69546
LANDSAT data multivariate distribution relative normality measure 77−78506
LANDSAT data per-field, classification, unsupervised clustering techniques 77−64437
LANDSAT digital data for forest vegetation and land classification, in Minnesota 77−78528
LANDSAT digital thematic maps, radiometric interpretive legend 77−78468
LANDSAT evaluation for land cover data in metropolitan areas 77−78538
LANDSAT image, digital anal. and appls. 78−65404
LANDSAT image anal. for terrain investigations in Florida 77−78530
LANDSAT image classification, least square error approach 77−78523
LANDSAT image photointerpretation/classification using negative spectral bands 77−78498
LANDSAT image principal component technique for studying structural basin, Spain 77−78521
LANDSAT image processing, pipelined systems, design 78−96329
LANDSAT imagery, computer aided and air-photo interpretation techniques 79−74976
LANDSAT imagery, discovery of meteorite impact crater in central Alaska 77−91136
LANDSAT imagery, photographic contrast enhancement 79−29896
LANDSAT imagery, photographic data extraction 77−33212
Landsat imagery, planimetric restitution using Zeiss Stereotop 80−56648
LANDSAT imagery for surface-coal-mine inventory 77−91320
Landsat imagery for terrain analysis 78−40691
LANDSAT imagery processing and enhancement 78−69545
LANDSAT imagery survey of Melaleuca problems 77−82049
Landsat images, digital differential rectification 80−41570
Landsat images of Earth, processing by digital techniques 77−25784
LANDSAT large area classifier MAXL4X 77−78534
Landsat MSS points location on maps, methods and accuracy 79−2389
LANDSAT multispectral data, training sample size effect on classification accuracy 77−78544
LANDSAT multispectral data classification algorithms 78−61629
LANDSAT multispectral images clustering scheme 78−32241
LANDSAT multispectral sensor image adaptive coding techniques 78−45060
LANDSAT ratio image dynamic range reduction technique 78−69547
LANDSAT sample selection training algorithm SEARCH 77−78535
LANDSAT spectral data classifications, atmospheric correction 78−69548
LANDSAT-1 digital image registration and cloud effect rectification 77−78490
LANDSAT-1 imagery for geological evaluation 77−33211
landslide investigation methods and data interpretation 77−82020
landslide prediction in San Francisco Bay region 77−70665
landuse imagery computer anal., change detection metrics and MIXELS 77−82070
laser techniques for rain impact and erosion recording 79−62610
Laterolog borehole resist. logging device, function and applications 80−85755
latitude measurement, effect of relativistic deflection of light *(Russian)* 78−40462
lava lake cooling model, numerical analysis method 77−64247
lava temp. meas. techniques and apparatus on Etna 77−25800
least-squares collocation for Earth figure and gravit. field determ. 79−48392
level surveying, atoms. refr. correction *(Russian)* 80−77127
levelling survey data, math. anal. for assumed const. vertical vel. *(German)* 80−82081
limestone diagenesis simulation, computer model based on Sr depletion 78−73358
line masses depth estimation from residual Bouguer anomalies, via Backus-Gilbert min. distance criterion 79−44257
lineament, joint and drainage densities, rapid determ. method 78−32255
linear inference theory, appl. to underparameterised Earth models 78−49000
linear inverse problems solution, positivity constraints, appls. 77−45178
linear inverse problems solution, positivity constraints, theory 77−45177
linear inverse theory with a priori data 79−53580
linear inversion, non-uniqueness resolution via a priori data appl. 79−44261
linear inversion, use of a priori data to resolve nonuniqueness 79−84502
linear prediction in least-squares scheme, algorithms 80−98464
linear transformation characts. of geophysical fields, props. *(Russian)* 79−35007
linearized inverse problems, mathematical methods 77−73871
local gravity anomalies interpretation, integral ratios *(Russian)* 78−85463
local seismic foci, soln. of inverse problem 79−53582
long grains method for palaeomagnetic field strength and direction 80−77148

geophysical techniques continued
long wavelength static estimation in common depth point data 77−17032
lossless layered media state space models 77−91065
lossless wave eqn. in layered media, canonical Bremmer series decomposition 77−91064
low Sun-angle photography, flight planning, interpretive techniques 77−78465
low-vel. zone inversion, Weichert-Herglotz integral 80−21829
low-velocity zone, parameters determ. as functions of focal depth 77−86828
lower mantle elec. cond., theory of EM induction in rot. conductive Earth 78−44764
machine processing of remotely sensed data, conference, West Lafayette, Indiana (1980 June 3 to 6) 80−82586
macroseismic data processing and interpretation 78−61583
magnetic and gravitational anomalies extrapolation, equivalence principle *(Russian)* 79−39926
magnetic and gravity anomalies, numerical interpolation schemes *(Russian)* 79−62622
magnetic and gravity contact surface, data anal. by space domain filter method *(Chinese)* 80−89933
magnetic anomalies, derivative harmonic function restoration *(Russian)* 80−85577
magnetic anomalies, interpretation by singular point method 77−53229
magnetic anomalies, interpretation with end-corrected Fourier transforms. 78−65418
magnetic anomalies, total field, of spherical ore-bodies, interpretation via zero-line method 79−39973
magnetic anomalies analysis, regional background separation *(Russian)* 78−40703
magnetic anomalies caused by long horizontal cylinders, direct interpretation method 77−52971
magnetic anomalies in deep crust, mineralogical constraints on Curie isotherms 78−44805
magnetic anomalies interpretation, computer modelling 79−34971
magnetic anomaly depth determ. and inverse problems 77−45165
magnetic anomaly due to 2-D assym. triangular prism, expression for total field 80−94457
magnetic anomaly interpretation, bidimensional inhomogeneous problem soln. via Cauchy integrals *(Russian)* 79−35013
magnetic anomaly inversion, generalised multibody model 80−98226
magnetic anomaly map of Republic of Djibouti, reduction techniques 80−61753
magnetic anomaly of thin dyke, curve fit by calculator program 80−98228
magnetic anomaly quantitative interpretation 80−26652
magnetic anomaly reduction to mag. pole *(Chinese)* 79−100963
magnetic anomaly sounding, estimation of cover thickness above magnetised mass *(Russian)* 80−105069
magnetic assessment technique for titanomagnetite in Waipipi ironsands, New Zealand 80−17254
magnetic data analysis and reduction, for satellite magnetometer data 80−77141
magnetic field meas., magnetotelluric sounding technique using SQUID devices 78−96322
magnetic field measurement, field difference method with noise reduction 80−21850
magnetic induced polarisation method, theory for conductive cylinder *(Chinese)* 80−104858
magnetic induced polarisation techniques 80−98461
magnetic interpretation for geological contact and thin dike 78−28333
magnetic measurement, in situ method, for igneous rock bodies 79−84521
magnetic measurement at high altitude, by high-sensitivity balloon-borne ring-core magnetometer *(Japanese)* 80−94608
magnetic measurements of solid samples, application in geophys. 80−98487
magnetic minerals, Curie temp., HF meas. method *(Russian)* 79−39992
magnetic palaeointensity determination, ARM correction method 79−34968
magnetic prospecting, inverse problem approximate soln. *(Russian)* 79−39927
magnetic prospecting, inverse problem soln., decomposition iteration method *(Russian)* 80−4134
magnetic prospecting, optical filtering of airborne and ground data 77−25797
magnetic regional anomalies interpretation procedure *(Russian)* 77−33199
magnetic sounding, anomaly field vertical intensity autocovariance function *(German)* 79−34746
magnetic sounding, magnetostatic field problem, soln. in high susceptibility case via method of subsections 80−105065
magnetic survey at Northeastern Japan, high-altitude *(Japanese)* 77−82019
magnetic surveying, integration of gradiometer data 80−105064
magnetic surveying using horizontal gradient vectors 78−28334
magnetic susceptibility anisotropy as rock strain indicator 77−78170
magnetic susceptibility sounding, meas. at Yerington mine, Nevada 80−51323
magnetic variation sounding, anomalies above inhomogeneities of Earth spherical model 77−13056
magnetic vector determination of rock specimen, statistical method 80−51556
magnetometer data transmission via telephone lines 77−13126
magnetometric and electrometric methods for landslide dynamics investigation 77−87091
magnetometric resistivity anomalies, two-dimensional struct., mag. field determ. method 80−12334
magnetometric resistivity method field test on plateau 77−40977
magnetometric resistivity methods, theory 79−53531
magnetosphere VLF signals, preprocessing on spacecraft 77−64609
magnetotelluric data, signal/noise ratio enhancement 77−53227
magnetotelluric data analysis: removal of bias 79−53530
magnetotelluric fields, calc. in horizontally-inhomogeneous media using finite differences method *(Russian)* 79−44102
magnetotelluric impedance function estimation 78−85731
magnetotelluric investigations, induction effects detect. methods appl. in Sakhalin and Yakutia *(Russian)* 79−39642
magnetotelluric meas. over horizontally stratified formations, stratigraphic interpretation method *(Russian)* 79−62620
magnetotelluric measurements, using lock-in signal detect. 78−81104
magnetotelluric measurements, with remote mag. reference 79−88245
magnetotelluric monitoring of geoelectrical resistivity changes 77−2103
magnetotelluric resistivity and phase soundings interpretation, graphical procedure 78−40473
magnetotelluric sounding, affected by resistivity freq.-dispersion 80−41368
magnetotelluric sounding, audio-frequency, case history at Cavendish geophysical test range 80−51324
magnetotelluric sounding, fields of vertical mag. dipole over vertically inhomogeneous Earth 79−34736
magnetotelluric sounding, fundamental model 80−77167
magnetotelluric sounding, interpretation method 77−44918
magnetotelluric sounding, multiple-reflection method appl. to inverse problem soln. 78−61581
magnetotelluric sounding, natural source obs. one-dimensional inversion 79−92479
magnetotelluric sounding and crustal elec. cond. anomalies 80−31008
magnetotelluric sounding curves in nonuniform field of linear sources, comparative anal. *(Russian)* 79−48395
magnetotelluric soundings, effect of field vertical components on impedance determ. *(Russian)* 78−48963
magnetotelluric tensor analysis, appl. to two-dimensional geological structs. 78−40471
magnetotelluric two-dimensional inversion 77−73629
magnetotelluric vars. in 10-1000 sec. range, processing *(Russian)* 79−84535
Mahalanobis' D^2 distance for sediment distinction *(Portuguese)* 78−61388
major element whole rock anal. using sample fusion technique with electron microprobe 77−64494
mantle heat flow, subtraction of crustal contrib. from surface flow 77−37161
map intensification from small format camera photography 79−25354
mapping and remote sensing by optical filtering 80−101458
maps of mine workings on microfilm, with topographic maps 78−32259
marine Bouger gravity calc. using processing density concept 79−74829
marine geophysical surveying, new techniques appl. 79−53560
marine gradient magnetic sounding method 79−62598
marine gravimetry, cross-coupling effect compensation by intersection point method 78−57340
marine refraction seismology, interpretation techniques 77−64230
marine sediments diffusion coefficients determ., resistivity techniques validity 79−92601
marine seismograms, source signatures debubbling 79−16692
maximum entropy method appl. to inverse problems, short data records anal. and Earth density determ. 77−64465
maximum entropy method for spectral analysis of digital data *(Japanese)* 77−17227
maximum entropy power spectrum anal., soln. to problem of spontaneous line splitting 77−45187
maximum entropy spectral anal., confidence limits 80−22284
maximum entropy spectral analysis, power estimation method 79−16691
maximum entropy spectral analysis, prediction filter error length determ. for artificial samples 79−66829
maximum entropy spectral analysis method for seismic waves *(Japanese)* 77−2260
maximum entropy spectral analysis of multiple sinusoids in noise 79−48579
metabasalts polaeotectonic affinities determ. via immobile trace elements, appl. to Scotland Palaeocene basalts 79−34816
metal oxide-SiO_2 systems, phase diagrams calc. from high press. phases stability study 79−90779
metal species, pollutants, identification and determ. by chromatographic-at. spectrosc. method 78−68972
metamorphic bathozones and bathograds, meas. of regional scale post-metamorphic uplift and erosion 78−81113
metamorphism temp. and press. determ. via garnets comp. and zoning 77−2148
meteorological real-time data acquisition and anal. 78−69466
microcrystal density determination technique, mag. fluids 80−85751
microdensitometry appls. *(Czech)* 79−30524
microearthquake location using max. likelihood processor 77−17033
microearthquake research, methods and meas. errors 79−39987
microgravity surveys, computer processing system 80−85575
microwave dielectric constant logging, EM wave propag. method 80−12558
microwave distance measurement, trilateration in German Bight *(German)* 80−8248
microwave holographic imaging through random aberrating media 77−3551
microwave monitoring Earth, from satellite, advantages 80−17409
microwave radiometry and devices *(Japanese)* 78−16212
microwave remote sensing, radiative transfer eqns. 80−21855
microwave scanning radiometry, appls. 78−73551
microwave sensing from satellites, appl. to land surface emissivity meas. 80−98485
microzonation methods and techniques used in Peru 79−88513
microzonation of continental shelf, high-resolution geophysical surveys 79−88515
mine workings, roof and walls condition study, radar appl. *(Russian)* 79−62602
mineral composition of rocks at great depths, prediction from longit. elastic wave vels. *(Russian)* 80−104956
mineral determination, IR spectra appl. 79−62589
mineral exploration techniques, changes 79−100979
mineral identification in rocks, mag. rot. hysteresis loss meas. 80−67428
mineral prospecting by tunable laser spectroscopy 77−60500
mineral remote sensing by near IR spectra, hydrothermally altered area 80−81871
mineralized zones, interception probability calc. *(Rumanian)* 77−29509
mineralogy, appl. of cathodolum. microscopy and spectrometry 77−69919
mineralogy, crystal gas-liquid inclusion meas. with microscope heating stage 80−76967
mineralogy, goniometry, from photographs or angle-true sketches 79−55619
minerals, anal. of small samples using X-ray quantometer 78−61112
minerals, elasticity meas. via Brillouin scatt., appl. to coesite 77−44978
minerals, mag. separation using supercond. mags. *(Czech)* 78−88923

geophysical techniques continued
minerals fluid inclusions obs., Raman laser microprobe analysis appl. 80−57390
minerals optical constants, derivation from measured reflectances, errors in two-media method 79−58100
minerals release-adiabat measurements, effect of viscosity 80−51388
minerals spatial isotope distributions, recovery from stepwise degassing data 79−34967
minimum entropy deconvolution for seismic reflectivity profiling 77−81817
minimum Entropy Deconvolution with an exponential transformation 80−17407
mining tectonical forecast maps, geoelectric bed sounding method *(Hungarian)* 80−105075
mixed Fourier Walsh transforms, appl. to seismic array processing 77−81819
modelling techniques, statistical tests for goodness of fit 78−57333
Moho, dip and strike determ. from array anal. 79−66821
Mohorovicic discontinuity relief, determ. methods *(Russian)* 78−48992
monitoring underground nuclear explosions, book 79−681
monochromatic and colour images by aero- and space methods 79−44252
monofrequency borehole traveltime survey 78−28328
Mossbauer spectroscopy, appl. to study of Fe diagenesis in sulphide rich sediment core 79−74917
mountain aerial photography, colour film types compared 77−29500
MPP-1 stationary precision proton magnetometer, direct calibration method 79−53535
multiband photography for geomorphology, soils and land use study, feasibility 78−12025
multibaseline, geodetic meas. technique, precision ground based 79−34987
multichannel systems, Wiener filter and maximum entropy method 79−92619
multidimensional Gaussian max. likelihood classifiers error probability estimation 77−78540
multifrequency synthetic detecting holography *(Chinese)* 77−64444
multilayered plasticine models for rock folding simulation 77−53024
multilevel syntax analysis for geological data compression 79−48569
multiple covering problem for large scale seismic network modelling 78−69540
multiple seismic wave suppression on seismograms 80−46281
multiple water reflections recorded at ocean bottom 78−57331
multispectral aerial imagery capabilities for military geographic information acquisition 77−82054
multispectral aerial photography, Khomas Trough region gossaniferous outcrop identification 77−5346
multispectral aerial photography, rock type identification in NW Cape Province, S.Africa 77−5345
multispectral data anal., ISURSL levels classification 77−78539
multispectral data clustering, interactive approach 77−78526
multispectral digital images, intensity variations and false colour display correlation 77−78514
multispectral images, region extraction and classification by entropy index 79−58130
multispectral imaging, geology appl. 79−34823
multispectral photography appl. using MKF-6 camera and MSP-4 projector 80−56633
multispectral remote sensing ratio image digital processing and interpretation 78−81461
multispectral scanner image rectification, practical experience 78−88940
multispectral scanner imagery rectification 78−88939
multispectral sensor for satellite, analytical design 80−77262
natural resource digital image anal. development in USA 78−96327
natural resources imagery data processing techniques *(Italian)* 77−82063
natural soil radioactivity monitoring with portable gamma ray spectrum 80−31148
natural surface polarisation imagery, remote sensing appl. 78−61625
neutron activation anal., using standard reference materials as multielement irrad. standards 78−80815
neutron activation anal. technique for Na/K ratios in fluid inclusions determ. 78−61568
neutron activation analysis, gamma-ray spectra prediction, detection limits, computational procedure 78−85242
neutron activation analysis for determ. of V in crude oil 78−20109
neutron activation analysis of geological materials 80−16747
neutron activation analysis of rare earth elements in rocks, optimum method 79−88491
neutron activation analysis of rare earth elements in rocks and minerals 79−88492
neutron activation method of In-determ. in pure sphalerites 79−87929
nonlinear analytical prolongation method, survey inverse problem appl. *(Russian)* 79−21037
normal incidence synthetic seismogram fine struct., inverse problems soln. 78−49152
NQR techniques, appls. to geosciences and mineralogy 80−67426
NRM, multicomponent, separation method 79−34805
NRM meas. of artificial rock samples with inhomogeneous magnetization 77−45174
nuclear 'in situ' methods used in hydrology and hydrogeology *(Rumanian)* 79−39982
nuclear accelerator spectrometry, appl. to ^{10}Be meas. in 1000 and 5000 yr Antarctic ice 79−2305
nuclear geophysical methods, geometric factor *(Russian)* 77−87121
nuclear geophysics, allowance for scattered gamma radiation *(Russian)* 80−105067
nuclear oil well logging using 14 MeV neutron-excited gamma-ray spectrometry 79−48581
nuclear techniques in exploration for energy related minerals and metal ores 77−37438
nuclear techniques in hydrocarbon well logging 77−37443
ocean bottom geology, underwater robot/manipulator development 78−77356
ocean wave geomag. fields, towed magnetometer investigation 80−3923
oceanic crust density section construction, appl. to NW Indian Ocean structures *(Russian)* 79−48431
oceanic crust studies, deep seismic profiling using refl. meas. *(Russian)* 79−39966
oil and gas formations, prediction prior to drilling *(Russian)* 79−39970
geophysical techniques continued
oil and gas well profiles, appl. of combined well-logging techniques *(Russian)* 78−40705
oil and gas-bearing sites, mathematical selection methods *(Russian)* 77−9560
oil composition analysis by means of cracking, permittivity thermal dependences obs. *(Czech)* 80−46289
oil prospecting, new seismic reflection techniques 78−73541
operational environmental satellite system, next phase planning, USA 79−5728
optical preprocessor, use in Earth-resources satellites 80−67430
optimal freq. filtering for interference systems *(Russian)* 79−58117
optimum two-dimens. linear digital filter, design principles *(Chinese)* 77−91281
orebodies location in mineworkings, muon hodoscope appl. 79−84491
ores, Ta chem.-spectral determ. 79−16075
orthogonalization of random variables, weather forecasting appl. 77−74203
orthonormal lattice filter−a multistage multichannel estimation technique 79−84497
orthophotography, history, advantages and uses 77−66995
palaeo-geothermometry, from metamorphism of sedimentary organic matter, appl. in Upper Rhine Graben 79−70800
palaeoclimatic research, status and opportunities 80−51527
palaeoclimatology, larval bivalve shell morphometry as temp. indicator 79−53510
palaeogeographic reconstruction, H_2S levels stagnation coeff. appl. 80−36291
palaeointensity determination of laboratory rock sample 80−61917
palaeointensity methods using AF demagnetisation and anhysteretic remanence, reliability 78−77352
palaeomagnetic analysis, effects of haematite reduction to magnetite 78−65277
palaeomagnetic data anal., least squares line and plane method 80−109259
palaeomagnetic data smoothing, objective method, comments 79−34975
palaeomagnetic data smoothing, objective method 78−28159
palaeomagnetic directional data sets, shape 79−39881
palaeomagnetic field intensity, determ. at heated rock contact by stepwise remagnetisation method 80−21619
palaeomagnetic field intensity determ. by remagnetisation in alternating field 77−9535
palaeomagnetic field magnitude, nonthermal nondetrital method using Sun-dried bricks 77−45176
palaeomagnetic field magnitude and direction during polarity transition, new technique 77−37429
palaeomagnetic inclination data analysis by statistical method 80−109101
palaeomagnetic intensity determ. by continuous thermal cycling 77−37425
palaeomagnetic intensity determ. by modified Thellier method 77−37426
palaeomagnetic intensity determ. by single heating method, roof tiles and rocks appl. 77−37427
palaeomagnetic intensity determ. for very old rocks, problems 77−37428
palaeomagnetic intensity determ. from sedimentary and igneous rocks by AF remag. 77−37432
palaeomagnetic intensity determ. methods using theoretical grain-size thresholds 77−37188
palaeomagnetic intensity determ. using anhysteretic remanent magnetisation 77−37430
palaeomagnetic intensity determ. using anhysteretic remanent magnetisation 77−37431
palaeomagnetic intensity measurement, conf., Grenoble, France (Aug. 1975) 77−37130
palaeomagnetic intensity measurement, sediment particle size var. rel. to DRM/ARM ratio 78−32067
palaeomagnetic meas., comparison of anhysteretic remanence and thermoremanence in magnetite 77−5191
palaeomagnetic meas., mag. declination and inclination errors in experimentally deposited specularite-bearing sand 80−90075
palaeomagnetic measurements, origin and stability of drilling induced remanence 77−33059
palaeomagnetic polar paths, graphical approach rel. to palaeomag. cycles and global tectonics 79−66618
palaeomagnetic polarities using cryogenic magnetometer 79−70743
palaeomagnetic records, running means calc. for Holocene short period secular geomag. vars. determ. 80−98221
palaeomagnetic sounding, inverse mag. problem numerical soln. *(Russian)* 79−34747
palaeomagnetism, converging remag. circles for separation of superimposed remanences 78−28348
palaeomagnetism, thermal demagnetisation rel. to superimposed magnetisation meas. *(French)* 77−37125
palaeomagnetism, Zijderfeld vector diagrams use in multicomponent magnetisation studies 80−17420
palaeopiezometry using recrystallized grain size 77−91317
paraffin model experiment of plate tectonics 77−13073
parameter sensitivity analysis method for differential eqn. models 78−81453
parameters of geophysical objects, interval estimation via identification methods 77−82024
peat bog and sapropel bed thickness meas. by radar 80−21860
perimeter survey by photogrammetric methods 79−25185
permafrost, shallow, mapping, EM methods 79−16694
permafrost thickness determ. in wells in N. Canada 77−66989
perturbation matrix method for propag. in irregular stratification 77−73869
petroleum exploration, marine seismic data for detrital sediments 78−96303
petrophysical props. of ultramafic rocks, using factor analysis 80−90087
phase-matched filters appl. to Rayleigh waves from seismic sources 78−45010
photogrammetric camera, distortion calibration using star images 79−35881
photogrammetric network densification by aerotriangulation *(German)* 77−60496
photogrammetric online processing, general sequential algorithm 77−78463
photogrammetry, high intensity dot grids appl. to accurate area determ. 80−17225

geophysical techniques continued
photogrammetry, least squares prediction by multiquadric and covariance functions 77−78464
photogrammetry, orientation, triangulation and digitisation, numerical methods 78−36312
photogrammetry, OTF/MTF standards 77−78471
photogrammetry, real-time, instrumentation for analytical video stereoscopy of extended images 78−88926
photogrammetry, SEM appls., simplfied numerical transform. for distortion correction *(German)* 79−17572
photogrammetry and EDP, appl. to mapping of geological joints 80−56470
photogrammetry using digitally controlled differential rectifiers *(German)* 77−60495
photomapping using earth terrain camera, Skylab photographs quality evaluation 77−2283
plastic detector, large-volume, for aerial gamma-ray spectroscopy 79−58126
polar ice CO_2 content measurement, for ancient atmos. composition 80−61891
polar motion determ., satellite Doppler tracking, MEDOC 80−101445
polarized waveform dectors, matrix and Stokes vector representations, teleseismic waves appl. 78−12008
polarography, amalgam, film, with accumulation, appl. to micro-, macro-object anal., review 78−61098
pollution monitoring and instrumentation 79−12301
polymetamorphic terrain primary age determ. 78−96168
polynomial expansions fitting, appl. to long-wavelength mag. anomalies over Canada 80−85594
position location and navigation, conf., San Diego, CA, USA, Nov. (1978) 79−25374
position meas., satellite surveyor MX 1502, microprocessor controlled ground based system 79−25377
potential field anomalies geodynamic interpretation, physically based source models *(German)* 79−34782
potential field data, constrained inversion, use of pseudohyperellipsoids 80−85752
potential field data, interpretation using information theory and cybernetics 77−73861
potential field data, wavenumber domain methods 80−51559
potential field data interpretation, generalized matrix inversion method 77−87087
potential field modelling, end corrections 80−85580
potential field studies, satellite data application to regional anomaly surveys 80−51558
potential field transformation from relief to single reference plane, Fourier anal. appl. *(Russian)* 78−53759
potential fields, statistical interpretation with covariance functions 77−73873
potential fields, two-dimens., filtration and transformation algorithms *(Russian)* 78−3968
potential fields, two-dimens. and three-dimens., in freq. domain, equivalence theorem *(Chinese)* 79−88478
potential fields analysis on sphere, use of stochastic functions theory 80−56338
potential fields due to vertical circular cylinder and dike, statistical anal. 79−34972
potential fields extrapolation numerical techniques *(Russian)* 79−74988
potential fields inclined dykes interpretation in wavenumber domain 79−92630
potential fields linear analysis, general theory *(Russian)* 79−35011
power density spectrum estimation from finite length signal 77−91337
power spectrum analysis, nested variance technique, space physics, appl. in FORTRAN 77−87275
precession, lunisolar, determ. via obs. of extragalactic radiosources 77−5129
precision levelling with two-fluid tiltmeter 77−21919
prediction of geophysical events, overview and recommendations 79−8703
predictive multiple wave filtering *(Russian)* 79−58115
pressure and temp. indicators, using margarite stability and compatibility relations 77−5183
principal components analysis, appl. to interpretation of National Uranium Resource Evaluation (NURE) aerial survey data 80−101438
production mapping with orthophoto digital terrain models 79−84545
prospecting, analysis of statistical distribs. rel. to seismic exploration for bauxite *(Russian)* 77−9561
prospecting, effectiveness of geophysical and geochemical methods, evaluation *(Spanish)* 77−9552
proton activiation analysis of B and Li local levels in minerals, rocks and ores 79−74477
proton magnetometer, synchronous polarisation method advantages *(Russian)* 77−60482
proton multiprobe and fission track techniques for element distrib. determ. in zircon 80−17261
pulse neutron logging in inhomogeneous beds, data interpretation theoretical bases *(Russian)* 79−44273
pulse-probe method of thermal cond. meas. 79−53533
pyroxene geothermometry and geobarometry, subsolidus phase relations in CaO-MgO-Al_2O_3-SiO_2 system 79−16440
quantitative image analysis, applic. to mineralogy *(French)* 79−5631
quantitative ion-microprobe analysis, geochem. appls. 79−34976
quartz c-axis fabrics anal., photometric method 80−101456
radar altimetry data, smoothing processes for Geos-3 data 80−4144
radar auroral substorms, signatures of auroral east-west motions 77−29535
radar auroral substorms, signatures of expansive and recovery phases 77−25812
radar meas. of snow drift *(Japanese)* 77−82032
radar mosaicing, side-looking mapping errors and their reduction 77−13135
radar probing for rock salt 78−96215
radar reflection factor data, cartesian interpolation and display 80−31136
radar remote sensing of Earth's surface, techniques, review 79−12294
radiation balance meas. as instrument design problem 77−41173
radiation budget meas. by satellite, climate appls. 80−109283
radio echo sounding through ice, obs. in W Dronning Maud Land, Antarctica (1974) 77−86838
radio methods, quasi-single freq. Doppler-Faraday technique 80−77128
geophysical techniques continued
radioactive tracer detection techniques, flow problems appl. *(Japanese)* 78−96320
radioactivity, secular equilib. investigation method 79−2381
radioactivity of large volume geological samples, absolute activity determs. 80−56643
radiocarbon dating, ^{14}C detect. via small van de Graaff accelerator 79−11844
radiocarbon dating, ^{14}C enrichment method 79−10220
radiography of geological specimens for determ. of α- and fission-activity 78−20540
radioisotope dating using cyclotron as mass spectrometer 77−64489
radioisotope detection with tandem electrostatic accelerators 80−61923
radiometric imaging from space, atmosphere effects problems 80−98323
radiometric meas. of radioactive ores, effective γ-ray attenuation coeffs. 77−25680
radiometry, multispectral , by tethered balloon, of plants and soils 78−3958
radiometry diagrams, statistical standardisation check *(Russian)* 78−69483
radiophysical methods for investigation of environment *(Russian)* 77−78435
rainfall simulation, for evaluation of surface mine spoils area restoration, Wyoming 77−49094
random data filtering, effects of detrending and smoothing 78−40685
random oscills., RMS level estimation, fast method 77−70857
rapid interpretation method for gravity anomalies caused by sedimentary basins 77−87110
rare earth elements, determ. in geological materials, using thermal and epithermal neutron activation 78−7797
rare-gas radioactive dating, evaluation of double-spiking procedure for K-Ar dating 77−60473
ray theoretical inverse methods in geophysics 79−53578
ray theoretical seismograms, construction methods 79−34761
Rayleigh dispersion function computations for unlimited freq. values 80−21837
real time detect. and location of seismic events in central California 77−73654
real-time multispectral feature classification by analogue CCD 78−24438
reconstruction technique algorithms appl. to subsurface EM profiling by HF meas. 77−45199
recrystallised grain size geopiezometer, applicability limits 78−85715
recursive derivation of reflection coefficients from noisy seismic data 78−73324
recursive filters for potential field data processing 77−2268
recursive multichannel max. entropy spectral estimation 78−53735
reduced three rosettes measuring method for ang. deviations determ. *(German)* 77−60497
reflection seismic recordings, minimum entropy deconvolution 78−81423
reflection seismograms, simultaneous spherical divergence correction and optimal deconvolution 80−98258
reflection seismograph data, maximum likelihood filtering 79−5453
reflection seismology, curved interfaces determ. in bidimensional inhomogeneous media via time fields method *(Russian)* 79−35010
reflection seismology, multiple reflections and head waves in Gulf of Suez 80−56400
reflection seismology, synthetic seismograms at non-vertical incidence 80−56401
reflection seismology, tool for energy resource exploration, book 78−96162
reflection seismology, use of kepstrum in signal anal. 78−81425
reflection seismology, wavefront synthesis for vel. estimation and downward continuation 79−16392
reflectivity meas. by radar and disdrometer, comparison for rain 79−53546
refraction seismology, time term method anal. 79−66838
regional evapotranspiration, determ. from upper air meteorological data 77−91171
regularization method and uniqueness problems in study of regional flat-layered structs. 78−49161
regularization method in mag. and gravity anomalies interpretation 78−49163
remanence direction from converging remag. circles, least-squares method 77−45182
remote inspection of ground sites, cost/effectiveness model 77−91319
remote sensing, agricultural cover types separability in spectral channels and wavelength regions 80−98468
remote sensing, appl. of space television survey to obs. of Carpathian disjunctive dislocations *(Russian)* 80−104958
remote sensing, appls. in SE Sumatra coastal environment 79−53556
remote sensing, appls. of technology 77−5349
remote sensing, atmosphere, temp. and emittance effects on data 77−78393
remote sensing, atmospheric effects on radiative transfer, conference, San Diego, California (1979 August 29 to 30) 80−62376
remote sensing, atmospheric light diffusion estimation using const. transmission function 80−4100
remote sensing, book 80−101675
remote sensing, clay soil sand content determ. from percent reflectance 80−56475
remote sensing, design and pot. of decision tree classifier 77−56745
remote sensing, Earth scene dynamics as viewed by satellite-borne mosaic sensor 80−90321
remote sensing, eqn. for pot. evaporation from soil, water and crop surfaces 77−64334
remote sensing, error probability estimation without ground truth and known a priori probabilities 77−56746
remote sensing, evaluation of atmospheric effect on aerospace information 80−4101
remote sensing, evaluation of LANDSAT image data for land-use mapping 80−101443
remote sensing, factor analysis approach to spectral interval selection 79−88503
remote sensing, geological faults and linear features detect. from LANDSAT images 80−77177
remote sensing, geological interpretation from composited radar and Landsat imagery 80−56647
remote sensing, image processing and information extraction 77−64438
remote sensing, introductory review 77−2286
remote sensing, Landsat digital image rectification system 77−56734

geophysical techniques continued
remote sensing, Landsat forest and range inventory of S.E.Texas counties 77−56748
remote sensing, multispectral information volume optimisation in natural formations studies 80−4118
remote sensing, principles and interpretation, book 79−12319
remote sensing, recent developments 77−23752
remote sensing, sampling designs to test land-use map accuracy 80−17226
remote sensing, selective radiant temp. mapping using layered classifier 77−56750
remote sensing, study of Earth by astronauts *(Russian)* 78−40795
remote sensing, survey of methods and appls. 78−77364
remote sensing, synthetic aperture radar, appl., technology trends 79−5655
remote sensing, thermal inertia imagery of Earth surface, model for calibration of survey 80−105083
remote sensing, track-type, sampling requirement estimation 77−78507
remote sensing, via new type programmable multichannel radiometer 80−77253
remote sensing, visual observations of environment from space *(Russian)* 78−40796
remote sensing and ranging systems from space, conf., Rome, Italy (March 1980) 80−105432
remote sensing by artificial satellite *(Japanese)* 79−74977
remote sensing by Skylab microwave radiometer 78−16273
remote sensing by stereo side-looking radar, accuracy anal. 80−56646
remote sensing data (multispectral), contextual classification 80−77149
remote sensing data interpretation, computer-assisted analysis techniques 78−7776
remote sensing image data processing/acquisition techniques 78−61627
remote sensing of atmosphere, land and sea props. 78−93015
remote sensing of Earth from space, role of 'smart sensors', book 80−62402
remote sensing of environment, automated digital data handling 78−3960
remote sensing of forestry, digital signal preprocessing and postprocessing aspects of data analysis, book contrib. 79−92634
remote sensing of global phenomena by automatic satellites 77−64457
remote sensing of layered random media, radiative transfer theory 80−36413
remote sensing of natural resources, use of photographic imagery 77−64454
remote sensing of near-surface soil moisture, theory for passive microwave technique 77−87105
remote sensing of random media, theory 80−51571
remote sensing of stratified media, pulse-spectrum technique, permittivity determ. 79−8722
remote sensing technology, Canadian advances 78−16170
remote sensing technology developments and appl. *(Japanese)* 79−8701
remote sensing using multispectral scanner, parametric model 80−77261
remote sensing using solid-state linear array appls., user-oriented data processing 80−4151
remote sensing using solid-state linear array technology 80−4150
remote sensing with SAMIR, satellite microwave radiometer 80−56638
remote-sensed data texture anal. in computerised picture processing 78−61628
remote-sensing data, computer elaboration and image processing 78−40690
remotely sensed data machine processing, symposium, West Lafayette, IN (1979 June 27 to 29) 79−88473
remotely sensed data processing, conf., West Lafayette, Ind., USA, June 1977 77−78488
resistance logging, continued fractions method appls. *(Russian)* 78−3971
resistivity anomalies over buried conducting dykes, model tank expts. 80−85582
resistivity curves, finite difference evaluation method 80−89937
resistivity curves of horizontally multilayered models, calc. methods 80−46283
resistivity finite-difference modelling, practical approach 79−29878
resistivity mapping using combined telluric profiling technique *(French)* 78−69285
resistivity meas., LF electromagnetic wave method for soil *(French)* 78−24394
resistivity modelling, arbitrary two-dimensional structures 79−92617
resistivity of Earth interior, in uppermost kilometres on continental areas 78−24219
resistivity profiles, electrode arrangement comparison 79−88486
resistivity sounding, buried electrode data interpretation using layered Earth model 79−29701
resistivity sounding, computer program for related Hankel transforms numerical integration 79−92599
resistivity sounding, dipole to Schlumberger curve transformation by digital linear filters 78−45015
resistivity sounding, direct, interpretation by accumulation of layers 80−101322
resistivity sounding, direct interpretation, developments 77−9530
resistivity sounding, filter determination, Wiener-Hopf least squares method 79−92621
resistivity sounding automatic interpretation 77−49192
resistivity sounding by bipole-dipole method, theory 80−101450
resistivity sounding interpretation, approx. method 77−41185
resistivity sounding interpretation without borehole control 77−9328
resistivity sounding master curves, rapid computation 80−51560
resistivity survey, noise elimination, fluctuating Earth currents 79−92480
resistivity survey, VLF, effects of topography, flight altitude, wavetilt phase and amplitude 79−84093
resistivity-logging measurements, formation anisotropy effects 79−92611
resistivity/induced polarisation (IP) soundings, appl. to saline water and fresh water zones delineation 80−104867
RESMAC seismic array, interactive epicentre location procedure 78−65395
resource management, conf., Alamogordo, NM, USA, 1978 78−69541
rinneite, Rb-Sr dating of potash salt deposits 80−67429
rock chem. weathering rate 80−77142
rock cleavage, morphological classification 80−21736
rock crack mapping by obs. of seismic velocity anisotropy 80−98253
rock deformability, determ. by in situ methods 80−17411
rock deformation measurement, expt. using transmitted light technique 77−86860

geophysical techniques continued
rock discontinuities, suggested methods for quantitative description 79−84513
rock dynamic strength determ., reflected shear wave technique 78−57344
rock formation and penetration zone elec. parameters determ., probes number and type *(Russian)* 79−39969
rock joint orientation meas. evaluation in terms of regional stress 77−64487
rock joints roughness determination, new laboratory method 78−96315
rock layers, adjacent, material const. determ. using seismic refl. *(German)* 80−105054
rock magnetisation, meas. of laboratory sample 80−46271
rock magnetism, domain structure obs. by Lorentz electron microscopy 80−72502
rock magnetism, stratified anisotropy diagnosis possibilities 77−33061
rock magnetism methods, rot. magnetisation acquired during demagnetisation process 80−36295
rock mass deformability determ., in situ tests 79−53341
rock materials, strength determ. in triaxial compression, suggested methods 78−81432
rock materials tensile strength determination, suggested methods 78−96314
rock mechanics, appl. of AE *(Japanese)* 78−56845
rock movement, suggested methods for monitoring using borehole extensometers 79−84512
rock movement monitoring using inclinometers and tiltmeters 78−28318
rock permeability est. techniques test *(French)* 79−34801
rock pore aspect ratio spectrum determ., seismic velocities inversion 80−51387
rock samples, fused, X-ray fluoresc. anal., fundamental parameter method 77−77820
rock samples, removal of rot. remanent mag. acquired during alternating field demag. 77−60474
rock samples, Sn determ. by neutron activation method 78−85258
rock specimens impulse response estimation, numerical method and appl. to laboratory data 79−80049
rock strain, estimation from deformed ellipsoidal objects, algebraic method 77−21766
rock strain determination using randomly oriented strain markers 78−3765
rock strength tests, irregular specimen versions 78−7791
rock stress meas., conference (Sydney, 11-13 August 1976) 77−9573
rock stress meas. using anelastic strain-virgin stress relationship 77−9416
rock stress measurement, borehole jack fracturing technique 77−64488
rock stress measurement, hydrofracturing method and recent field results 79−29885
rock stress relaxation method at Akabira coal mine 77−9423
rock stress release, improved method for underground openings 77−9424
rock structure analysis, acoustic method *(Russian)* 80−85760
rock thermal conductivity determ. from fragment meas. *(Rumanian)* 78−20563
rock thermal conductivity measurement, steady state plate method *(Chinese)* 80−56615
rock type discrimination, Landsat filters assessment using laboratory spectra information 79−16791
rocks, anal. of small samples using X-ray quantometer 78−61112
rocks, analysis, for C_2-C_9 hydrocarbons, gas chromatographic method 79−39226
rocks, ancient metamorphic, study, appl. of geophysical and geological data combined anal. *(Russian)* 79−8630
rocks, complex resistivity meas. by freq. domain method *(German)* 80−4001
rocks, edge-fracture anal. method 77−21765
rocks, finite and incremental deforms. determ. from planar subfabrics in S-tectonites 77−21767
rocks, finite strain anal. using lines with initial random orientation 78−20568
rocks, fracture propagation by transient cooling 79−84236
rocks, igneous, crack porosity calibration from thermal cycling cracks 79−29759
rocks, multiphase magnetizations, recognition and separation techniques 78−28349
rocks, petrographic description, suggested method 78−81431
rocks, polygonal strain markers adaption 78−20567
rocks, Sc determination by neutron activation analysis using ^{46m}Sc 79−79356
rocks, silicate, carbonate, trace element anal. using computerised automatic X-ray fluoresc. spectrograph 77−56320
rocks, stress meas. methods in Norway 77−9422
rocks and minerals, multielement analysis by photon or neutron activation 78−12018
rocks elastic properties determination, modified borehole jack method 78−81448
rocks experimental folding under confining press., drape folds partially scaled models 79−58127
rocks hardness and abrasiveness determ., suggested methods 78−96313
rocks jointing, distinguishing of regional directions from joint sets assoc. with individual structs. 77−86876
rocks magnetic components, separation from alternating field step demagnetisation data 79−16444
rocks magnetic susceptibility anisotropy meas. using inductive magnetometers 78−85541
rocks modal analysis, error assoc. with point-counting 78−32232
rocks sound velocity determination, suggested methods 78−81433
rocks tensile strength indirect measurements, new theoretical aspects 79−29883
rocks texture heterogeneity, study via dielectric const. and elec. resistance *(Russian)* 78−96195
S-wave vel. meas. in soil and bedrock using down-hole method 80−98458
sand, triaxial test, bifurcation anal. 79−70783
SAR/LANDSAT data set assembly and anal. 77−78493
satellite altimetry, appl. to ocean geoid spectrum determ. 80−3904
satellite altimetry, refinement of short arc adjustment model 77−60336
satellite and lunar ranging, future developments 77−64483
satellite data collection with Geostationary Operational Environmental Satellite 79−29977
satellite determined gravity results, geophys. and geodetic appls. 77−25634

geophysical techniques continued
satellite Doppler geodesy, appl. to Great Britain triangulation geocentric positioning 79−29695
Satellite Emission Radio Interferometric Earth surveying (SERIES), GPS geodetic system 79−100804
satellite geodesy, appl. to adjustment of N American horizontal datum 77−2079
satellite geodesy, role of orbit determ. in altimeter data anal. 78−77177
satellite gradiometry for geoid improvement in local areas 78−36295
satellite imagery, computer-generated gridding 77−21930
satellite imagery, filtering to remove cloud cover 77−56744
satellite images macrophotography, technique 79−29895
satellite laser tracking, latit., time and height var. meas. at single station 77−32976
satellite laser tracking data, horizontal refractivity gradient correction 77−91276
satellite laser tracking for polar motion, Earth tides and latitude determ. 77−56570
satellite multispectral data digital anal. for land use inventory/mapping 77−78541
satellite on-board processing for Earth resources data 78−61626
satellite range measurements, formula for refr. effects computation 78−73609
satellite remote sensing for Earth resources surveying 77−25788
scanning electron microscopy for mineralogy 80−82077
scattering from vegetation, first-order renormalization method appl. 77−87099
sea surface topography, altimeter data analysis by sequential filter 80−4145
seafloor surface geothermal survey, techniques and results *(Russian)* 78−40527
sediment and nutrient loadings to Lake Ontario calc., methodological arguments 78−77278
sedimentary rocks, acoustic anisotropy due to overburden press. 80−56455
sedimentary rocks, epithermal neutron activation anal. of Re 77−9153
sedimentation rates determ. in rapidly accreting salt marsh by ^{137}Cs dating 78−96247
sedimentology, ellipsoidal grain thin sections, Monte Carlo simulation 77−5332
sediments, α-spectrometric dating method, using ^{210}Po 78−28350
sediments thermal cond. meas. using probes with semiconductor temp. sensors *(Russian)* 78−65431
seismic air gun operational method, pulse generation 80−90234
seismic analysis, appl. of PAL, highly tutorial interactive pattern recognition program 77−81833
seismic analysis and discrimination, computer-aided 78−20530
seismic anisotropy investigations in USSR, techniques 77−49038
seismic array and network automatic detect. 77−9516
seismic array recorded signals, apparent vel. and azimuth meas., computer programs 79−84522
seismic body waves, apparent phase vel. determ. 78−16177
seismic body-wave inversion method for Earth struct., using travel time and amplitude data 80−109108
seismic boundary delineation, with respect to reflecting areas preassigned parameters *(Russian)* 79−74857
seismic boundary images, reconstruction using numerical models *(Russian)* 79−39923
seismic coda appls. to seismic wave damping studies *(Russian)* 78−11824
seismic coda of local earthquakes, synthesis method 77−73683
seismic common-depth-point stacking, appl. of multirate digital filtering approach to interpolation 79−29876
seismic critically refracted rays, numerical tracing 78−7783
seismic cross sounding, data interpretation via reflected wave method *(Russian)* 78−92796
seismic data, acoustic imaging, source receiver coincident profiles 79−92615
seismic data, common depth point ray modelling for three dimensional isovelocity layers 77−21914
seismic data, deconvolution with l_1 norm 79−88484
seismic data, iterative stacking algorithm for signal separation 79−92612
seismic data, migration in terms of spatial deconvolution 79−88256
seismic data, nonlinear sweep techniques 79−92616
seismic data, optimum mixed delay spiking filters appls. 78−77346
seismic data, simultaneous inversion methods and resolving power 79−16699
seismic data, single-channel white-noise estimators for deconvolution 78−77345
seismic data, stratigraphic sequences, differentiation by statistical anal. 79−92503
seismic data, suppression by long leg multiples by coherency weighting 79−92613
seismic data, technique for dispersion continuous representation 80−51334
seismic data, time varying prediction filtering 79−92614
seismic data analysis, appl. of wavefront curvature expression in layered medium 79−29712
seismic data analysis, migration by phase shift-algorithm for array processor 80−72638
seismic data colour TV display system 79−74995
seismic data deconvolution, overview 77−91060
seismic data deconvolution, review 78−53736
seismic data deconvolution techniques for extraction of reflectivity function from seismic trace, book contrib. 79−92635
seismic data deconvolution using homomorphic filtering 77−91063
seismic data filtering and smoothing, least-squared error, stationary and nonstationary 80−4158
seismic data inversion, appl. of revised Earth mass and moment of inertia 77−86735
seismic data migration, collocation formulation of wave equation migration 80−4126
seismic data migration by Fourier transform 78−77341
seismic data migration in two and three dimens., integral formulation 78−77342
seismic data processing, Karhunen-Loeve transform. appl. *(French)* 79−44258
seismic data processing procedure *(Russian)* 79−21036
seismic data spectral estimation, novel aspects 77−91336
seismic deconvolution, influence of phase prop. of random noise finite realisation 79−44254

geophysical techniques continued
seismic deconvolution and wavelet estimation 78−20542
seismic depth migration after stack, finite-difference method 80−98254
seismic depth migration before stack, finite-difference method 80−98255
seismic depth-time conversion with weighting *(Russian)* 77−45194
seismic discrimination, via dynamic spectral ratios with variable freq. bands 77−81834
seismic discrimination improvement for nuclear explosions and earthquakes using pattern recognition 78−40694
seismic event classification, extraction and use of broad-band P-wave pulse 77−81830
seismic event detection probability, direct estimation method 80−67347
seismic events correlation in time section, algorithm *(Russian)* 79−39962
seismic events identification, appl. of non-linear stochastic models 79−16396
seismic events visual correlation quantitative estimates based on min. average risk criteria *(Russian)* 79−44133
seismic exchange waves method, appl. to Cuba crust study *(Russian)* 79−44158
seismic exploration, apparent attenuation due to intrabed multiples 79−16393
seismic exploration, effect of multiple scatt. on wave field spectral comp. *(Russian)* 79−8607
seismic exploration, iterative identification of non-invertible autoregressive moving-average systems 78−81422
seismic exploration, nature of arc-shaped line-ups common depth point seismic profiles *(Russian)* 79−44134
seismic exploration, technique and processing, book 80−51975
seismic exploration, wave front eqn. and travel time in weathered layer 77−78122
seismic exploration of laterally inhomogeneous media, wavefront curvature theory 80−104908
seismic facies analysis 78−96151
seismic fan shooting and least-squares analysis of non-layered anomalous vel. zones. 79−57857
seismic fault location in underground coal seams 80−94613
seismic fields, decomposition algorithm from charact. numbers and vectors of spectral matrices 77−9370
seismic freq. selection for CDP method in regions with intense multiple waves *(Russian)* 78−12012
seismic gap quiescence duration determ. method 80−26627
seismic hazard and zoning maps, status and prospects in United States 79−44109
seismic hazard mapping in United States, prospects for geological data appl. 79−44110
seismic higher mode Rayleigh waves, study as individual seismic phases 79−62440
seismic holography, integral representations of space time functions *(Russian)* 78−85483
seismic holography, kinematic mutuality of reflected and refracted waves *(Russian)* 78−69298
seismic horizon recognition by factorial discriminant analysis *(French)* 77−41190
seismic images formation, systems based on two-point eikonal *(Russian)* 79−96740
seismic imaging 80−46130
seismic imaging by holography, techniques and appls. 79−66831
seismic imaging of faults in multi-moded coal seams 80−85778
seismic instrument response, parametric expression scheme 77−91286
seismic intensity mapping method and application to Sweden 80−105089
seismic interfering wave separation problem soln. *(Russian)* 77−91042
seismic interpretation, time-to-depth conversion for layered medium 78−3962
seismic inverse and spatial filtration by reflected wave method *(Russian)* 78−3970
seismic inverse problem appl. of control theory 79−2402
seismic inverse problem for two-dimensional velocity variations 80−21833
seismic inversion for boundary shape between two layer stacks 79−16684
seismic method for studying underground rock destruction 77−9419
seismic microvibration frequency analysis by 50 m interferometer 80−109276
seismic microzoning, mapping method based on subsoil conditions 79−44108
seismic microzoning methods, need for experimental evidence 79−88514
seismic moment, method of determination from seismological bulletin data 80−89980
seismic moment determ. for local earthquakes using coda charact. 77−9534
seismic moment tensor estimated by linear inversion method 80−31125
seismic multidimensional velocity generalisation technique, appl. to Black Sea NW shallow and nearby land areas *(Russian)* 80−105068
seismic multiple reflected signal attenuation, least squares estimation procedure 80−85596
seismic multiple waves, prediction filtering in non-ideal conditions *(Russian)* 79−44131
seismic noise sources mapping in geothermal regions 77−81828
seismic observations digital processing, steady numerical solns. *(Russian)* 79−53317
seismic P-waves, inversion of vel. anisotropy 77−49017
seismic pattern, automatic recognition 77−81831
seismic pattern recognition, fundamental problems 78−81428
seismic profiles, two-dimens., dip-domain migration 78−77343
seismic profiling, continuous, with two receiver systems, effective vels. determ. 80−31150
seismic profiling (vertical), travel-time curves, theory 80−94473
seismic profiling of Black and Azov Sea floor, methods 80−89970
seismic prospecting, common depth point vels. critical values for stratified homogeneous forms. *(Russian)* 79−39668
seismic prospecting, inverse kinematic case soln. in layered Earth using reciprocal points *(Russian)* 79−44268
seismic prospecting, inversion of refl. data 77−21915
seismic prospecting, minimisation of distortion caused by geophone-ground coupling 79−44256
seismic prospecting for coal, approx. diffr. theory for transparent half-planes 80−89974
seismic prospecting problem soln. *(Russian)* 79−74859
seismic ray series method and dynamic ray tracing system for three-dimensional inhomogeneous media 80−98456
seismic ray tracing, three-dimens. methods 77−73870

geophysical techniques continued
seismic ray tracing, two-point problem, adaptive finite difference method 80−98457
seismic Rayleigh channel waves for reflection method, dipping coal seam discontinuity obs. 78−69471
seismic raypath migration, using programmable pocket calculator 78−7784
seismic recordings, information quality and data processing techniques efficiency *(Russian)* 79−39666
seismic recordings, multiple wave suppression problem soln. 80−77147
seismic recordings, time-variable curvilinear anal. *(Russian)* 79−39946
seismic records, combined separation of interfering signals *(Russian)* 78−12011
seismic records, combined spectral anal. for determ. of geologic section props. *(Russian)* 78−40696
seismic records, surface multiples suppression 80−56402
seismic reflected wave travel times inversion 77−56595
seismic reflection, synthetic seismograms for case of receiver within reflectivity zone 77−86786
seismic reflection coefficients, determ. from waves 79−44115
seismic reflection data dynamic corrections, fast algorithm 78−3966
seismic reflection data inversion 78−96307
seismic reflection profiles of marine sediments, multivariate statistics tech. and cluster anal. 79−2385
seismic reflection profiling on land with controlled source 77−64450
seismic reflection recordings, control theory appl. to inverse problem *(French)* 77−87081
seismic reflection sounding, wave eqn. migration with absorbing boundary conditions 80−104907
seismic reflection traveltime data, computerised method for effective vel. 80−21832
seismic reflectivity method extensions 80−56640
seismic reflector parameter estimation by virtual image technique 78−40681
seismic refr. survey depth determination, program for pocket calculator 80−82088
seismic refracted wave correlation method, interpretation accuracy *(Russian)* 80−85758
seismic refraction, influence of vel. lateral vars. on interpretation 77−21686
seismic refraction method, vel. determ. and error anal. 80−90229
seismic refraction method, velocity inversion errors, computation and recognition 80−4132
seismic refraction parameters, nomogram for rapid computation 78−7785
seismic refraction surveying, offshore, nonexplosive energy sources *(Russian)* 78−53752
seismic refraction technique for geophys. surveying, teaching 79−97161
seismic refraction waves, time-distance curve analysis methods *(Japanese)* 77−17038
seismic refractor velocity determ., cause and nature of errors 80−56621
seismic risk in S.Europe through to India, using Gumbel's third distrib. of extreme values 80−21648
seismic sections, construction as Earth pictures using stacked recordings of controlled directional reception *(Russian)* 79−39960
seismic SH-waves propag. in stratified medium with local inhomogeneities, finite element treatment *(Russian)* 79−34763
seismic shocks, location with imperfect knowledge of seismic wave path hodographs *(Russian)* 79−35009
seismic signal detection and parameter estimation 79−92502
seismic signal separation from records by interference system spectral synthesis *(Russian)* 77−91043
seismic signals, detect. under conditions of limited information about signals and noise 77−9536
seismic signals, optimal multichannel filtering evaluation taking account of amplitude and phase jitter *(Russian)* 78−40697
seismic signals adaptive deconvolution 77−91062
seismic signals anal. by phase plane method, explosion technology 79−66843
seismic signals deconvolution, adaptive filter structs. 80−98451
seismic sounding, common-depth-point method, prestack migration method for deformed refl. layer 80−98251
seismic sounding, computer-aided data interpretation 77−41202
seismic sounding, data analysis method for wave eqn. migration 80−90233
seismic sounding, iterative ray tracing between boreholes for underground image reconstruction 80−98466
seismic sounding, normal moveout velocity, 3-D problem with curved interface 80−101336
seismic sounding, screening in media with inclined boundaries *(Russian)* 78−92794
seismic sounding, spectral characts. of refl. waves near bright spot anomalies *(Russian)* 79−53319
seismic sounding, wave-equation datuming technique, appls. and computations 80−51553
seismic sounding, weathering correction method 79−44255
seismic sounding of ocean crust, suppression of sea-floor multiples 80−90231
seismic source depths, improved determ. using seismic coda 77−81829
seismic source located by surface waves, reference point equalisation method 80−72648
seismic source props. determ. by seismograms linear inversion 78−65394
seismic spectral-ratio analysis, appl. to Moho depth determ. under NORSAR array 77−86814
seismic station magnitude correction determ. with selected references 77−33202
seismic station situated on anisotropic ground, body wave propagation *(Russian)* 80−31128
seismic stations calibration, appl. of crustal spectrum characts. *(Russian)* 78−49158
seismic stripping, appl. to deep refls. unravelling 79−34970
seismic strong motion prediction for pot. earthquake fault, barrier model 80−105053
seismic surface wave data inversion in source mechanism studies 77−33204
seismic surface wave dispersion, digital processing *(Chinese)* 78−24374
seismic surface wave dispersion function, computations for unlimited freq. values 79−74848
seismic surface wave group vel. determ., optimum filter 77−56736
seismic surface wave phase vel., partial derivatives calc. algorithm 80−4140
geophysical techniques continued
seismic surface wave processing using PDP-15 interactive graphics 77−81818
seismic surface waves, anal. using PDP-15 interactive graphics 78−81427
seismic surface waves analysis, new techniques appl. to Adriatic subplate averaged model 79−44159
seismic surface waves dispersion curves, partial derivatives calc. *(Russian)* 79−34764
seismic surface-wave ray tracing, appls. 79−66630
seismic survey data analysis, sequential anal. method 80−89981
seismic surveying, features of time sections in two dimensionally inhomogeneous media 77−44933
seismic surveys, establishment of zero time 77−21916
seismic surveys, residual static and crossdip corrections simultaneous estimation 79−92500
seismic techniques for crustal struct. study 77−45169
seismic three-component registrations, interpretation via orthogonal regression *(German)* 78−32017
seismic transverse waves in rocks, identification techniques 77−21682
seismic travel time inversion, for 3-D vel. struct., Backus-Gilbert method 80−21838
seismic travel time inversion, geometrical approach 80−3946
seismic travel time inversion 79−70891
seismic travel times in plane layered media, computation 77−41191
seismic travel-time curve analysis-using computer *(Japanese)* 77−17226
seismic travel-time inversion method, for earthquake location and vel. struct. 80−109109
seismic traveltime data nonlinear least-squares inversion 80−4124
seismic V_P/V_S as a potential hydrocarbon indicator 77−17102
seismic-vel. data analysis using interference methods *(Russian)* 77−45193
seismic vel. determ. by reflected wave method, thin stratification effects *(Russian)* 77−44936
seismic vel. estimation, arrival time functions and max.-likelihood detector 78−45013
seismic velocity analysis, accuracy of determ. kinematic parameters of regular events *(Russian)* 79−39944
seismic velocity anomaly mapping by graphical method 80−77146
seismic velocity determination, overlying sequence stratification effect *(Russian)* 79−39961
seismic velocity determination in formations with curved interfaces *(Russian)* 78−53748
seismic velocity of lower mantle, meas. using wide aperture array 80−105071
seismic velocity profiles, synthesis from geotechnical data 79−88516
seismic velocity-depth structure, using waveform inversion method 80−105060
seismic vertical profiling, horizontal stacking technique *(Russian)* 79−62619
seismic vibrator signals, non-sinusoidal, theory 80−82086
seismic wave filtering and group and phase vel. determ. 79−35005
seismic wave front control method in seismic surveys and shooting data processing 80−90238
seismic wave onset detection, algorithm for automatic seismometer *(Japanese)* 80−94476
seismic wave production by camouflet source, theory 80−101344
seismic wave reflection at wide angles, travel times, interpretation method 78−65202
seismic wave spectral analysis, total field structure anal., autocorrelation functions 80−4142
seismic wave time residuals, P waves, three-dimens. inversion 80−21849
seismic wave travel times, meas. via method of seismically conjugate points 77−9368
seismic wave vel. calc. using reflection amplitude 78−69296
seismic waveforms extrapolation, by Fourier methods 79−34978
seismic wavelet estimation, short-time homomorphic signal anal. appls. 78−81426
seismic wavelet estimation using short-time homomorphic signal 78−88930
seismic waves, absorpt.-conditioned transition functions estimation and props. *(Russian)* 79−53318
seismic waves, reflection coeffs. identification from noisy data 79−29718
seismic waves converted from P to SV in mantle, detect. technique 77−81810
seismic waves definition in far field, criteria *(Russian)* 79−39965
seismic waves group velocity, high resolution anal. appl. to explosion and earthquake 78−81111
seismic waves higher mode dispersion, meas. technique 79−39974
seismic waves two-dimensional refl. time-delay curve, approximation for arbitrary refl. surface *(Russian)* 79−44132
seismic waves velocities investigation, new methods using common-point obs. *(Russian)* 79−74981
seismic waves with different velocities, separation using nonlinear interference systems 77−78438
seismic wide-angle refl. data from expendable sonobuoys, display and processing 79−39896
seismic wide line profiling and two-dimens. version of CDP technique *(Russian)* 79−62615
seismic zoning, contrib. of geophysical methods, conference (Erice, Italy, 13-23 April, 1977) 79−44104
seismic zoning, earthquake elastic energy release, heat prod., and Earth inertia tensor changes 79−44106
seismic zoning map, new elements 79−44105
seismic zoning problems, effect of earthquake freq.-magnitude statistical parameters 79−44112
seismogram calculation, explosive source sounding of layered media 80−98250
seismogram construction and reconstruction, weighting factors 78−28330
seismogram inversion and pseudo velocity logs, lithology identification 77−87088
seismogram processing, for Rayleigh waves phase vel. investigations in middle Europe 79−44136
seismograms, digital processing, kinematic corrections *(Russian)* 79−39929
seismograms, iterative identification of noninvertible autoregressive moving average systems 77−81816
seismograms and images, automatic transform. to seismic sections *(Russian)* 78−49155
seismograph, long-period, transfer function determ., temp. effects 77−9518

geophysical techniques continued
seismological observatories and seismic instrument construction in Poland *(Polish)* 77−21911
seismology, admissibility of soln. to multilayered dynamic problem without consideration of multiples 77−73668
seismology, aftershock sequences relocation in Iran and Turkey, seismotectonic implications 79−44119
seismology, appl. of foam rubber model of stick slip earthquake 80−3947
seismology, appl. to Earth interior struct. determ., book 80−41962
seismology, automatic vertical time-depth curve approximation via successive layer detect. *(Russian)* 78−40700
seismology, comparative evaluation of methods for multiple waves suppression *(Russian)* 78−40515
seismology, complete microzonation procedure importance and existing methods reliability 79−34748
seismology, complex trace analysis and colour encoded data display 80−21646
seismology, correlation refraction method, appl. to granite terrain weathered zone 80−90230
seismology, deconvolution and synthesis of multi-segment seismic traces 80−77162
seismology, diffracted wave travel times determ. method 80−8432
seismology, directivity function method appl. to source parameters of central California earthquakes 77−2112
seismology, effective vels. for stratified-isotropic media with interfaces, ray technique *(Russian)* 79−62614
seismology, finite-difference migration for steep dips 79−92620
seismology, glorified optics technique for wave propag. in nonplanar struct. 79−66629
seismology, higher-order refl. moveout spectra computation procedure 79−92501
seismology, initial phase anal. of R-waves from great earthquakes 80−41405
seismology, interference method for lower mantle radial vel. anomalies identification 79−25209
seismology, inverse problems interpretation *(Russian)* 79−34762
seismology, inversion anal. of static displacement data for Alaskan earthquake (1964) 80−30998
seismology, multichannel subtracting filters synthesis *(Russian)* 78−49156
seismology, multidimensional polarization analysis 78−73528
seismology, noise-resistance of optically generated correlograms *(Russian)* 78−40699
seismology, optimal vel. anal. in common depth point method *(Russian)* 78−40698
seismology, P_n vel. anisotropy anal. by MOZAIC time-term method 77−49013
seismology, props. of supercritical reflected waves from essentially nonplane seismic boundary *(Russian)* 79−8606
seismology, rapid convolution and correl. *(Russian)* 79−39959
seismology, ray amplitudes calc. of body waves in laterally inhomogeneous media 79−44118
seismology, ray approx. for laminated heterogeneous media *(Russian)* 78−69482
seismology, refl. areas parameters, estimation allowing for amplitude charcts. correl. *(Russian)* 79−74856
seismology, self-adaptive wave train subtraction in linear and three-dimensional surveying *(Russian)* 78−40695
seismology, signals resolution from coherent and incoherent noise, operators efficiency *(Russian)* 79−39963
seismology, similarity criteria for comparative anal. of elastic waves propag. vel. 79−96742
seismology, single-station fault-plane solution method 79−44263
seismology, small Friuli (Italy) shocks local magnitudes from total durations 79−34750
seismology, summation base restriction in seismic section migration *(Russian)* 78−40701
seismology, two-dimens. modelling of multiple reflections 77−2264
seismology, variational approach to elastic wave propag. in anomalous layers 79−44260
seismology, vertical stacking as reflection filter 78−12007
seismology common depth point data digital processing technique *(Russian)* 79−74875
seismology data reduction, approximate realisation, new techniques 79−70898
seismology methods in China, and earthquake prediction *(Rumanian)* 80−8257
seismology multiple waves freq. selection appl. to wedging out zones separation *(Russian)* 79−8706
seismology of ocean crust, expanded spread and const. offset profiling 80−56632
seismology profiling of deep crust struct., 2-D scheme 80−72637
seismometer beamforming array, linear adaptive algorithm 80−21834
seismometer calibration, in situ, modified step method 77−87101
seismometers, automated high-precision amplitude and phase calibration 77−9519
SEM, and assoc. microanal. by X-ray dispersive spectrometry applic. to mineralogy *(French)* 79−5630
SEM, wet, live and frozen objects, review 79−26183
separation method for normal and observed geomag. field 78−69479
sequential scene matching using edge features 78−32239
sequential search for geophysical objects, expt. design *(German)* 77−29464
SH waves, complete theoretical seismograms generation 77−45179
SH waves, complete theoretical seismograms generation 77−45180
shatter cones, geometry and description procedure 80−51398
shear wave vels. from down-hole meas. 77−70849
shear waves computation by ray method 79−53532
short arc adjustment model technique for oceanic geoid determination, satellite altimetry 80−21830
short range distance measurement by EM phase comparison technique 77−87090
side-looking airborne radar, Earth surface remote sensing appl. 78−20561
siesmic reflection coefficient calc. from digital data *(German)* 77−70853
sieving method for concentrating pollens and spores from fine grained sediments 80−17402
silicate HV high-resolution electron microscopy 80−70096

geophysical techniques continued
silicate measurement in anoxic pore waters, effects of oxidation during sampling 78−61394
silicate mineral, identification and asbestiform varieties, election optical and X-ray techniques 80−8446
silicate minerals Raman spectra, microscopic samples molecular analysis 80−57391
silicate rocks, X-ray spectral fluoresc. anal. 78−3762
similarity theory, use in Soviet work on geophysical fluid dynamics *(Russian)* 78−16174
sinter mineral samples, analysis by electronic microsonde *(Croatian)* 79−29910
Skylab imagery, method to differentiate saline from non-saline rangelands 77−91322
Skylab remote sensing data, inflight performance evaluation by ground-based meas. 77−64455
Skylab S-192 conical scanner data digital processing 77−82046
Skylab S-192 conical scanner imagery geometric evaluation 77−82047
Skylab spectral channel evaluation for classification and thematic mapping 77−78500
SLAR imagery correction for flight path curvature distortion 79−53553
slates age studies, $^{40}Ar/^{39}Ar$ stepwise outgassing method applicability 79−29721
snow cover parameters, microwave radiometry determination 80−56652
soil, shear wave vel. meas. during standard penetration test 78−48978
soil, thermal conduction flux in situ meas., methods *(French)* 78−96331
soil, thermal diffusivity, Fourier anal. of temp.-depth profile 79−44264
soil, thermal neutron constants, calibration of moisture gauges 77−25804
soil 81e p=sp 79−66836
soil and winter wheat yield on Great Plains, Landsat data evaluation 78−65351
soil automatic identification from digital terrain data 77−73884
soil bulk resistivity, meas. method 78−24381
soil homogeneity evaluation by radionuclide tracer breakthrough curve interpretation 80−97821
soil hydraulic conductivity, numerical calc. from suction press.-moisture retention relation *(German)* 79−2297
soil moisture and component estimation from spectral polarisation 79−16678
soil moisture calc. methods *(Russian)* 77−29493
soil moisture content measurement by microwave radiometry, review 80−17425
soil moisture IR thermography remote sensing through agricultural crop 80−109147
soil pattern data from aircraft/LANDSAT scanners delineation by digital anal., Indiana 77−78496
soil profile fundamental period estimation 77−9359
soil section cutting 79−80040
soil specific thermal resistance meas., theoretical basis and apparatus *(Rumanian)* 79−5461
soil surface moisture determination, photographic method for polarised visible light recording 79−53557
soil survey, lowland England, moisture content and soil discrimination from air photos 79−88504
soil temp. prediction from winter period meteorological data 77−37418
soil water content, estimation via total solar reflectance and spectral band ratioing 77−60479
soil water sampling, water regimes near porous cup samplers 77−66942
soil-water system, γ-ray transmission studies, calibration 80−26629
soils, multielement determ. by computerised instrumental neutron activation anal. 77−44546
soils, thermal props., transient measuring method *(German)* 78−61619
solar radiation incident at Earth surface, estimation from geostationary satellite data 80−82006
solid Earth tides, Fourier anal. applied to short data length 80−30972
solute loading and chem. denudation rate mapping in Devon, England 78−69375
solute transport in soils, two-site adsorption-desorption model evaluation 77−41101
sonobuoy and teleseismic study of Gulf of California transform fault aftershocks 77−25651
sounding of horizontally stratified media, geophysical problems unification 80−56622
sounding techniques, fundamental functions for horizontally stratified Earth 77−21918
sourcing method based on U, Th determ. in obsidian 79−2239
space geodesy, twin probes method 79−25443
space technology and scientific satellites, conf., Rome, Italy (Mar. 1977) 77−82107
spark source mass spectrography, geochemical appl., element sensitivity, precision and accuracy 78−20544
spatial filtering of higher Rayleigh mode phase vels. 78−77187
spatial spectrum of random field, use of reference sensor in autoregression evaluations *(Russian)* 78−61578
spectral anal., recursive multichannel max. entropy method 77−91338
spectral anal. of natural seismic events using autoregressive techniques 77−29470
spectral analysis of time series *(Italian)* 77−70841
spectral analysis of total mag. anomalies of step model 79−5450
spectral estimation techniques for discrete time series 78−53734
spectral feature enhancement of Landsat data, entropy minimisation *(Italian)* 80−98473
sphalerite geobarometer, experimental extension to 10 kbar 78−85703
sphalerite geobarometry, regionally metamorphosed terrain appls. 77−2257
sphalerite geobarometry in Balmat-Edwards district, New York 78−65261
spherical harmonic analysis of geomag. field 78−49164
SPOT, experimental Earth observation system, features *(French)* 77−82097
stable isotope abundances in natural compounds, meas. standards 78−32246
stable operational processes appl. to inverse geophys. problems 78−85718
static potential data inversion, generalized linear inverse 77−40967
static potential fields data inversion, generalised inverse appl. 78−77350
statistical algorithm for interfering seismic wave correl. *(German)* 77−25787
statistical algorithms for magnetic and gravity anomaly interpretation 77−70856
statistical algorithms for scaling geophysical fields 78−73527

geophysical techniques continued
statistical methods for gravity data in intermediate layer density estimates 78−15946
statistical methods for seismic activity analysis 77−41201
statistical processing of time series, spectral estimators *(German)* 77−70852
statistical theory of interpretation of geophys. obs., problems 79−84510
STEM/X-ray microanalysis, across α/γ interfaces in Fe-Ni meteorite 80−105212
stereogram production in geology, FORTRAN program 77−9521
stereophotogrammetry, automatic, using structural pattern recognition techniques 78−61632
stereophotogrammetry, digital profile to contour convertor, display 77−9501
strain ellipsoid estimation for large clasts in deformed rocks, down-plunge viewing method 79−92610
strain history of Dalradian slide using deformed pebbles 80−4013
strain meas. laser interferometer methods *(Japanese)* 79−25346
strained rock units, stratigraphic thickness determ. 79−21034
strata pressure determ. from seismic velocity *(Hungarian)* 80−21840
stratigraphic correlation by principal components, effects of missing data 79−25350
stratigraphic interpretation, appl. of synthetic sonic logs 79−88483
stratum velocities determination using seismic data, iterative method convergence *(Russian)* 79−74982
stress meas. in surface rocks using new cylindrical jack 77−9575
stress state determ. in transversely isotropic rock mass 77−56752
strong-motion data management developments 79−62629
structural mapping using two methods, optimal combination *(Russian)* 79−62617
structure estimation from acoustic reflection meas. 78−7818
submarine sediment recognition, sonoprobe surveying *(Japanese)* 79−39985
subsidence and ground movement, holographic interferometry 78−57343
subsurface layered media parameters, estimation using linearised multiple refl. model 79−5691
subsurface probing, using dipole antenna radiation patterns, of a two layered medium 78−7788
subsurface probing with horizontal magnetic dipole e.m. interference fringes method 77−5336
subsurface radar for Earth's surface remote probing 79−8724
subsurface radar using video pulse for deep probing in Earth, pulse propag. in lossy media using LF window 80−74282
surface albedo change, monitoring by LANDSAT 78−32104
surface geology sensed by ground mode radiowave propag., glaciated area of USA 80−76979
surface map of 0.8 cm microwave emission, satellite remote sensing *(Russian)* 80−77145
surface texture analysis with thermal and near IR scanners 79−53554
surface UV reflectance meas. from airborne platform, techniques and instrumentation 80−98453
surface waves, phase vel. and attenuation simultaneous inversion, Love waves in W North America 78−85491
survey data, collocation method 80−77125
surveying, collocation with help of Gaussian algorithm *(German)* 79−79730
surveying, interpolation via groups of triangulation data points of different statistical characts. *(German)* 77−9321
surveying, linear least squares interpolation, numerical aspects *(German)* 77−9322
surveying, reduction of influence of theodolite vertical axis error on horizontal angle meas. *(German)* 79−44278
swelling examination method for minerals 77−53232
synthetic aperture radar imaging in geosynchronous orbit 78−65442
synthetic seismogram computation, new method 78−85711
synthetic seismograms, calc. for spherical waves normally incident on plane parallel absorbing layers *(Russian)* 79−39667
synthetic seismograms, computation for impulsive waves in spherically symmetric model 79−74849
synthetic seismograms (one dimensional), effect of subsurface sampling 80−72435
synthetic-aperture radar on satellites, digital processing techniques 80−61914
Tau Inversion method for Hawaiian Ridge vel. struct. determ. 79−62467
technology transfer, problems in practice 77−78510
tectonic dislocation detection using seismic refraction methods *(Russian)* 78−12010
tectonic dislocations prospecting in complex media, appl. to seismic surface waves correl. method *(Russian)* 79−8605
tectonic processes modelling, appl. of creep rupture obs. in cold ice sheet 79−2306
tectonic stress directions in Alpine regions, correl. with joint orientations 80−105052
tectonodynamic regionalisation, appl. to Earth crustal struct. in Crimea *(Russian)* 79−8616
tectonomagnetic events, detect. using empirical transfer functions 79−16374
tectonomagnetic experiments, noise reduction by multivariate linear regression 79−84515
tectonomagnetism, improved signal discrimination and volcanomag. effect at Kilauea, Hawaii 79−92629
telluric and magnetotelluric methods, comparison for sedimentary structures 78−3713
TEM, application to mineralogy, sample prep. methods *(French)* 79−5629
temperature meas., transistor sensors for electrical systems *(German)* 79−30468
temperature meas. in shallow holes, Salton Sea geothermal field test 78−11849
temperature-dependent magnetic cleaning 77−41204
terrain analysis FORTRAN program 77−9509
terrain classification using colour imagery, algorithms 77−78466
terrain data production using distributed processing 77−37413
terrestrial electricity, mapping of induced currents around Kenya Rift, comparison of techniques 77−73628
terrestrial heat flow apparatus, used in N.China survey *(Chinese)* 80−56416
terrestrial surface temperature sensing, emissivity correction for thermal radiation interpretation 80−82092
tests for clastic rock softening *(Japanese)* 78−49013

geophysical techniques continued
thematic classified LANDSAT imagery of Portland, Oregon, tabular data base 77−78537
theoretical seismograms, for crustal vel. models constaints in central United States 79−39693
theoretical seismograms calc., reflectivity method for buried source 79−48421
thermal conductivity measurement of soil by probe method, minimisation of errors 77−17259
thermal conductivity measurements on saturated rocks at permafrost temperatures using divided-bar apparatus 79−84232
thermal inertia mapping by IR imagery, mathematical model 80−109280
thermal IR remote sensing, ground truth meas. 77−91318
thermal IR scanner analogue data digital processing 77−82045
thermal IR scanning, appls. to geology and hydrology 79−8723
thermal radiation from randomly inhomogeneous stratified media, calc. methods *(Russian)* 78−96312
thermal radio emission polarimetry, loss matrix 79−21069
thermoluminescence dating, appl. to deep-sea sediment core 79−74871
thermoluminescence dating, appl. to volcanic plagioclases 80−98475
thermoluminescence dating of rocks, appl. to Hawaiian alkalic basalts 77−86832
thermoluminescence dating of sediments baked by Chaine des Puys lava flows 78−92808
thermoluminescence radiation dosimetry appl. to radioactive minerals prospecting 78−32244
thermoluminescence spatial distribution, using image intensifier technique 80−47115
thermoluminescent dating of geological objects, appl. of natural quartz dosimetric props. 79−12288
thermoremanent magnetisation microanalytical recognition in ash-flow tuff 80−72497
three-dimensional potential fields conversion and pseudo-gravit. field computation 77−82026
three-frequency computational method for two-layer CFS data 79−16688
tidal data processing, Tihany Observatory results 77−87097
tidal tilts, parallel recording through digital print-out and photorecording channels *(Russian)* 78−88785
tills, anal. via mag. props., appl. to Lake Huron E coast till 77−33057
tiltmeter observations, effect of atmospheric processes *(Russian)* 78−48957
time extrapolated eigenvector prediction for time series analysis 77−56757
time series, rest frame spectra deduction from spectra computed in moving frame 77−25795
time series alignment, new statistical approach 79−92623
time series analysis, by ARMA-modelling *(German)* 80−31129
time series filtering with time variant operators, convolution and Fourier transform 77−87082
time-domain EM method, optimum pulse shape selection 77−45167
time-domain wave-shaping filter weights computation 78−77351
tomography for refractive media 80−82114
topographic corrections to geothermal obs., analytical method 80−46282
topographic mapping, digital terrain model appls. 79−84544
total solar radiation at Earth's surface using satellite measurements 80−4147
trace element determ. in rocks, minerals, neutron activation anal., detector comparison appl. 77−81443
track registration of U in rock samples 78−73533
transient EM sounding records computer processing, meas. errors anal. *(Russian)* 79−44269
transient thermal conductivity meas., thermal contact resistance 78−53744
transmission synthetic seismograms, direct inversion 79−29877
trend analysis and interpolation theory, geophysical appl. 77−45684
triaxial tests, rock stress conditions and rupture characts. var. *(Chinese)* 79−74962
trilateration network, adjustments to account for meteorological conditions 80−77131
tsunami-generating earthquakes, ionosphere detect. method 79−44681
tunnel location by cross-borehole EM probing 77−78545
Turam method in prospecting, normal values calc. *(Spanish)* 77−9551
two dimensional dike, gravitational effect interp. by Fourier transform 78−3967
two dimensional quasioptimal filtering, efficiency for separating geophysical fields *(Russian)* 77−70585
two-dimensional gravimetric and magnetometric problem, analytic construction based on Poincare sweep model 80−21846
two-timing methods, appl. in statistical geophysics 77−73879
ULF geomagnetic pulsations, meas. using pairs of electrodes inserted into trees as receiving antennas 78−32249
ultrahigh pressure experiments, calibration via acoustic vels. ratio in NaCL 77−27945
uncontrolled thermographic mosaic compilation and videotape processing 77−29502
under-surface temp. pattern estimation by dynamic remote sensing *(Japanese)* 78−36315
underground optical waveguides for crustal deform. determ. 77−53230
underground quarries, EM detection *(French)* 78−96306
unit vectors, time series interpolation 79−92625
upper mantle, peridotite equilibration conditions determ. from geochemical parameters 77−2130
upper mantle seismic anisotropy, determ. via higher mode surface waves obs. 77−49015
upward continuation, appl. to long-wavelength mag. anomalies over Canada 80−85594
uraniferous materials prospecting, influence of disequilib. and ^{222}Rn amanation factor variability 79−62498
US wave attenuation meas. for studying phys. props. of soil *(Polish)* 77−9566
variational inequality method, ditch seepage appl. 78−81251
vegetation and crop development mapping, table look-up procedure 77−78531
vertical electric sounding curves, computer interpretation *(Russian)* 79−34741
vertical frequency effect sounding in induced polarization and galvanic resistivity methods 78−69284
Very Long Baseline Interferometry (VLBI), foundations and geodetic appl. *(German)* 78−45036

geophysical techniques continued
very long baseline interferometry appl. to geodesy and geodynamics 77−56767
via DGU-2 curve plotter 80−36422
vibroseis deconvolution 78−16171
Vibroseis deconvolution method, noise effects 80−90232
vibroseis operation, vibrator-ground forced oscillating system, reson. phenomena *(Hungarian)* 80−105074
vibroseis signal similarity, computerized anal. 78−20543
Vibroseis system, encoding techniques 78−69474
Vibroseis technique, signal design 77−41182
virgin land resources, remote sensing, appl. of aerial and satellite photography *(Chinese)* 79−53551
VLBI, appls. to geodetic meausrement and crustal deformation monitoring *(Japanese)* 80−21929
VLBI, general considerations of international systems *(Japanese)* 80−17501
VLBI, principles of measurement *(Japanese)* 80−21921
VLBI appl. to geodesy, Earth rot. and network geometry optimisation 78−92996
VLBI measurements, implications for N.American intra-plate crustal deformation 80−51379
VLBI using geostationary satellite link 79−29968
VLF surface mode propag. in geophys. exploration, wave tilt meas. 80−77139
volatile trace elements determ. by RNAA 79−44276
volcanic activity dust veil index formulation, source of apparent periodicity 79−92514
volcanic activity prediction, fumaroles He/CO_2 ratios appl. 80−26482
volcanic explosion energy and depth determ. 77−17064
volcanic rocks classification using Irvine and Baragar classification scheme, FORTRAN IV program 78−57203
water backscatter and absorption coeffs., simultaneous determ. 80−82074
water flow low velocities meas. with submerged floats 78−7813
water flow through rock specimen, average pore vel. meas. 79−5473
water table prediction, model-free statistical methods 77−25714
wave dielectric log curves in formations of limited thickness, interpretation *(Russian)* 79−74990
wave propag. in layered media with lateral inhomogeneities, modal methods 77−73676
weakly coupled geophysical systems, statistical anal. techniques 79−80428
weather data, asynchronous, method for reduction to a common time 80−85735
well logging, electric, geometrical factors determ. from electrostatic field successive approx. *(Chinese)* 80−105057
well logging, soln. for thermal neutron diffusion eqn. in medium with cylindrical hole 80−51548
well logging with short-lived radioactive source 79−53563
well mud logging, online data processing *(Russian)* 78−40706
well temperature measurement, bottom-hole temperature stabilisation model 80−51356
well-logging for density, γ-γ log with computerised instrumentation *(Hungarian)* 80−21843
wet soil complex permittivity meas. method at microwave 77−45184
wheat canopy reflectance, Suits' spectral model appls. 78−7811
wind stress on sea ice, meas. techniques and results *(Japanese)* 78−88842
X-ray diffraction, appl. to Saxony Granulites petrofabric anal. 80−21740
X-ray fluorescence analysis for Cu content determ. of cuprous ores *(Rumanian)* 77−29508
zircon minerals, Hf determ. by neutron activation anal. *(Russian)* 77−40615
β-ray quantitative microautoradiograhy, by X-ray emission microanal. 78−20545
^{26}Al, decay in marine sediments, meas. with cyclotron, dating technique 79−71819
$^{26}Al/^{26}Mg$ isobars, separation via negative ion mass spectroscopy 80−31146
Ar-K isotopic dilution method for absolute age determ. *(Rumanian)* 78−20562
$^{40}Ar/^{39}Ar$ age spectrum technique, excess ^{40}Ar identification 77−5152
$^{40}Ar/^{39}Ar$ dating, appl. of isochron diagrams 79−29873
$^{40}Ar/^{39}Ar$ dating by step-heating method, appl. to E.Iceland lava 80−36273
$^{40}Ar/^{39}Ar$ dating of cordierite bearing rock, effects of excess radiogenic ^{40}Ar 77−29456
$^{40}Ar/^{39}Ar$ radioactive dating, appl. to K-bearing sulphide minerals age determ. 79−29720
As determ. in ores of reduced heteropoly acids, photometric method 78−61103
Au, determ. in rocks, minerals by at. absorpt. spectrometry 77−29067
^{10}Be, distrib. in geophysical samples, meas. using tandem van de Graaf accelerator 80−61924
C isotope stratigraphy, appl. to late Miocene shallow marine sediments, New Zealand 80−26479
^{14}C absolute dating using low altitude European tree-ring calibration 78−16195
^{14}C beam prod. from natural sample, radioactive dating 79−25352
^{14}C dating, meas. of ^{14}C abundance vars. in wines with 11-year solar cycle, (1909 to 1952) 80−109249
^{14}C dating method using 20 keV Kr ion beam for objects <65000 yrs. *(Danish)* 80−8440
^{14}C dating of CO_2 sample with accelerator, blind meas. 79−25362
^{14}C dating of mg geological samples with electrostatic accelerators 79−25361
^{14}C dating of small samples via proportional counting 80−82102
^{14}C dating rel. to magnetic and other dating methods 78−57359
^{14}C measurement in tree rings, chemical pretreatment and ^{14}C radial flow 78−28346
Ca, determ. in lake sediments, by atomic absorption spectroscopy 78−95970
^{41}Ca radioactive dating, feasibility and appls. 79−21063
^{137}Cs dating of sediments, confirmation by algal stratigraphy in Rostherne Mere, Cheshire 79−12156
Fe, characterisation in environmental samples by Mossbauer technique 79−66433
Fe determinations, effect of surface changes in Pt crucibles 80−61192
Fe ore deposit integral charact. determ. from magnetic anomalies *(Russian)* 79−62621

geophysical techniques continued
Fe ores, grade, bulk density, porosity determ. by nuclear geophysical methods 79−48570
Ge, high-resoln. spectrometry for uranium assay in boreholes 79−53571
^{3}H in water, low-level meas., inter-laboratory comparison 78−44888
Hg ores, determ. of Hg content using ^{57}Co isotope and scintillation counter 78−20539
^{114m}In-EDTA complex, method of determ., use as tracer in hydrology 77−73458
K-AR dating, revised consts. rel. to geomag. polarity time scale for interval 0 to 5 m.y. BP 79−57851
K-Ar dating method for argillaceous sediments 79−8716
K-Ar dating using three-dimens. plots 79−62601
K-Ar isochron method for age of North Mountain Basalt, Nova Scotia 80−3960
K-Ar isochron method use and misuse, atmospheric ^{36}Ar contamination removal 77−66988
Mn nodules, accumulation rates from alpha track method 78−7610
Na determ. in rock, mineral samples, X-ray fluoresc. quantometer modification 78−61589
^{18}O, palaeotemperature determs., effects of post-depositional alteration of rocks 77−29455
$^{18}O/^{16}O$ as Archaean gneisses petrogenetic indicator, results of clastic metasediments meas. 78−20410
P determ. in ores of reduced heteropoly acids, photometric method 78−61103
Pb total in soil, comparative study of analysis methods 78−16221
^{210}Pb dating method for determ. of Lake Ontario sedimentation rates 78−73408
^{210}Pb determ. by direct gamma-ray meas. in lake sediments and air samples 77−5156
^{210}Pb determination in lake and marine sediments 79−48582
^{210}Pb, use as heavy metal tracer in Susquehanna River system 78−49046
Po haloes used for geochronology 80−56468
Pu borehole assay using delayed-neutron activation anal. 80−21419
^{237}Pu gamma-emitting tracer prep. by $^{238}U(^{3}He,4n)$ 77−34497
Ra monitoring for earthquake prediction *(Japanese)* 78−28181
Rb-Sr, ratio determ., by X-ray fluoresc., for radiometric age meas. 77−70356
Rb-Sr dating, appl. to discrete structural-metamorphic events in multiply deformed Precambrian terrain 79−57895
Rb-Sr dating, half-life determ. by absolute counting 77−26943
Rn gas concentration meas. using alpha sensitive plastic detectors for U exploration 80−94617
Rn gas concentration measurement using alpha sensitive plastic films for U exploration 80−94618
Rn groundwater monitoring systems for earthquake prediction 80−94467
Rn integrated emanation, mapping for gases long-distance migration detect. 78−85560
Rn mapping in U exploration, exclusion of ^{220}Rn signal 80−61916
Rn measurement in groundwater and springs for earthquake prediction 78−88924
Rn, moisture insensitive monitoring using solid detectors 79−31228
^{220}Rn integrated meas. of long-distance transport for U ore detection 80−98476
^{222}Rn alpha-scintillation counting, statistical counting error calc. 77−3211
^{222}Rn concentrations in water, rapid meas. with commercial liq. scintillation counter 78−28339
^{222}Rn gas detection using Track Etch system for U exploration 80−98488
^{222}Rn mapping in U exploration, use of mat to avoid hole drilling 80−82087
^{222}Rn scintillation counting, standard deviation estimation 77−79519
^{222}Rn tracer measurement in aqueous samples by decay product filtration 77−60476
Ru determ. in silicate rocks, preseparation procedure for neutron activation anal. 77−44547
$^{34}S/^{32}S$ ratio meas. using SO_2 and SF_6 methods, discrepancies 78−65405
Sn determ. in rocks by thermal neutron activation anal. 77−44552
^{90}Sr bremsstrahlung radiation meas. for well logging using Ge spectrometer 80−94619
U abundance in Himalayan plants, fission track method 80−101305
U analysis, in geological samples, delayed neutrons method *(Rumanian)* 79−88507
U at Oklo natural fission reactors, radiometric meas. and isotopic anal. *(French)* 80−21754
U boreholes, in situ assay using prompt fission neutron technique 77−37441
U determ. in natural water by ion exchange separation, delayed neutron counting 77−36847
U determination in whole rock samples by fission track method 77−73880
U exploration, LANDSAT data merged with geol. and geophysics data 80−56651
U exploration, meas. of ^{222}Rn concs. in Earth using nuclear track technique 79−53574
U exploration, prompt fission neutron logging technique, computer modelling 79−53566
U exploration, via Rn long-distance migration in Earth, subterrestrial fluid convection hypothesis 77−37246
U exploration with computer-processed LANDSAT data 78−7777
U in geological samples, rapid determ. using X-ray fluorescence anal. methods 79−88479
U ore assaying by delayed fission neutron process 79−53536
U ore bodies ground level radiometric surveys, overburden effects correction techniques 79−88485
U ore deposits, review of methods of prospecting *(German, English)* 77−21925
U ore grade direct determ. by photoneutron assay method 79−53570
U prospecting, airborne radiometric meas., ground conc. estimation 79−53575
U prospecting, quantitative determs. from gamma-ray logs, digital time series analysis 79−48580
U prospecting by γ-ray logging of borehole, factors affecting resolution 80−98463
U prospecting using microdistrib. anal. of Siwalik vertebrate fossils by nuclear Track Etch tech. 80−98489
U pulsed neutron logging, minimisation of neutron absorber effects 77−37446

geophysical techniques continued
U series dating, open system model appl. 79−29874
U series dating of travertine, appl. to Nahal Zin, Israel, archaeological sites 79−34781
U, Th determination in rocks, fission/α technique 77−29497
U-Pb age method, calc. of uncertainties of U-Pb isotope data 80−46269
$^{235}U/^{238}U$ ratio, non-destructive field meas. for geophysical prospecting 80−21862
^{235}U-fission track micromapping, exam. of U mobilisation processes in Precombrian sediments 80−98477
^{238}U concentration in ore, absolute determ. by gamma-ray spectroscopy 77−13133
Zr/Hf determ. in silicate rocks by neutron activation 78−20547

geophysics
see also Earth; erosion; geochronology; geodesy; geology; geomagnetism; geophysical aspects of cosmic rays; geophysical techniques; hydrology; meteorology; oceanography; radiation belts; rocks; seismology; solar-terrestrial relationships; space research; terrestrial atmosphere; time and latitude; upper atmosphere
Afar region, geological evolution and geophysics 79−5468
AGU conference, June 1979, Washington, DC, USA 80−8732
AGU Spring Meeting (Washington, D.C., 30 May-3 June, 1977) 77−78077
American Geophysical Union, 1976 Spring Annual Meeting (Washington, April 12-15) 77−32969
American Geophysical Union, 1980 spring meeting, Toronto, Canada (1980 May 22 to 27) 80−67926
American Geophysical Union, Fall 1976 Annual Meeting (San Francisco, 1976, December, 6-10) 77−32970
Annual review of Earth and planetary sciences, vol.5 77−64174
anomaly source models, statistical parameters rel. to pot. fields obtained by superposition *(German)* 79−34783
Antarctic research expedition *(Japanese)* 77−87117
applied geophysics, MSc programme in Nigeria 80−105463
Arctic geophysical review, introduction *(French, English)* 79−48452
Arctic geophysical review, summary 79−48456
Arctic Ice Dynamic Joint Experiment 77−33190
artificial satellite geodesy and geophysics appls., review 77−64183
Mid-Atlantic Ridge, geophysical and petrological constraints 78−85508
avalanches and landslides, reach and velocity *(German)* 77−53095
axisymmetric inertial fluid oscillations in cylindrical cavity during spin-up from rest 78−5750
Benard convection, very viscous fluid, theory 80−10236
British Trias, hydrogeophysical props. 77−41074
CAI, interactive computing with graphic display 77−21
Carpathian system, geophysical data and Earth structure *(Hungarian)* 77−86829
combination of observations in the identification of geophysical objects 77−64173
conducting sphere, rot. in mag. field relativistic, co-rot. frame 79−53714
conf. of American Geophys. Union, Dec. 1979, San Francisco 80−81890
conference, April 1980, Birmingham, England 80−56474
conference, New Delhi, India (Jan. 1979) 80−94912
conference, Nov. 1979, New Orleans, USA 80−81891
correlation functions for geometric models of geophysical data *(Rumanian)* 79−58124
cosmology and geophysics, book 79−12552
Cretaceous-Tertiary extinctions, possible terrestrial and extra-terrestrial causes 78−31999
E.Crimea, geophysical data rel. to deep crustal struct. *(Russian)* 80−104933
data acquisition using Fourier series and Markov processes *(Italian)* 80−109254
data storage by metallic carrier electroerosion via liquid pulsed discharge *(Russian)* 78−61563
Deep Sea Drilling Project Leg 37-1974, conference Edmonton, Canada, (May, 9176) 77−91069
Dobrogea, Rumania, geophysics and geology *(Rumanian)* 78−20419
Earth and planetary sciences, annual review (volume 7) 79−84070
Earth observation programme of ESA 80−109250
Earth-oriented research programme of ESA 80−109251
education, applied science CNAA degree course at Kingston Polytechnic 79−35454
educational course, for physics students 77−67155
Einstein's work in solid-state theory, geophysical importance *(German)* 79−86848
elastodynamics, numerical boundary integral eqn. method 79−63036
environment evolution, available elements during Earth history rel. to life evolution 79−80030
epithermal neutron fields in nuclear geophysics *(Russian)* 80−85658
Europe, tectonic and geophysical implications of preliminary heat flow map 79−70765
field configurations, analytical description in terms of differential geometry *(Russian)* 79−74986
fluid dynamical systems, statistical anal. and prediction 78−11901
fluid dynamics, boundary conditions imposed by stratified fluid 79−55404
fluid dynamics, mathematical theory, book 80−105443
fluid dynamics, specialist symposium, (Munich, 6 to 9 September 1977) 79−57951
fluid dynamics, use of similarity theory in Soviet work *(Russian)* 78−16174
fluid layer with rot. and mag. field, cell sizes at thermal convection onset 77−54991
folds, non-Newtonian 79−88349
geodetic meas. methods and geophysical appl. 79−66835
geodetic observatory at Graz-Lustbuhel, Austria, work and projects 80−77117
Geos satellite, first six months' obs. 78−61705
geothermometry and geobarometry, conf., University Park, Pennsylvania (October 1975) 77−2123
global problems of fluid dynamics 78−96173
gravitation and inertia corpuscular model, geophysical consequences *(Russian)* 79−40439
gravity corpuscular model, geological and geophysical consequences *(Russian)* 77−67367
Griffith crack-antiplane shear wave interaction at interface of two bonded elastic half-spaces, geophys., seismological appl. 80−92087
hydrogeological problems, geologic concept in geophysical research 77−9451

geophysics continued
hydrology, method of characts. with fixed net for slowly varying nonstationary flows *(German)* 79−5515
inflection surfaces, use in descriptions of folds 79−88324
International Magnetospheric Study, Satellite Situation Center 77−53197
inverse problem, non-linearity effects 79−8704
inverse problems, potential theory for interpretation 78−7557
S.Irish Caledonides, plate tectonics and evolution 77−5174
Japanese Islands region, geophysical data compilation *(Japanese)* 80−67332
Lomonosov Ridge Experiment (Lorex 79) in Arctic Ocean 80−77120
magma double-diffusive crystallization rel. to igneous layered rocks 80−90081
magnetothermoleastic waves, propag. in initially stressed conducting layer 79−63
marine geology and geophysics, 1967-77 review 77−64260
mathematical geophysics, 11th International Symposium (Seeheim, Germany, 18-27 August 1976) 77−73622
metamorphism, rate laws 79−16467
meteorite craters, geophysical and geomechanical aspects 80−17265
MHD, monograph 78−40816
MHD induction, simplest physical model of generator 78−71548
mineralized zones, probability and uncertain number theory appls. *(Rumanian)* 77−29509
NASA Earth and ocean dynamics programme 77−56733
natural resource digital image anal. development in USA 78−96327
natural slopes, failure surfaces propag. 79−39719
oceanography, geological, book 78−92845
Oklo fossil nuclear reactors, radiation damage of minerals 80−21751
Oklo natural fission reactor materials, thermoluminesc. props., effect of radiation damage 80−21750
orthodoxy and creativity at frontiers of Earth sciences, symposium, Hobart, Tasmania (1977 February 7 to 10) 80−62380
Otway region, S.W.Victoria, conf. (Melbourne, 1975 October 9) 78−20415
overdetermined systems of linear eqns., partially regulated solns. 79−66825
Pamir-Himalayas region, International working conf. on geological and geophysical studies *(Russian)* 77−73734
plasma, self-gravitating, with finite ion gyroviscosity, rotating layer instability 80−56706
plasticity theory of metals, appl. to geophysics 80−104955
plutonic rock, discrimination and spectral reflectance, visible and IR obs. 80−90083
potential fields, anal. of characteristic-components method in interface construction 77−44901
potential fields from arbitrary 2-, $2^1/_2$- and 3-dimensional bodies, wave-number domain expressions 79−5634
potential fields on sphere, stochastic props. study 80−56338
pressure solution thermodynamics, interction between chemical and mechanical forces 78−57194
Quetelet, A.L.J., life and spread of science in Belgium during 19th century *(French)* 78−65742
Rayleigh waves, magnetothermoelastic, with thermal relaxation, theory 79−62
regression eqns. connecting geological and geophysical parameters *(Russian)* 77−73733
research worldwide growth, 1967-75 period 77−66884
rockfalls, Surprise Valley, Jasper National Park, Canada 77−44998
Roosevelt Hot Springs thermal area, Utah 79−84260
search for intelligent life in Galaxy, geophysical importance 79−53736
Smithsonian Astrophysical Observatory laser tracking systems 77−64481
solid bodies, hydrostatic compression eqn., geophys. appl. 79−62489
solid-Earth geophysics, bibliography 77−2078
space and time dependent media, problem of nonreproducible data, ionosphere appl. *(German)* 77−64464
spiral structures, geophysical and astrophysical 80−77287
stability of geophysical flows 79−70884
statistical geophysics, appl. of two-timing methods 77−73879
thermodynamical Gruneisen gamma formulation 78−65264
time series, linear trend analysis 77−49151
tracer theory in geophys. systems, nonsteady state 79−5646
United Kingdom Geophysical Assembly, conference (Edinburgh, 12-15 April, 1977) 77−48987
University of Hawaii lunar ranging expt., geodetic-geophysics support programme 77−56569
upper atmosphere, ionosphere and magnetosphere, handbook 78−73557
Vajont rock slide (Italy, 1963) analysis, new approach 79−8633
Weddell Sea, geophysical studies (1978 Jan./Feb.) *(German, English)* 78−96188
Wharton Basin near Investigator Fracture Zone, geophysical study 78−40532
Mg SiO_3 melt, instantaneous struct. simulated by mol. dynamics 80−84049

geophysics computing
see also computerised instrumentation
accuracy of data processing by special purpose digital computers *(Russian)* 79−62587
acoustic signal coherence limits in random ocean environment 80−46193
ADIF, a FORTRAN IV program for solving the shallow-water equations 79−84493
aerial radiometric data anal. using line-intensity estimation code MAZAS 79−62627
aeromagnetic anomaly from remanently magnetised Precambrian schist belt, Karnataka, India harmonic inversion 79−44094
aerosols, size distrib. meas. by impactors, data inversion via nonlinear programming 77−2258
agriculture acreage estimates using LANDSAT data, interactive software systems 77−78504
agrometeorological data, information flow organization and processing automation 77−78430
air pollution, smoke plumes visual effects, computer simulation 79−66429
air pollution data analysis using combined interactive graphic presentation and clustering technique 79−83656
air pollution density distrib., flow pattern in Tanabe area, Japan, numerical anal. *(Japanese)* 78−96289
air pollution diffusion, Gaussian puff model simplification for real-time minicomputer use 77−81997

geophysics computing continued
airborne spectroradiometric data, and LANDSAT data, hydrothermal alteration mapping appl. 79−34973
algorithm for processing of observational series, ocean currents appl. *(Russian)* 78−65421
alternating EM field perturbs. by cond. inhomogeneities 79−39653
ambient air quality maintenance data system applied to coal-fired electric generating stations 80−3560
analytical plotters, props. and software aspects, photogrammetric appl. 78−40709
analytical stereoplotter, OMI AP/C4, photogrammetric appl., features 78−40715
analytical stereoplotting system, C-100 PLANICOMP, features 78−40711
anomaly detection, FORTRAN IV programs for statistical method appl. *(Rumanian)* 77−41214
apparent resistivity of perfectly cond. sphere buried in half-space, calc. 77−2269
aquatic sediment lipids, Recent and ancient 80−51583
atmopsheric precipitation probability forecasts, nonparametric technique based on pattern recognition algorithm 78−44946
atmosphere, horizontal trajectory computation based on surface geostrophic wind 77−37284
atmosphere, molecular absorption, Lowtran 3B model 78−85690
atmosphere acoustic forecasts production, method using digital computer 79−79960
atmosphere models, advection in flux formulations for variable grid models 77−29380
atmosphere parameters, retrieval from scanning multichannel microwave radiometer obs. 80−90261
atmosphere photon transport problems, modified Monte Carlo procedure 78−61560
atmosphere transmittance, algorithm accuracies 80−101429
atmospheric and oceanographic information processing system 77−78519
atmospheric boundary layer turbulence, multi-component linear digital simulation 78−61513
atmospheric diffusion, sensitivity anal. of partial differential eqns. 79−49178
atmospheric evolution over last 4.5 billion years, computer simulation 77−64396
atmospheric infrasound waves recording method and computer anal. *(Russian)* 78−65407
atmospheric IR transmission spectra, high resolution field meas. and computer code calc. 79−66798
atmospheric irradiance meas. from aircraft, computer simulation 77−70830
atmospheric pollution monitoring, centralised supervision system in Fos-Etang de Berre region 78−81410
atmospheric precipitable water, computation from upper air data 79−34886
atmospheric surface boundary layer, hot-wire meas. of wind and temp., Denmark 77−9458
atmospheric transmission, LOWTRAN 3B predictions for water vapour absorpt. 79−44245
atmospheric transmission LOWTRAN 3B predictions, long-path high-resolution 78−92972
atmospheric transmittance and radiance, high-resolution HITRAN and data compilation 79−66795
atmospheric transmittance and radiance, moderate-resolution, LOWTRAN code 79−66796
atmospheric transmittance model for variable-mixing-ratio absorbent gases 79−80011
atmospheric transmittance profiles calc. method 78−85696
atmospheric turbulence measurement, computerised instrumentation system 77−56761
aurora, double plasma layers, simulation 80−12590
autocorrelation coeffs. from irregularly spaced areal data 77−33191
automatic buoy systems, centre for data collection and processing *(Russian)* 77−78427
automatic contouring of faulted subsurfaces 77−45170
automatic information and control systems 79−71394
barrier island migration computer simulation 78−20384
bathymetric charts construction aboard ship, efficient method 78−45029
bifurcated cooling tower plume, math. model of drift deposition 79−58002
biostratigraphic correlation within IGCP Project 148 79−62501
biostratigraphic data quantification 79−62593
biostratigraphical correlation 79−62503
biostratigraphical logging methods 79−62594
biostratigraphy, range charts and no-space graphs 79−62504
biostratigraphy, temporal range charts 79−62595
biostratigraphy methods, comparison for assemblage zones 79−62502
body wave seismograms, simple computational method 79−84492
borehole logging, minicomputer appl. *(Russian)* 79−84538
Bouguer gravity model, interactive CRT display, for geology CAI 77−22
BULK: a computer program for calculating bulk-chemical analysis from mineral phases observed in thin section, FORTRAN IV program listed 79−2378
CAI in geology, conf., Syracuse, USA (Nov. 1975) 77−15
CAI in geology 77−16
Canadian mineral occurrence index 77−53205
Canadian Seismic Array Monitor processing system 77−9517
cartography, use of electronically controlled drawing machines *(German)* 78−20348
chimney stack sampling, traverse point location for HP calculator program 80−94139
CLAIR data system overview 78−57325
Clairaut eqn., connection to satellite geodesy and Jupiter 78−11795
climate data archiving and quality control by computer 80−61907
climate simulation, geophysical fluid system 78−81353
climatic change, computer modelling 79−92587
climatic data service for USSR 77−70838
climatic model experiments, simulated changes in albedo, surface roughness, surface hydrology, solar energy conversion effects 78−81354
climatological power spectra computation technique 77−91305
cloud droplet coalescence growth, fast computational method for Telford's theory 78−69486
cloud motions, automatic tracking system using weather satellite picture sequences 78−45022
cloud seeding, num. simulation technique 79−84519

geophysics computing continued
clouds and atm. phenomena, integrated automatic processing of obs. data 79−29907
coastal aquifer water flow analysis 80−26654
color map automatic digitisation, spectral classification scanner technique 80−17424
common depth area algorithms in complex seismic conditions *(Russian)* 77−44937
COMOD, program for standardizing mineral resource commodity data 78−20524
computation nets, significance in increasing efficiency of geologo-geophysical research 79−96835
computer-aided seismic anal. and discrimination, bibliography 77−81832
continental drift reconstruction 77−2261
continental margin sedimentation, computer simulation 78−15998
contour map aeromagnetic data computer processing 78−7819
contour maps, evaluation method for determ. relative accuracies 77−90989
contouring method using digital filter, bathymetry appl. 79−39894
convergence speed of a posteriori variance estimation *(German)* 79−100984
coupled vector systems of nonlinear parabolic partial differential eqns., soln., geophys. appl. 77−41468
crop identification and area estimation by computer aided LANDSAT data anal. 77−78503
crystallisation in layered intrusions formation simulation 77−33069
crystallographic data Cartesian translation 77−37196
cursor, aided-track, for improving digitising accuracy 79−29899
D-region, electron density profiles, statistical model 80−61964
data analysis using interactive satellite video display systems 79−58229
data bank model, appl. to geological data 77−53199
data management and analysis systems for hydrogeochemical reconnaissance 78−20520
data management systems in economic geology 77−53201
data processing, underground mapping reflection seismic method 78−96325
deep probing and refraction seismograms, computer processing *(Russian)* 79−84528
deep seismic data processing, digital techniques appl. *(Italian)* 78−40719
deep seismic profiling, Atlantic Ocean, automatic processing of bottom seismograph records 78−45030
dendrogram association analysis, FORTRAN IV program 77−5326
DENZ, computer program for toxic atmospheric gas dispersion calc. 80−45842
digital data spectral analysis, max. entropy method algorithm *(Japanese)* 77−17227
digital map revision 80−17422
digital radar data computer processing for High Plains Coop. Program (HIPLEX) 78−92989
digital seismic data processing, struct. anal. of graphs *(Russian)* 78−53749
digital seismic prospecting, in oil and gas bearing provinces of Ukrainian SSR 79−96836
digital signal processing appls. to seismology 79−29915
digital stereo mapping, flexible algorithm 79−84543
direct gravity formula for 1967 Geodetic Reference System 78−92775
discontinuous structural surfaces, regression program in FORTRAN 79−84495
discrete design 80−200
distributed data bases for structured data 77−53200
diversity indices computation from information theory 77−33076
drill hole or sample area-of-influence determ., FORTRAN IV program 77−5327
droplet image analysis by TV camera and table calculator via IEC-Bus 78−36337
DTA analysis, quantitative, curve-fitting, appl. to basalt 80−77144
dynamic clustering and strong patterns recognition, automatic classification appl. 78−28322
Dynasonde software, real-time data acquisition and display 80−36405
Earth's evolution and paleoclimatology−a computational model 79−58080
Earth crust vertical movements, computer-generated time-space domain presentation 79−80056
Earth interior mass distributions, modelling by gravimagnetic fields 79−96750
Earth resource management system, ER-MAN II, remotely sensed data analysis 77−82058
Earth Resources Observation System Data Center for Landsat data 78−36289
Earth tremors true velocities, determ. from seismograms 79−96743
Earth-ionosphere waveguide, program to compute EM fields in irreg. spheroidal model 80−94638
earthquake conditioning improvement by scaling the eqns. of condition 77−40998
earthquake coordinates determ. using Mir-1 computer of Urgent Reports Service 77−78440
earthquake hazard model for Reno, Nevada 79−88285
earthquake parameter determ. method *(Chinese)* 80−77126
earthquake prediction, data evaluation and exchange problem 80−3957
earthquake wave anal. program *(Japanese)* 77−86783
earthquake wave analysis program WAVE, DEMOS-E library program 78−92800
earthquakes, automatic recognition and timing from single traces 79−66822
earthquakes, epicentral parameters determ., software package 79−48585
earthquakes, modelling strong motions 79−88296
earthquakes computer simulation 78−48987
electrical sounding, theoretical apparent resistivity curves calc. *(Italian)* 78−40472
electron microprobe, automated, evolution of quantitative elementary point anal. in geosciences *(French)* 78−78046
EM modelling, finite element program package 77−73874
EM prospecting using interactive minicomputer 79−62604
EM sounding, two-dimensional resistivity and induced-polarisation data inversion 79−16695
EM sounding over permafrost region, computer-assisted anal. 77−2086
EM wideband freq. response conversion to transient response using segmented transform. 78−77349
emission spectrographic analysis system, minicomputer based, using scanning microphotometry 80−22436

geophysics computing continued
environmental γ radiation, variation during rainfall *(Japanese)* 78−36240
estuary mapping, classification algorithms for Landsat data 78−40567
estuary models of Tampa Bay, Florida, comparison 78−77269
Executive system for processing geological data 77−53212
experimental data components isolation, Fourier transforms appl. 78−36434
exploration geophysics, 48th Annual International SEG Meeting, San Francisco, CA (1978 October 29 to November 2) 80−8441
exploratory drilling exhaustion sequence plot program 78−57334
F_2-layer, computer program for peak electron densities in main trough region 78−28417
F-region, polar cap and auroral zone, math. model 78−65458
far IR atmospheric emission and absorption spectrum calc. program 79−35020
fast earthquake epicentre location program 77−73653
fast Walsh transform configuration program derivation, appl. to seismic data processing *(Chinese)* 80−21853
fault strain field, included rectangular fault in semi-infinite media 80−98261
feature subset selection in remote sensing 79−25337
filtration simulation, hybrid, use of electrically conducting paper with discretely distributed capacitance *(Russian)* 78−88850
flow, bed topography and grain size in open-channel bends calc. 77−37245
flow-meters, flume, two-dimens. numerical modeling 78−30388
flowmeter, flumes and weir, construction error compensation, computer anal. 78−30387
FLUCOMP numerical river flow model 80−26653
fluctuations generation with arbitrary power spectrum, algorithm 78−73927
fluorocarbon, atm., detect. using computer simulated IR solar spectra 77−53217
forecasting precipitation, evaluation of real time operation 79−88443
forest productivity study using LANDSAT data, computer training, USA 77−78527
forestland location in western Massachusetts, direct LANDSAT resource anal. 77−78529
FORTRAN program for lateral tracing of time-stratigraphic units based on faunal assemblage zones 79−62510
G-EXEC generalized data handling system, design philosophy 77−53210
GARNET, graphic analysis of resources by numerical evaluation techniques 78−20525
GARP Atlantic Tropical Experiment, telecommunication data, computer processing 77−2251
general objective data base system for distributed coopèrative researcher files 77−53213
geochemical data bank design and use 77−9508
geodesy, program development for automatic drafting system *(German)* 78−15952
geodesy, props. of Gauss-Helmert least-squares adjustment model *(German)* 78−61309
geodesy densification of ground control networks, computer program package *(German)* 80−94452
geodesy GEOS-3 altimetric data, short arc reductions 77−70583
geodetic data base, basic entities definition 78−65392
geodetic network adjustment, sparse symmetric matrices profile improvement algorithm 77−48989
GEOLOG technique for field observation recording and interpretation 78−7774
geologic index maps updating computerised file system 77−2252
geologic processes simulation for teaching 77−17
geologic strata simulation with FLYSCH 77−18
geological and geochemical data management and processing 78−57324
geological computer design 77−53211
geological data automatic contouring techniques review 78−7820
geological data management, conf., 1975, Nov., Paris, France 77−53198
geological history computation from field survey and map data in FORTRAN 77−9522
geological interpretation from composited radar and Landsat imagery, computer processing 80−56647
geological lineaments computer-assisted photointerpretation, perception method 78−7639
geological map automatic compilation system design *(Russian)* 77−41025
geological records, coding method based on data transmission theory *(Russian)* 80−17383
geological surveys, Quaternary, automation 77−53209
Geological Undersea Surveyor, Acoustically-Navigated, for Mid-Atlantic Ridge appl. 80−4120
geology, area and centre of mass rapid computation 77−9507
geology, compositional data Q-mode factor analysis 77−9503
geology, computer network appls., teleconferencing 77−53202
geology, optical-rose diagrams 77−9505
geology, PETROS data bank, igneous rock major element analyses 77−2249
geology, SELLO, FORTRAN IV program for skewed distributions to normality transform 77−9502
geology, stereograms production, FORTRAN program 77−9521
geology compositional data Q-mode factor analysis, extended CABFAC and QMODEL programs 77−9504
geomagnetic dynamo integrals, numerical evaluation code 79−34733
geomagnetic field intensity vector, components determ. from absolute value 79−53534
geomagnetic measurements and data processing, new methods 79−39988
geomagnetic pulsations, numerical frequency-time anal. 79−39990
geopotential, algorithms for computation using simple density layer 77−5128
Geos 3, altimetry data appl. to orbit determ. expt. 80−4226
graphic computing system linked with signal enhancement seismograph, description and application 80−4131
gravitational field of 3-dim. mass determ. 77−81781
gravity, anomalies separation from background field, FON computer program *(Russian)* 78−53757
gravity and magnetic anomalies due to homogeneous polyhedral bodies, analytical expressions 80−3894
gravity and magnetic anomalies of polygonal prisms, mag. terrain corrections appl. 77−2082
gravity and magnetic field interpretation, optimal computing scheme construction 77−33201
geophysics computing continued
gravity anomalies, geological reduction *(Russian)* 78−40467
gravity anomalies interpretation, algorithm for calc. gravit. attraction of models of structural features *(Russian)* 78−53758
gravity anomalies interpretation, computer modelling 79−34971
gravity anomaly data processing system, involving interactive computer graphics *(French)* 80−94610
gravity effects calc., of two-dimensional and three-dimensional bodies 78−3961
gravity field of three-dimensional masses, calc. algorithms 80−94451
gravity interp. data processing techniques, shortening operators 77−64179
gravity prospecting, determ. of parameters of low-amplitude struct. with oil (gas) deposits *(Russian)* 79−44271
gravity studies using the facilities of UMRCC and the Computer Graphics Unit 78−77878
gravity waves, one-dimens., finite-element and finite-difference techniques comparison 79−18902
gravity waves, two-dimens., finite-element and finite-difference techniques comparison 79−18903
gridded data convolution and padding algorithm 78−69475
ground control networks, computer calculation of approximate coordinates *(German)* 79−84088
ground control networks, computer program for reliability estimation *(German)* 79−84089
ground movement reconstruction from earthquake recording 78−49165
ground relief gravity effect, computer calc. *(Russian)* 79−39952
groundwater aquifer model *(German)* 79−53377
groundwater flow simulation with computer-controlled RC network 77−45045
groundwater seepage in porous elastic soils, numerical performance of finite element schemes 77−91162
groundwater singly dispersive convection, finite-difference simulation 77−37265
groundwater system, transport of chain decaying radionuclides 80−51019
groundwater with convective dispersion, finite element anal., book contrib. 79−34877
Hankel transforms, related, of orders 0 and 1, numerical integration by adaptive digital filtering, FORTRAN IV algorithms 79−92599
holes in interlacing channels, nonlinear model 79−39720
hybrid river models software support 80−56499
hydrogeological database charact. *(Italian)* 80−109255
hydrologic data networks, design 79−21022
hydrologic records analysis and comparison, statistical program suite 77−21819
hydrological forecasts, automatic processing of operational information 78−3842
hydrological processes simulation, using super-kurtic probability density function 80−26558
hydrology, drainage basins, computer analysis *(French)* 78−7786
hydrology, fractional Gaussian noise algorithms and rescaled adjusted range 79−16545
hydrology, simulation procedures for Box-Jenkins models 79−79907
hydrometeorological data acquisition, microprocessor appl. *(Italian)* 77−82067
hydrometeorological information, optimum conversion to digital form 79−29903
hydrometeorology, USSR research vessels, information acquisition and processing *(Russian)* 77−21909
hydrostatic ellipticity calculation algorithm 80−62055
identification, numerical taxonomy methods 79−84494
information storage and retrieval system with microcomputer for hail 80−17381
information system automation *(Slovak)* 77−56735
interactive data acquisition system for geotechnical meas. *(Italian)* 78−7771
interactive minicomputer array processing system for Earth science 77−78518
interactive with graphic display, for CAI 77−21
International Magnetospheric Study, data management 80−4206
interplanetary shocks interaction with Earth's magnetosphere, computer simulation 78−16243
interpretation problems, soln., correl. theory of homogeneous random fields appl. 79−100986
inverse filter which is optimum in error-distrib. sense, stability charact. 78−81424
inverse gravity problem, linear programming appls. 78−28331
inverse magnetic problem for inductive magnetisation and palaeomagnetic sounding, numerical soln. *(Russian)* 79−34747
inversion algorithm for simultaneous inference of stratosphere gas conc. determ. 80−82000
ionograms, minicomputer inversion procedure for electron density profiles calc. 77−41263
ionosphere incoherent scatter data, analytic partial derivatives for least-squares fitting 78−73581
ionosphere oblique sounding data, inversion method 77−41265
ionosphere radio drift meas. simulation and analysis by correlation methods 78−45033
ionospheric data processing, improvement of convergence of least squares method *(Russian)* 78−85700
K-index estimation by computer 78−36305
KEYBAM interactive computer programs for use with PETROS petrochemical data bank 78−20523
kinematic multiple wave analogues strongest families, parameter prediction algorithm *(Russian)* 79−39943
Kolmogorov-Wiener least-squares filters appl. to geophys. anomalies separation 78−61580
lake quality monitoring, multidate Landsat data extraction progrm 80−17299
land surfaces, erosional potentials generation from topographic information, LEAP programs 77−33075
land-use mapping by machine processing of LANDSAT-1 data 77−78467
land-use/soil survey data processing for resource planning 78−7804
landform erosion simulation program 80−85650
LANDSAT, Earth resource information 78−96330
LANDSAT agricultural monitoring program to monitor corn in Iowa 77−78495
LANDSAT computerised data anal. rel. to global development 78−36286

geophysics computing continued
LANDSAT data clustering, four-dimensional histogram approach 77−78524
LANDSAT data for geological studies in India, digital anal. 77−78511
LANDSAT data high-level computer processing 78−69546
LANDSAT data per-field, classification, unsupervised clustering techniques 77−64437
Landsat data processing, satellite motion, multispectral scanner *(Italian)* 78−4070
LANDSAT image anal. for terrain investigations in Florida 77−78530
LANDSAT image and digital terrain elevation data processing with parallax 77−29501
Landsat imagery for terrain analysis, computer analysis and picture processing programs 78−40691
LANDSAT imagery geologic processing software 78−20521
LANDSAT imagery processing and enhancement 78−69545
LANDSAT large area classifier MAXL4X 77−78534
Landsat remote sensing, computer-aided forest and range inventory of S.E.Texas counties 77−56748
LANDSAT sample selection training algorithm SEARCH 77−78535
LANDSAT-based two phase sampling for wheat acreage estimation 77−78502
landuse imagery anal., change detection metrics and MIXELS 77−82070
large-scale hydrodynamic system simulation programs 77−21799
levelling data, time-space domain representation, computer program 78−88932
LF atmospheric data anal. with PDP computer 77−82014
limestone diagenesis simulation, computer model based on Sr depletion 78−73358
linear prediction in least-squares scheme for max. entropy spectra, Fortran subroutines 80−98465
lithostratigraphic correl. of subsurface sequences 79−62509
lithostratigraphic correlation, automatic, pitfalls 79−62506
lithostratigraphy, parametric interpolation of digitized log segments 79−62507
Lowtran molecular absorption empirical transmission function analysis 79−76400
machine processing of remotely sensed data, conference, West Lafayette, Indiana (1980 June 3 to 6) 80−82586
macroseismic data processing and interpretation 78−61583
magnetic anomalies interpretation, computer modelling 79−34971
magnetic anomaly of thin dyke, curve fit by calculator program 80−98228
magnetic field reduction to pole, fast Fourier series algorithm 77−5333
magnetic prospecting, 3-D anisotropic body mag. field calcs. and algorithm 80−4141
magnetospheric plasma convection, numerical simulation 79−62679
magnetotelluric anisotropic data, inversion technique 77−60475
magnetotelluric sounding, natural source obs. one-dimensional inversion 79−92479
magnetotelluric two-dimensional inversion 77−73629
magnetotellurics, automatic data processing 79−80041
mantle, thermal convection, time dependent simulation 80−101352
marine pollution, data collection 80−3545
mass consistent atmospheric flux model (MASCON) for complex terrain regions 78−92964
mesosphere and lower thermosphere, O_2 and O distrib., effect of magnetospheric elec. fields 79−66850
meteor wind automatic meas. set, programming and systems interaction *(Russian)* 77−41247
meteorite explosion, Tunguska, Siberia, shock wave effects, model, computation 77−5507
meteorological data sets, form. from first GARP Global Experiment (FGGE) obs. 80−101437
meteorological information flow system *(Japanese)* 77−56754
meteorological information processing *(German)* 80−36363
meteorological information system for response to nuclear power station accidental release of radioactivity 80−16888
meteorological interactive software system, for image data analysis 80−36404
meteorological real-time data acquisition and anal. 78−69466
meteorological satellite visible and IR image data, computer processing 79−29864
meteorology, data editing and validation using interactive graphics 78−77330
meteorology, data processing of M-100 rocket soundings 77−53233
meteorology, isoline printing method *(Russian)* 77−53245
meteorology, objective computer classification of composite charts 78−3906
meteorology, operational forecasting using automated guidance 78−49147
meteorology, surface synoptic obs., automatic real-time quality control 78−92920
METEOSAT data processing system *(Italian)* 80−109275
microclimatology, process computer appl. thermal balance recording methods 80−82044
microearthquake network automatic data anal. 77−81820
microearthquake network data, automatic anal. 78−81412
microearthquake research, methods and computer programs 79−39987
microgravity surveys, computer processing system 80−85575
mineral discovery probability, quantitative fall-backs of naturalist classifications 77−53204
mineral exploration, computer uses, limitations and requirements 77−53207
mineral resource data bases 77−53203
Mineral Resources Development Centre, developing countries computer aid 77−53215
minerals electron microprobe data analysis, using FORTRAN IV programs 77−86878
minerals modal analysis, from raw point-count data, using MODES (FORTRAN IV) program 77−86880
Minsk 22 computer in shipboard subsystem, operation peculiarities *(Russian)* 78−16165
Mississippi River computerized data bank 78−73520
molasse basin formation simulation 77−9428
monsoon circulations numerical simulation 80−21812
Monte Carlo simulation of ellipsoidal grain thin section ellipses 77−5332
multispectral data anal., ISURSL levels classification 77−78539
multispectral scanner data processing mechanisation 77−56778
Muskingum constants evaluation, FORTRAN IV 80−31077
geophysics computing continued
National Coal Resources Data System of US Geological Survey 77−53208
natural channel flow simulation by computer-controlled RC network 77−45046
natural gas, He conc. periodic vars. determ., algorithm 79−62608
natural streamflow control coeff., analytical calc. method 79−39777
networks, three dimensional calculation *(German)* 79−84090
neutron activation anal. instrumental, in US Geological Survey (Reston) 79−11850
nightglow multislit spectrometer design, computer simulation 78−73542
ocean bottom seismic profiling system with computerised data handling 77−2140
ocean crust sounding, computer processing method of seismograph records 80−85605
ocean density profile remote sensing by acoustic pulses, numerical algorithm 77−70893
ocean density profile remote sensing pulses, numerical algorithm 78−20429
ocean dynamic data, acquisition and display by portable real-time minicomputer system 80−12552
ocean environmental data files, quick guide 80−12551
ocean mapping, bottom return signal model and signal processor simulation 77−2272
ocean tides mapping with satellites, computer simulation 79−39880
ocean waves generation, propagation and dissipation spectral simulation model 80−31060
oceanic tides, large scale computation, review 77−73762
oceanographic data, using computer-controlled surface contour radar 79−80063
oceanographic information, automation of collection, processing and anal. on small-computer base 80−101439
oceanographic research, data processing and anal. 80−94605
oceanographic research shipboard minicomputers appl. 79−53562
oceanography, acoustic reflection profile display using dot matrix plotter with minicomputer 77−9548
oceanography, coastal current flows, Po delta application *(Italian)* 77−70667
oceanography, data anal. by Naval Coastal Systems Center (NCSC) environmental measuring system 80−12570
oceanography, element abundance charts, construction method for tropical Atlantic *(Russian)* 77−60485
oceanography, intelligent terminals and calculators as alternative to minicomputer systems 80−12553
oceanography, microcomputer applications 78−36322
oceanography, microprocessor-assisted flow-through anodic stripping voltammeter 78−36324
oceanography, turbidity current flow, computer simulation 78−15997
oceanography graphic system for space-time series processing and anal. 78−3998
oil spill simulation in Florida Gulf outer continental shelf 78−73406
Omo River project (Ethiopia) data management system appraisal 78−57326
onshore borehole records, data bank system 77−53214
optical crystallography computer anal. of spindle stage data 78−85702
optical depth, integral of Voigt function 79−25468
optimal numerical filters fitted for noise damping, atm. circulation simulation appl. 78−92997
optimal sampling and anal. method 78−73530
ore reserve estimation, in three-dimensional deposite using FORTRAN IV Function Segment 77−87085
orientation data fitting to von Mises distribution, in FORTRAN 77−5201
PAL, highly tutorial interactive, pattern recognition program for seismic anal. 77−81833
palaeontology, statistically oriented teaching approach 77−19
parameters of geophysical objects, interval estimation via identification methods 77−82024
Parry arcs, computer simulation of hexagonal prism ice crystals 77−53190
particulate pollution in Delhi due to Indraprastha power plant 79−21000
PETPAK, computing package for petrologists 78−57323
petrologic modelling with extended Q-mode factor analyiss, interactive programs 77−33070
phase vel. determ. of fundamental Love and Rayleigh waves 77−37148
phase-matched filters appl. to Rayleigh waves from seismic sources 78−45010
photochemical smog, rate parameters and computer simulation 78−48677
photogrammetric online processing, general sequential algorithm 77−78463
photogrammetry and EDP, appl. to mapping of geological joints 80−56470
photovoltaic cell efficiency calc., using irradiance-transmittance solar spectrum 80−26137
plotting, 3-dimens., irregular to regular grid data conversion 77−5328
point-density measurements using WANG 2200C minicomputer with digitiser 77−33072
polynomial and Fourier trend surfaces computation 78−32245
potential field transformation from relief to single reference plane, Fourier anal. appl. *(Russian)* 78−53759
potential fields, two-dimens., filtration and transformation algorithms *(Russian)* 78−3968
power curve regression equations for Ohio River, statistical computer program 78−61472
power spectrum analysis, nested variance technique, space physics, appl. in FORTRAN 77−87275
power spectrum for equally spaced time series of finite length, computing methods 77−45190
Q-mode classification of large data sets, nonhierarchical, agglomerative, AGCL (FORTRAN IV) program 77−86941
quantitative cartographic analysis, SYMAP auxiliary programs, geoenvironmental appls. 79−70469
radar image simulation, point scatt. model, remote sensing appl. 79−12296
radioactive material release to atmosphere, calc. of consequences with TIRION-4 code 79−29494
radionuclide disposal, GARD computer program for geochemical assessment 79−31068
rain, heavy, basic characts. determ., max runoff calc. 79−29802

geophysics computing continued
rain cell radar monitoring, automatic detection and tracking algorithms 80−51544
random to grid methods comparison 79−62596
Rayleigh dispersion function computations for unlimited freq. values 80−21837
Rayleigh wave soln. algorithms multilayered half space 80−98260
real time detect. and location of seismic events in central California 77−73654
rectangular and triangular diagram printer-plotting FORTRAN routines 77−5325
reflected wave recordings, allowance for vel. inhomogeneities in CDP data processing *(Russian)* 79−84526
reflection seismic recordings, minimum entropy deconvolution 78−81423
reflection seismograms signal anal., use of kepstrum 78−81425
relative humidity of air, control, error anal., accuracy 77−10034
remote sensing, atmosphere, temp. and emittance effects on data 77−78393
remote sensing, computer-based technology 77−53249
remote sensing, data processing developments, review *(Japanese)* 78−7801
remote sensing, geological faults and linear features detect. from LANDSAT images 80−77177
remote sensing, max. likelihood estimation of signature transformation algorithm 77−78497
remote sensing, multispectral data interpretation algorithms 79−88481
remote sensing data anal. package using ERIPS and LARSYS programs *(Japanese)* 77−5340
remote sensing data interpretation, computer-assisted analysis techniques 78−7776
remote sensing system for nationwide data base mapping 77−78512
remote sensor automatic image processing 77−21931
remote-sensing data, computer elaboration and image processing 78−40690
remotely sensed data acquisition and processing, developing countries appl. 79−34963
remotely sensed data machine processing, symposium, West Lafayette, IN (1979 June 27 to 29) 79−88473
remotely sensed data processing, conf., West Lafayette, Ind., USA, June 1977 77−78488
remotely sensed data processing, system performance and cost estimation 77−78517
replicated diversity indices computation for random samples of specified size 77−37197
resistivity, magnetic and IP data interpretation techniques 78−85708
resistivity logging, direct problem soln. using graphic display *(Russian)* 78−69481
resistivity soundings over horizontal strata, man/computer interpretation system 78−45014
RESMAC, Mexican seismic array 77−5355
resonance radiation transport with varying Doppler width, thermosphere appl. 80−26737
river, tidal wave propag., nonlinear model 79−5512
river basin study model 80−31079
river pollution distribution determination by remote sensing, computer aided analysis 80−81512
river tidal computations, explicit-implicit water level model 78−44886
river water quality, math. deterministic model, Blackwater catchment appl. 79−66732
river water quality, math. deterministic model, formulation and description 79−66731
rivers, ungauged, distributed numerical model development for estimating runoff and sediment discharge 77−91178
rivers, ungauged, distributed numerical model for estimating runoff and sediment discharge 77−91177
rivers, ungauged, runoff and sediment discharge estimation, distributed numerical method comparison 77−91179
rock description, LSD02 computer-based system 77−33071
rock fracture in uniaxial compression, computer modelling *(Japanese)* 80−12379
rocks asymmetric folding, finite-element simulation 78−77222
rocks chemical analysis, biotite gneiss and amphibolite mode estimation, using FISK (FORTRAN) program 77−86397
rocks fabric development simulation, appl. to quartzite 78−49015
safety assessment of radioactive waste disposal into salt deposits, fault tree anal. appl. 78−55046
sample control and identification system, computer operated, for neutron activation anal. of soil 79−96402
satellite data availability from Environmental Data Service 78−36288
satellite imagery, computer-generated gridding 77−21930
satellite multispectral data digital anal. for land use inventory/mapping 77−78541
sea level fluctuations, hydrodynamic numerical modelling of Lagoon of Venice 79−34832
sea wave profile meas. by radar altimeter, computer simulation 77−5367
SEASAT-A satellite radar altimeter spaceborne microcomputer 79−75073
sedimentary sea bottoms, machine classification 79−92626
seismic anal. and discrimination 77−81815
seismic analysis and discrimination, computer-aided 78−20530
seismic array recorded signals, apparent vel. and azimuth meas., computer programs 79−84522
seismic data, iterative stacking algorithm for signal separation 79−92612
seismic data, noise-resistance of optically generated correlograms *(Russian)* 78−40699
seismic data, nonlinear interference anal., crust and mantle regional studies 79−25217
seismic data analysis, migration by phase shift-algorithm for array processor 80−72638
seismic data migration by Fourier transform 78−77341
seismic data migration in two and three dimens., integral formulation 78−77342
seismic data processing, Fourier transform wave filter appl. *(Chinese)* 79−96838
seismic data processing, Karhunen-Loeve transform. appl. *(French)* 79−44258
seismic data processing, petroleum industry appl., automation level analysis 78−28327
seismic data processing, predictive deconvolution method appl. 79−8725
seismic data processing algorithms, sign coding appl. *(Russian)* 79−62616
geophysics computing continued
seismic data processing procedure *(Russian)* 79−21036
seismic data teleprocessing global network 77−29255
seismic dispersion curves, methods of computing partial derivatives 77−37149
seismic events correlation in time section, algorithm *(Russian)* 79−39962
seismic horizon recognition by factorial discriminant analysis *(French)* 77−41190
seismic image distortions by refracting curved interfaces, correction algorithms *(Russian)* 79−58118
seismic observations digital processing, steady numerical solns. *(Russian)* 79−53317
seismic pattern, automatic recognition 77−81831
seismic pattern recognition, fundamental problems 78−81428
seismic prospecting, inverse kinematic case soln. in layered Earth using reciprocal points *(Russian)* 79−44268
seismic raypath migration, using programmable pocket calculator 78−7784
seismic recordings, information quality and data processing techniques efficiency *(Russian)* 79−39666
seismic recordings, time-variable curvilinear anal. *(Russian)* 79−39946
seismic reflected wave method for media with variable vels., inverse case *(Russian)* 79−84525
seismic reflected waves, interpolation algorithm for vel. determ. *(Russian)* 79−88494
seismic reflection data dynamic corrections, fast algorithm 78−3966
seismic refr. survey depth determination, program for pocket calculator 80−82088
Seismic Research Observatories, upgrading of worldwide seismic data network 77−5334
seismic risk analysis of lifeline networks 78−65192
seismic signals, detect. under conditions of limited information about signals and noise 77−9536
seismic sounding, wave-equation datuming technique, appls. and computations 80−51553
seismic sounding data interpretation 77−41202
seismic source depths, improved determ. using seismic coda 77−81829
seismic surface wave data inversion 77−37147
seismic surface wave dispersion, digital processing *(Chinese)* 78−24374
seismic surface wave dispersion function, computations for unlimited freq. values 79−74848
seismic surface wave phase vel., partial derivatives calc. algorithm 80−4140
seismic surface wave processing using PDP-15 interactive graphics 77−81818
seismic surface waves, anal. using PDP-15 interactive graphics 78−81427
seismic travel-time curve analysis using computer *(Japanese)* 77−17226
seismic wave field digital filtering allowing for ray diffraction *(Russian)* 79−88495
seismic wave onset detection, computing 79−80059
seismic waveforms extrapolation, by Fourier methods 79−34978
seismic wavelet estimation, short-time homomorphic signal anal. appls. 78−81426
seismic waves group velocity, high resolution anal. appl. to explosion and earthquake 78−81111
seismic waves refl. coeffs. for layered media, fast computer program 77−49186
seismogram processing, for Rayleigh waves phase vel. investigations in middle Europe 79−44136
seismograms, interpolation of digitized curves 77−40999
Seismological Service of Canada, instrumentation and data processing 79−39914
seismology, automatic vertical time-depth curve approximation via successive layer detect. *(Russian)* 78−40700
seismology, data processing hardware developments 77−60355
seismology, estimate of number of signals forming wave field *(Russian)* 78−49157
seismology, location of strong earthquakes using information processing 77−73856
seismology, multichannel subtracting filters for freq.-domain anal. *(Russian)* 78−49156
seismology, optimal vel. anal. in common depth point method *(Russian)* 78−40698
seismology, rapid convolution and correl. *(Russian)* 79−39959
seismology, time-to-depth conversion for layered medium 78−3962
seismology, Zoeppritz's amplitude eqns. and Knott's energy eqns., in FORTRAN 77−40988
seismology common depth point data digital processing technique *(Russian)* 79−74875
seismology data reduction, approximate realisation, new techniques 79−70898
Seto Inland Sea hydraulic model tidal flow pattern anal. *(Japanese)* 78−36314
severe weather computerised forecasting system 78−20498
siesmic profiles, two-dimens., dip-domain migration 78−77343
SIGMI user-oriented file-processing system for geological data 77−9506
Skylab S-192 conical scanner data digital processing 77−82046
soil, unsaturated, coupled heat and water movement prediction, math. model 78−61446
soil hydraulic conductivity, numerical calc. from suction press.-moisture retention relation *(German)* 79−2297
soil pattern data from aircraft/LANDSAT scanners delineation by digital anal., Indiana 77−78496
solar cooling performance predictions via stochastic weather algorithms 80−35642
solar energy simulations, typical weather determination 79−16614
solution flow prediction, computer models, appl. to U solution mining 79−88013
sonar, signal processing algorithms soln. with multi-microprocessor network 78−45044
spatial derivatives mapping 77−40965
spectral modal analysis, dynamic anal. program *(Japanese)* 77−86784
spectral multiplication, props. as viewed in physical space, meteorological appls. 80−94607
statistical algorithms for magnetic and gravity anomaly interpretation 77−70856
statistical algorithms for scaling geophysical fields 78−73527
statistical cluster analysis, using G-mode central method, FORTRAN V program 77−86879

geophysics computing continued
stratigraphic correlation conf. Syracuse, NY, USA (Oct. 1977) 79−62500
stratigraphic section correl. by continuous variables 79−62505
stratigraphic units correlation from geological maps 79−62508
stratospheric photochemistry, computer simulation 79−21481
streambank erosion, stereometric meas., volume computation 80−17421
strong-motion accelerograph data management 78−36332
strong-motion accelerograph data processing 78−36330
strong-motion earthquake accelerograph records, data management 79−62629
subsurface hydrology, finite element method using mixed explicit-implicit scheme 79−79900
surface patterns in theoretical geography 78−57156
synoptic weather information at USSR Hydrometeorological Centre 77−78366
synthetic seismograms using finite difference techniques 78−73326
tectonics, Australia-Antarctica, revised computer fits 77−53032
terrain analysis FORTRAN program 77−9509
terrain data production using distributed processing 77−37413
thematic classified LANDSAT imagery of Portland, Oregon, tabular data base 77−78537
theodolites, electrooptical and microprocessor-based *(Czech)* 78−77860
thermal IR scanner analogue data digital processing 77−82045
tidal flow, interlacing channels, nonlinear computer model 79−34828
tidal sea level extremes calc. using nonlinear programming method 77−78479
tides, spectral modelling, finite element method, appl. to M_2 tide in English Channel 78−61579
time series filtering with time variant operators, convolution and Fourier transform 77−87082
time-domain wave-shaping filter weights computation 78−77351
torsional waves, computation of complete theoretical seismograms 79−12289
transient EM sounding records computer processing, meas. errors anal. *(Russian)* 79−44269
transient groundwater flow simulation by hybrid computer 77−45044
triangulation direction finding network for atmospherics sources fixing, data transmission and reduction 79−100981
triggering digital seismograph with microprocessor 78−96308
TRIPLOT, APL program for plotting triangular diagrams 78−57335
tropical cyclone surge model, finite difference method 79−12132
troposphere, radio propag. characts. prediction using FORTRAN computer programs *(Italian)* 78−85666
troposphere, urban photochemistry, computer simulation 78−49085
tropospheric range correction algorithm 78−61591
tsunami wave propagation anal., 2-step explicit finite element method 78−40503
Turam method in prospecting, normal values calc. *(Spanish)* 77−9551
turbulence breakdown coefficient determ., influence of data treatment technique *(Russian)* 78−7690
turbulent atmospheric transport, Monte Carlo simulation, radioactive pollution appl. 78−61550
TUTOR, geology CAI, PLATO system 77−20
typhoon and hurricane areas, distrib. models of press. and wind over sea surface 79−62570
undersea acoustic signal coherence fluctuations 80−46191
underwater sound channels, ray calcs. using pocket programmable calculator and Incomplete Beta Function 79−68467
US Geological Survey RASS-STATPAC system for mangement and statistical reduction of geochemical data 78−20522
US National Earthquake Information Service seismic data acquisition 77−29446
Vela Seismological Network, use of Datacomputer 77−82013
Vela seismological network, use of datacomputer 78−81411
vertical electric sounding curves, computer interpretation *(Russian)* 79−34741
via DGU-2 curve plotter 80−36422
vibroseis signal similarity, computerized anal. 78−20543
VLF direction-finding techniques comparison for determ. whistlers exit point at ionosphere 80−26631
VLF waves obs. by GEOS-1 79−29943
volcanic rocks classification using Irvine and Baragar classification scheme, FORTRAN IV program 78−57203
volcanology, lava lake cooling model, numerical analysis method 77−64247
water resource problem with multiple objectives, interactive optimisation, Yodo River basin, Japan appl. 79−57516
water resources research 79−20892
water-data bank compilation, Adour-Goronne river basin *(French)* 79−66720
weakly coupled geophysical systems, statistical anal. techniques 79−80428
weather, numerical prediction review 78−69393
weather displays and data acquisition systems, minicomputer appl. 77−78431
weather forecasting as a problem in fluid dynamics 79−84359
weather forecasting by computer, Switzerland *(German)* 77−37317
weather forecasting processing of radar and satellite imagery data 80−109252
weather prediction, 1950 ENIAC computations 80−42030
weather simulation, matrix generalised eigenproblem developments 77−25760
well mud logging, online data processing *(Russian)* 78−40706
wind derivation from cloud motion fully automated method, Meteostat data comparison with gradient winds 80−109244
wind-wave interaction, two-layer flow, numerical simulation 78−92823
X-ray fluorescence of rock samples, major-element data processing, SORT, REORD and MW programs in FORTRAN 77−86398
XLFRAC: a program for the interactive testing of magmatic differentiation models, in FORTRAN IV 79−2377
zones of influence of linear geological structures, computation program 78−57202
Au ores, neutron activation and mathematical programming *(Rumanian)* 78−20565
Hg pollution, future content of oceans and European air, soil, and river sediments 79−8687
Mn nodule undersea mining data file, management and statistical anal. 77−53206
NaCl, rock salt, progressively mined soln. cavities, struct. behaviour 78−61409

geophysics computing continued
U exploration with computer-processed LANDSAT data 78−7777
U prospecting, pattern recognition appl. 77−66999

geopotential *see geodesy*

geothermal power stations
10 MW, San Diego (USA) expt. facility performance 79−48085
American Nucl. Soc. winter meeting 1977 78−58315
American Nucl. Soc. Winter Meeting 1977 78−82408
availability accounting in plant with flashing system *(Japanese)* 80−16780
binary cycle, hydrocarbon working fluid and operating conditions selection 79−48091
binary thermodynamic cycle with dual boiling for 5 MW pilot plant 80−97763
development, reviews 79−87965
dry hot rock hydraulic fracture characterisation acoustic instrumentation 77−33221
economics and risk assessment 80−30378
economics of electric power generation using geothermal resources 80−35635
electric power generation, development and utilisation prospects 80−66937
electric power generation technology, reviews 79−24883
electrical potential, near-term supply curve for elec. appls. based on prod. costs 80−61277
energy accounting study 80−76589
energy conversion process, thermodynamic considerations 80−16779
energy resources, in Great Britain 79−17166
energy utilisation, geothermal, rel. to nucl. energy *(German)* 79−52876
environmental problems, air and water pollution, subsidence, induced seismicity, blowouts, noise review 80−55797
flash cycle optimisation, analytical expression in terms of temp. only 80−40894
fluid transport in geothermal reservoir, rel. to ^{222}Rn conc. and emanation source 78−11832
fouling problem overcoming, use of novel heat exchangers 79−43740
France, extraction and utilisation of geothermal energy *(French)* 79−39276
future prospects for geothermal sources in world energy strategy 80−72012
geopressured geothermal energy production plant, environmental effects 80−97764
heat exchange in geothermal strata maintained by linear, ring batteries of wells 80−45630
heat exchanger, liquid-fluidised-bed, flow distribution models 79−52879
heat exchanger appl., liquid-fluidised bed, scale control and corrosion tests 79−48090
heat exchanger design, shell and tube 79−48089
heat exchanger fouling data analysis, using multivariate regression technique 79−52880
hot dry rock geothermal energy development program 80−55801
hot dry rock geothermal reservoir fracture mapping techniques 80−81419
hot dry rock project, Los Alamos Scientific Lab. *(German)* 77−91086
hybrid geothermal/coal fired power plant, site specific economic anal. 79−24887
Iceland, geothermal energy exploitation 78−57181
Imperial Valley, California, quadrupole resistivity survey of geothermal fields 79−84096
industrial appl., evaporation/crystallisation processes, feasibility assessment 79−48086
in Italy, survey *(Italian)* 79−24889
Nicaraguan geothermal resource utilisation 79−29448
optimum design conditions, Geysers Unit 16, Northern California (USA) 79−52877
Portuguese 1951-78 development, Azores area *(Portuguese)* 79−79373
preheating of feedwater, in hybrid fossil-fired steam plant 79−48084
Roosevelt Hot Springs thermal area, Utah, geothermal power prospect 79−84260
salt domes, using double-pipe heat exchangers 79−48087
site identification and development processes 79−12101
siting, planning and regulatory considerations in geothermal resource development 80−66935
space heating, system design and economic anal. 80−30379
steam, using fossil superheating, thermodynamic analysis 79−48088
steam cycles comparison, direct-flash and binary, effect of noncondensable gases 79−52878
steam pipeline network, numerical simulation 80−40822
steam plants, dry, separated or separated/single-flash, binary cycle, Italy, New Zealand, Japan, USA 80−61276
technological aspects of geothermal energy exploitation 80−55799
Hg emissions in air and water 77−73838

germanate glasses
absorption and emission of Ho^{3+} 79−11439
alkali germanate, Ge coordination number change *(Japanese)* 77−58958
alkali germanate, He permeability, diffusivity and solubility 79−51308
alkali germanate crystals and glasses, struct. and stability, IR spectra meas. 80−64911
alkali germanosilicate glasses, water extraction for making graded index optical fibres 80−28361
alkali lime germanosilicate glasses, optical absorpt. of transition metal impurities 80−2784
alkali lime germanosilicate GRIN fibre prep., losses and geometrical props. 80−69560
energy transfer between Bi^{3+} and Eu^{3+} using time resolved spectra 79−33748
fibre, elongation, force depend., deviations from linearity 80−45334
film, SiO_2 rich, prepared by modified CVD, refr. index behaviour 78−60526
formation on $MoSi_2$ surface following Ge additions *(German)* 80−71782
germanate glass: Tb^{3+}, luminesc. props. 79−33798
germanate glass:Bi^{3+}, time-resolved spectra, radiative and nonradiative processes 79−47501
high GeO_2 glass, zero material dispersion wavelength and waveguide props. 80−58733
iron germanate glass, ion-beam sputtering, excitation efficiency of atoms 78−19623

germanate glasses continued
lead germanate glass crystallisation study by infrared spectrophotometry 80−6499
nonisothermal devitrification kinetics 80−92465
optical, resistance to humidity and spotting agents 77−58404
optical fibres, refr. index and comp. data 77−79950
Raman scattering, low-freq., 6-700K, excess scatt. 78−23473
self-diffusion of O, theory 79−95214
vibrational spectra and glass structure 80−84732
X-ray scattering at small angles study 80−84071
Al^+ ion coordination study by $AlK_{\alpha 1,2}$ X-ray fluorescence spectra *(Japanese)* 78−7308
B_2O_3-GeO_2 system melts evaporation coeffs. 79−65180
B_2O_3-PbO-GeO_2-Fe_2O_3 glass, Mossbauer exam. of Fe valence states 79−78597
$BaGeO_3$-(0.25MgF_2.0.75YF_3)-Ga_2O_3 glass, synthesis and props. 80−25648
$BaGeO_3$-CaF_2MgF_2-$Ca_2Al_2GeO_7$($CaTiGeO_5$) systems, glass forming and props. 80−19717
BaO-Al_2O_3-GeO_2-MF_2 (M=0.45 CaF_2+0.55MgF_2), MgF_2 and CaF_2 effect on physicochem. props. 80−34876
BaO-B_2O_3-GeO_2, exam. of glass formation and physicochemical props. 79−4959
BaO-La_2O_3-GeO_2, exam. of glass forming region, properties and crystallisation 78−88454
BaO-PbO-GeO_2-MF_2 (M=0.45CaF_2+0.55MgF_2), MgF_2 and CaF_2 effect on physicochem. props. 80−34876
CaO-B_2O_3-GeO_2 system, physicochem. props., alkaline earth oxides effect 79−65827
CdO-B_2O_3-GeO_2 system, phase equilibria at 800°C, X-ray powder diffr. anal. 79−4956
CdO-GeO_2:Tl_2O photochromic glass for optical information retention media 80−33108
Cs_2O-SiO_2(-GeO_2) system glasses, X-ray diffr. anal., electron radial distrib. curves 78−87622
Cu^{2+} impurity near IR electronic spectra, effect of alkali contents 78−27267
$20Fe_2O_3$.80[$3B_2O_3$.(1−x)PbO.xGeO_2] glass, phys. props. 80−49119
Ge-Pb-Bi-O glass, photoelasticity, glass transition limits 79−33670
GeO_2 based glasses, IR transmitting materials, appl. in 1 to 6 μm range, mech. props., review 79−4250
GeO_2 doped silica, low loss single mode fibre, CVD *(Japanese)* 78−37979
GeO_2, neutron diffr. obs. using Harwell linac 78−22666
GeO_2, thermal conductivity 1.5 to 30K *(French)* 77−39704
GeO_2, thermal expansion at low temperatures 78−83982
GeO_2:Mn^{2+}, EPR, struct. of vitreous and crystn. states 77−48039
GeO_2:Pr^+, glass, optical homogeneous linewidths 80−7395
GeO_2-B_2O_3-SiO_2 optical fibres, optical transmission loss as function of drawing conditions 79−32038
GeO_2-K_2O, glass composition effect on solubility in H_2O 80−39303
GeO_2-K_2O(Na_2O)(Li_2O), glass, Raman spectra, struct. and crystn. 80−92463
GeO_2-Na_2O, DC cond. rel. to dielectric loss peak freq. 79−78621
GeO_2-Na_2O, glass composition effect on solubility in H_2O 80−39303
GeO_2-Na_2O, Na^+ partial dissociation investigated by elec. meas. 80−92716
GeO_2-Na_2O glasses, equivalent cond., temp. depend., weak electrolyte theory appl. 80−107475
GeO_2-Na_2O-BaO glass, rare earth doped, nonradiative decay and multiphonon relax. 77−85802
GeO_2-P_2O_5-SiO_2 graded-index fibres, effect of deposition rate on spectral loss 80−87485
GeO_2-P_2O_5-SiO_2 long spliced graded-index fibre transmission characts. at 1.27 μm 79−81536
GeO_2-$PO_{5/2}$ glass, struct. and props. *(Japanese)* 77−27837
GeO_2-PbO glasses, IR transmittance and thermal expansion, effect of oxides and fluorides 77−63405
GeO_2.B_2O_3.SiO_2 glasses, material and mode dispersion 77−19415
K_2O-BaO-GeO_2:Bi^{3+}, Nd^{3+}, absorpt. and excitation spectra, fluoresc. 77−90183
K_2O-CaO-BaO-GeO_2, calc. of network refraction and exam. of glass structure 79−4783
K_2O-GeO_2, struct., Raman scatt. obs. 80−1936
K_2O-GeO_2:tb^{3+}, Yb^{3+} glass, luminesc, cooperative sensitization correlated with Rayleigh scatt. intensity 78−52573
K_2O-SiO_2-GeO_2 digermanosilicate glass, Raman study of structure 79−77524
K_2O-SiO_2-GeO_2 metagermanosilicate glass, Raman study of structure 79−77523
K_2O-SiO_2(-GeO_2) system glasses, X-ray diffr. anal., electron radial distrib. curves 78−87622
La_2O_3-GeO_2-Ta_2O_3(HfO_2)(ZrO_2), vitrification, crystn. 77−15559
$La_2O_3GeO_2$-Ga_2O_3(B_2O_3), vitrification and crystallisation 77−15558
Li_2GeO_3 piezoelectric glass ceramic, recrystallisation, pyroelectric response, permittivity 80−80703
Li_2O-Al_2O_3-GeO_2, interdiffusion coeffs. of Li and Na 80−88369
Li_2O-GeO_2, struct., Raman scatt. obs. 80−1936
Li_2O-GeO_2 glass, synthesis, Ge coordination state 77−24271
Li_2O-GeO_2-Ga_2O_3, electrode props., dissolution kinetics 80−89387
Li_2O-SiO_2-GeO_2 digermanosilicate glass, Raman study of structure 79−77524
Na_2-S-GeS_2 system, glass formation, struct. and ionic conduction 80−54138
$Na_2Ge_2O_5$, crystn., from Na_2O-GeO_2 glasses, lattice constants 79−77527
Na_2O-B_2O_3-GeO_2 system glass-forming melts, mass spectrometry obs. of thermodynamic props. 80−97468
Na_2O-GeO_2, electric cond. and dielec. relaxation *(Japanese)* 78−19905
Na_2O-GeO_2, struct., Raman scatt. obs. 80−1936
Na_2O-GeO_2, structure toughness-composition relationship 80−104257
Na_2O-GeO_2, thermolum. rel. to coordination number 77−16405
Na_2O-GeO_2 glass, X-ray diffr. study of Ge coordination number 80−10503
Na_2O-GeO_2 glass, XPS meas. *(Japanese)* 80−16154
Na_2O-GeO_2 glasses, low temp. viscosity, as function of composition 78−38865
Na_2O-GeO_2 glasses, neutronographic study of Ge^{4+} struct. state 80−19711
Na_2O-GeO_2 glasses, struct. changes, X-ray diffr. study *(Japanese)* 78−91254

germanate glasses continued
Na_2O-GeO_2:Fe_2O_3 glass, $Fe^{2+(3)}$ impurity ions struct.-chem. state, Mossbauer data 80−40028
Na_2O-GeO_2-CoO, Co^{2+} ions activated, magneto-opt. study 79−65844
Na_2O-GeO_2-SiO_2 glass, density, refractive index, thermal expansion hardness, IR spectra, DTA *(Japanese)* 78−15535
Na_2O-GeO_2-Yb_2O_3, glass struct., Yb^{3+} ion segregation 78−87620
Na_2O-GeO_2(SiO_2), thermal expansion at low temperatures 78−83982
Na_2O-K_2O-GeO_2-SiO_2-As_2O_3 glass, water extraction for making graded index optical fibres 80−28361
Na_2O-SiO_2-GeO_2 digermanosilicate glass, Raman study of structure 79−77524
Na_2O-SiO_2-GeO_2 metagermanosilicate glass, Raman study of structure 79−77523
Na_2S-B_2O_3-GeO_2, darkening and fading in UV irradiation *(Japanese)* 77−36270
Na_2S-GeO_2, darkening and fading in UV irradiation *(Japanese)* 77−36270
Nd^{3+} doped, spectral behaviour under narrow-line excitation 79−33747
P_2O_5-GeO_2 glass, absorption spectrum of Nd^{3+} ion, chem. composition effects, group IV element effects *(Polish)* 78−10932
P_2O_5-SiO_2-GeO_2 graded-index optical fibre, UV induced losses 80−87518
$Pb_5Ge_3O_{11}$, crystn. via metastable phase 78−30543
$Pb_5Ge_3O_{11}$, single crysts., photoemission anamoly during ferroelectric phase transitions 79−47599
PbO-Bi_2O_3-GeO_2, exam. of glass forming and liquid phase separation regions, and optical props. 78−88453
PbO-GeO_2, glass, exam. of Raman spectra *(Japanese)* 79−19894
PbO-GeO_2, structure of anionic network, IR spectra 80−103256
PbO-GeO_2 glass, synthesis, Ge coordination state 77−24271
PbO-GeO_2 glass, XPS meas. *(Japanese)* 80−16154
PbO-GeO_2:Fe_2O_3 glass, $Fe^{2+(3)}$ impurity ions struct.-chem. state, Mossbauer data 80−40028
SiO_2:GeO_2 single-mode optical fabre fabrication 79−46050
SiO_2:GeO_2/SiO_2 glass fibre waveguide, γ-radiation optical stability 80−23799
SiO_2:GeO_2-P_2O_5 graded-index fibre, spectral loss characts. in long wavelength band 79−59811
SiO_2-B_2O_3-GeO_2, optical fibres, UV radiation-induced losses 80−87517
SiO_2-GeO_2, optical attenuation in IR region 77−75665
SiO_2-GeO_2, optical fibre, wavelength dispersive props. and comp. 78−33793
SiO_2-GeO_2, refr. index and density, comp. depend. 78−23424
SiO_2-GeO_2, synthetic, struct, IR spectra 79−42993
SiO_2-GeO_2-B_2O_3, prepared by modified CVD, refr. index behaviour 78−60526
SiO_2-GeO_2-B_2O_5-P_2O_5, optical waveguide glass, comp. determ., plasma emission spectra 80−87446
SiO_2-GeO_2-Li_2O(Na_2O)(K_2O), refractive index and density 79−51926
SiO_2-GeO_2-P_2O_5, graded-index fibre material dispersion evaluation using nanosecond pulse radiator 79−81520
SiO_2-GeO_2-P_2O_5,optical glass fibre, profile synthesis 77−27333
SiO_2-P_2O_5-GeO_2 optical fibres, CVD, losses, reactant impurity effects 80−87522
$SiO_2P_2O_5$-GeO_2, optical fibres, UV radiation-induced losses 80−87517
SnO-GeO_2 system, glass form., compound anal. 77−35486
SrO-B_2O_3-GeO_2 system, physicochem. props., alkaline earth oxides effect 79−65827
TeO_2-GeO_2 system, phase diagram, X-ray phase analysis, DTA and electron microscopy 77−15545
Tl_2O-GeO_2, glass, ^{205}Tl NMR 77−59470
Tm^{3+}, in oxide glasses, multiphonon relax. rates and fluoresc. lifetimes 77−77266
V_2O_5-GeO_2 glass, effect of thermal processing on elec. and thermal props. *(Russian)* 77−63814
V_2O_5-GeO_2-PbO, memory and threshold switching 78−23142
ZnO-La_2O_3-GeO_2, exam. of glass forming region, properties and crystallisation 78−88454

germanium
see also nuclei with .....
α-irrad., stopping power for fast channelled α-particles 78−79654
absorption edge, hydrostatic press. effects 77−43994
abundance in ordinary chondritic meteorites 80−8595
acceptor complex spectra, tunnelling H systems 80−89036
acceptor ground state, stress effects 80−34385
acceptor ground state, US attenuatin meas. *(Japanese)* 78−19105
acceptor levels, ionis. energy and IR absorpt. 79−78033
acceptor spectra, interpretation 78−43332
acceptors, transitions from second excited state, photocond. meas. 79−11082
acoustic phonon geometric propag., anisotropic continuum acoustics 77−4170
acoustic phonon propag. and interaction with electron-hole drops *(Russian)* 80−29336
acousto-optical deflector performance at 10.6 μm 80−102835
adsorbed metal atoms effect on surface electron props. 77−55597
adsorption of Ar, Kr and Xe on (111) plane, adsorpt. pot. 78−26768
adsorption of Cd on Ge (111), combined RHEED-mol. beam obs. 77−4255
adsorption of Cs on (111) surface, work function meas., adsorption site model 79−23839
adsorption of K and Cs on (111) surface, effect on surface elec. props. 79−90880
adsorption of N_2 and CO, adsorption potentials and trapped electrons role 79−90872
adsorption of O_2 on surface, degree of freedom of rot. and translational motion of O particles 79−23842
adsorption of O, enhancement by elec. field of polarity facilitating field-ion emission 79−65325
adsorption of oxygen, electron-beam enhanced reaction, AES meas. 77−4256
adsorption of water, neutralization of surface recomb. and fast capture centre 79−33184
adsorption-desorption kinetics of H_2, O_2 and other gases, catalysis 77−47684
Akhieser region, nonlinearity parameter and US attenuation coeffs., temp. depend. 79−37762
alkali halide: Ge^{2+}(Sn^{2+})(Pb^{2+}), T-centres, absorpt. spectra, energy level diagram 77−73157

germanium continued
alpha-particle damage, quadrupole nucl. interactions on ^{73}A nuclei, TDPAC meas. 77−36160
ambipolar hot-carrier size effect kinetics 80−107799
amorphous, 1 MeV electron irrad. influence on kinetics of crystallisation 77−89476
amorphous, annealing effect on absorpt. edge *(Korean)* 79−15142
amorphous, anomalous magnetoresist., hopping model 78−23117
amorphous, anomalous magnetoresistance 80−6877
amorphous, appl. of theory of AC and DC hopping cond. 80−54698
amorphous, crystallisation study 80−33889
amorphous, defects, band gap states 80−80215
amorphous, dislocation model 80−1929
amorphous, dislocation model 80−1930
amorphous, doped, electronic props. 77−1418
amorphous, doping, Schottky barrier and p-n junction form. by RF sputtering 77−8187
amorphous, doping effect and nature of localised states 78−14696
amorphous, effects of ion implantation on structure 78−55881
amorphous, elastic moduli, random network model, calc. 78−6119
amorphous, elec. cond. obs. of crystn. expt. verification of model 77−20475
amorphous, electron energy loss spectra, appl. of cylindrical electrostatic analyser *(French)* 77−55856
amorphous, electronic density of states, mol. liq. model 80−49581
amorphous, electronic struct., far infrared absorption 80−45051
amorphous, electronic structure and molecular liquid model 80−54133
amorphous, EPR 78−88167
amorphous, ESR and DC cond. 77−48032
amorphous, far IR absorption 78−88306
amorphous, first order transition to metallic liquid, calc. of transition temp., enthalpy and entropy 79−69227
amorphous, Ge-O removal in pre-crystallisation annealing 78−9957
amorphous, growth rate of crystallisation, Raman spectroscopy study 80−44227
amorphous, ideal network struct., electronic struct., tight-binding model 80−44485
amorphous, ideal surface, definition and characts. 80−107623
amorphous, impurity effects on hopping conductivity 79−65485
amorphous, ion-implanted, epitaxial regrowth on Ge 77−35835
amorphous, ionicity dependence of defect reactions and negative-U states in glasses 80−88511
amorphous, ionisation enhanced crystallisation, elec. cond. meas. 77−35481
amorphous, IR absorpt., first-order effective charges due to at. displacements 77−48164
amorphous, laser reordering of implanted amorphous layer 79−19270
amorphous, localised states, Cayley trees appl. 79−65373
amorphous, Mott's parameters for hopping cond., effect of annealing 77−69324
amorphous, O_2^+ ion implanted, influence on electrical and optical props. 77−89891
amorphous, optical absorpt. edge shape, band edge fluctuations 77−20880
amorphous, optical and microwave props. of microscopically inhomogeneous materials 77−77161
amorphous, optical props., lecture 78−31219
amorphous, possible ABB-type excitonic superconductor *(Chinese)* 80−7029
amorphous, pure and H doped, voids, atom probe FIM 80−49107
amorphous, pure and hydrogenated, Raman spectra 79−61358
amorphous, scatt. of 2 MeV He^+ 77−69954
amorphous, sputtered hydrogenated, transport and recomb. 78−10506
amorphous, struct., dislocation model 78−42911
amorphous, struct. and growth kinetics, topological principles 80−49123
amorphous, struct. models 79−37628
amorphous, thermoelec. power in phonon-assisted hopping regime, Coulomb effects 78−76097
amorphous, tunnelling states simulation and sp. ht. 79−37791
amorphous, two-band model, Thorpe-Weaire type, localisation near band edges 78−23050
amorphous, vibrational spectra, struct. model calcs. 78−22806
amorphous and crystn., contamination behaviour, XPS 79−1815
amorphous and polycryst. layers, sputtered, elec. cond. and thermoelec. power 78−2586
amorphous film, annealing, effect on localised states 79−4535
amorphous film, bright-field hollow cone images 80−75136
amorphous film, crystn. front velocity during scanned laser crystn. 80−107662
amorphous film, crystn. kinetics, elec. cond. obs. 77−62767
amorphous film, crystn. rel. to time and temp. 77−20206
amorphous film, crystn. transform. kinetics 78−22653
amorphous film, DC cond., Meyer-Neldel rule 78−64152
amorphous film, DC sputter deposited, effect of trapped Ar on minimum temp. for impulse stimulated explosive crystallisation 80−100422
amorphous film, disorder induced phonon absorpt. meas. using double-beam Fourier spectrometer 80−105725
amorphous film, effective medium theory and freq. depend of conductivity 79−24090
amorphous film, effects of alloying chalcogen atoms 80−49670
amorphous film, evaporated, non-destructive density meas. 80−6680
amorphous film, formation and stability criteria 79−10799
amorphous film, freq. response characts. 79−56334
amorphous film, high freq. cond., AC loss 80−49792
amorphous film, high freq. phonon scatt. 80−49328
amorphous film, hopping cond., thickness depend. 77−89887
amorphous film, in situ meas. of thermal EMP, by ultrahigh vacuum electron microscopy 79−26184
amorphous film, ion-implanted, regrowth 79−15043
amorphous film, large aligned grain solid-phase growth during scanned laser crystallisation 80−49100
amorphous film, laser pulse annealing 80−15006
amorphous film, LF vel. of sound for Young's modulus mode 77−35636
amorphous film, O depth profiling by SIMS 80−39480
amorphous film, optical consts. in near IR range *(Korean)* 79−8137
amorphous film, persistent photoconductivity, dangling bonds 80−84487
amorphous film, post nucleation growth, computer simulation 78−34729
amorphous film, temp. thermal conductivity 78−22994
amorphous film, ultra high vac. prep., DC elec. cond. 80−49721
amorphous film, vac. evaporated, density meas., microcrystalline model of struct. 80−2313
germanium continued
amorphous film, variable range hopping 78−76176
amorphous films, high elec. field cond. and magnetoresist. at 4.2K 80−49748
amorphous films, self-ion bombard., electronic props. 79−28422
amorphous films, structural relaxation and crystallisation 80−100170
amorphous Ge contact for electron or hole blocking on high-purity Ge detectors 77−54400
amorphous Ge-metal junction, current-voltage charact., contact material effect 80−44725
amorphous hydrogenated and cryst. IR spectra 79−61359
amorphous layer, comparison of laser and electron beam pulsed annealing 79−69374
amorphous layer, crystallisation anal. by cond. meas. *(French)* 77−72599
amorphous layer, epitaxial recrystn. by electron irrad., solar cell appl. 78−84079
amorphous layer, on single cryst. Si, heteroepitaxy by laser annealing 79−77952
amorphous layer on Ge bulk, photoemission during X-ray Bragg diffr. 78−47209
amorphous overlayer on ultrathin Pt film, effect on cond. 78−72284
amorphous solid dielectric loss meas. by submillimetric waveguide laser 79−33603
amorphous sputtered films, hydrogenated, photoinduced optical absorpt. 80−50362
amorphous thin film, fast crystn. and void precipitation in laser pulse annealing, TEM exam. 79−56086
amorphous thin films, crack networks of voids 78−2399
amorphous thin films prepared by vac. evaporation, density meas. 77−80714
amorphous vibr. props. calc. for models 77−84873
amorphous whisker growth 78−2400
amorphous/cryst. interface, supercond. mechanism 80−44783
anisotropic oxidation, ellipsometry meas. *(Russian)* 79−43451
annealing of radiation induced defects at about 6K 78−2162
anomalous avalanche breakdown 80−80284
anomalous muonium states 80−34841
anomalous transmission, in dislocation free single crysts., six wave diffr. of X-rays 79−14650
antireflection coating, two given wavelength design method 78−59102
atom, excited states, quadrupole moments, Sternheimer shielding factors 78−82630
atom, gas phase reactions with oxidisers, visible chem. laser development 79−948
atom, K-fluorescence yield meas. 77−3300
atom, L-shell internal excitation accompanying L-capture 80−95726
atom, $O^{2+,3+,4+,5+}$ induced K-shell X-ray production cross section, 7 to 24 MeV 77−61850
atom, reson. X-ray Raman scattering, IR divergence of Compton effect 78−21873
atom+H^+(D^+), K shell ionisation, nuclear Coulomb effect 80−91650
atom+O ion collisions, A=16, 18, K-X-ray production 77−23554
atomic scattering factor, anomalous X-ray scatt. obs. 77−55204
atomically sharp cracks, TEM study 80−71729
Auger LMM spectra, transition probabilities, term splittings and effective Coulomb interaction 77−44126
Auger recombination probability calc. for degenerate carriers 80−24944
Auger spectra, comparison with multiplet struct. calc. 78−31287
Auger spectra, LMM, rel. to L_{23} photoelectron spectra 77−77348
autofocusing of X-rays and γ-rays using Ge cryst. 79−12916
avalanche photodiode, cryst. orientation depend. of multiplication noise 79−80680
avalanche photodiode, reach-through, temp. depend. characts. 79−95482
backscattered energy spectra, charged particles energy losses 79−83086
ballistic phonon focusing singularities 79−99277
band structure, cluster type effect 77−28109
band structure, crit. points in E_0' region from ellipsometric data 77−80726
band structure of diamond like crystals, cluster-Bethe lattice model calc. 80−6713
band structure of ion implanted Ge, X-ray bremsstrahlung and photoelectron spectra investigation 80−2360
band structure under high stress, nonperturbative calc. 78−10344
band structure using modified Vejkovic, Slavic pseudopot. form factor 79−56121
bicrystal, cond., Hall effect and Shubnikov-de Haas oscills. 80−10984
bicrystal, conductive layer form. at boundary *(Russian)* 77−39983
bicrystal, dislocation core structure *(French)* 78−26571
bicrystal, high resolution electron microscopy obs. of dislocations 80−103347
bicrystal, two-dimensional electronic phenomena at He temp. *(Russian)* 79−56273
bicrystal cleavage plane, Shubnikov-de Haas oscills. *(Russian)* 78−64094
bicrystals, high angle tilt boundaries, TEM *(French)* 80−70224
bicrystals, low angle [011] tilt boundary 79−82239
bicrystals, [011] tilt boundary, grain boundary stability 79−82240
biexciton and trion existence, photolum. *(Russian)* 80−16088
black, selective absorber characterisation 80−80112
black, solar selective absorber surface 79−29484
bolometer, bare Ge, and Ge-diamond, operated at 4.2, 2.0, 1.2, 0.3 and 0.1K 80−77868
bolometer, cryogenic, for 20 to 500 μm spectral region 78−70187
bolometer, low-temp., characts. 79−30561
Bormann topograms, diffr. effects obs. during X-ray transmission through a cryst. with dislocations in slip planes 79−4310
bound electron states close to conduction band due to 60° dislocations 77−28141
bound exciton complexes, density functional calc. 80−10890
Bragg reflection in case of multiple X-ray scatt. 80−100127
bremsstrahlung spectra for 1 GeV electrons and positrons, planar and axial channelling *(Russian)* 77−32465
brittle, deform. during static indentation in single crystals 79−87714
brittle-ductile transition rel. to covalent bond metallisation *(Russian)* 77−56071
bulk hot-electron properties, review 79−99553
bulk modulus from local Heine-Abarenkov model potential 78−42949
capture of carriers by attractive centres 79−7836
carrier concentration variations using electrolyte electroreflectance, topographical features 79−99562

germanium continued
carrier distribution function 78−26856
carrier trapping in high-purity germanium 79−47104
channelled protons, theory of energy loss 78−38765
channelling of H^+ and He ions, backscatt. particles ang. distrib. 79−51174
charge carrier diffusion coeff. 78−84218
charge carrier UHF heating using lumped-capacitance resonators 80−20203
charge density calc., Gaussian relaxation method 77−39760
chemical etching processes, review 78−95832
chemisorption of atomic H, highly efficient electron accommodation, single cryst. *(Russian)* 79−78818
chemisorption of Cl_2, photoemission polarisation effects with synchrotron radiation 78−14580
chemisorption of Cl, chemisorpt.-site geometry from polarised photoemission 77−15684
chemisorption of Cl, cluster model calc., iterative EHT 77−32062
chemisorption of Cl, threefold co-ordinated site chemisorption, cluster model calc., extended Huckel theory 78−39178
chemisorption of CO(Cl), surface photoemission, adsorption gate geometry 78−73079
chemisorption of H_2 on (111) surface, calc. using Anderson Hamiltonian 77−55463
chemisorption of O_2 on (111) and (100) surfaces, CNDO calc. 77−55464
chemisorption of O(1s), XPS investigation 77−69170
chemisorption on semiconductor surfaces, book contrib. 80−107648
chemomagnetic effect, elec. cond. change due to surface recomb. of H atoms 77−8086
cleaved in liquid He, surface elec. cond. *(Russian)* 80−15588
coadsorption of K and O_2, rel. to work function, K thermodesorpt. spectra 78−79874
coated Ag film, electrical resistance and ageing *(Russian)* 80−103759
coating on Ag vacuum condensates, effect on ageing kinetics *(Russian)* 77−59340
coaxial detectors, n-type high purity, construction and performance 79−41075
coaxial detectors with reverse electrode, radiation damage resistance 79−41076
cold semiconductor, Mott transition 78−91616
compensated, impurity photocond. relax times 80−88592
compensated, sub mm radiation absorpt., temp. depend. 80−66331
compensated by thermal defects, recomb. and optical props. 80−64989
complanar X-ray resonator circulating beam, high symm. multiple wave configurations *(Russian)* 80−78875
complex with vacancy in Si, electron state calcs. 78−67980
composition of inclusions, single cryst. 77−15441
compressed electron hole plasma, luminesc. 78−72592
Compton profile anisotropy, pseudopot. calc. 79−28854
Compton profiles, directional, X-ray scattering factors and 1-electron density matrix 80−10458
Compton scatter, spatial spread meas., imaging with position-sensitive detectors 78−46214
concentration determ. in atm. and rainwater in Vizcaya, Spain *(Spanish)* 78−57264
condensation from gas phase, nucleation, growth and transform. of amorphous and crystalline solids 80−24745
conductivity, inhomogeneous mag. field effects 77−4374
conductivity of cleaved surface *(Russian)* 79−51654
contact angle meas. between melt and crystal during Czochralski growth 78−64461
covalent semiconductor, piezoresistance coeffs. of holes, temp. depend. 77−39847
creep and dislocation structure under tension *(Russian)* 78−19839
creep and self-diffusion activation energies 78−38772
cross-slip of single dissociated screw disclocations, double etching and X-ray topography studies 80−15104
crystal, channelling of 1 GeV protons, pions and deuterons 77−89488
crystal growth, equilib. between Ge and gas over melt 80−2938
crystal growth and segregation under zero gravity 79−43130
crystal struct. factor, at. scatt. factor, electron diffr. determ. 77−15291
cubic semiconductor, Zeeman split acceptor levels, calc. method 79−28322
current instabilities in semiconductors, theory and expts. *(Hungarian)* 77−39857
CVD, vapour transport rate, Ge-I_2 equilib. 700 to 1300K *(French)* 78−64476
cyclotron reson. linewidth in quantizing mag. field 77−15752
cyclotron resonance, exciton and electron-hole drop diffusion coeffs. 77−48055
cyclotron resonance, irradiation effects 78−72416
cyclotron resonance and radiative recomb. with laser excitation, book contrib. 80−11472
cyclotron resonance in strong elec. fields, classical theory 80−7172
cyclotron resonance line shape, 337 μm, 15-80K, n-type 78−6577
cyclotron resonance line width in quantizing mag. field 78−10336
cyclotron resonance linewidth investig. of electron scatt. in irrad. and annealed cryst. 77−55707
cyclotron resonance peaks under high excitation 77−48056
Czochralski growth system, time-depend. cryst.-melt interface shape 77−24280
dangling-bond surface states 78−43452
DC hopping, analytical formulae, degenerate hopping in wide bands 77−89761
deep dislocation states 80−24836
deep donor character of muons and protons 80−10911
deep impurity levels, activation energy 80−107742
defect annihilation process near 100°C 79−95047
defect form. under radiation-accelerated diffusion conditions 80−19854
defect state, fast donor, electronic struct. calc. 80−54641
defects, radiation effects 80−29016
deformation, annealing charcts., X-ray study 78−75713
deformed at relatively low temps., Hall effect 79−82612
degenerate, doped with nonmag. impurities, Kondo effect 78−14746
degenerate, scattering by light by phonon zero sound 79−56145
demand evaluation and supply comparison 80−33106
deposition of Ge or Si substrates by low energy mass analysed ion beam 79−33946
desorption kinetics of two-dimens. condensed phases of Ag on (111) surface 79−90882
germanium continued
detector, high purity, comparative study with Li drifted Si detector re. thyroid scanning 79−16275
detector, high purity, fast neutron damage 80−59526
detector efficiency determ. using a standard Marinelli beaker geometry 80−63450
detector for X-ray and gamma-ray spectroscopy, high-purity, preparation and properties 78−86723
detectors used for high resolution gas ray spectroscopy 79−6804
determination in optical waveguide glass by DC plasma emission spectroscopy 80−87446
diamagnetic excitons, fundamental absorption edge, Faraday config. 79−8144
diamond, Ge doping by diffusion at high temp. and press. 79−19273
diamond, P-T diagram, cryst. struct. stability 78−51886
dielectric band structure calc. 79−47034
dielectric const. associated with direct interband transitions 77−20817
dielectric function, effective, and exchange interaction effects, calc. 79−99494
dielectric function, microscopic static, tight-binding calc., ion-ion interaction and phonon dispersion 77−24528
dielectric matrix, microscopic inverse, local field correction and acoustic sum rule 77−84863
dielectric polarisation calcs., microscopic local fields 80−20582
dielectric properties, mean point value calc. 78−87930
dielectric props., submillimetre wave dispersive Fourier transform spectroscopy obs. 77−37915
diffractive focusing of spherical X-rays *(Russian)* 79−4207
diffusion and solubility in CdTe, 630-800°C 80−103519
diffusion in Al-Sn(Ag) liq. alloys, mech. *(Russian)* 80−15276
diffusion in Cu, isotope effect 78−2285
diffusion in Si, effect of dislocation struct. on migration rate 77−51551
diffusion of Ga along dislocations 79−82385
diffusion of stable Ge isotopes, isotope effect in Cu 79−60552
diode, influence of mechanical stresses on effective carrier diffusion length in base region 77−35987
direct gap recombination, at high excitation level and low temp. 79−38650
directional Compton profile meas., structural information 79−28855
dislocation electron image filtering in electron microscopy 80−75129
dislocation electron states, from press. depend. of photocond. 80−96819
dislocation energy band width, carrier lifetime anal. 77−11874
dislocation energy levels, Hall effect meas. 78−6328
dislocation ensembles motion in neutron irradiated covalent crystals *(Ukrainian)* 80−10579
dislocation interactions in Ge covered with dielectric film of SiO_2 or Si_3N_4 80−39472
dislocation levels, electron occupancy 77−15795
dislocation line movement at low stresses *(Russian)* 77−47462
dislocation mobility 77−76413
dislocation motion near surface 79−82219
dislocation states, optical excitation, photoconductivity meas. 77−69273
dislocation states, optical excitation 77−85265
dislocation structure, sessile Lomer dislocations in bicrystals *(French)* 77−55286
dislocation structure and impurity atoms diffusion, effects of ultrasound 77−69119
dislocation-induced elec. pots. appl. 79−82551
dislocations, associated electron states 79−82544
dislocations, lattice images 79−82215
dislocations and grain boundary struct., 3-4 Å resolution electron microscopy 78−38707
dislocations under high stress, stacking fault energies, TEM study 80−70202
dispersion law of indirect excitons 80−24805
dissociated dislocations, constriction correlation with jogs 80−79801
dissociated dislocations, statistics of kink formation 79−82207
dissolution by oxidation and solvation, hole injection effect 80−26051
donor energy spectrum, mag. field effect, submm. photocond. meas. *(Russian)* 77−43666
donor ion pot., small r behaviour of nonlinear Poisson eqns. 80−54652
donor polarizability, multivalley effective mass calc. 80−96817
donor-acceptor electron transfer at low temps., photocond. tail 78−84249
donor-bound excitons, far IR magneto-absorption, pseudo-acceptor model 77−63418
dopant behaviour in CdTe 78−22742
dopant distribution in cryst. growing from lightly doped melt 78−2039
doped, D^- band width, influence of resonances 79−11061
doped, electron or neutron irradiated, vibrational absorption 78−6718
doped, semiconductor-metal transition, modified screened impurity pot. 79−99500
doped polarisability of donors 78−14693
doping inhomogeneity, meas. by low field electrorefl. 77−11584
double injection characteristics under high voltages 79−51590
doubly deformed, dislocation interaction obs. 79−73172
dynamic interaction of screw dislocations with flat clusters of dislocations on other slip planes in monocrystals *(Russian)* 79−86800
E_1-optical struct. from electroreflectance spectra 78−43897
edge dislocation struct., lattice distortion and surrounding vacancy distrib. 77−19954
edge dislocations, energy spectra 80−70637
edge-type dislocations, energy spectrum 80−24842
education, forbidden energy gap meas. in Si and Ge p-n junctions 80−57027
effective masses of heavy and light holes, from ohmic mobility data 80−80160
effective screening function 78−10383
EHT calcs. of energy bands and pressure dependences *(Japanese)* 78−34747
Einstein force constants, harmonic and cubic, calc. 77−47515
elastic constants, third-order 79−51184
elastic moduli, drag coeffs. and Keating's parameters 79−73238
elastoresistive effects 79−60838
electric field gradient-elastic tensor components, acoustic NMR obs. 80−25229
electric field influence on exciton states, Stark effect 80−54617
electric quadrupole sum rules rel. to optical consts. 79−38036
electrical and optical props. at low temps. 80−39636
electrical conductivity, optically injected carrier density and temp. depend. 78−68046
electrode, cathodic charcts. rel. to halide ions 79−57238

germanium continued
electrode, electon injection in liq. NH_3 80−6977
electrode, photoemission into electrolyte solns. 77−24616
electrodeposited, X-ray, electrochem., and electrorefl. characterisation 78−14624
electrodes for HF laser suitable for optical studies of semiconductors 80−64061
electron and positron bremsstrahlung spectra *(Russian)* 79−91522
electron beam irrad., {113} faults, nature and origin 80−70258
electron beam irradiation, 2.3 MeV, positron annihilation exam. of radiation defects *(Russian)* 78−34542
electron beam irradiation, of crysts., changes of real struct., HVEM 80−103390
electron heating by nonuniform elec. field, I-V characteristics 77−47825
electron heating in inhomogeneous elec. field 78−2494
electron hole drop, surface energy calcs. 77−47741
electron hole drop diffusion const., hysteresis effect determ. 79−23902
electron hole drop far IR absorpt., damping, size effects, Mie theory 79−78685
electron hole droplets, intervalence band absorption 80−6742
electron hole drops, large, microwave heating and evaporation 79−28287
electron hole size distribution at pulse optical excitation 80−59883
electron interaction with many excitons 78−26823
electron irrad., defect growth, struct. rel. to temp. 77−11591
electron irrad., light-sensitive defects 80−24498
electron irradiated, energy levels 79−28316
electron irradiated in HV electron microscope, defect form. and interaction with dislocations 77−19990
electron mean free path, stopping and straggling 78−91367
electron MFP determ. by depth and ang. depend. of inelastically scatt. electron spectra 78−92154
electron microscope obs. of nonequilibrium walls *(Russian)* 78−14347
electron microscopy, high resolution image interpretation 78−14259
electron microscopy, multi-beam lattice images in (011) orientation 77−24252
electron mobility in Δ_{1c} minima, temp. depend. 79−65473
electron mobility is semiconductors based on dielectric function modification of Dingle pot. 79−60836
electron momentum distribution, anisotropy, positron annihilation *(Russian)* 78−84676
electron scatt. by charged impurities under cyclotron reson. conditions 77−63286
electron scattering, inelastic, 70-1400 eV, mean free path 78−84696
electron states associated with core region of 60° dislocation 78−39057
electron states below cond. band originating from dissociated 60°-dislocations, calc. using effective mass method 79−19546
electron transmission and absorpt. in bulk solids, 5 to 30 keV 77−89491
electron transmission and absorption at 0.6 to 4 keV, obs. 77−84818
electron-beam-controlled transmission of 10 μm radiation 79−81466
electron-hole correlation density depend., in electron-hole liq., under uniaxial stress 79−15090
electron-hole deep deform., accel. and luminesc. under influence of radiation press. 77−47739
electron-hole drop, giant, in inhomogeneously stressed cryst., IR absorpt. investig. 77−39785
electron-hole drop, interaction with crystal surface 78−79941
electron-hole drop, surface props. calc. 77−89711
electron-hole drop and exciton atmosphere 80−6748
electron-hole drop condensation nucleation phenomena, ultrapure sample 77−47744
electron-hole drop dispersion under strong optical stimulation, phonon interaction effects *(Russian)* 77−1723
electron-hole drop drag, interaction with thermal pulses 80−103631
electron-hole drop drag by ultrasound *(Russian)* 80−100437
electron-hole drop ejection from continuously generated electron hole liquid 79−78017
electron-hole drop flight, photolum. max. press. depend. 78−10977
electron-hole drop formation, nucleation phenomena 79−33240
γ-electron-hole drop formation, time delay 77−31952
electron-hole drop freq. depend. damping 80−88482
electron-hole drop interaction in stationary and alternating mag. field *(Russian)* 77−62845
electron-hole drop large, dynamical props., carrier relax. rate temp. depend. and pair density 80−75509
electron-hole drop luminesc., phonon wind induced anomalous depend. at low mag. fields 80−34980
electron-hole drop luminescence at high mag. fields 79−65390
electron-hole drop luminescence surface energy effect 77−48239
electron-hole drop magnetoplasma resonance 79−60722
electron-hole drop magnetoplasmas, radius-independent elec. and mag. reson. 79−73446
electron-hole drop magnetostruction 78−87912
electron-hole drop modulation of direct transition absorpt. coeff. 77−90153
electron-hole drop motion, phonon wind 80−10887
electron-hole drop motion 80−6744
electron-hole drop motion at low exciton densities 77−47865
electron-hole drop motion recorded by microwave probe meas. 77−76755
electron-hole drop movement under action of forces of mutual repulsion *(Russian)* 77−89710
electron-hole drop net negative charge, giant fluctuating photocurrent obs. 77−35963
electron-hole drop phase separation, due to uniaxial stressing 78−84145
electron-hole drop radius temp. depend. 77−76753
electron-hole drop recombination radiation due to heat pulse action *(Russian)* 80−16087
electron-hole drop recombination spectrum, low energy tail 77−59612
electron-hole drop shape in mag. field 79−42458
electron-hole drop transition to metallic condensed state, Hartree-Fock theory 79−56136
electron-hole drop velocities, excitation wavelength depend. 78−88358
electron-hole drop velocities as probe of phonons 78−68517
electron-hole droplet, attachment to donor 78−87916
electron-hole droplet, effect of nonlocal contributions to energy 77−69246
electron-hole droplet, motion damping, impurity and piezoelec. scatt. 78−67951
electron-hole droplet cloud, role of thermalisation phonons 80−49617
electron-hole droplet cloud formation, phonon wind, luminesc. obs. 80−45136
electron-hole droplet cloud kinetics, thermalisation phonons 80−88483

germanium continued
electron-hole droplet condensation, crit. point 80−49612
electron-hole droplet condensation model, phase diagram and surface tension 80−6734
electron-hole droplet magnetoresistance 78−14744
electron-hole droplet motion, phonon damping 77−85152
electron-hole droplet scattering of acoustic phonons, total scatt. rate and anisotropy 79−33241
electron-hole droplet shape under uniaxial stress 77−43518
electron-hole droplets, capillary-wave reson. investig. by US attenuation 77−8027
electron-hole droplets, conc. in mag. field, magnetoplasma absorpt. spectra meas. *(Russian)* 77−24854
electron-hole droplets, large uniaxial stress 78−47703
electron-hole droplets, luminesc. and absorpt. lineshapes, RPA theory 80−49613
electron-hole droplets, magnetoplasma reson. with submillimetre circularly polarised waves 77−89712
electron-hole droplets, percolation theory of cond., expt. 80−92896
electron-hole droplets, reson. scatt. of free carriers 78−2500
electron-hole droplets, surface props., SCF calc. 78−51904
electron-hole droplets, transient photoluminesc. intensities 78−88353
electron-hole droplets, variation of α_3 electron density at constant stress 79−47025
electron-hole droplets distrib., and phonon wind 80−103629
electron-hole droplets in high stress limit 78−10369
electron-hole drops, accel. by IR radiation field 78−95264
electron-hole drops, appearance of plasma at high excitation rates 78−26821
electron-hole drops, Auger recomb. 77−48240
electron-hole drops, Auger recomb. 78−39600
electron-hole drops, carrier density, plasma reson. determ. 77−24522
electron-hole drops, damping of motion by mag. field 77−69244
electron-hole drops, determ. of nonradiative decay rate at 1.6K 77−8143
electron-hole drops, far IR absorption 78−56467
electron-hole drops, far IR magneto-optical effects 78−84565
electron-hole drops, in superfluid He, threshold phenomena *(Russian)* 79−42462
electron-hole drops, inflammation radiation under action of ultrasound *(Russian)* 79−7788
electron-hole drops, IR absorpt. spectra 79−87423
electron-hole drops, IR magnetoplasma absorptions 80−6728
electron-hole drops, kinetics of spatial distrib. *(Russian)* 78−43312
electron-hole drops, laser Doppler velocimetry 77−43504
electron-hole drops, laser induced, deform. under high magnetic fields *(German)* 78−23027
electron-hole drops, luminesc. and transport props. 77−48241
electron-hole drops, magnetoplasma resonance *(Russian)* 78−79944
electron-hole drops, magnetoplasma resonance at arbitrary crystallographic orientation in mag. field 79−78018
electron-hole drops, motion in low mag. fields 79−23904
electron-hole drops, non-isothermal nucleation 80−44514
electron-hole drops, nucleation anal. 77−69243
electron-hole drops, periodic explosions under light and microwave heating 77−11950
electron-hole drops, phonon lifetime and acoustic attenuation due to phonon-assisted Auger recomb. 80−34462
electron-hole drops, photoluminesc. kinetics 78−23524
electron-hole drops, repulsive interaction and spatial distrib. 79−99488
electron-hole drops, resonant power absorpt., Alfven wave anal. 79−42569
electron-hole drops, rest friction *(Russian)* 79−42463
electron-hole drops, size distrib., light scatt. meas. 79−28292
electron-hole drops, size effect on far IR absorption and scatt. *(Russian)* 78−10903
electron-hole drops, spatial distrib., time and spatially resolved absorption at 3.4 μm 78−92075
electron-hole drops, surface struct. 78−60058
electron-hole drops, US absorpt. and recomb. radiation, 1.8 to 3.5K 77−31954
electron-hole drops at high mag. fields 79−60721
electron-hole drops formation, nucleation theories 79−33239
electron-hole drops interaction with phonons 80−6747
electron-hole drops net charge, photocond. and photoluminesc. for pure and doped examples 79−38589
electron-hole Fermi liquid, in ⟨111⟩-stressed Ge, unusual phase diagrams 79−63137
electron-hole fluid drift in crossed electric and mag. fields, photocurrent dynamics *(Russian)* 79−99487
electron-hole gas and liq. coexistence 78−14668
electron-hole liq. thermalisation between mag. field split valleys 80−25444
electron-hole liquid, ground state props. under ⟨111⟩ uniaxial stress 79−69428
electron-hole liquid, luminesc. under infinite uniaxial compression 78−87915
electron-hole liquid, MHD effects 80−80190
electron-hole liquid, pinch effect 78−87993
electron-hole liquid, range of energetic Auger electrons 79−90970
electron-hole liquid, RPA calcs. 80−6743
electron-hole liquid, strain-confined 77−47738
electron-hole liquid, strain-confined 78−10355
electron-hole liquid, strain-confined 80−6745
electron-hole liquid gamma, orientational depend. of shape in mag. field 77−66121
electron-hole liquid in magnetic fields, expt. and theoretical investigations, review 79−60720
electron-hole liquid theory, generalised RPA 78−87914
electron-hole plasma, coexisting phases 77−1374
electron-hole plasma, destruction of pinch channel by longit. mag. field *(Russian)* 77−80802
electron-hole plasma, helical instability excitation in strong mag. field *(Russian)* 77−69368
electron-hole plasma, high density, IR absorpt. at low temps. 78−92078
electron-hole plasma, high density, low temp. transport props. 77−47864
electron-hole plasma, ultrafast transient response, theory and expt. 77−80748
electron-hole plasma condensation, in supersaturated gas of free excitons 77−69242
electron-hole plasma phase transition 80−24803
electron-hole two component liq. phase diagrams under stress 80−29332

germanium continued
electron-hole-droplet cloud, photoluminesc. of laser excited surface, phonon wind 78−84146
electron-phonon interaction, internal strain and impurity elec. field effect 78−14418
electronic and struct. props., nonlocal pseudopot. calc. 80−34349
electronic charge density of valence electrons 77−1094
electronic energy bands of diamond-type crysts., appl. of EHT method 78−87907
electronic inversion channel anomalous Hall factors *(Russian)* 79−95467
electronic states associated with 60° edge dislocation 77−89724
electronic states of isolated negative donor ion, binding energy 79−65404
electronic struct. from SCF calc. using intersecting spheres model 78−51888
electronic structure, self consistent local description 80−20067
electronic structure, self-consistent localised description 79−42445
electronic structure of surface (111), atomic geometry effects, photoemission and electron energy loss spectra 77−85283
electronic subsystem heating by Dember field for ambipolar diffusion *(Russian)* 77−39898
electroreflectance, effect of surface and nonuniform fields 78−68511
electroreflectance, field reversal asymm. at direct gap 77−69802
electroreflectance spectra, meas. on Al-SiO_2-Ge struct. 77−1677
electroreflectance spectra, nonparabolicity effects of bands *(Russian)* 79−4791
electroreflection spectra, multioscillatory *(Russian)* 77−8590
energy band gap dilation and vibr. contrib. determ. 79−60703
energy bands and wavefunctions, localised orbital description 78−18942
energy gap, impurity conc. depend., calc. 80−80170
energy loss spectra of C^{2+} ions in Ge targets 80−65114
energy spikes due to heavy ion bombardment, semiempirical model 78−47453
energy-gap narrowing and state filling under laser irrad. 79−42441
entropy of fusion anomalies, deviation from Richard's rule 77−47601
epitaxial, on n-GaAs, with Ni overlayer, smooth and continuous ohmic contact form. by solid-state diffusion 78−68086
epitaxial, on Si, misfit, strain and dislocations, book contrib. 79−82499
epitaxial film, crystallographic imperfections 77−35826
epitaxial film, ion implantation and electron beam anneal effects on carrier conc. 80−75255
epitaxial film, ion sputtering, growth mechanism, struct., props. 77−31917
epitaxial film, misfit dislocations, determination of Burgers vector *(Russian)* 79−33207
epitaxial film, vac. deposited on GaAs, doping effect of annealed GaAs surface 80−65718
epitaxial film growth by hydride-iodide method 77−48343
epitaxial film on Si, influence of fragmentary struct. on galvanomag. effects *(Ukrainian)* 78−84327
epitaxial films, ohmic contacts for GaAs devices 78−88027
epitaxial films, structural perfection rel. to deposition conditions 78−43258
epitaxial growth, solid-phase, through PdGe layers, channelling and backscatt. obs. 77−85936
epitaxial growth from monogermane at 685°C 78−51833
epitaxial growth of Cd on Ge (111) 77−7986
epitaxial growth of very thin electron microscopy specimens 80−100793
epitaxial layer deposition by vacuum pyrolysis 78−52676
epitaxial layer on GaAs tetragonal distortion in heteroepitaxial layer, X-ray diffr. exam. 78−67922
epitaxial layers, on GaAs substrate, misfit dislocation multiplication mechanism 78−87673
epitaxial-diffusion p-n junctions, inductive props. in secondary breakdown 80−15598
epitaxy, in situ X-ray topography, misfit dislocations 78−47671
equation of state, under press. 78−75801
erosion by rain at subsonic velocities 77−70191
etching, HF ion-plasma, cryst. surface layers treatment and study *(Russian)* 80−16517
evaporated film, lattice parameters and phase transition temp., surface influence of glass substrates 78−94996
EXAFS, atomic phase shifts calc. nearest neighbour distance determ. 77−48276
EXAFS, in real space, struct. determ. 77−15273
EXAFS, new horizon in struct. determs. 79−19949
EXAFS amplitudes, many-body effects 80−97379
EXAFS at high press. 80−97376
EXAFS in photoelectron yield spectra 80−16123
excitation spectra of shallow acceptors, Zeeman effect, expt. 80−7381
exciton and electron-hole drop decay, far IR magnetoabsorption obs. 77−40252
exciton and electron-hole drop entrainment by nonequilib. phonons 80−6751
exciton condensate and electron-hole droplet, metastable state, effect of illumination and high-frequency heating 79−15097
exciton condensation, electron-hole drop investigation in UHF field, nucleation *(Russian)* 80−80193
exciton condensation, light scatt. by electron-hole drops 80−84435
exciton condensation, microwave breakdown, luminesc., book contrib. 80−11471
exciton condensation, microwave cond., book contrib. 80−11040
exciton condensation, microwave cond. below 1K, book contrib. 80−8997
exciton condensation, microwave exciton breakdown and luminesc., one- and two-photon excitation 77−31955
exciton condensation, microwave studies, book 80−10886
exciton condensation in electron-hole drops *(Russian)* 79−19522
exciton damping by phonons 77−1373
exciton droplets, energy condensation *(Russian)* 80−107712
exciton drops nucleation centres under conditions of inhomogeneous strain *(Russian)* 78−2429
exciton emission, phonon-assisted, temp. depend. of relative integrated intensities 77−1375
exciton energy gap and LA and LO momentum-conserving phonon energies 79−90965
exciton gas, entropy ionisation, luminesc. meas. 78−35196
exciton gas, plasma model *(Russian)* 77−11860
exciton luminescence polarisation in mag. field *(Russian)* 77−12436
exciton microwave breakdown, electron-hole drops, book contrib. 80−11041
exciton mol. by phonon-assisted two-photon absorpt., theory 78−48197

germanium continued
exciton mol. creation by pure and phonon-assisted two-photon transitions 78−63987
exciton recombination with emission of single phonon, luminesc. replicas, detect. and anal. 79−60728
excitons, influence of temp. on high freq. breakdown in presence of electron-hole drops 78−26820
excitons bound to acceptors, Auger transition rates 78−34778
extended X-ray absorption fine structure using real space transform, struct. determ. technique 78−23553
far IR magnetoabsorption, excitons, electron-hole drops and impurities 78−6664
far IR photoconductive detector speed, limitation 79−30550
far IR radiation amplification on hot hole population inversion *(Russian)* 80−16060
far-IR absorpt. spectra interpret. 77−40233
Faraday effect, due to intervalence band transitions 79−38521
Faraday effect, IR, standard measure of magnetooptical rotation of plane of polarisation 80−60551
Faraday rotation and ellipticity, interband transitions, comparison with Si 77−52048
fast particle irrad., Frenkel defect formation threshold energy 80−6404
faulted dipoles, high-resolution TEM study 80−103345
Fermi level, minority carrier conc., effective intrinsic conc., Einstein relation in n- and p-type 77−85209
FET, fabrication on high purity substrate 79−45579
field effect charact. rel. to surface inhomogeneity 78−26933
field-emission current-voltage charact., effect of earlier measurements 80−71579
film, A1-type and amorphous, complex refractive index and reflectance 77−52121
film, amorphous, ^{74}Ge ion implanted, defect struct. obs. 78−51848
film, amorphous, AC conductivity, anomalous freq. depend. 77−4456
film, amorphous, contamination anal. by AES 77−36828
film, amorphous, high field effects, 100-300K 77−24563
film, amorphous, influence of deposition parameters on e.p.r. 77−1586
film, amorphous, O ion implantation effects on absorpt. edge and elec. cond. 77−39970
film, amorphous, prep. conditions influence on supernetwork struct. 77−76709
film, amorphous, prepared by evap. or sputtering, AC loss meas. 80−65560
film, amorphous, thermally induced reversible switching, effect of charge in thermal resist. 77−20371
film, amorphous, thermoelec. power and structural investigs. using in-situ electron microscopy 77−76983
film, amorphous, two-dimensional variable range hopping cond. 80−10977
film, amorphous, vac. deposited, XPS and elec. props., evidence for polycryst. phase 77−28691
film, amorphous and crystalline, effects of Al and Cu alloying on elec. transport props. 79−51689
film, amorphous and crystalline, optical props. 77−16412
film, amorphous evap., structural aspects in electronic data interpret. 77−76977
film, amorphous or cryst., elec. resist., temp. depend. 77−39978
film, dense electron-hole plasma, negative differential resistance 77−89794
film, elec. props., prep. by DC sputtering *(Japanese)* 79−78237
film, elec. resist. and struct., post-deposition heat treatment effects 79−78229
film, electrical cond. during laser-induced crystallisation 79−47175
film, electron transmission, 1-5 keV, electron MFP 77−15472
film, electronic struct. charge on ordering, double beam photoemission 78−19634
film, electroreflectance effects 79−43055
film, epitaxial growth from noncondensed phases, kinetic anal. 80−54565
film, epitaxial growth on Si, interdiffusion, plasmon energy loss anal. 77−31916
film, evaporated amorphous, angle of deposition effects, electron microscopy 77−43451
film, fragmented struct., elec. cond., Hall coeff. and magnetoresist. meas. 77−15979
film, growth on graphite substrate by thermal reduction 78−18934
film, inert gas ion refl., semiempirical analysis, compared with expt., 10-30 keV 78−6823
film, long term stability of electrical res. rel. to ambient atmosphere changes 78−2597
film, optical characterisation, inversion method 78−11008
film, polycrystalline, structural and elec. props. 78−76173
film, prep. by low press. reactive deposition process 79−24449
film, used as absorbing surface in solar collector 78−5580
film, vacuum deposited, O^+ bombardment sputtering rates 78−88390
film, volume plasmons, EELS, line shape 79−90984
film bolometer, radiation loss from JFT-2 Tokamak, meas. 80−95141
film characterisation technique, APFIM, time-of-flight spectroscopy 80−75138
film coatings for Mo tips, film characterisation by atom probe FIM atomic clusters, voids 80−33863
film growth, epitaxial and amorphous, low energy ion beam deposition 77−28729
film growth kinetics under high adatom conc., surface diffusion parameters 77−28088
film on BeO, surface polariton dispersion relations 77−69390
film recrystallised by unidirectional solidification, GaAs film deposition 78−19671
films, adhesion to substrates, effect of Ar^+ ion irrad. 79−11047
films, adsorption of H_2O vapour, IR spectra 80−6628
films, evaporated, oxide layers 77−76927
films on semicondcuting substrates with diamond structure, computer model of autoepitaxial growth 79−95927
foil, thinning for electron microscopy 79−49217
foil, traversed by H^+ (He^+), energy loss and straggling meas. 78−95100
foil, [110] oriented, seven-beam lattice images of defects 80−107209
Foucault currents in electron-hole drops *(Russian)* 77−8030
four photon mixing, intense tunable IR generation 77−68239
four wave mixing, intense tunable IR source for photochemistry 77−88852
four wave mixing, tunable IR generation 79−98444
four-photon mixing IR source, for isotope separation in UF_6 77−54760

germanium continued
four-wave mixing, phase-matched, of CO_2 and NH_3 laser radiation, 16 μm generation 79−3745
Fourier transform interferometry, visible reflectivity spectra 77−33765
free carrier, intervalence band indirect absorpt., at high optically created carrier densities 79−42961
free-carrier plasma edge, fast transient spectroscopy 77−8558
free-exciton lifetime, influence of dislocations 78−60064
galvanomagnetic recombination effect in cast microconductors 79−19609
galvanomagnetic-recombination field effect, theoretical model 78−43420
gamma irrad. above threshold, defect formation impurity ionisation mechanism 80−6433
Gaussian basis sets, Ga, Ge, As, Se, Br, and Kr, HF calcs. 77−38611
n-Ge:As, photoemission, into electrolyte soln., energy diagram, Volta pots., voltage drop 77−62990
Ge:P, radiation-accelerated diffusion 80−6559
grain boundary, lattice imaging in electron microscope 78−6069
growth, chem. transport, transfer inversion using Mo catalyst 79−11517
growth by Czochralski and Stepanov methods, supercooling 78−3015
Gruneisen constant, temp. depend. 77−72667
Hall effect, influence of dislocations 79−82611
Hall effect, uniaxial deform. effects in n-Ge 80−65605
Hall effect anomalies in compensated samples 79−69535
Hall effect in finite specimens of arbitrary lifetime and trap content 78−72175
Hall effect noise, theory and expt. 78−39173
Hall mobility of majority carriers, charge carrier scatt. and compensation effect *(Russian)* 77−32026
heat capacity and phonon dispersion, using five force schemes *(Russian)* 77−62649
heat pipe meas. of corrosion and vapour press. 80−23878
heavily doped, dislocation vel., electronic effects 77−11547
heavily doped, electronic effects on dislocation velocities 77−62531
heavily doped, far IR props. of shallow impurity states 79−95786
heavily doped, microcreep breakdown 80−97549
heavily doped, multiplex AC hopping conduction 79−11122
heavily doped, negative magnetoresistance model, spin-up spin-down electron effective mass variations 79−95423
heavily doped, self energy of phonons 80−44277
heavily doped, vacuum hot pressing, effect on thermal, electrical props. 80−25594
heavily doped, vacuum hot-pressing, thermal and electrical props. 77−40400
heavily doped and compensated, photoluminesc. exam. 78−2902
heavily doped with Ba, second phase inclusions on melt growth 78−22751
heavy ion impact, meas. of life-time of inner-shell vacancy in recoiled Ge atoms 77−63513
HEED, virtual inelastic scattering estimated 78−26390
heterodiffusion due to H atom surface recombination stimulation, Cu, Zn, In coated *(Russian)* 80−59726
heteroepitaxial film, ethanol pulsed adsorption effect on elec. cond. 80−93014
HF breakdown of excitons effect on kinetic of electron hole droplets *(Russian)* 77−59260
HF field effect meas. 77−55556
high press. appl. by spherical diamond indentor, plastic deform. obs. method 78−35619
high purity, nature of large traps, expt. on p^+-n-n^+ struct. 78−19051
high purity melt, stability of oxide second phases 79−47898
high-purity, with Al, B and P, residual impurities, photothermal cond. 80−24965
high-purity dislocation-free, divacancy-hydrogen complexes 78−2449
highly degenerate multicomponent plasma thermodynamic props., electron-hole drop transition 80−33739
hole diffusion exam., Monte Carlo calcs. 78−6372
hole drag current in two-photon transitions due to EM wave momentum 79−15187
hole drift velocity, effect of impurity scatt. 78−60127
hole drift velocity, time-of-flight meas. 78−10444
homogeneous n-type, avalanche ionisation and current oscills. 77−15864
hopping conduction at intermediate impurity concs. 80−6840
hopping conduction in crystalline and amorphous samples, semiclassical theory 79−91052
hot electron diffusion coefficient anisotropy 77−76838
hot electron distrib. function, response to step changes in elec. field 80−24937
hot electrons, intervalley diffusion 78−84227
hot exciton dissociation by long-wavelength acoustic phonons, photocond. spectra 77−4300
hot hole distribution function, effect of impurity and hole hole scatt. 79−11139
hot hole distribution function at low densities 79−11138
hot holes, diffusion coeff.meas. 78−6387
hot light hole distrib. function and light absorpt. 79−60844
hot microdeformation, and simultaneous X-ray topography apparatus *(French)* 80−38871
hot phonon influence on energy relax. of high-density carriers 79−82608
hot-electron diffusion Boltzmann eqn. 77−51757
hot-electron diffusion coefficient 78−87982
hot-hole noise, mag. field effects 77−4415
IGFET cryogenic temp. operation 79−69604
illumination influence on surface cond. irreversible elec. cond. increase *(Russian)* 80−92963
immersed in liquid He, optical pumping to generate first and second sound 80−6581
impact ionisation by electrons and holes, threshold energy 79−38078
impact ionisation of shallow donor states, 4 to 7K 78−30936
impact ionisation theory Auger processer 80−49752
implantation damage due to mol. and atomic ions 77−59056
implantation damage for low-energy heavy-ion bombard., spike effects 77−59055
impurity anal. by photoelectric spectroscopy, review 77−24584
impurity breakdown field increase due to strong compensation 80−20204
impurity cloud form., anal. using heat treatment effects on light scatt. in pure crystals 80−15146
impurity conduction, evidence for correlated hopping at moderate impurity conc. 77−20317
impurity determ. in very pure sample by photoelectron spectroscopy 77−39888
germanium continued
impurity distribution ratio, melt growth conditions and doping level influence 77−12516
impurity ion potential, asymptotic corrections 77−47769
impurity ion potential, in spatially varying dielec. const. semicond., variational calc. 79−7800
impurity levels of H and muons 79−56162
impurity modes due to point defects, comparison with IR and Raman meas. 79−4386
impurity photoconductivity, temp. elec. field and impurity centre conc. effects 78−56190
impurity photoconductivity 79−82631
impurity precipitation from solid soln., neutron irrad. effect 80−29177
impurity spectral linewidth meas., free electron effects 80−71463
impurity-ion potential, electron-conductivity mobility, spatially variable dielectric function calcs. 79−78105
indentation hardness and semiconductor-metal transition 78−35499
indirect exciton excited states 78−30873
indirect excitons, photoexcitation spectra, 2.0-2.6 meV 77−44051
inelastic X-ray scatt. cross section accompanied by intermediate momentum transfer 79−24387
inelastic X-ray scattering cross-sections, energy-integrated separation of components 78−38587
inhomogeneous stressed, electron-hole drop light scatt. and absorption 80−108212
injection current in presence of electron and hole mobility gradients 77−69326
inter-valence-band absorption in electron-hole droplets 79−4515
interatomic force consts. from lattice vibrs. 77−20020
interband Faraday ellipticity 78−92052
interband Faraday rotation, Roth theory calcs. 77−52046
interface structural model between amorphous and crystalline phase 78−63941
interfacial tension, crystal-liquid determ. 78−75809
interimpurity radiative recomb. with phonon cooperation 77−16385
internal photoelectric effect, quantum efficiency 80−20254
internal photoelectric effect, spectral depend. of quantum efficiency 78−39150
internal Stark effect on impurity states, low-temp. magnet. absorption meas. 80−60636
internal strain rel. to strain tensor, group theory anal. 79−86835
intervalley electron-electron scattering effect on optical transitions 80−108267
intraband optical absorption of shallow acceptor impurities, sum rule 79−28793
intravalley carrier transfer, transverse photo-EMF for various absorpt. coeffs. 79−69551
intrinsic, soft X-ray spectra detector, for plasma diagnostics 77−51232
intrinsic γ detector, deep level defect connection with O content *(Russian)* 78−43331
inversion layer electron and hole mobilities, determ. for high purity Ge 77−76937
ion+Ge target collisions, quasimol. KX-ray spectra, Doppler shift 77−19044
ion beam irrad., defects prod. by individual displacement cascades, TEM study 80−70265
ion bombarded, radiation defect formation, atom-atom collision cascades modelling 80−10582
ion bombardment, energy distrib. of positive secondary ions and sputtered atoms 77−32485
ion bombardment-induced photon emission as function of target temp. 80−100698
ion implanted, ruby laser pulse effects 79−69125
ion implanted by O, effect on crystal struct. electroreflection method 77−84783
ion irradiated, accumulation and annealing of struct. defects, secondary emission obs. 78−2167
ion irradiated, Auger electron spectra struct., possible surface diagnostic methods 79−69946
ion-implanted, laser pulse annealing, TEM and channelling study 80−100264
ion-implanted amorphous layers, melting model for pulsing-laser annealing 79−56080
ionisation rates, cryst. orientation depend. 80−103700
ionised impurity scatt. limited mobility in semiconductors with spatially variable dielec. function 78−51986
IR absorption and scatt. by electron-hole drops 78−51903
IR absorption by laser-excited nonequilibrium holes *(Russian)* 79−95752
IR absorption coeff. by holes, temp. depend., effective mass *(Russian)* 80−50350
IR absorption spectra, exciton effects on intervalence band transitions 77−4297
IR detector based on carrier photon drag 77−74507
IR magnetoabsorption of free and bound excitons 78−52474
IR nonlinear material, laser induced surface damage 77−19266
IR optical characteristics and performance requirements 80−48363
IR optical material, prod. techniques and charact. 78−50873
IR photon drag detector, photosensitivity spectrum 79−12853
IR telephoto lens design, 8-14 μm region 77−39011
IR transparent materials, forward and backward scatt. data 78−59099
irradiation by 3.5 MeV electrons of high temp., carrier density and lifetime changes 77−4128
isomer shift values of implanted $^{133}Xe/^{133}Cs$, Mossbauer spectra 80−7240
J_1J_2 transition from LS, revised assignments for $d^9s^2p^2$, $d^9s^2p^3$ 79−45630
K-shell X-ray prod. by $^{14}N^+$ bombardment 80−91482
K-shell X-ray prod. for Br ions 79−47547
kinetic theory for electron hole condensation 77−85151
laser annealing, optical refl. meas. of melted layer 79−78796
laser beam acceleration of particles along cryst. channel axis 77−30677
laser crystallisation, for production of large grained sheets for solar cells 80−93570
laser damage, 10.6 μm CW CO_2 beam 77−63497
laser damage threshold at 10.6 μm, up to 10^{10} W/cm^2 77−50707
laser induced elec. damage, carrier removal, mobility degradation 77−80791
laser initiated etching 77−25308
laser interaction, multiple refls. contrib. to thermal runaway, heat cond. eqn. 80−33044

germanium continued
laser irradiated, in-depth and surface temp. meas. by Moire-Schlieren technique 80−53392
laser irradiation, photoacoustic detection 80−2901
laser irradiation effect on cohesion 80−50470
laser pulse annealing, induced nucleation, crystal growth 80−84966
laser pulse reflectivity, picosecond pulses from Nd:glass laser 79−18469
laser window, thermal lensing 77−72021
laser-induced bulk breakdown and free carrier generation, photocond. meas. 80−35018
lattice defects formed on γ-irrad., effect on elec. props. 80−19839
lattice dynamical calc. using extended Born-von Karman scheme 78−59889
lattice dynamics, extended Born-Von Karman scheme 77−27953
lattice dynamics, inversion matrix, approx. inversion 78−71797
lattice dynamics, pseudopot. calc. 77−43295
lattice dynamics of diamond type crysts., Keating's valence force field 78−79687
lattice dynamics of group IV elements with the local Heine-Abarenkov model potential 78−63821
lattice dynamics under press 80−92627
lattice dynamics using Born-van Karman model 79−73271
lattice energy, strong orthogonality, requirement in calcs. dealing with crysts. by geminal method 78−14307
lattice images of defects and radiation damage applics. 80−107210
lattice parameter determ. by X-ray multiple diffr. study *(Russian)* 80−10460
lattice parameter temp. depend. meas., Bond's method for single cryst. 77−24243
lattice stability, pseudopotential theory and problem of covalent bonding 77−55490
lattice thermal conductivity, contrib. due to correction term, generalised Callaway integral 77−28056
lattice thermal conductivity, contrib. due to correction term in Callaway integral 77−62693
lattice thermal conductivity, contrib. due to correction term, generalised Callaway integral 78−2318
lattice thermal conductivity, effect of Debye temp. var. 78−18850
lattice thermal conductivity three phonon processes 78−34662
LCAO band structure, overlap and distant neighbour effects 80−49585
LEED, and Auger spectroscopy study of (111) cleavage face 79−95249
LEED obs. of vicinal surfaces 78−14561
light diffraction, in solid, by intense acoustic waves, diffracted field 77−83808
light scattering, by pure single cryst., influence of photoexcitation 79−28780
light scattering due to microdefects 78−27248
lightly doped, movement of dissociated dislocations in diamond cubic struct. 78−59806
lightly doped, nonohmic impurity cond. 78−14738
liquid, coordination numbers, calc. in microinhomogeneous struct. model *(Russian)* 80−38902
liquid, electrical resistivity and thermoelectric power using t matrix approach 77−31988
liquid, solubility and activity of O_2, 1233 to 1397K 78−44109
liquid, surface tension exam., sessile drop method *(French)* 77−20162
liquid, wetting of Si surface in H_2+HCl 78−43210
liquid inclusion migration in temp. gradient field 78−18842
Lo-Hi junctions, avalanche injection delay and ionization rate at low electric field 79−95475
local field, microscopic electronic polarisation 80−25283
local IR transmission 80−7357
localised vacancy state 79−82543
localised vibrational modes of isolated impurities, Green's function method 77−39650
longitudinal intervalley EMF due to inhomogeneities 78−19045
low-field study of p^+nn^+ or p^+pn^+ structs. on forward direction 80−60072
luminescence, presence of trions, molecules and excitons above Mott density 77−80737
luminescence circular polarisation in mag. field, Landau levels paramag. splitting 77−32435
luminescence kinetics and electron-hole drop motion 77−77288
luminescence line shape of free exciton, electron-hole droplet binding energy 77−44041
lunar drill sample, neutron activation and radiochemical anal. *(German)* 80−51673
macroinclusion in strongly-doped single crysts. 77−47474
magnetic circular dichroism at E_1 edges 78−92051
magnetic field luminesc. lifetime, quantum oscills., phonon wind effects 80−93385
magnetic phase transition between electron-hole drops and free-excitons 78−6278
magnetic susceptibility of light and heavy holes 79−42734
magneto-impurity effect, review 79−91081
magnetoacoustic effects in the drag of electron-hole drops by phonons 78−68057
magnetoconductivity meas. at 9.3 GHz, using three-wave interferometer *(French)* 77−47844
magnetodipole resonance, 0.6 to 1.35 mm wavelength *(Russian)* 77−80736
magnetoluminescence of electron-hole liq. 80−29790
magnetophotoconductivity, exciton contribution 79−15180
magnetoplasma reson. spectra, electron-hole drop shape effects 79−1712
magnetoresistance four-probe method for free carrier density and mobility meas. 77−43626
magnetoresistance meas., transverse diffusion currents on source of error 79−7843
magnetoresistance of electron-hole liq., percolation model 80−96920
magnetoresistance of thin n-type plate, size effect 78−72179
magnetostriction of electron-hole drop 77−85540
magnetothermal conductivity at low temp. 79−28158
many-valley cubic semiconductor, elec. conductivity tensor, warm electron range 78−39123
many-valley semicond. anisotropic acoustoelectric effect, thermo-EMF anisotropy fluctuation depend. on ultrasound freq. 79−69562
many-valley semiconductor, anisotropic, kinetic theory of impact ionsation 78−14740
matrix isolated cluster, optical absorpt. 80−16045
mean excitation energy based alpha particle stopping power meas. 78−30678
germanium continued
mean square atomic displacements, in single crysts., X-ray determ. *(German)* 78−30726
mechanical strength in brittle fracture region, influence of Si and O impurities 79−87682
melt, structural factors, tetrahedral concs., neutron diffr. study *(German)* 80−19688
melt grown single crystals, preferred growth directions and perfection 79−77537
melt-grown, H multivalent acceptor complexes 77−55491
metal contacts, surface electron state spectrum, surface treatment effects *(Russian)* 80−34497
metal-insulator-semiconductor structure, DC cond. and Shubnikov-de Haas effect 80−11012
metallic, eqns. of state under high press. 79−60475
microdefect distribution due to dislocation injection, selective etching 78−2122
microflaw vol. conc. determ., etching method 79−24688
microhardness exam. using static indentation on single crystal 79−52517
microwave absorption by nonequilib. current carriers, book contrib. 80−11042
microwave cyclotron resonance lineshape, magnetoplasma interference effect, reinterpretation of excitonic polaron 78−43287
microwave exciton discharge, collision frequency, hot carrier temp. determ. *(Russian)* 79−65507
microwave power meter using contact between metallic probe and Ge crystal 77−37986
migration energy of intrinsic point defects in different charge states 77−89582
minority carrier recombination after proton and γ irrad. 80−65591
MIS, photocurrent spectra investig. of fund. absorpt. edge 77−4397
MIS photocapacitative IR detector 80−47106
MIS transistor, MIS struct., electrophysical characts. 79−82680
mobility calculations including low impurity conc. limit 77−28173
mobility of screw and 60° dislocation at low stresses 77−11554
mode Gruneisen coeff. at point X, effect of lattice softening 78−38804
model pseudopotential, band struct. calcs., liquid semicond. resistivity calcs. 80−20075
molten, acoustic vel. and adiabatic compressibility, temp. depend., MP to 1400K 77−15498
mosaic single cryst., neutron integrated reflectivities 79−86656
Mossbauer effect, ^{57}Fe isomer shift, quadrupole coupling and interat. distance correl. 78−52408
Mossbauer spectra, 2nd-order Doppler shift, 1-100K 79−91317
Mossbauer spectroscopy of defects, radiation damage and deep levels 80−59533
Mossbauer spectrum of ^{57}Fe, appl. of in-beam implantation method 78−25372
Mossbauer transition of ^{73}Ge, large E2 dispersive interference 77−40158
Mott distortion of the electron-hole fluid phase diagram, luminesc. meas. 79−42457
Mott excitons, energy level calc. by variational method 78−6282
Mott transition of exciton gas in equilib. with electron-hole droplets 77−4298
multicomponent exciton gas, composition calc. 80−49618
multiphoton absorption, saturation of transmitted intensity of CO_2 laser pulses 80−64111
multiply charged impurity centers, energy spectrum 79−69469
multivalley structure, helical instability *(Russian)* 79−47101
muon$^+$ depolarisation, post muonic stage *(Russian)* 77−48116
muon spin rotation, spin Hamiltonian and anomalous muonium states 80−71286
muonium, deep and shallow levels, electronic struct. 78−39051
muonium relaxation rates 80−75912
muonium state, anomalous 79−56677
n- and p-type dust, electrification 79−56276
n-type, γ-irrad., nonlinear steady-state recomb., nonequilib. carrier lifetime and density 80−20215
n-type, γ-irrad. and subjected to arbitrary excitation and rate, recombination 79−38101
n-type, anisotropy of thermal and convective noise, in magnetic field 78−34873
n-type, anomalously enhanced plasma diffusion transverse to mag. field 80−96931
n-type, carrier relax. time, mag. field effects, rel. to Hall effect 80−39608
n-type, cathodically treated, surface mobility of electrons 77−51801
n-type, compensated, impurity photoconductivity 78−10512
n-type, compensated, switching effect, injection mechanism of hot holes 77−69387
n-type, cond. in warm electron region, phenomenological theory 77−43586
n-type, cyclotro resonance line shape at 337 μm, obs. 77−39770
n-type, D^- state struct. rel. to photocond. expts. 80−59924
n-type, D^--band conduction 77−76821
n-type, deform. induced point defects, Hall coeff. meas. 80−19800
n-type, deformed, 0.1 eV optical transition, interpretation using electronic states theory for Si 77−20261
n-type, deformed, 1/f noise, resist., mobility, and carrier density 77−8161
n-type, degenerate, Brillouin scatt. by phonon zero sound in quantising mag. field 77−69847
n-type, direct identification of $L_3' \rightarrow L_1$ transition, electroreflectance 77−1689
n-type, dislocated, temp. dependence of photoconductivity, pressure influence 78−76109
n-type, dislocational microwave conductance anisotropy *(Russian)* 79−91092
n-type, doped, dopant distrib. from carrier drift distrib. in high elec. field 79−51140
n-type, drag effects, heated electron-phonon system 78−23078
n-type, effect of non-parabolicity in quantum mechanical treatment of cyclotron reson. 77−31937
n-type, elastically deformed, anisotropy of thermoelec. effect 78−19066
n-type, elec. cond., effect of shock waves *(Russian)* 78−87979
n-type, electron irrad., threshold energy for atomic displacement, carrier traps 80−29351
n-type, electron irradiated, annealing at 6K, Watkins model explanation 78−47427
n-type, electron irradiated, high temp. annealing, nonequilibrium carrier lifetime and Hall effect 77−4370

germanium continued
n-type, EM wave interaction with hot electrons in strong mag. field with Voigt config. 77−69367
n-type, H-linear planar Hall effects of hot electrons 78−76082
n-type, Hall coeff. and cond. mech. in intermediate conc. at He temps. 79−95422
n-type, Hall effect anomaly after 50 MeV electron irrad. *(Russian)* 77−43619
n-type, Hall mobility in fast electron irradiated samples 77−55551
n-type, Hall mobility in specimens in strong pulsed electric fields, instrum. for meas. Hall current 79−35779
n-type, heavily doped, extrinsic sp. ht. in metallic regime 78−59956
n-type, HF plasma oscills. in external mag. field 80−54731
n-type, high-field magnetoresist. and magnetothermal EMF in many-valley semicond. 77−43621
n-type, hopping magnetoresistance percolation analysis 79−38106
n-type, impact ionisation at 4-9.5K 80−10994
n-type, impurity breakdown field, temp. depend. 79−24263
n-type, internal stress effect on electron-phonon interaction, thermal cond. anal. 79−42468
n-type, IR absorption by hot carrier 80−40087
n-type, irradiation induced compensation, elec. meas. 77−85225
n-type, laser irrad., accumulation of defects, effect on elec. props. 80−107317
n-type, lightly doped, conductivity and Hall mobility 80−11016
n-type, lightly doped, heavily compensated by fast neutrons, electrical props. 77−89766
n-type, longit. piezoresist., in strong elec. field 78−56147
n-type, low temp. galvanomag. effects, shallow attractive traps 80−88575
n-type, magnetoresist. anisotropy, in quantizing mag. fields, under conditions of mixed scatt. 77−15877
n-type, magnetoresistance in strong UHF electric fields 77−1437
n-type, magnetothermal cond., 4.2K 80−24688
n-type, many-valley semicond., current-voltage characts., with multivalued depend. of current on elec. field 78−26876
n-type, many-valley semicond., elec. breakdown criteria 78−19046
n-type, microwave Faraday effect in strong mag. field 77−1662
n-type, Mott transition, dielec. enhancement and conduction electron screening 78−72073
n-type, noise, small signal conductivity and diffusion in strong elec. fields 79−11192
n-type, noise and hot carrier diffusion in mag. fields 79−11193
n-type, noise spectra of hot carriers 78−76083
n-type, phenomenological cond. relax. time, uniaxial stress and electron-electron scatt. effect. 77−15862
n-type, phonon conductivity and attenuation 77−4167
n-type, photocond., excited by CO_2 laser pulses, depend. on intensity 79−69548
n-type, piezo-thermal cond. calc. 77−15639
n-type, piezoresist. calc. 78−19036
n-type, piezoresistance under mechanical stress, rel. to cond. band minima 80−6836
n-type, piezoresistance with deform. axis, symm. rel. to all const. energy ellipsoids 77−55533
n-type, piezothermomagnetic analogue of Grabner effect 77−4378
n-type, plastically deformed, elec. cond., magnetoresistance, Hall effect study *(Russian)* 79−99568
n-type, spectra, light induced, electrolyte and Schottky barrier techniques of meas. 80−76046
n-type, subjected to high voltages, distrib. of injected carriers 79−56239
n-type, substrate for intrinsic GaAs, surface polaritons, hydrodynamical model 80−6752
n-type, surface electron mobility, Hall effect and cond. meas. 79−56281
n-type, thermo-EMF drag, anisotropy parameter *(Russian)* 77−80799
n-type, thermoelec. power in quantising mag. field, phonon-phonon interactions 80−107832
n-type, thermomagnetic tensor struct. 77−62952
n-type, transverse magnetoresist. effects on Hall voltage meas., theory 77−72870
n-type, uniaxially deformed, longitudinal magnetoresist. in quantising mag. field 79−15168
n-type, US attenuation by impurities 77−69047
n-type, US attenuation due to donors and acceptors 77−28223
n-type accumulation layers, effect of low-energy Ar^+ ion bombardment on electron scatt. 77−66205
n-type inversion layers, broken-symmetry ground states 77−47873
n-type resistance thermometer material for 14 to 300K *(Russian)* 80−49731
n-type single cryst. with dislocations, UHF cond. *(Russian)* 79−78128
N-type switching, thermal mechanism 77−85273
n-type uniaxially stretched along [111] axis, negative differential conductance 77−51759
nearest-neighbour atom mean-square relative displacements, EXAFS spectra 79−91532
negative differential cond., ambipolar size effect due to hot carriers 78−72185
negative electron affinity surface, with Cs and $Cs+O_2$ overlayers, thermal stability of work function 78−92167
negative electron diffusivity in high fields 78−30935
neutron irradiated, absorpt. edge 80−93320
neutron irradiated, capture of positrons by radiation defects 78−38756
neutron irradiated, Hall effect and magnetoresist. meas. 80−6883
neutron irradiated, positron annihilation, ESR and resist. meas. 80−15160
neutron irradiated, substitution of impurity atoms by self-interstitials, $Ge(n,\gamma)$ reaction 80−39166
neutron irradiation of n- and p-types at low temp., resistivity, annealing characts. 77−89481
neutron scattering using inclination method, dynamic oscills. obs. 78−42867
neutron-irradiated, positron lifetime 80−97374
noise, 1/f, mag. field influence, surface origin evidence 79−99592
noncollinear phase matched four photon mixing, CO_2 laser radiation 77−14778
noncrystalline, high-press. expts., quenchable products 77−19874
nonequilibrium carrier excitation by CO_2 laser radiation 77−89803
nonequilibrium charge carrier-mag. field interaction electron-hole drops, recombination *(Russian)* 80−75511
nonlinear absorption of CO_2 laser radiation by nonequilib. carriers 79−32000
germanium continued
nonlinear acoustics, third-order elastic const. meas. 80−33292
nonlinear mixing, non-collinear phase matched 4-wave, of CO_2 and NH_3 lasers 79−988
nonlinear optical reflection props. rel. to thermal effects 78−42371
nonlinear optical susceptibility, tight binding bonding orbital model 80−5784
nonlinear susceptibility, 10 μm, determ. by time resolved ellipse rotation 80−83633
nonlinear susceptibility, four-wave mixing at room temp. for tunable IR generation 80−9940
nonradiative transitions at impurity centre with participation of short-wavelength phonons 80−16099
nonuniform electron-hole liq., props. in high density limit 77−43505
nonuniformly deformed, electron-hole drop density depend. on size *(Russian)* 80−20092
nucleation of Cd on Ge(111), struct. and surface coverage, RHEED-mol. beam obs. 77−4265
ODMR using luminescence of electron-hole drops *(Russian)* 77−90072
one-sided abrupt junctions, distinction between avalanche and tunnelling breakdown 78−56211
optical absorption from indirect transitions at high mag. fields 79−47441
optical absorption in samples with 60° dislocations 78−39577
optical material, thermal expansion, 60-300K 78−33791
optical props. in 2.5-15 micron region 80−80775
optical pulse transmission, pulse-width depend. 78−55403
optical pulse transmission, pulsewidth depend., phonons and plasmons role 78−31198
optical requirements for thermal imaging lens 80−69495
optical saturable absorber, passive mode locking of TE CO_2 lasers 78−71127
optical saturation characts. over CO_2 laser spectrum 77−88869
optical SHG, elec. field induced, theory 80−69457
optical spectra in interband transition region, lattice disorder influence 79−43006
optical stimulation, electron-hole drops and appearance of dense plasma *(Russian)* 77−4688
optical surface modes calc. 77−59200
optical switch, picosecond pulse generation at 10.6 μm 79−7159
optical waveguide cladding, attenuation, mode props. 77−27351
optical windows, contaminated by NH_3, CO_2, CO, HCl, methane, cryo-cooled, IR transmission 79−32007
optically induced carriers, reflection switch for CO_2 laser 77−3609
oscillator strengths of dipole optical transitions in group III acceptor impurities 79−56823
oscillatory exciton breakdown, microwave cond. 80−103716
oscillistor, hysteresis effects and N-shaped V-I characts. 79−33306
oscillistor effect in strong mag. fields, ambipolar drift and breakdown 78−2511
oxidation of clean cleaved (111) surfaces, EELS and AES 80−3230
p^+-ν-n^+ structures, charge transport under impurity freezeout conditions 80−92965
p^+-ν-n^+ structures, large-scale trap characts. 80−92966
p^+-n shallow junction avalanche photo diodes, noise and quantum efficiency 79−87143
p^+-n-m and m-n-m structures, current-voltage characts. 77−1476
p^+-n-n^+ and p^+-i-n^+ structures, inhomogeneous, influence of longitudinal mag. field 77−1479
p-i-n avalanche photodiode, temp. depend. characts. 79−35835
p-i-n struct., Li ion drift thermal profile 77−51813
p-n junction, current filament form., fluctuations and thermal noise 77−69411
p-n junction, graded, volume EMF of hot carriers 77−47895
p-n junction, high-grade, temp. gradient zone melting in production 77−4747
p-n junction, hot photocarrier and hot electron effects 78−30980
p-n junction, I-V curve for microplasma breakdown, at. size difference effect 78−2550
p-n junction, IR radiation modulation, light absorption by injected current carriers *(Russian)* 80−10013
p-n junction, photo-EMF generation in saturation region 80−75635
p-n junction injection characteristics in strong elec. fields 77−76913
p-n junction with hot carriers, current-voltage characts. 79−91135
p-n junctions, impurity photoelec. effect 79−56300
p-n junctions with hot carriers, current amplification, elec. domain form. 80−6966
p-type, 2 mm wave radiation interaction with charge carriers *(Russian)* 78−87991
p-type, acceptor wavefunctions in spherical approx. and piezoresist. 80−29405
p-type, and n-type Ge converted to p-type by irradiation at 77K, defect form. mechanism 79−23651
p-type, anomalous magnetoresist. under uniaxial compression *(Russian)* 79−33302
p-type, bleaching, optical heating and cooling of electrons involving intrab- and transitions 79−10365
p-type, bleaching assoc. with intraband transitions in CO_2 laser radiation absorpt. 77−68244
p-type, broadband modulation of 3 μm light by 10 μm light 78−42389
p-type, carrier drag by photons, comparison with p-GaAs 79−11185
p-type, carrier heating by weak electric field 77−11927
p-type, carrier scatt. by ionised impurities, rel. to carrier mobility calc., 10-70K *(Russian)* 78−39103
p-type, compensated, submm and mm radiation absorpt., acceptor conc. depend. 77−28664
p-type, depend. of saturation intensity on impurity conc. and residual absorption at 10.59 microns 80−45125
p-type, detector-grade single crysts., impurity background 79−11088
p-type, differential relax. times and diffusivities of hot carriers 77−62936
p-type, diffusion coeff. for hot holes in mag. field 80−39614
p-type, dislocation microwave cond. and Hall effect meas. *(Russian)* 77−47848
p-type, dislocations, grown-in defects, electrical props., deep level transient spect., Hall effect 80−39524
p-type, electron bombard. at high temp., carrier lifetime and defect levels 77−55306
p-type, electrorefl. spectra, 2.1 to 2.3 eV, influence of light beam 77−90169
p-type, energy spectrum of impurities and effect of mag. field *(Russian)* 77−47770

germanium continued
p-type, free-carrier reson., photoconductivity spectra in submillimetre wavelength 79−15353
p-type, freq. depend. of effective temp. of hot carriers 79−11135
p-type, highly deformed, hole scattering 77−20309
p-type, hole conductivity anisotropy 77−4360
p-type, hole drift vel. in high field 79−95415
p-type, hole-hole collisions, effect on carrier mobility above 80K 80−6838
p-type, hopping transport at high mag. field and uniaxial stress 79−95412
p-type, hot hole relax., IR saturated absorption 77−28569
p-type, hot-hole relax. rates by saturation spectroscopy 77−65611
p-type, in DMF solns., electrochem., photoelectrochem., redox. pot. determ. 79−96322
p-type, in nanosecond recorder of 10.6 μ wavelength radiation 77−37990
p-type, infrared absorption and plasma reflection 80−97284
p-type, injecting contact, sign of developed hot-carrier thermo-EMF 77−55606
p-type, intervalence-band transitions, saturation, theory 80−75997
p-type, irradiation with fast electrons, defect distrib. with depth 80−19841
p-type, laser radiation excited, gradient EMF anisotropy 80−75604
p-type, lattice scatt. identified as cause of 1/f noise 78−64074
p-type, linear magnetoresist. in strong elec. fields 77−43632
p-type, magneto-microwave Kerr effect, expt., scatt. mechanisms 78−39139
p-type, negative magnetoresist. and Hall effect, press. and field depend. 80−70733
p-type, neutron irrad. quenched sample, lattice defects 79−19284
p-type, noise, energy relax. time and diffusion of hot holes 77−76839
p-type, noise calc. in strong elec. field using Monte Carlo method 80−15578
p-type, nonlinear IR absorpt., theory 79−65868
p-type, odd magnetoresist., ionised impurity scatt., theory 78−72178
p-type, odd magnetoresist. in strong elec. and mag. fields 79−51612
p-type, odd magnetoresist. of warm holes 77−43628
p-type, odd magnetoresist. under weak carrier heating conditions 80−96917
p-type, optical cooling and carrier heating, intraband photocond. meas. 79−11174
p-type, p-n junction with hot carriers in charge accumulation regime, influence of light on operation 79−51661
p-type, phonon thermal cond., 0.1-7K, Ziman model 77−35763
p-type, photoexcited charge carrier capture by shallow impurity centres *(Russian)* 80−15571
p-type, photon drag detector, performance in 2 to 33 μm range 79−35834
p-type, photon drag spectrum 77−32044
p-type, proton irradiated, kinetics of accumulation of radiation defects, minority carrier lifetime 79−10885
p-type, spectral depend. of drag of electrons by photons 79−42590
p-type, stretched along ⟨111⟩ axis, bulk negative differential cond. and current oscills., 78K 79−19601
p-type, strong uniaxial deform. at low temps., piezoresist. 78−19038
p-type, temp. depend. of noise and diffusion of hot holes 78−39174
p-type, test of electronic band struct. by laser-induced reson. 78−37949
p-type, theory of photon-drag effect, parabolic and anisotropic band-struct. approx. 78−47825
p-type, thermal conductivity, effect of uniaxial stress 79−23792
p-type, thermal conductivity meas. down to 50 mK, acceptor state exam. 77−80658
p-type, uniaxial compression influence on carrier heating by weak electric field 80−10978
p-type, uniaxially deformed, magneto-impurity oscills. of photocond. 78−34862
p-type 80−96883
p-type adsorption of Au, effect on I-V characteristics, field emission study 78−67925
p-type film, transverse magnetoresist. meas. 78−72293
p-type film on GaAs, cond., Hall effect and transverse magnetoresist., anisotropy 79−51697
p-type heteroepitaxial film 79−91171
p-type sheet, free carrier confinement for IR modulation 78−25969
partial dislocations, motion 79−82229
particle detector; high-purity, effect of crystal growth direction on energy resolution 79−45541
particles, grown in Ar gas, cryst. struct. and habit, electron microscope study 79−74071
particles, homogeneously nucleated, production and props. 77−56252
partly dissociated excitons and impurity atoms system, collisional processes, charge transport theory 80−44581
Pendellosung fringe shape depend. on specimen-film distance *(Russian)* 80−87994
phase conjugate reflection, pulsed 10.6 μm, via intracavity degenerate four-wave mixing 78−87097
phase conjugation, high refl., intracavity CO_2 laser techniques 80−78894
phase conjugation of 4 μm for single line and multiline radiation 80−83641
phase diagram of electron-hole fluid in low temp. photoexcited semicond. 77−69237
phonon assisted Auger recomb. in indirect gap semiconductors 78−39126
phonon boundary scatt., reduction of lattice thermal cond. 78−55921
phonon conductivity correction term and electron-photon scatt. relax. rate, appl. to doped and undoped samples 80−39369
phonon density of states determ. from sp. ht. 77−7809
phonon density of states from thermodynamic functions *(Russian)* 79−35631
phonon dispersion, microscopic screening 80−49324
phonon dispersion curves, appl. of deformable-ion model 78−59887
phonon dispersion relation, adiabatic bond charge model 77−69057
phonon drag of electron-hole drops in longit. quantizing mag. field *(Russian)* 78−64070
phonon energy variation under high press. band struct. changes, tunnel spectroscopy study *(Russian)* 80−2134
phonon imaging, ballistic, low-temp., rel. to focusing theory 80−10605
phonon scattering and dislocation effect on low temp. phonon cond. 78−51754
phonon scattering by electron-hole drops, deform. potential 78−10360
phonon transmission from incoherent radiator into cryst., anisotropic continuum acoustics 77−47521
germanium continued
phonon viscosity tensor 78−34570
phonon-phonon scatt. strength, thermal cond. in low- and high-temp. regions 77−43296
phonons, directional depend. of boundary scatt. mean free path 79−73354
photo-field cathode, ageing and surface state effects *(Russian)* 77−28703
photoacoustic effect, free flexural vibrs. damping 77−89813
photoacoustic effect, orientational depend. *(Russian)* 80−65167
photocapacitance current spectrum near fundamental absorpt. adge 77−28217
photocathodes, Au absorbed photofield emission current spectral investigation 80−29856
photoconductive IR detectors, microwave-biased, noise performance 80−9037
photoconductivity, carrier lifetimes in excited states of impurities *(Russian)* 77−76864
photoconductivity, inversion of magneto-impurity oscills. 77−15913
photoconductivity, magnetoimpurity oscills. 79−82626
photoconductivity in microwave range, carrier density determ. method 77−8148
photoconductivity spectra of shallow impurities 79−82625
photocurrent magneto-oscillations 80−6911
photocurrent oscillations in mag. field, intense excitation *(Russian)* 78−26915
photodetectors, pin- and avalanche diodes, characts. *(Swedish)* 78−89545
photodiode, spectral response and responsivity 78−29160
photodiode as IR detector, fabrication and performance 77−57388
photoelastic consts. determ. 78−68474
photoelectric spectra of impurity groups 79−82627
photoelectric spectra of remanent impurities 79−87125
photoelectric spectra of shallow impurities, mag. field effect 79−82624
photoemission relax. energies *(French)* 77−36357
photoemission spectroscopy of surface states and oxidation 77−55863
photoionisation cross-sections of valence s- and p-electrons *(Ukrainian)* 77−73211
photoluminescence, high excitation intensities, direct and indirect gap transitions 77−12429
photoluminescence, low-temp., of doped samples 77−69900
photoluminescence, role of intrinsic surface states 78−52571
photoluminescence decay from electron-hole drops in doped and undoped Ge 77−66532
photomagnetic effect, space inhomogeneous nonequilibrium carrier lifetimes *(Russian)* 80−71152
photomagnetic EMF, reson. struct., energy relax mechanisms 78−2515
photon drag and radiation press. in refractive media, subMM wavelength 80−60048
photon-drag detector submillimetric-wave performance 79−30547
photon-drag voltage nonlinearity at high laser intensity 78−19081
photopiezoelectric effect under elastic deform. 80−107856
photoresistor, Cu doped, liquid N_2 cooled, detectability 78−80019
photothermal conductivity, low temp. depend. 80−70756
picosecond optical absorption, at high optically created carrier densities 79−47462
picosecond optical response, effects of parametric scatt., energy-gap narrowing and state filling 80−11424
picosecond pulse transmission, enhanced transparency, press. tuning 77−88871
piezoreflectance, at E_1 and $E_1+\Delta_1$ edges, high mag. field 77−77245
piezoresistance, energy and momentum relax. of charge carriers 78−47786
piezoresistance, low-temp. dislocation cond. mechanism in plastically-deformed pure samples 80−15527
piezoresistive vibrating circular membrane, reflectance light modulation 80−97232
piezospectroscopic determ. of electron-phonon to hole-phonon interaction 79−95783
piezospectroscopy of group V impurities in Ge 79−99915
planar dechannelling of protons, (100) direction 77−20000
plasma, spectral lines 77−7515
plasma cloud drift velocity, at high elec. field 80−6887
plasma excitation, ultrafast optical props. 78−31248
plastic deformation, impurities and dislocations interaction, cond. *(Russian)* 79−47100
plastic deformation under laser irrad. rel. to diamond-type structure *(Russian)* 77−56023
plastically deform., dislocation state spectrum, photocond., elec. cond., and Hall const. meas. *(Russian)* 80−2362
plastically deformed, photocond. and absorpt. spectra, dislocation levels 77−28219
plastically deformed, photocond. produced by polarised light 79−82641
plastically deformed low temp. cond. *(Russian)* 80−6831
plastically deformed under high temp. creep conditions, elec. props. 80−92915
plate, (111), multiple X-ray diffr. expt., ambiguity in indexing Renninger diagrams 79−1370
plate, anisotropic cond. thickness depend., intervalley scatt. *(Russian)* 77−85352
plates, semicond., scribing marks rel. to sclerometric microhardness 79−15891
point defect creation by plastic deform., Hall const., electrical conductivity 78−6053
point defect form. due to γ-ray irrad., carrier density, mobility meas. 78−71759
point defects, review of characts. *(Japanese)* 77−89428
point defects formation, electron or γ-irradiation, reliable of questionable hypotheses 77−80501
polarisation of implanted ^{12}B 78−43653
polycrystalline epitaxial film, exam. of growth kinetics and props. 80−55304
positron annihilation, effect of vacancies 79−24385
positron thermalisation, theory *(Russian)* 78−84170
positronium formation at surface, positron beam irrad. 79−13845
powder, diamag., strong mag. particle form., mag. props., EPR *(Russian)* 80−54863
powder, elec. cond., temp. and press. depend. 77−8090
powder, electrodeposition from fused salts 80−2979
powder electrodeposition, from molten fluoride mixtures 80−60797

germanium continued
powder/Au electrode contact pot. difference, grain size depend. 80−44723
protective coating on Sn supercond. films, effect on excess elec. cond. 80−65741
proton and pion 15 GeV/c nucl. interactions under random and channelling conditions in single crystals 79−13348
proton bombardment damage, irrad. energy depend., channelling meas. 80−24511
proton energy loss, 0.1-1.0 MeV 80−42909
proton impact X-ray emission, ang. distrib. and polarisation fraction 78−56546
proton irradiated, defect study using X-ray diffuse scattering 79−95048
proton irradiation damage in high parity detectors 78−37508
proton stopping power meas. at 100 keV, using ion induced X-ray emission 78−48725
pseudopotentials, nonlocal 77−11848
pure, degree of compensation, capacitance meas., 4.2-150K 79−7624
pure and Li or O doped, shallow defects, PTIS meas. 80−24971
purification, second-phase inclusions after O_2 treatment, electron microscope obs. 77−43238
quartz:Ge, α-β phase transition, refr. index. meas. 78−83945
quartz:Ge, optical and piezoelectric props., ang. distrib. *(Russian)* 78−23404
quartz glass, Ge and B dopants, OH impurities, preform material and fibre optic waveguide struct. 80−64173
quenched n- and p-type, intrinsic defects migrating near 100°C 77−62670
quenching defects, fast and slow 78−39052
quenching temp. effect on annealing rate of quenched-in acceptors 79−82590
radiation damage by 0.5 to 10 keV ions 80−100285
radiation effects, high-temp., under HVEM obs. 77−89475
radiation piezoelec. effect, EMF generation under α-irrad. and uniaxial deform. 77−12320
radiation piezoelectric effect in single crysts. 78−19419
radiation pressure, photon drag effect in far-IR 80−50452
radiative electromagnetic effect, alpha-particle irrad., Hall effect, photoelectromagnetic effect 78−10434
Raman shift, effect of pressure 78−92064
reaction with S vapour, applicability of Kossel's crystal model 79−87833
reactor irrad., opt. props. 77−90137
read out, by SAW, optical image memory in slow surface states 77−79942
recombination at dislocations 79−38023
recombination characteristics used in design of semicond. devices *(Russian)* 79−42557
recombination into shallow donors, low temp., transient case 79−38092
recombination luminesc. spectra from hot and cold carriers in electron-hole drops 79−38608
recombination of nonequilib. carriers in presence of dislocations 79−82607
reconstructed (001)2 x 1 surface structure, LEED intensity calcs., dimer model variations 79−77875
reflectivity, nonlinear, picosec. laser pulses and electron-hole plasma 79−47463
reflectivity changes due to illumination by beams of unequal frequency 79−76749
refractive index, 95-298K, 2.5-12 μm 77−8535
refractive index and refl. changes due to intense laser irrad., surface heating effect 78−42372
refractive index dispersion 79−24280
refractive index meas. of single cryst. prism, interlaboratory comparison 78−54443
regrowth under laser irrad. 80−24481
relaxation dynamics and photoconductivity 79−51636
resistance thermometer, low temp., approx. of calibration curve 78−45620
resistance thermometer appls. below 0.1K 78−73999
resistance thermometers, characts. from 1 to 35K, ISU mag. temp. scale 78−81970
resistance thermometers, stability test at 20K 78−81971
resistance thermometry, interpolation method 80−22357
resistive sensing devices, temp. calibration and reproducibility, high mag. field effect *(Czech)* 80−37029
resonance Raman scatt. under uniaxial stress near E_1 gaps 79−42960
rough surface, polarisation angles, ellipsometric meas. 78−56449
S-type diode, photoelec. props. 77−24614
saturable absorber for CO_2 TEA laser mode locking 78−46694
saturable absorption isolator for CO_2 laser systems 77−19284
saturation spectra, tunable laser induced grating dip for sub-picosecond relax. meas. 77−75623
Schottky barrier, electronic struct., pseudopot. calc. 78−95364
Schottky barrier, electronic struct., pseudopotential method, jellium model 79−38162
Schottky barrier diode, lightly doped, IR response and extended HF model 77−80836
Schottky barrier electrorefl. under uniaxial stress, band struct. 77−48193
Schottky barrier junction, surface electron states spectrum *(Russian)* 78−84297
screened donor impurities, binding energy calc., anisotropic mass effect 78−10399
screw dislocation loops, shrinkage vel. and cross slip freq., activation energies *(German)* 78−43028
screw dislocations, effect of dislocation dissociation on localised electron and hole states 79−82546
self- and impurity diffusion 80−29213
self-diffusion, activation energy and entropy factors 80−88353
self-diffusion, dynamical recovery 80−29215
self-diffusion mechanism 79−90824
self-interstitials, vacancies of their clusters 77−80500
Sellmeier coeffs. temp. depend., nonlinear optics average power limit 79−50349
semiconductor detector material, purification, cryst. growth, ion implantation 78−47674
shallow acceptors produced by quenching 79−51523
shallow hydrogenic centres, ground states, isotope shifts, photoelectric spectrosc. 78−39055
shallow impurities, excited states, population and lifetime *(Russian)* 79−51532
shallow impurity bound states, IR spectroscopic obs. 77−39806

germanium continued
shaped crystal growth from melt, meniscus-controlled process 80−107075
shaped crystals, grown by Stepanov method, struct. perfection 78−2123
single cryst., ^{18}F penetration, charged particle activation anal. 80−93828
single crystal, anisotropic oxidation, ellipsometric obs. 77−70194
size effects in small electron-hole drops 79−82530
slab, intrinsic, longit. cond., influence of surrounding gas *(French)* 78−10448
slab in waveguide, microwave absorpt. due to geometric reson. of longitudinal-section elec. surface waves 80−39874
slow surface, states, optical excitation investigation 78−76129
slow surface states, optical image storage for $LiNbO_3$ SAW readout 77−23773
solid-liquid interfacial tension determ., glassy sphere nucleation by rapid cooling 77−51570
solubility and diffusion of Na, vacancy mechanism 77−89592
solution-melt Ge-Au drops, periodic instability of motion over cryst. surface 78−47260
solvent, LPE growth of GaP-GaS and Ga(AsP)-GaAs 78−88434
specific heat at constant volume, leading anharmonic contribs. 77−89549
spectral diffusion in acceptor-hole system at low temp., ultrasonic hole-burning expt. 80−92610
spectrally selective EM wave absorber, solar energy collector material, props. *(Dutch)* 78−50872
spherical particles in polyethylene matrix, extinction cross section 80−9807
spreading resistivity rel. to load applied to meas. probe 78−4647
stacking fault energies, dislocation struct. models 79−82205
stacking fault width determ. from 224 reflections with g.b=0 78−59722
stacking faults of dislocations, constrictions obs. using weak-beam electron microscopy 77−35576
static dielectric function, local field correction, tight-binding model 79−95355
stationary creep depend. on deform. stabilisation of material struct. *(Russian)* 80−100300
STEM, bright field single atom images with half plane detectors 78−66010
Stepanov method for large shaped single cryst. prod. 78−3014
Stepanov method growth, temp. distrib. in shaped single cryst. 78−2032
Stepanov method growth, thermal stresses in circular cross section single cryst. 78−2033
Stepanov method growth of strips, thermoelastic stress calc. 78−2034
stopping power nucl., in ferromag. Gd, transient mag. field 78−34555
strain-confined electron-hole liquid, density variation 78−34779
strain-confined electron-hole liquid, lifetime and radiative efficiency vs density 79−38000
strain-confined large electron-hole drop characteristics 80−65469
strain-narrowing of luminesc. line from excitons 79−24356
strained, crit.-point for electron-hole droplets 79−4516
strained crystal, annealing effect, recrystn. and struct. *(Russian)* 80−89252
stress-induced phase change in single cryst. 79−23720
stressed, α_1 and α_3 electron-hole droplet luminesc. 79−28820
stressed, metal-insulator transition, luminesc. 80−20695
stressed, recombination luminescence from hot carriers in electron hole droplets 78−6754
stressed cryst., props. of strain-confined electron-hole liquid 79−7787
strong microwave field effect on electron-hole drops, luminescence kinetics 79−87047
structure of annealed (111) surface 78−75916
substrate, {111} oriented, $CuInSe_2$ heteroepitaxy by flash evaporation, struct. 80−108333
substrate, CdS epitaxial layers on (111) face 78−18920
substrate, vacuum deposition of Al, press. and residual gas comp. influence on film struct. 77−16497
substrate for epitaxial growth of ZnSe 80−75469
substrate for GaAs solar cells, thin film shallow homojunction struct., quantum efficiencies 80−35677
superconducting film, A1-type, critical mag. field 78−31023
superconducting friction layer formed during friction between Ge and Pb *(Russian)* 78−52143
superconductor-semicond. device research, future prospects 79−28467
supercooling single crystal growth, structural and chem. inhomogeneities 80−93473
surface, (001)-(2×1), reconstruction-induced mean-square displacements 80−15343
surface, (100), Ar ion bombarded, determ. of atomic steps, LEED 78−63913
surface, (100), dimer reconstruction, photoemission obs. 80−80939
surface, (110), sublimation of deposited GeS film, LEED meas., structural transitions 77−59195
surface, (111)2×1, oxide layer, surface states detect optical reflectivity obs. 80−50368
surface, (111)2×1, surface electron states detected by external reflectivity 78−80036
surface, (111), adsorption of polar molecules, surface recomb. centre neutralization 79−38147
surface, (111), chemisorption of H_2, effect of surface states 78−51823
surface, (111), clean, double diffr. spots in RHEED patterns 79−90855
surface, (111), clean and O_2 adsorbed, photoemission yield spectroscopy of electronic surface states 79−91122
surface, (111), diffuse scatt. at high temp., RHEED study 80−80043
surface, (111), high resolution photoemission yield, surface states 77−69392
surface, (111), ion-bombarded and annealed, spectroscopic ellipsometry study 80−103543
surface, (111), Sn monolayer, induced 7×7 superlattice struct. 78−91521
surface, (111), spectroscopy of electron subbands 80−71422
surface, adatom indirect interaction, theory 80−44696
surface, atomically pure, optical consts. and temp. depends. 79−65823
surface, chemical channel of recombination 80−39656
surface, clean, geometrical struct. rel. to electronic props. 77−62719
surface, cluster model approach for electronic struct. 78−56205
surface, field penetration and band bending in high elec. fields 79−42613
surface, formation of sulphide layers in S vapour 79−7757
surface, Hall effect study, channel cond. *(Russian)* 80−92909
surface, high freq. cond. and cyclotron reson. 80−11273
surface, laser induced ionic desorption, mechanism 77−15686
surface, Lyman-α emission from proton bombard. 79−91503

germanium continued
surface, optical charging meas., 120-300K 80−49817
surface, RF etch sputtering under controlled atmosphere 77−44397
surface, self diffraction of light, mechanism, rel. to nonequilib. carrier behaviour 79−72685
surface, sulphide layer form. rate rel. to S_2 vapour press. 79−43152
surface, wetting by Sn, Pb rel. to cryst. orientation 78−43211
surface, X-irradiated, slow relaxation of surface states 77−62980
surface (100), chemisorption of H, expt. results compared with pairing model calcs. for Si (100) 78−34719
surface (100), density of states, simple modelistic treatment of virtual surface states 80−103739
surface (100), electronic struct., scattering-theory formulation 79−42607
surface (110) atomic struct. 79−69331
surface (111), 500 eV Ar^+ bombard., high temp. annealing, recovery, RHEED obs. 78−87723
surface (111), chemisorption of O_2, surface-molecule model 79−90885
surface (111), clean and CO-covered 80−10785
surface (111), electron struct., photoelec. props. 80−100493
surface (111), GeS film evaporation, thermogravimetric, electron microscopy investigs. 77−15715
surface (111), n-channel inversion layer, subband energies 80−11063
surface (111) clean, O_2 adsorption rate and electron work function 80−59779
surface contamination by exposure to DC-704 silicone liq., IR refl. spectra anal. 77−59630
surface dislocations, depth localization definition by HF gas-discharge plasma *(Russian)* 77−31664
surface during X-irradiation, oxide hydration degree determ. 77−24605
surface electron states, appl. of surface photovoltage spectroscopy 77−69391
surface electron states, relaxed self consistent pseudopot. calc. 77−47880
surface electron states, review of optical methods of detection 77−66191
surface electronic props. meas. by SEM, sand-blasting effect 77−62976
surface electronic state localisation, layer density of states calcs. 80−6931
surface electronic struct., self consistent pseudopotential calc. 78−47842
surface galvanomagnetic props. and relax. time energy depend. 78−43459
surface Hall effect and cond., electron, hole conc. and mobility *(Russian)* 80−44619
surface ion implanted far IR composite bolometers 79−30549
surface microwave cond. observations *(Russian)* 80−2447
surface mobility of irrad. sample, interpretation using two-layer model *(Russian)* 77−51804
surface phase transition, order-order type *(Russian)* 77−39728
surface recombination before and after laser annealing, 10-μm transmission meas. 80−1247
surface reconstruction-induced subsurface strain, theory 78−91516
surface reflectivity changes and moving diffr. grating efficiency 80−58662
surface scatt. of Ar atoms, energy accommodation coeffs. 77−90230
surface slow states conc. determ. by field effect meas. 77−28232
surface states, recomb. centres, regularities, electrolyte contact effects *(Russian)* 80−65652
surface states, recombination centre formation *(Russian)* 80−29459
surface states, Tamm-like and field sustained, model studies, localisation props. 78−64092
surface structure, LEED and spot photometric meas. 79−23811
surface structure and chemical state 77−15670
surface subjected to chem. excitation, nonequilib. electron effects 78−72239
surface with p-n junction, photovoltaic effect under conditions of surface recomb. of H atoms 77−66185
surfaces, electronic struct., tight-binding calc. 80−54755
swinging fringes, six wave diffr. of X-rays from dislocation free single crysts. 79−14649
thermal conductivity, calc. using numerical soln. of Boltzmann eqn. 80−44373
thermal conductivity, low temp. calc. for impure insulators 79−33128
thermal conductivity at high temperature 79−55857
thermal conductivity of semiconductors, quantum acoustical method, thermal phonon lifetimes 80−65312
thermal expansion coeff., optical mode Gruneisen const. 79−46820
thermal expansion coefficient and Gruneisen const. 77−59128
thermal expansion coeffs. meas., room temp. to 250°C 78−55416
thermal neutron cross sections, in single crysts. 80−19672
thermal rectification and negative differential cond. 79−42554
thermal relaxation time, laser heating effect at 1.3K , book contrib. 80−11519
thermo-EMF, bulk differential meas. 77−4380
thermodynamic functions and normalised moments 79−51279
thin crystal, SEM, contrast features, variation of specimen thickness 79−23508
thin films on glass substrates, annealing by Ar ion bombardment 80−80136
thin single crystal, (110) orientation, preparation technique 79−95930
threshold energy for displacement of atoms 78−47428
time dependent phonon irrad. of detector area from pulsed incoherent phonon radiator 78−38790
transition metal-Ge interfaces, planar, first phase to nucleate 77−62764
transmutation doped, high field magnetoresist. of hopping transport 78−10474
transmutation-doped, impurity cond., 1.5-4.2K 77−89758
transparent IR window design for uniform pressure loading 79−23088
trapping defects, deep level transient spectroscopy 79−47045
tree rings, long term environmental pollution histories, neutron activation analysis 79−92107
triglycine sulphate-Ge contact, thermal resist. 77−4226
twin lamellas formation due to deposition of metal contacts 78−10060
two photon absorption of light with optical transitions between heavy- and light-hole states 79−11421
two-band system, acoustic scatt., appl. to hole transport props. 79−60823
two-phonon difference absorption spectra 78−76452
two-photon transitions from deep neutral impurity centres, light absorpt. and drag effect 79−91478
ultra pure, composition and struct. of non-elemental acceptor and donor centres 78−39658
ultrafine multiply twinned particles, form. by gas-evaporation technique 78−63685

germanium continued
ultrafine particle, positron annihilation exam. 78−56542
ultrafine particles prep. by gas evaporation in Ar 78−34455
uniaxially compressed crystal, exciton molecule radiation *(Russian)* 80−108264
uniaxially deformed, cyclotron resonance of RF field heated hot holes, *(Russian)* 80−44925
uniformly deformed, free carrier cyclotron resonance, electron-hole drops *(Russian)* 80−71182
uniformly stressed, density and binding energy of electron-hole droplets, photolum. meas. 78−60062
US absorption, depend. on orientation 79−69197
US absorption in single crysts., dislocation investigation *(Russian)* 77−62589
US attenuation, temp. variation, 273K to 500K at 4 MHz *(Rumanian)* 79−77691
US attenuation and nonlinearity const., temp. depend. 78−43075
US Propagation in pure and n-type crysts., velocity and attenuation, second and third order elastic moduli 80−70325
vacancy, ideal, electronic struct., tight-binding calc. 79−4529
vacancy, tight-binding calc. 80−24844
vacancy formation and stability due to noncentral force 80−70192
vacancy formations, entropy and enthalpy, comparison of theory with quenching expts. 77−11872
vacancy paradox 78−59804
vacancy states, unrelaxed, appl. of local formalism 77−4313
valence band relaxation energies during XPS 78−39657
valence band splitting in mag. field, LCAO interpolation model *(German)* 77−59251
valence band struct. obtained by magnetophonon effect 77−76748
valence-electron radial and momentum distribs., X-ray form factors and Compton profiles 79−65956
valence electrons, XPS, LCAO and OPW calc. 77−12496
voltage-current curves, specimens of variable cross-section 77−8113
volume plasmon, cryst. orientation influence 80−80921
wavefront reversal, high efficiency 80−74436
waveguide, nonlinear third harmonic generation of submillemetre waves 80−44632
weak heating of electrons, cyclotron reson. conditions, quantising mag. field 78−39141
wedge shaped film, photovoltaic effect 77−1454
whisker growth from vapour phase 80−15426
whiskers nucleation, effect of machining support surface *(Russian)* 79−65352
work function, meas. by thermionic emission 78−19628
X-ray anomalous passage for four-wave diffr. *(Russian)* 77−35437
X-ray anomalous transmission at three-wave diffraction (220;202) *(Russian)* 78−34393
X-ray anomalous transmission at three-wave diffraction (220;202) *(Russian)* 78−34394
X-ray attenuation coeff., anomalous scattering factors and dispersion corrections rel. to photoeffect cross section 79−99980
X-ray attenuation coeffs. 25 to 50 keV, energy dispersive method 77−66557
X-ray Compton line shape, effect of valence state 77−8682
X-ray detector, Au contact layer thickness meas. 80−62627
X-ray detector, efficiency meas. 77−23368
X-ray diffraction, effect of dislocations on temp. depend. of integrated intensities 77−39513
X-ray diffraction, four-wave, intensification of Borrmann effect 77−39501
X-ray diffraction, six-beam anomalous transmission, interpretation from eigensolns. 77−19832
X-ray diffraction, six-wave, intensification of anomalous transmission 77−7635
X-ray diffraction, symmetrical six-wave ang. depend. of transmission coeff. 77−51264
X-ray diffraction, three and four wave, comparison of diamond type crysts. 78−67608
X-ray emission spectra formation, role of nonequilibrium electron density *(Russian)* 77−63490
X-ray linear absorpt. coefficients, in energy range 5 to 50 keV 79−73066
X-ray monochromatisation by Ge crystal diffraction 78−62277
X-ray production, K-shell, on N^+ impact 77−75090
X-ray scattering cross sections, inelastic, in case of small momentum transfer 77−27786
X-ray six-beam anomalous transmission pattern, computer anal. 77−4021
X-ray spectra and energy band struct. 79−69407
X-ray transmission, anomalous, in presence of four-wave diffr. 78−79494
XPS, inelastic mean free path in 700 to 1200 eV range, bulk method 80−20763
yield strength calc. 78−43062
yield stress from Hugoniot elastic limit and elastic consts. 79−83261
yields by reduction of $Al_2Ge_2O_7$ by C *(Russian)* 80−40737
zincblende structure group IVA covalent crystals, Murnaghan parameter estimates from Morse pot. 78−95014
zone refining, molten zone movement under influence of Peltier effect 78−44007
zone refining purification 78−39683
α-quartz:Ge, Ge^{3+} centres, dynamic interchange, EPR obs. 79−19776
γ-ray detectors, material props., appls., radiation damage 78−13392
Ag/In/Ge ohmic contact to GaAs, solid phase epitaxy formation 79−60658
Al:Ge, impurity low-field galvanomag. coeffs., 4 OPW calcs. 77−69304
Al/Ge multilayered superconducting films, crit. fields and crit. temps. 79−7945
Al/Ge/Al sandwich structs., interdiffusion effect on Ge film conductivity 79−23788
Al-Al_2O_3-(a-Ge)-Al, electron tunnelling into a-Ge, press. effect 80−49938
Al-amorphous Ge-nSi, photoelectric props. 80−70822
Al-Ge, alloy, dil., electron-irradiated, impurity-interstitial interaction 77−15449
Al-Ge (100) interfaces, MBE prep. and geometrical struct., total refl. X-ray diffr. study 80−49531
Al-Ge photovoltaic cell, charact. 79−40612
Al-Ge-Al(Cr)(Au), study of metal contact resistance and microstruct. 77−89880
Al-Ge(001) interface, struct., total-reflected X-ray diffr. 80−88441

germanium continued
Al-Si_3N_4-Ge, thermally stimulated depolarisation current meas. 80−88643
Al-Si_3N_4-SiO_2-Ge structure, small signal HF photo EMF meas. 78−52097
AlAs-GaAs:Ge double heterojunctions, efficiency of radiative recombination 77−77286
$Al_xGa_{1-x}As$:Ge, anneal-induced defects, photoluminesc. obs. 79−61422
$Al_xGa_{1-x}As$:Ge, shallow acceptor photoluminescence 80−76064
p-$Al_xGa_{1-x}As$:Ge layer on GaAs substrate, Hall and elec. cond. meas., Hall mobility 80−2402
p-$Al_xGa_{1-x}As$:Ge-p-GaAs:Ge-n-GaAs:Sn heterostructure solar cells, LPE growth techniques 80−66977
$Al_xGa_{1-x}As$:Ge(Te)(Zn), photo- and cathodolum., comp. depend. *(Russian)* 77−48215
$Al_xGa_{1-x}Sb$:Ge, doping of solid solns. during LPE *(Russian)* 77−85087
As:Ge film, amorphous, chemical modification of props. 80−49250
As_2S_3, vitreous, Ag, Cu, Sn and Ge impurities effect on electrophys. props. 77−76826
As_2Se_3:Ge, amorphous and single cryst., ODMR expts. 80−50230
As_2Se_3:X (X=Cu, Ag, Tl, I, Ge), effect of doping, NMR meas. 80−11282
Au-Ge Schottky diode, phonon energies, barrier heights, photovoltage spectra 78−64112
Au-Ge thin film couples, activation energy for interdiffusion, accelerated ageing studies 79−82671
Au-Ge-Au, room temp. interdiffusion 78−76161
Au-SiO_x-Ge, sandwich structure, exam. of image structure using mirror electron microscopy *(German)* 79−11019
CO_2 laser control using Ge and InSb 78−1203
Cd:^{67}Ge, elec. quadrupole interaction temp. depend., PAC meas. 79−42877
CdS-Ge solar cell heterojunctions, CVD fabrication, photovoltaic response 80−93878
CdS-Te-Ge heterojunction, prep. photosensitivity, and negative cond., 77K *(German)* 77−20413
CdSb:Ge, anisotropy of elec., mag. props. 78−34829
CdTe:Ge, mag. props. 78−56289
CdTe:Ge, negative thermally stimulated cond. 79−19621
CdTe-Ge heterojunction, photoelec. props., sensitivity in near IR region *(Russian)* 77−69405
channelled energy loss for positive and negative 2-15 GeV/c, kaons, pions and protons 79−3332
Co:^{67}Ge, hyperfine mag. fields at ^{67}Ge, TDPAC meas. 78−43701
Co:Ge, temp. anomalies of hyperfine fields 78−23265
^{57}Co ion implantation, Mossbauer spectra, dose depend. 79−82899
electron-hole drop explosive instabilities under microwave radiation 77−31951
$(Eu,Lu)_3Fe_5O_{12}$:Ga(Al)(Ca,Ge), bubble material, dynamic characterisation, comparison between transport and FMR methods 80−39833
in Fe meteorites, concs. rel. to chemical classification and nebular condensation 80−36594
Fe:^{67}Ge, hyperfine mag. fields at ^{67}Ge, TDPAC meas. 78−43701
$Fe(OH)_3$, coprecipitation with Cu, Ag, Au; Ge, Sn, Pb; Mn and Ca 79−70415
(Ga,Al)As:Ge, epitaxial layers, radiative recomb., compensation, cathodolum. study 80−66307
Ga-GaAs heterojunctions, electronic struct., tight-binding and pseudopot. models 79−42633
$Ga_{0.9}Al_{0.1}As$:Ge(Si) epitaxial layers, defect obs. by TEM 77−51618
GaAs on Ge thin film stacked multiple-bandgap solar cell structs., prep. using CVD techniques 80−94083
p-GaAs:Ge, (111) surface, LPE grown, cryst. struct., phys. and chem. props. by Auger obs. 79−73386
GaAs:Ge, cryst. and epitaxial layers, ion-implanted, elec. props. 79−99542
n-GaAs:Ge, film, substrate temp. depend. of Ge incorporation during MBE 80−76196
GaAs:Ge, impurity conc. profile by glow-discharge optical spectroscopy 80−49258
GaAs:Ge, ion implanted, elec. props., comparison with Sn, Se and Te ion implanted samples 77−39879
GaAs:Ge, ion implanted, laser annealing, ellipsometric and Hall meas. 79−73193
GaAs:Ge, ion-implanted, photoluminesc., deep emission centres 80−34965
GaAs:Ge, LPE, on semi-insulating GaAs, film-substrate interface characterisation 78−72017
GaAs:Ge, MBE layers, photoluminesc. 80−29803
GaAs:Ge, MBE layers, complex free-carrier profile synthesis 80−54266
GaAs:Ge, mol. beam epitaxy of n- and p-types 80−10839
GaAs:Ge, n-type layers, heavily doped, formation by multiple ion implantation 80−88187
GaAs:Ge, solubility and point defect-dopant interactions 79−90689
GaAs:Ge, stress depend. of donor-acceptor recomb. energy 79−15113
GaAs:Ge, VPE, doping, electrophysical characts. meas. 78−43493
GaAs:Ge, VPE, high purity, residual donors, photocond. expts. 77−85174
GaAs:Ge, vap. grown, diatomic complex donor and acceptor model 78−80003
GaAs:Ge,Se transmutation shallow donor transition obs. 80−59925
n-GaAs:Ge epitaxial layer, ion-implantation doped, anomalous behaviour of impurities 78−18669
GaAs:Ge film, MBE grown, heavily doped, elec. props. rel. to growth parameters 80−100537
GaAs:Ge LPE layers, luminesc. props. rel. to substrate quality 78−52583
GaAs:Ge MBE power FETs with Sn surface impurities 80−80374
GaAs:Ge p-n junctions by mol. beam epitaxy 79−56289
GaAs:Ge^+, ion implanted, laser annealing effect on elec. characts. 79−73195
GaAs:Te, Ge, compensated, activated cond. 77−76968
GaAs-Ge, heterostructure, zincblende-on-diamond type systems, MBE growth, (110) orientation as preferred orientation 80−80099
GaAs-Ge interface, abrupt, electronic struct., self-consistent calc. 77−24611
$GaAs_{1-x}Sb_x$:Ge, LPE and elec. props. 77−55896
GaAs:Ge, LPE layer growth, impurity effect on terrace form. 79−95288
$Ga_xIn_{1-x}As$:Ge LED, by LPE, radiation emitted at 1.02 μm 78−48235
$Ga_xIn_{1-x}As_{1-y}P_y$:Ge, epitaxial film, elec. and optical props. 79−11251
GaP:Ge, ENDOR study, superhyperfine interactions 80−93210
germanium continued
n-GaP:Ge, photomemory effect and thermal field impurity breakdown 77−20362
Gap-Ge, compensated, photosensitivity 79−19624
Ge $4p^2(^1S_0)$, collisional quenching 78−33463
p-Ge broadband passive isolator for CO_2 laser system, pulse shaping 78−46662
n-Ge, current carrier-dislocation interactions, resistance in UHF range *(Russian)* 80−54732
Ge, electron-hole drop binding energy, optical threshold studies 79−38652
Ge, electron-hole drop emission kinetics, effect of nonequilib. phonons, 4.2K 78−14674
Ge film, AC cond., up to 200 kHz, 100-300K, role of contacts 77−76970
Ge film, radiation damage in electron microscope 77−84794
Ge, film, vac. deposition onto low temp. substrate, cryostat *(Japanese)* 78−27403
Ge, high-doped single crysts., impurity atom distrib. changes around growth dislocations in thermocyclic treatment *(Russian)* 80−107307
Ge I, absorption spectra of outermost d-subshell 77−75086
Ge I, absorption spectrum, 1500-1900 Å 77−71769
Ge I, transition probabilities, $4p^2$-4p4d and $4p^2$-4p5s, 1900-4700 Å *(French)* 78−74600
Ge II, oscillator strength meas. and trends in group IV homologous ions 80−42991
Ge II, radiative lifetimes, calcs. and beam-foil spectra 77−75223
Ge II homologous ions series, Stark broadening trends 80−105157
Ge III, effect of pressure on the Raman shift 78−92064
Ge III isoelectronic series, $4s4p\,^1P$ lifetimes meas. 80−42998
p-Ge, IR light free hole absorpt., nonvertical optical transitions *(Russian)* 80−80802
Ge IV spectra, nonrelativistic oscillator strengths calc. 77−83538
p-Ge, Li-compensated, carrier capture 77−15792
n-Ge, minority-carrier injection and extraction 80−49767
p-Ge modulation of 3.39 μm abs. by CO_2 laser irrad. *(Japanese)* 80−74410
Ge, μ^+ meson polarisation, H impurity behaviour 77−20786
Ge, nonpolar semiconductor, IR free carrier absorpt., two short wavelength phonon scattering 79−78665
p-Ge, saturable absorption of picosecond CO_2 laser pulses 80−95956
n-Ge sensor, resist.-temp. characts., 50-125K 77−41602
Ge, supercond. at high press., crit. temp. 80−60130
Ge surface, line tension induced dislocation motion 79−82212
n-Ge, thermal phonon scatt., piezo-thermal cond. 80−70482
Ge, valence band effective mass strain depend. 78−51880
n-Ge, vel. component of hot charge carriers' thermoelectromotive force 80−44630
Ge XXIV, $2p^5$-$2p^4$3s($2p^4$3d) transitions in laser produced X-ray spectra 78−13460
Ge XXIV, spectra and energy levels of F isoelectronic series 79−93948
Ge XXIV, transitions between $1s^22s^2p^5$-$1s^22s^22p^4$3d and $1s^22s^22p^5$-$1s^22s^22p^4$3s configs. 79−26925
Ge^-, photodetachment cross-section, crossed beam meas. *(German)* 77−42298
Ge^+, and isoelectronic ions, excited-state energy level k-ordering, l-patterns 77−88406
Ge^{2+}, photon coherent scatt., cross sections 77−50410
n-Ge: Ga(P), uniaxial compression, 0.6-2.9 mm radn. absorpt. 79−82629
Ge:^{119m}Sn, impurity lattice dynamics, Mossbauer spectra, Debye temp. 80−84262
Ge:^{125}I(^{125}Te), implanted atom sites and quadrupole interaction, Mossbauer spectra 77−20758
Ge:^{57}Co, ion-implanted, Mossbauer study, annealing effects 80−7231
Ge:^{57}Fe, quadrupole interac. 78−92005
Ge:^{57}Fe study via conversion electron Mossbauer spectroscopy 77−55735
p-Ge:Ag, Sb, electron beam irradiation cond. characts. 80−19842
Ge:Ag(Ni), gamma ray effects on impurity states 80−96822
Ge:Al, acceptor levels, Zeeman splitting, far IR photoconductivity spectrum 78−43444
Ge:Al, limiting solubility, rel. to charge carrier conc. 80−24596
Ge:Al, solid solns. decomp. 80−15249
Ge:Al, Zeeman effect in excitation spectra, photoelectric spectroscopy 79−82633
Ge:Al(B), uniaxially stressed, photoionisation of acceptors, impurity photocond. meas. 78−10509
Ge:Al(B)(P), impurity ground state levels from photo-thermal cond. in mag. field 77−51699
Ge:Al(Sb) film, amorphous, ion implantation, effect on cond. 78−83839
Ge:As, containing dislocation loops, dynamic scatt. of X-rays, extinction effect 78−47384
Ge:As, D^- states investigated by long wavelength photoconductivity 78−6323
Ge:As, far IR transmission spectra, singlet-triplet optical transitions in ground states of donors 78−2887
n-Ge:As, heavily doped, luminesc. from electron-hole drops 77−81144
Ge:As, interaction of muonium with atoms 79−11373
Ge:As, many-valley semicond., donor binding energies, variational calc. 78−23041
Ge:As, moderately heavily doped, electron-hole drops photoluminesc. 80−7417
Ge:As, NMR, conduction electrons in impurity band, metal-nonmetal transition 79−78544
Ge:As, recomb. of donor bound excitons, luminesc. intensity decay 80−25441
Ge:As, thermally induced defects properties obs. 77−63692
Ge:As, uniaxially stressed, electronic Raman scatt. from valley-orbit transitions 78−15166
n-Ge:As closely compensated, photolum. of charge carriers localised in trails of density of states 77−77294
Ge:As(Bi), donor bound exciton luminesc. and absorpt. 80−29777
Ge:As(Ga), photoconductivity oscillation with respect to applied mag. field *(Russian)* 78−80026
Ge:As(P)(Sb), impurity photocond. spectra under uniaxial compression 80−44656
Ge:As(Sb), D^- states in mag. fields, photocond. spectra, and far IR absorption spectra 79−95370
n-Ge:As(Sb), far IR absorpt. spectra 79−91469
Ge:As(Sb), phonon-bound donor resonance scatt., donor-electron radius mag. field depend. 79−77847

germanium continued
n-Ge:As(Sb)(Bi), irradiated with fast electrons at 77K, investigation of 300K annealing stage 79−51155
Ge:As(Se^+), energy spectra, multivalley effective mass calcs. 77−59266
Ge:Au, capacitance oscillations, trap recharging waves 77−43614
n-Ge:Au, current oscill. damping in weak transverse mag. field 77−4365
Ge:Au, current-voltage phase shift, impedance of subthreshold domains 77−43609
n-Ge:Au, electron capture by negatively charged traps, effect on hot electron enrgy energy distrib. 78−43398
Ge:Au, gamma-irradiated and electron irradiated, elec. props. meas. 77−62950
Ge:Au, IR detector, impurity photoconductivity *(German)* 78−82036
p-Ge:Au, interaction of primary radiation defects with Au atoms, after irrad. and annealing 79−51145
Ge:Au, moving elec. domain, impedance 77−1429
n-Ge:Au, negative photocond., field and temp. depend. 77−43660
n-Ge:Au, negative photoconductivity 78−34863
Ge:Au, p-n junction, injection amplification of photocurrent 79−51663
Ge:Au, recomb. at repulsive centres, photocond. lifetime meas. 77−43617
Ge:Au, Sb, Hall mobility, temp. dependence 80−96919
Ge:Au, Sb 79−69577
Ge:Au, trap charge exchange waves *(Russian)* 78−34846
Ge:Au, unipolar injection influence on high frequency conductance 80−34474
Ge:Au,Sb, electron irradiated, Hall effect, photocond., and photomagnetic effect meas. 77−4369
p-Ge:Au,Sb,Hg(Zn), radiation-defect form., Au influence 80−92911
Ge:Au film strain gauges, press. sensor *(Japanese)* 80−105631
n-Ge:Au piezoresistance in presence of deep levels, stress anisotropy 80−10979
Ge:Au under laser illumination, non-equilibrium conduction 80−6896
Ge:B, epitaxial film, exam. of doping during chemical deposition from gas phase 79−1446
Ge:B, ion implantation and depletion at low temps., radiation and DC characts. 79−60392
Ge:B, single crystals, grown by Czochralski method, exam. of B distribution ratio and diffusion coeff. 79−95042
Ge:B(Al)(Ga), shallow acceptor spectral line intensities 80−88517
Ge:B(Al)(Ga)(In)(Tl), binding energy, excited state spectra, photolum., semi-empirical short range pot. 80−44534
Ge:B(P), ion implanted, laser-induced regrowth 79−69130
Ge:Ba, Ca, recomb. props. 78−56156
Ge:Ba distrib. pattern, partition coeff., limiting solubility and energy levels 77−15444
Ge:Ba(Ca), elec. props. and effect of impurities on γ-radiation defect formation 78−10088
Ge:Be, P, absorption of radiation, 0.6-2.8 mm, 4.2 to 20K 80−66332
Ge:Be single crystals, grown by Czochralski method, exam. of Be distribution ratios and solubility 79−95043
Ge:Be(Mg)(Ca)(Ba), positron annihilation ang. distrib 80−45165
n-Ge:Bi,O, plastically deformed, dislocation scatt. anisotropy, effect of state of O in Cottrell atm. 78−19028
Ge:Cd, compensated, complex oscillatory impurity photocond. spectrum 77−43656
p-Ge:Cd,Sb, electron irrad. at 300K, elec. props. 80−6435
Ge:Cu, anelastic relax., internal friction temp. depend. meas. 79−65143
n- Ge:Cu, characts. of radiation defects 78−55893
Ge:Cu, deep-level impurities, insulating props. 78−39124
Ge:Cu, degree of Cu contamination in heat treated Ge 80−2359
Ge:Cu, displacement of Ge-Cu inclusions in const. elec. field, 700-850°C *(Russian)* 77−15634
Ge:Cu, electron irrad. effects on carrier density, defect form. 80−19843
Ge:Cu, hot photoexcited holes at low temp. 78−30954
Ge:Cu, IR detector, impurity photoconductivity *(German)* 78−82036
Ge:Cu, low frequency oscillations 77−15872
Ge:Cu, press. effect on energy spectrum of carriers, elec. cond. and Hall coeff. expts. 79−23930
Ge:Cu, quenched, energy levels of thermal acceptors, annealing effect 78−34798
Ge:Cu, quenched, interaction between shallow-level defects and Cu atoms, Hall effect meas. 78−64002
Ge:Cu, solubility and behaviour of Cu, internal friction investigations 80−92678
Ge:Cu, surface waves at static domain boundaries *(Russian)* 80−80288
Ge:Cu photodetector, I-V characts. 78−19141
Ge:Cu short wavelength quenching of photoconductivity 78−26907
Ge:Cu(Sb), electron irradiation effects on elec. props. 78−6103
n-Ge:D^-; energy spectrum of D^- impurity band 77−51702
Ge:Fe, amorphous film or ion-implanted, comparison of ^{57}Fe Mossbauer data 77−40159
Ge:Fe, implanted, Mossbauer spectra, conversion electron, temp. dependence 80−40025
Ge:Fe, recoil implantation Mossbauer expt. in presence of external mag. field 80−44981
Ge:Ga, appl. of heat pipe to Czochralski growth, segregational behavior 79−61511
p-Ge:Ga, carrier heating by weak elec. field, hole-hole collision influence 78−72161
p-Ge:Ga, cryst. defects due to γ-irrad., annealing 79−55779
Ge:Ga, cryst. defects due to neutron irrad., elec. cond. and annealing 79−55789
p-Ge:Ga, dislocation density effect on carrier lifetime and deep recomb. centres 79−51598
Ge:Ga, effects of destabilising vertical thermal gradients on cryst. growth and segregation 78−52659
p-Ge:Ga, heavily doped, elec. resist., 40 mK to 300K 79−38071
Ge:Ga, heavily doped, structure defect evolution during heating *(Russian)* 78−43026
p-Ge:Ga, lattice defects induced by γ-irrad. 80−29051
Ge:Ga, magnetoacoustic resonance attenuation, Zeeman splitting of acceptor ground state 77−47869
p-Ge:Ga, photoemission into electrolyte soln., energy diagram, Volta pots., voltage drop 77−62990
Ge:Ga, resonant scattering of phonons by bound holes in temp. range 1 to 5K 80−75393
p-Ge:Ga, saturation behaviour at CO_2 laser wavelengths 78−1307
Ge:Ga, simultaneous multiline saturation at 10.6 μm 77−88868
Ge:Ga, uniaxially stressed, far IR photocond. meas. 78−10496

germanium continued
Ge:Ga,Sb, compensated, low temp. props. rel. to appl. in bolometry 80−31867
p-Ge:Ga far IR absorption and photoconductivity obs. 77−39899
Ge:Ga photoconductor detector performance in low optical background 77−37999
Ge:Ga photoconductors in low IR backgrounds 79−63305
Ge:Ga surface, antireflection coated, laser pulse damage resistance obs. 79−14020
Ge:Ga(In), resonant phonon interaction with localised acceptor levels 80−6784
Ge:Ga(In), shallow acceptor ground state, thermal cond. meas. 77−43540
Ge:H, amorphous, H content determ. by IR absorpt., gas evolution and nuclear reaction methods 80−44130
Ge:H, amorphous, H-states exam. 78−39059
Ge:H, interstitial impurity levels, pseudopot. calc. 80−44533
Ge:H, photoelec. spectra, acceptor and donor behaviour 80−29443
Ge:H amorphous films, photoemission spectra 80−50517
Ge:Hg, anomalous photocond. with 10.6 μm laser light *(Russian)* 77−47861
Ge:Hg, anomalous room-temp. impurity photocond. 78−39159
Ge:Hg, S-type diode, elec. props. 80−20299
Ge:Hg, Sb, influence of electron irradiation on elec. props. 77−20318
Ge:Hg photoconductive detector, laser damage thresholds calc. 78−90443
Ge:Hg S-type diodes, photoelec. props. 80−6964
p-Ge:Hg(Cu)(Cd)(Zn), deep levels, optical-phonon-assisted capture of carriers 79−51597
Ge:In, magneto-optical transitions between discrete levels of In acceptor, far-IR obs., 4.2K 78−2890
Ge:In (Sb) and pure cryst., kinetics of strain-confined large electron-hole drop and its clinging exciton system 80−75508
Ge:In(Hg), impurity characterisation from thermal carrier meas. 80−65595
Ge:inert gas, ion implantation, UV photoemission exam. 78−80457
Ge:Li, Cu p-n junctions, current stimulated LiCu complex formation, photocurrents 80−107897
Ge:Li, determ. of drift parameters of Li 78−17509
Ge:Li, diffusion study using ^{6}Li(d,α) reaction 79−5202
Ge:Li, dislocation free, anomalous transmission of X-rays *(Russian)* 77−15286
Ge:Li, long wavelength photoconductivity spectrum 77−43641
Ge:Li, supersaturated solid solns., decomp., surface impurity content 78−51681
Ge:Li, thermal cond., 0.4-20K, Li valley-orbit splitting 79−15111
Ge:Li,O, EPR and piezospectroscopy 80−25338
Ge:Li-O, donor complex EPR and photoelectron piezoelectric spectra, dynamic tunnelling 79−1711
Ge:metal, polycrystalline film, electron transport props. 79−99642
Ge:Mg, diffusion and p-type cond. 80−6419
Ge:Mg, energy level behaviour, Hall coeff. and elec. cond. meas. 80−34396
Ge:Mn, amorphous, cond. increase by Mn doping 78−72155
Ge:Mn, amorphous, EPR meas. 77−85559
Ge:Mn, impedance characts., near threshold of excitation of recomb. waves 77−69342
Ge:Mn, Sb, recombination waves, convective instability development 80−70721
Ge:Na (111) surface, O_2 adsorpt., work function, surface cond. changes meas. 78−79875
n-Ge:Ni, negative differential conductance of surface channels 79−11134
n-Ge:Ni, quasi-surface conduction effects on photocond. spectrum and IR quenching 77−1452
n-Ge:Ni, recomb. waves, current instabilities obs. 77−1431
n-Ge:Ni, recombination of hot electrons on Ni impurity centres 80−44612
n-Ge:Ni,Sb, transient response at 4K, nonequilib. carrier recomb. 77−43659
Ge:Ni compensated, hot electron recomb. anisotropy 78−39125
n-Ge:Ni p^+-n-n^+ structs., double-injection current-voltage characts. 80−60074
p-Ge:Nz, Sb, influence of electron irradiation in elec. props. 77−20318
Ge:O, Cu, amorphous thin film, impurity effects on struct. 80−107054
n-Ge:O, Czochralski growth, O content rel. to props., IR, Li precipitation determs. 77−15445
Ge:O, elec. props., O donor levels determ. 77−8123
Ge:O, elec. props., O interaction with point defects 79−11081
Ge:O, IR absorpt. at low temp. *(Chinese)* 80−108228
n-Ge:O, impurity-saturated, dislocation-free, anomalously high magnetoresist., vacancy effects 77−43629
Ge:O, slow thermal relax. of cond. rel. to donor complexes 80−70704
Ge:O ion implanted, O localisation determ. 79−95040
Ge:P, amorphous, electronic transport and photocond. 79−60834
Ge:P, bound-exciton luminesc. and absorpt. 79−87469
Ge:P, charact. temp. and lattice thermal cond. 80−59743
Ge:P, conc. depend. of diffusion coeff. at P diffusion 78−95185
Ge:P, doping of epitaxial layers, in chloride and hydride processes 78−43036
n-Ge:P, electric dipole excitation of spin resonance 77−4551
Ge:P, lattice thermal cond., role of electron-phonon interactions and peripheral phonons 78−79702
Ge:P, lattice thermal resistivity due to electrons 78−51756
Ge:P, peripheral phonons and phonon cond. 79−14973
Ge:P, phonon drag thermoelectric power at low temp. 80−107828
Ge:P, solubility and segregation of electrically active P 77−15442
n-Ge:P,Ga, compensated, uniaxially compressed, anisotropy of mm. and submm. wave absorpt. 78−19074
Ge:P(As), Ga, lightly doped semicond., electron-phonon scatt., role of compensation 79−60456
n-Ge:P(As), nonlinear optical susceptibility, Raman scatt. cross-sections for impurities 77−46759
Ge:P(Sb), growth atm. effect on struct. microdefect form. 80−20779
Ge:P(Sb)(Bi), γ-irrad., carrier trapping and recomb. at point radiation defects 80−107810
Ge:Pb, ion implanted, lattice reordering, channelling and sheet resist. meas. 77−35577
Ge:Pb, ion implanted damaged layer, laser induced reorder 80−84201
Ge:Pd and pure, photoelectric props., surface states *(Russian)* 80−60043
Ge:S, photoionisation cross section of deep impurity centres 78−56510

germanium continued
Ge:Sb, acoustic attenuation, uniaxial stress effects 78−59863
n-Ge:Sb, adiabatic approximation in transient donor recombination 80−49761
Ge:Sb, amorphous, electronic transport props. 80−44589
Ge:Sb, annealing stages of thermal defects, elec. meas. 77−55282
Ge:Sb, bolometer element, absorpt. spectra, bias depend. 79−30553
p-Ge:Sb, cryst. defects due to γ-irrad. 79−55779
Ge:Sb, cryst. defects due to neutron irrad., elec. cond. and annealing 79−55789
Ge:Sb, Czochralski growth, orientation depend. of impurity distrib. coeff. 79−69976
Ge:Sb, D^- states investigated by long wavelength photoconductivity 78−6323
n-Ge:Sb, deep levels obs., freq. depend. of capacitance of p-n junctions 77−4315
Ge:Sb, dopant distrib. rel. to direction of cryst. growth 77−51400
Ge:Sb, effect of degree of doping on surface state charact. 79−69577
n-Ge:Sb, electron irrad., impurity photoconductivity 77−15900
Ge:Sb, electron-hole drop lifetime, quenching temp. influence 80−59889
Ge:Sb, excited donor states, double optical transitions, reson. absorpt. meas. 80−93371
n-Ge:Sb, exciton absorption 78−6688
n-Ge:Sb, fast electron irrad. at 77K, radiation defect changes by annealing at 220K 79−37737
n-Ge:Sb, fast neutron irrad. effects on donor conc., and annealing 78−56107
Ge:Sb, γ-irrad., electron capture mechanism by radiation defects 78−26885
n-Ge:Sb, γ-irrad. effects on donor conc. and compensation by acceptors 78−56106
n-Ge:Sb, γ-irradiated, trapping and recomb. coeffs. 77−43616
Ge:Sb, heavily doped, anomalous magnetoresist., metallic impurity cond., down to 5 mK 79−65502
Ge:Sb, heavily doped, mass anisotropy, and multiple scattering effects 80−107802
Ge:Sb, heavily doped, scatt. of electrons 77−59283
Ge:Sb, heavily doped semicond., scatt. mechanism, resist, and Hall coeff. maxima 80−75586
n-Ge:Sb, high-field Hall effect spectroscopy 80−65600
Ge:Sb, impurity conductivities 78−91691
Ge:Sb, lattice thermal resist. due to bound state electrons 79−46850
Ge:Sb, limiting solubility, rel. to charge carrier conc. 80−24596
Ge:Sb, low temp. anomaly of impurity cond. 79−95428
Ge:Sb, low-freq., low temp. dielec. behaviour below metal-insulator transition 80−50250
Ge:Sb, moderately heavily doped, electron-hole drops photoluminesc. 80−7417
Ge:Sb, neutron irrad., carrier mobility theory and expt. 78−56166
Ge:Sb, neutron irradiated, hopping cond. between shallow defect levels 77−4347
n-Ge:Sb, neutron-irradiated, paramag. defects, analysis of EPR spectra 77−55703
Ge:Sb, Ni(Mn), recombination wave spectrum, two-level traps 80−96906
Ge:Sb, phonon thermal cond. calc. 78−71893
Ge:Sb, shock polarisation anisotropy in elastoplastic compression range 77−16244
Ge:Sb, solid solns. decomp. 80−15249
Ge:Sb, thermal defects, influence on radiation defect formation and annealing 77−55281
Ge:Sb, Zn(Hg), photoelec. props., 70 to 300K 80−65621
Ge:Sb,Au, photoelectronoc exam. of multilevel gold structure 77−69272
Ge:Sb,Cu, exactly compensated, impurity absorpt. and photocond. spectra 78−56189
n-Ge:Sb,Cu, exactly compensated, static photocurrent-voltage charact. 79−38131
n-Ge:Sb,Cu, exactly compensated, unipolar injection influence on photoconductivity 79−42592
Ge:Sb,Cu, high resist. compensated, impurity of photocond., pulsed unipolar injection carriers 80−92935
Ge:Sb,Cu, photoelec. props., fast electron irrad. effects 80−60036
Ge:Sb,In, lightly doped semicond., electron-phonon scatt., role of compensation 79−60456
Ge:Sb (As), isolated D^- states and D^- complexes in mag. fields 80−15473
Ge:Sb crystals, purification by zone recrystallisation with temp. gradient 79−4916
Ge:Sb electron irradiated, cond. switching effect 77−89820
Ge:Sb semiconductors, inhomogeneously strained, phonon resonance scatt., Kwok's theory method 79−60455
Ge:Sb(As)(Ga), fast-neutron irradiated, shallow radiation defect levels, electronic props. 78−23049
Ge:Sb(As)(P), implantation doping, annealing and doping profile determ. 77−19972
Ge:Sb(Au) cleaved surface, influence of impurities on local surface states 79−78150
Ge:Sb(Ga), fast electron radiation defects, 0.52 eV absorpt. band, impurity photocond. and Hall effect meas. 78−27273
Ge:Sb(In), film, electronic props. 78−84330
Ge:Si, impurity lattice modes due to single and paired defects 78−75780
Ge:Si, impurity modes and IR absorption 78−76506
Ge:Si radiation-produced vacancies and interstitials, annihilation processes 77−89432
Ge:Sn, ion implantation of radioactive ^{119}Sn 80−59495
Ge:Sn, Mossbauer spectra of ^{119}Sn impurity atoms 80−15935
Ge:Te, ion-implanted, thermally assisted Xe-flash annealing, Rutherford backscatt. meas. 79−10881
Ge:Te^+, ion implanted, alignment of irrad. induced defects, TEM obs. 80−15168
Ge:Zn photoresistor, current responsivity rel. to nonequilib. hole lifetime 80−60035
Ge:Zn^-, G and D lines, stress induced components 80−71447
Ge:Zn^{11} carrier lifetime, nonequilibrium, phase method for determ. 80−65629
Ge/Al thin film couples, accel. ageing 80−44726
Ge/GaAs (110) heterojunction, valence band discontinuity in XPS spectra, precise determ. 80−84834
Ge/Mo substrates, device quality epitaxial growth of polycrystalline GaAs 79−69988
Ge/Si ratio vars. along Reykjanes Ridge and Iceland 79−8617

germanium continued
Ge-Ag, thermocouple, DTA under hydrostatic pressure, appl. to TMMC phase behaviour 79−65186
Ge-Al_2O_3 composite film, optical props., appls. 77−754
Ge-Au-Ni trilayer film, interdiffusion obs., on annealing 78−2308
Ge-Au-Ni(Pt)(Pd) trilayered films, annealing, interdiffusion 78−22902
Ge-Au-Pd film, interdiffusion obs., on annealing 78−2308
Ge-Au-Pt film, interdiffusion obs., on annealing 78−2308
Ge-CdSe heterojunctions, epitaxial, azimuthal rotation 78−84085
Ge-CsI, narrow band interference filters for 8-15 μm 77−34951
Ge-Cu-Ge, layered struct., proton induced X-rays, impurity atom depth determ. 77−11582
Ge-electrolyte contact, current-voltage charact., effect of mechanical deform. 78−68082
Ge-Fe, laser annealing of implanted ^{57}Co sources, Mossbauer obs. 80−39139
Ge-$Ga_{1-x}Al_xAs$, MBE of ultra thin film superlattices on GaAs substrates, TEM study 79−37932
Ge-GaAs, (100) interface, electronic struct. calc. 80−49861
Ge-GaAs, crystallisation at superhigh cooling rates 80−54349
Ge-GaAs, heteroepitaxial systems, misfit dislocations obs. using HV electron microscopy 80−100242
Ge-GaAs, heterojunction, electronic structure 79−73572
Ge-GaAs, n-n isotype heterojunctions, fixed-interface-charge model 78−56215
Ge-GaAs, p-n heterojunctions, surface electron states 79−73578
Ge-GaAs, p-nn^+ junction, I-V charact., inverse branch, effect of dislocation defects *(Russian)* 79−15217
Ge-GaAs, surface reactions and interdiffusion, photoemission study 80−49532
Ge-GaAs (100) interface, electronic struct., scattering-theoretic approach 78−95340
Ge-GaAs (110), heterojunction chemistry, photoemission expts. 78−95244
Ge-GaAs (110) interface, relax., self-consistent pseudopotentials 78−30981
Ge-GaAs (110) interface, self-consistent calc. of interface states and electronic struct. 78−52066
Ge-GaAs (110) junction, interface states and electronic struct. 77−69408
Ge-GaAs abrupt (110) interface, electronic struct. 78−95339
Ge-GaAs abrupt interface, electronic struct., self-consistent wave mechanical calcs. 77−89837
Ge-GaAs abrupt interface, orientation depend. of interface dipole energies, XPS expts. 78−39196
Ge-GaAs heteroepitaxial system, dislocation struct. in stress measurements 80−29030
Ge-GaAs heterojunction, band discontinuities, angle-resolved UPS obs. 79−7878
Ge-GaAs heterojunction, electrostatic dipole shifts contrib. to valence band discontinuities 79−51657
Ge-GaAs heterojunction, elec. and recomb. props., interface defect effects 80−80365
Ge-GaAs heterojunction, interface geometry, model 80−49879
Ge-GaAs heterojunctions, effect of γ-radiation on current-voltage charact. *(Russian)* 80−2459
Ge-GaAs inter faces, heteroepitaxial, misfit dislocations, TEM obs. 79−23610
Ge-GaAs interface, electronic struct. of Ge overlayers on (100) GaAs 80−49880
Ge-GaAs interface, photoemission 80−25530
Ge-GaAs interface, surface and interface states of (111) surfaces 79−15206
Ge-GaAs interface, XPS obs. of electronic struct. 78−95341
Ge-GaAs p-n diode, microplasma breakdown 79−91140
Ge-GaAs p-n heterojunction, current fluctuations 79−11209
Ge-GaAs p-n junction, microparameters determ. 79−11216
Ge-GaAs structure, electronic struct., ang.-resolved photoemission obs. 80−49881
Ge-GaAs superlattice and interface, electronic struct. 78−52065
Ge-Ge (Sn) friction pairs, elec. cond. of Ge tribolayers at He temp. 79−87140
Ge-GeO_2, MIS struct., electrophysical charact. 79−82680
Ge-GeO_2, optical charging memory, influence of doping GeO_2 with metal ions *(Russian)* 79−24077
Ge-GeO_2 boundary, electrophysical parameters *(Russian)* 77−85327
Ge-GeO_2 MIS structure, growth of GeO_2 from liq. phase *(Russian)* 80−40273
Ge-GeO_2 mixtures, gasification kinetics and GeO form. mechanism *(Russian)* 80−21273
Ge-GeO_2 system, optical charge memory obs. 77−89871
Ge-I, gas phase equilib. comp. 77−36776
p-Ge-In injecting contact, sign of developed hot-carrier thermo-EMF 77−55606
Ge-In Schottky barrier interface, covalent bonding of metal atoms 77−20429
Ge-In_2O_3 heterojunction solar cells, photovoltaic and rectifying props. 79−1618
Ge-InAs based MIS struct., avalanche carrier multiplication 80−88566
Ge-$LiNbO_3$, acoustooptic modulator for CO_2 lasers 78−42365
Ge-$LiNbO_3$, layer struct., acoustoelectronic phenomena 77−55556
Ge-MBBA interface, electrorefl., IR transmission and frustrated total internal refl. 78−19513
Ge-metal film, polycryst., struct. props. determ. 79−4494
Ge-metal interface, internal photoemission mechanisms 80−60077
Ge-metal oxide, elec. props., molecular deposition method 80−34525
Ge-metal Schottky barrier photodetectors, near IR interband transitions and optical parameters 80−73449
n-Ge-metal Schottky barrier contacts, IR optoelectronic props., quantum detector appls. 80−75640
Ge-Mo amorphous semicond.-granular metal film system, elec. transport and thermopower 77−76984
Ge-N_2O, rate coeff. meas. for $Ge+N_2O \rightarrow GeO+N_2$ reaction 78−63110
p^+-Ge-n-GaAs abrupt heterojunction, reverse currents *(Russian)* 78−10542
n-Ge-n-GaAs isotype heterojunctions, modelling, charact. 80−103747
Ge-Na interfaces, interdiffusion, electron states, EELS study 80−50484
Ge-$Na_2S_2O_3$ interface anodic oxidation electron transfer 79−56304
p-Ge-nn^+-Si, heterojunction, γ-radiation effect on forward I-V characteristics *(Russian)* 78−72255
Ge-Pd system, kinetics of formation of Pd_2Ge and PdGe films 77−69197

germanium continued
Ge-pyrolytic SiO_2 system, carrier trapping, GeO_2 sublayer effect 78−91775
Ge-Sb, D^- complexes and band form., photocond. 78−84251
Ge-Sb, far IR emission stimulation by impact ionisation 80−66301
Ge-Sb, meas. of electron-hole drop size by light scatt. 80−44515
Ge-Si, solid phase heteroepitaxy 80−6670
Ge-Si, solid soln., local IR transmission 80−7357
Ge-Si, UHV-produced epitaxial structs., electrophys. props. 78−3060
Ge-Si and Ga-Al fractionation in Hawaiian volcanic rocks 79−12112
a-Ge-Si crystal interface, low resist. elec. behaviour 77−89843
Ge-Si n-n heterojunctions, photovoltaic response 78−14804
Ge-Si sandwich structure, sputter profiling, combined Auger-X-ray anal. 80−66909
Ge-Si_3N_4 system, potential barriers determ. from photoinjection carriers trapping 80−103756
Ge-SiO multilayer edge filter design, 3.2 to 4.9 μm range 78−87131
Ge-SiO_2, MIS struct., electrophysical charact. 79−82680
Ge-SiO_2-Al, vacuum heating effect on stability 78−64143
Ge-SiO_2-Si_3N_4, MIS struct., electrophysical charact. 79−82680
Ge-SiO_2-p^+Si tunnel junctions, for determ. of AC cond. of amorphous Ge 77−24608
Ge-Si(GaAs) heterodiodes, interfacial structural defects effect on avalanche breakdown 79−42644
Ge-type semiconductors, two-photon parametric excitation of phonons 80−29339
Ge-YIG layer structure, amplification of bulk magnetostatic waves 78−34972
Ge-ZnS p-n heterojunction, epitaxial, elec. props. *(Russian)* 78−88023
Ge-ZnSe, (100) interface, electronic struct. calc., scattering theoretic approach 80−6940
Ge-ZnSe, (100) interface, electronic struct. calc. 80−49861
Ge-ZnSe abrupt (110) interface, electronic struct. 78−95339
Ge-ZnSe heterojunction, change in interfacial microstruct. on high temp. annealing 77−28242
Ge-ZnSe heterojunction, elec. and photoelec. props. *(Russian)* 77−32070
Ge-ZnSe interface, electronic struct., self-consistent pseudopot. calc. 78−91747
Ge-ZnSe p-n heterojunctions, effect of interfacial condition on optoelectronic props. 79−24061
n-Ge-ZnSe:Mn^{2+}-$In_{2-x}Sn_xO_{3-y}$ thin film electrolum. cell with low-threshold voltage 80−84786
Ge+$^{10}B^{n+}$, 4-38 MeV, K-shell ionis., X-ray obs. 79−59549
Ge+$^{28}Si^{n+}$, K-shell ionisation, projectile charge state depend., theory 78−17786
Ge+Br_2, heterogeneous photochem. reaction kinetics, laser radiation intensity effect 79−66326
Ge+Br_2, surface reaction, rate-limiting step, ellipsometric and photochem. meas. 80−16730
Ge+Ge, quasimolecular K X-ray anisotropy and ang. distrib. 78−1073
Ge+Ge, symmetric collisions, MO-2pσ radiation anisotropy, quasimolecular nature 78−70924
Ge+$GeBr_4$, single crystal+vapour system, reaction kinetics and laws of soln., heat of adsorption 79−39196
Ge+N_2O, chemiluminesc. reaction, HTFFR kinetics study 80−76496
Ge+O_2(NO)(N_2O), reaction rate consts. at 350K 78−53186
Ge+OCS, GeS multiple collision chemiluminesc., intercombination systems 80−45505
Ge+S (vapour) reaction kinetics 78−35718
Ge_2, multiplet struct. and charge distrib. 79−26881
$GeCaF_2$, cosputtered composite semiconductors, selective solar energy absorbers 79−56876
$Ge_{1-x}H_x$, amorphous, atomic struct., X-ray study 80−49106
Ge(Li) commercial coaxial large-volume detectors, time charact. 78−9029
Ge(Li) detector, fast neutron damage 80−59525
Ge(Li) detector, gamma-ray activity of large vol. samples, determ. 77−90656
Ge(Li) detector, Monte Carlo photon transport simulation 79−81122
Ge(Li) well-type semiconductor detector, γ-ray spectrometry *(Japanese)* 79−89521
Ge($^3P_0$)+N_2O, reaction rate const. meas., in flowing afterglow 77−77731
^{32}Ge, origin of high and low freq. K-satellites in X-ray emission spectra 80−50466
Ge(3^3P_0)+O_2(Cl_2)(COS)(N_2O)(NO_2)(NO+Ar) oxidation reacts., gas phase, kinetics 78−92468
H^++Ge collisions, charge exchange 77−6922
In:^{67}Ge, elec. quadrupole interaction temp. depend., PAC meas. 79−42877
In-Ge:As, Schottky barrier tunnel junction, zero bias resistance, temp. depend. 78−72258
InSb:Ge, heat treatment effects on elec. props. 78−43411
InSb:Ge, ion-irrad., p-n conversion during heat treatment 80−96558
p-InSb:Ge, proton irrad. defects energy level scheme, transport props. meas. 80−96576
InSb:Ge, uniaxially compressed, anisotropy of elec. props. 78−19035
InSb:Ge annealing effect on electrical parameters, absorption spectra and photocond. 77−11939
Kr^{24+}+Ge, K X-ray prod., impact parameter depend. 78−58800
Mn-Ge multilayer neutron monochromator, neutron diffr. expts. 77−84589
n^+-n-pGe avalanche photodiode, noise factors, internal quantum efficiency 80−70803
N_2^++Group IV elements and oxides, XPS and UPS prod. determ. 78−73084
Ni:^{67}Ge, hyperfine mag. fields at ^{67}Ge, TDPAC meas. 78−43701
Ni-n-GaP:Ge contact, doping effect in elec. props. 80−6983
PbS-Ge heterojunction, influence of conduction band discontinuity on lux-ampere charact. 78−39200
Pd/Ge film on GaAs substrate, sintering, AES, Schottky barrier energy 79−69581
α-quartz:Ge,Ag^+, Ag-compensated Ge centre, EPR meas. 77−77098
Se:Ge, vitreous, crystallisation kinetics study by elec. cond. meas. 79−65526
Si, drift mobility and Hall coeff. factor of holes 78−43379
Si, dynamical recovery and self-diffusion 79−82379
Si, gamma-irradiated, number of Frenkel defects 78−14377
Si, highly excited, theory of electron-hole plasma 78−10363
Si, localised states due to isocoric donor impurities 77−76768

germanium continued
Si type semiconductor, interimpurity zero-phonon radiative transitions 78−15222
n-Si:Ge, electron induced defects, room temp. instability 80−29052
Si:Ge, P(B), impurity-pair diffusion, influence of elastic stresses 78−87824
Si:Ge, recryst. after implantation using different temp. and energy sequences 80−84196
Si:Ge, regrowth behaviour from backscatt. and channelling meas. 80−2300
Si:Ge,Sn, role of interelectronic correl. in paramag. props. of impurity-vacancy complex 77−62858
Si:Ge B, strain compensation, X-ray Bragg reflexion 80−39137
Si:P, Ge, simultaneous diffusion processes, elastic stress influence 77−89591
Si-Ge heteroepitaxial system, imperfections and morphology, electron microscope and electron diffr. obs. 79−42420
Si-Ge heterojunction form., microscopic aspects, EELS meas. 80−80368
Si-Ge junction, Si monocryst. and Ge film, elec. props. 79−51660
β-SiC, wetting by fused Ge, Sn and Pb 77−85016
p^+-$Si_{1-x}Ge_x$-nSi junction diodes, lattice misfit effects on I-V charact. 80−70804
Si_3N_4:Ge films, intrinsic stress rel. to deposition conditions 80−39467
SiO_2:Ge, vitreous, luminescence centres at 396 and 280 nm 80−103996
SiO_2:Ge optical fibre, single-polarisation single-mode, exposed cladding fabrication 80−58725
SiO_2:Ge silica-core fibre-optic waveguides, effect of B, P and OH on radiation response 79−50419
SiO_2:Ge, B, P, optical fibre, radiation induced optical absorpt. spectra, 0.4 to 1.7 μm region 80−58761
Sn:^{67}Ge, elec. quadrupole interaction temp. depend., PAC meas. 79−42877
Sn:^{67}Ge, quadrupole interaction temp. depend. 77−12264
surface, H atom recombination at surface, elec. cond. and chemomag. effect *(Russian)* 79−91125
W-Ge whisker diode, 337 μm IR detector *(French)* 78−8445
YIG:Ge, effects of nontrigonal cryst. field on spectroscopic props. of Fe^{2+} ions 80−92864
YIG:Ge, Fe^{2+} spectroscopic props., nontrigonal cryst. field effects 80−44553
YIG-Ge layered struct., anisotropy of EMF under nonlinear ferromag. reson. conditions 77−8417
YIG-Ge structure, profile and position of reson. galvanomag. effect curve 78−72242
Zn:^{67}Ge, elec. quadrupole interaction temp. depend., PAC meas. 79−42877
Zn:^{67}Ge, quadrupole interaction temp. depend. 77−12264
ZnP_2:Ge, optical absorpt. spectra in range 0.5 to 2.2 eV 80−66250
$ZnSO_4$ electrolytes containing Ge and Co, polarisation charact., exam. by cyclic voltammetry 80−104444

germanium alloys
see also Ge-Si alloys
α-Ag-Ge, superconducting transition temp. depend. on electron per atom ratio, lattice deform. 77−8222
alkaline earth-Ge, M_2Ge, occurrence struct. 78−38663
amorphous film, crystn. transform. kinetics 78−22653
effect of thermal treatment on superconducting props. 79−61016
film, sputtered, high press. induced shifts in supercond. transition temp. 77−85374
film, superconducting props. 79−38215
molten, struct. and charact. of interatomic interaction, X-ray diffr. meas. *(Russian)* 77−1070
rare earth alloys, $RGe_{2-y}Ni_y$ phases with AlB_2-type struct., lattice parameters 77−24292
rare earth alloys, RM_2Ge_2 (M=Rh,Pd,Ag,Ir,Pt,Au), cryst. struct. 80−1964
rare earth germanide, RFe_2Ge_2, magnetisation and Neel temp. 77−8310
rare earth germanides, RMn_2Ge_2, magnetisation, 4.2-1200K 77−8285
rare earth intermetallics, RMn_2Ge_2, cryst. struct. 78−59782
rare earth-Fe(Co)-Ge, $ThCu_2Si_2$ type, lattice parameters 78−51469
rare earth-transition metal alloys, $RM_2Si_{2-x}Ge_x$, magnetism and hyperfine interactions, magnetisation and Mossbauer effect studies 80−75892
synthesis from thermalised sputtering and changes in Tc and depend. of H_{c2} on temp. 79−56350
transition metal-Ge, RF cosputtered system, supercond. props. 77−51835
78 a/o Si-22 a/o Ge alloy, time and temp. behaviour 77−22543
Ag-Ge, α-phase alloy, thermopower at low temps. 78−84196
α-Ag-Ge, cold-worked, lattice imperfections, X-ray diffr. study 78−38732
Ag-Ge, liq., thermodynamics and short range order, mass spectra meas. 79−52740
Ag-Ge, liq., viscosity, temp. depend. *(French)* 78−59964
Ag-Ge, liq. eutectic, neutron diffr. determ. of struct. 77−51302
Ag-Ge, liq. eutectic, struct. by neutron diffr. 78−18537
Ag-Ge, liquid, neutron diffr. investig. of pair correl. function, coordination numbers 77−35467
Ag-Ge, liquid, surface tension exam., sessile drop method *(French)* 77−20162
Ag-Ge, thermal expansion, X-ray determ. 78−26697
Ag-Ge, thermopower at low temp., Fe impurities 79−65440
Ag-Ge (4.5 at.%), FCC, vapour-deposited, lattice imperfections, X-ray diffr. 78−72032
Ag-Ge alloy, α-phase, lattice sp. ht. calcs. 80−65246
Ag-Ge alloy, liq.-quenched, metastable phase formation and evolution 77−90338
Ag-Ge eutectic alloy, heat capacity meas. over temp. range 800-1200K *(French)* 80−88331
Ag-Ge eutectic alloy, X-ray spectral exam. *(Russian)* 77−63489
Ag-Ge eutectic alloys, unidirectional solidification, electron microscope study of twinning 79−61574
Ag-Ge liquid alloy, small angle neutron scatt. 79−64982
Ag-Ge system, atomic struct. and electronic props. *(Russian)* 77−20289
Ag-In-Ge alloyed contacts to GaAs 79−78174
Al-Ga-Ge, liq., enthalpy of form., direct reaction calorimetry, 713-1230K *(French)* 79−66336
Al-Ga-Ge, thermodynamic props. of mixing of binary systems, phase diagram 80−45275
Al-Ge, and Al-Ga-Ge, Al activity, EMF study, phase diagrams 79−83175
Al-Ge, band model of high temp. magnetism 78−26809

germanium alloys continued
Al-Ge, dil., deviation from Matthiessen's rule at high temps. 78−64025
Al-Ge, dil., deviation from Matthiessen's rule, 4-OPW approx. calc. 79−19574
Al-Ge, dil., Dingle temp. calc. 78−39005
Al-Ge, dil., electronic transport coeffs. for point defect scatt., 4-OPW calc. 79−42531
Al-Ge, dil., magnetoresist., temp. depend. 80−70682
Al-Ge, directionally solidified lamellar eutectics, specimen prep. for TEM *(German, English)* 78−95885
Al-Ge, effect of irrad. on the nucleation of incoherent precipitates 79−8303
Al-Ge, film, double supercond. transition in resistance-temperature and current-voltage charact., percolation theory 79−56365
Al-Ge, galvanomag. transport coeffs., Hall effect 79−91029
Al-Ge, internal friction and shear modulus after neutron irrad. at 80K 79−1468
Al-Ge, liq., enthalpy of form., direct reaction calorimetry, 713-1230K *(French)* 79−66336
Al-Ge, rapid quenching, struct. and decomp. 80−76244
Al-Ge, structural changes during superplastic deformation, grain boundary porosity *(Russian)* 79−83258
Al-Ge (0 to 8 wt.%), superplastic props. *(Russian)* 80−45345
Al-Ge (0.1 wt.%), channelling meas. of Al interstitial atom trapping by Ge atoms 80−59537
Al-Ge (0.2 at.%), exam. of interstitial trapping by X-ray diffuse scatt. 78−47363
Al-Ge (2 wt.%), averaged, plastic flow mechanism 77−48507
Al-Ge (2 wt.%), quenched and aged, deform. slip line obs. 78−51544
Al-Ge (4 wt.%), superplasticity exam. *(Russian)* 78−39836
Al-Ge (6.8 at.%), quenching from mushy state for production of metastable phases 80−35223
Al-Ge alloy, effect of high press. on phase equilibrium *(Russian)* 79−1844
Al-Ge alloy, Ge particle size, determ. by small- and wide-angle X-ray scatt. 78−19966
Al-Ge alloy, Ge precip., ion irrad., dose rate and temp. depend. 78−79642
Al-Ge dil. alloys, Hall coeff., residual resist., and relax. times 79−11107
Al-Ge eutectic alloy, X-ray spectral exam. *(Russian)* 77−63489
Al-Ge eutectic alloys in screened ohmic contacts for solar cells 80−94090
Al-Ge film, ion-implanted, percolation and superconductivity 78−26982
Al-Ge film, random percolation, elec. resist. meas. 79−28418
Al-Ge ion-implanted, enhancement of supercond. transition temp. 77−32103
Al-Ge thin film alloy, critical currents near metal-insulator transition 79−65626
Al-Ge-Sn, thermodynamic props. of mixing of binary systems, phase diagram 80−45275
AlGe (4 wt.%), struct. peculiarities of superplastic behaviour due to porosity 79−34111
Au/Au-Ge/GaAs structure, ohmic contact behaviour, alloying time effect 79−19659
Au-Ge, liquid quenched, exam. of phase decomposition 78−48371
α-Au-Ge, superconducting transition temp. depend. on electron per atom ratio, lattice deform. 77−8222
Au-Ge (27 at.%), metastable phase struct. determ. by electron diffr. 78−83780
Au-Ge contacts on GaAs, SEM and TEM obs. of struct. 80−100522
Au-Ge contacts to n-GaAs layers with SiO_2 overlayer, ohmic props. 80−2467
Au-Ge eutectic films, prep. of Au films with nm-sized pores by etching 80−16227
Au-Ge evaporated film, effect of substrate on conductivity 79−78213
Au-Ge film, evaporated, for ohmic contacts to GaAs, compositional stratification, effect of source material impurities 79−77951
Au-Ge ohmic contacts, laser alloying on GaAs 79−73583
Au-Ge system, struct. of metastable phases *(German)* 80−108430
Au-Ge/GaInAsP, ohmic contact, elec. charact. 80−80376
Au-Ge/Ni films on GaAs, alloying behaviour, microprobe AES and X-ray diffr. 80−54548
Au-Ge/Ni ohmic contact to GaAS, solid phase epitaxy formation 79−60658
Au-Ge-Ni/GaAs metal-semiconductor thermoelectric coolers, effects of contact resist. and dopant conc. 80−81481
Au-Ge-Si, influence of struct. on elec. resist. of glass forming alloys 80−65518
(Au-Ge)-Ni film, for contacts to n-GaAs, metallurgical investigation using inert substrate 77−85313
(Au-Ge)-Pt film, for contacts to n-GaAs, metallurgical investigation using inert substrate 77−85313
AuGe, ohmic contact to epitaxial GaAs, production by laser alloying 78−88026
AuGe/n-GaAs, SIMS study Au behaviour during annealing 78−75947
Au_xGe_{1-x}, liq., ang. distrib. of positron annihilation 77−55848
$Au_{0.77}Ge_{0.136}Si_{0.094}$, undercooled metallic melt, viscous behaviour 77−66037
$Au_{77}Ge_{13.5}Si_{9.4}$, heat of crystn. and viscous behaviour 80−75166
Cd-Ge broken lamellar eutectic composite, tensile and compressive props. 80−71694
$CdGeAs_2$, amorphous, thermal gradient expts., recrystn. 80−55438
$CdGeAsMn_x$ glass, recrystallisation 80−44133
$CeMn_2(Si_xGe_{1-x})_2$, $Ce(Mn_{1-x}B_x)_2Si_2$, (B=Fe, Cu) mag. props. 80−25134
Co-Ge, liq., elec. resist. and thermoelec. power using t matrix approach 77−31988
Co-Ge, liq. alloy, structure studied by X-ray diffr. *(Russian)* 79−77493
Co-Ge binary system, phase diagram rel. to that of Ni-Ge *(French)* 80−97463
Co-Ge eutectic alloys, X-ray spectral investig. of electron struct. 77−44087
Co-Ge-B, Co rich, phase diagram 77−8800
Co-Si-Ge system, X-ray diffr. exam., band struct. *(Russian)* 78−56623
$(Co_xFe_{1-x})_5Ge_3$, Mossbauer investig. of hyperfine field at Fe nuclei 77−20776
CoGe and TiCoGe, electronic struct., X-ray K- and L-spectra obs. *(Russian)* 78−11022
CoGe, Co_2Ge and $CoGe_2$, X-ray spectrum analysis, energy band struct. *(Ukrainian)* 77−52200
germanium alloys continued
Co_2Ge_3, $CoGe_2$, amorphous film, annealing effects on struct. and elec. resist. 77−85099
Co_5Ge_3 amorphous film, elec. resist., microstruct. and annealing 77−85188
Co_5Ge_3, phase and struct. charact. 77−36450
Co_5Ge_3, solid and liquid, physicochemical props. and structure 80−39548
$Co_2Mn_xFe_{1-x}Ge$, hyperfine fields of Fe impurities, Mossbauer effect meas. 78−31130
CoMnSi, $CoMnSi_{0.85}Ge_{0.15}$, mag. props. 79−42758
$CoMnSi_{1-x}Ge_x$, amg. props. 80−60270
Cr-Ge, dilute alloy, phase diagram of spin density wave states 79−24158
Cr-Ge amorphous films, annealing effect on elec. resistance and struct. 80−54667
Cr-Ge liquid and amorphous alloys, struct. props., cond., viscosity, surface tension *(Russian)* 80−54119
Cr-Ge system, phase diagram, thermal anal., X-ray diffr., microhardness, and electron probe anal. *(French)* 80−97462
Cr-Ge system, XPS, X-ray and neutron diffr. and mag. meas. to study chem. bonding and electronic struct. 80−60749
$Cr_{11}Ge_8$, Cr_3Ge, thermodynamic functions 77−84948
$Cr_{11}Ge_8$, CrGe, and $Cr_{11}Ge_{19}$ amorphous films, short-range order, electron diffr. obs. *(Russian)* 78−56050
$Cr_{12}Ge_{19}$, CrGe, thermodynamic props. 77−36779
Cr_3Ge amorphous films, short range order struct. *(Russian)* 78−30841
Cr_3Ge, band theory, semiself-consistent band calcs. 78−2406
Cr_5Ge_3, amorphous film, short-range-order struct., electron diffr. meas. 79−15047
$Cr_xPd_{82-x}Ge_{18}$, amorphous, RF sputtered, elec. resist. and magnetoresist., Kondo type behaviour 78−76066
$Cr_xPd_{82-x}Ge_{18}$ amorphous alloys, magnetoresist., mag. susceptibility, magnetisation 78−80148
Cu-Ag-Ge, Hume-Rothery glass form. 80−96449
Cu-Ge, α-phase, lattice sp. ht. calcs. 80−65246
Cu-Ge, conc. single crystal, yield region investigation, flow stress and obstacle charact. 78−3173
Cu-Ge, dil., impurity electron struct., self-consistent KKR Green's function calc. 79−78040
Cu-Ge, dil., magnetic susceptibility, impurities effect, free electron gas model 79−91206
Cu-Ge, dil., magnetic susceptibility, impurities effect, Fermi surface effects 79−91207
Cu-Ge, dil., Matthiessen's rule deviations above room temp. 79−91023
Cu-Ge, dil., optical props. and electronic struct. 78−35164
Cu-Ge, dil., point defect props., density functional approach 80−29013
Cu-Ge, dil. alloy, thermopower and resistivities, validity of Nordheim-Gorter relation 78−91671
Cu-Ge, dilute solid soln., exam. of recrystallisation and stored energy 78−52836
Cu-Ge, disordered, phonon dispersion curves, inelastic neutron scatt. study 79−51223
Cu-Ge, dissoc. dislocations pinning by Suzuki effect *(French)* 79−100223
α-Cu-Ge, Fermi surface, high resolution positron annihilation study 78−6261
Cu-Ge, lattice dynamical meas. and anal. *(Russian)* 77−62599
Cu-Ge, liq., hard-sphere struct. factors 77−51301
Cu-Ge, liq., mag. susceptibility, diamag. 78−72326
Cu-Ge, liq. alloy, thermodynamic activity meas. by Knudsen-cell mass spectrometry *(French)* 80−10684
Cu-Ge, liq. and solid, positron trapping 78−48255
Cu-Ge, microconductors, cast, struct. and physical props. exam 78−44232
Cu-Ge, primary coplanar slip, role in deform. of FCC crystals *(Japanese)* 77−52412
Cu-Ge, single cryst., dislocation motion obstacles, effective strength 80−15107
α- Cu-Ge, superconducting transition temp. depend. on electron per atom ratio, lattice deform. 77−8222
Cu-Ge, system, atomic struct. and electronic props. *(Russian)* 77−20289
Cu-Ge, thermal expansion, X-ray determ. 78−26697
Cu-Ge, thin films, elec. cond., Ge influence 79−82690
Cu-Ge (0.44 to 7.3 wt.%), concentrated single crystal, yield region investigation, CRSS, slip 77−48478
Cu-Ge (0.7 or 1.5 at.%), stacking fault energies, weak beam method of electron microscopy 77−19971
Cu-Ge (1 at.%), FCC crystal, stress-strain curve, stage I to stage II transition *(Japanese)* 78−19834
Cu-Ge (10-12 wt.%), intermediate ξ'-phase form. during deform. *(Russian)* 78−19747
Cu-Ge (2 wt.%), positron annihilation, photon ang. distrib. meas. effect of deformation, annealing temp. *(Russian)* 78−35220
Cu-Ge (5 at.%), single crystal, Bridgman growth, neutron diffraction topographic obs. of layer substructure 79−27938
Cu-Ge (8 wt.%), anelastic effect due to deform. twins *(Japanese)* 79−20095
Cu-Ge (8.7 at.%), pulse duration effects in shock hardening 77−12644
Cu-Ge (8.7 wt.%) pulse duration effects on shock hardening 78−80561
Cu-Ge (8.7 wt.%) shock hardening behaviour at very short pulse durations 78−80560
Cu-Ge alloy film, electron transport props. 77−76955
Cu-Ge alloys, equilib. defects *(German)* 79−86789
Cu-Ge codeposited film, elec. resist. and thermoelec. power, rel. to struct. 79−87168
Cu-Ge film, thermoelec. power, 80-350K 78−68096
Cu-Ge single cryst. containing heavily faulted regions, X-ray diffr. profiles 80−24462
Cu-Ge solid soln., isotope effect for Ge diffusion 78−2285
Cu-Ge-Fe, Mossbauer effect of Fe impurities 78−31131
Cu-Ge-Te system, DTA, crystallographic and metallographic analysis *(French)* 77−25019
Cu-Nb-Ge, phase relations and diffusion layer form. 77−36458
CuGe (1 wt.%), stress removal during annealing after hydrostatic extrusion 79−83215
$Cu_{0.87}Ge_{0.13}$, α-phase, photoelectron meas., impurity level 78−35247
Fe-Ge, amorphous, atomic struct., neutron diffr. study 80−59392
Fe-Ge, characteristic energy losses and optical props. 80−29834
Fe-Ge, dil., mag. hyperfine fields, Curie temp. and Mossbauer meas. 77−63190
Fe-Ge, dil., XPS meas. 77−63538

germanium alloys continued
Fe-Ge, interface struct. and growth mechanism from melt 79−14715
Fe-Ge, liquid alloy, thermodynamic mixing function determ. by mass spectrometric meas. 79−29025
β-Fe-Ge, mag. props. from X-ray, magnetisation and Mossbauer meas. 79−42755
Fe-Ge, solid and liq. paramag. props. *(Russian)* 77−66247
Fe-Ge amorphous alloys, radial distrib. funct., electron diffr. exam. 77−68922
Fe-Ge amorphous films, conversion electron Mossbauer spectra, mag. moments 77−16231
Fe-Ge melts, struct. determ. 79−41940
Fe-Ge system, cryst. growth forms and interface struct. 79−61515
Fe-Ni-Co-Mo-Ge alloy 40NKM, excess mag. noise after various thermomag. treatments *(Russian)* 80−29575
Fe-Ni-Ge, liquid alloy, H_2 thermodynamic interaction, solubility *(Russian)* 78−11202
Fe_3Al-Ge, ternary ordered solid soln., formation by substitution 77−43177
$Fe_{80}B_{20-x}Ge_x$, amorphous, effect of metalloids on mag. props. 79−11304
$Fe_{80}B_{20-x}Ge_x$, amorphous, mag. saturation, spin wave stiffness, temp. depend. 80−75741
$Fe_{80}B_{20-x}Ge_x$, amorphous, size effect of metalloids on mag. props. 80−84594
$Fe_{80}B_{20-x}Ge_x$ glass, magnetisation, Curie and crystn. temps. 79−87289
FeGe, cubic, spin reson., 4.2-300K, 3-35 GHz 79−38384
FeGe, hexagonal, low-temp. mag. struct., neutron diffr. meas. 78−95418
FeGe, hyperfine interactions of ^{119}Sn atoms, Mossbauer spectra *(Russian)* 80−29665
$FeGe_2$, amorphous film, annealing effects on struct. and elec. resist. 77−85099
$FeGe_2$, antiferromag., Fermi surface, stress effects, oscillatory magnetostriction and torque meas. 80−103616
$FeGe_2$, antiferromagnet, de Haas-van Alphen effect 79−4505
$FeGe_2$, collinear and canted antiferromag. structures 77−51887
$FeGe_2$, Fe_2Ge, optical consts., electron energy loss spectra meas. 77−90121
$FeGe_2$, Fermi surface press. depend., de Haas-van Alphen method 77−43478
$FeGe_2$, mag. struct., Mossbauer method 78−60268
$FeGe_2$, single cryst. perfection depend. on growth rate and direction 80−55284
$Fe_{1.67}Ge$, Mossbauer and X-ray expts. 79−1734
Fe_3Ge, ^{119}Sn mag. hyperfine interaction, Mossbauer spectra *(Russian)* 79−38420
Fe_3Ge amorphous films, short-range struct., electron diffr. obs. 77−24267
Fe_3Ge, mag. props. of cubic and hexagonal phases 77−8475
Fe_5Ge_3, collinear mag. struct. from Mossbauer effect meas. 77−63343
Fe_5Ge_3 film, electron diffr. study of struct. and microheterogeneity 77−85108
β-Fe_5Ge_3 formation in isothermal sintering, phase transition kinetics 80−89197
Fe_xGe_{1-x}, amorphous, conversion electron Mossbauer spectra down to 4.2K 80−7205
Fe_xGe_{1-x}, amorphous, mag. behaviour, rel. to Fe_xSi_{1-x} and Fe_xSn_{1-x} amorphous alloys 78−95478
Fe_xGe_{1-x}, amorphous alloy, short range order anal. 77−80423
Fe_xGe_{1-x} amorphous alloys, conversion electron Mossbauer spectroscopy 78−84504
Fe_xGe_{1-x} amorphous alloys, high field mag. meas. 79−82765
Fe_xGe_{1-x}, amorphous film, FMR meas. of mag. props., temp. and comp. depend. 77−69636
Fe_xGe_{1-x} amorphous film, low temp. conversion electron Mossbauer spectroscopy 78−48101
Fe_xGe_{1-x} amorphous film, XPS and Mossbauer exam. 79−56577
Fe_xGe_{1-x}, liq., ang. distrib. of positron annihilation 77−55848
$Fe_{80}P_{20-x}Ge_x$, amorphous, size effect of metalloids on mag. props. 80−84594
$(Fe_{1-x}V_x)_3Ge$, magnetic and X-ray studies 80−1966
Ga-Ge, liq., enthalpy of form., direct reaction calorimetry, 713-1230K *(French)* 79−66336
Ga-Ge-Sn, thermodynamic props. of mixing of binary systems, phase diagram 80−45275
Ga-Ge-Zn ternary alloys, thermodynamic props., EMF meas. 80−81033
GaAs/Au-Ge/Ni, Schottky barrier energy var. with interdiffusion 77−20435
Gd-Ge amorphous films, spontaneous Hall effect and elec. resist. 80−80251
GdCuGe, $Gd_6Cu_8Ge_8$ and $GdCu_2Ge_2$, magnetic props. 77−32180
$(Ge,Si)_{1-x}Y_x$, Y=H,B,P,..., amorphous struct., kinetically determined topological model 79−55666
Ge-Ag, exam. of structure using electron microscope *(Russian)* 79−14738
Ge-Al (1.15 wt.%), US wave vel. meas. for anal. of solid soln. breakup 78−23887
Ge-Al film, amorphous, EPR meas. 78−80212
Ge-Al film, elec. resist. and IR transmission, comp. and substrate temp. depend. 78−52112
Ge-Al(Cu), alloying effects on elec. transport props. of amorphous and crystalline Ge films 79−51689
Ge-Au eutectic alloys, field ion sources 80−97414
Ge-Ce liquid alloys, enthalpies of mixing, exothermal effects *(Russian)* 80−34192
Ge-Co, liq., enthalpy of formation meas. 80−30267
Ge-Cu, liquid, solubility of O_2 at 1373K, in equilibrium with GeO_2 78−44109
Ge-Cu (0, 23, 40 at.%), amorphous film struct. *(German)* 78−95391
Ge-Cu film, amorphous, EPR meas. 78−80212
Ge-Fe, liq., enthalpy of formation meas. 80−30267
Ge-FeS, density of alloys 77−51473
Ge-Ga, segregation of Ga due to barometric mol. diffusion in gravitational, centrifugal fields 78−14472
Ge-Ga (1.13 wt.%), US wave vel. meas. for anal. of solid soln. breakup 78−23887
Ge-Ga alloys, amorphous, far IR absorption 78−88306
Ge-Ga amorphous alloy, co-evaporated elec. and optical props. 80−70860
Ge-Ga liq. alloys, thermodyn. props. 78−26695
Ge-GaP system, phase analysis 78−23674
Ge-InP system, phase analysis 78−23674

germanium alloys continued
Ge-metal film, polycryst., struct. props. determ. 79−4494
Ge-metal films codeposited, amorphous and polycryst., struct. and elec. props. 80−24766
Ge-Mn, liq., calorimetric investigation of heats of mixing, and entropies of mixing 79−95165
Ge-Ni, amorphous, struct., EXAFS study 80−49110
Ge-Ni, liq., enthalpy of formation meas. 80−30267
Ge-Ni, smooth and continuous ohmic contact to n-GaAs 78−68086
Ge-rare earth alloys, nature of chemical interaction, X-ray emission, absorpt. and photoelectron study *(Russian)* 80−55261
Ge-Sb, eutectic alloy, exam. of morphology during solidification *(Russian)* 79−34022
Ge-Sb eutectic alloy, crystallisation in electric field *(Russian)* 77−52311
Ge-Sb liq. alloys, SRO 78−22632
Ge-Se-Fe films, metallic and semicond., amorphous, mag. and elec. props. 78−52319
Ge-Si-Sb solid soln., distrib. of components in universal furnace expt. in Soyuz-Apollo programme *(Russian)* 78−31381
Ge-Sn, liq. alloys, thermodyn. props. 77−51518
Ge-Sn barrier Josephson tunnel junctions 78−68114
Ge-Sn barriers, Josephson tunnelling 79−28468
Ge-Sn solid solution, cooling rate effect on partition coeff. of Sn between liq. phase and crysts. 77−12510
Ge-Sn-M, M=Cu, As, Sb, formation of Ge-based solid solns. during crystallisation 77−80625
Ge-Sn(In) melts, short-range order, radial atomic distrib. functions 79−86673
Ge-Te, Ge-As-Te molten system, metal-semicond. transition, cond. obs. *(German)* 77−1457
Ge-Te, liq. alloy, heat of formation, 1030-1150K 77−1943
Ge-Te alloy, liq., magnetic susceptibility 79−87232
$Ge_{0.6}Cu_{0.2}Au_{0.2}$ film, superconducting transition temp., resistivity meas. 77−43774
GeS-FeS, density of alloys 77−51473
GeSi alloy, composition determ. by ellipsometry 79−83537
GeTe, effect of phase transition on mech. and elec. props. 77−51746
Hf-Ge-B system, phase equilibria 78−35356
$HfGe_2$ film, supercond. obs. 77−72939
Ho_5Ge_4, mag. struct., neutron diffr. study 80−25093
In/Au-Ge ohmic contact to GaAs, solid phase epitaxy formation 79−60658
In-Ge film, random percolation, elec. resist. meas. 79−28418
La-Ge, amorphous, alloying effect on supercond. props. 79−60951
$LaGe_2$ film, supercond. obs. 77−72939
$LaGe_x$, specific heat in range $0.07 \leq T \leq 10K$, comp. depend. 78−43517
Mg-Ge, X-ray spectra, electronic struct. *(Russian)* 77−48279
Mg-Li-Ge, phase diagram, isothermal cross section *(Russian)* 80−20900
Mg_2Ge, L, electron-phonon interaction and phonon cond. at low temp. L n-type semicond. 79−14903
Mg_2Ge, semicond., electronic band struct., reson. Raman scatt. meas. 77−12384
Mg_2Ge, three-phonon relaxation rate and phonon conductivity 78−14416
Mg_2Ge, valence band, XPS meas. 77−8018
Mn-Ge, antiferromagnetic, NMR exam. 77−16193
Mn-Ge (10.3 to 15.5 wt.%), reversible memory of form, X-ray diffr. expts. *(Russian)* 79−5006
Mn-Ge (5 to 90 at.%) liquid alloy, electrical resistivity *(Russian)* 77−55509
Mn-Ge amorphous films, short-range order, electron diffr. obs. 80−39473
MnAlGe film, mag. domains and amorphous to cryst. phase transition, electron microscopy obs. 80−71129
MnGaGe film, mag. domains and amorphous to cryst. phase transition, electron microscopy obs. 80−71129
MnGe, amorphous, spin glass transition, AC susceptibility meas. 80−75779
Mn_2Ge_7, high-temp. phase, X-ray powder cryst. struct. *(German)* 80−39005
Mn_3Ge, elec. and mag. props. *(Russian)* 77−76792
Mn_3Ge, triangular spin ordering, weak ferromagnetism 79−47237
Mn_3Ge_2, $Mn_{11}Ge_8$, amorphous thin films, quasieutectic model, electron diffr. investigation of short range order 79−69013
Mn_3Ge_2, textured, thermal expansion, 158K transformation *(Russian)* 77−32196
Mn_5Ge_3-Mn_5Si_3, electrical resistivity meas., order-disorder transition 80−10945
MnNiGe, coupled nature of mag. and struct. transition under press. 79−8033
$MnNiSi_{1-x}Ge_x$, mag. props. 77−12118
$Mn_xPd_{82-x}Ge_{18}$ amorphous alloys, elec. resistivity and magnetoresistivity 79−51543
$Mn_xPd_{82-x}Ged_{18}$, amorphous alloys, mag. props. 78−91906
$Mn_5(Si_{1-x}Ge_x)_3$, magnetic and cryst. struct., ferromag. props. 77−59391
$Mn_5(Si_xGe_{1-x})_3$ solid solution, mag. ordering, magnetisation and neutron scatt. meas. 78−27023
Mo-Al-Ge, new compounds, structure and props. 80−39003
Mo-Al-Ge, phase equilibria, X-ray and microstructural anal. 80−93536
Mo-Ge, amorphous supercond. alloy, produced by coevaporation, struct. and supercond. 79−91179
Mo-Ge amorphous films, supercond. transition temp. and residual elec. resist. *(Russian)* 79−19680
Mo-Ge-B, phase diag., struct. of $Mo_{1.7}Ge_{0.3}B$ 77−52285
$MoGe_2$-Mo diffusion couple, nucleation of $Mo_{13}Ge_{23}$ *(French)* 77−55398
$Mo_{13}Ge_{23}$, nucleation in Mo-$MoGe_2$ diffusion couples *(French)* 77−55398
Mo_3Ge, A15 cpd., normal state, low temp. resist. 80−107762
Mo_3Ge, RF sputtered, supercond. crit. temp. 78−14853
Mo_3Ge, superconductivity, T_c related to disorder and density of states 79−15249
Nb-Al-Ge film, superconductor, high rate sputter deposition and heat treatment 77−36399
Nb-Al-Ge-Cu, rapidly quenched, comp. and phase equilib. 80−76235
Nb-Ga, A15 phase, chem. deposition on Hastelloy substrate, for superconducting tape *(German)* 80−104071
Nb-Ge, A-15 compound formation by ion implantation 78−51572
Nb-Ge, A15 struct. superconductor, high field transport props. TEM study 80−34574

germanium alloys continued
Nb-Ge, amorphous supercond. alloy, produced by coevaporation, struct. and supercond. 79−91179
Nb-Ge, amorphous supercond. alloy, resistivity, transition temp. 80−60126
Nb-Ge, compounds with A15 structure, films, TEM study *(French)* 80−80135
Nb-Ge, fast quenching of A15-phases *(German)* 77−36014
Nb-Ge, supercond., high press.-high temp. treatment, phase props. 77−28746
Nb-Ge, supercond. A-15 phase, supercond. transition temp. after ion implantation 80−49972
Nb-Ge, supercond. film, prep. and props. *(Russian)* 77−66218
Nb-Ge, superconductivity film prod. by electron beam sputtering *(Russian)* 78−15308
Nb-Ge, superconductor, phase diagram determ. using various methods up to temp. of 2200°C 79−8414
Nb-Ge, supersuperconducting transition temp., correl. with resist. anomalies and defect struct. 77−47920
Nb-Ge, thermal anal. of levitation-heated samples 79−2772
Nb-Ge, transition metal atom stabilised superconductivity 79−7924
Nb-Ge alloys, stoichiometry and phase equilibria, X-ray diffr. study *(French)* 79−70040
Nb-Ge and Nb-Ge-Si, A15 cpds., CVD prep. and supercond. crit. temp. 79−60949
Nb-Ge film, CVD and sputter deposited, critical current density and stability 77−28327
Nb-Ge film, coevaporated, supercond. critical temp. and struct. 77−28275
Nb-Ge film, phase transformations due to annealing, electron diffr. study 80−54551
Nb-Ge film, supercond., TEM expts., correl. of struct. and elec. props. 78−14628
Nb-Ge film, supercond., two-phase, tetragonal Nb_5Ge_3 phase identification by electron diffr. 77−89665
Nb-Ge film, supercond. transition temp., rel. to prep. conditions 77−36009
Nb-Ge supercond. thin film characterisation by ion scatt., ion-induced X-rays, and ion resonance 77−40617
Nb-Ge system, phase diagram determ. 79−38796
Nb-Ge system, reaction diffusion, electron probe anal. 79−28152
Nb-Ge vapour deposited films with T_c of ~20K, preps. *(Japanese)* 77−12048
Nb-Ge-C, phase equilib. and supercond. 80−50593
Nb-Ge-Cu, phase equilib. and supercond. props. *(Russian)* 80−40332
Nb-Ge-Ni, phase composition and superconducting props., influence of Ni *(Russian)* 80−20898
Nb-Ge-Si, A15 struct. superconductor, high field transport props. TEM study 80−34574
Nb-Ge-Si, compounds with A15 structure, films, TEM study *(French)* 80−80135
Nb-Ge-Si, Si effect on raising superconducting transition temp. in pelicular specimens *(Russian)* 78−23188
Nb-Ge-Si, supercond. state transition temp., influence of Si on alloy constitution *(Russian)* 79−78244
Nb-Ge-Si film, CVD, struct., comp., stability and homogeneity 80−15421
Nb-Ge-Sn A15 cpds., CVD, superconductivity 79−38222
Nb-Ge-Sn(Pt)(Ir), A15 cpds. prod. by liq. quenching, phase stability and supercond. props. 79−95538
Nb-Nb_3(Al,Ge) multifilamentary supercond., fabrication and props. 77−20480
Nb-Si-Ge, ductile amorphous, superconductivity 80−60131
Nb_3(Al,Ge), liq. quenched, supercond. props. 80−84580
Nb_3(Al,Ge) supercond., diffused layer critical current depend. on Cu before and after annealing *(Russian)* 79−69643
Nb_3(Al,Ge) superconducting wire, improved fabrication method 77−28763
Nb_3Al-Nb_3Ge-Nb_3Ga system, supercond. crit. temps. 77−8218
$Nb_3Al_{0.76}Ge_{0.24}$, supercond. props. of cold worked core wires an basis of A15 phases 77−85369
$Nb_3Al_{0.8}Ge_{0.2}$, supercond., sp. ht. meas. 77−28296
$Nb_3Al_{0.83}Ge_{0.21}$, A-15 phase, sp. ht. meas. 79−19689
$Nb_3Al_{1-x}Ge_x$, RF sputtering synthesis, supercond. transition temp. variation 77−81216
Nb_3(Ge,Si) A15 film, supercond. and structural props. 79−87177
Nb_3(Ge, X), X=Si, Ga, CVD tapes, supercond. props. at high mag. fields 79−38279
$NbGe_2$ single crysts., elec. resist. and superconductivity 79−38233
$NbGe_2$, superconducting transition temp. meas. of sputtered films and bulk 80−7019
$Nb_{0.82}Ge_{0.18}$, structural and supercond. props. press. effects 80−39700
$Nb_{1-x}Ge_x$, supercond., mag. field props. 80−54822
Nb_3Ge, A-15 diffusion layers, influence of additions of growth and supercond. props. *(German)* 80−11130
Nb_3Ge A15 cpd., bulk modulus 80−7611
Nb_3Ge, A15 cpd., normal state, low temp. resist. 80−107762
Nb_3Ge, A15 superconductor, rel. between transition temp. and density of states 79−15247
Nb_3Ge, amorphous and crystalline A-15 phases 78−83896
Nb_3Ge, amorphous film, supercond., flux flow resist., vortex pair dissoc. 80−88701
Nb_3Ge amorphous films, microstruct. X-ray small angle scatt. study 79−14685
Nb_3Ge, amorphous films, thermally-activated internal friction peaks, structural obs. 80−80147
Nb_3Ge amorphous films, X-ray diffr. analysis of microstruct. 78−72035
Nb_3Ge, amorphous nongranular thin superconducting film, thermodynamic and resistive transitions 80−34571
Nb_3Ge, anomalous resistivity, insight from band theory 78−60106
Nb_3Ge, α-particle irrad., supercond. transition width 78−23193
Nb_3Ge, α-particle irrad., relationship between density of states and supercond. transition temp. 79−42684
Nb_3Ge, bridge contact, Josephson effect 80−70906
Nb_3Ge, CVD, AC losses, temp. depend., 4-20K 77−28311
Nb_3Ge, CVD, hysteretic losses, precipitates and deposition temp. effects 77−28319
Nb_3Ge, CVD, impurity doping effect on supercond. crit. props. 78−52174
Nb_3Ge CVD tapes, supercond. props. at high mag. fields 79−38279
Nb_3Ge, CVD-prepared, high field props. and scaling 79−56455
germanium alloys continued
Nb_3Ge coevaporated film, high supercond. transition temp., nucleation and growth 80−76185
Nb_3Ge composite filament, continuous, high-strength, prep. and supercond. props. 77−28765
Nb_3Ge, composition effects on T_c 77−76993
Nb_3Ge continuous supercond. tape, prep. by CVD 77−80893
Nb_3Ge, crit. current density temp. depend. 77−47951
Nb_3Ge, DC sputtered films, annealing and mech. deform. effects on struct. and supercond. props. 79−38217
Nb_3Ge, density of states from critical field meas. 79−42690
Nb_3Ge, disordered superconductor, T_c depression by acoustic plasmon overdamping 80−7020
Nb_3Ge, effect of ^{16}O and ^{32}S ion irrad. and thermal recovery on T_c, residual resist. and slope of crit. field 79−56348
Nb_3Ge, electron energy loss spectra, AES and HEED investig. of surface 77−24635
Nb_3Ge, electron irradiation at cryogenic temps., effect on T_c and transport props. 78−52122
Nb_3Ge, electron-lifetime effects on props. 80−10951
Nb_3Ge, electronic struct. calcs. 79−47005
Nb_3Ge, electronic struct., electron-phonon interactions, and low temp. anomalies 79−60701
Nb_3Ge, epitaxial growth of polycryst. films with high supercond. transition temp. 77−63015
Nb_3Ge film, CVD, thermal expansivity, X-ray diffr. meas. 78−6166
Nb_3Ge film, CVD fabrication of supercond. tape for high-field magnets 78−95698
Nb_3Ge film, CVD on inside of Cu tube, AC losses 77−28312
Nb_3Ge film, critical current density and flux pinning 77−20510
Nb_3Ge film, EXAFS meas. 78−2935
Nb_3Ge film, electron beam co-deposited, prep. and supercond. crit. temp. 78−15310
Nb_3Ge film, far IR reflection and transmission spectra, room temp. 77−55792
Nb_3Ge film, growth by co-evaporation in O_2, critical temp. enhancement 77−28273
Nb_3Ge film, high-temp. supercond. phase stabilisation w.r.t. prep. conditions *(Russian)* 80−70871
Nb_3Ge film, in supercond. proximity sandwich, energy gap struct., appl. to electron-phonon spectra 79−56401
Nb_3Ge film, low temp. sputter deposition 78−48315
Nb_3Ge film, nucleation of high-T_c phase in presence of impurities 78−88054
Nb_3Ge film, prep. by coevaporation, supercond. props. 78−91830
Nb_3Ge film, prepared by cosputtering, supercond. props. 79−4634
Nb_3Ge film, sputtered, chemical composition versus lattice parameter a_o and supercond. transition temp. relations 77−43771
Nb_3Ge film, sputtered and evaporated, transition temp., critical field and current anisotropy 77−28328
Nb_3Ge film, supercond., intercorrelations between composition, lattice parameter a_0 and T_c 77−8217
Nb_3Ge film, supercond., electron beam codeposition in O_2, Cl_2 or air, phase diagram 77−28728
Nb_3Ge film, supercond., TEM obs. of microstruct. foil prep. method 77−55642
Nb_3Ge film, supercond., epitaxial growth on Nb_3Ir and Nb_3Rh substrates 78−80473
Nb_3Ge film, superconductive, crit. temp., resistivity, structure depend. on comp. 78−6470
Nb_3Ge film, superconducting, A-15 type, getter-sputtering with controlled additions of O 78−88427
Nb_3Ge film, superconductivity, relevance of mag. interactions, EPR study 80−100545
Nb_3Ge film, T_c var. with ^4He irrad. induced defects 77−8220
Nb_3Ge films, correl. between crit. current density and microstruct. 79−38277
Nb_3Ge films, form. of A15 phases by DC sputtering 79−38740
Nb_3Ge films, prep. by DC sputtering and solid state diffusion, supercond. props. and struct. 79−38212
Nb_3Ge, granular supercond., simple model for resistive-nonresistive transition 78−72298
Nb_3Ge, high pressure and temp. treatment effect on supercond. props. *(Russian)* 77−1512
Nb_3Ge, high T_c film with impurity expanded lattice, form. and stabilisation 79−56099
Nb_3Ge, high T_c films, electron tunnelling and AES anal. 79−28471
Nb_3Ge, high T_c supercond., anal. of X-ray traces 79−56098
Nb_3Ge, high-T_c supercond., apparent T^2-depend. of normal-state resist. and lattice sp. ht. 77−47921
Nb_3Ge, hysteretic losses in parallel AC and DC mag. fields 79−87217
Nb_3Ge, inhomogeneous superconductor, scaling laws for pinning forces 79−47214
Nb_3Ge, low fluence alpha irradiation, behaviour of supercond. transition temp. 78−43510
Nb_3Ge, low temperature electron, neutron irrad. effects on critical temp. *(French)* 80−75669
Nb_3Ge, metallic bonding, electronic states calcs. 78−79916
Nb_3Ge, metallic glass, internal friction peak obs. 78−79666
Nb_3Ge, neutron irradiated, A15 compound, recovery of T_c by annealing 78−52132
Nb_3Ge, ordered and disordered A15 phases, energy gaps, tunnelling 77−8235
Nb_3Ge, plasma energies, tight-binding energy-band model 78−84159
Nb_3Ge, RF and DC sputtered films comparison, O content effect 78−72022
Nb_3Ge, RF sputtered film, high superconducting transition temp. 77−59346
Nb_3Ge RF sputtered films, amorphous atomic scale struct. 80−84064
Nb_3Ge, resistivity and T_c measurement after low temp. neutron irradiation 78−52123
Nb_3Ge, sputter-deposited, superconducting T_c and phase relationship 79−56344
Nb_3Ge sputtered and evaporated, struct.-depend. anisotropy of supercond. crit. currents 79−38292
Nb_3Ge sputtered film, struct. and superconducting props. 77−28337
Nb_3Ge sputtered films, Ge surface segregation exam. by AES 79−56084
Nb_3Ge, sputtered on Cu, film-substrate interface obs. by electron microscopy 80−65398
Nb_3Ge, structural and supercond. props. press. effects 80−39700
Nb_3Ge, supercond., elec. resist., phenomenological model 77−43775

germanium alloys continued
Nb_3Ge, supercond., projected upper limits to crit. current density 77−36037
Nb_3Ge, supercond., single phase, sp. ht. meas., 4-29K 78−72307
Nb_3Ge, supercond. film, amorphous content, X-ray diffr. study, rel. to transition temp. 80−75668
Nb_3Ge, supercond. film, CVD, crit. temp., crit. current density 78−76204
Nb_3Ge, supercond. film, electron beam codeposition, synthesis and props. 78−72296
Nb_3Ge supercond. film, of high transition temp., US attenuation 80−49991
Nb_3Ge, supercond. film, prep. by chem. transport reaction, critical props 79−47635
Nb_3Ge, supercond. sputtered film, ion scatt., AES, depth profiling 77−11806
Nb_3Ge, supercond. tape, growth technique via amorphous state 78−84708
Nb_3Ge supercond. thin films, He- and Ar-irradiated, X-ray diffr. studies 80−29503
Nb_3Ge, supercond. transition temp., rel. to A15 phase stability 78−52137
Nb_3Ge, superconducting, high crit. temp., prep. *(Japanese)* 79−78914
Nb_3Ge, superconducting, optical props. and electron-phonon interactions 80−2510
Nb_3Ge, superconducting A-15 type compounds, transition temp., radii ratio and structure *(Chinese)* 80−44752
Nb_3Ge superconducting film, α-particle induced defects and stoichiometry 77−32101
Nb_3Ge superconducting films, tunnelling obs., X-ray and electron diffr. obs. 77−32123
Nb_3Ge superconducting film, CVD deposited, second phase (tetragonal Nb_5Ge_3) rel. to critical current 77−32131
Nb_3Ge superconducting film preparation and props. 79−11515
Nb_3Ge superconducting films, role of O_2 in form. of struct. *(Russian)* 79−60950
Nb_3Ge superconducting film, crit. temp. correl. with resist. relations and film struct. *(Russian)* 80−15646
Nb_3Ge superconducting films, high critical temp., optimum sputtering conditions 80−15647
Nb_3Ge superconducting films, quantitative Auger anal. 80−55740
Nb_3Ge, superconducting hybridisation and bonding, XPS exam. 78−2988
Nb_3Ge superconducting long tapes, CVD prepared, high current densities at 20 T 79−33436
Nb_3Ge, superconducting thin films, energy gaps from tunnelling meas. 80−25050
Nb_3Ge superconductivity film, Nb_5Ge_3 and NbO content, X-ray diffr. obs. 80−2515
Nb_3Ge tape, prepared continuously by CVD, props. 78−60257
Nb_3Ge tape, supercond., prep. by continuous CVD process 78−11121
Nb_3Ge tape conductors, strain depend. of crit. current density 79−38278
Nb_3Ge:H film, sensitivity of supercond. transition temp. to H content 78−47894
Nb_3Ge-based superconducting alloys, upper critical field temp. depend. *(Russian)* 78−10622
Nb_5Ge_3, 0.30K supercond. transition temp. meas. with 0.14K transition width 78−6468
Nb_xGe_y, film deposition by ion beam methods 78−72728
$Nb_3Ge_xAl_{1-x}$, ternary supercond. alloys, comp. variations 80−97022
$Nb_3Ge_{1-x}Ga_x$ CVD films, supercond. transition temp. depend. on lattice parameter 79−38219
$Nb_2Ge_{1-x}Ga_x(Sn_x)$ CVD films, supercond. props., 4.2 to 19K 79−42713
$Nb_3Ge_{1-x}M_x$ (M=Ga,Sn), pseudo-binary, scaling laws for supercond. crit. currents 79−24118
$Nb_3Ge_{0.8}Nb_{0.2}$, A-15 type struct. and order parameter 79−77552
$(Nb_{0.99}Mo_{0.01})_{1-x}Ge_x$, supercond. transition temp. and crit. field 79−38220
$(Nb_{1-y}Mo_y)_3Ge$ system, composite transition metal atom supercond. 77−39984
$Nb_3(Nb_{1-x}Ge_x)$, impurity stabilised A15 supercond., transition temp., lattice consts., specific heat 80−93026
Nb_3Sn, effect on critical temp. for supercond. of disorder, induced by α-particles 78−47897
$(Nb_{0.99}Ti_{0.01})_{1-x}Ge_x$, supercond. transition temp. and crit. field 79−38220
$(Nb_{0.99}Ti_{0.01})_{1-x}Ge_x$, supercond., mag. field props. 80−54822
$(Nb_{0.99}Zr_{0.01})_{1-x}Ge_x$, supercond. transition temp. and crit. field 79−38220
$(Nb_{0.99}Zr_{0.01})_{1-x}Ge_x$, supercond., mag. field props. 80−54822
$(Ni,Co)_3Ge$, Co effect on temp. depend. of yield stress 78−31487
$(Ni,Co)_3Ge$, single cryst., Co effects on temp. depend. of yield stress 77−4812
Ni-Ge, amorphous, atomic struct., neutron diffr. study 80−59392
Ni-Ge, band model of high temp. magnetism 78−26809
Ni-Ge, dil., ferromagnetic, hyperfine field and relax. time obs. of impurity heavy nuclei 80−75533
Ni-Ge, dil., mag. props. at elevated temps. 77−63089
Ni-Ge, liq., density and surface energy, temp. depend., 1000-1700°C *(Russian)* 77−15662
Ni-Ge, liq. alloy, thermodynamic activity, mass spectrometric determ. *(German)* 78−20052
Ni-Ge , defect-solute interactions and radiation-induced segregation 80−25705
Ni-Ge (1 to 9 at.%), twinning stress used to eval. stacking fault energy of pure Ni *(Japanese)* 78−59820
Ni-Ge (2 at.%), vacancy cluster form. during deform. positron lifetime meas. 79−56882
Ni-Ge alloys, liq., integrated emissivity, electric resistivity 78−43155
Ni-Ge binary system, phase diagram rel. to that of Co-Ge *(French)* 80−97463
Ni-Ge-Au evaporated contacts on GaAs, TEM obs. 80−75449
Ni-Ge-Au/GaAs cathode struct., with enhanced injection efficiency, contact resist. 77−20431
Ni-Pd-Ge, phase relationships and struct. 77−36451
$(Ni_xCo_{1-x})_3Ge$ single crysts., $L1_2$ struct., cross-slip 80−40459
NiGe, and Ni_2Ge, amorphous film, electron diffr. exam. of struct. 77−35828
NiGe, Ni_2Ge and Ni_3Ge, X-ray spectrum analysis energy band struct. *(Ukrainian)* 77−52200
$Ni_{0.625}Ge_{0.375}$, amorphous film, crystn. mechanism *(Russian)* 77−51623

germanium alloys continued
Ni_3Ge, amorphous film, electron diffr. exam. of struct. 77−35827
Ni_3Ge single crystal, cleavage fracture 79−61694
Ni_3Ge single crystal, yield stress, temp. and orientation depend. 77−90432
Ni_3Ge single crystals, orientation and temp. depend. of flow stress 79−5008
Ni_3Ge, temp. depend. of mech. props. *(Russian)* 79−38895
Ni_3Ge-Fe_3Ge solid soln., flow stress, transition from positive to negative temp. depend. 80−60906
Ni_5Ge_3, amorphous and cryst. films, opt. props. in interband absorpt. region 80−66315
Ni_5Ge_3, amorphous film, elec. resist., microstruct. and annealing 77−85188
Ni_5Ge_3, amorphous-crystalline transition, opt. and elec. charact. *(Russian)* 77−85191
Ni_5Ge_3, solid and liquid, physicochemical props. and structure 80−39548
$Ni_{74}Ge_{26}$, ordered BCC phases at high temp. 79−32948
Ni_xGe_{1-x}, liq., ang. distrib. of positron annihilation 77−55848
NiMnGe, crystal and spiral mag. struct., Neel temp., X-ray and neutron diffr. 77−16052
NiMnGe, mag. struct., and mag. phase transitions 77−63187
$NiPt_NGe_{N'}$, cryst. struct. *(German)* 80−44171
NpM_2Ge_2 (M=Cr, Fe, Co, Ni, Cu), Mossbauer and magnetisation meas. 77−1555
Pb-Ge amorphous films, supercond. transition temp. and residual elec. resist. *(Russian)* 79−19680
Pb-Ge thin film alloy, critical currents near metal-insulator transition 79−65626
Pd-Ge, metallic glass, theoretical studies on structural models 79−37633
Pd-Ge glass, short range order obs. for $Pd_{80}Ge_{20}$ and $Pd_{78}Ge_{22}$, EXAFS expts. 78−55815
Pd-Ge metallic glass, appl. of EXAFS methods for struct. determ. 79−37624
PdGe, dissociation in presence of Pd film 79−47892
PdGe, Pd_2Ge, growth kinetics and structure on Ge substrate 79−11514
Pd_2Ge, PdGe, growth kinetics on single cryst. and evaporated Ge 78−22985
$Pd_{21}Ge_8$, cryst. struct. *(German)* 78−18586
Pd_5Ge, cryst. struct. and cryst. binding *(German)* 78−42958
Po-Ge film, random percolation, elec. resist. meas. 79−28418
$PrCu_2Ge_2$, magnetic props. 77−32180
Re_5Ge_3, RF sputtered, supercond. crit. temp. 78−14853
Rh_2MnGe, ferromag. Heusler alloy, hyperfine mag. field meas. by TDPAC technique 79−78580
Rh_2MnGe, hyperfine mag. field at Cd impurity, TDPAC study 80−39905
Sb-Ge, unidirectionally solidified, exam. of compressive props. and struct. 78−68730
Sb-Ge (1.2 to 2.2 at.%), carrier transport, magnetoresistivity, field-dependent tensor study 80−39609
Si-Ge, solid soln., vol. effect on bulk modulus 80−24526
Si_xGe_{1-x}, amorphous, vibr. props. 79−23693
Sn-Ge, liquid alloy, exam. of activity and heat of mixing, using mass spectrometry 78−51706
$TaGe_2$, superconducting transition temp. meas. of sputtered films and bulk 80−7019
Tb_5Ge_4, mag. struct. and mag. transitions, neutron diffr. expts. 78−43564
Te-Ge eutectic alloy, glassy, crystn. mechanism 78−22836
Ti-Nb-Ge foils, β phase decomposition, electron microscopy struct. investigation *(Russian)* 79−83172
Ti-Nb-Ta-Ge (40,20,0.8 wt.%) foil, dispersion hardening, TEM and electron diffr. obs. *(Russian)* 79−1873
TiGe, and TiCoGe, electronic struct., X-ray K- and L-spectra obs. *(Russian)* 78−11022
TiGe, $TiGe_2$, Ti_5Ge_3, X-ray K- and L-bands, electronic struct. *(Russian)* 79−1797
Ti_xGe_y, interrelationship of X-ray charact. with physical props. *(Russian)* 77−1765
UGe_3, compensated metal, topological props. of Fermi surface, magnetoresist. meas. 78−6350
UGe_3, de Haas-van Alphen effect, band struct. calc. 78−72068
UGe_3, spin fluctuation phenomena, band struct. calcs. and de Haas-van Alphen meas. 77−20225
UGe_3, thermoelectric power, 5-300K 79−65444
UGeS, mag. props., 4.2-300K 78−10667
UGeSe, mag. props., 4.2-300K 78−10667
UGeTe, mag. props., 4.2-300K 78−10667
UIr_2Ge_2, cryst. struct. 80−1964
$(V,Fe)_3Ge$, solid soln. form. and supercond. T_c *(Russian)* 78−80512
$(V,Nb)_3Ge$ solid solns., supercond. T_c, absolute thermal EMF, microhardness 77−36006
V-Al/Cu-Ge composite superconductors, transition temp. and upper crit. field, heat treatment effects 79−38268
V-Al/Cu-Ge composite tape, transition temp., upper crit. field 78−68126
V-Ge, fast quenching of A15-phases *(German)* 77−36014
V-Ge-C, phase equilib. and supercond. 80−50593
V_3 Ge, superconducting filament formation near edge dislocation *(Russian)* 79−4635
$V_3(Fe,Ge)$, struct. and supercond. transition temp. *(Russian)* 79−7920
V_3Ge, A-15 compounds, interlattice displacements, elastic consts. 78−55906
V_3Ge, A-15 cpds., nucl. mag. relax. in normal and supercond. state 80−49993
V_3Ge, A-15 struct. supercond., microhardness, bonding 78−76199
V_3Ge, A15 cpd., hydrogenation effects on supercond. transition temp., lattice parameters 80−103772
V_3Ge, Anderson-Gruneisen parameter, from 3rd order elastic const. data 79−33059
V_3Ge, anisotropic thermal vibrations, lattice const. X-ray study 80−34164
V_3Ge, band theory, semiself-consistent band calcs. 78−2406
V_3Ge, bronze-processed, stress-induced enhancement of supercond. T_c 78−64159
V_3Ge, electron-phonon coupling and supercond. crit. temp. 79−33379
V_3Ge, electronic struct., electron-phonon interactions, and low temp. anomalies 79−60701
V_3Ge, electronic struct. calcs. 79−47005
V_3Ge film, T_c var. with ^4He irrad. induced defects 77−8220

germanium alloys continued
V_3Ge, forbidden Bragg refls., rel. to supercond. transition temp. 79−15251
V_3Ge, Gruneisen parameter and thermal expansion eval. at room temp. 80−70351
V_3Ge, low temp. props., mag. suscept. and resistance 78−19213
V_3Ge multifilamentary superconductor, formation by composite diffusion process, and crit. temp. determ. 77−85959
V_3Ge, phonon densities of states and Debye temp. calcs. 79−51212
V_3Ge, phonon density of states, temp. depend. 79−42183
V_3Ge, plasma energies, tight-binding energy-band model 78−84159
V_3Ge, resist. charact. in normal state 78−51963
V_3Ge, superconducting, high transition temp., sputtering 78−15309
V_3Ge, superconducting A-15 type compounds, transition temp., radii ratio and structure *(Chinese)* 80−44752
V_3Ge superconducting film, α-particle induced defects and stoichiometry 77−32101
V_3Ge, superconducting transition temp. and electron density of states 77−32105
V_3Ge, superconducting transition temp., correl. with resist. anomalies and defect struct. 77−47920
V_3Ge, third order elastic consts. 78−88490
$V_3Ge_xOs_{1-x}$, low temp. props. 79−99652
V(Nb)-Ge-Cu, rapidly quenched, comp. and phase equilib. 80−76235
V_3Si, supercond. tape, growth technique via amorphous state 78−84708
V_3Si-Ge, cryst. struct., supercond. T_c comp. depend. 78−51494
V_3Si-Ge solid soln., supercond. T_c and paramag. susceptibility *(Russian)* 77−59348
$V_3Si_{1-x}Ge_x$, elastic props., 77 to 290K, rel. to supercond. transition temp. *(Russian)* 80−66560
$V_3Si_{1-x}Ge_x$ solid soln., longitudinal and transverse US wave propag. rate, 4.2 to 300K *(Russian)* 80−103423
W-Ge-B, phase diag. 77−52285
YGe_2 film, supercond. obs. 77−72939
$YbNi_2Ge_2$, intermediate valence cpd., mag. susceptibility expts., 4.2-280K 78−39288
Zn-Ge, eutectic, stereomorphology using SEM, TEM and optical microscopy *(Russian)* 79−52187
Zr-Ge-B system, phase equilibria 78−35356
Zr-Nb-Ge, singularities of $\beta \rightarrow \omega$ transform. in alloy, with high content of β-stabiliser *(Russian)* 78−76644
ZrGe, film, supercond. obs. 77−72939
$ZrGe_2$, RF sputtered, supercond. crit. temp. 78−14853

germanium compounds
see also germanium alloys
binary, with chalcogenides and pnictides, at. vol. and semicond. props. 77−20089
bis-methyldigermyl chalcogenide, ^1H and ^{13}C NMR study, chemical shifts 80−71201
chalcogenide amorphous film, effects of alloying chalcogen atoms 80−49670
chalcogenides, screw dislocations in layer crystal growth from vapour *(Russian)* 80−1953
chalcohalide glasses of Ge-As-S-I system, acousto-optical parameters 77−36199
chloromethylgermane, polycryst., proton spin-lattice relax. times meas. 78−39430
germanate analogues of gehlenite, synthesis and physicochem. props. 79−43181
germanates, XPS *(Japanese)* 80−16154
halides, XY_4 molecules, force consts. by modified Redington and Aljibury method 80−69261
hexa(trifluoromethyl) germanium, gas and liq., IR and Raman spectra, normal coord. anal. *(German)* 79−72315
holomethylgermanes, internal torsion modes, inelastic neutron scatt. 77−19105
LPE growth, saturation magnetisation, collapse field, bubble diameter 78−95703
$M^IM^{IV}IO_6$, vibr. spectra (M^I=Na,K,Rb,Cs,NH_4; M^{IV}=Ge,Sn,Pb) 77−42325
metal-GeS-metal system, current-voltage characts., band struct. effects in field emission region 79−42667
monochalcogenides, interaction of outer s states 79−10825
monochalcogenides interaction of internal s states 79−10826
optical fibres, GeO_2-$B_2O_3SiO_2$, ageing effects of moisture on fatigue and tensile strength 80−66539
optical fibres, ultratrace impurities determ., and behaviour during production by CVD process *(Japanese)* 80−87505
$Pb_5Ge_3O_{11}$:Gd^{3+}, ESR spectra, electric-field effect and reversible permittivity 80−29614
phthalocyanine, elec. cond. temp. depend. 80−80271
sulphide compounds of Si, Ge and Sn, struct. and chem. bonding *(French)* 78−30580
tetra(trifluoromethyl) germanium, gas and liq., IR and Raman spectra, normal coord. anal. *(German)* 79−72315
tetrahalides, isotope shifts, Coriolis coupling and force consts., isotope substitution and matrix isolation 77−42322
tetrahalides of Gp.IV elements, M-X bond flexibility, by compliance scheme 80−37805
tetramethyl germanium, methyl reorient., lattice vibrs., neutron scatt. obs. 79−51016
transition metal germanium borides, metallic resist. mag. suscept. 79−42731
tri(trifluoromethyl) germanium halides, gas, liq. and solid, IR and Raman spectra, normal coord. anal. 79−72316
triphenylgermanium isocyanate, X-ray crystal struct. determ. and refinement 77−7708
tris(trimethylgermyl)phosphine, gamma irrad., free radicals, struct. and EPR spectra 80−29623
$3Al_2O_3$-GeO_2-SiO_2, reduction by C, mixed diffusional-kinetic regime *(Russian)* 80−66771
$3PbO.GeO_2$, X-ray and electron diffr. exam. *(German)* 80−11632
Ag-Ge-S glasses, X-ray determ. of struct. *(Japanese)* 80−10501
Ag-Ge-Te system, chalcogenide, phase equilibria and diagrams *(German)* 80−108418
$Ag_8GeS_6(Se_6)(Te_6)$, absorpt. edge investigs. at phase transitions 78−35149
Ag_8GeTe_6, optical props. and polymorphism 80−45082
Al-Ge-SiO solar selective absorber surfaces, optical behaviour at high temp. 80−101130

germanium compounds continued
$AlGe_3N_3$-GaAs structures and MISFETs based on them 79−60932
As-Ge-Se, and As-Ge-Se-Sb glasses, acousto-optic props. 77−27327
As-Ge-Se based glasses, refr. index, 1-11 μm 78−39520
As-Ge-Se chalcogenide glass, mode-guiding layer in IR microwaveguides 80−28329
As-Ge-Se system, synthesis and phys. props. of amorphous layers 77−52252
As-Ge-Se system glasses, alkali-free, optical absorpt. 79−65883
As-Ge-Te, chalcogenide glass, elec. cond. and dielec. const. 80−75567
As-Ge-Te glass, dielectric meas. 79−87382
As-S-Se-Ge semiconducting glasses, IR charact. *(Czech)* 80−25332
As-Se-Ge, amorphous film, relief-type hologram mode, hologram replication *(Japanese)* 78−78959
As-Se-Ge film, master for hologram copying 78−29912
As-Se-S-Ge chalcogenide glass films, appls. to passive optical waveguide components 79−37048
As-Se-S-Ge chalcogenide amorphous film, computer-generated holograms using electron beam irrad. 80−95846
As-Se(Te)-Ge, fabrication of amorphous semicond. thin films with graded band struct. *(Japanese)* 77−55623
As-Te-Ge chalcogenide films, thermally induced transformations, TEM obs. 79−94917
As-Te-Ge system glasses, thin films, effect of S, Se, Sb, Bi, Tl on volt-ampere characts. 77−15976
As-Te-Ge/n-Si, film on cryst., heterojunction, elec. and photovolt. props. 80−100514
As-Te-Ge-Si sandwich type amorphous films with metal electrodes, space-charge-limited switching, pre-breakdown characts. *(Japanese)* 77−69385
As-Te-Si-Ge amorphous chalcogenide semiconductor, thin film interface, elec. charact. *(Korean)* 80−97014
$As_{10}Ge_{15}Te_{75}$, glass, cond. and switching characts. 77−32054
$As_{10}Ge_{15}Te_{75}$:Ag glasses, elec. props. 79−91045
$As_{25}Ge_{10}Te_{65}$, chalcogenide glasses, dielectric relaxation 80−55027
$As_xGe_{10}Te_{90-x}$ glass, cond. and dielec. const. from 77 to 383K and from DC freq. to 5 MHz 79−23964
$As_{10}Ge_{15}Te_{75}Ag_x$ glass, elec. and dielec. props., Ag additions effect 80−65558
$(As_2S_3)_{1-x}(GeS_2)_x$ and $As_2S_3Ge_x$ glasses, struct. and vibr. spectra 79−91440
$(As_2S_3)_{1-x}(GeS_2)_x$, LF inelastic light scatt. meas. 78−15181
$(AsSI)_x(GeS_2)_{1-x}$ glasses, Raman and long-wave IR spectra obs. of struct. 79−51964
As_2Se_3-Ge glassy thin films, flash photoresponse 80−107863
As_2Se_3-$GeSe_2$ glass, bulk and impurity IR absorpt. 80−71455
As_2Se_3-$GeSe_x$-$SnSe_x$ (x=1,2), exam. of Sn valency and physical props. 79−4753
$As_{10}Se_{67.5}Ge_{22.5}$, film as master for PVC copied holograms 77−23632
As_4Se_5Ge glass, struct. changes, Mn^{2+} EPR expts. 78−79534
$As_{40}Se_{50-x}S_xGe_{10}$ film strip-loaded waveguide formed in graded-index $LiNbO_3$ planar waveguide 78−74965
$As_{10}Te_{75}Ge_{15}$, dielec. props. 77−63355
$(As_2Te_3)_{1-x}Ge_x$, amorphous, AC cond. magnitude and variation *(French)* 79−47095
As_4Te_5Ge glass, struct. changes, Mn^{2+} EPR expts. 78−79534
$As_{45}Te_{40}Ge_{15}$, amorphous, elec. cond. at room temp., contact effect 77−20354
$As_xTe_{90-x}Ge_{10}$, $As_{35}Te_{55}Ge_{10-x}Si_x$ glasses, elec. and optical props., comp. depend. 77−24555
$As_{35}Te_{28}Ge_{16}S_{21}$, chalcogenide semiconductor study of electric properties *(French)* 80−29414
$As_{0.3}Te_{0.48}Ge_{0.1}Si_{0.12}$, amorphous film, transient switching processes 78−84232
$As_{30}Te_{48}Si_{12}Ge_{10}$, chalcogenide glass film, charge screening length 79−23974
Au-Ge-Te ternary system, solid soln. in vicinity of GeTe, phase diagram *(French)* 77−85994
B_2O_3-PbO-GeO_2-Fe_2O_3 glasses, mag. props. and Mossbauer spectra, spero-mag. order at low temps. 80−80530
$BaGeF_6$, Group IV hexafluoride anion radical γ-irrad., EPR spectra 78−72411
BaO-GeO_2 system, phase equilibrium diagram 79−70047
BaO-GeO_2-Na_2O borosilicate core glasses for high numerical aperture fibres 80−69534
BaO-GeO_2-Na_2O-H_2O system, hydrothermal crystn., phase formation laws 79−46636
BaO-TiO_2-GeO_2, subsolidus equilibria 77−86014
$BaO.GeO_2.5H_2O$, X-ray cryst. struct. determ. *(German)* 79−69067
$Bi_{12}GeO_{20}$, Czochralski single crystal growth 79−1823
$Bi_{12}GeO_{20}$ substrate, for interdigital transducer *(Czech)* 80−19201
Bi_2O_3-GeO_2, melt struct. model 80−33870
Bi_2O_3-GeO_2, metastable phases form., crystn. conditions, melt viscosity and density effects 80−35167
$Ca_3Ga_2Ge_3O_{12}$, appl. as substrate for mag. bubbles 77−28418
$Ca_3Ga_2Ge_3O_{12}$, substrate, electron examination of microstruct. and microsegregation 78−67919
$Ca_2Ge_2(GeO_4)(Ge_4O_{12})$, cryst. struct., X-ray anal. 80−19783
$3CaGeO_3.H_2O$, synthesis, IR spectra 77−43986
$Ca_4(Ge_3O_{10}).H_2O$, cryst. struct. determ. 79−90627
CaO-SiO_2/GeO_2-H_2O system, phase relations, influence of Si/Ge isomorphous substitution 79−52180
$Ca_5[GeO_4]_2(OH)_2$ monoclinic cell struct., crystallographic consts. 79−82191
Cd-Te-Ge system, CdTe-Ge cross section 77−52298
$CdGeAs_2$, electron irradiated, change in electrical props. 79−7829
$CdGeAs_2$, phase matched fourth harmonic generation, cascade process contrib. 79−76761
$CdGeAs_2$, polarised IR reflectivity, optical modes, optical phonons 77−69836
$CdGeAs_2$, ternary semiconductor crystals for nonlinear optical applics. 78−33782
$Cd_{23}Ge_{12}As_{65}$, amorphous, threshold switching, expt. 80−49830
$Cd_6Ge_3As_{11}$, band gap, DC cond., elastic consts., and glass transition temp., pressure depend. 78−72064
$(CdGeAs_2)_{1-x}D_x$ amorphous films, property control in common target sputtering, elec. cond. 80−7494
$CdGe(As_{1-x}P_x)_2$, crystal growth, phase studies, optical props. 78−48305
$CdGeP_2$, cond. compensation by electron bombardment 79−15151
$CdGe(P_xAs_{1-x})_2$, glass, static current-voltage characteristics *(Russian)* 77−15925

germanium compounds continued
$CdGe_{1-x}Sb_xAs_2$ system, amorphous and cryst. phases, DTA and microhardness obs. 78−22835
Cl_4, He(II) photoelectron spectra, spectral intensity patterns 79−98152
Co-Ge-Te system, phase equilib. 80−20908
Co_2GeO_4, hydrothermal growth from CoO-GeO_2-H_2O 77−48329
$Co_2Ge_2Te_3$, struct., resist., and thermo-EMF 80−20908
$CoTe_2$-GeTe, phase diagram, from thermal, X-ray, microstructural analyses 80−55367
Cu-Ge-O, phase diagram and thermodynamics, electrochem. study 80−50617
Cu-GeO_2/BaO-Cu thin film, amorphous, effect of electroforming on conductance and capacitance 80−34537
$CuInS_2(Se_2)$-$GeS_2(Se_2)$, degree of solid solubility and phases charact. 78−35377
Cu_2S-GeS_2 and Cu_2S-SnS_2 systems dissoc. of ternary congruently melting cpds. 79−87832
$Cu_2S(Se)$-GeS, phase diagrams 78−44100
Cu_2Se-GeSe quasibinary system, phase diagram and struct. 77−8802
Cu_2Se-$GeSe_2$ and Cu_2Se-$SnSe_2$ systems, dissoc. of ternary congruently melting cpds. 79−87832
Cu_2Te-$GeTe_2$, phase equilib., microstructural, DTA investigs. 77−16560
EuS-Ga_2S_3-GeS_2, chalcogenide glasses, conditions of form. of glassy prod. *(French)* 80−100325
G_2-B_2O_3 melt, thermodynamic props. from mass spectroscopy 80−39318
$GE_{40}S_{60}$-Ag glass, EPR exam. 78−23334
Ga-Ge-Se chalcogenide glasses, rare earth element doped, elec. props. 80−96885
Ga-Ge-Te system, GaGeTe formation, peritectic decomp. and struct. *(French)* 77−85995
GaAs solar cell fabrication, using AMOS tech., single and polycrystalline cells 78−39935
GaAs-$Ge_{1-x}(GaAs)_x$ n-p heterojunctions, hydrostatic press. effect on elect. and photoelectric props. 80−20304
GaSb-GaAs-Ge system, props. and struct. 80−20232
GaSb-Ge eutectic alloy, effect of crystallisation rate on microhardness 79−96110
$(Ge,Pb)_{1-x}Mn_xTe$, mag. and elec. props. meas. 80−29534
Ge-As, p-T-x diagram 77−11669
Ge-As, supersaturated solid soln., dislocation form. during thermocyclic treatment *(Russian)* 80−3057
Ge-As-Se, amorphous film, condensation formation and struct. props. *(Russian)* 78−38629
Ge-As-Se, and Se-Ge glasses, for IR appl., prod. using H_2 distillation 77−32551
Ge-As-Se films, light irrad., heat treatment rel. to optical props. *(Russian)* 79−4858
Ge-As-Se glass, appl. to 8 to 12 μm thermal imaging system 78−25935
Ge-As-Se glasses, elastic moduli, US vel. and reson. freq. meas. 78−23756
Ge-As-Se IR transmitting glass composition, prep. and props. 80−69474
Ge-As-Se system glasses, thermal capacity, 300-600K 79−65210
Ge-As-Se-Te glasses for 8-12 μm IR optics 80−69475
Ge-As-Te, thin chalcogenide glass film, high-field switching effects 77−32052
Ge-As-Te glass, between metal electrodes, contact props. determ. 79−7908
Ge-As-Te glass, thermoelec. power and DC cond., temp. depend. 77−62955
Ge-As-Te system, glasses, magnetochemical exam. 78−88092
Ge-Bi-S system, semicond., elec. cond., glass transition temp. and optical absorption meas. 77−16329
Ge-Bi-S system glasses, opt. props. and glass transition temp. 77−77224
N-Ge-Bi-Se glass, elec. and optical props. 80−65550
Ge-Bi-Te system, thermal cond. change during phase transitions 80−100368
Ge-Fe amorphous films, mag. and elec. props. 79−51695
Ge-GaSb, metastable continuous solid solutions 79−8284
Ge-GeO_2, MIS struct., electrophysical charact. 79−82680
Ge-GeO_2, optical charging memory, influence of doping GeO_2 with metal ions *(Russian)* 79−24077
Ge-GeO_2 boundary, electrophysical parameters *(Russian)* 77−85327
Ge-GeO_2 MIS structure, growth of GeO_2 from liq. phase *(Russian)* 80−40273
Ge-GeO_2 mixtures, gasification kinetics and GeO form. mechanism *(Russian)* 80−21273
Ge-GeO_2 system, optical charge memory obs. 77−89871
Ge-I_2, equilibrium study 700 to 1300K, vapour transport rate of Ge *(French)* 78−64476
Ge-In-Ga system, microscopic and X-ray phase anal. 77−12606
Ge-In-Te system, homogeneity region, struct., electrophysical props. 78−44091
Ge-In-Te system, region of solid soln. of In in GeTe 77−51499
Ge-O cpds., bond lengths rel. to force consts. 77−46653
Ge-P-S glass system, EPR of intrinsic and Mn^{2+} impurity centres 80−88870
Ge-P-Se system, glasses, semicond., density, microhardness, softening point rel. to conc. 77−7674
Ge-P-Se system glasses, penetration by indentor, activation parameters, microhardness 79−43419
Ge-Pb-S, glassy, photoconductivity dependences applied elec. field 80−107857
Ge-Pb-Se-Te, glass form., DC cond., and mole volume 79−90560
Ge-S, amorphous, photocond., photo-induced ESR, optical edge shift 80−49809
Ge-S, Ge-S-Ag, amorphous prop. and origin of paramagnetic defects 79−10801
Ge-S, glass, ESR, model of paramag. defects 79−78517
Ge-S amorphous film, defect states, ESR 80−49670
Ge-S film, amorphous, photo-induced ESR and optical absorption edge shift 78−88374
Ge-S glass, melt-quenched photoinduced ESR, annealing behaviour and glass comp. depend. 80−71156
Ge-S glasses, Cu doped, thermal, structural and dielectric props. 79−60283
Ge-S glasses, EPR study 78−43644
Ge-S system glasses, thermal expansion coeff. and free vol. at transition temp. *(Japanese)* 79−55876
Ge-S-Ag glasses, bulk and film, EPR study 78−43644
Ge-S-Cu, phase separation in melt centrifugal quenching 80−25701
Ge-S-Ga amorphous thin film, memory switching effects 80−88605
germanium compounds continued
Ge-S-Ga(In) system glasses, photoinduced changes 80−24365
Ge-S-In, chalcogenide glass, determ. of glass phases, phys. props. meas. 79−23526
Ge-S-Sb glasses, microgravity effect on recrystn., optical and elec. props. 80−49127
Ge-S-Se, glass formation 80−103251
Ge-S-Se system, glass-forming, struct. and props. 80−19713
Ge-S-Te system, glass forming 80−19718
Ge-S(As)-Se, solubility, photostimulated changes 80−24602
Ge-Sb-S-I, chalcogenide glass film, prep. by laser evaporation, and characterisation 77−12533
Ge-Sb-Se glass, elec. props, comp. depend. 80−70697
Ge-Sb-Se glass, physical props., purification method for Sb, Se from surface oxides 78−46735
Ge-Sb-Se system glasses, thermal capacity, 300-600K 79−65210
Ge-Se, glassy, photoinduced photolum. fatigue *(Russian)* 78−60520
Ge-Se based glasses, refr. index, 1-11 μm 78−39520
Ge-Se films, laser-beam recordings by thermal creation of holes 80−35010
Ge-Se glass, effect of Ag electrodiffusion on volt-ampere characteristics 79−7869
Ge-Se glass, elastic props. under press., US interferometry 78−79658
Ge-Se glass, vibr. props., Raman and IR spectra obs. *(Japanese)* 77−43989
Ge-Se glass film, photoinduced absorpt. changes 79−87519
Ge-Se glass system, effect of changes in local surrounding of atoms on optical props. *(Russian)* 78−80414
Ge-Se glasses, radiative localised centres, photoluminesc. 79−83025
Ge-Se liquid solutions, glass-forming, viscosity 77−66036
Ge-Se system glasses, thermal expansion coeff. and free vol. at transition temp. *(Japanese)* 79−55876
Ge-Se-Fe films, metallic and semicond., amorphous, mag. and elec. props. 78−52319
Ge-Se-Fe phase system, amorphous films, mag. and elec. props. 79−51695
Ge-Se-Ga thin film, elec. cond., switching phenomena *(Polish)* 80−11120
Ge-Se-Ga(In) system glasses, vitreous phase struct. 77−76320
Ge-Se-Te amorphous alloys, prep. and calorimetric obs. 77−11675
Ge-Se-Te glasses, form. region, elec. props. 79−94904
Ge-Si, electron irradiation and annealing 77−55305
Ge-Si cpds., short-range order, effect on valence band and direct optical gap 77−59252
Ge-Si single crystals, heat treated, hot carrier thermo-EMF 77−24575
Ge-Si solid solution film, elec. props. in range 4.2 to 500K 77−8214
Ge-Si system alloys, growth by Czochralski method, morphology 77−15329
Ge-Si-S system, glass formation, transition temp., crystallisation and melting 80−100178
Ge-Sn-As system alloys, microstruct., X-ray phase and thermal anal. 77−32564
Ge-Te, exam. of new compound, using light microscopy and X-ray diffr. exam. 78−48383
Ge-Te alloy films, amorphous, semicond. props., refr. index, struct. study 78−26978
Ge-Te and Ge-Te-As system glasses, local struct., ^{119}Sn Mossbauer obs. 79−41968
Ge-Te binary glass, eutectic, DSC obs., thermodynamic and thermokinetic charact. 80−39309
Ge-Te film, electrical switching 77−4411
Ge-Te films, laser-beam recordings by thermal creation of holes 80−35010
Ge-Te Ge-As-Te molten system metal-semicond. transition, cond. obs. *(German)* 77−1457
Ge-Te system, microstruct. in phase transform. region 79−52177
Ge-Te system, phase equil. diagram, $GeTe_{1\pm x}$ region analysis by metallography, microhardness and DTA *(French)* 77−70034
Ge-Te-As-In quaternary compounds, elec. resist. of thin sheets, Mott's theory *(Spanish)* 77−69320
Ge-Te-As-In quaternary compounds, elec. props., Hall effect *(Spanish)* 77−69344
Ge-Te-As-In quaternary compounds, thin sheets elec. props., thermoelec. power *(Spanish)* 77−69358
Ge-Te-Se/Si amorphous film-cryst. heterojunction, electron-beam-induced current 79−24060
Ge+$GeBr_4$, single crystal+vapour system, reaction kinetics and laws of soln., heat of adsorption 79−39196
Ge+H^+, K-shell ionisation cross-sections calcs. 80−43165
$Ge_{1.5}$, high-resistivity, uniform and space charge polarisation, thermally stimulated depolarisation anal. 78−15085
Ge_xAl_{1-x} amorphous film junction, I-V and C-V charact. 77−85307
GeAs, oxidation, hardness and electromechanical polishing response 80−71776
GeAs+$Cl_2^1(Br_2)(I_2)$, high temp. Raman spectra, cryst. growth mechanism *(French)* 79−26999
$Ge_{100-x}As_x$ glass, elec. props. 77−76966
GeAsS, X-ray photoelectron spectra, valence electrons density of states *(Russian)* 79−15583
$Ge_xAs_xS_xSe_{100-3x}$ and $Ge_xTe_xS_xSe_{100-3x}$ glasses, IR absorpt. spectra 77−12378
$Ge_{33}As_{27}S_{15}Te_{25}$, chalcogenide thin films, coupled carrier theory test, high field conditions 80−100466
$Ge_{33}As_{27}S_{15}Te_{25}$ glass, switching, microstructural changes 79−65523
$Ge_{0.3}As_{0.7}Se_{0.5}$, IR optic materials, characteristics *(German)* 80−38081
$Ge_xAs_xSe_{100-2x}$, x=2.5 and 5.0, chalcogenide glasses, IR absorpt. spectra 77−24842
$Ge_{10}As_xTe_{90-x}$ glass, thermal cond., 100-500K, and sp. ht., 373-600K 77−20138
$Ge_{15}As_4Te_8$, film, influence of electric field on crystallisation kinetics 78−42914
$Ge_{15}As_4Te_{81}$ glassy film, nonlinear current voltage charact., Poole-Frenkel effect 80−7007
$Ge_{10}As_{40}Te_{40}I_{10}$, chalcogenide glass film, switching delay time 78−26926
$Ge_{10}As_{40}Te_{40}I_{10}$, threshold switch, high resist. state 77−15924
$Ge_{30}As_{17}Te_{30}Se_{23}$, antireflection coating for KCl, design, prep. and performance 79−14063
$Ge_{30}As_{17}Te_{30}Se_{23}$-$As_2S_3$, two-layer antirefl. coating, error considerations in design 80−74477
$Ge_xAs_xTe_xSe_{100.3x}$, glassy, IR absorpt. spectra 78−23448
n-$Ge_{20}Bi_{10}Se_{70}$ glass, preparation and elec. props. 79−74126

germanium compounds continued
$Ge_{20}Bi_xSe_{80-x}$, semicond. glass, resist., thermoelec. power, optical absorpt. 80−88555
$Ge_{20}Bi_xSe_{70-x}Te_{10}$, n-type semiconducting glasses, resistivity and thermoelectric power meas. 80−54695
$Ge_{20}Bi_xSe_{70-x}Te_{10}$, semicond. glass, resist., thermoelec. power, optical absorpt. 80−88555
$GeBi_2Te_4$, Hall const., thermoelec. power, and elec. cond. 80−29407
$GeBr_4$, electronic struct., Xα SW calcs. 80−102447
$GeBr_4$, fine struct. resolution in Raman-active fundamentals 79−42967
$GeBr_4$, liq., reference interaction site model and struct. 80−70106
$GeBr_4$, vac. UV absorpt. spectra, 130-270 nm 77−75183
GeC_x, amorphous, prepared by glow discharge method, elec. and optical props. 77−21035
GeCl, mol., UV spectra, band assignments and rot. consts. 80−997
$GeCl_2$, combined electron diffr. and mass spectra mol. struct. determ. 79−89783
$GeCl_4$, atomic phase shifts calc., appl. of EXAFS 77−48276
$GeCl_4$ hydrolysis and oxidation kinetics for graded-index fibre vapour phase axial deposition 80−48477
$GeCl_4$, liq. struct., oscill. amp., neutron diffr. study 79−46544
$GeCl_4$, liq. struct. by neutron diffr. 79−73089
$GeCl_4$, vac. UV absorpt. spectra, 250 to 115 nm 77−79628
$GeCl_4$, X-ray absorpt. spectra struct. 80−37819
GeF, $A^2\Sigma^+$ state, time-resolved fluoresc. 78−58732
GeF, use in chemical lasers 80−64004
GeF_2, force consts., mean amplitudes of vibr. 78−17647
GeF_2, vibr. anal., kinetic consts. method 80−18838
GeF_4, ($GeCl_4$), X-ray absorpt. spectra struct. 80−37819
GeF_4, cryst., Raman spectra at 77K, scatt. angle, polaritons and space group 78−23439
GeF_4, electronic struct., Xα SW calcs. 80−102447
GeF_4, $\nu_3(F_2)$ IR band contour, isotopically pure cpds., mol. consts. 77−61746
GeF_4, sign of rot. g-factor, mol. beam expt. 79−59600
GeF_4, X-ray absorpt. spectra struct. 80−37819
GeF_6^{2-}, bond order and Raman intensity, delta function eqn. 77−61693
$GeFe_2O_4$, single crysts., elec. and mag. props, optical absorpt. spectra 80−54719
$Ge_{0.8}(GaAs)_{0.2}$, metastable solid solns., decomp. kinetics 79−38789
$Ge_{1-x}(GaAs)_x$, metastable solid solution, fine struct. *(Russian)* 79−27960
$Ge_{1-x}(GaSb)_x$, metastable solid solution, fine struct. *(Russian)* 79−27960
$(Ge_{1-x}Ga_x)_{1-x}Te$, rhombohedral and cubic phases, transport effects 78−2481
GeH_2, centrifugal-distortion dipole moment, CO_2 laser spectroscopy 77−75331
GeH_2, struct. determ., restricted HF calcs. 80−87030
GeH_3^-, electronic struct., electron affinity, inversion barrier, ab initio SCF Gaussian basis calc. 80−63552
GeH_3-group containing mols., normal coord. anal. 80−9579
GeH_4, abundance in Jupiter atm. from IR spectrum anal. 78−61791
GeH_4, avoided-crossing molecular-beam spectroscopy, hyperfine and spin rot. const. and rot. g factors determ. 80−78671
GeH_4, crystalline, determ. of mol. symm. from IR spectrum 78−9969
GeH_4, Doppler-free optical double reson. spectroscopy using single-freq. laser and modulation sidebands 80−68274
GeH_4 force consts. by modified Redington and Aljibury method 80−69261
GeH_4, heat capacity, dielectric const., thermodynamic props. 78−83967
GeH_4, IR laser sideband obs., ro-vibr. struct., isotope shifts, line widths 79−72306
GeH_4, IR spectra, Jovian atm. absorpt. profile, computer simulation 78−81584
GeH_4, IR spectra of ν_3 band, molecular const. determ. *(French)* 77−462
GeH_4, IR-microwave double reson., rot. assignments 77−75190
GeH_4, laser sideband spectroscopy *(German)* 79−26975
GeH_4, Lorenz-Lorentz coeff., refr. index, crit. consts. and density depend. 78−92041
GeH_4, microwave spectra of Q-branch, rot. consts. 79−54845
GeH_4, ν_3 and 2 ν_3 bands, high resolution IR spectra, rel. to Jovian atm. 78−37636
GeH_4, ν_3 fundamental, theoretical absolute J-manifold intensities 78−74707
GeH_4, orbital valency force field 77−34779
GeH_4, possible microwave interstellar maser lines 78−41020
GeH_4, relativistically parameterized extended Huckel theory 79−49924
GeH_4, solid, IR spectra 77−36226
GeH_4, Stark effect, rot. transitions in vibr. ground state, isotope shift 79−27029
GeH_4, tetrahedral mol., force field calcs. 78−29734
GeH_4, ν_2 fundamental, isotope effect 80−43024
GeH_4, vibrational state rotational struct., CARS spectra *(Russian)* 80−99513
$^{74}GeH_4$ mol. vibr., IR and CARS spectra *(Russian)* 80−102509
$^{74}GeH_4$, transition moment for ν_3, rel. to Jovian atmosphere 79−72363
GeH_4:$SiHD_3$, symmetries of GeH_4 cryst. phases, IR spectra meas. 79−19886
GeH_4+Cl_2, HGeCl* chemilum. obs., vibr. levels 77−81406
Ge_2H_6, rot. barriers, MS-SCF-X_α calcs. 80−106267
Ge_2H_6, valence electronic struct., model pot. in floating spherical GO formalism 78−74563
$Ge(HAsO_4)_2.H_2O$, cryst. struct. 78−26552
$GeH_4(F_4)$, rot. mag. moment spectra, mol. beam mag. reson. obs. 77−14509
GeH_3NCS, liq. and solid, IR and Raman spectra 79−89663
$(GeH_3)_3P$, vibr. force fields and amplitudes zero point, structs. 77−54551
$Ge(HPO_4)_2.H_2O$, cryst. struct. 78−26552
$(GeH_3)_2S$, UV spectra, assignments 78−46359
GeH_3X, (X=F,Cl,Br,I), force fields and consts., Redington's method calcs. 80−58130
GeH_3X, mol. consts. calcs. 79−36606
GeH_3NCS, mol., IR, Raman and microwave spectra, $^{70,72,74}Ge$ and $^{1,2}H$ isotopes 79−89663
GeI_2, ^{127}I NQR freqs. meas. 80−58285
GeI_x, thermodyn. props. 78−23960
$(Ge_{1-x}In_x)_{1-x}Te$, rhombohedral and cubic phases, transport effects 78−2481

germanium compounds continued
$Ge_{1-x}Mn_xTe$, magnetic behaviour of Mn 78−14938
Ge_3N_4 CVD film prod. and Al-Ge-Ge_3N_4-Al structure V-I and V-C characteristics *(Russian)* 78−47893
Ge_3N_4 films, synthesis and principal props. 77−24960
Ge_2N_2O, pressure induced tetrahedral tilting and deform. 80−24415
Ge_2N_2O, time-of-flight neutron diffr. study 79−19200
$Ge_xNi_{1-x}O$, crystallographic and elec. props. 77−32011
GeO amorphous film, hologram recording, photochem. props. 79−64186
GeO amorphous semicond. films, photostructural changes by photomodulation ellipsometry 79−71510
GeO film, optical props., rel. to possible appl. in holography 80−29816
GeO, Franck-Condon factors and r-centroids of A-X band system 77−65513
GeO, mol., VUV photoelectron spectra, $X^2\Sigma^+$ state 79−72358
GeO, population inversion of electronic levels by oxidation, visible emission 78−13697
GeO, produced in Ge+N_2O reaction, kinetics of chemilum. emitter form. and quenching 78−63107
GeO, RKRV Franck-Condon factors and r-centroids, ($A^1\Pi$-$X^1\Sigma^+$) transition, pot. energy curves 78−29817
GeO, supermultilayer dielectric film, elec. strength *(Russian)* 77−85648
GeO, UV spectra of mol., rot. anal. 79−81210
GeO:Cr, dielectric thin film, transmission and EPR spectra 77−69676
GeO_2, amorphous, obtained by hydrolysis of $GeCl_4$, exam. of props. 79−95956
GeO_2 amorphous, phonon frequency distrib. 78−30723
GeO_2, α-quartz structure, compression mechanism 79−23673
GeO_2, band struct., tight-binding calc. 80−24796
GeO_2 doped gradient optical fibres, pulse dispersion *(German)* 80−74496
GeO_2, electronic struct., photoemission spectra calc. 77−35865
GeO_2, electronic struct. and densities of states, tight-binding calcs. 80−15447
GeO_2, film, optical and electrophysical props. *(Russian)* 77−85821
GeO_2 films, memory switching phenomena 79−82650
GeO_2, forbidden energy gap oxide semicond. crystals, review of spectroscopic props. 78−2876
GeO_2, free energy of form., EMF meas. 80−35566
GeO_2, gamma-ray generation of O vacancies and O diffusion 79−99358
GeO_2, glass, refractive index, effects of alkali oxide comp. changes *(Russian)* 78−22182
GeO_2, glassy high freq. vibr. bands, central force model 80−49330
GeO_2, hexagonal and glassy, X and γ-irrad., thermolum. and paramag. centres 77−63472
GeO_2, hexagonal needle crystals, vapour growth 78−52651
GeO_2, highly dispersed, produced by plasmochemical method, adsorption props. *(Russian)* 77−70275
GeO_2, hydrothermal growth from CoO-GeO_2-H_2O 77−48329
GeO_2 layers on evaporated Ge films 77−76927
GeO_2, melting curves at high press., rel. to SiO_2 extended phase diagram 77−11672
GeO_2 melts, density, viscosity, struct., at high and low press. 79−87431
GeO_2, muonium and positronium form. 79−56679
GeO_2, new high-pressure modification 78−75825
GeO_2 particles used for optical fibre fabrication, struct. props. 80−89167
GeO_2, photoemission and X-ray emission spectra calc. 77−89866
GeO_2, radiation damaged, paramag. point defects, F-centres, ESR, absorpt. spectra 78−80213
GeO_2, reduction processes by C, kinetic analysis, reaction products *(Russian)* 80−55644
GeO_2, standard Gibbs energy of formation, meas. by electrochemical method *(Japanese)* 79−83499
GeO_2, structural analysis, using fluorescence excitation *(German)* 80−38923
GeO_2, tetragonal, exciton struct. in UV absorption edge 78−48199
GeO_2, tetrahedral glass, Raman studies 78−71823
GeO_2, thermal conductivity, 1.5-30K *(French)* 77−39704
GeO_2, ultrathin layers on Ge substrate, ATR spectra, thickness depend., struct. obs. 80−55214
GeO_2, vitreous, band limits and vibrational spectra 79−73935
GeO_2, vitreous, LO vibrational modes, Raman and IR spectra 77−7819
GeO_2, vitreous, Raman cross sections, rel. to appl. in fibre Raman lasers 78−31176
GeO_2, vitreous, struct., contrasted with EXAFS obs. of $ZnCl_2$ liq. and glass struct. 80−70133
GeO_2, vitreous, struct. study using small-angle X-ray scatt. 80−84071
GeO_2:Al, Ga, EPR, transferred hyperfine interactions of impurity-related trapped hole centres 77−85568
GeO_2:Al, tetragonal, $[Al]^0$ centre, nuclear Zeeman and quadrupole effects 78−35035
GeO_2:Mn^{2+}, EPR, struct. of vitreous and crystn. states 77−48039
GeO_2:Pr^{3+} glass, optical homogeneous linewidths 80−7395
GeO_2:Sc^{3+}(Y^{3+})(In^{3+}), trapped-hole centres, ESR meas. 79−77597
GeO_2:Si, optical props. IR absorpt., UV reflection spectra 78−84619
GeO_2:V^{4+}, crystal field splitting from ESR and optical absorpt. results 79−47063
GeO_2:V^{4+}(Cr^{3+}), direct mechanism in supertransferred hyperfine interaction 79−23936
GeO_2-B_2O_3-SiO_2, glass fibre, pulse transmission meas. of zero material dispersion 77−88937
GeO_2-CdO system, phase diagram anal. by differential thermal, X-ray anal. 77−8805
GeO_2-Na_2O borosilicate glass fibre prod. by phase separation and leaching 80−69558
GeO_2-Na_2O-B_2O_3 glass forming melts, thermodynamic props. and vaporisation processes, mass spectrometric study 80−79926
GeO_2-P_2O_5-SiO_2 glass fibre, incorporation of OH in modified CVD process 80−50560
GeO_2-P_2O_5-SiO_2 graded index optical fibres optimised for 1.3 μm wavelength region, fabrication techniques *(Japanese)* 80−99888
GeO_2-R_2O_2 system cpds., R=La, Gd, Er, physicochem. characts. 80−97469
GeO_2-SiO_2, glass, evaporation by high temp. mass spectrometry 80−79927
GeO_2-SiO_2, pyrolytic film prep. 77−81223
GeO_2-SiO_2, reduction by C, mixed diffusional-kinetic regime *(Russian)* 80−66771
GeO_2-SiO_2 optical fibres fabrication, 21.2 km graded-index VAD fibre with low loss and wide bandwidth 80−53414

germanium compounds continued
GeO_4^{4-} compounds, vibr. pot. function, force consts., isotopic shifts, mean vibr. amplitudes 80−23395
GeO_4^{4-}, normal vib. freq. and force const. calcs. *(Russian)* 78−46318
GeO_4^{4-}, normal vibr. freqs. calc. 79−54837
Ge_3O_3, isotopically substituted, IR freq. and intensity patterns 78−21926
Ge_3O_3, matrix isolated, IR isotope freq. and intensity patterns 78−46338
$GeO_2.6Bi_2O_3$, IR and Raman spectra, vibr. anal. 78−76464
GeP, dissociation kinetics rel. to volatile component sublattice 77−84917
GeP, thermodynamic characts. 10-300K, interatomic bond elasticity 80−59677
GeP, thin films, vacuum-deposited, struct. characterisation 77−47691
$Ge(S,Se)_2$ glasses, comparison A_1 Raman line, microscopic origin 80−29740
$Ge_x(S,Se)_{1-x}$, chalcogenide, covalent non crystalline topology, short range order 80−15009
GeS (001), density of empty states, core-level EELS and photoemission spectra meas. 79−78145
GeS (001) surface, electronic struct., Auger and electron energy loss spectra meas. 77−59314
GeS, (001) surface struct., LEED expt. 78−84034
GeS, absorpt. spectra, electron-phonon interactions 80−80810
GeS, amorphous, UPS and XPS, valence band struct. 77−90247
GeS amorphous layers between Al electrodes, dielec. relax. currents, pot. distrib. 77−16250
GeS, angular resolved UV photoemission and band structs. 77−85144
GeS, anisotropic EXAFS, cryst. struct. determ. 80−66323
GeS, band system vibr. anal. 80−48009
GeS, cryst. struct. *(German)* 78−51484
p-GeS, crystalline, photoelectric props. 80−70769
GeS, density of valence states, tight binding calc. 79−77976
GeS, dielec. function, optical and electron energy loss spectroscopy 78−15189
GeS, electron-hole interaction in d-electron excitations, photoelectron and optical spectra 78−34776
GeS, electrorefl. spectra 77−16282
GeS, exciton luminescence 78−52555
GeS, far IR reflectivity spectra, lattice vibr. and dielec. const. 77−52068
GeS film, between Al(Zn)(Sn) electrodes, Schottky and Poole-Frenkel cond. mechanisms 80−54799
GeS film, deposited on Ge(110) surface, sublimation, LEED meas., structural transitions 77−59195
GeS, film, effective electron mass determ. 77−1506
GeS film, effective electron mass determ. from current-voltage characts. in thermionic region 77−85135
GeS film, photocond. kinetics 77−39897
GeS, film on Ge, evaporation, thermogravimetric, electron microscopy investigs. 77−15715
GeS formation, from reaction of monocryst. Ge with S vapour 79−87833
GeS, gas-phase single-cryst. growth, photoelec. props. 77−36381
GeS, GeS_2, SS 79−97683
GeS, growth parameter meas. during cryst. growth from vapour in closed ampules 79−19168
GeS, IR reflectivity meas. 77−8570
GeS, in metal-semicond.-metal struct., thermionic electron emission model 77−28260
GeS, interband transitions, intrinsic photocond., anisotropy 80−20244
GeS, layer cpds., Raman spectra, press. coeffs. and mode Gruneisen parameters 78−10891
GeS layers form. on Ge surface, S_2 vapour press. rel. to growth rate 79−43152
GeS, low temp. photoluminesc. 77−77287
GeS multiple collision chemiluminesc., intercombination systems from Ge+OCS 80−45505
GeS, orthorhombic, atomic pseudopots. 79−42453
GeS orthorhombic layer crystals, photolum. spectra 80−2851
GeS, orthorhombic single cryst., fine struct. in reflectivity 79−19903
GeS, phonon dispersion relations, neutron scatt. study 79−42182
GeS, photoelectron spectra, rel. to ionicities and phase transitions 77−69960
GeS, physical basis for Urbach's rule 80−93366
GeS, rot. spectra, Born-Oppenheimer approx., adiabatic corrections *(German)* 77−57994
GeS, Schottky barrier, photovoltaic props. 79−7854
GeS, Si doped and undoped, elec. cond. and thermally stimulated currents 80−20194
GeS, thin layer cryst., far IR transmission spectra 79−56870
GeS, Urbach's rule, absorption edges 80−97224
GeS, valence level photoelectron spectra 77−27114
GeS, XPS investig. of valence band struct. 77−48311
$^{72}Ge^{32}S$, $^{74}Ge^{80}Se$, $^{74}Ge^{130}Te$, rot. g_J-factor meas., $^1\Sigma$ ground state *(German)* 77−30865
GeS-GeSe, limits of solid soln. region, microstructural, X-ray and DTA meas. 78−47530
GeS_{11} glass, neutron irrad., thermal and elec. props. 79−19286
GeS_{15} glass, TSD evidence for ionic cond. 77−76598
$GeS_{1.35}$ glass, neutron irrad., AC elec. cond. 80−24924
$GeS_{1.5}$:Cu, interpretation of dielectric behaviour 79−33595
GeS_2, amorphous film, reversible and irreversible photostructural changes 79−74061
GeS_2, chalcogenide glass, hollow cluster model of atomic structure 80−6366
GeS_2, cryst. and glass, Raman spectra, struct. *(Russian)* 79−51966
GeS_2, energy gap and optical props. in IR region 79−51948
GeS_2 glass, melt quenched, reversible photostructural change, optical transmission spectra obs. 80−45109
GeS_2 glass, molecular to band-like modes 77−66012
GeS_2, glass, structure correlation range, Raman Brillouin light scatt. determ. 77−20857
GeS_2 glass, temp. and press. depend. of elastic props. 77−15476
GeS_2, glassy, high freq. vibr. bands, central force model 80−49330
GeS_2, high temp. phase, struct. relation with $GeSe_2$ *(French)* 77−51359
GeS_2, IR optic materials, characteristics *(German)* 80−38081
GeS_2, LF inelastic light scatt. meas. 78−15181
GeS_2, single cryst., IR polarised reflectivity spectra, 79−56775
GeS_2, thermal conductivity, 1.5-30K *(French)* 77−39704
GeS_2-GeS-Ag_2S glass, Ag diffusion, 50-120°C 78−18828
GeS_2-$GeSe_2$ cross section, $GeSe_2$ single cryst. growth 77−52305
GeS_2-Na_2S, glass, synthesis, elec. cond., Raman spectra, temp. and composition depends. *(French)* 79−14962
germanium compounds continued
GeS_8 glass, activation energies after neutron irradiation, elec. cond. and transmission coeff. 78−83850
GeS_x, amorphous, ionicity dependence of defect reactions and negative-U states in glasses 80−88511
GeS_x amorphous semiconductor, neutron irrad. effects on thermal parameters 77−11597
GeS_x glass, x=1.25 to 1.5, softening and crystallization kinetics 79−32906
GeS_x, neutron irrad., thermal and elec. conductivity and heat capacity 78−2165
$Ge_{1-x}S_x$ glasses, building blocks and bonds 80−54141
$Ge_{100-x}S_x$, amorphous film, effect of alloying chalcogen atom on elec. cond., optical transmission and ESR 79−78101
Ge_2S_3, electron irradiated, effects on elec., photoelec. and optical props. 80−49806
Ge_2S_3, glass form. and characterisation *(German)* 80−64913
Ge_2S_3, photoenhanced diffusion of Ag 79−65257
Ge_2S_3-Ag contact, photoinduced diffusion of Ag in amorphous semicond. film 80−49418
Ge_2S_3-Ge_2Se_3, glass, photoluminesc. spectra, solid soln. form. *(Russian)* 78−23525
$Ge_{25}S_{75}$:Mn, bond struct. and character in Ge-S system, EPR obs. 80−66014
$Ge_{30}S_{70}$ glass film, Ag photodoping sensitivity 80−39121
$Ge_{40}S_{60}$, $Ge_{25}S_{75}$ glasses, Mn^{2+} EPR spectra investigation 79−11340
$Ge_{40}S_{60}$ glass, Cu doped, EPR study 79−65713
$Ge_{40}S_{60}$:Mn (Ag)(Cu), bond struct. and character in Ge-S system, EPR obs. 80−66014
$Ge_{42}S_{58}$, amorphous, bulk and film forms, elec. props. and ESR study 80−103691
$Ge_{42}S_{58}$ glass, Cu(Ag)(I) impurity effect on e.p.r., dangling bonds 77−4553
Ge_xS_{1-x} glasses, sp. ht., 2 to 18K 79−65214
$GeS_2(O_2)$, thermal expansion at low temperatures 78−83982
$GeS(S_2)$ amorphous films, photostructural changes, UPS study 80−49550
$GeS(Se)_x$, x=1 or 2, ht. of transition determ. by thermography 78−22847
GeS_xSe_{1-x}, electrorefl. spectra 77−16282
GeS_xSe_{1-x}, form. of solid soln. and phys. props. *(Russian)* 77−1232
GeS_xSe_{1-x}, IR spectra, differential calorimetry, phase diagram *(Russian)* 78−52513
$Ge_{1-x}S_x(Se_x)$, bulk-quenched glasses, opt. freq. dielec. const., chem. ordering effects 78−23472
$GeS(Se)(Te)(O_2)$, K X-ray spectra, Ge atoms effective charge, energy-gap widths 77−28657
Ge_xSb_{1-x} amorphous film junction, I-V and C-V characts. 77−85307
$Ge_{20}Sb_{25}S_{55}$ glasses, optical props., absorption edge temp. depend. 80−2789
$Ge_{2.33}SbSe_5$:Fe, Fe effect on physiochem. props. of glass 80−24370
GeSe (001), density of empty states, core-level EELS and photoemission spectra meas. 79−78145
GeSe, amorphous, film, thermally induced effects, UPS study 80−104042
GeSe, amorphous, pair distrib. function, anomalous X-ray scatt. 80−49126
GeSe, amorphous, UPS and XPS, valence band struct. 77−90247
GeSe, amorphous film, optical properties 78−39620
GeSe, amorphous film, photocond. meas. 77−43647
GeSe amorphous films, blocking metal contacts characteris. and photo/EMF obs. 77−76924
GeSe amorphous films, photoconductivity measurements, recombination model 78−64061
GeSe amorphous films in Al-GeSe-Al structs., AC cond. and capacity, thickness depend. 79−65566
GeSe amorphouse sputtered film, DC and AC behaviour, effect of contact material 79−95513
GeSe, antiferromagnetic behaviour, res. to negative magnetoresistance effect 79−73719
GeSe, density of valence states, tight binding calc. 79−77976
GeSe, dielec. function, optical and electron energy loss spectroscopy 78−15189
GeSe, electrorefl. spectra 77−16282
GeSe, galvanomag. meas., anisotropy, metal to semiconductor transition 80−6847
GeSe, layer cpds., Raman spectra, press. coeffs. and mode Gruneisen parameters 78−10891
GeSe, low temp. photoluminescence 77−77287
GeSe, optical absorption edge meas. 77−63430
GeSe, photoelectron spectra, rel. to ionicities and phase transitions 77−69960
GeSe, rot. spectra, Born-Oppenheimer approx., adiabatic corrections *(German)* 77−57994
GeSe, single crystal, optical absorption 80−25383
GeSe, valence level photoelectron spectra 77−27114
GeSe, XPS investig. of valence band struct. 77−48311
GeSe/KRS-6, GeSe/NaF, IR multilayer partial mirrors effective from 1.3 to 16 μm 80−9978
GeSe-PbSe-AsSe, glass form., elec. cond., struct. defects, assoc. *(Russian)* 80−54145
GeSe-Si amorphous-cryst. heterojunction, energy band diagram construction 77−55602
$GeSe_2$, amorphous, film, thermally induced effects, UPS study 80−104042
$GeSe_2$ amorphous film, laser induced light absorpt. oscillation, exciton model 80−50446
$GeSe_2$ amorphous film, laser-induced oscillatory phenomena 80−84711
$GeSe_2$, amorphous film, photocond., photo-induced ESR, optical edge shift 80−49809
$GeSe_2$ amorphous layers, photoconductance meas. 80−65632
$GeSe_2$ amorphous semicond., DC conductivity, calorimetric, and X-ray diffr. meas. 79−78107
$GeSe_2$, and $Ge_{1-x}Se_x$, amorphous, struct. models 79−37628
$GeSe_2$ chalcogenide film, struct. changes due to laser induced transmittance oscill., SEM obs. 78−6240
$GeSe_2$, chalcogenide glass, hollow cluster model of atomic structure 80−6366
$GeSe_2$, cryst. and glass, Raman spectra, struct. *(Russian)* 79−51966
$GeSe_2$, drift mobilities of electrons and holes, photocurrent decay meas. 80−2424

germanium compounds continued
$GeSe_2$ evaporated films, optical absorpt. and thermally induced effects 79−42989
$GeSe_2$ evaporated films, struct. and thermally induced effects 79−41963
$GeSe_2$, exciton absorpt., transmission spectra of cryst., glasses and amorphous samples 79−15485
$GeSe_2$, far IR reflectivity meas. 77−28565
$GeSe_2$, far IR reflectivity spectrum, dielec. const. and lattice vibrs. 77−52069
$GeSe_2$ film, chalcogenide glasses band gap variation 78−90461
$GeSe_2$ film, glassy, self-controlled laser-beam chopping effect 78−60528
$GeSe_2$ film, light induced transmittance oscillations 77−81171
$GeSe_2$ film, light-induced light absorption changes 77−73181
$GeSe_2$ glass, photoluminesc. spectrum, rel. to cryst. forms 77−55819
$GeSe_2$, glassy, powdered and bulk, fatigue of photolum. 80−80855
$GeSe_2$, glassy and single-cryst., photoluminesc. at 77K 77−63456
$GeSe_2$, glassy photoinduced photoluminescence fatigue 79−28827
$GeSe_2$, IR and Raman spectra 78−95585
$GeSe_2$, LF inelastic light scatt. meas. 78−15181
$GeSe_2$, liquid, struct., investigation using neutron diffr. meas. 79−23514
$GeSe_2$ multimode layer cryst., far IR transmission and reflection spectrosc., comparative merits 80−76019
$GeSe_2$, optical absorption edge 78−43901
$GeSe_2$ powdered crystalline, photoluminescence intensity under continuous excitation 80−71480
$GeSe_2$, single cryst., IR polarised reflectivity spectra, 79−56775
$GeSe_2$, single crysts., 3 polymorphic forms, DTA, photolum., IR and Raman sepctroscopy 80−33923
$GeSe_2$, struct. rel. with $GeSe_2$ high temp. phase *(French)* 77−51359
$GeSe_2$-As_2Se_3-Sb_2Se_3 system glasses, vitrification and elec. cond. 79−50996
$GeSe_2$-As_2Se_3-Sb_2Se_3, quenched glass system, elec. cond., low temp. heat treatment effect 80−39586
$GeSe_2$-As_2Se_3-Sb_2Se_3, elec. cond. over wide range of temp. 80−88564
$GeSe_2$-As_2Se_3-$SnSe_2$ system glasses, vitrification and elec. cond. 79−50997
$GeSe_2$-PbSe-AsSe, glass form., struct. defects, elec. cond., assoc. *(Russian)* 80−54144
$GeSe_2$-$SnSe_2$-As_2Se_3, GeSe-SnSe-As_2Se_3, Mossbauer investigation 77−20052
$GeSe_2$-Te, phase diagram and vitrification region determ. by DTA, SEM, X-ray diffr. *(French)* 77−72565
$GeSe_4$ film, self-controlled laser beam chopping effect 78−31266
$Ge_{0.08}Se_{0.92}$, molten semicond., pseudogap, elec. cond. and optical absorption meas. 77−8160
$Ge_{0.45}Se_{0.55}$-As_2S_3, antirefl. coating, performance at 3.8, 5.3 and 10.6 μm 77−61964
$Ge_{1-x}Se_x$, ave. energy gap, optical freq. dielec. const. and refr. index 77−76739
$Ge_{1-x}Se_x$ film, EPR, elec. and optical props. meas. 78−48038
$Ge_{1-x}Se_x$ glass, refr. index comp. depend. and photo-induced variation 79−91398
$Ge_{1-x}Se_x$, photolum. and optical props. meas. 77−20908
$Ge_{100-x}Se_x$, amorphous film, effect of alloying chalcogen atom on elec. cond., optical transmission and ESR 79−78101
Ge_2Se_3, glass form. and characterisation *(German)* 80−64913
Ge_2Se_3, vitreous, evaporation kinetics and amorphous film deposition 80−97434
Ge_8Se_{92}, glassy and liq. states, elec. cond. freq. depend. 77−76856
Ge_xSe_{1-x}, $0<x<0.2$, crystallisation in amorphous bulk and thin films 78−55813
Ge_xSe_{1-x}, amorphous, AC cond. *(Korean)* 80−44591
Ge_xSe_{1-x}, amorphous, excitation spectra of photolum. fatigue and creation of paramag. centres 80−50402
Ge_xSe_{1-x}, amorphous, exponential absorpt. edge rel. to struct. 79−99902
Ge_xSe_{1-x}, amorphous, X-ray diffr. and local order modelling 80−49125
Ge_xSe_{1-x} amorphous film, photocrystallisation, elec. cond. meas. 79−32911
Ge_xSe_{1-x} amorphous film, photocrystn., elec. cond. and optical microscopy obs. 79−87024
Ge_xSe_{1-x}, amorphous semicond., elec. props. 78−84219
Ge_xSe_{1-x}, bonds and band struct. determ., tight-binding model 78−18959
Ge_xSe_{1-x} chalcogenide glasses, trap-controlled carrier mobility, time of flight meas. 79−4557
Ge_xSe_{1-x} chalcogenide glasses, drift mobility of optically injected carriers 79−19627
Ge_xSe_{1-x} glass, $1/3 \leq x \leq 1/2$, Raman scatt., local order 78−23442
Ge_xSe_{1-x} glasses, DC cond. and static dielectric const. meas. *(French)* 77−62925
Ge_xSe_{1-x} glasses, defect states, photoluminesc. and ESR obs. 79−61418
Ge_xSe_{1-x} glasses, optical props. and local struct. *(French)* 77−77162
Ge_xSe_{1-x} glasses, vibr. props. 78−2219
Ge_xSe_{1-x}, liq., kinematic viscosity, 300-600°C 77−31706
Ge_xSe_{1-x} melts, short-range order change with comp. and temp., anomalous density behaviour 77−11676
Ge_xSe_{1-x}, thin film Schottky diode, photovoltaic effect 77−15895
Ge_xSe_{1-x}, vitrification, liquid-solid phase diagram, viscosity var. *(French)* 77−72680
Ge_ySe_{1-y}, glass, bulk and film, IR transmission and reflectivity meas., struct. mode assignments 78−79537
α-Ge_ySe_{1-y}, photoluminescence and fatigue effects 78−84648
$(GeSe_2)_x(As_2Se_3)_{1-x}$, vibr. excitations of large atomic clusters, Raman and depolarisation spectra 77−20856
$(Ge_{1/3}Se_{2/3})_{100-x}Ni_x$, ESR, rel. to elec. cond. 80−7155
$GeSe_xS_{1-x}$ solid solutions, long-wavelength optical phonons, Raman spectra 80−25378
$GeSe(Se_2)$ amorphous films, photostructural changes, UPS study 80−49550
$Ge_{20}Se_{40}Te_{40}$ amorphous alloys, thermal crystn. study 78−26789
$Ge_3Se_2Te_4$ film, chalcogenide glass, freq. depend. of Hall effect 77−1436
Ge_4Se_5Te, amorphous layer, Poole-Frenkel controlled charge carrier transport, model of charged dangling bonds 80−49750
Ge_4Se_5Te amorphous layers, prep. and elec. props. 80−97436
$(Ge_{0.32}Se_{0.32}Te_{0.32}As_{0.4})_{100-x}Ni_x$, ESR, rel. to elec. cond. 80−7155
a-GeSi film with Mo contacts, AC performance *(German)* 77−63012
$Ge_{1-x}Si_x$, solid soln., local levels, matrix elements of valence band, perturbing pot. calc. 77−1395
Ge_xSi_{1-x}, Si X-ray emission spectra obs. *(Russian)* 77−1767
$Ge_{10}Si_{12}As_{30}Te_{48}$, monostable chalcogenide glass threshold switch, temp. meas. *(German)* 77−4412
germanium compounds continued
$Ge_7Si_9As_{39}Te_{35}Ga_{10}$, chalcogenide thin films, coupled carrier theory test, high field conditions 80−100466
$Ge_xSn_{1-x}S(Se)$, lattice parameters, optical energy gap and IR refl. 78−23021
$Ge_{0.5}Sn_{0.5}Te$ film, elec. and optical props. 77−12028
$Ge_{1-x}Sn_xTe$ film, amorphous, elec. cond. 80−93016
GeTE, density of valence states, tight binding calc. 79−77976
GeTe, amorphous, UPS and XPS, valence band struct. 77−90247
GeTe, amorphous film, annealing effects on resistivity, comparison with SnTe 77−66212
GeTe amorphous films, annealing effect on optical props. 77−72931
γ-GeTe, anisotropy of elec. props. 79−73515
GeTe, antistructural disordering 77−15402
GeTe based thermoelec. materials, creep mechanisms 77−16643
GeTe, bond orbital model of band struct. 80−59853
GeTe, concentration of carriers, rel. to stoichiometry 80−6847
GeTe, crystal binding energy 79−37650
GeTe, crystallisation in constant electric field, thermoelectric parameters 77−44146
GeTe, degenerate semiconductor, EPR experiments on Mn^{2+} 79−11339
α-GeTe, diffraction contrast between inversion domains and at boundaries in TEM 77−62457
GeTe, effect of phase transition on mech. and elec. props. 77−51746
GeTe, effective masses for cond., density of states 80−88472
GeTe, elec. cond. and microhardness, thermal cycling effect *(Russian)* 78−35485
GeTe, electron-phonon interactin induced phase transition 79−82338
GeTe, enthalpy and specific heat, 0 to 860°C, polymorphic transitions obs. 77−43350
GeTe, ferroelec. with strong cubic anisotropy, phase transition 77−52026
GeTe film, amorphous, evaporated and annealed, variable range hopping cond. 78−80077
GeTe film, amorphous, specific current noise power 77−66190
GeTe film, amorphous and crystalline, electron diffr. meas. 77−39748
GeTe film, elec. props. 77−51831
GeTe film, evaporated, electro-reflectance meas. 80−11496
GeTe, film, local order, electron diffraction study 79−77485
GeTe, film, semicond., supercond. energy gap and crit. field, tunelling meas. 77−24644
GeTe film 79−43055
GeTe films, elec. props. and struct., influence of annealing and condensation conditions 80−15388
GeTe, Hall coeff., temp. depend. rel. to order parameter 80−96921
GeTe, heterophase state, plasma refl. spectra, twinning domain distrib. study 79−69845
GeTe, heterophase state with nonuniform distribution of free carriers *(Russian)* 78−2849
GeTe, heterophase state with nonuniform free carrier distrib. 79−56798
GeTe, high pressure effects on hole conc. and thermoelec. props. 78−26894
GeTe, high temp. mass spectrometric obs. of vaporis. 77−76542
GeTe, interpretation of polymorphic transformations 80−15032
γ-GeTe, investigation by elec. resist., latent heat of phase transform. and plasma refl. of light 79−99317
GeTe, liq., neutron diffraction study 79−77485
GeTe, low temp. alloys, microstruct. obs. *(Russian)* 78−19768
GeTe, machining effects on electrophys. props. 77−86199
GeTe, matrix isolated absorpt. and emission visible spectra, electronic states 80−28026
GeTe, nonstoichiometric, homogenisation 78−44004
GeTe, oxidation, partial pressure diagram 79−83183
GeTe, oxidation kinetics 77−44380
GeTe, quenched, phase transitions and electrophysical props. 79−51250
p-GeTe, reflectance, and thermorefl. spectra 80−80814
GeTe, region of homogeneity 77−47582
GeTe, single cryst., hole mobility 78−6379
GeTe, stoichiometry deviations influence on mech. props., 25-500°C 80−103410
GeTe, structural transitions 77−51497
GeTe, supercond., metal-insulator transition, electron pairing, effect on optical props. 80−60139
GeTe, thermal expansion meas. at phase transition 78−18771
GeTe, thermoelectric materials, physico-chemical study 78−30945
GeTe, X-ray emission spectra, amorphous and cryst. struct. *(Russian)* 78−88385
GeTe, XPS investig. of valence and struct. 77−48311
GeTe:I, ferroelectric transition exam. 78−88264
GeTe:Mn, thermoelec. power, 2.5-25K, magnon drag effect 78−56169
GeTe-As_2Te_3 system, phase diagram, eutectic comp., thermographic and X-ray anal. *(Russian)* 77−63646
GeTe-Bi_2Te_3(Sb_2Te_3), thermoelectric materials, physico-chemical study 78−30945
GeTe-Ga_2Te_3, electrophys. props. 77−48403
GeTe-In, solubility, thermo-EMF coeff. meas. 78−43124
GeTe-MnTe, heat treatment effect on struct., elec. props. 80−54725
GeTe-MnTe-SnTe system, compds., GeTe phase transition temp., elec. props., thermal cond. 79−43220
GeTe-MuTe, temp. characts. of phase transition, MnTe influence 80−20926
GeTe-Sb_2Te_3, solid solutions, cond., density of states 80−88472
GeTe-Si amorphous cryst. heterojunction, energy band diagram construction 77−55602
$GeTe_x$ cermet specimens, density, 25 to 412°C, depend. on nonstoichiometry and annealing temp. 77−25004
$(GeTe)_x$-$(AgSbTe_2)_{1-x}$, thermoelectric props. of monolithic and pressed samples at 300K 78−80009
$(GeTe)_x$-$(AgSbTe_2)_{(1-x)}$, thermoelectric characts., temp. depend. 300 to 750K 79−78123
$Ge_{0.5}Te_{0.5}$, heat capacity in solid and liq. phases, enthalpy of form. *(French)* 80−35565
$Ge_{0.5}Te_{0.5}$, strucutral anal. by neutron diffr., radial distribution functions 80−15010
$Ge_{1-x}Te_x$, amorphous, localised gap states, variable range hopping 77−72866
α-$Ge_{1-x}Te_x$, anisotropy of elec. props. rel. to cubic phase transition and band struct. 77−76820
$Ge_{1-x}Te_x$, elec. cond., Hall effect in phase transition region 79−11113
$Ge_{100-x}Te_x$, amorphous film, effect of alloying chalcogen atom on elec. cond., optical transmission and ESR 79−78101
$Ge_{15}Te_{85}$, amorphous, splat cooled, thermoelectric props. 78−43426

germanium compounds continued
$Ge_{15}Te_{85}$, crystal-glass transition influence on local struct. 77−36163
Ge_xTe_{1-x}, amorphous, struct., quadrupole splitting of $^3/_2$ spin state of ^{125}Te calc. 77−65950
Ge_xTe_{1-x} amorphous matrix with Te crystallites, effect of annealing 77−24274
$Ge_{13.3}Te_{61.7}As_{19}$ film, amorphous, characts. of optical switching 78−18031
$Ge_{15}Te_{81}As_4$ film, amorphous, characts. of optical switching 78−18031
$Ge_{15}Te_{81}As_4$, influence of O_2 on phase separation of chalcogenide glasses 77−47354
$Ge_xTe_{10-x-y}E_y$, E=impurity, glass-crystn. transition, memory effect 77−47870
$Ge_{15}Te_{81}Sb_2S_2$ film, amorphous, characts. of optical switching 78−18031
$Ge_{15}Te_{81}Sb_2Se_2$, glassy and liq. states, elec. cond. freq. depend. 77−76856
$Ge_xTe_xSe_{100-2x}$, x=2.5 and 5.0, chalcogenide glasses, IR absorpt. spectra 77−24842
$Ge_{20}Te_2Se_{80-x}Si$, amorphous-cryst. heterojunctions 79−65546
$Ge_{15}Te_{81}X_4$ amorphous semicond. switches, fabrication technology *(German)* 80−7493
GeX_4, (X=Br,Cl), electron impact dissoc., low-energy reson. capture 78−9263
GeX_4, X=H, F, Cl, mol. force consts., parametric representation method 78−25503
GeX_n radical, (X=H,D; n=1,2,3), thermodynamic function in ideal gas state 80−14871
$Ge_xZn_{1-x}Fe_2O_4$, ferrimagnetism and ion distrib. 77−12103
InSb-Ge eutectic alloy, effect of crystallisation rate on microhardness 79−96110
$IrGe_{1.5}S_{1.5}(Se_{1.5})$, new skutterudite relation compounds, prep. and charact. 78−52700
$KH_3(Ge_7O_{16}).3H_2O$, cryst. struct. determ. 79−90628
La_2Se_3-Ga_2Se_3-$GeSe_2$ ternary system, phase diags., glass formation *(French)* 78−3109
LiF-NaF-KF-K_2GeF_6-GeO_2 fused mixture, for electrodeposition of Ge powder 80−2979
$Li_2Ge(GeO_3)_2(OH)_2$, cryst. struct. determ. 79−90629
Li_2O-GeO_2 glass, synthesis, Ge coordination state 77−24271
Li_2S-GeS_2, glass forming region, struct. and ionic cond. 80−88358
$Mg_2Si_xGe_ySn_{1-x-y}$ composite Te material with high figure of merit 77−28164
$N(CH_3)_4GeCl$, cryst. and powder diffr. data 80−24422
$(NH_4)_2GeP_4O_{13}$, cryst. struct. determ. *(French)* 77−51358
$Na_6Al_6(Si_{0.99}Ge_{0.01})_6O_{24}.2NaBr$, Ge-doped sodalite powders, UV absorpt. band 80−71452
Na_2CoGeO_4, hydrothermal growth from CoO-GeO_2-NaOH-H_2O 77−48329
$Na_4Ge_9O_{20}$, $Na_2GeO_3.H_2O$, hydrothermal growth from CoO-GeO_2-NaOH-H_2O 77−48329
Na_2O-B_2O_3-GeO_2 vitreous melts, thermodynamic props. from mass spectra 80−65253
Na_2O-GeO_2, glass, thermolum. rel. to coordination number 77−16405
Na_2O-GeO_2, thermal expansion at low temperatures 78−83982
Na_2O+GeO_2, molten mixture, EMF measurements 78−43144
Na_2S-GeS_2, synthesis, structure and ionic conduction *(French)* 80−65291
$Na_2S=GeS_2$, glass forming region, struct. and ionic cond. 80−88358
Ni-Ge-SiO, solar selective absorber surfaces, optical behaviour at high temp. 80−101130
Pb-Ge-S semiconducting glasses, far IR transmission and struct. 79−65855
Pb-Se-As-Ge, phase separation in melt centrifugal quenching 80−25701
$Pb_{1-x}Be_xTe$, anomalous resist. near ferroelec. phase transition 80−20196
$Pb_5Ge_3O_{11}$, pyroelectric radiation detector appl. *(Czech)* 79−40611
$Pb_5(Ge_{1-x}Si_x)_3O_{11}$, electrogyration, phase transition and dielectric props. 80−93269
$Pb_{1-x}Ge_xTe$, band struct., tunnelling obs. in MIS struct. 80−54795
$Pb_{1-x}Ge_xTe$, degenerate semiconducting ferroelectric, structural phase transition temp., mag. field effects 80−45017
$Pb_{1-x}Ge_xTe$, dielec. const. determ. near ferroelec. transition 78−88269
$Pb_{1-x}Ge_xTe$, electron-phonon interaction effect on ferroelec. transition 78−76416
$Pb_{1-x}Ge_xTe$ epitaxial layers, phase transition obs. by far IR reflectivity spectroscopy 79−33691
$Pb_{1-x}Ge_xTe$, ferroelec. phase transition, IR refl. and resist. meas. 80−11353
$Pb_{1-x}Ge_xTe$, ferroelec. constants, C-V and C-T characts. of abrupt p-n junctions 80−25323
$Pb_{1-x}Ge_xTe$, ferroelectric phase transition effect on forbidden band width 80−24794
p-$Pb_{1-x}Ge_xTe$ film, cyclotron reson. above and below struct. phase transition 80−88879
$Pb_{1-x}Ge_xTe$, mag.-field-induced displacive phase transition 80−50278
$Pb_{1-x}Ge_xTe$ magnetoplasma reflectivity and transmission spectra 80−71428
$Pb_{1-x}Ge_xTe$, n- and p-type, effective masses 80−44481
$Pb_{1-x}Ge_xTe$, phase transitions 78−60408
$Pb_{1-x}Ge_xTe$, Raman scatt. from soft TO-phonon modes 79−95773
$Pb_{1-x}Ge_xTe$ solid solns., phase transition influence on elec. props., 77 to 450K 80−103689
$Pb_{1-x}Ge_xTe$, solubilities, elec. and optical props. 77−35940
$Pb_{1-x}Ge_xTe$, TO phonon interaction with acoustic phonons near phase transition temp. 79−90776
$Pb_{1-x}Ge_xTe$:Ga, Fermi level stabilization, transport props. meas., 77-400K 78−56065
$Pb_{1-x}Ge_xTe$:Ga, influence of hydrostatic compression on elec. props. 79−73516
PbO-GeO system, pyroelec. and TSC props. 78−43798
PbO-GeO_2 glass, synthesis, Ge coordination state 77−24271
PbO-GeO_2 melt, thermodynamic study 77−59760
3PbO.2GeO, TSC in thermoelectret state during ceramic synthesis, pyroelec. currents and energy struct. of capture centres 80−55014
$RhGe_{1.5}S_{1.5}$, new skutterudite relation compounds, prep. and charact. 78−52700
Sb-Ge-Se system glasses, thermal capacity, 80 to 300K 79−42272
Sb-Ge-Se system glasses, activation energy of elec. cond. calc. 79−51568
$SbGe_xSe_y$ glasses with const. Sb content, heat capacity, thermal expansion, US vel. and elastic moduli 77−76574
Sb_2O_3-$SiO_2(GeO_2)$-Na_2CO_3-H_2O, crystallisation 77−12605

germanium compounds continued
SbSI-GeS_2 system glasses with and without antireflection coatings, optical props. 77−8595
Sc_2O_3-GeO_2-KF-H_2O system, scandium germanates crystallisation in high temp. aq. solns. 77−24942
Se-As-Ge, glass alloy system, annealed light irradiated, photoinduced absorption change, random network model 79−59773
Se-Ge, amorphous, elec. cond. at room temp., contact effect 77−20354
Se-Ge, amorphous, Raman spectra and average band gap 80−50327
Se-Ge, amorphous thin film, photocontraction rel. to surface struct. 80−49551
Se-Ge, chalcogenide glass, Raman scatt. and bond struct. 79−95772
Se-Ge amorphous system, AC elec. cond., near T_g, temp. depend. 80−49791
Se-Ge glass, lattice vibr. spectra, photostruct. change, far IR absorpt. 78−72494
Se-Ge glasses, extreme far IR absorpt. meas. 80−50318
Se-Ge system, amorphous, press. depend. of AC cond. 77−76858
Se-Ge-As, chalcogenide glass, self-diffusion, investigation using radioactive tracers 79−23770
Se-Ge-Sb alloy glass, crystn. kinetics 77−20057
Se-Ge-Te, chalcogenide glass, elec. cond. and dielec. const. 80−75567
Se-Ge-Te glass, dielectric meas. 79−87382
Se-Te-As-Ge glasses, absorpt. spectra, diffuse reflectivity loss correction 79−82995
Se-Te-As-Ge glasses, elec. transport 79−60833
Se-Te-Ge, amorphous, off-state thermal switching 79−65524
Se-Te-Ge system, amorphous, electrical transport, activation energy 79−95406
$Se_{0.84}Ge_{0.16}$ glass, sp. ht. excess rel. to far IR absorption 77−84874
$Se_{1-x}Ge_x$, amorphous, AC cond. magnitude and variation *(French)* 79−47095
$Se_{1-x}Ge_x$ amorphous film, photocontraction effect 79−46975
$Se_{75}Ge_{25}$, obliquely deposited amorphous films, photo-induced optical effects 79−56871
$Se_{12}Te_{49}As_{29}Ge_{10}$ semiconductor amorphous films, field effect, trapping 80−84472
Si-Ge, temp. depend. of ESR line intensity of surface centres 77−32246
Si-Ge alloy, hot-pressed, thermal cond., effect of grain size 77−31813
Si-Ge solid solns., p-n junctions, photoelec. props. obs. 77−1471
Si-Ge:As,P, heavily doped, electron scatt., Hall coeff., Seebeck coeff. and resist. meas., 4-300K 77−4379
Si-Ge-Br, heterogeneous system, equilib. gas phase composition, Si-Ge cryst. growth appl. 79−10820
Si-Ge-Br system, diffusion mass transfer 80−33911
Si-Ge-Te system glasses, structural and electronic transitions 77−76890
$SiCl_4$-$GeCl_4$-BCl_4 particulate layers consolidation, in fabrication of optical fibre preforms 80−60787
$Si_{1-x}Ge_x$ amorphous, ESR centres, effect of annealing 77−55701
Si_xGe_{1-x}, vibr. props. 77−4176
$Si_{12}Ge_{10}As_{30}Te_{48}$, amorphous, energy controlled switching obs. *(Japanese)* 78−34867
$Si_{12}Ge_{10}As_{30}Te_{48}$, chalcogenide glasses, direct obs. of switching filaments 77−24595
$Si_{12}Ge_{10}As_{30}Te_{48}$, chalcogenide glass threshold switches, turn-on state maintenance *(Russian)* 77−85271
$Si_{12}Ge_{10}As_{30}Te_{48}$, chalcogenide glass film, switching delay time 78−26926
$Si_{12}Ge_{10}As_{30}Te_{48}$ chalcogenide glass threshold switch conductivity in high ohmic state *(Russian)* 78−43502
$Si_{12}Ge_{10}As_{30}Te_{48}$ chalcogenide glass, switching in thin layers with semicond. electrodes 79−4586
$Si_{12}Ge_{10}As_{30}Te_{48}$, conducting filaments and switching phenomena 79−87134
$Si_{12}Ge_{10}As_{30}Te_{48}$, dark cond. and thermoelec. power, thermal activation energies interpret. 78−23123
$Si_{12}Ge_{10}As_{30}Te_{48}$, energy-controlled switching obs. 77−35973
$Si_{12}Ge_{10}As_{30}Te_{48}$ glass, thermally stimulated depolarization current meas. *(Japanese)* 78−34875
$Si_{12}Ge_{10}As_{30}Te_{48}$ glass, nonlinear I-V characts. 79−99557
$Si_{12}Ge_{10}As_{30}Te_{48}$ surface, heat treatment and electron bombard. effects. SEM obs., rel. to switching filament form. 77−47700
$Si_{12}Ge_{10}As_{30}Te_{48}$, threshold switch, high resist. state 77−15924
$Si_{12}Ge_{10}As_{30}Te_{48}$, vitreous, localised states role in cond. in high elec. fields 77−76841
$Si_{0.5}Ge_{0.5}O_2$, band struct., photoemission spectra calc. and meas. 77−35865
$Si_xGe_{1-x}O_2$, $0\leq x\leq 1$, XPS and UPS, electronic struct. 77−48318
$Si_xGe_{1-x}O_2$, amorphous, electronic struct. in Bethe lattice approx. 80−44487
$Si_xGe_{1-x}O_2$, amorphous, electronic struct. 80−80166
SiO_2:GeO_2 graded-index fibres, without index dip, fabrication by CVD method 78−9431
SiO_2:GeO_2 optical fibres intrinsic attenuation 78−30067
SiO_2:GeO_2 optical fibres, definitive profile-dispersion data over extended wavelength range 79−76828
SiO_2:P_2O_5, GeO_2 fibre, anomalous conc. profile of P_2O_5 and GeO_2 77−79943
SiO_2-FeO_2 particulate mass transfer mechanism in modified CVD, thermophoresis 80−2955
SiO_2-GeO_2 cored optical fibre, low loss 77−62072
SiO_2-GeO_2 particles, deposition props. in flame hydrolysis reaction for optical fibre fabrication 80−48470
$Si_{12}Te_{48}As_{30}Ge_{10}$ amorphous film, high-field transient conduction 78−43500
$Si_{12}Te_{48}As_{30}Ge_{10}$, amorphous film, elec. cond. mechanisms, temp. depend. *(Japanese)* 78−80078
$Si_{12}Te_{48}As_{30}Ge_{10}$ film, temp.-depend. of non-ohmic current and switching characts. 77−8158
$Si_{12}Te_{48}As_{30}Ge_{10}$ film, amorphous, transient cond. characts. in preswitching regime 77−32055
$Si_{12}Te_{48}As_{30}Ge_{10}$ film, amorphous, Poole-Frenkel cond. for centres with screened Coulomb pot. 78−19044
$Si_{12}Te_{48}As_{30}Ge_{10}$-Au, Schottky barrier props. 79−7897
$(SiTe)_{1-x}(GeTe)_x$, solid soln., mag. susceptibility meas. *(Russian)* 80−70933
SmCaGe garnet LPE bubble film, coercivity, thickness depend. 78−68324
$Sm_{0.3}Lu_{0.2}Tm_{0.2}Y_{1.45}Ca_{0.85}Fe_{4.15}Ge_{0.85}O_{12}$, LPE growth, saturation magnetisation, collapse field, bubble diameter 78−95703
$Sn_xGe_{1-x}Se$, ^{119}Sn Mossbauer and elec. conductivity study 79−19595

germanium compounds continued
$Sn_{0.9}Ge_{0.1}Te$, Mossbauer spectra, soft modes 80−20550
$Sn_{1-x}Ge_xTe$, evaporated thin films, characts. 79−60944
$Sn_{1-x}Ge_xTe$, solid soln. series, Mossbauer study 80−39985
$Sn_xGe_{1-x}Te$ ($0.62<x<0.91$), specific heat anomaly at struct. phase transform. 77−69095
$Sn_xGe_{1-x}Te$, ferroelec. semicond. structural phase transition, X-ray study 79−37836
$Sn_xGe_{1-x}Te$, structural transitions 77−51497
$SnS-GeS_2$, exam. of phase diagram using DTA *(German)* 79−11585
$SnSe-GeSe_2-As_2Se_3$ glasses, vitrification region and elec. cond. 80−15008
$SnSe_2-GeSe_2$, phase diag., electrophys. props. of solid solns. 77−52306
SnTe-PbTe-GeTe, alloy semiconductor, phase transition *(Japanese)* 78−91443
Te-As-Ge, RF sputtering, temp. and bias effects on comp. 77−40367
Te-Ge-As-Si amoprhous film, voltage controlled negative resistance type characts. 79−69614
Te-Ge-Sn(Pb), Te rich, structural phase transformation concurrent with glass crystallisation, thermal evidence 79−4965
Te-GeTe system eutectics, crystn. rate effect on electrophys. props. mutual solubility effect 80−60774
$Te_{40}As_{35}Ge_7Si_{18}$ film, threshold switching in relax. oscill. mode 77−69389
$Te_{40}As_{35}Ge_7Si_{18}$, amorphous, threshold switching, expt. 80−49830
$Te_{40}As_{35}Ge_7Si_{18}$ with pyrolytic graphite electrodes, threshold switching characts. 77−24593
$Te_{48}As_{18}Ge_6Si_{28}$ amorphous film, I-V curve, memory switching 79−69615
a-TeAsSiGe film with Mo contacts, AC performance *(German)* 77−63012
$Te_{39}As_{36}Si_{17}Ge_7P_1$ amorphous film, electroluminescence from on state 79−8188
$Te_{80}Ge_{20-x}A_x$ glasses, rapid melt cooled, glass transition and stability range 80−75170
$Te_{0.81}Ge_{0.15}As_{0.04}$, amorphous and cryst., sp. ht., 1-20K 78−22864
$Te_{81}Ge_{15}As_4$, Hall effect in electrically switched memory state 80−2403
$Te_{80}Ge_{12.5}Pb_{7.5}$, phase-separated system, overlapping effects of glass transition and crystn., DSC results 78−83739
$Te_{80}Ge_{15}Pb_5$, DSC sensitivity to controlled ageing in glass transition region 80−71673
$Te_{80}Ge_{20-x}Sb_x(Bi_x)$, DSC studies of struct. phase transformation 80−66505
TeO_2-GeO_2 system, phase diagram, X-ray phase analysis, DTA and electron microscopy 77−15545
Tl-Ge-Te, glass formation 80−103255
Tl_2O-GeO_2 system, structure of thallium I germanates *(French)* 80−79754
$(U, Pu)O_{2\pm x}$, gradient of U, Pu and O at surface 77−18665
$Y_{1.52}Eu_{0.3}Tm_{0.3}Ca_{0.88}Ge_{0.88}Fe_{4.12}O_{12}$, bubble translation vel., ion-implantation effects 78−68327
$Y_2O_3-Lu_2O_3-Eu_2O_3-CaO-GeO_2-Fe_2O_3-PbO-B_2O_3$ system, garnet crystn. fields 78−43995
$ZnGeAs_2$, photoelectron spin polarisations, electron level struct. 79−87557
$Zn_{1-x}Ge_xFe_{2-x}{}^{3+}Fe_{2x}{}^{2+}O_4$, double exchange magnetism, Mossbauer study 80−66087
$Zn_{1-x}Ge_xFe_2O_4$, spinel series, obs. by Mossbauer spectroscopy of electron hoppings 78−43754
$ZnGeP_2$ bandgap absorption edge, spectra, electron transitions *(Russian)* 80−97305
$ZnGeP_2$, birefringence, effects on hydrostatic pressure and temp. 80−45033
$ZnGeP_2$, cond. compensation by electron bombardment 79−15151
$ZnGeP_2$, single cryst., polarised light photocond., optical transparency anisotropy *(Russian)* 78−2518
$ZnO-GeO_2-MnO-B_2O_3$ wideband cathodoluminescent phosphor 80−55196

getters
see also electron tube manufacture; vacuum techniques
acetylenic material, solid, on $Pd-CaCO_3$ catalyst, H getter, hydrogenation rates 77−44510
Dispersalloy, Sn-Hg amalgam, γ_2 precip. suppression and gettering kinetics 80−71651
fusion reactor, MFTF, end loss region high energy plasma gettering 80−102343
fusion reactor, use of nonevaporable getter pumps 77−57745
intermetallic compounds development, 20-years research results 77−7843
liquid-metal-cooled reactors, radionuclide trap in primary circuit 79−93768
mass spectrometer leak detector, increasing sensitivity by selective gas accumulation 79−6215
metal-getter T recovery systems and T inventory in fusion reactor 77−38415
phenyl propargyl ether, dimerised, with $CaCO_3$-Pd catalyst, as H getter 77−18001
Serpukhov proton synchrotron ion-getter pumps, operation evaluation 77−83347
SORB-AC wafer getter pumps, fusion reactor appl. 80−18637
Sorb-ac wafer pumps, behaviour in plasma machines, review 78−70627
sputtering at low temp. 78−35305
Tokamak fusion test reactor, transient getter scheme 80−79584
vacuum outgassing material selection and treatment 78−81994
vacuum pump pressure range extension by getter pumps 79−67327
K, built in getter for scintillation proportional counter 78−29707
Ba film, initial reaction probability with O_2, water, CO and CO_2, AES obs. 80−61153
Ce chemical getter beds, T removal from inert gases, CTR appl. 78−41861
Ce, gettering of H, mass spectrometry and microgravimetry study, rel. to HTGR gas purification 80−73374
$Cs-SiO_2-Al_2O_3$ system interactions, getter development for radiocaesium 80−83208
GaAs:Au, back surface gettering 80−10758
GaAs:Cr, gettering by back surface mech. damage 80−10759
GaAs:Cr, semi-insulating, damage gettering of Cr during annealing of Cr and S implants 80−107304
Gd, gettering effect 79−63241
Gd small ion-getter pump 78−89487
La binary alloys, use as tritium extractors from breeder blankets 79−67946

getters continued
Li, liq., for efficient particle removal from Tokamak 77−38411
Li, liq., for Tokamak reactors, thermal and dynamic flow props. of falls 77−38412
Si, ion-implantation gettering effects, crit. microstructure 77−43229
Si, O_2 getter in Fe-Al alloys, internal oxidation prevention 77−12739
Si, solubility of Au, gettering by P 78−83961
Si, stacking-fault nuclei gettering by trichloroethylene oxidation 77−43226
Si wafer, Czochralski grown, interstitial O gettering 77−86196
Si wafer, stacking faults, preoxidation gettering by reverse side P diffusion-induced misfit dislocations 80−60988
Si:Ga, sealed tube diffusion, Au and Cu gettering behaviour 77−76445
Si:P, Au gettering by P diffusion and P-induced dislocations 78−91346
Ti, excimer laser gas purification 78−46617
Ti, film, CO surface contamination effect on deuteriding 77−35814
Ti, getter for TFTR Flexibility Modification, in-torus surface pumping 80−95451
Ti, getter pump, corrugated surface and pumping speed, fusion reactor application 78−74491
Ti, gettering of H, mass spectrometry and microgravimetry study, rel. to HTGR gas purification 80−73374
Ti, sorption of H_2 and N_2, gas-discharge device appl. 80−10796
TiD_2, film formed during simulated Tokamak gettering cycles, desorption 80−34296
Zr foils, dehydrogenation of V by annealing 80−96736
Zr, gettering of H, mass spectrometry and microgravimetry study, rel. to HTGR gas purification 80−73374
Zr/Al, getter for TFTR Flexibility Modification, in-torus surface pumping 80−95451
Zr-Al alloy, selective gettering action for partial H_2 press. meas. 77−87775
Zr-Al getter pump, for fusion reactor 77−57748
Zr-Al getter pumping in beam driven Tokamaks 78−50401
Zr-Al intermetallic compounds in SAES ST101 getter, surface anaL during stimulated pumping 79−67945

GFRP *see glass fibre reinforced plastics*

giant pulsations (earth) *see micropulsations*

giant resonances *see nuclear collective states and giant resonances*

giant stars
see also supergiant stars
0- and B-type, UV obs. of mass loss effects 77−17551
abundances in M3 and 13 globular clusters 78−93334
accretion of interstellar grains by red giants and C star spectrum 79−21284
AFCRL sources, identification of southern objects 77−33682
ages, determ. via photoelectric MgH+Mgb index 80−12753
Am stars, evolved, search for photometric variability on lower part of Cepheid instability strip 80−62145
λ Andromedae, high-press. transition region in model chromosphere 80−26847
Z Andromedae, symbiotic star, IUE obs. of UV spectrum 80−109450
angular diameters determ. from lunar occultation obs. 79−30054
angular diameters from lunar occultations 79−44475
R Aquarii, Mira variable, 14.9 GHz obs. 79−75210
R Aquarii, symbiotic long-period variable, spectrum of assoc. nebulosity 80−90450
R Aquarii, UBVRI polarimetric obs., orbital motion effect *(Russian)* 80−36646
R Aquarii, UV, visible and 85 GHz continuum obs. 80−85946
R Aquarii (M7+pec), late type variable star, IUE obs. of circumstellar emission 80−82370
β Aquilae, single G-type subgiant, UVB photometry 79−62823
R Aquilae Mira variable, 14.9 GHz obs. 79−75210
Ariel 1540−53, eclipsing X-ray binary pulsator, evidence for giant primary star 78−8151
asymptotic giant branch evolution of intermediate-mass stars, post-second dredge-up phase 80−72936
asymptotic giant branch evolution with steady mass loss 80−26846
asymptotic giant branch stars in globular clusters, spectra 79−8913
atmospheres, microturbulence rel. to evolution 78−81625
atmospheric structure, mol. effects 80−21999
α Aurigae, 1.25-3.25 μ airborne photometric obs. 78−40934
α Aurigae, angular diameter meas. with large altazimuthal telescope *(Ukrainian)* 79−96925
ζ Aurigae, eclipsing binary, Ca I 6752 Å circumstellar line obs. 77−17619
α Aurigae, high-press. transition region in model chromosphere 80−26847
ε Aurigae, spectrum outside eclipse 77−71129
α Aurigae, UV spectrum obs. by International Ultraviolet Explorer 78−96475
α Aurigae (Capella), extra-atmospheric obs. analysis 79−25647
α Aurigae (Capella), intense line emission in soft X-ray spectrum 78−93228
α Aurigae (Capella), model chromosphere 78−40931
α Aurigae (Capella), orbital motion determ. using phase effect detect. at CERGA stellar interferometer *(French)* 80−36508
axions, very low mass, astrophysical bounds and stellar-energy loss 80−109353
B-type, intrinsic colour indices 79−84794
B-type, search for weak interstellar lines in spectra 77−74124
B-type, uvby indices, empirical effective temps. and bolometric corrections 77−45429
Ba II stars, spectral energy distribs. from DDO photometry 79−92757
BD+12° 1919 (IV-202 in M 67), curve-of-growth analysis of red giant 77−29841
BD+29°3805, K-type giant, spectroscopic binary orbit 80−67790
BD-3°5357, eclipsing binary with hot subdwarf component 77−91574
beat Cepheids, model constraints 79−5831
binary stars, G and K-type giants Ca II H and K lines emission intensity 80−82420
α Bootis, 1.25-3.25 μ airborne photometric obs. 78−40934
α Bootis, angular diam. determ. for IR photometry 77−64760
α Bootis, angular diameter meas. with large altazimuth telescope *(Ukrainian)* 79−96925
α Bootis, comparison of predicted and observed spectral energy distrib. 80−46546
α Bootis, emission lines in UV spectra 79−71028

giant stars continued
α Bootis, He I 10830 Å emission obs., high-temp. chromosphere 79−48792
α Bootis, K giant, surface gravity and mass 77−53587
α Bootis, non-thermal vels. height variation 77−13344
α Bootis, search for Ti II 3080 Å multiplet emission 80−51769
η Bootis, soft X-rays detect. with imaging X-ray telescope 79−48953
α Bootis, spectrophotometric profile, 3200-3600 Å 80−62118
α Bootis, stellar gravity from metallic line profiles and effective temp. 77−64759
α Bootis (Arcturus), anal. of chromospheric O I spectrum 77−56923
A Bootis (Arcturus), atmospheric parameters determ. 78−20826
α Bootis (Arcturus), CO fundamental bands, inhomogeneous chromosphere 78−36561
α Bootis (Arcturus), effects of mag. mixing on C/N and $^{12}C/^{13}C$ ratios 80−105229
α Bootis (Arcturus), far UV spectrum, coronal temp. determ. 78−16407
α Bootis (Arcturus), line blanketing and atm. struct. 77−33483
α Bootis (Arcturus), line identifications in UV spectrum 79−25598
α Bootis (Arcturus), model-atmos. analysis of spectrum 77−29827
α Bootis (Arcturus), O and C abundances *(Russian)* 78−16420
α Bootis (Arcturus), spectral line asymmetry meas. rel. to Sun 80−51753
α Bootis (Arcturus), UV obs. of chromospheric emission line profiles 78−81620
α Bootis (Arcturus), variable mass loss and giant convective elements hypothesis 77−22213
α Bootis (Arcturus) (K2 IIIp), theoretical temp. minima and explanation of Wilson-Bappu effect 79−62825
bright giants, classical Cepheids and nonvariable supergiants, spectrophotometric comparison 80−56837
bright IR star monitoring at 2.7 μm 78−16433
38 Cancri, δ Scuti star, UBV photometric obs. of variability 80−22021
RS Cancri, late-type variable star, spectral energy distrib. and spectral types *(Russian)* 78−40958
UU Cancri, long-period eclipsing binary, radial vel. meas. 77−74096
RS Cancri, OH emission obs. 78−8026
α Canis Majoris B (Sirius B), coronal model constraints from historical pseudo red giant phase 79−2543
α Canis Majoris B (Sirius B) as historical red giant, search for surrounding nebulosity 78−93242
α Canis Minoris, flux spectrogram, UV line blending and wavelengths, spectral resolution influence 80−56811
Y Canum Venaticorum, C star, $^6Li/^7Li$ atmospheric abundance 77−33523
Y Canum Venaticorum, C star, IR spectrum between 1.2 and 30 microns 80−46544
ζ Capricorni, Ba star, white dwarf+giant, UV spectra obs. 80−105284
α Carinae (Canopus), periodic variable mag. field detect. 77−49381
R Cassiopeiae, late-type giant, possible H_2O thermal emission identification 78−81628
BM Cassiopeiae, long-period eclipsing binary, radial vel. meas. 77−74096
γ Cassiopeiae, N I interstellar absorption in γ Cassiopeiae direction, UV obs. 80−51823
WZ Cassiopeiae, semiregular variable star, variable CaCl absorpt. bands 79−88683
κ Cassiopeiae, spectral obs., coarse atm. anal. 77−33487
R Cassiopeiae, VLBI obs. of SiO maser in Mira variable 79−92779
CD-38°245, metal-deficient halo red giant, spectrum, photometry and Ca/H ratio 78−69797
ω Centauri, anomalous giant branch rel. to abundance vars. in dwarf spheroidal galaxies 79−5904
ω Centauri, JHK photometry of globular cluster, giant branch spread 78−16476
ω Centauri, near IR photometry, giant branch struct. 77−41397
ω Centauri, near IR photometry anomalous giant branch 78−16477
V748 Centauri (Centaurus X-4?), high-latit. eclipsing system, VBLUW photometry 79−44529
ω Centauri giant branch, mixing versus primordial abundance vars. 77−17640
EI Cephei, Am eclipsing binary, light curve anal. 77−33560
U Cephei, chem. comp. of secondary component of close binary system 79−35308
VV Cephei, Hα region spectra and system analysis 77−78823
T Cephei, long-period variable, radial-vel. obs. 79−88684
T Cephei, Me variable, Tc discovery 78−32483
β Cephei stars, search south of declination −20°, B-type giants and subgiants 78−61863
Cepheid masses from observations and pulsation theory 79−48802
Cepheids, double-mode, photoelectric radial vels. and BVRI photometry 79−88675
δ Ceti, period changes of β Cephei type star 78−32487
T Ceti, semiregular variable, Tc I absorpt. line obs. 78−28689
o Ceti, vars. in spatial distrib. of 11 micron radiation 79−5828
o Ceti (Mira), long-period variable, radial-vel. obs. 79−88684
o Ceti (Mira), mass loss rate determ. 79−48831
o Ceti (Mira), observing campaign around 1979 October 18 light max. 79−92786
o Ceti (Mira), spectropolarimetry 79−21302
o Ceti (Mira), strong TiO-related dia. vars. 78−16429
o Ceti (Mira), variable 2.6 mm CO emission obs. 78−12241
o Ceti AB, IUE obs. of UV spectrum 80−22027
circumstellar dust shells, IR obs. 77−41404
CIT 6 (IRC+30219), IR C star, CO obs. of mass outflow 80−12761
cool C stars, nearby, distances 78−49434
cool giant stars, narrow-band polarisation effects 78−16427
cool giant stars, neutral-ion spectral anomaly 78−7985
cool giant stars, obs. and anal. of CO at 5 μm 78−36569
cool Mira variables, shock waves accel. in photosphere 77−13352
cool stars, chromosphere mass loss determ. from Mg II UV line obs. 80−85935
cool stars, effective temps; ang. dias. and reddening determ. from 1 to 5 μm flux curves 79−44458
cool stars, local interstellar H and D Lyman α towards four objects 79−5886
cool stars, model depend. of detailed anal. 77−53590
cool stars, polarization across TiO bands and scattering envelopes 79−97005
cool stars, supersonic stellar winds and rapid mass loss 79−21268
cool stars, Ti isotopic abundance ratios 80−26840

giant stars continued
cool stellar wind models for late type stars 80−51733
core He burning stars, H profile, previous mixing and loops in H-R diagram 77−29792
R Coronae Borealis stars, long-term IR behaviour 78−96490
CRL 3099, highly evolved C star, IR photometry and spectrum 78−49436
CSV 6110 in Taurus, o Ceti type variable, visible obs. 80−67745
cyanogen distrib. in 47 Tucanae red giants 79−71025
V460 Cygni, cool C star, atmospheric $^{12}C/^{13}C$ ratio 78−93223
χ Cygni, diameter of Mira-type star from speckle interferometry 80−67728
31 Cygni, eclipsing binary, Ca I 6752 Å circumstellar line obs. 77−17619
CH Cygni, linear polarisation vars. rel. to circumstellar dust grains form. 78−69808
χ Cygni, long-period variable, radial-vel. obs. 79−88684
χ Cygni, Mira variable star, variable 2.6 mm CO emission obs. 78−12241
NML=V1489 Cygni, OH/IR star, 1612 MHz OH maser multibaseline VLBI obs. 80−12766
CH Cygni, red giant, mag. field interpretation for outburst 78−4250
R Cygni, S-type star, Keenan band identification problem, IR obs. 80−72946
α Cygni, supergiant, near UV spectrum 78−7991
CH Cygni, symbiotic star, binary model 80−62158
V1016 Cygni, symbiotic star, evidence for late-type component from IR variability obs. *(Russian)* 80−105263
CH Cygni, symbiotic star, IUE obs. during active phase 79−62846
CH Cygni, symbiotic star, rapid and slow light vars. 80−51792
α Cygni (Deneb), variable line profiles interpretation 77−64761
V1329 Cygni (HBV 475), symbiotic variable, photometric and spectroscopic history 80−62148
β Cygni A, close companion visual obs. 80−8663
Cygnus X-2, binary, radial vel. and orbital elements from visible spectra obs. 80−77519
degenerate star-red giant interacting binary stars, compressible fluid flow, accretion 80−67779
δ Delphini stars in Michigan Spectral Catalogue, uvbyβ photometry rel. to spectral types 80−4377
disk and halo objects, CN strength differences 80−51750
double shell source stars, He shell flashes 77−56909
in Draco dwarf galaxy, effective temp. from photometry and spectral obs. 80−72941
in Draco dwarf spheroidal galaxy, stellar colour magnitude diagram and proper motion 80−73029
ζ Draconis, line identifications in UV spectra 77−87384
in E and S0 galaxies, H_2O absorption at 2 μ 78−41034
evolution of red giants 77−26010
evolved stars expanding envelopes, CO thermal and maser emission 80−82334
extended atmospheres, sphericity effects in red giants, model study 80−22012
F, G, K-type stars, chromospheres, wave dissipation of mechanical energy 80−82340
F, G and K-type stars, chromospheric radiative losses in continuum 80−72924
F-, G- and K-type, in solar neighbourhood, absolute magnitudes 78−81632
Fornax dwarf elliptical galaxy, giant branch colour-magnitude diagram 80−4431
G and K-type giant stars, Li abundances 80−41819
G giants kinematics, influence on asymmetrical drift determ. 77−13403
G- and K-type, kinematical and photometric props. 77−29937
G- and K-type, theoretical colours, model atms. 79−12474
G- and K-type, theoretical colours from synthetic spectra 79−62827
G- and K-type giants, CNO abundances 77−5530
G- and K-type giants and supergiants, correl. between motions and CN anomalies 77−17566
G- and K-type giants in short period binaries 77−87394
G- and K-type stars, space motions 77−45430
G-K giants, low $^{12}C/^{13}C$ ratio explanation constraints 79−5817
G-K giants and C stars, origin of $^{12}C/^{13}C$ ratios freq. distrib. 77−78780
G-type, heavy-element abundance effect on classification 77−29834
galactic centre region, 2.2 μm spectroscopy rel. to giant stars IR flux 78−36686
galactic halo C star possible association with Magellanic Stream, visible obs. 80−77411
galactic X-ray sources, IR photometric obs., identifications, reddening 79−71155
μ Geminorum, 1.25-3.25 μ airborne photometric obs. 78−40934
γ Geminorum, companion to gamma-ray source CG195+4 78−32459
γ Geminorum, differential abundance anal. rel. to α Lyrae standard 80−82362
ε Geminorum, occultation by Mars, evidence for atm. tides 77−37550
β Geminorum (Pollux), chromosphere model 78−40931
1 Geminorum B, spectroscopic binary, orbit from photoelectric radial vels. 77−22269
GK giants, CN strengths, mixing and supermetallicity 77−56930
GL 3068, IR spectrum of C star 79−12469
globular cluster giant stars, blanketing differences meas. 80−4345
globular clusters evolved stars, CN strengths and UV excesses from DDO photometry 77−64753
globular clusters red giants, metal abundances in M92 and (M15) 79−92759
in globular star clusters, Ca II H and K-lines and abundance 80−72940
β Gruis (M2 II), S I emission obs. in EUV spectrum 80−82359
halo giant in north galactic cap, photometry and spectra 78−85942
halo red giants, contrib. to faint red stars at intermediate galactic latit. 78−32457
HD 10380, Population I giant, chemical anal. and comparison with high vel. stars 80−82352
HD 108078, spectroscopic binary orbit from photoelec. radial vel. meas. 80−77451
HD 116745, Population II F giant, extended static stellar atmosphere 77−60759
HD 122563, metal-deficient giant, atm. $^{12}C/^{13}C$ ratio, mixing 78−4201
HD 128220, peculiar spectroscopic binary, props. of giant component *(French)* 77−57014
HD 128279, cool halo star, abundances, reduction procedure and equiv. widths 77−49384

giant stars continued
HD 129494, new pulsating δ Delphini star, photometric obs. and luminosity 80−67750
HD 129708, bright short-period Cepheid with δ Delphini tube spectrum, photometric obs. 80−67751
HD 139216, unusual Balmer lines in M-type giant 79−80310
HD 147508, spectroscopic binary, orbit from photoelectric radial vels. 78−69839
HD 155989, spectroscopic binary, orbit from photoelectric radial vels. 79−21355
HD 170899, possible halo population giant star 80−26859
HD 175305, red horizontal branch star in general field, spectroscopic and photometric anal. 79−40189
HD 184279, B-type subgiant, variability 79−84804
HD 18474, G-type giant, rare earth's abundance *(Spanish)* 79−25605
HD 199892, spectrographic binary, spectrograms and orbital elements 79−21359
HD 20722, peculiar nebula surrounding K-type giant 79−58407
HD 22007 (primary of ADS 16681), spectroscopic binary, radial vel., orbit elements 80−67793
HD 2343, spectroscopic binary, orbit from photoelectric radial vels. 80−8656
HD 31908, freq. analysis of δ Delphini star 80−46581
HD 4174, peculiar M-giant, magnetic field 80−8631
HD 4174, symbiotic star, spectroscopic obs. 80−85945
HD 4174 (=EG Andromedae), peculiar M giant, UV spectra obs. 80−94798
HD 52788, freq. anal. of δ Delphini star 79−35276
HD 63791, probable metal-poor halo G-type giant field star 80−26859
HD 6497, high-dispersion analysis of Arcturus group member 77−29838
HD 65750, photometric vars. of red giant, obs. of surrounding refl. nebula IC 2220 78−36567
HD 76932, subgiant halo star, chem. comp. rel. to nucleosynthesis 78−81626
HD 8781, freq. anal. of low-amplitude δ Scuti star 80−46575
HD 90706, 90707, 100943, giant and supergiant Be stars in open clusters IC 2581 and NGC 3766, obs. 80−90445
HD 91805, spectrum anal. rel. to nature of Bidelman-MacConnell weak G-band stars 78−49432
HDE 232078, variable mass loss in metal deficient red giant 79−67010
HDE 245770 (Ariel 0535+26), optical spectrum of Be star 78−4227
heavy-element excess in late spectral class stars 80−26854
Henize 2-37, symbiotic star, steam obs. rel. to presence of Mira variable 78−40970
Henyey-type evolution code, appl. to stars with shell energy sources 78−61848
α^1 Herculis, absolute mass loss from circumstellar absorpt. lines in spectrum of visual companion 78−7997
OP Herculis, irregular variable, Tc I absorpt. lines obs. 78−28689
OP Herculis, late-type variable star, spectral energy distrib. and spectral types *(Russian)* 78−40958
τ Herculis, line identifications in UV spectra 77−87384
α Herculis, location of α^2 Herculis along line of sight 78−73739
g Herculis, M-type giant, atm. physical conditions 78−24512
high galactic latitude stars, division into giants and dwarfs by proper motion *(Russian)* 80−109431
high velocity giant stars, detailed chemical anal. 80−82352
high-luminosity stars in Hyades, Hα and O I 7774 Å photometric obs. 77−22286
high-luminosity thermally pulsing stars, surface comp. rel. to interstellar medium element enrichment 78−40917
HR 1105, He I 10830 Å line obs. *(Russian)* 80−17586
HR 2081, double-lined spectroscopic binary, radial vel. orbit and min. masses 80−51811
HR 3126, peculiar M giant in reflection nebula, mass loss 77−17558
HR 3153, young cluster M giant, mass loss 77−17558
HR 5161, spectroscopic binary star, radial vel. orbit 80−12781
HR 6388, spectroscopic binary, orbit determ. from photoelec. radial vels. 78−49482
HR 6392, double star with very high luminosities 77−45493
HR 6766, weak G-band star, light-element abundances 78−57548
HR 7083, spectroscopic binary, orbit from photoelectric radial vels. 78−32517
HR 8752, G-type supergiant, obs. of associated radio source 78−40942
Hyades giants, Be abundances 77−53584
W Hydrae, long-period variable, suspected Zeeman splitting in OH masers 80−36632
β Hydri, nearby subgiant star, XUV radiation upper limit 79−12471
III-106, CH star in globular cluster M22, CO in IR spectra 80−62131
intermediate-mass stars asymptotic giant branch evolution as function of mass and comp. 80−12749
internal mixing, rel. to strong CN phenomenon 78−53921
IR airborne spectrophotometry, 1.2-5.5 μm, spectra and absolute calibration 80−62117
IR bright stars in region of galactic centre, catalogue and photometry 80−77299
IR limb-darkening coeffs. for late-type giant model atmospheres 79−71029
IR sources in AFCRL Survey, subcatalogue 77−87283
IR spectral observations, of late-type giants *(Japanese)* 79−80307
IR stars, search for OH 18 cm emission 78−40949
IR stars, survey for circumstellar OH emission 79−48787
IR stars, very long baseline interferometric obs. of assoc. OH masers 77−53699
IR stars among AFGL/CRL sources, spectroscopic obs. 78−32599
IRC+10216, C star, near IR obs. of new mol. feature 79−92762
IRC+10216, C star, NH_3 obs. in circumstellar envelope 79−48793
IRC+10216, C star, possibility of detecting cyanoacetylene-d_1 (DC_3N) 78−69901
IRC+10216, circumstellar dust shell model rel. to IR energy distrib. 80−56972
IRC+10216, far IR obs. 77−29949
IRC+10216, molecular abundances in cool C star 80−4354
IRC+10216, spatial spectra from 2.2 to 20 microns, deviations from spherical symmetry 80−41911
IRC+10216, variable C star, IR obs. 80−90568
IRC+10374, IRC+10523, IR stars, H_2O maser emission detect. 80−62298
IRC+10420, IR emission lines from F-type supergiant star 78−4395
IRC+10°216, circumstellar methane in IR spectrum 78−57694
IRC+30219, variable C star, optical emission-line phase obs. 80−90569
giant stars continued
IRC +10216, C star, far IR size 80−82539
K giants, observational evidence for mass loss 77−56928
K-giants, z-motions in polar zones 77−17565
K-type, $^{12}C/^{13}C$ ratio correl. with Fe/H ratio 79−48798
K-type, colour excesses, interstellar dust grains distrib. determ. 79−40251
K-type, in galactic centre, dust grains heating, radiation model 78−36697
K-type, macroturbulence rel. to luminosity 79−96997
K-type, turbulence in normal and super-metal-rich stars 79−92756
K-type, upper photospheric temp. models, super-metal-rich and normal giants 79−21278
K-type giant stars, evidence of circumstellar shells 80−90420
K-type giant stars, Population I, CN strengths and $^{12}C/^{13}C$ ratios 78−93229
K-type giant stars, reddening determ. from David Dunlap Observatory (DDO) photometry 78−4222
K-type giant stars polulation at South Galactic Pole, CN anomalies and distances 80−8622
K-type giants, multivariate anal. of spectrophotometry rel. to atmospheric characts. 77−78772
K-type spectra, metallicity determ. problems 79−44474
L973, red giant in globular cluster M13, curve of growth anal. 79−48796
AR Lacertae, double-subgiant eclipsing binary, spectra, abundances 78−8044
AR Lacertae, eclipsing binary, photometric obs., intrinsic variation 77−22271
late M-type giants in elliptical galaxies, evolutionary synthesis of stellar population 78−57626
late type giants, departures from LTE ionization equilib. 78−4204
late type giants, gravit. phase transitions 77−49380
late type giants, nonlinear coupling between pulsation and convection 77−13356
late type stars, Ca II H and K lines and nearby continuum photoelectric calibration 80−36617
late-type, 1.25-3.25 μ airborne photometric obs. 78−40934
late-type, CO emission lines obs. from expanding molecular envelopes 77−22219
late-type, luminosity criteria 77−5527
late-type, position on Hertzsprung-Russell diagram 77−78792
late-type, space distrib. in nuclear bulge of Galaxy, ellipsoidal density model 78−86009
late-type, sphericity effects in extended atms., models 78−81617
late-type (K0 to M6) giant stars, effective temps. 80−46545
late-type giant model atmospheres, limb darkening coeffs. 78−20821
late-type giant stars in galaxy NGC 253, evidence from two-micron spectrophotometry 80−4442
late-type giant stars O I 7773 Å triplet obs. 79−35250
late-type giants, ang. dias. by lunar occultation technique 77−74048
late-type giants, near IR photometry with balloon-borne telescope 78−73713
late-type giants, near IR photometry with balloon-borne telescope 80−4357
late-type giants, semi-theoretical density profiles along galactic radius through Sun 79−35253
late-type giants in Hyades-like clusters NGC 2423, 2482, intermediate-band photometry 80−31289
late-type stars, anal. of balloon-borne near IR multicolour photometry 80−98654
late-type stars, balloon-borne near IR multicolour photometry 80−4356
late-type stars, Ca II emission V/R ratio rel. to mass loss 78−93208
late-type stars, He abundance effects on spectrum appearance 80−46540
late-type stars, near IR multicolour photometry from BAT *(Japanese)* 80−31298
late-type stars, search for C IV reson. doublet, TD1 satellite UV obs. 77−5526
CW Leonis, (IRC+10216), IR C star, intrinsic polarisation origin 80−67730
87 Leonis, lunar occultation ang. diameter 79−25599
R Leonis, Mira variable, CO and OH IR vibr.-rot. overtone bands 78−36574
R Leonis, strong TiO-related dia. vars. 78−16429
ρ Leonis, supergiant, expanding envelope OAO-3 spectra *(Russian)* 78−4224
υ Leonis (SAO 138298), angular diameter from lunar occultation obs. 78−45332
π Leonis lunar occultation obs. giving angular diam. 77−33493
in LMC, photometric luminosity calibration, visible obs. 80−94797
LMC central regions, stellar count-brightness ratios rel. to population struct. 78−89245
LMC disc stars, photographic and photoelectric photometry rel. to population struct. 77−33633
long period variables in globular clusters, high sensitivity search for main-line OH emission 80−62207
long-period variable and IR stars, discovery of new 1665/1667 MHz OH/IR sources 77−64763
long-period variable stars, maser activity rel. to Hδ emission, obs. 79−88685
long-period variable stars, OH maser lines struct. and saturation 78−93264
long-period variable stars, radial vel. obs. 79−88684
long-period variable stars in S.hemisphere, narrowband polarimetry 80−98666
long-period variables, CO and SiO millimetre line emission obs. rel. to circumstellar shell props. 78−49423
LS I +61°303 as optical counterpart for GT 0236+610 source 78−36568
luminous cool stars, atm. $^{12}C/^{13}C$ ratio 77−13336
XY Lyrae, late-type variable star, spectral energy distrib. and spectral types *(Russian)* 78−40958
δ^2 Lyrae, M-type giant, atm. physical conditions 78−24512
in M13, Na abundance var., evidence for protocluster gas inhomogeneities 80−82439
M22, comparison with ω Centauri, spectroscopic evidence 80−46617
M34, open cluster, spectral types of brightest stars 78−12311
M3, globular cluster, luminosity function 77−57069
M3, M13, M92, M67, giant stars IR photometry, bolometric magnitudes and effective temps. 78−57595
M5, M13, M3, globular clusters, giant stars chemical comp. 80−67695

giant stars continued
M5 giant branch, spectroscopic survey 78−16467
M67, radial distrib. of bright giants rel. to mass loss 77−13408
M71, globular cluster, giants IR colours, CO band strengths and physical parameters 79−25650
M92, globular cluster, giant star C and N abundances 77−87496
M92, globular clusters, luminosity function 77−57068
M 67, abundances of F 170 and F 244 giants 77−29890
M-type, atmosphere mass estimate *(Russian)* 79−21292
M-type, atmospheres physical conditions 78−24512
M-type, circumstellar envelopes, observational study 78−53939
M-type, circumstellar gas and dust shells, optical and IR obs. 79−21281
M-type, classification from spectral scans 80−62127
M-type, in solar neighbourhood, absolute magnitudes 78−81631
M-type, IR photometry 80−41823
M-type, IR spectrophotometry in Cassiopeia 79−88658
M-type, spectral type and luminosity classification from near IR spectrograms 79−16952
M-type circumstellar envelopes, high-dispersion spectra 79−92755
M-type giant stars, spectral energy distribs. and effective temp. scale 78−28678
M-type giants, near IR luminosity-sensitive spectral features rel. to M31 and (M32) 78−49431
M-type stars, observations in wavelength range 370 to 550 nm, energy distribution 79−84798
M-type temp. sequence based on TiO spectra *(Russian)* 78−20831
M-type variable stars, obs. in DDO photoelec. system, spectral classification 78−32463
maser emission, role of plasma effects in generating high-rel. and symmetric spectral features 80−31378
maser stars, search for water vapour absorpt. lines 77−78804
mass flow models for cool, luminous objects 79−5813
mass loss and convective overshooting influence on evolution 79−84789
mass loss before envelope ejection due to pulsational instability 80−72935
mass loss by cool stars, review *(German)* 79−16957
mass loss rates 77−91534
massive single stars, main sequence evolution with and without stellar wind 79−16936
massive stars, 10^3-10^4 M⊙ range, final evolution 77−87371
massive stars, gravity modes vibr. stability during H shell burning stage 77−56933
Medium-Amplitude Red Variables, UBVRI photometry 77−45438
Melotte 66, oldest open cluster, giant branch clump luminosity rel. to age 80−17621
Melotte 66, very old open cluster, confirmation of broad giant branch 78−32538
metal-deficient stars, CO obs. at 2.2 and 2.4 μm 79−58336
Mira type stars, luminosity props. from spectra and light curve elements 80−105253
Mira type variables, Me and Se types, UBV photometry 80−82375
Mira type variables atm., OH maser, IR line overlap pumping mechanism 80−72764
Mira variables, envelope pulsational instability rel. to planetary nebula form. 80−26928
Mira variables, IR Photometry and OH maser pumping efficiency 80−82379
Mira variables, mass loss and red giant stars evolution 77−17571
Mira variables, statistical anal. of galactic concentration *(German)* 80−4390
Mira variables, supersonic mass flow theory 79−35270
model envelopes, physical props. *(Portuguese)* 80−22014
molecular spectra of pure S stars 78−77554
N Monoceros region, two-micron IR objects survey 80−8555
MWC 342, emission line spectrum in 1974-75 period 78−57558
NGC 188, open cluster, anomalous giant branch 78−41001
NGC 188 red giants, photographic photometry and space distrib. 77−53430
NGC 6121 (M4), near IR photometry of metal-poor globular clusters 77−41398
NGC 654, young open cluster, membership obs. 77−29885
in NGC 7789, open cluster, DDO and UBV photometry rel. to metal abundances 77−53648
in NGC 7789, open cluster, metal abundance, He content and mass loss 80−31335
nonradial oscillations excitation in giants and supergiants 77−74049
nonthermal vels. in six giants and the Sun 78−4219
novalike object in Vulpecula, light curve, photometric and spectroscopic obs. 80−67758
OB stars, in Vela region, list of 166 objects 77−87280
OB stars in associations and young clusters, He abundance vars. *(Russian)* 77−82287
OH 0739−14, M-type giant in reflection nebula, IR obs. 80−46692
OH maser emission from late-type stars, UHF obs. 80−56826
optical emission from stars with IR excesses, intrinsic linear polarisation origin 78−96481
β Orionis, line blocking, reddening empirical effective temp. determ. 77−87389
U Orionis, Mira variable, relation between 1612 MHz flare and light curve 80−56844
λ Orionis, obs. of UV radiation scattered by interstellar dust 80−56918
π^5 Orionis, Orion OB1 association star, interstellar lines obs. by Copernicus 80−22050
U Orionis, outbursts in main line OH emission 79−101158
α Orionis, speckle interferometry diameter, limb darkening 77−91525
U Orionis, stellar OH maser VLBI obs. rel. to mag. field 79−25742
κ Orionis, supergiant, expanding envelope OAO-3 spectra *(Russian)* 78−4224
α Orionis (Betelgeuse), model atm., effective temp. 77−56935
δ Orionis A, UV spectrophotometry and optical polarimetry, stellar wind variability 79−21277
peculiar red giants, s-process abundance evolution in galactic disc 77−13449
peculiar red giants evolution, constraints from masses and space densities 80−22001
57 Pegasi, long-period pulsating variable, spectrographic and photometric obs. 79−21305
β Pegasi, M-type giant star, Mg II h and k emission obs. 78−53945
AG Pegasi, symbiotic binary system, UV and optical spectrum rel. to nature of components 80−109449
photometry in southern open clusters 79−12468

giant stars continued
19 Piscium, C star, violet spectrum line identification and radial vel. 80−82361
TX Piscium, disc brightness distrib. and envelope obs. from lunar occultation meas. 80−67725
planetary nebulae formation models, implications for Fe condensation 79−40238
planetary nebulae precursors, stellar wind model for nebulae refractory elements gas-phase abundances 80−109516
Population I giant stars, theoretical surface abundances 80−94796
ζ Puppis, Of-star, UV spectrum, line identifications 77−45441
L_2 Puppis, semiregular variable, Ca I uneven distrib. from narrowband polarimetry 80−98666
radii, finite extent of atmospheres rel. to colour indices 78−32450
red giant mean initial mass from visual binary data 78−49429
red giant model atmospheres, opacity sampled models grid 80−82348
red giant of 6 solar masses, envelope composition rel. to evolution 80−105237
red giant sequence in LMC faint clusters 80−94841
red giant stage of stellar evolution 80−12752
red giant stars, circumstellar shells chem. struct. 80−105242
red giant stars, evolutionary sequences 78−65611
red giant stars, meridional circulation and CNO anomalies 79−48786
very red giant stars in Fornax galaxy, discovery and BV photometry 80−51768
red giant stars in globular clusters M92 and NGC 6397, C abundances 79−48785
red giant stellar wind/circumstellar nebula interaction model of planetary nebula origin 78−36674
red giant variable stars, multiple periodic vars. 77−87427
red giant variables in M13, photometric investigation 77−74104
red giants, ^{14}C and neutrons prod. 77−26005
red giants, ^{22}Ne neutron source effects on Mg and Ne abundances 78−49430
red giants, CNO isotopes 77−87399
red giants, CNO isotopes rel. to main-sequence mixing 77−33475
red giants, convective He shells, s-branch nucleosynthesis during thermal pulses 80−90410
red giants, ejection of ^{13}C enriched matter rel. to interstellar $^{12}C/^{13}C$ ratio 77−9788
red giants, grain-gas interaction in envelopes 77−60760
red giants, in Draco dwarf galaxy, metal abundance determ. 79−17078
red giants, in globular cluster NGC 6624, optical and IR obs. 77−45498
red giants, in metal-rich globular clusters, near IR photometry 77−45503
red giants, in symbiotic star systems, evolution *(Russian)* 77−17616
red giants, IR radiation emission in final stages 80−72931
red giants, Li synthesis by spallation reactions 77−49366
red giants, mass loss from dynamically unstable envelopes 78−20824
red giants, spectra, TiO bands obs. and theory 78−96480
red giants, spectra and comp. *(Norwegian)* 77−71111
red giants and supergiants, mass loss 77−9743
red giants in 47 Tucanae, C and N abundances 79−97000
red giants in Draco dwarf spheroidal galaxy, metal abundance 80−73030
red giants in Galactic nuclear bulge, spectroscopy 77−26058
red giants in Galaxy nuclear bulge, areal density vars. from UBV photometry 78−53926
red giants in globular cluster NGC 6752, DDO photometry and spectra 79−71079
red giants in globular clusters, mass loss 78−93238
red giants in globular clusters, parametric approach to slope of giant branch 77−53649
red giants in halo globular clusters, abundances 79−5898
red giants in M5 (NGC 5094), intermediate band electronography 78−49490
red giants with neutron cores, energy sources *(Russian)* 78−93197
red variable star, possible optical candidate of 2S 1702−363, spectroscopic obs. 78−77566
red variable stars, amplitude extension and amplitudes limit 79−62836
red variable stars in globular cluster M22, light curves 77−64808
red variables, medium-amplitude, UBVRI obs. 77−82224
s-process element prod. in deeply mixed convective envelopes 77−33470
S-type, list of brightest stars in IR 77−41382
S-type stars, molecular spectra and model atmospheres 80−51764
S-type stars, possible presence of ZrO IR spectrum 80−62124
S-type stars distrib. and population-type characts. 79−88651
S-type stars in Southern Milky Way, objective prism survey and BVI photometry 78−61754
HM Sagittae, eruptive variable, IR variability rel. to symbiotic binary model 79−25614
HM Sagittae, symbiotic star, evidence for late-type component from IR variability obs. *(Russian)* 80−105263
FG Sagittae, UBV photometry and spectroscopic obs. 77−71119
AQ Sagittarii, C star, ang. dia. from lunar occultation meas. 80−22008
ξ^2 Sagittarii, lunar occultation obs. giving angular diam. 77−33493
RY Sagittarii, magnitude estimates for R Coronae Borealis-type star 77−78800
V879 Scorpii, M-type long period variable, visible obs. *(Chinese)* 80−85956
Sculptor dwarf spheroidal galaxy, abundance vars. on giant branch rel. to ω Centauri anomaly 79−5904
V367 Scuti, double-mode Cepheid in NGC 6649, anomalous open cluster 79−5866
δ Scuti subgiants, possible model 79−48809
Scutum Cloud direction, giant stars density functions from RGU photometry 79−35242
semi-Ba and Ba stars, heavy element abundance effect on spectroscopic luminosities 77−53586
SIMS, C and SC stars, new discoveries on southern, red-sensitive objective-prism plates 80−36511
Sk 160, optical counterpart of SMC X-1, VBLUW photometry 77−82277
slow novae and symbiotic stars, late-type components spectral classifications 80−94813
speckle interferometry for stellar diameter meas. *(Russian)* 78−40922
spectra of giants in distant satellites of Galaxy 78−40926
spectral energy distrib. of eight stars used as spectrophotometric standards 79−35147
spectral types in NGC 6633 open cluster 77−74108
spectral types of stars with unusual photometric indices 79−71033

giant stars continued
spectroscopic binaries, Ca II H and K line emissions in late-type giants and supergiants 77−91566
subgiants, F-, G- and K-type, Be abundance rel. to post-main sequence evolution 77−13333
subgiants, Hertzsprung-Russell diagram age and mass calibrations for H burning evolutionary stages 80−51744
super-metal-rich stars, evolution rel. to H-R diagrams of old galactic clusters 77−49370
supergiants, evolution with mass loss by stellar wind 78−4197
supermassive rapidly rotating stars, mag. field effect on pulsational stability *(Russian)* 77−82220
supermetallicity and the strong-lined binary systems 79−75204
symbiotic stars, binary model with super-critical accretion 77−45458
symbiotic stars, stellar wind and accretion rates rel. to subclasses 80−62144
symbiotic stars, survey at 1612 MHz 80−12774
symbiotic stars and slow novae, late-type components spectral classifications 80−94813
T626, red giant in open cluster M67, curve of growth anal. 79−48797
γ Tauri, ang. diameter determ. from lunar occultation obs. 80−62119
α and θ^1 Tauri, diameters from Hyades lunar occultations 79−75253
θ^1 Tauri, double star, lunar occultation obs. 79−67052
α Tauri, emission lines in UV spectra 79−71028
α Tauri, grazing occultations during 1979 visible from Scandinavia *(Swedish)* 78−69656
δ Tauri, Hyades giant, identification as spectroscopic binary 77−64794
α Tauri, search for Ti II 3080 Å multiplet emission 80−51769
α Tauri, semiempirical model photosphere from Fe I lines obs. 78−4202
α Tauri (Aldebaran), angular diameter from lunar occultation 79−40185
α Tauri (Aldebaran), Ca II K line high-resolution obs. 78−16408
α Tauri (Aldebaran), chromosphere model 78−40931
α Tauri (Aldebaran), radius from 1978 Aug. 26 occultation fast photometry 79−67005
α Tauri (Aldebaran), Ti isotopic abundance ratios 77−22212
α Tauri (K5 III), S I emission obs. in EUV spectrum 80−82359
RR Telescopii, symbiotic star, steam obs. rel. to preence of Mira variable 78−40970
47 Tucanae asymptotic giant branch stars, N anomaly anal. 79−48867
turbulent diffusion and $^{12}C/^{13}C$ abundance ratio 80−21993
undersize subgiant components in close binaries 79−44528
Ursa Minor dwarf spheroidal galaxy, abundance vars. on giant branch rel. to ω Centauri anomaly 79−5904
β Ursae Minoris, astrometric obs. (1953-61) for Pulkovo large transit instrument orientation parameters determ. *(Russian)* 79−96910
γ Ursae Minoris, high dispersion spectroscopy 80−41853
variable emission-line star in core of M15, spectrum, photometry and position 79−5840
α Virginis, β Cephei type pulsation characts. 80−56835
ε Virginis, equivalent widths of Fe lines for spectral anal. 77−78771
ε Virginis, Fe curve of growth split as function of atmospheric pressure 77−29794
ε Virginis, Fe spectrum, differential model atmosphere analysis 79−25604
ψ Virginis (SAO 139033), ang. dia. from occultation obs. 78−20825
21 Vulpeculae, new luminous long period δ Scuti star, photometry 80−31306
W92, possible gravit. contracting binary system in NGC 2264 young cluster 78−32462
weak G-band stars, CH and NH band strengths, atm. material from CNO cycle 79−8917
weak G-band stars, photometry and spectra 77−49386
weak-G band stars, Li abundance determ. 78−53948
X-ray binaries, double core evolution 79−84816
yellow giants in young open cluster Collinder 140, spectral classification and possibility of membership 80−62211
^{26}Al from red giants 80−67712
Ba II metal rich stars, Ba abundance implications 79−71024
Ba II stars, binary nature from visible radial vel. obs. 80−82355
Ba II stars, JHK photometry 77−74053
Ba II stars, uvby photometry rel. to s-process element enrichment 79−58337
Ba II stars and s-process calc. 80−56824
Ba stars, absolute magnitudes redeterm. 78−8006
Ba stars, DDO system photometry, luminosity anomaly 79−35246
C and M-type, distrib. in galactic nucleus and Magellanic Clouds 78−32460
C IV in stars hotter than B 1, Copernicus obs. 79−44463
C stars, $^{12}C/^{13}C$ ratios 79−35257
C stars, $^6Li/^7Li$ ratio, low-energy spallation model 78−40927
C stars, 3.9 micron absorpt. band identification 78−93231
C stars, determination of $^{12}C/^{13}C$ and N/C ratios in atm. 80−17580
C stars, form. of carbyne and cyanoacetylene in stellar atm. 80−67708
C stars, IR spectrophotometry in Cassiopeia 79−88658
C stars, JHKL photometry 80−46555
C stars, Li line formation 78−65615
C stars, polyatomic molecular line search in photographic IR 77−78786
C stars, search for HCN and CH maser emissions 80−51856
C stars, spectroscopic problems 80−56832
C stars, variable, IJHKL photometry obs. 80−98657
C stars and G-K giants, origin of $^{12}C/^{13}C$ ratios freq. distrib. 77−78780
C stars in Cygnus, new discoveries catalogue 80−46551
C stars in red globular clusters in Magellanic Clouds 79−101143
C/N abundances on first giant branch of NGC 6752 globular cluster 80−67719
C/O ratio in massive stars, core convection effects 80−17579
C_2^-, $A^2\Pi_u$-$X^2\Sigma_g^+$ lines, obs. in carbon stars 80−98661
CH stars in globular clusters, possible binary nature 80−82355
CNO abundances in G and K giants 78−7993
CNO abundances in red giant envelopes 77−29825
CO 2.3 μ band strength in weak-G-band stars 78−12228
CO absorption and effective temp. of giants in globular cluster ω Centauri 80−51749
CO emission from late-type giants, molecular envelopes and planetary nebula origin 78−40940
CO in giants in globular cluster, IR obs. 78−93339
$^{12}C/^{13}C$ ratio in giant and supergiant atms. 77−13337
Fe abundances in G and K giants from near-IR spectra 79−16944
He content of envelope, zero age horizontal branch loci 78−77551
He core flash, convection efficiency and mixing possibilities 79−48774
He core flash onset and $^{14}C(\alpha,\gamma)^{18}O$ in low-mass stars 80−51735
giant stars continued
He flash in stars with shell energy sources 78−89169
He shell flashes rel. to galactic He enrichment 77−45428
He stars, post-giant evolution 77−56947
Li in weak G-band stars, spallative origin 80−51752
O-rich late-type stars, 16 to 39 micron spectroscopy 80−22002
OH masers, interferometry and source struct. 77−53583
OH/IR stars, IR search and identifications 78−24510
OH/IR stars, new SiO transition detect. 78−53954
OH/IR stars, OH main lines masers inversion 78−28664
OH/IR unidentified Type II stars, galactic distrib. and kinematics from 1612 MHz survey 78−49450
SiO 86.2 GHz maser sources, polarisation props. 80−4449
SiO masers, J=1→0 ν=1 and 2 masers relative intensity and vel. 80−4339
Tc in late-type stars, spectral analysis 80−8623
Tc stars, search for TcO spectral bands 78−40935

Gibbs free energy *see free energy*

Gibbs function *see free energy*

Ginzburg-Landau theory
A-15 space group struct., phase transitions, renormalisation group theory comparison with Landau theory 80−6489
amorphous superconductor, high-κ, upper and lower crit. fields 79−4629
antiferromagnet, superfluid flow states, existence from Ginzburg-Landau theory *(Russian)* 78−72085
antiferromagnetic superconductor, isolated vortex line 80−70912
bond percolation problem in semi-infinite medium, Landau-Ginzburg theory 79−93068
CDW commensurate-incommensurate phase transition, 1-D electron-phonon system 78−14682
chain conductors, CDW ordering 78−79731
condensed matter physics, dynamic correlations, book 80−86046
Coulomb superconductor with inverse quasiparticle distrib., behaviour in mag. field 77−20490
critical dynamics far from equilib. 77−57295
critical region fluctuations *(Russian)* 79−75484
crossover and scaling at low temp. 77−61023
crystal growth, generalised kinetic eqn. 77−55249
degenerate semiconductors, heterogeneous state, first-order phase transition, Ginzberg-Landau method analogue 80−70372
diffusionless first order phase transform. eqns. appl. to liquid crystals and solids 78−30734
dipolar uniaxial ferromagnet, equation of motion, nonlinear response near critical point 79−99717
dirty superconductors, time-depend. Ginzburg-Landau eqns. near supercond. transition temp. 80−70886
dislocation structures, supercond. states 79−69627
dislocation systems, superconducting states, impurity effects *(Russian)* 80−11131
disordered systems, electron localisation and classical solns. in Ginzburg-Landau field theory 78−56108
dissipative structures in quasi-one-dimensional superconductors, soliton solns. 79−87186
distorted vortex lattice, generation of soln. to Ginzburg-Landau eqns. 79−56467
distorted vortex lattice, order parameter and mag. field appl. to flux pinning 77−77013
distorted vortex lattice, order parameter and mag. field appl. to flux pinning 77−77014
dynamic renormalisation group anal. for Ginzburg-Landau model, in large n limit 79−9193
dynamical symmetry breakdown at the two-dressed-loop level and beyond 79−294
dynamical symmetry breaking, extended structs., generation in field theory 77−6026
dynamics of spins interacting with quenched random impurities 77−40065
EBBA, nematic, linear and nonlinear relaxations of fluid dynamical motion 77−31585
effective potentials, Ginzburg-Landau model 78−52287
elastically coupled systems at marginal dimensionalities, crit. dynamics and stability 80−101769
electron-hole pairing quantum coherent phenomena *(Russian)* 77−80869
electronic density of states, exponential tail in random potential 80−65423
equation of motion and nonlinear response near critical point 77−15991
exciton dielectric, inhomogeneous current state phase transition, free energy *(Russian)* 80−84703
Fermi liquids at surfaces quasiclassical boundary conditions 80−4641
ferromagnet, critical dynamics under quenched random magnetic fields 79−4681
ferromagnet, disordered, phase transitions, mol. field and Landau-Ginzburg theories 80−93118
ferromagnetic superconductor, uniaxial, domain struct. parameters 80−39705
ferromagnetic systems, inhomogeneous, Ginzburg-Landau theory, free energy and Curie temp. 79−51789
ferromagnets, amorphous, itinerant electron model 79−73664
filamentary superconductor, upper and lower crit. fields 80−25053
film, crit. mag. field calc. using Ginzburg-Landau eqns. *(French)* 79−60999
finite superconductor, mixed state 79−99662
first-order phase transition, nonlinear relaxation, Ginzburg-Landau theory including fluctuations 79−35658
flux pinning force, derivation from a potential 78−68128
flux-line lattice and precipitates, elementary interaction force 78−10623
flux-line lattice instability due to planar imperfections 78−23218
gauge choice in superconductors, vortex line free energy formulation 77−51838
granular composite superconductors, Ginzburg-Landau theory, props. 80−88673
hard superconductor, flux trapping, penetration depth determ. 80−100572
heterogeneous superconductor, crit. temp. determ. *(Russian)* 77−76992
incommensurate-commensurate crossover 79−65170
inhomogeneous superconducting film, excess elec. cond. calc. 77−55637
inhomogeneous superconductivity 80−88672
intermediate state, domain struct. near penetration field 77−16009
Josephson junction transients, effect of order parameter relax. 79−56423

Ginzburg-Landau theory continued
Josephson tunnelling as probe of Ginzburg Landau theory 77−89905
Josephson tunnelling current, theory of cos ϕ term. 78−14890
kinetic potential and Maxwell construction in nonequilibrium chemical phase transition 77−87716
Kondo effect in type II superconductors, upper critical field and Ginzburg-Landau parameter 78−14874
Landau-Ginzberg ferromagnet, static and dynamic correl. functions near magnetization curve 79−15318
liquid crystal, nematic-smectic transitions, mean field theory 77−27992
liquid-solid phase transition, dynamic Ginzburg-Landau theory 80−44292
localised defects, one-dimens. model, nearly ferromag. system, solids near displacive phase transitions 78−71820
magnetic moment spatial distribution in single ground state systems with impurities 80−97074
magnetic superconductors, Ginzburg-Landau theory of two antagonistic order parameters 79−38242
master eqn., dynamical renormalisation group transform., Ginzburg-Landau model, kinetic Ising model 80−42170
metallic chain, weakly coupled, Ginzburg-Landau theory 78−91626
metastable microalloys, equilib. form. criteria 78−30762
microbridges, response times and low-voltage behaviour 79−65602
mixed phase of ideal material, transport current distribs. 79−61008
mixed state, two-dimensional, in type I supercond., mag. field effect 77−1523
mobility edge, analogy with spin glass problem 77−85164
mode propagation in superconductors near T_c 79−19682
multicritical points, fluctuation dynamics *(Russian)* 77−27977
N-particle Schrodinger eqn., alternative derivation of Ginzburg-Landau eqn. 78−60242
nematic liquid crystals, radial and circular disclinations *(Russian)* 77−11762
non-equilib. instability, k=0 hard mode transition, appl. of dynamic renormalisation group 79−21686
non-equilibrium superconductor, superparticle-acceleration eqn., normal current diffusion eqn. 78−47911
non-pure supercond., Ginzburg-Landau parameter 77−76997
nonequilibrium superconductivity, oscill. of order parameter caused by quasiparticle injection 79−42697
nonequilibrium superconductor, high-freq. AC process dynamics 80−88674
nonequilibrium superconductor, nonstationary intermediate state *(Russian)* 77−80883
nonlinear critical dynamics of spherical model 77−22506
nonlinear transient phenomena in supercond., Ginzburg-Landau eqn. generalisation 77−32110
one-component Ginzburg-Landau field, nonlinear crit. slowing down 80−27252
ordering alloys, nonlinear critical relaxation of the Ginzburg Landau field coupled to a conserved density 80−90803
origin, development and applications, importance w.r.t. other theories *(Slovak)* 77−63022
perturbation series for crit. behaviour near H_{c2} 77−8233
pion condensate props. in mag. field, superconductivity, mixed state *(Russian)* 80−49974
Pm3n space group struct., phase transitions, renormalisation group theory comparison with Landau theory 80−6489
proximity effect sandwiches, bifurcation theory and order of phase transition 78−84353
proximity sandwiches, thermodynamics of second order phase transitions 79−56408
pseudo-one-dimensional system, Ginzburg-Landau theory of phase transitions 77−15529
pure metals, supercond. theory, exact solns. 80−49981
quasi-one-dimensional metallic systems, crit. behaviour, Ginzburg-Landau theory 79−56147
quasi-one-dimensional systems, free energy of Ginzburg-Landau field, equiv. Hamiltonian 78−6293
random magnet 78−10704
rare earth cpds., $RMo_6S_8(Se_8)$ and RRh_4B_4, coexistence of supercond. and mag. ordering *(Russian)* 80−84542
renormalisation group equations in critical dynamics, scaling far from equilib. 77−28395
rotating superconductors, Ginzburg-Landau equations *(Russian)* 77−40009
scaling at low temps. in Ginzburg-Landau model 77−30121
scaling critical exponents with neglect of cutoff, dimensional anal. 79−93087
semi-infinite system, order-disorder transition 78−47500
small superconductor in magnetic field, first and second order phase transitions 80−2519
solitary waves in Ginzburg-Landau (ϕ^4) field theory and electron localisation in disordered one-dimensional systems 78−14646
spin glass, time dependent Ginzburg-Landau equation 79−61161
spin systems with quenched random impurities, dynamics, replicas and frustration approaches 80−34673
spin-glass phase, time-dependent Ginzburg Landau model 78−39340
strong-coupling superconductors, press. coeffs. of critical field, Ginzburg-Landau parameter, penetration depth 80−54833
structural phase transitions 80−92639
superconducting, periodic structures, crit. fields *(Russian)* 80−88700
superconducting contacts, critical currents, density, penetration depth 80−25059
superconducting current variation with gravitational field variation, general relativistic phenomenological theory 80−54827
superconducting filament, dissipative current carrying states 78−47906
superconducting filaments, phase-slip state theory 79−56371
superconducting film, inhomogeneous, pair-breaking current, Ginzburg-Landau theory 80−97029
superconducting film, resistive transition 80−7049
superconducting junction proximity sandwich, mag.-supercond.-mag., phase diagram 78−95399
superconducting microbridges, basic props. and appls. 77−26400
superconducting order parameter fluctuations, pair tunnelling, review 79−1642
superconducting order parameter perturbation flux pinning 80−103801
superconducting structure, dirty S-N-S sandwiches, boundary conditions, for Usadel eqns. and props. 79−60990
superconducting thin film, vortices, local mag. flux density and elec. current density 80−84572
Ginzburg-Landau theory continued
superconducting thin hollow cylinder, mag. field penetration, Ginzburg-Landau calcs. *(Russian)* 80−75674
superconducting vortices, interaction energy using constrained var. calc. 79−78256
superconducting weak links, low-voltage dynamical props., Ginzburg-Landau model 79−60982
superconducting weak links, order parameter and quasiparticle dynamic props. 80−100555
superconductirg thin films Cooper pains, photon scatt. on plasmons, Landau-Ginzburg theory 80−65738
superconductivity, phenomenological unifying approach to London and Ginzburg-Landau theories 80−103779
superconductor, critical temperature mag. field depend., strong diamagnetism *(Russian)* 80−7022
superconductor, dynamical electrical conductivity below transition temp. 78−2623
superconductor, inhomogeneous, equilibrium order parameter 78−2616
superconductor, quasi-one dimensional, lossless and dissipative current carrying states 77−32109
superconductor, strong-nonequilibrium, dynamic phase-slip centres and resist. state 80−88675
superconductor, type II, with normal inclusions, current density distrib., theory 80−80461
superconductor critical dimensions *(Russian)* 77−15990
superconductor resistive state, coherence length, penetration depth 80−97030
superconductor surface, ponderomotive phenomena theory magnetic forces *(Russian)* 77−12058
supereonductor-normal metal interface, boundary conditions and critical currents *(Russian)* 80−15665
superconductors, critical slowing down, dynamic-exponents, Ginzburg-Landau theory 80−103783
superconductors, effect of insulating pairing of electrons on mag. props. 80−15651
superconductors, mag. flux structures, book 79−91199
superconductors, nonequilibrium, BCS-Boltzmann and Ginzburg-Landau descriptions 79−65589
superconductors, resistive state, phase-slip centres, current-voltage characts. *(Russian)* 80−80437
superconductors, tilted vortices, mixed state features in surface layers *(Russian)* 80−29512
superheating field for finite κ calc. 77−12060
TCNQ salt, HMTTF-TCNQ, three-dimens. ordering, Ginzburg-Landau model for Peierls instability 80−20160
TCNQ-TSeF, model for phase transition and low-temp. phase 77−47734
thin cylinder in transverse mag. field, metastable supercond., Ginzburg-Landau eqns. 79−60961
time dependent eqns. for external time variable mag. field *(German)* 78−10596
time dependent superconductivity, one-dimensional, relax. oscills. of order parameter 79−28475
time-dependent model, critical dynamics near dimens. 2 77−61021
triplet superconductivity, incomplete Meissner effect 79−15255
TSeF-TCNQ, Ginzburg-Landau model for metal-insulator transition 78−6301
TTF-TCNQ, crit. behaviour near 53K phase transition, Ginzburg-Landau theory 79−33249
TTF-TCNQ, crit. behaviour near 53K transition, generalised Ginzburg-Landau theory 79−56147
type I superconductor, paramagnetic effects of two-dimensional mixed state *(Russian)* 79−51729
type II magnetism, existence discounted 78−47983
type II superconducting foil, effects of current-induced mag. field on flux flow 77−77012
type II superconductor, clean cubic, anisotropy of generalised Ginzburg-Landau parameters 79−4630
type II superconductor, dielastic interaction of flux line lattice with internal stresses of cryst. imperfections 78−56270
type II superconductor vortex state, elastic energy calcs. on high inductions 77−36030
type II superconductors, flux-line cutting 80−7055
type II superconductors, longitudinal currents in a system of Abrikosov vortices, Ginzburg-Landau eqn. anal. 80−70914
type II superconductors, thermodynamics near $H_{c2}(T)$ and scaling law 79−60968
type-II superconductors, anisotropic, lower crit. field 80−60153
uniaxial dipolar magnet, critical dynamics and statics 77−59422
uniaxial ferromagnetic superconductor, mag. domain struct. and mag. field penetration depth 79−65583
vacuum manifolds, gauge groups and topological invariants 79−237
vortices in supercond., solns. of Gorkov and Ginzburg-Landau theories 79−65624
weak link, short, with distinct chem. potentials at boundary 80−2528
weak links, interaction in stationary states 78−31020
ϕ^4-field model with image mass, spontaneous coherent state transition 80−99057
Al film, metastable current states, mean free path variation *(Russian)* 80−2538
Al, small particles, Josephson-coupled, local fluctuation effects 78−72308
Al strips, supercond., order-parameter relaxation meas. 79−47207
Al-formvar superconductive junction, Ginzburg's generalised jellium model 80−15663
Al-Formvar-Sn coupled films, Ginzburg's excitonic supercond. model 80−97039
$CeAl_2$, magnetic ordering, 24 component Ginzburg-Landau model 80−97095
CrN, mag. struct. and first-order antiferromag. transition 79−61132
$ErRh_4B_4$, ferromag. superconductor, vortex phase 80−80441
^{3}He, anisotropic superfluid phases, book contrib. 79−99387
^{3}He, Ginzburg-Landau free energy 77−28063
^{3}He, inert p-wave phases in strong coupling theory 77−31825
^{3}He, superfluid, chiral fields, in Ginzburg-Landau region 79−55991
^{3}He, superfluid, distortion in elec. and mag. fields, NMR shifts 77−35780
^{3}He, superfluid, particle like solitons *(Russian)* 77−80675
^{3}He, superfluid, planar textures, Ginzburg-Landau eqn. solns. 80−10729
^{3}He, superfluid, sp. ht. discontinuities, rel. to Ginzburg-Landau parameters 80−54459
^{3}He, superfluid A and B phases, vortex solns. *(Russian)* 77−11762

Ginzburg-Landau theory continued
^{3}He, superfluid A-phase, slab in mag. field, deformed textures 77−39718
^{3}He, superfluid A-phase, slab, nonplanar textures 78−51777
^{3}He, superfluid B-phase, domain struct., derived from Ginzburg-Landau eqns. 78−63896
^{3}He-A, superfluid, first order current induced textural transition 79−95237
^{3}He-A superfluid slab, magnetoelectric textures, capacitive meas. 78−22924
In film, metastable current states, mean free path variation *(Russian)* 80−2538
In superconducting films, metastable states, supercooling fields 80−97031
In-Bi, single spheres, supercond. props. 79−73617
In-Bi(Tl)(Pb), small κ supercond., phase transitions higher than second order 80−88668
$K_2Pt(CN)_4Br_{0.3}3H_2O$ incommensurate linear conductors correlation length in 77−80745
La_3S_4, high crit. mag. field supercond., elec. resist., sp. ht. and magnetisation 80−2532
Nb films, supercond. props. and electronic density of states *(Russian)* 79−28439
$NbSe_3$, two charge density wave locking 79−95350
Nb_3Sn bronze process, flux pinning scaling law depend. on strain 80−75696
Pb-In, containing Ag particles, flux pinning in superconducting matrix 80−2534
Sn film, metastable current states, mean free path variation *(Russian)* 80−2538
Sn, small particles, Josephson-coupled, local fluctuation effects 78−72308
Sn-Bi(Sb), small κ supercond., phase transitions higher than second order 80−88668
$TaSe_2$:Fe, competition between charge and spin density waves, Landau-Ginzburg theory 79−95352
TaS_2(pyridine)$_{1/2}$, upper and lower critical fields, supercond. props. from Ginzburg-Landau theory 79−56456
U_2N_2Te, and related cpds., crit. behaviour 78−43605
UPTe, and UAsTe, crit. behaviour 78−43605
V_3 single cryst., supercond., Ginzburg-Landau parameters, magnetisation meas. 78−2620
V_3Si, thermodynamic study, intrinsic type II superconductivity 79−47193

glaciology
age determ. of ice cores 77−2190
Alberta, ice-free corridor in Late Pleistocene, lake bottom core dating 80−26552
Alberta, southern and central regions, probable extent of Classical Wisconsin ice 78−36207
Alpine meltwaters, ion exchange influence on dissolved load 78−81228
Alpine permafrost environment, mass-wasting by rock glaciers 77−81934
N.America, depth contours of last ice age glacier, rel. to geomagnetism 78−53615
N.America, Plio-Pleistocene continental glaciation rel. to Pleistocene stages terminology 79−62470
S.America, southernmost part, glacial history 77−2188
N. American glacial history extended to 75000 years ago 78−77284
N.American ice sheet, flow pattern from erratic distrib. 80−90108
American Southwest, cryogenic deposits rel. to cold, dry full-galcial climate 78−57296
Ampere Glacier, Kerguelen Is., heat balance in ablation area 77−64335
Ampere glacier (Kergueler Is.), surface boundary layer *(French)* 77−56666
W.Antarctic, isostatic readjustment affecting ice grounding line 80−51445
Antarctic, terrestrial ages of Allan Hills meteorites rel. to ice sheet age 79−88631
Antarctic and Greenland ice sheets, creep instability analysis 79−84304
Antarctic deep ice cores, crystal anisotropy, US vel. studies 80−12440
Antarctic glaciation, Cenozoic evolution rel. to circum-Antarctic Ocean and global palaeoceanography 78−16063
Antarctic glaciation, triggering in N.Atlantic 80−61812
Antarctic glaciers, radio emission spectra in 0.8-8.5 cm band *(Russian)* 77−29333
Antarctic glaciers thermal radio emission, theory for random layered media *(Russian)* 77−33106
Antarctic ice, Pleistocene bimodal response 80−109177
Antarctic ice as supernovae recorder, NO_3^- produced by Γ- and X-rays 80−31314
Antarctic ice cap, preservation of meteorites 78−36541
Antarctic ice core, 30000 yr isotope climatic record 79−92586
Antarctic ice core, CO_2 content of atmos. 20000 yr BP 80−61891
Antarctic ice core, ice crystal size and shape *(Japanese)* 77−81944
W.Antarctic ice sheet, current thinning and Holocene retreat 80−67384
W.Antarctic ice sheet, deglaciation threat from CO_2 greenhouse effect 78−28296
W.Antarctic ice sheet, fluctuations in Antarctic Peninsula area 80−94549
E.Antarctic ice sheet during Early Miocenes, evidence from subglacial erupted rock 80−98287
Antarctic ice sheet thickness mapping by radar *(German)* 77−56770
Antarctic ice shelf, ice melting model 80−4036
E.Antarctic ice surge at ~95000 BP, climate and sea-level study 80−51444
Antarctic iceberg melting 78−88863
Antarctic Ocean, interdisciplinary studies 78−11915
Antarctica, glacial weathering rel. to silica budget of Antarctic waters 78−20436
Antarctica, glaciological significance of meteorite discoveries 80−8597
Antarctica, radioactive waste disposal, glaciological aspects 77−61523
aqueoglacial deposit lithology of E.Lithuanian upland *(Russian)* 78−16011
Arctic Canada, ice-sheet initiation and climatic influences of expanded snow cover 79−66724
Arctic Ice Dynamic Joint Experiment 77−33190
Arctic permafrost regions, seismic and resistivity obs. 77−41072
astronomical theory, teaching approach 79−84891
S.Atlantic, glacial and interglacial oceanographic conditions from $CaCO_3$ and radiolarian distribs. 80−72556
glaciology continued
N Atlantic continental slope, submarine canyons and valleys origin and development 77−21713
Atlantic Eurafrican continental margin, glacial eastern boundary current 78−81179
Atlantic Ocean, quartz distrib. relation to climate in last glaciation 80−8308
Australasia, Late Quaternary ice age climates 79−84470
Baltic Ice Lake levels, dating rel. to S.Finland Salpausselka moraines 79−20872
Barents Ice Sheet as a relay regulator of glacial-interglacial alternation 79−2309
Barnes Ice Cap, surge activity 77−91167
basal till depositional fabrics reflecting alignments during transportation 78−20440
Batura Glacier, Karakoram Mountains basic features 80−17300
Berendon Glacier, BC, Canada, movement, ice structures and medial moraine at confluence 78−61441
Bermuda, Late Pleistocene sea level vars. 78−73400
Bolivia, evidence for glaciation 3.27 Myr BP 79−34865
Brecon Beacons, S.Wales, Late Glacial deposits and landforms 80−105005
British Columbia, S central, late Pleistocene glacial and nonglacial stratigraphy 78−92804
Late Cainozoic, sea ice and glacial development in N.Hemisphere 80−90098
coastal California, late Quaternary climate and evidence for Ice Age refugium 78−57293
Canadian high Arctic, past glacial activity 78−81236
Canadian High Arctic ice caps, ice thickness meas. 78−61439
Canadian Rocky Mountains, Holocene glacial advances 80−8341
Caniapiscau River, Canada, shaping by ice during the last 6000 years *(French)* 80−12439
Chile, Quaternary glacial fluctuations 78−44980
cirques in Bear River Range, north-central Utah, numerical anal. 80−72510
climate model, sensitivity and role of cloudiness *(Russian)* 78−88902
climate model, zonal asymmetry in energy balance 80−12536
climate model with ice-sheet dynamics, stable periodic solns. 80−90210
climatic warming effect on W.Antarctic ice sheet 79−34864
Clyde Foreland, Baffin Is., last interglacial-glacial cycle, stratigraphy, biostratigraphy and chronology 78−61536
cold ice sheet, creep rupture obs. at depth 79−2306
Columbia Icefield, surveying techniques 78−61445
continental ice sheet, stochastically driven with planetary wave feedback, model 80−77025
continental ice sheet, thickness changes from Geos 3 altimetry 80−4051
continental ice sheet model, spectral response to insolation vars. 79−2300
continental ice sheet model, stability to insolation periodic vars. 78−28251
continental ice sheet var., model for N. Hemisphere 77−21814
continental ice sheets, erosion 79−25276
continental shelves, marginal longit. channels struct. and origin 77−64261
Corsica (France), Quaternary glacial deposits props. and chronology 78−57234
Crete, evidence for glacial and nival formations *(German)* 77−64359
cryosphere-climate coupling, feedback effects rel. to quasi-cycles in meteorology 80−109239
Cumberland Peninsula, Baffin Is., tors, felsenmeer and glaciation 78−61442
deluvial deposits in SE Lithuanian periglacial valleys and ravines *(Russian)* 78−16010
Devensian glaciation in Britain, effects on water balance, 50000 yr BP to present day 80−72566
Devon Island ice cap, Canada, theoretical and observed temp. profiles comparison 79−16524
Devon Island ice cap, NWT, artificial radioactivity layers 77−5250
dislocation processes and tensile crack formation in glaciers 78−20438
W Dronning Maud Land, Antarctica, radio echo sounding during (1974) 77−86838
early Northern Hemisphere glaciation, ^{18}O isotope and palaeomagnetic evidence 78−7752
Earth ice cover, latit. changes effects on zonal and global albedoes 80−17377
Earth rotation affected by deglaciation 80−85576
Eemian interglacial and deep sea O isotope stratigraphy 79−29770
NE Ellesmere Island, NWT, Canada, glacial geology and chronology 78−77233
EM sounding of ice, visit to Arctic and Antarctic Research Institute, Leningrad 80−4504
erosion, effect on terestrial heat flow palaeoclimatic and topographic corrections 79−34767
NW.Europe, appl. of extended ^{14}C time scale by isotope enrichment 78−77314
folds and gravity tectonics in ice and rocks 77−70658
glacial ice melting effects on Antarctic surface water 79−34866
Glacial Lake Agassiz, northern extent in E Saskatchewan 77−91161
glacier, sliding on plane strewn with hemispherical obstacles *(French)* 79−8640
glacier friction law, shadowing function of Gaussian probability curve *(French)* 79−8641
glacier motion, defect distrib.-stress relation 80−8334
Glacier Peak tephra in North Cascade Range, stratigraphy, distrib., rel. to glacial events 79−25247
glacier structure and flow rel. to elongated air bubbles in ice *(Japanese)* 78−88861
glacier surfaces layer, EM sounding 79−62768
glacier thickness meas. using dielectric permeability characts. 78−89500
glaciers, radar subsurface sounding 80−67437
glaciers structure, obs. by Forbes and Agassiz and dispute over priority 79−17181
glaciers thickness measurement, appl. to gravity surveys in glacier-covered regions 79−16697
glaciers-ocean-atmosphere global system, numerical modelling 79−84469
global mass and energy requirements for glacial oscills. rel. to mean ocean temp. oscills. 78−81351
Gondwana Late Palaeozoic glaciation, nature from anal. of garnets and other heavy minerals 79−100874

glaciology continued
Gondwanan glaciation, cyclothems, continental positioning, and climate change 79−62526
Great Lakes region, glacial lobe identification by till minerals 80−56465
W.Greenland, glacier response to climate change 80−61820
Greenland and Devon Island ice cores, O isotope profile of last 10^5 years 80−41470
S. Greenland firn layers, transuranic nuclides, depositional history 77−86953
Greenland ice, tree ring and tidal stresses rel. to climate periods 77−33178
Greenland Ice Sheet, atmospheric trace metals and sulphates 78−7667
Greenland Ice Sheet, Hg contents 78−65349
Greenland ice sheet, radio echo sounding, signal polarisation 77−56755
Greenland Ice Sheet impurities, past volcanism record 78−11855
Hawaii, glacial ages 80−56503
Hawaiian glaciation chronology, K/Ar and ^{14}C ages 77−33113
Holocene and latest Pleistocene cirque glaciations in Shuswap Highland, British Columbia, ages 78−92856
Holocene glacial and tree-line vars. in White River valley and Skolai Pass, Alaska 77−78251
Holocene period conditions, French research work review *(French)* 77−37247
Holocene retreat of W.Antarctic ice sheet, model 79−66725
hot water drill, open circuit, for hole drilling in cold glaciers 78−65402
hydraulic transients, as seismic sources in volcanoes and glaciers 79−100816
ice age, Antarctic ice-surge theory supported by sea level study 80−51525
ice age beginning, instantaneous glacierisation, albedo rate change and feedback effects 80−105006
Ice Ages, causes 79−20961
ice ages, influence of Earth albedo contrast due to continental drift 79−74950
ice ages, prod. by Earth albedo sudden change 79−44241
ice ages, prod. by Earth encounter with interstellar cloud 78−57292
ice ages and continental drift, theory 79−44209
ice ages and ecological catastrophes, prod. by Earth-comet close approach 78−53714
ice ages and thermal equilib. of Earth, comments 77−5313
ice ages global mass and energy requirements, rel. to mean ocean temp. oscills. 77−78404
ice cover, flexural-gravity wave development, longitudinal tension effects *(Russian)* 79−100855
ice DC resistivity and recrystallisation of glacier ice 80−36348
ice free convection melting in saline water 78−3835
ice I_h, grain boundaries, internal friction meas. *(French)* 79−55754
ice on Mt. Everest, mass spectrometric chem. anal. of D, ^{17}O and ^{18}O *(Chinese)* 80−77016
ice secondary and tertiary creep meas. by borehole closure rates 77−64339
ice sheets in polar regions, radio obs. appls. 78−81419
ice thickness meas., gravity profiling technique 78−32253
ice-sheet growth, energy requirement, comments and reply 77−21815
ice-wedge casts in NE county Wicklow, distrib. and struct. 78−69379
iceberg fluctuations in North Atlantic *(German)* 78−49038
icebergs, calving from floating glaciers by vibrating mechanism 78−81197
SW Iceland, glacial chronology from palaeomagnetism of Esja, Eyrarfjall and Akrafjall mountains 80−89950
Icelandic, thermal and physical characts. of subglacial volcanism 80−101350
icesheet growth rel. to subpolar warmth of N.Atlantic Ocean 79−66711
Indian Ocean, ecologic and palaeoclimatic implications of vars. of O. universa 77−9445
Indian Ocean, palaeotemps. during Brunhes epoch from sediment core study 80−12429
Indian Ocean middle latitudes, Subtropical Convergence fluctuations and Quaternary climates 77−13087
Infracambrian glaciogenic sediments from Sierra Leone 78−69378
inland ice sheet thinning due to Holocene warmth 79−34873
interfluvial area of Minija and Sventoji, marginal formations structures *(Russian)* 77−25708
interglacial chronology, Rocky and Mackenzie Mountains, ^{230}Th-^{234}U dating of calcite speleothems 78−36120
interglacial episode termination and Wilson Antarctic surge hypothesis 78−53669
isostatic adjustment and sea level, global finite element model 79−20800
Japan, late glacial age chronolgy from morainic features and Lake Biwa sedimentary sequence 79−34872
Jungfraujoch ice-cores, impurity determ. by neutron activation anal. 78−11920
Kandalaksha Bay, White Sea, crystalline basement struct. from seismoacoustic profiling 77−86854
Labrador Shelf, early deglaciation 79−79891
Lake District glacial sediments, pre-Devensian till 80−94523
Lake Huron E coast tills, palaeomagnetism, physical and lithologic props. and age 77−33057
Lake Ontario, Late Wisconsin sediments, aspartic acid racemisation and ^{14}C dating 78−73415
Lake Whittlesey, ice frontal position in eastern Erie basin 80−12436
land-ice slide, glacier-initiated, near Pylon Peak, British Columbia 78−36208
last (Eemian) interglacial, abrupt end in NE.France 80−21818
last Glaciation, glacial inception and disintegration 79−5534
last glaciation, rapid ice-sheet growth and glacial period initiation 80−51530
Late Cenozoic glacial periods, rel. to Gulf Stream vel. fluctuations 80−12432
late Pleistocene and Holocene climates, glacial retreat energy and dynamics and surface radiation 77−64416
Late Precambrian glaciations, Africa, nonsynchroneity 77−81940
Late Quaternary climatic changes, W.Africa, from deep sea sedimentation 78−73355
Late Quaternary climatic variations in NW.Africa from E.Atlantic Sediment Cores 77−2223
Late Quaternary deposits lithobiostratigraphic characteristics, Baltic Sea *(Russian)* 79−88332
Late Quaternary glacial-interglacial cycle rel. to North Atlantic surface ocean kinematics 78−16026

glaciology continued
Late Quaternary glaciation of eastern Queen Elizabeth Islands, N.W.T., Canada 77−2189
Late Quaternary sea levels, central British Columbia coastal area 78−73377
Late Wisconsin flood into Gulf of Mexico 79−29775
late-Wisconsin glaciation extent in NW.Greenland and N.Ellesmere Island, glaciological and geological evidence 78−57232
Laurentide Ice Sheet growth rate and sea level lowering 77−5214
Lewis Glacier, Mt. Kenya, ice core rel. to African climate 78−11931
Lida Plateau in Lithuanian SSR, palaeoperiglacial cover formations *(Russian)* 80−98367
Lithuanian upland and plateau palaeoperiglacial blanket deposit formation *(Russian)* 80−81882
Loch Lomond Stadial in British Isles 79−79887
Lys glacier, conditions of front in 1971, 1975 and 1976 *(Italian)* 78−85610
Mackenzie River catchment, Canada, asymm. transverse valley profiles 78−20446
Mahone Bay, Nova Scotia, Late Quaternary glacial erosion and sedimentation 78−77232
Malaspina Glacier, Alaska, general obs. 80−8336
Mamontova Gora, Siberian nonglacial stratigraphy and radiocarbon dates rel. to glaciations 78−44819
Marie Byrd Land ice sheet, surface-wave dispersion investigation by finite difference method 79−66631
mass balance of glaciers in N.American high arctic and volcanic dust influence 78−36214
Matanuska Glacier, Alaska, O isotope investigation of basal zone origin 79−79884
Matanuska Glacier, Alaska, pebble orientation in ice and deposits 80−98366
Mediterranean Sea, glacial palaeo-oceanography 79−16505
Mediterranean Sea, hydrological regime during glacial periods *(French)* 80−4040
meltwater electrical resistivity observations, water origin anal. 80−85689
meltwater from ice sheets, global changes in postglacial sea level: a numerical calculation 79−2289
meteorite impact crater, central Alaska, possible glacial origin 79−25249
Milankovitch theory and ice ages, interactive climate feedback 80−46251
Milankovitch theory of ice ages, evidence from palaeomag. chronology of S.Australian beach ridges 80−98307
Milankovitch theory of ice ages, study using simple climate-ice sheet model 78−40644
Miocene glacial-eustatic changes in world ocean, rel. to Messinian salinity crisis 77−91151
Mizuho Plateau, Antarctica, ice sheet flow and local mass budget 80−31068
Mizuho Plateau, ice sheet thinning, possible causes 78−57229
Mount Elgon (Kenya/Uganda border), deglacierisation date determ. 78−53670
Mt Uenshiridake, Hokkaido, glaciological and meteorological studies of snowpatch *(Japanese)* 77−81943
multiple glaciation in NWT from stratigraphy of caves 77−21803
natural clay permafrost, electrical props. 77−44967
Neogene explosive volcanicity, temperature and glaciation 80−26481
New Hampshire, Wisconsinan ice readvance, stratigraphic and structural band features 80−8335
New Zealand, late-glacial chronology rel. to radiocarbon dating of Quaternary loess deposits 78−24271
SW.Newfoundland, geomorphology and Quaternary geology 78−20400
Newfoundland, Late Wisconsinian glacitectonic struct. and post glacial permafrost 78−61440
Newfoundland fjords, gravel clasts rel. to glacial erosion of bedrock 77−17148
Norwegian-Greenland basin continental slope, submarine canyons and valleys origin and development 77−21713
nuclear techniques in hydrology, survey 77−37419
Ontario, Pleistocene glaciation chronology rel. to geothermal regime perturbation 79−57883
orbital changes of Earth in climate variation models 80−98441
Oshmyany Upland in Lithuanian SSR, palaeoperiglacial cover formations *(Russian)* 80−98367
palaeoclimatic inferences from former glaciers in Scotland and the Lake District 79−44243
palaeoclimatic research, status and opportunities 80−51527
palaeoclimatology, in world climate conference, Geneva (1979 February 11 to 23) 80−46727
palaeoclimatology and vegetation changes during 2000 years BP, from anal. of varved lake sediments 79−25279
palaeoglaciation due to solar radiation reduction *(French)* 79−34857
Pelee-Lorain moraine, SW.Ontario, influence on Point Pelee geomorphology 78−92857
permafrost, surface layer, EM sounding 79−62768
permafrost mapping by audiofrequency magnetotellurics 79−58102
permafrost thermal behaviour, surface heat balance simulation 80−67385
Peyto glacier, geological features *(French)* 77−37199
Pleistocene, ice fluctuations rel. to southern trade winds and oceanic upwelling during last 75000 years 78−57217
Pleistocene deglaciation, influence on true polar wandering 79−44079
Pleistocene drift, ice-marginal sedimentary, glacitectonic and morphologic features, Newfoundland example 78−57233
Pleistocene glacial cycles, Pacific palaeoclimatic stratigraphies comparative anal. 78−57295
Pleistocene glacial vars. 79−66787
Pleistocene glaciation on Daisetsu volcano, rel. to Lake Biwa stratigraphy 78−24323
Pleistocene ice fluctuations rel. to Earth orbit vars. 77−37346
pleistocene volcanism and glacial initiation 77−91088
Pleistocene-Holocene transition, W.Pacific, from stable isotopes anal. in deep sea carbonates 78−73354
Pliocene and Pleistocene glaciations rel. to Barents Ice Sheet, evidence from Barents Sea 78−57227
polar ice caps, albedo feedback rel. to energy-balance climate models stability theorem 80−56594
polar ice sheets, basal temps. 77−78250
polar ice sheets, total gas content rel. to surface elevation changes 80−4053

glaciology continued
polygonal patterned ground in central New Jersey, origin during Wisconsin glaciation 79−25248
polythermal glaciers, flow, surface wave anal. 80−46210
polythermal glaciers flow, detailed continuum model, preliminary anal. 78−85617
post glacial uplift mechanism, phase boundary reaction to medium press. changes 80−90058
postglacial tilting of Akpatok Island, Northwest Territories 79−57901
postglacial uplift of crust, mechanism 80−104943
Lake Precambrian glaciation, Port Askaig Tillite derivation rel. to Cambrian opening of Iapetus Ocean 80−98299
Late Precambrian glaciation in Adelaide Geosyncline, palaeomag. evidence for low-latit. glaciation 80−101325
Precambrian ice age, effects of Earth rot. rate vars. 80−4097
pressure melting within glacier, indicated by regelation ice chem. comp. 78−61447
quartz grains, from sub-glacial and assoc. environments, characterisation using SEM 79−25238
Quaternary glaciations along Qinghai-Xizang Highway *(Chinese)* 79−92538
Quaternary glaciations and stratigraphical positions in China *(Chinese)* 79−79885
Late Quaternary pingo remnants in central London 80−56502
Queen Maud Land, Antarctica, ice elevation map from balloon altimetry 79−53374
NE Queensland, last interglacial-glacial cycle, dry land precipitation sequence 78−40598
Quelccaya tropical ice cap, Peruvian Andes, climatic ice core records 80−8345
radar vertical probing of glaciers, signal depolarisation 77−9557
radionuclides decomposition in glaciers 80−40934
Rannoch Moor, radiocarbon dates and Loch Lomond Readvance deglaciation 77−13115
rapid glaciation in N.Hemisphere climatological conditions from oceanic evidence 80−90213
Robinson's Head moraine, W.Newfoundland, ^{14}C dating, rel. to postglacial sea level changes 78−20401
rock glacier in Yukon Territory, Canada, obs. of activity 80−56500
rock glacier types and their drainage systems, Grizzly Creek, Yukon Territory 79−25271
rock glaciers in southern part of Jasper National Park, Alberta, distrib. and characts. 78−77276
Ross Ice Shelf, Antarctica, artificial radionuclides depositional history 79−88027
Ross Ice Shelf (Antarctica), basal freezing, confirmed by core drilling 80−101393
Ross Ice Shelf project, glaciomarine mud 79−88366
Ross Ice Shelf Project in Antarctica *(German)* 77−70836
Ross Ice Shelf temperature in bore holes, ice thickening history 80−31072
Salpausselka moraines, S.Finland, dating rel. to Baltic Ice Lake levels 79−20872
S.Saskatchewan, Wisconsin deglaciation 80−4049
saturated rocks in permafrost, thermal conductivity meas. 79−84232
Scotia Sea, Antarctica, maximum ice extent on island groups 78−20450
sea level changes due to West Antarctic ice sheet fluctuations 77−86933
sea level during last 18000 years, retreat of Antarctic ice sheet 80−41455
sedimentation processes and patterns in glacier-fed lake with low sediment input 78−88849
Sierra Nevada, California, glacial deposits, relative dating techniques from weathering 80−8451
snout variations in France, survey by aerial photography *(French)* 77−33101
Spitzbergen, glacier thickness meas. from helicopter *(Russian)* 77−29336
steady flow of viscous nonlinear fluid (Glen body) around perfectly smooth sphere *(French)* 79−7387
Storbreen, S. Norway, fluctuations rel. to Little Ice Age palaeotemperatures 77−5312
strain heating and creep instability in glaciers and ice sheets 77−86954
sub-pingo water lenses, Tuktoyaktuk Peninsula, Northwest Territories, obs. 79−20873
subglacial lake, Antarctica, radar sounding 79−29798
subglacially precipitated calcite, $^{18}O/^{16}O$ palaeoclimatic implications 79−20897
Swiss Alps, observations of behaviour *(French)* 77−37248
Taylor Valley, Antarctica, Late Pleistocene glacial chronology and effect on global climate 80−8343
thermal radiation polarisation, of permanent snow fields, from meas. obtained from the 'Meteor' satellite 78−88870
thickness of glaciers, radar measurement technique 80−98369
tidewater glaciers, upwelling in stratified ocean due to melting 80−81897
till along Lake Huron east coast, age, mag., physical and lithological props., discussion 78−20404
till landforms, fabric anal. 77−44989
tills deposited in arid polar environments, characts. 77−91160
Tuktoyaktuk Peninsula, NWT, pulsating pingos 77−53080
underwater margins of W.Spitsbergen, glacial morphogenesis and sea floor morphology 80−26494
underwater obs. of glaciers by side-scan sonar 77−5270
upper ocean layer, global freshening during deglaciation 78−53658
volcanic eruptions beneath glaciers, landforms rel. to Mars 80−67616
water-free crevasses spacing in glaciers 80−21784
Late Weichselian ice sheet of N.Eurasia 80−90109
Wenkchemna Glacier, ablation complex and rock glacier, Canadian Rocky Mountains 79−5514
late Wisconsinan till sheets, Brantford-Woodstock area, S.Ontario, trend surface anal. 78−92858
late-Wurm Arctic Ice Sheet, rel. to N.Hemisphere glaciation 77−45132
Wurm glaciation, rel. to lake-level fluctuations since 30000 yr BP 80−51447
Wurm glaciation, temp. and precip. chronology for N.America NW coast region 80−98438
Wurm glacier of Val Tresa, melting rel. to Quaternary glaciolacustrine sediments dislocations *(Italian)* 79−8647
SE Yukon, unique stratigraphic record of late Tertiary-Quaternary events 79−62499

glaciology continued
$CaCO_3$ dissolution in deep sea sediments, rel. to palaeoceanographic reconstruction 79−25269
^{18}O in equatorial Pacific core, glacial time scales and climate 80−21817
^{18}O stratigraphy in deep-sea sediments, evidence for deglacial meltwater effect 78−85530
^{210}Pb from nucl. explosions in environment 78−21774

glass
for semiconductor glasses see amorphous semiconductors and chalcogenide glasses
see also aluminosilicate glasses; amorphous semiconductors; borate glasses; borosilicate glasses; chalcogenide glasses; germanate glasses; glass fibre reinforced plastics; glass fibres; glass industry; glass-metal seals; optical glass; phosphate glasses; phosphosilicate glasses; vitreous state; vitrification
β-eucrypite, glass-ceramics, internal stresses 79−15770
absorption spectrum of Nd^{3+} ion, chem. composition effects, group IV element effects *(Polish)* 78−10932
acetate glasses, radiation effects on transparency 79−57261
acoustic and dielec. props. at low temps., review 78−6128
acoustic emission, obs. during heating through glass temp. 80−84253
acoustic phonons lifetime at low temps. 78−26650
acoustic props. at low temps., ultrasonic attenuation, dielec. props. *(French)* 77−72658
activated, athermality criteria for laser appls. *(Russian)* 77−66485
additions to piezoceramics, effect on props. during hot pressing 79−24475
adherence, of polyurethane 78−83336
adhesion with rubber, propag. of cracks, effect of humidity 77−86133
adsorption, of Rn 80−10775
adsorption of ethoxysilanes, on BK 7 glass, IR spectra *(German)* 78−30834
adsorption of proteins, in detergent soln. 78−44401
ageing use, photothermal processing, sorptive and luminescence props. *(Polish)* 78−11250
air cooled, flat, duration of inelastic deformation 78−84908
alcohol glasses, X-irradiated, electron scavenging mechanism 77−56235
alkali, rapidly quenched, alkali ion cond. 80−107559
alkali and non-alkali, working props. during microfibre and ultrafine fibre prod. 79−24486
alkali metal glass, elec. cond. meas. method 79−66250
alkali metal oxide glass, composition dependence of activated processes, mixed alkali effect 79−77525
alkali resistance, to NaOH 80−21143
alkali silicate:Nd_2O_3, coloured, dichroism *(Polish)* 79−99919
alkali silicate, γ-irrad., paramag. SO_3^- radicals 79−42838
alkali silicate, internal friction, influence of red/ox ratio of multivalent ions 78−31447
alkali silicate, ionic motion, ^7Li NMR obs. 78−27107
alkali silicate glass, appl. of XPS, chemical shift *(Japanese)* 79−34416
alkali silicate glass, CuO doped, ESR spectra of Cu^+, quadrupole effects 78−64265
alkali silicate glass, isothermal mech. loss spectrum, appl. of Rheovibron 80−88260
alkali silicate glass, Li^+ motion, ^7Li NMR spectra, nucl. relax. 80−34804
alkali silicate glass, photochromism 77−43955
alkali silicate glasses, chem. stability, cations coordination, leaching vacancy mechanism 80−35526
alkali silicate glasses, chem. stability depend. on cation O_2 structs. 80−35527
alkali silicate glasses, high temp. relax. mechanisms 80−70134
alkali silicate glasses, secondary relax. transitions 80−88261
alkali silicate glasses, struct. and thermal props. 80−84075
alkali silicate glasses in aqueous solutions, leaching kinetics rel. to surface pot. 80−11803
alkali-alkaline earth nitrates, Raman spectra, vibr. perturbations effect 79−8132
alkali-alkaline earth silicate glasses, IR refl. spectra *(Japanese)* 78−52505
alkali-alkaline-earth silicate glasses, IR reflection spectra *(Japanese)* 78−19491
alkali-silicate glasses and melts, partial molar vols. 79−94915
alkali-SiO_2, low temp. heat capacity 80−49373
alkaline earth silicate glasses, morphology effects on props. 80−49118
alkaline earth-silicate glasses, elastic props. and struct. 77−24273
alkaline glass: tryptophan (tyrosine), γ-irrad., electron traps, stimulated luminesc. 78−11536
alkaline silicate glass, surface layers, plasticity and microcrack formation, electron microscopy *(German)* 80−40469
aluminate glasses, new families, light transmission, 0.4 to 6 μm 77−24843
ancient samples, trace element anal. by neutron activation, rel. to corrosion and devitrification 78−12801
anionic constitution of glass forming melts 78−2011
annealed and tempered, contact induced static fatigue 79−8376
annealing, optimum temp. curve, analogue model *(Polish)* 79−52279
annealing process, horizontal, flat glass, math. model 79−61615
applications, review 78−3306
aqueous, electron scavenging, hopping controlled time-depend. reaction rates 80−108723
aqueous glass, γ-radiolysis, photolysis of trapped electrons, quasi-free electron IR absorpt., luminesc. 77−21401
aqueous glass, laser excitation, bleaching of trapped electron absorpt. bands 79−43606
aqueous soln., stabilising excess electrons, DTA at cryogenic temps. 78−76889
atomic absorption determ. of MgO, CaO and BaO *(Polish)* 79−24872
atomic absorption spectroscopy 79−61919
automatic recording dilatometer *(Japanese)* 79−70291
ball mill grinding, wet and dry, rate const. *(Japanese)* 80−29895
ball rolling on adhesive viscoelastic material, contact area 79−52394
band structure and forbidden gap in glasses and amorphous semiconductors, review 78−75987
basaltic, expt. study of cationic diffusion of alkali and alkali-earth ions 78−95180
bead, impact fracture *(Japanese)* 78−92338
bead filled polymers, crazing characts., slope-discontinuity method 79−11712

glass continued
bead reinforced nylon, design parameters, fibre orientation effect 80−81141
bead reinforced polycarbonate, design parameters, fibre orientation effect 80−81141
bead-filled epoxy resin, elastic moduli, interfacial slippage effect anal. 78−76688
beads, porous deposit, NaCl mass transfer to stationary water region *(Japanese)* 77−25700
beads in polystyrene soln., suspension, time depend. viscoelastic behaviour 80−99982
beam, brittle bending fracture and emitted stress waves 77−73329
beam, rectangular, flexurally vibrating Timoshenko's shear coeff. 78−83866
bioactive materials, review 78−3698
bioceramic, SnO_2 coated, for artificial heart valves, mech. props. *(German)* 79−12028
birefringence dispersion, meas. with Babinet compensator using white light 78−27177
blister formation in He^+-implanted glass, effects of gas diffusivity 77−35604
bonded, electrets obs., under corona discharge and electron irradiation conditions *(Russian)* 79−4759
bottles, qualitative method for monitoring chemical corrosion 78−85068
brittle failure of electron bombarded glass 77−28909
brittle fracture, theory under nonisothermal conditions 79−64593
brittle fracture theory, nonisothermal conditions 80−21101
bubbles, form., condensate trace quantities determ., spectral anal. techniques *(Russian)* 77−36852
building product, nonmetallic, first crack determ. device, during load test *(Czech)* 80−45471
cabal glass:$SiO_2(TiO_2)$, microheterogeneity, and elec. cond. 78−83997
calibo glass, quantum efficiency of non-radiative energy transfer 79−33832
β-carotene glass, photoconductivity mechanism 79−28368
cation exchange interdiffusion, nonidealness 80−39362
ceramic, AE meas. under maintained load *(German)* 79−43315
ceramic, dispersion strengthened glass matrix 77−40425
ceramic, form. characts. in slag glasses 77−8794
ceramic, fracture stress rel. to flaw and fracture mirror sizes 79−11689
ceramic, low temp. heat capacity, glassy and devitrified states 78−22862
ceramic, machinable, machining techniques 78−77881
ceramic, nucleation and growth studies by small angle neutron scatt. 79−32913
ceramic, randomly oriented physical props. 78−48502
ceramic, second-order microstresses 78−27468
ceramic, surface prep. for Si thermosprayed coating 78−11367
ceramic, thermal expansion variation with ratio of phases and comp. 77−35719
ceramic mineralogy 80−60826
ceramic prep. by hot pressing and crystallisation of glass powder, mech. props. 78−15351
ceramic randomly oriented, physical props. 78−48501
ceramic rods, strengthened, residual stress determ. 78−23830
ceramic-glass protective coatings for Ti, synthesis and props. 80−25900
ceramic-glass-glass composites, crack growth, elec.-mech. analogue 80−85022
ceramics, machinable, vac. compatibility 79−93152
ceramics, transient heterogeneous nucleation of glass-forming systems 80−88042
chain molecular amorphous solids, stat. thermodynamics and mol. theory 78−26442
characterisation with analytical electron microscope 80−84068
chemical durability, thermodyn. approach 78−7063
chemical plating of glass ceramic with Ni and Cu 77−44379
chemical resistance for medical laboratory techniques 79−88926
chemically strengthened, ion exchange temp. and time influence on stress profiles and strengths 78−31417
chemically strengthened, stress profile determ. using scatt. light 80−30186
chemistry *(Japanese)* 78−6885
Cl ThO_2 glasses, thermal anal. *(French)* 78−14282
clean, bibliography 77−28922
cleaning and polishing by low press. high frequency induction plasma *(Russian)* 78−35578
co-acting (synergistic) flaws and strength 77−20168
colour centre form. by UV irrad., afterglow, thermolum. and EPR obs. 78−10047
commercial, high field cond., weak electrolyte theory appl. 80−107475
commercial glasses, viscosity and stress relax. in glass transition region 80−93589
complex raw material, hydrothermal prep. 80−104106
composite, stainless steel, reinforced glass matrix, anal. of damping of vibrs. 80−40413
composite glass shells, bonded joint efficiency during external hydrostatic pressure cyclic loading 79−57079
composition, patent information, automated retrieval system 79−24715
composition and props. for structural material 80−84944
compression cracking theory and failure of glassy materials 80−7677
compressive testing 77−16773
condensation surface, low-temp., interaction with Pb at. beam 78−19626
conduction and valence bands props., review 77−66106
conference, Albuquerque, NM, USA 80−82565
conference, Prague, Czechoslovakia (June 77) 78−2010
conference on noncrystalline solids, Clausthal, Germany (Sept. 1976) 78−22654
construction application, review 78−3307
contact interaction of glass-polyethylene pair under elastic strain, friction and γ-ray effects 80−40549
container forming, mould surface temp. meas. 80−82767
container processing for parenteral products 77−28923
containers, exam. of fragmentation 79−20148
controlled pore glass, pore struct., determ. by electron microscopy and Hg penetration 78−43165
coordination number of Co^{2+} and chem. composition of secondary and tertiary silicate glasses *(Polish)* 78−9960
cordierite glass ceramics, effect of TiO_2 and ZrO_2 content on phase sequence during heat treatment 78−48381
Corning 7070 glass, relative permittivity at 3 GHz 79−33591
corrosion, effect of EDTA, ethyl alcohol and sugar in leach soln., chem. durability 79−74269
glass continued
corrosion, effect of surface area to solution volume ratio 79−96167
corrosion, influence of complexing agents and nature of buffer soln. on chem. durability 79−74268
corrosion resistance when sintered with stainless steel 77−77608
crack front curvature and slow fracture in liquid decane 79−8375
crack propagation, by mech. and thermal stresses 78−75721
crown glass, particle impact angle effect on strength degradation 80−50709
crown glass impacted with sharp SiC particles, strength degradation of tempered surfaces 79−66183
crystal growth mechanism for glass forming systems 78−30555
crystallisation and nucleation of reheating 80−84078
crystallisation and opacity, exam. by high temp. viscometry and X-ray diffr. *(Polish)* 78−84875
crystallisation kinetics, processes in glass forming melts 80−64905
crystallisation of melts and glasses, nonisothermal, kinetics 79−94914
crystallisation-chemical composition relation, regressional analysis *(Polish)* 77−16535
crystallised, internal stress depend. of hardness 80−16439
cutting with conc. energy sources *(Russian)* 79−38994
dating by hydration layer thickness meas. by NMR 77−74567
decomposition, phase separation processes, diffusion coeffs. determ. *(Germany)* 78−39736
defect reactions, ionicity dependence, negative-U states 80−88510
defects, EPR characterisation 79−38379
defects obs., Raman microprobe-microscope appl. 80−62737
deformation in glass transition interval 79−66137
dense, mirror-to-flaw size ratio, comparison with polycrysts. 80−25841
density fluctuations from elastic dipoles at low temps. 78−79709
determination in glass-fibre reinforced cement, X-ray fluoresc. anal. 79−52840
developments for electrical industry appls. 79−78925
devitrificates, quantitative charact. of microstruct., electron microscope study *(Polish)* 79−100311
devitrificates, quantitative charact. of microstruct. *(Polish)* 79−91889
devitrification, heat treatment parameters determ. from viscosity changes *(Polish)* 80−40404
devitrified opaque technical, microstrength and hardness 80−89312
devitrified technical, bending strength, scale effect 80−89311
dielectric anomalies at very low temps., acoustic anomalies analogy 78−31146
dielectric instabilities in high permittivity glass 78−52433
dielectric relax. loss, two level Anderson Halperin Varma model 80−66106
dielectric relaxation, order parameter model appl. 80−108151
diffusion coefficient equation 80−103521
diffusion coloured layers containing Pb and Cu 77−36677
diffusion in glasses and melts 78−2017
diffusion profiles analysis, grinding and etching techniques comparison 78−26732
diffusion strengthening technique 78−31418
disclination lines, topological stability 80−33902
disilicate, piezoelectric glass ceramic, recrystallisation, pyroelectric response, permittivity 80−80703
dislocation theory 79−99298
disordered systems, mode softened unified theory 79−55637
dissolution rate control by H^+ mobility 77−55932
dosimeter glass, radiophotoluminescence intensity change by intense laser light 80−89050
DTA, transformation range *(French)* 77−72562
E-glass textile filaments, wetting characts. 80−80030
echoes and elec. dipole echoes at low temps. 79−69771
elastic moduli, device for temp. depend. meas. at low pressures 80−30183
elastic moduli measurement, laser-target technique, for wide temp. range 77−27497
elastometric glasses and porous network polymers, review of future developments 78−22657
electrical, magnetic, and optical props., conference, Troy, NY, USA (Aug. 1979) 80−105417
electrical conductivity meas. technique using thermally stimulated polarisation currents 79−99561
electrical properties 78−2479
electrical relax., Debye-Falkenhagen theory 80−108155
electrode, Mg-meso-tetraphenylporphine-coated, in photovanovoltaic cell *(Chinese)* 80−40865
electrodes, glow discharge tube 80−33834
electron irradiated, colour centre depth distrib. 79−73217
electron microscopy using electrostatic field *(German)* 78−82081
electron migration and spectral relax., random-walk model 80−80280
electron scavenging kinetics, random walk hopping model 79−74401
electronic processes theory, Mott's contrib. *(Slovak)* 80−6686
electrothermal props. in structural transform. zones *(French)* 80−88047
elementary defect creation during glassmaking, model 78−22668
enamel coating on C steel prod. by induction fusion method, heating rate of steel effect 80−11825
enamel coatings, effect of firing method on adhesion 79−24647
engineering, type 13v, strength under static and cyclic loads 79−43356
engineering materials, nature and props., book 78−72707
enstatite-type glass-ceramic, crystn. kinetics and mechanism 77−55241
entrapped liquid lenses at elastomer-glass interface, formation and geometry 77−85021
entropy, excess, compared to ordered crystalline form 80−38914
envelope for H_2 dissociator, used in atomic clock, AES obs. of degradation 77−61876
EPR of Fe^{3+}, line shape, H to g transforms. 77−12193
equilibrium glass-plastic pressure vessel of minimum mass with non-geodesic winding 77−50905
equilibrium thermodynamics, sp. ht., refr. index and glass transition *(German)* 78−83745
erevanit based glass, granulation and briqueting 80−60823
erosion impact of annealed 310 stainless steel, SEM and TEM study 78−64725
ESR, review 80−108049
etching, effect of temp., appl. to particle track visualisation 79−76290
etching rate temp. and conc. depend. 77−10533
ethanol glass, 4K γ-irradiated, presolvated electron photoconductivity 78−47827
ethanol glasses containing anion radicals of fluorene and isologs, γ-irrad., optical absorpt. and EPR obs. after photobleaching 77−44491

glass continued
excavation glass, layers and profiles of SiOH, CaOH, and KOH polyatomic ion groups special corrosion effect 80−81387
failure prediction technique derived from fracture mech. 77−7343
far IR anomalous excitation obs. 77−40245
fatigue, static, review 77−40441
feldspar electrotechnical porcelain, phase composition calc. 77−21111
film, Brillouin scatt. from surface phonons, SAW vel. and attenuation 78−95587
film, props., rel. to deposition conditions, appl. in semicond. devices 78−23612
film, RF sputtered, roughness parameters 77−69202
film deposition by vac. evap. struct. mech. and optical props. *(Czech)* 78−80469
film on plumbite-treated cotton, form. of coating at interface 79−15058
flat, dependence of creep, viscosity on cooling intensity, during quenching 80−20964
flat, dependence of microbrittleness on SO_3 conc. 78−84960
flat, strength and durability levels 80−66608
flat glass, commercial, birefr. due to laminar inhomogeneities 78−39731
flat glass in vacuum, exam. of temp. dependence of microhardness and microstrength 78−88532
flint, dense, nonlinear elastic props. *(French)* 80−34132
float, circular plates, thermoviscoelastic anal. of a thermorheologically simple material 80−10161
float, exam. of dynamic fatigue 78−80631
float, low-Fe, weathered, surface, characterisation 80−93666
float, stretching, one dimensional model 77−36442
float glass, attack by water, behaviour of Al traces *(French)* 80−89378
float glass, bending strength 78−23767
float glass, commercially produced, thermally toughened and untoughened, surface damage resistances on air and tin side 79−61612
float glass, heat transfer and temp. control in annealing, computer appl. 78−27543
float glass, Sn penetration depth meas. 77−76614
float glass, Sn penetration in bottom surface, synthesis 80−79993
float glass, toughening by ion exchange, selection of technology parameters 78−84757
fluorescence linewidth, anomalous of impurity ions in glass, theory 80−50404
fluorescence linewidth 80−34978
fluoride systems, fundamental condition for glass formation 80−44135
fluoride-opacified glass melt, time depend. of volatilisation losses 80−70381
formation from liquid state 78−2012
formation in various phosphate and carbonate systems 80−19708
forming processes, review 78−3090
Fourcault sheet glass, internal and surface temp. during heating *(Czech)* 79−42285
fracture, by impulse loading, splitting method tests strength properties 79−57118
fracture, electrical energy losses and causes, atm. humidity effect 80−55498
fracture, grinding and flaw geometry effect 77−56081
fracture and fatigue, crack tip radii influence 80−89335
fracture energy, direct meas. *(French)* 80−104376
fracture energy meas. by modified double cantilever method 77−73387
fracture mechanics studies, specimen *(French)* 77−73401
fracture processes, adsorption-sensitive, control and appl. 77−52468
fracture toughness, biaxial strength tests, finite element anal. 80−89431
fragments, discrimination between window, container glass fragments by EPR, forensic science appl. 79−11841
friction and wear against C and glass fibre reinforced PTFE and polyacetal 78−56783
future, manufacture, control, props. and appls. in year 2000 AD 78−3308
gamma-irradiated, trapped electron form., dose effect on conc., empirical eqn. 79−34325
gas bubble anal. using chromatograph 77−52694
gas content determ. by dynamic extraction method 80−61219
Gaussian size distrib. of rigid particles, AE anal. 78−62181
glass:Eu^{3+}, spectroscopic props. of excited states of ions, laser induced fluorescence line narrowing meas. 79−38641
glass:Mn^{2+}, EPR, low-field hyperfine struct. 78−95513
glass:Nd^{3+}, line narrowed fluorescence spectra and site dependent transition probabilities 79−38640
glass:Nd^{3+}, resonantly enhanced four-wave mixing in absorbing media *(Chinese)* 80−102764
glass:Nd^{3+}, spectral props. *(Chinese)* 80−60645
glass, deformation in glass transition interval 79−66137
glass-Al, layered target, reduced thermal cond., X-ray meas. 77−31523
glass-ceramic, machinable, elastic const. temp. depend. 80−79852
glass-ceramic composite, internal stress effects on mech. props. 77−21250
glass-ceramic/bone histological and mechanical bonding *(German)* 79−8569
glass-ceramics based on β-spodumene solid solns., dielec. const. calcs. 77−52008
glass-crystal transition energetics, Piloyan's method appl. 80−38916
glass-epoxy laminate, superconducting magnet insulators, gamma-ray radiation effects 80−24495
glass-metal composite, heat conduction, memory switching 80−96703
glaze, effect of CaO and MgO content on microstructure 77−21083
glaze-porcelain system, intermediate layer investig. by electron probe microanalysis 77−8965
glazes, opaque, with ZnO, microstruct. 79−60281
gradient composition, optical props. 80−88947
grazing discharge at air/glass interface, X-ray emission 80−33846
growth micromechanism in corrosive environment 80−108616
hardening, etching in hydrofluoric acid effect by low temp. ion exchange 77−44373
hardness testing, mechanical property determ. *(German)* 80−40669
heat resistance, determ. 80−24690
heat treated, thin foil prep. for TEM obs. 78−7154
heating, recording of pulsed EM radiation in RF band *(Russian)* 77−55837
high field conduction and ionic jump processes in single- and mixed-alkali glasses 78−38873
high-field ionic and polaronic cond., dielec. relax., Poole-Frenkel theory 80−100351
glass continued
high-level radioactive waste, charact. of glasses for solidification 79−63779
high-resistivity, uniform and space charge polarisation, thermally stimulated depolarisation anal. 78−15085
high-transmission, improved solar cell modules appl. 80−76636
homogeneity by Christiansen filter method 80−84066
homogeneity measurement by improved Shelyubskii method using press. 79−29302
hydrogen embrittling effects from acoustic emission meas. 80−11742
hydrophilic protective coatings 78−85019
hydrostatic forming, novel industrial appls. 77−44191
ill-condensed matter, summer school, Les Houches, France (July-Aug. 1978) 80−82561
impact damage, localised 77−44306
impact damage, strength, annealed and tempered flat glass 80−85025
indentation fracture in brittle rocks and glasses 77−41023
indentation process analysis using finite element method 77−12689
industrial, cylindrical tubular elements under internal and external press., deform. and failure resistance 78−35460
inhomogeneities and defects in glasses and their surfaces, detection using microbubbles, implantation technique *(German)* 78−47647
inorganic, calc. of microhardness and glass transition temp. 79−5059
inorganic, cylindrical shell, with initial geometric imperfections, precritical deform. under external hydrostatic press. 77−81306
inorganic, effect of liq. medium, on process of mechanical destruction 80−89283
inorganic, protective coating for anodized Al, solution deposited 79−34205
inorganic, shell, stress/strain state investigation under external hydrostatic press. 77−81370
inorganic, specific heat in anomalous region near vitrification temp., simple relax. model 77−43341
inorganic, struct. by X-ray scatt. diffr. obs. 80−84069
inorganic, thermal expansion coeff. rel. to phys. props. 80−49389
inorganic, viscosity and free vol. 79−94916
inorganic oxide glasses, internal friction, review *(Polish)* 79−95078
insulating, thermal, acoustic props., low temp. anomaly microscopic model 80−28921
insulating material, temp. depend. of elec. resist. determ., expt. *(Croatian)* 77−74426
interface chemistry with electrolyte solutions 79−79256
interface with anodic electrolyte solution, simultaneous transfer of different cations in elec. fields 78−30800
interferometer for 90° reflecting angle meas. *(German)* 78−164
internal friction 79−52286
internal friction and relaxation in vitreous solids *(French)* 77−72651
internal friction in region of transition to viscous-flow state 79−66101
internal microstresses in glass-ceramics 78−30542
internal parameters, ordering parameters, history function, rel. to glass transition 78−30738
ion activation, energy parameters determ. 80−24634
ion bombarded surfaces, spectral refl. 77−55308
ion bombardment, electromigration as deterioration mechanism 78−26601
ion microprobe anal., empirical sensitivity factor approach 79−74439
ion migration during ion exchange by electrolysis, relaxation effect 77−66759
ion motion and mixed alkali effect analysis 78−30793
ion-exchanged, anomalous stress profile, photoelastic meas. 78−90803
ion-exchanged glass, diffusion coeffs. of Tl^+ ions 77−89583
ionic conductivity, weak electrolyte theory 80−84322
IR emissivity calc., strongly absorbing media surface refl. 80−107452
IR total internal refl. spectrum, surface polaritons *(Russian)* 77−20861
isobaric thermal behaviour during heating and cooling, rate of recovery, one-parameter model 80−75165
Knoop hardness number is grinding *(Polish)* 80−97580
laminate 27-63S, shear fracture toughness charact., strain rate effects 77−8950
laser decoration technology 80−84810
laser fusion targets, plating methods 78−60862
laser fusion targets, vapour deposited coatings, surface finish obs. 78−60863
laser induced damage 80−66335
laser induced gas etching technique 77−63815
laser induced surface damage, free electron density meas. 77−40309
laser irrad. effects, SEM meas. *(German)* 80−24492
laser irradiated, damage accumulation kinetics 79−99991
laser irradiation, nondirectional glow prod. 78−52575
laser target, spherical-shell, energy absorpt., expt. determ. 80−54016
layer, absolute thickness meas. of dielectric material 79−67253
layer, thermal radiation spatial distrib. rel. to temp. field, internal reflect. 79−59913
layered glass/polymer/glass plate in temp. field, failure 80−43674
Libyan Desert Glass, redox form. conditions, EPR obs. of as-received and irrad. samples 78−28228
life testing under flexing load *(French)* 80−89432
light scattering by glass undergoing phase separation and homogenisation 79−24326
liquid phase separation, multicomponent glasses, thermodynamics 79−95173
liquid quenching equipment 78−84854
liquid-liquid immiscible regions, surface effects on energetics 80−33903
liquid-phase separated, phase comp., temp. depend. 80−16289
liquid-phase separated, struct., use of elec. methods 79−66249
low density, sintering, expt. study 77−85980
low density, sintering, pore size distrib. effect 77−85981
low density, sintering theory 77−81246
low energy atomic motions and anomalies at low temps. 78−30724
low loss compound-glass, for optical fibres 78−13798
luminescence, glass with nonequivalent optical centres, decay rate averaging 79−8178
lunar soil, Fe and Ti bands in glass fraction 77−49320
lunar soil, implications of Ti rich glass clod at Oceanus Procellarum 79−70970
magnetic susceptibility measurement, torsional reson. technique 80−82796
Mars surface, glass alteration as source of clay minerals 78−89097
mass transport phenomena and interpret. 78−26720
material processing facilities and expts. on Spacelab. 78−36431
material removal mechanism by free abrasive grinding 77−52510

glass continued
mechanical destruction role of relaxation processes 80−89282
mechanical properties, review 78−3162
mechanical strength fracture dynamics, behaviour forecasting *(French)* 77−73344
medieval, simulated, durability anal. using IR reflection spectroscopy 80−40777
melilith, crystn. temp. rel. to cryst. habit *(German)* 78−6017
melt, bubble behaviour during refining, math. model 80−81277
melt, electrical resistance calc. in electric furnace 77−66165
melt, multibubble dissolution 80−81371
melt, multiphase electric current field *(Czech)* 80−84310
melt, nucleation and cryst. growth in glass-forming melt 78−2016
melt, temp. field calc. by numerical implicit method 80−44342
melt, thermal inhomgeneity, method of determining 78−84756
melt, unified theory of chem. relaxation using light scattering or US absorption 79−16028
melt, vaporisation, high-temperature, transpiration apparatus 80−52231
melt quenching, kinetics of motion of crystal-melt interfaces 79−69040
melting, automatic control, adaptive subsystem 79−61553
melting, heat transfer, review 78−3084
melting, kinetic equation for interaction between grain material and liq. 80−84901
melting, new aspects, review 78−3087
melting furnace, elec., 14 ton/day 79−58693
melting furnaces, development and prospectives, review 78−3088
melting in fire-heated tanks, modelling *(Polish)* 80−96633
melting process, TV monitoring, equipment protection 79−58756
melting process model, for flameheated tank furnace melting *(Polish)* 80−70380
melting related to chemical composition, for glass manufacturing industry *(Czech)* 78−80505
melts, glass forming, exam. of isobaric-isothermal pots. in glass transition interval 79−7681
melts, specific weight, electrical conductivity, viscosity and surface tension meas. methods survey *(Slovak)* 80−47079
metal-glass material, relation between struct. and props., prod. by hot densification 78−11145
metal-glass mats. alloyed with Cu, powder prep. and props. 78−72912
3-methyl-pentane glass, trapped electrons, model 77−48661
methylcyclohexane glass, γ-radiolysis, electron tunnelling from matrix trapped biphenyl ions 79−29379
methylcyclohexane glass, trapped electrons, model 77−48661
methylcyclohexane glasses, γ-irradiated in presence of naphthalene, isothermal luminesc. 80−93388
3- methylhexane, glass, γ-irradiated, trapped electron-radical mag. energy transfer, ELDOR, cross relax. 77−16209
3-methylpentane glass, γ-radiolysis, electron tunnelling from matrix trapped biphenyl ions 79−29379
3-methylpentane glasses, γ-irradiated in presence of naphthalene, isothermal luminesc. 80−93388
3-methylpentane glassy matrix, localised electrons, cavity model 80−107743
2-methyltetrahydrofuran, glass, γ-irradiated, trapped electron-radical mag. energy transfer, ELDOR, cross relax. 77−16209
$(Mg_{0.88}Fe_{0.12})_2SiO_4$, natural peridot, shock-prod. olivine glass, TEM 78−10178
mica glass-ceramics, near perfect shape-memory solid 77−48492
microballoon, D_2 target fabrication for laser fusion *(Japanese)* 78−8971
microballoons, laser imploded dynamics, X-ray streak camera study 79−68937
microbeads, binary, inhomogeneity-packing density relations 78−92211
microbrittleness and strength depend. on chem. comp. 79−38937
microbubbles, method for polishing bubbles into hemispheres 78−95869
microcircuitry elements, thermoelastic phenomena *(Polish)* 80−93724
microelectrodes, Na^+ and K^+ selective, electrochemical props. 79−91957
microelectrodes, open tip glass, influence of diffusion, double layer, and glass conduction on elec. resistance 80−67300
micropipette, mechanics of pulling 80−56295
microsphere laser targets, He and H_2 permeation 77−83078
microsphere laser targets He and H_2 permeation 77−83079
microsphere reinforced, composite, mech. charact. calc. 78−64578
microspheres, interaction force meas. in dried atmosphere *(Japanese)* 78−20077
microstructure of glass and oxide glasses 78−88442
microwave tunnel echo in glasses *(Russian)* 79−65726
minimum life prediction, uncertainty 77−16665
mixed alkali glasses, IR reflection spectra *(Japanese)* 78−19491
mixed alkali silicate glasses, heat capacity *(Japanese)* 78−55954
models, math. and phys., of glass making process, review 78−3083
molecular water, IR spectra 77−43992
molten, design of level measuring gauge 79−29304
molten glass/water thermal interaction, nucl. reactor appl. 78−46149
monolithic glass, formation by chem. polymerisation 79−78926
Mossbauer absorption of Fe III of synthetic silicate glasses of geologic interest *(French)* 80−80658
mould heat transfer during pressing 78−80500
multicomponent, conc. distrib. in surface layer after contact with $AgNO_3$ melt, $AgNO_3/NaNO_3$ mixture 80−44372
multicomponent systems, phase behaviour, miscibility, tie lines 80−84294
narrow sandwich seal, correction factor for thermal expansion mismatch 78−75110
narrow sandwich seals, shape factor, finite element anal. 78−75111
nepheline syenite for high level radioactive waste storage 77−6541
network forming, oxide, internal friction *(Japanese)* 77−70096
neutron scintillating glasses activated by Ce^{3+}, luminesc. 79−38668
nitrate glass: Eu^{3+} struct. reorganisation in glass transition interval, polarised luminesc. obs. 80−45141
non-radiative recombination at valence-alternation pairs 80−89048
noncrystalline solids conf. Lyon, France (Dec. 1976) *(French)* 77−72560
nonequilibrium thermodynamics, diffusion and relax. processes *(German)* 78−83746
nonmetallic compounds, type A_xB_y, glass form. from melt 80−44140
nonuniformities and basic principles of struct. 79−41970
nuclear fission waste storage *(Dutch)* 78−29587
nuclear quadrupole spin-lattice relax., soliton-nucl. quadrupole moment interaction, temp. depend. 80−50220
nuclear spin lattice relax. in amorphous state, review 79−11354

glass continued
nuclear track detectors, track forming, stabilisation and development processes 78−17516
nucleating heterogeneities effect on glass form. 77−11487
oceanic basalt glass, noble gas comp. of neutron activated samples 79−74866
one-dimensional disordered harmonic system, heat capacity from spectral moments 79−28107
opal glass, chemically toughened, prep. and mech. strength *(German)* 80−89191
optical, refractive index, oscillator strength effect *(Japanese)* 77−28538
optical small angle polarisation modulation, by Faraday rot. in diamag. glass *(Korean)* 78−50918
optical waveguide, thick, highly multimode, for fabrication method 78−18043
optimal polynomials in calcs. of complex glass's properties 78−68026
order parameter model, vol. and enthalpy relax. 80−88008
organic, shear strength behind the front of a plane shock wave 79−15752
organic glass, creep under shear with superposition of hydrostatic press. 78−31482
organic glasses, hole burning, fluoresc., struct. 79−31588
organic liquids, glasses and glassy crystals, entropy of struct. disorder, rel. to mol. struct. 79−65219
organic matrices, electron spin-lattice relax. of radiation-produced Ag atoms, temp. depend., tunnelling relax. 79−34331
Ostwald ripening and its application to precipitates and colloids in ionic crystals and glasses [Review] 78−80548
oxide, elec. cond. and dielec. relax., correl. 78−79801
oxide glass:Cr^{3+} absorption and emission 78−6774
oxide glass, elec. cond. parameters rel. to charge carriers 77−35970
oxide glass, local in depth anal. by neutral beam SIMS 80−89565
oxide glasses:Sm^{3+}, optical transitions 79−61430
oxide glasses, charact. by magnetic resonance and optical absorption of metallic probe ions *(Japanese)* 79−95640
oxide glasses, fast ion transport 80−107470
oxide glasses, internal friction, H bond interpretation 80−92605
oxide glasses, ion-bombarded, optical line intensities 80−35037
oxide glasses, multivariant system of oxides and partial props. prediction from V-phenomenon 78−79540
oxide glasses, thermal expansion coeff. calc. from chem. comp. 77−11710
oxide glasses with Bi or Se granules, elec. props. and microstructure 78−2490
oxide-electrolyte interface, transition layer model 78−68895
panel, dynamic stresses and failure under inertial loading 77−56073
paramagnetic, Faraday effect in pulsed megagauss field 77−69804
partially devitrified, grain boundary diffusion, new percolation problems 78−18844
particle size influence on force moving particle in inhomogeneous elec. field, influence of field frequency 79−11795
particles impacting on metal barriers, piercing, stony meteorite simulation 78−89043
particulates, glass, removal mech. from solid surface 79−50676
peeling of rubber film, spontaneous creation of interfacial dislocations 78−73011
Permalloy-SiO_2-Schott glass, bubble propagation struct. 80−34719
permeability of He *(Japanese)* 79−7715
phase diagrams, user needs for materials processing 79−11594
phase separated, EPR rel. to struct., elec. and opt. props. 78−23333
phase separating, interpretation of temp. dependence of transport process 78−87806
phase separation, review 78−2015
phase separation and glass structure concept changes, review 77−65955
phase transform. in steep thermal gradients, apparatus 78−84767
phonon avalanches, exptl. conditions for obs. 78−71822
phonon echoes, backward-wave 77−76513
phonon echoes, spectral diffusion, and US saturation recovery 78−10149
phonon echoes and self-induced transparency 78−79710
photoacoustic spectroscopy 80−92611
photoelastic constant for chem. strenthening, circular plate compression method *(Japanese)* 80−93279
photoinduced dichroism in radiation coloured silicate glasses 79−69808
phototropic, kinetic investig. *(German)* 78−64868
plane layer, 0.07 to 1000 units, reflectance and transmittance 78−17860
plastic, engineering, nondestructive structural identification 78−92422
plastic, fatigue strength, loading frequency effect 77−52484
plastic, Young's modulus, expt. study 77−52389
plastic AG-4c, fatigue resistance under bending in H_2SO_4 *(Russian)* 79−34163
plastic coating, thick-walled, compressive strength evaluation method 79−15897
plastic-glass composite, thermoelastic residual stresses in shells of revolution, cut-out element method 80−38271
plate, flexure crack propag., expt. and anal. 78−80620
plate, in contact with rubber cylinder, elastohydrodynamic lubricant film form., expt. and theory 77−28910
plate, physically or chemically tempered, contact fracture resist., model 78−19895
plate, stress analysis of large deflection by finite element method 77−7307
plate flexure for concave spherical mirror fabrication 77−42583
plate impacted by glass spheres, localised impact damage 77−56089
plates, biaxially stressed, anal. of localised impact damage 78−68772
plates, effect of localized damage on energy losses, during impact by glass spheres 78−52973
plates, fast crack propagation meas. continuous stress meas., new method 78−73009
plates, thermally tempered, strength degradation 78−48505
plexiglas shell, orthotropic, cylindrical, interacting under straight angle, manufacture and strength 77−90417
plexiglas tube exposed to const. axial loads, deform. and creep, loading regime effect 77−90416
Plexiglass, spark press. field in solid dielectric 77−24233
PMMA, quartz- and glass-particle reinforced, abrasive wear 80−97594
PMMA glass, electron bombard. induced elec. discharge, electromech. effects *(Russian)* 77−32324
polished surfaces, environment sensitive, ellipsometric obs. 77−48559
polyisobutylene-glass adhesion bond, macroscopic contact form. 79−39113
polymer, thermodynamics of densification process 78−95723

glass continued
polymer bound glass article, rapid kinematic corrosion test, method and apparatus 79−39063
polymer coated, exam. using ion scattering spectroscopy and scattered ion mass spectrometry 78−60641
polymer coated glass, current leakage path form. by water diffusion 78−10535
polymeric glasses, amorphous object morphology, determ. by spatial filtering 77−58931
polymeric glasses, kinetic theory of brittle fracture 78−48526
polymerised, theorist's ideal glass, short, long range props., statistical thermodynamics 77−27834
porous, adsorbed water, proton spin-lattice relax. meas. by pulse NMR 78−84053
porous, adsorbed water molecule interaction with surface hydroxyls, IR spectra 78−43244
porous, catalytic activity in radiative thermal cracking of propane *(Russian)* 79−39205
porous, dissoc. adsorption of ethanol, IR obs. 79−23830
porous, free molecule flow and interdiffusion 79−32658
porous, struct. and texture rel. to heat treatment effects *(German)* 78−44140
porous, thermoosmotic flow, filtration, of water 78−53248
porous glass:In, effect of press. on transition temp. 80−97027
porous glass, irradiated, accumulation and decay of paramagnetic centres *(Russian)* 77−85570
porous glass optimisation for immobilised enzyme systems 77−12891
porous Vycor, adsorption of 1,1-diphenylethylene, reson. Raman spectrum, surface species identification 78−42066
porous Vycor, surface phonons, Raman and IR reflectivity spectra meas. 78−38931
porous Vycor glass, quenching by O_2 and NH_3, photoluminescence obs. 80−93773
powder, coupled with silane, Fourier transform infrared spectroscopy 78−60642
powder, light scatt., close particle packing 78−1161
powder additions to piezoelectric ceramic TsTBS-3, effect on mech. strength 78−31370
powder-water-oil system, cohesion of powder particles with water, rheological prop. *(Japanese)* 80−14647
powders, theoretical aspect of sintering 80−20883
preparation from metal-containing organic cpds., state-of-the-art 77−55922
preparation in unipolar HF discharge 80−1855
prestrain effect on dynamic modulus of elasticity and attenuation coeff. in nonconducting materials 80−29110
prestressed plate, contact induced failure 80−3172
Prigogine-Defay ratio for inhomogeneous system with single internal parameter 77−76578
protective glassy layers at 500°C for Cu passivation 78−76785
proton transport 80−79974
pulsed RF radiation produced by scratching *(Russian)* 78−19607
Pyrex, cation exchange and interdiffusion 80−80002
Pyrex, H at. recombination coeff. calc., catalysis appl. 77−48634
Pyrex, impact of small steel spheres 77−73338
Pyrex, indentation recovery, defect struct. produced by deformation 79−43275
Pyrex, ion bombardment, form. of cpds., IR spectrosc. exam. *(German)* 80−88173
Pyrex, isothermal compressibility to 20 kbar, inductance coil method 80−49302
Pyrex, near-surface H embrittlement, effect on deform. and fracture props. 79−29180
pyrex, plates, exam. of friction, wear and elastic constant mechanisms 78−87309
Pyrex, polished surfaces, environment sensitive, ellipsometric obs. 77−48559
pyrex, statistical analysis of Hertzian fracture using Weibull distribution function 80−66623
Pyrex, steady wear mechanism against Cu expt. study to confirm theoretical anal. 80−45404
Pyrex, stress intensity factors of surface cracks and fracture stress, acoustic meas. 79−47845
Pyrex, substrate, for Si evaporated semicryst. layer growth 79−82482
pyrex, surface, laser annealed, characterisation by ellipsometry 80−103544
Pyrex glass, Hertzian fracture under quasi-static loading 79−66142
Pyrex glass, sedimentation pot. meas. device and ζ pot. determ. *(Spanish)* 77−70236
Pyrex substrate, AES of Ni films, purity 77−8755
pyrex-H_2O(aq. KCl) systems, electrokinetic coeff. determ. from sedimentation pot. 80−3365
Pyroceram, enhanced failure by combined pulse and CW laser 79−29182
pyroelectric, low-temp. behaviour 78−56432
pyroxene slag glass ceramics, exam. of synthesis conditions, influence of catalysts 79−4942
quantitative analysis using SIMS 77−56285
quartz:Ag glasses, EPR of atomic Ag centres 79−15349
quartz, alloyed, for shape-formers in Si strips growth by Stepanov's method 79−78867
quartz, crystallisation in different gaseous media 77−24269
quartz, crystn., effect of fusion temp. and time 77−36441
quartz, fused, thermal cond., temp. depend. at low temps. 80−65322
quartz, hardened plate, internal stress and birefringence microanal. using optical phase microscope interference-polarisation 79−39109
quartz, particle track formation and minimal energy loss *(German)* 77−18757
quartz, struct. study using small-angle X-ray scatt. 80−84071
quartz, surface energy evaluation, by a microindentation method 80−16473
quartz, thin layer, interaction with gas-discharge plasma *(Russian)* 78−14178
quartz, Ti-doped, acoustic props., thermal stability 77−24356
quartz, water vapour influence on crystn. stability 77−36440
quartz based ceramic, organosilicon binder, spalling-resistant, prod. 80−40313
quartz glass, ^{252}Cf fission fragment tracks, electron microscope obs. 78−17526
quartz glass, effect of boundary refl. and selectivity of optical characts. on radiative-conductive heat transfer 78−1554

glass continued
quartz glass, effect of O vacancies and hydroxyl-group concs. on crystn. 77−16533
quartz glass, optical breakdown by sharply focused laser beam 79−69776
quartz glass track detectors, nuclear phys. spectrometric appls., track diameter 78−17466
quartz glass-ceramics, atm. influence on sintering rate 79−38784
quartz glass-water suspensions, electrolytes effect on viscosity, pH and zeta pot. props. 79−34365
quartz glasses, viscosity rel. to crystallisation 77−24386
quartz glasses of various grades, natural luminescence and lattice vacancies *(Russian)* 77−28625
quenching, horizontal, technological parameters rel. to optical properties 80−45264
quenching, stress distrib. calc. using finite element anal. 79−66087
radiation stability origin *(Russian)* 77−55300
radioactive waste, high-level, leaching of radioactivity from glass blocks buried below water table 77−65312
radioactive waste containment, alpha-particle effects *(French)* 77−26849
radioactive waste immobilisation using glass 80−42812
radioactive waste storage, high-level waste glass 77−6540
rain erosion mechanisms of brittle materials 79−34154
Raman scattering, low-freq., 6-700K, excess scatt. 78−23473
Raman scattering by defects 77−8580
Raman scattering meas. of silicate glasses containing sulphate 77−69818
rare earth elements, use in glass and ceramics *(Polish)* 80−97455
rare earth glasses, R_2O_2S-Ga_2S_3, (R=La to Nd), exam. of preparation and props. *(French)* 78−80504
rare earth oxide (R_2O_3)-M_xO_y glassy systems (M=Ti,Nb,Ta), rapid quenching by laser beam, exam. of composition and crystallization 78−52856
rare earth-gallium sulphide system glasses *(French)* 77−19877
raster technique for automatic checking for defects in sheets 78−23883
reaction cured glass insulation coating, space shuttle, combined load testing at 1100°C 79−34261
redox number 79−29392
reflectivity, quantitative meas., undergrad. lab. expt. 78−49624
refractive index, freq. depend., use of dispersion formulae 79−65825
refractive index during annealing, nonlinear structural relaxation model 78−44234
refractories, glass-making, progress, review 80−40303
refractory, obtained by hot pressing of gels, crystallisation *(French)* 78−11193
relaxation kinetics, Prigogine-Defay ratio 77−20042
relaxation of props. during isothermal swell period, method of calc. 78−67654
relaxation phenomena, review 78−2014
relaxation phenomena and Raman spectroscopy, review of developments 78−22665
resin impregnated glass tape, friction and rheological props. 77−63806
rod, optimum sample shape for compression testing, failure 80−71756
rods, partially leached, contact-damage resist. 80−50707
rolled, metal wire reinforcing 80−104107
rolling friction on rubber, humidity influence 79−79118
rupture behaviour, long-term strength, thermofluctuation theory *(Russian)* 80−40536
scintillating glasses, effects of temp. on pulse height and cond. 77−10547
segment, resting on elastic ring, structural strength 80−14630
set point, of glass in glass-metal seals 80−108423
sheet, laminated struct., effect of prod. method 79−61555
sheet, laminated struct. and homogeneity, mech. agitation effect 79−61554
sheet, striation form. mechanism 79−61751
sheet glass, chemical resistance to water testing by surface cond. meas. *(Polish)* 79−70271
sheets, large scale, exam. of bending strength under uniformly distributed load 79−29135
shell, built-up, local strengthening influence on supporting capacity 80−71714
shell, cylindrical, bearing capacity under axial compression 80−76323
shell, for laser fusion targets, plasma polymerisation coating method 78−60859
shell, laser compression, two-dimens. effects *(Russian)* 77−4124
shells with metallic inserts, structural strength 80−35283
shock wave, implosive spherical, produced by laser pulses, shadowgraphic detection 80−87529
silica, phosphorus containing, optical absorp. characts. of hydroxyl radicals 77−14800
silica glass, ball mill grinding, rate constant determination *(Japanese)* 78−95828
silica glass, ball mill grinding, wet, dry, rate constant determination *(Japanese)* 78−95827
silicate: Yb_2O_3 glassy film, Yb laser spectral microanalysis 80−76585
silicate, ^{57}Fe-doped, 2-parameter distrib. analysis of Mossbauer spectra using general inversion method 80−66079
silicate, alkali, oxidation reduction equilibria and optical absorption of Cu ions *(Japanese)* 77−12824
silicate, assignment of IR reflection spectra *(Japanese)* 78−10902
silicate, containing ZnO and TiO_2, thermal capacity 80−88335
silicate, dangling bond states 80−24846
silicate, decomp. in alkaline aq. soln. by ion exchange 77−48637
silicate, elastic modulus temp. depend., metal oxides effect 79−61637
silicate, EM pulse radiation, under symmetrical bending 80−45350
silicate, fracture toughness 79−57190
silicate, glasses corrosion by aq. solns. 78−64752
silicate, high temp. microscopy investigation of softening temp., viscous flow, angle of contact *(Polish)* 77−55242
silicate, IR refl. spectra resulting from phase separation *(Japanese)* 78−39542
silicate, light scattering, comp. effect 79−99899
silicate, linear variation of secondary ion yield *(French)* 80−108763
silicate, neutron diffr. determ. of struct. 78−79533
silicate, stressed state investigation by NDT using UHF waves 78−11460
silicate, surface and near surface struct. 78−87850
silicate, thermooptical constant, depend. on chem. comp. 79−99861
silicate binary glasses, SiKα and SiKβ X-ray emission spectra 77−24272

glass continued
silicate glass: Cr^{3+}, optical props., 88-273K, energy levels in crossing region 78−6709
silicate glass: Er^{3+}, $^4I_{13/2}$ level relax. 79−87476
silicate glass:Eu^{3+}, fluorescence linewidth, anomalous, theory 80−50404
silicate glass:Nd^{3+}, electronic excitation spatial diffusion meas. by degenerate four-wave mixing 79−64274
silicate glass, hydrated, proton and ^{23}Na wide-line NMR study 80−84659
silicate glass, hydration in steam atmosphere 80−85211
silicate glass, hydration thermodynamics 80−81313
silicate glass, IR reflection spectra relation to corrosion state of surface *(Japanese)* 78−88554
silicate glass, low voltage electron microscopy of heated surfaces using C replica technique 80−25974
silicate glass, mechanical stress field influence on structural mobility 80−103421
silicate glass, nonactivated, far UV image recording, colour centre formation *(Russian)* 77−5950
silicate glass, space charge distrib. after 2.1 MeV electron irrad. *(Russian)* 77−69772
silicate glass, thermodynamic theory of structural relaxation *(German)* 80−38929
silicate glass corroded by moisture, IR refl. spectra change *(Japanese)* 78−53013
silicate glass darkening due to UV radiation from laser produced plasma jet 78−52598
silicate glass defect liquidation in vacuum meas. method 77−41627
silicate glass film, etching characts. in CF_4 plasma 77−90474
silicate glass. IR reflection spectra change due to moisture corona *(Japanese)* 78−19914
silicate glasses:Cu^{2+}, near IR electronic spectra, effect of alkali contents 78−27267
silicate glasses:Cu^{+}, effect of UV irrad., absorption bands 78−31222
silicate glasses, carbon tetrafluoride plasma etching characteristics 77−77616
silicate glasses, elastic moduli calc. 78−60696
silicate glasses, exam. of chemical stability, in alkali solns. 78−88557
silicate glasses, fused, cone cracks around Vickers indentations 79−29189
silicate glasses, indentation form. and fracture 79−66147
silicate glasses, industrial, elastic and shear moduli depend. on temp. 78−11254
silicate glasses, ion-microprobe determ. of Li diffusion 78−53649
silicate glasses, longit. and transverse elastic wave vels., temp. and comp. variations 80−88258
silicate glasses, low temp. synthesis, exam. of formation conditions, structure, and props. 78−88441
silicate glasses, low-energy excitations and hypersonic props., Brillouin scatt. meas., 1.7 to 15K 77−90160
silicate glasses, mixed-alkali, thermal expansion 77−4186
silicate glasses, model of struct. element, calc. of physicochem. props. 79−69016
silicate glasses, Na ion mobility, OH content effect 79−99359
silicate glasses, natural, fusion processes, EPR study 80−85659
silicate glasses, phonon echoes at low temp., coherent acoustic echo generation 79−65163
silicate glasses, polishing, surface characts. using grazing X-ray reflection *(French)* 80−65353
silicate glasses, polyalkali effect 77−24270
silicate glasses, redox equilibria of multivalent ions 78−26447
silicate glasses, relation between IR reflection spectra and corrosion state *(Japanese)* 78−23850
silicate glasses, stabilised, exam. of stress relaxation and deformation 78−92292
silicate glasses, stress corrosion cracking in N_2, CO_2, Ar, HCl, H_2SO_4 79−34171
silicate glasses, struct. and phase transform. 78−64538
silicate glasses, surface energy calc. from wettability data 77−35804
silicate glasses, swelling on proton, deuteron and He ion bombardment 78−67750
silicate glasses, viscosity-temp. relation 80−2187
silicate glasses containing AsO_4^{3-} ions, fining mechanism, Raman scatt. obs. 77−12379
silicate glasses containing iron, switching and memory effects 77−8155
silicate glasses fluctuation microcavities, vol., calc. 79−65000
silicate glasses from igneous rocks, high temp. thermal props. 77−33055
silicate glasses with high oxide modifier concs., property-comp. relns. 78−67655
silicate melt inclusions in volcanic rocks, samples of early magmatic liquid 77−37202
silicate reference material for silicate, gamma radiation detector 80−78454
silicate thermoplastic pigments for glassware, chem. resist. 79−61755
silicate triplex glass, produced by polymerisation, effect of monomer purity 79−24485
silicates, matrix effects in secondary ion emission 80−76125
silicon tetramethoxide, prep. from metal alkoxide, props. as precursor of oxide glass 78−48700
simple molecule glass, dielec. relax., 4-77K 77−73109
SIMS quantitative analysis, accuracy 79−39266
single-component, structure, crystallite and disordered-network hypotheses, review 79−41964
sintered glass-ceramics prep. from calcined simulated high level radioactive waste 77−28770
sintered powder porous bodies, liq. penetration mechanism *(Japanese)* 80−53853
Sitall, microcrystalline glass, exam. of frictional props. under end-end rubbing 80−16488
sitall base composites, antifriction props. 77−77591
sitall coatings in Li_2O-Na_2O-CaO-SiO_2 system, heat treatment effects on tech. characts. 78−84853
Sitall-based composite mat., grinding 77−63822
slow neutron action on glasses and vitreous ceramic and cryst. materials *(Spanish)* 80−57816
soda glass, ageing effect of HF discharge on conductivity and dielec. const. 78−39138
soda lime glass, microparticle impact, high speed photography obs. 78−44223
soda-lime, chemically modified, water contact angle, adhesional wetting 77−55426
glass continued
soda-lime, impact of small steel spheres 77−73338
soda-lime, liq. drop collisions, simulation of erosion in rainfield 77−56113
soda-lime, surface, damage due to impact of small glass and steel spheres 78−52994
soda-lime and reactor waste glasses, reaction with water, characterisation using ^{15}N H profiling method 79−54519
soda-lime glass, depth profiles of Na and Ca by SIMS and AES 78−51805
soda-lime glass track detector etching in NH_4HF_2, NaOH and KOH aq. solns. 79−26816
soda-lime-silicate glass, dynamics of fracture mirror boundary formation 77−86132
solidification kinetic eqn., derivation from heat transfer and viscosity eqns. 80−25679
sound insulation properties, most effective window configurations 80−87655
space flight applications in materials science 79−47885
specific heat, time-depend., at low temps. 79−60520
specific heat anomaly at low temp. 77−80631
specific heat at low temps. 77−11703
specific heat time depend., rel. to US props., at low temps. 78−59957
specimen containers, thin-walled silica glass, technique of construction 80−31724
spectral behaviour under narrow-line excitation, of Nd^{3+} doped ED-2 glass 79−33747
spectral diffusion, ultrasonic, low temp. 78−18709
spectral diffusion 78−59914
Spectrofloat glass, theoretical anal. of optical transmission and refl. props. 77−90120
sphere mixture, polydisperse system, AE anal. 78−62180
spinel transparent glass ceramics, colour centre form. due to alkali metal vapour and X-ray irradiation 79−87316
spinodal decomposition, review 80−96657
β-spodumene-mica glass ceramic, thermal expansion thermal shock and moduli of rupture and elasticity 78−60736
β-spodumene-mica glass ceramics, phase evolution and TiO_2, MgF_2 additive effects, exam. 78−44089
spontaneous echoes, spectral diffusion decay 80−84270
spreading of high-press. polyethylene melt, index 79−37902
stained, deterioration by atmospheric corrosion and micro-organisms 80−93664
static fatigue, reexamination of limit 77−90458
statistical mechanical model at low temps. 79−65686
steel antioxidation protective glass enamel cladding exam. of development 78−85031
strain intensity criterion for crack branching in brittle mats. 78−55592
strain interactions, low-temp. props. 79−42269
strength and failure predictions 77−21256
strength degradation from impact with spheres 78−27663
strength test, biaxial, use of Weibull statistics 78−68798
stress analysis, oblique incidence light scattering, birefringence *(Polish)* 80−71374
stress in working zone under biaxial compression, Moire-band method 77−81369
stress intensity factors by double torsion method, crack growth *(French)* 77−73345
stress relaxation meas. device 77−63845
stress-strain diagrams, anal. and classification of low deforming materials by their behaviour under stress 79−15753
strip, surface temp. field during annealing in tower of vertical drawing system 78−11242
structural analysis, using fluorescence excitation *(German)* 80−38923
structural relaxation, order parameter model 78−83740
structural relaxation, order parameter model *(German)* 80−44146
structural transformations, temp. effect on chem. equilib. 79−94912
structure, influence of thermal history *(German)* 80−38930
structure, NMR investig. techniques 78−23358
structure, review 78−2013
structure, X-ray neutron and electron diffr. studies, review 77−65954
structure and thermodynamics of glass-forming systems *(German)* 80−38924
structure determ. using EXAFS 80−45169
structure formation during crystallisation, Mossbauer obs. 77−48106
structure of glass-forming systems *(Russian)* 80−38925
structure of simple inorganic amorphous solids, review 80−15004
substrate, adherence of Ti and Cr films 80−7496
substrate, adhesion and hydrophilicity of glow-discharge-polymerised propylene coating 79−15829
substrate, c-axis oriented AlN film, low temp. growth by RF reactive planar magnetron sputtering method 80−76175
substrate, Cr film on with ZnS or MgF_2 underlayer, thermal strength, recrystn. influence 79−87748
substrate, for Mn_3O_4 film form. from Mn^{2+} ions in water *(Japanese)* 80−45411
substrate, glow discharge effects on surface props. and struct. 78−85201
substrate, SnO_2:Sb film, elec. props. 80−88652
substrate, subbing for AgBr layers, effect on photographic characts. *(Bulgarian)* 78−78016
substrate, surface temperature measurement, heated through Ga 79−97390
substrate, thermal expansion, rel. to thermal cycling stability of Pb film tunnel junction 79−87200
superionic conduction mechanisms 80−84321
surface, difluorodichloromethane thermochem. treatment, mech. props. 80−40565
surface, glow-discharge treated, adhesion of vacuum deposited oxide *(Russian)* 77−44372
surface, interdiffusion of H^* and alkali ions, extended Boksay-Doremus theory 80−34254
surface, N atom recomb., Langmuir-Rideal mechanism 80−7853
surface, physical chemistry 78−60854
surface, physical chemistry exam. 78−2018
surface, sputtering with inert gas ions 78−64438
surface anal. by AES 78−60013
surface comp. profiles by Auger spectroscopy and ion etching 77−90223
surface conductivity, effect of impurity adsorption *(German)* 78−30971
surface conductivity at solid/liq. interface 79−78152
surface contamination by H_2, shortening of ultracold neutron storage time 78−17461

glass continued
surface damage by abrasive contact, effect on strength 80−85066
surface flaw density, statistical determ. 78−11310
surface flaws, decoration technique 78−14547
surface fluctuation, obs. by laser-induced damage of Au evaporated film 77−1279
surface heating by laser, optical temp. meas. 79−55911
surface layer, structure and processes *(German)* 80−38928
surface model, causal relation, separation of inner glass and conc. of impurities on surface *(German)* 78−30817
surface modification by chemical and electrochemical methods *(Polish)* 77−86213
surface properties and contact angle after treatment with glow discharge and heating 80−21139
surface removal of stearic acid monolayers with organic solvents 77−28924
surface resistance changes during dew form. initial stages 77−11777
surface stress measurement, using opt. waveguide effect of chem. tempered glass *(Japanese)* 80−45473
surface textures and defects, exam. using liq. crysts. 80−6364
surface treatment, improvement in mech. and optical props. recent progress *(Japanese)* 79−79141
surface treatment effect, on chemical polishing time of crystal products 78−92436
swelling, blistering, 140 keV p, d and He ion irrads., porosity effects 77−35603
symmetry and topology concepts for spin glasses and other glasses 79−28541
systems with anisotropic g-tensor, EPR spectra, extra absorpt. peaks 79−51839
tank furnaces, physical models, selection criteria for liquids to simulate melted glass 79−8263
Taylor wire prod. by rapid quenching 78−44045
technical, STL10, A-1, A-3, A-6, 13V, statistical features of strength characts. 79−43353
technology and applications, review of advances 77−66618
tektites and natural glasses, N concs. 80−41446
tellurite, rare-earth activated, polarised luminesc. 78−48224
tellurite glass:Nd^{3+}, spectral behaviour under narrow-line excitation 79−33747
tellurite glass:Tm^{3+}, eigenstates and radiative transition probabilities calcs. 77−77265
tellurite glasses: Ho^{3+}, nonradiative relax. 77−24881
tellurite glasses, binary, struct. and props. *(Japanese)* 79−32917
tempered, density and refractive index variation 78−64564
tempered, spontaneous fracture due to NiS inclusions, exam. of behaviour mechanics 78−71294
tempered, stress meas. in surface, indentation technique 77−44341
tempered, surface residual stresses from indentation fracture mechanics 77−90439
tempered discs, meas. of nonuniform distribution of residual stresses 78−95865
tempered plate, stress state model and heat transfer rate determ. 78−60684
tempering, stress and structural relaxation 78−64574
tensile and impact strength, effect of surface damaging and annealing *(Czech)* 79−74227
tensile fracture stress pulse emission in glass rods 77−15486
tensile strength of threads and foils, dimensions depend. *(Russian)* 77−59852
ternary, composition-thermal expansion relationships 78−18801
ternary oxide systems, metastable two liquid tie line calc. 78−92246
tetrahedral glass AX_2, band limits and vibrational spectra 79−73935
textolite-glass shell, NDT 78−11471
textolites, three layer construction diagnostics of physicomech. props. 77−73254
thermal, acoustic, and dielec. props. at low temps. 79−65164
thermal behaviour during heating or cooling, retardation kinetics 77−4049
thermal cond. rel. to diffusion process due to phonon-defect interaction 80−34259
thermal conductivity, sitalls and glass, at various stages of heat treatment 79−60562
thermal conductivity and diffusivity, temp. depend., glass microscopic bead struct. material *(Russian)* 79−37885
thermal conductivity effect of strain at 0.1K 77−89602
thermal diffusivity, meas. by constant-rate heating method *(Japanese)* 80−6570
thermal expansion at low temps., rel. to alkali halides 80−96672
thermal expansion coeff. rel. to chem. composition *(Japanese)* 79−51285
thermal insulation props. for low temp. appl. *(German)* 77−27463
thermal radiative properties from 0.32 μm to 206 μm 79−69268
thermal stresses, temporary and residual, monitoring by semiautomatic heating polariscope-polarimeter 78−16833
thermally tempered sheet and plate, surface stress meas. using optical waveguide effect 80−25967
thermopolishing, by use of low temp. plasma radiation *(Russian)* 80−45406
thickness automatic measurement by laser beam 80−82744
thin layer thermal conductivity meas., radiometric method 79−94475
thin-film geometry, harmonic generation of surface-plasmon nature, off-synchronous treatment 79−18475
toughened, stress corrosion characts., exam. 78−71295
toughened, stress corrosion characts. 78−19912
toughened, stress relaxation, 200 to 600°C 78−19800
toughened, stress relaxation, at temp. below annealing range *(Czech)* 79−43305
toughened glass, 200 to 600°C stress relax., anal. *(Czech)* 78−79661
track detectors, effects of pre-irradiation and condition on etching 80−37702
transition elements, 3d, ESR for valency assessment, appl. to ceramics and glass industries *(German)* 80−34757
transmission and other props. 80−84712
transparent glass-ceramics, microstruct. and props. 78−59960
transparent materials, defective surface layer formation during abrasion, laser-induced breakdown *(Russian)* 78−53007
trapped electrons, electron-phonon interaction 79−78697
tunnelling system, broadening mechanism 79−28701
two dimensional steady flow problems, numerical soln., finite element method 79−23296
glass continued
two-phase, struct. and texture, electron microscope study 79−64999
Twyman effect in plane-parallel plates, effective surface tension *(Russian)* 77−31867
ultimate strength, and max. breaking rate 80−25863
ultrasonic NDT techniques, low-frequency 78−80690
US detector applications 78−33974
US drilling of workpiece, structural alterations 78−48555
US propagation at ultralow temperatures 77−39635
US properties, review 77−69048
US properties and short-time sp. ht. relationship 79−60440
US relaxation, linewidth and anomalous dispersion 77−39636
vibrational modes, conjecture effect of small anharmonicity 79−95112
vibrational spectra and glass structure 80−84732
Vickers indentation, slow surface crack growth 77−12688
viscoelastic properties, comparison with Lennard-Jones model 80−84983
viscoplastic, gas-vapour interlayer problem 80−49490
viscosity, as function of temp., computer calc. 79−29100
viscosity, role on glass form. *(French)* 77−55931
viscosity, temp. depend. at const. struct. temp. 80−65271
viscous deformation during heating and cooling 80−89314
viscous flow, examination of mechanism 78−87805
viscous flow of frozen struct. glass, consequences of valence configuration flow theory 80−39335
visible light scattering, anomalous and normal, in liq.-phase separated glasses 80−20654
volcanic glass and sanidine/plagioclase feldspars, Pb partitioning 79−74867
Vycor, finite size scaling of sp. ht. of sorbed ^4He 79−56015
Vycor, porous, adsorption of carbonium ions, reson. Raman spectra 78−84571
Vycor, positronium-surface interaction in pores 78−27347
Vycor, preferential adsorption of ^4He from ^3He-^4He mixtures 78−84023
Vycor glass, porous, adsorbed NH_3 Raman scatt. 80−11948
water resistance of glassware, rapid meas. method 79−61812
wear, acoustic emission obs., effect of ion aggregates in Rebinder-Westwood environment 78−48536
white Cl-containing slag glass-ceramic, synthesis with nonsulphide catalyst 78−52748
white-surface, spectral reflection coeffs. and colour coordinate comparison 77−71358
window, melts, glass-transition temps. from viscosity temp. depend. 80−34113
window glass, knots and cords, EPMA characterisation 80−84085
window glass, temp. depend. of coeff. of thermal expansion rel. to const. fictive temp. 78−67839
workability rel. to melting history, microstruct., apparent liquidus temp., mechanical props. 80−11633
X-ray absorption spectrometry of local order around Fe 80−79701
X-ray diffraction microcamera for analysis of cryst. defects in glasses 77−60002
X-ray fluorescence analysis of ancient glass, sample prep. 77−34064
X-ray reflectance of polished surfaces, depend. on refr. index distrib. of superficial layer *(French)* 77−28643
X-ray transmission, circular waveguides of curved Pb glass capillaries 78−86395
Young's modulus determination, using static compression, tension, and dynamic loading 78−83867
Zachariasen's rules, Madelung constant, and network topology 79−27926
Zerodur, glass-ceramic, thermoelastic props. 78−27550
$16Na_2O.12CaO.72SiO_2$, self-diffusion of Ca^{2+} ions *(Japanese)* 78−6173
Ag halide:Cu^{2+} photochromic glasses, darkening mechanisms, from flash photolysis and EPR studies 77−16156
Ag vacuum deposited coating on glass, strength 80−55505
AgI-Ag oxysalt high cond. glasses, struct. obs. 79−32908
AgI-Ag_2MoO_4 pseudobinary system, superionic cond. glasses, comp. depend. of ionic cond. 80−75380
AgI-Ag_2O-MoO_3, superionic conducting glass, IR spectra and struct. 79−10804
AgI-Ag_2O-MoO_3 glass glass superionic cond., struct. and transport props. 80−88602
AgI-Ag_2O-MoO_3 glassy electrolyte galvanic cells 80−104513
AgI-Ag_2O-MoO_3 system, glass form. with high ionic conductivity 77−89379
$AgPS_3$-AgX (X=I, Br), glass-forming regions, struct. model *(French)* 80−100464
Al coated glass microballoon targets for laser implosion expt., search for shell disintegration 80−33792
Al vacuum deposited coating on glass, strength 80−55505
AlF_3 based glasses, chem., thermal and optical props. *(French)* 80−70139
AlF_3-M_2F glasses, M=alkaline earth, density-of-states and structural forms, Raman spectra study 80−97255
Al_2O_3-glass mixture, microstructural changes and shrinkage during sintering 80−25640
$Al(PO_3)_3$-NaF-LiF, mixed-alkali effect 80−19715
Au vacuum deposited coating on glass, strength 80−55505
BaO-Fe_2O_3-Na_2O glass, mag. props. 78−88123
BaO-Fe_2O_3-(Na_2O) glass, rapidly quenched, mag. and ferrimag. props. 80−75744
BaO-K_2O-Na_2O-ZnO-SiO_2, corrosion and microhardness, effect of detergents 80−16518
BaO-K_2O-VO_2-SiO_2, glass, elec. cond. rel. to ion polarisability, polarons 80−49729
BaO-$La_{0.6}O$-VO_2-SiO_2, glass, elec. cond. rel. to ion polarisability, polarons 80−49729
BaO-SiO_2, effect of high-dose X-rays and reactor radiation 80−19838
BaO-SiO_2, Nd^{3+} luminesc. quenching by transition metal and rare earth ions 80−25449
BaO-SiO_2 glass ceramic, nucleation, effect of electric fields 78−83742
BaO-SiO_2 glass ceramic, growth and nucleation kinetics 80−7528
BaO-SiO_2 glass-ceramic, crystallisation mechanism 79−90559
BaO-SiO_2-Fe_2O_3 permanent mag. ceramics, exam. of phase diagram, using X-ray analysis, optical microscopy, electron probe anal., and thermal analysis *(German)* 79−29012
BaO-SiO_2-TiO_2, molten, ionic elec. cond., TiO_2 effects *(Japanese)* 77−51532
BaO-TiO_2-Cr_2O_3, new compound, phase relations *(Japanese)* 78−6911

glass continued
$BaO-V_2O_5-CuO$, $P_2O_5-V_2O_5-CaO-CuO$ glasses, EPR, Cu impurity effect on elec. props. 79−51849
$BaO-V_2O_5-CuO$ semiconducting glasses, impurity effects, elec. resist. and EPR study 80−103692
$BaO.2SiO_2$ spherulitic growth and recrystallisation 77−4046
$3BaO.5SiO_2$ glass, nonisothermal devitrification kinetics 80−92465
BeF_2 glass, durability in water 79−95171
$BeF_2:Eu^{3+}$ glass, luminesc. of Eu^{3+}, transition probabilities 80−80845
$BeF_2:Eu^{3+}$ glass, struct. and optical props. 80−84067
$BeF_2:Eu^{3+}$ glass, struct., Monte Carlo simulations 80−96448
$BeF_2:Pr^+$, glass, optical homogeneous linewidths 80−7395
$BeF_2-KF-CaF_2-AlF_3:Nd^{3+}(Er^{3+})$, multiphonon relax., fluoresc. obs. 78−15219
$BeF_2-KF-CaF_2-AlF_3-EuF_3$ fluoroberyllate glass, Eu^{3+} fluoresc. linewidth 80−66285
$BiO-SiO_2$ films, on Si, dopant distrib. pattern study using chem. etching 79−86812
Bi_2O_3 based glasses, IR transmitting materials, appl. in 1 to 6 μm range, mech. props., review 79−4250
Bi_2O_3-based glass, in ZnO-glass-ZnO struct., current-voltage characts. and TSC *(Russian)* 77−69404
Bi_2O_3-PbO, glass, cond. meas. using complex impedance anal. *(French)* 80−92707
$Bi_2O_3-TiO_2-Nb_2O_3$, subsolidus phase equilibria 77−55954
C fibre reinforced glass, SiC fibre coating, hot pressing production method *(German)* 78−95724
C, thickness imposed thermal diffusivity gradient 78−14521
Ca metasilicate crystallisation kinetics 77−11486
$CaO-(CaF_2)-Al_2O_3$, IR absorption spectra and X-ray emission spectra obs. *(Japanese)* 77−52075
$CaO-Fe_2O_3-SiO_2$ glass, struct. behaviour at melting, Mossbauer exam. 79−10802
$CaO-MnO-SiO_2$ system glasses, vitrification and crystallisability 77−7853
$CaO-SiO_2$ glass, solid reactions, study by hot stage electron microscope *(Japanese)* 78−12798
$CaO-SiO_2$ glass, trimethylsilylation method for silicate ion anal. *(Japanese)* 80−71975
$CaO-SiO_2$ glass, two phase region, expt. and thermodynamic data 80−16288
$CaO-SiO_2$ glass prep. by gel method 80−100824
$CaO-SiO_2$ system glasses, IR absorpt. struct. obs. of phases and struct. 80−34918
$CaO-SiO_2-Fe_2O_3$ glass, Mossbauer spectra 80−15850
$CaO-SiO_2-Fe_2O_3(MgO)$, melt, CaO dissolution *(Japanese)* 78−6909
$CaO-SiO_2-NiO$ systems Ni ions anal. by ESCA *(Japanese)* 80−40787
$CaO-SiO_2-NiO-MgO$ glass melt, interaction of NiO and MgO, elec. cond. and IR spectra obs. *(Japanese)* 80−24632
$CaO-SiO_2-ZnO$ continuous unidirectional crystn. of fibrous metasilicates from melt 78−95739
$10CaO.15Na_2O.75SiO_2$ glass, thermal cond., temp. depend. at low temps. 80−65322
$CdGe_{1-x}Sb_xAs_2$ glass, DTA, microhardness meas. *(French)* 77−72564
$CdO-Bi_2O_3-Al_2O_3$, glass formation and IR transmission *(Japanese)* 80−54146
$CdO-SiO_2$ glasses, photochromism *(Japanese)* 78−15140
$CeO-SiO_2$, molten and glassy state, X-ray diffr. determ. of struct. *(Japanese)* 78−9936
CoO-containing glass, effects of γ-rays, electron beam and neutron flux on transmissivity *(Japanese)* 77−73156
Cr vacuum deposited coating on glass, strength 80−55505
$CsF-BeF_2$ glass, anion conductivity, transport number radiometric meas. 79−86923
Cs_2O containing glass, electrolysis, vac. prep. of pure Cs 77−8773
Cs_2O profiled silicate glass, residual stresses 80−2107
$Cs_2O-MgO-SiO_2$ system, glasses, crystn. prods., composition, props. 79−41961
$Cs_2O-SiO_2(-GeO_2)$ system glasses, X-ray diffr. anal., electron radial distrib. curves 78−87622
$Cs_2O.4SiO_2$, behaviour of VO^{2+} as spectroscopic probe 79−78510
Cu/glass-polymer compound powders, prep. and corona charging props. *(Japanese)* 78−19679
Cu-Cd-Cl stretched photochromic glass, polorisation effects 79−95729
Cu-to-glass adhesion 77−44386
CuO-containing glass, Cu^+ diffusion and oxidation 80−79980
Eu^{3+} fluoresc. lineshape in glass, temp., time and conc. depend., two-phonon Raman scatt. 78−64406
Eu^{3+} spectral line inhomogeneous broadening, electron excitation migration *(Russian)* 77−48200
$Eu_{0.14}Si_{0.31}O_{0.55}$ glass, optical, magnetic, and magneto-optical props., chemical clustering 79−42951
$Eu_{0.14}Si_{0.31}O_{0.55}$, insulating amorphous mag., optical, mag., and magneto-optical props. 79−61344
(Fe, Ti) silicate glasses, optical absorption and Mossbauer spectra 80−55136
Fe-C(C-B)(C-Si), splat cooled, formation of metastable crystalline phases and glasses 78−88461
Fe-containing glass-ceramics, effect of Mn_2O_3 on strength 77−48380
Fe-glass porous material, wear resist. under dry friction 80−25876
Fe-glass-Cu sintered material, Cu effects on strength 77−77443
$Fe_2O_3-Na_2O-BaO$ glass, mag. props. 4.2-295K, mictomagnetism *(French)* 80−39782
$Ga_2O_3-R_2O_3:Nd^{3+}$ glass, prep., characts., X-ray diffr., absorpt. and thermal anal. obs. *(French)* 78−19704
$Ga_2O_3-SiO_2-X_2O$ (X=alkali metal), acid resist. 80−21140
Ga_2S_3 glass *(French)* 80−71369
$Gd_2O_3-Al_2O_3$ glasses, crystallization 79−50998
GeO_2-SiO_2, glass, evaporation by high temp. mass spectrometry 80−79927
hexamethylphosphoramide:Li glass, metallic condensation of Wannier-Mott impurity states 78−2420
$HfF_4-BaF_2-LaF_3$ glass system, IR transmitting, synthesis and props. 80−71623
$HfF_4-BaF_2-ThF_4-(ZrF_4)$ glass system, IR transmitting, synthesis and props. 80−71623
$K_2CO_3-SiO_2$ glass forming batch, Raman spectroscopy 78−64519
$K_2CO_3-SiO_2-As_2O_3$, laser Raman spectrosc. study of ions in quenched reaction mixtures 80−25357
$KF-BeF_2-DyF_3$ system, $KBe_2F_5-DyF_3$ cross section phase diagram, vitreous phases struct. 77−24383
glass continued
$KF-PbO-SiO_2$, shear wave velocity and its temp. depend. *(Japanese)* 78−30702
$KNO_3-Ca(NO_3)_2$ glasses, radiation products and recombination 79−57261
$KNbO_3$ glass, quenched, ionic cond., appl. as solid electrolyte 79−1522
K_2O glasses, partially leached, dehydrated surface reaction with water 80−3406
$K_2O-BaO-CaO-SiO_2$ glass-Nichrome-CaF_2 multicomponent self-lubricating coating, prep. by plasma spraying, and props. 80−40604
$K_2O-BaO-SiO_2$ glass, rare earth ion activated, spectral intensity, effect of number of 4f electrons 78−84602
$K_2O-CaO-BaO-SiO_2$, calc. of network refraction and exam. of glass structure 79−4783
$K_2O-CaO-SiO_2$ glass, composition-density relationship 77−90326
$K_2O-CaO-SiO_2$ glasses, Auger analysis, alkali signal decrease 80−61189
$K_2O-Li_2O(Na_2O)-SiO_2$, heat of mixing *(Japanese)* 78−10195
$K_2O-MgO-SiO_2$ glass, crystalline phase precipitation during crystallisation early stages, DTA *(Japanese)* 78−42919
$K_2O-Na_2O-BaO-SiO_2$ glass, corrosion kinetics in aqn. KOH, transition metal oxide addition effects 77−56125
$K_2O-PbO-PbF_2-SiO_2$, shear wave velocity and its temp. depend. *(Japanese)* 78−30702
$K_2O-PbO-SiO_2$, effect of DC on corrosion of SnO_2 electrodes 80−85075
$K_2O-PbO-SiO_2$, glass, mech. and optical props. *(Russian)* 77−20860
$K_2O-PbO-SiO_2$, powders, ion exchange during leaching in HNO_2 79−100358
$K_2O-PbO-SiO_2$, structural units, Raman spectroscopy 77−20847
K_2O-SiO_2, AES obs. of K^+ electromigration to surface under electron bombardment *(French)* 79−33869
K_2O-SiO_2, effect of high-dose X-rays and reactor radiation 80−19838
K_2O-SiO_2, influence of electric charge phenomena on AES *(French)* 80−50478
K_2O-SiO_2 diffusion-controlled cryst. growth 77−19876
K_2O-SiO_2 glass, IR reflection spectra change due to moisture corrosion *(Japanese)* 78−19914
K_2O-SiO_2 glass, improvement in water resist. by ion exchange 78−85012
K_2O-SiO_2 glass, Raman scattering of dissolved CO_3^{2-} ions 78−27848
K_2O-SiO_2 glass 80−33897
K_2O-SiO_2 glasses, Auger analysis, alkali signal decrease 80−61189
K_2O-SiO_2 glasses, IR reflection spectra, computer resolution *(Japanese)* 77−69832
K_2O-SiO_2 system glasses, ionic cond. correl. with chem. pot. 77−89581
$K_2O-SiO_2(-GeO_2)$ system glasses, X-ray diffr. anal., electron radial distrib. curves 78−87622
K_2O-SiO_2glass, structural analysis, using fluorescence excitation *(German)* 80−38923
$K_2O-SrO-SiO_2$, influence of composition on electrical conductivity 77−11723
$K_2O-SrO-SiO_2$, O_2 self diffusion exam. by proton activation anal. 79−65241
K_2O-TeO_2 glass, radiational EPR centres, struct. model *(Russian)* 77−28426
$K_2O-TiO_2-SiO_2$ glass, Si-O bonding, SiKβ X-ray fluorescence and IR spectra 80−10500
$K_2O-TiO_2-SiO_2$ system, vitreous, struct. obs. using neutron scatt. 78−22667
$(K_2O)_x(SiO_2)_{1-x}$ glass, pure and with As_2O_3, Raman study of As 80−84733
$K_2O.SiO_2$ glass, X-ray diffr. *(Japanese)* 80−19720
$K_2O.2WO_3$ glasses, X-ray diffr. study of struct. *(Japanese)* 77−11489
$K_2O.3CaO.BaO.xSiO_2$, property-comp. relns. 78−67655
$K_2O.4SiO_2$, behaviour of VO^{2+} as spectroscopic probe 79−78510
$K_2SO_4-ZnSO_4$ glass, transition metal ion doped, visible spectra 79−51990
$K_2SO_4-ZnSO_4$ system, glass formation and phase diagram study, physical props. 78−27500
$KTaO_3$ glass, quenched, ionic cond., appl. as solid electrolyte 79−1522
$LaF_3-BaF_2-ZrF_4(-MF)$, M=Na, Li, glassy transition, refr. index, density and molar refr. 80−1937
$La_2O_3-SiO_2$, glass synthesis by hot pressing of gels 79−15637
$La_2O_5-Na_2Si_2O_5$ molten glasses, surface tension and density, 900-1500°C 80−15334
La_2S_3 glass *(French)* 80−71369
$La_2S_3-Ag_2S-Ga_2S_3$ glass system, prep., thermal and elec. props. *(French)* 80−89192
Li concentration as function of depth using $^7Li(p,n)^8Be$ 77−35582
Li disilicate glass, radiation induced centres, EPR exam. 78−35033
Li glass NE-912, neutron detection efficiency *(Russian)* 80−27901
$Li_2B_2O_4-LiFe_5O_8$ glass, rapidly quenched, mag. and ferrimag. props. 80−75744
LiCl, deuterated aq. glasses, pulse radiolysis, trapped electron reactions 79−24804
LiCl, deuterated aqueous glasses, pulse irrad., trapped electron yield 79−20385
$(Li_{0.63}Na_{0.37})_2O.2SiO_2$, short range struct. by pulsed neutron scatt. 80−59396
$LiNbO_3$ glass, quenched, ionic cond., appl. as solid electrolyte 79−1522
$LiNbO_3-SiO_2:Fe_2O_3$ glasses, Li^+ ion cond. 80−107471
LiO_2-2SiO_2, glass, devitrification with ageing 78−79536
LiO_2-2SiO_2 glass, alkali motion ionic thermocurrent study, polarised impurity-vacancy dipole relaxation study 79−77806
$LiO_2-CaO-SiO_2$ phase equilibria 78−64528
$LiO_2-Na_2O-CaO-SiO_2$ glass-ceramic coating, high temp. effects on steel substrate 79−61776
LiO_2-SiO_2 glass, improvement in water resist. by ion exchange 78−85012
LiO_2-SiO_2 glass ceramic mineralogy 80−60826
$Li_2O-2SiO_2$ glass, DTA study, Kissinger plot 80−84084
$Li_2O-2SiO_2$ glass, ionic cond. under DC potential 79−28134
$Li_2O-3SiO_2$ glass, crystallization 79−74141
$Li_2O-(Al_2O_3)-SiO_2$ glass-ceramic, crystallisation mechanism 79−90559
$Li_2O-Al_2O_3$, rapidly quenched glasses, Li ion cond., elec. cond. 80−100346
$Li_2O-Al_2O_3(Ga_2O_3)(Bi_2O_3)$, quenched glasses, crystn. and ionic cond. 80−33899
$Li_2O-BaO-SiO_2$ glasses, elec. cond., room temp. to 450°C 80−107473
$Li_2O-Bi_2O_3$, rapidly quenched glasses, Li ion cond., elec. cond. 80−100346
$Li_2O-Fe_2O_3-SiO_2$ glass, struct. and crystallisation behaviour 78−83738

glass continued
Li_2O-Ga_2O_3, rapidly quenched glasses, Li ion cond., elec. cond. 80−100346
Li_2O-$Na_2O(K_2O)$-SiO_2, heat of mixing *(Japanese)* 78−10195
Li_2O-SiO_2, corrosion behaviour in aq. solns. of Al compounds 80−66679
Li_2O-SiO_2, crystn. and phase separation, positron lifetime and annihilation lineshape meas. 78−23550
Li_2O-SiO_2, glass ceramics, phase transformation processes 80−3025
Li_2O-SiO_2 glass, bulk crystn., SEM and optical microscope studies 80−44142
Li_2O-SiO_2 glass, crystallisation and phase separation 79−10803
Li_2O-SiO_2 glass, crystallisation study 79−90567
Li_2O-SiO_2 glass, cryst. nucleation, test of classical nucleation theory 80−1939
Li_2O-SiO_2 glass, protonated, field-driven guest proton redistrib. 80−107474
Li_2O-SiO_2 glass, thermotransport props. 80−79985
Li_2O-SiO_2 glass, water content effect on crystal nucleation and growth 79−55670
Li_2O-SiO_2 glasses, crystn. kinetics from amorphous X-ray scattering study 80−38919
Li_2O-SiO_2 glasses, Li self-diffusion, mass spectrometric method 80−79982
Li_2O-SiO_2(-TiO_2) glass, crystn., kinetic study using differential scanning calorimetry 80−44138
Li_2O-TeO_2 glass, radiational EPR centres, struct. model *(Russian)* 77−28426
Li_2O-TeO_2 glasses, struct., IR reflection spectra 78−68516
($LiO_{1/2}$-$NaO_{1/2}$)-$2SiO_2$ glass, alkali motion ionic thermocurrent study, polarised impurity-vacancy dipole relaxation study 79−77806
$Li_2O.2SiO_2$ glass, kinetics of crystal nucleation, effect of Pt and other impurities 78−88440
$Li_2O.2SiO_2$ glass and glass-ceramic, fatigue props. in various environments 79−91820
$Li_2O.2SiO_2$ glass and glass ceramic, Auger electron signal decay, crystn. effects 80−25503
$Li_2O.2SiO_2$ melt, bubble form. during unidirectional solidification *(Japanese)* 79−70057
$Li_2O.2SiO_2$, short range struct. by pulsed neutron scatt. 80−59396
Li_2SiO_3 glass pH meter electrode performance *(German)* 80−40695
Li_2SiO_4, piezoelectric glass ceramic, recrystallisation, pyroelectric response, permittivity 80−80703
$Li_2Si_2O_5$ glass, steady state crystal nucleation rate 79−90564
$Li_2Si_2O_5$ glass, steady state crystal nucleation rate 79−90565
$Li_2Si_2O_5$-Li_2SO_4 glasses, electrical cond. and Raman study of struct. *(French)* 79−65482
$Li_2Si_2O_5$-TiO_2 glasses, struct. and crystn. investigation using Raman spectra 80−38918
$LiTaO_3$ glass, quenched, ionic cond., appl. as solid electrolyte 79−1522
^{6}Li glass scintillators, appl. as neutron detector, problems and consequences 79−9968
x.MnO.(1−x)[19TeO_2.PbO], glass, antiferromag. behaviour, mag. props. 80−50072
Na conductive glass-Na amalgam interface, electrochem. obs. 78−76870
Na determ. by (p,γ) reacts., target excitation yields determ., appls. 77−44545
Na diffusion model, single alkali silicate glass 77−84990
Na silicate glass temp. depend. of rate of nucleation of acicular crystals 77−19875
Na_2-SiO_2 glass, prep. by metallic-organic derived method, phase separation 78−56610
Na_2-SiO_2-MgO glass, melt viscosity and IR meas. to study MgO behaviour *(Japanese)* 78−14495
NaBaZn glass, Eu^{3+} centre symm. 80−100447
$NaClO_4$ glass, radiation induced trapped electrons, photobleaching, H form. 77−44494
NaF-BeF_2 glass, anion conductivity, transport number radiometric meas. 79−86923
NaF-SrF_2-CrF_3, glass transition, crystn. and melting temps., optical transmission *(French)* 80−64910
($NaNO_3$-$Mg(NO_3)_2$):Nd^{3+}, glass, cryst., absorpt. luminesc. spectra, term struct. of Nd^{3+}, bonding 77−8624
NaO-CaO glass, melting speed, effect of struct. and grain shape *(Polish)* 79−29002
NaO-CaO-SiO_2 glasses, fluorinating agents effect on comp. and surface struct. 80−35364
NaO-SiO_2, glass, distrib. of different O ions, molar refractivity meas. 80−33897
NaO_2-SiO_2 glass track detectors, nuclear phys. spectrometric appls., track diameter 78−17466
Na_2O glasses, partially leached, dehydrated surface reaction with water 80−3406
Na_2O-2CaO-3SiO_2 glass, cryst. nucleation and growth, viscosity, thermodynamic props. 80−84079
Na_2O-$2SiO_2$ glass, alkali motion ionic thermocurrent study, polarised impurity-vacancy dipole relaxation study 79−77806
Na_2O-$2SiO_2$ glass, numerical optimisation of ESR V^{4+} spectra 79−38370
Na_2O-$2SiO_2$ high expansion glass, chemical durability improvement by ion exchnage 78−48361
Na_2O-$3SiO_2$ glass, high-temp. thermolum., colour centre absorpt. 80−16110
Na_2O-$3SiO_2$:Fe^{2+}, Fe^{3+} glasses, Mossbauer and ESR spectra and internal friction 80−100865
Na_2O-(BaO)-SiO_2 glass, chemical durability of surface, heat treatment effect 79−52405
Na_2O-(CaO)-SiO_2, corroded, quantitative anal. by IR frequency shifts 78−19909
Na_2O-(CaO)-SiO_2, diffusion controlled attack by aq. solns. 80−81218
Na_2O-Al_2O_3-SiO_2 glass, He migration 77−7902
Na_2O-Bi_2O_3-TiO_2, subsolidus phase equilibrium at 1000 degrees C 78−48384
Na_2O-Ca glass powders, mixed with CO_3 compounds, cellular-struct. glass fabrication 80−108382
Na_2O-Ca_2O-SiO_2 glass, crack nucleation about pointed indentations 79−91779
Na_2O-CaO, enhanced failure by combined pulse and CW laser 79−29182
Na_2O-CaO, wettability, effect of cleaning procedures 80−65336
Na_2O-CaO glass, (K_I,V) diagram determ. *(French)* 80−108558
Na_2O-CaO glass, abrasion-resistant, high strength 80−76369
glass continued
Na_2O-CaO glass, atomic absorption spectroscopy 79−43656
Na_2O-CaO glass, crack nucleation during indentation, micromechanics 80−30069
Na_2O-CaO glass, impacted with sharp SiC particles, strength degradation of annealed surfaces 79−61760
Na_2O-CaO glass, shear deform. under pyramidal indentations 80−84989
Na_2O-CaO glass, strength and failure predictions 77−21256
Na_2O-CaO glass phlogopite mica powders, composite fabrication, cellular struct. 80−84902
Na_2O-CaO glass tube, fracture by field assisted ion exchange 78−68771
Na_2O-CaO_2-SiO_2 glass, stressed, chemical reaction in water vapour 79−91819
Na_2O-CaO-Bi_2O_3-SiO_2, electro-conducting glass-ceramic production by ion-exchange and reduction treatment 79−1616
Na_2O-CaO-FeO-Fe_2O_3-MnO-SiO_2 glass, alkaline durability 78−23842
Na_2O-CaO-SiO_2, Al-coated glass, electron bombarded, SIMS analysis 79−66376
Na_2O-CaO-SiO_2, corroded glasses, electron microprobe analysis 77−4956
Na_2O-CaO-SiO_2, crack nucleation around plastic indents 78−92327
Na_2O-CaO-SiO_2, double torsion specimens, compliance and fracture load as crack length function 78−48508
Na_2O-CaO-SiO_2, dynamic hardness testing, pendulum attenuation, yield stress obs. 79−24699
Na_2O-CaO-SiO_2, elastic moduli meas., laser-target technique, for wide temp. range 77−27497
Na_2O-CaO-SiO_2, evaluation of crack resistance and crack velocity, using controlled fracture experiments 78−72881
Na_2O-CaO-SiO_2, expt. errors in estimating time to failure 77−16666
Na_2O-CaO-SiO_2, foil, exam. of surface plasticity, and cracks, by electron microscopy 78−68733
Na_2O-CaO-SiO_2, formation of colour centres, linear absorption of UV radiation 80−103328
Na_2O-CaO-SiO_2, fracture mirror form. 77−48541
Na_2O-CaO-SiO_2, fracture initiation, influence of temperature and composition 79−100246
Na_2O-CaO-SiO_2, glass, surface indentation effect on mech. strength, and thermal stress resistance 78−48463
Na_2O-CaO-SiO_2, glass, light scatt. rel. to heat treatment *(German)* 78−84598
Na_2O-CaO-SiO_2, glass, surface charge in aqueous electrolyte soln. 79−29245
Na_2O-CaO-SiO_2, grain-cleaning procedures effect on crushed glass chem. durability tests 80−66678
Na_2O-CaO-SiO_2, Hertzian fracture characts., comp. influence 78−31522
Na_2O-CaO-SiO_2, ion-exchanged, mixed alkali effect rel. to elec. cond. 78−34653
Na_2O-CaO-SiO_2, lifetime predictions, dependence on crack propag. eqns. 78−72882
Na_2O-CaO-SiO_2, molten glass, self-diffusion of Ca ions 78−10202
Na_2O-CaO-SiO_2, Na surface conc. determ., by $^{23}Na(p,\alpha)^{20}Ne$ reaction 77−20171
Na_2O-CaO-SiO_2, origins of acoustic emission in fracture 78−72889
Na_2O-CaO-SiO_2, particle track detector appl., for neutron dosimetry *(Czech)* 78−66425
Na_2O-CaO-SiO_2, plates, exam. of Hertz crack branching 78−72887
Na_2O-CaO-SiO_2, proof testing 80−108654
Na_2O-CaO-SiO_2, rain erosion mechanisms 79−34154
Na_2O-CaO-SiO_2, refining in glassmelting process 78−27467
Na_2O-CaO-SiO_2, soda-lime glass, hydration 79−87877
Na_2O-CaO-SiO_2, transition from slow to fast crack propag., effect of different liquids 78−23828
Na_2O-CaO-SiO_2 glass, optical props. characteris. in 0.006 to 22 eV region 77−16328
Na_2O-CaO-SiO_2 glass, K_{IC} eval. by double torsion technique 77−90444
Na_2O-CaO-SiO_2 glass, soln. of commercial refractories, 1200-1350°C 78−95821
Na_2O-CaO-SiO_2 glass, water content effect on crystal nucleation and growth 79−55670
Na_2O-CaO-SiO_2 glass, optical absorpt. comparison with 3d transition elements *(French)* 79−65819
Na_2O-CaO-SiO_2 glass, SIMS anal. of aq. corrosion profile 79−66182
Na_2O-CaO-SiO_2 glass, surface viscous flattening kinetics, sinusoidal profile decay method 79−79139
Na_2O-CaO-SiO_2 glass, annealed and tempered, fracture strength studies under dynamic conditions 79−96132
Na_2O-CaO-SiO_2 glass, corrosion in alkaline soln. *(Japanese)* 79−96174
Na_2O-CaO-SiO_2 glass, sharp contact cracking, residual stress effects 79−100245
Na_2O-CaO-SiO_2 glass, electronic struct. and optical props. 80−2790
Na_2O-CaO-SiO_2 glass, microprobe anal. of corroded surface 80−7704
Na_2O-CaO-SiO_2 glass, effect of phase on liquids and gas diffusion *(German)* 80−38931
Na_2O-CaO-SiO_2 glass, fractographic anal. of delayed failure 80−45387
Na_2O-CaO-SiO_2 glass, vol. relaxation and thermal history during forming process 80−70130
Na_2O-CaO-SiO_2 glass, leaching studies by sputter-induced photon spectrometry 80−80004
Na_2O-CaO-SiO_2 glass, molten, metal ion diffusion and redox behaviour, electrochemical studies 80−81332
Na_2O-CaO-SiO_2 glass, redox phenomena evaluation in melting-fining process, SO_2 evolution 80−84900
Na_2O-CaO-SiO_2 glass, high-vel. liq. impact, oblique impact anomaly 80−89329
Na_2O-CaO-SiO_2 glass, hot erosion plastic flow and fracture 80−89354
Na_2O-CaO-SiO_2 glass microbubbles, permeation eccentricities of He, Ne and D-T 78−47598
Na_2O-CaO-SiO_2 glass rods, prediction of thermal fatigue resist. 78−84955
Na_2O-CaO-SiO_2 glass foils, HVEM in-situ straining expts. 80−104216
Na_2O-CaO-SiO_2 glass:Fe, Mossbauer spectra of Fe^{2+}, Fe^{3+} impurities *(French)* 79−51893
Na_2O-CaO-SiO_2 glasses, Auger analysis, alkali signal decrease 80−61189
Na_2O-CaO-SiO_2 molten glass, electrolysis reactions 80−89496
Na_2O-CaO-SiO_2 sheet glass, pristine and scratched, fracture behaviour during bending 78−23829
Na_2O-CaO-SiO_2 soda-lime-silica float glass surface mass transport mechanisms at high temperatures *(Japanese)* 80−54479

glass continued
Na_2O-CaO-SiO_2:Cr^{3+}, absorpt. spectra, Fano antireson. and vibronic Lamb shift 80−71458
Na_2O-CaO-SiO_2:UO_2, energy spectrum of UO_2 ions, fluoresc. and absorption spectra 77−66531
Na_2O-CaO-SiO_2-Cr_2O_3, Raman spectra obs. of Cr^{VI} 77−52076
Na_2O-CaO-SiO_2-Cr_2O_3 glass, redox equilibria of Cr ions, impurity effects 80−89477
Na_2O-CaO-SiO_2-Fe_2O_3 molten glass, optical props., temp. depend. *(French)* 80−100667
$2Na_2O$-CaO-$XSiO_2$ glass, He mobility, interconnectivity, miscibility limits, effect of morphology 78−67864
$2Na_2O$-CaO-$3SiO_2$ glass, cryst. nucleation rate, viscosity, heat treatment 80−84081
Na_2O-CaO(Al_2O_3)-SiO_2 glass, composition-density relationship 77−90326
Na_2O-Cs_2O-SiO_2 glasses, thermal diffusivity, heat capacity and thermal cond., laser flash method study 80−65310
Na_2O-Fe_2O_3-SiO_2, Mossbauer spectra, crystallisation study *(Russian)* 79−19816
Na_2O-Fe_2O_3-SiO_2, partially crystallised, mag. props. 78−23302
Na_2O-Fe_2O_3-SiO_2 glass and crystals, leucite type, Mossbauer ESR study of Fe^{3+} distrib. 79−65774
Na_2O-FeO-Fe_2O_3-SiO_2, chemical durability at different pH values 78−72902
Na_2O-GeO_2(TiO_2)(SnO_2)(ZrO_2)(ThO_2)-SiO_2 glass, density, refractive index, thermal expansion, hardness IR spectra, DTA *(Japanese)* 78−15535
Na_2O-K_2O-CaO-SiO_2, chemical durability, mixed alkali effect 79−8377
Na_2O-K_2O-SiO_2, Na diffusion 78−26724
Na_2O-K_2O-SiO_2 glasses, optical absorption of Ni (II) complex, complex co-ordination change, annealing effects 79−69870
Na_2O-K_2O-SiO_2 glass melt, interdiffusion coeffs. of Na^{2+}, K^{2+}, temp. depend. 80−44348
Na_2O-K_2O-SiO_2 melts, Na^+ and K^+ diffusion and interdiffusion processes 80−34221
Na_2O-Li_2O(K_2O)-SiO_2, heat of mixing *(Japanese)* 78−10195
Na_2O-PbO-SiO_2, molten glass, reactions with conducting materials 80−85186
Na_2O-PbO-SiO_2 glass-ceramic composite, directionally crystallised 80−107058
Na_2O-SiO_2, (5.3, 94.7 wt.%), liq.-phase separated, struct., heat treatment effect 80−16359
Na_2O-SiO_2, crack front shape corrections for crack velocities in double torsion specimens 79−91778
Na_2O-SiO_2, disilicate glass, reaction with Fe, Mossbauer effect 78−11190
Na_2O-SiO_2, disilicate glass, Fe ion introduction, Mossbauer effect 78−11191
Na_2O-SiO_2, effect of annealing on absorbed H_2O action on temp. spectra of internal friction 78−88487
Na_2O-SiO_2, effect of high-dose X-rays and reactor radiation 80−19838
Na_2O-SiO_2, enthalpy data 79−95183
Na_2O-SiO_2, fusion process study, EMF meas. *(French)* 80−89190
Na_2O-SiO_2, glass, devitrification with ageing 78−79536
Na_2O-SiO_2, ion bombardment, form. of cpds., IR spectrosc. exam. *(German)* 80−88173
Na_2O-SiO_2, Na_2O-CaO-SiO_2 glasses, thermal capacity meas. at low temps. 80−44334
Na_2O-SiO_2, structure toughness-composition relationship 80−104257
Na_2O-SiO_2, torsional deform. above Tg under low stresses 80−25804
Na_2O-SiO_2 (96 wt.%) glasses, thermally stimulated polarisation and depolarisation current techniques for studying ion motion 80−6541
Na_2O-SiO_2 glass, acoustic and thermal Gruneisen parameters 80−59608
Na_2O-SiO_2 glass, bridging to non-bridging ratio and correl. to glass density and refr. index, ESCA study 80−84832
Na_2O-SiO_2 glass, bubble gas comp. change 80−79946
Na_2O-SiO_2 glass, coated with SnO coeff. of friction and fracture toughness 78−80657
Na_2O-SiO_2 glass, conduction and dielec. loss mechanisms, paired interstitialcy model 80−107468
Na_2O-SiO_2 glass, electronic struct. and optical props. 80−2790
Na_2O-SiO_2 glass, evaporation by high temp. mass spectrometry 80−79927
Na_2O-SiO_2 glass, IR reflection spectra change due to moisture corrosion *(Japanese)* 78−19914
Na_2O-SiO_2 glass, influence of $p(O_2)$ on Na vaporisation at 1345°C 80−6502
Na_2O-SiO_2 glass, internal and surface struct. by X-ray scatt. 80−84074
Na_2O-SiO_2 glass, magnetooptical props. 78−80318
Na_2O-SiO_2 glass, microcracking about NiS inclusions, fracture mech. description 80−89333
Na_2O-SiO_2 glass, molten, metal ion diffusion and redox behaviour, electrochemical studies 80−81332
Na_2O-SiO_2 glass, OH^- content effect on mech. and other props. 80−89337
Na_2O-SiO_2 glass, pulsed EPR study of Cu 78−84479
Na_2O-SiO_2 glass, scoring, deform. and fracture mech. approach 80−89332
Na_2O-SiO_2 glass, stability at high press., X-ray diffraction obs. *(German)* 78−92251
Na_2O-SiO_2 glass, tunnelling recomb. luminesc. 80−2875
Na_2O-SiO_2 glass, vitreous coating, adhesion to Fe-Ni alloy 79−20336
Na_2O-SiO_2 glass containing halogens glass formation 80−103254
Na_2O-SiO_2 glass drops, quenched from liq. state, thermally treated, density profile 80−81085
Na_2O-SiO_2 glass melt, dissoln. of O_2 and CO_2 gas bubbles 80−79945
Na_2O-SiO_2 glass surface anal., effect of electron bombardment during AES on composition 79−83065
Na_2O-SiO_2 glasses, Auger analysis, alkali signal decrease 80−61189
Na_2O-SiO_2 glasses, elementary electronic excitations, refl., luminesc., and photoemission meas. 80−84778
Na_2O-SiO_2 glasses, Na_2O effect on Si-O bonds *(Japanese)* 78−42918
Na_2O-SiO_2 glasses, struct., mol. dynamic calcs. 80−24366
Na_2O-SiO_2 glasses, water reactions at elevated temps. and press. 80−81312
Na_2O-SiO_2 melt, diffusion coeffs., electron microanal. meas. of Na and Si concs. 77−31790
Na_2O-SiO_2 melts, cryoscopic struct. study 80−14994
Na_2O-SiO_2 sp. ht., 2-20 K and expansion coeff., 2-30K comp. effects 77−20097

glass continued
Na_2O-SiO_2 system glasses, ionic cond. correl. with chem. pot. 77−89581
Na_2O-SiO_2 vitreous system with relaxating structure, spinodal decomposition 78−75553
Na_2O-SiO_2:Au+CeO_2, Au particle nucleation 80−81066
Na_2O-SiO_2:Ce (III) and (IV), u.v. absorpt. 77−4658
Na_2O-SiO_2:Cu^{2+} glass ESR and optical absorption 79−77526
Na_2O-SiO_2:CuO glass, gamma-irradiated, EPR and optical spectra 80−103885
Na_2O-SiO_2:Fe_2O_3 glass, $Fe^{2+(3)}$ impurity ions struct.-chem. state, Mossbauer data 80−40028
Na_2O-SiO_2/$AgNO_3$, exam. of ion exchange equilibria 79−5178
Na_2O-SiO_2/$AgNO_3$, thermodynamic characteristics of ion exchange process 79−8452
Na_2O-SiO_2-CaO:Fe_2O_3, Mossbauer spectra, isomer shift and quadrupole splitting *(Korean)* 79−51889
Na_2O-SiO_2-CoO, Co^{2+} ions activated, magneto-opt. study 79−65844
Na_2O-SiO_2-CuO, γ-irrad., CuO effects on EPR 80−84645
Na_2O-SiO_2-Fe_2O_3, glass, X-ray absorpt. spectra, effective co-ordination charges 80−84805
Na_2O-SiO_2-MgO melt, elec. cond. meas., MgO behaviour *(Japanese)* 78−75857
Na_2O-SiO_2-MgO(CaO)(BaO) glasses, elec. cond., room temp. to 450°C 80−107473
Na_2O-SiO_2-NaCl system glass, phase relationships and diagrams 79−66048
Na_2O-SiO_2-NaF, elec. cond. of melt, and IR absorpt. spectra of glassy phase *(Japanese)* 77−62657
Na_2O-SiO_2-NaF system glass, phase relationships and diagrams 79−66048
Na_2O-SiO_2-NiO systems Ni ions anal. by ESCA *(Japanese)* 80−40787
Na_2O-SiO_2-Pr_2O_3(Ho_2O_3) glass, magneto-optical props. 79−65894
Na_2O-SiO_2-SnO_2 (TiO_2) glass, exam. of Na^+ self diffusion, elec. conductivity, and viscosity 78−87819
Na_2O-SiO_2-Tb_2O_3 magnetooptical study 80−88976
Na_2O-SiO_3, Raman spectra obs. of Cr^{VI} 77−52076
Na_2O-SnO_2-ZrO_2-SiO_2, chemical stability in NaOH and Na_3CO_3 solns. 80−16532
Na_2O-TeO_2 glass, radiational EPR centres, struct. model *(Russian)* 77−28426
Na_2O-TeO_2:Ho^{3+}(Er^{3+})(Yb^{3+}) glass, luminesc. quenching by OH and OD *(Russian)* 79−28839
Na_2O-TiO_2-SiO_2, elec. props. and energy gap 78−26921
Na_2O-TiO_2-SiO_2 glass, IR refl., Raman and EPR spectra, struct. *(Russian)* 78−2860
Na_2O-TiO_2-SiO_2 glass, Si-O bonding, SiKβ X-ray fluorescence and IR spectra 80−10500
Na_2O-TiO_2-SiO_2 glass, co-ordination of Ti, X-ray emission spectra study 80−84072
Na_2O-WO_3 glass containing transition metal ions optical absorption 78−27254
Na_2O-ZrO_2-SiO_2 glass, treated with 2 N solns. of $NaCO_3$ and NaOH, surface layer comp. 80−35366
Na_2O-ZrO_2-SiO_2 system, corrosion in NaOH and Na_2CO_3 solns. at 90-150°C 79−66187
NaOH glass, radiation induced trapped electrons, photobleaching, H form. 77−44494
NaOH·CrO_4^{2-}(NO_2^-), electron tunnelling, pulse radiolysis 80−108722
NaOH:$Fe(Cn)_6^{3-}$, electron tunnelling, pulse radiolysis 80−108722
$5Na_2O.Fe_2O_3.8SiO_2$, glass crystallisation study by Fe^{3+} EPR and Mossbauer spectra 80−64904
$Na_2O.2SiO_2$ glass, diffusion of Ag into surface layer from $AgNO_3$ melt 80−44371
$Na_2O.2SiO_2$, short range struct. by pulsed neutron scatt. 80−59396
$Na_2O.4SiO_2$, behaviour of VO^{2+} as spectroscopic probe 79−78510
$25Na_2O.75SiO_2$ glass, thermal cond., temp. depend. at low temps. 80−65322
Na_2SiO_2-CaO glass, thermostimulated and tunnel luminesc. 80−45157
Na_2SiO_3 glass pH meter electrode performance *(German)* 80−40695
$25Na_2O.75SiO_2$ glass, ionic cond. meas. 79−33110
Nd:glass, Fourier-transform photoacoustic spectroscopy 79−9246
Nd:glass laser with numerical programmed control *(Russian)* 80−91811
Nd_2O_3-SiO_2 glass, exam. of spectroscopic and luminescent props. 78−88364
Ni spheres in glass matrix, brittle composites, fracture 79−66141
Ni-7070 pyrex glass boundary, 9 MHz Stoneley wave generation 79−82433
$NiFe_2O_4$ precipitation process from silicate glass, ESR study, effective g value, transition temp. 80−25194
$NpBa_6Zr_{12}F_x$ glass, Mossbauer spectrum 80−11304
Pb bismuthate glass, IR transmission props., density 79−74127
Pb crystal glass melting, elec. furnace 79−58691
Pb glass, secondary electron emission yield, reducing and heat treatment conditions *(German)* 79−56894
Pb glass counter, automated calibration system 80−106233
Pb multicomponent glasses, alkali evaporation, mass spectrometry study, thermal anal. 79−74464
Pb-glass Cherenkov detector for high-energy gamma rays 77−3222
PbO containing crystal glasses, viscosity, effects of Li_2O, BaO, ZnO, MgO and SrO 80−19973
PbO containing crystal glass, viscosity-temp. depend., glass transition, and softening point 80−24637
PbO cryst., chem., electrochem. corrosion *(French)* 79−20232
PbO glass, mechanochemical reduction 77−52628
PbO glass, strength, effect of HNO_3 etching 77−56124
PbO glass, thermal focusing of elliptically shaped optical beams 79−18489
PbO-Bi_2O_3-Al_2O_3, glass formation and IR transmission *(Japanese)* 80−54146
PbO-K_2O-SiO_2, O tracer diffusion above transform. temp. 79−28120
PbO-K_2O-SiO_2(-Al_2O_3), corrosion in acid, leaching kinetics 78−92378
PbO-Si-O, general features of reaction 79−11819
PbO-SiO_2, absorpt. spectra of Cu^{2+} ions and interpret. 78−27276
PbO-SiO_2, absorpt. spectra of Nd^{3+} ions and interpret. 78−27277
PbO-SiO_2, charge trapping and dielec. breakdown, radiation-induced, microphase separation 78−23399
PbO-SiO_2, corroded in acid, IR reflectance spectra 77−20846
PbO-SiO_2, corrosion in acid, conc. profile meas. 78−92379
PbO-SiO_2, EPR of Cu^{2+}, V^{4+}, and Mn^{2+} 78−39392
PbO-SiO_2, glass on Si, emission mode of SEM 79−28226

glass continued
PbO-SiO_2, IR and Raman spectra interpreted in terms of struct. 78−27213
PbO-SiO_2, leaching behaviour in dil. HNO_3, ellipsometry and AES obs. 78−23846
PbO-SiO_2, melt, elec. cond. and struct. 80−88020
PbO-SiO_2, melt, polymer equilibria 80−88019
PbO-SiO_2, optical coating for GaAs-$Al_{1-x}Ga_xAS$ laser 78−71113
PbO-SiO_2, reaction with PbO thin layers on surface 78−34660
PbO-SiO_2, structure toughness-composition relationship 80−104257
PbO-SiO_2, surface flattening kinetics by sinusoidal profile decay method *(Japanese)* 80−34284
PbO-SiO_2 (70 wt.%) glasses, thermally stimulated polarisation and depolarisation current techniques for studying ion motion 80−6541
PbO-SiO_2 and Na_2O-PbO-SiO_2 system glasses, radiative paramag. and optical absorpt. centres 77−8402
PbO-SiO_2 and PbO-SO_3-SiO_2 system glasses, struct. and IR absorpt. spectra 79−41967
PbO-SiO_2 binary glasses, Pb depth profiles after acid etching, α-particle backscatt. 79−79343
PbO-SiO_2 films, on Si, dopant distrib. pattern study using chem. etching 79−86812
PbO-SiO_2 glass, acoustic and thermal Gruneisen parameters 80−59608
PbO-SiO_2 glass, distrib. of different O ions, molar refractivity meas. 80−33897
PbO-SiO_2 glass, electronic struct. and optical props. 80−2791
PbO-SiO_2 glass, modifier release in acid soln. 79−43450
PbO-SiO_2 glass, reduced channel-plate, variable range hopping conductivity 80−107466
PbO-SiO_2 glass, trimethylsilylation method for silicate ion anal. *(Japanese)* 80−71975
PbO-SiO_2 glasses, constitution of silicate groupings 77−7676
PbO-SiO_2 glasses, density-of-states and structural forms, Raman spectra study 80−97255
PbO-SiO_2 glasses, elec. cond. and dielec. behaviour 80−44361
PbO-SiO_2 glasses, high temp. ESR of Fe(III) 80−60410
PbO-SiO_2 glasses and crystal, silicate anion constitution 79−48023
PbO-SiO_2 reduced glass, electron backscattering 77−85855
PbO-SiO_2 surface mass transport mechanisms at high temperatures *(Japanese)* 80−54479
PbO-SiO_2 system, IR and Raman spectra, heat treatment conditions effect 79−66088
PbO-SiO_2 wall added to SPEAR Mk. I mag. detector 78−37494
PbO-SiO_2-Fe_2O_3(0,2,10 wt.%), conduction process 77−8096
PbO-SiO_2-NiO-MgO glass melt, interaction of NiO and MgO, elec. cond. and IR spectra obs. *(Japanese)* 80−24632
PbO-SiO_2-TiO_2, molten, viscosity *(Japanese)* 78−18819
PbO-SiO_2-(CaO)(MgO)(BaO)(NiO)(CoO), melt, PbO activity *(Japanese)* 78−6907
PbO-SiO_2-(CaO)(SrO)(BaO)(NiO), melts, density *(Japanese)* 78−6908
PbO-SiO_2(-Al_2O_3), corrosion in acid, leaching kinetics 78−92378
$(PbO)_x(SiO_2)_y$ glass, vibrational spectroscpic exam. 79−11417
PbO.SiO_2 film, formation mechanism on Si, X-ray spectral anal. 79−87008
2PbO.SiO_2, glassy, DTA obs. of crystn. kinetics 77−89381
2PbO.SiO_2 melt, coding rate influence on constitution of silicate anions, crystn. kinetics 80−103248
$PbSiO_3$ and Pb_2SiO_4, vitreous, free energy of form. at elevated temps. 79−43195
Pt coatings on glass, quartz, ceramic or sitall, method 77−44376
Pt-Au glass-bonded printed thick-film conductor, adherence fracture energy 77−9037
S, glass, catalytic crystallization in organic media at room temp. 77−84657
Sb-containing glasses, ^{121}Sb Mossbauer spectra 77−20764
Sb-O-Cl(Br)(I), glass-forming regions 80−88057
Sb_2O_3 glass, X-ray diffr. anal. of struct. 78−87621
Se, glass, catalytic crystallization in organic media at room temp. 77−84657
SiC-fibre reinforced glass, fabrication, thermal expansion, flexural and fracture toughness 80−40319
SiO_2 based, packaging of radio-active waste appl. *(French)* 79−71910
SiO_2 based glasses, highly absorbing anomalous IR absorption at low temps. 78−43871
SiO_2 based glasses, IR transmitting materials, appl. in 1 to 6 μm range, mech. props., review 79−4250
SiO_2 based melt, Na vaporisation, H_2O vapour effects 77−55353
SiO_2, densified, enthalpy variation, heat of dissolution obs. *(French)* 79−34015
SiO_2, E′-centre model, IR absorption spectra 79−37634
SiO_2, fused, photoelastic coeffs., freq. depend. 77−4619
SiO_2, fused, slide glass surface, Ca^{2+} ion deposition as inhibitor to alkaline attack 80−50737
SiO_2, fused, surface crystn. by Li^+ ion implantation and annealing 80−89383
SiO_2 fused glass, coherent elec. echoes 79−61300
SiO_2 glass, AES anal. *(French)* 79−39236
SiO_2, glass, acoustic and thermal Gruneisen parameters 80−59608
SiO_2 glass, crystallinity positron annihilation study 78−72629
SiO_2 glass, electron microscopic determ. of struct. 79−90561
SiO_2 glass, electronic struct. and optical props. 80−2790
SiO_2 glass, formation by hydrolysis of $Si(OC_2H_5)_4$ with NH_4OH and HCl soln., and characterisation 80−71622
SiO_2, glass, HF phonon phase vel. meas., below 1K, tunnelling model 77−7818
SiO_2 glass, heat treatment study by positron annihilation 78−55812
SiO_2 glass, low loss optical fibre, radiation-induced IR absorpt. 80−87521
SiO_2 glass, molecular to band-like modes 77−66012
SiO_2 glass, monolithic, low temp. synthesis by SiO_2 gel pyrolysis 79−43194
SiO_2 glass, monolithic, low temp. synthesis 80−40318
SiO_2 glass, phonon scatt., $>10^2$ GHz, by supercond. junction spectrosc. 80−10625
SiO_2 glass, porous, adsorption of inorganic cations, in distilled water medium 79−24814
SiO_2 glass, porous, below-freezing pt. adsorbed layer, istohermal adsorption and dimensional changes obs. 78−75925
SiO_2 glass, Raman spectra of dissolved molecular H_2 and D_2 79−33707
SiO_2 glass, relax. times of mol. OH^- ions at very low temps., elec. dipolar echoes 79−78616

glass continued
SiO_2 glass, sputter yield peak ang. var. 77−32484
SiO_2 glass, Suprasil I, electric dipole moment distrib. of values 79−61299
SiO_2, glass synthesis by hot pressing of gels 79−15637
SiO_2 glasses, spectral emittance at high temps. 80−96674
SiO_2, ion bombardment, form. of cpds., IR spectrosc. exam. *(German)* 80−88173
SiO_2, ion implanted, radiation effect on chem. stability 77−1158
SiO_2, molten, struct., X-ray radial distrib. anal. 78−67651
SiO_2, optical waveguide form. by low energy electron irrad. 77−7189
SiO_2, planarised sputter deposition 78−75959
SiO_2, specific heat at low temp. depend. on thermal treatment 80−54401
SiO_2, strengthened by ion exchange and quenching, brittle destruction theory 80−45398
SiO_2, thermal capacity meas. at low temps. 80−44334
SiO_2, three-component glass, liq. phase separation, with two oxide modifiers 80−103250
SiO_2, transparent prep. from $Si(OC_2H_5)_4$ *(Japanese)* 79−70038
SiO_2, vitreous, Fe^{2+} absorpt. spectra in polarised light and struct. position 79−43007
SiO_2, vitreous, III-V analogues and bonding topology 79−73102
SiO_2, vitreous, low temperature heat capacity enhancement model 80−75369
SiO_2, vitreous, O and Si diffusion-controlled processes 80−79981
SiO_2, vitreous Brillouin scatt., 35 GHz phonon vel. and absorpt. below 1K 80−100664
SiO_2:OH^-, vitreous, elec. dipolar echoes 78−52430
SiO_2-based, O self-diffusion theory 79−95214
SiO_2-based, tunnelling systems, intrinsic elec. dipole moment, coherent elec. echo obs. 80−29705
SiO_2-based surface struct. and topography study using emission electron microscope 77−1285
SiO_2-CaO-Na_2O, layers near surface, anal. using SIMS 80−88041
SiO_2-CaO-Na_2O-M_mO_n systems, M=Zr, Sn, Ti, Al, La, Ta, P, Mn, Fe, Pb, Cr, water, alkali, acid resist., chem. durability 79−34162
SiO_2-glass, high-temp. strain relax., optical correlation spectroscopy 77−65951
SiO_2-glass fibres, struct. anal. using X-ray diffr. and optical microscopy 77−65952
SiO_2-glasses, radial distrib. functions 80−44136
SiO_2-K_2O, thermodynamic approach to ionic conds., statistical model of chem. potential 79−46833
SiO_2-K_2O-CeO_2-Sb_2O_3, polychromatic glass, Sb^{4+} centre, EPR obs. 79−87317
SiO_2-Li_2O, layers near surface, anal. using SIMS 80−88041
SiO_2-Li_2O-K_2O-ZnO glass ceramic, prep., phase transformations and physical props. 80−45299
SiO_2-Li_2O-Li_2SO_4, glass-forming region, struct. and ionic cond. 80−84320
SiO_2-M_2O (M=Na,K) glasses, temp. depend. of elastic modulus 80−40410
SiO_2-Na_2O, thermodynamic approach to ionic conds., statistical model of chem. potential 79−46833
SiO_2-Na_2O (Li_2O), phase separation detection 77−1890
SiO_2-Na_2O alkali glass, grain-cleaning procedures effect on crushed glass chem. durability tests 80−66678
SiO_2-Na_2O glass, fracture initiating flaws, depth meas., crack propag., SEM exam. 78−48494
SiO_2-Na_2O glass, Na^+ diffusion 78−91478
SiO_2-Na_2O surface, $Ca_3(PO_4)_2$ film form., bonding to bond 80−85212
SiO_2-Na_2O-BaO glass, rare earth doped, nonradiative decay and multiphonon relax. 77−85802
SiO_2-Na_2O-$CaCO_3$ sheet glass, rupture upon local contact loading 80−50725
SiO_2-Na_2O-CaO, electrochemically coloured, chemical composition and structure of surface layers 78−84758
SiO_2-Na_2O-CaO (13, 11 wt.%) glass, phase separation, SiO_2 purity effect 80−44144
SiO_2-Na_2O-CaO glass, phase separation characts., melting atmosphere effect 80−44141
SiO_2-Na_2O-CaO:Fe(As)(Cr) glasses, optical absorpt. changes on heat treatment 78−31224
SiO_2-Na_2O-CaO-MgO, glass hardened plate, internal stress and birefringence microanal. using optical phase microscope interference-polarisation 79−39109
SiO_2-Na_2O-CaO-MgO float glass, surface SnO_2 distrib., ellipsometry and XPS study 80−84346
SiO_2-Na_2O-CeO_2-Sb_2O_3, polychromatic glass, Sb^{4+} centre, EPR obs. 79−87317
SiO_2-Na_2O-K_2O water glass with polyethylene filler, thermogravimetric and thermomechanical anal. 79−20020
SiO_2-Na_2O-Nd_2O_3 glass, magneto-optical props., absorpt. spectrum 80−88969
SiO_2-Na_2O(Li_2O) glasses, bonding of Si-O exam. by X-ray emission spectra 78−52594
SiO_2-PbO system glass, thermal capacity, temp. depend. 79−95181
SiO_2-PbO-K_2O glass, reflection spectra 78−88325
SiO_2-RO-Na_2O-Li_2O (RO=MgO, CaO, SrO) glass-ceramic coating, optimisation of props. by selective oxide action 80−55552
SiO_2-TiO_2, US vel. and absorption 80−107380
SiO_2-TiO_2 glass phonons, IR and Raman spectra meas. 79−91447
SiO_2-TiO_2 system, physicochem. props. of glasses with low thermal expansion coefficient 77−35718
SiO_2-TiO_2 system, true solid soln. existence obs. 77−36475
SiO_2-TiO_2-Na_2O, optical absorption coeff., 2.1-3.3 eV 77−77240
SiO_2-TiO_2(Al_2O_3)(ZrO_2), noncrystalline film form., IR study *(Japanese)* 77−59634
SiO_2-ZnO-Na_2O-Li_2O, glass-ceramic coating, optimisation of props. by selective oxide action 80−55552
SiO_2-ZrO_2-Li_2O-Na_2O based crystallisable glasses composition and properties 80−50731
SiO_3:B, P films doped by pyrolisis and ion implantation, IR absorpt. obs. of impurity conc. 77−72802
SiO_2(-TiO_2) glass prep., melting *(Polish)* 80−40316
$((SiO_2)_{45}(CaO)_{55})_{65}$ (Fe_2O_3)$_{35}$ glass, effect of melt atmosphere on mag. props. 78−68299
$Si_2O_6(OH)_2^{6-}$ group, electronic struct. calcs. 78−67971
SnO-SiO_2 glass, exam. of immiscibility 78−75837
SnO-SiO_2 glass, struct., X-ray density, IR obs. 79−46574
SnO_2 coated glass, surface elec. breakdown 80−25303

glass continued
SrO-SiO_2, effect of high-dose X-rays and reactor radiation 80−19838
SrO-SiO_2-Fe_2O_3, permanent mag. ceramics, exam. of phase diagram, using X-ray analysis, optical microscopy, electron probe anal., and thermal analysis *(German)* 79−29012
Tb^{3+} ions in silicate glass, photoluminesc. and optical absorption spectra 79−19919
TeO-V_2O_5 glass system, X-ray diffr. study 79−10805
TeO_2, ferroelectric glass, phase transition, permittivity, electrochromism, photochromism 80−80719
TeO_2-Al_2O_3-WO_3 glass, rare earth doped, nonradiative decay and multiphonon relax. 77−85802
TeO_2-Fe_2O_3 system, atomic arrangement, neutron diffr. data 78−83743
TeO_2-Fe_2O_3 system, glass structure 79−90562
TeO_2-Li_2O glass:Nd^{3+}, highly doped, spectroscopic props. and CW laser action *(French)* 79−41385
TeO_2-Li_2O glassy system, struct. recomb. model 80−19707
TeO_2-MoO_3-M_nO_m, glass formation range 78−71680
TeO_2-MoO_3-V_2C_5, phase comp. determ. using X-ray diffr., electron microscopy and DTA *(German)* 80−88046
TeO_2-V_2O_5 glass threshold devices, reversible monopolar switching 80−2434
TeO_2-V_2O_5-Fe_2O_3 system, phase equilib. and analysis, primary crystn. fields 77−66628
TeO_2-V_2O_5-$Li_2O(Na_2O)(K_2O)(Cs_2O)(Ag_2O)$, glass, IR spectra of crystalline phases 79−38536
TeO_2-WO_2 glass, dipole correlations, capacitances and TSC meas. 79−28670
TeO_2-WO_3-R_nO_m, glass formation range 78−71680
Ti-molten glass system, interactions and wetting, EPR anal. 78−14542
TiO_2 devitrified glass, Raman spectra 79−78677
TiO_2-SiO_2, semicond. glass, small polaron hopping cond. 78−60126
TiO_2-SiO_2, semicond. glass, optical props. 78−60412
TiO_2-SiO_2 glass form. by low temp. chem. polymerisation 80−84899
TiO_2-SiO_2 glass system, Raman and hyper-Raman light scatt. spectra 80−66187
TiO_2-ZrO_2-SiO_2 amorphous film, alkali resistance, refractive index, IR spectra *(Japanese)* 78−23546
Tl_2O-SiO_2, glass, ^{205}Tl NMR 77−59470
U glass, fission track dating, error analysis 80−95503
UO_2^{2+} glass, Nd^{3+} or Ho^{3+} doped, fluoresc. appl. in improved planar solar convertor 80−40904
V_2O_5 containing glass, electronic cond., effect of random glass struct. 79−23972
V_2O_5, splat-cooled, crystallisation, high-press. effects 78−9956
V_2O_5-As_2O_3-RO, R=Ba, Ca, Pb, semicond. glass, electronic props. 80−88557
V_2O_5-BaO-K_2O-ZnO glasses, elect. props. and struct. 80−15547
V_2O_5-CuO-BaO, unpaired electron localisation, ESR study 80−66026
V_2O_5-TeO_2 system, vitreous, struct. obs. using neutron scatt. 78−22667
V_2O_5-V_2O_4-$BaZnO_2$ glass, V ion states, mag. and elec. props. 80−88556
Y_2O_3-AlN-SiO_2 oxynitride glasses, elec. props. 80−80267
Yb:glass, luminesc., low temp. energy transfer 80−2837
Zn-glass, friction, loading time effect *(Japanese)* 78−34095
ZnO-PbF_2-SiO_2, shear wave velocity and its temp. depend. *(Japanese)* 78−30702
ZnO-PbO-B_2O_3, exam. of glass formation and its props. 79−8283
ZnS-Na_2O-K_2O-SiO_2, form. using electric furnace, furnace design 80−11620
ZrF_4 glasses, elec. props. *(French)* 78−75868
ZrF_4:Eu^{3+} glass, luminesc. of Eu^{3+}, transition probabilities 80−80845
ZrF_4-BaF_2-MF_n (M=Na, Ca, Ln, Th, n=1, 2, 3, 4), vitreous phases, network formers, modifiers and stabilisers *(French)* 80−64909
ZrF_4-BaF_2-ThF_4-NaF(RF_3) (R=rare-earth) glass system, anion cond. 80−70460
ZrF_4-BaF_2-ThF_4(LaF_3)(NdF_3)(PrF_3), F^- ion cond. glasses, cond. process 80−107477
ZrF_4-based glasses, elec. transport props. 80−79983
ZrF_4-ThF_4-BaF_2:V^{3+}(Cr^{3+}) glasses, absorpt. spectra *(French)* 79−99918
ZrF_4-ThF_4-NdF_3(LaF_3), phase equilibrium, vitreous phase struct., charact. temp., optical props. *(French)* 79−11587
ZrF_4-ThF_4BaF_2, IR-transparent, synthesis using reactive atm. processing technique 80−100826
ZrF_4ThF_4-BaF_2 system, new fluoride glass, optical props. *(French)* 77−36443
ZrO_2 glass, melting depend. on minute components, surface crystallisation 80−84278
ZrO_2, glaze, liq. phase separation rel. to cryst. in glassy phase 80−103252

glass fibre reinforced plastics
ABS, glass-filled, deform. and fracture behaviour, 293-353K 77−56077
acoustic emission 80−104294
acoustic emission investigation of deformation and fracture 77−16756
ageing by boiling in water, effect on physicomech. props. 80−60892
aluminoborosilicate glass fibre reinforced epoxyphenol and phenolformaldehyde, strength props., binder effects 79−5028
asbestos cement/glass reinforced plastics hybrid composites, tensile strength *(Italian)* 77−56024
automated production methods 80−25651
bakelite matrix laminate, internal stresses occurring during production 79−66034
bending tests, specimen size and shape selection 77−52575
birefringent orthotropic composite models, stress freezing 78−19799
bottoms, with a filler, rigidity 80−15183
brittle coating analysis of orthotropic materials 79−27606
bulk moulding compound, flow state, closing speed effect *(Japanese)* 80−55469
cemented joint of cylindrical shell with cover, stressed state 80−69668
centrifuged laminate, fracture characts. determ. *(German)* 79−38967
chopped glass fibre reinforced polyester E, types SMC-65(-25 and -30EA), moisture absorpt. 80−93799
chopped glass fibre reinforced polyester resin, deformation and thermoset cure effect on heat cond. during molding 79−86325
complex stress-state conditions, mech. props., method for studying 80−50799
compressive creep of filled polycarbonate *(Japanese)* 77−8888
compressive fracture mode 77−21251
coupling agent/matrix interface investigation by Fourier transform IR spectroscopy 80−20884

glass fibre reinforced plastics continued
crack growth in steel wire reinforced polymer with glass fibre matrix-toughening components 77−56076
creep behaviour, polyester laminates, glass fibre-reinforced, due to natural weathering 79−66107
creep calc. in nonstationary temp. distrib., temp.-time analogy 77−70132
creeping tests on flat specimens in liq. media, clamping device 78−7126
cross-ply laminate, constrained cracking 78−19870
crossply glassfibre, cantilever beams, nonlinear damping for nonsinusoidal strain 79−47762
curved panels, expt. snap buckling under lateral loading 77−59849
cyclic strength in complex stressed state 80−3181
cylindrical laminated plastic shell, mech. behaviour 77−58567
cylindrical shells, compressive and flexural strength *(Japanese)* 80−81115
cylindrical shells, temp. stresses developing during polymerisation 80−40326
damage assessment by stress wave emission and dynamic mech. meas. 78−11461
deformation, relation between matrix vol. changes and mech. props. 80−11715
deformation conc. around openings due to pulse loading 78−23799
design criteria 80−25970
design of panels for strength and stiffness 79−61601
deterioration in water, hydraulic press. effect *(Japanese)* 80−55470
deterioration in water, immersion time effect *(Japanese)* 80−55471
dielectric const./mechanical strain relation, microwave study 77−32650
dome, anal. and expt. stress anal. 78−72813
dynamic stress concentration around defects, discrete model 80−30024
E-glass fibre reinforced epoxy, eval. of tensor polynomial and Hoffman strength theories 78−19830
E-glass type fibre, silane coupling agent deposited on surface, hydrolysis and drying effect on siloxane bonds 80−85072
elastic moduli meas., effect of deform. rate *(German)* 78−64796
elastic props. 77−70090
electric connector moulding compound, low press. diallyl phthalate, props. 78−52750
epoxide matrix, winding in transverse direction, creep and thermal expansion 79−96093
epoxide resin, light polarisation exam. of stress 78−68857
epoxy, braided filament reinforced, damage summation in nonstationary cyclic loading 80−60969
epoxy, fatigue, time and temp. depend. 80−21095
epoxy, fracture mechanics 80−35294
epoxy beams, dynamic mech. behaviour, meas. and analysis 77−28844
epoxy cross ply laminates, transverse cracking and long. splitting, strain effects 79−61723
epoxy cross-ply laminates, multiple transverse cracking 78−95800
epoxy cylinder, imperfect, buckling under combined loading 80−7620
epoxy laminate, failure, fractographic study 79−96111
epoxy laminate, general fatigue failure criterion and test program 80−7658
epoxy laminate, glass-fibre reinforced, with circular holes, tensile fracture 80−25789
epoxy laminate, mech. strength meas., comparison with theory, tensor polynomial failure criterion 78−39886
epoxy laminates, exp. determ. of nonlinear shear behaviour 80−66575
epoxy matrix, brittle coating stress anal. technique 79−43528
epoxy matrix, buckling 78−44166
epoxy matrix, cryogenic tensile, compressive and shear props. 78−6983
epoxy matrix, fatigue damage in cyclic bending 79−100256
epoxy matrix, filler shape, orientation distrib. and interaction effects on Young's modulus *(Japanese)* 78−39735
epoxy matrix, internal moisture condition effect on strength 79−15736
epoxy matrix, laminate, metallization by Cu and chem. treatment by H_2CrO_4 *(German)* 80−93670
epoxy matrix, multilayer circuit board, holographic interferometry appl. to real-time studies of heat effects 79−91873
epoxy matrix, room temp. curable, mech. props. and thermal conductivity 78−68669
epoxy matrix, short aligned fibres, mech. charact., SEM and optical obs. 78−72761
epoxy matrix, strength in twisting, stretching and transverse bending 80−11622
epoxy matrix, struts for superconductive storage magnets, mech. props. 80−25824
epoxy matrix, thermal cond., diffusivity and sp. ht., determ. 80−24613
epoxy matrix, unidirectional, hygroelasticity, angular depend. 80−50663
epoxy matrix, unidirectional, strength distrib. 78−68735
epoxy matrix, vacuum hardened shell, strength and deform. charact. eval. 78−48528
epoxy matrix laminate, tensile testing, monitoring cond. effect on stress wave emission data 79−87814
epoxy pipe, radiometric inspection by image analysing systems 77−90532
epoxy resin, destruction by diffused water 78−48511
epoxy resin, destruction by freezing or boiling of phase separated water 78−48512
epoxy resin, dynamic Young's modulus and internal friction 80−25754
epoxy resin, local defect effect on strength 77−90317
epoxy resin laminate, sliding behaviour against Cu or Al spheres at cryogenic temps. 80−66671
epoxy resin matrix, crack form. *(German)* 78−19887
epoxy resin matrix, mech. props. 78−64582
epoxy resin-cemented glass joint, temp. relationship of fracture toughness 80−3196
epoxy resins, expt. exam. of fracture by peeling method *(Russian)* 80−71761
epoxy-aniline matrix, laminate, work required to rupture along interfaces 79−43413
epoxy-based, heat ageing effect on thermophys. props., 10-400K 77−59161
epoxy-phenolic binder, exam. of short cycle fatigue strength under compression 80−11759
epoxy-phenolic matrix, cyclically deformed under shear, energy dissipation, static tensile-compressive stress effect 80−104225
epoxy-polyamide, single lap joint, tension-shear strength *(Japanese)* 78−11494
epoxy/Al alloy bonded joint, mean strength, moisture effects 79−20106
epoxy/E-glass continuous fibre composite type 3M Scotchply, complex moduli, comparison of meas. with estimated bounds 80−93590

glass fibre reinforced plastics continued
exam. using ion scattering spectroscopy and scattered ion mass spectrometry 78−60641
fabric reinforced polyester, biaxial stress failure surface under static and fatigue loading 78−72836
failure due to deform., optical investigation method *(Russian)* 80−35437
failure under compression, tension and bending 79−96142
fatigue, flexural properties, unidirectional GRP, transverse direction 79−66138
fatigue and flexural strength 79−8364
fatigue damage, early detection by NDT, applic. to ±45° glass/epoxy and ±45°/0° graphite/glass/epoxy 77−28951
fatigue damage accumulation obs. using diffuse light transmission *(Russian)* 78−19896
fatigue damage in notched samples 78−15496
fatigue damage monitoring of processes damaging elec. insulating materials 80−97673
fatigue fracture kinetics studied by diffusion scatt. of luminous fluxes 80−76446
fatigue life, determ. from reheat temp. 79−61724
fatigue lifetime prediction based on cumulative damage 80−11776
fatigue processes, review 80−81176
fatigue props. and flexural rigidity *(Japanese)* 80−55510
fatigue strength, tensile, low cycle, anisotropy 77−66697
fatigue strength in shear in plane of reinforcement 77−32690
fibre orientation, effect of injection speed 79−4944
fibre reinforced epoxy, transverse shear effect on compressive strength 80−40439
fibre volume fraction determ., using photodiode scanning technique 78−48578
fibreglass, mechanoluminescence during monoaxial stretching 78−68742
fibreglass, structural, compression testing method 78−23895
fibreglass nonmagnetic He cryostat construction 79−67309
fibreglass/epoxy composites, laminates, rings, tubes, thermal contraction at low temps., report 80−19968
fibreglass/epoxy laminate curing by microwave heating 77−77457
filament wound column, effect of end conditions on critical loads 77−59873
filament wound tube, US defect detection 80−7734
filled resin matrix, elastic moduli, analytical method of determ. 79−100201
flat stressed state, strength and deformation props. function of reinforcement struct. 80−19866
flexural fatigue props. *(Japanese)* 79−20171
fracture mechanics appl. to static and fatigue failure 78−19898
fracture process investigation using scanning electron microscope fitted with hydraulic tensile straining stage 79−54227
fracture strength, time depend. probabilistic failure model 80−40477
glass fabric laminate, nontransparent dielectric, laser emission reflection and destructive action *(Russian)* 79−74031
glass fibre reinforced epoxy, as electrical insulation for Tokamak toroidal field coils, mech. props. 78−64610
glass fibre reinforced epoxy, exam. of interlaminar shear stress distribution 79−43308
glass fibre reinforced polyester, creep life, effect of liquid environment and increased temp. *(Russian)* 77−16723
glass fibre-reinforced polyester cross-ply laminates, effect of resin failure strain on tensile props. 78−3212
glass fibres-resin interface studies 80−93531
glass reinforced polyamide 6, fatigue strength after heat treatment, ageing and coating of Al-containing lacquer *(Polish)* 80−89347
glass textolite cylindrical shells, parallel wound, feasibility of diagnosing strength 78−67157
glass-C fibre reinforced epoxy, thermal cond., diffusivity and sp. ht., determ. 80−24613
glass-carbon fibre-reinforced composite disc, rot. strength 79−74198
glass/MoS_2 reinforced PTFE, fibre orientation effect on friction and wear 79−79125
high temperature, properties, brief review 77−25092
high work of fracture composites, prep. and mech. tests 80−81029
hybrid, tensile strength, statistical analysis 77−63624
hybrid C and glass fibre, fracture energy 78−95801
hybrid C fibre and glass fibre reinforced plastics, review of physical properties 80−55496
hybrid glass fibre/C fibre reinforced epoxy-phenolic, elastic characts. prediction 80−108491
impact tensile fracture energy *(Japanese)* 78−39888
impact tensile strength obs. *(Japanese)* 78−23781
injection moulded GFRP distortion meas. by holographic interferometry 79−79020
injection moulding, flexural anisotropy 79−61659
insulating materials, fatigue behaviour, influence of superposition of elec., mech. and environmental stresses 80−97590
interlaminar crack growth during fatigue 80−11763
interlaminar fracture energy 80−55495
interlaminar shear strength determ., anal. of methods 77−86107
ionising radiation effects on mech. props. of fibre-filled polyethylene *(Russian)* 77−59736
Kinel, mech. props., 20 to 300°C *(French)* 77−56018
laminate, comparison of single and multi-hole bolted joint strength 79−91739
laminate, failure process 78−31529
laminate, fatigue strength rel. to test frequency 79−8362
laminate, fatigue strength under normal and interlaminar shear stresses 80−11758
laminate, mixture law of tensile and fracture strength and variation *(Japanese)* 79−43337
laminate, post-failure behaviour, no stress conc. 77−28895
laminate, stress anal. finite element modelling 79−59924
laminate crack resistance under prolonged loading 77−21276
laminate in plane-stress state, strength depend. on reinforcement struct. 78−23796
laminates, damage accumulation during tensile loading 79−83262
laminates, failure in compression 80−11755
laminates, failure models, reinforcement struct. effect 80−66641
laminates, load carrying capacity, interlaminar imperfections influence *(German)* 79−100218
laminates, strength and deformability, artificial ageing effect 80−60893
laminates, strength anisotropy rel. to organic fibre reinforced plastic laminates 80−19872
laminates, stress, strain anisotropy, tensor calculus *(Polish)* 77−12678
laminates, US evaluation of hygrothermal effects 80−7730
load-time history anal. in instrumented Charpy test *(Japanese)* 80−55511
long-term strength evaluation, parametric methods efficiency 80−40662
mat reinforced polyester resin laminate cantilever, bending fatigue strength, cyclic freq. effect *(Japanese)* 80−55507
mechanical charact. under compressive load *(Japanese)* 78−92301
mechanical properties and residual stresses in wound components of glass-C fibre composites 77−52436
mechanical properties measurement, use of electrical resistance strain gauges, effects on props. 79−43541
metal/glass fibre reinforced plastic vessel, with damaged reinforcing layer, carrying capacity 78−39876
microstructure rel. to mech. props. 80−11685
microwave determ. of mech. strains, anisotropic props. in millimeter range 77−9023
monolithism and reliability conditions 78−48364
multicomponent composites, mech. props. 79−52329
multilayer shells with rubber fillers, exam. of stability under axial compression comparison to theory 80−7643
NDT of strength after immersion in hot water 77−90530
non woven epoxy laminates comparison with paper phenolic and woven glass epoxy 78−35635
Nylon 6, unidirectionally reinforced, mech. props. and fracture 77−21252
Nylon 6 matrix, unidirectional short fibre reinforcement, tensile and impact strength 79−91734
nylon matrix, design parameters, fibre orientation effect 80−81141
optical transparency conditions, interparticle interference effects 78−23428
optimal reinforcement for cylindrical shell subject to temp. field 77−84148
organosilane coupling agent interphase of glass-fibre reinforeced plastics, molecular organisation 80−44195
orthotropic cylinder, nonuniform, thermoelastic stresses 77−7312
orthotropic laminates, torsion strength and shear modulus determ. 80−92587
PET, glass fibre filled, order-disorder transitions during extrusion 80−50633
phenol resin matrix effect of thermal loading on physicomech. props. 79−24622
pin-bearing strength, stacking sequence effect 77−70105
pipe, on-line US inspection 77−86263
pipe, subject to external press., layering 77−52485
pipe, thin walled, finned, stress anal. and load bearing capacity 80−81100
plastic, thermal cond. meas. rel. to temp., heat cond. problem soln. 79−37887
plastics, reinforced, chem. process appl. 80−40322
plate, under vibr. load, strength testing, device 79−29318
plates, 3-layered, optimisation 80−20996
PMMA matrix, unidirectional short fibre reinforcement, tensile and impact strength 79−91734
polyacetal matrix, friction and wear against glass and steel 78−56783
polyacetal mouldings, shape testing, projection of optical gratings *(German)* 79−29322
polyamide, GFPA 66, rel. strain meas. during creep in liq. environments 80−30046
polyamide 6, glass fibre reinforced, fatigue fracture types under circular flexural loading *(German)* 79−70170
polyamide 6, response function characterization of thermal state in dynamic testing 79−18680
polyamide 6 matrix, fatigue under rotary bending *(German)* 79−15782
polyamide thermoplastic, stiffness and strength 78−27600
polycaproamide, viscoelastic, linearity conservation 80−108492
polycarbonate matrix, creep crack growth *(Japanese)* 78−39887
polycarbonate matrix, design parameters, fibre orientation effect 80−81141
polycarbonate matrix, dynamic fracture toughness, absorbed energy and crack propagation velocity *(Japanese)* 80−16447
polycarbonate matrix, fatigue crack propag., mean stress effect *(Japanese)* 79−66151
polyester, 90° cross-ply laminates, multiple transverse fracture and cracking 77−8913
polyester, compressive fatigue tests at cryogenic temps. 80−25870
polyester, thermoset moulding, cure cycle effect on mech. props. 80−45369
polyester, unidirectionally reinforced, damage summation in nonstationary cyclic loading 80−60969
polyester laminates, glass fibre reinforced, enhanced elasticity, chem. resist. tests *(Polish)* 80−60901
polyester matrix, behaviour under bending load *(Japanese)* 79−38904
polyester matrix, crack growth micromechanism in corrosive environment 80−108615
polyester matrix, fatigue behaviour 80−25856
polyester matrix, filament wound pipe, winding angle effect on failure 79−43379
polyester matrix, greenhouse sheets, ageing behaviour, natural and artificial weathering *(German)* 80−81226
polyester matrix, internal reinforcement joints under static and fatigue loading 79−91776
polyester matrix, plate struct., skeletal member effect on stiffness and strength, finite element anal. 79−91733
polyester matrix, single loop joint, tension-shear strength *(Japanese)* 78−11494
polyester matrix, struts for superconductive storage magnets, mech. props. 80−25824
polyester matrix, vacuum hardened shell, strength and deform. charact. eval. 78−48528
polyester matrix filament wound pipe, failure 78−44192
polyester matrix tube, strength under biaxial loading 79−38892
polyester resin, interfacial bond strength, effect of surface treatment 77−21303
polyester resin, reinforced with glass chopped strand mat and woven roving fabric, fracture toughness and crack-growth meas. 79−83299
polyester resin, unsaturated polymerisation by UV irrad. *(German)* 79−100367
polyester resin composites, microstructure 79−37625
polyester resin matrix, crack form. *(German)* 78−19887

glass fibre reinforced plastics continued
polyester resin/glass fibre discs, rotating strength, stress distrib., failure criterion rel. to mould process 78−76701
polyester/E-glass chopped fibre composites types PPG SMC-R25 and PPG SMC-R65, complex moduli, comparison of meas. with estimated bounds 80−93590
polyester/E-glass hybrid chopped/continuous fibre composite type PPG XMC-3, complex moduli, comparison of meas. with estimated bounds 80−93590
polyethylene matrix, melt, rheological props. 79−37273
polyethylene-glass fibre composites, gamma-irradiated filler 80−66840
polymer matrix, compressive strength 78−64609
polypropylene, design stress data, w.r.t. time, temperature and composition effects 79−96098
polypropylene, injection moulded discs, struct. and mech. props. 78−19706
polypropylene matrix, unidirectional short fibre reinforcement, tensile and impact strength 79−91734
polyurethane foam matrix, fracture toughness, modulus increase 78−44196
polyurethane foam/glass reinforced plastic/Al, sandwich construction, non-symmetric, flexural fracture 79−74233
PTFE matrix, friction and wear against glass and steel 78−56783
punching shear tests under static and impact loadings *(Japanese)* 80−55512
radial orientation of reinforcement for high strength shell 79−95994
radial reinforcement effectiveness rel. to tangential reinforcement 77−28777
rectangular fibre reinforced plastic pressure vessel *(Japanese)* 78−11197
reliability determ. 78−1568
residual strength, hygrothermal history effect 77−77513
resin beams with glass fibres, crack propag. expt. 78−15521
resin matrices and their contribution to composite properties 80−81028
resin selection, for marine appl. 79−96035
ring, exposed to press., transverse prop. effect on bearing capacity 77−86177
rings, filamentous and layered, outer pressure, stratification *(Russian)* 78−31489
rolling-in effect on physicomech. props. 78−23658
roving glass cloth fibre reinforced plastic, fracture mech., time depend. *(Japanese)* 80−55508
roving glass cloth fibre reinforced polyester resin cumulative damage fatigue *(Japanese)* 77−8941
roving glass cloth reinforced polyester resin laminate cantilever, bending fatigue strength, cyclic freq. effect *(Japanese)* 80−55507
satin woven glass cloth fibre reinforced plastic, fatigue life under random loading *(Japanese)* 80−55509
semifinished product nonlinearity model, force anal. of winding 78−63325
shear characteristics of tubular specimens, strain gauge and clamp 80−85114
shear strength determ., comparison of methods 77−90527
sheet moulding compound, influence of cure time restrictions, on minimum weight design of double layer panels 80−11623
sheet moulding compound, material, process and performance 80−81032
shell reinforced around hole, deformability meas. 80−16371
shell subject to local load, experimental theoretical analysis of state of stress and strain 77−4822
shells, cylindrical, stability during nonsteady heating and transverse flexure 80−40445
Shrinkage stresses in glass/resin composites 78−19869
silane, coupling agent on E-glass fibre, structure, Fourier transform infrared spectroscopy 78−60643
silane, coupling agent on porous silica, Fourier transform infrared spectroscopy 78−60642
sloping cylindrical shell, reaction during nonstationary loading 77−1857
sound absorpt. materials, effects of outdoor exposure 77−88985
specimen preparation for testing, three-layer cylindrical with syntactic foam base 80−3267
steel pin radially reinforced laminated rings, mech. props. 80−11714
stiffened shell residual stress formation 79−100108
strain disintegration under repeated static load 80−11756
strength, influence of form of reinforcement on spread of data *(Japanese)* 79−11672
strength, of composites renforced in two directions 80−19288
strength dispersion, statistical anal. *(Japanese)* 79−61655
strength geometry 77−70123
strength in biaxial compression in three planes of symmetry 77−59874
strengthening under biaxial tension 78−23797
stress analysis, brittle coating technique 80−35299
stress conc. effect on spread of strength and fatigue life *(Japanese)* 79−96117
stress luminescence, volume resistivity effects *(Japanese)* 78−43943
stress/strain conc. round hole, Moire fringe study 77−28964
stringed musical instrument resonant plates, use of synthetic materials 80−102937
structural inhomogeneity and strength 79−43358
technique for applying to metal structures 80−6289
Teflon-glass fabric double layer material join with epoxy-resin, adhesion strength determ. method 77−77681
temperature distrib. in components 78−1559
temperature-force depend. of lifetime 78−23795
Textolite, method of stressed state study during hardening 79−57191
thermal activity, prediction of struct. charact. and physicomech. props. 77−63872
thermal conductivity, diffusivity and sp. ht., 80-300K *(German)* 79−10990
thermal conductivity, temp. depend. 77−43393
thermal conductivity and diffusivity, 2-15K 77−24457
thermal conductivity measurement, rel. to temp., heat cond. problem soln. 79−37887
thermal conductivity of fibreglass composite, with complex spatial struct. 80−6571
thermal expansion, thermal and elect. cond., 2 to 290K 79−60528
thermal expansion coeff. and glass transition temp., thermal stress effect 78−14484
thermal inspection, one sided for separation of parts 79−79206
thermoelastic consts. for cross wound shell 80−14577
thermophysical props., 10-300K *(Russian)* 77−89390
thermoplastic resins, perfomance at elevated temperatures obs. 79−95067

glass fibre reinforced plastics continued
thermoplastic-based sheet materials, flexural anisotropy and stiffness assessment 80−76442
thermoplastics, short-fibre-reinforced, 100-s creep modulus prediction, at small strains 78−15473
thermosetting polymers, mech. props., 4.2-300K 77−25160
thick-walled shell, crack prevention during heat treatment 77−52376
thickness measurement 79−63189
three-dimensional structure, elastic and strength charact., effect of high modulus and hollow fibres 77−4803
transverse flexural vibration, statistical charact. of logarithmic decrement 77−7334
tube under cyclic pressurisation 78−68761
tubular specimen manufacture, apparatus 79−15906
two-layer tube, stressed state 79−64513
unidirectional glass-plastic, fracture dynamics 80−100906
unwinding resistance of hardening layers, fibre tension effect 77−32691
US inspection, dry-entry ultrasound transmission, through polyurethane 77−90563
vinyl ester matrix, axial fatigue failure sequence and mechanism 78−68773
vinyl ester matrix, fatigue life-limiting parameters 80−11746
vinyl ester thermoset moulding, cure cycle effect on mech. props. 80−45369
viscoelastic shell, thick-walled, deform. in post critical stage 77−58566
VMP fibre reinforced epoxide binder, structure and strength, effect of fibrous filler tension 78−68751
winding device for mech. test specimens prep. 78−7138
wound martensitic steel welded composite vessels, glass fibre reinforced plastic wound, struct. strength 80−97552
wound struct., scale factor rel. to strength 80−3135
woven and chaotically reinforced, expt. laws of physical props. distrib. 77−70025
woven epoxyphenol glass plastic, creep prediction during random changes in load, ambient temp. and humidity, computer calc. 77−70121
woven-roving type, high-speed punching, failure mechanisms 80−85143
yielding behaviour of plate with circular hole *(Japanese)* 79−8323
Young's modulus, heat treatment and heating temp. effect 80−35233
Young's modulus determination, dynamic high-speed method *(German)* 80−85123
Al/polyurethane foam/glass fibre reinforced plastic *(Japanese)* 78−56707
C glass fibre hybrid plastics, review of mech. props 79−20107
C/glass reinforced epoxy resin, hybrid effects, conditions for positive or negative effects vs. rule of mixtures, mech. props. 78−68769

glass fibres
see also fibre optics; optical fibres
acoustic materials, fibrous glass and mineral fibre development 80−33341
alkali boroaluminosilicate system, self-focusing fibres with aperture of 0.18 80−87548
alkali lime germanosilicate GRIN fibre prep., losses and geometrical props. 80−69560
alkali-$PbSiO_3$ optical fibres, high aperture, double-crucible preparation 78−1450
aluminosilicate, crystn. during heat treatment 79−52258
attenuation less than 5 db/km, using special deposition method *(German)* 77−34940
book, current topics in material science 80−46747
caustics, occurrence in the drawdown zone of silica fibres 77−66617
ceramics, manufacture using waste glass fibres 80−40304
chemical durability in alkali, powder method of testing *(Polish)* 78−7065
chemical purity in glass fibres for communication appl. 79−41437
clad-glass fibres, thermal stresses 80−107360
colloidal particles in gap between fibres, electroconcentration effect 80−11895
commercially available, charact. for fibre optical appl. 77−83983
connector for single-fibre cables, epoxyless 79−86253
connectors developments, standardised, for mass production *(French)* 79−86257
cooling during drawing 79−52253
crack growth during dynamic fatigue and effect on strength loss for tensile loading 80−89334
CVD, high deposition rate method using He gas 77−11055
data transmission appl., propagation principles *(German)* 79−81529
doped silica glass, optical fibre, ultimate low loss window 77−11023
drawing, neck-down shape prediction from furnace temp. distrib. 78−5594
drawing from compound glasses, using double-crucible and glass-plastic methods 79−3815
drawing of smooth fibres, diameter control improvements 78−1445
drawing process, characterization and control 80−58826
drawing process, extensional instabilities 80−89258
drawing using ZrO_2 induction furnace 78−1446
E-glass fabric, acid-treated, elec. resistivity studies 79−70178
E-glass fibre, coupled with silane, structure, Fourier transform infrared spectroscopy 78−60643
E-glass fibre, pore size distrib. anal. method 79−87805
E-glass fibre strength, effect of forming and ageing atmos. 78−92283
E-glass type, silane coupling agent deposited on surface, hydrolysis and drying effect on siloxane bonds 80−85072
elastic moduli, thermal history depend. *(Japanese)* 80−45333
elastic stresses in glass fibre preforms 79−64343
fabric composite, phosphate binders effect 78−44075
fabrication by improved CVD method 78−1448
fibre-optic communication in industry, appls., glass fibre props., connectors 80−87550
fibre-optic glass manufacture using polypropylene sump pumps 80−14410
fibreglass, mechanoluminescence during monoaxial stretching 78−68742
fibreglass insulating materials, radiative heat transfer rel. to optical props. 80−100367
filter paper, macerated, measurement standard for suspended solids in water 79−8454
filtration materials for radiation protection 80−5341
flaw generation, by indentation fracture technique 80−81156
flexural fatigue and surface abrasion 78−15504
forming process, charact., anal. techniques 80−58827
glass wool, fibrous material acoustic wave absorpt. props. 80−28378

glass fibres continued
high-strength, epoxy-acrylate coated, static and dynamic fatigue, tensile strength 79−1906
homogeneous, large aperture bundle tied by helix of metal or glass filament, light propag. anal. 78−87154
laser drawing limitations on optical fibres 78−1447
lightguide fibre, prototype drawing fascility 80−64229
lightguide fibre preform manufacture using modified CVD process 80−64228
manufacture process using CVD *(German)* 78−33933
melt spinning process anal. *(Japanese)* 79−78911
metal coating of optical fibres, for strengthening and surface protection 78−30103
microbrittleness and strength depend. on chem. comp. 79−38937
microscopic glass fibres and spheres, production and charact. for microanal. 79−24487
multicomponent optical glass fibre, profile synthesis 77−27333
optical, epoxy-acrylate coated, strength and static fatigue 78−1386
optical, fatigue failure probability 79−32045
optical, flaw generation and strength, dust particle effects 77−23741
optical, high-temperature fatigue strength and OH^- stress-induced corrosion 78−1387
optical, light focusing, charact. and appls. *(Hungarian)* 77−784
optical, low-loss, for optical communication, fabrication technologies state of art 79−10420
optical, preparation methods and performance factors 80−69557
optical, similarities with waveguide transmission, scalar approx. *(German)* 77−34942
optical, smooth fracture faces manufacture using incandescent wire 78−38098
optical, step-index, nearly elliptical, with high eccentricity, fabrication for studying modes 80−95989
optical, tensile strength 79−46062
optical, tensile strength testing, Weibull statistics 78−59128
optical, UV-cured, epoxy-acrylate coated, environmental effect on long-term strength 78−5582
optical channel for nanosecond pulse transmission 77−62064
optical communication appl., system components construction and operation *(German)* 79−18553
optical communication glass fibre development and prospects 78−9453
for optical communucations, colloquium, London, England (Jan. 1979) 80−67930
optical fibre, fracture surface anal. 80−58754
optical fibre, strengthening by molecular stuffing 80−58830
optical fibre, UV cured epoxy acrylate coated, zero stress ageing effect on strength 80−58753
optical fibre, vapour phase materials and processes, review 80−58825
optical fibre communication advances, materials and techniques 80−102853
optical fibre drawing, fluid-dynamic stability analysis 77−11053
optical fibre technology and information transmission props. *(German)* 80−10010
optical fibreguides, for lightwave communication, fabrication and characterisation 80−50586
optical fibres, fatigue failure prediction, appl. of fracture mech. theory 79−998
optical fibres, mech. reliability 80−91909
optical fibres, production for fibre optics, exam *(Polish)* 78−83130
optical fibres, tensile strength and static fatigue, analysis using Weibull distribution for optimum design 80−85011
optical fibres in communications, mats. props. 77−3666
optical fibres with high tensile strength prep. 78−63211
optical glass fibre development, large-core, for military appls. 80−48451
optical glass fibre manufacture, double-crucible and plasma methods 77−50763
optical graded-index fibre vapour-phase axial deposition method, fibre characteristics 80−58824
optical losses rel. to imperfections 77−88949
optical transmission systems appls. *(German)* 80−69516
optical waveguide applications 78−1332
optical waveguide communication, state-of-the-art review 77−62052
optical waveguides, materials systems, fabrication and charact. 77−19394
performance specification for optical communication *(Dutch)* 78−83112
phosphate glass optical fibres, transparent in UV region, manufacturing 78−87113
plastic-coated, fused silica, ageing and static fatigue 79−46067
preparation, appl. in Portland cement reinforcement, alkali resistance 80−81019
production methods for optical communications, review *(German)* 80−23813
quartz, internal stress and birefringence microanal. using optical phase microscope interference-polarisation 79−39109
reinforced Al, highly deformed, microstruct. and mech. props. *(German)* 80−55489
reinforced cement, review of reinforcing theory, ageing, stress/strain relations 78−44165
residual stress meas. by strain gauge, metrological charact. 77−120
resin interface studies 80−93531
resin-coated optical fibre, tensile strength tests *(German)* 78−33871
semi-automatic machine for hot splicing glass fibres for optical communication 80−23818
silica, epoxy acrylate coated, tensile strength >500 ksi, km length prod. 77−11052
silica, fused, surface flaws obs., fracture strength 77−14793
silica, stimulated Raman emission, 1-1.3 μm source 77−42568
silica optical fibres, ageing polymer-coated fused specimens in pH solns., tensile strength and dynamic fatigue 79−46063
silicate glass, optical loss, effect of manufacturing conditions 77−21085
silicone and glass clad compound glass optical fibre comparison 80−69533
single-mode optical fibres with different B_2O_3-SiO_2 compositions 78−1392
soda lime silica glass optical fibres, low OH content, low loss 78−37975
spring steel cutter for glass fibres 80−48468
stimulated Raman scattering, cascade effects *(Russian)* 77−23714
strength, forming conditions influence 80−20882
stress in glass fibers induced by the draw force 79−47737
surface composition of E and A fibres, effect of ageing, reduction, exam. using X-ray photoelectron spectroscopy 79−20223
surface struct. effect in solubility in water *(Japanese)* 80−34198
surface tension of fibres, evaluation 78−47657
tape permittivity dependence on binder content 77−59506
technology and applications, review of advances 77−66618
tensile strength, statistics, for optical communications *(German)* 80−38121
tensile strength and fatigue 77−3662
tensile strength meas. using chain-loading fibre tensometer *(Japanese)* 80−55610
thermal behaviour *(Japanese)* 79−77780
thickness meas. and control system in production *(German)* 80−10052
ultrafine and microfibre prod., working props. of alkali and non-alkali glasses 79−24486
vapour phase axial deposition, OH content reduction by flame hydrolysis control 80−48474
waveguides fabrication, mech. props. 77−23766
zirconosilicate glass strength, stiffness and Young's modulus, effect of cement environment 77−44335
Al_2O_3-SiO_2, clad with B_2O_3-SiO_2 effect of drawing tension on residual stresses 78−64554
As_2S_3 glass fibre, elongation, force depend., deviations from linearity 80−45334
B_2O_3 glass fibre, elongation, force depend., deviations from linearity 80−45334
BaO-GeO_2-Na_2O borosilicate core glasses for high numerical aperture fibres 80−69534
β-$CaSiO_3$ fibre, continuous unidirectional crystallisation from melt 78−95739
GeO_2 glass fibre, elongation, force depend., deviations from linearity 80−45334
GeO_2-Na_2O borosilicate glass fibre prod. by phase separation and leaching 80−69558
GeO_2-P_2O_5-SiO_2 glass fibre, incorporation of OH in modified CVD process 80−50560
Hg vapour lamp light output increase by use of fine quartz or glass fibres *(Dutch)* 77−62028
Li_2O-SiO_2-P_2O_5 glass ceramic fibres, heat treatment, crystn., tensile strength 80−84995
Na_2O-B_2O_3-SiO_2 glass fibre, plastic coating influence on strength 80−58697
Na_2O-B_2O_3-SiO_2 glass fibre, plastic-coated, liq. N_2 strength 80−58707
Na_2O-B_2O_3-SiO_2 glass, low-loss GRIN fibres, double-crucible prod., loss and bandwidth meas. 80−69559
Na_2O-B_2O_3-SiO_2 low-loss optical fibre prep. by double crucible technique *(German)* 78−33929
Na_2O-B_2O_3-SiO_2:GeO_2 medium-loss graded-index preform fabrication by phase separation and leaching *(German)* 78−33930
$Na_2O.SiO_2$ fibre, reactivity to atmospheric moisture below annealing range, internal friction measurement 78−92288
SiO /GeO_2, single-mode, numerical aperture effects on optical and mechanical props. 80−69548
SiO_2, coated silica fibres, tensile strengths of 1 km lengths 78−1384
SiO_2 fibre lightguides, fused, zero stress strength reduction and transitions in static fatigue 80−87523
SiO_2 fibres, fused, drawn from rods, oxy-H_2 flame, prep., strength, dia. var. 80−102868
SiO_2 fibres, fused, failure predictions based on fatigue strength 78−71293
SiO_2, fused silica fibres, high-strength epoxy-acrylate coated, dynamic and static fatigue 78−1385
SiO_2 glass fibre, elongation, force depend., deviations from linearity 80−45334
SiO_2 glass fibre, plastic-coated, liq. N_2 strength 80−58707
SiO_2 glass fibre drawing, caustic curves in solidified drawdown zones 77−39117
SiO_2 glass fibres, exam. of phase separation effect on internal friction 78−88455
SiO_2, prep. from $Si(OC_2H_5)_4$ *(Japanese)* 79−70038
SiO_2, silica, synthetic, tubing and fibre fabrication using SiO_2-B_2O_3, for optical fibre waveguides 79−50462
SiO_2 silica glass fibre CVD manufacture and characteristics 80−28345
SiO_2 vitreous fibres, relax. props. near glass transition interval 80−34137
SiO_2:F, silica fibres, numerical aperture and attenuation, drawing from preforms 78−1449
SiO_2/P_2O_5, single-mode, numerical aperture effects on optical and mechanical props. 80−69548
SiO_2-Al_2O_3-B_2O_3, glass fibre, water and acid resistance 80−11799
SiO_2-GeO_2/SiO_2 load bearing optical cable, geophys. appls. 80−91923
SiO_2-glass fibres, struct. anal. using X-ray diffr. and optical microscopy 77−65952
SiO_2-Na_2O-CaO-MgO, internal stress and birefringence microanal. using optical phase microscope interference-polarisation 79−39109
SiO_2-ZrO_2-Al_2O_3-CaO-Na_2O-K_2O-Li_2O, chemical resistant glass for glass fibres 80−21128
$SiO_2$$B_2O_3$-$K_2O$-$Al_2O_3$-$As_2O_3$ glass fibres containing metallic granules, tensile strength, Young's modulus, DC conductivity 80−30023
ZrO_2-SiO_2 glass fibre prep. form metal alcoholates 78−6886
ZrO_2-SiO_2(-Na_2O) glass fibres, prep. from metal alkoxides, resistance to NaOH soln. 80−97454

glass industry
air pollution, review 78−3936
applications of gauges and optical projectors 80−21249
automatic control of glass melting, adaptive subsystem 79−61553
electric furnace, muffle type, automation of temp. regime 77−61068
electric furnace for glass prod. 80−11620
fibre reinforced plastics, automated production methods 80−25651
fibre-optic glass manufacture using polypropylene sump pumps 80−14410
forming machines, review 78−3091
glass balls production, drop feeders automation 79−61556
glass making system, continuous, energy balance 80−89189
glassware dimensional and sidewall inspection using digital camera and computer 78−16890
heat exchange monitoring between flame and glass surface in furnace 77−26298
IR thermometry, readings interpretation 80−82765
magneto-hydrodynamic phenomena, of mixing in the glass industry *(Polish)* 80−64647
melting furnace, elec., 14 ton/day 79−58693

glass industry continued
melting furnace, gas consumption through ports, monitoring and control system 79−58692
melting furnace, resist. between electrodes calc. 79−58690
melting optical glass in Pt crucibles, power supply freq. convertors 79−72728
melting process, TV monitoring, equipment protection 79−58756
microelectrode puller for reproducibility 77−48967
models, math. and phys., of glass making process, review 78−3083
ophthalmic lens surface working machinery 80−28363
optical fibre drawing, split beam CO_2 laser heat source 77−19465
radiation pyrometer, use in automatic control of molten glass temp. in feeders 77−49729
raw materials and batch prep., review 78−3085
refractories for glass making, progress, review 78−3089
sheet glass, laminated struct., effect of prod. method 79−61555
sheet glass, laminated struct. and homogeneity, mech. agitation effect 79−61554
tubing diameter meas., using radionuclide methods *(Czech)* 77−5803

glass-metal seals
see also electron tube manufacture
annealing effect on internal stresses 80−40389
compound parabolic concentrator heat transport to storage 79−62102
ductile wire-through-glass seal, stress anal. 77−84161
fibreguide to metal hermetic seal, using Cu tube component 78−83120
finite element anal. of stresses, photoelastic meas. 79−29197
hermetic seal, optical fibre-to-metal, construction 78−83078
interface study by Auger spectroscopy 80−76587
Kovar protective coating, Ni-In alloy, electrodeposition, surface preparation and testing *(Italian)* 80−40621
phosphate glass-Al alloys seals, elec. and mech. props., glass transition 80−81018
pressure-mode soft-metal vacuum seal, for glass and ceramics 80−17952
set point, of glass in glass-metal seals 80−108423
soda-lime glass to Fe-Cr seal, field-assisted bonding, SIMS anal. 79−34399
stress relaxation meas. device 77−63845
vacuum seals for $MgFl_2$ windows 78−94457
Si-glass IR cell, for ultrahigh vacuum and temp. 79−6134
W electrode, method for sealing into quartz 79−71463

glass transition
abietic acid, transverse US wave propag., glass and liquid transition region 80−79883
acids, conc. aqueous, amorphous protonic conductors, DC cond., glass transition and elec. relax. meas. 78−2290
acrylonitrile-vinylidene chloride copolymers, temp. variation with comp. 79−79247
Adam-Gibbs theory, for conc. polymer soln. 78−83353
$AgPS_3$-AgX (X=I, Br), glass-forming regions, struct. model *(French)* 80−100464
n-alcohol-Lewis base mixtures, glass transition temp. composition depend. 77−66015
aliphatic alcohols, glass transitions, cellulose blotter/torsion pendulum technique, for relax. determ. 80−54357
alkali halide aq. solns., homogeneous nucleation glass form., press. depend. 78−51649
alkali metaphosphate, M_2O-R_2O_3-P_2O_5 (R=Y or rare earth), glass transition temps. and coeffs. of linear thermal expansion 80−88343
alkali metaphosphate glasses, low frequency Raman scattering and glass transitions 79−95745
alkaline earth glasses, RO-Al_2O_3, -P_2O_5, R=Mg, Ca, Sr, Ba, exam. of electron beam irradiation effects 79−4253
alkaline earth metaphosphate, MO-R_2O_3-P_2O_5 (R=Y or rare earth), glass transition temps. and coeffs. of linear thermal expansion 80−88343
alkyl halides, depolarisation thermocurrent obs. of main relax. around glass transition 78−27158
alternating copolymer of styrene and N-substituted maleimides, NMR relax. studies of mol. motion 77−85608
amorphous polymer, super-glass transition processes, damping process 80−24573
amorphous solid, glass transition temp. rel. to low temp. phonon mean free path 79−51226
asphalt, glass transition temp. and viscosity 79−77045
atom-glasses, hard sphere model of glass transition 79−4399
binary liquid mixture, glass transition temp., composition depend., theory 77−76531
bispenol-A epoxy resin, glass transition temp., effect of absorbed water, PMR line width 79−90766
butadiene acrylonitrile elastomers, props. in glass transition range *(Polish)* 79−42223
butanediol-1,3, viscoelastic props., digital correlation Brillouin scatt., in glass transition region 78−2865
cellulose acetate-dimethylphthalate gel, mech. props., substitution effect *(Russian)* 79−23291
chain molecular amorphous solids, stat. thermodynamics and mol. theory 78−26442
chalcogenide glasses, struct. and growth kinetics, topological principles 80−49123
chitin (poly-N-acetyl-D-glucosamine), dynamic mech. behaviour, effect of water 80−97522
chitosan (poly-D-glucosamine), dynamic mech. behaviour, effect of water 80−97522
chlorobenzene-cis-decalin, mixtures, dielec. const. and loss tangent in liq. and solid phases 80−100628
chlorobenzene-cis-decalin mixtures, phase transitions and dielec. behaviour study in 77-330K 80−29680
cholesteryl oleate (linoleate), solid-solid transition, glass transition, cryst. nucleation temps., DSC obs. 78−34604
composite material, model 77−84901
composition dependence 78−59936
configurational properties of liquids near glass transition 78−26662
copolymer globule model, orientationally-ordered liq. cryst. state *(Russian)* 80−59389
deformation in glass transition interval 79−66137
dichloromethane-decalin glass, mol. dynamics, from dielec. loss meas., 107-148K, 293K 78−76379
elastin, hydrated, dielectric relax. 79−5247
elastomer, relaxation processes, statistical description *(Russian)* 79−23229

glass transition continued
epoxide network polymers, glass-transition and chem. struct. *(Russian)* 78−51653
epoxide resin cured with aliphatic dicarboxylic acids, fatigue behaviour *(Japanese)* 79−79092
epoxide resins, amine-hardened, heat distortion, glass transition temps., chem. cure 80−44302
epoxy polymer, glass microsphere-filled, glass transition temp. *(Russian)* 79−24489
epoxy resin, cure history effect on dynamic mech. props. 80−54356
epoxy resin, meas. of glass transition temp., linear viscoelasticity 80−29157
epoxy resin, plastic deform. mechanism 80−97534
epoxy resin, rubber modified, positron annihilation 80−29825
epoxy resin, time-temp. superposition of creep data, linear viscoelastic props. 80−30045
epoxy resin cross linked with aliphatic polyamines, struct. and dynamic mech. props. *(Japanese)* 80−38956
epoxy resin/particle composites, particle size effect in thermal expansion, filler effects on T_g 80−84305
epoxy resins, relationship between struct. and mech. props. *(Japanese)* 78−31438
epoxy-rubber glass transition rel. to filler, cooling rate 79−4403
equilibrium thermodynamics, sp. ht., refr. index and glass transition *(German)* 78−83745
ethanol, plural glass-transitions, thermodynamic functions 78−38820
ethanol-water system, metastable states, hydrates existence and props., low temp. 78−71835
ethylene-vinyl alcohol copolymer, drawn samples, annealing effect around T_g temps. on shrinkage and mol. orientation 80−79712
ethyleneterephthalate-ethylene glycol copolyester/15% polyglycol, semicryst. melting and glass transitions 80−49346
extruded, glass transition temp., melting pt., DTA 78−2235
ferroelectric, ion-ion interaction due to soft phonon modes 79−99838
fluorocarbon ether bibenzoxazole polymers of low glass transition temp., preparation and charact. 79−51006
frozen structure glass, viscous flow, valence configuration flow theory 80−39335
glass bead-reinforced epoxy resin composite, bulk and shear elastic props. 78−6959
glass fibre, thermal behaviour *(Japanese)* 79−77780
glass fibre reinforced polymer, thermal expansion coeff. and glass transition temp., thermal stress effect 78−14484
glass forming and props. 80−19717
glass-forming liquids, relax. times, temp. depend. 78−83924
hard-sphere model, relax. effects 78−38821
hydrocarbons, glass transitions, cellulose blotter/torsion pendulum technique, for relax. determ. 80−54357
inorganic glasses, microhardness and glass transition temp. calc. 79−5059
internal parameters, ordering parameters, history function, rel. to glass transition 78−30738
ionic polymer, role of electrostatic forces in glass transition temp. 77−84908
kinetics, linear nonequilib. thermodynamic theory 78−67815
liquid, low mol. weight, glass transition temp. and crit. props. 80−39265
liquid, low mol. wt., universal reduced glass transition temp. 80−38895
liquid-glass transition, glass transition depend. on heating and cooling rates 80−79920
liquids, glass transition rel. to press. depend. of viscosity 80−34171
lubricant, glass transition, light scattering study 79−29228
lubricant, glass transition rel. to elastohydrodynamic lubrication 79−29227
lubrication film temp. and traction, rel. to solidification and glass transition temp. 79−28041
macromolecules, linear, heat capacities, scanning calorimetry meas. 80−61134
melts, glass forming, exam. of isobaric-isothermal pots. in glass transition interval 79−7681
metal alloy glasses, polymer model, glass temp. correlations 80−6361
metallic glasses, free vol. theories of glass transition 78−14284
metallic glasses, structure, stability and prod., elec., mag. and mech. props., review 80−44134
metallic glasses, Young's modulus/thermal props. correlation 78−6961
mixed amorphous system, correlation of Tg 80−24574
molecule glass, simple, dielec. relax., 4-77K 77−73109
multipolymers, glass transition rel. to phase separation 78−91270
Nafion, densities and expansion coeffs. as function of various parameters 80−79711
nitrate glass: Eu^{3+} struct. reorganisation in glass transition interval, polarised luminesc. obs. 80−45141
nitrocellulose-nitroglycerine propellant, glass transition temp., thermomech. anal. meas. 79−14917
noncrystalline solids, chem. bond stiffness, rel. to thermodynamic and kinetic props. *(French)* 77−72561
NR, glass-rubber transition, time-temp. superposition, shear creep compliance meas. 80−88309
nylon 6, effect of moisture content on glass transition temp. and Young's modulus 79−4401
nylon 6 (polycaproamide), salted, glass transition temp. and elastic modulus, moisture effect 80−103465
nylon 6-inorganic salt mixtures, glass transition temp. 80−19921
nylon 6-LiCl mixtures, DC cond. and struct., Lill effects 80−44149
phenolformaldehyde resin, sp. ht. obs. *(German)* 78−75845
phenolic novolac resin-rubber mixture, glass transition, mixing ratio effect *(German)* 79−77732
phosphate glass-Al alloys seals, elec. and mech. props., glass transition 80−81018
photographic migration images, liquid developed, fixing and abrasion resistance 80−4792
phthalocyanine polymer, dynamic mech. props. and fracture energy 80−100866
pitch, coal-derived low-volatile residues, glass transition, rheological props., DSC anal. 80−39331
plasticised cellulose acetate sheet, post-yield fracture 80−25859
PMMA, amorphous, reorientational relax., 6-165°C, polarised laser beam scatt. correlation 78−2864
PMMA, biaxially oriented, shrinking kinetics in transform. range 78−27588
PMMA, glass-rubber transition, time-temp. superposition, shear creep compliance meas. 80−88309

glass transition continued
PMMA, piezobirefringence, optical and mech. relaxations, temp. depend. 80−34885
PMMA, secondary loss peaks, effect of structural features 79−11649
PMMA, solid, mol. relax., photon correl. spectroscopy 77−90159
poly(4-methyl pentene-1), US props., glass transition, Gruneisen parameters 80−54316
poly(4-methyl-1-pentene), semicrystalline, bulk and film, glass transition temp. 79−42982
poly(di-n-heptyl itaconate), alkyl side chain independent relax., double glass transition 80−59636
poly(N-vinylcarbazole), glass transition temp., mol. wt. relation 80−19922
poly-2-hydroxyethyl methacrylate, glass transition temp., water content and tacticity effects 79−37817
poly-ε-caprolactone-PVC blends, morphology 79−69019
poly-ε-caprolactum, semicryst. melting and glass transitions 80−49346
poly-N-n-alkymaleimides, glass transition temp. 77−65956
poly-tetramethyl-p-silphenylene-dimethylsiloxane block copolymers, crystn., morphology, kinetics 79−14695
polyacrylonitrile and copolymers with polyisobutylene, specific heat and glass transition temp. meas. *(German)* 78−34603
polyalkyleneoxide polymer, proton nuclear mag. relaxation *(Rumanian)* 78−91977
polyalkylmethacrylates, vitreous, thermal cond., press. and temp. depend. 78−2315
polyamide-12 plasticized with sulphonamides, relaxation props. *(Russian)* 80−55031
polyamides, 1,3-cyclohexanebis(methylamine) based, thermal props. and glass transition temp. 80−39264
polyarylate organosiloxane polyblock copolymer, struct., props., phase conversion *(Russian)* 79−65010
polyarylate-arylenesulfone oxide block copolymer, glass transition, melt and soln. viscosity *(Russian)* 79−55915
polyaryloxyphosphazene copolymers, thermal, morphological and rheological props. 80−103265
polybutadiene, carboxyl-terminated, glass transition temp., thermomech. anal. meas. 79−14917
polybutadiene, cross linked, deform. below T_g, radical form. and crazing 79−52307
1,2-polybutadiene, dynamic viscoelastic props. in curing process 80−76298
polycarbonate, γ-irradiated, dielec. behaviour and glass transition 80−97182
polycarbonate, amorphous US vels. from Brillouin scatt., room temp. to 250°C 79−91454
polycarbonate, bisphenol A, WAXS pattern, temp. effect and thermal history 80−93583
polycarbonate, rel. to sorption of water and its effect on dielec. behaviour 79−11383
polycarbonates, glass transition pt., calorimetric determ. *(Polish)* 79−51241
polyelectrolyte, plasticised, effect of ion placement and struct. on props. 79−7679
polyester-polyurethane semi-interpenetrating networks, mech. props., morphology 80−45362
polyesteramides, glass transition temp. determ. by DTA 79−4402
polyesters, photoreactive, synthesis and struct.-prop. relations 80−7826
polyether ester-PVC blends, annealed, dynamic mechanical and sonic velocity behaviour 80−25740
polyether-polyester elastomers, differential scanning calorimetry, crit. points *(Japanese)* 80−75344
polyether-polyester elastomers, differential scanning calorimetry by using poly(oxy-1,4-butylene glycol) as soft segment *(Japanese)* 80−79916
polyethylene, amorphous, glass temp. 77−66017
polyethylene, amorphous linear, glass transition temp. by torsion braid anal. 79−73296
polyethylene, crystallisation of thick film from glassy state by annealing 80−54151
polyethylene, high and low density, depolarisation thermocurrent study, relax. modes rel. to glass transitions 80−7263
polyethylene, linear, glass transition temp. 80−15225
polyethylene, linear, glass transition temp. upper limit, ^{13}C Fourier transform NMR 79−14918
polyethylene, relax. phenomena, −30 to 200°C, premelting and glass transition 78−51440
polyethylene, TSC study of deuteration 80−20581
polyethylene oxide, relax. phenomena, −30 to 200°C, premelting and glass transition 78−51440
polyethylene oxide, solid state relaxation, DSC study 78−9962
polyethylene terephthalate, glass-rubber transition determ., small-angle X-ray scatt. 78−95145
polyethylene terephthalate CO_2 permeability above and below glass transition 79−73340
polyisobutylene, EPR, correlation with glass transition 79−11348
polyisobutylene and copolymers with polyacrylonitrile, specific heat and glass transition temp. meas. *(German)* 78−34603
polyisobutylene melt, thermodynamic constitutive eqns., adiabatic deform. expts. 78−1620
trans-1,4-polyisoprene crystals, press. effect on growth rate 80−88064
polymer, amorphous, translational motion and lattice vibr. obs. by Raman scatt., T_g phenomena 78−23469
polymer, amorphous, under press., glass transition phenomena, model 79−23706
polymer, conformational sp. ht. determ. method 78−14474
polymer, electrochromic dye probe for softening around T_g 80−84724
polymer, glass transition, fluctuation theory and thermodynamics *(German)* 79−51242
polymer, glass transition due to plastic deform., high-molecular linear polymer of narrow molecular mass distrib. 79−96065
polymer, glass transition elevation by entanglements 78−83926
polymer, glass transition kinetic nature, sp. ht. 79−10929
polymer, glass transition temp., dilatometric and dielectric relaxation data 80−6497
polymer, glass transition thermodynamics, fluctuation theory approach *(German)* 79−33078
polymer, glass transition under high-press., dielec. loss method obs. *(Russian)* 78−71841
polymer, glassy, ageing, scanning calorimeter meas., theoretical prediction 79−10810
polymer, high mol. wt., glass transition temp. and crit. props. 80−39265

glass transition continued
polymer, mol. wt. depend. 79−95144
polymer, polydisperse, glass transition temp., mol. mass depend. 80−92656
polymer blends, two-component, glass transition, calorimetric investig. *(Russian)* 80−39268
polymer filled, internal stresses influence on glass transition temperature 80−10645
polymer film, glassy and rubbery, isotope effect in H_2 and D_2 diffusion, T_g region behaviour 80−84327
polymer glass, isobaric vol. and enthalpy recovery, transparent multiparameter theory 80−24375
polymer glass, isothermal struct. relax., in high elasticity transition region, mol. model *(Russian)* 78−87629
polymer glass, sp.ht. discontinuity at glass transition 80−19954
polymer glass temp., correl. to dilute soln. dielec. relax. rates 78−10175
polymer glass temperature, rel. to cohesion energy and vacancy form. energy *(German)* 78−22670
polymer glass transition, dynamic props., mol. model *(Russian)* 78−87777
polymer glass transition, temp., conform. effects 78−83925
polymer glass transition T_g rel. to ESR parameter T_{50G}, mol. interpretation 78−67817
polymer glass-transition point meas. apparatus using vibration meas. of immersed plate *(Russian)* 78−71842
polymer glasses, aged, enthalpic state determ. by scanning calorimetry 80−6528
polymer glasses, thermodynamics of densification process 78−95723
polymer latex film composite, glass transition temp. determ. using thermomech. curves 80−75342
polymer mixing, heats 80−61132
polymer mixtures, compatible, glass-transition temps. 79−46789
polymer network formation, pre-gel intramol. reaction and gelation, shear moduli and glass transition 80−45501
polymer properties of glass transition, conformational effects anal. 79−69231
polymer reactions, two phase, below glass transition temp., limiting conversions 78−88632
polymer transitions, domain size effects 79−69232
polymeric cryoprotectants in preservation of biological ultrastruct., aq. soln. low temp. states 78−65157
polymers, crosslinked, specific characts. *(German)* 78−75585
polymers, effect of glass transition temp. on thermal props. *(German)* 78−30742
polymers, elec. resist., corresponding states relationship 80−59704
polymers, glass transition, positron annihilation studies, review 78−95614
polymers, irradiated, crosslinking density effect on glass transition *(German)* 80−34175
polymers, molecular wt. effect, thermodynamic theory 80−19920
polymers, pure liquid, electric field dependence of the glass temperature 79−86875
polymers, solid, mech. deform., model 79−20120
polymers, solidification, as dissipative process 80−65205
polymers, transient current nature 78−80278
polyolefin, amorphous, thermostimulated creep, 77-350K 79−69185
polyolefin, amorphous, thermostimulated creep and glass transition 79−69186
polyolefins, amorphous, compensation temp., thermostimulated creep 79−14919
polyoxyethylene-glutaric acid eutectic, melting and crystn. 80−28924
polyoxymethylene, dielec. relax., 90-300K, 400-10^4 Hz, behaviour near T_g *(Russian)* 77−69770
polyoxymethylene, low-strain deform., transmission electron microscope exam. 79−5013
polyoxymethylene, relax. phenomena, −30 to 200°C, premelting and glass transition 78−51440
polyoxymethylene, transitions and relaxation spectrograph 80−65204
polyoxymethylene copolymers, solid, mol. motions, 4-315K, dynamic-mech. study 79−4258
polyphenylene oxides, high temp. ageing effect on struct. and props. *(Japanese)* 77−70078
polypropylene, Halen and Daplen, semicryst. melting and glass transitions 80−49346
polypropylene, TSC meas. of relax. modes, apparent double glass transition 80−11323
polypropylene fibres, γ-irrad., microstruct. changes in glassy-high elastic state transition *(Rumanian)* 80−49347
polypropylene fibres, EPR during glass transition, γ-irrad. 79−8445
polypropylene oxide, complex with metal salt, glass transition temp. 79−69234
polysiloxane dizwitterionomers, mech., dielec. relax., effect of H_2O sorpt., thermal history 80−50261
polystyrene, amorphous, press. effect on glass transition and glassy state 78−26674
polystyrene, anionic, kinetic parameters assoc. with glass transition temp., calc. 80−49345
polystyrene, atactic, isothermal internal friction meas. of glass transition 79−74191
polystyrene, end group modified, chain dynamics studied by fluorescence depolarization 80−19724
polystyrene, glass transition temp. rel. to solvent crazing 77−12681
polystyrene, glass-rubber transition, time-temp. superposition, shear creep compliance meas. 80−88309
polystyrene, glass-transition temp., mol. wt. effect, thermodynamic theory 80−19920
polystyrene, glassy atactic, struct. anal. from small-angle X-ray scattering 79−73109
polystyrene, glassy state, relax., free vol. fluctuations effect 80−19722
polystyrene, microcryst. cellulose filled, glass transition temp. shifts 78−95144
polystyrene, mol. wt., distrib. rel. to glass transition temp., ESR spin-probe investig. 79−8041
polystyrene, photon correlation spectroscopy near glass-rubber relaxation 79−47464
polystyrene, plasticizer effect on electric strength 80−29688
polystyrene, polarised Rayleigh scatt. near glass-rubber relax., photon correl. spectroscopy 80−40124
polystyrene, ref. std. material testing, evaluation, glass transition temps., instrumental effects 79−4404
polystyrene + poly(2,6,-dimethyl phenylene oxide), isotactic, crystallisation and melting 78−18554

glass transition continued
polystyrene amorphous film, cyclically fatigued, molecular behaviour 80−35310
polystyrene glasses, transition temp. and thermodynamic state 78−75819
polystyrene-chloranil molecular complex, glass-rubber and liquid-liquid transitions 80−45002
polystyrene-polyisoprene block copolymers, low mol. wt., glass transition temp., DSC investig. 77−7854
polystyrene-SiO_2, glass transition rel. to filler, cooling rate 79−4403
polystyrenes, anionic, TSC obs. of T_g and T_{II} transitions 80−84686
polysulphone, glass and melt, PVT props., glass transition 79−14911
polytetrahydrofuran films, elec. characts. under AC 80−40062
polytrifluoroethylene, dielectric relax. processes above and below glass trans. *(Japanese)* 80−55028
polyurethanes, cross-linked, mol. mobility and struct., thermomechanical and NMR obs. *(Russian)* 80−69285
polyurethanes based on toluene di-isocyanate, struct.-prop. relns. 78−80509
polyvinyl cyclohexane, head-to-head, prep., characterisation 79−70036
polyvinyl fluoride, dielectric support for glass transition 78−2239
polyvinyl fluoride, glass transitions, Ar permeability and diffusion obs. 79−32919
polyvinyl fluoride, relax. phenomena, −30 to 200°C, premelting and glass transitions 78−51439
polyvinylacetate melt, thermodynamic constitutive eqns., adiabatic deform. expts. 78−1620
polyvinylbutyral, elec. and dielec. props., mol. wt. effect on charge storage 80−97192
polyvinylidene fluoride, γ-irradiated, low temp. internal friction 78−83874
polyvinylidene fluoride, dielec. props. and phase transitions *(French)* 80−55008
polyvinylidene fluoride, film, piezoelec. relax. 79−87394
polyvinylidene fluoride, glass transitions, Ar permeability and diffusion obs. 79−32919
polyvinylidene fluoride, relax. phenomena, −30 to 200°C, premelting and glass transitions 78−51439
Prigogine-Defay ratio, rel. to order parameter theory 78−2232
propane-(1,2)diol: $^{57}Fe^{2+}$, dil. solution, Mossbauer exam. of struct. relax. at glass transition 77−66016
PV, glass-rubber transition, time-temp. superposition, shear creep compliance meas. 80−88309
PVA, microcryst. cellulose filled, glass transition temp. shifts 78−95144
PVC, different stereoregularities, heat treatment effect on glass transition temp. and c_p changes 79−4985
PVC, glass-rubber transition, time-temp. superposition, shear creep compliance meas. 80−88309
PVC, glass-rubber transition determ., small-angle X-ray scatt. 78−95145
PVC, heat capacity and thermodynamic props., 6 to 375K obs. 78−79779
PVC, tensile and indentation behaviour, durability tests, glass transition 79−5017
PVC, thermal and dynamic glass transition temp. relation *(German)* 78−14450
PVC block copolymers, physical props. and morphology 79−82166
PVC-ethoxymethylmelamine blends, dynamic mech. props. *(Japanese)* 79−96063
PVC-vinylchloride system, glass transition, vinylchloride influence *(German)* 80−79917
relaxation memory effects, exactly soluble one-dimensional model 79−1398
rubber, natural, stretching effects on glass transition, sp. ht. obs. *(German)* 78−79753
rubber, natural, thermal properties depend. on temp. and press. 79−95223
selenide systems, binary, glass transition behaviour, model, comp. depend. 78−26673
simple glass forming materials, universal nature of two relax. processes in region of glass transition 77−84907
soft core model of simple liquids self diffusion, glass transition 78−67634
soft-sphere model, mol. dynamics study 80−49343
sorbitol, relax. processes, optical probe obs. 79−47430
spin-glass alloys, magnetoresistance, Boltzmann formalism calcs. 80−88540
styrene-acrylonitrile copolymer swelling, glass transition and crazing, polar group incorporation 78−85017
styrene-butadiene copolymers, elec. strength meas. rel. to glass transition 78−15096
styrene/MMA copolymers, struct. and rheology 80−1444
supercooled amorphous state, Gaussian core model 79−73101
supercooled liquid-amorphous phase boundary, empirical criterion, Monte Carlo simulation 79−1496
temperature, determ. from expansion and elec. cond. temp. depend. 80−19967
temperature, domain size dependence 77−89525
temperature, rel. to mol. wt. 80−34176
o-terphenyl, liq. and glassy, dynamics of dissolved ferrocene, Mossbauer obs. 80−55000
tetrabenzo[a, cd, j, lm]perylene evaporated film, crystn., time depend. as function of purity 80−88449
thermodynamics of glassy state with multiple order parameters 78−14283
transition interval, theory, physical meaning *(German)* 78−22834
tricritical points, symm., in binary mixture of polymeric glass 79−82320
trimethylphosphate, plastic and hard crysts., liq., nucl. spin-lattice relax. mol. motion 78−48065
viscous liquid, glass forming, stabilisation calc. 80−39267
viscous liquid, glass transition, mol. mechanism for thermodynamic second order transition 78−2237
viscous liquid, glassy state, effect of fictive temp. on dielec. relax. 79−24256
viscous liquids, glass transition, nonconfig. contribs. to excess entropy 80−92654
water, normal and heavy, glass-transition temp., crystn. temp., and dielec. const. 80−15229
wet resin, glass transition model 77−84901
window glass melts, glass-transition temps. from viscosity temp. depend. 80−34113
AgI-Ag_2O-P_2O_5 system, glass form. and superionic cond. characts. 78−26722

glass transition continued
$AgPO_3$-Ag_2SO_4, new Ag^+ and Li^+ ion glass conductors, glass transition, Raman spectra *(French)* 79−47094
$AgPO_3$-AgX (X=I, Br), glass-forming regions, struct. model *(French)* 80−100464
As-Se, relation between glass-transition temp. and optical memory-eraser temp. 80−10650
As-Se system glasses, thermal expansion coeff. and free vol. at transition temp. *(Japanese)* 79−55876
As-Te-Ga system, glass-forming region and props. 80−25674
As_2S_3, relation between glass-transition temp. and optical memory-eraser temp. 80−10650
As_2Se_3-$GeSe_x$-$SnSe_x$ (x=1,2), exam. of Sn valency and physical props. 79−4753
$Au_{0.77}Ge_{0.136}Si_{0.094}$, undercooled metallic melt, viscous behaviour 77−66037
B_2O_3 and alkali borate glasses, Raman study at high temps. 80−93306
B_2O_3, glassy, influence of annealing on transition region 80−44145
BeF_2 glass transition, Monte Carlo study 80−75343
CaO-MgO-Al_2O_3-SiO_2, glass-ceramic prep. by hot pressing and crystallisation of powder 78−11192
$CdGe_{1-x}Sb_xAs_2$ system, amorphous and cryst. phases, DTA and microhardness obs. 78−22835
$Cd(NO_3)_24.1H_2O$-$CoCl_2$, melt viscosity, equivalent conductivity, glass transition temp. 78−75855
$Cd(NO_3)_24.1H_2O$-$NiCl_2$, melt viscosity, equivalent conductivity, glass transition temp. 78−75855
Cu-Zr (50 or 54 at.%), splat-quenched, glass transition and crystn. temps. determ. 78−22659
EuS-Ga_2S_3-GeS_2, chalcogenide glasses, conditions of form. of glassy prod. *(French)* 80−100325
$Eu_xSr_{1-x}S$, insulating spin glass, mag. props. 80−2589
(Fe,Co)PBAl, metallic glass, viscous flow, alloying effect 78−79793
Fe-B(-Si)(-Ni), amorphous alloy, anelastic relaxation 79−4997
Fe-Ni-P-B(C), amorphous alloy, anelastic relaxation 79−4997
Fe-P-Al(Si)(B), amorphous alloy, anelastic relaxation 79−4997
$Fe_{40}Ni_{40}B_{20}$ glass, phase transform. during isochronal annealing 78−14451
$Fe_{32}Ni_{36}Cr_{14}P_{12}B_6$ metallic glass, effect of pre-ageing on glass transition temp. 80−100326
$Fe_{40}Ni_{40}P_{14}B_6$, metallic glass, acoustic emission generated during viscous flow 78−39853
$Fe_{40}Ni_{40}P_{14}B_6$, metallic glass, glass transition, viscous flow and differential scanning calorimetry meas. 80−96635
$Fe_{40}Ni_{40}P_{14}B_6$, Metglas 2826, hot forming 80−84980
Ge-As-Se system glasses, thermal capacity, 300-600K 79−65210
Ge-Pb-Bi-O glass, photoelasticity, glass transition limits 79−33670
Ge-Pb-Se-Te, glass form., DC cond., and mole volume 79−90560
Ge-S system glasses, thermal expansion coeff. and free vol. at transition temp. *(Japanese)* 79−55876
Ge-S-Te system, glass forming 80−19718
Ge-Sb-Se system glasses, thermal capacity, 300-600K 79−65210
Ge-Se system glasses, thermal expansion coeff. and free vol. at transition temp. *(Japanese)* 79−55876
Ge-Se-Te glasses, form. region, elec. props. 79−94904
Ge-Te binary glass, eutectic, DSC obs., thermodynamic and thermokinetic characts. 80−39309
$HNO_3.H_2O$, devitrification crystallisation, fast Raman and wide-line NMR obs. *(French)* 79−73915
H_2SO_4 glass, γ-irrad., trapped H ESR, vol. relax. effects 79−52703
$(KCN)_{0.5}(KBr)_{0.5}$, lattice dynamics neutron scatt. obs., glass phase formation 80−15207
K_2SO_4-$ZnSO_4$ system, glass formation and phase diagram study, physical props. 78−27500
La_2Se_3-Ga_2Se_3-$GeSe_2$ ternary system, phase diags., glass formation *(French)* 78−3109
Li_2O-Al_2O_3-SiO_2 glasses, viscosity, thermal expansion, glass transform. temp., and refr. index 79−42282
Li_2O-Al_2O_3(Ga_2O_3)(Bi_2O_3), quenched glasses, crystn. and ionic cond. 80−33899
$LiPO_3$-Li_2SO_4, new Ag^+ and Li^+ ion glass conductors, glass transition, Raman spectra *(French)* 79−47094
$Li_{x+2}P_xO_{3x+1}$, polyphosphate, melting and crystallisation 80−70376
MgO-Al_2O_3-SiO_2, glass ceramic, structure and props. *(German)* 80−38927
$NaNO_3$-KNO_3-$Ca(NO_3)_2.4.09H_2O$ melt, mixed alkali effect 80−34219
$NaNO_3$-$TlNO_3$-$Ca(NO_3)_2.4.09H_2O$ melt, mixed alkali effect 80−34219
Na_2O-B_2O_3-SiO_2 glass, phase separated, HCl leaching rate and microstruct. 79−29242
Na_2O-CaO-Bi_2O_3-SiO_2, electro-conducting glass-ceramic production by ion-exchange and reduction treatment 79−1616
Na_2O-GeO_2(TiO_2)(SnO_2)(ZrO_2)(ThO_2)-SiO_2 glass, density, refractive index, thermal expansion, hardness IR spectra, DTA *(Japanese)* 78−15535
$Na_2S_2O_3.5H_2O$, glass transition, theory 77−84890
NiPBAl, metallic glass, viscous flow, alloying effect 78−79793
$(Ni_5Pd_5)_{82}P_{18}$ amorphous alloy, glass transition temp. 77−84909
PVF_2, film, static and dynamic pyroelectric coeffs. from 90-370K 79−99827
PbO containing crystal glass, viscosity-temp. depend., glass transition, and softening point 80−24637
PbO-B_2O_3, solder glass, thermal reduction of Cu^{2+} and Cu^+:Cu^{2+} effect on thermal props. 78−15350
Pd-Ni-P, metallic glass, viscous flow, alloying effect 78−79793
$Pd_{0.775}Cu_{0.06}Si_{0.165}$, undercooled metallic melt, viscous behaviour 77−66037
$Pd_{77.5}Cu_6Si_{16.5}$ metallic glass, diffusion of Au 78−55983
$Pd_{77.6}Cu_6Si_{16.5}$, metallic glass, viscosity meas. from rates of thermal transformations 78−26713
$Pd_{48}Ni_{32}P_{20}$, metallic glass, viscosity meas. from rates of thermal transformations 78−26713
$Pd_{80}Si_{20}$, amorphous, structural changes with neutron irrad., X-ray scatt. obs. 80−33898
Pt-Ni-P, metallic glass, viscous flow, alloying effect 78−79793
$Pt_{45}Ni_{30}P_{25}$, metallic glass, viscosity meas. from rates of thermal transformations 78−26713
Se, amorphous, kinematic transform. study by DTA 79−27921
Se, amorphous, struct., DSC and X-ray diffr. expts. 78−22662
Se, amorphous film, dielec. activity obs. near glass transition temp. 80−75933

glass transition continued
Se amorphous films, structural relax., viscosity, creep, heat capacitors, and IR spectra meas. 79−42424
Se amorphous layers, dielectric relax. in glass transition range, ageing 79−82923
Se amorphous layers, substrate range depend. on dielec. relax. in glass transition temp. 79−69773
Se and Se-As, amorphous, dipolar activity at glass transition temp., AC method 77−66454
a-Se, hole form. energy, heating time and cooling rate depend. 79−41958
Se, vitreous, elastic coeffs. about glass transition temp. US study *(French)* 80−19865
Se:As, amorphous, pure and doped, photoelectronic preps. in glass transition region 79−4583
Se:As, amorphous film, dielec. activity obs. near glass transition temp. 80−75933
Se-Ge amorphous system, AC elec. cond., near T_g, temp. depend. 80−49791
SiO_2 fabric, structural stability rel. to brittleness, X-ray diffr. and IR spectrosc. studies 80−96634
SiO_2 vitreous fibres, relax. props. near glass transition interval 80−34137
SiO_2-Al_2O_3-MgO-TiO_2 glasses, internal friction during crystn. 79−52285
Te rich ternary chalcogenides, glass transition temp. predictions 78−38823
$Te_{80}Ge_{12.5}Pb_{7.5}$, phase-separated system, overlapping effects of glass transition and crystn., DSC results 78−83739
$Te_{80}Ge_{15}Pb_5$, DSC sensitivity to controlled ageing in glass transition region 80−71673
$Te_{80}Si_{20-x}Pb_x$ glasses, phase separation, double T_g presence 80−88306
Tl-Ge-S system, glass forming 80−19716
$TlAsS_2(Se_2)(Te_2)$, elec. cond. and thermopower in solid and liquid states 77−89764
$TlPO_3$, vitreous and polycrystalline, NMR and IR exam. of cation motion 77−66041
$ZnCl_2$, liq., glass, cryst., sp. ht. meas., glass transition temp. rel. to press. 77−66029

glasses *see glass*

glassy state *see vitreous state*

glide, dislocation *see slip*

globular star clusters
absorption-line strengths, comparison with elliptical and S0 galaxies 80−4430
age and chemical comp. determ., review *(Polish)* 78−61751
age and distance determ. using subdwarf photometry results 80−82435
age differences 79−80340
ages, effects of He settling in low mass stars 80−73013
ages and composition, rel. to fundamental knowledge about galaxies evolution 80−90488
AM-1, possible intergalactic globular cluster, description 79−25651
AM-2, possible faint globular cluster, description 79−25651
ANS UV obs. in 1550-3300 Å range 77−91598
asymptotic giant branch stars in globular clusters, spectra 79−8913
axial ratio and major axis position angle, UBVR obs. 77−17642
binary stellar systems, tidal disruption and coalescence 78−93330
black hole, stellar distrib. Fokker-Planck eqn. 79−21364
black hole ang. momentum reduction by star capture 77−29874
black holes, central, self-consistent potentials for dynamical simulations 80−26915
black holes rel. to gamma- and X-ray bursts *(Russian)* 77−17721
blue horizontal branch clusters, ANS far UV photometry 79−71080
blue stragglers rel. to anomalous Cepheids 77−45451
brightness and density distrib., two parameter generalised isochronous models 80−67807
capture by galactic nuclei, as result of dynamical friction 78−16547
ω Centauri, ω a absorption and effective temp. of giants 80−51749
ω Centauri, anomalous giant branch rel. to abundance vars. in dwarf spheroidal galaxies 79−5904
ω Centauri, anomalous horizontal branch rel. to clusters RR Lyrae stars period-amplitude relation 79−67019
ω Centauri, Ca abundance of RR Lyrae variables 79−16962
ω Centauri, cluster membership determ. for V65 and V78 78−73743
ω Centauri, eclipsing binary V78 light curve anal. in freq. domain by automatized Fourier technique 80−22039
ω Centauri, giant stars blanketing differences 80−4345
ω Centauri, JHK photometry, giant branch spread 78−16476
ω Centauri, near IR photometry, giant branch struct. 77−41397
ω Centauri, near IR photometry anomalous giant branch 78−16477
ω Centauri, search for new variables 78−61895
ω Centauri, SEC Vidicon photometry of main sequence 80−90491
ω Centauri, spectroscopic obs. of RR Lyrae variables 79−5824
ω Centauri, UBV photometry of RR Lyrae stars 78−73719
ω Centauri giant branch, mixing versus primordial abundance vars. 77−17640
ω Centauri region, faint filamentary nebulosity obs. near globular cluster 80−56914
centre regions, stellar collisions, binary star components periodic collisions 78−8061
classification, physical mechanism for Oosterhoff dichotomy 77−78837
close binaries and the evolution of star clusters 79−5863
close binary stars, incidence rel. to nature of cluster X-ray sources 77−41396
close binary stars form. by two-body tidal capture 77−33556
close binary systems in globular clusters, possible existence 79−44530
colour-magnitude diagram, rel. to subdwarf stars thirteen-colour photometry 79−92767
core collapse, theory 79−84829
core collapse of spherical cluster, approx. theory 78−49486
core evolution, effect of gravithermal catastrophe 80−67804
cores evolution, life and death matters 79−25653
death rates, present and past 78−28733
diffuse object, detect., in galactic centre direction *(French)* 79−8959
distance determ. south of $\delta = -22°$, 77−26030
distribution and consumption rate of stars around massive collapsed object 77−45497
distributions in M31 and Galaxy 79−12513
dust patches, UBVR photometric obs. 78−81662
dynamic evolution, review of obs. and numerical theories 78−77585
dynamical evolution, Fokker-Planck eqn. numerical integration 80−36675

globular star clusters continued
dynamical evolution test computations 77−49445
dynamical evolution with changing gravit. const. 79−17030
dynamical nonlinear stability of spherical stellar systems 80−31336
dynamics during gravit. encounters between Local Group galaxies 77−57098
E3 (ESO-037-SC 01) dying globular cluster, photometry and stellar content rel. to tidal truncation 80−105291
element abundance survey 77−87489
ellipticities of RR Lyrae star systems 77−60805
equilibrium statistical mechanics of gravitating systems with energy cutoff 78−93326
equilibrium statistical mechanics of relativistic systems with energy cutoff 78−93327
Eridanus, faint stellar system discovery on ESO Schmidt plates 78−20887
evolution and origin of galactic halo stars 79−58388
evolution of ellipticities 77−13406
evolution rel. to three-body gravitational scattering 79−44344
evolutionary structure of large star clusters 79−48866
extraterrestrial intelligence, search of OH and H_2O lines 80−56725
flare stars, large-scale winds driven by mass loss, effects on interstellar matter 78−32464
formation and evolution 77−26031
galactic, colour excess ratio, rel. to interstellar absorpt. law 78−28797
galactic, orbital evolution due to dynamical friction 78−24529
galactic, radial motions rel. to galactic halo model 79−67068
galactic, UBV colour-magnitude diagrams, catalogue bibliography 78−24531
galactic bulge, ages rel. to RR Lyrae stars spectra 77−26012
galactic centre region, clusters expected number density 78−32535
galactic centre region, globular clusters IR studies 80−82434
galactic disc clusters, removal by dynamical friction 79−35367
galactic gas-to-dust ratio determ. from globular cluster obs. 79−88747
galactic globular cluster system flattening, interstellar extinction effects 79−48908
galactic globular clusters, basic morphological data 79−92815
galactic globular clusters, basic parameters 77−91593
galactic globular clusters, orbital eccentricities 77−71132
in Galaxy, number of clusters *(Russian)* 79−17036
gas flow, time-dependent flow models 78−12304
gas flow and contents, numerical study 80−8666
gas outflow models including photoionisation 78−93338
GCl 0422−213, distant globular cluster in Eridanus, preliminary photometry and spectroscopy 80−17624
giant branch slope, parametric approach 77−53649
giant stars, Ca II H and K-lines and abundance 80−72940
giant stars, cluster membership determ. via photoelectric MgH+Mgb index 80−12753
gravothermal catastrophe enhancement in two-component isothermal spheres 78−4297
gravothermal catastrophe of finite amplitude 79−2476
halo cluster compositions and galactic halo formation 79−5898
heavy element abundances in galactic halo, radial gradient 79−92857
Hodge 11, in LMC, colour-magnitude diagram, metal abundances 78−69850
horizontal branches extent, role of forced mixing at He shell flash 80−56818
horizontal-branch A-type stars, astrophysical parameters determ. 79−62829
hot horizontal branch stars, theoretical B−V colour indices and bolometric corrections 79−58327
IC 4499, periods and light curves of RR Lyrae stars 79−44490
inhomogeneous spherical gravitating systems dynamics, simplest hydrodynamic models 80−17620
integrated colours, of globular clusters in the Galaxy, Fornax and (M31) 78−16469
integrated IR photometry, colours and interstellar reddening 80−67575
integrated IR photometry and wide field techniques 80−67574
integrated IR photometry using wide field photometer 80−62029
intermediate-mass stars asymptotic giant branch evolution as function of mass and comp. 80−12749
interstellar reddening in direction of low latit. clusters 77−22299
isothermal cores, stability limits 80−46622
isothermal two-component clusters, equilib. series and secular stability 79−48870
kinematic and dynamical differences between two groups 78−8069
Kron 3, SMC globular cluster, identification with X-ray source (4U 0026−73) 79−5919
late core collapse in gravitating systems, theory 80−22048
late-type stars, He abundance effects on spectrum appearance 80−46540
Liller 1, optical candidate for X-ray burster MXB 1730−335, IR bursts detect. 79−44640
Liller 1 (=MXB 1730−335), unsuccessful search for IR bursts 80−98740
Liller I (MXB 1730−333), unusual burst in K-band (2.2 μm) 80−62319
LMC, instrumental colour-magnitude diagrams for 24 stellar clusters 77−22279
luminosity as extragalactic distance indicators 77−91641
luminosity distr-bution of clusters in M31 80−36708
RR Lyrae pulsators as He indicators 80−51778
RR Lyrae stars, transitional period-luminosity depend. 77−53614
in M104 galaxy, radial distrib. and total number 77−74140
M10, M12 , M71, M92, radial vels. from meas. of stars in fields 78−41004
M10 and M12, obs. star distribs. rel. to gravitational disturbance 78−69849
M13, astrometric cluster membership probabilities from old proper motions 79−88708
M13, astrometric obs. for stellar proper motions and membership probabilities 79−75252
M13, Calculated and observed integral magnitudes comparison 79−97043
M13, central region, colour-magnitude diagram 77−53656
M13, curve of growth anal. of L973 red giant star 79−48796
M13, globular cluster, two colour photographic photometry of variable stars 77−87492
M13, M92, M15, globular clusters, weak G-bands in giant stars 77−78778
M13, photometric investigation of red variable stars 77−74104

globular star clusters continued
M13, search for faint nearby radiosources 78−32531
M13 red giants, proteocluster gas inhomogeneities from Na abundance var. evidence 80−82439
M15, BVR area photometry 78−85983
M15, dynamical models without black hole 78−32536
M15, faint stars photometry rel. to main sequence intrinsic width and luminosity function 77−78834
M15, globular cluster, Kustner 1082, hot ultrashort period Cepheid *(Chinese)* 77−67096
M15, globular cluster, obs. of hot ultrashort period Cepheid *(Chinese)* 77−71121
M15, globular cluster, optical struct. of core 77−13412
M15, globular cluster, search for radio emission from ionized H 77−13410
M15, low Ar abundance meas. in planetary nebula (K648) 80−82443
M15, member star K1082 suspected ultrashort period variable star 80−26883
M15, nucleus brightness profiles of X-ray globular cluster 78−69848
M15, surface brightness distrib. from electronographic obs. 78−85981
M15, X-ray globular cluster, search for O III 5007 Å forbidden line emission 78−36644
M15 core, Hα and continuum obs. 79−17031
M15 core, variable emission line star obs. 79−5840
M19, photograhic obs. of Population II Cepheids and RR Lyrae stars 78−41002
M22, blue variable obs. 78−85945
M22, Ca abundance of RR Lyrae variables 79−16962
M22, CH star obs., CH and Cn anomalies 78−8001
M22, CO in IR spectra of III-106 CH star 80−62131
M22, comparison with ω Centauri, spectroscopic evidence 80−46617
M22, globular cluster, light curves of red variables 77−64808
M22, membership and other problems 78−32537
M2 (NGC 7089), faint stars photometry and colour-magnitude diagram 80−101623
in M31, colour excesses rel. to galaxy gas-to-dust, ratio 78−8120
M31, former globular clusters considered as H II regions *(Russian)* 80−31347
M31, globular clusters colour indices, rel. to interstellar absorpt. law 78−28796
M31, identification of H II regions and distant galaxies previously considered as globular clusters *(Russian)* 78−12370
M31, search for globular clusters in disc and minor axis fields 78−32568
M31, UBV photometry of star clusters 79−62879
M33, identification of star clusters, list of 58 candidates 79−9002
M3, dynamical study based on photoelectric radial vels. of individual stars 79−75251
M3, globular cluster, luminosity function 77−57069
M3, globular cluster, RR Lyrae stars multiperiodic vars. 77−87430
M3, inner structure, photoelec. scanning method *(Italian)* 78−93343
M3, M13, M15, UBVR photometric obs., dust patches 78−81662
M3, M5, M13, M15, equidensity curve meas. *(Russian)* 79−97041
M3, stellar proper motions, membership and cluster internal motions 80−8665
M3 and 13, abundances in cluster red giants 78−93334
M3 H-R diagram compared with southern high-velocity stars 79−25600
in M49, giant elliptical galaxy, globular clusters space distrib. 78−93393
M4, globular cluster, colour-magnitude diag. 77−37629
M4, globular cluster, UBV photometry of RR Lyrae stars 77−78802
M4, metal abundances of RR Lyrae stars 79−58351
M4, variable star discoveries *(Chinese)* 80−77418
M53, search for faint nearby radiosources 78−32531
M55, globular cluster, colour-magnitude diagram 77−64812
M5, globular cluster, bright variable star obs. 77−91590
M5, M13, M3, giant stars chemical comp. 80−67695
M5, proper motions, membership and internal motions 80−41864
M5, spectroscopic survey of giant branch 78−16467
M5 (NGC 5904), intermediate band electronography of red giants 78−49490
M69, metal-rich globular cluster, photometric calibration 77−91592
M71, giant stars IR colours, CO band strengths and physical parameters 79−25650
M92, C abundances in red giant stars 79−48785
M92, globular cluster, age difference from old open cluster (NGC 188) 77−56912
M92, globular cluster, C and N abundance variations in horizontal branch 77−87495
M92, globular cluster, giant star C and N abundances 77−87496
M92, globular cluster, membership and internal motions 77−17634
M92, globular clusters, luminosity function 77−57068
M92, M15, abundances in clusters red giants 79−92759
M92, struct., automated plate reduction techniques 77−41394
M 15, globular cluster, period behaviour of RR Lyrae stars 77−45444
M 15, nature of emission-line variable in cluster core 80−77458
Magellanic Clouds, masses determ. for globular clusters 79−5867
Magellanic Stream origin 77−91648
mass loss from stars 78−93238
mass-energy-mean density relationship of dust-poor stellar systems 80−22049
massive black holes, dynamical evolution 78−4302
massive black holes, stellar density cusp 78−4303
metal abundance and reddening from photometry obs. 80−67800
metal abundances, rel. to galactic populations and Galaxy evolution 78−96545
metal-poor-stars, spectral energy distrib. and Fe/H ratio 78−53937
metal-rich, near IR photometry 77−45503
metal-rich horizontal branch stars, evolution 77−45466
metallicity effects on integrated colours, calibration 78−89227
metallicity function *(Russian)* 78−28732
Mira variables around globular clusters, freq. distrib., cluster membership 80−36676
models, props. based on stellar evolution and cluster structure 80−62210
MXB 1730−33 X-ray burster, possible optical counterpart 77−33694
MXB 730−335 X-ray source association, IR obs. 77−9776
N-body calculations, statistical results depend. on N 79−80339
N-body spherical system, stellar consumption rate by black hole *(Russian)* 77−91562
NGC 1261, colour-magnitude diagram 80−17623
NGC 1261, globular cluster, Oosterhoff type I system, variable star obs. 77−53651
globular star clusters continued
NGC 1851, 6624, abundance gradients spectroscopic investigation 80−82437
NGC 1851, globular cluster, radial vel. of evolved star UV5 as X-ray source candidate 77−74158
NGC 1851, Hα absorption of UV5 and core 78−61896
NGC 1851, H I detect., 21 cm line obs. 78−45368
NGC 1851, He abundance determ. for star UV5 78−49441
NGC 1851, NGC 1904, globular clusters, radio and X-ray obs. 77−26028
NGC 1851, periods and light curves for 19 RR Lyrae variables 78−73714
NGC 1851, unsuccessful search for H I 79−5873
NGC 1851, X-ray globular cluster, central region struct. 77−45501
NGC 1851, X-ray globular cluster, UV energy distrib. from OAO photometry 80−73009
NGC 1851 and 6441, globular clusters, X-ray bursts sources, SAS 3 obs. (1977, July and August) 77−74160
NGC 1852, red globular cluster in LMC, planetary nebula obs. 77−17668
NGC 1854, LMC blue globular cluster, photographic photometry 77−74107
NGC 1868 in LMC, BV photometry of metal-poor intermediate-age cluster 80−51814
NGC 188, old open cluster, age difference from globular cluster (M92) 77−56912
NGC 1904, globular cluster, BV photometry 77−13415
NGC 1904 (M79), UBV photometry, colour-magnitude diagram 78−32528
NGC 2209, LMC cluster, metal abundance 78−8122
NGC 2298, globular cluster, variable stars photometry 77−13353
NGC 2419, globular cluster, variable star obs. 77−60804
NGC 2420 and 47 Tucanae comparison rel. to galactic evolution 77−45499
NGC 2808, photoelectric UBV and DDO photometry 78−45369
NGC 3201, globular cluster, BV photometry 77−2458
NGC 3201, globular cluster, UBV photometry of bright stars 77−60803
NGC 362, globular cluster, BV photometry 77−13416
NGC 419, in SMC, nearby C- and M-type stars, cluster membership 80−26921
NGC 419 in SMC, C star content 78−53962
NGC 4590, metal poor globular cluster, BV photometry 77−64813
NGC 5053, haloglobular cluster, photometric study 77−74103
NGC 5128 (Centaurus A), globular clusters deficiency 80−26986
NGC 5272 (=M3), discovery, V mags. and spectrum 79−71050
NGC 5272 (M3), novalike object photometry and identification as W Virginis variable 79−75224
NGC 5286, B photometry of variable stars, cluster membership 78−32534
NGC 5824, assoc. with bright transient X-ray source Centaurus XR-4 78−12420
NGC 5927, metal rich cluster, colour-magnitude diagram 80−36678
NGC 5946, 6440, 6624 fields, UBVR photometric sequences 79−88702
NGC 5986, obs. of variable stars, periods and light curves 79−5868
NGC 6121 (M4), near IR photometry of metal-poor globular clusters 77−41398
NGC 6121 (M4), RR Lyrae stars UBV photometry 80−22018
NGC 6144 and neighbouring region, photometric obs. 80−51816
NGC 6224, X-ray globular cluster, photometry of nucleus 77−37628
NGC 6235, colour magnitude diagram, BV photometry 80−90483
NGC 6256, probable galactic globular cluster, BV photometry 78−77583
NGC 6266, colour magnitude diagram, distance and metallicity 78−61894
NGC 6356, photometric obs. of Mira variables 78−32530
NGC 6366, metal-rich globular cluster, colour magnitude diagram 77−5462
NGC 6397, age from main sequence turnoff, BV photometry 80−90484
NGC 6397, C abundances in red giant stars 79−48785
NGC 6397, globular cluster, metal poor late-type stars and early A-stars, radial vels. 77−17638
NGC 6397, globular cluster weak G-bands in giant stars 77−78778
NGC 6397, metal-poor globular cluster, BV photometry of 399 stars 77−82292
NGC 6397, vel. dispersion meas. using TV detector and cross-correl. techniques 78−16305
NGC 6401, globular cluster, discovery of nearby faint planetary nebula 77−49461
NGC 6440, 6541, 7099, surface brightness, star density and colour profiles 80−12783
NGC 6440, surface photometry of cluster core 80−82436
NGC 6522, nearby Population II Cepheid, dist. 80−82396
NGC 6528, globular cluster, colour-magnitude diagram for field stars 77−87483
NGC 6528, metal-rich globular cluster, colour-magnitude diagram from UBV photometry 80−4406
NGC 6535, photometric study of variable stars 78−32529
NGC 6541, UBV photometry, metallicity and distance 79−35316
NGC 6584, new variable stars 80−62137
NGC 6624, globular cluster, binary star model for X-ray source 3U 1820-30 77−33701
NGC 6624, globular cluster, recurrent X-ray bursts from 3U 1820−30 77−60806
NGC 6624, optical counterparts of X-ray burster in core 80−67801
NGC 6624, optical studies of X-ray source 78−93335
NGC 6624, UBV photometry of X-ray globular cluster 78−93337
NGC 6624 (3U 1820-30), globular cluster, optical, IR and X-ray obs. 77−45498
NGC 6638, Mira and RR Lyrae variable obs. *(French)* 78−16475
NGC 6656, metal-poor globular cluster, BV photometry of 374 stars 77−82291
NGC 6712, X-ray globular cluster, identification with Ariel 1850−08 77−13414
NGC 6717, colour-magnitude diagram, distance and metallicity 80−46624
NGC 6752, blue horizontal-branch stars photometry 78−49488
NGC 6752, evidence for white dwarfs 78−93233
NGC 6752, first giant branch, C/N abundances 80−67719
NGC 6752, main sequence form UBV photometry 79−71079
NGC 6934, variable stars photometry 80−56891

globular star clusters continued
NGC 7078 (M15), X-ray globular, spectra of two-hour variable UV-bright star (M15-K1082) 79−88681
NGC 7099, metal-poor globular cluster, UBV photoelectric photometry 78−77584
Pal 12, metal-rich globular cluster in outer galactic halo, optical and IR obs. 80−105290
Palomar 10, discovery of 123 new Mira variable stars 78−40837
Palomar 2, distance and structural props. 80−62213
Palomar 5, remote globular cluster in galactic halo, chem. comp. 77−87482
periodicity investigation at 21 cm 80−82529
perturbations of spherical cluster in general relativity, variational principle 79−53860
planetary nebulae, detection rates in globular clusters 80−26950
Pleiades, flare star spatial distrib. using recovery method *(Russian)* 80−94722
populations uniformity 77−53654
pre-horizontal branch evolution and Oosterhoff dichotomy in globular clusters 78−69784
prestellar gas, element separation by gravitational diffusion 79−21386
primaeval entropy fluctuations and gravit. clustering 78−28867
radial colour distributions, integrated UBV photoelectric photometry 79−25648
radio continuum obs. at 2.7, 4.8 and 10.7 GHz 80−101619
radio sources in globular clusters, optical identifications 79−62923
radiosources detect. in globular cluster fields 79−17114
radiosources obs. 77−87484
relaxation degree and evolution, appl. of N-body system numerical integration 80−67808
Reticulum, structure, star counts 78−12309
six-colour photometry rel. to interstellar reddening and metal abundances 77−13407
SMC, atlas of variable stars, clusters, emission regions and supergiant stars, book 79−44619
SMC, UBV photometry of open, intermediate and globular clusters 79−17033
SMC star cluster colour magnitude diagrams and stellar identification charts 80−73014
southern clusters, surface-brightness profiles rel. to struct. and stellar content 79−71078
southern globular clusters, gas content upper limits 80−22047
space distrib. 77−87481
space distribution, rel. to dynamics and galactic struct. 79−2560
spatial distrib. of stars, recovery method *(Russian)* 80−94722
spatial struct. rel. to distance to galactic centre 77−37625
spherical stellar system, distrib. of stars around massive central black hole 78−65660
star counts 77−33578
star density distribution of red and blue globular clusters of LMC 79−92811
star distrib. around massive black hole for unequal star masses 78−8062
statistical mechanics of gravitating systems 79−35311
steady state distrib. of stars near massive compact body *(Russian)* 78−16481
steepest descent technique and stellar equilibrium statistical mechanics, stability 78−65659
stellar evolution in horizontal and asymptotic branches 78−81613
stellar systems with continuous mass spectrum, necessary condition for equilib. 78−93328
stochastic tidal disruption 78−12303
strip photometry application, multicolour obs. 78−89229
structural parameters and integrated magnitudes 80−46623
structure, automated plate reduction techniques 77−41394
structure and content 77−91597
subcritically accreting black holes, model for X-ray sources in globular cluster cores and X-ray burster sources 80−12779
subsystem space distrib. and population in Galaxy 77−53689
Terzan 2, identification with X-ray burst source XB 1724−31 79−5919
theoretical isochrones, tables 79−71081
theoretical isochrones with decreasing gravit. const., Dirac's multiplicative cosmology 78−16586
thermodynamic equilibrium states, frozen in pot. waves 79−67070
tidal disruption of galactic globular clusters, rel. to clusters mass function and space distrib. 80−105294
tidal radii, limiting radii of direct and retrograde satellite orbits 79−88572
time independent flow models 77−37624
47 Tucanae, abundance gradients from spectroscopic obs. 79−40228
47 Tucanae, C and N abundances of red giant stars 79−97000
47 Tucanae, chemical comps. of stars 80−46620
47 Tucanae, colour-magnitude diagrams for inner regions 78−57598
47 Tucanae, cyanogen distrib. in red giants 79−71025
47 Tucanae, globular cluster, UBV photometry 77−37630
47 Tucanae, membership and metallicity of three RR Lyrae stars 80−62206
47 Tucanae, metal-rich globular cluster, UBV photometric study 77−57065
47 Tucanae, N anomaly anal. 79−48867
47 Tucanae, spectral inhomogeneities in faint stars 78−93340
47 Tucanae (NGC 104), CN vars. in upper main-sequence stars 80−94794
two component Emden sphere model, theory 80−22045
UBVI colour excesses 77−13417
W Ursae Majoris metal-poor systems, evolution to globular cluster ages 79−25628
UV energy distributions of galactic globular clusters, Orbiting Astronomical Observatory photometry 80−73009
UV spectroscopic meas., central surface brightness distribs. 79−67067
(V-K) colour rel. to metal abundance 77−87485
variable stars in clusters, problems 78−81641
in Virgo cluster of galaxies, distance modulus 77−74149
in Virgo cluster of galaxies, globular clusters luminosity distrib. 78−12308
Virgo galaxies globular clusters, luminosity function and Hubble const. new determ. 79−92902
white dwarf formation rate 80−4346
white dwarfs formation rate 78−28674
winds, nova-driven, rel. to intracluster gas Hα emission 78−57596
in WLM galaxy (A2359), BV photometry and absolute magnitude 77−82302
globular star clusters continued
X-ray binaries in dense stellar clusters, dynamical effects 79−97098
X-ray burst sources, identifications with globular clusters 78−12427
X-ray burst sources, massive central black hole model 78−49566
X-ray burst sources in globular clusters, neutron stars hypothesis *(Russian)* 78−16480
X-ray bursts, effects of thermal limit for spherical accretion 78−45430
X-ray obs. with ANS 77−26029
X-ray source, evolution of 100 M⊙ black hole in binary 78−61932
X-ray source, locations 79−97102
X-ray source formation by collisions of compact and normal stars 78−28854
X-ray source globulars, UBV photometry 78−16468
X-ray sources, appl. of QSO black tide model 77−78884
X-ray sources, equatorial positions determ. 80−105292
X-ray sources, long-term variability 79−2579
X-ray sources, models 78−81706
X-ray sources in globular clusters, review 78−12428
X-ray sources obs. in M31 80−26979
X-ray stars in globular clusters 78−20916
zero age horizontal branch stars, expected location 78−77551
C stars in red globular clusters in Magellanic Clouds 79−101143
CH star content, possible binary nature 80−82355
CN strengths and UV excesses of evolved stars from DDO photometry 77−64753
CNO burning and zero age horizontal branch stars location 78−12201
CO and JHK photometry, comparison with E and S0 galaxies 78−36684
CO in giants in globular cluster, IR obs. 78−93339
$^{12}C^{16}O$ emission, unsuccessful search at 2.6 mm wavelength 78−41000
Fe/H abundances of extreme Population II stars in globular and dwarf galaxies 78−40939
H II in cores, evidence 78−8065
H II optical search 78−12305
H_2 mass upper limit from CO 2.6 mm transition obs. 79−17029
H_2O maser emission search 79−30094
He abundance in galactic globulars 78−45370
He abundance var. 80−56894
OH main line emission from globular clusters, high sensitivity search 80−62207
TiO band strengths in metal-rich clusters 78−49487
TiO band strengths in metal-rich clusters, reddening and metallicity determ. 79−40227
glossaries
dictionary of astronomy, book 80−22151
dictionary of physical sciences 77−41428
fibre-optic technology for interconnection designers 78−46800
geological terminology (3 vols.) *(Russian)* 80−22150
geology 78−88833
mass spectrum dictionary for library searching 79−89031
solar and solar-terrestrial physics, illustrated glossary 78−57537
speech understanding system, structure of lexicon 79−64422
glow discharge lamps *see discharge lamps*
glow discharge microphones *see microphones*
glow discharges
Abel's integral eqn., least squares finite element method appl. 79−25830
abnormal, positive ion kinetics in cathode fall 79−14626
adhesive bonds breaking under high vacuum, light and electron emission, spectral comp. obs. 80−55190
air, DC point-to-plane elec. discharge, temp. patterns, Michelson interferometry 80−54061
air, domain instability, average velocity and disappearance time estimation 80−44062
air, effect on nucleation characts. of Au on polymer substrates 79−77963
air, flowing, negative ion density increase with press. 80−28821
air, glow discharge plasma, electron energy balance 77−43092
air, non-self-sustained discharge plasma ionisation instability obs. 78−71609
air flow glow discharge, voltage, current oscills. 79−55585
air flow with transverse mag. field 78−71562
air glow plasma, X-band heterodyne generation by microwave mixing 77−35391
anomalous glow discharge Faraday dark space, electron vel. distrib., Langmuir probe meas. 80−44040
anomalous glow discharge transition to nozzle hollow cathode discharge 78−67531
atmospheric positive streamer corona, primary wave emission, secondary electron emission 80−44008
atom-ion collisions, in hollow cathode discharge, limit angle, corpuscular diagnostics 79−55454
atomic and ionic spectral line excitation in cathodic region *(Russian)* 78−63611
atomic fluorescence spectrometry, hollow cathode lamp, pulsing conditions optimisation 78−65972
attachment instability suppression by rot. elec. field 79−64954
back discharge, flashover meas., streamer or steady glow mode, dust layer effects 78−59708
benzene, junction barrier, inelastic electron tunnelling 77−72916
benzene, plasma polymerisation in glow discharge, thin film IR and free radical EPR obs. 80−2964
breakdown, temporal development of electrode pot. 80−44003
breakdown and extinction, tube wall role 80−44002
butane RF plasma, initial etching prior to deposition of C 79−66224
cathode, hollow, in Ne and He *(Russian)* 80−28856
cathode fall, steady one-dimens. microscopic theory *(French)* 78−1930
cathode region microscopic model 78−67524
cathode spot excitation, dielectric stimulator, pulsed gas discharge switch 77−19802
cathode surface heating by high pressure glow discharge, catastrophic bridging 78−87574
cathodic sputtering atomisation for AAS 78−44415
characteristics meas. for sputtering appl. 78−72726
cleaning effectiveness rel. to base material atomisation rate *(Russian)* 80−20797
CO, in glow flow discharge, electronic states, excitation mechanism 80−53040
constricted discharge in transverse air flow 80−24278
corona in atmosphere, review 78−26363
corona to glow discharge transition mechanism, morphologic discussion 79−99014

glow discharges continued
crossed field tube for high power on-off switching 77−24222
crossed-field type, electron energy distrib. diagnostics 79−27851
Cu^+ hollow-cathode laser, IR output depend. on He-Ar press. ratio 80−48223
current transport at the surface of a hollow cathode, current distrib. technique 80−54048
current-voltage characteristics, in longit. mag. field 78−18471
current-voltage characts. in narrow capillaries 80−1871
cylindrical hollow cathode negative glow, fast electron angular distrib. obs. 78−67529
cylindrical hollow-cathode discharge, optimum press., discharge parameters effects 77−55194
DC, time-depend. cataphoretic gas separation with end volumes 80−79603
DC and UHF field energy transfer to glow discharge plasma electrons 78−67539
DC glow discharge in tube with walls of different catalytic activity 80−100103
detector for millimeter rad., cyclotron reson. effect on sensitivity 78−62222
diagnostics, instantaneous triple-probe method for direct display of plasma parameters in low density continuum plasma 80−84000
diagnostics with electric probes, sputtering appl. 78−71537
diatomic molecular gas, electronic excitation rate, vibr. temp. influence 80−19633
dielectric surface creep discharge photon intensity rel. to charge transport 78−67561
diffuse discharge, HV, anode drop meas. in transverse air flow 77−39483
diffusion welding, surface treatment by glow discharge effect 78−7089
Earth, electrochemical glow discharge and aerosol anomalies before earthquakes 79−16407
edge structure of laterally spreading short glow discharges 80−59328
electrolysis, power supply unit, current regulator 77−39489
electron beam generation, pulsed, high power, gas dynamics appl. 78−63515
electron beam welding, of Al alloys, appl. 79−73052
electron collision rates and distribution functions in O_2 glow discharge 79−10631
electron gun, cold cathode, for pulsed ionisation of high-pressure CO_2 laser 79−27269
electron gun, glow-discharge type, with plane-frustrum cold cathode, charcts. 79−7495
electron gun use of glow discharge lamp for Auger spectroscopy 77−31027
electron temperature in glow discharge in transverse mag. field, spectrosc. method meas. 80−87855
electron velocity distribution function, obs. 77−76236
electron velocity distribution function relax., periodic behaviour in highly modulated elec. field 79−64935
electron-beam-sustained discharge, plasma contraction by mag. field of current 80−100115
electronegative gas glow discharge, plasma instability boundary conditions *(Russian)* 80−38739
EM MM-wave detection properties, in mag. field 80−70059
emission spectrometry, current developments *(Japanese)* 78−86356
ethylene, junction barrier, inelastic electron tunnelling 77−72916
ethylene plasma polymerisation by magnetron discharge 79−33995
externally maintained, by intense electron beam, N_2 oxidation, collective interaction 79−32841
flat discharge with convective cooling, plasma column thermal instability 77−24232
fluorocarbon, plasma polymerising and etching, mass spectrometric obs. 77−32790
forward ionisation waves rel. to acoustic phenomena 78−75282
furnace, DC glow discharge, for high-rate carburizing of automotive components 79−83370
fusion plasma experiments, vacuum developments 79−63260
gas discharge, magnetron geometry, mag. field and press. effects 77−43090
gas gap subject to pulsed ionising radiation, volt-amp characts. 78−51377
gas mixture, self sustained volume photoionisation discharge existence conditions 80−79610
gas temp. meas. in glow discharge in capillary using thermocouples *(Russian)* 78−59694
gas temperature measurement from mol. emission spectra in glow discharge 79−55558
gaseous inclusions in insulating solid, elec. strength and degradation 78−83631
glass substrate, glow discharge effect on surface props. and struct. 78−85201
glass-electrodes, glow discharge tube 80−33834
glow discharge detection, gas breakdown theory 78−58035
glow polymerisation, thin organic polymer coating technique *(German)* 77−12774
graphite hollow cathode glow discharge C conc. determ. 80−44032
Grimm lamp, glow discharge, for emission spectrographic anal. of binary alloys *(Japanese)* 79−99015
Grimm lamp structure and use in emission spectrochem. analysis of metals *(Japanese)* 78−27867
high current, stabilisation methods, used for diffusion bonding 80−38221
high press. probe meas., current-voltage characts. 79−90466
high voltage, in electron gun regime 79−86638
high-voltage flow discharge as electron gun 77−62428
hollow anode-cathode discharge, voltage, anode geometry and pot. effects 79−99017
hollow arc cathode, with highly ionised dense plasma, props. 79−64951
hollow cathode, glow discharge, current balance and secondary electron emission 80−75108
hollow cathode, state of equilib., spectroscopic meas. 80−19647
hollow cathode, with plane-parallel geometry, current and radiation mechanisms 78−18474
hollow cathode discharge, electron temp meas. 78−67445
hollow cathode discharge, H_2 prod. in H_2O vap. plasma 78−75441
hollow cathode discharge, with quadrupole mass filter, ion form. and handling 79−12878
hollow cathode discharges for gas lasers, review 80−99717
hollow cathode effect based on cathode fall theory 77−35413
hollow cathode effect with axial elec. field *(French)* 79−60209
glow discharges continued
hollow cathode gasdynamic jet carrying excited metal atoms as spectral light source and chemical reactor 79−46493
hollow cathode tube, high current metastable atoms production 80−10445
hollow sintered cathode spectral lamp *(Rumanian)* 79−17509
hollow-cathode discharge, external cathode type, morphologic study 79−60207
hollow-cathode discharge, in N_2, H_2 or Ar, ion mass composition 79−68969
hollow-cathode glow discharge, fast electron current, electrostatic vel. analyzer diagnostics 79−27856
hollow-cathode glow discharge with static stepped V-I characteristic *(Russian)* 78−75443
homopolar devices, rotation of DC glow discharge, Doppler shift of spectral lines 80−33838
HV, electrode surface effects 79−64955
HV, theory 80−19629
HV glow discharge as plasma electron source, charcts. 80−44031
HV pulsed discharge, electron beam production 80−9072
hydrocarbon cracking; C stripper foil irradiation lifetime 79−76249
illumination effects on electron distribution functions 78−34378
Inconel 625, nitriding in N_2-H_2 glow discharge 80−16590
Inconel 625, surface treatment of plane and hollow components in glow discharges 79−1923
inert gas, origin of visible continuum radiation, bremsstrahlung theory 77−62421
inert gas, striation current conditions 79−55595
inert gas halide lasers, e-beam sustained, glow discharge stability 79−55117
inert gases in U hollow cathode tube, time resolved optogalvanic effect 79−37564
infinite, dense gas homogeneity, theory 77−51253
initial value region for boundary value problem 77−39496
inorganic thin films, plasma-promoted deposition 79−78896
instability in N_2-CO_2, non self sustained ionisation source, mechanism 80−38819
intermediate pressure, voltage-current characts. 79−55604
ion etching device for SEM samples 80−82847
ion flux, strong mag. field, low press., double probe meas. effects *(German)* 77−31534
ion plating, evaporation sources, gaseous media, and transport modes 80−80984
ion plating, inert gas handling 79−69994
ion source using HF glow discharge, temp. and electron density profile meas. *(German)* 78−70221
ionic siliciding, diffusion layer prod. on Mo 78−23855
ionisation instability, stabilising effect of turbulent transport processes *(Russian)* 78−59698
ionisation overheat instability in alternating fields, h.v. pulse stabilisation *(Russian)* 78−91175
ionization-diffusion oscillations in glow discharge plasma, rel. to stepwise ionization 78−1927
ionizing waves, propagation 78−38565
Langmuir probe characteristics at low plasma densities, numerical analysis 78−63592
laser discharge stability, high-power mol. laser, book contrib. 77−50650
lasing, in glow discharge, excitation freq. calc., electron upflux, book contrib. 77−50648
lateral propagation mechanism and velocity of anomalous discharge 79−82111
lateral spread of short glow discharges 79−46501
LEP, electron positron storage ring, vac. chamber, glow discharge surface cleaning 80−58010
light sources, reproducibility for emission spectroscopy 78−3429
low press. discharge, attractive forces on electrodes 80−49041
low pressure plasma system, design and operating characteristics 79−64880
magnetoplasma column in waveguide, wave packet bifurcation 77−7556
Mars, dust clouds and frictional generation of glow discharges 77−78708
mass spectroscopic source combination with quadrupole mass filter for solids anal. 78−61075
metal ion lasers, hollow cathode 80−99708
metal vapour production by sputtering in hollow-cathode discharge 80−1868
metals, H permeability, general transport eqn. 80−54426
methane, ion-molecule reactions in glow discharge, mass spectrometric obs. 78−63627
MHD gas movement near anode spots 80−1869
microarc atmospheric pressure glow discharge, operating characts, obs. 79−82106
molecular discharge, externally sustained, thermal instability 77−58915
molecular discharge heat instability mode, mol. relax. vel. const. determ. *(Russian)* 78−5959
molecular gases, non-self sustaining discharge for CW laser excitation, review 78−42849
molecular-gas discharge in a rotating electric field 79−77444
moving striations, phenomenological model including external cct. 79−19113
negative glow plasma, contact electrode charging time meas. 78−67525
nitrided steel surface wear-related topography 78−60847
non self-sustained, detachment process effects 78−59713
nonequilibrium plasma chemical reaction kinetics 78−76863
nonselfsustained, comp. and stability, peeling-off, ionisation and recomb. effects *(Russian)* 77−11414
PDX vacuum vessel, glow discharge conditioning 80−79607
periodically pulsed, theoretical model of cataphoresis 79−34313
phototube, gas-filled, rise time spectral depend., appl. to EM radiation detector miniaturisation 78−86318
plasma, corpuscular diagnostic method of metastable atoms, review *(Czech)* 80−24241
plasma, non-LTE, props. and at. processes, medium to high press. 80−59170
plasma, optogalvanic effect analysis using rate eqns. in modified Schottky formalism 79−23421
plasma diagnostic techniques appl. to glow discharge characterisation 78−71536
plasma etching and plasma deposition, glow discharge phenomena 79−69993
plasma etching characts., effect of dark space in RF glow discharge 79−15830

glow discharges continued
plasma line emission intensity calc. and meas. 78−67526
plasma polymerisation, pulsed RF discharge 77−56227
plasma polymerisation by glow discharge method, formation mech. *(Japanese)* 80−61094
plasma sheath breakdown to glow transition in plasma filled gap 80−100105
polyhexamethyldisiloxane thin film form. in glow-discharge flow system 78−68631
polymer film growth *(German)* 78−35343
polymer layer, glow deposition rate obs. in DC discharges 78−68633
polymer thin film growth by glow discharge polymerisation, temp. depend. 78−68632
polymerisation, double probe meas. and contamination effects 77−70300
polymerized dielectric thin films deposited by glow discharge, time-dependent props. 77−63564
population inversion in transverse flowing gas, discharge struct., from optical meas. 78−78992
positive column, ionisation waves, half subharmonic excitation 80−44006
positive column analysis, oxygen 79−55577
positive column of glow discharge of electronegative gas, molecular excitation and ionisation by electron collisions 80−49031
positive column stability in stationary regimes 79−41893
positive corona from two interacting thin points in air 80−49040
positive glow corona along a cylindrical rod between two parallel plates 80−38768
positive point to plane discharge, determ. of basic quantities during glow to arc transition 79−32837
positive-ion distribution in a strong electric field, steady state kinetic eqn. 80−33844
pulsed DC glow discharge, cataphoresis eqns. 78−67506
pulsed glow discharge, externally maintained, by electron beam 78−79490
pulsed HP glow discharges, time-resolved electron-neutral collision frequency meas. 77−39498
pulseless corona, space-charge limited current flow, computer solutions of Poisson and current continuity equations 79−86627
quartz glass surface, action of glow discharge *(Russian)* 80−25886
Re-sputtering and implanting sputtered atoms during deposition 80−16137
reactive oscills. freq. eqn. derivation, numerical calc., He,,Ne expts. 77−1027
RF plasma excitation, appl. to ion plating 79−69995
RF sheath in self-sustained plasmoids, size and disappearance analysis 80−44026
RF sputtering, impedance matching networks, experimental and design information 80−50555
RF sputtering system, Langmuir probe study of glow discharge at various freqs. 80−55294
secondary electron emission at discharge tube wall 77−27762
secondary electron emission in cathode fall region of discharge tube wall 80−44001
secondary electron emission mechanism 77−19800
self-quenching streamer discharge in a wire chamber 79−63869
sheath RF impedance, scatt. and ionisation effects 79−86630
simulated combustion gases, mode and sparking characts. of back discharges, NO conc. effects 80−6301
spark chambers, parallel plate, efficiency characteristics calc. 78−33393
spatial control, pulsed high-pressure preionisation stabilised discharges 80−79606
spectrochemical analysis with glow-discharge lamp *(Japanese)* 78−85262
spectroscopic light source, characts. using Ar(He) carrier gas, Al(graphite) cathodes 78−82047
sputter ion plating technique 79−83142
sputtering, alloy surface topography obs., Stewart-Thompson theory 78−43977
sputtering, plasma characts. by Langmuir probe technique 80−80929
sputtering and reactive effects in a stainless steel tube during glow discharge treatment 78−70141
sputtering characteristics of E×B discharges *(Japanese)* 77−68889
sputtering DC discharge, electron density and temp. profiles, Langmuir probe meas. *(French)* 78−30482
sputtering diagnostics, optical spectroscopy 78−72666
sputtering discharge, production and energy distrib. of H atoms present in traces *(French)* 77−24229
stability, rel. to transition to arc 79−10740
stability of normal and other discharges with parallel resistance, anal. 77−11416
stainless steel, reduction of H by Ar glow discharge, rel. to ultra cold neutron storage 80−104459
stationary, contraction dynamics in air flow *(Russian)* 78−87511
steel, industrial, surface chem. characterisation by SIMS, glow discharge spectrometry and other techniques 80−66907
steel, shafts, type 45, fatigue strength improvement after glow discharge treatment 80−108573
steel, stainless, nitriding in glow discharge in crossed electric and magnetic fields 80−16578
steel, surface cleaning in glow discharge, ion bombardment effect *(Russian)* 78−95848
steel nitridation process *(Russian)* 77−11412
steel surface hardening, ion-carbo-nitriding in CO-N_2-H_2 gas mixtures, expt. *(Japanese)* 80−71670
sticking instability in air flow *(Russian)* 78−38559
streamer breakdown, discharge growth calcs. for two-dimens. geom. case 80−24286
striations, large amplitude, electron conc. variation 77−89342
striations, running and stationary, stepped discharge current effect *(German)* 79−90487
styrene, plasma polymerisation in glow discharge, thin film IR and free radical EPR obs. 80−2964
substrate prep. for film deposition using glow discharge techniques 79−24438
superdense, effect of transverse magnetic field on ion concentration 80−87972
superheat-ionisation stability, stabilised by RF elec. field 79−19112
superheating ionisation instability with rot. elec. field 80−79611
surface treatment, struct. changes in vacuum deposited metal coatings *(Russian)* 79−15852
surface treatment of glass, effect on surface props. and contact angle 80−21139

glow discharges continued
TE glow discharge, influence of fluid-dynamic phenomena 78−71619
temperature measurement, using electronic rot.-vibr. mol. spectra *(Russian)* 78−71575
tetrafluoromethane-H_2 glow discharge, plasma etching of Si and SiO_2 surfaces 79−98922
threshold current for glow to arc transition 77−27771
transition to arc 78−26369
transversely inhomogeneous, stability, equiv. cct. theory 78−51373
transversely inhomogeneous discharges, equivalent circuit treatment 77−62419
travelling striations, controlled by current modulation 79−82118
trigatron gap, transient glow discharge obs. and simulation *(Japanese)* 77−43097
tube impedance with and without metal cover 78−67508
tube shape, flow velocity, effect on electron temp. of medium pressure positive column 79−64941
turbulent flow, 20 to 200 m/s air current *(Russian)* 77−65921
unconstricted positive column of high-vel. gas flow 77−35426
vacuum technology, medium, high and ultrahigh, conf., Oxford, England (Apr. 1978) 79−63242
VUV source, laser induced two photon blackbody radiation from He atoms in glow discharge 78−58102
welding heat source, appls. review 79−73051
AgBr evaporated layer response in ionisation semiconductor photographic system *(German)* 80−101859
Al sheet surfaces, chem. characterisation by SIMS, glow discharge spectrometry and other techniques 80−66907
Al storage ring vacuum chambers, glow discharge processing versus bakeout 78−70658
Al-Cu-Si, effect of sample conditions on sputtering and intensities, emission spectrochem. anal. using glow discharge *(Japanese)* 80−21349
Ar, after-arc phenomena *(Japanese)* 77−58916
Ar, $Ar+O_2$, ground surface ion bombardment of stainless steel in DC glow discharge 78−95098
Ar, cathode dark space ionisation avalanche with cold cathode *(Russian)* 80−84013
Ar, cylindrical hollow cathode, ignition and breakdown expts. 78−91169
Ar discharge, optogalvanic and excited state photoionisation signals, space charge effects 80−14947
Ar, discharge sudden contraction, effect of gas heating 79−27859
Ar, gas temp. meas. by fluoresc. spectroscopy 78−18467
Ar, glow discharge, spectral line excitation, cold cathode region 77−84552
Ar, hollow cathode discharge, ion mass composition 79−68969
Ar, imprisonment of reson. rad. in cold cathode region 78−59703
Ar, ion flow mass-energy relations, near hollow cathode 77−84563
Ar negative glow fast electron density rel. to discharge pressure and current 78−67528
Ar, positive column, progressive and regressive ionisation waves *(French)* 80−43905
Ar, sputtering, metastable and reson. states density meas. *(French)* 80−14955
Ar-CO, positive ion spectra, ion clusters obs. 80−64807
Ar-He with different potential cathodes expt. *(Russian)* 77−39484
Ar-hexamethyldisiloxane, glow discharge positive column ion mass spectra identification 80−38834
B+Ar(Kr)(Xe), B emission line broadening in glow discharge lamp 77−3304
C bonding to Tokamak walls, XPS studies 80−80942
C oxides, glow discharge, excitation and ionisation mech., elec. and optical obs. *(Russian)* 78−59695
C steel joints, with interference, increasing supporting capacity, by electrophysical methods, exam. 78−85055
CO loss in glow discharges in CO, CO-He and CO-N_2-He mixtures 77−19788
CO, vibr. relax. at glass surface, glow discharge meas. 79−18409
CO-He glow discharge, positive column, ionisation processes 80−79618
CO-He-O_2, species concentrations in glow discharge and afterglow, mass spectra, laser conditions 78−14241
CO_2 dissociation obs. in flow system with cylindrical hollow cathode 78−66674
CO_2 dissociation obs. in hollow-cathode glow discharge 78−70946
CO_2 gas laser, glow discharge electron irrad. rel. to output characts. 79−64198
CO_2 glow discharge, acoustic wave influence on F^- forward ionisation wave 78−67521
CO_2 glow discharge chemical processes and rate coefficients 78−63626
CO_2, initial rate of decomposition in volume discharges 79−50905
CO_2 laser, convective-cooled, fast-flow, pulse discharge stability 78−94389
CO_2 laser, glow discharges at high press., voltage-current characts. 78−87036
CO_2 laser discharge, TEA, glow form. and glow-to-arc transitions, high speed camera obs. 78−25846
CO_2 laser gas mixture, vol. photo-preionisation by VUV radiation 80−87966
CO_2 laser mixtures, high press., collision freq. 77−55184
CO_2 TEA laser, optimum operational conditions with double discharge at atm. pressure *(Bulgarian)* 78−33720
CO_2 waveguide lasers, high-power, high-press., photoionisation-stabilised 78−46641
CO_2:N_2:He plasma, lasing action, gain limiting attainment possibility 79−89884
CO_2-He, species concentrations in glow discharge and afterglow, mass spectra, laser conditions 78−14241
CO_2-N_2 electroionisation laser mixture, ionisation instability of semi self maintaining discharge 80−63971
CO_2-N_2-H_2, non-self-maintained glow discharges at atm. pressure, elec. characteristics and energy exchange 78−71606
CO_2-N_2-H_2O fast flow discharge laser, output power time depend. 80−99697
CO_2-N_2-He gas mixtures, fluorescent IR radiation from glow discharge 78−94386
CO_2-N_2-He gas mixtures, time-of-flight meas. of electron transport parameters 78−94387
CO_2-N_2-He laser mixtures, self-sustained glow discharges, low ionisation pot. organic additives effects *(French)* 77−88694
CO_2-N_2-He mixture volumetric glow discharge formation at atm. pressure 78−71615

glow discharges continued
CO_2-N_2-He system, CO_2 TEA laser discharge development, high-speed-camera investigation 79−55109
CO_2+N_2+He, glow discharge positive ion species identification *(Russian)* 80−84014
Cd vapour laser, hollow-cathode white light, new design concept 80−87405
Cd-Ar low-pressure discharge column, energy balance obs. 78−67504
Co_2:He:N, glow discharge instability in afterglow 80−6313
Co_2-N_2-He, pulsed discharge with temp. and density gradient in cathode sheath 79−41899
Cr coatings, plasma-chemical deposition using transport reactions *(Russian)* 80−16191
Cu, Doppler-free laser spectroscopy in hollow cathode discharge 80−9537
Cu glow discharge sputtering redeposition, in noncond. compound chem. anal. 77−77860
Cu hollow-cathode emission spectra, 200 to 430 nm 79−72264
Cu II laser with cylindrical hollow cathodes, UV performance 80−102709
Cu, surface, electron stimulated desorption, glow discharge treatment 79−65964
Cu/CuCl double pulse laser, continuous glow discharge appl. 80−1190
CuBr laser, tunable dye laser radiation, gas temp. atomic density meas. technique 79−82037
Fe group elements, singly ionised, charge transfer, rel. to laser action 80−74246
Fe, hollow-cathode emission spectra, 200 to 430 nm 79−72263
Fe surface hardening, ion-carbo-nitriding in CO-N_2-H_2 gas mixtures, expt. *(Japanese)* 80−71670
Fe-Ar low press. flow discharge, axial density profiles of sputtered cathode atoms 80−49029
H glow discharge, electron macroscopic props. *(Russian)* 80−92403
H, penetration of Mo cathode in glow discharge, point defect depend. 79−41903
H-isotope enrichment using low-temp. glow discharge technique 78−66675
H_2, hollow cathode discharge, ion mass composition 79−68969
H_2, ion flow mass-energy relations, near hollow cathode 77−84563
H_2 plasma, endothermic reduction of BCl_3 in thermal plasma and nonequil. plasma discharge 78−15671
H_2, stationary and moving layer relationships *(German)* 80−24289
H_2-Ar hollow cathode discharge, effect of additional gas ionisation by oscillating electrons *(Russian)* 77−31536
H_2-He, hollow cathode effect in cylindrical geometry *(French)* 80−33842
H_2-He(Ne), H Balmer line excitation by recomb. *(Russian)* 77−46516
H_2-N_2 glow discharge, positive column, electron energy-distrib. spatial variation 77−47294
H_2-N_2 hollow cathode effect discharge 79−86639
H_2-SiH_4, emission spectroscopy of SiH 80−69984
HCl, dissoc. excitation in flowing afterglow, Cl form., light emission 78−90115
He, 2^3P level population relax., laser absorpt.-perturbation meas. 78−59706
He, 3^3D level, fine struct. changing collisions in glow discharge 80−58346
He constricted glow discharge, space charge double layer influence obs. 78−67492
He, cryogenic discharge, interferometer meas. of neutral gas temp. 78−1924
He cryogenic glow discharge, effect of laser radiation (10.6 μm) 80−64803
He, electron behaviour in cathode fall, Monte Carlo simulation 78−1941
He, fast electron energy distrib. in positive column and negative glow 80−38764
He flowing discharge, glow/arc transition and cathode-zone wave structure obs. 78−75475
He glow discharge, n=3 sublevel quenching and energy transfer, laser perturbation method 80−44060
He glow discharge plasma, ionis. waves in positive column 80−1876
He glow discharge with constriction, electrokinetic and optical characts. axial distribs. *(Russian)* 77−80393
He, high press., time resolved electron-neutral collision freq. 77−55184
He hollow-cathode discharge, Ba^+ and Sr^+ formation 78−67527
He I, low-press., quenching of singlet states by N_2 80−49030
He, intermediate press., positive column conc. of ions and metastables 80−44017
He, laser-induced Raman emission source at 569 and 637 Å 79−46024
He, low press., excitation transfer and quenching of n=3 excited states 80−38743
He low-current discharge, metastable atoms, radial density distrib. obs. and calc. 78−67495
He, nanosecond discharge in weakly ionised plasma, existence of two phases 80−24277
He, negative glow electron energy distrib., appl. to hollow cathode lasers 77−19790
He, negative-luminesc. plasma, electron energy distrib. from line intensities and probe obs. 80−49033
He short glow discharge, lateral spread 79−46501
He, spectroscopic element detector for gas chromatography 78−31721
He, usual glow and hollow-cathode discharges, negative glow, spectroscopic obs. 77−72516
He-CO, positive ion spectra, ion clusters obs. 80−64807
He-CO_2-Cs, quenching cross section of resonant Cs(6P) state by CO_2 mols. 80−43860
He-Cd, glow discharge, collision rates calcs. 77−68882
He-Cd, usual glow and hollow-cathode discharges, negative glow, spectroscopic obs. 77−72516
He-Cd vapour excitation in hollow cathode discharge 80−64815
He-$Co_2(O_2)$ volume discharge, electron recombination and attachment 77−19799
He-Cu hollow cathode laser, three phase excitation 80−48279
He-Na mixture, low-pressure discharge, radial cataphoresis obs. 78−67507
He-Ne, glow discharges, AC cataphoresis meas. using light spectrometry 79−60096
He-Ne, striation current conditions 79−55595
He-Ne gas laser, glow discharge electron irrad. rel. to output characts. 79−64198
He-Ne glow discharge, passive freq. charact. 79−50915
glow discharges continued
He-Ne mixture, cataphoretic gas separation in DC glow discharge with end volumes 80−79428
He-Zn laser, negative glow and positive column discharges comparison 78−1217
He_2, 600 Å emission continuum struct., in 700-900 Å region in glow discharge 80−95641
Hg low-pressure pulse-modulated discharge optical and electrical parameters 78−67491
Hg vapour discharges, high-press., e-beam initiated, laser absorpt. meas. 80−92412
Hg-TlI, lamp, chem. comp., temporal and spatial evolution 78−87532
K, discharge plasma, anomalous bright 5730 Å band excitation mechanism 78−67475
Kr, DC glow discharge excited atoms, radial conc. distrib. obs. 78−67494
Kr discharge, electron energy distrib. function, electrical characts. investig. 80−24279
Kr hollow cathode discharge, multiply charged and mol. ion prod. and loss 79−46499
Kr, hollow-cathode glow discharge with gas flow 78−67532
Kr-Cl_2 mixture, glow discharge positive column, electron energy distrib. and rates of inelastic processes, negative Cl ions form. 80−19632
Kr-Xe, glow discharges, AC cataphoresis meas. using light spectrometry 79−60096
KrF, 0.8 J multi-atm. laser, glow discharge characts. 78−58992
KrF excimer laser, water dielec. Blumlein-driven fast elec. discharge pulser 79−10318
KrF laser, e-beam sustained, glow discharge stability 79−55117
KrF X-ray-preionized high-pressure laser, discharge vol. press. depend. 79−18403
Mo cathode, H_2 discharge, FCC surface layer form., electron diffr. obs. 77−55311
Mo electrodes, in glow discharge, H penetration and diffusion 77−7629
Mo, glow-discharge surface treatment, struct. defect prod. 77−63832
N cooled discharge plasma electron energy distrib. function 78−63633
N glow discharge, volt-ampere charact. in gas flow *(Russian)* 80−106991
N, glow discharge instability in afterglow 80−6313
N glow discharges surface coronas and photopreionisation stability, demonstration 80−105475
N, nonequilibrium plasma, thermocouple diagnostics 80−103188
N-O mixtures, positive glow corona in quasi-uniform fields 80−100104
N_2, barrier discharge, struct., spectral anal. *(Russian)* 77−21463
N_2 DC glow discharge, nitridation of Mg surfaces, 0.3-5 torr, mechanism 78−3370
N_2, DC glowing discharge rel. to microwave discharge, electron energy distrib., probe meas. *(Russian)* 77−47280
N_2 DC metastable atoms prod. 80−38758
N_2, electronic states excitation and population in glow discharge 77−487
N_2, flowing discharge, characts. depend. on initial conditions 78−51378
N_2, glow discharge, DC, low-press., translational/rot. temps. relation 78−38454
N_2, glow discharge, decay instability and contraction, interferometric and photographic obs. *(Russian)* 78−59696
N_2, glow discharge, ionis. mechanism 78−13613
N_2 glow discharge, semi-self maintained, stability *(Russian)* 79−27845
N_2 glow discharge, variable current penetration mechanism 79−55584
N_2, high press., time resolved electron-neutral collision freq. 77−55184
N_2, hollow cathode discharge, ion mass composition 79−68969
N_2, in CO_2 laser, electron beam-ionis. optical pumping characts. 77−75477
N_2 ion flow mass-energy relations, near hollow cathode 77−84563
N_2, mol. excitation, in glow discharge and afterglow 78−63623
N_2 molecular plasmas, electron kinetics *(German)* 78−91171
N_2, neutral components comp., mass spectroscopy study *(Russian)* 80−10439
N_2, non-self-maintained glow discharge ionisation instability, vibr. states excitation calc. 77−19805
N_2 plasma, beam and glow discharge type, macroscopic props., kinetic eqns. 80−43864
N_2 plasma, electronic excitation levels in gas-discharge 80−24280
N_2, plasma, pulsed discharge, component conc. radial distrib. determ. *(Russian)* 77−21462
N_2, RF plasma, gas rotational temp. determ. 79−90458
N_2^+ Meinel system, high resolution spectrum to 11 250 Å 80−99497
N_2-H_2 mixture, glow discharge, ionisation and excitation obs. 78−67505
N_2-Ne, positive column, electron vel. distrib. function *(German)* 78−1885
N_2-Ne glow discharge, energy balance, ionis. collisions *(German)* 78−34263
N_2-Ne glow discharge, kinetic eqn., transport coeff., collision freq., mean energy *(German)* 78−34261
N_2-O_2 gas mixtures, highly transient gas discharges, obs. 79−37562
N_2-O_2 mixture transient discharges, RF techniques 80−70067
$N(^2D,^2P)$ metastable production by electron collisions in DC glow discharge 80−59274
NH_3 glow discharge, electron energy distrib. and negative ions *(Russian)* 79−7499
NH_3, positive glow discharge, N_2^{2+} radiation intensity distrib. obs. *(Russian)* 78−30512
N_2O-He, species concentrations in glow discharge and afterglow, mass spectra, laser conditions 78−14241
Na, low press. depleted discharge, recomb. struct. 79−94837
Nb-NbO_x-Pb Josephson tunnel junctions, fabrication using FR glow discharge oxidation 80−34559
Ne discharge, ionisation wave, phase instability and disintegration obs. 78−67518
Ne, excited atoms concentration determ., comparison with HF discharges *(Russian)* 80−70050
Ne, glow discharge, ionisation waves, regular and irregular, correlation meas. 78−1917
Ne, glow discharge, turbulent ionisation waves, correlation meas. 78−67519
Ne glow discharge plasma, coherent on-resonance self-focusing of optical pulses 79−41427
Ne, hollow cathode discharge, role of Penning ionisation of minor species 79−86633
Ne hollow cathode discharge tube, spectral line intensities, rise time 80−103212
Ne, luminesc. discharge, loss mechanisms *(French)* 78−9877

glow discharges continued
Ne medium-pressure discharge, electron temp. radial profile meas. by electron-atom bremsstrahlung continuum 78−67497
Ne, moving striation modes, numerical calc. 79−1365
Ne, negative glow discharge recomb. at. excitation *(Russian)* 77−76225
Ne, Nonlinear mixing of two unstable coherent ionization waves 79−86573
Ne, positive column, radial distrib. of excited atoms *(French)* 78−14237
Ne, RF discharge, emission modulation due to fast electron distrib. time variation 79−41900
Ne, reson.-absorpt. plasma of glow discharge positive column, Ne superradiation pulse variation 78−71489
Ne short glow discharge, lateral spread 79−46501
Ne stationary discharge with diffuse recombination, limit current and multiple states 78−67498
Ne_2 voltage change due to laser irrad., 572-654 nm 78−63605
Ne^+, radiating ions, velocity distrib. symm. in hollow cathode discharge, charge and momentum transfer 79−73054
Ne-Al large diameter hollow cathode discharge, near IR Al II laser transitions 80−102715
Ne-Ar, glow discharges, AC cataphoresis meas. using light spectrometry 79−60096
Ne-Cu hollow-cathode laser discharge sputtering obs. 78−66800
Ne-He DC glow discharge electron density decay, microwave cavity obs. 78−91167
Ne-O_2, DC glow discharge, Ne I spectral line intensities 78−74610
Ne-Xe glow discharge, negative flow charge exchange excitation of Xe^+ levels 80−38857
Ne+Kr(Xe) and Ne+Kr+Xe glow discharge, Kr^+ and Xe^+ excitation in negative luminesc. *(Russian)* 77−68883
O atom concentration, in O_2, (CO)(CO_2) glow discharge, mass spectrometric determ. *(Russian)* 78−87512
O atom production and removal in DC glow discharge 79−77432
O bonding to Tokamak walls, XPS studies 80−80942
O glow discharge atomic radial distribution obs. 78−67501
O plasma, high-temp. oxidation of SiC 77−25174
O_2 (inert gas), surface modification of polymer, ESCA obs. 78−3438
O_2, DC, particle concs. calc. 80−1859
O_2 discharge, Au-O bond energy, glow discharge mass spectrometry obs. 80−64808
O_2 discharge, transition metal-O bond energy, glow discharge mass spectrometry obs. 80−64808
O_2 gas-discharge plasma, interaction with Si surface 78−83840
O_2 glow discharges, current modulated, O atom production and removal rates 79−90477
O_2, low press. and current, theory 78−87560
O_2, positive column contraction characts. 79−90483
OH radicals in glow discharge, rot. levels distrib., temp. meas. 78−47169
P, amorphous film, prepared by chemical transport in glow discharge, electronic props. 79−24011
SF_6, discharge and oscill. due to axial injection of impulsive electron beam 80−59316
SF_6 gas, dispersion relation of spontaneous oscill., unstable regions 80−1875
SF_6 glow discharge, non-linear effects on self-exciting wave 78−83633
SF_6 plasma interaction with solid polymer, emission-spectra 80−87960
Si etching in fluorocarbon glow discharge, chemical aspects 79−86631
Si, glow discharge film decomposed from silane, on amorphous substrate, elec. cond., RHEED study 80−20044
Si:As, ion implanted, glow discharge optical spectroscopy 78−22755
Si:B, RF glow discharge sputtering damage centres, barrier formation 79−33329
Si-F-H amorphous solar cells, DC glow discharge fabrication 80−72041
SiH_4, low pressure, plasma parameters, relevance to Si film deposition 80−44030
SiO_2 etching in fluorocarbon glow discharge, chemical aspects 79−86631
SiO_2, substrate, glow discharge effect on surface props. and struct. 78−85201
SiO_2, surface reactivity modification by Ar/O_2 plasma treatment 78−64890
Ta_xN_y, FCC, formation in ionised glow-discharge 77−52266
TiC abrasion-resistant coatings, glow discharge assisted CVD 79−83392
Tl-Hg, UV preionised discharge, possible excimer laser 79−55119
TlI-Hg, excimer band emission from electron beam initiated discharge 80−78841
TlI-Xe, excimer band emission from electron beam initiated discharge 80−78840
U, hollow cathode discharge, opto-galvanic spectroscopy-electron temp., isotope ratio analysis 79−77437
U, sputtered, absorpt. spectra in hollow cathode glow discharge 80−32643
UI, absorption line shape change, pulsed hollow cathode source *(French)* 80−47927
^{238}U ($^5L^0_6$) from hollow cathode lamp, laser absorpt. spectroscopy *(French)* 79−59402
Xe, plasma column in flashtube, characts. and parameters 80−54053

GO calculations
ab initio effective core pots., reduction of all electron to valence electron calcs. 77−14361
ab initio LCAO-HF-concentrated GO crystal-orbital program 77−55471
ab initio molecular fragment calculations with pseudopotentials 79−93905
ab initio pseudopotential for FSGO calcs., appl. to Li compounds 77−75043
acetylene, and cation, SCF MOGO calc. of electronic struct. 77−34556
acetylene, average mol. polarisability, Frost model wavefunctions calcs. using p-type Gaussians 78−41924
acetylene, ground and triplet states, electronic and geom. struct. 78−94184
acetylene, magnetic susceptibility, frost model wavefunctions with p-type Gaussians 80−5477
alkali halides, electron momentum distrib. and Compton profiles 79−13631
alkali halides, geometries, force consts., charge distribs., FSGO model pot. calcs. 77−88379
alkanes, solvent effects, quantum mech., macroscopic electrostatic contribs. 77−30801
alkyl chlorides, proton affinity correl., ab initio SCF calc., MINDO/3, STO and G basis sets 78−33421

GO calculations continued
allene, transition state for internal rot., HF/STO-3G calcs. with correlation energy corrections 78−25430
allyl cation and radical, ab initio non-paired spatial orbital wavefunctions 77−26968
amide C-N bond character, metal ion bonding effects 77−6801
amides, geometry from ab initio calcs. 80−23338
atoms, Fermi contact interaction, spin density calcs., Hiller Sucher Feinberg identity 80−69061
atoms, first row, polarisation functions for Gaussian basis sets 78−5126
benzene, electronic struct., mag. susceptibilities, ab initio calcs. 78−74571
benzene, FSGO calcs. of orbital energies locations, dipole moments, charge distribs. 77−67976
benzene radical anion, ab initio MO calcs., struct. 79−18113
biological molecules, ab initio calcs., small Gaussian basis sets 79−59341
bis(fluoroxy)difluoromethane, ab initio MO calcs. of geometry, torsional barriers 78−90313
bromomethane, ab initio SCF MO calcs., ionis. pots., dipole moment, config., electronic props. 78−1104
1,3-butadiene, FSGO calcs. of orbital energies, locations, dipole moments, charge distribs. 77−67976
carbonyl fluoride, vibr. transition moments and force fields, gaussian basis set calcs. 79−81152
carbonyl to oxacarbene rearrangement, conformation, ab initio SCF MO calcs. 77−32780
cartesian Gaussian functions, one- and two-electron integrals 78−37538
chloromethane+Cl^-, S_N2 reaction, local orbital description, ab initio FSGO method 78−76842
Compton profile, single- and double-gaussian FSGO model 77−88504
correlation energy, Gaussian geminal basis set calcs. 77−57885
diamond, ab initio calcs. of struct. using FSGO method 77−80753
diamond, electron density, bulk and surface atoms, from ab initio model calcs. 79−4590
diatomic molecule nucl. mag. shielding using LCAO MO functions and gaussian expansion 79−36548
diazomethane, electronic struct., least energy dissoc. path to CH_2 and N_2 products 78−5131
difluorobenzenes, X-ray and UV photoelectron spectra, ionis. pots., ab initio GO calcs. 77−61795
dimethyl ether, low-lying excited states, improved virtual orbitals calcs. 77−14372
dimethylether, equilib. struct., ab initio SCF calcs. 77−3265
dipeptide, struct. and bonding, ab initio calcs. 79−53039
effective convergence to complete orbital bases and at HF limit through systematic Gaussian primitive sequences 80−14065
electron affinity, variation-perturbation approach 77−54513
electron density contours from FSGO model wave functions, nonbonded radius of atoms, mol. anisotropy of polarisability 79−85897
electron density of states, quantum shift, Gaussian random pot. 78−18941
electron repulsion integrals, computation involving Gaussian basis functions 78−58572
electronegativity, nonempirical scale, ab initio FSGO wavefunction calcs. 77−26966
ellipsoidal Gaussian basis functions, integral formulas and test calcs. 77−23420
ethane, valence electronic struct., model pot. in floating spherical GO formalism 78−74563
ethylene, ab initio GO calc. 78−94187
ethylene, and radical ion, SCF-MO calc., bonding and electronic struct. 77−38610
ethylene, average mol. polarisability, Frost model wavefunctions calcs. using p-type Gaussians 78−41924
ethylene, dipole moment derivatives, IR vibr. intensities, STO-3G, 4-31G, calcs. 77−6750
ethylene, magnetic susceptibility, frost model wavefunctions with p-type Gaussians 80−5477
ethylene, planar, V-N vertical transition, SCF and correlation energies 77−68032
ethylene+H⇌ethyl radical, pot. energy surface, analytic function 79−11779
ethylene radical cation, electronic states assignments, ab initio SCF CI calcs. 77−10584
ethynyl radical, vertical electronic spectrum, CI calcs. 77−34656
exchange interactions of atoms in paired orbital approx. 77−88521
extended even-tempered orbital bases for atomic and mol. calcs., systematic approach 80−32591
first row atom-H molecules, ellipsoidal Gaussian basis in MO theory 79−93919
first row atoms, Gaussian basis sets, uniform quality, ab initio calcs. 78−5116
first-row atom, uniformly balanced constrained gaussian basis tests 77−65423
floating spherical Gaussian orbital calculation, ab initio pseudopotential, hydrocarbons 77−83496
floating spherical GO calcs. of electron momentum distribs. and Compton profiles 77−30933
floating spherical GO open-shell calculations, double gaussians, first row atoms and ions 78−94182
1-fluoro-2-propanol, conformational energies and rot. barrier, ab initio calc. 79−31390
fluorobenzene radical anion, ab initio MO calcs., struct. 79−18113
fluoroxyperoxytrifluoromethane, ab initio MO calcs. of geometry, torsional barriers 78−90313
formaldehyde, electronic excited states, GO calcs., $\pi \rightarrow \pi^*$ transition 79−22616
formamide, hydration by H_2O mol., point charge model 77−34569
FSGO calculations, tetrahedral Gaussian lobe functions and Cartesian Gaussian basis sets 79−22587
furan, FSGO calcs. of orbital energies, locations, dipole moments, charge distribs. 77−67976
$G_n(a)$ auxiliary function calc. in Gaussian orbit-orbit integrals 77−23414
Gaussian basis sets, Ga, Ge, As, Se, Br, and Kr, HF calcs. 77−38611
GAUSSIAN-70, integral labelling technique 77−10583
Gaussian-70 MO program, LCAO-SCF eqn. soln., population anal., appl. 78−70742
geminal basis set optimisation, with crude SCF reference state 77−57885
generator coordinate method 78−29731
geometry optimisation, Newton-Raphson method algorithm 77−10612

GO calculations continued
glyoxal, $^3n\pi^*$ states, ab initio STO-3G CI calcs., ΔE_{SCF} transition energies 78−94194
group IV hydrides, pseudopot. FSGO calc. 79−22591
H-bonded and H-like bonded systems 78−9068
H-bonded complexes-first row hydrides, ab initio calcs. *(French)* 80−5479
Hartree Fock atomic orbitals, approximation by Gauss functions 77−67985
heterobenzenes, electronic struct., π electron mag. susceptibility anisotropy 79−59353
histamine monocation, FSGO calcs. of orbital energies locations, dipole moments, charge distribs. 77−67976
homonuclear diatomics, equilib. geometries, Gaussian-based model pot. calcs. 78−94183
homopolar tetrahedral solids, Gaussian relaxation method of density of states calc., appl. to Ge 77−39760
hydrides, first row, localised MOs, size-energy relation, at initio LMO GO calcs. 77−50351
hydrides, first-row, pseudopot. calcs. using FSGO 78−9062
hydrides, second row, ab initio calcs. using FSGO basis, mol. parameters correlation 78−901
hydrocarbon radicals, ab initio calc. of spin densities 79−93938
hydrocarbons, double-zeta quality ab initio mol. fragment calcs. with pseudopots. 79−85879
hydroxymethylene radical cation stability, CH_2O^+ isomers, ab initio MO study 80−42965
integrals involving continuum orbitals, numerically oriented evaluation method 77−61673
intermolecular integrals, calc. using truncated Gaussian expansions of atomic orbitals 77−88520
large molecule, ab initio calcs. using mol. fragments, floating spherical Gaussian basis sets characts. 77−42233
large molecules, mol. fragment basis, generalisation, for ab initio calcs. 80−91438
lithium acetylene, SCF MOGO calc. of electronic struct. 77−34556
lithium ethylene, SCF-MO calc., bonding and electronic struct. 77−38610
methane, FSGO calculations using pseudopotentials 77−26971
methane, Gaussian basis sets, quality studies 79−59345
methane, H-X bond position, correlation with electronegativity 78−9069
methane, localisability in MO calcs., measured by absolute overlap and 2nd moment dispersions 78−74557
methane, localised molecular orbitals, HF theory 79−97980
methane derivatives, stabilisation of planar tetracoordinate C, substituent effects, RHF/STO-3G calcs. 77−6671
methanol, equilib. struct., general valence force field, ab initio calcs. 77−3265
methanol, low-lying excited states, improved virtual orbital calcs. 77−14372
methyl fluoride, vibr. transition moments and force fields, gaussian basis set calcs. 79−81152
methyl glyoxal, $^3n\pi^*$ states, ab initio STO-3G CI calcs., ΔE_{SCF} transition energies 78−94194
methyl lithium, equilib. geometries and electronic states, FSGO calcs. 79−10019
methylene+$H_2 \rightarrow CH_3+H$, triplet methylene abstraction, partial open shell FSGO calc. 78−80719
molecular correlation energy calc., appl. of Gaussian geminal 78−41960
molecular energy gradient, ab initio HF program 79−89606
molecular geometry optimisation in mols. with second row atoms 77−42232
molecular orbital methods, speed and accuracy, comparison of methods 79−41106
molecular polarisability, selection of Gaussian basis sets 78−58865
molecular polarisability calcs., basis set with external elec. field perturbation depend. 77−38740
molecular vibrational wave functions, semiclassical Gaussian basis set method 80−9583
molecular wavefunctions, transcorrelated method 77−61678
molecule, 1st row, geometry optimisation, using bond function augmented basis sets 78−905
molecule, total energy of molecule, local spin density functional approx., LCAO SCF calc. 79−93920
molecules, bond contributions to electronic energies, ab initio STO 3G calcs. 77−6669
monoelectric operators with modified Gaussian functions, expectation values 79−6820
multi-centre integrals, Racah algebra, Talmi transformation 79−45626
naphthalene, anion, cation and triplet, GO LCAO MO calcs. of electronic struct. 78−25416
negative ions, electronic structure, stabilisation calcs. using big mol. Gaussian SCF/CI program 79−18121
nuclear magnetic shielding constants calc. by GIAO method using Gaussian functions 80−1001
open-shell systems, FSGO calcs. with model pots. 78−33413
orbital amplitudes of nuclei, extrapolation procedure, gaussian basis set and nucl. cusp eqn. 78−74560
partial at. charges calc. from ab initio mol. electrostatic pots., appls. 78−70739
phenyl cation, singlet, triplet state mol. geometries, energies, ab initio UHF STO calcs. 77−6672
polyethylene, conform. stability, 1-electron levels, long-range effects calcs. 80−28123
polyethylene, one-, three-dimensional, energy band struct., ab initio calcs. 79−95330
polymer, FSGO model, X-ray diffr. struct. factor calcs. 77−46660
propene, force constants, SCF ab initio calcs. 77−34780
pyridine, FSGO calcs. of orbital energies, locations, dipole moments, charge distribs. 77−67976
pyrrole, FSGO calcs. of orbital energies, locations, dipole moments, charge distribs. 77−67976
Rayleigh-Ritz method, convergence of Slater, Gauss and two-electron functions 77−65419
refractory compounds, electron struct. and phys. props. 80−54585
resonant states, complex basis functions methods 79−6887
RHF energy values calcs., influence of mol. integral errors 77−50354
saturated hydrocarbon polymers, conform. stability, 1-electron levels, long-range effects calcs. 80−28123
second row atoms, contracted Gaussian basis sets for mol. calcs. 80−83264
GO calculations continued
second-row hydrides, equilib. geometry, FSGO model pot. calcs. 77−50347
sparse s and p type Gaussian basis set LCAO MO SCF calc., mol. props. 80−23306
spherical Gaussian basis sets, for relativistic Hartree-Fock calcs. 80−32595
tetrahedral Gaussian lobe functions 79−6825
3,3,4,4-tetramethyldiazetine, photoelectron spectra, ring size effects on azo group ionis. pots. 77−61793
thiocarbonates, mol. struct., S-substitution effect *(French)* 80−23335
thionitrates, mol. struct., S-substitution effect *(French)* 80−23335
third-row hydrides, core d-electrons, FSGO struct. optimisation method 77−50382
transition metal atoms, first-row, 3d orbital calcs. using Gaussian basis sets 77−65422
trifluoroacetic acid, ab initio MO calcs. of geometry, torsional barriers 78−90313
uniform quality basis sets 77−34555
vinyl isocyanate, and vinylcyano ether, geometry and conform., ab initio minimal STO-3G MO calcs. 80−23337
vinylcyano ether, and vinyl isocyanate, geometry and conform., ab initio minimal STO-3G MO calcs. 80−23337
water, NMR shielding constants of ^1H and ^{17}O, paramag. contrib., triple perturbation theory 79−101?7
water molecule, nucl. spin-spin coupling consts. geometric approx. 79−59380
X-ray crystallography, Fourier transforms of Gaussian orbital products 78−38573
Al, single vacancy formation energy calc., SCF-LCGO modified solid state scatt. theory 80−54637
AlH, valence excited states, pot. curves 78−41973
$Al^{3+}(H_2O)n$ (n=1,2,4,6), FSGO-pair-pot. calcs. *(German)* 80−74278
Ar, solid, energy bands, depend. on choice of exchange-correlation pot. 80−70607
ArHCl, ab initio FGO calc. 78−50467
BH, localisability in MO calcs., measured by absolute overlap and 2nd moment dispersions 78−74557
BH, mag. field depend. susceptibility, gauge invariant GO calc. 78−1100
BH, mol. spectroscopic consts., FSGO calcs. 77−6758
BH_3, localisability in MO calcs., measured by absolute overlap and 2nd moment dispersions 78−74557
BH_4^-, electron momentum distribution and Compton profiles, FSGO calcs. 80−87032
$B_2H_5^+$, FSGO ab initio calc. of geometry, CNDO/2 calc. 78−41943
B_2H_6, electron momentum distribution and Compton profiles, FSGO calcs. 80−87032
B_2H_6, quadratic valence force field, rel. to ethene 79−3382
$B_3H_8^-$, electron momentum distribution and Compton profiles, FSGO calcs. 80−87032
B_4H_{10}, electron momentum distribution and Compton profiles, FSGO calcs. 80−87032
$(BHNH)_n$, band structure, ab initio calcs. 79−23895
$(BH_2NH_2)_n$, band structure, ab initio calcs. 79−23895
BN, cubic, energy band and piezoelec. calcs. 78−72071
$B_3N_3H_6$, electronic struct., mag. susceptibilities, ab initio calcs. 78−74571
B_2O_3, bipyramidal struct., stability, ab initio SCF-MO calcs. 80−99446
Be compounds, electronic structure, configs., energy, bonding, of small mols. and complexes 78−13420
Be, correl. energy, Gaussian geminal basis set calcs. 77−57885
Be, ground state energy, split valence GO basis set SCF calc. 77−34554
BeH_2, localisability in MO calcs., measured by absolute overlap and 2nd moment dispersions 78−74557
BeH_3, FSGO model of mol. struct., energy terms 79−63904
$Be^{2+}(H_2O)_n$, (n=1,2,3,4,6), FSGO-pair-pot. calcs. *(German)* 80−74277
C, polarisation functions for Gaussian basis sets 78−5126
CH_2, FSGO LCAO calc., bond angles 77−34557
$CH_3(CH_3^+)(CH_3^-)$, HF, GVB and CI calcs. 77−75063
CH_2SiH_2, ab initio GO calc. 78−94187
C_2N_2, and $C_2N_2^+$, electronic struct. UV and PE spectra 80−23304
CO, ellipsoidal Gaussian basis functions, integral formulas and test calcs. 77−23420
Cl^-, contracted Gaussian basis sets for mol. calcs. 80−83264
Cl-containing systems, core Auger and core electron binding energy shifts, ab initio LCAO SCF MO UHF calcs. 77−30777
$ClF(ClF_2^-)(ClF_3)$, localised MO ab initio calc., Gaussian orbital ab initio calc. 80−14083
F_2, valence electronic states, $^1\Pi_u \leftarrow X^1\Sigma_g^+$ absorption spectrum 79−63920
FBO, electronic struct. calcs. 77−30772
FH, numerical coupled HF hyperpolarisabilities, basis set depend. 79−76357
F $(H_2O)n(n=1,2)$, FSGO-pair-pot. calcs. *(German)* 80−74278
F_2S_2, electronic struct. and stability of isomers, gaussian SCF MO calc. 79−93921
Ge_2H_6, valence electronic struct., model pot. in floating spherical GO formalism 78−74563
H, Fermi contact interaction, spin density calcs., Hiller Sucher Feinberg identity 80−69061
H^-, electronic structure, stabilisation calcs. using big mol. Gaussian SCF/CI program 79−18121
$H+C^{2+}(C^{3+})(N^{2+})$, radiative charge transfer, rate coeffs., pot. energy curves 77−88554
H^++CO ($^1\Sigma$), ground state pot. energy surface, ab initio SCF calc., protonated equilib. geometry 80−83301
H_2, Compton profile, correl. Gaussian wave function calc. 79−81241
H_2, D_2, photoionisation, body-frame Hund's case b description 78−94295
H_2, electric dipole polarisability, many-body perturbation theory calcs. 78−21839
H_2, mag. field depend. susceptibility, gauge invariant GO calc. 78−1100
H_3^+, $^2\Sigma_u^+$ excited level, GO SCF calcs. 77−46507
$H_3^+ + H_2 \rightarrow H_5^+ \rightarrow H_2 + H_3^+$, ab initio GO pot. surface, C_{2v} symmetry 77−25252
H_4 and H_4^+, H_4^- ions rectangular configurations, stability, SCF MO LCAO calcs. 77−42235
H_4, FGSO open-shell calcs. 79−10025
H_4, ground and excited states, SCF MO CI calcs. 77−6693
HCN^+, photoelectron spectra of third electronic state, ab initio calc. of pot. energy surface 78−70871

GO calculations continued
$H_2CN^+H_2 \rightarrow HCN^+H+H_2$, ab initio GO SCF pot. energy surface, saddle point, reaction path 77−50379
HCl^-, reson. states by electron impact, GO and SCF+CI methods, dissociation channels 77−71883
HF, Auger transition energy calcs. 77−34704
HF, ellipsoidal Gaussian basis functions, integral formulas and test calcs. 77−23420
HF, H-X bond position, correlation with electronegativity 78−9069
HF, low lying states, GVB and CI calcs. 77−14362
HF, mag. field depend. susceptibility, gauge invariant GO calc. 78−1100
HF, spectroscopic consts., FSGO calcs. 77−6758
HF+formyl fluoride, multiple site reactivity, ab initio GO supermol. calc. 78−11498
$(HF)_2$, intermol. pot. function, ab initio 6-3½G calc. 79−18254
H_2^+He, total energy, interat. dist., geometric configurations, LCAO MO SCF calcs., stability, binding energy 77−42236
HO-H...OHX, X=H, CH_3, NH_2, OH, F, H-bonds, electron donor substituted, mol. orbital calc. 78−13422
H_2O, core ionis. pot. of O, basis set depend. 78−17821
(H_2O), electron affinity, ab initio SCF calcs. 79−76343
H_2O, equilib. struct., ab initio SCF calcs., general valence force field 77−3265
H_2O, H-X bond position, correlation with electronegativity 78−9069
H_2O, localisability in MO calcs., measured by absolute overlap and 2nd moment dispersions 78−74557
H_2O, localised MO, basis set depend. 79−36525
H_2O, low-lying excited states, improved virtual orbital calcs. 77−14372
H_2O, nucl. mag. shielding and susceptibility, SCF calcs. 77−14351
$(H_2O)_2$, coherent X-ray scatt. profile calcs. 77−61765
HOF, nucl. mag. shielding and susceptibility, SCF calcs. 77−14351
HPO, mol. struct. and props., ab initio, calc., Gaussian lobe orbital 78−62713
HS_2, rotamers, electronic and geometrical structs., ab initio floating GO basis calcs. 78−74572
H_2S, ground and excited states, SCF and CI calcs. 77−414
H_2S_2, electronic struct. and stability of isomers, gaussian SCF MO calc. 79−93921
$(H_2S)_2$, hydrogen bond, proton transfer, pot. energy surface 77−67977
He, quantum-mechanical calculations 77−14350
He_2, intermol. forces, Gaussian basis function calcs. 78−21993
$HeNe^+$, collisional form., excitation, pot. energy curves calcs. 77−6697
KF, ab initio SCF MO energy, dipole moment and polarisability 80−1085
KrF, electronic states, ab initio CI calcs., spin-orbit coupling, pot. curves, dissoc. energy, dipole moments 77−38619
Li compounds, electronic structure, configs., energy, bonding, of small mols. and complexes 78−13420
Li, Gaussian basis sets, uniform quality, ab initio calcs. 78−5116
Li_2, floating spherical Gaussian orbital, Hartree-Fock-Roothaan and pseudopot. calcs., comparison 78−46262
Li_3, spin density, Gaussian basis set 78−33427
LiF, ab initio SCF MO energy, dipole moment and polarisability 80−1085
LiH, crystalline, surface struct., floating spherical Gaussian orbital method calc. 77−1281
$LiH, LiHe^+$ and $LiHe_2^+$ systems, ab initio SCF LCAO calcs. of stability and spectroscopic consts. 77−71748
LiHH system, pot. surfaces, nonempirical GO calcs. 77−42374
$Li(H_2O)^+$, coherent X-ray scatt. profile calcs. 77−61765
LiH_2O^+, geom., electronic struct. FSGO model calcs. 78−82614
$Li^+(H_2O)_n$, (n=1,2,3,4,6), FSGO-pair-pot. calcs. *(German)* 80−74277
LiN_2, geom., electronic struct. FSGO model calcs. 78−82614
$LiNH_3^+$, geom., electronic struct. FSGO model calcs. 78−82614
$Mg^{2+}(H_2O)n$ (n=1,2,4,6), FSGO-pair-pot. calcs. *(German)* 80−74278
N, polarisation functions for Gaussian basis sets 78−5126
N_2, excitation energies, eqn. of motion-Green's function calcs., 3rd order contribs. 77−65417
N_3^-, theoret. electron density distrib. cf. expt. density distribs. of NaN_3 and KN_3 77−46489
NH, mol. spectroscopic consts., FSGO calcs. 77−6758
NH_3, GO AO exponents optimisation and scaling effects on mol. props. 77−65424
NH_3, H-X bond position, correlation with electronegativity 78−9069
NH_3, IR absorption band integrated intensities, ab initio and LMO studies 80−23458
NH_3, LCAO-MO-SCF calcs., analysis of Gaussian basis sets rel. to one-electron props. 78−55122
NH_3, localisability in MO calcs., measured by absolute overlap and 2nd moment dispersions 78−74557
NH_3-lithium halide complex, ab initio calcs., Li bond rel. to H bond 77−14343
N_2H_2, $N_2H_2^+$, ab initio calcs., electronic struct., geometries relative energies 77−46487
N_2H_2+ethylene reaction, H transfer, ab initio SCF GO calcs. 77−44469
NO_2, optimisation of diffuse Gaussian exponents 79−3364
NO_2^-, optimisation of diffuse Gaussian exponents 79−3364
NOF and ONF, ab initio calcs. of geometry and electronic struct. 79−76342
$Na^+(H_2O)n$ (n=1,2,4,6), FSGO-pair-pot. calcs. *(German)* 80−74278
NbC crystals, electron energy spectra 80−49568
Ne, 1s and 2s photoionis. cross sections, L^2 calc. 80−951
Ne, atomic interaction energy, basis set effects in SCF calcs. 77−83678
Ne, L-shell photoabsorption cross-section, moment theory and finite basis pseudospectra calcs. 79−63938
Ne, solid, energy bands, depend. on choice of exchange-correlation pot. 80−70607
Ne_2, pair polarisability tensor, extended Gaussian basis set, perturbation coupled HF calc. 77−75058
O, polarisation functions for Gaussian basis sets 78−5126
O_2, $a^1\Delta_g$ and $b^1\Delta_g^+$ state, MCSCF wavefunctions 78−37561
OH_n, ab initio LCAO SCF calcs. of ionisation pot., electron, proton, H and hydride affinities 77−88387
P^-, contracted Gaussian basis sets for mol. calcs. 80−83264
$Pd(CO)_4$, ab initio LCAO MO SCF results invalidate pseudopot. calc. 77−6675
S^-, contracted Gaussian basis sets for mol. calcs. 80−83264
SF_2, ab initio LCAO MO SCF calcs., elec. struct., mol. props. 77−14344
SO_2, SF_2, SO_2F_2, bond function parameter transferability 77−30770

GO calculations continued
SiH_4, Gaussian basis sets, quality studies 79−59345
Si_2H_6, bond lengths, photoelectron spectrum, mol. orbitals calcs. 78−5132
Si_2H_6, valence electronic struct., model pot. in floating spherical GO formalism 78−74563
Si_2H_6O, geom. and electronic struct., ab initio MO calc. 79−97972
Ti (0001) film, electronic struct., Fermi level, surface states, GO calcs. 80−6927
V, energy bands, Compton profile, optical cond., SCF LCAO calcs. Gaussian orbitals 78−47698
$V(CN)_5NO^{3-}$, struct., FSGO calcs. 78−70736
$V(CN)_6NO^{4-}$, struct., FSGO calcs. 78−70736
Xe, relativistic Hartree-Fock calcs. using spherical Gaussian basis sets 80−32595
Zn_2, ab initio SCF LCAO MO calcs., contracted basis set effects 77−83495
ZrC crystals, electron energy spectra 80−49568

gold
see also nuclei with .....
5d and 4f subshells, photoionisation partial cross-section, energy depend. meas. 80−29850
(110) surface, proton reflection, influence of channelling 80−54295
adatom beam scatt. expts. on NaCl and KBr (100) surfaces 79−77924
adatom on Pt, surface diffusion, FIM expts. and Morse potential calcs. 78−34717
adatom on Pt, surface diffusion energies 79−77923
additive-free hard Au for electric connectors and PCB contacts 80−108718
adhesion of epoxy resins to surface 77−4888
adhesion to Cu, surface treatments and surface impurities 77−15701
adsorbed layer, surface diffusion on W, spreading behaviour 79−99421
adsorbed layer on W, effect on field emission energy distrib. 77−8730
adsorbed on AgBr dispersion in gelatin, transient absorpt. spectra, latent image form. and decay 80−66837
adsorbed on Ge, effect on photofield emission current 80−29856
adsorbed on Si, thermal expansion and at. vibr. singularities 77−89635
adsorbed on W (100), electron field emission revealing unmasked surface reson. 79−15595
adsorbed on W field emitter, (110) and (211) planes, effect on work function 77−12503
adsorption, of Pb, formation of $AuPb_2$ epitaxial layer, LEED, AES study of $Au/AuPb_2$ interface 78−71988
adsorption, of Xe and CO on (100), LEED, AES, EELS, surface pot. 77−15691
adsorption, on Si (111), 2-dimens. condensed layer, isothermal desorption spectroscopy 77−69181
adsorption and chemisorption of CO, high resolution UPS 78−39666
adsorption and early stages of condensation on W single cryst. surfaces 78−6212
adsorption and field-desorption on GaAs and GaP surfaces, FEM studies 80−34304
adsorption of O_2, Auger spectra 78−87879
adsorption of O_2 on (111) and polycrystalline surfaces, LEED, AES and energy loss spectra 80−34310
adsorption of Pb on (320) and (311) surfaces, LEED and AES obs. 79−86998
adsorption of water and Hg, work function change 77−7966
adsorption of Xe, electronically excited atoms coupling to cond. states 77−89642
adsorption on Ge, effect on I-V characteristics, field emission study 78−67925
adsorption on glass surface, AES study, electron bombardment effects 80−65380
adsorption on platinised Pt electrodes in aq. HCl 78−56914
adsorption on Re low index planes, FEM 78−14597
adsorption on Ta(100), model 77−1321
adsorption on W, field emission microscopy exam. of work function, correlation with LEED and RHEED meas. 78−35276
adsorption on W (100), effect on surface reson. 79−65983
AES, valence band spectra, solid-state and atomic features 78−72646
AES and characteristic energy loss spectra, expt. and interpretation 78−27354
aggregated film, optical props., 0.35-1 μm 77−66548
aggregates, solid, aerosols, dynamic shape factors meas. 80−61165
alloying with GaAs, SEM and optical study 80−70820
alpha particle backscatt. Rutherford spectra anal. 80−50497
alpha particle energy loss straggling 80−42902
amorphous, bombard. by Au ions, collision cascades, computer simulation 79−46731
amorphous film, getter sputtering at 25K 79−38741
analysis in electroplating solution, electrochemical, in presence of cyanide ions 77−1965
analysis of trace elements using vidicon spectrometer 77−21453
angle resolved XPS, temp. independence 79−19975
angular-dependent studies on some prototype vertically and laterally inhomogeneous samples 78−95655
anode, chem. dissolution in aq. alkaline cyanide, electron stoichiometry 80−40697
anodic dissolution in aqueous alkaline cyanide 79−20375
anodic electrodeposition from liq. NH_3 solns. 79−28957
anthracene-Au interface exciton luminescence Frenkel exciton metallic quenching *(Russian)* 80−50421
assay-activation analysis of rock, use of Au and Ag standards based on phenolformaldehyde resin 78−3419
atom, 4f X-ray photoabsorpt. structs. 77−18826
atom, α-particle impact K-shell ionisation, 40 to 110 MeV 78−17752
atom, ab initio effective core pot., Dirac-Hartree-Fock and Hartree-Fock calcs. 78−33426
atom, Compton scatt. of 1.12 MeV γ-rays by K-shell electrons 77−54539
atom, D matrix isolation spectroscopy using sputtering apparatus 77−26407
atom, effective ionisation cross section determ. for H, Li, Na, Cu, Ag, Au and Fr, classical theory *(Russian)* 77−30998
atom, electron impact, relativistic, L-shell ionis., $L\beta/L\alpha$ branching ratio energy depend. 79−98228
atom, electron impact ionisation, K-shell, doubly differential cross section meas. 79−98226
atom, electron impact L-shell ionis., 300-600 keV 77−50542

gold continued
atom, electron impact M-shell ionisation, 60-600 keV, absolute cross sections meas. 80−83493
atom, ESCA spectra for outermost electronic shells 77−1970
atom, excitation by FKα and AlKα ESCA sources 78−53301
atom, incoherent γ-ray scatt. by K-shell electrons 77−83560
atom, inner-shell ionis. by relativistic electron and positron impact 77−6933
atom, isolated, above alkali halide (100) surface, potential energy 77−89650
atom, isolated in mol. matrix, absorption spectra 79−22724
atom, K-shell electrons, Compton scatt. of 1.12 MeV gamma-rays 77−68016
atom, K-shell electrons, Compton scatt. of 1.12 MeV gamma-rays, energy distrib. meas. 77−68017
atom, K-shell X-rays, energy shifts and excitation mechanism 78−41990
atom, L-shell electron impact ionisation, X-ray production cross sections 77−19095
atom, L-subshell ionisation cross-section ratio by ion beam impact, projectile charge and vel. depend. 77−6920
atom, L-subshell ionisation with high vel. positive ions 79−50122
atom, nuclear K-X-ray satellites, Z=50-83, by α-bombard., 17.5-22.5 MeV 80−42984
atom, oscillator strengths, relativistic HF, core-polarisation model pot. 78−86818
atom, photoelectric cross section, derived from total absorpt. cross sections 77−10646
atom, photoelectric cross sections for 323 keV gamma rays 77−88432
atom, Rayleigh scattering at 59.34 keV through 60° to 150° 77−83547
atom, relativistic 1s wavefunctions test, using exptl. Compton profiles 80−32600
atom, relativistic effective core pots., appl. to AuH and AuCl ab initio calcs. 78−86767
atom, stabilized, contact HFS const., matrix shifts 77−42254
atom, total to K-shell photoelectric cross section ratios, 145 to 662 keV γ-rays 77−54545
atom, transition probability of valence shells, relativistic pseudopot. calc. 78−86803
atom, valence orbitals, Dirac-Fock scheme, direct and indirect relativistic effects 78−41969
atom, VUV absorption spectrum, photoionis. cross section, Fano parameters 79−93947
atom, X-ray production cross sections for protons, fluoresc. obs. 80−102476
atom total to L-shell photoelec. cross section ratio 77−30836
atomic cluster, on W support film, computer simulation of phase contrast 80−100150
atomic X-ray spectra, parity violation, from electron-nucleus weak currents *(Russian)* 79−22642
atomistic images of field ion microscopy at high temps. 78−55792
Au-CdTe contacts, photo-effect in the 77-300K range, barrier height estimation 80−107850
Auger spectra, $N_{4,5}N_{6,7}N_{6,7}$ and $N_{4,5}N_{6,7}O_{4,5}$ 80−89094
backscattering of fission products 80−16138
backscattering of H and He atoms, ang. and energy distribs. 80−76123
band structure, self-consistent relativistic calc. 80−75501
bicrystal, core structs. of misfit dislocations in grain boundaries, TEM 78−14360
bicrystal, dislocation networks in twin boundaries in TEM obs. 78−51556
bicrystal, grain boundary thickness, meas. using X-ray techniques 80−34011
bicrystal, thin, tilt boundary migration and facet development 78−2379
bicrystalline, electron diffraction on networks of grain-boundary and interphase dislocations *(Russian)* 79−73168
bicrystalline film, lattice imaging of low angle tilt boundaries by TEM 78−79620
bicrystalline thin films, epitaxially grown, preferred inclinations of ⟨100⟩ grain boundaries 80−103367
bicrystalline thin films, faceting of [001] grain boundaries 80−70222
bicrystals, interaction of lattice dislocations with grain boundaries, electron microscope obs. 78−51579
bicrystals, large-angle twist grain boundaries, X-ray diffr. obs. 79−90672
bicrystals, periodic ⟨111⟩ twist grain boundary structs., electron diffr. obs. 79−65100
binding energies, stable phase and elastic constants calc., appl. of reson. model pot. 77−69263
biological specimen prep. for SEM 79−5421
black film, structural composition and its influence on optical props. 78−56530
black solar absorbing film, particulate nature 77−39003
Bloch waves, corresponding atomic and mol. orbitals, in HEED 79−27880
capture cross section in n-type Si, MOS struct. expts. 78−91772
cathodoluminescence, film and polycryst. samples, low energy electron irrad., visible and UV emission 78−2921
CESR linewidth and g-shift in presence of spin-orbit perturbation, spin-phonon scatt. 77−63285
CESR meas. 77−24743
channelling, reson. excitation of H- and He-like ions 78−43058
channelling of B^{4+}, C^{5+}, N^{6+}, O^{7+}, F^{8+} and F^{7+}, reson. coherent excitation 79−51178
channelling of H^+, planar channelling and blocking profile, transfer matrix method 78−22780
channelling of He^+ in thin single cryst., coherent electronic excitation 78−22778
chemisorbed CO layer, mag. phase transition obs. *(Russian)* 77−77083
chemisorption, of H(O), on electrode, volume of adsorbed species, temp. and press. effects 78−84060
chemisorption of O_2, catalytic effect of Ca, AES study 79−15021
chemisorption of O_2, on (111) surface, AES investig. 77−55446
cluster, FCC cluster, 40 kV electron scatt. dynamic effects 77−79721
clusters on alkali halide surface, size depend. of valence bands, XPS study 80−65647
coalescence of small clusters on NaCl substrate at room temp. 78−18935
coated Cu, corrosion by thermal degradation products of chloroprene and silicone rubber 79−47801
coated diffraction gratings, UV light polarisation at grazing incidence 78−87129
coated surface, reflectivity in soft X-ray range 78−45221

gold continued
coating, sliding wear resistance 77−12708
coating for radioactive source backing, spontaneous resistance variations 77−54386
coating on Cu crystals, effect of coating on Cu fatigue behaviour 78−72850
coating on Si substrate, amorphous Si whisker growth characts. by SiH_4 thermal decomposition 80−34342
coating on Sn-Ni alloy electrodeposits, corrosion resist., appl. as elec. contact material 77−77633
coating on steel for watch part finishing, ion plating *(French)* 78−23879
coincidence grain boundary, lattice displacement, electron images 77−80516
coins, surface anal. by X-ray fluoresc., SEM and scanning Auger spectroscopy 80−89552
colloidal, stability and Hamaker const. determ. 79−87883
condensation kinetics, on KCl 80−88453
condensation kinetics on KCl substrate, evolution of size distrib. function 79−28243
condensation of Pb on Au (100) 78−91569
condensation on Si (111), AES obs. of very first stages 78−14633
condensed film on NaCl, ion bombarded, film growth, thermally stimulated exoelectron emission 80−50537
conduction electron g-factor meas. 77−35859
conduction electron scatt. from vacancies 77−76735
conduction electron scattering, quenched and annealed crysts., de Haas-van Alphen Dingle temp. meas. 77−89688
conduction electron spin props., g-factor, de Haas-van Alphen oscill. amplitudes 77−35858
conduction-electron spin flip by phonons, expt. data anal. 79−61219
contact films, dissociation of GaAs and $Ga_{0.7}Al_{0.3}As$ during alloying 79−79357
contact for n-GaAs, ohmic, planar, formation and props. 79−15223
contact for n-type Si, current load capacity meas. *(Czech)* 77−89846
contamination of Si and SiO_2 wafers during plasma etching 80−19831
convoy electrons from solids, ion vel. and Z and target material depend. 78−84692
core level binding energy and density of states from first atomic layer, XPS meas. 79−87563
core-electron excitation edges 80−66345
corrosion in H_2SO_4 solutions, effect of pH 79−70344
Coster-Kronig N_{45}-$N_{67}X$ transitions, semi-empirical Auger electron model and obs. 77−85889
critical temp. determ. by exploding wires method, liquid metal enthalpy 78−6149
crowdions, prop. anal. using Frenkel-Kontorova model 79−42056
crystal lattice projection, in ⟨111⟩ direction, from electron microscope image by multiray calc. 79−94855
crystal structure stability, collinear three-ion interaction theory 80−49173
crystallite, surface decoration, depletion zone anal. along KCl slip step 79−90868
crystallites, formation in flowing Ar system, density, size distrib. and size dispersion 78−88415
crystallites, surface migration on alkali halides 78−26783
crystallites, vacuum deposited on MgO (111) surface, in-situ TEM obs. of mobility 77−76686
curvature factor, interpretation of de Haas-van Alphen oscillation amplitudes 79−47000
curved crystal, planar channelling effects for relativistic protons and π^- mesons, deflection effects 79−77656
cyclotron mass and Fermi velocity meas. by de Haas-van Alphen effect 77−76734
DC reactive sputtering, glow discharge mass spectrometry and X-ray diffr. 79−38701
Debye temperature var. at high temp. *(French)* 78−63831
Debye Waller determ. from modified Cheveau model 78−59918
Debye-Waller factor temp. parameter 78−30725
Debye-Waller factors, modified ang. force model 77−66013
decoration, obs. of grain boundary segregation in NaCl bicrysts. 77−68982
decoration, obs. of graphite surface behaviour under various vacuum conditions 78−75915
decoration of additively coloured NaCl:OH^-, form. and decay of defect clusters and elec. double layers 79−10850
decoration of electron beam cleaved MgO surface 77−47657
decoration of KCl:Pb cryst. surfaces 80−15144
decoration of solid-melt interface of NaCl-LiCl mixed crystals, obs. of high temp. phases 80−15026
defects, atomic arrangements around, dynamic obs. of atom movement 80−39108
deformed, annealing kinetics of vacancies, elec. cond. meas. and computer simulation 78−47353
deformed, annealing kinetics of vacancies *(Japanese)* 80−88139
deformed, exoelectron emission and electron energy distrib. 80−7481
deformed bars, cold rolled, exam. of microstruct. by thin foil TEM 78−88502
dental fillings, cause of dose perturbation in radiation therapy 80−12265
deposit location in Canton Bousquet, Quebec *(French)* 77−53051
deposited on alkali metal substrates, calc. binding energy of Au atoms to substrate 79−33208
deposition at high rates from organic plating baths *(French)* 80−66441
deposition by ion beam sputtering, composition and stress state 77−89674
deposition of Pb, on Au substrate, quantitative Auger electron spectroscopy, substrate and instrumental effects 80−71523
deposition on CdS, Schottky diodes and MIS devices, surface treatment effects, SEM obs. 80−54794
deposition on ceramics with Cr interlayer 77−20202
desorption on Si (111), kinetics of two-dimens. phases on single cryst. substrate 78−14598
determination, in Italian chondritic meteorites, by destructive neutron activation anal. 78−12172
determination by gamma ray differential absorpt., in thin Ag objects 80−85227
determination in rocks, minerals by at. absorpt. spectrometry 77−29067
dielectric const. by multiangle reflection meas., optical props. 79−95723
diffraction grating, concave, Au-coated, polarisation anomalies 80−69519
diffusion, grain boundary, of Cu and Pd, determ. using AES data 77−11742

gold continued
diffusion, light activated reactive, into As_2S_3 film 77−55393
diffusion, self- and Co impurity, temp. depend. of isotope effect 78−47563
diffusion and electric transport in glassy As_2S_3, effect on elec. and opt. props. 77−76623
diffusion barrier formation, at metal-semiconductor or metal-metal interface using laser annealing 80−80373
diffusion coefficient of H, steady-state flow method 80−10795
diffusion in amorphous As_2Se_3 77−51549
diffusion in Cu, diffusion coefficient temp. depend. *(Russian)* 77−84987
diffusion in Er, anisotropy, interstitial solute diffusion mechanism 80−29223
diffusion in $Ga_xIn_{1-x}P$, epitaxial film, effect of intrinsic impurities 78−87825
diffusion in GaP, interimpurity interaction effect on distrib. profiles of impurities diffusing simultaneously 77−76451
diffusion in In solder for GaAlAs DH laser, deterioration anal. 80−33019
diffusion in p-Si:Cu, influence of Cu 77−62679
diffusion in Pt at low temp. 78−30789
diffusion in semicond., B, temp. depend. of coeffs., mechanism 77−7898
diffusion in Si, enhancement by photo- and electron-irrad. 77−27901
diffusion in solid Pb, ultra-centrifuge study 78−47593
diffusion mobility of gas bubbles in Au 80−39357
diffusion of Co and Fe, 700-1050°C *(Russian)* 77−80651
diffusion of Cr along grain boundaries, analytic and numerical solns. 77−4274
diffusion of Cu, 75-150°C, AES, device appls. 77−1262
diffusion of H and D, in situ growth of stable oxide barriers 78−75883
diffusion of Ni and Cu, relative diffusion rates 77−80652
diffusion of Pd and Pt, 700-1000°C *(Russian)* 78−91484
diffusion on atomically clean Si (111) surface 78−72037
diffusion through electroplated Pt film, AES obs. 79−14968
diffusion/oxidation of underlying Cu, rate-controlling step 80−34240
discontinuous film, elec. cond. and current noise, temp. depend. meas. 78−56245
discontinuous film, light absorpt. spectra, dielec. function calcs. 79−51507
discontinuous film, optical transmittance 78−56529
discontinuous films, on sapphire substrates, electrical noise, high temp. behaviour 80−54807
dislocation free bicrystal, DSC dislocation network generation in coherent twin boundary 77−62544
dispersed particles in NaCl, age hardening of surface, double decoration obs. 79−11634
Doppler factor, comparison between calculated values and measured results 78−54811
drops, VLS growth of TiP whiskers on drops 79−4497
dynamical factors calcs., by multi-slice dynamical diffr. methods 79−23505
EHD emitted ions, energy distrib. 79−61503
elastic constants, third-order 79−51184
elec. resist. and vol. change due to lattice vacancy 79−51101
electrical contact surface, lubrication by plasma-deposited thin films of fluorocarbon polymer 80−89157
electrical contact to semiconductor, spark welding method, for elec. meas. *(German)* 79−49215
electrical resistivity, 5.2-40K, deviation from Matthiessen's rule 79−99526
electrical resistivity, press. variation 78−84193
electrical resistivity, pseudoharmonic effect of phonons 80−34414
electrical resistivity, temp. depend. data 80−51967
electrical resistivity 79−38042
electrical resistivity deviations from Matthiessen's rule due to dislocations 79−65425
electrical resistivity of dislocations, calc. *(Russian)* 78−60117
electrically exploded foils, heating and burst phenomena 77−39488
electrochemical behaviour in nucl. reactor radiation field 77−52650
electrochemical electrode, photoemission-into-electrolyte 79−74390
electrode, adsorption of metal ions, kinetics, surface struct. 78−79873
electrode, adsorption of pyridine, angle-resolved Raman spectroscopy 80−52991
electrode, amalgamated, electrochem. capacity meas. by potentiodynamic technique 80−40704
electrode, deposition of Cu monolayer in underpotential region, RHEED investig. 80−54539
electrode, diffusion into polymer film 79−77821
electrode, electrochem. oxidation of alcohols using alkaline electrolytes *(German)* 78−15681
electrode, electrochem. oxidation of N_2H_4 and methylhydrazine, appl. to gas monitoring 79−39248
electrode, emersed, electrorefl. spectra 79−28788
electrode, evaporation rate from cathode spot in vac. arcs. 80−49024
electrode, single cryst., (100), solid and thin-layer differential-pot. capacity curve with NaF aq. soln. *(French)* 79−47932
electrode, solid electrolyte roughness rel. to interface impedance 77−4437
electrode, thermal diffusion into amorphous semiconductor thin film, α-particles backscatt. obs. 78−10228
electrode pot. effects on surface plasmon excitation 78−15149
electrode surface, adsorbed Br_2, anisotropy of optical props. 80−60534
electrode/Ge powder contact pot. difference, grain size depend. 80−44723
electrodeposit, struct., texture, influence of As on brightness *(Bulgarian)* 78−79862
electrodeposit, struct., texture, influence of substrate *(Bulgarian)* 78−79863
electrodeposited, hard, hardening mechanisms, grain size effect 80−35302
electrodeposited and sputtered, hard, reactive softening, X-ray diffr. studies 80−100414
electrodeposited coating, Cu diffusion under high temperature, influence on contacts performance *(Czech)* 78−91486
electrodeposition, heavy metal ion induced depolarisation effects 77−16511
electrodeposition, in 2 μm layers 79−74104
electrodeposition, surface prep. of Be-Cu 78−7100
electrodes, drift and thermal diffusion in amorphous semicond. thin films, α-particle backscatt. meas. 79−4434
gold continued
electrodes, partially covered with photoresists. layer, ferricyanide reduction 78−85236
electroless deposition, substrate structure influence 77−8771
electroless plating on GaAs for fast characterisation of epitaxial layers 79−33347
electromigration and deform. 78−2286
electromigration and residual resistivity of ^{57}Co 78−71881
electromigration in Pb, 165 to 270°C 80−29221
electromigration in Pb 77−69116
electron backscattering, X-ray prod., energy distrib. calc. 79−38698
electron beam energy losses 78−91368
electron capture into continuum states of fast channelled protons, Gaussian flux peaking calcs. 79−86827
electron diffraction phenomena, rocking curves 78−14251
electron diffraction study, ECP contrast, Bloch wave model 80−96419
electron emission induced by low energy light ions 79−61482
electron emission spectra produced by exploding wire photon sources, yield and energy meas. 78−31299
electron inelastic mean free paths and energy losses, electron gas statisitcal model 79−46733
electron irradiated, exam. of vacancy migration energies, annealing kinetics 78−47571
electron irradiated, interstitials and their clusters, diffuse X-ray scatt. study 80−33997
electron irradiated, low temp., Frenkel defects, diffuse X-ray scatt. study *(German)* 79−23601
electron mean free path, 60-140 eV 77−62909
electron mean free paths and stopping powers calc. using statistical model 77−19996
electron microscopic examinations, HV, nearly aberration-free lattice images for single crysts. 79−32865
electron range, low-energies continuous-slowing-down approx. and range straggling calcs. 80−39183
electron scattering cross sections, 300 to 1200 keV 78−9922
electron transmission and absorpt. in bulk solids, 5 to 30 keV 77−89491
electron transmission and absorption at 0.6 to 4 keV, obs. 77−84818
electron tunnelling from particle, polarised light emission and plasmons 79−51685
electron-ion pseudopot., form factor, liquid elec. cond., phonon dispersion 78−34785
electron-phonon interaction determ. from current-voltage curve at 1.5K *(Russian)* 77−47789
electronic density of states, cluster approx., compared with photoemission spectra 79−60675
electronic energy loss of H, D, and He below 20 keV 80−42906
electronic props., pseudopotential calc. 78−51960
electronic stopping function for He^+ and Li^+, 50-300 keV 79−69169
electroplate, delineation of hard from soft by etching 78−3292
electroplate on Cu, water vap. adsorption 77−69168
electroplated, microstruct. and hardness, effect of thickness and deposition conditions 80−20057
electroplated, polyphosphate, citrate-phosphate and sulphite baths, comparison w.r.t. internal stress and grain size 79−7756
electroplated, thickness meas. by beta-ray backscattering *(Slovene)* 78−6860
electroplated layer, dropwise steam condensation, thickness depend. 79−46791
electroplating, pulsed potentiostatic deposition from Au(I) sulphite solns. 78−15321
electroplating, selective, on Pd-Ti conductor patterns, Si IC manufacturing appls. 79−95951
electropolishing for electron microscopic examination 78−35589
electroreflectance of single cryst. electrodes, obs. in aqueous solns. 80−25342
electroreflectance spectra of monocrysts., anisotropic surface effects 79−8123
emittance, calc. from spectral radiative and reflecting props. 77−35730
energy band structure, X-ray emission spectra, APW calc. 80−92811
energy band structure, X-ray N-emission spectra, relativistic APW calcs. 80−70596
energy losses and straggling for H^+ and He^+ beams *(Russian)* 80−84226
energy reflection coefficient for 5 to 10 keV He ions 78−95639
epitaxial film growth with ionised beams and surface imperfections 77−32529
epitaxial films, grain boundary struct. evolution during recrystn., interface energy effect *(Russian)* 80−15387
epitaxial growth, cluster mobilities, in-situ electron microscopes obs. 80−15407
epitaxial growth and nucleation on NaCl during ion bombardment 79−11024
epitaxial growth in NaCl with continuous C-intermediate film 78−84102
epitaxial growth on Pd, alloying effects 77−62785
epitaxial layer, electron channeling pattern, large angle, generation and appl. 80−100296
epitaxial layer, grain boundaries, electron microscope obs. 79−11025
epitaxial layer on NaCl substrate, electrotransport inferred from void growth rate *(German)* 80−10699
epitaxial layers, sandwiching of biopolymers, electron microscopy specimen prep. 78−36080
epitaxial particles, high resolution dark field electron microscopy 77−85111
epitaxial particles, high resolution TEM topographical images 77−43439
epitaxial single-crystal film occluded DNA molecule electron-microscopic contrast 79−57568
epitaxially grown bicrystal, on (001) Fe substrate, interfacial dislocation behaviour 77−51622
epitaxially grown double layers on vacuum deposited Fe, interfacial dislocations 78−30847
epitaxy on W (001) 78−60041
epitaxy on W (110), LEED and AES 77−69198
EPR, quadrupole interaction 78−48027
equation of state, low temp., appl. to thermal expansivity 79−60476
ESCA laterally inhomogeneous sample, ang. and spatial depend. intensity 79−74468
etching, prior to deposition of C, in RF butane plasma 79−66224
evaporated, 890 GHz surface resistivity meas. by pyroelectric detector 77−39915
evaporated film, adsorbed CO, enhanced Raman scatt. mechanism in ultrahigh vacuum 80−107645

gold continued
evaporated layer, secondary electron energy distrib. and work function *(French)* 79−99993
evaporated layer growth on V{100}, total current spectroscopy 77−36329
evaporated metal nuclei on C, SiO_2 films, atm. contamination, AES meas. 77−4264
evaporated particle, high resolution electron holography with field emission electron microscope 79−30614
EXAFS, $L_{2,3}$, determ. of s and d contrib. 77−44086
EXAFS at L-edges of heavy elements 79−47543
fast electron multiple scattering, and inner secondary electron generation 77−1160
FCC, atomic defects, computed electron microscope images 78−26392
FCC, dynamical study for Gruneisen parameters 77−47594
FCC, Gruneisen parameters, effect of temp. variation 78−22812
FCC, props. of vacancies and divacancies 80−10545
FCC, stacking fault, antiphase boundary energies, investig. methods, review *(French)* 79−42080
FCC, thermal expansion coeffs., Morse pot. calcs. 79−77775
Fermi surface and thermoelec. power, de Haas-van Alphen calc. 79−4503
Fermi surface anisotropy meas. by positron annihilation 77−20222
Fermi surface orbit integrals, tetrahedron method, cyclotron mass orientation depend. 80−44476
film, (001) surface atomic steps obs. using TEM 77−20173
film, (111), sputtered, surface struct., HV electron microscopy and theoretical model 78−22981
film, absolute work function meas. by field-emission retarding-pot. device 77−59322
film, adatom surface diffusion at low temps., elec. resist. study *(French)* 80−65376
film, aggregated, absorpt. peaks, collective oscills. of electrons 78−80428
film, air corona discharge, thermal energy positive ion extraction 80−38801
film, Al/copper phthalocyanine/Au cell, photoexcitation, doping, energy loss mechanisms 79−99573
film, angular depend. UPS, surface electronic struct. 79−83095
film, annealing curves, size effect parameter determ. from Mayadas Shatzkes theory 77−76962
film, beam splitter phase coatings, for producing phase quadrature interferometer outputs 78−77974
film, chem. deposition on Si, form., struct. 78−34723
film, contact reaction with amorphous Si 79−23846
film, Cr and Si low temp. diffusion, CO effect 80−100361
film, damping and vel. of longit. elastic waves at 9.4 GHz 80−10596
film, deposition on NaCl by ion beam sputtering, initial growth features 79−77962
film, deposition on polymer substrates, effects of glow discharge on nucleation characts. 79−77963
film, deposition with sputter gun 77−44162
film, detection of faceting on (h,k,0) surfaces by diffr. in electron microscope at 100 kV 78−43273
film, diffusion of Ag along grain boundaries, scanning Auger microscopy obs. 78−22897
film, discontinuous, centre-to-centre particle distrib. determ. 80−96761
film, discontinuous, degradation under MeV heavy ion bombard., Rutherford scatt. and TEM obs. 79−24397
film, discontinuous, high temp. elec. cond., model 79−78220
film, discontinuous, morphology and size distribs. of islands, electron microscope obs. 77−62766
film, discontinuous, optical absorption 77−69927
film, discontinuous, optical transmittance, effect of island morphology 78−84673
film, discontinuous, substrate radiation damage effect on resist. and strain gauge stability 79−95520
film, discontinuous, vac. evaporated on C and SiO, struct. and elec. cond. 80−39686
film, domain size and internal strain, studied by electron diffraction line broadening 78−30840
film, dynamic recoil implantation, in Si 79−14833
film, early growth stages on amorphous C, cluster migration obs. 79−77964
film, effect of high DC density stressing on pre-existing voids 80−24770
film, electrical resistivity, influence of metallic adsorption *(French)* 79−19677
film, electron beam transmission, reflection, and absorp., $35 \leq E \leq 70$ keV 77−39754
film, electron bombarded, transition radiation 77−85828
film, electron emission and electroluminesc. 77−90257
film, electron inelastic scatt. mean free paths, synchrotron radiation photoelectron spectra meas. 78−76587
film, electron transmission, 1-5 keV, electron MFP 77−15472
film, electron transmission, calc. 80−60724
film, electroreflectance effects 79−43055
film, electrotransport-induced failure site, minor constituents effects 79−23763
film, ellipsometric obs. of optical props. 79−78776
film, energy losses of 20-40 keV electrons 78−92153
film, energy losses of electrons, microcalorimetric meas. 80−59543
film, epitaxial growth, characterisation of [001] tilt boundaries 78−84097
film, epitaxial growth, effect of electron bombard. of NaCl substrate, TEM and AES obs. 79−90916
film, epitaxial growth, whisker form. 77−76713
film, epitaxial growth on Ag(111) surface, LEED meas. 78−14632
film, epitaxially grown, struct., LEED, AES, resist. and X-ray diffr. analysis 77−59223
film, evap., temp. change and gas adsorpt. effect on opt. consts., ellipsometric obs. *(German)* 80−89081
film, evaporated, DC elec. resist. 80−29487
film, excess (1/f) voltage noise 79−42598
film, excess vacancy diffusion to free surfaces and voids, resist, decay 79−65237
film, grain boundary, electromigration, tracer meas. 77−31802
film, granular, transmission and reflection spectra, validity of sum rule 80−97358
film, growth kinetics of icosahedral particles *(French)* 77−24494
film, growth on C replica stripped from pure and doped NaCl single crysts., elec. memory expts. 77−76691
film, growth on clean and contaminated GaAs (001) surfaces 78−26785
gold continued
film, in mag. field up to 40 kOe, microwave skin effect 77−12032
film, inert gas ion refl., semiempirical analysis, compared with expt., 10-30 keV 78−6823
film, inertialess glow induced by picosecond laser pulses *(Russian)* 80−100714
film, influence of predeposited island film on crystallisation of continuous films 78−18930
film, influence of target texture on backscatt. yield of 2 MeV ^4He particles 79−4875
film, integrated condensation coeff. on NaCl cleavage faces, Rutherford ion backscatt. obs. 80−59827
film, interaction with adsorbed dye mols., absorpt. and luminesc. 80−103981
film, interface reaction with n-type $Ga_{0.7}Al_{0.3}As$ and GaAs 80−39482
film, ion bombarded, surface craters induced by displacement cascades 80−107344
film, ion plated, defect growth structs., SEM obs. 80−24768
film, ionic sputtering and AES anal. *(French)* 78−76959
film, laser absorpt. vs. temp., calorimetric meas. 79−98423
film, low temp. void growth and resistivity decay 78−10302
film, Maxwell stresses at charged surface from elastoresistance 80−49957
film, MBE and field emission deposition on III-V semiconductors, comparative study 79−87016
film, microporosity induced by nucleation and growth processes, TEM expts. 78−10303
film, modifications of optical and elec. props. as function of struct. during deposition 79−78777
film, modulated surface-plasmon reson. in situ meas., O_2 adsorpt. 77−77311
film, multiple attenuated total reflection spectroscopy, initial growth process 79−19490
film, nonohmic characts. and electron emission 80−60066
film, on α-quartz substrate, optical consts. evaluation from surface polariton dispersion 78−48249
film, on Ag, optical constants, 4000-6000 Å, using surface plasmon optical excitation 77−69925
film, on Ag(111), thickness and optical consts. using surface plasmon excitation 79−47533
film, on amorphous C and Si substrates, dispersion force contrib. to adhesion *(French)* 80−59842
film, on C/Ag system, epitaxial growth in ultra high vacuum 77−1336
film, on CdS, bonding and interdiffusion, XPS obs. 80−80000
film, on complementary cleavage planes of TGS, morphology, electron microscope obs. 79−15031
film, on corundum with intermediate Cu and Cr layers, struct. obs. 77−28084
film, on Cu, ion-induced intermixing 80−15420
film, on glass or quartz, laser-induced damage, determ. of surface fluctuation of slide 77−1279
film, on MgF_2 and SiO substrates, internal stresses correl. with struct. 79−87026
film, on NaCl, preferential epitaxy induced by electron bombard. or elec. field 80−10824
film, on Ni, AES anal., influence of ion bombardment on depth resolution 77−20210
film, on sapphire substrate, nucleation, growth and postdeposition thermally induced epitaxy 79−77946
film, on Si, coincidence site phase boundaries 78−67927
film, on Si, early growth by ion-beam sputtering 77−44158
film, on Si, specific high-angle boundaries *(Russian)* 77−76678
film, on Si, use of sputtering for layer removal 79−78813
film, on Si (100) substrate, growth and struct., LEED and AES obs. 79−51457
film, on Si and CaF_2 substrates, interphase coincidence boundaries 79−1560
film, on Si or CaF_2, oriented crystn., formation of coincidence orientations on interphase boundary 79−90922
film, on W substrate, chemisorbed N_2 effect on crystallite growth, FEM obs. 79−46976
film, on W substrate interface struct., FIM obs. 80−65384
film, on ZnS crystal for composition control, calc. of defect conc. 78−95052
film, optical and elec. props. in situ determ. during deposition 77−59341
film, optical characterisation, inversion method 78−11008
film, optical consts. meas. via automatic ellipsometer without phase plate 77−53970
film, optical dielec. const. in visible region, 300 to 1.5K 77−90211
film, optical props., theory including electron surface scatt. 80−29817
film, photoelectron emission, intershell interaction influence on 3d and 5d branching ratio 80−104038
film, polycrystalline, temp. depend. of Drude absorption 79−78779
film, quantum size effect, field emission study 80−70849
film, refr. index, obs. using automated Fourier-Stokes analyser ellipsometer system 78−49886
film, self-supporting thermotransmission meas. 1.8 to 3.5 eV 78−27343
film, simulation of transmission of 1-keV electrons 77−12475
film, single layer and multilayer systems, thickness determ. by X-ray fluoresc. 80−68180
film, spike effects of heavy ion sputtering 80−35034
film, sputtered, hardness and ductility 79−87025
film, sputtered, physical props. 79−77938
film, surface roughness effects on the energy dispersion of backscattered protons 79−24403
film, surface step structure imaging by dark field electron microscopy 80−15346
film, surface-plasmon modulated-reson. for adsorption studies 79−83045
film, thermal phonon radiation into α-quartz substrates 79−42363
film, threshold current density and incubation time to electromigration 78−14643
film, transmission sputtering 78−52613
film, transparent, secondary electron emission of 10-100 keV electrons 77−32477
film, twin boundary struct. and migration, atomic scale electron microscopy obs. 80−107276
film, ultrathin, quench-condensed, two-dimensional elec. cond. 78−39233
film, ultrathin evaporated, acoustoelectric meas. of electron mobility and diffusion 80−65707
film, ultrathin islands, band structure formation 77−85893

gold continued
film, unbacked, optical constants by transmission interferometry 79−78778
film, unbacked, optical consts. meas. by transmission interferometry 79−78768
film, unsupported, simultaneous meas. of refractive index and thickness *(French)* 77−55842
film, vac. deposited on V, Au or amorphous C substrates, surface pot. and work function 79−42672
film, vacuum deposited, internal stress and its depend. on gas adsorption 80−6683
film, vacuum deposited, O^+ bombardment sputtering rates 78−88390
film, vacuum deposited, surface struct., HEED meas. 78−6234
film, vacuum deposited on Cu, sputtering yield by substrate Auger meas. 79−95889
film, van der Waals energy of interaction with heavy alkali atoms 77−11829
film, vapour deposited, attenuation and phase vel. of SAW interacting with charge carriers 79−46136
film, vapour deposited, voids 77−69194
film, vapour deposited on polymer, ageing, adhesion, elec. cond., electrochem. pot. *(Russian)* 79−33362
film, vapour-deposited (001), surface struct. and lattice const., TEM obs. 77−1326
film, very thin, on MgO (001) surface, AES obs. 79−33870
film, void growth in early stages of ageing and electromigration 78−38991
film, void size and number prediction 79−28256
film, whisker growth due to high current densities 77−69191
film, work function changes upon water contamination 80−44705
film (001) surface, computer modelling of high resolution TEM images 80−6330
film adhesion on oxide or glass with interposed fluoride film 78−19667
film bicrystal, grain boundary dislocations in plane matching boundaries 80−39110
film bicrystals, exam. of low energy planes for tilt grain boundaries 78−51551
film characterisation technique, APFIM, time-of-flight spectroscopy 80−75138
film coatings for Mo tips, film characterisation by atom probe FIM atomic clusters, voids 80−33863
film continuity, observations by Auger spectroscopy 78−64433
film deposition, thermal effects, influence on internal stress meas. 80−96767
film depositon on GaP and GaAs for constructing surface-barrier photodetectors 77−77423
film electrode, electrochem. adsorpt. of O_2, elec. resist. obs. *(French)* 79−29372
film electrodeposition, substrate effects on film props. 80−81329
film growth, optical and elec. prop. meas. during deposition *(French)* 77−70007
film growth on mica substrate, surface defects and heterogeneous nucleation 78−47684
film growth on Mo (110) surface, AES, LEED, thermal desorption study 80−80130
film growth on Si(100), LEED and X-ray texture anal. 79−99452
film on α-quartz, SAW velocity/temp. dependence 77−31861
film on (100) Si, measurement of SAW dispersion and thickness using acoustic microscopy 80−53575
film on Al, optical reflectance and absorpt. obs. 80−7426
film on Cr adhesion layer, etching, SEM anal. of abnormal undercutting 79−5075
film on Cu, oxidation exam. by ion scatt. spectra 79−79153
film on oxidised Si with metal adhesion layer, ageing props. 77−11820
film on Si, SAW dispersion and film thickness meas. 80−10769
film on Si substrate, solid-solid reactions 78−95369
film room-temp. plasma chemical transport deposition 79−78894
film sandwiches, recovery kinetics and early stages of diffusion, DC resist. expts. 79−77971
film surface, Cu and Ag contamination, AES obs. 80−24763
film with micron-size pinhole, low energy electron scatt. 79−81351
films, (111), sputtering in high voltage electron microscope 80−35027
films, condensation on alkali halides, growth, struct., stability *(French)* 78−38989
films, discontinuous, electroluminescence obs. 80−103998
films, in situ meas. in ultrahigh vac. at low temp., optical reflectivity and transmissivity, DC resistivity *(French)* 78−39617
films, on Al, Ni, EUV reflection efficiencies 79−14073
films, optical props. meas. rel. to electron surface scatt. theory 80−29818
films, thickness meas. standards for Rutherford backscatt. 79−40529
films on barrier-layer photocells, spectral distrib. of transmission coeffs. 77−1744
films on GaAs:Cr substrates and LPE layers, Cr redistrib. during annealing 80−15312
fine particles, adhesion, role of twinning and surface energy, TEM obs. 78−72009
fine particles, adhesion and sintering, TEM exam. 78−44053
fine particles, gas evaporation technique for prep., X-ray diffr. study 80−75327
fine particles, gas evaporation technique of prep., X-ray diffr. study, charact. temp. 80−75328
fine particles, prep. by gas evaporation technique, crystal habit 77−52239
fine particles, vacuum deposited, morphological features using TEM weak-beam dark-field technique 80−15410
fine particles, vacuum-deposited, degree of faceting during sintering 80−84411
flow stress during cutting 77−59881
foil, 8 ns laser pulse-target interactions, ion-expansion struct. 79−14575
foil, average thermal neutron flux determ. method 78−73112
foil, coherent twin boundary, electron microscopy *(Japanese)* 79−82130
foil, electrodeposition of alpha activity, use in Si surface barrier detector 78−82565
foil, electron scatt., appl. of Monte Carlo type calc. *(French)* 77−7636
foil, electron scattering, most probable transmitted scatt. angle calc. *(French)* 77−68901
foil, electron spectra from α-particle and fission product passage 77−24918
foil, H and H^+ neutralisation at solid surface 79−74043
gold continued
foil, heating by high-energy relativistic focused electron beam *(Russian)* 77−1154
foil, integral ang. distrib. of D^+, D_2^+ and D_3^+ ions 79−93894
foil, neutron activation cross sections meas. for generalised intermittent irradiation, fusion machines appl. 78−58283
foil, proton energy straggling determ., at 0.35, 1, and 1.75 MeV, γ-emission reactions 79−4354
foil, radiation damage, in situ study by HV electron microscopy 78−6101
foil, sputtering in a high voltage electron microscope 77−36328
foil, X-ray induced electron emission, secondary electron energy distrib. 77−59669
foil, X-ray induced electron emission 77−4713
friction props. of surface films in air and high vacuum 78−60850
g-factor, determ. from de Haas van Alphen meas. 77−11847
galvanic coatings, corrosion by org. insulant thermal destruction products *(Ukrainian)* 77−52525
gas phase, He I photoelectron spectra, photoionisation cross section meas. 79−98051
getting, of Au in Si by P diffusion and P-induced dislocations 78−91346
grain boundary structure, high resolution HVEM 80−103360
grain boundary structure, TEM 80−100255
grain boundary thickness obs. using electron diffr. techniques 80−79811
Gruneisen number and nonlinearity const., elastic moduli data, US attenuation 80−65165
Gruneisen parameters, 10-100K, phonon wave vector depend. 78−38801
Gruneisen parameters, dynamical study using modified Bhatia model 79−37797
hardness, temp. depend. 77−40440
heat content between 300.05 and T (T from 400 to 1000K) drop calorimetry *(French)* 80−10682
heat pipe meas. of corrosion and vapour press. 80−23878
heated thin film in liquid ^4He at 0.1K, temp. for large energy flux 79−55981
heavy ions with energy 0.4-0.9 MeV/A, stripping by C foils, straggling, foil behaviour 78−33351
HEED, band theory, zone axis crit. voltage effect 78−83659
high current density plated, Co diffusing out, oxidation kinetics 78−92393
high-resolution spectroscopy in far UV 77−66484
high-temperature meas. and calibration appl., above 1000°C *(Rumanian)* 80−47061
high-Z disc targets, 1.06 μm laser radiation interaction 80−6269
hollow cathode laser, ion laser transitions 80−69366
immersion plating on Al, adhesion and contact resist. 79−39033
implantation in Fe, effect on corrosion by H_2SO_4 soln. 80−71793
implanted ion detection by X-ray emission anal. in TEM 78−51575
inner electron wavefunction, meas. using Bragg scatt. of 412 keV gamma-radiation 79−14734
p-InSb-Au, surface barrier, structure, photosensitivity spectrum 79−51674
interatomic pair potential, phonon spectra 80−33927
interatomic potentials from experimental phonon spectra 78−75621
interdiffusion with SiO_x and Al_2O_3 films 77−85000
interface with dilute ^3He-^4He mixture interface, Kapitza resist., dynamic meas. 79−28188
interstitial, calc. images and diffraction patterns 80−100152
intraband optical conductivity, electron-electron scatt. 78−35166
ion, spectra from beam-foil excitation and Tokamak produced plasmas 79−54828
ion bombarded, Ar^+ ions, time-of-flight spectra of sputtered atoms 80−89103
ion bombardment, analysis of obs. shadow pattern 77−32488
ion bombardment, ang. distrib. of relfected keV ions 79−65127
ion bombardment, by Ar^+, focused ejection 80−104028
ion bombardment-induced photon emission as function of target temp. 80−100698
ion etching, dispersion coeff. determ. *(German)* 80−40597
ion imaging of thin specimen 79−99035
ion implantation damage, spike threshold, TEM 79−90705
ion implanted, ellipsometry, 1.8-5.5 eV, dielec. function 78−6697
ion implanted Cu single crystals, pulsed electron beam irrad. 80−65019
ion irradiated with Bi^+ and Bi_2^+, cascade energy density effect on defect cluster type 80−107340
ion plating process 79−66186
ion scattering, energy and mass spectra of scattered 8 keV Ar^+ ions and desorbed species 77−32487
ion scattering energy spectra by TOF and electrostatic analyser methods, comparison 79−2895
ion sputter cleaning, in EM 80−101895
ion stopping power systematics, Z_1-oscills. 79−65130
ion tracklength in mica 78−38767
ions, beam-foil spectra from 20 to 238 MeV energy, 5 to 60 nm, lifetime meas. problems 80−9722
IR absorption coefficient, temp. depend., 3 to 30 μm 78−74953
irradiated, self-interstitial type defects, combined single-double alignment channelling backscatt. 78−34561
irradiated with electrons and neutrons, positron annihilation meas. *(German)* 77−62563
island condensate, on LiF or NaCl, nucleation kinetics, influence of ionised atoms 77−11816
island film, on NaCl cleaved surface, growth, effect of perp. elec. field *(German)* 77−76697
island film, on SiO_x, growth and struct., effect of perp. elec. field *(German)* 77−76696
island film, role in oriented crystallisation of Ag on active a-C 79−7762
island film real structure and electrical conductivity obs. 79−77948
island films, forming process, I-V charact., and switching 79−11242
island films on CaF_2 in acidic medium, morphological changes, C replica method 77−1286
island structure on GaAs, effect on photoelec. memory effect 77−55570
Kambalda (W.Australia) komatiite sequence, Au, Pd, Ir and Ag in interflow sedimentary rocks 79−20830
L_{III}-edge X-ray absorpt. reson., chem. environment effects 79−72256
laser, pulse stimulated emission with discharge excitation 77−79810
laser, vapour, 627.8 nm UV emission, average output power and efficiency 79−45933
laser microprobe emission spectroscopy, matrix effects 77−16870
laser radiation absorptance at 1.064μm 79−87528

gold continued
lattice dynamics, energy wave number charact., by reson. model 80−10612
lattice dynamics, ion-ion and ion-electron interactions 80−49321
lattice dynamics, modified Bhatia model, phonon dispersion, Debye-Waller factor temp. depend. 77−31729
lattice dynamics, modified CGW model calcs., phonon dispersion, sp. ht. and equiv. Debye temp. 78−10135
lattice dynamics on Kreb's model 80−59594
lattice images, obs. with a field emission electron microscope 79−14659
lattice location in Zn, gamma-spectral study 80−80227
lattice vibration and electron press., central pair pot. model calc. 78−75749
lattice vibrations and ideal elec. resistivity 79−46770
layers, thickness determ. by laser microprobe and flame atomic absorpt. 80−27355
Lifshitz constant for calc. of van der Waals force between two solids *(French)* 80−107658
liquid, field emitted ions, energy distrib. 79−61501
liquid, ion source fabrication and emission characts. 80−68995
liquid-forming agent in vapour-liq.-solid growth of Si 78−42935
liquid-forming agent in vapour-liq.-solid growth of Si 78−42936
local pseudopotential, phonon frequencies, binding energy and liq. metal resist. calc. 77−20216
low density target, laser-prod. plasma, resistive inhibition of suprathermal electrons 80−87916
low energy sputtering by Ar and Xe ion bombardment 78−15269
low-angle tilt boundaries, edge dislocation serration and dissociation 77−72621
luminescence spectra due to slow electron bombard. 78−10995
in mafic and ultramafic rocks from Mid-Atlantic Ridge, Pd, Ir, and Au contents 77−91073
magnetic susceptibility, Animalu transition metal model pot. invest. 80−75711
magnetoresistance, of quenched and annealed metal, defect scatt. 79−4981
matrix isolated atoms, matrix influence, theory 78−46288
matrix isolated atoms, matrix influence, theory 78−46290
matrix-isolated, matrix-induced changes in opt. spectra 77−57913
mean excitation energies from α-particle stopping power meas. 79−13615
mean excitation energy based alpha particle stopping power meas. 78−30678
melting curve to 60 kbar press., reinvestigation 80−39260
metal beam epitaxy, high temp. high purity sources 79−43156
metallic film, anomalous stopping power effects 80−65102
metallised amorphous GeSe junctions, electrical contact effects on properties *(German)* 80−93010
metallised coating on polyethylene terephthalate film, fracture under laser irrad. *(Russian)* 80−76333
metallography 78−3289
migration in GaAs, ESCA study *(French)* 78−75885
migration in Si, electron bombardment effects 80−100362
mirror, laser damage, temp. depend. of absorptance, vaporisation and vap. heating 79−81471
mirror film, ultraclean DC sputtered, optical props. 77−50748
MNOS structure, Au-diffused, with chem. oxidised ⟨100⟩ substrate Si-SiO_2 interface traps 77−62995
mobility of small crystallites on KBr cleavage planes 79−23857
moderator surface preparation for increased slow positron yield 80−61011
molecular ion cluster emission in SIMS, parity rule applics. *(French)* 80−63882
molecule, VB calcs., wave functions, interatomic distance and dissoc. energy values 77−57883
monodisperse sol, ordered struct. obs. 78−3384
monolayer, on W(001), elec. struct. 78−72236
MOS capacitor, Au-doped, bulk and interfacial prop. determ. using quasi-equilibrium and linear voltage ramp techniques 79−95501
MOS transistors doping, Au surface-state energy levels 80−11092
Mossbauer effect on ^{119}Sn and ^{197}Au meas. 78−15080
Mossbauer spectra, 2nd-order Doppler shift, 1-100K 79−91317
multiphoton photoeffect, induced by single selected ultrashort laser pulses, anomalies 77−28692
multiphoton photoeffect, new effect due to ps laser pulses 78−80452
multiply twinned particles, internal and surface struct. by electron microscopy 80−84189
muonium formation, μ^+ beam on thin foil array, μ^+ decay spectra 77−75346
neutron activation anal. in Bi 79−57336
neutron damage, defect clusters 80−34067
neutron damage calcs., deuteron break-up source, sputtering appl. 77−35593
neutron radiotherapy, 14 MeV, skin-sparing, effect of metal sheets 78−35923
neutron sputtering yield determ. 77−36319
neutron yield calcs., electron beam incidence 78−95622
nucleation, on KCl, nucleus growth mechanism and kinetics, electron microscope obs. 77−62780
nucleation of evaporated Te films on Au oriented islands 78−2388
nucleation on KCl, collective behaviour, monatomic step influence 77−15719
nucleation on NaCl:Fe(Mn), surface imperfection effects 77−15699
nucleation on NaCl from new vapour source, temporal and electron micrograph obs. 79−77954
nucleation on organic substrates, ion bombard. effects 78−75965
nuclei interaction on KCl (100) surface 77−89670
nucleus formation and growth, effect of intermittent deposition 79−23853
optical constant meas., 100 to 1000 eV using transmission gratings 80−93258
optical constants, dispersion, temp. depend., Kramers-Kronig calcs. *(Russian)* 77−69796
optical constants direct determination, d absorpt., reflectivity 77−69791
optical constants meas. by transmission interferometry 77−69790
optical transition radiation, bombardment by 29 MeV protons 78−2938
ore, leaching, effects of ultrasonics and their appls. 78−92214
ore, Witwatersrand Basin, fluid inclusion study 77−86891
ores, neutron activation and mathematical programming *(Rumanian)* 78−20565

gold continued
oriented single crystal substrate for epitaxial growth of Sb electrodeposits 78−43267
overlay film on quartz for SAW device temp. compensation 80−79043
overlay on Al foil, impedance-match expts. using laser-driven shock waves 80−29119
overlayer, on GaP photoelectrode 78−14812
overlayer on GaSb surfaces, adatom interactions, photoemission obs. 79−33898
overlayer on n-GaP photoelectrodes, potential, I-V curves 77−89848
pair potentials calc., appl. to point defect props. 80−19798
paramagnetic, conduction electron spin transmission 77−69693
particle, micro-area electron diffr. using electron holography 80−49055
particles, light scatt. spectra, size and shape effects 77−44015
particles, Mossbauer fraction from Gaussian potential 78−47489
particles, nucleation centres in polyethylene terephthalate crystn. 79−15658
particles, small single cryst., habit plane characterisation 80−79733
particles, small vapour deposited multiply twinned, struct. anal. using TEM 79−82488
particles, vapour deposited, struct. by TEM imaging techniques 79−77566
particles, vibrations associated with twins 80−100253
particles condensed on NaCl surface, electron diffr. pattern interpretation, computer simulation *(French)* 77−76700
pentagonal symmetry, icosahedral struct. *(French)* 80−79729
phonon density of states determ. from thermodynamic functions *(Russian)* 77−7800
phonon dispersion, binding energy, compressibility, pseudopot. calc. 77−4164
phonon dispersion, lattice phonons three body interaction model 79−99280
phonon dispersion, model pseudopotential method 79−23685
phonon dispersion relation in resonant model potential 80−6473
phonon dispersion relations, screened shell model 78−83894
phonon dispersion relations and Debye-Waller factor calcs. 78−51630
phonon frequency determ. in noninteracting band scheme 78−47483
phonon limited electrical resistivity, temp. depend. 80−24876
phonon resistivity, low temp. 78−79978
phonon spectra, self-consistency condition for force const. models 80−44264
phonon-limited elec. and thermal resistivity 79−42517
photionisation and electron impact ionisation relationship, mean free paths 79−22672
photoelectric cross section in region 187 to 662 keV 79−69952
photoelectric cross sections, from total absorption cross sections, 5 to 130 keV 79−26947
photoelectric cross sections of low energy photons 78−46309
photoelectron count rates, using VUV He reson. line radiation source in UHV apparatus 78−89602
photoelectron spectra, bulk and surface, rel. to band struct. 80−20770
photoemission, location of transitions in k space along lines of high symmetry 79−47594
photoemission, polarisation and ang. dependencies 77−12495
photoemission, primary and secondary yields using low-energy monochromatic X-rays 80−35053
photoemission from indirect optical excitations 79−43103
photoemission spectrum for exploding wire radiator source, Boltzmann eqn. soln. 79−26949
photoemission spectrum from d-bands, ang. depend. obs. 77−12492
photoemission study of bulk and surface electronic struct. 79−4894
photographic emulsion sensitisation by S and Au 78−16869
photographic emulsion sensitisation during latent image formation, nature of sensitivity specks 77−82637
photographic emulsion sensitization mechanisms 79−20419
photoionisation, relative cross-section meas. by X-ray detection 78−33369
photon activation analysis of coins and art objects 78−349
photoneutron yields released by incident electrons, improved calc. 80−27630
piezoelastic modulator for 10.6 μm radiation using Au clad amorphous Se optical waveguide 78−66956
planar and axial channelling of protons, numerical simulation 79−65132
planar channelling of α-particles, stopping power of solids 78−51602
plasma, high-density, high-temp., radiative opacity, particle beam fusion system 80−10365
plasma impurity, radiation loss effects on Tokamak expts. 78−22465
plasma impurity X-ray emission, in H_2 DIVA Tokamak 79−32820
plasma production, electron beam irrad. of foil, mag. enhanced deposition 79−86591
plated layer thickness meas., ^{195}Au nondestructive method 79−96244
plated Ni powder for electroplating conductive pastes 79−95957
platelets, (1$\bar{1}$1), Fe epitaxial growth, dislocations 80−96760
plating assessment for printed circuits 79−43163
polyacetylene-Au, ohmic contact *(Japanese)* 80−96888
polycrystalline, dislocation relaxation under high pressure 79−77605
polycrystalline, low energy H^+ scatt., computer study 77−36338
polycrystalline film, RF bias-diode and triode sputtered, resist. and microstruct. 78−80072
polycrystalline foil, sputtering yield meas. by UHV microbalance with ion gun *(Japanese)* 80−17951
polycrystalline wire, internal oxidation of impurities 78−83842
positron annihilation, 4.2-500K, Doppler broadening meas. 78−43957
positron annihilation characteristics, 27 to 592K 79−91523
positron annihilation characteristics, effect of temp. 78−64427
positron annihilation measurements, monovacancy and divacancy parameters 77−35550
positron annihilation rates, electron-electron and electron-positron correl. effects 78−76548
positron lifetime and annihilation lineshape from 4.2K to MP 77−20272
positron-vacancy interactions, equilib. temp. depend. of positron annihilation 78−76547
powder, ultrafine, sintering, coalescence growth stage 80−89174
precipitation in Si supersaturated soln., Hall effect meas. 77−89465
primary electron backscatter yield using material model parameters 80−39184
proton beam uniaxial channelling-blocking and single-alignment channelling-backscatt. anal. 77−84816
proton diffusion, config. and activation energies 79−37878
proton impact, blocking profile calcs. 78−18694
proton irrad. at 0.3K, resistivity annealing 77−76475

gold continued
proton irradiated, radiation-annealing effects in energetic displacement cascades, film resist. meas. 78−26603
proton stopping cross sections, 350 to 650 keV backscatt. technique 79−4352
pseudopotential, fitted to elastic data 78−75705
pseudopotential nonlocal model 78−14659
quenched, vacancy cluster form., effect of Sn, Cu impurities 77−62546
quenched and annealed, conduction electron scattering 78−47774
quenched polycryst., vacancy loss at grain boundaries 80−59477
quenched single crysts., vacancies, diffuse scatt. and resist. obs. 80−33994
radiation-stimulated dissociative diffusion in Si model 79−23785
radioactive waste disposal method including encapsulation in thick gold layer 78−74441
range and range straggling of heavy radioactive ions 78−22776
range distributions for 25-200 keV $^{14}N^{+}$ ions 80−103405
range of $^{27}Al^{+}$ ions, meas. by (p,γ) reson. broadening 79−46729
rare earth ferromagnet, mag. hyperfine field interaction, ^{197}Au Mossbauer effect 77−8463
recoil ranges of ^{18}F in Au by irradiation of O_2 with ^{3}He and ^{4}He particles 80−71931
reflection of H, D and He ions 78−95640
reflective coatings, refr. index, UV polariser mirror coating appl. *(Russian)* 77−34928
refractory thin film systems, interdiffusion obs. by combination of scattering techniques 80−65308
residence time on KBr and NaCl surfaces, time-of-flight meas. 80−10788
residual resistance ratios for pure Au, size correction 77−43742
resistivity and thermoelec. ratio, electron-electron scatt. contrib. 80−70670
resistivity and thermoelectric ratio at low temp., 0.04 to 7K 79−73497
resonance self-shielding factors, depend. of Doppler factor 78−17439
resonant and nonresonant conduction-electron-spin transmission 80−75857
resonant model potential, energy depend. 78−18952
rod, tensile loaded, internal friction and Young's modulus measuring equipment, inelastic phenomena exam. *(Hungarian)* 79−52546
scattering and radiation damage for 14 MeV neutrons and 10 to 20 MeV protons 77−15458
Schottky barrier to II-VI and III-V semiconds., comparison with $(SN)_x$ and HgSe as contact materials 77−85312
Schottky barrier with III-V and II-VI semiconds., correl. of barrier height with anion electronegativity 77−20430
secondary electron emission, Boltzmann eqn. appl. *(French)* 80−55238
secondary electron spectra, low energy peaks interpretation 78−39638
secondary ion emission, energy spectra, 0-55 eV, contamination levels 79−15573
SEM, contrast of electron channelling patterns, estimation from low index refl. 78−9921
SEM, electron channelling patterns 78−83697
semiempirical, relativistic oscillator strengths including core polarisation for p-, s-, d-series 78−74609
sensitivity speck, formation during ripening, nature and role 79−39171
shock compressed, thermal energy relaxation 77−69043
Si:Au, step junction, mathematical model *(Rumanian)* 79−87148
single cryst., thin films and bulk, anisotropic X-ray emission 80−108303
single particles, high resolution electron microscopy using BeO specimen supporting films 77−27793
sliding charact., friction and wear *(Japanese)* 78−56778
small particles, embedded in gelatin, phonon spectrum, Mossbauer obs. 77−43921
small particles, in polyester matrix, optical scattering spectra 79−73961
small particles, size effects studied by electron energy loss anal. 79−47567
small particles, size-effect modifications of Debye-Waller factor 77−84877
small particles, transition cluster-solid state 79−33593
sol, grain boundary struct. obs. and boundary diffusion 78−51552
sol crystals, grain boundary struct. and boundary diffusion obs. *(Japanese)* 78−15721
solar absorber, SiO_2 thin film with embedded Au particles 80−81490
solar absorption, Au black optical props. rel. to structural composition 79−83630
solar black, optical props., microstruct. influence 79−42937
solar black, struct. comp. and optical props. 78−27339
solid metal embrittlement of Ti-Al-V-Sn (6,6,2 wt.%) 80−16551
solid solubility in Pb, elec. resist. meas. 80−39298
sols, acoustically induced birefringence 80−93274
solubility, in $CdTl_2Se_4$, microhardness method 80−96650
solubility in Ge-Si solid soln., thermodynamic calcs. 79−86890
solubility in Si, gettering by P 78−83961
space-charge generation props. in Si MOS struct. 80−2475
spectral determination by scintillation method in geological samples 79−70391
spectral distrib. of X-ray braking radiation, due to electrons, calc. using Monte Carlo method 78−56538
spectral emissivity in 1-10 μm range at 100 to 400°C 77−11713
spherical crystal, drop grown from melt, RHEED obs., superstructs. 78−43225
spin polarised LEED from (110) surface 78−18508
spin properties of conduction electrons 79−46999
spin-orbit projected d density-of-states 78−38999
spin-polarised LEED from low-index surfaces 78−14556
sputtered layer on metal collector, thickness distrib. meas. by electron backscatt. 78−18927
sputtered with 15 or 30 keV H^{+}, He^{+} and Ar^{+} ions, energy and angular distrib. 78−95625
sputtering, by point defects, time-of-flight spectra 79−47573
sputtering and chem. attack by H ions of 100 eV energy 78−95635
sputtering by fast neutrons 77−36316
sputtering by fast neutrons 79−61470
sputtering by low energy H^{+}, Rutherford backscattering technique 80−40198
sputtering coating in oil-contamination free vacuum for SEM 79−12784
sputtering coefficient depend. on Ar^{+} ion dose 77−59661
sputtering of Au foil by fission fragments 78−2968
sputtering process study on Au, Al, Si targets, Rutherford backscatt. technique 77−8703
sputtering with Xe^{+}, Xe^{2+}, nonlinear effects 80−20748

gold continued
sputtering yield, transmission, for 6.8 MeV Au^{+} bombard. 77−1808
sputtering yield at low energy for light-ions 78−19620
sputtering yields for ions over 15-135 keV 79−56899
sputtering yields for light ions 79−87537
sputtering yields of D^{+} and Ar^{+} ions using matrix isolation spectroscopy 79−78809
stacking fault tetrahedra, critical nucleation temp. 78−26581
stacking fault tetrahedra formation, quenched-in vacancy clustering, continuum model 79−77594
stepped surface, edge atom dipole moments 78−14791
stopping cross section meas., ^{4}He, 0.5 to 21. MeV 79−4353
stopping of channelled ions 77−51424
stopping power for 0.3 to 2.0 MeV ^{4}He ions 79−60415
stopping power for 0.3-1.5 MeV protons 79−55801
stopping power for 28 MeV α-particles, re-evaluation 78−79651
stopping power for ^{107}Ag, ^{109}Ag and ^{150}Sm 80−70284
stopping power for MeV H^{+}, D^{+}, $^{4}He^{2+}$, $^{7}Li^{3+}$ ions, deviations from Bethe formula 78−26612
stopping power meas. for 4-5 MeV/N ^{16}O, ^{40}Ar, ^{65}Cu, and ^{84}Kr 78−70720
stopping power of He ions <30 keV 77−10546
stopping power of heavy ions at 50-500 keV 77−76478
stopping powers, low energy, determ. by TOF techniques 79−45594
stopping powers, projectile range for Z=8-20, 0.0125-12.0 MeV/nucleon 78−83856
stopping powers and backscatt. charge fractions for 20-150 keV H^{+} and He^{+} 80−42907
stopping powers for 28.8 MeV α-particles 77−80556
stopping ratios of 50-300 keV H^{+}, He^{+}, $^{7}Li^{+}$, and $^{8}Be^{+}$ 80−42903
subshell photoelectron branching ratio meas. using synchrotron radiation 80−66397
4-subshell photoionisation cross section, energy depend. from Auger and photoelectron spectra 80−35057
substrate, (001) orientation, growth of Ni thin films *(French)* 80−44446
substrate, c-axis oriented AlN film, low temp. growth by RF reactive planar magnetron sputtering method 80−76175
substrate, Fe epitaxial growth, temp. effect on morphology 78−26798
substrate, for vacuum deposited Fe, interaction layer formation mechanism 80−54559
substrate, for VPE Pt, crit. thickness of pseudomorphic film growth, substrate size depend. *(Russian)* 80−29286
substrate, interaction layer at interface with vacuum deposited Fe film 79−99433
substrate, periodic arrays of misfit dislocations during epitaxial growth of Cu and Pd, electron diffr. 78−51857
substrate, polymeric films, ESCA, sample charging phenomena 80−20764
substrate for evaporated Be thick films, secondary electron emission 80−104022
substrate for Fe epitaxial layer, misfit dislocation obs. 79−73415
superconducting transition temperature estimated 78−43358
surface, ^{4}He backscatt., Rutherford scatt. cross section correction test 80−66369
surface, (100), adsorbed Br, EELS obs. 80−50483
surface, (100), normal and reconstructed, electronic struct. changes, ang. resolved photoemission obs. 80−25520
surface, (100), reconstruction, superstruct., model 80−103551
surface, (110), electron spin polarisation in LEED 78−83692
surface, adsorbed C^{+} layer removal, by 20-30 keV Ar^{+} bombardment, in plasma 77−76103
surface, atomic interplanar spacing determ. from simulation of channelling expts. 77−80563
surface, cadmium arachidate monolayer, reson. surface plasmon reflection 78−56536
surface, chemisorption of I, AES and LEED study 80−100405
surface, clean, hydrophilic nature 80−80029
surface, electroreflectance spectra 80−55066
surface, energy spectra of charge state fractions of backscattered H and D 77−8705
surface, H(He) positive ions impact, backscattering, fraction reflected 80−60741
surface, He, Ne, and Ar ion irrad., 0.05 to 3 MeV, orientation of fast ions excited in surface collisions 79−4876
surface, high energy ion backscatt., computer simulation *(German)* 77−59664
surface, iodide ion adsorption, depend. on electrode crystallographic orientation 79−15020
surface, O single layer, ferromag. props. *(Russian)* 78−64256
surface, resonant absorpt. of sound *(Russian)* 78−95216
surface, sputtering with 15 and 30 keV H^{+}, He^{+} and Ar^{+} ions *(German)* 79−24407
surface, with Ag monolayer, adsorbed pyridine giant Raman effect 80−63637
surface (100), characterisation of reordered and normal surfaces by LEED, AES and EELS 78−34687
surface (100), disordered, diffuse LEED intensities obs. 79−4462
surface (110), (1×2) and (1×3) superstructures, LEED study 80−20024
surface (110), electroreflectance, surface state contrib. 80−80755
surface (110), reconstructed, LEED anal. 79−77878
surface (111), anomalous surface superstruct., UHV electron microscope obs. 80−10760
surface (111), Bi^{3+} desorption, struct. changes kinetics 80−54500
surface (111), interfacial photoemission into electrolyte, 3.4-5.0 eV, vectorial volume effect 77−36375
surface (111), relativistic effects on LEED intensities 79−7737
surface atoms, XPES, core level binding energy, density of states 79−8224
surface composition anal., adsorbed layers, by ion-forwarded electron spectra 77−31850
surface decoration, on (111) Ag surfaces, by electrodeposition *(French)* 80−44445
surface decoration techniques, TEM and SEM study of localisation of decorating crystallites *(French)* 80−10470
surface dipole moment calc. 80−60060
surface electron states, photoelectron spectra meas., rel. to Au alloys 78−14781
surface electronic structure, XPS study 80−55259

gold continued
surface interaction with O_2 rel. to thermomag. effect in gas *(Russian)* 77−11302
surface phenomena, electron microscopy 80−103556
surface plasma resonance, effect of cadmium arachidate monolayer 77−90210
surface plasma waves, dispersion curves, attenuated total reflection spectra 78−88015
surface plasma waves 79−47151
surface plasmon obs. using X-ray emission 78−92146
surface proton and electron channelling on reflection 80−39193
surface reconstruction, physical realisation of two-dimensional Ising and X-Y model 80−15351
surface reflection and penetration of 25 eV to 10 keV He, T and H atoms 77−59657
surface resistivity, evaporated layer, at 890 GHz rel. to waveguide applic. 77−34004
surface state energy levels and diffusion at Si-SiO_2 interface 79−51652
surface state on (111), $E(k_{\parallel})$ relation, ang. resolved photoemission 78−76582
surface states, intrinsic, UV photoemission meas. 77−20983
surface valence state from surface tension props. 79−95462
surface-Cs adatom interaction, polarisation energy from opt. data 77−72792
surface-grazing scattering, 1 MeV Ar^+ beam, excited-state orientation depend. on scatt. angle 77−61847
surfaces, separated by N_2 Knudsen gas, thermomag. effects, low temp. 78−30405
surfaces, Van der Waals forces computation 79−15204
surfaree (101), disordered, diffuse LEED intensities, statistical disorder theory 79−4463
target, microwave laser irrad., plasma form., inhibited electron thermal cond., laser intensity threshold Z-depend. 80−48928
TEM exam. of ion damage in FCC metals 78−87727
thermal conductivity at high press. meas. 78−95283
thermal expansivity, simple eqn. of state appl. 77−27970
thermal modulation reflectance spectrum, temp.-dependent shift 77−81121
thermal properties and Gruneisen parameter, Toya's first principle approach 78−38806
thermal radiative properties at cryogenic temps., comparison with model predictions 77−15604
thermal resistivity, temp. depend calc., free electron approx. 77−66152
thermoelectric power at low temps. of pure samples 77−76798
thermoelectric power determ. 77−24549
thermomodulation spectra of high-energy interband transitions 80−108226
thermopower temp. depend. 79−65436
thickness meas. of Au and Ni layers on Cu substrates simultaneously 80−13041
thin crystal, anomalous transmission of high energy electrons *(Japanese)* 77−43117
thin disc prep. and electropolishing for TEM 78−88601
thin film, discontinuous, high resist., Hall effect meas. 80−65716
thin film, elec. resist., effect of annealing In electrodes 80−80416
thin film, electromigration, adhesion layer effects 80−96685
thin film, in Si detector, electrical contact at He temp. 78−37019
thin film, influence of coalescence on growth kinetics 79−46981
thin film, self-sustaining, electron mean free path meas. 80−92883
thin film, vac. deposited, Auger spectroscopy 80−2952
thin film (001), surface struct., high resolution TEM 80−100383
thin film bicrystal, annealing twin form. by boundary dissociation 79−47729
thin film bicrystal, diffraction effects from inclined grain boundaries 80−103362
thin films, cryst. ripening rel. to heat treatment *(German)* 80−3109
thin films, material transport instabilities accompanying ageing *(German)* 80−7601
thin foil, enhanced electron energy deposition heated, soft X-ray vacuum UV spectra 80−80901
thin foil, growth of stacking fault tetrahedra 80−19815
thin foil, spatial resolution of X-ray microanalysis 80−101065
thin foil thickness meas. using ^{148}Gd and ^{241}Am alpha-particles 79−30417
thin layers, diffusion rate of H_2, N_2, Ar, CO_2, air, and O_2 80−100359
thread, pull-off force with respect to Pt thread, in air, influence of elec. charge 79−11196
tilt boundary, $\Sigma=11$, simulated and observed struct., vibr. of individual atoms at grain boundary 80−88167
tilt boundary, small- and large-angle [001], X-ray diffraction study 79−82238
trace anal. with portable X-ray analysis 78−49160
transmission sputtering by $Ag^+(Ar^+)(He^+)$ ions 79−4885
twinned crystals, epitaxial growth on KCl crystals, electron microscopic study of microstructure 78−91566
twist boundaries, large angle [001], atomic struct. determ. by computer modelling and X-ray diffr. study 80−70162
ultrafine particles, optical props. 78−19481
UPS, band struct. 77−16455
UPS, expt. methodology aspects 77−90245
UPS examination, temp. effects 78−68604
vacancy and divacancy diffusion 79−82377
vacancy annihilation, to dislocations, computer simulation *(Japanese)* 80−88205
vacancy clustering of S 77−4100
vacancy clusters, equenching and ageing, electron microscopy study 78−76671
vacancy diffusion along single edge dislocations, computer modelling *(Russian)* 77−47612
vacancy model, electron statistical, formation energies determ. 77−76390
vacancy properties 78−47326
vacancy size effect, surface energy in small particles and bulk specimens 80−75223
vacuum condensation, on mica, saturation density of nuclei 78−18932
vacuum condensation on KCl, spatial distribution of nuclei 78−18931
vacuum deposited layer on KI, nucleation and growth 79−61516
vacuum deposition, on (100) surfaces of Kbr, KCl and NaCl substrates with colloidal centres *(Rumanian)* 78−60579
vacuum deposition on dielectric substrates, ellipsometric and electron microscopic meas. 79−74011

gold continued
vacuum evaporated particle coalescence behaviour on doped alkali halides 79−77961
valence band Auger spectra 78−76563
valence bands, angle-resolved photoemission determ. 80−108323
valence bands, angle-resolved photoemission meas. using synchrotron radiation 77−24930
vapour brightness amplifier at 627.8 nm, for projection microscope 80−83616
vapour deposited coatings, mean thickness at which films reach continuity 79−51459
vapour deposition, improvement of adhesion, line definition, contact resistance and semiconductor properties by sputter-etching 79−43145
vapour properties above 3000K, by pulsed-electron-beam meas. 77−15567
Volmer-Weber mode of epitaxy, deposition on KCl and MgO, post-nucleation phenomena 79−77955
VPE, nucleation on NaCl, role of surface steps 78−79902
VPE on W (110), alignment of (111)FCC-(110)BCC epitaxial metal pairs 79−19488
wear, atmos. press. effect, rel. to fatigue 77−70189
wear coefficients determ. using pin-on-cisc apparatus 80−76366
wetting and adherence of Na_2O-B_2O_3 glass on surface 80−24714
wetting by water, hydrocarbon contaminant effect, macroscopic continuum model 77−85018
wire, microparticle trigger discharges and impact damage in HV vacuum insulated gap 77−24227
wire, thermal cond., 0.8-10K 77−89748
wire, ultrapure, cryst. forms of hillocks and voids formed by electromigration 77−31811
work hardened, Hasiguti peaks, spectrum and recovery, impurity effects *(French)* 77−66670
X-ray absorption, discontinuities and limits, chem. combination effects 80−93435
X-ray cathode, secondary electron energy distrib. excited at 277 and 1487 eV 77−8716
X-ray cross sections, L-shell, proton induced, 1 to 3 MeV range 79−1799
X-ray Debye-Waller factors, CGW vs. DAF models 79−37794
X-ray fluorescence and at. absorpt. analysis of Sarawak Au artifacts 80−85229
X-ray induced desorption of gases from surface 77−35813
X-ray M_5 absorpt. limits 78−6812
X-ray photoelectron spectra ang. depend. *(German)* 78−72679
X-ray photoemission, electron yield, 30-90 keV 77−8726
X-ray production by 9.5 to 41.8 MeV Fl ions, total L-shell cross-sections 77−85847
X-ray production surface impact of F^{n+} and Si^{n+}, Lα X-rays 79−69907
XPS, achromatic X-ray source, spectrum iterative deconvolution, doublet and valence band 78−72689
XPS, angle-resolved, from valence levels, Brillouin zone averaging 78−48285
XPS, angular-dependent, meas. on single cryst. 77−40329
XPS, D-orbital directed emission 77−40328
XPS, electron level binding, energy determ., and spectrometer calibration method 77−16458
XPS, electronic struct. 80−7464
XPS, of polycryst., appl. of monochromated spectroscopic UV discharge lamp 78−89601
XPS of valance bands, ang. depend. 77−44122
Ag film, epitaxial growth on isolated Au patches covered with amorphous C layer 80−40270
Ag, ion beam plating using mass analysed ions, SIMS and AES expts. 78−19673
Ag/Au thin film couple, interdiffusion mechanism 77−20132
Ag-Al_2O_3-Au structure, electrorefl. meas. *(French)* 80−50366
Ag-Au, pseudoalloy behaviour at interfaces, grain boundary diffusion 80−6567
Ag-Au thin film couples, polycrystalline, low temp. diffusion, resist. obs. 79−4435
Ag-Au thin films, interdiffusion, pore formation, stress effects, adhesive effects *(Russian)* 79−82502
Ag-Cu composite wires, size effect and interface contribution to diamagnetism 77−69490
Ag+H^+, L-shell ionisation at large scatt. angles 78−90283
Al/Au/Al layer configuration, electron energy deposition meas. 77−24338
Al-Al_2O_3-Au device in Cl_2 atmosphere, current-voltage charact., press. depend. 80−65704
Al-Al_2O_3-Au sandwich conduction props. 78−2580
Al-Al_2O_3-Au(Al), capacitance, water sorption effects 77−43738
Al-AlN-Au; voltage controlled negative resist., O_2 press. effect 78−72281
Al-Au bimetal thin film interdiffusion zone, intermetallic phase form kinetics, 70-160°C 78−75891
Al-Au couple, electroformed, nonohmic charact. and electron emission 80−60066
Al-Ge-Al(Cr)(Au), study of metal contact resistance and microstruct. 77−89880
Al-GeSe-Au, effect of contact material on DC and AC behaviour of sputtered amorphous GeSe film 79−95513
Al-SiO_2-Au, thin layer struct., electroluminesc. *(French)* 78−76531
Al-SiO_x-Au, MIM struct., electroformed, struct. and elec. props., 4-300K 79−78206
Al-SiO_x-Au cathode, emitted electron energy distrib. 78−52645
Al-tetracene-Au cell, depletion layer, LF capacitance meas. 79−56328
$Al_xGa_{1-x}As$:Au, LPE film, impurity levels, elec. and optical props. meas. 78−26862
Al_2O_3 to Au solid state reaction bond, effect of ambient atmosphere 78−67914
Al_2O_3-Au, cermet coatings, solar energy photothermal conversion, Bruggeman effective medium theory 79−83627
As-Se:^{197}Au, glassy, Au impurity influence, elec. cond., optical absorpt. and Mossbauer meas. 77−24558
a-As_2Se_3-Au contact sandwich, response to voltage step in dark and with illum. 77−69431
Au (111)/Ag (111) thin film system, diffusion processes 79−77843
Au bicrystals, struct. of grain boundaries using diffr. techniques 80−59478
Au decoration, of individual Ag crysts. by ion bombardment *(German)* 79−69164

gold continued
Au diffusion, and elastic strain, influence on O_2 state in Si *(Russian)* 79−69181
Au, grain boundary struct. anal. by HVEM *(Japanese)* 80−15109
Au, grating, extreme off-plane mounting, X-ray efficiency calc. 78−45757
Au, ground and excited states, pot. energy curves, relativistic effects calcs. 79−31416
Au I, absorpt. spectrum obs., 1300 to 1900 Å 78−62751
Au I, relativistic oscill. strengths 77−14388
Au II, ion laser transitions in He-Au mixture, 253.3 to 763.5 nm 77−7071
Au island epitaxial films, on (111) surface of fluorite, discrimination of twin orientation 79−46983
Au, K-shell photoionisation, cross section meas. K X-ray-photoelectron coincidence method 79−72285
Au, optical props., dielec. function, void model, sample effects 80−76048
Au, photoelectron spectra, occupied surface-state bands in sp gap 79−43094
Au thin films, electron diffr. investigation of Debye temp. 80−88420
Au, ultra-microhardness testing for vacuum deposited film and bulk specimen 78−79910
Au vacuum deposited coating on glass, strength 80−55505
Au, vapour deposited particles, with hexagonal profile, struct. determ. using TEM imaging 79−77567
Au^-, electrochemical generation, oxidation, standard pot., in liq. NH_3 79−100386
Au^+, self-sputtering, DIVA, metal-impurity, confinement, discharges 80−28843
Au:N, difference in conc. distribs. between implanted N^+ and N_2^+ ions 77−80529
Au/(Zn-)phthalocyanine/Al(In), photovoltaic effects, dark elec. props. of rectifying cells 79−4604
Au/(Zn-)phthalocyanine/Al(In), photovoltaic effects, illuminated thin-film cell props. 79−4605
Au/Ag couple, diffusion induced stresses and plastic deform. 78−26736
Au/Al thin film, Al diffusion studied by attenuated total reflection method 80−92722
Au/Au-Ge/GaAs structure, ohmic contact behaviour, alloying time effect 79−19659
Au/AuPd, bicrysts., in situ relax. of interphase interfaces 80−39455
Au/Cr layered films, microstruct. and interdiffusion during ageing, 423 to 573K 79−46965
Au/Cu, bilayers, interdiffusion phenomena, lattice dislocations, TEM obs. 80−59736
Au/Cu, double layer film, oxidation *(Japanese)* 80−61010
Au/Cu, initial epitaxial growth at room temp. 80−59829
Au/Fe/Au superimposed layers, influence of O_2 on interdiffusion, controlled-atmosphere electron microscopy 77−51552
Au/GaSb (110) interface, heat-treated, struct. and chem. state, angle-resolved XPS 80−97400
Au/Hg probe for C-V meas., work function difference between probe and Si 80−2450
Au/In film structure, interdiffusion at room temp. 77−39703
Au/In proximity effect bridges, finite size array 79−78270
Au/In proximity effect bridges, square arrays, transition temps. 80−84557
Au/n-TiO_2 Schottky diodes, I-V and C-V characts. 80−96988
Au/Ni(Ni-P), interdiffusion, backscatt. study 80−79991
Au/oxide/n-GaAs struct., photocurrent relax. 80−92978
Au/Pb thin film couple, room temp. interdiffusion study 79−28154
Au/Pd, bicrysts., in situ relax. of interphase interfaces 80−39455
Au/Pt interface, diffr. studies of conc. variations 79−42322
Au/Pt/Cr films, diffusion of Si, depth anal., optical and Rutherford backscatt. meas. 79−10981
Au/Pt-Ir contact, spectral characts. of VLF noise allowing for logarithmic creep *(Russian)* 77−85301
Au/Si interface, X-irradiated, dose profiles 79−24388
Au/SiO-B_2O_3/Al, emitted electron energy distrib. *(French)* 80−39681
Au/Sn evaporated film, interdiffusion, X-ray diffr. and ion backscatt. obs. 79−33121
Au/Sn films, evaporated, microstructure and texture, TEM obs. 80−39481
Au/Sn thin film couples, evaporated, TEM study 80−59832
Au/Ti thin film, temp. and humidity effect on interdiffusion 79−51317
Au/ZnSe:Mn/n-GaAs low threshold thin film DC electrolum. cell, pulse-excited characts. 80−76081
Au-Ag, contact PD, electron interferometric meas. 77−32069
Au-Ag, thin film, double layer system electron beam effects during sputter profiling AES obs. 79−65347
Au-Ag bilayers, conc. profile by AES, interdiffusion coefficient determ. *(French)* 78−84077
Au-Ag film system grain-boundary diffusion at low temp., meas. by surface accumulation method 79−77839
Au-Al thermocompressional contacts, diffusional zones, phase growth during annealing *(Russian)* 80−75389
Au-Al/GaAs interfaces, atomic interdiffusion, soft XPS studies 80−65302
Au-$Al_{0.5}Ga_{0.5}As$ -GaAs heterojunction Schottky-barrier solar cells, barrier height enhancement 80−85284
Au-Al_2O_3 cermet film, dense regular, optical props., rel. to appl. as selective solar absorber 79−79408
Au-Al_2O_3-Al, solid-state anodisation of Al by vapour infusion, oxide growth rate 80−11830
Au-Al_2O_3-Al system, influence of mech. modulation on elec. transport 80−2481
Au-Al_2O_3(Al_2O_3-MgO) cermet selective surfaces for evacuated solar collectors 79−43785
Au-$Al_xGa_{1-x}As$ interface, Auger depth profiling 77−89657
Au-AlGaAs-GaAs heterojunction Schottky barrier solar cells, barrier height enhancement 80−94071
Au-amorphous GeSe-Au structs., AC cond. and capacity, thickness depend. 79−65566
Au-As_2Se_3 contact, model of charge injection 78−68088
Au-As_2Se_3 sandwich cell, origin of dark currents 77−76920
Au-Au_2P_3 system, eutectic temp. 80−59628
Au-B-Au systems, elec. field effect on B film struct. 80−20050
Au-C, light ion large angle scatt. in weakly screened Rutherford region 80−84823
Au-$Cd_{0.175}Hg_{0.825}Te$ contacts, photo-effect in the 77-300K range, barrier height estimation 80−107850

gold continued
Au-CdF_2, metal-semiconductor contact, capacitance and photocurrent, barrier height 77−85321
Au-CdF_2 Schottky diodes, degradation 79−23969
Au-$CdIn_2S_4$ surface-barrier diodes, mech. of current flow 78−56228
Au-CdS, Schottky junction, surface defects, photovoltaic, piezoelectric and V-I characteristics *(French)* 80−49898
Au-CdS junction diodes, chemically etched CdS cryst. surfaces effect on barrier layer 80−44722
Au-CdS Schottky barrier, piezoelec. effect due to mech. bending 77−69779
Au-CdS-Al structure, interfacial phenomena, complex impedance meas. *(French)* 79−42668
Au-CdS(GaP) Schottky diode, elec. props. under stress 79−15222
Au-CdS(Se)(Te) contacts, electronic states, vacuum UV photoelectron spectra 80−70827
Au-CdTe Schottky barriers, quantum photoelectric yield, theoretical anal. 77−39939
Au-CdTe Schottky barriers, defect effects 79−60921
Au-CdTe Schottky-barrier diodes, fabrication and characterisation *(German)* 80−89151
Au-CdTe-Au structure, as spectrometric detector of nucl. radiation 77−54460
Au-CdTe-Au structure, current transport props. 80−80408
Au-CeF_3-Al MIM struct., dielec. props. temp. irreversibility *(Czech)* 80−15616
Au-Cr bifilm, resistivity and struct. changes under heat treatment, diffusion effects 77−1497
Au-Cr bilayer system, optical mechanical and corrosion properties 77−32707
Au-Cu_2O Schottky barrier solar cells, surface anal. using AES 79−43759
Au-dielectric cermets, optical constants, incl. proximity effects 78−56446
Au-dye-amorphous SiO_2-Au struct., dye-sensitised steady-state photocond. 80−107924
Au-$Ga_{1-x}Al_xAs$ Schottky diodes, band struct. from I-V, C-V meas. 80−96989
Au-$Ga_{1-x}Al_xAs$ variable-gap surface-barrier struct., photoelec. effect 80−39634
Au-$Ga_{1-x}Al_xSb$ Schottky barriers, barrier height 80−96986
Au-GaAs, film-substrate interface alloying behaviour, electron microscopic study 79−60652
Au-GaAs, photosensitivity losses, field and spectral depend. 80−2452
Au-GaAs (110) Schottky barriers on ordered and disordered GaAs surface, props. 78−95360
Au-GaAs interface, atomic modulation of interdiffusion, effect of reactive Al monolayers 80−49432
Au-GaAs interface, electronic struct., photoemission meas. 77−20385
Au-GaAs MIS solar cells, effects of thin oxide layers on characts. 80−89624
Au-GaAs polycrystalline Schottky barriers, transition with grain size from electrode-limit to bulk-limited cond. 80−65676
Au-GaAs Schottky barrier, photocurrent, recomb. losses *(Russian)* 80−2470
Au-GaAs Schottky barrier diode, X-band applications 77−8192
Au-GaAs Schottky barrier diode, Richardson const. 77−20424
Au-GaAs Schottky barrier solar cells, effect of interfacial oxide layer on cell characts. 80−61365
Au-GaAs Schottky barriers, PES and depth profiling obs. 79−42641
Au-GaAs Schottky-barrier diodes, fabrication using LPE 77−40357
Au-GaAs solar cell, practical antireflection coatings 77−763
Au-$GaAs_{1-x}P_x$, surface-barrier struct., photodetectors of visible and UV radiation 77−20437
Au-GaInAsP, rectifying contact, elec. characts. 80−80376
Au-GaS, Schottky-barrier electroreflectance spectra under uniaxial stress 79−56767
Au-GaSb contacts, interface struct., technology rel. to elec. props. *(German)* 77−72915
Au-GaSb Schottky barriers, PES and depth profiling obs. 79−42641
Au-GaSb structure, metal-semicond. interaction, soft XPS meas. 78−60203
Au-GaSb surface barrier struct., elec. and photoelec. props. 78−56229
Au-Ge, amorphous, junction, current-voltage charact. 80−44725
Au-Ge Schottky barrier photodetectors, near IR interband transitions and optical parameters 80−73449
Au-Ge Schottky diode, phonon energies, barrier heights, photovoltage spectra 78−64112
Au-Ge thin film couples, activation energy for interdiffusion, accelerated ageing studies 79−82671
Au-Ge-Au, room temp. interdiffusion 78−76161
Au-He CW mW-level laser source at 280 nm 80−43352
Au-He discharges, new ion laser transitions in near IR region, CW excitation 79−59673
Au-$In_{1-x}Ga_xSb$, photovoltaic effect and Schottky barriers 80−49897
Au-InP, Schottky barriers, electroreflectance spectra 77−43698
Au-InP, Schottky diodes, behaviour under heat treatment 79−78172
Au-InP boundary, Schottky barrier height, interfacial layer effects 78−14824
Au-InP Schottky barriers, PES and depth profiling obs. 79−42641
Au-InP Schottky diodes, barrier height study 78−52088
Au-InS Schottky-barrier diode, tunnelling current due to thermionic-field emission 79−33340
Au-InSb Schottky-barrier, photovoltage, temp. effects 77−69415
Au-In(Sn) double layer, quantum size effect *(French)* 77−20466
Au-MgO cermet film, dielectric const. and selective solar absorption 78−2937
Au-Mo-Si multiple layer structure, bombarded with P ions, calc. of P ion profile in substrate *(Russian)* 79−55771
Au-n-$Al_xGa_{1-x}As$-n-GaAS Schottky barrier solar cells, prep. and props. 80−26140
Au-n-AlGaAs-n-GaAs Schottky-barrier solar cells, band readjustment effect 80−81458
Au-n-$Ga_{1-x}Al_xAS$, Schottky barrier height as function of AlAs content 79−65535
Au-n-$Ga_{1-x}Al_xAs$-n-GaP narrow-band variable-gap surface-barrier photoedetector 80−96944
Au-n-GaAs Schottky diodes, interface state density model 77−39937
Au-n-Si Schottky barrier solar cells, recombination in space charge region 80−61351
Au-n-Si-p-Si structure with wavelength depend. photocurrent sign, photodetector 79−12849

gold continued
Au-O bond energy glow discharge, mass spectrometry obs. 80−64808
Au-oxide-GaAs struct., steady-state and transient photocurrents 80−6994
Au-oxide-n-GaAs MIS structures, reverse bias influence on photocurrent 80−107921
Au-oxide-n-GaAs structs., reverse-bias depend. photocurrent, photoionisation of surface states 80−20323
Au-p-n-Si Schottky barrier solar cell, photovoltaic characts., barrier heights, carrier mobility 79−83601
Au-$Pb_xSn_{1-x}Te$-Au structure, third harmonic variations at 77K and 300K 78−84313
Au-PbTe-Au, semiconductor thin films, random noise measurements 80−15629
Au-Pd-Au sandwich, obs. of strongly enhanced mag. susceptibility 80−93076
Au-polymer-Al system, short-circuit current with temp. variation 77−32090
Au-Pt composite coating for steel inner vac. liner of fusion reactor 77−30669
Au-Pt epitaxial film system, mismatch dislocations obs., electron microscopy 77−4268
Au-sapphire interface, effect on shear strength of adsorbed species 80−49485
Au-Sb thin film interdiffusion 77−59152
Au-semiconductor system, room temp. interfacial reaction, AES obs. 78−18913
Au-Si, film-substrate system, relax. effects, internal friction meas., temp. range 20 to 900°C 78−18886
Au-Si, spatial origin of electrons in internal photoemission struct. *(French)* 78−91770
Au-Si (polyethylene) interfaces, algorithm for energy deposition of X-rays 77−28648
Au-Si boundary, Schottky barrier height, interfacial layer effects 78−14824
Au-Si contact, O determ. by SIMS, nuclear reaction and Rutherford backscatt. anal. 79−4482
Au-Si interface, critical Au-film thickness obs. for room temp. interfacial reaction 80−75390
Au-Si interface, electron energy loss and AES meas. 80−89096
Au-Si interface, valence band and core levels, Si diffusion, alloy form., photoelectron spectra obs. 80−45205
Au-Si internal photoemission struct., spatial distrib. of excited electrons *(French)* 78−23166
Au-Si Schottky contact elec. props. rel. to AES 77−85322
Au-Si Schottky-barrier, formation process anal., V-I characts. *(French)* 78−91768
Au-Si surface barrier diode, photosensitivity in spectral range, 1-6 eV 77−89850
Au-Si system, transition layer struct. form. and heat treatment influence, amorphisation obs. 80−54529
Au-Si thin film double layer, silicide form., electron diffr. study 80−80005
Au-Si_3N_4-GaAs-GaP structures, as elec. controlled optical transparencies, optical processing use 77−85339
Au-Si-Al structure electrode mass transfer and switching with memory 78−95389
Au-SiO_2 codeposited film, optical, elec., mechanical and corrosion props. 77−32708
Au-SiO_2-Si structures, electron and ion emission from MOS field cathodes *(German)* 77−12499
Au-SiO_2-Si system, oxide film 16-36 Å thick, tunnel currents 80−70842
Au-SiO_2-Si targets, electron beam induced charge carriers in SiO_2 *(German)* 77−12007
Au-SiO_2-n-Si solar cells, comparison of majority- and minority-carrier silicon MIS solar cells 80−85280
Au-SiO_2-nSi, tunnelling MIS struct. 80−92995
Au-SiO_x-Au diode and triode struct., angular distrib. of emitted electrons 77−69429
Au-SiO_x-Au evaporated thin film sandwich, circulating and emission currents 80−11102
Au-SiO_x-Ge, sandwich structure, exam. of image structure using mirror electron microscopy *(German)* 79−11019
Au-SiO-Au structure AC conductivity, bulk and interface effects 80−54798
Au-Sn film, evaporated, interdiffusion and phase formation, in situ He ion backscattering meas. 78−22901
Au-Sn layer system, on glass, thin film interdiffusion 77−20134
Au-SnNi-Au ohmic contacts on n-GaAs 78−35319
Au-tetrathiotetracene-Al systems, dark cond., photocond. mechanisms rel. to contact phenomena *(Russian)* 78−52103
Au-$Ti_{0.3}W_{0.7}$, thermal annealing study of metallisation on Si 80−80134
Au-Ti/n-GaAs contacts, interdiffusion and Schottky barrier height variations 77−89849
Au-TiC, multilayer struct., microhardness and elec. resist. 80−2950
Au-W/n-GaAs contacts, interdiffusion and Schottky barrier height variations 77−89849
Au-W-GaAs Schottky barrier, elec. and chem. props., AES 80−96973
Au-WO_3, electrochromic cermet, optical and electrical props. 79−33674
Au-WO_3 cermets, electrochromism 77−90129
Au-WO_3 electrochromic cermets, resist. and optical density meas. 79−8201
Au-Y_2O_3-Y junctions, migration of Au rel. to voltage-controlled negative resist., SIMS obs. 79−91157
Au-zinc phthalocyanine-Au junction, microstruct. characterisation by TEM method 78−95241
Au-Zn_3P_2 Schottky diodes, influence of additional laser illumination on photoresponse spectra 77−89852
Au-Zn_3P_2 surface barrier diode, wavelength-modulated photoresponse spectra 77−12004
Au-ZnO-In metal-semicond. diode, electrolum. spectra 79−99948
Au-ZnS electrolum. Schottky barrier diode, S^+-implanted, blue emission 80−76082
Au-ZnSe:Ga(Al), Schottky diode, wavelength modulated photoresponse spectra 78−6714
Au-$ZnSiP_2$, Schottky contact, production and props. 79−7901
Au+^{208}Pb, 5.8 MeV/amu, Pb K-shell excitation probability 78−5338
Au+^{3}He(^{4}He) L-subshell ionisation, Coulomb deflection effects 78−22020
Au+$^4He^{2+}$, L-shell ionis. probability, X-ray prod. 79−18276
Au+Ag adsorbed layers on Si, dispersed struct. formation 78−22952
gold continued
Au+Al_2O_3, solid-state reaction, bonding, temp. depend. 78−48695
Au+$Au^{x+}(Br^{x+})(Cl^{x+})$, differential single-scatt. cross sections at MeV energies 78−33570
Au+e, atomic field bremsstrahlung, absolute cross section meas. 77−50529
Au+H^+, atomic K-shell ionis., X-ray emission 79−18280
Au+H^+, K-shell ionisation, 7-15 MeV, relativistic effects 78−82830
Au+H^+, L X-ray production cross sections, 0.3-1.8 MeV, expt. rel. to PWBA prediction 80−53115
Au+H^+, L-shell ionis., 0.5-3.5 MeV, X-ray emission obs. 77−54528
Au+H^+, L-subshell ionisation cross-sections, X-ray meas. 77−46520
Au+H^+, L-subshell X-ray prod., cross-section meas. 77−46575
Au+H^+, relativistic K-shell ionisation cross-section meas. 78−33593
Au+H^+ ionisation, induced L-shell alignment 80−32813
Au+$H^+(D^+)$, L-subshell vacancy production, Coulomb deflection effects 80−9711
Au+$H^+(He^+)$ interactions, backscatt. ions energy spectrum, computer simulation of ion motion 79−43088
Au+He^{2+}, high energy ionis. probability, semiclassical approx. with relativistic Hartree-Fock function 79−6998
Au+I, noncharacteristic X-ray emission, self-consistent relativistic many-electron correl. diagram 77−19023
Au+I, relativistic effects in variable-screening model 77−14516
Au+I, slow collision, M MO radiation anisotropy 79−72269
Au+I collisions, average ionisation probability of Au meas. 77−68005
Au+Kr^{n+}, K-L level matching, X-ray obs. 79−63948
Au+light and heavy ions, L-shell X-ray production and subshell ionisation cross sections meas. 80−91637
Au+Xe,4.7 MeV. u^{-4}, meas. of shape and absolute value of $1s\sigma$ excitation probability 79−13816
Au^++X, X=H, H_2, He, C, N, O, cross-section, closure-Born approx. 78−66630
Au^{n+}+H, single electron capture cross-section 79−59560
Au^{n+}+H_2, single electron capture cross-section 79−59560
Au_2, ground state, ab initio effective core pots., relativistic effects calcs. 79−31377
Au_2, Harris-Pohl selected valence electron split-shell MO calcs. 80−91439
Au_2^+, ab initio SCF calcs. using relativistic effective core pot. 80−95524
AuI isoelectronic series, oscill. strengths, relativistic HF calcs. 79−98034
^{79}Au+^{19}F(^{28}Si), target Lα X-ray prod., projectile charge state depend. 79−47549
^{195}Au, diffusion coeff. in liq. Cu 79−95196
^{197}Au Mossbauer isomer shifts, book contrib. 79−87356
^{198}Au, hepatic fractional clearance of colloids as meas. of effective blood flow 79−66547
^{198}Au, use in ovarian carcinoma treatment 80−36087
^{199}Au, carrier-free extraction from neutron-irradiated ^{198}Pt, medical appls. 79−2130
Au(111)/Ag(111) thin film system, diffusion processes, diffused Ag composition profile 79−90832
Be/Au/Be layer configuration 77−24338
Be-Au, ohmic contact to GaP, metallurgical struct. 77−1485
Br adsorpt. on Au electrode, specular reflect. investig. 78−61047
C/Au/C layer configuration, electron energy deposition meas. 77−24338
CC ^{198}Au, pancreas scanning, extension of the subtraction technique 79−66506
CO_2 laser bimetallic mirror coating vacuum sputtering technology 80−35086
CaO:Au, electroluminesc. meas. 80−40162
CaO:Au, thermoluminesc., following UV excitation, 290-500K 77−40292
$CdInGaS_4$:Au, single crystal, thermostimulated conductivity *(Russian)* 79−11142
CdS-Au structure, work function of {0001} faces of CdS, effect of piezoelec. props. 78−23164
CdSb:Au, solubility, thermal anal., microhardness, microstruct., elec. characts. 77−16557
CdSe:Au impurity light absorpt. for current control in negative resistance region 80−11052
$CdSnAs_2$-Au, surface barrier junction, elec. props., temp. depend. 80−65686
CdTe-Au system, phase diagram rel. to doping 80−16282
$CdTl_2Se_4$:Au, doping effect on surface tension of melt and cryst. microhardness 80−49464
$CdTl_2Se_4(Te_4)$:Au, elec. cond., density, dielectric const., changes on fusion 80−88553
Cr/Au metallisation system, corrosion inhibition using intermediary Pd layer 79−79155
Cr-Au film structure, on Si interdiffusion 77−39698
Cu, photoelectron spectra 77−73218
Cu:Au:C, surface, obs. at very low accel. voltage (200 V-1 kV) by SEM 80−10764
Cu/Au+0.03 at.% Fe, thermocouple characteristics, in mag. field at low temps. *(Russian)* 78−54365
Cu/Sn-Ni/Au tricouples, electrodeposited, interdiffusion obs. 80−84331
Cu-Au, dil., impurity diffusion, mass depend. of energy factor of isotope effect 78−30795
Cu-Au interdiffusion, Cu contact tarnishing 78−7098
Cu-Au thin film system, interdiffusion coeff. from cond. and Auger anal., 25 to 250°C 77−59154
Cu-Au thin films after accelerated ageing, failure by Kirkendall porosity 80−6675
Cu-Au-Cu, thin films, sandwich struct., bombarded by 3-15 keV Ar^+ at angle of incidence of 30°, sputtering yield coeff. 79−65968
diffusion in Pb-Pd, Pb-Ag, de-enhancement by impurities 80−19990
Fe:Yb(Au), radiation-damage evolution, influence on lattice-location meas. 80−6426
Fe-Au (111) bicrystal films, misfit dislocations obs., for 500°C substrate temp. 77−51624
Fe-Au bimetal epitaxial films, examination of interaction at temps. ≥600°C 80−75482
$Fe(OH)_3$, coprecipitation with Cu, Ag, Au; Ge, Sn, Pb; Mn and Ca 79−70415
films, vac. condensed at oblique vapour incidence, oriented cryst. growth, electron diffr. study 80−97432
GaAs:Au, back surface gettering 80−10758
GaAs-Au, quenching of exciton luminesc. by surface elec. field 80−29801
GaAs-Au, Schottky barrier energy var. with interdiffusion 77−20435

gold continued
n-GaAs-Au Schottky barrier diode, thermally assisted tunnelling currents 77−20412
n-GaAs-Au(Al) Schottky diodes, interface state density model 77−80840
n-GaP, Au-coated semicond. electrode, photoelectrochem. behaviour in water 77−21399
GaP:Au, diffusion, solubility, and electrotransport of Au 78−91489
GaP-Au, Schottky barrier, layer formation, elec. and optical props. 78−91766
GaP-Au, Schottky barrier, stress effects on elec. props. 80−34512
Ge:Au, capacitance oscillations, trap recharging waves 77−43614
Ge:Au, cleaved surface, influence of impurities on local surface states 79−78150
n-Ge:Au, current oscill. damping in weak transverse mag. field 77−4365
Ge:Au, current-voltage phase shift, impedance of subthreshold domains 77−43609
n-Ge:Au, electron capture by negatively charged traps, effect on hot electron enrgy energy distrib. 78−43398
Ge:Au, gamma-irradiated and electron irradiated, elec. props. meas. 77−62950
Ge:Au, IR detector, impurity photoconductivity *(German)* 78−82036
p-Ge:Au, interaction of primary radiation defects with Au atoms, after irrad. and annealing 79−51145
Ge:Au, moving elec. domain, impedance 77−1429
n-Ge:Au, negative photocond., field and temp. depend. 77−43660
n-Ge:Au, negative photoconductivity 78−34863
Ge:Au, p-n junction, injection amplification of photocurrent 79−51663
Ge:Au, polycrystalline film, electron transport props. 79−99642
Ge:Au, recomb. at repulsive centres, photocond. lifetime meas. 77−43617
Ge:Au, Sb, Hall mobility, temp. dependence 80−96919
Ge:Au, Sb 79−69577
Ge:Au, unipolar injection influence on high frequency conductance 80−34474
Ge:Au,Sb, electron irradiated, Hall effect, photocond., and photomagnetic effect meas. 77−4369
p-Ge:Au,Sb,Hg(Zn), radiation-defect form., Au influence 80−92911
Ge:Au film strain gauges, press. sensor *(Japanese)* 80−105631
n-Ge:Au piezoresistance in presence of deep levels, stress anisotropy 80−10979
Ge:Au under laser illumination, non-equilibrium conduction 80−6896
Ge:Sb,Au, photoelectronoc exam. of multilevel gold structure 77−69272
Ge-Au film, polycryst., struct. props. determ. 79−4494
Ge-Au-Ni trilayer film, interdiffusion obs., on annealing 78−2308
Ge-Au-Ni(Pt)(Pd) trilayered films, annealing, interdiffusion 78−22902
Ge-Au-Pd trilayer film, interdiffusion obs., on annealing 78−2308
Ge-Au-Pt trilayer film, interdiffusion obs., on annealing 78−2308
H^++U(Ni)(Au)(Sn), 4.88 GeV, K-vacancy production cross sections 77−19036
He-Au, UV ion laser, dominant transition at 280 nm 79−942
He-Au mixture, Au II ion laser transitions, 253.3 to 763.5 nm 77−7071
He-Au UV laser, spectral range, threshold, power output 78−66809
Hg-Au, minigrid optically transparent thin-layer electrode 77−70305
I ion+Au collisions, mol. M-X-rays, self-consistent relativistic HF-Slater many electron correl. diagrams 77−14567
$I^{43+}+Au^{69+}$, $I^{25+}+Au^{51+}$, correlation diagrams, inner-shell vacancy prod., characteristic X-rays 77−83503
p-InGaAsP-Au, Schottky barrier height comp. depend., photoelec. meas. 77−20433
InP-Au Schottky contacts, interfacial oxide layers used to increase effective barrier height 79−7896
InSb-Au contact system, low temp. alloyed contact formation 80−100519
InSb-Au Schottky barrier, photovoltaic spectra and magneto-optical transitions, Landau levels and excitons 77−47858
KBr:Au^-, optical absorpt. bands and MCD, electron-lattice interaction 80−108236
KCl crystal, surface elementary steps interaction with Au particles 80−39400
KCl:Au, EPR and optical absorpt. 78−39397
KCl:Au^-, absorption bands and MCD, electron-lattice interaction 77−55808
KCl:Au^-, absorption band shape in D-mode model 79−47485
KCl:Au^-, fluorescence, stress and mag. field depend., Jahn-Teller effect and relax. processes 77−48220
KCl:Au^-, Jahn-Teller effect 78−64015
MgF_2-Al film substrate tunable external-reflector retarder, computer based anal. 80−53407
MgF_2-Au, cermet coatings, solar energy photothermal conversion, Bruggeman effective medium theory 79−83627
MgO-Au cermet film, high intensity electron bombard. effect on secondary electron yield 77−81184
MgO-Au cermet film, selective black absorbers 77−1747
NaCl:Au, EPR and optical absorpt. 78−39397
NaCl-Au system, sliding and rolling electrification 78−14796
Na_2O-B_2O_3:Au glasses, Au solubility, oxidation state and opt. absorpt. 80−44321
Nb_3Sn-Au, supercond. tunnel junction with microshort circuit, nonlinear phenomena 78−14898
Ni:Au, ion-implanted, laser irrad. effect 80−108306
Ni/Au film on silicon vacuum deposited, electron impact mass spectrometric exam. of surface contaminants 78−75957
Ni-Cr/Au films, interdiffusion processes and oxidation phenomena 80−59735
$^{16}O^{8+}$+Au K-shell ionis., δ-ray emission 77−79557
Pb:Au, type II superconducting film, penetration depth meas. 77−28285
Pb-SiO_2-Au tunnel junction, obs. of conductance anomalies 78−26968
PbI_2-Au, light sensitive, internal photoelectric emission 80−107910
$Pd_{77.5}Cu_6Si_{16.5}$:Au metallic glass, diffusion of implanted Au 78−55983
Pt-Au, thick film, adherence meas. and evaluation 80−50813
Pt-Au bimetallic films, electron diffraction on networks of grain-boundary and interphase dislocations *(Russian)* 79−73168
Pt-Au film couple, diffusion of Au, depend. on annealing ambient, AES exam. 77−1261
Pt-polymer-Au capacitor, electroforming, negative resist., electron emission 80−80406
RbCl:Au, EPR and optical absorpt. 78−39397
RbCl:Au^-, optical absorpt. bands and MCD, electron-lattice interaction 80−108236
Si (111)-Au interface, chemically driven intermixing, UPS study 80−50533

gold continued
Si (111)5×1 Au surface struct., RHEED 77−62452
n-Si, diode with Au traps, negative differential conductance 79−11221
Si wafer contaminated, Au redistrib. during growth of oxide or phosphosilicate glass 77−4121
Si:Au, (111) surface impurity, ESCA obs. 78−52640
Si:Au, amphoteric centre, struct. bonding of deep level defects 80−88506
Si:Au, autoradiographic detection of getter effect, Ar ion implantation 78−38739
Si:Au, C-V curves of MIS diode used to examine trapping levels 80−65697
Si:Au, deep impurities, book contrib. 78−10403
Si:Au, deep-level impurities, insulating props. 78−39124
Si:Au, degeneracy factor of acceptor level 78−51927
Si:Au, diffusion, effect of C concentration 78−10076
Si:Au, diffusion of Au anal. 79−23786
Si:Au, diffusion-induced defects, X-ray triple cryst. diffractometry 80−2213
Si:Au, EPR spectrum, strong nucl. quadrupole effect 80−93172
Si:Au, electron and hole capture, DLTS obs. 80−49661
Si:Au, electron capture cross section, energy level of Au acceptor centre 78−51926
Si:Au, gamma-induced trapping levels 79−87059
Si:Au, heavily doped, gradual p^+-n junctions, trap levels *(French)* 80−34392
Si:Au, IR absorption and elec. resist. meas., impurity centres 79−38580
Si:Au, impurity diffusion and distribution obs. by neutron activation analysis *(Japanese)* 77−84787
Si:Au, impurity induced internal friction, impurity centre symmetry 79−73252
Si:Au, impurity photocond., for IR electrophotographic system 77−24589
Si:Au, influence of carrier heating on exclusion 77−8110
Si:Au, method of determining content of impurities with deep levels 80−2056
Si:Au, neutron irradiated, penetration of Au into Si 78−59984
Si:Au, nonequilib. population of electron states and photomemory of surface pot. 78−56206
Si:Au, O(H), film, amorphous, elec. cond. meas. 80−80423
Si:Au, p^+-n junction, quantitative study of Au atoms by TSC method 80−2458
Si:Au, P-induced point defects influence on Au gettering mechanism 80−65030
Si:Au, photoionisation cross-sections and energy levels 79−87060
Si:Au, photomag. effect 77−4401
Si:Au, precipitation of solid soln., effect of gamma irradiation 80−59515
Si:Au, recoil implantation from thin surface films, backscatt. obs. 78−63783
Si:Au, surface doped with metal impurities, water adhesion energy *(Russian)* 77−89620
Si:Au, thermally stimulated capacitance method fitting anal. 79−47107
Si:Au Ar ion implant gettering obs. by MOS and Rutherford backscatt. techniques 80−39119
Si:Au deep level parameter determ. by isothermal capacitance transient spectroscopy 80−88507
Si:Au diodes, diffused, influence of gamma irradiation, Au levels monitored 77−66199
Si:Au donor and acceptor centre obs. using IR absorpt. and dynamic nucl. polarisation with optical pumping 80−54639
Si:Au n^+p diodes, deep level transient spectroscopy, system effects and data anal. 79−99501
Si:Au p^+-i-n^+ diode, double injection switching, effect of trapped space charge 77−1473
Si:Au p^+-i-n^+ diode, I-V characts., recomb. centre influence 78−19134
Si:Au p^+-n junction, small area, acceptor level conc., determ. from TSC curves 80−75631
Si:Au planar extrinsic IR detector, use of multiple internal refl. for increased sensitivity 80−77862
Si:Au surface, electronic props. 77−66194
Si:Au use in weakly absorbed nucl. radiation detectors 77−67947
Si:Fe, interstitial form., Au dopant effect 80−29611
Si:Ga, Cu, Au, gettering of Cu and Au during Ga diffusion 78−91350
Si:Ga, sealed tube diffusion, Au and Cu gettering behaviour 77−76445
Si:P, Au, diffusion of Au obs. 77−51550
Si:P, Au, neutron irradiated, distrib. of P and Au determ. 78−79627
Si:P, Au, radiation-doped, influence of growth defects on elec. props. 79−69144
a-Si/Au barrier, capacitance and cond. 80−2469
Si/Au interface, X-ray dose enhancement, Monte Carlo calcs. 79−22484
n-Si-Au, evaporated contact photoelectric props. *(Russian)* 78−43473
Si-Au, interface study using EELS 80−97391
Si-Au, ohmic contact to GaP, metallurgical struct. 77−1485
p-Si-Au, Schottky barrier IR detector 77−37985
Si-Au contacts, Schottky barrier heights and interface states 77−85317
Si-Au Schottky barrier solar cell fabrication, doping of a-Si 80−50969
Si-Au Schottky diode, X-ray effects on elec. props., irrad. induced diffusion 77−4439
Si-Au Schottky diode, X-ray irradiated, radiation-accelerated diffusion of Au in Si 78−26952
Si-Au Schottky diodes, role of O in formation mechanics 79−42639
Si-Au-P system, partition coeff. of P, temp. depend. 79−43158
Si-Au-Si, Auger line intensity, contrib. of backscattered electrons 79−65962
Si-SiO_2 interface, Au conc., effective impurity doping 78−52094
Si-SiO_2 interface, Au doping, trap distribution 80−20319
Si-SiO_2-Au Schottky barrier solar cells, back-illuminated, theoretical performance 80−61345
SiO_2:Au, implanted atom, X-ray photoemission obs. 78−39050
SiO_2:Au, XPS line broadening and extra-atomic relax. energies 80−71561
$Si_{12}Te_{48}As_{30}Ge_{10}$-Au, Schottky barrier props. 79−7897
Sn/Au thin film diffusion couples, Kirkendall void form. 80−96698
Ta-Ta_2O_5-ZnS:TbF_3-Au thin films, MIS struct., DC electrolum. obs., Poole-Frenkel effect 78−88038
Te-Au thin film interface, evolution, switching effects *(French)* 80−6660
Ti/Au thin films, effect of Cl_2 on elec. resistance, Ti atom migration and preferred orientation 80−34530
Ti-anodic oxide-Au, electronic cond. *(French)* 79−95512
Ti-Pd-Au metallisation, patterning by plasma etching of Ti 78−27677
Ti-TiO_2-Au diode, spectral photoresponse and I-V characts. 80−15617

gold continued
Ti-W/Au metallisation on Al, temp. stability, barrier props. 79−23868
TiC film, Au-dispersed, struct., hardness and wear rate 77−77493
TiC-Au film, prep. by activated reactive evaporation, struct. and mech. props. *(Japanese)* 78−3252
U-Au conglomerates, Witwatersrand type, significance of diagenesis for origin 79−84265
(W-Au)-SiO_2-Si:B MOS transistor, ion implantation effect on threshold voltage 78−34903
Xe ion+Hg vapour (Au foil) collisions, quasimol. M-radiation 77−14566
^{136}Xe+Au, 625 MeV, probability of forming 1sσ vacancies 78−25681
Y-Y_2O_3-Au junction, defect struct. and local conduction 78−26970
ZnO:Au^{2+}, phosphors, emission spectra, impurity effects 77−32420
ZnS:Au, phosphor, 'blue' and 'green' centre form. *(German)* 79−38665
ZnS:Au,Al phosphors, luminesc. excitation spectra and exciton struct. 80−55164
p-$ZnSiAs_2$:Au(Tl)(S), photoluminesc., radiative recombination 77−24883
ZnTe:Au, elec. field and impurity conc. effect on ionisation energy 80−88514
ZnTe:Au, impurity identification and characterisation, capacitance, luminescence and IR absorption 80−60639

gold alloys
see also gold compounds
alkali metal-Au alloys, elec. props. 78−84187
charge density perturbations, ^{197}Au isomer shift obs. 77−20771
deposition by ion beam sputtering, composition and stress state 77−89674
dilute, conduction electron-local moment interactions using dHvA wave-shape anal. 79−77981
dilute, containing rare earth impurities, magneto-transport props. 78−68015
dilute, virtual bound states due to 4d- and 5d-transition metal impurities 80−70667
electrical resistivity, deviations from Matthiessen rule and scattering anisotropy 78−76051
electrodeposits for electronics industry, characts. 78−52695
electroplating, comparison with Sn-Pb alloy *(French)* 80−89158
internally deformed struct. as source of homogeneous linear struct. 78−26497
Mossbauer isomer shifts of ^{197}Au, theory, book contrib. 79−87357
mutual alloying behaviour of the elements straddling the line Li-Mg-Cu-Au in the long periodic table 78−84769
photoelectron spectroscopy, bonding investig. 80−55263
Pt-Au, chemisorption of H_2 and CO, effect of surface segregation 77−51601
rare earth alloys, RAu_2X_2 (X=Si,Ge), cryst. struct. 80−1964
rare earth alloys, $RAuNi_4$, (R=Gd, Tb, Dy, Ho, Tm, Yb and Er), mag. props. 77−20595
rare earth intermetallics, RAu_2, mag. props., 4.2-300K 79−7972
rare earth intermetallics, $RAu_{3.6}$, ordering temps. and effective moments 78−60283
rare earth intermetallics, RAu_3 (R=Gd, Tb, Dy, Ho, Er, Tm), mag. props. *(German)* 79−51761
rare earth-Au, amorphous, mag. and transport props. 80−34605
rare earth-Au, dil., Mossbauer exam. of mag. hyperfine field at ^{197}Au impurity 78−88244
rare earth-Au alloys sputtering, negative ions origin and effects 78−60574
rare earth-Au-In, Fe_2P type phases 77−70033
rare earth-gold amorphous alloys, R_4Au, anisotropy versus exchange 80−34624
surface electron states, photoelectron spectra meas., rel. to Au 78−14781
Ag-Au, calibration line introduction for comp. determ. by AES 79−56892
Ag-Au, composition changes under ion bombardment, scanning Auger microprobe obs. 79−83076
Ag-Au, corrosion in HNO_3 80−85091
Ag-Au, determ. of surface versus bulk composition, low energy ion scatt. spectroscopy 77−1284
Ag-Au, deviations from Matthiessen's rule 78−10420
Ag-Au, dil., elec. quadrupole interactions on ^{111}Cd probe nuclei, time differential PAC meas. 78−15066
Ag-Au, dil., low temp. elec. resist. 78−51964
Ag-Au, ion irrad., surface segregation and selective sputtering, AES expts. 79−7740
Ag-Au, liquid, surface tension *(Japanese)* 79−19431
Ag-Au, nucleation and growth on substrates 79−77956
Ag-Au, order-disorder transforms., s-band model 79−60502
Ag-Au, residual elec. resist., pseudopot. calc. 80−6813
Ag-Au, sputtering, ion yield depend. on alloy comp. 77−20976
Ag-Au, sputtering by 6 keV Xe^+ ions, energy distribs. 78−43969
Ag-Au, surface comp. after sputtering, AES obs. 77−55858
Ag-Au, surface enrichment, AES meas. 77−1283
Ag-Au, surface layer, effect of Ar^+ bombardment, AES and SIMS 80−25504
Ag-Au, surface segregation, ion scatt. spectroscopy meas. 79−82423
Ag-Au, temp. depend. of elec. field gradient, TDPAC meas. 77−32304
Ag-Au, thermoelectric power determ. 77−24549
Ag-Au, vacuum-deposited monocryst., internal friction, 200-3000 Hz, 20-850°C *(Russian)* 77−21197
Ag-Au (1 and 20 at.%), grain boundary energy and struct., solute atom effects 77−47465
Ag-Au (50 at.%), thermal expansion and lattice parameters, temp. depend. 78−91456
Ag-Au alloy, Auger exam. of preferred sputtering 77−44106
Ag-Au alloy thin film electron microprobe analysis *(French)* 77−32856
Ag-Au alloys, EMF meas. employing Ag-β-Al_2O_3 *(German)* 80−104307
Ag-Au system, surface segregation 79−69330
Ag-Au-Ay thin films, diffusion induced grain boundary migration 79−77833
Ag-Au-Cu, sputtering and AES 80−50503
Ag-Au-Cu, surface composition change on sputtering with 2 keV Ar ions 80−66365
Ag-Au-Pd, liquidus and solidus surfaces 78−60649
Ag-Cu eutectic composite wire, HF conductivity and skin effect 79−33305
Ag-Cu-Au, effect of additions on eutectic and peritectic temp., of binary alloys 78−84801
Ag-Pd-Cu-Au dental alloy, age-hardening characts. 79−87646

gold alloys continued
Ag-Sn alloys containing Au, splat cooled ribbons, electron microscope exam. 78−39987
Ag-Sn-Au, dental amalgams, effect of small additions of Au, struct. and corrosion study 79−20718
AgAu, ion bombardment by alkali-metal sputter ion source *(Japanese)* 79−54734
AgAu, mols., VB calcs. 77−57883
AgAu, quenched, short range order effects on specific heat 80−29181
AgAu, recovery and formation of mixed dumbbells after thermal neutron irradiation 79−69161
AgAu, sputtered neutral mass spectrometry using post-ionisation in microwave plasma 78−92579
$Ag_3Au_{1-x}Cu_x$, phase relations, X-ray diffr. and differential thermal anal. 80−108395
$Ag_{0.6}Au_{0.4}Mn$, dil., effect of mean free path on strength of RKKY interaction 78−39291
$Ag_{1-x}Au_xYb_y$, thermopower and resistivity 79−65457
$Ag_xAu_{1-x}Zn$, resistivity and X-ray diffr. 78−47283
Ag_3Sn, containing Au, etching technique for alloys and amalgams 78−3291
Al-Au, electronic structure exam. by soft X-ray and X-ray photoelectron spectroscopy 77−85136
Al-Au, growth kinetics of plate precipitates 77−66649
Al-Au, growth kinetics of plate shaped precipitates 78−6932
Al-Au, growth kinetics of plate shaped precipitates 78−6933
Al-Au, growth kinetics of plate-shaped precipitates 78−6934
Al-Au, growth kinetics of plate-like precipitates, vol. diffusion controlled growth 78−6935
Al-Au, interdiffusion *(Czech)* 77−62684
Al-Au, liquid alloys, exam. of Si diffusion *(Russian)* 79−28118
Al-Au, precipitate plate growth kinetics 79−15679
Al-Au (0.2 wt.%), precipitation mechanism and creep behaviour 80−3058
Al-Au bimetal thin film interdiffusion zone, intermetallic phase form kinetics, 70-160°C 78−75891
Al-Au melt, Si solubility *(Russian)* 77−66024
Au/Au-Ge/GaAs structure, ohmic contact behaviour, alloying time effect 79−19659
Au/AuPd, bicrysts., in situ relax. of interphase interfaces 80−39455
Au/Zn/InP Schottky barrier diode, fabrication and elec. props. 79−33348
Au-^{171}Yb, dil., nuclear induced resistivity drop 78−10431
Au-^{174}Yb, dil., nuclear induced resistivity drop 78−10431
Au-3d transition metal alloys, UPS study, localised states 80−93449
Au-Ag, appl. of self-consistent cluster Bethe lattice study of two-band alloy model 80−29303
Au-Ag, bicryst. thin film couples, interphase interfaces, TEM 80−70540
Au-Ag, cold worked, impurity conc. rel. to internal friction Bordoni peak, solid soln. hardening mech. 80−16363
Au-Ag, deposition on alkali halide, kinetic nucleation model 77−85118
Au-Ag, dilute, low temp. thermoelec. power, electron diffusion and phonon drag 77−20301
Au-Ag, liquid alloy, surface energy meas. by const. temp. method on solid alumina 78−6208
Au-Ag, mech. damping 78−31444
Au-Ag, optical spectra, 0.5-6 eV, d-band struct. 77−48168
Au-Ag, plastic deformation, energy storage efficiency 77−4807
Au-Ag, radiation damage and diffusion 80−24645
Au-Ag, surface segregation 79−77873
Au-Ag, thermal conductivity, data anal. and synthesis 78−95284
Au-Ag, thin film struct., Rutherford backscattering spectrometry, signal overlap subtraction 80−50486
Au-Ag (13 at.%), thermopower standard in mag. field 79−78081
Au-Ag (35 at.%), dechannelling of energetic He ions at dislocations 80−70275
Au-Ag alloys, SRO and ordering energy *(Russian)* 77−65964
Au-Ag film, thermoelectric power and resist. meas., MFP and Fermi surface meas. 77−51826
Au-Ag single phase alloy, sputter yields 79−87546
Au-Ag-Cd, γ-ray PAC of ^{111}Cd, nearest neighbour contrib. to elec. field gradient 77−36161
Au-Ag-Cd, martensitic transformation, preceding struct. anomaly 78−68692
Au-Ag-Cd alloys, martensitic phase transition, elastic anomalies and mode softening 79−91647
Au-Ag-Cd pseudobinary alloys, thermodynamic study of order-disorder and martensitic transform. 78−48399
Au-Ag-Cu, chem. surface anal., low energy ISS compared with SIMS 78−64908
Au-Ag-Cu, optical props. study using automatic nulling spectroellipsometer 80−55058
Au-Ag(Cu), surface segregation, electronic theory, density of states, cluster-Bethe-lattice approx. 80−49369
Au-Al, liq. alloy, thermodynamic activities and enthalpies 80−19960
Au-Al system, influence of current on phase form. in diffusion layer *(Russian)* 78−52826
Au-Al-In solid soln., elastic strain energy depend. of supercond. T_c 79−38229
Au-Be, contact form. for semicond. devices by ionised-cluster beam deposition 77−32528
Au-Bi, liq. alloys, Bi activities, ht. of mixing 77−4921
Au-Cd, behaviour of Cd d-bands, comparison with Hg and Ag alloys 79−37972
Au-Cd, charge-transfer and valence-band behaviour using ^{197}Au Mossbauer and X-ray photoemission spectra 79−60695
Au-Cd (47.5 at.%), effect of cooling rates on stress-strain behaviour 78−76721
Au-Cd (47.5 at.%), modified 2H and 9R martensites 78−14366
Au-Cd (47.5 at.%), single cryst., temp. and press. derivatives of elastic consts. near martensitic phase transform. 77−63667
Au-Cd alloy, α and ζ phase, low temp. sp. ht. 78−18789
Au-Cd system, cryst. struct. of $AuCd_3$ and existence of $AuCd_{\sim 5}$ phase *(German)* 77−25020
Au-Cd(Ga)(In) alloy, UPS exam. of valence bands 79−19511
Au-Co, dil, local moments, third harmonic de Haas-van Alphen wave shape anal. 78−84127
Au-Co, dil., valence and core level spectra, XPS study 80−84838
Au-Co, dil. alloy, crystalline electric field and spin-orbit splitting, NMR results 77−32274

gold alloys continued
Au-Co, dil. alloy, de Haas-van Alphen obs. of spin dependent scatt. by mag. pairs 77−32007
Au-Co, electrodeposit, characterisation by ^{57}Co-^{57}Fe Mossbauer spectroscopy 80−39989
Au-Co, electrodeposit, Mossbauer meas. of Co chem. state 80−39990
Au-Co, electron scatt., spin-orbit effects 80−65533
Au-Co, electron scatt. by mag. impurity pairs, de Haas-van Alphen obs. 77−66162
Au-Co, electroplated, 'polymer' inclusions, chem. identity obs. 79−37931
Au-Co, liq. alloys, partial struct. factors 80−1919
Au-Co, liquid alloys, ^{59}Co NMR studies 79−95660
Au-Co, liquid alloys, struct. determ. by X-ray diffr. 78−6006
Au-Co, liquidus line determ. by mag. meas. 80−60250
Au-Co, molten, US vel. meas., compressibility and partial struct. factors determ. 77−69045
Au-Co electrodeposit, Co-hardened, state of Co in as-deposited material, Mossbauer obs. 80−15397
Au-Co electrodeposit, Co-hardened, characterisation by Mossbauer spectroscopy, Co precip. formation 80−80108
Au-Co electrodeposit, struct. and hardness characts. 79−28245
Au-Co electrodeposits, Co hardened, chemical state of Co, Mossbauer emission spectra 79−90897
Au-Co electrodeposits, Co hardened, high temp. film formation 79−91848
Au-Co electrodeposits, heating effect on microstruct. and surface topography 77−43456
Au-Co film, co-evaporated, struct. and ohmic behaviour 79−87021
Au-Co melts, struct., compressibility, X-ray and neutron diffr. 77−11614
Au-Co solid solution, mag. susceptibility 79−61081
Au-Co solid solution, mag. props., freq. depend. suscept. maximum 79−69655
Au-Cr, conc. spin glasses, thermopower 80−65538
Au-Cr, cosputtered films, optical props. 0.2 to 6.1 eV 77−32454
Au-Cr, dil., elec. resist., generalised phase shift anal. of Kondo effect 80−75556
Au-Cr, dil., spin glass, elec. resist., press. and conc. effects 78−52278
Au-Cr, dil. alloys., elec. resist., deviations fro Matthiessen's rule 80−75541
Au-Cr alloy, quantitative Auger electron anal., sputter-yield ratio 77−44096
Au-Cr alloy pressure gauges, annealing effects 78−49854
Au-Cr alloys, Cr conc., quantitative Auger electron analysis 77−85852
Au-Cr Kondo alloy, effect of press. on resistivity. 78−79978
Au-Cr pressure gauge, technological processing 77−49740
Au-Cr-GaAs Schottky-barrier diodes, effect of γ-radiation on current-voltage charact. *(Russian)* 80−2459
Au-Cr(Mn), spin glass alloy, elec. resist. 77−8067
Au-Cs, liq. alloy, mag. susceptibility rel. to ionic charact. 77−1536
Au-Cs(Mg)(Rb)(Zn), charge transfer, Mossbauer effect ^{197}Au isomer shifts, XPS valence-band spectra 80−2676
Au-Cu, cold worked, impurity conc. rel. to internal friction Bordoni peak, solid soln. hardening mech. 80−16363
Au-Cu, dielectric const. by multiangle reflection meas., optical props. 79−95723
Au-Cu, dil., electron irradiated, interstitials and their clusters, diffuse X-ray scatt. study 80−33997
Au-Cu, dilute, low temp. thermoelec. power, electron diffusion and phonon drag. 77−20301
Au-Cu, Ising FCC and antiferromag., mag. phase diagram, ordering, Monte Carlo calc. 80−103833
Au-Cu, optical spectra, 0.5-6 eV, d-band struct. 77−48168
Au-Cu, oxidation kinetics of Cu out of Au soln. at 50-150°C 80−21171
Au-Cu, preferential sputtering 79−83080
Au-Cu, refr. index and absorpt. coeff., 1-5 eV *(Russian)* 78−60484
Au-Cu, residual elec. resist., pseudopot. calc. 80−6813
Au-Cu, short-range order and energy of ordering, diffuse X-ray diffr. meas. *(Russian)* 77−43174
Au-Cu, surface comp. after sputtering, AES obs. 77−55858
Au-Cu, surface comp. as function of temp., AES expts. 78−95212
Au-Cu, surface conc. profile and surface energy 80−84350
Au-Cu, thermal conductivity, data anal. and synthesis 78−95284
Au-Cu (50% at.), pretransitional fluctuations *(French)* 80−2160
Au-Cu film, elec. resist. and temp. coeff. of resist. 77−39968
Au-Cu solid soln., spectral determ. of comp. using UHF plasmotron as source 79−52812
Au-Cu-Ag, phase transform. effect on mech. props. *(Russian)* 78−3122
Au-Cu-Ag dental alloy, age-hardened, struct. and morphology 78−92272
Au-Cu-Ag-Pd (35.4, 17.8, 9.7 at.%), dental alloy, age-hardenable, TEM obs. 77−21156
Au-Cu-Cr, thin layer, deposited on glass or Si substrate, X-ray microanalysis *(French)* 80−50902
Au-Cu-Fe spin glass alloys, impurity mag. resist. meas. 80−59972
Au-Cu-Ga, solid soln., phase systems, valence electron density effects *(French)* 78−19724
Au-Cu-Ni, computer characterisation, exam. of phase equilibria and miscibility gap 79−11561
Au-Cu-Ni(Ag), phase precipitation on domain boundaries *(Russian)* 78−39777
Au-Cu-O surface, quantitative Auger analysis using relative sensitivity factors 78−7295
β-Au-Cu-Zn, martensitic transformation temps. ageing and quenching effect 79−47687
Au-Cu-Zn-Ni (13, 3.4, 8.5 wt.%), white gold, metallographic structure after cold rolling, effect of heat treatment, recrystallisation *(French)* 79−52238
Au-Dy, dil., hyperfine interaction of Γ_8 quartet, Mossbauer expt. 78−43718
Au-Dy, dil., hyperfine interaction, Mossbauer study, Kramers quartets 80−66083
Au-Er, dil., cold-worked, EPR expts. 80−39864
Au-Er, dil., EPR at 100 mK to 1K 80−66028
Au-Er, ESR studies 80−108064
Au-Er film, stress-induced g-shift, ESR meas. on Er 77−51951
Au-Fe, alloy with mixed types of order, uniform mag. phase diagram 79−78368
Au-Fe, anomalous Hall effect, asymm. scatt. of itinerant electrons 77−43569
Au-Fe, competing interactions in FCC alloys 78−95453
Au-Fe, conc. spin glasses, thermopower 80−65538
Au-Fe, dil., approach to saturation of magnetisation 78−56293
gold alloys continued
Au-Fe, dil., contact charge density, internal conversion meas. 79−56630
Au-Fe, dil., crit. dynamics 80−60325
Au-Fe, dil., in supercond. proximity, localised bands 78−10613
Au-Fe, dil., ion implanted, phase comp., Mossbauer study 80−7244
Au-Fe, dil., local mag. moments, neutron scatt. study 79−61058
Au-Fe, dil., local moments, third harmonic de Haas-van Alphen wave shape anal. 78−84127
Au-Fe, dil., thermopower, interconfig. fluctuations 79−65412
Au-Fe, dil., valence and core level spectra, XPS study 80−84838
Au-Fe, dil. alloy, transverse magnetoresist. in spin glass regime 80−34417
Au-Fe, dil. alloys, spin glasses, modified bond model calcs. 79−33489
Au-Fe, finite mag. clusters near percolation conc. 78−72371
Au-Fe, impurity spin dynamics in magnetic glasses at low frequencies *(French)* 78−88126
Au-Fe, Kondo system, magnetisation, Mossbauer expt. 77−77028
Au-Fe, liq., thermodynamic mixing effects, mass spectrometric meas. eval. *(German)* 77−59123
Au-Fe, long range mag. order 77−63215
Au-Fe, mictomagnet, freq. depend. of susceptibility max. 78−95445
Au-Fe, polygonisation, recrystallisation, precipitation microstruct. without external plastic deform. 79−43276
Au-Fe, spin glass, mag. moment dynamics, neutron diffuse scatt. meas. 77−69584
Au-Fe, spin glass, quench-condensed film, reduced MFP influence on elec. resist. 77−69306
Au-Fe, spin glass, spin relaxation rates, neutron scatt. study 79−47235
Au-Fe, spin glass, transition temp., freq. depend. 80−97113
Au-Fe, spin glass behaviour in low DC field 77−66373
Au-Fe, spin glass in low DC field, mag. viscosity, time decays of remanences 78−64209
Au-Fe, spin glasses, alternating susceptibility 80−65912
Au-Fe, spin-glass, characteristic temps. 79−38348
Au-Fe, spin-orbit coupling and electron scatt. 80−2370
Au-Fe, spin-orbit electron scatt. near percolation limit, anomalous Hall effect meas. 79−73492
Au-Fe, very dil. alloy, Kondo temp. 78−91688
Au-Fe (Mn)(Co), spin glass transition and anomalous Hall effect 79−61162
Au-Fe (1 at.%), spin glass, specific heat 80−60355
Au-Fe (1-7 at.%), extraordinary Hall effect, near ferromag. percolation limit 79−19575
Au-Fe (14.5 at.%), spin dynamic exam. by diffuse magnetic neutron scatt. 77−8320
Au-Fe (15 at.%), small angle neutron scatt. study 79−47293
Au-Fe (16.2 at.%), cluster glass, mag. small angle neutron scatt. 80−50111
Au-Fe (17 at.%) alloy, fission fragment irrad., simulation of neutron effects 77−80549
Au-Fe (20 at.%), mag. virtual bound state alloys, XPS of core states 79−47588
Au-Fe (22 at.%), ferromag. phase, AC susceptibility near T_c 78−43575
Au-Fe (3.1-10.4 at.%) spin glass alloys, high field magnetisation curves 80−11213
Au-Fe (4 at.%), spin glass energy relaxation of remanent magnetisation at low temp. 79−87271
Au-Fe (4 at.%), spin glass, magnetisation and energy relax. below T_g 80−65921
Au-Fe (40 at.%), discontinuous precipitation reaction at grain boundaries 79−87642
Au-Fe (4.2 at.%), spin glass, DC magnetisation, field depend. 80−97103
Au-Fe (4.4 and 4.8 at.%), isotropic spin glass behaviour and transverse magnetoresist. 77−15830
Au-Fe alloy, dil., Mossbauer exam. in spin glass regime 79−61289
Au-Fe alloy, spin glass, neutron scatt. 78−68265
Au-Fe alloy film, mag. susceptibility max. 79−24173
Au-Fe alloys, magnetism and atomic clustering 80−103810
Au-Fe alloys, spin correlations, neutron diffr. meas. 80−80482
Au-Fe film spin glass, low temp. resistivity, mean free path effects 78−80163
Au-Fe ion implanted alloy, Mossbauer conversion electron scatt. 80−88898
Au-Fe solid soln., diffusion coeffs., Mossbauer spectra 77−12260
Au-Fe solid soln. alloys, reson. and relax. effects 79−82865
Au-Fe spin glass, energy flux associated with remanent magnetization relaxation *(French)* 80−7110
Au-Fe spin glass, long-time relax. processes, heat capacity expts. 77−66374
Au-Fe spin glass, susceptibility cusp, influence of Fe clusters 79−61163
Au-Fe spin glass alloy, neutron scatt. study 79−61179
Au-Fe spin glasses in low DC fields, susceptibility and thermoremanence 77−77063
Au-Fe-Ni layer coating, Fe and Ni conc. meas. by X-ray diffr. *(German, English)* 80−34330
Au-Fe(Co)(Mn), spin glass, residual resistivity conc. depend. 80−2382
Au-Fe(Mn) dil. spin glass alloy, impurity-impurity interaction press. depend., resistivity meas. 77−20308
Au-Ga, dil. alloys, dHuA meas. and phase shift analysis of electronic scatt. anisotropy 77−35932
Au-Ga, liq. alloys, Ga activities, ht. of mixing 77−4921
Au-Ga, resist. and supercond. meas., electron-phonon interaction and Coulomb pseudopot. determ. 78−43358
Au-Ga based contacts to GaAs alloyed in As_2 beam 79−95495
Au-Ga dil. alloys, electronic struct. 79−37974
Au-Ga liq. alloys, ΔG^E of mixing from ht. of melting and sp. ht. of cpds. 77−4920
Au-Ga-In solid soln., elastic strain energy depend. of supercond. T_c 79−38229
Au-Gd, dil., conduction electron-local moment exchange interaction meas. 80−60191
Au-Gd, dil., crystal-field splitting of localised Gd^{3+} moments, ESR obs. 79−82869
Au-Gd, dil., fine struct. splitting, magnetisation meas. 79−56498
Au-Gd, dilute, thermoelec. power, crystal field and interaction effects 77−66158
Au-Ge, liquid quenched, exam. of phase decomposition 78−48371
Au-Ge, ohmic contact for n-GaAs, formation and props. 79−15223
α-Au-Ge, superconducting transition temp. depend. on electron per atom ratio, lattice deform. 77−8222

gold alloys continued
Au-Ge (27 at.%), metastable phase struct. determ. by electron diffr. 78−83780
Au-Ge contacts on GaAs, SEM and TEM obs. of struct. 80−100522
Au-Ge contacts to n-GaAs layers, with SiO_2 overlayer, ohmic props. 80−2467
Au-Ge eutectic films, prep. of Au films with nm-sized pores by etching 80−16227
Au-Ge evaporated film, effect of substrate on conductivity 79−78213
Au-Ge film, evaporated, for ohmic contacts to GaAs, compositional stratification, effect of source material impurities 79−77951
Au-Ge ohmic contacts, laser alloying on GaAs 79−73583
Au-Ge system, struct. of metastable phases *(German)* 80−108430
Au-Ge/GaInAsP, ohmic contact, elec. characts. 80−80376
Au-Ge/Ni films on GaAs, alloying behaviour, microprobe AES and X-ray diffr. 80−54548
Au-Ge/Ni ohmic contact to GaAS, solid phase epitaxy formation 79−60658
Au-Ge-Ni/GaAs metal-semiconductor thermoelectric coolers, effects of contact resist. and dopant conc. 80−81481
Au-Ge-Si, influence of struct. on elec. resist. of glass forming alloys 80−65518
Au-Ho nuclear orientation thermometer for use from 1-30 mK 79−17419
Au-In, charge-transfer and valence-band behaviour using ^{197}Au Mossbauer and X-ray photoemission spectra 79−60695
Au-In, electrodeposited from acid cyanide electrolyte, exam. of wear and corrosion resistance 78−80482
Au-In liq. alloys, ΔG^E of mixing from ht. of melting and sp. ht. of cpds. 77−4920
Au-In-Pb, $AuIn_2$-In-Pb portion of phase diagram 77−32562
Au-In(Sn), HCP ζ-phase, magnetic susceptibility 78−47946
β'-Au-Mg, de Haas-van Alphen effect, relativistic LMTO bandstructure, Fermi surface 79−37959
Au-Mg, high resolution electron microscope and electron diffr. investigation, obs. of $Au_{15}Mg_4$ monoclinic phase 80−1968
Au-Mg, long-period superstructures, electron diffr. obs. 79−94959
Au-Mg (18 at.%), superstruct. determ., electron microscope obs. 78−75630
Au-Mn, band profile, density of states, quantum defect-Green's function calcs. 80−54599
Au-Mn, conc. spin glasses, thermopower 80−65538
Au-Mn, dil., ^{52}Mn γ-ray anisotropy down to 3 mK, Kondo and relax. effects 77−81034
Au-Mn, dil., nuclear orientation of recoil implanted ^{52}Mn 78−43716
Au-Mn, dil. spin glass, thermopower, rel. to spin glass freezing temp. 78−79983
Au-Mn, orthorhombic struct., electron diffra. and electron microscopy obs. 80−15052
Au-Mn, spin-orbit coupling and electron scatt. 80−2370
Au-Mn alloys, equiatomic region of phase diagrams crystallographic and mag. exam. 78−52755
Au-Mn alloys, reversible and irreversible DC magnetisation in spin glass regime 80−65908
Au-Mn system, AABB struct., experimental evidence for occurrence 78−63698
Au-Mn-Cr(Pd) alloy, ferro- to non-mag. transform. 77−12117
Au-Mn(Cr)(Fe), dil., spin glass state and Kondo effect, nucl. orientation of ^{54}Mn 78−6514
Au-Mn(Fe)(Cr), spin glass, anomalous Hall effect 78−30908
Au-Ni, composition modulated foils, layer struct. and mech. props. 79−95300
Au-Ni, dil., valence and core level spectra, XPS study 80−84838
Au-Ni, fast liq. quenched, anomalous sp. ht. near ferromag. crit. comp. 77−80947
Au-Ni, heat capacity, 1.5 to 15K 78−95452
Au-Ni, liquid alloy system, determ. of thermodynamic props. using Knudson effusion method, phase diagram calc. *(German)* 78−51707
Au-Ni, mag. clustering 79−7977
Au-Ni, magnetisation and sp. ht., ferromag., paramag. and crit.-conc. regions 79−38330
Au-Ni, modulated struct. form. by spinodal decomp., lattice imaging electron microscopy obs. 79−95996
Au-Ni, preferential sputtering 79−83080
Au-Ni, supermodulus effect, one-dimens. modulated structs. 79−95068
Au-Ni, surface segregation, strain effects 80−80042
Au-Ni (15 at.%) film, evidence of modulated struct., TEM exam. 78−87887
Au-Ni (30 at.%), singularities of struct. state, diffuse electron and X-ray scatt. *(Russian)* 79−4945
Au-Ni bimetallic cluster, segregation and short range order props. at boundaries 79−29071
Au-Ni foil, composition-modulated, elastic modulus enhancement 77−52382
Au-Ni solid soln., creep 78−15475
Au-Ni-Cu phase diagrams, thermodynamic calc. *(Korean)* 78−68672
Au-Ni-Cu-Zn, white gold, metallographic struct., heat treatment and plastic working effect 80−40403
Au-Ni-O surface, quantitative Auger analysis using relative sensitivity factors 78−7295
Au-Ni(Pd)(Pt), surface composition determ. 79−69328
Au-Pb-In solder joints, layer growth, ageing 77−32764
Au-Pd, bicryst. thin film couples, interphase interfaces, TEM 80−70540
Au-Pd, biological specimen prep. for SEM 79−5421
Au-Pd, disordered, shaft range order diffuse scatt., electron diffr., interpretation 77−84596
Au-Pd, He(I) photoelectron spectra, 5d band 79−33892
Au-Pd, surface comp. changes under ion bombardment, AES study 80−55250
Au-Pd, thermal conductivity, data anal. and synthesis 78−95284
Au-Pd (1(50) wt.%), quenched, vacancy annihilation and short-range order formation, elec. resist. 80−108487
Au-Pd alloy, on rock salt, epitaxial growth and struct. 77−20211
Au-Pd alloy, surface comp., polishing, cleaning and Ar sputtering effects 77−72763
Au-Pd coating for radioactive source backing, spontaneous resistance variations 77−54386
Au-Pd dil. alloys, electronic states, virtual bound states model *(French)* 77−62809
Au-Pd-Pt-Ag, composition-property diagrams, mathematical models for diagrams *(Russian)* 79−11554

gold alloys continued
Au-Pd-Zn system, quasibinary section phases investig. 77−12596
Au-Pd(Pt), elect. resistivity, temp. depend. between 1.6 and 4.2K *(German)* 79−28337
Au-Pt, cold worked, impurity conc. rel. to internal friction Bordoni peak, solid soln. hardening mech. 80−16363
Au-Pt (60 at.%), solid soln. neutron small-angle scatt. study of phase decomp. 79−15646
Au-Pt-Pd-Ag-Cu, commercial dental alloy, age-hardening characts. 80−89235
Au-rare earth, dil., magnetoresist., quadrupole scatt. effects 78−39096
Au-rare earth, dil., magnetotransport props., theory 78−39097
Au-Rh(Y)(Zr)(Nb)(Pd), dil., Friedel d-reson. scatt. and elec. resists. 80−44566
Au-Sb, charge-transfer and valence-band behaviour using ^{197}Au Mossbauer and X-ray photoemission spectra 79−60695
Au-Sb, liq. alloys, ΔG^E of mixing from ht. of melting and sp. ht. of cpds. 77−4920
Au-Sb thin film interdiffusion 77−59152
Au-Si, amorphous sputtered film, elec. props. 78−68006
Au-Si, liq. alloy, thermodynamic activity meas. by Knudsen-cell mass spectrometry *(French)* 80−10684
Au-Si, melt, thermodynamic study of phase diagram *(French)* 78−27482
Au-Si eutectic melt, wetting of quartz 77−31840
Au-Si film, elec. resist. decay and struct. change on exposure to air 77−72924
Au-Si formation at thin film interface, electron diffr. study 80−80005
Au-Si interface, valence band and core levels, Si diffusion, alloy form., photoelectron spectra obs. 80−45205
Au-Si-Mn, amorphous spin glass film, mag. susceptibility 79−42775
Au-Sn, charge-transfer and valence-band behaviour using ^{197}Au Mossbauer and X-ray photoemission spectra 79−60695
Au-Sn, liq. alloys, ΔG^E of mixing from ht. of melting and sp. ht. of cpds. 77−4920
Au-Sn, zeta and AuSn phases, heats of form. and heat contents 80−60837
Au-Sn (100 ppm Sn), vacancy clusters, quenching and ageing, electron microscopy study 78−76671
Au-Sn alloys, surface comp. by Auger spectroscopy, sputter cleaning 77−59648
Au-Sn evaporated films, comp. and annealing behaviour, 20-400°C 77−76695
Au-Sn liquid, optical reflectivity spectra of virtual bound states 80−89021
Au-Sn liquid alloys, Sn activity *(Japanese)* 78−6901
Au-Sn(Bi)(Ga)(Ni), elec. resist. in liquid and solid state *(Russian)* 79−51549
Au-Sn(Cu), dil., quenched vacancy cluster form. 77−62546
Au-Tb, dilute, thermoelec. power, crystal field and interaction effects 77−66158
Au-Te, charge-transfer and valence-band behaviour using ^{197}Au Mossbauer and X-ray photoemission spectra 79−60695
Au-Te, elec. field gradients and charge transfer, Mossbauer spectra 80−25268
Au-Te, liq. alloys, ΔG^E of mixing from ht. of melting of sp. ht. of cpds. 77−4920
Au-Te, thermodynamic props., calorimetric meas. 78−20051
Au-Ti, dil., virtual bound states, optical absorption meas. 78−2891
Au-Ti/SiO_2/p-Si MOS struct., interface state distrib., DC tunnelling spectra determ. 80−75611
Au-Ti/n-InP Schottky diode, elec. characts. and barrier height 77−59329
Au-Tl (29 to 100 at.%), thermal analysis, exam. of phase diagram 78−88445
Au-Tm, dilute, thermoelec. thermoelec. power, crystal field and interaction effects 77−66158
Au-transition metal, residual resistivity, effect of 4d and 5d transition metal impurities 79−60791
Au-transition metal alloys, ^{197}Au Mossbauer isomer shift cellular atomic model 80−84673
Au-V, dil., ^{51}V CW NMR line width anal., RKKY broadening 78−15033
Au-V, dil., Kondo alloy, spin dynamics, nuclear spin relax obs. 78−68155
Au-V Kondo alloys, mag. susceptibility and NMR Knight shift in conc. independent region 77−77027
Au-Y, dil., conduction electron-local moment exchange interaction meas. 80−60191
Au-Y, dil., hyperfine interactions, $^{87}Y^m$ nuclear orientation meas. 78−43715
Au-Yb, dil., EPR at 100 mK to 1K 80−66028
Au-Yb, dil. alloy, high field nuclear relax. of ^{173}Yb, anisotropic cond.-electron exchange 77−8434
Au-Yb alloys, dil., nucl. reson. of ^{173}Yb local moments 79−65763
Au-Yb dilute, NMR investig. of anisotropic cond. electron exchange 77−63309
Au-Yb thin films, ESR spectra, strain effects 80−71172
Au-Zn, (55 to 88 at.%), equilib. diagram, X-ray diffr. obs. 80−25660
α-Au-Zn, disordered, shaft range order diffuse scatt., electron diffr., interpretation 77−84596
Au-Zn, liq., thermodynamic props. *(German)* 80−49386
Au-Zn, molten, EMF meas. of activities using ZrO_2 solid electrolytes *(Japanese)* 80−88339
α-Au-Zn, superconducting transition temp. depend. on electron per atom ratio, lattice deform. 77−8222
Au-Zn/p-$Ga_xIn_{1-x}PyAs_{1-y}$, specific contact resist. 80−84509
Au-Zn(Cu), electrolytic thinning for use in transmission electron microscopy 78−57918
(Au-Ge)-Ni film, for contacts to n-GaAs, metallurgical investigation using inert substrate 77−85313
(Au-Ge)-Pt film, for contacts to n-GaAs, metallurgical investigation using inert substrate 77−85313
Au_xAg_{1-x}, density of states and resist., CPA calc. 80−24780
$Au_{52.5}Ag_xCd_{47.5}$, pseudoelastic behaviour associated with thermoelastic martensitic transform. 80−16304
AuAl formation by thin film interactions, identification by X-ray diffraction 79−99442
$AuAl_2$ superconductive device to provide reference temps. below 0.5K 79−63220

gold alloys continued
$AuAl_2(Ga_2)(In_2)(Sn_2)(Sb_2)(Te_2)$, core-level binding energy shifts and charge transfer 80−25268
Au_3Cd, order-disorder phase transform., X-ray diffr. anal. *(Russian)* 80−45297
Au_3Cd, sputtered epitaxial films, order-disorder reaction obs. 78−84092
Au_3Cd_5 and Au_5Ce_8.h, cryst. struct. and binding type *(German)* 79−86742
AuCd.r, cryst. struct. determ. 77−84699
AuCu II, periodic antiphase struct. *(French)* 79−14937
AuCu II, rational and irrational long period struct. 79−95175
AuCu II plates, growth mechanisms 77−48423
AuCu II plates, growth mechanism 79−56976
AuCu, mols., VB calcs. 77−57883
AuCu, optical constants direct determination, d absorpt., reflectivity 77−69791
AuCu-Al thin film bilayer system, phase formation, backscattering spectra 80−96728
$AuCu_3$, ordered, band struct. and optical props. at 30K 79−60696
$AuCu_3$, quantum theory of order-disorder transition energy 77−62640
$Au_{1-x}Cu_x$-Fe, dil., resistance maximum 79−61056
Au_3Cu, ht. of order-disorder transform., differential microcalorimetry *(French)* 78−57950
$Au_3Cu_{1-x}Ag_x$, phase relations, X-ray diffr. and differential thermal anal. 80−108395
AuFe alloy films, mag. susceptibility, Fe concentration and annealing depend. 79−61119
AuFe, Ising spin glass, calc. of wavevector depend. susceptibility 77−63223
AuFe, spin glass, anomalous magnetoresistance 79−78077
AuFe spin glass, μ^+ zero-field spin relax. probe for spin dynamics 80−97177
AuFe, spin glass freezing above ferromag. percolation limit 78−52264
$Au_{1-x}Fe_x$, $0.14<x<0.28$, ferromagnetism study by specific heat meas. 80−7121
$Au_{85}Fe_{15}$, and $Au_{82}Fe_{18}$, mag. props. 80−84592
$Au_{92}Fe_8$, apparatus for measurement of initial paramagnetic susceptibility 79−54160
AuGa, and $AuGa_2$, supercond. transition temp. and crit. field 79−38232
$AuGa_2$ film, supercond., mag. susceptibility and Knight shift press. depend. 77−43777
$AuGa_2$ type supercond., mag. impurity and press. effect on crit. temp. *(Russian)* 78−23189
$AuGa_3$, supercond., press. depend. of thermodynamic props., theor. *(Russian)* 77−51843
AuGe, ohmic contact to epitaxial GaAs, production by laser alloying 78−88026
AuGe/n-GaAs, SIMS study Au behaviour during annealing 78−75947
Au_xGe_{1-x}, liq., ang. distrib. of positron annihilation 77−55848
$Au_{0.77}Ge_{0.136}Si_{0.094}$, undercooled metallic melt, viscous behaviour 77−66037
$Au_{77}Ge_{13.5}Si_{9.4}$, heat of crystn. and viscous behaviour 80−75166
AuIn-Pb pseudobinary system, DTA 78−23667
$AuIn_2$, pulsed NMR expts, rel. to performance as nuclear refrigerant 79−61259
$AuIn_2$ superconductive device to provide reference temps. below 0.5K 79−63220
AuLi, vibr. freq. determ., IR spectra, matrix depend. 77−75146
AuMg, B2 intermediate phase, slip system, ordering energy and atomic size ratio depend. 80−59471
$Au_2(Mn,Z)_2$, Heusler alloy, (Z=Al, Cu, Ga, In or Zn), magnetic order and coupling 79−38303
AuMn, mag. struct., phase transition, and magnon spectrum, random anisotropy effects 80−88722
AuMn, mictomagnetic, Hall and magnetoresist. effects 78−43361
AuMn, ordered, vacuum deposited epitaxial films, orientation control by external stress 80−100426
$Au_{11}Mn_4$, electron diffraction and microscopy obs. 78−75512
$Au_{11}Mn_4$ ordered phase formation, electron diffr. and microscopy study 80−107418
$Au_{11}Mn_4$, ordering, electron diffr. and high resolution TEM obs. 78−71707
Au_3Mn thin films, electron diffr. study 80−92793
Au_4Mn, atomic short range order and pair interaction, neutron diffr. exam. 78−22695
Au_4Mn, electron irrad. in electron microscope, radn. ordering 79−86818
Au_4Mn, fully ordered, microstruct., high resolution electron microscopy 79−1439
Au_4Mn, heat treated, short-range order, diffuse X-ray diffr. study *(German)* 80−88092
Au_4Mn, high resolution dark field electron microscopy exam. of ordering 79−7615
Au_4Mn, magnetic anisotropy const., anomalous field depend. 77−12113
Au_4Mn, magnetocrystalline anisotropy temp. depend. 77−51900
Au_4Mn ordered alloy, coincidence sites in domain boundaries, high resolution TEM obs. 78−71708
Au_5Mn, ordered, coincidence sites in domain boundaries, high resolution TEM obs. 78−71708
Au_5Mn_2, electron microscope exam. of ordering 78−63697
Au_5Mn_2, monoclinic, ordering, high resolution electron microscopy 79−43290
Au_5Mn_2, phase transformations and domain structures *(French)* 78−27509
Au_5Mn_2, variants in domain struct. 77−43224
Au_2MnAl, Heusler alloy, Mossbauer, determ. of Au hyperfine field 77−4586
Au_2MnAl, Heusler alloy, ferromag., NMR meas. 78−76320
Au_2MnIn, Heusler alloy, ferromag., NMR meas. 78−76320
AuMnSb, ferromag. Heusler alloy, mag. hyperfine fields at Au and Sb sites, Mossbauer spectra 77−32303
$Au_{35}Ni_{65}$, vapour quenched amorphous alloy, atomic arrangements 80−100173
$AuPb_2$, epitaxial layer, formation during Pb absorpt. on Au, LEED, AES study of Au/$AuPb_2$ interface 78−71988
$(Au_xPb_{1-x})_{1-c}Fe_c$, ferromag. and spin glass ordering 78−56335
Au(Pd)-Zn, martensitic transformation, Hall coeff., specific elec. resistivity and X-ray powder diffraction 78−72774
$(Au_{1-x}Pd_x)Ga_2$, supercond. transition temp. and crit. field 79−38232
$Au_{50-x}Pd_xZn_{50}$, $(0\leq x\leq 15.02)$ β'-phase, Hall effect and elec. cond. 80−107768
$AuSb_2$, pyrite structure, Raman scatt., phonon frequencies 77−40235
gold alloys continued
AuSi, wetting and reactions on α-Al_2O_3 77−85022
$Au_{1-x}Si$ amorphous metallic films, optical props. as function of composition 79−95865
$Au_{1-x}Si_x$, amorphous film, spectra 0.01-6.2 eV, $0.13\leq x\leq 0.5$ 78−68574
$Au_{1-x}Si_x$, liquid, elec. resistivity as function of temp. and comp. 79−56188
Au_3Si, room temp. dissociation 78−35672
$Au_{35}Si_{65}$, amorphous vacuum-deposited and liquid-quenched films, diffusion and crystn. 80−84094
$Au_{81}Si_{19}$, optical refl., 0.5 to 6 eV, hall coeff. and elec. resist. 80−29755
$Au_{81.4}Si_{18.6}$, glass forming alloy, Gibbs free energy change on crystallisation 80−25676
Au_xSi_{1-x} amorphous alloy, crystallisation, elec. cond. study 80−103246
Au_xSi_{1-x} amorphous films, phys. studies 80−75476
$Au_{75}Si_{19}Fe_6$, apparatus for measurement of initial paramagnetic susceptibility 79−54160
Au_4Si.m, metastable phase, substruct. unit cell *(German)* 80−88091
AuSn, optical props., 0.5-5 eV 78−39522
AuSn, XPS, electronic struct. 80−7464
$AuSn_4$-Sn, eutectic struct., faceting and morphological regularity 79−61573
$AuSn_4$-Sn, unidirectionally solidified, X-ray diffr. anal. of crystal struct. 78−91308
$Au_{1-x}Sn_x$ liq./solid alloy, resist. and percolation 80−6804
Au_4V, effect of structural changes on phys. props. 78−31400
Au_4V, partially disordered, magnetisation distrib., polarised neutron diffr. study 79−47244
Au_4V single crystal, ordered, mag, props., domain models 80−39770
$Au_{100-x}Zn_x$, $(47\leq x\leq 52)$, β'-phase, Hall effect and elec. cond. 80−107768
Au_3Zn, R_2-phase, long period domains, transmission, scanning and optical microscopy obs. 79−38801
Au_4Zn, electropolishing for electron microscopic examination 78−35589
Au_4Zn, long period ordered alloy, selective radiation damage in electron microscopy 78−10092
Au_4Zn, modulated struct. phenomena, survey 79−95033
Au_4Zn, ordered alloy, long period superstructure study, electron microscopy, diffr. 78−10059
Au_4Zn, ordered alloy, long-period antiphase boundary struct., growth mechanism 79−19262
$Au_3Zn(Cd)$, long-range ordered, periodic antiphase domain boundary struct., X-ray diffr. obs. 79−95028
Be-Au, dil., quadrupole interactions and lattice location, ^{197}Hg TDPAC and Mossbauer expts. 78−43726
Be-Au, ohmic contact to p-InP, low contact resist. 80−65677
$Ce_{30}Au_{20}$, amorphous, cryst. field effects and mag. interactions, magnetisation and transport props. meas. 78−68191
$Ce_{80}Au_{20}$, metallic glass, mag. ordering and cryst. field effects, speromagnetism 80−80531
$CeAu_2Si_2$, ^{29}Si NMR and mag. susceptibility 79−61246
Co-Gd-Au film, amorphous, Hall effect 77−85347
$Co_{1-x}Au_x$, amorphous, elec. resist., temp. depend., spin wave contrib. and resist. minimum 78−51961
Cr-Au, matrix sensitive and insensitive factors evaluation using quantitative AES 79−24395
Cr-Au alloys, dil., elec. resist., 77-700K 78−64035
Cs-Au, disordered, min. metallic cond. 79−95372
Cs-Au, electron diffusion thermoelectric power calc. 77−28161
Cs-Au, ionic melts, elec. props. 79−99338
Cs-Au, liq., electronic struct., effects of short-range order 77−15755
Cs-Au, liq., exptl. evidence for ionic elec. transport 77−51534
Cs-Au, liq., metal-nonmetal transition and change in electronic and mag. props. 77−51790
Cs-Au, liq., molar vol. meas. 80−59546
Cs-Au, liq. alloys, ionic conductance 77−1251
Cs-Au, liquid, metal-insulator transition, mag. susceptibility, Knight shift, theory 80−44672
Cs-Au alloy, cryst., UV photoemission investig. of band struct. 77−24923
Cs-Au liq. alloy, formation of localised electronic states, NMR obs. 80−93201
Cs-Au(Sb), liq. alloys., mag. susceptibility and electronic struct. 77−1537
CsAu, band struct. and charge distrib., semicond. and metallic behaviour 77−20238
CsAu, electronic struct., XPS meas. 79−69403
CsAu, molten, equimolar, structural evidence of ionic nature 80−64882
CsAu, NMR line shape, Knight shift, X-ray diffr. study, struct. props. 78−68402
CsAu, optical absorpt. in liq. and solid 79−61397
CsAu, photoelectron spectroscopy and energy bands calc. 78−76581
$Cs_{1-x}Au_x$, liq., metal-nonmetal transition, electronic theory 78−79930
Cu/Au planar interface, formation of ordered phases CuAu and Cu_3Au 79−82392
Cu-Ag-Au, coherent phase diagram, theoretical calc. 80−70373
Cu-Al spherical crysts. grown from drop of melt, topography 80−84353
Cu-Au, (0.02-5 at.%), cold worked, internal friction peaks 79−11652
Cu-Au, calc. of coherent phase diagram, using cluster variation method 79−11564
Cu-Au, cold worked solid solution, flow stress and activation volume 80−16393
Cu-Au, corrosion in HNO_3 80−85091
Cu-Au, critical voltage effect *(Japanese)* 78−91206
Cu-Au, dil., dose depend. of impurity detrapping stages after electron irradiation 78−51582
Cu-Au, dil., electron high dosage source for residual resistance specimens and irradiation expts. *(German)* 78−21274
Cu-Au, dil., enhanced lattice sp.ht. 78−51699
Cu-Au, dil., magnetoresist., temp. depend. 80−70682
Cu-Au, dil., Matthiessen's rule deviations above room temp. 79−91023
Cu-Au, dil., O_2 solubility, thermodynamic and residual resist. study 78−59952
Cu-Au, dil., optical props. and electronic struct. 78−35164
Cu-Au, dil., thermal neutron irradiated, isochronal resist. recovery, 30-400K 79−19287
Cu-Au, dose depend. of recovery after thermal neutron irrad. 77−69011
Cu-Au, elastic modulus and internal friction during plastic deform., dislocation props. determ. 80−35244
Cu-Au, elec. resist., pseudopot. calc. *(Russian)* 78−2460

gold alloys continued
Cu-Au, HV electron microscopy, crit. voltages depend. on comp., temp. and short-range order 80−100146
Cu-Au, long-range ordered, periodic antiphase domain boundary struct., X-ray diffr. obs. 79−95028
Cu-Au, order-disorder transform, influence of strain energy 78−84796
Cu-Au, permeation of H and D, in situ growth of stable oxide barriers 78−75883
Cu-Au, plastic deformation, energy storage efficiency 77−4807
Cu-Au, surface anal. by LEED and AES 77−69153
Cu-Au, surface structures, LEED obs. 80−10761
Cu-Au, vacancies and divacancies, quenching effects and elec. resist. meas. 80−39072
Cu-Au (4 at.%), anneal hardening mechanism 80−60879
Cu-Au (50 at.%), ordered, influence of elastic stresses on mech. props. *(Russian)* 78−92298
Cu-Au alloys, electron density at Cu nucleus 79−54408
Cu-Au alloys, vacancy and divacancy migration activation energies, elec. cond. meas. 80−88140
Cu-Au dilute alloys, thermopower and resistivities, validity of Nordheim-Gorter relation 78−91671
Cu-Au film, aged, strength failure due to Kirkendall porosity 79−77969
Cu-Au film, optical props. of ordered and disordered alloys 77−20945
Cu-Au film, short wavelength composition modulation, interdiffusion exam. 77−72723
Cu-Au off-stoichiometric alloys, long period superlattice 79−55699
Cu-Au solid soln., Cu rich, meas. of interdiffusion, intrinsic and tracer diffusion coeff. 78−47608
Cu-Au solid soln., Cu rich, elastic const. 79−87681
Cu-Au system, grain boundary adsorption thermodynamics *(Russian)* 80−44317
Cu-Au system, theory of interphase and antiphase boundaries 79−83174
Cu-Au system, two-phase mixtures, long-period superlattices 80−84140
Cu-Au-Cu thin film, diffusion induced grain boundary migration 79−77833
Cu-Au-Fe, ferromag. ordering in FCC γ-Fe precipitates, Mossbauer study 80−71267
Cu-Au-O alloys, dil., O-metal interactions, activity coeff. meas. at 1423K 80−93792
Cu-Mn-Au spin glasses, anisotropic exchange interactions, effect of non-mag. impurities 80−80534
Cu-Ni/Au-Ni multilayer films, ohmic behaviour, use as strain gauge 80−65713
Cu-Ni/Au-Ni multilayers obtained by co-evaporation in UHV, ohmic stability and TCR 79−78226
Cu-Ti-Cu, wetting of Al_2O_3, alloying effects 80−107617
(Cu-Au)-Co, single crysts., solid soln. and particle strengthening, superposition 80−97495
$Cu_3Ag_{1-x}Au_x$, phase relations, X-ray diffr. and differential thermal anal. 80−108395
Cu_3Al-Al_2O_3 dispersion hardenend, short range order, quenching effect on yield stresS 78−35399
CuAu, calc. of elastic interaction between locally transformed regions with screw and edge dislocations 78−83844
CuAu, electrical resistivity meas. to detect phase changes 77−48425
CuAu, exam. of streaming due to intrinsic fluctuations 79−11602
CuAu I, ordered equiatomic, lattice specific heat meas., Debye temp. 80−54396
CuAu, mag. susceptibility and electronic struct. of ordering *(Russian)* 80−11161
CuAu, order-disorder transform., band theory for internal energy 79−19539
CuAu, ordered, vacuum deposited epitaxial films, orientation control by external stress 80−100426
CuAu, quenched, short-range order X-ray diffuse scatt., microdomain model anal. 79−96043
CuAu, thermal-neutron damaged, I_D and I_E recovery substages 77−35590
CuAu type structures, interstitial atom redistrib. in octahedral and tetrahedral interstices *(Russian)* 77−55280
CuAu-type superstructure, interaction of reacting dislocations *(Russian)* 78−83814
$Cu_{1-x}Au$, neutron scatt., selection rules for phonon mass operator 79−28065
Cu_3Au, 5-100 keV Cu^+ ion bombardment, displacement cascades, TEM investig. 77−11601
Cu_3Au alloy, dynamics of ordering clusters in thermal non-equilib. state 79−51257
Cu_3Au, alloys, superlattice-fringe imaging theory, images formed from two beams 80−79649
Cu_3Au and $CuAu_3$, band theory of order-disorder transforms. 79−60501
Cu_3Au, antiphase domain growth, quantitative comparison between theory and expt. 79−77606
Cu_3Au, antiphase domain growth 80−55346
Cu_3Au, atomic rearrangements during fast and thermal neutron irradiation 79−42114
Cu_3Au, compound formation rel. to heat of mixing 80−55689
Cu_3Au, Debye-Waller factor measurement in anal. of diffuse scattering data 79−23494
Cu_3Au, deformation twinning 77−63717
Cu_3Au, dislocation slip band mobility, critical stress 80−2032
Cu_3Au, disordered [001]-orientated single crysts., plastic deform., TEM and slip line studies 80−97541
Cu_3Au, displacement cascades prod. by Cu^+ bombardment 79−99251
Cu_3Au, dynamics on transitional ordering process from disordered to ordered state 79−4267
Cu_3Au, effects of temp. an order-depend. elec. resist. 77−31992
Cu_3Au, elec. resistivity, temp. depend. 79−47078
Cu_3Au, electrical resistivity and LRO, energy gap formation in Fermi surface 80−88533
Cu_3Au, eqn. of state, applicability of semiempirical function of binding energy *(Russian)* 77−15533
Cu_3Au, fast neutron irrad., displacement cascades 78−83852
Cu_3Au, flow stress 77−21231
Cu_3Au, heavy-ion or neutron bombardment, disordered zone form., TEM diffr. contrast 77−11600
Cu_3Au, heterophase fluctuations near order-disorder transform., X-ray and neutron diffr. 77−73272
Cu_3Au, interaction between superdislocations of opposite signs gliding in parallel planes *(Russian)* 77−80506

gold alloys continued
Cu_3Au, long-range order parameter from electron micrograph thickness fringes 77−65938
Cu_3Au, mag. susceptibility and electronic struct. of ordering *(Russian)* 80−11161
Cu_3Au, meas. of ordering instability 79−38818
Cu_3Au, mechanical damping in terms of Granato-Lucke theory, comparison with leaded and unleaded brass 78−95772
Cu_3Au, metastable states domain existence, phase transition ordering energy, press. effect *(Russian)* 80−45303
Cu_3Au, neutron irrad., displacement cascades, direct obs. method 80−107335
Cu_3Au, ordered and disordered, cavitation induced erosion 77−16743
Cu_3Au, ordering process, cluster size evolution 78−39766
Cu_3Au, partial sputtering yields 77−8696
Cu_3Au, radiation disorder model of phase stability 80−16297
Cu_3Au, superdislocation motion resistance due to atoms in incorrect positions *(Russian)* 79−99189
Cu_3Au, surface effects on order-disorder phase transition 77−76556
Cu_3Au, TEM diffr. contrast of dislocation loop 77−24253
Cu_3Au thin films, fine-grained and disordered, low temp. ordering 80−97433
Cu_3Au type antiferromagnet Ising lattice, finite entropy at T=0, phase transition 77−89958
Cu_3Au, under irradiation, microstructural-based estimate of disordering 80−2067
Cu_3Au, X-ray and inelastic neutron scatt. investig. of spinodal ordering 77−77473
Cu_3Au-Co, single crystal, overaging mechanism 79−20081
Cu_3Au-Co, underaged, ordered and disordered single crystal, hardening mechanisms 78−3134
Cu_3Au-Co single cryst., precip. hardening *(German)* 80−84946
Cu_3Au-Cu_3Pd(Pt), quasibinary system, order-disorder transform., superlattice form. 80−2159
Cu_3Au-Ni, antiphase domains morphology 80−108460
$Cu_{81.5}Au_{18.5}$, meas. of ordering instability 79−38818
CuAuI superlattice, (101) lattice twinning mode assoc. with ordering transition 77−15431
Cu_2AuPd, struct., TEM and electron diffr. meas. 78−38666
$Cu_3Au(-xCo)$, x=0.64 and 1.5 at.% Co, LRO 78−18584
$CuMnAu_x$, hysteresis, spin orbit scatt., effect on anisotropy in spin glass state, rel. to Au impurity conc. 80−71095
$DyAu_2$, long-duration pulsed mag. field appl. to magnetisation meas. 79−61183
$DyAu_6$, mag. props. temp. depend. *(French)* 77−51879
$Er_3Au_3Sb_4$, mag. suscept. meas., 4 to 300K 79−51742
$EuAu_5$, cond. electron spin polarisation 77−63136
Fe-Au, dil., size effects on mag. hyperfine fields at non-mag. impurities 78−43586
Fe-Au layers, amorphous ferromag., elec. transport phenomena and reson. scatt. *(German)* 77−72847
Fe-Mo-Au, orienting of precipitating Au particles by external elastic stress 77−73279
$Fe_{1-x}Au_x$, amorphous, elec. resist., temp. depend., spin wave contrib. and resist. minimum 78−51961
$Fe(Pd_{1-x}Au_x)_3$, mag. struct. ferro-antiferromagnetism coexistence *(Russian)* 79−82759
$Fe(Pd_{1-x}Au_x)_3$ ordering alloys, mag. props., 4.2 to 500K *(Russian)* 79−47301
$Fe_{25}Pd_{50}Au_{25}$, atomic ordering influence on mag. props. and elec. resistance *(Russian)* 80−7551
GaAs/Au-Ge/Ni, Schottky barrier energy var. with interdiffusion 77−20435
Gd-Au amorphous films, spontaneous Hall effect and elec. resist. 80−80251
Gd-Co-Au, sputter deposited amorphous alloy, substrate bias, magnetic anisotropy, annealing 78−48006
Gd-Co-Au amorphous film, domain wall dynamics near compensation point 79−1696
Gd-Co-Au amorphous magnetic films, domain wall obs. by Lorentz electron microscopy 77−80979
Gd-Co-Au film, ferrimag., amorphous, coated with Permalloy films, mag. props. 79−1695
$Gd_{80}Au_{20}$, amorphous ferromag., critical phenomena and mag. props. 77−85469
$Gd_{80}Au_{20}$, amorphous ferromag., mag. and transport meas. 77−89930
GdAuSn, mag. props. 77−85439
GdCoAu amorphous film, bias field depend. of domain drag propagated bubble domains 79−78471
a-GdCoAu films, perpendicular anisotropy temp.depend., Lorentz microscopy 77−28419
Ge-Au eutectic alloys, field ion sources 80−97414
Ge-Au film, codeposited, amorphous and polycryst., struct. and elec. props. 80−24766
$Ge_{0.6}Cu_{0.2}Au_{0.2}$ film, superconducting transition temp., resistivity meas. 77−43774
Hg-Au, liquid dilute amalgams, elec. cond. and thermoelec. power 78−51976
Ho-Au, dil., hyperfine interaction of Ho^{3+}, nuclear orientation expts. 78−43717
$HoAu_3$, mag. phase diagram 80−75761
$Ho_3Au_3Sb_4$, mag. suscept. meas., 4 to 300K 79−51742
In/Au-Ge ohmic contact to GaAs, solid phase epitaxy formation 79−60658
In_4Au_9, γ-brass with P cell, struct. determ. 77−24290
La-Au, amorphous, alloying effect on supercond. props. 79−60951
La-Au, splat-quenched, Mossbauer effect and elec. resist., amorphous struct. 80−84676
La-Au liq.-quenched alloys, Mossbauer spectra, struct. 80−15841
La-Gd-An, amorphous, high Gd content, bulk mag. props. 77−59426
La-Gd-Au, amorphous, mag. field depend. of resist. minima 77−59275
La-Gd-Au, amorphous spin glasses, mag.-cluster description 79−42776
La-Sm-Au, amorphous, surface effects on Sm valence, XPS and X-ray absorption meas. 80−108325
$La_{1-x}Au_x$, supercond. splat cooled amorphous alloy, sp. ht. 78−19182
$La_{100-x}Au_x$, amorphous film, stability, supercond. temp. and residual resistivity 79−4636
$La_{18}Au_{22}$, amorphous, evidence for short wavelength cutoff in fluctuation spectrum 78−68113
$La_{76}Au_{24}$, disordered ribbons, production of quenched samples using arc furnace 80−71612

gold alloys continued
$LaAu_2Si_2$, ^{29}Si NMR and mag. susceptibility 79−61246
$La_{80-x}Gd_xAu_{20}$, amorphous dil. alloy, RKKY interaction, magnetisation meas. 77−32207
$La_{80-x}Gd_xAu_{20}$, amorphous, supercond. and spin-glass regime, magnetisation and resist. meas. 77−36011
$La_{80-x}Pr_xAu_{20}$, amorphous, mag. and supercond. props. 80−75713
Li-Au, electron diffusion thermoelectric power calc. 77−28161
Li-Au, liq. semicond. electronic struct., resist. and thermoelec. power meas. 77−47712
MgO-Au cermet films, for selective black absorbers 79−29483
γ- Mn-Au, magnetic struct. for compositions near onset of antiferromag. ordering 77−63111
γ-MnAu, antiferromag., phase diagram, X-ray diffr. and Young's modulus meas. 80−71024
$MnAu_2$, helical antiferromagnetic compound, optical props. and electronic struct., visible and IR obs. *(French)* 80−45101
$MnAu_2$, helical antiferromag., optical absorpt., density of states 80−66224
$MnAu_2$, optical consts., 0.5-3.5 eV, intra-and interband absorpt. *(French)* 78−10916
$MnAu_4$, domain struct. exam. by powder method *(German)* 78−91883
Nb_3Au, A-15 struct. supercond., microhardness, bonding 78−76199
Nb_3Au, BCC, density of states, comparison with A-15 78−80095
Nb_3Au, supercond. diffusion layer prep. 79−1834
Nb_3Au, X-ray $M_{IV,V}$ emission bands *(Russian)* 80−45170
Nb_3Au, XPS of valence electrons meas. 77−21003
$Nb_{\sim 3}Au$, upper crit. field 79−82729
Ni-Au, amorphous film, ferromagnetic, anomalous Hall resist. 77−15832
Ni-Au, dil., orientation depend. of surface segregation, AES and SEM obs. 78−71908
Ni-Au, electronegativity and core electron binding energy shifts of Au 77−15346
Ni-Au, local environment effects, magnetisation decrease 79−65664
Ni-Au, oxidation in air, 50-150°C, film growth obs. using AES and contact resist. 80−3242
Ni-Au alloys, surface segreg., surface energy and solute strain energy effects 77−72760
Ni-Au film, amorphous, magnetoresist., in fields up to 80 kG 77−39823
Ni-Au-Fe, liq., activity of iron at 1573K 77−70328
Ni-Cr-Ti-Al/Au-Ni brazed joint, high temp., AE under elev. temp. and loading *(German)* 78−31597
Ni-Ge-Au evaporated contacts on GaAs, TEM obs. 80−75449
Ni-Ge-Au/GaAs cathode struct., with enhanced injection efficiency, contact resist. 77−20431
NiAu, dil., disordered, virtual bound states, reson. model pot. theory 79−23934
$Ni_{1-x}Au_x$, amorphous, elec. resist., temp. depend., spin wave contrib. and resist. minimum 78−51961
$Ni_{1-x}Au_x$-Co, dil., hyperfine field and isomer shift, precip. process, Mossbauer expts. 80−25267
$Ni_{1-x}Au_x$-Co, dil., Mossbauer effect, mag. hyperfine field 80−20528
Pb/Au/Pb, Josephson junction, oxide formation process, ellipsomesric meas. *(Japanese)* 80−11561
Pb-Au, dil., solute resist. meas., multiple point defect form. 78−10433
Pb-Au, interstitial and substitutional distrib. 80−84204
Pb-Au (0-0.0918 at.%), lattice parameter changes due to Au dissolution 79−77558
Pb-Au (2.5 wt.%) film, In diffusion, alloy form. 78−22899
Pb-In/Au, Josephson junction, oxide formation process, ellipsomesric meas. *(Japanese)* 80−11561
Pb-In-Au, film, supercond. penetration depth 78−72306
Pb-In-Au, series-connected Josephson tunnel junctions, fabrication procedure diagnostics 78−47909
Pb-In-Au alloy, Josephson junction electrode materials, strain relax. 79−38255
Pb-In-Au base electrode film Josephson junctions, tunnel barrier oxide struct. 80−65750
Pb-In-Au Josephson tunnel junctions, strain relax. effects 79−65617
$Pb_{1-c}Au_c$, liquid alloys, local fluctuations and quadrupolar relaxation 80−66060
PbInAu film, RF plasma oxidised, surface analysis using ESCA 80−50742
Pb−(Au) (0.1 and 0.2 wt.%), single crysts., yield strength depend. at 77K on Av conc. 80−55479
Pd-Ag-Au, lattice parameters and thermal expansion coeffs., X-ray diffr. meas. 79−99121
Pd-Ag-Au, temp. effect on lattice parameters and thermal expansion 78−51473
Pd-Au, alloys-H solid solutions, superconducting transition temp. behaviour *(Russian)* 80−70879
Pd-Au, electronegativity and core electron binding energy shifts of Au 77−15346
Pd-Au, low temp. thermoelectric power 79−47084
Pd-Au film on $BaTiO_3$ dielectric ceramic substrate, interaction between film and substrate during sintering 79−33958
Pd-Au:$H_2(D_2)$, thermodynamic props. at 555 and 700K, vibr. freqs. and excess entropies 80−29186
Pd-Au-Ag ternary system, isoparametric curves and Wegard's law plots 79−47657
Pd-Au-Si, amorphous films, RF sputter deposition, composition and thermal behaviour 80−55292
Pd-Au-Si, influence of struct. on elec. resist. of glass forming alloys 80−65518
Pd-Pt-Au alloys for low-temp. precision resistors 79−69490
$Pd_{1-x}Ag_{1-x}$-Au, dil., electron density at Au, Mossbauer reson. 78−39473
PdAu (4.7 at.%), effect of alloying on activation energy of H_2 diffusion 80−107571
PdAu, dil., disordered, virtual bound states, reson. model pot. theory 79−23934
PdAu wires, sorption of H_2 78−43239
$(Pd_{1-x}Au_x)_{0.99}Co_{0.01}$, mag. hyperfine interaction for impurity Co atoms *(Russian)* 80−7078
$(Pd_{0.8}Au_{0.2})D_{0.04}$, lattice location of D, ion channelling obs. 78−67708
$(Pd_{0.8}Au_{0.2})D_{0.04}$, thermal vibr. temp. depend., ion channelling exam. 78−47457
$Pd_{1-x}Au_xH_c$, search for superconductivity 77−8221
$(Pd_{80}Au_7Si_{13})/Fe_{30}$, compositionally modulated amorphous film, diffusion, struct. relax. 80−103518

gold alloys continued
$(Pd_{0.67}Fe_{0.33})_{1-x}Au_x$, ordering effects on mag. props. *(Russian)* 78−47942
PdH_x-Au, dil., electron density at Au, Mossbauer reson. 78−39473
$Pr_xLa_{80-x}Au_{20}$, amorphous, low temp. excitations, specific heat 80−100337
Pt/Au alloy surface chemistry, sample morphology effects 78−7233
Pt-Au, amorphous struct. produced by Au implantation, spinodal decomp. TEM obs. 78−31379
Pt-Au, dil., recovery spectrum after thermal neutron irrad., Au effect and defect conc. depend. 80−65057
Pt-Au, electronegativity and core electron binding energy shifts of Au 77−15346
Pt-Au, grain boundary permeation 79−65253
Pt-Au, ion-irradiated, self-interstitial migration in stage II recovery, FIM obs. 77−59140
Pt-Au, miscibility gap, thermodynamic anal. *(German)* 79−91629
Pt-Au, solid soln., magnetic props. and lattice parameters *(German)* 79−87236
Pt-Au, surface comp. and catalysis, AES and thermal desorption meas. 79−46898
Pt-Au, surface segregation using atom-probe FIM 79−77883
Pt-Au, surface segregation, comp. depth profiles meas. using atom-probe field ion microscope 80−100380
Pt-Au (100), chemisorption of H_2 and O_2 and their interaction, UPS investig. 77−51600
Pt-Au (4.0 at.%), ion irradiated, direct obs. of vacancy struct. of (220) platelet 78−51534
Pt-Au glass-bonded printed thick-film conductor, adherence fracture energy 77−9037
Pt-Au thick film conductor, glass bonded, adherence, fracture energy, Al_2O_3 substrate effects 77−56075
Pt(Au), ion irradiated alloys, stage II recovery 78−47440
$Pt_{90}Ir_5Au_5$, $Pt_{80}Ir_{10}Au_{10}$, low temp. sp. ht. 79−73320
PtMnSn, ^{197}Au and ^{119}Sn hyperfine fields, Mossbauer expt. 78−72439
$Pt_{86}Rh_9Au_5$, $Pt_{74}Rh_{17}Au_9$, low temp. sp. ht. 79−73320
Rb-Au, electron diffusion thermoelectric power calc. 77−28161
RbAu, NMR line shape, Knight shift, X-ray diffr. study, struct. props. 78−68402
RbAu, photoelectron spectroscopy and energy bands calc. 78−76581
Sb-Au, amorphous film, elect. resist. 78−95390
Sb-Au amorphous film, quench condensed, struct. and stability 79−99459
Sb-Au amorphous films quench-condensed, resistivity and Hall effect meas. 79−99638
Sc-Au, dil., elec. field gradient, Mossbauer meas. 80−80665
Si-Au, (LMM) Auger electron emission by keV Ar^+ bombardment 79−95880
Si-Au, amorphous, ESR linewidth var. with temp. and comp. 77−48033
Si-Au, solid soln., influence of precip. on relax. of ^{29}Si nucleus 80−11287
Si-Au alloys, direct synthesis by inplantation of Au^+ *(Japanese)* 79−28006
Si-Au amorphous film, metal-nonmetal transition, elec. cond., thermoelectric power meas. 79−47132
Si-Au amorphous system, optical absorpt., IR photocond. 79−42582
Si-Au eutectic alloys, field ion sources 80−97414
Si-Au films, quenched condensed, elec. resist. and supercond. 80−54669
Si-Au system, ion implanted induced giant gettering, annealing effects 80−88221
$Si_{1-x}Au_x$ amorphous films, IR absorpt. spectra 80−16034
$Si_{100-x}Au_x$, amorphous, dielec. anomaly, rel. to nonmetal-metal transition 78−2791
Sm-Au, amorphous, surface effects on Sm valence, XPS and X-ray absorption meas. 80−108325
SmAu, diode sputtering, negative ion MFP 78−95641
SmAu, significance of negative ion formation in sputtering and SIMS anal. 78−72663
$SmAu_6$, mag. props. temp. depend. *(French)* 77−51879
Sn-Au, amorphous film, elec. resist., temp. depend. 79−91159
Sn-Au, amorphous film, optical props. 79−69895
Sn-Au, liquid alloy, exam. of activity and heat of mixing, using mass spectrometry 78−51706
Sn-Au film, amorphous and polycrystalline, thermopower meas. *(German)* 77−80857
TbAu, amorphous, magnetisation characts., 5 to 300K, hysteresis cycle *(French)* 77−80965
$TbAu_3$, mag. phase diagram 80−75761
$TbAu_6$, mag. props. temp. depend. *(French)* 77−51879
$Tb_3Au_3Sb_4$, mag. suscept. meas., 4 to 300K 79−51742
Te-Au, dil. liq. alloy, elec. cond. at high temp. and press. 78−87959
Te-Au film, metastable supercond. alloys, produced by low temp. ion implantation 80−88670
Te-Au film, supercond. by ion irrad. 80−34544
Ti-Au, (9.9 wt.%), eutectoid system, $\beta \rightarrow \alpha_m$ transform., nucleation kinetics 80−97474
Ti-Au, existence of β to α_m phase transformation 78−44123
Ti-Au, thermodynamics and kinetics of β to α_m transformation 78−84795
Ti-Cu-Ni-Au metallisation systems, in 85°C 78% RH SO_2 contaminated environment, performance 79−74304
Ti-Pd-Cu-Ni-Au metallisation systems, in 85°C 78% RH SO_2 contaminated environment, performance 79−74304
Ti-Pt-Au, nonalloyed ohmic contacts to n-GaAs by pulse-electron beam annealed Se implants 80−2466
TiAu, dil., disordered, virtual bound states, reson. model pot. theory 79−23934
Ti_3Au, self-consistent LMTO band calcs. 79−37954
$Tm_3Au_3Sb_3$, mag. suscept. meas., 4 to 300K 79−51742
V_3Au, effect of atomic ordering on XPS of valence bands 77−52224
V_3Au, supercond., electronic density of states and T_c changes with atomic ordering 78−91800
V_3Au, XPS of valence electrons meas. 77−21003
$Y_3Au_3Sb_4$, cryst. struct., X-ray diffr. meas. 77−47378
YbAu, mag. susceptibility, thermally excited interconfiguration crossover 77−16042
$YbAu_2$, surface effects on valence 78−91746
$YbAu_2$, surface electronic structure, XPS study 80−55259
$YbAu_2$, valence transition at surface of Yb 80−70652
$YbInAu_2$, intermediate valence cpd., mag. susceptibility expts., 4.2-280K 78−39288

gold alloys continued
YbPt-YbAu system, valency state, Yb behaviour *(French)* 80−45277
Zr-Au (0.3 and 0.2 wt.%), irradiated, backscattering meas. of Zr self-interstitial atom trapping by Au 77−69014
$ZuCuZn_2$, martensitic transition, shear elastic const. meas. 77−28810

gold compounds
see also gold alloys
DNA-Au (III) interaction, rate consts., activation energies, pH, spectrophotometric obs. 80−30228
eutectics, HgTe-PbTe and Au-PbTe, prep. and thermoelectric behaviour charact. 80−107774
tetrachloroaurates, ^{35}Cl NQR freqs., correl. with crystallographic data 79−33559
AgI-AuI, pseudo-binary phase diagram 78−76637
$AlCl_3$, intercalation compound with graphite, reduction by H_2 *(French)* 78−27820
$(Au, Ag)Te_2$, calaverite, Te atom splitting and modulated struct. 79−99145
Au (I) compounds, electronic config. and nucl. quadrupole interaction, atomic SCF Hartree-Fock calcs. 79−60777
Au complex, paramag., ^{197}Au mag. and elec. hyperfine interactions 78−39471
Au complex, TTF-bisdithiolene complex, spin Peierls transition 77−4523
Au complexes, electronic config. and elec. field gradient, relativistic HF method 80−54664
Au mixed valence complexes, quasi-one-dimens., elec. props. at ultrahigh press. 78−2470
Au-As, system interactions due to heat treatment, backscattering anal. 79−91719
Au-B system, interactions, product chem., phase, struct. anal., book contrib. 78−47305
Au-Cl system, high temp. vaporisation chemistry incl. form. of vapour complex species 79−47963
Au-Ge-Te ternary system, solid soln. in vicinity of GeTe, phase diagram *(French)* 77−85994
Au-InP, MIS Schottky barriers, interfacial parameters determ. 79−95505
Au-Sb, system interactions due to heat treatment, backscattering anal. 79−91719
$AuAg_3Te_2$, petzite, X-ray cryst. struct. refinement 79−46634
AuBr, α, I, P and BCC forms, transitions 78−38836
AuBr, I and P forms, growth by vap. transport, cryst. struct. 78−38676
AuBr, spectra and luminesc., 100 to 200K *(Russian)* 77−69911
$AuBr_3$, spectra and luminesc., 100 to 300K *(Russian)* 77−69911
$AuBr_4^-$, harmonic force field, mean vibr. amplitudes, cation effect 77−3335
$Au(CN)_2$, adsorption on activated charcoal, kinetics 79−82457
$Au(CN)_2^-$, electrochemical reduction kinetics 78−73052
AuCa radicals, rotational analysis for near IR bands *(French)* 77−61741
AuCl, ab initio effective core potential studies, relativistic effects 79−93933
AuCl, luminesc., excitons 80−2839
$AuCl_3$, intercalation with graphite *(French)* 78−42982
$AuCl_4^-$, harmonic force field, mean vibr. amplitudes, cation effect 77−3335
$AuCl_4^-(Br_4^-)$, mean vibr. amplitudes and force field, Muller approx. 77−10659
$AuClO_4$, X-ray cryst. struct. determ. 80−1973
AuF_3, ^{19}F NMR chemical shift, crystal chemistry 78−87645
AuF_6^-, produced from fast $Cs+(AuF_5)_n$ collisions, ionisation cross section energy depend. 80−81300
AuH, AuCl, relativistic effective core potentials, ab initio calcs. 78−86767
AuH, AuLi, AuCu and AgAu, VB calcs., wave functions, interatomic distance and dissoc. energy values 77−57883
AuH, gaseous, dissociation 79−91925
AuH, relativistic (non-relativistic) HF one-centre expansion calcs. 80−52908
AuI, elec. cond. 79−42302
AuO, electronic spectra in rare gas matrix 78−996
Au_2O_3, X-ray absorption, discontinuities and limits, chem. combination effects 80−93435
Au_2O_3, X-ray cryst. struct. determ. 79−69074
Au_2P_3, melting temp., Au_2P_3-Au eutectic temp. 80−59628
Au_2P_3, polyphosphides with weak Au-Au interactions, cryst. struct. determ. by X-ray techniques 79−37674
$Au_7P_{10}I$, polyphosphides with weak Au-Au interactions, cryst. struct. determ. by X-ray techniques 79−37674
Au_2S, concentration specks, latent image formation 79−34334
$AuS_4C_4(CF_3)_4.TTF$, 1-dimens. mag. props. 77−66271
AuSi radicals, rotational analysis for near IR bands *(French)* 77−61741
$AuTe_2$ growth at Te-Au thin film interface, evolution, switching effects *(French)* 80−6660
AuTeI, cryst. struct. 78−51504
$AuTe_2I$, Fermi surface determ. by Shubnikov de Haas effect 77−51639
AuV, gas, bond dissoc. energy, from high-temp. mass spectra of V-Nb-Mo-Au 79−45860
AuX_4^{n-}, X=Cl, Br, n=1, 2, force consts., bond polarizability 78−5201
^{197}Au Mossbauer isomer shifts, book contrib. 79−87356
$Cs_2Au^IAu^{III}Cl_6$, influence of high hydrostatic pressure on cryst. struct. in pressure range up to 52×10^8 Pa 79−51249
$Cs_2Au_2Cl_6$, ^{197}Au Mossbauer high press. study of mixed valence compound 78−52387
$Cs_2Au_2Cl_6$, electronic state of Au at high press., Mossbauer spectra 80−60467

goniometers
aberrations correction, expt. criteria for use of deconvolution methods 78−18492
angle pickup, using precision variable resistor 80−47047
annular photoelectric goniometer sensitivity calc. 78−41327
autocollimation goniometer, reading error 78−16829
bakable UHV, precision three-axis goniometer 78−70673
case hardening depth meas. using ultrasonic goniometer, corner reflection method, book contrib. 79−100325
cone-and-plate rheogoniometer for stress meas. in aqueous polymer solns. 80−1496
crystal analyser optical alignment for X-ray fine spectral structure study 77−18148

goniometers continued
crystal channelling measurements, experimental system, components, capabilities 77−22617
crystal cutting apparatus 80−86275
crystal goniometric setup with electronic control system consisting of Kharkov linear electron accelerator 80−68976
crystal mounting on ends of fibres using a controlled method 78−93663
crystal orienting device for ESR studies 77−82581
crystal structure, gamma-ray diffraction applications 80−14972
electromechanical, for total motion knee goniometry 77−52902
electron microscopy, goniometer for use in high resolution objective lens pole-pieces 79−58844
ELF/VLF goniometer receiver, remote, unmanned, in Antarctica, UHF telemetry link 80−21854
ellipsometer attachment 80−90883
goniospectrophotometer, high angular resolution recording, for visible and UV 78−45671
GUR-5, for small-angle X-ray scattering meas. 78−74115
high pressure cell using miniature diamond anvil 80−237
high resolution goniometer for EM 10 electron microscope 77−74561
image analyser comparative tests 79−14106
interferometric, mes. of angles *(Czech)* 78−49794
interpolating indexing instrument for UDP-025 goniometer 78−74119
IR goniometric refractometer, construction and test results 79−71513
joint motion meas. by triaxial electrogoniometer, for human prosthesis design 78−11781
laser alignment of crystal face perpendicular to axis of rot. 77−15283
limbs motion analysis appl., prosthesis microcomputer control 80−51138
Lucke texture goniometer with computer control X-ray pole figure plotting appl. 78−18500
moire pattern detection by solid-state dynamic self-scanned photocell array 79−32084
multiblade-tool angles meas. using shadow-section method 79−71410
NDT, failure prevention, test methods and equipment *(German, English)* 79−52560
neutron diffraction on vertical axis goniometer, high temp. diffr. furnace 77−58926
neutron time-of-flight spectrometer goniometer, performance 77−26931
nuclear reaction cross section and channelling expts. 78−21801
optical goniometer accuracy effect of atm. turbulence 78−55461
opticoelectronic phase goniometers compared to opticoelectronic amplitude goniometers 79−71412
optoelectronic linearity and sensitivity ranges increase 80−23786
polishing device, universally adjustable goniometer 79−2755
pulsed FT NQR spectrometer, automation for single crystal Zeeman studies 80−66066
quartz, doubly rotated plates, angle-of-cut goniometry 79−54098
retroreflector photometric and goniometric accuracy 80−86375
single crystal surfaces, alignment for precise grinding and electropolishing 78−4604
spectral reflectometry of 0.1 mm surface elements appl. *(Japanese)* 78−89527
testing of aspherical surfaces on goniometer 79−76895
texture goniometer alignment of Schulz reflection technique, method for testing 80−81272
texture goniometer for analysis of rocks 80−26630
topography settings, white beam X-ray, for cryst. defects, synchrotron radiation 2-axis spectrometer 78−67619
total luminous flux meas. on radiometric base, goniophotometer 80−42250
triaxial, for human joint rotation meas., theoretical justification 79−92417
ULF, techniques for locating Pc 1 geomagnetic pulsation sources *(French)* 79−70890
ultra high vac. manipulator with six degrees of freedom 78−18509
ultrahigh vacuum system, for channelling backscattering experiments *(Japanese)* 79−26061
US, for measurement of surface stress in steel 79−15947
US, surface wave appl., corner reflection method 79−100324
verification prism manufacture and recertification 77−27392
very perfect crystals, topography and goniometry 78−30516
Weissenberg goniometer, integrating, for X-ray structural analysis of single cryst. 77−43113
Weissenberg Rheogoniometer, addition of polarizing microscope 79−68838
Weissenberg rheogoniometer, computerised calib. and meas. of Newtonian fluids 78−87323
Weissenberg rheogoniometer, human vitreous viscoelasticity meas. 79−92266
Weissenberg rheogoniometer, R-17, axial compliance reduction for viscoelastic fluids 80−106859
whistler analyser, semiautomated, using spectrum analyser and programmable tracking filter 79−74975
X-ray, for fine metal fibre stress/strain curves determ. *(German)* 78−92413
X-ray, linear position sensitive proportional counter tests *(French)* 77−31557
X-ray, portable *(German)* 77−194
X-ray, zero deviation *(German)* 79−58854
X-ray diffraction, used in cutting of dielectric crystals 79−80592
X-ray diffraction characterisation, highly collimated beam, appl. to Si 78−9912
X-ray diffraction studies, goniometer system for large specimens 77−76248
X-ray diffractometer, double-crystal, design features, appl. 78−49948
X-ray goniometer, for producing accurately oriented cryst. faces 79−37591
X-ray goniometer, for stress measurement in single crysts. and coarse-grained specimens 80−64837
X-ray powder diffractometry goniometer, with temp. control *(French)* 80−79631
X-ray spectrometer, double-crystal, dynamic feedback system for stabilisation 79−97482

GP zones *see Guinier-Preston zones*

grain boundaries
for grain boundary diffusion, see diffusion in solids; for gain boundary segregation, see segregation
see also bicrystals; subboundary structure; twin boundaries
acoustic emission during tensile tests, H_2 assisted fracture 79−100257

grain boundaries continued
adamantane, crystalline, lattice and sub-grain boundary self-diffusion coeffs. meas. 78−6179
adsorption-induced interface decohesion, pair bonding theory 80−88166
aggregate, polycrystalline, grain boundary sliding contrib. to total strain 77−25114
β- and β''-Al_2O_3-Na_2O, fast ion conductors, TEM obs. 79−86920
alkali halides, exposed to US waves, dislocation multiplication in original stage 78−47383
alloy, drag 78−51550
alloy, precipitation hardened, containing narrow soft zones at grain boundaries, fracture toughness 77−77553
alloy, solid soln., grain boundary mobility 79−46676
alloy decomposition kinetics, Johnson-Mehl-Avrami (JMA) formula appl. 80−16263
alloys, decomposing, internal friction peaks in grain boundary model *(Russian)* 78−35418
alumina, polycryst., compressive strength, microplasticity 77−36620
anelastic relaxations and magnetic aftereffects in solids, conf., Katowice, Poland (Jan. 1978) *(Polish)* 79−96072
anisotropic insulators, interaction of point charge and interface 79−69584
anisotropic media, stress fields of dislocation arrays *(German)* 79−23615
athermal motion 79−14819
Au film, diffusion of Ag along grain boundaries, scanning Auger microscopy obs. 78−22897
austenitic stainless steel, recrystallisation transformation energies, α' to γ, effect of Si content and deformation by rolling *(French)* 77−48433
Bauschinger effect, grain boundary contrib. 79−47759
bicrystal, elastic incompatibility stresses *(Japanese)* 80−107361
bicrystal, electron diffr. from near coincidence twist boundaries 79−7526
bicrystals, grain boundary anal. using TEM 79−28003
bicrystals, near-coincidence twist boundaries, electron diffr. obs. 79−90675
α-brass, bicrystal, grain boundary fracture at intermediate temp. *(Japanese)* 79−15774
β-brass, bicrystal and tricrystal stress strain behaviour 77−36607
α/β brass, grain boundary sliding and intergranular cavitation during superplastic deformation 79−5009
brass, interface boundaries, TEM procedures for struct. 80−19814
brass, interphase boundaries, struct. 80−19813
brass, plastic flow, rate controlling mech. at high temps. 77−81308
α-brass, stress corrosion cracking in single and bicrystals 77−4866
brass α-β two-phase bicrystals, interface sliding studies 80−54248
β-brass bicrystals, shear-incompatible, grain boundary contrib. to Bauschinger effect 80−97550
brittle materials, influence of structural parameters on fracture toughness 79−96133
broken twist boundary, model 78−47394
bronze-steel, phase composition and struct. of diffusional interlayer in fusion zone, X-ray analysis 78−56821
cavities, star-shaped unstable growth 79−46679
cavity growth anal. during superplasticity 80−60923
cavity growth controlled by surface diffusion, numerical study 79−90668
cavity nucleation, by plastic deform., at grain boundaries 79−29127
cavity nucleation at second phase particles in grain boundaries 78−59819
ceramic, ferrimag. or ferroelec., microstructure and physical props. 78−72756
ceramic, grain boundary segregation 78−15410
ceramic, plastic deformation, grain and grain boundary processes 77−4814
ceramic materials, fine-grained, cyclic plastic deform. as cuase for thermal expansion hysteresis 80−89290
ceramics, high performance, review and fabrication methods 77−8785
chloranil pellets, thermally stimulated discharge current and dielectric studies 80−93236
coatings, defects and their effect on props. 80−39474
coherency loss in modulated structures, approx. criterion 77−48391
cohesion, segregation effects 78−15411
coincidence grain boundary, lattice displacement, electron images 77−80516
coincidence site lattice, differential geometry 79−28000
coincidence site lattice model 80−54255
coincidence site lattices, and pattern shift lattices *(French)* 79−69035
coincidence-site lattice interfaces 80−15381
coincident site lattices theory *(Russian)* 78−2141
computer simulations, of twins and grain boundaries, methods in X-ray topography 79−23484
computer-simulated grain boundaries, effects of rigid body translations 79−60386
continuum model for diffusion in region with multiple diffusivity 79−77801
coupled grain boundary sliding and migration, computer modeling 78−87687
Cr-Mo, martensite to ferrite transform. by fatigue deform. *(French)* 79−66056
crack, stress depend. of growth rate during creep 77−80575
crack growth, estimation of creep rupture time *(Chinese)* 78−83325
crack-tip slip band blocked by grain boundaries, simple model 79−50665
creep, diffusional, grain boundaries as point defect sources or sinks 79−37757
creep, grain-boundary sliding controlled, grain rolling, superplasticity 77−90399
creep, high temperature, role of dislocations 78−43065
creep and growth, irradiation induced, solute effects on defect precip. rate 80−88252
creep and growth, radiation induced, fundamental mechanisms 80−92596
creep crack growth, model based on vacancy diffusion along grain boundaries 78−75716
creep damage and the remaining life concept 80−59574
creep fracture, failure mechanism involving grain boundary sliding and brittle crack extension 80−97557
creep fracture model, plastic growth of cavities at tip of grain boundary wedge cracks 77−52446
crystal orientation, determ. by zone axis method, appl. to grain boundaries, TEM 80−103226
crystal orientation, zone axis method *(French)* 80−44215

grain boundaries continued
crystalline grain interfaces, distrib. functions, boundary conditions 77−55503
crystalline materials, struct. of grain boundaries using diffr. techniques 80−59478
cubic materials, intergranular structures, geometrical approach, review *(French)* 80−59482
cubic structures, symmetry of coincidence site lattices *(Russian)* 80−79807
Debye-Sears cell lattices, DSC-1 and DSC-2, computation of coincident and near-coincident cells 77−84746
decohesion, exchange type soft solute segregation in hard hosts 80−54258
decohesion energy, solute adsorption influence 80−65009
defect diffusion, radiation effects 78−87827
diamond grain configuration in high temp. creep and fatigue 77−21221
diamond lattice, Burgers vestor of grain boundary dislocations *(Russian)* 79−73176
diffraction, optical analogue using simulated models 78−38723
diffusion at low temperature, anal. of surface accumulation method for film systems 79−77838
diffusion induced grain boundary migration 79−77833
diffusion phenomena, vacancy-impurity complexes effect, appl. to nonequilib. segregation near grain boundaries *(Russian)* 80−44350
diffusional crystal growth mechanisms 80−3059
diffusional growth of grain boundary crack 78−47471
diffusive cavitation of grain interfaces, non-equilib. models 79−46668
dislocation absorption 77−80538
dislocation and diffusion creep transition 80−88253
dislocation behaviour at advancing grain boundary during recrystallisation 77−7734
dislocation elimination by recrystallisation *(German)* 78−51559
dislocation interactions, electron microscopic obs. 78−34517
dislocation mechanism, of grain boundary crack nucleation, and growth under low cyclic stresses 80−19811
dislocation model, relative rotation of unconstrained polycrystals 77−27896
dislocation source during high temp. deform. *(Russian)* 78−15453
dislocation spreading 78−38729
dislocation struct. 77−55283
dislocation structure, atomistic computer simulation 79−60383
dislocations, Burgers vector determ. using electron microscopy 78−34720
dislocations, Burgers vector identification from electron microscopic images 80−19807
dislocations, effects on grain boundary processes of the steps in boundary plane 80−79785
dislocations, impurity influence on spreading temp. of grain boundary dislocations 79−77609
dislocations and lattice transformations, book contrib. 80−107242
drift diffusion under influence of stress fields 79−77835
Duralumin, effect of alloy purity and ageing on fracture mechanism, and resultant toughness 79−5049
Earth mantle peridotites, stress estimates from structural studies 78−69330
edge dislocation interactions in infinite array, elastic energy 78−55871
edge dislocations, atomistic study of structure 80−15110
elastic field of dislocation networks and grain boundaries 79−60362
elastic interaction with point defects 80−59483
elastically loaded polycrystal, stress state by contact problem theory 80−14573
electric cells, metal/β-alumina/metal, complex admittance diagrams, grain boundary effect *(French)* 80−45653
electrical resistivity, dislocation model 77−76800
electroceramic development involving grain boundary structural analyses *(Japanese)* 77−85977
electromigration, general anal., composition profiles from steepest descent methods 78−67849
electron dynamical diffraction from periodic arrays of dislocations 78−83669
electron micrograph, computer simulation for crystal defect identification 78−30525
electron microscopic study of grain boundary dislocations *(Hungarian)* 79−55751
electron microscopy images of coincidence grain boundaries 78−30639
electron solid, two-dimens., defects and implications for melting 80−39076
electronic structure, development of analytical electron microscope 80−86521
energies, discrete dislocation anal. 79−51115
energy and fine struct., surface dislocation model 79−28002
energy-misorientation relationship use in modelling grain boundary defects and props. 80−84188
engineering materials, intergranular fragility index 80−66637
engineering materials relation between deform., rupture, power-law creep 79−5020
entropy computation in computer simulation 78−30647
epitaxial film, interfacial boundaries and transition regions *(Russian)* 80−103596
equilibrium segregation of dil. solutes to grain boundaries, free surfaces, interphase interfaces 78−31411
fatigue crack initiation, rel. to grain boundaries, stress gradients and cross slip 77−27890
FBR oxide fuels, dynamic response of grain boundary cavities to stress and temperature changes under conditions of continuous gas generation 80−66544
FCC crystals, deform. faceting of large-angle grain boundaries TEM 77−65984
FCC metals and alloys, grain boundary energy and self-diffusion, effect of solute segregation 78−15412
FCC polycrysts., under hydrostatic pressure 80−107356
FCC/BCC partial coherent, boundaries, computer modelling 79−46669
ferrite-austenite (α-γ) interface, Fe self-diffusion compared with grain boundaries diffusion 80−65306
ferrites, soft and microwave, grain-size effects on mag. props., review 78−64222
ferroelectric ceramic, elec. and thermoelec. props. of grains and grain boundaries 78−43382
ferromagnetic domain wall dynamics, soliton theory appl., grain boundary effects 79−82813
ferromagnetic domain wall dynamics and soliton theory, coercive force determ. 79−42796

grain boundaries continued
field ion microscopy, developments, lattice imperfections 79−67445
field-ion microscopy, appl. to grain boundary dislocation studies 79−73170
film, multiple grain boundaries and surface diffusion 77−4276
film, rel. to effect of surface condition on diffusion at low temp. 78−91469
film systems, grain boundary diffusion, book contrib. 79−1526
FIM techniques, appl. to metallurgical problems, review 78−35620
finely crystalline materials superplasticity, rel. to displacement along grain boundary *(Russian)* 80−15184
finite solid, dislocations, disclinations and grain boundaries 80−2019
fission fuel grain boundary loss terms, use in fission gas release and swelling models 80−63257
fission product release, enhanced by grain boundary diffusion 78−4986
fluorite, use of proton irrad. to reveal growth and deform. features 80−84216
fracture, intergranular, at elevated temps. 77−48545
fracture, intergranular, low temp. mechanism 78−60795
fracture mechanism in various temperature and stress intervals *(Russian)* 79−24600
fracturing device for ion microprobe analyser, and appl. to grain boundary segregation 77−21341
free surface segregation, rel. to grain boundary segregation 80−71657
fusion reactor metals, He embrittlement, grain boundary cavity model 80−34075
GaAs, polycrystalline, grain boundary resistance meas. effect on solar cell performance 80−93891
general theory, microscopic derivation in crystal 79−1441
Gibbs thermodynamic anal., interaction with vacancies *(Russian)* 80−2034
glass, partially devitrified, grain boundary diffusion, new percolation problems 78−18844
glide dislocation interaction with intrinsic boundary structure 78−87686
grain and phase boundaries between crystals, conf., Konigstein, Germany (Oct. 1977) 78−72762
grain rearrangement, solids wth hexagonal grain struct. 78−84896
granular mats., stress-strain relations, intergrain slip 80−16374
graphite, grain boundary scattering effect on temp. depend. of electroresistivity, galvanomagnetic effect *(Russian)* 78−56148
graphite, silicized, fracture analysis, deform. 78−15530
groove evolution in presence of evaporation 78−14364
groove profile, effects of surface free energy anisotropy 79−7734
grooving under action of surface diffusion and evaporation or corrosion 80−39397
grooving under influence of evaporation or corrosion 79−28179
ground surface profile, crest and trough height distrib., Monte Carlo simulation *(Japanese)* 79−34180
ground surface profile power spectrum, Monte Carlo simulations *(Japanese)* 79−34179
hard magnetic material, coercive field, planar defect influence 77−24710
Hastelloy, H_2 embrittlement in H_2S environments, impurity segregation effects 80−71724
high angle, thermally activated movement 79−33002
high-angle, nature of dislocations, calcs. 78−14361
homogeneous material, 2D defects, interface problems 79−46674
hot-pressed with crystn. grain boundary phases 78−95716
hydrostatically compressed crystals, crack nucleation mechanism 79−10893
ice bicrystal, anisotropy of migration and faceting of grain boundaries 79−60381
ice I_h, internal friction meas. *(French)* 79−55754
ice-water interface, surface tension meas. by grain boundary groove method 77−24481
II-VI cpds., solar cell applic., role of grain boundaries and lattice mismatch 77−77377
Incoloy 800, degree of sensitisation vs. minimum Cr at grain boundaries 79−47721
Incoloy 901, foil prep. for TEM exam. 80−88001
Inconel, caustic stress corrosion cracking resistance, processing variables effect 80−71796
Inconel 600, effects of ageing and misorientation on intergranular corrosion *(Japanese)* 79−79158
Inconel 600, S penetration leading to sulphide form. *(French)* 79−74306
Inconel 600, thermal treatment, grain boundary microstruct. and SCC resistance 80−71675
Inconel 617, creep, morphological changes of carbides, affect on creep props. 80−108509
Inconel X-750, deform. and fracture characts., 24-816°C 80−108551
interaction with disperse inclusions of soluble phase, theory *(Russian)* 77−80513
interfacial cohesion, adsorption-induced losses 80−65010
interfacial diffusion effect on nucleation kinetics at grain and interface boundaries 77−35761
interfacial structure effects on high temp. mechanical behaviour 80−59480
intergranular fracture during power-law creep 79−96105
intergranular fracture energy, effects of segregated impurities, to grain boundaries 79−38928
intergranular orientation relationships by Kikuchi electron diffr. 80−15116
internal boundaries of large and small misfit, interrelationship 77−62542
internal friction in magnetics, elastic moduli anomalies *(Russian)* 77−35633
internal friction peaks, activation energy determ. *(Russian)* 77−43276
interphase boundary structure in solids, investig. 80−15112
intrinsic structure, in grain boundaries and boundary mobility 80−103368
ionic materials, grain boundary, diffusion, space-charge contrib. 77−55386
irradiation creep due to dislocation and glide 77−69009
irradiation growth, contrib. of grain shape to anisotropy 80−92556
laser optical simulation of diffr. from distorted lattices 79−23612
lattice dynamics studies of grain boundary structs., method and appl. to stability 80−49237
lattice resolution analysis, of coincident-site boundaries of electron microscope images 80−33861
leucosapphire crystals, block boundary energies 78−55877
liquid phase sintered systems, particle coalescence probability estimation 80−104086
liquid phase sintering, elementary mechanisms, soln.-reprecipitation 80−50571
liquid phase sintering, role of grain and phase boundaries 78−72747
LMFBR transient fuel behaviour, effect of grain boundary fission gas 79−54532
low-angle grain boundary dislocations, periodic clustering, TEM 79−46681
martensitic nucleation mechanism, FCC→BCC and other martensitic transforms. 77−36503
material transport rate and stress distribution during grain boundary diffusion driven by surface tension 79−61525
melting transition, grain-boundary, in two-dimensional lattice-gas model 80−59634
metal, annealing, struct. and grain boundary mobility 79−47728
metal, creep movement of dislocations, effect of stress distrib. at grain boundaries *(Russian)* 78−27564
metal, damping capacity rel. to struct. defects *(Russian)* 77−44283
metal, diffusion welding, migration of oriented intergranular boundary with pores *(Russian)* 80−84943
metal, dislocation elec. resist. and reson. scatt. 77−43550
metal, effect on bulk material props. 80−34004
metal, flow stress, subgrain size and subgrain stability of elev. temps. 77−86094
metal, fracture under influence of high power US waves *(Russian)* 79−5034
metal, grain boundary diffusion, temp. depend. and activation energy 78−95191
metal, grain boundary elements, FIM *(German)* 77−27894
metal, grain boundary groove migration at solid-liquid interface, simulation and with camphene 78−52789
metal, hardening due to increased subgrain boundary stability 78−52934
metal, He-containing, high temp. embrittlement model 79−83320
metal, high temp. creep, remarks rel. to zero creep method 77−12671
metal, induced elastic interaction of dilatation centres with grain boundaries *(Russian)* 80−84205
metal, low energy 77−27895
metal, low energy grain boundaries 77−84764
metal, migration obs. using FIM 78−79617
metal, polycryst., Bauschinger effect and mutual restriction between grains 78−52895
metal, polycrystalline, binding energy spectrum approach to grain boundary segregation 78−15409
metal, resistomatic studies of lattice defects review *(Japanese)* 78−59799
metal, stress conc. caused by grain boundary sliding under power law creep 78−60732
metal, textures and collective props. of lattice defects, external surfaces, grain boundaries 77−62543
metal, thermodynamic props. of grain and phase boundaries, review *(German)* 79−34012
metal film, elec. cond., size effect 78−76162
metal film, grain boundary electron scatt. in total film cond. model 80−7004
metal film, grain boundary resist., three-dimens. model 80−7003
metal film, grain boundary scattering model 79−15234
metal film, polycryst., superimposed effects of three arrays of scattering planes on electrical conductivity 80−80412
metal film, resist., temp. coeff. of resist., and Hall coeff. in grain boundary cond. model 80−39683
metal film, temperature coefficient of total resistance 80−70853
metal film, with grain boundary scatt., thermoelec. power, Fuchs-Sondheimer eqns. 78−52108
metal powders sintering, at 1 to 10 MPa, melting mechanism *(German)* 80−35122
metal wire, influence of grain boundaries on high temp. creep *(German)* 78−72812
metallic bicrystals, residual resistance theory, diffusivity, disorientation effects *(Russian)* 80−49875
metallic conductivity, polycrystalline, grain-boundary scatt. model 80−88530
metallic epitaxial layer, electron microscope obs. 79−11025
metallic film, grain boundary electron scattering by effective mean free path 78−84320
metallic film, strain gauge factor anal. 78−6458
metallic films, grain boundary scatt., Hall coeff., theory 80−88649
metallic films, monocrystalline, size and grain boundary effects in elec. cond. 78−76164
metallic materials, fatigue life distrib. theoretical obs. near fatigue limit 80−59569
metallic systems, coincidence site lattice model, failure for grain boundaries 79−60384
metallic thin films, grain boundary and surface scatt., statistical model 80−103762
metals, BCC, tilt boundaries, struct. 80−84184
metals, FCC, (001) twist boundaries symmetry and struct. 79−82242
metals, FCC, twist boundaries, struct. invest. using computer simulation technique 80−84185
metals, FCC and BCC, grain boundary struct., and segregated impurity sites, computer simulation 79−73173
metals, grain boundaries, struct. and props. recent developments 79−99217
metals, grain boundary structure, description of as polyhedra packing 79−10863
metals, mechanical props., testing and modelling 80−25811
metals, polycrystn., creep damage and cavity growth, assessment using density meas. 80−104217
metals, pure and alloyed, grain boundary relaxation model, *(Russian)* 80−39107
metals, resistance fluctuation spectroscopy, power spectrum of density fluctuations 79−65428
metals and alloys, grain and phase boundary model *(German)* 79−99216
metals and alloys, relaxation, rel. to defect struct. *(Russian)* 78−19801
Meyrick criterion, for incidence of discontinuous precipitation and grain boundary enrichment ratio 79−78983
mica, deformed, syntectonic nucleation of new grains 79−65102
micromechanical modelling of interacting creep processes in polycrystals 78−30205
microscopic derivation of theory of extended objects in crysts. 79−37704

grain boundaries continued
microstructure alterations and texture form. in normal grain growth, computer simulation 79−90679
migration, effect of solute atoms 79−28124
migration, group mechanism *(Russian)* 77−80514
migration, TEM obs. on mechanism 80−79812
migration in presence of grain-boundary coalescence of inclusions *(Russian)* 78−26579
migration kinetics, atom diffusion across boundary, theory 80−79809
migration under influence of high hydrostatic press. 77−68981
migration vacancy generation, and drag force 80−15090
misfit dislocations, core structures, TEM obs. 79−90673
misfit dislocations, core structures, TEM obs. 79−90674
misorientation, across low-angle boundaries, meas. 79−82237
molecular dynamics studies, use of coincidence lattice theoretical model 78−30645
MX type reactor fuels, microscopic swelling meas., effects of grain boundary migration 78−66348
mylonites, grainsize reduction and grain boundary sliding rel. to flow strength 80−21721
Nimonic EhI437B, heat resistant, true breaking stress in rapid air stream 79−66163
Nimonic PE16, abnormal grain growth after cold working and annealing 79−74176
Nimonic PE16, grain boundary carbide precipitation kinetics 77−52332
non-cubic lattice, coincidence site lattices 77−72625
nuclear ceramics, grain boundary energy to surface energy ratio, as determ. from pore geometry 80−34291
nuclear fuel, gas release and swelling, operational model, grain boundary gas 80−95346
nuclear fuels, fission gas precipitation into intra- and intergranular porosity, theory 80−57849
nuclear reactor fuel, transient fission gas behaviour, exptl. and analytical results 79−59190
nuclear reactor fuel transient heating conditions, mobility of fission gas bubbles 79−59189
nuclear reactor transient fuel behaviour, modelling of grain boundary fission gas effects 79−59169
offsets during creep 77−7735
p^+-n, n^+-p solar cell structures on polycrystalline material, performance 80−89640
pearlitic steel, P internal friction peak *(Russian)* 78−38774
periodic grain boundary struct., interaction with lattice dislocations 79−51117
Permalloy film magnetometer, mag. props. and LF noise 78−48005
Permalloy-Cu(Al) two-layer films, mag. anisotropy, grain boundary diffusion *(Russian)* 80−71122
permeation of grain boundaries in solids, appl. to Au and Cr in Pt 79−65253
phase boundaries in first-order phase transitions, dynamics stability 80−107403
phase transitions, appl. of TEM 79−68988
photovoltaic cell, grain boundary effects on performance 79−83603
photovoltaics and absorber/reflectors, diffusion, chemical reactions, contamination, AES and SIMS 80−72066
piezoelectric semiconductor, piezoresist. of grain boundaries 78−51995
plane coalescence, at grain boundaries 80−70221
plane matching by lattice imaging electron microscopy, direct obs. 78−6072
plane matching secondary relaxations, electron microscopy high angle, plane matching secondary relaxations, electron microscopy 80−103363
plasticity 80−65135
point defects, stress induced absorpt. and emission by grain boundaries 80−39081
polycrystal, US scatt. by grains 80−2122
polycrystalline film couples, diffusion during recrystn., numerical simulation 79−77844
polycrystalline films, grain boundary reflection coeff. thermal expansion effect on resistivity temp. coeff. 79−91162
polycrystalline heterostructure solar cells, grain boundary effects 78−52063
polycrystalline materials, diffusion controlled stress rupture 77−32681
polycrystalline materials, effect of grain boundary sliding on anelasticity 80−96592
polycrystalline materials, high temp. creep, role of grain boundary sliding 80−34128
polycrystalline metals, effect of grain boundary sliding on steady creep 80−96590
polycrystalline metals, elec. cond., statistical model for grain boundary effects 80−6814
polycrystals, Bi segregation embrittlement 79−83318
polycrystals, containing stationary or migrating grain boundaries, diffusional across transport 79−77832
polycrystals, models for constrained cavity growth 80−44251
polyethylene, theory of adhesion to alkali halide crystals, allowance for boundary dislocations 77−70280
polymers, X-ray diffr., lateral grain boundaries 79−14700
polystyrene latex, colloidal crystal, grain boundary struct. and boundary diffusion obs. *(Japanese)* 78−15721
polystyrene latex, grain boundary struct. obs. and boundary diffusion 78−51552
pore shrinkage, diffusional mechanisms 79−28131
porous structure, shrinkage kinetics, boundary slip and superplasticity 77−36611
power law creep, grain boundary and interphase boundary sliding 79−61643
precipitate hardened material, intergranular cavity growth inhibition 80−50677
precipitation reactions, determ. of struct. aspects, electron microscopy 80−103359
properties, with reference to impurity effects *(Dutch)* 80−96544
quantum field theory of crystals and extended objects, review 79−42164
quartz resonator, growth sector boundaries 77−39595
random close packing based model 78−95058
recrystallisation, phase boundary motion, heat release effect, self-consistent treatment 80−103449
recrystallisation nucleation, model for strain induced grain boundary migration 79−46675
refractory metal, generalised model for prediction of periodic trends in sintering activation 78−64498
grain boundaries continued
refractory metal films, evaporated, optical props., rel. to struct. 80−55211
relative orientation of two crystals from analysis os spot diffr. patterns 77−47305
relaxation peak parameters, calcs. 80−2117
resistivity calc. by pseudopotential method *(French)* 79−51539
sapphire, Czochralski crystals, formation of low angle grain boundary macrostruct. 78−47392
sapphire filaments in Al_2O_3:MgO matrix, single cryst. boundary migration 80−44369
sapphire ribbon crystals, EFG growth and charact., voids, grain boundaries and dislocations 80−103283
scanning optical microscopy examination of grain boundaries of polycryst. solar cells 78−79618
secondary boundary formation during crystn. *(Russian)* 77−59767
segregation; combined X-ray microanal. and lattice fringe imaging determ. 79−15681
segregation, computer simulation using Mie type interatomic pot. 80−54259
segregation, grain boundary, equilib. impurity conc. *(Russian)* 80−103478
segregation, ion microprobe mass analyzer appl. *(Japanese)* 77−25233
segregation, T-t dependence of temper brittleness 77−36617
segregation, two dimensional compd. form. and precipitation 78−15408
segregation, X-ray spectral analysis method, for element distrib. determination 80−21337
segregation at grain boundaries, critical assessment 80−75362
segregation equilibrium upper limit, at grain boundaries 77−84763
segregation kinetics, theory 80−11649
segregation theory, in terms of surface adsorption analogues 78−15407
segregation-induced embrittlement of grain boundaries 79−83318
self limiting discharge propagation over cathode surface 79−41889
semiconducting ferroelectric glass-ceramics, dielectric dispersion *(Russian)* 79−8097
semiconductor, polycryst., electronic processes at grain boundaries under optical illum. 77−55561
semiconductor, polycrystalline, elec. cond. model 77−11908
semiconductor, Poole-Frenkel effect, grain boundary barriers 79−11137
semiconductor, with grain-boundary barriers, thermally stimulated and isothermal discharges of capacitor across semicond. 78−2582
semiconductor bicrystal, charge carrier interface recomb., photocond. meas. method 79−99431
semiconductor defects, spectroscopic techniques to study of electronic props. 80−84446
semiconductor film, polycrystalline on optical props. grain boundary effects 80−80890
semiconductor film-substrate boundary, epitaxial interface form. and transition regions 80−10821
semiconductor structures, grain boundary barriers, sudden change in current 78−56246
semiconductor thin films, polycryst., barrier-limited cond. 79−95527
semiconductor thin films and heterojunctions, grain boundary and interdiffusion studies, AES and SIMS 79−77842
semiconductor with grain boundary barriers, thermal breakdown 78−39171
semiconductor with grain-boundary barriers, elec. cond. 77−55523
semiconductors, grain-boundary resist., DC voltage depend. 79−82597
semiconductors, polycryst., opto-electronic processes at grain boundaries 77−43667
semiconductors, polycryst., with low angle grain boundaries, residual cond. 80−15525
semiconductors, polycrystalline, electrical conductivity theories *(Czech)* 79−42537
semiconductors with grain-boundary barriers, boundary states' energy struct. influence on elec. cond. 79−11147
sink strengths for thin film surfaces and grain boundaries 80−88207
sintering, appl. of stereological charact. of interface interaction 77−63589
sintering, final stage, steady state diffusion models, testing of models by numerical simulation 79−4428
sintering, surface redistribution by grain boundary diffusion 80−84871
skeletonization in quantitative metallography 80−101002
sliding, of grain boundaries containing particles during diffusional creep 79−37712
sliding, stresses and deform. 78−68739
sliding and intercrystalline fracture in high temp. creep *(Czechoslovakian)* 77−32642
sliding and its accommodation during creep and superplasticity 77−40436
sliding model 80−75237
slip band theory, model for creep based on dislocation climb at grain boundaries 79−37756
snow, growth mechanism with specific grain boundary 79−23547
snow, wet, grain clusters obs. 80−26553
soap foam, arrangement of cells in a net rel. to grain sections of polycryst. 80−70225
sol crystals, grain boundary struct. and boundary diffusion obs. *(Japanese)* 78−15721
solar cell with large grain polycryst. material, enhanced carrier collection at grain-boundary barriers 79−92081
solar cells, polycryst., influence of grain boundaries electronic structure on diode characts. 80−94068
solar cells, polycryst., recomb. at grain boundaries, effect on photoresponse 80−108796
solar cells, semiconductors, direct gap 79−92075
solid solution, grain boundary self-diffusion co-eff. meas. in single phase 77−7886
solid-liquid metallic binary alloy, interfacial tension, chem. adsorption and temp. depend. 80−59777
solid-phase reaction kinetics, intercrystallite diffusion role 79−33106
solid-solid interface chemistry, characterisation, theory 80−75448
soliton-like features, molecular dynamics computer simulation study 79−77610
stainless steel rod adaptor, failure anal. in Fast Burst Reactor 77−54307
steel, 12Kh1MF, fracture in creep at temp. near 0.5 MP *(Russian)* 77−32675
steel, alloy, Cr-C (12, 0.2 wt.%) growth of grain boundary ferrite allotriomorphs, photoemission electron microscope exam. 78−88468
steel, alloy, embrittlement during tempering *(Russian)* 77−90436

grain boundaries continued
steel, alloy type, photoemission electron microscope obs. of high temp. precip. behaviour 80−108456
steel, austenitic, annealed, Ni ion bombardment, swelling temp. depend. effect of He implantation 80−29080
steel, austenitic, Cr-Ni (18,12 wt.%), containing coarse grain boundary precipitates, thermomechanical treatment 78−27545
steel, austenitic, Cr-Ni-Mn (21, 4, 9 wt.%), heat resistant, grain boundary reaction, effect of alloying elements *(Japanese)* 77−52331
steel, austenitic, grain boundary sliding, exam. by tensile creep tests 78−76715
steel, austenitic, Kh17N13M3T, activation characts. of rupture, 630-730°C, Sb and Nb microalloying effects *(Russian)* 79−5033
steel, austenitic, Mn-V-C, discontinuous precipitation, grain boundary struct. effect 79−29068
steel, austenitic, precipitation hardened, ductility of grain boundaries and crack propag. *(German)* 78−52834
steel, austenitic 316, grain boundary, sliding, grain size depend. 77−25108
steel, austenitic 316, grain boundary sliding, creep strain and stress depend. 77−25109
steel, austenitic and duplex 308 stainless, mech. of intergranular corrosion and pitting corrosion 79−91846
steel, austenitic Cr-Ni (18,12 wt.%), containing coarse irregular carbide precipitates along grain boundaries, ductility 78−60718
steel, austenitic Fe-Mn-V-C, ageing characts., discontinuous precip. nature 80−84940
steel, austenitic heat resistant, zig-zag grain boundaries, strength 77−73308
steel, austenitic heat resisting, creep rupture props., effect of grain- and grain boundary-strengths 80−97573
steel, austenitic heat-resisting, deformation and fracture rel. to grain-boundary reaction nodules 78−80591
steel, austenitic stainless, Cr-Ni (18, 10 wt.%), ^{59}Fe self-diffusion in ferrite/austenite interface *(French)* 80−19975
steel, austenitic stainless, embrittled by α-particle irrad. 77−69015
steel, austenitic stainless, extrinsic grain boundary dislocations, effect on $M_{23}C_6$ precipitate nucleation 79−51118
steel, austenitic stainless, extrinsic grain boundary dislocation spreading 79−57004
steel, austenitic stainless, grain boundary as dislocation source during high temp. deform. *(Russian)* 78−15453
steel, austenitic stainless, grain boundary migration during high temp. creep, TEM exam. 78−88509
steel, austenitic stainless, grain boundary struct. changes during initial stages of recrystallisation 77−36559
steel, austenitic stainless, grain boundary struct. during recrystn. and grain growth 80−76270
steel, austenitic stainless, He implanted 1.4970, high temp. fracture 77−86186
steel, austenitic stainless, interaction of grain boundary dislocations with precipitates during high temperature creep 80−16384
steel, austenitic stainless, low-cycle fatigued at high temps., crack obs. 77−1874
steel, austenitic stainless, Ni-alloyed, Cr_2N precipitation, interface struct. and morphology 80−11644
steel, austenitic stainless, recrystallisation, TEM obs. *(Japanese)* 79−52269
steel, austenitic stainless, structural inhomogeneity, electron and optical microscope exam. 78−72827
steel, austenitic stainless, temper embrittled, type 304, Auger spectroscopic exam. of grain boundary surface phases 78−76741
steel, austenitic stainless, type 316, effect of hold times on fatigue life, explanation in terms of grain boundary sliding damage 78−72851
steel, austenitic stainless, type 347 and 316, voids at grain boundaries near creep fracture surfaces 79−83311
steel, austenitic stainless, type 800, tensile creep props. rel. to inter-granular microstruct. at 800°C, TEM study 79−38885
steel, austenitic stainless, V alloyed, creep inhibition at grain boundaries, dislocation struct., TEM study 79−43346
steel, austenitic stainless, V alloyed, creep mechanism 77−48514
steel, austenitic stainless B-containing, decomp. of solid solns., effect of cooling conditions 77−44256
steel, austenitic stainless FV548, neutron irradiated, Si-rich phase occurrence of M_6C phase 80−15156
steel, austenitic stainless type 304, time-depend. fatigue, mechanistic model 80−100925
steel, C, X-ray line fitting by Gram-Charlier distrib., appl. to tension test *(French)* 79−15689
steel, C (0.2 and 0.45 wt.%), spheroidization at 680 to 690°C, struct. changes *(Russian)* 78−15431
steel, C-Mo-P, intergranular fracture and grain boundary segregation, P, H, Mo effects *(Japanese)* 79−15775
steel, C-Ni-Cr (0.6, 1, 1 wt.%), grain boundary segregation of S, N, P, As, Sb and Bi *(Japanese)* 78−15405
steel, carbon type, hydrogen press. effect on morphology of hydrogen attack 80−85052
steel, cast high-strength, local integranular fractures, formation mechanism *(Russian)* 78−95795
steel, continuously cast, tensile strength and ductility above 800°C 80−55476
steel, Cr, brittleness onset during high-temp. tempering *(Russian)* 77−81276
steel, Cr, ferritic, corrosion morphology, electrochem. pot. and Mo additions effect *(French)* 80−45439
steel, Cr (1.7 and 2.5 wt.%), segregation of S and P to prior austenite grain boundary, stress effect *(Japanese)* 77−55962
steel, Cr-Mo (1, 0.5 wt.%), heat treated creep failure, role of stress state 79−5047
steel, Cr-Mo (2.25, 1.0 wt.%), temper embrittlement, effect of Mn, Si, comp. and carbide precip. 80−85037
steel, Cr-Mo (2.25, 1 wt.%), damage accumulation and microstruct. changes during creep 80−3129
steel, Cr-Mo (2.25, 1 wt.%), interrelationship between creep deform. and creep rupture 79−61664
steel, Cr-Mo (2.25, 1 wt.%), SCC and temper brittleness, P grain boundary segregation effect 80−55571
steel, Cr-Mo (2.25, 1 wt.%), small changes effect in impurity elements, creep life 80−25790
steel, Cr-Mo-V, rupture ductility rel. to cavitation, density and SEM obs. 79−34142
grain boundaries continued
steel, Cr-Mo-V low-alloy, prior austenite grain boundary embrittlement by B 80−66657
steel, Cr-Ni-C (3, 1, 0.6 wt.%), grain boundary sulphide precip. and hot ductility *(Japanese)* 80−71654
steel, Cr-Ni-Mo, 'light spots', fractographic anal. 79−29204
steel, Cr-Ni-Mo, combined B and rare earth metal additions effect on microstruct. impact strength and hardness 79−38963
steel, Cr-V (1.5, 0.5 wt.%), ferritic, effect of temp. and microstruct. on creep damage 79−5023
steel, CrNi, etchability of austenite *(German, English)* 80−11860
steel, dual phase HSLA, compositional anal., TEM 80−85253
steel, embrittlement by impurity segregation 79−8367
steel, etchant for revealing austenite grain boundaries 80−85098
steel, Fe-Si coated grain oriented sheet, grain detection 78−11470
steel, ferrite nucleation, appl. to B hardenability 78−27505
steel, grain boundary segregation of C, atom probe FIM study 80−37134
steel, grain boundary strengthening mechanism 80−35207
steel, hardenability, role of B and P segregation 80−97486
steel, high speed, tempered, etching reagents for austenite grain boundaries 78−80704
steel, high strength, sulphide stress cracking props., density and distrib. of intergranular sulphide effects 79−74291
steel, high-strength, 80 kg/mm^2 class, effects of metallurgical factors on susceptibility of stress relief testing *(Japanese)* 79−43458
steel, high-strength low alloy, H_2 attack, 350-510°C 80−97636
steel, impact and tensile props., Si effects 79−24614
steel, inclusion, grain boundaries and H_2 attack, fracture analysis 77−32695
steel, intergranular failure, role of grain boundary composition 79−20155
steel, low alloy, low C grain boundary proeutectoid ferrite formation, direct obs. method 80−3074
steel, low alloy, quenched and tempered, formation of stony fracture during forging 79−79059
steel, low alloy, temper embrittlement and ternary equilib. segregation 80−60958
steel, low alloy ferritic, sub-micron cavity nucleation, SEM obs. 78−95753
steel, low C, C content effects in corrosion fatigue in nitrate solns. *(Russian)* 78−56811
steel, low C, struct. changes during decarburisation in intercritical temp. interval *(Russian)* 77−25075
steel, low C, tempered, lath martensite, Ni (5 wt.%), microstruct./yield strength relationship 77−21234
steel, low impurity, peritectic transformations, influence on initial struct., solidification, grain boundaries *(Russian)* 80−66621
steel, low-C, structural, with Zr impurities, grain boundaries, AES 79−24524
steel, manageing 300 grade, serrated flow in austenitic state 80−30041
steel, maraging, effect of thermal cycling (γ to and from α) on props. 80−20986
steel, maraging, Hart's model in hydrogen embrittlement 79−24621
steel, maraging, Ni (18 wt.%), fatigue crack initiation and propag. in earlier stage *(Japanese)* 77−8937
steel, maraging, Ni (18 wt.%), grain boundary precipitation, scanning Auger electron obs. 78−3132
steel, martensitic, fatigue crack form. associated with cyclic slip deform. along prior austenite grain boundaries 78−60831
steel, mild, hot shortness mechanism, surface enrichment of residual elements and oxidation *(Chinese)* 79−74230
steel, mild, sheet, with low Al content, annealing, AlN recrystn., precipitation kinetics *(French)* 79−20083
steel, Mn-Ti-B-rare earth, distrib. of B *(Chinese)* 78−84811
steel, multilayered with types St2kp and 10Kh18N10T, secondary recrystallisation props. *(Russian)* 80−66533
steel, N_2 effect on grain boundary migration rate during secondary recrystallisation *(Czech)* 77−59812
steel, Ni-B, B effect on temperability and microstructure 79−15710
steel, Ni-Co-Mo-Ti, hot formed, recrystallization and grain boundary precipitation effect on mech. props. *(German)* 79−66073
steel, Ni-Cr, intergranular segregation of P in austenite, grain boundary coherency depend. 78−84761
steel, Ni-Cr, SCC, grain boundary impurity effect 80−30150
steel, Ni-Cr, temper embrittlement, intermediate tempering treatments 80−60944
steel, Ni-Cr, temper embrittlement by Sb, Ni, Cr effects 77−36628
steel, P segregation, effect on brittle fracture after quenching and tempering *(Russian)* 80−81145
steel, pearlitic, struct. variations under plastic strain and subsequent heating, cementite decomp. *(Russian)* 80−84954
steel, quenched, adsorption of P on austenite grain boundaries rel. to tendency to delayed fracture of type 18Kh2N4VA *(Russian)* 80−45378
steel, quenched, tempered, intergranular failure during fatigue crack growth 79−8357
steel, Si, highly-oriented domain and grain obs. methods, using ferromagnetic colloid technique 80−11856
steel, Si, with coating, grain-oriented, domain pattern measurements *(Japanese)* 79−38353
steel, Sn (1.5 wt.%) and Mn-Mo (3, 0.4 wt.%), specimen fracturing device for ion microprobe analyser, to grain boundary segregation 77−21341
steel, stainless, 0Kh12G14N4Yu2, effect of plastic deform. on biphase struct. 78−44176
steel, stainless, 316, creep and rupture, 525 to 900°C, creep rate 79−11678
steel, stainless, 316, creep and rupture, 525 to 900°C, rupture and ductility 79−8327
steel, stainless, corrosion and grain boundary penetration on exposure to coal gasification environment 80−61003
steel, stainless, Cr-Cu (17, 0.6 to 1.1 wt.%), texture 80−84957
steel, stainless, Cr-Mn (21, 14 wt.%), grain boundary precipitation and fracture *(Japanese)* 79−100149
steel, stainless, creep ductility, sigmal phase influence 80−55478
steel, stainless, ferritic, Ti stabilised, exam. of grain boundary structure *(Russian)* 79−15662
steel, stainless, Frank-Read dislocation source obs. in grain boundary 77−84756
steel, stainless, grain boundaries, electron microscope obs. *(Russian)* 79−4311

grain boundaries continued
steel, stainless, grain boundary ledges, contrast phenomena identification 78−51555
steel, stainless, He ion irrad., fracture behaviour, in-situ HV electron microscopy 80−29089
steel, stainless, liq. Li corrosion rate expressions, 600-1000°C 80−93682
steel, stainless, martensitic new etchant to reveal prior austenite grain boundaries 78−3290
steel, stainless, martensitically ageing, techniques for revealing microstruct. characts. 79−70241
steel, stainless, proneness to intergranular corrosion, plasticity change tests 77−73366
steel, stainless, radiation-thermal treatment, N_2O_4 coolant action, intergranular corrosion *(Russian)* 78−58357
steel, stainless, sensitization, C content and ferrite morphology effect 80−89400
steel, stainless, sensitized, direct evidence of Cr depletion near grain boundaries 77−90358
steel, stainless, type 304, grain boundary sliding in isothermal and thermal fatigue *(Japanese)* 78−84979
steel, stainless, type 304, hydrogen assisted cracking, martensite formation on deformation effects 79−52362
steel, stainless, type 304, TEM study of dislocation emission from grain boundaries 79−66121
steel, stainless, validity of coincidence site lattice model of grain boundary struct. 79−51120
steel, stainless 304L, sintering, effect of grain growth and boundaries on shrinkage rate 77−36419
steel, stainless austenitic, low alloy 316, high temp. plasticity, B addition effects *(Russian)* 77−28852
steel, stainless casts, creep ductility, Auger spectroscopy study 80−60917
steel, stainless ferritic, drawability, mech. props., and grain boundaries in 08Kh16AMT and 08Kh18T1 80−35270
steel, stainless SUS 316, creep fracture at elevated temps. vacuum environment effect *(Japanese)* 77−8942
steel, stainless type 304, AES of stoichiometric Cr carbides and carbide precipitates at grain boundaries 80−3055
steel, stainless type 316, in-situ HVEM studies under ion beam irradiation 80−103396
steel, temper embrittled, grain boundary failure model for intergranular fracture modes 80−25825
steel, type A508, Cl 2, microcrack formation during stress-relief annealing of a weldment 78−80629
steel, very low C, delamination study by impact testing 78−3218
steel austenitic stainless 316, grain boundary sliding, temp. depend. 77−25110
steel intercrystalline stress corrosion cracking in a $Ca(NO_3)_2$ soln. *(German)* 80−30130
steel low C, γ-α transform. kinetic rel. with self-diffusion characts. *(Russian)* 78−67850
steels, C, quenched and tempered, struct.-prop. relationships 80−7599
steels, heat-treated, nature of high sensitivity to stress raisers 80−21051
steels, martensitic-ferritic, austenitic, microdefect accumulation during creep, effects of heat treatment, hardening 79−24550
stereology of allotriomorphs 77−44211
straight bar bending strength, brittle fracture energy conditions *(Russian)* 80−58974
stress induced drift diffusion, appl. to creep and growth of grain boundary voids 78−72811
structure, differential geometry 80−54253
structure, review 77−4110
structure and energetics 78−14359
structure model, polyhedra packing 78−47393
subgrain growth by boundary migration 77−76417
succinonitrile, grain boundary groove shapes, at a solid/liquid interface 79−65101
succinonitrile, grain boundary groove shapes, at solid/liquid interface appl. to Arbel-Cahn theory 79−69114
superplastic deformation, grain boundary form., dislocation density and diffusion parameters 79−65099
superplastic deformation, grain rearrangements 78−83828
superplasticity, region I characteristics 80−107357
surface discontinuity, annealing by surface diffusion 79−23812
surface dislocations, minimum energy configuration 80−49235
surface dislocations, universal concept, rel. to disclinations and grain boundaries 80−100231
surface science in metallurgy, review 79−42388
surface waves, derivation from general boundary theory 79−1442
surface-moving grain boundary interaction, anal. *(Russian)* 78−67721
TEM, modified O-lattice for CSL and DSC lattice determ. 79−55752
TEM, weak-beam, of nearly transverse boundaries 77−19854
TEM analysis, CSL condition determ. 80−15117
TEM determ. of Burgers vectors for grain boundary dislocations 78−87680
p-terphenyl polycrystalline layers, AC cond. 80−44746
textured matrix, grain growth, theory *(Russian)* 77−81273
theory as independent crystal imperfections, plastic rotation, boundary continuum *(Russian)* 79−82236
thermoelectric materials, extruded materials with tetradymite struct., primary and in situ recrystn., elec. props. 79−43266
thin film, influence of grain boundary migration on diffusion behaviour 80−88460
thin film bicrystals, dislocation interaction, with grain boundaries during plastic deform. electron microscopy technique 80−54281
thin polycrystalline films, rate of mixing depend. on grain boundary struct. 80−107578
three-dimensional epitaxial crystallite nucleation at substrate grain boundaries 77−76707
tilt boundaries, differential geometry of tensor quantities 78−10058
tilt grain boundaries, stress-induced migration in cubic crysts. 80−44252
time-defect densities in tilt boundaries of f.c.c., b.c.c., h.c.p., crystals 78−2142
TNT, creamed, dimensional stability, irreversible thermal expansion 79−73316
transition, cell-preserving, space group theory of translation, twin and translation-twin boundaries 77−19892
transition metal oxides, ⟨100⟩ coincidence twist boundaries energy 80−107270
d-transition metals, impurity integration with large-angle grain boundaries 80−39148
tunnel MIS solar cells, grain boundary effect on performance 79−79394
grain boundaries continued
twist boundaries, differential geometry 77−27893
twist disclinations, differential geom. 79−14805
two-phase anisotropic medium, interfacial dislocation, stresses, displacements and energy calc. 80−79786
type II superconductor, flux-line lattice instability due to planar imperfections 78−23218
TZM-Mo alloy, mech. props., effect of exposure to high temp. He containing O_2, room temp. study 80−93639
unified theory of grain boundaries 79−7616
vacancy adsorption on internal boundaries, rel. to recrystalln. and precip. 78−10084
X-ray diffraction line broadening, of crysts. containing small angle boundaries, Warren-Averbach anal. 79−37578
Zircaloy, micrograin superplasticity at 850°C 78−23758
Zircaloy-2, irradiation growth, reaction rate theory calcs. 80−88212
Zircaloy-4, creep damage at LWR temp. 79−52312
Zircaloy-4, stress-relieved and cold-worked, stress relaxation in bending at 673K 80−93609
Zircaloy-4/stainless steel, diffusion bonding in presence of Fe intermediate layer 79−10987
ZnO-based varistor, grain-boundary segregation, thin film X-ray spectroscopy obs. 80−35185
Ag and Ag-Au(Bi), grain boundary energy and struct., solute atom effects 77−47465
Ag epitaxial films, grain boundary struct. evolution during recrystn., interface energy effect *(Russian)* 80−15387
Ag, FCC, polycrystalline, deformation-strain curve description using substruct. parameters *(Russian)* 79−87690
Ag film, epitaxial growth, characterisation of {001} tilt boundaries 78−84097
Ag film, Ge coated, electrical resistance and ageing *(Russian)* 80−103759
Ag film, void growth, TEM obs. 80−59833
Ag foils, polycryst. and bicrystals, grain boundaries, ^{119}Sn Mossbauer anal. 80−7229
Ag, grain boundary energy misorientation, hydrostatic press. effect, press. induced struct. phase transformations 80−54257
Ag, implanted grain boundary cavities effect on cavity growth kinetics and creep fracture 78−52935
Ag, large grain boundary cavity coalescence during tension creep 78−52894
Ag particles, lattice defect influence on size effect 78−88329
Ag, surface self diffusion coefficient, O_2 pot. effect *(Japanese)* 78−60014
Ag thin evaporated films, rel. between microstruct. and excess free energy, TEM 80−70427
Ag thin films, deposited by cathodic sputtering using high-resolution electron microscopy, voids obs. 80−49557
Ag, thin-film bicrystals, planar lattice defects and migrating grain boundaries interaction 80−79835
Ag, wires, polycryst., internal friction and rigidity modulus, O removal from grain boundaries 78−3160
Ag/Al thin film couples, diffusional alloying, Kiessig X-ray interf. obs. 80−10713
Ag/Au thin film couple, interdiffusion mechanism 77−20132
Ag-Al (26 at.%), massive transform, $\beta \rightarrow \zeta$, crystallography and morphology 80−97475
Ag-Al polycryst. thin-film couples, interaction process 79−51443
Ag-Au, pseudoalloy behaviour at interfaces, grain boundary diffusion 80−6567
Ag-Cu (6.2 at.%), tricrystalline specimen, discontinuous precipitation, specific grain boundary energy *(German)* 77−86039
Ag-Cu (6.2 at.%), tricrystalline specimens, fine lamellar discontinuous precipitation *(German)* 78−52822
Ag-Cu (6.2 at.%), tricrystalline specimen, discontinuous precipitation, thermodynamics *(German)* 79−34043
Ag-Cu eutectic and off-eutectic alloys, thermal stability 77−25077
Ag-MgO (0.1 wt.%), intergranular cavity growth at elev. temps. 79−66068
Ag-S solid solution, grain boundary segregation and S diffusion in Ag 80−25700
Ag-Sn (0 to 6%), equilibrium intergranular segregation and diffusion 78−43130
AgCl bicrystal, grain boundary slip simulation 78−3176
Al, ⟨111⟩ tilt boundaries kinetic properties 78−34522
Al alloys, 7075-T6, H_2 effects and Cd segregation to grain boundaries 78−84764
Al alloys, thermomech. treatments, effects on microstruct. 80−100858
Al, bicrystal, ⟨100⟩ oriented, plastic deform. 78−19812
Al bicrystal, estimation of grain boundary torque 77−7736
Al, bicrystal, faceting of migrating ⟨110⟩ coincidence boundaries 79−46680
Al, bicrystal, fatigue crack initiation, crystal boundary effects *(Japanese)* 78−92328
Al, bicrystal, liquid metal induced grain boundary fracture, relative orientation effects 77−36690
Al bicrystal, migration of special ⟨110⟩ tilt boundary 79−46670
Al bicrystal, plastically deformed, slip heterogeneities 80−79858
Al, bicrystal, varying purity, breakaway of grain boundary from adsorbed impurity 77−31678
Al, bicrystal having $\Sigma 7$ and $\Sigma 21$ coincidence tilt boundary, plastic deform. *(Japanese)* 79−66116
Al bicrystals, [011] low-angle tilt boundaries, high resolution electron microscopy 80−34012
Al bicrystals, faceting of migrating ⟨110⟩ coincidence boundaries 80−34013
Al bicrystals, isoaxial, fatigue crack initiation in grain boundary affected regions *(Japanese)* 80−89338
Al bicrystals, stress induced migration of ⟩112⟩ symmetric tilt boundaries *(Japanese)* 80−15311
Al, boundary dislocations gliding, on coincidence boundaries, TEM study 79−82224
Al, coincidence site lattice and DSC dislocation network model of high angle grain boundary structure 80−54260
Al, cold rolled, commercial purity, initial stages of recrystallisation, TEM obs. 79−56999
Al, compressed, nucleation and recrystallisation study by electron microscopy and Kikuchi diffr. 79−52236
Al, computer simulation, of ⟨110⟩ tilt boundaries, struct. and symmetry 79−37713

grain boundaries continued
Al, computer simulation of tilt grain boundaries 78−30642
Al, creep at intermediate temps., in situ study of cell boundary evolution, HVEM 78−48480
Al crystals, TEM meas. of excess vol. of grain boundaries 80−15111
Al, deformed in tension, elec. cond. changes at 78 and 283K, grain boundary effect *(Japanese)* 80−30029
Al, diffusion in migrating interfaces 79−19390
Al, diffusion of Zn along grain boundaries, effect of grain boundary struct. *(Japanese)* 77−15628
Al, dislocation generation from grain boundary, in situ obs. 78−51547
Al, elastic grain boundary responses, thermodynamic props., computer calc. 77−39593
Al epitaxial films, grain boundary struct. evolution during recrystn., interface energy effect *(Russian)* 80−15387
Al, FCC, polycrystalline, deformation-strain curve description using substruct. parameters *(Russian)* 79−87690
Al, fatigue, high temp., cyclic grain boundary migration phenomena 80−85053
Al, fatigue crack initiation, pre-existing subgrain effect 80−97565
Al film, electron transport, grain boundary scatt. 79−60937
Al film, grain boundary diffusion of Cu 78−2303
Al, film, photoelectron-grain boundary scatt. in Al-SiO_2-Si struct. 78−64120
Al film, polycryst. heat conductivity depend. on thickness, block boundary density *(Russian)* 79−82689
Al, film, single cryst., defects, residual gas effects, TEM obs. 77−39587
Al film, vacuum deposited, O_2 contamination effect on form., grain boundary barrier layers 79−82487
Al film, vacuum evaporation growth, impurity presence, effects *(Hungarian)* 80−7495
Al film on GaAs, plasma oxidation, AES and TEM 77−77621
Al film on single cryst. Si slices, long-term tests 79−33346
Al films, deposited on calcite substrate, grain boundary scattering, elec. resistivity meas. 79−65096
Al foil, electron diffr. effects and images from inclined grain boundaries 79−82241
Al, fracture mechanism 80−100903
Al grain boundaries energy, evaluation in dangling-bond approx. 80−54256
Al, grain boundary migration, TEM obs. on mechanism 80−79812
Al, grain boundary sliding and deformation mechanism maps 80−3128
Al, isoaxial bicrystal, deformation behaviour, study by photoelastic coating and moire methods *(Japanese)* 78−11294
Al, periodic grain boundaries struct., computer simulation 77−89448
Al, periodic grain boundary struct., geometrical anal. 77−89449
Al, plastic deform. of poly- and single-crystals, AE study 79−24579
Al, plastically deformed, spreading of extrinsic grain boundary dislocations 78−43023
Al, polycryst., annealed, special grain boundaries in equilib. struct. *(Russian)* 80−29982
Al, polycryst. in annealed and creep conds., dislocation interactions with grain boundaries 79−42067
Al, polycrystalline, movement of 3-fold nodes of boundaries in high temp. creep 80−89317
Al, pure, creep, grain size effect on rate at 408K 77−52428
Al, pure, cubic, spatial orientation *(Russian)* 77−11567
Al, quenched, irradiated, and quenched plus irradiated, grain boundary hardening 80−3162
Al, single crysts., misfit recrystn. dislocations formation study during recrystn. by X-ray synchrotron topography 79−38849
Al, subgrain coalescence, grain boundary recrystallisation nucleation 80−3094
Al, symmetrical high angle boundaries computer simulation 77−51389
Al, symmetrical high-angle tilt boundary energy calcs. 77−27892
Al, thermal desorption of oxide film, influence of grain boundaries and recrystn. 80−61023
Al, tilt boundary, $\Sigma=5$, struct. and atomic vibr., computer simulation 80−70223
Al, validity of coincidence site lattice model of grain boundary struct. 79−51120
Al wire, grain boundary internal friction after recrystn. annealing *(Russian)* 80−66561
Al, Zn diffusivity along grain boundaries, grain boundary struct. effects 77−20128
Al-Al_2O_3, dispersion hardened, creep *(Czech)* 80−108463
Al-Al_2O_3 alloys, dilatometric method for studying relaxation of conc. of defects 77−55288
Al-Cu, effect of alloy purity and ageing on fracture mechanism, and resultant toughness 79−5049
Al-Cu, intergranular morphology of θ' precipitates, angle between grain boundary/precipitate plane 78−48413
Al-Cu, single and two phase, superplastic behaviour 80−11709
Al-Cu (0.5 wt.%), evaporated layers, electromigration, linewidth depend. 80−65277
Al-Cu (3.5 wt.%), precip. on stationary and non-stationary grain boundaries 78−84820
Al-Cu (4 wt.%), non IPS geometric surface relief effects associated with diffusional phase transform. 77−32575
Al-Cu (4.5 wt.%), cast alloy, ductile intergranular fracture 77−28908
Al-Cu (5 wt.%), fatigue strength, coarse precipitation effect *(German)* 79−91660
Al-Cu alloy bicrystals, neutron irrad. effects on grain boundaries, intergranular fracture and precip. 77−48520
Al-Cu thin film couple, interdiffusion, AES obs. 80−6569
Al-Cu-Zr (6, 0.3 wt.%) superplastic, grain boundary sliding 79−83254
Al-$CuAl_2$ aligned, fracture, effect of growth speed, orientation, environment 77−28907
Al-Fe, dil., defects and phases, Mossbauer studies 80−40004
Al-Fe dil. alloy, bamboo struct., grain boundary internal friction peak 79−43306
Al-Ge, structural changes during superplastic deformation, grain boundary porosity *(Russian)* 79−83258
Al-Li, cold worked neutron irrad. alloys, He bubble behaviour, microstruct. changes 77−54359
Al-Li-Mn (2.8, 0.3 wt.%), recrystallised sheet, fracture behaviour, SEM and TEM study 80−97566
Al-Mg, grain boundary dislocation identification, TEM obs. 77−62534
Al-Mg, recrystallised, grain boundary dislocation identification by computer simulation of TEM image *(Japanese)* 77−47457
Al-Mg alloys, overheating effects on microstruct. and props. 77−63698

grain boundaries continued
Al-Mg_2Si (0.95 wt.%), excess Si effect on ductility 78−27580
Al-Mg_2Si (1 wt.%) secondary recrystallisation by grain boundary unsewing 79−1886
Al-Mg-Si alloys, cast, precip.-rich zones on grain boundaries, soln. heat treatment conditions effect on mech. props. 80−104176
Al-Mg-Si alloys, ductile intergranular fracture mechanisms, void formation and nucleation 80−108578
Al-Mn (1.8 wt.%), cold-rolled, precipitation and recrystallisation 78−27540
Al-Mn-Si, recrystallisation and precipitation 78−52824
Al-poly-Si Schottky-barrier solar cells, grain boundary effects on electrical behaviour 80−85279
Al-Si (0.57 at.%), Si precipitate dissolution kinetics 80−84935
Al-Si-N-O system, comps. corresponding to β'-sialon phase reaction hot-pressing 80−84891
Al-SiO_2 interface, stress and microstruct. via TEM 78−26797
Al-Sn, (<0.28 wt.%) corrosion behaviour in 16% HCl 78−85054
Al-Ti-B alloys, phase comp. and distrib. of components, X-ray obs. *(Russian)* 79−52164
Al-Zn, dil., grain boundary diffusion 78−91475
Al-Zn, grain boundary reaction sites, determ. of struct. aspects, by electron microscopy 80−103359
Al-Zn, plastic deform. effect on struct. transform. at elev. temp. *(Czech)* 79−79044
Al-Zn-Fe-Si, Fe and Si effects on precip., TEM and X-ray diffr. obs., ageing at 90°C 77−48439
Al-Zn-Mg, cavitation during superplastic deform. *(Japanese)* 78−15464
Al-Zn-Mg, grain boundary surfaces, plasmon loss satellites in Auger spectra 78−15261
Al-Zn-Mg, grain boundary segregation, AES meas. 78−72781
Al-Zn-Mg, plastic instability rel. to grain boundary failure at low temps. 78−56702
Al-Zn-Mg, stress corrosion cracking, grain boundary precipitate size and distrib. electron microscopy study *(Japanese)* 79−79159
Al-Zn-Mg (2.2, 4.7 at.%), precipitate free zones, X-ray microanal. 80−108768
Al-Zn-Mg (6, 2.5 wt.%) alloy, ledge formation due to reaction with slip bands 79−57089
Al-Zn-Mg alloy (6, 3 wt.%), grain boundary segregation, AES exam. 78−39783
Al-Zn-Mg alloys, grain boundary segregation, implications to stress corrosion cracking 80−84936
Al-Zr (0.22 wt.%), hardness and struct. changes during prolonged ageing at 350, 400 450°C *(Japanese)* 79−52281
Al-ξ(AlAg) eutectic and off-eutectic alloys, thermal stability 77−25077
$Al_2Be_4(Si_6O_{18})$, beryl single crysts., growth defects study using X-ray topography *(French)* 79−37710
AlGe (4 wt.%), struct. peculiarities of superplastic behaviour due to porosity 79−34111
Al_2O_3, acceptor-dominated polycrystn., cond. and creep 79−78109
Al_2O_3 bicrystals, grain boundary obs. 80−39106
Al_2O_3, fine grained, basal slip and nonaccommodated grain boundary sliding 80−60916
α-Al_2O_3, grain boundary segregation, electron microscopy 80−103361
Al_2O_3, grain boundary thickness obs. using electron diffr. techniques 80−79811
α-Al_2O_3, growth and adhesion on Pt-Al alloys 77−8994
γ-Al_2O_3, magnetically quenchable positronium-like systems 79−87065
Al_2O_3, polycrystalline, creep and grain boundary sliding 77−36576
Al_2O_3 polycrystalline, effects of space charge, grain-boundary segregation and mobility differences on conductivity 80−79979
Al_2O_3, sintered, containing $MgAl_2O_4$ precipitates, Mg distribution at grain boundaries 78−80498
Al_2O_3, sintered, MgO-enhanced densification, test of second phase and impurity segregation models 78−64511
Al_2O_3:MgO, grain boundary segregation of Ca and Mg X-ray spectrosc. and STEM study 80−107269
B″-Al_2O_3-Na_2O, bulk and grain boundary ionic cond. from conductance and capacitance meas. 80−2204
β-Al_2O_3-Na_2O, grain boundaries and ionic cond. 79−23620
β-Al_2O_3-Na_2O, single cryst. and polycryst., elec. props. 77−72714
β-Al_2O_3-Na_2O doped with transition metal ions, complex plane anal. of impedance and admittance 80−70452
Al_2O_3-SiO_2 (3 wt.%), J-integral meas. at high temps. *(German)* 80−93624
Al_2O_3-TiC sinter products, grain size meas. by combination etching process 79−74331
Au bicrystal, core structs. of misfit dislocations in grain boundaries, TEM 78−14360
Au bicrystal, grain boundary thickness, meas. using X-ray techniques 80−34011
Au, bicrystal, thin, tilt boundary migration and facet development 78−2379
Au, bicrystalline, electron diffraction on networks of grain-boundary and interphase dislocations *(Russian)* 79−73168
Au bicrystalline film, lattice imaging of low angle tilt boundaries by TEM 78−79620
Au, bicrystalline thin films, faceting of [001] grain boundaries 80−70222
Au bicrystals, interaction of lattice dislocations with grain boundaries, electron microscope obs. 78−51579
Au, bicrystals, large-angle twist grain boundaries, X-ray diffr. obs. 79−90672
Au bicrystals, periodic ⟨111⟩ twist grain boundary structs., electron diffr. obs. 79−65100
Au, diffusion/oxidation of underlying Cu, rate-controlling step 80−34240
Au electrodeposited coating properties obs., Cu diffusion under high temperature *(Czech)* 78−91486
Au epitaxial films, grain boundary struct. evolution during recrystn., interface energy effect *(Russian)* 80−15387
Au, epitaxially grown bicrystalline thin films, preferred inclinations of ⟨100⟩ grain boundaries 80−103367
Au film, epitaxial growth, characterisation of [001] tilt boundaries 78−84097
Au film bicrystal, grain boundary dislocations in plane matching boundaries 80−39110
Au film bicrystals, exam. of low energy planes for tilt grain boundaries 78−51551
Au, grain boundary struct. anal. by HVEM *(Japanese)* 80−15109

grain boundaries continued
Au, grain boundary thickness obs. using electron diffr. techniques 80−79811
Au, polycryst. film, RF bias-diode and triode sputtered, resist. and microstruct. 78−80072
Au, quenched polycryst., vacancy loss at grain boundaries 80−59477
Au, serration and dissociation of edge dislocations in low-angle tilt boundaries 77−72621
Au sol, grain boundary struct. obs. and boundary diffusion 78−51552
Au, struct. obs., high resolution HVEM 80−103360
Au, structure, TEM 80−100255
Au, thin film bicrystal, diffraction effects from inclined grain boundaries 80−103362
Au, tilt boundary, small- and large-angle [001], X-ray diffraction study 79−82238
Au, tilt boundary, $\Sigma=11$, simulated and observed struct., vibr. of individual atoms at grain boundary 80−88167
Au/AuPd, bicrysts., in situ relax. of interphase interfaces 80−39455
Au/Pd, bicrysts., in situ relax. of interphase interfaces 80−39455
Au-Ag film system grain-boundary diffusion at low temp., meas. by surface accumulation method 79−77839
Au-Fe, polygonisation, recrystallisation, precipitation microstruct. without external plastic deform. 79−43276
Au-Fe (40 at.%), discontinuous precipitation reaction at grain boundaries 79−87642
$BaSrTiO_3$, model for 1/f excess noise 79−99591
n-$BaTiO_3$, ceramic, expt. and theoretical investigation of grain-boundary resist. 79−56235
n-$BaTiO_3$, ceramic, systematic expt. and theoretical investigation of grain-boundary resist. 79−56236
$BaTiO_3$ ceramics, grain boundary pot. barriers, cathodoluminesc., electron probe anal. 80−2864
$BaTiO_3$ ceramics, PTC-type, grain boundary study using TEM 80−107267
$BaTiO_3$, defect chemistry and elec. cond. improved positive temp. coeff. model 77−39859
$BaTiO_3$, donor doped, elec. props., effect of kinetic processes 78−64042
n-$BaTiO_3$, grain boundary resistivities 77−80782
$BaTiO_3$, polycryst., elec. resist. anomaly in phase transition region 78−43381
$BaTiO_3$:SnO_2, transition temperature shift, resistivity anomaly obs. *(Korean)* 77−39856
$(Ba_{1-x}Y_x)TiO_3$ ceramic, resistivity rel. to dopor dopant content 79−65474
Be, brittle-ductile transition, intergranular embrittlement *(Russian)* 78−3208
Be, creep mechanism 77−36586
Be, polycryst. plasticity, cleavage strength, ductility transition temp. 80−44250
BeSiN ceramics, glass free grain boundary 79−90671
Bi, epitaxial film, magnetoresist., carrier scatt. at grain boundary planes and surfaces 77−32095
Bi, polycryst., grain boundary scattering effect on temp. depend. of electroresistivity, galvanomagnetic effect *(Russian)* 78−56148
Bi_2MoO_6, superplasticity during phase transitions 80−108498
$Bi_{0.5}Sb_{1.5}Te_3$ film, effect of struct. on thermal cond. 79−28257
Bi_2Te_3 film, effect of struct. on thermal cond. 79−28257
$Bi_2Te_{3-x}Se_x$ films, thermal cond. depend. on grain size, phonon-boundary scatt. 79−69304
Bi_2WO_6, superplasticity during phase transitions 80−108498
C film, vac. condensed, graphitisation, electron microscopy 80−40265
CaF_2, press forged, mech. and optical props. 80−38079
CaO sintering, Cr_2O_3 addition effect *(Czech)* 80−45258
Ca_2SiO_4, bredigite-larnite rock from Scawt Hill, electron microprobe anal. 78−68952
Cd, low angle boundary decomp., dislocation struct. control *(Russian)* 78−3142
Cd, polycrystn., annealed, effect of hydrostatic pressure on grain size, growth and boundary mobility 79−37717
Cd-Zn eutectic and off-eutectic alloys, stability 77−25077
Cd_3As_2 film on NaCl substrate, vacuum deposition, growth morphology, microstructure 80−75479
$Cd_xHg_{1-x}Te$, X-ray topographic assessment 79−37716
CdS, cryst. grown from melt under press., microstruct. 77−59019
CdS epitaxial film, with grain-boundary barriers, field characts. of elec. cond. 77−55626
CdS polycrystalline film, pot. barrier at grain boundaries from Hall effect *(Russian)* 77−32094
CdS polycrystalline films, high strain sensitivity 80−93017
CdS-Cu_2S, thin film heterojunction, form. of Cu_2S thin layers along grain boundaries 79−56294
CdS-$CuInSe_2$, solar cell, grain boundary effects on performance 79−83603
CdS-$CuInSe_2$ solar cells, grain boundary and interface recomb. effects 79−39311
CdS(Se), small-angle boundaries, SEM obs. 80−24456
CdTe, film grown by hot wall epitaxy, elec. props. 79−82696
(Co,Cr,Ni)-TaC, eutectic alloy, directionally solidified, struct. defects, autoradiographic investig. *(Russian)* 77−25038
(Co,Cr)-$(Cr,Co)_7C_3$, eutectic alloy, directionally solidified, struct. defects, autoradiographic investig. *(Russian)* 77−25038
Co film, electromigration exam. from structural changes and resistance increases 77−20213
Co film, low-angle grain boundary struct. *(Russian)* 79−42807
Co, HCP-FCC transition, mag. domain behaviour, Lorentz electron microscopy 77−80958
CoNiZn ferrites, Fe excess, complex permeab. var. with annealing temp. 77−89979
Co_5Sm, magnetic domains, nucleation and pinning, magneto-optical Kerr effect 80−39811
Cr containing Cr_2O_3, film struct., oxide percentage determ. and temp. coeff. of resist. 80−103607
Cr film, evaporated, on die-cast Zn, microstruct. and intrinsic stresses, substrate temp. effects 78−10304
Cr-Au film structure, on Si interdiffusion 77−39698
Cr-MIS solar cells, on polycryst. Si, grain boundary effect and conduction mech. 80−93894
Cs-Rb(K)(Na), solute atom-grain boundary interaction energy, electron-statistical calcs. *(Russian)* 79−73175
Cu -Sn (0.05 at.%), grain boundary relax., misalignment angle effect *(Russian)* 78−3159

grain boundaries continued
Cu alloy, creep fracture prediction, intergranular damage meas. 77−21268
Cu alloy, mobility of boundaries, transition metal addition effects *(Russian)* 77−21160
Cu alloys, appl. of SEM to brittleness study 78−3214
Cu annealed and cold rolled, with bamboo structure, exam. of grain boundaries as vacancy sources in diffusional creep 78−88508
Cu, appl. of SEM to brittleness study 78−3214
Cu, bicrystalline thin films, characterisation of [001] tilt boundaries 80−75473
Cu bicrystals, effect of grain boundary on tensile deformation *(Japanese)* 78−88495
Cu bicrystals, grain boundary sliding and intergranular fracture studies 78−75717
Cu coating, bias sputter parameters effect, hollow cathode 77−40369
Cu, coincidence site lattice and DSC dislocation network model of high angle grain boundary structure 80−54260
Cu, crack nucleation and stage I propag. in high strain fatigue, microscopic and interferometric obs. 78−52936
Cu, crack nucleation and stage I propag. in high strain fatigue, mechanism 78−52937
Cu, cracks in earlier stages of fatigue, fractography *(Japanese)* 77−8924
Cu, creep damage and cavity growth, assessment using density meas. 80−104217
Cu crystals, two-phase, recrystn. retardation, particle size, spacing effects 80−89242
Cu dilute alloys, compositional changes in oxide thin films, Auger electron microanalysis *(Japanese)* 77−21319
Cu, disperse Al_2O_3 particles and matrix struct..effect on H-embrittlement *(Russian)* 78−3207
Cu, elastic grain boundary responses, thermodynamic props., computer calc. 77−39593
Cu, electrochem. overgrowths, role of substrate dislocations and grain boundaries in nucleation and growth 79−51454
Cu, evaporated film, grain boundary grooving and hillock form. 79−69381
Cu, FCC, polycrystalline, deformation-strain curve description using substruct. parameters *(Russian)* 79−87690
Cu foil, role of grain-boundary porosity in superplasticity *(Russian)* 78−56690
Cu, foil recrystallisation during annealing in high voltage electron microscope, grain growth *(Russian)* 79−100159
Cu, foils, faulted defect formation by moving boundaries 80−107281
Cu, formation of H_2O vapour bubbles, effect as intergranular creep fracture 80−71722
Cu, grain boundaries, nucl. gamma reson. *(Russian)* 79−8080
Cu, grain boundaries effect on thermal cond. 79−51546
Cu, grain boundary anal. by TEM, CSL condition determ. 80−15117
Cu, grain boundary character, revealed by etching and slip line continuity 79−33001
Cu, grain boundary migration, TEM obs. on mechanism 80−79812
Cu, grain boundary morphology effect on void form. 78−48533
Cu, grain growth rate, 520-970°C *(Russian)* 80−29972
Cu, grain-boundary sliding component in high temp. fatigue 80−50706
Cu, high purity, creep cavitation topology, high temperature region *(Czech)* 80−65138
Cu high purity, grain boundaries as dislocation sources in premacroyield strain region 79−34096
Cu, internal friction, impurity effect *(Russian)* 79−87677
Cu, intrinsic struct. electron diffr. anal. 80−84186
Cu, ion bombarded, cone form. and associated surface features 77−59054
Cu, lattice and grain boundary diffusion of P, exam. of diffusion rates by tracer sectioning technique 78−79817
Cu, near $\Sigma 9$ grain boundary, structure and dislocation interactions 80−79808
Cu, near $\Sigma 9$ grain boundary, props., identification by image matching of Burgers vectors 80−79810
Cu, near $\Sigma 9$ grain boundary properties, boundary dissociation 80−100251
Cu phthalocyanine, grain boundary struct., crystallographic planes 80−103366
Cu, polycryst., creep and fracture behaviour, effects of prestrain and O 80−97544
Cu, polycryst., grain boundary orientation determ. by struct. protonography *(Russian)* 78−38726
Cu, polycryst., grain size and high-temp. yield strength 80−7641
Cu, positron lifetime as a function of grain size 77−15427
Cu single crystal, large angle grain boundaries formed during cold work, TEM obs. of orientation relationships 79−90678
Cu, single crysts., ⟨110⟩ oriented, tensile deformed, HVEM of recrystn., recrystallised state 80−89256
Cu, single crysts., temp. depend. on grain boundaries energy and struct. 79−37718
Cu, sintered, appl. of stereological charact. of interface interaction 77−63589
Cu, sintered single crystal on flat single crystal, energy misorientation relationship of grain boundaries 79−60377
Cu spheres, on Cu single cryst. surface, grain boundary energy anisotropy using gravitational torques 79−60385
Cu spheres, rotation and translation during sintering onto a substrate, grain boundary energy SEM study 79−38759
Cu, structure of high-angle (001) CSL twist boundaries 79−46677
Cu, twist boundary structure, plane translations 79−69113
Cu, validity of coincidence site lattice model of grain boundary struct. 79−51120
Cu wire, residual elec. resist., size effect and grain boundary contribs., heat treatment effects *(Russian)* 78−56126
Cu-Al, cold worked solid soln., anneal hardening, grain boundary effects 78−48420
Cu-Al (14.3 wt.%), ^{110}Ag diffusion in β/γ_2 interphase boundary 80−79989
α-Cu-Al (15 at.%) alloys, effects on low temp. neutron irrad. induced point defects behaviour 77−43251
Cu-Al-Co, precipitate-free zones near grain boundaries, growth kinetics, TEM obs. 80−40368
Cu-Al-Ti, formation of modulated structure rel. to barrier nucleation of new phase *(Russian)* 77−32580

grain boundaries continued
Cu-Au system, grain boundary adsorption thermodynamics *(Russian)* 80−44317
Cu-Au thin films after accelerated ageing, failure by Kirkendall porosity 80−6675
Cu-Be (1.8 wt.%) alloy, discontinuous precip. form. and growth, TEM obs. 80−104169
Cu-Be (2 at.%), plastic deform. and dislocation substruct. 80−76307
Cu-Be (2 wt.%), alloying addition effects on grain boundary reaction *(Japanese)* 80−49236
Cu-Bi, grain boundary thickness obs. using electron diffr. techniques 80−79811
Cu-Bi (0.0115 wt.%), embrittled, grain boundary faceting, TEM study 79−27998
Cu-Bi (0.02 wt.%) alloy, intergranular fracture, Kossel X-ray diffr. in SEM obs. 80−108579
Cu-Bi alloys, embrittled grain boundary obs. using STEM, Cu-SiO_2 comparison 78−38730
Cu-Bi alloys, grain boundaries, electron microscopy 77−12694
Cu-Bi alloys, grain boundary segregation 79−61596
Cu-Bi foil, electron diffr. effects and images from inclined grain boundaries 79−82241
Cu-Cd (1.0 wt.%), yield stress and flow stress 80−97524
Cu-Co (2.48 wt.%), two-phase, surface meas. study of grain boundary sliding during creep 77−81299
Cu-Cr alloy, laser irrad., structural changes *(Russian)* 80−100247
β-Cu-In, unidirectionally transformed eutectoid, lamellar microstructure, influence of grain boundaries on thermal stability 78−72795
Cu-Ni (40 at.%) alloy, grain boundary migration, intergrain liq. layer effects *(Russian)* 77−15633
Cu-Ni bimetallic thin film, effect of microstructre on interdiffusion 79−77840
Cu-Ni film system, time depend. diffusion coeffs., grain boundary and dislocation effects 77−80656
Cu-Ni textured alloys, grain boundary effusion of Ni to surface 79−90680
Cu-Ni-Al, grain boundary reaction under isothermal ageing at 623 to 973K *(Japanese)* 79−70090
Cu-Ni-Be (30, 0.5 wt.%), grain boundary reaction after ageing and quenching, obs. *(Japanese)* 79−70089
Cu-Ni-Be-(Al) (30,0.5,(0.2-2) wt.%), Al addition effect on grain boundary reaction *(Japanese)* 80−54254
Cu-Ni-Fe (26,8 wt.%), microduplex struct. form., recrystn. annealing *(Japanese)* 78−76659
Cu-Ni-Nb (30, 0.9 at.%), precipitate free zones, X-ray microanal. 80−108768
α-Cu-Ni-Zn-Pb, fire cracking, effect of pores and impurities 79−29207
Cu-Sb, dil., grain growth rate, 520-970°C *(Russian)* 80−29972
Cu-Sb solid solution, dil., FCC, intergranular solid shortness mechanism *(Russian)* 79−5032
Cu-Si alloy, correl. of periodicities in diffr. patterns and images from grain boundary 78−14362
Cu-transition metal alloy, internal adsorpt. and mag. susceptibility, grain size effects *(Russian)* 78−19759
α-Cu-Zn(Al) fracture behaviour, effect of deform. temp. and alloying content *(Japanese)* 79−20159
Cu_3Au thin films, fine-grained and disordered, low temp. ordering 80−97433
CuCl, interface supercond., piezoelec. hypothesis 80−60128
CuCoNi ferrite magnetoacoustic oscills. rel. to microstruct. 77−85536
Cu_xO, film, thermoelec. power, activation energy variation with electrode spacing in DC sputtering 78−76099
Cu_2S-CdS thin film solar cells, Cu_2S layer separation, struct. 79−95282
Er_2O_3, of Hf, vol. and grain boundary diffusion coeffs., tracer sectioning technique 79−7712
Fe, adsorbed S effects on surface reaction kinetics and surface self-diffusion 78−7234
Fe, Armco, corrosion and mechanical behaviour in liquid Li 78−53036
Fe based alloys, solute segregation to grain boundaries 78−72780
Fe, bicrystal, vapour grown, statistical analysis of grain boundary angles 77−47470
Fe, cast, US flaw detection by boxcar integration 80−89437
α-Fe, cavitation and sliding distrib. changes during creep at 500°C 78−6991
α-Fe, cavity formation at grain boundary-subboundary interactions 77−86040
Fe, chemically induced grain boundary motion, in Zn atmos. 78−38724
α-Fe, creep life, meas. by microstruct. changes 78−35443
α-Fe, deformation induced intergranular creep cavitation 78−31473
Fe, diffusion and solid solubility of Sb, 773-873K, ion backscatt. anal., rel. to intergranular embrittlement 78−71880
Fe, embrittlement, fracture mode transition as function of grain boundary sulphur 80−55520
Fe, FCC, grain boundary struct. and energy, computer expt. 78−30643
Fe film, low-angle grain boundary struct. *(Russian)* 79−42807
Fe, free surface and grain boundary O_2 and S chemistry 80−75410
Fe, grain boundaries, electron microscope obs. *(Russian)* 79−4311
γ-Fe, grain boundary diffusion of Ni 79−23787
Fe grain boundary grooving by N contaminated liquid Li, corrosion mech. 77−6522
α-Fe, grain boundary segregation of C, N_2 and C Auger spectroscopy 78−72778
Fe, gray, Mg bearing, high strength, eutectic grain determ. by Si reverse liquation 79−15886
Fe, microcracks formed by H_2 precipitation, SEM and TEM obs. *(Japanese)* 79−70071
Fe, oxidation and domain structure, electron microscope exam. *(Russian)* 79−1437
Fe, polycrystalline, fracture surface singularities under single loading conditions *(Russian)* 80−50696
Fe polycrystals, grain misalignment, electron microscope determ. *(Russian)* 80−103358
Fe, pure, hydrogen-charged, initial cracking obs. 80−108580
Fe, pure, initial grain boundaries effect on cold-rolling and annealing textures *(Japanese)* 80−35205
Fe, pure, mech. props. at low temps. 78−44219
Fe, pure, Sn and Cr diffusion, effect of boundary struct., autoradiography study *(Japanese)* 80−49419
Fe, segregation of ^{119m}Sn at grain boundaries, Mossbauer effect 78−15414

grain boundaries continued
Fe, thin foil, extrinsic grain boundary dislocations, low C content influence 80−107273
α-Fe-(Ni,Mn,Cr,Mo,W)-P (1 wt.%). grain boundary segregation, temper brittleness, AES study *(Japanese)* 79−78981
Fe-Al-Si (6.22, 9.63 wt.%), bending test under high press., high temp. 80−85057
Fe-C, proeutectoid ferrite nucleation kinetics at austenite grain boundaries 80−55405
Fe-C (0.11, 0.23, 0.42 wt.%), grain boundary ferrite allotriomorphs, growth kinetics 77−44244
Fe-C (0.25 wt.%), austenitising temp. effect on proeutectoid ferrite reaction kinetics, scanning Auger microprobe exam. 78−44144
Fe-Ci (3 wt.%), local magnetisation losses, grain orientation effect 80−88817
Fe-Co (33 wt.%), oxidation and domain structure, electron microscope exam. *(Russian)* 79−1437
Fe-Co-V (2 wt.%), gamma phase 77−36514
Fe-Cr, grain-boundary segregation of carbon, electrochemical study 79−100147
Fe-Cr (28 wt.%), intergranular corrosion and anodic polarization at grain boundary groove *(Japanese)* 79−15869
Fe-Cr (9 wt.%), extrinsic grain boundary dislocations, low C content influence 80−107273
α-Fe-Cr alloys, recrystallised, C segreg. effects, TEM *(French)* 77−28828
Fe-Cr-Ni based alloys, Ni^+ ion and neutron irradiated, γ′ particle redistrib. and phase stability 79−78977
γ-Fe-Cu, lattice and grain boundary diffusion of Cu 79−23765
Fe-Mn (3 wt.%), Sn diffusion along grain boundaries, micro-Auger spectroscopy 77−11740
Fe-Mn(Ni), fracture mechanism in various temperature and stress intervals *(Russian)* 79−24600
Fe-Mo (4.1 wt.%), substructs. developed during steady state creep at 1100-1200K, TEM obs. *(Japanese)* 79−38900
Fe-Ni, α→γ conversion, electron microscope and X-ray spectral microanal. 79−78966
Fe-Ni, coercive force depend. on grain struct. and inclusions 77−20635
Fe-Ni (3 wt.%), grain boundary segregation microanal. using X-ray (STEM) and AES 78−87685
Fe-Ni (4 wt.%), extrinsic grain boundary dislocations, low C content influence 80−107273
Fe-Ni system, Ni addition effects on activated sintering of Fe powder compacts 77−4756
Fe-Ni-Al (18.2 wt.%) aged, fracture toughness and mode, grain size depend. 77−12700
Fe-Ni-C, intercrystalline embrittlement in tempered martensite, elimination by reaustenitization *(Slovak)* 80−108548
Fe-Ni-C, role of strain in deform. induced martensitic transform. *(Japanese)* 78−92263
Fe-Ni-C (24, 0.5 wt.%), recovery and recrystallisation of stable austenite after hot rolling *(German)* 77−32591
Fe-Ni-C (31.9, 0.02 wt.%), metallographic study of austenite grain size effect on martensite kinetics 79−1863
Fe-Ni-Cr alloy 800, minor alloying element effect on creep, ageing microstruct. 78−27572
Fe-Ni-Mn, martensite, aged, grain boundary embrittlement 79−96144
α-Fe-P, grain boundary adsorption of P, internal friction *(Russian)* 77−32609
Fe-P, P equilib. grain boundary segregation 79−38835
Fe-P (0.14 wt.%), cavity formation at grain boundary-subboundary interactions 77−86040
Fe-Si, (3wt.%) alloys, grain boundary anal.,, scanning AES 79−43256
Fe-Si, coated, effective domain and grain obs. methods and Fe losses 80−34675
Fe-Si, glissile and twinning dislocation motion temp. depend., influence of grain boundaries *(Russian)* 77−47452
Fe-Si, internal friction, domain boundary area *(Russian)* 79−24562
Fe-Si (2.35 wt.%), misorientation dependence of grain boundary segregation, Auger spectroscopy exam. 78−76629
Fe-Si (2.9 wt.%), spatial orientation *(Russian)* 77−11567
Fe-Si (3 wt.%), behaviour of disperse inclusions, influence of recrystn. processes *(Russian)* 80−66519
Fe-Si (3 wt.%), breaking stress grain size and grain boundary energy during onset of reversible temper brittleness *(Russian)* 77−32673
Fe-Si (3 wt.%), chemical comp. and hot rolling effect on brittleness *(Czech)* 80−50712
Fe-Si (3 wt.%), containing B, grain boundary segregation, AES evidence 77−86046
Fe-Si (3 wt.%), grain oriented tape-wound core, dynamic domain size var. and Fe losses 77−12146
Fe-Si (3 wt.%), hysteretic losses, domain struct. and cryst. defects 79−19747
Fe-Si (3 wt.%), recrystallisation along grain boundaries *(Russian)* 78−6942
Fe-Si (3 wt.%), rel. to role of solutes in secondary recrystn. 77−86043
Fe-Si (3 wt.%), temp. depend. of migration rate of secondary recrystallisation grain boundaries *(Russian)* 79−1436
Fe-Si (3wt.%), hardening under dynamic load, grain boundary effect 77−12674
Fe-Si alloy, deformed by slip, polygonal boundary form. *(Russian)* 79−24534
Fe-Si alloys, polycrystalline, domain struct. at grain boundaries *(Russian)* 77−51917
Fe-Si-B-N-S, B, S, N effects on grain boundary segregation and grain growth inhibition, review 80−3047
Fe-Sn, grain boundary embrittlement by Sn segregation, Mossbauer study 80−7239
α-Fe-Sn alloy, grain boundary hardening and segregation 80−55417
Fe-Sn system, Sn binding state, using segregated ^{119m}Sn, Mossbauer anal. *(Japanese)* 80−20525
Fe-Ti (0.15 wt.%), Ti distrib., segregation, FIM anal. 80−84200
Fe-Ti alloys, kinetic trapping model for H_2-induced grain boundary cracking 79−29164
Fe-V(Cr)(Mn)(Ni), unlimited component solubility, intercrystallite internal adsorption *(Russian)* 80−39294
Fe-Zn, chemically induced grain boundary motion 78−38724
$Fe_{40}Ni_{40}B_{20}$ glass, phase transform. during isochronal annealing 78−14451
α-Fe_2O_3, crystalline grain growth during heat treatment 78−11252

grain boundaries continued
Fe_3O_4, finely dispersed, electronic phase transition, cond. and DTA meas. 78−91736
GaAs, epitaxial layers, grain boundaries, deep level transient spectroscopy study 80−49234
GaAs epitaxial layers on polycryst. GaAs substrates, LPE growth charcts. 80−75471
GaAs, film, selective anodisation, grain boundary edge passivation 79−11711
GaAs, grain boundaries, extended Read model 80−96543
GaAs, grain boundaries investigation using DLTS techniques, photovoltaic material appls. 80−92539
GaAs, polycrystalline, carrier transport at grain boundaries 80−29411
GaAs Schottky barrier solar cells with grain boundary edge passivation 79−83592
GaAs solar cell, polycryst., grain boundary passivation by oxidation, AES, SIMS and XPS obs. 80−81467
GaAs thin film polycrystalline Schottky barrier solar cells, grain boundary chemistry 80−94067
GaAs thin film polycrystalline solar cells, grain boundary edge passivated 80−94069
GaAs:Se(Zn) polycrystalline film, Hall effect, resistivity meas. 80−96911
n-GaAs/K_2Se-K_2Se_2-KOH/C liq. junction cell, effect of Ru ion chemisorption on grain boundaries 80−55879
GaP, green cathodolum. from cryst. defects, SEM, TEM study 80−80870
GaP on GaAs substrate, heteroepitaxial layers, stuct. defects *(German)* 79−23865
GaP, SEM, cathodoluminesc., impurity and defect detect. 78−83695
$Gd_xZr_{1-x}O_{2-x/2}$, elec. cond. of ceramic solid solutions 80−107554
Ge, bicrystal, dislocation core structure *(French)* 78−26571
Ge, bicrystal, two-dimensional electronic phenomena at He temp. *(Russian)* 79−56273
Ge bicrystals, [011] tilt boundary, grain boundary stability 79−82240
Ge bicrystals, high angle tilt boundaries, TEM *(French)* 80−70224
Ge bicrystals, low angle [011] tilt boundary 79−82239
Ge, dislocations, lattice images 79−82215
p-Ge film, fragmented struct., elec. cond., Hall coeff. and magnetoresist. meas. 77−15979
Ge film, polycrystalline, structural and elec. props. 78−76173
Ge, grain boundary, lattice imaging in electron microscope 78−6069
Ge, high resolution electron microscopy, dislocation and grain boundary struct. 3-4 Å resolution 78−38707
Ge, polycrystalline thermal-imaging lens, optical requirements 80−69495
Ge single crystals, constitutional supercooling growth conditions, structural and chem. inhomogeneities 80−93473
H_2, form. in Al-Zn-Mg after water vapour embrittlement 78−15564
$HUO_2PO_4.4H_2O$, role in high proton cond. 79−77809
$(Hf_xZr_{1-x})_{80}Nb_{20}$, β-decomposition, effect of Hf additions 79−8304
n-$Hg_{0.61}Cd_{0.39}Te$ single crystals, flicker noise due to grain boundaries, meas. 79−1611
In film, vacuum evaporation growth, impurity presence, effects *(Hungarian)* 80−7495
InBi, single cryst. zone melting growth and etching 79−34189
In_2O_3-SnO_2 thin film, Hall mobility, temp. depend., grain boundary effects 80−75658
n-InP film, polycrystalline, elec. props. 77−76965
InP, large size single crysts., synthesis, solute diffusion technique, low-angle boundaries obs. 79−33917
InP p-n junction, grain boundary etching 80−96541
InP thin films for photovoltaic devices 80−93972
p-InSb, excess In, polycryst. thin film, elec. transport props., non-stoichiometric effect 79−95528
Ir, brittle fracture, impurity segregation to grain boundary effects 78−64637
Ir-W (0.3 wt.%), P segregation to grain boundaries, effect on high temp. ductility 78−95754
Ir-W (0.3 wt.%), polycrystn., brittle fracture TEM study 79−61715
Ir-W (0.3 wt.%): Al(Fe)(Th)(Ni)(Rh), effect of additions on grain boundary composition 79−83309
Ir-W (0.3%), grain boundary comp., trace element additions effect 80−66661
K-Rb(Cs)(Na), solute atom-grain boundary interaction energy, electron-statistical calcs. *(Russian)* 79−73175
KBr bicrystal, Ag^+ injection transport and grain boundary mobility, electrodecoration obs. 80−2214
KBr bicrystal, grown from melt, interfacial substructure, impurity effects 77−4263
KCl bicrystals, grain boundary migration kinetics, effect of solutes 78−43185
KCl, cryst., etch hillocks on (100) cleavage planes 77−4109
KCl, Czochralski-grown, creep and struct. changes, 77-300K *(German)* 77−28862
KCl, doped, grain boundary diffusion, space-charge contrib. 77−55386
KCl:RbCl, $SrCl_2$, laser window material, prep., grain boundary stability 77−46774
KCl-KBr, dislocation rosettes, diffusion origin 78−83820
KCl-KBr mixed crystals, microhardness studies, nonlinear depend. on composition 78−83872
KCl-NaCl, dislocation rosettes, diffusion origin 78−83820
$KMg_3AlSi_3O_{10}F_2$, dislocations, subgrain boundaries, X-ray diffr. topography study *(Chinese)* 80−88149
FCC-Li, symmetrical high-angle tilt boundary energy calcs. 77−27892
LiF, hardening under dynamic load, grain boundary effect 77−12674
LiF, press forged, mech. and optical props. 80−38079
LiF, strong reorientation resulting from creep, X-ray obs. 79−100228
LiF, thermal phonon scatt. by low angle grain boundaries 78−67795
$LiNbO_3$, imaging of photorefractive effects by double cryst. X-ray refl. topography 78−39521
Li_2O-SiO_2-P_2O_5 glass ceramic fibres, heat treatment, crystn., tensile strength 80−84995
Mg alloy, MA12, structural state effect on life and in fatigue crack generation in air and in vacuo 79−87728
Mg, grain boundary diffusion creep 78−11291
Mg, grain boundary struct., Kikuchi electron diffr. obs. 80−15116
Mg-Al (0.8 wt.%), grain-boundary sliding component in high temp. fatigue 80−50706
Mg-Al (5, 7, 9 and 11 at.%,) discontinuous precipitation growth kinetics 77−63677
grain boundaries continued
Mg-Al (9 wt.%), ageing via cellular reaction, microanal., cell boundary vel. meas. 78−11230
Mg-Ce, workability, aging charcts. and tensile strength 80−55416
Mg-La, workability, aging charcts. and tensile strength 80−55416
Mg-Mn-Ce, structural changes and deformation during superplastic flow 78−15472
Mg-Mn-Ce alloy, MA8, dislocations at grain boundaries and grain-boundary glide 78−64605
Mg-Mn-Ce alloy, superplastic deform., role of grain boundaries 78−19843
Mg-Zr alloy, cavitation during diffusion creep 77−44296
$Mg_{1.86}Al_{1.67}Si_{2.47}O_{3.19}N_{3.81}$, 12H polytype, intergranular phases and compositional variations 80−79645
MgF_2 film, vac.-deposited, origin of mech. stress 79−90925
MgF_2 film, vacuum deposited, rel. to tensile stress, meas. and calc. 79−87027
MgO bicrystal, fracture mechanism obs. 77−44339
MgO, boundary segregation of Ca, Fe, La and Si 79−70069
MgO, compressive stress-strain behaviour at high temps. 80−25774
MgO, defect aggregation and thermal-electric breakdown, TEM obs. 79−42069
MgO, polycrystalline, grain growth and grain boundary migration, pore effects *(Japanese)* 78−19701
MgO polycrystals, ultrafine-grained, creep microstruct. 80−35246
MgO single crystal, cathodolum. in SEM 79−1440
MgO, subgrain boundaries form. obs. by TEM, diffusion coeff. determ. 80−79817
MgO, ultrafine grained Fe doped, high temp. creep 79−15727
Mg_2Si0_4, etch pits in cleaved faces, revealing low angle boundaries 79−14818
Mg0 bicrystals, electron microscope exam. of secondary grain boundary dislocations in high angle twist boundaries 80−6415
Mn-Al permanent magnets, defect structure, mag. props. TEM obs. 78−91902
Mn-Zn ferrites, grain boundary exam. using TEM and AES 80−107268
MnZn ferrite, MoO_3 addition effect on grain growth kinetics and densification 79−61550
MnZn ferrites, doped; determ. of grain boundary composition, using Auger spectroscopy *(German)* 79−23618
MnZn ferrites, Ti substituted, mag. permeab. meas., grain boundary comp. AES obs. 78−95473
MnZn soft ferrites, commercial grade, microstruct. rel. to mag. props. 80−34009
MnZn-ferroferrites, sintered, microstruct., TEM study *(Dutch)* 80−2036
Mo alloys, intercryst. fracture in ductile-brittle transition region, local internal stresses effect 80−81200
Mo, atomic structure of grain boundaries 79−33003
Mo, block boundary dislocation struct. singularities under high temp. steady state creep conditions *(Russian)* 79−90670
Mo, C doped sheet, electron beam welded, low temp. ductility 79−87685
Mo, cast state, interaction nature between C, O_2 and N_2, influence on struct. and props. *(Russian)* 79−70114
Mo, competition between interstitial atoms during segregation at grain boundaries, AES obs. *(Russian)* 77−25008
Mo filament, coated with thin Ni film, creep and recrystn. *(Russian)* 78−19822
Mo film, evaporated, grain size and resist. 80−88650
Mo film, sputtered, elec. resist., annealing and struct. effects 80−60109
Mo, grain boundaries, electron microscope obs. *(Russian)* 79−4311
Mo, grain boundary segregation of O, atom probe FIM study 80−37134
Mo, grain structure characteristics analysis using Quantimet-720 79−52496
Mo, mech. props., effect of exposure to high temp. He containing O_2, room temp. study 80−93639
Mo, O segregation at grain boundaries, obs. by atom imaging probe 78−21276
Mo polycrystals, grain misalignment, electron microscope determ. *(Russian)* 80−103358
Mo sheet, 45° brittleness due to partial recrystallisation, 45° crack formation and propagation *(Russian)* 79−100238
Mo, single crystals, creep deformed, Burgers vectors, block boundary dislocation struct. *(Russian)* 79−77603
Mo, sintered, grain boundary segregation of S and N 79−56982
Mo, vacancy diffusivity from width of grain boundary void denuded zone 77−47615
Mo-O system, grain boundary segregation and intergranular fracture 80−55516
Mo-O-C system, grain boundary segregation and intergranular fracture 80−55516
Mo-W alloy type MW25N, crystallisation form, globular dendrites, grain boundaries *(Russian)* 80−66494
Mo-W bilayer films on Si substrates, silicides formation, marker expt. 79−99376
Mo-Zr alloys, TsM-6, Zr segregation at grain boundaries, carbide precipitation, X-ray spectral anal. *(Russian)* 79−74154
Na-K(Rb)(Cs), solute atom-grain boundary interaction energy, electron-statistical calcs. *(Russian)* 79−73175
$Na_2Al_2Si_3O_{10}.2H_2O$, natrolite, cleavage etching in acidic and neutral media 80−6407
NaCl bicrystal, grain boundary segregation, Au decoration obs. 77−68982
NaCl, effect of annealing and neutron irrad. on block struct. 80−29061
NaCl, halite, dynamic recrystn. during compression creep, geophys. appl. 80−25772
NaCl, high-temp. deformed, dislocation grain subboundaries *(Russian)* 80−96534
NaCl, impurity precipitation and grain boundary diffusion 80−107567
NaCl polycryst. containing Al_2O_3 dispersion, diffusive creep 80−97531
NaCl, thermal phonon scatt. by low angle grain boundaries 78−67795
NaCl:Ba, Ba precipitation at dislocations, kinetics, ionic cond. meas. 79−60510
NaCl:Ca crystals, surface recrystn., moisture effect 80−84950
$NaNO_3$, crystallite boundary structural instability during solidification *(Russian)* 78−95738
β-Na_2O-CaO-Al_2O_3, impurity conc. at grain boundaries, AES obs. 77−35570
Nb alloy, VN2AE, influence of nitriding on heat resist. and brittleness *(Russian)* 79−8380
Nb, bicrystal, flux pinning by grain boundaries 79−24114

grain boundaries continued
Nb, electromigration *(Russian)* 77−7909
Nb, high purity, faceting of boundaries 78−83826
Nb, pure, cubic, spatial orientation *(Russian)* 77−11567
Nb/Cu-Sn-Mg, superconductor, effect of Mg addition to Cu-Sn matrix 80−25028
Nb-Fe(Co)(Ni)(Os), alloying element influence on strength, ductility, surface and grain boundary energies *(Russian)* 79−74234
Nb-Zr-C, structural depend. of elasticity limit fracture features *(Russian)* 79−29171
Nb_3Al superconductors, sputter deposited, BCC to A15 transition, microstruct. investig. 78−27512
Nb_3Ge films, magnetron sputtered preps. and microstruct. 79−38276
NbN film, ultrathin granular, zero dimensionality and Josephson coupling 78−10612
Nb_3Sn, crit. current ang. depend., prep. conditions effect 77−47949
Nb_3Sn, diffusion-processed layer, texture meas. 79−82726
Nb_3Sn filament, crit. current stress induced degradation 77−24658
Nb_3Sn, flux density gradient determ. by Faraday effect 80−107969
Nb_3Sn, TEM of radiation damage 79−65122
Nb_3Sn, thin film, TEM microanalysis 80−104491
$NdGa_5O_{12}$ wafer, dislocations, etch pits and birefr. obs. 78−83818
$Nd_xZr_{1-x}O_{2-x/2}$, elec. cond. of ceramic solid solutions 80−107554
Ni alloy, recryst. after hot deform. *(German)* 80−25716
Ni alloy, rolled, annealing texture *(Russian)* 77−21159
Ni alloys, recrystallised, grain boundary inheritance and props. 77−59816
Ni coating, electron beam evaporated, ductility and struct. 78−11439
Ni, diffusion of H_2 in single- and polycrystals at 60°C, grain boundary effects *(German)* 80−2211
Ni, diffusion welding, migration of oriented intergranular boundary with pores *(Russian)* 80−84943
Ni, effects of grain size on resist. anomaly near Curie point *(French)* 77−4318
Ni, electrochem. overgrowths, role of substrate dislocations and grain boundaries in nucleation and growth 79−51454
Ni, FCC, polycrystalline, deformation-strain curve description using substruct. parameters *(Russian)* 79−87690
Ni film, low-angle grain boundary struct. *(Russian)* 79−42807
Ni, foil, polycryst., channelling micrographs using accelerators, defects investig. 77−11445
Ni, grain boundaries, mobility, effect of impurities *(Polish)* 79−96073
Ni, grain boundary cavities growth under applied stress and internal pressure 80−29032
Ni, grain boundary defect structure, hardening effects, TEM 80−103365
Ni, grain boundary internal friction, B solid solubility as function of grain size 80−60903
Ni, grain boundary ledge density, effect on flow stress 78−48465
Ni, grain boundary ledges, contrast phenomena identification 78−51555
Ni, grain boundary migration during recrystallisation after cold drawing 77−73289
Ni, grain boundary sliding and deformation mechanism maps 80−3128
Ni, inner layer of high temp. oxide scale, metallographic obs. 80−3240
Ni, oxidation, high temp., effect of C on cavity form., SEM study 80−97638
Ni, oxidation, role of grain growth 77−81337
Ni sheet, surface, adsorbed ^3H, ethylene-^{14}C determ., autoradiography method 77−63989
Ni, splat quenched, gaseous impurities effect on struct. 77−4042
Ni, stress corrosion susceptibility, S segregation effect, Auger spectrosc. study 80−61019
Ni, structure of high-angle (001) CSL twist boundaries 79−46677
Ni, substrate surface effects on C deposition 77−28721
Ni, surface self-diffusion in presence of adsorbed halogens *(French)* 80−24723
Ni, vacancy diffusivity from width of grain boundary void denuded zone 77−47615
Ni, vol. and grain-boundary diffusion of Ag *(Russian)* 78−67863
Ni/Fe layers, interdiffusion, Auger sputter profiling obs. 79−46848
Ni/Pt double layers on Si substrate, silicide formation 78−84010
Ni-Al, grain boundary diffusion in migrating boundaries 79−46830
Ni-Al_2O_3 alloy, electron beam evaporated, struct. and mech. props. 78−11114
Ni-B, grain boundary internal friction, B solid solubility as function of grain size 80−60903
Ni-base superalloy, effects of grain boundary carbides on creep and back stress 80−3130
Ni-base superalloys, powder metallurgical, creep-rupture at intermediate temps. 80−97568
Ni-based superalloys, TEM obs. of cellular transformation products 80−3045
Ni-Co-Cr superalloy, powder produced, necklace struct. development 80−40395
Ni-Co-Cr-Mo-Al, Astroloy, extruded powder metallurgy superalloy, recrystallisation study 79−4976
Ni-Cr, microstruct. effects in low-cycle fatigue tests 77−56108
Ni-Cr, Ni rich, discontinuous precipitation *(German)* 79−91653
Ni-Cr, wrought, fatigue at high temp., microstruct. assessment 79−29208
Ni-Cr (2 wt.%), role of hydrostatic pressure on sintering of creep cavities 79−28980
Ni-Cr (20 wt.%), volume and grain boundary diffusion of Ni and Cr, C effect *(French)* 79−95203
Ni-Cr austenitic alloy, oxidation mechanism, intergranular diffusion effect *(French)* 80−81229
Ni-Cr-Co based alloy, IN-738 turbine blades, hot isostatically pressed investment castings, effect of heat treatment on grain boundary struct. 80−89270
Ni-Cr-Co superalloy IN-792, crack growth resistance, metallurgical effects 77−36655
Ni-Cr-Mg alloy, KhN70VMTYu, Mg effect on grain boundary struct., props. 79−19261
Ni-In, FCC crystals, exam. of volume transform. kinetics of cellular precipitation 79−11625
α-Ni-In, solid solution, lamellar microstructure, influence of grain boundaries on thermal stability 78−72795
Ni-Mo (20.8 wt.%), order, heat treatment effects 80−40406
Ni-S, dil. alloy, AES of grain boundaries *(French)* 80−50477
Ni-Si, intergranular segregation of Si, electron energy loss spectrometers, X-ray anal. *(French)* 79−8388
grain boundaries continued
Ni-Si (12.7 at.%), heterogeneous precipitation at internal and external surfaces during Ni ion irradiation 79−77647
Ni-SiO composite film, acoustic damping capacity and struct. *(Russian)* 77−59070
β-Ni-Zn, eutectoid decomposition kinetics *(German)* 77−8819
Ni-Zn ferrite, grain size depend. of grain boundary sliding *(Japanese)* 80−15120
Ni-Zn ferrite, high temp. behaviour of grain boundaries under bending stress *(Japanese)* 77−1875
Ni-Zn ferrites, polycrystalline, grain boundary slip *(Japanese)* 77−63764
Ni_3Al and $Ni_3(Al, Ti)$, S segregation to grain boundaries 78−48410
$Ni_xFe_{3-x}O_4$, DC and low freq. cond. and influence of microstruct. 80−70699
NiO, ⟨001⟩ tilt boundary relative energy 80−29033
NiO, ⟨100⟩ coincidence twist boundaries energy 80−107270
NiO, grain boundary thermal grooving, mass transport, self-diffusion coeffs. 80−44217
NiO, self-diffusion of Ni, 700-1400°C, rel. to Ni oxidation mechanism 78−27681
NiO, single crysts., annealed, dislocation arrays in low angle tilt boundaries, TEM study 79−37707
NiO-Al_2O_3 system, concurrent meas. of vol., grain boundary and surface diffusion coeff. 77−55399
NiO_2 single crystals, welding, optical and SEM study 79−65097
Ni_xO, film, thermoelec. power, activation energy variation with electrode spacing in DC sputtering 78−76099
$Ni_{0.5}Zn_{0.5}Fe_2O_4$ coarse grain polycryst. ferrite, diffusional creep *(Japanese)* 80−104238
PLZT, ferroelectric domain struct. obs. by SEM and optical microscopy *(Japanese)* 78−15136
Pb and Pb-Tl (2.5 wt.%), grain boundary sliding, grain size and stress effects 78−27571
Pb, cyclic grain boundary migration during high temp. fatigue 80−39111
Pb, film, hillock formation by grain boundary sliding 80−107673
Pb film, thermal strain, strain relax. mech. 79−42427
Pb film, vac. deposited, thermal strain depend. on thickness and grain size 79−90926
Pb, grain boundary self diffusion, microtome serial sectioning anal. 80−79975
Pb, polycrystalline film, electron diffr. evidence by off coincidence grain boundaries 77−47469
Pb thin films, thermal strain, multiple cycling to 4.2K effects 79−90918
Pb-In alloys, flux pinning at grain boundaries 80−34572
Pb-In alloys, vortex pinning on grain boundaries *(Russian)* 77−89910
Pb-In-Au alloy, Josephson junction electrode materials, rel. to strain relax. 79−38255
Pb-Sn, unidirectionally solidified eutectic, lamellar microstructure, influence of grain boundaries on thermal stability 78−72795
Pb-Sn (62 wt.%), intercrystalline and interface boundary sliding, tensile tests, SEM obs. 79−38886
Pb-Sn eutectic, directionally solidified, perfection and stability of lamellar struct. *(French)* 77−77468
Pb-Tl, sliding and its accommodation during creep and superplasticity 77−40436
$Pb_3Fe_2WO_9$, perovskite ferroelec., characts. of dielec. polarisation, influence of oxidation and reduction 77−8496
PbS, chemically deposited film, photosensitivity, effect of morphological struct. 79−82647
$PbSe_xTe_{1-x}$ epitaxial layers, growth, struct., elastic strain and Hall mobility 77−15717
$Pb_{1-x}Sn_xTe$, large non-seeded single cryst. growth by sublimation method, and characterisation 79−78860
PbTe film, elec. transport props., grain boundary pot. 79−42679
PbTe films, thermal cond. and elec. props., 4.2 to 300K 79−28162
n-PbTe, low temp. elec. cond. 80−20227
Pt, elec. cond., impurities on grain boundaries 79−87076
Pt-Au bimetallic films, electron diffraction on networks of grain-boundary and interphase dislocations *(Russian)* 79−73168
Rb-K(Cs)(Na), solute atom-grain boundary interaction energy, electron-statistical calcs. *(Russian)* 79−73175
Sb, semimetallic film, elec. cond., grain boundary scatt. effects 80−103766
Sb-Sn (8 at.%) alloy, grain boundary migration, intergrain liq. layer effects *(Russian)* 77−15633
Sb_2S_3, film, defect struct., electron microscope mode 79−28224
Sb_2S_3 spherolite crysts., direct lattice resolution obs. of defect struct. 80−107255
Sc_2O_4, polycryst., form. conditions of anion vacancies, phase comp. 80−54220
Si, bicrystals, grain boundary states and varistor characts. 80−24829
Si, CVD film, transport props. 79−24089
Si CVD grown polycrystal recrystallisation 78−64560
Si, CVD on graphite, zone melting, grain boundary conc., rel. to solar cell efficiency 77−85945
Si, CVD polycryst. solar cell, grain boundary effects rel. to dopant conc. 77−7744
Si, cast, growth structure and photovolt. props. of solar cells 80−94008
Si, cast polycryst. p-n junction solar cell, hydrogenation effects 80−93916
Si, dendritic film growth on alumina, solar cell appls. 77−77432
Si, enhanced conductivity in plasma hydrogenated films, thermionic emission 80−70692
Si epitaxial layers on metallurgical-grade polycryst. substrates, characteris. 79−28967
Si, epitaxial regrowth and grain struct. of Al metallisation on ⟨100⟩Si 78−79901
Si films, ribbon-against-drop process, physical and chemical characterisation 80−92798
Si, grain boundary defects in thin semicrystalline material 80−93889
Si, grain boundary elec. props./impurity correl. using surface anal. of multigrained samples by SIMS and AES 80−79816
Si, ion implanted, damage struct. obs. using TEM and cross section specimens 80−107298
Si, multigrained, grain boundary elec. and compositional props., surface anal. 80−76575
Si, multigrained, impurity segregation to grain boundaries, AES and SIMS obs. 80−65027

grain boundaries continued
Si, neutron transmutation doped, zero-bias resist. of grain boundaries 78−76072
Si, orientation anal. of polycrystalline samples 79−1438
Si, phonon scattering at low-angle grain boundary 79−77708
Si, poly crystalline, electronic behaviour of grain boundaries, solar cell appl. 80−92859
Si, polycryst., elec. and photovolt. props., grain size effects 80−49800
Si, polycryst. films, transport props. and grain boundary charact. by TEM 80−50980
Si, polycryst. p-n junction solar cells, grain-boundary and intragrain recombination currents 80−81442
Si, polycryst. p-n solar cell, influence on recombination 80−93913
Si, polycryst. solar cell, effect on device charact. 80−93914
Si, polycryst. solar cell, relative orientation of grains and nature of grain boundaries 80−93915
Si, polycrystalline, grain growth study 78−92188
Si, polycrystalline, grain boundary effects on minority-carrier diffusion length and solar-cell efficiency 79−48124
Si, polycrystalline, grain boundary obs. by TEM, solar cell appl. 80−72057
Si, polycrystalline, large grain size, gross defects effect on effective carrier lifetime 77−80793
Si, polycrystalline, neutron transmutation doped, grain boundary zero-bias resistance 79−15153
Si, polycrystalline, passivation of grain boundaries 79−56158
Si, polycrystalline, phenomenological model for mobility 80−65564
Si, polycrystalline, solar cells, grain-boundary hydrogenation technique for improvement 80−85273
Si, polycrystalline barrier heights and passivation of grain boundaries 80−93890
Si, polycrystalline Czochralski-grown, MIS solar cell characterisation using scanned laser response exam. 80−93884
Si polycrystalline film, effect of defects/grain boundaries on photovoltaic mech. 80−93883
Si resistors, polycryst., elec. props. in nonlinear regime, grain boundary trapping model 79−38204
Si ribbon crystal evaluation for solar cells 77−76813
Si ribbon grown by capillary action shaping technique, electron channelling analysis 77−76418
Si ribbons, capillary action shaping tech., lifetime charact. 78−34847
Si, ribbons produced through capillary action shaping, elec. and struct. characts. 78−47804
Si, semicrystalline layer, deposited on stainless steel and Pyrex glass, growth conditions and props. 79−82482
Si, sintered, grain boundaries, TEM obs. 80−15118
Si solar cells, low-cost sheet fabrication structural defects, effect on electronic props. and cell performance 80−50977
Si solar cells, polycrystalline p-n junctions, recombination currents, physical models 80−93892
Si, thermionic electron emission, from defect states at grain boundaries 79−91559
Si:Al, polycryst. film, grain boundary diffusion, Auger sputter profiling 80−75388
Si:As, polycrystalline, As segregation at grain boundaries, elec. props. meas. 80−75259
Si:O, O rich polycryst. film, carrier transport 78−80076
Si:P, polycryst. films, elec. props., EPR, defect states, doping effects 80−75660
Si:Sb(P)(B)(Ga), low angle boundary formation, in single crysts., effect of impurities on cryst. growth conditions 80−11555
Si/Al and Si/Al-Si(Cu), rel. to Si regrowth minimisation through overlying Al or Al alloy film 80−70569
Si-Al system, Si regrowth minimisation methods in Al films 80−15384
Si-Al-O-N, high-temp. fracture and diffusional deform. mechanisms 80−40509
Si-Al-O-N ceramic, grain boundary desegregation and intergranular cohesion 80−100872
Si-Al-O-N system, stable phase cryst. struct. and microstruct. obs. using TEM 80−108421
Si-Fe, domain and grain obs. using ferromag. colloid technique 80−11219
Si-metal contact, transport theory of Schottky barriers 80−80372
SiAlON, prepared from siliceous sand and Al powder, hot pressing, steatite contamination effects *(Japanese)* 80−93528
SiC, high-temp. creep interpretation by deform. mapping techniques 77−21230
SiC, hot pressing, addition of B, B_4C and Al_2O_3 77−24999
β-SiC, polycryst., ^{30}Si self-diffusion 80−100350
β-SiC, sintering, B transport and lattice parameter change 80−108370
Si_3N_4, engng. ceramic, lattice resolution studies 78−27510
Si_3N_4, hot-pressed, impurity phases, TEM obs. 79−8260
Si_3N_4, hot-pressed with crystn. grain boundary phases, prep. 78−95715
Si_3N_4, MgO-fluxed, hot pressed, grain boundary phases 78−27464
Si_3N_4, reaction-bonded and hot pressed, deform. and fracture during creep 79−38916
Si_3N_4, thin intergranular phase, imaging by high-resolution electron microscopy 79−90895
Si_3N_4 with Y_2O_3 and Al_2O_3 additions, hot pressed, exam. of mech. props., grain boundary crystallization 79−20009
Si_3N_4:$(MgO+Al_2O_3)(Y_2O_3)$, hot-pressed and sintered, microstruct. and impurity distrib. 80−49261
Si_3N_4-Al_2O_3, hot-pressed with crystn. grain boundary phases, prep. 78−95715
Si_3N_4-Al_2O_3, hot-pressed with crystn. grain boundary phases 78−95716
Si_3N_4-MgO, compressive creep, source of viscoelastic effect 80−50675
Si_3N_4-MgO (5 wt.%), microstructural changes during gas pressure sintering *(Japanese)* 77−12589
Si_3Ni_4, hot pressed, MgO fluxed, grain boundary phases, lattice fringe imaging obs. 79−11540
Si(111):Pb ion implanted amorphous layers, recrystallisation, impurity out-diffusion model *(Chinese)* 80−88363
Sn, binding state of atoms segregated at boundary of Fe and Fe alloys, Mossbauer study 80−7232
Sn film, evaporated on cooled substrate, grain boundary scatt., depend. on annealing temp. 79−65561
Sn film, polycrystn., grain boundary scattering rel. to annealing temp. 79−65560
Sn-Ni electrodeposited equatonic alloy, cryst. struct., X-ray, electron diffr. anal. 80−79748
grain boundaries continued
Sn-Pb eutectic, strain rate sensitivity of flow stresses, grain boundary sliding during superplastic, non-superplastic deform. 80−7645
SnO_2-polySi solar cells, fabrication, grain size effects on device parameters 80−94045
Te film, polycryst., hole mobility, influence of tunnelling through barriers on grain boundaries 77−43748
Te, screw dislocation substruct. studied by torsion expt. 79−10859
ThO_2-CaO electrolyte, grain boundary effects in cond. region 77−8156
α-βTi alloys, high strength, heat-treated weldments, intergranular fracture 80−21097
α-Ti, cold rolled, primary recrystn., in situ investig. in HVEM 80−104185
Ti, metallographic specimen prep. for chem., mech. electrolytic polishing 78−80705
α-Ti, S, C and Cl diffusion, AES meas. 78−51735
Ti, surface and grain boundary free energy, zero-creep determ. 79−4313
Ti, type 70A, containing 0-6000 ppm ^3He, sensitivity of tensile props. 80−39197
Ti-Ag (10 to 17.5 wt.%), eutectoid system, $\beta \rightarrow \alpha_m$ transform., nucleation kinetics 80−97474
Ti-Al (14 at.%), with precipitate free zones, tensile props., grain size effects 77−16690
Ti-Al (14.4 at.%), void form. and solute segregation under Ni ion irradiation 79−42122
α-βTi-Al-Sn-Zr-Mo (6, 2, 4, 6 wt.%), deformation associated with surface cracks and α particles 79−79107
Ti-Al-Sn-Zr-Mo (6,2,4,6 wt.%) fusion weldment, substruct. characts. 80−84183
Ti-Al-V, containing 0-6000 ppm ^3He, sensitivity of tensile props. 80−39197
Ti-Al-V (6,4 wt.%), surface and grain boundary free energy, zero-creep determ. 79−4313
Ti-Al-V (6,4 wt.%) superplastic deform. 78−31471
Ti-Al-V-Sn (6, 6, 2 wt.%) weldments, heat treated, transangular fracture 80−40524
Ti-Al-V-Sn (6, 6, 2 wt.%), fatigue crack growth, cyclic freq. and microstruct. influence 80−55515
Ti-Al-V-Sn (6,6,2 wt.%) fusion weldment, substruct. characts. 80−84183
Ti-Au, (9.9 wt.%), eutectoid system, $\beta \rightarrow \alpha_m$ transform., nucleation kinetics 80−97474
Ti-V-Si (30, 1 at%), quenched and aged, hardness, tensile behaviour and phase transform. 79−11646
α_m-Ti-X (X=Ag, Au, Si), precipitation mechanisms and Meyrick theory of cellular reaction initiation 79−74163
TiC-steel alloy, struct. form. during sintering, strength, rel. to heat treatments 77−59717
TiO_2:Si(Fe)(Mn)(Cr)(Ni), anodes, low breakdown voltage due to electron tunnelling via grain boundaries 79−74407
UO_2 and UO_2-Ni, surface, grain boundary and interfacial energies 78−21649
UO_2, high burnup nuclear fuels, relation between fission product release and fuel microstruct. 80−57845
UO_2 irradiated, grain edge porosity growth 79−19285
UO_2, nonstoichiometric, surface and interfacial props. 77−69161
UO_2 nuclear fuels, fission gas release at high burn-ups 80−57852
UO_2, resolution of fission gas from grain edge bubbles, porosity effect 79−85607
UO_2, surface energy *(German)* 79−7742
UO_2, swelling and gas release at low and intermediate temps. 77−50241
UO_2, transfer of fission gas between grain faces and edges 78−79815
UO_2-(Ni), surface, grain boundary and interfacial energies 78−71905
$UO_{2+\alpha}$, ternary sintering diagram, grain boundary diffusion 79−59234
V, different grain sizes, room temp. microstrain *(German)* 77−36614
V-Be diffusion couple, ion backscatt. anal. 77−35752
V_3Ga, diffusion-processed layer, texture meas. 79−82726
V_3Ga layer on bronze, diffusion of Ga *(Russian)* 80−65297
V_3Si, H_{c2} anisotropy in high field, grain boundary flux pinning 78−43532
V_3Si, neutron irrad., grain boundary pinning, field-depend. change of crit. current density 80−65759
W, block boundary dislocation struct. singularities under high temp. steady state creep conditions *(Russian)* 79−90670
W, cast state, interaction nature between C, O_2 and N_2, influence on struct. and props. *(Russian)* 79−70114
W, competition between interstitial atoms during segregation at grain boundaries, AES obs. *(Russian)* 77−25008
W, distribution of C, effect of grain boundary free energy *(Russian)* 77−90351
W filament, coated with thin Ni film, creep and recrystn. *(Russian)* 78−19822
W foil, electron diffr. effects and images from inclined grain boundaries 79−82241
W, grain boundary migration initiated by high hydrostatic press. 78−51554
W, incoherent twin boundary microfaceting on annealing, field ion microscope determ. 79−77608
W, recrystallisation of commercially pure and doped wire drawn to high strain 79−100165
W, single crystals, creep deformed, Burgers vectors, block boundary dislocation struct. *(Russian)* 79−77603
W, texture and grain boundary struct., primary misorientation function 79−1877
W, texture and grain boundary struct., primary misorientation function 79−1875
W, texture and grain boundary struct., primary misorientation function, expt. deform. 79−1876
W wire, AKS-doped, second phase particle obs. by TEM, SEM and atom probe microanalysis 80−108457
W, wire, doped, heavily drawn, recrystallisation 77−16609
W, wire, doped, high temp. creep behaviour 78−88499
W, wire, exam. of grain boundary segregation, using Auger spectroscopy, new technique 78−80551
W wires, KSiAl doped cavity formation *(German)* 78−31524
W, with impurities, effect on high temp. plasticity *(Russian)* 79−79057
W-Cr alloys, segregation of Cr to gain boundaries, field ion microscope investigation 77−8816
W-K-Si-Al doped wires, heavily drawn, fibre struct., annealed 79−56993
W-Mo, vapour deposited, long-term strength and thermocyclic creep 80−16405

grain boundaries continued
W-Ni powder compacts and wires, recrystallisation, influence of omnidirectional press. *(Russian)* 77−8849
W-Th, atomic structure of grain boundaries 79−33003
WC-Co, STEM anal. of grain boundaries 80−79644
WC-Co and WC-Co-TaC-TiC-NbC cemented carbides, microstructure, high temp. deformation, uniaxial plastic compression 80−40451
YIG, deformed at high temp., subgrain boundaries and dissociations of dislocations, TEM obs. 79−90658
Zn, activationless motion, group co-operative transition mechanism 80−2039
Zn alloys, anodic corrosion in seawater 77−77628
Zn, background damping in vicinity of grain boundary peak 77−28843
Zn bicrystal, diffusionless motion of grain boundaries, 200-405°C 79−19264
Zn bicrystals, $\langle 10\bar{1}0\rangle$ tilt, misorientation depend. of grain boundary sliding 80−15119
Zn bicrystals, grain boundary slip in deform. 80−34008
Zn film, RF sputtered, carrier reflection coefficient determinaton 79−42674
Zn, grain boundary detachment from adsorbed impurity, conc. depend. 78−2144
Zn, grain boundary nonactivated motion vel., orientation depend. *(Russian)* 80−84180
Zn, hot rolled, grain boundary fine structures, TEM exam. 78−76680
Zn, incompatible bicrystals, effect of grain boundaries on mech. props. *(Japanese)* 78−39798
Zn, low angle boundary decomp., dislocation struct. control *(Russian)* 78−3142
Zn, Zn-Sn and Zn-Sn-Pb, intergranular and solid-liquid interfacial tensions 77−36452
Zn-22 wt.% Al superplastic eutectoid alloy tensile deformation obs. *(Japanese)* 79−90714
Zn-Al, dislocation slip peculiarities during superplastic deform. 79−20102
Zn-Al (0.4 wt.%), intergranular slip during in situ superplastic deform. 80−96538
Zn-Al (1.1 wt.%) superplastic alloy, grain size determ. *(Czech)* 80−81118
Zn-Al (22 wt.%), positron diffusion and trapping at grain boundaries 80−39157
Zn-Al (22 wt.%), superplastic, of very high purity, cavitation 79−24586
Zn-Al (22 wt.%) eutectoid, superplastic, grain size effect on plastic deform. at room temp. *(Japanese)* 78−31462
Zn-Al (22 wt.%) superplastic alloy, grain growth texture 80−81075
Zn-Al alloys, dislocations obs. in superplastic deformation 78−51549
Zn-In(Bi) interfacial tension and microstruct. 79−74132
$Zn_{1-x}Cd_xS$, reactively sputtered polycryst. film, cond. mechanism and grain boundary barriers *(French)* 77−76972
ZnO based varistors, nonlinear cond. theory 79−78192
ZnO ceramic, nonohmic, drift phenomena of capacitance and current 80−39587
ZnO, ceramic varistor, physical props. of elec. barriers by AES and electron microscopy 77−20326
ZnO ceramic varistors, I-V characts., single grain junction meas. 79−15225
ZnO ceramics, microstructural evaluation 79−55750
ZnO, segregation of Li_2O at grain boundaries 78−64513
ZnO varistor ceramics, current-voltage characts., inhomogeneities and single barriers 80−80273
ZnO varistors, statistics and grain size effects on breakdown characts. 80−34010
ZnO:Ba, Co, rare earth metal varistors, microstructure-prop. relations 80−100249
ZnO-Bi_2O_3 varistor, grain boundary segregation, STEM study 79−78980
ZnO-Bi_2O_3-Sb_2O_3-Co_2O_3-MnO_2-Cr_2O_3, nonohmic ceramic, microstruct. exam. 78−47292
ZnO-grainboundary-ZnO junction in ceramic varistor, capacitance-voltage characts. 80−65689
ZnS, cryst. grown from melt under press., microstruct. 77−59019
ZnS film, vac.-deposited, origin of mech. stress 79−90925
ZnS, twist boundary struct., atomic scale electron microscopy obs. 80−107276
ZnSe, electron beam induced current study of grain boundaries by SEM 80−59479
ZnSe, single crysts., grown from melt under Ar pressure, defects form. 79−4312
ZnTe, elec., SEM and TEM studies of impurity segregation during long annealing 80−30001
ZnTe:Li, diffusion investigation by SEM and TEM 80−10706
Zr alloys, creep and growth, irradiation induced, rate theory approach 80−89294
Zr alloys, creep and growth, irradiation induced, microstruct. depend. 80−93602
Zr base alloys, irradiation growth, dislocation model 78−51595
α-Zr, grain-boundary sliding component in high temp. fatigue 80−50706
Zr, irradiation growth, reaction rate theory calcs. 80−88212
Zr-Nb microduplex alloys, struct. and props. 78−3170
Zr-Ru(Pd), heat treated, mech. props. and struct. 78−80571
Zr-Sn, grain-boundary migration during fatigue at 600 to 775°C 80−16443
β-Zr-Sn, zircaloy-2, exam. of grain boundary sliding 78−79616
Zr_3Al, $L1_2$ phase yield strength 78−19811
Zr_3Al, ordered polycrystals, ductile fracture 78−64641
ZrC, high-temp. strength, affecting factors 77−63794
ZrC_x, micro X-ray spectral anal. of boundary zones 79−8301
ZrO_2:CaO, polycrystalline, grain boundary enhanced interdiffusion, flux density eqn. 80−29220

grain boundary diffusion *see diffusion in solids*

grain growth
alloy, binary, theory for initial stage of grain growth and unmixing kinetics 78−19714
alloy, coarsening by temp. cycling 79−29111
alloy, cubic, computer simulation of formation of tweed and modulated structs. 79−96029
alloy, solid state reactions, effect on microstruct. 79−29015
alloy, two-phase, recrystallisation mechanisms 79−47708
anomalous, mathematical simulation *(Russian)* 77−55972
Astroloy, grain coarsening by critical strain annealing 79−47711

grain growth continued
Babbitt grade Bk-2Sh, improvement in antifriction layer props. by impulse discharge *(Russian)* 79−1917
coarsening kinetics by ledge mechansism 79−46805
computer simulation, of steady-state and dynamic grain growth and grain size distribs. 79−38836
computer simulation of normal grain growth 79−11546
discontinuous, pore drag 77−44203
eutectic, irregular, branching limited growth 80−81042
FBR oxide fuels, dynamic response of grain boundary cavities to stress and temperature changes under conditions of continuous gas generation 80−66544
grain boundary cavities, star-shaped unstable growth 79−46679
grain growth 77−36520
Inconel 718, grain growth during sintering 80−97449
Johnson-Mehl and cellular microstructure, comparative analysis, computer simulation 80−54392
kinetics of normal grain growth 80−71661
lenticular martensite growth by transformation wave propag. 80−81055
liquid phase sintering, elementary mechanisms, soln.-reprecipitation 80−50571
LWR fuel rods containing fission gas, grain growth 79−67866
massive transformations, free energy, microstruct., growth and nucleation 77−4776
metal, oxidation kinetics, effects of control of scale structure 77−16751
metal, sintered compacts, residual pore effect on grain size distrib. 77−85961
metals, grain struct. form. during two-dimensional recrystallisation, simulation on electronic calc. machine *(Russian)* 79−87666
mica, deformed, syntectonic nucleation of new grains 79−65102
microstrùcture alterations and texture form. in normal grain growth, computer simulation 79−90679
migration of grain boundaries, group mechanism *(Russian)* 77−80514
Nimonic PE16, abnormal grain growth after cold working and annealing 79−74176
nucleation, criterion for dynamic recrystallisation during hot working 78−52852
platelet growth and stereological characterization of plates 80−55404
powdered compact, densification model with simultaneous grain growth 78−80486
recrystallisation, conf., Leeds, England (April 1978) 79−47706
recrystallisation, in situ studies, appl. of X-ray synchrotron topography 78−35610
rolling, critical reduction, effect on chemicothermal treatment processes 77−70073
sapphire filaments in Al_2O_3:MgO matrix, single cryst. boundary migration 80−44369
secondary nucleation, influence of crystal brittleness and degree of supersaturation using in growth *(Italian)* 78−23836
single crystal growth during massive transformations 78−56629
sintering, liquid phase, computer simulation of chemically driven grain growth 80−55427
sintering, packing fraction effects *(German)* 78−64494
snow, wet, grain clusters obs. 80−26553
soap foam, arrangement of cells in a net rel. to grain sections of polycryst. 80−70225
steady state grain growth, concept of sweep constant 79−38837
steel, 18H2N4WA, hot-worked, kinetics of austenite grain growth, rel. to deformation degree *(Polish)* 80−45322
steel, 18Kh2N4MA, Co effect on struct., and mech. props. 78−44147
steel, 30N9K4, effects of Mo, V, and N on grain growth, tempering, hardenability, strength and toughness 78−44202
steel, 36NKhTYu, ageing to produce ultrafine grains, discontinuous precipitation *(Russian)* 77−81277
steel, alloy, Cr-C (12, 0.2 wt.%) growth of grain boundary ferrite allotriomorphs, photoemission electron microscope exam. 78−88468
steel, alloy structural, anomalous grain growth 80−20984
steel, austenitic, Cr-Ni (25, 20 wt.%) recrystallisation and sigma phase formation 80−35211
steel, austenitic, grain growth in 16G2S. 16G2SF, AND 09G2SF, As effect 77−70060
steel, austenitic, high-speed, austenite grain growth, W addition effects 79−20085
steel, austenitic stainless, estimation of grain growth time dependence, activation energy 78−72787
steel, austenitic stainless, grain boundary struct. during recrystn. and grain growth 80−76270
steel, austenitic stainless, grain growth kinetics, effects of C content and rolling *(French)* 77−81269
steel, C, austenitic, recrystallisation and grain growth obs. with photoelectron microscope 79−47730
steel, C, recrystallization annealing, grain growth, effect of type of deform. 80−100847
steel, Co (2 wt.%), effect of Co on pearlite growth 77−90359
steel, constructional, austenite grain shape eval. method 78−35607
steel, Cr (25 wt.%) recrystallisation annealing, surface structure investigation in polarised light 77−28947
steel, Cr-Ni (16,14 wt.%), Si effect on texture, grain growth after rolling or recrystallisation *(French)* 77−55986
steel, extra-mild rimming, thin sheet, grain growth in the recrystallisation *(French)* 79−70074
steel, Fe-Cr-C, austenitizing temp. effect on microstruct. and mech. props. 80−16341
steel, ferritic stainless, type 444 welds, ductility loss mechanism 80−85002
steel, low C, ferrite grain nuclei form. during polymorphic transform. *(Russian)* 80−50626
steel, low C, Mn, recrystallisation and grain growth in hot rolling 79−47714
steel, low C, Ti-stabilized, recrystn. texture development 79−83231
steel, low-alloy, austenite grain growth, role of V, Nb, N alloying additions 77−44255
steel, low-C, structural, with Zr impurities, grain boundaries, AES 79−24524
steel, medium C, static and dynamic stress effect on hardenability and grain growth *(Korean)* 78−35404
steel, mild, sheet, with low Al content, annealing, AlN recrystn., precipitation kinetics *(French)* 79−20083
steel, multilayered with types St2kp and 10Kh18N10T, secondary recrystallisation props. *(Russian)* 80−66533

grain growth continued
steel, N_2 effect on grain boundary migration rate during secondary recrystallisation *(Czech)* 77−59812
steel, Nb,(V),(Al), hot-rolling, laboratory simulation, recrystn. of austenite 80−97512
steel, Nb, high and medium C, austenite grain growth 78−11249
steel, pearlitic structural, austenite grains, growth rate during heating 80−100860
steel, stainless, austenitic grain growth, annealing twins role 79−57016
steel, stainless, grain growth after deform. by rolling, C effects on kinetics *(French)* 77−28866
steel, stainless, maraging, grain growth, temp. effect 79−57019
steel, stainless 304L, sintering, effect of grain growth and boundaries on shrinkage rate 77−36419
steel, transformer, textural barriers to grain growth after cold rolling and annealing *(Russian)* 78−39796
steel, type 37KhN3MF, austenite grain growth depend. on structural inheritance *(Russian)* 79−61582
steel, unkilled deep drawing sheets, influence of N content on recrystn. *(German)* 80−40376
steel, W-Mo, sintered high-speed, naphthalenelike grain form., quenching effect on fracture toughness 80−30103
steel fibre reinforced Ag, exam. of recrystallisation behaviour *(German)* 78−84849
steel ShKh15, austenite, grain growth, melting procedure effects 77−12650
steels, low alloy, grain boundary anal.,, H_2 embrittlement, scanning AES 79−43256
strengthening phase particle distrib., quantitative analysis 78−15629
subgrain growth by boundary migration 77−76417
superalloy, hot consolidation of rapidly solidified powders, review 79−33965
superplasticity, region I characteristics 80−107357
supported metal catalysts, particle growth, models 77−8830
supported metal catalysts, particle growth, obs. of Pt on alumina 77−8831
texture development in grain growth, computer simulation 79−96036
texture formation during anomalous grain growth *(Russian)* 77−55984
textured matrix, theory *(Russian)* 77−81273
TNT, creamed, dimensional stability, irreversible thermal expansion 79−73316
Ag, grain growth in strained {110}<112> low stacking fault FCC crystals after artificial nucleation 79−91722
Ag halogenide, grain form. and growth in metastable soln. *(Russian)* 77−34048
Ag, sintering and grain growth, effect of Sb solute addition 78−84730
Ag, tensile deformed, dynamic recrystn. *(German)* 80−84959
AgBr emulsion, model system, Ostwald ripening obs. 77−2707
Al and Al-Mn (1 wt.%), subgrain growth during annealing after cold work 78−56656
Al, cold rolled bicrystal, plane grain growth anisotropy 79−91686
Al, deformed, struct. and recrystallisation transmission Kossel diffr. obs. 77−52340
Al, pure elec. cond. grade, substructural developments during recovery, Sandstrom's model validity 79−74187
Al, recrystallisation kinetics after small deform. and grain growth *(Czechoslovakian)* 77−32592
Al-Cu alloy, vacuum deposited thin film, abnormal grain growth before melting transition and subsequent struct. change 79−60663
Al-Mg_2Si (1 wt.%) secondary recrystallisation by grain boundary unsewing 79−1886
Al-Ni (6 wt.%) alloy, misorientation between subgrains, second-phase particles role, STEM microdiffr. obs. 80−104415
Al-SiO_2, Al-SiO_2(SiO)-Si, solid-state reaction mechanism 77−52623
Al-Ti-C, grain refinements study using centrifugal force *(Japanese)* 79−20035
Al-Zn (22 at.%), rel. to segregation, X-ray scatt. expts. *(French)* 79−96032
β''-Al_2O_3, conductive, Li_2O stabilised, sintering and annealing 77−59724
Al_2O_3, sintered, MgO-enhanced densification, test of second phase and impurity segregation models 78−64511
Al_2O_3 substrates, grain growth during sintering 80−40302
Al_2O_3, translucent, fabrication by high press. sintering 78−11167
Al_2O_3:Fe, pore form. during oxidative annealing, grain growth slowing 80−100856
Al_2O_3-MgO, MgO addition role in sintering 79−91608
Al_2O_3-MgO-Cr_2O_3, effect of Cr_2O_3 on surface grain growth 79−23815
β''-Al_2O_3-Na_2O solid electrolyte, heat treatment effects on ionic cond. and microstruct. 80−65293
BC, sintered, struct. and props. 80−104181
BN, cubic struct. form. from hexagonal struct. at high press., catalytic effects *(Japanese)* 77−90308
BaO.n Fe_2O_3, magnet, effect of SiO_2 on texture and densification behaviour *(German)* 79−24631
$BaTiO_3$, thin film, obtained by modified doctor blade method grain orientation *(Japanese)* 77−77455
$BaTiO_3$:La, Sb, second phase effect on elec. and mag. props. 80−60986
$BaTiO_3$:Mn, polycrystn., annealing effect on transition temps. 80−3100
$BaTiO_3$-PbO-B_2O_3, liquid phase sintering, effect on props. *(German)* 79−33980
$(Ba_{1-x}Y_x)TiO_3$ ceramic, resistivity rel. to donor dopant content 79−65474
Be, ultra fine-grained, recrystn. after deform. 79−52239
α-brass, defect removal, obs. by positron annihilation 78−84677
$CaTiO_3$, perovskite, raw material activity and firing conditions as factors in sintering and grain growth 79−83161
Cd electrodeposition on Cu electrode, conditions for granular growth 80−55310
Cd, polycrystn., annealed, effect of hydrostatic pressure on grain size, growth and boundary mobility 79−37717
Cd-$CuCd_3$, off-eutectic alloys, controlled grain growth *(Japanese)* 77−55958
CdSe thin film transistor on Cr substrate, cryst. struct., substrate defect effects 80−70563
Co-Sm magnets, H_2 atm. sintering effect on mag. props. 77−85504
Cr, interaction with dense stream of N ions, metallography, microhardness, specific volume *(Russian)* 80−15169
Cr_2O_3, active, block growth in crystallisation 77−85972
Cr_2O_3, grain growth during sintering *(Japanese)* 80−16261
Cu, defect removal, obs. by positron annihilation 78−84677
grain growth continued
Cu, foil recrystallisation during annealing in high voltage electron microscope, grain growth *(Russian)* 79−100159
Cu, grain growth during isothermal annealing *(Russian)* 79−52259
Cu, grain growth in strained {110}<112> low stacking fault FCC crystals after artificial nucleation 79−91722
Cu, grain growth rate, 520-970°C *(Russian)* 80−29972
Cu, high purity, recrystallisation kinetics *(Russian)* 78−11238
Cu, recrystallisation kinetics after small deform. and grain growth *(Czechoslovakian)* 77−32592
Cu, recrystallization annealing, grain growth, effect of type of deform. 80−100847
Cu, recrystallization diagram for fine grained metal in region of small deform. *(Czech)* 77−59811
Cu single crysts., deformed, HVEM study of recrystn. texture 80−104179
Cu-Be (2 wt.%), alloying addition effects on grain boundary reaction *(Japanese)* 80−49236
β-Cu-In, unidirectionally transformed eutectoid, lamellar microstructure, influence of grain boundaries on thermal stability 78−72795
Cu-In eutectoid, coarsening at 829K 79−1885
Cu-Sb, dil., grain growth rate, 520-970°C *(Russian)* 80−29972
Dy, recrystallisation *(Russian)* 77−24946
Er_2O_3-Ta, oxide grain growth at interface 77−81245
Fe, (100) [001], texture development by recrystallisation and normal grain growth 78−27539
Fe alloy, (110) [001] texture development by recrystallization and normal grain growth 77−32594
γ-Fe alloy, supersat. solid soln., recrystn. inhibition by cold rolling 77−73286
Fe, cast-Mg, 78−44149
Fe, grain growth, normal and abnormal, statistical distrib. of linear grain sizes 80−93581
Fe, grain growth kinetics under 2 to 10% tensile deform. 77−40435
Fe, interaction with dense stream of N ions, metallography, microhardness, specific volume *(Russian)* 80−15169
Fe, pure, grain growth, abnormal, kinetics 79−24537
Fe, zone refined, strained, substructural changes during annealing *(Slovenian)* 78−84845
Fe-C (4.3 wt.%), splat cooled, amorphous phase form. and crystn. 77−15323
Fe-C-Si(Co), eutectoid alloy, Si and Co addition effects on pearlite growth rate 77−16575
Fe-Co-Si (4,1.5 wt.%), textured, mag. props. 80−35200
Fe-Cr (17.3 wt.%), oxidation at 1000°C, alloy grain growth effect 78−7075
Fe-Cr-Al, elec. heating alloy, effect of rare earth additives on quality *(Chinese)* 78−84825
Fe-Cr-Al(-Y) alloys, oxide grain morphology and growth mechanism 80−3239
Fe-Cr(W)-M, (M=Si,Mo,Ni,Mn,P,Cr), cellular growth of S-pearlite formed by carburisation 80−108486
Fe-Cu alloy, vapour-deposited, struct. and thermal stability 78−43265
Fe-M, (M=Cr,W,Mo,V,Ti), morphology and growth kinetics of δ-pearlite formed by carburisation 80−108485
Fe-Ni, secondary recrystallisation singularities *(Russian)* 80−66528
Fe-Ni (50 wt.%), secondary recrystallization 78−23723
Fe-Ni alloys, graim growth texture 79−91687
Fe-Si, (3wt.%) alloys, grain boundary anal.,, scanning AES 79−43256
Fe-Si, grain oriented, with unique inhibition system for texture development 77−90366
Fe-Si, recrystallization, in situ studies, appl. of X-ray synchrotron topography 78−35610
Fe-Si (3 wt.%), Al-bearing, grain-oriented, N_2-H_2 annealing effect on texture, mag. props. 77−12714
Fe-Si (3 wt.%), AlN-inhibited, Se effect on primary grain recrystallisation 77−12715
Fe-Si (3 wt.%), behaviour of disperse inclusions, influence of recrystn. processes *(Russian)* 80−66519
Fe-Si (3 wt.%), containing B, grain boundary segregation, AES evidence 77−86046
Fe-Si (3 wt.%), grain growth inhibition by MnS spherical particles with size distrib. 80−35218
Fe-Si (3 wt.%), grain oriented, MnS-AlN-inhibited, precipitate morphology 77−12648
Fe-Si (3 wt.%), grain oriented, mag. props., effect of decarburizing *(Chinese)* 80−103821
Fe-Si (3 wt.%), orientation distrib. in primary recrystallised textures, mag. permeability 77−12712
Fe-Si (3 wt.%), secondary recrystn., struct. inhibition, permeability improvement 77−12713
Fe-Si (3wt.%), grain-oriented, secondary recryst., grain growth inhibition 80−89245
Fe-Si steel, high permeability, processing effect on recrystn. and deform. 77−12716
Fe-Si-B, high induction alloy, improving mag. props. by adding B to coating 79−83338
Fe-Si-B, melt C content effect on grain growth and induction 80−35351
Fe-Si-B-N-S, B, S, N effects on grain boundary segregation and grain growth inhibition, review 80−3047
Fe-Si-B-S, grain-oriented, high induction, B and S addition effect on magnetic props. *(Slovak)* 79−4697
Fe-V(Cr)(Mn)(Ni), unlimited component solubility, intercrystallite internal adsorption *(Russian)* 80−39294
Fe_4N growth kinetics in Fe-N system *(Korean)* 80−93540
α-Fe_2O_3, crystalline grain growth during heat treatment 78−11252
Ge, amorphous film, large aligned grain solid-phase growth during scanned laser crystallisation 80−49100
Ir-W (0.3 wt.%), grain growth, temp. and time effects 79−100186
$LiNbO_3$-CdO, CdO addition effect on sintering 79−83157
Mg, recrystallisation after cold rolling 78−72790
MgO (:CaO) powder compacts, grain growth microstruct. changes on sintering, SEM study 79−78918
MgO, polycrystalline, grain growth and grain boundary migration, pore effects *(Japanese)* 78−19701
MgO-C dispersion, creep, effect of C on grain size and growth 79−100213
(Mn,Zn)Fe_2O_4:Si, Ca, Ti, second phase effect on elec. and mag. props. 80−60986
Mn-Al-C, fine-grained cast struct., remanence and coercive force 80−60365

grain growth continued
MnZn ferrite, MoO_3 addition effect on grain growth kinetics and densification 79−61550
MnZn ferrites, doped; determ. of grain boundary composition, using Auger spectroscopy *(German)* 79−23618
MnZn ferrites, impurity induced exaggerated grain growth 78−92222
$MnZnFe_4O_8$, duplex struct. formation during sintering, grain growth study 79−11541
Mo filament, coated with thin Ni film, creep and recrystn. *(Russian)* 78−19822
Mo film, evaporated, annealing behaviour, SEM obs. 80−65397
Mo wire, struct. and high-temp. creep, dopant elements influence 80−66603
NaF, sintering, relation between densification and grain growth 77−12585
Nb-Zr-N biphase alloy, recrystallization annealing 80−104180
Ni alloy IN-738, Y_2O_3 (1.5 wt.%) addition, mechanical alloying 77−40427
Ni, alloying, influence on recrystn. and grain growth *(Russian)* 80−81071
Ni coating, electron beam evaporated, ductility and struct. 78−11439
Ni, defect removal, obs. by positron annihilation 78−84677
Ni, polygonisation, high press. grain growth, dislocation struct., electron microscopic obs. 77−16613
Ni, pure, anomalous grain growth 80−20984
β_1-Ni-Al, elastic softening and electron diffr. anomalies prior to martensitic transform. 77−8825
Ni-based alloys, binary, ternary, complex, TiC additions, effects 78−92305
Ni-based-Ta(Cn,N) hard metals, isostatic hot pressing influence on mechanical properties 78−92219
Ni-Co-Cr-Mo-Al, Astroloy, extruded powder metallurgy superalloy, recrystallisation study 79−4976
α-Ni-In, solid solution, lamellar microstructure, influence of grain boundaries on thermal stability 78−72795
$Ni_{36}Fe_{32}Cr_{14}P_{12}B_6$, metallic glass, crystallisation 79−77520
NiZn ferrites under high press., grain growth *(Chinese)* 78−52825
$Ni_{0.36}Zn_{0.64}Fe_2O_4$, normal grain growth 78−72796
PLZT, exam. of grain growth in hot pressing, and liquid phase sintering 79−33981
Pb, anomalous grain growth 77−8855
Pb, film, thermal strain, strain relax. above room temp. 80−59841
Pb-Ca-Sn alloys for battery grids, proposed phase diagram, grain struct. development, corrosion phenomena 77−16546
Pb-Sb, improvement in antifriction layer props. by impulse discharge, impulse discharge treatment *(Russian)* 79−1917
Pb-Sn, controlled solidification, monograin growth, selection and struct. *(French)* 77−16568
Pb-Sn, unidirectionally solidified eutectic, lamellar microstructure, influence of grain boundaries on thermal stability 78−72795
Pb-Zn, off-eutectic alloys, controlled grain growth *(Japanese)* 77−55958
$Pb_5Ge_3O_{11}$, ultrafine-grained crystallized from glass, ferroelectricity 78−39508
Sc_2O_4, polycryst., form. conditions of anion vacancies, phase comp. 80−54220
Si film, growth on SiO_2 substrate by pyrolysis of SiH_4 77−89678
Si, polycryst., CVD, recrystn. on heating 80−80107
Si, polycryst. manufacturing methods for photovoltaic energy prod., solar cells, grain growth from melt *(Dutch)* 78−52661
Si, polycrystalline, grain growth study 78−92188
Si:Al(B), polycrystn., CVD grown, recryst., influence of dopants on grain growth and size 80−54575
Si:O, CVD layer, RHEED study of surface crystallinity, annealing effect on structure 79−69371
Si:P, heavily ion implanted, polycrystalline, grain growth 79−19477
SiC-AlB_2 (0.61 to 1.2 wt.%), hot pressed, microstruct. 80−93563
Sm_3NbO_7, grain growth kinetics 77−85969
SnO_2, heat treated film, electrical conductivity 77−8211
$SrFe_{12}O_{19}$, ferrite, powder effect of SiO_2 during sintering, exam. of grain growth and phase diagram *(German)* 79−24473
$SrFe_{12}O_{19}$:Si, Sr, second phase effect on elec. and mag. props. 80−60986
$SrO.6Fe_2O_3$, ultrafine, microstruct. development during sintering, mag. props. 79−70022
TaC, ultrafine grain, high pressure hot pressing 79−70024
Te film, evaporated, predeposited Ag, Sn, Bi, Al and Se nucleation centres effect on grain growth 77−4739
Th blanket pellets, grain growth kinetics 78−86613
ThO_2, ceramic oxide, thermally stimulated depolarisation currents, grain size and growth determ. 79−65792
α-Ti, cold rolled, primary recrystn., in situ investig. in HVEM 80−104185
Ti, pure, rapid grain growth 80−16343
Ti, rolling and recrystallisation texture formation *(Russian)* 77−59802
Ti sintered, struct. stability, effect of dispersed refractory compound inclusions 77−28825
Ti-Al-V (6, 4 wt.%), superplastic, mech. behaviour and hardening charcts. 79−83269
Ti-Al(Mo), swaged and recrystallized, grain growth 80−3092
Ti-coated C steel, effect of heat treatment on struct. and props. 77−56159
Ti-Mo-Zr-Sn (11.5, 6, 4.5 wt.%), metastable beta III phase, recrystallization and grain growth 80−3091
TiC, sintering and grain growth, metallographic anal. 80−25642
TiC-Co(Ni), grain growth kinetics *(French)* 77−44252
TiC-Ni, particle growth quantitative anal. by metallography and stereology 77−77684
TiC-Ni-Mo(W), cemented carbides, grain growth, metallographic obs. 77−24982
UO_2 equiaxed grain growth modelling 80−13589
UO_2, grain growth, in-reactor and lab. testing 79−74184
UO_2 grain growth studies, grain size and activation energy meas., rel. to nuclear fuel evaluation 79−93808
UO_2, sintered pellet, isothermal grain growth kinetics 77−18663
W, enhanced low temp. sintering, temp. sensitivity causes 77−36418
W filament, coated with thin Ni film, creep and recrystn. *(Russian)* 78−19822
W, recrystallisation of commercially pure and doped wire drawn to high strain 79−100165
W wire, struct. and high-temp. creep, dopant elements influence 80−66603
grain growth continued
W-K-Si-Al doped wires, heavily drawn, fibre struct., annealed 79−56993
W-Ni, liquid phase sintering, microstruct. meas. 78−44054
W-Ni liquid alloys, sintered, coarsening of W grains, exam. 78−56598
W-Ni powder compacts and wires, recrystallisation, influence of omnidirectional press. *(Russian)* 77−8849
W-Ni system, grain growth and densification during liquid phase sintering 79−38760
WC-Co, grain growth kinetics *(French)* 77−44252
Y, recrystallisation *(Russian)* 77−24946
Zn electrodeposited on polished Fe, reaction rate in solid state *(Japanese)* 78−15322
Zn, electrodeposition, on Ni surface, nondendritic granular deposit form. 77−59968
Zn-Al (22 wt.%), eutectoid, low stress and superplastic creep behaviour 80−81120
Zn-Al (22 wt.%), superplastic eutectoid, concurrent grain growth and deformation mechanism 79−74222
Zn-Al (22 wt.%) superplastic alloy, grain growth texture 80−81075
ZnO, additives effects on sintering and grain growth 78−80497
ZnO, fully dense, grain growth 80−93526
ZnO:Bi, Sb, Co, second phase effect on elec. and mag. props. 80−60986
Zr, rolling and recrystallisation texture formation *(Russian)* 77−59802

grain refinement
steel, 35Kh3MFS, strengthening involving austenite fine grain processing *(Russian)* 77−52358
steel, austenitic, 16H2NMB, struct., texture and mech. props. of product of transform. 78−92273
steel, brittle fracture resist., fractography and grain refinement 77−60024
steel, C, bainitic hardenability, overheating effect 79−38866
steel, C, type 25KhN3MFA, forgings, austenite grain refining 79−38864
steel, Cr-Mo (2.25, 1 wt.%), weld metal, high temp. crack growth, effect of tempering, prestrain and grain refinement 78−27622
steel, Cr-Mo and Cr-Ni-Mo, V effects on recrystallisation *(Russian)* 77−66654
steel, high-speed, grain size effect on wear charcts. 77−59944
steel, low alloy, coarsening at high temp. of small carbide particles dispersed in ferrite 77−52335
steel, low alloy, ferritic-pearlitic, carbonitride hardening 80−104174
steel, low C, ferrite grain nuclei form. during polymorphic transform. *(Russian)* 80−50626
steel, low-alloy, austenite grain growth, role of V, Nb, N alloying additions 77−44255
steel, low-C and low-alloy types, Nb effect on cold resist. 79−38954
steel, maraging, grain refinement due to cyclic heat treatment 78−52971
steel, maraging, structural recrystallisation, alloying element effects 77−70080
steel, martensitic, Cr-Ni, grain refining and phase transforms. effect on plasticity *(Russian)* 78−39837
steel, structural, 35KhN1M2F, forgings, struct. inheritance during ht. treatment 78−23735
steel 30khGSNA, low alloy, quenched, grain refinement influence on impact strength *(Russian)* 80−20974
supercooled, struct. refinement mech. *(Russian)* 80−20975
β-Ti-Mo (15wt.%) metastable alloy, strength enhancement 77−66650
Al castings, grain refinement by gas-generating mold coatings containing hexachloroethane 79−83355
Al, during unidirectional solidification, effects of addition of powdered cpds. *(Japanese)* 78−35395
Al, effect of Al_3Ti, TiC and B 78−52828
Al-Ti alloy for use in aircraft, work hardening *(French)* 80−97502
Al-Ti-Si phase diagram, calc., interpretation of grain refinement results 78−84781
Al-TiB_2-Si, Si effect on grain refinement *(German)* 79−91656
Al-Ti(-Si), nucleation entropy and grain refinement 79−91627
Al-Zn (40 wt.%), grain refinement by thermal cycling 78−3149
Al-Zn (40 wt.%), mechanical properties after thermal cycling 78−3150
Al-Zn-Mg-(Zr), low cycle fatigue, grain refinement effect 77−44345
Al-Zn-Ti(Mn), mech. props., Ti or Mn addition effect *(Korean)* 80−93613
Al-Zr (1-13 wt.%), rapidly quenched, extended solid solubility, grain refinement and age-hardening 80−76266
Be, containerless grain refinement using BeO in space environment, melting and solidification 79−47673
Cr, interaction with dense stream of N ions, metallography, microhardness, specific volume *(Russian)* 80−15169
Cu, grain refinement of dynamic recrystallisation during hot working *(Japanese)* 77−52345
Cu-Al_2O_3, dispersion-strengthened, vapour-deposited, rel. to tensile creep 78−11115
Cu-In, thermally cycled, effect on mech. props. and microstruct. 79−4987
Cu-Si-Ni, undercooled, grain refinement 79−34079
Fe, interaction with dense stream of N ions, metallography, microhardness, specific volume *(Russian)* 80−15169
Fe-Ni-C (31, 0.1 wt.%), kinetics of deform. induced martensite, shock loading and grain refinement effects 78−15395
Fe-Ni-C (31, 0.1 wt.%), metastable austenite, fractography 77−59919
Fe-Si (3 wt.%), current pulse effects on struct. at crack tip *(Russian)* 77−44332
Mo-Zr-C alloys, carburising and annealing effects *(Russian)* 77−59828
Ni, supercooled, struct. refinement mech. *(Russian)* 80−20975
steels, Cr-C-Mn(Ni), struct. prop. rel., design of struct. steels for high strength and toughness 80−97491
Ti-Al-V (6,4 wt.%), β-annealed, subsurface fatigue crack initiation 80−108553
Ti-Zr-Mo alloy, effect of O_2 on elec. resistivity, microhardness, mech. props. 77−56092
$TiAl_3$ crystals dissolution in pure Al liq., grain refinement of α-Al solid-solution by Ti addition 80−35178
α-U, pseudo-single cryst. and polycryst., low temp. sp. ht. 78−83972

grain size
see also grain growth; grain refinement
acoustic emission during tensile tests, H_2 assisted fracture 79−100257
β- and β''-Al_2O_3-Na_2O, fast ion conductors, TEM obs. 79−86920
alloy, austenitic, mechanical changes after electrolytic quenching *(Russian)* 80−50653
alloy, cold-worked, particle size and strain determ. from X-ray diffr. profiles 78−88588

grain size continued
alloy, splat-quenched, grain size, isothermal transform. 77−77463
alloys, rapidly quenched crystalline, struct., and heat treatment effects 80−76292
alumina, grain size and fracture toughness, effect of fracture toughness test methods 78−72883
annealing twins density, photoemission microscopy 80−35208
aqueoglacial deposit lithology of E.Lithuanian upland *(Russian)* 78−16011
austenitic steel, 45G17Yu3, structure and loss of strength after hot deform. by rolling *(Russian)* 78−39794
austenitic thin gauge plates by US backscattering *(German)* 79−91878
average grain volume meas. and topological parameters by serial section analysis 77−36705
Baltic underwater coastal slope sand grain size and mineral composition *(Russian)* 80−76963
basaltic andesite dykes, Iritono, central Abukuma plateau, plagioclase grain size 78−7618
basalts, mag. grains effect on remanent magnetisation 77−37191
beaches, SE Rio de Janeiro state, sediment textural charact., grain size *(Portuguese)* 78−81144
body loading with cracks, energy conditions for brittle failure *(Russian)* 80−96234
α-brass, acoustic harmonic generation by long-range dislocation motion 79−42150
α-brass, fatigue crack propag., role of dislocation substruct. 80−60963
brass, recrystallization during induction heating 80−97511
brittle crack, plane, crit. size *(Russian)* 77−44329
brittle fracture relationship 78−80651
brittle materials, grain size dependence of microcrack initiation 80−40505
brittle materials, influence of structural parameters on fracture toughness 79−96133
brittle solids, microfracture resulting from anisotropic shape changes 80−88254
C2, C3 carbonaceous chondrites, grain size and petrography 79−2529
calcite rocks, experimentally deformed, texture development 79−83230
calculation, in space filling geometries from measurable 2D parameters, computer simulated model verification 79−38838
[CC] Ag−(100)InP, metal-semicond.cathode contact, metallurgical, physical, chemical processes 80−107911
cemented carbides, binder grain size 80−44401
ceramic, ferrimag. or ferroelec., microstructure and physical props. 78−72756
ceramic materials, fine-grained, cyclic plastic deform. as cuase for thermal expansion hysteresis 80−89290
ceramics, coarse-grained, dimensional anal. of grain size depend. of fracture strength 80−70299
ceramics, crack propagation, microstructural aspects 79−15771
ceramics, effects on room temperature fracture energy and on tensile strength 78−88533
ceramics, fine-grained, US attenuation and velocity obs., 5 to 500 MHz 77−39634
ceramics, polycrystn., porosity, twinning and grain-size depend. on spontaneous cracking 80−44253
ceramics, polycrystn., strength-grain size relations 79−79081
ceramics containing metastable tetragonal ZrO_2, grinding induced tempering 80−89260
coatings, defects and their effect on props. 80−39474
Constantan, fatigue, grain size effect 77−21260
corundum ceramic, roughness depend. on initial grain size of alumina *(Polish)* 78−30816
Cr-Ni-Mo-V, austenite form. during heating, influence of recrystn. during tempering *(Russian)* 80−104188
crystallisation in capillary tubes, grain diameter distribs. 79−41999
crystallite dimensions determ. using synchrotron radiation X-ray diffr. photographs 80−24313
deposited film thickness and grain size determ. on non-conductive SEM specimens 78−77170
deposition by ion beam sputtering, composition and stress state 77−89674
diamond, synthetic powder, thermal cond. 80−96702
dislocation density, depend. on extent of plastic deform. and grain size *(Russian)* 78−22715
dislocation substructure strengthening and thermomechanical processing, conf., Las Vegas, USA, Feb. (1976) 77−84760
electrophotographic two-component developer discharge and contact interaction *(German)* 78−62258
EPIQUANT, automatic structure analyser 80−85116
exploding wire, structural inhomogeneity and MHD sausage instability, arc chains, grain size and annealing 79−41904
ferrite, microwave mag. props., grain size effect 78−10722
ferrite, transform. kinetics, grain size, alloying element effect, carbide precip. 80−93560
ferrite powder, grain size meas. by electron microscopy, sample prep. *(German)* 78−56833
ferrites, soft and microwave, grain-size effects on mag. props., review 78−64222
gelatin in nuclear photoemulsion, effect of pulsed elec. field on physical and mech. props. *(Russian)* 78−869
grain growth, steady-state and dynamic, computer simulation 79−38836
graphite, spheroidal, microstruct. in Mg cast iron, rel. to polishing and annealing treatments 77−56160
haematite, degree of reduction, potential relaxation due to cracks *(Russian)* 80−66770
haematite, grain size and coercive force from high temp. AF demag. 77−37189
haematite reduction to magnetite, stress development mechanism *(Russian)* 80−93553
Hastelloy X, creep, effect of He environment and grain size *(Japanese)* 77−48488
Hastelloy X, grain size effect. creep and creep-rupture *(Japanese)* 80−16382
heterogeneous duplex grain structure in 304 austenitic stainless steel, US spectroscopy 80−30204
hydrothermal etching method 80−50790
ice, Antarctic, cryst. size and climatic record down to last ice age 80−94544
II-VI cpds., solar cell applic. role of thin film growth morphology and grain size 77−77377
grain size continued
Inconel 617, creep, morphological changes of carbides, affect on creep props. 80−108509
Inconel 718, grain growth during sintering 80−97449
inhomogeneous materials, with ellipsoidal inclusion, and polycrystals, elastic deform. 78−15451
instability zone rel. to new phase preformation and nucleation 78−10169
iron, pure, tensile deformation behaviour under high pressure *(Japanese)* 80−16381
kinetics of normal grain growth 80−71661
linear polycrystal, grain length statistics *(German)* 79−86872
lunar regolith fine fraction, Luna-24 slow positron probe 80−26762
lunar soil, comparative modal petrology and phase chem. of >20 μm and <20 μm fractions 79−84688
magnetic colloid, theoretical estimates fo equilibrium chain lengths 79−79309
magnetic colloid, theory of large agglomerates 79−79310
magnetite, particle size effect on palaeointensity determ. 77−37186
magnetite and Fe, grain-size thresholds, palaeointensity determ. appl. 77−37188
Manicouagan impact melt, Quebec, stratigraphy, chemistry and grain size var. 78−81164
materials testing in welding by grain struct. comparison *(German)* 77−86273
measurement, NDT deep-drawing steel sheet and band, method and instrum. *(German)* 78−85059
metal, cold worked, grain size depend. of dislocation density 79−7614
metal, cold-worked, particle size and strain determ. from X-ray diffr. profiles 78−88588
metal, deposition condition relationship with struct. and props. 78−11369
metal, flow stress, subgrain size and subgrain stability of elev. temps. 77−86094
metal, plastically deform. X-ray diffr. data, moment method *(Czech)* 78−31593
metal, sintered compacts, residual pore effect on grain size distrib. 77−85961
metal, weld pool solidification under EM agitation 79−24510
metal film, vacuum deposited, grain struct., influence of impurities and alloying elements *(Russian)* 78−56048
metal growth in space, theoretical models, comparison with ground expts. 78−84786
metallic film, strain gauge factor anal. 78−6458
metallic films, size effects, resistivity derivation 78−76163
metallic thin film, polycryst., plastic flow, dislocation slip 79−82505
metallography, quantitative methodology *(French)* 80−30205
metallography, semiautomatic recording apparatus 79−87767
metals, aspects of impact testing, grain size effect on critical impact velocity 79−79111
metals, polycrystn., creep damage and cavity growth, assessment using density meas. 80−104217
metals and alloys, BCC lattice, crit. embrittlement temp., struct. parameters effect *(Russian)* 80−66618
meteorites, matrix textures and grain size distribs. in unequilibrated ordinary chondrites 77−87340
microstrains distrib. in macroinhomogeneous fields *(Russian)* 80−21018
monocrystal surface layer damage depend. on abrasive working parameters *(Russian)* 80−76368
multiphase alloy deposits, microstruct. effects 79−28254
mylonites, grainsize reduction and grain boundary sliding rel. to flow strength 80−21721
natural compounds, surfaces, X-ray image processing appl. *(French)* 78−41379
nearest-neighbour size correlation with grain size *(French)* 77−8843
Ni alloy KhN45Yu, strength properties, dispersity of struct. effect 80−55486
Nimonic 115, superalloy, critical strain model for creep fracture 77−32648
Nimonic 80A, rapidly solidified, struct. and initial precipitation, field-ion and TEM study 79−78982
nondestructive measurement of grain size and anisotropy, model 170 instrument 79−11753
nucl. echo signals, cryst. anisotropy *(Russian)* 79−99790
nuclear fuel, gas release and swelling, operational model, grain boundary gas 80−95346
olivine in Japanese peridotites, subgrain sizes rel. to uppermost mantle differential stress lateral var. 80−98275
one-dimensional polycrystalline structure, computer simulation *(German)* 77−68935
Ostwald ripening kinetics, depend. on particle vol. fraction 79−46806
oxide ceramics, dependence of props. on raw materials, exam. using ceramic magnets as model *(German)* 79−4936
Permalloy corrosion resistance enhancement 79−79150
photographic emulsion, grain size, uniform, sensitivity spread contributory factors 78−16864
photographic film, fogging effects diagnosis, use of granularity meas. 79−47952
photographic film grain size and transmittance influence on fluctuation and diffraction spectra *(German)* 80−4788
photovoltaic cell, grain boundary effects on performance 79−83603
plasma sprayed coating, ultramicrostructure and porosity 79−82500
polycrystal, elastoplastic, grain size effect on deformation curve *(Russian)* 79−51191
polycrystal, US scatt. by grains 80−2122
polycrystalline film, singularities of recrystallisation *(Russian)* 78−2382
polycrystalline films, grain boundary reflection coeff. thermal expansion effect on resistivity temp. coeff. 79−91162
polycrystalline materials, freq. and grain size dependency of US attenuation 80−50783
quartz, dislocation struct. in deformed grains, etching technique 77−39590
quartz beach sand, spectral reflectance/grain size relationship 78−16005
quartz ceramic, SiO_2-Cr_2O_3-TiO_2, creep and porosity, for ceramics with different structures 80−21011
quartzite, grain boundary and struct., analogue expts. using ice 80−21718
random arrays of grains, spectral properties 80−12727
rare earth-Co, 2-17 comp., permanent magnet props. 77−8348
recrystallisation, in situ studies, appl. of X-ray synchrotron topography 78−35610
relationship between ferrite and austenite grain size 80−3001

grain size continued
Rene 95, Ni based superalloy, effect of grain size and gamma prime size, on fatigue crack propag. 78−64686
rocks of crystalline basement, grain size in ductile deform. zones and mylonites 79−53344
sand, grain size rel. to rhomboidal lattice struct. on beaches 77−37178
sapphire filaments in Al_2O_3:MgO matrix, single cryst. boundary migration 80−44369
sedimentary rocks, sieve size statistics from grain meas. 77−70645
sediments of Point Pelee, SW.Ontario, grain size rel. to geomorphology and origin 78−92857
single-phase structure, nonuniform, grain size quantitative rating, exam. of system used 78−85072
skeletonization in quantitative metallography 80−101002
soap foam, arrangement of cells in a net rel. to grain sections of polycryst. 80−70225
soil, Martian, fine-grained component model based on Viking lander data 78−85882
stainless steel, machine faceted, low-energy ion erosion studies 80−80923
stainless steel aged by discontinuous precipitation mechanism ultrafine grain and mech. props. *(Russian)* 77−70053
steel, 0Kh16N15M3B type, He ion irradiation effect on struct. and mech. props. 78−19848
steel, 10Kh11N20T3R, brittle fracture susceptibility rel. to grain size *(Russian)* 77−59901
steel, 18 Kh2N4MA, grain size effect on mech. props. 78−44207
steel, (0.36 wt.% C) Ni-Cr-Mo, electroslag refined, fracture toughness and fatigue behaviour 80−81171
steel, A533 B, fatigue crack propagation, grain size and temp. effects 78−56727
steel, alloy, austenitic, grain size, tempering effect on brittle fracture susceptibility 80−55534
steel, alloy, Cr-Cu-Mn-C, HT80, effect of grain size on sensitivity to reheat cracking *(German)* 78−72856
steel, alloy, maraging, 18% Ni, effect of solution and ageing treatments, on microstruct., tensile props., fracture toughness 78−80648
steel, alloy 36NKhTYu, deformation resistance, grain size effect *(Russian)* 78−11271
steel, alloy 40Kh, sulphide cracking resistance, strengthening method influence 80−55577
steel, alloy structural, anomalous grain growth 80−20984
steel, austenite, pipe, ultrasonic testing of grain size 78−44313
steel, austenite decomposition, controlled rolling rel. to substruct., props. 79−29014
steel, austenite grain size eval. technique 80−25933
steel, austenite hot deformation influence on phase transformations 80−7606
steel, austenitic, 30KhGSA, grain size before quenching rel. to mech. props. 79−24553
steel, austenitic, 316, creep failure at 625°C, grain size effect 78−27631
steel, austenitic, fracture toughness props. of A533B, prior austenite grain size effect 78−60780
steel, austenitic, grain boundary sliding, exam. by tensile creep tests 78−76715
steel, austenitic, intercrystn. corrosion and mech. props., inflence of Cr, N and Nb *(German)* 80−50747
steel, austenitic, Kh17N13M3T, activation characts. of rupture, 630-730°C, Sb and Nb microalloying effects *(Russian)* 79−5033
steel, austenitic, neutron irradiated, He absorption 77−51414
steel, austenitic, type 70, cold brittleness structural depend., fracture mechanisms *(Russian)* 80−97571
steel, austenitic 18KhGT, carburising in vac., rate, austenite grain size, C distrib. 79−20277
steel, austenitic 316, grain boundary, sliding, grain size depend. 77−25108
steel, austenitic 316, grain boundary sliding, creep strain and stress depend. 77−25109
steel, austenitic grain size rating methods, comparison 78−85074
steel, austenitic stainless, Cr-Ni (25, 25 wt.%) grain size, temp. and stress influence on creep 80−30021
steel, austenitic stainless, grain size effect on softening *(Russian)* 78−23731
steel, austenitic stainless, microstructural effects on US attenuation 78−11455
steel, austenitic stainless, Ni-alloyed, Cr_2N precipitation, interface struct. and morphology 80−11644
steel, austenitic stainless, yield strength, effect of N_2 additions and grain size, solid soln. strengthening 77−52430
steel, austenitic stainless Kh18N10T, strength properties, dispersity of struct. effect 80−55486
steel, C, cementite formation and properties 80−45313
steel, C, contact fatigue strength, effect of austenite grain size 79−100254
steel, C, fracture, effect of cementite *(Russian)* 78−7037
steel, C, martensites, fractography, facets classification *(Slovak)* 79−20173
steel, C, microstructural inhomogeneity, influence on formability and fracture 80−11682
steel, C, recrystallization annealing, grain growth, effect of type of deform. 80−100847
steel, C, relax. resist. rel. to struct. 78−23788
steel, C, strain ageing contribution to fatigue hardening 78−23817
steel, C, type 25KhN3MFA, forgings, austenite grain refining 79−38864
steel, C, yield point determ. rel. to grain size, deform., ageing and temp., dislocation theory *(Serbian)* 79−34120
steel, C and HSLA, grain size and substruct. control by alloying and thermomech. treatment, review 80−3082
steel, C content effect on annealing texture, plastic anisotropy and mechanical props. 80−29976
steel, C-Mn, corrosion in acidic soln., metallurgical factor effects 79−70206
steel, CC Ti-C, threshold fatigue behaviour, effect of grain size and yield strength 79−91790
steel, comp. and ferrite grain size influence on Ludwik eqn. constants *(German)* 80−81107
steel, constructional, austenite grain shape eval. method 78−35607
steel, continuously cast, tensile strength and ductility above 800°C 80−55476
steel, Cr and Ni-Cr, cyclic re-austenitizing 80−35222
steel, Cr-Al (12, 6 wt.%), ferritic stainless, high temp. treated, strengthening mechanisms 80−3106
grain size continued
steel, Cr-Mo, cast and forged, difference in mech. props. 77−48465
steel, Cr-Mo, grain size effect on ductile brittle transition 79−24615
steel, Cr-Mo (10-14, 2-6 wt.%), heat-resist., creep-rupture strengths 80−104271
steel, Cr-Ni-Cu (14, 5, 2 wt.%), phase transform. and props., preliminary heat treatment effect 79−79011
steel, Cr-Ni-Mo-V, quenched, morpholgoy, structural constitution after austenite form. by heating *(Russian)* 78−68709
steel, Cr-Ni-Ti-B, grain size effect on mech. and struct. props. *(French)* 80−45361
steel, creep rate mismatch interaction in stress relief cracking 80−97578
steel, determ. of austenite grain size 79−74332
steel, duplex ferrite-martensite, microstructure resistance optimisation 80−40482
steel, eutectoid, mech. behaviour, thermomech. treatment effects 80−84970
steel, fatigue life, structural parameters and chem. comp. effects, rel. to test parameters 77−59928
steel, ferritic stainless, type 444 welds, ductility loss mechanism 80−85002
steel, grain boundary strengthening mechanism 80−35207
steel, high alloy Cr-Mo-W, splat quenched, formation of metastable austenite 80−84974
steel, high Mn, austenite grain size, effect of rolling and V, Ti and Zr additions *(Korean)* 77−12632
steel, high purity, low S content, for tough semi-finished products in nuclear power plant *(German)* 80−45393
steel, high Si dual-phase, mech. props and microstruct. anal. 80−40444
steel, high speed R6M5K5, excess carbide size and distrib. effect on grain size 77−90356
steel, high strength alloy, near threshold fatigue crack growth, prior austenite grain size effect 78−39903
steel, high-speed, grain size effect on wear characts. 77−59944
steel, high-speed tool, properties, powder metallurgy prep. method *(Czech)* 80−60800
steel, high-strength, 80 kg/mm^2 class, effects of metallurgical factors on susceptibility of stress relief testing *(Japanese)* 79−43458
steel, hypoeutectoid, fracture toughness, effect of Widmanstatten ferrite 80−35315
steel, low alloy, ferritic, As effect on grain size 77−70062
steel, low alloy, low C grain boundary proeutectoid ferrite formation, direct obs. method 80−3074
steel, low alloy, medium strength, SEM obs. of fracture surfaces, cleavage fracture model 77−36649
steel, low alloy, SNCM 8, quenched, tempered, prior austenite grain size effect on stress corrosion cracks *(Japanese)* 79−66215
steel, low alloy, St 52-3, structural, fracture toughness, fatigue precracking and grain size effect 78−60782
steel, low alloy effect of grain size, and amount of pearlite on fracture resistance 79−100255
steel, low C, brittle fracture of notched specimens, ferrite grain size and notch geometry effects 78−19860
steel, low C, dual phase structures (martensite and ferrite), effect of martensite composition on content, mech. props. 78−76717
steel, low C, ductile-brittle transition behaviour, grain size effects 78−52942
steel, low C, grain size effect on fatigue strength, high temps. 78−68759
steel, low c, grain size influence on size of brittle transgranular shear facets 80−35327
steel, low C, high cycle fatigue, crack initiation model *(Japanese)* 80−104258
steel, low C, impact and tensile props., effect of Si 77−36526
steel, low C, lower yield stress, grain size effects, Petch slope, temp. depend. *(Japanese)* 78−39852
steel, low C, notched specimens, brittle fracture stress, effect of ferrite grain size, notch acuity and notch length 79−20187
steel, low C, prior austenite grain size, effect on near threshold fatigue crack growth 78−92341
steel, low C, prior austenite grain size, effect on near threshold fatigue crack growth 78−92342
steel, low C, type AISI 1018, microstruct. effects on fatigue crack growth 79−61718
steel, low C, unnotched specimens, brittle fracture beyond general yielding tensile-torsional stresses 77−56096
steel, low C type 08KP, plastic deform. depend. on grain size *(Russian)* 80−66580
steel, low Si, martensite struct. and mech. props. *(Korean)* 80−93614
steel, low-alloy, oxidation resist., N effect 80−66706
steel, low-alloy, recrystallisation after hot deformation 77−44268
steel, low-C electric sheet, struct. and coercive force after second cold rolling 77−44270
steel, low-C martensitic, Ni addition influence on toughness and ductile-brittle transition 80−30099
steel, maraging, 18% Ni content, exam. of age hardening-grain size relationships 78−84833
steel, maraging, 18 wt.% Ni, tensile props., effect of aged struct. and austenite grain size 77−48511
steel, maraging, effect of thermal cycling (γ to and from α) on props. 80−20986
steel, maraging, Ni-Co-Mo (18, 8, 5 wt.%), fatigue strength charact. *(German)* 77−21241
steel, maraging, prior austenite grain size effect on tensile ductility and fracture toughness 79−100226
steel, martensitic grain size effects in H_2 assisted cracking, austenitising 77−28901
steel, microalloy V-Nb, V, Nb effects on strength and formability of cold rolled sheets 77−55979
steel, microalloyed, types V1599, V1600, V1286, NbCN precipitation in undeformed austenite 80−89230
steel, mild, fatigue limit, effect of grain size, cold work, temp., loading frequency 77−32685
steel, mild, grain size depend. of cleavage fracture toughness 79−8359
steel, mild, microstructure effect on cleavage fracture stress 79−8358
steel, mild, tensile deformation, behaviour under high pressure *(Japanese)* 80−16381
steel, mild, with different grain sizes, surface strengthening by high frequency loading *(Czechoslovakian)* 77−28934
steel, Mn-Ti-B-rare earth, distrib. of B *(Chinese)* 78−84811
steel, Nb,(V),(Al), hot-rolling, laboratory simulation, recrystn. of austenite 80−97512

grain size continued
steel, Ni, cryogenic fracture toughness enhancement through grain refinement 77−36651
steel, Ni, struct. change of hot-worked austenite during post-deform. holding 80−35228
steel, Ni-Co-Mo-Ti, microfractographical features, embrittlement and grain size influence on fracture behaviour *(German)* 80−30053
steel, Ni-Cr, P doped, tempered martensite embrittlement 80−30089
steel, non-oriented, texture and mag. props., effect of Mn and S content 77−86047
steel, pearlitic eutectoid, cleavage fracture, grain size effect 78−60784
steel, pearlitic eutectoid, crack initiation and effective grain size for cleavage fracture 80−30085
steel, pearlitic structural, austenite grains, growth rate during heating 80−100860
steel, pearlitic/ferritic, pearlite interlamellar spacing and grain size effect on US attenuation 79−34230
steel, powder forged, fatigue, surface treatment effect 80−85048
steel, ShKh15, carbide particle size and pearlite grain size changes during deform. and hot working *(Russian)* 78−6946
steel, stainless, 15Kh25T, embrittlement at 400 to 550 degrees C, grain size and cooling rate effects 78−44203
steel, stainless, dislocation struct. adjacent to fatigue crack tips 77−36643
steel, stainless, ferritic, corrosion resistance improvement by Mo and Ti additions 77−90505
steel, stainless, maraging, grain growth, temp. effect 79−57019
steel, stainless, shock loaded, residual martensite obs. 80−104414
steel, stainless, type 316, 20% cold worked, exam. of creep 78−72817
steel, stainless 304, shock loading response, grain size effect 77−36601
steel, stainless AISI 316, fatigue crack growth, effect of grain size on threshold stress intensity 78−44216
steel, stainless ferritic, 10 to 30 wt.% Cr, ductile-brittle transition temp. 80−30095
steel, stainless recrystallisation of thin bands, heating time investig. 79−38848
steel, stainless type 304, fabrication-related sensitisation 80−60887
steel, stainless type 304, shock hardening, anomalous residual, at short pulse duration 80−20942
steel, structural, brittleness susceptibility rel. to heat treatment 79−24620
steel, structural, C10, C15 and St52-3, grain size dependence of low yield point *(German)* 78−56689
steel, structural, classification according to ductile-brittle transition temp. 78−11298
steel, structural, grain size depend. of yield stress in homogeneous deformation range *(German)* 80−30013
steel, structural, second phase particle effects on impact strength 80−108581
steel, structural, unalloyed, brittle fracture, grain size and precipitate thickness effect 78−60786
steel, structural recrystallisation, phase and struct. transformations during heating 77−55990
steel, tool, martensitic hardened, reagent for revealing austenitic grain size 80−21207
steel, tool, quenching procedure effect on distortion, tool life 80−50657
steel, transformer, formation of perfect cubic texture in thin sheets *(Russian)* 78−80557
steel, type 20Kh deformed, austenite grain size, inheritance effect with quenching and tempering 80−60881
steel, type AC/HT-2, grain diameters, US attenuation 80−89429
steel, ultrahigh strength, effects of strength and grain size on near-threshold fatigue crack growth 78−64704
steel, US determ. 78−40015
steel, W-Mo-Co, high-speed tool, struct. and props., cooling rate effect at primary crystn. temp. 80−76241
steel, white layers forming at high rates of friction, struct. props. *(Russian)* 79−15800
steel, yield point charact., grain size effect *(German)* 78−72810
steel austenite, recrystallisation diagrams, heating, plastic deform. rel. to struct. 79−20067
steel austenitic stainless 316, grain boundary sliding, temp. depend. 77−25110
steel boiler tubes, Cr-Ni-Mo, austenisation conditions effects obs. 80−3151
steel grain size spread, quantitative rating method 78−85073
steel low C, effect of grain size on transition behaviour and bending speed correl. *(Japanese)* 79−8345
steel Ni-Cr, Sb doped, temper embrittlement susceptibility, intercritical heat treatment effect 78−64570
steel OKh18N10T, subjected to low temp. thermal cycling, rel. to. temp. depend. of yield point *(Russian)* 78−48489
steel St.3kp, ductile-brittle transition temp., variation with grain size 78−27640
steels, austenitic stainless, crack propag. rates under high-temp. low cycle fatigue conditions 80−21088
steels, C, quenched and tempered, struct.-prop. relationships 80−7599
steels, cleavage fracture model at low temperatures *(German)* 80−35293
steels, solute segregation and intergranular fracture 80−60957
steels, structural St 37-2, cleavage fracture, report 80−25868
steels, tool, cold hydrostatic extrusion rel. to struct., props. 79−20068
steels, ultrahigh C, superplastic, mech. behaviour at elevated temps 80−21028
steels 2Kh13 and 20Kh1M1FTR, sulphide cracking resistance, strengthening method influence 80−55577
steels 4Kh4VMFSSh and 45Kh3V3MFSSh, grain size, hot deform. and austenitising effects 80−76286
straight bar bending strength, brittle fracture energy conditions *(Russian)* 80−58974
structural steel, microstruct. and brittleness, rel. to austenizing and heat treatments 77−56091
subgrain imaging, in bulk specimens to study localised plasticity using SEM 80−66609
submarine basalts, grain size, rel. to changes in mag. signal of oceanic crust 77−90995
superplastic alloys, grain size effect on maximum strain rate sensitivity 79−100227
superplastic deformation, grain arrangements 78−83828
superplasticity, mechanism rel. to hyperfine grain struct. 78−84930
supralinear photographic emulsions, radiobiological aspects 80−26290

grain size continued
αTi, work hardened in tension, developed of internal strain *(French)* 78−76716
titanomagnetites, hysteresis props., grain size and comp. depend. 77−37187
transition metal nitrides of group IV-V, laser irrad. action, erosion strength *(Russian)* 77−56112
TV equipment, grain size determination and structural classification by visual comparative method *(German, English)* 80−35461
two phase polycrystals, grain size stability and switching, dislocation climb and glide, computer model 78−75715
Udimet 700, creep, rupture, grain size effects 77−21229
water-sediment interface US reflection with bidirectional displacement 78−60017
wax-graphite composite, specific capacitance, temp. and grain size depend. 80−50286
X-ray absorption anal., particle size effects 77−16882
X-ray diffractometrical sub-structure analysis *(German)* 77−68894
X-ray line broadening, polyphase or non-cubic materials, thermally induced strains 77−4809
Zircaloy, micrograin superplasticity at 850°C 78−23758
Zircaloy-2, pressure tubes, irrad. creep and growth, anisotropy factors 80−97536
Zircaloy-4, β-transformed, flow stress and dynamic strain ageing 80−3101
ZrO_2 powders, stabilised, for plasma spray-coatings 80−20869
Ag, annealing twins rel. to stacking fault energy 79−33006
Ag, graining, comparison with colour image *(German)* 79−29380
Ag halide emulsion props., Tl^+ ion influence 79−100413
Ag halide photography and xerography compared *(Japanese)* 78−24876
Ag halogenide, grain form. and growth in metastable soln. *(Russian)* 77−34048
Ag-halide microcryst., space charge characts. 78−15097
Ag-Mn, annealing twins rel. to stacking fault energy 79−33006
Ag-Sn (6,11 at.%) alloy, splat-quenched, X-ray diffr. study of microstruct. 77−8860
AgBr homogeneous emulsions, iodide influence on photographic props. 79−44959
Al alloy, AK4-1, hot-worked, struct. states and recrystn. *(Russian)* 78−19778
Al alloys, fatigue crack initiation, computer simulation 80−100893
Al alloys, fracture, grain size effect 78−60781
Al alloys, preliminary forging effects on struct. and mech. props. of extruded sections *(Russian)* 78−80564
Al and Al-alloy films, struct. induced electromigration failure, Monte Carlo calcs. 80−49405
Al attenuation-equalising filters, diffr. phenomena in diagnostic radiography 79−39486
Al, cold rolling of 1100 plates, substruct. development 80−108476
Al conductor alloys, subgrain-strength relationship, effect of alloying and processing 77−32606
Al, creep behaviour, at high temp., influence of oxidation 80−97538
Al, fatigue crack propag., grain size effect *(Japanese)* 78−39889
Al film, lattice and bulk heat capacity meas. for normal and supercond. states 80−92684
Al film, nucleation-grown, RF sputtered, Mayadas-Shatzkes cond. 77−1498
Al film, vacuum deposited, 7 to 65 μ thick, morphology and purity determ. 77−76699
Al films, N_2^+ and O_2^+ ion bombardment, structural and phase changes 80−2094
Al, high purity, cyclic torsional deform., factors influencing ductility 77−56031
Al, high purity, deformed at 573K, stress reductions effect on creep behaviour 79−74216
Al, plastic deform. of poly- and single-crystals, AE study 79−24579
Al, polycrystalline, acoustic emission energy release, grain size and flow stress depend. 80−11722
Al, polycrystalline, deform. sub-struct., effect on tensile props. *(Japanese)* 78−11279
Al, polycrystalline aggregate, various grain sizes, specimen thickness effect on mech props. 79−61645
Al, pure, creep, grain size effect on rate at 408K 77−52428
Al, pure, grain size effect *(Japanese)* 77−59911
Al, pure elec. cond. grade, substructural developments during recovery, Sandstrom's model validity 79−74187
Al, single and polycrystals in torsion, superplasticity *(Russian)* 78−3180
Al, splat-cooled, grain-size distrib. function, TEM study 80−40396
Al, sputtered and electron gun evaporated films, grain size and orientation obs. 78−10308
Al, tensile flow stress at room temp., grain size and strain effect 77−77528
Al thick probes, neutron transmission curves near Bragg-edge for grain size and texture eval. *(German)* 80−71667
Al/Ge multilayered superconducting films, crit. fields and crit. temps. 79−7945
Al-Bi(Cd)(Pb)-Ti, containing low-melting pt. inclusions, mech. props. 80−93632
Al-Cu (0.5 to 4.6 wt.%), cathode foil for electrolytic capacitors, relationship between comp., struct., and etchability 79−74314
Al-Cu-Si, effect of sample conditions on sputtering and intensities, emission spectrochem. anal. using glow discharge *(Japanese)* 80−21349
Al-$CuAl_2$, directionally solidified eutectic alloy, effect of heat treatment 77−55977
Al-Fe, cast, influence of Zr on precipitation, solidification and grain size *(Rumanian)* 78−84813
Al-Fe (0.5 wt.%)-Ti-Cr, Ti, Cr addition effects on toughness/microstruct. relationship *(Japanese)* 77−48525
Al-Ge, structural changes during superplastic deformation, grain boundary porosity *(Russian)* 79−83258
Al-Ge (0 to 8 wt.%), superplastic props. *(Russian)* 80−45345
Al-Mg (2 wt.%), hardening and fracture characts., β-phase dissolution role 80−81178
Al-Mg (2.4 wt.%) alloy, solution-treated, grain size effects on fatigue strength 77−4839
Al-Mg alloys, relationship between props. and nonequilib. phase diagram 79−96000
Al-Ni (6 wt.%), fine-grained, deform. in tension and torsion 80−85008
Al-Ni-(Mg) (6, 0.3 wt.%), fine grained, Luders' band deform. 77−77527
Al-Si, DC magnetron-sputtered, residual gas influence on props. 80−80968

grain size continued
Al-SiO_2 interface, stress and microstruct. via TEM 78−26797
Al-Zn, precipitation struct. and phys. props. effect of miscibility gap *(German)* 78−92265
Al-Zn-Mg, plastic instability rel. to grain boundary failure at low temps. 78−56702
Al-Zn-Mg (6.0, 2.5 wt.%), aged, grain, size depend. of fracture toughness 78−48495
Al-Zn-Mg-Cu age-hardened alloys, fatigue crack propagation rel. to grain size in vac. and NaCl soln. 80−16538
Al_2O_3 hot pressed, high density, effect of grain size on grinding 78−39723
Al_2O_3, hot pressing, microstruct., texture 80−40299
β''-Al_2O_3, Li_2O-stabilised, hot-pressing 80−40298
Al_2O_3, microhardness as function of grain size 79−79084
Al_2O_3 plasma-sprayed, struct. and thermal diffusivity 79−86932
Al_2O_3 polycrystalline, effects of space charge, grain-boundary segregation and mobility differences on conductivity 80−79979
Al_2O_3, sintering behaviour and props. of 24 aluminas *(German)* 79−4932
Al_2O_3, translucent, fabrication by high press. sintering 78−11167
Al_2O_3, vacuum condensate, struct. and mech. props., second phase effect *(Russian)* 80−71705
Al_2O_3:Fe, pore form. during oxidative annealing, grain growth slowing 80−100856
Al_2O_3-BaO, fracture *(German)* 77−28882
Al_2O_3-Cu composite, vapour deposition, microstruct., texture and surface topography 77−70001
β-Al_2O_3-Na_2O, AC impedance, microstruct. and strength 80−100349
β''-Al_2O_3-Na_2O solid electrolyte, heat treatment effects on ionic cond. and microstruct. 80−65293
Al_2O_3-Na_2O-LiO_2 (8.8, 0.75 wt.%) exam. of Na^+ resistivity as function of temp. grain size model 78−80654
β''-Al_2O_3-NaO-LiO_2, stabilised, effect of phase composition, grain size, on Na ion cond. 78−47582
Al_2O_3-TiC sinter products, grain size meas. by combination etching process 79−74331
Al_2TiO_5, grain size pseudobrookite oxide, microcracking relations 79−29194
Au, electrodeposited, hard, hardening mechanisms, grain size effect 80−35302
Au, electroplated, polyphosphate, citrate-phosphate and sulphite baths comparison 79−7756
Au film, sputtered, rel. to hardness and ductility 79−87025
Au, optical props., dielec. function, void model, sample effects 80−76048
Au-Co electrodeposits, heating effect on microstruct. and surface topography 77−43456
Au-Fe (17 at.%) alloy, fission fragment irrad., simulation of neutron effects 77−80549
B fibre, US inspection, immersion method 80−66757
B, zone melting, solar energy appl., struct. and elec. props. 77−16492
B-B_4C materials, hot-pressed, elastic modulus and flexural strength rel. to grain size and porosity 79−79018
BC, sintered, struct. and props. 80−104181
$BaFe_{12}O_{19}$, effect of impurity concentrations, and sintering conditions on grain size *(German)* 79−23630
BaS:Bi phosphors, polycrystalline, effect of grain size on thermolum. 79−61446
$BaTiO_3$, ceramic, effect of grain size on nonlinear dielec. props. 77−8522
$BaTiO_3$, doped-undoped ceramic composites, sintering behaviour 79−100094
$BaTiO_3$, effect of phase transformation on fracture behaviour 78−48507
$BaTiO_3$, polycrystalline ferroelectric, grain-size dependent props. 80−71352
$BaTiO_3$, vacuum condensates on US irrad. substrates, props. 77−66466
$BaTiO_3$:Dy ceramic, sintering, grain size, characterisation and props. 77−55923
Be, deformation strengthening, microstruct. and impurity effects 77−4791
Be, grain size effect on mech. props. *(Russian)* 79−47749
Be, polycryst., plasticity and cleavage, yield and flow stresses 80−44249
Be, polycryst. plasticity, cleavage strength, ductility transition temp. 80−44250
Be, RF sputtered film, props. rel. to deposition conditions 77−39965
Be, rolled ingot, with duplex microstruct., basal texture of two grain size distrib. 77−36556
Bi, film, evaporated, elect. and elastoresistance props. 79−33367
Bi film, surface defects and struct., electron microscopy and elec. props. *(French)* 80−15415
Bi_2MoO_6, superplasticity during phase transitions 80−108498
$Bi_{0.52}Sb_{1.48}Te_3$, microstructure rel. to thermoelec. props. 77−85249
$Bi_2Te_{3-x}Se_x$ films, thermal cond. depend. on grain size, phonon-boundary scatt. 79−69304
$Bi_2Te_{3-x}Se_x$, microstructure rel. to thermoelec. props. 77−85249
Bi_2WO_6, superplasticity during phase transitions 80−108498
C and low-alloy steel inherent austenitic grain size determ., exam. of methods used 78−85071
CaF_2, strength-controlling fracture energy depend. on flaw-size to grain-size ratio 80−81152
$CaSO_4$:Dy, α and γ thermoluminescence response comparison 79−85814
Cd, grain size effect on acoustic emission generated during plastic deformation 78−80609
Cd, polycrystn., annealed, effect of hydrostatic pressure on grain size, growth and boundary mobility 79−37717
Cd, warm rolled, texture and grain size depend. of tensile props. 80−71720
Cd-B(W) particulate composite, dispersion hardening, grain size and texture strengthening 77−8840
Cd-Zn (1.5 wt.%), warm worked, effect of grain size, texture, on mech. props. 79−4988
$Cd_xHg_{1-x}Te$ film, vacuum departed, struct. and elec. props. 77−59344
$Cd_xHg_{1-x}Te$, vac. evap. film struct. rel. to carrier scatt. 77−85116
CdS, chem. sprayed film, struct. and morphology 78−72020
CdS film, chemically deposited, cond. depend. on thickness, grain size, annealing time *(Russian)* 77−8210
CdS, film for solar cells, struct. and elec. props., thickness depend. 78−72289
CdS, polycrystn. layers on CdS substrate, electron microscope study of surface struct. 78−22940
grain size continued
CdS-Cu_2S solar cells, microstructural study of heterojunction materials 80−93978
CdS-$CuInSe_2$, solar cell, grain boundary effects on performance 79−83603
CdSe evaporated films, struct. and epitaxy, TEM, RHEED, and X-ray diffr. obs. 79−77939
CdSe film, vac. deposited, elec. resist. and surface changes by laser annealing 80−2491
CdSe film, vacuum deposited, struct., resist. and Hall mobility 77−76974
CdSe thin film transistor on Cr substrate, cryst. struct., substrate defect effects 80−70563
CdTe, laser window material, vap. deposition, mech. props. 77−46776
CeO_2 coating of laser optical components, electron microscope obs. 80−43342
β-Co, creep at low stresses 79−79028
Co-Mo alloy electrodeposits, codeposited impurities rel. to H_2 permeation, props. 79−19493
Cr, and Cr alloys, cast, B additions effect on struct. and props. *(Russian)* 78−19891
Cr, evap. film, refl. and struct. 78−72021
Cr film, on mild steel, hardness and protective props., rel. to grain size 78−11436
Cr film, vacuum-evaporated, with A-15 struct., prep. and characterisation 77−62768
Cr film vacuum deposition on glass display panels 78−39694
Cu alloy, fatigue cavitation, high temp. 77−36658
Cu and Cu-Al alloys, polycryst., effect of grain size, specimen thickness, on mech. props. 78−84945
Cu, anisothermal annealing, effect on props. of MOOB bands 78−23719
Cu based materials, sputter deposited at high rate, microstruct. and props. 78−22988
Cu, bidirectional twisting, effect on elongation and ductility changes 77−44315
Cu, cementation, characterisation of nucleation and growth from aq. soln., TEM and SEM study 79−28972
Cu, cold worked, grain size effects on short-term strength *(Russian)* 78−56693
Cu, commercial, pure, vacuum environment end grain size effects on creep rupture props. at elevated temps. *(Japanese)* 80−81162
Cu, creep damage and cavity growth, assessment using density meas. 80−104217
Cu crystals, two-phase, recrystn. retardation, particle size, spacing effects 80−89242
Cu electrodeposit, US agitation effect on hardness, porosity and grain size, work-hardening 77−60075
Cu, fatigue crack propag., role of dislocation substruct. 80−60963
Cu film, annealing effect on grain size 78−72015
Cu film, strain coeff. of resist., film thickness and grain size depend. 77−55620
Cu film, vacuum deposited, rel. to thickness depend. of breakdown stress *(Russian)* 77−59238
Cu, grain size effect on acoustic emission generated during plastic deformation 78−80609
Cu, high-purity, grain size and strain rate influence on mech. behaviour, precursors existence 80−85016
Cu mirror, microstruct. effect on Ag overlayer deposition, 10.6 μm reflectivity 77−42543
Cu pin, heavily deformed surface layer after dry sliding against steel ring, TEM obs. 77−60033
Cu, polycryst., grain size and high-temp. yield strength 80−7641
Cu, polycrystalline aggregate, various grain sizes, specimen thickness effect on mech props. 79−61645
Cu, positron lifetime as a function of grain size 77−15427
Cu, recrystallization annealing, grain growth, effect of type of deform. 80−100847
Cu, recrystallization diagram for fine grained metal in region of small deform. *(Czech)* 77−59811
Cu thick probes, subthermal neutron transmission curves, for Bragg grain size and texture eval. *(German)* 80−71667
Cu, thick sputter deposit, microstruct., tensile props. 77−40461
Cu, wire, recrystallisation *(German)* 77−86055
Cu-AL(Zn), effect of original grain size on struct. and props., after deformation and annealing 78−44178
α-Cu-Al, stress-strain behaviour, effect of grain size and composition 77−56038
Cu-Al, two-phase Cu-rich alloy, influence of microstruct. on stress-strain behaviour 80−7631
Cu-Al (13 at.%), polycrystalline aggregate, various grain sizes, specimen thickness effect on mech props. 79−61645
Cu-Al (3 wt.%), annealing twins density, photoemission microscopy 80−35208
Cu-Al (5.5, 7.3, 6.3 and 2.5 wt.%), Hg embrittlement under cyclic loading 77−86225
Cu-Al (9.3 wt.%), in torsion, deformation temp. depend., superplasticity due to grain size, dislocation density *(Russian)* 79−74200
Cu-Al_2O_3 dispersed composite, electron beam deposition, struct. characterisation 77−44197
Cu-Al_2O_3 dispersed system, electron beam evaporated thick film, struct./prop. relations 77−44198
Cu-Al-Ni-Fe-Mn, cast Ni-Al bronze, fracture metallography 78−27597
Cu-base alloy formed by high rate sputtering 78−11368
Cu-based alloys, deposition condition relationship with struct. and props. 78−11369
Cu-Cd (1.0 wt.%), yield stress and flow stress 80−97524
Cu-In, thermally cycled, effect on mech. props. and microstruct. 79−4987
Cu-Ni-Cr system, coarsening in the ($\gamma_1+\gamma_2$) region, metallographic study 78−84762
Cu-Pb thin film couple, interdiffusion and recrystallisation, grain size effects 77−76625
Cu-Sb, peculiarities in temp. behaviour of internal adsorption *(Russian)* 79−55890
Cu-Si-Ni, undercooled, grain refinement 79−34079
Cu-transition metal alloy, internal adsorpt. and mag. susceptibility, grain size effects *(Russian)* 78−19759
α-Cu-Zn(Al), solid soln., intermediate temp. embrittlement *(Japanese)* 79−20158
Cu-Zr alloys, isothermal transformation diagram 80−20902
Cu_3Au, flow stress 77−21231

grain size continued
CuCoNi ferrite magnetoacoustic oscills. rel. to microstruct. 77−85536
$CuFeS_2$, natural chalcopyrite, defect struct., TEM 77−62535
$CuInS_2$ films, RF sputtered, growth and props. 80−80124
$CuInTe_2$, vac. deposited film, growth, struct. and elec. charact. 77−69995
CuZn32 bands, mechanical props. anisotropy after annealing at variable heating rates 77−90364
Fe alloy, low, (110)[001] oriented, mag. charact. 77−1879
Fe, Armco, Bauschinger effect, computerised evaluation method 80−93625
Fe, Armco, grain size and strength depend. on nonmetallic inclusions *(Russian)* 80−100894
Fe, Barkhausen effect, grain size depend. at 300K and 77K *(German)* 77−16113
Fe, cast, austenitic grain size determ. 80−81255
Fe, commercial, ductile-brittle transition temp., variation with grain size 78−27640
Fe, creep at 77, 295K, formation of five struct. 80−60926
Fe, dynamic hot densification, degree of deformation 77−63585
Fe electrodeposited foils, microstruct., internal stress and mech. props. 80−20807
Fe, eutectic grain in grey Fe, method of size determ. 77−72529
Fe foil, electrodeposited, phys. and mag. props. 79−91275
Fe, grain growth, normal and abnormal, statistical distrib. of linear grain sizes 80−93581
Fe oxides, haematite and wustite, structural changes during reduction by $CO-CO_2$ mixtures 77−60110
Fe powder, sintered and hot pressed, effect of porosity, grain size on magnetic props. 79−96159
Fe, pure, effect of H_2 on relaxation 77−52391
Fe, pure, initial grain boundaries effect on cold-rolling and annealing textures *(Japanese)* 80−35205
Fe, remagnetisation processes, temp. and grain size depend. *(German)* 78−14987
γ-Fe, S diffusion, grain size effect 79−86930
Fe thick probes, subthermal neutron transmission curves, for Bragg grain size and texture eval. *(German)* 80−71667
α-Fe, yield point behaviour in homogeneous plastic deformation *(German)* 80−35248
Fe-Co-V(-Ni), annealing effect on microstruct. rel. to mag. and mech. props. 80−89267
Fe-Cr-Ni (20,15 wt.%), low cycle fatigue life under hold time conditions, grain size effect 77−77577
Fe-Cr-Ni austenitic alloys, environment sensitive cracking, metallurgical variables effect 80−35391
Fe-Cr-(C), oxidation, grain size and growth effects *(Japanese)* 77−48583
Fe-Cu alloy, vapour-deposited, struct. and thermal stability 78−43265
α-Fe-Fe_3C alloys, ground surface layer exam. of props. 78−84840
Fe-Mn, warm rolled, rel. contribs. of texture and grain shape to props. 79−91705
Fe-Mn (1 at.%), strain age hardening 80−108472
Fe-Nb-C (0.04, 0.02 wt.%), strengthening, hot rolling *(Chinese)* 79−100154
Fe-Ni, secondary recrystallisation singularities *(Russian)* 80−66528
Fe-Ni (25 wt.%), and single phase, solidified from undercooled melt, mech. props. 77−48540
Fe-Ni-Al (18.2 wt.%) aged, fracture toughness and mode, grain size depend. 77−12700
Fe-Ni-Al-Co-Cu-Ti YuNDK type, S effect on mech. props. 80−60927
Fe-Ni-Al-Cu (25, 14, 4 wt.%), alloy YuND4, effect of Ti addition on structure, mag. props. 80−15714
Fe-Ni-C (31.9, 0.02 wt.%), metallographic study of austenite grain size effect on martensite kinetics 79−1863
Fe-Ni-C (31.9, 0.02 wt.%) alloy, hardness of martensite-austenite mixtures 80−60959
Fe-Ni-C (31.9,0.02 wt.%), determ. of number and size distrib. of martensitic plates 80−76255
Fe-Ni-C austenite, effects of strain rate grain size, temp., on yield stress 78−72821
Fe-Ni-Cr coating, electrodeposited, exam. of passivity 78−80655
Fe-Ni(-Mo), formation of austenite structure in relation to α to γ transformations 79−100142
Fe-Si, grain oriented sheet, AC hysteresis, surface struct. and elastic stress effects 80−88791
Fe-Si, recrystallization, in situ studies, appl. of X-ray synchrotron topography 78−35610
Fe-Si (3 wt.%), breaking stress grain size and grain boundary energy during onset of reversible temper brittleness *(Russian)* 77−32673
Fe-Si (3 wt.%), effect of heating rate during primary recrystn. on props. after secondary recrystn. 78−84837
Fe-Si (3 wt.%), grain growth inhibition by MnS spherical particles with size distrib. 80−35218
Fe-Si (3 wt.%), yielding phenomena at high temp. *(Japanese)* 77−48489
Fe-Si alloys, polycrystalline, domain struct. at grain boundaries *(Russian)* 77−51917
Fe-Si(6.5 wt.%) ribbon, prep. by rapid quenching and mag. props. 80−45251
Fe_2O_3, haematite, fine-grained, hard viscous remanent magnetisation 77−56623
Fe_3O_4, magnetite, grain size limits for pseudosingle domain behaviour, rel. to palaeomagnetism 80−11215
Fe_3Pt austenitising conditions on M_s temp. 80−81088
Fe_2TiO_5, grain size pseudobrookite oxide, microcracking relations 79−29194
GaAs, film, solar cell on large grains 79−100528
GaAs, ion-implanted, laser pulse annealing of amorphous surface layer, TEM 80−55436
GaAs LPE on polycrystalline Mo 79−43157
GaAs large-grained solar cell film recrystallisation 79−38737
GaAs, polycryst. Schottky barrier solar cells, effect of grain size on efficiency 80−50968
GaAs, polycryst. solar cells, thin film growth and grain size, effect on cell efficiency 80−81471
GaAs polycrystalline film growth for solar cells 79−33941
GaAs-Au polycrystalline Schottky barriers, transition with grain size from electrode-limit to bulk-limited cond. 80−65676
$GaAs_{1-x}P_x$, chemical transport and crystal growth in closed tube *(Japanese)* 78−39673

grain size continued
Ge film, polycrystalline, structural and elec. props. 78−76173
Ge powder/Au electrode contact pot. difference, grain size depend. 80−44723
Ge-metal film, polycryst., struct. props. determ. 79−4494
Ge-Si alloys, hot-pressed, fine-grained, boundary scatt. of phonons, lattice thermal cond. 80−107583
Ge-Si alloys, hot-pressed, fine-grained, boundary scatt. of phonons, theory 80−107584
InAs, thin film prep. and elec. props. 79−1633
p-InP, RF sputtering on CdS and other substrates, and grain size obs. 77−90272
$In_{2-x}Sn_xO_{3-y}$-poly Si SIS solar cells 80−97787
IrO_x, electrochromic, oxidation state changes and struct. 80−100950
Li-Zn ferrite, mag. and microstruct. props., effect of V_2O_5 addition *(Japanese)* 77−28415
LiF:Mg, effects of grain size on thermolum. and thermally stimulated exoelectron emission 79−15536
$Li_{0.5}Fe_{2.5}O_4$, effects of low-melting additive on struct. and dielec. props. 77−85494
$Li_{0.5(1-x)}Mn_xFe_{2.5-0.5}O_4$, rectangular hysteresis loop, microstruct. form. 77−12718
$Li_2O-Al_2O_3-SiO_2$ glass, crystallised, grain size and internal strain 80−103259
Mg alloy, MA12, structural state effect on life and in fatigue crack generation in air and in vacuo 79−87728
Mg-Al spinel ceramics, mech. strength, non-stoichiometry and microstruct. *(Japanese)* 80−21054
Mg-Si (5 wt.%), thermally induced strains, X-ray line broadening 77−4809
$MgAl_2O_4$, strength-controlling fracture energy depend. on flaw-size to grain-size ratio 80−81152
$MgCa(CO_3)_2$, dolomite, partial thermal decomp. into MgO and $CaCO_3$, product cryst. growth 80−108706
Mg_2Cu sorption capacity, grain size distrib., and compactness for H_2 storage appl. 79−74547
$MgFe_2O_4$, sintered, cation ordering, grain size effects 78−39763
Mg_2Ni sorption capacity, grain size distrib., and compactness for H_2 storage appl. 79−74547
MgO, compressive stress-strain behaviour at high temps. 80−25774
MgO, hot pressed, microstruct. influence on microhardness 79−38971
MgO, polycryst., creep diagrams inc. ambipolar diffusion and grain size 77−73304
MgO, pore distrib. and grain size in intermediated sintering stage *(Japanese)* 79−74124
MgO:LiF, accretive recrystallisation during hot pressing 77−36421
MgO-C dispersion, creep, effect of C on grain size and growth 79−100213
$MgTi_2O_5$, grain size pseudobrookite oxide, microcracking relations 79−29194
$MgTi_2O_5$, thermal diffusivity, grain size and microcracking effects 78−10233
Mn film, variation of elec. resist. with deposition conditions, grain size determ. 77−43746
Mn film, variation of resist. with deposition rate, grain size determ. 77−43747
Mn-Al-C, fine-grained cast struct., remanence and coercive force 80−60365
MnZn ferrite fabricated by hot isostatic pressing, recording head appl. 80−35139
MnZn ferrite powder prep., wet method 80−89180
MnZn soft ferrites, commercial grade, microstruct. rel. to mag. props. 80−34009
Mo alloy TsM-6, creep rate in vacuum, grain size effect 80−108514
Mo, evap. film, refl. and struct. 78−72021
Mo film, evaporated, grain size and resist. 80−88650
Mo film, on SiO_2/Si substrate, effect of heat treatment after deposition on internal stress 78−22973
Mo film, sputtered, elec. resist., annealing and struct. effects 80−60109
Mo form MoF_6 by H_2 reduction, 500 to 1200°C *(Russian)* 80−7516
Mo, grain structure characteristics analysis using Quantimet-720 79−52496
Mo laser mirror, optical and metallurgical characterisation 80−33129
Mo, layer, grain size depend. on thickness *(Czech)* 77−47695
Mo sheet, shock-induced intergranular cracks 79−57087
Mo, shock deformation twinning, shock press., pulse duration and grain size effects 79−5021
Mo, sintering, effect of Ni activator grain size 77−63590
Mo-C-Zr-B (0.004, 0.12, 0.002 wt.%) effect of grain size, cellular dislocation structure, on mech. props. *(Russian)* 79−34105
Mo-Ti-Zr, alloy TZM, polycrystalline, anal. of elastic anisotropy and microyielding 80−30050
Mo-ZrO_2 dispersion hardened, rolled, grain struct. and props. 77−77492
Mo_2B_5, monocryst., grain size, abrasive and strength props. 80−11787
NH_4Cl-H_2O, solidification microstructs., effect of reduced gravity 80−96632
$(NH_4)_{10}[W_{12}O_{40}(OH)_2].H_2O$, thermal polycondensation 79−14924
$(Na,Li)NbO_3$ ceramic, optimum prep. conditions and characterisation 78−3079
NaCl, halite, dynamic recrystn. during compression creep, geophys. appl. 80−25772
NaCl polycryst. containing Al_2O_3 dispersion, diffusive creep 80−97531
NaF powder, porous, of skeleton struct., grain size effect on strength *(Russian)* 77−24991
$Na_2O-Fe_2O_3-SiO_2$, glass, partially crystallised, rel. to mag. props. 78−23302
Nb, CVD, kinetics and microstruct., pressure and temp. depend. 80−11569
Nb, creep rate in vacuum, grain size effect 80−108514
Nb film, sputter-deposited on stainless steel, electron microscopy and ESCA 77−52554
Nb, granulated film, critical current temp. depend. *(Russian)* 80−103803
Nb-Ge film, coevaporated, supercond. critical temp. and struct. 77−28275
Nb_3Al, liq. quenched, microstruct. and supercond. props. 77−72957
NbC, vacuum condensate, struct. and mech. props., second phase effect *(Russian)* 80−71705
Nb_3Ge CVD supercond. tape critical current anisotropy obs. 79−33372
Nb_3Ge, RF and DC sputtered films comparison, O content effect 78−72022

grain size continued
Nb_3Ge, sputtered on Cu, film-substrate interface obs. by electron microscopy 80−65398
NbN, granulated film, critical current temp. depend. *(Russian)* 80−103803
Nb_3Sn, filamentary superconducting composite, TEM 77−80887
Nb_3Sn film, electron beam codeposited, growth morphology and tensile props. 78−10301
Nb_3Sn, grain size in A15 reaction layers 78−14911
Nb_3Sn, high-rate sputter-deposited, effect of oxygen on microstruct. 80−20343
Nb_3Sn, monofilaments, radiation-enhanced diffusion growth, crit. current density 80−65758
Nb_3Sn multifilamentary composite supercond. wires, transverse sections prep., ion milling, TEM obs. of grain size 80−101000
Nb_3Sn, powder metallurgically produced, microstruct. characts. 80−89233
Nb_3Sn, superconducting, formed from Cu-Sn alloy, props. 79−42709
Nb_3Sn-Cu multifilamentary composite wire, Nb_3Sn filament morphology and grain size 80−100855
Ne, solid, lattice thermal cond. 0.5 to 10K, dislocation densities, average grain sizes 78−79830
Ni, (99 wt.%), annealing twins density, photoemission microscopy 80−35208
Ni coating, electron beam evaporated, ductility and struct. 78−11439
Ni, creep at 77, 295K, formation of five struct. 80−60926
Ni, creep rate at low stresses, effect of grain size 80−71707
Ni, effects of grain size on resist. anomaly near Curie point *(French)* 77−4318
Ni electrodeposit on Cu, growth and microstruct. 77−11823
Ni electrodeposits, struct., electrolyte anions influence 80−20056
Ni, inner layer of high temp. oxide scale, metallographic obs. 80−3240
Ni, powder, correlation between specific surface area and technological props. 78−64503
Ni powder, porous, relationships between mech., physical, and microstructural characts. 80−20846
Ni, pure, anomalous grain growth 80−20984
Ni, shock hardening, anomalous residual, at short pulse duration 80−20942
Ni, shock-loaded, residual strengthening, effect of grain size, dislocation cell size and deform. twin spacing 79−91744
Ni, textured galvanic layers, grain size determ., matrix and twinning orientations *(Russian)* 77−43461
Ni, thick sputter deposit, microstruct., tensile props. 77−40461
Ni, work hardening, grain size effects 77−16605
γ,γ'-Ni-Al alloys, irrad. effects on precip. 77−8829
Ni-Al films, evaporated, grain size and microstruct. 80−15423
Ni-Al_2O_3 alloy, electron beam evaporated, struct. and mech. props. 78−11114
Ni-base wrought superalloy, creep and stress rupture behaviour in air and vacuum 80−60918
Ni-based alloys, binary, ternary, complex, TiC additions, effects 78−92305
Ni-Co (10 wt.%), cast single phase, solidified from undercooled melt, mech. props. 77−48540
Ni-Co-Al alloys, continuous precip., SEM, TEM, X-ray diffr. study 80−89220
Ni-Cr machine steel, austenite grain size effects on mech. props. *(Russian)* 77−44292
Ni-Cr-Co superalloy IN-792, crack growth resistance, metallurgical effects 77−36655
Ni-Cr(20 wt.%), oxidation at elevated temps., struct. effects *(French)* 77−59994
Ni-Cu (30 wt.%), cast single phase, solidified from undercooled melt, mech. props. 77−48540
Ni-Mo alloy electrodeposits, codeposited impurities rel. to H_2 permeation, props. 79−19493
Ni-P, electrodeposited films, amorphous and crystalline, electron microscopy, in-situ crystallisation 79−11043
Ni-ThO_2 dispersion strengthened, high temp. strength, grain size and shape effects 77−48447
Ni-V, dil., oxidation behaviour at 1200°C 77−77636
Ni-Zn ferrite, grain size depend. of grain boundary sliding *(Japanese)* 80−15120
Ni-Zn ferrites, hot-pressed, key props. 78−15348
Ni_3C films, form. by carburisation, characterisation 80−34337
NiO, stress relief and plastic flow in temp. range 1323-1473K 80−89302
NiZn ferrite, magnetic props., porosity and grain size effects 77−36095
$Ni_{0.36}Zn_{0.64}Fe_2O_4$, normal grain growth 78−72796
$Ni_{0.5}Zn_{0.5}Fe_2O_4$ coarse grain polycryst. ferrite, diffusional creep *(Japanese)* 80−104238
Pb and Pb-Tl (2.5 wt.%), grain boundary sliding, grain size and stress effects 78−27571
Pb, film, hillock formation by grain boundary sliding 80−107673
Pb film, vac. deposited, thermal strain depend. on thickness and grain size 79−90926
Pb, strength loss in supercond. state, size factor effect *(Russian)* 80−88677
Pb-In (40 wt.%), solid soln., single phase, superplastic behaviour 80−21048
Pb-Sb-Te-Cu-Sn, influence of specimen and grain size on mech. props. *(Russian)* 77−81297
Pb-Sn, eutectic, superplastic behaviour, grain size effect 80−7635
$Pb(Fe_{1/2}Nb_{1/2})O_3$-$La_2O_3(CeO_2)$ ferroelec. ceramics, electrophysical props. 78−35099
$Pb_3Ge_2O_7$, vacuum condensates on US irrad. substrates, props. 77−66466
$Pb_{0.8}In_{0.2}$, superconducting, flux-flow noise 79−95556
$Pb_{0.8}Sn_{0.2}Te$ crysts., Bridgman grown, X-ray perfection study 80−107018
n-PbTe, cold hydroextrusion, plastic deform. rel. to thermoelec. props., struct. 77−11945
PbTe, continuous epitaxial film, grain size, growth cond. depend. 78−26786
$Pb(Zr,Ti)O_3$ films, ferroelec., ion beam deposition sputtered from multicomponent targets 80−80974
$Pb(Zr_{0.52}Ti_{0.48})O_3$, polycrystalline ferroelectric, grain-size dependent props. 80−71352
Pd sponge powder, sintering shrinkage kinetics 80−29900
PdGe, Pd_2Ge, growth kinetics and structure on Ge substrate 79−11514
$Pr_{0.75}Sm_{0.25}Co_5$ magnets, struct. and props. sintering temp. depend. *(Russian)* 79−82819

grain size continued
Pu, $\beta\rightarrow\alpha$ and $\gamma\rightarrow\alpha$ transforms., microstructures and kinetics 77−25048
$239PuO_2$, stoichiometric, high-temp. deformation 80−81111
Sb, film, microrelief, electron microscope obs., grain size and condensation rate 77−55469
Si, cast, growth structure and photovolt. props. of solar cells 80−94008
Si continuous polycrystalline films on C substrates 78−64490
Si film, growth on SiO_2 substrate by pyrolysis of SiH_4 77−89678
Si, film, polycryst., for photovoltaic appl., grain size effects 78−72034
Si, growth of large grain polycryst. layers on graphite substrates by CVD on liquid layers 80−55849
Si, laser annealed layers, grain size distrib., Raman obs. 79−73189
Si, orientation anal. of polycrystalline samples 79−1438
Si, polycryst., elec. and photovolt. props., grain size effects 80−49800
Si, polycrystalline, grain boundary effects on minority-carrier diffusion length and solar-cell efficiency 79−48124
Si powder, effect on microstructure and mechanical props. of Si_3N_4 *(German)* 79−4998
Si ribbons, roller quenching method of prep., grain sizes and carrier conc. 80−40275
Si, self-implanted layer, grain size, laser irrad. energy density depend. 78−72012
Si solar cell parameters, grain size dependence 80−94049
Si, solar grade, directionally solidified using C crucibles, TEM study 79−47617
Si:Al(B), polycrystn., CVD grown, recryst., influence of dopants on grain growth and size 80−54575
Si:As(B), ion-implanted, scanned laser and electron beam annealing 79−73182
Si:O, O rich polycryst. film, carrier transport 78−80076
Si-Al system, Si regrowth minimisation methods in Al films 80−15384
Si-Ge alloy, hot-pressed, thermal cond., effect of grain size 77−31813
Si-Ge alloy, thermoelec. material, lattice thermal conductivity rel. to grain size and carrier conc. 78−91495
Si-SiO_2-Mo-Si_3N_4-Al MNOS structures with metal grains, charge transport at SiO_2-Si_3N_4 interface 80−65693
SiC, hot pressing, addition of B, B_4C and Al_2O_3, role of grain boundaries 77−24999
SiC, strength-grain size relation, surface finish effects 77−81333
Si_3N_4, CVD, effect of deposition parameters 77−55272
Si_3N_4, hot pressed with different grain struct., mech. props. 79−61700
Si_3N_4, reaction-bonded, quantitative microstructural analysis 79−100092
Si_3N_4-$Y_2O_3(CeO_2)$, hot pressed, sintered, microstruct., flexural strength and fractographic anal. 80−40293
SiO_2 fused powder, difference between white and black silica, devitrification rates 80−28918
Sm-Pr-Co alloys, mag. props. and struct., comp. depend. *(Russian)* 80−20430
$Sm(Co_{0.85}Fe_{0.05}Cu_{0.10})_z$, coercive force meas. 77−4530
Sn/Au thin film diffusion couples, Kirkendall void form. 80−96698
Sn-Ni electrodeposited equatonic alloy, cryst. struct., X-ray, electron diffr. anal. 80−79748
SnCaV garnet polycrystal, ferrimag. resonance loss rel. to grain size 77−85581
SnF_2, phase transitions 80−100329
SnO_2-polySi solar cells, fabrication, grain size effects on device parameters 80−94045
$SrFe_{12}O_{19}$, exam. of factors affecting reaction kinetics, thermal analysis *(German)* 79−24471
$SrO.6Fe_2O_3$, ultrafine, microstruct. development during sintering, mag. props. 79−70022
$SrTiO_3$, vacuum condensates on US irrad. substrates, props. 77−66466
Steel, type 34Cr4, post-hotforming recrystallisation condition, use of NEOPHOT 2 and EPIQUANT 80−84949
TC-Co, nearest-neighbour size correlation with grain size *(French)* 77−8843
Ta, CVD, kinetics and microstruct., pressure and temp. depend. 80−11569
Ta, deposition parameters, struct., and elec. props. 77−81222
Ta epitaxial layers, formation conditions influence on struct. *(Russian)* 80−20045
Ta film, planar-magnetron-sputtered, phys. and elec. props. 80−6673
TaC, ultrafine grain, high pressure hot pressing 79−70024
Te film, evaporated, crystallinity and electronic props., annealing effect 77−85107
ThO_2, ceramic oxide, thermally stimulated depolarisation currents, grain size and growth determ. 79−65792
(Ti,V)C, activated reactive evaporation deposited films, annealing study, microstructure 80−24762
Ti, acoustic harmonic generation by long-range dislocation motion 79−42150
Ti alloys, fatigue crack propagation resistance, grain size effect, exam. 80−11765
α-Ti, commercial purity, static strain ageing 77−86061
Ti, commercial-purity, Portevin-Le Chatelier effect, mechanism 77−8886
α-Ti, fatigue crack growth, influence of grain orientation, SEM study 80−108550
Ti, grain size effect on acoustic emission generated during plastic deformation 78−80609
Ti, grain size effect on yield stress and work hardening at 295 and 575K 78−64593
Ti, vacuum deposited, cryst. struct. and elec. props. 78−79908
Ti-Al (14 at.%), with precipitate free zones, tensile props., grain size effects 77−16690
Ti-Al age-hardened alloys, fatigue crack propagation rel. to grain size in vac. and NaCl soln. 80−16538
Ti-Al-H, H effect on mech. props. and lattice constants 80−21036
Ti-Al-Sn (5, 2.5 wt.%) alloy, fatigue under combined alternating bending and torsional stresses 77−8923
Ti-Al-V (6,4 wt.%), effects of grain size on superplasticity, deformation mechanisms, microstructural characteristics 79−52323
Ti-Al-V (6,4 wt.%) superplastic alloy, maximum attainable ductility 80−60919
Ti-Al-V-Sn (6, 6, 2 wt.%), fatigue crack growth, cyclic freq. and microstruct. influence 80−55515
Ti-Al-(V) (6,4 wt.%), hot salt stress corrosion susceptibility, microstruct. effects 77−36688
Ti-Al(Sn) alloys, thermal and athermal solid solution strengthening 77−4787
Ti-Mn, superplastic, microduplex grain struct. stabilisation 78−44058

grain size continued
α-β Ti-Mn alloys, etching and electropolishing to reveal α and β-grain size 78−3254
β-Ti-Mo-V-Fe-Al (8,8,2,3 wt.%), metastable, high cycle fatigue crack initation, grain size effect 77−86145
Ti-Zr-Mo alloy, effect of O_2 on elec. resistivity, microhardness, mech. props. 77−56092
TiB_2 thick film on low C steel substrate, CVD in US field, crystallite size 80−84854
TiB_2, TiC, vacuum condensate, struct. and mech. props., second phase effect *(Russian)* 80−71705
TiC, activated reactive evaporation deposited films, annealing study, microstructure 80−24762
TiC, deposited by activated reactive evaporation, TEM and hardness 79−23872
TiC-Ni composite coating, activated reactive evaporation prep., structure 77−44393
TiN-Ti_2N, activated reactive evaporation formed deposits, microstructure, transformation depend. on depositing conditions 80−24761
TiO_2, rutile, film, CVD in $TiCl_4$-H_2O system 77−12541
UO_2, grain growth, in-reactor and lab. testing 79−74184
UO_2 microspheres, prep. from $UO_3(NH_3)_2$, exam. of mech. and physical preps. 79−6758
UO_2, sintered pellets, relationship between intercept length and grain diameter 78−52743
UO_2, sintering, use of NH_3, grain size changes 77−55920
UO_2, stoichiometric, sintering diagram *(Rumanian)* 79−87602
(V,Ti)C+Ni cermet, binder grain size 80−44401
V, different grain sizes, room temp. microstrain *(German)* 77−36614
V, hydrogenated, grain size depend. of tensile strength 77−36657
VC-TiC, deposited by activated reactive evaporation, TEM and hardness 79−23872
V_3Ga, grain size in A-15 reaction layers 78−14911
VO_2, reactively sputtered film, influence of manufacturing parameters on film struct. and props. *(French)* 77−81218
V_3Si, grain size in A-15 reaction layers 78−14911
Va, creep rate in vacuum, grain size effect 80−108514
W alloy, determ. by acoustic method 78−72961
W fibres, dependence of fine struct., on processing parameters 79−34082
W, metal-ceramic, mech. props. and structural nonuniformity 79−15705
W-ThO_2 composite, struct., lamination tendency, effects of method of manuf. 78−68653
W_2B_5, monocryst., grain size, abrasive and strength props. 80−11787
WC-Co, nearest-neighbour size correlation with grain size *(French)* 77−8843
WC-Co alloy, transverse rupture strength rel. to grain size and strain rate, 400° to 900°C *(Japanese)* 78−48486
WC-Co carbide, crack paths, SEM study *(Japanese)* 80−50710
WC-Co cemented carbide, carbide grain size effect on strength rel. to structural defects 77−32689
WC-Co cemented carbides, high temp. transverse rupture strength, effect of domain size of binder phase *(Japanese)* 78−92329
WSi_2, sputtered, props. for MOS IC appl. 80−70831
$Y_3Fe_{5-x}Al_xO_{12}$, permeability spectra rel. to microstruct. 80−71100
$Y_3Fe_{5-x}Gd_xO_{12}$, permeability spectra rel. to microstruct. 80−71100
Y_2GdIG film, amorphous, mag. bubbles obs. and structural transformation 80−75824
YIG, open die hot pressing, spin wave and FMR line width 80−89170
YIG, permeability spectra rel. to microstruct. 80−71100
Y_2O_3, grain size depend. of fracture energy, SEM study 79−34130
Y_2O_3, strength-controlling fracture energy depend. on flaw-size to grain-size ratio 80−81152
Zn, ductile-brittle transition pressure, grain size effect *(Japanese)* 78−60745
Zn, oriented polycrystals, tensile behaviour under hydrostatic press. *(Japanese)* 77−52417
Zn, phosphate coating, effect of grain size on film formation kinetics 79−34203
Zn polycrystals, deformation, grain sizes effect at room temp. *(Czech)* 80−45359
Zn-Al (0.4 wt.%), grain size effect on acoustic emission generated during plastic deformation 78−80609
Zn-Al (10,22,50wt.%), low temp. mech. props. plastic deformation, glissile dislocation nucleation *(Russian)* 80−11695
Zn-Al (1.1 wt.%) superplastic alloy, grain size determ. *(Czech)* 80−81118
Zn-Al (22 wt.%), eutectoid, low stress and superplastic creep behaviour 80−81120
Zn-Al (22 wt.%) eutectoid, superplastic, factors affecting ductility 77−86097
Zn-Al (22 wt.%) eutectoid, superplastic, grain size effect on plastic deform. at room temp. *(Japanese)* 78−31462
$ZnFe_2O_4$, duplex struct. formation during sintering, grain growth study 79−11541
ZnO films, texture and grain size rel. to chem. spray deposition parameter 77−31921
ZnO sputtered films, undoped and Ga doped, props. rel. to deposition conditions 80−107935
ZnO varistor ceramics, current-voltage characts., inhomogeneities and single barriers 80−80273
ZnO varistors, statistics and grain size effects on breakdown characts. 80−34010
ZnO:Ba, Co, rare earth metal varistors, microstructure-prop. relations 80−100249
ZnO_2, polycrystn., determ. of crystallographic orientation of grains 79−69049
Zr alloys, acoustic emission during tensile testing 77−90433
Zr-base alloys, annealed specimens, irradiation growth 80−49276
Zr-Nb (2.5 wt.%), annealed, irradiation growth at 353K 79−46710
Zr-Nb (2.5 wt.%), pressure tubes, irrad. creep and growth, anisotropy factors 80−97536
Zr-Nb microduplex alloys, struct. and props. 78−3170
β-Zr-Nb(Cb) alloys, anneal hardening and flow softening 79−78993
Zr_3Al, $L1_2$ phase yield strength 78−19811
ZrC, high-temp. strength, affecting factors 77−63794
ZrO_2, containing metastable tetragonal phase, stress induced phase transform. effect on props. 78−68683
ZrO_2, crystallisation from $Zr(OH)_4$, effect of water vapour, heat treatment and grain size *(Japanese)* 79−19170
ZrO_2, crystallisation from $Zr(OH)_4$, influence of water vapour *(Japanese)* 79−78865
grain size continued
ZrO_2, destabilisation by phosphoric acid, cubic to monoclinic transition, effect of temp., grain size, chemical composition 79−20037
ZrO_2, partially stabilized, processing defects 80−97558
ZrO_2, stabilised, fabrication by hot petroleum drying method, X-ray diffr. and thermal anal. study 80−40297
ZrO_2 stabilised with Y_2O_3, ultrafine grained, fabrication and flexural strength 77−1829
ZrO_2, ZrB_2, vacuum condensate, struct. and mech. props., second phase effect *(Russian)* 80−71705
ZrO_2-CaO (12-19 mole%), AC elec. behaviour, 300-900°C, grain size, electrode material, and sintering effects 78−34649
grain structure *see crystal microstructure*
grain subboundaries *see subboundary structure*
grammars
contrastive linguistics, P-struct. C-struct. grammar 78−69959
multilevel syntax analysis for geological data compression 79−48569
parser for segmenting continuous speech into pseudo-syllabic nuclei 80−91985
web, Earth resources satellite picture model applic. 77−37466
gramophones
signal rate of change, distribution meas. 80−79083
tone arms, bending vibrations and their avoidance *(Japanese)* 80−33329
Granato-Lucke theory *see dislocation damping*
granular materials
see also granular structure
abrasive, failure and strength characts. in US field, test unit 80−85112
abrasives, granular composition changes due to wear *(Russian)* 79−79115
acceleration waves, influence of void compaction and material non-uniformity 77−68472
balance laws for granular material mixtures 77−19581
bentonites, granulation, appl. to deactivation of radioactive waste waters *(Russian)* 77−38369
body submerged in granular layer, heat and mass transfer 78−94536
bronze powder, granulated, porosity of starting mat., zinc stearate additive, effects on sintering kinetics 77−63599
capacitive dispersion field transducers for granular material exam. 78−85078
capacitive grain moisture meter Standard Specimens 77−82481
cohesionless granular materials, flow at high deformation rates and low stress levels 78−90810
compacting of density hardening granular materials 79−32283
compressibility and force transmission, discrete probabilistic model 78−15448
continuum theory, uniqueness and stability 77−40518
cracks, stress concentrations and shapes, Fourier transform methods 80−83761
crushing strength determ. apparatus 79−70260
deformation, mixed characteristic problem 80−23914
density measurement, plane strain conditions, acoustic method *(Polish)* 80−62635
density measurement by pycnometry 80−69903
detective quantum efficiency and granularity rel. to quantum noise 79−21829
dilatant granular materials, initial planar deformation 79−41591
double sliding free rotating model 78−38384
dynamic flow rates, meas. apparatus 80−14860
elastic layer underlain by smooth rigid base, surface load 77−14905
elasto-viscoplastic-viscous theories of granular and porous media, soil mechanics appl. 79−76982
elastohydrodynamic traction, granular behaviour 80−103008
erevanit based glass, granulation and briqueting 80−60823
erosion by airflow, expt. and theory 77−942
ferrite powder, grain size meas. by electron microscopy, sample prep. *(German)* 78−56833
fine particle granulometric analysis, sieve and pulse methods *(German)* 80−22502
fine particles materials technology, fabrication and appls. *(Japanese)* 77−70016
flow, due to gravity, in chutes and channels, of cohesionless material 79−64753
flow, micropolar continuum theory 79−35565
flow around heated cylinder, thermal wake and separation point 77−31302
flow from parallel sided bins, thickness of shear zone 80−81279
flow round obstacles 80−103064
fluidised beds, dehydration of solutions and suspensions, rel. to granulation 80−81373
fractal dimension characterisation, textured and structured particle profiles, dilation logic appl. 79−58673
glass particulates, removal mech. from solid surface 79−50676
grain orientation in sheared dispersion, appl. to sedimentary and igneous rocks 80−3420
granular layer on elastic foundation, axisymmetric contact problem 79−27600
granules ejected in air stream, parameters of motion under gravity 77−15103
griseofulvin tablets, tensile strength and disintegration times 77−60027
heat conduction eqns. *(Russian)* 77−75767
heat transport coefficients, contacting particles in noncond. medium 78−59261
HF conductivity, theory *(Russian)* 78−23124
hot isostatic pressing in sheaths, process parameters calc. 80−84874
inhomogeneous granular solid, one dimens. accel. waves, speed, amplitude 78−87288
inspection of part quality, coarse struct. materials, LF US methods 80−81264
localised internal heating, thermodynamic theory 80−19230
mechanics, continuum and statistical approach 79−59923
metal, dielec. const., Maxwell-Garnet and effective medium theories 77−47760
metal, granular superconductivity, instability 80−103796
metal, inhomogeneous granular, superconductivity 80−103795
metal, selective solar energy absorption, particle shape depend. 78−71162
metal granules, form. mechanism study during centrifugal atomisation of rotating blank 80−100798
metals, supercond. transition, increased resistance rel. to quasi-particle tunnelling 80−88689

granular materials continued
model laws, especially for silo models 78−38383
modelling by steel spheres, packing density coeff. 78−84916
multipole-stresses theory, phys. foundation, application 77−45
packing parameters, calc. from particle size anal. results 80−19294
particulate material, stress dependent behaviour 77−90398
particulate material deformation mechanism as Markov process *(Japanese)* 80−14562
plane plastic flow, expt. test 78−34027
plastic flows, microscopic frictional effects, J_2-flow potential and yield function 80−64384
plasticity theory, invariants depend. models 78−34026
polyethylene pellets, falling in air in pipe, equilib. region press. drop, friction factor 78−63479
polymers, compression, stress state 80−10218
random packing, statistical mech. considerations 80−104088
rocks, mechanical heterogeneities rel. to flow cleavage form. 79−57934
rocks, thermal conductivity of granular media, results for greisen and granite *(French)* 78−11880
rolling, granule kinematics 80−84875
separation of minerals using supercond. mags. *(Czech)* 78−88923
shear deformation, entropy model 80−84233
shear deformation, microscopic and macroscopic exam., stress/strain charcts. calc. *(Japanese)* 80−11691
shear modulus, rel. to void ratio *(Japanese)* 79−32401
sheared particulate beds, mass transport kinetics in, Markov chains appl. 79−60057
shock waves, 1-dimens. in uniformly distributed granular material, porosity discontinuity 78−83285
size analysis, irregular shape particles, from acoustic emissions 79−61825
slag as road banking material *(Japanese)* 78−31612
slip in flowable zone, stress distrib., internal friction 79−99261
spheres at high pressure, contact stresses and spreading resistance 78−71296
stress and strain cells 79−32416
stress-strain relations, intergrain slip 80−16374
stress-strain relations, no intergrain slip, elastic zone 79−34087
thermal and elec. cond. calcs. 77−50865
thermal conductivity, effective, theoretical bounds 77−58541
thermal conductivity, wetting effect 78−47611
thermal conductivity meas. with spherical probe. *(German)* 77−5830
thermal conductivity prediction of heterogeneous mixture, digital simulation technique 78−87247
thermal diffusivity measurement, constant rate heating method *(Japanese)* 80−6572
thermal insulation for buildings, heat conduction in disperse media *(Hungarian)* 79−1056
thermoelasticity theory, granular materials 80−42066
thin film, optical characterisation *(French)* 79−11402
trace elements determination by thermal and epithermal neutron activation *(Portuguese)* 80−7874
vibration test rig for wear meas. of granules 78−56840
void compaction and material nonuniformity, influence on acceleration waves, addendum 78−83280
wave propagation in granular medium, theory 77−23909
wave pulses, finite, 1-D 80−43642
Ag granular film, plasma reson. absorpt. by incident light 79−28850
Al alloy AK5M2 granules, rolling speed effects 78−60604
Al alloy granules, lubricants for rolling 80−60980
Al alloy melts, centrifugally atomised, granule size distribution 79−100080
Al alloys, rolling, temp. and speed effects 79−70015
Al and Al alloy granules, hot rolling, angle parameters and forward slip 80−25601
Al_2O_3-B_2O_3-SiO_2, alkali glasses, granulating mechanism for medical use 80−40315
Al_2O_3-$ZrSiO_4$, granular corundum-zircon refractory, development 80−66462
$CaHPO_4$, powder and granules with starch mucilage binder, surface topography variation under compression 80−80998
CdS-In, photosensitive granular superconductor 79−78246
Cr_2O_3-ZrO_2 granules, from spray drying of suspensions 80−104100
Fe-Al_2O_3 granular films, superparamagnetism and relax. effects 80−71118
Fe-SiO_2(Al_2O_3)(ZrO_2) granular films, superparamag., Mossbauer effect 80−7131
MgO, granular, first-order stresses due to thermal shock 77−40409
Nb granular films, ratio of supercond. transition temps. 80−84529
NbN, thin film, phase transition between incoherent and coherent supercond. states 79−56394
Ni film, granular, tunnelling of spin-polarised electrons and magnetoresist., exchange effects 77−12024
PuO_2 fuel, reproducible fabrication 77−77452
SnO_2, from rocks, quantitative determination by Mossbauer effect *(Rumanian)* 78−49178
ZnO-glass-ZnO structure, with Bi_2O_3-based glass and granular ZnO layers, current-voltage charcts. *(Russian)* 77−69404
ZrO_2 products from granules, props., prep. method effect 80−25628
ZrO_2, sintering of granular masses, stabilized with CaO and Y_2O_3 78−44064

granular metallic thin films *see discontinuous metallic thin films*

granular structure
see also granular materials
balance laws for granular material mixtures 77−19581
glass tip, surface and crystallographic struct. using field-ion and electron microscopy 80−10767
Ni alloy KhN45Yu, strength properties, dispersity of struct. effect 80−55486
photographic emulsion, photon noise rel. to granularity 77−2708
single-phase structure, nonuniform, grain size quantitative rating, exam. of system used 78−85072
speed-granularity relations for X-ray and γ-ray exposures 79−21828
steel, austenitic stainless Kh18N10T, strength properties, dispersity of struct. effect 80−55486
LiMnSc ferrites, role of intergranular microstresses in control of coercive force 77−20640
SmB_6 films, crystn., struct. and elec. resist. 77−63559

granular structure continued
W powders, influence of geometrical props. on compaction *(Russian)* 80−20818
ZnO ceramics, microstructural evaluation 79−55750

graph theory
see also directed graphs; trees (mathematics)
angular momentum expressions reduction by matrix arithmetic, computer method, perturbation calcs. 77−26126
antisymmetrization wave function by method of group functions 77−3278
aromaticity, reson. energy in graph theory 80−91412
atom, open-shell, 1st order transition matrices calc., graphical method in RPA 80−47846
atomic hyperfine struct. quantum beats, intensity profile, ang. momentum theory graphical method 78−25497
biological multistate systems, freq. of cyclic processes 80−108834
block graph structural number, determ. by cut-set method *(Polish)* 77−33829
bond graph and linear graph relation 77−17749
bond graph fluid line models for inclusion with dynamic systems simulations 80−27136
boranes, polyhedral, bonding topology, graph-theoretical interpretation 78−33408
borate glass melts, struct. determ. using graph theory 79−64980
branching of mol. skeletal forms, algebraic characterisation 77−38625
Brownian motion of rot. body, graphical method 77−13702
carbocations, degenerate $(CH)_N^+$ type, permutation description *(German)* 79−45658
carboranes, bonding topology, graph-theoretical interpretation 78−33408
cellular system growing, graph generation by parallel rewriting 79−66458
circuit based graphs for renormalized perturbation theory 79−71266
classical fluids, graph theoretic techniques 78−71662
combinatorial graph complexity, measure 77−71176
conjugated heterocycles with single heteroatom, stability, graph theoret. approach 77−38604
conjugated hydrocarbon, graph theoretical formulation of London diamag. 80−27919
conjugated molecule, with proper axis of rot., MO calcs., graph theory appls. 79−76329
conjugated molecules, alternant, with one heteroatom, stability, graph theory calcs. 77−3253
conjugated systems, nonparametric resonance energies, graph theory and MO 77−61681
cosmic rays, ultra high energy, discussion *(French)* 80−21879
Coulomb bridge graphs in $2+\epsilon$ dimensions 80−24131
degenerate energy levels, adiabatic and time-independ. perturbation theory diagrammatic anal. 79−2642
diagram technique for basis functions, transformation, appl. to group-subgroup basis, cryst. tensors 77−26127
diagrammatic many-body perturbation theory applicable to arbitrary model spaces 80−47844
dielectric charge carrier drift simulation using stochastic graphs 80−15539
diffraction pattern of selected area, indexing, graphical technique, for teaching 78−54132
dimer config. enumeration, n-dimensional theory, graph paths 78−54315
duality of interaction models 77−9849
eigenvalues of graphs with twofold symmetry (molecular configuration) 79−72437
electron correlation, variational description, loop driven graphical unitary group approach, $SO_2(2^1A')$ appl. 80−47903
electron correlation problem, graphical unitary group approach, appl. to ketene 79−76324
electron g-factor, sixth order contributions, anal. evaluation of graphs 77−6066
electron gas, interacting, elec. cond. 78−95276
electronic wavefunction, correlated, graphical unitary group approach, abelian point group symmetry utilisation 79−68193
field problems, multi-terminal representations appl., graph theoretical field model 80−90689
finite chemical graphs, characterisation by isomorphism invariant 79−13623
finite element anal., combinatorial approach to flexibility method 77−2528
fluid, classical, short-range struct. universality, bridge functions 80−10478
fluid, polar, equilib. theory, graph theoretical treatment 78−6002
fluorocarbon-hydrocarbon mixtures press. second virial coeff., graph theory prediction 80−43823
fluorocarbons, press. second virial coeffs., walks on graphs method 80−7841
functional dependences, expt. determined, analysis method using osculating curves 79−93109
Gaussian model of imperfect gas, possible transition 77−80260
Gaussian polymer molecule config., large mol. Kirchhoff matrix reduction 79−13850
Gaussian polymer molecule config., stars and random regular nets, distrib. functions 79−13849
genetic net, stable dynamics logical probability models 79−74638
graph-like state of matter, electrical cond. of random networks, gelation and elasticity 78−65875
heteroconjugated molecules, π-electron props., graph theory anal. 79−89586
hydrocarbons, mol. graphs, eigenvalues 77−26996
hydrocarbons, press. second virial coeff., graph theory prediction 80−43823
hydrocarbons, press. second virial coeffs., walks on graphs method 80−7841
hypernetted chained equation, series soln., simple chain recursion method 78−65861
infinite conjugated polymers, π-electron energy and energy gap, topological calcs. 80−91713
intense field QED in continuous medium, appl. to Thomson scatt. and Cherenkov radiation 80−27435
ionised system theory, general Mayer graph estimates, long range behaviour 79−46424
king and domino polynomials for polyomino graphs, lattice dynamics appl. 77−71278
low-temperature series expansions, algebraic techniques 79−17352

graph theory continued
magnetic fields, multiterminal representations 79−68345
many electron correl. problem, unitary group approach via spin algebra graphical methods 80−47902
master eqns., discrete, struct. of exact solns. 78−77821
master equation for time evolution of Markov process, network representation 77−5642
matter, graph-like state, LCGI schemes, expt. data statistical anal. 78−15696
maximal rectilinear crossing of cycles 77−64916
Mayer graphs, general, two root-points, rigorous estimates and appl., long range behaviour 78−4565
Mayer graphs with n-root points, improved estimates with appl. 79−67222
mesh analysis using graph theory, generalised procedure, teaching 80−101681
metal clusters, bonding topology, graph-theoretical interpretation 78−33408
MO coefficients, symmetrical analysis and calc., eigenpolynomials 78−29729
mode-coupled multimode fibre transfer function 79−10409
modelling and formulations 79−67165
molecular, graphs, search for self-avoiding paths 79−59336
molecular energy levels 80−58123
molecular homeomorphism, structural, between nuclear pot. and electronic charge density 80−42968
molecular orbitals, atom self-polarisability, electrophilic substitution reactions 77−9076
molecular orbitals, graph theory, equality conditions *(Chinese)* 79−93910
molecular structure ordering, graph theoretical basis 79−59326
molecular structure-property and structure-activity correlations, graph theoretical anal. 79−26868
molecular topology, branching, distance matrix, information theoretic calcs. 78−25405
molecule, heteroconjugated, LCAO MO graph-theoretical formulation 78−890
molecules, axially symmetric, graphic study, no atom on symmetry axis *(Chinese)* 79−36792
molecules, topological props. of bond order 77−75041
monomer self-associating systems, nonideal, graphical anal. by equilibrium ultracentrifugation 80−41335
numbered complete graphs, unusual rulers, and assorted applications 79−9074
one dimensional system with phase transform., exact linear renormalisation 78−32769
orbit-orbit interaction, new tensor expansion, matrix and graphical forms 80−14064
orthopositronium decay rate, $O(\alpha)$ corrections, graph theory 77−31029
Penrose graphs, scatt. process representation 78−49983
Percus-Yevick equation, series soln., simple chain recursion method 78−65861
permutation matrices using graphical methods of spin algebras, Serber coupling 79−6833
perturbation theory, diagrammatic, appl. to N_2, CO_2, BF 80−58131
plasma, equilib. and stability, mag. shear effects, graphical technique 80−14925
polar fluids, fluctuations and inequalities 79−7538
polycyclic conjugated molecules, π-electron energy contrib. of ring, rel. to linear analogue 77−30787
polycyclic structure fragment searches 79−50156
polymer chains, Forsman's equations, graph theory appls. 78−55265
polymeric conjugated hydrocarbons, energy gap estimation, graph-theoretical approach 80−24789
quantum chemistry, spin-free, alternacy, quantum no. assignment 79−9988
quantum electrodynamics, Theiss' regularisation procedure appl. 80−9129
quantum theory graphical spin algebra, differential operators 77−60964
reconstruction problem 78−16621
relativistic field equations for half odd integer spin and unique mass, graph theoretical methods 78−62290
simultaneous linear eqns., topological soln. 80−31483
spacetime code, quantum topology 78−36859
star mayer graphs, ninth order, three-space lattice symmetry coeffs. *(Russian)* 78−29064
structural chemistry, trivalent graphs with 10 vertices 78−38644
structural similarity in molecules, graph theory recognition 79−50157
superposition of numerical graphs, functional changes *(Ukrainian)* 78−89293
Temperley-Nagle identity for graph embeddings 79−147
water-resource development project design, optimal apportionment scheme appl. *(French)* 80−77019

graphic equipment, computer *see computer graphic equipment*

graphics, computer *see computer graphics*

graphite
(0001) surface adsorption of Xe, monolayer liquid and solid struct. 80−65400
ablating Jovian probe heat shield, C vaporisation into nonequilib. stagnation point boundary layer 79−1264
absorbed Kr mono- and bilayers on graphite, two-dimens. struct., neutron diffr. study 79−42393
acceptor compounds, band struct. model and electrostatic effects 80−92814
acceptor intercalation cpds., C_nBr and C_nNO_3H, electronic struct., quantum-magnetothermal oscills. 80−44478
acceptor intercalation cpds., modulated electronic struct. 79−95310
acidic surface oxides, struct. investigation using diazomethane 79−52404
additive to lubricant, effect on operating performance of sintered materials 80−11785
adhesion and wettability by groups VIII metals *(Russian)* 80−20008
adhesive properties of melted Al, Ga and In, 300 to 1200K *(Russian)* 77−15663
adsorbed ^{3}He, NMR relax. times below 4.2K 78−38898
adsorbed Ar, Kr, overlayer-substrate spacing, LEED determ. 80−103579
adsorbed Ar monolayer, equilib. config. and lattice consts. 80−54524
adsorbed Ar monolayer, heat capacity 80−6636
adsorbed Ar monolayer, lattice spacing and isosteric heat below 50K, LEED obs. 80−34303
adsorbed Ar monolayer, neutron diffr. study 78−34705

graphite continued
adsorbed benzene, diffusive motion on basal planes, neutron scatt. study 79−42385
adsorbed butane, intramol. and surface vibr. modes, inelastic neutron scatt. obs. 77−72780
adsorbed butane, struct. and dynamics, neutron scatt. study 78−87870
adsorbed dense monolayer on graphite cleavage face, phase transition 78−56034
adsorbed ethane submonolayer, struct. and melting, elastic neutron scatt. 80−29266
adsorbed H_2 monolayers, H_2 dynamics 79−66341
adsorbed inert gas, phase transitions using Landau model 79−69243
adsorbed Kr, submonolayer films, mol. dynamics simulation 80−88425
adsorbed Kr, X-ray diffr. from 2-D solid 78−75498
adsorbed Kr monolayer, disregistry transition 78−30825
adsorbed Kr monolayer, solid, commensurate to incommensurate transition 80−80079
adsorbed Kr monolayers, commensurate-incommensurate transitions, low temp. theory 80−103582
adsorbed layer of O_2 on film, mag. susceptibility 78−43241
adsorbed layer of tetramethyltin, nature of 2 D diffusion 80−84372
adsorbed layers of O_2, heat capacity meas. 80−49511
adsorbed methane monolayer, two-dimens. diffusion by mol. dynamics method 79−90873
adsorbed methane on graphite basal plane, first order melting transition, triple point 80−2269
adsorbed methane submonolayer, two types of two-dimens. fluid, diffusion coeff. 79−37920
adsorbed methanol, proton mag. relax. times obs. 77−51590
adsorbed molecular monolayer formation time at contact spots in friction 77−43425
adsorbed monolayer of Kr, gas to condensed phase transition 77−7968
adsorbed N_2 monolayer, phonon dispersion curves for postulated four sublattice struct. 78−47667
adsorbed neopentane, quasi two-dimens. fluid, NMR 80−102525
adsorbed rare-gas monolayer, commensurate-incommensurate transition 79−69244
adsorbed tetrafluoromethane layer, adsorption isotherms, crit. temps. *(French)* 80−34312
adsorbed trimethyl tin chloride, orientation on graphite, recoilless gamma reson. 77−76663
adsorbed two-dimensional O_2, props. calc. 80−103568
adsorbing Ar, orientational epitaxy in slef-consistent phonon approx. 79−95261
adsorption, of Ar, on Xe-plated surface, virial coeffs. and interatomic pots. 77−9125
adsorption, of first layer of Ar 55 to 62K 79−28197
adsorption, of inert gases, 2-dimens. condensation, crit. temps. 80−20032
adsorption, of inert gases, solidified layer struct. and density *(French)* 78−18893
adsorption, of $N_2(H_2)$, orientational ordering, theory 80−2262
adsorption, of O_2, mag. phase transition, theory 78−38811
adsorption, on methane, phase transitions and orientational order, mol. field theory 79−95257
adsorption and desorption of Xe on (0001), kinetics using AES 77−72782
adsorption and dissociation of O_2, CNDO/2 calcs. 79−28206
adsorption and migration of O_2, CNDO/2 calcs. 79−28205
adsorption film spreading pressure, direct meas. 77−15692
adsorption from Ar-N_2 liquid soln., mol. dynamics calc. 80−59806
adsorption of ^{3}He, mag. props., 2-D gas behaviour 78−47631
adsorption of ^{4}He, selective, on (0001), level crossings 80−71556
adsorption of Ar, Lennard-Jones 9:3 adsorptive system, Percus-Yevick and hypernetted chain theories 80−20030
adsorption of Ar, Monte Carlo calcs., grand canonical ensemble, long-range corrections 78−30826
adsorption of Ar, multilayer adsorbed films, mol. theory 80−80058
adsorption of Ar, orientational ordering of incommensurate monolayers, LEED obs. 78−95233
adsorption of Br_2, EXAFS 77−43430
adsorption of CH_4, Xe, Kr, substrate deform. meas. 80−54520
adsorption of cyclohexane, conformers *(Italian)* 77−55439
adsorption of H_2, 63 to 90K *(French)* 77−11791
adsorption of H_2, dynamics, neutron scatt. exam. 79−60641
adsorption of H, effect of non-orthogonality between localised orbitals of adsorbed atom 77−43435
adsorption of H(D), on (0001) surface, vibr. spectrum, at. beam scatt. obs. 80−92779
adsorption of He, surface band splitting, theory 80−60058
adsorption of inert gas microcluster, temp. depend., mol. dynamics study 80−80056
adsorption of inert gas monolayers, nonregistered-registered phase transition 79−77894
adsorption of inert gases, modified Buckingham pot., virial coeff. anal. 79−65312
adsorption of Kr, neutron diffr. obs. 77−72789
adsorption of Kr submonolayer, melting, X-ray scatt. obs. 78−95234
adsorption of methane in first monolayer domain, thermodynamic props. *(French)* 80−29275
adsorption of methane-d_4 on graphon, neutron scatt. exam. 79−60640
adsorption of N_2, Ar, monolayer two-dimensional phase change, calorimetric investig. 77−47669
adsorption of ND_3 on graphon, neutron scatt. exam. 79−60640
adsorption of neopentane-d_4, on graphon, neutron scatt. exam. 79−60640
adsorption of NH_3(methane) (neopentane), NMR pulsed field gradient method, diffusion coeff. meas. 80−15362
adsorption of NO, crit. and triple point temps. of first adsorbed layer 78−91548
adsorption of NO, monolayer melting and polymorphism 78−84063
adsorption of O_2, graphical determ. of entropy of adsorpt. *(French)* 77−11790
adsorption of O_2, partially localised, partially mobile monolayer films, adsorption isotherms 80−107646
adsorption of o-H_2 (p-D_2), NMR, orientational behaviour, weak crystal field 78−75935
adsorption of paraffin molecules, struct. and dynamics, empirical interatomic pots. 79−99417
adsorption of Xe, Kr, finite size effect and temp. depend., multicritical phase diagrams 79−42372
adsorption of Xe and Kr, first layer study 79−73397
adsorption on graphite, Mossbauer obs. 80−18060

graphite continued
aerosol particles, urban, graphitic C as optically absorbing component, photoacoustic meas. 79−96493
AES, obtaining density of states information from self-deconvolution of Auger band-type spectra 78−92150
AES electrode, mass transfer in channel, effect on calibration graph *(Russian)* 77−86428
AES/APS self-convolution inversion, FFT and digital signal processing 79−71430
AGR moderators, graphite oxidation and coolant chemistry 80−42774
alkali graphite intercalation compound, evidence for alkalilike cond. bands 80−45201
alkali graphite intercalation compounds, evidence for alkali-like conduction band, UPS study 80−45208
alkali intercalated graphite, C XVV Auger lineshape anal. 80−104019
alkali intercalation cpds., selection rules and restricted valence band self-convolution for KVV Auger transition 80−29832
alkali metal-benzene ternary intercalation compounds thermal and X-ray anal. *(French)* 78−27434
alkali metal-graphite lamellar cpd., reversible intercalation of tetrahydrofuran 80−16211
alkali metals in graphite, organic molecule effects, aromatic hydrocarbons *(French)* 78−27433
arc, in Ar flow, meas. of anode voltage drop 80−84022
arc anodes, fibre layers, props. and cooling behaviour 79−52245
artificial, electrophys. props. 77−51745
artificial, residual macrostresses 77−16642
artificial single crystals, failure under action of laser emission, exam. *(Russian)* 80−10573
ATJ, ultrahigh vac. compatibility, outgassing characts. 79−81080
ATJ-S, strain response to mixed tension and compression loading 78−26032
ATJS type tensile strength, oxidation effects up to 2500K 80−3209
atomic absorption graphite furnace analysis, matrix interferences reduction with L'vov Platform, Pb analysis 79−92020
atomic thermal motions, comparisons at 300K based on X-ray neutron and phonon spectrum data 79−7657
atomiser for flameless atomic absorption spectrophotometer, disc form, exam. 78−54463
Auger electron appearance potential spectroscopy *(Japanese)* 80−50473
Auger KVV and XPS valence band spectra 78−11028
band struct. determ. by angle-resolved photoemission 80−45203
band structure, calc. based on rigorous cellular method 77−15762
band theory, Fermi surface constructed, ab initio energy band calc. 77−11841
band theory, press. effects on Fermi surface 77−85131
BC-graphite body, hot pressing, props. *(Japanese)* 79−78923
bending strength, surface roughness effect at high temp. *(Japanese)* 79−70131
bending strength testing, quality improvement 79−52581
body, heating in high-temp. gas flow, numerical soln. 79−37318
bonding effects 78−26482
breeder reactor, effect of cladding coating and internal pressurization on fuel-cladding interaction, rod overall length change 79−54581
burning permeable surface, accel. flow, turbulent heat/mass transfer 78−38417
calorimeter, multisection, for energy distrib. in high current relativistic electron beam 77−46456
calorimeter in water phantom for absorbed dose meas. 80−74032
carbographite mats., elec. cond. temp. depend. 77−43592
carbon fibres, graphitised, Br_2 and ICl intercalation and its removal 79−43561
carbyne form. in atm. of C stars and W Hydrae 80−67708
carbyne forms, of C, in natural graphitic formations in Ceylon and California 79−77450
carrier mobility, temp. depend. determ. from magnetoresist. expts. 80−11009
cast Fe, flaky graphite, damping capacity 77−8869
catalytic gasification using Pt, Ir, Pt-Ir, small bimetallic particle identification by controlled atm. electron microscopy 79−83502
cathodes for glow discharge and hollow cathode spectroscopic light sources 78−82047
cellular method calc. for nonspherical potential 78−56063
Ceylon, randomised X-ray powder diffraction patterns, adjustable sample holder 80−6317
chemical sputtering by H^+ ions 77−36341
chemisorption, of O_2, influence of Fe as impurity 80−96732
chemisorption, of O, CO-NDO calcs. 78−75937
chemisorption of atomic H, regular phases 78−38965
chemisorption of CO, CNDO calc. using cluster model 80−54522
chemisorption of H_2, substrate relax. effects 77−7962
chemisorption of H, cryst. orbital NDO calcs. 77−7965
chemisorption of H, regular phase, CO-NDO approx. 77−15681
chemisorption of N periodic overlayers, CO-NDO calcs. 79−7745
chromatographic columns, efficiency rel. to particle size 78−92536
circumstellar graphite grains, form. around Wolf-Rayet star (HD 193793) 80−31301
circumstellar graphite grains in front of Wolf-Rayet star HD 193793, photometric evidence 80−26861
cloth erosion by 20 keV H_2^+ and He^+ ions 79−46725
coarse grained, fracture toughness *(German)* 80−76358
coated heat sink materials for fusion appl., thermal shock testing 80−18651
coated with W, substrate for CVD of GaAs, film prep., props. and solar cell characts. 79−28930
coating on crucible used in melting U, use of Y_2O_3 77−32712
coke source inference from neutron small angle scattering meas. 77−74923
collective modes, theory for layer cpds., appl. to electron energy loss data 77−47754
colloidal graphite, in mag. field, optical transmission meas., polarisation depend. 78−31712
colloidal suspension in water, dichroism in homogeneous elec. field 79−8122
combustion product radial distrib., electric field effects 79−100374
composite, graphite particle-Al alloy, prod. by pellet method and mech. props. 78−27454
composite aircraft structures, flaw detection by US methods 78−44288
composite material, with ZrB_2 and SiC additions, prep., props., struct. 77−28775
composite materials, survey 78−56609

graphite continued
composites containing refractory carbides, electrochem. etching for microscope section preparation 77−28949
Compton profiles, momentum densities, comparison with glassy C 80−2895
condensation and compression of Ar monolayers, LEED obs. 79−77906
condensation and compression of Ar monolayers on basal plane 79−65316
conference, Baden-Baden, Germany (June 1976) 78−43990
constructional, fracture toughness testing methods 78−7129
contact interaction with Ni and Fe at high press. and temp. *(Russian)* 79−11722
contact interaction with WO_3 film on W, interference effect *(Russian)* 79−11721
contact reaction with electrolytic Mn, Co, Ni and Fe 80−15342
corrosion by CO_2, CO production radiolytically induced gas pressure effects 80−106115
corrosion in PBHTGR process heat reactor following massive air ingress *(German)* 80−83181
cosmic dust, influence of Fe on graphite nucleation 80−26927
crack propag., temp. and environment effects 78−56794
crack propag. kinetics 79−66161
cracks, jump determ. from specific failure and elastic energy 79−87712
creep irradiation expt., design, operation, initial results 77−42067
creep rig, high temp. 77−44423
crucible material, Cu-Nb alloy prep. 80−84879
crystalline, thermoelec. power, anomalous phonon drag effect 78−19065
crystallisation from molten metal solns. *(Chinese)* 79−91634
CTR material, the ion injection effect 78−34557
cups for solid sample introduction into eletrothermal atomiser 80−62734
CVD anisotropic thick hollow cylinder, residual stress due to uniform cooldown 79−42423
CVD of TiB_2 coating 80−21131
cylindrical thin shell, thermal shock, fundamental heat cond. soln. 78−29575
damage function in neutron irrad. up to 15 MeV 80−34059
deformation, crack and fracture behaviour, SEM exam 80−11706
deformation, nonlinear, of thermally stressed disc 78−6964
deformation and fracture mech., high temp. effects 77−63763
degassing rate measurement for fusion reactor appls. 80−102306
desorption, CH_4 release 79−51420
desorption of Li permeating graphite membrane, identification of CLi_3 79−34392
desorption of surface oxides, kinetics 78−60025
development and irradiation program for PBHTR appls. 80−5245
diamagnetism with quasilinear dispersion law, orbital susceptibility, valence bands *(Russian)* 80−80475
diametral compressive strength, comparison with uniaxial tensile strength *(Japanese)* 78−72947
diamond-graphite equilib. line, from synthesis and graphitisation of diamond 78−24811
diffraction of He atoms by (0001) basal face, bound state resonances 79−47575
diffusion coeffs. of Br_2, HNO_3, and $PdCl_2$ 79−42310
diffusion of Cs 77−7901
diffusion of H_2 and N_4 through powder compacts, time-lag analysis 78−2301
diffusion of Sr, lab. determ. 77−7900
dispersed Al-Si, wear characts. *(Korean)* 80−93658
dispersed particles in cast Al alloys, seizure resist. of composite alloys 80−89360
dissolution rate in molten Si, Fick's law calc. 79−99319
doped, electronic struct., energy spectrum, HMO LCAO calcs. 77−43539
double plasma arc, rotation in graphite tube 78−71599
E_{2g} mode splitting, two-phonon spectrum 78−92077
Earth upper mantle, graphite abundance rel. to plate tectonics 80−81845
EBR-II fission product control, cover-gas cleanup system and graphite trap 79−9791
elastic constant softening 79−51190
elastic constants, self-consistent calcs. 77−27933
electrical conduction, anisotropic, rel. to stacking disorder 80−34437
electrical conduction in c-direction, rel. to struct. perfection 79−38069
electrical conductivity *(German)* 78−23089
electrical conductivity press. depend. calcs. using band model 77−28171
electrical resistivity, pyrographite, during electrochem. insertion of H_2SO_4 *(French)* 80−2437
electrochemical insertion of $BF_3(C_2H_5)_2O$ *(French)* 78−27438
electrochromic effect, reversible 80−29718
electrode breakdown voltage dependence on adsorbed gases 78−75465
electrode for electric discharge sintering, metal powder+punch electrode reactions 78−11148
electrode reactions with molten glass 80−85186
electrodes for inversion voltamperometry with alternating current 79−70333
electron beam induced deposition from adsorbed CO, CO_2 or methane on W, AES obs. 77−89651
electron channelling, γ-ray spectra *(Russian)* 79−61280
electron elastic reflection angular characteristics., low primary energy 80−29835
electron energy loss spectra, 0.02-2 eV 78−39642
electron energy loss spectra, extended fine struct. in K-ionis. edge 79−47566
electron energy losses, wave-vector depend. 77−51688
electron irradiation of single crystal, threshold energy for displacement damage 77−76461
electron microscope, imaging of isolated individual sheets 79−2890
electron microscopy, controlled-atmosphere, specimen temp. meas. using opt. pyrometry 78−93690
electron spatial absorbed-dose distrib. for 25 MeV beam 77−88289
electron-phonon interactions, rel. to elec. transport 80−34156
electron-spectroscopic analysis of neutron-irradiated pyrographite 80−63261
electronic energy band parameters, depend. on temp. press. and acceptor conc. 77−62818
electronic properties of various modifications 80−49592
electronic props., self consistent LCAO calc., point vacancy in 2-dimens. cryst. 78−51932
electronic props., self-consistent LCAO calc. 78−51887
electronic struct., exact exchange HF calcs. 80−65438
electronic structure, X-ray absorption and emission, XPS 77−16431

graphite continued
electrothermal atomiser using graphite braid, for at. absorpt. spectrosc. 79−34377
emulsion chamber, cosmic gamma-ray prod. spectra 79−29959
energetic deuteron irradiated surface struct. quantitative meas. 78−95210
energetic ion sputtering, appl. of AES-SIMS (IMA)-FDS combined systems to physical and chemical processes 78−95636
enthalpy of solution at 1320K, heat of transformation from diamond 78−59945
epitaxial films of diamond-graphite, deposition on diamond substrate 77−4271
epitaxic derivatives, program (AIDED) for automatic indexing, appl. to graphite lamellar compounds 79−50927
epoxy composite, hydrothermal ageing 77−21189
epoxy composite laminate with third phase reinforcement, static and impact behaviour 77−40447
epoxy laminate, fatigue residual strength degradation model and theory of periodic proof tests 77−70158
epoxy laminate, mixed mode fracture, fracture strength 77−70156
epoxy laminate containing holes, high temp. tensile strength 77−25105
epoxy-graphite composite, for spacecraft communication antenna fabrication 78−4063
epoxy/graphite composite and cured epoxy resin, thermal expansion and swelling 80−92450
epoxy/graphite laminate, T300/5208, proof testing under cyclic tension-tension fatigue 80−81249
epoxy/graphite laminates, statistical fatigue, high load effect 80−93642
EPR, effect of motional averaging, anisotropy, skin effect rel. to heat treatment and neutron irradiation *(French)* 80−34752
EPR meas. rel. to temp., crystallite orientation, paramag. suscept. 78−35023
exfoliated, adsorbed Ne, vapour press. meas., 15-30K 79−69350
exfoliated, adsorption of benzene, −70 to −5°C *(French)* 79−33177
exfoliated, adsorption of cyclohexane, −25 to −70°C *(French)* 79−33178
exfoliated, sp. ht. low temp. meas. 79−73317
exfoliated, third sound meas. in ^{4}He superfluid film coupled with isothermal adsorption 80−20005
expanded, thermal insulating props., furnace appls. *(French)* 78−44345
extraction of N_2 from Ta powder, by vacuum hot extraction method, effect of graphite *(Japanese)* 78−84729
failure criterion, J-integral critical value 78−84999
failure energy of polycrystalline sample considered as heterogeneous medium, porosity effect 79−96138
far IR magnetospectroscopy of Landau level structure 79−73906
fast neutron flux effect on irradiation damage 78−22768
fatigue, cyclic, influence of stress cycle and neutron irrad. 79−52335
fatigue behaviour, Goodman diagram determ. 77−56078
femoral cement-free implant, mechanical strength tests *(German)* 79−8570
fibre, electrical hazards 79−91111
fibre, surface anal. by XPS and polar/dispersive free energy anal. 80−65340
fibre, transversely isotropic moduli 79−83246
fibre, Type-A, surface comp. and energetics 77−70024
fibre epoxy composites, eutectic coating moisture barriers 80−81228
fibre epoxy laminates, low thermal expansivity, design considerations 80−81031
fibre filled phthalocyanine composites, cure cycle investigation 80−81030
fibre filled polyimide composite laminates, space environment, phys. and mech. response 80−81140
fibre filled polyimide composite prepreg laminates, room-temp. ageing effect 80−81093
fibre reinforced Al, mech. props., comparison with B-Al composite 77−52470
fibre reinforced Al, temp. and press. effect on interface chemistry, mech. prop. meas. 78−64595
fibre reinforced composites, damage by moisture, diffusion anal. 80−81227
fibre reinforced epoxy, notched, fatigue initiation 77−52471
fibre reinforced epoxy, single ply, thickness effect of percolation and cond. 80−92953
fibre reinforced epoxy composite, moisture profile meas. using nucl. reaction anal. 80−55760
fibre reinforced epoxy composites, exposed to high temp., degradation of tensile and shear props. 80−81113
fibre reinforced epoxy matrix laminates, microscopical anal. 78−3288
fibre reinforced glass, impact damage tolerance and reliability 80−81177
fibre reinforced polyimide composites, friction and wear behaviour 79−52381
fibre reinforced Sn-Pb investment castings, tensile strength 77−48487
fibre/epoxy laminates, free edge induced failure 80−11775
fibres, elec. resist., mech. props. after nitration 77−32698
fibres, HM, surface comp. and energetics 80−54480
fibres, structure obs., Raman microprobe-microscope appl. 80−62737
filled polyvinyl furfural, contact area, filler effect 79−57040
filled PTFE, carbon aspect ratio effect on friction and wear characts. 77−59945
filled rubber, performance assessed against steel structures under water lubrication conditions 80−21123
film, low-temp. thermometer 77−49734
film, relativistic excitations by inelastic electron scatt. 77−1463
film, secondary electron emission and EELS rel. to plasmons 80−50481
film for solar selective surfaces, effect of Cu, Ag or Ni substrate 78−74952
finite-size crysts. first- and second-order Raman scatt. 79−95759
fission reactor core, impurity migration, proton microprobe obs. 79−52803
fluoride, chemical reactivity, rel. to lubrication appl. 79−66349
fluorides, $(CF)_n$ and $(C_2F)_n$, prep., struct., discharge characts., electrode props. 80−89502
foam, thermal props. 77−48689
foil, thickness determ. by TEM using diffr. and energy loss anal. 78−29088
formation on C-Ni(Co)(Fe) solid solns., high-temp. metallography investig. 79−29306
fracture, effective specific work of, evaluation method 79−57170
fracture, stress gradient effect 78−92321
fracture criterion 77−48552
fracture mode criterion, combined, disk test study *(Japanese)* 79−66153
graphite continued
fracture toughness meas. by diametral compressive testing method 80−35495
fracture toughness measurement, by disc test comparison with stress analysis of disc test 78−92432
frequency distribution based on unfolding technique 80−92619
friction of graphitised and ungraphitised C materials in P_2O_5 vapour, 300-600°C 79−79116
fusion reactor applications, mechanical constitutive laws for irradiation behaviour 80−32448
fusion reactor first wall appl., radiation damage 79−86822
fusion reactor limiters for ISX-A expt. 80−32457
fusion reactor liner, thermal response 80−32456
fusion reactor liners, thermal fatigue tests 80−32460
fusion reactor material, 0.6, 3.5 MeV He^+ irrad., surface erosion, porosity effects 77−35602
fusion reactor wall, microexplosion of pellet, energy deposition 78−54890
galvanomagnetic and thermomagnetic effects at low temp. 80−44618
galvanomagnetic effects, low field data and free carrier densities 78−87986
galvanomagnetic effects, temp. and field dependencies 78−64050
galvanomagnetic effects, trigonal warping of constant energy surfaces 78−87987
galvanomagnetic properties, anomalous, in quantum limit 80−39604
galvanomagnetic properties, in strong mag. field 79−23986
galvanomagnetic properties, temp. depend. between 4.2 and 298K 77−32024
gamma photons penetration, 6 MeV, expt. benchmark data and computed data comparison 80−5256
gas-solid interface, electronic struct. HFR calc. 80−54745
gasification, Fe-catalysed, electron, microscopy 80−104358
GCFR core-catcher crucible, material compatibility for UO_2-316 stainless steel graphite system 79−59171
Grafoil, $^{15}N_2$ monolayer adsorpt., reson. photon scatt. 80−34832
Grafoil, ^{4}He crit. superflow, two-dimens. random bond model 80−15319
Grafoil, absence of substrate nucleation of BCC ^{3}He, 30-320 mK 79−19422
Grafoil, adsorbed Br_2 config. investig. by EXAFS 77−51602
Grafoil, H_2 adsorbed layer orientational props., mean field theory 80−15361
Grafoil, NMR expts. on confined liq. ^{3}He 79−51371
Grafoil, nuclear spin relax. and atomic motion of adsorbed ^{3}He 79−51369
Grafoil coated with monolayer Ar, sp. ht. of adsorbed submonolayer ^{4}He film 79−51379
Grafoil substrate, NMR obs. of magnetisation of ^{3}He 79−51370
Grafoil surface with adsorbed ^{3}He, ground state, thermodynamic anal. 79−19421
grain boundary scattering effect on temp. depend. of electroresistivity, galvanomagnetic effect *(Russian)* 78−56148
grains, in Venus atmosphere, as source of UV absorpt. 78−20665
graphite, effective specific work of fracture, evaluation method 79−57170
graphite, pyrolytic, galvanomag. effects, effect of fast neutron irradiation 80−34465
graphite, US inspection apparatus for complex profiles 79−5109
graphite, zone-axis pattern maps 80−100137
graphite⇄diamond equilib. transition press. 78−34617
graphite monofluoride, self-consistent semi-empirical LCAO calcs. of electronic band struct. 77−85142
graphite monofluoride, surface alteration by interaction with Ar^+ and Xe^+ beams 78−91347
graphite nitrate, charge transfer, ionic salt model 79−11780
graphite-air mixture steady and oscill., mean heat transfer 80−89536
graphite-$AlCl_3$, well-staged, Raman and IR spectra 80−50339
graphite-alkali metal intercalation cpds., IR, active lattice mode obs. 80−45072
graphite-AsF_5 intercalated species, fractional ionisation and identification 80−97397
graphite-AsF_5 intercalation compounds, de Haas-van Alphen effect, charge transfer rate 80−54595
graphite-B_4C, neutron shielding materials, long term radiation effects 80−9413
graphite-Br_2, in-plane intercalate lattice modes, Raman scatt. 79−42163
graphite-Br_2 intercalation cpds., EXAFS study 80−71515
graphite-Br system, intercalation threshold, ellipsometric investigation 78−26760
graphite-diamond, shock induced transform. anal., post shock graphitisation 80−79933
graphite-epoxy composite, open-section stiffened compression panel, buckling and struct. efficiency 77−35061
graphite-epoxy hybrid laminates, low level Charpy impact response 78−11333
graphite-$FeCl_2$($FeCl_3$) intercalation cpds., lattice dynamics, Mossbauer spectra 80−15925
graphite-$FeCl_3$ intercalation complex, IR and Raman spectra study of optical modes 79−56797
graphite-HNO_3 intercalation compound, in-plane elec. resistivity 80−34435
graphite-HSO_3F intercalation compound, Raman spectral study *(French)* 80−60581
graphite-ICl residue compounds, struct., X-ray diffr. 78−47287
graphite-K inclusion compounds, paramagnetism after treatment by π or n donors *(French)* 78−10749
graphite-K intercalation compounds, Fermi surface, transport and supercond. props. 79−65367
graphite-$SbCl_5$(F_5) intercalation compounds, elec. resist., comp. and temp. depend. *(French)* 77−62971
graphite-SbF_5(Cl_5) intercalation compounds, compacts, elec. resistivity, C fluorination 80−34493
graphite-SbF_5 intercalation compounds, elec. cond. and opt. reflectance 77−62970
graphite-tissue interface, neutron stopping power, air/nitrogen gaps 80−26353
graphite-UF_6 intercalation compounds, NMR exam. 78−39416
graphite/epoxy thermal deformation characts. test, mirror telescope appl. 77−78636
graphite/polyimide laminates, effect of ply stacking sequence and orientation on residual stresses 77−52378
graphitic carbons, particle emission rel. to morphological changes during sublimation 77−47566

graphite continued
graphitized C black, continuous phase transitions of adsorbed Kr monolayers 78−34698
graphitized C black, virial coeff. theory of Kr adsorption 78−34697
growth shape in Fe-C melts, S and Mg effects 79−38817
Hall coefficient in mag. field range below 1.2 kOe 77−15871
halogen-graphite intercalation compound, calorimetric study of order disorder transform. 79−52206
heat strength calc. for power reactors 79−36331
high density, erosion in molten Si rel. to cryst. growth technology 78−3244
high temp. bulk, B poisoned, thermal neutron spectra meas. 79−54465
high temperature behaviour, over 2600K, polymorphic carbyne forms 79−7575
high-current, graphite cathode vaporisation, composition and temp. spectral determ. 78−14228
high-field galvanomagnetic props. 77−62941
highly oriented, pyrolytic surface, polarised reflectivity spectra at near normal incidence, surface prop. effects 79−15481
honeycomb extended lattice VB theory, long range order spin pairing 80−52136
HTGR fuel and graphite structure stress analysis methods and programs *(Japanese)* 78−74434
HTGR fuel element graphite, determ. of ^{90}Sr diffusion coeffs. 79−67869
HTGR fuel elements, neutron irradiation behaviour of graphitic matrix materials 79−19283
HTGR structural material development *(German)* 78−25297
HTR fuel compact, suitability testing 78−29631
impurity analysis, laser emission spectroscopy, material evaporation, auxiliary spark gap effects 79−87924
in cast Fe, fine cryst. struct. on tempering *(Russian)* 80−96476
insertion compound, graphite-HSO_3F *(French)* 79−52635
intercalaction compounds, action of alkali metals *(French)* 78−27431
intercalaction compounds with alkali metals, large anisotropy and stage depend. 80−44795
intercalate with SbF_5 and AsF_5, optical reflectance 78−35163
intercalated with AsF_5, HNO_3 and $SbCl_5$, Raman scatt. in low stage cpds. 80−20638
intercalated with AsF_5, mag. spin susceptibility, density of states at Fermi energy 79−7966
intercalated with AsF_5, quantum oscillatory phenomena 80−107823
intercalated with Br_2, Fermi level, far IR magnetorefl. expts. 77−40228
intercalated with Cs, melting and staging, X-ray scatt. obs. 79−19180
intercalated with DNO_3, mol. dynamics, NMR line shape and spin-lattice relax. 79−28631
intercalated with $FeCl_3$, vibrational excitations, polarised Raman spectra 79−19888
intercalated with nitrate, galvanomagnetic props. 78−76092
intercalated with $PdCl_2$, $RuCl_3$ and $OsCl_3$, synthesis and cryst. struct. 79−8253
intercalated with potassium, electronic band struct. calc. 78−6255
intercalated with SbF_5, elec. cond. 77−43549
intercalates with alkali metals, basal plane elec. resist. 80−44685
intercalates with K, staging classical model variations, EXAFS results 80−45166
intercalation acceptor lamellar cpds., charge distrib. and transport props. 79−95411
intercalation by HNO_3, chemistry 79−43564
intercalation by metals, effects on C-C band lengths *(French)* 77−28994
intercalation by $TiCl_4$ 80−40675
intercalation compound, $C_{24}Cs$, positional and orientational correlations 80−33970
intercalation compound, C_6Li, charge distrib. 78−34743
intercalation compound, C_6Li energy band struct. 78−30861
intercalation compound, $C_{8.8}K$, mag. susceptibility fluctuations near supercond. transition temp. 79−78259
intercalation compound, C_8Rb, elastic and inelastic neutron scatt. 78−30597
intercalation compound, elastic coherency strain 79−60306
intercalation compound, graphite-$AlCl_3$, electrochemical characterisation method 80−55666
intercalation compound, graphite-K, effect of H addition on superconducting transition temp. 80−70872
intercalation compound, interaction between one or two s orbitals *(French)* 80−65440
intercalation compound, LiC_6, ^7Li NMR *(French)* 78−35050
intercalation compound, RbC_8, first stage intercalation cpd., X-ray crystallographic obs. *(French)* 79−32966
intercalation compound and AsF_5, metallic optical reflectance meas. 78−6683
intercalation compound KC_{24}, prep. by reduction of aromatic compounds 80−3306
intercalation compound LiC_6, synthesis method and reflectivity spectrum 79−15600
intercalation compound with AsF_5, high elec. cond. 78−26838
intercalation compound with AsF_5, lamellar, highly two dimensional synthetic metal, room temp. elec. cond. 78−6349
intercalation compound with AsF_5 resist. and magnetoresist. 79−99590
intercalation compound with $AuCl_3$, reduction by H_2 *(French)* 78−27820
intercalation compound with Br_2, stage 2, Raman spectra 80−80787
intercalation compound with $FeCl_3$, form., effect of added O, Cl, and water vapour *(German)* 79−52634
intercalation compound with $FeCl_3$, layered, lattice modes, Raman spectra 79−95785
intercalation compound with $FeCl_3$, Mossbauer spectra 80−20538
intercalation compound with $FeCl_3$, stage 1, dielec. response and intraband plasmon dispersion 80−59902
intercalation compound with halogens, ionisation 78−26489
intercalation compound with HNO_3, HNO_3 mol. orientation, model 80−24432
intercalation compound with K, C_8K, supercond. props. 80−44755
intercalation compound with K, dielec. function, EELS study 80−45183
intercalation compound with K, KC_{24}, anisotropic mag. susceptibility and phase transitions 79−19370
intercalation compound with Li, LiC_6, sp. ht. meas., 4-300K 80−44332
intercalation compound with Rb, superlattice struct., electron diffr. study 80−75214
intercalation compound with SbF_5, texture 78−31355
intercalation compounds, a-axis conductivity model 78−10435
graphite continued
intercalation compounds, acceptor type, elec. cond. theory 80−44686
intercalation compounds, anisotropy of elec. props. rel. to chem. bond struct. 80−24888
intercalation compounds, band struct. model, dynamical dielec. function, reflectivity 80−34348
intercalation compounds, C_8M, (M=K, Rb, Cs), Breit-Wigner line shape anal., Raman spectra 80−50336
intercalation compounds, C_nK, de Haas-van Alphen effect, cyclotron reson., and transport props. 80−44479
intercalation compounds, C_nK, electronic struct. and elec. props. 80−44471
intercalation compounds, charact. by electron inelastic scatt. anal. 79−95055
intercalation compounds, characterisation by electron energy loss spectra 79−95054
intercalation compounds, coherency strains and staging 80−44167
intercalation compounds, conf., La Napoule, France (May 1977) 78−27428
intercalation compounds, dispersion relations of intercalate modes 80−34379
intercalation compounds, electronic props., conductivity and optical reflect. *(German)* 80−49837
intercalation compounds, electronic props. in dil. limit 77−47714
intercalation compounds, electronic props. review 78−30860
intercalation compounds, electrostatic interactions and staging, nonlinear Thomas-Fermi eqns. 80−107732
intercalation compounds, Fermi surface and transport props., LCAO model 80−80159
intercalation compounds, galvanomagnetic and optical data, electronic structure 77−51634
intercalation compounds, high elec. cond., engineering appl. 80−70780
intercalation compounds, interband Landau level transitions, magnetorefl. 77−52095
intercalation compounds, K-point effective masses and Fermi level shifts, magnetorefl. study 80−50305
intercalation compounds, KC_8 and CsC_8, polarised refl. spectra 78−31213
intercalation compounds, low energy optical transitions, refl. spectra and X-ray diffr. 80−25371
intercalation compounds, mag. susceptibility, tight-binding model 80−44796
intercalation compounds, magnetic resonance determ. of oxidation state 78−35051
intercalation compounds, nomenclature 80−1948
intercalation compounds, props. and appls. 78−71711
intercalation compounds, Raman scatt. and IR refl., review 80−45066
intercalation compounds, struct. and order-disorder transforms. 78−71710
intercalation compounds, struct. and phys. props., symposium, San Jose, USA (March 1979) 80−62379
intercalation compounds, two-dimensionality, structural phase transitions 80−19938
intercalation compounds, X-ray charact. 80−19780
intercalation compounds, X-ray struct. factor meas. applications 80−54207
intercalation compounds and cathodes 78−27780
intercalation compounds $C_{12}Cl$ and $C_{16}Cl$, form. and struct. *(French)* 80−40674
intercalation compounds $C_{24}K$, order-disorder transition, X-ray study 80−33922
intercalation compounds LiC_6 and LiC_{12}, electronic struct. calcs. 80−70613
intercalation compounds of graphite-Na-N-H *(French)* 79−52633
intercalation compounds struct., elec. props. 78−27446
intercalation compounds with acceptor molecules, CESR 78−48042
intercalation compounds with alkali metal, interlayer screening and mag. susceptibility 80−44794
intercalation compounds with alkali metals, electronic props. 80−45202
intercalation compounds with alkali metals and halogens, intralayer crystal struct. and order-disorder transform. electron diffr. 78−26540
intercalation compounds with alkali metals and halogens, physical props. 78−31050
intercalation compounds with AsF_5, and SbF_5, synthesis and elec. props. 80−70781
intercalation compounds with AsF_5, elec. and meas. with high anisotropy 78−26837
intercalation compounds with Br_2, ICl and IBr, Raman scatt. 77−12390
intercalation compounds with Br, K, ^{13}C NMR spectra 80−66048
intercalation compounds with Br, magnetoreflectivity in high fields under press., energy band parameters 79−61346
intercalation compounds with $FeCl_3$, intercalation kinetics 78−31354
intercalation compounds with $FeCl_3$, prep. *(French)* 78−27445
intercalation compounds with $FeCl_3$, struct., expt. data for domain theory 78−30596
intercalation compounds with H_2SO_4 and sulphuric oleums, elec. resist. evolution 80−45518
intercalation compounds with HNO_3, differential scanning calorimetry investigation 79−42234
intercalation compounds with ICl, anomalous sp. ht. due to order-disorder transform. 79−42235
intercalation compounds with K, electronic props., de Haas-van Alphen effects and Fermi surfaces 80−75498
intercalation compounds with K, electronic props., resistivity, Hall effect and magnetoresistance 80−75585
intercalation compounds with K, Rb, Cs, resistivity anomalies and phase transform. 78−26839
intercalation compounds with K, Rb, or Cs, phase transitions, resistive anomalies, electronic props. 79−95405
intercalation compounds with K and Cs, low temp. sp. ht. 78−71868
intercalation compounds with K and Cs, low temp. specific heat meas. and XPS 78−26693
intercalation compounds with K and tetrahydrofuran *(French)* 78−26692
intercalation compounds with Li, nucl. relax. times 80−44947
intercalation compounds with Li, prep. from Na-Li melts *(French)* 80−2970
intercalation compounds with metal fluorides, prep. and props. 80−40686
intercalation compounds with metal halides, acceptor sites 80−49218

graphite continued
intercalation compounds with Rb, Raman scatt. from in-plane lattice modes 78−15168
intercalation compounds with Rb, Raman scattering 78−35130
intercalation compounds with $SbCl_5$, K and bisulphates, development as reagents in organic synthesis 78−27444
intercalation compounds with SbF_5, carrier density from ^{19}F NMR line shapes 80−25224
intercalation cpds., electronic props. 78−34744
intercalation mechanisms and physical chemistry 78−27430
intercalation of Br_2, oxidation and residual Br effects 79−43565
intercalation of chlorides in chlorosulphonic acid *(French)* 78−27436
intercalation of $FeCl_3$, form. kinetics and microstruct. *(German)* 79−43560
intercalation of layered structures, crack propag. theory 80−97559
intercalation of metal chlorides and bromides 78−27435
intercalation process with Br_2 78−63965
intercalation rate, effect of graphite struct. 78−31356
intercalation with AsF_5, EPR, NMR and X-ray diffr. obs. 80−19775
intercalation with $AuCl_3$ *(French)* 78−42982
intercalation with Cs(K) donor atoms, Raman scatt. 78−10890
intercalation with Eu and Yb, struct. 80−44184
intercalation with Hg and alkali metal 80−44183
intercalation with $TlBr_3$ *(German)* 79−43563
intercalation with $TlCl_3$ *(German)* 79−43562
intercalcation compound, metallic electronic props. and correl. with chemistry 80−44567
interclation with Li, Raman scatt. study 80−88999
interfacial impedance of graphite electrode/graphite-βZnS mixture electrode in acidic aq. soln. *(Japanese)* 77−52648
interfacial tension determ. between C saturated liquid Fe by buoyancy meas. *(German)* 80−34273
intergalactic pyrolitic graphite whiskers, absorpt. effects rel. to cosmic microwave background 80−94866
internal strain rel. to strain tensor, group theory anal. 79−86835
interstellar grains temperature, effect of IR optical consts. 78−12324
interstellar graphite grains, H_2 form. on surfaces 79−21367
interstellar graphite grains rel. to 2175 Å feature, implications of C depletion meas. 80−17638
interstellar porous graphite grains, rel. to 2200 Å extinction hump 80−62228
interstitial C atom, INDO calc. *(French)* 80−39068
ion bombarded, light gases, structural study using TEM 80−92570
ion bombarded with H^+, D^+ and He^+ ions, Raman scatt. and SEM anal. 77−35609
ion irradiated, MeV He ions, exptl. study of effects 79−4341
ionisation chamber, ionisation error due to porosity 80−52829
ionisation chamber with CO_2 filling, Monte Carlo anal. of fast neutron irradiation 78−82583
IR active optical vibrations, IR reflectivity meas. 77−69837
IR optical properties, refl. data and complex dielec. function 78−10889
IRC+10216, circumstellar graphite dust shell model 80−56972
irradiated, lattice expansion, vacancies and interstitials contrib., bond order role 80−65042
irradiated, microporosity, elec. resist., length, struct. changes 78−43051
irradiated, thermal cond. at elevated temps. 79−28163
irradiated, ultimate tensile, bending and compressive stength charact. 78−15479
irradiation creep 77−42066
irradiation induced creep, UKAEA reactor group studies 77−42065
irradiation testing of reference grades with greater dimens. stability 80−42776
irradiation-induced temp.-change effects, semiempirical model calc. 80−42775
isomer shift values of implanted $^{133}Xe/^{133}Cs$, Mossbauer spectra 80−7240
isotropic, nonlinear stress/strain relationship effect on band strength 79−20119
isotropic graphite materials, resist. to deformation and fracture under complex stress conditions 80−16479
K-shell cross section for 80 kV electrons 79−55798
Knudsen cells heated by radiation, emissivity *(Japanese)* 80−13073
lamellar compounds, ^{13}C NMR studies 80−44936
lamellar compounds with Li, K, Rb, HNO_3 and SO_3, EPR studies 80−44902
lamellar derivatives, KC_{24}(tetrahydrofuran)$_m$, (m=1 and 2), ^1H NMR study 80−44932
lamellar graphite in cast iron, tensile strength, reactor appl. 77−57718
laminate, fibre reinforced composites, moisture diffusion, 3-D Fick's law 78−10218
laser emission spectroscopy, quantitative microanalysis of reactor graphites 80−81384
laser pyrolysis in He or H_2, products exam. 79−20356
laser vaporised surface, free jet expsn. of vapour 78−1703
lattice atom displacements near end of implanted μ^+ tracks 78−55890
lattice dynamics of adsorbed Ar and N_2 monolayers 78−75946
lattice vibrations, long wavelength, Raman and IR reflectivity spectra 78−75746
lattice vibrations 78−34574
layer materials, SXAPS interpret., cond. band self-convolution model, cryst. field splitting 78−23558
layered, electronic band struct., direct evaluation by angle resolved photoemission 77−51652
layered material prep. and growth, book contrib. 78−19647
lonsdalite→graphite phase transform. mechanism, electron diffr. expts. 79−28099
low energy ion sputtering, theory 79−28880
low field Hall coefficient, effect of warped energy surfaces 78−68043
magnetisation in mag. fields up to 150 kG at 4.2K, diamag. props. 77−32156
magnetisation in strong mag. fields, filled band contrib. 77−32157
magnetoreflection under press., Landau level transitions 80−50303
magnetoreflectivity in high fields under press., energy band parameters 79−61346
Magnox reactors, moderator corrosion, coolant comp. effect on radiolytic graphite/CO_2 reaction 77−6489
Magnox reactors, moderator corrosion protection, H_2 injection into Wylfa reactor I coolant gas 77−6490
material properties, neutron irrad. effects, model 79−10880
mechanical failure in lab. tests, fracture mech. approach, finite element stress anal. 77−4149
graphite continued
mechanical props., high temp., review 79−38897
melting point rel. to press. 78−24811
metal chloride intercalation compound, reduction 78−27821
microhardness changes, effect of annealing and neutron irradiation 77−8861
microporous graphite compact, anomalous diffusion of N_2, time-lag and transient-state kinetic analysis 78−34655
minority carriers and H-point magnetorefl. spectra 77−63398
mixed-field γ meas. with nonhydrogenous Rossi counter 80−9430
moderator, fast neutron irrad. damage, chem. rate theory applic. effect of annealing and thermal equilib. defect concs. 77−67804
moderator, fast neutron irrad. damage theory and modifications 77−67805
moderator, neutron small angle scatt., thermal and radiolytic oxidation effect, porosity size distrib. 79−17977
moderator structure design and manufacturing specification 80−23110
monofilaments, use as in-line electron beam energy monitors 77−61159
monolayer on graphite, neutron scatt. studies 80−107655
monolayer on graphite, sp. ht. and u.p., size and steric effects 77−85073
monolayer on Ni (110) surface, oxidation mechanism 80−101037
monolayers, dissolution into (110) face of Ni, 600-913K 80−49504
MPG-6, thermoelectric material, thermal cond. meas., 1100-2000K 78−24798
negative magnetoresistance in small-sized block samples *(Russian)* 80−49779
neutron damage annealing and C_{44} shear modulus in irradiated graphite, stored at room temp. 80−2080
neutron damage at 1200°C, fusion reactor first-wall appl. 79−93829
neutron detection, health physics monitor 77−83116
neutron effects on shrinkage 80−37456
neutron induced changes, exam. of lattice consts. elastic modulus, elec. cond 79−95053
neutron irrad., porosity changes, neutron small angle scatt. investig. 78−34544
neutron irrad. damage, chem. rate theory applic. 77−27913
neutron irradiated, annealing of radiation damage 79−1465
neutron irradiated, effect on quantum limit Shubnikov-de Haas oscills. 78−95304
neutron irradiated, EPR, rel. to electronic struct. *(Japanese)* 78−19326
neutron irradiated, polycryst., low temp. sp. ht. anomalies, spin-spin interactions 79−15307
neutron irradiated, thermoelec. and thermomag. effects 77−59296
neutron irradiation, electron transport, annealing study 80−39165
neutron irradiation behaviour of isotropic nuclear graphite 78−18683
neutron irradiation effects on thermal shock resist. and fracture toughness of HTGR graphites *(Japanese)* 80−66622
neutron penetration, Monte Carlo calculations for 30, 45 MeV *(Japanese)* 80−18677
neutron pulse die away, trapped neutron pseudo-decay consts. meas. at 77, 194K 77−42007
neutron pulse propag., effect of transverse stack dimensions in graphite assemblies 77−54272
neutron pulse propag., interf. effect of cold neutrons 77−54273
neutron pulse propag. dispersion and diffusion parameters for graphite assembly 77−54271
neutron radiation damage in PBR, mech. props., stress fields *(German)* 77−34387
neutron radiation damage of graphite rods and vitreous silica blocks 80−29070
neutron scatterer in open tangential reactor channel, intense monochromatic beam prod. 77−71712
neutron wave propagation in graphite pebble bed system *(German)* 77−6481
neutron-irradiated, crystal struct. recovery, ESR obs. *(Japanese)* 77−43254
neutron-irradiated, sp.ht., 0.4-4.5K, rel. to localised spin transition 77−28389
NGC 6888, ring nebula, evidence for graphite dust 77−29905
nitrate, structural ordering in intercalation compounds 78−26539
nitrate intercalate, X-ray obs. *(French)* 78−27440
nitrates, elec. props. perpendicular to layers, resistance, magnetoresistance, charge transport mechanisms 80−80268
NMR spectra 79−51862
nodule form. in cast Fe, graphite nodule form., ion microprobe mass anal. appl. 79−43295
nodule growth, kinetics and rate controlling process *(Japanese)* 80−35203
nonlinear deformation, theoretical-exptl. correl. of material models 77−32626
notch sensitivity, 20 to 2800°C 80−76353
nuclear, change in ratio of thermal expansion coeffs. at elevated temps. 79−42283
nuclear, CO formation at initial stages of H corrosion 78−11355
nuclear, prestressing effects on nuclear graphites 78−14482
nuclear fuels with graphite matrix, characteris. including thermal stress fracture 77−46294
nuclear fusion reactor materials development trends 77−46401
nuclear grade, unirrad. and neutron irrad., compressive stress effect on Young's modulus 77−61503
nuclear graphite: Ba impregnated, sorption of Cs, thermodynamic modelling of multicomponent sorption behaviour 80−102243
nuclear reactor materials, radiational size stability, effect of technological factors 79−26527
nucleation, role of pre-heat treatments *(Japanese)* 80−35220
nucleation on surface of solid solutions *(Russian)* 80−40360
optical probe of lattice dynamics 78−35131
orientation, exam. of preferred functions 80−1945
oriented non-spherical particles, polarisation characts. 79−81362
oxidation, corrosion resistance, bend strength, assessment for rotary glass fibre making apparatus 78−64753
oxidation, standard Gibbs free energy change, electrochemical determ. 77−29041
oxidation kinetics near 1000K 77−48616
oxidation loss and wettability of inorganic fluxing materials for crucible manuf. *(Japanese)* 78−84755
oxidation resistance, effect of P cpds., metal impurities and struct. defects 77−81331
oxide coating protection effectiveness estimation 77−86198
particle-Al alloy composite, improved damping capacity and machinability 77−4786

graphite continued
particles, diamag. levitation, Brownian-motion press. gauge appl. 78−24807
permeability, effect of neutron irradiation 79−71900
phase contrast electron microscopy of holes and steps 77−38063
phase equilibrium, with diamond, thermodynamic stability, effect of particle size 79−65184
phase transition to graphite under shock wave loading *(Chinese)* 79−82337
phonon dispersion, temp. depend., 4K-1500°C, neutron spectroscopy 78−59906
phonon dispersion relations calc. 79−90740
phonon thermal conductivity, rel. to elec. cond., possible supercond. 80−49434
photoelectron escape depths determ. from X-ray photoelectron spectra 78−27368
photoemission, book contrib. 77−44133
photoemission, C 1s core-electron line shape, excitonic effects, Fermi energy and hole density of states 80−29848
photoemission, primary and secondary yields using low-energy monochromatic X-rays 80−35053
physisorbed ^{4}He superlattices, ground-state energy, variational calc. 80−24710
piezoreflectivity, 3 to 6 eV 79−47472
plate sample holders for XPS 80−11972
Poco AXM-5Q1, thermal and elec. transport props., 4-3000K 78−6375
point defects and self diffusion 78−63758
polyacetylene-graphite, ohmic control *(Japanese)* 80−96888
polyethylene membrane (graphite charged) electrode, electron transfer *(French)* 78−27778
polygranular, flexural strength after heat treatment porosity correl. 80−84996
polyphenylquinoxalines, graphite filled, behaviour during friction 80−40553
porosity effect on strength variation 78−31369
porous, heating in air atmosphere, spectral emissivity 80−19969
powder, model for testing liq. cryst. method for detection of small objects in optical microscopy 80−9034
powder, reduction of $MgCr_2O_4$ *(Japanese)* 77−56225
powder electrodes for electrolum. anthracene diode 77−69917
powder mixture with 30 wt.% Si, reaction hot pressing 78−60592
powder-cushion gripping to promote good alignment in tensile testing 78−92418
powder-mixed $CaSO_4$:Dy Teflon TLD discs for beta dosimetry 77−86639
precipitates in quenched Ni-C alloy, TEM structural examination *(Russian)* 78−68695
precipitation from Ni-C (1.8 at.%) TEM obs. 77−52334
pressure effects on structure, polymorphic transitions, X-ray diffr. anal. 79−1859
properties near sublimation temperature, low current carbon arc appl. 79−50901
proton bombardment at 52 MeV, neutrons and photons penetration 80−27821
PTFE/graphite bond in H_3PO_4 environment, electrochemical exam. of joint failure 78−60979
pulsed neutron wave propagation expt. using electron LINAC *(Japanese)* 80−78345
pyrographite, highly ordered, paracrystn. nature, bimodal statistics anal. 79−77451
pyrographite, initial stress state, neutron irrad. effect 80−97555
pyrographite, IR spectral emissivity at high temperatures 80−103505
pyrographite, Si-containing, high-temp. treatment effects 77−40429
pyrographite, surface struct., amorphisation, secondary electron spectra and AES 79−43077
pyrolitic, Ar^+, N^+ and He^+ ion bombardment numerical discussion of flaking 78−52947
pyrolitic, oriented ellipsoidal voids, small-angle X-ray scatt. 78−64429
pyrolytic, behaviour of implanted D and He 78−95071
pyrolytic, compressed, annealed, low temp. electron irrad., elastic const. meas. *(French)* 78−43050
pyrolytic, diffusion of Nb, 1450 to 1950°C 77−39693
pyrolytic, doped with B^{11}, neutron irrad. damage at 60°C 79−90702
pyrolytic, elastic and inelastic scatt. of Mossbauer γ quanta *(Russian)* 79−61287
pyrolytic, extrinsic defect effect, on a-axis electrical resistivity, exam. 78−47784
pyrolytic, ion bombard., flaking, stress fields around penny-shaped cracks 78−52946
pyrolytic, ion bombarded, surface deformation *(Japanese)* 78−18879
pyrolytic, IR reflectance and dielec. props. meas. 77−55781
pyrolytic, irregular end-plane sections for rot. ring-disc electrode 78−92488
pyrolytic, N_2^+ active ion bombardment, SIMS obs. 79−16034
pyrolytic, neutron irrad., Raman spectra, point defects 77−69834
pyrolytic, neutron irrad. at low temp., thermal cond. recovery *(French)* 77−62566
pyrolytic, sputtering yield meas. on first wall materials of thermonuclear fusion devices *(Japanese)* 77−85865
pyrolytic, stress-annealed, binding to evaporated Ni 77−59210
pyrolytic, structural factor effect on strength 79−66135
pyrolytic, thermal expansion coeff. rel. to temp. 78−43147
pyrolytic C coating within pores 79−41035
pyrolytic commercial, high-temp. thermal and mech. props. 80−75372
pyrolytic crystals, surface topography, bombarded with Ar^+, N^+, He^+ ions 78−6820
pyrolytic graphite, magnetoresistance positive-negative transition *(Russian)* 80−96923
pyrolytic graphite, thermal diffuse scatt., Mossbauer γ-ray diffr. 80−40026
pyrolytic graphite c-axis longitudinal magnetoresistance in quantum limit 78−47814
quantitative X-ray phase analysis of graphite content in C 79−52820
quartz-graphite junction, thermal cond., 6 to 95K, junction rectification 78−63890
radiation absorption cone, for laser energy meas. by optical calorimetry *(Slovak)* 79−40572
radiation alteration over wide range of neutron flux and irradiation temp. 80−29072
radiation creep 77−42064
radiation damage and its relevance to reactor design 79−33016
graphite continued
radiation damage by $^4He^+$, depth depend. and current density effects 80−2091
radiation damage dosemeter, GAMIN 78−29657
radiation damage effect on erosion by H 78−21640
radioactive waste encapsulation appl. *(German)* 78−33281
Raman scatt. and luminesc. 78−23460
Raman spectra, second order, obs. of anomalously sharp feature 77−81103
Raman spectra of carbons and graphite, new lines, exam. 78−48169
Raman spectra of ground natural graphite, grinding influence 79−42956
reactive diffusion in Zr, interaction kinetics 79−42318
reactive sputtering by H^+ ions, target temp. depend. *(Russian)* 77−4707
reactor, fracture toughness up to 2600°C 78−68760
reactor, strength and deformation under conditions of cyclic variations in load and temp. 79−43355
reactor, T behaviour *(German)* 77−24442
reactor, thermal shock fracture toughness eval. by arc discharge heating 78−72835
reactor grade, irrad. creep, 850 to 1100°C 78−44167
reactor H_2O-graphite system, neutron rethermalisation 79−97806
reactor material, laser microemission spectroscopy for local determ. of impurities *(German)* 78−7161
reactor material, stress and strain determ. depend. of mech. charact. on temp. and fluence 79−40998
reactor material, ultrasonic nondestructive testing *(Japanese)* 79−43520
reactor materials, determ. of macro and mesoporosity by stereometric anal. *(German)* 79−3205
reactor UO_2-graphite interaction in operating fuel elements 77−18669
recompressed expanded, thermal conductivity, elastic moduli, density effects *(French)* 78−26744
reflectance meas. in visible spectrum 77−77241
reflectivity in near IR and hydrostatic press. 79−91423
reflectivity in near IR under hydrostatic press., lineshape anal. 79−91424
reflectors in PBR with OTTO fueling, neutron effects, stress anal., cooling measures *(German)* 77−34368
reinforced epoxy, laminated plate under tension, stacking sequence and lay up angle effect on free edge stresses round hole 78−88524
reinforced organic composite, graphite, or C-C, ablation, mathematical modelling 79−41564
reloadable creep facility for tensile or compressive expts. 77−42070
residue compounds, nitrate-type, phys. props. 78−10199
resistivity and magnetoresistance, 4.2 to 293K 80−100459
resistivity measurements for intercalation compounds, contactless 80−37054
RF plasma utilisation in sputtering and surface reactions 78−84714
ribbon, interlayer interaction effects on diamagnetism London theory 78−52201
ring, eccentric, under radial thermal load, stress state 80−76351
scattering and selective adsorption of H_2 (D_2) on (0001) surface 80−71553
scattering of and interaction with ^{4}He 80−60732
self focusing high current relativistic electron beam for structural and chemical transformations *(Russian)* 80−15190
shape, in cast Fe, influence of interfacial energy 80−16360
shell, thin, cylindrical, orthotropic, thermal stresses and displacements due to instantaneous thermal shock 80−92060
shock compression, polymorphic transform. kinetics 79−86838
shock wave, prod. by explosion, vel. meas. 80−59074
silicized, fracture analysis, deform. 78−15530
single crystal, from Fe-C melt, morphology 78−42932
sintered powder, energy losses, secondary electron spectra, AES, and EELS 79−99997
sliding against C, dusting wear regime 80−97595
slow electron elastic reflection charact. 80−25507
solar selective absorbers, graphite on Cu, interf. films deposited on diffr. gratings 79−14103
sols, peptized and unpeptized, structure determ. by neutron diffr. and small angle scatt. 80−40748
solubility in ferrite, high temp. vacuum metallography determ., 545 to 750°C *(Russian)* 77−55359
sound waves, giant quantum attenuation 80−54741
spatial distribution of particles in cast Fe, metallographic study 78−92419
specific heat anomalies around 1.45K in 13.7 T mag. fields 79−42270
specimens for irrad. in reactor core and reflector channels, ampules for handling 77−50220
spectral emittance, meas. at temp. up to 3000°C 77−22550
spheroidal, formation in metal-C system due to high-angle boundaries, X-ray diffr., TEM and SEM obs. *(Russian)* 80−81065
spheroidal, microstruct. in Mg cast iron, rel. to polishing and annealing treatments 77−56160
spheroidal, presence of magnesium studied with electron probe microanalyser *(Ukrainian)* 80−26072
spheroidization, effect on fatigue strength of cast Fe *(Japanese)* 78−64626
spheroidization in cast Fe, Mg residue effects *(Korean)* 79−43286
spherol crystals, morphology and growth 78−18567
sputtering, physical and chemical, by H_2 and He, 600 to 7500 eV 77−36340
sputtering by low energy H and D 78−95630
sputtering yield, use as first wall material 78−95629
standard reference material for thermal conductivity measurement 79−27496
strain measurement, 298 to 3000K, new optical technique 78−85063
strength and struct., conf., Bath, London, England (Apr. 1979) 80−82566
stress-strain diagrams, anal. and classification of low deforming materials by their behaviour under stress 79−15753
stress/strain behaviour, exam. with high temp. short time testing facility 78−53051
stressed materials, mech. charact. analysis using acoustic emission *(German)* 79−15881
structural, impact toughness, reln. to compressive strength 78−88605
structural graphite, radiation dimensional stability, variations 79−71896
structural transformation to diamond probability under high temp. and press. *(Chinese)* 80−65220
substrate, $(Ta,Ti)B_2$ CVD coating, hardness meas., SEM study 80−24760

graphite continued
substrate, (Ti,Zr)B_2 CVD coating, hardness meas., SEM study 80−24760
substrate, Kr absorpt. system, monolayer regime phase diagram 80−49507
substrate, Nb CVD coatings, grain struct. depend. on temp. 80−25574
substrate, NMR relax. times of adsorbed ^{3}He 79−51374
substrate for ^{4}He film growth, vap. press. meas. 80−70499
substrate for adsorbed methane submonolayer, structural transitions between epitaxially ordered phases 80−96740
substrate for inert gas monolayer, transition from localised to nonlocalised state 77−11787
support films, 2 nm, prep. for high resoln. electron microscopy 77−87880
support for Ag particle film, particle motion rel. to heating in gaseous environments 78−34695
surface, ^{4}He low-energy scatt., inelastic effects 80−100738
surface, (0001), He atom scatt., bound state reson., interaction pot., band struct. effects 80−29840
surface, (0001), He atom scatt., gas-surface pot. 78−48267
surface, adsorbed benzene, melting and orientation, NMR study 80−100403
surface, adsorbed CO, fluid-registered solid transition 80−59796
surface, adsorbed Cs, dissolution, lamellar cpd. form. *(French)* 80−100399
surface, adsorbed He, band struct. and thermodynamic props. 80−80349
surface, adsorbed inert gas at. excitation spectrum 78−71943
surface, adsorbed Kr, Potts lattice gas, renormalisation-group treatment 78−67908
surface, anisotropic He-C pair interaction for He atom near surface 80−96738
surface, asymptotic interaction with He, H, and H_2 79−99429
surface, basal face Kr monolayer, fluid-registered solid transition 80−49491
surface, basal plane, selective adsorption of ^{3}He and ^{4}He 80−6650
surface, CO_2 laser beam-irrad., shielding time 79−55530
surface, conditioning by atomic H 80−93665
surface, Fe_2O_3 amorphous layer, Mossbauer spectra, superparamag. props. 80−60474
surface, He scattering, bound state reson. and inelastic effects 79−28876
surface, hypervel. particle impact simulation, using high-power pulsed laser 77−44094
surface, Kr monolayer commensurate-incommensurate transition, X-ray scatt. 79−73382
surface, laser-induced impulse 79−43071
surface, luminesc. accompanied by ion implantation 80−60683
surface, methane adsorption, orientational phases, Monte Carlo calc. 80−2263
surface, methane-d_4 monolayer films, neutron diffr. studies of phases 80−96739
surface, motion of Fe particles 79−90850
surface, physisorbed Xe monolayer, dynamical and thermal props. 80−34292
surface, rare gas adsorbed monolayers, nonregistered-registered phase transition 80−39414
surface, reaction with H_2, mol. beam-surface expt., quasi-equilib. treatment 77−86376
surface, wettability, surface tension, contact angles of liqs. 79−37901
surface (0001), 2-dimens. condensed layer isothermal desorption spectroscopy 77−69181
surface (0001), absorbed Xe or Kr monolayer, liq. state model 77−69185
surface (0001), inelasticity in He scatt. 80−76127
surface (002), phase diagram of adsorbed O_2 monolayer 79−73401
surface alteration by interaction with Ar^+ and Xe^+ beams 78−91347
surface behaviour under various vacuum conditions, Au decoration obs. 78−75915
surface cleaning, air cleavage and UHV cleavage, obs. using Au decoration 78−80665
surface contamination by H_2, shortening of ultracold neutron storage time 78−17461
surface diffusion of 2-dimens. hypercrit. fluid methane, neutron scatt. obs. 77−20193
surface energy determ. using high temp. vacuum metallography *(Russian)* 77−15677
surface erosion by 100 keV $^4He^+$ and 200 keV H_2^+ 78−23569
surface erosion by ion bombardment crystal anisotropy effect 78−23845
surface heating by laser, optical temp. meas. 79−55911
surface homogeneity, changes on gasification, N adsorption study 79−51396
surface interaction and band struct. effects for He derived from scatt. data 78−92162
surface interaction with Cs, study of surface diffusion, computer simulation 78−30837
surface interaction with He atom 80−34316
surface morphology changes after irrad. with energetic He ions 78−21767
surface reaction with Be, Be_2C layer formation 77−36786
surface with adsorbed Ar monolayer, substrate-induced strain and orientational ordering 79−82460
surface with N_2 overlayer, orientational ordering, neutron scatt. meas. 80−10783
surface-Xe (Kr) adatom interaction polarisation energy from opt. data 77−72792
suspension, particle size distrib. function electrooptical diffusion method for determ. 80−8956
suspension in He, high-temp. power plant coolant, efficiency enhancement *(Russian)* 79−68549
suspension in liq. dicyclopentadiene, CO_2 laser pulse induced chem. reactions 80−66821
suspensions, particle shape influence on light absorpt. in mag. field 80−60549
synergistic effect of electrons on atomic H activity 80−106112
synthetic graphite materials, radiation defects, review 77−47494
target in air, refl. of CO_2 laser radiation, plasma layer form. 80−25500
targets for use in LAMPF high intensity beams 79−68107
TEM, sources of background X-radiation 80−101908
temperature calibration standards using graphite-halogens, TEM appl. 80−86510
tensile strength of threads and foils, dimensions depend. *(Russian)* 77−59852
graphite continued
thermal conductivity, effect of porosity 80−65314
thermal conductivity, near 100 mK, rel. to appl. in cryostat construction 77−82535
thermal diffusivity, high temp., meas. by radial flash method 80−52227
thermal shock on a finite orthotropic thin shell 79−68587
thermal shock resistance and fracture toughness during graphitising heat treatment *(Japanese)* 80−71843
thermal shock resistance and fracture toughness meas. *(Japanese)* 79−91868
thermal vib. amplitudes from integrated intensities corrected for TDS 78−67780
thermal-neutron spectra calc. 77−26824
thermionic cathode, Cs-coated 79−11494
thermocouple, in-situ graphite-Si ribbon, calibration and meas. accuracies manufacture 79−97386
thermodynamic properties in HTGRs, accident anal. *(German)* 78−25315
thermoelectric power, low temperature, anomaly rel. to phonon drag 80−65610
thermoelectrical, and thermomag. props., cylindrical band model 80−39616
thickness, high temperature gauge calibration using Re+p cross section data 77−23054
thin film, surface struct., high resolution phase contrast electron microscopy imaging 80−103224
time and spatially resolved at. absorpt. anal. 80−40760
Tokamak, TFR, variable-radius Mo and graphite limiters 78−63600
Tokamak fusion reactor, mag. limiter plate, electron irrad. and thermal shock 78−66416
Tokamak fusion reactor blanket design concepts at BNL 77−3164
Tokamak reactor ISSEC 78−41860
trifluoromethanesulphonate intercalate, prep. by anodic oxidation 78−27439
tritium effects, first wall controlled thermonuclear reactor conditions, simulation 79−647
two-dimensional lattice vibrations calcs. 80−2126
ultrasound method for impregnation by low melting point metals *(Russian)* 78−46876
uniaxial tensile creep capsules with continuous strain registration 77−42071
unipolar arc damage in hot, dense D plasma 79−3235
urban aerosols, optically absorbing component identification as graphitic C 79−34939
vacancy and substitutional impurities, moderately-large-embedded-cluster approach 80−49663
vacuum gap electrode surface sorption, mass spectroscopic obs. 78−75466
valence charge density 77−84694
Van der Waals film adsorbed on graphite, two-dimensional phase transitions 80−107653
Van der Waals interactions, in and between layers of atoms 77−84695
vapour cloud, laser-prod., temp. conditions investig. 80−59290
vitreous, disintegration by fluorophosphate optical glass melt 78−30101
wall and limiter material for Tokamaks, induced desorption diffusion and gas production by 100 eV electrons and ions 79−675
Wannier functions and density matrix determ. in terms of localised orbitals 78−2408
water reaction with pyrolytic graphite surface 78−15707
wax-graphite composite, specific capacitance, temp. and grain size depend. 80−50286
wear, thin layer activation meas. technique, assessment 78−92366
wetting, by molten Al, effects of US 79−15629
wetting by pyroceramic melt, lining material 77−1831
wires, SbF_5-intercalated/Cu composite, elec. cond. 80−44687
X-ray attenuation coefficients, in range 0.40 to 1.54 Å 79−32855
X-ray K-absorpt. edge, EELS meas. 78−56551
X-ray monochromator crystal, TDS, Mossbauer obs. *(German)* 77−16230
X-ray photoelectron diffraction, influence of radiation damage 79−19970
X-ray plasmon scattering from small particles at zero k 80−11505
X-ray spectroscopy of single crysts., use of polarised radiation 78−8481
X-ray spectrum in region of Raman band 80−7436
XPS, high energy cond. and valence band states 78−39664
Al composite development using liquid infiltration technology 77−24986
Al-graphite adhesion and contact angle, effects of metal additives *(Japanese)* 78−60008
Al-graphite two-dimensional shield, neutron penetration meas. 79−3245
Al-Si casting alloys, graphite-dispersed, mech. props. and wear resist. 77−4857
α-Al_2O_3/graphite mixtures, high corrosion resistance refractory materials, fracture anal. *(French)* 79−70137
Ar, momentum density of electrons, two-gamma positron annihilation determ. 77−69211
Ar-graphite system, effects of dynamic coupling 80−10771
AsF_5-graphite intercalation compound nature 80−103308
B coatings on surface, fusion reactor appl. 80−23147
B_4C-graphite, irradiation-induced dimens. changes, rel. to HTGR conditions 78−8905
Be_2C-graphite-UC_2 fuel development for pulsed reactors 79−67856
Br-graphite, intercalation cpd., magnetothermal oscill. and charge-density waves 80−11199
Br_2-graphite systems, adsorbed and intercalated, EXAFS 78−72638
C black, graphitised, adsorbed methane, rot. tunnelling, neutron scatt. obs. 79−15000
C diffusion from graphite to W coating prevention, in metal-graphite layer structure of X-ray tube *(German)* 80−105759
C graphitic, imperfectly ordered ultramicrostruct. characts. direct imaging feasibility by high resolution electron microscopy 79−77463
C K-edge fine struct. 80−66325
C-graphite materials, fluidised bed, carburising of metals, diffusion saturation 79−20276
C-graphite materials for HTR and fusion reactors 80−73928
C+CO_2 reaction, kinetics at low press. and hydrogen inhibition 77−63950
C+CO_2 reaction, Langmuir-Hinshelwood kinetics at intermed. press. 77−66766
C_8AsF_5 intercalation compound, NMR and static mag. susceptibility meas. 78−88214
$C_8^+AsF_6^-$, synthesis of first stage graphite salt, relationship to first stage graphite/AsF_5 intercalate 79−24738

graphite continued
CBr_x, graphite intercalated, de Haas-van Alphen effect and cyclotron reson. 80−44479
$C_8Br_xCl_{1-x}$ intercalate, crystallographic, elec., mag. props. 80−107184
$C_{24}Cs$ and $C_{36}Cs$, graphite intercalated, ordering of intercalant layers, X-ray diffuse scatt. 80−44182
C_8Cs, intercalation cpd., theory of order-disorder phase transitions 80−19908
$C_6Eu(Yb)(Ba)$ intercalation compounds, three dimensional continuous melting 80−59631
$(CF_x)_n$, fluorinated graphite, ^{13}C NMR and ^{19}F NMR spectra 80−15808
$C_{6.6}FeCl_3$ intercalation compound, charge transfer, acceptor sites, XPS study 80−49218
C_8FeCl_3, behaviour with H_2 and CO, effect of activation 79−43623
$C_{12n}K$, graphite intercalated, two-dimens. structurally disordered phases, X-ray diffr. profiles 80−44181
C_8K graphite intercalation compound, band structure calc., charge transfer effect 80−6692
$C_8K(Rb)$, graphite intercalated, phonon dispersion relations and Raman spectra 80−44272
C_6Li, intercalate ordering in first stage graphite-Li 80−6380
C_8Li, theory of order-disorder phase transitions 80−19908
$C_8^+MF_6^-$, (M=Os,Ir,As), struct. and elec. props. 80−70183
$C_{11.3}NiCl_{2.13}$ intercalation compounds, cryst. struct. *(French)* 80−33947
CO_2 permeability meas. up to 41 bars 80−29176
$C_{12}^{2+}PtF_6^-$, struct. and elec. props. 80−70183
$C_{24}Rb$, intercalated graphite, resistivity and specific heat anomalies 80−107440
$C_{24}Rb$, graphite intercalated, de Haas-van Alphen effect, cyclotron reson., and transport props. 80−44479
$C_{24}Rb$, intercalated graphite, order struct. determ. by neutron scatt. 80−107143
C_8Rb, intercalation cpd., theory of order-disorder phase transitions 80−19908
$nC(graphite)+U(g)\rightarrow UC_n$ (n=1 to 6), enthalpy changes obs. 80−7842
Cr_3C_2, form. from Cr_2O_3/graphite mixture in H_2 atmos. *(Japanese)* 78−92225
CrO, reduction by powdered graphite, mechanism 77−4748
Cs desorption, release into nucl. reactor coolant 80−18431
Cs graphite, structural ordering in intercalation compounds 78−26539
Cs sorption kinetics modelling 80−102244
Cs-Graphite, interaction ordered and disordered cpd., Raman spectra 80−11393
CsC_8 intercalation compound, cryst. atomic struct. study *(French)* 79−42021
Cu/graphite-SbF_5 wire composites, synthesis and elec. props. 80−70781
Cu-graphite, brushes, friction and wear under severe sliding conditions against steel 79−38991
Cu-graphite starter brushes, effect of high velocities, current densities on wear, friction 78−88544
D^+ bombardment, surface damage, sputtering, SE, study 80−32459
Fe, cast, flake and nodular, heterogeneous nuclei and graphite chemistry 79−55896
Fe, cast, heated in CO atm., obs. cracks around graphite flakes *(Japanese)* 78−84974
Fe, cast, Mg, despheroidising effect of Bi, Sn on graphite in alloy 78−56670
Fe, cast, spheroidal graphite effects of Si and C on mechanical props. *(Korean)* 79−66114
Fe, cast, US study of sections undergoing deform. or thermal cycling 80−104285
Fe, cast, with spheroidal graphite, crystn. *(German, English)* 80−97473
Fe, cast hypoeutectic, Ce distrib. in graphite grains 80−100279
Fe, exam. of graphite and cast Fe dissolution during sintering 79−33969
Fe-C-Mg, cast iron, graphite phase obs. *(Russian)* 77−59744
Fe-graphite, intercalate, prod. by slow electrochemical reduction *(French)* 78−27437
Fe-graphite, sintered, diffusion layer form. 79−100299
Fe-graphite porous sintered, determ. of impregnation depth with polycaprolactam-finely divided Cu metallic polymer 79−70272
Fe-S-C (1,3 wt.%), sulphidised Fe-graphite bearing materials, sintering, struct. form. 78−60601
$FeCl_2$-graphite, intercalation compound, formation by reduction of Fe(III) compounds with $Fe(CO)_5$ 78−63721
$FeCl_3$ intercalate, direct imaging, HVEM 80−84037
$FeCl_3$-graphite, intercalation compound, Fermi level lowering and core exciton spectrum, EELS study 79−74036
$FeCl_3$-graphite intercalation cpd., electronic excitation spectrum, high resolution EELS meas. 80−45182
$FeCl_3$-graphite intercalation compound, dielec. function, band struct. EELS study 80−49643
$FeCl_3$-intercalated graphite, plasmon spectra 79−38011
HNO_3-graphite intercalation cpd., proton relax. meas., two-dimens. system model 77−51968
K-intercalated graphite (stage-1), electron energy loss expts. and band struct. theory 79−100001
KC_{24}, intercalated graphite, struct. phase transitions, X-ray diffr. 79−65189
KC_8, intercalated graphite, electronic and cryst. struct. 80−44472
KC_8 intercalation compound, H_2 chemisorption *(French)* 79−43624
$KC_8H_{2/3}$, H_2 chemisorption *(French)* 78−27432
Kr-plated graphite, possible Ising transition in ^4He adsorbed monolayer 80−34298
Li-graphite intercalation compounds, synthesis, elec. and optical props. 79−74108
Li-pyrographite intercalation cpds., synthesis and elec. resist. 79−91601
LiC_6, intercalated, charge-transfer and non-rigid-band effects 80−44496
LiC_6, intercalated graphite, band struct. determ. by angle-resolved photoemission 80−45203
LiC_6, intercalation compound, electronic struct., XPS meas. 80−59850
MgO film, graphitic C detected by surface Raman spectra 80−2297
MoF_6-graphite intercalation cpd. 78−27441
N_2^++Group IV elements and oxides, XPS and UPS prod. determ. 78−73084
Na-graphite intercalates, preparation, struct. 80−103307
NaCl-graphite interface, elec. cond. 78−52060
Ni-C-Ce, overmodification *(Russian)* 80−40432
Pt-graphite catalyst, H adsorption, ESR obs. 79−24818
RbC_8, intercalated graphite, band struct. determ. by angle-resolved photoemission 80−45203

graphite continued
SiC protective coatings, on graphite for HTR, corrosion *(German)* 78−3248
SiC-B eutectic alloys, struct. of crystallising graphite 79−38829
Th-graphite fusion blanket assemblies, neutronic calcs. using 14 MeV source 79−59262
UO_2 molten, interactions with steel and graphite 79−49700
UO_2 pellets-graphite-Zircaloy cladding, evaluation of graphite lubrication 80−32342
UO_2/Zircaloy pellet/cladding interaction, eval. of lubrication of graphite 79−67857
UO_2-graphite interactions, effect of stainless steel, temperature on reaction rate 79−59172
WF_6-graphite intercalation cpd. 78−27441
Xe-plated, adsorption of Ne, virial coeffs. 78−18904
ZrB_2-SiC-C(-V)(-Nb), refractory cermet, hot pressing and oxidation resist. 80−3231
ZrC growth on surface via activated cementation *(French)* 77−52552

graphitisation
anthracene, mesophase formation during carbonisation under pressure 77−44182
aromatic hydrocarbons, carbonisation of heterocyclic cpds. catalysed by $AlCl_3$ 77−63572
artificial carbons, graphitisation shrinkage kinetics 77−48385
bulk mesophases, electron microscope obs. 78−44035
catalytic, three-phase, of phenolic resin C by Ni particles 78−68922
catalytic effect of S, 1400-2000°C 77−28735
charcoal, catalytic graphitisation by gaseous species from Ca 80−11872
coke, anisotropic spheres obtained during needle coke form., struct. obs. 77−63573
coke, effect of addition of borides on hot-pressing 80−40282
coke, partially graphitised, K intercalation-desorpt. cycle rel. to stacking faults 78−47396
cokes, acicular and spherulitic, high pressure effects on graphitisation 77−36414
cokes, graphitised, Raman spectra, effective Debye parameter, magnetoresist. 78−44231
crystal growth and graphitization 80−89165
diamond synthesis by graphitisation of carbon materials at high press. and temp., Ni influence 80−60795
diamond tools on steel, graphitisation due to clean surface reactions 78−85008
3,5- dimethylphenol formaldehyde resin carbon, catalytic graphitisation from various metals 80−11871
film, work function, heat treatment 78−64563
glassy C, graphitisation kinetics 79−52246
graphite based composite material, with ZrB_2 and SiC additions, prep., props., struct. 77−28775
graphite-diamond, shock induced transform. anal., post shock graphitisation 80−79933
kinetics within first min. of heat treatment 77−66596
Mering-Maire's analysis, paracrystn. nature of pyrolytic C 79−77451
mesocarbon microbead, heat treatment under high pressure 77−28736
mesophase formation during carbonisation under pressure 77−44182
naphtha tar pitch, mesophase formation during carbonisation under pressure 77−44182
nucleation, role of pre-heat treatments *(Japanese)* 80−35220
petroleum feedstocks and cokes, graphitisability 80−93580
phenanthrene, mesophase formation during carbonisation under pressure 77−44182
phenol formaldehyde resin carbon, catalytic graphitisation from various metals 80−11871
phenolic resin carbon, by Al powder, catalytic mechanism 77−28734
pyrolysis mechanism, electron microscopy, DTA, IR, ESR obs. 78−56593
saccharose char, catalytic graphitisation *(French)* 77−28739
steel, alloy, low C, effects of pre-treatment on graphitisation behaviour *(Japanese)* 78−84860
steel, high C, graphite nucleation on surface *(Russian)* 80−40360
steel, low alloy structural, pre-treatments to enhance graphitisation, dilatometric and optical microscopy study *(Japanese)* 79−78992
texture change on ht. treatment under press. 78−60687
XPS anal. of Ar and ^{57}Fe ion-bombarded 77−11769
C, catalytic, by various metals 80−3401
C cathode in Al reduction cell, intercalation props. 79−43559
C fibre, graphitisable, prepared by benzene decomp., stepwise heat treatment, TEM expts. 77−85950
C fibre reinforced glassy C composite, graphitisation 79−15643
C fibre reinforced Ni, struct. and strength change at high annealing temp. *(Russian)* 79−66076
C fibres struct. and physical props. effects of B additions and heat treatment temp. 78−68715
C film, vac. condensed, graphitisation, electron microscopy 80−40265
C films, surface struct., graphitisation, secondary electron spectra and AES 79−43077
C foil, ion irrad., crystallographic transform. 79−55794
C foil, ion irrad., graphitisation rel. to lifetime, relevance to beam-foil spectroscopy 80−15166
C, glassy, graphitisation, density change 78−44142
C, graphitisable, catalytic graphitisation by Cr, Mn and Mo oxides 80−89166
C, graphitisation, cooperative accelerating effect of $CaCo_3$ and N_2 80−55429
C mats., stages 77−81235
C, nongraphitizable, catalytic graphitization by Cr_2O_3, MnO_2 80−97440
C, pyrolytic, by Ni, rates and activation energy 79−57010
C, structure change, during thermal ordering, radiation disordering 80−54283
C, turbostratic, formed in phenolic resin C by catalytic graphitisation of dispersed Ni, TEM study 79−77466
C/C composite with S-modified pitch binder precursor, carbonisation and mech. props. *(German)* 77−44183
C-C composites, existence diagram and properties *(French)* 78−64517
Co-C alloys, graphite nucleation on surface *(Russian)* 80−40360
Fe, cast, white, freezing rate and Si content effect on graphitisation *(Japanese)* 77−56009
Fe, white cast, migration of C to the surface, solubility *(Russian)* 80−92720
Fe-C (synthetic diamond) role of diffusion of graphitisation in phase interaction 77−36449

graphitisation continued
Fe-Mg, cast, ferrite-based, graphite nucleation on surface *(Russian)* 80−40360
Ni-C alloys, graphite nucleation on surface *(Russian)* 80−40360
Re:C, work function, graphitic layer formation 80−96966
graphitising
nodule growth, kinetics and rate controlling process in graphite *(Japanese)* 80−35203
steel, graphitised, elastic modulus and internal friction, temp. depend. 80−35242
steel, hypereutectoid, form. of surface graphitisation centres *(Russian)* 79−11720
steel, hypoeutectoid, alloying effect of graphitisation *(Japanese)* 79−52270
FE, cast, growth of graphite crysts. from δ-containing Fe-C melt *(German)* 78−3148
Fe, cast, alloyed and unalloyed, microsegregation thermodynamics 80−76261
Fe, cast, corrosion in uninhibited alcohol/water coolants, and graphitization 78−44248
Fe, cast, graphite content determ. by X-ray diffr. method 80−100977
Fe, cast, modular graphite form., Ce effect *(Japanese)* 77−56000
Fe, cast, nodular graphite form. by Bi and Pb additions *(Japanese)* 77−63693
Fe, cast, nodular graphite form. by Ar, N_2 or CO_2 gas bubble suspension *(Japanese)* 77−63694
Fe, cast, rare earth-Mg, metallurgical and technological features, appl. in China *(Chinese)* 78−84851
Fe, cast, S and Mg effect on nodular graphite form. *(Japanese)* 77−56001
Fe, cast, unalloyed and alloyed, addition effects on struct., thermodynamics of microsegregation 79−8305
Fe, cast, white, graphitisation, effect of hot impact deform. 78−19780
Fe, cast, white, graphitisation during heat treatment *(Russian)* 80−20971
Fe, cast nodularisation of graphite by Ce, Y, La, Ti, and Zr additions *(Japanese)* 77−55999
Fe, pure, on heat treatment *(German)* 77−59818
Fe-C, graphitisation, interfacial segregation effects 77−52373
Fe-C melt, graphite cryst. growth rate rel. to supersaturation *(German)* 77−55940
Fe-C system, liq.-solid equilib. at high press., influence of graphitising elements *(Russian)* 78−56613
Fe-C-Si, cast, graphite nodularization during annealing, Mg and S effects *(Japanese)* 80−81087
Fe-C-(Si)(S) alloys, graphitisation during heat treatment *(Russian)* 80−20971
Fe-Cu(-C), alloyed with graphitising elements, geometrical thermodynamics *(Russian)* 79−52261
Fe_3C, cementite, modified by rare earth metal and alloying additions, thermal stability *(Russian)* 78−56663
graphs
see also Bode diagrams; nomograms
alloying behaviour and compound form. graphical rep. 77−19895
atomic spectra, quantum defects and ionis. pots., graphical procedure for students 80−7
computer programs for high-school expts. 78−86094
digital seismic data processing, struct. anal. of graphs *(Russian)* 78−53749
electromagnets design aids, laboratory type *(Czech)* 79−88985
equilibrium constants determination, projection map technique 78−53240
G-convolution of n-point functions in quantum field theory 80−18065
groundwater chemical geothermometer, Na-K-Ca temp. with Mg correction 80−51357
histogram plotting, FORTRAN program 'HIST' 78−77876
hydrocarbons, saturated, topological orbitals, graph theory and ionis. pots. 78−82615
isomers, structural formulae, graphs generation by computer *(Russian)* 79−49967
lens paraxial eqn. dimensional analysis 80−74462
Mayer graphs, general, rigorous estimates and applics., uniform upper bands 77−82363
metal, plastic strain graph plotting at high strain rates by cutting method 77−90521
molecules, graphical struct., matrix descriptions 77−38737
ocean current meter data, graphic presentation 78−45055
optical system design, multi-layer, using equivalent films *(Czech)* 78−90486
polyhedra characteristic eqns. of graphs, symmetry factoring 77−83517
robust feature matching through maximal cliques 80−99671
selective information distribution system for international scientific cooperation *(Russian)* 79−179
surge wave height determination, graphical method 80−56485
tube bank efficiency in cross-flow, graphoanalytic method *(Russian)* 79−7365
gratings (diffraction) *see diffraction gratings*
gratings (optical) *see diffraction gratings*
gratings (spectra) *see diffraction gratings*
gravimeters
see also geodesy
AFGL absolute system, progress report 79−92607
in artificial Earth satellites, basic mechanical principles *(German)* 80−101461
Askania type gravimeters, sensitivity determ. rel. to gravity tidal changes at Poltava *(Russian)* 78−88782
Askaniya gravimeter, phase distortion in tide registration *(Russian)* 78−4011
automated GMN-K gravity meters, marine testing *(Russian)* 79−39953
automated gravimetric titrator, U meas. 79−85609
calibration, based on inclination method 77−91313
Canadian precise gravity networks for crustal movement studies, instrument evaluation 79−79724
counter rotation circuit nonlinearity *(Russian)* 79−88497
cross-coupling effect compensation, by intersection point method, marine gravimetry 78−57340
Eotvos effect variations allowance in gravimetric studies, data processing 79−74969
external temperature variations effects on CG-2 type gravimeter readings *(Chinese)* 79−88476
gas gravimeter use for variable linear acceleration meas. 78−77875
gravimeters continued
gradiometer, moving-base, surveys and interpretation 78−77344
gradiometer systems for lunar gravity meas. 80−94730
gradiometers in artificial Earth satellites, basic mechanical principles *(German)* 80−101461
GS-12 No.185, design and circuitry *(Russian)* 78−4010
gyroscope appl. to gravity meas. in ocean, horizontal platform using electrostatically suspended gyroscope *(Chinese)* 79−100976
haemofiltration control system *(German)* 79−5403
HF, calibration and sensitivity 78−7812
La Coste and Romberg model D, scale factor determ. 78−85724
LaCoste and Romberg gravimeter, vibration characts. *(Japanese)* 78−65400
LaCoste and Romberg gravimeter platform, horizontal accel. effects 80−4129
LaCoste and Romberg inertial navigation system for gravity meters 77−82022
LaCoste-Romberg G-258 gravimeter, instrumental improvements for μGal meas. 79−92606
LaCoste-Romberg model D and G, digital voltmeter reading evaluation 79−96830
laser ballistic gravimeter, meas. of absolute acceleration due to gravity 80−12569
Liebscher method of gravit. constant determ., theoretical analysis *(German)* 77−29465
marine digital gravity meter, computing unit design *(Russian)* 79−39936
marine spring gravimeter, GMN automatic equipment *(Russian)* 77−45197
microgravimetric network for secular gravity studies in Scotland 78−36298
Mossbauer gravity meter for mineral exploration 77−37444
networks, adjustment *(German)* 79−44084
noise due to atm. pressure fluctuations 77−44894
portable absolute gravimeter development with few parts in 10^9 accuracy 79−80054
portable absolute gravimeter for nontidal gravity vars., plans 79−92605
resonant gravity gradiometers, electronic cooling 79−49222
sea gravimeter trials on Halifax Test Range, NW.Atlantic 77−2267
seabed gravimeter with TV observation system *(Russian)* 77−70869
superconducting, continuous gravity meas., atm. press. effects 79−79725
superconducting gravimeter, general struct., detection system and precision *(Chinese)* 79−34995
superconducting gravity gradiometers 79−29868
torsion gravimeter, suspended mass vibration damping *(Russian)* 78−4015
transportable apparatus for absolute meas. of gravity 79−66823
gravimetric instruments *see gravimeters*
gravimetry *see density measurement; weighing*
gravitation
see also general relativity; gravitational collapse; gravitational red shift; gravitational waves; quantum field theory of gravitation; Schwarzschild metric; unified field theories
ϕ^4 theory, renormalisation of energy momentum tensor 77−6019
absolute space time theory, criticism 78−86210
absolute space time theory, reply to criticism 78−86211
absorption of gravit. force and tidal forces *(German)* 77−41524
acceleration, absolute determ. method 79−71187
acceleration of freely falling particle in stationary gravit. field *(Russian)* 77−53808
acceleration of two massive bodies, for teachers 78−81766
affine manifolds, 3-D, existence of metric 80−82695
analogue of electromagnetic induction *(Russian)* 79−21609
angular momentum of stationary gravitating systems 79−88851
angular scattering of spinor charged particles by a Kerr-Newman field 80−94996
anholonomic coords. and tidal gravitational field of planet 79−34723
anisotropic Bianchi II cosmological models with matter and electromagnetic fields 79−48976
anisotropic parametrised post-Newtonian gravitational metric field 77−5720
anomalous Einstein coefficients representation with effective space-time metric *(German)* 77−82118
appl. to double star attraction *(Italian)* 80−8531
astronomical bodies, mag. field, cosmological interpretation 80−46714
astrophysical plasmas in mag. and gravitational fields, MHD separation of high energy plasma 80−67547
asymmetric Maxwell theory, additional universal inverse square forces 80−27149
asymptotic flatness of spacelike infinity 78−45532
asymptotically flat gravit. field, Hertz pot. and radiation fields 77−60994
attraction between two quickly moving bodies, energy depend. 77−2597
attraction of rectangular parallelepiped 78−7556
attraction of right polygonal prism 77−82439
attraction of vertical right circular cylinder, rel. to gravity data interpretation 77−60343
attractive potential of planet of arbitrary oblateness 77−91424
axially symmetric Brans-Dicke solutions for Einstein's field eqns. 80−90753
axially symmetric fields of gravitation, covariant decomposition of field eqns. *(German)* 79−80473
axisymmetric accretion flows very near black holes and Rosen-collapsed objects 80−12778
axisymmetric gravit. fields, review 77−17881
axisymmetric gravitational fields, internal symmetries 79−88849
axisymmetric gravitational fields, nonlinear differential eqn. giving exact eigenfunction solns. 78−77779
axisymmetric stationary gravitational field, classification scheme 77−5722
axisymmetrical body, translational-rotational motion in gravitational field of sphere, averaging methods applic. *(Russian)* 78−21049
background depend. approach, quasistatic limit 77−9937
background depend. approach, relativistic gravitational eqns. 77−9938
Backlund transformations of axially symmetric stationary gravitational fields 79−40421
Bars-MacDowell eqns., Einsteinian solns. 78−41221
baryon gravitational annihilation as type of radioactive decay *(Russian)* 77−26470
Bel-Petrov field classification, algorithm 78−93566

gravitation continued
Bel-Robinson superenergy tensor, tetrad description of gravit. field 77−57236
Bhabha-Gupta field coupled to external EM and gravitational fields, causality 78−4767
bi-metric theory of gravit. 77−17889
bi-metric theory of gravitation, props. of rotating neutron stars 80−90466
bi-metric theory rel. to gravitational red shifts 79−35119
Bianchi type I cosmological soln. in new gravitational theory 79−88775
Bianchi type I space-time gravitational field, particles eqn. of state 80−77664
bimetric gravitation and cosmology 77−17352
bimetric gravitation theory, appl. to binary pulsar (PSR 1913+16) 78−45347
bimetric gravitation theory, cosmological basis, closed universe 78−65844
bimetric gravitation theory, cosmological model 77−33710
bimetric gravitation theory, existence of incompressible matter 77−33329
bimetric gravitation theory, fields due to finite-size charged body 79−88862
bimetric gravitation theory, fields due to point charge 79−88861
bimetric theory, conservation laws 80−4616
bimetric theory, degenerate stellar mass *(Russian)* 79−12466
bimetric theory, extremality props. of mass calc. 78−120
bimetric theory, flat metric election 80−62004
bimetric theory, inertial and gravitational masses 77−13666
bimetric theory, neutron star mass limit 77−78813
bimetric theory of gravit. 78−24713
bimetric theory of gravitation, cosmological models 77−41424
bimetric theory of gravitation, viability, gravitational radiation from neutron star binaries 79−35611
bimetrical formalism in general relativity, gravitational field description *(Russian)* 77−45750
Birkhoff's theorem generalisation 80−27187
black hole entropy, sense or not 80−52092
black hole equilibrium in radiation filled cavity 80−52093
black holes, gravit. mirror effect as possible detect. technique *(Russian)* 78−40987
black holes, particle creation in gravit. field 77−17614
black-body radiation and thermal equilibrium in static gravitational field 79−67238
black-hole evaporation unified gravit. and electromag. field theory 78−53979
Bondi-Hoyle-Lyttleton model of gravitational accretion, stability 77−82120
brachistochrones, tautochrones, evolutes, and tesselations, for teaching 79−25798
Brans Dicke theory, dust distrib. in nonrigid rotation 79−93020
Brans Dicke theory, plane symm. static fields 80−114
Brans-Dicke and Sen-Dunn theories of gravitation, spherically symm. static conformally flat solns. 79−44825
Brans-Dicke axisymmetric stationary vacuum fields 77−33921
Brans-Dicke cosmologies, linear density perturbation 77−22336
Brans-Dicke cosmology, the cosmological term 78−24582
Brans-Dicke fields generated from Einstein's vac. fields 79−30308
Brans-Dicke fields generated from Einstein's vacuum fields, 'rod solution' 79−71326
Brans-Dicke Maxwell field eqns., class of exact solns. 77−13668
Brans-Dicke Maxwell fields, static Weyl solutions 79−85033
Brans-Dicke static axially symmetric Maxwell fields 79−97278
Brans-Dicke static spherically symmetric field, EM potential of test point charge 79−85041
Brans-Dicke theory, charged particle field 78−65849
Brans-Dicke theory, cosmological solns. for homogeneous isotropic universe 78−96579
Brans-Dicke theory, cylindrically dust distribs. in rigid rotation 78−62136
Brans-Dicke theory, generalised static EM fields 80−12972
Brans-Dicke theory, static and non-static solns. 78−32744
Brans-Dicke theory and general relativity, distinction, physical equivalence of theories 77−57240
Brans-Dicke theory for irrotational barotropic models with stiff matter, exact solns. 80−95018
Brans-Dicke theory of gravit., freq. shift of radiation from exploding/collapsing object 79−67210
Brans-Dicke-Maxwell nonstatic cylindrically symmetric fields 79−49138
canonical formulation of gravitational theory, generally covariant space-time separation *(Russian)* 77−41513
Cartan's theory, generalisation of spin-spin interaction 79−9169
Cartan spacetime, pseudoscalar action 79−12691
cartesian operator algebra for expansion of tensor quantities and equations in a spherically symmetric background 79−44821
causality and relativity 78−81901
cavity, vanishingly small, gravitational field inside matter 80−95012
central field, interstellar flyby missions, relativistic effects 78−61729
charged black hole, evolution of scalar perturbations near Cauchy horizon 79−35608
charged black hole interaction with EM waves, decoupled eqns. for Debye potentials 77−22261
charged body free fall motion in gravit. field, field energies and equivalence principles 78−49740
charged dust equilibrium distrib., classical Brans-Dicke theory 79−12694
charged particle, gravitational mass derivation 80−4597
charged particle field eqns. in gravity theory, static spherically symmetric solns. 79−85031
charged particle gravitational field, general spherically symmetric metric 77−53806
charged particle self-interaction in black hole gravitational field 79−97275
charged perfect fluid, stationary gravitational fields 78−24709
charged tachyon, gravitational field 78−54282
circular disc gravit. attraction 77−52959
classical field theory 79−80375
classical fields gravitational coupling, decomposition method extension 78−127
classical gravity with higher derivatives, massive excitations 78−65845
classical non-Abelian gauge theories in the space of reference frames 80−31977
clusters of galaxies, dynamical props. from nonlinear gravitational instability theory 77−87557

gravitation continued
cold ultradense config. in Brans-Dicke theory 78−4546
collisionless gravitating systems, gravitational pot. nonlinear eqns. determ., astrophysical appl. 80−67560
colour geometrodynamics, eightfold way, review 80−95243
composite rotating plasma, gravitational instability, including Larmor radius, Hall currents, collisions 77−60591
conformal anomalies in curved space-time 77−26210
conformal anomalies using dimens. regularisation in general metric 77−57454
conformal flatness and the Schwarzschild interior solution 79−30333
conformal gravity as a gauge theory 79−49144
conformal invariance of world lines of particles with non-zero rest mass *(Russian)* 77−2575
conformal supergravity, props., gauge theory 78−78085
conformally flat Einstein-Maxwell spaces, Newman-Penrose formalism 80−62559
conformally flat space-times of divergence free Riemann tensor 78−41220
conformally invariant gravit. theory, astrophysical appl. 77−82428
conformally invariant gravitation theory and space-time singularities 77−74286
conformally invariant theory non-singular cosmologies 77−22337
continuity equations, for transverse multipole amplitudes, EM and gravitational fields 79−58609
continuum field theory, convergence to general relativity 80−46875
corpuscular model, geological and geophysical consequences *(Russian)* 77−67367
corpuscular model of gravitation and inertia, geophysical consequences *(Russian)* 79−40439
correspondence principle, energy aspect, in gravitational theory *(Russian)* 77−2576
cosmic matter-antimatter asymmetry and gravitational force 80−90586
cosmic microwave background, residual fluctuations, gravitational effects 80−62332
cosmological anisotropic dust filled model, closure result 77−37676
cosmological models, homogeneous, using Einstein's theory of gravitation 79−12547
cosmological particle pair creation as above barrier reflection, WKB approx. 79−80377
cosmological soln. with matter for new gravitational theory 80−86021
cosmologies with varying gravity, theories and effects 77−60858
cosmology, general relativity, big bang model, nucleosynthesis, scale covariant theory, review 78−73789
cosmology, simulation of two-dimensional gravit. system dynamics rel. to Universe large-scale struct. form. 80−98749
cosmology, space-time metric, quantised field influence, external grav. field *(Russian)* 80−86027
cosmology based on the quantisation of space and time *(Danish)* 80−8724
Cosserat continuum in space with torsion *(Russian)* 78−24715
coupled inertial and gravitational effects in the proper reference frame of an accelerated rotating observer 79−93007
covariant 'in-out' formalism for creation by external fields 79−107
covariant gravitational theory using Yang-Mills fields *(German)* 79−21615
covariant theory, field eqns. and eqns. of motion, Newtonian approx. *(German)* 78−29029
covariant theory of gravitation, curvature quantities, Yang-Mills type field *(German)* 77−53816
covariant theory of gravitation, Einstein field eqns. reformulated *(German)* 77−53817
curved space-time, conformal coupling of gravitational wave field to curvature 80−68105
cylinder, longitudinal vibrs., gravity effects 78−34061
cylindrical gas system, rotating and self gravitating, thermodynamic instability 80−82191
cylindrical wave solutions of a scalar-tensor theory of gravitation in a Lyra manifold 79−21633
cylindrically symmetric self gravitating fluids, with press. equal to energy density 79−58591
de Sitter gauge theory for gravitation *(Chinese)* 79−80487
De Sitter symm. space, gravit. interaction and spinning electron eqn. 78−103
decoupled eqn. solns., EM and gravitational perturbation eqn. soln. construction 78−70029
deflection of light, meas. at 1919 May 29 solar eclipse 80−67553
deflection of light *(French)* 80−94710
differential constants of motion for free gravitating particle systems, Newtons theory 79−9166
differential forms in general relativity 79−44818
dimensional analysis in metric relativistic theories 77−30067
dimensionless coupling constant magnitude and cosmogony 77−33714
Dirac electron mean motion in gravit. field 77−22478
Dirac eqn. De Sitter gauge transformation, gravit. field interaction 77−67563
Dirac equation as basis for unified treatment of electromagnetic and gravitational theory 78−8314
Dirac particles in Minkowski space with torsion 78−57824
Dirac-spinor form of Maxwell's eqns., polarised light beams in gravitational fields 78−50696
Doppler effect, gravitational, explored using geostationary satellite 80−109351
duality and Backlund transforms. 80−12971
dually charged perfect fluid, stationary gravitational fields 77−49654
dynamical space and gravitation, geometrical framework, Mach's principle 80−95001
dynamical space and gravitation within a purely geometrical framework including Machian ideas 78−93587
dynamics in galaxies, gravitational instability of loosely wound spiral density wave 80−85998
early big bang, asymptotic freedom, rel. to cosmic microwave background isotropy 80−46712
early Universe, horizon problem and the broken-symmetric theory of gravity 80−62344
early Universe, possible gravithermal origin of cosmic inhomogeneities 80−56986
Earth, external gravitational field, determinative and stochastic descriptions 79−34730
Earth gravitational field, local vanishing due to left turning motion *(Japanese)* 80−98798

gravitation continued
Earth-Moon system origin determ. and lunar palaeotides 79−40098
education, g radial variation, comments 77−82343
education, gravitational fields, brachistochrones and isochrones 77−87596
education, should Einstein's or Newton's theory be taught in secondary schools? *(Hungarian)* 79−88780
educational problems, programmable pocket calculator 78−4438
Einstein's dust equations, non-radiative solns. 77−13643
Einstein's field eqns., information on local physical conditions 78−21017
Einstein's field eqns. on curved background metric, approximation method 78−109
Einstein's field theory with teleparallelism and Dirac's electrodynamics *(German)* 79−40418
Einstein's gravitational field eqns., finite element method soln. 80−86177
Einstein's theories extended, book 80−22164
Einstein's theory of gravitation, review 80−90745
Einstein's theory of gravitation generalised using tetrad field to avoid singularities 78−57833
Einstein's theory of gravity, special formulations *(German)* 79−58605
Einstein black hole, existence, local instantaneous symm. of space-time, variable vel. *(Chinese)* 77−13381
Einstein eqns. new family of solns., connection with spinning mass fields 77−30061
Einstein field equations, covariant splitting, spherical symmetry models *(German)* 79−21616
Einstein gravit. field eqns., static solns. and Birkhoff's theorem 79−71340
Einstein gravitational eqns., integration by inverse scatt. method, soliton solns. *(Russian)* 79−25940
Einstein gravitational light deflection in astrometry 77−17359
Einstein gravitational theory, rel. to origin of matter in universe 78−20918
Einstein symposium, Berlin, Germany (Mar. 1979) 80−90596
Einstein theory, axisymmetric scalar-tensor gravit. field 77−33917
Einstein-Cartan's theory with anticommuting variables in Dirac's Hamiltonian formalism 79−49125
Einstein-Cartan and Einstein theories of gravity, effective equivalence 78−24703
Einstein-Cartan equations, solns. 78−8299
Einstein-Cartan generalised field eqns., spin field 77−22472
Einstein-Cartan generalised theory, field eqns. and contracted Bianchi identities 79−12681
Einstein-Cartan theories, first-order, classification problem, generally invariant Lagrangians *(Czech)* 80−42129
Einstein-Cartan theory, charged fluid spheres, exact solns. 79−2687
Einstein-Cartan theory, cold matter static spherical configurations 78−49308
Einstein-Cartan theory, junction conditions 77−30058
Einstein-Cartan theory, spherically symm. static solns. with completely polarised Cosserat medium 80−95021
Einstein-Cartan theory, static fluid spheres, field eqn. analytic solns., neutron stars 79−2688
Einstein-Cartan theory, static spherically symmetric solns. 78−89387
Einstein-Cartan theory, with anticommuting variables, quantisation in Diracs Hamiltonian formalism 79−93017
Einstein-Cartan theory as Poincare symmetry gauge theory 77−22463
Einstein-Cartan theory of gravitation, generalized 78−73895
Einstein-Cartan theory of gravitation, homogeneous isotropic cosmological model *(Russian)* 77−49510
Einstein-Cartan theory of gravitation in a Hamiltonian form 78−93581
Einstein-de Sitter model and metric, book contrib. 80−22248
Einstein-Infeld-Hoffman theory, Lagrangian formalism to fifth order and gravitational waves 77−67354
Einstein-Maxwell, homogeneous fields admitting transitive group of motions 79−40437
Einstein-Maxwell eqn. soln. for spherical shell charged dust distrib. 77−2574
Einstein-Maxwell eqns., exterior stationary axisymmetric solns. 79−21622
Einstein-Maxwell eqns., generation of Lewis solns. from Weyl solns. 79−93019
Einstein-Maxwell eqns. with axial symmetry, exact solns. 80−118
Einstein-Maxwell equations, axisymmetric stationary exact solns. 79−25952
Einstein-Maxwell equations, solns., causality violation in rotating universe 79−44828
Einstein-Maxwell field equations, charging transforms 80−95017
Einstein-Maxwell field equations, connection approach 79−88860
Einstein-Maxwell fields, equilib. and global integrability conditions 77−30070
Einstein-Maxwell fields, Kerr-NUT metric 78−89382
Einstein-Maxwell fields, static and axially symmetric, comment on soln. 79−71339
Einstein-Maxwell fields, stationary solns. by combining Demianski algorithm with Kinnersley method 80−90758
Einstein-Maxwell instantons charge quantization 79−80489
Einstein-Maxwell nonstatic-source free symmetric coupled zero-mass and EM fields 79−63111
Einstein-Maxwell null field metric, exact cosmological solns. 79−67122
Einstein-Maxwell scalar eqns., axial symmetric field singularities 79−71327
Einstein-Maxwell space times, momentum and angular momentum in H-space 79−49137
Einstein-Maxwell space times, symmetry mappings 79−49139
Einstein-Maxwell stationary field eqns. 80−98840
Einstein-Maxwell system of eqns., EM field four-vector gauge 79−88864
Einstein-Yang-Mills equations, canonical connections on Riemannian symmetric spaces 80−95004
Einstein-Yang-Mills theory, gauge theory and symmetry 77−22464
Einsteins assembly of test particles, reconstruction in Minkowski space-time 79−30303
Einsteins gravitation theory, use of exterior forms 80−17845
Einsteins gravitation theory as a gauge field 79−26209
elastic homogeneous sphere in its own gravit. field, general relativistic calc. 77−67344
electrodynamic and gravitational effects of Proca stresses in astrophys. 78−93098
electrogravitational conversion cross sections in static EM background fields 78−24711
gravitation continued
electromagnetic interpretation, contribution to classical theory *(Rumanian)* 80−68109
electromagnetism and gravitation field equations, metric-affine gravit. framework 78−45547
electron gravitational interaction, QED corrections 77−30305
electron-ion plasma, equilib. and stratification in gravit. field *(Russian)* 79−29988
electrons, negative energy, explanation of inertia *(German)* 79−88842
electrostatic potential in Reisser-Nordstrom gravitational field 79−30335
electrothermodynamical theory, gravitational field shielding *(Rumanian)* 80−68107
electrovac solns., axially symm., source of gravit. and EM fields 77−60987
elementary particle magnetic layered theory, including gravity 77−30353
elementary particle theory, unified description *(German)* 77−41803
EM and gravitation fields in flat space time, relationship, hierarchy hypothesis 77−5732
EM propagation between physical source and constant vel. receiver in vacuo 80−105502
EM wave diffraction by large star 77−5724
EM wave focusing effect, short-wave limit imposed by lens star gravity field asphericity 79−58604
EM waves, gravit. deflection and polarisation plane rot. in non-Minkowskian spacetime 79−35115
embedding classical fields in QFT, electrodynamics, Yang-Mills theories, gravit. appls. 78−54223
energy conservation and the principle of equivalence 79−54018
energy from quadratic Lagrangian with torsion 78−115
energy-momentum gravitational pseudopotential and Kerr-Schild metrics 77−2573
entropy, gravit. field source rel. to black hole thermodynamics and time asymmetry 77−2451
equations of motion, Heisenberg and classical, force term, spin-curvature coupling 80−57158
equivalence, massive bodies of electromag. struct. *(Russian)* 79−21610
equivalence principle according to Mach 79−44823
equivalence principles in electromagnetism 77−30083
Ernst equation two connection, operator bundles, for axially symmetric gravitational fields 80−31646
etergy-momentum tensors, characterization in gravitational field eqns. 79−88846
Euclidean gravity, self-dual solns., Einstein eqn. solns. 79−85037
expanding universe, galaxy correls. time evolution, gravit. instability, model 79−17145
extended supergravity, gauge internal symmetry 77−38115
external gravitational potential, approx. with closed systems of trial functions 80−101310
external torsion and the electromagnetic force 79−17306
f-dominance of gravity in SIS two-tensor theory 78−36915
f-g gravity theory, exact spherically symmetric solns. 79−319
Fermi universal coupling and gravit. in general relativity 77−79
field eqn., higher order derivs. and spherically symmetric static solns. *(Chinese)* 80−42108
field equations from Lagrangian density, post-Newtonian approx. 77−17888
field theory, ten-dimensional manifold of local inertial reference frames 80−46903
field theory with point particles and zitterbewegung 77−57262
fields whose brachistochrones and isochrones are identical curves, for teaching 79−25807
fifteen parameter conformal group, geometry and isomorphism 79−9154
finite range tensor gravitation 80−27200
Finsler space, second curvature tensor 79−17318
Finsler space, volume concept anal. of gravitational field *(Russian)* 77−13670
Finsler spaces, gravitational field theory 80−12962
fluid spheres, charged, exact solutions 77−30069
formalism, using vector field 78−89385
fourth-order field eqns., Weyl-Eddington theories 78−121
Free vector field in a homogeneous space with torsion 80−90759
freely falling object in reference frame of accelerated rotating observer 78−54259
Friedman models, particle creation from vac. 77−5603
Friedmann cosmological models, fermion pair creation by gravit. field and singularity *(Russian)* 78−93493
fundamental mechanics, thermodynamics and gravitation (book) 80−41964
galaxies, gravitational potential, three dimens., generalised model 80−109551
galaxies, local gravit. instability of double gas disk 80−8691
galaxy halo effect on galaxy warp precession 80−82508
galaxy pair, interacting, zero relative vel. surfaces in gravit. field 80−67881
gaseous rotating cylinders, thermodynamic stability anal. by linear series 78−81618
gauge field actions and their principle bundle formation *(Chinese)* 79−71331
gauge field theories 79−80493
gauge field theory, gravitational considerations and red shift *(Japanese)* 79−80484
gauge group deformations, generalised Gupta program, review 80−12957
gauge theories, difficulties assoc. with variational principles 77−17884
gauge theory, special relativistic limit 80−22256
gauge theory, spherically symmetric star model *(Chinese)* 77−67086
gauge theory in Hamiltonian classical mechanics, EM and gravitational fields 80−13202
gauge theory of de Sitter group, fundamental length parameter 77−64990
gauge theory of gravitation, restrictions 77−17893
gauge theory of Poincare group 80−86189
gauge-invariant perturbations on most general spherically symmetric space-times 79−71322
Gauss-Bonnet and Bianchi identities in Riemann-Cartan type gravitational theories 80−86190
general covariant group, nonlinear realisation, invariant theoretical consideration 79−35612
general physics and heat, book 79−25814
general relativity, caustics and singularities, gravitational converging effects 80−77654
general relativity, classical fields with spin 78−8298

gravitation continued
general relativity, vacuum field equations, fifth dimension, ratio of EM to gravitational force 80−77679
general relativity reformed as a gauge theory in spinor affine space-time 77−22470
general scalar-tensor theory, rel. to time-varying gravit. const. and cosmic He abundance 79−92667
general scalar-tensor theory with constant G 78−21041
general symmetric structure including attraction and repulsion *(Chinese)* 77−64913
generalised theory, general covariance, correspondence and inertial isotropy 77−2591
generalized problem of three centres, external variant appl. 80−109087
generally invariant Lagrangians for the metric field and other tensor fields 79−71317
geocentric gravitational constant determ. from near-Earth satellite laser ranging 79−34724
geomagnetic dynamo, gravit. powered model 79−84102
geometric gravity Lagrangian, SP(4) and general coord. transforms. 78−70039
geometric unification of classical gravitational and EM interactions 80−57165
geometrised gravitational theory, energy-momentum tensor 79−25958
geometrized theories of gravitation 79−21636
geometrodynamics, e.m. and gravitational fields combination *(German)* 77−76
geophysical effects of corpuscular theory of gravitation *(Russian)* 79−62427
ghost neutrinos in Einstein Cartan theory 80−52108
global superenergetic quantities, uniqueness in general relativity and Einstein-Cartan theory 80−4595
good cut equation 80−95006
gravi-inertial reference system, props. *(Russian)* 77−53810
gravi-inertial reference systems, in spaces with pure gravit. radiation *(Russian)* 77−53809
gravi-magnetic hypothesis reconsidered 79−44362
gravitation-electromagnetism unification, Planck length, five dimensional principal U_1 bundle theory *(Chinese)* 80−86181
gravitational acceleration meas. using phonograph turntable 79−44687
gravitational field and force derivation using Faraday's and Maxwell's ideas of electromagnetic waves *(French)* 80−68106
gravitational field at spatial infinity asymptotically Minkowskian space-times 80−46885
gravitational field eqn. solution by functional method 80−17847
gravitational field struct. at spatial infinity, asymptotically Euclidean spaces 80−46884
gravitational field with absolute parallelism struct., integrable covariant energy-momentum conservation law 80−8873
gravitational instability in presence of suspended particles and rot. 79−64633
gravitational interaction, spin, rotation and quantum effects, review 80−37203
gravitational radius, equilib. of gravity and elec. forces 80−57152
gravitational solitons 79−44838
gravitational theories generated by groups of transformation and Dirac's large number hypothesis 79−12677
gravitational theory of matter 79−21627
gravitational-inertial field of Universe, generalised metric tensor theory 78−89275
gravitism and new astrophysical school of thermodynamics 79−29986
gravity mass invariance 78−57778
gravity theories with propagating torsion 80−57161
gravodynamics, post-Newtonian effects rel. to Einstein effects in general relativity *(German)* 78−16286
gravothermal catastrophe 78−81536
gyroscopic precession, starlight aberration, calcs. in stationary metrics 78−54284
Hamilton-Dirac 3+1 anal., effect of gravit. interaction on classical field 77−82399
Hamiltonian for Einstein-Dirac field 77−71428
harmonic mappings of Riemannian manifolds to gravit. fields 77−49648
heat transfer in direction of gravitational force *(German)* 77−80049
heavy guided photon in gravit. field 80−67949
Hilbert's metrical matter tensor generalisation of Einstein's field eqns. 78−21040
historical background for teachers, gravitation as Newton saw it 78−4436
history of gravitational and unified theories, book contrib. 80−22259
horizons in gravit. theory with scalar field, existence *(French)* 77−67340
Hoyle-Narlikar conformal gravitation, cosmological tests 80−56698
hyperbolic orbits, differential eqns. *(Russian)* 77−78622
hypermomentum and Riemann constraint microscopic violation in general relativity 77−87678
hypermomentum in hadron dynamics and gravit. 78−41487
ideal fluid, charged by vector field, self-gravitating distribs., Einstein-Cartan theory 80−95020
inaccuracy consequences computation, for orbits in Earth's gravitational field 78−40460
incompressible flow influenced by gravitation, hydrodynamic soln. 79−41648
indistinguishability of neutrino field and stokesian fluids 79−30159
induced forces on mass particle in gravit. field 80−22240
inertia and gravitation in general relativity 78−8317
inertial frame dragging effect, and contrib. of matter to gravit. constant, Brans-Dicke theory 79−67206
inertial induction in open universe 77−57255
inertial-gravitational field, physical significance and geodesic principle 77−67362
information theoretical aspects of gravit. field, space-time fluctuations 77−57266
inhomogeneous local gauge transformations in spacetimes with torsion 79−71330
instantons, soln. of classical Einstein eqns. 77−30066
integer spin zero-rest-mass field, irreducible representation of Lorentz group 80−68110
interacting gravitational and electron fields, Hamiltonian formulation, canonical form 79−17301
interaction energy of ellipsoidal bodies 79−44355
interior Brans-Dicke equations for static perfect fluid 78−4547

gravitation continued
interplanetary submicron grain orbits, gravit. attraction, radiation press. and electrodynamics 79−8879
interstellar giant molecular clouds, gravit. field probing 80−62242
inverse square law, deduction from Newtonian cosmology *(Italian)* 80−8722
inverse square law, null expt. proposal 79−71346
inverse square law forces, problem soln. using 'unit radius' 77−60923
inverse square law from Kepler's laws, Cartesian coords., for teaching 77−33802
inverse square law test at laboratory distances 80−82706
inverse square law test in laboratory 80−31657
isothermal-Kruskal coordinates and Einstein's equations 79−63106
isotropic Universe, kinetics of small perturbations *(Russian)* 78−54102
isotropic Universe, kinetics of small perturbations *(Russian)* 78−54103
isotropic universe, kinetics of small perturbations *(Russian)* 78−65731
Jacobi's virial eqn. soln. for celestial bodies 79−8832
Johann Georg von Soldner and the gravitational bending of light, with an english translation of his essay on it published in 1801 79−17176
Jordans 5-D unified theory of gravitation, Ehlers-Harrison type transform 80−8882
Kerr gravitational field effect on optical images 77−45480
Kerr NUT solution from flat space time by Backlund transformation 80−52098
Kerr solution superposition, Tomimatsu-Sato solution 80−31634
Kerr-like neutrino-gravitational solutions 80−95240
Kerr-Newman geometry, coupled gravit.-e.m. perturbation 78−8305
Killing horizons around a uniformly accelerating and rotating particle emitting gravitational radiation 80−105557
Kilmister-Yang model, minimal differential eqns. 77−33922
kinetic-theory of gravitational systems 77−5748
L-A pair of coupled eqns. for gravitational and EM fields *(Russian)* 79−88859
laboratory test sensitivity, beyond geometrical optics limit 79−85053
Lagrangians in flat space-time 80−86169
Lane-Emden equation, spherically symmetric soln. 80−46890
large numbers hypothesis and the Einstein theory of gravitation 79−21477
Lee's derivative of geometrical objects, tetradic transform. *(Russian)* 79−93024
Legendre series summation, recursive procedure, gravit. potential evaluation 80−31486
lens action by massive galaxy, QSO 0957+561 AB, flux var. and image splitting 80−27008
lens action of intervening galaxy on double QSO 0957+561 AB, IR spectrum 80−77510
lens effect, appl. to twin QSOs 0957+561 A, B 80−12827
lens effect, EM wave diffr. in Schwarzschild space-time 80−90750
lens effect, evidence from double quasar (Q 0957+561) 80−27005
lens effect, focusing by slowly rotating relativistic spherical mass 80−105155
lens effect, high-intensification regions 79−25463
lens effect, rel. to 3C 303, QSO group in cluster 77−78878
lens effect, rel. to quasar image doubling assoc. with absorpt. systems 80−22112
lens effect and pregalactic halo objects 80−17484
lens effect as applied to double QSO 0957+561 80−82533
lens effect for double quasar 0957+561, 6 cm VLA obs. 80−101647
lens effect formed by spherical galaxies, multiple image prod. 80−90532
lens effect interpretation of QSO 0957+561 A and B, evidence from direct imaging 80−17686
lens effect of moving black hole 77−33549
lens effect of spherically symm. mass distrib., optical scalar eqns. 77−64637
lens effect with allowance for diffraction, anal. *(Russian)* 78−32743
lens hypothesis, appl. to triple QSO (PG 1115+08) 80−86012
lens hypothesis applied to double quasar 0957+561A, B 79−88762
lens in double quasar 0957+561A, B due to intervening galaxy, IR obs. 80−73065
light beam of variable flux, gravitational influence 78−21037
light bending, new theory of photon and energy based on two primitive particles 79−67145
light bending by Sun, vars. caused by solar activity *(French)* 80−56795
light deflection, Sun semidiameter appl. *(German)* 80−46531
light deflection (Einstein effect), prospects of observation at solar eclipse (1981 July 31) *(Russian)* 80−51651
light deflection by gravit. field, work of Johann Georg Soldner (1776-1834) 78−81787
light deflection by solar gravit. field, effect on meas. of Gorky latit. *(Russian)* 78−40462
light deflection by Sun, principle of equivalence calcs. 78−81729
light deflection in close double stars, mass meas. *(French)* 79−62753
light deflection in gravit. fields, rel. to meas. of parallaxes of objects at cosmological distances 78−53796
light propagation in Kerr metric, geometrical optics appls., analytical results 77−29637
light propagation in nonlinear electrodynamics in generalised gravitational theory 77−5727
light rays, bending by Sun's gravit. field, effect on clock and local latit. corrections 78−7878
linear field theories, conservation of source strength, superpotentials 77−5726
linearised GL(4) gravities, dynamical structure 78−65846
linearised gravitational field, perturbed characteristic functions appl. 80−4614
linearized Einstein theory, twistors, plane fronted impulse wave backgrounds 79−30329
linearly expanding universes in Jordan-Brans-Dicke theory 80−46711
liquid metal tube flow, turbulence, heat transfer, thermogravitation effect 78−71315
local conserved currents in unified field theory 79−17307
local supersymmetry, geometric interpretation 77−38096
locally de Sitter invariant theory *(Chinese)* 77−26219
locally rotationally symmetric cosmological model containing a nonrotationally symmetric electromagnetic field 79−30161
logarithmic correction to post-Newtonian gravitational law for planetary motion 77−70986
Lorentz invariant theory, spin-1/2 particles interacting with gauge fields 80−22257
Lorentz-covariant model of the system of two gravitating particles 80−8865

gravitation continued
Lorentz-covariant theory of gravitation 80−8881
Lorentz-invariant theory, results for red shift, light deflection, perihelion shift *(German)* 78−29030
lunar motion and Earth shrinking effects 80−46182
lunar tidal acceleration determ. from laser range meas. 78−69718
Mach's inertial interaction to produce gravitational force 77−2589
Mach's principle, gravity and inertia, Leibniz invariant theory 77−41426
Mach's principle, modification of general relativity theory *(German)* 79−88843
Mach's Principle, relative motion and fundamental numbers 77−9943
Mach's principle equivalence principle, violation, for teachers 78−61998
Machian approach 78−29032
Machian argument in Friedmann models of Universe 77−74168
Machian framework, purely geometrical, for describing gravity and inertia 79−44651
magnetic fields generated near rapidly rotating gravitating bodies 78−46487
magnetic monopole, energy tension and gravitational field *(French)* 80−52075
magnetism analogy 78−65851
magneto-dipole configurations in general relativity 80−67539
magneto-gravitational effect *(Russian)* 77−9935
magneto-gravitational instability and suspended particles 77−45302
magnetoplasma stability against EM perturbations in presence of gravit. field 77−41295
Malin's gravit. field eqns. 77−13667
Mansouri-Chang gravitation theory, no hair theorem for black holes 79−49145
mapping function in W_4-fields *(Russian)* 78−24716
marginally bound dust collapse, time functions in numerical relativity 79−71321
Marinov's absolute space-time theory, gravit. freq. shift 78−21042
Mars, moment of inertia and isostasy 77−33390
mass attraction of sphere and circular plane *(Hungarian)* 79−17206
mass defect in Reissner-Nordstrom metric, charge conservation *(Chinese)* 80−86182
mass defect in Reissner-Nordstrom metric *(Chinese)* 80−27186
massive quantum scalar field coupled to gravit. field, stress-tensor trace anomaly 77−41768
massive scalar field in curved background, vacuum expectation value of stress tensor 77−13658
massive scalar field in Einstein universe, vacuum stress tensor, finite-temp. effects 77−41769
massive spin-2 particles, strong gravity in Einstein space 77−60988
massive Thirring model connection 79−12624
massive vector fields and black holes 78−96499
massless boson fields, group theory 77−34098
massless scalar and EM field equations interacting with gravit. field, particle-like solns. 79−54290
mathematical principles, classical to relativistic evolution, book 80−22162
matter and light wave interferometry in gravitational fields 80−94997
matter terms in gravit. theory, minimal prescription method 79−25916
maximal extension of nonsingular soln. in generalised theory of gravit. 78−41214
Maxwell's equations, gravitational analogue 79−63108
Maxwell equations in Riemann-Cartan space, spin-torsion coupling const. 80−82697
Maxwell-Einstein theory, local supersymmetry 77−2582
McLauren cool discs, equil. and stability w.r.t. perturbations, gravitating mass effect *(Russian)* 79−92860
measurement theory, interrelation of quantum theory and gravitation 78−54235
meta universe, tachyon energy and momentum, contribution to gravitational field 77−45760
metric existence in 2-D affine manifolds 79−85039
metric theories, appl. to gravit. dipole radiation from binary systems 77−60589
metric theory, without minimal coupling of matter and gravitational field 77−13671
metric-affine gravit. theory, vol. preserving and canonical transform. 79−44826
metric-affine theory as gauge theory of affine group 78−32746
metric-affine theory of gravit., intrinsic hypermomentum current components, hadron dilation, shear and spin 78−12632
metric-affine unification of gravity and gauge theories 79−63109
metric-torsion gravitational theories, charge conservation 78−45544
metric-torsion gravitational theories 77−87668
metrical connection in space-time, Newton's and Hubble's laws 78−57435
micro- and macro-gravitational fields, relationships, physico-geometrical remarks 79−63103
microscopic, as Yang-Mills field 79−44829
minicompact objects according to the bimetric theory of gravitation 79−49140
momentum transfer in gravitation theory 80−4601
monkey/hunter problem and possible solutions 79−75306
Moon, gravitational field, model based on Luna 10, 12, 14, 19 and 22 data 78−45249
multipole anal., time-depend. relativistic, definition of multipole moments 77−65087
negative mass and positive mass matter, hypothetical coexistence, causal paradoxes 80−82685
neutral gravitating fermion system, equilibrium states 80−31692
neutrino-generated static space-times 80−52107
neutron interference, gravity and inertial effects, principle of equivalence at quantum level 80−77669
neutron matter, equilib. config. allowing for nuclear and gravit. interactions *(Russian)* 77−18462
neutron optics, gravitational effects and applicability of Fermat's principle *(Russian)* 79−13376
neutron star, cold, binding energy and stability 79−17006
neutron stars, max. mass in new theory of gravitation 77−33545
Neveu Schwarz Ramond model, complete action for spinning string, field eqns., constraints 77−13943
new general relativity, geometry translation group gauge theory 77−79020
Newman-Penrose form of gravitational Lagrangian 78−24717
Newton's law, deductive and inductive nature, for teaching 78−24617
Newton's law, introduction of a repulsive force 78−73839

gravitation continued
Newton's law, linear depend. of mass *(Italian)* 79−12706
Newton's laws of motion, planets and rocket dynamics, for schools 78−12509
Newton and mutual gravitation of fixed stars 78−20
Newtonian connection, nontrivial extension of Galilei group *(French)* 78−36916
Newtonian cosmology, extension to whole of space *(Italian)* 79−21475
Newtonian cosmology, universe energy conjecture *(Italian)* 79−21474
Newtonian cosmology and universal gravitation constant *(Italian)* 79−21473
Newtonian gravitation, appl. to motions of perihelia of inner planets orbits 80−67531
Newtonian gravitation and cosmology for unbounded Universe *(Italian)* 80−12836
Newtonian gravitation and mechanics, cosmological appls. *(Italian)* 80−12835
Newtonian gravitation implications for cosmological var. of gravit. const. and solar luminosity 80−82182
Newtonian gravitational systems of specified ang. momentum, improbability of collisions 79−53706
Newtonian gravitational theory, continua and particle dynamics 79−6038
Newtonian interaction between particles satisfying Dirac eqn., Einstein-Sciama force 78−32745
Newtonian mechanics and expansion of the universe *(Italian)* 79−21472
Newtonian potential of homogeneous cube 77−13680
Newtonian theory, tensor pot. and Cartan's four-dimens. represent. *(Russian)* 77−49658
Newtonian theory and its generalisation 79−80485
Ni's theory of gravity for massive neutron stars 78−4273
non-gravitational foci and apexes, of paths with common launching point and common apsidal distances 79−16804
non-linear coupling of quantum theory and classical gravity 80−27389
non-relativistic theory satisfying general relativity tests 77−79016
non-Riemann geometrizable effects in the gravitational one-body problem 79−85016
nonintegrable phase factor, Aharonov-Bohm proposal 78−129
nonisotropic systems near liquid-vapour critical point, similarity hypothesis, gravitational effects 80−17913
nonlinear de Sitter symmetry and restricted space-time regions 79−85043
nonlinear EM effects induced in vacuum by gravitational interaction 79−44827
nonlinear interaction between monochromatic wave and particles in gravitating system *(Russian)* 77−82285
nonlinear Lagrangian theories 77−67364
nonlinear laser spectroscopy, gravitational effects 79−67391
nonlinear theory in flat space, equivalence principle for massive bodies of EM struct. 80−46899
nonlocal spinor field theory of matter 79−49141
nonmathematical review of gravitational capture 80−26734
nonminimally coupled gravitational and EM fields, Lagrangian 79−71328
nonstationary gravitational field, creation of fermion pairs *(Russian)* 77−74635
nonsymmetric field struct., generalised gravit. theory 77−74296
nonsymmetric field structure determined space time geometry for gravitational theory 79−85045
nonsymmetric theory, Cauchy initial value problem 80−86168
nonsymmetric unified field theory, physical interpretation and light propag. 79−21618
Nordstrom Reissner metric, generalised, exact soln. 77−82430
normal modes of self-gravitating fluids in perturbed configurations, perturbational-variation procedure 78−32336
NP 0531, Crab pulsar, distrib. modelling of rotating matter and gravit. field *(Ukrainian)* 80−12775
null experiment to test inverse square nature 80−52116
null formalism, eqns. of motion, two-body problem 77−9927
null gravidynamics, initial value problem and Dirac-bracket relations 78−77781
null radiation gravitation deflection by relativistic spherical masses 79−58600
numerical simulation of 3-dimens. gravitating systems of colliding masses 77−9654
NUT metric in background of Einstein's static universe 78−93565
one-dimensional self-gravitational system, equilib. statistical mechanics 78−36922
oscillations of a gravitating and rotating uniform liquid sphere 79−44082
parametrised post-Newtonian parameters, results from strain-tide spectroscopy 78−73301
parametrized post-Newtonian approx., Rastall's gravit. field eqns. 78−36894
parity violation in the neutron's gravitational interaction 79−58617
particle creation in curved space-time, back reaction effect 77−49645
particle creation in generic external fields, particle definition 78−8498
particle detection and creation for scalar quantum field in curved space-times 77−67597
particle dynamics in special relativity 78−93529
particle motion in external gravitational field, Schwarzschild metric calc. *(German)* 77−9923
particle motion in gravitational field, special theory of relativity *(Russian)* 77−45691
particle production rate in gravitational fields *(Russian)* 77−91423
particle rest mass variability, theory and constraints from solar system expts. 77−45781
particle-classical field interaction, appl. to linearised gravitation and symmetric electrodynamics 79−5992
particles and fields conference, Argonne, IL, USA (Oct. 1977) 78−78130
particles in external gravitational fields, relativistic dynamics *(Russian)* 78−12614
Pauli eqn. for particle in metric and EM fields *(German)* 77−78997
perfect fluid cosmology with geodesic world lines 79−25775
perihelion precession as Machian effect 77−26098
perihelion precession rate in system of two charged masses 78−73897
perturbing celestial bodies, non-spherically symm. gravit. fields, tidal potential study 80−12654
photogravitational restricted three-body problem, Lagrangian points 80−26725

gravitation continued
photon decay in curved space-time, Hubble red shift and solar limb effect explanation 79−35606
photon energy shift, possible antigravity in gravitational red shift 79−12673
photon motion in gravitational field of rotating cylinder 79−25937
plane waves in the bimetric gravitation theory 78−93583
planetary gravitational field, kinetic eqn. soln. for gas 78−16322
planetary gravitational fields, inform. theory appl. 78−53835
planets, differential rotation, gravitational effects 79−8862
Poincare gauge theory, spacetime torsion 77−13672
Poincare gauge theory with Weyl-type Lagrangian and gravitation 78−4545
point charge relativistic free fall motion under weak gravitational field 80−42057
Poisson's eqn. numerical soln. for flattened centrally condensed objects, stellar models 79−35110
polar g-values 78−81727
polarised radiation from vicinity of black hole, gravity effects 77−82440
post-Newtonian charged n-body problem, centre of inertia and coord. transforms. 79−93025
post-Newtonian n-body problem in gravitation with PPN parameters γ and β, centre of inertia 79−17325
potential calculation, via Stokes eqn. 79−62428
potential energy, polytrope of index 5, proof of its finiteness 78−40920
potential of prescribed family of orbits, Szebehely eqn. solns. 78−40808
potential theory, time varying, comparison with general theory of relativity 79−30305
predictive relativistic mechanics for gravitational interaction, approx. solns. 77−2541
predictive relativistic mechanics of gravitating masses 79−25914
prestellar gas, element separation by gravitational diffusion 79−21386
projection tensor formalism for stationary axisymmetric gravitational fields 79−25947
propagating torsion and gravitation 79−35615
PSR 1913+16, binary system, test of relativistic effects *(Dutch)* 80−62172
pulsars and gravitational spin precession 78−12264
Q 0957+561 A,B, UV spectra and gravit. lens interpretation 80−82537
QED in an external gravitational field, S-matrix evaluation, pair prod. 78−82131
QED in external gravitational field, S-matrix construction 78−78116
QED with scalar gravitational field interactions, nonelimination of divergences 78−93834
quadratic density distrib., figure theory, fifth approx. eqns. soln. 79−25470
quadratic Lagrangian in space with torsion *(Russian)* 78−24714
quadratic Lagrangians, solns. of field eqns. *(Russian)* 77−67
quadratic Poincare gauge theory of gravitation, short range confining component 78−89388
quadratic theory, Fridman's problem *(Russian)* 78−65847
quadratic theory, gravitational field eqns. *(Russian)* 77−45753
quadratic theory, Schwarzschild problem *(Russian)* 77−45754
quantisation, Ward identities and Green's function eqns. 77−67552
quantisation method for gravitational field *(French)* 79−30341
quantisation of matter without quantising related fields 80−105525
quantised gravit. charge and fine-struct.-const. calc. 77−26524
quantum field theory in curved space-time, Feynman propagator 77−45961
quantum field theory renormalisation in curved space-time, Schwinger's method appl. to gravit. interaction 77−49834
quantum interference, gravitational and rotational effects 77−45734
quark binding, explained by strong gravity with cosmological const. 78−4820
quark confinement, relevant cosmological f-g fields 80−86659
quasar 0957+561, radioastron. obs. of assumed double quasars 80−105381
quasars, gravitational screens and superluminal separation 80−51896
quasars 0957+561 A, B, twin quasistellar objects or gravit. lens theories 79−67114
quasimonochromatic radiation propag. in static gravit. field *(Russian)* 77−70992
quasimonochromatic radiation propag. in stationary gravit. field *(Russian)* 77−70993
quasistationary conc. systems without rotation, gravitational field *(Russian)* 77−45768
$R+R^2$ theory of gravity, with torsion, Brikhoff theorem, vacuum field eqn. solns. 79−71337
radiating cylinder, gravitational field anal. 79−30332
radiating fluid spheres in general relativity 79−71323
radiating non-twisting charged systems, gravitational field 79−40430
radiowave focusing in interstellar medium, model *(Russian)* 78−81905
ray gauge, pure gravity 78−8313
reduced gravitational field eqns., on algebraically special space times with twisting rays 79−30302
reference coordinate system concept, development history *(German)* 77−13642
regular solns., modified theory *(German)* 79−88844
Reissner naked singularity, spontaneous pair creation 78−24990
Reissner Nordstrom singularity, spherically symmetric clusters of charged particles 79−12672
Reissner-Nordstrom black hole, coupled gravit.-EM perturbation anal. 77−26022
Reissner-Nordstrom black hole, stationary interacting fields 78−24710
Reissner-Nordstrom black holes, instability of the Cauchy horizon 79−67201
Reissner-Nordstrom geometry, forced perturbations 78−8303
Reissner-Nordstrom gravitational field, electric dipole *(Russian)* 79−21611
Reissner-Nordstrom perturbations, coupled Einstein-Maxwell eqns. 80−68108
Reissner-Nordstrom-de Sitter metric, the third law, and cosmic censorship 79−35609
relativistic electromagnetic fluid flows, geometrical aspects 79−72950
relativistic energy momentum localisation, general theory 77−9928
relativistic force equation, appl. to determ. of light bending and red shift in grav. field *(Afrikaans)* 79−97270
relativistic gravitating particles with cylindrical symmetry, calc. of averages in equilib. system *(Russian)* 78−73904
relativistic gravitation energy, tetradic formalisms and localisability *(German)* 78−12630
gravitation continued
relativistic gravitation from massless systems of scalar and vector fields 80−12969
relativistic gravitational potential, relation to mass-energy 80−22239
relativistic massive particles, gravitational deflection, general relativistic anal. 80−46767
relativistic particles motion and radiation in electric and mag. fields, gravitational field effects *(Russian)* 79−97269
relativistic star, curved space-time, vac. stability, polarisation, phase transition 77−49290
relativistic theory, static solutions and Poincare press. 80−31648
relativity, 6-D, gravitational effects, Schwarzschild metric, orbital precession 80−62550
relativity, seven-dimensional, 4-D gravity coupled to Yang-Mills fields 80−82699
repulsive gravitational forces, possible clustering mechanism 77−37674
revolving body, gravitational pot. representation by finite system of mass points *(Russian)* 80−72757
Riemann gravitational theory, cosmic time asymmetry *(German)* 79−35610
Riemannian fourfold, gravitational field eqns. 77−57242
Riemannian metric description, of gravit. and EM interactions 78−36904
riemannian-Maxwellian invertible structures in general relativity 80−4618
Rosen's bimetric theory, eqns. of motion 77−13665
Rosen's bimetric theory, two-body problem 77−37796
Rosen's bimetric theory of gravity, orbital topoography and other astrophysical consequences 78−54274
Rosen bimetric theories, background Killing vectors, conservation laws 80−52099
Rosen bimetric theory, polytropic spheres 80−105563
Rosen bimetric theory, stationary axial-symmetric fields 79−96906
Rosens bimetric theory, appl. to slowly rotating neutron stars 79−85042
Rosens bimetric theory of gravitation, gravitational radiation and ultimate speed 80−52087
Ross theory, vacuum field solns. 79−128
rotating body gravitational field, stationary motions of material point *(Russian)* 77−58545
rotating cylinder gravitational field, equations of motion of material particles and photons 79−9157
rotating finite bodies, motion eqns. in extended parametrised post-Newtonian formalism 77−64628
rotating gravitating gas disc, explosive instability *(Russian)* 77−87260
rotating infinite cylinder, exterior solns., everywhere singular metric 77−60986
rotating permanently magnetised sphere, EM field in inertial and comoving reference frames 79−71316
rotating radiating body, nonstationary soln. of Einstein eqns. 77−22450
rotating stratified ellipsoids of revolution, effects on inertial frame dragging 79−2573
Sakharov's thoery of gravitation 79−25950
Saturn, external gravit. field, tidal perturbs. due to rings, mass of rings calc. 79−35189
Saturn's rings gravit. field 77−87320
Saturnian system, gravit. potential 79−75152
scalar field, anisotropic, with cosmical time 79−88847
scalar field, gravitational peculiarities 80−31623
scalar field theories, refractive index and Fresnel formula applied to empty space 77−30082
scalar fields, non-null eigenvalues 79−21623
scalar metric torsion gravitational theories, comment 79−21632
scalar particle in gravitational field, high energy dispersion *(Russian)* 77−45994
scalar tensor theories, plane wave solns. in Einstein-Maxwell theory 77−33919
scalar tensor theories and generalised geometries 77−2587
scalar tensor theories and variable rest masses 80−36916
scalar-metric and scalar-metric-torsion theories 77−74295
scalar-particle prod. near anisotropic universe singularity due to gravit. field 77−91421
scalar-tensor theories, Palatini variational principle 77−2592
scalar-tensor theories, sufficient condition for Birkhoff's theorem 77−57261
scalar-tensor theory, Birkhoff's theorem for EM field 77−17892
scalar-tensor theory, cylindrical wave solns. 77−60996
scalar-tensor theory, naked singularity 79−8826
scalar-tensor theory, plane symm. solns. of field eqns. 77−33920
scalar-tensor theory, plane-symmetry solns. 78−70035
scalar-tensor theory, single action determ. 77−79018
scalar-tensor theory, static conformally flat soln. 79−93018
scalar-tensor theory in Lyra manifold 78−36917
scalar-tensor theory with negative coupling const. 77−2590
scale covariant gravitation theory, rel. to stellar vel. dispersion age depend. 78−65661
scale covariant theory, appl. to gravit. const. var. 79−92666
scale covariant theory, conformal transformation of Einstein eqns., astrophys. appls. 77−79019
scale covariant theory and galaxy group virial masses 80−98728
scale covariant theory of gravitation, astrophys. appls. 78−16710
scale-covariant gravitation and electromagnetism, variational principle 79−85027
scale-covariant gravitation theory, appl. to stellar dynamics 80−26913
scale-covariant gravity theory, electrodynamics involvement 80−109350
scale-covariant theory, galaxy and QSO magnitude/red shift relations 80−56980
scale-covariant theory, radio source counts and models in G-varying cosmology 80−56981
scale-covariant theory, thermodynamic relations and 3K background radiation 80−56979
scattering of zero rest mass plane waves 78−4542
Schwarzschild black hole, focusing gravit. mirror effect 80−46602
Schwarzschild black hole, gravit. field effect on polarised radiation from orbiting point source 77−67109
Schwarzschild black hole, plane EM wave diffraction, Poynting vector near horizon 80−22250
Schwarzschild space-time, vacuum polarisation induced by gravitation 80−82410
screening effect rel. to Earth tides obs., assessment *(Russian)* 78−88787
self-consistent variational theory, Machian model 80−67558

gravitation continued
self-gravitating fluids in perturbed configurations, normal modes rel. to convection 78−32337
self-gravitating gas-particle suspension, magneto-gravitational instability, with conduction 79−29989
semiclassical field theory of gravitation, renormalisation scheme 80−68117
Sen-Dunn theory, vacuum field solns. 79−128
shear-free and acceleration-free fluids in Einstein's theory of gravitation *(German)* 77−22467
shock waves in general relativity, geometrical struct. 79−71297
short-range repulsion, model *(Russian)* 80−46388
singletons and massless, integral-spin fields on de Sitter space 80−110
singularities, effect of self-induced torsion of Dirac sources 79−21626
singularity problems in electrodynamics and gravitational theory, soln. 80−8534
SL(2,C) gauge theory 77−13669
SL(4), common symm. group of EM and gravit. interactions 77−34112
SO(3,2) gauge theory, geom. of Einsten-Cartan theory 79−75425
SO(4,2) conformal group as gauge group, Yang-Mills-like Lagrangian 80−62560
soft graviton emission in scatt. processes, linearised gauge theory 78−49746
solar system, particles gravit. interaction rel. to development 77−91451
solar system, relativistic effects verification, comparison of obs. results with theoretical data *(Russian)* 79−80209
solid bodies, general expansion of force function 78−7877
solid bodies in solar system, gravitational potential 78−77550
some thermodynamical remarks on the theory of gravitational field 78−81899
source strength of matter, cosmological problem 77−82119
space of uniform mass distribution, geometrical descript. *(Hungarian)* 78−21043
space probe tests of gravitational theories 79−71345
space time permeated by compressible, thermally conducting self-gravitating field, props. 79−71315
space-like geodesics in fields of charged mass point and uncharged static cylinder 77−53805
space-time, general relativity 80−68104
space-time homogeneous models with torsion 79−58607
space-time structures, classification 77−30057
spatially homogeneous universes which admit source-free magnetic fields 80−12973
spatially homothetic cosmological models 79−25771
spherical bodies, gravit. effect on motion of axisymm. body 77−13222
spherical cavity in an Einstein Universe 80−95013
spherical symmetric field, spin ang. momentum tensor calc. 80−42107
spherically symm. Einstein-Yang-Mills-Higgs system, canonical formalism 77−87892
spherically symmetric accretion of gas with self-gravitation 79−8834
spherically symmetric charged dust distrib., Brans-Dicke theory, Schrodinger eqn. soln. 79−12693
spherically symmetric charged dust distrib., Einsteins theory generalised to Brans-Dicke theory 79−2694
spherically symmetric objects, electrostatic and gravitational field determ. 77−71253
spin 1/2 particle, gravitational field around it 78−45529
spin 3/2 fields quantisation in presence of external gravitation 77−22446
spin strings theory, EM waves propag. *(Russian)* 78−81906
spin-2 field theory of gravity, locally Lorentz invariant 77−5725
spin-3/2 axial anomaly, Feynman graph, point splitting, topological and zeta function methods 78−93588
spin-orbit effect in classical two-body Hamiltonian 77−68386
spin-spin contact interactions in Einstein and Einstein-Cartan-Sciama-Kibble theories 77−5719
spinning masses, generalisation of Tomimatsu-Sato solns. 77−49652
spinning masses, gravitational fields, exact solns. with arbitrary integer deltas 77−67351
spinning particles, eqn. of motion in post-Newtonian approx. of Einstein-Cartan theory 79−25954
spinning particles interacting with gravit. field 77−71261
spinor field and gravitational field interactions, classical theory 78−93569
spinor field cosmological models, Einstein-Cartan theory of gravitation 78−32618
spinor-type fields with linear, affine and general coordinate transformations 79−25949
spinors and Petrov types, field classification 77−67339
spontaneous particle creation in strong gravitational field, semiclassical theory 78−54281
star with neutron core, gravitational equilib. relativistic treatment 78−57570
stars, late-type, gravit. phase transitions 77−49380
static and stationary axially symmetric fields, Kerr, NUT and Bardeen metrics *(German)* 80−52073
static fluid spheres in Einstein-Cartan theory 79−35604
static gravitational solitons, singularities, horizons, field behaviour at infinity *(Russian)* 80−73229
static plane-symmetric solutions in Brans-Dicke and Sen-Dunn scalar-tensor theories 77−17891
static plasma polarisation in Schwartzschild gravitation field *(Russian)* 79−16825
static spherical shell of matter, line element calc. 77−30065
static spherical sources of scalar, EM and gravitational fields *(Russian)* 78−12613
static spherically symmetric distrib. of charge, complete field, charged dust appl. 78−21026
static spheroidal charged dust distribs., metrics 79−71318
stationary axially symmetric Brans-Dicke-Maxwell fields 80−52100
stationary axially symmetric field eqns. soln. 78−29010
stationary gravit. fields, general electrovacuum *(Hungarian)* 77−22469
stellar gravitational field, effect on interstellar medium equilib. configs. stability 80−82448
stellar unstable gravity modes, asymptotic representation 78−28656
stochastic gravitational fluctuations in a self-consistent mean field theory, review 80−90734
stratified space of absolute parallelism, gravit. field *(Russian)* 77−71259
stress-tensor trace anomaly of field in curved spacetime 77−64983
string direct interaction, gauge-invariant theory, gravit. interaction 77−41804
gravitation continued
strong equivalence principle, post-Newtonian SO (1,3) Yang-Mills theory 80−68113
strong gravitational coupling, effect on nuclear force in nucleon-nucleon interactions 78−514
strong gravitational field and general relativity 80−67548
strong gravity and elementary particle theory in general relativity 78−8315
strong gravity and particle mass spectrum 77−30351
strong gravity const. determ. from pion mass difference 77−22715
strong gravity equations, spin and torsion effects, rel. to spin of Universe 79−97116
strong gravity model, energy-momentum complex construction 77−9939
SU(1, 1) spin coeffs. for space-like symmetry 77−53807
SU(2) gauge theory, sypersymm. breaking by pseudoparticles, supergravity implications 78−24959
superconducting current variation with gravitational field variation, general relativistic phenomenological theory 80−54827
supergravitation, calibration invariance *(Russian)* 78−4548
supergravity, 2-loop divergence, with external gravitons on-shell cancellation 77−49659
supergravity, appl. of superspace goemetry of Fermi and Bose coords. 77−26143
supergravity, classical solns. 78−122
supergravity, coupling to scalar multiplet 77−67366
supergravity, extended, U(N) invariance 77−61003
supergravity, extended, with gauge internal symmetry in de Sitter space 77−79021
supergravity, extended, with SO(4) symmetry 77−64991
supergravity, gauge field quantisation 77−2735
supergravity, geometry of superspace, vector-spinor matter 78−49744
supergravity, local supersymmetry in (2+1) dimens., differential forms. 78−49980
supergravity, locally invariant supersymmetric gauge field theory 78−49742
supergravity, minimal set of auxiliary fields, gauge algebra closure 78−49743
supergravity, space-time spin struct., and Hamiltonian constraint square roots 77−49663
supergravity, superspace formulation 77−30084
supergravity, surface integrals as symmetry generators 77−74634
supergravity and cosmological const. 77−74171
supergravity and gravity unified geometric theory 77−41521
supergravity coupled to massive self-interacting scalar multplet, spontaneous symmetry breaking 77−74633
supergravity theories, algebraic simplifications 77−87681
supergravity theory, spin 3/2 field eqns., commutator algebra 77−81
supergravity with axial-gauge invariance 77−41790
supergravity with Majorana spin 3/2 gauge fields and supersymmetry 77−17894
supermassive stars, possible dynamical stabilization by shadow gravitational potential 77−33338
supersymmetric nonlinear σ-model in 4-D, coupling to supergravity 78−49981
supersymmetry and supergravity 77−61212
supersymmetry nonlinear realisation in anti de Sitter space 77−87915
tachyons in bi-metric gravitation theories, causal tachyons 78−21038
telescopic principles in the theory of gravitation *(German)* 79−40416
temperature of a gravitational field 79−85055
tensor theory in curved metric on flat background 79−75426
tetrad gravitational field, weak principle of equivalence and gauge theory *(Russian)* 78−62135
tetrad potentials gauge, reference systems with Newtonian time *(Russian)* 78−89378
tetrad theory, and extended translational invariance *(Russian)* 77−53822
tetrade theory, rel. to expansion and rot. momenta of large cosmical masses *(Russian)* 77−17351
theory of gravitation and electromagnetism from Bohm-Aharonov expt. 79−85028
theory of motion, electromagnetism, gravitation 80−105500
theory testing by lunar laser ranging and planet radar ranging 77−53823
three body problem, Lagrange equilateral triangle, Euler collinear solns., generalisation to nongravit. forces 78−54178
time dilation, gravit., according to absolute space-time theory 77−43
time-varying Newtonian gravity and universal motion 77−2598
Tomimatsu-Sato generalised gravitational fields, limits 78−21022
torsion, Hojman-Rosenbaum-Ryan-Shepley dynamic theory, and Eotvos-Dicke-Braginsky expts. 79−71336
torsion effect on macroscopic gyroscope 80−98830
torsion enables metric to allow gravit. field 78−73902
torsion field, propagation eqns. for bodies with spin and rotation 80−77670
torsion gravitational theories, spinning particle motion, Lagrangian theory 79−12692
torsion potential, coupling strength, experimental bounds 80−73249
torsion potentials, self consistent in Einstein-Cartan theory 79−12690
torsion singularities, Bianchi-V cosmology with Proca field 77−67149
torsion theory, attractive spin-spin contact interaction 78−8312
trace anomalies in a two-dimensional de Sitter metric and black-body radiation 78−65841
transformation groups for resolution of partial differential eqns., appl. to gravity, quantum mech. and heat transfer *(French)* 79−49099
translatory-rotary motion of gravitating spheroids *(Russian)* 78−73841
Treder's tetrad theory, field eqns. deducible from variational principle *(German)* 78−16709
Treder's tetrad theory, polar particles *(German)* 77−41520
turbulent flow and heat exchange, gravitational field influence 79−86427
two-body gravidynamics 79−71683
two-body problem in linearised gravity 80−86160
two-body spin-independ. system, simplified form for Hamiltonian and Lagrangian 77−17829
two-tensor field theories for hadron-lepton gravit. interactions, interaction term 77−87932
two-tensor gravitation from covariant inverse problems of variational calculus 77−74278
type-N gravitational field with twist 78−45534
unification and proton quasistability, gravitational and fine struct. consts. *(Russian)* 80−77680
unified actions for gauge fields and gravitation *(Chinese)* 79−17305

gravitation continued
unified field theory, five-dimensional theory of interacting scalar, electromagnetic, and gravitational fields 80−105833
unified field theory, nonsymmetric, metric hypothesis, spinor analysis 80−68404
unified gauge theories and gravitational cut-off, renormalisation group method 77−18213
unified gauge theory of gravit., e.m., mag. monopole fields 77−57263
unified theory of gravitation and electromag., Weyl-Dirac theory with torsion 80−52106
uniform rotating sphere, five parameter internal gravit. field family *(Russian)* 80−95008
Universe, closed or open, Fornax system density profile, strong gravitational interactions 80−90587
Universe, gravitational-inertial field, crit. systems struct. 80−8720
Universe and microcosm, gravitational-inertial field theory 80−8721
universe models with Rastall's theory of gravity 78−41100
vacuum, particle-free state and group representations, stratification and C*-algebra *(Russian)* 78−81896
vacuum gravitational field with two-dimens. group of motion *(German)* 77−22466
vacuum polarization effects on radiative opacities in a strong magnetic field 79−85032
vacuum state, influence of gravitation and cosmological effects on symmetry breaking *(Chinese)* 78−65858
vacuum stresses induced by accel. of infinite plane cond. for massless scalar and EM fields 77−30071
vacuum with spin in the ECSK-theory of gravitation 79−44830
Vaidya's metric, complexification, radiative and nonradiative, parts of energy-momentum tensor 80−68093
variable quasars and active galactic nuclei, strong gravity effect on light curve 79−16812
variational principle for gravitational equations of the Bianchi identity type 80−4599
vector graviton and metric fields *(Chinese)* 79−71324
vector-tensor field of gravitation, a simple model 79−71325
velocity of gravit. interaction 78−21045
viscous fluid cosmological model in general relativity 78−61944
Weyl's class of static vacuum solutions for axially symmetric gravitational fields 80−68089
Weyl's geometry appl. 78−65843
Weyl and Papapetrou axisymmetric space-time as geodesics of hyperbolic complex plane 79−49126
Weyl metrics, pseudo 80−95002
Weyl-Dirac theory with torsion, complex Dirac field, conservation equations 80−68112
white dwarf luminosity in scale covariant theory of gravity 79−80303
Yang's gravit. field eqns., reduced spinor formalism *(Chinese)* 78−119
Yang's gravitation theory, homogeneous cosmological models 79−17304
Yang-Mills gravity dynamics homogeneous and isotropic world models 78−45543
Yang-Mills struct. of gravit. final state of collapsing matter 77−60984
Yang-Mills-Einstein eqn. pseudoparticle solns., gravit. effect on Yang-Mills topology 77−82682
Zee's broken symmetric gravity theory 80−62558
zero-rest-mass fields, boundary conditions at past null infinity 78−24661
e^+e^- pair creation in strong EM fields, gravitational effects 80−42376
Ne-Xe gas discharge, LF oscillations, modulation by gravitation and inertia forces 77−11429

gravitational acceleration *see gravitation*

gravitational collapse
see also black holes; cosmology
anisotropic, mag. field strength var., MHD approx. calcs. 77−11283
aspherical, matter associated perturbations, linear Einstein field and conservation eqns. 79−5843
asymptotic freedom and dense baryonic matter 79−62738
axially symmetric star, general relativistic collapse, initial data 80−85960
axially symmetric stationary black hole states of Einstein gravitational theory 77−37614
axion production, astrophys. implications of new light Higgs boson 79−22007
axisymmetric accretion flows very near black holes and Rosen-collapsed objects 80−12778
axisymmetric gravitational collapse with escaping neutrinos, Einstein's field eqns. 80−26888
baryons, gravitational annihilation, radioactive decay 77−6075
bimetric general relativity theory 80−85853
black flash model of QSOs and Seyfert nuclei 78−57673
black hole, charged, interior evolution final state 80−8648
black hole, generation of pairs by collapsing body *(Russian)* 77−13234
black hole recoil due to gravitational radiation reaction, spherical and nonspherical collapse 80−85969
black holes, accretion disc as quasar and galactic nuclei power source 78−57667
black holes, existence of gravit. field outside black hole 79−9158
black holes, growth in dense stellar systems with evaporation of stars 80−62178
black holes, Hawking's effect, quantum field theory applied in curved space-time 78−12268
black holes, small mass, spin effects on formation in Einstein-Cartan theory 77−71125
Bok globules, collapsing cloud models 80−62216
Bonnor electrovac counterparts of Tomimatsu-Sato solns. of Einstein eqn. 78−57835
Brans-Dicke theory of gravit., freq. shift of radiation from exploding/collapsing object 79−67210
charged fluid sphere, gravitational collapse 80−31637
charged media, general relativistic Lagrangian dynamics *(Russian)* 78−7874
classical and quantum, problems *(Russian)* 77−87258
classical and quantum, problems *(Russian)* 78−53815
classical and quantum collapse problems *(Russian)* 77−56822
classical problem, nonlinear differential eqns., solns. 78−93099
cold white dwarf, numerical integration of general relativistic eqns. 77−17568
collapsing relativistic stars, linearised odd-parity radiation 78−93297
collapsing shell, Schwarzschild-de Sitter space-time, thermodynamics and radiation 80−17607
gravitational collapse continued
conference, singularities in general relativity, Waterloo, Canada (Aug. 1977) 80−31405
cosmic censorship, mathematical formulations 80−31619
cosmic censorship hypothesis and the positive energy conjecture 80−31618
cylindrical general relativistic collapse, numerical study results 78−93585
dense stellar systems, fates 79−25652
dust, thin spherical shell, around black hole, dynamics, Russner-Nordstrom geometry 78−77481
dust ball, nonsingular collapse in quantum conformal geometry 79−97284
dust cloud in Corona Austrina, mm wavelength obs., nonhomologous collapse, rel. to star form. 79−30102
dust lanes in galaxies rel. to spiral structure 79−92849
dust shell, charged, spherical, gravitational collapse, maximal time slicing condition 80−67554
Earth core, gravit. settling rel. to core energetics and geomag. field generation 77−73638
Einstein's eqns. for dust, gravit. collapse and radiation 78−99
Einstein's gravitational equations, local and global modifications 78−61719
Einstein equations, [(2+1)+1]-formalism, apparent horizons in space-time with rotational Killing vector 80−73222
Einstein Maxwell equations, static axisymmetric interior soln., mag. support against gravit. collapse 78−16288
Einstein static universe, generalised, equilib. configs. for perfect fluids 77−45748
Einstein-Cartan theory, bounce of spheres 78−93572
Einsteins gravitational equations, non-static source of Taub solns. 78−4537
equivalence principle, gravitational collapse, and the classical particle problem 79−25927
evolving systems instability, elastic stability theory and catastrophe theory approaches 78−44442
falling through black hole into another universe, theory 78−32748
finite-particle scheme for three-dimens. gas dynamics 78−67218
form factors α and β product asymptotic limit for celestial bodies 79−84653
free-fall sources of gravit. radiation, failure of quadrupole formula 80−51647
Friedmann cosmological model, classical and quantum gravit. collapse problems *(Russian)* 77−87257
Friedmann cosmological model quantisation, geometrical-dynamical anal. *(Russian)* 77−64636
galactic active centre, relativistic astrophys. *(Russian)* 77−13233
galactic chemical evolution at initial rapid-collapse phase 78−69870
galactic nuclei, gravit. instability of nuclear disc formed from stellar mass loss 80−67858
galactic spiral structure, gaseous theory of origin 80−82517
galaxi formation, anisotropic gravit. collapse 78−4344
galaxies and galaxy clusters, relaxation from aspherical initial conditions 78−96538
galaxies formation, pregalactic evolution model 79−92863
galaxies formation by gravit. instability, role of ang. momentum 80−98722
galaxy and star formation theories, gravitational instability role *(Czech)* 80−41718
galaxy formation, dynamical development and struct. of six collapsing models 79−25710
gas cloud, three-dimens. collapse and fragmentation 78−77552
gas clouds, inhomogeneous, one-dimensional collapse, role of small perturbations *(Russian)* 80−36497
gas clouds, rotating isothermal, fluid-in-cell method 77−5523
gas clouds spherical gravitational collapse, unsteady hydrodynamics 78−45212
gas flows, selfgravitating, thermodynamic processes and radiation, numerical method 80−14848
gaseous sphere contraction vel., virial-based soln. 79−48665
gauge-invariant perturbations on most general spherically symmetric space-times 79−71322
general relativity, geometrical factors *(Russian)* 77−73944
geometric quantization and gravitational collapse 80−90752
globular cluster cores evolution, life and death matters 79−25653
globular clusters, late core collapse in gravitating systems 80−22048
globular clusters, present and past death rates 78−28733
globular star cluster core evolution, effect of gravithermal catastrophe 80−67804
globular star clusters, isothermal cores, stability limits 80−46622
gravitational compression of a body within the approximation of the special theory of relativity 80−4611
gravothermal catastrophe and negative specific heat of self-gravitating systems 78−93593
gravothermal catastrophe of finite amplitude 79−2476
gravothermal instability in two dimensions 78−89395
hadron system, rel. to contraction of closed oscillating Universe *(Russian)* 80−4466
homogeneous collapsing star, orthogonal vector and tensor harmonics, matter and field asymmetries 79−5841
horizon instability in perturbed scalar field *(Russian)* 78−53816
ideal fluid, general relativistic dynamics *(Russian)* 77−49287
interacting EM and gravitational perturbation in gravitational collapse with charge and small asymmetries, interacting EM and gravitational perturbation 80−105274
interstellar clouds, collapse dynamics and models, rel. to star formation 78−32566
interstellar clouds, rotating, nonaxisymmetric collapse theory rel. to protostar form. 80−85927
interstellar clouds, rotation, axially symmetric collapse and protostellar form. 80−77380
interstellar clouds, structure and evolution under external pressure 78−61898
interstellar clouds collapse and star form., suppression by interstellar gas heating 80−105349
interstellar clouds cooled by C atoms and ions, critical mass for gravit. instability *(Russian)* 80−12801
interstellar CO clouds, contraction and fragmentation 80−67838
interstellar cold gas clouds with mag. field gravit. contraction, star form. 78−8102
interstellar cylindrical clouds, two-dimensional collapse calcs. 79−40247
interstellar gas clouds, molecule form. 77−78848

gravitational collapse continued
interstellar gas clouds, non-uniform collapse stability 80−101631
interstellar gas clouds, spherically symm., effect of H_2 form. 80−101628
interstellar gas clouds gravit. collapse, caustic and critical times for one-dimens. model 78−93367
interstellar grain cloud, gravit. collapse rel. to star form. 78−69788
interstellar grain clouds gravit. contraction, star form. 77−53575
interstellar large globules, struct. and dynamics 80−62246
interstellar magnetic clouds, gravit. collapse 77−13420
interstellar magnetised gaseous discs, gravitational instability 80−4424
interstellar medium, gravit. collapse and star form. in shock-compressed layers 78−40919
interstellar medium, influence of initial vel. fields upon star form. 80−21985
interstellar nonrotating magnetic gas clouds collapse, numerical calcs. 80−105299
interstellar rotating clouds, protostellar formation, numerical methods and tests 80−56902
interstellar spherically symmetric radially moving clouds, spectral line shapes 78−20865
interstellar turbulent 80−56910
inverted black holes, anisotropic collapse, static vacuum, electrovacuum field struct. 80−67776
Kerr and Tomimatsu-Sato metrics from group transformation, rot. vacuum soln. 78−65838
Kerr black hole, gravitational perturbations 79−44819
Klein Gordon equation, massless, bound states in Kerr metric 79−35600
Lifshitz-Khalatnikov time functions in gravitational collapse 80−31615
low freq. gravit. radiation, from collapsing systems 79−71314
magnetized stars and gas clouds, whistler mode radiation during collapse 78−28509
magnetofluid, self-gravitating, local behaviour of congruences 78−89384
marginally bound dust collapse, time functions in numerical relativity 79−71321
massive cold star, appl. of stability predictions through a succession of folds 79−76991
massive neutron star, fermionic matter, coupled Dirac-Einstein eqns., self consistent soln. 78−73731
massive star core collapse, eqn. of state and composition near β equilib. 80−82335
massive star cores, supernova explosion from shock heating 80−56863
massive stars, Homestake long-range neutrino detector research program 79−80107
massless scalar field in a de Sitter universe and its thermal flux 79−127
massless scalar particle creation, classical and quantum gravit. collapse *(Russian)* 79−9039
mathematical physics, success and failure viz. Kolmogorov-Arnold-Moser theorem, gravit. collapse, singularities, matter stability *(German)* 78−65744
naked singularities, event horizons, and charged particles, test particle motion in Reissner-Nordstrom field 79−71684
naked singularities and cosmic censorship, current situation 80−31621
naked singularity solutions, gravit. collapse with axial symm., geodesics, particle orbits 78−41215
neutrino flux from quark matter at core of collapsed stars 80−22028
neutrino viscosity in collapsing stellar cores 78−61875
neutron star formation, competition between neutrino and gravitational radiation 77−49421
neutron stars mass upper limit for stability against black hole form. 78−96498
non-linear transport equations: Properties deduced through transformation groups 80−4680
noncrossing timelike singularities of irrotational dust collapse 80−31617
nonlinear electrodynamics, Birkhoff's theorem analogue *(Russian)* 78−54273
nonrelativistic para-Fermi gas, thermodynamic and mag. props. 79−25974
nonsingular gravitational collapse, Yang-Mills cosmos 79−21621
nonuniform configuration, classical and quantum gravitational collapse *(Russian)* 78−7873
observer falling freely into nonrotating black hole distant stars distrib. evolution *(Polish)* 80−26897
odd-parity perturbations, junction conditions on spherically symmetric space-times 80−42127
Oppenheimer-Snyder solution, Newtonian analogue 77−73945
optical appearance of collapsing star 80−4391
oscillating universe, expansion and collapse stages 77−87579
oscillatory collapse, exact soln. *(Russian)* 77−87256
parity nonconservation and stellar collapse 79−92789
particle creation by singularities in asymptotically flat spacetime 78−54260
particle creation in gravit. collapse, absorpt. effect 77−91420
perfect fluid, vorticity, general relativity theory 77−11282
perturbed spherically symmetric collapsing star, initial value problem in quasi-Newtonian background 79−5842
photon emission from gravitationally intense cylindrical bodies 78−57840
planet form., behaviour of system of particles at high press. 77−87261
plasma, rotating, effect of suspended particles on gravit. instability 80−109347
pre main sequence stars, rapidly rotating, evolution in gravit. contraction phase 80−62133
pre-galactic H gas cloud, local stability, linear perturbation anal. 80−82513
predictability breakdown, principle of ignorance 77−17356
presolar nebula collapse 79−58281
primordial black holes formation 80−12776
protogalaxies, rot. and star form. rate 79−35374
protostellar cloud, rotating, collapse and stability, turbulent viscosity effect 80−109510
protostellar cloud, solar-type star form. with spherical symmetry 80−85930
protostellar cloud and formation of solar-type stars in spherical symmetry, accretion shock effects 80−62107
protostellar clouds, rotating, ring form. during dynamic collapse 80−56820
protostellar envelopes of masses 3 M⊙ and 10 M⊙, struct. and hydrodynamic evolution 80−36616
protostellar rotating gas clouds, fragmentation 80−51827
pulsar, quasar and X-ray source obs. 80−36657
quantum field coupled to Schwarzschild-de Sitter metric, vacuum energy-momentum tensor 80−52091
gravitational collapse continued
quantum fluctuations in gravitational collapse and cosmology 78−49571
quantum fluctuations near the classical space-time singularity 80−8893
quantum uncertainty in final state 77−82433
quasars, physical props. of collapsed objects with large central gravit. redshifts 77−5588
quasispherical spacetimes of Szekeres, collapse without gravit. radiation 78−28510
quasistationary collapse of slowly rot. nonhomogeneous bodies in general relativity 77−49289
radiation detection, astrophysical sources, resonant mass, laser interferometer and Doppler ranging methods 80−68122
Rayleigh-Taylor convective overturn in stellar collapse 80−41815
Reissner-Nordstrom black holes, instability of the Cauchy horizon 79−67201
relativistic EM fluid flows, geometry 79−58601
relativistic non-ideal hadron gas universe, gravit. collapse *(Russian)* 79−44650
relativity, general, zitterbewegung, atoms with point particles 80−57147
rotating 2 M⊙ Fe-O star *(Russian)* 78−4199
rotating axisymmetric collapsing source, soln. of Einstein's field equation for enveloping radiating zone 79−2682
rotating black hole formation by dust cloud gravitational collapse 79−2557
rotating black holes, instabilities of massive scalar perturbations 79−54026
rotating gas cloud, binary system form., three-dimens. hydrodynamical anal. 78−65494
rotating gas cloud collapse, equatorial ring formation, Lagrangian method 78−12628
rotating gas clouds, gravit. axisymm. adiabatic collapse 78−7875
rotating stars, 7 and 10 M⊙ stars evolution with time-depend. redistrib. of ang. momentum 78−36553
rotating systems, Einstein equations 80−68101
Saturn, gravitational contraction history 77−33405
Schwarzschild geometry, nonlinear scalar field dynamics 79−275
Schwarzschild space-time, vacuum polarisation induced by gravitation 80−82410
self gravitating fluids with cylindrical symmetry 80−12970
self similar collapse of isothermal spheres and star formation 77−53568
shape instability of collapsing sphere, pressure stabilisation 80−8537
shear free collapse 79−97013
singularities, review 77−57238
singularities and rule of unanimity 78−4529
singularity theorems and universe rejuvenation 78−32616
spacetime singularities 78−8291
spherical accretion in point mass gravitational field, selfsimilar flow *(Russian)* 78−28498
spherical gravitational distrib. in ideal liq., classical and quantum theories *(Russian)* 78−49311
spherical star without rotation, gravitational collapse study *(French)* 79−93016
spherical static fluid, interior solns., appl. to collapsed stellar objects 77−57245
spherically symmetric fluid, general relativity, equation of state, no slow uniform contraction 80−62544
stable heavy neutrinos, dynamical interactions and astrophys. effects 79−5743
star, collapse triggering by thermonuclear burning in degenerate C core 78−65608
star clusters, evolution, Fokker-Planck eqn. numerical integration 80−36675
star collapse generating gravitational radiation, strength estimate 80−46584
star core, shockwave prod., neutrino transport effects 80−94818
star core collapse to neutron star, electron neutrino and antineutrino emission, spectral calcs. 80−109454
star formation, protostellar cloud ang. momentum problem, mag. breaking 80−82342
stars, collapse theory 80−77389
stars, criteria for mass ejection 77−33534
stars, enhanced gravit. radiation recoil 77−33336
stars, equations of state 79−97014
stars, mass loss during collapse rel. to slow rot. 78−49426
stars, neutrino ang. momentum losses 77−56916
stars, neutrino bursts and gravit. waves, proposed search for correl. 78−77567
stars, neutrino damping of nonradial pulsations 77−56999
stars, neutrino radiation for hot neutron star form. rel. to envelope outburst problem 78−45350
stars, rate of collapses in Galaxy 77−71122
stars, relativistic collapsing, radiation, linearized even-parity EM and gravit. radiation 79−75228
stars, second order perturbations with rotation, gravitational waves 80−56816
stars, slowly rotating, gravit. collapse, supernova explosion, neutron star or pulsar remnant 78−96472
stars rotating sphere, free collapse 78−93325
static scalar field, possibility in Schwarzschild metric 77−45765
stellar collapse, adiabatic hydrodynamics and shock wave propag. 80−56861
stellar collapse, effects of nuclear forces, partition function and dissoc. 79−48833
stellar collapse, ellipsoidal models and gravit. radiation 78−45317
stellar collapse, hydrodynamics 78−45318
stellar collapse, neutrino trapping effect on nucl. dissoc. 80−90407
stellar collapse and the black hole limit from a dynamical view 79−30081
stellar collapse to neutron stars and black holes, computer generation of spherical spacetimes 80−46385
stellar collapsed core, neutrino prod. of bypassed isotopes, neutrinos role in nucleosynthesis 79−40182
stellar collapsing core, role of neutrino dissipation 79−101166
stellar compression into disc, gravit. radiation *(Russian)* 77−13325
stellar core, collapse rel. to gravitational waves emission 79−92664
stellar core, ellipsoidal model calcs., gravitational and neutrino radiation 79−53802
stellar core, neutrino prod. and interaction with ejected envelope ^{26}Mg, ^{26}Al prod. *(Russian)* 80−77285
stellar core, secondary indications of collapse 80−62177

gravitational collapse continued
stellar core collapse, neutrino prod. and inelastic scatt. by nuclei at extreme temps. 80−36488
stellar core collapse, neutrino trapping 78−32437
stellar core collapse, neutrinos conservative scatt. and electron scatt. rel. to thermalisation 79−92659
stellar core collapse, Thomas-Fermi model of warm nuclei 80−51648
stellar core collapse, vacuum neutrino oscills, inhibition by high matter density 80−36496
stellar core collapse and overturn with Rayleigh-Taylor unstable gradient 80−94819
stellar cores, homologous collapse, perturbations effects 80−94779
stellar evolution, terminal stages in QCD 77−78773
stellar evolution, weak interactions and supernova outbursts 77−87464
stellar gravitational collapse, neutronisation and lepton escape rel. to hydrodynamics 80−77388
stellar N-body systems, two-body tidal dissipation rel. to core collapse 78−93329
stellar systems with continuous mass spectrum, necessary condition 78−93328
strong gravitational field and general relativity 80−67548
supermassive star, expanding, and contracting dust shell, Einstein's theory of gravit., black hole formation 78−12088
supermassive star collapse to black hole, Einstein eqns., numerical soln. 80−41851
supernova collapse, eqn. of state at subnuclear densities 80−77278
supernovae with neutrino degeneracy 78−40977
tachyonic matter in the gravitational collapse, book contrib. 79−44822
thermal props. of self-gravit. plane-symm. gas 77−13323
thermodynamic equilib. of gravitating sphere in Lyra's geom. 78−65840
uniform gravitational collapse, lepton pair creation, macroscopic gauge theory of gravity 78−81724
universe, closed, gravitational collapse and ultimate fate 79−75303
unstable isothermal spheres, collapse, star form. appl. 78−32332
W3 molecular cloud core, collapse and rot. 80−94843
warm neutron degenerate matter, eqn. of state 79−84810
weak neutral current, effects in stellar collapse, review, book contrib. 78−85964
Weyl singularities, stability of nakedness 80−46896
ν emission in gravitational collapse, Liouville line element 78−57437
Fe-O stars collapse, physical and mathematical formulation and computational method 77−87369
Fe-O stars with masses of 2M⊙ and 10 M⊙, gravit. collapse 78−20815

gravitational constant
bimetric gravitation theory, cosmological model and var. of gravit. const. 77−33710
binary pulsars, relation between speed ups and variation of gravitational constant 78−73728
Brans-Dicke closed space cosmology, exact soln. for radiation-filled era 78−93488
calibration theory and gravitational const. variation in early universe *(Russian)* 80−17706
changes and planetary expansion limits 78−28155
cosmological change of gravitational const. rel. to Earth struct. 77−73626
cosmological limit on possible var. 78−93492
cosmological parameters rel. to gravitational const. 79−48974
cosmological variation, effects on solar luminosity 80−82182
cosmologies with variable past gravit. constant and macroscopic masses, solar and stellar tests 77−45619
cosmologies with varying gravit. const., theory 78−57705
Dirac's large number hypothesis, fundamental const. variability 77−67153
Dirac cosmology, effect of gravit. const. var. 77−22334
Earth momentum of inertia, effects of gravit. const. vars. 78−49302
experimental determ. at distances around 10 m 79−85051
experimental determination using pendulum with two degrees of freedom 77−67371
finite-struct. and gravit. const. in unified theories 77−41802
fundamental constants, calcs. in various theories 77−30354
fundamental constants, self-consistent values *(German)* 79−12758
G-varying cosmology, galaxy and QSO magnitude/red shift relations 80−56980
G-varying cosmology, radio source counts and models 80−56981
G-varying cosmology, thermodynamic relations and 3K background radiation 80−56979
G-varying cosmology and cosmic microwave background spectrum 80−86020
gauge field theory of gravitation, cosmological implications 79−44839
in gauge theory of de Sitter group, fundamental length parameter 77−64990
Gaussian gravitational constant variation, determ. from visual binary stars obs. *(Russian)* 79−44537
general relativity, observability of physical quantities, inertial mass, gravitational constant, planetary motion 80−56700
general relativity test, planets observed by astrometric and radiometric methods 78−45552
geocentric gravitational constant, evaluation from Viking Doppler and range data 80−3891
geocentric gravitational constant (GM), determ. from satellite-satellite tracking data 80−3911
geocentric gravitational constant determ. from near-Earth satellite laser ranging 79−34724
geophysical determ. of Newtonian gravit. const. 78−81098
Hoyle-Narlikar conformal gravity, cosmological effects of gravit. const. var. 80−56698
inertial frame dragging effect, and contrib. of matter to gravit. constant, Brans-Dicke theory 79−67206
measurement, balance appl., thermal noise effect 78−65906
measurement, kilogram as standard mass unit *(German)* 77−22532
measurement using evacuated torsion balance 77−49707
Moon tidal acceleration, no evidence for changing gravit. const. 79−16849
Newtonian cosmology if G varies 77−17730
Newtonian cosmology with diminishing gravitational constant 78−54100
Newtonian cosmology with time-varying constant 78−65733
Newtonian cosmology with varying gravitational constant, alternative approach 78−54101
renormalisational, and fermion pair creation in nonstationary gravit. field *(Russian)* 79−17323

gravitational constant continued
Sakharov's thoery of gravitation 79−25950
secular decrease rel. to Earth expansion, evidence from Mercury 77−32972
secular variation rate, palaeontological evidence 77−45307
stellar clusters, theoretical isochrones with decreasing gravit. const., Dirac's multiplicative cosmology 78−16586
stellar evolution with variable gravitational constant, Universe age effects 79−30052
theoretical determination, integration of test body eqns. of motion *(German)* 77−67370
theoretical isochrones for stellar evolution with variable G, Brans-Dicke theory 79−67125
time dependence 80−90771
time variation, effect on evolution of dynamical systems 78−24459
time variation, influence on cosmic He abundance 79−92667
time variation, rel. to form. times of rich clusters of galaxies 78−69892
time varying Newtonian gravity, Q in cosmology 78−77634
time-varying force law in Newtonian theory, rel. to Earth thermal history 78−93592
torsion balance determ., thermal noise limitation 78−16714
two-body problem, with decreasing gravit. const. 77−13219
vacuum polarization and non-Newtonian gravitation 80−62896
value, constraints from obs. of white dwarfs 79−25464
variation, cosmological light element abundance constraint, comment on errors 80−72767
variation, Dirac's Large Numbers Hypothesis 79−16819
variation, effects on star clusters dynamical evolution 79−17030
variation, implications of cosmic large numbers coincidences 79−48969
variation, impossibility in Newtonian physics 78−69675
variation, rel. to Sun and Moon accels. and origin of mountains 79−8592
variation, summary of obs. evidence 79−12759
variation of gravitational const. rel. to earthquake periodicity 78−3724
variation with cosmological time, anal. using scale covariant theory 79−92666
variation with time *(Norwegian)* 78−69674
variations, effect on stellar evolutionary tracks 80−82186
varying to cosmology with primordial star generation 78−61946

gravitational experiments
20 kg gravitational wave antenna, Brownian noise at 4.2K, upper limit for gravit. radiation at 8580 Hz 77−37800
accelerometers, gravitational wave detection, and general gravit. expts. 78−45555
antenna, design for use at 3 mK 77−82435
antenna for gravit. waves, quality factor meas. 78−8330
antenna sensitivity, quantum mech. anal. *(Russian)* 79−75436
antenna small perturbation meas., optimum strategy 77−82438
astronomy, gravit. waves detect. techniques 77−67368
asymmetric rotator as detector for monochromatic gravitational waves *(Russian)* 79−85054
birefringence induced by gravitational waves, new detector 79−97291
black holes, observational status 79−97019
cardiopulmonary readjustments in passive tilt 80−56084
Cavendish experiment at large distances *(Russian)* 80−27207
cavity transducer for subatomic mech. vibr. 77−82436
coherence effects in neutron diffraction and gravity experiments, review 79−58616
constant measurement using evacuated torsion balance 77−49707
control requirements, experiments in space 80−8896
cooled gravitational wave antennas, explanation of expt. obs. 78−54280
correlation techniques, poss. detect. of gravit. waves 78−89393
counter-orbiting drag-free satellites in Earth polar orbit, general relativity test and geodetic meas. 77−22047
critical phenomena experiments, gravity effects in fluids near the gas-liquid critical point 79−58667
cryogenic gravitational wave antenna, initial operation of 390 kg system 79−67217
cryogenic Weber-type gravitational wave antenna, obs. of mechanical Nyquist noise 77−30078
data analysis algorithms 79−67216
Deep Space Net spacecraft tracking technology, appl. to experimental gravitation 80−8895
deflection of polarised radiation, improved upper limits 77−2596
detector, statistical anal. of recorded data 78−21047
detector efficiency, elastic body and conducting charge 77−17899
detector of gravitational waves, appl. of photon-graviton resonance, technical problems, expt. possibilities 78−73905
detectors for gravitational rad. 79−93033
disc antenna response to scalar and tensor waves 77−30079
Earth artificial satellites motion, relativistic effects 79−2465
Earth gravit. shift by direct atomic-time-scale comparison 77−33925
Earth stain-tides, spectroscopy rel. to parametrised post-Newtonian parameters 78−73301
Earth tides observations, gravity screening effect assessment *(Russian)* 78−88787
Einstein's theory verification, expts. in space, review 79−6042
Einstein effect (gravitational deflection of light), obs. at solar eclipse (1981 July 31) *(Russian)* 80−51651
elasto-optical detection of gravitational waves 80−126
EM detector, two-level, parametric, anal. of operation 79−6041
EM tunable gravitational wave detector 79−137
emission, props., detection of gravit. waves, comparison with EM waves 78−21030
equivalence principle, test using neutron elec. dipole moment 77−57265
equivalence principle test, precession of fermions in mag. field *(Norwegian)* 77−64986
equivalence principle test using space-borne clock 79−49152
femur, rat, influence of hypergravity on compressive strength 80−3690
femur strength, rat, rel. to growth, bone-length, gravity 80−16978
force on freely falling electrons, meas. apparatus 77−30080
Fujii's gravitational theory, test 78−4550
Gaussian spindle gravitational wave antenna and single antenna anticoincidence expts. 77−41523
general relativity effects on some modern technological developments *(German)* 79−58615
general relativity test, planets observed by astrometric and radiometric methods 78−45552
general relativity test, precision ring laser interferometry technique 80−52117

gravitational experiments continued
general relativity tests, successes and limitations *(Danish)* 77−64985
gravitational const. experimental determ. at distances around 10 m 79−85051
gravitational radiation, detection possibility, Doppler tracked spacecraft 78−45549
gravitational radiation detection *(Japanese)* 78−77792
gravitational wave antennas, use of low-noise preamplifier 78−243
gravitational wave astronomy, review 79−92664
gravitational wave detection, low temp. antenna designs 77−17900
gravitational wave detection by compact EM systems *(Russian)* 78−49747
gravitational wave effects as relativistic particles 79−75424
gyroscope, high accuracy all angle readout using quantised flux 77−26223
heterodyne gravitational wave detector, sensitivity 77−41298
high precision clock appl. 77−74301
Hoyle-Narlikar conformal gravitation, cosmological tests 80−56698
Hughes-Drever expt., and theories of gravitation 78−21046
interaction forces at separations around 10 meters 80−17857
inverse square law, null expt. proposal 79−71346
inverse square law test in laboratory 80−31657
inverse-square-law of gravit. forces 78−8331
laboratory experiments, required technology, noise sources 77−64987
laser detector of gravitational waves *(Russian)* 78−77794
lens effect, search for secondary radio image of source 3C 303a 77−78878
Lense-Thirring effect, relativity test, counter-orbiting satellites 78−45554
light bending by eclipsed Sun, star field obs. *(French)* 78−20634
light deflection, effect on Sun semidiameter meas. *(German)* 80−46531
local field and gravitational radiation experiments 80−46948
low flux radiation, meas. technique using EM fields 77−30075
Maryland-Argonne gravit. radiation detector, anal. of 1973-74 data 77−22476
mass variations obs., periodic, using electromechanical vibrating system 80−47020
Maxwell's eqns. in matter, covariant formulation 78−57798
microwave cavity gravitational radiation detectors 79−21647
Munich-Frascati expt., final negative results 79−8830
neutron interference fringes due to gravitational potential, role of gravity in quantum mechanics 80−62495
NP 0532, Crab pulser, gravitational radiation obs., energy flux upper limit 80−36655
null experiment to test inverse square nature 80−52116
parity violation in the neutron's gravitational interaction 79−58617
photon clocks 77−37801
precision in gravit. expts. 78−8333
present evidence, future expts. for general relativity 79−93031
prototype Nb gravitational radiation antenna, microwave parametric accelerometers 79−44841
PSR 1913+16, binary pulsar, orbital period changes as test of metric theories of gravit. 77−60589
PSR 1913+16, binary pulsar, relativistic observable effects 80−77438
quadrupole mass-detector, in field of weak plane gravitational waves *(Russian)* 79−21645
quantum effects in gravit., expt. tests 77−87684
quantum nondemolition meas. of harmonic oscillators, gravit. wave detection 78−41198
quartz antenna, Q-factor 79−35623
radiation detection, Ar laser interferometer appl. 79−101076
radiation detection, astrophysical sources, resonant mass, laser interferometer and Doppler ranging methods 80−68122
radiation detection by Doppler tracking of spacecraft 79−30345
radiation detection method, elastooptical antenna, photoelastic effect 80−46947
radiation detector, limits to meas. of displacement 78−86215
radiation detectors, and waves, review 79−126
radiation detectors, implications of extension to noise theory for RF SQUIDs 77−87685
radio signal retardation by solar gravity, Viking expt. results 80−36933
radiowave deflection by Sun, General Relativity test 77−70994
red shift meas. using Mossbauer effect in ^{67}Zn and ^{181}Ta 78−24905
relativistic experiments in gravitational fields, review 80−42135
relativity experiments with clocks 80−46950
relativity gyroscope expt., high accuracy test facility 77−30077
resonant antennas for gravitational radn., electromech. tuning 79−97290
resonant gravitational wave antenna with linear motion detector, ultimate sensitivity limit 77−13679
resonant mass gravitational radiation detectors, quantum limits 79−63123
Rome group 389 kg gravitational wave antenna, operation information 80−90769
satellite, orbits near Jupiter and Saturn, post-Newtonian effects 79−101054
scale covariant gravitation theory appls. 77−79019
seismometer detection of gravitational waves 80−86196
small cryogenic gravitational-wave antenna, meas. at 1.5K 79−21646
space-time curvature meas., sensitivity of gravitational radiation antenna 78−45553
spinning particles, in grav. fields, effects on motion 80−46952
SQUID coupled to piezoelectric transducer, detection of gravitational waves 78−21218
star clusters, dynamical evolution as test for gravit. const. change 79−17030
stars, neutrino bursts and gravit. waves, proposed search for correl. 78−77567
superconducting shielded gyroscope, mag. torque 77−13678
theoretical significance of gravit. expts. 78−8332
thermoregulation in unrestrained rats during and after exposure to 1.5-4 G 80−45857
torsion balance for G, thermal noise limitation 78−16714
tunable detector for gravitational radiation, design parameters 80−86195
tunable free mass gravit. wave detector 79−71347
velocity of gravit. interaction 78−21045
velocity of gravitational effects, meas. by Roll-Krotkov torsion balances *(German)* 78−81912
VLF radiation, search, rel. to interplanetary radiowave phase scintillation 79−70995
wave antenna, Nb-sapphire RF superconducting resonator, fabrication and props. 79−51704

gravitational experiments continued
wave antenna, superconducting accelerometer using Nb-on-sapphire RF resonator 79−49210
wave antennas, gravitational, with and without piezoelectric ceramics, elec. equivalent circuits 78−73915
wave detection, action on free-mass detector *(Russian)* 77−26222
wave detection, test bodies in plane wave field *(Russian)* 77−26221
wave detection, using flux gradient accelerometer, working model tests 77−26274
wave detection prospects, instrumental aspects 79−138
wave induced IR emission from polar crystals 77−45769
wave observations, recent advances *(Chinese)* 79−97292
Weber cylinder response in different gravit. theories 77−2585
white dwarfs mass-radius relation, constraints on gravit. const. 79−25464
wideband laser-interferometer gravit. radiation expt. 78−41223
X-band supercond. cavity accelerometer for gravitational wave antenna 77−30076
Al alloy disc, quality factor of vibr. rel. to gravit. radiation detector 78−75093

gravitational radiation *see gravitational waves*

gravitational red shift
see also cosmology
bi-metric theory of gravitation 79−35119
clusters of galaxies, red shift of traversing light, photon prop. 77−29642
CoD−38°10980, white dwarf, gravit. redshift meas. 78−24511
cosmological model without big-bang, gravitational origin for universal red shift *(German)* 80−51927
cosmological red shift, Doppler and gravitational components using Birkhoff's theorem 78−86041
Earth's rotation effect on gravitational shift, verification 77−2579
EM system free fall, equivalence principle, red-shift and Eotvos expt. 77−64982
equivalence principle and gravit. redshift 77−9944
o^2=40 Eridani B, gravitational redshift white dwarf redshift 79−62868
experiments, high precision clock appl. 77−74301
four-body forces and red-shift, gravit. clocks 77−61001
gauge field theory, gravitational considerations and red shift *(Japanese)* 79−80484
general linear nonmetric theory *(Russian)* 77−33339
isotropic red-shift, rel. to shear-free and acceleration-free fluids in Einstein's theory of gravitation *(German)* 77−22467
Kerr-type particle, uniformly accelerating and rotating, Schwarzschild, Rindler and Kerr surfaces 80−85855
Lemaitre Universes, Jeans instability 78−12445
light velocity and gravitational potential, Laplace's deduction of differential aberration *(German)* 78−57838
local relativistic red-shift effect 78−28788
Lorentz-invariant theory, results for red shift, light deflection, perihelion shift *(German)* 78−29030
massive spheres, maximum central redshift 77−13229
measurement using ^{67}Zn and ^{181}Ta Mossbauer expts. 78−24905
neutron stars, mass-radius relation, obs. constraints, dense matter eqn. of state 80−46597
neutron stars, mass/redshift relation rel. to struct. 77−78812
Newtonian non rotating cosmological model *(Spanish)* 79−48978
O-type stars, radial vels. and K-term rel. to gravit. red shift 77−56922
OQ 208, red shift difference between broad and narrow emission lines 79−67100
photon energy shift, possible antigravity in gravitational red shift 79−12673
pulsars and compact X-ray sources, gravit. redshifted γ-rays, neutron star mass constraints 78−4274
QSO absorption redshift systems, central gravitational redshift model 79−25753
QSOs, gravit. red shifts rel. to broad lines profiles 78−16566
quasars, gravit. and Doppler redshifts, interpreted as massive black holes ejected from galaxies 80−46695
quasars, Hoyle-Fowler model, photon emission critical angle 80−31383
quasars, physical props. of collapsed objects with large central gravit. redshifts 77−5588
relativistic force equation, appl. to gravit. red shift *(Afrikaans)* 79−97270
rotating star, interior Kerr metrics, tests 78−28666
scale covariant gravitation theory appls. 77−79019
Schwarzschild sphere, static config. with core and envelope 77−22058
second-order effect, possible expt. 77−22477
Seyfert galaxies, gravit. red shifts rel. to broad lines profiles 78−16566
solar spectrum, convective correction to measured wavelengths 78−93181
space-time experiments, potential of an orbiting interferometer 79−35624
star, cold, massive, rest-mass density and redshift 80−56859
static Universe model with two centres, red shift explanation 78−57706
Sun, Fe I line meas. 80−90391
sunspot umbrae, material motions and gravit. red shift obs. 77−45374
thermodynamic equilib. of gravitating sphere in Lyra's geom. 78−65840
van Maanen's star, astrometric study of Sproul plate series, radial vel., gravit. redshift 78−40936
white dwarf stars, rot. and gravit. redshift 77−29816
white dwarfs, visual surface brightness relation appl. 78−81624
white dwarfs H line asymmetries and gravitational redshifts 77−17556

gravitational waves
see also gravitons
absorption by excited vacuum-space time 77−67355
absorption in water mols. 80−82189
antenna, active resonant, for gravitational radiation, sensitivity and noise 79−30346
antenna, design for use at 3 mK 77−82435
antenna, instrumented with reson. capacitor transducer, sensitivity 78−45553
antenna for gravit. waves, quality factor meas. 78−8330
antenna small perturbation meas., optimum strategy 77−82438
antenna theory 77−9934
antenna transducer cct., appl. of artificial cold resistor 78−32750
antennas, magnetic pick-up transducer theory 79−85052
anti-gravity generation due to counterclockwise turning of gyroscope *(Japanese)* 80−12980
astronomy, gravit. waves detect. techniques 77−67368
astronomy, gravitational waves sources and detectability 79−92664

gravitational waves continued
asymmetric rotator as detector for monochromatic gravitational waves *(Russian)* 79−85054
asymptotic de Sitter space, grav. field eqn. solns. 79−9163
asymptotically flat gravit. field, Hertz pot. and radiation fields 77−60994
atomic, transitions induced by gravitational radiation *(French)* 78−29026
axially symm. two body problem in general relativity, free fall, gravit. energy flux 77−71254
axially symmetric two-body problem, Bondi mass loss, quadrupole formula failure 80−42120
background gravitational radiation spectra in early state of the Universe *(Russian)* 80−36745
background radiation, detection using spacecraft Doppler tracking 79−80494
background radiation, possible detection by Doppler tracking interplanetary spacecraft 80−67914
Bel-Petrov field classification, algorithm 78−93566
Bianchi type VII homogeneous cosmological models 77−17734
Bianchi type-I universe, tensor perturbation equations, derivation 79−124
bimetric theory of gravitation, viability, gravitational radiation from neutron star binaries 79−35611
binary neutron stars, evolution, gravit. radiation and mass transfer 77−78821
binary pulsar, gravit. radiation rel. to pulsar period secular change 77−5542
binary pulsar PSR 1913+6, dissipative effects connected with gravitational radiation, indirect evidence 79−75236
binary star, close low-mass, evolution with mass exchange and gravit. radiation losses 77−53631
binary star gravitational radiation, limits on finite size effect 77−33337
binary star radiation, relativistic corrections and spectrum fine structure 80−90479
binary stars, effect of gravit. radiation on evolution and spins 78−12292
binary stars, gravit. dipole radiation in alternative metric theories of gravitation 77−60589
binary stars, gravit. waves interaction, tidal reson. 78−93089
binary stars, gravit. waves tidal generation from orbiting Newtonian stars 78−4284
binary stars, low mass, gravit. radiation and evolution 77−57030
birefringence induced by gravitational waves, new detector 79−97291
black hole, charged, EM and gravit. waves propag. 77−87470
black hole, nonrotating, gravit. waves from test particle on plunging trajectory 80−4246
black hole, rapidly rot., reson. oscills. and gravit. radiation 77−9766
black hole, Reissner-Nordstrom, coupled gravitational and EM perturbs., scatt. matrix, energy conversion, quasi-normal modes 80−67775
black hole collisions, generation of gravitational radiation 77−13663
black hole collisions and scatt. gravit. radiation, zero frequency limit 77−64980
black hole fields, MHD relativistic processes 78−12280
black hole in external mag. field, relativistic particle radiation 80−22035
black hole interactions, gravitational radiation emission 79−125
black hole recoil dur to wave emission 80−85969
black holes, Gibbs-Duhem relation from Weinholds geometric approach 80−57153
black holes, irreverisble thermodynamics, fluctuation-dissipation theorem 77−60791
black holes, rotating, reson. freqs. of free oscills. rel. to gravit. waves 80−105271
boost required for zero flux, gravit. and EM compared 78−29027
boundary coupling of gravitational wave and EM radiation in cavity 78−54267
Cauchy problem formulation for Einstein eqns., coordinate conditions, reference frame theory 80−57150
Z Chamaeleontis, cataclysmic binary, possible gravit. radiation emission 80−4386
charge black hole scatt., gravit. to EM conversion, low-freq.-limit cross section 77−25935
classical force measurements, quantum restrictions *(Russian)* 80−62566
classical gravitational bremsstrahlung, wave generation 78−93093
close binary stars, low mass, evolution, gravitational wave emission influence 80−82425
close binary stars, orbital ang. momentum loss by gravit. radiation, mass transfer rates 78−40991
collapsing relativistic stars, linearised odd-parity radiation 78−93297
collapsing stars, enhanced gravit. radiation recoil 77−33336
collapsing systems, low freq. gravit. radiation 79−71314
colliding plane gravitational waves 79−40431
colliding plane gravitational waves 80−101741
collisional EM-gravitational waves, Szekeres so!n. generalisation 80−46893
collisions involving EM and neutrino waves in general relativity 77−17886
compact stars, gravit. radiation rel. to evolution of homogeneous ellipsoidal figures 77−33333
concentric EM resonator, gravitational wave radiation *(Russian)* 77−45772
conformal two-structure as the gravitational degrees of freedom in general relativity 79−17292
conservation equations and the gravitational symplectic form 79−2679
conservation laws and gravit. radiation, total stress-momentum definition 77−79014
contact binary stars of low mass, gravit. radiation emission rel. to evolutionary fate 77−2453
conversion of gravitational waves into electromagnetic waves by a moving charge 78−93584
cosmic coherent avalanche catastrophies, gamma-freq. graviton radiation 78−85844
cosmological field of high press. gravit. radiation, energy 78−57837
cosmological gravitational waves, prod. of temp. fluctuations in primordial background radiation 78−65728
cosmological model, with gravit. and scalar waves 79−53949
cosmological models, exact solns. 79−88771
cosmological origin and consequences 80−109569
cosmological particle creation classical analogue, WKB approx. 79−30160
covariant definitions of gravit. radiation, comparison *(Russian)* 77−53820
gravitational waves continued
covariant theory of short waves in gas in gravitational field *(Russian)* 77−62370
Crab pulsar, gravit. radiation revised estimate 78−32501
Crab pulsar, upper limit for gravit. radiation energy flux 78−73730
cryogenic gravitational wave antenna, initial operation of 390 kg system 79−67217
cryogenic gravitational wave antennae, sensitivity 79−12705
cryogenic Weber-type gravitational wave antenna, obs. of mechanical Nyquist noise 77−30078
crystalline solids, HF radiation by normal modes 77−2586
curvature collineation for the field of total radiation 79−21606
curved space-time, conformal coupling of gravitational wave field to curvature 80−68105
cylindrical general relativistic collapse, numerical study results 78−93585
cylindrical gravitational-wave antenna, eigenfrequencies determ. 77−45771
cylindrical wave solutions of a scalar-tensor theory of gravitation in a Lyra manifold 79−21633
data analysis algorithms for wave expts. 79−67216
data analysis for Weber-type expt. 79−58614
data simulation for Weber-type expt. 79−54031
detectability of advanced gravitational radiation, emission mechanisms 79−6033
detection, astrophysical sources, resonant mass, laser interferometer and Doppler ranging methods 80−68122
detection, low temp. antenna designs 77−17900
detection, quantum nondemolition meas. schemes 79−67218
detection, use of relativistic particles 77−9940
detection, using flux gradient accelerometer, working model tests 77−26274
detection antennas, resonant, optimum filtering and sensitivity 80−8545
detection by compact EM systems *(Russian)* 78−49747
detection by Doppler tracking of spacecraft 79−30345
detection by resonant antennas, theory 79−44840
detection method using harmonic oscillator coupled to weak classical force 80−77684
detection possibility, Doppler tracked spacecraft 78−45549
detection prospects, instrumental aspects 79−138
detector, statistical anal. of recorded data 78−21047
detector, using DC SQUID 80−46949
detector efficiency, elastic body and conducting charge 77−17899
detector of gravitational waves, appl. of photon-graviton resonance, technical problems, expt. possibilities 78−73905
detectors, use of low noise preamplifier 78−243
detectors for gravitational rad. 79−93033
dielectric tensor and magnetic permeability in the weak field approximation of general relativity 80−90751
disc antenna response to scalar and tensor waves 77−30079
dispersion in cold matter 80−12967
duality and Backlund transforms. 80−12971
effect on fine-scale anisotropy of cosmic microwave background 78−81535
effect on orbital motion, evidence for inhomogeneous Universe 80−61998
Einstein's eqns. for dust, gravit. collapse and radiation 78−99
Einstein's eqns. for stationary axisymmetry 79−71311
Einstein eqns., exact classical wave solns. 80−8864
Einstein eqns., plane wave solutions 78−70022
Einstein-Infeld-Hoffman theory, Lagrangian formalism to fifth order and gravitational waves 77−67354
Einstein-Maxwell equations, EM and gravitational wave spacetimes, similarity solutions 80−57154
Einstein-Maxwell fields in asymptotically null-spherical coords., news functions 78−12631
Einstein-Maxwell theory, cosmological model with gravitational, electromagnetic, and scalar waves 80−86188
Einstein-Rosen gravitational wave superenergy tensor 80−62554
elastic medium, gravit. and acoustic waves, relativistic eqns., neutron star appl. 78−24712
elastic solid, effect of gravitational waves, oscills. *(German)* 78−81904
elastic spacetime rel. to black holes and gravitational waves 78−73625
elasto-optical detection of gravitational waves 80−126
electromagnetic fields conformal to non-empty space-times 79−30331
electromagnetic interpretation, contribution to classical theory *(Rumanian)* 80−68109
electrothermodynamical theory, gravitational field shielding *(Rumanian)* 80−68107
elliptically polarized, interaction with field of mag. dipole *(Russian)* 78−49738
EM detection, anal. as perturbed boundary-value problem 77−13677
EM detection methods 80−95024
EM detector, two-level, parametric, anal. of operation 79−6041
EM phenomena induced by weak grav. fields, possible gravitational wave detector 80−82692
EM spherical cavity resonator, amplitude of standing gravitational waves *(Russian)* 78−73906
EM tunable gravitational wave detector 79−137
EM wave emission by charged particle in gravit. wave field *(French)* 77−67353
emission, props., detection of gravit. waves, comparison with EM waves 78−21030
emission from rotating and precessing rigid bodies, simple model, appl. to pulsars 79−97271
emission of gravit. radiation by quantum mech. harmonic oscill. 77−33918
emission solns. from rotating and precessing rigid bodies 80−57151
energy density of gravit. field *(Chinese)* 77−82427
energy in Einstein general relativity 80−4610
energy loss in scattering problems, Einstein quadrupole formulae 78−89379
energy momentum in general relativity 79−21607
energy-momentum gravitational pseudopotential and Kerr-Schild metrics 77−2573
energy-momentum in general relativity 79−75423
equations of motion and radiation reaction 80−73232
experimental precision, gravitation and general relativity 78−8333
experiments, high precision clock appl. 77−74301
exponential amplification in gravitational field of ultrarelativistic rotating body 78−93594
external gravity field calc., signal processing approach 78−24708

gravitational waves continued
extraterrestrial pulse radiation, gravit. wave detector parameters *(Russian)* 77−9942
fields of identical tensor dimensions, correspondence *(Russian)* 78−65839
first quantitative evidence of the gravitational wave *(Chinese)* 79−80483
free-fall sources of gravit. radiation, failure of quadrupole formula 80−51647
freely-falling bodies, gravit. radiation 77−41518
galactic supernovae, seismic detection of gravit. radiation *(Russian)* 77−13371
galaxy tidal deformation by primordial gravitational waves, numerical simul. 79−92865
gauge-invariant perturbations on most general spherically symmetric space-times 79−71322
Gaussian spindle gravitational wave antenna and single antenna anticoincidence expts. 77−41523
general relativity, gravitational radiation and invariants of curvature tensor 78−57836
general relativity experimental verification, planetary orbit and gravity wave searches *(Russian)* 77−9941
generalised Peres space-time plane wave-like solns. of weakened field eqns. 78−57827
generation, linear momentum flux to higher orders 77−57258
generation by stellar encounter, bremsstrahlung formulae 78−4096
geometrical spacetime perturbation theory: regular first-order structures 79−2678
geometrised gravitational theory, energy-momentum tensor 79−25958
geometrized theories of gravitation 79−21636
gravitational conductors, waveguides, and circuits 80−36920
gravitational emission detectors, optimum quantum meas. *(Russian)* 78−45556
gravitational energy loss in scattering problems 80−73244
gravitational field and force derivation using Faraday's and Maxwell's ideas of electromagnetic waves *(French)* 80−68106
gravitational field stochastic fluctuations 79−44837
gravitational radiation, collapsed objects and exact solns., Einstein Centenary Summer School, Perth, Australia, 1979 January 80−105434
gravitoelectric antennas, direction sensitive, using uniformly moving charged particle beam 79−9164
graviton production by cosmological background, role of conformal (non) invariance 79−49131
gravitons in Minkoswki space-time, review 77−87683
harmonics, generation, plane-wave solns. of Einstein eqns. 77−13664
Hawking radiation of scalar and Dirac quanta from a Kerr black hole 79−30334
high frequency gravitational and electromagnetic wave coupling 78−8304
high frequency waves in dissipative fluid 79−12671
ideal fluid sphere moving in gravitational background, eqn. of motion, gravitational radiation 79−85026
impulsive gravitational waves collision, vac. Einstein eqns. soln. 78−21029
inertia and gravitation in general relativity 78−8317
interaction between plane strong EM wave and weak gravit. wave *(Russian)* 77−45774
interaction of plane gravitational waves with variable polarization 80−95010
interaction with elec. field of cloud of charged particles *(Russian)* 78−37169
interferometer detection, quantum mechanical radiation press. fluctuations 80−90770
intrinsic coupling between gravitational wave and quantised EM radiation 78−54268
isolated N-body system, gravitational radiation in higher multipole moments 80−42119
isolated perfect fluid, gravit. radiation, higher multipole moments 78−16707
isotropic universe, gravit. perturb. propag., using general relativistic kinetic theory 78−20920
Kerr black hole, gravitational perturbations 79−44819
Kerr black hole, low-freq. radiation from infalling particle 80−62176
Kerr black hole, tidal interactions and gravit. radiation 78−4276
Kerr-Schild generalised metric and Einstein-Maxwell fields 78−77783
Kerr-Schild metric description *(French)* 77−71255
Killing horizons around a uniformly accelerating and rotating particle emitting gravitational radiation 80−105557
Landau damping of small amplitude transverse traceless gravit. waves 79−49130
laser detector *(Russian)* 78−77794
laser detector for possible gravitational wave recording 79−40442
laser displacement sensor, appl. to gravitational radiation detect. 80−101747
LF gravitational radiation and redshift discrepancies for distant clusters of galaxies 77−71148
linearised gravitational radiation field, mag. components, measurability anal. 80−36921
linearized Einstein theory, twistors, plane fronted impulse wave backgrounds 79−30329
local field and gravitational radiation experiments 80−46948
local relative motion in general relativity 80−42123
long-wave primordial gravit. radiation, interaction with galaxies 80−17661
low flux radiation, meas. technique using EM fields 77−30075
magnetisable liquid, thin layer instability 79−41762
Maryland-Argonne gravit. radiation detector, anal. of 1973-74 data 77−22476
massive black hole ejection from galaxies, quasar-galaxy association 77−22263
matter and light wave interferometry in gravitational fields 80−94997
maximal background spectrum for extragalactic sources 77−9825
measurement at 1.5K, with small cryogenic gravit. wave antenna 79−21646
mechanism for mass transfer in OY Carinae 80−82385
microwave cavity gravitational radiation detectors 79−21647
microwave noncontacting accelerometer for gravitational wave antenna, supercond. cavity 77−30076
multipole expansions of gravitational radiation, review 80−73240
Munich-Frascati expt., final negative results 79−8830
n-body system radiation flux 77−22468
neutron hot perfect fluid relativistic stars, asymptotic eigenfrequency distrib. for even parity perturbations 78−49668
neutron star binaries formation rel. to gravit. radiation 79−35291
neutron star formation, competition between neutrino and gravitational radiation 77−49421
neutron stars, gravitational wave amplitudes and asymptotic eigenfrequencies distrib. for even modes 79−17300
neutron stars, rapidly rotating, gravit. radiation 78−65646
neutron stars formation, neutrinos and gravit. waves emission 78−12266
Newman-Penrose formalism and its application in general relativity, review *(Russian)* 79−21595
news theorem, gravitational counterpart of Poynting theorem 77−74291
Newtonian spheroid, homologous oscill., gravit. radiation, appl. to stars 80−46533
noise, from spontaneous prod. of gravitons, energy density distrib. *(Russian)* 79−12551
nonexistence in physical systems 79−80482
NP 0532, Crab pulser, gravitational radiation obs., energy flux upper limit 80−36655
observations, recent advances *(Chinese)* 79−97292
odd-parity perturbations, junction conditions on spherically symmetric space-times 80−42127
orbiting point masses, post-Newtonian gravit. radiation 77−13226
particle falling into Kerr black hole, high-freq. gravit. and EM radiation 78−16452
particle motion in the field of a Kasner-type bare singularity with complex or equal indexes *(Russian)* 79−49132
particle scattering, asymptotic behaviour near past null infinity 77−53819
particles in circular orbits around rot. black hole, gravit. waves emission 79−17009
periodic gravitational waves, focusing effects *(Russian)* 79−6032
perturbations and gauge conditions 80−82693
perturbations of analytic background metric 78−8302
perturbations of general type-D metrics, separation of wave eqns. 77−64975
plane, system of test bodies *(Russian)* 77−26221
plane, test bodies, action on free-mass detector *(Russian)* 77−26222
plane electromag. waves interaction, general relativity soln. *(Russian)* 79−21605
plane wave interaction, optical scalars and invariants of curvature tensor 77−17887
plane wave solutions stationary generalisation general relativity theory *(Russian)* 80−12968
plane waves in the bimetric gravitation theory 78−93583
plane without singularities, collisions 80−31640
plane-fronted, integrals of wave equations in space time *(Russian)* 78−89380
Poincare gauge theory of gravitation 79−75434
point masses in unbound orbits, gravit. radiation, Newtonian limit 78−4541
polar crystals, gravit. wave induced IR emission 77−45769
polarisation in Yang's gravitational field *(Chinese)* 80−17850
possible detection using correlation techniques 78−89393
post-Newtonian gravitational bremsstrahlung, theory 78−40811
postlinear formalism for gravit. wave generation 78−114
primordial waves, resonance with gravitationally bound systems 79−58599
propagation of gravitational waves in expanding universe 78−73787
prototype Nb gravitational radiation antenna, microwave parametric accelerometers 79−44841
PSR 1913+16, binary pulsar, appl. of bimetric gravit. theory 78−45347
PSR 1913+16, binary pulsar, as gravitational wave source, progress report 79−75234
PSR 1913+16, binary pulsar, confirmation of existence of gravit. waves *(French)* 79−80495
PSR 1913+16, X-ray and timing meas. correlations, grav. radiation, gas cloud friction 80−62171
pulse wave in spatially homogeneous universe, Einstein eqn. soln. 80−42121
pure radiation fields and gravitational waves 80−77673
quadrupole mass-detector, in field of weak plane gravitational waves *(Russian)* 79−21645
quadrupole test particle as detector of gravit. waves, eqns. of motion in general relativity 77−82426
quantum effects and regular cosmological models *(Russian)* 80−27206
quantum nondemolition meas. for gravitational radiation anal., oscillator-apparatus coupling 79−2711
quantum nondemolition meas. of harmonic oscillators, gravit. wave detection 78−41198
quartz crystal gravitational radiation antenna, Q factor 78−16715
quasi-stellar objects, gravitationally pumped masers model 78−54071
radiating systems, gravit. field, twisting free type II metrics 77−71256
radiation, detection, review *(Japanese)* 78−77792
radiation, linear theory of gravity approach 80−42118
radiation damping, solvable model 80−73243
radiation damping, space dimens. depend. *(German)* 80−52086
radiation damping and fast motion approx. 77−13662
radiation detection from stellar collapse 78−24707
radiation detection method, elastooptical antenna, photoelastic effect 80−46947
radiation detector, limits to meas. of displacement 78−86215
radiation detectors, and waves, review 79−126
radiation detectors, implications of extension to noise theory for RF SQUIDs 77−87685
radiation formula 80−98838
radiation from collapsing relativistic star with rotation 80−56816
radiation from weak field source 77−45770
radiation of dipole sources, Maxwell's eqns. analogue, appl. astrophysics 77−13536
radiation reaction force in weak gravitational field, coordinate system depend. *(Russian)* 80−62553
recoil, analogy with enhanced EM radiation recoil 77−33876
refractive index, interaction of gravit. waves with elastic body *(Russian)* 77−2584
Reissner-Nordstrom black hole, reflection and absorpt. of EM and gravit. waves 79−44820
Reissner-Nordstrom geometry, scalar waves, approx. scheme 80−52089
relative displacements of free test particles in fields of strong gravitational wave 77−74293

gravitational waves continued
relative motion detection in gravitational field 79−75422
relativistic astrophysics, Einstein's theory *(German)* 79−80213
relativistic corrections of gravit. force, radiation damping 79−97272
relativistic experiments in gravitational fields, review 80−42135
relativistic Kepler problem, field asymptotic behaviour in infinite past 79−88575
relativistic Kepler problem, orbits with gravitational radiation damping, behaviour in distant past 79−88574
relativistic particle falling into black hole, EM and gravitational radiation *(Russian)* 80−52097
relativistic particle interactions 79−75424
relativistic physics, gravitational radiation, Albert Einstein's papers *(Polish)* 79−75313
relativistic theories of gravitation, expt. testing using spacecraft-Doppler detection 78−77793
relativity, general, zitterbewegung, atoms with point particles 80−57147
relfection from compact stars 78−49314
research, current status and future prospects 80−73254
resonant antennas for gravitational radn., electromech. tuning 79−97290
resonant gravitational wave antenna with linear motion detector, ultimate sensitivity limit 77−13679
resonant mass gravitational radiation detectors, quantum limits 79−63123
retarded soln. of Einstein field eqns., spatially compact source 77−5723
Riemannian spaces, Lie derivatives and deviation eqns. 80−46876
Robinson's theorem, shear free condition 78−93586
Rome group 389 kg gravitational wave antenna, operation information 80−90769
Rosen's theory rel. to binary pulsar PSR 1913+16 77−26021
Rosens bimetric theory of gravitation, gravitational radiation and ultimate speed 80−52087
rotating bar, gravitational field, and forced oscill. of resonant antenna 80−52090
rotating model for radiation and radiation-reaction force of free-falling charge 78−8301
rotating stars, nonaxisymmetric collapse and gravit. wave radiation 78−36553
rotating stars stability and gravit. radiation 78−93210
Sakharov's thoery of gravitation 79−25950
scalar and EM wave eqn. solns. in gravit. and EM waves metric 78−8307
scalar tensor theories, plane wave solns. in Einstein-Maxwell theory 77−33919
scalar waves in Schwarzschild metric, approx. scheme 79−54025
scattering, from vacuum black holes 78−65648
scattering of zero rest mass plane waves 78−4542
Schwarzschild black hole, prob. distrib. of incoming radiation 78−8300
Schwarzschild black hole, scatt. of gravit. waves, low freq. limit 78−16456
Schwarzschild black hole in ext. mag. field, radiation emitted by relativistic particles 78−96501
seismometer detection of gravitational waves 80−86196
self-excited oscillators, gravitational waves and limiting stability *(Russian)* 78−45540
shock waves from Einstein eqns. eikonal approx. 78−116
shock waves in general relativity, detection 77−5710
single soliton cosmological waves, Friedmann cosmological model background *(Russian)* 80−17708
singular hypersurfaces, asymptotic regularisation as alternative to distrib. 80−36923
singularities at real points of H space 80−98831
slow-motion approximation in radiation problems 80−73242
solitons with axial symmetry *(Russian)* 79−93030
source energy change for gravitational wave emission in Einstein theory 79−21608
sources, and use as expt. test of general relativity 79−93032
sources of gravitational radiation, conf. proceedings (Seattle, 24 July-4 Aug. 1978) 80−36778
space-matter tensor, algebraic classification 78−29009
space-matter tensor algebra in general relativity 79−12656
spectrum at low freqs., theory 79−44350
spherically symm. mass, eqn. of motion and gravit. radiation 77−17879
spherically symmetric electrostatic field superposed with EM wave, gravitational radiation emission *(French)* 77−57257
spherically symmetric scalar waves, gravitational self-interaction *(Russian)* 79−9165
spin 1/2 plane waves interacting with rot. body, gravitational scatt. helicity depend. *(German)* 80−52088
spinning rod, energy and ang. momentum effect on rigidity 77−30068
spinning rod, gravitational radiation 78−62137
SQUID application to measurements in fundamental physics 79−26087
SS 433, lifetime against gravit. radiation in ultra-close binary system model 80−4384
stars, neutrino bursts and gravit. waves, proposed search for correl. 78−77567
stars, relativistic collapsing, radiation, linearized even-parity EM and gravit. radiation 79−75228
stars, rigidly rotating, secular instabilities due to gravit. radiation reaction 80−4342
stars, rigidly rotating, secular instabilities in general relativity due to gravit. radiation reaction 80−4341
stars, rotating Newtonian, secular instability to gravit. radiation and viscosity 78−53922
static gravitational solitons, singularities, horizons, field behaviour at infinity *(Russian)* 80−73229
stationary charged C-metric 80−17849
statistical formulation of gravitational radiation reaction 80−90749
stellar collapse, ellipsoidal models and gravit. radiation 78−45317
stellar collapse, gravit. radiation burst 77−53571
stellar collapse origin, wave strength estimate 80−46584
stellar collapsing core, roles of gravit. radiation and neutrino dissipation 79−101166
stellar compression into disc, gravit. radiation *(Russian)* 77−13325
stellar model, gravit. radiation from collapsing rot. gaseous ellipsoid 77−53572
stellar models, secular instability of Maclaurin spheroids due to gravit. radiation and viscosity 77−17538
stellar source, Z Chamaeleontis possibility 80−90439
stochastic background, energy density upper limit from pulsar timing meas. 80−36743
stochastic background detection using Doppler tracking of spacecraft 80−67913
SU(2,1) generation of electrovacs from Minkowski space 79−75427
superconducting accelerometers, gravitational wave detection, and general gravit. expts. 78−45555
supernova neutrino bursts, gravit. radiation generation 78−81642
supernovae, gravit. radiation generation by escaping neutrinos 78−93092
supernovae, neutrino damping rel. to gravit. radiation 77−56999
tidal radiation, appl. to body in field of black hole 78−4540
time symmetric advanced and retarded solns. 77−57259
time symmetric gravitational waves evolution, initial data, apparent horizon 78−12626
torsion of spacetime included in a quadratic Lagrangian 78−8316
torsions in Riemann Cartan space times, U_4 reinterpretation, gravit. radiation solns. 78−45537
Trautman's radiation condition 80−73241
tunable detector for gravitational radiation, design parameters 80−86195
tunable free mass gravit. wave detector 79−71347
twistor Hamiltonian anal. of massive scatt. 77−37792
twistor space, Kahler struct. in asymptotically flat space-time with gravit. radiation 77−26218
ultralong waves from binary stars, detection opportunities 79−5746
ultrarelativistic black-hole encounters 79−30330
universal anisotropy and gravit. waves, effect on microwave background fluctuations 78−28866
universe models containing matter and gravitational radiation 77−87679
upper limit for gravit. radiation at 8580 Hz, meas. with 20 kg antenna 77−37800
Vaidya background, gravitational perturbations 77−74292
Vela pulsar, gravit. radiation revised estimate 78−32501
VLF, search, rel. to interplanetary radiowave phase scintillation 79−70995
wave propagation in prestressed nonlinear elastic solids, relativistic theory, gravit. wave detectors 79−1124
weak, interaction with rot. mag. dipole field *(Russian)* 78−36912
weak gravitational wave, influence on two point-masses bound system 80−21903
weak plane, radiation of freely gravitating charge *(Russian)* 78−89381
weak plane gravitational wave action on two connected masses 80−17851
Weber cylinder response in different gravit. theories 77−2585
white dwarfs, rapidly rotating, gravit. 78−65646
γ-ray transient event of supernova remnant, indirect evidence for gravit. waves 80−105270
Al alloy disc, quality factor of vibr. rel. to gravit. radiation detector 78−75093
Ar laser interferometer used in antenna system 79−101076

gravitons
axial anomaly for Majorana spin 3/2 loop with external gravitons in supergravity 78−8580
Brownian motion theory of quantum mechanics 79−12699
causal unification of relativity, gravitation and quantum mechs. 77−33923
complex pp waves and the nonlinear graviton construction 79−130
composite model, double self-dual condition 79−97287
composite model of the graviton 79−35621
cosmic coherent avalanche catastrophies, gamma-freq. graviton radiation 78−85844
covariant quantisation of gravitation 78−8327
dual theory space-time geometry, graviton coupling to fermion string 77−18242
duality of gravitation in the quantization problem 79−30344
Einstein equation solutions on nonsingular positive deinite metric 79−49150
emission, props., detection of gravit. waves, comparison with EM waves 78−21030
exact masslessness from quantum gravity canonical formalism 79−80492
gauge field theory, sourceless, impossibility of geon analogues 78−361
general gauge graviton loop calculation 80−27204
ghost free axial gauge, infrared gravitons 79−67214
gravitational solitons 79−44838
gravitational solitons with axial symmetry *(Russian)* 79−93030
graviton-matter interaction, Zitterbewegung interpretation 80−122
isotropically expanding universes, effect of graviton creation 78−16588
massless spin 3/2 field, irreducibility 79−35620
Minkowski space-time, gravitational interactions, review 77−87683
neutrino cosmology, open universe with neutrino and graviton dominance 77−17731
noise, from spontaneous prod. of gravitons, energy density distrib. *(Russian)* 79−12551
nonlinear, unprimed spinor description 80−8892
nonlinear graviton-photon interaction in Einstein-Maxwell space-time 79−30338
nonlinear realisation of general covariance group, massless tensor graviton and massive vector tordion 79−54030
pair production by gravitational waves in field of black hole 77−22474
pair production in early Universe, effective pot. approach 78−24587
pairing model, dynamical method for generating gravit. 78−70042
PCAC, dimensional derivation of gravitational correction 78−21371
perihelion anomaly, general relativity and quantum gravity 77−22473
photoproduction, static mag. dipole field due to steady currents, radiative corrections 78−62138
Planck energy nonconserving fluctuations and strong forces 80−57551
post-Newtonian charged n-body problem, centre of inertia and coord. transforms. 79−93025
pregeometry, gravity with composite metric 79−35619
production by cosmological background, role of conformal (non) invariance 79−49131
quantum effects and regular cosmological models *(Russian)* 80−27206
quantum field theory of electrostatic potential in gravitational field 78−54270
quantum gravity, dynamics, trapping of physical gravitons 80−31652
quasi-stellar objects, graviton to photon conversion model 78−54071
regular isotropic cosmological model, graviton generation *(Russian)* 77−22338
renormalisation and 1/N expansion, graviton propagator calc. 78−8320
rest mass, lunar ranging data anal. by Seelinger's theory 79−6040
rest massless, gravitational field equations of fourth order and supersymmetry 79−12674

gravitons continued
scalar fields, improved gravit. coupling 79−49151
second viscosity in early Universe 77−74169
self-energy, general gauge calc. 79−133
soft graviton emission in scatt. processes, linearised gauge theory 78−49746
spinning rod, gravitational radiation 78−62137
spinor theories in curved space-time, nonlinear invariances 79−54029
strong gravity, supersymmetric theory for f- and g-gravitons and massive gravitinos 78−62141
strong gravity and Dirac numbers 78−21372
strong gravity and elementary particle theory in general relativity 78−8315
supergravity, 2-loop divergence, with external gravitons on-shell cancellation 77−49659
supergravity, Bianchi identities and supercovariant derivative 80−17852
supergravity, Hamiltonian formulation 78−24722
supergravity, S-matrix difficulties, graviton elastic scatt. amplitude 79−135
supergravity, weak field approx. *(Russian)* 80−27201
supergravity coupled to massive self-interacting scalar multplet, spontaneous symmetry breaking 77−74633
trace anomaly for 4- and 6-dimensions integrated energy momentum tensor, single loop divergences 79−2709

gravity
see also gravitation
5° mean gravity anomalies, recovery from ATS 6/Geos 3 satellite to satellite range-rate obs. 80−41366
Δg field conversion to complete gradient *(Russian)* 77−70587
absolute meas. at Potsdam *(Russian)* 78−69274
absolute measurement, transportable apparatus 79−66823
acceleration meas. using falling ball, teaching 78−28896
active margin, gravity and struct., British Columbia and Washington 79−92516
African plate, gravity rel. to mantle convection pattern and stress system 77−81859
E.African Rift, cross-cut by volcanic chain in N.Tanzania, gravity survey 80−98301
air turbulent flow in heated channel, effect of gravitational field 80−64533
airborne gravimetry, topographic corrections for gradients 77−40966
central Alaska, Bouguer anomaly map rel. to plate tectonics 80−51380
algorithm for determ. of field of 3-dim. masses 77−81781
E.Alps, gravity and mag. field transformations *(German)* 79−70735
E.Alps, mag. and gravity anomalies correls. *(German)* 79−53327
E.Alps crustal struct., gravimetric model for HD-profile (Vicenza to Innsbruck) 79−34765
anholonomic coords. and tidal gravitational field of planet 79−34723
anomalies, appl. to Mohorovicic discontinuity relief determ. *(Russian)* 78−48992
anomalies, approx. design for modelling, algorithms *(Russian)* 78−85464
anomalies, approx. theory *(Russian)* 78−28338
anomalies, automatic interpretation for 2-dimens. masses 77−41188
anomalies, conformal deform. method for singular points determ. *(Russian)* 79−39934
anomalies, derivative harmonic function restoration *(Russian)* 80−85577
anomalies, due to phase boundary distortion in mantle 77−52963
anomalies, Falkland escarpment and Agulhas fracture zone, boundary between oceanic and continental basement 77−21700
anomalies, geological reduction *(Russian)* 78−40467
anomalies, Geos 3 satellite altimeter data 80−21612
anomalies, interpretation, Kolmogorov-Wiener least-squares filters appl. 78−61580
anomalies, linear anal. *(Russian)* 78−53755
anomalies, logarithmic pot. from anomalous masses of variable density 77−52961
anomalies, magnetic and gravitational equivalence of extrapolation *(Russian)* 79−39926
anomalies, new interpretation theory 79−84509
anomalies, numerical interpolation schemes *(Russian)* 79−62622
anomalies, recovery from Geos 3 altimeter data 80−3896
anomalies, singular points interpretation 79−92622
anomalies, source depth estimation, spectral method 79−92631
anomalies, source depths 77−44892
anomalies, spectrum of 2-D and 3-D bodies rel. to magnetic anomalies *(Chinese)* 80−56342
anomalies, stratified bodies, separation technique *(Russian)* 79−39933
anomalies, surface deformation and mantle convection 77−44893
anomalies, surface harmonic expansion coeffs. from orthogonal collocation calcs. 80−81801
anomalies analysis, regional background separation *(Russian)* 78−40703
anomalies analysis in Atlantic and W.Europe, influence of window functions on prediction *(German)* 77−86749
anomalies and Puerto Rico Trench origin 78−11861
anomalies calc. for regular homogeneous perturbing bodies *(German)* 78−69478
anomalies caused by sedimentary basins, rapid interpretation technique 77−87110
anomalies due to faults, general expression for Fourier transform 78−61300
anomalies due to finite inclined dykes, interpretation using Fourier transform. 77−53223
anomalies due to homogeneous polyhedral bodies, analytical expressions 80−3894
anomalies due to rectangular prismatic bodies, spectral anal. 77−53222
anomalies extrapolation in structural gravity prospecting *(Russian)* 79−39951
anomalies in Altai Sayan folded region USSR, due to deuteroorogenic stage complexes 80−101327
anomalies in NW Indian Ocean, appl. to oceanic crust density section construction *(Russian)* 79−48431
anomalies interpretation, algorithm for calc. gravit. attraction of models of structural features *(Russian)* 78−53758
anomalies interpretation, calc. of gravit. attraction of vertical right circular cylinder 77−60343
anomalies interpretation, graticule spacing and depth discrimination 77−53224
anomalies interpretation, NW.Black Sea 79−39633
gravity continued
anomalies interpretation, separation from mag. anomalies of comparable horizontal dimensions 80−94606
anomalies interpretation, Tikhonov's regularization method 78−49163
anomalies of arbitrary bodies, FFT method for rapid computation 77−41186
anomalies of cylindrical bodies, separation of gravity and magnetic effects *(Russian)* 77−9325
anomalies of mag. and gravity field, anal. by unitary method 80−89932
anomalies of polygonal prisms, mag. terrain corrections appl. 77−2082
anomalies of two idealised bodies, theoretical transforms 79−5441
anomalies prediction using collocation and known density information 80−26626
anomalies rel. to intraplate seismicity 78−53606
anomalies separation from background field, FON computer program *(Russian)* 78−53757
anomalies with periodical struct., data interpretation 77−78433
anomalous fields, stochastic harmonic analysis 79−35003
anomalous gravity fields interpretation, computer modelling 79−34971
anomaly, direct computation by equiv.-point method and simplified cubic spline 78−7780
anomaly calc. at Tsumeb mine, S.W.Africa 78−3700
anomaly covariance function, local characts. 80−98212
anomaly data processing system, involving interactive computer graphics *(French)* 80−94610
anomaly due to geologic contact, Fourier transform method for horiz. profile 80−94447
anomaly due to inhomogeneous magnetization distrib., computation 78−7779
anomaly due to subsurface struct., automatic deconvolution 80−85574
anomaly estimation, least squares collocation 77−90983
anomaly estimation using Geos-3 altimeter data without precise satellite orbits 77−64178
anomaly in Wilkes Land, Antarctica, evidence for possible hypervelocity impact crater 77−17059
anomaly interpolation to regular network nodes *(Russian)* 78−15945
anomaly interpretation, direct and inverse problems soln. for hemispherical bodies *(Russian)* 79−35012
anomaly interpretation, pot. fields linear anal. *(Russian)* 79−35011
anomaly interpretation methods for Pripyat trough studies *(Russian)* 77−91293
anomaly interpretation using statistical algorithms 77−70856
anomaly of two-dimens. body, line integral method calc. 80−56335
anomaly probing by satellite-to-satellite tracking 77−56768
anomaly reduction to a sphere *(Russian)* 77−86744
anomaly source models, statistical parameters rel. to pot. fields obtained by superposition *(German)* 79−34783
anomaly survey data analysis, curve-matching optimisation method *(Chinese)* 80−89935
E Antarctic craton sedimentary basins from seismic, mag., gravity and radar obs. 77−21733
anti-gravity generation due to counterclockwise turning of gyroscope *(Japanese)* 80−12980
arbitrarily shaped three dimensional body 77−44908
Archean granitic area, Ontario, Bouguer gravity maps 77−5127
Arctic basin, seismic and gravity profiles 77−33030
Arctic regions, free-air gravity anomalies from 60°N to North Pole 79−48391
Asama and Kusatsu-shirane Volcanoes, Japan, Bouguer anomaly and gravity changes *(Japanese)* 79−70733
aseismic ridges, isostasy anal. 80−3971
Ashkhabad geodynamic test field, nontidal gravity vars. 79−92466
central Asia, seismic risk zones from gravimetric data 77−70608
asteroid belt, gravit. potential and effects on planetary orbits, analytical method 79−75082
asymmetrical body, convergence of gravit. pot. expansion in spherical harmonics 78−24479
N. Atlantic, sea floor spreading and early opening, mag. and gravity data 78−65247
equatorial Atlantic (7 to 10°N), gravity field rel. to fracture zones lithospheric struct. *(Russian)* 80−104932
Atlantic fracture zones in equator region, gravimetric model 80−72483
N.Atlantic Ocean, detailed gravimetric geoid 79−62422
Atlantic Ocean south of Bermuda, geophys. survey within Mesozoic mag. anomaly sequence 80−26492
S.Atlantic oceanic crust in Mesozoic and subsequent evolution, mag. and gravity data 80−21699
N.Atlantic region, gravity anomalies, regional elevation and deep struct. 79−16421
Atlantic type continental margins, struct. from geophysical meas. 77−21702
atmospheric processes, effect on tiltmeter and gravity obs. *(Russian)* 78−48957
attenuated white noise statistical gravity model 80−30977
Australia, geophysical profile along 29°S 80−72460
Australia, gravity field models rel. to mantle convection and subcrustal stresses 80−72484
Australia, isostasy and evolution of compensation mechanism 78−65252
Australia, isostatic compensation of topography 80−72479
Australia, ocean loading effects on tidal gravity 78−28151
Australia, reconnaissance gravity survey 77−44889
Australia and Papua New Guinea, absolute gravity, 1979 obs. 80−72407
Avalon zone, Atlantic Canada, extent determ. from mag., seismic and gravity data 80−12384
Badra area of Iraq, gravity investigation 79−34729
NE.Baikal region, regional gravity anomalies, interpretation 80−98217
Baikal rift zone, gravity anomalies rel. to continental rift form. *(Russian)* 80−12364
Baiśoara mine, gravity anomaly rel. to ore body distrib. *(Rumanian)* 78−20347
Banda Arc, gravity profiles rel. to continent-island arc collision 79−84211
barometric pressure vars. influence on gravity 77−44894
base points, repeated meas. accuracy estimation *(Chinese)* 80−76892
bedrock topology and groundwater, gravity exploration in glaciated areas 77−91289
Benue Trough, Nigeria, gravity field rel. to tectonic evolution 80−21701
Black Sea transverse rise, geological and geophysical data 78−3754
boiling, under increased gravitation, heat exchange mechanism, bubble form., review 77−46895

gravity continued
Bonnet Plume Basin, Yukon Territory, Canada, gravity profile anal. as aid to coal basin evaluation 80−76898
borehole gravimetry, estimation of dip and lateral extent of beds 78−7782
borehole gravity date, accuracy 79−5632
borehole gravity observations, terrain effects 80−98462
Bouguer anomaly theory and misconceptions 78−61302
Bouguer formula of 1749, appl. to gravity corrections derivation 79−29692
Bouguer gravity model, interactive CRT display, for geology CAI 77−22
Bouguer reduction of gravity anomalies using log data *(Russian)* 79−84082
Bouguer regional anomalies, appl. to deep geological struct. study *(Russian)* 78−48958
British Isles 80−109086
Cabo-Ortegal mafic/ultramafic massif, emplaced nappe, gravity data 80−21689
Cainozoic volcanic centres of N.Africa, gravity links rel. to E.African Rift 79−34722
Caledonian granites in Britain, negative gravity anomalies rel. to geothermal pot. 79−74486
Canadian precise gravity networks for crustal movement studies, instrument evaluation 79−79724
Cape Verde archipelago, underlying crustal struct. from seismic, mag. and gravity data 77−17052
Caracas, gravity-tide meas. rel. to Pasadena magnitudes of earthquakes 80−51344
W.Carpathian gravity low, depth and origin 79−88230
Caspian Sea, gravity meas. from aeroplane *(Russian)* 78−40704
cavity effect in tunnels of various cross-sections, theory *(Russian)* 78−88784
celestial bodies, Stackel harmonic potential in elliptic and parabolic cylindrical coordinates 79−96898
Chagos-Laccadive Ridge (Indian Ocean), geophysical study 77−44952
changes meas. with supercond. gravimeter 79−79725
China, gravity field rel. to convection generated stress concentration and Tangshan earthquake 79−92507
E.Churchill Province, gravity anomalies rel. to Andean-type tectonism 80−36222
collocation and least squares methods for data handling 79−29870
complex fields interpretation via minimisation method, automated system appl. *(Russian)* 79−35006
composite gravity fields in three-dimensional space, singular points numerical characts. determ. *(Russian)* 79−96833
conference on satellite Doppler tracking and geodetic appl., London, England (Oct. 1978) 80−77264
contact surface parameters, determ. using space domain filter method *(Chinese)* 80−89933
contacting surface depth and shape determ., random and sytematic errors *(Russian)* 79−39935
contour maps, optical filtering 77−25797
contouring irregularly spaced data 77−64180
corpuscular model, geological and geophysical consequences *(Russian)* 77−67367
Coso Range, California, aeromagnetic and gravity surveys 80−89943
cylindrical body of finite length, gravity pot. *(French)* 77−78079
damped and constrained least squares method with application to gravity interpretation 79−66830
data inversion by compressed mass plane method *(Chinese)* 77−64175
data processing techniques, generalised method 77−53247
data reduction for geological interpretation *(Russian)* 79−84537
data reduction on arbitrary surface in regions of high topographic relief 78−61298
Dead Sea Rift and adjoining areas, gravity and density distrib. 79−57893
Dead Sea Rift and N.Israel, mag. and gravity obs. and interpretation 80−98233
deep asymmetry of Earth, inertia rel. to convection currents 80−98269
deflection of the vertical at Tokyo 80−17228
direct and inverse problems soln. using approximate equivalence method *(Russian)* 77−70586
direct gravity formula for 1967 Geodetic Reference System 78−92775
dispersion, close-packed, two-dimens., gravity effect on thin film drainage 79−86486
disturbance covariance functions, upward continuation integrals 78−85468
downward continuation problem, soln. by initial value method *(German)* 77−86750
Earth, coordinates of gravit. field stationary points 78−53805
Earth, global gravity field compared to geomagnetic potential 80−104854
Earth, gravit. field perturbations rel. to secular motion of Moon mean longit. and perigee 77−78679
Earth, gravit. harmonics from artificial satellites shallow reson. orbits 78−40805
Earth, gravity field fine struct. via. twin probes method 79−25443
Earth, GRIM 2 gravit. pot. model determ. and evaluation *(French)* 79−8587
Earth, precision orbit computations for Starlette satellite 78−65478
Earth 30th order harmonics from resonant inclination variations of ten satellites 79−84071
Earth actual gravity field isoparametric and isozenithal type representations 79−53297
Earth anomalous gravity effects during 1976 April 29 annular eclipse *(Chinese)* 79−2174
Earth bodily tide and yielding due to tidal loading 78−36091
Earth crust, investigation via combined gravity and seismic methods *(Russian)* 79−74987
Earth crust and upper mantle global density 79−62592
Earth density model, based on gravimetric data *(Russian)* 80−31009
Earth figure and gravit. field determ., least-squares collocation method 79−48392
Earth gravitational field, influence of atmospheric masses 79−57841
Earth gravitational field, regularising algorithm for numerical model construction *(Russian)* 77−44899
Earth gravity anomalies and tectonics, review 80−98593
Earth gravity field, Fourier transform anal. and relation to geoid anomalies 80−3897
Earth gravity field anomalies sources, depths determ. 79−16366
Earth gravity field meas., satellite systems comparison 79−53298
gravity continued
Earth gravity intensity variations, use of AChF-3 pendulum clock 80−104856
Earth gravity potential, spherical harmonics theory 80−30973
Earth potential, generalisation of Laplace expansion to Earth's surface 77−60337
Earth rotation axis precession angle, effect of harmonics in gravit. pot. of Earth, Moon and Sun 78−48953
Earth tidal gravity at Aburatsubo Crustal Movement Observatory 80−101316
Earth tidal potential, multiple expansion 79−12062
Earth tide gravity maps for W.Europe 77−9317
Earth tides anal. in Peking region before 1976 July 28 Tangshan earthquake *(Chinese)* 80−3892
Earth tides observations, monthly data set anal. *(Russian)* 78−88786
Earth topographic surface anomalies, determ. by cosmic methods 80−56337
Earth variable gravitational and geomag. pots., effects of bumpy core-mantle interface 79−79771
Earth-Moon system tidal friction, changing Earth moment of inertia 80−81803
earthquake sources exhibiting anelastic vol. changes, gravity effects 78−57176
East Africa, isostatic compensation 79−8623
education, Earth's interior and const. gravity models 77−45645
education, Earth as point mass, conical shell derivation 77−78928
effect on artificial satellite inclination, first order theory error determ. 80−17475
effects on seismic surface waves 80−8252
N Egypt, shear zones from gravity data 78−28208
Eolian Islands, S. Thyrrenian Sea, basement structural trends from aeromagnetic and gravimetric data 78−40519
Eotvos effect variations allowance in gravimetric studies, data processing 79−74969
estimation technique using FFT, inertial navigation systems appls. 79−25376
eucrite parent body, gravity and size from melt/solid segregation 79−40144
Europe, absolute meas. 78−85469
W.Europe, tilt and gravity obs. of Earth tides, spatial analysis 79−66602
external gravitational field, determinative and stochastic descriptions 79−34730
external gravitational potential, approx. with closed systems of trial functions 80−101310
faulting and gravitational energy 79−84121
Fennoscandian land uplift gravity lines 79−92474
field interpretation, optimal computing scheme construction 77−33201
finite length theoretical anomalies, Fourier transforms 78−61299
Finland, meas. at Fennoscandian land uplift gravity lines 79−92472
flow of gases, liquids and bulk solids, common eqn. represent. and exptl. test 80−38477
fluid, simple, light scatt., gravity effects on crit. exponents determ. 80−20650
Fourier analysis of gravimetric and magnetometric anomalies *(Rumanian)* 79−58123
fracture zones, vertical deflections *(German)* 79−84087
free air anomalies, 5°×5°, by satellite-to-satellite tracking method 80−72408
free air anomalies in world's oceans rel. to residual elevation 77−78081
g determination, student expt., linear least squares data anal. 78−45450
Gamburtsev graphical method for three-dimens. anomaly calc. 77−41203
Garm geodynamic test field, repeated gravity obs. 79−92465
GDR, 1970-6, small range gravity meas. 79−92469
general techniques and applications 77−56567
generalized problem of three centres, external variant appl. 80−109087
geocentre position variation determ. using geostationary satellite obs. 80−82083
geocentric gravitational constant, evaluation from Viking Doppler and range data 80−3891
geocentric gravitational constant (GM), determ. from satellite-satellite tracking data 80−3911
geodetic networks, optimisation *(German)* 78−15950
geoid, longitude-averaged meridional profile of pear-shaped section 80−94450
geoid and potential coeff. determ. from gravity data, atmospheric correction 77−17017
geoid improvement in local areas, satellite to satellite tracking appl. 79−62423
geological gravity anomalies, model calcs. *(Hungarian)* 80−21605
geophysical potential fields on sphere, stochastic props. study 80−56338
geopotential, 15th-order resonance effects of Nimbus 1 rocket (1964-52B) 78−65168
geopotential, correl. with mantle heat flow 77−37161
geopotential, evaluation of 14th order harmonics 79−29694
geopotential, harmonic coeffs., determ. error *(Russian)* 79−5439
geopotential, Neuman problem stable soln. 77−52964
geopotential, satellite data application to regional anomaly surveys 80−51558
geopotential, simple layer model and resonant effects on satellite orbits 79−16364
geopotential, spherical harmonic potential coeffs., use of area means 80−94449
geopotential 14th order harmonics evaluation from satellite resonant inclination vars. 78−48954
geopotential 29th order harmonics from Ariel 1 orbit at 29:2 reson. 77−56572
geopotential appls. of $\beta/2$ orbital reson. of artificial satellites 79−53296
geopotential determ. by satellite laser tracking 77−64184
geopotential determination, upward and downward continuations, geodesy and topography effects 80−21603
geopotential expansion in nonsingular orbital elements 77−90988
geopotential field, 28th degree and 27 th order terms from mean elements of US Navy navigation satellites 79−48642
geopotential fields singularities localization in three dimens. space 79−74968
geopotential from gravity measurements, levelling data and satellite results 80−101313
geopotential harmonic coefficients, determ. from China 2 rocket (1971-18B) orbit 80−4231
geopotential harmonics, mantle convection and stress field under Pacific plate calc. 77−9393

gravity continued
geopotential improvement from satellite and surface data (Goddard Earth Models 7 and 8) 77−32977
geopotential models, accuracy 79−25183
geopotential representation 77−44885
geopotential second derivative var. sign, variometer meas. *(Russian)* 78−69278
geopotential second zonal harmonic, secular perturbation of artificial satellite motion in coordinates 79−62720
geopotential solutions GEM 9 and 10, gravity model improvement using Geos 3 80−3909
geopotential with point mass anomalies, modelling approach 78−40465
Ghana, gravity mapping and interpretation 77−78080
glacier ice thickness meas., gravity profiling technique 78−32253
glacier-covered regions, gravity surveys 79−16697
global correl. of topographic heights and gravity anomalies 78−15953
global gravity anomalies and two-scale mantle convection 77−17067
global gravity anomalies rel. to two-scale mantle convection 78−85528
global soln. including alimetry 80−3914
gradients, vertical and horizontal, measured by gravimeter, relative precision 79−84500
gradients calc. using auxiliary coupling eqn. *(Russian)* 77−86745
gravimagnetic anomalies, interpretation on basis of pots. classes with inverse problem finite form 80−21847
gravimagnetic fields, anomalous pot. fields appl. to Earth interior mass distribs. modelling 79−96750
gravimeter network adjustment, equiprobable interval method of sample classification 79−29889
gravimetric and deep seismic sounding, data interpretation *(Russian)* 79−39937
gravimetric density formula for Earth of spherical shells 78−61303
gravimetric geoid over Alps, and tectonic interpretation *(French)* 79−66600
gravimetric geoids, comparison with Geos 3 altimetric geoid 80−3898
gravimetric observations, effect of the Honkasalo term in tidal corrections 80−21602
gravimetric plethysmography for leg blood flow meas. 80−36176
gravimetric problems, soln. by numeric method *(Russian)* 80−30976
gravitational and geomag. fields correl., rel. to bumpy core-mantle interface 77−2085
gravitational logging and role in combined geological and geophysical research *(Russian)* 77−70868
gravitational potential energy spherical harmonic eqn. 80−21613
gravity anomaly from masses distributed over infinite regions, interpretation theory 80−82103
gravity perturbation due to ocean tide, series computation 80−104857
ground relief gravity effect, computer calc. *(Russian)* 79−39952
W.Gulf of Oman, gravity profiles rel. to tectonics 80−8279
Haicheng earthquake, 1975 February 2, associated gravity field vars. *(Chinese)* 78−61332
Hankel inversion of gravity profiles, numerical procedure 80−56619
Hawaiian-Emperor seamount chain, gravity and bathymetry rel. to oceanic lithosphere isostasy 79−39688
Hellenic Arc, gravity data rel. to dynamic model 77−21734
horizontal infinite trapezoidal prism, gravity effect, Fourier spectrum 77−87095
hypercircle method in the problem of a case-bonded cylinder in the gravity field 78−45484
N Iceland, gravity and height vars. during present rifting episode 80−90060
Iceland, gravity vars., 1965-75 period 78−40466
W.Iceland shelf, central volcanoes, magnetic and gravity evidence 77−37180
IGSN 71, long range meas. with LaCoste-Romberg gravimeters 77−52957
N.E. India, and N. Burma, seismicity, gravity and tectonics 77−25654
India, Bouguer gravity anomaly map and tectonics 80−61791
N.E.India, gravity field anal. 78−7559
Indian geopotential anomaly, seismic and gravity data anal. 80−90037
Indian Ocean, 1×1° gravimetric geoid compared with GEOS-3 radar altimeter geoid profiles 79−16365
inertialess charged particles, collection on circular cylinders by elec. forces and gravitation 78−44400
inertialess charged particles, collection on elliptical and irregular cylinders by elec. forces and gravitation 78−68924
infinite polygonal cylinders, inverse gravity problem 78−53607
interference fields separation, statistical algorithms *(German)* 77−29462
intermediate layer density, statistical methods for gravity data 78−15946
interpretation, simple gradient method for geological contact 78−28332
inverse gravimetric problem, appl. of simplex method 77−56740
inverse gravimetric problem, direct soln., trap method 79−58101
inverse gravimetric problems, parametrisation 80−104855
inverse gravimetry problem, three-dimens., trial and error method of soln. 79−62607
inverse gravitational edge effect problem, non-uniqueness resolution via a priori data appl. 79−44261
inverse isostatic problem, global soln. for Pratt and Airy hypotheses 80−3893
inverse log.-potential problems, integral and functional eqn. analysis 77−40968
inverse problem, appl. of linear programming, basic numerical techniques 79−53581
inverse problem, assembling principle for constructing solns. *(Russian)* 77−44898
inverse problem, harmonic moments of masses as initial approx. *(Russian)* 78−3701
inverse problem, linear programming appls. 78−28331
inverse problem, non-linearity effects 79−8704
inverse problem, unified least-squares method 77−73872
inverse problem for gravity anomaly, least-squares soln. 80−98214
inverse problem of gravit. and mag. prospecting, approximate soln. *(Russian)* 79−39927
inverse problems, nonlinear eqn. soln., Tikhonov algorithm 77−41200
inverse problems, potential theory for interpretation 78−7557
inverse problems, stable soln. in a class of convex bodies 77−64181
ionosphere, gravity effect on instability formation conditions in F-region 79−96858
Iraq, subsurface geology in W.Karbala, gravity interprets. 77−73731
Irish gravity map, trend surface anal. 77−2080
isostasy at midocean ridge crests 80−31022
gravity continued
isostasy investigation, correl. coeffs. between elevations and Bouguer anomalies 77−86850
isostatic anomalies in petroleum gravimetric prospecting *(Spanish)* 77−9319
isostatic disturbances, rel. to elastic stresses in lithosphere 77−81842
isostatic gravity anomaly, evolution of ocean-continent boundary at passive continental margins 77−81777
central Israel, gravity evidence for pre-Late Jurassic east-west fossil continental margin 79−34766
Izu Peninsula, Japan, crustal uplift, Mogi model, related gravity change *(Japanese)* 78−96165
Izu Peninsula, Japan, earthquake swarm epicentres distrib. rel. to Bouguer anomaly *(Japanese)* 78−96144
Izu Peninsula, Japan, gravity change assoc. with earthquake swarm *(Japanese)* 78−96123
Izu Peninsula, Japan, gravity obs. rel. to Jan. 1978 quake *(Japanese)* 80−41394
J_2-field, periodic solns. of equatorial satellite *(French)* 78−45205
James Bay gravity survey rel. to Kapuskasing Gneiss Belt, Ontario 78−48959
Japan, nontidal gravity changes during earthquake activity 79−92471
Japan, ocean tides effects on M_2 gravity tides 77−60342
Japanese and Izu-Bonin Islands junction, gravity meas. 77−78085
Japanese island arc volcanic rocks, relation between chemical comp. and gravimetric data 78−32102
Japanese Islands region, topography and gravity anomalies data compilation *(Japanese)* 80−67332
Jharia coalfield of India, survey of struct. and geol. 80−76972
Juan de Fuca Ridge crest, E.Pacific, tectonic topography compensation 80−56448
Jupiter, figure parameters and gravit. moments 78−65547
Jupiter and Galilean satellites, gravity field from Pioneer 10 and Pioneer 11 tracking data 77−37554
Jupiter dynamical oblateness, rel. to optical oblateness 77−29715
Jupiter gravitational moments, effects of dense core 80−98603
Kenya, gravity data catalogue, Bouguer anomaly maps 78−48956
Kenya rift valley, geophysics 77−86825
Kiglapait layered intrusion, three-dimensional gravity analysis 79−84072
Kilauea volcano, Hawaii, three-dim. crust and mantle struct. 78−28205
King's Trough, NE.Atlantic Ocean, struct. from bathymetric, seismic and gravity data 78−49005
Krafla Caldera, NE Iceland, gravity and elevation changes caused by magma movement 80−90052
Krivoj Rog basin (Krivbas) underground workings, gravity anomalies interpretation *(Russian)* 78−85466
Kupjansk-Novoazovskoe profile quasiperiodic gravity anomalies and structural confinement *(Russian)* 78−85465
Kuril Trench, gravity profiles rel. to lithosphere elastic-perfectly plastic bending 78−73341
Kusatsu-shirane Volcano, Japan, 1976 steam explosion, geophys. obs. *(Japanese)* 79−70773
La Soufriere, Guadeloupe, gravity changes around volcano 79−92468
Labrador Trough, N.Quebec, gravity survey 77−44888
Laccadive uplifting zone, crustal struct., gravity field modelling *(Russian)* 80−3966
Lake Biwa, Japan, secular gravity change meas. 78−40463
Laramide Wind River uplift, Wyoming, USA, gravity and seismic refl. data 80−21679
lateral density inhomogeneities, min. depth 78−7596
Liaoning Province, China, crustal struct. from gravity data *(Chinese)* 77−5142
Liaoning Province, China, crustal thickness from gravity and seismic obs. *(Chinese)* 80−12349
Ligurian Sea area, crustal and upper mantle structure from seismic and gravity data 78−65209
loading of large reflector antenna, structural design 78−57448
local anomalies interpretation, integral ratios *(Russian)* 78−85463
local changes resulting from deformation 79−48389
local field faults, effect on cloud distribution 78−32136
local physical frames transformation, decomp. theorem, geodetic interest 77−78082
local vectors connection in actual gravity field of Earth, model field, disturbing pot. 78−61297
logging data, appl. to interior density distrib. determ. *(Russian)* 78−92999
Los Angeles basin SW block, gravity field rel. to thermal subsidence and petroleum generation 80−3967
low-amplitude structure with oil (gas) deposits, parameters from gravity test data *(Russian)* 79−44271
lumped coeffs. of 14th and 28th order from Interkosmos 9 and 10 orbital inclination changes 78−20342
lunar Apennines and regional surroundings, gravity data rel. to isostatic state 78−77503
lunar gradient mapping from Lunar Polar Orbiter, simulation 77−41329
lunar gravity field, harmonic anal. 77−87290
lunar gravity field, long-term Keplerian rate method 77−87291
lunar impact craters struct. from gravity models 77−64674
lunar mascon maria, evidence for isostasy 77−37524
lunar surface gravimetric surveying process optimization 79−8846
M_2 ocean-tide corrections to tidal gravity observations in Western Europe 77−86737
Manicouagan impact crater, gravity study and upper crust density contrasts 78−81170
mantle, density inhomogeneities beneath oceanic trenches, island areas and marginal seas from gravity data 80−21676
mantle (lower), density anomalies derived from geophys. data 80−89927
mantle two-dimensional flow beneath accreting lithosphere, effects on gravity field 79−12102
marine Bouger gravity calc. using processing density concept 79−74829
marine gravity modelling, considerations of indirect effect (geoid undulation effect) 80−3907
Mars, coordinates of gravit. field stationary points 78−53805
Mars, generalised figure size and orientation *(Russian)* 78−40857
Mars, global topography harmonics and Bouguer gravity anomaly map 78−85880
Mars, gravity field, combined Viking and Mariner 9 results 78−20688
Mars, gravity map, Viking Orbiter 2 results 79−58291
Mars, spherical harmonic representation using short-arc technique 77−73999
Mars deflections of the vertical rel. to triaxial ellipsoid 77−73997

gravity continued
Mars gravitational figure, global and regional props. 79−62784
Martian gravity field, comparison of results obtained from Viking 1 and 2 and Mariner 9 80−8577
mass equivalence, gravitational compass, and grad. meas. in gravitational field 80−86076
mean anomalies (550 km squares) and mean geoid heights 79−88233
mean anomalies in 550 km squares 77−90994
mean anomalies on sphere, implied geoid undulations 80−21614
mean anomaly block size relation with spherical harmonic representations 78−28154
mean anomaly block sizes and spherical harmonic representation, comment 80−30979
E.Mediterranean, crustal struct., sedimentary layers 78−69311
W.Mediterranean, gravity and bathymetry rel. to tectonics 77−32973
E.Mediterranean gravity anomalies, volcanic activity rel. to tectonic development 78−69318
E Mediterranean regional vertical tectonics from gravity obs. 77−5172
E.Mediterranean Sea, gravity data rel. to tectonic elements and crustal struct. 78−44801
Mercury, gravity field harmonics rel. to internal convection 78−12127
meteorite craters, gravity inverse problem rel. to geomechanical evolution 80−17265
meteorite impact structure, Gosses Bluff, Australia 80−72520
Michigan Basin deep borehole, gravimeter survey 79−39634
microgravimetric network for secular gravity studies in Scotland 78−36298
microgravity surveys, computer processing system 80−85575
microseisms influence on terrestrial quartz gravity meters, mechanism *(Russian)* 79−39967
Mid-Atlantic Ridge, median valley model from gravity obs. 80−90071
Mid-Atlantic Ridge fracture zone, gravity field rel. to deep crustal architecture *(Russian)* 79−96747
Mississippi embayment, regional positive gravity anomaly 77−78084
Moon, coordinates of gravit. field stationary points 78−53805
Moon, density model consistent with topographic, gravit., librational and seismic data 77−45332
Moon, gravit. field perturbations rel. to secular motion of Moon mean longit. and perigee 77−78679
moon, gravity meas., gradiometer systems on polar orbiting satellite 80−94730
Moon, harmonic anal. and Bouguer gravity map 77−60634
Moon, mass point model of gravity field 77−87289
Moon, origin of moments of inertia differences 78−45247
Moon, results from anal. of VLBI and laser data 77−29672
Moon gravitational potential, third and fourth harmonics rel. to coordinate system for selenodetic reference network *(Russian)* 80−72797
Mount Carmel, struct. and extension into E.Mediterranean, marine geophys. survey 77−33026
mud volcano in Trinidad, gravity anomaly model 80−56442
mutual gravitational potential of N solid bodies, harmonic coeffs. expansion 79−12390
nanogravity survey in Canada rel. to tectonic movement detect. due to groundwater movements 77−33038
Narmada-Son lineament, extension towards Murray Ridge 78−15985
Nelson River anomaly, SE.Saskatchewan, seismic survey 78−28153
Neumann problem for potential in toroidal coords. for axial symmetry 77−64182
Nevada, interpretation of gravity surveys in Grass and Buena Vista Valleys 80−41365
new gravity system, changes in international gravity base values and anomaly values 80−51317
Newcastle upon Tyne University, England, new gravity base 79−29693
NE Newfoundland, geophysical and geological trends on continental shelf 77−5145
Newfoundland, gravity zoning 77−52965
Newfoundland Basin, gravity survey rel. to Mesozoic evolution 78−32045
NE.Newfoundland continental shelf, gravity survey rel. to Charlie Fracture Zone 77−25664
non-Newtonian fluid, free convection from vertical plate, variable gravity force effect 77−42878
non-tidal vars. over large territories 79−92464
nonlinear analytical prolongation method, survey inverse problem appl. *(Russian)* 79−21037
nontidal gravity field change rel. to liquid core inhomogeneity 79−92463
nontidal variations as exemplified by Hungarian depression nature *(Russian)* 79−8621
Nootka Fault Zone, new plate boundary off W.Canada, gravity anomalies 79−92518
normal ellipsoid three-dimens. field, numerical computation 79−8590
normal ellipsoidal three-dimens. field, first-order numerical calc. 77−52960
normal gravity minus radial component, accurate formula 78−65170
normal potential and gravity of levelled ellipsoid *(Russian)* 78−69276
Nova Scotia, gravity and tilt obs. rel. to improved ocean tide models 78−92821
Nova Scotia crustal struct. and NW.Atlantic M_2 tide from tilt and gravity obs. 78−40464
ocean gravity anomalies, recovery from Geos 3 altimetry data 80−3905
oceanic block ridges, gravity field 77−81780
oceanic geoid computations, accuracy 80−21608
oceanic isostatic thermally-expanded ridge crests, gravity signatures 79−66604
odd zonal harmonics determ. using modified equations 78−92773
odd zonal harmonics from Cosmos 248 eccentricity oscill. analysis 78−81100
oil-gas province basement, gravity field studies *(Russian)* 80−85759
otolith membrane, variable gravity model 80−85573
NW Pacific, gravity, data rel. to upper mantle struct. and deep processes 77−37160
S.W.Pacific, gravity anomalies and main tectonic units 77−17078
NW Pacific Ocean, gravimetric geoid 77−73624
E.Pacific Rise, gravity meas. rel. to oceanic crust props. and origin 80−101360
palaeogravity since late Precambrian kimberlite nodule data 78−24217
Palmdale uplift, gravity changes and thrust faulting 78−44757
Peking-Tientsin area, China, crustal struct. from gravity data, rel. to seismicity *(Chinese)* 78−61357
perturbing gravitational potential calc., approximation of Stokes and Vening-Meinesz eqns. allowing for initial data errors 80−101459
gravity continued
perturbing potential, calc. by Stokes eqn. 79−62428
plane and axially-symmetric potential problems 77−52962
planet external potential, determ. using gravity vector anomaly *(Russian)* 77−33375
planet physical surface, appl. of satellite model of gravit. pot. 79−62774
planet surface gravit. potentia, satellite model error estimation 79−96935
planetary gravitational spectra from direct measurements 80−30978
planetary gravity field modeling from spacecraft tracking data 79−21132
planetary tidal friction rel. to Solar System stability 80−82233
planets gravitational spectra, determ. from planetary orbiters tracking 80−41744
polar/equatorial density effects 80−46758
Poltava, tidal changes in force of gravity (1973 to 1976) *(Russian)* 78−88782
Poplar Bay, Lac du Bonnet, Manitoba, possible meteorite impact crater 77−17150
potential and field anomalies due to thin mass layers 77−44897
potential coeffs, to degree 52 from 5° equal area gravity anomalies 78−69273
potential derivatives evaluation using Bernstein multidimens. inequality *(German)* 78−93081
potential field anomalies, profiles and synthetic magnitude *(Rumanian)* 79−57845
potential field anomalies, transformation error functional minimisation *(Russian)* 77−13053
potential field anomalies geodynamic interpretation, physically based source models *(German)* 79−34782
potential field data, constrained inversion, use of pseudohyperellipsoids 80−85752
potential field data interpretation, generalized matrix inversion method 77−87087
potential field modelling, end corrections 80−85580
potential field transformation from relief to single reference plane, Fourier anal. appl. *(Russian)* 78−53759
potential fields, accuracy of linear transformations in presence of interference 77−44900
potential fields, anal. of characteristic-components method in interface construction 77−44901
potential fields, analytic continuation for plane problem 77−56568
potential fields, source strengths and centres 80−85581
potential fields, statistical interpretation with covariance functions 77−73873
potential fields, two-dimens. and three-dimens., in freq. domain, equivalence theorem *(Chinese)* 79−88478
potential fields, two-dimensional, singular points determ. *(Russian)* 79−39925
potential fields due to vertical circular cylinder and dike, statistical anal. 79−34972
potential fields extrapolation numerical techniques *(Russian)* 79−74988
potential fields from arbitrary 2-, $2^1/_2$- and 3-dimensional bodies, wavenumber domain expressions 79−5634
potential fields inclined dykes interpretation in wavenumber domain 79−92630
potential fields interpretation, statistical algorithms *(German)* 77−29461
potential on mobile base, second derivatives determ. *(Russian)* 79−39954
potential problem, orthogonal functions in sphere *(French)* 78−36090
Potsdam plumb-line, hydrologic influence on long-period motions *(Germany)* 78−57222
power spectrum, rel. to lateral density anomalies in upper mantle 77−29261
profile interpretation, linear inverse problem 77−73875
profile inversion by polynomial method 78−69476
prospecting, accuracy, meas. spacings and contour intervals calc. techniques *(Russian)* 79−44272
prospecting problem appl. of nonsmooth function minimisation methods 77−41180
Proterozoic crust, gravit. instability inferred from mantled gneiss dome pattern 80−81848
Pyrenees, central southern region, gravity gliding and compressive nappes 78−69342
quasi-periodic vars. rel. to earthquakes and crustal structure *(Russian)* 78−69275
N.Queensland, Australia, crust struct. from gravity survey 80−72458
Raft River Valley, Idaho, surveys of geothermal system 79−84307
Rayleigh scattering linewidth near pt., simple fluid, gravity effect 77−85735
Rayleigh scattering near crit. pt., nonzero beam diameter and gravity effect 77−85737
Rayleigh scattering near crit. pt., nonzero beam diameter effect, and gravity effect 77−85736
recurrence relations for integrals of associated Legendre functions 79−29690
regional anomalies, interpretation via mechanical modelling of crustal structs. form. *(Russian)* 78−49154
regional anomalies in Soviet Union, statistical processing *(Russian)* 79−84081
residual Bouguer anomalies, line masses depth estimation via Backus-Gilbert min, distance criterion 79−44257
residual gravity anomalies interpretation *(Russian)* 79−88232
SE.Reunion Island, gravity survey *(French)* 80−56334
Reykjanes Ridge, gravity anomalous south of 60°N rel. to evolution between 40 and 12 Myr BP 80−90069
Rhinegraben area, gravity anomalies and geothermal implications 80−104852
Rhinegraben area, matter transfer in upper mantle effect on gravity field 80−104927
Rhinegraben zone, nontidal gravity vars., local studies 79−92470
Rocky Mountain Trench near Radium, BC, gravity evidence against high angle fault 77−44940
Rumania, first order network accuracy *(Rumanian)* 77−32979
Rumania, gravity correl. with geothermal regimes 79−70768
Rumania, lithospheric microplates rel. to regional gravity anomalies *(Rumanian)* 78−20380
Saguenay area, Quebec, gravity survey 77−52958
W.Sakhalin shelf, NW.Pacific, Faye-Bouguer anomalies 77−32975
satellite determined gravity results, geophys. and geodetic appls. 77−25634

gravity continued
satellite orbit, time regularisation of Adams-Moulton-Cowell algorithm 78−45208
satellites gravity measurements, basic mechanical principles of gravimeters and gravity gradiometers *(German)* 80−101461
Saturn, effect on Pioneer 11 trajectory, mass determ. from carrier freq. Doppler shift 80−82294
Saturn, external gravit. field, tidal perturbs. due to rings, mass of rings calc. 79−35189
Saturn, figure parameters and gravit. moments 78−65547
Saturn, gravit. quadrupole moment rel. to maintenance of rings 78−53869
Saturn, influence of rings on gravitational field *(Russian)* 77−74008
Saturn gravitational moments, effects of dense core 80−98603
Scandinavia, Blue Road area, crustal model and isostatic state 77−64240
sea mounts, S.Indian Ocean, gravity models *(French)* 79−74884
sea-mount loads affecting crust, isostatic compensation and geoid anomalies 80−109132
second derivative method formulae evaluation by Fourier transform 79−100987
second-degree sectorial harmonic reson. motion of satellite 78−24452
secular var. effects, orthometric corrections to relevelling data *(German)* 80−56341
secular var. on Carpathian Geodynamic Test ground *(Russian)* 77−90992
secular variation in Mexico unconfirmed for 1971-78 period 79−84074
secular variations, correl. with anomalous local atm. press., USSR *(Russian)* 78−53612
secular variations, due to water quantity vars. in lithosphere *(Russian)* 78−53609
secular variations, in Caucasus, correl. with geological struct. and seasonal hydrogeologic vars. *(Russian)* 78−53611
Shap granite, English Lake District, constraints on struct. and emplacement, gravity and mag. survey 78−44817
short-wavelength variations, flat Earth model utilising satellite motion 80−98216
shortening operators used in gravity interp. data processing techniques 77−64179
Singhbhum, India, gravity field anal. 78−32001
sinusoid variation detect. near Moscow and Sukhum *(Russian)* 77−86747
Skeleton Lake, Ontario, Canada, evidence for Palaeozoic impact crater 79−92553
sounding data, upward and downward continuation as inverse problems 79−44262
South Pole gravity tides, long period, 1970 obs. 80−21611
Spain, residual anomalies rel. to geology *(Spanish)* 78−88781
spatial analysis of upward continuation of potential field data 79−74828
spherical functions analysis, contrib. to numerical development *(German)* 78−61311
spherical harmonic coefficients of Earth's field, orthogonality 80−104881
spherical harmonics expansion of potential, convergence 78−81097
standards for gravity surveys 77−48990
standards for modern gravity surveys 78−7558
stars, uvbyβ photometric system calibration in terms of temp. and gravity 78−4198
static potential data inversion, generalized linear inverse 77−40967
static potential fields data inversion, generalised inverse appl. 78−77350
statistical algorithms for scaling geophysical fields 78−73527
statistical geodesy, mathematical struct. and appls. 79−29696
statistical gravity disturbance model, three-dimensional, algebraic errors correction 78−96125
statistical model from gravity anomalies and HB_1 model 78−61306
statistical three-dimens. gravity disturbance model 77−44891
Strait of Juan de Fuca, magnetic and gravity anomalies, geology 77−52973
subduction zone, gravity regime of descending lithosphere, effect of subduction angle 78−77206
Sun, gravit. field perturbations rel. to secular motion of Moon mean longit. and perigee 77−78679
surface gravity anomalies, rel. to geodetic boundary value problem soln. 79−62424
surface gravity var. rel. to irregular rotation of Earth 79−92473
surveying, modern standards 77−17016
surveys, two-dimensional and three-dimensional bodies 78−3961
Tashkent Palaeozoic crystalline basement, tectonic struct., gravity survey *(Russian)* 78−53610
Taylor expansion of theoretical gravity formula 79−100807
telluroid, definition 78−65171
terrain relief effect on gravimetric meas., polyhedron approx. 80−3895
Thelon metamorphic front, cryptic suture in Canadian Shield 77−53023
thermoelastic plane Lamb's problem with gravity 77−29241
thermoelastic steady state response to moving load, effect of gravity and temp. 77−23871
three-dimensional body, external gravit. field analytic continuation into interior *(Russian)* 79−34731
three-dimensional masses, gravity field calc. 80−94451
three-dimensional potential fields conversion and pseudo-gravit. field computation 77−82026
three-dimensional statistical gravity disturbance model 77−90991
tidal gravity in Gt. Britain 80−94446
tidal gravity measurements, comparison with self-consistent equilib. ocean tides 78−96218
tidal loading from integrated Green's functions 80−89928
tidal variations, ocean tides effect 79−53359
tide amplitude factor, phase lag at Beijing, China *(Chinese)* 80−8246
time variations of gravity and height *(German)* 78−15949
transworld tidal gravity profile 78−57160
truncated plate, gravity gradient determ. 77−44890
SW.Tunguska syneclise, platform structure from gravity surveys 80−98289
Tweeddale, negative gravity anomaly rel. to newly discovered granite batholith in Southern Uplands 79−92541
two dimensinal vertical fault, gravity approx. and interp. 78−61301
two dimensional dike, gravitational effect interp. by Fourier transform 78−3967
two-dimensional gravimetric and magnetometric problem, analytic construction based on Poincare sweep model 80−21846
two-dimensional gravimetry problem with variable mass density, equivalence theorems 78−85467
gravity continued
two-dimensional masses, field calc. using analytical continuation *(Russian)* 78−69277
two-dimensional triangular prism, gravity effect, Fourier transforms 78−3703
Ukraine, crusted struct. from combined deep seismic sounding and gramimetry data 80−21845
Ukrainian Precambrian Shield, deep fractures analysis *(Russian)* 79−20773
Ukrainian Shield, comparison of gravity and heat model with deep seismic survey profile *(Russian)* 78−48991
United States, regional free air gravity anomalies and tectonic obs. 79−57906
upper mantle liquid partial melts, liq. distrib. affected by gravity 80−81851
$V_{zz}(V_\Delta, Z_a)$ anomalies over stratified bodies, interpretation analytic method *(Russian)* 79−39968
variation with time 80−8247
variations, rel. to gravitation and inertia corpuscular model *(Russian)* 79−40439
variations before and after 1975 Haicheng and 1976 Tangshan earthquakes 79−57842
variations during preseismic crustal deformations 79−70734
variations with time of gravity and altitude, meas. via N.W.Europe gravity base network *(German)* 78−15948
vector, inertial navigation, covariance analysis of periodic traversing 80−95087
vector gravity survey, inertial navigation system appl. 79−29914
Venus, gravity field from Pioneer tracking 80−46439
Venus intended gravity meas. by Pioneer Venus Orbiter 77−73996
vertical gradient calc. methods 79−16689
vertical gradient meas. for detect. of small geological and anthropogenic forms, discussion 78−61575
vertical gradient meas. for detection of small geological and anthropogenic forms 77−17223
vertical gradients and crustal movements, precision meas. 79−92467
vertical gravity gradients, charts for quick determ. using horizontal plates *(Spanish)* 79−100982
viscous slab gravity flow, cumulative strain and boundary effects 77−81862
Walvis Ridge, S. Atlantic, gravity anomalies and origin 80−21682
Wilkes Land, Antarctica, large gravity anomaly, no evidence for meteorite crater 80−26512
Wolf Creek crater, Western Australia, gravity investigation 79−100838
Yellowknife supergroup, Northwest Territories, volcanic rock density determ. from gravity obs. 80−98320
Zambia, Bouguer anomaly map rel. to tectonics and struct. 77−40969
Zambia, gravity rel. to elevation 77−81782
Fe ore deposits from gravity and magnetic anomalies, determ. accuracies *(Russian)* 79−84536

gravity meters *see gravimeters*

gravity waves
accelerating shear flow, internal gravity waves 79−32628
acoustic gravity waves, atmospheric, harmonic generation 78−88956
acoustic gravity waves, computation in realistic atm. model 80−90164
acoustic gravity waves, quasi-simple wave solns. 77−75930
acoustic gravity waves role in generation of spread-F and ionospheric scintillation 79−66868
acoustic-gravity wave propag. in diffusively separated atmosphere 79−74933
acoustic-gravity waves, dispersive eqns. obtained by kinetic eqn. method *(Russian)* 78−85620
acoustic-gravity waves in upper atmosphere, diffr. around spherical Earth 78−4016
acoustic-gravity waves in Venus thermosphere 80−17520
acoustogravity wave generation in Earth's atmosphere 79−66776
acoustogravity waves, ionospheric disturbances accompanying earthquakes and explosions 80−36451
aerodynamic drag of sea surface, role of high freq. gravity waves 80−26536
Alberta hailstorm, gravity wave patterns 77−21827
Alfven-acoustic-gravity wave propag. and reflection, compressible, inviscid, perfectly conducting isothermal fluid 77−51124
almost-highest wave, simple approx. 79−90268
amplitude of diurnal waves rel. to Earth rotation rate *(French)* 80−8245
atmosphere, acoustic gravity wave generation by meteors *(Russian)* 77−91340
atmosphere, acoustic-gravity waves, relaxational dissipation 78−4018
atmosphere, acoustic-gravity waves generated by horizontally-moving sources *(Russian)* 80−21795
atmosphere, acoustic-gravity waves generation by ionosphere press. oscills. 78−77296
atmosphere, circulation associated with cold front, moist case 79−2334
atmosphere, equatorial, penetrative cumulus convection, gravity waves and travelling ionospheric disturbances 78−36361
atmosphere, equatorial gravity waves generation 78−36232
atmosphere, equivalent gravity wave formalism for tides in joint presence of friction and rot. 79−66847
atmosphere, gravity and buoyancy waves, rel. to stellar extinction oscills. 80−56606
atmosphere, gravity waves generated by shear layers 77−2195
atmosphere, gravity waves generated during solar eclipse 78−88887
atmosphere, gravity waves generation by HF acoustic waves, Cherenkov radiation *(Russian)* 77−17265
atmosphere, gravity-inertia oscills. in nonlinear flows, suppression 78−11955
atmosphere, internal gravity waves generated by penetrative convection 77−2196
atmosphere, internal gravity waves rel. to sound attenuation *(Russian)* 77−3693
atmosphere, internal solitary waves, obs. 79−8656
atmosphere, internal waves generation and breaking over ocean 78−44901
atmosphere, internal waves momentum flux and orographic scatt. 79−8663
atmosphere, layer structs. response to gravity waves 78−81290
atmosphere, marginally unstable interfacial gravity waves in boundary layer *(French)* 78−92888

gravity waves continued
atmosphere, mean motion induced by transient inertio-gravity waves 80−105029
atmosphere, MHD wave propag. in presence of rot. and variable mag. field 79−40024
atmosphere, near-surface internal gravity waves rel. to tropospheric wind *(Russian)* 77−33141
atmosphere, nonlinear gravity wave-critical level interaction 79−1205
atmosphere, nonlinear interaction with mean flow 79−53463
atmosphere, orographically scattered gravity waves 77−67057
atmosphere, production during 1976, October 23 solar eclipse 77−17181
atmosphere, propag. in tropical zone 77−78376
atmosphere, rate of wave energy transfer to upper atmosphere mean flow *(Russian)* 77−13101
atmosphere, ray tracing, tornadic storms and hurricanes warning system 78−73448
atmosphere, relaxational dissipation, basic formulation 78−4017
atmosphere, Rossby gravity wave propagation in latitudinally sheared zonal flows 78−16124
atmosphere, Rossby wave packet, vertical propag. in dissipative medium *(German)* 78−36220
atmosphere, squall line formation, nonlinear process 78−81323
atmosphere, theoretical props. of acoustic-gravity waves 77−33270
atmosphere, thermally forced Rossby and gravity waves, frictional effects 77−78384
atmosphere, trapeze instability modified by mean shear flow 77−5301
atmosphere, travelling ionospheric disturbances 80−82128
atmosphere, turbulence and internal waves spectra in stably stratified boundary layer *(Russian)* 78−81297
atmosphere, wave generation and frontal collapse 78−77300
atmosphere, wave overreflection and shear instability 79−53450
atmosphere, waves and thermospheric winds *(French)* 77−53256
atmosphere and oceans, wave disturbances 78−32209
atmosphere during 1976 October 23 Australian total solar eclipse 79−92558
atmosphere generation by movement of solar terminator, rel. to ionospheric electron densities 77−91348
atmosphere gravity wave-meanflow interaction, indication in radar obs. 78−81282
atmosphere Na layer, gravity waves and tidal oscills., lidar obs. 78−88955
atmosphere propagation, modified forward- backward scheme for two-grid-interval noise in numerical model 80−26575
atmosphere surface layer, calc. of mean velocity and temp. profiles *(Russian)* 80−8415
atmospheric boundary level, gravity wave-critical level encounter, calc. 80−26583
atmospheric circulation, forced by heating, transient mass flow adjustment 79−53455
atmospheric equatorial waves, nonlinear interactions 77−66961
atmospheric gravity wave generation and breaking over ocean 80−26571
atmospheric gravity wave sources, review 80−26572
atmospheric internal wave component identification on airglow charts, multiple-point method 78−73526
atmospheric tides, thermal exciting energy, numerical anal. 79−70833
aurora-generated gravity waves dynamic effects on midlatit. ionosphere 80−17438
auroral electrojet, acoustic gravity wave spectra 78−4033
auroral electrojet, generated gravity waves, Joule heating and Lorentz force effects 78−28393
auroral electrojet, gravity waves and infrasound generation, Joule heating and Lorentz force 79−66866
auroral origin of medium scale gravity waves in neutral composition and temperature 79−74998
barotropic waves, large amplitude, interaction with ambient shear flow, critical modes 77−80175
billows, gravity and geostrophic waves, exact solns. 79−34908
Boussinesq axisymmetric wave 78−22358
breaking, and Kelvin-Helmholtz instability 79−81847
breaking gravity-wave flow near tip, time-dependent free-surface flows 80−83808
buoyant flow, thermally driven, equations of motion 79−23334
capillarity-gravity waves, third-order reson. interactions 78−34148
capillary wave form. on gravity water waves, model eqn., surface tension, viscosity 78−83421
capillary waves generated by steep gravity waves, meas. 78−59409
capillary-gravitational waves, asymmetric, plane forced, wave shape on liquid surface of const. depth *(Russian)* 79−86448
capillary-gravity waves, 2-dimens. wave packet 77−35154
capillary-gravity waves, exact eqn. numerical soln., closed bubbles 80−14715
capillary-gravity waves, linear problems 78−51178
capillary-gravity waves in two-layer fluid *(Russian)* 79−39733
capillary-gravity waves in viscous fluid 78−51177
capillary-gravity waves on ocean bottom, development and stability *(Russian)* 78−16033
capillary-gravity waves produced by moving press. distrib. 80−69859
Cauchy integral-equation method, steady water wave problem numerical soln. 79−10574
cnoidal wave, existence downstream after flow under sluice gate 79−86403
compressible and incompressible fluids 80−14714
compressible atmosphere, vertically rotating, critical levels 80−6073
compressible flow, acoustic gravity waves travelling wave solns. 80−48721
creeping waves, on shallow water, numerical investigation 78−90928
critical level flow, viscous stabilization 77−45074
critical point hydrodynamics 78−59361
deep ocean, fine struct., internal gravity waves and wave breaking meas. and models 78−85578
deep water, finite-amplitude steady irrotational inviscid waves 80−64575
deep water gravity waves, bifurcation and symmetry breaking, four wave interactions 80−69855
deep water gravity waves, two-dimens. nonlinear wave eqn., exact envelope soliton solns. 80−43725
deep water waves prod. by local disturbance 77−72314
density wave theory for normal spiral galaxies, review 80−67873
density wave theory of spiral galaxies 79−48939
development in two-layer fluid *(Russian)* 80−12421
diffraction of hydrodynamic surface gravity waves at vertical obstacles *(Russian)* 77−55012
gravity waves continued
directional gravity wave spectra and surface currents, remote sensing with dual freq. radar 78−96323
dispersion relations in sheared, stably stratified flow 77−27577
dissipation of interfacial and internal long gravity waves, Korteweg-de Vries eqns. 80−90686
double boundary-layer model of mass transport in progressive interfacial waves 79−10573
ducting in thermosphere 78−77378
ducts, eddy motions induced by water waves and periodic flows 80−33679
E_s-layer, h-type at Uppsala, downward generation by internal gravity waves 78−81497
E_s-layers, mid-latitude, gravity wave heating, rel. to electron temp. gradients 78−28397
E-region, gravity waves durign winter anomaly from lower thermosphere daytime neutral wind meas. 78−45071
E-region, polar electron density fluctuations, gravity wave interpretation *(French)* 80−46334
Earth atmosphere, acoustical-gravity waves interaction and self-action in plane waveguide *(Russian)* 78−36221
Earth core, internal gravity waves and inertial oscills. 77−91082
Earth liquid outer core, theory 80−36274
energy production and dissipation in thermosphere 79−74997
equatorial electrojet, effects of gravity wave winds and wind shears 77−5388
F_2-layer, travelling disturbances prod. by gravity waves, Hooke perturbation formula testing 79−40005
F_2-layer of mid-latit. ionosphere, internal gravity waves day and night effects 79−58150
F-region, high latit., gravity waves obs. using fixed freq. sounding 79−25390
F-region, nonstationary nighttime disturbances produced by internal gravity waves 78−73565
F-region, travelling disturbances, frequency of occurrence over Waltair, India 79−40011
F-region, wavelike vars. in path of totality of 1976 October 23 solar eclipse 79−66865
F-region electron content and atmospheric gravity waves at high magnetic dip station 77−53277
finite amplitude gravity-capillary waves on deep water 80−74898
fluid wave propag., gravit. instability, rot. and streaming effects 79−37293
free surface flows under gravity, exact selfsimilar solns. 80−48725
free-surface flows, stream functions variational principle, finite element anal. appl. 79−64675
galactic density waves, nonlinear growth *(Chinese)* 79−97085
gas-streamlined liquid film, quasiharmonic motion development in vertical flow 77−55014
generation and frontal collapse, comments and reply 79−88423
generation in two-layer linearized model, initialization methods 77−86971
gravity waves, long period, on beach, generalised KdV-eqn., soln. 78−92844
gravity-capillary surface waves, nonlinear interactions 78−18310
gravity-capillary waves, reson. three-wave interaction, perturbation method 77−68608
gravity-capillary waves with edge constraints 79−68732
Green-Naghdi model for water of var. depth 79−48514
growth and equilib. of short waves in wind-wave tank 78−1679
hydromagnetic stability of compressible fluid 79−32689
hydromagnetic-inertial-gravity waves, propag. in magnetic-velocity shear 79−55422
Indian Ocean, evidence for continuous spectrum of equatorial waves 80−98331
induced airglow Brunt-Vaisala oscills. 79−53603
induced atmospheric pressure field above spectrum of surface gravity waves 80−92168
induced wind field determ. using phase path meas. 78−16178
inertio-gravity waves in zonal shear flow in equatorial ocean 80−26520
infinite depth fluid, steady free surface gravity-capillary waves, integro-differential formulation 80−6072
instabilities of finite amplitude gravity waves in deep water, superharmonics 78−38349
instabilities of finite amplitude gravity waves in deep water, subharmonics 78−38350
interfacial gravity waves, form. by submerged vorticity regions and fluid inhomogeneities 79−64682
internal, buoyant-parcel motion 78−55655
internal, propag. in shear layer, discontinuity form. 79−32543
internal, resonant over-reflection from Helmholtz velocity profile 79−50740
internal gravity wave break on slope *(Japanese)* 79−81909
internal gravity wave breaking on slopes *(Japanese)* 80−100005
internal gravity wave reflection from shear layer 77−42854
internal gravity waves, conservation law 77−15047
internal gravity waves, long, large amplitude, propagation in stratified fluid 79−37333
internal gravity waves and upper atmosphere emissions 80−105093
internal inertia-gravity waves in tropical stratosphere 80−41497
internal nonlinear waves in stratified fluid in closed basin 78−75159
internal wave modulation and stability 77−37231
internal waves in stratified flow around source run off system *(Ukrainian)* 77−68658
internal waves in stratified pipe flow 77−23971
ionosphere, acoustic gravity waves reson. coupling with ionisation waves in mag. field 77−25832
ionosphere, E_s-layers form. by gravity waves generated in region of solar terminator 79−12337
ionosphere, electron content quasiperiodic fluctuations during 1976 April 29 partial solar eclipse 78−24407
ionosphere, electron density latit. vars., internal gravity waves 78−32269
ionosphere, equatorial, elec. fields generated by gravity wave winds 77−53283
ionosphere, equatorial, gravity waves rel. to total electron content fluctuations 78−36360
ionosphere, generation of inhomogeneities, effects on geomag. pulsations 78−45143
ionosphere, generation of small-scale inhomogeneities by internal gravity waves 78−45100

gravity waves continued
ionosphere, gravity waves due to total solar eclipse, detect. by radio technique 77−91364
ionosphere, gravity waves rel. to radio waves phase path changes 79−35043
ionosphere, height depend. of travelling disturbances wave-normal depression and amplitude 79−40006
ionosphere, obs. of gravity waves assoc. with Hurricane Eloise 79−66872
ionosphere, press. oscills. transfer to neutral atmosphere during substorms 79−58158
ionosphere, propag. of acoustic gravity waves, explosion excitation *(French)* 78−12042
ionosphere, S. hemisphere gravity wave obs. using total electron content technique 79−21096
ionosphere, spatial resonance mechanism for equatorial spread-F irregularities drifting patches 79−21095
ionosphere, topside, large scale wave-like struct. at low and middle latits. 77−21985
ionosphere, total electron content meas. during 1976 Oct. 23 solar eclipse over Australia, rel. to induced gravity waves 78−49210
ionosphere, travelling disturbances, possible correl. with jet stream activity 78−69601
ionosphere, travelling disturbances characts. over Thumba 78−69590
ionosphere, travelling disturbances determ. by Faraday rot. modulation 79−21101
ionosphere, VLF atmospherics anomalies, rel. to Calcutta rainy days 80−82127
ionosphere, wave detect. from periodic fadings in VHF satellite transmissions during solar eclipse 77−33277
ionosphere F_2-region, meteorological perturbations due to gravity waves at sunspot minimum *(Italian)* 79−29922
ionosphere F-region, gravity waves, obs. during tornado outbreak (1974, April 3) 78−85753
ionosphere plasma interaction with gravity waves, elec. field and current prod. 80−61957
ionosphere waves in D- and F-regions, temporal vars. 80−8483
ionospheric, lower, layer structs. response to gravity waves 78−81290
ionospheric acoustic-gravity waves, Doppler sounding, rel. to storm detection and prediction 79−2326
ionospheric disturbances due to gravity waves generated by 1973 June 30 solar eclipse 77−21993
ionospheric effects of sudden commencement assoc. gravity wave 78−57385
Keller's solitary wave, capillary force effect 77−72313
Kelvin-Helmholtz instabilities and radiating waves, excitation by gravity wave-critical level interaction 79−88427
Lake Huron, Saginaw Bay, Georgian Bay and North Channel, gravit. oscills. 77−60435
linear, reciprocity principles 77−75931
linear wave-current interaction, energy propag. stopping 77−47029
liquid waves propag. over permeable bed *(Polish)* 78−38353
liquid with superficial film and diffusion effect *(French)* 78−75156
long and short surface waves interaction 77−41049
long-period, on fluid of rapidly varying depth, differential eqns. 78−9647
long-period gravity waves in ice-covered sea 80−67372
magnetic-velocity shears, linear wave motions 77−58799
mass transport theory for ocean bottom boundary layer *(Russian)* 78−16036
mass transport velocity in progressive gravity waves, double boundary layer model 77−78217
mesopause, energy characts. of internal gravity waves obs. by OH emission *(Russian)* 79−12324
mesopause, internal gravity waves rel. to OH emission 78−12031
mesophere, heating effects of gravity waves induced by Earth's diurnal rotation 78−40613
mesophere, wave effects on dynamics 79−53464
mesosphere, acoustic-gravity waves propag. 77−25734
mesosphere, acoustic-gravity waves propagation 78−44912
mesosphere, Arctic, vertical temp. and density patterns anal. as gravity waves 79−16622
mesosphere, equatorial, waves and winds over Jicamarca from multiheight radar obs. 78−36230
mesosphere, equatorial, wind fluctuations at gravity wave periods 78−36229
mesosphere, gravity waves obs. from vertical vels. radar obs. at temperate latits. 79−16572
mesosphere, mid-latit. internal gravity waves 77−5298
mesosphere, tides and gravity waves at mid and low latits. 78−36231
mesosphere, wave-field calc. 77−17186
mesosphere, winter, partial reflection drift obs. 77−64393
mesosphere internal gravity waves, propag. range *(Russian)* 79−16575
mesosphere wave component in partial refl. obs. 80−81993
MHD gravity waves, dispersion on running stream of inviscid elec. cond. liq. 78−59502
MHD gravity-capillary waves in liq. film falling by permeable bed 78−67277
MHD-gravity waves, over-reflection in stratified flow 77−11207
middle atmosphere, VHF radar obs. 80−105032
middle atmosphere dynamics, review 80−17338
modulation of internal gravity wave packet, resonance with mean motion 78−5761
mountain waves of finite amplitude evolution and stability 78−44929
neutral atmospheric motions effects on two-stream irregularities in equatorial electrojet 79−16742
nightglow temps., internal gravity wave effects 78−45066
non-stationary capillary-gravity waves in a shear flow *(Russian)* 79−34849
nonlinear deep water gravity waves, random inhomogeneous field evolution 80−69857
nonlinear dispersive waves, fourth order envelop eqn. 77−89135
nonlinear energy transfer in a narrow gravity-wave spectrum 79−100873
nonlinear energy transfer infinite depth wave spectrum 80−53801
nonlinear free surface flow digital simulation by boundary integral eqn. method 78−92850
nonlinear propagation of wave-packets on fluid interfaces 77−47032
nonlinear Schrodinger eqn., Fermi-Pasta-Ulam recurrence 79−10579
nonlinear Schrodinger eqn. exact solns., gravity wave appl. 79−77147
nonlinear surface waves with gravity or surface tension restoring forces 78−22357
nonresonant second-order interaction of waves, generation of deeply penetrating gravity-like oscill. 78−28508
gravity waves continued
nonstationary effects of gravity waves on ion formation in lower ionosphere 78−73567
nonviscous liquids, free surface flow, gravity waves with surface tension depend. on impurities *(French)* 79−90267
normal mode initialisation technique, variational nonlinear, atm. gravity waves appl. 79−5584
ocean, air-water interface, effects on gravity waves 79−57947
ocean, beta dispersion of inertial waves 79−70810
ocean, equatorial, zonal internal waves, math. model *(Russian)* 79−12119
ocean, gravity and Rossby waves dispersion relations 79−2280
ocean, influence of rot. on surface gravity and internal waves 79−2281
ocean, interference with EM current meter recordings 77−78456
ocean, internal gravity waves, rel. to low-freq. acoustic fluctuations 77−50809
ocean, long gravity wave forcing by finite depth effect on nonlinear wave packet 79−48510
ocean, mass and momentum diffusion by internal gravity waves 77−13086
ocean, monomolecular slicks drift response to wind and wave action 78−69364
ocean, nonlinear gravity wave-critical level interaction 79−1205
ocean, nonlinear internal waves allowing for rotation 80−26534
ocean, random wave field, directional energy distrib. influence on dispersion relation 77−86921
ocean, strong interaction with turbulence *(Russian)* 77−81904
ocean, surface and internal gravity waves generated by baric disturbances *(Russian)* 78−77252
ocean, surface/internal waves energy transfer model 77−923
ocean, trapped edge waves in presence of irregular coastline 78−44853
ocean, wind generated gravity waves, saturation range in freq. spectrum 77−60399
ocean gravity wave growth by modulated wind stress 77−17119
ocean inertial oscills. radiation damping, wind mixed layer turbulence 79−39730
ocean internal nonlinear gravity-inertial waves in stably stratified layer 77−21785
ocean internal short-period waves generation by shear flow instability 79−2273
ocean internal tidal oscills. spatial characts. from temp. meas. 78−61434
ocean internal wave field, equilib. mechanisms 78−44852
ocean internal wave generation by advecting atmospheric fields 77−53066
ocean internal wave generation in geostrophic current by atmospheric pressure disturbances *(Russian)* 79−100853
ocean internal wave spectra analytical representation 77−41056
ocean internal waves, shear distortion of orbital vels. 77−78208
ocean internal waves, shear instability *(Russian)* 78−69352
ocean internal waves interaction with small-scale surface turbulence *(Russian)* 78−44845
ocean random gravity wave in deep water, statistical pressure props. 77−2155
ocean random gravity wave mathematical representation 80−46198
ocean short surface wave transformation by inhomogeneous currents *(Russian)* 77−73753
ocean surface gravity waves, nonlinear theory, derivations 77−60387
ocean surface gravity waves, nonlinear theory, interp. and appls. 77−60388
ocean surface gravity waves during Tropical Storm Delia, directional spectra and kinematics 79−48506
ocean surface waves, low freq. noise prod. in deep ocean 78−81184
ocean surface waves, triple roots and curved caustics 78−40584
ocean unsteady gravity wave dissipation *(Russian)* 77−78194
ocean wave detection by microwave radar, gravity-capillary wave modulation 78−77333
ocean wave groups, vels. and refr. laws verification 78−85575
ocean wave-current random interactions in water of varying depth 77−37238
ocean waves, directional spectra, remote sensing by microwave radar 78−57364
oceanic short-period internal gravity waves, nonstationary features rel. to thermocline oscills. *(Russian)* 78−16024
one-dimensional, finite-element and finite-difference techniques comparison 79−18902
orbital motion of particles in steep, irrotational gravity waves in deep water 80−1614
oscillations of two liquids separated by membrane *(French)* 78−87355
oscillatory boundary layer, on bed beneath gravity waves, laser Doppler anemometry 78−90929
over-reflection of horiz. propag. gravity waves by vertical shear layer 79−10577
NW.Pacific Ocean, edge waves obs. *(Russian)* 78−44841
N.W.Pacific Ocean, temp. fluctuations in internal gravity waves freq. range 77−49081
parallel flow normal modes in inviscid stratified fluid with propagation at infinity 80−24071
parallel or swirling stratified shear flow, internal gravity and axisymmetric waves 79−86446
parametric instabilities in internal gravity waves 77−19615
particle trajectories in steep, symmetric gravity waves 80−6071
periodic finite amplitude waves on rot. fluid surface, numerical method 77−51071
periodic gravity waves, integral relations, equivalence to Bernoulli's eqn. 79−68731
permanent wave structs. on an open two layer fluid 78−59411
permanent wave structures and resonant triads in a layered fluid 79−37377
plane wave reflection over variable depth water 77−15051
planetary boundary layer, internal gravity waves in time-varying stratification 78−3864
plates, eddy motions induced by water waves and periodic flows 80−33679
progressive capillary-gravity waves, energy and momentum integrals 79−94637
propagation in random media, oceanic appls. 79−5987
radiating instabilities and resonant overreflection 79−53433
radiowave wind obs. of waves during 1976 over Saskatoon 79−79935
random, dispersion relation experiment, wind-wave flume 79−72904
random, dispersion relation theoretical framework, wind waves 79−72903

gravity waves continued
ripples, wind-generated, gravity waves effects, Doppler meas. 77−62264
running stream, capillary-gravity wave problem 79−23333
sea bottom, mass transfer, horizontally 2D bodies effect 78−11909
sea surface gravity waves refraction, coastal, for flat inclined ocean bottom *(Russian)* 77−33084
secondary vorticity in internal waves 79−72899
self-gravitating fluids, definition of g-modes and p-modes 77−41291
shallow seas, nonlinear stationary internal and surface waves propag. 80−17292
shallow water, numerical computation of steep gravity waves 80−1615
shallow water model, dynamics rel. to normal mode initialization 77−86984
shape and breaking in stratified shear flow 78−34147
short gravity-capillary waves modulation by longer-scale periodic flows 80−57106
short ocean waves in finite depth waters, wave packet instability 80−81908
small amplitude water waves, uniqueness in region of varying depth 80−1613
solar atmosphere, acoustical-gravity waves interaction and self-action in plane waveguide *(Russian)* 78−36221
solar atmosphere, evidence for trapped gravity waves 80−72898
solar atmosphere, gravity waves generation by HF acoustic waves, Cherenkov radiation *(Russian)* 77−17265
solar atmosphere, MHD-gravity wave critical levels 78−77531
solar atmosphere, penetrative instabilities theory in presence of thermal dissipation 80−109406
solar atmosphere magnetoacoustic gravity waves 77−29752
solar atmospheric oscillations, power, phase and coherence spectra 79−8897
solitary, nonlinear oblique interactions 77−23970
solitary, resonant interaction between three waves 77−27543
solitary wave evolution for very weak nonlinearity 79−10575
soliton fission in channel of varying width 80−46816
spectral decomposition of short gravity wave systems 80−36319
spectrum evolution affected by internal wave *(Russian)* 80−21776
spin and angular momentum in gravity waves 80−53798
spiral density waves in galaxies, response of stellar orbits 79−44570
sporadic-E wavelike oscills. due to atm. gravity waves 79−101002
stably stratified shear flow in channel, internal gravity wave packet mean flow 79−98740
standing waves, finite amplitude, on finite-depth perfect liq. surface *(Russian)* 78−75155
standing waves, large amplitude on deep water, numerical computation 80−24042
standing waves of finite amplitude on surface of ideal liquid of finite depth 79−81906
steady gravity-capillary waves on deep water, weakly nonlinear waves 79−77153
steep, almost-highest wave, matching and anal. extn. 78−46991
steep progressive gravity wave, rounded crest, transcendental eqn. 77−56643
steep surface wave deformation, growth of normal mode instabilities 79−1206
steep water waves, surface tension effects 80−38424
steep wind waves, amplitude modulation 80−103036
stellar penetrative atmosphere, convective, gravity and acoustic instabilities 79−84783
Stokes' coeff., new relns. 79−41698
stratification effects in boundary layer flow over hills 78−53707
stratified Boussinesq fluid, turning-level dynamics of internal waves 77−15092
stratified compressible flow, inhomogeneous acoustic-gravity wave eqn. 77−80174
stratified fluid flows, transient solns. 77−35196
stratified fluid with finite depth, internal wave eqn. governing long gravity waves 79−97217
stratified fluids of finite depth, weakly-nonlinear, long internal gravity waves 79−77148
stratified inviscid Boussinesq fluid, instability of internal gravity wave 77−68663
on stratified liquid, linear initial-boundary value problems 77−39301
stratified ocean, vertical struct. of oscills., numerical calc. 79−39751
stratosphere, gamma-ray quasi-periodic intensity variations rel. to internal gravity waves *(Russian)* 80−90177
stratosphere, generalised Lagrangian-mean description of wave/mean flow interaction 80−109214
stratosphere, lower, radar meas., of gravity waves 78−44917
stratosphere, lower, radar meas. of gravity waves 78−81292
stratosphere, mixed Rossby wave, QBO shear effects 79−88413
stratosphere, wave spectra resembling turbulence rel. to turbulent transport estimates 79−79981
stream function relationships, variation approach 80−36318
surface, free, irrotational flow, time-dependent 80−83807
surface, incident on submerged horizontal plate 78−5758
surface gravity wave, wind-wave generation, bispectral contrib. 78−49033
surface gravity wave diffraction by cylinders *(Russian)* 77−68605
surface gravity wave packet development when moving over an uneven bottom 79−41700
surface tension restoring forces on gravity waves in narrow channels 80−28568
surface wave diffraction, in shallow water, optimal control problem *(Russian)* 80−74896
surface wave diffraction at underwater axisymmetry obstacle, polynomial approx. *(Russian)* 79−77143
surface wave diffraction by arbitrary obstacles *(Ukrainian)* 80−48722
surface wave diffraction over underwater channel of varying depth *(Russian)* 80−79333
surface wave horizontal asymmetry *(Russian)* 80−74897
surface waves, interaction with arbitrarily disposed submerged inhomogeneities *(Russian)* 80−79334
surface waves, multi-dimensional packets 78−42624
surface waves, tsunami wavelength, wave equation soln. 78−90927
surface waves, vertical asymmetry over a limited depth *(Russian)* 80−79337
surface waves diffraction, ray methods 78−40574
surface waves under gravity, uniformly analytic initial domains 79−72901

gravity waves continued
terrestrial atmosphere acoustic-gravity waves, generation mechanisms *(Russian)* 78−85621
thermally stratified rot. fluid, secular spin-up, expt. and numerical study 79−77217
thermoconvective waves in horizontal gas layer 77−7407
thermosphere, comp. effects in acoustic gravity waves 77−21959
thermosphere, correl. with tropospheric lightning 79−84557
thermosphere, dissipation and diffusion effects on gravity waves propag. 77−13141
thermosphere, gravity wave activity effects on photochem. and comp. 80−41583
thermosphere, gravity wave generation, propag. and dissipation 79−2405
thermosphere, gravity wave spectra propag. 79−66848
thermosphere, internal gravity waves, rel. to tropospheric weather systems 77−91339
thermosphere, lower, gravity waves detect. by French incoherent scatter facility 78−81478
thermosphere, lower, tides and gravity waves interaction rel. to thin shear turbulent layers 78−65444
thermosphere, mid-latit. internal gravity waves 77−5298
thermosphere, minor species relative phase and amplitude response to gravity waves 79−58140
thermosphere, short periodic gravity waves propag. theory 78−49185
thermosphere, source in tropospheric jet stream *(French)* 78−69554
thermosphere, vertical energy flux from medium scale gravity waves generated by jet stream 78−81479
thermosphere, wave propag. in diffusively separated atmosphere 80−12580
thermosphere, wave-induced diffusion effects on acoustic-gravity waves 78−61637
thermosphere and mesosphere, travelling neutral disturbances and minor constituent particle mass 78−49189
thermosphere heating during magnetic storm, dynamic energy transport from high to low latits. 80−26657
thermosphere medium scale gravity waves, sources in meteorological jet stream, exptl. study 79−21088
thermosphere over S. Australia, waves in lower region 78−36348
thermosphere wave effects on dynamics 79−53464
thermosphere waves, review 77−45211
tidal data processing, Tihany Observatory results 77−87097
tornadic storms on 1976 January 13, assoc. gravity waves 80−41515
transient waves generated by a moving oscillatory pressure on a sloping beach 80−56476
trapped coastal waves on equatorial beta plane 79−20846
travelling gravity-capillarity surface waves, on liq. film falling past permeable bed 78−87351
travelling ionospheric disturbances, daytime effect on radioastronomical intensity meas. and interferomety 80−67450
travelling ionospheric disturbances, in F1 region, phase path technique obs. 80−36436
troposphere, buoyancy waves, Doppler radar obs. and theoretical model 79−84367
troposphere, gravity waves and LF oscills. in tropics 80−12496
troposphere, gravity waves generated by shear flow instability 80−31098
troposphere, gravity waves nature and role 79−92575
troposphere, ground level gravity waves occurrence in SE.Australia, microbarographs obs. 78−73439
troposphere, internal gravity waves generated by jet streams 77−25737
troposphere, viscous internal gravity waves and low freq. oscills. in tropics 77−87003
troposphere-ionosphere coupling during 1973 November 20 isolated tornadoes 79−70851
two-dimensional, created against vertical cliff, uniform asymptotic soln. 78−67210
two-dimensional, finite-element and finite-difference techniques comparison 79−18903
two-dimensional, initial boundary value problem in terms of stream function 77−7409
two-layer 'shallow water' model 80−59061
two-layer fluid, weakly nonlinear solitary long gravity waves 78−83419
upper atmosphere, gravity wave emission from moving sources 77−60504
upper atmosphere, gravity waves and travelling ionospheric disturbances from electron density power spectra 78−28394
upper atmosphere, gravity waves interaction with $O_2(^1\Sigma)$ airglow 79−29918
upper atmosphere, internal gravity waves meas. in meteor zone 77−25806
upper atmosphere, internal gravity waves rel. to hydrodynamic accelerators *(Russian)* 78−16225
upper atmosphere, internal gravity waves rel. to non-LTE radiative transfer in CO_2 15 μm band *(Russian)* 78−36341
upper atmosphere, interpretation of experimental data on internal gravity waves *(Russian)* 78−16224
upper atmosphere, neutral waves determ. from AE satellite meas. 79−58139
upper atmosphere, possible effect on Loran-C 100 kHz signals 80−109304
upper atmosphere, vertical winds effects on medium scale internal gravity waves propag. 79−75004
upstream difference method 80−106806
Venus atmosphere, internal gravity waves 79−5770
viscous or perfect incompressible fluids, gravity waves with surface tension and capillarity strain *(French)* 77−65749
viscous thermally conducting layer, internal gravity wave damping *(Russian)* 77−11201
water, capillary-gravity waves, nonlinear modulation 77−11206
water, surface gravity water propag., wave action and set-down on shear current 78−90920
water of arbitary uniform depth, integral props. of steep waves 77−70683
water surface waves, phase speeds of upwind and downwind travelling waves 80−98332
water wave, steady, numerical soln. using Riemann Hilbert method 80−33618
water waves created against cliff, development 80−72530
water-wave diffr. by semi-infinite vertical barrier on rotating Earth 78−83417
wave-slope spectra in capillary-gravity range, increasing wind, laser beam meas. 77−3836

greasing *see lubrication*

Green's function methods
see also CPA calculations; KKR calculations
1f-shell nuclides, optical pot. imag. part, isotopic features 79−9535
$\lambda\phi^{2N}$ quantum field theory, Green's function approximation scheme 77−13862
$\lambda\phi^4$ theory, renormalised perturbation theory, Green's function calc. by R operation 78−54570
σ models, nonlinear, perturbative approach to symmetry restoration 80−37163
σ models, nonlinear, soft mass renormalisation of 1/N expansion 80−47164
Σ_3 perturbation method using Green's functions for mol. calcs. 78−55123
ϕ^3 4-D model, existence 79−97261
ϕ^3 interaction, four-dimensional Green's function model *(Russian)* 78−77775
$g\phi^4$ field theory, strong coupling expansion, appl. to $g\phi^{2N}$,$g(\bar{\psi}\psi)^2$ and QED 79−58880
ϕ^4 model, Altman's contractor techniques, appl. to nonlinear integral eqns. for Green's functions 79−45005
$g\phi^4$ theory, asymptotic series sum of perturbation theory, Green's function method *(Russian)* 79−54271
($\hbar\omega$,2e) reactions, Green's function method and correlated electron motion 77−88431
a giant resonance theory in the 1p1h+2p2h+continuum approximation 79−67628
acoustic emission and plate Green's function 77−50798
acoustic field analysis, two-dimensional *(Japanese)* 79−81591
acoustic field in stratified media of variable viscosity, Green's functions 80−4545
acoustic radiators, directivity pattern calc. from near-field sound meas. 78−83149
acoustic wave diffraction by thick slitted screen 79−68455
actinide, compounds, f-electron systems with fluctuating valence, phase transitions 80−6789
actinides, electronic struct., Hubbard's alloy approx. 79−73665
adatom density of states, impurity atom effects 80−92958
adatom interaction with solid substrate, effect of mechanical stress on chem. pot. 80−10784
adatoms, anisotropic long range elastic interaction between adatoms 79−33185
adatoms, electron state at high coverages 79−28400
N.Adriatic Sea, Green's function of Laplace's tidal eqn. 80−17291
adsorbates, photoexcitation theory rel. to angle-resolved UPS and surface EXAFS 80−39426
adsorbed layer, nonuniform charge distribution, phase transitions, Hartree-Fock calcs. 80−54525
adsorption, coherent potential approximation 79−33193
adsorption of atoms on metals, Green's function formalism for studying electronic struct., local density of states calc. 80−107884
aerodynamic stability of Timoshenko bar, time- and space-harmonic balance *(German)* 80−83812
alkali halide, U-centre pairs, localised modes 77−7813
alkali halide crystals, defect modes due to substitutional anion-pair and cation-pair impurities 80−92540
alkali halides, local and reson. modes due to hydide ions, U-centres and additive cation impurities 79−77710
alkali halides, mixed, U-centre localised modes 80−100319
alkali halides, vibration modes due to single ion impurities 79−51225
alkali iodides, U-centres 79−46775
alkali metal atoms, laser three-photon absorpt., ionisation cross-sections *(French)* 78−5182
allene, ionis. pots., Green's function method 77−14608
alloy, one-dimensional, electronic struct. 79−69391
alloy, ternary, ordered, Green's function treatment, disorder transition 77−15540
alloy band structure, two-band alloy, multiband theory 79−37952
alloys, binary with long and short range order, electron energy spectrum calcs. *(Russian)* 79−99471
alloys, disordered binary, crit. US attenuation 79−99272
alloys, force-and-mass disordered, average local-information transfer approx. 80−88290
alloys, local density of states and local environment 79−82509
alloys, substitutional, self consistent cluster theory for off diagonal disordered systems 80−84272
allyl-radical, pi-electron system, appl. of UHF Green's function method 77−61684
amorphous magnetic materials, spectral density functions 79−47269
amorphous semiconductor superconductivity feasibility model *(Russian)* 78−80092
an inhomogeneous Schrodinger equation and its solutions in scattering theory 79−63073
analytic regularization in an arbitrary number of dimensions 79−26215
Anderson localisation, real-space renormalisation approach 80−2364
Anderson localisation, real-space renormalisation group theory, decimation method 80−88461
Anderson model, asymmetric, t-matrix approx., ground state 80−20061
Anderson model, non-orthogonal elec. resist. 80−59947
Anderson-Mott transition, crit. dimensionality 80−10876
anharmonic crystal, lattice dynamics and stability, self-consistent phonon theory 79−51209
anharmonic crystal, lattice dynamics and stability 78−6129
anharmonic crystals, neutron scatt. cross-section, sublattice displacement effects 79−77460
anharmonic oscillator, analytic theory of continued fractions, Green's function 79−6019
anisotropic crystals, infinite rectilinear dislocation, vibrs. 80−44210
anisotropic ferromagnet, one-magnon light scatt., temp. depend. 77−52063
anisotropic ferromagnet with biquadratic exchange, crit. temp. 77−12124
anisotropic Heisenberg ferromag., inhomogeneous dynamic susceptibility tensor 80−39729
anisotropic insulators, interaction of point charge and interface 79−69584
anisotropic media, scalar macroscopic field construction by method of images 78−32697
anisotropic paramagnet, statistical mechanics using second order Green's function theory 80−25074
anisotropic $S=^1/_2$ ferromagnet, reson. susceptibility, statistical mech. theory 77−8413

Green's function methods continued
antiferromagnet, 1-dimens., two-spin IR absorpt., Green's function and classical moments theories 77−40025
antiferromagnet, dil. paired, bond dilution problem, CPA theory 79−78389
antiferromagnet, one-magnon light scatt., effect of anisotropy 79−33676
antiferromagnet, one-magnon light scatt. from spin-flop and paramag. regions, effect of anisotropy 79−33677
antiferromagnet, quasi-two-dimens., nonreson. HF field absorpt. *(Russian)* 77−63287
antiferromagnet, two-magnon Raman scatt., temp. effects 77−48178
antiferromagnet, uniaxial S=1, effect of cryst. field anisotropy 77−28344
antiferromagnetic insulator, magnetothermal resist. 77−35767
antiferromagnetic metal, with paramag. impurities, Neel temp., impurity conc. depend calc. 78−68232
arbitrarily shaped dielectric body inside waveguide, three-dimensional anal. 78−71005
aromatic compounds, intersystem crossing theory, El-Sayed rule extension, anomalous rate consts. 77−30911
aromatic hydrocarbons, intersystem crossing mechanism, rate consts. 77−65497
asymptotic behaviour in renormalisable QFT, Green's functions 78−70254
asymptotic estimates in perturbation theory and complex instantons 79−6273
asymptotic estimates in quantum field theory, Lipatov method 79−21895
atmospheric pollution, dispersion, transformation and deposition 79−83663
atom, electron, impact, inelastic scattering in laser field, Green's function method calcs. 79−94086
atom, K-shell electron elastic photon scatt., high-energy calcs. 77−431
atom, with two internal vacancies, characts. calc. by Green function method *(Russian)* 78−50450
atom, with two internal vacancies, chem. shift of characts. *(Russian)* 78−50451
atom surface scatt., reflection and sticking coeffs., short range forces, low energy limit 80−40208
atom-solid elastic scatt., iterative integration scheme using Green function 77−48294
atomic and molecular structure, electron correl., pair theory 79−54774
atomic calcs., use of Coulomb GF in various representations 77−57907
atomic electron scattering, in laser field, many-body problem 79−31679
atomic electron scattering, many-electron correlations 77−42409
atomic energy level isotopic shifts and nuclear polarisation *(Russian)* 78−13444
atomic excited states, field theoretic approach 79−68199
atomic ground state correlation energies, Green's function calcs. 77−75061
atomic HF and correlation energies, relativistic corrections and dipole matrix, calc. 77−26981
atomic hyperfine interactions, modified delta-function pot. 79−3378
atomic multiphoton inoisation probability, Green's function model pot. 78−25498
atomic ordering, appl. of Green's temp. functions *(Russian)* 79−51051
atomic polarisability of two atoms of large separation *(Russian)* 79−76481
atoms, electron coincidence ionisation spectra, Green's function anal. 79−31714
atoms, electrostatic electron interactions, relativistic calcs. 77−57894
atoms, eqn. of motion-Green's function and config. interaction methods comparison, appls. 80−47841
atoms, ionisation pots., electron affinities, Rayleigh-Schrodinger and Green's function calcs. 77−75075
atoms, multiphoton ionisation, Green's function method calcs. 79−89650
atoms, multiphoton ionisation, reson. cross-section, very-narrow-bandwidth source 78−55150
atoms on semi-infinite linear chain, chemisorption theory and superoperator formalism 80−93800
Auger electron spectra of atomic Fano resonances 80−93454
augmented quantum field theory, systems containing derivative coupling and/or vector fields 79−63367
averaged Maxwell equations in severe random nonuniformities 80−69298
axial vector current anomaly in gauge field theory Green's function calc. *(Russian)* 80−27412
axially symmetric Helmholtz eqn., fundamental solution 78−77722
axisymmetric transducers, with various boundary conditions, single integral computer method for Green's function 80−87591
backward potential scattering at high energies *(Chinese)* 79−9143
band structure, deformation potentials calc. 79−1568
band structure, phase shift changes effect, sensitivity factor 77−72810
BCC crystal lattice containing interstitial atom in split config., reson. and localised vibrs. *(Russian)* 80−84268
beam, homogeneous, initial boundary value problem of transverse vibr. 79−41601
Bethe-Goldstone time-depend. first-order theory, short range correl., transition moments 78−25449
bilocal fields, ϕ^3 vertex, unitary S-matrix 78−62323
binary alloys, acoustic modes in random and correlated alloys, order-disorder transform. 80−65189
biological Bose condensation, and time threshold for biological effects 79−100664
black hole+heat bath, thermal equilib. possibility, thermal Green functions 78−12275
black holes, odd-parity perturbations, normal modes 77−17612
Bleustein-Gulyaev wave transmission characts. at corner 77−59197
Bloch electrons, weak magnetism, spin and spin-orbit interactions *(Russian)* 79−33443
Boltzmann equation, numerical soln., local Green's function method 79−97327
bonded wedge shaped stamp apex singularity, Green's functions for elastic half space 80−64489
book, mathematical methods for physics 77−45670
Borel transform and the renormalization group, review 79−26238
Bose gas, one dimensional, long wave asymptotic multi particle Green functions *(Russian)* 80−77700
Bose liq. near lambda point, Green function anal. 77−87689
Bose system, density and current correlation functions *(Japanese)* 79−54046
boson, rainbow approach of scalar model *(Russian)* 80−68436
boson condensation, solvable quantum field theoretic model 77−57447

Green's function methods continued
boson system, interacting, self consistent theory without anomalous propagators 77−33942
bound spectrum by action-angle variables path summation 77−30038
bound states of two dimens. O_N model at finite temps. 78−41409
boundary-value problems, book 80−28
branched cracks in 2-D, numerical soln. 79−46269
Brillouin scattering, resonant, analogy to modulation spectroscopy *(Japanese)* 78−68526
Brillouin scattering by Love waves, theory 80−66212
Brillouin scattering by oblique-incidence acoustic phonons, lineshapes 78−72534
Brillouin scattering by Stoneley waves, elasto-optic and surface ripple mechanisms 80−71435
Brillouin scattering from surface waves, appl. to Si, GaAs and Al 80−40125
Brueckner expansion, embedding in Green's function theory for nuclear matter binding energy 79−22220
butatriene, ionis. pots., Green's function method 77−14608
C_n method in spherical geometry, appl. to transport problems 79−22362
C-CD, insulator-semiconductor interface, electrostatic field, Green's function calc. 77−76933
Cauchy problem, linear eqns. with const. coeffs., absolute instability, 3-dimens. 79−12622
causal function in many body problems, analytic props. *(German)* 77−45787
causality and dynamical pictures in finite temp. Green's function 77−79219
cavity, scalar Green's function, numerical calcs. using integral eqn. *(French)* 79−32110
cavity normal modes and normal freqs., Green's function numerical study *(French)* 79−32111
CDW commensurate-incommensurate phase transition, 1-D electron-phonon system 78−14682
charge density waves, Hubbard model calc. *(Russian)* 79−65395
charge density waves, unidimensional generalised Hubbard model *(Russian)* 79−65396
charge imbalance relaxation freq. depend. near superconducting T_c 80−93030
charged particle, soft photon contrib. to Green's function, IR asymptotics, gauge transform. *(Russian)* 77−57438
charged particle in field of quantised plane wave *(Russian)* 79−890
charged particle scatt. in quantising mag. field 80−46853
charged particle scattering in homogeneous mag. field, transition amplitude 79−10218
charged scalar particle in field of running electric wave *(Russian)* 79−889
chemical kinetics, sensitivity analysis, numerical Green's function procedure 79−100334
chemical kinetics sensitiviy anal. 79−20343
chemical reactor, falling-film gas-liq. type, mathematical model 79−86526
chemisorbed atom, electronically adiabatic vibr. state lifetime 77−72768
chemisorbed layer, depend. of work function in order-disorder phase transition 79−19460
chemisorption, superoperator formalism, appl. to Anderson-Newns model 80−26047
chemisorption on metal, intra-adsorbate Coulomb correl. and surface struct. roles 78−71979
chemisorption on metal, intra-adsorbate Coulomb correl. and surface struct. roles 78−71980
chemisorption on model insulator 77−85072
chemisorption on real infinite systems, Green's function formalism 79−19461
chemisorption site determ., by angle-resolved UPS 78−71970
chemisorption substrates with complex band struct., new technique 78−71961
classical and quantum lattice systems critical lengths and critical temp. estimates 79−56556
classical EM wave diffraction by a thin periodic slab, rigorous approach 78−82890
classical motion of extended charges, eqn. of motion energy balance determ. 79−10250
classical operators, eigenvalues 77−26228
classical oscillators, parametrically excited, appl. to plasma interactions 80−33729
cleaved crystal, surface electronic Green's functions in terms of the bulk Green's function via random-walk theory 79−60898
closed time path Green's functions, transform. props. *(Chinese)* 80−105491
coherent function of radiation source field in unbounded scattering medium *(Russian)* 78−1160
collective excitation, SBO Green's function eqns. 79−99492
collinear atom-diatom inelastic scatt., Green functions method 78−25660
Coloumb excitation of atoms by fast protons, proton energy loss depend. on impact parameters *(Russian)* 80−53123
coloured null flags and para-Fermi fields 77−5993
compact simple Lie group, Green's function, group manifold and path integral *(German)* 80−37169
complex pole calc. by variational technique 80−98822
complex poles residues of outgoing Green function, eigenfunction expansion involving resonant states 77−82885
complicated level systems, high-temp. series expansion 77−51863
composite media, generalised Fourier expansions, homog. equations 78−77712
composites, short-fibre, unidirectional, effective thermal cond. bounds 80−92727
concentric domains, two dimensional heat equation general solution *(German)* 80−99918
condensed matter physics, dynamic correlations, book 80−86046
conductivity equations analysis, computer-aided, field disturbances in conducting fluid modelling *(Russian)* 78−231
connected-kernel multifermion Bethe-Salpeter equations 80−32005
core holes, localised-delocalised relation, ionis pot., Green's function method 77−75064
cosmic ray interplanetary steady-state transport eqn. soln. 77−87214
Couette flow, linearised stability 77−31279
Coulomb Green's function, nonrelativistic analytic props. of eikonal approx. 80−32038
Coulomb Green's function Sturmian expansion, Goldstone diagrams and reduction theorems 78−898
Green's function methods continued
Coulomb Green function for extended, uniformly charged nucleus 79−13199
Coulomb problem, zero-energy 78−62097
Coulomb scattering, Green's functions, integral eqns. soln. 77−37789
Coulomb T-matrix, modified integral eqn. using Green's functions 79−35976
coupled channel multiparticle scattering theories, Green function eqns., factorisation props., spurious solns. 78−82323
coupled thermoelastic problem, formal soln. 80−4529
coupled thermoelastic problem, Green's function soln. 79−72818
coupling parameter trajectories 78−8519
covalent crystal, dynamical correlation effects on quasiparticle Bloch states 80−88499
covalent semiconductors, electronic struct. of localised defects, review 80−44535
CP^{n-1} multi-instanton fields, quantum fluctuation 80−329
crack emanation, from circular hole in infinite sheet, Green's function methods 80−92084
cracks, emanating from fastener holes 78−67118
critical dynamics, classical systems, Fokker-Planck description 78−21057
crystal, point defects, anisotropic cubic elastic Green's tensor function, elastic energy coeff., Algol 60 program 77−11537
crystal impurity centres, quadratic Stark effect, quantum mech. band shape calcs. 77−69863
crystal slab, 3-D, surface states, relativistic Green matrix method, muffin-tin potential 80−80345
crystal surface states, calc. by relativistic Green matrix method 79−47139
crystal vibrational modes, surface atom freq. spectrum, mean correl. displacements *(French)* 78−2206
crystal with long range impurity states, electron spectrum *(Russian)* 79−56167
crystals, matching Green function method 77−85129
cubic crystal, new type of long-wavelength surface vibrs., Green's function method study 78−26758
cubic ferromagnet, magnetic crystal, semi-infinite, impurity states, Green's function method *(Russian)* 79−51647
cubic lattice, Green's function determ. 78−62162
cut-off potential, asymptotic energy behaviour of Green function 80−27165
cyclopropane, ionis. pot., many-body Green's function method 77−67972
cylinder, direct and inverse scatt. problems, Dirichlet boundary conditions 80−95774
cylinder, perfectly conducting, space charge appls. *(French)* 78−25770
cylindrical body heated by moving heat source, heat cond. and temp. distrib. Green's function derivation 77−42681
cylindrical light beam diffr. on wideband US signal 78−50698
damped oscillator 79−80467
DC resistivity as functional of generalised dynamical susceptibilities, solid state model 79−28330
decoupling procedure in Green's function method, sum rules for de Gennes' model *(Russian)* 78−56434
defect vibrations, resonant and localised 77−1200
defects in solids, density matrix evaluation in self-consistent method 80−29349
density matrices, generalised integrals, Green's functions 77−79029
density matrix, asymptotic high temperature expansion 78−54115
DFB waveguide laser theory, Green's function approach 78−5504
diagrammatic Green function technique appl. to cryst. field systems with exchange 78−68130
diatom+diatom, ang. momentum decoupling approximations and factorisation 79−72397
diatomic molecule, effective quasiparticle pot. 79−49940
diatomic molecule, overtone intensities in reson. Raman scatt. 80−48001
diatomic molecule, vibr. Green's function and two-photon dissociation, appl. to H_2^+ 80−28075
diatomic molecule in strongly interacting solvent, IR band shape, field theoretic methods appl. 79−27038
diatomic molecules, model pot. for calc. of multiphoton processes 77−508
Dicke model phase transition, thermodynamic Green's function method 80−5715
Dicke model with external fields, simple Green function approach, lack of phase transition 78−9353
dielectric crystals, externally deformed, phonon transport eqn. 77−27956
dielectric function, time-dependent Hartree-Fock formalism 79−69448
dielectric susceptibility, mol. cryst. with extended defects, exciton contrib. 77−55486
diffraction problem, non-homogeneous media, non-stationary problem 80−22211
diffusion of particle, scatt. length 77−13629
diffusion processes, general, path integral formulation 77−33844
dilute alloy, method of orthogonal operators 79−33254
dilute alloys, transitional and noble metal impurities in simple metals, electronic struct. 77−43528
dilute binary alloys, formation energy, lattice relax. and zero-point vibrations 78−83771
dilute binary alloys, formation energy, lattice relax. and zero-point vibrations 78−87646
dimensional anal. in renormalised perturbation theory 78−24950
dimensionally renormalised Green's functions, massless particles theories 77−13839
dimensionally renormalised Green's functions, massless particles theories 77−13840
1,5-bis dimethylamino pentamethinium perchlorate, refl. spectra calcs. 77−85154
Dirac distributions, perturb. of self-adjoint Hamiltonians, Green's functions and wavefunctions, scattering theories 80−62514
direct reactions, semiclassical theory, complex paths and uniform approximations 77−71244
dirty superconductors, time-depend. Ginzburg-Landau eqns. near supercond. transition temp. 80−70886
discontinuities across characteristic surfaces of field eqns. 79−93279
dislocation, thermal vibrs., mean-square displacement, double-time Green function technique 79−19345
dislocation anisotropic theory, isotropic limit, cryst. with dislocation pile-up 79−46656
dislocation displacement field in elastic half-space *(Russian)* 79−51107
disordered alloy, self-consistent boundary site approx. in cluster theories 79−19500

Green's function methods continued
disordered alloys, density of states, and their moments 77−11837
disordered chains, electronic props. 80−2363
disordered crystals, two-time Green's functions 80−6480
disordered electronic systems, spin interaction effects, loop expansion and exact relations among local gauge invariant modes 80−80221
disordered Heisenberg spin model, magnetisation calc. 80−60167
disordered lattice, phonon modes, lattice Green function expansion method 80−79900
disordered one-dimensional lattice systems, diffusion and hopping conductivity 80−59991
disordered one-dimensional system, electron density of states and Peierls transition *(Russian)* 80−29304
disordered semiconductors, resonance Raman scatt. 79−11419
disordered substitutional alloy, mag. props., Heisenberg model 79−38342
disordered system, elec. cond., tight binding approx. Kubo formalism 79−60778
disordered system, electron density of states asymptote in a random field 80−44489
disordered system, ensemble averaged Green function, analytic approx. 77−11842
disordered system, orbital mag. susceptibility of conduction electrons 78−76217
disordered system with n orbital per site, Lagrange formulation, hyperbolic symm., Goldstone modes 80−80222
disordered system with n orbitals per site, n=infinity limit 79−60768
disordered system with n orbitals per site 1/n expsn. 79−90999
disordered systems, coarse-grained quantities and short-range order 78−75787
disordered systems, short-range order and off-diagonal randomness 78−75782
disordered systems, systematic approach, averaged Green functions calc. 80−80150
distorted one dimensional system with bond disorder, electron density of states, CPA calcs. 80−24778
distributed thermocouple theory, electric pot. field, Green's function soln. 79−93138
distribution functions and Green functions *(Russian)* 78−65890
domain structure, theory, band model of ferromagnetism approach 77−80954
domain wall dynamics, eddy current dominated, and magnetisation losses 80−88778
domain wall velocity, damping parameter meas. from low field microwave excitations 80−34676
driven damped oscillator, path integral treatment 79−80457
dual string model, Green's function struct. 77−18243
dwarf stars, scaling hypothesis, relativistic statistics and critical mass 79−16960
dynamic Jahn-Teller effect in ESR spectra, Green's functions calcs. 80−84643
dynamic system, classical quantisation conditions with stochastic behaviour anal. 80−8922
dynamical properties of solid surfaces, analytic approach 78−71929
Dyson eqn., exact soln. for mean value of Green's function 78−4559
Dyson eqn. and Ward-Takahashi identities of closed time path Green's functions *(Chinese)* 79−80759
Dyson eqn. approx. anal. for Green's function mean value *(Russian)* 77−74201
(e,2e) molecular knockout reactions via electronic struct. calcs., Green's function methods 77−88577
early Universe, EM and gravit. Green's functions 78−73786
Earth crust viscoelastic deform. by finite quasi-static sources, Green functions 79−39686
Earth oscillations, split normal modes, theoretical amplitude and Green's dyadics 80−101341
earthquake aftershocks as Green's functions 78−44787
earthquake modelling in homogeneous half-space 79−12078
education, composite potential well, energy level determ. using Green's function factorisation theorem 79−97148
education, Schrodinger eqn. for free particle, wave packet spreading in coord. representation 80−17736
effective electron-electron interaction in a group-theoretical diagram technique 79−28303
effective fields on nucleus allowing 2p2h config., Green's function method eqns. 79−6361
Eguchi-Hanson instanton, TP inversion in quantum gravity, appl. to scatt. theory 79−58613
eikonal approximation, Green function and density of states in field of randomly distributed impurities 77−8052
elastic fracture mechanics problem, two-dimensional, anal. 79−23272
elastic half-space, epicentre solns. for pt. multipole sources 79−81798
elastic infinite plates clamped along inner curvilinear edges 78−38191
elastic plate of epitrochoid shape, transverse displacement 79−17220
elastic plates, semicircular, displacement due to concentrated force at a point, Green's function technique 80−58904
elastic spheroidal Earth, Green's function for deformation eqns. 77−81779
elastic surface waves, surface effects theory 79−90171
elastic surface waves at hexagonal surface and interface, thermodynamic and dynamical props. 79−69338
elastic system, composite, interface flaw, appl. of dynamic Green function method 77−84153
elastic wave interaction defects of finite vol. and defect mutual interactions 78−32676
elastically bent crystal, dynamical Bragg diffr. of X-rays 79−14639
elasticity, micropolar continua, static problems, nonhomogeneous eqn. of equilibrium, Green's functions and Fourier transforms 80−58905
elasticity, nonlocal theory, stationary boundary problems, reciprocity principle and Green's tensors 80−68046
elasticity, variational formulation of integral eqns. *(French)* 77−72181
elastostatic strip and wedge, Green's functions, bi-linear forms and eigenfunction completeness 79−97205
electric dyadic Green's function, direct derivation 77−14641
electric field dyadic Green's functions in source region 80−43229
electric field evaluation in source region using tensor Green's function 77−75363
electric potential problems, solution, appl. 77−82370
electrical conductivity of homogeneous materials, theory relating to Kirchhoff's method of determ. 79−64170
electrically and mag. polarised matter in waveguide, EM field, Green's function method 78−1123
electrodynamics, asymptotic estimates of higher approx. *(Russian)* 78−12584
electromagnetic diffraction, transient and time harmonic, by a semi infinite cone 78−5392
electromagnetic field problems, investigation of numerical soln. 80−14271
electromagnetic scatt., time depend., boundary value formulation, integro-differential eqns. 78−66726
electromigration, driving force, weak charge solutions 79−55917
electron+ion scattering, Schwinger's variational principle, Rydberg states 80−78713
electron conductivity in random pot., diffusive mode existence 79−65421
electron density of states of a crystal and infinite cluster 80−10850
electron eigenstates in ordered and disordered ensembles of scatterers 79−99466
electron energy states, anisotropic Green function method *(Russian)* 78−38998
electron gas, one-dimens., with backward scatt., soliton Green's functions 78−10386
electron gas with surface, Green function theory, exchange and correlation effects 77−8164
electron in coherent EM field, null-plane formulation, Volkov soln. expansion 77−13898
electron in Coulomb field, operator Green's function 78−46500
electron in random field in 4-ε dimensional space 78−47756
electron propagator theory for mol. electron binding energies and photoionis. intensities 80−47848
electron transfer, intramol., electron propagator method 77−34560
electron transport in anhomogeneous anisotropically scatt. medium, medium Green's function 80−27244
electron tunnelling, two band calcs., Gamow formula applications 80−54665
electron-atom scatt., polarisation potential 78−42228
electron-hole plasma, two particle state influence on dielectric function 79−56154
electron-hole system spectrum, in one-dimens. infinitely deep pot. well *(Russian)* 78−67944
electron-ion system, effective ion interaction and force consts. 80−65185
electron-positron system in mag. field, thermodynamic pot. 78−8341
electronic local density of states, determ. using cluster Bethe lattice method 77−11868
electronic structure of solids, appl. of fast self-consistent cluster calc. for large systems 79−82513
electronic structure of solids, singularities 78−10320
electrostatic, boundary value problem of four strips inside grounded cylinder 79−13862
electrostatic potential and derivatives of infinite length cylinders *(French)* 80−28140
electrostatic potential problems in anisotropic media, theorems development *(Spanish)* 77−71901
electrostatic two-dimensional problem anal. 77−31043
Eliashberg equations, soln. by means of N-point Pade approximants 78−6475
elliptical differential equation, harmonic functions generalisation *(Ukrainian)* 77−49560
EM beam in circ. cylinder, reciprocity theorem *(French)* 78−42260
EM exploration, target near dipping contact, response modelling 79−8595
EM field calculation using integral eqn. method *(Russian)* 78−82887
EM field in unstable medium, estimation of dyadic Green's function using random current source 79−94129
EM wave direct scattering from one-dimensional inhomogeneous media, anal. 79−10244
e.m. wave propag. problems 77−19139
EM wave scatt. by dielectric cylinder, new Green's functions and integral eqns. 80−48123
EM wave scatt. by grid of parallel cylindrical wires with finite cond. 80−53190
EM wave scatt. from dielectric infinite cylinder embedded into another 79−59620
EM waves near conducting boundary, multiple scatt. expansions and mode distribs. 77−42465
empirical parametrisation of electronic structure 78−91585
energy deposition of fast ions in plasma, Green's function calc. methods 79−14559
energy level calcs. for cryst. with vacancies or substitutional impurities *(Russian)* 78−56101
energy-representation, semiclassical Green's function 80−90692
equations of motion Green's function methods, higher order terms, ionisation pots. 80−52891
equations of motion Green's function methods, higher order terms, ionisation pots., CI comparison 80−52892
equations of motion-Green's function, third order contrib., appl. to N_2 77−65417
equations of motion-Green's function methods, wave function approach 77−65416
equilibrium characteristics in the condensed state with the nearest-neighbours interaction *(Russian)* 79−12726
ethylene, ionis. pot., Green's function method and CI calcs. 79−13839
ethylene, ionis. pots., Green's function method 77−14608
ethylene imine, ionis. pot., many-body Green's function method 77−67972
ethylene mol. Green's function Σ perturbation method for mol. calcs. 78−55123
ethylene oxide, ionis. pot., many-body Green's function method 77−67972
Euclidean Dirac field, local structure, Green's function method 80−68347
Euclidean Green functions, quantum fluctuations of instantons 79−26220
excitation energies in atomic and molecular electronic systems calc., using renormalised Dyson equation *(Japanese)* 80−83295
exciton absorption, linear impurity conc. approx., validity criterion *(Russian)* 80−49620
exciton energy levels, influence of exciton gas and electron-hole plasma 80−96795
excitons in electron-hole plasma, dynamical screening and self-energy 79−15093
excitons near hard walls, energy levels 79−78014
expansion into eigenfunction set 80−22205

Green's function methods continued
exponential functions, chiral and gravitational 79−97490
exterior linear elliptic problem, numerical method, appl. to 2-dimens. wave resistance 80−28485
Fabry-Perot, and confocal resonators, comparison of diffraction formulas 78−87077
face centred orthorhombic lattices, matrix elements 77−5767
FCC lattice, defect modes due to substitutional impurities, Green's function anal. 77−62600
FCC metals, dynamics of multiple interstitials and interstitial impurity complexes 78−75775
Feller eqn., generalised, boundary condition solns. 78−62167
Fermi glass, theory for localised electrons 77−39807
Fermi liquids at surfaces quasiclassical boundary conditions 80−4641
Fermi system, excitons in electron-hole plasma 79−90969
Fermi systems, review of methods in quantum field theory 78−8338
Fermi weak interaction theory, consistent renormalisation scheme, Yang-Mills theory parallel 78−66071
Fermion contribution to instantons 78−78079
fermion Green's functions, functional integral representation construction 79−21941
fermion system, two-body propagations with dynamic effective interactions 77−41896
fermion system, two-body propagators with dynamic effective interactions, s-channel 77−41897
fermion systems, quasipartic renormalisation of memory function approach for response functions 78−8345
ferrimagnet, uniaxial two-sublattice, energy spectrum, magnetisation, and crit. field, Green function method 80−25060
ferrimagnets, one-magnon light scatt., temp. dependence, two-sublattice systems 78−31061
ferroelectric, displacive, inelastic neutron scatt. cross section determ. 77−31737
ferroelectric crystal, displacive, effect of elec. field on thermal cond. 77−85002
ferroelectric crystal, optical absorpt. coeff. calc. 78−10851
ferroelectric semiconductor phase transitions, self consistent approach 77−52028
ferroelectric spontaneous coherent state transition, chaotic phases approx. *(Russian)* 79−4776
ferromagnet, anisotropic, Green-function theory 77−16025
ferromagnet, anisotropic, theroy of light scatt. 77−90161
ferromagnet, dipolar crit. temps. 77−89962
ferromagnet, dynamical props. of flat parallel domain struct. *(Russian)* 78−6499
ferromagnet, impurity spin critical dynamics 80−2593
ferromagnet, isotropic, second-order Green's function theory 80−2578
ferromagnet, itinerant, spin waves, appl. of self consistent many-body theory 79−73702
ferromagnet, itinerant electron, angle-resolved photoemission, temp. depend. of single-hole Green's function 80−76142
ferromagnet, magnon-phonon interactions, Heisenberg exchange red. 80−80494
ferromagnet, noncond., Green function, contrib. of bubble graphs due to dynamic and kinematic spin wave interactions 77−51894
ferromagnet, randomly anisotropic, long wavelength mag. excitations 78−84406
ferromagnet, S=1, variation of Curie temp. with small uniaxial anisotropy 77−85448
ferromagnet, singlet-triplet, Dyson eqn. derivation 80−107974
ferromagnet, surface and bulk nucl. spin waves, Green function formalism 80−70984
ferromagnet, tight binding model, surface magnetisation 80−103807
ferromagnet, uniaxial with arbitrary spin and second order single ion anisotropy 78−84379
ferromagnet, uniaxial with single-ion and exchange anisotropies, magnetisation in transverse mag. field 78−56277
ferromagnet, with liq.-like disorder, excitations 79−61084
ferromagnetic alloys, itinerant electrons, magnon stiffness const. 77−63155
ferromagnetic degenerate semiconductor, magnon spectrum near instability of homogeneous state 79−28516
ferromagnetic Fermi-liquid model, electron-impurity system hydrodynamics, elec. cond. 80−103835
ferromagnetic film, of cubic symmetry, depend. of Curie temp. on thickness and boundary conditions 78−19287
ferromagnetic polariton linewidths, theory 78−87918
ferromagnetic resonance, line width, inhomogeneous broadening, magnon scatt. 78−35043
ferromagnetic resonance line, uniform, at finite temps., dislocation broadening 78−19334
ferromagnetic s-d model, electronic spectrum struct., moments method 80−97052
ferromagnetic semiconductor, mag. polaron stability 80−96803
ferromagnetic slab, finite thickness, magnetostatic theory of response functions, appl. to Brillouin scatt. 79−61083
ferromagnetic slab, finite thickness, spin correl. functions 80−80522
ferromagnetic slab, light scattering from bulk and surface spin waves, theory 80−71389
ferromagnetic surface-rearranged thin films, spinwave spectrum, derivation from generalisation of Bogoliubov canonical transform. 79−69702
ferromagnetic systems, singlet-triplet, excitation spectrum, double-time Green's functions 80−84603
ferromagnets, random, large exchange interaction, Green function theory 78−6537
Feynman rules for lattice gauge theory of quark confinement, Green's functions, review 78−93850
field equations, higher order, Green's functions limit props. 77−34085
field problems in multilayer composites, produced by line charge 78−29875
film, electron energy spectrum allowing for arbitrary one-dimens. internal field *(Russian)* 77−69212
film, spherical, van der Waals' forces contrib. to thermodynamic props. 77−15724
film, spherical van der Waals' forces contrib. to thermodynamic props. 77−15724
film, surface density of states calc. within tight-binding scheme 77−55594
film deposition, adatom diffusion and capture by clusters, random-walk problem 78−2385
films, thin, quantised, electronic energy spectrum *(Russian)* 80−44688

Green's function methods continued
finite electron no. system, approx. Green's-functions algebraic formulations 80−47849
finite temp., dynamical pictures and causality 79−63144
finite temperature vacuum excitations for relativistic field theories with dynamical symm. breaking 77−5994
fluctuation EM field of infinite medium with spherical inhomogeneity, finite temp. Green's functions 78−1126
fluid dynamics, micropolar, potentials and Green's functions 80−96286
fluorite structured crystals, high temp. disorder and elastic consts. 78−30689
foreign gas broadening, translational heat-bath model, variational methods 78−9124
formamide, photoelectron spectrum, Green's function calcs., satellite lines 80−28061
formic acid, ionis. and photoelectron spectra, inner valence electrons 78−82784
free electron laser, quantum theory for strong fields 80−83583
free particle Green's function, Gaussian matrix elements 79−2667
fully symmetric nonlinear theories, Green's function methods, SCF theory 77−61180
$g\phi^4$ theory, strong coupling limit of Green functions, anharmonic oscillator appl. 78−78071
G-convolution of n-point functions in quantum field theory 80−18065
gas, one-dimens., of hard rods, exact nonlinear driven response 78−22447
gauge dependence of spectral functions 80−37191
gauge supersymmetry, spontaneously broken, quantum loops UV finiteness 79−21919
gauge theories, U-gauge Green's functions construction, with spontaneous symmetry breaking and Slavnov identities 79−235
Gel'fand-Levitan kernel for 3-D Schrodinger eqn. 80−36892
general quantum field theory, nonlinear program 77−10189
generalised axisymmetric Poisson eqn., separable cases, Green-Dirichlet problem in circle 77−22383
generalised density matrices and Wigners distribs. 77−82455
generalised Wilson expansions in dimensional renormalisation 78−86403
generating coefficients for lattice Green's functions, appl. to FCC cryst. 77−1185
generating functional for gauge-invariant Green's functions 79−63355
geoelectric sounding, controlled-source DC pot. problem by self-pot. Green's function 80−77136
glass melt, multibubble dissolution 80−81371
gluon operator coefficients in electroproduction 79−58926
Goldstone system with off-diagonal disorder, analytic Green's functions using pseudofermion approx. 79−60466
grain boundary drift diffusion under influence of stress fields 79−77835
graphite intercalation compound, interaction between one or two s orbitals *(French)* 80−65440
gravimetric tidal loading computation 80−89928
gravitational attraction between two quickly moving bodies, energy depend. 77−2597
gravitational multi-instanton scalar fields, Greens functions 79−85050
gravitational wave generation, postlinear formalism 78−114
Green's function, moving lossy media, transformation of wave eqaution 77−82398
Green's function in nonrenormalisable massless $\phi^6_{3+\epsilon}$ theory, removal of cutoff, vertex functions expansion 78−45772
gyrotropic medium, Green's function and field of moving charges 80−58445
Hamilton-Jacobi equation solns. in Coulomb pot. and quasiclassical approx. 80−46765
harmonic oscillator, three-dimens., Green's function of Schrodinger eqn. 80−73211
harmonic oscillator, time-dependent 80−8826
HCP lattice with substitutional impurity, defect Green's function and T matrix 79−42191
heat conduction, anisotropic medium homogeneous in cylindrical regions, steady-state anal. 77−58526
heat conduction, boundary value problems, soln. 80−79106
heat conduction, in monoclinic anisotropic system, various boundary conditions, temp. field soln. 77−58525
heat conduction in anisotropic media, anal. solns. for bounded regions 77−84117
heat conduction in axisymmetric body-duct configuration 79−32185
heat conduction in half-space with cutting, Green's functions of boundary-value problem *(Russian)* 78−18145
heat conductivity eqns., soln. of boundary value problems by Green's function method *(Russian)* 78−63267
heat conductors with randomly varying boundaries, Green's functions *(German)* 79−32188
heat equations, Green kernels and domain perturbation 79−68563
heat loss of internally heated body to peripheral flow, oblique derivative boundary conditions 79−72778
heat transfer in composite solids with heat generation 79−76949
heavily doped semicond., electronic sp. ht. and transport coeff., influence of band-tail parameters 79−14941
heavy ion optical pot., long range absorpt., from Coulomb distorted states and Green's functions 78−29494
heavy quark dynamics in non perturbative QCD vacuum 79−80795
Heisenberg, ferromagnet, nearly two-dimensional and nearly one-dimensional thermodynamic props., Green's function investigation 79−15275
Heisenberg anisotropic antiferromag., spectrum and correlation functions 79−28499
Heisenberg anisotropic ferromagnet, Bogoliubov inequalities, inhomogeneous dynamic susceptibility, single particle matrix Green's function 79−95564
Heisenberg anisotropic ferromagnet, collective Green function, longit. susceptibility *(Russian)* 79−65631
Heisenberg anisotropic ferromagnet, longit. correl. function, generating Green functions 78−6500
Heisenberg antiferromagnet, anisotropic, excitations at finite temp., CPA calcs. 79−95562
Heisenberg antiferromagnet, anisotropic, spectrum and correl. functions in spin-flop phase in generalized HF approx. 78−39283
Heisenberg antiferromagnet, Green function theory 80−107975
Heisenberg antiferromagnet, second order Green's function 78−43545
Heisenberg antiferromagnet, uniaxial, props. by Green's function method 77−85406
Heisenberg chain, dimerised, spin dynamics 77−20528

Green's function methods continued
Heisenberg ferromagnet, consistent linearised Green's function theory for $s=1/2$ 79−4685
Heisenberg ferromagnet, anisotropic, collective Green's function, dynamical RPA 80−70925
Heisenberg ferromagnet, biquadratic exchange, Green's function method, Hamiltonian and Curie temp. 80−15675
Heisenberg ferromagnet, cubic, with next nearest neighbour interactions, two-magnon bound states 80−70977
Heisenberg ferromagnet, Curie temp., decoupling of Green functions 77−12133
Heisenberg ferromagnet, diagram techniques for Greens functions with spin operators 78−91836
Heisenberg ferromagnet, disordered, pair effects in bond model 79−78290
Heisenberg ferromagnet, higher order corrections to spectrum 78−80222
Heisenberg ferromagnet, isotropic with biquadratic exchange 78−39344
Heisenberg ferromagnet, longitudinal dynamic susceptibility 78−64181
Heisenberg ferromagnet, spin waves at low temp., method of variational derivatives 79−24152
Heisenberg ferromagnet, spin-wave renormalisation, $S\geq 1$ 80−71070
Heisenberg ferromagnet, with biquadratic exchange 77−63060
Heisenberg ferromagnet, with biquadratic exchange interaction 78−34999
Heisenberg ferromagnet 80−25064
Heisenberg ferromagnet mixed crystal, mag. props. 80−34579
Heisenberg ferromagnet system, temp. Green's function sum rules *(Chinese)* 80−31678
Heisenberg ferromagnet with biquadratic exchange 79−38338
Heisenberg ferromagnet with biquadratic interactions 77−55653
Heisenberg film, spin-one isotropic, quadratic interactions, quadrupolar-paramag. T_c 78−64210
Heisenberg film, spin-one isotropic, with biquadratic interactions, phase transition 77−20611
Heisenberg isotropic ferromagnet, first-order Green's function theory 77−36046
Heisenberg magnet, correlation theory of static and dynamic properties 80−65765
Heisenberg model with one-ion anisotropy, closing relns. for Green's functions 78−2642
Heisenberg spin-$^1/_2$ ferromagnets, 1st order Green's function theory 78−72323
Heisenberg-biquadratic and Blume-Emery-Griffiths interactions dipolar and quadrupolar susceptibility 78−76257
Helmholtz's reciprocity theorem, invalidity for scalar wave field propag. 80−31527
Helmholtz and Green's theorems, integral eqn. methods, static equivalence principle 78−57090
Helmholtz eqn. within wedge 79−9130
heterogeneous dielectric, Dirichlet problem, Green's function method 78−37782
heterojunction superlattice, energy spectrum 78−6259
heterojunction superlattices, Green's function of electron in periodic field 80−49857
hexagonal continuum infinite half-space, elastic Green's function 79−63038
hexagonal crystal, surface contrib. to low temp. sp.ht. 77−1233
HF approximations, thermodynamic Fermi systems 80−4642
Higgs-Kibble mechanism, superfield theoretical treatment 78−89616
high density plasma interaction with a strong EM wave, Green's function method calcs. 80−48885
homopolar crystals, imperfect, lattice dynamics 80−59601
Hubbard and similar models, functional Fourier transform 80−84416
Hubbard antiferromag. semiconductor, electron correlations, weak coupling 78−67969
Hubbard model, conc. depend. of Hall and Verdet coeffs. 80−80240
Hubbard model, electrical conductivity calculation, dielectric function and plasma oscillations 78−64020
Hubbard model, electron correlation, self consistent theory 79−60673
Hubbard model, extended, optical absorpt. spectra 77−20812
Hubbard model, functional derivative study, perturbation method and first-order approx. 77−43465
Hubbard model, functional derivative study, self-energy correction, self-consistent eqn. 77−43466
Hubbard model, Green's function, functional-derivative study 80−75483
Hubbard model, Green's function determ. using group theoretical diagram method 77−62791
Hubbard model, quasi-particle energy in weak correlation regime 79−28305
Hubbard model, Ward identities, particle number conservation, analytical structure of self energy 78−79913
hybrid integral eqn. method, appl. to ship waves 79−32540
hydrogenic Green's functions, reduced, power moments, and 2nd-kind Green's functions 79−85891
hydrogenic one particle Green's function power moments, 1s-type orbital reduction 78−9051
III-V semiconductor surfaces and interfaces, Green's function technique, tight binding approx. 80−49855
image charge pot. at interface of two semi-infinite media, Thomas-Fermi soln. 79−87155
image methods for constructing Green's functions and eigenfunctions for domains with plane boundaries 80−94979
imploding wire array, mag. field study 79−55021
impure crystals, vibrs. in average local information transfer approx. 79−46774
impurity cluster pairs, lattice localised modes 79−33058
impurity electron level position depend. on interaction with bands, Wannier representation calcs. 80−54653
impurity states, calc. using Green's function method, non-orthogonal basis set *(Russian)* 79−15119
inelastic positron scatt. in electron gas, plasmon excitation 80−92843
infinite cracked isotropic sheet, under symmetric loads, Green's functions for stresses, stress intensity factors and displacements 80−99967
infinite finite temperature baryon matter, Green's function formalism, quantum correction 78−13000
infrared behaviour of electron Green's function, renormalisation group use 79−35977
instantaneous Coulomb interaction in SU(2) Yang-Mills QCD 80−396
instantaneous Coulomb interaction in SU(2) Yang-Mills QCD 80−22574
instanton calculations using dimensional regularisation 79−2908
Green's function methods continued
instanton Green functions and tensor products 79−54252
instanton quantum fluctuations, in 2-D nonlinear theories *(Russian)* 80−4868
instantons, gravitational, flavour currents of QCD, Green's functions, foam-like structure of space-time 80−62825
insulator-metal transition, electron-phonon interaction, electronic transport props. 77−89702
insulator-metal transition, role of electron-phonon interaction in narrow-energy-band solid 77−89701
integral characteristics of the electron structure of crystalline surfaces 78−64078
interacting Bose gas, T=0K, self-consistent description 80−80015
interacting electron system, orthogonality catastrophe 80−6757
interacting many-level system, thermodynamics, from RPA Green's functions 78−43549
interface state models, appl. of Green's function matching procedure 77−59320
interface-atom mean-square displacements, elastic continuum theory 77−89632
interfaces, multiple, Green's functions, factorisation method 80−54760
ion impact on solids, multiple scatt. at small angles, approximation formula *(Russian)* 77−4706
ion source, of mass spectrometer, EI/FI modes pot. distrib. calcs. 77−74553
ionic crystal, anharmonism effect on exciton peak broadening in absorpt. spectra *(Russian)* 80−97317
ionic crystal, surface lattice dynamics, Green function approach 77−31865
ionisation potentials, sum rule, Manne Åberg theorem connection, many body Green's function formalism 80−27930
Ising field theory, 2-D, $T<T_c$, three point function string structure 79−270
Ising field theory 2-D, $T<T_c$, Green's function strings in n-point functions 79−271
Ising field theory in mag. field, cut breakup in two point function 79−272
Ising model, transverse field dynamic behaviour 78−22814
Ising model with transverse field, commutator and anticommutator Green functions 78−76211
Ising model with transverse field, method of two-time Green's functions 80−2543
Ising model with transverse field in paramagnet 78−68138
Ising paramagnet in transverse field 77−8260
Ising transverse paramagnet, Dyson eqn. 79−82736
isotopically disordered ferroelectric cryst., thermal cond. 77−76628
isotropic elastic strip, vibration excitation by surface and volume forces 79−32355
isotropic Heisenberg ferromagnet, localised spin-wave modes, biquadratic exchange effects 77−51896
isotropic strip with transverse crack, Green's function for stress intensity coeff. *(Russian)* 77−35093
itinerant electron ferromag., Ward-Takahashi identities, zero temp. case 79−73669
itinerant ferromagnet, effect of planar defects on electronic struct. and mag. ordering 79−99672
Jahn-Teller cooperative T−(e+t) systems, pseudo spin thermal cond. 80−34406
Jahn-Teller cooperative T-(e+t) system, thermal cond. 80−70479
jet noise source distrib., from far-field cross-correlations 77−84039
Josephson contacts with semicond. layer, critical current *(Russian)* 79−99661
Jost function and S-matrix for pot. of general form., Schrodinger eqn. soln. in hypergeometrical functions *(Russian)* 78−81870
Jost solutions and Green's functions for the three-dimensional Schrodinger equation 79−71277
junction growth mechanism during friction *(Japanese)* 79−32391
Kerr metric, stationary axisymmetric test fields 77−41515
kinematical multi-level exciton schemes 78−39028
Klauder augmented quantum field theory, ϕ^4 model 78−78094
Klauders augmented quantum field theory, Green's function formalism, Yukawa model, σ-model 79−6277
Klein-Gordon charged particles, perturbation theory for non-equilibrium stat. Green's functions 80−31994
Klein-Gordon particles, charged, quantum kinetic theory, Feynman rules and thermal eqn. 80−57177
Kondo lattice and Kondo effect 79−78312
ladder model of QCD, hadron struct. 80−37213
ladder vertex function and screened pot. rel. to Green's function calcs. 77−5754
large molecular systems, local pot. surface and charges, parametrisation scheme for quantum mechanical computation *(German)* 80−18793
Lehmann-Symanzik-Zimmermann formulas in a gauge-independent path-dependent formalism 79−21942
Levinson theorem and its generalization in relativistic quantum mechanics *(Chinese)* 79−92988
light diffraction, Ewald extinction theorem and Green function method for semi-infinite dipole cryst. 79−23683
light double scattering from Brownian particles, depolarised correlation function 77−10839
light wave propagation in lens systems 80−78947
light-cone finite normal products 78−86408
limit $\hbar\to 0$ in quantum field theory, rel. to scatt. amplitudes, differential cross section *(Russian)* 77−61202
linear and homopolar electric and magnetic fields calc. *(Russian)* 77−53745
linear conductor, localized mag. moment formation and one and two impurity sites 80−50087
linear crystal with thermal gradient, electronic Green's function 78−64019
linear equation associated with solitons, Green's function using scatt. theory 78−4507
linear hemitropic micropolar isotropic elastostatics 78−49661
linear physical field, propagator expansion in power series of coupling constant 79−30647
linear second order equations with periodic coefficients *(Russian)* 79−58528
linear second order systems 79−12578
linear stochastic systems, field quantum theory dynamics *(Russian)* 78−16722

Green's function methods continued
Liouville-Green approximation, general connection formulae in complex plane 79−9083
Lippmann-Schwinger eqn., trinucleon bound-state problem 78−33156
liquid, mol. assembly, iterational soln. to integrodifferential eqn. 79−77473
liquid metal, electroconductivity in mag. field *(Russian)* 78−39085
liquid metal, electron momentum density, perturbed Green's function method 78−60052
liquid metal, tight-binding model, effective medium approx. 77−15756
liquid metals, strong binding model, electronic density of states, Green's function calcs. *(Russian)* 80−70111
Lloyd formula and muffin-tin CPA local density of states 80−70577
loaded thin circular plate stability criterion 78−77700
local bound states, existence conditions in weak fields, stationary Schrodinger eqn. calcs. 80−36904
local formalism for very large bonded systems 77−4313
local impurity states, existence, levels, Green function, tight-binding calcs. 78−67981
local method for heat conduction and fluid flow problems 77−79420
localised crystal, quantum theory, causal Green's functions 79−42338
localised defects in solids, self-consistent approach to electronic struct., appl. to Si vacancy 79−78043
Lorentz invariance of quantum field theory of electric and mag. charge 78−33010
Love waves, dispersion eqns. in transversely isotropic layer on isotropic elastic material 79−14308
low frequency asymptotics, reduced description of nonequilibrium states *(Russian)* 77−5760
lung, analytic model, Green's function for convection-diffusion eqn. 78−11684
Luttinger model, preservation of sum rules for 1p-Green function 77−9956
macromolecular force constants refinement in normal coord. calcs. 77−31035
magnetic Debye crystal, with magnon-phonon coupling, crit. changes in vibr. modes 79−95094
magnetic dilute alloy, two-impurity spin correl., self-consistent treatment 77−24672
magnetic electron gas induced by van Vleck ion, spin polarisation 79−56176
magnetic film, surface spin waves and surface anisotropy effects at finite temp. 79−78452
magnetic impurity in metal, Ward relation between vertex function and one-electron Green's function 79−61052
magnetic system with cryst. field pots., Green's function theory and high temp. series expsn. 80−15673
magnetic systems with dipolar and quadrupolar pair interactions 77−63222
magnetisation of uniaxial ferromagnets with single ion anisotropy in transverse field 77−32143
many body problems, real time Green's function 78−57855
many body systems and functional integrals 79−80506
many fermion energy calculations 78−66238
many-body problem in relativistic meson field theory, book contrib. 80−357
many-particle Green diagram, group theory anal. 78−28992
many-particle system, generalised diffusion processes 78−73942
mass spectrometer sample line diffusion processes 78−64907
massive propagators in instanton fields, Green's functions, quantum chromodynamics 79−49390
massive spin-1 particles in external symmetrical tensor field, quantisation and noncausality 80−105790
massless QCD, instanton contribs. to fermion Green's functions 79−22037
massless QED, appl. of conformal symmetry for calc. gauge invariant Green's functions 79−63394
massless spinor field/massive pseudoscalar field interaction, mass perturbation around exact soln. 79−63368
massless Thirring model, saturating field configurations for two point Green's function 79−35923
matrix Pade approximants, applics. in pot. theory 79−78
maximal variational principle for transport theory 78−62166
mean field perturbation theory, path integral formulation 78−12803
mechanical response and the initial value problem 79−2620
metal, BCC, chemisorption of monolayer of atoms, charge in density of states determ. 77−47682
metal, Dimple, temperature dependent multi-ion interactions 78−22691
metal, effects of large scale voids on thermal magnetoresist. 80−10946
metal, electron field emission, energy distrib. 77−1788
metal, FCC, (100) surface, chemisorption-induced interaction between electronic levels of two-level adsorbate 80−39644
metal, quasimagnetic impurity, exact solution of Wolff's model 78−56105
metal, surface relaxation, lattice statics calc. 78−63925
metal crystal with and without surfaces, asymptotic displaced charge round impurities 79−95364
metal surface, dynamic image pot. for tunnelling electrons 80−49874
metal surface, narrow band, self consistent model calc. of electronic states 78−95333
metal surface, with substitutional disorder, electronic density of states 78−23145
metal surface electronic density of states, random distribution of impurity atoms 78−6424
metal surface region, electrostatic energy and screened charge interaction for different Fermi surface shape 80−70631
metal surfaces, electronic spectrum of ordered monolayers 77−85293
metal-insulator transition, Hubbard model, Poisson approx. to functional approach 80−96790
metal-insulator transition, Ising model, for transition temp., Green's function calc. 79−15084
metal-metal interface, simple, electronic props. 78−72234
metal-vacuum-metal point contact junction characts., Green's function calc. 80−103744
metals, amorphous and liquid, electronic states, average spectrum 80−49579
metals, CFC, frequency spectra, and correlated spectral density between bulk atoms 79−19330
metals, dynamical props. of point defects, book contrib. 80−103317
metals, HCP, vacancy and interstitial config. 79−65071
Green's function methods continued
metals, phonon limited resistivity, anharmonicity, Debye Waller factors, multiphonon terms 80−49691
metals, point defect diffusion controlled reaction theory, book contrib. 80−103318
metals, point defect relaxation volumes, dipole tensors and Kanzaki forces 80−54222
methyl radical, hyperfine coupling, in ground and excited states, Green's function calcs. 77−6692
microelasticity, construction of static and dynamic Green tensors 77−27470
micropolar Cosserat media, theory of disclinations 78−38698
micropolar thermoelasticity, Green formula for infinite domain with cavity 79−30241
microstrip anisotropic electrostatic field problems, Green's function technique 78−70998
microwave bundle transmission, plasma column, dielectric const. and r depend. *(Russian)* 77−3983
MIM junction, tunnelling, tight-binding Green function calc., disorder effect 78−10577
MIS structure, calc. of surface electron states 80−15611
mixed crystal, line profile of absorpt. and Raman spectra, calc. 78−48183
mixed crystal, theory of lattice vibr., conditionally averaged Green functions 77−1190
mixed valence metals, elementary excitation damping, electron specific heat 79−95180
mobility edge, analogy with spin glass problem 77−85164
mobility edge behaviour, particle in random potential, divergence of Green's function 80−34409
mobility edge problem, continuous symmetry 80−10939
molecular aggregates, optical spectra, near strong coupling limit, Green's function model 77−83774
molecular crystal, dipole plasma oscillations, Bose-Einstein condensation of excitons *(Russian)* 78−84155
molecular crystal, dipole plasma oscillations, scattering of light 79−33723
molecular crystal, quasi-one-dimensional, exciton wave scatt. by impurity 79−78012
molecular crystal, two-phonon resonances, bound states absorpt. coeff. 78−47486
molecular crystal, two-phonon resonances, bound-states, general theory 78−47485
molecular crystals, Raman scatt. from external orientation vibrations 79−95776
molecular crystals, weakly disordered theory of time evolution of exciton coherence 80−65455
molecular electronic continuum, reson. Raman scatt., anal. model 77−65475
molecular electronic struct., UHF Green's function method, appl. to allyl-radical 77−61684
molecular force field determination, Green's function method, ambiguities 80−960
molecular ground state correlation energies, Green's function calcs. 77−75061
molecular resonant Raman scatt., strong vibronic coupling limit, Green's function 77−83605
molecular vibrational analysis, Green's function method, mixing parameter matrix determ. 79−31494
molecule, one-particle Green's function with multiconfiguration reference states 79−31363
molecule, relativistic Green function 77−20214
molecule, XY_2 type, chem., perturbation of force field 79−76417
molecules, electron coincidence ionisation spectra, Green's function anal. 79−31714
molecules, eqn. of motion-Green's function and config. interaction methods comparison, appls. 80−47841
molecules, ionisation pots., electron affinities, Rayleigh-Schrodinger and Green's function calcs. 77−75075
molecules, vertical valence ionis. pot., many-body Green's functions 78−22051
Molien function of a symmetric group 80−8857
moment method for solution of two Pocklington type integral equations 78−55279
momentum autocorrelation functions from classical Green's functions. [Teaching] 78−61976
momentum matrix element calc. using Green's function method 77−1351
monotony properties and inequalities for Green's functions for multipoint boundary value problems 79−30202
Monte Carlo method for quantum hard spheres radial distrib. function 79−54005
Mossbauer impurity atoms trapped by vacancies, resonance energy shift 80−25265
Mossbauer spectrum, magnetic ion exchange interaction effects 79−95696
Mott's formula for thermopower and for Wiedemann-Franz law 80−84462
moving lossy media, transformation of wave equation for telegraphy 77−82398
multilayered elastic body embedded in infinite material, acoustic wave scatt. theory 80−69584
multiphoton excitation, collisionless, of large mol. kinetic eqns. 79−54914
multiple scattering of classical EM waves by fixed dielectric obstacles, Fredholm's method 78−71008
multipoint boundary-value problem, maximisation of Green's function 77−37733
multishell method, exact calc. of cluster in effective medium 78−10319
$(N \pm 1)$ particle system resonances dilated Green's function approach 79−71295
N distinguishable particles, rel. to single-particle density matrix, perturbation expansion 80−54635
N nonrelativistic pairwise interacting particle scatt., $(N \geq 4)$, soln. uniqueness 79−75379
N-body scattering equation approach using pole decomposition of Green's function 80−62540
n-point functions in local quantum field theory 77−13877
naphthalene $^1B_{2u}$ resonance pairs, energy denominator depend. of excitons absorpt. 77−39783

Green's function methods continued
narrow gap semiconductor, resonant scatt., Green's function method and CPA 80−6827
narrow-band solids, real and imaginary-time Green's functions for HF and narrow-band limits 79−56112
neutron diffusion, multidimensional, nodal Green's function method 79−59106
neutron diffusion theory, angular effects in toroidal diffusion, one-group homogeneous diffusion model 79−22351
neutron total cross section fluctuations, shell model approach using Greens function, resonances 79−22283
neutron transport problems in spherical geometry 77−54277
noble metals, electronic props. of dil. impurities, exact Green function treatment 77−62856
nodal Green's function method for multidimensional neutron diffusion calculations 80−47547
noise active suppression, Green's operator for nonsteady problem 77−27426
non-Abelian gauge theories in a background field, Green's functions 79−75689
non-Abelian quark-gluon theory, energy-momentum tensor 77−38122
non-homogeneous elastic medium, sudden twisting of penny shaped flow 78−87302
non-standard perturbation theory for Green functions, nuclear spin eqns. appl. *(Russian)* 79−45
nonequilibrium superconductors, microscopic and Boltzmann eqn. approach 80−15649
nonlinear scalar interactions, 1/N expansion 78−16903
nonlinear singular perturbation problem on a semi-infinite interval 78−94631
nonperturbative Green's function approach to quantum field theory 77−34079
nonpolar fluid, excessive electrons near crit. points 80−92836
nonpolar molecular crystal phonon sidebands, Green's function mol. model 79−37779
nonrenormalisable massless $\phi^6{}_{3+\epsilon}$ theory, renormalisation of regularised theory 78−45771
nonrenormalisable model, non-cutoff Euclidean Green's function in four dimens. space-time 79−21898
nonrenormalizable quantum field models in four-dimensional space-time 79−110
nuclear compound state g-factors and moments of inertia, temperature Green's function method *(Russian)* 77−74757
nuclear energy level single-particle strengths 77−41875
nuclear matter, dispersion relations, HF method for hard core interactions *(German)* 78−54713
nuclear matter, thermal conductivity calc. based on relativistic quantum field theory 79−75886
nuclear matter calculations, Brueckner and Green's function theories, ground state props. 78−8750
nuclear multiple scatt. theory, spectator expansion of full Green's operator 78−17162
nuclear reactor, coupled cores, calc. of buckling variation and neutron flux, Green's function method 78−74421
nuclear relaxation, low temp. stimulated by paramagnetic impurity 79−33563
nuclear single particle states 77−30533
null plane quantum field theory, two-time Green's function props. 78−93
$O(N)\psi^4$ interaction, strong coupling limit, rel. to renormalizability of chiral field 78−386
off shell scattering amplitude, S-matrix, pot. scatt., Mittag-Leffler expansions of Green's function, convergence 78−73874
off-diagonal disorder, exactly solvable 77−80719
one-dimensional antiferromagnet, with antisymmetric exchange, Green's function theory 79−15290
one-dimensional conductors, libron effects on electron spectrum, theory 80−96854
one-dimensional crystals, matching conditions, Bloch functions, logarithmic derivatives 80−15475
one-dimensional electron system, distorted, dynamical elec. cond. calc. 80−59962
one-dimensional electron-phonon system, renormalisation *(Russian)* 78−43314
one-dimensional Frohlich model dynamics, Green's function anal. 80−20170
one-dimensional model with four-fermion interaction particle mass *(Russian)* 77−41781
one-dimensional random Glauber model, magnetisation relax. 80−80523
one-dimensional sine-Gordon system, kinks 80−46969
optical dispersive resonators with system of reflective gratings *(Russian)* 80−96029
optical fibres, step index, mode conversion due to scattering from off-axis inhomogeneity 80−10045
optical waveguide, scattering from arbitrarily located inhomogeneity 78−87161
optical waveguide mode conversion analysis appl. 77−27344
optically anisotropic media, Green's function *(German)* 80−93255
orbit determination for cosmic object, Green's functions appl. 80−61992
orbital magnetic susceptibility, effects of impurities 77−47962
order-disorder antiferroelectric, simple model dynamics, diagram method formulation *(Russian)* 80−40070
ordered adlayers, density of surface states, Green's function calc. method 77−85291
ordered adlayers, electronic struct. 79−38142
ordered overlayers, on FCC metal surface, electronic struct. calcs. 79−60906
ordering solid solution, many particle correls. coupled Green function eqns. *(Russian)* 77−72675
oriented orbitals, photoemission cross-sections, surface Green function formalism 80−93453
$P(\phi)_2$ gauge invariant massive theory 78−41403
Pade approx. and low-energy Lagrangian field theory 77−61220
paramagnet, electron state density for narrow-band model with Coulomb interaction 80−10852
paramagnet, velocity of sound, temp. depend. modification due to spin-phonon interaction, phonon relax. 78−19303
partial wave, use in Schrodinger equation for Dirac bubble potential 79−80456
particle-hole propagator, order analysis 77−38602
path integral formalism, barrier penetration effects on wave functions and energy spectrum 78−62117
path integral quantisation in nonrelativistic quantum mechanics *(Japanese)* 79−9138
Peierls systems with dil. impurities, microscopic theory of pinning effect 77−15837
perovskites, d-band, surface electronic props., π-bands exam. 79−38145
perturbation theory as effective mass formalism 78−28915
perturbation theory for strong interaction, appl. to molecular crystals *(Russian)* 77−15528
perturbed Hartree-Fock calculations, with reduced Green's functions, theory 77−14338
phase space Green's function, using Wigner operator eigenfunctions and eigenvalues 78−24728
phonon dynamics 78−79704
phonon scattering at multilevel impurities, dispersion, damping, Green's function calc. 79−14892
phonon scattering by paramag. ions with S=1 in cryst. field of uniaxial symm. 77−76496
phonon scattering by paramagnetic ions, Zeeman levels in absence of zero field splitting 77−15508
phonon-magnon bound state, temp. depend. 79−78349
photoelectrons in crystals, scatt. by impurity centre, multipole wavefunctions 79−42490
photoemission, external, many-body apsects 78−72703
photon propagator and pair production in steady electric field *(Russian)* 79−9320
piezoelectric photoacoustic detection, theory and expt. 80−90904
piezoelectric semiconductors, acoustic phonon-conduction electron interaction, Brillouin scatt. theory 77−40255
piezoelectric surface waves on semiinfinite crystal, asymptotic expressions 78−51812
piezosemiconductor film, surface-mode acoustic wave amplification 79−46907
planar thermoelastic contact problems, Green's function for exterior contact 80−38350
planar thermoelastic contact problems, Green's function for interior contact 80−38351
plasma, cyclotron harmonic absorption via the Green's function for the mode conversion-tunneling equation 78−75296
plasma, immersed H elementary excitation spectrum, exchange and polarisation effects 80−43892
plasma, inhomogeneity spreading in weakly ionised current-carrying plasma 78−71445
plasma, Langmuir turbulence, large-scale, renormalisation group method 80−38650
plasmas, lifetime and level shift of bound states 77−62331
plasmon-plasmon interaction in many-electron system, equation of motion approach 79−87052
plasticity equations, new functions framework *(French)* 79−21549
plates, thin rectangular elastic, response using Greens functions 80−1424
point defects, basis sets for study using Green's function methods 79−90994
point defects, elastic interactions in semi-infinite medium 80−39146
point force soln. for infinite transversely isotropic solid 77−45701
Poisson's equation for isolated source distribs., computer soln. using finite mesh, Green's function 78−35
polar crystal, hot electron transport, eikonal approx. for energy loss 77−1426
polar crystal, hot electron transport, loss to single phonon modes 77−1427
polar semiconductor, TO phonon-helicon coupling 79−73539
polariton Fermi-resonance, EM wave dispersion 80−2344
polarization Green's function with multiconfiguration self-consistent-field reference states 80−37724
pollution dispersion-convection equation, soln. for bay with currents 77−91157
polycrystalline material, scatt., lattice representation 78−65774
polyethylene, perdeuterated, skeletal vibr. spectrum 78−23445
polyethylene molecule, fractured, local electron level calc. 80−14263
polymer, defect solid, local and resonance vibrations, appl. to deuterated polyethylene 79−99287
polymer, vibrational spectra of chain, Green's function anal. 78−18724
polymer, vibrational spectra of chain, Green's function anal., Fourier method for perfect infinite chain 78−18725
polymers, adsorption of molecules, Green matrix local impurity SCF calcs. 80−92778
polypeptides, unordered, circular dichroism, Green operator method 77−14467
Pomeron propagator representations 77−10199
post yield solutions for fracture mechanics analyses of cracks emanating from elliptic holes 79−68643
potential method appl. in mechanics 78−16634
potential problems, non-local, Perey effect, WKB method 80−68077
potential problems, numerical solution, integral equations without Green's function 78−20950
predissociating harmonic oscillator, relative line widths and level shifts 80−23469
preequilibrium decay models and quantum Green's functions 79−9542
prolate spheroidal models of humans in near field of short electric dipole, irrad. 80−104639
proximity-effect sandwiches, exact double-layer Green's function 79−1646
pseudoparticle fields, propagation functions 78−54556
pulsed field, due to electric dipole and perfectly conducting wedge 77−54652
QCD_2, fermionic Green function and functional determinant, closed representation 80−13269
QCD_2, massless, fermionic Green's function and determinant 80−22560
QCD, Green's functions for composite particles 79−85262
QCD, two dimens., renormalisation group functions 78−29242
QCD vacuum, effects on hadronic currents, instantons, e^+e^- annihilation and precocious scaling 79−332
QED, A_0=0 gauge, propagation of fermions 79−71669
QED, conformal-invariant, Ward identity of dilation current 80−68401
QED, Green's function in external elec. field and combination with mag. field and plane-wave field 80−101964
QED, renormalisation constants, small mass behaviour 77−2780
quadrupolar systems, excitation spectra from Green's function methods 78−56278
quadrupolar-coupled quasi-Heisenberg system, Green's function theory of phase transitions 79−38340

Green's function methods continued
quantum chemistry, electronic struct. calc., improving Σ perturbation approach 79−13642
quantum dynamics, sensitivity anal. 79−67178
quantum effects in systems with accelerated mirrors 80−22508
quantum field theory; scalar field interactions, in Green's function formalism 77−57436
quantum field theory, coupling const. dispersion relations 77−45987
quantum field theory, derivatives of the renormalisation consts. 77−65111
quantum field theory, Euclidean approach in curved spacetime, functional anal. 80−27181
quantum field theory, lattice-limit definition of functional integrals 80−27396
quantum field theory, modified renormalisation conditions 80−9089
quantum field theory, nonperturbative generating functionals for Green's functions 80−73588
quantum field theory, $P(\phi)_2$ Green's functions 77−10160
quantum field theory, relativistic, reconstruction of local observable algebras from Euclidean Green's functions 78−54522
quantum field theory of solids, book 77−31922
quantum field theory on cone, Green functions, diffusion kernels 77−18161
quantum fluctuations and particle struct. in field theory model 79−30659
quantum gauge anomalies axial vector current derivation method calcs. *(Russian)* 80−62863
quantum gauge supersymmetry, props. of globally supersymmetric Green's functions 79−63352
quantum liquids and crystals, computer modelling 80−54472
quantum mechanical eqn. of Kadanoff and Baym, time reversal noninvariance 79−17332
quantum mechanical many-body problem, vertex function and crossing symmetry 80−62515
quantum mechanical particle in random potential, inverse participation ratio in $2+\varepsilon$ dimens. 80−36908
quantum physics, Green's functions, book 79−65147
quantum process probability in external gravitational fields, Green's function calcs. 80−36931
quantum statistical mechanics, thermodynamic Green's functions, eikonal approxs. 77−9958
quantum statistical Monte Carlo method, Green's function path integrals with hard boundaries 79−67223
quantum system, intermediate states spectrum, Sturm expansions of Green's functions 79−9132
quantum system, normal phase-space coords. 77−45738
quark currents, fermion collective motions, Green's functions 79−93348
quasi-one-dimensional electron-phonon system, electron jump effect on phase tansition *(Russian)* 80−92673
quasi-one-dimensional solid, CDW distorted, macroscopic dielec. function 80−39515
quasi-two-dimensional dirty superconductor, nonstationary Josephson effect *(Russian)* 80−100556
quasipotential eqn. for wavefunction, QED derived by Fock-Podolsky method 77−65127
R-matrix coupled channel propagation equations 79−54273
radial reduced Coulomb Green's function 80−31559
radiative heat transfer, integral theory with anisotropic scatt. and general boundary conditions 78−32339
radiative transfer albedo problem in inhomogeneous isotropically scatt. atmospheres 80−36398
radiative transfer in noncoherent anisotropically scatt. plane-parallel slab *(Russian)* 78−61723
radiative-conductive heat transfer in plane-parallel layer 78−22256
Raman excitation profiles and mol. spectra synthesis, vibronic and exciton-in-mol. theory 78−42076
random dielectric, mean pot. and field 78−55271
random systems, localisation 80−80218
random-walk theory and correl. functions in classical statistical mechanics 77−5768
randomly driven system, strong coupling expansion for classical statistical dynamics 80−105568
rare earth metals, electronic struct., Hubbard's alloy approx. 79−73665
Rayleigh wave attenuation by point defects 79−73251
reaction-diffusion problem, nth order, asymptotic anal. 79−11764
reactor boundary changes, generalised perturbation theory 78−4980
reactor heat conduction and fluid flow, local Green's function method for initial value problems 79−89359
reactor noise, neutron multigroup theory, calc. of second order correl. functions *(German)* 79−89390
Reggeon calculus, asymptotic behaviour, quantum corrections, above critical intercept 77−45990
Reggeon field theory, ordered phase, Pomeron Green's function definitions 78−4807
Reggeon quantum mechanics, Hamiltonian formulation, S-matrix, pomeron Green functions 78−16951
relativistic composite particle scatt., quasipotl. approach 78−404
relativistic free-electron in uniform mag. field, Green's function of Dirac eqn. 80−18098
relativistic KKRZ theory of energy bands of heavy solids 79−82512
relativistic two-body problem, 3-D formulation in terms of rapidities 78−49985
renormalised perturbation theory, model of 3-D nonlinear field, free of UV divergences 78−54567
renormalization in a symmetry-broken theory 79−93291
resolvent operator expansion, generalised method, Schrodinger eqn. soln. appl. 80−86126
resonance Raman scattering and luminescence of excitons in self-trapping process 80−20689
resonant Brillouin scattering via exciton-polaritons, theory 80−50353
resonant far IR absorption by impurities 78−6715
resonant tunnelling current for general junction pot. barrier 79−51656
Rindler, de Sitter and Schwarzschild spaces, Greens function thermal props., renormalisation 79−2686
ring plates, stability under compressive stresses *(Russian)* 77−54873
RKKY interaction and conduction electron polarisation, Green's function and multiple scatt. formalism 78−91859
Robertson-Walker universe, finite temp. effects 78−45440
rotating fluid, waves due to sources and internal boundaries 79−37323
rotating system, finite temp. QFT 80−73599

Green's function methods continued
rough surface, dispersion relation for surface plasmons, quantum mechanical approach 78−72099
RPA and pairing vibration approximations, multiple basis set calcs. 77−5755
Saint-Venant torsion problem, classical, integral and functional eqns. 78−57780
SAW attenuation due to thin film finite conductivity and air loading 77−31154
SAW interdigital transducers, quasi-static anal. 80−69621
scalar electrodynamics, Green's function perturbative expansion higher orders 77−87923
scalar field with isospin, IR asymptotic behaviour of one fermion Green's function 79−89067
scalar Helmholtz equation, integral formulations 78−36796
scalar macroscopic fields in anisotropic stratified media, Green's functions 79−58544
scalar microwaves propagation in medium with severe random nonuniformities 80−69297
scalar QED, Green's functions in external elec. field *(Russian)* 79−49434
scalar quantum field theories, noncanonical self-coupled, functional eqns. 77−65104
scattering by several fixed scatterers integral eqns. in wave mech. 77−78996
scattering properties of arbitrarily-shaped lossy dielectric bodies of revolution 78−22072
scattering theory with different state spaces of perturbed and free system 79−40406
Schrodinger eqn., radial, general pot. props. for soln. by hypergeometric functions 80−4581
Schrodinger eqn. with random potl., cure. Green's functions 78−86
Schrodinger equation, discrete-time, Green functions, k-transforms 80−46859
Schrodinger equation with an anharmonic oscillator potential 80−27163
Schwinger-DeWitt expansion, boundary terms, flat space results 78−77815
screw dislocations, inelastic neutron scatt. 78−75774
screw dislocations, phonon dispersion curves of localised modes, inelastic neutron scatt. 77−72661
self consistent RPA for three body forces in Fermi systems 78−89810
self-dual gauge field, Green function 78−82099
semi-infinite array of identical potentials, surface effects and electronic density of states 78−54110
semi-infinite Heisenberg ferromagnet, macroscopic theory of response functions and appl. to light scatt. 80−20410
semi-infinite isotropic elastic medium, reson. scatt. of Rayleigh waves by mass defect 80−20025
semi-infinite solid, elementary excitations in surface region 79−60618
semi-infinite transversely isotropic materials, Green's function solutions 79−46205
semiclassical expansion of the anharmonic-oscillator propagator 79−63072
semiconductor, chemisorpt. of H_2, Anderson model, including correlation and overlap effects 77−76662
semiconductor, defect electronic struct., SCF method 80−80208
semiconductor, degenerate magnetic, mag. excitations, light scatt. 77−63161
semiconductor, electron correlation and bound excitons 77−85150
semiconductor, ferromagnetic, longitudinal response function 77−72831
semiconductor, hole scatt. from impurity pots. in spherical-band approx. 77−76803
semiconductor, impure, exciton absorpt. line shape calc. *(Russian)* 78−10934
semiconductor, light scatt. spectra, interference effects 79−82977
semiconductor, tetrahedral, electronic struct. of point defects, surfaces and interfaces, Green's function scatt. theoretic method 79−33258
semiconductor, two-dimensional electron-hole systems in high mag. fields, phase transitions 80−49608
semiconductor, Zincblende struct., localised vibrs. due to defect complexes, Green's function study 80−79896
semiconductor alloy, disorder scatt., Green's function calc. 77−11906
semiconductor defects, electronic structure and lattice distortion, Green's function methods *(French)* 80−59917
semiconductor film, Wannier-Mott exciton states *(Russian)* 78−79943
semiconductor films, exciton light absorption coefficient *(Russian)* 80−71504
semiconductor surface, chemisorption of mol. complexes, bond orbital model *(German)* 80−59807
semiconductor under intense laser field, scatt. theory, extension to non-equilibrium state of thermodynamic double time Green functions 79−43040
semiconductor/adsorbate system, local density of states calcs. *(German)* 80−60062
semiconductors, degenerate, resonance Raman scatt. 80−80781
semiconductors, disordered, light induced stationary non-equilibrium distribution of electrons, balance equation 80−39528
semiconductors, force variation due to charged defects 80−92634
semiconductors, van Hove critical point region, electron-phonon interactions, dispersion law 80−70344
semiconductors and insulators, role of electron-hole interaction in optical spectra, review 80−45113
semiconductors with direct band gaps, exciton-polariton interactions, Green's function approach 80−92831
semimetal, mixed superconducting-excitonic insulator phase, diamagnetism, virtual intraband transitions 80−2520
semimetal, simultaneous Cooper and insulating pairing, physical states 80−93036
shell of revolution, Green's function of steady heat cond. operator 79−86319
Signorini's problems, reciprocal variational inequalities soln. 79−41585
simple liquid, dynamical structure factor and Green's functions 79−4228
simple metals, ground state energy, structural expansion 80−88497
sine-Gordon soliton, adiabatic behavior in presence of perturbations 79−49093
singlet ground state system, line shape of mag. excitations, diagrammatic expansion calc. 77−69482
singularity at corner of wedge shaped punch or crack 78−83252
slab geom., transmission and reflection coefficients in the slowing down region 80−13005
Slavnov-'t Hooft identities in Mandelstam's formalism 78−45776

Green's function methods continued
SO(3) gauge invariant theory, quantisation, spontaneous broken gauge theory, S-matrix gauge independ. 79−269
solar coronal magnetic field models, validity of Green's function solns. 80−21970
solar force-free mag. field calc. with constant α, exact solns. 77−33438
solid sheet with selective optical props., combined radiative and conductive heat transfer 78−90672
solid solution, nondiagonal disordered system, excitation spectrum 80−15429
solid state systems, electron localisation and spectra 79−15110
solid surface, Rayleigh wave scatt. from mass defect 77−20177
solid surface, theory, book 80−36787
solids, relativistic Green function 77−20214
soliton field theory, construction of Green's functions from an exact S matrix 79−71629
solution, electronic excited state transport, Green function soln. 79−68994
spatially disordered systems, Anderson localisation and metal-insulator transition 80−59926
spatially dispersive semi-infinite media, polariton Green's functions, refl. spectra 77−85154
spectral forms and renormalization group equations of the Schwinger model 79−63357
spectral line broadening by foreign gas, translational heat bath model, T-approx. 78−9125
spin and pseudospin lattice systems, Green's functions diagrammatic technique 78−8355
spin and pseudospin lattice systems, Green's functions diagrammatic technique, Pauli operators 78−8356
spin half field theory in Rindler space, Green's functions 78−12826
spin susceptibility for itinerant electrons with energy dependent effective interactions 78−19209
spin susceptibility of a many electron system 77−69465
spin systems, disordered, commutator and anticommutator Green's functions 79−51792
spin-systems, double-time Green functions method, thermodynamics 79−15313
spinor and scalar particles in mag. field *(Russian)* 78−49997
spinor field quantisation 78−45777
spinor fields in an Einstein universe, finite temp. effects 79−21614
spinor Green's function in Einstein universe, vac. averaged stress-energy tensor 78−41217
spontaneously broken supersymmetic model at high temperature, Green's function props. 79−26257
statistical description of nuclear compound states, temp. Green's functions method *(Russian)* 78−17115
Stekloff type boundary-value problems, Green's functions, asymptotic formulae *(Russian)* 77−22379
stochastic acceleration of particle in random pot., renormalised canonical perturbation theory 77−27233
stochastic differential eqns., Green's function soln. by hierarchy method, closure approx. error 80−149
stratified ocean of finite depth, water wave problem, Green's function soln. 79−48489
streaming, uniform, past fixed semicirc. infinite strip 79−23299
stress intensity factors FOR X-formed arrays of cracks 78−67121
stress singularity at the corner of a wedge-shaped crack or inclusion 79−46268
stressed crystal, point defect interaction with dislocation 77−80537
strong correlated system, single particle Green's function calc. of elec. cond. 80−20142
strong simple harmonic motion in isotropic layer over isotropic elastic material 79−23239
strong-coupling limit of renormalisable interacting quantum fields 78−49968
strongly interacting solvents, IR band shapes, solvent-induced chirality, field theoretic Green's function method 79−27037
subsonic and supersonic aerodynamics, SOUSSA computer code 78−71352
superconductive tunnelling, extension of Feuchtwang method 78−68121
superconductor, 2-dimens. fluctuation-induced cond. above crit. temp. 78−10608
superconductor, two-band, with nonmagnetic impurities, transition temp. 78−2607
superconductor-metal-insulator-metal-superconductor system, Josephson current, weak supercond. *(Russian)* 80−54842
superconductor-normal metal interface in a finite geometry 79−33404
superconductors, magnetic impurity low temp. behaviour, transition temp., specific heat, free energy 80−88691
superconductors, spin susceptibility of conductivity electrons, spatial dispersion *(Russian)* 79−51719
superconductors, two-band, crit. current density depend. on external mag. field *(Russian)* 80−88707
superconductors, zero-gap dirty, cond. electron spin resonance theory 80−103888
superconductors with impurities and Kondo effect, Green's function calcs. 77−89894
superconformal algebra, two-point and three-point Green's functions of scalar superfield 77−30280
supergraph anal., gauge supersymmetry, S-matrix 80−27422
superspace, auxiliary mass BPHZ renormalisation procedure 78−16902
surface, (e,2e) reactions, theory 78−39640
surface, effects of roughness on dynamical props. 78−75923
surface, Green function method for electronic struct. and vibr. modes calc. 78−88012
surface, lattice force constant determination 78−71933
surface and interface electron states, one-dimensional model, Green's function soln. *(Russian)* 77−59311
surface and interface problems, Green's function and generalised phase shift 79−60895
surface atom mean-square displacements, elastic continuum theory 77−76655
surface density of states in tight-binding formalism 78−10530
surface diffusion and spin polarisation, 2-D CIDEP, asymptotic Green's function method appl. 80−91584
surface electronic structure from matching Green function method 78−88013
surface Green's function formalism for N-interfaces 78−39179
surface Green's function matching, physical and physicochem. appls., review 77−78954
Green's function methods continued
surface physics, partial differential eigenvalue eqn. 80−6929
surface reconstruction of two band crystal, model for CsCl structure 78−14544
surface reconstruction of two band crystal, total electronic energy, change calc. 78−14543
surface wave, scattering, by submerged sphere 78−34145
surface waves, finite depth rotating fluid, Green's function anal. 79−37324
surface waves, perturbation anal. of attenuation and dispersion 78−47653
surface waves in anisotropic cubic cryst. 80−70518
surface-skimming bulk wave excitation, analysis 80−53519
surfaces states of semi-infinite s-p hybrid diatomic linear chain 77−4419
susceptibility relationship to correlation length, renormalisation group calc., anomalous-dimension crossover function 79−42780
Takagi model, critical and tricritical behaviour using double-time Green's functions 77−45816
TCNQ, lattice softening mechanism 80−6481
temperature Green's function for tunnelling model, new contraction method 79−35635
tensor expansions for harmonic vector wave eqn. in spheroidal coord. systems 78−41171
tetrahedral XY_4 type molecule, change in mean square amplitude 77−57963
thermal blooming, theoretical aspects of compensation 78−32226
thermal stresses due to moving heat sources *(Polish)* 78−18184
thermodynamic Green's function, perturbation theory 77−26266
thermoelastic deformations of half space, Earth strains and tilts 78−36092
thermoelastic dielectrics, reciprocity theorem for dynamic problems 79−37165
thermoelasticity in solid symmetrical bodies of revolution, thermal transients, finite element analysis *(Spanish)* 79−23208
thermosphere, structure and dynamics rel. to tides and diffusion waves 79−35026
thin disordered film, electronic energy spectrum calcs. extended Halpern Green's function technique 80−20066
thin film heterostructure, energy spectrum study 80−70787
thin film on substrate, normal Brillouin scatt. by acoustic phonons 80−20648
Thirring model, symm., anomalous dimens. and Schwinger term 77−87900
Thirring model with SU_n symmetry, scale invariance 79−9288
Thomas-Fermi eqn. solns., iterative method 79−9185
three body problem, Green function hierarchy 79−75941
tight-binding Green's functions for surfaces, thin films, and solid interfaces using random-walk theory 80−54753
time-dependent Onsager problems, soln. 79−20457
tissue induced EM power distribution in closed environment 80−3725
TMMC, one-dimens. magnet, local magnon modes 80−65829
trace and dilatation anomalies in gauge theories 78−4790
transient and time-harmonic dyadic Green's functions for perfectly conducting cone 79−18334
transient flow in porous media, Green's function appl. 79−72935
transition metal, chemisorpt. of H_2, Anderson model, including correlation and overlap effects 77−76662
transition metal, chemisorption of ordered atomic layers, HF Green's function formalism and phase shift technique 80−24733
transition metal, chemisorption of ordered overlayers with C(2×2) and (2×1) structs. 79−46925
transition metal (001) surface, model, chemisorption, coverage depend. of adsorption behaviour 78−71976
transition metal impurities in transition and noble metal hosts, electronic struct. 78−75990
transition metals, chemisorption of light gas atoms, on (100) surface, model calcs. 77−11797
transition metals, electronic props. of dil. impurities, exact Green function treatment 77−62856
transition metals, liq., electronic struct. and transport props. 80−29314
transmission characts. of optical waveguides with periodic external force 80−99873
transport noise, Green's function procedures 80−17902
transport theory integral eqn. soln. in Green's function formalism, scatt. amplitudes 80−4566
trigonal crystals, ferroelectric phase transition, renormalisation group theory 80−55052
turbulent convection of scalar fields, probability density functions relax. 79−27622
two body scatt., non-relativistic, variational matrix Pade approximants *(German)* 78−54247
two dimensional periodic lattice, electron ordering, CDW-disordered state transition, Hubbard model *(Russian)* 80−6754
two-body scatt. T matrix in real-time formalism 78−41230
two-centre scattering amplitudes, var. determ. 77−78998
two-dimensional boundary-value problems of small amplitude waves in finite water depth, num. analysis method 77−9444
two-dimensional quantum plasma in mag. field, exchange energy 77−72904
two-electron ions, ground state, quadratic Stark effect 80−37775
two-particle bound state, lifetimes and level shifts 78−75265
two-particle Green's functions, bound states and poles 78−16694
two-particle-hole Tamm-Dancoff approximation (2ph-TDA) equations for closed-shell atoms and molecules 78−70937
two-phase transversely isotropic elastic materials, Green's function solns. 80−58912
two-sublattice biquadratic systems, phase transitions 79−99710
type II antiferromagnet with bilinear and biquadratic coupling, magnetic excitons in cubic cryst. field 79−78353
type II superconudctor, of flux-line lattice 77−32128
underwater sound, theoretical and numerical Green's function field soln. in plane multilayered medium 80−33314
unidirectional wave motions, book 78−77730
unitary groups, functional integral representation *(Russian)* 79−9309
unsteady subsonic and supersonic pot. aerodynamics for complex config. aircraft 77−72320
valence electron photoionisation, ionisation pot. and spectral intensities 78−70883
van der Waals force in cond. media, fluctuating electrodynamics 78−30876
variable-depth function for ocean shelf edge tides 80−81915

Green's function methods continued
variation-iteraction soln. of Hartree Fock eqns., Green's integral operator, SCF formalism 79−6842
variational Green's function, finite element soln. to second order boundary value problem 77−71193
vector spherical harmonics of unit hyperboloid in Minkowski space 78−32732
velocity dependent pot. uncoupled Schrodinger eqn. soln. using Green's technique 78−69998
vertical ionisation potentials calculation, CNDO adapted approx. 80−18799
vibrating piezoelectric solid, perturbation theory for linear electroelastic eqns. 79−1739
vibronic theory of ferroelectricity 79−19854
virtual surface states, Green function theory 80−80342
viscous incompressible liquid, heat conductivity problem *(Russian)* 80−69897
Ward identity, conformally invariant form, Green's function and two conserved currents 78−86421
Ward Takahashi identities soln. 79−241
wave functions, relation between phase function and Green's function 80−105543
wave propagation in inhomogeneous media, backscatter folding series *(Russian)* 78−73862
weak ferromagnet, with easy plane anisotropy correl. functions and magnetisation, temp. depend. *(Russian)* 80−84581
Wick's theorem, relation between canonical and Fokker-Planck dynamics 79−17329
Wroblewski relationship, scaling phenomena, renormalisation group eqns. *(Chinese)* 79−92986
X-ray absorption spectra, remote fine structure, multiple-scatt. model 77−28644
X-ray dynamical scatt., numerical calc. of Green's functions 77−80396
X-ray projection topographs, calc. method, intensity profiles for dislocation images 79−14638
X-ray traverse topographs, computer simulation on basis of Green function method 80−49044
X-Y ferromagnet, S=1, with uniaxial anisotropy, Curie temp. 79−78425
X-Y model, second order Green's function theory 80−54913
XPS, angle-resolved, role of electron diffraction 78−64446
XY_2 linear symmetric mols., chem. perturbations, Green's function calcs. 80−63866
XY_3 pyramidal molecules, change in mean square amplitude values, calc. 78−55158
Yang-Mills and gravitation, Ward identities and Green's function eqns. 77−67552
Yang-Mills fields, instantons, tensor products of instantons *(Russian)* 79−67477
Yang-Mills pseudoparticles, fermion Green's functions 78−54548
Yang-Mills theory, large order calcs. 78−8511
zero-component field theories, high order behaviour without n→0 limit 79−75438
zincblende (110), surface relaxation 79−38143
ZnS:V^{2+}, impurity states by Green's function method 80−92855
e^+e^- annihilation cross sections, operator approach, one-photon approx. 80−47315
π-electron systems, self-consistent many-body theory 78−25432
Ag, deformation potentials for isotropic strains 79−42506
Ag, electronic and mag. structure calcs. of mag. impurities 80−80213
Ag-transition metal, dil., mag. impurities, electronic struct., KKR-Green's function calc. 80−65783
AgBr:Li^+(Na^+), impurity induced IR absorpt. 80−7386
AgBr-Li^+(Na^+), local mode freqs., Green's function calc. 80−39237
Al, liquid, electron momentum density, correlations and ionic potentials 78−60052
Al-Ag, force-and-mass disordered alloys, vibrs., average local-information transfer approx. 80−88290
Al-Fe, dil. solid soln., vacancy-trapped Mossbauer impurity Debye Waller factor 80−60468
Ar, solid, lattice dynamics calc. using Kihara hard core pot. 77−1193
Ar, vacancy, electronic structure, Green's function theory 80−39525
Ar:Ne, localised mode due to Ne impurity, Green function technique 77−1201
Au-Mn, band profile, density of states, quantum defect-Green's function calcs. 80−54599
B_2O_3, vibrational force consts. and B-O bonding, Green's function method 77−14406
BX_3, (X=Br, Cl, F), ellipticity of symm. force field, force consts. 78−17646
BaF_2, F^- interstitial and substitutional trivalent captions, phonon reson. and IR absorpt. 80−84752
C, vacancy, tight-binding calc. 80−24844
C^- predissociations, anal. line profile and energy shifts, linear pot. approx. 77−6871
C^+ predissociations, anal. line profile and energy shifts, linear pot. approx. 77−6871
C^+ predissociations, Fano line profiles, linear pot. calcs. 77−6872
C_2, electron affinity, vibr. struct. in radiative electron attachment spectra 77−88592
CO adsorbed on Ni, valence band photoemission, SCF MO CNDO calc. 80−100754
CO_2, valence shell ionis. spectra, theory and dipole (e-2e) spectra expts. 79−76522
CS molecule, calc. of HeI photoelectron spectrum, ionisation pot., vibr. struct. 77−3415
CS_2, photoelectron spectra (He II), Green's function anal. 79−27031
CaF_2, F^- interstitial and neighbours, mean-square displacements 80−29011
CaF_2, Frenkel defect, entropy of form., Green function calc. 80−19898
CaF_2, impurity modes due to interstitials, Green function formalism 80−24554
CaF_2, phonon resonances associated with vacancy 80−19893
$Cd_{1-x}Hg_xTe$, lattice dynamics of low conc. of Hg atoms, perturbation model impurity description 79−55853
$CePd_3$, mixed valence cpd., theory of inelastic mag. neutron scatt. 79−15284
ClO_2F, pyramidal type mol., force field comput. using Green's function procedure 80−23407
$Co(C_5H_5NO)_6(ClO_4)_2$ [$(BF_4)_2$], X-Y antiferromagnet, Neel temp., spin correlation functions 80−60345
Green's function methods continued
Cr antiferromagnetic with nonmagnetic impurities, mag. susceptibility using two band model 80−2559
Cr, band struct., X-ray emission bands, self-consistent calc. 77−28104
Cr_2O_3, magnon energy temp. renormalisation calc. 77−1531
Cs, elec. dipole approx. and elec. quadrupole resons. allowed in multiphoton absorpt. *(French)* 78−5190
CsBr, (110) surface, electronic struct. of valence bands calc. *(Russian)* 80−75621
CsCl, (110) surface, electronic struct. of valence bands calc. *(Russian)* 80−75621
CsI, (110) surface, electronic struct. of valence bands calc. *(Russian)* 80−75621
CsI, isotope diffusion 78−75875
$CsNiF_3$, one-dimens. magnet, local magnon modes 80−65829
Cu, deformation potentials for isotropic strains 79−42506
Cu, electronic and mag. structure calcs. of mag. impurities 80−80213
Cu, entropy factors for vacancy formation and migration 78−75866
Cu, surfaces and twin faults, electronic states calc. by surface Green's functions 80−39647
Cu-Al, change in force constant due to volume effects 78−75778
Cu-Al, impurity concentration effects 78−75777
Cu-Be, impurity concentration effects 78−75777
Cu-Ni(Zn)(Ga)(Ge), dil. impurity electron struct., self-consistent Korringa-Kohn-Rostoker Green's function calc. 79−78040
Cu-Si, change in force constant due to volume effects 78−75778
Cu-Si, impurity concentration effects 78−75777
Cu-transition metal, dil., mag. impurities, electronic struct., KKR-Green's function calc. 80−65783
CuBr:Cl(I), lattice-dynamical study of impurity modes 80−29129
CuCl:Br(I), lattice-dynamical study of impurity modes 80−29129
CuI:Br(Cl), lattice-dynamical study of impurity modes 80−29129
p-D_2, order parameter temp. depend. 79−42242
p-D_2, order-disorder phase transition 78−79726
$ErCo_2(Fe_2)$, mag. excitations, RPA theory 80−65830
Eu chalcogenides, cond. band spin struct. 80−71577
EuSe, mag. phase stability, theory 77−63183
α-Fe vacancies, formation entropy, diffusion const., determinant and Green's function methods 79−77595
Fe-Co, electron energy spectrum calc. by Green function method *(Russian)* 77−35860
Fe_3O_4, doped, electron correls. above and below Verwey transition, Green function theory 77−51687
Ga(As,P):N, intermediate range model of N states 79−73467
GaAs, electronic states of neutral vacancies 77−11875
GaAs, polaritons, surface nonlinear interaction theory 78−42379
GaP, electronic states of neutral vacancies 77−11875
GaP, electronic structure of neutral phosphorus vacancy, empirical pseudopotential 79−78042
GaP:N, electron binding by N pairs 79−90990
GaP:N, electronic energy levels calc., optimisation 79−28315
GaSb-InAs system, (110) surface and interface electronic struct. 80−100494
Ge, impurity modes due to point defects, comparison with IR and Raman meas. 79−4386
Ge, localised vacancy state 79−82543
Ge, localised vibrational modes of isolated impurities, Green's function method 77−39650
n-Ge, phonon conductivity and attenuation 77−4167
Ge, vacancy, tight-binding calc. 80−24844
Ge:Si, impurity lattice modes due to single and paired defects 78−75780
Ge-Si, dil. alloy, IR absorpt. and first-order Raman scatt. due to single and paired impurity atoms 79−82976
Ge-Si, impurity concentration effects 78−75777
H atom, Green's function path integral soln. 79−67187
H chemisorption on metal substrate, model including image charge effects 79−73405
H, dipole static polarizability for any state, modified Coulombic Green's function Sturm expansion 79−7031
H, electron impact, in laser field, Born-Oppenheimer approx. calcs. 79−54973
H, electron scatt., polarisation potential 78−42228
H, excited S-states, static dipole polarisabilities, Green's function calcs. 77−6696
H, first-order wave functions, computer calcs. using Green's functions 78−41934
H, ground-state, freq.-depend. multipole polaris., reduced Green's functions 78−1097
H, Stark broadened line shape, unified Franck-Condon-JWKB method 77−10635
H-bond, dynamical model, Green function method 77−65447
H_2, liq. metal, electron kinetic eqn. with exchange, elec. resist. 79−15131
H_2 mol., Green's function Σ perturbation method for mol. calcs. 78−55123
o-H_2, order parameter temp. depend. 79−42242
o-H_2, order-disorder phase transition 78−79726
H_2 vertical ionis. pot., many-body Green's function calcs. 80−102439
H_2^+, dynamic polarisability, electronic states two centre Coulombic Green's function, continuous spectrum exclusion 78−82626
H_2^+, polarisability, internuclear distance depend., excluding continuous spectrum 77−10581
HCN, HNC ionisation potential, electronic structure 77−3260
HCN, ionis. and photoelectron spectra, inner valence electrons 78−82784
H_2CS, ionis. pot., many-body Green's function method 77−67965
H_2O, many electron Green's function calcs. optical pot. 80−58126
H_2O, many-body Green's function, electronic mol. props. 78−25417
H_2O, vertical ionis. pot. calc. from one-body Green's function 77−42440
H_2S, gas-phase, states in valence photoelectron spectrum 78−94284
H_2S, inner valence electron ionisation calcs., photoelectron spectra obs. 78−82619
H_2S, ionis, pot., many-body Green's function method 77−67965
He isoelectronic series, static dipole polarisability, reduced Green's functions, HF calcs. 77−71750
He, isoelectronic series 79−3358
^{3}He, exact Green function eqns., extraordinary phases 77−47642
^{3}He, superfluid, transport parameters, Kubo formulae and BCS-Green's functions 80−88382
^{3}He, superfluid B-phase, gap parameters and collective modes in strong mag. field 80−15325

Green's function methods continued
^{3}He-^{4}He mixtures, superfluid transition temp., Green's function calc. method 77−72735
^{4}He, HCP, ground-state props. 80−44389
HoZn, spin wave spectrum, Green function analysis 78−2666
H(p,x), direct and charge transfer scattering processes, second quantisation 80−78289
In pnictides, mixed, impurity induced Raman scatt. spectra 80−88983
InP, electronic structure of neutral phosphorus vacancy, empirical pseudopotential 79−78042
InSb, phonon assisted cyclotron resonance exact sol. of integral eqn. for Green's function 79−61227
K halides, surface lattice dynamics, by Green's function method 78−71936
KBr, defect modes due to H^--D^- pair impurities 80−59602
KBr, electronic states at (100) surface, accounting for spin-orbit interaction *(Russian)* 78−91750
KBr:Rb, U-centre modes, Green's function method calc. 77−24372
KCl, defect modes due to H^--D^- pair impurities 80−59602
KCl, electronic states at (100) surface, accounting for spin-orbit interaction *(Russian)* 78−91750
KCl:Cs^+(I^-), low-temp. heat capacity enhancement due to impurities 80−107442
KCl:F^-(Br^-)(I^-), U-centres, local defect modes, Green's functions calcs. 80−44280
KCl:Kbr(KI), enhancement in sp. ht. due to anion impurities 79−51274
KCl:Na^+(Rb^+)(Ag^+), entropy changes associated with point defect form. calc. 77−7741
KCl:Pb^{2+}(0.005% Pb), A band fine structure, electron-phonon interaction 78−60491
KCl:Tl, energy level scheme, mol. orbital model 80−10912
KDP type crystals, ferroelec. phase transition, Greens function theory *(Chinese)* 79−56740
KF(Cl)(Br)(I), surface lattice dynamics, Green function method 78−34693
K_2FeF_4, Raman scatt. in two dimens. antiferromagnet 78−19488
$K(H_{1-x}D_x)_2PO_4$, polar mode softening and elastic anomaly temps. 79−28067
KH_2PO_4, and isomorphs, ferroelectric transition and Curie temp., soft mode effect, Green's function anal. 79−24269
KH_2PO_4, Green's function theory of ferroelec. phase transition 77−85669
KH_2PO_4 type crystals, transverse elec. susceptibilities 80−50273
KH_2PO_4 type ferroelectrics, Green's function theory of phase transitions with pseudo-spin-lattice coupled mode model 80−71354
KH_2PO_4-KD_2PO_4 mixed cryst., dielec. polarisation, Green's function anal. 77−52011
KI, electronic states at (100) surface, accounting for spin-orbit interaction *(Russian)* 78−91750
KI, gap modes due to impurity pairs 77−62602
KI, gapmode calc. using Green's function technique, effect of uncertainty in eigendata 78−79708
K_2MnF_4:Zn(Mg)(Ni), local magnetisation, NMR and Green's function study 80−65870
$K_3Mn_2F_7$, antiferromagnet, two magnon Raman scatt., linewidth, compared to calc. 78−15164
$K_3Mn_2F_7$, two magnon Raman scatt., magnon dispersion, susceptibility, Green's function methods 80−50340
$KNiF_3$:Mn^{2+}, isotropic Heisenberg ferromagnet, localised spin-wave modes, biquadratic exchange effects 77−51896
Kr, solid, lattice dynamics calc. using Kihara hard core pot. 77−1193
Li, hyperfine coupling, in ground and excited states, Green's function calcs. 77−6692
Li_3, binding energy, Wigner-Seitz pot. calcs. 77−83512
LiF, cross relaxation of β-active ^{8}Li nuclei *(Russian)* 80−103895
LiH, many electron Green's function calcs. optical pot. 80−58126
LiH, many-body Green's function, electronic mol. props. 78−25417
Mg, single crystal, Green's function method of lattice statics, monovacancy 78−55865
Mg, vertical ionis. pot. calc. from one-body Green's function 77−42440
MgO, intrinsic surface states at (100) and (110) surfaces 78−91740
Mo (001) surface, surface states and photoemission 79−60887
Mo, band struct., X-ray emission bands, self-consistent calc. 77−28104
Mo-Re (5 at.%), enhanced lattice sp. ht. due to LF reson. modes 78−14882
Mo(001), surface electron struct., matching Green function method calcs. 78−88014
N_2 adsorbed on Ni, valence band photoemission, SCF MO CNDO calc. 80−100754
N_2, excitation energies, eqn. of motion-Green's function calcs., 3rd order contribs. 77−65417
N_2, ionisation pot. calc. by equations-of-motion, Green's function method, critical analysis 77−30762
N_2, ionisation potential, Green's function-eqns. of motion calcs., third order terms 78−41926
α-N_2, mol. cryst., theory of time evolution of exciton coherence 80−65455
N_2, shake-up peak positions and intensities calcs. using eqns. of motion Green's function method 78−86910
α-N_2, solid, anharmonic lattice vibrations calcs. 78−71812
N_2, solid, gamma-phase, anharmonic lattice vibr. 79−33705
$ND_4D_2PO_4$, cryst., transverse and longit. elec. susceptibilities, modified Ising model calcs. 80−97203
N_2F_2, trans- and cis-isomers, photoelectron spectra, Green's function calc. 77−83650
NH_3^+, ionisation pot. of ^{2}E state, Jahn-Teller effect 78−62948
N_2H_2, isomers, photoelectron spectra, vibr. struct., ionisation pots., Green's function calcs. 77−75213
$NH_4H_2PO_4$, cryst., transverse and longit. elec. susceptibilities, modified Ising model calcs. 80−97203
NO_2, valence shell ionis. spectra, theory and dipole (e-2e) spectra expts. 79−76522
N_2O_4, photoelectron spectrum interpretation 79−22761
NaCl-type crystals, donor levels due to dislocations, calc. 80−6771
Nb, band struct., deformation potentials calc. by Green's function method 79−1568
Nb, band struct., X-ray emission bands, self-consistent calc. 77−28104
Nb-H system, lattice dynamics, local frequency spectrum, mean thermal displacement of H 80−59604
Ne, vacancy, electronic structure, Green's function theory 80−39525
Ne, vertical ionis. pot. calc. from one-body Green's function 77−42440
Green's function methods continued
Ne, vertical valence ionis. pot., many-body Green's functions 78−22051
Ni (001), chemisorption site determ. for S and CO, angle-resolved UPS 78−71970
Ni, band struct., cryst. pot. anisotropy effect *(Russian)* 80−88474
Ni, liquid, electronic struct. and transport props. 80−29314
Ni(001), surface electron struct., matching Green function method calcs. 78−88014
OF_2, photoelectron spectra, ionisation energies, ab initio many-body Green's function calc. 79−89709
ONF_3, vibr. anal. using Green function 77−57962
P_2, electron affinity, vibr. struct. in radiative electron attachment spectra 77−88592
PH_3, inner valence electron ionisation calcs., photoelectron spectra obs. 78−82619
PN, photoelectron spectra, ionisation pot., vibr. struct., Green's function method 77−61799
Pd:H, electron density of states of interstitial H 77−47766
Pd-H system, lattice dynamics, local frequency spectrum, mean thermal displacement of H 80−59604
RbCl, U-centre local modes calcs. 77−62603
RbH_2PO_4, acoustic longit. mode coupling to order parameter and effect on ferroelec. phase transition 79−51914
SF_2, photoelectron spectra, ionisation energies, ab initio many-body Green's function calc. 79−89709
S_2N_2, photoelectron spectrum, interpretation, Green's function calcs. 80−87175
Si (111), (e,2e) reactions, theory 78−39640
Si, deep-level point defects, effective-mass nature 80−59922
Si, defects, divacancy and split 100 interstitial, electronic structure calc. 80−65494
Si, energy spectrum of Fe group impurities 79−23932
Si, ideal vacancy, self consistent Green's function calc. 78−91640
Si, laser annealing, nonlinear dynamic transport processes 80−93437
Si, localised defect, self consistent Green's function calc. 80−10919
Si, optical spectrum, many particle effects, band struct. 80−89024
p-Si, phonon conductivity and attenuation 77−4167
Si vacancy, defect electronic energy levels calc., optimisation 79−28315
Si vacancy, electron states, Anderson negative-U system 80−96820
Si, vacancy, self consistent Green's function method 80−24843
Si, vacancy, tight-binding calc. 80−24844
SiO, valence ionis. energy, calc. including correl. effects 79−68185
SiO_x system, cluster plus effective medium tight-binding study 79−33216
Sm compounds, mixed valence, metals or small gap insulators, two-band Hubbard Hamiltonian 80−34399
Ta-H system, lattice dynamics, local frequency spectrum, mean thermal displacement of H 80−59604
Ti, band struct., cryst. pot. anisotropy effect *(Russian)* 80−88474
Ti complexes, cryst., amorphous, coordinated H_2O, mol. force field ellipses, mol. force consts. 77−34609
TiO, energy band struct. and density of states *(Russian)* 80−44493
Tl halides, polar semicond., binding energy of Wannier excitons 77−69232
V, band struct., X-ray emission bands, self-consistent calc. 77−28104
V-H system, lattice dynamics, local frequency spectrum, mean thermal displacement of H 80−59604
VO, energy band spectrum, APW and Green's function method calcs. 79−7783
VO, energy band struct. and density of states *(Russian)* 80−44493
W (001), chemisorption of H, HF Green's function formalism and phase shift technique 80−24733
Xe, solid, lattice dynamics calc. using Kihara hard core pot. 77−1193
Zn-Mn(Cr), dil, mag. anisotropy, Hartree-Fock calcs. 80−11162

grinding
abrasive tool with filler, increase in grinding efficiency *(Russian)* 80−7687
active abrasive conc. determ. by static method based on etch figure stars count 80−74544
adsorption-sensitive fracture processes, control and appl. 77−52468
Alnico 5 alloy, S and Ti additions effect rel. to non-metallic inclusions, coercive force and grindability 80−89375
aspheric axisymmetric lens figuring, wear pattern prediction 77−27398
aspherical surface prod., review 77−7224
autunite, random layer structure by grinding, X-ray powder patterns 77−78174
ball mill grinding, effect of Vickers hardness and rate const. of spec. surface increase *(Japanese)* 77−52259
ball mill grinding, rate constant determination *(Japanese)* 78−95828
ball mill grinding, wet, dry, rate constant determination *(Japanese)* 78−95827
ball mill grinding rate constant, under size increase feed rate effect *(Japanese)* 79−28974
brass, delamination effects during grinding 79−52470
breakage distribution, in batch grinding, mathematical model determination 78−92416
camera optical component fine diamond grinding on modernised equipment 79−46092
carbides, sintered, sample prep. for metallographic structural anal. 80−13048
ceramic, polished section prep. using pedepin *(German)* 78−19983
ceramic, rate constants of wet and dry ball mill grinding *(Japanese)* 80−29895
ceramic material specimens, prep. with Pedemax-Planopol automatic grinder and polisher 79−74333
ceramics containing metastable tetragonal ZrO_2, grinding induced tempering 80−89260
cermet grinders with fillers, performance 77−72103
comminution of solids under hydrostatic pressure, technique 78−52702
computer-controlled polisher for small-tool fabrication of mirrors 80−14496
contact area determ. of grinding tool with blank 80−64221
control of diameter, laser-based noncontact gauging systems appl. 79−2745
copper porphyrins, mag. susceptibility and EPR, sample grinding effects 80−60420
corundum, grinding, effect of grinding wheel material, particle size, temp. *(German)* 79−43173
corundum, grinding material, review *(Polish)* 80−29917
crystal, single, jig for precise orient. and grinding *(Czech)* 79−26047

grinding continued
crystal turning in common lathe 78−18482
cutting mechanism model 79−79124
cylindrical lens surface generation, grinding and polishing machinery design 80−79023
diamond, electrolytic grinding, magnetic field effect 80−11790
dressing effect on grinding performance, review 80−16502
elastic and plastic behaviours, role in grinding *(Japanese)* 80−100868
elastic tools for finishing optical components with noncircular cylindrical surfaces 80−28368
fibre optic elements, damaged layer struct. after diamond grinding and polishing 79−7220
fracture and deform. mech., SEM obs. *(Japanese)* 79−15620
glass, ancient, X-ray fluoresc. anal., importance of sample prep. 77−34064
glass, blanks, stresses and birefr. changes with dimensions 78−30100
glass, diffusion profiles analysis, grinding and etching techniques comparison 78−26732
glass, fracture, grinding and flaw geometry effect 77−56081
glass, GLS, surface radiation strength, grinding and polishing press. effect 77−72104
glass, Knoop hardness number is grinding *(Polish)* 80−97580
glass, material removal mechanism by free abrasive grinding 77−52510
glass, rate constants of wet and dry ball mill grinding *(Japanese)* 80−29895
glass, strength under linear tension, bending, torsion and compression of type K8 79−14062
glass finishing with small-grained diamond grinding wheels *(German)* 80−38137
graphite, ground natural, Raman spectra, grinding influence 79−42956
hard and brittle materials, microsection prep. technotron and polishing systems *(German, English)* 80−11859
hard ceramics, precision grinding device for radioactive tracer diffusion studies 78−41291
heat flux, distrib. *(Russian)* 79−79132
information criterion for selecting the number of points in workpiece monitoring 79−67274
large high-precision prism grinding, use of 3G-71 lathe 80−102872
Large optical component grinding and polishing condition selection 79−81579
large optical components, automated apparatus for grinding 80−102869
large spherical surfaces with annular tool 78−18074
laser mirrors, optical fabrication techniques 77−65600
lens, individual meniscus-type, coarse grinding errors 79−50458
lenses, as student lab. project 77−5614
lenses surface, spectacle type, using automatic and semi-automatic machines *(French)* 80−58822
machine wheel life modelling, group method of data handling 80−58987
magnetic collimator mirrors, grinding and polishing processes *(German)* 79−71433
Magnico alloy, with Si, Nb, Ti effect of Ub on mag. props. and grindability 77−63811
metal, coated abrasive belt grinding, relation between wear of grain cutting edge and material removal 80−16507
metal, wear, grinding and erosion, microsphere form. mechanism 79−79123
metal grinding in oxidising medium, electromechanical processes *(Russian)* 79−79149
metal powder, milling conditions effect on densification during pressing and sintering 78−11149
metal surface replica production, nondestructive mech. and electrolytic grinding and polishing *(German, English)* 77−48607
metallographic specimens, grinding and polishing apparatus 78−23889
metals, submicroscopic surface relief after finishing 79−29276
microchannel plate surface finishing using liquid 78−90544
minerals, industrial, finest grinding methods *(German)* 79−8256
mirror, paraboloid, off-axis section, fabrication by stressed mirror polishing 80−99886
mirror surface manufacture on pyroceramic blanks 77−62079
monolithic component glasses and rigid sintered fibre-optic elements, microcrack form. during grinding 78−87175
optical aspheric rotationally symm. surface generation, computer control 77−27395
optical blank grinding and polishing, for LAT primary mirror 78−90541
optical blank shaping by free grinding method, system of allowances 78−46849
optical component manufacturing of low stiffness plates 78−71236
optical crystals, finishing using diamond cup grinding wheels *(German)* 80−19112
optical elements, high speed production line design 77−27397
optical fibre, grinding and polishing productivity, diameter depend. 77−62067
optical glass, kinematic relationships in automatic glass grinding and polishing machines *(Czech)* 79−32096
optical glass, semiautomatic machines kinematics *(Czech)* 78−63208
optical glass, surface layer structure after grinding and polishing, Kr sorption meas. 77−31122
optical glass, variation of diamond tool working ability 77−7225
optical glass ceramic, (sital) surface operation parameters, selection using bending strength tests 79−32101
optical glass diamond grinding kinetics 80−64224
optical surface shaping, contact problem soln. 80−33260
optical surface shaping, contact problems 80−74540
optical surface shaping by successively corrected mask method 78−18076
optical surfacing, struct. of fine ground surface 77−27393
optical workshop machines, kinematic relationships *(Czech)* 78−50953
particle size measurement techniques, rapid response, online methods, continuous industrial processes appl. 78−89429
particles, small, impossibility of comminution by compression 78−52709
pellet precision grinding and high-speed polishing using synthetic material 78−50958
physical theory, eqn. of state *(Russian)* 79−74267
Polirit granules for polishing, evaluation of disintegration degree 77−11057
polycarbonate, decomposition by H_2SO_4 and grinding by ball mill, exam. of molecular chain scission *(Japanese)* 78−64827
polycarbonate, degradation behaviour by vibratory ball mill *(Japanese)* 78−39732
polymers and elastomers, cryogenic grinding technique 77−32555
grinding continued
polystyrene, degradation behaviour by vibratory ball mill *(Japanese)* 78−39732
porcelain, strength eval. after grinding 77−52518
porous materials, effects of different methods of prep. on reproducing surface 80−60995
porphyrins, metal-free, EPR, sample grinding effects 80−60420
powder, dry ball milling, breakage parameters variation with ball and powder loading 80−80999
powder, moist, granulation on vibrated chute *(Japanese)* 78−95710
powder, ultra fine, surface roughness effect on formation by rotating friction mill *(Japanese)* 78−95709
powder, work index estimation during grinding *(Japanese)* 78−19680
powders, ultra fine prod. by rotating friction mill, mechanism in initial wear region *(Japanese)* 80−25589
PVC, mech. comminution in fine struct. changes in porosity, density, specific surface area *(German)* 78−35345
quartz, grinding and surface treatment by ball mill in cetyl alcohol *(Japanese)* 80−25890
quartz, ground single crystal, stressed surface layer depth *(Russian)* 79−79133
quartz, mechanically activated, reactivity *(German)* 79−29395
quartz, quantitative X-ray anal., standardisation, milling effect on degree of disorder *(German)* 78−11176
quartz ground surface, structure features of dull layer 77−54763
quartz powdered, thermal effects of Fe contamination, adsorbed H_2O, annealing on DTA 79−100161
rare earth-Co alloys, ferromagnetic intermetallic compounds, comminution charact: 77−12564
rare earth-Co alloys, powdered, fine grinding in gastight attrition mill 79−33967
Reciprocating motion for fine diamond grinding 78−71237
residual stresses determ., ground and lapped metal surfaces 79−34211
residual stresses rel. to grinding and cutting directions, X-ray diffr. obs. *(Japanese)* 78−23847
rod mill, for wet grinding of igneous rock at temps. up to 400°C 80−37012
semiautomatic machines, kinematic ratios calc. *(Czech)* 78−79146
single crystal surfaces, grinding and electropolishing using simple goniometer 78−4604
sintered material, porosity effect on temp. generated during grinding 78−35530
Sitall-based composite mat., grinding 77−63822
small grinding and polishing tool control by computer 79−98516
small nonsymmetrical aspheric surface fabrication, using grinding or polishing minipad 79−64365
spherical lens generator, sphericity and fracture control 77−27394
spherical optical component, cutting process for coarse grinding, optimisation 79−32103
steel, alloy, fatigue strength and fracture, diamond grinding effect 80−55532
steel, grinding, effect of hardness, texture, and bond of grinding wheel, temp. effect *(German)* 79−43459
steel, grinding effect with Elbor wheel 78−48540
steel, high speed, wheel loading meas. using neutron-activated workpieces 79−5070
steel, low C, fatigue endurance limit, metallurgical technology and mech. treatment effect 80−55536
steel, martensitic cracks form. mechanism obs., impingement cracks and strain influence *(Japanese)* 78−56747
steel, medium C, ground, residual stresses, X-ray evaluation 80−79863
steel, mild, fatigue strength, effect of grinding surface *(Japanese)* 77−48533
steel, Mn (16 to 20 wt.%) metallographic analysis method 80−50791
steel, sintered, high speed, with Ti(C,N) additions 78−11160
steel, stainless, 316, surface finish effect on low-cycle fatigue at 400°C 79−29277
steel, type 12Kh2N4A, belt grinding, struct. transformations 80−30169
steel, unhardened, grinding by Si_3N_4-based abrasive material 78−35529
steel 40 kH, wear resistance in oil abrasive environment, various grinding methods *(Russian)* 77−70184
steel 40Kh, surface working effects on crack resist. *(Russian)* 78−56734
steel bearing, surface-ground, residual stress fatigue property comparison 80−60975
steel cutting and grinding, surface adsorption effects 78−39938
steel ShKh15, fatigue strength and residual stress distrib., machining method effects 78−31528
steel stainless, solar energy collector optical props. rel. to heat treatment 78−94455
surface profile, crest and trough height distrib., Monte Carlo simulation *(Japanese)* 79−34180
surface profile power spectrum, Monte Carlo simulations *(Japanese)* 79−34179
temperature measurement, dynamic calibration of synthetic diamond thermoelectrodes 77−55985
thermophysical analysis *(Russian)* 78−48549
thin and polished section preparation status and trends *(German)* 80−28360
thread grinder, high precision, laser interferometric auto-correcting system 80−90830
ticonal, grindability improvement, thermomagnetic and heat treatments 77−16625
transition metal borides, abrasive props. 77−63808
vibratory mill, prod. of small amounts of finely divided unoxidised mat. 78−68646
vibratory tools, hand-arm energy dissipation and accel. levels 78−96116
Zircon ceramic, exam. of development and fabrication 80−11608
AgCl, surface layer stress distrib. after mech. treatment, polarisation-optical obs. 78−18887
Al, wheel loading meas. using neutron-activated workpieces 79−5070
Al_2O_3, abrasive, wear in simulated hot grinding 78−56784
Al_2O_3, crystallite size and lattice distortion, determination using X-ray line broadening analysis, appl. to ceramic powders 79−8261
Al_2O_3, grinding and polishing, quantitative control and optimization *(German, English)* 80−35460
Al_2O_3, grinding material, grain shape optimization *(Polish)* 80−29916
Al_2O_3 hot pressed, high density, effect of grain size on grinding 78−39723
Al_2O_3 suspensions, grinding method influence on rheology and suitability for high-density sintering 79−29001

grinding continued
β-B, abrasive props. 77−63808
C, dense hard-type solids prep. from petroleum coke powder by grinding 79−20002
Ca halophosphate luminophors, grinding influence on thermolum. 79−95854
CaF_2, press-forged laser window, polishing, cleaning and grinding 79−59849
$CaSO_4$:Dy phosphor powder, effect of grinding on thermoluminescent sensitivity 79−33852
β-Ca_2SiO_4-CaO-SiO_2 paste, hydration, compression strength and composition 80−50584
$Cd_xHg_{1-x}Te$ single crystal, photoconductivity spectral distrib. rel. to surface condition 79−78136
CdS, magnetic susceptibility, grinding-induced states 79−61040
CdSe, magnetic susceptibility, grinding-induced states 79−61040
Co, superalloy, attritious wear in grinding 77−32696
Cr, powder comminution method effect on props. of TiC-steel+Cr composite 78−15341
Cr-Fe (30 wt.%) alloys, refined fine comminution 78−60598
Cu phthalocyanine, grain boundary struct., crystallographic planes 80−103366
Fe, Armco, ground, residual stresses, X-ray evaluation 80−79863
Fe complex, pyridine-n-oxide perchlorate, Mossbauer spectra, site distortions enhanced by grinding 80−15883
Fe-Pt, plastic deform. effect on struct. singularities and mag. props. *(Russian)* 80−44892
GaAs, peculiarities of plasma region reflection, effect of surface treatment methods *(Russian)* 79−69827
GeTe, machining effects on electrophys. props. 77−86199
InP substrates, HCl etching speed and polarity obs., with aid of laser beams *(Slovak)* 78−56575
InSb, X-ray topographic evidence of asymmetrical pre-yield behaviour 80−75229
K_2O-Al_2O_3-B_2O_3-SiO_2, glass, ESR exam. of paramagnetic centres formed during mech. destruction by grinding 78−88188
La-N-C system, metallographic investigation *(German, English)* 77−52600
LaB_6, US comminution of refractory compound powders 78−23656
LiF ground surface, structure features of dull layer 77−54763
MgF_2, mech. props. anisotropy effect 77−797
MgO, anisotropy of grinding damage, chem. polishing and etching 79−47793
MgO, powder activation during grinding 77−90300
MnBi particles, effect of grinding on coercivity 77−36098
Mo sputtering for laser mirror refurbishment 80−14498
Nb-N(O)(C) system, specimen prep. for metallography *(German, English)* 80−89439
Nb_xC powders, plastic deform. characts. on vibratory milling 78−11183
Ni, powder, subjected to vibratory milling, exam. of plastic deformation, recrystallisation, sintering 80−16234
SiC, abrasive, wear in simulated hot grinding 78−56784
SiC, attritious wear 77−32696
SiC, grinding, effect of grinding wheel material, particle size, temp. *(German)* 79−43173
SiC, grinding material, grain shape optimization *(Polish)* 80−29916
α-SiC monocrystalline grains, mech. props. and grain separation *(Polish)* 80−40554
SiC, US comminution of refractory compound powders 78−23656
SiO_2, fused material removal mechanism by free abrasive grinding 77−52510
SnTe, mechanochem. and thermal oxidation comparison, Mossbauer obs. 80−104310
SrF_2, press-forged laser window, polishing, cleaning and grinding 79−59849
SrO.HfO_2(ZrO_2), US comminution of refractory compound powders 78−23656
$SrTiO_3$ electro-optic crystals, mechanical grinding and polishing 80−48471
Ta-N(O)(C) system, specimen prep. for metallography *(German, English)* 80−89439
Ti alloys, grinding, effect on surface struct. 80−25878
Ti-Al-V-(Sn), surface finishing effect on internal stresses, X-ray study *(German)* 79−34210
TiC-Fe-Cr powder mixture, exam. of milling condition effects 80−16237
$TlCl_3$.$(TlCl)_3$, labelled, exchange of Tl ats. rel. to γ-irrad., heat treatment, grinding 78−92470
U ore, ^{222}Rn release 78−89970
V-N(O)(C) system, specimen prep. for metallography *(German, English)* 80−89439
W, polishing technique as prep. for TEM 80−71851
W, powder, subjected to vibratory milling, exam. of plastic deformation, recrystallisation, sintering 80−16234
WC, electrochemical grinding, effect of mag. field 77−86214
WC-Co, quantitative charact. of surface damage by electrochemical grinding 79−47836
WC-Co (10 to 30 wt.%) transverse rupture strength, residual stresses due to surface grinding effects 77−63789
Y_2O_3, effect of roasting temp. of $Y_2(C_2O_4)_3$ on crushing, compressibility, sintering props. 77−8790
Y_2O_3, translucent ceramic, prep. effect on struct. and props. 79−87601
Y_2O_3, US comminution of refractory compound powders 78−23656
Zn ferrite, production by mechanochemical reactions by grinding in ball mill 79−20014
ZnO, adsorpt. of H_2O vapour, annealing and grinding effects 78−68656
ZnO, ground powder, X-ray Fourier anal. *(Japanese)* 78−39727
ZnO powder, effect of dry grinding in EPR and catalytic activity *(Japanese)* 80−84640
ZnO-B_2O_3, glass, ESR exam. of paramagnetic centres formed during mech. destruction by grinding 78−88188
ZrC, US comminution of refractory compound powders 78−23656
ZrO_2, metastable, tetragonal, strengthening by surface grinding 80−71777
ZrO_2, near-surface phase transforms., effect of grinding and polishing 78−15557
ZrO_2, produced by coprecipitation with stabiliser, sintering 77−66614
ZrO_2 products from granules, props., prep. method effect 80−25628
ZrO_2, wet vibro-grinding with surfactants, superhigh density sintering suitability 79−33989
grinding continued
$ZrSiO_4$, mechanochemical effect by mechanical grinding *(Japanese)* 78−84754
$ZrSiO_4$, sintering, effect of grinding and additives 78−48356
grinding mills *see grinding*
ground electrodes *see earth electrodes*
ground services, aerospace *see ground support systems*
ground support equipment
see also aircraft communication; navigation; telemetering equipment
Mars 6 descent vehicle radio signal parameters meas. by retranslation method 77−67020
meteorological rocket telemetry system *(German)* 77−64606
Pioneer Venus occultation experiment, radio science data generation 80−67492
Seasat-A satellite synthetic-aperture-radar processor, England (Oakhanger) sited 79−21128
SIRIO satellite down link propagation expts. in Finland 79−84338
SIRIO satellite reception, atten. meas. during first year at Deutsche Bundespost Earth station at Leeheim 79−84335
SIRIO satellite signal propag. meas. by Netherlands PTT ground station, and equipment 79−84344
SIRIO satellite transmissions near 11.6 GHz at Slough UK, meas. 79−84333
space science instrument testing, modular, CAMAC based computer controlled ground support equipment 79−25434
Viking Ground Reconstruction Equipment for facsimile picture recording 77−38051
ground support systems
see also aircraft communication; navigation; telemetering systems
aeronautical meteorology, progress and challenges 78−53692
artificial satellite attitude determ. system, Taiyo (1975-014A) *(Japanese)* 77−17319
communications satellite system measurements 78−61712
CTS biomedical communications expt., selection of Earth terminal parameters 77−48898
GEOS, IUE and METEORSAT Earth Station antennas, design, charcts. *(German)* 77−56764
GEOS, IUF, and METEOSAT ground stations, weather obs., Earth exploration *(German)* 77−56763
geostationary orbit determ., by single-ground-station tracking 80−109329
International Ultraviolet Explorer (IUE), ground data processing system performance 78−96383
International Ultraviolet Explorer (IUE) spacecraft, instrumentation and ground control 78−96382
Ionosphere Sounding Satellite appl., operation planning and data anal. *(Japanese)* 79−16799
Ionosphere sounding satellite control, automated system 77−60572
Ionospheric Sounding Satellite, automated control system *(Japanese)* 77−78607
Ionospheric Sounding Satellite, command system *(Japanese)* 77−78609
Ionospheric Sounding Satellite, summary of control centre *(Japanese)* 77−78606
Ionospheric Sounding Satellite, telemetry receiving system *(Japanese)* 77−78610
Ionospheric Sounding Satellite control, data recording and anal. system *(Japanese)* 77−78611
Ionospheric Sounding Satellite control, tracking system *(Japanese)* 77−78608
IR Astronomical Satellite (IRAS), ground operations and data processing 79−80193
meteorology, aviation weather, automation in prediction procedures 78−49080
Meteosat ground facilities, European/W.Indian network *(French)* 78−45183
Meteosat image processing 78−36297
Ondrejov laser satellite-tracking station, site evaluation 78−36418
OSO-8 UV spectrometers, computer-controlled mission operations 80−41723
passive ground-based electro-optical detection of artificial Earth satellites 79−62717
Pioneer Venus, Unified Abstract Data Library and Quick Look Data Delivery System 80−67494
Pioneer Venus Multiprobe entry phase, telemetry recovery 80−67493
SAS-3 X-ray astronomical satellite, programmable format telemetry system 77−2328
satellite solar cell panel monitoring by ground station telemetry 79−62003
Spacelab, high rate data handling in space and on ground, multiplexing system 79−21138
Spacelab, payload data path from user input (on-board) to user ouput (laboratory) 79−21137
UK-6 satellite, computer command system 79−25440
Voyager, telecommunications system and broadcast from Jupiter 80−26715
weather service, future trends 78−53694
grounded anode amplifiers *see cathode followers*
grounded collector amplifiers *see emitter followers*
grounded plate amplifiers *see cathode followers*
grounding *see earthing*
groundwater
accumulation zone of mineralized water in salt-bearing sections, vertical electric sounding *(Russian)* 78−11807
E.Africa, meteoric water ^{18}O content rel. to Pleistocene climatic changes 77−56723
alluvial aquifer, Galerkin-finite element simulation of recharge 78−81263
alluvial aquifers, relations between geophysical and hydraulic parameters *(Italian)* 77−53079
annual discharge vars. into railroad tunnels 77−78268
folded Appalachians, meteoric water circulation rel. to thermal springs origin and heat flow meas. 80−41414
aquifer, flow in fractured porous media 77−91173
aquifer, partially confined, uniform eqns. for nonstationary filtration 77−70693
aquifer, temp. field due to hydrothermal convection, numerical calcs. 80−90105
aquifer, viscoelastic model appl. to subsidence due to pumping 77−91175
aquifer characteristics, sensitivity anal. rel. to linear programming management model 78−11936

groundwater continued
aquifer computer model *(German)* 79−53377
aquifer delayed yield, theory 80−61830
aquifer delayed yield resulting from soil water hysteresis 80−61834
aquifer fluid flow when charged with hot water from fault zone 79−74921
aquifer hydrology, inverse problem by statistical approach 80−105011
aquifer parameters, invariant imbedding and identification 79−57992
aquifer parameters calc. method using sparse data 80−61826
aquifer permeability and storage identification by artificial recharge hybrid simulation 77−45043
aquifer recharge from ephemeral streams in arid regions 79−5521
aquifer response to tidal forcing and 1964 March 28 Alaskan earthquake 78−73407
aquifer simulation of groundwater, Canterbury, New Zealand 77−53093
aquifer storage capacity determ., well tide eqn. 80−21785
aquifer transmissivity calc., statistical approach to inverse problem 80−61827
aquifer vars. rel. to transmissivity and storage, models 79−16537
aquifer water extraction leading to land deformation 80−105003
aquifers, convection, effect of temp. depend. viscosity and thermal expansion 79−32662
aquifers, effects of drought in England and Wales, 1975-6 period 78−88866
aquifers, hydraulic characts. 77−9450
aquifers, hydrodispersive transfer 80−98374
aquifers, pollutant prop., experimental study *(French)* 77−41105
aquifers, pollution transfer charact. evaluation using tracers *(French)* 77−41104
aquifers, thickness mapping from geoelec. soundings 78−3712
aquifers, transport model parameters determ. 78−61463
aquifers used for fluid storage, head gradient control 78−11944
aquifers with horizontal and vertical fractures, elec. macroanisotropy coeff. calc. 77−52976
arenaceous aquifers, matrix conduction props. 77−64347
arid terrain, soil zone chemistry in cyclic wetting and drying 79−62529
artesian wells drilled in permafrost, temp. field, efficiency of heaters for ice plugging prevention 77−78242
artificially fractured rock, heat transfer agents flow patterns 80−17239
Athabasca Oil Sands area, Alberta, groundwater temps. 79−62465
Atlantis II Deep, geothermal brine system 80−94526
audiomagnetotelluric investigations in geothermal areas 79−84097
Baikal region hot springs *(Russian)* 80−94551
N.Baja California, groundwater rel. to submarine hydrothermal activity 78−61431
Boisson spring waters, physiological props. of dissolved ^{222}Rn 79−48292
borehole in karat dolomite aquifer, vertical groundwater flow 80−81938
boundary integral eqn. method for two-dimens. steady groundwater problems 79−16718
bounding wells to counteract preexisting groundwater movement effects 79−2324
Broadlands geothermal field, New Zealand, boiling curves 78−85516
calcite-depositing spring, chemical vars. and calcite precipitation 79−44202
carbonate chemistry of chalk water from Givendale, E.Yorkshire 79−66719
casing depths and solute travel times to wells 79−2321
Caspian Sea, submarine groundwater runoff contrib. to biogenous elements balance 80−31073
cavernous aquifer, thermal convection currents 77−64340
Cerro Prieto geothermal field, conf. at San Diego, (Sept. 1978) 80−94911
Cesano geothermal field, Italy, geological study 80−76975
Cheleken Peninsular geothermal waters, USSR, search for superheavy nuclei 79−96781
chemical geothermometer, Na-K-Ca temp. with Mg correction 80−51357
chemical migration of radionuclides in soil 80−17144
climate, soil and vegetation, annual water balance dynamics 79−79896
climate, soil and vegetation, soil moisture movement in liquid phase, model 79−79894
climate, soil and vegetation, water balance dynamics 79−79893
coastal aquifer, single potential soln. for regional interface problems 77−41080
coastal aquifer of Israel, nitrate and chloride pollution, single-cell model 77−5265
coastal aquifer water flow analysis 80−26654
coastal aquifers, Bahia, Brazil, study using resistivity surveys 79−57977
Columbia Plateau, groundwater at time of basalt flow intrusion 80−81881
column drainage through porous media, moving boundary problems, theory and numerical analysis 78−81252
computer assisted management *(German)* 79−57989
confined, form. rate of chem. composition 80−46207
confined aquifer unsteady flow, boundary integral methods 80−61828
confined-unconfined aquifers, numerical study 77−41081
contaminant arrival distribs. as general evaluation requirements 79−16533
contaminant arrival distribs. for steady flow in heterogeneous systems 79−16535
contaminant arrival distribs. in transient flow systems 79−16536
contaminant location/arrival time/outflow distribs. for steady flow 79−16534
contaminated groundwater zone control by underground impermeable wall, radioactive waste site *(Japanese)* 79−34446
contamination, Holt County, Nebraska, USA 80−12033
continental geoid fluctuations, effect on groundwater and environment 78−36215
contour mapping in Venice, stochastic interpolator method, theory 80−8353
contour mapping in Venice, stochastic interpolators method, results 80−8354
convection, simple theoretical and expt. study, geophysical appl. and analogies 80−24018
convection of water adjacent to horizontal impermeable surfaces, similarity solns. 78−11940
convective dispersion, finite element. anal., book contrib. 79−34877
convective dispersive equation, movement of chemical pollutants in groundwater, model 80−16855
convective instabilities in vertical fractures and faults 80−21786
cooling of infinite sill (igneous intrusion) 79−20787
groundwater continued
Cortaro Basin, S.Arizona, inverse method appl. 80−98371
crack propagation due to hydrostatic press. 80−72505
crustal fracture, fluid-filled, mechanical interaction with Earth surface 79−79779
crustal fracture water, radioisotope long-term vars. rel. to earthquake prediction 79−62451
Dead Sea rift valley brines, Sr behaviour 80−17295
delayed aquifer yield as a phenomenon of delayed air entry 79−84325
density distrib., horizontal and vertical, piezometric level determ. 78−49043
desaturating geothermal reservoir, numerical modelling 80−12363
dissolved ^{14}C, initial activity determ., new model and review 80−8458
distributed parameter system identification using doubly cubic spline, underground aquifer appl. 78−69391
Diyala catchment, Iraq, water balance between Derbendikhan and Himrin dams 80−12462
drainage basin parameters, patterns of variability, India 79−39769
drainage runoff hydrograph calc. for loamy soils in Lithuanian SSR 79−39781
Dutch sedimentary deposits, prospecting using resistivity method 77−9527
dynamic aquifers with stochastic forcing function, analysis 79−2319
dynamics in plane regions during time varying seepage and evaporation *(Russian)* 79−79878
Earth tide effects on flows in horizontal permeable elastic layers connected to wells 78−7666
earthquake precursory changes of groundwater Rn content 80−94467
earthquake precursory Rn changes, in shallow subsurface of New York State 80−94463
earthquake precursory Rn changes, Izu-Oshima-kinkai earthquake (1978) 80−94472
earthquake prediction, changes in chemical composition, subterranean waters and gases *(Russian)* 79−84163
earthquake prediction methods, conditions and hydrodynamics of underground water *(Russian)* 79−84162
earthquakes initiated by seasonal rainfall, S.California 80−85615
Edwards carbonate aquifer, Texas, U isotopes fractionation rel. to aquifer oxidation/reduction 80−98362
EM freq. sounding in Tunisia 77−9529
emulsion containing water from crack detection processes using penetrating agents, purification *(German)* 79−5517
England, decreasing wetness in 1969-77 period 78−65377
evaporation from soil, water and crop surfaces, eqn. for remote sensing 77−64334
evaporite deposition from groundwater mobilised salt, coastal sabkhas, Libya 80−81883
exploration in hard rock terrain 77−41075
extraction in southcentral Arizona, rel. to faulting 79−57979
fault slip stabilisation by coupled deformation-pore fluid diffusion 80−56378
filtration characteristics, multiple functions of filters in thermistor meas. *(Polish)* 78−40716
fingero-imbibition phenomena with varying phase density, two parameter singular perturb. soln. 79−29789
finite element Galerkin method for groundwater flow calc. 78−89320
fissured aquifer with free surface level, unsteady flow to pumped well 79−16547
Florida, water chemistry and mass transfer in artesian aquifer 78−49057
Floridan Aquifer, dolomitisation of sediments 79−53346
flow, free boundary problem 77−66933
flow, fresh-salt water interface, mixing zone *(Japanese)* 78−11927
flow, investig. using In-EDTA tracer and neutron activation anal. 78−11921
flow, numerical predictions by method of characts. 77−29342
flow, one-dimens. unsaturated-saturated problem, two-dimens. view 79−5525
flow, unconfined, tunnel opening, 2-D finite element anal. 78−11922
flow 2-dimens. eqns. soln., iterative methods 77−64351
flow anal. by finite element method 78−92871
flow anal. by finite element method 78−92875
flow digital simulation, finite element method 78−93018
flow equation, computational efficiency and Taylor expansion derivation 79−88383
flow in aquifer with consolidation, Theis soln. deviations 77−64344
flow in deformable porous media, algorithm 79−2323
flow in unconfined aquifers, integro-differential eqns. 79−5522
flow in unsaturated noncohesive soil, modelling *(Polish)* 77−70709
flow model using finite element method 78−92874
flow models for statistically homogeneous porous formations 80−12448
flow parameters, spatial variability and uncertainty, geostatistical technique 80−8352
flow pathways determ. from satellite altitudes, apparent radiance data appl. 79−16522
flow pattern in soil using equation of mean 80−81958
flow rear lakes, numerical simulation 79−2322
flow simulation with computer-controlled RC network 77−45045
flow systems, three-dimens. modelling 79−84318
flow through inhomogeneous porous media, analytical theory 77−62301
fluid convection, appl. to Rn long-distance migration 77−37246
fracture water radioisotope abundances for earthquake prediction 79−44124
fracture water radioisotope vars. and earthquake prediction 79−44204
fracture waters in Ukrainian Shield, search using geothermal survey peculiarities *(Russian)* 80−104935
fracture zone water of N.Kirgizia, He content and U series isotopes 77−33108
free water surface behaviour, porous media, appl. to earth dam seepage 80−8349
free water surfaces mapping methods *(French)* 79−96771
freshwater-brine mixed solution, chemical speciation of Cd, Cu, Pb and Zn 78−20409
frost heave in Tomakomai, Hokkaido, 1976 to 1977 *(Japanese)* 78−92860
Galal Badra Basin, Iraq, water deficit 80−26565
Galapagos Rift hydrothermal fields, struct. and morphology of seafloor 80−72489
Galerkin finite element procedure for analyzing flow through random media 79−81967
geochemical nature, Giji and Kian, watersprings in southern Okinawa, Japan *(Japanese)* 79−96783

groundwater continued
geomorphological studies for exploration of groundwater in Rajasthan desert 79−53375
geopressured geothermal wells production characts. 78−81223
geothermal aquifers, reservoir lifetime and heat recovery factor, for urban heating 79−74492
geothermal areas in Iceland, H-water isotope thermometer appl. 78−69384
geothermal energy, review 79−29447
geothermal energy extraction from penny-shaped reservoir made in hot dry rock 80−108784
geothermal energy investigations in Sweden 79−74488
geothermal energy prospects in Brazil 79−74487
geothermal energy resources, low enthalpy, in Denmark 79−74489
geothermal energy resources in Oregon, USA, elec. and EM sounding obs. 80−97761
geothermal exploration in Iceland, volcanological methods 79−74877
geothermal field parameters, convection theory 79−66663
geothermal fluid buoyancy, CO_2 effect 79−44203
geothermal fluids, exploration via seismic noise sources mapping 77−81828
geothermal reservoir, liquid dominated, fault zone controlled charging model 80−81935
geothermal reservoir, transient steam flow, Kawah Kamojang, Java 80−77018
geothermal reservoir exploitation, finite difference modelling 80−55798
geothermal survey of Namekawa and Ubayu spas, Japan *(Japanese)* 77−70619
geothermal systems, natural convection in porous media, review 79−1194
geothermal systems, sulphate-water O isotope thermometry 78−69383
geothermal tracing with atmospheric and radiogenic noble gases 78−69502
geothermal water, possible presence of superheavy elements *(Russian)* 79−13358
geothermal water, pressure-temp. curves under conditions of New Zealand geothermal field 77−51488
geothermal water-rock association in Massif Central, France, ^{87}Rb-^{87}Sr systematics 77−60373
geothermal waters, fluorite solubility equilibria 77−60368
geothermal well water, chemical analyses at Coso, California 80−90104
geothermally active fault zone, water convection 80−19375
geothermometer using Na/Li ratio in geothermal waters *(French)* 79−53369
geothermometry, chemical and isotopic techniques 78−69501
geyser vent, pre-boiling convection, mathematical model 80−31067
geysers, lab. models rel. to natural phenomena 78−69373
granite, failure expts., pore press. stabilisation 80−90079
Grant Mineral Belt, New Mexico, effects of U mining and milling 77−56657
Grass Valley, Nevada, USA, microseisms in geothermal exploration 80−21647
gravity exploration in glaciated areas 77−91289
gravity secular variations, due to water quantity vars. in lithosphere *(Russian)* 78−53609
gravity-induced cross-formational flow of formation fluids, red earth region, Alberta, Canada 79−84317
Great Lakes, water table fluctuations rel. to W. Lake Michigan shoreline erosion 79−5542
Guaymas Basin, Gulf of California, basaltic sill intrusion into sediments, hydrothermal activity 80−46154
Hakone volcano, Japan, thermal structure and energy balance 79−74878
Hawaii Geothermal Project, groundwater geochem. study 80−72567
Hawaiian geothermal areas, compositions 77−64331
head gradient control in aquifers for fluid storage, comments and reply 79−5533
heat flow anomalies in sulphide deposits due to groundwater flow *(Russian)* 78−15978
heat transfer with liquid filtration into shattered rocks 79−81962
Heidelberg, groundwater U conc. rel. to world rivers natural U content 79−44208
heterogeneous multiaquifer systems, iterative quasi-three-dimens. finite element model 79−79905
hillslope hydrographs using finite element method 77−70696
Himalayan geothermal belt *(Chinese)* 79−79759
hodograph method, use of reference function 79−84323
hot brines from French Dogger, metastable S species and trace metals 79−62527
hot Limagne spring reservoir temp. estimation *(French)* 80−41462
hot spring and drill hole water, geothermal reservoir temp. determ. using O isotopes 78−69382
hot spring water, dissolved Al concs. in France *(French)* 79−74913
hot spring water chemical constituents, Mt. Akagi region (Japan) *(Japanese)* 78−16072
hot springs, Japan, heat output vars. rel. to earthquakes *(Japanese)* 78−96241
hot springs Mt. Akita-Komagatake area, Japan, F content measurement *(Japanese)* 80−31074
hot water springs in N.Spain, trace elements concs. *(Spanish)* 77−49097
hydraulic conductivity, numerical calc. from suction press.-moisture retention relation *(German)* 79−2297
hydrologic cycle, rel. to nuclear waste disposal 78−94103
hydrologic influence on long-period motions of Potsdam plumb-line *(Germany)* 78−57222
hydrothermal alteration in active geothermal fields 79−5535
hydrothermal alteration mapping, airborne spectroradiometric data anal. and LANDSAT data appl. 79−34973
hydrothermal alteration of hot spring deposits 80−76974
hydrothermal alteration of volcanic rocks at Matagami, geochemistry rel. to massive sulphide genesis 78−77231
hydrothermal flows, two-phase, in permeable media, struct. 80−85693
hydrothermal system, temp. measurement scale based on chem. comp. of gas fraction 80−98277
hydrothermal system in Long Valley caldera, results from mag. model 77−86846
hydrothermal systems, transport phenomena assoc. with cooling plutons 78−36206
hydrothermal systems transport phenomena, nature of rock porosity 78−36205
Iceland, D tracing in hydrothermal systems 78−69386
groundwater continued
Iceland high-temperature geothermal systems, aquifer chemistry 78−96245
imbibition in 2-phase flow through porous medium with capillary pressure 79−20884
imperfect borehole, hydromechanics and stationary filtration *(Russian)* 79−88375
Imperial Valley, California, quadrupole resistivity survey of geothermal fields 79−84096
India, Wenner electrode obs., seasonal and salinity depends. 79−92551
Indian radioactive thermal spring water D content, mass spectrometric anal. 79−39765
induced recharge in Ganges Basin, alternative methods for water supply 80−81952
infiltration into frozen soil 78−16077
ionic diffusion in naturally-occurring aqueous solns., use of activity coeffs. in transition-state models 78−57224
irrigation, connection between soil and groundwater 80−26554
irrigation detection in the Loire-Britanny river basin *(French)* 79−96774
S.Israel, isotopic comp. of formation waters from deep drillings 77−86945
Izu Peninsula, Japan, groundwater geochem. in crustal uplift area, rel. to earthquake prediction *(Japanese)* 78−96242
Izu-Oshima-kinkai earthquake, Jan. 1978, groundwater chem. and temp. changes *(Japanese)* 80−46134
Izu-Oshima-kinkai earthquake, Jan. 1978, precursory groundwater level changes *(Japanese)* 80−41391
Jharia Gondwana sedimentary basin, India, groundwater movement rel. to geothermal meas. 80−98276
Kalahari Basin, geoelec. survey 78−3830
Kalamos springs, Greece recharge area determ., environmental isotope study 79−53393
karst depressions, areal growth rates, ages 79−48484
karst waters and karstic rocks tidal movements 77−86940
karstic limestone terrain, Texas, USA, drainage history and aquifer 80−56501
karstified aquifer in Donaueschingen, W.Germany 80−26564
Kingskettle, Scotland, phenol and cyanide leaches into groundwater from gasworks site 79−88020
Krafla caldera, NE Iceland, groundwater mass flow rel. to gravity and elevation changes 80−90052
Lake Assal (FTAI), geothermal zone, geochemical and expt. studies 78−69314
Larderello field, secondary changes in composition of geothermal fluids 78−69387
leaky aquifer, approx. differential eqn. 78−81242
leaky aquifer analysis, finite element method soln. 78−93017
leaky aquifiers, integrodifferential eqns., numerical method of unlimited appl. 78−11935
level var. on central San Andreas fault 77−91023
levels rel. to landslide stability *(Russian)* 77−25683
limestone diagenesis simulation, computer model based on Sr depletion 78−73358
lithosphere elastic expansion caused by groundwater depletion 80−31010
macroscopic dispersion in porous media, controlling factors 78−11938
management, finite element discrete kernel generator 78−92873
management, system response function hierarchy 77−64346
management by decomposition 77−64345
Massif Central hot springs, France, alkaline earth ions acquisition, rel. to geothermometry *(French)* 79−29788
medium with low initial water saturation, end effect in two-phase flow 80−33656
migration during soil freezing, obs. *(Japanese)* 78−88862
Milk River aquifer, Alberta, isotope and ion geochemistry 80−8351
modified Richards' eqn., oscill. of numerical soln. 78−81243
motion into dilatant zone, electrokinetic and mag. anomalies prod. 79−39658
movements, detect. by gravity survey rel. to tectonic movement detect. 77−33038
mud volcanoes, Copper River Basin, Alaska, composition of emitted gases 79−84308
multi-layered geothermal reservoir, natural convection 80−8347
multicell aquifer model calibration, iterative method 80−8456
multiple fluid in three dimensions, vortex theory 80−14709
Nasu hot spring, F content *(Japanese)* 79−8648
natural recharge, math. modelling 78−11934
Nepal, geothermal springs 80−72476
New Brunswick, resistivity and induced polarisation (IP) survey for delineating saline water and fresh water zones 80−104867
non-steady flow problem in two-layer porous medium 78−81260
nonlinear laminar flow into eccentrically placed well 77−66929
nonlinear laminar flow into well in porous aquifer 78−7670
nonsteady flow through tunnel opening, reductive finite element/Crank-Nicolson anal. 78−92861
Norris Geyser, Yellowstone Park, USA, microseisms of geothermal area 80−104909
occurrence in trappean terrain of Sholapur district, Maharashtra, influence of groundwater divide 79−8649
ocean floor hot spring created by drill hole 80−55951
oilfield brines from Kansas and Colorado, Sr isotopic comp. 78−57225
oxidation-reduction sequences in ground water flow systems 79−84303
Palmdale, California, groundwater diffusion rel. to P-wave millisecond travel time vars. 79−57863
Palmdale, California, groundwater rel. to crustal resist. changes 79−16373
perched water table detection using EM telemetering systems 80−26655
permafrost, effect of seepage flow on thawing and freezing 79−1241
phosphate fertilizers, leaching from agricultural soils to groundwater 79−20901
phreatic aquifers between two open channels, transient anal. 77−78284
phreatic flow over sloping semipervious layer 79−16532
physicochemical characts. vars. around Asama Volcano, Japan, rel. to volcanic activity *(Japanese)* 79−70814
pixe analysis of water with detection limits in the ppb range 79−48005
pollutant, hydrodynamic dispersion in soil *(Italian)* 77−41071
pollutants, radioactive tracers appl. *(French)* 80−7995
pollutants from underground coal gasification 78−92865
pollution below Dharwar, India 78−69380
pollution from septic tile field 77−29338

groundwater continued
pollution of surface and underground waters, isotopic tracing *(Italian)* 77−53078
pore fluid stabilization of weakening fault zone, earthquake precursory effects 79−84145
pore water pressure changes in sand deposits during earthquakes 79−88308
porous media, miscible or immiscible displacements, identification and modelling 78−69392
porous stratum, plane stationary flow, temp. field calc. using Lauwerier formula analogue 80−38485
prospecting in Africa, geophysical techniques 80−61818
prospecting techniques used in Armenia volcanic region 80−85753
quality, coal gasification potential impact 79−87949
quality in GFR, survey results *(German)* 79−62539
radar subsurface sounding of groundwater in deserts and glaciers 80−67437
radio-nuclide transport in soil, conc. profile in groundwater, waste storage problems *(German)* 79−74556
radioactive liquid waste disposal in deep aquifers in USSR 79−29489
radioactive waste, low-level commercial disposal sites, trench water survey 79−85629
radioactive waste burial sites, hydrogeologic conditions, groundwater modelling 80−21550
radioactive waste geologic repositories, computer anal. of long-term radiation hazards 80−18483
radioactive waste migration, groundwater environment, hydrodynamic dispersion in transport models 80−17146
radioactivity, determ. of bulk α and β radioactivity *(Rumanian)* 79−88346
radioactivity in Arizona water, baseline values 78−81230
radioactivity of Bulgarian spring waters *(Russian)* 77−41098
radiochemical analysis for Rn in groundwaters appl. to Christchurch artesian wells 77−82039
radioisotope applications in agriculture, hydrology, medicine industry etc., booklet 78−35947
radionuclide chain migration 78−85616
radionuclide migration in groundwater from accelerator earth shields 79−48194
radionuclide movement from hypothetical nuclear waste repository, groundwater modelling 80−16853
radionuclide sorption from shallow land disposal of low level radioactive waste 80−16851
radionuclide transport, 1-D computer simulation 80−51019
radiotracer studies at Mangi for subsoil hydrological investigations 79−34869
Raft River geothermal reservoir, Idaho, USA, borehole geophys. study 80−21672
Raft River Valley, Idaho, surveys of geothermal system 79−84307
rain infiltration into soil, theory *(German)* 80−90102
Ranney wells waters, interconnection with River Sava determ. by environmental T meas. 78−20447
recharge mechanism, Los Naranjos area, Mexico, using environmental isotope methods 80−12458
removal from Polesine area, surface subsidence study 78−28233
resistivity in layered structure with unconfined aquifer 79−79734
N.Upper Rhine Graben, negative height change causes *(German)* 79−34727
Rhinegraben geothermal anomaly at Landau oil-field, model 80−98281
river discharge volume after marsh reclamation, theory 80−36349
Roosevelt Hot Springs, resistivity sounding, EM and Schlumberger 79−84095
Roosevelt hot springs, Utah, seismic noise study 80−56399
Roosevelt Hot Springs thermal area, Utah, geothermal power prospect 79−84260
Roosevelt Hot Springs thermal area, Utah, heat flow and hydrothermal alteration enthalpy 80−90008
salinity and ionic strength determination method 80−109176
salinity and river basin salt balance management 77−78276
saltwater intrusion into unconfined coastal aquifer, finite element soln. 80−105004
sampling procedure 77−41215
saturated-unsaturated flow in deformable porous media, numerical model 77−91181
saturation, rel. to density log standard material comp. influence on readings *(Russian)* 79−74989
saturation rel. to dissolved carbonates in Edwards artesian aquifer, Texas 78−73416
seepage and groundwater flow, numerical analysis, book 79−100884
seepage flow, Boussinesq eqn. solns. 79−2320
seepage from free surface of triangular channel, variational inequality method 78−81251
seepage in porous elastic soils, numerical performance of finite element schemes 77−91162
semipervious stratified aqu. layers, hydrogeological parameter determ. *(Russian)* 78−32236
shallow aquifers detection using thermal infrared imagery 79−84326
soil filtration problems, finite element method *(Russian)* 79−88374
soil fluid flow with free or artesian surface 78−92872
soil hydraulic conductivity var. of Wisconsin soil series 78−81250
soil moisture, basic hydrophys. charact., determ. method 80−85696
soil moisture IR thermography remote sensing through agricultural crop 80−109147
soil moisture movement and groundwater recharge by T tagging technique 78−61438
soil water absorption, as runoff loss during spring-floods 80−109178
soil water diffusivity, scaling using universal consts. 80−8371
soil water flow modelling, finite difference and Galerkin techniques 78−81249
solutes, movement through aqueous fissures in porous rock 80−94553
solution flow prediction, computer models, appl. to U solution mining 79−88013
solution mining of U ore, environmental impact, groundwater restoration 79−88012
solution mining of U ore, Environmental Protection Agency requirement for underground injection 79−92101
spring runoff from arable land and saline soils *(Russian)* 77−21811
spring water, quantitative index of physio-chemical characteristics, appl. to Central Apennines 77−66931
spring water discharge rel. to local geomagnetic var. 77−2097
springs in W.Nevada, water chemistry determ. 77−9455

groundwater continued
St. Lucia, Sulphur Springs geothermal field model 80−94494
stability of solid freezing front 78−63844
steady replenishment *(German)* 77−66930
steady state flow models, theory and numerical props. 77−78483
steam-water counterflow in porous media, model, geothermal systems appl. 79−79879
stochastic analysis of one- and three-dimens. subsurface flows 79−5520
storm response timing, runoff model 77−37274
strategy for integration of groundwater resources in regional planning 80−41472
stream hydrograph, major base flow components identification and separation 79−79898
stream-connected aquifer system, lumped parameter stochastic model 78−81241
stream-well-aquifer system groundwater flow anal., linear system models 78−77289
streams draining granite terrain, S.Carolina, dissolved Fe as groundwater component indicator 80−12444
sub-pingo water lenses, Tuktoyaktuk Peninsula, Northwest Territories, obs. 79−20873
subsurface environments, fate of pollutants, math. modelling 77−56658
subsurface flow, stochastic anal. of spatial variability 79−84321
subsurface hydrology, finite element method using mixed explicit-implicit scheme 79−79900
subsurface nuclear waste disposal, groundwater modelling 80−16852
subsurface water chemistry study, coring and squeezing technique 78−57332
Superior Province, Canada, groundwater rel. to crustal resist., magnetotelluric sounding results 79−57882
supplies in Himalayan region of Uttar Pradesh, influence of droughts 77−56708
Tarmanskii Marsh, influence of human activity on hydrological and thermal regimes 78−92864
Tehran groundwater pollution by detergents 78−61453
teledetection methods *(French)* 79−96776
S. central Texas, effect of Balcones Faults on groundwater movement 78−53672
Texas-New Mexico Permian Basin seismicity rel. to hydrocarbon recovery operations 80−36256
N.Thailand, hot springs and geothermal gradients 80−94495
thermal convection, two-phase, in porous layer, flow visualisation study 79−72930
thermal convection in porous medium 77−33109
thermal domes, CO_2-rich mantle fluid heating possibility 79−66659
thermal fluids of Abano region, N.Italy, sources and circulation paths 79−20883
thermal spring water in Rumania rel. to Neogene volcanism *(Rumanian)* 78−20451
thermal water occurrences in Trans-Pecos, Texas 79−74923
thermohaline flow, horizontal instability in porous medium layer 79−77239
time series, trend of hydrographs 80−85687
total N content trace anal. 77−5253
transient aquifers, modified optimisation method for parameters estimation 78−61462
transient groundwater flow simulation by hybrid computer 77−45044
Turkey, karst water resource development 80−61821
Turtz mine, ^{3}H tracer investigation *(Rumanian)* 77−53251
Tuscany hot springs, geochemical and isotopic abundances rel. to geothermal areas location 77−49049
Tuwa spring water, activity ratio and separation of $^{223}Ru/^{226}Ra$ 78−86962
two-dimensional flow, calculation methods 79−100875
two-dimensional isoparametric Hermitian element for field problem soln. 77−60914
two-dimensional unconfined saturated flow, boundary integral solns. 78−77291
two-phase interface and free surface equations in groundwater flow 79−48527
unconfined aquifer, groundwater mounds growth affected by in-transit water 79−84327
unconfined aquifer on sloping bed, steady state flow, finite element study 79−16531
unconfined aquifers, packer, slug and recovery tests 79−79904
underground water mineralisation, reliability anal. of geophys. estimation *(Polish)* 77−73862
underground water movement tracing using halogen tracers and NAA 79−88014
underground water resources in Belgium *(French)* 77−25712
NE.United States, effects of soil Al leaching response to acid precip. 80−12442
unsaturated zone hydrology, United States educational effort 78−81224
unsteady filtration with unknown boundary, nonlinear integro-differential eqn. 80−43769
unsteady flow, mathematical models and parameter determ. *(Chinese)* 79−57976
unsteady flow beneath strip oceanic islands 77−5257
unsteady flow from tunnel opening, reductive finite element anal. *(Japanese)* 78−96251
unsteady flow in 2-D at horizontal plane *(Chinese)* 80−46205
unsteady flow in porous medium with sloping impervious bedrock 80−12459
USSR, correl. between underground water regime and seismicity *(Russian)* 80−104913
W.Utter Pradesh, ground water extraction potential 78−32130
velocity determ. using natural He, radioactive waste storage study 80−82111
velocity determ. using organic solute-mineral surface interactions 80−98492
Venice, subsidence rel. to groundwater withdrawal, model 79−5519
vertical movement, correction to terrestrial heat flow meas. 80−3969
Wairakei thermal region, thermal water transport of major rock constituents 77−81844
warm springs of S.Island, New Zealand, laumontite potential 79−62528
water resource finite element anal., conf. at London, England 1978 78−92867
water table lowering rel. to relevelling in Rhine Graben *(German)* 79−34726
water table mound geometry under recharge basins 77−5267

groundwater continued
water table movement modelling using dynamic filtration *(Russian)* 78−88850
water table prediction, model-free statistical methods 77−25714
water table response to sequence of recharges 78−11937
water table var. on Gdansk coast rel. to precipitation *(Polish)* 79−25281
waterbearing strata, hydrodynamic parameters *(Russian)* 79−16526
well in confined aquifer of variable thickness, flow problem, soln. 79−20888
well water levels at Funabara and Kakigi, Japan, rel. to earthquakes *(Japanese)* 78−96241
wells, flow anal. by finite element method 78−92870
wells and aquifer development, siting using electrical resistivity meas. 77−9528
wells of Greater Chicago area, dead water, ^3H anal. 78−16062
wells tapping deep unconfined aquifers, water level fluctuations, atm. press. effects 80−81953
wetland mapping in New Jersey and New York 78−77265
X-ray spectrometry, data interpretation, online system using multivariate statistical anal. and pattern recognition 80−3461
Yellowstone thermal waters, subsurface boiling and dilution effects on isotopic comp. 78−49048
C isotope geochemistry of small groundwater system, NE. Ontario 79−84324
^{14}C anomaly in regional carbonate aquifer, Great Basin, Nevada 77−45042
CO_2 meas. correction to C isotopic comp. for CO_2 outgassing effects during pH meas. 79−66718
CO_3^{2-} chemistry of groundwater from tropical tower karst, S.Thailand 79−79906
^{14}C and T meas. in Eaton River Basin and Mirabel area, Quebec 78−28249
^{14}C content, possible subsurface prod. rel. to dating 80−85690
^{14}C dating, mass transfer and isotope evolution theory 79−20882
Cl^- content, appl. to Miocene aquifer isopermeability map 78−81256
F content in hot spring waters, Kohu City, Japan *(Japanese)* 79−70821
He survey in S.India for structural mapping, water sample obs. 80−8261
He/Ar and N_2/Ar ratio vars. in fault zone groundwater air bubbles for earthquake prediction 78−88803
Hg levels in soil and water in Israel and Sinai 77−29337
Hg, neutron activation anal. for low levels in water 79−70503
I^-, anal. in groundwater by X-ray fluorescence spectrometry 80−45829
$^{18}O/^{16}O$, groundwater seepage, control Kentucky karst 80−8370
^{226}Ra leaching from contaminated soils, investigation of Ra bearing soils from Port Hope, Ontario 79−20900
$^{87}Rb/^{87}Sr$ studies of waters in geothermal area, Cantal, France 78−61443
Rn conc. in underground waters and soil-air around Asama Volcano, Japan *(Japanese)* 79−70813
Rn concentration continuous monitoring using ionisation chamber 79−21068
Rn concentration in underground waters from landslide zone, Narao district, Japan 78−11918
Rn content, continuous meas. method for earthquake prediction 77−44935
Rn in geothermal reservoirs 78−69381
Rn measurement in groundwater and springs for earthquake prediction 78−88924
^{222}Rn concentration in N.Carolina groundwater supplies rel. to stomach dose and conc. standards 78−85612
S isotope exchange between sulphate and sulphide in acid solns., expt. determ. at 300°C and 1000 bars 78−62937
SiO_2 geothermometer temp. of groundwater rel. to regional heat flow, United States 79−74876
Sr isotope ratio of Israel groundwater, for ancient seawater composition 80−61804
U determination in environmental waters by epithermal neutron activation 79−53010
U, genesis of Proterozoic deposits, source of mineralizing fluids, Australia 79−84270
U in natural waters, field meas. technique 78−85705
U in percolating fluids 79−84226
U movement during higher grade metamorphism rel. to movement of water 79−84274
^{234}U excess, ageing effect in confined waters, comment 77−5252
^{234}U excess, ageing effect in confined waters, comment 77−9449

group theoretical schemes
bound proton-neutron system, basis functions and collective states 79−67688
bound proton-neutron system, operator averaging technique, recurrent construction of collective variables 79−67689
colour scheme interpretation, new phenomena in charged-current neutrino reactions 77−2817
covariance group in presence of external EM fields 77−65114
covariance group representation of elementary particles in presence of external EM field 77−65115
E based vector-like unified theory, group theoretical anal. of symm. breaking 77−87929
finite isospin groups for hadron classification, expt. consequences 79−360
hadron isospin classification, same finite group for mesons and baryons *(Chinese)* 80−62887
hadron mass, instanton effects on light quark spectroscopy, MIT bag model 78−62372
homogeneous 16-vertex model, symm. group Lorentz similarity transformation interpretation 79−9300
Hughes-Yadegar algebra, group theoretical derivation, symm. algebra of H atom 77−17766
instanton, group theoretical aspects 79−97494
jet decay models, group-theoretical and four-momentum variables 80−73684
kinematical symmetry groups and state spaces, classical and quantum physics 80−52008
meson-meson scattering, resonating group calcs., low energy limit 78−424
nucleus, model density matrix, $U_{3(n-1)}$-irreducible decomposition 79−67692
octonion algebra, unified theories with orthogonal groups 77−46005
reductions in integrable systems *(Russian)* 80−91017
relativistic eikonal physics, group theoretical approach 77−82694

group theoretical schemes continued
relativistic particle classification, representation theory, 8 nonisomorphic simply connected covering groups of O(3,1) 77−46008
SO(4,1) sourceless gauge field eqns., classical solns. 79−2921
SU(3) representation theory, connection with SU(3) particle classification schemes, Weyl character formula 77−34101
symmetries of 6j coefficients 78−86423
U(3(n-1)) scheme, translationally invariant wave function, proton-neutron states, electromag. transition operators 77−41906
unitary analytic representations of SL(3,R)*, operator formalism method 77−45983
unitary scheme, two-particle fractional parentage coeffs. 77−41905

group theory
see also Clebsch-Gordan coefficients; crystal symmetry; elementary particle theory; group theoretical schemes; Lie groups; renormalisation; SU_n theory
3j symbols, T coeffs. and D function *(Russian)* 77−30055
3j-coeff., symmetries 78−41181
6j coefficient canonical parameters 77−26128
6j symbol calculation for compact groups 80−8856
σ model representation of Yang-Mills theory as a spontaneous violation *(Russian)* 80−13220
Σ models of spontaneously broken symmetries 78−399
A15 structure, O_h^3-Pm3n, group theory of phase transition 78−9992
Abelian group functions, algebraic conditions 79−54007
Abelian groups, Cauchy sequences 79−35519
Abelian transformation group spectrum with positive entropy 77−37722
abstract averaging theorem 77−2510
adamantane, deuterated single plastic cryst., normal modes and librations, group-theoretical anal. *(French)* 79−14905
additivity, rapidity, relativity, teaching 80−41984
adsorbed monolayers, groups of sites used in statistical calculations, Bethe's method *(French)* 77−70334
affine algebraic groups, automorphisms 79−17269
affine symplectic group, generating functions 78−41149
algebra (CCR), quasi-free states and automorphisms 77−5686
algebraic approach to hadrons without seeing quarks 80−9143
allowable representations of appropriate small groups, calc. of system coords. and physical props. 79−2595
ambiguity group for classical canonical transforms, role in quantum mechanics 80−8839
analytic continuation in decay-scattering systems, singularities as model basis 80−8850
analytic continuation of a group of eigenvalues 79−6010
Anderson localisation, real-space renormalisation group theory, decimation method 80−88461
angular momenta addition 77−71228
angular momentum group of four quarks 78−16980
anisotropic constitutive equations and Schur's lemma 78−89337
anisotropic harmonic oscillator, accidental degeneracy of energy levels 78−8263
anisotropic harmonic oscillator, n-dimens., accidental degeneracy, semi-direct product representation 78−4506
anti-commutative, self-inverse matrices and transformations in eigenvalue problems *(Chinese)* 80−101951
application to quantum statistical mechanics, Markovian eqns., transportation theory 78−21063
asymptotic reduction products of representations of covering group of SU(1,1) 78−58137
asymptotic series by H^0 strictly singular perturbations 80−62498
atom, unitary group generators representation matrices calcs. 78−78610
atomic and molecular physics, dynamical groups 80−42362
autonomous dynamic systems, limit cycles and one parameter transformation groups 78−49641
Bargmann-Wigner and Weyl spin-3/2 fields, spinors, chiral operator 80−31981
Bargmann-Wigner eqns., SO(4,2) covariant formulation 78−37126
bi-local model, Poincare group and position operator 78−93844
Bianchi type VIII spatially homogeneous cosmologies 77−17729
bifurcation from rotationally invariant states 78−77671
bilateral classes, classification scheme for elements of groups 80−68020
biorthonormal systems, Parserval's identity 78−16669
Bloch electrons in magnetic field, quantum numbers 80−96768
body-fixed frames and angular momentum projection operators 80−86122
Bondi-Metzner-Sachs group, lifting of projective representations 78−21028
boost matrix elements of the homogeneous Lorentz group 79−92975
boranes, polyhedral, bonding topology, graph-theoretical interpretation 78−33408
Borel multipliers for the Bondi-Metzner-Sachs group 80−18088
Bose fluid, interacting, renormalisation group approach 78−45562
boson and classical systems normal forms, annihilation and creation operator, linear canonical transformations 80−22275
boundary-value and eigenvalue problems of domains without classical symm., possible appl. of group representations 77−13571
boundary-value and eigenvalue problems of domains without classical symm., second and third type, group representations 77−13572
Boussinesq equation, group theoretical approach 80−82914
branching rule for restriction from SO(7) to G_2 78−16624
Bravais lattices, new group theoretical deriv. 79−77540
C* approach to math. foundations of statistical mechanics 77−26226
C*-algebra, complete positivity and asymptotic abelianness 77−60892
C*-algebra automorphism groups with spectrum condition, lifting problem 77−5621
canonical anticommutation relations with compact gauge group, quasilocal algebra 79−89069
capillary-porous body, nonlinear heat/mass transfer problem, soln. using invariant groups 78−55688
carboranes, bonding topology, graph-theoretical interpretation 78−33408
Carter separable spacetimes, characteristaion 78−36867
causal A-statistics 80−22504
Cayley quantum theory, new aspects in eight-dimens. Clifford algebra 80−8846
chain $D_5 \supset C_5$, 6j, 9j symbols, 3jm factors 80−27171
charmed weak current group struct., chiral $SU_4 \times SU_4$ breaking 77−65118
chemical bond transferability, group or loge functions 78−41939
chemical dissipative structures, bifurcation, symmetry and influence of elec. field 80−81289

group theory continued
chemical network, nonlinear pattern as transform. group symmetries 78−27878
chemical potential, algebraic theory for usual gauge group 80−31661
chemistry teaching, pedagogical approach to direct product represent. 80−17771
classical groups, invariant operators 79−21585
classical lattice system group analysis 77−67385
classical lattice systems of arbitrary spin, group structure 77−33958
classical systems with infinite set of conservation laws 80−86102
Clifford group, one-dimens. representation *(Russian)* 79−54281
coherent states and projective representation of the linear canonical transformations 80−82662
cohomology groups with coefficients in sheaves of holomorphic functions, vanishing theorems 79−49405
collective Hamiltonian subdynamics and collective states, geometric approach 80−8904
collective models, algebraic formulation, collective and intrinsic submanifolds 80−73811
colloquium, lattice theory, Szeged, Hungary (Aug 1974) 77−60890
combinatorial, algebraic and topological representations of groups, semigroups and categories, book 80−57016
commutation relation [A, B]=−icI for one parameter unitary groups 78−65811
commuting operators, R(3) scalars for quadrupole phonon state classification 80−62876
commuting tensor operators, and state labelling problem for SO(4)⊃P 78−28980
compact groups, tensor representation 77−5625
complete symmetry group of forced harmonic oscillator 80−90705
completely integrable systems and symplectic actions 79−44712
complex electron configurations, quasispin method, mixing configurations 80−42953
complex mass and field operator for unstable particle 80−9105
complex multidimensional ball, equivalent projective unitary group of analytic transformations *(Japanese)* 78−12534
conditional probability of a generalised probability theory, quantum mech. foundations 80−12949
conference, group theoretical methods in physics, Austin, Texas, USA (Sep. 1978) 80−4474
conference, group theoretical methods in physics, Netherlands, (June, 1975) 77−17862
conference, group theory and application to spectroscopy, Nova Scotia, Canada (Aug. 1978) 80−41947
configuration space basis state generation, U(n) matrix elements 80−86120
conformal group, quantisation and Kepler problem 77−17872
conformal invariance and gauge vacuums 78−8530
conformal invariance in quantum mechanics 77−2730
conformal invariance of relativistic equations for arbitrary spin particles 79−30649
conformal invariant 2- and 3-point functions for tensor fields with arbitrary spin 78−49977
conformal relativity, unified description of bradyons and tachyons based on dynamical SO(4,2) 77−67352
conformal space-time group, invariant tensors for maximal subgroups 79−85239
conformal spinors, $O_{2,4}$ transformations in $E_{2,4}$, components obeying Dirac eqn. 78−45504
conformal transformations, unitary implementability 79−21965
conformal transformations in spinor space-time 79−30674
conformal transformations in superspace 78−70295
conformally covariant spinor field equations 79−22004
conservation laws of general relativity, gravit. gauge group $SL_{2,C}$ 77−22456
contact conformal transformations, finite, nonrelativistic 78−36815
continuous stochastic semi-group resolvent, Laurent series appl. 77−53759
Coulomb coupling, strong, group SO(2,1), Klein Gordon eqn. 77−17837
coupling coeff., general theory 79−88829
covariance group in presence of external EM field 77−18211
covariant σ models, first order system of differential eqns. 80−31978
covariant coherent states for quantized systems with nilpotent symmetry group *(German)* 78−73865
covariant observables and instruments 80−8842
crystal, ordering phase-transform. group theory anal. *(Russian)* 80−103287
crystal field theory, finite symmetry adaptation in spectroscopy 80−43032
crystal irreducible problems, use of Clebsch-Gordan reduction 78−2052
crystal point groups, basis functions for irreducible representation, appl. to morphic effects on IR and Raman spectra *(Japanese)* 79−4265
crystal rotational symmetry, and tensor props., 1-, 2- and 4-fold principal symmetry, trigonal, and hexagonal groups 80−100193
crystal rotational symmetry, and tensor props., method for group $3(3_z)$ 80−100192
crystal symmetry, cubic harmonics, $l \leq 17$ Cartesian coords. 77−51338
crystal tensor components, unitary groups appl., and phase transition selection principles 79−46589
crystal wave functions, symm. transformation, computer programs, symmetrisation procedure 78−10315
crystallographic space groups, irreducible linear representation, image struct. 80−6377
cubic harmonic functions, actual forms to 16th order, quantisation axis in [111] direction 77−60971
cubic harmonics computation, using point groups and an algorithm 78−20994
cyclic transformations, symmetrical anal. of stable groups, graphical procedure 80−101943
D_{2d} crystals, structural phase transitions, soft modes, group theory 80−92638
D_k^+ series, finite SL(2,R) representation matrices, all subgroup reductions 77−49556
de Sitter groups, continuous subgroups 78−28910
de Sitter groups SO(4,1) and SO(3,2), complex quaternions and spinor representations 78−36887
de Sitter space, conservation laws from action principles in five-space 77−22451
de Sitter space, dynamics of free particle systems 78−20958
decay processes and dynamical subgroups 80−8848
group theory continued
decay-scattering systems, resonances and their eigenfunctionals in Friedrich's model 80−8847
defect dynamics, closure of governing eqns., plastic state theory 79−37702
deformation of symplectic structure and quantization 80−8853
degenerate three dimensional local and quasi local vibration spectral distributions 80−29138
Delaunay rotation stereohedra types for 3×432 group 80−38984
diagram approach to character formulas for finite and compact groups 80−36888
diagram technique for basis functions, transformation, appl. to group-subgroup basis, cryst. tensors 77−26127
Diff R^N group, unitary representation 79−93303
differential equation symmetries, method of obtaining, relation to separable coord. systems 77−17781
differential equations, generalization to transformation groups *(Russian)* 79−92991
dilations as propagators of Hilbertian varieties 79−9189
dilute linear Heisenberg chain, partition function and irreducible representation of permutation groups by HLISP 78−34945
dipolarly coupled spin pairs, correlation function and relaxation time, group theory approach 78−48068
discontinuous groups, Siegel domain of second kind *(Japanese)* 80−51999
discrete mechanical systems, group method of determining parameters *(Russian)* 77−71205
double group theory, half-shell and two-level system, optical polarisation 78−49594
double group theory, half-shell and two-level systems, rot. and half integral spin states 78−45447
double groups and projective representations, Clebsch-Gordan coeffs. calcs. 79−92977
double groups and projective representations 79−88833
double space groups O_h^6 (Fm3c) and O_h^8 (Fd3c), selection rules 80−10518
dual covariance algebras, duality 77−17748
dual current vertex, group theoretical struct. 78−74229
dynamic critical phenomena closed-form differential renormalisation group generator 78−86413
dynamic renormalization group, phenomenological fitting 79−75471
dynamical group quantisation 78−4520
dynamical groups for the motion of relativistic composite systems 80−9115
dynamical semigroup for time evolution of finite system 77−30045
dynamical semigroups, dilations, open quantum mech. system embedded in closed system 77−2508
dynamical systems, new class of crystal models, symm. props. 77−19888
dynamics in state space, Heisenberg equations 77−37782
E_6 model of particle interactions, asymptotically free model 78−24922
E_8 group, branching rules, Kronecker, products 80−27438
education, group representation theory, intuitive approach 77−87592
education, group theory of covariant harmonic oscillators, interacting quarks 78−61970
education, plane rotator, degenerate perturbation theory, Zeeman and Stark effects 79−9059
education, renormalisation group theory, second order phase transitions, undergraduate statistical physics 78−62012
effective electron-electron interaction in a group-theoretical diagram technique 79−28303
Einstein-Maxwell equations, coupled, general soln., Ernst-Maxwell eqn. depend. on arbitrary harmonic function 77−74
Einstein-Maxwell field, symplectic structure 78−29028
electron correlation problem, graphical unitary group approach, appl. to ketene 79−76324
electron diffraction, many-beam dynamical theory 77−15290
electronic wavefunction, correlated, graphical unitary group approach, abelian point group symmetry utilisation 79−68193
elementary particle theory and group theory, book 77−67589
EM field theory, spinor representation of Maxwell's eqns., algebraic props. 80−86097
EM field theory, spinor representation of Maxwell's eqns. 80−86096
Emden-Fowler eqns., nonlinear boundary and eigenvalue problems by group methods 79−71224
empirical data tables, equivalent transformation *(Russian)* 79−9208
energy spectrum of extremal invariant states 78−24
entropy of density matrix, definition with respect to observable 78−45586
entropy prod. for quantum dynamical semigroups 78−57883
EPR, symmetry adaptation and operator equivalents *(French)* 78−91924
ergodic properties of an operator obtained from a continuous representation 78−89305
ergodic theory in von Neumann algebras 80−9104
Euclidean fermion-boson systems on lattice, appl. to field theory 78−45559
exceptional groups and elementary particles 77−18191
exotic spinors in supercond., charge depend. of quantised flux and Josephson current 79−33400
extended integrity bases of finite groups 79−40349
factored irreducible symmetry operators 77−26197
faithful irreducible representation for subgroup contained in S_7 78−25
faithful normal states on von Neumann algebra 77−17760
fermion system thermodynamics, appl. of class of dissipative evolutions 80−46960
fermion systems, infinite, irreversible dynamics 77−82451
fermion systems, inverse temps. with eqn. states, automorphism group 80−82712
ferroelastic second-order transitions, cryst. unit cell modification, group theoretical anal. 79−37830
ferroelectrics, improper and incommensurate phase transitions, neutron scatt. studies 80−75974
ferromagnetic material, polycryst., magnetic texture anal. 80−108002
ferromagnets, uniaxial, US attenuation and kinetic coeffs. near crit. point, renormalisation group theory 79−4715
Feynman diagrams, appls. in advanced quantum theory, book 80−22157
fibre bundle with Cartan connection, group contraction 77−74573
fibre bundles, Poincare group canonical representation, Lagrangian formalism 79−30678
fibre bundles, pseudoconvexity 77−29998
fibre bundles and topology 80−105793

group theory continued
field theory, massless equations, first-order, conformally covariant 78−29265
fifteen parameter conformal group, geometry and isomorphism 79−9154
finite group having two generators and two relations 77−87626
finite group induced representations 77−2507
finite group representations, method of commuting operators *(Chinese)* 78−8257
finite groups, weight and step operators 77−78953
finite groups with faithful irreducible rational represent. of prime odd degree *(Ukrainian)* 77−37723
flavour and colour quark groups, unitary symmetry links 80−9151
flavour conservation, natural, in neutral weak currents, symm. $SU_2 \times U_1 \times U_1'$ model 78−12858
flexible Jordan admissible algebra, dimens. seven, hadron physics appl. 78−93792
Flodmark-Blokker method for irreducible representations of crystallographic space groups 80−6376
fluid layer, selection mechanisms for convective motion pattern form. 78−54316
Fokker-Planck eqn., quantum dynamical semigroups 77−61034
Foldy Wouthuysen transform. group content, nonrelativistic limit for arbitrary spin 79−75387
forced convection in presence of external mag. field, similarity soln. group theoretic approach 79−77266
fundamental group unitarity *(Russian)* 77−53739
G_2, weight multiplicities 78−78105
GL(4,R) unitary representations 79−44
Galilean semi-group for more general theory of symmetries, isolated quantum system 78−49718
Galilei group conformal extensions, reln. to Schrodinger group 78−36877
Galilei to Poincare algebra transformations 78−36793
Galilean formulation of spin, Clifford algebras and spin groups 78−57736
gauge equivalence of representations of symmetry groups in quantum mechanics 78−77752
gauge group and p-wave phases of superfluid ^{3}He 79−23798
gauge group theory of combined gravitational and e.m. interaction 77−80
gauge theories, exact gauge symm. group, ang. momentum operator, mag. monopole props. 77−2764
gauge-covariant conformal transformations 79−12946
Gaussian generalised stochastic fields, Markov property 80−22287
Gel'fand bases, permutation representation for symmetric groups 80−73619
Gel'fand invariants for unitary, orthogonal and symplectic group 78−32651
Gel'fand lattices, exponential of, and irreducible representations of U(n) 77−60897
Gel'fand states of representations of U(n) and the Gel'fand lattice polynomials 80−86608
Gelfand-Naimark z-basis, infinite-component field-theoretic model 77−82661
general lattice systems and surface tension, group struct. 80−4675
general light cone frame, from Galilei group to Lorentz group, appl. to Schrodinger-Pauli eqn. 77−61187
general relativity, space-like infinity, conformal structure 78−8293
general relativity conformal groups, appl. *(French)* 80−101
generalised isomerisation modes 77−68135
generalised Poincare group, reduction of irreducible unitary representations with respect to subgroups 77−30281
generalised symmetry algebras for para-Fermi fields 79−30676
generalised vector field equations, symmetry group *(Russian)* 77−79206
generalized Galilei groups in classical dynamics 79−30221
generating functions for characters of group representations and their applications 80−8840
generators of infinite direct products of unitary groups 78−24677
genetic diagrams for groups of orthogonal matrices O(n) 77−29988
geometric quantization and internal symmetry 80−42089
geometrical optics, appl. of group theory 78−25944
geophysical elastodynamics, group theoretical formulation, seismic sources 77−78126
Gibbs space, group theoretic aspects 77−33971
Gln basis labelling, Racah algebra identification with S_N 80−8835
graded G-structures on differential manifold 80−8858
gradient formula for the group U(2l+1) in nuclear collective model theory 78−37300
gradient formula for the $O(5) \supset O(3)$ chain of groups 78−78285
gravitation, gauge theory, spinor formalism 80−90762
gravitation, metric-affine theory as gauge theory of affine group 78−32746
gravitation theory, de Sitter gauge invariance and spinor calculus 80−12978
group chain $D_{4d} \supset D_4 \supset C_4$, 6j symbols, 3jm factors 80−46848
group representations, appl. to boundary value and eigenvalue problems of domains without classical symmetry 77−13580
group symmetries in nuclear struct., book 80−41963
group theoretical construction of two-dimensional models with infinite sets of conservation laws 80−99056
group theory, space and point group factorization, appl. to crystallography and spectroscopy 79−60295
groupoids, inductive, of finite cyclic rings *(German)* 80−6375
hadron gravitational interaction, band spinor representation of GL(n,R) 78−50000
Hamilton G-spaces, quantisation of A-bundles 77−26139
Hamiltonian evolution, sufficiency condition, semigroup formalism 77−30047
harmonic anal. on Lorentz group as dynamical relativistic Fourier anal. 77−82406
harmonic oscillators, complete symmetry group 80−46856
Hartree-Fock basis, unitary group decomposition of Hamiltonian operators 79−80889
HCP lattice with substitutional impurity, defect Green's function and T matrix 79−42191
heat storage, periodic, heat-carrying fluid and storage material transport kinetics 79−3901
heat-conduction eqn., nonlinear group props., inverse problems soln. 77−75770
Helmholtz eqn., 2D, group theory in approx. soln. of boundary problem *(Russian)* 77−49557
group theory continued
Hilbert spaces, nested, spectral props. in class of operators and group representations 78−4459
historical development and appl. *(French)* 80−25
HMO characteristic polynomial construction, group-theoretical rules 77−23432
homogeneous Lorentz group, chirality, Weyl spinors 78−93810
homogeneous Lorentz group SO(3,1), boost matrix elements and Clebsch-Gordan coeff. 78−4505
homotopy groups of condensed matter physics 78−63752
Hubbard model, Green's function determ. using group theoretical diagram method 77−62791
Hughes-Yadegar algebra, group theoretical derivation, symm. algebra of H atom 77−17766
hyperboloids, wave eqn., O(2,2) symm., separation of variables 78−77679
hyperfunctions and asymptotic symmetries 78−8218
hypermomentum in hadron dynamics and gravit. 78−41487
icosahedral group, isoscalar symbols and symmetrised coupling symbols 80−57510
impact-parameter group, realisation on cone functions *(Russian)* 78−45817
imprimitivity systems, quantisation and superselection rules 80−4592
incommensurate crystal phases, symm. props., superspace groups 80−75195
induced projective representations of finite group, cryst. symm. appl. 78−4461
infinite macrosystems in standard representation, dynamical symmetries 80−4590
inhomogeneous symplectic group, role in framework of Wigner isomorphism *(French)* 79−12589
instantons and embeddings in gauge field configurations, group theoretic study 80−4878
instantons of Yang-Mills eqn., rank 2 stable vector bundles 78−45774
integral geometry and geometric probability, book 77−60910
integral transforms, alternative forms using hyperdifferential operators 77−49570
intelligent states, computation of Clebsch Gordan coeff. 78−62101
intelligent states, group-theoretic study and computation of matrix elements 78−62100
interfacial roughening transition, renormalisation group theory 79−2734
internal Galilei group for a two-particle system 79−75406
intrinsic $SO(2,1) \times GL(1,R)$ invariance of Dirac eqn. 78−93826
invariance groups for class of countable systems of first-order partial differential eqns. 78−49635
invariance groups of Dirac and Kammer-Duffin-Petiau eqns. 77−67320
inverse problem in abstract relativistic scatt. theory 80−4894
IO(n), lowering and varing operators and normalisation consts. 79−58569
ionic grouping theory of electro-optical and nonlinear optical effects of crystals *(Chinese)* 78−27183
irreducible representations of finite groups, independ. sets of basis functions 78−41134
irreducible representations of groups with subgroup of index 2 78−57733
irreducible tensor operator methods in strong-field coupling 79−7811
irreversible processes and dissipative systems in quantum theory 80−8906
Ising lattices, position-space renormalisation-group transformations, problems and proofs 78−93619
Ising planar ferromag. model, spinor algebra and odd operators 78−45570
ISO(n), explicit determ. of representation functions 80−31561
isotropic harmonic oscillator, n-dimensional, noninvariance group 78−8264
IU(n), lowering and varing operators and normalisation consts. 79−58569
IU(n) and IO(n) invariant operators and their eigenvalues 79−30194
IU(n) group, matrix elements of irreducible representations *(Russian)* 78−54149
j symbols and jm factors for all dihedral and cyclic groups 79−92968
Jordans 5-D unified theory of gravitation, Ehlers-Harrison type transform 80−8882
K-harmonics method, group of canonical transformations 78−50106
Kaluza-Klein bundle, unified theory 80−37153
Kepler problem, 1-D, invariant *-product quantisation 80−17831
Kepler problem, global symmetry anal. 77−5662
Kepler problem, Lorentz and anti-de Sitter group 78−36817
kerr-Schild geometry, spinors, and instantons 79−35601
KMS states and ang. momentum, extension 79−75439
Koornwinder's polynomials and representations of the conformal group 79−63343
Korteweg-de Vries type eqns., group-theoretical interp. 80−77624
Kostant-Souriau geometric quantization of nuclear collective models 80−9247
ladder operators of group matrix elements 80−31555
Lagrangian formulation for noninteracting high spin fields, Lorentz group representations 77−49825
laminar boundary layer, optimal control, group theoretic approach 79−32452
laminated composite shells, mixed isoparametric finite element models 77−78979
lattices, distributive, bounded, Baer semigroup coordinatisation using idempotent residuated mappings 80−73280
Lee's derivative of geometrical objects, tetradic transform. *(Russian)* 79−93024
Lie groups, octonion/quaternion hypercomplex numbers, nine-vectors and real world 78−37151
ligand fields calcs., strong and intermediate fields, tensor algebra 80−42922
linear chain model, symmetry-adapted, layer dynamics of high-symmetry crystals 80−34148
linear Jahn-Teller systems, continuous group invariances, icosahedral systems 80−49677
linear Jahn-Teller systems, continuous group invariances 78−60092
linear semi-group stability and stabilisation problems *(Chinese)* 79−35521
liquid crystal phase transitions, second-order, Landau thoery, group-theoretical arguments 80−29154
liquid crystals, continuous symmetry groups 79−32902
liquid crystals, thermotropic, struct., two-dimens. order, and symm. props., review 79−86698

group theory continued
liquids and solutions, comparison of mono- and multi-molecular correlation functions *(French)* 79−50971
local class field theory generalisation using K-groups, Abelian extensions 79−44799
local symmetry groups and fermion families 79−13030
Lorentz group, linear representations and matrix element computation formulas 79−58571
Lorentz group, matrix elements of boost of unitary representations in basis $SO(3.1)\supset SO(2.1)\supset SO(2)$ 80−4507
Lorentz group, relativistic partial wave anal. for particles with spin 79−93319
Lorentz group, relativistic semigroup and tachyons *(Russian)* 77−82386
Lorentz group, unitary irreducible representation of O(3,1) *(Russian)* 77−29986
Lorentz group, use to derive props. of Wigner 3j-symbols 77−33837
Lorentz group in oscillator realisation 78−77755
Lorentz group linear representations and their matrix elements 79−93306
Lorentz group O(2,1), coupling of continuous representations 79−49078
Lorentz groups, homogeneous and inhomogeneous, teaching method to illustrate difference 80−17766
Lorentz invariant multiparticle amplitudes, massive particle relativistic kinematics, spinor amplitudes 78−41156
Lorentz type internal symmetry 78−50005
low rank group enveloping algebras, reduction and generating function 80−86601
M_4 factorisation, spinor algebra, Dirac equation geometrical, interpretation 80−62838
M(2) group representations in terms of Lame, Mathieu and parabolic functions 77−45675
M-C-O deformation modes, no. and symmetry determ., group theoretical method, for teaching 78−11
magnetic bubble materials, magnetoelastic interactions 80−65976
magnetic circular dichroism, one-electron reduced matrix elements 80−45048
magnetic crystals, spin arrangements, symmetry, wreath groups 80−88724
magnetic materials, symm. restrictions on constitutions eqns., group theoretical procedure 77−55255
magnetic monopole, group theoretical approach 77−71434
magnetic resonance, symmetry adaptation and operator equivalents *(French)* 78−91924
magnetic space group, reality criterion for corepresentations 78−22677
magnetic space groups, minimal supergroups 77−85417
magnetic structure, group theory description, single irreducible group representation *(Russian)* 80−44804
magnetic structure, neutron diffraction patterns, group theoretical, exchange Hamiltonian symm. anal. *(Russian)* 79−65648
magnetic structure determ., group theory approach to neutron diffr. pattern interpretation *(Russian)* 79−51749
magnetic structure elastic polarised neutron scatt. atomic mag. moments 80−29531
magnetic structure symm. anal. in neutron studies periodicity changes at mag. phase transitions 79−99680
magnetic structures, neutron diffr., symmetry anal., group theoretical group anal. of exchange Hamiltonian 80−29527
magnetic structures, neutron diffr. anal., group theory approach, mag. lattice determ. *(Russian)* 79−47236
magnetic structures, symmetry anal. in neutron studies, phase transition concept 79−99679
magnetic symmetry, improper symm. and Neumann's principle 78−38646
many-electron interaction in crystals, symmetry group basis 77−51682
many-particle Green diagram, group theory anal. 78−28992
Maslov index, explicit construction, applications *(French)* 77−17875
mass changing cosmology, solar evolution and neutrino flux 78−45441
massive gauge fields, complete spontaneous symm. breaking, asymptotic freedom, symplectic and G_2 groups 78−62305
massless boson fields 77−34098
massless fields with continuous spin, quantisation 78−4525
mathematical foundations of dimensional analysis and the question of fundamental units 80−42086
Maxwell's equations, O(3,1) approach 78−36846
mechanics, symmetry of materials, transformation of coords. in constitutive eqn. 80−53621
Melosh transformation, Dirac eqn., group theoretical anal. 77−2749
Melosh transformation, Eriksen like form, group theoretic interpretation 80−8859
metal clusters, bonding topology, graph-theoretical interpretation 78−33408
methane, hyperfine struct., Racah finite group algebra appls. 78−78617
methane, vibration-rotation energies of harmonic and combination levels 80−47962
metric-affine theory of gravit., intrinsic hypermomentum current components, hadron dilation, shear and spin 78−12632
minimal EM coupling in elementary quantum mechs., group theoretical derivation 78−54590
minimal uncertainty states for rotation and allied groups 78−4501
modular group and dimer problem, Ising model 77−5763
molecular, symmetry coordinates construction, arbitrariness limitation 78−55252
molecular and solid state problems, point group coupling, coeffs., props. and application 80−43033
molecular cation, rearrangement pseudorotation modes, reaction mechanisms, permutation theoretic anal. 78−44369
molecular CI matrix elements eval. for canonically ordered basis 79−31420
molecular crystals, group theory anal. of lattice vibrs. 77−80590
molecular electronic struct., group function model 78−62700
molecular point groups, infinite, complete reduction of representations, mol. vibrs., electronic states appls. 78−94206
molecular symmetry adaption, diagonalisation of overlap matrix 79−26877
molecular symmetry adaption, force const. matrix of symmetric mols. 79−26878
molecular symmetry adaption, representations on symmetric polyhedra 79−31368
molecular systems with spatial point symmetry, unrestricted Hartree-Fock group theoretical struct. 80−37741
molecular vibr. level classification by Longuet-Higgins group 80−43030
group theory continued
molecules, interacting, rigid, HF, self-consistent nonorthogonal group function approx. 79−31430
molecules, relations between matrix elements in relativistic Hartree-Fock-Roothaan theory 79−36521
Molien function, new algorithms, space group representations 77−72575
Molien function of a symmetric group 80−8857
Molien generating function calc., irreducible representation of cryst. space group 77−72576
momentum-dependent nuclear potential, group-theoretical derivation of matrix elements 77−26588
monodromic Galois groups of the sextic equation of anisotropic elasticity 79−97207
multicluster production, multiplicity distribs., group-theoretical approach 77−2800
multidimensional equipartition psychophysical scale existence conditions 77−53738
multispinor Lagrangian, symm. group 78−58115
n-component compressible model with cubic anisotropy, critical behaviour RG calc. 78−145
N-level system, generator of completely positive dynamical semigroups 78−45513
Nambu-Goldstone realisations of dynamical groups and nonlinear eqns. *(Russian)* 78−89632
nematic-isotropic transition, nature, field renormalisation group formalism study 78−87775
network structures of a system coded by groups 80−81286
Neumann, completely positive maps, semigroup generators 78−93545
neutron inelastic scattering, simplified group theoretical selection rules 77−24247
Newton-Wigner position operator derivation 80−98821
Newtonian connection, nontrivial extension of Galilei group *(French)* 78−36916
NMR spectroscopy, eigenvalue-eigenvector problem 80−43074
non-Abelian gauge group theory, relationship with solitons 80−4549
non-Abelian solvable finite groups, spin systems, self-duality conditions 80−101944
non-ferroic phase transitions, group theoretical methods 80−70388
non-linear transport equations: Properties deduced through transformation groups 80−4680
nonAbelian gauge groups, dual charge, mag. monopoles *(Chinese)* 77−34076
nonassociative algebra, bibliography 80−36793
noncompact group, soluble gauge theory 80−32013
noncompact groups, equiv. problem to 2-centre integrals in quantum mechanics *(Russian)* 78−89367
nonholonomic systems of higher order, Mangeron-Deleanu eqns. in Poincare-Chetaev variables 77−33853
nonLie method for mathematical physics eqns. group props. investigation 80−36832
nonlinear evolution eqns., conservation laws, group theoretical derivation 80−57520
nonlinear functional equations, group representation theory and branch points 77−67195
nonlinear realisation of symm. groups using differential geometry 77−60899
nonrelativistic algebraic models, gauge invariance, causality props. 78−62319
nonsymmetric unified field theory, metric and local invariance group 80−90754
nuclear 3-cluster systems, resonating group method 78−50108
nuclear collective model, group theory and quadrupole vibrs. 77−57610
nuclear quadrupole surface vibr. model in body-fixed coords. 77−18450
nuclear reaction theory applications, survey 77−18503
nuclear structure problems, algebraic variational method 77−18451
nuclear structure Sp(2,R) model, connection with α-particle model for ^{8}Be 77−65207
nucleon-nucleon interaction matrix, irreducible basis of representations of group O(n-1) 77−6271
O(2,1) group representations in terms of Lame, Mathieu and parabolic functions 77−45675
O(2,1) representation spaces calc. 77−49555
O(3,1) Lorentz group, generating functions, integrity bases *(French)* 80−105803
$O(3)\otimes U(1)\otimes U(1)$ internal symmetry in massless vector field theory *(Russian)* 80−22531
O(3) irreducible representation bases, for systems with finite symm. group 77−9902
O(3) shift operators, general anal. 79−94
O(3) symmetry, dynamical, appl. to circ. oscillator, Cartesian and polar wave functions connection *(Russian)* 79−49073
$O(4)\otimes O(2,2)$ representations in quantum mechanics two centre problem *(Russian)* 79−21590
$O(5)\supset O(3)\times O(3)$, basis states using modified boson operators 78−4554
O(n) shift operators, normalisation coeffs. 78−57738
octahedral group, symmetry-adapted functions, calc. of rotation matrices using recursion relation 80−31482
octonionic structures in particle physics 80−9147
orbital correspondence anal. in max. symm., appl. to spin-forbidden processes 78−78631
ornamented bells, group theoretical approach to warble 77−80032
orthogonal and symplectic groups, algebraic identities among infinitesimal generators 78−32703
orthogonal groups, finite, generalised integrity bases and counting rules for numerator invariants and covariants 79−49014
orthogonal groups, raising, lowering weight operators 78−57737
orthogonal groups, spinor representations 77−33838
OSp(4,1) invariant fermionic σ model, graded orthosymplectic geometry 79−54277
para-Fermi quantization in the representation of SO(n) 80−86554
permutation group outer-product reduction coeffs., rel. to SU_n group CG coeffs. *(Chinese)* 78−49631
permutation matrices using graphical methods of spin algebras, Serber coupling 79−6833
permutation representations, epikernels and phase transitions 77−47545
permutation symmetry, geometrical approach 78−21001
permutational symmetry of many particle states 80−57128
phase transition classification scheme, equitranslational transitions 79−17374
phase transition theory, renormalization group method 77−80601

group theory continued
phase transitions, group theoretical methods rel. to problems of classical Landau theory 80−73292
phase transitions, renormalisation group theory rel. to hamiltonian symm. *(Russian)* 77−11666
photon position operator, Galilean components 77−33906
physical and chemical systems in relation to struct. and substructs. 80−42921
physical symmetry groups, subgroups and invariant EM fields and potentials 80−8841
planar approx. to field theory through limit of large internal symmetry group 78−45519
plasma, Vlasov-Poisson system, self-similar group theoretic solns. 78−26242
plastic crystal, orientational disorder, group theory method 80−107091
plastic crystal, orientational dynamics, neutron scatt. data interpret. using functions derived from group theory 80−107092
plethysm problem of $U((n+1)(n+2)/2) \supset SU(3)$ 77−29987
Poincare, space-time symmetries of (2+1) dimens. lattice Dirac eqn. 78−4799
Poincare algebra representation reduction by Gallilei algebra 80−86605
Poincare and Galilei groups, quantum mechanics 78−49701
Poincare and Galilei groups in arbitrary dimensional spaces 78−77672
Poincare generators corresponding to lightlike irreducible unitarity representations 77−18193
Poincare group, irreducible representations of groups containing subgroup of finite index 80−68384
Poincare group, irreducible unitary representation, velocity operator 78−32713
Poincare group, phase space representation, relativistic particle mechanics appl. 80−8784
Poincare group, representation by gauge theory monopole solns. 78−16925
Poincare group P(1,3), translation operator matrix elements for relativistic particles *(Russian)* 79−40696
Poincare group representations for relativistic extended hadrons 79−89099
Poincare group representations in the free quantum field framework *(German)* 78−77772
Poincare group representations on phase space 79−88827
Poincare invariance without Poincare group 79−12992
Poincare subgroups, role in high energy physics models 79−97530
Poincare subsymmetry, associated invariant EM field *(French)* 77−61209
Poincare-like groups, Kronecker product, decomp., general construction method 78−45460
Poincare-like groups, Kronecker product decomposition, appl. to Weyl group 78−49632
point clusters, classification of symmetric coordinates, method 80−57203
point clusters, classification of symmetric coordinates, rectangular tetrahedron and cube examples 80−57204
point groups, character formulae for isoscalar factors 79−22858
point groups, continuous, characters and representations 80−36809
point groups, continuous, reduction of representations 80−36808
point groups, continuous, reduction of representations 80−36810
point groups, Racah coeffs., isoscalar factors, character formulae 77−13568
point groups for rigid molecular frames 77−18815
Polish groups, continuous unitary projective representations, Bondi-Metzner-Sachs group 77−17770
Polish groups, splitting and representation groups 78−36874
polymer molecules, irreducible representations of symmetry groups 79−3603
polymer physics applications 77−19124
polynomial irreducible tensors, generating functions 78−49633
polynomial irreducible tensors for point groups 79−2593
polynomial tensors for double point groups 79−40681
postgraduate textbook for physicists 77−41455
presymmetry in relativistic quantum mechanics, absence of kinematics 80−8843
presymplectic Hamilton and Lagrange systems, gauge transformations and the Dirac theory of constraints 80−9106
primitive spinor model *(Russian)* 79−21522
programmable procedure for generating many-particle states 80−27169
projected basis set for the irreducible representation $\{2^{N/2-S}, 1^{2S}\}$ of U(n) 78−77668
projective symmetries of dynamical systems, infinitesimal symm. transforms of vector field 78−32650
projective unitary-antiunitary representations determ. of factor systems 77−17768
pseudo Coulomb problem, group O(2,1), irreducible representation 80−73209
pseudo-groups applied to symmetry and defects ordered media 80−10541
pseudo-Jahn-Teller effect, cubic, linear, rotational invariance 80−15482
pseudo-oscillators, group theory 80−22226
pseudo-Riemannian curvature spaces, group struct. 78−57829
pseudosymmetric crystals, isovector struct. theory, Cochran struct. 80−88076
QFT, asymptotically free models with Yang-Mills fields, symplectic groups framework 79−2940
quadratic Hamiltonians in phase space and their eigenstates 80−86127
quantisation, geometric, representation spaces 78−36869
quantisation, group-induced, in central mechanics problems 78−36866
quantisation appl. of group extensions 77−37765
quantum chemistry, spin-free, alternacy, quantum no. assignment 79−9988
quantum chemistry, spin-free, particle-hole and pairing symmetries 79−6812
quantum dynamical semigroups, approach to equilibrium 78−49710
quantum dynamical semigroups, irreducible and ergodic props. 77−64956
quantum dynamical semigroups and spin multipole relaxation in isotropic surroundings 78−86813
quantum field theory and group algebra 77−18183
quantum fields in Lorentz basis 80−86565
quantum harmonic oscillator Brownian motion, quantum dynamical semigroup formalism 77−30100
quantum Markovian processes 78−29049
quantum mech. motion group, completeness theorem 78−4519
quantum mechanical problem of particle motion, field of two Coulomb centres *(Russian)* 79−92992
group theory continued
quantum mechanics, description of operators 80−8820
quantum mechanics, group representation theory, intuitive approach for teaching 79−25804
quantum N-level systems, approach to equil. for completely positive dynamical semigroups 77−30048
quantum spin systems, Fermi systems and group extensions in Weyl quantisation procedure 80−8905
quantum theory, physical geometry, group manifold 80−105522
quantum theory and structures of time and space conference, Starnberg, W.Germany (July 1978) 80−27044
quasifree completely positive semi-group generator for nonequilibrium statistical mechanics 79−25963
quasisymmetry (P-symmetry) groups in crystallography, semidirect products method 78−51457
quaternions and subluminal and superluminal Lorentz transformations, book contrib. 79−44724
radiation statistics, group theoretical approach 79−86129
Raman scattering, irreducible tensor operator for 32 cryst. point groups 77−8572
real-space renormalisation giving differential renormalisation-group eqns., two-dimens. triangular Ising lattice 78−65881
recoupling coeff. and isoscalar factors, for chain of compact topological groups 78−20939
recoupling coefficients, subgroup factorisation 78−66
recoupling coefficients of the general linear group in bases adapted to shell theories 78−77670
recoupling coefficients of the symmetric group involving outer plethysms 78−77669
reduction symmetry method in crystal field theory 80−70656
relativistic field eqns., geometric and algebraic foundation of spinor formalism 78−37128
relativistic particle classification, representation theory, 8 nonisomorphic simply connected covering groups of O(3,1) 77−46008
relativistic quantum mechanics, Galilean limit, group contraction, probabilistic interpretation 78−77760
relativistic quantum mechanics, semigroup 80−27180
relativistic symmetry group of spin and particle number 77−64971
relativity, general, spinors and Petrov types, field classification 77−67339
relativity groups, symmetry breakdown and bundle representations 80−86610
renormalisation group, invariance props. of crit. exponents 77−22512
renormalisation group and dynamic crit. phenomena, appl. to lattice dynamic 77−22515
renormalisation group approach to scaling, phys. appl. 78−49634
renormalisation group eqn., algebraic anal, 77−74575
renormalisation group eqns. for gauge field theory with multiple coupling consts. 78−360
renormalisation group transforms, optimal variational approx. 77−87699
renormalisation groups and critical phenomena in graduate level text 77−102
representability conditions for rotationally invariant density matrices, group theory appl. to generation 79−88870
representation generating theorems and interaction of improper quantities with order parameter 80−4682
representation groups for semiunitary projective representations of finite groups 80−12933
representation theory, quasistandard bases of permutation group, Gelfand bases of unitary group *(Chinese)* 78−12832
resonances in quantum mechanics over phase space, group theory aspects 80−8852
Riemannian spaces, connections and spinor connections associated with finite groups of transformations 79−44842
rigged Hilbert space and decaying states 80−4591
rotation group irreducible representations, spin-1/2 representation, teaching approach 79−58488
rotation group realisations, orbital ang. momentum and massless particles 77−37776
SL(3,R), linear representation on Banach space 79−2592
scalar particle 77−57151
scattering cylinder of finite conductivity, symmetry group and natural resonances 79−45888
Schrodinger eqn. with screened Coulomb pot., group theory approach 77−87655
Schrodinger group projective representations 77−37773
selection rules, for crystals with imperfections, subgroup method *(German)* 80−38980
semi-group for vision lateral inhibition process modelling 78−65010
semiclassical soliton solns. in quantised field theories 80−4874
semigroup generation by second-order hypoelliptic differential operators 78−65755
semigroups, dual, w*-infinitesimal operators *(Japanese)* 77−41454
semirigid molecules, Stark effect, isometric groups, elec. dipole moments theory 78−29815
sequential decays of open quantum systems 80−8851
Shubnikov space group, PUA representations 77−87625
Shubnikov space groups, selection rules 79−9075
SI units, group props., dimensionality 80−17746
SI units, group props. 80−17745
sine-Gordon equation, one dimens., group of invariance, dimens. anal. method 78−54528
singular holonomy group 78−41206
singular spin harmonics 79−97529
site symmetry approach to hybridized orbitals 77−13552
$SL_4(R)$, unitary multiplicity free representations 80−82907
SL(2,C), new nonlinear realisations 79−88828
SL(2,C) gauge theory of gravitation 77−13669
SL(2,C) unitary representation decomposition induced by SU(1,1) discrete series 79−21967
SL(2,R), universal covering group, Plancherel formula 80−68393
SL(2,R) acting on quaternions, spectrum of $r^{-(s+2)}$ type potentials 80−57125
SL(2,R) and solitons 78−57748
SL(2,R) approach to Schrodinger spectral problem with pseudosingular potential 80−8845
SL(3,R), relativistic spin selection rules 77−61215
SL(3,R) symmetry, coupling of self-conjugate systems 79−97228
SL(4), common symm. group of EM and gravit. interactions 77−34112
Slater determinants coupling for construction of K-harmonics, computer oriented method 77−57612

group theory continued
slow neutron scatt. by rotating systems of identical nuclei *(Russian)* 80−14968
smooth distribution group and Schrodinger equation in $L^p(R^n)$ 79−97227
SO_3 monopoles, spherical symm. limits on mag. charge, gauge independent proof of Guth-Weinberg theorem 77−30231
SO(2,1), Lorentz group in oscillator realisation, integral transforms, matrix elements 80−57513
SO(2,1), plane waves on the impact parameter group *(Russian)* 79−2668
SO(2,3), decomposition into irreducible representations 79−89080
SO(2n+1) group, tops and finite-rotation matrices in odd-dimensional spaces *(Russian)* 80−101952
SO(3,2) gauge theory, geom. of Einsten-Cartan theory 79−75425
SO(3), static finite energy solns. of gauge fields with separated radial variable 77−45956
SO(3) group representations in terms of Lame, Mathieu and parabolic functions 77−45675
SO(3) isotropy subgroups and Higgs pots. 78−37132
so(4,2) algebra, six-dimens. canonical realisations 80−99066
SO(4,2) infinite component fields, model of composite relativistic defects 80−18071
SO(4,C) group vector parametrisation, elementary particle theory problems 77−45976
SO(4), relativistic, three-particle bound states, wave function calcs. 78−8558
SO(4) group and Lame eqns. of second order 77−45676
SO(4)-invariant pseudo-Jahn-Teller system with equal coupling 80−15029
SO(n,1), unitary irreducible representation, invariant scalar products 80−57514
SO(n), Weyl coeff. 78−45503
SO(n) groups, (n>5), representation theorem 78−86407
SO(n) symmetric tensor representations, analytic functions on complex cone 77−60895
SO(n-1,1) representation matrix elements, computation formulas 79−43
SO(r,s), symmetry properties of embedded space-times 79−44814
solid, internal strain rel. to strain tensor, group theory anal. 79−86835
soluble one particle models, point interactions with several centres 80−4518
solution of the Dirac equation with anomalous magnetic moment 78−82133
Sp(2n) down to Sp(2n−2), missing label operators 80−62877
Sp(2n) symplectic group, degenerate irreducible representations 80−57512
Sp(3,R) model for nuclear collective rot. states 77−26600
space and field, group struct. *(Russian)* 77−13650
space group representations, complex conjugation 79−90583
space-field geometry anal., fundamental eqn. soln. *(Russian)* 77−53752
space-time conformal group, metric tensors 78−93816
space-time groups, discrete subgroups of Poincare group 77−17767
special symmetries of jm factors and j symbols 79−84989
spectral subspaces of 1-parameter groups of automorphisms 77−17761
spherical tensors, cubic normal components *(French)* 77−41452
spin orbit interaction, origin 79−91008
spin permutation group, representation matrices 78−28976
spin permutation group representations, transformation matrices, graphical approach 77−71224
spin representation of orthogonal group, superfield interpretation 77−49874
spin system, isotropic, N-component, with long- and short-range interactions, crit. behaviour 78−76256
spin systems, group theory anal. of thermodynamic limits 77−74343
spin-orbit coupling, charge and spin density wave effects 79−91009
spinor electrodynamics, anomaly free and axially coupled, bilinear gauge renormalisation 79−307
spinor field geometrodynamical superspace, quasi-catastrophe theory 78−41137
spinor fields, conformal, dimensions, scale invariance 80−27394
spinor functional determinate in Yang-Mills potential, upper bound of 1 79−311
spinor gauge field in spinor space-time formalism 78−41401
spinor geometry for Friedmann space, space-time quantisation *(Russian)* 77−33909
spinor norm, new formula 78−62048
spinor soliton stability 79−97532
spinor space, quantum phenomena 79−17192
spinor theory via involutions, Lorentz group representation appl. 80−86607
spinor-type fields with linear, affine and general coordinate transformations 79−25949
spinors in Hilbert space 77−13569
spontaneous symmetry breaking, general mathematical aspects *(French)* 77−17772
spontaneous symmetry breaking, induced representations 80−5464
spontaneously broken symm. projective geometry and group contraction 78−8551
stationary states of quantum dynamical semigroups 79−12632
statistical sum calc. by coherent states method *(Russian)* 77−13691
stereoisomer generation, specification and enumeration, config. symmetry group appl. 80−1079
structural phase transformations, translational symmetry changes 77−62500
structural phase transition induced refractive index changes in crysts. 80−16000
structure, extension characts. 79−35522
structure, extension cubic automorphism 79−35523
Sturmian operator, four Euclidean conformal group struct. 80−8844
SU(2,2) induced representations and twistors 78−8229
SU(4)⊃SU(2)×SU(2), commuting missing labels operators, equivalent sets 77−60896
SU(6) description of collective nuclear states 77−54134
subalgebra of similitude algebra and invariants 77−29983
superalgebra with spinor-vector generator, Goldstone spin 3/2 particle, Higgs effect 77−49876
superconformal algebra for Thirring and scalar superfields 79−40682
superconformal group and quark-like fermionic coordinates 80−9145
superconformal group in flat superspace 77−2763
superconformal transformations group 79−2953
group theory continued
supergauge and gauge transformations, spinor equation admitting an infinite group 79−71645
supergravity group structure 79−21619
supergravity groups, struct., complex conjugated superspace general covariance groups 79−6036
supergroup transformation, paraGrassmann algebra of relativistic fields 79−45029
supersymmetry irreducible representations direct product reduction, rest frame *(Russian)* 77−61216
symmetric criticality principle 80−102
symmetric gauge fields 78−362
symmetric group theory and Waller-Hartree spin-free method 78−41908
symmetric groups, generation algorithms 80−98813
symmetries, first integrals, splittability of dynamical systems 78−36795
symmetries and statistics in many-particle systems, group theory aspects 77−18452
symmetries in indefinite metric spaces 77−33907
symmetries of 6j coefficients 78−86423
symmetry and phase transitions, inverse Landau problem 77−47544
symmetry breaking, wave function choice, effect on predictions, DKP formalism view 80−9120
symmetry groups of completely integrable eqns. *(Russian)* 77−82365
symmetry groups of field equations for spin 1/2 79−21568
symmetry groups of nonrigid molecules as generalized wreath products and their representations 80−48013
symplectic group assoc. with canonical commutation relns., complex extension of representation 77−17769
symplectic groups. explicit decomp. of tensor products 79−17191
symplectic manifolds, reduction through consts. of motion 79−49020
T_4 translation group gauge theory, Einstein's theory of gravitation 77−13660
teaching of group theory, from common objects to mols. 78−32631
tensor fields invariant under subgroups of the conformal group of space-time 79−2603
ternar semigroups of continued representation of metric spaces *(Russian)* 77−22372
thiourea, incommensurate phase, soft modes, condensation of even-order harmonics 80−103313
thiourea, phonon modes near order-disorder transforms., hard-core modes due to pseudospin-phonon coupling 80−44285
three pion states, permutation group S_3 irreducible representation 79−17635
three-nucleon system, fractional-parentage construction of wave function 77−14041
time evolution in equilibrium states without time automorphism 79−12722
Tomita-Takesaki theory, classification of type III factors 77−17756
tops and d-functions in even spaces *(Russian)* 80−4508
transition metal complex, ligand field problems 80−42920
transition metal complexes, ligand field spectroscopy, selection rules, intensity enhancement of forbidden transitions 80−45049
transition metal symmetric clusters, exchange multiplets and operators, group theoretic method 79−7955
transition metal systems, ESR studies, polarised absorption, ligand field model, group theory applications 80−43077
translation-invariant quantisations phase space algebraic structs. 77−17846
tree-space finite rotation matrix 78−36792
triangular Ising model percolation props., renormalisation group anal. 78−93620
triviality of continuous multipliers for the real line 79−44767
twisted products for cotangent bundles of classical groups and Stiefel manifolds 78−49680
twistor flag spaces as phase spaces of conformal particles 79−97239
twistor theory, particle models 80−13278
twistors and geometric quantisation theory 79−104
two-dimensional supersymmetric models, group theoretical construction 80−99069
two-electron atom, doubly excited states, classification 77−14373
$U(2)\sigma C^{2\times2}$, representation theory, generalised Bessel functions 80−98818
U(3), canonical resolution of multiplicity problem, constructive soln. 77−17874
U(3)⊃SO(3) chains of groups, irreducible single row representation 77−71458
$U(4)\supset D^{3/2}[SO(3)]$, chains of groups, irreducible single row representation 77−71458
U(n), multiplicity free Wigner and Racah coeff. 80−31556
U(n) boson polynomials, appl. to physical problems 80−4890
U(n) lowering operators 78−8216
U(p,q), matrix elements and Casimir operators of discrete series representations 79−97238
uniaxial spin systems, quasiclassical method appls. 80−8931
unified description of symmetry groups *(Russian)* 78−41436
unified field theories, E_7 group generators, 3jm factor calcs. 79−93330
unified theories, quantised Grassmann variables, colour and flavour degrees of freedom 77−49891
unified theory of gravit., electromag., based on conformal group SO(4,2) 77−2594
uniqueness of number operators for certain symmetries 78−20987
unitary group, branching rules for subgroups 78−45462
unitary group approach to molecular electronic structure, review 80−5467
unitary group formulation of Hartree-Fock theory 80−4589
unitary group generators and permutations, CI matrix elements, algebraic method 80−37725
unitary group generators and permutations, CI matrix elements, graphical method 80−37726
unitary group irreducible representation subduction coeffs. 80−37723
unitary group representations, appl., book 79−30198
unitary groups, functional integral representation *(Russian)* 79−9309
unitary-antiunitary group representation, type and standardform 79−54008
unitary-antiunitary group representations 80−98809
universal metaplectic structures and geometric quantization 79−25881
unrestricted Hartree Fock equation, in mol. systems, group theoretical classification of solns. 79−36522
unstable fermion system, semigroup law, canonical description 80−8907
unstable particles, dynamical spin spreading 80−9117

group theory continued
unstable quantum states and rigged Hilbert spaces in nonrelativistic scatt. theory 80−8849
vacuum gravitational field with two-dimens. group of motion *(German)* 77−22466
variational principle for Z_+^N action on compact space 77−53825
vector constants and their algebras for classical Hamiltonians 79−56
vector groups, multiplier representation, translation-invariant traces, Fourier anal. 79−6023
velocity operator for irreducible unitary representation of Poincare group, identification 77−49873
vibrating symmetric system under nonlinear forces, group representation theory 77−2536
visual hallucination patterns, mathematical theory of neuronal activity 80−35892
von Neumann algebra of type III, structure, crossed products 77−17757
wave and Dirac operators, conformal group representations 77−33895
Weyl's commutation relation, implied generalized statistics 77−82408
Weyl gravitational fields, generalisation under action of isometry group of complex hyperbolic plane 79−49126
Wigner rotations and associated matrices for Dirac particles 77−2761
Wigner-Weyl isomorphism, group theoretical aspects and basic props., $E^{(2)}$ symmetry group 78−62089
XY_4 molecules, tetrahedral, vibration-rotation energies of harmonic and combination levels 80−47962
Young operators invariance groups, Pauling numbers 77−18774
Yukawa potential bound states, Sturmian group theoretical approach 80−8825
H atoms, two-photon transition matrix elements, group theory calc. 78−62776
ϕ^6 theory, Gell-Mann and Low renormalisation group appls. 78−29224
π^+, π^0, Santilli's model for hadron constituents number, computation simple approach 80−42389
^{12}C $J^\pi=0^+$ isoscalar levels, α-particle model with group theoretical methods 77−74766
Cd_3As_2 type crystals, symmetry props. of energy bands 80−39500
$(H_2O)_2$, tunnelling-rotational energy levels, group theoretical classification 77−54549
^{3}He, superfluid, 5-d spin theory 80−49450
^{3}He, superfluid, topological classification of line singularities in cylindrical pore 79−4447
^{3}He, superfluid, topology of non-singular textures using relative homotopy groups 78−84021
$IrBr_6^{2-}$, Raman tensor patterns, vibr. reson. Raman scatt., group theoretical calcs. 78−986
$KMnF_3$, IR-active phonons in tetragonal phases 80−2748
^{6}Li+n, 12 and 20 MeV, resonating group method exam., effective internuclear potential 78−50159
^{16}O, band system generation by infinitesimal operators of subgroup Sp (2,R) 78−50109
PbTe, standard representation of Bloch spinors using phase convention 79−51473
SCl_2, electronic struct., group theoretical and CNDO/2 calcs. 78−33419
SCl_4, electronic struct., group theoretical and CNDO/2 calcs. 78−33419
S_2Cl_2, electronic struct., group theoretical and CNDO/2 calcs. 78−33419
SO(2), infinite-well pot., for teachers 77−33791
$ZnSeO_4.6H_2O:Cu^{2+}$, crystal struct. orientational degeneracy removal scheme, space groups, ESR spectra 78−47267
$ZrSe_3$, long wavelength optical phonons, Raman scatt. and IR refl. 80−34921

Gruneisen coefficient
acetone-chloroform (-iodomethane) ($-CS_2$), liq. mixture, excess Gruneisen parameter, intermol. interaction 78−67635
acoustic Gruneisen parameter for high-temps. in Earth's interior 79−39691
adamantane, mol. cryst., thermal expansion coeff. and Gruneisen coeff. 77−84952
alkali halide, Anderson-Gruneisen parameter evaluation 80−24617
alkali halide, dielec. const., press. depend. from Szigeti relations, Gruneisen const. of transverse optical mode 79−19828
alkali halide, interaction potential, Gruneisen parameter, compressibility 78−14304
alkali halide, lattice props. from interorbital-distance-related-repulsion approach 78−22809
alkali halide, transverse optic mode Gruneisen parameter and dielectric props. 77−31747
alkali halide crystal, Gruneisen parameter, vol. depend. anal. 80−2135
alkali halide crystals, anharmonic effects 79−99290
alkali halide crystals, long wavelength optical mode frequencies and Anderson-Gruneisen parameter 80−65182
alkali halide elastic dielectrics, Gruneisen parameter, effective ionic charge volume derivative 80−84273
alkali halide high-pressure submillimetric-wave spectra 79−33694
alkali halides, cryst., pot. parameters, Hellman function calcs. 80−2181
alkali halides, optic mode Gruneisen parameters 78−43088
alkali halides, Poisson ratio and Gruneisen parameter, vol. depend. anal. 80−96614
alkali halides, static dielectric behaviour, vol. depend., many-body interactions effects 78−2786
alkali halides, transverse optic mode Gruneisen parameter 80−39244
alkali hydride, repulsion interaction 78−26488
alkali hydrides, bulk props. prediction from molecular behaviour 78−51468
alkali hydrides, lattice props. from interacton pot. energy function 80−100199
alkali hydrides, thermodynamic props. calc. using ionic pots. 78−10155
alkali metal, atomic props., accuracy of description depenxence on pseudopotentials *(Russian)* 78−38997
alkali metal, bulk properties, computer simulation 78−30729
alkali metal, lattice vibr. and Gruneisen parameter 78−59917
alkali metal, thermal expansion, elastic constants, phonon freq. anisotropy *(Russian)* 79−1516
alkali metal, thermal expansion and Gruneisen parameters 78−38857
alkali metal halides, interionic repulsive short-range interaction pot., lattice energy calc. 80−96466
alkali metals, equation of state and vol. depend. of thermodynamic props., pseudopot. theory 78−18738
alkali metals, Gruneisen parameter, temp. variation 80−107396
Gruneisen coefficient continued
alkali metals, Gruneisen parameter and temp. depend. of elastic consts. 80−39317
alkali metals, Gruneisen parameters, influence of press. on lattice anharmonicity and temp. depend. 80−79905
alkali metals, Gruneisen parameters calc. using non-central force model 77−1242
alkali metals, mode Gruneisen parameters, ab initio calc. 77−20091
alkali metals, thermal properties and Gruneisen parameters, employing model pot. 78−71815
alkaline earth chalcogenides, crystal parameters calcs. using repulsive interaction pot. 79−37795
alkaline earth chalcogenides, interionic repulsive short-range interaction pot., lattice energy calc. 80−96466
alkaline earth metals, liq., pseudo-Gruneisen parameter, temp. depend. 77−7873
alkaline earth oxides, cohesive and thermophysical props., role of three-body interactions 80−92477
alklai halide, optic mode Gruneisen parameters and strain derivatives, Born-Mayer and Sziegti model 78−55929
Anderson Gruneisen parameter, expression 77−76517
Anderson-Gruneisen function exam. 79−55855
Anderson-Gruneisen parameter, heavy metal halides 78−79715
Anderson-Gruneisen parameter effect of anharmonicity 78−79714
Anderson-Gruneisen parameter for 16 cubic symmetry crystals 80−24556
Anderson-Gruneisen parameter for cryst. of cubic symmetry, determ. using elastic moduli 78−79713
Anderson-Gruneisen parameter for cubic crystals 78−79672
aqueous non-electrolytes, excess internal pressure and Gruneisen parameter behaviour 80−88015
BCC crystal, elastic constants, thermal expansion and bulk modulus 80−6452
benzene-ethylene dichloride (-CCl_4), liq. mixture, excess Gruneisen parameter, intermol. interaction 78−67635
bicyclo[2.2.2]octane, thermal expansion coeff., Gruneisen parameter 77−76581
binary liquid mixtures, excess Gruneisen parameter and intermolecular interactions 77−20082
biocyclo[2.2.2]octane, mol. cryst., thermal expansion coeff. and Gruneisen coeff. 77−84952
bond anharmonicities, Gruneisen parameters and pressure-induced frequency shifts 80−107397
α-brass, Gruneisen parameter determ. using thermoelastic effect 79−28068
bulk moduli, Wachtman's eqn., and temp. depend. 78−75799
caesium halides press. depend. of effective ionic charge 80−96462
carbon tetrachloride-benzene, liq. mixture, excess Gruneisen parameter, intermol. interaction 78−67635
chalcogenide crystals with FCC structure, Moelwyn-Hughes parameter appl. to calcs. 77−80437
chloroform-acetone, liq. mixture, excess Gruneisen parameter, intermol. interaction 78−67635
cubic and non-cubic solids, Gruneisen parameters, vol. depend. 80−29145
cubic metal, vol. and temp. depend. of phonon frequencies, Gruneisen parameters calc. 77−15514
cubic pure metals, thermal expansion coeffs., Morse pot. calcs. 79−77775
diamond, Gruneisen spectroscopic mode parameters via Raman spectra 77−7876
Earth's thermal properties, derivation from seismic data 79−96753
Earth core Gruneisen parameter, reevaluation 79−39685
Earth interior, Gruneisen coeff. formulation rel. to thermal model 78−15982
Earth interior, Gruneisen parameter rel. to generalised eqn. of state 78−96194
Earth lower mantle Gruneisen parameter, evidence for approximation $\gamma\rho$=const. 80−3970
Earth mantle and core, Gruneisen parameter, melting curve and adiabatic gradient 80−90028
elastic deformation, thermodynamics of, eqn. of state for solids 80−96589
electron irradiated solid, dynamic and dosimetric characts., laser and holographic interferometry obs. *(Rumanian)* 80−90886
equation of state, appl. to atomic solids and solid and liquid polymers 78−30733
ethylene dichloride-benzene, liq. mixture, excess Gruneisen parameter, intermol. interaction 78−67635
fundamental Earth physics appls. 78−36125
geophysical appl. 78−65264
globular hydrocarbons, cohesive energy and Gruneisen parameter calcs. 79−19183
glycerol($-d_3$), single cryst., glassy, and supercooled, polarised Raman spectra, anharmonic multiphonon interactions 79−91419
harmonic approx., theoretical evaluation by Legendre polynomial expansion 78−59916
homovalent disordered solid alloy, entropy-vol. correlation 78−63868
Invar, magnetic and thermal anomalies 80−34603
iodomethane-acetone, liq. mixture, excess Gruneisen parameter, intermol. interaction 78−67635
ionic crystal, repulsive short-range interaction pot., lattice energy calc. 80−96466
ionic crystal, thermodynamic props. calc., pot. energy function approach 80−54407
ionic crystals, Anderson-Gruneisen parameter, interaction approach 80−88291
ionic crystals, interatomic forces, Gruneisen and Anderson-Gruneisen parameters 80−79904
Landau theory for pressure-induced phase transitions 79−34807
liquid, disorder parameter-pseudo-Gruneisen parameter relation 78−34411
liquid, Gruneisen parameter rel. to Rao's acoustical parameter 80−92581
liquid state, semi-empirical eqn., temp. and lattice distortion parameter depend. 77−31785
liquids, pseudo Gruneisen parameter, modified semiempirical calcs. 79−90799
melting, dislocation model, appl. to FCC cryst. 78−26658
melting theory, thermodynamic basis of Lindemann's law 78−18743

Gruneisen coefficient continued
metal, allotropic transform., anharmonicity, effects due to thermal expansion and Gruneisen parameters 79−52207
metal, b.c.c., modified Cheveau model for lattice waves, phonon dispersion and Gruneisen parameter 77−1189
metal, complete thermodynamic eqns. of state 80−24561
metal, Gruneisen ratio, rel. to Poisson ratio press. depend. and shock data 77−11712
metal, low temp. phonon resist. 77−62888
metal, rel. to press. depend. of Poisson ratio 77−47504
metal, thermodynamic properties, outer electron contributions *(French)* 78−43091
metal, vacancy formation parameters and Gruneisen constant 78−22709
metals, generalised Gruneisen tensor from solid nonlinearity parameters 80−84275
metals, Gruneisen parameters, interatomic forces, pseudopot. calc. 80−44165
metals, Morse potential appl. in molecular-metallic framework 80−79742
methane, solid, phase II, Raman spectrum, vol. and temp. depend. 80−97260
methane, solid, thermal expansion coefficient and Gruneisen parameter 78−47540
Mie-Gruneisen equation of state, appl. to planetary interiors 78−29072
Mode-Gruneisen parameter dispersion curves CC ^{4}He, FCC high-density cryst., lattice dynamics by inelastic neutron scatt. 79−1539
naphthalene-d, press. depend. of lattice freqs. at 100K 79−46768
Nb carbides, nonstoichiometric, elastic props., 20-2000°C 77−12661
noble metal, Gruneisen parameter temp. variation calc. 78−51638
octafluoronaphthalene, phase transitions at elevated press., Raman and mid-IR spectroscopy obs. 80−45062
organic liquids, thermodynamical Gruneisen parameter, press. depend. 78−14479
oxide glasses, thermal expansion coeff. calc. from chem. comp. Gruneisen const. 77−11710
oxide minerals, elastic constant systematics 79−69177
phase transformation, press. induced, Gruneisen parameter and eqn. of state determ. 80−90031
picrite, calculation using measurement of US vel. 80−41436
PMMA, amorphous, tunnelling models and thermal expansion below 4K 79−73326
PMMA, Gruneisen const. and thermal props., temp. depend., 4-300K, Brillouin scatt. obs. 80−100662
Poisson ratio volume depend., Debye theory 78−22785
poly(4-methyl pentene-1), US props., glass transition, Gruneisen parameters 80−54316
polyalkaneimide, mech. and thermophys. props. at liq. He temps. 80−3117
polycrystal elasticity theory, role of Gruneisen elastic parameters 79−95070
polyethylene, X-ray diffr. at press. up to 14000 kg cm^{-2}, 298K 77−35492
polyethylene cryst., unit cell variations with temp. and high press. 78−47250
polymers, glassy, Gruneisen const. calc. from thermoelastic meas. 79−14945
porous solid, generalised p-α model, eqn. of state, sound vel. 80−65154
pressure dependence meas. method and apparatus 77−35714
pressure effects on phonon dispersion spectrum and Gruneisen coeff. 77−43287
pressure induced phase transitions, influence on Gruneisen parameter 79−1497
pure material, in two-phase solid-liq. melt regime, eqns. 77−55342
quartz, fused, vol. depend. of Gruneisen const. 79−23670
α-quartz, Gruneisen constants for optical modes, neutron irrad. and press. effects *(Russian)* 78−22815
quartz, Gruneisen parameter at high press. 80−8299
quartzite, Gruneisen parameter at high press. 80−8299
quench-condensed films, superconducting transition temp., elastic stress and strain effects 80−70883
resistivity strain coeff. calcs. 80−100449
semiconductor, Anderson-Gruneisen parameter, bulk modulus temp. depend. 78−10154
shock waves in material with linear shock wave-particle vel. relation 77−69042
silicate minerals, elastic constant systematics 79−69177
simple liquids, internal pressure and cohesive energy density, Gruneisen parameter 80−88007
simple liquids, thermodynamic props. and solubility parameters 78−2265
solid, anharmonic parameter, $\gamma\beta$T, interpretation *(French)* 80−34160
solid lattice thermodynamics, two-temp. Debye approx. *(Russian)* 80−77728
solid matter behind wave front, eqn. of state *(Chinese)* 79−82308
solids under press., simple model for Gruneisen parameter and adiabatic compressibility 77−11706
steel, martensitic, Gruneisen parameter determ. using thermoelastic effect 79−28068
strain driven thermoelastic instability toward brittle fracture 80−103415
TCNQ salt, TSeF-TCNQ, electrical conductivity, press. depend. 77−51729
thermal pressure in solid and eqn. of state, computer simulation 78−34593
thermoelastic meas. method 80−107581
transition metals, electronic Gruneisen parameter 79−82297
uniaxial crystals, third-order elastic consts., Anderson-Gruneisen parameter evaluation 80−65119
US nonlinearity parameter for solids, relationship with Gruneisen parameter 80−74561
US parameter for nonconducting cubic crystals 78−87744
volume dependence of Poisson and Gruneisen ratios 77−43351
water, thermodynamical Gruneisen parameter, press. depend. 78−14479
Zerodur, glass-ceramic, thermoelastic props. 78−27550
Ag, FCC, dynamical study for Gruneisen parameters 77−47594
Ag, FCC, Gruneisen parameters, effect of temp. variation 78−22812
Ag, Gruneisen parameters, 10-100K, phonon wave vector depend. 78−38801
Ag, Gruneisen parameters, dynamical study using modified Bhatia model 79−37797
Ag halides, anal. of cryst. binding and Anderson-Gruneisen parameters 80−15040
Ag halides, dielectric behaviour and optic mode Gruneisen parameters 79−10907
Gruneisen coefficient continued
Ag, X-ray Debye temp. and isobaric Gruneisen coeff., anharmonicity effects 77−62654
Ag-Mn, dil., anomalous thermal expansion below 50K 78−51710
AgBr, dielectric behaviour under hydrostatic press. 78−52420
AgBr-AgCl mixed crystal, elastic consts., temp. and press. derivatives 77−11620
AgCl, dielectric behaviour under hydrostatic press. 78−52420
β-AgI, thermal expansion, 4 to 270K 80−79961
Al and its alloys, dynamic determ. of Gruneisen coeff. 77−24418
Al, electronic Gruneisen parameter in shock Hugoniot eqn. of state 80−10635
Al, FCC, dynamical study for Gruneisen parameters 77−47594
Al, FCC, Gruneisen parameters, effect of temp. variation 78−22812
Al, Gruneisen coeff. depend. on specific volume, phonon spectra calcs. 79−65165
Al, Gruneisen parameter behaviour at high press. 78−83899
Al, Gruneisen parameter determ. using thermoelastic effect 79−28068
Al, Gruneisen parameters, dynamical study using modified Bhatia model 79−37797
Al, low temp., coeff. of linear thermal expansion 79−23694
Al, low temperature lattice parameters and Gruneisen parameter 78−38658
Al, melting curve and Gruneisen coeff. at high press. 80−65200
Al, shear constants, press. effect up to 2500 atm., −196 to 25°C 77−31710
$Al_{10.4}Ga_{0.08}V$, low temp. thermal expansion 78−95167
Al_2O_3-SiO_2-Cu_2O glasses, Grueneisen's constant of low expansion 79−77779
$Al_{10}V$, low temp. thermal expansion 78−95167
alkali halides, interatomic forces, Born model anal. on US data 78−55833
Ar, solid, vol. depend. lattice dynamics, pseudo-harmonic approach 79−99260
$As_2S_3(Se_3)$, thermal expansion at low temperatures 78−83982
As_2Se_3 glass, mech. props. var. due to high press. phase change 77−76481
Au, FCC, dynamical study for Gruneisen parameters 77−47594
Au, FCC, Gruneisen parameters, effect of temp. variation 78−22812
Au, Gruneisen parameters, 10-100K, phonon wave vector depend. 78−38801
Au, Gruneisen parameters, dynamical study using modified Bhatia model 79−37797
Au, thermal properties and Gruneisen parameter, Toya's first principle approach 78−38806
Au-Cd (47.5 at.%), single cryst., Gruneisen parameters from press. derivatives of elastic consts. near martensitic transform. 77−63667
B, liq., thermoelastic props. near melting point 80−19862
BN, Raman scatt. exam. of high press. effects on force const. anisotropy 79−38542
BP, sp. ht., Debye temp., compressibility and Gruneisen coeff. meas. 78−63865
BaF_2, Raman spectra, 15 to 1300K, anharmonic vibr. effects 77−43990
$Ba(NO_3)_2$, Born-Mayer interaction pot. and lattice props. 79−37858
$Ba(NO_3)_2$, press. derivatives of elastic-moduli, ultrasonic velocity meas. 78−95102
$BaTiO_3$, pot. functions of ions 80−19885
$BaTiO_3$, X-ray diffr. intensities, anomalous temp. depend. *(Russian)* 79−1484
Bi, Gruneisen parameter, high press. phase transitions 79−60467
Bi, liquid, eqn. of state parameters rel. to Earth core energetics 77−15536
CO_2, solid, high press. mol. libration calc. with Kihara core pots., Gruneisen parameter and lattice 80−65173
CS_2-acetone, liq. mixture, excess Gruneisen parameter, intermol. interaction 78−67635
CaBr(Cl)(I), Gruneisen γ and other thermodynamic props. at zero and elevated press. 78−43142
CaF_2 (fluorite), Gruneisen parameter at high press. 80−8299
CaF_2, Raman spectra, 15 to 1300K, anharmonic vibr. effects 77−43990
Cd, resistivity, existence of Einstein type phonon mode 79−42519
$CdCr_2S_4$, thermodyn. props. 78−51703
CdTe, temperature variation in bulk moduli in solids 79−73237
$CdTl_2Te_4$, single and polycryst. samples, linear expansion, heat capacity and thermodynamic props. 80−103489
Ce, high pressure phase transition, anomalous Gruneisen parameter behaviour 80−79934
Co, Anderson-Gruneisen parameter, temp. depend., third-order elastic consts. calc. 79−46776
Co, thermal expansion and bulk modulus 77−31788
Cr, linear expansion coefficient, at low temp. 78−83977
Cs halides, Gruneisen and Anderson-Gruneisen parameter determ. 80−59611
Cs phonon freqs. and Gruneisen parameter, model pseudopotential calc. 77−35643
CsBr, thermodynamic props., lattice dynamical calc. 77−20090
CsI, thermodynamic props., lattice dynamical calc. 77−20090
$CsNiCl_3$, linear-chain antiferromag., low temp. thermal expansion 80−39326
Cu, elastic moduli rel. to Gruneisen elastic parameters 79−95070
Cu, FCC, Gruneisen parameters, effect of temp. variation 78−22812
Cu, Gruneisen parameter behaviour at high press. 78−83899
Cu, Gruneisen parameter determ. using thermoelastic effect 79−28068
Cu, Gruneisen parameters, 10-100K, phonon wave vector depend. 78−38801
Cu, Gruneisen parameters, dynamical study using modified Bhatia model 79−37797
Cu halides, anal. of cryst. binding and Anderson-Gruneisen parameters 80−15040
Cu I, press.-induced phase transitions, Raman scatt. obs. 77−43995
Cu wire, corrosion in $AgNO_3$ soln., elec. resist. variation, rel. to Gruneisen parameter 78−11404
Cu-Fe, force constant change with pressure, relative Mossbauer fraction 80−34163
Cu-Mn, dil., anomalous thermal expansion below 50K 78−51710
CuBr, press. depend. of Raman scatt. meas., Gruneisen parameters determ. 77−24845
CuBr, specific heat and lattice dynamics 79−37798
$CuBr_xI_{1-x}$, disorder-induced TA Raman lines 79−73929
CuCl, polycryst., thermal expansion meas. at low temps. 77−55367

Gruneisen coefficient continued
CuCl, press. depend. of Raman scatt. meas., Gruneisen parameters determ. 77−24845
$CuCl_xBr_{1-x}$, disorder-induced TA Raman lines 79−73929
CuI, press. depend. of Raman scatt. meas., Gruneisen parameters determ. 77−24845
CuI, specific heat and lattice dynamics 79−37798
Cu_2O, thermal expansion at low temp. 78−59959
p-D_2, far IR absorpt. in ordered state 79−91430
D_2, solid, equation of state, at high pressure 79−46781
D_2, solid compressed, anomalons double peaked one-phonon for IR obsorption, Gruneisen const. calc. 79−56788
Dy, paramag., rel. to anomalous thermal expansion, up to 273K 79−7967
Er, Anderson-Gruneisen parameter, temp. depend., third-order elastic consts. calc. 79−46776
Er, lattice dynamics, thermal expansion, bulk modulus calcs. 77−20022
F, liquid, hard sphere model with attractive interactions 80−96434
Fe, Gruneisen parameter behaviour at high press. 78−83899
Fe, highly pure, phonon contrib. to elec. resist., 1.6-298K 78−84194
Fe in Earth's core 78−61361
Fe, liquid, at Earth outer core conditions, Gruneisen γ function determ. 79−84186
Fe, purification, recrystn. temp. and elec. resistivity *(Japanese)* 80−100780
Fe, thermal props. at high-press. (150 GPa), from shock-wave expts., Earth core struct. 80−21683
Fe-Ni, Invar alloys, anomalous thermal expansion coeff. *(Japanese)* 79−65225
Fe-Ni alloys, anomalous thermal expansion, Gruneisen eqn. 78−83980
Fe-Ni Invar anomalies, low spin to high spin transition 79−56558
GaAs, lattice vibration, thermal expansion and pressure effect 80−39233
GaP, thermal expansion below room temp. 80−79963
GaS, infrared optical props., polarisation depend., vibr. modes 80−100658
GaSb, lattice vibration, thermal expansion and pressure effect 80−39233
ε-GaSe, Raman scatt., hydrostatic press. effect 80−84745
Ge, effect of pressure on the Raman shift 78−92064
Ge, Gruneisen constant, temp. depend. 77−72667
Ge, lattice dynamics under press 80−92627
Ge, mode Gruneisen coeff. at point X, effect of lattice softening 78−38804
Ge, phonon energy variation under high press.: band struct. changes, tunnel spectroscopy study *(Russian)* 80−2134
Ge, thermal expansion coeff., optical mode Gruneisen const. 79−46820
GeO_2, thermal expansion at low temperatures 78−83982
GeS_2 glass, temp. and press. depend. of elastic props. 77−15476
GeS_2, thermal expansion at low temperatures 78−83982
GeS(Se), layer cpds., Raman spectra, press. coeffs. and mode Gruneisen parameters 78−10891
O-H_2, far IR absorpt. in ordered state 79−91430
H_2, solid equation of state, at high pressure 79−46781
^{4}He, HCP, lattice dynamics, neutron-inelastic-scattering obs. 79−33154
^{4}He, HCP, pulse echo expts. 78−38910
^{4}He, solid-fluid, eqn. of state, melting props. under press. 80−96721
Hf, HCP, lattice dynamics, thermal and elastic props., model 80−34155
HfO_2-TiO_2, thermal expansion coeff. and dynamic response to pulsed energy deposition 78−26705
Hg, liquid, eqn. of state parameters rel. to Earth core energetics 77−15536
Hg, thermodynamical Gruneisen parameter, press. depend. 78−14479
HgTe, 1.5 to 30K, thermal expansion and heat capacity meas. 80−59681
Ho, bulk modulus, thermal expansion, third order elastic constants 77−84875
In, Gruneisen parameter behaviour at high press. 78−83899
InP, depend. of phonon spectrum on hydrostatic press., Raman spectra 80−93315
InSb, lattice vibration, thermal expansion and pressure effect 80−39233
InSb, thermal cond., elec. cond., and thermoelec. power, press. depend. 80−59744
InSb, US attenuation and Akhieser loss, temp. depend. 79−86842
K, BCC, temp. var. 78−6137
K, Gruneisen parameter, press. depend. 80−65184
K, mode Gruneisen parameters, neutron scatt. obs., 4.5K, 0.001-4.1 kbar 77−4179
K, mode Gruneisen parameters, calc. 77−4180
K, phonon frequencies, normal mode Gruneisen parameters, pseudopot. calcs. 79−42184
KBr, Gruneisen parameter, high press. phase transitions 79−60467
KBr, mode Gruneisen parameters, acoustic phonon dispersion relations 79−42201
KCN, crystal props., log potential model calc. 78−63829
KCN, polymorphism, high pressure, Raman spectra 78−88302
KCl, thermodynamic props., lattice-dynamical calc. 77−35715
KCl-KBr mixed system, Gruneisen coefficient evaluation 80−39240
$KNbO_3$, cubic, temp. depend. of intensity of X-ray interference 80−59613
$K_2Pt(CN)_4Br_{0.3}.2.7D_2O$, under hydrostatic press., compressibility, neutron diffr. 79−46742
Li, BCC, temp. var. 78−6137
^{6,7}LiH(D), cryst., cohesive energy, force const., lattice freq., Debye temp., Gruneisen parameters, calc. 78−91293
LiIn, from thermal expansion and sp. ht. of $LiAl_{1-x}In_x$ 78−22869
$LiNbO_3$, X-ray diffr. study of lattice dynamics parameters *(Russian)* 79−65156
$LiTaO_3$, X-ray diffr. study of lattice dynamics parameters *(Russian)* 79−65156
Lu, lattice dynamics, heat capacity, thermal expsn. 79−86857
Mg, melting temp. under shock loading 77−47553
Mg_2Sn, third-order elastic constant, low temp. limit of Gruneisen parameter 79−73280
Mn_2SiO_4, tephroite, thermal expsn., 25-850°C, Gruneisen parameter determ. 79−60527
Mo, linear expansion coefficient, at low temp. 78−83977
MoS_2(2H), lattice dynamics, Coulomb and quasi-harmonic effects 80−39245
α-N_2, solid, thermal expansion and Gruneisen coeff. *(Russian)* 79−10969
α-N_2, temp. depend. of IR spectra, Gruneisen parameters determ. 80−84730
NH_3, ND_3, crystals, rotation mol. motion *(Russian)* 78−87762
NH_4Cl Raman spectra, pressure effects 80−97268
Na, BCC, temp. var. 78−6137
Na, Gruneisen parameter, press. depend. 80−65184
NaBr, heat capacity, Gruneisen parameters, 2 to 20K 80−29180
NaCN, crystal props., log potential model calc. 78−63829
NaCl, elastic props. at press. up to 9 GPa, ultrasonic wave velocities 79−95073
NaCl, eqn. of state, effect of Gruneisen parameter 79−51233
NaCl, Gruneisen coeff. press. depend. up to 33 kbar 77−35714
NaCl, Gruneisen γ and other thermodynamic props., vol. depend. 77−76577
NaCl, thermodynamic props., lattice-dynamical calc. 77−35715
$NaClO_3$ temperature variation in bulk moduli in solids 79−73237
NaF, heat capacity, Gruneisen parameters, 2 to 20K 80−29180
Na_2O-B_2O_3 glass, negative thermal expansion, LF Guneisen parameter, numerical analysis 77−11707
Na_2O-$GeO_2(SiO_2)$, thermal expansion at low temperatures 78−83982
Na_2O-SiO_2 glass, acoustic and thermal Gruneisen parameters 80−59608
Na_2O-SiO_2 glass, low temp., comp. effects 77−20097
NbO_2, semicond., thermal expansivity 80−34213
Ne, phonon dispersion relation, Gruneisen parameters at high press. 79−42179
Ne, solid, phonon-dispersion, mode Gruneisen parameters and elastic consts. 77−11651
Ni, low temp., coeff. of linear thermal expansion 79−23694
Ni, Ni-Co, low temperature lattice parameter, Gruneisen parameter 77−76357
NiS_2, high press. effect on mag. transition temps. 78−91866
noble metals, evaluation at Gruneisen number and nonlinearity const., elastic moduli data 80−65165
Pb, electronic thermal Gruneisen parameters 80−39242
Pb, Gruneisen parameter and binding energy, model pot. calcs. 77−51517
Pb, Gruneisen parameter behaviour at high press. 78−83899
Pb, Gruneisen parameters and thermal expansion coeff. 79−33103
Pb, liq., thermodynamic characterisation, by isobaric expansion meas. 80−103494
Pb-In, superconductive, electron tunnelling under hydrostatic press. 77−51850
$Pb_5Ge_3O_{11}$, ferroelectric, anharmonic effects in low freq. symm. modes, Raman study 80−25365
$Pb_5Ge_3O_{11}$, lattice dynamics parameters anisotropy, X-ray diffr. study 80−59612
$Pb_5(GeO_4)(VO_4)_2$, $Pb_5(SiO_4)(VO_4)_2$, and Pb_5GeO_{11}, elastic nonlinearity and acoustic losses 80−59554
$Pb(NO_3)_2$, press. derivatives of elastic-moduli, ultrasonic velocity meas. 78−95102
PbO-SiO_2 glass, acoustic and thermal Gruneisen parameters 80−59608
$(PbSe)_{1-x}(SnTe)_x$, lattice dynamic props., Gruneisen parameters *(Russian)* 78−83984
$PbTiO_3$, X-ray interference intensity temp. depend., lattice ion vibr. *(Russian)* 80−20601
$PbZr0_3$, X-ray interference intensity temp. depend., lattice ion vibr. *(Russian)* 80−20601
Pd, electronic Gruneisen parameter calc. 79−11055
Pd-H alloys, thermal expansion, low and room temp., electronic and lattice components 77−63026
Pd-H(D), thermal expansion and lattice anharmonicity 9 to 270K 80−39241
Rb, BCC, temp. var. 78−6137
Rb phonon freqs. and Gruneisen parameter, model pseudopotential calc. 77−35643
RbBr, phonon freqs. at 80, 290, 370K, neutron inelastic scatt. study, comparison to Gruneisen parameters 78−51631
RbCN, crystal props., log potential model calc. 78−63829
RbCl, Gruneisen parameter, high press. phase transitions 79−60467
RbCl, thermodynamic props., lattice-dynamical calc. 77−35715
$RbMnF_3$, antiferromag., mag. props. 79−8032
Re, Anderson-Gruneisen parameter, bulk modulus and compression curves 78−30690
Ru, Anderson-Gruneisen parameter, temp. depend., third-order elastic consts. calc. 79−46776
Ru, lattice dynamics, sp. ht., thermal expansion 79−82363
Ru, lattice dynamics, thermal expansion and bulk modulus 77−59079
Se, trigonal or amorphous, thermal expansion and Gruneisen coeffs., 10-300K 78−22870
Se-Ge glass, rel. to photostruct. change of lattice vibr. spectra 78−72494
Si, generalised Gruneisen parameter elements determ. using uniaxial press. for inelastic neutron scatt. 77−35442
Si, Gruneisen coeff. from stress-induced phonon energy meas., inelastic neutron scatt. 79−82298
Si, lattice dynamics under press 80−92627
Si, stretched, lattice vibr. anharmonicity, influence of stress on elastic moduli, Raman spectra 80−80791
Si, structural props. using electron-ion Hamiltonian using density-fundamental methods 79−82177
Si, temp. depend. 77−72667
Si, temperature variation in bulk moduli in solids 79−73237
Si, thermal expansion coefficient and Gruneisen const. 77−59128
Si, thermal expansion coeff., optical mode Gruneisen const. 79−46820
α-SiC, wurtzite type cryst., temp. depend. of one phonon Raman spectra, Gruneisen parameters 77−66500
SiO_2, amorphous, tunnelling models and thermal expansion below 4K 79−73326
SiO_2, fused, US study by harmonic generation, elastic consts., Gruneisen parameters 78−83735
SiO_2, glass, acoustic and thermal Gruneisen parameters 80−59608
SnI_4 crysts., dynamical props. of ^{119}Sn by Mossbauer spectroscopy 77−59495
SnI_4, Raman spectra, temp. and press. meas. and lattice dynamical calcs. 78−56472
SnTe, low-temp. sp. ht., thermal expansion and Gruneisen parameter 77−15601
p-H, solid, constant volume heat capacity and eqn. of state, temp. depend. 80−65334
$SrF_2(Cl_2)$, Raman spectra, 15 to 1300K, anharmonic vibr. effects 77−43990
$Sr(NO_3)_2$, 261-740K, X-ray diffr. obs. 77−35720
$Sr(NO_3)_2$, Born-Mayer interaction pot. and lattice props. 79−37858

Gruneisen coefficient continued
$Sr(NO_3)_2$, press. derivatives of elastic-moduli, ultrasonic velocity meas. 78−95102
$TaSe_2$ (2H), thermal and elastic props., X-ray diffr. exam. 79−37754
Tb, third order elastic consts. and thermal expansion 77−80569
TeO_2, paratellurite, stress induced changes in Raman spectrum 78−39540
Th, electronic thermal Gruneisen parameters 80−39242
ThO_2, temp. depend., lattice vibrational frequencies in range 298-2300K 78−79712
α-Ti, plastic deform., anharmonicity, and Gruneisen parameter 80−88246
Ti, thermal expansion coeff. and Gruneisen const., 6 to 300K *(Russian)* 79−51281
Ti-Fe, force constant change with pressure, relative Mossbauer fraction 80−34163
TiO_2, interionic repulsive short-range interaction pot., lattice energy calc. 80−96466
Tl halides, anal. of cryst. binding and Anderson-Gruneisen parameters 80−15040
TlBr, dielectric behaviour under hydrostatic press. 78−52420
TlCl, dielectric behaviour under hydrostatic press. 78−52420
UC, temp. depend. of Gruneisen parameter and lattice vibr. freq., between 298 to 2500K 80−29142
UN, temp. depend. of Gruneisen parameter and lattice vibr. freq., between 298 to 2500K 80−29142
UO_2, elastic props. at high press., US meas. 77−4141
UO_2, temp. depend., lattice vibrational frequencies in range 298-2300K 78−79712
V-Fe, force constant change with pressure, relative Mossbauer fraction 80−34163
V_3Ge, Anderson-Gruneisen parameter, from 3rd order elastic const. data 79−33059
$V_3Ge(Si)$, Gruneisen parameter and thermal expansion eval. at room temp. 80−70351
V_3Si, Anderson-Gruneisen parameter, from 3rd order elastic const. data 79−33059
V_3Si, thermal expansion, 20-300°C, using differential push-rod dilatometer 80−39320
W, linear expansion coefficient, at low temp. 78−83977
W, shock compression, 1223K, re-exam. of expt. data 77−55320
WC-Co, elastic moduli and their press. derivatives 79−83248
Y, thermal and elastic props. 79−33027
$Y_3Fe_{5-x}Al_xO_{12}$, $Y_{3-x}Gd_xFe_5O_{12}$, linear expansion 77−48024
YIG, thermal attenuation of US waves, 500-1000 MHz 77−84854
$ZnIn_2S_4$, Raman scatt., hydrostatic press. effect 80−84745
ZnO, wurtzite type cryst., temp. depend. of one phonon Raman spectra, Gruneisen parameters 77−66500
α-ZnP_2, lattice parameters and thermal expansion, 80-320K, X-ray obs. 80−75373
ZnS, cubic, thermal vibr. temp. depend., anharmonic models 80−92618
ZnS, phonon dispersion under extreme press. and metallic transform., Raman spectra meas. 78−10895
ZnS, wurtzite type cryst., temp. depend. of one phonon Raman spectra, Gruneisen parameters 77−66500
ZnS(Se)(Te), thermal expansion and lattice dynamics under press. 80−100316
ZnSe, lattice vibration, thermal expansion and pressure effect 80−39233
ZnSe, phonon dispersion under extreme press. and metallic transform., Raman spectra meas. 78−10895
ZnTe, 1.5 to 30K, thermal expansion and Gruneisen parameter meas. 80−59681
ZnTe, lattice vibration, thermal expansion and pressure effect 80−39233
ZnTe, phonon dispersion under extreme press. and metallic transform., Raman spectra meas. 78−10895

GTO calculations
acetaldehyde, lowest Rydberg state, multiphoton ionisation spectra 80−83435
acetylene, near HF dipole polarizability, using EFV GTOs 79−31395
alkanes, ab initio calcs. using FSGO, internal rot. 78−82639
atom total energies, RHF calc., GTO basis sets for heavier elements 77−61686
atomic collisions, momentum transfer phase factors, mol. integral evaluation with travelling GTO basis set 79−22778
atomic integral calculations, permutational approach using spatial symmetry 79−36515
benzene, ground, singlet and triplet states, ab initio VB STO, GTO calcs. 77−75060
benzene, monosubstituted, ring protonation and C_{1s} binding energies, STO-3G calc. 79−29336
chemical shifts, H atoms, expectation values, GTO functions calcs. *(German)* 77−42340
chemisorbed atoms, theory, CI calcs. *(German)* 78−31707
Compton profiles using Gaussian expansion of at. orbitals, appl. to He, Ne, Ar, Kr, Na, and Al 80−945
contracted Gaussian basis set for correl. wave functions, appl. struct. and energies 80−52881
contracted Gaussian type orbital basis set 80−23297
contracted Gaussian-type orbital basis sets, test with and without outer orbital splitting 80−47872
cusp conditions, for props. at nucleus 79−3351
diatomic molecules, electric polarisabilities, EFV GTO basis set 78−50661
diatomic systems, nonadiabatic coupling matrix elements by Hellmann-Feynman theory and HF 80−83263
electric-field-variant orbitals, at. and mol. elec. props. 78−37543
ethylene, near HF dipole polarizability, using EFV GTOs 79−31395
Gaussian-lobe orbitals, ang. depend., anal. of standard p- and d-orbitals 79−6851
Gaussian-lobe orbitals, ang. depend., axial GLO sets, theory 79−6852
Gaussian-lobe orbitals, ang. depend., polyhedric lobe edifices 79−6853
heat of reaction, basis set of effect and approx. natural orbitals in SCF CI GTO calcs. 78−76904
HEED, many beam problem, use of Gauss-type orbitals and plane waves 78−83661
hydrogenic functions, Gaussian expansions involving few variational parameters 80−91420
hydrogenic Gaussian lobe functions 80−74102
lone pair orbital explicit representation, augmented contracted Gaussian basis set 78−25423

GTO calculations continued
methane, coord. bond calcs. 80−58129
methane, elec. dipole polaris., near Hartree-Fock value, using EFV GTOs 77−88591
methane, elec. dipole polarisability, coupled and uncoupled Hartree-Fock calcs. 77−34539
methanol, coord. bond calcs. 80−58129
methyl fluoride, coord. bond calcs. 80−58129
methylamine, coord. bond. calcs. 80−58129
methylene ion, pot. energy surfaces of excited states, ab initio GTO SCF CI calcs. 78−58602
minimal Gaussian basis set, for at. and mol. calcs. 80−47874
molecular correlation energy, perturbation calc. using Gaussian-type germinals 78−17578
molecular electrostatic potentials influence of polarisation functions 79−839
molecular geometry, basis set effect and approx. natural orbitals in SCF CI GTO calcs. 78−76904
molecular ionisation potential, quark influence, ab initio SCF calcs., appl. to H_2O and SO_2 79−10058
multicentre integrals of derivative spherical GTOs 80−91432
quadrupole polarisability, using elec. field variant GTO basis set 79−76359
rare earth atoms, Gaussian basis sets calcs. 80−63541
roughening transition, self-consistent calc. of statics and dynamics 79−27939
silanes, ab initio calcs. using FSGO, internal rot. 78−82639
transition metal atoms, third row, contracted Gaussian type orbital basis set 80−23297
valence electron studies using atomic Fues potential, homonuclear diatomics 80−78544
Z-depend. of optimum gaussian orbital exponents, gaussian exponent rule 79−3361
Al, vacancy electronic struct. LCGO calcs., solid state scattering theory 79−78044
BH, variation-perturbation minimal Gaussian geminal basis sets correl. energy calc. 78−78629
BH_3-ethylene complex, semiorthogonalised orbitals, integral approx. scheme 80−83262
$BeBH_5$, H bridged system, floating spherical Gaussian model 80−78518
CoO, ab initio SCF and CI calcs. on d-d transitions, CoO_6^{10-} cluster d-electron localisation 77−35897
Cu_2 contracted Gaussian-type orbital basis sets, test with and without outer orbital splitting 80−47872
$CuCl_4^{2-}$, charge distrib. and ligand field splitting calc. 77−62879
CuO, ab initio HF-MC-SCF with GTO basis set, dissoc. energy and bond length 80−47890
F^-, static electric dipole polarisability 79−76332
F_2, LCAO-GTO $X\alpha$ calc., rel. to other LCAO calcs. 80−52871
GeH_3^-, electronic struct., electron affinity, inversion barrier, ab initio SCF Gaussian basis calc. 80−63552
H_2 $^1\Sigma_g^+$ ground state, hybrid Slater-Gaussian-type 1s orbitals calc. 77−38605
H_2, correlation energy, perturbation calc. using Gaussian type germinals 78−17578
H_2^P, Temple lower bound mol. orbitals, GTO calcs. 78−41935
$H_2+e^-\rightarrow H_2^*+e^-$, Gaussian basis Glauber approx., elastic and vibrorotational excitation cross sections 80−58399
$H_{3^{2+}}^+$ pot. surface, GTO config. expansion 79−26907
H_3^+, Temple lower bound mol. orbitals, GTO calcs. 78−41935
HCN, dipole moment derivative, sign anomaly, CGTO ab initio calc. 78−74795
HCN, SCF ab initio ground state pot. energy surface, geometry, rel. to HCN^- 78−78646
HCN^-, SCF ab initio ground state pot. energy surface, geometry, rel. to HCN 78−78646
HF, elec. dipole polaris., near Hartree-Fock value, using EFV GTOs 77−88591
HF, NMR shielding consts. and mag. susceptibilities, coupled HF with extended GTO basis 80−5480
HF, nuclear spin-spin coupling const., finite perturbation calcs. 78−78616
HF, variation-perturbation minimal Gaussian geminal basis sets correl. energy calc. 78−78629
H_2O, elec. dipole polarisability, coupled and uncoupled Hartree-Fock calcs. 77−34539
H_2O, elec. dipole polaris., near Hartree-Fock value, using EFV GTOs 77−88591
H_2O+Li^+, ab initio GTO calc. of vibr. intensity changes of spectroscopic parameters 78−58583
He_2, pair polarisability correl. effects, SCF-CI-GTO-SO calc. 78−82651
He_2^{2+} $^1\Sigma_g^+$ ground state, hybrid Slater-Gaussian-type 1s orbitals calc. 77−38605
HeH^+, Temple lower bound mol. orbitals, GTO calcs. 78−41935
I, GTO basis sets, Hartree-Fock-Roothaan calcs. 79−97973
In, GTO basis sets, Hartree-Fock-Roothaan calcs. 79−97973
Li H^-, mol. orbital calcs., diffuse functions for basis sets, electron affinity 78−25436
Li_3, potential energy surface and config., RHF CI calc. 77−34562
$LiBH_4$, H bridged system, floating spherical Gaussian model 80−78518
$LiBeH_3$, H bridged system, floating spherical Gaussian model 80−78518
$LiCH_5$, H bridged system, floating spherical Gaussian model 80−78518
LiH, correlation energy, perturbation calc. using Gaussian-type geminals 79−10042
LiH, NMR shielding consts. and mag. susceptibilities, coupled HF with extended GTO basis 80−5480
LiH, variation-perturbation minimal Gaussian geminal basis sets correl. energy calc. 78−78629
Mg_2, $X^1\Sigma_g^+$ state, pot. curve, coupled pair many electron theory calc. 79−89621
N_2, correlated electron density using AHF GTO wavefunctions 80−23313
N_2, energy band calc. by linear combination of muffin tin orbitals method 77−4283
N_3^-, low-lying excited states 79−31425
NH, fine struct. in $X^3\Sigma^-$ and $A^3\pi$ states, STO and GTO calcs. 77−6679
NH_3, elec. dipole polarisability, coupled and uncoupled Hartree-Fock calcs. 77−34539
NH_3, elec. dipole polaris., near Hartree-Fock value, using EFV GTOs 77−88591

GTO calculations continued
$NaCl^-$, mol. orbital calcs., diffuse functions for basis sets, electron affinity 78−25436
NaH^-, mol. orbital calcs., diffuse functions for basis sets, electron affinity 78−25436
$NiCl_4^{2-}$, charge distrib. and ligand field splitting calc. 77−62879
NiO, ab initio SCF and CI calcs. on d-d transitions, NiO_6^{10-} d-electron delocalisation 77−35896
O_2, photoexcitation and photoionisation cross sections, HF Gaussian method 80−53064
O_2, RH-GTO-MCSCF calc., 1s photoelectron spectra, multiplet intensity ratio 78−5134
OH^+, fine struct. in $X^3\Sigma^-$ and $A^3\pi$ states, GTO and STO calcs. 77−6679
PH, fine struct. in $X^3\Sigma^-$ and $A^3\pi$ states, GTO and STO calcs. 77−6679
PH_3, NMR shielding consts. and mag. susceptibilities, coupled HF with extended GTO basis 80−5480
SH^+, fine struct. in $X^3\Sigma^-$ and $A^3\pi$ states, GTO and STO calcs. 77−6679
Sb, GTO basis sets, Hartree-Fock-Roothaan calcs. 79−97973
Si (111), chemisorbed Cl layer, SCF LCAO band struct. calcs. 78−88010
SiH_3X (X=H, F, NH_2, OH), coord. bond calcs. 80−58129
SiO_2, mol., ab initio SCF calcs., ground state stability, struct., vibr. freqs. 78−86781
Sn, GTO basis sets, Hartree-Fock-Roothaan calcs. 79−97973
TE, GTO basis sets, Hartree-Fock-Roothaan calcs. 79−97973
Xe, GTO basis sets, Hartree-Fock-Roothaan calcs. 79−97973

Gudden-Pohl effect *see electroluminescence*

guided electromagnetic wave propagation
see also guided light propagation; waveguides
anisotropic media, gyroelectric or gyromagnetic, EM wave propag. *(French)* 77−10813
atmosphere, radio refractive index structure in transitional boundary layer 78−57268
coaxial cylinders separated by dielectrics *(Russian)* 78−17845
concentric line with helical inner conductor, EM field and phase constants 79−86112
concentric line with helical inner conductor, wave impedance and attenuation consts. 79−86113
cyclotron resonance, Doppler effect, anomalous, amplification of slow waves in electron beam, obs. 80−78463
cylindrical inhomogeneity in homogeneous medium of infinite extent, guided EM field numerical computation 80−14274
dielectric film refractive index meas., synchronous angle integrated optical method 80−15976
dielectric three-ply system with space heterogeneity, surface EM waves *(Russian)* 78−55288
diffraction excitation and smoothly inhomogeneous layer of ionospheric waveguides, guiding props. 80−36449
Earth-ionosphere round-the-world echo signals, height factor estimate from expt. results 77−13159
Earth-ionosphere waveguide, mode conversion coeffs. for VLF propag. below stratified anisotropic ionosphere 77−53143
Earth-ionosphere waveguide, VLF propag., multimode nature effects on correlation factors *(Russian)* 77−70745
Earth-ionosphere waveguide concepts, appl. to numerical study of satellite reception of VLF signals 80−90282
Earth-ionosphere waveguide model, inverse propag. problem soln. 79−58154
Earth-ionosphere waveguide propag., rel. to geomag. storm sudden commencement preliminary reverse impulse 80−8477
education, waveguides, quantisation of radiant energy 78−36757
ELF propag. in nonstratified Earth-ionosphere waveguide, integral eqn. method 80−61959
ELF propagation in Earth-ionosphere transmission line, rel. to ionospheric profiles 78−36234
EM transmission structures, relativistic foundation and network formalisms 80−58446
equivalence principle for EM transmission through filled slit of arbitrary cross section 80−9787
evaporation ducts, polarisation depend. of transient signals 78−57269
frequency selective surfaces, EM wave scatt. from periodic screens, waveguide and optics appls. 80−87278
gas dielectric waveguides, with resonances in walls 77−65639
HF peculiar lunar echoes, guided wave propag. in ionosphere and magnetosphere 78−93032
HF transionospheric long range propag. from satellite, obs. at Florence 78−36396
inhomogeneous dielectric waveguide propagation, generalised WKB solns. 77−75385
inhomogeneous media, horizontally polarized wave transmission and trapped waveguide modes 78−9297
ionosphere, diffraction trapping of HF waves by waveguide 78−53772
ionosphere, rel. to Pc 1 source regions 77−25881
ionosphere, short radiowaves ducted propag., large-scale inhomogeneities effects 79−62657
ionosphere distant HP propagation, role of near-critical rays 79−53619
ionosphere polar electric field, horizontal transmission to equator 80−8478
ionosphere waveguide, ray trajectories with allowance for permittivity weak disturbance 80−61966
ionosphere waveguide propagation, excitation by ground based sources *(Russian)* 78−32283
ionosphere waveguides, excitation of electromagnetic modes, using Lorentz lemma method *(Russian)* 78−32284
ionosphere waveguides, excitation problem, using asymptotic method *(Russian)* 78−32285
localised RF fields, duct propag. along inhomogeneous magnetoplasma column 79−46453
locally striated medium, normal waves, short wavelength asymptotics 77−65558
lossy ferrimagnetic slab, model spectrum 79−86111
microwave ducting in inhomogeneous troposphere, anal. 79−39818
microwave EPR self-induced transparency in free radical powder, waveguide propag. 77−24747
MIS structure, MM wave modification by surface carrier scatt., surface pot. depend. 80−44736
multilayer lossless dielectric loaded waveguide, transient field distribution 80−23604

guided electromagnetic wave propagation continued
partially filled plasma waveguide, dipolar modes, field and power density distributions 77−7555
plasma, hot collisional uniaxial, guided waves, TM mode dispersion rel. 80−53995
plasma-filled cylindrical waveguide, nonlinear EM wave propag. 77−991
plasmapause as a VLF waveguide 77−87193
radio waves, propag. in natural waveguides 77−78328
radio waves scattered by meteor trails, trapping by ionospheric ducts 80−4172
radiowave propagation, ray trajectory props. in irregular ionospheric waveguide 80−90284
radiowave propagation in troposphere waveguide, effect of elevated M-inversion 80−90195
random, periodic structure, statistical properties, eigenfunction 77−75392
rectangular waveguide partially loaded with magnetised planar ferrite, e.m. wave propag. 77−576
rectangular waveguides, EM field calc. *(Russian)* 78−82884
reflection from moving boundary between two dielectrics in waveguide 77−584
rotating dielectric column in circular waveguide 78−1133
Schumann resonances, expt. data appl. to atmosphere and lower ionosphere elec. cond. profiles evaluation 80−36360
Schumann resonances and elec. cond. of atmosphere and lower ionosphere, reson. freqs, and ELF attenuation 80−31099
selflocalised EM fields in dense plasma 78−75350
semiconductor, EM beam self-focusing 79−18488
semiconductor, MM wave guiding and control by surface plasmons 80−103713
SHF beyond-the-horizon signals, evaporation duct influences 78−92935
strip transmission line in magnetic field, normal mode dispersion 77−28552
surface EM waves, excitation efficiency of prism and grating coupling techniques 77−61902
surface wave electromagnetic scattering from notches in ground plane covered by dielectric slab 80−87277
surface wave scattering, metallic strip on reactive surface 77−75394
thin wire in air filled tunnel, planar boundary limit 77−3522
thin wire in circular tunnel, quasi-static limit for propagating mode 77−54653
TM modes guided in dielectric slab deposited on conducting substrate 79−72458
trifurcated parallel-plane plasma waveguide 77−84448
troposphere, ducted EM wave propagation, roots of modal eqn. 80−72607
troposphere, radio refr. index struct. parameter height distrib. and duct thickness 78−73491
troposphere nonuniform radio wave guide, coupled mode anal. 80−94587
troposphere waveguide, propag. of atmosphere radiothermal radiation *(Russian)* 79−88406
tropospheric ducting environments, case studies of beyond horizon propag. 77−41132
two-dimensionally inhomogeneous media, Maxwell eqns. decoupling 79−41302
wave equation solutions decaying at prescribed rate with respect to time 77−58230
wave retardation by large diameter helices, theory, expt. 79−32787
whistler-mode waves guidance through plasmasphere 78−93054
whistlers, effect of Earth-ionosphere waveguide propag. on polarisation and arrival angles 79−100924
whistlers, low-latitude, conditions of duct trapping 79−84586
X-ray propagation through capillaries, surface roughness influence 79−49349
SiC with dielectric coating, surface polaritons, waveguide modes 80−80195

guided light propagation
see also optical waveguides
acousto-optical beam deflector design, fabrication, and applications 77−19433
acoustooptic guided wave Bragg diffr., phased SAW array in $LiNbO_3$ 77−58439
amplitude modulated laser beam prog. in random inhomogeneous medium, phase fluctuation anal. 78−87017
anisotropic diffraction by bulk acoustic waves 77−23784
anisotropic inhomogeneous guiding media, rel. between phase and group indices 78−9320
anisotropic layered medium, rel. between phase and group indices 77−39042
asymmetric-slab optical waveguide losses due to refractive index inhomogeneities 78−1381
beam eqn. integration for randomly curved cylinder with variable refractive index *(Russian)* 77−31139
beam propagation through lenslike medium of complex permittivity 77−11009
Bragg diffraction grating, guided light refl., deflector appl. *(French)* 77−65621
Bragg reflection in planar dielectric waveguides with periodic thickness modulation 77−79970
caustic patterns for melt zones in solidified glass samples, symmetric cases 79−22892
caustic patterns for melt zones in solidified glass samples, asymmetric cases 79−22893
cladded optical fibre, parabolic-index core and homogeneous cladding, propag. characts. of modes 77−11013
codirectional coupled waves representation 78−1150
convex dielectric thin film fibre optical modes, conformal mapping 77−83996
cruciform section optical fibre in single material 77−39046
curved const. cross section lightpipe, steady state and transient solns. 77−62068
curved waveguide, with parabolic refr. index profile over cross section, light propag. 80−19104
curved waveguide, with refr. index varying over cross section, light propag. 80−19103
cylindrical fibre with symmetric index distrib., matrix analysis 77−84001
dielectric branching waveguide mode order convertor 78−1379
dielectric fibres of arbitrary cross-section, fundamental mode propag. 80−43443
diffused optical waveguide numerical analysis and applications 78−1377
exponentially decaying gain medium, waveguiding 78−50774

guided light propagation continued
ferrite-dielectric optical waveguide, azimuthally magnetised, theoretical characteristics *(Russian)* 78−22211
ferrite-dielectric optical waveguides, longitudinally magnetised, theoretical characteristics *(Russian)* 78−18061
fibre, dielectric, of noncircular cross sections, fundamental mode propagation computing 79−76874
fibre, graded-core, propagation characts., numerical description 77−23758
fibre, graded-index, geometric optics approach to light acceptance and propag. 77−23756
fibre, multimode, propag. modelling, effects of mode conversion due to microbends *(French)* 77−23760
fibre, single mode, pulse fluctuations, propagation 80−87475
fibre, transfer function meas., baseband frequency response *(French)* 77−79919
fibre, with coherent dielectric core cladding, transverse and hybrid modes structure 79−14091
fibre in circular arc, meridional rays, geometrical optics *(German)* 77−39048
fibre mode analyser using refraction from oblique section 77−88952
fibre transmission problems *(French)* 77−79918
fibre with parabolic index profile, guided modes 77−39041
fibre-optic index-difference dispersion and bending loss/wavelength relationships 78−1367
fibre-optic scattering loss dependence on launching condition, lossy-layer model 78−5577
in fibres, propag. theories, results from International workshop Lannion, Sept. 1976 *(French)* 77−11018
fibres, ray approach *(French)* 77−79916
field wave front correction, emitted from fibre lightguide *(Ukrainian)* 78−83081
film, refr. index and thickness determ. using guided optical waves 78−74049
film properties measurement using guided optics techniques 79−99958
flat glass, commercial, birefr. due to laminar inhomogeneities 78−39731
focused light ATR method, appl. to guided waves on grating 78−74992
gain-guiding stripe-geometry DH semiconductor laser oscillation characteristics 79−45945
gain-guiding stripe-geometry DH semiconductor laser small-signal modulation characteristics 79−45946
Gaussian light beams in thin films 78−33817
glass, chem. tempered, surface stress meas. using opt. waveguide effect *(Japanese)* 80−45473
glass, phase separated, opt. props. of elongated phases 78−27179
glass, thermally tempered sheet and plate, surface stress meas. using optical waveguide effect 80−25967
glass fibres, light propag. in a large aperture bundle, tied together by a helix metal or glass filament 78−87154
glass fibres, multimode, calc. *(German)* 77−62070
graded-index optical fibre, with near parabolic-index profiles, mode dispersion 79−76873
graded-index slab waveguide TE mode analysis 77−72087
grating coupler, chirped and curved, for focusing beam 80−78979
helical constant cross section lightpipe, varying refr. index, radiation transport 77−65640
hologram recording and read-out with evanescent field of guided waves 77−10869
holographic grating on metal with dielec. coating, polarisation anomalies 77−62058
inhomogeneous medium, two-dimens., light propag. problems rel. to thermogasdynamic waveguide development 80−32914
integrated grating circuit for guided-beam multiple division fabricated by electron-beam direct writing 80−91934
integrated optical system, guided optical mode interaction with SAW 78−42465
IR surface wave propag. along metal surface *(Russian)* 79−68441
IR waveguides, bending effect on power transmission 77−19430
irregular thermodynamic guide mean energy density of light beam 77−83976
laser beam waveguide propag. in frozen gaseous layers at 4.2K 80−64168
laser waveguide mode propag. in nonlinear amplifying medium 77−58308
lens-like media, propagation constant, variational method 77−27347
light transmission mechanism in optical fibres, communications appl. 80−43469
lipid bilayer, planar, light guide effect, bilayer spectrosc. appls. 79−29509
metal-clad diffused optical waveguide propagation losses 77−84000
metallic surface, single curved, TE wave propag. 78−37967
modes in uniform and imperfect guides, statistical analysis *(French)* 77−79914
multi-dielectric slab, W type structure, optical transmission props. 77−42615
multilayered media, refl., interference theory 77−65567
multimode fibre optical pulse delay and broadening 77−83998
multimode fibres, pulse propag. 77−789
multimode irregular fibres, ray statistics *(Russian)* 77−88913
multimode optical fibre transmission, perturbation soln. 78−1380
multimode optical fibres 78−30051
oblique input end-face lightguides 77−75684
optical fibre, immersed in high-index surrounding medium, attenuation 77−42614
optical fibre, partial coherence propag. 77−72070
optical fibre transmission, conference, Williamsburg (1977) 78−1382
optical fibres, baseband freq. meas., interpretation 78−46777
optical fibres, elliptical selectively excited, near-field distrib. 80−48401
optical fibres, multimode effect of microbending on propag. *(French)* 80−53406
optical fibres, phase modulation of coherent light using HF sound 78−87142
optical fibres, transmission technology, progress review 78−1330
optical waveguide, asymmetric slab, mode conversion analysis, Green's function method 77−27344
optical waveguides, single-mode ring-type *(Russian)* 80−38104
periodic optical waveguides of lenslike media with complex permittivity 77−83997
periodic stratified medium, general theory 77−65565
planar lipid bilayers as light guides, elec. field induced scatt. 80−48148
guided light propagation continued
plastic calorimeters, light guides containing fluorescent radiation converter 79−740
polygonally bounded waveguides, hybrid finite element analysis 77−27358
pulse propagation in pipes, model 78−30068
radially stratified fibres, 4×4 matrix method for propag. characts. calc. 77−34931
randomly distorted multimode optical fibres, step index fibres *(French)* 80−74470
randomly gradient fibres with irregular bends, optical mode propagation and scattering 78−1325
ray tracing through deformed glass rods with radially graded RI 79−64338
retinal receptors, human, modal pattern stability, with wavelength, inhomogeneous waveguide model 79−8504
rod outer segment and interstitial matrix of rat, refr. index difference determ. using waveguide parameter 79−5277
round optical fibers, transmission props. of radial offsets, EM analysis 79−81566
scintillation counters, light guide design for timing meas. 77−38554
SELFOC fibre, non-Gaussian laser beam propag. 78−1335
signal transfer properties influenced by stress birefringence, multimode fibres *(German)* 77−62044
by single curved surface 78−71196
solitons in the theory of guided lightwaves 80−58760
spatially periodic media, modal theory 77−7218
statistically irregular focusing fibre, losses 77−46804
stochastic wave propagation, ambiguity function 78−69993
symmetrical rib optical waveguide fundamental modes 77−23744
thin-film optical waveguides *(Polish)* 78−33849
underground lens line, coupled to atmosphere, turbulence struct. by statistical anal. 77−7008
underground optical waveguide beam distortion by air convection 77−62063
very narrow conducting stripe lasers, symm. and asymm. waveguiding 79−36896
wave mutual focusing in media with quadratic nonlinearity 78−30033
GaAs, epitaxial layer, 1.06 μm two-photon absorption coeff., guided wave meas. 78−46707
GaAs-$Al_{0.2}Ga_{0.8}As$ periodic layered media, optical surface waves 78−43946
LiF film, guided wave excitation by fast electrons 79−24384
$LiNbO_3$ film on Al_2O_3, optical guided wave mode conversion by Love waves 79−46055
$LiNbO_3$ laser beam/SAW mode conversion 79−46056
$LiNbO_3$, leaky SAW and guided light Bragg interaction, theoretical anal. 78−72484
$LiNbO_3$, optical waveguide, diffr. of modes by standing elastic surface waves *(Russian)* 78−1343
Si film, optical characterisation from guided wave optics 78−48245

Guinier-Preston zones
alloy, role of anisotropy in elec. resist. of Guinier-Preston zones 77−36515
alloys, radiation effects on ageing and precipitation, review 80−29956
ellipsoidal zone model of X-ray scatt. *(French)* 77−84568
glass ceramic, nucleation and growth studies by small angle neutron scatt. 79−32913
heterogeneous nucleation theory appl. to precipitate nucleation 78−48412
nucleation, heterogeneous theory, appl. to precipitate nucleation at Guinier-Preston zones 77−36509
particle size distribution influence on exta-resist. of coherent precips. 80−49689
steel, ferritic, with interstitial N, continuous precipitation and clustering 80−7585
ternary alloy, metastable miscibility gap determ. by small angle scatt. 77−28780
X-ray small angle scattering, for extra-resist. calcs. 80−92873
X-ray small-angle scattering, rel. to elec. resist. 79−19125
Al alloy 7075, precipitation hardening, toughness and microstruct. *(Japanese)* 78−15509
Al alloys, age-hardenable, precipitation and dissolution processes, positron annihilation and X-ray small-angle scattering comparison 80−89238
Al alloys, age-hardening, resistivity charge by low temp. deform., GP zone cutting *(Japanese)* 78−84831
Al-Ag, low-conc. alloy, spinodal curve and metastable miscibility gap 77−63680
Al-Ag, precipitation study by internal friction *(French)* 80−35190
Al-Ag, type-II superconductor, torque oscillations in mag. field *(Russian)* 80−103800
Al-Ag (15 wt.%), precipitation hardenend cyclic stress-strain response 78−35412
Al-Ag (1.03 at.%) alloy elec. resist. meas. above room temp., Ag atom configuration correlation 78−35534
Al-Ag (4 wt.%), scattering of conduction electrons, effect of size and internal struct. of GP zones *(Japanese)* 77−21149
Al-Ag (5 wt.%), Guinier-Preston zone struct., correl. function *(Russian)* 77−12627
Al-Ag(Cu)(Zn), electrical resist. of Guinier-Preston zones during age-hardening 77−72848
Al-Cd hypomonotectic alloy, rapid solidification and decomposition 80−50638
Al-Cu, decomposition of Guinier-Preston zones *(German)* 80−30014
Al-Cu, elastic interaction energy calcs. for Guinier-Preston zones 79−11617
Al-Cu (1.7 at.%), EXAFS study of precipitation 79−100151
Al-Cu (3 wt.%), stress aged, GP zone struct. by X-ray diffuse scatt. meas. *(Japanese)* 80−71653
Al-Cu (3 wt.%) single cryst., stress aging, oriented precipitation *(Japanese)* 80−71652
Al-Cu (3.71 wt.%), stress oriented precipitation of Guinier-Preston zones and θ′ 78−52809
Al-Cu (3.97 wt.%) alloy containing Guinier-Preston zones, high resolution lattice images 80−107114
Al-Cu (4 wt.%), AE during deform., effect of ageing at 170°C 78−64597
Al-Cu (4 wt.%), aged to contain Guinier Preston zones, crystallographic fatigue crack growth 78−60832

Guinier-Preston zones continued
Al-Cu (4 wt.%), enhanced precipitation under electron irradiation in HVEM 78−52818
Al-Cu (4 wt.%), naturally aged, early stages of G.P. zone form. 77−90355
Al-Cu (4 wt.%), precipitation sequence of metastable phases, NMR meas. 78−23713
Al-Cu (4 wt.%), relationship between enthalpy, yield strength, and size of Guinier-Preston zone *(French)* 78−19767
Al-Cu (4 wt.%), reversion charact. *(Japanese)* 77−21150
Al-Cu (4 wt.%), size distrib. and form. mechanism of GP zones *(Japanese)* 77−25054
Al-Cu (4 wt.%), supersaturated and aged conditions, high strain deform. 80−60907
Al-Cu (4 wt.%) alloy, reversion characts. *(Japanese)* 79−56989
Al-Cu (4 wt.%) alloy, reversion process of Guinier-Preston zones, ^{63}Cu NMR obs. 80−60871
Al-Cu (4.3 wt.%) alloy, containing Guinier-Preston zones, high resolution lattice images 80−107115
Al-Cu (4.3 wt.%) alloy, lattice electron micrograph interpretation 79−86659
Al-Cu (5 wt.%) alloy, ageing during relax. of elastic stresses, X-ray diffr. expts. *(Russian)* 77−59821
Al-Cu alloys, Cu precipitate detect. by positron annihilation, GP zone development 80−3051
Al-Cu alloys, dil., EXAFS spectra 80−2898
Al-Cu alloys, Guinier-Preston zones study by stress ageing 79−100152
Al-Cu samples (0.5, 2.0 and 4.0 wt.%) polycryst., precipitation, positron annihilation and TEM 80−50639
Al-Cu single cryst., hardening due to oriented GP zones 80−55414
Al-Cu-Mg (1.3, 1.3 at.%) alloy, natural ageing, meas. of quenching vacancy dislocation loops 79−15704
Al-Cu-Mg (2.6, 0.4 wt.%), Fe, Si, Mn and Ti addition effects on age-precipitation *(Japanese)* 80−20937
Al-Cu-Mg alloy, struct. of Guinier-Preston zones *(Russian)* 79−1870
Al-Cu-Si-Mg (4, 0.8, 0.8 wt.%) alloy, GPB zone formation during room temp. ageing 77−44263
Al-Li (6.72 at.%), δ' coherent solvus determ. on ageing at 20 to 200°C, X-ray scatt. 77−25056
Al-Li alloy, annealing of vacancies and ageing, resist. and TEM obs. 77−21172
Al-Li alloy, thermal anal. of precipitation 78−15417
Al-Li system, δ' coherent miscibility gap determ. by small-angle X-ray scatt. 77−77483
Al-Mg, elastic and anelastic props. in relation to Guinier-Preston zones, US investigation *(French)* 79−38833
Al-Mg, Guinier Preston zone study by neutron diffr. *(French)* 77−28819
Al-Mg, single crystal, radiation of elastic constants 78−11263
Al-Mg alloy, AL24M, decomp. kinetics and ageing mechanism *(Russian)* 80−45269
Al-Mg alloys, initial decomposition exam. by X-ray diffr. *(Russian)* 77−77482
Al-Mg solid solns., decomposition studied by ultrasonic meas. of elastic props. 80−35184
Al-Mg supersaturated solid soln., spinodal decomposition at 20°C *(French)* 77−85987
Al-Mg-Ag, age effect on age hardening *(Japanese)* 78−52831
Al-Mg-Si, Guinier-Preston zones, inception and effect on ageing, review *(Hungarian)* 79−11627
Al-Mg-Si alloys, DTA exam. of zone form. and other solid phase conversions 77−86057
Al-Si (9 wt.%), precipitation hardening during isothermal ageing 80−29969
Al-Zn, age hardenable precipitation and dissolution, positron annihilation and X-ray scatt. 80−16314
Al-Zn, dil. alloy, ageing and reversion, annealing curves, X-ray obs. 78−88485
Al-Zn, formation of Guinier-Preston zones, and their limit temp. *(Japanese)* 78−84861
Al-Zn, GP zones, effect of Si, Ag, Mg on transport props. 77−16588
Al-Zn, G.P. zone form., temp. limit 80−16317
Al-Zn, Guinier-Preston ellipsoidal zone model of X-ray scatt. *(French)* 77−84568
Al-Zn, Guinier-Preston zone form. kinetics study using linear localisation probe *(French)* 78−15413
Al-Zn, Guinier-Preston zone reversion, thermoelectric power meas. *(French)* 79−20058
Al-Zn, Guinier-Preston zone struct., absolute SAXS meas. *(Japanese)* 79−70072
Al-Zn, resistivity anomalies in Guinier Preston zones *(French)* 78−6937
Al-Zn, resistivity calc. for age-hardened alloy 77−73284
Al-Zn 6.8 at.%, Guinier-Preston zones *(French)* 79−87640
Al-Zn (0.041 to 4.4 at.%), clusters, electrical resistivity meas. *(Japanese)* 77−21168
Al-Zn (10 wt.%), ageing at low temp., solute conc. fluctuation effects *(Japanese)* 79−4969
Al-Zn (10 wt.%), ageing at low temp., effects of fluctuation of solute conc. 80−76287
Al-Zn (10 wt.%), ageing at low temp., effects of fluctuation of solute conc. 80−76288
Al-Zn (10 wt.%), ageing behaviour, calorimetric study 80−45328
Al-Zn (15 at.%), structural changes during post ageing between 125°C to 215°C 80−40399
Al-Zn (15 wt.%), calorimetric ageing study 80−45330
Al-Zn (2 and 4 wt.%), ageing and elec. cond. reversion *(Japanese)* 79−4983
Al-Zn (30 wt.%), metastable phases, transformation kinetics, quenching rate effects meas. 77−55960
Al-Zn (30 wt.%), precipitation sequences and transformation kinetics, X-ray diffr. and TEM obs. 77−55959
Al-Zn (6.8 at.%), decomposition, electron microscope study *(French)* 77−40422
Al-Zn (6.8 wt.%), effects of ageing temps. on microhardness and resistivity *(Japanese)* 78−35408
Al-Zn (6.8 wt.%), Guinier Preston zones internal struct., study by X-ray diffusion, α_R phase comparison *(French)* 80−66472
Al-Zn (7 at.%), liquid quenched, early stage phase separation, exam. 78−68698
Al-Zn (70, 30 wt.%), decomp. study, 25-160°C *(Czech)* 80−89225

Guinier-Preston zones continued
Al-Zn (8-25 wt.%), solid solns., residual resist. during clustering 80−97483
Al-Zn alloy, metastable phases formed at 200°C, room temp. stability 80−16315
Al-Zn alloy, resist. and X-ray small angle scatt. during GP zone form., theory *(French)* 79−29070
Al-Zn alloys, relation between microhardness and average radius of Guinier-Preston zones 78−95811
Al-Zn alloys, room temp. decomp. of metastable phases precipitated at 200°C 78−84814
Al-Zn-Fe-Si, Fe and Si effects on precip., TEM and X-ray diffr. obs., ageing at 90°C 77−48439
Al-Zn-Mg, decomp. kinetics and ageing mechanism *(Russian)* 80−45269
Al-Zn-Mg, decomposition calorimetric study *(German)* 79−74165
Al-Zn-Mg, metastable miscibility gap determ. by small angle scatt. 77−28781
Al-Zn-Mg, plastic instability rel. to grain boundary failure at low temps. 78−56702
Al-Zn-Mg, solid soln. decomp., 20 to 200°C 79−38830
Al-Zn-Mg, zone comp. and contrib. to elec. resist. 80−16316
Al-Zn-Mg, zone composition change during ageing 79−29110
Al-Zn-Mg (3.2, 2.2 wt.%) alloy, GP zone reversion, η' of formation, quant. investig. 77−4784
Al-Zn-Mg (4.5, 2 to 3 at.%) solid state reactions by interrupted continuous heating 80−25737
Al-Zn-Mg (4.5 at.%, 2 or 3 at.%), decomposition behaviour during continuous cooling, XSAS and TEM examination 80−16264
Al-Zn-Mg (4.8, 1.2 wt.%), quenched, Guinier Preston zones formation 80−45273
Al-Zn-Mg (5.9, 2.9 wt.%), ageing effects on microstruct. 80−16306
Al-Zn-Mg alloy, Ag addition and pre-precipitation treatment, influence on GP zone growth 80−71658
Al-Zn-Mg alloy, melting point *(Hungarian)* 77−25078
Al-Zn-Mg alloy 7075, effect of thermal and mechanical pretreatments, on Guinier-Preston zone 78−39817
Al-Zn-Mg alloys, decomp. kinetics from Young's modulus obs., microprocesses *(German)* 78−64522
Al-Zn-Mg alloys, decomposition kinetics, resistivity meas., extended jump model 78−84766
Al-Zn-Mg alloys, extra-resistivity of coherent precipitates 80−3050
Al-Zn-Mg alloys, precipitation behaviour *(German)* 78−39780
Al-Zn-Mg type 7N01-T4, weld, SCC in NaCl-H_2O_2 soln. *(Japanese)* 80−108631
Al-Zn-Mg-Ti, Ti effect on microstructure during ageing 78−64568
Al-Zn-Mg(3.2, 2.2 wt.%), deform. strengthened by Guinier Preston zones 77−52343
(Al-Mg-Si)-Al_2O_3, SAP type, ageing 79−96055
AlZnMg alloy, precipitation hardened, strength 78−39786
Cu-Al-Co, precipitate-free zones near grain boundaries, growth kinetics, TEM obs. 80−40368
Cu-Be, electrical resist. of Guinier-Preston zones during age-hardening 77−72848
Cu-Be (0.99 wt.%), direct obs. of small Guinier-Preston zones 78−72776
Cu-Be (2 wt.%), precipitation sequence, TEM obs. 80−108450
Cu-Be alloys, CuBe precipitation 80−29966
Cu-Be-Co (1.8, 0.2 wt.%), TEM obs. of precipitates, ageing charact. *(Korean)* 77−66648
Fe-Ni-Co-Mo alloys, struct. transform. produced during tempering 77−86058
KCl, pure and Ba-doped, rel. to γ-irrad. effects on intensity distrib. of diffuse X-ray scatt. 77−24329
Ni-Be (2 wt.%), high-temp. radiation embrittlement, mechanical tests and TEM *(Russian)* 77−44331
Ti-Nb-Ta-Ge (40,20,0.8 wt.%) foil, dispersion hardening, TEM and electron diffr. obs. *(Russian)* 79−1873
TiO_2, iron bearing, exsolution of Fe_2O_3 79−61597

Gunn devices
see also Gunn diodes
negative conductance, temp. and bias voltage depend. 77−51756
planar, high-bit-rate pulse regeneration and modulation of injection lasers 79−59731
planar elements, stationary domains 79−56238
tunnelling and negative resistance phenomena in negative conductance microwave devices, book 78−26947
GaAs, epitaxial layers on conductive substrate, elec. characterisation 78−91790
GaAs, maximum electric field in high-field domain 78−79996
GaAs transferred electron devices, ohmic contacts 78−52082
InP, maximum electric field in high-field domain 78−79996
InP, relationship between microwave efficiency and metallurgical state of cathode contact 80−6981

Gunn diodes
amplifying Gunn diodes, nonlinear effects 79−51622
anode domain disappearance dynamics, computer simulation calcs. 80−6859
domain instabilities in transverse mag. field 79−23981
domain instability at near-critical dopant conc. 79−23980
frequency multiplier, for superhigh frequencies, high multiplication factor 78−4636
gas analyser with acoustooptic detector and semiconducting generator based on Gunn diode *(Russian)* 80−101141
high-field domain dynamics anal. using stroboscopic SEM 79−56232
high-field domains, obs. at 1 GHz by picosecond pulse stroboscopic SEM 77−85228
III-V semiconductors, p-n heterostructures, epitaxial growth techniques, appl. to electronics, review 80−54770
impact ionisation of deep levels, effect on time-averaged I-V characteristics *(Russian)* 77−62935
injection-laser optial repeater *(Russian)* 77−83974
microwave oscill. generation at two freqs. 80−65614
multidomain mode due to charge inhomogeneities 80−70714
population inversion condition 77−77251
static domain form. 77−8111
two-dimensional, cathode-slanted planar, domain dynamics, study using strobosocopic SEM 79−23978
n-GaAs, AuGe contact, total resist. meas., temp. dependence 78−76146
n-GaAs epitaxial film, pure and Cr doped, heavy electron trapping, Gunn oscills. 80−6857

Gunn diodes continued
GaAs, epitaxial growth for microwave devices *(French)* 77−48360
GaAs epitaxial layer high power Gunn diode developement and fabrication 80−16199
GaAs epitaxial layers, photocond. high field effects on carrier capture and recomb. 77−43646
GaAs LSA diodes, current controlled LPE for optimum doping profiles 78−35318
GaAs, peak electron vel. and threshold field temp. depend. 77−32075
GaAs planar Gunn device, domain dissolution for wide range of doping 77−8109
GaAs, velocity-field charcts. at 35 GHz, impurity conc. var. 77−85306
GaAs:Si, transferred-electron devices by low-level ion implantation 80−92543
n-$Ga_xIn_{1-x}Sb$ Gunn diode, high field domain charcts. 80−59992
$Ga_xIn_{1-x}Sb$, transferred-electron effect, and device performance estimation 78−19049
InP, relaxation LSA mode obs. 77−8102

Gunn effect
see also limited space charge accumulation; negative resistance effects
current instabilities in semiconductors, theory and expts. *(Hungarian)* 77−39857
current instability due to Bragg scatt., travelling dipole domains, fluctuations 78−26874
higher polymer films, steady Gunn type oscillations, origins *(French)* 79−28351
history of hot electron physics 78−26869
III-V semiconductor, transferred electron effect 77−39855
III-V semiconductor n-channel inversion layers, subband struct. and gate-controlled Gunn effect 77−76929
mode selection and Gunn domain 77−85230
nonequilibrium steady states, distrib. functions and phase transitions 77−61041
semiconductor, basic shape of Gunn domain using $\mathcal{J}$ operator 77−55535
transient behaviour of Gunn domains and associated equivalent circuits 78−19043
two-dimensional semiconductor, Gunn instability 78−84305
$Al_xGa_{1-x}As$, graded-gap crystal, voltage-current characteristics 79−69613
$Ga_{1-x}Al_xAs$, velocity saturation and cond. band struct. under press. 78−26863
GaAs, carrier generation-recomb. processes 79−38080
GaAs devices and their use for generation and freq. conversion of microwave oscillations 80−15534
n-GaAs, diffusion coeff., Monte Carlo calc., rel. to trapped domain behaviour 78−56152
n-GaAs epitaxial film, pure and Cr doped, heavy electron trapping, Gunn oscills. 80−6857
GaAs Gunn domain appearance and movement, SEM obs. 77−80785
GaAs, Gunn effect, equal-areas rule 80−107798
GaAs, IR field induced Gunn oscills. 78−30956
GaAs, influence of strong transverse mag. field on Gunn effect 80−6854
n-GaAs, limiting freq. of Gunn effect in polyharmonic LSA mode 80−6856
GaAs, three level cond. band struct., uniaxial stress effects, resist. and Gunn effect threshold meas. 77−85137
GaAs, three-level conduction band struct. obs. 77−15764
n-GaAs, transferred electron effects under hydrostatic pressure 77−32018
n-GaAs, transferred electron effects under hydrostatic press. 78−26871
GaAs:O, slow domains, origin 78−60132
$Ga_xIn_{1-x}Sb$, electron vel. field charcts., microwave heating method 79−91058
$Ga_xIn_{1-x}Sb$, transferred-electron effect, and device performance estimation 78−19049
$InAs_{1-x}P_x$ epitaxial layers, sub-threshold velocity-field charcts., intervalley separation 77−63010
$InAs_{1-x}P_x$, high field instabilities, press. and comp. depends. 78−26873
$In_{1-x}Ga_xSb$, drift velocity of electrons 77−20327
n-InP, high field props. under high press. 78−26872
InP, relaxation LSA mode obs. 77−8102
InP, transferred electron effect 77−39855
n-InP, transferred electron effects under hydrostatic press. 78−26871
n-InP, transferred electron instabilities, hydrosttic press. effect 80−6869
n-InSb, charcts. of Gunn effect 77−55538
n-InSb, Gunn domains, direct probe meas. 78−26877
n-InSb, Gunn effect, influence of impact ionisation 80−44609
n-InSb, hydrostatically compressed, instabilities of current, Gunn effect meas. 77−1432
n-InSb, influence of mag. field on hot electron effects 78−2493

Gunn effect devices *see Gunn devices*

Gunn oscillators
injection laser integration with Gunn oscillator on semi-insulating GaAs 78−71232
magnetoresistance measurements of electron mobility and modulation noise 77−62948
GaAs, magnetoresistance meas. of mobility and noise 77−62948
n-$Ga_xIn_{1-x}As_yP_{1-y}$, transferred electron oscill., threshold field 77−85227
InP, magnetoresistance meas. of mobility and noise, contact effects 77−62948
InP, ohmic contacts by thin film epitaxy 79−38159

guns, plasma *see plasma guns*

gyration *see rotation*

gyrators
see also network analysis
waveguide gyrator, thin-film, theoretical analysis 78−25993

gyromagnetic effect
see also gyromagnetic ratio; magnetic resonance
density gradient effect on magnetic gyrotropy 79−94730
ferrimagnetic slab magnetised in arbitrary direction, magnetostatic mode characteristics 78−2670
ferrites, saturation magnetisation meas. of gyromagnetic materials of microwave frequencies *(German)* 79−67357
gyroscope, coupled to rotating ring, Barnett effect 78−86260
rare earth compounds, gyromagnetic resonance, study of magnetism *(Danish)* 79−15359
$Sm_xTb_{1-x}FeO_3$, gyrotropic props. and birefringence, in spin reorientation range 80−7324
YIG thin film gyromag. waveguide, on GGG substrate, optical propag. props. Faraday effect 80−74513

gyromagnetic ratio
see also g-factor; magnetic resonance
L-alanine:Cu(II), EPR and ligand-ENDOR measurements 80−44907
alternating magnetic field amplitude meas. *(French)* 80−73332
electron, g-2 experiments as a test of special relativity 79−58539
electron, high-γ g-2 meas. for special relativity test 79−58540
even-even nuclei, backbending mechanism anal. *(Chinese)* 78−78247
g-2 experiments as a test of special relativity 79−58539
garnets, ferro- and paramag., gyromag. ratio determ. by magneto-optical method *(Russian)* 77−32356
light cone formulation and Galilean symmetries 77−13962
light-cone formulation for arbitrary spin particles 77−13961
muon, g-2 experiments as a test of special relativity 79−58539
nuclear cranking model, HF calcs. of gyromagnetic ratio and moment of inertia 79−93482
proton, in weak field, review of results of last 15 years 78−57887
proton, meas. in weak mag. field at NPL 80−105678
proton, meas. techniques used at NPL based on ampere realization 80−98940
proton, used for absolute meas. of ampere 80−98941
proton in strong mag. field in water, meas. method 79−40527
QED, gyromagnetic ratios for muon and electron 80−22548
special relativity experimental test from high-γ electron g-2 meas. 79−58540
e gyromagnetic ratio in Coulomb field 80−82870
W^{+or-} bosons, lowest order g-2 Weinberg-Salam model, Feynman diagrams 80−47291
CaF_2, high resolution double NMR at low gyromag. ratio 78−25577
$Eu_zY_{3-z}Ga_tFe_{5-t}O_{12}$, epitaxial garnet films, props. at compensation points 80−39823
H^+, gyromag. ratio and fine struct. meas. by meas. distance between wires, using laser interferometer 80−74253
$KMgF_3:Cr^{2+}$, dynamic Jahn-Teller effect 77−66416
Pr compounds, Van Vleck paramagnets, mag. props., anisotropy from NMR anal. 80−54862
SiC, laser Raman spin-flip scatt. from excitons, luminesc. 80−80786
YIG: Ca_x(Mg), films, microwave losses induced by Fe^{4+} ions, ferromag. reson. study 79−1715
ZnTe, magneto-optical effect, I_2 bound exciton 77−12432
ZnTe:Na(Li), spin flip acceptor scatt., transition selection rules 79−61380

gyroscopes
see also navigation
active re-entrant Sagnac system fibre optic approach to rotation sensing, active re-entrant Sagnac system 80−10038
angle velocity meas., precision increase, using structural redundancy *(Russian)* 78−49804
angular drift rate standard, aircraft gyroscope accuracy increase 79−71421
anti-gravity generation due to counterclockwise turning of gyroscope *(Japanese)* 80−12980
artificial satellite equipped with two gyroscopes, planar oscills. 79−62714
astatic, natural frequencies, elastic cardan suspension *(Russian)* 78−51056
astatic, with hysteretic type interframe correction *(Russian)* 77−23864
astatic gyroscope with elastic cardan suspension, dynamics *(Russian)* 78−63273
asynchronous cardan mounted gyroscope, stability of stationary motion *(Russian)* 77−62147
autonomous sytems, invariance of kinetic and potential energy *(Ukrainian)* 79−50577
axisymmetric rotating mass, gyroscope precession 78−8238
ball bearing surface CVD coating expts. 79−83366
Barnett effect, in gyroscope, coupled to rotating ring 78−86260
body dither laser gyro, scale factor nonlinearity 78−79062
cardan suspension, geometric interpretation of condition for regular precession *(Russian)* 78−86148
cardan-suspended, under small vibrations, resonance phenomena anal. *(Russian)* 77−53889
contactless, influence of nonconservative moments on precession *(Russian)* 79−80421
control moment, single-gimbal, geometric theory 79−21738
corrected gyrocompass asympotic stability *(Russian)* 79−10457
cryogenic, rotor suspension conditions *(Russian)* 79−30459
deformable gyroscope in non-Euclidean space, classical non-relativistic theory 77−30004
direction, azimuthal drift correction *(Russian)* 80−73349
drift, elastic deform. effect on rot. gimbals with base vibr. *(Russian)* 77−14894
drift velocity for gyro in gimbaled support *(Russian)* 79−32230
dry-friction periodic relay system analysis *(Russian)* 79−10455
dynamically tuned, drift anal. and compensation method *(Russian)* 77−53890
dynamically tuned precession, linear acceleration effect on stability *(Russian)* 78−62193
Earth orbiting, rot. motion according to general relativity 79−84651
education, gyroscopes, rolling and suspended, ang. momentum demonstration 79−9061
eigenvalue problems solution, with real symmetric matrix of same dimension 80−12895
electrostatic, geometry of suspension, max. rigidity case 78−62072
electrostatic suspended gyroscopes, electrofield torque due to offset of envelope assembly *(Chinese)* 80−43225
electrostatically suspended, on horizontal platforms, gravity meas. in ocean appl. *(Chinese)* 79−100976
equations of motion, hydrodynamic interpretation *(Russian)* 77−31300
error analysis for gyroscope subject to spatial vibration, shock absorber effect *(Russian)* 78−13892
fibre gyroscope, possible integrated optics soln. 80−10041
fibre laser gyroscopes 77−46728
fibre optic, phase nulling gyro 79−72719
fibre optic laser gyro signal detection and processing technique 79−37037
fibre optic ring interferometer gyroscope, Fresnel drag effect 78−79142
fibre optic rotating sensor, Sagnac interferometer preliminary results 80−10040
fibre optic rotation sensor, all-waveguide configuration, key element tests 80−58796
fibre optic rotation sensor with low drift 80−69530
fibre optical gyroscope, Sagnac or Fizeau effect 79−72669

gyroscopes continued
fibre-optic interferometer applications, thermally induced nonreciprocity 80−58665
fibre-optic rotation sensor construction and laboratory test 79−98497
flexible coupling, parameters calc. *(Russian)* 79−97376
floating gyroscope with vibrating base, perturbing moments *(Russian)* 80−40
flotation integrating gyroscope, dynamic errors 79−93135
forced rotation, arrangement dynamics *(Russian)* 80−86284
frame behaviour on movable foundation, eqns. of motion solution *(Russian)* 77−50876
free, reorientation, kinetic moment control under influence of orthogonal moments *(Russian)* 79−80423
general relativity prediction of deviation in Earth orbit, detection possibility 78−45550
guidance systems performance improvement, permanent magnets flux stability enhancement 80−50144
gyro-horizon compass, stability conditions *(Ukrainian)* 77−72144
gyrocompass levelling and setting for gyrostabilised platforms *(Russian)* 80−52190
gyrocompass optimal alignment *(Russian)* 79−67293
gyrodampers, passive satellite attitude control system appl. 78−96379
gyrohorizon with harmonic and random swinging, error anal. *(Russian)* 78−62194
gyrooptical compass, signal measurement time *(Russian)* 80−33007
gyropendulum, aperiodic single rotor 80−14561
gyrostabilizer, nonlinear suspension bearing, dynamic error *(Russian)* 78−75063
gyrostat, ang. mom., kinetic energy, and generalised inertia forces 77−19517
gyrostat, nonregular precessions in a Newtonian central field *(Italian)* 78−81825
gyrostat, symmetric satellite, uniaxial stabilisation at libration points 80−14560
gyrostat inertial motion, ang. velocity hodographs *(Russian)* 78−86137
gyrostat inertial motions, hodograph eqns., dividing motion *(Russian)* 78−86138
gyrostat motion, analytic props. of soln. *(Russian)* 78−86132
gyrostat motion time-optimal damping under random perturbations 77−68379
gyrostat with fixed point, lateral inertial imbalance effect on spin stability 79−32229
gyrostatic bodies, control of motion by means of gyroscopes *(Italian)* 78−12549
gyrotachometer, error autocompensation at angle vibr. of base *(Russian)* 78−16782
gyrotron, freq. characts. determ. *(Russian)* 79−14241
heavy, periodic motion anal. by Poincare's small parameter method *(Russian)* 77−23863
Hooke's joint, dynamics with non-orthogonal flexure axes 79−182
Hooke's joint gyroscope, response to linear vibration 79−54124
hydrodynamic suspension, spherical, axial decentralising force analysis and obs. *(Russian)* 77−72147
industrial weighing 80−42217
inertial systems constructed on double-gyroscope frame base, generalised models *(Russian)* 78−28937
Kovalevskaya gyroscope, new class of motions 80−68037
kovalevski hodographs of gyroscope angular velocity in the Delone case *(Russian)* 79−63013
Lagrange, system of n, stability of uniform rotation *(Russian)* 78−86136
Lagrange gyroscope, stationary out-of-balance, stabilisation *(Russian)* 79−63019
Lagrange gyroscope motion, geometrical investigation, hodograph curves *(Russian)* 79−63015
Lagrange gyroscope type body, periodic solns. to eqns. of motion *(Russian)* 78−86142
Lagrange gyroscopes, system of two, stability of regular precessions *(Russian)* 77−62145
Lagrangian hodographs of ang. velocity *(Russian)* 78−86133
Lagrangian moving ang. velocity hodograph *(Russian)* 78−86134
laser, accuracy increase by automatic output signal correction *(Russian)* 80−215
laser, Litton LC-2717, for missile appls. 79−72598
laser engineering and appls., conf., Washington, USA (May-June 1979) 80−1216
laser gryoscope, using passive ring resonator 77−88828
laser gyro, integrated 3 axis design 80−1268
laser gyro, multilayer light scatt. 78−33764
laser gyro, positive scale factor correction 77−34894
laser gyro, tutorial review 80−1266
laser gyro, Zeeman, beat-note sensitivity 80−53340
laser gyro evaluation plan and test results 80−9934
laser gyro performance analysis using fast Fourier transforms 80−9933
laser gyro technology 77−75598
laser gyros, low-scatter low-loss mirror prod. 80−1272
laser gyroscope, accuracy limit *(Russian)* 79−10343
laser gyroscope, concepts and status 77−88827
laser gyroscope, operation principle 79−23007
laser gyroscope, passive ring resonator, for inertial rot. meas. 77−58352
laser gyroscope, structure and basic characts. 79−23006
laser gyroscope applications 79−23008
laser gyroscope with induced mode locking, limiting sensitivity 79−59744
laser inertial rotation sensors, conf., San Diego USA (Aug. 1978) 80−1265
laser vibratory gyroscope, steepness characts. and S/N ratio anal. *(Russian)* 78−59070
Levi-Civita theorem generalised to gyroscopic systems *(French)* 77−71202
Mach-Zehnder heterodyne interferometer as gyroscope 77−82594
moment of forces on truncated rotor, edge effect *(Russian)* 80−28135
motion, elementary discussion 78−16605
motion in cardan suspension, investigation *(Russian)* 78−73985
motion in Newtonian gravitational field, averaging method *(Russian)* 78−65766
motion of a gyroscope with a cavity filled with a viscous liquid *(Russian)* 79−18696
motion picture camera gyroscopic stabilisation system, anal. of dynamics and accuracy *(Russian)* 80−95173
motion rigidity *(Russian)* 79−9099
multigimbal Hooke's joint gyroscope, damping and mistuning effects 79−54126
multigimbal Hooke's joint gyroscope, dynamics 79−54125
multiturn fibre Sagnac interferometer, shot-noise-limited inertial rotation meas. 80−1349
nonholonomic error *(Russian)* 78−63272
nonrigid cardan suspension, shock absorber parameters choice *(Russian)* 78−89473
optical, drift compensation method *(Russian)* 79−63206
optical fibre, based on Sagnac effect, background and development *(German)* 80−48431
optical fibre interferometer gyroscope 80−1348
optical fibre ring gyroscope, optimum sensitivity limits 80−10039
optical fibre ring interferometer, Fresnel drag in single-mode fibres 79 37035
optical fibre ring interferometer, reciprocity of birefr. single-model fibres 79−81513
optical fibre ring interferometer gyroscope, nonreciprocity noise, fibre dispersion meas. 80−1346
optical fibre rotation sensor, laboratory performance evaluation 80−1347
optical fibre-ring interferometer, polarisation analysis 79−64333
optical fibres, low-loss single-mode, elliptical and circular core, laser gyro appl. 80−1344
optical fibres, progress and components, review *(French)* 80−69524
optical rate sensor, discrete component Sagnac effect, error sources 80−1342
optical rotation rate sensors, Air Force appls. 80−9932
optical rotation sensor, passive ring cavity, drift performance 80−1343
optical waveguides for laser gyro applications 80−1345
optical-fibre ring interferometer, gyroscope applications, sensitivity 79 50379
optimal control of moving bodies, use of Bulgakov normal coords. method *(Russian)* 79−9104
parameter meas., mechanical spring simulation under working conditions 79−67263
passive optical rotation sensors using guided waves, developments 80−58781
passive resonant ring laser gyroscope design 80−99768
pendulum-gyroscopic platform stabilised in inertial space, autonomous determ. of coords. *(Ukrainian)* 78−65760
phase-nulling fibre optical laser gyro 79−36949
platform drifting rate, fixed-angle method for analyzing measurement errors 79−80609
pointing and stabilisation by fine control of secondary mirror 77−82124
precession, starlight aberration, calcs. in stationary metrics 78−54284
precession demonstration 80−73155
precession-correction monitoring, expt. planning 79−71422
precessional equations, admissibility of passage *(Russian)* 79−30219
principle resonance of gyroscope on elastic suspension *(Russian)* 79−30461
quasi-stationary motions of a heavy gyroscope in gimbals *(Russian)* 80−41
Raytheon laser gyroscope using MnBi magnetic mirror 78−79064
Raytheon multioscillator ring laser gyroscope 78−79063
reaction to impulsive torque, description for teaching 78−24604
relativity gyroscope expt., high accuracy test facility 77−30077
repeater, angular digitiser construction principle *(Russian)* 80−73311
resonance motion in free suspension *(Russian)* 79−10460
resonant motion of gyroscope with contactless suspension on vibr. support *(Russian)* 78−51054
resonant regimes, with damping system on vibrating base *(Russian)* 77−71312
response of slightly damped gyroscopic systems 80−52012
ring laser, empirical model for drift estimation 79−72605
ring laser appl. 80−1238
ring laser gyro, anomalous dispersion and gas flow effects 79−98430
ring laser gyro, dispersion and gas flow effects 80−1267
ring laser gyro, military appl. 78−42370
ring laser gyro, two-mode, four-mode soln. to locking problem 80−1270
ring laser gyro, two-mode, multioscillator approach to locking problem 79−59742
ring laser gyro *(German)* 80−53337
ring laser gyro technology at Rockwell 80−1271
ring laser gyroscope, accuracy limit, model calc. 80−1241
ring laser gyroscope, nuclear radiation vulnerability 80−9935
ring laser gyroscope, Raytheon four freq., mag. mirror, Faraday and Zeeman biassing 80−1269
ring laser gyroscope for missile guidance using magneto-optic bias mirror 78−79061
ring laser gyroscopes, multioscillator approach to locking problem 78−79042
rotation, precession, gyroscopic motions of body with fixed point *(Italian)* 77−13601
rotor scanning laser based vibration detector *(Russian)* 80−22351
Sagnac effect fibre ring gyro with electronic phase sensing 80−1350
Sagnac fibre-ring interferometer gyro with electronic phase sensing 79−17472
satellite gyrostat, optimal stabilisation of relative equilib. positions *(Russian)* 77−39213
satellite with 2-degrees-of-freedom gyroscope, stability *(Russian)* 77−39212
satellite with gyroscope in Newtonian field *(Russian)* 77−39211
satellite-gyrostat reorientation, optimal attitude control 80−61980
satellites, spin-stabilised, effect of orbital eccentricity and nodal regression on gyroscopic motion 78−45206
seismometer appl., vertical component meas. *(Japanese)* 78−4006
seismometer applic., horizontal component meas. *(Japanese)* 77−5351
seismometer for vertical seismic motion meas. *(Japanese)* 79−96842
separatrix motions of a Lagrange gyroscope *(Russian)* 79−63014
shock absorber selection parameters, forced vibrations 80−43659
single-rotor corrected gyrocompass motion subject to random parametric disturbance *(Russian)* 79−10456
singularly perturbed equations, appl. to study of gyroscopic systems 77−57183
solid body orientation control by an excess number of power gyroscopes *(Russian)* 79−80419
speed-optimal EM correction of magnetised rotor *(Russian)* 79−9227
spherical floating gyroscope, perturbing viscous friction moment in suspension due to vibr. *(Russian)* 78−13893

gyroscopes continued
SQUID appl. to nuclear gyros and magnetometers, high stability and sensitivity 80−98949
stabilisation of gyrostat in Newtonian force field *(Russian)* 77−851
stability conditions for centre of mass in ang. vibr. *(Russian)* 79−80420
stability of gyroscope in Cardan suspension on rot. base *(Russian)* 77−852
stability of Staude's permanent rot. with damping 78−21126
stability with gas lubrication spin axis bearings *(Chinese)* 79−63205
standards for metrological support 79−67262
strong field precession of slowly spinning gyroscopes, generalisation from d'Alembert's principle 78−40812
superconducting, to test Einstein's general theory of relativity 80−8897
superconducting, trapped-flux spin-down torques 78−57941
superconducting gyroscope, development of London moment readout 79−26090
superconducting gyroscope, high accuracy all angle readout using quantised flux 77−26223
superconducting shielded gyroscope, mag. torque, for tests of gravit. theories 77−13678
surveying and geophysical measurements with inertial rotation sensors 80−12571
symmetric gyroscope motion, differential eqns. stabilisation procedure including perturbing torques 80−4244
terrestrial gyrocompass, dry friction anal. *(Russian)* 78−77899
testing under operating conditions using system with astrocorrections 79−71413
triaxial electrostatic, error anal. *(Russian)* 79−88947
tuned elastic suspension, dynamical characts. 80−79133
two-axes indicating gyrostabiliser stability anal. *(Russian)* 78−54360
two-degree-of-freedom with free rotor, behaviour 77−41595
two-rotor gyrocompass intercardinal error anal. *(Russian)* 79−30460
two-stage force gyroscopes, artificial satellite altitude control *(Russian)* 79−30458
two-step float-operated, parameters selection *(Russian)* 79−97377
unsteady oscillations reduction using inner gimbal-base elastic damping coupling *(Ukrainian)* 77−30143
vertical, param. and mean square error calc. method *(Russian)* 77−33982
vertical gyroscope theory, nonlinear problem *(Russian)* 78−51053
vibrating rotor gyroscope, sensitivity increase *(Russian)* 79−27503
vibration meas. and control, optical methods *(Russian)* 80−8983
vortex rate gyro, dynamic response characteristics, ang. rate meas. 78−21125
weight reduction in left turning due to spontaneous symmetry breaking *(Japanese)* 80−98798
Zeeman multioscillator ring laser gyro, props. 79−72604

H-centres
alkali fluorides, ESR study of interstitial atomic H centres 79−56609
alkali halide, crystal, irradiation-induced defects 80−107316
alkali halide, irrad., colloidal centre growth, model 77−19946
alkali halide crystals, radiation damage products, impurities and colour centres *(German)* 78−10086
alkali halides, defect form., model of excitonic mechanism 78−38696
alkali halides, divalent cation doped, irradiated, first-stage F-centre prod. 80−107231
alkali halides, doped, F-centre accumulation efficiency temp. depend. 77−76394
alkali halides, F-centre accumulation, radiation induced, temp. depend., F-H annihilation effects 80−59460
alkali halides, interstitial motion during radiation damage and sputtering processes 80−54230
alkali metal halides, F-colouring role of impurities 80−64995
alkali metal halides, irradiated, annealing 78−92494
diamond, type Ib, electron irradiated, migration of N, optical absorption meas. 78−56505
diamond, vacancy enhanced N aggregation, electron irradiation effects IR spectra 80−70245
diamond, vibronic bands at 2.498 eV (H4), 2.417 eV and 2.536 eV, absorpt. and luminesc. under stress 77−85758
diffusion-controlled defect recombination, quasi-steady radius, tunnelling and elastic interaction *(Russian)* 80−10908
halides, vacancy-interstitial pair prod. by electron-hole recomb. 79−4530
ionic crystals, radiation defect accumulation temp. depend. 80−19803
KBr(I):D, inelastic light scattering of localised vibration of interstitial H atom in alkali halides 80−88998
primary F-H pair, annihilation probability of components in thermoactivated motion *(Russian)* 78−14340
quartz fibre, ESR and IR obs. of microinhomogeneities 77−8401
radiation-tunnel decay of an H′ centre 80−103327
BaF_2, undoped, H-centre prod. by reactor neutron irrad., optical absorpt. meas. 77−59010
CaF_2, undoped, H-centre prod. by reactor neutron irrad., optical absorpt. meas. 77−59010
CuCl, defect and impurity bands, lattice consts. 80−54638
KBr and KBr:Sr X-irradiated, optical investig. of Br_3^- centres 77−16348
KBr, colour centre form. under polarised UV irrad., dichroism in absorption spectra 80−107232
KBr, defect accumulation under electron irrad. at 4K 80−107233
KBr, diffusion-controlled defect recombination, quasi-steady radius, tunnelling and elastic interaction *(Russian)* 80−10908
KBr, efficiency of creation of X_3^- centres in X-rayed alkali halides *(Russian)* 78−71731
KBr, electron irrad., F-centre formation kinetics, interstitial stabilisation mechanism 79−69103
KBr, electron irradiated, defect accumulation kinetics of low temps. 80−10577
KBr, excitation of thermolum. near liq. He temp. 80−40171
KBr, H-centre struct., hyperfine interactions 78−79611
KBr, radiation-induced F-centre accumulation efficiency *(Russian)* 79−69102
KBr, recomb. in ionic crysts., defect interaction 80−84206
KBr, recomb. in ionic crysts., defect interactions 80−84207
KBr, self-trapped exciton form. via thermally induced defect reactions 80−60687
KBr, X-irrad., activation energy and thermal diffusion 78−72606
KBr:Li(Na), low temp. radiation hardening mechanism, single halogen interstitials as hardening agent, Ha annealing 79−23634
KBr:Rb, H-centre interaction with Rb^+ ion 78−75662

H-centres continued
KBr:Rb^+, elastic interaction of H-centre with impurity, dynamic effects 77−76396
KCl crystal, F-H centre formation by opt. conversion of self-trapped excitons 78−91335
KCl, efficiency of creation of X_3^- centres in X-rayed alkali halides *(Russian)* 78−71731
KCl, F- and H-centre production by nonradiative decay of self-trapped exciton 78−23042
KCl, H-centre struct., hyperfine interactions 78−79611
KCl, X-irrad., activation energy and thermal diffusion 78−72606
KCl, X-ray irradiated, first-stage F-centre prod. 80−107231
KCl:Ca,H, ENDOR studies of localised vibrations of substitutional atomic H 78−80248
KCl:H, dichroic H- and U-centres by polarised bleaching of interstitial H 80−29766
KCl:I^-, H, fluorescence of interstitial H-centres 79−73987
KCl:I(Br), colouration under two-photon excitation, absorption spectra 78−84618
KCl:Li,H optical and EPR exam. of H centre, $(LiH)^+$ absorpt. spectra 79−99920
KCl:Li^+, restricted interstitial motion of $H_A(Li^+)$ centre, ESR and uniaxial stress expts. 77−48053
KCl:Na,Br, EPR of interstitial and diinterstitial $BrCl_2^{2-}$ centres 77−81007
KCl:$SrCl_2$, H_{Na} annealing, X-ray irrad., H centre capture by IV dipoles 78−10927
KCl:Tl^{2+}, hole mechanisms of H- can F-centre production, thermolum. obs. 77−16407
KI, recomb. luminesc. of H-centre and F-centre electrons *(Russian)* 78−80402
KI, self-trapped exciton form. via thermally induced defect reactions 80−60687
$KMgF_3$, struct. of H-centre, low-temp. EPR meas. 77−12202
LiF:Na^+ H_A-centre struct., hyperfine interaction 78−79611
LiF:OH, neutron irrad., interstitial H-centres, ESR obs. 80−93175
MgF_2, EPR of electron irrad. induced F interstitial H- and H_A-centres 77−77099
MgF_2, gamma- or neutron irradiated, ESR meas. on hole centres 77−12201
MgF_2, pulse electron irrad., H-centre migration 79−7601
MgF_2, transient absorption and luminesc. following electron beam excitation 77−69920
MgO, radiation induced O interstitials, EPR meas. 78−55866
NaCl crystals, electronic and hole centres and surface, quantum-chemical calcs. 80−65489
NaCl, efficiency of creation of X_3^- centres in X-rayed alkali halides *(Russian)* 78−71731
NaCl, quantum-chem. calcs. of electronic and hole centres and surface 80−20118
NaCl, self-trapped exciton form. via thermally induced defect reactions 80−60687
NaF:K^+, γ-irradiated, $H_A(K)$ centres, EPR obs. 77−69689
RbCl:Ca,H, ENDOR studies of localised vibrations of substitutional atomic H 78−80248
RbCl:I, H, fluorescence of interstitial H-centres 79−73987
SrF_2, undoped, H-centre prod. by reactor neutron irrad., optical absorpt. meas. 77−59010

H I regions
21 cm emission within 10° of galactic centre, broadband obs. 77−78853
21 cm line, profiles and brightness temps. rel. to galactic shocks 78−54042
21 cm observations, comparison with UV and optical absorpt. line meas. 78−24532
21 cm observations of region 348°≤l≤12°, (+3°≤b≤+17°) 78−45377
1331+170, quasi-stellar object, 21 cm absorpt. detect. at Z≈1.8 79−75292
absorption column density rel. to ^{12}CO emission intensity, EHF meas. 79−35319
absorption lines high-resolution mapping in direction of NGC 2024, M17, W49 and Orion A 78−81667
AO 0235+164, BL Lacertae-type object, VBLI obs. of redshifted H I absorpt. 80−46658
Bok globules, search for neutral H 77−29904
bright southern galaxies, H I obs. 77−57084
Canes Venatici I galaxy group, neutral H obs. of NGC 4136, 4144, 4190, IC 4182 and (DDO 133) 79−84853
Cassiopeia A direction, evidence for HCN absorpt. assoc. with H I clouds 80−101624
Cepheus OB3 association, H I expanding shell rel. to supernova-induced star form. 78−12306
Circinus galaxy, H I 21 cm line obs. 77−33652
cloud model, intragalactic factor in external objects apparent distrib. 78−96552
clusters of galaxies, H I broad band emission search 80−46667
cold diffuse cloud towards 3C 225.0, UHF and EHF obs. 80−105311
cool clouds, kinematics and distrib. from 21 cm. obs. towards H II regions 79−44577
Cygnus H I supershell, connection with Cygnus X-ray superbubble 80−90575
Cygnus Loop, H I shock excitation rel. to high-rel. gas Hα emission 80−41873
Cygnus X, H I 21 cm line emission maps of field containing G78.2+2.1 SNR 80−56917
30 Doradus, supermassive nebula, motions of neutral and ionised material 77−71137
in dwarf spheroidal galaxies, upper limits to H I content 78−57633
early solar nebula, isotopic anomalies injection 79−101094
in early-type galaxies, 21 cm line obs. 78−45401
in early-type galaxies, accretion from gas-rich dwarf galaxies 80−31349
elliptical and lenticular galaxies, gas content 78−16544
elliptical galaxies, H I detect., upper limits 77−53685
elliptical galaxies, H I emission search, gas content determ. 80−46657
elliptical galaxies, search for H I emission 78−65681
extended continuous stream in galactic anticentre, 21 cm obs. 80−90524
extended envelopes round spiral galaxies, 21 cm obs. 80−90520
extended H I regions around spiral galaxies, probe for galactic struct. and intergalactic medium 78−12354

H I regions continued
external galaxies, diffuse [O I] emission and Hα lines, warm interstellar gas 78−4312
extragalactic diffuse H I clouds as probes of hot intergalactic medium 77−5568
G46.8−0.3 direction, H I absorpt. vels. rel. to supernova remnant distance 79−84833
G48.6+0.0 direction, H I absorpt. 78−85996
G74.9+1.2 direction, H I absorpt. rel. to distance of supernova remnant and point source 77−64864
galactic 21 cm emission-absorpt. survey, two component interstellar medium model 79−40256
galactic 21 cm line obs. for southern hemisphere 80−85987
galactic 21 cm line obs. in 348°≤l≤360°, −22°≤b≤−1° region 77−60824
galactic absorption spectra in direction of extragalactic radiosources 78−24541
Galactic Centre, decimetric H recomb. lines obs. rel. to nuclear H I disc 77−82310
galactic centre, expanding H I features rel. to nuclear eruptive phenomena 78−57647
galactic centre, H I distrib. and kinematics, model 79−17079
galactic centre region, H I 21 cm line survey 78−12361
galactic centre region, H I absorpt. obs. 77−45560
galactic centre region, neutral H survey 79−88722
galactic centre region, shock wave model of kinematic features of H I and molecules 77−91629
galactic disc, H I absorpt. meas. in seven low-latit. pulsars 80−101606
galactic H I, high angular resolution emission spectra, self absorpt. and other charact. 79−35350
galactic H I 21 cm line survey, low latits. 20-42° galactic longit. 78−57637
galactic H I absorption, obs. of struct. on small ang. scales 80−22051
galactic H I at |b|≥10°, southern sky survey 77−64830
galactic H I between l∼294° and 331°, kinematics rel. to Cepheids 79−48910
galactic H I cloud struct. in interarm region 79−21445
galactic H I distrib. outside solar circle 79−21421
galactic H I distrib. small scale struct., obs. of 3C 10 and 3C 58 78−45383
galactic H I regions, 42 cm absorpt. search rel. to protons mag. monopole struct. limits 79−53717
galactic H I regions, contrib. to diffuse soft X-ray brightness distrib. 79−53942
galactic H I regions, emission-absorpt. obs. from Arecibo 78−57610
galactic H I regions, location with respect to galactic plane 77−74127
galactic H I shells and supershells 79−53861
galactic H I spectra analysis 79−44605
galactic longitude-velocity map 78−86023
galactic nucleus, H I contour maps 79−35386
galactic plane, warping by LMC 77−45540
galactic rotation curve from H I maps, mass distrib. 78−96529
galactic spiral structure from H I 21 cm obs., linear theory, nonreson. region 79−88738
galactic structure from H I 21 cm surveys 79−44611
galactic survey, photographic presentation 80−62241
galaxies, H I 21 cm line widths correl. with absolute magnitude and type 79−5900
galaxies, H I profiles appl. to mass determ. 80−56937
galaxies, H I survey of 500 southern objects 77−33650
galaxies, lenticular, photographic obs., morphology and H I content *(French)* 79−2570
galaxies, nearby, H I profiles obs. 80−41895
galaxies, warped H I discs obs. 77−5567
galaxies, warped H I layers 78−16543
in galaxies peripheral regions, ionising background radiation effects on H I density 78−65729
in galaxies primordial protoclusters, search for H I emission at z=3.33 and (4.92) 78−41066
Galaxy, 21 cm obs. rel. to rot. curve accounting for interstellar gas expansion *(Russian)* 79−48938
Galaxy central region, improved H I data rel. to barlike model of inner Galaxy gas distrib. 80−67845
Galaxy disc, interstellar matter z-distrib. rel. to local galactic force field 80−62271
Galaxy H I subsystem, rot. curve *(Russian)* 80−36724
giant molecular cloud near M17, H I abundance, 21 cm obs., chem. evolution 79−21383
globular clusters, southern, H I and OH emission upper limits 80−22047
H2027+19, Delphinus soft X-ray source, model, X-ray obs. 80−90576
HD 50896 sightline, Copernicus UV obs. rel. to neutral gas props. 77−26036
heating, mechanical, by supernova blast waves, theory 80−36682
Heeschen cold cloud, assoc. with southern dark dust clouds 77−13434
Heiles Cloud 2, obs. of H I self absorpt. 77−29901
high galactic latitude H I emission, time variable 21 cm line profiles correction 80−51844
high galactic latitudes, H I temp. distrib. 77−22293
high positive velocity clouds, spatial and vel. struct. 77−13442
high velocity clouds, evidence against intergalactic interpretation 77−41399
high velocity clouds at low galactic latits., H I absorpt. 78−49506
high velocity clouds in anticentre direction, preferred to companion galaxy hypothesis 77−29941
high velocity clouds origin *(Russian)* 78−49492
high velocity H I clouds, fine struct. 77−29898
high-latitude H I clouds, obs. in OH 18 cm lines 80−67841
high-velocity clouds, fine struct., H I 21 cm obs. 79−30113
high-velocity H I, implications of interstellar absorpt. features 79−48891
high-velocity H I cloud near M33, obs. rel. to M33 H I tail 80−12815
high-velocity H I clouds, intergalactic interpretation and adiabatic theory of galaxy form. 80−46677
high-velocity H I clouds, map 80−26923
hot H I regions, heating by photoelectrons from O^- ions 78−36666
HVC 132+23−211, small high-velocity cloud, detailed struct. 78−89241
IC239, H I distrib. determ. 79−53910
IC 10, H I emission obs., unusual kinematics 79−67098
IC 10, irregular galaxy, giant H I envelope obs. 79−67094
in IC 342, Scd galaxy, H I large-scale struct. obs. 80−67857
IC 342 companion galaxy, H I mass 80−36712
H I regions continued
IC 443, supernova remnant, H I cloud and jet obs. 77−33592
IC 443, supernova remnant, H I shock excitation rel. to high-rel. gas Hα emission 80−41873
IC 443, supernova remnant, negative vel. H I condensations obs. 78−54016
II Zw 70/II Zw 71, compact galaxies, H I maps, tidal interactions 78−96531
interarm region and gas layer parameters, 21 cm line obs. 79−9007
intercloud winds, theory from two-phase interstellar medium model 78−85991
intergalactic H I in spectra of large-red shift quasars, consequences of neutrino rest mass *(Russian)* 80−105414
intergalactic neutral clouds, collisions with galactic discs rel. to interstellar super-rings form. 80−98717
intermediate latitude H I absorption, aperture synthesis obs. 79−12503
intermediate-velocity gas, UV obs. rel. to dynamically associated H I and H II regions 78−36655
interstellar clouds, non-linear relationships between N(Ca II), N(K I) and N(H) 79−92832
ionisation fronts, D-type, as phase transitions 77−33594
ionisation fronts, narrow radio recomb. lines emission 77−29940
in large galaxies, mapping survey, 21 cm obs. 80−94870
in late-type galaxies, H I obs. rel. to integral props. derivation 78−86015
Leo galaxy triplet (NGC 3623/7/8), H I distrib., 21 cm line obs. 79−44623
Lindblad's expanding H I ring, rel. to supernova hypothesis for extinctions at end of Cretaceous 78−32500
in LMC, super-giant H I+H II shells obs. 78−86012
local H I cloud, latit.-dependent line-shift field 77−74128
local interstellar gas in southern sky, single 21 cm component study 79−84834
local spiral arm, fine struct. 77−57091
low-latitude negative velocity clouds in galactic anticentre, distance 77−45506
Lyman α intensity, lower values 78−36675
Lyman-α 1216 Å flux rel. to physics of interstellar medium 77−2459
Lynds 1778/1780, H I and OH emission obs. in dark nebula 80−17628
in M101, extended H I envelope obs. 79−62904
M101, H I distrib. and motions in giant spiral galaxy 79−44613
M101 companion galaxies, integral props. from H I meas. 78−49532
inner M101 galaxy group, H I obs. 80−67885
in M31, gas-to-dust ratio determ. 78−8120
in M31, gravit. effects of M32 on H I disc and spiral arm pattern 79−21408
in M31, H I emission in NE.region, 21 cm obs. 80−90537
in M31, H I high-resolution obs. and major axis vel. plots 78−41057
M31, H I in outer regions 78−16532
M31, H I sheets ejected by M32, multiple disk radial vels. computer simulation 78−16523
M33, H I distrib. obs. and spiral struct. 80−56948
M33, H I large-scale struct. 78−96539
M33 direction, H I 21 cm emission/absorpt. obs. 80−62262
M33 H I tail, obs. rel. to adjacent high-vel. H I cloud 80−12815
M51 system, extended H I obs. 78−89253
in M81, spiral galaxy, gas dynamics 80−105336
M81 and 82 interacting galaxies, H I 21 cm obs. 77−45561
M82, Irr II galaxy, high angular resolution H I study 77−33626
M82, irregular galaxy, aperture synthesis obs. of H I emission 79−17077
in M 31, H I density distrib. rel. to spiral struct. morphology 78−65690
in Magellanic Stream, fine struct., 21 cm obs. 80−90523
Magellanic Stream, high sensitivity obs., small-scale struct. 79−35385
Magellanic Stream, tidal origin 77−64834
Magellanic Stream, turbulent wave of Magellanic clouds in galactic halo 78−8125
morphology of H and trace gases, review 77−26070
neutral clouds, influence on intercloud medium ionisation by single O star 77−9782
in new galaxy in Circinus, H I distrib. and vel. field 77−41409
NGC1023, H I distrib. determ. 79−53910
NGC2805, 2814, 2820 and IC2458, H I 21 cm obs. of close galaxy group 79−53917
NGC 1023 galaxy group, H I obs. and possible intergalactic H I cloud discovery 80−67886
NGC 1052, elliptical galaxy, field, H I emission mapping and line profiles 80−98719
NGC 1052, elliptical galaxy, H I obs. 78−69873
NGC 1052, H I detect. in elliptical galaxy 78−41041
in NGC 1569, dwarf irregular galaxy 80−90538
NGC 1851, globular cluster, H I detect., 21 cm line obs. 78−45368
NGC 1851, globular cluster, unsuccessful search for H I 79−5873
NGC 2146, peculiar spiral galaxy, extensive H I obs. 77−17676
NGC 253, Sc galaxy, aperture synthesis obs. of H I distrib. 77−74131
NGC 2623, interacting galaxy, H I absorpt. and emission obs. 79−17087
in NGC 2915, southern galaxy, H I content from radio obs. 77−67126
in NGC 2974, 4015, 5846, elliptical galaxies, H I contents 79−62906
NGC 300, spiral galaxy, aperture synthesis obs. of H I, outer plane warping 79−53905
NGC 3628, detection of emerging H I plume at 21 cm wavelength 78−54038
NGC 3904, elliptical galaxy, H I content from 21 cm line 77−87545
NGC 3962, elliptical galaxy, large scale H I distrib. 79−80347
NGC 4038/39, interacting galaxy pair, H I kinematics and distrib. 79−35365
NGC 4151, Seyfert galaxy, 21 cm line obs. 77−57087
in NGC 4214, barred Im galaxy in Canes Venatici I group, H I obs. 79−92862
NGC 4248, galaxy, H I obs. 78−4358
NGC 4278, elliptical galaxy, H I content meas. 77−22312
NGC 4278, elliptical galaxy, H I detect. 78−4342
in NGC 4565, warped Sb galaxy, H I distrib. 21 cm obs. 80−109542
NGC 4594, Sombrero galaxy, H I content, stellar rotation curve, mass-to-light ratio 77−53680
NGC 4631 group of galaxies, intergalactic neutral H rel. to tidal interactions model 78−54059
NGC 4631/NGC 4656, interacting pair of galaxies, neutral H aperture synthesis obs. 78−54043
NGC 4636, elliptical galaxy, H I content from 21 cm line 77−87545
NGC 4636, elliptical galaxy, H I emission detect. 78−32570

H I regions continued
in NGC 4636, elliptical galaxy, large-scale distrib. 78−45400
NGC 4736, spiral galaxy, H I distrib. and vels. from 21 cm study 77−57090
NGC 4945, spiral galaxy, H I absorpt. obs. 77−33651
NGC 5367, young star cluster assoc. with H I loop 77−82294
in NGC 5383, barred spiral galaxy, H I vel. field and 21 cm flux density 78−24549
NGC 5474, peculiar Scd galaxy, H I distrib. and kinematics 80−8683
NGC 6822, irregular galaxy, interferometer study of H I assoc. with optical core 78−20889
NGC 7538 and Sherpless 159, H II region/mol. cloud complex, H I aperture synthesis obs. 80−90510
in NGC 925, barred spiral galaxy, high-resolution H I obs. 80−105329
in Nilson dwarf galaxies, H I survey statistical props. 79−92851
nonplanar H I assoc. with Perseus spiral arm, 21 cm obs. 78−16489
North Polar Spur, H I ridge and X-ray emission ridge rel. to supernova remnant models 80−105370
open clusters, H I upper limits 79−30095
origin from supernovae explosions 80−67877
Orion A, C recomb. lines and H I clouds obs. 78−57605
Orion Nebula, radio obs. of nearby H I distrib. and vels. 80−105322
PHL 938, quasar, continuum spectrum reddening and dust/gas ratio 78−96561
PHL 957 (quasar) direction, limits on H I emission 77−91659
QSOs, absorption lines shortward of Lα emission, redshifts, origin in moving H I clouds 79−9025
quasars of high redshift, search for 21 cm absorpt. 80−4453
R-type ionization front approaching contact discontinuity 78−49510
radial vels. in LMC, catalogue 79−101089
radio galaxies, search for H I clouds 78−12316
radioastronomical spectra 21 cm line, radial vel. contour maps 80−17626
radiofrequency recombination lines, computation of b_n factors 77−64832
in ring galaxies, H I survey 79−5901
ring galaxy A0035 (Cartwheel), H I 27 cm line obs. 77−64852
in RMB 56 (1216+141), compact blueshifted galaxy, H I content meas. 78−16527
S0 galaxies, H I obs. 77−2466
in S0 galaxies, radio continuum and H I obs. 77−87549
in Sa spiral galaxies, H I study 80−98714
Sagittarius A, aperture synthesis obs. of H I absorpt. 77−26037
Sagittarius dwarf irregular galaxy, H I obs. 78−20887
in Seyfert galaxies, H I spectra and distrib. survey 79−8988
Sharpless 159 and NGC 7538, H II region/mol. cloud complex, H I aperture synthesis obs. 80−90510
Shostak high-velocity cloud, H I obs. 78−32575
small cold H I clouds, discovery during search for narrowband 21 cm radiation 77−29661
in small galaxies, accurate 21 cm H I spectra 79−35382
solar neighbourhood, galaxy counts/H I column densities relation, latit. depend. effect interpretation 80−26953
solar vicinity, H I clouds, kinematics from Nancy 21 cm absorpt. survey 79−8971
southern open clusters, search for interstellar H I 80−46619
southern sky, H I column density as function of position 80−4420
spectra towards extragalactic radio sources, 21 cm emission, and absorpt. obs. 80−94854
spectral profile, N.galactic hemisphere, Gaussian anal. 80−17643
spiral galaxies, H I clouds distrib. and motions, colour pictures of Doppler shifts 77−17383
spiral galaxies, in Virgo cluster, H I deficiency *(Russian)* 79−21438
spiral galaxies, nearly edge-on illusionary warps in H I discs 78−65682
spiral struct. of galactic inner parts from 21 cm line and stellar data 77−82304
Stephan's Quintet, H I emission search 79−30136
in Stephen's Quintet, broadband 21 cm H I emission 80−109554
supernova remnants, expanding H I clouds entrainment by presupernova stellar wind 80−62249
supershell formation from OB associations interaction with interstellar medium 80−82468
survey, contour maps, 21 cm obs. 80−85986
Taurus dark cloud, gas temps. and motion 77−78851
Taurus HL-1, small H I velocity bridge, 21 cm obs. 78−28755
transition probabilities and absolute oscillator strengths for C I, O I and N I absorpt. 77−49448
turbulent plasma, maser effect in H I 21 cm line *(Russian)* 79−88727
in unseen galaxies, 21 cm obs. and limits on space density 77−29925
velocity field in galactic centre region, axisymmetric kinematic model 79−17101
Virgo cluster spiral galaxies, H I deficiency from 21 cm obs. 80−62277
Vulpecula-Delphinus, new H I feature discovery *(Russian)* 80−46654
W33, H I shell obs. 77−64871
W58, galactic star-forming region, obs. of assoc. mol. cloud and H I region 80−67810
Zw 1400+0949 cluster (NGC 5416 group), galaxies H I mass/luminosity ratios 80−22090
H and C radio recomb. lines obs. in H I regions and assoc. H II regions 77−17659
H to H_2 transition region in interstellar clouds, H_2 photodissoc. 79−25672
K I, quadratic depend. of column density on N_H 78−20872
Na I, quadratic depend. of column density on N_H 78−20872

H II regions
abundance gradients from photoelectric spectrophotometry in 3700-7400 Å range 78−41036
AFGL IR sources in revised catalogue, identifications from 3.5-12.5 μm obs. 79−25659
Allen's obscured IR source in NGC 2264, spectrophotometric anal. 79−21370
anisotropic H II regions with axial symmetry, models 78−85993
aperture synthesis obs. 77−87507
AS 501, compact H II region, OH main-line maser emission obs. 80−67716
association with O-type stars, rel. to galactic struct. and stellar spectral type 80−105236
Barnard Loop, Hβ obs. 79−80346
Barnard Loop Nebula, far UV imagery 77−29911
in barred spiral galaxies NGC 1313, 5236 and 7552 visible obs. 80−82510

H II regions continued
Becklin-Neugebauer source in Orion, 3.3 to 5.5 microns spectrum 80−12796
binary H II region in galaxy VV 8, obs. rel. to galaxy rot., mass and surface brightness obs. *(Russian)* 79−48937
in bright galaxy nuclei, metal abundances and star form. 80−98708
in 3C 120, Seyfert galaxy, H II regions network spectrophotometry 80−67890
3C 391, supernova remnant, direction, evidence for extended H II region from 1.4 and 10.7 GHz obs. 80−4417
Carina I and II H II regions, far IR obs. 79−25657
Carina Nebula, extinction determ. from open cluster UBV photometry obs. 80−90513
Carina nebula, struct. and rel. to η Carinae 77−87520
η Carinae, assoc. open cluster Trumpler 15, age and reddening from UBVRI obs. 80−90487
η Carinae nebula, spectral obs. at 4 microns 78−4237
Cartina Nebula, O-type stars on line of sight, extinction law, photometry obs. 80−105240
Cassiopeiae A supernova remnant and surrounding H II region, γ-ray generation 80−85989
central H II regions in compact galaxy RMB 56 (1216+141), obs. 78−16527
Cepheus A mol. cloud, OH maser lines obs., star form. region 80−36691
Cepheus IV star formation region, continuum and recomb. lines, SHF obs. 80−90501
Champagne model of gas dynamics 79−35331
charge transfer of C^+ and S^+ in diffuse nebulae 80−77463
chemical composition of galactic and extragalactic H II regions 78−93359
chemical evolution, O and N abundance 80−46680
circumstellar H II regions, form. rel. to dynamical evolution of protostellar clouds 77−17543
clumping factor measurement, appl. to M33 H II regions 78−20870
colliding ionization fronts, shells in H II regions 78−4329
compact, two-component dust models for near IR emission 77−33600
compact dust-bounded H II regions, rel. to IR objects and maser sources 77−26032
compact H II region formed during 10 M⊙ protostellar envelope hydrodynamic evolution, struct. 80−36616
compact H II regions, fine struct. IR line emission 78−16482
compact H II regions, IR obs. in 3.4 to 33 microns range 77−22287
compact H II regions, large beam IR obs. 78−16488
compact H II regions, radiative shock front thermal instability 80−67821
compact H II regions, review of radio obs. 78−16507
compact H II regions assoc. with OH masers, CO obs. 77−57078
compact H II regions at sites of newly formed OB stars, obs. of nearby H_2O masers 78−12390
compact H II regions in areas of DR 21, W75N and K3-50, IR line obs., extinction determ. 80−12788
compact H II regions in irregular galaxy NGC 6822, new discoveries 80−51854
compact H II regions near class I OH maser sources, IR obs. 77−45525
compact H II regions near Type I OH maser sources, obs. 78−8094
compact H II regions near type I OH masers, obs. 79−25671
compact inhomogeneous, radio recomb. line and continuum emission theory 79−62885
compact IR sources assoc. with H II regions and molecular clouds, polarimetry 78−41019
compact IR sources assoc. with southern H II regions 77−45515
compact region near Herbig-Haro objects 7-11, 22 GHz obs. 80−73019
compact regions, far IR obs., (40-150 μ) 79−62883
Cone nebula region, continuum source 6 cm map and formaldehyde kinematics and distrib. 80−4418
Crab Nebula, magnetoparametric instabilities 78−61727
Crab Nebula, mapping and total flux determ. at 1 mm wavelength 77−49460
Crab Nebula, possible γ-ray line detect. 77−49458
Curtis-Schmidt thin prism survey for extragalactic emission line objects, Univ. of Michigan list I 77−71012
Cygnus X region, mapping and physical parameters 77−9783
Cygnus X region, maps of calibrated surface brightness of (Hα+N II) 77−78854
Cygnus X region, riddle of γ Cygni radio source resolved 78−28809
dense H II condensation in NGC 2175, obs. 78−20883
dense radio H II regions distrib. in inner Galaxy, kinematic models 80−12813
density fluctuatons, statistical approach 80−77468
diameters and emission as extragalactic distance indicators 77−91641
diameters of giant regions rel. to luminosity of parent galaxies 79−8973
dielectronic recombination through the forbidden levels, low density and T_e highly ionised plasma 80−43850
30 Doradus, absorpt. by foreground H I in LMC 78−24541
30 Doradus, central object R 136, struct., colour, mass, photometry obs. *(German)* 80−67825
30 Doradus, in LMC, Wolf-Rayet stars discovery 79−16980
30 Doradus, interstellar and nebular lines towards central object (HD 38268) 80−51839
30 Doradus, IR survey, 2 μm sources in central region 78−32544
30 Doradus, nebular complex, photographic obs. 77−33606
30 Doradus, supermassive nebula, motions of neutral and ionised material 77−71137
30 Doradus, uvbyR surface photometry 77−91600
30 Doradus complex, in LMC, UV reddening law 78−96516
30 Doradus direction, unique interstellar Ca II K-line profile obs. 80−51850
30 Doradus nebula, Balmer line photometry 79−62888
30 Doradus nebula, in LMC, interstellar Ca II and Na I obs. 80−46643
30 Doradus nebula, variability of R 136 central star *(German)* 77−45448
30 Doradus nebular complex, chemical comp. and struct. obs. 80−62226
30 Doradus region, far UV extinction anomaly 78−45386
30 Doradus region, in LMC, interstellar extinction and stellar population 78−96517
30 Doradus region, in LMC, radio model 78−96523
30 Doradus region, UV absorpt. by interstellar gas in stellar spectra 80−85978
double-charge transfer processes in gaseous nebulae 79−30112
DR15, galactic H II region, obs. at 408, 1407 and 2695 MHz 80−94881

H II regions continued
DR 21, CO J=2-1 isotopic line obs. at 230 GHz 77−33590
DR 21, ethynyl radical abundance and distrib. 78−65664
DR 21 (W75), continuum obs. at 3.9 mm 79−35333
DR 21-W75, high-resolution, far IR obs. 77−33589
dust, effect on H II regions struct. 77−33588
dust content, review 78−16508
dust distrib. in giant extragalactic H II regions 79−35320
dust grain props. *(Italian)* 79−48897
dusty H II blisters, appearance at radio and IR wavelengths 80−85979
dusty H II regions, non on-the-spot (OTS) models 78−85995
dusty H II regions, photoelectric yield of insulating dust grains 80−90507
dynamic evolution of dusty H II region 79−88719
dynamical evolution of spherical gas-dust nebulae including diffusion effects 79−80342
effects on molecular clouds 79−5880
electron temperature gradients with distance from galactic centre 79−88744
electron temperatures, determ. from radio recomb. line obs. at 22 GHz 79−35334
electron temps. and He abundance 79−21389
element abundances, model anal. of ionisation correction formulae 78−57623
elemental abundances, empirical determ. method test 78−61908
emission line objects in LMC *(French)* 78−69875
emission nebulae, association with Trapezium type multiple systems 80−67781
evolution, ionization fronts struct. 78−12330
excited H, decametric range radio lines search *(Russian)* 80−12822
expanding gas shells in Canis Major R1 and OB1 associations 78−93336
extended low brightness regions, H166α recomb. line at 1425 MHz 80−90512
extended regions, recomb. line emission obs. in galactic plane 77−13433
extragalactic, observed IR flux 77−87501
extragalactic distance indicators, obs., struct. considerations 79−40231
extragalactic H II regions, spectra anal. and models 80−73024
extragalactic metal rich nebulae, abundance determ. errors 80−82461
far IR fine structure line obs. 80−62253
far IR fine structure lines, obs. of [O III] 88.35 microns and [O I] 63.2 microns 80−12794
fluxes and parent galaxy diameters rel. to extragalactic distance scale 79−44576
forbidden line emission spectrum, effects of motion of hot exciting star 77−78845
G0.5−0.0, far IR obs., luminosity, colour temp., optical depth 78−41012
G0.7-0.0 (Sagittarius B2), struct. and He abundance 78−45380
G12.2−0.1, radio and IR obs. of OH/H_2O source 78−57620
G316.8−0.1, CO obs. at 115 GHz, star form. region 79−35353
G333.6−0.2, 2 μm line emission detect. 78−54017
G333.6−0.2, G298.2−0.3, southern compact H II regions, IR emission lines obs. 78−96522
G333.6−0.2, IR Line and continuum spatial study 77−49455
G333.6−0.2, Ne II 12.81 μm forbidden line obs. at high resolution 80−85983
G333.6−0.2, S III 18.7 μ fine-struct. forbidden line obs. 77−37637
G339.2−0.4, radio recombination line obs. of low-excitation H II region 80−46650
G37.7+0.1, double recombination line galactic thermal source, obs. at 1400 and 2371 MHz 78−69897
G45.1+0.1, 8-13 μm spectrophotometry of compact H II region 78−65672
G45.5+0.1, compact H II region, IR sources photometry 78−4396
G48.6+0.0, galactic H II region, direction, H I, OH and H_2CO absorpt. line meas. 78−85996
G49.5−0.4, giant H II region, $^3He^+$, probable detect. and significance 79−25689
G49.5−0.4 (W51), high resolution obs. at 5 and 15 GHz 78−54065
G75.84+0.4, IR photometry and spectrophotometry 79−62889
G 0.7−0.0 (Sagittarius B2), interpretation of radio recomb. line emission 77−17651
G 31, in Carina spiral feature, assoc. with young open cluster (NGC 3324) 77−22282
G 339.6−0.1, high resolution map at 1415 MHz, possible assoc. with 4U 1642−45 79−71143
galactic, aperture synthesis obs., quick look survey 78−12329
galactic, H I and He I ratio recomb. line survey at 10.2 GHz 79−48874
galactic, O III 51.8 μm forbidden emission line obs. 79−25685
galactic, obs. at 5 GHz 78−4327
galactic and extragalactic, mid IR and radio continuum flux density relation 79−21382
galactic and in spiral galaxies, ring-like distrib. *(Russian)* 78−93424
galactic anticentre direction, associated stars photometry and spectra rel. to outer Galaxy struct. 80−22079
galactic centre, 2.2 μm spectroscopy rel. to ionised gas distrib. 78−36686
Galactic Centre, decimetric H recomb. lines obs. rel. to ionised gas disc 77−82310
galactic centre, expanding H II arc and nuclear turbulent ionised gas 78−57647
galactic centre, extended thermal component, broad-line H94α emission 78−77598
galactic centre, far IR obs. 78−41012
galactic centre, H II regions rel. to cosmic ray positrons annihilation 79−44309
galactic centre, ionising agent of extended thermal radio emission 79−97059
galactic centre, IR obs. of compact H II regions 78−24551
galactic centre direction, H200β line detect. 77−78868
galactic centre region, compact radio continuum sources obs. 79−21430
galactic core, H II obs. in near IR 79−53864
galactic extended low-density H II region, rel. to star form. and diffuse IR emission 79−17047
galactic Hα background emission, high spatial and spectral resolution pictures 80−56897
galactic H II large scale distrib., recomb. line surveys 78−16539
galactic H II regions, CO obs. rel to Galaxy rot. curve to R=16 kiloparsecs 79−97081
galactic H II regions, forbidden S III 18-71 micron emission obs. 79−97046
galactic H II regions, location with respect to galactic plane 77−74127

H II regions continued
galactic H II regions around l=111°, aperture synthesis obs. 77−64827
galactic new H II regions and exciting stars, obs., rel. to spiral struct. 78−61900
galactic nucleus, 6 cm recomb. line emission vels. 78−69885
galactic plane, H II regions assoc. with far IR emitting dust at galactic longit. (l^{II}=27.5°) 80−62231
galactic plane towards PSR 1858+03, obs. rel. to pulsar distance 77−64785
galactic southern H II regions, mapping at 1415 MHz 79−53899
in galaxies, H II region dias. applicability to Hubble constant determ. 80−41887
in galaxies, H II regions rel. dispersions as distance indicators 80−31360
in galaxies, nearby, ionised gas thermal emission contrib. to radio continuum radiation *(German)* 80−109544
in galaxies NGC 300 and NGC 1365, comp. 80−4441
in galaxy NGC 3631, H II regions survey rel. to spiral struct. 77−45538
in galaxy nuclei, contrib. to nuclei bright line emission 80−109552
galaxy pairs, tides rel. to H II regions distrib. 80−46664
gas dynamics, galactic extended low density region components 80−36694
gas dynamics, two-dimensional axisymmetric calcs. 80−12791
gas properties from spectral line surveys 79−5879
gaseous nebulae, riddle of spectra, history 80−8676
giant extragalactic H II regions, vel. dispersion meas. 79−44606
giant H II complexes in galaxy NGC 6946, radio continuum emission 77−41407
giant H II regions, in A0035, large southern ring galaxy 77−45559
giant H II regions, radio maps interpretation 78−85994
giant H II regions in galaxies central regions, form. by explosions in galactic nuclei 80−56951
giant H II regions in Magellanic Clouds, monochromatic photographs 77−45516
giant regions in NGC 4038-9 interacting galaxies 79−97053
GL 490, GL 2591, obscured IR objects, K-band obs. rel. to H II regions models 79−92828
globules, time evolution 77−17661
Gum Nebula, temp. and density vars. *(French)* 80−26951
H II/OH maser regions, heating by ion streams 80−56912
HD 153919, X-ray source, IUE UV spectrum obs. rel. to circumstellar H II region 78−96569
HD 50896 sightline, Copernicus UV obs. rel. to H II regions props. 77−26036
Herbig-Haro objects, radio obs. and nearby compact H II regions 80−51756
HFE 64-70, 100 μm objects in Cygnus X, identifications with H II regions 77−17663
high-radiofrequency observations, comparison with far IR emission 78−49497
hot plasma clouds, contrib. to diffuse soft X-ray brightness distrib. 79−53942
Hubble V, in irregular galaxy NGC 6822, 21 cm continuum emission obs. 78−20889
IC 1318, giant H II region, large-scale line splitting discovery 78−96521
IC 1318 b and c and 5070, N II 6584 Å forbidden line profiles of giant H II regions 79−67081
IC 1318 nebular complex in Cygnus X region, light extinction 80−51835
IC 133, in galaxy M33, H_2O maser emission detect. 77−29926
IC 1396, bright rims, high resolution 1415 and 4830 MHz obs. 79−71092
IC 1396, three dimens. model from 2695 MHz high resolution map 80−105316
IC 1396 (Sharpless 131), 2695 MHz continuum map 80−105310
IC 1795, HF C I recomb. line emission obs. 78−28748
IC 1795, interaction with edge of W3 mol. core 80−94843
IC 1795 (W3), N II forbidden line unusual profiles over giant H II region 80−46645
IC 1795 (W3), UBV photometry of field stars 77−57082
IC 1795/1805, H II regions IR luminosity compared with exciting star total luminosity 78−96519
IC 1795/1805/1848 region, 2695 MHz map 77−17658
IC 1805, 1848, giant H II regions, physical anal. from radio obs. 80−36695
IC 1805, radio identification of IR object assoc. with passage of shock front 78−93369
IC 1848 A, bright-rimmed mol. cloud, IR source obs. rel. to star form. 79−5810
in IC 342, H_2O maser emission detect. 78−45417
IC 5070/NGC 7000 complex, 28 W catalogue and sources at 610 MHz 80−105308
inhomogeneities in high excitation H II regions, effects on spectra 78−54007
intermediate-velocity gas, UV obs. rel. to dynamically associated H I and H II regions 78−36655
ionisation and temperature structure, influence of star, gas density and chemical comp. 78−61911
ionisation front, shocked gas dynamics rel. to sequential form. of subgroups in OB associations 80−98696
ionisation fronts, D-type, as phase transitions 77−33594
ionisation fronts, narrow radio recomb. lines emission 77−29940
ionisation of low-density intercloud medium by single O star 77−9782
ionisation structure in inhomogeneous region 80−17644
ionisation-shock fronts hydrodynamic linear theory 80−17625
ionization front, oblique refraction 78−54025
ionization front time evolution 77−17654
IR emission, airborne obs. using Michelson interferometer 77−73966
IR emission, models for dusty and diffuse regions 78−41010
IR emission of dusty H II regions 79−71091
IR line emission, airborne obs. 78−93353
IR obs. at 10 μ using ESO 3.6 m telescope 79−35337
IR obs. of H II regions in M33 galaxy 78−61923
IR observations, 1-1000 μm wavelength 79−67084
IR sources, multiple systems in molecular clouds 79−101180
in irregular and blue compact galaxies, spectrophotometry rel. to chemical comp. and evolution 80−36711
isophotal diameters rel. to extragalactic distance scale 79−44575
K3-50, compact H II region, 2 to 4 micron spectrophotometry 77−13422
K3-50, ionized gas, IR and optical spectrophotometric meas. of compact H II region 79−53870
K3-50, optical nebula, radio obs. of assoc. H II regions 78−16554

H II regions continued
line intensities, data compilation 79−88721
in LMC, far IR obs. 78−81671
in LMC, four super-giant H II shells obs. 78−86012
LMC, giant H II ring obs. rel. to energetic stellar winds 78−77593
LMC, H II regions distrib. rel. to spiral struct. 77−29924
LMC, UV surface brightness meas., TD-1 sky survey 79−71125
LMC H II regions, ANS UV obs. of exciting stars 79−71017
Local Group galaxies, H II regions morphology and distrib. 78−16541
low density region round 36 M⊙ star, evolution calc. 77−60814
Lyman continuum photons selective absorpt. by dust 78−28759
β Lyrae, H II region radio emission rel. to nature of secondary component 78−36638
M101, spectra of H II regions, comp. gradient across spiral galaxy 78−65683
in M104 (Sombrero galaxy), absence rel. to mass spectrum of star formation 77−17675
M16, O III 5007 Å forbidden line profiles from core 79−8976
M17, aperture synthesis obs. at 5 GHz 79−35342
M17, dusty H II region, stellar optical polarisation meas. 78−45379
M17, far IR obs. rel. to H II region interaction with mol. cloud 80−22053
M17, far IR spectrometry 77−53668
M17, high resolution radio and far IR maps compared 79−75263
M17, large-scale vel. components, insect-eye Fabry-Perot obs. 78−93380
M17, near IR slit scans of Kleinmann-Wright IR source in mol. cloud 80−105300
M17, radio brightness distrib. at 3.5 mm wavelength 77−64837
M17 (NGC 6618), 21 cm obs. of components and structure 78−49508
M17 (Omega Nebula, W38, NGC 6618), S III, O III, N III, IR obs. 80−90495
M17 (Omega Nebula), O III 51.8 μm forbidden emission line obs. 79−25685
M17 SW, obscured IR point source spectroscopic anal. 79−48878
M1-67 possible H II region, internal motions 79−92841
M1-78, possible young H II region, struct. at 15.4 GHz 78−41025
in M31, correl. with spiral struct. in UV image 80−98716
M31, former globular clusters considered as H II regions *(Russian)* 80−31347
M31, Hα survey, catalogue of 981 H II regions 78−40840
M31, identification of H II regions and distant galaxies previously considered as globular clusters *(Russian)* 78−12370
M31, reddening of 22 H II regions 79−71082
in M33, contrib. to 4850 MHz radiocontinuum emission 78−28783
in M33, emission regions catalogue 80−46416
in M33, H_2O maser emission detect. 78−45417
M33, ionisation of interarm medium 77−67131
M42, Brackett-alpha emission in Becklin-Neugebauer object region 78−36657
M42, far IR polarisation obs. 77−53663
M42 (Orion Nebula), X-ray obs. by Astronomical Netherlands Satellite 78−28852
M43, emission nebula around NU Orionis, radio and IR obs. 78−54012
M51, thermal emission from bright H II regions 77−74135
in M82, stimulated recomb. line emission obs. 77−41408
in M82 nucleus, Brackett-line obs. 79−25704
in M83, H II regions spectral characts. and chemical abundances 80−56927
M8, Dragon dust cloud obs., isophotometry 78−36673
M8, IR map 77−64817
M8, large-beam near IR and 24 GHz obs. 79−48882
M8, new IR-CO source obs. 77−64818
M8, radio recomb. line obs. at 5 and 10 GHz 79−84832
M8 (Lagoon Nebula), far IR obs. 80−4413
in M 31, distrib. rel. to spiral struct. morphology 78−65690
Magellanic Clouds, chem. comp. of H II regions, photoelec. spectrophotometry 78−77607
Magellanic Clouds, H II regions chem. comps. 78−93381
in Magellanic Clouds, model nebulae anal. rel. to chemical comp. determ. 80−22085
Magellanic Clouds, spectrophotometry of nebulae suitable as standards 78−12350
magnetic fields, search for Zeeman effect in RF recomb. lines 77−60809
in Markarian 325, irregular galaxy, emission clumps observational props. 80−67869
Markarian 59 , supergiant H II region in SBm galaxy NGC 4861 spectrum and struct. 80−98705
middle IR polarisation by dust, model 79−67078
Milky Way near l=333°, 8.87 GHz obs. 80−22102
in molecular clouds, evolution, effect of O-type star winds 80−94846
morphology of H and trace gases, review 77−26070
multiple-component H II regions, radio recomb. lines press. broadening 80−4419
N160A, N159D (MC76, MC77), in LMC X-1 region, 2 cm obs. 80−51875
N51D, bubble-like nebula in LMC, internal motions obs. 80−105295
N 59, nebular complex in LCM, filter photography 79−17052
nebular complexes, physical parameters of thermal radio sources 77−57101
newly formed H II regions in interstellar dark clouds, physical props. from radio continuum interferometry 80−105301
in NGC 1068, interpretation for emission line data 80−90519
NGC 1499, nebula parameters determ. from decametre wavelength obs. *(Ukrainian)* 79−40243
NGC 1499 (California Nebula), CO obs. along ionisation front 78−24537
NGC 1499 (California Nebula), Hα obs., ξ Persei as exciting star 77−33622
NGC 1566, Sbc galaxy, spectrophotometry of nucleus and nine H II regions 80−51824
NGC 1977/Orion molecular cloud interface, radio recombination line obs. 79−25658
NGC 2024, HF C I recomb. line emission obs. 78−28748
NGC 2024, interstellar $^{16}OH/^{18}OH$ abundance ratio obs. 78−54024
NGC 2024, near IR obs. 79−58393
NGC 2024, search for linear polarisation in radio recomb. lines 80−41872
NGC 2024, study of nearby partially ionised interstellar medium 77−57077
NGC 2024 (Orion B), recomb. line obs. 77−29895
NGC 2024 (Orion B) nebula, CO J=2 to 1 line obs. 80−8673

H II regions continued
NGC 2024 (W12), 21 cm obs. of components and structure 78−49508
NGC 2175, identification with cosmic gamma-ray source (CG189+1) 77−91669
NGC 2237, Rosette Nebula, decametric obs., brightness temp. contours 78−57615
NGC 2237 (Rosette Nebula), H II region obs. in absorption at 12.6 and 25 MHz *(Russian)* 78−41024
NGC 2264, classification of optical, IR and radio obs. data 80−67818
NGC 2264, N II forbidden line unusual profiles over giant H II region 80−46645
NGC 2359, radial vels. and internal motions in ring-type nebula 78−81678
in NGC 2366, dwarf galaxy, visible and radi obs. 80−77475
in NGC 2403, galaxy distance rel. to H II regions size 77−2471
NGC 2467 nebular complex, internal motions 77−22304
NGC 281, CO and H_2O obs. 78−28740
NGC 281, obs. of shock in region of shock-induced star form. 79−25688
in NGC 2997, morphology and hot spots around nucleus of galaxy 80−62282
in NGC 3310, peculiar spiral galaxy, near nuclear H II regions exploratory investigation 80−62235
NGC 3372, location of η Carinae 80−4383
NGC 346 in SMC, very early O-type star discovery 79−5820
NGC 3603, interstellar λ4430 band obs. 78−32555
in NGC 4314, barred spiral galaxy, distrib. from UBV surface photometry of central region 80−77482
in NGC 4449, irregular galaxy, H II region interaction with extraordinary supernova remnant 80−56895
in NGC 4594 (Sombrero Galaxy), H II regions and ionised interarm gas detect. 78−36685
in NGC 5128, H II regions discovery by multicolour photography 79−53913
in NGC 5128 (Centaurus A), high-resolution spectroscopy and tubelike model of dust band 80−56945
in NGC 5128 (Centaurus A), obs. by picture processing anal. 79−53907
NGC 5291, massive gas-rich peculiar lenticular galaxy in IC 4329 cluster 79−71127
NGC 5471, in galaxy M101, gas and stellar mass determ. *(Russian)* 78−93426
NGC 604, 5471, giant extragalactic H II regions, IUE UV spectra 80−77467
NGC 604, in M33, SNRs rel. to content of high mass stars 80−31340
NGC 604, in M 33, core-halo struct. 80−85984
NGC 604 in M33, [S III] obs. and N/S abundance gradients 78−8083
NGC 6052, complex galaxy, supergiant H II regions rel. to late-type spirals collision 80−8681
NGC 6334, CO detailed struct. in assoc. mol. cloud complex 78−4324
NGC 6334, H_2O masers mapping and star form. 80−73025
NGC 6334, nearby H_2O maser discovery 79−21369
NGC 6334 and 6357, distances from early type star photometry 78−85998
NGC 6334 complex, 1 mm continuum map of cool IR sources 79−21390
NGC 6357A, O III 51.8 μm forbidden emission line obs. 79−25685
NGC 6888, ring nebulae around Wolf-Rayer star HD 192163, spectra of filaments and smooth gas *(Russian)* 80−90515
NGC 7000, N II 6584 Å forbidden line profile of giant H II region 79−67081
NGC 7000 (North America Nebula), rocket UV imagery 80−82440
NGC 7000/1C 5070 complex, 28 W catalogue and sources at 610 MHz 80−105308
NGC 7000/IC 5070 (North American/Pelican) nebular complex, obscuration and excitation 78−36667
NGC 7538, IRS 1, formaldehyde maser, SHF band obs. 80−67822
NGC 7538 (IRS 1+2), compact H II region, 2 to 4 micron spectrophotometry 77−13422
NGC 7538 and Sherpless 159, H II region/mol. cloud complex, H I aperture synthesis obs. 80−90510
NGC 7538 region, IR study 79−84842
NGC 7793, late-type galaxy, ionized gas phys. conditions and mass-luminosity distrib. 80−26967
NGC 7822 (W1) optical studies of kinematics rel. to supernova remnant struct. 78−54028
North America and Pelican Nebular Complex, struct., visual extinction map 80−22063
northern H II regions, 10 MHz absorpt. obs. 77−13485
observational properties rel. to planetary nebulae 80−109539
Omega Nebula (M17), O I 63 μm forbidden emission line obs. 79−25684
ρ Ophiuchi dark cloud, radio continuum radiation model rel. to exciting stars 77−33585
origin from supernovae explosions 80−67877
Orion, shock fronts and expansion rel. to OMC CO vel. features 80−41880
Orion A, C recomb. lines and H I clouds obs. 78−57605
Orion A, H_2O maser source outburst obs. *(Russian)* 80−105320
Orion A, H I absorpt. lines high resolution mapping 78−81667
Orion A, radio brightness distrib. at 3.5 mm wavelength 77−64837
Orion A, radio meas. of electron temp. distrib. at 22 GHz 77−87558
Orion A, SiO and H_2O maser obs. 78−8085
Orion ionisation-front IR source, effect of multiple grain components on 10 μm silicate feature 78−36659
Orion molecular source, CO J=2-1 isotopic line obs. at 230 GHz 77−33590
Orion Nebula, 2.1 μ H_2 emission , high spectral resolution obs. 78−20878
Orion nebula, ^{30}SiO detect. 78−8097
Orion Nebula, C abundance from visible and IUE obs. 80−82451
Orion nebula, C and Mg abundances from UV spectrum 80−41882
Orion Nebula, C I IR forbidden emission lines obs. 78−85987
Orion Nebula, C recomb. line mapping 78−20866
Orion Nebula, chem. comp. from emission line obs. 77−49456
Orion Nebula, dimethyl ether emission detect. 79−53862
Orion Nebula, double Herbig-Haro object 77−26006
Orion Nebula, ethynyl radical abundance and distrib. 78−65664
Orion Nebula, Fabry-Perot high-resolution O I 8446 Å mapping 79−35344
Orion Nebula, far UV imagery 78−4326
Orion Nebula, fine-struct. lines obs. and elemental abundances 80−4410

H II regions continued
Orion Nebula, forbidden Cl II and forbidden Fe II near IR high resolution mapping 80−62217
Orion Nebula, forbidden line and optical continuum electron temps. comparison 79−30105
Orion Nebula, forbidden line wavelengths *(French)* 77−64829
Orion Nebula, gaseous depletion *(Italian)* 79−21396
Orion Nebula, H_2 emission from shock-heated region in molecular medium 78−4321
Orion Nebula, H_2 emission interstellar extinction meas. 79−25668
Orion Nebula, He ionisation struct. and abundance, SHF obs. 80−105315
Orion Nebula, high resolution map at 33 μ 78−28757
Orion Nebula, high-vel. features driven by stellar wind from θ^2 Orionis A 79−8978
Orion Nebula, IR obs. by Fourier transform spectroscopy 78−61747
Orion Nebula, IR polarisation, preferential extinction in Kleinmann-Low nebula 78−4311
Orion Nebula, IUE obs. of UV continuous spectrum 80−90499
Orion Nebula, large proper motions of nebular features and faint star 78−12349
Orion Nebula, linear polarisation obs. 78−45392
Orion Nebula, low-luminosity X-ray sources obs., assoc. with star form. 80−26959
Orion Nebula, near IR Fourier spectroscopy 77−57071
Orion Nebula, near IR Fourier spectroscopy of weak lines 79−35328
Orion Nebula, near IR photography with vacuum-cold camera 80−90341
Orion Nebula, O I 63 μm forbidden emission line obs. 79−25684
Orion Nebula, O III 51.8 μm forbidden emission line obs. 79−25685
Orion Nebula, OH masers obs. 78−16493
Orion Nebula, optical evidence for stellar wind bubbles 79−88724
Orion Nebula, optical linear polarisation meas. 77−45536
Orion Nebula, photoelectric photometry of central region 77−33624
Orion Nebula, photographic obs. in Hα, Hβ and He I 10830 Å lines 78−81669
Orion Nebula, physical conditions from optical and radio lines obs. 77−45524
Orion Nebula, polarisation at 11.1 and 19.6 μm meas., aligned absorbing grains 80−36690
Orion Nebula, radio obs. of nearby H I distrib. and vels. 80−105322
Orion Nebula, search for H_2 ground state S(2) line 79−8961
Orion Nebula, search for vibrationally excited H_2 emission 78−93346
Orion Nebula, SO 36 GHz emission line detect., rel. to mag. fields 80−46642
Orion Nebula, spectrophotometric obs., ion abundances, and thermal balance 77−67121
Orion Nebula, spherical model, emission spectrum 77−53666
Orion Nebula, struct., radio obs., partially ionized gas 79−21379
Orion Nebula, submillimetre emission obs. 80−36685
Orion Nebula, temp. gradients, obs. and model 78−8077
Orion Nebula, vibrationally excited H_2 78−8076
Orion Nebula (NGC 1976), long-slit spectroscopy in rocket UV 80−105297
Orion Nebula peripheral regions, spectrum obs. rel. to element depletion and ionisation 80−36686
Orion Nebulae, IR studies of ionization front 79−75261
Orion region, struct. in radiocontinuum 78−49549
λ Orionis, absorption shell and core 78−77590
λ Orionis A, far UV flux, emission line obs. of surrounding H II region 78−93303
peculiar H II regions with nonthermal radioemission, supernova shell interaction *(Russian)* 77−91610
Perseus Arm H II regions, high-resolution radio maps 78−32549
Perseus arm H II regions, spectrophotometry and reassessment of galactic abundance gradients 80−22055
photoionisation models, for third period elements 80−46640
photoionisation models for gaseous nebulae with optically thin condensations 80−36693
photoionization models for gaseous nebulae 79−21392
V Puppis, eclipsing binary, circumstellar H II region 77−13385
in R-associations, obs. of free-free emission from embedded B-type stars 80−26851
radial vels. in LMC, catalogue 79−101089
radiative losses and gains 77−37639
radio recombination line obs., of C and H from 10 regions 78−93360
radio recombination line obs., review *(Russian)* 77−57080
radio recombination line source model, electron temp. and density inhomogeneity 79−92830
radio recombination lines, high-n, Zeeman splitting 80−58210
radio recombination lines, narrow, prod. around X-ray source 79−8972
radio sources, ang. dias. meas. errors 79−12534
RCW 107 (NGC 6164/5), ionisation struct. 77−45526
RCW 122, CO obs. at 115 GHz, star form. region 79−35353
RCW 36, H_2CO and OH obs. in nearby mol. cloud 78−69862
RCW 38, CO obs. at 115 GHz, star form. region 79−35353
RCW 38, nearby faint early-type stars UBV photometry 80−4352
RCW 38, RCW 57, interstellar $^{16}OH/^{18}OH$ abundance ratio obs. 78−54024
RCW 48-49, discovery of strong H_2O maser emission 77−57102
relationship to CO clouds, blister model 79−25681
Rosette Nebula (NGC 2237/2246), new physical parameters from 6.5 GHz obs. 80−4414
S104, 609 MHz aperture synthesis obs. 78−57618
S106, NH_3 obs. of nearby mol. cloud 79−84840
S106, radio obs. of assoc. mol. cloud, CO, HCO^+, HCN, OH and formaldehyde lines 78−61906
S106 and S235, aperture synthesis obs., star form. regions 78−36672
S106 IR, S235 B, obscured IR point sources, spectra rel. to circumstellar compact H II regions model 80−12795
S130, CO obs. of mol. cloud assoc. with bright rim near VY Canis Majoris 78−24536
S132, distance of exciting stars 77−2424
S132, radio continuum emission from giant H II region 79−8974
S140, far IR emission obs. from assoc. mol. cloud 77−33611
S159, CH obs. 78−28751
S187, H109α recomb. line obs., core envelope type struct. 79−8965
S206, galactic nebula, model for struct. 78−12326
S232, mag. field strength meas. 80−51840
S252 (NGC 2175), galactic nebula, aperture synthesis obs. 77−64828
S252 (NGC 2175), mol. line obs. of star-forming complex 80−4411

H II regions continued
S255, CO emission small-scale struct. from lunar occultation obs. 80−46637
S88B, Hα knot, optical radio and IR obs. of vicinity 77−74115
S 213, assoc. with Berkeley 11 open cluster 80−94840
Sagittarius A, far IR obs., luminosity, colour temp., optical depth 78−41012
Sagittarius B2, 2.2 μ obs., origin in field stars 77−29908
Sagittarius B2, ^{30}SiO detect. 78−8097
Sagittarius B2, far IR obs., luminosity, colour temp., optical depth 78−41012
Sagittarius B2, He abundance problem 78−49496
Sagittarius B2, high vel. H_2O maser features obs. 77−9779
Sagittarius B2, high-resolution, far IR obs. 77−33589
Sagittarius B2, NH_2D microwave detect. 78−20880
Sagittarius C, far IR obs., luminosity, colour temp., optical depth 78−41012
Sh2-149, near IR photography with vacuum-cold camera 80−90341
Sh2-156 (IC 1470), morphology, excitation and structure 80−67826
Sh 2-158 (NGC 7538), bright high excitation galactic nebula, morphology, excitation and kinematics 79−40241
Sharpless 106, assoc. Trapezium system 79−44566
Sharpless 106, excitation and nature of bipolar nebula from IR obs. 79−48888
Sharpless 106 IR sources, 8-13 micron spectrophotometry 80−105305
Sharpless 115, evolved region, struct., UHF obs. 80−105313
Sharpless 119, search for continuum radio emission from Calar Alto IR objects 77−41418
Sharpless 140, near IR slit scans of compact IR source (S140/IRS 1) 80−105300
Sharpless 155 nebula and Cepheus OB3 association, thermal radio emission obs. 78−96514
Sharpless 159 and NGC 7538, H II region/mol. cloud complex, H I aperture synthesis obs. 80−90510
Sharpless 232, new background planetary nebula PN 173+3.1, visible obs. 80−105309
Sharpless 235A, optical, radio and IR obs. 80−4415
Sharpless 254, 255 and 257, triple emission nebula in Orion, obs. 77−13430
Sharpless 88A-B and 106, compact H II regions, optical obs. 79−8969
Sharpless H II regions, assoc. H_2O maser emission detect. 80−62298
Sharpless H II regions, small-scale struct. at 4.995 GHz, high-resolution catalogue 78−61755
Sharpless small H II regions, radio line and continuum obs. 77−87509
shock fronts from OB-type stars H II regions, role in interstellar clouds form. 80−109506
shock waves, ion recomb. initiation 77−64825
small H II regions with exciting stars, radio maps 80−62224
SMC, abundances in 10 H II regions 78−4320
SMC, atlas of variable stars, clusters, emission regions and supergiant stars, book 79−44619
southern H II regions, 1 mm continuum obs. 79−8968
southern H II regions, NH_3 obs. 78−69863
southern H II regions models from radio recomb. line data 77−33620
southern hemisphere IR sources, search for H_2 2.1 μ emission 80−22059
southern sky, obs. in 2-20 MHz range 77−45563
spectrophotometry of compact H II regions from 4 to 8 microns 79−35321
in spiral galaxies, charact. rel. to disc radio continuum flux 77−13460
in spiral galaxies, counts rel. to galaxy distance and luminosity 80−82484
in spiral galaxies, interpretation of line intensity gradients across discs 77−13459
star formation regions, H II regions membership rel. to population categories and mol. clouds evolution 80−17645
star formation through accretion shock, model for H II blisters 80−21994
stellar wind bubbles effects on density gradients 77−74112
Stromgren zones around young stars, implications of EHF continuum obs. 80−51766
T Tauri nebula, ionisation and emission line spectrum calc. 80−67820
theoretical spectra for compact regions *(Russian)* 78−4337
time evolution effect of collisional ionisation 77−53664
Tycho supernova remnant, search for fossil Stromgren sphere 78−36661
unusual large-scale motions 78−16509
velocity dispersions in giant H II regions rel. to linear diameters 77−33595
visible spectra, emission lines due to dust 79−53874
volatile dust effects *(Italian)* 79−21394
in VV 126, multicomponent interacting galaxies, visible spectroscopy obs. *(Russian)* 80−77494
in VV 794, photographic and spectral obs. *(Russian)* 80−77493
W12 (NGC 2024), H I absorpt. lines high resolution mapping 78−81667
W28 A_2, RATAN-600 2-13 cm wavelength obs. *(Russian)* 80−17642
W33, H II complex, high resolution obs. at 2.8, 6, 18 and 21 cm wavelength 78−57619
W33, near IR slit scans of compact IR source in mol. cloud 80−105300
W33, recomb. lines as evidence for cool H II region with mass flow 78−49501
W35, W43, low-freq. radio recomb. lines studies 78−32589
W3, 10.5 GHz recombination line map 77−60817
W3, 8 to 13 micron spectrophotometry of compact sources 77−57070
W3, accurate H_2O maser source positions 78−4332
W3, dusty H II region, stellar optical polarisation meas. 78−45379
W3, far IR spectrometry 77−53668
W3, identification with cosmic gamma-ray source (CG135+1) 77−91669
W3, IR maps from 4.9 μm to 20 μm 78−49495
W3, VLBI synthesis obs. and struct. of OH maser W3(OH) 80−105368
W3(OH), H_2O vapour maser turn-on 78−36677
W3(OH), high vel. water maser features obs. 80−31339
W3(OH), rapid time vars. of H_2O maser source, models 79−17058
W3(OH) and surrounding diffuse ionised gas, radio recomb. line obs. 78−93371
W3 (OH), non-metastable NH_3 absorption at 23.1 GHz, first obs. 78−65677
W3 complex, CO, CS and HCN obs. LF obs. 80−82446
W3 complex, mapping of source parameters 79−58392
W3 IRS 1, fine structure line radiation, dust UV opacity 80−90505
W3 molecular cloud complex, model from mol. obs. 80−94843

H II regions continued
W3 region, near IR obs. of far IR sources G133.8+1.4 (W3N) and G133.982+1.14 (BS4) 80−22058
W3-W4-W5 complex, CO emission mapping 79−17059
W3/W4/W5 region, 1420 MHz continuum survey 78−16497
W3/W4/W5 region, heavy optical obscuration obs. 80−62301
W40, OH 18 cm lines obs. 78−4318
W40 and W48, near IR and CO mm wavelength obs. 78−65667
W43, radio emission obs. 77−17724
W48, 18 cm obs. of OH source 78−28812
W48, H 85α recomb. lines obs. 78−28762
W48, OH emission and absorption, spatial distrib. in H II region *(Russian)* 80−36733
W49, high-resolution, far IR obs. 77−33589
W49, stimulated Raman scatt. and high vel. H_2O maser features 77−49463
W49 A, H_2O masers and H II regions obs. at 23 GHz 79−71136
W49 A, struct. deduced from mol. and recomb. line obs. 77−33665
W49 N, VLBI obs. of high vel. H_2O maser emission 77−26038
W49A, H I and C I radio recomb. lines obs. 77−64821
W49A, high sensitivity Hnα radio recomb. line obs. 80−26998
W49A, W51A, H109α recomb. line, aperture synthesis obs. 80−105314
W49A, W51A, W51B, Arecibo obs. of H166α and C166α recomb. lines 77−22300
W4, excitation by open cluster Ocl 352 80−94843
W51, CO J=2-1 isotopic line obs. at 230 GHz 77−33590
W51, detect. of impact broadening of recomb. line 78−28741
W51, first optical detection, rel. to galactic spiral struct. 78−61900
W51, H II region-molecular cloud complex, cold gas flow 79−97048
W51, O III 51.8 μm forbidden emission line obs. 79−25685
W51, structure and vel. characts. of H II regions 79−71139
W51, W49, airborne for IR spectroscopic obs. rel. to dust cloud model 80−36684
W51 (IRS 2), compact H II region, 2 to 4 micron spectrophotometry 77−13422
W51-IRS 2 and W49 NW, IR spectra obs. 80−90497
W51A, W3 (Main), W49A, continuum obs. at 3.9 mm 79−35333
W51B, H I and C I radio recomb. lines obs. 77−64821
W58, galactic star-forming region, obs. of CO assoc. with H II region complex 80−67810
W58, IR obs. of H II regions and dust clouds near K3-50 77−49457
W75 maser sources, 1667 MHz line profile features 79−5914
W75-DR 21 region, structure of CO in molecular cloud complexes 78−89232
W80 (Pelican Nebula), CO obs. of expanding mol. shell surrounding H II region 80−105296
W 3, study of nearby partially ionised interstellar medium 77−57077
W 51, far IR spectrometry 77−53668
W 51 region, possible detect. of Na I 17 cm hyperfine emission 78−8139
weak emission image tube spectrophotometry, precision of meas. *(French)* 79−88601
weak shocks, properties 78−93348
wide spectrum H_2O source detect. at 22 GHz 77−74120
CH, obs. of 3.3 GHz ground state transitions 78−77592
CH radio emission, obs. 77−87512
CO obs. at 115 GHz in southern H II regions 77−87506
$^{12}C^{16}O$ and $^{12}C^{18}O$ J=2→1 transitions obs. 80−73022
Cl chemistry, as H ionisation source 79−40245
Fe abundances in gaseous nebulae, from forbidden Fe III and Fe VI lines intensities 78−53806
H and C radio recomb. lines obs. in H I regions and assoc. H II regions 77−17659
H I absorption profiles, kinematics and distrib. 79−44577
H I absorption profiles towards 11 galactic H II regions 79−12499
H I radio recombination lines, quasiclassical anal. 78−28511
H radio recombination line obs. from Arecibo 79−48880
H-like ions, departure coeffs. from thermodynamic equilib., rel. to radio-sources recomb. lines 79−76369
H_2O maers, obs. with resolution of 0.0008 arcsec 77−74154
H_2O maser lines very-high-velocity satellite features generation by stimulated Raman scatt. 78−73746
H_2O masers associated with compact H II regions in Sagittarius B2 77−13486
H_2O masers in H II regions, time variability 77−82296
H_2O masers in H II regions, time vars. obs. 79−88725
H_2O sources, spectra and autocorrel. anal. 78−65713
H110α recombination lines and formaldehyde, obs. towards bright rims in diffuse nebulae 77−87510
H137β/109α intensity ratio, interpretation 80−31344
Hα/[N II] ratio in H II regions *(Italian)* 79−21395
He abundance from 15 and 22 GHz recombination line obs. 80−98703
He II abundance and IR excess 78−86000
Hnα radio recombination lines, profile in static ion field 77−78629
Hnβ radio lines profiles in static ion field 79−62740
N,O abundances in gaseous nebulae 78−8093
O III, forbidden 88 μm line emission from H II regions and galactic centre 78−49503
O/H abundance ratio determ. in Galaxy from H II regions radio obs. 80−36692
OH 43.79-0.13, radio obs. of assoc. H II regions 78−36669
OH 48.61+0.02, radio obs. of assoc. H II regions 78−36669
OH and H_2O masers, radial vel. struct. 77−33617
OH and H_2O masers assoc. with compact H II regions, model 78−81666
OH main line masers in compact regions, magnetic field and inversion mechanism 79−48884
OH, radio lines absorpt. obs. in galactic radio sources 78−54068
OH type I maser sources, model 80−90556
OH weak masers detect. in H_2O masers direction 77−33618
S abundance from S III 6312 Å forbidden line, using ionization correction scheme 78−54018
SiO masers search at 7 mm wavelength 78−4215

hadron classification schemes
16-plets of mesons, mass relations, algebraic approach to broken SU(4) 77−38097
$^3P_0$ generalised model, reln. to Melosh transform. 78−12885
admissible complete sets in ladders U(6,6) symmetry 78−8626
anisotropic superfluidity of hadronic matter 79−13090
baryon classification in straton model *(Chinese)* 79−22075

hadron classification schemes continued
baryon classification in SU(4) charm symm. model, mag. moments 77−61257
baryon configuration mixing in 70 1^- multiplet of SU(6)×O(3), decoupling conditions 77−38142
baryon spectrum, P-wave excitations of quarks in bag model 77−13925
baryonic $(56,1_3^-)$ supermultiplet and new ΔD35(1925) reson. 77−82718
baryonium spectrum classification based on duality and unitarity 78−45869
boson nonets mass relations in broken SU(3) plus SU(2), mass of 9th pseudoscalar meson 77−38144
charm baryons, mass splitting and weight diagrams 79−26314
charm classification in SU(4), quark-lepton analogy *(Norwegian)* 77−34137
charmed baryons, spectrum in SU(4) breaking 15-plet dominance scheme 77−74663
charmonium spectroscopy, explicit soln. of wave eqn. for arbitrary power pots. 80−403
chiral SU(4)×SU(4) representation mixing, algebraic struct. 77−34102
diquark clustering in baryon spectrum, $(56,1^-)$ and $(70,0^+)$ multiplets 78−41503
EAS, hadron interaction model and mass spectrum *(Russian)* 79−96873
elementary particle classification, selection maps for quantum logics 78−29320
even-wave harmonic oscill. theory of baryon decay 78−45853
filling U(4) multiplets by hadrons *(Russian)* 79−22076
finite isospin groups for hadron classification, expt. consequences 79−360
graded algebras, finite dimensional irreducible representations, appl. to (Sp(2n); 2n) 79−49074
hadron building blocks, pionic mass intervals in narrow and S-state resonances 80−105875
hadron classification, quark model, SU(4) symmetry 78−12861
hadronic structure functions and form factors in low-order QCD with Migdal regularization 79−30720
Lie group framework for composite particles and mass spectrum 79−97608
mesons in O^{++} nonet, quark struct. 77−49906
new particles, scheme with colour-antisextet quarks 77−10225
nonlocal structures, shell effects 80−52391
particle spectrum, series classification 77−74652
pseudoscalar meson mixing problem, SU(4) spectral function sum rules, chiral symm. 77−38143
quark-line rule for hadron nonets, review 79−26304
sequential particle order, fundamental concept for hadron physics 79−80762
sequential particle order, fundamental concept for hadron physics, S-matrix theory 79−80763
SO_4 symmetry for classification of dibaryons and baryoniums 79−97531
strong interaction formalism with internal coords., partial unification of quantum theory and SU(3) classification 77−65137
SU(4) 20-plet of vector mesons *(Russian)* 78−58220
SU(5) symmetry with beauty quark, baryon and meson mass spectra 79−45079
SU(6)×SU(3) as classification group for baryons, Poincare group and quarks 77−18246
SU(6)⊃SU(3)⊗SU(2) Wigner coefficients 79−97607
SU(8) classification 79−80808
SU(8) mass relations among $J^P=1^{12}{}^+$ and $3/2^+$ baryons 77−71499
SU(8) symmetry and the baryon mass spectrum 79−80814
topological expansion for baryons and mesons, Veneziano scheme 78−70335
trilocal structures, expansions 80−57460
unified theory with right handed currents, SU(6) based vector-like gauge theory, proton stability 77−49890
unitary analytic representations of SL(3,R)*, operator formalism method 77−45983
Λ' existence, ninth $I=0$ $J^P=1/2^+$ baryon, asymptotic level realisation of SU(3), hyperon semileptonic decay anal. 77−18245
$N\bar{N}$, baryonium, internal struct. *(Norwegian)* 79−36032
$q^m\bar{q}^n$, multiquark hadrons, bag model anal. 77−34127
$qq\bar{q}\bar{q}$ mesons, spectra and decay couplings anal. in bag model 77−30331

hadron current
see also current algebra
$\Delta S=0$ weak hadron neutral current, quark parton model, νN and e^+e^- interactions 78−12859
charged second class currents, model 77−213
chiral solutons and current algebra 79−40680
exchange current affairs in electron scatt. off nuclei 79−71846
G-parity nonconservation, ev ang. correlation for allowed beta-decay 78−17151
geometrodynamics for quarks and hadrons, current definition and nonconservation 78−45809
meson exchange current theories 79−71798
metric-affine theory of gravit., intrinsic hypermomentum current components, hadron dilation, shear and spin 78−12632
neutral current struct. 78−24994
neutrino interactions and six-quark model, right hadronic currents *(Russian)* 77−82736
neutrino reactions at high energy, weak interaction props. and hadron struct. investigation, book contrib. 79−30727
nonleptonic decays of ordinary and charmed hadrons, vector-like model 78−41545
nonleptonic weak interactions, irregular G_u-parity term, hadronic currents 77−2770
nuclear currents, microscopic anal. of elementary particle description 78−82304
pomeron current model for diffraction dissociation 78−4843
QCD vacuum, effects on hadronic currents, instantons, e^+e^- annihilation and precocious scaling 79−332
reduction formula and non-leptonic decays in light-front formalism 78−12911
second class nucleonic currents and elementary particle structure 77−18200
semi-leptonic weak interactions, book contrib. 78−78162
single quark transition model, parity violating charmed hadron decays, current-current interaction 78−12907
SU(4) σ model with massive gauge fields 77−10184
three triplet quark model with observable colour, hadron weak current, $\Delta T=1/2$ rule *(Russian)* 78−74219

hadron current continued
unified gauge theories of weak currents of hadrons 79−80786
weak, models with 4 and 6 quarks *(Russian)* 77−74616
weak charged V-A current 78−74179
weak interactions, vectorlike model with right handed mixing 78−416
weak neutral currents, light-cone algebra anal. 79−6311
ed inelastic scatt., electrodisintegration at high energy and momentum transfer, exchange currents 79−6342
K nonleptonic decays, without dynamics enhancement *(Russian)* 79−30733
μ radiative capture, appl. to nuclear spin and isospin doublets 78−82320
$\nu(\bar{\nu})N \rightarrow \nu(\bar{\nu})\gamma X$, hadron neutral current, parton model *(Russian)* 78−45910
$\nu_\mu(\bar{\nu}_\mu)N$ quasielastic scatt., cross sections, effect of second kind weak hadron currents *(Russian)* 77−82734
νp high energy interactions, vector meson diffr. prod., charged and neutral current 78−54625
$^{12}C(\mu^-,\nu_\mu\gamma)^{12}B$, appl. of μ^- radiative capture to nucl. spin and isospin transitions 78−86511
$^2H(n,\gamma)$, slow neutrons, mesic interaction current, isobaric resonance *(Italian)* 78−25179

hadron decay
see also baryon decay; meson decay
cascade generation, 100-10000 GeV, anomalous effects *(Russian)* 78−70366
charmed hadron decay in SU(3)×U(1) gauge model of weak interactions, quark triplets 77−2789
charmed hadrons, $\Delta C = \Delta S$ decays 78−45912
constituent quarks in SU(3) and SU(6), current algebra., hadron decays, review, book contrib. 80−47259
diquonium decay into mesons, exact selection rules for chromo-harmonic potl. 79−13054
direct photon emission from excited bosons and e^+e^- collisions, relativistic oscillator model 78−37208
fireball decay in statistical-bootstrap theory 78−436
fireballs, quantum-statistical chain decay, pion clusters 78−430
flavour changing self energies, contrib. to $\Delta S = 1$ hadronic weak decays 79−71713
Gell-Mann-Okubo formula, total widths of unstable hadrons 78−45805
hadron lepton model interpretation of particle resonance states 80−4957
hadron production, coherent and inclusive, due to hadron-nucleus collision 80−83100
hadron-hadron collisions, fragmentation processes, treatment in quark models 79−58940
hadrons as compounds of bradyons and tachyons, ground state and decay anal. 78−58156
meson and quark distribution functions, quark cascade model 79−36033
multparticle decay theoretical models for heavy hadrons containing charmed quarks 78−70344
neutral charmed particle, direct obs. of pair decay in 400 GeV/c proton interaction 79−85299
neutrino decay and quantum number conservation laws *(Russian)* 79−348
new short-lived particle weak decay, possible evidence in pN GeV/c collision *(Russian)* 77−74728
nonleptonic 20+15 dimens. weak interactions 79−71746
nonleptonic decays of ordinary and charmed hadrons, vector-like model 78−41545
pp collisions, high energy, fireball mass, rapidity, spin distribs. 80−57645
pseudoscalar transitions between high-spin reson. 78−8666
quark model and SU(4) 78−62366
quark sea, percentage in hadron bags under constraint of quark-line rule 78−24998
quarkonium decays into heavy quarks 79−58943
resonance, EM decay and excitation, review, book contrib. 80−47300
$SU_3 \times U_1$ calibrating theory, weak and EM interactions appl. *(Russian)* 79−35964
SU(3)×U(1) gauge models, generalised mixing and CP violation in hadron decays 78−41473
SU(6) scheme of relativistic quark model, hadron electromag. and weak form factors 78−41500
weak decay processes in charm scheme of subhadronic constituents 78−25012
μ production by decay of hadronic shower, EM production of trimuons in deep inelastic muon scatt. 80−22619
ν sources, right hand weak currents and direct neutrinos *(Russian)* 77−82699
p decay modes in SU(5) and SO(10) theories 80−13301
$\bar{p}p \rightarrow \bar{\Delta}^{++}\Delta^{++}$, 3.6-12 GeV/c, cross sections and decay, parity exchange contribs. from quark model 79−13146

hadron-deuteron interactions
see also hadron-deuteron scattering; hyperon-deuteron interactions; meson-deuteron interactions; proton-deuteron interactions
absorption cross-section, 200 GeV/c, screening correction 78−21468
Coherent Tube Model for very high energy inelastic interactions of deuterons 77−18347
complex ang. momenta method and increase in effective longit. distances *(Russian)* 79−49541
hadron struct. anal. 78−45955
inelastic screening, form factor at $t \neq 0$ 80−91070
mass spectrum deformation of hadronic system, in coherent production on d *(Russian)* 79−93394
multiparticle reactions on deuterons, multiperipheral parton model anal. to rescatt. 79−22154
polarised deuteron, h+D→p+X, S and D wave functions, nuclear core hypothesis 78−62417
triple-Pomeron coupling and high-energy deuteron break-up 79−22153
d breakup, exotic final state interaction, intermediate Δ, ΔN threshold parameters 78−50043
d+nucleus→π+X, inelastic rescatt. contrib. to cumulative meson prod. *(Russian)* 77−61334
dd→π^0X, large transverse momentum, π^0 prod. cross section, ISR energies 79−3055
Nd, differential cross sections, Coulomb penetration factor in DWBA calc. *(Chinese)* 80−27603
Nd→3N, impulse approx. and cutoff radius *(Russian)* 78−12925
Nd→(Nπ)d, Drell Hiida Deck mechanism for particle dissociation on a composite target 79−93465

hadron-deuteron interactions continued
nd→($p\pi^-$)d, 26.6 GeV/c coherent interaction, peripherality of nucleon diffr. dissoc. 79−45108
nd→($p\pi^-$)d, diffr. dissoc. and interactions of diffractive produced systems 79−45107
nd breakup reaction, Reid soft-core pot. calcs. at 22.7 and 46.3 MeV 77−74860
Nd disintegration cross-section, variable cut-off radius in impulse approx. type models *(Russian)* 79−22276
nd→nnp, inelastic scatt. mechanism at moderate energy *(Russian)* 78−41723
nd→pnn, 800 MeV, quasielastic charge exchange, p spectra meas. 78−70389
nd→pπd, interference phenomena in coherent production, nucleon diffractive amps., helicity-flip 80−47329
D+hadron, inclusive π, N spectra in high energy hadronic reactions, d fragmentation region *(Russian)* 78−54809

hadron-deuteron scattering
see also hadron-deuteron interactions; hyperon-deuteron scattering; meson-deuteron scattering; proton-deuteron scattering
Amado model for nd scatt., NN exchange cuts in second Born amplitude 77−2790
inelastic shadow correction for hadron+deuteron elastic scatt., complex cut integral 78−70347
Nd scattering, parity non-conserving effects, predictions 79−93448
rescattering, rel. to momentum form. time rise *(Russian)* 80−52528
dd, gluon distribution 80−82939
dd collisions, 4.3, 6.3, 8.9 GeV/c, d spectra high momentum struct., multiple NN scatt. model 78−89727
nd, three-body Amado-Lovelace eqn. at positive energies, anal. soln. 78−16938
nd elastic scattering, perturbation calcs., Faddeev eqns., Reid soft core pot. 78−33177
nd elastic scattering at 180°, neutron energies 200 to 800 MeV 78−12927
nd quartet scatt., many-body theory *(Russian)* 77−38190
nd scattering, 14.4 MeV, parity nonconserving asymm. 78−21449
nd scattering amplitudes, 14.4 MeV Faddeev eqns. variationl soln. *(Russian)* 79−85321
nd scattering in high-partial waves, on-shell theory 78−41565
$^2H(n,n)^2H$, polarised n, 12 MeV, analysing power, similarity with (p,p) scatt. 78−70514

hadron electroproduction
σ_L/σ_T electroprod. data, colour excitation, proposed direct inclusive leptoprod. tests 80−52514
an asymptotic connection between processes of deep inelastic scattering and inclusive annihilation 79−22105
asymptotic freedom and local duality 77−71518
axial vector form factor from current algebra, π PCAC and covariant threshold electroprod. amps. 80−414
baryon resonance electroproduction, review of expt. information 77−22745
baryon resonances, EM transitions, multipole moments in single quark transition model 80−62985
Bjorken scaling violation models with new scaling rule 79−26305
broken $SU(6)_w$ analysis of electroproduction 79−93436
causality, Regge behaviour, proton electroprod. struct. function, Bjorken limit of sum rule 77−67662
charge correlations from residual hadrons using electroprod. data 79−3032
charmed meson prod. in quark exchange model 78−8600
charmed meson produced in e^+e^- annihilation 80−91106
charmed particle prod. in e^+e^- annihilation 78−78199
cumulative π, electroproduction from d, effect of rescatt., scaling effects *(Russian)* 78−74265
deep inelastic electroproduction struct. funct., Abelian gauge field effects 79−71754
deep inelastic hadron electroproduction, charge retention, quark-parton and jet models 79−45090
deep inelastic processes book contrib. 78−82222
deep inelastic quantum chromodynamic charm leptoproduction 79−54312
differential section of e scattering by boson of arbitrary spin *(Russian)* 78−25049
duality between resonances and free quark-antiquark pairs 79−63448
e^+e^-→hadrons, 9.4-10.4 GeV, three Υ states, mass spacings, lepton pair widths 80−68465
electroproduction, spin-dependent, sum rules, test of relativistic constituent quarks 78−25050
flavour singlet coefficient functions, QCD corrections, sum rules for pol. electroprod. 80−47301
fragmentation functions beyond leading order in QCD 80−13282
gluon fragmentation functions from quark jets 79−49453
gluon operator coefficients in electroproduction 79−58926
hadron, fragmentation from heavy quark partons 78−8603
hadron EM interactions, book 80−46748
impulse approximation in QCD, partons p_t distrib., appl. to deep inelastic electron scatt. 78−62368
inclusive, determ. of quark fragmentation functions ratios 77−54079
inclusive, local duality and precocious scaling 77−2842
inclusive electroproduction, final state hadrons, Regge-Mueller anal. 77−38176
inclusive electroproduction of hadrons, virtual photon prod., quark fragmentation region 78−54634
inclusive electroproduction particle ratios on H and D targets 77−18291
inclusive prod. in current fragmentation region 79−30741
jet production by a gluon source in QCD 79−22056
jets in high energy collisions 79−45114
K inclusive electroproduction, K/π and K^+/K^- prod. ratios 78−37217
Landau's hydrodynamic model, further aspects 78−82173
meson, spinless, pair prod. in e^+e^-, two photon processes at high energy 77−71524
meson electroprod. test of Compton amplitude duality 77−30388
meson electroproduction in correlating quark rearrangement model 80−86666
narrow resonance, 2.5-3.0 GeV/c^2 mass region in e^+e^- 77−2852
narrow resonance search in 2.5-3.0 GeV mass range in e^+e^- 77−2851
narrow resonances, search in 2520-2990 MeV mass region in e^+e^- 77−2850
new colour quantum number 77−87927

hadron electroproduction continued
new particles observed in e^+e^- annihilation 80−95283
nucleon structure functions, Bethe-Salpeter eqn. approx. soln. in quark-gluon model 77−54080
nucleus-electron hadron electroproduction 78−66267
parton model, transverse momentum cutoff 77−10215
physical pion low energy electro- and photoprod., Ward identity, chiral symmetry breaking struct. 80−5003
physical pion low energy photo- and electroprod., photoprod. phenomenology, quark mass 80−5004
pion, inverse electroprod. in $\pi^-p \rightarrow e^+e^-n$ 276 MeV, model independ. anal. *(Russian)* 77−61317
pion electroproduction, quark-parton model consistency 77−79254
polarised coincidence electroprod. scaling laws 77−49975
proton electroproduction struct. function, elastic form factor, scaling function, causal representation 79−13138
pseudomesoniums, spectroscopy, prod. and decay props. 79−45058
QCD, charm contrib. to electroprod. struct. functions 78−58170
QCD, transverse momentum of jets in electroprod. of hadrons 78−62367
QCD higher order effects in spin-dependent deep inelastic electroproduction 80−13281
QCD jet dynamics, hadron and photon prod. at large transverse momentum 79−45077
QCD structure function relation between deep inelastic ν reactions and polarised electroprod. 80−37221
quantum chromodynamics, electroprod. of charmed particles *(Russian)* 78−45878
quark-lepton interactions and $\bar{e}$-e ($\bar{p}$-p) annihilation 77−22746
quark-parton model, deep inelastic scatt. 77−79270
Regge behaviour of electroproduction structure functions in asymptotically free theories 78−25025
resonance excitation amplitudes and symmetric quark model 77−79272
resonance states below 2.2 GeV observed in e^+e^- annihilations 78−78197
rising hadronic cross section effects on EM processes, generalised vector dominance formulation 78−93868
scale breaking parton model for electron and neutrino deep inelastic scatt. 78−66122
scaling, model-independent. anal. 77−5999
spectral representation for nucleon form factors in electroprod. process 78−12914
Sterman-Weinberg improved jet formula 79−63447
Sterman-Weinberg jet formula corrections for e^+e^- annihilation from QCD perturbation theory 79−36086
structure function scaling props. and Gross-Neveu model anomalous dimens. 77−67660
structure functions, studied using light cone expansion via O_4 symm. 77−41845
three-jet prod. in large momentum transfer reactions, perturbative QCD theory 79−93373
unified formulae for EM decays, electroprod., e^+e^- hadron pair prod. for arbitrary spin 77−57535
VDM, generalised, electroprod. and photoprod. of vector mesons 78−41519
vector meson electroprod. in deep inelastic e and μ scatt. 78−78184
virtual Compton amplitude, anal. model 77−22739
weak and EM interactions at high energy [conf. Les Houches, France (July 1976)] 79−80785
$b\bar{b}$ prod. and decay in e^+e^- data at PETRA 79−63492
$\check{c}c$ $\bar{q}q$ states, decay, hadronic and photo-prod., e^+e^- annihilation prod. 80−99092
D and D* production near 4 GeV in e^+e^- 77−82754
D meson prod. and decay in e^+e^- at 4.03 , 4.41 c.m. energy 77−87989
Δ(3,3) region, low hadronic mass, Δ, τ, and nucleon axial vector form factors 78−74259
e(μ)N, deep inelast. scatt. from polarised targets 78−25053
ed, charged pion forward electroprod. at $Q^2=1.0(GeV/c)^2$, $\pi^\pm$ cross section ratio 79−93434
ed→hadrons, inclusive distrib. of hadrons from deep inelastic scatt. 79−89167
e^-e^+ annihilation, >2 GeV, production of charmed particles and charged τ lepton, review 78−17006
$e^-e^+ \rightarrow$hadrons, finite energy sum rules in QCD 79−40754
$e^+e \rightarrow X(hX)$, bound states and asymptotic limits for QCD in 2-dimens. 79−71716
e^+e^-, 27-4, 27.7 GeV/c, hadron prod./muon prod. cross section ratio, thrust distrib., average spherocity 80−426
e^+e^-, annihilation, production of new particles, J/ψ, ψ' and τ props. 80−5008
e^+e^-, annihilation, weak neutral currents of quarks hadron prod. cross section P-odd depend. *(Russian)* 79−93445
e^+e^-, hadron production, inclusive study, momentum distrib., energy and multiplicity 80−57613
e^+e^- 80−63010
$e^+e^- \rightarrow$ hadron jets, 13-31.6 GeV, planar events evidence, transverse momentum and broadening 79−93441
$e^+e^- \rightarrow$ hadrons, dual unitarisation and quartz model 77−10272
$e^+e^- \rightarrow$ hadrons, scaling and quark struct. 80−425
$e^+e^- \rightarrow$ hadrons, string model investigation 79−58946
$e^+e^- \rightarrow$ jets, in Υ and Υ′ region, sphericity and charged multiplicity 80−428
$e^+e^- \rightarrow$ jets, on-shell QCD quark form factor from two particle correlations 80−86740
$e^+e^- \rightarrow$3 jets, integer charge quark model, gluon jets 80−91101
$e^+e^- \rightarrow$3 jets, three gluon coupling in perturbative QCD 80−105913
$e^+e^- \rightarrow$4 jets, differential 4-jet acoplanarity distribs., QCD predictions, heavy quark prod. 80−78083
e^+e^- annihilation, 10 to 40 GeV, hadron multiplicity 80−63007
e^+e^- annihilation, 13-31.6 GeV, charged particle multiplicity growth, cross section 80−37286
e^+e^- annihilation, 3.6-5.8 GeV, inclusive D and K meson prod. cross sections 79−93439
e^+e^- annihilation, 4 and 7 GeV, $\bar{n}$ and $\Sigma^\pm$ prod., cross sections 79−63494
e^+e^- annihilation, charge current asymmetry as QCD test, neutral gluons 80−57616
e^+e^- annihilation, fine energy scan for narrow states between 29.9 and 31.46 GeV 80−22627
e^+e^- annihilation, gluon jets and heavy quarkonium prod., QCD test, ψ prod. 80−42479

hadron electroproduction continued
e^+e^- annihilation, gluon jets, multiplicity and ang. distribs. asymmetries 80−91105
e^+e^- annihilation, hadron and lepton prod., τ-lepton decay, $K^\pm$, p, $\bar{p}$ yields, quark flavours 80−73725
e^+e^- annihilation, hadron final state props. at 13 GeV and 17 GeV 79−63491
e^+e^- annihilation, hadron jets transverse momentum and ang. distribs. from QCD 79−40793
e^+e^- annihilation, hadron multiplicity distribution, Regge like parton model *(Russian)* 80−78100
e^+e^- annihilation, hadron prod. total cross section, CM energies 1.4-2.0 GeV 80−57619
e^+e^- annihilation, hadronic final state charge current asymmetry, QCD test, neutral gluons 80−37289
e^+e^- annihilation, heavy quark jet ang. distribs., quark mass, QCD anal. 80−42481
e^+e^- annihilation, high energy, secondary hadron transverse momentum, QCD anal. 80−37285
e^+e^- annihilation, higher order QCD corrections 80−47316
e^+e^- annihilation, jet ang. distrib., QCD correction 80−42482
e^+e^- annihilation, jet azimuthal ang. correlations in QCD 80−9179
e^+e^- annihilation, Λ_c charmed baryon prod., branching ratio, inclusive cross sections 80−37280
e^+e^- annihilation, meas. of gluon spin 79−30701
e^+e^- annihilation, overlapping resonances 77−2848
e^+e^- annihilation, prod. of orbitally charmed hadrons, free quark model anal. 79−22120
e^+e^- annihilation, QCD and semilocal duality (hadrons/$\mu^+\mu^-$) cross section ratio 80−78085
e^+e^- annihilation, QCD and jet acollinearity, quark-gluon coupling 80−105914
e^+e^- annihilation, quark jet fragmentation into mesons and baryons, chain decay model 80−63001
e^+e^- annihilation, single particle and multiparticle inclusive prod., QCD high energy predictions using methods of cut vertices 79−89128
e^+e^- annihilation, three-jet analysis, minimisation of sum of squares of transverse momenta 80−63008
e^+e^- annihilation and deep inelastic reactions, jet anal., thrust distrib., summing leading logs 80−63004
e^+e^- annihilation and quark fragmentation functions, Monte Carlo quark-parton model 79−22119
e^+e^- annihilation channel, differential dispersive theory of ψ/J 78−45933
e^+e^- annihilation to hadrons, overlapping resonances with variable channel struct., ψ prod. 79−22118
e^+e^- annihilation with polarised beams 79−36111
e^+e^- baryon-antibaryon prod. neutral current effects in Weinberg model 77−18310
e^+e^- calorimetric experiments, γγ processes, tests of QCD 80−22628
$e^+e^- \rightarrow$charmed mesons, decoupling of highly excited vector mesons 77−87986
e^+e^- collisions, jet prod. and two-photon annihilation, hadron spectra 80−91121
$e^+e^- \rightarrow \Delta X$, polarisation effects in nonperturbative parton model, scaling 80−105912
$e^+e^- \rightarrow e^+X$, QCD predictions for deep inelastic scattering on an electron 79−63493
$e^+e^- \rightarrow e^+e^-$ +hadrons, double equivalent-photon approx. *(Russian)* 79−403
$e^+e^- \rightarrow e^+e^-$ qg($q\bar{q}$)+ jet, γγ initiated 3 jet events in QCD 80−102057
e^+e^- events, hadron/μ-pair cross-sections, struct. near 4 GeV 77−248
$e^+e^- \rightarrow F^*\bar{F}^* \rightarrow F\gamma_1\bar{F}\gamma_2$, photon ang. correlations and prod. amplitudes 80−47319
e^+e^- final states, $q\bar{q}$ decay, semiclassical model, vacuum polarisation by colour field 80−63011
$e^+e^- \rightarrow \gamma$+hadrons, γ-spectra and QCD anal. 78−8678
$e^+e^- \rightarrow \gamma$+hadrons, high energy, lepton radiation and γ struct. functions, quark parton model 80−32113
$e^+e^- \rightarrow \gamma^* \rightarrow \gamma$+hadrons, QCD predictions 80−63009
$e^+e^- \rightarrow \gamma^* \rightarrow$hadrons, hadron calorimetric meas., QCD predictions, gluon emission 80−91102
$e^+e^- \rightarrow h_1h_2X$, polarised electrons, structure functions, γ* partial widths *(Russian)* 77−61308
$e^+e^- \rightarrow h^\pm X$, at CERN ISR with x=0 77−18303
$e^+e^- \rightarrow h^\pm X$, violation Bjorken scaling, momentum fluctuation, range of timelike photon 79−3033
$e^+e^- \rightarrow H\bar{X}$, associated production of gluonic jets and heavy mesons 78−93892
$e^+e^- \rightarrow hX$, high energy predictions from perturbative QCD 80−42417
$e^+e^- \rightarrow$hadron jet, 3 to 17 GeV, including charm threshold and upsilon resonances, review 80−47321
$e^+e^- \rightarrow$hadron jets, 30 GeV, strong coupling constant and QCD test 80−37283
$e^+e^- \rightarrow$hadron jets, 7.7-31.6 GeV, two particle ang. correlations 80−47318
$e^+e^- \rightarrow$hadron jets, QCD, Monte Carlo model 80−27514
$e^+e^- \rightarrow$hadron jets, quark helicities, neutral current vector and axial couplings 80−32114
$e^+e^- \rightarrow$hadron jets, test for planar events in QCD 79−40794
$e^+e^- \rightarrow$hadron jets, two fireball model anal., Monte Carlo method *(Russian)* 80−37288
e^+e^- hadron production at 13, 17 GeV CMS, first observation with PLUTO detector 79−36088
e^+e^- hadronic annihilation, 22-31.6 GeV, top threshold, sphericity and thrust distrib. 80−429
$e^+e^- \rightarrow$hadrons, 12, 30 GeV_γ jets, quark fragmentation and coupling constant, QCD comparison 80−105915
$e^+e^- \rightarrow$hadrons, 12, 30 GeV, π,k,p,$\bar{p}$ production 80−105916
$e^+e^- \rightarrow$hadrons, 13-31.6 GeV, gluon bremsstrahlung evidence, seagull effect, one sided jet broadening 80−430
$e^+e^- \rightarrow$hadrons, 1.35 to 2.125 GeV, hadronic cross sections 79−58968
$e^+e^- \rightarrow$hadrons, 1.42-3.09 GeV total CM energy, total cross section 79−93440
$e^+e^- \rightarrow$hadrons, 33-35.8 GeV, new quark flavour search, cross sections and thrust 80−86736
$e^+e^- \rightarrow$hadrons, 400 GeV, search for narrow reson. states near 6 GeV 77−74699
$e^+e^- \rightarrow$hadrons, azimuthal correlations, quantum chromodynamics anal. 78−70382

hadron electroproduction continued
e^+e^-→hadrons, below 2 GeV, comparison of QCD sum rules with expt. 79−49458
e^+e^-→hadrons, cross-section constraints in asymptotically free theories with anomalous dimens. 77−30393
e^+e^-→hadrons, D semileptonic branching ratio at $\psi''(3770)$ 78−45934
e^+e^-→hadrons, energy correls. in QCD, asymptotically free perturbation theory 79−63497
e^+e^-→hadrons, higher order QCD corrections 80−95280
e^+e^-→hadrons, jet behaviour, review 80−52524
e^+e^-→hadrons, jet struct. in the energy range 3.1-9.5 GeV 78−89725
e^+e^-→hadrons, jets from heavy quarks, QCD perturbation theory 80−63012
e^+e^-→hadrons, manifestation of heavy leptons, decay props. *(Russian)* 77−26537
e^+e^-→hadrons, multiplicity, scaling, inclusive spectrum, simple hadron cascade model 78−66135
e^+e^-→hadrons, neutral and weak currents anal. 77−26533
e^+e^-→hadrons, new flavour search at PETRA 80−37282
e^+e^-→hadrons, non-perturbative QCD vacuum, total cross section corrections 80−86735
e^+e^-→hadrons, planar events, gluon jet identification 80−47317
e^+e^-→hadrons, R problem, QED and QCD corrections, quarks and leptons 80−95281
e^+e^-→hadrons, relative total hadronic cross section meas. 79−54346
e^+e^-→hadrons, reson. behaviour around 1820 MeV 77−65163
e^+e^-→hadrons, search for narrow resonances in 1.45-1.92 GeV mass region 78−89724
e^+e^-→hadrons, semiinclusive hadron prod., quark fragmentation function corrections, QCD 80−63013
e^+e^-→hadrons, three-jet events and QCD test at PETRA 79−97631
e^+e^-→hadrons, total cross sections, c.m. energy range 1.92 to 3.09 GeV 79−45094
e^+e^-→hadrons, Υ, Υ', Υ'' states, mass differences, leptonic width ratio 80−68466
e^+e^-→hadrons ($\mu^+\mu^-$), Υ(9.46) muonic branching ratio, total and leptonic width 80−86703
e^+e^- inclusive hadron prod., neutral weak currents 78−50041
e^+e^- inclusive hadron prod., polarisation and p nonconservation asymmetries, π, $K^\pm$, $D^\pm$ prod. 80−78084
e^+e^- interactions, review 79−80833
e^+e^-→jets, energy cone distrib. around jet axis, QCD anal. 80−86732
e^+e^-→jets, exclusive calcs. for QCD jets, Monte Carlo approach 80−105911
e^+e^-→jets, high energy, $q\bar{q}$ pair conversion model, seagull effect 80−5007
e^+e^-→jets, jet ang. momentum, ang. distrib., oblateness and invariant mass, QCD calcs. 80−73722
e^+e^-→jets, particle ratios from quark statistical model 80−73724
e^+e^-→jets, t-quark pair prod. effects in annihilation, Kobayashi-Maskawa model 80−86733
e^+e^-→jets, two photon four jet anal. 80−27513
e^+e^- jets, two-particle distribs. from single-particle fragmentation functions, effects of heavy quark flavours 80−68468
e^+e^-→multihadrons, PETRA energies, total cross section and average multiplicity 80−22626
e^+e^-→multihadrons, planar three jet events, gluon bremsstrahlung, strong coupling constant 80−57617
e^+e^- narrow angular jets, QCD and hadron phenomenology, cones or tubes 80−13320
e^+e^-→nπ, jet struct., lightlike (zero mass) quarks anal. 79−63496
e^+e^-→$p\bar{p}$, 1925-2180 MeV total energy, form factors and cross sections 80−427
e^+e^-→$\pi^+\pi^-$(K^*K), $\sqrt{s}$=1.5 GeV, EM timelike form factors for π and K 80−91089
e^+e^-→$\pi^+\pi^-\pi^0$, 1.45-1.875 GeV, ω behaviour at 1.55 GeV 80−82984
e^+e^-→$\pi^+\pi^-\pi^0$, 750-1100 MeV, ω and ϕ meson interference 80−105910
e^+e^-→$\pi^+\pi^-\pi^+\pi^-$, 1.45-1.875 GeV, ρ behaviour at 1.55 GeV 80−82984
e^+e^-→$\pi^\pm$X, weak neutral-current effects 77−13968
e^+e^-→ψX, estimate of inclusive ψ and $\psi\eta_c$ prod., QCD anal. of cross section 79−85308
e^+e^-→$q\bar{q}g$, (3g), jet-mass spectra, perturbative QCD 80−63006
e^+e^-→$q\bar{q}g$, long. polarised beams, beam-event asymmetry, massless QCD null result 80−91104
e^+e^-→$q\bar{q}\gamma$, IR and collinear divergences, cancellation in one-loop corrections to QCD cross sections 79−40730
e^+e^- resonance production above charm threshold 77−79275
e^+e^-→ρ^0X, 1.45 to 1.61 GeV 79−63489
e^+e^-→ρe, transition form factors, dispersion theory 79−63495
e^+e^-→three jets, acoplanar angle relative to beam polarisation, vector/scalar gluons 80−63005
e^+e^-→Υ(9.46), electronic width determ., energy spectra for hadron inclusive production 79−26339
e^+e^-→VX, polarisation states and differential cross sections for πA_1 and $\rho^+\rho^-$ *(Russian)* 80−102059
e^+e^-→vector mesons, colour quark model for new reson. above 4 GeV 78−17033
electroproduction with |t| from 0.125 to 1.3 GeV^2 77−79274
eN, scaling violation, Callan-Gross relation, colour excitation 77−65159
eN→eX, form factors and structure functions, review, book contrib. 80−47294
eN→e+hadrons, E<2 GeV, formalism, review, book contrib. 80−47312
eN→eπ_fX, test of soft-pion theorem in inclusive pion electroprod. 79−17739
eN→e$\pi^\pm$X, ^{1}H, ^{2}H targets, π^+/π^+ ratio, Q^2 to 4 GeV^2 77−74693
eN→e$\pi^\pm$X, sum rules for polarised N 78−89718
eN→eπN, π form factor determ. 78−66128
eN inelasticcatt., low energy pion electroprod. and hadron form factors, book 79−85306
eN→pX, ^{1}H, ^{2}H targets, forward protons to Q^2=9.5 GeV^2 77−74690
e^-N, inclusive pion production due to $\gamma q \to \pi q'$ process, quark-parton model *(Russian)* 80−78073
e^-N→e^-Nπ, electromag. and weak process from weak neutral current interaction *(Russian)* 78−45928
ep, 20.5 GeV, inclusive π^0 electroprod. in deep inelastic region 80−52520
ep deep inelastic scatt., density matrix appl. to scaling props. 78−8673
ep→e$K^+\Lambda^0$, scalar transverse separation 77−71520
ep→e$K^+\Sigma^0$, scalar transverse separation 77−71520

hadron electroproduction continued
ep→eΛX, electroprod. of forward Λ baryon near/along virtual photon direction 79−22116
ep→e+hadron+x, parton picture from QFT, structure function scaling behaviour 79−402
ep→epϕ, Q^2 depend. of diffractive slope, decay ang. distrib., vector dominance model 79−89169
ep→epπ^0, $-k^2$=0.88 $(GeV/c)^2$, comparison with various models 77−18294
ep→epπ^0, coincidence electroproduction of single neutral pions in the resonance region at q^2=0.5 $(GeV/c)^2$ 79−89168
ep→epπ^0, elastic π^0 electroprod. above resonance region, cross section, direction 78−62412
ep→hadrons, inclusive distrib. of hadrons from deep inelastic scatt. 79−89167
ep inelastic scattering, charged hadron multiplicities, inclusive π^- distribs. 78−41552
ep scatt., longitudinal cross section and asymmetries for jets in leptoproduction 80−32106
$e^-\pi$→e^-+hadrons, spectator interaction effects in large $p_\perp$ deep inelastic processes 79−93427
eq parity violating neutral current couplings, model independent anal. 79−17737
η prod., 4-5.2 GeV, F, F* masses determ. 77−87988
K^0 prod. in e^+e^- annihilations, 3.4-7.6 GeV 77−87987
K_s^0e prod. in e^+e^-, charmed particle weak decay 77−2853
N(1420), $SU(6)_w$ fits in baryon photo- and electroproduction 77−46057
p electroprod. struct. function and constituent-particle scatt. 78−45931
p inclusive electroproduction in fireball model 78−41554
π, pair production in two-photon e^-e^+ events 77−71523
π electroprod., light cone dispersion sum rules, axial vector currents 78−41556
π electroproduction inclusive processes, quark fragmentation function ratio determ. 77−61294
π inclusive electroproduction, quark-parton model comparison with expt. data 78−37218
π prod., test of quark parton model 77−57488
π production, theoretical anal., fixed-t dispersion relations 77−22743
π^0 electroproduction, test of quark parton model 78−8672
π^+, electroproduction at threshold, weak form factor 79−22107
π^+ electroproduction, transverse and longitudinal cross-section separation, pion radius 77−38179
π^+ prod. on ^{27}Al and ^{51}V 78−21543
$\pi^\pm$, quark-parton model, fragmentation functions 79−13136
ρ^0 prod., parity violating effects 80−9178
e^+e^- annihilation, 30 GeV, inclusive K^0 prod. $K^0K^+/\mu^+\mu^-$ prod. ratio 80−91103
e^+e^- annihilation, quark jets, transverse momentum profile 80−57621
e^+e^- annihilation jet invariant mass in QCD 79−85307
e^+e^-, high energy interactions *(Chinese)* 80−78074
ep→enπ^+, forward π^+ electroprod. in Δ(1232) resonance region 79−22115

hadron-hadron interactions
see also baryon-baryon interactions; hadron-hadron scattering; meson-baryon interactions; meson-meson interactions
η_q prod. cross section ratio in quark parton model *(Korean)* 80−27466
additive quark parton model, hadronic fragmentation distribs. 78−8711
angular momentum, average for two-body system, lower bound 77−57514
asymptotic behavior of multiplicities in theories with Koba-Nielsen-Olesen scaling 78−78083
baryonic and electric charge distribs. in multiparticle prod., quark-parton model 77−79285
baryonium interactions, string model, dual amplitudes *(Russian)* 78−54620
bremsstrahlung model of Brodsky and Gunion, comments 79−93362
centauro, Geminion and multipion events, quark matter hadronisation, prod. cross sections 80−47331
central rapidity region, asymptotic and nonasymptotic energies, Reggeon field theory, nonleading terms 77−10185
CERN ISR, facility and hadron physics program review 80−873
charge transfer in multiparticle prod., quark-parton behaviour during collision 77−57490
charge transfer in the uncorrelated cluster production model *(Russian)* 79−40755
charged-particle multiplicities in high-energy collisions 77−34194
charm particles, inclusive production cross sections, correlating quark rearrangement model 79−54320
charm prod. cross section and particle lifetimes, Monte Carlo anal. 78−89679
charm production, mass scales, in deep inelastic processes, parton model, generalised VDM 77−13930
charmed meson productions in hadronic and EM hadron interactions 79−13143
charmed particle production, η_c, ψ and other $c\bar{c}$ bound states 80−63036
cluster model, field theoretic, multiperipheral production, Feynman scaling violation 80−57576
clusters in hadron multiple production processes 79−49545
complex momenta eikonal approx., hadron-nucleus collisions at asymptotically high energies *(Russian)* 78−74294
conference on hadron struct. and lepton-hadron interactions, Cargese, France (July 1977) 80−4473
cosmic ray hadron-nucleus high-energy interactions, models from slow particle characts. 79−80177
cosmic ray interactions, 10 to 100 TeV, anal. of emulsion chamber events 79−62705
cosmic rays, models of hadronic collisions rel. to EAS computer simulation 78−57415
diffractive bumps, gluonic excitation Regge trajectories from bag and dual models 79−2978
diffractive phenomena, review 77−57552
dihadron mass continuum and narrow resonance prod. in p-Be, 400 GeV interaction 78−33178
dilepton ang. distribs., QCD and quark model anal. 79−80801
dilepton prod. during hadronic collision space-time evolution, quark-parton model 79−2980
dilepton production and scaling 77−50031
dilepton production in hadronic collisions, review 79−49547
dimensional counting and Landshoff, multihadron reactions at large transverse momentum 78−33092

hadron-hadron interactions continued
dimuon continuum origin and space-time evolution of hadron collisions 77−88015
direct γ production at large p_T, high energies 77−71547
Drell-Yan annihilation, threshold effects and quark masses 77−54076
Drell-Yan conjecture in asymptotically free theories 79−17689
Drell-Yan contrib. to lepton pair prod., incident hadron $q\bar{q}$ correlation function 78−89668
Drell-Yan dynamics, lepton pair from $q\bar{q}$ collision, energy scaling breakdown 78−54610
Drell-Yan muon prod., QCD correction uniqueness 80−78032
Drell-Yan trigger, hadronic prod. of dilepton pairs and muons 78−37182
dual unitary approach of associated strange and charm prod. 77−41824
elastic quark-quark scatt. model, relations for hadron pairs 78−66092
electromagnetic pair prod., equivalent-photon method *(Russian)* 79−26353
EM corrections to hadron charge exchange and backward scatt. *(Russian)* 79−3028
exclusive, intermediate energies, parameter for transversity measurement 77−30398
extended particle model, dynamical theory of hadron interactions 77−87936
extended quark model, large p_T hadron prod. 78−29342
fireball dimension determ. in hadron collisions, Bose-Einstein correlations 79−22069
flavour transfer in quark and gluon exchange, Pomeron models 77−49917
forward hard scattering in hadron-hadron collisions in the energy region $\sim 10^{14}$ eV 80−86773
forward jet production meas. in high transverse momentum hadron-proton collisions 80−101989
four-hadron isobar model 79−26263
fragmentation as probe of hadron dynamics 78−45956
fragmentation processes, treatment in quark models 79−58940
generalised hydrodynamical models 79−89131
gluon fusion model, hadronic charm prod. 78−66081
hadron+hadron→meson+X, quark elastic scatt. as high transverse momentum meson source 77−57575
hadron+nucleus interactions, Fermilab energies, inclusive rapidity distribs., parton-cascade model 78−37252
hadron+nucleus interactions, yields of projectile fragments, quark model calcs., A-depend. 78−41499
hadron calorimeter expts., asymptotic power laws, QCD and parton model predictions 80−57560
hadron collective interaction, particle inclusive spectrum properties, space-time model 79−40808
hadron constituent model discrimination using large transverse momentum data 78−12881
hadron induced multiparticle reactions, S-1500 GeV, resonance prod. correlations, jet model *(German)* 80−91118
hadron production, multiplicity distribution, Regge like parton model *(Russian)* 80−78100
hadron-hadron, in H, AL, inclusive particle distribs., QCD predictions 80−99112
hadron-hadron 3-jet collisions, charge conjugation asymmetries and trilinear gluon coupling 80−105934
hadron-nuclei collisions, statistical mechanism of multiparticle prod. 77−46155
hadron-nucleon, correl. length between created particles, multiple prod. case *(Russian)* 77−6187
hadron-nucleon forward amplitudes, Reggeon exchange absorptive corrections 79−40765
hadron-nucleon inelasticity coeff., high energies, A-dependence *(Russian)* 77−6166
hadron-nucleus, absorptive part of scatt. amplitude, multiparticle prod., Glauber theory 78−37248
hadron-nucleus, pseudorapidity distribs., 24 GeV/c-4 TeV, energy and target depend. 80−91115
hadron-nucleus, rapidity distrib., 22.8, 50, 400 and ≳1000 GeV in emulsion, multiperipheral models 80−91117
hadron-nucleus (nucleon), relativistic secondary multiplicities, constituent quark rescatt. 80−63034
hadron-nucleus collisions at high energy, expt. data review 77−50120
hadron-nucleus fast interaction, particle density fluctuations *(Russian)* 77−6167
hadron-nucleus high energy reactions, multiple prod., parton-hadron cascade model *(Russian)* 78−17066
hadron-nucleus inelastic collisions, multiplicities, ang. distrib., hydrodynamic and parton models *(Russian)* 77−250
hadron-nucleus interaction, multiple particle prod., absorptive part of scatt. amplitude *(Russian)* 78−17164
hadronic atom, HN interactions, multiple scatt. expansion for level shifts 78−70978
hadronic bremsstrahlung models, ordinary and charge conserving, causality and unitarity breakdown 77−57486
hadronic large p_T reactions, K^+ and K^- prod. as model test, hard quark scatt. 79−40735
hadronic massive lepton pair prod., theory review, Drell-Yan model 78−89752
hadronic total cross sections, soft and hard components, model anal. 79−49546
hard collisions, calorimeter trigger, Ochs-Stodolsky scaling law derivation, parton model 79−17775
hard processes, large rapidity separation of baryonic number, partons, and dual topology 80−95255
hard scattering models, large transverse particle prod., cross section constraints from opposite side rapidity distribs. 78−29360
harmonic oscill. model, reson. total widths 77−38119
heavy quark mesons, inclusive hadronic prod. *(Russian)* 80−86770
high energy, impact parameter props. from σ_{tot}, σ_{el} data 77−6183
high energy collisions, variables and optical concepts, review 80−444
high energy hadron-nucleus interactions, mean slow particle multiplicity mass depend. 80−102081
high energy hadronic collisions, similarities, universality prop., reaction mechanism 78−33090
high energy inelastic collisions, product ang. distrib., semi-empirical formulae 79−54362
high energy inelastic hadron reactions, π prod., scaling law, fireball model 78−74287
high energy interactions and cosmic ray components in the atmosphere 79−62707
hadron-hadron interactions continued
high energy lepton pair prod. with pol. hadrons, P and C violations 80−99068
high-energy hadron-nucl. interactions 78−45957
high-energy hadronic collisions, classical space-time concepts 78−70420
high-energy inclusive spectra near phase-space boundary using quark fragmentation model 78−89658
high-mass diffraction in the supercritical region 79−22081
hydrodynamical description of the missing-mass clusters 79−71728
hydrodynamical model of multiparticle prod., scaling solns. 78−8616
Hypercharge-exchange reactions, exchange degeneracy breaking and Regge cuts 77−71494
inclusive $3\pi^-$ correlation functions, Mueller scheme with Bose-Einstein statistics 78−93915
inclusive cross section of symmetric hadron pairs produced, hard scatt., parton model and QCD 80−63052
inclusive lepton pair prod., invariated helicity struct. funcions anal. 79−13172
inclusive lepton pair prod., P violation, quark-parton model in Weinberg-Salam theory, QCD 80−37217
inclusive processes, large momentum transfer, quark counting, EM form factors 80−68498
inclusive processes, multiplicity and scaling, resonance production, additive quark model, SU(6) theory, review 80−63043
inclusive production of hadrons in particle-particle collisions at high energies, scaling low 78−54656
inclusive production of heavy particles, p_T depend. 77−22817
inclusive spectra of secondary pions, Feynman scaling and statistical model 80−42502
isobar model, angular crossing relations, Euclidean approx., meson+nucleon inelastic scatt. 79−13019
isospin-spin polarisations, dynamical characts. 80−32035
jet analysis, QCD calcs. and phenomenological models 80−52523
jet and lepton-pair production in high-energy lepton-hadron and hadron-hadron scattering 79−17729
jet struct. in hadronic lepton pair prod. ang. energy cross section, QCD 79−75806
jet structure, two-jet events, glueball-Pomeron identity, dual field theory 80−63051
jet structures of leptons, quarks and gluons, perturbative QCD, process dependence 80−68470
jet studies and large transverse momentum collisions, review 79−22143
jets, loading particles, in large transverse momentum events, quantum number effects 79−89198
KNO scaling, automodel behaviour of multiplicity distrib. as function of inelasticity factor *(Russian)* 79−89213
Kopylov-Podgoretsky-Cocconi formulation modification for hadron-hadron collisions 80−78044
large, small momentum transfer regions, transition point for s-depend. 77−30339
large p_T hadronic collisions, QCD sensitive test, quark and gluon jets 80−57647
large p_t inclusive interactions, scaling behaviour of γ/π prod. cross section ratio, models testing 77−50032
large p_T jet prod. in hadronic collisions, QCD calc. for inclusive cross section 78−86439
large p_T proton inclusive prod., quark-quark elastic scatt. 79−17773
large transverse momentum and large mass production in hadronic interactions review of theoretical models 79−89115
large transverse momentum particle and jet prod., QCD approach 79−17761
large transverse momentum processes, high energy collisions, review *(Russian)* 79−26351
large- and small-p_T production, momentum conservation events 77−71539
large-p_T reactions, transverse quark polaris., quantum chromodynamics test 79−17741
leading charge flow in high energy inelastic hadron collisions 77−50020
lepton and photon production in hadron collisions, review 79−405
lepton pair prod., thermal parton model 79−13075
lepton pair prod. in hadron-hadron collision 78−66138
lepton pair production, QCD and hard-scatt. model, spin-spin asymmetries 80−63014
lepton pair production, $q\bar{q}$ annihilation within same hadron, structure function anal. validity 80−57622
Lepton pair production cross section using Drell Yan formula, sum rules, moments 78−54611
lepton pair production in hadronic collisions, parton model and scaling approach 78−82150
lepton prod. with large transverse momentum, SU(6) parton model 78−89673
lepton prompt prod. in hadron collisions, cluster model, e/π ratios 77−2886
linear chain decay, pion coherence, Bose-Einstein symm. 77−49921
local thermodynamic equilibrium *(Russian)* 80−9155
low transverse momentum fragmentation processes, quark-gluon struct. of hadrons 80−22561
low-mass lepton pairs from hadron and neutrino beams, meson annihilation model 79−93401
massive μ pair prod. in hadron-hadron collisions, asymptotically free parton model 77−13936
massive μ pair prod. in hadronic collisions, ang. distrib, quark-partons+gluons model 77−82706
massive lepton pair transverse momentum distrib. in hadron collisions, QCD predictions 79−9391
mean charged multiplicity, energy depend., modified Heisenberg calcs. 79−40806
mean multiplicity of secondary particles in hadron-nuclear interactions, multiple scatt. theory *(Russian)* 80−68502
meson resonances, low energy, narrow 78−29341
Monte Carlo quark-parton model for multiparticle and low mass dimuon prod. 79−30697
multi-particle and inclusive reaction at high energies, review 79−17777
multi-particle production processes via hadron interactions, review 78−33024
multicluster production, multiplicity distribs., group-theoretical approach 77−2800
multiparticle data, reaction mechanism search and classification 77−88016
multiparticle prod. charge distribs. and fluctuations, Monte Carlo quark-parton model 79−93363

hadron-hadron interactions continued
multiparticle prod. in hadron-hadron collisions, scaling and multiperipheral model, review *(Russian)* 77−2875
multiparticle prod. in high-energy hadron-nucleon interactions 77−34192
multiparticle prod. in quark-parton model, Monte Carlo method 78−41607
multiparticle prod. long range correls. and parton model 77−82712
multiparticle production description by Chapman-Kolmogorov eqns. 78−12882
multiparticle production model for high energy hadronic collisions 79−80790
multiparticle production processes, correls. due to energy-momentum conservation, uncorrel. jet model 78−41601
multiperipheral theory, unitarity condition and Reggeon theory *(Russian)* 77−30348
multiple hadron production and struct. from 10 GeV to 10 TeV interactions 80−57653
multiple production of elementary particles, dispersion analysis *(Russian)* 77−30450
multiplicities in hadronic and current induced reactions, e^+e^- annihilation, clustering 77−46070
multiplicity, semi-empirical formula 78−58210
multiplicity dependence on impact parameter from elastic scatt. *(Russian)* 77−26544
multiplicity distribs., multicomponent description of energy depend. at high energy *(Russian)* 79−80859
multiplicity distribs. and normalised cumulants 77−38185
multiproduction on nuclei, nature of pomeron 77−87955
neutral-cluster model, charge-transfer distribs. in high-energy hadron collisions 77−82713
neutron stars, determ. from pulsars and compact X-ray sources 80−77442
non-Abelian gauge theory, colour model, high-energy hadron interactions 77−45973
nondiffractive, rescattering by dipole pomeron *(Russian)* 77−13947
nuclear high-energy collisions, hadronic mass spectrum 78−33049
nucleus+hadron, cluster model of hadronic interactions, intermediate energy secondary nucleons prod. *(Russian)* 78−17062
overlap function in high energy collisions of composite objects 77−6087
partial inelasticity coefficients in hadron interactions with various targets *(Russian)* 80−68483
particle ratios and lepton prod. at large p_T, parton model 77−67620
parton model, hard and soft processes in small p_T inclusive reactions 78−41599
parton model of large transverse momentum meson prod., logarithmic corrections to Bjorken scaling 77−71483
perturbative QCD, recent progress 80−42418
phase shifts, stability in spherically symmetric pot., Coulomb-strong interference 77−74237
photon and lepton hadroproduction, QCD test 79−17745
photon production, $AB\rightarrow\gamma\gamma X$, scaling and quark mass dependence, quark parton model 80−73749
polarised hadron-hadron high-$p_\perp$ collisions, weak effects 77−30457
polarization phenomena in hadronic reactions, review 80−52527
Pomeron, low-energy, coupling to hadron energy-momentum tensor trace 77−18248
pomeron building mechanism, in fragmentation region 78−89687
pomeron current model for diffraction dissociation 78−4843
Pomeron two-gluon exchange model, quark counting, hadron-size effects for total cross sections 77−57495
prompt lepton sources from hadronic collisions 80−73726
proton-hadron high energy collisions, hadron struct. 79−67614
QCD, hadronic charm production, cross section and charmed quark mass 79−36017
QCD, jet production, large transverse momentum 80−42503
QCD analysis of jets recoiling against large transverse momentum muon pairs 79−9416
QCD and Feynman-x depend. of lepton pairs produced in hadron collisions 79−36036
QCD and short range nuclear phenomena 80−91060
QCD appl. to meson and jet prod. 79−45076
QCD hadronic μ pair prod., gluon gauge depend., struct. func. calc. 79−80810
QCD prediction for ang. distrib. of dileptons in hadron collisions 79−26300
QCD quark-gluon plasma, hadronic prod. of leptons, photons and ψ *(Russian)* 78−89672
QCD quark-gluon plasma, hadronic prod. of leptons, photons charm and ψ 78−89669
QCD test, prod. of heavy quark flavours in hadronic interactions 77−45957
quantum chromodynamics, hadroprod. of lepton pairs and real photons 78−50056
quantum number distribs. and fluctuations in multiparticle prod., quark-parton model 78−82249
quark attenuation and recombination in nuclear matter, hadron-nucleus reactions 80−52601
quark fragmentation function, determ. of parameters 80−13261
quark fragmentation functions for inclusive hadron production, Regge formalism 80−68462
quark recombination mechanism in multi-hadron production 80−18114
quark-parton cascades in nuclei and secondary hadron spectra from hadron-nucleus collisions *(Russian)* 80−57623
rapidity distribution symmetry axis in hadron-hadron and hadron-nucleus collisions 77−57569
Regge complex-pole model 77−41871
Reggeon calculus, hadron-nucelus total and inelastic cross-sections 77−34193
relativistic self-trapping of hadrons 78−21405
s-channel resonance model based on peripheral resonances, exotic peaks 80−91069
s-channel unitarity correl. of elastic scatt. and inclusive k_T^2 distrib. 79−26258
scale invariant variable *(Russian)* 78−82227
scaling law, universal 80−18082
scaling law in strong interactions 78−41606
selection rule as extension to OZI and FWR rules 78−29343
sequential decay model for hadron-hadron multiparticle prod., appl. to nuclear matter 78−46021
small p_T hadronic collisions, jets, quark, fragmentation universality and rising rapidity plateaus 79−40734

hadron-hadron interactions continued
soft hadron-nucleus collisions, two chain parton model description 80−82944
soft hadronic collisions and fragmentation on nucl. targets, quark dynamics 79−22063
soft hadronic processes, quark-parton model test for inclusive cross sections 79−17776
soft photon expansion and theorem, bremsstrahlung cross section 79−17728
space-time description of hadronic diffraction 77−87960
strange and charm particle prod., conserved vector currents for gluons 77−74617
strong interactions, introductory book using potential theory 77−223
structure function relations, lepton pair processes at large transverse momenta 78−82214
subnuclear structure concept via dilepton prod. in hadronic collisions, historical review 79−93365
temperature origin in high energy strong interactions, large transverse accel. 78−37186
temperature parameter for thermal-like emission spectra, fluctuations 80−68482
three hadron systems, resonance peaks, Brayshaw mechanism validity 80−73732
three large p_T jets, hadronic prod., perturbative QCD anal., processes and formalism 80−42508
total cross section, anal. of Pomeron-f complex 78−483
transverse momentum behaviour of hadrons, multihadron systems, and lepton pairs 79−45121
transverse momentum distribs., small and large p_T behaviour, new particle-wave duality 79−45081
transverse quark polarization in large P_T reactions and e^+e^- jets 79−63410
tranverse-momentum spectra, mass depend. calc. 78−45958
two-particle correlations involving neutral strange particles, at 250 GeV/c 78−82242
uncorrelated jet model at high energy, quantum statistics, soft pion prod. 78−16995
universal multihadron jets, quark interactions 77−38132
vector meson inclusive prod. cross section in hadron-nucleon collisions, parton transversal motion *(Russian)* 79−67617
vector meson production, 6 GeV, anomalous interaction mediator, e^+e prod. data anal. *(Chinese)* 77−67664
violation of Feynman scaling, central region, fragmentation, mixed two component model 77−26551
wave packets and the space-time structure of production processes 79−36048
weak interactions, right handed currents effects in QCD 79−13016
$B\rightarrow\psi X$, weak decay predictions, B identification in hadronic collisions 79−93408
D-meson emission, two-gluon charm form. *(Russian)* 77−71489
$D\bar{D}$ production in large p_T hadronic collisions, $e\mu$ and eK correlation study 79−40772
e/π ratio at low p_T in high energy hadronic collisions, possible $Q\bar{Q}\rightarrow e^+e^-X$ mechanism 79−71687
e^+e^- pair prod. calc., high energy internal conversion of bremsstrahlung photons 79−420
$hh\rightarrow\mu^+\mu^-$+jet+X, QCD anal. of recoiling jets and angular effects in large q_T pair prod. 79−45078
$h_1h_2\rightarrow l\bar{l}X$, massive lepton pair prod., polarisation and spin effects 80−105929
$hN\rightarrow\gamma(\mu^+\mu^-)$+jet+hadrons, gluonic jets, prod. mechanism *(Russian)* 79−58986
J/ψ, inclusive production cross sections, correlating quark rearrangement model 79−54320
μ pair prod., QCD ang. correl. 78−49976
μ pair production in hadron-hadron collisions, gluon effects, QCD predictions 78−78148
$\mu^+\mu^-$ prod., QCD high energy predictions using methods of cut vertices 79−89128
$\mu^+\mu^+$ production, small transverse momentum distrib., QCD soft gluon bremsstrahlung effects 79−75723
$q\bar{q}\rightarrow g\mu^+\mu^-$, large q_T muon pairs ang. distribs. in perturbative QCD 79−85275
Be+hadrons, 200 GeV/c, high transverse momentum jets and single particles 77−61329

hadron-hadron scattering
see also baryon-baryon scattering; hadron-hadron interactions; meson-baryon scattering; meson-meson scattering
additive eikonal quark model anal. of various hadron-hadron cross-sections 77−26493
asymptotic theorems, review *(Czech)* 78−29357
axiomatic restrictions on scatt. amplitudes, quantum theory 78−32967
colour distribution in high p_T qq scatt., colour singlets 80−4940
correlational anal. of inelastic hadronic processes, multicluster mechanism *(Russian)* 78−89684
diffraction scattering, convergent polynomial expansion, scaling 79−45096
diffractive, determ. of density oscillations within hadrons 77−22689
diffractive phenomena, review 77−57552
eikonal model of hadronic matter distribution of particles and nuclei 79−26317
elastic hadron-hadron diffraction scatt. processes, scaling, conformal mapping without spurious cut 80−82992
elastic scatt. systematics at high and intermediate energies 77−22717
EM corrections to hadron charge exchange and backward scatt. *(Russian)* 79−3028
extrapolation method for perturbative expansion of S-matrix, high energy hadron collisions, ϕ^4 model calcs. 78−394
fermion scattering, comment on radiative corrections in large Higgs mass limit 79−67557
geometrical model for scatt. at ultrahigh energies, existence of dips 79−89191
geometrical models, energy depend. anal. 77−41806
gluon fragmentation, polarised 80−82988
hadron-hadron total cross-sections to 300 GeV/c, phenomenological anal. 77−38206
hadron-proton amplitudes, real parts from 3-universality 77−49926
hadronic colour induced Van der Waals force consequences 78−45863
hadronic diffraction, elastic scatt. as tunnelling phenomenon, dual model relation 80−57575

hadron-hadron scattering continued
hadronic high momentum transfer scatt., spin meas. and polarisation review 79−63498
hadronic interiors, meas. and charge distrib., hadronic diffraction scatt. 80−73817
high energy hadron-hadron scatt., Jost-Lehmann-Dyson representation, light cone singularities 78−17049
iteration models, elastic reactions beyond diffraction peaks 78−93839
large angle, power automodel asymptotic behaviour *(Russian)* 78−17050
large angle elastic factorisation in quark model *(Russian)* 77−57497
large momentum transfer behaviour in two-body scatt., hadron quark struct. 77−22690
large-angle scattering, quasi-potential approach, pre-asymptotic effects 80−68484
low energy scatt., anal. of internal quark-gluon eigenstates, Wigner-Eisenbud formalism 79−63525
polarisation meas. at high energies 78−884
proton-hadron elastic scatt., Chou Yang droplet model anal., form factors 78−21464
quark dynamics in low energy hadron-hadron scatt. 79−93366
quark model discrete mass eigenstates and hadron-hadron low energy scatt. 80−42415
radiative corrections in charge-exchange and backward hadron scattering 79−17727
rescattering by dipole pomeron *(Russian)* 77−13947
s-channel unitarity correl. of elastic scatt. and inclusive k_T^2 distrib. 79−26258
scaling of differential cross sections, model independ. aspects 77−256
SU(1,3), dynamical group for non-charmed hadron scattering states 80−62883
supersymmetry, field theory, fermion (meson)-meson scatt., high energy behaviour 79−295
t-channel diffractive scatt., elastic peak and hadron size 79−45083
three-hadron physics, book 77−45980
total absorption model extension to include phase and spin 77−57507
two-body SU(3) quark model for all angles 77−49916
two-component Pomeron and hadron total cross-sections 79−17697
unitarity relation, corrections to soln. for hadron elastic scatt. amplitude *(Russian)* 77−74723
waveparticle duality, hadron constituents 80−9136

hadron interactions *see hadron-deuteron interactions; hadron-hadron interactions; lepton-hadron interactions; photon-hadron interactions*

hadron leptoproduction
see also baryon production; hadron electroproduction; meson production
anomalous current fragmentation in high-$p_\perp$ leptoproduction 79−13134
asymptotically free gauge theories, scaling violations in leptoproduction 78−4769
charm production, mass scales, in deep inelastic processes, parton model, generalised VDM 77−13930
current induced reactions, conf. 77−34106
deep inelastic hadron leptoproduction on nuclei, inclusive hadron final states 78−54741
deep inelastic hadronic final states, sum rules, quark parton model 77−87981
deep inelastic lepton-hadron scatt., semiinclusive hadron prod., quark fragmentation function corrections, QCD 80−63013
deep inelastic leptoprod., ang. energy flow, perturbative QCD predictions 80−9176
deep inelastic leptoproduction, normalising the renormalisation group anal., QCD twist effects 80−86690
deep inelastic leptoproduction data, Wilson coeffs. from struct. functions 77−61292
deep inelastic leptroproduction, meson bound state contrib. to σ_L/σ_T 80−78029
diquark jets in leptoprod. and large p_T reactions, fragmentation functions 78−82149
fragmentation functions of heavy quarks into hadrons, ν reactions, e^+e^- annihilation appls. 79−3013
hadron final states in deep inelastic processes, parton model 77−34128
inclusive leptoproductions, scaling violation, colour-octet model effect 79−13077
jet fragmentation universality in lepton processes 78−434
jet production mechanism in lepton-hadron interactions, cascade and uncorrelated jet models 80−52516
large Q^2 transverse quark polaris., quantum chromodynamics test 79−17741
lepton+hadron, deep inelastic scatt., QCD event states, 3-jet events 80−52515
lepton+nucleon, jet analysis, QCD calcs. and phenomenological models 80−52523
lepton+nucleon, jet structure, cascade model and jet model 80−42471
lepton+nucleon, quark and gluon jets, Breit frame, QCD 80−62995
lepton-hadron relation, neutrino induced dimuon and trimuon events 78−25032
nuclear leptoproduction, phenomenological model 79−63660
nuclear targets, quark-nucleon inclusive cross section, heavy lepton pairs 80−57607
nucleus+lepton, coherent and inclusive prod. of hadrons with low P_T, Coulomb excitation and decay of projectile 80−83100
perturbative QCD, $\sigma_s(q^2)$ meas. in deep inelastic scatt. 80−4949
QCD, leptoprod. and Drell-Yan processes beyond leading approx., Bjorken scaling 79−6323
QCD and jets in leptoproduction 79−45059
QCD calc. of three-jet processes in leptoprod. and hadronic μ-pair prod. 78−21338
QCD perturbation theory and final-state jet measures 79−89117
QCD predictions for inclusive and semi-inclusive leptoprod., hadron ang. distribs. 79−13041
QCD predictions for jet transverse momentum in leptoproduction 79−63442
quark cascade model, appl. to meson spectra in e^+e^- annihilation 78−41482
quark fragmentation functions in inclusive hadron muoproduction 79−67565
quark fragmentation into mesons, statistical model, vector meson contrib. 78−54639
scale breaking parton model for electron and neutrino deep inelastic scatt. 78−66122
spin-depend. leptoproduction, light-cone model 77−2772

hadron leptoproduction continued
target-mass effects in hadronic lepton-pair production, hadronic mass corrections to Drell-Yan formulae 79−89139
totally inclusive leptoprod., scaling anal., target mass corrections in QCD parton model 80−102052
universal multihadron jets, quark interactions 77−38132
$e\bar{e}\rightarrow\gamma\gamma\rightarrow q\bar{q}$ 79−49531
$e^+e\rightarrow e^+\pi^+\pi^-\gamma$, virtual electrons bremsstrahlung photon, Feynman diagrams, Weizsacker-Williams approx. 80−52484
e^+e^-, jet analysis, QCD calcs. and phenomenological models 80−52523
e^+e^- annihilation, multihadron prod., phenomenology 77−34170
$e^+e^-\rightarrow$hadrons reson. struct. in 1700-1950 MeV region 77−65164
in deep inelastic scattering, quark jet as trigger for gluon jet 80−62996
$lp\rightarrow l'hX$, azimuthal depend., parton model calc. 78−93887
$\mu^\pm$-nucleus 150 GeV deep inelastic scatt. in nuclear emulsions 79−17893
$\mu N\rightarrow\mu\psi X$, diffractive and non-diffractive ψ leptoprod. in QCD 80−424
$\mu^-N\rightarrow$hadron shower, charm-pair production effects 80−73748
μp deep inelast. scatt., DD 50-250 GeV EM corrections, *(Russian)* 78−25048
$\mu p\rightarrow K_s^0X$, 225 GeV, deep inelastic scatt., strange neutral particle prod. 80−105902
$\mu p\rightarrow\Lambda^0(\bar{\Lambda}^0)X$, 225 GeV, deep inelastic scatt., strange neutral particle prod. 80−105902
ν deep inelastic scatt., four flavour quark model, asymptotic freedom 78−45905
$\nu(\bar{\nu})$ interactions, charm model of weak interactions, parton model anal. 77−6106
$\nu(\bar{\nu})N$, 30-100 GeV, invariant-mass struct., possible new hadron prod. 77−2816
$\nu(\bar{\nu})N$, hadronic system charged particle multiplicities and transverse momentum distribs. 78−78165
$\bar{\nu}$-nucleus charged current interactions 79−22275
$\bar{\nu}N$, neutral current charm particle prod. search 80−22600
$\nu N\rightarrow$hadron shower, charm-pair production effects 80−73748
$\bar{\nu}p$ charged current jet size, comparison with e^+e^- jets 80−22599
$\tau\rightarrow\nu_\tau+$hadron(s), decay modes and ν_τ-mass 80−63057
$Ne+\nu_\mu(\bar{\nu}_\mu)$, inclusive prod. of hadrons, preliminary data 78−89853

hadron-nucleus reactions
see also hyperon-nucleus reactions; meson-nucleus reactions; nucleon-nucleus reactions
backward production on nuclei and the tube model, comments 80−52544
baryonic inclusive spectra in hadron-, photon- and HI-nucleus collisions, fireball model 80−86892
cascade model, space-time model, extension to photon- and lepton-nucleus collisions 80−68633
charged particle multiplicities, description unification 79−75986
cluster cascade model, single particle distributions and two-particle correlations 80−18300
collective tube model, multiparticle prod. off hadrons and nuclei 80−5112
cosmic ray hadron-nucleus high-energy interactions, models from slow particle characts. 79−80177
cosmic ray interactions, 10 to 100 TeV, anal. of emulsion chamber events 79−62705
cumulative hadron production off nuclei, parton recombination model 79−71773
deep inelastic electro-creation by polarised vector mesons *(Russian)* 80−102209
Drell Hiida Deck mechanism for particle dissociation on a composite target 79−93465
emulsion nuclei, 50-400 GeV/c, multiparticle prod., multiple scatt. model anal. 79−67782
emulsion nuclei, He nuclei emission in 7.5 to 200 GeV hadron interactions *(Russian)* 80−9325
existence of slowly moving sources, vel. depend. frictional sources 79−6690
fast proton backward emission mechanism *(Russian)* 79−63706
Fermi model for high multiplicity compound nucleus decay 80−22799
Fermilab energies, inclusive rapidity distribs., parton-cascade model 78−37252
fireball cascade model analysis of multiparticle production on nuclei 79−89283
hadron-hadron, in H, AL, inclusive particle distribs., QCD predictions 80−99112
hadron-nucleus (nucleon), relativistic secondary multiplicities, constituent quark rescatt. 80−63034
hadron-nucleus interaction, multiple particle prod., absorptive part of scatt. amplitude *(Russian)* 78−17164
hadron-nucleus interactions, secondary particle multiplicity, one-cluster model *(Russian)* 78−17165
heavy nucleus, coherent and inclusive prod. of hadrons with low P_T, Coulomb excitation and decay of projectile 80−83100
high energy, secondary particle multiplicity distrib. anal. *(Russian)* 79−59095
high energy, simple space time description, zero parameter model 80−47479
high energy collisions, book contrib. 79−21889
high energy hadron-nucleus interactions, inclusive prod., quark-quark elastic scatt. model 78−45858
high energy hadron-nucleus interactions, mean slow particle multiplicity mass depend. 80−102081
high energy hadronic collisions, similarities, universality prop., reaction mechanism 78−33090
high energy particle interactions on nuclei, review 80−42658
high energy reactions, multiple prod., parton-hadron cascade model *(Russian)* 78−17066
high-energy, correlation between fast target protons and hadron+nucleon collisions 78−41681
inclusive π, N spectra in high energy hadronic reactions, d fragmentation region *(Russian)* 78−54809
inclusive inelastic scatt. in phase space, quantum thoery 80−32247
independent particle model, extension to spectator-participant model for central heavy ion reactions 80−73861
inelastic diffraction, antishielding phenomenon *(Russian)* 79−97734
KNO scaling, automodel behaviour of multiplicity distrib. as function of inelasticity factor *(Russian)* 79−89213
leading particle spectra on nuclear targets and multi-chain model 80−73829
massive lepton pair production as a test of models for particle production on nuclei 80−102213

hadron-nucleus reactions continued
mean effective mass number for big hadron model, knock-out proton and pion contamination 79−63704
mean multiplicity of secondary particles in hadron-nuclear interactions, multiple scatt. theory *(Russian)* 80−68502
mean normalised multiplicity target depend. at high energy 80−47454
multi-chain model, recoil nucleon effect 80−83124
multihadron production in nuclear matter and hadron struct., space-time description, review *(Russian)* 80−68571
multiparticle production, multiplicities, cross sections and ang-distribs. 80−86768
multiparticle production model for high energy hadronic collisions 79−80790
multiparticle production of nuclei, intranuclear cascading of secondaries 78−66262
multiple production, expt. results, review *(Russian)* 79−3118
multiplicity distrib. in hadron-nucl. collisions 78−62514
multiplicity of relativistic charged particles, 20-400 GeV *(Russian)* 80−5191
nucleus+hadron, cluster model of hadronic interactions, intermediate energy secondary nucleons prod. *(Russian)* 78−17062
optical pot. eqns. for low and moderate energies *(Russian)* 80−63214
projectile fragment yields, quark model calcs., A-depend. 78−41499
proton inclusive spectra in nuclear high energy collisions 78−70557
pseudorapidity distribs., 24 GeV/c-4 TeV, energy and target depend. 80−91115
QCD and short range nuclear phenomena 80−91060
QCD hard scatt. off nuclear targets 79−63444
quark attenuation and recombination in nuclear matter, hadron-nucleus reactions 80−52601
quark-parton cascades in nuclei and secondary hadron spectra from hadron-nucleus collisions *(Russian)* 80−57623
quark-parton model *(Russian)* 79−22066
quasielastic cluster knock-out, multiplicities 78−46042
rapidity distrib., 22.8, 50, 400 and ≳1000 GeV in nuclear emulsion 80−91117
secondary particle multiplicity distribution in nuclei, 200 and 800 GeV *(Russian)* 78−89879
soft hadron-nucleus collisions, two chain parton model description 80−82944
soft hadron-nucleus reactions at high energies, theoretical model 79−17870
soft hadronic collisions and fragmentation on nucl. targets, quark dynamics 79−22063
spatial temporal development, nuclear hadronic cascades 80−63040
super high energy, pseudorapidity distrib. characts. 80−5170
total cross-sections, moments of nucl. densities 78−78252
transverse momentum distrib. of secondary hadrons *(Russian)* 78−29444
universal descript. of ang. distrib. 78−17188
virtual mesons effect on hadron-nucleus reactions, book contrib. 80−472
nN in nuclei, 200 GeV/c, inclusive backward prod., collective tube model 80−47338

hadron-nucleus scattering
see also hyperon-nucleus scattering; meson-nucleus scattering; nucleon-nucleus scattering
absorptive part of scatt. amplitude, multiparticle prod., Glauber theory 78−37248
diffraction cross-sect., effects of centre of mass correls. 78−93977
elastic scatt., explicit formula in eikonal approx. 80−42665
fast proton backward emission mechanism *(Russian)* 79−63706
Glauber amplitude corrections *(Russian)* 78−41683
Glauber model, implications for inelastic hadron-nucleus scatt. 79−75930
Glauber model anal. of hadron scatt. probe of neutron density 78−66196
Glauber model leading corrections, Watson multiple collision series summation 79−85557
high energy particle interactions on nuclei, review 80−42658
isoscalar dipole strength excitation in GQR region by inelastic electron and hadron scatt. 80−47448
meson exchange current effects 79−26380
mesonic degrees of freedom 79−26412
multiple, enhancement of Bose-Einstein symmetrisation effects 78−58271
multiple scattering nature, experimental test proposal 79−63702
planar diagrams and appl. of Abramovsky-Gribov-Kancheli relations *(Russian)* 79−93670
reggeon parton spacetime struct. Koplik-Mueller paradox *(Russian)* 80−42730
virtual mesons effect on hadron-nucleus reactions, book contrib. 80−472
$(\alpha,\alpha X)$, 1 GeV/N, inclusive hadron-nucleus cross-sections, multiple scatt. series 80−13519

hadron photoproduction
see also baryon photoproduction; meson photoproduction
baryon resonances, EM transitions, multipole moments in single quark transition model 80−62985
baryon resonances and electromagnetic couplings 79−9384
baryon spectroscopy and photoproduction couplings using new baryon wavefunctions 80−102016
bubble chamber expts., use of laser beams 77−38521
charm photoprod. with linearly pol. photons, QCD calcs., gluons 80−68464
charm production, mass scales, in deep inelastic processes, parton model, generalised VDM 77−13930
diffractive high energy processes, review, book contrib. 80−47309
double equivalent-photon approx. *(Russian)* 79−403
hadron EM interactions, book 80−46748
high p_T hadronic jet photoprod., QCD anal., quark and gluon jets 80−42474
higher order QCD jets in photoproduction 80−99087
jet struct. at large transverse momentum 78−82225
large $p_\perp$ photoproduction, gluon fragmentation function extraction, scaling 80−105853
large p_T inclusive photoprod. and hard scatt. model 79−9417
nondiffractive processes, review, book contrib. 80−47313
nuclear shadowing, hadron photoproduction on nuclear targets H-U, 1.0 to 10.5 GeV 77−82748
photons, effect of large intermediate masses in hadron-mediated photon-nucleus interaction 80−27625
QCD, photoprod. of heavy quark flavours 78−21384
resonance, EM decay and excitation, review, book contrib. 80−47300

hadron photoproduction continued
resonance region, experimental review 77−22738
rising hadronic cross section effects on EM processes, generalised vector dominance formulation 78−93868
shadowing in hadronic photoproduction cross section in C, Cu, Pb, 20 to 185 GeV 79−30823
total cross sections for E>4 GeV, review 78−78186
total cross-section, VDM and Lipkin's 'third component' 77−82745
vector boson pair photoprod., theoretical cross sections 80−57610
$\bar{c}c$ $\bar{q}q$ states, decay, hadronic and photo-prod., e^+e^- annihilation prod. 80−99092
$\bar{D}^0$ prod. and decay in high energy photon interaction, mass and decay time 80−42478
e^+e^- collisions, jet prod. and two-photon annihilation, hadron spectra 80−91121
$e^+e^-\rightarrow e^+e^-+2$ jets, $\gamma\gamma\rightarrow q\bar{q}$ contrib. to cross section, QCD corrections 80−78106
$e^+e^-\rightarrow e^+e^-qg(q\bar{q})+$ jet, $\gamma\gamma$ initiated 3 jet events in QCD 80−102057
e^+e^- initiated $\gamma\gamma$ processes, charged pair prod., $f^0\rightarrow\gamma\gamma$ width 80−91123
$\gamma^*\gamma^*\rightarrow 2$ jets in e^+e^-, parton model QCD corrections for doubly deep processes 80−73758
$\gamma\gamma$ collision, deep inelastic, helicity method 80−22606
$\gamma\gamma\rightarrow$hadrons, 1-5 GeV, hadron prod. cross sections 80−37315
γN, exclusive photoprod. reactions, Okubo-Zweig-Iizuka rule 80−95277
γN, inclusive pion production due to $\gamma q\rightarrow\pi q'$ process, quark-parton model *(Russian)* 80−78073
γp cross-section observed increase, jets as source, QCD and vector-meson dominance model 80−22620
$\gamma p\rightarrow h^+X$, large p_T photoprod., perturbative QCD test 80−37276
$\gamma p\rightarrow h\bar{X}$, quark jet model and total cross section 79−13133
$\gamma p\rightarrow\pi^+n$, 600-1875 MeV, pol.p and γ, G and H polarisation parameters 80−99105
$\gamma p\rightarrow X$, strong interaction model anal., review, book contrib. 80−47310
$\gamma\pi$, hadron photoprod. and saturation of sum rules *(Russian)* 79−49529
Λ-multi π peaks in photoprod. data, charmed baryon weak nonleptonic multibody decay interpretation 77−34153
μ^+N, 280 GeV/c in Fe, Ψ virtual photoprod. 80−37279
$\rho'(1600)$ meson resonance from 2- and 4-pion distribs. in photoproduction data 80−95279
C, total hadronic photoprod. cross sections, 12-30 GeV 79−9379

hadron production
see also baryon production; hadron leptoproduction; hadron photoproduction; meson production
annihilation cross section of $e^+e^-\rightarrow$hadron near $N\bar{N}$ threshold *(Russian)* 79−85311
asymptotic behavior of multiplicities in theories with Koba-Nielsen-Olesen scaling 78−78083
bremsstrahlung, grand partition function determ. 78−33041
C Ne+$\nu_\mu(\bar{\nu}_\mu)$, inclusive distrib. of produced hadrons 78−89854
cascade model, comparison with hadron prod. in quark fragmentation region 79−22065
charged current ν and $\bar{\nu}$ interactions, hadron prod. at high energy, quark parton model 79−36058
charged-particle multiplicities in high-energy collisions 77−34194
charmed particle prod. by neutrinos, light-cone algebra 77−18274
cluster concept in multiple hadron prod. 78−66177
coherent prod. at 200 GeV/c in π-nucleus 77−18360
composite model of quarks, large P_T hadron prod. 78−62472
correlation integrals, partially exclusive 77−71550
cosmic ray hadron families, characts. calc. rel. to elementary act model depend. 79−80160
cosmic ray high-energy gamma-quantum and hadron families, Monte Carlo studies 79−80158
cosmic ray showers, ang. distrib. and multiplicity 78−36412
cosmic-ray-nucleus reactions, hadron multiple prod., muon time-correl. meas. *(Russian)* 77−14133
cumulative production on nuclei, mechanism *(Russian)* 77−6332
density of produced particles, hadron- and nucleus-nucleus collisions in quark model 77−67681
dihadron prod., A depend. of prod. cross sections for massive dihadron states 78−33180
dihadron production spectra prediction using quark model and Chao-Yang statistics 79−89124
Drell Hiida Deck mechanism for particle dissociation on a composite target 79−93465
elastic quark-quark scatt. model, relations for hadron pairs 78−66092
EM mass differences and struct. 80−27502
extended quark model, large p_T hadron prod. 78−29342
factorization breaking in deep inelastic neutrino hadron production in perturbative QCD 79−80820
Feynman scaling, multihadron prod. through intermediate reson. 78−78152
Feynman-Wilson gas, statistical model for multiparticle physics 79−22071
fragmentation in quark combinatorics, hadron prod. processes *(Russian)* 78−89671
gluon-gluon interactions, hadron prod. and σ(total) growth at high energies 80−91049
hadron+hadron, cluster model, field theoretic, multiperipheral production, Feynman scaling violation 80−57576
hadron+hadron, jet analysis, QCD calcs. and phenomenological models 80−52523
hadron+hadron inclusive cross section of symmetric hadron pairs produced, hard scatt., parton model and QCD 80−63052
hadron+nucleus interactions, yields of projectile fragments, quark model calcs., A-depend. 78−41499
hadron EM interactions, book 80−46749
hadron inelastic scatt., secondary hadron multiplicity distribution, Regge like parton model *(Russian)* 80−78100
hadron interactions, inclusive, large momentum transfer, quark counting, EM form factors 80−68498
hadron interactions, local thermodynamic equilibrium *(Russian)* 80−9155
hadron mean charged multiplicities, universality in particle and nuclear collisions 77−54086
hadron-hadron collisions, fragmentation processes, treatment in quark models 79−58940
hadron-nucleus collisions, transverse momentum distrib. of secondary hadrons *(Russian)* 78−29444

hadron production continued
hadron-nucleus inelastic collisions, multiplicities, ang. distrib., hydrodynamic and parton models *(Russian)* 77−250
hadronic phase transitions, evidence from present data phenomenology 79−45006
high-energy, multi-eikonal theory 77−6098
high-energy cosmic-ray components in atmosphere, scaling features 78−93062
high-energy hadron-nucl. interactions 78−45957
hydrodynamic model, scaling and logarithmic multiplicity of secondary hadrons *(Russian)* 77−10221
inclusive and semi-inclusive scaling-in-the-mean functions 78−4880
inclusive hadron and lepton prod. in statistical model 77−18353
inclusive hadron poduction, quark fragmentation and triple Regge models, quark decay functions 80−62921
inclusive processes, multiplicity and scaling, resonance production, additive quark model, SU(6) theory, review 80−63043
inclusive production of large-transverse-momentum hadrons and hadron pairs 79−89310
inclusive spectrum produced at large-transverse-momentum *(Chinese)* 78−12935
jet phenomenon and Lorentz deformation 80−105806
jet prod., Lorentz deformation 80−27420
jet studies and large transverse momentum collisions, review 79−22143
KNO scaling for high-energy multiplicity distribs., distrib. functions 77−18237
large p_T hadron jets, correlating quark rearrangement model 79−2997
large p_T hadron prod. off nuclei, QCD parton model, nucleus as gluon filter 79−89110
large p_t hadron production, lowest subprocess model, two body reactions 78−4887
large p_T production and hard rearrangement of quarks 79−63454
large Q_T transverse momentum lepton pairs and hadron jets prod., reaction mech., perturbative QCD 79−2999
large- and small-p_T production, momentum conservation events 77−71539
long-range correl., overlapping independent emission 78−82141
many-hadron production at low $P_\perp$, basic concepts and models, review 79−6331
multihadron production in matter connection with hadron quark-glue model 79−356
multihadron production in nuclear matter and hadron struct., space-time description, review *(Russian)* 80−68571
multiparticle data, reaction mechanism search and classification 77−88016
multiparticle production of nuclei, intranuclear cascading of secondaries 78−66262
multiple generation processes, multiparticle correlations *(Russian)* 79−75807
multiple hadron generating models, transition to KNO scaling *(Russian)* 79−22051
multiple hadron production and struct. from 10 GeV to 10 TeV interactions 80−57653
multiple prod. on ^{2}H, rescattering anal., parton model 77−87945
multiplicity distrib. scaling law at high energies 77−54083
multiplicity of particles produced in hadron-nucleus high-energy interactions 78−4933
multiproduction on nuclei, nature of pomeron 77−87955
neutral-cluster model, charge-transfer distribs. in high-energy hadron collisions 77−82713
nonleading particles, inclusive prod. distrib. 77−2880
nonperturbative QCD effects at large momentum transfers, e^+e^- annihilation to hadrons 78−82226
nuclear collisions, hadron prod. in quark-parton model 78−12868
nuclear high-energy collisions, hadronic mass spectrum 78−33049
from nuclei incoherent-multiple-collision effects 77−50037
nucleus+hadron, coherent and inclusive prod. of hadrons with low P_T, Coulomb excitation and decay of projectile 80−83100
ocean, neutrino detection by nonlinear sound generation by hadron showers 80−36465
polarisation in hadron cumulative prod. and large transverse momentum processes *(Russian)* 78−74293
pp collisions, high energy, fireball mass, rapidity, spin distribs. 80−57645
QCD, hadron prod., large-transverse-momentum correl. 79−63438
QCD, hadron prod. at large transverse momentum 77−87949
QCD, hadroprod. of heavy quark flavours 79−22062
QCD, high P_T hadron prod. in pionisation region and vacuum singularity *(Russian)* 80−86772
QCD gluon contribs. to large p_T reactions 78−41504
QCD hadron jets, branching processes, multiplicity distrib., KNO scaling *(Russian)* 80−101998
QCD jets, Markov branching processes 80−27463
QCD multijet model, universal quark-jet fragmentation in soft hadronic reactions 80−13285
QCD perturbation theory, quark decay functions, heavy hadron prod. 78−62364
QCD predictions for large p_T hadron prod. by polarised hadrons 78−82148
quantum cluster decomposition of hadronic final state, stochastic theory of multiple hadron prod. 78−41507
quantum number distribs. and fluctuations in multiparticle prod., quark-parton model 78−82249
quantum particles in a stochastic linear potential and the temperature of hadrons 80−32087
quark colour correlations *(Russian)* 79−93382
quark fragmentation functions for inclusive hadron production, Regge formalism 80−68462
quark jet fragmentation 79−45063
quark-parton cascades in nuclei and secondary hadron spectra from hadron-nucleus collisions *(Russian)* 80−57623
quark-parton distributions model, large transverse momentum hadrons, logarithmic scale breaking 78−16989
quark-parton model, with scaling violations, large p_T processes anal. 78−45927
quarkonium decay, gluon jets and gluonic resonances, QCD test 78−93841
relativistic nuclei collisions, multi-hadron prod. mechanism 80−57763
rescattering frm deuteron, rel. to momentum form. time rise *(Russian)* 80−52528
RPA scheme in multihadron production processes, high energy, strong correls. 78−41506
s-dependence of proton fragmentation by hadrons, 30-250 GeV/c 78−74291
s-dependence of proton fragmentation by hadrons 4-24 GeV/c 78−74290
scale-invariant solution in hydrodynamic theory of multiple production *(Russian)* 78−45896
secondary hadron multiplicity distribs., hadron prod. mech. universality test *(Russian)* 79−93477
sequential jet decay described by an Inonu-Wigner contraction of the Lorentz group 79−17695
shower particles average number in 300 GeV p-nucleus emulsion interactions 77−50018
statistical theory of hadron multiple prod. *(Russian)* 77−67625
stream generation by quarks and gluons, transverse impulse *(Russian)* 79−85280
string junction model, large p_T hadron prod. 78−62380
SU(2) quark diagram struct. of prod. amplitudes 77−22662
temperature of hadronic spectra and black solitons 77−26498
thermodynamical quark bootstrap, hadron prod. 77−30336
topological approach to high-energy large transverse momentum interactions 79−22057
two photon processes, manifestation strength of colour below and above colour threshold 80−381
uncorrelated-jet model at large-p_T, momentum conservation role 77−54082
universal multihadron jets, quark interactions 77−38132
d target, deformation of mass spectrum of hadronic system *(Russian)* 79−93394
e^+e^- annihilation, expts. at LEP 79−97613
e^+e^- annihilation, jets, colour-singlet subsystems, large rapidity gaps 80−68469
$e^+e^-\rightarrow e^+e^-(\mu^+\mu^-)(\tau^+\tau^-)$, high energy colliding beams, Mark J detector study 80−95282
$e^+e^-\rightarrow$hadrons, 53 GeV^2, $\pi^\pm$ and $K^\pm$ cross sections, scaling 78−78201
$e^+e^-\rightarrow$hadrons, high energies, two-fireball model, jet problem *(Russian)* 77−82756
$e^+e^-\rightarrow$hadrons, neutral weak current effects 77−49987
$e^+e\rightarrow$hadrons, weak interaction effects, ang. distrib. charge asymm. baryon longitudinal polarisation *(Russian)* 77−30397
e^+e^- inclusive annihilation, many-hadron final states 78−29339
$K^-p\rightarrow\Sigma^-\pi^+(\Sigma^+\pi^-)(\Lambda\pi^+\pi^-)$, study in K^-d bubble chamber, in the c.m. energy range, 1.6-1.74 GeV 80−13331
μN scattering, 2.8-4.5 GeV, struct. functions and charge ratios 78−74264
μp charged current interactions, hadron production, quark-parton model comparison 79−40769
μ^+p inclusive hadron distribs., scaling props., quark-parton fragmentation 77−61296
$\nu_\mu(\bar{\nu}_\mu)$N, prod. of hadrons with new quantum numbers, quark parton model *(Russian)* 77−82735
$\bar{\nu}_l$l→hadrons, amplitudes, cross sections, V-A theories 77−10239
νN→hadron+hadron neutral current prod. in Weinberg model *(Russian)* 77−6111
$\nu p\rightarrow\mu^-$+jet, greater than 10 GeV, jet props. 79−45084
p-nucleus shower particle multiplicity distribs. at 6.2-300 GeV. scaling hypothesis 77−50019
pN collision, 200 GeV/c, production of long-lived hadrons and leptons, antinuclei production 80−13342
pN→hadron shower, charm-pair production effects 80−73748
pp, 200, 300, 400 GeV, hadron prod. at large p_T invariant cross section 79−40926
$p\bar{p}$, hadronic jets, possible intermediate bosons 80−18149
pp, jet thrust spectrum, 3-jet structure, QCD calc. 80−47333
pp, multihadron production, gluon matter hadronisation 79−45047
pp hadron prod. at large p_T, multiplicities, quark model *(Russian)* 77−262
pp→hadrons, phase transition in Feynman-Wilson analogue fluid, multiplicities, plateaux, cross-sections 80−73744
pp→hadrons, scaling violation in fragmentation region in quark model, 10^6 GeV *(Russian)* 79−3051
pp interaction two-body correlations at high-energy 77−54124
pp interactions, hadron prod. 23.4 to 63.4 GeV, charged multiplicity density for various p_T 78−70414
pp interactions, multiplicity distributions associated with charged hadron prod., ISR energies 79−3053
pp→pX, 205 GeV/c, leading p spectrum, random walk hypothesis, geometric bremsstrahlung model 80−68493
pp→π+X, high p_T jet prod., QCD perturbation theory 79−89209
pp rapidity distrib., rising plateau from longit. phase-space 77−88017
pp→$W^\pm\gamma$X, mag. moment parameter meas. 79−97640
π^-n, 40 GeV/c, two-particle charged and γ rapidity correls. 77−18335
π^-p, charged multiplicity with strange particle prod., 4.9 to 205 GeV/c 77−18334
π^+p, angular correl. reson. prod. effect at 16 GeV/c 77−88014
Be+p, 400 GeV/c, two hadron correlation at large transverse momenta 78−46060
Be+p, high mass symmetric hadron and pion pair prod., scaling props. 79−22291
Be+p collisions 400 GeV, meas. of dihadron mass continuum and search for narrow resonances 78−33178
Be(p,X), 200, 300, 400 GeV, hadron prod. at large p_T invariant cross section 79−40926
Be(p,X), 400 GeV/c, nucleon number depend. of inclusive dihadron prod. 79−49626
Be(p,$h^\pm$), 200 to 400 GeV, inclusive production of large-transverse-momentum hadrons and hadron pairs 79−89310
^{2}H+p, 200, 300, 400 GeV, hadron prod. at large p_T invariant cross section 79−40926
Pb(p,X), 400 GeV/c, nucleon number depend. of inclusive dihadron prod. 79−49626
Ti(p,X) 200, 300, 400 GeV, hadron prod. at large p_T invariant cross section 79−40926
W(p,X) 200, 300, 400 GeV, hadron prod. at large p_T invariant cross section 79−40926
Y→3g, angular patterns and front-back moments, QCD 80−73702

hadron scattering *see hadron-deuteron scattering; hadron-hadron scattering; lepton-hadron scattering; photon-hadron scattering*

hadronic atoms
see also mesic atoms
absorptive line shape hadronic atoms 77−83767
antiprotonic, black sphere model for line widths, WKB approx. 77−14618
antiprotonic atoms, X-ray transition energies, strong interaction and $\bar{p}$ mass meas. 78−25759
antiprotonic atoms of light nuclei and isotopes, $\bar{p}$-n strong interaction effects 78−29867
antiprotonic H, meas. on bound $N\bar{N}$ systems 79−68336
antiprotonic H atoms, first obs. of L X-rays 78−90111
Coulomb levels shift *(Russian)* 79−45870
education, hadronic atom strong interaction induced level widths and shifts, WKB calc. 77−78923
hadronic colour induced Van der Waals force consequences 78−45863
level shifts, multiple scat. expansion 78−70978
low-energy hadron-nucleus interaction theory 78−70977
momentum space method for hadronic atoms including relativistic hadron-nucleus reactions 79−872
nuclear interactions of strange particles and resonances, conf. Warsaw, Poland (Ict. 1976) 78−70406
pionium, isospin anal. of energy shifts 78−62961
$p\bar{p}$ atom, ground state energy displacement *(Russian)* 79−89813
protonium, atomic X-ray yields 1s and 2p level shifts and widths, cascades, calc. 80−78730
protonium annihilation widths from coupling channel boundary condition model 79−36803
review, significance of exotic atoms to particle physics 78−9282
sigma atoms, strong shifts, atomic level widths, decay modes 79−86083
$\bar{p}$ atoms, meas. on bound $N\bar{N}$ systems 79−68336
$\bar{p}p$, isospin anal. of energy shifts 78−62961
$p\bar{p}$ atom, influence of $n\bar{n}$ channel on props., nuclear level shifts *(Russian)* 80−69270
$\bar{p}p$ nP bound states, black sphere model for linewidths 78−42252
$p\bar{p}$ system, possible evidence for narrow bound states below threshold, mesonic struct. 78−62443
$\pi\mu$, production and detection from K_L^0 decay 79−81306
Σ^- atoms, meas. of strong interaction effects 78−42251
Σ^- atoms 79−93452
Σ^- hyperonic atom, nuclear capture rate calcs. using $\Sigma^- p \rightarrow \Gamma n$ amplitude 78−62962
ΣN effective complex pot. from Σ-atoms and scatt. lengths 80−57717
H, isospin anal. of energy shifts 78−62961
H-quark interaction, var. method calcs. 78−37771
He with bound quark, atomic spectral lines calc. 79−86092
^{3}He, isospin anal. of energy shifts 78−62961
^{4}He-$\bar{p}$, X-ray spectrum, energies and relative intensities for 3d and 2p levels 78−70979

hadrons
see also baryon resonances; baryons; hadron classification schemes; hadron current; hadron decay; meson resonances; mesons
absolute stability, quark mixing and discrete symm. considerations 78−33036
abundance of stable particles prod. in early Universe 79−44653
charmed hadron masses, from effective quark masses, sum rules 80−4965
closed systems with nonconservative internal forces, Lie admissible quantisation, hadron struct. 80−37174
cosmic ray flux composition at mountain altitudes *(Russian)* 80−61973
cosmic ray hadron interactions, transverse momenta at 10^{14} to 10^{15} eV in Pamir expt. 79−80170
cosmic ray hadron-nucleus high-energy interactions, models from slow particle characts. 79−80177
cosmic ray hadrons, ultrahigh energy interactions scaling deviations and modified models 79−80172
cosmic ray hadrons of tens of TeV energies, energy characts. of gamma-ray quanta produced 79−80148
cosmic rays EAS, hadron component sensitivity to fragmentation range in inclusive spectra 79−84614
diffractive dissociation model, quark states 79−75752
distribution of masses of leptons and hadrons 80−99093
dynamical theory of quark confinement and hadron spectrum 77−82701
EAS, burst size and hadron energy, Durham array obs. 77−73917
EM characteristics, bag model *(Russian)* 79−93380
extended hadrons, Lorentz deformation props., O(4) and light-cone coordinate systems 80−68354
extended hadrons, stochastic description 78−431
form factors, axiomatic local constraints *(Russian)* 78−58190
form factors, structure functions and charge radii from parton model *(Russian)* 79−93381
form factors in quantum chromodynamics, asymptotic form *(Russian)* 78−17021
form factors in terms of inelastic Jost functions for hadrons consisting of quarks 77−2831
geometrical approach 80−91065
gravitational collapse of hadron system, rel. to contraction of closed oscillating Universe *(Russian)* 80−4466
gravitational interaction, band spinor representation of GL(n,R) 78−50000
hot hadronic matter in early universe, relativistic eqn. of state 78−45438
lh theory of leptons and hadrons, unification in GA_{4R} gauge 80−86639
light hadronic spectroscopy, expt. and quark model interpretations, review, book contrib. 80−68438
magnetic dipole transition, quark anomalous mag. moments *(Russian)* 80−82975
mass sum rules, SU_3 subalgebras of SU_6, quark flavours 80−9152
microstructure, relativistic quantum dynamics inside de Sitter microuniverse 80−27480
multilocal fields in relativisitic quantum field theory 78−37125
new elementary particles, quark and composite models *(German)* 80−57570
non-ideal hadron gas, eqn. of state appl. to universe Friedmann model *(Russian)* 79−44649
nontopological solitons, hadron appl. 80−47191
parton struct. and diffraction scatt. for soft processes 79−344
proto-matter hadronic nature from ang. momentum-mass relation for cosmic bodies 80−77528

hadrons continued
QCD model, asymptotically free field theory, anomalous dimensions of composite particles 80−73665
relativistic harmonic oscillators and hadronic struct., 1st year graduate quantum mechs. 78−61971
relativistic non-ideal hadron gas universe, gravit. collapse *(Russian)* 79−44650
rotational states 80−22596
solitons, nontopological, and appls. to hadrons 78−32968
space-time properties, unified gauge theory of gravitational and strong interactions 80−95016
spin, relation to isospin, strangeness and charm 80−37183
spin 1/2 wave equations irreducible under Poincare group, degenerate to Dirac eqn. 78−21332
strong gravity, field equations, strong interactions, de Sitter microsphere idea of hadrons 80−68111
structure functions for quarks, gluons, hadrons in QCD 79−54318
superfluidity, anisotropic, of hadronic matter, analytic formulation 80−105869
superheavy, instantons in quark plasma *(Russian)* 79−36039
wave-particle duality, hadron constituents 80−9136
Yang-Mills pots., Van der Waals force and fermion motion 80−52465

haemodynamics
see also blood
abdominal cavity organs, circulation hydrodynamics in presence of extracoporeal perfusion 77−29172
adrenocortical steady-state characts., blood flow and ACTH conc. 77−81517
ambulatory blood pressure recording in man, transducer and perfusion system 79−53271
aneurysm, pulsatile pressure and flow distrib. using latex fusiform models 77−21547
aneurysm detection using bioacoustic signal processing techniques 78−28120
angiograms, digital, comparison of methods of meas. blood flow *(German)* 79−39468
angiography, computerised, anal. and visualisation of blood dynamics and motion of organs 80−8170
animal research, totally implantable directional Doppler flowmeters 80−67293
antipyrine, radioiodinated, prep. and stability for use in local blood flow determs. 80−94366
aorta, dog, simulation via adaptive model 79−11964
aorta, root of, functional anatomy and deform. props. 80−67136
aorta entrance, flow anal. 78−69124
aorta model, canine, finite element soln. of Navier-Stokes eqn. 79−29550
aorta model, two chambered, viscoelastic, press. estimation in ascending and descending aorta 78−77076
aortic and mitral valve prostheses, in vitro flow visualisation 77−86703
aortic arch atherosclerotic formations effect on blood mass flow distrib. 80−16995
aortic arch principle separation region, depend. on freq., amplitude and rate of flow 77−52831
aortic blood pressure, harmonic signal anal. by computer 77−52899
aortic coarctation distal flow profiles 78−44528
aortic concave-convex pivoting disc valve prosthesis, hydrodynamic evaluation 79−84027
aortic dynamics in man, analogue simulation model 78−80903
aortic flow at zero load in myocardial ischaemia 77−37003
aortic leaflet valve prosthesis, optimal design and longevity anal. 77−90958
aortic pressure meas. using intact unmodified intra-aortic balloon 78−31844
aortic regurgitation rel. to thoracic impedance cardiogram, dog expt. 77−40890
aortic shear stress reduction by cardiac pacing 78−40239
aortic stenoses modelling 79−79581
aortic stenosis, expt. model, turbulent vel. meas. 77−21550
aortic stenosis, turbulent wall press. meas. in exptl. model 78−3538
aortic valve, closing behaviour, model 79−53170
aortic valve, human, finite element stress analysis 77−44699
aortic valve, vortex motion and induced pressures 79−62288
aortic valve model time-depend. laminar incompressible flow through spherical cavity 77−9217
aortic valve opening, haemodynamics 78−20208
aortic valve prostheses, hydrodynamic losses eval. 80−72378
aortic valve prosthesis, Hancock porcine xenograft, comparison of models 242 and 250 77−56532
aortic valve prosthesis, Reul-Ghista optimal tri-leaflet, in vitro performance tests 79−92432
aortic valve prosthesis, wall shear stress in Bjork-Shiley and Starr-Edwards types in vitro *(German)* 78−81067
aortic valve prosthesis water hammer pulse effect *(Japanese)* 78−3676
aortic valve replacement with subcoronary ball valve, early expts. 77−56524
aortic zero-load flow, sensitivity and afterload independence 77−56394
apexcardiogram, math. model of endogenous thoracic forces 78−31849
arterial, US meas. of velocity patterns, using pulsed Doppler velocity meter 78−15855
arterial bifurcation, steady convective diffusion model 77−21546
arterial bifurcation models, viscous energy dissipation for steady flow 78−40218
arterial blood flow, one-dimensional unsteady eqns., soln. by method of characts. 79−92251
arterial blood flow, shock wave formation, math. model 79−5305
arterial blood pressure, indirect noninvasive automatic meas. device 77−44771
arterial blood pressure, non-invasive transducer for continuous meas. 77−44817
arterial blood pressure noninvasive monitoring by US imaging and phono cuff-sphygmomanometry 80−36180
arterial blood pressure preprocessor 79−83979
arterial branchings models, laser ultramicroscopic investig. of three-dimens. flow 78−35876
arterial compliance, elec. analogue of variable compliance 80−41097
arterial curvature sites anal. of unsteady component of pulsatile flow 77−56408
arterial diagnosis, appl. of impedance plethysmography 77−56508
arterial diameter meas. using US transit-time micrometer 78−7410

haemodynamics continued
arterial dynamics, model of multilayered shell with fluid flow 77−29171
arterial dynamics in mammals, similarity principle 78−44532
arterial elasticity, transcutaneous assessment by US Doppler flowmeter 77−77948
arterial elasticity determ. and transcutaneous continuous pressure monitoring analysis 79−53179
arterial flow, bifurcating flow model 79−55418
arterial flow lipid transport model 78−44552
arterial haemodynamic transfer function calc. from Doppler US flowmeter waveforms 78−61235
arterial haemodynamics evaluation using venous US catheter-tip technique 77−44730
arterial impedance estimation, systemic, from cardiac catheterisation data 78−11691
arterial impedance plethysmographic signal quantitative interpretation 79−57742
arterial insufficiency detect. and quantification using impedance plethysmograph 78−31957
arterial mean pressure, effect of changes on short-term pressure wave struct. 79−29539
arterial models, preparation method for flow studies *(German)* 79−53166
arterial pathology discrimination from angiograms 79−16274
arterial physio/pathological data from transcutaneous CW Doppler-shifted US 77−44731
arterial pressure automatic determ., using microprocessor based instrument, Dinamap 78−96108
arterial pressure automatic indirect monitor 80−56231
arterial pressure modulator for perfusion circuit of isolated organ *(French)* 78−81004
arterial pressure regulation rel. to baroreceptor Na sensitivity 77−48818
arterial pressure waves, physiological interpretation of spectra, heart rate, respiration waves 79−29540
arterial pressure-flow relationships in anaesthetised dog 78−69120
arterial pulsatile blood flow, linear theory *(Chinese)* 79−39427
arterial pulse wave vel. meas. by Doppler shifted US and EM flowmetry 78−69229
arterial pulse waves, effects of transmural press. and muscular activity 80−104616
arterial steal haemodynamics 80−101206
arterial stenoses, fluid mechanics 80−35948
arterial stenosis, in vivo and model expts., flow-induced wall vibrs. 78−3535
arterial stenosis, math. model 80−72202
arterial stenosis and stenotic atherosclerosis, dynamic press.-flow diagrams 80−3658
arterial stenosis detection by transcutaneous pulsed Doppler method 77−44732
arterial stenosis model, pulsatile flowfield downstream 80−17001
arterial stenosis models, initiation of turbulence, steady and pulsatile flow 79−79577
arterial system, elastic non-uniformity using hydraulic model 77−29164
arterial system, forward and backward wave calc. 79−57697
arterial system and cardiac activity, optimum tuning model *(German)* 79−16225
arterial system characterisation in time domain 78−40213
arterial system impulse response determ. 79−79594
arterial system least energy regulation 78−53434
arterial system math. model, press.-flow relationships 78−53435
arterial system model validity, quantitative evaluation 80−61599
arterial system nonlinear model validation 79−96600
arterial system total compliance computer from input impedance 80−41096
arterial systolic blood pressure monitoring, circulation model 77−60224
arterial tonometer, microprocessor based 78−31955
arterial US scanner, colour coded differential velocity display 79−34617
arterial vasa vasorum deformation/hydraulic resist. study *(Japanese)* 78−3544
arterial vein grafts, acute and chronic studies of vel. profiles 77−52832
arterial velocity flow system, transmission-line model 77−44715
arterial wall axial deformation and anisotropy obs. 79−83833
arterial wall empirical linear response models 77−90831
arterial wall motion determ. using Doppler US system 78−15876
arteries, small, isolated, perfused, method for simultaneous elec. and mech. recording 80−101300
arteries with longit. ridges, flow field and mass transport anal. 77−44702
arteries with nonlinear elastic modulus, press. pulse propag. 78−44550
arteriosclerotic flow models, velocity fluctuation and shear stress obs. *(German)* 79−16226
artery, finite deform. elastic model, large amplitude oscills. 77−37000
artery, math. model for calc. of flow from measured press. 78−31831
artery avascular region O transport analysis 77−40691
artery pressure-radius relationships, comparison of elastic tube models 77−64077
artery pressure-radius relationships, comparison of theory and expt. for rubber tube 77−64078
artificial, blood pumps, leaflet valve manufacturing technique *(German)* 79−84002
artificial circulation system electrical control *(Spanish)* 78−3680
artificial exchange organ, effect of flow channel thickness on surface-induced blood damage 79−39439
artificial heart, atrial charact. estimation using analogue simulation 77−44846
artificial heart, control system, anal. of effectiveness of algorithm using aortic blood press. as regulated parameter 80−3864
artificial heart, driven by automatic driving system 78−7541
artificial heart, non-invasive determ. of instantaneous cardiac output and dynamic performance 77−44845
artificial heart, pneumatically driven, cardiac output meas. 78−44729
artificial heart, simulation of fluid dynamics *(Japanese)* 79−43954
artificial heart, transfer function governing ventricular ejection in assisted circulation 80−104817
artificial heart and assisted circulation apparatus, hydrodynamic test bench rigs 79−48372
artificial heart blood pump ventricle, mech. driven, visual study of flow field 77−56539
artificial heart test system, simulation of artificial ventricle and mock circulatory system 77−52933

haemodynamics continued
artificial heart valve, butterfly type with occluder, canine exp. results 77−81665
artificial heart valve closing element surface pressure distrib. 79−57811
artificial heart valve element, visual representation of flow *(Russian)* 77−32926
artificial kidney, evaluation using systems anal. 78−36074
artificial kidney, extracorporeal blood correcting unit 78−7535
artificial kidney, single-needle dialysis, factors affecting blood flow 78−31972
artificial kidney, wearable, monitoring instrumentation 77−64154
artificial mitral valves, insufficiency, press. and work losses *(German)* 78−88764
artificial organ blood manifold hydrodynamics and thrombotic problems 79−79588
artificial ventricle, all-pneumatic system, cardiovascular dynamics simulation 78−81082
assisted circulation, phase control, biological triggering signals 77−78044
assisted circulation methods and apparatus, classification 77−81653
atherogenesis, haemorheology-fluid dynamical factor *(Japanese)* 80−12171
atherogenesis at branching sites, steady laminar flow field 77−21553
atherosclerosis, simulated, US assess., in-vitro and in-vivo comparisons 79−96639
atrial and/or arterial blood pressure servo control in expt. animals 78−31986
atrial contraction, model anal. of contrib. to ventricular filling 80−85424
atrial pacing stress test quantification, normal, abnormal values, coronary artery disease in man 78−85449
atrio-aortal left ventricular bypass, haemodynamics in calf *(German)* 78−88763
auxiliary blood circulation pump, electronic control circuit 77−78050
baroreceptor activation reactivity to noxious stimulation reduction, hypertension implications 80−61596
Baylor left ventricular bypass pump, calf expts. 78−73295
beagle pup haemodynamic changes associated with growth, US obs. 77−25505
beat-to-beat stroke volume estimation from pulmonary arterial pressure contour 79−53178
bifurcation, particle paths and stasis in unsteady flow 78−20206
bifurcation pressure measurements, glass models 79−25021
bioengineering, international conf., Cape Town, S.Africa (April 1977) 79−20695
Bjork-Shiley aortic prosthesis, in vitro vel. meas. using laser-Doppler anemometer 80−17196
blood circulation simulation development 77−66825
blood flow, renal, using externally monitored ^{131}I-hippurate uptake 77−2036
blood flow in artery, pulsatile flow 80−106845
blood flow measurement, UDP-30 arterial US pulse Doppler flowmeter 80−104805
blood flow measurement by US Doppler method, computer-aided determ. of angles *(German)* 78−80931
blood intermittent pump with linear motor drive *(German)* 79−5401
blood pressure, industrial noise effects on man, cardiovascular disease risk factors 79−5321
blood pressure, volume, heart rate and cardiac function regulation *(Japanese)* 77−40688
blood pressure control model 77−21557
blood pressure control system dynamic behaviour identification 79−2097
blood pressure instruments, direct systolic/diastolic meas., review 78−69234
blood pressure instruments, noninvasive arterial meas. using US Doppler effect 78−69167
blood pressure monitor/conditioner, noninvasive cuff device 77−73605
blood pressure transducers, technical evaluation 79−44002
blood pump, pulsatile, stabilisation of unsteady ball valve motion 78−44708
blood pump implantations in animals, regulation mechanisms in circulation and fluid balance *(German)* 78−81064
blood stream meas., use of US probes and Doppler technique *(German)* 79−2113
blood ultrafilter design analysis 77−64152
blood velocity measurement, instantaneous, ultrasonic Doppler system appl. *(Dutch)* 78−31832
blood velocity noninvasive meas. in large vessels, broadband pulsed Doppler US system 78−61224
blood-flow velocity estimation, Kalman filters for Doppler ultrasonic meas. 79−62325
body tilts, passive, forearm and finger blood flow responses 80−8084
bone, healing fracture, blood flow rel. to ^{85}Sr uptake 80−72187
bone blood flow, meas. with a ^{133}Xe washout method 80−72288
bone blood flow determ., comparative study of $^{99m}TcO_4$ and ^{131}I-iodo-antipyrine 78−28046
bone imaging radiopharmaceutical local accumulation model 78−24127
bone revascularisation processes study method, local blood flow dynamic anal. using ^{85}Sr 80−81684
brachial arterial pressure, monitoring by modified phono-sphygmomanometry procedure 77−2065
brachial artery blood flow measurement, noninvasive ultrasonic Doppler technique 77−86570
brain, radioisotopic activity, 4-dimens. reconstruction using 200-element detector array of Ge 78−11732
brain blood flow display on colour TV using computerised picture processing technique *(Swedish)* 77−44780
brain blood flow meas. in the cat 79−83887
brain capillary, microkinematic obs. of blood velocity *(Russian)* 79−5366
brain O_2 and CO_2 tension dynamics, math. model 77−36965
brain O_2 transport, nonlinear Monte Carlo simulation, hybrid computer implementation 78−40131
branch-to-trunk area ratio, effect on transition to turbulent flow, cardiovascular system appls. 80−67108
branching vessels, flow visualisation using water model 77−25477
breast tumour detection by US Doppler blood-flow signals 80−46001
bubble detection and flow evaluation 79−34612
burnt skin heat and water losses, thermal modelling 78−31790
canine cardiovascular changes associated with age, US obs. 77−25504
capacitoplethysmography for heart and lung meas. *(Japanese)* 78−53465

haemodynamics continued
capillary blood flow, long-term effects of ^{60}Co gamma and fission spectrum neutrons, mouse 78−80927
capillary blood flow and transcapillary fluid exchange, methematical model 77−29173
capillary blood volume flow determ. by improved photoplethysmograph, Hemorheograph 78−31934
capillary flow conductivity index dependence, calc., approx. method *(German)* 78−7376
capillary permeability determ. from multiple indicator data, effects of finite red cell permeab. 78−44483
capillary-tissue diffusion in multicapillary system, anal. 79−2095
cardiac, left ventricular mural force changes rel. to myocardial pump performance 80−8092
cardiac, prostheses problems *(French)* 79−34590
cardiac assist devices, in-series, digital afterload phase angle controller 77−44843
cardiac assist system, intrathoracic, self-sufficient instantaneous haemodynamic control 77−44842
cardiac assistance, in-series, by intra-aortic balloon pumping, haemodynamic responses, computer model 79−96711
cardiac assistance, performance criteria for optimisation 79−74782
cardiac bidirectional shunt quantification, thermodilution method 80−3837
cardiac blood flow meas., computerised system 80−36051
cardiac blood flow visualisation, clinical usefulness of US pulsed Doppler technique *(Japanese)* 79−96638
cardiac contraction dynamics study 78−44523
cardiac effects of increased lung vol. and decreased pleural press., man 80−41073
cardiac ejection fraction and wall motion, comparison at rest and during isometric exercise 80−30857
cardiac function, reliability of noninvasive methods for meas. during exercise 79−16231
cardiac in-series assistance using balloon pump, effects on left ventricular afterload/aortic power dissipation 78−3669
cardiac left ventricle blood flow field off-line computation from Doppler US velocimetry 79−62324
cardiac left ventricular ejection fraction from gated images count rate 79−29605
cardiac left ventricular function obs., radioisotope angiography 79−74749
cardiac muscle mechanics, relation with zero-load aortic flow 79−29548
cardiac output, influence on intrapulmonary shunt 80−8086
cardiac output and blood flow meas. using indocyanine green and microspheres 77−77925
cardiac output and right ventricular residual fraction determ. with rapidly responding pH sensor 77−40860
cardiac output and shunt calc. from dye dilution curves using automated catheterisation system 78−81023
cardiac output and shunts, automatic computation from indicator dilution curves 79−48359
cardiac output calculations by N_2O technique, corrections for press. and temp. 77−16948
cardiac output computerised monitoring by transthoracic admittance plethysmography *(Japanese)* 77−86693
cardiac output control mechanism modelling *(Japanese)* 78−69133
cardiac output determ. by Stewart-Hamilton method, computer algorithm 77−86691
cardiac output estimation by N_2O rebreathing method in adults and children 77−12953
cardiac output estimation during exercise by rebreathing technique, automated system 77−37090
cardiac output estimation from aortic pressure curves, simulation model 79−53177
cardiac output estimation from isotope dilution and residue detect., time-varying flow and vol. effects 80−101194
cardiac output flow wave calculator *(Japanese)* 77−70489
cardiac output meas. by US transoesophageal probe 79−92315
cardiac output measurement, continuous electronic thermodilution meas. 77−40859
cardiac output measurement, in vitro comparison of six commercially available thermodilution systems 78−77135
cardiac output measurement, simplified saline conductivity method 79−92318
cardiac output measurement, tracer transport model accounting for recirculation 77−36978
cardiac output measurement error due to nonuniform dye distrib. 77−36979
cardiac output regional distrib., non-invasive determ. using ^{201}Tl 78−31890
cardiac pacing, symposium, Tokyo, Japan (Mar., 1976) 77−81666
cardiac probe, microprocessor-based, for gated equilib. and beat-by-beat left ventricle function 79−62396
cardiac response sensitivity to time relationship between vibr. and cardiac cycles 77−56407
cardiac shunt detection with the short-lived radioactive gases 80−94357
cardiac stroke volume and systolic time interval adjustments during bicycle exercise 80−3679
cardiac stroke volume meas. from impedance, rel. to aortic flow waveform 77−86522
cardiac synchronised augmented pulsation pressure concept, prototype 77−78058
cardiac valve dynamics, fluid physics appls. *(French)* 79−34589
cardiac work, anal. using general energy equation of thermodynamics 78−20207
cardio-pulmonary system, thermal indicator heat and mass transfer, pulsatile flow 79−25018
cardio-pulmonary system, thermal indicator heat and mass transfer, pulsatile flow 79−25017
cardiology, radioisotope sequential meas. of ventricular vols. and cardiac output 80−94319
cardiopulmonary readjustments in passive tilt 80−56084
cardiopulmonary stress test data acquisition and control systems 79−79673
cardiopulmonary stress testing in children 80−30911
cardiosynchronisation method for assisted circulation apparatus, problems 78−7534
cardiotomy circuit, factors affecting haemolysis 78−36073
cardiovascular and respiratory system dynamics *(French)* 79−34585
haemodynamics continued
cardiovascular computerised modelling, pressure regulation in hypertension 79−88098
cardiovascular computerised monitoring in medical intensive care unit 78−20304
cardiovascular control dynamic test method evaluation, model considerations *(German)* 77−52813
cardiovascular effects of positive-pressure ventilation in normal subjects 80−41081
cardiovascular flow disturbance, US detection 77−60231
cardiovascular flow disturbance detection by pulsed US Doppler velocimeter autocorrelograms 77−25526
cardiovascular function, effects of normal and loaded spontaneous inspiration 80−56088
cardiovascular measurements, conf., Bellingham, USA (Sept. '78) 80−31419
cardiovascular modelling of pressure regulation effects, hypertension 77−73539
cardiovascular modelling to study effects of pressure regulation: hypertension 79−25027
cardiovascular monitoring in the coronary care unit 78−20308
cardiovascular parameters correl. with freq. components of oesophageal phonocardiogram 77−52836
cardiovascular response to acute aquatic and treadmill exercise in the untrained rat 80−8085
cardiovascular shunts, detection and quantitation with commonly available radioisotopes 80−94356
cardiovascular simulator for the undergraduate physics laboratory 79−84889
cardiovascular system, analogue circuit and compartmental model, normal and defective states 79−57700
cardiovascular system, early adaption to simulated zero gravity 80−3827
cardiovascular system, haemodynamic obs. in awake rabbits during hyperbaric He-O_2 exposure 80−101200
cardiovascular system, identification and parameter estimation 80−35947
cardiovascular system, mathematical models and identification problems 80−89780
cardiovascular system as fluid cct., elec. network analogue 80−30759
cardiovascular system simulation by elec. compartmental model 79−5388
carotid arterial disease evaluation using noninvasive photoplethysmography 78−40390
carotid arteries, normal and stenosed, local Doppler audio spectra 80−30811
carotid artery disease, blood velocity analysis during pulsed Doopler US imaging 77−29189
carotid artery disease, US detection techniques 79−11989
carotid artery imager, CW Doppler US and spectrum analyser 79−57731
carotid artery Na kinetics 3-compartment model, incorporation of diffusion effects 78−27996
carotid artery occlusive disease detection, by supraorbital photoplethysmography 77−40731
carotid artery pressure, noise-resistant trigger cct. 77−48889
carotid back pressures in conjunction with cerebral angiography 80−98119
carotid bifurcation scanner, differential velocity display with colour coding 77−21588
carotid bifurcation tomographic scanner, US Doppler colour coded vel. display 77−25529
carotid obstruction detect. by supraorbital opacity pulses 80−51200
carotid thrombosis, canine model, ^{131}I fibrinogen for clot detect. 78−85363
carotid-vertebral circulation exam. by variable range-gated directional Doppler technique 77−29188
Casson fluids flow in non-circular ducts, appl. to haemodialyser 79−20563
catheter flow probe for left ventricular source parameters meas. 79−92324
catheter pressure meas., transducer smearing correction using microprocessor based discrete deconvolution 80−67275
cell-vessel wall interaction, fluid dynamic aspects 80−97998
central venous pressure and blood volume distrib., abdominal pressure model 79−92282
centrifugal blood pump for cardiac support 78−44709
cerebral angiography, brain O_2 tension response, using animal model 77−52872
cerebral angiography, cortical pO_2 and K^+ dynamics rel. to contrast agent neurotoxicity 78−35954
cerebral artery walls, rheoencephalogram parameters vs. mech. props. 78−3547
cerebral bifurcations geometry, human, effect of static distending press. 80−94259
cerebral blood flow, atraumatic meas. by ^{133}Xe *(French)* 77−37039
cerebral blood flow, colour functional imaging 77−5067
cerebral blood flow, confidence limits with positron emission tomography system 79−11994
cerebral blood flow, linear computer model 79−92288
cerebral blood flow, meas. in pig by ^{133}Xe clearance technique 80−94421
cerebral blood flow, regional distrib. during exercise in dogs 80−101197
cerebral blood flow, tissue pO_2 and pCO_2, continuous and simultaneous meas. 79−57829
cerebral blood flow, total and regional, effect of cerebral extracellular fluid acidity 80−67123
cerebral blood flow and O_2 uptake, correl. with dominant EEG freq. 77−5095
cerebral blood flow automated analyser for ^{133}Xe studies 77−86597
cerebral blood flow computer for use in angiogram theatres 78−73227
cerebral blood flow control in hypercapnia, model 79−100641
cerebral blood flow determination, computer assisted method for multi-exponential curve fitting 78−20246
cerebral blood flow dynamic charact. in sinusoidal hypoxia, goat 79−100652
cerebral blood flow dynamics, computer model 79−83837
cerebral blood flow estimation in newborn infant, noninvasive technique 77−90949
cerebral blood flow meas., lateral counting corrections 79−8536
cerebral blood flow meas., regional, computer program description 77−5098
cerebral blood flow meas. in animals using ^{14}C-ethanol 80−41205
cerebral blood flow meas. using NMR 77−40730

haemodynamics continued
cerebral blood flow noninvasive meas., analytical problems 80−41208
cerebral blood flow noninvasive regional meas. and computer analysis 78−35948
cerebral blood flow parameterisation, scintiangiography meas. 79−25025
cerebral blood flow regional meas., cyclotron prod. of ^{77}Kr 77−56468
cerebral blood flow system using H_2 clearance method 78−40457
cerebral blood volume meas. by ^{11}C-labelled carboxyhaemoglobin 80−8134
cerebral collateral circulation, simulated on computer model 77−36995
cerebral cortex, brain function rel. to blood flow 79−43988
cerebral cortial blood flow transients in cat. meas. technique using tissue heat transfer 79−92457
cerebral flow meas. by radioisotope clearance, radiation scattering effect 78−3600
cerebral gas exchange, perfusion and diffusion limitations 80−45940
cerebral infarction, abnormality of Xe brain/blood partition coeff. and blood flow 80−97993
cerebral perfusion image processing, minicomputer system 77−29200
cerebral regional blood flow, computerised monitoring system for stroke patients 79−79626
cerebral regional blood flow and vol. meas., intravenous isotope method 77−86610
cerebral regional blood flow assessment by continuous carotid infusion of ^{81m}Kr 78−20254
cerebral regional blood flow meas., ^{133}Xe inhalation method with on-line computer 77−40734
cerebral regional blood flow meas. by ^{133}Xe clearance 79−83912
cerebral regional blood flow meas. by ^{133}Xe inhalation, anal. method comparison 78−44604
cerebral regional blood flow meas. with ^{133}Xe, functional landscapes in brain 78−85356
cerebral regional blood volume, variations meas. by computerised axial tomography 79−29583
cerebral regional O_2 distrib. model during continuous inhalation of $^{15}O_2$, $C^{15}O$ and $C^{15}O_2$ 78−65108
cerebral tissue perfusion rate determ. from ^{15}O activity decay after photon activation 80−26341
channel, with diverging walls, blood streaming viscous-convected inertia effect 77−52828
cheek pouch epithelium, tumour-bearing, radiation-induced vascular alterations, Syrian hamster 80−17016
chest radiograph optoelectronic processing for pulmonary venous hypertension detect. 79−74754
chest radiology, introduction to physiological aspects 79−25071
choroidal blood flow, non-invasive meas. 77−40704
choroidal blood flow meas., theoretical basis using radioactive inert gas 79−92349
circulation augmentation, end-diastolic air compression boot 80−101291
circulation control physiology study *(Japanese)* 77−36969
circulation evaluation by nuclear medicine 79−70605
circulation single channel theograph anal. *(Russian)* 79−29545
circulation-assist, steady state anal. of press. and flow 80−17193
circulatory arrest, prolonged, visual evoked potentials during hypothermia 79−16204
circulatory assist device using blood pumping by mag. field 77−56518
circulatory clinical model matching techniques 79−53176
circulatory disorders, pelvis and legs, programming method for angiography 79−34646
circulatory regulation by artificial heart *(Japanese)* 77−36971
circulatory system polynomial model *(Japanese)* 77−70488
circulatory variables, power spectra of spontaneous variations 79−29538
computer angiography, new tool for X-ray functional diagnostics 79−79640
computer system SYSCORMORAM for haemodynamic and cineangiographic data treatment 78−81030
computer-aided monitoring after open-heart surgery, appl. to adrenaline effects meas. 78−81059
computerised tomography, cylindrical, appl. to intact circulatory system 77−77971
conference, London, England (May 1980) 80−94925
constant pressure resevoir for organ perfusion 80−94437
continuum model of blood flow, book contrib. 80−3706
control system for manipulation of press. or flow in unanaesthetised animal 77−48983
convection, forced, from hot-film probe in reversing flow, finite-difference soln. 80−12177
coronary, analysis by circulation model, using hybrid simulator *(Japanese)* 77−5021
coronary artery blood flow thermographic visualisation during by-pass surgery 79−53265
coronary blood flow, calc. from myocardial clearance of systemically administered ^{133}Xe 77−16967
coronary blood flow meas., precordial counting collimator 77−77967
coronary bypass surgery, left ventricular function and myocardial metabolism evaluation by atrial pacing 77−81646
coronary flow model, of horse, method of charact. calc. 77−86524
coronary haemodynamic parameter estimation using elec. analogue 77−37092
coronary perfusion pressure programmable control circuit 79−92278
coronary regional intravascular resist. determ. 78−31853
coronary sinus blood flow on-line computerised assessment by thermodilution 78−81024
Couette flow, blood suspension aggregation *(French)* 80−97991
counterpulsation, external, computer anal. using nonlinear math. model of cardiovascular system 77−2069
counterpulsation dynamics simulation, rel. to heart assist. blood pump 80−16996
counterpulsation operating mechanisms for assisted circulation 79−48371
couple stress fluid pulsatile flow through circular tubes 79−62275
creeping flow in closed cylindrical cavity, numerical calculation 80−16976
curved tube, pulsatile flow visualisation 78−44546
cutaneous flow meas., laser beam Doppler shift method, instrument 78−28030
CW Doppler flow meas., perivascular transducer effect on accuracy 77−90825
data processing in intensive care unit *(French)* 77−40903
deep venous thrombosis detection by plethysmography 77−40884
defibrillating trapezoidal waveforms, haemodynamic responses 80−72370

haemodynamics continued
deformable valved tube, viscous fluid flow in presence of gravity 77−25500
diagnostic method based on distorted signal 77−41540
dialyser performance improvement by osmotic flow induction 77−48946
dialysis and ultrafiltration, staged tortuous microcapillary system 77−37107
dielectrography methods and apparatus, recording capacitance changes due to blood vol. fluctuations 78−57046
diffusion of O_2 and CO_2 through blood flowing in channel 77−60303
digital automatic blood pressure recorder *(Japanese)* 78−24168
directional blood velocity waveform, Doppler preprocessors 79−34611
discrete-time Doppler frequency meter for blood flow imaging 79−57704
disease prognosis, appl. to haemorrhagic shock, nonlinear dynamical model 79−83838
distensible tube damping effects on turbulent flow, cardiovascular system implications 80−103076
dolphin, lung collapse and intramuscular circulation during diving 80−81643
Doppler blood flowmeter modulation *(Japanese)* 79−2115
Doppler signal centre freq. estimation using quadrature zero-crossing counter, US blood flowmeters 78−31879
Doppler sonographic flow meas. over small cross-sections in vitro and in vivo *(German)* 78−88729
Doppler US blood velocity meas., phase-locked loop technique 78−61234
Doppler-shift blood-velocity waveforms, real-time spectrum analyser 79−88145
double-boundary vessels, flow calcs. using finite-difference transforms 78−44526
drug elimination interactions, physiological flow model in rat 80−81628
drug-carrying microspheres, intravascular mag. guidance 78−73188
echo-Doppler, range-gated, pulsed, review and evaluation 79−96642
echocardiography, pulsed Doppler, variable sample vol. dimension 80−76816
education, Bernoulli's eqn. and Hagen-Poiseuille's law, capillary bed representation 80−57039
education, fluid mechanics of coronary artery bypass surgery 77−78911
elasticity, appl. of large deform. anal. to arteries and left ventricle 77−5018
electric admittance blood flow monitor, clinical evaluation 80−81759
electric impedance, clinical appl. for arterial insufficiency study 79−83878
electrical characteristics of flowing blood 80−36053
electrical impedance pulse in limbs, origins, separation of blood vol. and resist. change 77−40891
electrical resistivity changes of flowing blood *(Japanese)* 79−2015
electrical simulation of human arterial system 77−25501
electromedical devices of the angiohaemodynamical catheterisation laboratory 80−85515
electron microscopic anal. of liver acinus, double embedding technique 80−3885
electronic sphygmomanometer, direct and indirect methods for blood pressure meas. 79−25125
ellipsometric monitoring of mol. and cellular biological processes in vitro 77−48852
EM blood flowmeter, comparison of dynamic calibration methods 78−40362
EM flowmeters 77−78008
erythrocyte filtration through polycarbonate filter determ. method *(German)* 79−79708
erythrocyte flow behaviour, particle motion in ghost cell conc. suspensions 80−3605
erythrocyte sedimentation rate, for teaching 78−49610
erythrocyte tank-treading motion in a shear flow, model 80−104568
exercise physiology in teenagers and asthmatic children 80−12170
external counterpulsation, optimal phase shift determ. model 79−29557
external iliac arterial bed, LF dynamics meas. in unanaesthetised baboon 77−36998
extracorporeal blood circulation apparatus, tabulated data 77−78045
extracorporeal heart-lung bypass, mechanical support of circulation *(Japanese)* 77−40690
Fahraeus effect and cell screening rel. to dextran-induced aggregation 79−62273
Fahraeus effect and cell screening rel. to volume flow rate 79−62272
fat emboli detection by Doppler US flowmeter digital signal processing 77−25525
femoro-popliteal by-pass graft, flow in idealised models 79−39429
ferrofluid seal, for blood flow statis during surgery, hydrostatic loading 77−13031
fibre optic catheter, for intravascular press. and sound meas. 78−44638
fibre-optic microfluorimeter for animal haemodynamic and pharmacokinetic meas. 79−92455
filtration through capillary wall 77−32936
finger electrode system, tetrapolar elec. impedance plethysmography meas. 77−81608
finger instantaneous arterial press. meas. method 80−56245
finger-tip transducer for meas. digital vol. pulse, skin-resist. response and ECG 77−86729
fish, blood flow meas., use of laser Doppler velocimeter *(Japanese)* 79−84052
flow, peripheral, meas. by elec. impedance technique 79−70601
flow, quantitative meas. by constant infusion of short-lived isotopes 80−17088
flow and tracer uptake in normal and abnormal canine bone 80−17072
flow calc. by indicator dilution, pulsatile error analysis 77−60225
flow detection in human heart, US pulsed Doppler flowmeter system, microcomputer based 80−104690
flow distribution within the myocardium *(Japanese)* 79−96590
flow disturbances, main pulmonary artery rel. to ascending aorta, man 80−45929
flow imaging with nucl. mag. reson. spin echoes 78−85330
flow in channel, O_2 uptake 77−81516
flow in collapsible tubes 79−25020
flow in straight and curved capillary glass tubes 80−61607
flow meas. from US Doppler signals, on-line computer system decoding 78−3570
flow meas. using implantable pulsed Doppler flowmeter, dogs 77−90966
flow measurement, Doppler US flowmeters, optimum vel. resolution 77−957
flow measurement, intact circulation, X-ray filming, video techniques, review 77−52822

haemodynamics continued
flow measurement by CW Doppler technique using implantable transducers, accuracy 77−25537
flow measurement by laser Doppler system *(Swedish)* 80−51199
flow measurement from freq. analysed US Doppler signal 78−44573
flow measurement in dynamic phantom using ^{81}Rb-^{81m}Kr and NaI detector 77−66843
flow measurement using NMR and flat crossed-coil detector 78−40284
flow measurement using X-ray fluoresc. *(French)* 77−37033
flow measurements by NMR of the intact body 80−81680
flow model, hydrodynamic study with blood simulant 79−25023
flow model for blood type suspensions in circular tube 79−29543
flow restriction in rat small intestine, crypt survival after X-irradiation 79−11979
flow sensing in conscious rats, multichannel pulsed Doppler technique 78−44577
flow speed and quantity determ. from digital angiograms *(German)* 78−92690
flow telemetering system using implantable CW Doppler US flowmeter, IC appls. 78−11749
flow telemetering using implantable CW Doppler US vel. meter, IC 77−86565
flow visualisation methods for in vitro cardiovascular flow studies 77−56409
flow-velocity meas. by US techniques, Kalman filter appls. 79−100686
flow/pressure relationships, when to meas. flow or hold flow const. 77−77926
flowmeter, cylindrical crossed-coil NMR, for noninvasive measurement 79−62328
flowmeter, directional Doppler, carotid artery stenosis diagnosis, stroke prevention appl. 77−52823
flowmeter, directional Doppler device, transducer design 77−25535
flowmeter, implantable bidirectional pulsed Doppler, for animal research 78−44749
flowmeter, implantable Doppler design with phase-locked loop 78−31873
flowmeters, digital 2D full range Doppler velocity meter for cardiovascular diagnosis 78−88731
flowmetry, noninvasive, in upper limbs of patients with arteriovenous dialysis fistulas 80−21562
forced oscillations in large vessels of circulatory system, dog's arterial blood flow anal. 78−85329
friction, effect on parietal microenvironment 80−16973
gamma-camera adaptive gating device for heart synchfonisation 78−31898
gas bubbles, behaviour when subjected to oscill. press. 80−97984
gas catheters, flow-dependent, in vivo calibration 79−16330
glomerular filtration rate and renal plasma flow, simultaneous meas. by radioisotope clearance 77−56458
gravimetric plethysmography for leg blood flow meas. 80−36176
haemodialysis, effects of blood and dialysing soln. flow rates on efficiency 78−36053
haemodialysis, single-needle, recirculation anal. 80−41320
haemodialysis by extra corporeal ultrafiltration method, parameter estimation of vascular bed 79−84015
haemodialysis ultrafiltration, transient characts. governing eqn. 78−36075
haemodialysis with hollow fibre membranes, flow maldistribution effect on performance 80−26248
haemofiltration control system *(German)* 79−5403
haemofoil mitral valve, results of flow visualisation expts. 80−104632
haemoperfusion devices, comparative studies, press. drop and flow uniformity tests 80−35929
haemoperfusion through fixed-bed adsorber 78−31976
heart, ellipsoidal model, appl. to left ventricular contractions study 80−104608
heart, minimal O_2 consumption and optimal contractility, theoretical approach 79−74694
heart and muscle, apparent source resistance 79−25005
heart congenital defect evaluation from dynamic tracer meas. 78−40378
heart contraction mechanism, modelling 80−72204
heart disease, haemodynamical parameters optimal control 79−53182
heart motion kinetic anal., force-displacement relation 78−40222
heart rate and blood pressure biofeedback, literature review 80−21484
heart rate and blood pressure biofeedback theoretical models review 80−16974
heart relaxation parameters, digital anal. of isovolumic press. fall, dogs 80−94276
heart shunt diagnostics by radioisotope angiography, anal. by PASD computer program 78−20250
heart synchronized gamma-camera gating for haemodynamic status evaluation 79−53232
heart valve prostheses, fluid shear stress 77−90833
heart valve prostheses, rel. to vol. flow rate 77−25597
heart valve prostheses development 77−56523
heart valve prosthesis, theoretical limit to flow design 77−60302
heart valve prosthesis, tilting disc type, computer prediction of thrombogenic sites 77−44834
heart valve prosthesis design, role of simulation studies 79−12033
heart valve prosthesis mean press. gradient meas. under in vitro pulsatile flow 77−56531
heart valve prosthesis testing 77−56530
heart valves, artificial, implanted cause of thrombus formation 77−78047
heart valves, blood flow, vortex method calcs. 80−72189
heart valves, diseased and prosthetic, assessment of haemodynamic function 77−48830
heart valves, fluid-mechanical study 79−53171
heart valves, vortex-grid method 80−41105
heat transfer in tissue, Pennes model vs. Wulff model 77−40635
hepatic effective blood flow, meas. by fractional clearance of ^{198}Au-colloids 79−66547
hepatic scintiangiography, patient positioning techniques 78−20259
hepatobiliary dynamic flow study using ^{99m}Tc 79−53217
Hiemenz flow, pulsatile, struct., and temporal variation of wall shear stress near stagnation point 77−62303
high-resolution blood flow imaging system using binary phase coded pseudonoise sequences 79−57703
Hippuran transit times in kidney, renogram deconvolution 78−40317
hollow fibre dialyser, mass transfer 80−66873
human retinal blood flow meas. by laser Doppler velocimeter 79−79623

haemodynamics continued
HYDRA hybrid analyser appl., use of sequential transcoder *(Czech)* 77−21668
hydrodynamic generator for blood flow simulation 79−79706
hydrodynamic properties of human blood plasma 77−73538
hydromechanical simulation facility 79−20708
hypertension classification using non-parametric technique 77−21558
hypertension in end-stage renal failure, math. model 78−31829
hypertensive crisis, press. control. closed loop control of sodium nitroprusside infusion 78−44688
hyperthermia, role of blood flow 80−3596
hypertrophy criteria in VCG of children with Fallot's tetralogy 78−7503
hypopnea consequent to reduced pulmonary blood flow in the dog 80−45941
iliac arterial bed of unanaesthetised baboon, LF dynamics 79−83816
iliac artery, blood flow values in conscious humans using angiocinedensitometry 79−25022
impedance cardiography, problems 80−41285
impedance plethysmography, influence of erythrocyte vel. 78−61238
in-series cardiac assist devices, expt. and theoretic observations 78−36063
incompressible three-dimensional internal flows, finite difference soln. of Navier-Stokes eqns. 77−58795
indicator dilution measurements of flow parameters in curved tubes and branching networks 77−66824
indicator-dilution meas. of flows and vols. in patients with transposition of great vessels 78−61209
indirect pressure meas. in pony using oscillometric method 78−36085
inert gas exchange, mathematical lung models, effects of common dead space 80−67126
inert gas transport in the microcirculation, isobaric supersaturation risk 80−45939
infant circulation model after surgical correction of transposition of great arteries 77−44713
infarcted left ventricle, source impedance and internal reactive power 77−37007
inferior vena cava hydrodynamics, passive mechanical model, negative resistance effects 77−81521
instantaneous blood flow meas., X-ray imaging using cine/video densitometric data 79−34598
internal carotid artery, canine, under const. load regime, mech. props. 77−90843
intestine, exteriorised, influence of blood flow on temp. distrib. in the mouse 79−48219
intra-aortic balloon heart assist device fluidic drive system 78−53566
intra-aortic balloon pump simulator for dynamic demonstration and teaching 77−56537
intra-aortic balloon pumping, flow obs. and model expts. on blood damage 77−81664
intra-aortic balloon pumping efficacy evaluated by nonlinear cardiovascular system model 78−44732
intra-aortic balloon support, prognostic indices, rel. to left ventricular assist device use 77−56536
intracardiac blood flow measurement, noninvasive ultrasonic technique 77−86569
intracardiac shunt noninvasive quantitation using cardiovascular sound complexes 78−48918
intracorporeal long-term blood pumps, design criteria and physiologic performance criteria 78−40430
intravascular mean vel. meas. using crosscorrel. technique 80−81763
intravascular O_2 measurement, current-to-voltage convertor 79−34684
intravascular O_2 sensors, Monopolar, in vitro evaluations 79−34683
intravascular radioactive tracers, calc. of residence time distribs. in fields of external registration 80−72291
intravascular thrombus induction in vivo using localised hydrodynamic shear stresses 80−97997
intravenous fluid overload, cardiopulmonary effects, radiologic manifestations 79−92259
IR noninvasive monitoring of cerebral and myocardial O_2 sufficiency and circulatory parameters 78−44583
ischaemic episode, computerised continuous beat by beat anal. and rational plots 79−62394
ischaemic heart disease studied by cardiac pacing 77−81628
Korotkoff sounds possible origin from steady press. flow in compressed arteries 80−81639
laminar blood flow, gas and heat transport, platelet and protein diffusion 78−92669
laminar boundary layer flow past two dimens. slot 78−5724
laser Doppler anemometer, directionally sensitive two-component, velocity meas. in artery casts 80−75004
laser Doppler blood velocimetry *(Japanese)* 80−94310
laser Doppler spectroscopy, biology appls. 79−66598
laser Doppler velocimeter signal analysis for pulsatile arterial flow meas. *(Japanese)* 79−2156
laser instrumentation system for simultaneous meas. of transcutaneous O_2 and skin blood flow 80−26321
laser irradiated tissue, significance of blood flow in temp. calcs. 80−55993
laser irradiated tissue, significance of blood flow in temp. calcs. 80−104563
left heart and systemic circulation, 2-stage identification scheme 80−41071
left heart bypass, partial and subtotal systems compared 77−81660
left ventricle, effects of external pressures on pressure-volume relation 79−11954
left ventricle, model study of isovolumic and non-isovolumic contracts 80−85428
left ventricle and systemic vascular bed model parameter estimation 77−21548
left ventricle ejecting beats, estimation of hydromotive source press. 80−76776
left ventricle ejection fraction meas., scintillation camera deadtime 79−62355
left ventricle model, diastolic pressure-vol. relations and wall pressure distrib., fibre extension 80−8079
left ventricle model parameter estimation, global search algorithms *(French)* 78−3529
left ventricle pressure distribution 77−37006
left ventricle prosthesis, pneumatically regulated, in-vitro/in-vivo performance 78−3681

haemodynamics continued
left ventricle time-varying capacitance model, driving energy and cardiac O_2 consumption *(Japanese)* 80−21486
left ventricular aneurysm, triaxicardiometric criteria 79−39586
left ventricular assist device, diaphragm-type, factors affecting pumping dynamics 78−44706
left ventricular assist device, intrathoracic, with biolised blood-contacting surfaces 78−7540
left ventricular assist device testing using calf model 78−73296
left ventricular bypass performance, influence of power waveform 78−40433
left ventricular diastolic press.-area curves, shifting with positive end-expiratory press. 80−104604
left ventricular ejection fraction determ., comparison of three radionuclide techniques with contrast angiography 78−31889
left ventricular ejection fraction determ. by equilib. radionuclide angiography 80−12227
left ventricular flow pattern index of pumping efficiency 79−96601
left ventricular function, correlation with myocardium deformation 79−16244
left ventricular function, effects of intracoronary nitroglycerin, computer anal. 79−70575
left ventricular function, normal and abnormal, vel.-strain relationship 78−69119
left ventricular haemodynamics during respiration, dog expts. 80−81635
left ventricular performance, respiration effects model 80−3670
left ventricular performance characteristics in trained and sedentary dogs 80−97969
left ventricular performance parameters rel. to max. dZ/dt 80−101159
left ventricular turbulence 77−48834
left ventricular work requirements to exercise before and after artificial heart implantation 77−44847
left-heart haemodynamics, mathematical model 78−65074
left-ventricular ejection fractions meas. by equilib. radionuclide angiography 80−12226
leg, lower, external compression effect on venous blood vol. 80−97989
light beating spectroscopic instrument for continuous meas. of tissue blood flow 80−41160
limb blood flow automated monitoring system using venous occlusion admittance plethysmography 78−31937
limb blood flow meas. by elec. admittance plethymography, evaluation of theory and accuracy 78−31936
linear tube, axially symmetric wave motion of viscous liquid, haemodynamics model 77−73537
liver, perfusion, normal and partially hepatectomized rat, in vivo meas. using ^{99m}Tc S colloid 79−79636
liver membrane potential in situ, effect of blood flow changes 78−48772
local circulatory system characterisation by CW Doppler US flow meas. 78−57109
lung, atelectatic, mechanism of decreased blood flow 80−45931
lung, quasi 1 dimensional unsteady fluid flow eqns. study 80−3691
lung, regional distrib. of (dV/dt)A/(dQ/dt) in man, at rest and with exercise, meas. with ^{81m}Kr 79−16232
lung, regional function, short-life radionuclides, review 79−53211
lung circulation, density dilution method appl. to obs. of fast osmotic fluid shifts 80−104781
lung function, regional, electroplethysmograph 77−21647
lung haemodynamic resistance longit. distrib. 77−36996
lung lobe, dog, responses to lobar venous occlusion 80−30743
lung numerical modelling, human 78−80911
lung parameter measurement, rebreathing technique for small lung vols. 77−36994
lung perfusion determination by dilution principle with expiration detection of indicator *(German)* 78−85326
lung perfusion determination using O isotopes and dilution principle *(German)* 78−85327
lung physiology and chest radiology 79−25072
lung tissue volume and blood flow, rebreathing methods for determ. 79−20569
lung transport and metabolic processes, indicator-dilution study 77−44711
lung vascular permeability after microemboli, effect of platelet depletion, sheep obs. 80−97972
lung ventilation and perfusion scintigrams, computer aided diagnosis 79−88181
lung ventilation-perfusion ratio recovery from inert gas data 77−40829
lung ventilation-perfusion ratio resolution of inert gas data 77−12943
lung vessel pressure-diameter behaviour, pigs, effect of parenchyma and length changes 80−67116
magnetic field effect on microcirculation in frog interdigital membrane 77−32935
magnetic measurement of cardiac bloodflow 78−44517
magnetocardiogram and cardiac output meas. with integrated system 80−104709
magnetocardiography in weak DC ambient magnetic fields 79−79567
maintenance haemodialysis, circulation study *(Japanese)* 77−40689
mass transfer in semi-cylindrical hollows, electrochemical measurements 79−23365
mass transport to walls of stenosed arteries rel. to Reynolds number and blood flow separation 80−41093
maternal-placental blood flow model with vel.-depend. permeability 78−40224
Mayer waves, history and methodology 79−29537
mean arterial pressure, noninvasive automatic determ. 79−57796
measurement, future appls. and prospects 77−78010
measurement of central venous-, pulmonary artery end-diastolic- and pulmonary capillary wedge-pressure 77−90955
mechanical haemolysis fluid dynamics, rel. to artificial heart valves 80−97999
mechanical heart computer simulation 79−70709
mechanics of blood flow 80−76778
mechanopressography, left-ventricular, noninvasive intrinsic assessment of pumping efficiency 80−72203
medical diagnostics problems of computer applications *(German)* 79−20696
mesenteric artery Na distrib. in early salt-induced hypertension 78−27999
metabolic and thermoregulatory effects of acute ^{60}Co γ-radiation in myomorph rodents 79−88134
metabolites, dynamics of depend. sorption by C sorbents 77−70487
haemodynamics continued
methods for quantitative meas. and localisation of peripheral arterial occlusive disease 79−96640
microcirculation autoregulation mechanistic theories, computer simulation 78−27995
microcirculation flow dynamics meas. using video microscope 77−78009
microcirculation mathematical modelling 79−2094
microcirculation O_2 distrib. during and after arteriolar occlusion 78−44529
microcirculation regulation study *(Japanese)* 77−36972
microcirculation semiquantitative demonstration using US noninvasive meas. method *(German)* 78−85348
microcomputer-based blood-pressure recorder *(Japanese)* 80−67139
microcomputer-based pulmonary wedge pressure measurements 80−26391
microkymography, flow vel. meas. in microvascular bed after exdotoxin administration *(German)* 78−77173
microprocessor-based tilting bed for blood pressure control 80−26412
microprocessor-controlled cardiac output meter 80−36162
microthermopolar fluids in circular pipe, Hagen-Poiseuille flow 80−24092
microvascular filtration, comparison of characts. in isolated and intact lungs, dog expts. 80−97974
microvascular pressure measurement, capacitive modulation of micropipet impedance 77−37080
microvessels, influence of plasma layer on steady blood flow 78−27978
microwave heating of tissue, effect of surface cooling and blood flow 78−57038
minicomputer-based scheme for turbulence measurements with pulsed Doppler ultrasound 80−26435
mitral valve, conditions of closure 80−85439
mitral valve, natural, human, turbulent flow 77−36975
mitral valve replacement, prediction of postoperative systolic left ventricular wall stress 78−40427
model for phasic press. and flow in large arteries 80−94254
modelling of motion in large vessel partly replaced by prosthesis 77−64082
models, numerical integration method for improving soln. stability 78−69118
monitoring cart, self-diagnosing microcomputer-based design 78−31943
monitoring of blood vol. change in menstruation, vaginal photoplethysmographic transducer 78−92733
monitoring system for stroke patients 80−26394
monitoring technique in late pregnancy toxaemia 77−81602
monitoring transducer for blood temp., during extracorporeal circulation 78−44639
multichannel analyser, microprocessor-controlled, transfer of blood pressures and neural activities for computer anal. 80−72356
multinephron kidney equations, numerical soln. 79−83822
multiple indicator-dilution study of saturable uptake of metabolised substance in dispersing organ 78−27998
multiple noncritical stenoses, fluid dynamics expt. 77−90844
muscle blood flow meas. by ^{133}Xe clearance, CdTe semicond. detector system 78−40305
muscular hyperemia, study technique using ^{133}Xe 79−5351
myocardial blood flow, ^{133}Xe studies, theoretical, technical and practical aspects 80−94355
myocardial blood flow, meas. by fractional uptake of ^{84}Rb and microspheres 79−34656
myocardial blood flow and haemodynamic responses to exercise training, dog expts. 80−3678
myocardial blood perfusion and transport modelling using inert-tracer techniques 77−5121
myocardial contractility, real time meas. by analogue computer with digital displays *(Japanese)* 79−44015
myocardial fibre shortening velocity dependence on inotropic and haemodynamic conditions 78−31833
myocardial interaction between ventricles 77−12946
myocardial perfusion evaluation by coded aperture tomographic technique 80−21537
myocardial perfusion index calculator for prediction of subendocardial ischaemia in cardiac surgery 77−40915
myocardial regional blood flow from dynamic anal. of ^{201}Tl 79−70627
myocardial regional function and coronary blood flow study during ischaemia in baboons, telemetry system 78−44752
myocardial regional perfusion, tomographic scintigraphy 78−3584
myocardial uptake of ^{201}Tl, correl. with local perfusion, dog expts. *(French)* 80−104740
myocardium, contractility determ., anal. of differential quotients 79−34584
myocardium prosthetic, haemodynamic results 79−84019
Navier-Stokes equations, finite element soln. 80−94269
neonatal peripheral circulation, human, characterisation by US pulsed Doppler technique 80−76815
neonatal whole body γ-irrad. in growing dog, plasma renin activity and arterial press. 80−41132
neonate blood pressure meas., noninvasive technique 77−48916
neuronal activity and focal blood flow coupling in experimental seizures 80−40989
NMR blood flowmeter *(Japanese)* 80−51202
NMR flat crossed-coil detector for blood flow meas. 79−83880
noisy blood flow meas. pulsed US spectral analysis 79−57705
non-Newtonian fluids, particle movement, appl. to dyeing and haematology *(German)* 78−87369
nuclear medicine conference, Karlovy Vary, Czechoslovakia (May, 1979) 80−12840
numerical analysis of blood flow in heart 78−15854
numerical solution, flow through deforming tube 80−104614
organ blood flow determ. using radioactive microsphere technique, PDP-11 interactive program 78−20247
organ blood flow measurements, effect of instantaneous partition coeff. of Xe 80−101256
oscillatory flow, Fahraeus-Lindqvist effect 80−3668
oscillatory flow in thin-walled curved elastic tubes 77−56397
oscillatory frequency effects in plane wavy conduit flows 78−20209
oxygenation in complex coiled silicone rubber tubes 77−60304
oxygenation using coiled tubes 78−40422
oxygenator using microchannel membrane, transport and flow phenomena 78−69253
parietal friction meas. by pulse type Doppler velocimeter 80−17206

haemodynamics continued
particle flow behaviour in branching vessels models, vortices in 90° T-junctions 80−16971
patient parameters monitoring by SOLO, an interactive minicomputer based bedside monitor 80−26392
pattern classification of patients with essential hypertension 77−25583
perfusion, meas. by heated thermocouple probes' temp. transients anal. 79−96598
perfusion and intraaortic balloon pumping system, Biopul's-3 78−7536
perfusion measurement in capillary beds, two-regime model of heated thermocouple probe 77−5110
perfusion pulse attenuation in dog autoregulation 78−44545
perfusion pump EM drive, features 78−7532
perfusion rate determ. from temp. perturbation, unbiased minimum variance linear estimator 79−92283
perfusion rate measurement by dynamic thermal dilution 77−40883
peribronchial fluid pressure rel. to vascular and airway press. and interstitial oedema 80−97971
perimicrovascular fluid pressure estimation in isolated perfused dog lung lobes 80−30750
peripheral circulation evaluation, noninvasive techniques 80−56163
peristaltic motion of blood in vessel with actively deforming wall, numerical simulation 80−72205
physical principles, comparison of meas. methods *(German)* 78−92735
placenta, human, detect. of pulsatile flow in situ by impedance meas. 80−104799
placental blood flow evaluation, comparison of ^{113m}In and ^{133}Xe intravenous injection methods 78−28043
plasma filtration from whole blood, effect of various parameters 78−48826
plasma radio-Fe kinetics in man, effect of plasma Fe conc. 79−25019
platelet adhesion obs. in flow chamber 79−79589
platelet aggregate formation in region of separated canine blood flow 78−27989
platelet aggregation studies using TEXAC whole picture analysis 79−25133
platelet stimulation under influence of high shear stresses in tube flow 80−97996
platelet transport between blood and artificial filtering surfaces 78−40423
plethysmogram detection and its clinical usefulness *(Korean)* 79−62380
plethysmograph, automatic venous occlusion device 80−17176
plethysmography, elec. admittance, blood flow meas., evaluation of theory and accuracy *(Japanese)* 79−43979
plethysmography, impedance, sampling field in the human calf 79−57740
plethysmography over past 30 years 78−31933
plethysmography using Hg strain gauge, in evaluation of efficacy of nitroglycerine paste 77−40905
plethysmography using Hg-in-rubber strain gauge, temp. drift error and compensation 77−52900
plettysmography system, simultaneous multifinger meas. 80−21516
polyox WSR-301, posterior rat extremity perfusion, hydrodynamic friction lowering 79−79586
post-stenotic turbulent wall pressure fluctuations, spectral and temporal characts. 80−16994
posthaemorrhage blood volume control model for intravenous fluid therapy 77−40697
potentiophotometric platelet aggregation meas. by turbidity change 80−36061
pressure, human, noninvasive meas. *(Japanese)* 80−94395
pressure, indirect meas., meaning of max. oscills. point in cuff press. 80−94396
pressure, indirect meas. method, review 80−94383
pressure, systolic and diastolic, rel. to pulse transit time 79−29541
pressure ambulatory recordings, minicomputer processing 80−89887
pressure and flow-rate signals, canine, cross correlation by freq. plane filtering 80−32919
pressure and pulse rate, system for determ. long term variations 79−57792
pressure automated control in dogs using microprocessor 80−81797
pressure automatic monitoring, long-term, minicomputer system 80−101276
pressure continuous recording in ambulant hypertensives, computer anal. 79−62390
pressure control, mechanical-chemical balloon implant 79−20712
pressure direct measurement for intensive care and operations, computerised correction system 78−44635
pressure drop across aortic heart valves, steady and pulsatile flow 79−74707
pressure during sleep, model of influence of vestibular system 77−25410
pressure for extracorporeal circulations, elec. sensor *(German)* 78−92721
pressure indirect meas., occluding cuff design criteria 77−64146
pressure meas. instrument for newborn infants 79−92406
pressure meas. techniques, Medicor electromanometry 77−90943
pressure measurement, automatic, device for linear press. change in cuff 77−48902
pressure measurement, blood gas anal., silicone rubber catheter operating mechanism *(Japanese)* 78−61273
pressure measurement, Hg manometer contactless readout and recording cct. 77−81603
pressure measurement, new air release valve design 77−60266
pressure measurement, noninvasive techniques 80−41298
pressure measurement errors in cuff methods, Korotkov and impedance plethysmography techniques 77−40886
pressure measurement in baboons, direct vs. indirect methods 77−29233
pressure measurement in cardiology, computer aided anal. *(Swedish)* 77−44779
pressure measurement with portable systems using Korotkov sounds, meas. accuracy 80−76855
pressure monitor, semiautomatic, using electronic sphygmomanometer 78−20300
pressure monitor, systolic-diastolic, using display stabilising circuit 78−40364
pressure monitoring systems simulator 79−83963
pressure noninvasive meas. techniques for rhesus monkeys and beagle dogs 77−44871
pressure radiotelemetering, cardiovascular response to dynamic/static exercise monitoring 78−3633

haemodynamics continued
pressure recording, simple method for fidelity improvement, Korotkoff sounds 80−76811
pressure recording transducer, arterial and venous 79−34708
pressure sensor, catheter-tip, with on-chip compensation and signal processing 77−44818
pressure transducer for student use, using hybrid IC 78−8186
pressure transducers in clinical use 79−96692
pressure transistor device, high sensitivity, quasi-digital 79−79675
pressure wave propagation in arteries 80−96228
pressure waves, forward and backward, total-occlusion method for anal. 80−56257
pressure-flow relationships in rat mesentery microvessels *(Japanese)* 80−21485
pressure-induced tissue breakdown, fundamental problems 78−31838
prosthetic aortic heart valves, wall shear stress meas. in near vicinity 79−83829
prosthetic aortic valve, Bjork-Shiley, steady flow in vitro vel. 78−44735
prosthetic aortic valves, press. drops under steady and pulsatile flow, in vitro meas. 78−44731
prosthetic cardiac valve, concave-convex pivoting disc two-dimensional model 79−84028
prosthetic circulatory device fluid mechanics and haemolysis, review 80−46101
prosthetic disk valves, max. opening rel. to aortic blood flow characts. 80−108941
prosthetic heart and mock circulatory system, math. model 78−81080
prosthetic heart valve, disc-type, in vitro meas. of fluid stresses 77−52833
prosthetic heart valve, disk-type, numerical soln. for steady axisymmetric flow 80−35952
prosthetic heart valve design flow evaluation using finite difference transforms 78−44733
prosthetic heart valve flow pattern visualisation by laser technique 78−44734
prosthetic heart valves, disc, ball and tilting disc types, fluid stresses in vitro 78−81078
prosthetic heart valves, insufficiency, pressure loss and energy loss obs. *(German)* 79−83818
prosthetic heart valves, insufficiency and pressure loss in mitral position 79−20717
prosthetic heart valves, pressure-flow relationship and dynamic behaviour 79−25158
prosthetic heart valves, rigid leaflet and caged-ball types, diastolic ventricular mechs. 78−81079
prosthetic heart valves, vel. profiles under steady flow conditions 77−56410
prosthetic mitral valve, pressure drop and flow pattern obs. 79−92430
prosthetic ventricle and valve evaluation, flow visualisation data anal. 78−40425
prosthetics, haemodynamic design considerations 78−40428
pulmonary, quasi one-dimens. unsteady nonlinear fluid flow eqns. soln. 80−41104
pulmonary air emboli, effect of ventilation with different gas mixtures 78−27991
pulmonary and recirculation parameter identifiability following sequential bolus inputs of ^{133}Xe 78−44605
pulmonary arterial blood flow dynamics, nonlinear anal. 78−44527
pulmonary arterial circulation process nonlinearity 77−12944
pulmonary arterial compliance effect on pulmonary blood flow distrib., analogue simulation 78−44553
pulmonary arterial hypertension meas., Bubble Ultrasonic Resonance Pressure method 79−92313
pulmonary arterial press. rel. to thoracic baseline impedance, intravascular fluid vol. meas. 77−40888
pulmonary arterial pressure, noninvasive estimation in dogs using ^{133}Xe images 80−41184
pulmonary artery blood press. anal. algorithm 78−40376
pulmonary artery press. estimation using pulse wave velocity 80−12203
pulmonary blood flow, method for noninvasive bedside determ. 80−81762
pulmonary blood flow, noninvasive meas. using PDP 12 digital computer 79−70685
pulmonary blood flow, spatial distrib. in dogs with PEEP ventilation 80−72191
pulmonary blood flow, spatial distribution in dogs in increased force environments 78−92664
pulmonary blood flow estimation, Ljung's algorithm sensitivity 80−56107
pulmonary blood flow in isolated perfused dog lung lobes, effect of oedema 80−97975
pulmonary blood flow redistrib. in PEEP ventilated dogs 80−8083
pulmonary blood pressure, flow and vol. in man, effects of sitting up 79−88103
pulmonary capillary blood flow in dogs, atraumatic meas. 78−7552
pulmonary capillary permeability inferred from lymph and multiple-indicator expts. 77−44604
pulmonary circulation, human, behaviour during head-up tilt 79−39433
pulmonary contusion and flail chest, effects on perfusion and O_2 exchange 80−67119
pulmonary flow meas., static and dynamic testing of plethysmograph and pneumatic differentiator 78−28150
pulmonary gas exchange model, effect of ventilation-perfusion, diffusion-perfusion ratios *(French)* 79−8516
pulmonary haemodynamic effects of lung inflation, graded hypoxia in conscious sheep 79−83824
pulmonary haemodynamics meas. using US oesophageal probe 78−35902
pulmonary microvascular response to haemorrhagic shock, resuscitation and recovery 80−3674
pulmonary physiology, pathology, and ventilation-perfusion studies 79−29613
pulmonary pressure-flow curves measured by a data-averaging circuit 80−61725
pulmonary regional perfusion, comparison of ^{81M}Kr continuous intravenous infusion, ^{99M}Tc macroaggregates 79−39477
pulmonary responses to elevated cerebral spinal fluid pressure in the dog 79−88108
pulmonary right-to-left shunting, quantitation by double indicator and O_2 techniques 77−12951
pulmonary vascular disease, resist. model of arterial morphology and mechanics 77−36997

haemodynamics continued
pulmonary vascular interdependence in excised dog lobes 80−97976
pulmonary vascular resistance, longitudinal distrib., and lung inflation in hypoxia 80−56086
pulmonary vascular response to hypoxia, online impedance analysis system 77−52943
pulmonary vascularity computerised texture features rel. to catherisation parameters 80−8154
pulmonary venous pressure estimation from routine chest radiographs using hybrid optical-electronic system 78−44657
pulmonic arterial stenosis, intravascular press. and vel. fluctuations 80−94260
pulsatile blood flow in arteriole of frog web 80−16964
pulsatile flow, laminar-turbulent transition, appl. to blood flow *(French)* 77−5022
pulsatile flow, micropolar fluid model 77−7359
pulsatile flow, momentum correction factor 77−81524
pulsatile flow disorder, poststenotic blood velocity meas. in dogs 79−8521
pulsatile flow in arteries simulation, utilitarian approach 80−3669
pulsatile flow in channel of small exponential divergence, flow separation 77−86528
pulsatile flow in curved tube, axial velocity profile meas. 80−41088
pulsatile flow in porous channel, heat transfer 77−19604
pulsatile flow of dusty fluid through constricted channel 79−14468
pulsatile flow studies in a model of the human aortic arch 80−104633
pulsatile flow through tube containing rigid and distensible sections, num. soln. technique 77−56419
pulsatile laminar flow, velocity meas. for flow in 90° branch, appl. to atherogenesis 78−38277
pulsatile pressure waves of finite amplitude in elastic tubes, water expt. 77−27596
pulsatile viscous flow through diseased coronary arteries of man 77−90835
pulsative flow, digital simulation by finite element method 78−92670
pulsative flow, effects on blood elec. impedance *(Japanese)* 80−21513
pulse rate, blood press. and rate-press. product automatic meas. during rest and exercise *(German)* 78−35974
pulse wave propagation in arteries, initial stresses and muscle activity effects 80−12172
pulse wave propagation in arteries 80−41099
pulse wave vel. meas. in man, effect of arterial tree anatomical struct. 79−53180
pulse wave velocity, digital meter *(Japanese)* 79−39546
pulse-wave velocity measurement in humans *(German)* 80−81751
pulsed Doppler blood velocity meter readout 78−69158
pulsed Doppler flowmeter, development and cardiac appls. *(Japanese)* 80−36037
pulsed incompressible flow, stability *(French)* 77−5023
pulsed NMR studies of biological water 80−35930
pump, controlled high pressure, for heart support systems *(German)* 79−8580
pump, experiences with miniaturised press.-controlled servo *(German)* 78−88762
pump regulation electropneumatic servo operation *(German)* 79−8579
pumping ability of left heart rel. to end-diastolic vol. and inotropic state 78−31851
racial differences in blood pressure control 80−30757
radial arterial deformation meas. based on impedance rheography 78−3545
radioisotope uptake of bone-seeking radioisotopes in normal bone rel. to blood flow 80−94320
radioisotope venography, lower extremity, recognition of systemic portal shunts 80−94329
radiolabelled microspheres, use in meas. of regional blood flows during $+G_z$ stress 80−81786
radionuclide cardiology, dynamic phantom 80−12232
radionuclide mean clearance time transverse section imaging 78−73222
radiotracer flow measurement, automatic bolus injector 77−9238
radiotracer methods for laminar flow in small channels, liq. tracer method 77−58816
radiotracer methods for laminar flow in small channels, response model 77−58814
radiotracer methods for laminar flow in small channels, tracer-sphere method 77−58815
rate-dependent left bundle branch block patients, atrial pacing expts. 79−44019
recirculation maths. and cardiac output meas. 77−56404
red blood cell ADP release at high shear stresses 80−98002
red blood cell mechanical disruption 80−98001
red blood cell micromechanics in viscometric flow 80−98000
red blood cell speed absolute meas. in retinal vessels, using laser Doppler velocimeter 79−83884
red blood cells, hydrodynamic and diffusion considerations in rapid mix expts. 80−40982
red cell flexibility, whole blood filtration technique using 5 μm pores *(German)* 78−57030
red cells in dilute suspensions, turbulent flow and effect on O_2 uptake kinetics 77−60223
reduced hydrodynamic drag of normal human blood 78−61210
regional blood flow during simulated diving in the conscious Weddell seal 80−72194
regional flow, assessment by intravenous injection of ^{99m}Tc pertechnetate 80−104732
regional myocardial perfusion determ. from H_2 washout curve 79−92459
renal arteries model, human, qualitative and quantitative flow studies *(German)* 80−21483
renal artery stenosis, effect on renovascular hypertension 80−108934
renal artery with deformed vascular wall, blood flow 78−65063
renal autoregulation, math. model of transient adjustments 77−90842
renal blood flow measurement using externally monitored ^{131}I-hippurate uptake 77−2036
renal branch unsteady blood flow simulation 78−27983
renal diagnosis by blood circulation angiocinedensitometry *(German)* 79−2127
renal differential function in dogs using ^{99m}Tc-dimercaptosuccinic acid 79−79639
renal function, identification techniques 79−96658
renal function studies, combined in vitro-in vivo radionuclide procedure, technical aspects 77−90884

haemodynamics continued
renal responses in unrestrained dogs during explosives detect. implanted telemetry 77−32927
renal vascular resistance and I washout during renal angiography 77−77927
renal/iliac flow telemetering from exercising dogs, implanted CW Doppler flowmeters 77−90822
renovascular hypertension, computer-assisted static/dynamic imaging evaluation as screening test 79−79635
respiration, human, managment of artificially ventilated patients 79−70576
respiration dynamic model eqns., explicit solns. and periodic functions *(French)* 79−79574
respiratory system, human, mechanics of regulation 80−41102
respiratory tracer gas nonlinear computer anal., non-invasive meas. method 79−62395
respiratory transport, haemoglobin struct. 79−57576
response to ventricular pacing 77−81525
retina, blood flow, photon correlation velocimetry 77−90828
retinal blood flow, laser Doppler meas. 78−69174
retinal internal circulation visualisation using Purkinje's methods 78−69043
RF EM noninvasive transcutaneous measurement technique *(Italian)* 78−85352
rheography, integral method and electrode for exertion function tests 77−77995
rheological and thermophysical fluid props., physicochem. composition depend. 78−80902
rheoplethysmograph type RPG-202 79−92405
rheoplethysmography, for study of artery function *(French)* 77−37075
rheoplethysmography with occlusion, for study of vein function *(French)* 77−37076
right-to-left shunting determ., suitability of radiopharmaceuticals 77−37048
sarcoma, rate, temp. effect on microvascular haemodynamics during early growth 80−72188
sclerotic arteries, shear stresses in pulse flow *(French)* 79−92249
self-excited oscillator, analysis from distorted signals 77−48831
semilunar leaflet contrib. to turbulent blood flow 80−3666
separation regions in curve tube junctions modelling aortic arch 78−44547
shear flow, thixotropic fluid appl. *(Russian)* 78−87365
shear-induced augmentation of O_2 transfer 80−94274
shock waves in fluid-filled distensible tubes 80−94272
sickle blood cell rheology, pressure-flow curves 77−25503
sickle cell blood in capillaries, flow resistance, O_2 consumption effect model 78−48821
signal acquisition and processing in clinical cardiac catheterisation lab. 77−44768
simulation, numerical, of oscillating flow through sclerotic arteries, finite element anal. 80−26246
simulator for heart valve testing 77−52932
skeletal blood flow, implications for bone-scan interpretation 80−72199
skeletal muscle, canine, blood flow and O_2 uptake obs. in acute anaemia 80−45930
skeletal tracer kinetics, ^{99m}Tc(Sn)methylenediphosphonate uptake in canine tibia rel. to blood flow 80−56192
skin, perfusion, quantitative meas. with ^{133}Xe 80−81707
skin, pig, blood flow clearance changes after single X-ray doses 79−29567
skin blood flow, human, modelling of thermal effects 79−24959
skin blood flow, reflex control by skin temp., role of core temp. 80−85427
skin blood flow meas. by ^{133}Xe, radiation dose 77−16994
skin blood volume pulse, radiation effects, humans 77−5029
soft tissue perfusion rel. to stress, appl. of skin temp. meas. to pressure sore prevention 77−48923
soft tissue temp. increases due to US Doppler blood flowmeters, thermographic meas. 79−62294
solution of high mol. wt. polymers in blood, effect on flow, press. reduction 77−86527
sphygmanometer, Omron's 77 model, accurate meas. 79−74773
sphygmomanometer, random-zero design with variable height reservoir 78−35986
sphygmomanometry, automatic indirect methods, equipment 77−81616
spleen microcirculation, open and closed circulation, rabbit 79−20573
steady flow of incompressible fluid through axisymmetric constriction *(French)* 77−58789
steady pressure drop at various haematocrits, effects of obstruction, in vitro determ. 77−56415
stenosed tube, numerical solns. of Navier Stokes problems 80−16975
stenosed valve, energy losses in flow calcs. 80−41082
stenoses model disorder distal, steady and pulsatile flow 79−57688
stenosis model, flow disorder to mild stenoses in simulated pulsatile flow 78−44551
stenosis model, pulsatile flow downstream 79−92279
stenosis model, turbulence development in pulsatile flow through partially occluded tubes 78−44531
stenosis model, turbulence in water flow system 78−44530
stenosis with upstream roughness, press. and vel. fluctuations 77−56416
stenosis with upstream roughness, pressure and velocity fluctuations 77−40687
stenotic flow, vascular anal. model 79−79593
stenotic flow models, fluid dynamic wall interactions 77−56414
stochastic systems theory, appl. to blood pressure control 80−81522
strain gauge plethysmograph, automated 2-channel 79−29648
stroke volume calc. from transthoracic impedance plethysmogram 78−7381
subcutaneous vasculature histological changes in mouse after single 250 kV X-ray doses 77−73549
sublobar atelectasis and regional pulmonary blood flow, pig expts. 80−81633
superior vena caval pathway obstruction diagnosis following Mustard's operation, transcutaneous Doppler US 79−70596
supersaturation by counterperfusion and diffusion of inert gases 77−90829
supraorbital Doppler evaluation of blood flow in vascular surgery 79−88144
surface EMG and fatigue, muscle temp. and blood flow 80−94199
surface tissue, two-phase theory for circulatory influence on heat transfer 80−104564

haemodynamics continued
synchronised diagnostic and treament techniques 80−61727
systalic blood pressure monitor, type SCS-501 *(Japanese)* 77−70565
systemic arterial bed, quantitative evaluation by parameter estimation of a simple model 80−56094
systemic vasculature, importance of non-linear contribs. 78−44549
systolic time intervals during $+G_z$ accel., appl. to cardiovascular function estimation 77−5087
telemetered cardiovascular changes with free-ranging and treadmill exercise in dogs 77−90821
telemetry system, implantable, single-freq.for monitoring blood pressure 77−86688
temperature gradients in low-flow vessels, appl. to blood temp. distrib. 78−27990
tendon capillary bundles, intermittent flow obs., bullfrog, guinea pig 79−100649
tensile loading, transient, response of blood 80−104618
testicular perfusion imaging, [^{99m}Tc] sodium pertechnetate study, method and obs. 80−12238
thermal properties of tissue, thermistor meas., influence of blood vessels using simulation model 77−40962
thermocouple probe, spherical heated, for perfusion meas. 79−92456
thermography as a means of blood perfusion measurement 80−56167
thermoregulation of rabbit head, facial vein myogenic mech. 80−97869
thixotropic fluid, shear flow, oscillatory Couette flow, apparent viscoelasticity 79−90288
thoracic electrical impedance, cardiac-associated changes in man 79−25128
thoracic electrical impedance sensitivity to blood volume changes 79−34543
three-dimensional problem numerical solns. 78−40238
thrombophlebitis diagnosis, reliability of Doppler and impedance techniques 78−77144
thrombophlebitis patients, venographic, impedance and Doppler US findings 78−48919
thromboresistance of biomaterial, influence of implantation techniques *(German)* 80−3861
thrombosis detection by US, plethysmography and phlebography 78−7435
tissue heat balance, relationship between blood perfusion, metabolism and temp. 80−108852
tissue microwave heating models, surface cooling and blood flow effects 78−7388
tissue perfusion measurements made with thermal diffusion probe, effect of probe geometry 80−104802
total artificial heart haemodynamic study 79−84018
transapical left ventricular bypass with continuous blood filtration 77−48940
transcapillary water movement resulting from non-oncotic osmotic forces 78−44548
transcutaneous blood flow measurements using pseudorandom noise Doppler system 80−36035
transcutaneous EM flowmetry meas. using steady mag. fields 80−41158
transendothelial albumin transport in steady state pipe flow at high shear rates 77−32939
trauma in extracorporeal oxygenation, conf., Stolberg, Germany (Nov. 1978) 80−94922
true volumetric US flow meas. technique 77−90824
tumour blood flow, meas. by photon activation, ^{15}O decay technique 80−104755
tumour blood flow changes due to microwave hyperthermia 78−24116
tumour blood flow rel. to radiation and drug response 80−67114
turbulence detection using pulsed US Doppler method 77−40724
turbulence measurements in straight connectors for extracorporeal blood circulation 80−81641
turbulent flow measurement with pulsed Doppler US 77−40871
two-fluid model for flow through small diameter tubes 80−3667
unsteady flow curved elastic tube model, data for circulatory path physiology and assist devices 80−16998
unsteady flow in contracting or expanding pipe 77−86523
unsteady viscous flow in curved elastic tube, Fourier analysis 79−92281
unsteady viscous flow in non-uniform channels, numerical anal. 77−52830
US blood flow imaging model eqns. and implications 79−48308
US blood flow meas. using random noise, target model and optimal receiver 77−21589
US blood flow spectral anal. using coherent optics 78−53459
US blood flow spectrum, coherent optical anal. 77−40722
US blood flow velocimeter, MTI filter, with inherent A/D 79−16263
US blood flowmeter, noninvasive Doppler device 77−44733
US blood flowmeters, early history 77−77946
US carotid arteriography, real-time, vel. profile imaging 78−24108
US correlation technique for blood flow meas. 77−36968
US digitiser/processor for extraction of clinical parameters from Doppler-shift waveforms 80−36042
US Doppler blood flowmeter, geometrical spectrum broadening anal. 77−86567
US Doppler blood velocimeters, max. freq. detector 79−53201
US Doppler flow measurement, effects of geometrical spectrum broadening 77−40725
US Doppler flowmeter, new modulation method 80−45989
US Doppler flowmeter average frequency processor 79−83873
US Doppler flowmeter spectra for asymm. transducers 78−31880
US Doppler shift signal processing, maximum frequency follower 79−62320
US Doppler signal LF spectral analysis for blood flow model 79−62312
US Doppler spectra, transit time and geometrical broadening 78−44576
US Doppler spectragrams refreshed display and haemodynamic parameter meas. 80−41152
US Doppler velocimetry for 3D blood flow meas. 78−88730
US Doppler-shift arterial flow signals, Fourier anal. 77−29187
US Doppler-shift waveforms, physiological interpretation 80−89814
US flow meas., in objective determ. of human $+G_z$ accel. tolerance 78−3619
US flow measurement using Doppler techniques *(French)* 80−26303
US flow meter *(Japanese)* 78−31875
US flow signals in tumour detect. 78−3571
US flowmeter data processing, transfer function modelling of arteries 78−61225
US FM blood vol. flowmeter processing technique 78−31878

haemodynamics continued
US implantable CW Doppler blood flowmeter, optimal system design 78−53460
US implantable IC CW Doppler flowmeter 78−31877
US mean frequency Doppler modulator performance, blood flow meas. appl. 80−45991
US pulsed Doppl transoesophageal method for aortic haemodynamics meas. in humans 80−30808
US pulsed Doppler flowmeter, vel. accuracy and range resolution 77−77945
US pulsed Doppler technique for quantitative blood flow meas. 80−45990
US pulsed Doppler techniques for cardiovascular meas. 77−77947
US range-gated echo Doppler techniques for cardiac output and aortic flow meas. 78−40276
US synchronized pulsed Doppler blood flow and dimension meas. in conscious dogs 79−62318
US system for blood press. anal. during treadmill stress testing 80−81674
US transesophageal meas. of human haemodynamic parameters 80−41146
US vascular imaging, Doppler method, improvement 78−24106
valveless elastic tube, pumping effect, model *(German)* 78−59493
vascular bed modelling, optimal dialysis appl. 80−30758
vascular beds, optimum modelling using indicator-dilution measurements 77−40686
vascular compliance interaction with const. vascular taper 77−36999
vascular diagnostic system using US Doppler vel. detectors 77−29190
vascular interface system for automation of haemodynamic monitoring and therapy 78−81054
vascular murmurs, model studies of origin and character 77−56398
vascular pressure measurement systems, calibration 79−96691
vascular stenoses, steady flow through, model 79−70563
vascular stenosis detection using flow continuity and turbulence, US Doppler method 77−40723
vascular system, haemorheology and two-phase flow *(French)* 79−34586
vascular system, US Doppler imaging, book contrib. 80−36045
vascular tree structures, optimisation of diameters and bifurcation angles 78−11683
veins, simulation of collapse 78−44535
velocity in abdominal aorta and common iliac artery of man 80−16972
velocity meas., absolute, US Doppler method *(Japanese)* 79−43974
velocity meas., real time multichannel US Doppler signal analyser 77−73551
velocity meas., US Doppler velocimetry, experimental appls. *(French)* 79−34610
velocity meas. by hot-film anemometer *(Japanese)* 79−29678
velocity meas. in microvessels using video correl. system 78−53543
velocity measurement using catheter, cross correl. technique 78−80943
velocity measurement using laser Doppler microscope 79−62329
velocity measurements in vicinity of aortic prostheses 79−74706
velocity profiles, US MTI meas. 80−36033
velocity profiles in small tubes, effect of red blood cells 79−25014
velocity waveform frequency analysis, invasive and noninvasive meas. near stenosis 77−56417
venoarterial indicator-dilution curves, improved correction of distortion 79−25013
venous blood flow visualisation using dynamic leg scintigraphy with large field-of-view scintillation camera 78−73215
venous flow, mech. oscills. ultrasonic Doppler study 80−108931
venous flow, US determ. of cross-sectional shape of elastic tubes 77−25506
venous occlusion plethysmography for the detection of venous thrombosis 80−56268
venous return curves from Valsalva maneuvers 79−53174
venous return resistance, meas. in awake calves using total artificial heart 77−52941
venous system visualisation combined with press. meas., technique and equipment 80−36094
venous volume and local haemodynamics in calf, effect of positive external press. 78−11688
venous volume measurement, eval. of elec. impedance plethysmography 77−40885
ventilation-perfusion ratio, practical considerations of multiple inert gas elimination technique 77−56411
ventilation-perfusion ratio distrib. determ. from inert gas data with enforced smoothing algorithm 78−61208
ventilation-perfusion ratio distribs., graphical assessment from inert gas elimination data 77−52834
ventilation-perfusion ratio intraregional maldistribution simulation 78−31834
ventilation-perfusion relationship in young healthy awake and anesthetised-paralysed man 80−67120
ventilator-patient coupling, effects of positive press. ventilation on cardiac output and pulmonary arterial flow 78−31852
ventrical, left, haemodynamical parameters meas., frame rate requirements 79−100715
ventricle, spherical, dynamic press. distrib. 79−70562
ventricular aneurysms, mechanical behaviour, mathematical model 79−11953
ventricular function computer simulation, development of model and parameter estimation 78−53439
ventricular functionanalyser, microprocessor-based 80−26402
ventricular mean transit time, right, using radiocardiography 77−2040
ventricular wall dynamics and obs. on blood flow 78−80896
vessel rheological props. and haemodynamic parameters meas. *(French)* 79−66587
yessel simulation, ideal fluid small oscillations, mass forces in elastic shell 79−77253
vessel wall motion, US Doppler shift meas. 77−25538
vessel walls, ion permeability 77−32934
video-tracking of micro-circulation, appl. of bit-slice processors *(German)* 78−88749
viscoelastic tube, viscous fluid wave propag., asymptotic formulae and numerical results 79−34595
viscosity factors in severe nondiabetic and diabetic retinopathy 78−65069
viscosity variations associated with hyperlipoproteinaemia, rel. to cardiovascular risk factors *(German)* 78−57031
viscosity-temperature relationship, human plasma and serum 79−20564

haemodynamics continued
viscous flow in collapsible tubes of slowly varying elliptical cross-section 77−64076
volume expansion effects, gas cavities 80−67134
volume flow quantitative estimation with transcutaneous Doppler US 80−36052
X-ray computed tomography, 3-dimens., of heart, lungs, and circulation 79−53224
CO_2 pressure, end-tidal and arterial diff. obs. 80−72193
CO_2 pressures in dogs during acute hypercapnia, arterial-expired differences 80−72198
^{60}Co effects on blood press. and performance in monkeys rel. to dose-rate 77−81540
^{60}Co exposure effects in monkeys rel. to performance decrement 77−81541
^{59}Fe tracer data analysis program and kinetics model *(German)* 79−5342
^{113m}In-labelled transferrin, use in meas. of blood vols. in rat, rabbit 80−3878
O_2 diffusion in blood, analysis of carrier facilitated transport in heterogeneous media 77−39360
O_2 mass transport and regulation, microelectrode and math. modelling study 78−44534
O_2 partial pressure meas. in cat cerebral cortex 79−83826
O_2, steady state diffusion in red blood cell and model suspension 77−40644
O_2 transmural transport to retina, mathematical model 79−34583
O_2 transport from pulsatile viscous blood flow to diseased coronary arteries of man 78−40220
$^{81}Rb/^{81m}Kr$ ratio as radioactive tracer study of organic bleeding *(Dutch)* 80−3807
^{99m}Tc-EHDP accumulation in canine tibia, meas. method 78−20245
^{133}Xe washout curve discriminant analysis for lower extremity vascular impairment 78−35949

haemoglobin *see proteins*

hafnium
see also nuclei with .....
abundance determ. in silicate rocks, meteorites and lunar samples by neutron activation 78−20547
abundance in stony meteorites 79−92731
atom, even config., parametric calcs. 78−82631
atom, partial level density, statistical props. of atomic energy levels 78−70732
barrier metal for sintered Pt-GaAs contacts 77−8193
calciothermic, electrorefining 78−68647
corrosion in buffer soln., revealed by impedance and potential meas. 79−96182
diffusion in Er_2O_3, vol. and grain boundary diffusion coeffs., tracer sectioning technique 79−7712
electrode, surface oxide film, impedance and pot. behaviour 80−61001
electron field emitter, temp. drop meas., allotropic transform. temp. 80−2931
electron structure and soft X-ray emission spectrum, RAPW calcs. 79−91536
electronic excitations, charact. energy loss meas. up to 50 eV 80−60723
emittance at 400 to 850K and normal spectral reflectance at room temp. 77−20813
film, optical absorption meas. using synchrotron radiation, 20-250 eK 77−12457
film, RF sputtered onto sapphire, high stress in graded interfacial layers, AES meas. 77−43446
film on Si substrate, ion-beam induced silicide form. 79−46718
HCP, elec. field gradient 78−14698
high temperature thermophysical properties 78−91404
HTGR pebble bed core, initial heterogeneous poisoning by B and HF 80−22981
implantation of Si, Al, Hf, Ta into InP and GaAs, form. of protective oxide 78−79622
with interstitial O, quantitative TEM obs. of small agglomerates 80−107227
isochromat spectroscopy using SXAPS equipment 79−95877
L-subshell ionisation cross section, branching ratios, fluoresc. yield, Coster-Kronig factors 80−43166
lattice dynamics, phonon dispersion, mode softening 80−107390
lattice dynamics, thermal and elastic props., model for HCP Hf 80−34155
liquid, viscosity at melting point, free energy *(Russian)* 80−92699
neutron detector using (n,γ) on ^{157}Gd, ^{177}Hf foils, proportional chamber detection of conversion electrons 78−37517
nuclear target preparation from HfO_2 reduction by Ca 80−18746
oxidation, microstructural study *(French)* 80−45436
oxidation in flow conditions at 1000 to 6000K 78−11445
polymorphic transition, emission images obs. in temp. range 1800-2100°K 80−100836
reactor cooling and heat recovery appl. *(Italian)* 78−4978
RF sputter deposition, ion bombardment and ion implanation 80−25564
secondary ion emission, energy spectra, 0-55 eV, contamination levels 79−15573
separation from Zr, new process 78−6875
solar abundance from Hf II spectral lines obs. 77−17518
solid state phase transformation $\alpha \rightarrow \omega$, exam. of phase transformation kinetics under static, and dynamic pressures 78−80541
solvent extraction and complex formation with tridentate organophosphorous compounds 78−76853
surface, decomp. of hydrocarbons, O or N surface segregation effects 80−55654
thermal diffusivity meas., 300 to 1000K, Lorenz number determ. 80−29384
thermotransport and thermopower of O_2 78−76055
vacuum technology appl., melt processing and appl. *(Hungarian)* 80−55318
valence band XPS, correl. to supercond. 79−65980
X-ray fluorescence analysis, simultaneous determ. of Zr and Hf trace elements in soln. 80−97752
Zn-salt, molten system, separation of Hf and Zr 80−11884
$BaTiO_3$:Hf, crystal field distortion by stacking faults, PAC meas. 80−11306
β-Hf, electrotransport and diffusion of Ta impurities *(German)* 78−87826
α-Hf, electrotransport of O impurities *(German)* 78−87826

hafnium continued
Hf III, multiconfig. Dirac-Fock theory, relativistic SCF method 77−3282
Hf IV, 6s $^2S_{1/2}$-6p $^2P^\circ_{1/2,3/2}$ transition, relativistic oscillator strengths, influence of core polarisation 80−58132
Hf IV, one-electron spectra energy levels and line lists 79−49953
Hf XLV X-ray spectra from laser produced plasmas 80−42981
Hf-Ge planar interface, first phase to nucleate 77−62764
HfI, at spectrum, g-values, Zeeman effect, LS-coupling, ionisation pot. 77−3292
^AHf, A=179,180, absolute atomic masses 79−89228
^{179}Hf, nucl. quadrupole moments and hyperfine struct. in ground multiplet ^3F 77−83520
Pt:^{181}Hf, interaction of implanted impurity with radiation induced lattice defects, TDPAC meas. 80−24494
SrS:Hf, phosphor fluoresc. spectra, host lattice defect 77−12416
SrS:Hf phosphor, activation energy and freq. factor calcs. from glow curves 77−12451
SrS:Hf^{4+} phosphors, phosphorsc. decay curve 77−63450

hafnium alloys
see also hafnium compounds
absorption of H_2 79−77754
metatectic reaction prediction 79−29020
noncubic metal-Hf, dil., ^{178}Hf Mossbauer transition, electric quadrupole interaction 80−39928
Ag-Hf film, optical absorption spectra meas. 77−85823
Co-Cr-Al-Hf, high temp. oxidation 78−11432
Co-Hf, dendritic segregation 80−76260
CoCrAl-Hf, Hf effect on oxidation 78−44275
Co_2HfAl, Heusler alloy, paramag. state NMR and susceptibility meas. 79−65643
Co_2HfAl, hyperfine fields of Fe impurities, Mossbauer spectra 80−71255
Co_2HfSn-Fe, dil., Heusler alloy, Fe hyperfine fields, Mossbauer obs. 78−68424
$Co_2HfSn(Al)$, ferromag., hyperfine fields meas. by NMR 77−63315
Cr-M, optimum alloying with rare earth metals, Ti, Zr, Hf, Nb, Ta 78−68651
$Cu_{40}Nb_{30}X_{30}$ (X=Ti, Zr, Hf), superconductors with metastable ordered structs. 80−108484
Fe_2Hf, ferromagnetism in hexagonal and cubic compounds 77−36074
$(Hf,Zr)V_2$, phase transition, sp. ht. anomalies meas., 70-150K 77−35691
Hf, 0.3 wt.% Zr, melting pt. and radiance temp. meas. by pulse heating method 77−53914
Hf-Al-C, phase diagram and lattice constants, X-ray diffr. method 80−89207
Hf-B, abrasive props. 80−16489
Hf-Be, coupled phase diagrams and thermochemical descriptions 80−25656
Hf-Co, phase diagram, X-ray diffr., thermal anal. and metallography obs. 78−60652
Hf-Co-Ga system, crystal atomic struct. and phase equilibria *(Ukrainian)* 78−84772
Hf-Cr-Ga, X-ray microanalysis of phase equilibria *(Ukrainian)* 78−6898
Hf-Cu, amorphous, thermal stability, crystn., DSC and elec. resist. study 80−107060
Hf-Fe, amorphous, thermal stability, crystn., DSC and elec. resist. study 80−107060
Hf-Fe alloys, oxidation 79−52460
Hf-Fe(Co)(Ni)(Cu), oxidation of intermetallic phases 79−100298
Hf-Ge-B system, phase equilibria 78−35356
Hf-Ge-Ga, X-ray microanalysis of phase equilibria *(Ukrainian)* 78−6898
Hf-H, diffusion in hydride phase, exam. 80−29204
Hf-Ir, dil., elec. field gradient at ^{193}Ir, Mossbauer meas. 80−66090
Hf-Mo, high temp. phase diagrams 77−44217
Hf-Mo-C, isothermal section of phase diagram at 1400°C, X-ray phase analysis determ. 79−34006
Hf-Mo-C, phase diagram, crystallisation patterns of partial system Mo-HfC-Hf 77−12598
Hf-Mo-C, phase diagram and crystallisation of partial system Mo-HfC-C 77−12599
Hf-Mo-C system, isothermal section of phase diag. at 1700°C 78−68674
Hf-N, solid soln. hardening, impurity cluster and interstitial mechanisms 77−36523
Hf-Nb (30 to 50 at.%) exam. of beta phase decomposition processes 78−76674
Hf-Nb-Ga, phase equilibria X-ray study at 800°C *(Ukrainian)* 79−95998
Hf-Ni (65 to 80 at.%), phase diagram and cryst. struct. of intermediate phases 79−52170
Hf-Ni-H, catalytic activity, exam. by conversion of toluene, and bicyclic aromatic hydrocarbons 80−30276
Hf-Ni-H, catalytic props. 80−30274
Hf-Ni(Co), amorphous, formation, decomposition and elec. transport props. 80−20143
Hf-Ni(Cu)-Ga, alloys, phase diagrams and cryst. struct. *(Russian)* 80−25658
Hf-O, solid soln. hardening, impurity cluster and interstitial mechanisms 77−36523
Hf-Ta, dil., hydrostatic and uniaxial compression, elec. field gradient at Ta, time differential PAC meas. 77−69739
Hf-Ta, prep. by carbide-oxide reaction 77−12554
Hf-Ti, binary continuous solid solution, elec. resist. and thermoelec. power behaviour 79−69492
Hf-V, superconductivity and metallurgy of C15 materials 79−4610
Hf-V foil, rapidly quenched and heat treated, supercond. props. 80−54852
Hf-Zr, binary continuous solid solution, elec. resist. and thermoelec. power behaviour 79−69492
Hf-Zr (3 wt.%), $\alpha \rightarrow \beta$ transform. temp. and entropy, emissivity 77−48424
Hf-Zr-Ga, phase equilibria X-ray study at 800°C *(Ukrainian)* 79−95998
Hf-Zr(Sc), thermopower composition depend. 79−65445
$HfAl_3$, anomalous growth in thin films, AES, TEM and He backscatt. meas. 77−43462
HfC-HfB_2, wear in vacuum, role of boride phase 80−21113
HfC-$HfBr_2$, preparation and high temp. antifriction props. 79−1918

hafnium alloys continued
$HfCo_6$, saturation magnetisation, Co mag. moment and electron transfer 77−73005
$Hf_{1-x}Co_x$, amorphous alloys, thermal stability, elec. cond. enthalpy 80−100172
$Hf_{1-x}Fe_x$ amorphous alloys, formation, crystallisation and electrical resistivity 80−96838
Hf_2Fe, moment form. on H_2 absorpt. 79−87343
$Hf(Fe_{1-x}Co_x)_2$, mag. props., Mossbauer spectra and magnetisation meas. 80−39948
$HfFe_{2-x}Si_x$, Laves pseudo-binary compound, cubic C15 phase stabilisation 77−39559
$HfFe_{2-x}Si_x$, Mossbauer spectra, hyperfine interactions 80−15862
$HfFe_2Si_2$, cryst. struct. 77−31633
$HfGe_2$ film, supercond. obs. 77−72939
$HfMn_2$, Curie-Weiss law depend. of susceptibility, mag. props. *(Russian)* 79−65655
$Hf_{0.65}Nb_{0.35}$, superconducting alloy, transition temp. and flux line pinning 77−43772
HfNi, hyperfine critical exponents, TDPAC meas. of bulk meas. 77−8465
$HfNi_3$, α and β modifications, X-ray cryst. struct. determ. 79−7578
Hf_3Ni_7, X-ray cryst. struct. determ. 79−4270
Hf_8Ni_{21}, single-cryst., X-ray cryst. struct. determ. 79−4269
$Hf_3Ni_2Si_3$, struct., lattice consts., space group, X-ray Weissenberg camera data 78−47284
$HfPt_3$, corrosion resist. and elec. cond., bulk and film samples 78−72285
HfV_2, C-15 struct., phase transitions, elec. cond., crystal lattice parameters *(Russian)* 80−54826
HfV_2, C15 Laves phase, supercond. and stoichiometry 78−39245
HfV_2, C15 supercond., dielec. transitions, temp. depend. of resist. and mag. susceptibility, 4.2-300K 79−38136
HfV_2, dielectric phase transition, elec. resist. temp. depend. 79−65525
HfV_2, elec. resist. and mag. suscept., anomalous temp. depend. 79−69491
HfV_2, latent heat of structural transform. 80−24589
HfV_2, supercond., dielec. phase transition *(Russian)* 78−64168
HfV_2, supercond., Young's modulus and internal friction meas. 79−11654
HfV_2, supercond. compound, thermal expansion at low temp. 78−76189
$HfV_2H_{2.1}$, proton NMR relax. time and Knight shifts, diffusional activation energies meas., sorption props. 80−75871
HfV_2H_x and HfV_2D_x, composition depend. of supercond. crit. temp. 77−20482
$HfV_2H_x(D_x)$, superconducting transition temp. var., isotope effect 77−12047
Hf_xZr_{1-x}, elec. quadrupole interactions at ^{181}Ta impurities, TDPAC meas. 78−76364
$(Hf_xZr_{1-x})_{80}Nb_{20}$, influence of Hf additions to $Zr_{80}Nb_{20}$, beta decomposition anal. 79−8304
$Hf_{1-x}Zr_xV_2$, lattice consts. at 4K and room temp., phase division at x=0.4 78−51474
$Hf_{0.5}Zr_{0.5}V_2H_x(D_x)$, enhanced supercond. transition temp. on H(D) additions 78−80083
Lu-Hf, elec. field gradient at ^{175}Hf nuclei aligned at low temps. 79−82884
Mo-Hf (0.3 wt.%), strength, plasticity and microhardness, internal nitriding effect *(Russian)* 80−40433
Mo-Hf-B-C, low C, sheet, strength 77−1859
Mo-Hf-C, superior powder metallurgy die alloys for isothermal forging mech. props. 79−74201
Mo-Hf-C-Ni, electrochemical phase composition anal., precip. of HfC phase *(Russian)* 80−20901
Mo-Hf-N, exam. of phase equilibria *(Russian)* 79−29018
Mo-HfC, eutectic formation of regular struct., crystn. *(Russian)* 80−66496
Mo-HfC-C, projection of solidus surface, partial system of Hf-Mo-C 77−1834
Nb-Hf, dil., neutron irradiation at 4.6K, influence of impurities on defect prod. 79−55790
Nb-Hf, single cryst. elastic consts. 77-298K 78−84879
Nb-Hf (26 at.%), mixed state, ultrasonic velocity meas. 79−60974
Nb-Hf (38 at.%) superconductor, peak effect, summation problem, mag. history flux pinning force 80−20362
Nb-Hf-N, exam. of phase equilibrium using electron microscopy and X-ray analysis *(Russian)* 79−15654
Nb-Hf(26 at.%), mixed state, magnetoacoustic attenuation 77−4473
Nb-W-Hf-C, quenched from liquid state, formation of nonmetallic inclusions *(Russian)* 79−57007
Nb_3Sn, current carrying capacity increase by Hf addition 80−7056
Ng-Hf-C(N), phase comp. after casting and annealing, precip. 79−56983
Ni alloy Mar M200, directionally solidified Hf additions, effect of vol.% γ' on creep rupture 78−27526
Ni-Cr-Si (10, 1.8 wt.%), Zr, Hf, La or Sm alloying additions effect on oxidation resist. 77−63831
Ni-Hf, wetting of AlN, effect of alloys exam. 78−80710
Ni-HfO_2 (3 wt.%), dispersion hardened alloy VDU-2, thermal and mech. treatment 77−90376
Ni-W-Co-Cr, superalloy MAR 200, with Hf, cellular composite prod. by isothermal dendrite ripening 78−44150
Pt-Hf, high temp. thermodynamic props. 77−63633
Sc-Hf, binary continuous solid solution, elec. resist. and thermoelec. power behaviour 79−69492
Sm-$HfCo_7$ alloy, rare-earth electron transfer 77−40028
Ta-W-Hf, embrittlement, effect of composition 77−21247
Ta-W-Hf, small-angle electron scattering in TEM from lattice strains accompanying precipitation 79−14658
Ta-W-Hf (8,2 wt.%), T-111, O_2 absorption, effect on lattice parameter and specimen dilation 78−83958
Ti-Hf-O system, $\omega(0)$ phase form. 79−11553
Ti-Mg-ZrC, sintered, friction and wear props. 79−70019
Ti-Zr-Hf disordered solid solns., thermal cond. 79−15132
Ti(Zr,Hf)-Gd-B system, phase equilib. 80−11629
V-Hf-Nb(Zr), multifilamentary, superconducting props. improvement 79−38267
V-HfV_2-HfCr_2-Cr, phase diagram *(Russian)* 77−52288
V_2(Hf,Zr), Laves phase compounds, electrical resistivity, temperature dependence 78−76047
V_2(Hf,Zr), NMR and mag. susceptibility, density of states determ. *(Russian)* 80−66053

hafnium alloys continued
V_2Hf base Laves phase compound tapes, supercond. props., prep. 77−40011
V_2Hf, struct. transform. at low temp., X-ray diffr. anal. *(Russian)* 80−45298
V_2Hf, supercond., fast neutron irrad. effects on T_c 77−55633
$V_2Hf_{1-x}Ta_x$, C15 supercond., electronic and lattice props. 78−68110
V_2HfZr, C-15 cryst. struct. supercond. props. 78−64173
$V_2Hf_{1-x}Zr_x$, normal and supercond. state, transition temps., mag. susceptibility and specific heat determ. *(Russian)* 80−60132
$V_{2-x}Nb_3Hf$, NMR of ^{51}V and mag. susceptibility, 20-300K *(Russian)* 80−93192
V_3Si-Hf solid soln., supercond. T_c and paramag. susceptibility *(Russian)* 77−59348
W-C-Hf, vacuum melted, phase composition, struct. and props. 78−31403
W-Hf-C, cubic solid soln., form. and props. 78−48348
W-Hf-C, phase equilib. 80−55348
$(Zr,Hf)Fe_2$, mag. hyperfine field at Hf sites, TPDAC meas. 79−82901
Zr-Hf, electrophys. props. *(Russian)* 80−39551
Zr-Hf (2.2 wt.%), high temp. oxidation in flowing O_2, 873-1173K 80−93687
Zr-Hf (2.2 wt.%), oxidation kinetics in flowing CO_2, 873 to 1173K 80−16596
Zr-Hf (2.2 wt.%), oxidation kinetics in flowing CO_2 at high temp. 80−47575
$Zr_xHf_{1-x}V_2$, polycrystalline superconductor, resist. and mag. susceptibility, transition temp., temp. depend. 80−25113

hafnium compounds
see also hafnium alloys
halides, XY_4 molecules, force consts. by modified Redington and Aljibury method 80−69261
refractory carbides, borides and nitrides, wetting by and interactions with liq. metals 80−54473
tetrahalides, struct., force field and Coriolis const. calcs. 78−86843
tetrahalides of Gp.IV elements, M-X bond flexibility, by compliance scheme 80−37805
vitamin B_{12}-^{181}Hf complex, γ-ray PAC expt., crystal and liq. 79−39341
$AlHfTaO_6$, powder X-ray diffr. data 79−99155
Er_2O_3:HfO_2, polycryst., Er self-diffusion 80−29207
Fe-HfB_2-MoS_2, self lubricating coatings, exam. of props. 79−96217
Fe-HfC-MoS_2, self lubricating coatings, exam. of props. 79−96217
HfO_2, polycrystalline, monoclinic, elastic props. at room temp. 78−27548
HfO_2, powder, preparation technique for highly sinterable powder 78−39714
HfO_2, vacuum deposited film, use in multilayer reflector for near UV 77−34924
$HfSe_2$, optical phonon modes and localised effective charges, reflection spectra 78−76453
Hf complex, Hf-EDTA, aqueous solns., rotational diffusion, TDPAC study 80−34837
Hf complex, tetrakis (tropolonato) hafnium (IV), mol. interactions in solid, perturbed γ-γ ang. correl. obs. *(French)* 79−8076
Hf complex, with N-benzoyl N-phenyl hydroxylamine, mol. reorientation in soln. 77−16218
Hf-C-N-O-H, solid solns. of H, exam. of props. 80−29172
Hf-H, diffusion in hydride phase, exam. 80−29204
Hf-M-B systems (M=Rh,Ir), phase equilib. and cryst. structs. 80−15072
Hf-O, phase props. 77−40415
Hf_3As, cryst. struct., X-ray diffr. pattern intensity profile 80−49201
HfB_2, mag. susceptibility temp. depend. *(Russian)* 79−82749
HfB_2, oxidation in O_2 atmosphere, exam. 80−11814
HfB_2, single crystal growth *(Japanese)* 79−65987
$HfB_{2.035}$, ht. capacity, 5-350K 77−47590
$Hf(BH_4)_4$, host cryst., excited state assignments and E-symmetry ground state, near IR MCD obs. for $U(BH_4)_4$ 80−66153
HfC, adsorption of Cs(K), adsorpt. energy, thermionic emission 77−7978
HfC, bond energy and ionization efficiencies from SIMS 79−24400
HfC CVD coating, on W-ThO_2 and SiC filaments, effect on high temp. mech. props. 78−15347
HfC coated emitters, thermionic emission props. *(Japanese)* 77−40322
HfC electronic structures calc. and obs., by APW method and X-ray photoelectron spectroscopy *(Japanese)* 79−15074
HfC, etchant for revealing microstructure 80−85097
HfC, generalised susceptibilities and electronically driven phonon anomalies 79−42208
HfC, high-temp. supercond., role of electronic struct. in obs. phonon anomalies 77−24363
HfC, micropowder, abrasive props. 77−63821
HfC, pressing regime influence on high-temp. creep *(Russian)* 80−100852
HfC, quasi-self-consistent energy band structures using relativistic KKR calcs. chemical bonding 79−51484
HfC, reactive RF sputtering in N_2, HfN film deposition 79−78886
HfC, single crystal growth by plasma heating 78−60569
HfC, X-ray emission band exam. and electronic struct. 77−8689
HfC:Ta, perturbed ang. correlation spectra, elec. quadrupole interaction 80−15916
HfC-HfB_2, reactions, cpd. formation and props. 78−23685
HfC-TaC alloys, microhardness rel. to valence electron conc. 77−86130
HfC-TiC, phase diag. calc. 77−90329
HfC-TiC, pseudobinary systems, phase diagrams, computer calcs. 78−44092
HfC-W(Mo), thermionic emission, surface structural characts. after prolonged use, work function variation 80−20758
$HfC_{0.968}$, ht. capacity, 5-350K 77−47590
HfC_x, complex phases with NaCl struct., microhardness rel. to electronic structure 77−90438
HfC_x, electron energy spectrum and phys. props. in homogeneous region *(Russian)* 77−31941
$HfC_{1-x}N_x$, elect. resist. *(German)* 79−38064
HfC_xN_{1-x}, electronic struct., theoretical approach 80−54584
HfC_xN_{1-x}, X-ray valence photoelectron spectrum, 4f signal calc. 80−66391
$HfC_xN_yO_z$, valence band XPS, correl. to supercond. 79−65980
$HfCl_4$-CsCl melt, equilib. phase diagram and vapour press., equilib. reaction 77−66764

hafnium compounds continued
$HfCo_2$:Ta, perturbed ang. correlation spectra, elec. quadrupole interaction 80−15916
HfF_4, mol. struct. and vibr. freqs., gaseous electron diffr. obs. 80−32836
HfF_4-BaF_2-LaF_3 glass system, IR transmitting, synthesis and props. 80−71623
HfF_4-BaF_2-ThF_4-(ZrF_4) glass system, IR transmitting, synthesis and props. 80−71623
$HfFe_2$:Ta, perturbed ang. correlation spectra, elec. quadrupole interaction 80−15916
$HfGeO_4$, nuclear quadrupole interactions, TPDAC meas. 79−82902
HfH_4, Dirac-Fock one-centre calcs. 77−88380
HfN coating on cemented carbide tools, machining evaluation 79−29253
HfN, electronic struct., relativistic energy band struct. calc. 80−34354
HfN on stainless steel, activated reactive evaporated coatings, high rate deposition, microhardness 80−25580
HfN, RF sputter deposition, ion bombardment and ion implanation 80−25564
HfN, vibr. IR spectrum, mol. consts. 79−68230
HfN, X-ray emission band exam. and electronic struct. 77−8689
HfN_n, effect of equilib. N_2 press., 10^{-2} to 100 atm, on MP 77−36465
$HfNi_{1.8}Si_{3.2}$, X-ray determ. of crystal struct. *(Russian)* 77−76361
$HfO+BaCO_3$, mechanism, effect of polymorphic transitions 79−11605
HfO_2, chem. induced elec. field gradient, perturbed ang. correl. obs. 78−80257
HfO_2, correcting coatings, u.v. transmission cutoff 77−760
HfO_2 crystallite growth from oxide plasmas, growth morphology 80−59417
HfO_2, dielec. and thermophys. props. 77−52009
HfO_2 dispersed Ni, recrystallisation during annealing, O_2 partial press. effects *(Russian)* 78−3140
HfO_2, electronic excitations, charact. energy loss meas. up to 50 eV 80−60723
HfO_2 film, CVD growth, struct., elec. and optical prop. characterisation 77−55891
HfO_2 film, growth by thermal decomp. of β-diketonate complexes, charcts. 79−100055
HfO_2, high pressure polymorphism 80−59429
HfO_2 laser coating, UV damage obs. 80−33056
HfO_2, monoclinic, microcracking, elasticity, internal friction, thermal expansion meas. 79−29195
HfO_2, obtained by vapo-condensation, exam. of structure and phase props. *(French)* 79−19489
HfO_2, optical coatings, laser damage resist., spectral depend. 77−62022
HfO_2, plasma deposition of crysts. and their characterisation 80−20800
HfO_2 protected Al mirror, high refl. 8 to 12 μm, normal to high incident angles 78−79090
HfO_2 reduction by Ca 80−18746
HfO_2 single crystals, Y_2O_3 stabilised, optical props., impurities and annealing conditions influence 79−52399
HfO_2, stabilised, low temp. induced centres, ESR meas. 78−72409
HfO_2, stabilised comps., elastic props. rel. to porosity and temp. 80−81096
HfO_2, thermal anal. using solar heating *(Ukrainian)* 79−77725
HfO_2, vac. deposited, near UV multilayer reflector 77−39014
HfO_2, Y_2O_3-stabilised, solid soln., Raman scatt. anal. of struct. transform. 78−88312
HfO_2, zero and low coeff. of thermal expansion 80−39325
HfO_2:Er_2O_3(Y_2O_3)(Eu_2O_3), elastic props., sonic reson. meas. 80−7612
HfO_2:M^{n+}, M=Ce, Pr, Tb, Eu impurity valence transitions 77−51694
HfO_2/SiO_2 mirror coatings, light scatt. and optical strength in UV range 80−106595
HfO_2-Al_2O_3, phase diag., 1500-2250°C 77−85998
HfO_2-CaO(MgO) elec. field gradient at ^{181}Ta, TDPAC meas. 79−33577
HfO_2-CeO_2, solid solutions 77−16549
HfO_2-Cr_2O_3 system in Ar medium, phase equilibria, 1600-2500°C *(Russian)* 77−55953
HfO_2-Eu_2O_3, phase composition in HfO_2-rich region, X-ray anal. 77−12609
HfO_2-Eu_2O_3, phase equilibrium, 960 to 1900°C, X-ray anal. 78−23688
HfO_2-EuO_2 system, liquidus determ. from thermal anal. *(Ukrainian)* 79−96007
HfO_2-Gd_2O_3, phase relations 78−72769
HfO_2-$KHnO_2$($KScO_2$), ionic cond., lamellar struct. *(French)* 77−1257
HfO_2-La_2O_3 system, phase form. and relations, phys. props. 79−43218
HfO_2-MgF_2, interference coatings perpared by electron beam evaporation, UV optical strength 79−59779
HfO_2-MgO system, intermediate phases existence, X-ray diffr. and IR obs. 79−38805
HfO_2-PrO_x, phase equilibria and physicochem. props. in range 1000 to 1800°C 79−100117
HfO_2-R_2O_3 solid solns., prep., crystn., R=Nd,Sm,Dy,Yb 78−42909
HfO_2-rare earth oxide, cubic solid soln., lattice parameters 79−82186
HfO_2-SiO_3, layer for dielectric mirror, for KrF excimer laser *(Japanese)* 79−72588
HfO_2-Sm_2O_3, X-ray diffr. obs. of phase relations 79−61566
HfO_2-TiO_2, phase relations and thermal expansion 77−21121
HfO_2-TiO_2, thermal expansion coeff. and dynamic response to pulsed energy deposition 78−26705
HfO_2-TiO_2 system, liquidus determ. from thermal anal. *(Ukrainian)* 79−96007
HfO_2-TiO_2 system, zero and low coeff. of thermal expansion 80−39325
HfO_2-V(Ta), eutectic system, metallography *(Russian)* 77−66629
HfO_2-Y_2O_3, solid soln., diffuse X-ray scatt. by vacancies 78−71728
HfO_2-ZrO_2 refractory, sublimation *(Russian)* 78−47513
HfO_4^{4-}, normal vibr. freqs., force consts. calc. *(Russian)* 77−6759
$HfOCl_2$, aqueous solns., rotational diffusion, TDPAC study 80−34837
$HfO(H_2PO_4)_2.H_2O$, chem. induced elec. field gradient, perturbed ang. correl. obs. 78−80257
$(HfO_2)_y(In_2O_3)_{1-y}$, bulk resistivity 77−35936
$(HfO_2)_{0.9}(Y_2O_3)_{0.1}$:$Cu^{2+}$, ESR at room temp., spin Hamiltonian parameter determ. 77−16167
HfP_2O_7, chem. induced elec. field gradient, perturbed ang. correl. obs. 78−80257
HfS, equilibria, nonstoichiometry and elec. props. temp. depend. *(French)* 78−64053
HfS_2, enthalpy and specific heat, temp. depend. 80−54406
HfS_2, growth by I_2 vapour transport using temp. oscill. method 77−77355
HfS_2, intercalation-induced shift of absorpt. edge 79−82999
HfS_2, layer compound, expansivities and thermal degradation 77−89554
hafnium compounds continued
HfS_2, optical props. modulation spectroscopy, indirect absorpt. edge 77−52117
HfS_2, vacuum UV reflectivity spectra, cond. band model 77−44012
HfS_3, one-dimensional semicond., Raman spectra meas. 80−50345
HfS_3, quasi one-dimens., optical phonon anisotropy, IR spectra study 80−40112
$Hf(SO_4)_2$, elec. quadrupole interaction, TDPAC technique, coincidence system 80−93216
$HfS_3(Se_3)$, phonon study of chemical bonding 80−20645
$Hf_3Sc_4O_{12}$, cryst. struct. determ., powder X-ray diffr. exam. 77−4083
$HfSe_2$, layer type dichalcogenides, reflectivity 6 to 40 eV, electronic deep level excitation 77−55801
$HfSe_2$, vacuum UV reflectivity spectra, cond. band model 77−44012
$HfSe_{2-x}Te_x$, elec. resist. and mag. suscept. studies 80−44599
$HfSi_2$, thermal expansion, microhardness, Debye temp. meas. 77−35717
$HfSi_2$, work function rel. to phys. props. 77−47887
$HfSiO_4$, Raman spectrum interpretation, lattice vibrs. 77−48160
$HfSiO_4$:U^{4+}(U^{3+}), opt. spectra 78−88334
$Hf_xTa_{1-x}C$, thermal cond. and diffusivity, 1000-2200°C, elec. cond. 78−91491
$Hf_xTa_{1-x}C_y$ solid solns., mag. susceptibility, 20-1300K *(Russian)* 78−39287
$HfTe_{2-x}$, elec. resist. and mag. suscept. studies 80−44599
HfV_2D_4, disordered solid solution, order-disorder transition 80−88321
HfV_2O_7:^{181}Ta, EFG temp. depend., TDPAC 77−59488
HfX_4, (X=Cl,Br,I), He I and He II photoelectron spectra, ionis. energy, chem. bonding 78−46394
HgO_2-Y_2O_3, solid soln., elastic and photoelastic props., Mendelstam-Brillouin scatt. 78−6693
$K_2Hf(MoO_4)_3$, synthesis and struct. 77−36386
$K_8Hf(MoO_4)_6$, X-ray structural investigation 78−79597
La_2O_3-GeO_2-HfO_2, vitrification, crystn. 77−15559
$La_2Zr_2O_7$-$La_2Hf_2O_7$ system, cryst. struct., phase diagram 78−83806
$Li_{1-x}Hf_{2-x}Ta_x(PO_4)_3$, new solid ionic conductors 77−35953
$(NH_4)_3HfF_7$, longitudinal decoupling of quadrupole interaction 78−39456
Nb-HfN, BCC solid soln., nitride solubility, alloying effects *(Russian)* 79−51262
Nd_2O_3-HfO_2 system, phase relationships 80−35169
Ni-Cr-HfO_2, dispersion-strengthened, hot rolling effects on props. *(Russian)* 77−59797
Ni-HfO_2(2.14 wt.%), dispersion hardened, HfO_2 particle size effect on struct. and mech. props. *(Russian)* 80−20944
Sc_2O_3-HfO_2, cubic solid soln., lattice parameters 79−82186
SrO.HfO_2, US comminution of refractory compound powders 78−23656
$Ta_{0.97}Hf_{0.03}S_2$ (1T), charge density waves, ESCA, XPS investigs. 77−12490
$Ti_{1-x}Hf_xSe_2$ mixed cryst., elec. resist. and phase transition temp. 80−24928
$YHfTaO_6$, powder X-ray diffr. data 79−99155
Y_2O_3:HfO_2, elec. cond. and O ion mobility 80−34490
Y_2O_3-HfO_2, cubic solid soln., lattice parameters 79−82186
Y_2O_3-HfO_2 system, solid soln. form. mechanisms 79−11579
ZrC-HfC, pseudobinary systems, phase diagrams, computer calcs. 78−44092
ZrO_2-HfO_2, monoclinic solid soln., ceramic prep. and use 80−55338
ZrO_2-HfO_2-CaO, cubic solid solutions, thermal expansion 77−15598
half adders *see adders*
half-lives (radioactive) *see radioactive decay periods*
half wave rectification *see rectification*
half wave rectifiers *see rectifiers*
halides
see also compounds of individual elements, e.g. "tungsten compounds" and "organic compounds"
see also alkali metal halides; halogens
activators for cementation at Zr/graphite *(French)* 77−52552
alkali halide crystals, kinetic shape stability loss in faced cavities in diffusion zone 79−55916
alkaline earth fluorides, thermolum. glow-peak shapes 77−28639
Anderson-Gruneisen parameter, heavy metal halides 78−79715
aryl halides, mol. beam photodissoc., fragment translational energy distrib. 77−50481
bromides, and mixtures, molten, elec. cond., density, viscosity, surface tension, review 77−80638
cubic fluoride lattice, π-electron spin density due to Cr^{3+} ion 80−49683
electrophotoionised discharge, inert gases-halide mols. laser mixtures, current voltage characts. 80−38821
F-centre form. photochem., review 78−63763
fluoride crystals, nonlinear refr. index, 1064 nm 78−30005
fluoride perovskite- and tysonite-type, upper valence bands, tight binding calc. 77−80730
fluoride systems, fundamental condition for glass formation 80−44135
fluorides, muon Coulomb capture ratio 78−62959
fluorite structure, retarded ionic motion 80−88361
Group IA element halides, bond order correl. with dissoc. energy 80−32596
Group IIIA element halides, bond order correl. with dissoc. energy 80−32596
group IIIA metal halide, UV photodissoc., metal-atom resonance-line lasers 80−58529
Group IIIA metal tetrahalide ions, vibr. anal. 80−63608
group IV halides, pot. consts. calcs. 79−36605
Group IV tetrabromides, intramol. force fields and mean vibr. amplitudes 80−106316
heavy metal diatomic halides, Wasastjerna pot. function, force consts. internuclear separations and binding energies 80−14187
heavy metal halides, atomis. energy, electron affinity, mean amplitude of vibr. *(German)* 79−51045
hexahalides, shapes and other props. 78−82647
hydrogen halides, rot. relax. rate consts., information theoretic synthesis 79−86044
hydrogen halides rot. relax. with inert buffer gas, comment 80−69221
hydrogen halides rot. relax. with inert buffer gas, reply 80−69222
inert gas halide excimer laser, electron beam excited, efficiency 80−53278
inert gas halide lasers, operation and use in photochem. 80−9860
inert gas halide lasers, use in mol. photolytic dissoc. obs. of Se_2 80−11935
inert gas halides, triatomic, optical emission 78−66558

halides continued
inert gas monohalides, hyperfine interactions, struct., valence bond calcs. 78−66473
iodides, ^{127}I and ^{129}I Mossbauer isomer shifts, book contrib. 79−87360
iodides and mixtures, molten, elec. cond., density, viscosity, surface tension 77−80638
ion+solvated positron, competitive reaction in water, ang. correl. obs. 79−61846
ion adsorption at Bi/H_2O interface, zero charge pot. conc. depend. 80−40706
ion transport 78−63878
ionic crystals, cohesive energy calc. 80−6384
ions, in soln., positronium formation, Doppler broadened annihilation line shapes 80−45164
lamellar, polymorphic phase changes of adsorbed NO 77−31900
liquid, inorganic, Moelwyn-Hughes parameter calc. from US data 80−59375
metal fluoride-graphite intercalation cpds., prep. and props. 80−40686
metal halide (oxide) dissociation energies, calc. from chemiluminesc. reactions, temp. depend. rate const. correction 77−40524
metal halide discharges, horizontal burning, parameter meas. techniques 80−38802
metal halide layered materials, prep. and growth, book contrib. 78−19648
metal halide vapour lasers, kinetic model 79−94222
metal halide vapour lasers using gas-discharge tubes 79−64251
metal halide vapours, quantum efficiency of fluoresc. excited by photodissociation 79−81421
metal halides, bond distances and cohesive energies calcs. 80−18783
metal halides AC discharge, TlI, InI and NaI impurities, atomic plasma characts., a priori method 80−44034
metal-rich compounds, pnictides, chalcides and halides, struct. and bonding, review 79−46626
mixed metal chloride acousto-optical props. *(Russian)* 78−60419
MX_2 and MX_3 mols., vibr. freq. and geom. struct. 80−1081
NMR spectra of halogen nuclei, shielding and quadrupole coupling consts. 78−84487
octahedral ions and molecules of 2nd and 3rd row metals, force consts. 77−54548
perovskite systems, ABX_3, cryst. chem., X-ray diffr. 78−95042
positronium halides, $[X^-; e^+]$, electronic struct., annihilation characts., HF calc. 77−50567
positronium halides, $[X^-; e^+]$, electronic struct., annihilation characts., HF calc. 77−50568
pressure and temp. dependence meas. using tesla discharge as spectroscopic source 80−274
structures, and cryst. chem. of halide compounds of type $A_2B^+B^{3+}X_6$ 79−46639
transition metal dihalides, layer struct., lattice dynamics, calc. 80−65177
trihalides, D_{3h} point group, mol. consts., struct. effects 79−54992
vacancy-interstitial pair prod. by electron-hole recomb. 79−4530
Ag iodobromides, spectral absorpt. curves, density, wavelength and temp. depend. 78−16871
CuCl crystal resonant Raman scatt. and luminescence competition *(Japanese)* 80−80770
H halides, polarisability, correl. with mol. dimens. 80−23288
PF_5 dopant for polyacetylene 80−88171
XeF(Cl)(Br)(I), covalent and ionic states, spectroscopic props., ab initio CI calc. 78−90092

Hall constant *see Hall effect*

Hall effect
1/f noise, mobility fluctuations 80−92950
1/f-noise in Hall voltage 79−24039
AC ferromagnetic Hall effect in electron-impurity system, itinerant electron model 77−47796
actinide, transport props. and sp. ht., role of optical and acoustic phonons 77−15821
actinides, lattice vibrs. role in phys. props. determ. 77−28158
algorithm for calc. of impurity concentration from sheet resistivity and sheet Hall coefficient data 80−70246
alkali metal tungsten bronzes, inhomogeneous, numerical simulations of Hall effect 77−43551
alkali metal-NH_3 solution, Hall effect and cond. at metal-nonmetal transition 78−2530
alkali metal-NH_z solutions, metal-nonmetal transition Hall mobility, electrodeless meas. 78−56194
alloy, amorphous, magnetic, transport props. 79−73485
alloy, binary, Hall coeff. sign change origin 77−69302
alloy, concentrated, electrical resist. and Hall coefficient, temp. depend. 78−39093
amorphous ferromagnet, thermal cycling and annealing, critical behaviour 79−42790
amorphous metals and alloys, review of transport props. 79−4546
amorphous semiconductor, substantially doped, electronic props., review 79−87175
amorphous semiconductors, doped, electronic props. 78−19030
amorphous semiconductors, Hall mobility by modified relaxation time approx. 80−24950
amorphous semiconductors, hopping carriers, AC cond. and DC Hall mobility 80−44585
amorphous semiconductors, review of expt. data 79−51606
Anderson transition in mag. field, weak field cond. and Hall effect 80−6726
anthracene, excess electron and excess hole cryst., band struct., drift and Hall mobilities, depend. on press. 79−60709
automatic resistivity, Hall mobility and thermopower meas. *(Polish)* 77−41638
binary alloys, charge transfer and transport props. in tight-binding model 79−82577
bipolar conductivity investigs. using ohmic and acoustoelec. currents in Hall effect 77−32027
bipolar semiconductor, strong EM wave propagation, effect of generation-recombination processes *(Russian)* 79−78115
bone apatite, Hall coefficient dependence on mag. field, obs. 79−92248
borides, hexa- and di-, electronic structs., elec. props., book contrib. 78−47701
bubble-domain materials, amorphous, Hall-effect hysteresigraph for coercivity measurement 79−73786
carrier conc., temp. depend., computer data anal., effect of band parameter errors *(Russian)* 78−52006

Hall effect continued
chalcogenide glass, charged dangling bond model reassessment 77−72813
chalcogenide glass, elec. cond. mechanism, review of developments 78−26854
chalcogenide glasses, multicomponent, Hall-thermopower sign anomaly 77−35957
charge-transfer solid, quasitone dimens., Hall effect and transverse mobility 77−4326
chemisorption on metal films, use of external mag. field, review 78−72003
coefficient, direct formula derivation 77−72852
conducting continua containing inhomogeneous inclusions, fields in presence of Hall effect *(Ukrainian)* 77−31986
conducting liquid flow on moving porous plate with Hall effect 79−18964
constant current generator, wide-range, for Hall meas. appl. 77−82545
contactless Hall coeff. meas. in materials of small Hall angle in skin depth regime 78−86303
contactless measurement of sheet conductivity and mobility of semiconductor wafer by using eddy current 80−62693
Couette flow, unsteady, Hall effects 77−15127
covalent semiconductor, Hall effect sign in hopping cond. 77−72872
critical behaviour near percolation threshold *(Russian)* 77−28152
crystal symmetry, cubic and non-cubic, distinguished by weak field galvanomagnetic meas. 80−60009
crystals of low symmetry and axially symmetric, Hall and thermoelec. effects *(Russian)* 79−95427
degenerate semiconductor, film, with unlike surfaces, theory of kinetic effects *(Russian)* 79−51694
degenerate semiconductor, Sondheimer oscills., asymptotic behaviour 78−19059
degenerate semiconductors, hot electron transport in parabolic energy bands, kinetic theory, transport coeffs. 80−29412
diamond:B, epitaxial layer, charge transfer and acceptor state 78−19169
diamond:Li, ion implantation, Hall effect and elec. cond. meas. 80−15526
diamond, electron irradiated, photocurrent and Hall current, 290 and 4.2K 79−87129
diamond, ion-doped with Li electron transport 80−92917
diamond, irradiated, Hall current meas. by split electrode method 77−1435
diamond, semicond., electron irrad., charge carrier mobility 77−11921
diamond, semicond., energy band struct., elec. and optical props., review 77−35862
diamond, type Ia, electron irrad. effect on photocond., acceptor centre form. 77−47853
dilute magnetic alloy, cond. electron scatt. asymm. 77−62916
dilute magnetic alloy, reverse Kondo effect, magneto-transport theory 80−15509
dilute magnetic alloys, transport props. from Suhl's dispersion relations 77−62891
diode design review, intense mag. insulated ion diodes 78−9857
discovery 80−27099
disordered and ordered systems, theoretical review 79−51605
disordered materials, inhomogeneous, numerical simulations of Hall effect 77−43551
disordered system, DC Hall effect in hopping region 77−66174
disordered system, Hall mobility due to hopping-type cond. 79−15167
disordered system, phononless HF Hall effect 78−87953
disordered system of two level atoms, Hall and Faraday effect theory 79−51601
disordered systems, conf., Cambridge, England (May, 1978) 79−51604
disordered systems, elec. cond. and Hall mobility, theory 80−54697
disordered systems, hopping Hall mobility 77−72846
disordered systems, theory of Hall effect in hopping region 77−47836
disordered systems, theory of Hall effect in hopping region 77−51713
education, Hall effect, positive voltage interpretation by electron motion 78−69945
electrical contacting method, Au wire-semiconductor, spark welding, for elec. meas. *(German)* 79−49215
electrical resistivity, Hall coeff. of samples dual to van der Pauw samples 79−88984
electrolytes, dil. solns., Hall const., ion solvation and dynamics *(French)* 77−4910
electrolytes, dilute solns., Hall effect 77−20337
Fermi systems, disordered in two dimensions, interaction effects 80−75655
ferrite-semiconductor structure, resonance galvanometric phenomena in semicond. 78−87989
ferroelectric crystal without centre of symmetry, photo-Hall effect *(Russian)* 78−60152
ferromagnet, itinerant electron, magnetoresist. and anomalous Hall effect due to electron-phonon interactions 80−70680
ferromagnet, low-field magnetoresistance and domain drag 78−68014
ferromagnet, scattering-independent contribs. to Hall cond. 78−51957
ferromagnetic binary alloys, anomalous Hall effect *(Russian)* 79−42521
ferromagnetic metal, anomalous Hall effect 79−87084
ferromagnetic metal, anomalous magnetooptic effects near Curie temp., s-f exchange model 80−2736
ferromagnetic metal, atomic layers, Pauli paramagnetism to band ferromagnetism transition thickness depend. 78−72377
ferromagnetic metal, two-band model ordinary Hall effect and spin-depend. phenomena 79−19577
ferromagnetic metals, domain wall motion, voltage generation 80−34679
ferromagnetic semiconductor, anomalous Hall effect, s-f model 78−10478
ferromagnetic semiconductors, carrier mobility, electron-two magnon scatt. Hall effect 78−51992
film, electrophysical properties measurement apparatus 78−4654
film, evaporated, galvanomag. and mag. props., thickness depend. 78−23181
film, metallic, electron transport phenomena *(Czech)* 77−51827
film with unlike surfaces, magnetomorphic oscills., generalised Sondheimer model 78−56243
films, elec. and galvanomag. props., microstruct. 80−70859
finite systems containing traps, Hall effect, two-carrier one-dimens. transport anal. 80−44614
flowing electrolyte, Hall effect, student expt. 79−21501
Fokker-Planck eqn., kinetic effects due to detailed equilibrium violation, elastic scatt. *(Russian)* 80−31687
n-GaAs, persistent photocurrents, Hall effect anal. 79−87130

Hall effect continued
galvanomagnetic phenomena, difficulties in nonlinear theory 79−11151
galvanomagnetic transducers, steady pressure effects 77−79129
graphite, galvanomag. props., temp. depend. between 4.2 and 298K 77−32024
graphite, galvanomagnetic and thermomagnetic effects at low temp. 80−44618
graphite, Hall coeff. in mag. field range below 1.2 kOe 77−15871
graphite, high-field galvanomagnetic props. 77−62941
graphite, low field Hall coefficient, effect of warped energy surfaces 78−68043
graphite, neutron irradiation, electron transport, annealing study 80−39165
graphite, pyrolytic, galvanomag. effects, effect of fast neutron irradiation 80−34465
graphite intercalated with nitrate, galvanomagnetic props. 78−76092
graphite intercalation compounds, electronic props. in dil limit 77−47714
graphite intercalation cpds., Fermi surface and transport props., LCAO model 80−80159
graphite intercalation cpds. with K, Rb, or Cs, phase transitions, resistive anomalies, electronic props. 79−95405
graphite-K intercalation compounds, electronic props., resistivity, Hall effect and magnetoresistance 80−75585
Hall cross in perpendicular inhomogeneous mag. field 79−81323
heat treatment effects on elec. props. 78−43411
heavily doped semicond., electronic sp. ht. and transport coeff., influence of band-tail parameters 79−14941
heavily doped semiconductor, scattering mechanisms resist. and Hall coeff. maxima 80−75586
heterogenous gyrotropic media electrodynamics, antisymmetric repciprocity principle conditions fulfilment *(Russian)* 80−74287
HgCdTe/CdTe, limited diffusion volume photodiode, characterisation 80−75627
historical review applications 80−31477
hopping conductivity in ordered and disordered solids, review 77−15851
Hubbard model, Green function method, conc. depend. of Hall and Verdet coeffs. 80−80240
hydrocarbon fuels, universal formula for elec. cond. of combustion-products plasma 79−19004
hydrocarbon fuels combustion prod. plasma with alkali impurity, elec. cond. 79−55466
hydromagnetic flow over a conducting thick porous plate with Hall effects 79−64789
hydromagnetic thermal instability of rotating fluid layer, Hall current effects 79−27699
III-V semiconductors, props. and optoelectronic device appls. 79−74088
III-V semiconductors transport parameters, review 79−19587
impurities, conc. of C, O, Si 78−59832
impurity bands and inversion layers 79−51609
impurity scattering in mag. field 80−44559
incompressible viscous fluid, MHD flow past accelerated plate, Hall effects 80−92275
inhomogeneous conductors, cond. anisotropy and Hall effect near percolation threshold 80−107755
inhomogeneous continua with Hall effect, elec. fields and effective conductance tensor *(Ukrainian)* 77−50590
inhomogeneous media, galvanomag., stratified, elec. fields 80−63888
inhomogeneous medium, Hall coeff., computer simulation 77−24597
inhomogeneous semiconductor, nonequilibrium carrier mobility 77−15879
inhomogeneous system, with spherical inclusions, Hall coeff. and average carrier density 79−69533
p-InSb:Ge, single cryst. field dependence of Hall effect, cond. and carrier mobility *(Bulgarian)* 78−34848
n-InSb, anomalous Hall effect, stress depend. 80−65598
n-InSb, Hall mobility of free electrons, determ. using radioelectric effect 77−69327
InSb, thin film, Hall mobility of carriers at room temp. 79−65568
interband scattering conditions, anomalies of Hall effect 78−6403
Invar, elec. transport props. and Invar features *(Russian)* 78−14710
Invar, single crysts., Hall effect and transverse magnetoresist., 4.2-120K *(Russian)* 77−59277
inversion layers, effective-medium theory in two-dimens., appl. to macroscopic inhomogeneity model 79−95504
inversion layers, models 79−51682
Kapton, pyrolysed, cond. polymer, transport and mag. props. 80−96887
layer semiconductor system, theory of Hall effect 79−69589
layered struct., interaction of spin waves with hot carriers, transport coeff. for weak and arbitrary Hall effect 79−15291
layered structure metals, transport props., book contrib. 77−43566
liquid in rot. system, Hall effects on MHD Couette flow and heat transfer 79−41681
liquid metal, electroconductivity in mag. field *(Russian)* 78−39085
liquid metal, theory 77−47797
liquid metals, simple, Hall effect, theory 78−23073
liquid metals and alloys, cond., Hall coeff. and thermoelec. power, tight-binding model 77−47798
liquid semiconductors, Hall effect measurement 80−65594
low temperature depend. of elec. resist., mag. suscept., heat capacity, Hall const. *(Russian)* 78−30900
magnetic alloys, dil., in finite mag. field, Suhl's dispersion eqns. 77−24673
magnetic domain drag effect in presence of variable mag. field or variable transport current 79−78433
magnetic field prod. and meas. 78−8425
measurements to 40 kbar under hydrostatic pressure in piston-cylinder device, 150 to 300K 79−67337
measuring cell, for liquid metals and semiconductors obs. 77−5866
metal, asymmetric electron scatt., anomalous Hall effect in ferromags. *(Slovak)* 78−79986
metal, compensated, with closed Fermi surface, temp. depend. 77−8074
metal, ferromagnetic, Nernst-Ettingshausen effect, rel. to Hall effect and thermoelec. power 79−56199
metal, irrad., containing self-interstitials and vacancies, electronic transport props. 78−60105
metal, kinetic effects at high anisotropic strains, elec. transport props. meas. 78−54384
metal, liq., tight binding theory of transport props., Ishida-Yonezawa approx. for single-band model 78−84190

Hall effect continued
metal anisotropic normal metal, linearised Boltzman eqn., Hall effect coeffs. 79−1595
metal film, Hall coeff. in mean free path model 79−11240
metal film, resist., temp. coeff. of resist., and Hall coeff. in grain boundary cond. model 80−39683
metal-like phases, carrier conc. and mobility, interrelation *(Ukrainian)* 79−95386
metallic films, grain boundary scatt., Hall coeff., theory 80−88649
metallic glass, prep. and phys. props. development 80−81003
metallic glasses, electronic structure, neutron scatt., elec. resist., Hall coeff., mag. susceptibility and XPS 78−23013
metallic rare earths, conference, St. Pierre-de-Chartreuse, France (Sept. 1978) 80−12844
metallic thin films, Hall coeff., temp. depend. 79−95516
metallic thin films, size effect conductivity in transverse mag. field, Hall coeff. *(French)* 78−91787
metals, electron theory and cond. props., contrib. of Sir Rudolf Peierls, 1928-1935 80−57054
metals, ferromag., elec. cond. review 77−31993
metals, inhomogeneous, magnetoresist. and Hall coeff. 79−95387
metals, nearly-free-electron, holelike Fermi surface, Hall coeff. and magnetocond. tensor 79−4547
MHD, forced flow through horizontal channel, Hall effect, buoyancy force effects 80−53871
MHD, Hall effect on unsteady flow due to rotating infinite disc 78−18354
MHD, thermodiffusive mixture flows, Hall and ion-slip effects, uniqueness theorem 78−87415
MHD accelerator, thermodynamic props., mag. field strength, Hall currents in arc region 77−65917
MHD accelerators, electrodynamic characts. 80−64788
MHD channel, two-dimens. flow in entrance region with Hall and ion slip currents 77−42968
MHD channel flow heat transfer, Hall effect and ion slip 77−80220
MHD channel with Hall and ion slip currents, forced convective heat transfer 80−33823
MHD convective flow through channel with conducting walls, Hall effects 78−5802
MHD convective flow through porous channel with Hall and wall conductance effects 80−74993
MHD convertor, current concentration due to Hall effect, elimination by variable resistive electrodes 77−80378
MHD Couette flow, Hall and ion-slip effects, heat transfer 79−94726
MHD Couette flow, Hall effect in rot. system 80−74991
MHD Couette flow with Hall currents, stability, numerical soln. 77−72360
MHD devices, plasma ionization instability, dynamic suppression, switching modelling 80−59308
MHD flow, due to impulsively started plate, transverse mag. field 78−1747
MHD flow, past porous flat plate 78−14093
MHD flow induced by oscill. disc in rot. fluid 79−18968
MHD flow over oscillating porous plate, Hall current and rot. effects 78−5803
MHD flow over porous plate, Hall effect 78−51246
MHD forced convection in channel bounded by plate and permeable bed, Hall effects 80−69934
MHD free and forced convective flow between porous plates with Hall effect 79−41763
MHD generator, characteristics improvement, using current parallel to magnetic field 80−1751
MHD generator, Faraday type, current profile optimisation, electrode cond. profile 78−94939
MHD generator current density and elec. field dependence on plasma thermodynamic pulsation *(Polish)* 77−80268
MHD oscillatory flow past flat plate, Hall current effects 79−98816
MHD Poiseuille flow in annular channel with radial mag. field, Hall effect 78−67276
MHD rotating channel of parallel plates, Hall effects on hydromagnetic flow and heat transfer 77−42926
MHD wave propagation in anisotropic media, electrical dissipation effects *(Japanese)* 78−87445
microwave Hall mobility measurement 79−54154
MIS structure, charge-transfer, surface mobility and Hall mobility determ. 78−23175
mixed powder materials, mixing rule of Hall carrier mobility *(German)* 78−52008
α-MnS, elec. props. meas. 78−87971
mobility measurement in specimens in strong pulsed electric fields 79−35779
molybdenum chalcogenides, multicomponent, physical props. 80−84577
monocarbides of subgroups IVa and Va, kinetic props., review 78−47613
MOS structures, total dose effects on surface state density, carrier conc. and mobility 77−20443
MOS structures with superthin gate dielectric, hole mobility in inversion layers 80−29482
MOS transistor, Au-doped, Au surface-state energy levels 80−11092
MOSFET, two-dimens. electron gas, determ. of fine struct. const. based on quantised Hall resist. 80−96997
MOST channels, quasi-Fermi level gradient distrib., Hall voltage 80−29481
MOST struct., gamma irrad., interface states and carrier mobility 79−73593
negative effective mass carrier contribution to EMF, sign *(Russian)* 78−26886
noble metal-rare earth alloy, dil., magnetotransport props., theory 78−39097
noble metals containing rare earth impurities, magneto-transport props. 78−68015
noise, explained as carrier mobility fluctuations 77−62949
non-transition elements and alloys, supercond. transition temp., Hall const. correl. 79−47186
noncrystalline systems, theory 79−51610
nonhomogeneous semiconductor, galvanomagnetic effects 79−91077
nonlinear conductor, odd-symmetry two-dimens. Hall effect in alternating elec. field 80−80303
normal-superconducting composites, magnetoresistance and Hall coeff., classical theory 80−84547
partially ionised gases, magnetic inductive effect, Hall coefficient 77−19662

Hall effect continued
partially ionised plasma, thermal instability, Hall currents 78−63551
Penning discharge, Hall crit. mag. fields 79−27146
phonon inelastic interband scatt. in transport effects 77−43552
plasma, current-conveetive instability, stabilisation by mag. field *(Russian)* 77−3930
plasma, nonequilib., two-temp., expanding in disc-shaped channel, hypersonic MHD interactions 80−10368
plasma, rot. theta-pinch mechanism, MHD anal. 77−24135
plasma, rotating Hall plasma, self gravitational instability, MHD stability 80−14890
plasma, stationary periodic waves with Hall dispersion, magnetohydrodynamic approx. *(Russian)* 77−27661
plasma, turbulence effect on Ohm's law 78−22463
plasma accelerator, closed Hall current discharge, anode sheath struct. 77−76215
plasma accelerator, ion current oscills. *(Russian)* 79−98995
plasma accelerator, open single lens Hall current type, characts. 77−55178
plasma channel flow, coaxial, compressive, viscous, thermal and elec. cond. effects *(Russian)* 77−3927
plasma flow in accelerator (compressor) coaxial channel, two-dimens., simulation 80−19566
plasma Hall accelerator, azimuthal drift current, induction meas. method 79−23465
plasma stability, Hall current and gyroviscosity effect 80−75041
plate with finite Hall electrodes, accuracy of relaxation soln. for potential problem 79−33303
poly(p-phenylene), AsF_5 doped, highly cond. charge transfer complexes, elec. and optical props. 80−70778
polyacene quinone radical polymers, two-dimens. variable range hopping 79−51608
polyacetylene:AsF_5, Hall effect meas. 80−24955
polyacetylene film, heavily doped with AsF_5, conductivity and Hall effect meas. 79−28353
polycrystalline layer, carrier conc. and effective Hall mobility 77−4375
polycrystalline substances, use of Hall and Seebeck effects in phys. parameter determ. 77−12023
polyphthalocyanine, amorphous, linear polymer, Hall effect meas. 79−23989
polypyrrole films, electrochemical prep., chem. and phys. characterisation 80−70708
powder combinations, compressed, mixing rules concerning Hall effect and Hall mobility *(German)* 78−84234
protein-methylglyoxal complex, electronic props., energy band cond. 79−24936
pyridinium pentasilver hexaiodide, solid electrolyte, contrib. of non-Brownian motion to transport props. 80−70453
pyrocarbon, Hall effect and conductivity of specimens deposited at 2000 and 2200°C 78−23112
quantum diffusion in crystals 78−18820
randomly inhomogeneous cond. medium in mag. field 80−19558
rare earth amorphous alloys, transport props. 80−20152
rare earth chalcobismuthites, $RBiTe_3$, prep., elec. props., and crystallographic date 80−59981
rare earth metals, 80-1000K 77−43572
rare earth metals, mag. and transport props. 79−69658
rare earth metals, XX 80−15504
rare earth tungsten oxide bronzes, metallic, elec. props. meas. 78−30906
rare earth-Au(Cu), amorphous, mag. and transport props. 80−34605
rare earth-Co systems, anomalous Hall effect and Kerr rotation obs. 77−11897
rare earth-transition metal amorphous film, Kerr and Hall effect meas. 77−24722
rare earth-transition metal amorphous thin films, mag. potential distribution and wall velocity meas. 80−34725
rare-earth-Co films, extraordinary Hall effect meas. 78−6459
rhombic distortion of cryst. lattice at low temp. 78−2253
semiconductor, amorphous and liq., Hall conductivity in random-phase model 80−65599
semiconductor, bounded, transport effects when a current passes along an energy inhomogeneity 79−7845
semiconductor, defect interactions, radiation physics *(Russian)* 79−46702
semiconductor, donor levels, anomalous press. effects, Hall const. meas. 77−51693
semiconductor, dynamic conversion of light beams, by phase shifted free-carrier holograms 78−46547
semiconductor, effective conductivity tensor, effect of spherical anisotropic inclusions 77−55546
semiconductor, enhanced electrodiffusion purification in mag. field, GaAs epitaxial film appl. 80−66409
semiconductor, galvanomagnetic-effects in strong elec. field 78−56163
semiconductor, Hall current method generalisation to arbitrary magnitude mag. fields *(Russian)* 80−29421
semiconductor, Hall effect in finite specimens of arbitrary lifetime and trap content 78−72175
semiconductor, homogeneous, Hall effect noise 78−39173
semiconductor, impurity characterisation from thermal carrier meas. 80−65595
semiconductor, influence of nonhomogeneous mag. field 77−39882
semiconductor, intrinsic, quantum theory of transverse galvanomag. phenomena, model of two standard bands *(Russian)* 77−62945
semiconductor, irradiated, Hall mobility, dark and photo-conductivity calc. 78−47835
semiconductor, magnetoresistance quantum limit for impurity scatt. 79−91083
semiconductor, near intrinsic magnetoresist. effect determ. of carrier density and mobility 78−2501
semiconductor, nondegenerate nonpolar, quantum theory of magnetophonon reson. 77−28200
semiconductor, partly disordered, with mobility threshold, transport props. and thermoelec. parameters 80−34449
semiconductor, piezogalvanomagnetic effects measurement at low temps., apparatus with stabilised dynamic load 77−67458
semiconductor, polycrystalline, phenomenological theory of Hall effect 79−11160
semiconductor, resolution of transport equation, by linearisation *(French)* 78−79989
semiconductor, Seebeck and Hall coeffs. Lorenz number, anisotropy, theory *(German)* 80−65608

Hall effect continued
semiconductor, transverse magnetoresist. effects on Hall voltage meas., theory 77−72870
semiconductor, type I zero-gap state, Nernst-Ettingshausen and Hall effects 80−44622
semiconductor, zero gap, collisionless, anomalous Hall effect 79−23988
semiconductor epitaxial layer, free-carrier density determ. by Hall meas., surface and interface depletion corrections 79−91170
semiconductor film, carrier mobilities and doping conc., Hall meas. in MISIM struct. 77−76975
semiconductor film, cell for measuring electrophys. parameters over wide temp. range 77−51830
semiconductor film, polycryst., Hall and drift mobilities 79−95531
semiconductor heteroepitaxial film, electrical characterisation, book contrib. 79−82699
semiconductor materials temperature dependence meas., using automatic device 80−52270
semiconductor melts, metallic cond. at high temp. 80−49832
semiconductor or insulator, theory for flow of Hall current in sample of arbitrary shape 79−73532
semiconductor plasma, unstable EM wave propagation, hot carriers, Hall effect, calc. 80−39620
semiconductor resistivity and Hall effect meas., nondestructive four-electrode characterization 80−49743
semiconductor thin film, carrier redistribution in strong crossed elec. and mag. fields *(Russian)* 77−72927
semiconductor thin films, Hall effect and magnetoresist. determ. in weak and strong mag. fields by four-probe method 79−60853
semiconductor with disordered regions, carrier mobility, theory and expt. 78−56166
semiconductor with superlattice, electron dispersion in direction of axis of superlattice 80−39612
semiconductor-ferrite layer structure, influence of Hall effect on spin wave spectron and amplification by current 79−11308
semiconductors, amorphous, doped, electronic props. 80−80283
semiconductors, amorphous, electronic transport mechanisms and coeffs. 80−80282
semiconductors, drift mobility and Hall factor, nonpolar optical scatt. mechanism 79−51579
semiconductors, elec. props., mag. field effect determ., method 80−44623
semiconductors, electron scattering by deep level impurities 80−10968
semiconductors, even dynamic photoelectric Hall effect 78−91708
semiconductors, galvanomagnetic effects in high mag. fields, for electron scatt. by optical phonons 80−2405
semiconductors, heterogeneous, anisotropic, Hall coeffs., Hall mobility, carrier density *(Russian)* 80−70734
semiconductors, high temp. conductivity and Hall effect meas. 77−87786
semiconductors, impurity electron scatt., resonance scatt., Hall and drift mobility 80−65487
semiconductors, kinetic effects at high anisotropic strains, elec. transport props. meas. 78−54384
semiconductors, mobility-fluctuation description of 1/f noise 80−84496
semiconductors temperature dependences meas., automated installation 80−31792
semimetal, degenerate, quantum theory of transverse galvanomag. phenomena, model of two standard bands *(Russian)* 77−62945
semimetals, Hall coefficient and magnetoresist. of interacting two carrier system 79−69530
p-Si, electron irrad. effect on Hall mobility temp. depend. 80−60011
p-Si, interstitial Fe and thermal defects, Hall effect and resist. meas. 79−82200
solar cells, thin film polycrystalline materials, resistivity and Hall effect meas. 80−93899
solid state physics, 1925-33 80−57066
SOS films, surface recomb. profile and transport parameters 79−33357
SOS MOS devices, hole mobility under residual stress, Hall meas., valence band struct. 78−88039
spatially inhomogeneous system, galvanomagnetic effects *(Russian)* 78−72129
spin glass, Hall effect anomaly conditions 78−68267
spin glasses, anomalous Hall effect including Kondo effect in molecular field approx. *(Russian)* 80−34424
superconducting transition temperature, empirical correl. with Hall coeff. 79−78247
superlattice semiconductor, odd photomagnetoresistance effect 79−95425
TCNQ salt, HMTSeF-TCNQ, temp. and press. depend. 77−35929
TCNQ-HMTSeF, large Hall effect obs. below room temp. 78−6364
Tl-Te melt system, semicond., Hall effect 78−56164
toroidal discharge, investig. 80−38701
transition metal, Hall coeff., force correlation function method 79−91028
transition metal carbides, 3d metal, interatomic interaction 79−1569
transition metal chalcogenides, quasi-one-dimens., elec. mag., and supercond. props., review *(Russian)* 80−93022
transition metal diborides, 3d metal, interatomic interaction 79−1569
transition metal dichalcogenides, 2H polytype, Hall coeff. sign reversals 77−80795
transition metal intercalates of Ni and Ta dichalcogenides, Hall coefficient and resistivity 80−39610
transition metal mononitrides, 3d metal, interatomic interaction 79−1569
transition metal oxides, 3d metal, interatomic interaction 79−1569
transition metals and alloys, 3d, Hall effect, electron scatt. processes 80−34419
transition metals and alloys, noncrystalline 78−95280
TTF-TCNQ, Hall mobility using Faraday rot. method at 9.3 GHz 77−47801
two dimensional disordered systems, Hall effect at low freq. 80−107819
two-component layered system, with interpenetrating components, thermoelec. and galvanomag. props. 78−79982
two-dimensional binary mixture, effective medium theroy of cond. and Hall effect 79−95380
type II superconductor influence of structure defects on resistive and Hall effects *(Russian)* 79−33419
unsteady MHD flow in rotating system, Hall current effects 80−33704
Van der Pauw meas. method, contact position and sample geometry influence *(German)* 78−233
Van der Pauw method, meas. of resistivity and Hall constant 77−67467
VHF power measurements using Hall effect *(Polish)* 80−95112
W-dichalcogenide, valence band nature, elec. and mag. props 78−39014
Z-pinch gas discharge, Hall effect influence on plasma dynamics 77−51218

Hall effect continued
zero gap semiconductors, electron scatt., thermoelec. power and Hall effect at low temp. 80−44628
Ag, pure and low density defect conc., low field Hall coefficient determ. at low temp. 77−43568
Ag-Au(Cd), deviations from Matthiessen's rule 78−10420
Ag-In_2S_3-Si layered struct., Hall effect, I-V characts., surface states *(Russian)* 80−97001
Ag-Mn, spin glass, anomalous Hall effect 78−30908
Ag-Mn dilute, magnetoresist. and Hall effect, field-depend. electron scatt. 77−43581
AgBr(Cl), evidence for population inversion of hot electrons 79−91085
αAgI, solid electrolyte, contrib. of non-Brownian motion to transport props. 80−70453
$AgInS_2$, and $AgIn_5S_8$, spray pyrolysis, film struct., elec. and optical props. 80−71592
AgN_3, high-resist. explosive cpd., elec. and galvanomag. props., temp. depend. 80−103728
$(Ag_{x/2}Pb_{1-x}Sb_{x/2})Te$ solid solns., Hall coeff., thermoelec. power, and thermal cond., 100 to 500K 79−82614
β-Ag_2S, electrogalvanic and elec. props., and range of existence *(French)* 78−43175
Ag_2S, transport props., 700-1500K 78−47796
Ag_2Se, electronic and electrogalvanic props. in α-phase region *(French)* 80−107820
$Ag_2Se(Te)$, single cryst. growth by chem. transport, and characterisation 77−36380
Ag_8SnSe_6, cryst., Hall effect investigation of polymorphic transform. 80−39605
p-Ag_2Te, electrophysical props. 77−39842
Al alloy, dil., Hall coeff., calc. by 4-OPW approx. 78−76052
Al, anisotropic electron scattering, Hall coefficient, path integral calc. 79−91027
Al, anomalous nucl. acoustic reson. signals 77−20732
Al, impurity low-field galvanomag. coeffs., 4 OPW calcs. 77−69304
Al, low-field galvanomag. props., Fermi surface and defect struct. effects 77−4323
Al, magnetomorphic oscillations, magnetoresist. and Hall coeff. meas. 77−28159
Al, nuclear acoustical reson., 20-80K, Hall coefficient in high mag. field 79−8058
Al, with dilute pt. defects, thermopower, Hall effect and magnetoresist. 79−65458
Al-Ag(Ga)(Ge) dil. alloys, Hall coeff., residual resist., and relax. times 79−11107
Al-Cr, Al-Mn, Al-Cr-Mn, dil. alloys, Hall coeff. and elec. resist. 77−11898
Al-Cr(Mn), anisotropic electron scattering, Hall coefficient, path integral calc. 79−91027
Al-Cu, dil., anisotropic scattering of conduction electrons on dilute Cu impurities 79−47082
Al-Ga(Ag), dil, Hall coeff. by OPW Fermi surface model 80−6816
Al-Ge, galvanomag. transport coeffs., Hall effect 79−91029
Al-In_2S_3-Si layered struct., Hall effect, I-V characts., surface states *(Russian)* 80−97001
p- (AlGa)As:Zn, MBE grown, elec. props., shallow junction solar cell use 79−91175
$Al_xGa_{1-x}As$, compensated, electron mobility temp. depend. 80−96868
n-$Al_xGa_{1-x}As$, electrical props. 78−6381
$Al_xGa_{1-x}As$, Hall effect, press. temp. and composition depend. 80−49775
$Al_xGa_{1-x}As$ MBE layers, ionized beam doping, elec. and optical characts. 79−37721
$Al_xGa_{1-x}As$, measurements to 40 kbar under hydrostatic pressure in piston-cylinder device, 150 to 300K 79−67337
p-$Al_xGa_{1-x}As$:Be layer, MBE growth, Be doping and diffusion, elec. and optical props. 77−51397
$Al_xGa_{1-x}As$:Cu(Ag)(Au), LPE film, impurity levels, elec. and optical props. meas. 78−26862
p-$Al_xGa_{1-x}As$:Ge layer on GaAs substrate, Hall and elec. cond. meas., Hall mobility 80−2402
$Al_xGa_{1-x}As$:Mg doping characteristics, elec. props., effective hole masses 79−78117
$Al_xGa_{1-x}As$:Te, epitaxial film, elec. cond. and Hall coeff. rel. to donor levels 77−24630
Ar induction HF discharge plasma in crossed fields, with Cs seeding, Hall parameter 79−55465
Ar-Cs plasma, HF induction discharge, Hall effect *(Russian)* 77−43101
$As_2(S,Se,Te)_3$ glasses, Hall mobility composition depend. 78−68042
As_2Se_3, amorphous, DC Hall effect, elec. cond. mechanism 78−23121
Au, thin film, discontinuous, high resist., Hall effect meas. 80−65716
Au-Co, electron scatt., spin-orbit effects 80−65533
Au-Fe, anomalous Hall effect, asymm. scatt. of itinerant electrons 77−43569
Au-Fe, spin-orbit coupling and electron scatt. 80−2370
Au-Fe (Mn)(Co), spin glass transition and anomalous Hall effect 79−61162
Au-Fe (1-7 at.%), extraordinary Hall effect, near ferromag. percolation limit 79−19575
Au-Fe alloys, spin-orbit electron scatt. near percolation limit, anomalous Hall effect meas. 79−73492
Au-Mn, spin-orbit coupling and electron scatt. 80−2370
Au-Mn(Fe)(Cr), spin glass, anomalous Hall effect 78−30908
AuMn, mictomagnetic, Hall and magnetoresist. effects 78−43361
Au(Pd)-Zn, martensitic transformation, Hall coeff., specific elec. resistivity and X-ray powder diffraction 78−72774
$Au_{50-x}Pd_xZn_{50}$, $(0 \le x \le 15.02)$, β′-phase, Hall effect and elec. cond. 80−107768
$Au_{81}Si_{19}$, optical refl., 0.5 to 6 eV, hall coeff. and elec. resist. 80−29755
$Au_{100-x}Zn_x$, $(47 \le x \le 52)$, β′-phase, Hall effect and elec. cond. 80−107768
α-B, rhombohedral, elec. cond., thermoelec. power, and Hall coeff. 80−6843
BC, EPR, book contrib. intensity correl. with elec. cond., Hall coeff., book contrib. 78−48041
Ba-ferrite, hard magnetic, temp. range 308.5 to 354K 79−38109
Ba-ferrite, temp. range 303 to 353K 79−42564
$BaFe_{12}O_{19}$, Hall effect, magnetisation and elec. resist., 30 to 80°C 77−51766
$BaPb_{1-x}Bi_xO_3$, superconducting props., Hall coeff. and elec. resist. meas. 80−84531

Hall effect continued
$BaTiO_3$, transport and optical props., small polaron hopping theory 79−47096
BeTeI, cryst. struct., semimetallic nature, elec. resist. and Hall coeff. meas. 77−28788
Bi film, carrier conc., mobility and 1/f noise 80−44748
Bi film, carrier conc. and mobility, resist., galvanomag. and thermoelec. meas. 78−52111
Bi film, in situ meas., MFP and specular scatt. parameter determ. 78−2589
Bi film, kinetic props. of electrons 77−63011
Bi, Hall effect and helicon reson. at high mag. fields 79−60861
Bi, magnetotransport props. in quantising mag. fields 77−20340
Bi, powdered mag. resistance *(German)* 79−28358
Bi-Cd alloy liq., Hall coeffs. 78−14711
Bi-In alloy, liq., Hall coeffs. 78−14711
Bi-Sb, semiconducting solid solution, forbidden band width Sb-conc. depend. 77−66117
Bi-Sb, Shubnikov-de Haas effect and semimetal-semicond. transition in high mag. fields 80−44674
Bi-Sb alloy film, amorphous nature, AC and DC cond. and Hall coeff. obs. 80−11114
Bi-Sb alloy film, elec. resist., magnetoresist., Hall coeff., 4.2K, conc. depend., anomalous size effect *(Russian)* 77−89884
Bi-Sn alloy, liq., Hall coeffs. 78−14711
$Bi_{0.88}Sb_{0.12}$, semiconducting transport props., 2 to 100K 80−59989
$Bi_{1-x}Sb_x$ epitaxial layers, effect of film thickness on elec. props. *(Russian)* 79−11244
$Bi_{1-x}Sb_x$ epitaxial thin films, galvanomag. props. in semimetal and semicond. regions 79−11254
$Bi_{1-x}Sb_x$ film, low temp. anomalies of elec. props. and quantum size oscillations 79−65571
n-$Bi_{1-x}Sb_x$, Hall effect in strong mag. fields 79−69532
$Bi_{1-x}Sb_x$, semicond.-semimetal transition, temp. and press. depend. of transport props. 78−76120
$Bi_{1-x}Sb_x$, thin film, elec. props., composition variations *(Russian)* 79−7841
$Bi_{1-x}Sb_x$ thin films, elec. props., 4.2-300K, Hall coeff. meas. *(Russian)* 79−24087
$Bi_{0.52}Sb_{1.48}Te_3$-Te, phase-equilibrium boundary, Hall coeff. meas. 78−44094
$Bi_{2-x}Sb_xTe_{3-y}Se_y$ solid solution, density-of-states effective mass, carrier mobility temp. depend. 80−24931
p-BiSe, single crystal, synthesis and elec. props. 77−16490
p-Bi_2Se cryst. growth, elec. props. 77−8748
n-Bi_2Se_3, cryst. nonparabolic cond. band., IR refl. and Hall voltage meas. 77−31940
n-Bi_2Se_3, IR, reflectance, Seebeck coeff. and Hall voltage meas. 79−60692
n-Bi_2Se_3, single cryst., new aspect of carrier scatt. 80−49707
Bi_2Se_3:Hg point defects in crystal lattice, Hall coefficient and IR spectra determ. 80−55129
Bi_2Te_3, galvanothermomag. props. up to 14 kbar 77−47829
n-Bi_2Te_3, galvonomagnetic props., influence of hydrostatic press. 79−73536
Bi_2Te_3, Shubnikov-de Haas effect and Hall coeff., high press. effect 77−51767
Bi_2Te_3-Sb_2Te_3, Bi:Sb=1:2, 2:1, solid soln. deviation from stoichiometric cross section 79−43221
Bi_2Te_3-Sb_2Te_3 film, cond., galvanomag. Seebeck and Nernst-Ettingshausen effects under press., band model 77−47907
Bi_2Te_3-Sb_2Te_3 solid soln., deviation from stoichiometric cross section 78−35362
BiTeI, elec. props., crysts. grown from melt in excess iodine 79−4907
BiTeI-SbTeI solid solns., form., crystn., elec., thermal props. 78−44003
$Bi_2Te_{2.7}Se_{0.3}$, magnetoresistance and Hall EMF meas., using AM method 80−52278
$Bi_2Te_{2.88}Se_{0.12}$, solid soln., single cryst. growth and doping, thermoelec. efficiency and Hall coeff. 79−33921
$Bi_2Te_{3-x}Se_x$ films, surface band struct. and scatt. mechanism 80−34535
$Bi_2Te_{3-x}Se_x$ solid solution, Hall effect anisotropy parameter, thermoelectric power, depend. on carrier density 79−69536
C, amorphous, elec. cond. and Hall effect, temp. depend. 78−60141
Cd, Hall effect and elec. resist., temp. depend. 78−64030
Cd, Hall resistivity, importance of intersheet scattering 77−76794
Cd-Sb, near CdSb, Hall coeff., resistivity 79−56216
Cd-Sb thin film prep. by vacuum deposition, elec. props. 78−92194
$CdAs_2$, synthesis, microstruct., hardness and elec. cond. 79−51268
Cd_3As_2, band structure, Kane model, magneto-Seebeck and Hall data 77−62821
Cd_3As_2, electron effective mass. temp. depend., Hall effect and thermoelec. power meas. 80−39613
Cd_3As_2 films, amorphous, elec. resist., Hall mobility, temp. depend., cond. mechanism 77−76982
$Cd_3(As_xP_{1-x})_3$, thermoelectric power and Hall effect., mag. field depend. 78−10484
p-$CdCr_2Se_4$:Ag, electrical props., 100-300K 80−54692
$CdCr_2Se_4$:Cu, elec. props., temp. depend. *(Russian)* 78−72181
n-$CdCr_2Se_4$:In, electrical props., 93-168K 80−49713
$CdCr_2Se_4$:In, ferromag. semicond., carrier mobility, electron-two magnon scatt. Hall effect 78−51992
$Cd_{0.93}Cu_{0.07}Cr_2Se_4$, single cryst., Hall EMF depend. on temp. 79−7848
$CdF_2:Ge^{3+}$, Ce^{3+}, in semicond. state, elec. cond. and Hall meas. 78−10443
$CdGeAs_2$, optical and elec. props. 79−19590
n-$CdGeAs_2$:In(Te), resist. and Hall coeff. meas., influence of press. 77−47810
$CdGe_xAs_2$ glass, conductivity and Hall effect for x=0.1 to 0.8, 300 to 600K 77−69347
$Cd_xHg_{1-x}Te$, elec. characts., impurity effects 80−92890
$Cd_xHg_{1-x}Se$, 77-400K *(Russian)* 78−2485
$Cd_xHg_{1-x}Se$, carrier mobility, 4.2 to 300K, scatt. mechanisms 79−4561
$Cd_xHg_{1-x}Se$, Hall coeff. and electron mobility, band parameters 79−73506
$Cd_xHg_{1-x}Se$ mixed cryst., electron mobility and electron scatt. 78−95296
$Cd_{0.1}Hg_{0.9}Te$, polycrystalline thin film, correlation between structure and 1/f noise 78−39234
n-$Cd_{0.245}Hg_{0.755}Te$, magnetophonon reson. and quantum oscillations 77−39902
$Cd_xHg_{1-x}Te$ film, vacuum departed, struct. and elec. props. 77−59344

Hall effect continued
$Cd_xHg_{1-x}Te$ compressed sintered slabs, Hall coeff. and microstructure obs. *(Russian)* 78−10475
$Cd_xHg_{1-x}Te$, electron irradiated, elec. and recomb. characts. 78−39113
$Cd_xHg_{1-x}Te$, epitaxial graded-gap layers, elec. transport props. 77−85358
$Cd_xHg_{1-x}Te$ films, epitaxial growth, optical, elec., and photoelec. props. 79−11512
$Cd_xHg_{1-x}Te$, fine-graded gap struct., electrophysical props. *(Russian)* 78−60144
$Cd_xHg_{1-x}Te$, graded-gap layers, galvanomag. props. at low temp. and in weak mag. field 80−75664
p-$Cd_xHg_{1-x}Te$, Hall const. variation with comp. after annealing in Hg vapour 77−15868
$Cd_xHg_{1-x}Te$, IR detector appls., prep., elec. props. *(German)* 78−86332
$Cd_xHg_{1-x}Te$, low temp. piezoresistance, Hall effect, elec. cond., plastic flow 80−6844
$Cd_xHg_{1-x}Te$, photomagnetic and galvanomagnetic effects in quantising mag. fields 80−20223
$Cd_xHg_{1-x}Te$, resistivity, Hall effect and magnetoresist. in strong elec. field 77−28199
n-$Cd_xHg_{1-x}Te$, single crystal, scattering mechanism on intensity of 1/f noise 80−39642
$Cd_xHg_{1-x}Te$, solid solns., role of stoichiometry defects 77−47813
$Cd_xHg_{1-x}Te$, strong elec. field effect on galvanomagnetic effects 79−11159
CdO, influence of initial compacting press. on elec. resis. Hall coeff. 80−20872
Cd_3P_2, energy band struct. and electron mobility at low temp. 79−37984
CdS, 200 keV electron induced defects, low temp. annealing 77−80796
CdS, epitaxial film, structural and electron transport props. 79−82481
CdS film, dark cond., negative temp. depend. 78−47892
CdS film, Hall effect meas. 79−65570
CdS film, on Si, structural and transport props. 78−6463
CdS film, prep. by hot wall technique, morphology and semicond. props. 79−95292
n-CdS, polaron effective mass, DC Hall effect meas. 78−39037
CdS polycrystalline film, pot. barrier at grain boundaries from Hall effect *(Russian)* 77−32094
CdS single cryst., temp. depend., 800-1200K *(Russian)* 77−80797
CdS, single crystal, growth by modified Piper-Polich method, props. *(Japanese)* 79−100036
CdS sprayed films, elect. and optical props. 78−39241
CdS:$CuCl_2$, sintered film, dopant conc. effects on carrier mobility 78−2484
CdS:Cu(Cl) polycrystalline films with residual conduction, kinetic phenomena *(Russian)* 77−15981
CdS:In film, flash evaporated, prep. and elec. props. 80−20792
CdS:Li chemically deposited filter, elec. props. 80−11113
n-CdS:Te, grown from Te soln., elec. props. 79−65475
n-CdS(Se), bipolar photocond. and acoustoelectric current 79−19636
CdS_xSe_{1-x}:In film, flash evaporated, prep. and elec. props. 80−20792
p-CdSb, elec. props. at low temp. 77−62866
CdSb, monocrystalline film, prep., elec. props. 79−43159
CdSb:Ge, anisotropy of elec., mag. props. 78−34829
CdSe, electrical cond. near metal-insulator transition 79−73550
CdSe film, Hall voltage meas. 77−69434
CdSe film, vacuum deposited, struct., resist. and Hall mobility 77−76974
p-CdSe, Hall density and mobility, in Se vapour atm., 600-1100K 78−52014
p-CdSe layers, ion implantation prep., elec. props. 79−51699
CdSe, pulsed Hall photoeffect, transient processes in scattering of carriers 80−15546
CdSe:In, epitaxial layer, effect of activator distribution on conductivity 78−43047
CdSe:Ti, optical and elec. investig. of shallow donor levels, reson. states 77−63437
$CdSnAs_2$, electron induced defects, p- to n-type cond. inversion, Hall meas. 77−24557
p-$CdSnAs_2$, Hall effect, thermo EMF, thermomagnetic effects 80−107822
p-$CdSnAs_2$, heavily doped, elec. transport props. under elastic deformation 80−96915
$CdSnAs_2$, hydrostatic press. effect on resist. and Hall coeff., band struct. 77−47808
n-$CdSnP_2$, Hall coeff. and elec. cond. meas., 24-900K 80−54721
n- $CdSnP_2$, Hall mobility of electrons meas., 120-300K 77−4373
$CdSnP_2$, Hall mobility of holes 78−52015
$CdSnP_2$:Cu, deep centres, emission transitions, polarisation *(Russian)* 78−84650
p-CdTe, bipolar photocond. and acoustoelectric current 79−19636
CdTe, bipolar photoconductivity exam. 78−6410
CdTe detectors, depletion layer extension 78−41891
CdTe epitaxial layers on GaAs, cryst. struct. and phys. props. 79−33202
CdTe film, photogenerated carrier transport props. 80−88590
n-CdTe, Hall effect and resist., close and distant donor-acceptor pairing effects 77−39881
CdTe, high-resistivity, irradiation effects on carrier transport and trapping process 78−2164
p-CdTe single crysts., photoreversal of Hall effect 77−43631
p-CdTe:Cl, deep level characterisation, gamma-ray detector parameters 77−39802
p-CdTe:Cl, influence of gamma-irradiation on elec. props. 77−62951
CdTe:Cl, influence of lattice defects on electrical behaviour 78−2497
CdTe:Cl, localisation of electrons, temp. depend. of cond. and Hall effect 78−14732
CdTe:Cl, semi-insulating, Hall effect and cond. meas., carrier mobility 77−39849
CdTe:Cl, semiinsulating, Hall effect and elec. cond., impurity levels 77−55532
CdTe:Cl, single cryst., photo Hall effect obs. 78−76094
CdTe:Cu films, impurity behaviour, Hall mobility and hole density meas. 80−80420
CdTe:Fe, annealed, magnetically ordered, Hall effect and photocond. 78−19060
CdTe:Ge, dopant behaviour 78−22742
CdTe:p, defect model, from Hall effect meas. 77−43620
CdTe-HgTe, neutron irrad. rel. to elec. props. 79−15141
CdTe-HgTe, semicond. solid solns., effect of reactor irrad. on electrophys. props. 77−51744

Hall effect continued
$CdTl_2Te_4$, Hall and thermo-EMF coeffs., in solid, liquid states 80−54704
$Cd_{3-x}Zn_xAs_2$, cryst., two-band and impurity conduction, 1.8 to 370K 78−19057
$Cd_{3-x}Zn_xAs_2$ press. and temp. depend. of Hall coeff. 77−69349
$CeAl_2$, skew scatt., evidence of cryst. field effect, Hall effect meas. 78−2466
$CeCoSi_2$ film, Hall effect and magnetoresist. *(Russian)* 80−11109
$Ce_{1-x}La_xAl_2$, extraordinary Hall effects, 4.2-300K, cryst. field interaction 78−79980
$Ce_{3-x}S_4$, $Ce_{3-x}Sm_xS_4$, elec. cond. mechanism, thermoelec. power, Hall and absorpt. coeffs. 77−24559
Co films, electromigration and Hall effect 77−62664
Co, liquid, Hall effect, band struct. and exchange scatt. 80−80250
Co, random close packed, normal Hall effect meas. 77−35924
Co-Gd-Mo amorphous films, resist. and extraordinary Hall effect, thermal annealing effect 80−70852
Co-Gd-Mo(Au) alloy film, amorphous 77−85347
Co-Ni, anomalous, residual coeff. calcs. using coherent pot. method *(Russian)* 80−80249
Co-Pd, transfer phenomena and association with electronic struct. *(Russian)* 79−91017
Co-Pd alloys, 0-70 at.% Pd, conc. depend. of anomalous Hall field and resistivity *(Russian)* 78−14713
$CoAs_3$, prep. and characterisation 77−77356
$CoCr_2Te_4$, cryst. growth, struct., elec. props., Hall effect 78−43416
$Co_{1-x}Fe_xSi$, elec. and optical props. 80−49740
$Co_{1/3}NbS_2$, intercalate, metallic cond., Hall effect and mag. props. 77−76789
$Co_{40}Ni_{40}B_{20}$, spontaneous Hall effect and resistivity 79−19576
CoP_3, prep. and characterisation 77−77356
$Co_xPd_{80-x}Si_{20}$, amorphous, structural and mag. heterogeneities 80−80484
Co_2RhS_4, mag. semicond., mag. and elec. props. 80−93121
CoS_2, galvanomagnetic effect of single cryst. 80−96912
$Co(S_xSe_{1-x})_2$, galvanomag. effects, obs. and interpretation 80−70726
$CoSb_3$, prep. and characterisation 77−77356
$CoSnTe_2$, thin films, metallic elec. props. 79−78212
Cr, Hall coeff., mag. field depend. at low temp. 77−20296
Cr-Al, temp. depend. of Hall coeff. 79−33280
CrB_2, crystal growth by floating-zone method, elec. and mag. props. 77−1801
$Cr_{1-x}Mn_xSi_2$, semicond. props. 78−79992
$CrSe_2$, layered, phys. and elec. props. 80−44594
Cr_3SeTe_3, anomalous Hall effect 77−69351
$CrSi_2$, semicond. props. 78−79992
Cs-NH_3 solution, metal-nonmetal transition, cond. density and Hall coeff. meas. 77−51789
Cu, electron-phonon interaction, scatt. and transport props. 79−91037
Cu film, electron transport props., struct. defects role 77−40117
Cu, monocryst., Hall resist., anisotropic temp. depend. rel. to Fermi surface 77−62897
Cu polycrystalline plate, electric current distortion effects 77−72853
Cu, quenched, Hall coefficient, relaxation times, Fermi surface 80−84460
Cu, Sondheimer oscills. in elec. resist. and Hall effect meas. 77−11896
Cu-Ag film, amorphous resistivity, Hall coeff., thermopower and annealing kinetics 77−43744
Cu-Al(Ge)(Sn) alloy films, electron transport props. 77−76955
Cu-Mn, dilute, magnetoresist. and Hall effect, field-depend. electron scatt. 77−43581
Cu-Mn, spin glass, anomalous Hall effect 78−30908
Cu-Ni, comp. modulated alloy films, transport props., 10 to 300K 79−95515
Cu-Ni thin films, ferromag., Hall effect meas. 80−80428
$CuCr_2Se_4$, crystal growth from melt, exam. of props. 80−55283
$CuCr_2Se_{4-x}Br_x$, elec. resistance, Hall const., magnetoresistance singularities *(Russian)* 79−91078
$Cu_{0.67}Cr_{1.78}Se_{2.67}Br_{1.34}$, Hall emf., temp. depend. 79−7846
$Cu_yCr_2Se_{4-x}Br_x$, ferromagnetic semicond., Hall effect 80−60012
$Cu_yCr_2Se_{4-z}Br_x$, degenerate ferromag. semicond., resist. minimum 79−73517
$CuCr_2Se_4(S_4)(Te_4)$, binary and ternary solid solns., mag. and elec. props. 80−2407
$CuGaSe_2$, cryst. struct., X-ray powder data 77−39565
$CuGaSe_2$ single crysts., Hall effect and resist., acceptor states 80−10975
$CuGaSe_2$ single crystals, elect. and optical props. for solar cell appl. 80−10981
$CuGaSe_2$ thin films, on GaAs substrates, structural and elec. props., photoluminesc. meas. 79−65564
$CuGaTe_2$, elec. and optical props. 80−6829
$CuGdTe_2$, synthesis and elec. props. 78−26529
CuH dilute alloy, Hall coefficient, relaxation times, Fermi surface 80−84460
$CuInS_2$, optical and elec. phenomena 78−39605
$CuInS_2$:Cd(Zn), elec. props. 77−62927
$CuInSe_2$, acceptor levels, elec. props. study 80−39578
$CuInSe_2$, n- and p-type, elec. resist. and Hall effect, 80 to 500K 79−87096
$CuInSe_2$ thin films for solar cells, radiofrequency sputtering technique, elec. props. 80−93487
$Cu_4Mn_2S_4(Se_4)(Te_4)$ spinel, prep. and elec. props., 100 to 650K 79−43127
$Cu_2Mo_6S_8$, normal state and superconducting property measurements 78−91660
$Cu_xMo_6S_8$, Hall effect and magnetoresistivity 78−95400
$Cu_xMo_6S_8$, normal-state electronic props., Fermi surface and supercond. parameter derivations 79−60850
Cu_2O:Mn, photomemory mobility components, charged centre conc. 80−103725
Cu_2S, defect models of different allotropic varieties, thermal reactions of Hall coeff. *(French)* 77−47448
Cu_2S film, reactively sputtered, Hall effect meas., 90-300K 80−15541
Cu_2S, low temp. modification, elec. props. 77−8092
Cu_2S, polycryst. thin films, struct., optical and elect. props. for solar energy appl. 80−10837
Cu_2S, rel. to band models of Cu_2S-CdS heterojunctions *(Japanese)* 78−23154
Cu_2S:Cd(Zn), effects of doping on elec. and optical props. 78−38743

Hall effect continued
$Cu_{2-\delta}S$, $Cu_{2-\delta}Se$ and $Cu_{2-\delta}(S,Se)$, ionic and electronic cond., thermopower and Hall coeff. 77−20117
Cu_xS films, magnetron reactive sputtering deposition and elec. props. 79−78884
$Cu_{2-x}Se$, elec. props. and band struct. 79−73513
$Cu_{2-x}Se$, electrical activity of Cu vacancies 80−39606
$Cu_{2-x}Te$, electrical activity of Cu vacancies 80−39606
$Cu_{2-x}Te$, x=0 to 0.3, elec. cond., Hall const., carrier mobility, conc., thermoelec., density, lattice parameter 77−11915
$Cu_{0.75}VS_2$, cryst. struct. and phys. props. *(French)* 78−14328
Dy film, Hall effect meas. in para- and ferromag. regions 77−55622
$DyAg_{1-x}In_x$, elec. and Hall resist. 80−96844
Dy_2S_3, semimetallic, elec. and thermal transport meas. 78−10442
Er, Hall const. and elec. resist., 80-700K *(Russian)* 78−60110
Er_2Te_3, films, prep., elec. props. 78−43494
Eu chalcogenides, anomalous Hall effect, spin correlations, analysis 77−20344
Eu chalcogenides, anomalous Hall effect, impurity scatt. 78−39131
EuB_6, correlation between mag. struct. and elec. props. 77−63192
EuB_6, Hall effect and resistivity data, ferromagnetic ordering temp., pressure depend. 80−60010
EuB_6, mag., transport and thermal props. 79−73738
EuB_6, pure single crystals, magnetic and electric props. 80−11260
EuB_6, resist., Hall effect, and magnetoresist. under hydrostatic press., 4.2 to 300K 80−96879
$EuB_{6-x}C_x$, pure and doped, mag. and transport props. 80−54689
$EuBi_2Te_4$, elec. cond., Hall, thermo-EMF coeffs. determ., 300-1100K 78−43386
$EuGa(In)_2X_4$, X=S,Se,Te, prep. and props. 77−85214
EuO, hydrostatic press. effects on elec. resist. in temp. range 3 to 300K 79−23968
EuO, photoelectron anomalous transport phenomena 78−23114
EuO:Gd, elec. cond. under hydrostatic press., Curie temp. 80−96881
EuO:Gd, pure and doped, elec., mag., and optical props. rel. to electronic conc. 80−96880
EuO(Se), complex elec. cond. anomalies 80−107812
$EuSb_2S_4(Se_4)(Te_4)$ elec. cond., Hall, thermo-EMF coeffs. determ., 300-1100K 78−43386
EuSe, dynamical conductivity in high mag. fields 79−78118
EuSe, Hall effect, elec. cond. and magnetoresistance temp. depend. 79−33296
EuTe, magnetic impurity states, mag. and transport props. 80−96913
Fe, amorphous film, Hall effect and magnetisation *(Russian)* 77−35922
Fe and Fe-Ni Metglas alloys, ohmic and Hall resist. 100-700K, mag. behaviour 80−80254
Fe film, amorphous and polycrystalline, Hall effect, resistivity and mag. moment 78−91786
Fe film, Hall resist., effect of N impurity codeposition 78−64146
Fe films, thickness variations in extraordinary and spontaneous Hall coeffs. 80−97013
Fe, liquid, Hall effect, band struct. and exchange scatt. 80−80250
Fe, mag. breakdown and Hall resist., theory and model calcs. 80−75552
Fe-Au layers, amorphous ferromag., elec. transport phenomena and reson. scatt. *(German)* 77−72847
Fe-C, dil., Hall-field electrotransport of C, effective valence numbers 79−28148
Fe-Co, anomalous, residual coeff. calcs. using coherent pot. method *(Russian)* 80−80249
Fe-Co-Si-B sputtered amorphous thin film, coercivity, galvanomagnetic props., resistivity 80−29578
Fe-Cr-Al, Kanthal films, vac. deposited, evaporation characts., comp., struct. and elec. props. 80−88646
Fe-N alloy, dil., galvanomag. effects, 4.2-250K 78−87964
Fe-Ni, (35 wt.%), transport props. and Invar features *(Russian)* 78−51973
Fe-Ni, anomalous, residual coeff. calcs. using coherent pot. method *(Russian)* 80−80249
Fe-Ni based amorphous alloys, Hall and ohmic resistivities 79−91013
Fe-Si amorphous film, Hall const. and magnetoresistive effect 78−52105
Fe-V(Cr)(Mo)(W)(Ti)(Nb) alloys, split bands evidence from sp. ht. and elec. transport data 77−24515
$Fe_{80-x}Co_xB_{20}$, spontaneous Hall effect and resistivity 79−19576
$(Fe_{1-x}Co_x)_{78}Si_{10}B_{12}$, amorphous, Hall effect and magnetoresist. *(Japanese)* 77−85199
$FeCr_2S_4$, elec. and galvanomag. props. 78−23111
$FeCr_2S_4$, pure and doped, CVD grown, surface struct., elec. props. and band struct. 79−4905
$Fe_{1-x}Cu_xCr_2S_4$, Hall effect and magnetoresist. 79−78119
$Fe_{1/3}NbS_2$, intercalate, metallic cond., Hall effect and mag. props. 77−76789
Fe_xNbSe_2, transport props. and mag. ordering 80−65527
$Fe_{40}Ni_{40}B_{20}$, amorphous ferromag., resist. and galvanomagnetic props., rel. to magnetisation 78−14712
$Fe_{80-x}Ni_xB_{20}$, spontaneous Hall effect and resistivity 79−19576
$Fe_xNi_{80-x}B_{20}$ and $Fe_xNi_{80-x}P_{14}B_6$ metallic glasses, low temp. resist. and galvanomag. effects, mag. state influence 80−84461
$Fe_xNi_{80-x}B_{20}$, $Fe_xNi_{80-x}P_{14}B_4$, amorphous, voltage meas. *(Croatian)* 79−11102
$Fe_xNi_{80-x}B_{20}$, $Fe_xNi_{80-x}P_{14}B_6$, amorphous ferromag., galvanomag. props. 79−56196
$Fe_{32}Ni_{36}Cr_{14}P_{12}B_6$, Metglas 2826A, Hall resistivity, effect of thermal cycling and annealing 78−56125
$Fe_{40}Ni_{38}Mo_4B_{18}$, metallic glass, mag. and transport props. 80−39752
$Fe_{27}Ni_{53}P_{14}B_6$, amorphous, Hall resist. and mag. props., short range order effects 80−34422
$Fe_{40}Ni_{40}P_{14}B_6$, $Fe_{32}Ni_{36}Cr_{14}P_{12}B_6$, amorphous, press. and temp. depends. 77−66155
$Fe_{40}Ni_{40}P_{14}B_6$, metglas 2826, amorphous, Hall resistivity, thermal cycling and annealing effects 79−38050
$Fe_{29}Ni_{49}P_{14}B_6Si_2$, Metglas 2826B, Hall, elec. resist., magnetisation and heat capacity meas. 78−68019
$(Fe_{1-x}Ni_x)_{78}Si_{10}B_{12}$, amorphous, Hall effect and magnetoresist. *(Japanese)* 77−85199
Fe_2O_3, haematite, weak ferromag., Hall effect mag. field depend. *(Russian)* 77−11937
$Fe_xPd_{80-x}Si_{20}$, amorphous, structural and mag. heterogeneities 80−80484
$FeRh_2S_4$, mag. semicond., mag. and elec. props. 80−93121
Fe_3S_4, galvanomagnetic props., resist. and Hall effect meas., 4.2-300K 80−54673

Hall effect continued
$Fe_{3+x}Si_{1-x}$, electron transport 78−91669
n-GaAS, plastic deform. effect on elec. props., dislocation level 77−28178
GaAS:Cr, mag. field depend. of single carrier parameters, mixed cond. anal. 79−91043
$Ga_{1-x}AlAs$:Zn, acceptor energy level and elec. props. 80−65482
$Ga_{1-x}Al_xAs$ epitaxial layer, elec. cond., Hall effect, band struct. 80−49964
$Ga_{1-x}Al_xAs$, LPE growth and characterisation 80−50566
$Ga_{1-x}Al_xAs$, non-shallow levels and cond. band struct. from Hall carrier conc. meas. 80−39607
$Ga_{1-x}Al_xAs$:Si, LPE, phase diagram, Hall effect meas., carrier conc., donor ionisation energies 77−72803
$Ga_{1-x}Al_xAs$:Si, Si determ., spectrochem. method, photoluminesc. spectra, Hall effect meas. *(German)* 77−77851
$Ga_{1-x}Al_xSb$, melt growth and elec. props. 79−65999
n-$Ga_{1-x}Al_xSb$, transport phenomena in low and high mag. fields 78−80007
GaAs, annealing rel. to stoichiometry deviation, Hall effect, electron microscope meas. 77−24410
GaAs, automatic electrochemical Hall mobility profiling 79−99615
GaAs, compensated, electron mobility temp. depend. 80−96868
GaAs, compensated, magnetoresist. and Hall effect 77−66176
GaAs compensated VPE thin film, electron Hall mobilities 80−107932
n-GaAs, conversion to p-type after 1 MeV electron irrad. 79−77636
GaAs, current controlled negative resist. at low temps. 78−39133
GaAs, cylindrical and spherical localised inhomogeneities in mag. field, anomalous elec. prop. calcs. 80−44621
GaAs, defect clusters induced by γ-rays and neutrons, effect on elec. props. 80−29408
GaAs diffusion of ion implanted Be, SIMS and electrical profiling 78−47605
GaAs, dual implantation of C^+ and Ga^+, sheet resist. and Hall effect meas. 78−67728
GaAs, elec. effects of dislocations 79−82586
p-GaAs, electronic props. 78−68040
n-GaAs, epitaxial, high temp. carrier transport 80−65725
n-GaAs, epitaxial film, defect clusters, charge-carrier mobility temp. depend. anal. 80−54701
GaAs, epitaxial layer, effective doping density, comparison of Hall and magnetoresistance meas. 77−11938
n-GaAs, epitaxial layers, electrical parameter determ. by graphical method *(Russian)* 77−15975
GaAs, epitaxial layers, elec. characterisation 78−91791
GaAs, epitaxial layers, MBE grown, Hall mobilities, substrate temps. 80−20335
GaAs epitaxial layers on polycryst. GaAs substrates, LPE growth characts. 80−75471
n-GaAs, heavily doped, impurity-band cond., DC cond., Hall mobility, and magnetoresist. meas. 80−49733
GaAs, high press. electron transport props., three band model 80−15516
GaAs, high-purity, residual donors, ionisation energies determ. 78−6333
p-GaAs, impurity band Hall mobility 80−70730
n-GaAs, LPE, deep trapping centre characterisation by Hall and photo-Hall meas. 80−88578
GaAs, low temp. gamma irrad., donor-acceptor pair formation 79−69158
GaAs, MBE, growth temp. depend. and characts. 79−28946
GaAs MBE epilayers, photoluminesc. and elec. characterisation 80−11500
n-GaAs, mechanism of cyclotron reson. induced cond. 78−43396
GaAs, melt grown, improve elec. and luminesc. props. after short time heat treatment 77−63452
GaAs, model relating elec. props. to impurity concs. 77−51697
GaAs, negative differential mobility and geometrical magnetoresist. calc. 77−43624
n-GaAs, photo-Hall effect meas. of ionised impurity scatt. 78−56182
GaAs, photoelectric memory effect, effect of metallic island struct. on surface 77−55570
GaAs, point defects, laser annealing 80−107224
n-GaAs, proton irrad., E_p=30 MeV, defect form., orientation depend. 78−55898
GaAs, semi-insulating, cond. mechanism, model explaining temp. depend. of elec. props. 79−51571
GaAs, semi-insulating, conduction model 80−10986
GaAs, semi-insulating, surface layer thermal conversion mechanism, Hall effect meas. 80−49772
GaAs, semi-insulating, thermal conversion, Hall effect and luminesc. meas. 78−6405
GaAs, semi-insulating, undoped and Cr-doped, compensation mechanisms, Hall effect and optical absorpt. meas. 80−84477
n-GaAs, shallow donors, elec. cond. and Hall coeff. meas. 77−11942
GaAs, shallow donors, screening, energy spectrum of electrons and cond. mech. 79−7831
n-GaAs, three valley band struct., high temp. Hall mobility 80−29318
GaAs, two dimensional impurity bands, Hall mobility 79−95509
GaAs, unintentionally doped layer grown by MBE, elec. props. 79−91167
GaAs, VPE, electron Hall mobility meas., attempted correlation with growth parameters 78−43417
GaAs, VPE by single flat temp. zone method, elec. props. 79−95526
GaAs, VPE film growth in Ga-$AlCl_3$-H_2 system, O_2 injection effect 79−100057
n-GaAs VPE layers, Hall mobility, effect of Cu contamination, photolum. expts. 80−54810
GaAs VPE layers for FET devices, impurity characterisation 80−29491
n-GaAs vapour phase epitaxial film electrophysical props. rel. to growth temp. *(Russian)* 80−49961
GaAs:Ag, diffusion of Ag at 1000°C, profiles, Schottky barrier and Hall effect meas. 80−54435
GaAs:Be, annealing effect during MBE 78−79898
GaAs:Be, ion implanted, elec. profiling and optical activation expts. 77−89457
p-GaAs:Be, ion implanted, annealing characts., defect cond. profiling, electron diffr. obs. 79−4318
p-GaAs:Be layer, MBE growth, Be doping and diffusion, elec. and optical props. 77−51397
p-GaAs:C, ion implantation efficiency, elec. profile and compensation level meas. 77−27880

Hall effect continued
GaAs:Co, epitaxial layers and bulk, diffusion and elec. activity of Co 79−56333
GaAs:Cr, Be, ion-implanted, semi-insulating, carrier mobility and conc. temp. depend. 77−76808
GaAs:Cr, epitaxial layers, MBE grown, Hall mobilities, substrate temps. 80−20335
GaAs:Cr, FET, influence of Cr on mobility of electrons 80−92910
GaAs:Cr, Mg, ion implanted, elec. meas. and optical activation studies 79−86806
GaAs:Cr, optically excited, Hall effect meas. 77−20343
GaAs:Cr, parameters determ. using cond., Hall-effect and magnetoresist. meas. *(Slovak)* 78−47802
GaAs:Cr, photoconductivity and photo Hall spectra 78−19091
p-GaAs:Cr, semi-insulating, illumination effect on mobilities 77−32043
GaAs:Cr, semi-insulating elec. compensation, Hall and resist. meas. 77−62855
p-GaAs:Cr, semi-insulating photoelectronic analysis 77−80804
GaAs:Cr, semi-insulating, characterisation by photoelectronic data 78−68051
p-GaAs:Cr, semi-insulating, mobilities and carrier concentrations, temp. depend. 80−70702
GaAs:Cr, semiinsulating, hole recomb. domains, Hall mobility and photocond. 77−15867
GaAs:Cr, Zn(Se) shallow impurity implantation, elec. props. after annealing 80−24465
GaAs:Cr,Zn, implanted, doping profiles after laser annealing, elec. props. 80−2058
p-GaAs:Cu, impurity photocond. and absorpt. coeff., Hall meas. 80−6770
GaAs:Fe, for FET, VPE and characterisation 78−19672
n-GaAs:Ge, film, substrate temp. depend. of Ge incorporation during MBE 80−76196
GaAs:Ge, ion implanted, elec. props., comparison with Sn, Se and Te ion implanted samples 77−39879
GaAs:Ge, LPE, on semi-insulating GaAs, film-substrate interface characterisation 78−72017
GaAs:Mg(C)(Te)(Ge), ion implanted, laser annealing, ellipsometric and Hall meas. 79−73193
GaAs:Mn epitaxial layers, fabrication and electrical props. 77−80859
GaAs:O, deep level, Franck-Condon shift, photocond. and Hall effect study 80−70642
GaAs:O, impurity photocond. in high elec. field, 90K, and photo-Hall effect 78−19095
n-GaAs:O film, influence of O on elec. props. 79−11252
GaAs:Se, Ga, dual species ion implantation, elec. characts. 80−103377
GaAs:Se, implanted, annealing with O-free CVD Si_3N_4 encapsulant 78−83834
GaAs:Se^+, implanted semi-insulating, pulsed electron and laser beam annealing effects on elec. characts. 79−73196
GaAs:Se(Zn) polycrystalline film, Hall effect, resistivity meas. 80−96911
GaAs:Si, accelerated growth rate effect on MBE, Hall mobility and photolum. meas. 80−104067
GaAs:Si, Cr, carrier concs. from Hall effect, microscopy, localised vibrational modes absorption meas. 78−56104
GaAs:Si, electron irradiated, LPE layers and Bridgman crysts., IR absorption and Hall meas. 77−16345
GaAs:Si, film, conversion of type of conduction stimulated by ion bombardment 77−4457
GaAs:Si, ion implantation, thermal annealing, Hall meas., SIMS atomic profile meas. 80−75243
GaAs:Si, ion-implanted, annealing with Nd:glass laser 79−73194
n-GaAs:Si, optically enhanced Hall mobility meas. 77−39884
GaAs:Si, pulsed laser annealing of implanted layers, defect structure and Hall effect meas. 79−69118
GaAs:Si epitaxial films, elec. and photoelec. props., impurity distrib. 80−7006
n-GaAs:Si LEC crystal, carrier conc., B acceptor centres, Hall meas. and IR spectra 78−6717
GaAs:Si layers, MBE growth, elec. and optical props., doping characts. 80−10819
GaAs:Sn epitaxial layer, electronic props. and epilayer-substrate interface props. 77−89886
GaAs:Sn(Be) MBE films, elec. characterization 79−91168
n-GaAs:Te, elec. cond. and Hall coeff. temp. depend. meas., three band model 79−33287
GaAs:Te, heavily doped degenerate semicond., anomalous increase in Hall voltage 79−61053
GaAs:Te, ion implanted, laser annealing 79−73192
GaAs:Te, recombination barrier, dark cond., photocond., and Hall mobility meas. 80−15559
GaAs:Zn, Se, double doping during LPE, exam. of elec. cond. and Hall effect 79−4923
GaAs:Zn MBE layers, ionized beam doping, elec. and optical characts. 79−37721
GaAs-$Al_xGa_{1-x}As$ differentially doped heterojunction interface, two-dimens. electron gas obs. 80−49886
GaAs-$Al_xGa_{1-x}As$ heterojunction interface, two-dimensional hole gas obs., Shubnikov-de Haas meas. 80−80357
GaAs-$Al_xGa_{1-x}As$ multilayers, two-dimens. transport at high mag. fields 80−65724
GaAs-AlGaAs:Si heterojunction interface, two-dimens. electron gas, Hall effect and cyclotron reson. meas. 79−65530
GaAs-GaCu:Tl, cathode luminescence spectra, Hall effect, cryst. defects 80−76087
GaAs-GaAlAs multilayer struct., Hall mobility enhancement 80−100511
GaAs-ZnSe, solid solution crystals, grown by Bridgman method, exam. of resistivity and Hall effect 79−95919
$GaAs_{0.6}P_{0.4}$:Be, implanted annealing studies, elec. resist., Hall effect meas. 78−84213
$GaAs_{1-x}P_x$ based structs., carrier conc., mobility calcs. from Hall effect meas. 78−60138
$GaAs_{1-x}P_x$, electron irrad., radiation defects annealing 80−29059
$GaAs_{1-x}P_x$, N trap bound state, Hall effect determ. 78−19055
$GaAs_{1-x}P_x$ solid solution, disorder scatt. Hall mobility meas. 77−69350
$(GaAs)_{1-x}(ZnSe)_x$, LPE growth, resist., Hall effect and cathodoluminesc. meas. 77−28270
$Ga_{1-x}In_xAs$:Mn grown by LPE, elect. props. 80−100541
GaInAsP, VPE growth and props. 80−16194
$Ga_{1-x}In_xP_{1-y}As_y$, carrier compensation and alloy scatt. 80−29490
Hall effect continued
$Ga_{0.3}In_{0.7}Sb$, negative differential mobility and geometrical magnetoresist. calc. 77−43624
$Ga_xIn_{1-x}Se$, fabrication, struct., elec. and optical props. 80−44180
$Ga_{1-x}Mn_xSb$ alloys, mag. phase transition obs. 78−52248
$Ga_{1-x}Mn_xSb$, elec. cond., mag. susceptibility, Hall const., and thermo-EMF, 80 to 1000K *(Russian)* 80−88549
GaN, epitaxial growth on sapphire substrates, elec. props., X-ray diffr. anal., photoluminescence spectra 79−4919
GaN film, thermoelec. power and Hall coeff. meas. 77−55627
GaP, electron irrad., radiation defects annealing 80−29059
n-GaP, epitaxial layers, electrical parameter determ. by graphical method *(Russian)* 77−15975
GaP, heteroepitaxial CVD on Si, dual process, film characts. 77−16503
p-GaP, LPE layers, Hall effect 78−91704
GaP layers, LPE growth, elec. props., residual impurities 79−38202
GaP:Cu, elec. and optical props., rel. to doping and heat treatment 80−16056
GaP:Ni, Hall effect and absorpt. spectrum investig. of acceptor level 77−44033
GaP:s, elec. props. following 1.7 MeV electron irradiation 78−80005
n-GaP:S electrical properties investigation *(Japanese)* 77−39840
GaP:Sn, LPE growth from Sn soln., elec. resist. and Hall coeff. meas. 78−2593
n-GaP:Te, doping parameters calc., by means of Hall data analysis 78−51925
GaP:Te, Hall effect and elec. cond., 80-400K 78−91705
n-GaP:Te, LPE layers, Hall effect 78−91704
GaP:Zn, Hall effect and elec. cond., 80-400K 78−91705
p-GaP:Zn, Hall effect determ. of hole mobility temp. depend., scatt. mechanisms 77−4364
GaP:Zn, implanted, elec. profiling using anodic oxidation in N-methylacetamide 80−54690
GaP:Zn, Sn doped epitaxial layers, Hall const., hole mobility and conc. 80−15143
GaP:Zn,O, Auger coeff. from luminesc. decay and Hall effect 77−48226
GaP:Zn,O, Auger coeff. from luminesc. efficiency and Hall effect 77−48227
GaP-Si, heteroepitaxial growth, electronic and optical props. 80−104075
$GaS_xSe_{(1-x)}$, Bridgman-grown, electrical props. meas. 78−84216
GaSb and $GaSb_xAs_{1-x}$ films, MBE growth and elec. props. 79−23863
GaSb, bulk and epitaxial, IR reflect. meas., carrier conc. and mobility determ. 80−80769
GaSb, carrier density depend. on impurity conc., multiple doping effects 77−8047
GaSb, defect concentration determ. model, Hall effect 80−103385
p-GaSb, elec. cond., Hall effect, mobility and carrier concentration *(Russian)* 79−19603
GaSb film, polycrystalline, Hall mobility 80−97015
n-GaSb, galvanomagnetic effects 78−72172
GaSb, LEC growth, Hall coeff. 80−89133
GaSb, sputtered films, on GaAs, growth, Hall effect, impurity levels 80−20334
GaSb, undoped, intrinsic acceptors, parameters determ. 79−51515
GaSb:Fe, shallow acceptor level, electrical meas. 79−11087
GaSb:Gd(Yb), elec. props., dopant effects 79−87115
GaSb:Mn(Sm), struct., thermo EMF, galvanomag. props. rel. to dopants, eutectic $Mn_{0.6}Ga_{0.4}Sb$ form. 77−15869
GaSb:S, cond. and Hall coeff. relax., impurity config. model 80−6786
n-GaSb:Se, resonant and bound impurity states, Hall effect and resistivity press. depend. 77−28143
n-GaSb:Te, elec. transport mechanism in cond. band from Hall mobility and transverse mangetoresist. meas. 79−73531
n-GaSb:Te, Hall coeff., carrier conc. and mobility, elec. cond., 290 to 550K *(Russian)* 79−19604
GaSb:Te,Zn(Te,Mn), prep. and electrophys. props. 79−87116
p-GaSb:Zn, hole transport props. from 77 to 300K 79−73530
GaSe, Hall mobility anisotropy 78−68041
p-GaSe, resist. and Hall-mobility meas. at 77-850K 77−59295
GaTe, Hall mobility, resistivity anisotropy 79−11150
p-GaTe, scatt. by homopolar optical phonons, Hall effect meas. 77−28197
GaTe, transport properties under hydrostatic pressure 80−75589
p-$GaTe_xSe_{1-x}$, resistivity and Hall effect meas. 77−24556
Gd-Co amorphous film, DC or RF sputtered, mag. props., He^+-backscatt. investig. 77−20650
Gd-Co film, amorphous, Kerr and Hall loops 77−89996
Gd-Co film, sputtered from segment target, composition and mag. props. 78−27062
Gd-Co sputtered films, preparation process, props. 77−59688
Gd-Mn(-Co) alloys, amorphous, ferrimag. props. and Hall effect 79−73692
Gd-Ti(V)(Cr)(Mg)(Nb)(Ge)(Si)(Au) amorphous films, spontaneous Hall effect and elec. resist. 80−80251
Gd-transition metal, amorphous film, galvanomag. effects, Hall detector 77−89882
$GdAg_{1-x}In_x$, elec. and Hall resist. 80−96844
$GdAl_2$, ferromagnetic, extraordinary Hall effect 80−39560
GdCo film structure, dependent on substrate type *(Russian)* 80−24747
$Gd_{1-x}Co_x$, film, resistivity, Hall effect, domain wall density 78−76169
$(Gd_{1-x}Co_x)_{1-y}Ar_y$ amorphous mag. film, elec. and mag. prop. depend. on Ar 80−80410
GdFe film structure, dependent on substrate type *(Russian)* 80−24747
$Gd_{18}Fe_{82-x}Ni_x$, amorphous film, mag. and galvanomag. props. 77−24715
Gd_2GeSe_5, elec. props., 300 to 1100K 79−51585
$Gd_xLa_{1-x}Al_2$ ($x<0.05$), Hall effect measurements 80−44569
GdN, and $GdN_{1-x}O_x$, mag. interactions 80−60218
GdN, mag. interaction and carrier conc. 80−71005
$GdN_{1-x}O_x$, magnetic interaction and carrier conc. 80−71005
Gd_xNi_{1-x} sputtered amorphous films, mag. props. and Hall meas. 78−95488
Gd_2S_3, semimetallic, elec. and thermal transport meas. 78−10442
$Gd_xY_{1-x}Al_2$ ($x<0.05$), Hall effect measurements 80−44569
$(Ge,Pb)_{1-x}Mn_xTe$, mag. and elec. props. meas. 80−29534
n-Ge, anisotropy of thermal and convective noise, in magnetic field 78−34873
n-Ge, anomaly of Hall effect after 50 MeV electron irrad. *(Russian)* 77−43619
Ge, before and after alpha-particle irrad. radiative electromagnetic effect 78−10434

Hall effect continued
Ge bicrystal, cond., Hall effect and Shubnikov-de Haas oscills. 80−10984
Ge, bicrystal, two-dimensional electronic phenomena at He temp. *(Russian)* 79−56273
n-Ge, carrier relax. time, mag. field effects, rel. to Hall effect 80−39608
Ge, charge carrier scatt. and compensation effect on Hall mobility of majority carriers *(Russian)* 77−32026
Ge, compensated by thermal defects, Hall effect anomalies 79−69535
n-Ge, deform. induced point defects, Hall coeff. meas. 80−19800
n-Ge, deformed, 1/f noise, resist., mobility, and carrier density 77−8161
Ge, deformed at relatively low temps., Hall effect 79−82612
Ge detector; high-purity, effect of crystal growth direction on energy resolution 79−45541
Ge, dislocation energy levels, Hall effect meas. 78−6328
p-Ge, dislocation microwave cond. and Hall effect meas. *(Russian)* 77−47848
p-Ge, dislocations, grown-in defects, electrical props., deep level transient spect., Hall effect 80−39524
Ge, drift mobility and Hall coeff. factor of holes 78−43379
Ge, electron irrad., light-sensitive defects 80−24498
n-Ge, electron irradiated, high temp. annealing, nonequilibrium carrier lifetime and Hall effect 77−4370
Ge, electronic inversion channel anomalous Hall factors *(Russian)* 79−95467
Ge epitaxial film, ion implantation and electron beam anneal effects on carrier conc. 80−75255
Ge, epitaxial film, ion sputtering, growth mechanism, struct., props. 77−31917
Ge epitaxial film on Si, influence of fragmentary struct. on galvanomag. effects *(Ukrainian)* 78−84327
Ge film, amorphous, vac. deposited, XPS and elec. props., evidence for polycryst. phase 77−28691
Ge film, elec. props., prep. by DC sputtering *(Japanese)* 79−78237
p-Ge film, fragmented struct., elec. cond., Hall coeff. and magnetoresist. meas. 77−15979
Ge film, polycrystalline, structural and elec. props. 78−76173
p-Ge film on GaAs, cond., Hall effect and transverse magnetoresist., anisotropy 79−51697
n-Ge, H-linear planar Hall effects of hot electrons 78−76082
n-Ge, Hall coeff. and cond. mech. in intermediate conc. at He temps. 79−95422
Ge, Hall effect, influence of dislocations 79−82611
n-Ge, Hall effect, uniaxial deform. effects 80−65605
n-Ge, Hall mobility in fast electron irradiated samples 77−55551
Ge, heavily doped, vacuum hot-pressing thermal and electrical props. 77−40400
P-Ge, heteroepitaxial film, galvanomagnetic effects, influence of mechanical stresses 79−91171
Ge, high purity, carrier trapping 79−47104
Ge, high-purity dislocation-free, divacancy-hydrogen complexes 78−2449
Ge, hydrogen multivalent acceptor complexes 77−55491
Ge, irradiation by 3.5 MeV electrons at high temp., carrier density and lifetime changes 77−4128
n-Ge, laser irrad., accumulation of defects, effect on elec. props. 80−107317
n-Ge, lightly doped, compensated by disordered regions, conductivity and Hall mobility 80−11016
p-Ge, negative magnetoresist. and Hall effect, press. and field depend. 80−70733
Ge, neutron irrad., Hall effect and magnetoresist. meas. 80−6883
Ge, optical excitation of dislocation states 77−85265
p-Ge, piezo Hall effect meas. 80−96883
n-Ge, plastically deform., dislocation state spectrum, photocond., elec. cond., and Hall const. meas. *(Russian)* 80−2362
Ge, plastically deformed under high temp. creep conditions, elec. props. 80−92915
Ge, point defect creation by plastic deform., Hall const. electrical conductivity 78−6053
Ge, relax. time energy depend. and surface galvanomag. props. 78−43459
Ge, shallow acceptors produced by quenching 79−51523
Ge, surface, Hall effect study, channel cond. *(Russian)* 80−92909
n-Ge, surface electron mobility, Hall effect and cond. meas. 79−56281
Ge surface Hall effect and cond., electron, hole conc. and mobility *(Russian)* 80−44619
n-Ge, transverse magnetoresist. effects on Hall voltage meas., theory 77−72870
Ge, trapping defects, deep level transient spectroscopy 79−47045
p-Ge:Ag, Sb, electron beam irradiation cond. characts. 80−19842
Ge:Al, limiting solubility, rel. to charge carrier conc. 80−24596
Ge:Au, gamma-irradiated and electron irradiated, elec. props. meas. 77−62950
Ge:Au, Sb, Hall mobility, temp. dependence 80−96919
Ge:Au,Sb, electron irradiated, Hall effect, photocond., and photomagnetic effect meas. 77−4369
p-Ge:Au,Sb,Hg(Zn), radiation-defect form., Au influence 80−92911
Ge:Ba(Ca), elec. props. and effect of impurities on γ-radiation defect formation 78−10088
Ge:Be single crystals, grown by Czochralski method, exam. of Be distribution ratios and solubility 79−95043
p-Ge:Cd,Sb, electron irrad. at 300K, elec. props. 80−6435
Ge:Cu, electron irrad. effects on carrier density, defect form. 80−19843
Ge:Cu, press. effect on energy spectrum of carriers, elec. cond. and Hall coeff. expts. 79−23930
Ge:Cu, quenched, interaction between shallow-level defects and Cu atoms, Hall effect meas. 78−64002
Ge:Cu(Sb), electron irradiation effects on elec. props. 78−6103
Ge:Ga, cryst. defects due to neutron irrad., elec. cond. and annealing 79−55789
Ge:In(Hg), impurity characterisation from thermal carrier meas. 80−65595
Ge:metal, polycrystalline film, electron transport props. 79−99642
Ge:Mg, energy level behaviour, Hall coeff. and elec. cond. meas. 80−34396
Ge:O, elec. props., O donor levels determ. 77−8123
Ge:P, amorphous, electronic transport and photocond. 79−60834
Ge:P, solubility and segregation of electrically active P 77−15442
Ge:Sb, annealing stages of thermal defects, elec. meas. 77−55282
Ge:Sb, cryst. defects due to neutron irrad., elec. cond. and annealing 79−55789

Hall effect continued
n-Ge:Sb, electron irrad., impurity photoconductivity 77−15900
n-Ge:Sb, γ-irrad. effects on donor conc. and compensation by acceptors 78−56106
Ge:Sb, heavily doped semicond., scatt. mechanism, resist, and Hall coeff. maxima 80−75586
n-Ge:Sb, high-field Hall effect spectroscopy 80−65600
Ge:Sb, limiting solubility, rel. to charge carrier conc. 80−24596
Ge:Sb,D^-, impurity band spectrum, Hall coeff. interpretation 77−51702
Ge:Sb(Au) cleaved surface, influence of impurities on local surface states 79−78150
Ge:Sb(Ga), fast electron radiation defects, 0.52 eV absorpt. band, impurity photocond. and Hall effect meas. 78−27273
Ge-Si alloy, epitaxial growth by getter sputtering, characts. 79−28915
Ge-Si solid solution film, elec. props. in range 4.2 to 500K 77−8214
Ge-Si:Sb, energy spectrum of Sb 80−34382
Ge-Si:Te, solid solns., donor states energy spectrum 80−88516
Ge-Te-As-In quaternary compounds, elec. props., Hall effect *(Spanish)* 77−69344
n-$Ge_{1-x}Al_xAs$:Te, long-lifetime photocond. effect obs., Hall effect meas. 77−89795
$GeBi_2Te_4$, Hall const., thermoelec. power, and elec. cond. 80−29407
$GeFe_2O_4$, single crysts., elec. and mag. props, optical absorpt. spectra 80−54719
$(Ge_{1-x}Ga_x)_{1-x}Te$, rhombohedral and cubic phases, transport effects 78−2481
$(Ge_{1-x}In_x)_{1-x}Te$, rhombohedral and cubic phases, transport effects 78−2481
$Ge_3Se_2Te_4$ film, chalcogenide glass, freq. depend. of Hall effect 77−1436
$Ge_{0.8}Si_{0.2}$, elec. cond., density of states, impurity and temp. depend 80−65568
$Ge_{0.5}Sn_{0.5}Te$ film, elec. and optical props. 77−12028
γ-GeTe, anisotropy of elec. props. 79−73515
GeTe, effect of phase transition on mech. and elec. props. 77−51746
GeTe, Hall coeff., temp. depend. rel. to order parameter 80−96921
GeTe, high pressure effects on hole conc. and thermoelec. props. 78−26894
GeTe, quenched, phase transitions and electrophysical props. 79−51250
GeTe-MnTe-SnTe system, compds., GeTe phase transition temp., elec. props., thermal cond. 79−43220
$(GeTe)_x$-$(AgSbTe_2)_{(1-x)}$, thermoelectric characts., temp. depend. 300 to 750K 79−78123
α-$Ge_{1-x}Te_x$, anisotropy of elec. props. rel. to cubic phase transition and band struct. 77−76820
$Ge_{1-x}Te_x$, elec. cond., Hall effect in phase transition region 79−11113
He-Cs discharge plasma, high freq. oscills. in crossed elec. and mag. fields *(Russian)* 77−15189
$Hg_{1-x}Cd_xSe$, (x=0 to 0.15), Shubnikov-de Haas oscillations, influence of level broadening 79−11155
HgCdTe, electron irradiated, high temp. defects 79−78122
HgCdTe, Magneto transport anomalies at low carrier densities, Wigner crystallisation 80−20222
n-HgCdTe, photocond., Hall mobility and resist. 80−34478
HgCdTe, zero gap, unusual high electron mobility and related phenomena 79−82601
n-$Hg_{0.785}Cd_{0.215}Te$, slightly compensated, transport props. of photo-excited carriers 78−47832
$Hg_{0.79}Cd_{0.21}Te$, ion implanted, elec. props. 80−20184
$Hg_{1-x}Cd_xTe$, carrier conc., Hall effect, photocond., IR spectra meas. 80−49771
$Hg_{1-x}Cd_xTe$, epitaxial layers, elec. properties in the range 4.2 to 300K *(French)* 80−65721
$Hg_{1-x}Cd_xTe$ epitaxial layers, elec. props. 80−96910
$Hg_{1-x}Cd_xTe$, ionized intrinsic pt. defects, effect on carrier density 77−47835
$Hg_{1-x}Cd_xTe$, LPE growth and characterisation 80−50565
$Hg_{1-x}Cd_xTe$, long-term Hall-type conversion by vacancy diffusion at room temp. 79−65498
$Hg_{1-x}Cd_xTe$, props. and appls., book contrib. 77−39834
$Hg_{1-x}Cd_xTe$, semiconducting phase, acceptor states and galvanomagnetic effects 80−11017
$Hg_{1-x}Cd_xTe$, semimetallic and semicond., Hall coeff., anomalous temp. depend., 4.2 to 70K 80−65604
$Hg_{1-x}Cd_xTe$, zero-bandgap state induced by press., galvanomag. props. 77−47725
$Hg_{a-x}Cd_xTe$, (x<0.16), semimetallic phase, acceptor states and galvanomagnetic effects 80−6882
$Hg_xCd_{1-x}Te$, Hall effect and elec. cond., carrier density and mobility temp. depend. 77−4341
$HgCr_2Se_4$, electronic props. rel. to departure from stoichiometry 80−100472
$HgCr_2Se_4$, ferromag. semicond., transport props. 78−68039
$HgCr_2Se_4$, n-type ferromag. semicond., galvanomagnetic props. 80−70727
HgI_2, photoexcited, Hall effect, magnetocond., and cyclotron reson., carrier mobility and effective mass 77−59294
$Hg_{1-x}Mn_xTe$, acceptor reson., states in high mag. field 80−49668
HgSe, CVD crysts., electrophys. characts. 77−85910
HgSe, epitaxial growth on CdSe, struct. and electrophysical props. 77−12540
HgSe, point defect model rel. to elec. props. and phase diagram 77−4339
HgTe, acceptor reson., states in high mag. field 80−49668
HgTe, contrib. of resonant states to conductivity 79−51577
HgTe, electron conc. temp. depend., 1.6 to 32K, Hall effect and cond. meas. 80−24952
HgTe film, vac. deposited, elec. props., 78-420K 80−11119
HgTe, heteroepitaxial growth by close-spaced technique of confined type *(Japanese)* 77−24967
HgTe, mobility of electrons and holes, 4 to 100K 80−107821
HgTe, uniaxially compressed, anomalous magnetoresist. and band crossing 79−65501
HgTe, vacancy doping, effect on elec. characts. 79−82595
HgTe, vacancy doping by off-stoichiometry, influence on transport props. 78−55862
HgTe:Cu(In), dopant interactions 77−47834
$HgTe_xSe_{1-x}$, solid soln., intrinsic carrier density and energy band struct. 78−39134
Ho, field and temp. depend., 4.2-150K, singularities *(Russian)* 80−29387
Ho, Hall const. and elec. resist., 80-700K *(Russian)* 78−60110

Hall effect continued
Ho-Sm alloys, field and temp. depend., 4.2-150K, singularities *(Russian)* 80−29387
In, electron MFP, conduction electrons injected from ferromag. 79−15135
In film, evaporated, resist., Hall effect and light transmittance, use as semitransparent electrode 77−39966
In, Hall field, reversal, 6-280K 78−72135
In, transverse magnetothermoelec. props. 78−47768
n-InAs, electron mobility dependence on conc. Hall effect at 300K 78−47794
InAs epilayers in MOS, Hall coeff. rel. to mag. field in multilayer model 78−2575
InAs, exam. of decomposition of donors 79−1605
InAs film, DC sputtering, struct. and elec. props. 77−66567
InAs, heteroepitaxial, charge transport obs. by gate-voltage-controlled meas. on MOS struct. 77−47912
InAs heteroepitaxial layers, VPE grown, effect of $AsCl_3$ mole fraction on elec. props. 79−11255
InAs, heteroepitaxial layers, $AsCl_3$ mole, fraction and substrate orientation effects on elec. parameters 80−39690
InAs, intrinsic point defects, nature and influence on electrophys. props. 78−79609
n-InAs, Shubnikov-de Haas transverse kinetic coeffs., quantum oscills. 80−49778
InAs surface layers, oscillatory transport coeffs. 78−64136
InAs, surface potential and surface states rel. to n-, p-, compensated n-type behaviour 77−15932
InAs, thin film prep. and elec. props. 79−1633
n-InAs, transport props., influence of higher energy bands, calcs. 79−19598
n-InAs, undoped, electron irrad., Hall coeff., elec. resistivity, optical absorption 77−89479
n-InAs, VPE layers, on GaAs substrate, electronic profile 79−95525
InAs:Cd, Te, donor-acceptor interaction, elec. cond. and Hall coeff. meas. 80−59988
InAs:Cd,Te interaction between impurities, effect on elec. props., Hall effect. 80−19832
n-InAs:Cr, Czochralski growth of high-resist. single crysts. 77−66587
InAs:Mn, NMR, magnetoresist., Hall effect and mag. susceptibility meas. 78−26888
InAs:Zn,S,(Se)(Te), exam of microhardness, Hall effect as function of dopant 79−95038
InAs-GaSb superlattices, semicond.-semimental transition obs. 80−49882
$(InAs)_{1-x}(CdSe)_x$ solid solution, elec. props. 79−15146
$InAs_{1-x}Sb_x$, epitaxial film, carrier recomb., elec. and optical props. 79−15164
$In_{0.53}Ga_{0.47}As$, Hall mobility and Hall factor, temp. and donor conc. depend. 80−49773
$In_{0.53}Ga_{0.47}As$, interband magnetoabsorption study, quasi-Ge model application 80−50304
p-$In_{0.53}Ga_{0.47}As$:Zn on InP, elec. and optical props. 80−75662
InGaAsP-InP lattice-matched heterojunction, LPE growth and characterisation 77−21041
$In_{1-x}Ga_xAs_yP_{1-y}$, Hall mobility, comp. depend. 80−75587
n-$In_{1-x}Ga_xP$ solid solns., electron scatt. mechanisms *(Russian)* 79−4568
$In_{1-x}Ga_xP_{1-y}As_y$ LPE films, hot electron and magnetotransport props. 78−26977
$In_{1-x}Ga_xP_{1-y}As_y$ lattice-matched epitaxial layers, LPE growth on GaAs(100), characterisation 80−75465
$In_xGa_{1-x}P_yAs_{1-y}$, electron effective mass and Dingle temp., Shubnikov-de Haas oscills. 80−59859
$In_{1-x}Ga_xSb$ films, elec. props., preparation 80−100473
InO_3:Sn film, prep. by spray hydrolysis, struct., elec. and optical props. *(Japanese)* 79−42678
In_2O_3 films, electron beam evaporation, elec. and optical props. *(Japanese)* 80−60784
In_2O_3 films, reactively evaporated, elec. props. 80−84521
In_2O_3, reactive ion plating onto insulating substrates, and elec. and optical props. 79−87588
In_2O_3, thermally evaporated film, struct. and elec. props. 80−104066
In_2O_3:Sn, film, HF sputtered, cond., Hall mobility, oxidation, charge carrier density 78−72287
In_2O_3:Sn films, doping profiles and elec. props., appl. to optoelectronic devices 79−38203
In_2O_3:Sn films, pure and doped, prod. by ion plating, elec. and optical props. 80−2488
In_2O_3-SnO_2 thin film, Hall mobility, temp. depend., grain boundary effects 80−75658
In_2O_3-SnO_2-CdTe:P, p-n homojunction solar cell, elec., photovoltaic props., photoluminescence 80−81463
In_2O_3-SnO_2-InP solar cell junctions, efficiency, InP surface props. 80−85288
n-InP, 10-300K ,thermal activation energy and influence of compensation 78−72171
n-InP, compensated, elec. props., space-charge effects 80−65569
InP, electron transport props., mag. field and temp. depend. 80−92888
n-InP, epitaxial, Hall effect, electron mobility and density, temp. depend. 78−72288
InP, epitaxial layer, effective doping density, comparison of Hall and magnetoresistance meas. 77−11938
p-InP film growth, by close space vapour transport, elec. charact. 79−28944
InP, growth and props. 79−1822
n-InP, γ-ray and electron irrad., annealing of radiation point defects, elec. cond. and Hall coeff. meas. 80−65051
n-InP, impurity and minimum metallic cond. in mag. field 80−103731
InP, ion implanted, anodic oxidation and elec. carrier conc. profiles 79−70185
InP, n-type conductive regions produced by ion implantation 78−10067
InP, negative differential mobility and geometrical magnetoresist. calc. 77−43624
n-InP, room temp. electron irrad., Hall coeff. meas. 77−89478
InP, synthesis solute diffusion grown, elec. props., photoluminesc., etch pit profiles 79−4914
InP, weak field Hall mobility and Hall mobility and Hall ratio 78−23116
InP, Zn diffused single-crystal, substitutional dopant and hole conc. meas. 80−75260
InP:Co(Cr)(Fe), Hall and resistivity meas. 80−10990

Hall effect continued
InP:$S^+(Se^+)$, ion-implanted VPE layers, laser annealing, elec. and struct. anal. 79−73199
InP:Sn, LPE growth from Sn soln., elec. props., 80 to 300K 79−11250
p-InP:Zn, 300K, mobility, hole conc. 78−14745
InS, prep., and elec. and optical props. 77−77361
n-InSb, acoustomagnetoelec. effect, 20-120K, sign reversal obs., and Hall mobility 77−24592
n-InSb, anomalous Hall effect at high mag. field 77−15876
n-InSb, compensated cryst., influence of surface cond. on Hall coeff. and elec. resist. 79−69579
p-InSb, deformed, giant negative magnetoresistance 78−87990
p-InSb, elec. instability and oscills. of transparency in transverse mag. field 78−6407
InSb, electrical effects of dislocation, galvanomag. props. 78−23119
n-InSb, electron gas degeneration in strong mag. field 77−66173
InSb, electron irradiated, kinetics of changes in carrier density 79−56228
n-InSb, electron mobility at 77K in avalanche regime 79−33295
p-InSb, excess In, polycryst. thin film, elec. transport props., non-stoichiometric effect 79−95528
InSb film, degenerate, concs. and ionisation energies of defect levels, Hall effect meas. 79−91087
p-InSb film, elec. transport props. 78−72291
n-InSb film, low energy electron irrad. effect on elec. props. 80−7009
InSb, film, transverse 1/f noise and signal-to-noise ratio of related Hall elements, comment 79−99593
InSb, film, transverse 1/f noise and signal-to-noise ratio of related Hall element 79−99594
InSb films, melt-grown, point defect effect on elec. props., 77-300K 80−2502
n-InSb, galvanomag. props. at low temp., carrier localisation, metallic impurity cond. 77−28195
n-InSb, galvanomagnetic props. at low temp., mag. field induced metal-nonmetal transition 77−76845
InSb, galvanomagnetic props. of annealed single crystals 80−96909
InSb, gamma irradiated, changes in energy spectrum of impurity spectrum 78−51937
n-InSb, Hall coeff. and magnetocond. in mag. freeze-out regime 79−60849
n−InSb, Hall effect and magnetoresist. in mag. freeze-out region 79−15165
n-InSb, Hall effect and magnetoresist. in extreme quantum limit, stress depend. 80−11021
InSb, Hall plates, temp. and pot. distribs. determ., temp. depend. cond. effect 79−60851
p-InSb, high press. effect on elec. props., 50-300K 77−47807
InSb, high-purity specimen irradiated at 80K, transport prop. and defect annealing 78−95307
InSb, impact ionisation and magneto-transport, high crossed elec. and mag. fields 80−107797
p-InSb, influence of plastic deform. on elec. props. 80−103711
InSb, intrinsic and n-type, elec. cond., carrier wave instability in elect. and mag. fields 79−82617
p-InSb, ion bombardment using 30-80 keV ions, isochronous annealing, elec. props. obs. 79−19295
InSb, ion irrad., isothermal annealing effects 80−6424
InSb, low temp. electron mobility, theory and expt. 77−89759
p-InSb MIS struct., field effect studies 80−80386
InSb, magnetic freeze out *(Japanese)* 78−39130
InSb, magneto-surface transport props. 77−43693
n-InSb, magnetotransport experiments, surface treatment induced effects 80−34468
InSb, micron size Hall probe for precision mag. field mapping 79−75558
p-InSb, negative magnetoresist. under press. 80−20224
p-InSb, negative piezomagnetoresist. and Hall effect meas., antiferromag. order form. 78−19061
InSb, photoresistor in mag. field, increased responsivity 78−39162
InSb, polycryst. film, Hall and drift mobilities 79−95531
InSb recrystallised thin films on mica substrate, elec. props. 80−70867
n-InSb, Shubnikov-de Haas transverse kinetic coeffs., quantum oscills. 80−49778
n-InSb, sign change of Hall effect, in quantum limit 77−15875
InSb, thin films, electrophysical props. obs. 80−103765
InSb thin films prepared by ion beam epitaxy system *(Japanese)* 78−22976
n-InSb, transverse magnetophonon reson., oscillatory amplitude and damping 78−47813
n-InSb, undoped, press. induced slow relax. of free electron conc., Hall coeff. meas. 77−47833
InSb, undoped and Te-doped, anomalous impurity segregation, Hall and mass spectrum meas. *(Chinese)* 80−59501
p-InSb, uniaxially stressed, elec. cond., Hall coeff. and photocond. at 15K 77−47828
n-InSb:Cr, deep impurities, elec. cond. and Hall coeff. meas., 4.2 to 120K 80−107791
InSb:Cr, press. effects on transport props. 78−56146
InSb:Cr, Zn and InSb:Zn, impurity centre behaviour, impurity conc. and Hall coeff. meas. 80−65490
InSb:Cr,Zn, transport props. meas. 77−1424
InSb:Cr:Zn, Hall coeff. in static and pulsed mag. fields 79−15169
p-InSb:Cu(Ag), ionisation energy of multiply charged impurities, compensation effects 78−18996
p-InSb:Cu(Zn) film, heavily doped, ionized impurity scatt., Hall effect and DC cond. meas. 79−99643
InSb:Ge annealing effect on electrical parameters, absorption spectra and photocond. 77−11939
p-InSb:In, two-phase polycryst. films, negative magnetoresist. 80−11011
InSb:Mn, NMR, magnetoresist., Hall effect and mag. susceptibility meas. 78−26888
InSb:S, ion implanted, Hall effect meas. 77−20342
InSb:S(Se)(Te), reson. states and reson. scatt., elec. props. 80−49738
InSb:Te, heavily doped degenerate semicond., anomalous increase in Hall voltage 79−61053
n-InSb:Zn, Zn diffusion out of implanted layers, Hall effect meas. at 77K 79−10984
InSb-MnSb eutectic alloy, temp. depend. of conductivity and Hall effect, field depend. of Hall coeff. 77−24566
$InSb_{1-x}Bi_x$ disordered solid solns, ionisation energy of fluctuation levels 78−72116

Hall effect continued
n-In_2Se, influence of hydrostatic press. on elec. cond. and Hall coeff. 77−55552
In_2Se_3-Cu_2S system, electrophys. props., influence of 1-4% Cu_2S 80−20219
In_4Se_3 layer crystal, three-dimensionalization of transport effects 79−73514
p-In_6Se_7, electrophysical props. 110 to 400K, Hall mobility *(Russian)* 77−35867
In_6Se_7, single cryst. prep. and electrophys. props. 79−43129
InTe thin films, flash evaporation, electrical props. 80−65722
IrP_2, prep. and characterisation 78−39679
K, Hall coeff., 4.2 to 16K 80−44570
K, Hall effect, temp. depend. 78−64029
K, high-field Righi-Leduc effect lattice thermal cond. 78−34825
K, magnetoresistance anomalies due to inhomogeneities, examination 78−56130
K, Righi-Leduc and Hall coeffs. meas., ^4He temp. range 77−66156
$KNbO_3$, elec. and thermoelec. singularities due to small polaron hopping motion cond. transition 79−42565
$KTaO_3$, photoconduction in ferroelectrics 78−91720
$KTaO_3$, pure and Gd_2O_3 doped, elec. cond. and sp. ht. 79−78097
$(La,Gd)Al_2$, reverse Kondo alloy, transport props. at finite mag. field 80−6812
$La_{1-x}Eu_xB_6$ solid solutions, cryst. lattice defectiveness, mag. susceptibility and elec. conductivity 80−15083
LaB_6 film, structure, stoichiometry, elec. properties 78−60043
$La_{0.8}Ga_{0.2}$, amorphous, Hall effect at 4.2, 78K and room temps. 79−60797
$La_{1-x}Ga_x$, amorphous foil, Hall coeff. meas. 80−20153
La_2GeSe_5, elec. props., 300 to 1100K 79−51585
$La_{0.65}Pb_{0.35}MnO_3$, transport props. near Curie points 78−88100
$La_{1-x}Sr_xVO_3$, semiconductor-metal transition, Anderson localisation, Hall mobility and 1/f noise meas. 79−78142
Li ferrite, electrical cond., thermoelectricity, magnetoresistance meas. 78−19039
Li, Righi-Leduc and Hall coeffs. meas., 2 to 120K 77−66156
Li-B (0-60 at.%), density, elec. resist. and Hall coeff. 78−39089
Li-NH_3 system, inhomogeneous, numerical simulations of Hall effect 77−43551
LiAl, anomalous elec. resistivity near critical composition 80−103673
LiAl, transport props., rel. to semimetallic band struct. 80−88581
$LiNbO_3$, reduced, electron Hall mobility, photo-Hall meas. 77−8121
$LiNbO_3$:Fe, optical damage induced by laser light, X-ray irrad., carrier mobility effects 79−33657
$LiNbO_3$:Fe, photovoltaic effect and charge transport mechanism 79−38123
Li_2O-Fe_2O_3-Pr_6O_{11}(Er_2O_3)(CeO_2)(Eu_2O_3), Hall effect and magnetoresist. 78−34849
Lu, Hall coefficient meas., 80 to 1000K 80−49694
Mg, Hall effect and elec. resist., temp. depend. 78−64030
Mg, Hall resistivity, 1.7-300K, up to 2 T, cyclotron motion breakdown 77−89751
Mg-Gd(Ho), dil., magnetoresist., anomalous Hall effect 80−15502
MgMn ferrite, electrical cond., thermoelectricity, magnetoresistance meas. 78−19039
MgO-Si_3N_4, hot-pressed, electrical props. 78−39136
Mn-Bi film, with perpendicular anisotropy, galvanomag. props., hysteresis loops 77−20464
Mn-Zn ferrite, extraordinary Hall effect 79−51615
$MnAs_{0.95}P_{0.05}$, anisotropy of elec. cond. and Hall effect 80−92908
$MnAs_{1-x}P_x$ mixed crystals, metallic magnetically ordered, Hall effect 80−65536
Mn_3B_4, Hall effect-temp. depend. mag. struct. effects *(Russian)* 77−51764
$Mn_{1-x}Fe_xSi_{1.7}$, solid soln. system, temp. depend of conductivity and thermo-EMF, conc. depend of Hall const. 77−11913
Mn_3Ge, elec. and mag. props. *(Russian)* 77−76792
$Mn_{1/3}NbS_2$, intercalate, metallic cond., Hall effect and mag. props. 77−76789
MnO, Hall mobility of photoelectrons 77−69352
$(MnTe)_{1-x}$-$(As_2Te_3)_x$ solid solns., thermoelec. props. 79−42567
$(MnTe)_{1-x}(Bi_2Te_3)_x$ ($x \leq 0.05$) solid solution, electrophys. props. 80−24925
MnZn ferrite, temperature dependence of Hall mobility 78−30944
$Mn_{1.18}Zn_{0.06}Co_{0.01}Fe_{1.75}O_4$, transport props. near Curie points 78−88100
Mo, Hall effect, effect of electron-phonon scatt. anisotropy *(Russian)* 80−10947
Mo, longwave dopplerons, nonlocal Hall effect, surface impedance, size effect *(Russian)* 80−80253
Mo, transverse galvanomag. and thermomag. coeffs. 77−20298
Mo-dichalcogenide, valence band nature, elec. and mag. props. 78−39014
Mo-Permalloy, galvanomag. props. 77−39822
Mo_2B_5 and MoB_4, thermal, elec., and mag. props. 80−20187
MoS_2, elec. cond. and Hall coefficient temp. depend. 77−28180
$MoSe_2$, elec. cond. and Hall coefficient temp. depend. 77−28180
$MoSe_2$:Nb(Re), layered, elec. props., semicond.-metal transition 77−11922
$MoTe_2$, elec. cond. and Hall coefficient temp. depend. 77−28180
$Mo_{0.5}W_{0.5}Se_2$ single cryst. vapour growth, characterisation 80−93466
Na, Hall coefficient, quasiclassical Boltzmann eqn. calcs. 80−103678
$NaNbO_3$, elec. cond., Hall mobility, thermoelec. coeff. 79−82584
$NaNbO_3$, elect. cond. mech., resist., Hall coeff. and thermoelec. power meas. 80−65603
$Na_xVS_2(Se_2)$, mag. and elec. props. rel. to struct. transitions 78−91848
Na_xWO_3, degenerate electron gas, Friedman effect, review 77−20242
Na_xWO_3, metallic, transport props. near metal-insulator transitions 77−24596
Nb, Hall and Nernst-Ettingshausen effects, temp. depend. *(Russian)* 77−85198
Nb-N(-H) system, electrophys. props. of nitrides and hydronitrides 77−85215
Nb-Sn, A15 compounds, Hall coeffs. 79−33281
$NbS_2(Se_2)$ intercalation complexes with 3d transition metals, mag. and metallic transport props. 80−44814
$NbSe_2$-Fe, dil. alloy, magnetotransport and superconductivity 77−55516
$NbSe_3$, CDW linear chain metal, two band model in ohmic region 79−38056
$NbSe_3$, conductivity anisotropy and transverse magnetoresistance 79−38055
$NbSe_3$, linear-chain metal, Hall effect meas. 78−76058
$NbSe_3$, oscillatory magnetotransport, Fermi surface anisotropy, Hall effect, g-factor, Dingle temp. 78−51975
$NbSe_3$, two band model and galvanomagnetic study 80−20176
$NbSe_2$(2H), low field magnetoresist. and anomalous transport props. 80−65602
$Nb_{1-x}V_xSe_2$, elec. and mag. anomalies at CDW transition 80−107722
nbSe_2 (2H) single crystal, elec. resistivity, effect of hydrogen intercalation *(Russian)* 78−84338
NdAl, ferromagnetic, extraordinary Hall effect 80−39560
Nd_xCo_{1-x} film, amorphous, mag. props. meas. 78−68312
Nd_xFe_{1-x} film, amorphous, mag. props. meas. 78−68312
Nd_2GeSe_5, elec. props., 300 to 1100K 79−51585
Nd_2S_3, semimetallic, elec. and thermal transport meas. 78−10442
Ni alloys, anomalous Hall effect meas., two current model 77−62906
Ni alloys, normal Hall effect at 4.2K, two-spin current model interpretation 77−15829
Ni, ferromagnetic, Hall effect, anomalous, rel. to scatt. processes 80−44572
Ni film, CO adsorption effect on galvanomagnetic and magnetic props. 78−43490
Ni film, evaporated, elec. resist. and galvanomagnetic props. 80−80411
Ni film, evaporated, galvanomag. and mag. props. 78−23180
Ni film, evaporated, oscill. due to CO adsorption 77−1496
Ni film, few atomic layers thick, transition from Pauli paramag. to band ferromag. 80−44885
Ni film, vac. deposited on liquid-He-cooled sapphire, galvanomag. props. 79−95519
Ni films, evaporated, effect of CO adsorption on galvanomag. and mag. props. 79−33363
Ni films, evaporated, effect of CO adsorption on galvanomag. and mag. props. 79−33364
Ni foil, hydrogenated, thermoelectric and Hall effects 79−65559
Ni foils, hydrogenated, thermoelec. and Hall effect 78−43364
Ni, liquid, Hall effect, band struct. and exchange scatt. 80−80250
Ni, magnetoresistance anisotropy, planar Hall effect 79−23947
Ni-Al (6.3 at.%), influence of localised order on thermo-EMF and Hall-EMF *(Russian)* 78−6951
Ni-alloy, anomalous Hall effect, contribution from skew scattering and side displacement of two-current model 79−56198
Ni-Au, amorphous film, ferromagnetic, anomalous Hall resist. 77−15832
Ni-Cr alloys, low temp. transform. mechanism, electrophys. props. obs. *(Russian)* 77−59777
Ni-Cu, ferromagnetic, Hall effect, anomalous, rel. to scatt. processes 80−44572
Ni-Cu alloy, magnetoresistance anisotropy, planar Hall effect 79−23947
Ni-Fe, film, anomalous Hall and Nernst-Ettingshausen effect, contribution of phonon and impurity scatt. *(Russian)* 78−64145
Ni-Fe-Cr, extraordinary Hall effect, elec. and mag. meas. at 77 and 300K 80−34421
Ni-rare earth intermetallics, RNi_3, amorphous alloys, mag. and transport props. 79−42513
$Ni_{1-x}Co_xS_2$, elec. cond., thermoelec. power and optical meas. 80−59986
$Ni_{1-x}Cr_xS$, elec. transport, mag. susceptibility and DTA meas. 80−96954
Ni_3(Fe,M), M=Cr,Mo,W, elec. resist., temp. depend. anomalies, Hall and Nernst-Ettinghausen effects *(Russian)* 80−10942
Ni_3(Fe,M), M=Cu, Cr, Mo, W, kinetic phenomena rel. to ordering and electron struct. *(Russian)* 78−76043
Ni_3Fe, effect of alloying with Cr, Mo, W or Cu *(Russian)* 78−39095
$Ni_3(Fe_{1-x}Nb_x)$, temp. and conc. depend. of anomalous Hall effect *(Russian)* 80−70674
Ni_3Mn film, anomalous behaviour of Hall effect *(Russian)* 77−28262
$Ni_{1/3}NbS_2$, intercalate, metallic, cond., Hall effect and mag. props. 77−76789
NiO, Hall effect anomaly, sign reversal at 600K 80−100471
NiS_2, weak ferromagnet, galvanomagnetic effect 79−11148
NiS_2, weak ferromagnetic semiconductor single crystal, elec. and magnetic props. 77−85226
$NiS_{2-x}Se_x$, elec. cond., thermoelec. power and Hall effect meas. 80−65561
$Ni_{0.5}Zn_{0.5}Fe_2O_4$, Hall mobility, elec. cond. and carrier conc., 30 to 180°C 77−51765
Pb film, near supercond. transition temp., Hall effect 79−42698
Pb-Sn-Te, solid solution, scattering mechanism of carriers 80−49710
$Pb_{1-x}Cd_xS$, epitaxial, resist. and Hall coeff., substrate temp., thickness and comp. depend. 78−72290
$Pb_{1-x}Cd_xS$, metastable epitaxial films, elec. props. 78−26979
$Pb_{1-x}Ge_xTe$ solid solns., phase transition influence on elec. props., 77 to 450K 80−103689
$Pb_{1-x}Ge_xTe$:Ga, Fermi level stabilization, transport props. meas., 77-400K 78−56065
$Pb_{1-x}Ge_xTe$:Ga, influence of hydrostatic compression on elec. props. 79−73516
PbI_2 (2H), electronic transport and cyclotron reson. 79−28369
$Pb_{40}In_{60}$, mixed state supercond., Hall and Ettingshausen effects, vortex entropy transport 80−44780
$Pb_{1-x}In_xTe$, $0.01 \leq x \leq 0.2$, elec. cond., Hall coeff. liquid He temp. 78−47815
$Pb_{1-x}In_xTe$, impurity-state conduction and temp. depend. of transport coeffs. 78−47795
$Pb_{1-x}Mn_xTe$ (x=0.005, 0.001, 0.05), solid solns., exam. of electrical and thermal props. 79−1599
$PbMo_6S_8$, Hall effect and magnetoresistivity 78−95400
$PbMo_6S_8$, normal state and superconducting property measurements 78−91660
$PbMo_6S_8$, normal-state electronic props., Fermi surface and supercond. parameter derivations 79−60850
PbO_2 and pyrolusite compressed powder mixtures, mixing rules concerning Hall effect and Hall mobility *(German)* 78−84234
PbO_2 pressed powder, Hall voltage and change of cond. in transverse mag. fields 79−4567
p-PbS, dispersion law investigation, valence band density of state effective mass 79−95314
PbS film, polycryst., chem. deposition from soln. and characterisation 78−72743
PbS, low carrier conc., prep. and props. 77−39846
PbS, nonstoichiometric, increase of rest pot. with p-type semicond. character 78−56170
p-PbS, struct. of valence band, transport processes study 80−20081

Hall effect continued
PbS:Tl, Hall and Seebeck coeffs., Hall mobility, impurity states 80−15545
PbS:Tl, self-compensation of acceptors by vacancies, Hall coeff. meas. 80−92913
PbS_xS_{1-x} epitaxial film, Hall mobility meas., surface charge transport 77−20473
PbSe film, influence of pot. barrier on thermoelec. props., elec. cond., Hall coeff. and Nernst-Ettingshausen coeff. 78−39239
PbSe, Hall effect and elec. cond. under strong anisotropic pressure 77−55549
PbSe, valence band struct., Hall and transverse Nernst-Ettingshausen effects, optical absorption 79−11064
PbSe:Tl, elec. props. and IR reflection 78−6686
PbSe:Tl, high temp. elec. and optical props., impurity states 79−60854
PbSe:Tl, impurity states, optical absorption and Hall effect meas. 78−18995
PbSe:Tl, scatt. of holes and phonons by impurities 78−19068
PbSe:Tl, self-compensation of acceptors by vacancies, Hall coeff. meas. 80−92913
$PbSe_{0.5}S_{0.5}$, valence band struct., absorpt. spectra, elec. props. 80−44505
$PbSe_xTe_{1-x}$ epitaxial layers, growth, struct., elastic strain and Hall mobility 77−15717
$Pb_{1-x}Sn_xGe$:In, press.-induced transition to gapless state, galvanomag. effects 78−19108
$Pb_xSn_{1-x}O_2$:Sb films, DC sputtered, elec. props. 80−80426
$Pb_{0.59}Sn_{0.41}Se$, struct. phase transition, temp and hydrostatic press. influence, Hall effect, resistivity *(Russian)* 78−51675
$Pb_{1-x}Sn_xSe$, band struct. and transport props., hydrostatic press. effects 80−15452
$Pb_{1-x}Sn_xSe$, displacive transition, temp. and press. depend., elec. meas. 80−10672
$Pb_{1-x}Sn_xSe$ epitaxial film, Hall mobility meas., surface charge transport 77−20473
$Pb_{1-x}Sn_xSe$, film struct. and elec. props. 77−80708
$Pb_{1-x}Sn_xSe$, n- and p-type, with band inversion, study of transport phenomena 80−49741
$Pb_{1-x}Sn_xSe$, transport phenomena in solid solutions with band inversion 80−107792
$Pb_{1-x}Sn_xSe$, valence zone struct. effect on mobility/inherent conc. ratio *(Russian)* 79−73437
$Pb_{1-y}Sn_ySe$, electron-irradiated, elec. and recomb. props. 79−56227
$Pb_{0.76}Sn_{0.24}Tc$, background radiation, influence on elec. props. 80−20226
PbSnTe, electron irradiated, high temp. defects 79−78122
PbSnTe, Magneto transport anomalies at low carrier densities, Wigner crystallisation 80−20222
$Pb_{0.41}Sn_{0.59}Te$, Hall coeff., elec. cond. meas. 80−44615
$Pb_{0.56}Sn_{0.44}Te$, press. induced ferroelec. phase transition 79−65809
p-$Pb_{0.65}Sn_{0.35}Te$, transport coeffs. and dispersion law 80−44629
$Pb_{0.72}Sn_{0.28}Te$, Hall effect and elec. cond., 77 to 480K, energy band struct. 77−76817
$Pb_{0.72}Sn_{0.28}Te$, Hall mobility, temp. and carrier conc. depends. *(Russian)* 77−39877
$Pb_{0.78}Sn_{0.22}Te$:In, low current carrier conc., Hall effect, lattice constant 79−82603
$Pb_{0.78}Sn_{0.22}Te$:In epitaxial layers, dislocation density, Hall effect, conductivity, photoeffects 80−25024
$Pb_{0.8}Sn_{0.2}Te$, LPE layers, carrier conc. variation with annealing and growth temp. 77−39878
$Pb_{0.8}Sn_{0.2}Te$, single cryst. and epitaxial film, far IR refl. spectra, carrier density, Hall const., and plasma freq. 80−20629
$Pb_{0.8}Sn_{0.2}Te$:Cd, defect struct., Hall effect and solubility meas. 77−11571
$Pb_{0.8}Sn_{0.2}Te$:Cd, influence of Cd doping on high field magnetoresist. and Hall effect 80−75590
n-$Pb_{0.82}Sn_{0.18}Te$, conduction band struct., determ. by Shubnikov-de Haas meas. 78−2504
$Pb_{0.82}Sn_{0.18}Te$ epitaxial films, surface transport of carriers at 77K 79−28419
$Pb_{0.82}Sn_{0.18}Te$, film, effect of hydrostatic pressure on props. 80−70862
$Pb_{0.82}Sn_{0.18}Te$, Hall mobility, scatt. mechanisms, temp. and carrier conc. depend. 77−55548
$Pb_{0.82}Sn_{0.18}Te$, layers on mica substrate, Hall constant peculiarities 80−75588
p-$Pb_{0.82}Sn_{0.18}Te$, mag. susceptibility, inversion layers effect *(Russian)* 77−72996
$Pb_{0.82}Sn_{0.18}Te$, narrow-gap, Hall effect quantum oscillations *(Russian)* 77−4377
$Pb_{0.82}Sn_{0.18}Te$ solid solution, energy band spectrum characts., Hall effect meas. 77−76737
p-$Pb_{0.82}Sn_{1.8}Te$, Hall coeff. sign-inversion temp. 78−52010
$Pb_{1-x}Sn_xTe$ film, effect of mechanical strains on elec. props. 77−58621
$Pb_{1-x}Sn_xTe$, band struct. changes due to displacive phase transition, Hall coeff. meas. 80−10671
$Pb_{1-x}Sn_xTe$, Cd-In diffusion, changes in elec. props. 78−91348
$Pb_{1-x}Sn_xTe$, correlation between elec. props. and crystalline environment 77−80773
$Pb_{1-x}Sn_xTe$, diffusion of Cd, Hall effect, cond. and solubility meas. 79−69292
$Pb_{1-x}Sn_xTe$, effective mass of holes, thermoelec. power, Hall coeff., carrier conc. 79−65371
$Pb_{1-x}Sn_xTe$, electron-irradiated, elec. and recomb. props. 79−56227
$Pb_{1-x}Sn_xTe$, energy spectrum under hydrostatic pressure 79−65381
$Pb_{1-x}Sn_xTe$, epitaxial layers, carrier lifetime meas. 79−42559
$Pb_{1-x}Sn_xTe$ film, deposition, elec. and piezoresist. props. 78−6465
$Pb_{1-x}Sn_xTe$ film, pure and Bi doped, polycryst., struct., elec., optical props. 79−42542
$Pb_{1-x}Sn_xTe$ film, sputtered, for IR detector appl. elec. and optical props. 80−35084
n-$Pb_{1-x}Sn_xTe$, galvanomag. effects, alloy scatt., 4.2K 77−39880
p-$Pb_{1-x}Sn_xTe$, galvanomagnetic and oscillatory effects under press. 79−69413
p-$Pb_{1-x}Sn_xTe$, LPE layer, carrier conc. and mobility 79−99639
$Pb_{1-x}Sn_xTe$ narrow gap solid alloys, hole Fermi surface, galvanomag. and oscill. effect obs. *(Russian)* 77−69345
$Pb_{1-x}Sn_xTe$, solid-liq. phase equilib. above 750°C 79−82316
$Pb_{1-x}Sn_xTe$, thermoelectric effects, characteristics at low temps. 80−107831
$Pb_{1-x}Sn_xTe$, valence band struct., Hall effect meas. 78−39016
$Pb_{1-x}Sn_xTe$:Cd, Cd diffusion obs. using Hall mobility and Cd solubility expts. 78−26584

Hall effect continued
$Pb_{1-x}Sn_xTe$:In, dielectric state, avalanche breakdown in strong elec. fields *(Russian)* 80−92901
$Pb_{1-x}Sn_xTe$:In, energy spectra modifications due to comp. changes and press. appl. 80−10915
$Pb_{1-x}Sn_xTe$:In, Hall const. depend. on temp., autocompensation, band gap temp. depend. explanation 79−69527
$Pb_{1-x}Sn_xTe$:In, Hall effect and photoconductivity *(Russian)* 80−103720
$Pb_{1-x}Sn_xTe$:In, high temp. Fermi level position 79−90948
$Pb_{1-x}Sn_xTe$:In, with low carrier conc., transport phenomena 80−49783
$Pb_{1-x}Sn_xTe$:In epitaxial layers, growth, elec. props., and luminesc. 80−54542
$Pb_{1-x}Sn_xTe$:In film, anomalous elec. props. 78−10477
$Pb_{1-x}Sn_xTe$:In(Ga)(Al), elec. props., dopant influence 79−51599
$Pb_{1-x}Sn_xTe$-PbTe heterostructures, MBE produced on mica and $LiNbO_3$, elec. props. study 80−88629
$Pb_{1-x}Sn_xTe_{1-y}Se_y$, narrow-gap solid soln., lattice parameter, energy gap and Hall mobility of carriers 79−73154
PbTe, and its alloys, microhardness meas. as function of applied load, elec. props. exam. 78−48493
PbTe, diffusion of Cd, Hall effect, cond. and solubility meas. 79−69292
PbTe, effect of pressing and sintering, study of induced defects by SEM 80−59983
p-PbTe, energy band struct. and scattering of holes 80−10874
PbTe epitaxial films, carrier recomb. and deep levels, photocond., Hall effect, and luminesc. meas. 79−38024
PbTe, epitaxial layers, carrier lifetime meas. 79−42559
PbTe film, elec. transport props. 79−42679
PbTe film, electronic thermal cond. and thermoelec. power 80−93018
n-PbTe film, epitaxial, hot electron transport effects 77−12035
PbTe film, ion-implantation-induced lattice defects 77−68985
PbTe films, thermal cond. and elec. props., 4.2 to 300K 79−28162
n-PbTe, Hall effect of hot electrons 77−55547
PbTe, high field drift vel. and Hall coeff. 78−26875
PbTe, ion implantation induced damage and reson. levels 80−49255
PbTe, ion-implanted, doping profile evaluation by Hall effect and sheet resist. meas. 78−59831
n-PbTe, LPE layer, carrier conc. and mobility 79−99639
PbTe layers, quality control of carrier conc. using Hall effect graphical representation 77−1500
n-PbTe, low temp. elec. cond. 80−20227
n-PbTe, low temperature electrical transport, Hall effect 80−84478
PbTe, Magneto transport anomalies at low carrier densities, Wigner crystallisation 80−20222
PbTe, uncontaminated films on mica sustrates, elec. props. obs. 77−76967
PbTe, uncontaminated films prepared by mol. beam deposition, elec. props. meas. 78−15316
PbTe:Bi(Sb)(Cr)(Ag), thermoelec. props., thermal and elec. cond. 79−82616
PbTe:Cd, Cd diffusion obs. using Hall mobility and Cd solubility expts. 78−26584
PbTe:Cd, defect struct., Hall effect and solubility meas. 77−11570
PbTe:In, electron mobility, temp.-independent part, Hall effect and elec. cond. meas. 80−92914
PbTe:In, Shubnikov-de Haas oscillatory effects, quasilocal impurity level 80−92912
PbTe:In based solid solutions, impurity states, elec. props. 79−87054
n-PbTe:In(Cu) epitaxial films, elec. transport props. 80−75659
PbTe:Ti, effect of impurities on transport props. 79−11158
PbTe:Tl, influence of Tl impurity states 80−20121
PbTe:Tl, thermoelectric power, elec. cond., Hall coeff. and optical absorpt. coeff. 80−39584
PbTe:Zn, defect struct., Hall effect and solubility meas. 77−11572
PbTe-based solid solns., 79−23990
$PbTe_{1-y}Se_y$:In, high temp. Fermi level position 79−90948
Pd based alloys, extraordinary Hall effect 78−76053
Pd-Co, dilute, extraordinary Hall effect meas., 2-250K 80−34420
Pd-Co, normal Hall effect *(Russian)* 80−103676
Pd-Fe, normal Hall effect, temp. and conc. depend. *(Russian)* 77−80763
Pd-Fe, normal Hall effect *(Russian)* 80−103676
Pd-Ni, normal Hall effect *(Russian)* 80−103676
Pd-Ni alloys, kinetic props., anomalous Hall coefficient *(Russian)* 77−76791
Pd-Si, amorphous, struct., crystn. and Hall effect meas. 80−75178
Pd-Si(-Cu), amorphous, Hall effect meas. and electronic struct. 80−75551
Pd-Si(−Cu), glassy, liq. and cryst., mag. and elec. props. 77−66249
Pd-W, elect. resist., mag. susceptibility, Hall coeffs., in plastically deformed state and after annealing *(Russian)* 79−66174
Pd_2Si film on Si, metallic, resist. and Hall mobility meas. 78−47886
$PrAl_2$, ferromagnetic, extraordinary Hall effect 80−39560
Pr_2GeSe_5, elec. props., 300 to 1100K 79−51585
Pt-Fe(Co)(Mn), dil., skew scatt. Hall effect, magnetoresist. and mag. anisotropy, orbital magnetism of impurity 80−70678
$PtSb_2$, high field elec. props., impact ionisation 80−96892
Rb, Righi-Leduc and Hall coeffs. meas., 2 to 120K 77−66156
$RbAg_4I_5$, solid electrolyte, contrib. of non-Brownian motion to transport props. 80−70453
$RbAg_4I_5$, superionic conductor, absence of Hall effect for Ag ions 77−31805
Rb_xWO_3, phase transitions, supercond. transition temp. and elec. props. 79−28431
Rb_xWO_3, resistivity, Hall effect and Seebeck coeff. from 1.5 to 300K 80−6879
Re, elec. resist. and Hall effect at low temp. *(Russian)* 78−47760
Re single crystal, 4.2K, under 12 kbar press. *(Russian)* 77−80762
Ru, electronic structure and mag. breakdown, galvanomag. props. obs., 1.3-20.4K 78−91600
Ru, giant thermopower oscillations due to magnetic breakdown trajectories 79−60688
Ru, magnetoresistance and Hall effect under mag. breakdown conditions *(Russian)* 79−95389
RuP_2, prep. and characterisation 78−39679
$(SN)_x$, elec. cond., galvanomag. effects 79−91091
$(SN)_x$ film, Hall effect, elec. cond. and magnetoresist. meas. 78−84314
$(SN)_x$ single crystals, galvanomag. effects 79−19582
Sb, carrier density at press. up to 80 kbar, magnetoresist. and Hall effect obs. 79−73534

Hall effect continued
Sb-Au amorphous films quench-condensed, resistivity and Hall effect meas. 79−99638
$Sb_{1.5}Bi_{0.5}Te_3$ solid solution, temp. influence obs. *(Slovak)* 78−30946
Sb_2S_3, galvanomag. props. and elec. resist., temp. depend. 78−43419
$(Sb_2Se_3)_{0.7}(Bi_3Se_3)_{0.3}$, solid soln., prep. and elec. properties of layered crystals 80−70762
Sb_2Te_3, mag. and elec. props., carrier excitation 78−43395
Sb_2Te_3, stoichiometric, Hall effect and thermoelec. power studies 80−100470
Sc-H, conc.-temp. depend. at room temp. of elec. resist. thermo-EMF, mag. susceptibility, and Hall coeff. 80−29382
Se-Te-Sb glasses, electronic transport 80−88579
p-Si, $^{49}BF_2$ ionised mols. obtained by implantation of 78−31003
n-Si, A-centre ionisation energy change due to uniaxial deform. 78−71733
Si, amorphous, doped, drift and Hall mobility, photocond. 79−65477
Si, amorphous, substantially doped, electronic props., review 79−87175
Si, amorphous film, RF plasma deposition from $SiCl_4$-H_2, characterisation 80−66435
Si, amorphous films, halogenated and hydrogenated, elec. and optical props. 80−97016
n-Si, carrier relax. time, mag. field effects, rel. to Hall effect 80−39608
n-Si, carrier scatt. anisotropy, Hall mobility calcs. 77−24552
p-Si, deformed, 1/f noise, resist., mobility, and carrier density 77−8161
Si, diffusion coeff. of Se, by sheet Hall coeff. meas. 79−46843
Si, dislocation energy spectrum, appl. of EPR and elec. meas. 79−82547
Si, drift mobility and Hall coeff. factor of holes 78−43379
n-Si, effective mass from intraband Faraday rot. and Hall effect 77−52049
p-Si, elec. props. and thermal defects, influence of high temp. treatment 79−69531
p-Si, electron irrad., influence of acceptor impurity conc. and irrad. temp. on defect formation 79−19281
Si, electron irrad., limiting position of Fermi level, elec. cond. and optical absorpt. meas. 79−65484
n-Si, electron radiation defect annealing, negative stage, Hall coefficient, defect levels 79−90701
Si epitaxial film, correlation between electrooptical and electrical props., IR absorpt. spectra *(Russian)* 78−60453
n-Si epitaxial layers on oppositely conducting substrates, two layer Hall coeff. meas. technique 80−80297
p-Si, fast electron irrad., Hall mobility, temp. depend. 78−56165
Si film, elec. props., effect of amorphous to polycryst. transition 79−28425
Si film, on sapphire, carrier distrib. effects 77−51818
n-Si films on sapphire, crystalline defects effect on elec. props. 77−20470
p-Si, galvanomagnetic effects 79−33297
n-Si, γ-irrad, (E_{max}=100 MeV), carrier recomb. 78−56158
n-Si, γ-irrad., galvanomagnetic effect anisotropy rel. to layer inhomogeneity 79−33299
Si, Hall effect, influence of dislocations 79−82611
n-Si, heavily doped, carrier conc., comparison of expt. and theory, screening effects 77−85216
Si, high-resistivity, characterisation by Hall meas. 78−10480
Si, hot holes negative Hall effect 79−87118
n-Si, inhomogeneous impurity distrib., elec. props., effect of γ-irradiation 77−55550
Si, inversion layer, Hall effect meas. 78−56199
p-Si, inversion layer, screening effect and quantum transport in strong mag. fields 78−19155
n-Si inversion layers, electronic g-factor, spin-split Landau levels 80−80346
Si inversion layers, Hall effect, consistency with presence of macroscopic inhomogeneities 79−51681
Si inversion layers, stress and intersubband correlation 78−60227
n-Si, irrad. with 1.2 GeV electrons, temp. depend. of Hall coeff. 79−51156
Si, LPE using Ga_xAl_{1-x} solvent, resist. and Hall mobility 77−36411
Si large grain films on metallurgical Si substrates, Hall mobility 80−61357
p-Si, laser irrad., accumulation of defects, effect on elec. props. 80−107317
n-Si, layer impurity distrib., γ-ray and neutron irradiated, transverse magnetoresist and Hall effect meas. 78−19058
Si, MOS inversion layers, Hall effect 78−64118
n-Si MOS inversion layers, Hall cond. meas. 80−39676
Si MOSFET n-channel, Hall meas. on trap states at 77K 80−44732
Si, negative differential mobility and geometrical magnetoresist. calc. 77−43624
Si, neutron irrad., Hall effect and magnetoresist. meas. 80−6883
n-Si, neutron irradiated, charact. of changes in mobility 78−39135
n-Si, neutron or γ-irrad., elec. props., in strong elec. fields 79−95416
Si, neutron transmutation doping, ^{31}P conc. meas. 80−19833
Si on sapphire, gettering effect by O implantation, Hall and Rutherford backscattering meas. 79−65103
Si on sapphire, residual strain effect on elec. props. *(Japanese)* 80−84522
Si on sapphire thin film, Hall effect, magnetoresistance *(French)* 80−65601
Si, point defects, laser annealing 80−107224
Si, polycryst. CVD film electrical props. 78−6466
Si, polycryst. films, transport props. and grain boundary charact. by TEM 80−50980
Si, polycryst. rods, p-n junction appls. and transport props. 79−99612
Si, polycrystalline, Hall mobility 80−60006
p-Si polycrystalline films on graphite substrates *(French)* 78−64154
Si, precipitation of Au, supersaturated soln., Hall effect meas. 77−89465
Si, proton irrad., efficiency of form. and nature of defects, Hall meas. 80−6444
Si, radiation defects, influence of dislocations on accumulation, elec. props. 80−92558
Si ribbons, roller quenching method of prep., grain sizes and carrier conc. 80−40275
Si ribbons for solar cells, ultra high speed growth, elec. props. 80−89162
Si, spin dependent recomb. at dislocations, EPR and photocond., Hall effect meas. 79−38095
Si, thermal donor energy levels, Hall effect meas. 78−6335
Si, thermal donor generation in temp. range 600-800°C 79−11121

Hall effect continued
Si, thermally induced donors due to heat treatment and Fe contamination 79−78035
Si, two dimensional impurity bands, Hall mobility 79−95509
p-Si, X-irrad., subthreshold defect prod., Hall meas. of carrier conc. and photocond. spectra 77−89470
Si:O, electrical activity due to heat treatment, Hall effect meas. 80−15543
Si:Al, acceptor levels, IR spectra 78−67972
p-Si:Al, diffusion and incorporation of dopant in closed system, elec. props. 77−59026
Si:As, CW CO_2-laser annealing, comparison with thermal annealing 80−84193
Si:As, elec. activation of implanted As during low temp. anneal, Hall effect meas. 78−51571
Si:As, ion implanted, annealing charact., elec. props. 77−19974
Si:As, polycrystalline, As segregation at grain boundaries, elec. props. meas. 80−75259
Si:B, ion implanted, comparison of range and range straggling 77−55293
Si:B, polycryst., effect of laser annealing on struct. and elec. props. 79−11243
Si:B film, sputter-deposited, elec. props., struct., SEM and TEM obs. 79−95298
Si:BF_2^+, anomalous migration of F and electrical activity of B 78−34654
Si:BF_2^+(Si^+,B^+), recrystallisation of implanted amorphous layers, elec. props. 79−55762
p-Si:B(Al), radiation defect form. and annealing study using Hall effect, cond. and carrier diffusion length 80−84214
Si:B(P), dislocated crystals, DC conductivity, Hall effect, energy spectrum 78−10400
a-Si:B(P), Hall effect and impurity cond. 77−72871
Si:B(P), ion implanted, polycryst. annealing charact. 77−24324
Si:Fe, B thermally activated Fe interstitial, elec. and kinetics props. *(German)* 80−34035
Si:Fe, photoconductivity and Hall effect 79−4579
Si:Fe^0 interstitial localisation, EPR spectrum 79−1582
Si:Ga, neutron irrad., Hall effect meas. of shallow donor levels 80−20124
p-Si:Ga, neutron transmutation counterdoped, shallow defect levels, Hall effect and photocond. obs. 79−87055
Si:Ga (Al)(In) extrinsic detector material props. 77−89797
Si:Ga^+, impurity distrib. profiles using SIMS and Hall effect method 79−69152
p-Si:Gd, irradiated, elec. props. 79−51613
Si:Gd, radiation defect form., effect of Gd impurities, elec. and optical meas. 78−71764
Si:In, C, 0.111-eV acceptor level, X-level defect conc. from IR absorpt. and Hall meas. 79−51512
Si:In, dopant energy levels, Hall meas. interpretation 80−107736
Si:In, doping conc., meas. by Hall, C-V and junction breakdown methods 79−14824
Si:In, electron irrad., Hall effect meas. 80−2401
Si:In, neutron irrad. to compensate for residual B, photocond., IR focal plane array 78−67727
Si:In, new acceptor level 77−66136
Si:In, photoelec. props. meas 77−89804
Si:Li, precipitation centres, elec. cond., Hall effect meas. 78−48417
n-Si:Mg, energy levels and degeneracy ratios determ. by Hall effect meas. 79−90993
Si:Na ion implanted, Hall effect temp. depend., electron surface density and mobility 80−11018
Si:O, effect of interstitial O on elec. props. 77−76846
p-Si:P, annealing behaviour, recovery, surface carrier density and Hall mobility meas. 77−32012
Si:P, annealing characteristics at low temp., elec. props. 78−63781
Si:P, carrier mobility and distrib. rel. to annealing, 400-910°C 78−79995
p-Si:P, defect energy levels, ion implantation effects, Hall coeff., sheet resist. meas. 77−85173
Si:P, diffusion-doped laser irradiation effects, electrical reactivation of P 80−39124
Si:P, electrical conductivity oscillation, effect of dislocations 78−6388
Si:P, Hall effect 78−72176
n-Si:P, heavily doped, carrier conc., Hall coeff. and elec. cond. meas. 77−8094
n-Si:P, heavily doped, elec. cond. and Hall effect meas., impurity effects 78−19032
Si:P, heavily doped, glow-discharge-produced, elec. and optical props 80−2497
Si:P, heavily doped semicond., scatt. mechanism, resist, and Hall coeff. maxima 80−75586
Si:P, implanted, pulsed electron beam annealing, Hall effect and sheet resist. meas. 80−34467
Si:P, incoherent light flash annealing, elec. props., backscattering spectra 80−97504
Si:P, ion implanted, laser and thermal annealing, elec. cond. and Hall effect meas. 79−69145
n-Si:P, low-compensated, Hall factor, electron-phonon interactions 79−4570
Si:P, measurement techniques for determining P densities 80−75262
Si:P, neutron transmutation doped, radiation damage exam., elec. props. 78−95080
Si:P, neutron transmutation doping, elec. props. rel. to neutron fluence 80−96555
n-Si:P, piezoresist. under strong uniaxial elastic deform. 77−15858
Si:P, polycryst., grown in epitaxial reactor at 800°C, characterisation 77−1815
n-Si:P,V, degeneracy ratios and impurity levels of V, resist. and Hall effect meas. 77−20260
Si:P CVD films, ion-implanted, doping effect on elec. props. 80−2495
Si:Sb, epitaxial film, growth by mol. beam technique 80−2292
Si:Sb, ion implanted, annealing, Sb behaviour above solid solubility, Hall effect meas. 80−88200
Si:Se, energy levels, resistivity and Hall coeff. 79−69528
Si:Se,B(Ga)(Al)(In), diffusion of Se, solubility and ionization levels, Hall effect and photocond. meas. 79−42486
Si:Sn, thermal conductivity, Hall mobility depend. on Sn conc., phonon-defect scatt. 80−29232
Si:Ti, deep level impurity, Hall meas. 80−6768
Si-Al-Al_2O_3 system, solid phase Si regrowth on sapphire 80−100413

Hall effect continued
Si-epitaxial film, ionised-cluster-beam deposited, cryst. and elec. characts. 80−70553
Si-Ge, heavily doped vacuum hot-pressing, thermal and electrical props. 77−40400
Si-Ge:As,P, heavily doped, electron scatt., Hall coeff., Seebeck coeff. and resist. meas., 4-300K 77−4379
Si-SiO_2, two layer system, P^+-ion penetration tails, expt. and computer anal. 80−75249
$Si_{(6-Z)}Al_ZO_ZN_{(8-Z)}$ 78−39136
SiAs, cryst. growth from melt, elec. props. 80−76170
n-SiC, 6H polytype, expitaxially grown, electronic props. meas. 77−39975
n-SiC (6H), density of states effective mass determ., high temp. meas. of elec. props. 79−15073
SiC (6H), epitaxial film, electronic props. 79−60942
β-SiC, cubic, elec. props. 78−51996
SiC, cubic, magnetoresistance and Hall mobility, field and orient. depend. *(Russian)* 77−69346
SiC polytypes, localisation of cond. band minima in Brillouin zone, Hall coeff. 80−20082
Si_3N_4, hot-pressed, electrical props. 78−39136
SiO_2, amorphous, elec. cond. mechanism, review of developments 78−26854
Si(100) inversion layers, magnetoelec. and piezoresist. evidence for mobility domains 77−4447
SmB_6, mixed valent, large low-temp. Hall effect and resist. 80−39611
SmB_6, mixed valent semicond., transport props. and electonic struct., review 80−96877
Sm_2GeSe_5, elec. props., 300 to 1100K 79−51585
$Sm_xLa_{1-x}B_6$, solid solns., exam. of structure, elec. props. 80−39290
SmS film, semicond. and metallic modifications, elec. props. 77−32098
SmS, Hall effect near semicond.-metal transition 77−62968
SmS, semicond., anomalously high magnetoresist., Hall coeff. and elec. resist. meas. 78−10479
SmS, semicond.-metal transition, cond. band type, deform. pot. determ. 79−69417
Sn, galvanomagnetic props., temp. depend. meas. in single cryst. 80−96850
$Sn_{1-x}Ge_xTe$, evaporated thin films, characts. 79−60944
$Sn_{1-x}Mn_xTe$, $0.02<x<0.08$, transport and magnetic properties, low magnetic field 79−99569
$Sn_{1-x}Mn_xTe$, electronic struct., transport props., mag. ordering effects 80−65441
SnO_2 doped films for spectral-selective surfaces, refl. and elec. props. meas. 79−74013
SnO_2 film, reactor irrad. induced changes in elec. props. 77−28267
SnO_2, reactive ion plating onto insulating substrates, and elec. and optical props. 79−87588
$Sn_{1-x}Pb_2Te$, elec. and struct. props. of epitaxial layers *(Russian)* 78−64147
$Sn_{1-x}Pb_xTe$, film, production under quasi-equilibrium conditions 80−45241
SnSSe, electron mobility, elec. cond. and Hall effect meas. 78−80004
$SnS_{2-x}Se_x$, electron mobility elec. resist. and Hall constants 79−28346
SnSe, electronic props., region of existence *(French)* 77−35885
SnTe, annealed, iodide method of prep., props. meas. 80−71591
SnTe, film, heat treatment in air, effect on struct., props. 79−11037
SnTe, Hall coeff., temp. depend., interpretation 78−87988
SnTe, isothermal meas. of galvanomag. and thermomag. effects *(Russian)* 78−56160
SnTe:Mn, ferromag.-ordering, transverse magnetoresist. and Hall effect meas. 77−85240
SnTe-MnTe, degenerate semicond., anomalous Hall effect 80−29420
SnTe-PbSe, semicond. film, growth, phase composition, condensation temp. rel. to cond. type 77−28266
$SrTiO_3$, pure and Nb doped, heat treated, Hall effect, electrical cond., optical absorpt., defect states 78−47812
$SrTiO_3$:B layers, ion implanted, conductive props. Hall mobility, defect energy levels 79−82693
TCNQ salt, $TEA(TCNQ)_2$, thermopower sign anomaly and Hall effect 79−56205
TTF-TCNQ, DC Hall effect meas. 77−89753
Ta film, RF sputtered, thermoelec. power, Hall coeff. and struct. props. 77−43743
Ta:N film, triode sputtered, struct.-related cond. props. 79−78225
Ta-Ti-N, reactive sputtered film, elec. props. 78−84336
TaS_2 (1T), Hall effect 79−38103
TaS_2 (4Hb) layer cpd., oscillatory magnetotransport obs. 77−85241
TaS_2 intercalation complexes with 3d transition metals, mag. and metallic transport props. 80−44814
TaS_2-Fe, dil. alloy, magnetotransport and superconductivity 77−55516
$TaS_{2-x}Se_x$ (1T), transport props. 80−103710
$TaS_{2-x}Se_x$ layer compound, Hall coeff., 4-200K 78−95305
1TTaS_2(Se_2), Hall effect meas., 1.4-360K 80−44616
$TaSe_2$:Fe, competition between charge and spin density waves, Landau-Ginzburg theory 79−95352
$TaSe_2$/(2H) layer cpd., oscillatory magnetotransport obs. 77−85241
$TaSe_2$-Fe, dil. alloy, magnetotransport and superconductivity 77−55516
$TaSe_3$, oscillatory magnetotransport, Fermi surface anisotropy, Hall effect, g-factor, Dingle temp. 78−51975
$Ta_xTi_{1-x}Se_2$, cryst. struct. and elec. props. 79−47133
$TbAg_{1-x}In_x$, elec. and Hall resist. 80−96844
$TbAg_{1-x}In_x$, mag. and transport props. 78−43572
$TbAl_2$ ferromagnetic, extraordinary Hall effect 80−39560
Te, a-edge dislocated crystals, mobility anisotropy 80−107781
Te, deformed and annealed crystal, Hall coeff., depend. on stress 79−7847
Te, energy gap under press., elec. resist. and Hall effect meas. 78−30926
Te evaporated film nucleation on Au oriented islands, Hall mobility meas. 78−2388
Te film, annealing effect on elec. cond. and Hall effect 77−8213
Te film, elec. props. effect of deposition rate 78−14844
Te film, evaporated, crystallinity and electronic props., annealing effect 77−85107
Te film, field effect meas. 77−43757
Te film, Hall consts., thickness depend. of mobility 79−87171
Te film, on TGS substrate, ferroelec. field effect 79−42675
Te film, thermally evaporated, elec. cond., Hall voltage and thermoelec. power 77−47913

Hall effect continued
Te film condensed on mica, struct. and electrophysical props. 80−39688
Te films, elec. props., 77 to 450K, thermal width of band gap 79−51698
Te, films, elect. and galvanomag. characts. 79−33365
Te, galvano- and thermomagnetic effects 78−30939
p-Te Hall effect meas. at high elec. fields 77−66175
Te, lightly doped, galvanomagnetic props. in fields up to 140 kOe 78−91707
Te, mag. inversion of Hall effect *(Russian)* 77−4376
Te, oriented films, semiconducting props., Hall coeff., band structure 80−70854
Te, piezo-Hall effect from 4.2 to 77K 77−76848
Te, piezoelectrical free-carrier scatt. by screw dislocations, Hall effect and cond. meas. 80−24926
Te, screw-dislocation-induced scatt. and acceptor states, galvanomag. and optical expts. 77−28142
Te, thin evaporated films, 130 Å, temp. depend. of elec. props. 79−95529
Te, two types of carriers 80−60013
Te, undoped, elec. cond., magnetoresist. and Hall meas., hydrostatic press. effect 77−47830
Te, warm hole conductivity 78−72160
Te:Cu films, elec. transport props. 80−60120
Te:Sb, 96 to 500K, cond. Hall const., hole mobility, conc., dislocation effects *(Russian)* 78−64039
Te:Sb, impurity states and impurity conduction, hydrostatic pressure 80−39521
Te:Sb, surface carrier effects on Hall mobility at low temp. 77−80794
$Te_{81}Ge_{15}As_4$, Hall effect in electrically switched memory state 80−2403
Th_3As_4, prep. and semicond. props. 78−23087
Th_3As_4-U_3As_4 solid soln., electronic props. 80−34469
Ti, film, elec. resist. Hall effect and absolute differential thermoEMF *(Russian)* 79−24083
Ti, vacuum deposited, cryst. struct. and elec. props. 78−79908
TiC-ZrC, solid soln., conc. and temp. dependence of props. 80−39736
TiN films, reactively RF sputtered, struct. and elec. props., substrate bias effects 80−96763
TiN layers investigation for solar-cell contacts 80−81461
TiN-CrN system solid solns., electrophys. and galvanomag. props., energy spectra 77−15847
TiN-MnN, solid solns., electrophys. props. 77−35914
TiO_2:Zr, electronic conduction, temp. depend. 77−8099
TiS_2, evidence for semicond. props., Hall coeff., refl., cond., thermoelec. power 80−20220
TiS_2, resistivity, Hall effect and mag. suscept. 78−79991
TiS_2, semicond. charact. under press., in-plane resist. and Hall coeff. meas. 78−23086
TiS_2, transport props. and semicond. nature 80−44598
TiS_2, transport props. under press. 79−95410
$TiSe_2$, CDW transition temp. and transport props. pressure depend. 79−99550
$TiSe_2$ impurity effects on elec. props. 80−80263
$TiSe_2$, semimetal, electronic props., superlattice form. 77−15532
$TiSe_2$, semimetallic charact. under press., in-plane resist. and Hall coeff. meas. 78−23086
$TiSe_2$, transport props. under press. 79−95410
$Ti_{1-x}V_xS_2$, resistivity, Hall effect and mag. suscept. 78−79991
$Ti_{0.99}V_{0.01}Se_2$, negative mgnetoresist. and nonlinear cond. 79−87105
$Ti_{0.99}V_{0.01}Se_2$, negative magnetoresist. and nonlinear cond. 80−44617
$Ti_{1-x}V_xSe_2$ ($0\leq x\leq 0.1$), elec. resist. and Hall effect 80−2386
Tl-Bi system, phase transitions near Tl_3Bi, elec. props. meas. 80−35181
Tl-S melts, Hall effect 77−85239
Tl_2O_3 single crystal, elec. cond., cryst. grown from vapour in air 77−85219
Tl_2O_3, single crystal, elec. cond., annealing at 923K in O_2 effects 77−85220
TlTe single crystal, resistivity, Hall coeff., magnetoresistance, thermoelec. power 78−43418
Tl_2Te_3, exam. of electrical props., density and viscosity, for solid or liquid states 79−95431
Tl_2Te_3, exam. of electrical props., in solid, liquid state 80−54686
Tl_2Te_3:Ag(Sn), effect of dopant on electrical props., density and viscosity, for solid or liquid states 79−95432
Tm, Hall coefficient meas., 80 to 1000K 80−49694
TmSe, far IR refl. and DC resist., 1-300K, interconfig. fluctuation effects, and Hall meas. 78−35136
Tm_xSe, magnetoresist. and Hall effect, stoichiometry effects 80−65597
U film, condensed on cold substrate, electronic props. *(Russian)* 79−7912
V-Si, A15 compounds, Hall coeffs. 79−33281
VH_x, reluctance, Hall effect 79−38102
VN-CrN system solid solns., electrophys. and galvanomag. props., 77 to 1300K 77−24567
VN-Mn, solid solns., electrophys. props. 77−35914
VO_2, film, semicond.-metal transition, carrier density, mobility and Hall meas. 77−43751
VO_2, metallic phase, electronic props., plasma freq., Hall coeff. 78−84195
VSe_2, CDW states, correl. mag. and transport props. 79−73494
VSe_2, metallic behaviour obs., anomalous elec. and mag. props., temp. effects 77−15819
VSe_2, press. depend. of CDW transitions, role of Coulomb correlations, elec. props. 78−87927
V_3Si, Hall effect, 77K to superconducting transition temp. 78−43359
V_3Si single crysts., elec. resist. and Hall coeff., temp. depend., 17-300K *(Russian)* 77−69292
$V_xTi_{1-x}S_2$, elec. and mag. props. 79−65504
$V_xTi_{1-x}Se_2$, cryst. struct. and elec. props. 79−47133
W, alternating sign Hall effect and doppleron spectrum 78−79981
W, longwave dopplerons, nonlocal Hall effect, surface impedance, size effect *(Russian)* 80−80253
W, temperature dependence 78−91666
W_2B_5 and WB_4, thermal, elec., and mag. props. 80−20187
WS_2-NbS_2 system, compds., elec., antifriction props. 79−38066
WSe_2, elec. cond. and Hall coefficient temp. depend. 77−28180
Y-Mn(-Co) alloys, amorphous, paramag. props. and Hall effect 79−73692
Yb, film, amorphous and cryst., transport props. rel. to band struct. *(Russian)* 77−12026
$YbB_{6-x}C_x$, pure and doped, mag. and transport props. 80−54689
$YbGa(In)_2X_4$, X=S,Se,Te, prep. and props. 77−85214

Hall effect continued
Yb_2Te_3, films, prep., elec. props. 78−43494
Z-pinch, noncylindrical, dynamics and particle accel. mechanism 77−76170
Zn, analysis at high temp. 78−2465
Zn, Hall effect and elec. resist., temp. depend. 78−64030
Zn, Hall effect and phonon scattering in pure crystal 79−23948
Zn, Hall effect coeffs. at high temp. calc. 79−1595
Zn, monocryst., electron motion, Hall effect and Fermi surface 77−47793
$ZnAs_2$, homogeneity region and electrophys. props. 80−60833
Zn_3As_2:Cu(Te), single crysts., gas phase growth, elec. props. 79−15598
$ZnCr_2Se_4$, electroconductivity, thermoelectromotive force, Hall effect *(Russian)* 80−70694
$ZnGeP_2$, synthesis, charact., applic. to laser windows *(French)* 78−80467
$Zn_xHg_{1-x}Se$, band struct. and scattering mechanism, determ. from transport coeffs. 77−59254
$Zn_xHg_{1-x}Se$, galvanomagnetic effects, Shubnikov-de Haas oscill. determ. of band struct. 80−6884
$Zn_xHg_{1-x}Te$, impurity influence on thermomagnetic effects and elec. cond. 79−60856
ZnO accumulation layers, Hall mobility and work function, correl. 78−60185
ZnO CVD epitaxial layer, highly conductive layer, cond. and Hall coeff. obs. 79−51696
ZnO, epitaxial layers, influence of deposition conditions on luminescence, electrical props. 79−99924
ZnO films, RF sputtered single-cryst., on sapphire, struct. and SAW props. 80−80105
ZnO, polar faces, space charge layers, anomalous electron mobility 77−62981
ZnO powder, O_2 partial press. and illumination effects 79−51607
ZnO single csytals quantised accumulation layers, Hall mobility of electrons 79−60909
ZnO sputtered films, undoped and Ga doped, props. rel. to deposition conditions 80−107935
ZnO surface extreme accumulation layers due to He^+ ions 77−72909
ZnO, surface phenomena, interpretation by compensation model 78−95323
ZnO-ZnS powder mixtures, elec. cond. and Hall effect meas., percolation effects 79−7828
ZnO-ZnS powder mixtures, Hall effect and elec. cond. 79−51607
Zn_3P_2, elec. cond., Hall effect, P interstitial effects 80−84465
Zn_3P_2, single crystal, growth, electronic and device props. 80−25551
p-Zn_3P_2, temp. dependence of resistivity and Hall constant 77−35937
n-ZnSe crystals, electron scatt. mechanisms, high mobility 80−34433
n-ZnSe, impurity band, Hall effect, elec. cond., mobility and magnetoresist. expts. 77−35888
ZnSe, pure and Cu doped, elec. props. after heat treatment in Zn or Se vapour 79−99505
n-ZnSe, purified by annealing in molten Zn, Hall mobility and polaron coupling 77−85243
ZnSe, residual cond., recomb. of photoexcited carriers, Hall coeff. 80−75605
ZnSe single cryst. for LED, heat treatment effects on elec. props. 80−29406
ZnSe:Al(As), and pure single cryst., defect struct., Hall effect and Zn self-diffusion meas. 79−1427
ZnSe:Al(As), high temp. electron mobility, lattice scatt. and ionized impurity scatt. 79−91042
ZnSe:Al(Mn), elec. and luminesc. props. 77−39844
ZnSe:Ga, defect struct., Hall effect and resist. meas. 79−1428
ZnSe:In, heavily compensated, galvanomag. props. and thermopower 79−51600
ZnSe:In, heavily doped, Hall effect and DC cond. expts., compensating acceptors 78−52013
ZnSe:In, heavily doped, impurity band cond., Hall coeff. and cond. expts. 78−72147
ZnSe(:Ga)(Al), effect of thermal treatment and doping on elec. props. 77−85223
$ZnSiAs_2$, cryst. growth and elec. props. *(French)* 77−76815
p-$ZnSiAs_2$:Au(Tl)(S), photoluminesc., radiative recombination 77−24883
$ZnSiP_2$, effect of crystal growth method, on physical props., effect of doping on physical props. *(German)* 79−52094
n-$ZnSiP_2$, lattice limited Hall mobility, nonpolar optical scatt. mechanism 79−51579
$ZnSiP_2$:Ga, effect of doping conc. on elec. cond. and Hall coeff. 78−76077
n-$ZnSiP_2$:Ga, elec. cond. and Hall meas., 77 to 1000K, scatt. mechanisms 79−11153
ZnTe, effect of quenching on electrical props. 79−1920
ZnTe, elec. active intrinsic defects, Hall meas. of carrier conc. 77−51700
Zr-C disordered systems, Hall effect depend. on composition conc. 79−95459
Zr-H, inhomogeneous system, time changes of Hall voltage 79−87080
Zr-Hf, mag. susceptibility, elec. cond., Hall conc. thermoEMF conc. depend. *(Russian)* 80−39551
Zr-Ti, alloy, mag. susceptibility, elec. cond., Hall conc. thermoEMF conc. depend. *(Russian)* 80−39551
ZrB_2, self-consistent band struct., XPS, reflectance, NQR, Hall effect and density of states meas. 80−107689
ZrC-C, disordered, Hall const. anomalies 79−56277
ZrS_3, quasi one-dimens. semicond., elec. transport props. 80−107790

Hall effect devices
carrier mobility meas. instrum. for specimens in strong pulsed electric fields using Hall current method 79−35779
cervical dilation measurement in human parturition 77−48851
cross in perpendicular inhomogeneous mag. field 79−81323
depth measuring apparatus for borehole logging 79−5643
double AC Hall effect system for profiling semicond. impurities 77−37924
extensometer for simple shear meas. in polymers 79−23286
fluxmeter using Hall probe for magnetic field detection down to 10^{-3} T 80−244
generator, integrated, magnetic field meas. appl. *(German)* 80−52276
generator, magnetic field force meas. appl. *(German)* 78−253
generator characts., influence of nonhomogeneous mag. field 77−39882
magnetic field meas. appl., development trends *(Italian)* 79−80650

Hall effect devices continued
magnetic field measurement, Hall effect device method 78−41336
magnetic field measurement at low temp., probe characts. 78−37003
magnetic field monitor 77−67477
magnetic field sensor for superconducting cable, magnetisation anisotropy meas. in hysteresis loss using Hall sensors 80−17966
magnetic field sensors up to 23 T, comparison of InAs, InSb and GaAs probes 77−10066
magnetic flux meas. for grain detection in Fe-Si sheets 78−11470
magnetisation intensity, meas. method for ferromag. material in static mag. field 77−49751
magnetometer, system for calibration and checking in 0.3 to 6.0 T range 80−17964
magnetometers for rocket attitude meas. 79−21148
noise intensity in generator geometry, two-dimensional theory 78−6420
photovoltaic cell, theoretical anal. 79−66408
plasma accelerator, using Cd vap. 78−71553
plasma accelerator, with extended accel. zone, ion stream modulation at exit 78−79480
probe for induction meas., in small dimension magnetic loops *(Hungarian)* 78−4665
probe temp. compensation for spark source mass spectrometer 77−12846
probes for small mag. field detection, temp. matching 79−40592
pulsed induction discharge, Hall effect 79−64833
radio hologram recording using linear Hall detector multipliers in mm range 77−639
SHF power meter based on Hall effect in semiconductors 78−238
speed meas. devices survey, industrial appl. *(French)* 79−93105
superconducting magnet, device for energy loss meas. 79−71489
$Cd_xHg_{1-x}Te$ film, elec. props. for Hall effect device applics. 77−59344
Gd-transition metal, amorphous film, galvanomag. effects, Hall detector 77−89882
InAs thin film Hall element, CVD, H_2O transport agent 77−40377
InSb films, transverse 1/f noise and S/N ratio of related Hall elements 79−42597
InSb, Hall plates, temp. and pot. distribs. determ., temp. depend. cond. effect 79−60851
InSb ultramicro Hall element for magnetic bubble field distrib. meas. 79−56585

Hall effect transducers
ammeter appl., DC, for up to 50 kA 80−31793
collective accelerator magnetic field meas. apparatus 79−31354
compensation-point Hall effect temperature sensor 78−93679
Daresbury Laboratory automated magnet field meas. facility 79−30509
electrical steel sheet, magnetostriction meas. using Hall effect transducer *(German)* 80−13111
flow meas., recording and control appl., rotametric device *(Rumanian)* 80−48826
generator for EPR spectrometer magnetic field regulator *(Polish)* 78−41340
high-energy physics magnet meas. 79−31353
II-VI semiconductor film appls. 78−23621
linear position transducer, with improved linearity, jaw movement meas. appl. 77−44765
linearity improvement of type TLMK Hall probes *(Slovak)* 80−82795
liquid level measurement and regulation using megohmmeter and op. amp. *(Rumanian)* 79−40532
magnetic field monitor, operational principles *(Polish)* 79−85130
magnetic induction gauge consisting of 3 Hall transducers 80−105682
ocean surface wind wave related turbulence meas. by impellor current meter array 80−46301
phase shifters for fluorometer, high temperature flow meters appl. 79−8459
piezogalvanomagnetic effects measurement in semicond. at low temps., apparatus with stabilised dynamic load 77−67458
probe, KEK main ring, dipole magnets field meas., B-clock system 77−83308
probe, with improved accuracy and linearity, for measuring mag. field applied to ions traversing mass spectrometer 79−88987
probes for defect field meas. 78−53155
remote meas. of axial/radial components of magnetic fields in conducting coils 78−93659
small Hall effect transducer potential, elec. field and majority carrier density distrib. 79−67290
strong mag. field measurement for ferromag. materials 80−4745
superconducting magnets excited by AC, energy loss meas. device 79−2796
weak magnetic field meas., voltage sensitivity 77−57370
$Cd_xHg_{1-x}Te$ thin film Hall probes for high mag. fields 79−30452
HgTe thin film Hall sensor fabrication 80−2951
InSb, single cryst. micro element, mag. bubble stray field meas., expt. 77−40097

Hall generators *see Hall effect devices*

halogens
see also astatine; bromine; chlorine; fluorine; halides; iodine
air pollution gauge, apparatus based on secondary emission of Pt 80−85320
alkali atom+halogen molecule, electron contact, model system *(Dutch)* 79−50111
(alkali atom)$^+$+(halogen atom)$^-$, recombination 78−7192
alkali metal:halogen, charge transfer excitations 79−95815
alkene-halogen, matrix isolation vibr. spectroscopy, complex form. studies 78−62952
atom, 1s hole states, ionisation, ab initio SCF calcs. 78−17568
atom, ^{2}P state, pot. energy surface complex intersection 77−77736
atom, Sternheimer shielding functions calcs. 79−76352
atom (^{2}P)+inert gas atom (^{1}S), coupled channel study, rel. to elastic approx. 79−81255
atoms produced in IR photodissoc., hydrogen halides form., IR chemiluminesc. 77−63932
chemi-ionisation reactions of Ca, Sr, Ba, and Yb with halogens and interhalogens 77−32791
chemisorption on Na, surface chemiluminesc., MO description 79−43048
chemisorption on W, UV photoelectron spectrosc. study 80−7854
chemisorption on W (100) substrate, adatom charge and binding energy, self-consistent calc. 77−62734
desorption kinetics from Nb, Mo, Ta, and W, pulsed ion beam method 80−34300
determination, by emission spectrograph, surrounding gas effects *(German)* 77−44571

halogens continued
determination, in terrestrial, meteoritic and lunar samples, rel. to cosmochemical processes 78−12111
determination of halogen content of Earth by gamma-ray spectroscopy and radioactivity meas. 80−76945
diatomic isovalent sequence, free-mol. electronic transition intensity consts., systematics 78−42137
diatomic molecule, 1s hole states, ionisation, ab initio SCF calcs. 78−17568
dimers, mol. beam. elec. deflection obs. 80−53080
excimer lasers, book contrib. 79−81417
excimer lasers, review 77−34877
exothermic trihalogen Borne-Bunker reaction, long lived intermediates, comment 78−92464
exothermic trihalogen Borne-Bunker reaction, long lived intermediates, reply 78−92465
graphite intercalation compound with halogens, ionisation 78−26489
halide anions, in gas, photodetachment cross-sections, OPW and APW calcs. 77−38607
halogen-metal vapour lasers, average lasing power 79−936
inert gas halogen excimer laser principles, performance and applications 78−55342
inert gas-halogen mixture, ion form., ion-mole. reactions, mass spectra 77−61841
inert gas-halogen mixtures, UV laser output from elec. discharge after X-ray preionisation 79−64205
interhalogen dimers, mol. beam. elec. deflection obs. 80−53080
interhalogen trimers, mol. beam. elec. deflection obs. 80−53080
leak detector, reduction of background effects by means of chromatographic columns 78−70110
lunar samples, Li and halogen contents 77−60638
metal vapour lamp, additive partial pressure determ. from self-reversed spectral line maxima 78−67476
metal-halogen arc lamp, nonequil. comp. developed by slow chem. reactions *(Hungarian)* 77−47288
molecule, master eqn. theory, dissoc. rate consts. 77−77742
molecule+alkali atom, ion pair form., trajectory model 77−16800
molecule+alkali dimer, thermal chemi-ionisation reactions, products, energies 77−63903
molecule+$K_2(Cs_2)$, thermal energy mol. beam chemi-ionisation 77−9065
molecule+K, ion pair form., vibr. energy depend. 79−34287
molecule chem. radiative collisions *(Russian)* 78−23942
molecules, van der Waals dimers, PCILO calcs. 79−36542
negative ions, electron spin polarisation in photodetachment 78−25495
negative ions source 77−41729
positron, scatt., low energy, semiempirical polarisation pot. calcs. 80−9736
pressure and temp. dependence meas. using tesla discharge as spectroscopic source 80−274
projection lamps and light fittings *(German)* 77−58408
short-arc lamp for Super 8 cinefilm projector appl. using rare-earth halogens 80−62747
solid, intermolecular bonding influence on nucl. quadrupole interaction tensor 77−62882
solid, melting curves, Lennard-Jones Devonshire theory 80−65201
supersonic atomic and molecular beams, nozzle source 77−31028
surface ionisation, on LaB_6, using ion source 78−60538
underground water movement tracing using halogen tracers and NAA 79−88014
XPS in transition metal coordinate compounds, inner shell binding energies 78−21973
Al+halogen chemiluminescent reactions 77−9086
H(D)+X_2, (X=F,Cl,Br,I), exoergic collinear reactions, impulsive energy release model 77−90591
X^- (X=Cl,Br,I), in atm. press. flames, form. and removal kinetics 77−52642

Hamidashi effect *see ferroelectricity*

hand tools
air tools, noise evaluation standards 80−23855
IC wiring tools for laboratory use 78−86073
optical fibre end preparation 77−88907
substrate core sampler, lightweight low-friction, ecological survey appls. 80−95090

handling, materials *see materials handling*

handsets (telephone) *see telephone sets*

Hanle effect
alkali metal, resonance levels relax., hyperfine struct. effect 77−38725
atomic and laser spectroscopy, book 77−79554
atomic collisions, relaxation coefficients, meas. method *(French)* 78−58771
atoms, level crossover signal distortion by radiation capture 77−3327
$^3\pi\pi^*$benzaldehyde, zero field splitting and sublevel decay rates, deuteration and host effect 80−37750
compact non-LTE radiative transfer theory 78−61728
diatomic molecule, ground state, opt. prod. and orientation, review *(Russian)* 79−27046
diatomic molecule, two identical 3-level atoms, excitation spectrum 80−23476
excited atom, alignment in gas discharge, Hanle effect 80−23378
excited atoms, orientation in elec. field *(German)* 78−25472
gas laser, atomic constants and collision cross sections determ. by level crossing 78−50763
ground state atoms+excited atoms, anisotropic collision rate 79−76488
inert gas, at. excited states in discharge, Hanle effect 79−76394
laser techniques, vis. and UV, small mols., electronically excited states, book contrib. 78−9277
lifetime meas. in atoms, mols., ions 77−30832
magnetometer, one-component Hanle effect, with feedback, stability and operating range 78−82011
magnetometer freq. optimisation, computer anal. and expt. 77−18057
quantum magnetometer with Hanle effect, three layer superconducting shield 77−53962
Raman scattered light, Hanle effect influence 80−83323
semiconductor, donor-acceptor pair luminesc. polarisation with optical orientation 77−24895
two-level atom, Hanle resonances for J=0 to J=1 transition 77−18855
two-photon transitions, Hanle effect, saturation resonances 77−30842
Ar, $3p^55p$ config. aligned in discharge, interf. signals, lifetimes and collision cross sections 78−70796

Hanle effect continued
Ar, collisional depolarisation of selectively excited 2p levels *(French)* 78−86830
BO_2, $A^2\Pi_u$-state, Hanle effect, press. and Zeeman broadening 79−18239
Ba $(5d6p)^3D_3$ state, lifetime meas. by dye laser spectrosc. 80−78577
Ba atomic beam, light-shift induced zero-field level crossing, optical Hanle effect 80−52947
Ba I, light shift induced zero-field level crossing 80−58220
Ba II, Hanle effect, $^2P_{3/2}$ lifetime determ. 77−18852
Ba, reson. line, density depend. 77−23473
Ba^++Ba, $6p^2P$ level lifetimes, depolaris. cross-sections, Hanle effect obs. 79−26943
BeF_2, radiation induced defects, nuclear Hanle effect 78−43734
Br_2, $B\ ^3\Pi_{0u}^+$ Hanle effect 77−75234
CS_2, fluorescence due to laser excitation, Hanle effect 78−25628
Ca, 4s4p $^1p_1$ level Hanle effect density depend., lifetime 80−91494
Ca II, Hanle effect, $^2P_{3/2}$ lifetime meas. 77−18852
Ca+He, $^1P_1$ level lifetime, Hanle measurement 80−23365
CaF_2, radiation induced defects, nuclear Hanle effect 78−43734
CaF_2:Eu^{2+}, circular polarisation in luminesc. and optical orientation 78−6740
Cd, 6^3P_1 level, relax. of alignment and population 78−70795
Cd, (5s7s), (5s6d), (5s7d) configs., triplet state lifetimes *(French)* 77−3326
Cd, (ns nd)$^1D_2$ states, Hanle effect, alignment destruction by collisions *(French)* 78−5324
Cd II, Hanle effect, $^2P_{3/2}$ lifetime determ. 77−18852
Cd II+He, relax. consts. for depolarising collisions 77−19239
Cd, P_1 state resonance fluoresc. in rot. mag. field 77−42271
CdS crystals, electron-hole plasma, carrier optical orientation 80−100689
CdS, exciton resonant secondary emission spectrum temporal evolution 79−51499
Co I, excited levels lifetimes meas. by zero field level crossing method 78−5178
Cs Hanle effect magnetometer characteristics and evaluation results 77−79586
Eu chalcogenides, paramagnetic, optical orientation of 4f electrons 77−69799
EuS, ferromag. semicond. film, Hanle effect, optical orientation time consts. meas. 77−40214
p-GaAs, electron-nuclear spin coupling, low field, under optical pumping conditions 77−77126
H_2, electron impact excitation, two-step, Hanle effect obs. 78−25730
He I, heavy ion impact excitation, alignment relax. of nonresonant levels *(French)* 77−61842
He I 1s3d levels, cascade-free lifetime meas., using He^++He 35 keV collisions 78−58607
He I D_3 line, Stokes parameters for quiescent prominences, Hanle effect quantum theory 78−85924
He I D_3-line polarization in solar prominences, level-crossings effect 80−94772
^{3}He, dynamical Hanle effect, line halfwidth, sensitivity threshold, signal to noise ratio *(Russian)* 77−54541
^{3}He, stationary effect 77−23474
He(2^3S_1)+Ca(Sr)(Ba), coherent $^2P_{3/2}$ levels excitation by Penning ionis., Hanle effect 80−5520
Hg II, $6p^2P$ and $6p^2D$ levels, radiative lifetimes meas. 80−78576
Hg, lifetimes and cross sections of depolaris. collisions of laser working levels 79−76387
Hg-Cd, sensitised fluoresc., anomalous Hanle effect 79−81186
Hg+Cd, quantum beats under transfer of orientation 79−98206
Hg+He(Xe), collisionally induced coherence, orientation and alignment, transfer among 6s6d levels 78−74747
Hg+Zn(Cd), sensitized fluoresc., orientation and alignment transfers *(French)* 79−13808
^{199}Hg, Hanle resonance in radio-frequency fields 80−91508
Hz, 3d complex, radiative lifetimes, hyperfine constants 78−70873
In I, $6^2S_{1/2}$ state lifetime meas. by Hanle effect method 78−90097
K_2, $B^1\Pi_u$ state lifetimes, Hanle effect 78−90218
K_2, optically aligned ground state, Hanle effect obs. 79−36707
Lu I, 5d6s(^{3}D)$6p^2D_{3/2}$ state, Stark effect, level crossing obs. 77−75098
Mg, Hanle effect density depend., $3s4p^1P_1^0$ level, and oscill. strengths 79−72282
Mg II, Hanle effect, $^2P_{3/2}$ lifetime meas. 77−18852
Mg, reson. line, Hanle effect, density depend. 79−6917
N_2, $B^3\Pi_g$ state, Hanle effect on rot. level 77−58090
NO_2, $^2B_2$ state, fluoresc. anomalous mag. depolaris. 78−21962
NO_2, coherence time rel. to radiative lifetime, theory 79−18240
NO_2 Hanle effect, nonstationary states in molecular spectroscopy, level splitting 80−23465
NO_2, Hanle effect, using Doppler reduced laser excitation 78−25627
Na, 3^2P-states, orientation and alignment relax. 79−76395
Na, Hanle effect for $3^2S_{1/2} \rightleftarrows 3^2P_{1/2}$ transition 77−42287
Na, magnetically induced SHG, intensity saturation 80−1273
Na, optical pumping, Hanle effect 78−33475
Na_2, optically aligned ground state, Hanle effect obs. 79−36707
Ne, velocity diffusion, saturated absorpt. obs. of Hanle effect 77−61716
Ni I, UV lines, oscillator strengths from hook method and absorpt. meas. in furnace 80−83319
Rb $5^2P_{3/2}$ state, Hanle effect intensities 78−66521
^{85}Rb, $5^2P_{3/2}$ state, Hanle effect *(French)* 78−42018
S_2, selectively excited, coherence retention during rotationally inelastic collisions 77−46622
Sm, Hanle effect expt. on $4f^66s6p^7F_1$ level 80−43004
Sr, $5p^2\ ^1D_2$ level lifetime 79−63960
Sr II, Hanle effect, $^2P_{3/2}$ lifetime determ. 77−18852
Sr+He, $^1P_1$ level lifetime, Hanle measurement 80−23365
SrF_2:Eu^{2+}, circular polarisation in luminesc. and optical orientation 78−6740
Tl I, $6s^26d^2D_{3/2}$ state, hyperfine struct. interaction const., mean lifetime 77−42286
Xe, $6p_{01}$ level, peculiar signal in Hanle effect 78−25487
Xe, lifetimes and cross sections of laser levels 77−75480
Zn, (ns nd)$^1D_2$ states, Hanle effect, alignment destruction by collisions *(French)* 78−5324
Zn II, Hanle effect, $^2P_{3/2}$ lifetime determ. 77−18852
Zn, triplet state lifetimes, (4s6s), (4s5d), (4s6d) configs. *(French)* 78−5175

hard soldering *see brazing*

hard-sphere fluids *see classical theories of fluid structure; liquid theory; quantum theories of fluid structure; statistical mechanics*

hardening
see also dispersion hardening; quench hardening; radiation hardening; solid solution hardening; surface hardening; work hardening
alloy structural steel, electron fractographic pattern of fatigue fracture under cyclic loading 77−56094
alloys, apparatus for rapid hardening from liquid state 80−76275
anisotropic hardening of initially orthotropic materials 80−33488
austenite, hot-worked, subgrain struct., X-ray diffr. and electron microscope obs. *(Russian)* 79−15698
BCC crystals in tension and compression, theoretical latent hardening 80−24459
β-brass, martensitic, transform hardening and energy dissipation 77−21141
brass single crystal, intracrystalline slip bands in high temp. creep *(Czech)* 79−77604
cold rolling mills, roll service life, rehardening by heat treatment 80−16347
concrete, plastic-brittle behaviour, hardening and softening constitutive eqns. 77−21270
concrete, strain rate effect on strength and deform. during hardening process *(Japanese)* 80−93616
corundum-based refractory lining specimen, thermal softening assessment *(Russian)* 79−83237
crystal plasticity, hardening law for slip systems 79−33030
cubic crystals, compression test, double slip kinematics 80−65005
cyanate bath, soln. mechanism of Fe and Cr 79−39271
cyclic elastic-plastic dynamic analysis by finite element method 77−33864
cyclic hardening, of hardenable metals and alloys, algorithm *(Bulgarian)* 80−70296
cyclic thermoplasticity, finite element analysis by subvolume technique 77−42749
defect superlattices, hardening influence, computer simulation *(Russian)* 79−83206
dislocation mobility in inhomogeneous stress field, hardening effects 80−70219
ductile-fibre composites, strengthening effects of brittle zones 77−8946
elastic-plastic initial value problem, iterative numerical integration 77−62170
elastic-plastic struct. cyclic thermomech. loading 79−7299
elastic-viscoplastic materials, hardening parameters 78−46895
elastoplastic anal. using ASKA program system, bending, isotropic/kinematic hardening 78−63312
elastoplastic material, variational inequality 78−63320
elastoplastic structures under cyclic loads, small displacement finite element analysis 77−62171
epoxide resins, amine-hardened, heat distortion, glass transition temps., chem. cure 80−44302
epoxy composites, with different degrees of hardening, bulk-creep prediction 80−104223
epoxy resin, hardening, mechanical and dielectric losses 78−48115
epoxy resin curing, elastic moduli changes, US wave propagation monitoring technique 79−20305
FCC alloy, hardening by spinodal modulated structure 80−60874
fcc crystals in tension, latent hardening, eqns. for tension and compression 79−77671
Fe, pure, lattice hardening due to H_2 charging, during tensile testing 79−66156
ferroelectric ceramic, defect effects on mech. strength 78−64332
gelatin hardened layer structuralisation, kinetic anal. using swelling 78−62255
glass, photoelastic const. for chem. strenthening, circular plate compression method *(Japanese)* 80−93279
glass fibre reinforced plastic, unwinding resistance of hardening layers, fibre tension effect 77−32691
glass fibre reinforced polyester and epoxy resin, vacuum hardened shell, strength and deform. charact. eval. 78−48528
glass fibre reinforced Textolite, method of stressed state study during hardening 79−57191
glass hardening, etching in hydrofluoric acid effect by low temp. ion exchange 77−44373
gypsum, strength changes on setting *(Japanese)* 77−36619
heat resistant material, long term loss of strength 80−71751
hydride forming, metals and alloys, phase hardening 78−52833
inelastic deformation, hardness law 78−46896
iron, Armco, effect of low temps. and heat treatment on growth rate of fatigue cracks 79−57027
isotropic material in plane stress, piecewise linear theory, plasticity 80−43622
$L1_2$ ordered alloys, latent hardening 77−16676
liquid photopolymer materials, mathematical modelling of layer thickness and exposure parameters *(Russian)* 80−62784
M_s changes on phase hardening 78−23708
metal, hardening due to increased subgrain boundary stability 78−52934
metal sytems, mech. prop. improvement by pulsed laser generated shock wave 77−48443
metals, BCC, low temp. softening 79−34113
metals, supercooling on homogeneous crystn. *(Russian)* 80−19914
methylundecanhydride hardened phenol formaldehyde resin, hardening kinetics and mech. losses 80−66520
Permalloy, high permeability, effect of hardening additions on mag. props. *(German)* 79−28566
phosphate containing materials, technological prod. processes, review 80−97452
plane strain problem of hardening and softening plastic materials, theory 78−83869
plastic, Vicat softening temp., meas. instrument *(German)* 77−63871
plasticity, polycrystalline, based on dislocation processes, probabilistic approach 78−26621
Polimal 142, polyester moulding material, hardening *(Polish)* 80−66523
polycrystalline plasticity, probabilistic approach, appl. 78−26622
polyethylene, highly oriented, fibre composite model 78−3183
polyethylene, highly oriented fibre composite, self-hardening, tensile props. 77−55939
polyethylenepolyamine hardened epoxy resin, hardening kinetics and mech. losses 80−66520

hardening continued
polymer, magnetic field, nonuniform const., effect on props. during hardening 78−11235
polymer solns., shear and normal stress behaviour, flow hardening *(German)* 78−67165
polymers, cross-linked, with different degrees of hardening, bulk-creep prediction 80−104223
polyurethane cement, viscosity and shear strength, components influence *(German)* 80−93729
Portland cement, absorbed H_2O, pulsed NMR study 80−84665
PVC plastisols, thermally hardened, rheological props. *(German)* 79−29154
rigidly plastic media with hardening, shock-loaded, dislocation model and elastoplastic waves 79−86379
rings, plastic, large deforms., plasticity and hardening effects 80−43627
rock, plastic-brittle behaviour, hardening and softening constitutive eqns. 77−21270
shell stability during axial compression, hardening beyond elastic limit 80−99931
silicate glass, high temp. microscopy investigation of softening temp., viscous flow, angle of contact *(Polish)* 77−55242
siloxane rubber, energy investigation of softening during deform. 77−4819
soil, anisotropic hardening model, cyclic loading appl. 79−16441
steel, alloy, hardened, electrochem. characts. and stress corrosion cracking, ageing and cold treatment effects 80−108639
steel, alloy, surface quality improvement, thermomech. treatment 80−61020
steel, alloy, type 52100, exam. of microstruct. and fracture, as function of austenitising in temp. range 800 to 1100°C 78−76673
steel, austenitic, martensitic transform. effect on hardening kinetics and fracture resist. of friction surface of 45Kh12G8 and 110G13 *(Russian)* 80−50727
steel, austenitic, metastable, 0Kh14AG12M, Cr-Mn and Cr-Mn-Ni, phase transform. kinetic effect on mech. props. *(Russian)* 79−34024
steel, austenito-martensitic, struct. changes during plastic deform., mutual influence of phases *(Russian)* 80−30015
steel, C, bainitic hardenability, overheating effect 79−38866
steel, C, hardened by HF current, mech. testing method 80−61053
steel, C, isoforming and warm rolling, effect of mech. props. 80−11673
steel, C type 45, martensitic needle size, effect on mech. props. after induction hardening 80−11672
steel, cast, high tensile strength, heat treatment 80−16358
steel, Cr, tempering resist., mech. props., Cu addition effect 79−79012
steel, Cr with metastable austenite, wear resist., temp. effect 80−76370
steel, Cr-Mo (9,1 wt.%), austenitized in $\gamma+\delta$ phase field, secondary hardening and tempering 78−11247
steel, Cr-Mo-Ni-WV (6, 4, 3, 2 wt.%), tempering and secondary hardening, TEM obs. *(Chinese)* 80−104245
steel, Cr-Mo-V, 1% Cr, chem. comp. and struct. effect on deform. props. *(German)* 79−1888
steel, Cr-Mo-V, combined Cr-Mn addition effects on hardenability 78−7046
steel, Cr-Ni (14, 5 wt.%), tempering resist., mech. props., Cu addition effect 79−79012
steel, Cr-Ni-Mo, dynamic and static softening behaviour at hot forming temp. *(German)* 80−25728
steel, Cr-V, hardened sping, surface finish effect on fatigue strength *(Japanese)* 79−61708
steel, die type 5KhNM, stressed state effect on softening 79−66168
steel, hardened, martensite struct. characts., Cu and Al additions effect *(Russian)* 78−19709
steel, heat treatment with induction heating, 78−92285
steel, high hardenability carburising, accelerated annealing technique 78−84857
steel, high speed, hardened, for drills, mech. and cutting props. 79−43407
steel, high strength, failure stress, structural relationships 80−81190
steel, high-alloy die, electrothermal treatment 80−29996
steel, high-temp. isothermic combined heat treatment and mech. working influence on struct. and mech. props. of 60S2 *(Russian)* 80−20969
steel, high-temperature thermomechanical treatment, holding after deform. effect on strengthening 79−38868
steel, hot worked and rapidly worked, secondary hardening problems *(German)* 80−3083
steel, induction hardened sheet, inhomogeneity and distrib. of residual stresses effect on fatigue *(Japanese)* 78−31518
steel, Kh15N5AM3, combined heat treatment and mech. working *(Russian)* 77−55997
steel, lattice hardening and anomalous softening caused by electrolytic H_2 charging *(Japanese)* 79−43398
steel, lattice hardening due to dissolved H_2 77−8952
steel, lattice hardening/softening due to dissolved H_2 77−77581
steel, low alloy, softening of heat affected zone under postweld tempering 77−21196
steel, low alloy and C, hardened and tempered parts, nondestructive magnetic inspection 78−95889
steel, low alloy and C, hardened and tempered parts, nondestructive magnetic inspection 79−1929
steel, low C, cyclic plasticity and low cycle fatigue life 80−21058
steel, low pearlite, low alloy, low temp. strength props., heat treatment 77−12658
steel, low S, ESR, overheating effect on toughness 78−52860
steel, martensitic, Cr (12 wt.%), temper embrittlement 79−87722
steel, martensitic, fatigue life, low-cycle, temp. and strain rate effects 80−85056
steel, martensitic 12% Cr, temper embrittlement 80−66650
steel, medium C, deform. hardening, plasticising action of Sn-Zn melts 80−55415
steel, metastable alloys, singularities of $\alpha \rightarrow \gamma$ transform. and hardening *(Russian)* 79−52210
steel, mild, fatigue softening and hardening detected from Barkhausen noise 80−76428
steel, Mn, type 35SGM, magnetic, electrical, and mech. props. after tempering and hardening 79−66086
steel, Mn-Ni-Mo, PWR pressure vessel, irrad. induced embrittlement, chemical composition effect *(French)* 79−20195
steel, molten, heat loss during solidification hydrodynamic eqns., hardening front kinetics *(Russian)* 80−55385
steel, silchrome, thermomech. hardening 78−23736
steel, sintered Cu, hardenability *(Japanese)* 77−48527

hardening continued
steel, sintered type M2 high speed, heat treatment response and cutting props. 78−15336
steel, stainless, 304, beam, elastic-plastic response to impulse loads 79−34118
steel, stainless, Cr-Ni, maraging, effect of Mo, Co additions on hardening 78−84835
steel, stainless, tempering after air hardening from rolling heat *(German)* 80−93571
steel, stainless type 304, shock hardening, anomalous residual, at short pulse duration 80−20942
steel, statistical distrib. of mech. props., and life characts. exam. 78−64606
steel, structural 15Kh2NMFA, use of linear and nonlinear fracture mech. for crack propagation resist. determ. 79−5056
steel, thermal etching displaying hardening structure 77−40487
steel, tool, cutting blades, heat treatment in fluidised bed, hardening 79−20087
steel, tool, martensitic hardened, reagent for revealing austenitic grain size 80−21207
steel, TRIP, strength and plasticity rel. to thermomech. treatments 77−44281
steel, ultra-high strength, strengthening, props. and characts. *(Korean)* 79−24607
steel, wear resist., mech. props. and struct. effects 80−35338
steel *(German)* 80−100869
steel 10GN2MFA, effect of low temps. and heat treatment on growth rate of fatigue cracks 79−57027
steel 45, effect of low temps. and heat treatment on growth rate of fatigue cracks 79−57027
substructure strengthening mechanisms, dislocation charact. 77−84761
technology, automobile industry 79−96048
thin walled bearing races eddy current inspection of hardening and tempering quality 78−95892
thin walled tubular specimens, plotting hardening curves based on torsion tests 77−56180
tool steel transformation hardening by CO_2 laser 80−16483
transition metalloids, t-matrix theory of thermal and nonstoichiometric softening 79−86788
two phase materials, plastic strain and meas. stress hardening rate 77−52449
two-phase materials, strength contributions 77−52448
vicalloy-2, high heating rate effect on mag. props. *(Russian)* 77−81328
visco-plasticity problem with hardening, finite element anal. *(French)* 79−46222
viscoplasticity with hardening, quasi-variational problems *(French)* 77−14913
wear resistant material, US welding effect on struct. *(Slovak)* 79−74185
Ag FCC crystals, compressively activated slip, theoretical latent hardening 80−65128
Al alloy, low-cycle fatigue strength, isothermal hardening effect 79−38863
Al FCC crystals, compressively activated slip, theoretical latent hardening 80−65128
Al single cryst., latent hardening in tension 80−60878
Al, strength changes on US treatment in programmed loading *(Russian)* 77−32583
Al-Cu-Mg-(Ag), effect of addition on fatigue microstructure relationships 80−40483
Al-Mg-(Ag), effect of addition on fatigue microstructure relationships 80−40483
Al-Ni (63.6 at.%), elastic softening and electron diffr. anomalies prior to martensitic transform. 77−86078
Al-Zn (6.8 at.%), hardening during spinodal decomposition *(French)* 79−66035
Al-Zn-Mg (4.5, 2.5 wt.%), composition effect on stress corrosion and mech. behaviour 78−27684
Al-Zn-Ti(Mn), mech. props., Ti or Mn addition effect *(Korean)* 80−93613
Au, electrodeposited, hard, hardening mechanisms, grain size effect 80−35302
$CdO-WO_3-H_2O$, interconnection between kinetics of structure formation and chem. reactions 78−53198
Cr-Mn-Si steel, heat-treatment quality, higher harmonics of EMF obs. 78−60941
Cu, deformation hardening by shock front, quasiisentropic compression, front width effects 79−100209
Cu, polycrystalline, intracrystalline slip bands in high temp. creep, comparison with brass single crystal *(Czech)* 79−77604
Cu, polycrystalline, recovery and recrystn. kinetics 80−81081
Cu single cryst., latent hardening in tension 80−60878
α-Cu-Al, stress-strain behaviour, effect of grain size and composition 77−56038
α-Cu-Al (0.5 to 10 at.%), latent hardening and dislocation density 78−19853
Cu-Al martensite, temper hardening, study by TEM, DTA, microhardness and yield strength meas. 79−43260
Cu-Al(Au)(Ga)(Ni)(Pd)(Rh)(Zn) (4 at.%), anneal hardening mechanism 80−60879
Cu-In, thermally cycled, effect on mech. props. and microstruct. 79−4987
Fe cast, Mg, austenite isothermal transform., Sn addition effect 79−87611
Fe, cast, nodular, hardenability, isothermic transition *(Czech)* 77−59778
Fe, high purity, H induced softening *(Japanese)* 79−78988
Fe, lattice hardening and anomalous softening caused by electrolytic H_2 charging *(Japanese)* 79−43398
Fe, lattice hardening due to dissolved H_2 77−8952
Fe, lattice hardening/softening due to dissolved H_2 77−77581
Fe, softening caused by electrolytic H charging *(Japanese)* 80−35197
Fe-C, dil. alloys, softening, conventional and in situ expt. 79−47744
Fe-C, dilute alloys, softening, conventional and in situ expt., HVEM obs. 79−47743
Fe-Cr-Co-Mo, microstruct., hardness, mag. props., influence of isothermal tempering and heat treatment 79−79129
Fe-Ni, hardening by plastic deform. during polymorphic transform., struct. mechanics for γ-phase form. *(Russian)* 77−90344
Fe-Ni, hardening by plastic deform. during polymorphic transform., mechanical props. *(Russian)* 77−90345
hardening continued
Fe-Ni (28 at.%), martensitic transformations, Mossbauer scattering evidence of soft modes 80−93223
Fe-Ni-Ti, shape recovery depend. on hardening *(Russian)* 79−83259
Fe-Ni-V, effect of low temp. ageing on props. during high temp. ageing *(Russian)* 78−39811
Fe-Si (3 wt.%), single crystals, cyclic deformation oriented for single glide 79−100224
Fe-Si (3wt.%), hardening under dynamic load, grain boundary effect 77−12674
α-Fe-Sn alloy, grain boundary hardening and segregation 80−55417
Fe_2O_3 haematite platelets, growth and cross-connection in consolidation of haematite pellet *(Chinese)* 80−104186
GaAs:Si, hardening by solute-vacancy pairs 77−4794
LiF, hardening under dynamic load, grain boundary effect 77−12674
Mg alloy MA12, thermally strengthened, fatigue cracking in air and vacuum *(Russian)* 78−35481
Mg cast iron, effect of heating temp. on microstruct. and mech. props. 77−56005
MgO-spinel concrete, cast, hardening by elec. heating 80−21258
Nb alloy SVMTs, high-temp. ageing, struct. and morphology of hardening phases *(Russian)* 80−40390
Nb, neutron bombarded, defect size distrib. influence on hardening *(Russian)* 80−10580
Ni, creep, effect of AC mag. field, 1.5-4.2K *(Russian)* 79−11657
Ni, deformation hardening by shock front, quasiisentropic compression, front width effects 79−100209
Ni, high-purity, softening of strained single crystals *(Russian)* 80−40499
Ni, shock hardening, anomalous residual, at short pulse duration 80−20942
Ni, thermal softening, influence of alternating mag. field *(Russian)* 78−23312
Ni, US deformation at low temps. *(Russian)* 79−11656
β_1-Ni-Al, elastic softening and electron diffr. anomalies prior to martensitic transform. 77−8825
Ni-Al (1.18 wt.%), substruct. hardening effect, depend. on mechanism controlling creep rate, 700°C 79−20144
Ni-Cr Nimonic alloys, mech. props., high-temp. irrad. effects 80−100885
Ni_3Al, substitutional soln. and defect hardening mechanisms 77−21155
NiO, doped and pure single crystals, plastic deform. 77−36578
Pb-Sn(Bi) alloys, dil., impurity effects on softening at T_c *(Russian)* 78−23220
PbO glass, mechanochemical reduction 77−52628
Pd, H phase hardened, recrystallisation study 80−60883
Ta, Ta-Re, Ta-Re-N, deformed at 77K, dislocation substruct. 77−32647
α-Ti alloy, rolled, elastic stiffness and Bauschinger effect accompanying anisotropic hardening *(Russian)* 80−40435
Ti-Al-V, rolled, elastic stiffness and Bauschinger effect accompanying anisotropic hardening *(Russian)* 80−40435
Ti-Al-V (6, 4 wt.%), superplastic, mech. behaviour and hardening characts. 79−83269
U, γ- and β-hardened, recrystallisation, effect of impurity distrib. 78−70602
V alloys, strengthening in internal oxidation *(Japanese)* 78−11493
V, structural changes in single crystal under single electric impulse discharge *(Russian)* 79−65086
V-Zr-C-Y alloy weld metal, hardening phase precipitates examination, TEM appl. 80−7576
V_3Si single cryst., creep deform. 80−71695
W fibre reinforced Cu composite, hardening in two-phase material 77−52448
W-Re alloy, effect of thermal prehistory on resistivity meas. 78−3241
Zn-Al-Cu (18, 4 wt.%), plastic deform. at room temp., superplastic props., tensile strength *(Czech)* 80−45360
Zr polycrystalline, low-temp. alternating deformation and annealing, yield stress, elec. cond. variation *(Russian)* 79−74199
β-Zr-Nb(Cb) alloys, anneal hardening and flow softening 79−78993

hardness
see also abrasion; hardness testing
activation volume determ. by means of change in hardness 79−18836
Al alloy AK4-1, acoustic investigation of ageing 79−34083
Al alloy blend 6061, isostatically computed powder, effect of heat treatment temp. on tensile strength and hardness 79−61720
alkali metal halides, microhardness and atomic vibr. freq. relation 80−75297
alkali metal halides, revised values of van der Waals energies 77−72579
alkali-halide crystals, plastic deformation, effect of solid film coatings *(Russian)* 77−25167
alloy, austenitic, mechanical changes after electrolytic quenching *(Russian)* 80−50653
alloy, hard, powder mixtures, porosity and hardness during pressing, u.s. vibration effects 77−1821
alloy, selective stripe, electrodeposition and hot flow techniques, metallurgical characteristics 80−50567
alloy hard, binary carbide with Ni-Mo binder, physicomech. props. 77−90461
alloys, FCC base hard materials, low temp. toughness *(Japanese)* 80−100916
alloys, ion implantation in tribology and corrosion science, overview 79−14830
alloys, $L1_2$ ordered, temp. depend. of hardness 80−30104
alloys, magnetic, amorphous, magnetic strip appl. *(German)* 77−16700
alumina deposition by activated reactive evaporation, microhardness 77−44176
aluminate glasses, new families, light transmission, 0.4 to 6 μm 77−24843
Armco iron, kinetics of form. and struct. of thermodiffusional protective coatings 77−56158
arsenides (Ti, V, Cr, Mn, Fe, Co, Ni, Cu, Zn, Ga, Ge), oxidation, hardness and electromechanical polishing response 80−71776
austenite, quenched and tempered, effect of bainitic decomp. products on mech. props. 77−56007
ball mill grinding, effect of Vickers hardness and rate const. of spec. surface increase *(Japanese)* 77−52259
bellows type expansion joints, in LMFBR, Na test, hardness distribution rel. to welding boundary *(Japanese)* 79−67850
bitumen, phys. props. and constitution, effect of air blowing 77−44384
bone, Haversian plate in man, microhardness 78−48825

hardness continued
boride coatings, high temp. resist. and struct. 79−39008
boride coatings on Ni alloy, thermal stability, exam. of coating 78−44271
borides, metallic, sintering, review, book contrib. 78−48359
borides, ternary, struct. classification, props., book contrib. 78−47309
borides (Ti, V, Cr, Mn, Fe, Co, Ni), oxidation, hardness and electromechanical polishing response 80−71776
brass, high-speed strain effect on struct. and props. *(Russian)* 77−59855
α-brass, plane stress ductile fracture, prestrain effects 80−108532
α-brass, polycrysts., deformed in tension or rolling, anneal hardening *(Japanese)* 80−93564
brass, recrystallization during induction heating 80−97511
brittle abrasive material, rating capability for elastic deformation 78−56680
bronze, sintered, Zr addition effects on struct., hardness, wear resistance *(Russian)* 77−70019
butyl rubber vulcanisation with resins, mech. props. *(Polish)* 79−74129
carbides (Ti, V, Cr, Mn, Fe), oxidation, hardness and electromechanical polishing response 80−71776
cast iron, kinetics of form. and struct. of thermodiffusional protective coatings 77−56158
cast iron, white, high Cr-Mo, fracture toughness 80−50726
cemented carbides, physical and chem. nature 80−76265
ceramics, microstructure dependence of mechanical behaviour 78−88533
ceramics and brittle solids, abrasive wear, role of plastic deform. and fracture 80−108594
chemisorption modification of strength of solids 79−51423
coal, variations with maceral and orientation 79−24605
cold work in tension, strain rate effect on stored and dissipated energies 77−86111
covalent crystal, resistance to microindentation 78−60753
crack tip stress and strain *(Chinese)* 79−73249
cubic crystals, scratch hardness, anisotropy 79−96130
cutting tools, diffusive wear, mag. field effect 80−60985
CVD on quartz substrate from gas mixture of $TaCl_5$-BCl_3-H_2-Ar 80−29880
dental stones, effect of particle size on hardness and scratch resistance 79−79077
dentin, human, effects of irradiation on wear resistance, microhardness and acid solubility 79−96634
diamond, hard conducting C ion implanted layer, resistivity 77−15974
diamond, natural, micromechanical characteristics 79−20190
diamond, natural microhardness 78−35504
diamond, optically active centre effect on strength props. 80−40462
diamond, synthetic, carbonado type, struct. and microhardness 78−84994
diamond, yield stress from Hugoniot elastic limit and elastic consts., Knoop hardness 79−83261
diamond powder, consolidation by thermal decomposition of methane and benzene 80−66448
diamond powder, sintering with Co binder 78−27450
diamond-Co, sintered together, remanent magnetism 79−99731
diamond-like C film, plasma stream condensation with RF pot., props. 79−15612
die filling and densification in hot extrusion forging of porous preforms 78−23645
die steels for cold plastic working, powder metallurgy, characts. 78−68649
dislocation interaction, force between dislocation, and misfitting ordered particle, calc. 78−83815
elastic-plastic, hardness and fracture 78−34090
elastomer compound O-rings for service in hot water, evaluation 79−29257
electroboronizing, Al effects on hardness and wear resistance *(Korean)* 77−73356
electron beam curing, beam voltage effects on mech. props. and chem. struct. 77−70201
ferrite, hot pressed, powders, influence of CoO and CuO alloying on physicomechanical characts. *(Russian)* 77−66600
fibre optic light guide, single fibre, microhardness 77−62051
fibre-reinforced hard alloy, effect of microstruct. on impact strength 77−56099
fibrous composite, residual stress form. during hardening 78−1575
flat glass in vacuum, exam. of temp. dependence of microhardness and microstrength 78−88532
frictional electromagnetic clutch material, sintered, friction, hardness, wear props. 78−11339
glass, devitrified opaque technical, microstrength and hardness 80−89312
glass, indentation process analysis using finite element method 77−12689
glass, inorganic, calc. of microhardness and glass transition temp. 79−5059
glass, Knoop hardness number is grinding *(Polish)* 80−97580
glass, mechanical properties, review 78−3162
glass, strength degradation from impact with spheres 78−27663
glass, tempered, stress meas. in surface, indentation technique 77−44341
glass surface, difluorodichloromethane thermochem. treatment, mech. props. 80−40565
glass-ceramics, transparent, microstruct. and props. 78−59960
glasses, crystallised, internal stress depend. of hardness 80−16439
graphite, irradiated ultimate tensile bending and compressive strength charact. 78−15479
graphite, microhardness changes, effect of annealing and neutron irradiation 77−8861
graphite, pyrolytic, structural factor effect on strength 79−66135
graphite particle-Al alloy composite, prod. by pellet method, and mech. props. 78−27454
graphite-epoxy hybrid laminates, low level Charpy impact response 78−11333
graphite/epoxy laminates, stress wave damage 80−93611
hardfacing alloys in impact abrasive loading, wear resistance, temp. effects 79−87737
hardness, elastic moduli, density, cryst. temp., mech. props., for flywheel appl. *(Dutch)* 78−52878
hardness, elec. cond., photo emission, and mag. props. *(Norwegian)* 79−32909
Hayes alloy no.716, Fe-Cr-Ni-Co-W-Mo-Si-C-B (26, 22, 12, 3.5, 3, 1.2, 1.1, 0.4 wt.%), hardfacing alloy 80−100802
hexaboride single crystals, microhardness meas. 80−21087

hardness continued
high-alloy bearing, LTMT effects on ht. resist. and contact fatigue resist. 77−44354
high-alloy die steel, heat resistance and crushing strength, low-temp. thermomech. treatment effects 77−52372
high-C steel, strength characts. with controlled hardenability after bulk-surface hardening 77−56156
history, factors affecting, relation to other mech. props. 79−92916
ice single crystal, rel. to friction of steel ball *(Japanese)* 78−88537
III-V semicond. plates, scribing marks rel. to sclerometric microhardness 79−15891
III-V semiconductor, surface microhardness depend. on surface treatment method 78−15560
impact welding process, fundamental parameters 80−97679
Incoloy 800, creep rupture ductility, 500 to 600°C, hardness and metallurgic exam. 79−43435
Incoloy 800, from KFA experimental duct at 700°C and 480 d in DRAGON reactor, mech. props. before and after contamination 79−47777
Incoloy 800, mechanical props., heat treatment and appl., conf., Petten, Netherlands (March 1978) 79−43296
Inconel, type 706, precipitation and creep rupture behaviour, optical and TEM study 79−74158
Inconel 617, microstruct., mech. props., thermal ageing effect 77−36557
Inconel 625, plasma nitriding, hardness meas., Rutherford backscatt. surface anal. 80−45442
indentation analysis, relation of hardness, toughness and brittleness 79−100249
indentation hardness, the effect of mechanical stresses *(German)* 78−95794
indentation hardness and hot pressing, calc. methods 80−58981
indentation hardness and microhardness test methods for plastic deform. *(Hungarian)* 80−97664
indentation hardness number conversion table analysis 79−11736
interstitial compounds, electronic structure and useful phys. props. 77−89683
intertransition metal compounds, hardness and oxidation resist. 77−63773
ion irradiated, radiation-induced damage, microhardness and lattice consts. meas. 78−2170
ion-implanted alloys, surface props. effects and appls. 80−79824
ion-nitrided steel surface structure and hardness, heat treatment effects *(Japanese)* 79−87718
Knoop indentation, for measuring microhardness near worn metal surfaces 79−60613
laminate, residual stress form. during hardening 78−1575
laser CVD, film physical props. and applications 80−93493
Ll_2 ordered alloys, positive temp. depend. of strength, phase destabilization 80−81203
martensitic steel, abrasive wear resistance, effect of tempering strain martensite 77−56116
melt-spread coating, microhardness of transition layers formed on Fe-group metals by Al alloy melt 78−60879
metal, abrasive wear resistance rel. to physicomechanical props. 79−91804
metal, fatigue testing at US frequency, hardness change 77−44440
metal, hard, brittle, correlation between wear, crack resistance and stress intensity factor *(German)* 77−36666
metal coatings, obtained by vacuum evaporation and sputtering, mech. props. rel. to prep. conditions 77−59239
metal mechanical property effects on frictional behaviour 80−55548
metal-metalloid amorphous systems, thermal instability, crystn. characts. 77−4044
metallic glass, hardness, elastic moduli, density, cryst. temp., mech. props., for flywheel appl. *(Dutch)* 78−52878
metallic glasses, strength and stiffness 77−8899
metallic glasses manufacture, struct. and stability *(Norwegian)* 79−14687
metallic oxide powders and mixtures, hydrostatic pressing, density and hardness variation 79−70029
metals, surface sliding damage, no lubrication, materials depend. *(Japanese)* 78−56780
$Mg_{70}Zn_{30}$, amorphous alloy 77−27835
monocrystal surface layer damage depend. on abrasive working parameters *(Russian)* 80−76368
mutual alloying behaviour of the elements straddling the line Li-Mg-Cu-Au in the long periodic table 78−84769
Nb-O, effect of O_2 on penetration of Li at 400°C 79−11719
nephrite, mech. props. 77−44295
Ni-Cr-Mo-Ti-Al, quenching and ageing effects on props. of type 36NkhTYuM8 79−52275
Nimonic alloy, effect of annealing on hardness, carbide phase strengthening *(Russian)* 79−34137
nitrided layer, fracture toughness determ. from hardness impressions *(German, English)* 80−97575
non-magnetic material wear in presence of magnetic field 80−60982
olivine, hardness var. with temp., rel. to polycryst. yield stress 80−26500
optical, struct. and mechanical properties 79−76772
optical glass strength limit rel. to Knoop microhardness 79−72641
Permalloy, solid boriding for mag. head appl., wear resist. and microhardness 80−21172
Permalloys, wear by magnetic tape, AES *(Japanese)* 78−39916
piping, high frequency fatigue testing under symmetrical and asymmetrical loading 77−86246
plastic elasticity, hardness, creep, and relaxation meas. with Vickers indenter by electroacoustic method *(German)* 78−48584
plastic zone, direct meas. in side grooved fracture toughness specimens 78−68864
plastics and reinforced plastics, tabulated data as design guide 77−21087
platilon UO1, use in artificial blood pumps, fatigue resist. and mech. props. 79−84026
plexiglass, red, gamma dose meas. by optical absorpt., elec. conductivity, and mechanical hardness 78−55045
PMMA, estimation of activation parameters in sclerometric tests 80−66625
polyethylene, chain-extended, oriented, microindentation hardness 78−76728
polyethylene, filled, mech. props., cyclic heating effect 80−55526
polyethylene, high density, hydrostatic extrusion conditions effect 77−63722
polyethylene-glass fibre composites, gamma-irradiated filler 80−66840

hardness continued
polyethyleneterephthalate film, influence of crystallisation on adhesive and cohesive props. 79−56100
polymers, abrasive wear resistance rel. to physicomechanical props. 79−91804
polymers, hydrostatic extrusion effects on subsequent mechanical behaviour 77−90392
polymers, wear in thermally stressed state 80−3202
polypropylene, fracture exam. using microscopic obs. *(German, English)* 79−20186
polypropylene, thermal stabilizer content effect on props., processing and ageing *(Polish)* 79−70099
polystyrene, atactic, indentation recovery 80−84988
polythene, ultraoriented, microhardness, extrusion conditions effect 80−50704
porous material, wedge indentation hardness, slip line field theory 77−86128
Portland cement-fly ash, physico-mech. props., SEM and X-ray diffr. anal. 79−74239
powder, temperature effect on flow and tensile strength 79−61668
powder, work index estimation during grinding *(Japanese)* 78−19680
PVC, crosslinked, mech. and thermal props. with plasticisers *(Japanese)* 79−15741
PVC, tensile and indentation behaviour, durability tests, glass transition 79−5017
pyrographite, Si-containing, high-temp. treatment effects 77−40429
quartz dental composites, acrylic acid grafted on particles by gamma-radiation 80−66840
quasi binary eutectic systems, with inclusive phases, hardness, transform., decomposition *(Russian)* 80−97572
rare earth compounds, binary, regression eqns., for calc. props. from electron struct. 80−39498
rare earth gallium borates, high temperature crystallisation, composition, struct., props. 80−40253
rare earth glasses, R_2O_2S-Ga_2S_3, (R=La to Nd), exam. of preparation and props. *(French)* 78−80504
rare earth metals, elastic props., connection with electron struct. *(Russian)* 80−19895
rare earth oxides, anisotropy of single cryst. *(French)* 77−52489
rare earth RNb_3O_9, synthesis and physicochem. props. 77−90304
rare earth titanates, $R_2Ti_2O_7$, synthesis and phys. props. 79−43128
rare earths, elastic and mechanical properties, review 79−70132
(rare-earth) $Fe_3(BO_3)_4$, cryst. growth from soln.-melt, props. 80−108337
Recalloy, Fe-Nb, semihard magnetic alloy, magnetic props., hardness, microstruct. 78−56660
refractory coatings, deposited by electron evaporation, struct. and props. 79−23871
refractory compounds, hardness, methods of increasing by prod. method 80−25643
refractory materials, group IVa and Va, slip, microhardness comments 78−84967
refractory wear-resistant coatings, composite struct. develop., props. 77−63618
reinforced magnetically hard material, fibre-reinforced, porosity and impact strength 77−55916
residual stresses in indentation, exptl. verification 77−21249
rocks hardness and abrasiveness determ., suggested methods 78−96313
rolls in hot strip mills, contact fatigue failure 80−60950
sand, resin-coated, curing effects on physicomech. props. *(Korean)* 78−60855
sapphire :Ti^{4+}, deformation history effects on precipitation hardening 79−83209
satellite, hardness and erosion resistance to aqueous SiO_2 slurry 79−43441
scale dependence *(Russian)* 77−52556
semiconductor, ternary chalcopyrite, microhardness, empirical bond approach 77−69031
semiconductor, tetrahedrally bonded, microhardness, empirical bond approach 77−69030
sharp contact cracking, residual stress effects 79−100245
silicate glasses, indentation form. and fracture 79−66147
Silumin, AlSi10Mn, struct. and mech. props., Na modification effects 77−63786
single crystals, dislocation mobility under conc. loads at indentations 79−95015
snow, hardness and particle shape effects on drifting phenomena *(Japanese)* 78−88856
sodium tartrate tetrahydrate, gel-grown single crysts., charact. 77−90261
soft metal, effect of loading time on contact area *(Japanese)* 78−6230
spinel ferrites, electrical resistivity and hardness 77−43596
stainless steel rod adaptor, failure anal. in Fast Burst Reactor 77−54307
steel, 18% Ni maraging, hardness, effect of soln. treatment and inclusions 78−23805
steel, 18Kh2N4MA, Co effect on struct., and mech. props. 78−44147
steel, 30Kh3SNMBF, α-phase nucleation and growth, influence of supercooled austenite state *(Russian)* 77−48435
steel, 30N9K4, effects of Mo, V, and N on grain growth, tempering, hardenability, strength and toughness 78−44202
steel, 37Kh12N8G8MFT, precipitation hardening, hardness meas. and electron microscope exam. *(Russian)* 79−38843
steel, 4340, quenched, tempered, and austempered, effect of plastic strain followed by ageing on elastic limit 78−31446
steel, adhesive wear, heat treated load effect 78−11344
steel, AISI 4340, positron lifetime and X-ray particle size meas. during high cycle fatigue 79−5053
steel, Al-Cr-Mo, nitride hardened rollers, surface fatigue resistance under pure rolling and sliding-rolling contacts 79−79184
steel, alloy, fretting corrosion, exam. of secondary structures 79−100292
steel, alloy, high C, amorphous, produced by rapid quenching from melt, hardness and strength 78−59764
steel, alloy, high-speed, struct. changes investigation by hot hardness and quench dilatometry *(French)* 80−76249
steel, alloy, maraging, 18% Ni, effect of solution and ageing treatments, on microstruct., tensile props., fracture toughness 78−80648
steel, alloy, type 11Kh18M, eutectic carbide composition change due to heating 80−16353
steel, alloy, U20Kh6T2D, structural transformations during heat treatment, and wear resistance 78−88484
steel, alloy, W-Mo-Cr-V, blanks welded to steel 45, optimal high temp. tempering 80−16351
steel, alloy cast, optimal alloying, carburising effect 80−50771
hardness continued
steel, alloy high-C, amorphous, mech. props. and thermal stability 80−76361
steel, austenite, abnormal decomposition kinetics and mechanism *(Russian)* 80−55344
steel, austenitic, aged, stress induced martensitic transform., mech. props. *(Russian)* 79−87632
steel, austenitic, high Mn, abrasive wear resistance *(Korean)* 77−25162
steel, austenitic, KO 34 samples, electron beam welded, Charpy test expts. *(Hungarian)* 80−104252
steel, austenitic, Mn strain hardening at room and low temps. *(German)* 79−38845
steel, austenitic heat resistant, zig-zag grain boundaries, strength 77−73308
steel, austenitic heat resisting, creep rupture props., effect of grain- and grain boundary-strengths 80−97573
steel, austenitic solid solution, chem. evaluation of B and its correlations with hardenability and hardness *(German)* 79−39230
steel, austenitic stainless, biphase, ferritic, ageing and thermomech. treatment effects on struct. and props. 80−35226
steel, austenitic stainless, Cr-Ni, Mn and Mo effect on mech. props. rel. to treatment 79−96039
steel, austenitic stainless, Cr-Ni-Mo-Mn, Mo, Mn and ageing effects 78−35413
steel, austenitic stainless, electron beam welding effect, on mech. props. of steels 310L, 316, 21-6-9 78−48498
steel, austenitic stainless, grain size effect on softening *(Russian)* 78−23731
steel, austenitic stainless, type 321S12, fatigue cycling in R=−1 loadings 80−35317
steel, austenitic stainless, unlubricated, friction, wear and microstruct. of types 304, 316 and Nitronic 60 80−108589
steel, ball bearing with modified chem. comp., improved rolling contact fatigue 78−64732
steel, brittle transition temp. comparison of arc, gas-pressure and friction-pressure welded alloy by hardness measurements *(Japanese)* 79−11691
steel, C1020, dual phase, mech. behaviours and structs. *(Korean)* 80−25779
steel, C, developments, properties and fabrication processes *(Dutch)* 77−70021
steel, C, fatigue failure in type 45, strength charact. 79−52373
steel, C, fretting fatigue damage, SEM exam. 78−88541
steel, C, hard patch of rubbed surface, tempering effect *(Japanese)* 78−7054
steel, C, induction hardened, surface durability, optimum case depth 80−30137
steel, C, ion nitriding, wear resistance *(Japanese)* 77−63828
steel, C, pore formation in surface layers, during As diffusion redistrib. 80−49421
steel, C, prestrain effect on non ductile transition temp. and bending speed relationship *(Japanese)* 78−84919
steel, C, quenched and tempered, ductility, effect of hydrostatic press. 78−44190
steel, C, rubbed surface, continuous hard layer *(Japanese)* 77−52501
steel, C, type S15CK, tufftrided, fatigue strength at elevated temp., under reversed axial strength *(Japanese)* 78−84980
steel, C hot dipped aluminised, phase composition anal. of alloy layer by X-ray, electron probe and hardness meas. 79−34192
steel, C type 45 hardened layer structure and props. with intensive spray cooling and hardening 79−38859
steel, C-Mn, corrosion cracking, role of microstresses and crystal lattice stresses *(Russian)* 77−25190
steel, C-Mn-(Cr), structural changes during stress cycling after heat treatment and cold rolling *(Russian)* 78−19787
steel, carburised, fracture resistance 79−24612
steel, carburised, transform. of residual austenite, mag. field effects *(Russian)* 80−29952
steel, carburized, fractography of fatigue fractures 77−86137
steel, carburized, point contact sliding 79−87738
steel, carburized fatigue, non-martensitic struct. effect, rel. to mean stress and residual stress *(Japanese)* 78−7024
steel, cementite precipitation from binary alloys, hardness and Mossbauer effects 77−70054
steel, cold drawn wire, anisotropic fracture *(Russian)* 77−1867
steel, cold worked, original struct. effect on softening during heating 80−60882
steel, cold-formed, low pearlite, Nb alloyed, Nb effects, precipitation, recrystallisation *(German)* 77−8832
steel, commercial C, stress corrosion cracking susceptibility in liquid NH_3 *(Japanese)* 78−11411
steel, Cr-Al (12, 6 wt.%), ferritic stainless, high temp. treated, strengthening mechanisms 80−3106
steel, Cr-C (13, 0.15 wt.%), bainitic transform. *(German)* 78−11218
steel, Cr-C (18, 0.9 wt.%), cavitation, abrasion resistance, effect of unstable austenitic struct. *(Russian)* 77−16695
steel, Cr-Mo (2.25, 1.0 wt.%), temper embrittlement, effect of P, Sn, comp. and carbide precip. 80−85036
steel, Cr-Mo (2.25, 1.0 wt.%), temper embrittlement, effect of Mn, Si, comp. and carbide precip. 80−85037
steel, Cr-Mo-V, excessive temp. effect on creep behaviour, structure and hardness *(German)* 80−30054
steel, Cr-Mo-V (1.35, 1.0, 0.25 wt.%) exam. of mech props, comparison with mathematical model predictions *(Czech)* 79−91740
steel, Cr-Ni, effect of tempering under load on mech. props. 80−16354
steel, Cr-Ni (1.47, 1.48 wt.%), lath martensite microstruct. and props., cold rolling effect 80−55422
steel, Cr-Ni-(Mn), mech. props. at low temp. 77−70118
steel, Cr-Ni-Mo, combined B and rare earth metal additions effect on microstruct. impact strength and hardness 79−38963
steel, Cr-Ni-Mo, handbook data for type 34KhN1M 79−78960
steel, Cr-Ni-Mo-V-Nb (12,8,1,1.5,0.4 wt.%) Ce addition effects on strength and hardness *(Russian)* 78−15454
steel, Cr-Ni-Nb, LKh16N4B, high temp. frictional charact. 80−21118
steel, CVD coating temp. effect on hardness and dimens. stability 77−40470
steel, deformation under mutual indentation in contact with Li melt *(Russian)* 77−59853
steel, duplex ferrite-martensite, microstructure resistance optimisation 80−40482
steel, effect of laser irrad. in inert gas atm. *(Russian)* 79−38935

hardness continued
steel, electric field effect on strength, hardness 80−50714
steel, eutectoid, anisothermal strain with phase transform., effect on tensile strength *(Russian)* 80−40431
steel, eutectoid, fatigue crack tip props. in rotary bending and cyclic torsion 77−32668
steel, eutectoid, mech. behaviour, thermomech. treatment effects 80−84970
steel, fatigue limit estimation when subject to bending loads 77−21281
steel, fatigue strength, statistical prop. *(Japanese)* 79−20169
steel, Fe-Cr-C, austenitizing temp. effect on microstruct. and mech. props. 80−16341
steel, ferritic martensitic, effect of ductility of second phase on ductile fracture 78−19847
steel, grinding, effect of hardness, texture, and bond of grinding wheel, temp. effect *(German)* 79−43459
steel, Hadfield, containing Ni, carbide precipitation, heat and cold work effects *(Korean)* 77−77484
steel, hardness, rel. to tensile and impact strength 77−90428
steel, hardness, tensile and impact props. correlation, at low temps. *(Japanese)* 77−52413
steel, heat-resistant, martensitic, Kh12NMFB weldability 80−20987
steel, high alloy Cr-Mo-W, splat quenched, formation of metastable austenite 80−84974
steel, high C, high alloy, $M_{23}C_6$ type carbides, effect of alloying elements on defect struct. and hardness 80−16481
steel, high C chrome type 9Kh2, cold rolling rolls, hardness determ. 79−87713
steel, high Cr, V additions effect on brittleness near 475°C *(Russian)* 78−19890
steel, high speed, AISI M2 and M7, fracture toughness 77−86141
steel, high speed, hardened, for drills, mech. and cutting props. 79−43407
steel, high speed, props. after electroslag remelting 80−104139
steel, high speed, sintered, and wrought, type T6 strength and toughness 80−30102
steel, high speed, type R6M5K5, secondary and red hardness of marquenching 80−16350
steel, high speed tool rapidly quenched, exam. of solidification struct. 78−39758
steel, high speed type M-50 and 18-4-1, fracture and fatigue 80−16457
steel, high strength, hypereutectoid, low alloy, microcrack frequency and fracture toughness rel. to martensitic struct. *(Czech)* 77−70163
steel, high-speed, low temp. mag. cycling effects on ferromag. struct. 80−100928
steel, high-speed, N effects on struct. and props. 77−59799
steel, high-speed, sintered, refractory carbide additions effect on hardness and cutting performance 77−66608
steel, high-speed tool, properties, powder metallurgy prep. method *(Czech)* 80−60800
steel, high-strength tool steel D7KhFN, remelting effect on mech. props. 80−76284
steel, hot rolled, M1 tool type, microparticle distributions and mech. response 77−44279
steel, HSLA, V effect on mech. props. *(Korean)* 80−29987
steel, hypoeutectoid Widmanstatten struct. form., contrib. to the laws *(Slovenian)* 78−84817
steel, inclusion chemistry control for machinability enhancement 80−85067
steel, ion-softnitriding of type S15C with N_2-H_2-CH_4 mixture, mech. props. of surface *(Japanese)* 79−61780
steel, ionic nitriding, layer hardness obs. 80−45414
steel, KhVG, annealed, mag. inspection of hardness and struct. 80−7750
steel, low alloy, bainite transform. behaviour, struct., toughness 78−27513
steel, low alloy, type 3sp, effect of temp. at end of rolling on mech. props., and coercive force 78−72799
steel, low alloy, type 4340, quenched and tempered, effect of plastic strain followed by ageing, on torsion fatigue resistance 78−92360
steel, low C, austenite transform., TTT diagrams 77−70031
steel, low C, cyclic loading, change in mech. props. rel. to heat treatment 80−104282
steel, low C, hardness correl. with macrostress intensity under plastic strain 79−87708
steel, low C, Mb-Nb, reheated, quenched, tempered, microstruct. 77−36550
steel, low C, mech. props. determ., NDT methods 79−29176
steel, low C, microhardness of nonmetallic inclusions and metallic matrix 79−96127
steel, low C, normalised, plastic deform., using microhardness and grain strain meas. 77−4810
steel, low C, tufftrided, fatigue strength ahd microstructure change by reversed stressing *(Japanese)* 78−15511
steel, low pearlite, Nb microalloyed, ageing at 600°C, mech. props. *(German)* 77−36542
steel, low-C, kinetics of void development in fracturing A533B tensile bars 80−76357
steel, maraging, 0Kh6N8M7S, effect of Cr, Ni and Mo on hardness 80−21093
steel, maraging, ageing kinetics and struct. of N12K7M5TYu, effect of high temp. deform. of austenite *(Russian)* 80−84960
steel, maraging, Co-Ni-Mo (20,15,5 wt.%), environmentally assisted fracture 77−52547
steel, maraging, effect of thermal cycling (γ to and from α) on props. 80−20986
steel, maraging 18%Ni, calorimetric anal. of ageing *(Japanese)* 80−89264
steel, martensitic, ageing of 05kh3N2MD2, hardness depend. on tempering temp. *(Russian)* 79−24544
steel, martensitic, Cr-Ni-Co-Mo-Ti, Kh12N8K5M3TYu, ageing of C free martensite *(Russian)* 79−1884
steel, martensitic, tempered, C and low alloy, hardness, effect of alloying additions 78−27629
steel, martensitic low C, development and props. *(Russian)* 80−20933
steel, medium C, isothermally quenched, high-temp. deform. effects on struct. and props. *(Russian)* 80−25760
steel, medium C, microalloying with V and Ti, effect on hardness and structure 80−11750
steel, medium C, type 35 laser treatment effect on struct. and mech. props. 79−39041
hardness continued
steel, medium C quenched, tempered, relation between wear and work surface layers *(Japanese)* 77−52499
steel, microhardness changes under high-press. and laser irrad. *(Russian)* 77−59903
steel, middle and low C, clad plate, inhomogeneity and residual stresses, heat treatment effects *(Japanese)* 78−6955
steel, mild, fatigue crack initiation 77−86163
steel, mild, fatigue life, effect of H_2S and SO_2 gas 79−15871
steel, mild, high temp. fatigue, effect of temp. variation 78−64685
steel, mild, point contact sliding 79−87738
steel, mild, semi-killed, tempering, effect of microstruct. and hardness 77−21184
steel, Mn-Cr, blank hardened, shot peening effect on bending fatigue strength *(German)* 78−35402
steel, Mn-Cr, normalised, shot peening effect on bending fatigue strength *(German)* 78−35401
steel, Mn-Cr-B (1.46, 1.03, 0.003 wt.%) 80−55422
steel, Mn-Cr-V, crack propag. resist. at hardness indentation, and fracture toughness *(German)* 79−29220
steel, Mn-Cr-V, structural changes during solution annealing *(Czech)* 78−84864
steel, NC6, cementite network separation, kinetics *(Polish)* 80−25698
steel, neutron irradiated press. vessel material, small angle neutron scatt. meas. 79−13428
steel, Ni-Co-Cr, high-strength medium C, Cr effect on props. 80−76339
steel, Ni-Co-Mo (17.55, 8.02, 4.92 wt.%) maraging, lath martensite microstruct. and props., cold rolling effect 80−55422
steel, Ni-Cr temper embrittlement by P 77−40448
steel, Ni-Cu-Mo-C, powdered, influence of cooling rate after sintering on preps. 79−95969
steel, Ni-Mn (16, 2 wt.%), 40N16G2, single crystal, stabilisation and destabilisation mechanisms *(Russian)* 78−23732
steel, Ni-P plated, electroless, fatigue strength and plated layer microstruct. *(Japanese)* 80−93645
steel, pearlitic, wear behaviour rel. to basic material props. 80−108592
steel, plastic deformation zone, caused by crack, extent determ. with microhardness, surface roughness, measurements *(French)* 80−7682
steel, powder forged for carburizing appl., core props., mech. props. 78−15339
steel, quenched, verification of change of props. in mag. field 78−52985
steel, quenched surface layer hardness rel. to adsorption contact fatigue *(Ukrainian)* 80−40478
steel, quenched-tempered, relationship between half value breadth and hardness *(Japanese)* 77−52366
steel, rapid, surface modification by ZrB_2 treatment 79−66203
steel, rare earth additions, effect on physicomechanical props. 77−12639
steel, stainless, AISI 304, dislocation substruct. around fatigue cracks, SEM obs. 78−15516
steel, stainless, cold plastic deform. effect on struct. and props. 80−29113
steel, stainless, electrohydraulic effect and struct. changes *(Russian)* 78−23783
steel, stainless, ferritic, Ti stabilised, exam. of grain boundary structure *(Russian)* 79−15662
steel, stainless, laser generated stress waves, effect on hardness 79−69192
steel, stainless, maraging, high strength, notch toughness, effect of ageing *(Japanese)* 78−11311
steel, stainless, stress corrosion cracking and microhardness, effect of bombardment by He^+, Ni^+ and Cr^+ 80−85087
steel, stainless, type 304, physicomechanical and wear props., influence of ion implantation and overlay coatings 80−40603
steel, stainless, type 316, modelling effects of fast neutron irradiation in mech. behaviour 80−84234
steel, stainless, type AISI 321, surface damage and mech. changes after H atom irrad. 80−39182
steel, stainless austenitic, low alloy 316, high temp. plasticity, B addition effects *(Russian)* 77−28852
steel, stainless wear by magnetic tape, Auger spectroscopy exam. *(Japanese)* 78−39916
steel, structural, type St3S, hardness, random functions 80−76329
steel, surface Si reinforced type U8, metastable phase, composition, struct. *(Russian)* 80−92599
steel, surface structural changes on exposure to plasma, etch resistance *(Russian)* 79−83234
steel, tempered StE70, water quenched, residual stress field in centrally welded plates *(German)* 78−72794
steel, Ti-V, Ti and V effects on precipitation, hardness and annealing *(German)* 77−55968
steel, tool, blanking punch, chipping behaviour *(Japanese)* 79−100250
steel, tool, M2, laser surface melted, heat treatment effects on struct. 79−70086
steel, tool, quenching procedure effect on distortion, tool life 80−50657
steel, tool, thermal treatment effect on abrasive wear resistance 78−92369
steel, tool, W-Mo, heat treatment effect on props. 80−50656
steel, tufftrided, fatigue strength under reversed torsion *(Japanese)* 79−61707
steel, tufftrided, S15CK smooth specimens, fatigue strength, strengthening mechanisms *(Japanese)* 78−27609
steel, type 1Kh17N2, white zone formation and props. during friction in vac. *(Russian)* 80−40542
steel, type 4340, deformation study, positron lifetime and hardness correlation 79−87649
steel, type 55SM5FA, formation of hardened layer during burnishing 78−85046
steel, types 60G, ShKh15, structural changes near holes and inclusions due to pulsed currents *(Russian)* 80−108459
steel, ultrahigh C, heat treated, mechanical properties and microstructure 79−57012
steel, unkilled deep drawing sheets, influence of N content on recrystn. *(German)* 80−40376
steel, US critical angle reflectivity, near-surface metallic prop. gradient effect 80−70516
steel, W, high C, amorphous, rapidly quenched from melt, mech. and thermal props. 79−38874
steel, W alloy, microstruct. and hardness, splat quenching effect 80−76293
steel, wear resistance during abrasive wear, comp. and struct. effects 80−35337

hardness continued
steel, white layers forming at high rates of friction, struct. props. *(Russian)* 79−15800
steel, X-ray and microhardness meas. at high strain rates *(German)* 78−3184
steel 1Kh18N9T, physico-mech. props. after boring in metallic melts *(Russian)* 78−56736
steel 20, diffusion coating for protection against H_2 effect on mech. props. 78−31589
steel 45 microstruct. and hardness after electron bombardment 79−38956
steel austenitic Cr-Ni-Be, cellular precipitation *(Japanese)* 78−11229
steel bearing, surface-ground, residual stress fatigue property comparison 80−60975
steel bearing parts, magnetic inspection of heat treatment quality 78−73007
steel bearing rings, optimisation of thermomechanical working parameters *(Russian)* 80−93579
steel gas nitrosulphurising, S25C, wear property 80−50729
steel hardness and ductility variations and micrographs rel. to heat treatment and phase diagram obs. 79−87609
steel R6M5, tempering after quenching with rapid heating 77−56002
steel rollers, case-hardened, nitrided, surface failure, durability 78−84959
steel St3, kinetics of form. and struct. of thermodiffusional protective coatings 77−56158
steel SW7M, low-cycle fatigue at high hardness levels *(Polish)* 80−89323
steels, C, quenched and tempered, struct.-prop. relationships 80−7599
steels, heat treatment of 30KhN2MFA and 40Kh, nondestructive mag. quality control method 80−108662
steels, high-purity and commercially based, containing 10 wt.%W or 5 wt.%Mo, tempering behaviour 80−7600
steels, nitrided age-hardened, for blanking punches, chipping resist. props. *(Japanese)* 80−89340
steels, solute segregation and intergranular fracture 80−60957
steels, tool, cold hydrostatic extrusion rel. to struct., props. 79−20068
strengthening by modified ausforming 78−76665
strontium calcium tartrate tetrahydrate, gel grown mixed single crystals, defect characterisation 80−2027
styrene-butadiene-styrene block copolymer, with reinforcing resins, effect of styrene domain structure 79−83317
sulphides (Fe, Co, Ni, Cu, Zn), oxidation, hardness and electromechanical polishing response 80−71776
surface, mech. and corrosion props. improvement using US energy *(Rumanian)* 79−15821
surface energy evaluation, by a microindentation method 80−16473
transition metal borides, refractory, single cryst. prep. methods and characterisation, book contrib. 78−48296
transition metal carbides, complex phases with NaCl struct., microhardness rel. to electronic structure 77−90438
transition metal carbonitrides, physicochem. props., comp. depend. 80−55370
transition metal refractory materials, slip and microhardness 78−3211
transition metal silicides, group IV, thermal expansion, microhardness, Debye temp. meas. 77−35717
transition metal-metalloid glasses, struct., elec., supercond., and mech. props. 80−6365
TZM-Mo alloy, mech. props., effect of exposure to high temp. He containing O_2, room temp. study 80−93639
vacuum deposited films, mech. props. 78−75968
vitreous metaphosphates 80−25864
α-W_2C, polycryst., plastic behaviour at ambient temp. *(French)* 79−1435
wear mechanism review 78−72891
weld, heat affected zone extraction and testing of flat, microtensile specimens *(German)* 77−9017
white Fe castings, morphology of eutectic M_3C and M_7C_3 80−108427
wire for high-speed matrix printers *(Japanese)* 80−55540
work hardening, indentation hardness to yield stress ratio glide processes 77−40426
Zircaloy-2, hot-pressed, influence of diffused C on structure and oxidation 80−61016
α-Zr, ω phase proportion during high press. deform. *(Russian)* 79−74147
α-Zr, crystalline anisotropy determ. by hardness meas. *(French)* 79−20157
AG, hardness, temp. depend. 77−40440
Ag alloy, ceramet contact, Brinell and Vickers hardness number comparison 79−38978
Ag composite, SiC whisker-reinforced, prep. aboard Skylab. 78−84741
Ag, dispersion strengthened with MgO particles, electrical contacts appl. *(Slovak)* 78−31544
Ag, ultra-microhardness testing for vacuum deposited film and bulk specimen 78−79910
Ag-CdO cermets, coprecipitated carbonates and hydroxides, physicomech. props. 80−25706
Ag-Cu, metastable solubility lines on Ag side 78−39737
Ag-Ga solid soln., internally oxidised, hardness *(Japanese)* 78−60744
Ag-Ni, two ductile phase alloy, exam. of softening behaviour after cold rolling 78−72847
Ag-Pd alloy, for use as wire-spring relay contact material 79−52278
Ag-Sb-S, prep. and props. of glasses in the system 77−20053
$AgAsS_2$-$AgSbS_2$ system, thermal, microstructural X-ray phase anal. 77−32565
$AgPS_2$, single crystal, prep. and structure 77−35524
$Ag_4P_2S_7$, single crystal, prep. and structure 77−35524
Ag_3Sn-Hg, metallic powder-liquid system, correlation between hardness and evolution and sintering states 80−25614
Al alloy, 51S, modified by misch metal, for space appl. 80−55466
Al alloy, fretting corrosion, exam. of secondary structures 79−100292
Al alloy 7001, ageing effect on hardness and tensile props. rel. to delay time till quenching 78−92286
Al alloy anodic oxide film hardness, effect of pH and metallic additives *(Japanese)* 77−56146
Al alloy D16AT, fatigue life, struct. and microhardness, working conditions effect 80−55525
Al alloys, electric field effect on strength, hardness 80−50714
Al alloys, laser generated stress waves, effect on microstruct., hardness and strength 79−69192
hardness continued
Al, alloys, thermomechanical working effect on mech. props. *(Russian)* 77−21181
Al alloys 7075-T6 and 2024-T3, crack propag./wear rate relationship 78−3232
Al, cyclic loading, change in mech. props. rel. to heat treatment 80−104282
Al, fatigue induced dislocation struct. and hardening, exam. *(Japanese)* 78−64624
Al, laser strengthening, struct., hardness and dislocation density *(Russian)* 80−76399
Al, microhardness under high hydrostatic press., meas. by microindentation 80−3182
Al, physicomechanical and wear props., influence of ion implantation and overlay coatings 80−40603
Al, stress-strain curve from continuous indentation test 77−90396
Al, tribological investigation using two-cylinder tribometer *(German)* 77−25164
Al, vacuum condensate, struct. and mech. props. depend. on deposition conditons 80−15417
Al-Ag (up to 40 at.%), exam. of anelastic phenomena and structural state 78−76693
Al-Al_2Cu, aligned eutectic, precipitation, TEM and microhardness meas. 78−27529
Al-Al_4C_3, dispersion hardened physical props. meas. *(German)* 78−31415
Al-C, dispersion hardened, effect of processing parameters on mech. props. 80−20826
Al-Cr, rapidly solidified, crystalline and amorphous structures 77−44274
Al-Cr (3 to 11 at.%), cooling rate effect on solidification struct. and mech. props. *(Japanese)* 78−39755
Al-Cu (4 wt.%), θ'-phase precipitation, characterisation of stages 79−56984
Al-Cu (4 wt.%), with θ' precipitates, relation between elastic limit and hardness *(French)* 79−5018
Al-Cu films, deposition rate, mol. beam incidence angle influence on struct., film props. *(Russian)* 79−60646
Al-Cu-Mg, dil. alloys, ageing response *(Korean)* 77−28832
Al-Cu-Mg/mica particulate composite mech. props. 80−100919
Al-Cu-Mn (1-5.2, 0-0.6 wt.%), N alloying and comp. effect on mech. props. *(Bulgarian)* 80−71719
Al-Cu-Sn (3.4, 0.28 wt.%), Mossbauer anal. of Sn behaviour during ageing 78−31431
Al-Cu-Zn alloy, ageing, X-ray and electron diffr. meas. *(Russian)* 78−39806
Al-$CuAl_2$, directionally solidified eutectic alloy, effect of heat treatment 77−55977
Al-Cu(Zn, Ag, Mg_2Si), intermediate precipitates, stability, X-ray, elec. resist. and hardness study 80−3063
Al-Cu(0-10 wt.%) sintered compacts, mech. props. rel. to sintering 80−76210
Al-Ge alloy, effect of high press. on phase equilibrium *(Russian)* 79−1844
Al-Li (10 at.%), struct. changes on annealing, 25-500°C, Li atoms role 80−35183
Al-Li solid soln., decomposition exam. by secondary ion ion emission *(Russian)* 78−68696
Al-Mg, ageing process, effects of Ag additions and pressure *(Russian)* 80−45321
Al-Mg (5 wt.%), hardness-flow stress rel. during strain-controlled bending fatigue 79−74245
Al-Mg-Ag, age effect on age hardening *(Japanese)* 78−52831
Al-Mg-Li alloy, 01420, surface layer props. *(Russian)* 78−80674
Al-Mn alloys, study of solidification by rapid cooling *(Japanese)* 78−88459
Al-Ni (3.6 at.%) alloy, quenched from melt, distortion of matrix caused by coherent precipitates, electron diffr. meas. 77−59791
Al-Si, unidirectionally solidified eutectic alloy grow at different rates, Vickers hardness 77−36654
Al-Si (1 wt.%), hardness-flow stress rel. during strain-controlled bending fatigue 79−74245
Al-Si eutectic alloy, hardness rel. to tensile and compressive strength 79−52354
Al-Si-Mg alloys, Si content and Mg addition effect on mech. props., Na treatment *(Korean)* 79−38901
Al-steel mixture, wear resistant, produced by compaction by discrete shock waves 80−84882
Al-W(Mo)(Nb), struct. and props. of alloys obtained from granules 80−50717
Al-Zn, precipitation struct. and phys. props. effect of miscibility gap *(German)* 78−92265
Al-Zn (15,16,18 at.%) alloys, coherency spinoidal curve position determ. 77−52281
Al-Zn (18 at.%), position of coherency spinodal curve 78−23660
Al-Zn (6.8 wt.%), effects of ageing temps. on microhardness and resistivity *(Japanese)* 78−35408
Al-Zn alloys, preprecipitation, elec. resist., microhardness meas., dislocation-growth distortion interactions *(Japanese)* 77−25053
Al-Zn alloys, relation between microhardness and average radius of Guinier-Preston zones 78−95811
Al-Zn-Mg, duplex ageing effect on tensile props. 79−91721
Al-Zn-Mg, type 7075-T651 plate, thickness direction inhomogeneity of mech. props. and fracture toughness 80−100892
Al-Zn-Mg (5,2 wt.%), TEM of early stages of precipitation 77−40423
Al-Zn-Mg alloys, precipitation behaviour *(German)* 78−39780
Al-Zn-Mg granules and bands rolled from them, heat treatment 80−100862
Al-Zr (0.22 wt.%), hardness and struct. changes during prolonged ageing at 350, 400 450°C *(Japanese)* 79−52281
(Al-Mg-Si)-Al_2O_3, SAP type, ageing 79−96055
α-AlB_{12}, prep. and electrothermal props. 80−20863
AlC_xN_y, refractory deposit, prep. by thermal decomp. of Al dialkylamides and characterisation 80−11572
$AlMgB_{14}$, prep. and electrothermal props. 80−20863
AlN-Al_2O_3 composites, hot-pressed 77−52275
α-Al_2O_3, annealing, stable hardened subsurface layer form. 77−56128
Al_2O_3, crack initation threshold, SEM and acoustic emission study 79−70157
Al_2O_3 film, RF sputtered by planar magnetron, phys. props. 77−43448
Al_2O_3, fracture toughness meas. using Knoop indentation method *(German)* 80−25830

hardness continued
Al_2O_3 hard anodic coatings, effects of cellular structures 78−11448
Al_2O_3, ion condensing metal plasma stream, coating microhardness, chemical reactions 79−42426
Al_2O_3, microhardness as function of grain size 79−79084
Al_2O_3, sintered, correlation between wear, crack resistance and stress intensity factor *(German)* 77−36666
Al_2O_3:Cr_2O_3(Ti_2O_3), dopant influence on struct. and mech. props. 80−24471
Al_2O_3/Al clad powder prep. and physicomech. props. 79−29010
Al_2O_3-B_2O_3-P_2O_5 glasses, formation and props. 78−83737
Al_2O_3-Cu composite, dispersion-strengthened, hardness, tensile strength and struct. 77−70063
Al_2O_3-Nb composites, influence of gas impurities on solid-state bonding on annealing 80−11739
Al_2O_3-SiO_2 glasses, thermally toughened, residual compressive stresses evaluation 78−31523
$Al(PO_3)_3$-LiF system glasses, microhardness and US vel. 79−99274
$Al(PO_3)_3$-NaF system glasses, microhardness and US vel. 79−99274
Al_2O_3, corundum, abrasive, evaluation of brittleness, contact endurance by cyclic microhardness 79−15890
As-Sb-S-I system glasses, vitrification and volt-ampere characts. 77−31756
As-Se glassy film, photostimulated changes in microhardness 77−15723
As-Se-Bi, semicond. chalcogenide glasses, crystallisation and electrophys. props. 78−9955
As-Te-In, glass-forming, density and microhardness 80−103257
$AsSe_{1.2}$:Fe, Fe effect on physiochem. props. of glass 80−24370
As_2Se_3 bulk glass, physical parameters anisotropy, cooling effects 77−36545
As_2Se_3-$GeSe_x$-$SnSe_x$ (x=1,2), exam. of Sn valency and physical props. 79−4753
As_3Se_2 films, microhardness data for number of illumination-annealing cycles 79−24378
$AsSe_{1.1}Te_{0.2}$:Fe, Fe effect on physiochem. props. of glass 80−24370
$AsSe_{1.5-x}Te_x$ glasses, physical props. 78−68028
Au, electrodeposited and sputtered, hard, reactive softening, X-ray diffr. studies 80−100414
Au, electroplated, microstruct. and hardness, effect of thickness and deposition conditions 80−20057
Au film, sputtered, hardness and ductility 79−87025
Au, hardness, temp. depend. 77−40440
Au, ultra-microhardness testing for vacuum deposited film and bulk specime.ı 78−79910
Au-Co electrodeposit, struct. and hardness characts. 79−28245
Au-Cu alloy, internal oxidation, calorimetric meas. 79−43258
Au-Cu-Ag dental alloy, age-hardened, struct. and morphology 78−92272
Au-Ge-Te ternary system, solid soln. in vicinity of GeTe, phase diagram *(French)* 77−85994
Au-Mg alloy, internal oxidation, calorimetric meas. 79−43258
Au-Pd-Pt-Ag, composition-property diagrams, mathematical models for diagrams *(Russian)* 79−11554
Au-plating, additive-free, electronic appls. props. 80−108718
Au-TiC, multilayer struct., microhardness and elec. resist. 80−2950
Au_4V, effect of structural changes on phys. props. 78−31400
B films, prep. by H reduction of BCl_3, struct. and hardness 80−54543
B modifications, exam. of physical props. and electron structure 79−94954
B, preparation and purification, physical characterisation *(French)* 80−16189
β-B, rhombohedral, Knoop hardness and room temp. resist., rel to purity 80−21084
B, zone-refined effect of Ni doping on conductivity type, microhardness and metallographic obs. 77−31682
B-C system, region of existence of B_4C phase 78−76636
B_4C, mech. and thermal props. 80−21083
B_4C, melting and phase homogeneity range 80−20911
B_4C, metallography and Knoop microhardness *(French)* 78−76730
BN, hardness rel. to temp., phase compositions 78−60752
BN, polycryst. cubic, props. 80−21013
B_2O_3-V_2O_5-P_2O_5, glass, mech. and elec. props 80−84228
B_6O, mech. and thermal props. 80−21083
BP coatings, on Mo by CVD and their composition and microhardness 79−28942
BP epitaxial film 77−11629
$B_{13}P_2$, epitaxial, micro-Vickers hardness number 77−40444
Ba hexaferrites, mech. and mag. props. 79−70151
BaF_2:Y^{3+},Gd^{3+} production and mech. props. 79−72638
BaO-K_2O-Na_2O-ZnO-SiO_2, corrosion and microhardness, effect of detergents 80−16518
$BaR_2(MoO_4)_4$, R=rare-earth, struct., optical, mech., spectral and physicochem. props. 80−84161
$BaSO_4$, single cryst., neutron bombard. effect on struct. 78−63793
$Ba_xSr_{1-x}Nb_2O_6$, growth defects 78−38640
Be bronze BrB2, quenched deformed, substruct. and props., effect of prerecrystallisation annealing *(Russian)* 78−60677
Be, surface hardening by B ion implantation 80−16604
$BeAl_2O_4$, Czochralski grown single crystal, hardness, thermal expansion, concl., elastic const. 79−52353
Bi, recrystn., effect of Sb, Sn and Pb 78−52841
Bi, whiskers, hardness, elec. props. *(Russian)* 78−51874
Bi:Sb, solid soln. struct., growth rate effects 77−52246
Bi:Ti(Sn)(Pb)(Ag), microhardness anisotropy 80−21079
Bi-Sb (1.2-7 at.%) solid solns., microhardness of single crystals 77−28886
Bi-Sb (5-12 at.%), single cryst. cleavage plane, microhardness parameters depend. 78−35486
α-brass, defect removal, obs. by positron annihilation 78−84677
C, amorphous film, spin resonance, IR spectra, microhardness 80−71157
C, dense hard-type solids prep. from petroleum coke powder by grinding 79−20002
C, diamond-like, produced by RF glow discharge of hydrocarbon gases, props. and coating rates 80−21146
C film, diamond-like, ion deposited, hardness and mech. stability 80−2314
C film, diamond-like, plasma condensed, mech. props. 79−90924
C film, sputtered glassy, prep., mech. and struct. props. 77−66588
C, glassy, prep. from liq. phenolformaldehyde resin, TEM obs. 79−83145
C, vapour-deposited, transparent and hard insulating layer, struct. and props. 80−10830

hardness continued
CC TaC based hard metal, non-stoichiometric sintering, mech. props. 80−25616
$CaCO_3$ calcite, neutron irrad. effects 77−39617
$CaEuAl_3O_7$, mechanism of solid-phase reactions of formation and physicochem. props. 77−52622
$CaHPO_4$, powder and granules with starch mucilage binder, surface topography variation under compression 80−80998
$Ca_5(PO_4)_3OH$ bioceramic, material props. 80−93523
$CaTaRO_6$, (R=La, Nd, Gd, Sm, Er, Lu), synthesis and physicochem. props. 79−52139
Cd-Zn (Ag), annealed, work softened, exam. of crystallographic texture, hardness 78−80559
$CdAs_2$, synthesis, microstruct., hardness and elec. cond. 79−51268
$CdGeP_2$, growth from melt solution in Cd, microhardness 77−44139
$CdGe_{1-x}Sb_xAs_2$ glass, DTA, microhardness meas. *(French)* 77−72564
$CdGe_{1-x}Sb_xAs_2$ system, amorphous and cryst. phases, DTA and microhardness obs. 78−22835
$Cd_xHg_{1-x}Te$, determ. of slip planes by dislocation etching 79−82220
$Cd_xHg_{1-x}Te$, dislocation motion, effect of lattice defects on microhardness *(Russian)* 80−70220
$Cd_xHg_{1-x}Te$, surface microhardness depend. on surface treatment method 78−15560
$Cd_xHg_{1-x}Te$, thermally activated slip, microhardness temp. depend. *(Russian)* 78−34567
$Cd_xMg_{1-x}Se$ single crystals, melt grown, struct. and microhardness anisotropy 79−86836
CdS, surface layer, photomechanical and photoplastic effects 79−99264
CdSb:Au, solubility, thermal anal., microhardness, microstruct., elec. characts. 77−16557
CdTe, grown by chem. transport, morphology, struct. and microhardness *(Russian)* 78−22729
CdTe-CdS solid solution phase diagram *(Russian)* 79−100120
CdTe-Co(Mn) systems, reaction of components, DTA, microstruct. and microhardness obs. 79−38804
$CdTl_2Se_4$:Au, solubility meas. by microhardness method 80−96650
$CdTl_2Se_4$:Au(Ag)(Cu), doping effect on surface tension of melt and cryst. microhardness 80−49464
$Ce_2(SO_4)_3.9H_2O$, grown from solution, exam. of Raman spectra and physical props. 79−52104
Co based metallic glass, B and P glass former additions, elastic consts., flow behaviour correlations 78−44154
Co-$(Cr,Co)_7C_3$ eutectic, oxidation effect on toughness and strength 80−89404
Co-Al-Nb, monovariant directionally solidified eutectics, struct. and mech. props. *(Russian)* 78−92254
Co-Cu, electrodeposited alloy, struct. and physicochem. props. 78−35327
Co-Fe, morphology and certain props. of α-and η-phase martensite *(Russian)* 77−1838
Co-Fe amorphous alloys, high permeability props. *(Japanese)* 77−51927
Co-Fe-Si-B, amorphous alloys, substitution effect on mag. props. 79−69695
Co-Ge binary system, phase diagram rel. to that of Ni-Ge *(French)* 80−97463
Co-Ni-Cr-Nb, effect of Fe addition on precipitation behaviour 80−29962
Co-Ni-Mo-C, amorphous alloys, med. props. and thermal stability *(Japanese)* 80−85049
Co-Ni-Zn, diagram of state, crystalline lattice consts., microhardness *(Russian)* 80−66479
Co-powder, isostatic compaction, mech. and elec. props. *(French)* 80−40285
Co-Sb-Te ternary system, crystn., heat treatment and phase equilib. 79−52156
Co-Ti (9 at.%), decomp. kinetics, elec. resist., hardness, and saturation magnetisation during ageing *(Russian)* 80−50587
Co-Ti-C, secondary precipitation and allotropic transform., TEM obs. 80−108453
Co-Ti-Fe (3, 1 to 2 wt.%), spinodal decomposition 80−100839
Co-transition metal, transition metal additives influence on struct., specific resistance, microhardness, mech. props., magnetic props. 79−29078
Co-X-Co (X=Cr,Mo,W) systems, crystn. temp. and hardness 79−77529
Co-Zr, amorphous phase form. in Zr-poor region, hardness and fracture strength *(Japanese)* 80−84914
CoB-based boride coatings on Co base alloys, microstruct. and mech. props. 78−11427
CoB_{12}, growth from melt and phys. props. 80−20782
CoO single crystals, strain rate deform. characts., yield stresses and work hardening 77 to 1400K 80−60939
$Co_{75}Si_{15}B_{10}$, amorphous, crystallisation study *(Japanese)* 78−9959
$Co_{75}Si_{25-x}B_x$ glass, mag. moment, Curie temp., and microhardness, metalloid comp. depend. 77−55665
Cr, CVD protective coating on steel, struct. and carbide form. 77−40387
Cr coatings, ion-plated, deposition parameter influence on struct. and hardness 79−82485
Cr, deposited by high rate sputtering, mech. props. 77−36630
Cr electrodeposits, estimation by X-ray diffraction method 77−36708
Cr film, evaporated, on die-cast Zn, deposition rate depend. 78−10304
Cr film, on mild steel, hardness and protective props., rel. to grain size 78−11436
Cr film, preparation by decomp. of bis-arene cpds., struct. and phys. props 80−60785
Cr foil, laser irradiated, low-angle X-ray scatt., angular block misalignment and hardness *(Russian)* 80−103413
Cr, interaction with dense stream of N ions, metallography, microhardness, specific volume *(Russian)* 80−15169
Cr steel, austenite, abnormal decomposition kinetics and mechanism *(Russian)* 80−55344
Cr-$(Cr,Co)_7C_3$ eutectic, oxidation effect on toughness and strength 80−89404
Cr-AlN, dispersion strengthened, hardness and oxidation rate, 1000 to 1500°C *(Russian)* 78−15574
Cr-C facing alloys, effect of B on phase composition and facings props. during abrasive wear 80−21117
Cr-C(N) coating, deposited by hollow cathode discharge, characterisation 78−11371
Cr-Ce-N, Ce and N effects in ductile-brittle transition, microstruct., hardness, *(Russian)* 78−35497
Cr-Fe alloy (up to 50%), hardness, oxidation and electronic constitution 80−30154
Cr-Ge system, phase diagram, thermal anal., X-ray diffr., microhardness, and electron probe anal. *(French)* 80−97462

hardness continued
Cr-La-V-Nb-Ta, La, V, Nb Ta effect on hardness and strength *(Russian)* 79−34050
Cr-Mo, structural carbonitrided at low temps., rotating bending fatigue strength *(Japanese)* 77−48534
Cr-Nb-Mo alloy system, comp. and temp. depend. alterations in mech. props., phase diagram interpret. *(Russian)* 80−85045
Cr-Ni steel, carburised, effect of atm. during heating to quenching temp. on austenite decomp. 77−56157
Cr-V-Ce-N, (2.4 to 2.6, 1.7 to 2.3, 0.005 to 0.23 wt.%) V effect on hardness, and ductile to brittle transition temp. *(Russian)* 79−34138
Cr-X-C amorphous alloys, (X=Fe, Co, Ni, Nb, Mo and Ta), crystn. temp. and hardness 79−73133
CrC, plasma sprayed coating 78−68835
CrN, deposition by hollow cathode discharge process, and hardness 79−24452
Cr_2O_3-Al_2O_3 solid soln., Vickers micro-hardness 80−66629
CsH_2PO_4, microhardness, expt. determ. 79−24603
CsI, mechanical props., effect of impurities 77−69034
CsI:Na^+, cryst., mech. props. assessed from yield stress and microhardness 79−15748
Cu alloy, fretting corrosion, exam. of secondary structures 79−100292
Cu and Cu-Si, deformation and fracture under dynamic loading 78−35442
Cu clad steel, bond strength through intermediate Zn *(Korean)* 79−66213
Cu coating, bias sputter parameters effect, hollow cathode 77−40369
Cu, cold rolling, mechanical props., ageing, annealing, recrystallisation, plastic strain *(Russian)* 80−35202
Cu, cyclic loading, change in mech. props. rel. to heat treatment 80−104282
Cu, defect removal, obs. by positron annihilation 78−84677
Cu, deformation under mutual indentation in contact with Pb-Bi eutectic melt *(Russian)* 77−59853
Cu electrodeposit, US agitation effect on hardness, porosity and grain size, work-hardening 77−60075
Cu, electrodeposited coating, annealing effect on struct. and microhardness *(Russian)* 78−76668
Cu foil, laser irradiated, low-angle X-ray scatt., angular block misalignment and hardness *(Russian)* 80−103413
Cu, hardness, temp. depend. 77−40440
Cu, hardness-flow stress rel. during strain-controlled bending fatigue 79−74245
Cu, powder, sprayed, effect of start props. in struct, and porosity of sintered products *(Czech)* 77−85960
Cu, rolled at room temp. and 200°C, variation in props., hardness and X-ray meas. *(Russian)* 77−73285
Cu solid soln., wear 78−3233
Cu, strip, formed by high deform., mech. props. charact. *(Russian)* 78−27534
Cu, swaged, inhomogeneous work hardening *(German)* 80−76267
Cu, tribological investigation using two-cylinder tribometer *(German)* 77−25164
Cu, ultra-microhardness testing for vacuum deposited film and bulk specimen 78−79910
Cu, vacuum condensate, struct. and mech. props. depend. on deposition conditons 80−15417
Cu, X-ray and microhardness meas. at high strain rates *(German)* 78−3184
Cu-Al, internally oxidised, structural, elec. and mech. charact. 78−60761
Cu-Al, two-phase Cu-rich alloy, influence of microstruct. on stress-strain behaviour 80−7631
Cu-Al, vacuum condensate, struct. and mech. props. depend. on deposition conditons 80−15417
Cu-Al (11.6 wt.%), mech. props., tempering temps. effects 78−76669
Cu-Al martensite, temper hardening, study by TEM, DTA, microhardness and yield strength meas. 79−43260
Cu-Al_2O_3, composite coatings, prep. by precip., props. 78−23841
Cu-Al_2O_3 coatings, electrodeposited, dispersion hardened, exam. of props. 79−34181
Cu-Al_2O_3 dispersed system, electron beam evaporated thick film, struct./prop. relations 77−44198
Cu-Al_2O_3 electrodeposits, dispersion hardened, props. 79−28258
Cu-Al-Fe, mech. props. rel. to heat treatment 80−50682
Cu-Al-Fe-Mn (10,3,2 wt.%), phase comp. struct., continuous cooling from β-phase effect 79−24499
Cu-Al-Mn, partial decomp. of β_1 phase, effect on mag. props. and martensitic transform. *(Russian)* 80−45306
Cu-Al-Si, Si effect on mech. props. and microstructure *(Korean)* 79−38903
Cu-Be (2 wt.%), plastic deformation influence on ageing, granular microhardness *(Russian)* 80−55474
Cu-Be alloy, notched specimen, static and dynamic behaviour 78−27634
Cu-Be-Co (1.8, 0.2 wt.%), TEM obs. of precipitates, ageing charact. *(Korean)* 77−66648
Cu-Be-Co (2,0.3 wt.%) alloy, heat treatment, influence of tempering on hardness, tensile props. transform diagram *(French)* 78−31384
Cu-Cd-Se system, Cu-CdSe cross section and props. of cpds. formed 78−27491
Cu-Fe, precipitation processes during aging, TEM, resistivity, hardness study *(Japanese)* 80−35221
Cu-Fe system, ageing and reversion phenomena study 80−89274
Cu-ferrous alloy, hard inclusion composite exam. of wear resistance props. 79−34153
Cu-In, unidirectionally transformed, mechanical props. 78−48492
Cu-Ni-Al, ageing charact., optical TEM, X-ray, hardness obs. 79−29079
Cu-Ni-Al, grain boundary reaction under isothermal ageing at 623 to 973K *(Japanese)* 79−70090
Cu-Ni-Be (30, 0.5 wt.%), grain boundary reaction after ageing and quenching, obs. *(Japanese)* 79−70089
Cu-Ni-Be-(Al) (30,0.5,(0.2-2) wt.%), Al addition effect on grain boundary reaction *(Japanese)* 80−54254
Cu-Ni-Fe (26,8 wt.%), microduplex struct. form., hardness meas., optical and electron microscopy *(Japanese)* 78−76659
Cu-Ni-Mn (20,20wt.%), structural transform., X-ray and hardness study *(French)* 78−39760
Cu-Ni-Sn spinodal substitute for Be-Cu alloy 80−35217
Cu-Ni-Ti, ordering within precipitates, TEM obs. 80−108461
Cu-P-Se system, glasses, semicond., density, microhardness, softening point rel. to conc. 77−7674

hardness continued
Cu-Sn (16.5 wt.%), Vickers hardness, stress induced martensite from γ phase 79−70066
Cu-Sn-Ni alloys, mech. props. after thermomech. treatment 79−79009
Cu-Sn-P (5, 1-5 wt.%), effect of P on friction and wear charact. 80−16494
Cu-Ti, deform. effect on precipitation and recrystallisation, electron microscope study 77−70115
Cu-Ti, Zr effects on cellular precipitation 77−16587
Cu-Ti (Zr), strength improvement by thermomechanical treatment *(Japanese)* 78−48426
Cu-Ti (3.5 wt.%), aged by US strain, struct. and props. *(Russian)* 80−21003
Cu-Ti (3.5%), coherent precipitates, US irrad. effect on struct. and hardness *(Russian)* 77−48446
Cu-Ti (5 wt.%), effect of cold work on ageing behaviour, study by elec. resist. and hardness meas. *(Japanese)* 79−78991
Cu-Ti alloys (0.5 to 4.0 wt%) ageing charact. determ. 79−20089
Cu-Ti-Fe (0.7, 0.9 wt.%) film, dispersion-strengthened, form. by high rate magnetron/plasmatron sputtering, and props. 80−25715
Cu-Zn (36 wt.%), hardness-flow stress rel. during strain-controlled bending fatigue 79−74245
$CuAl_2$, Knoop hardness meas. on single cryst. faces 79−37696
$CuCd_2GaTe_4$, semiconductor, physicochem. and transport props. 77−59762
$(CuInTe_2)_{1-x}$-$(2ZnTe)_x$, phase diagram and cryst. growth of $CuZn_2InTe$ from $ZnCl_2$ flux 80−16287
Cu_2O, slip systems, Kroop hardness anisotropy meas. 77−31714
Cu_3P, single crystal, prep. and props. 80−40250
$Cu_2S(Se)$-Ge(Sn)S, phase diagrams 78−44100
$Cu_{46}Zr_{54}$, devitrification effect on mech. props. 80−30082
$Cu_{56}Zr_{44}$ metallic glass, devitrification and its effect on mech. props. 80−33893
Dy, substructural changes during plastic deform., stress-strain diagrams and microhardness meas. *(Russian)* 79−52296
Er, substructural changes during plastic deform., stress-strain diagrams and microhardness meas. *(Russian)* 79−52296
EuB_6, growth by soln. method, struct., mech. and elec. props. 80−16168
Eu_2O_3, large single crystals, production and props. rel. to structural anisotropy *(French)* 77−36396
(Fe, Ni, Co)-Si-B, amorphous, compositional effect on struct. changes, after heating up to 700°C, exam. *(Japanese)* 78−48433
Fe alloy granule reinforced Cu M2 wear resistance in rubbing with lubrication 80−16490
Fe alloy granule reinforced Cu, friction in vacuum 80−25880
Fe, Armco, cyclic deform. in presence of H_2 *(Russian)* 77−16728
Fe, Armco, microstruct., effect of strain rate on change, due to tension-compression 78−80614
Fe, Armco, microstruct. and hardness after electron bombardment 79−38956
Fe based metallic glass, B and P glass former additions, elastic consts., flow behaviour correlations 78−44154
Fe, cast, grey, tensile strength, surface area to volume ratio effect *(Japanese)* 80−45389
Fe, cast, hardness, wear resist. and struct., electron irrad. effects 79−96126
Fe, cast, high Cr, phase composition, mech. props. rel. to heat treatment 79−29108
Fe, cast, high Cr, wear resistance improvement 77−70186
Fe, cast, influence of Y and Sb on microhardness and lattice spacing of ferrite *(Russian)* 80−19748
Fe, cast, mech. props., demodification influence of isothermal holding and Mg additions *(Bulgarian)* 79−15707
Fe, cast, mech. props., effect of repeated heating and cooling *(Japanese)* 77−59907
Fe, cast, Mn, wear resist. and hardening, struct. effect 79−87734
Fe, cast, point contact sliding 79−87738
Fe, cast, spheroidal graphite, graphite size effect on mech. props. *(Korean)* 78−11278
Fe, cast, spheroidal graphite effects of Si and C on mechanical props. *(Korean)* 79−66114
Fe, cast, spheroidal graphite, degree of normalization effect on mech. props. *(Korean)* 79−87664
Fe, cast, spheroidizing effect of Mg and Ce modifiers 80−35193
Fe, cast, white Cr alloyed, wear resistance, effect on abrasive hardness 78−64722
Fe film, thermally evaporated, contamination effects obs. 80−49545
Fe, friction at elevated temps. 78−15548
Fe, interaction with dense stream of N ions, metallography, microhardness, specific volume *(Russian)* 80−15169
Fe, isochronous annealing recovery, in cold rolled and explosively formed samples 79−100166
Fe, microhardness of single crysts. effect of temp. on dislocation structure *(German)* 79−52357
Fe powder, sponge and atomized types, steam oxidation, pore closure and surface hardness 80−45441
Fe powder, ZhGr1.0, optimisation of heat treatment in salt bath 77−28756
Fe, sintered, metallographic meas. of pore size, effect on mech. props. 78−19685
Fe, splat-quenched, microhardness and martensite 80−76359
Fe-Al (1 to 4 wt.%), effect of nitriding on surface structure and props., and on diffusion layer *(Russian)* 79−34197
Fe-Al(Cr)(V)(Ti), hardness after nitriding, metallographic, electron microscopic and microprobe anal. 78−51608
Fe-Al(V)(Ti), nitrided, struct. and props. 78−19950
Fe-B, rapidly solidified, metastable phases *(German)* 79−29045
Fe-B_2metallic glass, hardness, elastic moduli, density, cryst. temp., mech. props., for flywheel appl. *(Dutch)* 78−52878
Fe-B metallic glasses, density, mech. and thermal props. 78−31432
Fe-B metallic ribbons, correl. between quenching temp. and mech. and mag. props. 80−89373
Fe-B ribbon, microhardness, and static coercive force, melt overheating effect 80−84978
Fe-B_4C sintered material, mech. props. and struct. charact. 79−100084
Fe-C, softening of high purity Fe, by C, due to double kink nucleation *(French)* 78−84949
Fe-C (0.16 wt.%), hardness-flow stress rel. during strain-controlled bending fatigue 79−74245
Fe-C-Mn (0.5, 0.6 wt.%), powder forged, mech. props. 80−21096

hardness continued
Fe-C-Ni-Cr(Cu), dynamically hot pressed, mech. props., additives effect 78−60620
Fe-CaF (6 and 9 wt.%), sintered, elevated temp. mech. props. 77−28878
Fe-Co-Mo-C, amorphous alloys, med. props. and thermal stability *(Japanese)* 80−85049
Fe-Co-Mo-Nb(Ta) semihard mag. alloy, mag. props., thermal expansion, elec. resistivity and hardness *(Japanese)* 80−88789
Fe-Cr, friction at elevated temps. 78−15548
Fe-Cr, role of C in transform. by heating in ($\alpha+\gamma$) phase *(French)* 78−52798
Fe-Cr (13 wt.%)+polycarbosilane, powder metallurgy, charcts. 77−85962
Fe-Cr-Al-Y (Y-Al_2O_3)(Y_2O_3), preparation and exam. of mech. props. 78−52720
Fe-Cr-Co permanent magnets, phase diagram, miscibility gap 77−89984
Fe-Cr-Co-Mo, microstruct., hardness, mag. props., influence of isothermal tempering and heat treatment 79−79129
Fe-Cr-Mo alloy castings, thick-section, factors affecting 80−108374
Fe-Cr-N (5.9, 0.5 wt.%), martensitic, tempered, fine struct. 77−25079
Fe-Cu, modulated microstruct., continuous cooling effect, hardness and electron microscope obs. 79−87665
Fe-Cu (2 wt.%), furnace cooled, ageing and steam oxidation 78−23744
Fe-Fe_2O_3 composite films, structural props., microhardness, 250 to 700K 78−84095
α-Fe-Fe_3C alloys, ground surface layer exam. of props. 78−84840
Fe-Mn, γ to α transition on cooling, struct. and microhardness investig. *(Russian)* 77−44246
Fe-Mn alloy, splat-quenched, martensite formation obs. 77−44247
Fe-Mn-C (11.5, 0.2 to 1.6 wt.%), water quenched, effect of C on phase composition, abrasion, plasticity *(Russian)* 78−35445
Fe-Mn-Ni-C, age hardenable, struct. and strength 77−8844
Fe-Mn-Ti alloys, austenitic, precipitation strengthened 80−25714
Fe-Mo (13-20 at.%) binary alloys, spinodal decomp. on ageing, TEM and X-ray diffr. study 80−97503
Fe-Mo-CaF (15, 9 and 6 wt.%), sintered, elevated temp. mech. props. 77−28878
Fe-Nb (3.1 wt.%), semihard mag. alloy, Recalloy, mag. props., elec. cond. *(Japanese)* 78−10723
Fe-NbC, exam. of phase diagram, and mech. props. *(Russian)* 79−20028
Fe-Nb(Ta)-Co, Recalloys, semihard mag. alloys, mag. and elec. props., hardness, thermal expansion *(Japanese)* 79−5066
Fe-Ni (32 wt.%), electrohydraulic effect and struct. changes *(Russian)* 78−23783
Fe-Ni base amorphous alloy, crystallisation 77−84660
Fe-Ni base metallic glasses, microhardness charact. of stability under annealing 79−57011
Fe-Ni-Al-Co-Cu-Ti YuNDK type, S effect on mech. props. 80−60927
Fe-Ni-C (24, 0.5 wt.%), recovery and recrystallisation of stable austenite after hot rolling *(German)* 77−32591
Fe-Ni-C (31.9, 0.02 wt.%) alloy, hardness of martensite-austenite mixtures 80−60959
Fe-Ni-C alloy, splat-quenched, martensite formation obs. 77−44247
Fe-Ni-Co coating electrodeposition optimum conditions *(Russian)* 79−83292
Fe-Ni-Co-W(Mo) (18.65, 8.99, 4.87 wt.%), ageing charcts., 380-530°C 80−60876
Fe-Ni-Cr (40, 15.8 wt.%), precipitation and creep rupture behaviour, optical and TEM study 79−74158
Fe-Ni-Cr-Ti-Al, with thermoelastic control coeff., comp. and heat treatment influence on props. *(French)* 80−81074
Fe-Ni-Mo, small angle X-ray scatt. study, pre-precipitation phenomenon obs. *(French)* 78−19757
Fe-Ni-Mo-C, amorphous alloys, med. props. and thermal stability *(Japanese)* 80−85049
Fe-Ni-Ti (27.4, 2 to 3 wt.%), aged, stress induced martensitic transform., mech. props. *(Russian)* 79−87632
Fe-Ni-V, austenite, martensite elec. cond. depend. on heating *(Russian)* 79−70177
Fe-Ni-V alloy, ageing of martensite *(Russian)* 78−39808
Fe-Ni-WC hard alloy, struct. and props. 79−79007
Fe-Ni(Mn)-Al-C, form. of ductile Ni_3Al by split quenching, mech. props. 79−100197
Fe-Si (3 wt.%), (110)[001] oriented single crystal, form. of rolling and annealing texture 77−16608
Fe-Si (3.72 wt.%) fatigue failure in vacuum and air 78−68789
Fe-Si-Al, Sendust, 12 μ thick film prep. by sputtering, mag. and other props. 77−55888
Fe-Si-Al, Sendust, ribbon-form, prep. by rapid quenching, mech. and mag. props. 80−71611
Fe-Si-Al Sendust alloy ribbon form, rapid quench prepared, elec. cond., coercive field, permeability 79−83151
Fe-Si-Al-Ni alloy, Super Sendust, Ni content and thermomag. treatment effects 77−4861
Fe-Si(Cr)(Ni)(Mn)(C), alloy layers formed by reaction with molten Al, X-ray, EPMA anal., hardness meas. *(Japanese)* 78−72926
Fe-Ta alloy, mech. drawn and aged, exam. of electrical resistivity, hardness, microstruct., and mag. props. *(Japanese)* 78−48545
Fe-TiC pseudofused composite magnetoabrasive powders, props. 80−100926
Fe-Ti(Nb), internally nitrided, mech. props. 77−44307
Fe-V (1 wt.%), nitrided and annealed, struct. 77−8998
Fe-VC alloys, struct. and mech. props. 79−52171
Fe-V(Nb)-N, precipitation study, 550 to 600°C *(German)* 77−90350
Fe-W system, damping capacity of Gentalloy, internal friction, mech. and mag. props. 79−77679
Fe-W-C, eta carbides at 1250°C 77−36506
Fe-W-C-Cr, eta carbides at 1250°C 77−32581
Fe-W-Cr-Mo system, mag. and mech. props. rel. to production methods *(Japanese)* 80−71107
Fe-W-Cr-Mo-Co with austenitic phase, magnetic and mech. props., cold working and ageing effects *(Japanese)* 78−60678
Fe-X-MoS_2 (X=WC, HfC, Al_2O_3, ZrO_2, HfB_2, ZrB_2), self lubricating coatings, exam. of props. 79−96217
Fe-Zn, quenched, martensite struct. and hardness, electron microscope exam. *(Russian)* 80−66619
Fe-Zr, amorphous phase form. in Zr-poor region, hardness and fracture strength *(Japanese)* 80−84914
FeB_x coatings on steel, formed by B diffusion, pack cementation process, microstruct. and mech. props. 78−15592

hardness continued
$Fe_{80}B_{20}$, hardness, elec. cond., photo emission, and mag. props. *(Norwegian)* 79−32909
$Fe_{80}B_{20-x}Si_x$, metallic glass, mech. and mag. props., depend. on metalloid content 79−91213
Fe_3C, microhardness and charact. hardness 79−52376
$(Fe_{1-x}Co_x)_{80}P_{13}C_7$ amorphous alloy, soft mag. material, props. 77−4533
$(Fe_{1-x}Co_x)_{75}Si_{15}B_{10}$ amorphous alloy, soft mag. material, props. 77−4533
$(FeNi)_{80}B_{20}$, glass, elastic consts. 79−83249
$Fe_{40}Ni_{40}B_{20}$ glass, phase transform. during isochronal annealing 78−14451
$Fe_{80-x}Ni_xB_{20}$ and $Fe_{80-x}Ni_xP_{14}B_6$ amorphous alloys, microhardness correl. with mag. props. 80−88826
$Fe_{80-x}Ni_xB_{20}$, $Fe_{80-x}Ni_xP_{14}B_6$, amorphous, microhardness meas., dependence on mag. props. *(Croatian)* 79−11688
$Fe_{65}(Ni_{1-x}Cr_x)$, microhardness and specific heat, depend. on Cr content *(Russian)* 79−100240
$Fe_{32}Ni_{36}Cr_{14}P_{12}B_6$ metallic glass, crystn. kinetics by TEM 80−75186
$Fe_{40}Ni_{40}P_{14}B_6$, amorphous, annealed and unannealed, temp. depend. of flow stress and ductility 79−29119
$Fe_{40}Ni_{40}P_{14}B_6$, hardness, elec. cond., photo emission, and mag. props. *(Norwegian)* 79−32909
$Fe_xNi_{80-x}P_{14}B_6$, and $Fe_xNi_{80-x}B_{20}$ glass, microhardness, correl. with mag. props. 79−57085
Fe_2O_3, plasma sputtered coatings, oxide dissociation, coating props., struct. and composition *(Russian)* 80−54577
Fe_xO_y film, thermally evaporated, contamination effects obs. 80−49545
$Fe_{80}(P_{13}C_7)_{20-y}B_y(Si_y)$, density, microhardness, and crystn. temp., comp. depend. 80−84093
$Fe_{78}Si_{10}B_{12}$, amorphous alloy crystallisation study *(Japanese)* 78−9959
GaAS, microhardness and charact. hardness 79−52376
GaAs:Cr(Te)(Zn), dopant influence on hardness 77−84777
GaAs-Si eutectic alloy, effect of crystallisation rate on microhardness 79−96110
GaP, mech. props. and photomechanical effect 77−84833
$(GaP)_x(ZnSe)_{1-x}$, solid solution, reaction of Zn with Se during Czochralski growth and LPE 79−8238
GaSb-Ge eutectic alloy, effect of crystallisation rate on microhardness 79−96110
GaSe sputtered film microhardness, influence of gas discharge *(Russian)* 80−49560
Ga_2Se_3-FeSe, phase diagram, elec. cond., mag. susceptibility 80−88301
Gd-Fe(Co), thin amorphous system, resistance and hardness, chemical comp. and temp. effect 80−15625
Ge crystal, crack initation threshold, SEM and acoustic emission study 79−70157
Ge, plates, semicond., scribing marks rel. to sclerometric microhardness 79−15891
Ge, semiconductor-metal transition and indentation hardness 78−35499
Ge, single crystal, exam. of microhardness using static indentation 79−52517
Ge, yield stress from Hugoniot elastic limit and elastic consts., Knoop hardness 79−83261
Ge:Al, limiting solubility, rel. to charge carrier conc. 80−24596
Ge:Sb, limiting solubility, rel. to charge carrier conc. 80−24596
Ge-GaP system, phase analysis 78−23674
Ge-InP system, phase analysis 78−23674
Ge-P-Se system, glasses, semicond., density, microhardness, softening point rel. to conc. 77−7674
Ge-P-Se system glasses, penetration by indentor, activation parameters, microhardness 79−43419
Ge-S-In, chalcogenide glass, determ. of microhardness 79−23526
Ge-S-Se system, glass-forming, struct. and props. 80−19713
Ge-Sb-Se glass, physical props., purification method for Sb, Se from surface oxides 78−46735
Ge-Te system, phase equil. diagram, $GeTe_{1\pm x}$ region analysis by metallography, microhardness and DTA *(French)* 77−70034
GeO_2-$PO_{5/2}$ glass, struct. and props. *(Japanese)* 77−27837
$Ge_{2.33}SbSe_5$:FE, Fe effect on physiochem. props. of glass 80−24370
$GeSe_2$-$SnSe_2$-As_2Se_3, GeSe-SnSe-As_2Se_3, Mossbauer investigation 77−20052
GeTe, elec. cond. and microhardness, thermal cycling effect *(Russian)* 78−35485
GeTe, nonstoichiometric, homogenisation 78−44004
GeTe-MnTe, heat treatment effect on struct., elec. props. 80−54725
Hf-O, phase props. 77−40415
HfC-HfB_2, reactions, cpd. formation and props. 78−23685
HfC-$HfBr_2$, preparation and high temp. antifriction props. 79−1918
HfC-TaC alloys, microhardness rel. to valence electron conc. 77−86130
HfC_x, electron energy spectrum and phys. props. in homogeneous region *(Russian)* 77−31941
HfN on stainless steel, activated reactive evaporated coatings, high rate deposition, microhardness 80−25580
HfO_2-Cr_2O_3 system in Ar medium, phase equilibria, 1600-2500°C *(Russian)* 77−55953
$HfSi_2$, work function rel. to phys. props. 77−47887
$Hg_{1-x}Cd_xTe$, segregation, compositional characterisation 80−107434
Hg_2X_2 (X=Cl, Br, I), calomel family, single crysts., microhardness using Vickers method 80−25848
Ho, substructural changes during plastic deform., stress-strain diagrams and microhardness meas. *(Russian)* 79−52296
$HoAlO_3$, Czochralski growth and props. 77−48335
InAs, exam. of decomposition of donors 79−1605
InAs, individual solubilities and cosolubilities of Zn, Cd, Te, microhardness 77−16552
InAs, single crystal, exam. of microhardness using static indentation 79−52517
InAs:Zn,S,(Se)(Te), exam of microhardness, Hall effect as function of dopant 79−95038
InAs-CdTe, preparation, microhardness rel. to component interactions 77−24350
InAs-CdTe quasi-binary system, temp.-comp. diagram, physicochem. and thermodynamic analysis 80−104127
InP, microstructs. assoc. with hardness indentations 78−80627
InP, plastic deform. and scratch microhardness meas. 78−27583
InSb-Ge eutectic alloy, effect of crystallisation rate on microhardness 79−96110
InSe-SmSe system, microhardness and electrophys. props. 79−87093
p-In_6Se_7, electrophysical props. 110 to 400K, microhardness *(Russian)* 77−35867

hardness continued
In_2Te_3-PbTe system, phase diagram, elec. props. 78−35361
KBr, quenched single cryst., hardness var. with load 80−76337
KBr-KI, mixed crysts., microhardness, theory 80−75298
KCl, hardness increase mode, effect on dislocation mobility 79−51114
KCl, Knoop microhardness anomaly on (001) planes 79−38942
KCl:Ba(Ca)(Sr), microstruct. and hardness, impurity distrib. effects 79−24529
KCl:Ca^{2+}, Z_1-centre thermolum. 80−80879
KCl:Pb, impurity distrib., light scatt. and microhardness study, heat treatment 80−96562
KCl-KBr, mixed crysts., microhardness, theory 80−75298
KCl-KBr mixed crystals, microhardness studies, nonlinear depend. on composition 78−83872
KCl(Br)(I), single cryst., quenched, microstruct. around indentations 80−7628
$KD_{2x}H_{2(1-x)}PO_4$ crystals, plastic deform. and mech. props. 79−79035
KH_2AsO_4, microhardness, expt. determ. 79−24603
KH_2PO_4 crystals, plastic deform. and mech. props. 79−79035
KH_2PO_4, microhardness, expt. determ. 79−24603
KI, load relaxation studies 79−79016
K_2O-PbO-SiO_2, glass, mech. and optical props. *(Russian)* 77−20860
K_2O-PbO-ZnO-B_2O_3-SiO_2, corrosion and microhardness, effect of detergents 80−16518
K_2SO_4-$ZnSO_4$ system, glass formation and phase diagram study, physical props. 78−27500
La, $(SO_4)_3.9D_2O$, soln. growth, struct., props. 77−77363
LaB_6, growth by soln. method, struct. mech. and elec. props. 80−16168
LiF, deform. mech. map. 77−81298
LiF, electron irradiated, mech. characts. 78−26595
LiF, estimation of activation parameters in sclerometric tests 80−66625
LiF, hardness anisotropy obs. 79−79085
LiF, hardness increase mode, effect on dislocation mobility 79−51114
LiF, Knoop microhardness anomaly on (001) planes 79−38942
LiF, load relaxation studies 79−79016
LiF, ultra-microhardness testing for vacuum deposited film and bulk specimen 78−79910
$LiNbO_3$, single crystal, exam. of microhardness using static indentation 79−52517
Li_2O pellets, neutron irrad., microstruct. and Vickers mircohardness meas. 79−8339
Li_2O-B_2O_3-P_2O_5, glass, mech. and elec. props 80−84228
$LuAlO_3$, single crysts., prep. and phys. props., X-ray struct. anal. 79−4298
Mg cast iron, effect of heating temp. on microstruct. and mech. props. 77−56005
Mg-Al(-Zn), solute-vacancy binding energies from hardness meas. 78−39789
Mg-Ga (6 wt.%), precipitation, lattice const., ageing effects *(Chinese)* 79−43279
Mg-Li-Al (31, 1 at.%), heat treated, precipitation 80−40364
Mg-Ni-S, electroforming, mech. props. rel. to heat treatment 80−35133
Mg-Tb, (up to 45 wt.%), phase diagram, and mech. preps. 80−16277
Mg-Zn (5 wt.%), age hardening, X-ray diffr. anal. *(Chinese)* 80−104173
Mg-Zn metallic glass, hardness, elastic moduli, density, cryst. temp., mech. props., for flywheel appl. *(Dutch)* 78−52878
MgF_2, ultra-microhardness testing for vacuum deposited film and bulk specimen 78−79910
MgO, anisotropy of grinding damage, chem. polishing and etching 79−47793
MgO briquets, prep. by shock compaction and characteris. 79−43178
MgO, hardness anisotropy obs. 79−79085
MgO, hardness increase mode, effect on dislocation mobility 79−51114
MgO, hot pressed, microstruct. influence on microhardness 79−38971
MgO, Knoop microhardness anomaly on (001) planes 79−38942
MgO, lattice misorientation and displaced vol. for microhardness indentation 78−64617
Mg_2SiO_4, microhardness variation, exam. using Vicker indentor 80−25849
Mn-B system, microhardness and phase analytical studies 79−24502
Mn-Ga, Elinvar charact. *(Japanese)* 79−61638
Mn-Ni-Ti (Zr) systems, and mech. props. thermal expansion for different heat treatments *(Japanese)* 79−29123
Mn-Ni-Ti(Zr), non-ferromagnetic Elinvar-type alloys 79−24566
Mn-Ni-V(Nb)(Ta), nonferromagnetic Elivar type, mech. props. meas. 77−48473
Mn-Pt, Elinvar props., −150 to 500°C *(Japanese)* 77−52385
Mn-Pt, exam. of Elinvar props., from −150 to 500°C 78−76684
Mn-Y-Zn-Cd alloy,phase equilibria, plastic deformation, microhardness *(Russian)* 80−40334
Mn_2As-Mn_2Sb, structural and magnetic props. determ. 78−76248
MnB_{12}, growth from melt and phys. props. 80−20782
$Mn_{46}Co_{54}$, amorphous alloy prep. by high-rate sputtering, struct. and prop. characteris. 79−24462
Mo alloys, dispersion-strengthened, plastic deform. and hardness, temp. depend. 80−3087
Mo, deformed, dislocation-free channels prod. by heat pulses, electron microscope obs. and hardness meas. *(Russian)* 79−52251
Mo, dislocation structure evolution near electro-eroded crater *(Russian)* 80−100237
Mo flame sprayed coatings, comp., microstruct. and mech. props. 80−16598
Mo form MoF_6 by H_2 reduction, 500 to 1200°C *(Russian)* 80−7516
Mo laser mirror, optical and metallurgical characterisation 80−33129
Mo, macroscopic heterogeneity of plastic deform., metallographic examination *(Russian)* 79−100210
Mo, mech. props., effect of exposure to high temp. He containing O_2, room temp. study 80−93639
Mo, microhardness and charact. hardness 79−52376
Mo, microhardness meas. of dislocation structure inhomogeneity in electromachining crater zone *(Russian)* 80−16326
Mo, neutron irradiated single crystals, vacancy reactions in III recovery 79−73220
Mo powder, influence of powder reduction processes on props. 80−89175
Mo single crystal, effect of prior ultrasonic working on hardness, crystal orientation and creep resistance *(Russian)* 79−34056
Mo-(Zr+V+C) (1.1 wt.%) alloy, phase composition, carbide phase microhardness *(Russian)* 80−60834
Mo-Al-Ge, new compounds, structure and props. 80−39003
hardness continued
Mo-B, Mo-B-Fe(Ni), microalloying influence on mechanical props., cold rolling, plasticity *(Russian)* 80−40502
Mo-based metallic glass development 80−89172
Mo-Hf (0.3 wt.%), strength, plasticity and microhardness, internal nitriding effect *(Russian)* 80−40433
Mo-Ti (up to 5.48 wt.%), internal nitriding, hardness, nitride type, precipitation *(Japanese)* 79−79157
Mo-Ti-Zr (0.5, 0.7 wt.%) alloy TZM, props. and appl. *(German)* 80−21040
Mo-Ti-Zr alloy TZM, fatigue and plastic flow, irradiation effects 77−52466
Mo_2B_5-based alloys, mech. props., rel. to appl. as electrodes in electrospark machining 80−21174
MoN_x, ion condensing metal plasma stream, coating microhardness, chemical reactions 79−42426
$MoSe_2$ coating, on Mo, support annealing influence on orientation, texture and hardness *(Russian)* 80−20961
$MoSi_2$ on Mo, coating by local heating 77−81335
$MoSi_2$-$CrSi_2$, phase equilib., struct. and props. 80−50608
$NH_4H_2AsO_4$, microhardness, expt. determ. 79−24603
$NH_4H_2PO_4$ crystals, plastic deform. and mech. props. 79−79035
$NH_4H_2PO_4$, microhardness, expt. determ. 79−24603
NaCl, crack initation threshold, SEM and acoustic emission study 79−70157
NaCl, deform. mech. map. 77−81298
NaCl, dislocation rosettes around Vickers diamond pyramid indents, quenching effect 80−11740
NaCl, hardness increase mode, effect on dislocation mobility 79−51114
NaCl, Knoop microhardness anomaly on (001) planes 79−38942
NaCl, load relaxation studies 79−79016
NaCl, single crystal, temp. anisotropy of plasticity and brittleness 78−3198
NaCl:Ca, microhardness and thermoluminescence, hardness-quenching temp. variation 80−29813
NaCl:Ca(K), impurity state from heat treatment on microhardness 77−80532
NaCl:Eu, secondary Eu phase dissolution, EPR and optical absorpt. study 80−96655
NaCl:X (X=Ca, Sr, Ba, Mg, K, Li, Tl, Ag), impurity conc. effect on mech. and elec. props. 78−47469
NaCl-$BaCl_2$ 1%, oriented growth of $BaCl_2$ phases, morphology 77−80627
NaCl-Ca, single crysts., load-microhardness curves, heat treatment, impurity effects obs. 78−30694
NaCl-NaBr, mixed crysts., microhardness, theory 80−75298
NaF, load relaxation studies 79−79016
Na_2O-B_2O_3, microhardness and boric oxide anomaly 77−36624
Na_2O-B_2O_3-P_2O_5, glass, mech. and elec. props 80−84228
Na_2O-B_2O_3-SiO_2 glass-Ni compact, indented, strength and fracture toughness 80−93636
Na_2O-CaO glass, crack nucleation during indentation, micromechanics 80−30069
Na_2O-CaO glass, shear deform. under pyramidal indentations 80−84989
Na_2O-CaO-MgO-Al_2O_3-SiO_2, corrosion and microhardness, effect of detergents 80−16518
Na_2O-GeO_2(TiO_2)(SnO_2)(ZrO_2)(ThO_2)-SiO_2 glass, density, refractive index, thermal expansion, hardness IR spectra, DTA *(Japanese)* 78−15535
Na_2O-NaF-CaO,ZnO_{1-x}-Al_2O_3-SiO_2, opal glasses, strength, surface composition 80−30066
Na_2O-SiO_2 glass, scoring, deform. and fracture mech. approach 80−89332
Na_xWO_3, bronze, composition-dependent microhardness, rel. to bonding 79−24606
Na_xWO_3, hardness anisotropy, comp. depend. 79−29181
Nb CVD coatings on graphite, grain struct. depend. on temp. 80−25574
Nb, cold-rolled, deform. zone geometry and texture gradients 77−48452
Nb, microhardness and charact. hardness 79−52376
Nb, oxidation in imperfect vac., solute O_2 level change and ductility loss 79−52452
Nb, pure, reaction with gas residual in vacuum, physicomech. props. effect 80−16587
Nb, recovery and recrystallisation, fast neutron irradiation effects 77−70069
Nb-alloys, reaction with gas residual in vacuum, physicomech. props. effect 80−16587
Nb-Ga, phase system form. and stability of A15 phase 77−90347
Nb-Ge system, phase diagram determ. 79−38796
Nb-Ir(Rh) system glasses, form., crystn. and microhardness, resist. obs. 80−89178
Nb-Ni metallic glass, hardness, elastic moduli, density, cryst. temp., mech. props., for flywheel appl. *(Dutch)* 78−52878
Nb-Ti-Al alloy, effect of heat treatment on strength and elastic props. 77−55976
Nb-Ti-O system, phase equilib., microstruct., thermal, and X-ray anal. 77−8806
Nb-Ti-Ta alloys, metallurgical anal. and crit. current densities 79−38286
Nb-Y, and Nb, mech. props., neutron irrad. and Y scavenging effects 77−90394
Nb_3Au, A-15 struct. supercond., microhardness, bonding 78−76199
NbB_2, single crysts., hardness anisotropy and slip 80−21085
NbC coating on C steel and Armco Fe, deposition, struct. and props. 79−52462
NbC, deformation behaviour during rubbing in wide temp. range 80−16486
NbC, microhardness and charact. hardness 79−52376
NbC single cryst., Vickers microhardness, slip mechanism 80−71732
$NbC_{0.86}$, single crystal work function, thermionic emission and contact pot., microhardness and binding 79−19649
Nb_3Ir, A-15 struct. supercond., microhardness, bonding 78−76199
Nb_3Sn, A-15 struct. supercond., microhardness, bonding 78−76199
Nb_3Sn-Cu multifilamentary wires, in situ prep., supercond. and mech. props. 79−38768
Nd-Gd-Te alloys of R_2Te_3-T_3Te_4 region, physicochem. props. 78−52017
$Ni_{75}Si_8B_{17}$, amorphous alloy, crystallisation study *(Japanese)* 78−9959
Ni, 200, high temp. cyclic deformation and hardening 80−21055
Ni alloy EI867, heat resistant, mech. props., effect of prolonged elevated temp. 77−21194

hardness continued
Ni alloys, recrystallised, grain boundary inheritance and props. 77−59816
Ni, B-containing diffusion layer formation *(Russian)* 77−48570
Ni, B-containing multicomponent diffusion layer formation *(Russian)* 77−44400
Ni based alloys, hot hardness and oxidation resistance meas. 78−31588
Ni coating, self lubricating containing oxides, carbides and borides on steel 80−21189
Ni coating hardness rel. to sulphamate electrolyte selection *(Bulgarian)* 78−88552
Ni, defect removal, obs. by positron annihilation 78−84677
Ni, dislocation structure evolution after hydroextrusion *(Russian)* 80−96530
Ni, dispersion strengthened, high-temp. cyclic deformation 80−21056
Ni electrodeposition from alkaline citrate electrolytes, coating impurity quantities and props. *(Russian)* 79−8252
Ni electroless plating, effect of ultrasonic irrad. 79−33953
Ni, grain boundary defect structure, hardening effects, TEM 80−103365
Ni, hardness after-effect studied by anelastic relaxation 80−66570
Ni powders, stereological appl. in study of compacting process, elec. and mech. props. *(French)* 80−40286
Ni, rolling texture, athermal softening *(Russian)* 77−66655
Ni single crystal, stretched, electron microscope exam. of deformation cell structure during polygonization *(German)* 80−7651
Ni sputtered coating microstructure on mechanically activated cathode *(Russian)* 79−91586
Ni-Al film, co-evaporated, comp.-depend. struct. and morphological changes 79−87020
Ni-Al_2O_3 cermet, fabrication and mech. characts. 79−38781
Ni-Al-Mo (12.7, 21.6 wt.%), directionally solidified eutectic composite, precipitation 80−108454
Ni-Al-Si, β-phase stability *(Russian)* 78−39738
Ni-Al(-Si), diffusion, lattice parameter, microhardness, and constitution, effect of Si additions *(Russian)* 80−84316
Ni-based-Ta(Cn,N) hard metals, isostatic hot pressing influence on mechanical properties 78−92219
Ni-C-W-Cr(-Mo), Vickers hardness and crystallisation temp. 80−16361
Ni-Co-Cr-Mo-Al, Astroloy, extruded powder metallurgy superalloy, recrystallisation study 79−4976
Ni-Cr (20 wt.%), high temp. frictional characts. 80−21118
Ni-Cr (33 at.%), US deform. effect on short range order form. *(Russian)* 78−39839
Ni-Cr (33.3 at.%) alloy, ordering after US deform., microhardness and elec. resist. meas. *(Russian)* 79−20113
Ni-Cr alloy, structural changes, during thermal stress cracking, X-ray and microhardness meas. *(Russian)* 78−35496
Ni-Cr-Al-Ti alloy type ZhS6U, effects of heat treatment in high vel. gas streams on props. 79−57025
Ni-Cr-Fe-Mo-Co (21.41, 19.28, 8.64, 2.16 wt.%), Hastelloy alloy X, exam. of thermal stability 78−84865
Ni-Cr-Mo-C hardfacing alloy, hardness and abrasive wear resistance 79−79117
Ni-Cr-P, amorphous, corrosion behaviour, immersion tests and electrochem. meas. *(Japanese)* 80−85085
Ni-Cr-W-C(Si) hardness, corrosion resistance, wear resistance tests in 10% HCl *(German)* 78−92368
Ni-Cr-W-Co-Ti heat resistant alloy ZhS6K, fatigue resistance, heat treatment and protective coating effects 77−81320
Ni-Cr-W-Mo-Ti-Al alloy KhN67MVTYu, heat treatment effect on mech. props. 77−70082
Ni-Cr(Mo), solid soln., US effect on mech. props. *(Russian)* 78−23819
Ni-Fe-Mo-Cu (79, 16, 4.3, 0.7 wt.%) K-state formation, physical props. exam. 78−47761
Ni-Fe-Nb (Mo), magnetic alloy, TEM and X-ray obs. *(Chinese)* 80−24401
Ni-Fe-Nb alloys, mag. permeability and struct. *(Chinese)* 78−84450
Ni-Fe-Nb-Al (11.2, 8.09, 79.66 wt.%), modulated struct. growth process rel. to ageing *(Chinese)* 80−66541
Ni-Fe-Nb-Al alloys, mag. permeability and struct. *(Chinese)* 78−84450
Ni-Fe-Nb-Al(-Mo), wear resisting mag. head material, mag. props. and struct. 80−35350
Ni-Fe-Nb-Mo (11.42, 6.92, 1.54 wt.%), Hardperm, high magnetic permeability alloys 77−8361
Ni-Ge binary system, phase diagram rel. to that of Co-Ge *(French)* 80−97463
Ni-Mo-C(-Cr)(W), Vickers hardness and crystallisation temp. 80−16361
Ni-P (8 wt.%), protective coating for wear and corrosion resistance of steel 77−21329
Ni-P-Al_2O_3 (SiC), composite deposit electrodeposition *(Russian)* 78−35326
Ni-SiC(WC), dispersion hardened coating, chemically deposited using electroless baths, exam. of protection props. 79−34208
Ni-Ta (70, 30 wt.%) metallic glass, struct. and crystn. *(Russian)* 80−70136
Ni-Ti mech. memory alloys, tensile props. *(Korean)* 77−63724
Ni-Ti-P, amorphous, corrosion behaviour, immersion tests and electrochem. meas. *(Japanese)* 80−85085
Ni-TiO_2 electrochem. composite coating phase composition and microhardness factors *(Russian)* 79−91598
Ni-Zn ferrites, hot-pressed, key props. 78−15348
Ni-Zr, amorphous phase form. in Zr-poor region, hardness and fracture strength *(Japanese)* 80−84914
Ni-ZrO_2, thin layers, vapour deposited, dispersion strengthened, exam. of struct., mech. props. 78−80554
β'-NiAl, ordered, hardness after-effect studied by anelastic relaxation 80−66570
$Ni_{36}Fe_{32}Cr_{14}P_{12}B_6$, metallic glass, crystallisation 79−77520
$Ni_{36}Fe_{32}Cr_{14}P_{12}B_6$ metallic glass, mech. props. and thermal stability 80−76362
NiO:Mn, microhardness, plasticity, ageing effects 79−43291
Ni_2P, CVD on Mo plate, microhardness and resist. to chem. attack 79−66009
α-Np, deform. modes around hardness indentations 77−20009
P_2O_5-Al_2O_3-Na_2O-K_2O-Li_2O-(CaO+MgO) glass system, ion exchange effect on mech. props. 80−30229
$P_2Se_xS_y$ glass, thermophysical props., 303-413K, struct. interpretation 78−47615
P_2Se_xSy glass, vitrification temp., elec. props. and hardness meas. *(Russian)* 77−28177
hardness continued
PVC-Cu, particulate composite, mech. props. effect of particle size 78−95799
Pb-Al_2O_3 composites, mech. alloyed, hot hardness meas. *(Japanese)* 78−84830
Pb-Sb battery grids, ageing behaviour obs., effects of casting and cooling 79−100517
Pb-Sn(Cd)-Te, microhardness meas. as function of applied load, elec. props. exam. 78−48493
PbO-B_2O_3 glasses, microhardness 80−66612
PbS sputtered film microhardness, influence of gas discharge *(Russian)* 80−49560
PbS-Sb system alloys, phase diagram, composition depend. of microhardness and thermo-EMF 77−25028
$Pb_{0.95}Sr_{0.5}(Zr_{0.53}Ti_{0.47})O_3+Nb_2O_5$, optimum comp. for soft ferroelectric ceramic 77−43938
PbTe, microhardness meas. as function of applied load, elec. props. exam. 78−48493
PbTe:Ga, location, behaviour of Ga, electrophysical props. meas. 79−38016
PbTe-InTe system, phase interactions and solid soln. form., physicochem. and elec. characteris. 80−104129
PbTe-SnTe solid solns., directional solidification 77−44149
Pd electrodeposited layers, props., deposition parameters influence *(German)* 80−20808
Pd-Ti, hydrogenation, lattice spacings, microhardness and mag. susceptibility meas. 79−77557
RbH_2AsO_4, microhardness, expt. determ. 79−24603
RbH_2PO_4 crystals, plastic deform. and mech. props. 79−79035
RbH_2PO_4, microhardness, expt. determ. 79−24603
Re coating on cemented carbides, CVD, hardness *(German)* 78−64777
Re-Zr-V, constitutional diagram *(Russian)* 79−56956
Re+rare earth oxide cermets, prep. and props. 78−27466
ReO_3, hardness anisotropy, comp. depend. 79−29181
Re_xSi_3, X-ray cryst. struct. determ., microhardness rel. to Re content 80−84142
Sb-Se-I, phase diagrams of various cross-sections 78−44093
$SbS_xSe_{1-x}I$ layer elec. and ferroelec. props., mech. stress effects *(Russian)* 80−50279
Si crystal, crack initation threshold, SEM and acoustic emission study 79−70157
Si, high O conc., electrical and mechanical props., influence of heat treatment 77−35934
Si, local mechanical defects, annealing and effect on autoepitaxial growth *(Russian)* 80−7701
Si, near (111) surface, SEM study of scratches and fracture initiation by pointed indenter 80−71734
Si, plates, semicond., scribing marks rel. to sclerometric microhardness 79−15891
Si semiconductor-metal transition and indentation hardness 78−35499
Si, single crystal, exam. of microhardness using static indentation 79−52517
Si, yield stress from Hugoniot elastic limit and elastic consts., Knoop hardness 79−83261
Si-Al(Ti)C, sintered, exam. of props. 80−25644
Si-Y-Al-O-N glasses, compositional anal., hardness depend. on N_2 content 79−34129
SiB_4, mech. and thermal props. 80−21083
SiC (6H), slip systems and plastic deform. at high temp., Knoop hardness meas. 79−87683
SiC, abrasive, evaluation of brittleness, contact endurance by cyclic microhardness 79−15890
SiC, chem. stability, mech. and thermal props. rel. to appls. 80−21103
SiC, effect of crystallographic anisotropy on Knoop microhardness 80−66626
SiC fibre reinforced Ni-Cr alumina coated fibres, hot pressed, annealed, IR study 78−60623
SiC, phase transition under isostatic press., microhardness meas., −196 to 1700°C 79−19318
SiC, polycrystn., crack initation threshold, SEM and acoustic emission study 79−70157
SiC, reaction densified, controlled surface flaw initiated fracture 77−8919
SiC single cryst., reaction-bonded and hot pressed, hardness and wear behaviour 79−38970
SiC single crystal, hot hardness and creep behaviour 79−100247
SiC-B_4C eutectic, directional solidification, growth and mech. props. 79−91638
SiC-Ni based superalloy reaction, at elevated temps. 80−3287
SiN_x, film by magnetron sputtering, composition, hardness and optical props. 78−3047
Si_3N_4 amorphous films, CVD mech. and thermal props. *(Japanese)* 77−90280
Si_3N_4, CVD, Vickers microhardness, effect of deposition parameters 77−56079
Si_3N_4, fracture toughness meas. using Knoop indentation method *(German)* 80−25830
α-Si_3N_4, hardness anisotropy 78−95804
Si_3N_4, hot-pressed, fracture in bending *(Japanese)* 79−79113
Si_3N_4, pyrolytic, prep. by CVD, bulk and coatings, exam. of electrical, optical and physical props. 79−95935
Si_3N_4, pyrolytically-deposited, engng. significance 79−38746
Si_3N_4, reaction-bonded and hot pressed, hardness and wear behaviour 79−38970
α-Si_3N_4 single crysts., growth, morphology, hardness and slip system 79−83112
Si_3N_4 with Y_2O_3 and Al_2O_3 additions, hot pressed, exam. of mech. props., grain boundary crystallization 79−20009
SiO_2, vacuum deposited, 7-10 μ, microhardness and structure 78−19669
SiO_2-Na_2O-CaO-MgO-Fe_2O_3-Al_2O_3-SO_3-Sn thermally polished, exam. of strength of surfaces 80−25887
SiO_2-Na_2O-K_2O water glass with polyethylene filler, thermogravimetric and thermomechanical anal. 79−20020
SiO_2-$PO_{5/2}$ glass, props. and struct. *(Japanese)* 77−27837
SiO_x film, durable optical, ion plating onto plastics, optical and mech. props. 80−38141
SiTe-GaTe, thermo-EMF, elec. cond. and solubility 77−20346
$SmB_4(B_6)$, growth by soln. method, struct. and mech. props. 80−16168
SnO_2 film, pure and Sb doped, transparent cond., prop., characts., stability, struct. *(Japanese)* 78−47889

hardness continued
$SnSe$-Sb_2Se_3 system, phase diagram, differential thermal, microstruct., X-ray phase and microstructure anal. 77−16555
SnTe, annealed, iodide method of prep., props. meas. 80−71591
SnTe-Tl_2Te, phase and elec. props. 77−48406
strengthened by lattice transformations, mech. props. study *(Japanese)* 79−43332
(Ta,Ti)B_2 on graphite, CVD coating, hardness meas., SEM study 80−24760
Ta, film, CVD on silica, struct. and mech. props. 77−24965
Ta-Ir(Rh) system glasses, form., crystn. and microhardness, resist. obs. 80−89178
Ta-N (0.6 to 6.5 at.%), supersaturated solid soln., precipitation 79−96028
Ta-O solid soln., interstitial ordering and precipitation at 100 to 270°C, exam. 78−52813
Ta(C,N)-Ni-HfC(HfN)(Mo_2C)(VC), sintering, prod. of hard metals 78−11155
TaC-TaB_2, phase diag., solubilities, reactions 77−63643
TaN film, growth by CVD, microhardness and corrosion resist. 77−36404
Ta_2O_5, reactive DC sputtering deposited films with magnetron-plasmatron, mechanical elec., optical props. 80−25566
$TaSi_2$-$CrSi_2$, phase equilib., struct. and props. 80−50608
$Ta_{16}W_{18}O_{94}$, characterisation of thermally contracting tungstates 78−63869
Ta_2WO_8, characterisation of thermally contracting tungstates 78−63869
$Ta_{22}W_4O_{67}$, characterisation of thermally contracting tungstates 78−63869
Tb-Sn-Se system, cross section Tb_2Se_3-$SnSe_2$ phase diagram, physicochem. anal. 79−87621
Tc, temp. depend. of hardness and hot plastic strain *(Russian)* 79−74202
Te, synthetic, optical props. in visible spectrum and microhardness meas. *(French)* 77−28590
Te-based eutectics, crystn. rate effect on electrophys. props. mutual solubility effect 80−60774
Te-Bi_2Te_3 oriented eutectic, microhardness, influence of size of phases *(Russian)* 78−92322
Te-Sb_2Te_3 oriented eutectic, microhardness, influence of size of phases *(Russian)* 78−92322
$TeSe_{19}$ glass, crystallisation kinetics 77−35484
Th-Fe (20 to 70 at.%), amorphous alloy, electrical resistivity and thermal stability 80−33901
(Ti,Cr)B_2, sintering kinetics and props. 80−100811
(Ti, Cr)B_2-based alloys, densification of powder mixtures by hot-pressing, elec. and mech. props. 80−20812
(Ti,V)C, activated reactive evaporation deposited films, annealing study, microstructure 80−24762
(Ti,Zr)B_2 on graphite, CVD coatings, hardness meas., SEM study 80−24760
Ti, (0.9998), positron lineshape parameter and hardness rel. to annealing temp. 80−3281
Ti alloy, VT16, decomp. of α'' martensite during continuous heating *(Russian)* 78−48370
Ti alloy, VT16, decomposition of metastable β-phase *(Russian)* 78−68710
Ti alloy OT4, high plasticity effect 80−35272
Ti alloy VT20, phase composition and structure effect on mech. props. 79−38958
Ti alloys, β-annealing and controlled rate quenching effects 78−80568
Ti alloys, correl. with strength 79−87707
α-βTi alloys, high strength, heat-treated weldments, intergranular fracture 80−21097
Ti base alloys, melt-extracted polycryst., mech. props. 80−76360
Ti diffusion coated cast Fe, wear resistance 79−52459
α-Ti, diffusion of O_2, 700 to 950°C, lattice parameter and microhardness meas. *(French)* 79−86929
Ti, industrial grade structural changes during polygonization *(Russian)* 78−19779
Ti, interaction with N_2 at elevated temp., kinetics and mechanism of reaction 77−12741
Ti ion planted coating on steel 77−70217
Ti, laser generated stress waves, effect on microstruct. hardness and strength 79−69192
Ti, neutron irradiated, relation between microstructure and recovery behaviour 77−15456
Ti, physicomechanical and wear props., influence of ion implantation and overlay coatings 80−40603
Ti, plastic deform. dynamics, mech. characts. and phys. props., effect of O_2 *(French)* 80−45353
Ti sintered, struct. stability, effect of dispersed refractory compound inclusions 77−28825
Ti, tribological investigation using two-cylinder tribometer *(German)* 77−25164
Ti-Al, elec. spark Al doping of VT-18, surface struct. and props. *(Russian)* 80−76398
Ti-Al-H, H effect on mech. props. and lattice constants 80−21036
Ti-Al-Mo-Zr alloy VT9, Cu-Cr(Ni) coated, plastic deform. and diffusion annealing effect on props. *(Russian)* 78−35425
Ti-Al-V (6,4 wt.%), porous compacts, determ. of effective stress in hot pressing 80−100807
Ti-Al-V-Cr-Zr-Mo (3, 8, 6, 4, wt.%), phase transforms. 79−100113
Ti-Al-Zr (3,3 wt.%), W alloying addition effects on mech. props. *(Russian)* 77−59860
Ti-Al(Cr), interaction with N_2 at elevated temp., nitridation behaviour 77−12742
Ti-Be-Si glass ribbons, physical and mech. props. 78−95767
Ti-coated C steel, effect of heat treatment on struct. and props. 77−56159
Ti-Cr-B system, self-propagating high temp. synthesis, crystallochemical and mech. props. 80−20861
Ti-M-V-Cr-Mo, RMI 38644, shock loaded, age hardening 79−29112
Ti-Mn base beta alloys, H effect on stability solid soln., hardness *(Japanese)* 77−81261
β−Ti-Mo, thermal instability, hardness and tensile deform. *(Japanese)* 80−71703
Ti-Mo (16 at.%), effect of H impurities on lattice spacing, hardness, and plastic strain *(Russian)* 79−11664
Ti-Mo-Zr-Sn (11.5, 6.0, 4.5 wt.%), mech. property, microstruct. relationships 80−84961

hardness continued
β-Ti-Mo-Zr-Sn(11.5, 6, 4.5 wt.%), metastable phase III, microstruct. and age hardening response 80−84945
Ti-N_2, condensate formed by plasma flow precipitation in vacuum, cryst. and surface props. *(Russian)* 80−100788
Ti-Nb (4.32 wt%), high temp. oxidation kinetics under 1 bar pressure, 1255-1471K 80−89410
Ti-Nb-W, 20 to 1000°C, isothermal section, X-ray anal., microstruct., hardness, cond., transform. *(Russian)* 77−55947
Ti-Nb-Zr-Ta, superconducting props. comp. depend., stress effects and precipitation behaviour, X-ray scatt. 80−93059
Ti-Ni-Si metallic glass, prep., thermal and mech. props. 78−64497
Ti-Ru (0.05 to 90 wt.%) hardness, thermal EMF, electrical conductivity, in annealed or quenched state *(Russian)* 77−55998
Ti-Ta (4.37 wt%), oxidation kinetics, 1258-1473K, and at pressure of 0.013, 0.133 and 1.0 bar 80−89411
Ti-transition metal, transition metal additives influence on struct., specific resistance, microhardness, mech. props. 79−29078
Ti-V-Si (30, 1 at%), quenched and aged, hardness, tensile behaviour and phase transform. 79−11646
βTi-V-Si (40, 1 at.%), Si effect of precipitation and age hardening 77−63676
Ti-Zr-Mo alloy, effect of O_2 on elec. resistivity, microhardness, mech. props. 77−56092
α-Ti-Zr-W, effect of W impurity on mech. preps. 80−16392
Ti_3Al, phase transitions and physical props. 77−25068
Ti_2AlC, Ti_3AlC, TiC, phys. props. 77−43602
Ti_2AlN, prep. and props. 77−28745
Ti(B,N), CVD coating on cutting tool 79−61802
TiB_2 coating, on WC-Co alloy cutting plates, hardness and struct. 80−21175
TiB_2 coatings, prep. by CVD and interaction with substrate 79−24680
TiB_2, erosion resistant boride coating on Ti and Ti alloys 79−20290
TiB_2, hardness of sintered material 78−60636
TiB_2 high temp. hardness of single crystals *(Japanese)* 77−48522
$Ti_{50}Be_{40}Zr_{10}$ glass, mech. props., X-ray diffr. exam. 78−11292
TiC, activated reactive evaporation deposited films, annealing study, microstructure 80−24762
TiC, ageing and ordering phenomena *(Russian)* 78−39807
TiC coatings, on cemented carbides, struct. and hardness 80−59771
TiC coatings on steels and hard alloys 80−76414
TiC, deformation behaviour during rubbing in wide temp. range 80−16486
TiC, deposited by activated reactive evaporation, TEM and hardness 79−23872
TiC film, Au-dispersed, struct., hardness and wear rate 77−77493
TiC, frictional characts. and contact-zone deform. in homogeneity range 80−66673
TiC, laser CVD, coating characterisation 80−93494
TiC, micro-Vickers hardness, up to 1500°C 77−28890
TiC, microhardness and charact. hardness 79−52376
TiC single crystal, micro-Vickers hardness meas. up to 1500°C *(Japanese)* 78−23804
TiC single crystals, growth from vapour by modified hot wire method, temp. effect on habit 79−61509
TiC-Au film, prep. by activated reactive evaporation, struct. and mech. props. *(Japanese)* 78−3252
TiC-B, struct. and mech. props. 80−55461
TiC-Cr_3C_2(Cr_3C_2-WC), powder mixture, steel bonded, exam. of sintering behaviour 78−52712
TiC-Ni composite coating, activated reactive evaporation prep., structure 77−44393
TiC-steel composite, effect of method of Cr additions on props. 78−15341
TiC-TiB_2, friction characts., comp. depend., 20-1000°C 80−3203
TiC-TiB_2, preparation and high temp. antifriction props. 79−1918
TiC-TiB_2, strength and antifriction props. over wider range of concs. 80−50673
TiC-TiN, hardness var. charact. in homogeneity field 80−3192
TiC-TiN, physicochem. props., comp. depend. 80−55370
TiC-VC(Nbc)(YaC), comp. depend. 77−28772
TiC-WC-TaC carbide mixture in plasma reactor *(German)* 77−1819
TiC_x, electron energy spectrum and phys. props. in homogeneous region *(Russian)* 77−31941
TiC_x film, formation by hollow cathode discharge reactive deposition process, on mild steel sheet 79−24451
TiC_xN_y film, on C steel, Vickers hardness and adhesion strength 79−65338
$TiCrB_2$-Ni(Ni-Mo) systems, interphase reactions, electron probe anal., metallography and hardness exam. 80−2990
TiI_4, thermal diffusivity, near FCC to BCC transition 80−59740
TiI_4:C, deep doping during ion-beam welding, microhardness meas. 79−19294
TiN, CVD growth in US field, effect on adherence and hardness 77−59696
TiN layers formation, on steel substrate, microchardness and structure obs. *(Hungarian)* 80−2965
TiN, reactive ion plating with auxiliary discharge deposition conditions influence on film props. 80−20801
TiN-Al_2O_3, exam. of sintering and densification kinetics, and physical props. 79−95986
TiN-Ti_2N, activated reactive evaporation formed deposits, microstructure, transformation depend. on depositing conditions 80−24761
TiN_x, deposition by hollow cathode discharge process, and hardness 79−24452
TiN_x, ion condensing metal plasma stream, coating microhardness, chemical reactions 79−42426
Ti_3N_4 plasma condensation on steel and carbide *(Russian)* 80−20796
TiO-ZrO_2, pseudo binary system, effect of Ti addition on struct. and props. of zirconia 79−11583
TiO_2, reactive DC sputtering deposited films with magnetron-plasmatron, mechanical elec., optical props. 80−25566
TiO_2, sintering, hardness, density, elec. cond. and colour *(Japanese)* 78−68659
TiO_x film, durable optical, ion plating onto plastics, optical and mech. props. 80−38141
$TiSi_2$-$CrSi_2$, phase equilib., struct. and props. 80−50608
Ti_xSi_y, work function rel. to phys. props. 77−47887
Tl-Bi-Sb-Te system, peritectic reactions in $TlBiTe_2$-$TlSbTe_2$ cross section, crystn. character 80−108406

hardness continued
Tl-Sn-Te system equilibria, polythermal and isothermal cross sections obs., ternary cpd. form. 80−104128
Tl-Te, phase equilibrium exam., using DTA, X-ray diffraction, and hardness 79−1846
Tl_3AsS_4, crystal growth by Bridgman-Stockbarger method, exam. of props. 79−11506
$TlGaS_2$-$TlGaSe_2$, phase and composition-property diagrams 80−55366
$TlInS_2$-$TlInSe_2$, phase and composition-property diagrams 80−55366
Tl_2S-Ag_2S system, phase equil., DTA, X-ray and microhardness obs. 79−38803
Tl_2S-SnS, phase equilibria exam. 80−55369
Tl_2S-Tl_2Se(Tl_2Te), exam. of phase equilibria, using DTA, X-ray phase analysis and microhardness 79−4953
Tl_3Se-SnSe(PbSe) systems, phase equilib. 79−52181
$TlSe.As_2Se_3$, $Tl_2Se.As_2Se_3$, γ-irrad. effects on mech. props. 77−80567
TlTe, melt, elec. cond., surface tension, microhardness, influence of impurities 80−88551
Tl_2Te, melt, resistivity, surface tension, microhardness, influence of impurities 80−88552
Tl_2Te-HgTe(HgSe) systems, phase diagrams 79−87620
Tl_5Te_3-Tl_4SnTe_3-Tl_4PbTe_3, phase equilib., DTA, SPA and microhardness meas. 80−96628
U-Al, transform. and struct. changes, cooling, cooling rate effect *(Korean)* 77−63660
UO_2 microspheres, prep. from $UO_3(NH_3)_2$, exam. of mech. and physical preps. 79−6758
US-UC-UC_2 system, potential nuclear fuels, phase solid soln. studies, prep. and props. exam. 79−40996
$US_xN_yO_z$, neutron diffraction exam. of structure 78−79777
$(V,Nb)_3Ga$, $(V,Nb)_3Ge$ and $(V,Nb)_3Si$ solid solns., conc. depend. 77−36006
(V,Ti)C+(Ni,Mo) cermet systems, performance through hardness vs crack resist. plots 79−79099
V and V-Mo, mechanical properties, O, N_2 and C addition effects 79−52356
V cathodic deposition, from crude V, V_2C and VC, hardness meas. *(Japanese)* 79−78908
V-Ga-Cu, phase diagram *(Russian)* 77−25014
V-Mo, effect of ion plated Mo on corrosion in liquid Na, mech. props. 78−53020
V-Ni-Al, phase equilib., elect. cond., hardness *(Russian)* 77−66627
V-Zr-N quasi-binary section, long term hardness to compare heat resistance 78−3223
VC, damage sustained during neutron irradiation 77−1841
VC-TiC, deposited by activated reactive evaporation, TEM and hardness 79−23872
VC-TiC coating, high rate deposition by activated reactive evaporation, and characterisation 78−11372
VC_x coating, C steel vanadisation by CVD 80−44454
V_3Ge, A-15 struct. supercond., microhardness, bonding 78−76199
$V_{3-x}M_xGa$, M=Ti, Cr, Mn, Fe, Co, Ni, cryst. struct. and microhardness meas. 79−86740
δ-VMn, ordering and disordering behaviours 77−48428
V_2O_5 single cryt. microhardness and anisotropy of mech. props. *(French)* 80−50713
V_3Si, A-15 struct. supercond., microhardness, bonding 78−76199
(W, Mo)C, hard-facing applications, effect of Mo on struct and hardness of WC 80−108474
W fibre, KSiAl doped, recrystallisation, Li diffusion effects, hardness, strength, microstructure meas. *(German)* 78−64644
W fibre reinforced Ni, high temp. stability 77−48372
W, microhardness and charact. hardness 79−52376
W, strength, temp. depend. 77−1871
W-Al_2O_3 cermet films, oxide evaporation deposited on Mo, Ti, Al_2O_3 substrates, struct., props. 80−25581
W-Cu-Co(Ni), electrical contact material, comparison of Co and Ni effects *(Korean)* 78−10539
W-Cu-(Ti)(Zr), exam. of mech. props. as function of temp., composition, and oxidation props. 80−16472
W-Fe-Co, sintering and mechanical props. *(Japanese)* 80−21086
W-Hf-C, phase equilib. 80−55348
W-Ni-Fe, W-Ni-Fe-Mo (Mn), sintering and mechanical props. *(Japanese)* 80−21086
W-Ni-Fe(Co)(Cr), structural characterisation *(French)* 77−56074
W-Os system films, condensation temp., conc., and phase comp. effect on struct. and props. *(Russian)* 80−24749
W-Re film, obtained by electron beam volatilisation and vac. condensation, props. *(Russian)* 77−24490
W-WC, activated sintering, mech. props. *(Korean)* 78−60622
WB_{12}, growth from melt and phys. props. 80−20782
W_2B_5-based alloys, mech. props., rel. to appl. as electrodes in electrospark machining 80−21174
WC, deformation behaviour during rubbing in wide temp. range 80−16486
WC, plasma sprayed coating 78−68835
WC-Co, developments, properties and fabrication processes *(Dutch)* 77−70021
WC-Co, exam. of effect of continuous carbide phase, on hardness, and deformation 78−52974
WC-Co, VK type hard alloy, influence of residual stresses on static strength 77−1862
WC-Co alloys, P additions, effect on hot pressing, hardness and wear resist. 78−11162
WC-Co cemented carbide, indentation fracture, operative fracture mode survey 77−70183
WC-Co cemented carbides, effect of Co form and distrib. in prep. starting mixture 78−44072
WC-Co cemented carbides, rel. between Palmqvist indentation toughness and fracture toughness 79−70155
WC-Co hard alloys, hot pressed, mech. props. 79−100260
WC-Co hard metal, stress conc. factor and stress intensity factor, rel. to wear *(German)* 78−11335
WC-Co powder, prep. by direct carburisation of WO_3 in presence of Co_3O_4 80−50573
WC-Co-Cu, interdiffusion up to 1120°C 78−11492
WC-TaC-Co, cemented carbide, strength improvement by hot isostatic pressing 78−84969
WC_x formation during pyrolysis of WCl_6 and toluene, coating props. 77−36682

hardness continued
W_6Co_6C cemented carbide substrate, TiC CVD coating, structure, composition and hardness exam. 78−11425
WCuB prep. by infiltration of W skeleton by CuB, hardness meas. *(German)* 78−64508
$W_{50}Fe_{50}$ glassy alloy, refractory, triode sputtered 80−75185
WSi_2 on W, coating by local heating 77−81335
Y-Si-Al-O-N glass, prep. and props. 80−25647
$Y_3Al_5O_{12}$ crystals, variation of microhardness anisotropy with heat treatment 79−56053
$YbAlO_3$, single crysts., prep. and phys. props., X-ray struct. anal. 79−4298
YbB_6, growth by soln. method, struct. and mech. props. 80−16168
Zircaloy, dispersion and spheroidisation treatment of δ ZrH, effect on corrosion resistance 79−76072
Zn, wear resistant coating, effect of surface-active substances in electrodeposition on props. *(Russian)* 78−11359
Zn-Al (22 at.%), heat treatment and straining effect on fracture and corrosion 79−87672
$ZnAs_2$, homogeneity region and electrophys. props. 80−60833
Zn_3As_2-ZnSe(ZnTe) solid solutions, single cryst., phase equilib. and props. 80−16283
ZnO (0001) surface, hardness, electrolyte pH and bias voltage effect 78−47654
ZnO ($10\bar{1}0$) surface bias voltage effect on hardness, charge exchange near dislocations 78−52078
ZnO, chemomechanical effects 79−82431
ZnO-$Al_2O_3SiO_2$, transparent glass-ceramic, microstruct., physical props., crystallisation ht. treatment depend. 78−80506
ZnS, ultra-microhardness testing for vacuum deposited film and bulk specimen 78−79910
ZnS:Ag, struct. and mech. props. 78−22753
ZnS-ZnSe single cryst. grown from melt, anisotropy of mech. props. and struct. 77−24303
ZnSe+CeTe⇄CdSe+ZnTe ternary mutual system, phase equilib. 79−52179
α-Zr, polycrystalline, cyclic deformation *(Japanese)* 78−68757
Zr, structural changes during plastic deform. *(Russian)* 77−8880
Zr-Cr-B system, self-propagating high temp. synthesis, crystallochemical and mech. props. 80−20861
Zr-Dy dil. alloys, plastically deformed, mech. props. and microstruct. *(Russian)* 79−20112
β-Zr-Mo-(Al)(Ti)(La), metastable, deform. induced transform. 78−52805
Zr-N_2, condensate formed by plasma flow precipitation in vacuum, cryst. and surface props. *(Russian)* 80−100788
Zr-Nb (2.5 wt.%), fuel cladding, anisotropy after creep and irradiaton 78−7001
Zr-Nb (2.5 wt.%), seam welding tubing, microstruct. in weld region 79−61621
Zr-Nb (2.5 wt.%), strain ageing 77−77511
Zr-Ru(Pd), heat treated, mech. props. and struct. 78−80571
Zr_3Al, cold worked, annealing effects 77−36535
Zr_3Al, ordered polycrystals, hardness and flow stress relationship 77−44309
ZrB_2, microhardness and charact. hardness 79−52376
ZrC based cermets, strength and gas-abrasive wear resistance 77−25163
ZrC, microhardness and charact. hardness 79−52376
ZrC, single cryst. growth by modified hot-filament method, cryst. morphology and microhardness 79−19983
ZrC-C, CVD, microhardness and microstruct. 77−8916
ZrC-NbC-MoC_{1-x} alloys, physicomech. props., comp. depend. 79−66097
ZrC-ZrB_2, friction charact., comp. depend., 20-1400°C 80−3203
ZrC-ZrB_2, preparation and high temp. antifriction props. 79−1918
ZrC-ZrB_2, strength and antifriction props. over wider range of concs. 80−50673
$ZrC_{0.84}$, single crystal work function, thermionic emission and contact pot., microhardness and binding 79−19649
$ZrH_{1.9}$, neutron irrad. induced defects, nature and thermal stability 77−50246
ZrN, microhardness and resist. to brittle fracture 79−87715
ZrN-Al_2O_3, exam. of sintering and densification kinetics, and physical props. 79−95986
ZrO_2, near-surface phase transforms., effect of grinding and polishing 78−15557
ZrO_2, partially stabilised, toughening mechanism 77−56084
ZrO_2/Al clad powder prep. and physicomech. props. 79−29010
ZrO_2-CaO, stabilised microspheres, structure, mechanical props. *(Russian)* 80−100379
ZrO_2-Nd_2O_3(Sm_2O_3)(Dy_2O_3) eutectic, unidirectional solidification, microstruct. and crystallographic characterization 80−35176
ZrO_2-Y_2O_3, stabilised microspheres, structure, mechanical props. *(Russian)* 80−100379
$ZrSi_2$, work function rel. to phys. props. 77−47887

hardness testing
abrasive material, brittleness and contact endurance eval. by cyclic microhardness 79−15890
accelerated method for long-term strength determ. 77−40494
analysis of recording and performance 77−86278
automatic loading device for microhardness testing on PMT-3 tester 77−77668
ball insertion curves, effect of load appl. on indices 78−60903
bicylindrical indentor, for microhardness meas. 80−40642
Brinell press attachment for testing at 250 to 300°C 78−56842
brittle, single crystal, exam. of microhardness using static indentation 79−52517
cemented carbide, simple evaluation method 77−32748
clastic rock softening characteristic tests *(Japanese)* 78−49013
colorimetric method for high frequency treated bandsaw blades 79−74325
cubic single crystals, hardness meas. by spherical indentation 80−16622
curved surfaces, HRC hardness determination method 77−63852
deadweight standard Rockwell hardness testing machine, design and performance 78−88592
device, attachment for automatic appl. of identations 77−1907
diamond indenters, microhardness meas. technique, rel. to quantifying bonding changes 79−24606
equipment for production line inspection 79−29320
fatigued steel brittle transition temp. meas. *(Japanese)* 79−87797

hardness testing continued
film, diamond indentation and draw tester for meas. of ultra-adherence 78−72944
filmed structures, hardness and adhesion meas., scratch technique 80−50805
gauges, PMT-3 and PMT-5, comparison of metrological props. 79−20317
glass mechanical property determ. *(German)* 80−40669
griseofulvin tablets, tensile strength and disintegration times 77−60027
impact testing machine operating over wide range of deform. rates 78−3271
indentation, elastic contact problem, automatic anal., point-matching method 77−31213
indentation depth measurement 79−83418
indentation tester, vertical displacement, for compacted powders, plastics and foodstfuffs 80−58988
indentation testing, mech. characts. calcs. inc. elastic strains *(Russian)* 78−95863
induction hardened parts, high frequency, heat treatment quality inspection 78−48598
Knoop-indentation, used for determination of self-contained stress *(German)* 80−21200
mechanical anisotropy evaluation, using hardness test *(Polish)* 78−48575
metal, hardening temp. determ. using pulsed laser 78−72942
metal, stress/strain diagram determ. by spherical punch *(German)* 78−76803
metal contact, strain in microrelief ridge 77−44443
metallic materials, dynamic hardness testing, energy meas. principle 80−21241
metals, alloys hardness testing, depth of impression meas., automated 79−15892
metals, NDT of hardness using applied EM transducer 77−56178
metals, review 79−87773
microhardness, Knoop numbers, correction factors, elastic recovery 78−72952
microhardness, meas. method for diagonals of diamond pyramid impression 78−7117
microhardness, methods comparison *(Chinese)* 80−11850
microhardness meas. by ball dropping/recoil velocity ratio 77−81363
microhardness tester recording the indentation diagram 79−57173
microscope, laboratory standard for hardness impression meas. 79−21808
nondestructive hardness test, determ. of elastically homogeneous struct. elastic limit 77−66719
oscillating spring mass system, exam. of system and plastic penetration depth change *(German)* 78−31592
penetrating, deformation of sphere and rough plane obs , in contact with normal load *(Japanese)* 77−19575
plastic deformation, hardness meas. test method *(Hungarian)* 80−97664
plastic pipe *(Japanese)* 77−60017
plastics, automatic hardness testing apparatus, display *(German)* 80−66742
plastics, penetration hardness testing, exam. of thermal effects *(German)* 78−76801
plate impact experiments, optical alignment of impact faces 77−45876
polymer materials, NDT, rigidity and hardness from acoustic, thermal, optical and dielectric props. *(Russian)* 77−48601
portable instrument for hardness determ. by Rockwell technique 77−63854
Rockwell diamond indenters, meas. method rel. to standards 79−66251
scale dependence *(Russian)* 77−52556
scale effect during indentation, role of elastic strains *(Russian)* 79−39062
sclerometric tests, estimation of activation parameters for materials 80−66625
scratching method 80−25953
semiconductor plate, relationship between scribing mark and sclerometric microhardness 79−15891
steel, acoustic hardness testing 79−39088
steel, austenitic, KO 34 samples, electron beam welded, Charpy test expts. *(Hungarian)* 80−104252
steel, crankshaft forgings, by type NChG instrument 78−53133
steel, heat treated small parts, electromagnetic hardness inspection 79−34241
steel, hot-rolled high quality sheet use of stat. maths. for NDT determ. of mech. props. 79−11749
steel, mild, semi-killed, tempering, effect of microstruct. and hardness 77−21184
steel, notched bar impact test specimens, strain hardening distrib. *(German)* 77−60004
steel, stainless austenitic, by Vickers test, precipitation hardening and N_2 effects obs. *(Rumanian)* 77−55973
steel, stress and strain intensity, determ. after plastic deform. using microhardness meas. 80−40641
steel 78−53114
steel 40 G, coercimeters with attached electromagnets used for quality control 80−108672
steel parts, cylindrical, hardness inspection by EM method with higher harmonics 78−23891
steel SS-41, plastic working with vibr., US hardness tester 78−53044
steel tubing, cold rolled, nondestructive mag. method for determ. of mech. props. 78−23903
steels, eutectoid 79−15889
surface layers and microvolumes, physical and mechanical props., continuous indentation calcs. *(Russian)* 80−40629
tempered glass discs, meas. of nonuniform distribution of residual stresses 78−95865
thin crystals and films, nondestructive microhardness testing of near-surface layers 80−71829
tube, thin-walled, Rockwell hardness determ. 78−7125
ultra-microhardness tester, for expts. on vacuum deposited films 78−53161
Vickers hardness meas. of curved-surface components 78−80699
Al alloy, sintering of powder metallurgy parts, metallographic exam. and hardness testing 77−4752
base materials, sclerometric determ. of hardness 77−77670
CdS, (10$\bar{1}$0) face, deformed zones around microimprints 78−23812
$CdTl_2Se_4$:Au, solubility meas. by microhardness method 80−96650
Cr-Mn-Si steel, heat-treatment quality, higher harmonics of EMF obs. 78−60941
hardness testing continued
Fe, cast, grey, eddy current test for hardness certification 80−7733
Fe electrodeposited coatings, microhardness, Ha_5 design appl. 79−39069
Fe, pig, white, mech. props. meas. *(French)* 80−104370
Fe-W-Cr-Mo-Co (18,12,3,x wt.%) alloy, cold working effect obs. *(Japanese)* 77−40428
Na_2O-CaO-SiO_2, dynamic hardness testing, pendulum attenuation, yield stress obs. 79−24699
PdAl-Fe(Ni), phase diagrams, eutectic points and solubility *(Russian)* 80−40333
Ti alloys, hardness meas., peculiarities 79−87774
W, single crysts., microhardness anisotropy determ. by scratching 77−77669
Y_2O_3, plasticity, microhardness testing, indentation, plastic deform. temp. depend. *(French)* 78−56713

harmonic analysis
see also waveform analysis
aeromagnetic anomaly from remanently magnetised Precambrian schist belt, Karnataka, India harmonic inversion 79−44094
analytic function determ. from conjugate harmonic 79−71227
approximation method for anthropomorphic mechanism compensating synergy *(Slovenian)* 77−64920
atmospheric O_3 total amount at Belsk, Poland, harmonic anal. 78−92883
atmospheric pollution and natural radioactivity diurnal waves *(Rumanian)* 79−21009
atmospheric waves in Mediterranean area, zonal harmonic anal. 77−78380
aurora, southern oval, spherical harmonic analysis 78−81487
auroral pulsations, harmonic anal. 79−8736
biharmonic eqn. finite element approx., dual iterative method 77−2524
biological signals, aorta blood pressure, computer analysis 77−52899
cantilever vibration of cantilever-electro-piano *(Japanese)* 79−18634
circuit with variable mutual inductance, canonical equations appl. *(German)* 77−60901
climatology, anal. of 500 mb geopotential height in N.Hemisphere 77−5311
clinometric obs. at Khristoforov (1973-5 period) *(Russian)* 78−3704
conformal partial wave analysis and harmonic analysis in general, book 78−28917
cooling tower supporting columns and reinforcing rings, displacement analyses 78−38187
CRI waveform display, Fourier analysis using SR56 calculator 78−36986
dynamical relativistic Fourier anal., harmonic anal. on Lorentz group 77−82406
E-region ionospheric drift meas. over Udaipur 78−16233
Earth's gravity potential, convergence of spherical harmonics expansion 78−81097
Earth gravity field, harmonics from artificial satellites shallow reson. orbits 78−40805
Earth gravity field, model improvement using Geos 3 (GEM 9 and 10) 80−3909
Earth gravity field, numerical development of spherical functions *(German)* 78−61311
Earth gravity potential, GRIM 2 model determ. and evaluation *(French)* 79−8587
Earth potential, generalisation of Laplace expansion to Earth's surface 77−60337
Earth surface tidal tilts, harmonic anal. and atmospheric press. fluctuations influence *(Russian)* 78−88790
elastic displacement fields, representation by three harmonic functions 79−97208
elastic waves in anisotropic media, asymptotic equipartition of kinetic and strain energy 80−92081
elliptical differential equation, harmonic functions generalisation *(Ukrainian)* 77−49560
EM field problem with a non-linear condition 79−18326
EM induction in rot. conductive Earth, spherical harmonic coeff. 78−44764
EM wave scatt. theory, using vibrator with nonlinear contact 80−1110
exosphere temperature, global model based on Fabry-Perot interferometer meas. from OGO-6 satellite 77−53265
FKSZ stars, astrometric obs. and systematic differences spherical harmonic anal. *(Russian)* 79−44336
geodesy, uniformly distributed data harmonic anal. for global systems geocentric origins comparison 79−57839
geodetic boundary value problem, surface harmonic series soln. 79−62424
geoid, gravimetric, for N.Atlantic, spherical harmonic model 79−62422
geomagnetic activity indices, magnetospheric modulation, harmonic anal. of Km, Kn and Ks 78−40468
geomagnetic daily variation in low latits., anal. 78−36098
geomagnetic Dst space-time patterns during individual mag. storms 77−13184
geomagnetic external spherical harmonic coeffs., solar cycle var. 80−85592
geomagnetic field, definitive spherical harmonic model and secular var. for 1965 78−96133
geomagnetic field, solar cycle vars. of first-degree spherical harmonic components 80−85593
geomagnetic field anal. 78−49164
geomagnetic field models based on total intensity meas., effect of obs. errors 77−9335
geomagnetic potential, series expansion in spherical functions at surface of ellipsoid 77−13057
geomagnetic secular acceleration, spherical harmonic model 79−88249
geomagnetic variations in Japan, monthly mean lunar daily variations, 1958-1973, harmonic anal. 79−96739
geomagnetic vars. in 13-30 year per-od range 78−15962
geopotential, harmonic coeffs., determ. error *(Russian)* 79−5439
gravitational fields of Earth, Moon and Mars, harmonics rel. to stationary points coordinates 78−53805
gravitational potential at planet physical surface, satellite model applicability 79−62774
gravitational potential of asymmetrical body, convergence of expansion in spherical harmonics 78−24479
gravity, anomalous fields, stochastic harmonic analysis 79−35003
gravity, tidal changes at Poltava, 1973 to 1976, harmonic anal. *(Russian)* 78−88782

harmonic analysis continued
gravity anomalies at Earth topographic surface, two-parameter spherical harmonics expansion 80−56337
gravity mean anomaly block sizes and spherical harmonic representation, comment 80−30979
group representations and appls., book 78−32652
instant Fourier transform based on harmonic anal., real-time appls. 77−22402
internal friction peak shapes, harmonic analysis for relax. processes investig. 79−52284
ionosphere F_2-layer, analytic description of geometric parameters maps by spherical functions 79−53616
Ising model 77−30112
Laplace eqn., half plane representations and harmonic continuation 77−22391
lipid bilayer nonlinear electric effects studied by harmonic anal. 78−24188
lunar daily geomagnetic variations at Sabhawala and Hyderabad, harmonic anal. 79−44097
lunar gravity field, harmonic anal. 77−87290
lunar relief and selenoid deform. 80−72800
lunar topography and gravity, harmonic anal. 77−60634
magnetospheric modulation of geomag. activity, harmonic anal. of am, an and as indices 79−66605
Mars global topography, harmonics and geophysical implications 78−85880
mechanical light modulator, harmonic anal. of noise spectrum 78−1362
meteor stream radiant distrib. using spherical harmonic analysis 78−20648
mixed boundary value problem in three dimens. 77−71184
mixed problems in theory of harmonic functions, Monte Carlo method appl. 79−10464
Moon gravitational potential, third and fourth harmonics rel. to coordinate system for selenodetic reference network *(Russian)* 80−72797
multidimensional contour resolution into components 79−84941
mutual gravitational potential of N solid bodies, harmonic coeffs. expansion 79−12390
neutron transport, spherical harmonics approximations 77−3065
nonlinear dispersive and dissipative wave propagation 77−74231
nonlinear multidegree-of-freedom system, superdivision harmonic oscillations due to fourth order nonlinearity 77−57175
ocean tides analysis 77−87080
oceanic tides, semidiurnal waves determ. via obs. of artificial satellites trajectories *(French)* 79−8634
overlapping spectral component separation using harmonic analysis *(Russian)* 77−45895
palaeomagnetic field, time-averaged, anomalies rel. to lower mantle 78−11808
paleomagnetic field configuration, anal. appl. to reconstruction of Pangaea during Permian period 77−56577
perturbation theory for strong interaction, appl. to molecular crystals *(Russian)* 77−15528
physical systems instabilities, variational principles for complex eigenvalues 79−21527
plane eikonal eqns., class of complete integrals 77−49562
planet surface gravit. potentia, satellite model error estimation 79−96935
planetary gravitational spectra from direct measurements 80−30978
plate, elastic, under tension stress conc. due to surface pit 78−83243
plate, thick, containing eccentric spherical cavity, transverse bending stresses 78−63288
pulse-excited systems for nondestructive materials testing, using eddy current method *(Czech)* 79−39071
quantum statistical mechanics, local harmonic approx. 77−53832
reactor lattice epithermal neutron spectra, spherical harmonics anal. 78−21619
relativistic Boltzmann equation 79−17367
ring current magnetic field characts., spherical harmonic analysis 80−101493
Schrodinger equation, nonlinear, constrained harmonic motion 80−77625
Schumann resonance problem, convergence of zonal harmonic series 79−2348
seismic Rayleigh waves of period 50 seconds, group vel. distrib. in Pacific Ocean 78−65197
Shubnikov-de Haas quasi-periodic oscill. curves, harmonic analysis, computer method *(Russian)* 78−39132
simple harmonic waves in infinite nonhomogeneous elastic medium, diffr. by Griffith crack, rigid strips 77−54913
sine-Gordon equation, nonlinear, constrained harmonic motion 80−77625
singular spin harmonics 79−97529
solar daily geomagnetic variations at Sabhawala and Hyderabad, harmonic anal. 79−44097
solar large-scale magnetic field, harmonic anal. rel. to coronal holes 77−64713
solar magnetic fields, spherical harmonic anal. and coronal field high resolution mapping 77−56892
solid harmonics, addition theorems 78−28914
spherical and spheroidal harmonics 78−4463
spherical harmonic expansion method for data sampled on sphere 79−2602
spherical harmonic gradient formula, generalisation 79−17271
Stackel harmonic potential, expressions in elliptic and parabolic cylindrical coordinates 79−96898
steady state response of systems with spatially localised non-linearity 77−84135
SU*(4), elementary representations and intertwining operators 79−301
surface loads, reciprocating dynamic stresses produced in elastic half space 78−9562
surface wave, scattering, by submerged sphere 78−34145
tensor spherical harmonics, appl. to Navier equation of dynamic elasticity 80−98296
tensor spherical harmonics on S^2 and S^3 as eigenvalue problems 79−17324
thermal-motion correction for bond angles, harmonic approx. 78−55777
thermogenesis, harmonic analysis and inverse filter 80−27304
tidal dynamics of Irish and Celtic Seas 79−25254
tidal sea level extremes calc. using nonlinear programming method 77−78479
tilt meter observations harmonic anal., influence of S_1 diurnal meteorological wave *(Russian)* 78−88788
Toda lattice equation, nonlinear, constrained harmonic motion 80−77625
US scatt. by single objects 80−99892
vector and spin-weighted functions, induced representations 77−29991
weather satellite data, complex demodulation 78−49177
^{16}O, Hamiltonian matrix analysis, base model of orthogonal scheme for 0^+ state 79−63610

harmonic generation
see also optical harmonic generation
acoustic gravity waves, atmospheric, harmonic generation 78−88956
antiferromagnet, first-order orientational phase transition, second acoustic-harmonic generation 78−27067
beam-plasma system, three wave coupling 77−19726
α-brass, acoustic harmonic generation by long-range dislocation motion 79−42150
cold plasma, strongly turbulent, second harmonic generation 77−55133
cubic ferromagnet, second magnetoacoustic harmonic generation *(Russian)* 79−42816
dirty superconductors, third harmonic response to weak EM field near transition temp. 79−38249
DPPH, dil.; saturated spin system, spin decoupling effect and variation of dipolar energy reservoir temp. 80−88877
electrometer ferroelectric second-harmonic modulator design 77−82549
electron cyclotron instabilities, multi-harmonic, theory 78−87442
electron plasma, strongly turbulent, EM scattering 77−55150
EM wave propagation, nonlinear, in strong mag. fields, second harmonic generation 80−77988
EM wave scatt. theory, using vibrator with nonlinear contact 80−1110
exact solution to simple harmonic generation 79−75354
fluid and isotropic solid acoustic harmonic generation 77−27417
free charge carriers in solids, high order harmonic generation 77−76804
II-VI semiconductors, SHG efficiency at 77K under high field condition 80−84470
Lamb wave propag. on isotropic plates, second harmonic acousto-optic interaction 80−34886
laser plasma, struct. features of 2 ω_0 and 3/2 ω_0 harmonics *(Russian)* 77−11366
longitudinal elastic waves, harmonics generation 77−79991
magnetoelastic crystal, cubic, acoustic SHG, static magnetisation effects *(Russian)* 78−56362
magnetoelastic media, acoustic SHG 77−36109
magnetoplasma, plasma wave generation and SHG by Gaussian EM beam 79−37479
magnetoplasma, third harmonic generation by Gaussian EM beam 78−83572
MBBA, US propag., nonlinear effects 77−59069
metals, higher sound harmonic generation in momentum nonlinearity regime *(Russian)* 78−38783
microwave frequency in bounded magnetoplasma 80−48897
piezoelectric cryst., excitation and energy flux of acoustic harmonic 79−15404
piezoelectric semiconductor, second acoustic harmonic generation of acoustoelectronic waves 77−43669
piezoelectric semiconductor, US parametric amplification effects, contributions to nonlinear material coefficients 80−34144
piezosemiconductors, second harmonics of acoustoelectric current 80−80329
plasma, EM beam self-focusing and harmonic generation 77−19714
plasma, inhomogeneous, generation of higher harmonics of resonant radiation 80−106880
plasma, SHG by Gaussian beam 78−91112
plasma, strong inhomogeneous, second harmonic generation of e.m. wave from plasma reson. region *(Russian)* 77−995
plasma discharge, second harmonic generation by surface waves 79−1306
plasma nonlinear wave phenomena, collisional and weakly collisional cases 77−11346
plasmas, CO_2 laser produced, picosecond development of high harmonic emission 79−90391
power line harmonic VLF radiation, transmitter-induced amplification in magnetosphere 78−96360
pulse shape of second harmonic generated by two level system 78−60327
quartz, shear elastic waves, conical refr. and collinear interaction 77−62588
ruby, two level spin system, second harmonic generation, time depend. 79−65719
ruby, two-photon spectroscopy of reson. three-level spin system, reson. shift 79−82864
SAW, for detection of mol. films 77−80688
SAW, harmonic generation at unbonded interfaces and fatigue cracks 78−90562
SAW, parametric mixing and harmonic generation anal. 79−50489
SAW generation, linear and nonlinear growth 79−56057
SAW harmonic generation, overlap-integral anal. 79−55259
scanning acoustic microscope, nonlinear imaging of edge 78−38158
second harmonic generation, nonequilib. media 78−77726
second harmonic generation in finite amplitude SAW, anisotropic media *(French)* 80−34285
second harmonic SAW generation in devices involving semiconductor coupling 79−46148
semiconductor, ionic, nonlinear intraband absorpt. and harmonic generation 78−33779
semiconductor, n-type, surface wave SHG 79−60860
semiconductor, second harmonic generation by hot electron and electron transfer effects, optimum conditions 79−41491
semiconductors, theory of parametric amplification, rel. to SHG 77−69382
semimetals, higher sound harmonic generation in momentum nonlinearity regime *(Russian)* 78−38783
SHG in elec. field 77−11962
SHG in magnetoactive plasma by internal source *(Russian)* 77−58868
simple harmonic generation: an exact method of solution 79−25872
solar emission, harmonic generation and mm waves mixing for receiver *(Italian)* 77−49292
solar type III radio bursts, second harmonic radiation and related nonlinear phenomena 78−7958
submillimetric and IR laser absolute frequency meas. 77−79882
superconducting microbridges and tunnel junctions, half-harmonic generation at RF induced steps 79−56439
TGS, autostabilised state, elec. second harmonic generation 80−103921
TGS crystal, generation of second acoustic harmonics 78−18711

harmonic generation continued
TGSSe, autostabilised state, elec. second harmonic generation 80−103921
thin conductors, SHG and size cyclotron reson. 78−72186
two level spin system, second harmonic generation, time depend. 79−65719
two level system, microwave SHG, at. correlations and line shape 77−19219
two level system, microwave SHG, at. correlations and line shape 77−19220
two-photon resonant up-conversion, third harmonic generation 78−90453
X-ray phase-matched nonlinear interaction possibility in ideal crystals 79−41416
Al alloys, fatigue, microcrack development, acoustic SHG study 80−35440
Al_2O_3:Cr_2O_3, saturation effects by double-quantum transitions 78−80197
Bi, magnetoplasma waves, freq. doubling in propag. 79−28367
CdS, piezoelec. polycryst. film layer struct., acoustic harmonic generation 77−89812
Fe_2O_3, haematite, SHG, acoustic detect. of modulated sound wave *(Russian)* 78−43623
Ge waveguide, nonlinear third harmonic generation of submillemetre waves 80−44632
He, liq., first sound response, nonlinear, at 1, 3 10 MHz 79−46858
InSb waveguide, nonlinear third harmonic generation of submillemetre waves 80−44632
$LiNbO_3$, SAW, suppression of harmonic generation by ZnO thin-film loading 80−84355
$LiNbO_3$, y-z, x-z and $41^1/_2$-x cuts, SAW SHG, laser probing 77−31153
$(NH_4)_2SO_4$, SHG, 2.5 GHz, rel. to ferroelec. transition 77−59541
Sb_2S_3, dielec. and acoustic nonlinearity 78−15107
SbSI, dynamic dielectric nonlinearity, in microwave band 78−35109
SbSI, reversible characts. of generation of second microwave harmonic 78−39509
Si inversion layers, harmonic generation due to hot electrons 80−65694
SiO_2, fused, US study by harmonic generation, elastic consts., Gruneisen parameters 78−83735
TGS, ferroelec., elec. SHG in autostabilised state 77−85661
Ti, acoustic harmonic generation by long-range dislocation motion 79−42150
TiO_2:Fe^{3+}, microwave second harmonic generation and freq. conversion 80−50166

harmonic oscillators
1/N perturbation theory, large orders by inverse scatt. in 1-dimens., anharmonic oscillators 80−22214
ϕ^4 field, scaling limit in anharmonic oscillator 79−63341
action-angle variables in quantum mechanics 80−31543
adiabatic oscillator and related pots., spectral and scatt. theory 79−58568
adsorbed diatomic molecule, coupled-harmonic-oscillator model for vibr. modes 79−82461
Airy function basis for $(D_{1/4}{}^+ + D_{3/4}{}^+)$ oscill. representation of SL(2,R) 80−82919
anharmonic, large order perturbation expansion coeffs. of ground state energy 79−9139
anharmonic, mol. state stability, symmetry breaking for a non-linear Schrodinger equation 79−26867
anharmonic chain with nearest neighbour interaction, periodic permanent waves 79−150
anharmonic damped oscillator and coherent state representation 79−97236
anharmonic lattice, Gibbs states time evolution 79−54065
anharmonic oscill., classical versus quantum case *(Spanish)* 80−73210
anharmonic oscillator, 3-term recursion relations and quasienergies, WKB method, quantisation rules 79−97257
anharmonic oscillator, analytic theory of continued fractions, Green's function 79−6019
anharmonic oscillator, appl. to nonpolar dielecs. and displacive-type ferroelecs. 79−8087
anharmonic oscillator, calculation of instanton-anti-instanton contributions in quantum mechanics 80−68078
anharmonic oscillator, classical, variational method test, sp. ht., elec. susceptibility and oscillation freq. *(Portuguese)* 80−77611
anharmonic oscillator, computation of energy eigenvalues of Hamiltonian 80−12925
anharmonic oscillator, convergent perturbation series 79−88836
anharmonic oscillator, eigenvalues, eigenfunctions 78−36883
anharmonic oscillator, energy level asymptotic behaviour by coherent states method 78−81873
anharmonic oscillator, energy level calcs., double well potential summable series 80−17819
anharmonic oscillator, Feynman-Dyson series asymptotic expansion 80−62503
anharmonic oscillator, large order perturbation coeffs., asymptotic evaluation 80−82867
anharmonic oscillator, modified perturbation theories using Riccati eqn., energy eigenvalues 79−12644
anharmonic oscillator, moment recursions and the Schrodinger problem 79−35584
anharmonic oscillator, multipseudoparticles, perturbation theory in ground state energy calcs. 79−17622
anharmonic oscillator, nonergodicity and dynamical approach 80−52057
anharmonic oscillator, perturbation series 80−57137
anharmonic oscillator, perturbation theory, hypervirial theorems 80−105535
anharmonic oscillator, perturbation theory higher orders and struct. *(Russian)* 79−25904
anharmonic oscillator, perturbative approach 79−80464
anharmonic oscillator, quantisation conditions 80−42103
anharmonic oscillator, quantum mechanical, eigenvalues of secular eqns. 78−49698
anharmonic oscillator, statistical thermodynamics 77−13724
anharmonic oscillator, three-dimensional, radial Schrodinger eqn. 80−86144
anharmonic oscillator, time-dependent, Hamiltonian mechanics, Lie theory of extended groups 80−77982
anharmonic oscillator, trial Hamiltonians for quantum statistical treatment 80−77652
anharmonic oscillator system, hierarchy of evolution eqns. 80−68053
anharmonic oscillators, divergence of perturbation theory 79−75393

harmonic oscillators continued
anharmonic oscillators, nonseparable problem with exchange, classical limit 80−57120
anharmonic oscillators, partition function, statistical variation perturbation method 80−77648
anharmonic oscillators, quantum theory, independent to spherically coupled, level crossing 78−77747
anharmonic oscillators, single and coupled, with quartic coupling energy levels, quantum theory 79−35587
anharmonic oscillators, tight upper and lower bounds on perturbation coeffs. 79−85003
anharmonic oscillators, transition moments 78−12601
anharmonic oscillators in quantum mechanics, perturbation theory at large orders, ϕ^{2N} interaction 77−45735
anharmonic quartic oscillators, statistical mechanics 80−98817
anharmonic temperature factors, site symmetrised Fourier invariant treatment 79−33040
anharmonically coupled oscills., time depend. Hartree theory, susceptibility, absorpt. and Raman spectrum 80−58241
anisotropic harmonic oscillator, accidental degeneracy of energy levels 78−8263
anisotropic harmonic oscillator, n-dimens., accidental degeneracy, semi-direct product representation 78−4506
anisotropic harmonic oscillator group, quantum mech. representation 78−8262
approximate spectral decompositions associated with a family of harmonic oscillators *(French)* 79−44761
asymmetric top, oscill.-type coherent states 79−58579
asymptotic estimate of perturbation theory at large orders, anharmonic oscillator, Φ field theory 80−4585
asymptotic series expansion and complex classical trajectories 78−93557
atom+diatom collinear collision, refined Born approx. 78−74724
atom+excited harmonic oscillator, high-energy, energy transfer 79−68296
baryon resonance decay, l-broken $SU(6)_W$ model equivalence to relativistic harmonic oscillator quark model 78−41546
baryon resonance photoexcitation amplitudes, relativistic corrections, harmonic oscillator quark model 77−13935
baryonic state even wave harmonic oscillator theory, structure functions versus form factor 79−393
biharmonic oscillator, coincident energy levels, for teachers 79−40324
Bose-like oscillator, uncertainty relation for canonical variables 80−62539
bound states and energy spectrum, appl. to massless Klein-Gordon equation in Kerr metric 79−35600
Brownian oscillator, whiteness of quantum noise source 78−75
canonical transformation of the Hamiltonians quadratic in coordinate and momentum operators 79−84991
charged, interaction with transverse EM field mode 80−5712
charged linear harmonic oscillators, interaction between two one-dimensional oscillators 78−16963
charged particle in mag. field, phase operator 80−8827
classical, time-depend., dynamical invariant, algebraic derivation 80−12898
classical coupled dipole oscillators, optical props., normal mode treatment 79−36611
classical nonconservative systems, appl. of time depend. canonical transforms 80−17792
classical phase-space distribs. for approximating quantum states 79−63145
closed shell system, paramagnetism, harmonic oscill. model 77−58194
coherent multiphoton intense interactions, convergent perturbation anal. 80−1037
coherent states and lattice sums 79−2650
coherent states for general potentials, confining one-dimens. examples 80−4571
coherent states for general potentials, nonconfining one-dimens. examples 80−4572
coherent states for general potentials formalism 80−4570
coherent states for general pots. with harmonic oscillator props. 78−73883
coherent-state formalism in supercond. and Josephson-junction calcs. 79−51723
collective radiation and the near-zone field 80−37977
collinear atom-diatom inelastic scatt., Green functions method 78−25660
complete symmetry group of the one-dimensional time-dependent harmonic oscillator 80−46856
conserved quantities and symm. groups 78−28981
constrained system of free oscillators, nonlinear wave eqns. 80−77625
constraining forces, flexible and rigid 80−90773
continuous observation, quantum restrictions 79−97252
correlation coefficient and electron correlation 80−78552
correspondence principle for potential x^{2N} 80−42088
coupled, diagonalisation of general quadratic Hamiltonian 79−49158
coupled anharmonic oscillator energy levels, large quantum number behaviour, path integral method 80−91
coupled anharmonic oscillators, coherent state representation, perturbative soln. 79−17270
coupled anharmonic oscillators, level density, quantum theory 77−30044
coupled harmonic oscillators, natural freqs. from anal. geometry, for teaching 79−25806
coupled oscillater systems, stochasticity thresholds for chain of particles 79−80465
coupled oscillator model for opt. activity in Occupation Number Representation 79−31619
coupled oscillators, approx. and exact quantum energies and eigenfunctions 79−26961
coupled oscillators, macroscopic excitation relaxation 80−52135
coupled oscillators in stochastic electrodynamics 79−75373
coupled resonators, normal mode anal. 79−14327
coupled system, nonseparable, vibr. energy levels, semiclassical method 79−97224
covariant generalisation, two-body relativistic systems 78−69977
covariant harmonic oscillator with half integer spin, pseudoclassical model 78−16679
cranked, in coordinate space 78−25135
cranked deformed harmonic oscillator, wave functions, matrix elements, high spin nucleus appl. 78−25131
cranked harmonic oscillator pot., self-consistent condition 78−17122
curved space path integral, quantal Lagrangian and Hamiltonian for harmonic oscillators system 78−41193

harmonic oscillators continued
D-dimensional gr^4 anharmonic oscillator, space dimens. depend. 79−92983
damped, canonical approach, for teaching 80−17757
damped, differential eqn. soln., teaching appl. 79−62950
damped, eqns. of motion in quantum statistical theory, Fokker-Planck eqn. *(French)* 78−89399
damped, non-equilibrium quantum statistical mechanics, system quantisation 80−52070
damped, operator polynomials, divisors, perturbation theory 80−36905
damped harmonic oscill., action of retarded restoring force *(Italian)* 77−68381
damped harmonic oscillator, quantum friction in c-number picture 80−94980
damped harmonic torsional oscill., period and logarithmic decrement meas. 77−30142
damped particle motion, dissipation 79−63071
Debye lattice, thermal props., WINIMAX approx. appl. 80−49333
demonstration, normal modes, sinusoidal perturbation response, chart recorder 77−13539
diatomic molecule, rot. perturbed Morse oscillator, eigenfunctions and Franck-Condon factors 77−42309
diatomic molecule+diatomic molecule, collinear collision, anharmonicity effects 79−31656
dielectric friction in plasma, harmonic oscillator and rigid dipole dielectrics 80−53928
diffusion process modelling, equivalence of different methods 78−57818
dipole interaction of an oscillator with scalar field 80−94
Dirac phase operator nonexistence proof, number operator spectrum 80−86135
dispersive waves, nonlinear model eqn., parametric growth rate 79−12615
dissipation and quantum theory 79−63077
dissipative oscillator, time relaxation approx. anal. *(Russian)* 79−5997
dissipative systems, canonical quantisation, von Neumann equation 80−52132
dissipative systems, quantisation 77−22445
distorted wave Glauber approximation, Pauli eqn. soln. 78−57809
divergent series summation by order depend. mappings 79−88819
double anharmonic oscillator, asymptotic estimates and Borel resummation 79−85002
double humped fission barrier using biharmonic oscillator pot., penetrability calcs. 78−86524
double well anharmonic oscillator, no horn of singularities 78−73884
double well oscillator, nonlinear contribs. to the partition function 79−12963
doubly anharmonic oscillator, class of exact solns. 80−105531
doubly anharmonic oscillator, exact solns. 79−84998
driven damped oscillator, path integral treatment 79−80457
driven oscillator motion with nondecreasing input vels., use in inertia actuated fuse 78−59293
Duffing equation, randomly forced, Feynman's variational method 80−73201
dynamical symmetries and constants of motion for time-depend. oscill. 77−64943
dynamical symmetries in spherical geom. 79−40394
Dyson eqn., exact soln. for mean value of Green's function 78−4559
education, classical and quantum uncertainties, particle in box, harmonic oscill. and atom 79−25789
education, group theory of covariant harmonic oscillators, interacting quarks 78−61970
education, harmonic plane waves, particle displacement 80−73138
education, quantum mechanics, spherically symmetric pots., ladder operators, energy levels and degeneracy 78−62013
education, quantum mechanics and perturbation theory, perturbed harmonic oscillator *(Spanish)* 78−36786
education, spiral spring, (nonhelical) simple harmonic motion, Bessel functions, closed form solns. 80−57026
education, thermodynamic work and harmonic oscill. 78−49598
eigenvalues, coupled second-order differential eqns., numerical soln. method 80−94976
elastic three-body linear collision, inverse scatt. problem, for teaching 79−35468
EM field interaction, initial value problem 80−47223
energy eigenvalues of Coulomb and oscillator potentials, connections 79−12637
energy levels, ground and first excited states, $g\phi^4$ quantum field theory 80−62839
energy quanta, dissipation, linearly damped harmonic oscillator 80−68074
ensemble of oscillators with embedded impurity oscillator, absorption spectrum windows 79−6045
excited states, hypervirial relations, off-diagonal 80−37728
extrema, asymptotic analytic theory for Fokker-Planck processes 80−12992
extremum sufficient condition in classical action integral, eigenvalue problem, education 80−105462
extremum uncertainty product and sum states 78−24687
fast rotating nuclei, harmonic oscillator approx., moments of inertia and yrast lines 79−30765
Feynman's variational principle for real path integrals, generalisation 78−89365
extended Feynman path integral formula 80−36890
Feynman path integrals on/near caustics, semiclassical approx. using catastrophes 79−53992
Feynman path integrals with Gaussian measure, Laplace transform method 80−62522
finite harmonic oscillator chain with surface impurity, dynamics 80−59776
forced harmonic oscillator, complete symmetry group 80−90705
forced harmonic oscillator, Hamiltonian for time-depend. damping, for teachers 79−21495
forced harmonic oscillator, quantum mech., interaction 77−60951
forced oscillators, transition to stochasticity 79−84997
forced quantum oscillator equation, time-depend., soln. in coordinate representation 80−52044
forced van der Pol oscillator, relaxation oscills. 79−49089
four nucleon wave functions, Taylor series method 78−66223
Fourier transform, fractional order, appl. to quantum mechanics and electron motion in magnetic field 80−82665

harmonic oscillators continued
friction, stochastic quantisation, nonlinear Schrodinger equation 80−27164
friction in quantised Langevin systems, Schrodinger eqn., damped harmonic oscill. solns. 79−21570
$g\phi^4$ theory, strong coupling limit of Green functions, anharmonic oscillator appl. 78−78071
galvanometer, reflecting, with recording facilities, for teachers 78−16606
Gaussian quantum stochastic processes on the CCR algebra 80−12985
general anharmonic oscillator, eigenvalue calc. 79−6015
generalised harmonic oscillator bracket calculation program 79−53996
generalised one-dimens. oscillator, second order Wigner-Kirkwood semiclassical partition function and thermodynamic functions 80−62601
generalised Schwinger boson realisations and oscillator-like coherent states, rot. groups and asymmetric top 79−80743
generating functions calc. from characteristic functions 79−914
generating functions for integrals involving harmonic oscillator functions 79−35577
generator coordinate method 78−29731
generator coordinate method in natural state formalism, appl. to harmonic oscill. 77−17831
geometric quantisation, corrected Sommerfeld-Wilson rule 77−67318
geometric quantisation for multidimensional harmonic oscillators and Kepler problem, Maslov theory 80−17833
Gibbs ensemble, approach to equilibrium 77−41553
gr^{2N} anharmonic oscillator, perturbation theory 80−90712
gradient method in quantum mech., one-dimens. harmonic oscillator appl. 77−82831
graphical method for matrix determinant and inverse, generating functions for harmonic oscillator integrals 78−57732
gravitational wave detection method using harmonic oscillator coupled to weak classical force 80−77684
Green's function, bound derivation, appls. 79−58559
Hamiltonian formalism for harmonic oscillators and free fields 78−29005
Hamiltonian mechanics, Lie theory of extended groups 80−77982
Hamiltonians, quadratic, classes of quadratic invariants, interrelations and symmetries 80−31565
Hamiltonians, time depend. linear canonical transformations 77−74213
harmonic crystal properties in stationary nonequilibrium state 78−16752
Hartmann flows, resonant perturbations *(Russian)* 79−32685
heavy meson spectroscopy, centrifugal and harmonic oscill. pot. 79−17699
highly excited harmonic oscillator in crystal, damping 79−40408
Hilbert superspaces and Grassmann numbers, Fermi oscillator system appl. 80−95223
hydrogen bond absorption spectra, interaction between two harmonic oscills. 79−6929
hypervirial scaling iterative method 80−73196
infinite harmonic crystals, stationary nonequilib. states, existence, props. 77−55325
integrals of motion for hamiltonian of coupled harmonic oscillators, calculation program 79−58239
invariants for time-dependent harmonic oscill. 77−64942
inverse matrix diagonal and off diagonal elements, self energy perturbation theory 78−82607
inverted biharmonic oscillator potential, exact penetrability calcs. 77−2554
IR interaction with mols., classical/semiclassical theory 78−90164
isotonic, coherent state dynamics, energies 79−44794
isotonic oscillator, coherent states for nonharmonic potentials 80−52061
isotopic molecules, reduced partition function ratio, generalised finite polynomial approx. 78−66529
isotropic classical oscill. Lagrangian and Hamiltonian ambiguities, transform. props. 77−67270
isotropic harmonic and isotropic oscillators, hypervirial relations, giving recurrence relations for radial matrix elements 78−4502
isotropic harmonic oscillator, n-dimensional, noninvariance group 78−8264
isotropic harmonic oscillator in ang. momentum basis, algebraic formulation 80−94983
kinetic equations of coupled oscills., generalised Stratonovich method *(German)* 77−87686
kinetic formulation for random pots. 78−32756
kq representations in quantum mechanics 79−84990
Lewis Riesenfeld harmonic oscillator, unitary declension of dynamical symmetries 79−89074
Lewis Riesenfeld oscillator, dynamical symmetry breaking 80−47210
Lewis-Riesenfeld time-depend. harmonic osc., dynamical symmetries 80−4588
Lie algebras associated with classical relativistic planar motion in axisymmetric EM fields 79−49064
Lie-admissible deformation of self-adjoint systems 80−101941
linear harmonic oscillator on lattice, wave functions, energy eigenvalues, Pade approximant method 78−57817
linear quantum channel with thermal noise, quasiprobability distribs. 80−12984
linearly damped harmonic oscillator, quantisation 78−21068
linearly perturbed parameter dependent systems, energies calcs. 79−25893
Lorentz groups, homogeneous and inhomogeneous, teaching method to illustrate difference 80−17766
Lorentz-invariant minimum uncertainty product 79−6006
magnetoaerodynamic forces on oscill. circular cylindrical shell, simple harmonic motion 79−1257
magnetoelectric susceptibilities, phenomenological rules for computation 80−55068
Mathieu damped oscill., parametric random excit., moment stability 77−9869
matrix elements, generating functions 77−23407
meson masses calc. using harmonic oscillator pot. in Klein-Gordon eqn. 79−93392
meson masses in gauge theory with harmonic oscillator pot., coloured quark-gluon model 79−350
model for matter plus radiation system with quadrupole interactions, thermodynamic props. 79−49181
molecular predissociation model, level widths, shifts and curve crossing 78−90239
molecular vibration frequency change influence on Franck-Condon factors 80−106312

harmonic oscillators continued
molecule-molecule reaction, ergodic energy transfer, vibr. quantisation effects 78−85137
momentum autocorrelation functions from classical Green's functions. [Teaching] 78−61976
momentum-dependent nuclear potential, group-theoretical derivation of matrix elements 77−26588
Morse oscillator, anharmonic, position-momentum uncertainty products 80−68072
Morse oscillator, discrete spectrum in SO(2,1) algebra 80−42091
Morse oscillator, matrix elements calcs. with Sturm-Liouville eqn. eigenfunctions 79−2660
multiple well anharmonic oscillators and perturbation theory 79−49086
N-dimensional oscillator, time-depend., SL(N+2, R) symmetry group 80−46851
N-dimensional systems, exact time-depend. invariants 80−8824
Neother's theorem, time-dependent invariants and nonlinear equations of motion 80−12932
Newton and Heisenberg eqns. of motion relation, harmonic and anharmonic oscill. 79−6018
Noether's theorem and exact invariants for time-dependent systems 80−86114
non-adiabatic parametric excitation of oscillator-type systems 80−77643
nonlinear harmonic oscillator, perturbation theory 80−19272
nonlinear oscillator in harmonic force field, averaged quantum eqn. of motion 78−54232
nonlinear oscillator with a strange attractor 80−90
nonlinear oscillator with fluctuating parameters, dynamics, thermal noise 80−101729
nonlinear oscillators, 1-D, intramolecular vibr. energy transfer, quantal, classical and statistical behaviour 80−91641
nonlinear oscillators, Brownian motion, projection operator method, double well potential oscillator appl. 79−2723
nonlinear oscillators, multiple time scales expansion, theory and practice 79−92971
nonlinear quantum mechanics, appl. of Gauss tranformation to $^1/_2$ fields 79−63082
nonlinear quantum oscillator ensemble excited by external periodic force, statistics *(Russian)* 80−27213
nonlinear systems; Noether's theorem and invariants 80−52058
nonlinear systems, multi-degree-of-freedom, harmonic excitation, instability 80−73162
nonstationary quantum systems, SU(2) coherent states *(Russian)* 80−90693
nonstationery quantum systems, loss-energy states 79−75399
nuclei, axially symm., soln. of HF eqns. in coord. space 77−88060
numerical study of phase-integral connection formula 77−71230
odd anharmonic oscillators, perturbation theory 80−86106
off-diagonal operator equivalents, closed polynomial formula in terms of two-dimensional harmonic oscilltor 79−67186
one dimens. symmetrical quantum systems, exact local states 80−46870
one-dimens. chain with friction, discrete-continuous transition 77−849
one-dimens. chain with friction, discrete-continuous transition 77−850
one-dimensional chains, velocity correl. functions calcs. 77−82403
one-dimensional oscillator systems, density of states-frequency theorem 80−82602
one-particle quantum mechanics, duality between confining pots. and $(R+L_c^\infty)$ pots. 80−31574
open dynamic subsystem, nonlinear eqn. with fluctuating parameters derivation 80−94991
open system, exact master equation 77−71270
optical activity of large molecules from classical scatt. theory 77−31060
oscillating Hermite-Gaussian wave functions for harmonic oscillator Schrodinger eqn. 78−70004
oscillator basis for octupole collective motion in nuclei 78−70470
particle density in linear harmonic oscillator potential 79−92966
partition function and fermion equivalent evaluated using thermal zeta functions 77−41501
periodic Hamiltonian flows, generalised Bertrand's problem, isotropic harmonic oscillator 78−86131
perturbation expansion of classical one-dimens. Hamiltonian system 77−26167
perturbation theory, anharmonic oscillator, strong coupling regime, appl. to Φ_4^4 model 78−89622
perturbed oscillator energies, numerical calc. method 79−58580
perturbed oscillators with λx^M perturbation 80−27161
phase problem, transition moment, interaction energy, induced absorpt. and emission 80−31540
phase space, creation, annihilation operators 78−73871
phase space quantization of the linearly damped harmonic oscillator 79−35627
phase transitions, structural, first order, anharmonic oscillator model in (1+1) dimensions 80−86239
polyatomic molecules decomposition, pseudocanonical description of non-Boltzmann excited ensemble of oscillators 79−29331
position and momentum eigenstates, superposed coherent states 80−57135
potential scattering amplitude high energy behaviour in presence of confined channels 78−8268
predissociated two-channel model, resonances with complex rot. method 80−58327
predissociating harmonic oscillator, relative line widths and level shifts 80−23469
programmable calculators appls. in scientific calcs. 77−64940
projective symmetries of dynamical systems, infinitesimal symm. transforms of vector field 78−32650
q-equivalent particle Hamiltonians 78−93525
QCD hadronic spectrum, α-expansion method extraction, harmonic oscillator test 79−3009
quadratic Hamiltonians, exact propagators 78−49709
quadratic Hamiltonians, quadratic invariants and SU(n) symmetry group 78−36873
quadratic Lagrangian exact propagator 78−77762
quadrupole perturbation of harmonic oscill. pot. 77−60978
quantal time depend. oscillator with damping and perturbative force 80−82
quantal time depend. oscillator with losses, wave packet motion damping in quadratic field 80−86117
quantisation, non-equilib. statistical mechanics 77−5750
quantization of inequivalent classical Hamiltonians, damped oscill., for teaching 79−35466

harmonic oscillators continued
quantum, Brownian motion, quantum dynamical semigroup formalism 77−30100
quantum, derivation of new expression, for harmonic oscillator brackets 78−20997
quantum, stochastic electrodynamics approach 79−49077
quantum action angle variables 80−46842
quantum collective field method, planar limit appl., SU(N) theory and harmonic oscillators 80−57468
quantum damped oscillator, coherent states and reson., by Schrodinger eqn. 79−97251
quantum damped oscillator, master equation and pure state representations 80−8823
quantum dissipative system, nonlinear von Neumann equations 79−25976
quantum friction and statistical mechanics 80−77649
quantum Hamiltonian on lattice, estimation of eigenvalues 79−40669
quantum harmonic damping oscillator, loss energy states 78−49719
quantum harmonic oscill. chain, relaxation dynamics *(Russian)* 80−94992
quantum harmonic oscillator, Brownian motion, random walk, dissipative forces and coherent states 79−63086
quantum harmonic oscillator, driven and stochastically modulated, reduced eq. of motion 78−77764
quantum harmonic oscillator relaxation, Gaussian identities 78−4524
quantum harmonic oscillators, multidimensional, soln. with time depend. frequencies 80−8822
quantum mech. phase-space formulation, variational principle, harmonic oscill. ground state 77−2558
quantum mechanical damping 80−46862
quantum mechanical systems, moment method of eigenvalue and expectation value determ. 80−62534
quantum nondemolition meas., oscillator in coherent state 78−54228
quantum nondemolition meas. of harmonic oscillators, gravit. wave detection 78−41198
quantum nonlinear oscillator, quasiclassical theory of excitation time 79−40411
quantum oscillator, parametric instability 80−46866
quantum oscillator interacting with massless modes, correlation function long time limit 78−65814
quantum oscillators, matrix element diagrams 80−105455
quantum pendulum, representation of canonical relns. 80−42084
quantum systems, effective cooling 78−32728
quantum theory, B-S wave function for generalised four-dimens. harmonic oscill. *(Chinese)* 78−64
quantum-mechanical parametric amplification 80−42097
quantum-mechanical soln. of harmonic oscill. in box 77−13632
quartic, eigenfunction zeroes 80−73197
quartic anharmonic oscillator, non-perturbative soln. of eigenvalue problems 77−33900
quartic anharmonic oscillator, symmetry properties in generator coord. method 78−49699
quartic oscillator, semi-classical expansion 80−31592
quartic oscillator, zeta function 80−62532
quasi-classical quantisation of multidimens. systems, adiabatic invariants *(Russian)* 79−3343
radial matrix element generating function for mol. vibr. calcs. 77−18904
radial Schrondinger eqn., propag. method, appl. to close coupled eqns. 80−42096
radiative corrections, in random EM field stochastic electrodynamic treatment 77−45736
random excitation of harmonic oscillations of single degree of freedom systems 78−54175
randomly disordered linear chain, normal frequencies 78−36818
Ray-Reid invariants, appl. 80−82661
recoil corrections in electric gamma transitions 79−89263
relativistic, numerical eqns. from arithmetic basis of special relativity 77−57185
relativistic Bethe-Salpeter harmonic oscillator 80−32006
relativistic Hamiltonian mechs., position variables 80−27123
relativistic harmonic oscillator, fundamental mode calc. using own time coord. *(German)* 78−32729
relativistic harmonic oscillator for spin-1/2 particles in the Bethe-Salpeter formalism 80−91001
relativistic harmonic oscillator quark model, N and $\Delta(1236)$ form factors 78−93852
relativistic harmonic oscillators and hadronic struct., 1st year graduate quantum mechs. 78−61971
relativistic two-body interaction, exactly soluble system 78−16955
relativistic two-body interaction with radiation damping 77−30022
resonance Raman scatt. from mols., temp. effect, displaced harmonic oscillator model 80−23424
resonant interaction with ang. momentum oscill., exact soln. by means of Taylor expansion 77−33902
resonant scattering of laser pulses by a system of N atoms 78−74617
resonant stellar systems, formal third integral of motion *(Russian)* 77−82284
rotating, eigenvalues of radial Schrodinger eqn. 79−67184
rotating harmonic oscillator, eigenvalues 80−82675
rotating nuclei, selfconsistency conditions in cranked harmonic oscillator model, HF calcs. 78−58239
Schrodinger eqn., complete exact solution to the translation-invariant N-body harmonic oscillator problem 80−31558
Schrodinger eqn., discrete-time, linear harmonic oscill. 78−49717
Schrodinger eqn. numerical soln., teaching aid 78−8188
Schrodinger equation with an anharmonic oscillator potential 80−27163
Schrodinger time depend. eqn., solutions comparison 78−12596
semiclassical expansion of the anharmonic-oscillator propagator 79−63072
simplified anharmonic oscillators, energy levels 77−64961
SO(4,2) infinite component fields, model of composite relativistic defects 80−18071
soft mode instability mech. 80−86142
solitons, weakly damped, mechanical model, anharmonic oscillator in pot. well 78−86192
Sp(n,R) discrete series, harmonic oscill. eigenstates, nuclear collective model 78−71
spherical basis generating function from Talmi and Moshinsky-Smironv coeffs. *(French)* 80−86113
spin-oscillator coupled system, stochastic model for dynamics 77−22500

harmonic oscillators continued
spin-oscillator coupled system, stochastic model for dynamics, projection operator approach 78−77813
spinless particle moving in harmonic pot., magneto-optical props. 78−42106
spontaneous emission, master eqn. for harmonics oscillator system 79−17277
stars in thermal imbalance, vibr. stability in damped harmonic oscillator model 77−13320
statistical mechanics of waves in thermal equilib. 79−9175
stochastic action integral interpretation of quantum mechanical transformation function 80−77644
stochastic foundations of quantum mechanics, harmonic oscill. in stochastic electrodynamics 77−9910
stochastic quantum dynamics with dissipative forces 77−33891
stochastic transition, determination method 79−71366
sub-poissonian statistics of an anharmonic oscillator in thermal equilibrium 80−82669
superoperator method for oscill. interacting weakly with medium 79−40409
superoperator method for weak interaction of oscillator with non-particular medium 79−30290
supersymmetric relativistic oscillator, model 77−38086
symmetries and first integrals 80−22221
Talmi and Moshinsky-Smirnov coefficients in an harmonic oscillator basis *(French)* 80−94993
Talmi transformation, multicentre integrals, harmonic oscillator functions 79−93908
Talmi-Moshinsky harmonic oscillator bracket, simple analytic expression 80−86115
three body problem for general even power potential with applications 79−25900
three-dimensional, Green's function of Schrodinger eqn. 80−73211
time dependent, Noether's theorem 78−93554
time-dependent, derivation of infinite number of invariants and related auxiliary eqns. 79−67185
time-dependent, exact invariant determ., direct method 78−12597
time-dependent anharmonic oscillator, invariant Hamiltonian 79−44780
time-dependent harmonic oscillator, Lewis invariant generalisation 78−93560
time-dependent harmonic oscillator 80−8826
time-dependent harmonic oscillator type Hamiltonians, explicit invariants, Schrodinger wavefunctions 78−8259
time-dependent polynomial Hamiltonians, nonlinear transform. 79−40395
time-dependent three-dimensional harmonic oscillator, generalised invariants 77−49623
transformation groups for resolution of partial differential eqns., appl. to gravity, quantum mech. and heat transfer *(French)* 79−49099
transient beats, determ. using operational amplifier cct. 79−54
transition amplitudes for time dependent harmonic oscillators 80−94981
transitions between pseudostationary states, quantum treatment, damped oscill. with external perturbation forces 78−65
translation invariant harmonic matter, exact Schrodinger eqn. soln. 78−65802
truncated space calcs. of exact bound state energies 79−3090
two linear harmonic oscillators, coupled by interaction pot., SCF calc. 78−37625
two particle system, interaction through action-at-a-distance force, relativistic mechs. 78−66055
unbounded Hermitian operators, low-lying eigenstates, method 80−98812
uncertainty relations, covariant harmonic oscillator forms 79−9137
unimolecular dissociation dynamics, collinear triat. system, R-matrix method 79−70315
Van der Pol diffusion coupled oscillators, wave self-focusing and self modulation 80−90685
vibration-rotation interaction, estimate for eigenvalues 79−12628
vibration-vibration energy transfer, perturbed wave eqn. soln. 80−1051
vibrational level system relaxation, kinetic eqns. 79−92989
vibrational-translational energy transfer, forced harmonic oscill. model 79−59540
wave propagation in stratified media, matrix anal. 79−12618
wavefunctions, asymptotic behaviour 80−67979
Yang-Mills classical theory, conserved quantities 80−350
$\pi\pi \rightarrow \pi\pi$, operator dual model for bound relativistic quark based mesons *(Russian)* 79−9408
Θ_2^4 quantum field theory, numerical methods, anharmonic oscillator approx. 80−52390
$\Upsilon \rightarrow e^+e^-$, harmonic oscillator model, QCD gluon-bottom quark coupling 79−3016
$FeBr_4^-$, in various solvents, $^4A_1$ ^4E d-d band reson. Raman spectra, solvent depend., harmonic oscill. model 80−55085
$g\phi^4$ model, large-order behaviour of the 1/N expansion in zero and one dimensions 79−58862
$H+D_2$, collinear motion, energy transfer and dissociation, collision dynamics 80−99563
n-InSb, stationary energy transport velocity of light scattered from bunched solid-state plasma 79−95720
YAG, colour centres conceived as bound polarons 78−63990

harmonic oscillators (circuits)
Josephson oscillators, synchronisation props., single point junctions and chains 79−19703
magnetic field detector using second harmonic oscillation 79−54161

harmonics
see also harmonic analysis
AC and DC power lines, ELF radiation obs. 79−48609
cubic, product representation, Fermi surface determ. 77−13588
Earth torsional eigenfrequencies, effects of density and shear vel. discontinuities on asymptotic overtone struct. 77−78111
Earth torsional normal modes eigenfreqs., asymptotic overtone struct., model study 77−78110
Einstein-Maxwell equations, coupled, general soln., Ernst-Maxwell eqn. depend. on arbitrary harmonic function 77−74
forced oscillations experiment for students 80−17780
fusion reactor, TFTR, power line, variable freq. AC harmonic content 80−99293
gravitational waves, plane-wave solns. of Einstein eqns. 77−13664
Hough harmonic expansions for numerical integration of global barotropic primitive eqns. 77−78442

harmonics continued
induced telluric current and power harmonic radiation enhancement during sudden storm commencement 79−2184
multidimensional contour resolution into components 79−84941
nonlinear dielectric measurement by detection of third order harmonics *(French)* 77−67459
nonlinear sonic wave, excitation by quasi-monochromatic Alfven pumping 80−106649
nonlinear stochastic differential eqns. excited by Gaussian noise and harmonic disturbances 77−87631
quartz resonators, parameter calc. with energy trapping *(Russian)* 78−30141
rotating (kerr) black hole perturbations, spin weighted spheroidal harmonics 78−4277
rotationally symmetric mag. field expansions into zonal harmonic functions 79−31772
spherical harmonics and their poles, determ. 77−13575
spherical harmonics problems, identities 80−63515
SQUID magnetometers, AC-biased, macroscopically quantised, higher harmonics in Josephson effect 80−98952
steel, alloy, corrugated texture perfection, mag. anal. 80−88745
structural vibration testing, using electromag. forcing device, use of feedback to reduce harmonics 79−20298
underwater sound, second harmonic amplitude in water-saturated marine sediments 78−1476

Hartmann lines *see Luder's bands*

Hartree calculations *see SCF calculations*

Hartree-Fock approximation *see HF calculations*

Hartree-Fock calculations *see HF calculations*

Hasiguti relaxation *see anelastic relaxation; dislocation damping*

He *see helium*

headphones
see also earphones
equipment and services, 1979 video yearbook 79−14197
free field transmission meas., expts. with human observers and artificial ears *(German)* 80−79098
low freq. calibration, effect of leakage 77−62119
noise excluding audiometric headsets, perform. characts. 79−32157
piezoelectric, using high polymer film *(German)* 77−62128
Teflon-FEP, film, plate-electret, construction and use in condenser type headphone 80−5907

health effects of radiation *see biological effects of radiation*

health hazards
see also biological effects of radiation
60 Hz electric field effects on small birds and mammals 77−86538
148 MHz teratogenic potential in pregnant mice 79−70583
400 kV substation electric fields, long-term exposure, epidemiologic investigation *(French, English)* 80−21599
800 MHz portable transmitters, meas. of energy deposition in simulated human operators, comments and reply 79−57777
acoustic noise, biological effects other than hearing, review of animal expts. 79−5314
acoustic noise, impulsive, accuracy of measurement 79−18652
ACS Tenth Biennial Education Conference on Safety and Health in Academic Lab., recommendations 79−80387
actinide element movement through food chain 78−61264
actinide industrial dusts, lung clearance studies at NRPB 78−65137
actinide radioactive waste, biological hazards, consequences for LMFBR fuel recycling 80−86960
actinide separation in nuclear fuel and wastes, hazard assessment 79−85806
actinides, man-made, health effects compared to natural radionuclides 80−61647
aerosol, electrostatically charged, particle deposition in hollow cast of human larynx-tracheobronchial tree 79−43953
aerosol, reacting, sulphate and nitrate level calcs. 80−26056
air, trace elements, environmental health hazard aspects *(Czech)* 78−7756
air filters, portable electrostatic devices 80−36158
air pollution, toxic effects, exposure-effect diagram *(Dutch)* 78−49130
air pollution tolerance levels and norms, threshold values establishment *(Dutch)* 78−49129
airborne dust, field sampling techniques 79−12258
aircraft ambient and cabin air O_3 conc. simultaneous determ. 80−90198
aircraft noise, effects on mental health 79−5316
aircraft noise and premature birth 79−5324
airport control tower cab, optical design 80−58661
antennas, 10MHz to 1GHz radiation safety, ANSI and EPA recommendations 80−30765
aquatic life, protocols for evaluating effects of chemical substances 78−53604
asbestos, piezoelec. and ferroelec. rel. to asbestosis and model of carcinogenesis 77−78075
asbestos minerals, paragenesis, biological effects 77−81876
atmospheric aerosol characterization for particulate S, health effects 79−20984
background radiation and estimated risks from low-dose irradiation 80−46058
benzo(a)pyrene and C black combined aerosol form., rel. to air pollution and health hazards 78−80796
beta-rays, high-energy, hazards to eye lens and gonads 78−65131
biological safety cabinet design, testing 79−16362
biological shield removal, associated radiological protection problems 80−9431
biomedical electronics, recommendations for Spanish hospitals *(Spanish)* 80−72350
biomedical pressure cuffs, hazards in single-stage regulation 80−98160
bronchial cancer induction by α-emitting warm particles 78−96078
cancer, geomagnetism, weather and cosmic radiation 78−53615
cancer risk from $^{239}PuO_2$, max. permissible conc. in air 79−25108
cancers, genetic defects, resulting from use of various energy sources 79−16259
cancers and mutations, radiation levels and induced illnesses 80−76791
carcinogenetic hazard from natural background radiation in Japan 79−57720
carcinogenetic risk estimation, comparison of radiation therapy and chemotherapy 79−20592
Chalk River Nuclear Laboratories research in radiation biology, environment and radiation protection 78−61222

health hazards continued
chemical carcinogenicity, low-dose-rate extrapolation of animal data 77−56327
chemical laboratory, airborne contaminants monitoring, USA regulations 80−12869
chemical pollutants and radiation, comparative biological hazards 79−25035
chest radiography screening for employees in nuclear industry 80−26342
chlorobenzenes determination by gas chromatography with photoionis. detection, air and biological samples 80−35809
chlorofluoromethane, computer based policy analysis to reduce human health impacts 80−89698
Cicoil personal RF radiation hazard detector, evaluation 80−5337
CO dose meter for working places exposed to extreme peaks of CO contamination 78−81096
coal conversion technologies, health and environmental effects 80−81493
coal workers, localised-field magnetopneumographic meas. 80−104714
combustion aerosols, particle size distrib., health hazards 78−81394
computerised tomography, performance risk measures, information theoretic approach 80−8166
computerized tomography, performance risk measures, concepts 80−8165
cosmic ray nuclei, charge spectra (Z=30-40) obtained in Earth orbit 80−3828
cosmic rays, dosimetric significance at altitude of supersonic transport and in free space 78−20295
cosmic rays, geomagnetic shielding in Earth orbit 80−12626
crocidolite fibre fine structure rel. to pulmonary tissue immunoresponse 79−74824
decommissioning of commercial power reactors, environmental, economic and sociological effects 79−67901
decommissioning of commercial power reactors, technical feasibility, cost, environmental effects 79−67902
diagnostic radiology, Sweden, patient exposure and radiation risks 79−53248
dialysis equipment elec. hazards and safety 79−84010
dose comparisons in the effects of radiation and of chemical pollutants 79−88115
dust particles in atmosphere, effects and size distribution *(Dutch)* 79−52974
ear-defenders, active noise reduction system for aircrew flying helmets 79−18602
earthquake associated effects, microzonation 79−88272
earthquake evaluation, case history, Auburn Dam, 79−88284
earthquake hazard model for Reno, Nevada 79−88285
earthquake hazards warning, US Geological Survey's role 79−84488
earthquake risk deduction, microzoning 79−88290
EHV installation, biological/psychological effects 77−81535
electric and magnetic fields *(French, English)* 80−72209
electric current flow and EM radiation effects on human body 77−64084
electric power transmission systems and high-Btu gas pipelines, comparative eval. 80−104520
electric shock, instrument safety precautions, may result in health hazards 77−34001
electric shocks, 50/60-Hz AC, ventricular fibrillation tests on animals *(German)* 80−101154
electricity-producing plants, nucl. and fossil-burning 77−44880
electron accelerator, linear highfrequency, hazard factors and conditions for safe operation *(Czech)* 80−52794
electron linear accelerators, regulations, standards, and guidelines for use in medical radiation therapy 79−53258
electron microscope, conventional and HV, X-ray leakage 77−38066
electrosurgical hazard monitor 79−83882
electrosurgical safety precautions 79−92317
ELF submarine communication systems, land-based transmitting antenna elec. and mag. field hazards 80−35973
EM dominant reson. freqs. of human body 78−31857
EM fields, hazard quantification of field-man interaction in elec. shielded enclosures 80−85445
EM radiation, coupling between small thin-wire antenna and biological body 78−3548
EM radiation hazard instrums. 79−92378
EM radiation protection, in transmission stations, Polish and international regulations *(Polish)* 78−61263
EM waves biological effects, interdisciplinary and international contribs. 79−48288
embryo, human, radiation effects on pre-natal development 79−29566
emissions from alternative electricity generation fuel cycles, health hazards evaluation 78−11791
energy, environment and health, Failla Memorial Lecture, learning from nucl. experience 78−80982
energy generation, human health risk, comparison of conventional and nonconventional technologies 79−87956
energy sources, role of health physicist in development of safe sources 78−36088
energy technologies risk assessment, conventional vs. non-conventional (renewable) resources 79−52862
environment monitoring ground radioactive burial site *(Japanese)* 80−67015
environmental, ionising radiation, perspective 78−35896
environmental, nonionising radiation 78−35883
environmental actinides, pot. carcinogenic effects 80−30780
environmental modelling principles, radioactive effluent 79−79414
environmental monitoring and control 79−39328
environmental noise, conclusions and recommendations of conf. Gothenburg 1977 79−5325
environmental noise, health effects of noise exposure, review 79−5313
environmental noise, medical effects, Conf., Gothenburg, Sweden, 1977 79−5311
environmental noise, review of biological effects on humans 79−5315
environmental noise exposure, medical effects, review of basic considerations 79−5312
environmental particulates, anal., X-ray techniques 77−56322
environmental pollution, anodic stripping voltammetry anal. of samples 79−11836
environmental radioactivity near a radioactive waste disposal site 80−98148
epidemiology, causality, and public policy 79−97177
eye lens, human, microwave-induced hazardous non linear thermoelastic vibrs. 79−83853
fast neutron exposure, risk of leukemia 80−30782
health hazards continued
fault currents effects and protection 80−56330
female bladder aseptic catheterisation 79−79674
fetal exposure in diagnostic radiology 80−8133
fissile material supervision, aspects *(German)* 78−684
fission reactor occupational radiation exposure, ALARA inplant design, cost-benefit anal. 80−18547
fission reactor Pu fuel facility damage from high winds, risk anal. 80−63356
fission reactor radiation protection, ALARA, effectiveness of design modifications 80−18546
fission reactor radiation protection, ALARA, reactor inplant design, a regulatory viewpoint 80−23016
fission reactor radiation protection, ALARA objectives, reactor design for occupational exposure 80−23017
fission reactor radiation protection, ALARA occupational radiation exposure, utility design viewpoint 80−18548
floods, Arno River, Italy 79−88373
fusion power, radiological protection review 80−9411
fusion reactor blanket material impurity hazardous activity and dose rates, biological hazard pot. 80−102315
fusion reactors hazards assessment *(Czech)* 78−86681
gamma dose intensity in dwelling places, dose conversion factors *(Hungarian)* 77−77990
gamma sources in walls of dwelling rooms, exposure rate calc. 78−73260
gamma-ray activity in coals, rel. to power station choice 78−11746
gaseous effluent standards comparison for nuclear and fossil fuel power prod. facilities 80−32536
ground shaking, Salt Lake City, ground response maps 79−88287
Hanford workers dying from cancer and other causes, radiation exposures, Richland USA 78−15893
health physics in the Novazza (Bergamo, Italy) uranium mine *(Italian)* 79−74764
hearing damage to divers rel. to noise levels in hyperbaric chamber 77−62107
hearing protectors, attenuation-frequency characts. meas. using cadaver ears 79−11947
hearing protectors, circumaural type, objective meas. of attenuation 79−11948
hearing protectors, effectiveness meas. 79−14180
n-hexane induced changes in visual evoked pots. and ERG of industrial workers 80−45886
high electric field biological effects on human nervous systems 80−89739
Hiroshima mass radiologic gastric surveys, examinees' doses 80−89858
Howe Caverns, USA, doses to employees and public from Rn and Rn daughters 80−89859
HTGR, maximum pot. hazard of ultimate accident sequence initiated by PCRV leak 78−13278
human epidemiologic studies rel. to health effects of microwave radiation 80−35970
HV electric field induced in humans, determ. using moment method 77−86535
HV transmission line elec. and mag. field exposure effects and hazards 78−77083
immunological effects of auditory stress 79−5323
in-vivo activation analysis, diagnostic technique 80−56210
indoor natural radiation environment and dose distribution in man, multi-compartment models 79−12015
industrial deafness risk, British Government code of practice 78−55513
industrial hygiene training at Quinnipiac College, USA 79−84879
industrial noise, biological effects other than on hearing 79−5320
industrial noise, effect on blood pressure in humans 79−5321
industrial noise, health problems and meas. *(Hungarian)* 77−27424
industrial noise hazard control programme 78−9490
industrial plant noise, exposure control 79−14153
instant working level meter methods, mathematical evaluation 79−9918
ionisation smoke detectors, risks to humans 78−15909
ionising radiation, mortality of radiation workers 80−8108
ionising radiation, review of sources 79−88149
IR radiation from GaAs laser diodes, effects on human eye evaluation *(German)* 78−20241
Istanbul overall air pollution obs. 77−37398
laboratory fume hood performance evaluation by face velocity meas. 80−37011
laser applications for discotheque light effects, safety considerations with respect to output power and exposure time, regulations and recommendations *(German)* 80−101224
laser fusion research, safety aspects, control measures and protective eye-wear 77−40711
laser light, dosimeter for health physics evaluation of operating conditions at laser installations 80−76835
laser low-level prolonged exposure effects on visual function 80−3714
laser products, US Bureau of Radiological Health standards ref. 77−12955
laser radiation, calc. of max. permissible exposure levels 79−96666
laser radiation dosimetry, standardisation of practice 77−16998
laser radiation hazards and protection standards 80−46069
laser radiation of 1.54 μm wavelength, max. permissible exposure of human eye 79−11966
laser safety, basic classification concepts 79−39524
laser safety calc., for various viewing conditions 79−39447
laser safety considerations 77−77940
laser safety eyewear, filter glasses 79−39525
laser scanned visual displays, pulsed light data extrapolation 80−3713
laser-induced retinal morphological and functional changes and safe energy levels 80−3712
lethal diseases from ionising radiation, new index of risks 80−94294
leukemia risk from neutron exposure 79−39509
leukemias, nonlymphatic, rel. to adult exposure to diagnostic X-rays 80−67158
LF environmental noise annoyance, expt. study 77−36941
lidar for global wind meas. from satellite, eye-safety hazard 79−58231
lightning mechanism, types and biological effects 78−49081
linear accelerators, health physics aspects of 20 to 40 MeV operations 79−45482
LMFBR, Clinch River Plant, sensitivity for radiological consequences to var. in aerosol parameters 78−13294
LMFBR HCDA, radiological consequences, attenuation due to radiative cooling 78−13296
low dose ionizing radiation, health hazard estimates 80−61646
low irradiation dose risk evaluation *(French)* 79−89508

health hazards continued
low-dose radiation carcinogenesis 80−12198
LWR, occupational radiation exposure problems 77−18711
LWR and coal power stations, effects on ambient media from mining to waste disposal *(Spanish)* 77−75005
LWR plant, occupational radiation exposure, recommended limitations 79−59266
magnetic fields, static, possible effects on cancer 77−32914
mamography, risks, radiation dosage and picture quality, review *(German)* 80−36103
medical equipment safety, leakage currents meas. and minimising 78−11748
metal casting workplace lighting, vision problems, Swedish report *(Swedish)* 77−77896
metallic pollutants, study of movement in environment and biological chains *(French)* 77−41162
microwave and radiofrequency radiations exposure limits proposed, in Canada 79−5375
microwave biological effects, book 77−90850
microwave effects research, medical appls. and hazards, 1940-60 80−86066
microwave exposure hazard publicity 79−70582
microwave hazard probe calibration plane-wave power density meas. 77−71341
microwave induced thermal stresses in ocular lens of human eye 78−80914
microwave leakage during patient treatment 80−76820
microwave potentially hazardous radiation sources, review 78−73173
microwave radiation hazard assessment methodology for USA Army Radiation Protection Program 78−85389
microwaves appl., in industry, science and medicine 80−3754
microwaves as potentiating factor in cardiovascular disease in North Karelia, Finland 77−12959
microwaves in environment, human hazards 77−77938
millimeter range of wavelengths, personnel safety 79−92391
mineral dusts, electron microscope anal., environmental monitoring 77−81877
mineral dusts and asbestos fibres 77−86732
mineral dusts in environment 77−87068
mineral particulates, identification by selected area electron diffraction 77−90970
mixed-oxide fuel fabrication plant, large commercial, accident radiological risk assessment 78−17401
neutron yield calcs., electron beam incidence, radiation protection implications for accelerators 78−95622
NMR imaging, physiological effect threshold for RF and mag. fields 79−66484
NMR of tritiated samples, use of plastic tube insert 79−40546
noise, acoustically absorptive room boundaries, industrial plant noise abatement appl. 77−75741
noise, effect on hearing ability *(Chinese)* 79−62267
noise, occupational, hearing hazard obs. on heavy industry workers 77−81512
noise, occupational exposure, audiometric and audiologic services 77−64056
noise, occupational exposure, otolaryngologist's role in hearing conservation 77−64055
noise, physiological defensive activation 79−5318
noise, statistical estimation of percentage of overexposed noise-impacted workers 78−92671
noise dose criteria for setting hearing loss risk estimates for industrial noise 78−1504
noise level measurement techniques, industrial processes appl. 78−33955
noise-induced sleep disturbances and their effects on health 79−5317
non-ionising EM radiation, biological response research perspectives 79−48289
non-ionising radiation, hazards in the laboratory 79−57708
non-ionizing radiations, hazards 79−92390
nonionising electromagnetic radiation bioeffects research and related occupational health aspects 78−73172
nonionising radiation hazard definition problems 80−3823
nonionising radiation protection, international programme 80−3822
nonionising RF and microwave radiation hazards *(French)* 80−3824
nuclear energy industry, impact on human health and safety 77−25508
nuclear facility workers, mortality anal. 80−45981
nuclear fuel cycle, risk estimation, evaluation, and management 78−17350
nuclear fuel reprocessing and waste disposal, public issues 77−46375
nuclear high-level waste in underground repository, rel. to naturally occurring toxic minerals 78−15913
nuclear industry, radiation doses, health risks from various power sources 80−57899
nuclear medicine, intrainstitutional mobile, health physics considerations 79−8546
nuclear power, effect on the environment, general radiation level and waste product disposal 79−18051
nuclear power and low level radiation hazards 79−100681
nuclear power health risks, for teachers 79−35506
nuclear power plan in Holland, aspects *(Dutch)* 78−13252
nuclear power plant, impact and fate of released Cu on aquatic environments 78−7665
nuclear power plant siting evaluation, comparison with coal-fired power station *(Czech)* 78−50266
nuclear power production, radiation protection programme in Iran, trends 77−65337
nuclear radiation, public health aspects 77−75003
nuclear reactor, HCDA anal., effects on reactor struct., radiological consequences 77−71666
nuclear reactor accident, human exposure to radiation, biological consequences 78−7407
nuclear reactor accident risk calcs., models and data 80−47613
nuclear reactor design, reliability, risk assessment, power plant safety anal. 77−71665
nuclear reactor fission product release, evaluation of population hazards 77−14250
nuclear regulatory and safety technology, experience in transfer 77−65300
occupational doses in Ontario Hydro nucl. power program 77−88285
ophthalmic hazards associated with laser endoscopy 79−79598
organ-specific radiological impact of airborne effluents from model PWR and FBR reprocessing plants 80−3825
health hazards continued
organic effluent toxicity from nuclear fuel reprocessing, rel. to carcinogenecity 78−5005
organic micropollutants, adsorpt. on chrysotile and crocidolite, rel. to carcinogenic props. 78−80790
particle accelerators, radiological safety in design and operation, American National Standard 79−89511
permit-to-work certification scheme, for use in health building laboratories 80−22338
pesticide exposure effects on deep brain structures, filtered EEG spike obs. 77−44806
phosphate fertilizers, occupational dose from natural radionuclides 79−100751
polycyclic aromatic hydrocarbons, in particles from coke oven, size distrib., health hazards 78−36268
polynuclear aromatic hydrocarbons, atom. distrib. 78−3934
power generation, past and future, medical aspects 80−36219
power production, biological risk 80−98209
power stations environmental effects, nuclear and thermal comparison 77−71706
power-line elec. field interaction with human and animal organisms 79−66483
public health aspects of radiation 79−88141
α-quartz, collected on PVC membrane filters, X-ray diffr. determ. 77−70392
radar antenna radiation effects on maintenance and repair personnel investigation 77−81529
radar irradiation, impact on human systems 77−40710
radiation, ionising, risk associated with CT doses 80−61654
radiation, low-level, current estimates of hazards to human populations, review 78−57043
radiation, low-level, hazard to humans 79−11987
radiation, public health aspects 78−35895
radiation, risk to health assessment 80−41124
radiation and the environment, undergraduate course evaluation 78−1
radiation danger during manned space flights 80−41788
radiation danger in prolonged manned space flights 80−61711
radiation dose, X-ray and radioisotope examinations, children 79−16308
radiation exposure, perception of harm 80−85450
radiation exposure and other hazards, comparison of relative risks 79−2111
radiation exposure during human dental enamel anal. by proton irradiation 79−70608
radiation exposure meas., airport cargo workers 79−8544
radiation field measurements, Vermont Yankee Nuclear Power Station 79−9893
radiation hazards assessment, DNA repair and human cancer 80−41143
radiation hazards to personnel assoc. with diagnostic nucl. medicine 77−81587
radiation low level link with cancer deaths in atomic plant employees 78−85339
radiation monitoring instruments, evaluation and comparison 79−96667
radiation protection, health aspects of low-level radiation 80−26375
radiation research, lab. contamination in the early period 80−42031
radiation therapy, ^{137}Cs needle implants, miniaturized 79−11995
radiation therapy, estimate of risk due to unwanted neutrons by dose calcs. 80−81714
radiation worker health registry for AECL employees 79−88201
radiation workers, health considerations 80−98038
radioactive, low- and intermediate-level waste, risk anal. of road transport in Netherlands 78−17359
radioactive fallout effects of Nagasaki atomic bomb 78−85393
radioactive particle inhalation, acute effects, prognosis for survival in mammals 77−16956
radioactive releases from nuclear installations, eval. of accidental atmos. discharges 79−39529
radioactive solid waste, storage facility, radiological safety assessment 79−17995
radioactive waste, biochemical and chemical processes leading to radionuclide transport from low-level waste burial sites 80−101275
radioactive waste, commercial burial site, radionuclide dynamics and health implications 77−61618
radioactive waste, high-level and actinide contaminated, from fuel reprocessing, long-term radiotoxicity problems 77−61571
radioactive waste, non-fuel bearing components, engineered transport and burial system 77−61580
radioactive waste burial grounds, generic hazard evaluation 79−22418
radioactive waste disposal into deep ocean, hazard assessment 77−88233
radioactive waste in deepsea disposal sites, environmental surveys using submersibles 77−61617
radioactive waste material transportation, risk anal. 78−17357
radioactive wastes, long term disposal facility failure hazards, preliminary examination 79−54533
radioactivity incidents, national arrangements, review 80−102355
radioactivity of building materials and γ-radiation in dwellings 79−92095
radioactivity release to environment, late effects on population 78−15861
radiogenic cancer, estimate of life shortening per rem absorbed dose 79−11967
radioiodine release from U_3O_8 in O_2 and inert gas atm., chem. identities 77−57712
radioisotopes, resuspended, possible importance of short-term exposure 80−85501
radiological protection in medical establishments, pilot study 79−8552
rat metastatic growth effect of local tumour hyperthermia 78−24115
reactor loop, experimental, hazard and protection from tritium 79−36420
respirable fraction of airborne dust, performance characts. of samplers 78−53438
retinal damage by 325 nm He-Cd laser radiation 78−69136
retinal injury, thermally-induced, due to high optical-radiation doses 80−3710
retinal tissue damage, by single ultrashort laser light pulses 78−96065
RF and ionising radiation effects on personnel working with high power electronic systems *(Italian)* 77−21561
RF and microwave exposure, USA occupational safety and health standards 80−3727
RF and microwave radiation interaction with living systems, review of mechanisms 79−79602
RF and microwave radiations 77−77939
RF fields effects, legislation proposals for workers' protection 80−56223

health hazards continued
RF radiation effects and hazards 80−3709
RF radiation from portable and mobile telecommunication transmitters 77−40795
RF radiation hazards, engineering status review 77−9220
RF radiation levels in urban areas 78−40351
RF telemetry exposure effects on biosystems 77−86533
risk assessment from radiation 79−25116
risk estimation need 80−41361
Rn, atmospheric, accumulation in calcite caves 80−104531
Satellite Power Station microwave health and ecology programme 79−70443
seismic hazards. regional tectonics of Makran coast 79−88295
seismic risk, Taiwan 79−88277
seismic risk map, new proposal for Japan 79−88281
seismic risk procedures, application to microzonation problems, Los Angeles 79−88289
SEM laboratory, health and safety hazards 78−21295
sewage sludge land disposal, Mo hazard 77−33115
skin, α-irradiation, possibility of late effects, U miners 79−20584
soil residual contamination levels and decommissioning nuclear facilities, radiological criteria 78−11747
solar concentration system health hazards 80−3492
solar flare protons, radiation hazard in shielded spacecraft 80−8194
solar flares near-Earth radiation hazard, dosage estimation technique 80−67482
solar receiver radiative loss and eye hazard evaluation by Net-Radiometer 80−89673
solvents, film cleaning, survey 77−10130
spacecraft trace contaminant concentration, toxokinetic/toxodynamic model 79−83952
specific absorpt. rate over freq. range of prolate spheroidal models of humans and animals 79−100658
specular reflections by polaroid films, pot. eye hazard 80−85447
sports-related noise or trauma, effects on hearing 77−64057
static and LF mag. field biological effects and hazards 79−34579
static and low frequency magnetic fields, biological effects review *(Slovak)* 78−88722
surface fault rupture zoning in California 79−88293
technologically enhanced natural radiation, chemical problems, human exposure 79−96346
thyroid, high dose associated with adrenal scanning using ^{131}I 79−29629
transmission line AC EM fields, health effects regulation 80−94286
transport vibration prevention approaches 78−55506
transuranic elements in environment, recommendations for exposure of persons 79−93842
transuranic mobility in agricultural ecosystem 79−96668
transuranic transport from environment to man modelling 79−96669
transuranium elements, resuspension from contaminated surfaces 79−62376
transuranium radionuclides in the foodchains 79−74554
tritiated water, inhalation hazard from open containers 80−8240
UK population, sources of radiation exposure, review 80−36156
ultrasonographers, pot. hazard from previously administered radionuclides 80−98120
urban aerosols, characterisation and hazard assessment 77−41157
urban noise, effect on cardiovascular function in rhesus monkey 79−5322
urban noise, field study, noise sources, effects on humans 79−5319
urban-sited heating reactor, risk assessment 78−37423
US applications in obstetrics and gynecology, safety and pot. hazards, review 80−67170
US tissue characterisation practice and risk 79−48309
UV and IR radiation effects on eyes, safety measures *(Japanese)* 78−35881
UV and IR rays, effect on skin, safety measures *(Japanese)* 78−35882
UV emitting lamps, method for estimation of O_3 concs. in vicinity 80−81765
UV hazards and protection standards 77−81588
UV radiation from lamps, properties and harmful effects *(Swedish)* 80−35996
UV radiation standards for health and safety 78−74056
vibration, dual-axis whole-body movement, discomfort assessment 78−13842
vitrified high-level radioactive waste, associated hazards 78−13259
vitrified high-level waste, calcs. of radioactivity release due to leaching in final disposal 78−17360
water pollution and human health in developing nations 77−29339
welding fume particulate thoracic accumulation, assessment by magnetopneumography 80−101247
workplace carcinogens, respirator selection, US standards review 77−79076
X-ray baggage anal. equipment, radiation safety standards, Canada 79−2139
X-ray diffraction and fluorescence anal. equipment, radiation safety 79−12017
^{241}Am III retention and distrib. in neonatal beagle 78−28094
Ba isotopes, uptake and retention of ^{133}Ba and ^{140}Ba-^{140}La in mouse tissues, eye and skeleton doses 77−9276
CO_2 laser irradiation at 10.6 micron, irreversible damage threshold meas. 80−83627
CO_2, TEA lasers using amine additives, cyanide deposits prod. 77−71991
^{14}C, dosimetry and metabolism of low energy β-emitters 79−8551
^{14}C, formation, distrib. in nuclear fuel cycle *(Russian)* 80−5316
^{14}C production in reactors and explosions, population dose, health impact 77−14274
^{14}C released to atmosphere as CO_2, population dosimetry 78−35958
^{252}Cf, heavy metal shielding for neutron sources 79−9892
^{60}Co retention in mouse, rat, monkey and dog, at tracer levels 77−9271
Cs, radioactive, dynamics in herons inhabiting contaminated reservoir system 78−28092
^{137}Cs body burden in Japanese from 1967 to 1975 77−9283
HTO potential radiation dose to man, HT gas escape into forest ecosystem 78−96101
^{3}H biological half-life estimation in man, model 79−20689
^{3}H distribution in glycogen, haemoglobin and chromatin of mice drinking tritiated water 78−31910
Hg emissions from geothermal power plants 77−73838
Hg in human thumbnails, neutron activation anal. 77−64130
Hg vapour monitor, personal piezoelec. cryst. dosimeter 77−21672
health hazards continued
^{203}Hg-methyl mercury chloride retention in man after inhalation 77−9277
^{129}I, limits to radiological dose, dog retention data 77−60253
^{129}I, thyroidal burdens from dietary sources 77−44755
^{131}I population thyroid dose in USA after Chinese atm. nucl. weapons tests 78−77116
^{131}I therapy, review of contamination and exposure hazards 80−41257
^{131}I transport from pasture to milk, modelling Dresden-Monticello data 79−88203
$^{131}I_2$, $CH_3{}^{131}I$, radioactive, airborne, diffusion coeffs. 79−2142
^{79}Kr, kinetics after inhalation in man, rel. to internal dosimetry calcs. 78−28073
^{85}Kr, data on kinetics of total body retention and clearance after inhalation of ^{79}Kr 77−37121
^{95}Nb inhalation in beagle dogs, deposition and retention, dosimetry 78−35959
Pb, airborne, effects on children, Steinbuch's Lernmatrix appl. 77−44878
Pb compounds identification in urban aerosols, rel. to respiratory uptake 78−44991
Pb, from petrol engine exhaust, deposition on plant and soil surfaces 77−87063
Pb, scotopic vision deficits in young monkeys 77−56377
^{210}Po activity in Indian tobacco, meas. and lung dose calc. 77−9224
Pu as energy resource, availability, health hazards, nuclear weapon proliferation 77−46286
Pu, Manhattan project workers, 32-year medical follow-up 80−26379
Pu, toxicity, cancer risk. calc. 77−2025
Pu toxicity hazards, cancer fatalities 77−66864
Pu translocation from simulated wound sites in rat 78−77117
PuO_2-UO_2-Na aerosol, from LMFBR HCDA conditions, characterisation 78−94104
^{237}Pu, ^{239}Pu, citrate, early retention in mature beagles 78−96095
$^{238}PuO_2$, uptake by plants in polluted soil 79−5381
^{239}Pu,^{240}Pu, Danish cereal grains, variation of direct contamination 79−5382
^{239}Pu acute inhalation, early mortality and morbidity estimate 78−96079
^{239}Pu and ^{233}U droplets burning in air, aerosol generation investig. rel. to inhalation hazards 79−67959
^{239}Pu uptake by pea plants 77−9282
^{239}Pu, use in weapons and energy prod., radiological hazards, security 77−10492
^{241}Pu concentrations in Swedish reindeer lichens, radiochem. anal. 78−15912
^{226}Ra background levels in lower troposphere from coal burning 77−37361
^{226}Ra determination in water, sampling and meas. methods 77−9278
Rn and Rn daughters, background concs. in Canadian homes 80−104546
Rn and Tn, air concentration in dwelling places *(Hungarian)* 77−78409
Rn barrier, interior of building structs. foundations built on U mill tailings material 79−2138
Rn concentration in dwellings and influencing factors 80−108832
Rn, concentration of ^{222}Rn, ^{220}Rn and decay products in room air, exhalation, ventilation and deposition effects 78−73261
Rn daughter concentrations in air of dwellings in Great Britain 78−77118
Rn decay products, concs. in mine air 77−9280
Rn exposure and human disease, impact of energy conservation in residential buildings 80−56225
^{220}Rn and ^{222}Rn, decay products, diffusion coeffs. in air and Ar 79−90366
^{220}Rn decay products attachment to flowing aerosols using centrifuge 80−61167
^{220}Rn unattached decay products, diffusion coeff. depend. on ventilation and rel. humidity 77−9279
^{222}Rn daughters, meas. of low conc. in air 78−28308
^{222}Rn determination in air and water, sampling and meas. methods 77−9278
^{222}Rn short-lived daughter population exposure in Great Britain 78−35970
^{222}Rn, theoretical, evaluation of emanation under a variety of conditions 80−104545
SO_2, norm determ., technical meas. aspects *(Dutch)* 78−49131
SO_2 pollution electricity generation, policy options for control 80−51022
^{89}Sr distribution between bound and free forms, in vitro meas. of rat soft tissue 78−28095
^{90}Sr in milk and composite diet samples in India 77−86650
U mill tailings, meas. of surface Rn flux, effect of moisture content 78−5056
U mill tailings, radiation pathways and potential health impacts 79−85826
U mill tailings pile, health effect estimations 77−40800
U, miners Rn daughter inhalation and pulmonary cancer incidence 78−96080
U mining in Canada, health hazards associated with Rn daughter inhalation 79−88140
U ores, dusts and mill tailings, simultaneous determ. of ^{238}U, ^{234}U, ^{230}Th, ^{226}Ra, and ^{210}Pb 78−15736
UO_2 inhaled particle distrib. and clearance on first bifurcation and trachea of rats 78−73267
^{233}U and Pu fuels, relative occupational hazards 78−94101
^{187}W, absorpt., distrib. and milk secretion by dairy cow 77−9281

hearing
see also bioacoustics; ear; hearing aids; speech
absolute thresholds and kanamycin-induced hearing loss in guinea pig 78−57017
acoustic analysis, nerve paths, bandpass filter operation *(Italian)* 80−94218
acoustic biotope, neural representation 80−51116
acoustic biotope neural representation, stimulus event relations for sensory neurons 79−66475
acoustic filter components for ANSI standard psychoacoustic testing 78−83198
acoustic fluctuation strength models comparison 78−65033
acoustic impedance meter, tympanic membrane, deafness diagnosis appl. 77−25460
acoustic noise, duration effect on annoyance 79−14151

hearing continued
acoustic pressure field alongside manikin's head, rel. to in situ hearing aid tests 77−90805
acoustic reflex, in animals, influence on loudness of pulsed pure tones 78−92647
acoustic reflex, loudness, summation and critical bandwidth 77−2009
acoustic reflex, statistically based measure and relation to stimulus loudness 77−32907
acoustic reflex, threshold and growth 78−40185
acoustic reflex adaptation in humans 79−2082
acoustic reflex magnitude for homophasic or antiphasic binaural activating signals in noise 80−51117
acoustic reflex threshold for impulses 77−64052
acoustic reflex threshold temporal integration, instrumental effects 77−77910
acoustic reflex thresholds, comparison of three methods for predicting hearing loss 78−3511
acoustic trauma assessment in extended HF range, with impedance measurements 80−61592
acoustic-reflex dynamics for pulsed signals 79−20549
acoustic-reflex growth and loudness 80−35916
acoustical analysis of auditory system of crickets 79−92226
acoustical research into life sciences, review 80−97925
action potential latencies, narrow-band, in normal and recruiting human ears 79−43929
action potential tuning curves, normal and pathological human ears 78−20184
active noise reduction system for ear defenders 78−92748
adaptive psychophysical testing, group-vote rules 79−100626
additive masking effects of noise bands of different levels 78−57021
AM noise, rate and modulation thresholds detect. by mass 78−85320
AM tone, human auditory assessment of modulation freq. 78−3515
AM tones coding in chinchilla auditory nerve 80−97927
ambiguous word, event related pot. differences, principal component anal. 80−8070
amphibian middle ear dynamics using laser speckle interferometry 78−40198
anatomical and physiological basis of auditory information 79−11944
angle estimation and binaural processing in animal echolocation 78−40186
anthropometric manikin, effects of sound direction on eardrum response 79−96572
application of communication theory to acoustics, separation of sound carrier and modulating signal 80−79063
articulation development, possible nonlinear time varying control in feedback path 78−35870
articulation status and improvement for /r/ and /s/, delayed judgment speech-sound discrimination 78−65060
artificial head for head-related stereophonic recording, design *(German)* 78−40199
artificial mastoid type 4930 *(German)* 78−27970
asymptotic threshold shift in chinchillas exposed to impulse noise 78−57019
audibility and effective loudness of sirens and speech in automobiles 77−16935
audibility relative magnetic threshold meas. *(Croatian)* 78−11673
audible training aid for visually impaired infants, motion activated 80−36193
audiometer, automatic digital, for mass hearing examinations 80−33379
audiometer, Bekesy-type, for clinical use 78−3499
audiometer, pure-tone and speech, computerised *(Japanese)* 79−74774
audiometer, screening, and real-time computer techniques 78−81009
audiometers, principles, appls. and commercial models 78−44669
audiometers produced by Medicor Works 79−62384
audiometric facility at West Middlesex Hospital, London for standardised hearing tests 80−76858
audiometric procedures for industry 80−81621
audiometric testing, A-weighted equivalents of permissible ambient noise 78−69107
audiometric tests, automatic operation using a programmable system, hardware *(Italian)* 77−5006
audiometric zero proposal referred to IEC artificial ear 79−12039
audiometry, quiet and masked brief tone, normal and noise-induced hearing loss subjects 80−85415
audiometry using electric response *(Japanese)* 80−51183
audiomotorial reflex, provocation and registering techniques *(Croatian)* 79−53162
auditorium design criteria by subjective eval. *(Japanese)* 77−31180
auditory analysis mammal's cortex response, individual tone discrimination *(Italian)* 80−89765
auditory backward inhibition and concert halls 79−59892
auditory cortex and the pitch of complex tones 80−51122
auditory cortex of unanaesthetised monkey, vertical stereotaxic approach to elec. recording 80−72383
auditory filter, shape determ. from growth of masking 77−90806
auditory function, mathematical model *(Dutch)* 77−9213
auditory impairment danger from inpulse noise, CHABA and the Federal Republic of Germany comparison 80−45920
auditory nerve, effect of response suppression on exposure to 2-tone stimuli 80−51115
auditory nerve fibre response to cubic difference tone, in cat 79−2081
auditory nerve oscillating summed action potential, spike pattern and synchronisation, insect 78−40181
auditory nerve response from cats raised in low-noise chamber 78−53420
auditory nerve responses and cochlear microphonics in cats using pulsed US 78−61200
auditory neurons, discharge rate density function dynamics for various tone-stimulus intensities 79−88089
auditory physics, hearing theory physical principles 80−85410
auditory picture properties, psychological factors, radio broadcasting appl. *(Polish)* 77−77917
auditory sensitivity, loss following exposure to spectrally narrow impulses 79−96568
auditory space neural map, owl 79−8514
auditory uncertainty relations for various tone signals 79−100622
auditory-nerve fibre discharge patterns, representation of speech-like sounds 80−108912
auditory-nerve fibre encoding of 2-tone approximations to steady-state vowels 80−61582
auditory-nerve fibre responses to bandlimited noise, nonlinearities 80−61583

hearing continued
auditory-visual perception of speech with reduced optical clarity 80−35919
aural distortion product, growth rate and phase characts. at different freqs. 80−97930
aural reflex, influence on sound transmission in the inner ear *(Japanese)* 80−81620
aural reflex and noise susceptibility relationship *(Japanese)* 79−24998
autoregressive analysis, a method for detect. of EEG changes in newborns to tones 80−108982
averaged electroencephalic response to tone pips in normal-hearing and hearing-impaired subjects 78−65049
aviation medicine, visual, auditory and vestibular fitness standards (report) 79−11920
backward and forward masking interactions 77−36945
backward inhibition in concert halls, parallelism between vision and hearing 80−14521
backward masking, detection versus recognition 78−61201
band-limiting experiments, suppression and critical bands study 78−92641
barrier perception mechanism of blind people, auditory horizon and space orientation 80−67089
basilar membrane electronic model for evaluation of speech disorders 78−40206
basilar membrane motion in alligator lizard, relation to tonotopic organization and freq. selectivity 80−76753
basilar membrane motion linear and nonlinear models 77−90800
basilar membrane travel times, systematic errors in direct estimates 80−51124
bat, const. freq.-FM sonar signal processing in auditory cortex 77−12940
bat, moustache, aural representation in Doppler-shifted-CF-processing area 78−80892
bat, moustache, target range sensitive neurons in auditory cortex 79−83808
bat, Pteronotus suapurensis, long-latency 'subthreshold' collicular responses to emitted const.-freq. components 79−79562
bat Doppler echolocator, obs. of surroundings 77−70483
bats, binaural perception and resolving power, correlation interferometer model *(French)* 78−80883
behavioural, unit and AP thresholds, relationship in normal and abnormal ears 78−92642
bilabial stop consonants differing in voice onset time, noncategorical perception 78−11676
bilinguals, perceptual switching 78−11670
bimodal cues for speech loudness 80−10090
binaural analyser detector characts. of human auditory system, correlometer comparison 77−86506
binaural critical masking bands 80−21475
binaural detection at high frequencies with time-delayed waveforms 78−61196
binaural diplacusis, influence of intensity on pitch 79−34571
binaural dissimilarity and optimum ceiling shapes for concert halls, lateral sound diffusion 79−68489
binaural echo suppression, measurements 80−33385
binaural illusion 77−77916
binaural interaction, depend. on interaural line and amplitude differences in discrimination and detect. 78−92637
binaural interaction, model for subjective lateral position 78−92640
binaural interaction theory based on auditory nerve data, tone detect. in noise 77−36950
binaural interaction threshold 80−81619
binaural phasic effect, effect of masking noise bandwidth 78−20183
binaural processing of information on short sounds, neuronal model 78−80885
binaural signal analysis by cross correl. 78−27958
binaural stimuli, symmetric time-intensity traded, discrimination 80−35907
binaural summation of the loudness of pure tones 78−92638
binaural system, monaural information processing on short sounds, neuronal model 78−65031
binaural time discrimination 77−9206
biosonar signals, moustache bat, auditory information processing 79−11943
bone conduction vibrators, calibration force levels 78−65046
brain, mag. evoked field mapping 80−104705
brain auditory receptive fields, centre-surround organisation, owl 79−66476
brain stem auditory evoked potentials and blink reflex in quiescent multiple sclerosis 80−67091
brain stem electric response audiometry and middle ear effusion 80−56151
brain stem evoked responses, acoustically depend. wave V latencies 78−85318
brain stem potentials, monkey, mapping following monaural clicks 79−16211
brain stem responses, cat, effects of lesions 80−85407
brain stem responses, cat, intracranial and extracranial recordings 80−85406
brain stem responses in patients with acoustic neuromas 79−92235
brain stem transmission time and auditory nerve response 80−45917
brain-stem auditory evoked response in young and old adults, normal variability 78−77064
brainstem, lower, auditory mechanisms, book contrib. 79−2084
brainstem auditory evoked pot., human, sources 80−108919
brainstem auditory evoked potentials, human, freq. comp. 80−16956
brainstem auditory evoked pots., influence of nonpathologic factors 79−88079
brainstem auditory evoked responses, polarity of acoustic click stimuli, proposed standard 80−45986
brainstem auditory evoked responses in man, effect of stimulus rise-fall time and duration 77−12935
brainstem auditory on- and off-potentials in humans 80−16954
brainstem auditory on- and off-pots., latency determ. 80−94233
brainstem evoked response, effects of signal rise time and frequency 79−20552
brainstem evoked response, relationship of latency and amplitude with sound intensity 79−20551
brainstem frequency, response to waveform envelope periodicity 80−61590
brainstem population responses, inhibitory influence 80−104595

hearing continued
brief tones, detect. and discrimination in cats with auditory cortex lesions 79−88081
broadband compression for improved hearing procedures *(German)* 80−104591
bSR (wave V) and N_1 latencies in response to acoustic stimuli with different bandwidths 79−94400
caecilian ear, sensitivity, electrical potential of cochlea 77−36959
California consonant test development 78−27965
California sea lion, discrimination of pure tone intensities 77−25467
California sea lion, upper limit of underwater auditory freq. discrimination 78−69106
cat, response of collicular auditory neuron to human speech 78−92646
categorical perception, melodic musical intervals 78−53421
cellular model approach 78−44515
central auditory function in stutterers 79−20550
central denervation hypersenstivity in auditory system of cat 79−96575
central optimal processing for pitch of complex tones, general template 78−57016
cerebral activity model, audition coordination 80−85404
characteristic function equation for two-interval forced-choice experiments 80−97929
children, auditory thresholds, noise exposure and biological factors 79−16219
children's hearing levels, effect of road traffic noise, exp. study 79−20553
children's newly acquired phoneme articulation, right-ear auditory feedback control 79−57676
children's pure-tone detection, auditory sensitivity testing 80−35912
children auditory threshold meas., forced-choice adaptive procedure 79−29644
chinchilla, freq. discrimination study 78−92639
chinchilla, identification functions for synthetic VOT stimuli 78−57022
chinchilla, threshold shifts following 3 days noise exposure 78−88712
Chinese firemen, responses to noise 77−39157
circumaural headset for hearing testing, calibration 77−9211
click evoked compound action pots., guinea pig obs. 80−94231
click stimuli, psychophysical magnitude estimates rel. to electrophysiological responses in man 78−31817
click-evoked brainstem potentials in man using high pass noise masking 78−61193
click-evoked elec. brainstem responses in audiological diagnosis 79−92237
click-evoked electric brainstem responses, use in audiological diagnosis 80−104689
coarticulatory cue decoding rel. to age 80−51126
cochlea freq. selectivity sharpening models comparison 78−53418
cochlea frequency response and tectorial membrane, math. anal. 80−26240
cochlea hair cell tuning props. 77−64054
cochlea mechanics, modes and waves 79−92232
cochlea model, acoustic wave reflection and resonance 80−61581
cochlear, evoked mech. response and the auditory microstruct. 80−94223
cochlear, struct. and functional changes following US irrad. 80−89791
cochlear compound action pots., tuning curves and delay times 80−94230
cochlear fibre responses in guinea pigs with well defined cochlear lesions 80−94226
cochlear fluid mechanics, signal anal. by Hopf bifurcation 80−26241
cochlear mechanics, 5 decade or research 80−76749
cochlear mechanics, nonlinear behaviour in 2-tone responses 80−76751
cochlear micromechanics and anatomy, review 80−76750
cochlear microphonic and sound-elicited electrical impedance changes measured in scala media of guinea pig, spectral comparisons 79−96567
cochlear microphonic measured in scala media of guinea pig cochlea, spectral content 79−96566
cochlear microphonic responses, far-field, to continuous pure tones, cat scalp recordings 80−97924
cochlear models, 2-tone suppression and second filter 80−76752
cochlear models−1978 80−94221
cochlear nerve fibres, hysteresis of tuning curves 77−52806
cochlear nonlinear phenomena in two-tone responses 80−94225
cochlear nucleus neuron tonotopic organisation, evidence from masking of elec. by acoustic stimuli 78−44511
cochlear nucleus neurone response, model of phase struct. of bitonal stimulus 78−80887
cochlear partition vibration, recent views 80−81617
cochlear summating potentials, effects of crossed olivocochlear bundle stimulation 77−52800
coding of intensity and interaction of forward and backward masking 80−45918
coding of intensity nonlinearities within the context of temporal summation model 80−45919
combination tones, compatibility between psychophysical and physiological meas. 78−57014
combination tones and relation with suppression, psychophysical meas. 80−108910
combination tones at frequencies greater than the primary tones 80−61589
comfortable loudness levels for pure tones and speech 78−65050
community noise, scaling of loudness, noisiness and annoyance 77−11086
comparison with vision, broadcasting appl. *(Japanese)* 78−73155
compensation of difference tones and odd-order nonlinearity in ear *(German)* 79−79559
compound PST histogram rel. to neural activity in cochlear 80−94148
compound PST histograms, deconvolution 80−94146
computer simulated patients for teaching students of speech and hearing 79−17162
computer-synthesized noise, signal detection 80−21476
concert hall acoustic investigations, Gulbenkian Great Hall, Lisbon 79−14163
conditioning auditory stimuli and the cutaneous eyeblink reflex, human obs. 80−67090
conductive hearing loss in children rel. to negative middle ear press. 80−12164
conservation during occupational noise exposure, otolaryngologist's role 77−64055
conservation in military occupational noise environment 79−14154
consonant confusion patterns, effects of filtering and sensorineural hearing loss 78−73163
hearing continued
consonant confusions in patients with sensorineural hearing loss 77−25469
consonants auditory and visual similarity rating patterns anal. 78−48807
contingent negative variations, rel. to distraction-arousal hypothesis 77−5002
continuous sound variation evaluation *(German)* 77−77905
contralateral cueing effects in backward masking 80−61587
contralateral cueing effects in forward masking 80−89770
convolution equation solution, problems arising 80−94147
cortex unit response to synthesized formants, cat 80−67098
cortical auditory evoked responses under hyperbaric conditions 80−94237
cortical desynchronisation detected by power meas. of scalp EEG 77−81494
cortical event-related potential waveform, effect of stimulus sequence 77−2011
cortical evoked potential expts., freq. and amplitude modulated stimuli 80−94236
cortical evoked response audiometry, portable programmable tape recorder 77−60279
cortical slow negative waves following non-paired auditory and visual stimuli 80−3650
cortical slow negative waves following non-paired auditory stimuli 79−62266
cricket, directional information coding by descending interneuron 78−77066
crickets, auditory behaviour of hybrids, evidence for genetic coupling in animal communication 77−32913
critical bandwidth in patients with acoustic neuroma 80−16953
critical bandwidth in presbycusis 80−16955
critical rate for identification and information capacity *(Japanese)* 77−77914
cross-modal and intramodal matching tests, tape construction method 80−41334
damage, protecting all industrial workers against noise 80−45841
damage by noise, exposure meas. by monitoring sound press. within ear 77−52799
damage risk from sound levels and spectra of rock music 79−68517
deaf children, vocal pitch exercising apparatus 79−25001
deaf people, computer generated speech training patterns 80−51290
deafness detection using electronic aids 78−11760
deafness due to impact noise from industrial machinery 79−18599
decibel, definition, meter calibration and hi-fi equipment *(Spanish)* 79−54092
decision making, split-second, electrophysiological signs, auditory stimuli 80−89771
defect diagnosis using electro-cochleographic methods *(Dutch)* 80−3855
dereverberation process evaluation by normal and impaired listeners 80−91974
destructive interference applicability for personal sound protection *(German)* 77−66817
detectability of switching transients at onset or offset of brief sinusoidal signal *(Japanese)* 80−97943
detection of combined differences in freq. and intensity 78−35863
detection of intensity increments of narrowband noise signals, amplitude model 80−61591
detection of signals with identical energy spectra but different waveforms under conditions of signal uncertainty 80−51125
detection of single gap in white noise 79−43931
detection of temporally uncertain signals 80−67094
detection probability of continuous signal parameter change evoking blurred change of loudness 80−41054
detection probability of continuous signal parameter change evoking blurred change of pitch 80−41055
detection threshold for two tone complex 78−3504
dichotic chord perception, ear dominance, pure tones versus tone glides 79−92225
dichotic chords, effect of bone conduction on intensity independence 79−43928
dichotic chords perception, individual differences 79−88082
dichotic listening, laterality effects 78−3509
dichotic listening as diagnostic tool, computerised dichotic tape generation 78−92740
dichotic listening audio tapes preparation 78−57010
dichotic listening performance reliability using two response modes 78−27966
dichotic perception of English consonants, role of distinctive features 79−68508
dichotic two-response paradigm, random guessing model 78−61206
difference estimation, between successive sounds *(German)* 77−77904
difference limens and the subjective scale of loudness 80−41046
difference tone level perception 80−12157
difference tone perception at low freqs. 80−67087
differential electrical excitation of auditory nerve 80−67092
digital model of binaural hearing, stimulus-response characts. 78−20192
directionality in amphibia, neurophysiological basis 78−40197
discrimination of acoustic stimulus rise times, human, age attributes 79−92234
distance estimation of sounds presented through headphones 80−41048
distance perception in binaural hearing 78−61202
distorted speech perception, role of training 80−5881
distribution of hearing loss in population with ageing and exposed to noise 77−48815
divers in hyperbaric chamber, noise levels and hearing damage 77−62107
dolphins, critical interval of active hearing 77−40682
double-notch audiogram, interpretation 80−85413
dynamic difference limen determ., loudness discrimination for varying intensity sounds *(Japanese)* 80−97942
dynamic stimulation, pulsed tone detect. in presence of masker with time-varying interaural correl. 79−88080
ear, chemical and physical aspects *(Dutch)* 77−9188
ear dominance and sequential interactions for tones of different freq. 80−35909
ear dominance in dichotic chords and ear superiority in freq. discrim. 78−3502
ear level dependent freq. selectivity model *(German)* 77−64038
ear protectors, performance estimation 78−40192
ear response to the effects of repetition time, analogue simulation *(Italian)* 80−94217

hearing continued
early late arrivals for multidesktop distributed sound system in large room 80−38179
earmuff listening conditions, behavioural compensation limits for auditory localisation 77−36947
earphone cushion, comparison between one-piece model 51 and conventional two-piece MS-41AR cushion 80−51123
earphones, comparison of DT 48, TDH 49, and TDH 39 types 79−94438
earphones, stereophonic reproduction with control of special transfer functions through head movements *(German)* 78−20182
earplugs, real-ear noise attenuation and effectiveness 78−87199
echo detecting charact. of inferior colliculus neurons of unanaesthetised bats 77−70484
echo detection and target-ranging neurons, bat auditory system 79−62269
echolocation in bats and auditory system 80−108906
education, psychoacoustical expts. with all pass networks 79−25787
EEG, decision P350, waveform and neural mechanism, auditory click and elec. finger stimuli 80−61528
EEG, event-related potential changes in chronic alcoholics 80−67076
EEG, freq. following pots. in man, evaluation, masking and clinical studies 79−70553
EEG, operant conditioning of brain steady potential shifts in man 80−21466
EEG, slow potential shifts and decision P350 interactions, auditory and elec. stimuli 80−61529
EEG audiometry, objective anal. 79−100632
EEG averaged response, middle components, contralateral noise effect 79−96576
EEG averaged response, stimulus freq. and intensity rel. to middle components 77−52804
EEG contingent negative variation rebound effect, visual and auditory simuli 80−3648
EEG-EPograms, comparative freq. analysis 80−67269
EEG-EPograms, simultaneously recorded from various parts of brains of sleeping cats 80−16951
EEG-EPograms simultaneously recorded in various parts of the cat brain 80−12153
effects of sports-related noise or trauma 77−64057
electroacoustic impedance instruments, meas. of temporal charact. and filter response 78−3512
electronic models to simulate sensory distortions on speech perception by the deaf 78−3507
electrophysiological filtered click responses, short-latency, recorded from vertex and external auditory meatus 79−53156
electrophysiology, spectral analysis of cochlear and brain stem evoked potentials 80−16957
elephant, frequency range study 80−104596
emitted potentials and temporal uncertainty 79−34575
English consonant dissimilarity ratings by normal and hearing-impaired subjects 80−35914
event related potentials due to single stimuli, recognition by discriminant functions 77−9305
event-related desynchronisation, graphical display and statistical evaluation 78−24192
evoked brain potentials, comparison of signal components in auditory and visual pots. 78−44513
evoked brain stem pot., sex differences in amplitudes and latencies 80−89767
evoked brain stem pots., effects of analogue and digital filtering 80−89878
evoked brain stem response, cochlear processes affecting wave V latency 80−16958
evoked brainstem response, age and sex diffs. 80−94234
evoked cortical potential online detector 78−31952
evoked potential, age depend. 80−12163
evoked potential, as probe of hemispheric differences in cognitive processing 78−15847
evoked potential, human, automated recording and analysing complex 79−57780
evoked potential, theoretical investigations and clinical appl. 80−26234
evoked potential amplitude and contingent negative variation as function of inspired N_2O concs. 80−45916
evoked potential data, appl. of low-pass linear filters 79−84032
evoked potential data acquisition, dual-processor system 79−79712
evoked potential development in early childhood, longit. study 78−77061
evoked potential rel. to sensory discrimination task 80−3645
evoked potential scalp topography in auditory and visual go/nogo tasks 78−31818
evoked potentials, appl. in brain mechanism studies and diagnosis *(German)* 80−61535
evoked potentials, average, microprocessor-based system for studying 80−56150
evoked potentials, averaged, effects of active attention switching between ears 77−40680
evoked potentials, averaging and FM 79−34574
evoked potentials, effectiveness of earphone shielding for artifact control 79−57790
evoked potentials, event-related, in normal, mentally retarded and autistic children 80−85388
evoked potentials, event-related obs. in schizophrenics 80−85405
evoked potentials, freq. following responses in primary auditory and reticular formation structs. 80−12154
evoked potentials, interlab. vs. intralab. and intersession vs. intrasession variability 77−70570
evoked potentials, recording and evaluation procedure for neurophysiology and medical diagnostics *(German)* 80−26404
evoked potentials, scalp topography and waveform 77−25412
evoked potentials, time shifted, generation technique 79−16354
evoked potentials, use in pediatric diagnosis 80−26407
evoked potentials and sonomotor responses, evaluation of components and recording techniques 78−3498
evoked potentials during natural and drug induced sleep 80−35903
evoked potentials in discrimination tasks, scalp topography 77−52797
evoked potentials in EEG, meas. by adaptive matched filters *(German)* 78−88755
evoked potentials in normal human subjects, age-related vars. 78−77063
evoked potentials in the brain stem, anal. method 80−41297
evoked pots., differential changes, mouse obs. 79−100624
hearing continued
evoked pots., technique for separating endogenous from exogenous pots. 79−100794
evoked pots. with pseudorandom noise excitation, spectral anal. 79−83795
evoked resonances, comparison of narcoleptics, primary insomniacs and normal controls 80−61579
evoked response, hemispheric differences 77−90801
evoked response, primary inhibited elements, review 80−94235
evoked response audiometry, on-line statistical detect. of average pots. 78−69245
evoked response audiometry (ERA), window-ERA determ. of hearing thresholds *(German)* 77−70477
evoked response audiometry system for dogs, in dental instrument noise studies 77−29226
evoked response correlate of symbol and significate 79−25000
evoked response methodology in animals 80−46103
evoked response research on animals, exptl. design 77−78068
evoked response with homophasic and antiphasic signal and noise, masking level difference quantification 80−41045
evoked responses, computer driven bipolar stimulator 78−57011
evoked sustained potentials, nature of response 79−34572
evoked sustained potentials, stimulus relationships 79−34573
evoked-response data acquisition system, specification and design 80−56165
feature detectors for voice onset time, voiceless anal. channel 78−3505
feedback, effect on guitar playing intensity and speech prod. 78−85322
fiddler crab auditory and vibrational stimuli receptor, Barth's myochordotonal organ 77−77921
figural props. of auditory patterns 79−16214
filter-characteristics derived from direct-masking and pulsation threshold data with rippled-noise masker 77−90804
filtered click stimuli spectra used to evoke acoustic brainstem responses 80−85408
fish, problem of sound perception *(Russian)* 80−41043
fluctuating noise, effective sound level prediction *(Japanese)* 79−27462
fluctuating noise annoyance meas. using magnitude estimation method *(Japanese)* 79−27461
FM detection for low modulation freqs., theory 80−61586
FM processing, evidence for direction-specific channels in auditory system 79−96573
FM tone exposure and selective adaptation, evidence for information processing channel 79−74689
focused US for input of auditory information into aural labyrinth 78−40275
formant based speech code for severely impaired hearing subjects 77−64051
formant frequencies of steady-state and consonant-bound vowels, difference limens 78−53426
forward and backward masking, suppression effects 79−74690
forward masking, evidence of temporal processes 80−97932
forward masking with equal-energy maskers 80−35905
Fourier-Mellin transform and mammalian hearing 78−40187
frequency acoustic reflex, multiple probe meas. 80−56065
frequency compression for moderately hearing impaired subjects, speech intelligibility 78−20188
frequency discrimination, effects of leading tone *(Japanese)* 78−85324
frequency discrimination as function of freq. and sensation level 77−32910
frequency discrimination capacities in goldfish, phase-locking in saccular nerve fibres 78−88720
frequency discrimination for masked tones 80−76754
frequency discrimination for pulsed versus modulated tones 78−40194
frequency discrimination of a brief tone, effects of leading and trailing tones *(Japanese)* 80−97941
frequency following pot., appl. of least-square-fit technique 80−94149
frequency following potential, 500 Hz, kangaroo rat, evaluation with noise masking 80−108905
frequency following response and brainstem evoked response 80−94232
frequency following response sources in man 77−70479
frequency following responses in man, identification and separation 77−48810
frequency measurement based on neural timing 77−5011
frequency perception, colour as a pervading principle over pitch, rhythm, and form 80−56059
frequency selectivity, influence of non-linearity of hearing system *(German)* 77−73532
frequency selectivity in post-stimulatory masking, expt. method 79−53155
frequency selectivity of human auditory system, from acoustic reflex meas. 79−83797
frequency selectivity of single auditory nerve fibres in response to broadband noise 77−77906
frequency selectivity of the cochlea for formant peaks at high signal levels 80−97936
frequency transitions in cat vocalizations, investigation 79−96570
frequency vibrato at 440 Hz, pleasantness *(Japanese)* 78−15846
frequency-following potential components in man 78−77062
friction analyzers for [j] 77−77911
frog mid-brain auditory neurons, discharge rate density function 78−20191
fundamental freq. declination, perception 79−90091
fundamentals of hearing analysis, ear defects *(Italian)* 80−94216
fused auditory image, discrimination of perceived movement vel. in dichotic stimulation 77−52802
gap detection by chinchilla 80−108907
gerbil, LF neural and cochlear-microphonic tuning curves 78−88718
glycoproteins, fast axonal transport in guinea pig auditory neurons 80−104573
goldfish, information coding in single auditory nerve fibres 78−40184
green tree frog, female discrimination of intermediate sounds in synthetic call continuum 78−69109
group delay distortions in electroacoustical systems 78−69105
growth function for human response to large-amplitude impulse noise 79−16222
guitar strings, correl. of acoustic and subjective quality charact. 80−19173
hair cells, inner, role of in hearing 79−43932
hair cells, vertebrate, response latency 79−83794
handicap of hearing impairment and limited benefit of hearing aids 78−53424

hearing continued
harmonic-sensitive neurons, mustache bat auditory cortex 79−43933
head-related stereophonic recording techniques, dummy head method 78−61286
hearing level prediction from acoustic reflex thresholds in persons with HF hearing losses 80−76759
hearing protector attenuation: a perspective view 79−81619
HF audiometry, age and sex variations 80−16959
HF audiometry and noise-induced hearing loss 80−16960
HF audiometry and stapedius muscle reflex thresholds in juvenile diabetics 80−85411
HF auditory function evaluation system, 8-20 kHz 80−33384
Hi-Fi sound reproduction, listening tests in preference to acoustic measurements 79−83792
high-frequency auditory thresholds of infants and adults 80−97945
high-intensity noise, after-effects of exposure 79−74685
history of physiological acoustics, Ohm-Seebeck dispute and work of Helmholtz 77−57141
holographic interferometry with optical fibres, hearing mechanism obs. 80−76879
human, ipsilateral stimulus intensity, tympanometry 80−104592
human auditory system perceptual mechanism, dynamic vowels, dichotic fusion expts. *(Japanese)* 80−53569
human equivalent audibility thresholds for bone cond., age variation 78−96054
hypernasality quantitative evaluation using acoustic perception computer method 78−27971
identification by frequency range of surface waves in insects *(German)* 79−96580
impact sound loudness meas. *(Japanese)* 79−98546
impedance and tone screening of schoolchildren 80−108985
impedance changes elicited by tactile and electrocutaneous stimulation 80−56066
impedance matching by combined effects of outer and middle ear 79−96571
improved WKB calc. for 2D cochlear model 80−97928
industrial deafness risk, British Government code of practice 78−55513
industrial ear protectors, standardisation of testing, current developments 78−22225
industrial hearing protection, types and limitations 78−55509
industrial noise, effect upon threshold level 79−83801
industrial noise, fatigue and recovery of human acoustic stapedius muscle reflex 79−53159
industrial noise, health problems and meas. *(Hungarian)* 77−27424
industrial noise and hearing conservation 78−22223
industrial noise exposure, practical hearing conservation programme 80−12161
industrial noise hazard control programme 78−9490
industrial noise induced deafness and protective measures 78−22224
infants, discrimination of voiced stop consonants 78−61207
infants in incubators, measurement of noise exposure and possibilities of hearing damage 80−53545
inferior colliculus neurons, cat, response to binaural beat stimuli obs. 80−72179
inferior colliculus of immature mouse, plastic reinnervation, autoradiography with ^{14}C-deoxyglucose 79−92233
infrasound, atmospheric, detect. by homing pigeons 77−29156
inner ear, sound-induced resistance changes 80−81618
inner ear impulse response and basilar membrane modelling 79−34570
insect auditory nerve fibre, latency shift, neuronal time cue of sound direction 79−48274
insect auditory nerve oscillating summed action potential expt. 77−64039
intensity difference detect. between brief adjacent tonal stimuli 78−53427
intensity discrimination as function of freq. and sensation level 77−36944
intensity discrimination of band-noise signals as function of duration and bandwidth 78−27959
intensity discrimination with gated and continuous sinusoids 80−10094
intensity perception, effect of fixed standard on resolution in identification 78−88719
intensity perception, preceding stimulus effect on identification 80−51120
intensity perception, roving-level discrimination and resolution and bias edge effects 77−86509
intensity resolution and relation to loudness matching 80−108908
interaction of whole body vibration and impulse noise 80−61585
interaural discrimination, rel. to lateral position matching 77−86510
interaural intensity, difference thresholds 77−48813
interaural time diffs. in azimuthal plane 77−77909
intermodulation product pair, masking and growth 78−20185
interneurones, locust, time-intensity trading obs. 80−26238
intracochlear acoustic pressure measurements in guinea pigs 80−94228
intracochlear interference effect applicability for personal sound protection *(German)* 77−66816
ipsilateral acoustic reflex artefacts measured in cadavers 80−85414
ipsilateral acoustic reflex stimuli calibration 80−17170
lateral line microphonic response to high-level stimuli, analytical model 80−61580
lateralisation performance, acoustic integration at high freqs. 77−90802
lateralisation thresholds based on interaural time differences for three tone harmonic complexes 78−57008
laterality effect in isometric and isotonic labial tracking 79−57625
laterality matching data, regression interp. 79−5297
lateralization by freq. for repeating sequences of dichotic tone pairs 78−40188
lateralization in monkeys, examination of two cues serving directional hearing 80−12156
lateralization model and role of time-intensity tradings in binaural masking 78−3503
lateralization of complex waveforms, effects of fine structure, amplitude and duration 77−25463
lateralization of complex waveforms 80−97931
lateralization of dichotic signals with large interaural amplitude difference *(French)* 79−20547
learning under degraded listening conditions, accuracy and effort 79−96578
LF central masking, 200 Hz expt. investigation 77−64040
LF electric current stimulation of auditory and visual sensations 78−40261
LF environmental noise annoyance, expt. study 77−36941
hearing continued
LF hearing loss evaluation, simultaneous recording of brain stem and freq.-following responses 78−11665
LF masking patterns 77−36955
LF tone-burst stimuli, determ. of freq. following response, humans and cats 79−83796
linear amplitude change thresholds for continuous pure tone 79−92238
linear system model 80−51127
listener's perception thresholds, mono, stereo, pseudo-quadrophonic, quadrophonic systems study *(Polish)* 80−5906
localisation acuity in horizontal plane 78−85323
localisation in median sagittal plane, spectral cues 77−64041
localization, mathematical model 77−12933
localization of noise bands by Old World monkeys 80−97926
loss, age rel. to susceptibility in young and adult ears 77−9208
loss, statistical study of urban population not subjected to occupational noise *(French)* 80−81623
loss due to noise and sodium salicylate combined effects, obs. 77−52798
loss of hearing, aviation personnel 79−11945
loudness and power series transformation, preliminary model and meas. 78−57012
loudness comparisons between different types of stimuli 78−20186
loudness discomfort and most comfortable loudness levels, psychometric functions 77−25468
loudness discomfort level and acoustic reflex threshold for speech stimuli 80−76762
loudness discomfort level and acoustic reflex threshold for normal and sensorineural hearing-impaired subjects 80−76763
loudness enhancement and decrement in four paradigms 80−51119
loudness growth depend. on excitation pattern skirts 78−61195
loudness of complex sounds as a function of the standard stimulus and the number of components 79−5296
loudness of continuous and interrupted pure tones, effect of psychophys. method 80−76760
loudness of modulated tones *(German)* 80−94219
loudness of narrowband noise pulses 80−38194
loudness perception, for short-duration tones in masking noise 78−65047
loudness perception of signals of monotonically changing sound pressure 77−64044
loudness reduction of masker, non-simultaneous, and influence on pulsation threshold *(German)* 79−79560
low-frequency hearing loss, filtered speech, psychophysical tuning curves and masking 80−51121
low-frequency model of cochlea, anal. 80−97937
low-level pure tone masking, tuning curves obtained with simultaneous and forward masking 78−65042
magnetic auditory evoked response using SQUID 78−80889
magnetic evoked fields, human 79−16212
mammalian, psychophysical tuning curves and auditory thresholds after hair cell damage 79−96564
masked auditory threshold development in house mouse 77−77907
masked auditory thresholds for constant and gliding tones 79−2079
masked pure tone thresholds, influence of auditory fatigue 77−9207
masked speech intelligibility, influence of auditory fatigue 80−67096
masker interaction in pure-tone forward masking 80−97935
maskers effect on psychophysical performance in discrimination and detection 80−51118
masking, pure-tone forward, intensive and temporal effects 79−92227
masking, pure-tone forward, short-term spectral effects 79−92228
masking effects on articulation in normal speaking adults wearing palatal appliances 80−76766
masking effects on lip movements during speech 78−65061
masking level differences for temporal masking 77−64050
masking of tone-envelope irregularities by a tone of another frequency 79−34576
masking patterns of pure tones, nonlinearities *(German)* 77−21534
masking patterns of pure-tone maskers *(German)* 80−8069
masking period patterns, of AM pure tones *(German)* 77−2007
masking-level difference for repeated filtered transients 78−85321
masking-period patterns produced by VLF maskers, rel. to basilar membrane displacement 77−56383
mastoid, human, model of mech. system imitating acoustic props. 78−80886
matching information to brain, problems 80−51114
mathematical survey of modern theory of nonlinear systems applied to human hearing 78−40195
mechanism of production of summating potential, hair cell functional differences, elec. cct. model 80−72176
medical electronics, appl. to otology *(Japanese)* 80−67268
melody perception, computer program for music transcription 77−5009
microphonic sensitivity, investigation of overstimulation using differential recordings in guinea pig cochlea 79−92231
microwave auditory effect 78−24094
microwave auditory perception, contrib. of middle-ear structs. 80−67097
microwave auditory phenomenon, microwave pulse irrad. of animal brain matter 80−35968
microwave evoked auditory activity 77−60229
microwave hearing mechanism hypothesis, holographic assessment 80−72178
microwave induced auditory responses in mammals, using 3 GHz pulses 78−53444
microwave pulsed fields, evoked auditory sensations, some peculiarities 80−61636
microwave reception by brain, interaction with nerves 77−12958
microwave-induced, auditory sensations prod. by pulsed microwave irrad. 77−2010
microwave-induced auditory responses 80−61628
microwave-induced auditory signal freqs. and thresholds 78−40260
middle component AERs from neonates to low-level tonal stimuli 80−94220
middle-ear admittance development in hamsters 79−88088
middle-ear muscle contraction, influence on auditory threshold 78−85319
mispronunciations listening tests by segmenting speech into words 80−64308
model of auditory system from middle ear to primary auditory nerve 77−29158
model of creation of sound sensation varying with time 80−41053
models and signal processing, conf., Munster, Germany (Sep. 1978) 80−90610
monaural and between-ear temporal gap detection, single gaps 78−11669

hearing continued
monaural and binaural discrimination of intensity and freq. 77−86511
monaural and binaural signal detect., role of dynamic cues 77−36952
monaural sensitivity changes due to pinna, min. audible field meas. 77−48812
monkeys, species-specific perceptual processing of vocal sounds 79−79563
monosyllabic word discrimination, classroom acoustics effects 79−53160
movement-related tonal signal processing, left hemisphere superiority 80−35913
moving source localization, minimum auditory movement angle 78−31820
moving stimulus, detectability of varying interaural temporal diffs. 78−53422
multidimensional audio, meas. and hearing sound quality 79−64458
multifrequential impedance meas. 80−17031
multivariate anal. of subjective measures for sound in rooms *(Japanese)* 77−31179
music, acoustic component of Western consonance and disonance perception 78−90607
music, interaction of responses to braille and music rel. to cerebral lateralisation of haptic perception 78−7374
music pattern recognition, MACSIM self-learning network 78−7373
music perception, appl. of computer program 79−8513
music perception, programmable tone generator presenting melodic and harmonic patterns 77−56381
musical acoustics, review of recent work 79−76920
musical consonance, concept and psychoacoustic foundations *(German)* 77−5007
musical instrument timbre recognition, perceptive effects of data reduction *(French)* 80−28387
musical pitch of two-tone complexes and predictions by modern pitch theories 79−88083
musical pitch prediction from component freq. ratios, antomatic, using computer-algorithm 79−96574
narrow-band filtered speech perception 77−36956
neonatal acoustic reflex, static and dynamic impedance obs. 80−104597
nerve fibre bandwidths and critical bandwidths in cat 77−12932
nerve fibre model 80−94227
nerve firing rates, patterns for spoken digits 79−83802
nervous system activity analysis 80−30921
neural lateralisation of species-specific vocalisations by Japanese macaques 79−62268
neural mechanism system properties 78−40200
neural network modelling by computer simulation, spatial firing patterns 79−74686
neuron, characts. of digital model 78−3516
neuron, stochastic electronic model 77−48775
neuron receptive fields, owl 78−44512
neuron response to pulsed microwave irrad. in cat, microwave hearing 78−40259
neurone phasic sensitivity as function of sound signal freq. 79−57666
noise, effect on hearing ability *(Chinese)* 79−62267
noise, temporal gaps detect. as meas. of auditory sensation decay 77−36953
noise damage, temporary and permanent threshold shifts *(German)* 77−77902
noise dose criteria for setting hearing loss risk estimates for industrial noise 78−1504
noise effects, and acceptable levels and meas. *(Spanish)* 78−15857
noise effects, measurement and anal. *(French)* 79−81621
noise effects, specific and nonspecific, human hearing system *(French)* 77−21538
noise exposed workers, audiometric and audiologic services 77−64056
noise exposure, simulated work-week impulse, hearing loss 79−74687
noise from road traffic and sleep disturbance 77−42659
noise generator for auditory neurophysiological and psychophysical experiments 79−29676
noise hazard, occupational, obs. on heavy industry workers 77−81512
noise intensity discrimination, bandwidth and masker presentation effects 77−9209
noise loudness determ. methods *(French)* 77−34996
noise measurement standardisation *(German)* 78−9496
noise protection of occupationally exposed workers 79−92392
noise research index, for UK (1975/1976) 77−7257
noise stimuli, computer simulation of Poisson transduction 77−86512
noise-exposed subjects, test-retest reliability of repeated manual and Bekesy thresholds 80−81622
noise-induced hearing loss estimation tables 78−15848
noise-induced threshold shift and cochlear pathology in the Mongolian gerbil 78−65035
noise-induced vasoconstriction rel. to pattern A personality 80−35917
noncombination of pitch and loudness in multidimensional scaling 78−40193
nonlinear distortion in sound perception 77−5010
nonlinearities model described by active processes with saturation at 40 dB 80−56058
nonspectral pitch perception 77−9205
normal hearing threshold, depend. on clinical rejection criteria 79−88091
occupational impulse/impact noise exposure, review of current knowledge 80−79056
occupational noise exposure, permanent threshold shift, from an A-weighted Leq of 89 dB 78−92644
octave enlargement phenomenon and its origin 79−100633
Old World monkeys, localisation of pure tones 78−65038
optimal processor theory of aural processing in pitch of complex tones 78−57015
organisation difficulties as possible cause of reading backwardness 78−35869
otometry, combination with brainstem-evoked response audiometry 80−85417
paired-harmonic maskers and inharmonic maskees 78−40180
parakeet, auditory duration discrimination 78−65045
partial masking in Old World monkeys, masker bandwidth and band spacing effects 79−88085
pedestal experiments, formulae for predicting effect of signal on duration, pedestal level and quadrature addition 79−68524
perceived noisiness of intermittent sounds, humans 78−11672
perceptibility of phonetic features, in fluent speech 78−92635
perception nonlinear model with autocorrel. feedback 80−81615
perception of combined freq. and amplitude modulations 78−35864
perception of place and manner of articulation 77−48814
perception of uniform rhythm in sound impulse sequences, functional model 78−65032
perceptual effects of spectral modifications on musical timbres 78−65039
periodicity measures for repeated random auditory patterns 78−61197
peripheral and central auditory deficits of elderly subjects, use of hearing aids 80−17201
peripheral and central processes in selective adaptation of place of articulation in stop constants 78−3523
peripheral auditory adaptation, dependence on recording site 80−81613
peripheral auditory adaptation, guinea pig action potentials 80−89766
peripheral auditory system, anal., noise appls. 78−80888
peripheral feedback qualitative model 79−39422
personal hearing protectors, determination of effectiveness 79−14156
phase changes, audibility using different kinds of irradiation 77−2006
phase changes perception, role of combination tones, psychophysical and electrophysiological expt. 77−36948
phase locking in monaural and binaural neurons 78−88717
phase relations in internal representation of 2-tone octave complex 79−83790
phase spectra of steady three tone complexes, subjective effects 77−29153
phoneme boundaries, effects of adaptation 78−80884
phoneme discrimination of fricative consonants using automatic system 79−55286
phoneme recognition system based on human audition, psychophysical expts. 78−69115
phonemes processing, speed-accuracy study 78−20193
phonetic perception, effect of silence as a cue during word utterance 79−81650
physical principles of audiology, book 80−82592
physiological acoustics and health 80−96103
piezoelectric earphones, usefulness in recording brain stem auditory evoked pots. 80−94389
pitch and intensity changes, dynamic approach to perception 80−33378
pitch and masked threshold in octave complexes rel. to interaction in two-tone stimuli 77−52795
pitch and pitch discrimination of broadband signals with rippled power spectra 78−61199
pitch detection mechanism model 77−90811
pitch mixture of dichotic chords, effects of signal intensity and noise 78−3501
pitch of amplitude-modulated low-pass noise and predictions by temporal and spectral theories 80−67095
pitch of dichotic pure tones, model for relative salience 78−3500
pitch of noise signals, evidence for central spectrum 77−36942
pitch of vibrato tones 80−35911
pitch perception, dominant spectral region existence 77−32912
pitch perception, spatial and temporal cue analysis of complex tones hearing 79−2080
pitch perception mechanism for tones *(Japanese)* 80−12162
pitch perception of complex tones, role of temporal information *(Japanese)* 77−44691
pitch perception of musical sounds, dependence on degree of training in hearing *(German)* 79−74682
pitch ratings of harmonic series 78−20189
pitch shift of monaural pure tones caused by contralateral sounds 77−21536
pitch shifts following tone adaptation 79−20546
pitch strength meas. associated with ripple noise 78−88716
poststimulatory pitch shifts for pure tones 80−97934
power law transformation giving short term integrators producing time-intensity trades for noise bursts 78−40190
preadolescent children's voices, acoustic correlates of perceived sexual identity 80−10088
precedence effect, possible role in avoidance of interaural ambiguities 80−61588
precedence effect on word identification by normally and impaired hearing subjects 78−40189
precise perceptibility of original loudness through electroacoustic playback *(German)* 77−21535
primary auditory cortex of awake cats, single unit activity vs. amplitude of epidural evoked potential 80−35904
primary auditory neurons, preferred intervals in spontaneous activity 80−45921
primary neurons, comparative physiology 80−94224
protection, performance of custom-moulded earplugs 80−104774
protectors, attenuation-frequency characts. meas. using cadaver ears 79−11947
protectors, circumaural type, objective meas. of attenuation 79−11948
protectors, effectiveness meas. 79−14180
protectors, meas. of real-ear attenuation, SABS 572 1973 80−53581
protectors, meas. of real-ear attenuation by standardised test methods 78−1508
protectors, use of noise levels for assessing adequacy 80−104771
psychoacoustic and sound recording, book 77−826
psychoacoustic decision process, blurred nature effect on sound sensation 79−74683
psychoacoustic detection threshold of transient intermodulation distortion in recorded music 80−56060
psychoacoustic experiments using freq. and amplitude modulated stimuli 80−94236
psychoacoustical aspects of synthesized vertical local cues, computer synthesis 78−61198
psychoacoustical tuning curves, influence of pulsation threshold method 77−21533
psychoacoustics, mechanism of human hearing 79−83793
psychoacoustics and the perception of space, stereo reproduction appl. 79−100623
psychological and physiological acoustics, history (1920 to 1942) 77−45664
psychophysical 2-tone suppression, stimulus component level effects 80−61584
psychophysical 2-tone suppression as function of input level for $f_2/f_1>1.0$ 80−76756
psychophysical freq. resolution in cat as determined by simultaneous masking, relation to auditory-nerve resolution 80−35906
psychophysical investigation of divided time intervals shown by sound bursts *(Japanese)* 80−12160

hearing continued
psychophysical pitch biases related to vowel quality, intensity difference, and sequential order 79−5295
psychophysical tuning curves, relationship with suppression 80−12158
psychophysical tuning curves, restricting listening band to signal region 79−53158
psychophysical tuning curves for combination tones $2f_1$-f_2 and f_2-f_1 80−76755
psychophysical tuning curves for simultaneous and foward masking 78−53423
psychophysical tuning curves of chinchillas 77−12931
psychophysiological techniques applied to aircraft design and other operational problems 80−26384
pulsate brain stimulation in normal and deafened cats, temporal summation 80−12155
pulsed sinusoids with interaural temporal differences, lateralisation 77−36946
pure tone audiometry, comparison of ascending and bracketing methods 80−56323
pure tones detect. and recognition in noise 78−11668
pure-tone audiometric threshold rel. to age tables 80−35918
pure-tone audiometric thresholds, relation to age, comparative anal. of data 79−5299
pure-tone intensity discrimination, neural-counting model incorporating refractoriness and spread of excitation 80−35908
quadraphonic sound field analysis method and appl. *(Japanese)* 77−75730
quantisation and averaging 80−94145
race and sex variations in hearing threshold levels of N.Carolina industrial employees 80−97939
range effect in the perception of voicing 78−65044
rapid auditory processing in normal and disordered language development 77−5016
reaction time and absolute threshold in cat 77−36957
reaction times, for functional exploration of sensory, sensory-motor and auditory routes *(French)* 77−37077
reaction times for functional and nonfunctional hearing loss 77−56385
receptor pattern in herring 79−96579
reflex response as function of intensity and temporal charact. of pulsed stimuli 78−20190
reflex thresholds for noise stimuli 80−108916
residue pitch adaptation, monaural perceptibility meas. 78−57020
resolving capacity of human auditory analyser 78−69104
respiratory tracking of dichotically presented tonal amplitudes 78−27973
response properties of spiral ganglion neurons in cochleas damaged by direct mechanical trauma 80−67093
reverberant sound perception, masking level differences determ. 77−64049
review of physical aspects of hearing 77−90808
review of sound anal. by the ear 80−104593
rhythm perception in early infancy 77−48816
ripple noise pitch detection by human, adaptive model 78−73166
room acoustics and subjective sound perception, computer simulation *(Polish)* 79−7258
rotating tones and binaural beats 77−64043
roughness perception of amplitude modulated tones and noise 77−25462
Schroeder-Hall hair-cell model, further investigations 79−70554
selective attention, two-channel simultaneous freq. difference limen 77−52801
selectivity, two-stage lateral inhilation 77−56382
sensor perception measurement methods *(Russian)* 79−62270
sensori-neural impaired, effect of protection on speech intelligibility 79−81658
sensorineural hearing loss, freq. selectivity and speech discrimination 80−61593
sensorineural hearing loss effect on acoustic stapedius reflex growth functions 79−16216
sensorineural hearing loss effect on loudness discomfort level 79−96577
sensory evoked potentials in nervous system clinical disorders, book contrib. 79−2029
sensory-acoustical and bio-acoustical expts., theoretical aspects 77−70478
sentence comprehension, multiplicative effects for combined acoustic disturbances 80−35915
sentence information processing, EEG evoked response and CNV obs. 79−57626
serial-recall performance, effect of syntactic order, hearing impaired vs. normal subjects 78−27961
Shepard demonstration, decoupling of auditory pitch and stimulus freq. 78−40191
short-term recall, phonological interference effect 79−96537
shuttlebox side preference as mediated by pulsed microwave and conventional auditory cues 79−100634
signal central spectral pattern anal. based on cochlear neural timing and freq. filtering 79−5300
signal detection in psychoacoustics 78−3514
simulators of auditory and visual impairment, development project 79−83982
simultaneous and nonsimultaneous masking, observations of transition region 80−76757
simultaneous notes perception in polyphonic music 78−61191
simultaneous pure-tone masking, masking asymmetry depend. on intensity 78−65041
sine wave tones, effect of amplitude envelope on pitch 78−65034
single auditory nerve fibres, adaptation, saturation and masking 79−48273
skull and auditory ossicle vibr. anal., human preps., using holographic interferometry 80−67210
smoothing effect, generalised Talbot law appl. *(Russian)* 80−72177
sonar, bat, perception of echo phase information 79−83800
sonometry, sound audibility, serial noise from machines and equipment *(French)* 77−21537
sound amplitude modulation detect. by trained musicians 78−3517
sound differences in sensory space for sound reproduction engineering *(Russian)* 78−55521
sound duration effect on annoyance *(Japanese)* 77−50828
sound localization, pattern display panel 78−27969
sound quality, perceived, of sound-reproducing systems, investigated by multivariate techniques from experimental psychology 79−68536
sound sensation, partial relative sound evaluation arising from given feature or subfeature 79−74684
hearing continued
sound source location, physical effects, Haas effect *(German)* 79−57668
sound transmission from mech. part of nerve endings model 79−57667
sound variations subjective evaluation model *(German)* 77−52796
source elevation illusions, created by spectral manipulation using monaural hearing 78−3510
spatial freq. analysis within cochlea, meas. of stiffness gradient along basilar membrane 79−24995
spatial hearing problems, stereophony, quadraphony appl. *(German)* 79−16213
spatial orientation of animals, role of auditory mechanisms *(Russian)* 80−45915
speaker identification, effects of selected vocal disguises 80−10091
spectral estimates of auditory brainstem responses 80−30913
spectral integration 80−21477
spectrum pulse sequences, discrimination of PLC sequences 79−88086
speech, time-intensity trade, temporal speech-Stenger effect 77−25470
speech, word list formats in hearing tests 80−33370
speech comprehension ability of hard-of-hearing, calc. model *(Dutch)* 78−73165
speech discrimination functions for normal-hearing subjects 79−92240
speech discrimination in deaf subjects with cochlear implants, elec. stimulation of auditory nerve 80−108915
speech discrimination in infants, developmental changes 78−65048
speech discrimination scores, binomial variable model 79−53161
speech encoding in auditory nerve, effects of nonlinearities 80−108913
speech intelligibility, distinction between distinctive features and acoustic cues 78−11681
speech intelligibility, reverberation and noise effects in cases of presbyacusis 80−96139
speech intelligibility, temporal interruptions with and without intervening noise 77−32911
speech intelligibility and S/N ratio in high noise *(Japanese)* 77−73533
speech intelligibility in noise induced hearing listeners, effects of high-freq. compensation 80−38186
speech intelligibility measuring, hearing-impaired children 79−20554
speech intelligibility test, DIN 45621 recommendation, acoustics and phonetics, German test *(German)* 78−35867
speech interference level as predictor of face-to-face communication in noise 78−57018
speech perception, adults, overt and covert aspects 77−52803
speech perception, auditory and visual contribs. 77−16939
speech perception, discrimination of rise and decay times in tone and noise bursts 80−19166
speech perception, hemispheric specialisation, acoustic change rate, expt. obs. 80−104594
speech perception, order effect of acoustic segments of VC and CV syllables on stop and vowel identification 78−27967
speech perception, use of comfortable listening levels, effect of loudness level 79−2078
speech perception model used to evaluate speech recognisers 77−32905
speech processing by auditory nervous system 80−108911
speech reception threshold, reliability in the determ., psychometric function 80−61657
speech reception threshold for sentences as function of age and noise level 80−19169
speech recognition using spectral peaks *(Japanese)* 77−64053
speech-pattern learning in French and English children 78−57025
speechreading, use of residual hearing *(Japanese)* 77−81511
Sphenodon punctatus, ear anatomy and hearing 77−40681
squirrel monkey, temporary threshold shift from noise exposure 78−88715
Staggered Spondaic Word Test, lead and lag effects 77−5008
stapedial reflex in noenates 79−92236
stapedial reflex thresholds and tympanometric compliance values, age and sex variations 80−41049
stapedius reflex thresholds, aging and distortion product 79−100628
stapedius reflex thresholds, comments on effect of aging 79−100627
stapedius reflex thresholds, effects of aging 79−100625
steady-state vowel representation in temporal aspects of discharge batterns of populations of auditory nerve fibres 80−21479
stereo perception space, in intensive stereophony (quadrophony) *(Czech)* 79−68491
stereophonic equalisation of artificial heads without exact replication of eardrum impedance 80−81614
stereophony, importance of transients 79−88090
stereophony, reproduction of sound effects using microphone and headphones *(German)* 79−37106
stimulus dominance in fused dichotic syllables, category goodness hypothesis 80−33368
stimulus freq. effects on adaptation in auditory nerve fibers 79−43924
stimulus variability and auditory filter shape 78−3506
stimulus-onset asynchrony effect on dichotic performance of children with auditory-processing disorders 80−41044
stop consonant discrimination based on human audition 79−50528
stutterers' central auditory function, synthetic sentence identification test 79−96586
subjective analysis of acoustic noise *(German)* 79−46109
subjective duration and temporal masking patterns of broadband noise impulses 77−36943
subjective experiments (e.g. aircraft noise anal.), use of changeover designs 77−82380
subjective hearing event, directivity of loudspeaker *(German)* 78−79174
subjective loudness and its physical correlate 77−64037
subjective loudness measurement, affecting auditory factors *(Japanese)* 80−85409
subjective noise annoyance by low level sound 80−35902
subjective noise charact. comp. using PL/1 program 78−59192
subjective preference of sound with single early reflection 77−29154
subjective preference tests for musical sound fields with single echo 78−31819
susceptance tympanograms, asymmetry obs. 80−41051
switching phases rel. to freq. and duration of tone pulses, difference limens 77−48809
syllabic structure in words, auditory/vibratory perception by profoundly hearing-impaired children 78−27962
syllable perception with alternate formants presented to opposite ears 78−65043
syncopated auditory polyrhythms, discontinuous reversals in meter interp. 78−55528
synthesised musical instrument tones, perceptual evaluation 77−90807

hearing continued
synthetic /bdg/ identification by hearing-impaired listeners under monotic and dichotic formant presentation 80−58871
teleconferences, influence of vision on auditory direction when presenting speakers *(German)* 79−72762
tempo sensation of burst signals *(Japanese)* 77−77913
temporal auditory summation of pure tones in birds 79−70558
temporal factors and suppression effects in backward and forward masking 79−16215
temporal integration of two-component tone glides 79−16217
temporal masking, effects, critical band noise masker expts. 77−25458
temporal masking with pure tone masker 80−30732
temporal modulation transfer functions based upon modulation thresholds 80−21478
temporal order perception for vowels and consonant-vowel syllables 78−69108
temporal perception of sound events, subjectively uniform rhythm *(German)* 79−20548
temporal perceptions, effects of early auditory deprivation 80−76761
temporal recognition masking or interference 77−25464
temporal summation experiments, procedure and evaluation of results 77−29157
temporal switching between binaural information sources 78−53425
temporally variable sounds, procedure for loudness calc. 78−3508
temporary threshold shift and acoustic reflex, temporal charact. 78−27968
temporary threshold shift from transportation noise 79−90074
temporary threshold shift produced by varying noise exposures 77−64042
temporary threshold shifts in humans exposed to octave bands of noise 79−74688
Terhardt's pitch theory, examples in support 80−12159
threshold audiometry, computerized, optimum crossings and time-window validation 80−19187
threshold meas., comparison of two methods of manual audiometry 79−66477
threshold of octave masking test, interpretative obs. 80−56064
threshold shift in chinchilla from daily exposure to noise 77−36954
thresholds, auditory and acoustic reflex, effects of stimulus duration and stimulus off time 78−73164
thresholds of pain and hearing, cassette recorder noise and music levels *(German)* 80−81616
timbre differences, functional model *(German)* 80−30733
timbre differences between complex tones, investigation using method of triadic comparisons *(German)* 80−67088
timbre discrimination in musical patterns 78−88713
timbre of complex tones, physical and psychological factors *(Japanese)* 80−97944
timbre perception, review 78−77068
timbre-classification of complex tones. (The relation between subjective and physical parameters) 78−77060
time information direct use, place clues in white-spectra stimuli 77−90803
time-altered speech intelligibility rel. to age 77−52805
time-intensity trading ratios in lateralisation task 77−36958
tonal pattern discrimination, selective attention and learning under various levels of stimulus uncertainty 77−12934
tonal sequences perception and familiar melodies reproduction 77−36951
tonal signal lateralization and detection of interaural differences of time 79−43930
tone burst detect. in continuous and gated noise maskers 77−64045
tone detection and choice reacion times, cat, behavioural system and apparatus 78−20187
tone detection in pseudorandom noise, effect of masker level 79−92224
tone glides, temporal integration 78−57013
tone quality, descriptor charact. *(Japanese)* 79−24997
tone quality eval. expts. *(Japanese)* 79−24996
tone segregation by phase, phase sensitivity of single ear 79−88084
tone sequences ABAB, min. level and freq. differences for perceptual fission 77−56384
tone threshold, off-frequency listening and auditory-filter asymmetry 80−35910
tone-pitch duration threshold, influence of initial phase of short sinusoidal pulses 78−24077
tone-pitch threshold, analytic expression, function of frequency 77−60221
tone/noise combination effect on speech intelligibility rel. to aircraft noise 77−50824
tones, AM, dependence of fluctuation strength on sound parameters *(German)* 79−34569
tracking procedures for training and evaluating speech reception 78−61204
tractor cab noise affect on the hearing perception of drivers 79−83791
traffic noise, acoustical correlates of aversiveness 79−41511
traffic noise, annoyance testing *(German)* 77−19473
traffic noise nuisance in residential areas, individual responses 77−31167
transition length, effects on perception of stop consonants 78−92636
travelling waves and cochlear resonance 80−94222
trombones, trombonist's perception 78−90611
tuning curves of cochlear and brainstem responses in the guinea pig 80−108917
two tone suppression in backward masking 77−77912
two-tone aural nonlinearity, review 80−89768
two-tone interaction in octane complexes, investigation by pulsation-threshold method 78−20181
two-tone spectral resolution 78−11667
two-tone suppression, analogue in whole nerve responses 78−11671
two-tone suppression, in nonlinear model of basilar membrane 77−48811
two-tone suppression, phenomenological model 77−16936
two-tone suppression, stimulus freq. effect, physiological and psychophysical obs. 78−85317
two-tone suppression in cat auditory nerve, rate-intensity and temporal anal. 78−61194
two-tone suppression in forward masking, mechanism and freq. distrib. 80−108909
two-tone unmasking in forward masking procedure, perceptual cueing 80−97940
tympanic membrane perforation in cuts, LF hearing loss 78−53419
tympanometric asymmetry 78−27963
tympanometric screenings of 2-year-old children, repetitive obs. 80−85412
tympanometry, interactions among variables 78−27964
tympanometry in 3 year old children, seasonal influences 80−41052
tympanometry in 3-year-old children, correl. with findings at paracentesis 80−85416
underwater sound, psychophysical struct. 77−77908
unmasking produced by combination tones 79−96565
US pulse echo system using interaural localization 80−89769
vertex short latency acoustic responses in cat, factors affecting amplitudes and latencies 78−61192
vibrotactile speech training deaf aid, frequency analysis system 77−29214
visual effects of auditory deprivation, common intermodal and intramodal factors 80−89754
visual field displacements evoked by intense sound exposure, humans 78−85332
voice onset time and fundamental freq. cues in /zi/-/si/ distinction 77−2008
voice onset time discrimination 77−25466
voice qualities, multidimensional classification 78−92651
voicing distinction in initial stop consonants, dissociation of spectral and temporal cues 78−3519
vowel formation by profoundly deaf children, Argentine Spanish appl. *(Spanish)* 80−30734
vowel identification, excerpted from /l/ and /r/ contexts 77−9210
vowel perceived duration, temporal course 78−77065
vowel perception, temporal factors 77−25465
vowel recognition test for investigating sensitivity of vocal tract area functions 79−59887
whales, southern right, sound playback expts. 80−89772
white-noise nonlinear system anal., appl. to peripheral auditory system 80−108914
wind noise, expts. on human beings 78−92648
word discrimination scores, effect of marking by noise 80−41047
word perception, role of medial consonant transitions 79−81651
workplace noise exposure control, costs and benefits 77−23809
zebra finches, female, long-term recognition of father's song 79−83799
Zwicker's masking period patterns, computational model 78−88714
Ta-Al_2O_3 microelectrode array, design and fabrication 80−76868

hearing aids
ageing and use of hearing aids, performance with peripheral and central auditory deficits 80−17201
auditory training apparatus, individual for persons suffering from severe hearing loss 79−39590
bandwidth compression, limitations of voiced portion of speech 79−29668
children who wear individual hearing aids in British Columbia, Canada 80−41326
cochlear implantable prosthesis, information coding 80−46100
cochlear implantable prosthesis realisation rel. to IC technology 80−46099
compression aids, meas. of attack-release times 79−20707
computerized test system, signal processing techniques 78−30131
coupling device for transfer characteristics measurement *(German)* 77−75756
CROS aids, evaluation with unilateral listener 80−104812
deaf speech and hearing aids, vocoders, frequency lowering and lipreading cues 80−12309
directional microphones aids, effect in different acoustic environments 79−92239
electroacoustic freq. response, mathematical prediction 78−40408
EM hearing-aid receiver, experimental scheme for dynamic behaviour anal. 78−9518
filter, programmable, charact. *(Swedish)* 78−36055
free field pure tone audiometry as comparative system for aid assessment and fitting 80−108983
Glossynograph system for presenting printed text synchronously with speech for hearing-impaired persons 80−56153
handicap of hearing impairment and limited benefit of hearing aids 78−53424
history of acoustics, from Echo to 18th century *(German)* 79−76915
implantable *(Japanese)* 80−81774
implantable 8-channel stimulation system for labyrinthine deafness *(German)* 79−16347
implantable design, implantation procedures and chinchilla results 77−60295
implantable multichannel neural stimulator, custom IC fabrication 80−85534
implanted hearing stimulators 79−79561
in situ tests, appl. of acoustic press. field meas. alongside manikin's head 77−90805
intelligibility improvement in presence of noise for hearing impaired person, signal processing 77−11091
KEMAR manikin, use of larger external ear replica 79−70557
loop induced magnetic fields in classrooms for the hard of hearing, using orthogonality principle 77−61893
magnetic, meas. of audibility relative magnetic threshold *(Croatian)* 78−11673
measurement system comparison 78−65151
microelectrode arrays, photolithographic fabrication and neurophysiological performance 79−12034
multiple-electrode prosthesis for cochlear implantation in deaf patients 78−36061
Multipoint Electrotactile Speech Aid 78−40407
perceived sound quality obs. 80−41050
problems with use, implantable artificial middle ear 79−84009
programmable hearing aid with multichannel compression, speech discrimination tests, children 80−17202
quality judgments of speech signals processed by hearing aids, multidimensional scaling 80−97933
sound pressure in insert earphone couplers and real ears 78−65152
sound quality, perceived, investigated by multivariate techniques from experimental psychology 79−68536
speech communication, contribution of speech reading and hearing aids 79−25002
speech comprehension ability of hard-of-hearing, calc. model *(Dutch)* 78−73165
speech processing, linear amplification, AF peak clipping and HF carrier clipping 77−17007
speech translation system, real-time, for hearing impaired 78−7546

hearing aids continued
tactile hearing aid, portable with microprocessor control 79−84029
vocoder, portable, tactual, design *(Japanese)* 78−44691

heat
see also heat transfer; heating; latent heat; specific heat; temperature; terrestrial heat; thermal variables control; thermal variables measurement; thermodynamic properties; thermodynamics
convective fin heat loss, temp. depend. thermal cond. and tip heat loss 79−72780
demonstration, enhancement using coolant sprays 80−8761
fluctuations near crit. point 80−47005
history, reassessment of Rumford's theory 77−57292
intensity distribution inside absorbing-isotropically scatt. semiinfinite medium 78−32335
liquid and free-flowing materials, meas. using calorimeters 77−87765
open systems, definitions of heat, internal energy transfer by convection 80−69644
school physics, elementary presentation by theory of heat, thermodynamics, and thermometry *(Danish)* 80−4483
teaching demonstration, boiling phenomena when red-hot balls enter water of different temps. 78−24627
thermodynamic principles of heat-work transfer *(German)* 78−62171
water flow in channel with variable heat flux 77−62254

heat capacity *see specific heat*

heat conduction
see also thermal conductivity
ablation, multidimens., embedding in inverse heat cond. problem, finite difference method 78−94508
absorbing-scattering infinite slab, combined conductive and radiative heat transfer 78−71269
absorbing-scattering semitransparent planar layer, flat temp. waves 78−90683
analogue simulation using difference equations *(Japanese)* 78−1664
anisotropic media, anal. solns. for bounded regions 77−84117
anisotropic multiply connected media, deterministic and nondeterministic symbolic procedures 77−14878
anisotropic sheet with insulated hole, temp. distrib. 79−32202
anisotropic simple materials, transport coeffs., reciprocal relations 77−72708
anisotropic solid, arbitrary shape, three-dimensional soln. 77−58527
anisotropic to isotropic transformation 78−87231
annular rib cooled by boiling liq. on surface, heat cond. anal. 79−55315
annulus, off-centre, heat cond. soln. 77−7285
annulus, spherical, rot., forced thermal convection of viscous fluid 79−27634
ansiotropic medium homogeneous in cylindrical regions, steady-state anal. 77−58526
approximate solns. 78−26018
approximation analytic solutions, heat cond. in adjacent regions *(Russian)* 78−83212
axial wall conduction, with var. prop. convection, axial temp. distrib. calcs. 77−15010
axisymmetric body-duct configuration 79−32185
battery heat flowmeter, heat flux meas. using Kalman filter 79−37143
beam structures, thermally induced vibrations and heat conduction problem, numerical method 80−64427
bibliography of heat transfer 78−63425
binary gaseous mixtures, transient heat conduction 80−64670
binary mixture theory for thermal diffusion in unidirectional fibrous composites 78−87230
binary monatomic gas mixture, conductive heat transfer 79−94459
biological tissue around cryosurgical probe, Stefan-like problem analysis 77−17005
BIOT2, heat conduction, three-dimens. code *(Hungarian)* 80−43593
Biot's variational principle, consequence of invariance in thermal cond. 78−33988
Biot variational eqn. generalisation 80−43591
blast wave, with transport props., self-similar soln. 77−68621
bodies of revolution, heat cond. during nonaxisymmetrical heating *(Ukrainian)* 79−98591
bodies with wavy surfaces, thermoelastic contact, heat conduction 80−64492
body in variable property fluid, heat transfer 78−38170
boiling heat transfer during rewetting, one-dimens. cond. model 79−598
boundary layer of viscous heat cond. medium, acoustic streaming 79−86544
boundary value problems, error analysis of determined thermophysical characteristics 79−81687
boundary value problems, soln. 80−79106
boundary value problems, soln. for heat conductivity eqns. by Green's function method *(Russian)* 78−63267
boundary-value problems, numerical solutions *(Russian)* 78−55545
boundary-value problems for nonuniform media 78−63266
boundary-value problems for region with moving boundaries, analytical soln. methods, review 77−75768
in bounded and unbounded domains, continuous data-depend. results for general theory 77−68365
bubble and eddy heat diffusion in single phase flow 80−19477
bubble-liq. mixture with nonsteady interphase heat transfer, shock struct. 78−83424
building, thermal energy balance, method for including environmental modulation *(French)* 79−3900
building constrcution model, temp. changes 79−81684
building two-dimensional heat load, anal. by finite element method 78−71536
building with porous walls for air ventilation, heat transmission 79−4016
Burgers equation, sawtooth soln. decay 80−31529
calculation via electrical analogue, from elec. resist. 77−72128
calorimeter, scanning, with pyroelec. heat sensor, heat cond. eqn., model 77−10026
Cauchy problem, numerical proceedure 77−5644
cells of triangular lattice with central heat sink, nonsteady cond. 79−81683
chemical reaction, solid, endothermic, unsteady heat conduction, thermal conductivity change 80−76511
chemically active liquid in horizontal porous bed, convective instability 79−41769
chopped glass fibre reinforced polyester resin, deformation and thermoset cure effect on heat cond. during molding 79−86325
circular plate, quasi static thermal deflection 79−14259

heat conduction continued
closed cylindrical shell with insulated cross crack *(Ukrainian)* 78−90638
closed form solutions for cylinder 79−32186
coaxial cylindrical discs, radial heat flow 78−75032
combination of Lagrange and Euler methods 79−76941
combined heat transfer, state of the art review 80−79119
complex domain heat exchange, new soln. techniques 78−94509
composite bodies, nonstationary thermal conduction processes, numerical simulation *(Russian)* 80−92016
composite cylindrical rod, approx. one-dimens. thermal conduction 77−11117
composite material, heat conduction lattice model 79−81682
composite materials, numerical method calcs. 78−94522
composite media with complex geometry, pot. field problems 78−16663
composite medium with periodic surface temp., contact resistance, heat cond. using Heaviside operational method 78−9549
composite prismatic bars, doubly connected cross section, heat flow shape factors, anal. determ. 79−1068
composite regions, analytical soln., appl. to metallic nuclear fuel rod 77−7295
composite slab with variable cond., transient heat cond. anal. using collocation method 80−10106
composite wall, constant props., transient heat cond. problem *(French)* 78−87229
composites, Sturm-Liouville problem eigenvalue bounds 79−50568
compound prismatic bodies, stationary problems *(Russian)* 78−38168
condensed medium, semitransparent, plane layer radiative-conductive heat transfer 80−43590
condensing surface thickness effects, dropwise condensation 78−22250
conduction-controlled rewetting of hot surface, two-parameter relation 77−19605
conduction-convection problems, error growth for explicit difference schemes 80−92017
cone/plate system in fluid, friction heating and convection 78−87238
conjugate problems, finite difference solns. 80−19213
contact conductance theory, effect of multiple sources 79−76942
continuous heat source, sphere, boundary conditions of second kind, temp. field 77−23851
convective-conductive transient heat transfer, finite-element method 79−3888
convergent and divergent flows, turbulent boundary layer with press. gradient, Reynolds analogy 78−83382
converse problems, initial temp. distrib. determ. by optimal dynamic filtering 80−19208
cooling bodies, thermal stresses and temps. determ. by finite elements 77−14881
cooling fin with heat sink, design optimisation 79−1046
coupled conduction-turbulent convection in a circular tube 78−94691
coupled radiative and conductive transfer thermokinetics *(French)* 79−1095
coupled radiative plus conductive heat transfer, absorption coeff. temp. depend. allowance 80−74698
coupled thermomechanical phenomena, nonlinear transient anal. 79−32181
critical radius effect with a variable heat transfer coefficient 78−83205
cross flow heat exchanger, longit. wall heat conduction, numerical calcs. 78−90645
cryosurgery, math. and biophys. foundation 77−40920
cryosurgery instruments, effects of heat transfer material on working parameters 78−36037
cylinder, in vaporisable liq., temp. distrib. calcs. *(French)* 77−14874
cylinder, inverse heat cond. problem soln. for thermal consts. determ. 79−37142
cylinder, medium temp. control *(Russian)* 77−54856
cylinder, solid, temp. prediction method for inverse heat cond. problem 79−94449
cylinder, solid circular, const. surface cooling, temp. fields *(German)* 77−39195
cylinder, with 3-dimens. anisotropy 79−94458
cylinder comprising homogeneous elements, calc. of temp. field *(Russian)* 77−84110
cylinder immersed in liq., correct boundary conditions 78−38171
cylinders, vertical and coaxial, theory of convection, velocity profile and heat transfer 80−59036
cylindrical annuli, concentric, eccentric horizontal, natural convection heat transfer 79−55382
cylindrical body heated by moving heat source, heat cond. and temp. distrib. Green's function derivation 77−42681
cylindrical heat cond. eqn., implicit difference methods 79−41551
cylindrical mould, heat cond. with phase change 79−37108
cylindrical regions with noncircular boundaries, boundary value problem 77−89000
cylindrical shell mixed boundary value problem, integral eqn. 77−35
cylindrical shell of complex configuration, calc. of nonsteady thermal regime 78−1543
cylindrical transient inverse heat cond., numerical soln. 77−6501
Czochralski growth system, time-depend. cryst.-melt interface shape 77−24280
d^2S/dt^2, sign during thermal conduction 80−36959
Davies model of heat cond., entropy prod. in open quantum systems 79−88899
deformable solids with rough surface, stochastic problem of heat conduction and thermoelasticity *(Russian)* 78−38169
derivative boundary condition problems, steady state heat generative case 79−68545
differential equations, generalised differential operator appl. *(Hungarian)* 79−14202
differential equations solution, parabolic, with M-matrices, w.r.t. rate of convergence *(German)* 80−1405
differential equations solution, two-dimensional, inverse problems *(German)* 80−1404
diffusion process, parabolic boundary-value control problem, numerical treatment 77−847
diffusion process localisation in const. property media, heat conduction 80−58888
diffusivity measurement, using wave packet soln. and microprocessor-controller 78−73989
direct differential methods, review 80−64352
disperse media, effective thermal conductivity small Peclet no. 78−22254
dissociating gas in pipes, heat and mass transfer 80−24105

heat conduction continued
drop, evaporation in vap., slow viscous flow, heat flow asymmetry effect 77−75966
droplet evaporation on heated surfaces, theory 78−87785
drops, noncirculating, direct contact condensation 78−94548
dust laden gas in channel, combined heat transfer 78−91031
dynamical thermoplasticity, appl. of mathematical system theory 78−83271
dynamics problems of highly intensive heat transfer, solns. 80−87702
eccentric annulus, steady-state heat conduction 77−62132
education, heat conduction, generalized eqn., parabolic or hyperbolic soln. 78−36746
education, homogeneous ellipsoidal inclusions, general theorems, Poisson theorem, dielectric polarisation, conduction and elasticity 78−61979
effect of boundary refl. and selectivity of optical characts. on radiative-conductive heat transfer 78−1554
elastic bodies, formulation of field eqns. removing paradox of infinite signal propag. speed 77−35014
elastic heat conductors, second order response functions 77−68424
elastic material, non-linear, thermodynamic theory, considering thermal vel. waves 77−62189
elastic mixtures with long range spatial interaction 79−12600
electric current carrying leads, compensating for heat flows 77−7299
electrical analogy for nonstationary heat transfer through walls *(Slovene)* 77−39191
electrical circuit, slowly modulated dissipative steady state, dQ=TdS far from equilib. 78−81934
electrode units in MHD channel, temp. distrib. 78−59258
elliptic cylinder, interior value problem 79−37123
end-temperature in semi-infinite rod, distributed parameter optimal control problem 78−13886
energy transfer in a heat-conducting medium with arbitrary scattering of thermal radiation 78−94507
engineering calculation method, time derivative averaging of temp. 77−11110
equation solution regularity for non-rectangular plane domain *(French)* 77−67199
evolution equations for heat cond. with memory 80−38220
explosion, thermal, crit. parameters analysis 80−11891
explosive boundary condition problems, accuracy of approx. solutions *(Russian)* 80−99912
extended domain method 80−19209
F-region, vertical cond. rel. to neutral temp. and zonal wind during Joule heating 79−21084
fast reactor, HCDA, heat conduction calc., method of weighted residuals 79−635
ferrofluid, helical flow with heat cond. between coaxial porous tubes 79−23371
ferromagnetic suspension, heat transfer for shear flow conditions 79−46394
fibre reinforced composites, quasi-one-dimensional heat conduction, non-linear mixture theory 80−64335
fibre-reinforced composite, quasi-one-dimens. thermal diffusion, mixture theory 78−71271
fibreglass laminates, thermal NDT using liq. crysts. 80−93709
fibrous composites, stationary transfer, effective heat conduction coeffs. 80−64337
field-emission cathode peak current, size effect 80−29863
film boiling, conduction and radiation from flat plate *(German)* 79−72789
fin array, shrouded, with, without tip clearance, laminar heat transfer 79−55376
finite difference approach, convergence of iteration *(Russian)* 77−39197
finite elastic cylinders, Ritz solns. for axisymm. temp. and stress fields 78−38190
finite element anal. of conduction with moving boundary *(Russian)* 80−38216
finite element discretisation, two-dimens. stationary heat cond. using successive overrelaxation and conjugate gradients 78−83206
finite element explicit algorithm 77−46885
finite element formulation of cond. eqn. in general orthogonal curvilinear coords. 77−14882
finite element heat cond. in reactor solids, review and TEMPEL computer program 78−62593
finite element thermal transient problems, use of reduced eigenvalue method 77−3711
finite heat propagation rate, hyperbolic eqn. 77−14875
finned-pipe solar energy collector, optimal material distribution 79−83631
fins, nonlinear problems, 1-D conduction, initial value problem 80−83726
fins optimisation circular, with heat generation, using variational technique 77−65658
first principle of thermodynamics, for non-uniform temp. processes, mathematical formulation 79−71388
fission reactor evaporator, premature bend dryout phenomena, wall temps. 77−61499
fission reactor fuel, transient heat conduction problem in composite region, simulation capability of elec. heater *(Japanese)* 80−68772
fission reactor LOCA, AA 80−18528
flat layer of selective medium with semitransparent boundaries, radiative-conductive heat transfer 80−19227
flat plate, in forced flow, approx. method for heat transfer calc. 78−94682
flow, of liq., thermal markers for vel. field meas., error reduction 78−91036
fluid, convective heat transfer with alternating circulation, mathematical model *(Rumanian)* 79−14208
fluid, non-simple heat-conducting, thermodynamics 77−80057
fluid in contact with surface, transient temp. field, mesh refinement method 80−69825
fluid thermal conductivity meas., transient hot-wire technique, theory 78−65933
fluidised bed, high-temperature, radiant, conductive-convective components of external heat exchange 80−43709
fluidised bed, rate of heat transfer from freely-rising slug of hot gas 80−96307
fluidised beds, packed or quiescent, heat transfer from immersed heater 78−71391
fluids, Newtonian, eqns. of motion, initial value problem 80−62477
fluids with microstruct. and microtemp. 79−98705
forward Monte Carlo heat conduction, known-temp. boundary condition treatment 79−158
free convection loop embedded in heat conducting solid, heat transfer 80−96257
freeze-drying of food models, heat and mass transfer 79−1098
freezing/melting boundary, model for approx. calcs. 78−5630
frost growth rate prediction eqn. for cooled surfaces 78−87248
fuel droplets, mathematical models of transient heat flow 79−18673
fuel element transient heat transfer, temp. distrib. 78−17280
fundamental solution to heat cond. eqn. in two temps. asymptotic behaviour 79−94454
fusion reactor, blanket temp. variation with slab geometry 78−78495
gas, heat transfer between two concentric spheres with internal degrees of freedom 78−30399
gas, real, viscous, heat-cond., acoustic nonequilib. phenomena 78−47086
gas analyser, based on thermocouple vacuum gauge 80−61183
gas column, onset of oscillation due to heat conduction field 78−14027
gas column, onset of oscillations due to heat conduction, limiting condition 78−14028
gas flow, high-temp., heating of graphite body, numerical soln. 79−37318
gas layer, heat cond., radiation interaction in presence of band spectrum 79−55307
gas mixture above flat plate, mixed convection 78−5636
gas plane flows in presence of weak supply of energy *(Russian)* 79−32498
general inverse problem, appl. of dynamic programming 78−45475
general physics and heat, book 79−25814
generalised Legendre transforms, operational props. and appl. to heat transfer 78−59256
giant heat pulse, temp. distrib., classical Fourier and wave heat cond. eqns. 78−94518
Gibbs equation, generalised, heat fluctuations 79−76940
glass fibre reinforced plastic, thermal cond. meas. rel. to temp., heat cond. problem soln. 79−37887
glass-metal composite, heat conduction, memory switching 80−96703
governing principle of dissipative processes appl. 79−3884
granular material, dispersion of thermal waves 77−89001
graph theoretic field model, modelling and formulations 79−67165
graphite cylindrical thin shell, thermal shock, fundamental heat cond. soln. 78−29575
Gyarmati's principle for heat cond. eqn., formulation *(German)* 80−33420
H-function of two variables applic. 79−94450
half-space, plane Stefan problem soln., degenerate hypergeometric transformations method 79−86332
half-space with cutting, Green's functions of boundary-value problem *(Russian)* 78−18145
harmonic chain with random masses, transmission coeff. and heat conduction 79−80547
harmonic thermal flux monitoring quasistationary temp. distrib. 78−51040
heat and electrical transfer differential eqns. 78−67004
heat and mass transfer bibliography−Soviet works 79−23318
heat conducting thermoelastic materials, relativistic theory of wave propagation 80−83748
heat engine, irreversible, optimal config. 79−54085
heat evolution during cyclic deformation of a hereditary medium *(Russian)* 79−46227
heat flow eqn., different schemes 78−90627
heat storage, periodic, heat-carrying fluid and storage material transport kinetics 79−3901
heat transfer bibliography, Japanese works 79−23317
heat transfer on layered composites 78−71264
heterogeneous media, mean temp. field variations 79−68544
HGTR core, multiregional coupled conduction-convection model 78−94083
hollow cylinder, temp. and stress fields under action of periodic heat flux to inside surface 77−35013
hollow cylinder heated at inner surface, regular regime anal. 77−46882
hot-wire anemometer, sensitivity to stream temp. fluctuations, end cond. effects 78−34215
hybrid system, solution by partial differential eqns. 78−5745
hyperbolic equation, integral variational principle *(Russian)* 78−83213
hyperbolic equation, mol. kinetics basis 77−11109
hyperbolic equation application telegraph eqn. soln. 79−37122
hyperbolic heat-cond. eqn., Bubnov's derivation, comment 77−62134
implicit finite difference method, Romb, for numerical solution of hydrodynamic flow and heat conduction *(Russian)* 80−14725
inclined fluid layer, conduction and natural convection regimes *(French)* 78−42514
inclined infinite fluid layers, transition to transverse rolls, stability eval. 80−79299
incompressible heat-conducting relativistic fluid, four-vector form 80−33707
infinite diffusion velocity and causality in special relativity 79−63027
infinite plate with transverse circular cylindrical hole, internal heat generation 80−23872
infinite vertical fluid layer, transverse rolls transition from conduction regime, power series soln. 79−94611
infinitely thick slab subject to random surface temps., frequency response function, temp. variations 77−19511
ingot, temp. field calc. approx. by equiv. cylinder *(German)* 78−84788
inhomogeneous body with source, temp. field determ. by integral transformations 77−42703
inhomogeneous curved wall and hollow bodies, calc. by temp. field parabolic approximation *(Russian)* 78−46881
inhomogeneous medium, unsteady heat cond. eqn. soln. 79−94457
inhomogeneous region with imperfect thermal contact *(Ukrainian)* 77−68372
inhomogeneous slab, boundary-value problems 77−39204
inhomogeneous thermal conduction equations 78−70074
instantaneous propagation paradox 80−10109
integral equations, expansion in orthogonal system of Watson operators 77−11108
integral equations for problems in which heat transfer coeff. varies 77−14876
integro-differential eqn. asymptotic stability theorems 77−67216
interior algorithm for optimisation of forms *(French)* 77−72130
inverse boundary problem, soln. method 79−90111

heat conduction continued
inverse boundary problems, soln. using splines 79−90112
inverse boundary-value problems, finite difference method 78−63263
inverse boundary-value problems 77−42685
inverse heat conduction, integral solns., general anal. 79−81681
inverse heat conduction eqn., boundary conditions recovery, using Cauchy soln. and regularising algorithms 78−26016
inverse heat conduction problem, criteria for comparison of methods of soln. 79−68547
inverse heat conduction problem, finite difference soln., appl. ablation 77−46886
inverse heat conduction problems, iterative approach to soln. 80−10111
inverse heat conduction problems, numerical solns. 77−39193
inverse nonlinear problems, simulation methods 78−94513
inverse problem, finite-element method appl. 80−10112
inverse problem, Fourier eqn. Runge-Kutta integration 78−89417
inverse problem, integral eqns. calcs. 80−74695
inverse problem, thermal boundary conditions determ. 77−42686
inverse problem for exothermic body 78−42516
inverse problems, by 79−37120
inverse problems, integral eqns. soln. 77−42689
inverse problems, method of soln. 77−41465
inverse problems, similarity solns. 77−42688
inverse problems, soln. using specialised analogue computers 79−37121
inverse problems, stable solns. 77−42684
inverse problems, uniqueness theorems 77−42691
inverse problems soln., jet cooling appl. 80−10107
irradiated semitransparent surface, simultaneous radiative and conductive heat transfer, boundary conditions 80−74719
irreversible processes, thermodynamic in quality 77−61043
isotropic inhomogeneous medium, homogenisation for transient heat conduction 80−64338
isotropic nondeformable body with fading memory and high heat cond. 78−1545
Lagrange formalism, in heat conduction theory 77−50858
Lagrangian, for heat cond. with finite wave speed 78−94519
laminar flow, steady heat transfer between parallel plates, with conduction in wall 77−47003
laminar flow with internal heat source in channel, heat transfer 80−64532
laminar jet at wall, heat transfer 79−41725
laminar tube flow with varying wall temp., heat transfer anal. 78−38318
laminate, 3-phase, longitudinal heat propag. at high exciting freqs. 78−90684
laminated stack, thermal conductance theory 79−41556
laminates, anisotropic to orthotropic transform. 80−38217
Laplace eqn., appl. of integral eqn. method, heat conduction through layered media 77−68366
Laplace equations in thin regions, mixed boundary-value problem 77−35016
laser, Nd:YAG pulsed conductively cooled design 78−46647
laser light with time-varying intensity in optical medium, temp. field kinetics 78−59098
laser-evaporated material, quasisteady crater evolution, heat cond. anal. 77−48283
layer with high particle concentration, radiant component of heat cond. 79−86318
layered composites, heat conduction eigenvalue problems 80−74702
layered systems, heat conduction eqn. including radiation across gap, numerical soln. *(German)* 80−1407
linear, transient conditions, resoln. using finite integral transform. method *(French)* 80−38218
linear boundary inverse problems, soln. method 79−72777
linear conduction and contact temperature, a definition comparison *(German)* 79−90117
linear defining eqns. with thermal perturbation vel. 79−90114
linear harmonic chain, nonequilib. steady states, information theoretic approach 80−19214
linear heat conductor, conduction anal. with heat flux branching at boundaries 77−11107
linear theory of heat conduction with memory, uniqueness theorem 80−1401
linear thermal conduction eqn., errors of differential-difference approx. *(Russian)* 78−38173
linear thermoconsolidation, porous elastic solid containing compressible fluid 79−23186
liquid droplet evaporation, idealised models for preheat stage 78−94586
liquid metal, laminar convective heat transfer along cylinder 77−914
liquid metals, incipient boiling superheats, heat flux effects 80−74697
liquid-fluidised bed, radial heat conduction 77−42916
LMFBR, effective conduction mixing lengths for subchannel anal. of finite hexagonal bundles 78−13210
local Green's function method for heat conduction and fluid flow problems 77−79420
Lorentz gas, Fourier's law of heat cond. 79−58620
LWR, stationary boiling front in liquid film cooling of a vertical heated rod 79−45341
LWR fuel rod quenching, two-dimensional heat conduction model 79−93815
material systems containing aqua solns., heat cond. with freezing 79−50565
materials with memory, linear theory 79−14206
materials with memory, linear theory of heat cond., final value problem, existence, uniqueness theorems 78−59266
media with volumetric heat absorpt., thermal disturbances propag. 78−59259
melting, Landau problem, numerical soln. of bedding eqns. 79−14233
melting and solidification, formulated as heat conduction problem 78−91420
melting of semiinfinite solid, nonFourier heat cond. temp. distrib., interface location, small times 77−58542
melting surface, generalised Stefan condition, jump condition from surface thermodynamics 80−19216
metal, casting of slab, continuous, solidification interface shape 79−15656
metal, thermal wave, steady-state soln. 78−9527
metallic contacts, directional effects of heat flow, thermal rectification 77−58532
metallic joints, electrolytic tank appl. 78−83207
metals, unidirectional solidification, heat flow model 80−79914

heat conduction continued
MHD generator, cathode spot erosion, thermal conduction-diffusion 78−5955
MHD refractory materials, arc spot heat impact degradation *(Japanese)* 78−39819
microfluids, linear theory of chemically reacting mixtures 80−14777
microfluids 79−72776
micropolar current and heat conducting magnetically-saturated solid, field eqns. 78−36845
microthermopolar fluids in circular pipe, Hagen-Poiseuille flow 80−24092
minimum final distance and fuel problem of 1-D heat cond. system 78−59257
mixed boundary value problem, analytic soln. 80−5909
mixed boundary-value problems for rectangular domain with variable heat-transfer coeff. 77−7281
mixed method solns. for steady heat conduction 80−64333
modelling of mechanical system with external unsteady thermal action 79−37124
modified equations for wave number dependent relax. time 78−71259
molar molecule heat and mass transfer phenomena, generalised variational principle 80−79104
molecular-kinetic generalisation of the heat-transfer equation 78−67219
monoclinic anisotropic system, various boundary conditions, temp. field soln. 77−58525
Monte Carlo anal. of time depend. heat conduction with convective boundary conditions 78−680
Monte Carlo heat conduction using transport eqn. approximation 79−159
moving anisotropic rectangular slab, generalised Jacobi transform appl. 78−30149
moving boundary, asymptotic soln. of first boundary-value problem 77−46884
moving boundary problems, collocation method using B-splines, bubble expansion and collapse 77−7288
moving thermal contact problems, finite element soln. 78−26019
multi-dimensional solidification, dominated by thermal cond., similarity calc. method 80−38243
multicomponent solid body undergoing allotropic transform., fundamental deform. eqns. *(Russian)* 78−16645
multiconnected composite body, of complex shape, two-dimensional heat conduction 77−54859
multidimensional conduction phase change problems, effect of density change, enthalpy model 77−42699
multilayer disc system, temp. fields investig. 80−74696
multilayer domain, bounded, with local heat sources, analytic soln., integrated circuit appl. 79−94456
multilayer rectangular fins, conduction efficiency 78−63262
multilayer solids, soln. of heat conduction and thermoelasticity problems *(Russian)* 78−38177
multilayered cylinders, nonstationary temp. fields with rotational symmetry *(German)* 78−79190
multimedia problems, Monte Carlo soln. method 80−74704
multiphase heat conduction problem, finite-element free boundary formulation 77−62133
multiphase laminar flow with heat conduction, numerical soln., implicit difference method *(German)* 77−15110
multiply connected body, heat cond. 78−46882
non-Fourier, in thin surface layers 77−80048
non-local heat conducting fluids 77−50856
non-steady state thermal conductivity in multilayer sheets *(Russian)* 80−43596
nonclassical thermal cond. problem, nonstationary temp. regimes in plate *(Russian)* 79−59904
nonequilibrium problem, Chebyshev approx. for roots of eqn. 77−11112
nonhomogeneous thermal problems and Stefan single-phase problem in arbitrary domains 80−79102
nonhomogeneous transient boundary-value problem 77−42697
nonlinear, direct and reverse processes, mathematical modelling 78−94514
nonlinear, inverse problem, thermophysical characts. determ. 77−42721
nonlinear, unconditionally stable algorithms 77−23852
nonlinear, unsteady problems, application of comparison theorem to accuracy estimation 77−39196
nonlinear, with absorpt., similarity of nets method *(Russian)* 80−53603
nonlinear 2-D eqn. soln. *(Russian)* 79−37125
nonlinear boundary control problems, maximum principle *(German)* 78−9528
nonlinear conduction and volumetric heat source, thermal structures and fund. length 77−848
nonlinear diffusion equation, general class of similar solns., laser interactions, thermal cond. 77−37827
nonlinear Dirichlet problems, exponential decay estimates, elasticity and heat conduction 79−92939
nonlinear equations, class of solns. 78−63264
nonlinear Fourier eqn. soln., minorant-majorant aprox. 80−79105
nonlinear heat cond. eqn. soln. *(Russian)* 79−32187
nonlinear heat cond. problem with phase change, finite element anal. 78−75030
nonlinear heat conduction effect on shock wave fronts *(Russian)* 80−79352
nonlinear heat conduction eqn., group props., inverse problems soln. 77−75770
nonlinear heat conduction eqn. *(Russian)* 77−84112
nonlinear heat conduction eqn. analytic soln. *(Russian)* 77−84111
nonlinear heat conduction equation, soln. for Gaussian laser beam heating 79−69917
nonlinear heat conduction problems, soln. construction procedure, Kantorovich method 78−59264
nonlinear heat conduction simulation by analogue and hybrid computers 77−53768
nonlinear heat eqn. soln. by Picar's method *(Russian)* 78−51041
nonlinear heat transfer in solids, direct and inverse problems, approx. soln. method 78−94510
nonlinear inverse, analytical investigation methods 77−75771
nonlinear inverse problem, heat loads determ. 78−42515
nonlinear inverse problem, region with moving boundaries, generalised heat conduction eqn. 77−42692
nonlinear inverse problem, regularised numerical solns. 77−42693
nonlinear inverse problem soln. 79−94452

heat conduction continued
nonlinear Kalman filter for soln. of inverse heat cond. problem 80−19212
nonlinear problems, efficient soln. method using modified Crank Nicolson method 80−1402
nonlinear problems, method of successive intervals 77−42694
nonlinear problems, variational formulation *(Russian)* 80−74700
nonlinear radiating linear absorbing rod of finite length, asymptotic temp. behaviour 77−50859
nonlinear thermal diffusion equation, parameter calcs., numerical calcs. *(French)* 78−94584
nonlinear transient heat transfer, through multilayer wall *(Russian)* 77−23857
nonlinear unsteady, Laplace transform, small parameter, R-function and variational methods joint appl. 79−94451
nonlinear unsteady heat conduction, linearisation 79−81688
nonlinear unsteady heat conduction, variational principle 77−42698
nonstationary, nonlinear inverse problem, soln. uniqueness *(Russian)* 78−22245
nonstationary cond. of arbitrary shape bodies, three-dimensional solution by finite-difference method 77−75774
nonstationary heat conduction problem in presence of mass exchange, finite element anal. *(Russian)* 79−27492
nonstationary heat conduction process, optimisation, soln. 79−81686
nonstationary heat transfer phenomena, variational description 78−89416
nonstationary nonlinear heat-conduction problems, in absence of heat sources and sinks 80−19211
nonsteady differential eqn., numerical soln. 79−90110
nonsteady heat conduction in solid cylinder, analogue computer soln. *(Rumanian)* 77−68362
nonsteady heat conduction in variable temp. medium 77−84105
nonsteady heat fluxes, nonlinear differential eqns. 79−37116
nonsteady nonlinear thermal cond. of complex bodies, numerical method 78−59263
nuclear fuel rod gap conductance uncertainties deduced from fuel centre-line temps. 77−46308
nuclear fuel rod thermal characteristics, on-line simulation by elec. heated rod 77−46209
nuclear fuel thermocouple readings verification by transient response analysis 77−46309
nuclear reactor, Monte Carlo heat conduction solution using transport theory approx. 77−65260
nuclear reactor heat conduction problems with internal sources, Monte Carlo soln. 77−65259
numerical soln., Crank-Nicolson noise control 77−75769
numerical soln. oscillations, nonlinearity allowance scheme effect *(Ukrainian)* 78−90625
numerical soln. to heat cond. eqn., Laplace transform and FFT 78−57763
one dimensional distributed parameter system parameter and state estimation, heat conduction experimental result *(Japanese)* 80−83727
one-dimensional body, transient heat flux, spline identification method 79−37117
one-dimensional transient inverse heat conduction, accuracy and resolving power 79−94453
optimal control of body heating with max. temp. stress constraint *(Russian)* 79−14205
optimal control problem *(Russian)* 79−50567
orderable system, influence of heat cond. on spinodal decomp. 80−2169
orthotropic circular cylinders, steady and unsteady solutions 80−10110
packed beds, particle-to-fluid transfer coeffs., fluid diffusivities 77−31378
packed granular beds, conduction model 80−19206
parabolic differential eqns. soln. 79−90113
parabolic problem exact control finite element collocation method 77−26156
paraffin latent heat storage system theory and expt. 79−57484
parallelepiped with local energy source, approx. anal. of steady-state temp. field 77−11111
particle, spherical, transient heat-mass exchange 79−7276
passive solar buildings, thermal heat flow modelling using model expansion methods 80−45645
periodic system of narrow inclusions, effect on steady temp. field 78−63265
permafrost, two-dimens. temp. field with arbitrary temp. distrib. on subaerial surface 77−25703
phase change region, cond. and natural convection, numerical method 79−41563
phase changes subject to convection and radiation, perturbation solns. 79−76962
photomultiplier cooling by semiconductor microrefrigerators 78−57942
piecewise homogeneous body, heat cond. eqn., construction method *(Ukrainian)* 80−33414
piecewise-uniform plane, curvilinear cracks, integral eqns. of heat conductivity and thermoelasticity *(Russian)* 78−38250
piezoelectric slab. semiinfinite, heated, tangential elec. field excitation, soln. 77−14656
pipe, of variable thermal and elec. conds., elec.-heated, flow-cooled, temp. distrib. 78−90626
pipe flow, laminar with nonlinear wall heat fluxes, axial cond. 79−27636
pipe flow heat transfer, simultaneous wall and fluid axial conduction 80−74870
pipeline, nonstationary heat transfer to environment, soil temp. distrib. 77−84108
planar body, with circ. boundary and thermally insulated cracks, temp. distrib. 78−67002
planar solids, nonlinear heat transfer, direct, inverse appls. 79−98589
plane conductor, heated by current, effect of conductivity temp. depend. 77−42683
plane problems, exact and approx. solns. *(Russian)* 78−46883
plastic, thermal cond. meas. rel. to temp., heat cond. problem soln. 79−37887
plastic flow, effects of metastability 78−1579
plate, annealed in liquid media, numerical solutions of nonlinear problems 77−50857
plate, approx. soln. method for heat cond. problems 80−33415
plate, circular, thermally induced vibr. analysis 79−94524
plate, complex shape, temp. field during welding with moving heat source *(Russian)* 79−68553
plate, finite rectangular, superposition of boundary conditions in temp. distrib. eval. 77−14883
heat conduction continued
plate, heated surface, transient thermal process calc. for symmetrical heating *(Russian)* 78−83211
plate, infinite, asymmetric cooling, direct and inverse heat cond. problems 79−37113
plate, melting, inverse heat cond. problem soln. 79−37112
plate, thin, circ., quasistatic normal deflection due to time depend. heat-source distrib. 79−37145
plate with temp. depend. physical props., heat conduction initial stage 80−14544
Poiseuille flow, horizontal plane, heated from below, axial heat cond. effects on thermal instability 77−42825
polyamide 6 , glass fibre reinforced, response function characterization of thermal state in dynamic testing 79−18680
polyamides 6 and 66, response function characterization of thermal state in dynamic testing 79−18680
polyoxymethylene copolymers, response function characterization of thermal state in dynamic testing 79−18680
porous glass, investigation *(Russian)* 80−92145
porous materials, thermodynamics of non-equilibrium processes *(Hungarian)* 80−178
porous medium, deep evaporation characterisation, of water *(French)* 78−59468
porous reactors, with temp. depend. heat generation rate, element geom. effects 78−94738
potential function, inverse problem *(German)* 80−1406
potential theory, steady-state mixed problem, 3rd kind boundary conditions 77−65660
powder combustion theory, Stefan problem *(Russian)* 77−56230
problems, soln. method *(German)* 80−74705
problems soln. by method of finite elements 79−14204
heat-protective coating, temperature distrib., finite element anal. *(Russian)* 80−74701
quartz ceramics, thermal and temp. cond. in range 500-1900K 80−39370
quasilinear, finite difference methods appl. time spacing selection *(German)* 80−33418
quasilinear equations, approx. Galerkin method 80−33416
quasisteady mode with asymmetric boundary conditions 78−83208
quenching rates on hot surfaces, wetting of outer tube walls by water 77−82996
radial heat transfer, conduction, convection and heat of phase change 78−90700
radiant heat conduction problems, difference schemes *(Russian)* 77−7280
radiation boundary condition, implicit iterative soln. 78−5635
radiation-conduction problem soln. method, LMFBR meltdown accident anal. 80−19381
radiative heat exchange in black body system, conduction, radiation, scatt. and absorpt. 80−38239
radiative heat transfer problem solvability, radiation, scatt., absorpt. 80−33436
radiative plus conductive heat transfer, differential anal. method 80−74699
radiative-conductive heat transfer in plane-parallel layer 78−22256
radiative-conductive heat transfer in slab, steady-state problem 78−38181
radiative-conductive heat transfer in temperature-wave conditions 80−24020
radioactive waste vault, temp. distrib. anal. 79−636
random generalized solution to heat eqn. 77−84103
random heat conduction in solids, functional eqns. 78−83210
random heat eqn. soln. by iterative scheme 79−9195
random medium, method of time ordered cumulants 78−54320
Rayleigh-Taylor instability, thermal cond. and compressibility effects 80−79262
reaction zone propagation, combustion wave structure inversion in porous media 80−89494
reactor, fuel element nonlinear transient heat conduction, variational calc. 79−93685
reactor heat conduction and fluid flow, local Green's function method for initial value problems 79−89359
regenerators with hygrostatic materials, combined heat and mass transfer 79−81689
reinforced organic composite, graphite, or C-C, ablation, mathematical modelling 79−41564
reinforced plates, heat conduction and thermoelasticity eqns. *(Russian)* 77−75795
relativistic fluid, existence and unity of Cauchy problem solns. *(French)* 78−47070
relativistic fluid dynamics, extended thermodynamics 80−43803
relativistic heat conducting fluid, dispersion relation *(French)* 79−7419
relativistic inviscid heat conducting fluid, energy momentum tensor, evolution system 77−80233
relativistic thermo-viscous fluid dynamics, heat conduction and wave propag. 80−24107
relaxation theory of heat conduction and diffusion 77−35012
resistance furnace transfer function determ. for DDC *(German)* 77−3709
resistance thermometer sensor overheating, influence of meas. current *(Russian)* 79−26053
rewetting model using generalised boiling curve 79−9675
rigid conductors with nonlinear heat generation, thermal instability 77−27461
rigid heat conductors with memory, integrodifferential equation 79−37111
rigid wall-hot gas stream interaction, heat cond. eqns. soln. 78−79194
ring-shaped thin conductors, flow soln. in periodic problem by difference eqns. 79−94460
rock massif, nonstationary heat conduction near horizontal mine *(Russian)* 77−56620
rock melting drills, thermal analysis 77−17258
rod, current-carrying, steady-state heat conduction, perturbation soln. 78−5629
rod, expanding, conductive heat transfer computation, fast numerical technique 78−75029
rod, finite, insulated, unsteady heat cond. and temp. distrib., non-equilib. theory 78−67000
rod, heating, thermal cycle, control, optimal conditions rel. to response speed *(Russian)* 77−19510
rod, semi-infinite, temp. stresses 79−18714

heat conduction continued
rod, thermal conduction, dynamic behaviour of distributed systems *(Dutch)* 80−28407
rod, two-layered, temp. distrib., 1D approx. applicability 78−1544
rod with concentric heat generating core, temp. distrib. 79−32183
rotating circular cylinder, stresses and displacements due to axially non-symm. heating of lateral surface *(Polish)* 78−22248
rotating disc with axisymmetric surface heat source distrib., in laminar flow, heat transfer 79−46314
saturation theorems connected with the abstract wave equation 79−14207
self-modelling solution of heat conduction eqn. 77−14877
semi-infinite body, nonlinear heat cond. prob., parametric soln. 80−19207
semi-infinite cylindrical rod, temp. gradient at conical end, radiation effects 77−11106
semi-infinite solid with variable thermophysical props., heat cond. 80−23864
semi-transparent irradiated plate, combined conduction-radiation heat transfer, anal. soln. 78−75051
semiinfinite bar, heat conduction problem, hyperbolic eqn. soln. 80−19210
semiinfinite porous media, heat cond., phase transitions effects 78−94523
semiinfinite solid, with spherical inclusion, temp. field 78−94520
semiquantum liquids, viscosity and heat cond. temp. depend. *(Russian)* 80−34260
semitransparent thin cylinder, radiation-conduction heat transfer, light-guide approx. 80−96179
sheet conductor, induced eddy currents, IR meas. 80−37933
shell of revolution, Green's function of steady heat cond. operator 79−86319
shells of revolution, thin-walled, heated, temp. field, thermostatic control 78−67003
shock waves of arbitrary strength, with viscosity and heat conduction, stability 80−59076
simple materials, restrictions on heat conduction 78−63260
sinusoidal thermal perturbation transmission through wall, heat conduction and convection *(French)* 77−15007
slab, melting in contact with fluid, heat cond. prob. *(Japanese)* 80−53612
slab, time depend. thermal soln. 79−98592
slab, transient temp. distrib., differential operator method 77−31201
slab, with temp. depend. surface absorbance, laser heating 80−48545
slab with temp. depend. thermal cond., convective boundary, transient cond., finite difference method 78−75031
slab with temp. depend. thermal cond., optimal heating, finite element anal. 80−23863
sliding contact problems, heat conduction, temp. and heat source distribs. 79−98588
snow, frost, heat transfer, cond., radiation and water vapour diffusion model 78−94563
soil warming, waste heat from nuclear power station 78−37463
solar collector heat removal factor, axial conduction effects 80−7955
solar collector tube, bore heat flux and outside surface temp. variations 78−90629
solar collector/storage system, analysis 80−30390
solar energy collection, heat losses by conduction and convection, reduction techniques 79−79409
solar energy thermal storage, numerical simulation of energy transfer by conduction and radiation *(French)* 79−24916
solar flares *(Russian)* 79−35229
solar storage tank, buried, hemispherical, heat cond. to environment, series soln. 79−3891
solar wind, conduction microinstability onset and its consequences 77−87222
solid, thermophysical characts. temp. depend. determ. 77−42720
solid body in contact with high temp. gas flow 80−10108
solid sheet with selective optical props., combined radiative and conductive heat transfer 78−90672
solid surface response to high-power incident flux, with temperature dependent absorptivity 78−51038
solid with random conductivity, perturbation method, temperature field 79−46162
solidification, semiinfinite slab with const. boundary heat flux, transient interface position and temp. field 79−94481
solidifying ingot, temp., strain and stress distrib. *(Russian)* 77−25041
solidifying semitransparent cylindrical medium, thermal stresses, radiation and conduction 79−46200
solids, Lagrangian and Hamiltonian forms in heat conduction 80−79101
solitons, lattice thermal conductivity theory 80−46991
solitons, theory and applications 78−36811
Sommerfeld problem generalisation for one-dimens. ring 80−5908
sonic wave propagation, thermally conducting and radiating gases 78−42679
sphere, arbitrary volume heat source, boundary conditions of third kind 77−68364
sphere in saturated liquid, transient film boiling, liq. heat conduction effects on press. 77−84118
sphere inside spherical shell, nonstationary thermal conduction *(Russian)* 77−54861
spherical laser target hydrodynamic compression stability *(Russian)* 80−106159
spherical shell, heating by radial current, temp. field effect 78−33991
spherical source in heterogeneous continuum, thermal field 77−84106
stability in continuous media with heat/material sources/sinks 79−94455
stability of two temp. theory for heat conducting fluid motion 78−18303
stack of parallelograms, thin partition walls, steady temp. distrib. and heat flux 77−58535
stack of thin layers, in high vac., thermal contact cond. correlation 77−58536
static thermal contacts and unsteady cond., thermally equivalent model *(French)* 80−92027
stationary, in cylinder with piecewise-constant heat transfer coeff. on lateral surface 77−46883
stationary heat conduction in an anisotropic slab containing a crack 79−94470
stationary heat conduction in piecewise homogeneous bodies, generalised functions theory methods *(Ukrainian)* 80−23861
statistical distribution of particles over given volume 77−82467
steady-state, soln. using heat balance integral method 77−14880
heat conduction continued
steel, slab, transient temp. distortion due to thermocouple cavity 77−10016
Stefan multiphase problem, numerical algorithm 78−33989
Stefan problem of melting in annular duct with nonlinear outer boundary conditions 79−86329
Stefan problems, multidimens., numerical soln. 78−33987
Stefan variable-property problem, asymptotic solns. 79−37107
Stefan-like problems, soln. improvements 79−23181
stochastic theory of atomic chain coupled to two reservoirs 78−54319
structural approach, appl. to one-dimens. heat conduction 77−35015
structural elements, thin-walled, temp. fields calc., algorithm 79−37114
Sturm-Liouville system with discontinuous coeffs., direct soln. for vibr. and heat conduction 80−23930
sunspots, temperature distribution, anisotropic heat transfer *(German)* 77−45386
SUPERB general isoparametric finite element program 77−42682
superconducting composite media, effect of axial conduction and metal-helium heat transfer on local stability 78−91832
surface film, heat flux density and unsteady state temp. 78−75036
surface heat flux of body with nonlinear conduction 77−42687
surface heat flux reconstruction, heat cond. regularised soln. 79−37119
surface temp. meas. using contact thermometer, field meas. by liquid crystals *(German)* 79−58686
suspension of aligned ellipsoids, heat conduction 77−7286
synthesis of optimum boundary control *(Ukrainian)* 78−55544
system of heat exchanging bodies, boundary conditions identification methods 79−37115
system with variable heat transfer coefficients, thermal conductivity determ. 77−75772
temperature distribution of complex structure 77−42690
temperature distribution produced by a moving heat source 79−27488
temperature measurement error due to cond. along sensor leads, correction 77−13752
temperature measurement errors due to conduction along thermocouple leads 79−85136
temperature waves in rigid materials with memory 79−17238
thermal analysis, finite element method for temp. depend. parameters 79−32184
thermal conductivity, effect of asymmetry of heat flow rate 80−102959
thermal energy storage by latent heat of fusion *(French)* 79−3893
thermal gasdynamic testing, boundary conditions 80−23862
thermal insulation for buildings, heat conduction in disperse media *(Hungarian)* 79−1056
thermal perturbations in moving nonlinear media, convective spatial localisation, cond. coeff. depend. 80−106706
thermal properties, simultaneous evaluation, nonlinear estimation procedure 79−94478
thermal stability of chemically reacting heat conductors 77−68369
thermal storage unit, sensible-heat, solid, transient response 79−3892
thermal wave distributions, finite element calcs. 77−27459
thermally orthotropic plates, determ. of unsteady temp. distrib. by conformal mapping 79−55310
thermoconvective waves in a conducting and radiating fluid 80−19415
thermodynamic analysis of rigid heat conductors, hyperbolic heat conduction eqn. 80−64334
thermodynamics, second law, heat flow direction and Fourier inequality, comparative assessment 79−44896
thermoelastic anal. of finite orthotropic slab 79−1111
thermoelastic anisotropic bodies, generalised coupled thermoelasticity problem 77−89030
thermoelastic cylinder, thick walled with filler 77−84150
thermoelastic materials, heat conducting, relativistic theory of wave propagation 80−83748
thermoelastic periodic problems for infinite solid with disc shaped cracks, integral eqn. solns. *(Ukrainian)* 78−55559
thermoelastic stress in cylinders, Lanczos-Chebyshev method 80−33458
thermoelasticity, anisotropic, at low reference temp., linear coupled theory 80−59
thermoelasticity, appl. of orthogonal projection method 80−1403
thermoelasticity, uniqueness theorem and variational principle 80−92056
thermoelasticity models taking account of a finite heat propagation rate 79−94541
thermoelasticity problem with finite heat propag. vel., acoustic vibr. anal. 77−42770
thermoelectric convertor, generalised surface, quadratic form heat balance equations 79−83609
thermoelectric coolers, heat load estimation curves 78−45613
thermoelectric element, arbitrary shape, cooling efficency 78−67010
thermophysical parameters, determ., temp. fields anal. 79−37118
thermoviscoelasticity, heat liberation effect in deformable linear medium 80−33484
thick-walled construction, 2-dimens. stationary heat cond. problem soln. *(Russian)* 79−64484
third boundary-value problem, variational soln. 77−7282
three phase laminated composite, longitudinal heat propag. at low exciting freqs. 80−58889
three-dimensional, steady-state heat conduction in cylinders of general anisotropic-media 80−5910
time dependent transient, partial differential equation solution 80−106707
time invariant for heat cond. with finite wave speed 80−87704
time reversal problem for solids of spherical symmetry with heat generation and radiation 77−14873
time variable coeff. identification by soln. of nonlinear inverse problem 80−14545
transient, accuracy, stability and oscills., calc. methods 78−94516
transient, Laplace transform and boundary integral eqn. 77−72129
transient, nonlinear boundary conditions, integral method 77−39192
transient, one dimensional, early time, method of characts. numerical soln. 77−58524
transient, two-dimens., crit. time step for finite element solns. 78−71260
transient combined heat cond. and convection problem, explicit numerical soln. method 79−81869
transient conduction, two dimensional finite solid, temp. depend. conductivity 77−58528
transient convective turbulent heat transfer in tubes, thermal and hydrodynamic instability 78−83485
transient heat conduction, residual method with Lagrange multipliers 78−90630

heat conduction continued
transient heat conduction, soln. by ADI methods in r-θ geometry 79−14203
transient heat conduction, soln. of general nonlinear problem using electrical model *(Russian)* 77−54860
transient heat conduction and moisture migration problems, finite element approach 78−12653
transient heat exchange between a radiating plate and a high-temperature gas flow 79−94609
transient heat transfer between internally generating perfect conductor and semiinfinite solid, contact resistance *(German)* 80−1408
transient in finite slab with temp. dependent thermal cond. by orthogonal collocation method 78−33990
transient nonlinear problems, optimal reference temp. for thermophys. props. 78−94517
transient problem, generalised model of inhomogeneous system 78−94521
transient problems, finite element and matrix methods calcs. 78−94515
transient radiation-conduction heat transfer in selectively absorbing media 78−90670
transient radiation-conductive heat transfer in selectively-absorbing media 78−94572
transient temperature data for thermal parameters estimation, correl. ARIMA errors 79−76938
transient thermal stress problems, numerical anal. method 79−72810
transients with time depend. inputs, long time solns. 80−74703
transition boiling curves from quenching expts., two-dimens. model with axial conduction 79−19360
transparent turbulent gas flow past radiating plate, heat transfer anal. 77−35257
transport relaxation equations, reciprocity, boundary conditions 77−13719
triangular fin performance by the heat balance integral method 80−5911
truncated wedge of finite height 78−13884
tube, circumferential wall heat cond. effect on thermal boundary conditions 79−32200
tube wall, transfer functions determ., appl. to heat exchangers 77−7287
turbulent conductivity in stellar convection zones, effect of rot. 80−36612
turbulent flow near wall, effect of conduction error on hot wire meas. 79−7423
two parallel plates, heat conduction, gaseous molecules bimodal two stream relaxing distrib. *(Chinese)* 80−6097
two temperature theory of heat cond. fluids 78−26017
two-dimensional multiply connected regions of arbitrary shape and boundary conditions, temp. field calc. 79−86317
two-layer plate, random temp. fields and heat conduction, Monte Carlo method 80−33417
two-layer plate with separated suction, nonstationary temp. field 78−22255
two-layer thermal shielding, pulsed heat flow, temp. field 78−59260
two-phase medium, isotropic, heat distrib. eqns. *(Ukrainian)* 77−50863
two-phase medium, temp. field equalisation problem *(Ukrainian)* 77−50862
two-point boundary-value problems with eigenvalue parameter in boundary conditions 78−73830
unbounded plate with temp. dependent thermophysical parameters, calc. 80−79107
underground pipeline, unsteady heat loss, analytic expressions 78−83223
unidimensional, inverse Cauchy problem solution, coeff. identification *(German)* 80−33419
uniform layer with rectangular cut-out 77−39194
unsteady, heat flux solns. for converse problems 77−23853
unsteady cond. in circ. disc 77−65659
unsteady heat cond. in domains of irregular boundary, numerical expts. 78−51039
unsteady heat conduction accompanied by an endothermic solid reaction *(Japanese)* 79−76939
unsteady heat conduction equation, numerical soln. characts. at early times 78−79185
unsteady heat conduction in quarter plane, appl. to bubble growth 78−75045
unsteady heat transfer, between dense disperse material and internal object, 4th kind boundary conditions 77−42707
unsteady inverse problem, approx. anal. soln. 77−11113
upwindings of high order Galerkin methods in conduction-convection problems 79−3886
US appl. in metals heat conduction and convection 80−74723
variable relaxation heat propag., exact hyperbolic eqn. soln. 78−79184
variable thermal properties systems, perturbation methods calcs. 77−58522
variational formulations form in Langrangian of heat cond. problems 79−55309
variational Lagrangian irreversible thermodynamics of nonlinear thermorheology 77−27467
variational-difference schemes for nonregular grids 80−38219
viscoelastic fluid layer, convective instability, boundary thermal cond. independence 78−9659
viscoelastic media, deform. theory with account of thermodiffusion *(Ukrainian)* 78−67052
viscous binary mixture in porous medium, thermal conc. instability 77−35231
viscous fluid, smooth transition to convection 78−83396
viscous gas, with internal heat sources, thermoconvective stability *(Ukrainian)* 79−32495
viscous incompressible liquid, heat conductivity problem *(Russian)* 80−69897
viscous sublayer turbulent Prandtl no., wall heat cond. influence 79−94616
wall, perforated, relative effects of external and internal convection *(French)* 79−1248
wall, plane, nonsteady heat transfer, conjugate problem soln. 79−37128
wall, with sinusoidal modulation, algorithm *(French)* 78−42513
wall conduction, effect on heat transfer in turbulent flow between parallel plates 77−47007
wall temperature distributions, in regions of deteriorated heat transfer 78−83377
wall temperature with internal cond. and external convection, calc. method *(French)* 80−19215
wall with one-way heat flow, vertical inclined cavity stack 79−3899
heat conduction continued
wave equation for simultaneous heat and mass transfer in moving media 79−44747
wave propagation in viscous heat cond. gas, Gurtin type props. 77−27645
weakly absorbing material calorimetric meas., theory 79−76773
weakly absorbing solid medium, opacity fluctuations, heating by intense radiation and thermoelastic stresses problem 80−38048
welding, ultra pulse type, heat transfer characts. 79−1047
wire, electrically heated, steady state multiplicity 78−46880
Al alloy die casting, heat transfer coeff. 79−81685
CO_2-laser (long pulse)-plasma interactions, classical absorpt. and heat conduction in low-irradiance 80−75059
^{3}He-A, superfluid, instability of persistent currents and heat flow 80−15327
Li_2O pellets, neutron irradiated, temp. distrib. 80−86968
NH_2D, heat cond. gas, nonequilib. vel. distrib. function, laser absorption obs. 78−22448
Na vapour, heat cond., temp. discontinuity for dissociating gas 78−94887
Si, temp. rise induced by laser beam, nonlinear heat cond. 79−11487
heat content *see enthalpy*
heat convection *see convection*
heat dissipation *see cooling*
heat engines
acoustic, based on pistonless Stirling engine 80−19127
alloy with shape memory effect, working medium in heat engine *(Russian)* 78−48449
ambient thermal energy utilisation, use of clear night sky as a heat sink, for teaching 80−27082
Archibald rubber band heat engine, optimisation 79−5936
book, concepts and logic of classical thermodynamics, theory of heat engines 78−81938
Brayton cycle, indirect Brayton energy recovery system 80−35726
Brayton cycle isotope power system, for space appl. 79−48167
Carnot cycle, efficiency and irreversibility *(Spanish)* 80−176
chemically driven, finite time thermodynamics 80−76541
cold water pipe designs for ocean thermal energy conversion plants 80−45725
concentration difference energy engine and system developments for energy conversion storage and utilisation 80−40897
education, heat engines and external work, thermodynamics, conceptual expts. 78−49586
electrochemical heat engine for direct solar energy conversion 80−30519
energy analysis and viability of photovoltaic conversion and OTEC 80−61358
ferroelectric materials for dielectric power conversion, dielectric prop. anal. 80−80712
Fluidyne, modes of operation of a jet-stream Fluidyne 80−30534
fluidyne heat engine, pump op. low operating temp. 79−85206
free piston Stirling engines increase solar/thermal efficiency 79−96481
hydride engines, development, operating efficiency 80−30525
imperfect, extremals, time dependent thermodynamics 77−35025
irreversible, optimal config., dynamical treatment 79−54086
irreversible, optimal config. 79−54085
irreversible, second law of thermodynamics 77−101
irreversible, upper bounds for the work done 78−32783
irrigation pump Rankine cycle solar engine and wind turbine comparison 79−57448
Joule heat engine and pump, demonstration 80−105480
liquid based, thermodynamic principles 80−83730
low temperature energy conversion system, 55 to 93°C, operation of MARK I prototype 80−55883
magnetic Stirling cycle wheel, refrigerator and heat engine modes of operation 78−57964
marine two stroke compression ignition engines, heat exchange modelling 80−30529
marmem engines, martensitic transform. and shape memory effect 78−6920
memory alloy engine, efficiency 80−71648
metal hydride chemical engine for solar heat storage 80−61455
minimum entropy prod. and optimisation 80−85297
Ocean Termal Energy Conversion [OTEC], the Florida Current, thermal 80−26117
ocean thermal energy conversion, economic, social and environmental issues 80−30516
ocean thermal energy conversion, open cycle approach, plant design 80−30506
ocean thermal energy conversion, preliminary design of a cruising modular experiment 80−30505
Ocean Thermal Energy Conversion platform environmental impact assessment 80−45726
organic Rankine cycle engine R and D in Japan 80−35736
organic-fluid Rankine cycle for heat recovery at low temp. *(French)* 80−40895
osmo-hydro, a pressure retarded heat engine for prod. of elect. from low temp. waste heat 80−30528
OTEC, design and construction of a test plant 80−85298
OTEC, design of seacoast test facility, Hawaii 80−55888
OTEC, evaluation of alternative energy sources for the Guyana energy crisis 80−61270
OTEC, evaluation of bottom-fixed OTEC platforms on the edge of a continental shelf 80−55887
OTEC, NH_3 prod. 80−66988
OTEC, technology development, US DOE program review 80−94098
OTEC ocean engineering, status report 80−66989
OTEC plant development, an unfavourable analysis 80−55889
OTEC power plant, selection of working fluid (NH_3, propane and freon) 80−89665
OTEC power system development and environmental impacts 80−66990
OTEC R and D in Japan 80−35738
OTEC system performance study 80−104514
OTEC technology applied to light water fission reactors 80−52734
piston engine using $LaNi_5H_x$ as energy conversion medium, prototype 79−70458
pistonless engine capable of utilising solar energy, dynamics 78−71277
power and efficiency, irreversible heat flow 79−9198
pyroelectric high power density heat engine, dielectric losses, polarisation 80−80689
quantum open system model 79−44894

heat engines continued
Rankine cycle, radioisotope power system, emergency cooling by multifoil insulation melting 79−48168
Rankine cycle solar thermal power plants, operating experience 80−30523
Rankine cycle system, solar powered, digital simulation 79−52911
rotary expander engine, 250 hp, development program 80−30527
solar, pumping, irrigation, 7.5 W, with liquid piston, design and analysis 79−74537
solar cooling, Rankine-cycle systems, selection of working fluids 80−104515
solar engine for H prod., theoretical design 80−30598
solar fluidyne pump, design and operating charact., expt. test results 80−55890
solar powered automative transport utilising stirling heat engine 80−55824
solar powered regrigeration units 80−45729
solar pumps, using thermodynamic conversion 80−45728
solar pumps development, irrigation, 1978 status review 79−74506
solar Rankine cycle, pumping system perform. prediction model 79−70460
solar Rankine cycle air conditioner *(Japanese)* 80−72076
solar Rankine engine, pumping system applic. 79−70459
solar thermal pumps for water pumping 80−50942
solar-powered, 1 kW, reciprocating for rural appl. 79−74536
solar-powered, gravity-assisted heat engine based on dunking bird 80−89672
solid state heat engine, experimental demonstration of heat-to-electricity conversion within a dielectric 80−35707
solid-state engine with Nitinol memory material 78−59288
spacecraft nuclear dynamic power system, thermally-integrated 79−48166
spark ignition combustion engines efficiency, effect of mixture strength fluctuations 80−30526
Sterling, dynamics and control in a 15 kWe solar thermal electric generation plant 80−30522
Stirling, 500 to 2000 HP range, potential for stationary power appl. 79−48177
Stirling, computer and expt. simulation 79−48169
Stirling, design, isothermal second order calc. method 80−30533
Stirling, double acting four cylinder advanced engine concept (Advenco) 80−30542
Stirling, elementary design guidelines for power output, thermal efficiency, pressure ratio, cost 80−30530
Stirling, free piston, refrigerator performance charact. determ. 80−35722
Stirling, free piston engine technology development 80−30540
Stirling, free piston engines, closed-form solns. for a coupled ideal anal. 80−35721
Stirling, free piston module with hydraulic output for artificial heart blood pumps, engine dynamics anal. 80−35720
Stirling, free-piston, for solar thermal power plants 79−48174
Stirling, free-piston engine power conversion system utilising alternative fuel sources 80−55882
Stirling, miniaturised engine for artificial heart power 80−35724
Stirling, prototype liquid-piston free-displacer Stirling engine 80−35719
Stirling, solar energy conversion plants developments, for farm power needs in India 79−62024
Stirling, solar powered, for reverse osmosis desalination plant 80−55891
Stirling, stationary external combustion engines for combustion of coal and coal-based fuels 80−30535
Stirling cycle analysis, numerical methods accuracy evaluation 79−48170
Stirling cycle machine anal., choice of gas exchange model, performance criteria 80−30531
Stirling cycle machine anal. using nodal anal. techniques, review 80−30532
Stirling cycle machines optimisation, free piston design 79−48172
Stirling cycle power system, 1 kWe, isotope fuelled 79−48176
Stirling engine, performance charact. for Philips MP 1002 C engine 80−30537
Stirling engine combustion and heat transport system design alternatives for stationary power generation 80−30536
Stirling engine power conversion for MWe solar power system with parabolic concentrators 80−30561
Stirling engine powered heat activated heat pump development 80−35725
Stirling engine powered total energy system for recreational vehicle appls. 80−30538
Stirling engine technology in Japan 80−35739
Stirling engine with rhombic drive, effect of higher harmonics on preliminary design 80−35718
Stirling engine-driven gas heat pump system, energy efficiency 80−35740
Stirling engine/generator for on-site electric power generation, preprototype perform. testing 80−30539
Stirling free piston engine, development of a heat activated heat pump 80−30541
Stirling free piston engine technology and appls., design optimisation 80−35723
Stirling free-piston engine/linear alternator system, 1978 development status 79−48178
Stirling free-piston engine/linear alternator system, demonstrator engine design 79−48175
Stirling JPL laboratory research engine, computer simulation 79−48171
Stirling Laboratory Research Engine, preliminary test results 80−35717
Stirling laboratory research engine, preprototype design 79−48173
Stirling stroke controlled engine, variable angle wobble plate drive 80−30543
thermodynamics, mathematical formulation including negative absolute temps. 80−27250
β''-Al_2O_3-Na_2O, solid electrolyte, behaviour at high current density, sodium heat engine mode 80−61330
$LaNi_5$, appl. as H storage system for heat engines *(Ukrainian)* 78−67022
Na, using β-alumina ionically conducting ceramic, principle and thermal efficiency 79−48179
Ni-Ti, Nitinol memory material heat engine, comment on efficiency 80−3529
Ni-Ti, Nitinol memory material heat engine, reply to comments on efficiency 80−3530

heat exchange *see heat transfer*

heat exchangers
see also cooling towers
agitated vessels with bare and finned vertical tube baffles, heat transfer, power expenditure 79−1052
air chamber, thermostatic precision *(Japanese)* 79−35736
air cooled, characteristics of corrugated straight fin surfaces 78−18287
air cooled, heat transfer between fluidised bed and horizontal tube surface *(Japanese)* 77−58785
air-cooled, cross-flow heat exchangers, mean temp. difference calcs. 80−6054
air-water, greater operational efficiency of P-67 boiler 79−68710
all-Al heat exchangers, appls. of US soldering 77−58499
annular pipe heat exchanger, laminar flow heat transfer coeffs. 79−72779
artificial heart blood heat exchangers with radioisotopic power supplies 80−85532
bayonnet tube exchanger, optimum design 79−1083
blood heating/cooling, thermal design, equipment and blood props. considerations, appls. 78−92744
boiling crisis and press. drop, heat transfer enhancement devices 78−55638
brass cap cooling with liquid N_2, heat transfer 77−61071
BWR vertical separator superheater tube bundles, condensation heat transfer, noncondensing gas effects 80−47535
check calculations with parallel/mixed flow, standard expressions 78−67199
circulation loop, heat transfer 78−33994
coal-fired cored brick regenerative heat exchangers 79−1353
combustion 78−27761
compact heat exchanger evaluation *(German)* 80−53614
compact laminated fin heat exchanger, expt. determ. of hydraulic resistance and total pressure drop coeffs. *(Russian)* 79−58683
concentric, for dilution refrigerator 79−21756
condensate film flow on finned surfaces, heat transfer, heat exchanger design 78−75038
condensation augmentation, horizontal tube, using twisted tape inserts and internal fins 78−71265
condensation heat transfer in horizontal tube, effect of in-line static mixer 77−41626
cores, perforated surfaces, heat transfer augmentation 78−38402
corrosion behaviour evaluation, for heat exchanger appls. 80−85092
counter-flow, using heat pipes or thermosyphons, charact. 78−33993
countercurrent, dynamic response to temp. disturbance and step flow variations 79−1084
counterflow gas-liquid helium heat exchanger with copper grid 80−17947
counterflow heat exchangers for gas to gas appls., irreversibility concept 78−90699
cross flow heat exchanger, longit. wall heat conduction, numerical calcs. 78−90645
cross-flow, performance where overall heat transfer coefficient is variable 78−8401
cross-flow heat exchanger tube bank efficiency rel. to structure *(Russian)* 79−10448
cross-flow induced vibrations in tube bank, turbulent buffeting and fluid elastic instability 79−3958
cross-flow induced vibrations in tube bank, vortex shedding 79−3957
cross-flow-heat exchanger, model of thermal mixing process 79−1078
crossflow heat exchanger, approximate dynamic anal. by method of weighted residuals 80−92021
crossflow induced vibr. of tube banks 78−50245
cryogenic, transient performance of extended surfaces 77−30168
cryostat using supercrit. He coolant, for meas. on superconductors 77−30155
cryosurgery, self-contained apparatus 80−56271
curved tube bank vibration in turbulent transverse water flow *(Russian)* 80−33678
cylinder in cross flow, turbulence effect on heat transfer 79−1075
desalination units, evaporator-condenser, film-type, horizontal tube, configuration effect on heat transfer 80−53604
design, nomogram for heat transfer coefficient determ., water flowing in pipes or tubes 78−9641
design optimisation, w.r.t. heat transfer efficiency *(Russian)* 78−16789
dilution refrigeration with continuous countercurrent heat exchanger, theory 77−30152
dilution refrigerator, ^3He circulating, with more than one mixing chamber 77−30153
dilution refrigerator with sintered Ag powder heat exchangers, millikelvin range 77−30154
dispersed media, fluidised bed heat transfer 78−9704
double pipe heat exchangers, calc. of overall heat transfer coeff. 79−77109
double-pipe, geothermal power generation from salt domes 79−48087
duct, thermal entrance region, laminar forced convection, finite-element soln. 80−10118
dynamic analysis, digital algorithm for initial value problem 77−42727
electric heaters for nucl. applic. 78−86649
energy savings through the accurate prediction of heat transfer fouling resistances 80−61399
evaporation zone of heat pipes, heat exchange mechanism and vapour formation laws 80−24023
evaporative cooling and condenser efficiency and performance enhancement *(German)* 79−72781
evaporative thermal siphons for intensifying heat exchange 79−18682
film condensation of vapour in elec. field, heat exchange intensification 79−86331
fin and tube heat exchanger, heat transfer, water spray effects 79−193
fin array, shrouded, with, without tip clearance, laminar heat transfer 79−55376
finite element model, investigation of forced vibration response under elastic constraint 79−81786
finned heat pipe latent thermal energy storage system performance 79−57487
finned tube heat exchangers, improved design methods 80−95097
finned tubes bundle type, air flow heat transfer charact. investigation 78−21133
fixed bed heat regenerators, with heat losses and sources 79−188
flow, 3-dimensional, in bundle of rods *(Russian)* 78−37408

heat exchangers continued
flow and heat transfer around in-line tube banks with pyramidal roughness 78−18152
flow calorimeter for condensable gases, low temp. and high press., design and eval. 80−37033
flow calorimeter for condensable gases, low temp. and high press., computer program prediction and exptl. data comparison 80−37034
flow field computations in distributing collectors, MHD heat exchanger *(Russian)* 78−75227
fluid heating mantle using heat-exchanger principles 78−93665
fluidelastic vibration of tube arrays 78−94615
fluidised-bed, liquid, for geothermal plant appl., flow distribution models 79−52879
fluidised-bed, liquid, scale control and corrosion tests, geothermal power plant appl. 79−48090
fouling data analysis, for geothermal power plant appl., use of multivariate regression technique 79−52880
fouling in heat exchangers, review 79−3902
gas, in channels with lamellar surfaces and smooth ribs, flow resistance, heat exchange *(Russian)* 78−83218
gas and air flows, low velocities measurement, appl. 78−47078
gas cooled fast breeder reactors, roughening characts. of surfaces for improved heat transfer 77−18650
gas mixture turbulent concurrent double pipe heat exchanger equilib. and nonequilib. reaction 78−94856
gas turbine-HTGR system heat exchanger design 78−739
with gaseous carriers, compact heat transfer surface development 78−30296
GCHTR, steam gasification of coal using fluidised bed gasifier 77−83071
geothermal energy utilisation, fouling problem overcoming 79−43740
geothermal power plant appl., shell-and-tube design 79−48089
geothermal system, thermosyphon models for downhole heat exchanger appls. 79−57356
heat conduction in tube wall, transfer functions determ. 77−7287
heat flow calcs., algorithm *(German)* 80−1418
heat transfer augmentation techniques, impact on entropy generation 80−79118
heat transfer augmentation techniques for conservation of available work 80−103021
heat transfer coefficient, iteration-free calculation 78−1655
heat transfer conference, Aug. 78, Toronto, Canada 78−90624
high capacity, inexpensive construction 78−49826
high efficiency solar collector development 79−62051
high temp. heat exchangers, heat transfer improvements, radiation between walls, effects *(Japanese)* 78−87244
high temp. pebbles with periodically varying fluid temp., thermal stresses, heat storage capacity 78−26020
hockey stick heat exchanger, elbow centroid 80−9329
hot dry rock geothermal reservoir fracture mapping techniques 80−81419
hot wire anemometry method for the flow patterns in an array of heat exchanger tubes 79−90357
HTGR, passage walls heat transfer performance study *(Japanese)* 77−18687
HTGR Core Auxiliary Cooling System mathematical simulation 78−29570
HTGR heat exchanger, factors affecting performance of Cr_xC_y sprayed coatings 80−40609
HTGR radiative gas heat exchangers, radiation effects at high temps. 80−95338
HTGR steam generator or heat exchanger materials, compatibility with coolant circuit media 77−57721
HTR, metallurgical problems of intermed. heat exchanger 77−65256
humid materials, diffusivity and specific heat, transient temp. changes *(French)* 80−64355
hydrogen permeability of heat exchanger material, oxide protective layer formation meas. 78−8895
impinging jets, heat transfer, appl. to compact heat exchangers 79−1071
impulse chamber for intensifying heat exchange *(Russian)* 80−43597
indirect, thermodynamic calc., air conditioning system appl. *(German)* 77−23862
industrial plants, heat exchanger installations, heater min. furnace diameter determ. *(German)* 80−38234
interrupted plates type, Nusselt no. plate thickness depend. 78−87232
interrupted wall channels heat transfer and flow anal., appl. to heat exchangers 79−81883
Lamb wave equivalent US mode propagation in thin-walled tubing 79−68459
laminar convection, combined free and forced, in internally finned square ducts 77−51060
leak-proof heat exchanger for solar water heating systems 80−30524
linear heat transfer in wall *(Russian)* 79−98594
LMFBR heat exchangers, liquid metal temps. in pipes with wall fast flow discontinuities *(Spanish)* 77−74907
LMFBR sodium-water heat exchangers, design of expansion pipe-bend 77−30648
longitudinal and cross flow around heat exchanger tube bundles comparison, heat transfer efficiency aspects 78−94687
low-finned staggered tube bank, flow and heat transfer, high Re *(German)* 78−33996
measurement system, one and two loop *(Hungarian)* 80−31702
mechanically-produced unsteady boundary layer flow effect on convective heat transfer augmentation 78−71261
miniature cryogenic liquefier, heat exchange characts. 77−67440
models, approx. of dynamics of method of weighted residuals *(Japanese)* 78−67024
molten salt, thermal cond., heat storage, review *(Japanese)* 80−6573
monolithic deformable mirror/heat exchanger unit evaluation 80−33139
multipass, distributed temp. response transfer functions *(Japanese)* 77−33985
multirow dry or wet heat exchangers, simulation 79−191
multistage countercurrent fluidized-bed heat exchanger, optimal heating surface 77−89200
multitube type, operation, influence of deposits *(Rumanian)* 79−94467
N_2O refrigerator, thermodynamics and thermoelectric condenser design 80−108809
natural circulation loop with throughflow steady state soln. of flow rate and temp. 80−31742
network synthesis, mixed integer optimisation 78−30152
nuclear power reactor, austenitic stainless steel, appl. 77−3102
heat exchangers continued
nuclear power station heat exchangers, eddy current probe for nondestructive testing of transfer tubes *(Japanese)* 80−81246
nuclear power stations, three-loop, intermediate heat exchangers effectiveness determ. 80−608
nuclear reactor, HTR, hydrogen and tritium permeation through He heated tube walls 77−50250
nuclear reactor, potassium heat exchanger 77−46210
nuclear steam gasification of coal, test and development of heat-exchanger alloy 78−15589
nuclear steam generator, Cr-Mo low alloy steels suitability comparison 78−54834
oblique high-drag heat exchangers, turbulent flow and pressure losses 79−94710
ocean thermal energy conversion, OTEC system development, Conf. Houston, TX, USA (Nov. 1978) 79−83611
ocean thermal energy conversion, technology development program 80−30504
ocean thermal energy conversion (OTEC), biofouling effect on heat exchanger 78−44875
ocean thermal energy conversion appl., OTEC power systems, 1978 status and development trends 79−83614
ocean thermal energy conversion appl., US UTEC development programme overview 79−83613
ocean thermal energy conversion plant, 100 MW, systems aspects 78−96235
ocean thermal energy conversion plants, condenser and evaporator design improvements, use of internal and external flutes 79−61959
oil-cooling baffled shell-and-tube heat exchanger expt. 78−83395
optimal controller synthesis for a counterflow heat exchanger *(Polish)* 79−97384
optimal design 79−3895
optimum network design, thermodynamic combinatorial approach 80−66985
OTEC; analysis of a heat exchanger−thermoelectric generator system 80−35710
OTEC heat exchangers, $CaCO_3$ and scale formation 80−41461
paraffin plate heat storage element, fusion, periodic solidification, heat transfer kinetics *(French)* 80−40913
parallel and counter-flow, weighted residuals method and modal control 79−3898
particle layer deposition from gas dispersion turbulent flow in tubes, heat exchanger appl. 79−55409
passive solar heating systems, calc. of heat-transport-medium flow rate in heat receivers 80−99913
periodic flow thermal regenerator, transient performance 78−59389
periodic thermal storage, regenerator 80−35760
pinch temperatures in heat exchanger *(Japanese)* 80−62663
pipe expansion bend, Na-H_2O heat exchanger, bending-loadings determ. 77−80085
plate heat exchange systems, expt. frequency anal. *(Japanese)* 78−9642
plate type, cooling water fouling 79−1092
plate type, with hemispherical projections, heat transfer and drag 80−48560
plate-fin heat-exchange surfaces, convective heat exchange intensification 79−81691
plate-fin surfaces, performance ranking 79−32194
porous cylindrical board, temp. field and heat transfer efficiency 78−5793
Porous heat exchangers for continuous flow helium cryostats 78−16803
practical design for use in dilution refrigeration 78−41314
preheaters and evaporators, surface scale formation anal., heat transfer surface utilisation 80−48550
process heat recovery utilising heat pipe exchangers, design and performance 80−61398
process mathematical modelling *(Dutch)* 79−75525
pulsation bed of disperse material, heat exchange with horizontal tube bundle *(Russian)* 77−72137
quartz, heat treatment of dense moving layer, heat exchange development 79−20075
R & D on advanced heat exchangers in Japan, review 80−35737
radial tube bank vibration in transverse liquid flow *(Russian)* 79−81973
radiation, temp. distribution over wall thickness, model, boiler appl. 77−39210
radiation heat transfer effects in annular passages of heat exchangers *(Japanese)* 77−23239
Rapsodie and Phenix plants intermediate heat exchangers experience 78−82502
rational use of energy in houses *(Dutch)* 80−40836
rectangular curved channel hydrodynamics and heat transfer expt. 80−19398
recuperative, convective heat transfer, nonNewtonian carrier, conjugated problem 79−1086
recuperative, source/sink even model *(Hungarian)* 79−14226
refrigeration system, energy conservation estimates by second law anal. 80−45723
regenerative, behaviour at high temp., numerical model 77−62140
regenerative heater, high-temp., refined math. model 80−22365
regenerator, approx. soln. of regenerator eqn. 79−59918
rippled silica deposits, form. in heat exchanger tubes 79−1087
rotating heat exchanger, frictionless two-phase tube flow, centrifugal accel., choked flow 80−48792
rotating pebble bed heat exchanger for N_2 fixation using fusion energy heat source 80−32510
shallow fluidised bed heat transfer investigation 79−7404
shell and tube exchanger, electrochem. mass transfer modelling 79−1074
shell-and-tube heat exchanger, flow distrib. anal., rel. to CRBRP-IHX 77−42052
small flow-through cryostat for polarization microscope 78−86327
solar, thermal power system, open cycle air turbine *(French)* 80−45641
solar absorber-convertors block unit, thermal characts. experimental investigation 80−97801
solar collector heat pipe array with common heat exchanger 79−62038
solar collectors with multilayer cylinder heat exchangers, heat balance eqn. and thermal stress anal. 80−58977
solar concentrating collector optical efficiency, heat loss coeff. and heat removal factors 79−100483
solar energy appl., to refrigeration, H_2O-LiBr and NH_3-H_2O absorption cycles, design and optimisation 79−87974

heat exchangers continued
solar energy thermal storage by latent heat of fusion of mineral salts *(French)* 79−24915
solar installation for refrigeration and water heating, energy characts. 80−101124
solar thermal receiver utilising a small particle heat exchanger 80−30557
solar-powered solid-state heat transfer device based on photovolt. and Peltier effects 80−217
space heating, experimental installation, using solar absorbers, heat pumps, heat exchangers and measurement and control gear *(German)* 80−35741
spherical nozzles of high-temperature heaters, heat transfer calcs. 80−103022
steam turbine district heating plant, condensing and regenerating equipment 80−92029
steel, C, gas-flame spray deposited Fe-Si protective coating 80−61025
submerged tube surrounded by rigid tubes, hydrodynamic inertia coeffs. 77−7335
surface, optimisation using generalized geometric characteristic and mean vel. *(Russian)* 80−82760
surface selection methods 79−1070
surfaces, thermal efficiency determ. 79−27641
tap-water purification for home dialysis *(German)* 79−2160
temperature distrib. perpendicular to heat exchanger surface 79−32189
thermal mixing in cross-flow tube banks 79−1079
thermal modelling of heat exchanger for computer simulation 77−46904
thermal performance deterioration in cross flow due to flow nonuniformity 79−1082
thermal performance of in-line and staggered tube banks 79−7277
thermal regenerator, with variable mass flow rate, computer model 78−75047
thermal regenerator simulation numerical accel. 77−23855
thermal regenerators, packing materials, size and arrangements effects 79−190
thermal regenerators, periodic flow, transient performance 79−187
thermal storage, high temp., latent heat method using heat exchanger *(French)* 80−40912
thermionic, central station appl., design point selection, economic impact 79−48155
thermionic, design and testing of large convertor assemblies 80−40885
thermoelectric heat pumps, cross flow, anal. of operation and performance using mathematical model 80−107836
thermohydraulic irregularities in shell and tube flow exchangers, effectiveness 79−1072
three-fluid heat exchangers of two and three surfaces 79−10451
true vibrations numerical soln. 78−75094
tube bank duct acoustic resonances 78−90550
tube banks, flow-induced vibrs. 78−46929
tube banks in air crossflow, hydrodynamic vibration models *(Russian)* 78−46981
tube banks in cross flow, heat transfer 79−1077
tube banks in turbulent flow, heat transfer prediction 79−1080
tube bundle transient heat transfer and hydrodynamics with large flow and heat flux perturbations 78−83484
tube bundles, airside press. losses 79−1076
tube bundles, heat transfer to three dimens. flow 79−1073
tube in fin heat exchangers with rippled fins, optimal design for maximum heat transfer 80−6055
tubes in cross flow, local and average heat transfer 79−1081
tubular bundle type, with longit. drive, forced turbulent convection *(French)* 79−86333
tubular casing heat exchanger, effect of transverse baffles on heat exchange in inter-tube area *(Russian)* 78−45618
turbulent heat transfer from flat plates, facing curved wall effects *(Japanese)* 80−83799
ultra-compact, low cost, cryogenics appl. 79−35758
vertical evaporating circuit, heat exchange calc. and optimisation *(Russian)* 77−71321
VHTR heat exchangers, material criteria and selection 78−13232
VHTR system, material requirements for intermediate heat exchanger, rel. to creep-rupture tests 78−13235
vibrations of components in liquid and two-phase cross-flow 78−90770
vibratory contact with support plate, forces produced 77−88211
waste heat recovery using gas to gas heat exchangers 80−61400
water pulsating flow in heat exchanger effect of pulsations on heat transfer 79−94614
whole-body hyperthermia with oesophageal temp. feedback control 79−92423
wiped-film exchanger, local heat transfer coeff. 79−1051
wire-packed step heat exchanger for dilution refrigerators 78−54363
Cu, sintered, in contact with ^{3}He, thermal conductance, rel. to elec. resist., heat flow model calc. 80−10728
Cu, sintered exchange of heat with flow of superfluid ^{4}He 77−82526
Cu sintered exchangers for nuclear demagnetization refrigerator 79−58696
^{3}He/^{4}He dilution refrigeration operating principles and heat exchangers, review 79−67310
NaCl gas-droplet counterflow heat exchanger, numerical model *(French)* 80−61396
Ne+H_2 bubble chamber, heat exchange and temperature control system 77−6616
Ni-base alloys, creep, corrosion, and fatigue testing for appl. in nucl. process heat system 78−13237
SiC ceramic heat exchanger, cost-effective design 80−95341

heat flow *see heat transfer*

heat insulation *see thermal insulation*

heat losses
see also thermal insulation
absolute radiometer instrumental correction theory improvement 77−82585
atmospheric IR properties relevant to building envelope heat losses 80−58895
building envelope heat radiation losses and countermeasures 80−58894
building heat loss diagnostics, IR image evaluation requirements 80−86424
buildings, heat loss meas. using IR TV system 77−45837
collector long-term average performance prediction method 79−62116
electric current carrying leads, compensating for heat flows 77−7299
flat plate solar collector dynamic evaluation 79−62044
heat losses continued
flat plate solar collector efficiency and heat loss characteristic meas. 79−62064
gas blast circuit breaking arcs, radiative energy transfer 80−1416
heat balances of apartment house, in Dutch climate, energy conserving measures 79−61948
heat capacity measurement, high temp., modulation method, thermal losses compensation 79−85144
high vacuum, HV bushings, for cryogenic appl. 78−81977
honeycomb structured flat plate solar collectors compared 79−62046
hot water storage tank, heat loss rel. to thermal insulation *(Japanese)* 80−5918
IR effective emissivity meas. by natural cooling *(Japanese)* 78−29117
isotopic microgenerator design and construction optimisation due to min. power 80−108813
laser calorimeter types and techniques 80−69441
laser pumping system, thermodynamic calc. method 80−58551
liquefied gas, cold loss minimisation during transfer and storage 77−30165
microwave heating system for improving temperature uniformity in heated tissue 79−100795
plasmatron with interelectrode insert, output electrode turbulent heat transfer 78−71555
polymer melts, temperature measurement, thermocouple probe error correction 77−65034
PWR heat rate improvements, controllable loss system 79−67827
quasi-stationary Stefan problem for a hot pipeline in a frozen mass 79−23324
radiation shield, for cryogenic apparatus, thermodynamic optimisation 78−81982
recycle-flow calorimeter, 2 to 20 MPa 90 to 400K 80−42228
residential building heat loss estimation by aerial IR imaging 79−74586
slat solar collector natural convection obs. 79−62055
solar, water heater, low-temp., tubular heat receiver, temp. distribution, heat-balance differential equation solution 79−94464
solar collector, plate-in-tube, evacuated, theory and expt. 79−88004
solar collector honeycomb cell heat transfer interferometric meas. 79−62053
solar collector thermal performance test procedures 79−62066
solar collector thermal performance testing procedures *(Japanese)* 78−16795
solar collectors with plastic covers, radiation heat loss calc. 79−74538
solar concentrating collector optical efficiency, heat loss coeff. and heat removal factors 79−100483
solar distiller, multistage-inclined type, solar energy distribution determination 79−96423
solar energy collection, heat losses by conduction and convection, reduction techniques 79−79409
solar energy collection and storage, latent heat diode walls, space heating *(French)* 80−61298
solar energy collector design for low capital costs and least steady-state heat losses 80−104517
solar energy system performance rel. to duct and pipe losses 79−83633
solar energy systems, Conf., San Francisco, CA, USA, (Dec. 1978) 79−83635
solar flat plate collector cover system and absorber heat loss rel. to angle of incidence 79−62068
solar flat plate collector design and optimisation for Indian conditions 79−62087
solar power system, mathematical model, operating regimes optimisation 79−83562
solar receiver convective losses determ., using cryogenic heat transfer tunnel 79−83636
solar shallow pond performance with mirror on side away from Equator 79−62077
solar still, thermal losses to atmosphere, determ. 80−87707
solar water pump, for lift irrigation, modified design analysis 79−70440
solid, photoacoustic signal, heat loss influence 80−100308
space heating, all-year solar energy collection and storage system 79−62074
spacecraft heat rejection improvements using thermoelectric devices 80−108810
steady state salt gradient solar pond 80−35749
steel, molten, heat loss during solidification hydrodynamic eqns., hardening front kinetics *(Russian)* 80−55385
superconducting AC generator, heat losses in rotating liquid transfer union, simulation 77−84116
thermal sensation evaluation, comfort chart *(Japanese)* 80−81545
thermoelectric heat pumps, cross flow, anal. of operation and performance using mathematical model 80−107836
thermoelectric materials, thermal conductivity determ. heat losses, direct method 80−62662
Ar arc heating, high-pressure complex heat exchange expt. *(Russian)* 80−75112
NbTi solenoid, operating at 9 T in He gas 77−74461
Pt resistance thermometers, heat leaks effect anal. 80−57296

heat measurement *see thermal variables measurement*

heat of adsorption
activated chemisorption kinetics, differential heat of adsorption meas. 78−84062
aliphatic acids, thermodynamics of adsorption at air/aqueous soln. interface 80−10752
aliphatic alcohol, thermodynamics of adsorption at air/aqueous soln. interface 80−10752
alkali halides, of inert gases, variation 77−85049
BCC metal hydrides, geometric and electronic contribs. to thermodynamic props. 79−46815
binary alloys, surface conc. profile and surface energy 80−84350
butyl alcohol, pumping down curve, P(t), rel. to adsorption isotherm *(Japanese)* 80−52249
Cu, adsorption of CO, on (110), LEED, surface pot., IR spectra 77−66092
determination of gas-solid chromatography, for teachers 79−35497
ethane-C mol. sieve system, adsorptive pot. distrib., entropy, enthalpy 77−72778
exfoliated graphite, adsorbed Ne, vapour press. meas., 15-30K 79−69350
gas, on solid adsorbents, thermodynamics *(Rumanian)* 80−10786
gas-solid interface, flow microcalorimeter appl. 77−76665
graphite, adsorbed Ar monolayer, lattice spacing and isosteric heat below 50K, LEED obs. 80−34303

heat of adsorption continued
graphite, adsorption and migration of O_2, CNDO/2 calcs. 79−28205
heterogeneous surfaces, basis of Langmuir model, exponential distrib. adsorption energy, Freundlich eqn. *(German)* 78−30832
interaction parameter of adsorbed atoms on surface containing impurities estimated 77−15698
interstellar grains of H, heat of adsorpt. rel. to surface temp. and H_2 form. 79−21367
ionic crystal, adsorption of inert gases, initial heat of adsorption calc. 78−26773
ionic crystal, gas-solid interaction potential, adsorption sites and surface migration 80−24738
ionic crystal, phys. adsorption of nonpolar gases, localised and mobile phases, hopping adsorbates 80−24739
isosteric, determ. using contact pot. difference meas. 79−66347
isosteric heat of adsorption, adsorbate conc. depend. 80−59805
macromolecular layer, energy of interaction between two spherical particles 78−53271
measurement, dynamic characts. of adsorpt. calorimeter 78−24796
metal, adsorption of metal atoms, enthalpy calc. 80−100406
metal surfaces, replacement phenomena of chemisorbed gases, review *(Japanese)* 77−72779
metals, adsorption of S, thermodynamics of two-dimen. and three-dimen. sulphides 80−20036
metals, chemisorption of gases, book 79−69370
microporous adsorbents, experimental adsorption isotherms of characteris. of absorbents 77−69163
molecular sieves, bi-porous, sorption kinetics, expt. and theory comparison for batch systems 79−87873
molecular sieves, bi-porous sorption kinetics, math. models for systems with rectangular equil. isotherm 79−87872
molecular-statistical description, ensemble of excess systems 80−10776
multicentred adsorbed particles 77−60118
oriented overgrowths, pairwise interaction approach 77−62759
patchwise heterogeneous surface, applic. of extended model of associated adsorbate 78−14617
patchwise heterogeneous surface, thermodynamics of localised and nonlocalised adsorpt. 77−1299
pyridine, ethyl pyridine, heat of adsorpt. on sponge Fe, Fe_2O_3, CuO, adhesive wear, flow calorimetry 78−85193
Quantum theory of adsorption of isolated adatoms 78−22957
rare earth element submonolayer films, electronic phase transitions, heat of absorption 80−24736
refractory metals, heat of desorption of alkali metals 80−75430
simple metals, atomic chemisorption, atom-jellium model 78−84066
Spheron 6, surface group obs. using gaseous reagents, surface acidity evolution during heat treatments *(French)* 77−66767
stearic acid, heat of adsorpt. on Fe_2O_3 powder, surface area meas. by flow calorimetry 78−81974
submonolayer films on metallic surface, struct. and props. review 78−38972
surface, use of vacuum ultramicrobalance 79−71465
symmetrical adsorption thermodynamics, case of noninert adsorbent 80−80059
thermodynamics of gas adsorpt. 79−73396
transient ion desorption, work function, evap. rate, ion heat of adsorption 77−20198
transition metal, chemisorption of ordered atomic layers, HF Green's function formalism and phase shift technique 80−24733
transition metal (001) surface, model, chemisorption, coverage depend. of adsorption behaviour 78−71976
transition metals, heat of chemisorption of H_2 calc. 78−38959
Ag (111), Xe monolayer adsorption, statistical mech. 80−34306
Ag, adsorption of aromatic hydrocarbons, heat of adsorption, coating and fine struct. *(German)* 79−23844
Ag, of Cl_2, on low index surfaces, energetics and structures 79−82440
Ag, of O_2, isosteric heat of adsorption determ. 77−55453
Ag-Pd alloy, surface comp., AES expts., correl. with O_2 heat of chemisorpt. data 78−34684
AgBr, photographic emulsion, adsorpt. of Br^-, cyanine, thermodynamics 78−32908
Ag(111), adsorption of Xe, structural and thermodynamic studies 80−6640
Al_2O_3, adsorption of H_2O, energetics, effects of adsorption temperature on surface processes 78−60028
Al_2O_3, alumina, adsorpt. of saturated hydrocarbons, gas-solid chromatography based on compensation effect 80−26053
η-Al_2O_3, outgassed, of pyridines from n-heptane soln. 80−61154
Au, adsorption of Xe and CO on (100) 77−15691
C, activated and impregnated, temp. depend. adsorption of HCN 80−89522
CO on Pd, catalytic oxidation and chemisorption 77−70339
$Cd(OH)_2$, adsorption props. of surface, gas-chromatographic investigation 79−66343
CeO_2 in O_2 atmos., adsorption and elec. cond. props. 79−23836
$Co(OH)_2$, adsorption props. of surface, gas-chromatographic investigation 79−66343
$Cr(OH)_3$, adsorption props. of surface, gas-chromatographic investigation 79−66343
Cu (001), chemisorption of S, thermodynamics, AES study 79−82452
Cu (111), chemisorption of CO, IR spectra, LEED, and surface pot. meas. 80−39438
Cu (111), of CO, rel. to surface prep. 78−6223
Cu, adsorption and desorption of water vapour, relative humidity effects 80−49505
Cu film growth on amorphous C, energy characts., in situ electron microscope determ. 79−11027
Cu of Ag, pairwise interaction approach to adsorption of oriented overgrowths 77−62759
Cu-Ni alloy surfaces, chemisorption of CO, LEED, AES, thermal desorption, and work function meas. 79−90879
Cu_2O, adsorption and desorption of water vapour, relative humidity effects 80−49505
$DyFe_2H_x$, thermodynamic props., H_2 desorption isotherm meas. 80−89516
$ErFe_2H_x$, thermodynamic props., H_2 desorption isotherm meas. 80−89516
Fe film, polycryst., heat of adsorpt. of H_2 and D_2 78−91530
GaAs (110), adsorption of Cs 77−72794
Ge, adsorption of Ar, Kr and Xe on (111) plane, adsorpt. pot. 78−26768
Ge, of N_2 and CO, adsorption potentials and trapped electrons role 79−90872
Ge+$GeBr_4$, single crystal+vapour system, reaction kinetics and laws of soln., heat of adsorption 79−39196
H from metal hydride beds, hydride conversion and storage system chemical heat pump 80−72077
H-mordenite, of benzene *(German)* 79−90892
H_2, solid, H atom adsorpt. time and energy, hyperfine freq. meas. 79−50155
He isotopes on carbon black, effects of preadsorbed Xe 77−59172
^{4}He films adsorbed on graphite, transition temp., entropies, internal energies and heats of desorption, vapour press. meas. 80−2238
Hg, of water vapour, critical anal. of expt. data *(Spanish)* 79−82435
Ir (110), adsorption of CO, O_2, H_2, N_2, ethylene and benzene 78−38961
Ir (111) surface, chemisorption of O_2, dynamics 77−59211
$LaNi_{4.4}B_{0.6}$, H_2 absorpt. props. 80−88432
LiH, adsorption of He, ab initio calc. 78−38952
Mn film, vacuum-evaporated, H(D) uptake kinetics and energetics 80−88430
Mo, (112) face, Sr submonolayer adsorption 80−2271
NaCl, adsorption heat of Ar variation 78−26772
NaCl, of CO_2, gas-solid interaction potential, adsorption sites and surface migration 80−24738
NaCl, of methane, adsorpt. pot., localised and mobile phases, hopping adsorbates 80−24739
Ni (001), chemisorption of S, thermodynamics, AES study 79−82452
Ni (100) and polycrystalline surfaces, CO chemisorption, low energy SIMS and AES 80−34309
Ni films, CO-covered of H_2, isotherms, resist., work function changes 78−75926
Ni-Au alloys, surface segreg., surface energy and solute strain energy effects 77−72760
$Ni(OH)_2$, adsorption props. of surface, gas-chromatographic investigation 79−66343
Pd, of CO, UPS investig. of nature of chemisorption bond 77−51598
Pd wire, of H_2, heat of adsorpt., sticking probabilities 78−43240
Pd-D, crystallite size effects, simultaneous sorption and X-ray study 80−65237
PdAg wire, of H_2, heat of adsorpt., sticking probabilities 78−43240
Pt (111), adsorption of CO, XPS, UPS, thermal desorption, and work function meas. 79−77905
Pt (111) surface, of CO, LEED, desorption and work function meas. 77−72781
Pt, of Ba, vaporisation expts. on Pt-Ba cathodes 78−10272
Pt, of CO, effect of interactions on nature of chemisorption bond 77−51598
Pt, of Cs field-emission microscopy 78−51822
Pt(111), surface H-H interactions, heats of adsorption and desorption 78−18899
Re (10$\bar{1}$0) of k, electron-adsorption props. 79−33192
Ru (101), O_2 chemisorption, CO+O_2 interaction 77−73471
SiO_2, heat of adsorption of various mols. by IR spectroscopy 77−55447
SiO_2, P-doped amorphous, porous and hydrophilic, water adsorpt. and IR spectra obs. 80−80061
SnO_2, of water, adsorption anomaly rel. to pretreatment 79−28194
TiO_2, differential heat of chemisorption of H_2O 78−84052
TiO_2, rutile, pure and SiO_2-coated, adsorption of N_2 and Ar, 77.4K, microcalorimetry obs. 80−80062
W (001), chemisorption of H, HF Green's function formalism and phase shift technique 80−24733
W (100), adsorbed La, depend. of work function, heat of adsorpt. on surface coverage, contact potential study 78−67912
W (112), adsorption of La, contact pot. difference, LEED and field emission microscopy *(Russian)* 78−14618
W, adsorbed Sm, conc. depend. of lifetime and heat of adsorption of Sm atoms 79−69364
W, adsorption of La, specific characts. *(Russian)* 79−1543
W, of Cu, Ag and Pb, pairwise interaction approach to adsorpt. of oriented overgrowths 77−62759
W, polycryst. surface, heat of desorption of Cs 80−75430
W surface, of Cs ions, evap. isotherm from single cryst. faces 79−24829
W, with adsorbed Pd, field emission obs. of adsorpt., diffusion and self-diffusion 78−38945
ZnO 10$\bar{1}$0 surface, reaction of O_2, AES, LEED, EPR, desorpt., surface cond. and work function expts. 78−95950
ZnO, differential heat of chemisorption of H_2O 78−84052
ZnO, differential heat of chemisorpt. of CO_2, NH_3 79−52759

heat of combustion
calorimetric meas., two-cylinder equipment for solid, liquid and gaseous fuels meas. 77−79096
composite materials, surface, flame propagation velocity rel. to thermal props. *(Russian)* 80−7797
critical heat fluxes in internally heated annular channels 78−31637
inorganic solids, high energy irradiation, energy storage meas. 78−51581
polymer surface, flame propagation velocity rel. to thermal props. *(Russian)* 80−7797
polymers, correlation between flammability and heat of combustion *(Polish)* 78−53246
rare earth trifluorides, bomb calorimetric determ. of enthalpy of formation 80−50879
solid solution form. in heat of combustion process *(Russian)* 77−66765
TCNQ salt, TMPD-TCNQ, enthalpy of combustion, calorimetric meas. 77−52663
DyF_3, bomb calorimetric determ. of enthalpy of formation 80−50879
ErF_3, bomb calorimetric determ. of enthalpy of formation 80−50879
GdF_3, bomb calorimetric determ. of enthalpy of formation 80−50879
HoF_3, bomb calorimetric determ. of enthalpy of formation 80−50879
LaF_3, bomb calorimetric determ. of enthalpy of formation 80−50879
NdF_3, bomb calorimetric determ. of enthalpy of formation 80−50879
PrF_3, bomb calorimetric determ. of enthalpy of formation 80−50879
U, in F_2, standard enthalpy of formation of UF_6 79−96349

heat of crystallisation
Ω-caprolactam-ε-caprolactam polymers, vitrification, fusion, crystallisation *(Russian)* 77−47561
carbon tetrachloride, volume effect in metastability of crystalline phases on cooling 79−77716
chloroform, volume effect in metastability of crystalline phases on cooling 79−77716

heat of crystallisation continued
cyclohexane, volume effect in metastability of crystalline phases on cooling 79−77716
1,2-dichlorobenzene, volume effect in metastability of crystalline phases on cooling 79−77716
inorganic hydrates, applicability to heat storage material of latent heat type *(Japanese)* 78−23606
metallic glass, heat of crystn. and viscous behaviour 80−75166
metallic glasses, structures based on disclination-dislocation model 79−82159
polyethylene terephthalate, stretching, heat effects, struct. transforms. 79−15735
polymers, solidification, as dissipative process 80−65205
rare earth-3d transition metal amorphous alloys, crystallisation behaviour 80−49116
o-xylene, volume effect in metastability of crystalline phases on cooling 79−77716
As_2S_3:Ga system chalcogenide glasses, thermophysical and struct. props. 80−15007
As_2Se_3-As_2Te_3 glasses, differential scanning calorimetry obs. 77−43156
$Au_{77}Ge_{13.5}Si_{9.4}$, heat of crystn. and viscous behaviour 80−75166
$CsNO_3$-$Pb(NO_3)_2$, ht. of crystn. *(Russian)* 77−48418
Fe, glassy, heat of crystn., and bulk modulus, calc. using struct. model 78−51428
Ge, amorphous film, large aligned grain solid-phase growth during scanned laser crystallisation 80−49100
HfO_2-R_2O_3 solid solns., prep., crystn., R=Nd,Sm,Dy,Yb 78−42909
$NaNO_3$-$Pb(NO_3)_2$, ht. of crystn. *(Russian)* 77−48418
$NaNO_3$-$RbNO_3$-$Pb(NO_3)_2$, crystn. heat of eutectic, thermodynamic anal. *(Russian)* 77−63644
Pd-Au-Si, amorphous films, RF sputter deposition, composition and thermal behaviour 80−55292
Pd-Si amorphous films, RF and DC sputter deposition, composition and thermal behaviour 80−55292
$Pd_{77.5}Cu_6Si_{16.5}$, heat of crystn. and viscous behaviour 80−75166
Sb, thin layer, amorphous to crystalline phase transition *(German)* 77−69196
Se_xTe_{1-x}, amorphous, structural relaxation and crystallisation kinetics study by DTA 80−59394
Si, web dendritic ribbon growth, thermal analysis of solidification 78−72770
Zr-Cu, metallic glasses, glass transition temp., crystallisation temp., exothermal relaxation effect 79−52747
ZrO_2-R_2O_3 solid solns., prep., crystn., R=Nd,Sm,Dy,Yb 78−42909

heat of dissociation
acetone vapour, mol. assoc., monomer-dimer equilib., thermal cond. meas., MO calcs. 79−52647
alkali metal hexachloroniobates and hexachlorotantalates, thermodynamic props. from VP meas. 79−34345
azulene, multiphoton ionisation, mass spectra 80−63717
coronene trimer radical cation, spin densities in CH_3Cl_2-CH_3NO_2 solvent mixture, −100°C 80−5565
ethylene, planar dissociation, electronic rearrangement, states, bonds, ab initio multiconfigurational SCF calcs. 80−27937
iodomethane(-d_3)$^+$→CH_3^+(CD_3^+)+I, kinetic energy release distrib. meas. 77−1922
metal carbonyls, gaseous, metal-carbon bond, dissoc. energy and enthalpy of form. 78−44393
naphthalene, multiphoton ionisation, mass spectra 80−63717
struct. and props. exam. 78−92245
water, enthalpy of ionisation meas., reaction-solution rotating-bomb calorimeter 80−4717
water vapour, dissociated, thermodynamic props. *(Japanese)* 77−80263
Ag-Te-O, partial pressure diagrams 77−36681
AlF_3-MF(M=Li, Na, K, Rb or Cs), ion-molecule equilibria studied by mass spectrometric method, heats of dissoc. and form. calc. 80−104479
As_4, gaseous, atomisation enthalpy and enthalpy of form., mass-spectroscopic Knudsen cell method 78−80780
$AsBr_3$, electron impact positive ion form., appearance energy obs. 80−53151
$AsCl_3$, electron impact positive ion form., appearance energy obs. 80−53151
AsF_3(AsF_5), electron impact positive ion form., appearance energy obs. 80−53151
As_3Sb, As_2Sb_2, $AsSb_3$, and AsSb, gaseous, atomisation enthalpy and enthalpy of form., mass-spectroscopic Knudsen cell method 78−80780
$As_2Sb_2O_6$, $AsSb_3O_6$, and As_3SbO_6, gaseous, atomisation enthalpy and enthalpy of form., mass-spectroscopic Knudsen cell method 78−80780
BaPd, BaRh, gaseous, dissoc. energies, obs. and calc. values 78−58864
Bi, vapour pressure calc. from transpiration expts. on Mg-Bi and Pb-Bi alloys 77−76571
$DyFeO_3$, thermodynamic props. 79−77771
$Dy_3Fe_5O_{12}$, thermodynamic props. 79−77771
$FeSb_2$, heat capacity and thermodynamic props. from 5 to 1021.2K, heat of decomposition 77−90636
Ga_2Se_3, evaporation, thermodynamic props. 80−54365
GdS, vaporisation thermodynamics and dissoc. energy obs. 78−67822
GeO_2-SiO_2, glass, evaporation by high temp. mass spectrometry 80−79927
H_2SO_4-H_2O_2 cleaning soln. for Si wafers, thermal characts. 80−3225
$HgCl_2$+metallic Cu+neutral salt, heat of dissociation of complex salts 78−64887
$LaNi_{5-x}Fe_x(Cr_x)$, Fe and Cr electron hydride formation, X-ray and SEM obs. *(Japanese)* 79−43202
Li_2O, mass-spectrometric study of vaporization of solid and thermochemistry of gas 79−10940
LiOH(D)(T), thermal decomposition rates 530-690K, activation energy and enthalpy meas. 80−3321
Li_2(g), thermochem. props. 77−21410
$MgCr_2O_7.6H_2O$, dehydration, thermal decomposition, kinetics 79−11777
MoF_5, gas, thermodynamic stability 80−26041
NO, adsorbed on MgO, dimer form., heat of dissoc., EPR obs. 78−82755
Na_2O-SiO_2 glass, evaporation by high temp. mass spectrometry 80−79927
O_2-N_2, O_4 and O_2N_2 form., influence on N_2-induced O_2 absorption in Herzberg continuum 78−87429
$RuTe_2$, decomposition press. and thermodynamic props. 78−3366
S_n, properties of small aggregates rel. to metallic character of Te_n 78−86985

heat of dissociation continued
Sb_4, gaseous, atomisation enthalpy and enthalpy of form., mass-spectroscopic Knudsen cell method 78−80780
Sb_xSe_y (x=0 to 4; y=1 to 4) molecular species formed in vaporisation of solid $SbSe_3$, thermodynamic props. 80−11943
Se_n, properties of small aggregates rel. to metallic character of Te_n 78−86985
SiO(g), enthalpy of formation and dissociation energy, time-of-flight mass spectra 77−16859
$SrAg(PO_3)_3$, physicochem. characts. 77−52302
TaS_2, decomp. press. and enthalpy of decomposition 79−66042
Te_n, small aggregate, metallic character 78−86985
$TiO_{(g)}$, $TiO_{2(g)}$, thermochemistry, mass spectrometry 77−16857
UC_n (n=1 to 6), formation and atomization energies by high temp. mass spectrometry 80−7842
UF_4-MF (M=Na or K), ion-molecule equilibria, heat of form. and dissoc. and electron affinities determ. 80−104480
W_2As_3, decomp. press. and enthalpy of decomposition 79−66042
Zn-Te-O, partial pressure diagrams 77−36681

heat of formation
actinides and alloys, metallurgical props. rel. to electronic struct., energies calc. method 77−20221
aliphatic perfluorocarbons, electron attachment, fragmentation 0-12 eV 80−5618
alkali halide, static dielectric const. temp. depend. 78−43770
alkali halide solid solns., lattice parameter and heat of form. 80−79739
alkali halides, Schottky defect correl. of form. enthalpy and melting point 78−43015
alkali metal binary intermetallic cpds., OPW calc. of struct., bonding and stability 77−43169
alkali metal cyanide, lattice energy calc. from hydration enthalpy 77−35506
alkali metal fluoroaluminates, dissoc. enthalpies, mass spectrometric determ., heat of form. 80−97720
alkali metal heteronuclear diat. mol. form., equilib. consts., enthalpy changes 78−25750
alkali metal nitrates, standard heat of formation, electron affinity 78−91295
alkali metal oxides, M_2O^+, $M_2O_2^+$, M_3O^+, $M_3O_2^+$, heats of formation 80−16715
alkali metals, dil. binary solns., heat of formation 78−75840
alloy, cohesive energy, semiempirical model, heat of form. expressions 80−70160
alloy, heat of formation within density functional formalism 79−57283
alloy, nonlocality and energy of form. 79−20459
alloying tendencies and impurity heats of soln. 79−28102
anilines, substituted, in benzene, dielectric relax. and mutual viscosity, obs., enthalpy of formation 79−38449
anthracene, chemical thermodynamic props. 80−21312
azide salts, univalent, enthalpy of form. of radical, direct minimisation eqns. 77−62501
benzaldehyde, proton affinity, MINDO/3 results compared to ICR obs. 78−1103
benzyl radical, MINDO/3-FORCES, geom. of heat of formation 78−66472
binary alloy including transition metal, prediction model 77−56246
binary alloy melt, influence of associate formation on thermodynamic quantities 79−66329
brass, calorimetric investigation of thermodynamic props. 79−52172
cast iron-steel mixture, interaction of Zr, formation reaction thermodynamics *(Russian)* 80−55645
conjugated hydrocarbons, conformational analysis and heats of form. by force field method 77−60105
Coordination equilibria in non-aqueous solvents. I 80−66860
cresols, ideal gas thermodynamic props. 78−75250
defects, or inhomogenities, entropy of formation equation validity 80−79960
dicyanoketene, and isomeric forms, heat of form., ab initio STO-3G calcs. 80−58190
divalent transition metal halides, Coordination equilibria in non-aqueous solvents. I 80−66860
EPR of thermally induced defect 77−81005
formic acid, fragmentation, fragment structs. and energies calcs. 80−74124
formyl radical, -d_0, (-d_1), first ionis. pot., photoelectron spectrosc. determ. 80−48039
fusion of metals, vacancy theory 80−44299
gas phase chemical reactions in atmosphere, evaluated kinetic and photochemical data 80−101671
group IIIa dihydrides, structs. and stabilities 80−107146
haloalkanes, max. overlap approx., heat of form. and dipole moment 78−94198
heterocyclic molecules, ionisation pot. and heat of form., IOC-ω method 79−31733
hydrocarbons, conjugated, heat of formation and reson. energies 80−7839
hydrocarbons, nobenzoid, ionisation pot. and heat of form., IOC-ω method 79−31733
II-IV-V_2 semiconductors, heat of formation from spin-orbit splitting in valence bands 77−31985
InAs, gas-phase epitaxy, prep. thermodynamics, use of partial pressure diagrams 79−79279
inert gases, solid, long-range many-body interaction and monovacancy heat of form. 80−38996
intermetallic hydrides, interstitial site occupation by H atoms, quantitative model 80−96517
intermetallic molecules, diatomic, enthalpy of form. by model description 79−83497
intermetallic phases, B2 struct., substitutional and triple defects, enthalpies of formation 80−96520
ion+molecule, entropy change, enthalpy of form., equilib. consts., thermochemistry 80−30233
IV-VI compound layered materials, prep. and growth, book contrib. 78−19651
ketene, photoionis., ion fragmentation kinetic energy 78−9206
ketene-d_0,-d_2, mol. ion reactivity, vibr. energy effects, mass spectrometric obs. 77−44470
liquid alloy, binary, interatomic forces, thermodynamic props. and alloying 77−47324
liquid alloy, model predictions 78−35351

heat of formation continued
liquid alloy, thermodynamic props. rel. to struct. 77−1237
metal hydrides use as energy conversion media, review *(Japanese)* 80−55934
metal ions complex formation with carboxylic acids in aqueous soln. *(Italian)* 77−48669
metal-semimetal alloy, phase diagram computation from thermodynamic functions 80−40329
metallic dimers, formation enthalpy 79−74411
metallic melts, three-component, enthalpies of form. *(Russian)* 79−51277
metallic soln., association 78−15373
metallic system, compound formation rel. to heat of mixing 80−55689
metals, adsorption of S, thermodynamics of two-dimen. and three-dimen. sulphides 80−20036
methane, photoionis., ion fragmentation kinetic energy 78−9206
methanol, and $-d_{1,3,4}$, thermodynamic props. struct. and spectroscopic data 77−39396
methanol, polymers, structs., binding energies, LCAO SCF MO calcs. 77−83498
4-methylene-cyclohexadiene-2,6-one-1, proton affinity, MINDO/3 results compared to ICR obs. 78−1103
mischmetal-$Ni_{5-x}Al_x$ ternary alloys, Al addition effects on structural and H_2 absorpt. props. 79−52761
MNDO semiempirical calcs. accuracy rel. to current MO methods 80−47893
molecular cations, heats of formation determ. from core electron binding energies 77−86346
molecular complex, bond lengths and heat of form., INDO calc. 79−54783
nonstoichiometric compounds preparation probability thermodynamic approach 77−31611
nontransition element/alkali metal systems, direct calorimetric exam. 78−84775
nontransition metals, binary alloying tendencies 78−2261
nontransition metals, electronegativity parameters of theory of heats of alloy form. 79−74412
organic compounds, heat of formation, dissociation energy from dynamic electronegativity *(Chinese)* 79−96351
organic molecules, improved IOC-ω technique 77−14336
phenanthrene, chemical thermodynamic props. 80−21312
phenol, ideal gas thermodynamic props. 78−75250
phenyl ion from chlorobenzene ion fragmentation 80−25998
phenylcarbene, singlet and triplet ground states, rearrangement to cycloheptatrienacarbene, MINDO/3 calc. 78−13430
quantum-defect theory of heats of formation and struct. transition energies 78−55830
radical, MINDO/3 unrestricted open-shell calcs. 77−23429
rare earth (III) complexes, cysteinates, thermodynamics of form. 80−89515
rare earth and actinide halides and oxides, stability study, energy difference between trivalent and tetravalent metal states 78−79553
rare earth carbonates, carbonates, standard ht. of formation determ. 78−53239
rare earth compounds, binary, regression eqns., for calc. props. from electron struct. 80−39498
rare earth dihalides, cation valence changes, rel. to stability and enthalpy of formation 79−91000
rare earth gallium borates, high temperature crystallisation, composition, struct., props. 80−40253
rare earth intermetallics, RGa_2, AlB_2-type struct., electron transfer, bonding, heat of form. theory 78−92499
rare earth mononitrides, heat of vaporisation and standard heat of form. 77−52664
rare earth nitrides, Knudsen cell vaporization, vaporization enthalpies 79−10936
rare earth oxides, polyatomic gaseous, atomisation energies and stand. ht. of formation determ. 77−54622
rare earth trifluorides, bomb calorimetric determ. of enthalpy of formation 80−50879
rare earth-B, RB_2, thermochemistry and stability 80−97723
rare earth-transition metal Laves phase, thermodynamic exam. of formation 77−1241
reaction paths, heat of formation, MINDO/2(3) forces method 78−9078
refractory compounds heat of formation determ. using self-propagating high-temp. synthesis 80−3392
refractory metal-Al_2O_3 systems, vaporis. at elevated temp., mass spectrometric obs. 79−29388
semiconductor, atomic displacements and enthalpy of vacancy formation 78−38690
semiconductor, binary, estimation of heats of formation from melting temp. 78−27810
semiconductors, chemical thermodynamics, review 80−55692
superheavy elements E116 and E114, theoretical chem. 77−32824
thermodynamic equation for liquidus line of narrow homogeneity range compound 77−35716
thiospinels, thermodynamic stability, enthalpy of form. 79−52737
transition intermetallic cpds., CsCl struct., charge transfer and heat of form. 78−22689
transition metal alloy, model predictions 78−35351
transition metal alloy, quantum theory of heat of formation 79−86907
transition metal alloy, tight binding theory of heat of formation 79−28110
transition metal alloys, heat of formation theory, tight binding approx. 79−43618
transition metal alloys, sigma phase, from tight-binding Hamiltonian 77−59750
transition metal alloys, tight binding theory, moments approach 79−61891
transition metal alloys 80−7849
transition metal compound form., Miedema's empirical theory, microscopic basis 80−45541
transition metal diborides, heats of formation derived from theoretical bonding model 79−65027
transition metal dichalcogenides, of CdI_2-type, crystallographic parameters correlation to heats of formation and reduced length 79−27963
transition metal hydrides, binary, heats of form. 80−97725
transition metal hydrides, electronic struct., heat of formation, single particle lifetimes, Dingle temp. meas. 78−51923
transition metal iridium intermetallics, enthalpies of form. 77−12595
transition metal nitride formation by N_2^+ ion+metal reaction 79−96363
transition metal-group IIIB alloys, relationship between struct. and thermodynamic props. *(German)* 78−91307
transition metal-Yb(Ce) alloys, valence state of Yb and Ce 79−77545
transition metals and alloys, metallurgical props. rel. to electronic struct., energies calc. method 77−20221
trifluoroformamide, thermal dissoc., shock wave study 79−34284
tropone, proton affinity, MINDO/3 results compared to ICR obs. 78−1103
TTF-TCNQ, cryst. binding energy, enthalpy of form., calorimetric 77−52663
unstable compounds, free energy of formation calcs., FORTRAN program for ternary phase equilibria. 80−10683
vacancies, entropy of formation due to anharmonic effects 77−62521
vinyl radical, MINDO/3-FORCES, geom. of heat of formation 78−66472
Wood's alloy, liq. enthalpy effects when solute is added 80−39314
yttrium carbonates, standard ht. of formation determ. 78−53239
Al_2O_3, heat of formation 79−91982
Ag-Bi, metastable phases *(German)* 77−16543
Ag-Te, liquid alloys, Ag_2Te solid compound, calorimetric, investigation at high temp. 79−61893
$AgPO_3$-AgI glass system, solution calorimetry, enthalpy of formation *(French)* 78−64527
$Ag_2S(Se)(Te)$, solid and liquid, mass spectrometric obs. of VP, heats of form., comp. 79−42266
$Ag_2S(Se)(Te)$, thermodynamic props., growth of single cryst. by chem. transport reaction 77−36380
Al, monovacancy thermodynamic parameter calcs., temp. dependence 78−2114
Al-B, enthalpies and free energies, effusion and mass spectra, phase diagram 78−23665
Al-Ga-Ge liquid alloys, enthalpy of form., direct reaction calorimetry, 713-1230K *(French)* 79−66336
Al-Ge liquid alloy, enthalpy of form., direct reaction calorimetry, 713-1230K *(French)* 79−66336
Al-Li-Mg, estimation of isothermal sections of phase diagram 79−11567
AlB_2, thermochemistry and stability 80−97723
Al_4C_3, vaporis. thermodynamics, 1321-1607K 80−66859
AlF_3-MF(M=Li, Na, K, Rb or Cs), ion-molecule equilibria studied by mass spectrometric method, heats of dissoc. and form. calc. 80−104479
AlO_2 molecule, mass spectrometric study 80−89563
α-Al_2O_3, atomic disorder, dominant type 78−63757
Al_2O_3, high temp. gas phase equilib. formation enthalpy, dissoc., mass spectra 78−23925
β-Al_2O_3-Na_2O ^{23}Na asymmetry parameter, temp. variations 80−6540
AmOCl, vapour phase hydrolysis of $AmCl_3$ using ^{241}Am and ^{243}Am 77−29037
Ar-HCl, van der Waals mol., far IR spectra 77−79611
As_4, gaseous, atomisation enthalpy and enthalpy of form., mass-spectroscopic Knudsen cell method 78−80780
$AsBr_3$, electron impact positive ion form., appearance energy obs. 80−53151
$AsCl_3$, electron impact positive ion form., appearance energy obs. 80−53151
$AsF_3(AsF_5)$, electron impact positive ion form., appearance energy obs. 80−53151
As_3Sb, As_2Sb_2, $AsSb_3$, and AsSb, gaseous, atomisation enthalpy and enthalpy of form., mass-spectroscopic Knudsen cell method 78−80780
$As_2Sb_2O_6$, $AsSb_3O_6$, and As_3SbO_6, gaseous, atomisation enthalpy and enthalpy of form., mass-spectroscopic Knudsen cell method 78−80780
As_2Se_3-Sb_2Se_3, phase relns. 77−21118
Au-Si, melt, thermodynamic study of phase diagram *(French)* 78−27482
Au-Sn, zeta and AuSn phases, heats of form. and heat contents 80−60837
Au-Te, thermodynamic props., calorimetric meas. 78−20051
Au-transition metal alloys, ^{197}Au Mossbauer isomer shift cellular atomic model 80−84673
B-containing mols., MNDO calcs. for ground-state 77−88391
B_4C, enthalpy of formation, 1320K, appl. of high-temp. solution calorimetry 79−11814
B_2O_3, bipyramidal struct., stability, ab initio SCF-MO calcs. 80−99446
Ba-H_2 system, equilib. H_2 press. and enthalpy of forml of BaH_2 79−86893
$BaBr_2$-$BaCl_2$, vap. mixture, ion-mol. equilib., heat of form. of ions 80−26039
$BaCl_2$-$BaBr_2$, vap. mixture, ion-mol. equilib., heat of form. of ions 80−26039
$BaSc_2O_4$, synthesis, thermal stability, emissivity, reduction processes 77−8791
$Ba_3Sc_4O_9$, synthesis, thermal stability, emissivity, reduction processes 77−8791
$BaTiO_3$, thermodynamic props. 77−39680
Ba_2TiO_4, $Ba_6Ti_{17}O_{40}$, standard Gibbs free energy of formation, EMF meas. at 673K 80−85207
$Ba_3(VO4)_2$, determination of enthalpies of formation, from heats of solution 80−2182
Ba_3WO_6, Ba_2WO_5, and $BaWO_4$, chem. thermodynamics, galvanic cell study 80−21315
$BaZrO_3(s)$, evaporation and standard ht. of formation 77−25302
Bi-Gd(Th) systems, heats of form. 80−89517
Bi-S liquid soln., S activities meas. by EMF method *(Japanese)* 80−70425
Bi-Se system, high-temp. calorimetry *(French)* 77−44501
BiLi, gas phase thermodynamics, Knudsen effusion mass spectrosc. 80−100057
Bi_2O_3, energies of formation, solid-state electrochemical techniques 80−6527
β-$Li_xV_2O_5$ bronzes, thermochemical study 80−55691
C/H containing species, MINDO calc. *(German)* 78−82646
C-containing mols., MNDO calcs. for ground state 78−911
CCO radical, heat of form. calc., geometries excitation energies and vibr. freq. calc. using POL-CI wave functions 80−89512
CH_3CO^+, heat of form. from acetone cation+ketene proton transfer 77−90592
$C_2H_4F^+$, in reaction $CH_3F^{+\cdot}+CH_3F \rightarrow C_2H_4F^+ + HF + H^\cdot$ 77−63889
CN^-, enthalpy of formation and electron affinity 77−35506
CN^- ion, gaseous, heat of form., solvation, proton affinity calc. 77−1092
CN^-, proton affinity, enthalpies of form. and soln. 77−47375

heat of formation continued
$CO_2^+ + CO_2$, $(CO_2)_2^+$ formation, exothermicity lower limit, photoionisation of supersonic mol. beam 78−46406
$CO(H,Cl)_3^-$, heats of form., from formyl fluoride gas phase data 77−63900
$CO(H,F)_3^-$, heats of form., from formyl fluoride gas phase data 77−63900
$CO_2.CO_2^+$ + ethylene, rate coeffs. and product distribution determ., dissoc. energy and heat of form. 80−97693
CO_2(g), standard enthalpies of solution and formation, standard Gibbs energies of formation and standard entropy 79−57285
CS, enthalpy of form. determ. from CS_2 photoionisation mass spectral investigation 79−94044
CS, heat of form calc. 80−102581
CS, heat of formation from electron impact dissoc. of CS_2 and OCS 78−73074
CSe, atomisation energies, enthalpy of form. 78−33631
CSe_2, atomisation energies, enthalpy of form. 78−33631
CSe_2, photoionis. mass spectroscopic obs., Rydberg states props. 77−46604
$CaCu_5$, γ-phase in Ca-Cu system, calorimetric determ. of enthalpy of form. *(French)* 80−84915
$CaGa_2O_4$ and $CaGa_4O_7$, cryst., thermodynamic parameters of reactions of form., thermodynamic stability 80−108726
$Ca(O_2)_2$, standard heat, entropy and free energy of form. 79−87869
$CaSO_3$, thermal decomp., enthalpy of form. 77−73460
Cd-As, liq. alloys, thermodynamic props. and cpd. formation 77−1238
Cd-Pb-Sn melts, enthalpies of form. *(Russian)* 79−51277
$CdCr_2Se_4$, evap., mass spectra 78−53238
$CdGeP_2$, CdP_2, Cd_3P_2 77−90634
CdS, solution growth, using Te solvent 79−65993
CdS(Se), reaction with Sn chalcogenides, thermodynamic anal. 80−40728
CdSb, free energy, thermodynamic functions 79−77768
Ce^+, CeI^+, CeI_2^+ and CeI_3^+ formed by electron impact in CeI_3 vapour 77−23567
Ce-Bi, heat of formation, calorimetric meas. 78−44392
$CeFeO_3$, enthalpy of formation determ. from heat of oxidation, calorimetric investig. 77−25300
Ce_2O_2S, free energy of formation and nonstoichiometry of CeO_2 79−83498
$Cl^+ + CO \rightarrow O + CCl^+$, reaction cross section, heat of form., mass spectrometric obs. 79−61843
$ClNO_3$, standard enthalpies of form. determ. *(German)* 78−53235
ClO_2, standard enthalpies of form. determ. *(German)* 78−53235
ClO_4^-, single ion props. by lattice energy minimisation 78−83769
Cl_2O, standard enthalpies of form. determ. *(German)* 78−53235
CmOCl, ht. of formation from vapour phase hydrolysis of $CmCl_3$ 78−20062
Co-Ga system, exam. of thermodynamics of α and β′ phases 78−71870
$Co_{1-x}Al_x$, ordered β-phase, enthalpy of formation are defect struct. descript. 80−89519
CoO, Co_3O_4, free enthalpy of formation, solid oxide electrolyte galvanic cell method 78−23959
Co_3S_4, $Cu_{0.5}Co_{2.5}S_4$, $CuCo_2S_4$, spinels, ht. of formation 78−53237
Cr-Ge, thermophysical props., at elevated temp. 80−103493
$CrAl_2S_4$, thermodynamic stability, enthalpy of form. 79−52737
Cr_xC_y, enthalpy of form. and combustion 77−36784
CrF_2, thermodynamic props. meas., electrochem. method 77−7874
$Cr_{11}Ge_8$, Cr_3Ge, thermodynamic functions 77−84948
$Cr_{12}Ge_{19}$, CrGe, thermodynamic props. 77−36779
Cs_2CO_3 and Cs_2SO_4, ionic equil., mass spectra obs., heats of reaction and form. of ions 79−87867
CsCl, enthalpies of solution and formation 79−61892
Cs_2NpBr_6, prep., cryst. struct. and enthalpy of formation 78−10014
$CsPO_3$, form. from dihydroorthophosphate dehydration, reaction thermodynamics 79−52643
Cu based dilute alloys, enthalpy of formation and excess entropy 80−55347
Cu, monovacancy formation enthalpy 79−65217
Cu, vacancy form. enthalpy, positron annihilation meas. 80−97371
Cu-In alloy, thermodynamics, calorimetric exam. *(French)* 77−21105
Cu-In liquid alloy, thermodynamic props., potentiometric exam. *(French)* 77−59126
Cu-In liquid alloys, heat of form meas. *(Korean)* 77−9116
Cu-Si, melt, enthalpy of formation at 1370K 80−26042
Cu-Sn, self-diffusion of Sn, correl. with other props. *(Russian)* 79−23764
$CuCo_2S_4$, $Cu_{0.5}Co_{2.5}S_4$, spinels, ht. of formation 78−53237
Cu_xF_x, (x=2-5), heats of formation at 900K 78−31674
$CuGaO_2$, Gibbs free energy of formation, 680-1000°C 77−36489
$CuGa_2O_4$, Gibbs free energy of formation, 680-1000°C 77−36489
CuH, electronic struct., heat of formation, single particle lifetimes, Dingle temp. meas. 78−51923
$CuSe_2$, CuSe, Cu_3Se_2 and Cu_2Se, thermodynamic props., 298 to 420K *(Russian)* 77−69098
$CuZr_2 + H_2$, 550 to 850°C, absorption isotherms, thermodynamics 79−87841
Dy-Bi, heat of formation 77−86349
DyF_3, bomb calorimetric determ. of enthalpy of formation 80−50879
DyF_3, thermodynamic props., galvanic cell meas. 80−21316
$DyFe_2H_x$, thermodynamic props., H_2 desorption isotherm meas. 80−89516
$DyFeO_3$, thermodynamic props. 79−77771
$Dy_3Fe_5O_{12}$, thermodynamic props. 79−77771
$DyTaO_4$, heat of form. by adiabatic calorimetry 79−83494
$ErCO_3Y^{3-}$, (Y=ethylenediaminetetracetate ion), formation constants *(French)* 80−104458
ErF_3, bomb calorimetric determ. of enthalpy of formation 80−50879
ErF_3, standard enthalpy of formation 79−91990
ErF_3, thermodynamic props., galvanic cell meas. 80−21316
$ErFe_2H_x$, thermodynamic props., H_2 desorption isotherm meas. 80−89516
$ErTaO_4$, heat of form. by adiabatic calorimetry 79−83494
Eu_2O, Eu_2O_2, Eu_2OS, dissoc. energies and ht. of formation 77−47569
EuS, Eu_3S, EuS_2, Eu_2S_2, Eu_2OS, dissoc. energies and ht. of formation 77−47569
$EuTaO_4$, heat of form. by adiabatic calorimetry 79−83494
F compounds, ground states, mol. parameters, MINDO calcs. 78−41955
F_3^+, heat of formation, from OF_2 core electron binding energies 77−3417
Fe-Co ordered alloys, enthalpy of form. 78−48376
Fe-Co-Cr, heats of form. adiabatic calorimeter determ. 78−35713
Fe-Mn-C system, Gibbs energy, high temp. phase relations 78−80779
Fe-Mo system, thermomech. props. 80−89208
Fe-Sn liquid alloy, conc. depend. of enthalpy of form., conc. depend. *(Russian)* 78−44081
Fe-W(-O)(-C), Gibbs energy of form. of phases *(German)* 80−97724
$FeCl_2$, adsorbed monolayers, gamma-ray reson. 77−8478
Fe_2Mo, standard Gibbs energies, enthalpies, entropies of formation 78−61042
Fe_3Mo_2, standard Gibbs energies, enthalpies, entropies of formation 78−61042
$FeMoO_3$, standard Gibbs energies, enthalpies, entropies of formation 78−61042
γ-Fe_2O_3, heats of transition by quantitative thermography 77−9110
Fe_xO, standard free energy of formation, by EMF method with solid oxide electrolyte at low temps. *(Japanese)* 80−88338
α-, γ-FeOOH, heats of form. of Fe_2O_3 by quantitative thermography 77−9110
FeS_2, marcasite and pyrite phases sp. ht., thermodynamics of transform. 77−28016
$Fe_{0.9}S$, ferrimag. transition, mag., thermodynamic props., kinetics 79−47280
Ga/rare earth systems, direct calorimetric exam. 78−84775
Ga-Ge liquid alloy, enthalpy of form., direct reaction calorimetry, 713-1230K *(French)* 79−66336
Ga-Te, alloys, liq., thermodynamic functions, struct. 78−40075
Ga-Te, solid and liq. alloys, thermodynamic props. 80−35567
GaAs-HBr chemical vap. transport system, thermochem. data 78−6854
Ga_2Se_3, evaporation, thermodynamic props. 80−54365
GdF_3, bomb calorimetric determ. of enthalpy of formation 80−50879
GdF_3, standard enthalpies of formation 79−24810
$GdTaO_4$, heat of form. by adiabatic calorimetry 79−83494
Ge-Co, liq., enthalpy of formation meas. 80−30267
Ge-Fe, liq., enthalpy of formation meas. 80−30267
Ge-Ni, liq., enthalpy of formation meas. 80−30267
Ge-Te, liq. alloy, heat of formation, 1030-1150K 77−1943
GeI_x, thermodyn. props. 78−23960
GeO formation from Ge-GeO_2 mixtures, gasification kinetics *(Russian)* 80−21273
GeO_2, free energy of form., EMF meas. 80−35566
GeO_2, standard Gibbs energy of formation, meas. by electrochemical method *(Japanese)* 79−83499
$Ge_{0.5}Te_{0.5}$, heat capacity in solid and liq. phases, enthalpy of form. *(French)* 80−35565
H-bond complex formation, enthalpy change due to electronic excitation, spectroscopic determ. 78−92496
H-bonded systems, MINDO/3 geom. optimis. calcs., heats of form. of monomer and dimer 79−31399
H-containing mols., MNDO calcs. for ground state 78−911
$H + ICl \rightarrow HCl(\nu,J) + I$, IR chemiluminesc. 78−23962
HCO_3^-(aq), standard enthalpies of solution and formation, standard Gibbs energies of formation and standard entropy 79−57285
HF-cyclic ethers H-bonded complexes, calorimetry, IR spectra and MO calcs. 79−52738
HF-HCl, SCF energy hypersurface, stationary points, thermodynamics of form. 80−102436
$H_{1.6}MoO_3$ bronze, form., kinetic, thermodynamic investig. *(French)* 80−45247
H_xMoO_3, thermochemistry and electrochemical behaviour 79−100427
HNO^+, vertical spectra, heat of form., ab initio MRD-CI calcs. 79−49934
HOCO and HOCO*, thermochem. props., 100-300K 78−27805
HOCl, ab initio MRD CI calc., electronic spectrum, dissoc., heat of reaction, formation 78−21857
HSO, thermochem. props. 79−5173
^3He, entropy of vacancy formation 79−33156
HgS(Se), reaction with Sn chalcogenides, thermodynamic anal. 80−40728
HgSe, point defect model rel. to elec. props. and phase diagram 77−4339
$HoCO_3Y^{3-}$, (Y=ethylenediaminetetracetate ion), formation constants *(French)* 80−104458
HoF_3, bomb calorimetric determ. of enthalpy of formation 80−50879
HoF_3, enthalpy of formation by calorimetry 80−7843
HoF_3, thermodynamic props., galvanic cell meas. 80−21316
$HoTaO_4$, heat of form. by adiabatic calorimetry 79−83494
I_2 solid charge-transfer complexes, determ. of thermodynamic form. values 80−45540
In-Sb, metallic soln., association 78−15373
In-Te system, thermodynamic props. 77−12821
InI_x, x=1,2,3, thermodynamic props. 77−40572
In_2O_3, standard Gibbs energy of formation, meas. by electrochemical method *(Japanese)* 79−83499
InS(Se)(Te), fused, charge transfer nature 77−89757
InSb-Sn(Pb)(Bi), metallic soln., quasibinary alloy, association 78−15373
In_2Se_3, vapour press. temp. depend., heat of evap. and form. 80−59642
IrS_2, thermodynamic props. by effusion technique 77−40570
K_2CO_3 and K_2SO_4, ionic equil., mass spectra obs., heats of reaction and form. of ions 79−87867
K_3CrO_4, enthalpy of form. 78−53236
$K_{0.3}MoO_3$, thermochemistry 77−77801
β-$K_{0.27}V_2O_5$, heat of form. and sp. ht., 450 to 900K 80−61129
La-In, heat of formation meas. using differential direct isoperibol calorimeter 77−21101
La-In alloys, cohesive and superconducting props. from electronic struct. calcs. 79−99113
La-Sb, expt. determ. for various phases, 300K 79−91988
$LaAlO_3$ perovskite electrolytes for high-temp. fuel cells 79−29467
$LaCuO_2$, enthalpy of formation and high temp. stability from EMF of galvanic cell 80−11942
La_2CuO_4, enthalpy of formation and high temp. stability from EMF of galvanic cell 80−11942
LaF_3, bomb calorimetric determ. of enthalpy of formation 80−50879
LaIr(g), thermodynamic stability, high-temp. mass spectra obs. 80−7781
LaM_2-Gd, M=transition metal, correl. between g-shift and stability, EPR study 80−88874
$LaNi_{5-x}Al_x$ ternary alloys, Al addition effects on structural and H_2 absorpt. props. 79−52761

heat of formation continued
LaO, chemiluminescence due to bimolecular oxidation of La metal 77−29011
Li-Sb(Bi), thermodynamic props., 355-600°C 78−34634
Li_2, Li_3(g), thermochem. props. 77−21410
$LiAlCl_4$, fast ionic conductor, thermodynamic and phase props. 80−89211
$LiAlCl_4$, solid and molten electrolyte, thermodynamic stability 80−107447
$Li_{0.5}Al_{2.5}O_4$, spinel struct. magnetodielectrics, free energy of form. 79−83493
$LiBF_4$, thermal decomposition, equilib. decomposition press. and enthalpy of form. 79−91983
Li_2C_2, heat of formation, at. absorpt. spectrometric determ. *(Russian)* 78−15699
$Li_{0.5}Fe_{2.5}O_4$, spinel struct. magnetodielectrics, free energy of form. 79−83493
$Li_{0.5}Ga_{2.5}O_4$, spinel struct. magnetodielectrics, free energy of form. 79−83493
LiH_2 and LiH_2^+ binding energies, LiH_2 ionis. pot. and form. heat 79−94042
Li_2MoO_4, Li_2MoO_7, $Li_2Mo_3O_{10}$ and $Li_2Mo_4O_{13}$, thermodynamic props. 77−12822
Li_3N, heat capacity 5 to 350K, thermochem. props. to 1086K 78−92500
Li_xO_y, gaseous, mass-spectrometric study of thermochemistry 79−10940
$LiPO_3$, form. from dihydroorthophosphate dehydration, reaction thermodynamics 79−52643
LiV_2O_5, needle cryst. form. by reduction of molten Li_2O-V_2O_5, semicond. props. *(Japanese)* 78−3030
β-$Li_{0.27}V_2O_5$, heat of form. and sp. ht., 450 to 900K 80−61129
Li_3VO_4, enthalpy of formation 79−99333
Li_2ZrO_3, thermal decomposition, enthalpy of formation 298.15K 78−61003
Li_4ZrO_4, thermal decomposition, enthalpy of formation 298.15K 78−61003
Li_8ZrO_6, thermal decomposition, enthalpy of formation 298.15K 78−61003
Mg-Ga alloys, form. enthalpies and excess entropies, differential scanning calorimetry *(German)* 79−51278
Mg-Ga system, thermodynamic props. of metastable and glassy phases *(German)* 79−52743
$Mg(AlH_4)_2$, prep., thermal decomposition, molar heat capacity, heat of form. 80−3325
$MgCl_2$, anhydrous, aqueous 80−7844
$MgCu_2$-$MgZn_2$ system, heats of form. of Laves phases *(German)* 79−66337
$MgUO_4$, standard enthalpy of formation, high-temperature thermodynamic functions 78−27811
$Mg_3(VO_4)_2$, determination of enthalpies of formation, from heats of solution 80−2182
Mn, vaporization, thermodynamic study by Knudsen-cell mass spectrometry, enthalpies of form. 79−10937
Mn-Ge, thermophysical props., at elevated temp. 80−103493
Mn-Si liquid alloy, vapour-pressure meas. using torsion effusion method 79−42215
Mn_5C_2, enthalpy of formation at 1320K, from enthalpy of soln. expts. 78−59945
$Mn(CO)_5Cl(Br)(I)$, thermodynamic props. tabulation 79−24808
MnSe, and $MnSe_2$, thermodynamic props. 80−19958
MoF_5, gas, thermodynamic stability 80−26041
MoF_6(l), enthalpy of form. by soln. calorimetry 79−47962
MoO_2, Gibbs energies of form., form. enthalpies and standard entropies 79−52742
Mo_4O_{11}, Gibbs energies of form., form. enthalpies and standard entropies 79−52742
Mo_3Sb_7, Sb decomp. press. and enthalpy of form., Knudsen effusion meas. 79−87840
N-containing mols., MNDO calcs. for ground state 78−911
NH, heat of formation, review and new value 79−70362
NH_2 radical, heat of form., a diabatic electron affinity, from proton affinity meas. 79−91987
N_2H_2, $N_2H_2^+$, ab initio calcs., electronic struct., geometries relative energies 77−46487
N_2H_4, heat of form. determ. by electron impact dissoc. 78−61040
$(NO)_{2_g}$ heat of form., UV spectrum temp. depend. 78−64872
NOH^+, vertical spectra, heat of form., ab initio MRD-CI calcs. 79−49934
Na, monovacancy thermodynamic parameter calcs., temp. dependence 78−2114
$NaAlCl_4$, relative enthalpy to 573K and standard enthalpy of form., molar enthalpy of fusion 80−50878
NaAu(Ag), mol. dissoc. energy, third law enthalpy and heat of formation, mass spectra 78−40033
$NaBrO_3$, lattice parameters, thermal expansion, defect formation energy 78−79786
Na_2CO_3(s), $NaHCO_3$(s), standard enthalpies of solution and formation, standard Gibbs energies of formation and standard entropy 79−57285
NaF-ScF_3 system, ionic equilib., mass spectra 78−7222
NaI:Ca^{2+}, pure and doped, lattice defects, entropy and enthalpy of formation and migration 80−96687
$NaMo_6O_{17}$, thermochemistry 77−77801
Na_2O-B_2O_3, vitreous and cryst., enthalpy of form., calorimetric study 80−66861
Na_2O-B_2O_3-SiO_2/$AgNO_3$, thermodynamic characteristics of ion exchange process 79−8452
Na_2SO_4, liq., standard free energy of formation from 1160 to 1220K 78−56911
β-$Na_{0.27}V_2O_5$, heat of form. and sp. ht., 450 to 900K 80−61129
Nb-H system, enthalpy and entropy changes for non-stoichiometric hydride formation 79−52741
Nb_3Al, prep. by reduction of Nb_2O_5 and Al_2O_3 by CaH_2, thermodynamic calc. 80−100809
Nb_2(g), dissoc. energy, heat of form., Knudsen effusion mass spectrometric determ. 79−81297
Nd-Ga, heat of form. and soln., calorimetric meas. *(Russian)* 78−27806
Nd-Sb, heat of formation meas. 77−90635
$NdCO_3Y^{3-}$, (Y=ethylenediaminetetracetate ion), formation constants *(French)* 80−104458
NdF_3, bomb calorimetric determ. of enthalpy of formation 80−50879
NdF_3, enthalpy, entropy, heat capacity and Planck function from 5 to 350K 80−15257
heat of formation continued
NdF_3, enthalpy of formation 80−93789
Ni, positron lifetime meas., 4.2 to 1700K, monovacancy form. enthalpy 80−97370
Ni-Al, electronic, mag., and cohesive props. 80−44491
Ni-Co-Cr system, heats of formation and of transformation 80−50599
NiAl, thermal defects, dilatometric study *(Japanese)* 80−15092
$Ni_{98}M_2$, M=impurity metal, formation of MH(D)-complexes 80−65236
$(Ni_{1-y}Y_y)_3Al_{1-x}Sc_x(Ti)_x$, quarternary gamma prime ($L1_2$) pseudobinary props. revealed by ionicity modified pair model 78−19725
$Ni_{0.71}Zn_{0.29}Fe_2O_4$ and $Ni_{0.57}Zn_{0.43}Fe_2O_4$, form. kinetics 79−83159
O-containing mols., MNDO calcs. for ground state 78−911
OH, UV light absorpt. at 3080 Å, for Gibbs free energy of mol. 79−100425
$Os(CO)_5$, chem. thermodynamics 78−18799
PbLi, gas phase thermodynamics, Knudsen effusion mass spectrosc. 80−100057
PbO-$PbSO_4$ system, thermodynamic study of solid and liq. phases *(French)* 77−35667
PbO-TiO_2, solid phase reactions, thermodynamic anal. 77−12603
$PbSiO_3$ and Pb_2SiO_4, vitreous, free energy of form. at elevated temps. 79−43195
PbTe, enthalpy of formation *(Russian)* 80−15267
PbTe, thermodynamic props. 77−28023
PbTe-PbSe system, thermodynamic props. 80−11635
PbTe-SnTe, solid soln., enthalpy of formation *(Russian)* 80−15267
Pd-H system, enthalpy and entropy changes for non-stoichiometric hydride formation 79−52741
Pd-Ni(Co)(Cr), liquid alloys, enthalpy of form. *(Russian)* 77−56244
PdH, electronic struct., heat of formation, single particle lifetimes, Dingle temp. meas. 78−51923
PdO, free energy of form. using impedance dispersion analysis 80−108728
PrF_3, bomb calorimetric determ. of enthalpy of formation 80−50879
Pu alloys, binary, enthalpy of form., atomic model approach, correl. with phase diagrams 77−21415
PuN, high-temperature enthalpy, heat capacity 79−24809
PuOCl, heat of formation from vapour phase hydrolysis of $PuCl_3$ 78−20062
rare earth oxide-Nb_2O_5 system, phase formation thermodynamics 77−86348
RbCl, enthalpies of solution and formation 79−61892
$RbPO_3$, form. from dihydroorthophosphate dehydration, reaction thermodynamics 79−52643
$Re(CO)_5Cl(Br)(I)$, thermodynamic props. tabulation 79−24808
$Ru(CO)_{5(g)}$, chem. thermodynamics 78−18799
$RuTe_2$, decomposition press. and thermodynamic props. 78−3366
S_2O, photoionis. mass spectrum, heat of form., dissoc. energy 77−46605
SO_2Cl^- and $(SO_2)_2Cl^-$, heats of formation, determ. by mass spectroscopic technique 80−76540
Sb-Ce system, heats of form. 80−89517
Sb_4, gaseous, atomisation enthalpy and enthalpy of form., mass-spectroscopic Knudsen cell method 78−80780
Sb_2O_3, energies of formation, solid-state electrochemical techniques 80−6527
Sb_2O_3, standard Gibbs energy of formation, meas. by electrochemical method *(Japanese)* 79−83499
Sb_2O_3-SiO_2(GeO_2)-Na_2CO_3-H_2O, crystallisation 77−12605
ScM, (M=Ru,Rh,Pd,Ag,Mo), self-consistent local density functional calcs., LMTO method 79−11059
ScP, thermodynamics and high temp. vaporisation 80−88310
ScRh, gaseous, dissociation energies, high temp. mass spectrometric determ. 80−93790
$SeBr_4$, enthalpy of formation determ. 78−80777
$SeCl_4$, enthalpy of formation determ. 78−80777
Si-Al-B-O-N, calc. of phase diagrams from data set 80−55362
Si-Al-Zr-O-N, calc. of phase diagrams from data set 80−55362
$SiBr_m$, (n=1,2,3) heats of formation, mass spectrometric determ. 80−89511
SiC, pellet, rise in temp. involving reaction sintering 77−12555
$SiCl_2$, enthalpy of formation, thermochem. stability 77−58185
$SiCl_4$ physical and thermodynamic properties, rel. to Si technology 79−65218
SiCl(g), heat of formation, mass spectrometric determ. 78−15694
$SiCl_2$(g), heat of formation, mass spectrometric determ. 78−15694
$SiCl_3$(g), heat of formation, mass spectrometric determ. 78−15694
SiF, heat of form. mass spectrometric determ. 78−76900
SiF_2, heat of form. mass spectrometric determ. 78−76900
SiF_3, heat of form. mass spectrometric determ. 78−76900
$SiFH_3$, heat of formation, mass spectrometric determ. 78−7221
SiF_2H_2, heat of formation, mass spectrometric determ. 78−7221
SiF_3H, heat of formation, mass spectrometric determ. 78−7221
$SiHBr_3$, heat of form., mass spectrometric determ. 79−20455
SiH_2Br_2, heat of form., mass spectrometric determ. 79−20455
SiH_3Br, heat of form., mass spectrometric determ. 79−20455
Si_3N_4-Al_2O_3-AlN, isothermal sections, free energy of formation 80−55363
SiO_2-Al_2O_3-Si_3N_4, isothermal sections, free energy of formation 80−55363
SiO(g), enthalpy of formation and dissociation energy, time-of-flight mass spectra 77−16859
$SmTaO_4$, heat of form. by adiabatic calorimetry 79−83494
Sn-La(Ce)(Y) systems, heats of form. 80−89517
$SnSe_2$, sublimation, temp. depend. of equilib. constants 80−88312
SnTe, enthalpy of formation *(Russian)* 80−15267
SnTe, standard free energy of form. 79−57287
Sr^+, hydration, gas phase clustering mass spectra, thermodynamics, bonding 77−16814
Sr-H system, equilib. H_2 press., enthalpies of soln. and formation determ. 80−107428
SrO, enthalpy of solution, enthalpy of formation, 298.15K, from heat of soln. meas. 78−61041
$SrTiO_3$, thermodynamic props. 77−39680
$Sr_3(VO_4)_2$, determination of enthalpies of formation, from heats of solution 80−2182
Ta_3As, arsenic decomp. pressures and enthalpy of form. 77−70329
$Tc(CO)_5Cl(Br)(I)$, thermodynamic props. tabulation 79−24808
Te-In alloys, direct reaction calorimetric study, 737 to 1340K *(French)* 80−49382
Te-Tl, liquid alloy, thermodynamic investigation, enthalpy of form. and phase diagram 77−59756

heat of formation continued
Th-C-N system, existence of new β'ThCN' phase, struct. and thermodynamic study *(French)* 80−92499
Th-Os(Ir) system, phase diagram and thermodynamic props. *(German)* 79−47958
ThC_n(n=1 to 6), Knudsen effusion mass spectrometric investigations, enthalpies and heat of formation calcs. 80−66858
ThH_2, $ThH_{3.75}$, heat capacity and thermodynamic props. to 1000K 78−91451
Ti-Fe, equiatomic, heats of form., influence of short-range order *(Russian)* 80−81354
Ti-Ir alloys, Ti-rich, thermodynamic study at high temp. using Knudsen cell mass spectrometry 80−45539
Ti_2NiO_x (x=0 to 0.5), hydrogen characts., thermogravimetry/DTA meas. 79−52760
TiO, chemiluminesc., dissoc., heat of form., in metastable Ti collisions with O_2, N_2O, NO_2 77−40534
TmF_3, thermodynamic props., galvanic cell meas. 80−21316
U-C-N system, high temp. X-ray diffr. exam. of structure *(French)* 78−72765
$U^+ + N_2(D_2)(CD_4)$, endothermic reactions, heat of formation 77−73444
UB_2, thermochemistry and stability 80−97723
UC_n (n=1 to 6), formation and atomization energies by high temp. mass spectrometry 80−7842
UF_4-MF (M=Na or K), ion-molecule equilibria, heat of form. and dissoc. and electron affinities determ. 80−104480
UF_5, thermochem., heat of formation, dissoc. energy, ionis. pot. 77−70326
$UF_5 \rightarrow UF_5AU_2F_{10}$, dimerisation equilib. of gas phase, 600-870K 79−87838
UF_6, standard enthalpy of formation of gas and solid 79−96349
UH_3, UD_3, dissoc., isotope effect 80−26174
UH_4, thermochem., heat of formation, dissoc. energy, ionis. pot. 77−70326
$UO_2^{2+}{}_{(aq)} + UO_2NO_3^+{}_{(aq)}$, ground and excited state interaction, struct., thermodynamic functions, photochemistry obs. 80−32779
γ-UO_3, standard enthalpy of formation 78−88654
UO_2Br_2, and hydrates, standard enthalpies of formation and solution 79−24811
$(UO_2)_2Cl_3$, prep. and cryst. struct. 78−38674
UO_2F_2, standard enthalpy of form., from enthalpy of soln. in HF 77−48677
UO_2I_2, and hydrates, standard enthalpies of formation and solution 79−24811
α-UO_2SO_4, enthalpies of soln., form. determ. 78−27813
UO_2SeO_3, enthalpies of soln., form. determ. 78−27813
β-UO_2SeO_4, enthalpies of soln., form. determ. 78−27813
V-Ge, thermophysical props., at elevated temp. 80−103493
VSb_2, free-energy, heat and entropy of formation, 430-600°C *(Ukrainian)* 80−7837
VSi_2, thermodynamic props. determ. using ternary phase equilibria 78−91449
V_3Si, thermodynamic props. determ. using ternary phase equilibria 78−91449
V_5Si_3, thermodynamic props. determ. using ternary phase equilibria 78−91449
Y-Ni, liquid alloys, enthalpy struct. *(Russian)* 78−27474
Y-Sb compounds, heat of form. meas. 77−36783
Y-Si melts, enthalpy of formation and dissolution, microinhomogeneous struct., interatomic interactions *(Russian)* 80−34206
$YFeO_3$, dissociation press. and Gibbs energy of form. 79−11816
YM_2-Gd, M=transition metal, correl. between g-shift and stability, EPR study 80−88874
$YNi_{5-x}Al_x$ ternary alloys, Al addition effects on structural and H_2 absorpt. props. 79−52761
YbF_3, standard enthalpies of formation 79−24810
$YbTaO_4$, heat of form. by adiabatic calorimetry 79−83494
Zn-Ca, liquid alloy, exam. of thermodynamic props., using EMF method *(Russian)* 79−34003
$ZnAl_2S_4$ and $ZnCr_2S_4$, thermodynamic stability, enthalpy of form. 79−52737
$ZnGeP_2$ dissoc. press., vapour comp. and press., thermodynamic characts. 77−24934
$Zn_{1+x}O$, nonstoichiometry investig., 400 to 1200°C 77−11543
ZnP_2, sublimation 80−34181
ZnS, solution growth, using Te solvent 79−65993
ZnS(Se), reaction with Sn chalcogenides, thermodynamic anal. 80−40728
ZnSb, enthalpy of formation *(Russian)* 80−35564
ZnSe, solution growth, using Te solvent 79−65993
$Zn_3(VO_4)_2$, determination of enthalpies of formation, from heats of solution 80−2182
Zr iodides, gaseous, generated by HI+Zr reaction, enthalpies of formation 79−20458
$ZrCl_3$ disproportionation reaction sequence, and Zr lower halide formation enthalpies 79−15973
$Zr(HPO_4)_2$, amorphous, crystalline, enthalpy of formation 80−6518
$Zr(V_{1-x}Co_x)_2$, heat of form., relation between electronic struct. and H_2 storing props. 80−76662

heat of fusion
alkali halide, melting mechanism, vol. and enthalpy changes 79−55866
alkali metal salts, heat of melting and activities using cryoscopic data 77−40573
alkali nitrates calc. of heat of fusion using quantum mechanical relations 80−6491
atomic and plastic crystals, melting transitions, thermodynamic props. 80−96452
benzene, melting temp. and latent heat 79−55869
binary solid-liquid equilibria, student experiment, phase diagram computer program 78−89285
biphenyl, melting temp. and latent heat 79−55869
bis-4-n-alkylphenyl tetrafluoroterephtalates, synthesis and mesomorphic props. *(French)* 79−86679
bis-4-nalkyltetrafluorophenyl tetrafluoroterephtalates, synthesis and mesomorphic props. *(French)* 79−86679
Ω-caprolactam-ε-caprolactam polymers, vitrification, fusion, crystallisation *(Russian)* 77−47561
carbon tetrachloride, freezing and melting of stable and metastable phases 77−27984
catalase crystal lattice stability 77−25380
ceramic, calc. 77−43348
COC, prep., cryst. state, and mesophases 79−95143
4-cyanotetrafluorophenyl 4-n-alkylbenzoates, synthesis and mesomorphic props. *(French)* 79−86679
differential scanning calorimetry, theoretical melting curves anal. 78−16799
2,6-dioxaadamantane, plastic phase, transition and fusion thermodynamics, DSC meas. 78−75603
dodecylamine $(-NH_2)/H_2O_2$ and deuterated cpd., liquid crystal, phase relationships, isotope effects 79−19358
EBBA, fusion of metastable solid cryst. forms 79−14678
element, melting, vol. change, simple model 79−55865
ethane, solid, thermodynamic props. between double solid-to-solid transition and triple point temp. 78−75828
ethanol, plural glass-transitions, thermodynamic functions 78−38820
ethylene-CO copolymer, highly alternating, melting and internal motion 77−51474
eutectic molten salt mixtures, enthalpy of fusion estimation for energy storage *(French)* 79−24914
finned heat pipe latent thermal energy storage system performance 79−57487
fusion of metals, vacancy theory 80−44299
glass, melting in fire-heated tanks, modelling *(Polish)* 80−96633
heterogeneous system, melting, enthalpy and phase relations *(Czech)* 80−45543
2,4-hexadiynyl-1,6-bis(p-toluenesulphonate), programmed temp. and DSC obs., cryst. forms and polymerisation kinetics 79−43583
latent heat-of-fusion energy storage: experiments on heat transfer from cylinders during melting 80−6492
melting and boiling points vs. Coulomb pot., parabolic behaviour 80−70375
metal, calc. 77−43348
metal, diffusion, correlation with entropy of fusion 78−43109
metal, thermophysical properties meas. by submicrosecond-pulse-heating method 80−52220
metallic glass, heat of crystn. and viscous behaviour 80−75166
metals, entropies and heats of fusion 80−103458
metals, Hume-Rothery's class I, Engel-Brewer theory and related phys. props. 78−2059
metals, purification and thermodynamics, possibilities in space environment 79−46816
methane, melting transitions, thermodynamic props., positional disordering energies 80−96452
nematic eutectic-forming binary system, melting behaviour 77−89526
nematogens, enthalpy of fusion 78−22645
nylon-11, folded-chain crystal, pressure-induced crystallisation from melt, annealing 77−84671
nylon-12, folded-chain crystal, pressure-induced crystallisation from melt, annealing 77−84672
nylon-6 pressure-crystallised, annealing under pressure 77−84670
organic eutectic, heat of fusion and excess thermodynamic functions 78−3104
2-oxa-6-thiaadamantane, plastic phase, transition and fusion thermodynamics, DSC meas. 78−75603
2-oxaadamantane, plastic phase, transition and fusion thermodynamics, DSC meas. 78−75603
paraffin latent heat storage system theory and expt. 79−57484
PET, thermodynamic equilib. melting parameters, effect of annealing 78−71837
phase change material, melt time and heat flux relations, appl. to thermal energy storage 79−74546
phase change region, cond. and natural convection, numerical method 79−41563
phase transition liberated heat used in laboratory thermostat 78−195
1,4-cis-polybutadiene, stereoregular, recrystn. in partial melting temp. region *(Russian)* 80−6495
polycarbonate fibre, highly-oriented, drawing behaviour and mech. props. 78−76708
polydiphenylsiloxane, thermodynamics of fusion 80−84280
polyethylene, high density, effects of draw rate and temp. on necking stress *(Japanese)* 79−91757
polyethylene, MP, heat of fusion, degree of crystn. determ. by differential scanning calorimetry *(Russian)* 77−62489
polyethylene, single, polycryst., ^{60}Co-γ irrad., effect on melting behaviour 77−15548
polyethylene, solid-state extruded, exam. of props. 80−11669
polyethylene crystals in suspension, heat of fusion 79−87870
polyethylene oxide blends, thermal and mechanical props. 79−11679
polymer, crystalline, necking stress, thermodynamically derived equation *(Japanese)* 79−91758
polyvinylidene fluoride, crystallisation, α-polymorph equilib. melting point, heat of fusion determ. 77−4054
potassium n-alkanoates, thermal behaviour, differential scanning calorimetry obs. 80−92650
PVC, enthalpy determ. of order 79−7556
p-quaterphenyl, melting temp. and latent heat 79−55869
p-quinquephenyl, melting data and liq. cryst. transitions 79−55869
rare earth metals, thermodynamic props. determ. form US vel. meas. 78−55912
semiconductor melts, estimate of positional component of entropy of fusion, cluster model 77−55349
simple solid family of phase states *(Russian)* 80−15216
skin freezing temperature, human finger 77−21486
solar energy thermal storage by latent heat of fusion of mineral salts *(French)* 79−24915
square-well fluid, eqn. of state and thermodynamic props. 77−7834
steel, Ni-Co-C (9, 4, 0.2 wt.%) enthalpy, sp. ht. to 2000K 79−10960
p-terphenyl, melting temp. and latent heat 79−55869
thermal storage, high temp., latent heat method using heat exchanger *(French)* 80−40912
thermal storage by sensitive, latent heat,, dynamic model *(French)* 80−40917
Thermocrete heat storage material development 79−57483
2-thiaadamantane, plastic phase, transition and fusion thermodynamics, DSC meas. 78−75603
transition metals, thermophysical data at high temps., submicrosecond-pulse-heating method 80−103459
s-triazine, sp.ht. 130-380K, melting enthalpy and solid-state transition 79−46812

heat of fusion continued
two-phase Stefan problem when latent heat of fusion →0 *(French)* 79−71382
Ag halides calc. of heat of fusion using quantum mechanical relations 80−6491
Ag_3AsS_3, proustite, heat of melting 78−43106
Ag_2SO_4, enthalpies of transition and fusion 79−10925
Al ingot, dendrite arm spacing through heat flow control 77−73267
AlF_3, enthalpy of fusion from meas. of mixing with liq. Li_3AlF_6 and Na_3AlF_6 77−40569
Ar, melting transitions, thermodynamic props., positional disordering energies 80−96452
AsI_3, enthalpy, entropy of melting 78−34598
$Au_{77}Ge_{13.5}Si_{9.4}$, heat of crystn. and viscous behaviour 80−75166
$AuM_{(2)}$ cpds., M=Ga,In,Sn,Sb,Te, and derivation of ΔG^E of mixing for liq. alloys 77−4920
B, rel. to thermoelastic props. near melting point for liq. B 80−19862
Be, transformation enthalpies for α-β and β-liquid transitions 77−35690
BiI_3, enthalpy, entropy of melting 78−34598
$3Bi_2O_3.5B_2O_3$, viscosity, molar volume of melt and enthalpy of fusion 79−10924
$CaCl_2.6H_2O$ heat of fusion system for solar energy storage 80−16846
$CaCl_2.6H_2O$, heat transfer props. for heat of fusion energy storage 80−76654
CdSb, free energy and heat of formation 79−77768
$CdSnAs_2$, solubility in Sn melt, temp. depend., enthalpy of melting 80−59658
Co, amorphous and liquid, density of electronic states 79−23881
CoB, thermophysical props., 296-2000K 78−14477
Cr, thermal vacancies, energy of form. and conc. 80−29014
Cs-CsCl, liq. mixture, enthalpy of fusion, Gibbs energy of mixing and excess entropy 80−19947
CsCl-CuCl, phase transform. heats, DTA obs. *(Russian)* 80−55698
Cu-Al, heat capacity of phases, 233 to 800K, heat of transform. and entropy 77−47589
CuF_2, thermochemical props. 78−31674
CuTlS, melting heat and melting entropy *(Russian)* 80−70374
DI, thermodynamic properties 78−47517
FeB, thermophysical props., 296-2000K 78−14477
$Fe_{40}Ni_{40}P_{14}B_6$ glass, viscosity near T_g, using rapid heating, and fusion characts. 80−70438
Ga-Te, solid and liq. alloys, thermodynamic props. 80−35567
Ge, amorphous, first order transition to metallic liquid, calc. of transition temp., enthalpy and entropy 79−69227
HI, thermodynamic properties 78−47517
^3He, melting, specific heat, entropy, latent heat 78−75904
Hg, melting line determ., latent heat method, high press. 77−37903
Hg-Tl, phase limits, determ. by enthalpy functions along liquidus *(French)* 80−84911
In, heat capacity and enthalpy of fusion, 300-1000K 79−14939
In-Cd, soft mode, latent heats and entropies of fusion 79−46786
In-Tl, soft mode, latent heats and entropies of fusion 79−46786
InAs, heat and entropy of melting, assessment by quantitative thermography 77−15550
InSe, $InSe_{1.2}$, In_2Se_3, molar heat capacity and enthalpy of transition, 129 to 920K range 77−29030
Ir, thermophysical props. at temps. up to 7000K 80−103497
KCl-CuCl eutectic fused salt, potential as intermediate temp. solar heat transfer and storage medium 80−101135
LiCl, microcrystal, melting, mol. dynamics simulation 80−65199
$Li_{x+2}P_xO_{3x+1}$, polyphosphate, melting and crystallisation 80−70376
γ-Mn, enthalpy of fusion at 1386K 80−6490
Mo, liquid and solid, thermophysical props. 78−75808
MoF_5, prep., melting temp., vapour density, press., enthalpy of fusion, meas., assoc. 78−38813
$NaAlCl_4$, relative enthalpy to 573K and standard enthalpy of form., molar enthalpy of fusion 80−50878
Na_2O-2CaO-3SiO_2 glass, cryst. nucleation and growth, viscosity, thermodynamic props. 80−84079
Na_2O+GeO_2, molten mixture, EMF measurements 78−43144
NaOH fusion for heat storage, heat utilisation for turbo-alternator unit *(French)* 80−40915
Nb, liq. and solid, enthalpy meas. by levitation calorimetry 80−103499
PbS, heat of entropy of fusion 77−72701
PbSe, enthalpy, heat capacity, 300 to 1480K 79−60523
PbTe, thermodynamic props. 77−28023
Pd, liq. and solid, thermophysical props. 78−75808
$Pd_{77.5}Cu_6Si_{16.5}$, heat of crystn. and viscous behaviour 80−75166
Pt, thermodynamic characterisation, by isobaric expansion meas. 80−103494
RbCl-CuCl, phase transform. heats, DTA obs. *(Russian)* 80−55698
SbI_3, enthalpy, entropy of melting 78−34598
Sc_2O_3, fission and phase transition enthalpies 79−99299
Se, monoclinic to trigonal conversion, thermodynamic stability and associated investigs. 80−24592
$SrAg(PO_3)_3$, physicochem. characts. 77−52302
TcF_6, heat capacity, entropy Gibbs energy, 2.23-350K 78−38852
Te-In system, enthalpies of fusion, peritectic decomp. and allotropic transition, DTA *(French)* 80−76226
$ThCl_4$, thermodynamics of vaporisation and melting 79−60492
$TlNO_3$, boiling and melting pts., heats of transformation, solid-solid transformation 78−91441
UF_4, vaporisation behaviour 80−84283
V, thermophysical props. at temps. up to 7000K 80−103497
WO_3, fusion enthaply data from alkali tungstates liq. mixtures, mizing enthalpies at 801, 950°C 79−10949
Y_2O_3, calorimetric meas. of enthalpy, heat of fusion, heat of high temp. phase transition 77−28020
Y_2O_3, fission and phase transition enthalpies 79−99299
α-$ZnCl_2$, sp. ht., melting, heat of fusion determ. 77−66029

heat of mixing
alcohol-solvent, associated, excess free energy and enthalpy of mixing 78−31680
alcohols, vapour-liq. equilib. and heats of mixing, simplified group method anal. 80−96637
alkali fluoride-LnF_3(Ln=Y, La, Yb) binary liquid mixtures, thermochemistry 80−45538
alkali halides, binary liq. mixtures, freezing pt. depression 77−43312
alkali halides, molten salt mixtures, enthalpy of mixing, theory, Monte Carlo calcs. 77−72691

heat of mixing continued
alkali tungstates liq. mixtures with WO_3, mixing enthalpies at 801, 950°C 79−10949
alkali-alkali dilute alloys, lattice relax., energy of mixing 77−84936
alkanes, mixtures, order, enthalpy of mixing, calorimetric obs. *(German)* 78−18773
alkanes, vapour-liq. equilib. and heats of mixing, simplified group method anal. 80−96637
alloys, enthalpy of mixing, 'const. vol. alloy' formulation 79−28111
benzene-cyclohexane (methane) vapour mixture, excess enthalpy meas., appl. of differential-flow mixing calorimeter 78−12700
benzene-cyclohexane mixing enthalpy, using isothermal dilution calorimeter 77−41615
benzene-n-decane-n-tetradecane, molar enthalpies of mixing *(German)* 79−42253
benzene-n-heptane-n-tetradecane, molar enthalpies of mixing *(German)* 79−42253
benzene-p-xylene, excess vol., enthalpies, Gibbs free energies 80−44335
benzene-toluene-n-tetradecane, molar enthalpies of mixing *(German)* 79−42253
binary alloy melt, influence of associate formation on thermodynamic quantities 79−66329
binary and ternary systems, pred. of isothermal vapour-liquid equilibria, heat of mixing, viscosity 77−31761
binary liquid mixtures nonidealities, optimal representation 79−42248
binary vapours 80−93791
brass, liquid, thermodynamic props. *(German)* 80−66482
t-butyl alcohol, struct. determ. from vibr. spectra, H-bonding and heat of mixing *(Russian)* 78−3368
chemical equilibrium, entropy differences and statistical effects, symmetry corrections and entropy of mixing 79−21480
chloroalkanes, vapour-liq. equilib. and heats of mixing, simplified group method anal. 80−96637
chloroform-methanol mixtures, thermodynamic props. 79−87865
component interaction parameters, enthalpy and mixing energy *(Russian)* 80−54382
cubic margules solution model, miscibility gap and crit. point behaviour 78−59925
cyclohexane+n-hexane, effect of pressure on excess enthalpies at 298.15K 78−48689
cyclohexane+toluene, binary liq., viscosity and excess free energy of mixing 78−51680
cyclohexane-benzene (methane) vapour mixture, excess enthalpy meas., appl. of differential-flow mixing calorimeter 78−12700
cyclooctane+toluene, binary liq., viscosity and excess free energy of mixing 78−51680
2,2-diethoxypropane with heptane, benzene and carbon tetrachloride, excess enthalpy *(French)* 78−11542
dilute binary alloys, formation energy, lattice relax. and zero-point vibrations 78−83771
dilute binary alloys, formation energy, lattice relax. and zero-point vibrations 78−87646
disperse ore in a gas flow, mixing stage calcs. *(Russian)* 80−106829
ether-water mixtures, miscibilities, enthalpy of mixing, solvation *(German)* 78−18779
ethyl alcohol, solution, struct. determ. from vibr. spectra, H-bonding and heat of mixing *(Russian)* 78−3368
ethylbenzene+toluene, binary liq., viscosity and excess free energy of mixing 78−51680
ethylene + N_2, gaseous, excess enthalpy, determ. by flow calorimetry 78−91057
excess enthalpy and excess entropy functions derivation by direct method from TX phase diagram, heats of mixing calc. 80−75366
formic acid+acetic acid, liqs., mixing enthalpy 79−60515
furfural-water interface, anomalous mass transfer, coupling of heat and mass transfer 77−80626
gases, ideal, entropy of mixing, Gibbs paradox, indistinguishability 80−57226
glass-forming multicomponent systems, phase behaviour, miscibility, tie lines 80−84294
IIIiV semiconductor solid solutions, interaction parameters 78−51688
liquid, cohesive energy density, surface and interfacial tension and heat of mixing 77−55431
liquid, saturated, low press. enthalpy function, corresponding states and pseudocriticals 78−31672
liquid mixture, nonideality, prediction and meas. of thermodynamic excess functions 78−27818
metallic soln., association 78−15373
metallic system, compound formation rel. to heat of mixing 80−55689
methane-benzene (cyclohexane) vapour mixture, excess enthalpy meas. appl. of differential-flow mixing calorimeter 78−12700
methane-ethane liq. mixture, phase equilib., heat of mixing, vol. change, data evaluation 80−15233
methanol-pyridine base systems, excess enthalpies of mixing 79−42255
molten salts, enthalpy of mixing, theory, Monte Carlo calcs. 77−72691
nonideal mixtures, vap.-liq. equilib. data correlation eqn., heat of mixing 78−30763
partition coefficients, theoretical calc. of isovalent impurities with due regard for excess entropy of mixing in solid soln. and melt 79−65015
poly(2,6-dimethyl phenylene oxide) enthalpy of mixing with polystyrene 78−14471
polyethylene-polyoxymethylene mixtures connection of melt thermodynamic props. with solid state struct. *(Russian)* 80−54152
polymer mixing, heats 80−61132
polymer protonated and deuterated mixtures, partial miscibility 80−107037
polymer soln., dil. flow microcalorimetry, heat of mixing 77−56247
polymers, equation of state *(German)* 79−82309
polypropylene-chloroform (chloromethane), χ-parameters, heat of mixing, vap. press. and microcalorimetric meas. 78−34626
polystyrene solution in benzene, thermodyn. interaction coeff. determ. 78−3367
polystyrenesulphonates, in dioxane-water mixtures, heats of dilution meas. 80−59655
polystyrenesulphonic acid, in dioxane-water mixtures, heats of dilution meas. 80−59655
TCNQ anion radical salts, solid solns. phase transition, heats of mixing 78−47519
ternary, prediction from binary vap.-liq. equilib. and mixing data 79−73312
tetraalkyltin compounds, heats of mixing meas. 78−15693

heat of mixing continued
toluene+ethylbenzene (cyclohexane) (cyclooctane), binary liq., viscosity and excess free energy of mixing 78−51680
transition metal-group IIIB alloys, relationship between struct. and thermodynamic props. *(German)* 78−91307
2,4,6-trimethyl pyridine-aliphatic alcohols, molar excess enthalpies and vols. 79−42254
water-methanol, heat of mixing, high-press. calorimetric obs. *(German)* 78−16797
Ag-Bi, liq. alloys, thermodynamic investigation 80−70428
Ag-Li, solid and liquid alloys, calorimetric investigation of mixing enthalpy *(German)* 78−52773
Al-Ga, enthalpy of mixing, 'const. vol. alloy' formulation 79−28111
Al-Ga-Ge, thermodynamic props. of mixing of binary systems, phase diagram 80−45275
Al-Ga-In system, thermodynamic anal. 79−60512
Al-Ga(In) systems, thermodynamic anal. 79−60512
Al-Ga(In)(Sn), interpretation of metallic phase diagrams, entropy of mixing 79−42274
Al-Ga(Sn), ab initio calcs. of partial enthalpy and result for enthalpy of mixing 79−43197
Al-Ge-Sn, thermodynamic props. of mixing of binary systems, phase diagram 80−45275
Al-In, enthalpy of mixing, 'const. vol. alloy' formulation 79−28111
Al-Sc, solid solubility and residual resist. 79−51265
Al-Sn liquid alloys, heats of mixing and activities calcs. 79−42264
Al-Tl, enthalpy of mixing, 'const. vol. alloy' formulation 79−28111
Al-Zn, miscibility gap, spinodal region, thermodynamic data transferability *(German)* 79−20027
Al-Zn system, R-phase, mixing free enthalpy approx. calc. 77−1832
AlF_3-Li_3AlF_6(Na_3AlF_6), solid-liquid and liquid-liquid enthalpy of mixing meas. 77−40569
AlSb-Bi system, molten, enthalpy change due to mixing *(German)* 79−86892
AlSb-InSb(GaSb), liq., mixing enthalpies *(German)* 79−77755
Am-La, solubility, heat of mixing and vaporisation of Am, 1200 to 1600K 80−15232
Ar-He, heat of mixing, low press., theories comparison 78−26230
Ar-Kr, liq. mixture, excess thermodynamic props. 78−75836
Ar+methane, enthalpy of mixing, 123 to 145K and 2.03 to 9.12 MPa 77−70330
Au-Fe, liq., thermodynamic mixing effects, mass spectrometric meas. eval. *(German)* 77−59123
Au-M, liq. alloys., M=Ga, Bi, activities of Ga and Bi, ht. of mixing 77−4921
Au-Ni, liquid alloy system, determ. of thermodynamic props. using Knudson effusion method, phase diagram calc. *(German)* 78−51707
Au-Zn, liq., thermodynamic props. *(German)* 80−49386
$BaCO_3$, soln. kinetics and activation heat *(German)* 79−16031
Ba_2TiO_4, $Ba_6Ti_{17}O_{40}$, standard Gibbs free energy of formation, EMF meas. at 673K 80−85207
β-$Li_xV_2O_5$ bronzes, thermochemical study 80−55691
CO-He, heat of mixing, low press., theories comparison 78−26230
Cd-In-Sb, liq. alloy, Cd thermodynamic activities, Gibbs free mixing enthalpy *(German)* 80−45279
CdF_2-KF(LiF)(NaF), liquid mixture, enthalpy of mixing 78−48684
$Co_xMg_{1-x}O$ system, thermodynamic investigation, 1100 to 1300K *(German)* 80−107430
Cr-rare earth alloys, liquid phase, topology in diagrams of state *(Russian)* 80−54121
Cr_2O_3-Al_2O_3 solid solution, electrochemical determ. of activity 78−44391
Cs-CsCl, liq. mixture, enthalpy of fusion, Gibbs energy of mixing and excess entropy 80−19947
Cu dilute binary solid solutions, enthalpies of mixing and excess free enthalpies *(French)* 80−107427
Cu-Ni-Sn, liq. alloy, calc. and anal. of mixing enthalpies *(German)* 80−44325
Cu-Ni-Sn, liq. alloy, mixing enthalpies determ. using a SETARAM high temp. calorimeter *(German)* 80−44324
Cu-Pb (Fe), liq., thermodynamic props. *(Polish)* 80−89199
Cu-Sn liquid alloys, thermodynamic meas. 78−52765
Cu-V alloy, phase equilib. diagram exam. *(French)* 77−21100
Cu_2Se-Cu_2Te, intermolecular interaction, thermodynamic anal. of dissociation pressure 80−53088
Fe-C system, mixing variables, activities and entropies calc., short range order model *(German)* 80−25655
Fe-Cu liquid alloy, heats of mixing, mixing entropies *(Russian)* 80−65224
Fe-Ge, liquid alloy, thermodynamic mixing function determ. by mass spectrometric meas. 79−29025
Fe-Mn, thermodynamic props. *(Czech)* 77−85990
Fe-Ni solid soln., thermodynamic study 78−6904
$2FeO.SiO_2$-$2MnO.SiO_2$ melt, free energy of mixing 79−61572
$2.33FeO.TiO_2$-$2.33MnO$-TiO_2 melt, free energy of mixing 79−61572
Ga-Ge-Sn, thermodynamic props. of mixing of binary systems, phase diagram 80−45275
Ga-In-Sb system, phase diagram calcs. in Ga+In rich region 80−60842
Ga-In(Al) systems, thermodynamic anal. 79−60512
GaSb-Bi system, molten, enthalpy change due to mixing *(German)* 79−86892
GaSb-InSb(AlSb), liq., mixing enthalpies *(German)* 79−77755
Ge-As, p-T-x diagram 77−11669
Ge-Ce liquid alloys, enthalpies of mixing, exothermal effects *(Russian)* 80−34192
Ge-Mn, liq., calorimetric investigation of heats of mixing, and entropies of mixing 79−95165
Ge-Sn, liq. alloys, thermodyn. props. 77−51518
HCl-Xe, liq., enthalpy of mixing, calorimetric meas. 80−59661
HNO_3 cycle process for ocean thermal energy extraction 78−53660
HgTe-CdTe, mixing energy and short-range order, diffuse X-ray scatt. 77−28006
In-Sb, metallic soln., association 78−15373
In-Sb liquid alloy, calorimetric investigation, rel. to association equilibrium *(German)* 77−16862
In-Sb liquid alloy, mixing enthalpy, temp. depend. *(German)* 80−84298
In-Zn, liq., Zn activity meas. by Knudsen torsion-effusion method, enthalpies, entropies of mixing 79−10950
InAs-AlAs, phase diagram plotting by DTA and thermodynamic calc. 77−86016
InSb-Bi system, molten, enthalpy change due to mixing *(German)* 79−86892
InSb-Sn(Pb)(Bi), metallic soln., quasibinary alloy, association 78−15373
K-Rb, internal energy, heat of mixing, entropy, dielectric function 80−88340
$KO_{0.5}$-$NaO_{0.5}$-SiO_2 liquid, heat capacity of mixing at 1000K 79−77765
K_2O-Li_2O(Na_2O)-SiO_2 glass *(Japanese)* 78−10195
K_2O-SiO_2, vap. press., thermodynamic props. and phase diagram at high temps. 78−83932
K_xO_y, thermodynamic props. 80−29184
$K_2O.nB_2O_3$ (n=6, 4, 3), heat of soln. *(Japanese)* 77−77802
Kr+ethene, liquid mixture thermodynamic excess functions 78−48690
Li-Pb, liq. alloy, enthalpies of mixing, calorimetric study *(German)* 80−2170
Li-Pb liquid compound forming alloy, entropy of mixing 80−88328
Li_2O-Na_2O-P_2O_5, heat of soln. *(Japanese)* 79−34350
Li_2O-Na_2O(K_2O)-SiO_2 glass *(Japanese)* 78−10195
$Li_2O.nB_2O_3$ (n=6, 4, 3), heat of soln. *(Japanese)* 77−77802
Mg-Ca(Sr)(Ba), liquid, thermodynamic charact. *(German)* 77−59757
Mn-Cu(Sn), liquid alloys, thermochemistry 79−56962
Mn-Si, liq. thermodynamic props., rel. to alloy form. 77−7875
Mn-Si liquid alloy, vapour-pressure meas. using torsion effusion method 79−42215
MoO_3-MO system, M=alkaline earth metal, eutectic coordinates on phase diag. 77−44227
N_2-He, heat of mixing, 2-15 bar *(French)* 79−7436
Na-Cs, internal energy, heat of mixing, entropy, dielectric function 80−88340
Na-Cs, liq., struct. factor, free energy of mixing, and electrochem. pot., thermodynamic calc. 80−96436
Na-Ga liquid alloy, thermodynamic props. 79−37854
Na-Ga liquid alloy, thermodynamic props. of mixing derivation method 80−54385
Na-K, internal energy, heat of mixing, entropy, dielectric function 80−88340
Na-K liquid alloy, small angle X-ray scatt. study, conc.-fluctuation structure factors 80−54120
Na^+-K^+-F^--SO_4^{2-}, asymmetrical reciprocal molten salt system, excess enthalpies 80−30268
$NaO_{0.5}$-CaO-SiO_2 liquid, heat capacity of mixing at 1000K 79−77765
Na_2O-Li_2O(K_2O)-SiO_2 glass *(Japanese)* 78−10195
Na_2O-SiO_2 glasses and liquids, enthalpy data 79−95183
Na_2O-SiO_2/$AgNO_3$, thermodynamic characteristics of ion exchange process 79−8452
Na_2O+GeO_2, molten mixture, EMF measurements 78−43144
$Na_2O.nB_2O_3$ (n=6, 4 or 3), heats of soln. *(Japanese)* 77−77802
Na_2XO_4, (X=S, Cr, Mo, W), anal. and calc. of binary and ternary phase diagrams 80−88299
Ni-Ge, liq. alloy, thermodynamic activity, mass spectrometric determ. *(German)* 78−20052
Pb-Bi liquid alloy, Pb and Bi diffusivities, temp. and conc. depend. *(German)* 80−84311
Pb-Fe(Cu), liq., thermodynamic props. *(Polish)* 80−89199
PbO-$PbSO_4$ melts, thermodynamics, determination of free energies of mixing at 1253K 78−83976
Pd-Te liquid alloys, thermodynamic activities *(German)* 79−29022
Rb-Hg liquid amalgams, thermodynamic props. determ. from conc. cell EMFs 77−1246
Se-Te crystallised glasses, struct. transforms. and IR spectra 80−19712
Si-B system, liq., surface tension, density, and oxidation kinetics, 1410-1700°C 80−20011
SiO_2-K_2O, thermodynamic approach to ionic conds., statistical model of chem. potential 79−46833
SiO_2-Na_2O, thermodynamic approach to ionic conds., statistical model of chem. potential 79−46833
Sn-Ge(Au), liquid alloy, exam. of activity and heat of mixing, using mass spectrometry 78−51706
Ti-O system, O/Ti<1, high-temp. thermodynamics using Tian-Calvet microcalorimetry 78−85190
Tl-Te alloy, liq., bond equilib. theory for electronic props., thermochemistry 77−89365
Zn-bearing binary substitutional solutions, thermodynamics 80−44337

heat of reaction
see also heat of combustion; heat of dissociation; heat of formation
alkali dimer+halogen mol. (IBr)(ICl) thermal chemi-ionisation reactions, products, energies 77−63903
alkali fluoride-LnF_3(Ln=Y, La, Yb) binary liquid mixtures, thermochemistry 80−45538
alumina-acrylic composite bone cement 79−79689
anthracene anion radicals, enthalpy of disproportionation, calorimetric determ. technique 79−96296
automatic heat flow calorimeter for heats of reaction meas. 78−54373
basis set effect, and approx. natural orbitals, SCF CI GTO calcs. 78−76904
binary alloys, activity of most oxidizable element *(French)* 79−61868
difluorodiazine, cis-trans isomerisation, mechanism and kinetics, CNDO/2 study 77−90589
2,2-dimethoxypropane, enthalpy of hydrolysis meas., microprocessor-controlled system 80−22361
4,7-dioxaoctanal, equilib. anionic polymerisation, −90 to −68°C, polar substituent effects 78−88631
enthalpimetry, direct injection, inverse technique 78−92569
ethylene, reaction heat, HF limit energies, correlation energy 79−8447
exothermic reaction, criticality, Frank-Kamenetzki parameter 79−66335
fluid, reacting spheres, kinetic theory 78−35668
fluoroform(-d_1)-trimethylamine-Ar(Kr), cryospectroscopic IR study of association 77−468
hydrocarbons, C_1, C_2 and C_3, heats of reaction, inner and outer shell electron energies contribs. 79−66331
tris(hydroxymethyl)aminomethane, microprocessor-controlled system for precise meas. of temp. changes 80−22361
ion $(H_2O)_n$+H_2O⇄ion$(H_2O)_{n+1}$, standard free energies of reaction 79−34348
isopropyl vinyl ether, chem. initiated soln. polymerisation and radiation-initiated bulk polymerisation 79−91952
linear free enthalpy relation validity, thermodynamic foundation *(German)* 79−34351
linear mols., π orbital electron energy contrib. to reaction heat 80−76539

heat of reaction continued
lumped parameter system, with two parallel reactions, steady state multiplicity 77−60103
metal, standard free enthalpy of oxidation meas. *(French)* 79−61867
methyl isocyanide, unimol. isomerisation to methyl cyanide 79−24725
mischmetal-Ni-Al alloys, enthalpy change on hydride formation 79−95168
n-octanal, equilib. anionic polymerisation, −90 to −68°C, polar substituent effects 78−88631
oxidation-reduction reactions in undifferentiated Earth, thermal effects 79−25218
polycaprolactam characteristics dependence, at equilibrium state, on polymerisation conditions, in closed system *(Japanese)* 78−95928
propylene, electron impact ionisation and dissoc. 80−37894
pyrolysis, of single solid particle accompanied by consecutive reactions, vol. reaction model 79−47896
reactive closed-space vapour transport, simplified theory 80−15396
solubility of H_2 in YCo_5 and YNi_5 *(Russian)* 78−15356
spinels, entropy of cation transitions 79−11812
tetracene anion radicals, enthalpy of disproportionation, calorimetric determ. technique 79−96296
tetramethyl orthocarbonate, enthalpy of hydrolysis meas., microprocessor-controlled system 80−22361
thermochemical analyser, continuous flow, high sensitivity 79−92022
thermogravimetric methods, review 78−3408
transition metal compounds, $(M,M')Cr_2S_4$ and $(M,M')S$, where M,M'=Mo,Co,Zn,Cd, solid-state equilib. *(German)* 77−36486
trimethyl orthoacetate, enthalpy of hydrolysis meas. microprocessor-controlled system 80−22361
tris(hydroxymethyl)aminomethane, standard for soln. calorimetry, enthalpy of react. in HCl determ. 77−73462
Al_4C_3, vaporis. thermodynamics, 1321-1607K 80−66859
AlN+Ni(Co)(Fe), reactions at sintering temps. 79−74377
AlO_2 molecule, mass spectrometric study 80−89563
B(I) hydrides, ab initio calcs., proton and hydride affinities 79−10029
BaBr, BaCl gas equilib. mass spectra, dissoc. energy 77−65543
$BaTiO_3$-$Ba_{1/2}NbO_3$, defective solid solns., reduction 77−81395
$CH_2+H_2\rightarrow CH_4$, MINDO/3-FORCES calc., acativation energy and enthalpy of reaction 78−66472
$CH_4^+\rightarrow CH_3^++H$, MINDO/3-FORCES calc., activation energy and reaction enthalpy 78−66472
CaBr, gas equilib. mass spectra, dissoc. energy meas. 77−65543
CaO-$Ca(OH)_2$ reversible hydration-dehydration for solar energy storage 80−97810
CaO-ZrO_2 solid soln., thermodynamic investig., by EMF method 77−36485
Cs_2CO_3 and Cs_2SO_4, ionic equil., mass spectra obs., heats of reaction and form. of ions 79−87867
$CuFeO_2$, oxidation, thermogravimetric obs. 77−86203
$(Fe, Mn)O_x$, thermodynamic characts. deduced from Wustite reaction *(Italian)* 77−48401
G_2-B_2O_3 melt, thermodynamic props. from mass spectroscopy 80−39318
GeP, dissociation kinetics rel. to volatile component sublattice 77−84917
HOCl, ab initio MRD CI calc., electronic spectrum, dissoc., heat of reaction, formation 78−21857
$H_3O^+.nH_2O$ cluster ions, stability, assoc. and dissoc. 77−60055
$H_3S^+.H_2O$ cluster ions, stability, assoc. and dissoc. 77−60055
$H_3S^+.nH_2S$ cluster ions, stability, assoc. and dissoc. 77−60055
Hg-U system, thermodynamic props., vap. press. and EMF expts. 79−91625
K_2CO_3 and K_2SO_4, ionic equil., mass spectra obs., heats of reaction and form. of ions 79−87867
K_xO_y, thermodynamic props. 80−29184
$LaMnO_3$, stoichiometric manganite form. reaction, thermodynamic characts. 80−108727
$LiCrO_2$, evaporation, as a corrosion product in compatability experiment of Li_2O pellets with Fe-Ni-Cr alloys, mass spectrometric study 79−73301
$MgBr_2$-ABr (A=Cs, Rb, K, Na, Tl), thermochemical and struct. investigation *(German)* 79−1423
MgO, dissociation energy in range 2020 to 2160K 77−549
Mo complex, dithiocarbamate, model for molybdoenzymes, thermochem. meas. 77−86365
Na^+-K^+-F^--SO_4^{2-}, asymmetrical reciprocal molten salt system, excess enthalpies 80−30268
$NaO+NaO_2\rightarrow Na_2O+O_2$, in Na chemilum. obs. of $Na+N_2O$ 77−63916
NaOBr, solns., as reagents in enthalpimetric determs. 78−68954
O_2 bomb calorimeter modification for liquid metal reaction enthalpy meas. 79−201
$O_2+F^-(Cl^-)(Br^-)(I^-)$, 0.2-100 eV, reaction differential cross sections energy depend. meas., exoergicity 77−63902
$^{18}OH+CO_2(CO)$, evidence for at. exchange 79−47910
PbS-CdSe, phase boundary processes 78−71857
Sb_xSe_y (x=0 to 4; y=1 to 4) molecular species formed in vaporisation of solid $SbSe_3$, thermodynamic props. 80−11943
Si_nH_{4-n}, enthalpies of formation, effusion mass spectrometric meas. 80−26043
SiO_2/InP interface formation, thermodynamic considerations 80−100529
$SnSe_2$, rel. to p-T projection of phase diag. of SnSe-Se 78−27485
SrBr, gas equilib. mass spectra, dissoc. energy meas. 77−65543
$Ta+SF_6\rightarrow TaF_x$, x=1-5, thermochemical props. of TaF_x 79−100424
Te-$TeBr_4$ system, Gibbs free energy of reaction, electrochem. e.m.f. expts. 79−91991
Te-$TeCl_4$ system, Gibbs free energy of reaction, electrochem. e.m.f. expts. 79−91991
Te-TeI_4 system, Gibbs free energy of reaction, electrochem. e.m.f. expts. 79−91991
Ti-Co(Ni) alloys, absorpt. of H_2, press.-composition-temp. relationships, enthalpy, entropy 80−2267
Ti-Co(Ni) alloys, absorpt. of H_2, thermodynamic parameters calc. 80−2268
VO_2+I_2 transport react., thermochem., appl. to MoO_2:V cryst. growth 79−43116
$Zn(g)+H_2O(g)=ZnO(s)+H_2(g)$, standard Gibbs free energy of reaction 79−11815

heat of solution
alkali metal-H, liq. and solid, mol. orbital approach, solvation energies 77−4201
alkali metals, liq., calc. of enthalpy of soln. of nonmetals and elec. resist. 77−55225
alloying tendencies and impurity heats of soln. 79−28102
BCC transition metals, solubility of C 78−71861
chemical impurities, entropy and enthalpy of solution 78−51691
Compton scattering determ. method 78−83974
crystal growth from solution, mechanism role of solvent-solute interactions, surface entropy factor 77−24281
dextran fractions, production, characterisation and solution properties 80−59368
2,7-dialkoxynaphthalene, H_2O and D_2O solns., solubility and ht. of soln. 79−66333
1,4-dialkylbenzene, H_2O and D_2O solns., solubility and ht. of soln. 79−66333
diamond, enthalpy of solution at 1320K, enthalpy of diamond-graphite transform. 78−59945
flow calorimeter cell for measuring heats of solutions of solids 77−10027
flux equations, heat of transport and heat of soln. 79−99323
furfural-water interface, anomalous mass transfer, coupling of heat and mass transfer 77−80626
graphite, enthalpy of solution at 1320K, enthalpy of diamond-graphite transform. 78−59945
KCl-$BaCl_2$ system, solid solns., phase diagram, enthalpy of soln., vibr. entropy. 78−39751
metal, spherical solid model for muon and H in metals 79−78601
methyl iodide, dissolution into aqueous NaOH solns., fission reactor accident conditions 77−88236
polycarbonate, highly hot-drawn, mechanical prop. and phys. struct. changes 78−14293
polyconjugate system, interrelation between physicochem. props. and microstruct. 78−55816
polyethylene oxide, aq. salt soln., meas.-based thermodynamic quantities 78−75525
rare earth carbonates and chlorides in standard ht. of formation determ. 78−53239
ribonuclease A, enthalpy of soln. in aqueous consolute solns. 79−24939
ribonuclease A, lyophilized, heat of soln. depend. on H_2O content of solid 79−24938
solid solution, heterovalent, use of expt. data to estimate energy of soln. 80−54380
supersaturation evaluation, in cryst. growth from soln., heats of soln. use 79−46584
tetraethylammonium triiodide, solvent effects on electronic transitions of I_3^- 77−27080
transition metals, BCC, H impurity, calc. 78−6160
transition metals, solubility of H_2 and bulk modulus 78−55950
tris(hyroxymethyl)aminomethane, water solution calorimeter, determination of energy equivalent 78−23961
water, enthalpy of ionisation, 273 to 323K, from HCl neutralisation meas., sp. ht. changes 77−48676
Wood's alloy, liq. enthalpy effects when solute is added 80−39314
yttrium carbonates and chlorides in standard ht. of formation determ. 78−53239
AgCl, solubility in methanol+water mixtures 77−47579
$AgCl_xBr_{1-x}$, binary melt, Ag solubility, temp. and conc. depend. 80−10677
Al, heat of soln. of H, electron charge distrib. calc. 78−51689
Al, heat of solution of H, spherical model 80−96656
Al, impurities heat of solution, pseudopot. calc. 77−51393
Al:H, impurity energies and geometrics, self-consistent jellium calc. 79−99507
Al-Ag-Cu alloy precipitation and heat of evolution, microcalometric obs. *(Japanese)* 78−15406
Al-Mg, liquid alloy energy of soln. pseudopotential calcs. *(Russian)* 79−66330
Ar-He(Kr)(Ne), solubility in Ar, and related functions, three-body forces 79−10776
As-S glasses, heat of solution in alkaline soln. 79−91989
B_4C, enthalpy of formation, 1320K, appl. of high-temp. solution calorimetry 79−11814
$BaCO_3$, soln. kinetics and activation heat *(German)* 79−16031
$Ba_3(VO4)_2$, determination of enthalpies of formation, from heats of solution 80−2182
Bi-Se system, high-temp. calorimetry *(French)* 77−44501
β-$Li_xV_2O_5$ bronzes, thermochemical study 80−55691
CN^-, proton affinity, enthalpies of form. and soln. 77−47375
CO_2(g), standard enthalpies of solution and formation, standard Gibbs energies of formation and standard entropy 79−57285
CoO-SiO_2 system, enthalpies of soln. rel. to high press. phases stability, calorimetric study 79−90779
CsCl, enthalpies of solution and formation 79−61892
Cu-Au system, grain boundary adsorption thermodynamics *(Russian)* 80−44317
$CuCl_xBr_{1-x}$, binary melt, Cu solubility, temp. and conc. depend. 80−10677
FeO-SiO_2 system, enthalpies of soln. rel. to high press. phases stability 79−90779
Ge-Si, phase diagrams near melting point, Helmholtz free energy, heat of solution 80−70379
H_2SO_4-H_2O_2 cleaning soln. for Si wafers, thermal characts. 80−3225
Hf-Be, coupled phase diagrams and thermochemical descriptions 80−25656
KBr, KI, KIO_3, and KIO_4, enthalpies of soln. in water 80−50880
KCl, standard for soln. calorimetry, enthalpy of soln. in H_2O determ. 77−73462
KCl, water solution calorimeter, determination of energy equivalent 78−23961
K_2O, determination of enthalpy of solution in PbO-B_2O_3 mixture 79−95166
$K_2O.nB_2O_3$ (n=6, 4, 3), heat of soln. *(Japanese)* 77−77802
$LaNi_5$, of H, rel. partial absorption (desorption) enthalpies 80−50881
$LaNi_5$-H, thermodynamics of solution of H at small content 77−21104
Li, of H, entropy and enthalpy of solution 78−51692
Li-LiH system, liquid Li, dilute solns., equilib. H press., solubility, heat of soln., CTR materials 77−14266
Li_2MoO_4, Li_2MoO_7, $Li_2Mo_3O_{10}$ and $Li_2Mo_4O_{13}$, thermodynamic props. 77−12822
Li_2O-Na_2O-P_2O_5, heat of soln. *(Japanese)* 79−34350
$Li_2O.nB_2O_3$ (n=6, 4, 3), heat of soln. *(Japanese)* 77−77802
Mg, H_2 dissolution, resistometric study under press. 80−70417

heat of solution continued
Mg, heat of soln. of H, electron charge distrib. calc. 78−51689
α-Mg, solubility of H_2 77−25024
Mg:H, impurity energies and geometrics, self-consistent jellium calc. 79−99507
$MgBr_2$-ABr (A=Cs, Rb, K, Na, Tl), thermochemical and struct. investigation *(German)* 79−1423
$MgCl_2$ in HCl and in pure water 80−7844
MgO, solid solubility of Sc_2O_3, Al_2O_3, Cr_2O_3, SiO_2 and ZrO_2 80−15247
MgO solution in UO_{2+x}, shell model calcs. of enthalpy, computer program for formation energies 79−42251
$Mg_3(VO_4)_2$, determination of enthalpies of formation, from heats of solution 80−2182
γ-Mn, enthalpy of fusion at 1386K 80−6490
Mn, enthalpy of solution at 1320K, enthalpy of form. of Mn_5C_2 78−59945
Mn, solubility of N_2, 650-1030°C, 13-25 at.% N range 79−90783
$Mn_{0.6}Ni_{0.4}$, liq., soln. enthalpies of C and Mn, enthalpy determ. for graphite-diamond transform. and Mn_5C_2 form. 78−59945
Mo-N solid solution, exam. of enthalpy of solution, variation with temp. 79−10947
Mo-Nb solid solutions, enthalpy of soln. of H meas. 80−2166
NH_4NO_3 aqueous solution, enthalpies of dilution and relative apparent molar enthalpies, dissociated soln. case 80−50876
NH_4NO_3, standard enthalpy of soln. in water, standard thermodynamic state search 80−50877
Na, of O(N)(C)(H), entropy and enthalpy of solution 78−51692
Na-K, liquid alloy energy of soln. pseudopotential calcs. *(Russian)* 79−66330
$NaCO_3$, enthalpies of dilution 79−57284
Na_2CO_3(s), $NaHCO_3$(s), standard enthalpies of solution and formation, standard Gibbs energies of formation and standard entropy 79−57285
NaCl, aqueous soln., direct calorimetric meas. of enthalpies, at high temp. and pressure 79−57286
NaCl-water-tetrahydrofuran system, heat. of soln. meas. using Calvet microcalorimeter *(French)* 77−44504
$NaHCO_3$, enthalpies of dilution 79−57284
$NaNO_2$, enthalpy of soln. and dilution, obs. 78−80781
Na_2O, determination of enthalpy of solution in PbO-B_2O_3 mixture 79−95166
$Na_2O.nB_2O_3$ (n=6, 4 or 3), heats of soln. *(Japanese)* 77−77802
Nb-H(D) system, solubility, entropy and enthalpy, isotope effects 77−20069
Nd-Ga, heat of form. and soln., calorimetric meas. *(Russian)* 78−27806
NpI_4, heat of solution in aq. HCl acid 79−83495
Pa, body-centred tetragonal metal, enthalpy of soln. 78−48686
Pd, solubility of S, 600-1000°C, H_2-H_2S gas phase composition depend. *(French)* 78−87791
Pd-Ag-H, alloys, 25-50% Ag, thermodynamic props., 555-700K 79−65216
Pd-Cu, H solubility enthalpy and entropy, effect on elec. cond. 77−35699
Pd-Ni(Co)(Cr), liquid alloys, enthalpy of form. *(Russian)* 77−56244
$Pd_{0.9}Ag_{0.1}$:H(D), free energy, enthalpies of soln. 78−15692
Pu-O system, partial molar enthalpy of solution of O 77−47578
RbCl, enthalpies of solution and formation 79−61892
Si:P, epitaxial layer, vapour phase grown, temp. dependence of dopant inclusion, differential molar solution enthalpy *(German)* 79−52128
Si-Ge system, phase diagram, lattice const. var. effects 80−97470
SiC, solubility, partition coeff. of Be 79−10951
SiO_2 glass, densified, enthalpy variation, heat of dissolution obs. *(French)* 79−34015
SiO_2:Na^+, heat treated, heat of immersion in H_2O, organic compds. 80−3396
Sr, enthalpy of solution, 298.15K, rel. to SrO heat of formation determ. 78−61041
Sr-H system, equilib. H_2 press., enthalpies of soln. and formation determ. 80−107428
SrO, enthalpy of solution, enthalpy of formation, 298.15K, from heat of soln. meas. 78−61041
$Sr_3(VO_4)_2$, determination of enthalpies of formation, from heats of solution 80−2182
Ta-H, dil. soln., high temp. thermodynamics 78−43128
Ta-O, dil. soln., high temp. thermodynamics 78−43128
Ti-Be, coupled phase diagrams and thermochemical descriptions 80−25656
Ti-Be-Zr, coupled phase diagrams and thermochemical descriptions 80−25656
α-Ti-O solid soln., hexagonal, thermodynamics 78−3098
Ti-O system, O/Ti<1, high-temp. thermodynamics using Tian-Calvet microcalorimetry 78−85190
$TiCr_{1.8}$, H and D soln., enthalpy, solubility and mol. vibr. determ., comparison with soln. in metals and binary alloys 80−79951
U, heat of solution in aq. HCl acid 79−83495
UCl_4, heat of solution in aq. HCl acid 79−83495
UO_2Br_2, and hydrates, standard enthalpies of formation and solution 79−24811
UO_2F_2, standard enthalpy of form., from enthalpy of soln. in HF 77−48677
α-UO_2SO_4, enthalpies of soln., form. determ. 78−27813
UO_2SeO_3, enthalpies of soln., form. determ. 78−27813
β-UO_2SeO_4, enthalpies of soln., form. determ. 78−27813
$YFeO_3$, solubility in aq. KOH under hydrothermal conditions 77−39677
$Zn_3(VO_4)_2$, determination of enthalpies of formation, from heats of solution 80−2182
Zr-Be, coupled phase diagrams and thermochemical descriptions 80−25656
ZrH_x, self-diffusion of T, autoradiographic study, energy of soln. in H sublattice *(Russian)* 80−2194
$Zr(HPO_4)_2$, amorphous, crystalline, enthalpy of formation 80−6518

heat of sublimation
anthracene, chemical thermodynamic props. 80−21312
anthracene, optical determ. of vapour conc., vap. press. and heat of sublimation 78−22840
biphenyl cryst., nonbonded atom-atom interact. model, low freq. vibr. modes 77−1188
carboxylic acids, crystals, empirical interatomic potential functions 79−7567
interatomic interaction and plasmon energy, rel. to heat of sublimation 77−69267
heat of sublimation continued
metals, FCC, sublimation energy in pair potentials calc., appl. to point defect props. 80−19798
phenanthrene, chemical thermodynamic props. 80−21312
rare earth metals, preparation methods and properties, review 79−69969
rare earth mononitrides, heat of vaporisation and standard heat of form. 77−52664
simple solid family of phase states *(Russian)* 80−15216
TCNQ, enthalpy of sublimation and vapour press. meas. 80−92661
tetrafluoromethane, intermolecular pot., lattice energy and heat of sublimation 80−38995
thianthrene, heat of sublimation, cryst. lattice and polarisation energy 79−32941
transition metal alloyed with metalloids, glass transition temp. 80−24371
TTF, enthalpy of sublimation and vapour press. meas. 80−92661
TTF, heat of sublimation, cryst. lattice and polarisation energy 79−32941
TTF-TCNQ, enthalpy of sublimation and vapour press. meas. 80−92661
Ag, vaporization, thermodynamic props. determ. by mass spectroscopy 78−22841
AlI_3, UV absorbance, dimer-monomer dissoc. equilib., vap. press. of solid 78−13511
Ar, phase transition, anharmonic cryst.-gas transition 80−6510
Ar, solid, internal energy, determ. from vapour pressure 78−91435
β-B, rhombohedral, sublimation, 1823 to 2253K, torsion-effusion and mass spectroscopic meas. 77−39673
Cu film growth on amorphous C, energy characts., in situ electron microscope determ. 79−11027
Cu, vaporization, thermodynamic props. determ. by mass spectroscopy 78−22841
CuF_2, thermochemical props. 78−31674
DX, X=Cl, Br, I, thermodynamic properties, phase transitions 78−47518
$DyCl_3$, vapour press. and sublimation thermodynamics, mass loss effusion meas. 80−88313
Er, vaporisation, heat of sublimation, meas. 80−103471
$EuBr_2$, vaporisation thermodynamics, enthalpy sublimation 78−22837
EuS, 2nd and 3rd law 78−2248
Fe, segregation of impurities, physico-chemical aspects *(Czech)* 80−60866
$GdCl_3$, vapour press. and sublimation thermodynamics, mass loss effusion meas. 80−88313
GdS, vaporisation thermodynamics and dissoc. energy obs. 78−67822
HX, X=Cl, Br, I, thermodynamic properties, phase transitions 78−47518
I_2, heat of sublimation, laser photometric meas. 79−5942
K_2SO_4, mass spectrum obs. of vaporisation, vapour comp. and press., transition and form. heats 80−19933
Kr, solid, internal energy, determ. from vapour pressure 78−91435
Li_3N, vaporisation, studied by Knudsen effusion method 80−92662
Nb, Knudsen effusion mass spectrometric determ., $Nb_2(g)$ form. 79−81297
$PrCl_3$, sublimation press. and thermodynamics, mass loss effusion meas. 79−99307
$PuO_{(2)}$, spectroscopic data rel. to thermodynamic functions 80−34208
$PuRu_2$, intermetallic cpd., sublimation thermodynamics 80−96639
S, orthorhombic-monoclinic heat of transition, by mass spectral determination of sublimation heat 79−73302
Se, molecular cryst., Se-Se nonbonded pot. parameters derivation from heat of sublimation 79−27945
SmF, vaporisation, sublimation, Knudsen effusion method 80−6508
$TbCl_3$, vapour press. and sublimation thermodynamics, mass loss effusion meas. 80−88313
$ThO_{(2)}$, spectroscopic data rel. to thermodynamic functions 80−34208
$UO_{(2)(3)}$, spectroscopic data rel. to thermodynamic functions 80−34208
Xe, solid, internal energy, determ. from vapour pressure 78−91435

heat of transformation
see also heat of crystallisation; heat of fusion; heat of sublimation; heat of vaporisation
n-alkane, order-disorder phase transition bits. calc. 77−72684
N,N′-bis(p-alkoxybenzylidene)-α,α′-bi-p-toluidines, nematic phase, synthesis, thermodynamic props., gas-liq. chromatographic anal. 79−90763
4″-n-alkoxyphenyl biphenyl-4-carboxylates, liq. cryst. props. 79−82150
alkyl cyanobiphenyls, pretransitional behaviour, alkal chain length depend., light scatt. in isotropic phase 80−44301
4-4-n-alkyloxybenzoyloxy-benzylidene-4′-cyanoanilines, reentrant nematic and smectic phases 80−88308
N-4-n-alkyloxybenzylidene-4-n-alkylanilines, smectic polymorphism, calorimetric study 80−88307
2-4-n-alkylphenyl-5-(4-n-alkyloxyphenyl)-pyrimidines, smectic polymorphism, calorimetric study 80−88307
aragonite-calcite, effect of impurities, DTA 78−51662
benzene-hexa-n-hexanoate, phase transitions and mesophase form., sp. ht. and IR spectra, 13 to 393K 80−79955
benzylideneanilines, thermal parameters for cryst.-mesophase and cryst.-cryst. transitions 77−11679
biphenylbenzoates, synthesis, mesomorphic, and thermodynamic props. 80−44117
carbon tetrachloride, cryst. phase transformations at atm. pressure *(French)* 77−84920
Carnot cycles, transform. temp. and latent heat under applied stress, rel. to shape memory effect 77−28874
cholesteryl myristate, polymorphism of blue phase, DTA and microscopy meas. 79−37819
cholesteryl myristate, smectic A-cholesteric transition, tricritical behaviour, DTA and DSC study 80−65206
cholesteryl nonanoate, polymorphism of blue phase, DTA and microscopy meas. 79−37819
cholesteryl oleate (linoleate), solid-solid transition, glass transition, cryst. nucleation temps., DSC obs. 78−34604
copper phthalocyanine α-β phase transform., heat of transform., DTA investig. *(German)* 78−30754
crystal orientational disordering, thermodynamic props., stat. mech. model 80−96453
discotic mesophases, solute-solvent interactions, effect on phase transition 80−10490
dodecylamine ($-NH_2$)/H_2O_2 and deuterated cpd., liquid crystal, phase relationships, isotope effects 79−19358
EBBA, phase transition enthalpies, 1 bar to 2.5 kbar 78−75814

heat of transformation continued
ethane, solid, thermodynamic props. between double solid-to-solid transition and triple point temp. 78−75828
ferrocene, cryst., stable low-temp. phase 80−34185
graphite to diamond transformation, 1320K, from enthalpy of soln. expts. 78−59945
4-n-hexyloxybenzilidene-4′-n-propylaniline, liq. cryst. phases, thermal and structural studies 78−1989
p-n-hexyloxybenzylidene-p-aminobenzoic acid, liq. cryst. phase transitions, X-ray diffr. and DSC meas. 79−86877
ionic cryst., polymorphic transition due to disordering, calc. of lat. ht. of transition 79−14724
lipid membrane order, mol. theory 79−66452
liquid crystal mixture phase equilibria and transition temperatures 78−63845
liquid crystals, phase transitions up to 3 kbar, transition enthalpy, entropy 77−20051
martensitic transformation, stress induced, in single cryst., thermodynamic anal. 79−43249
MBBA: 4-methoxybenzaldehyde, pure and doped, nematic-isotropic transition temps., appl. to purity control 79−55872
MBBA, nematic-isotropic transition, isothermal compressibility and thermal expansion coeff. meas. 79−99301
MBBA, volume meas. and phase transitions at high press. 79−90764
mercury carboxylates, phase transitions, DTA 79−90759
mesomorphic mixtures, binary phase diagrams, thermodynamic props., diamag. anisotropy 78−95139
metamagnetic phase diagram, determ. method 78−68254
5-methyl-1-thia-5-azacyclooctane-1-oxide perchlorate, single cryst. transform., evidence for intermediate state 80−88078
nematic-isotropic phase equilibria, Flory-Huggins theory appl., heat of transition 77−4187
nematic-isotropic phase transition and short range orientational order 77−27832
nematic-isotropic phase transition at high press., thermodynamics *(Russian)* 78−87778
nematic-isotropic transition, thermodynamic props. calc. 80−103464
nematic-smectic A-smectic C Lifshitz point 77−69077
4-nitrophenyl-4′-alkoxybenzoates, incommensurate smectic A phase 80−10647
p-n-nonyloxybenzylidene-p-aminobenzoic acid, liq. cryst. phase transitions, X-ray diffr. and DSC meas. 79−86877
ordered cubic alloys, reversible martensitic transformations 78−27516
N-pentanol-Na-N-octanoate-water system, partial molar enthalpies 78−75543
phase boundary motion, heat release effect, self-consistent treatment 80−103449
p-phenylene bis (p-substituted benzoates), cryst.-nematic transition, mol. struct. effects, DTA 78−47504
picric acid-o-bromoaniline binary system, phase diagram and DC elec. resist. 77−15546
polycaprolactam film, subjected to 9 kV elec. discharge, X-ray obs. *(Russian)* 79−23536
polymeric thermotropic liq. crysts., mesogenic elements and flexible spaces in main chain 79−60269
pyrazine, cryst. phases, entropy changes and struct. implications 80−54397
radial heat transfer, conduction, convection and heat of phase change 78−90700
rare earth alloy-hydrogen system, $R^1_xR^2_{1-x}H_2$-H_3, phase transitions 78−18767
rare earth dicarbides, solid solns., phase transformation, strain energy 78−51672
semicarbazide hydrochloride, phase transition, IR spectra and thermal study 79−37833
solid solutions, congruent transformation pt., regular soln. theory 79−60477
steel, Ni-Cr, enthalpy of martensitic transform. 77−63670
TBBA/4-n-pentylphenyl-4-(4-cyanobenzoyloxy)benzoate, mixture, possibility of smectic A-smectic A transition 79−95132
TCNQ anion radical salts, phase transitions, solid solns., thermodynamic props. 77−47571
terephthalylidene-bis-(4-n-alkylanilines), smectic polymorphism, calorimetric study 80−88307
tetra-n-pentylammonium salts, molten, thermodynamic props., cation struct. 79−55639
thermal energy storage using plastic crystal phase transitions 79−57480
triphenylene, hexasubstituted, thermotropic mesophases 79−86681
vanadyl phthalocyanine-copper phthalocyanine mixed crysts., α-β phase transform., heat of transform., DTA investig. *(German)* 78−30754
water, characteristic IR emission due to latent heat of transform. 77−31754
xylideneaniline-p′-benzonitri 80−44328
$AgFeSe_2$, thermographic investigation of phase transitions *(Russian)* 80−10661
$AgFeTe_2$, thermographic investigation of phase transitions *(Russian)* 80−10661
$AgNa(NO_2)_2$, Landau behaviour of sp. ht. close to nearly tricritical ferroelec. phase transition 78−10861
Ag_3SI, superionic conductor, ordered phase struct. 78−83792
Ag_2SO_4, enthalpies of transition and fusion 79−10925
$Ag_2Se(Te)$, thermodynamics of phase changes *(Russian)* 77−73459
As, condensed layers, low temp. allotropic phase transition *(Russian)* 80−54553
AuBr, α, I, P and BCC forms, transitions 78−38836
$AuCu_3$, quantum theory of order-disorder transition energy 77−62640
Au_3Cu, ht. of order-disorder transform., differential microcalorimetry *(French)* 78−57950
$BaTiO_3$, thermodynamic props. 77−39680
Be, transformation enthalpies for α-β and β-liquid transitions 77−35690
CdP_2, Cd_3P_2, polymorphic transitions 78−23699
CrAs, heat capacity, enthalpy increments, thermodynamic props., 5 to 1280K 78−91450
$CrSb_2$, heat capacity and thermodynamic props., mag. transition, enthalpy of decomposition 78−43591
Cu-Al, heat capacity of phases, 233 to 800K, heat of transform. and entropy 77−47589
Cu-Al(In), lamellar eutectoids, calorimetric determ. of interfacial enthalpy 78−60668
CuCl, ismorphic transitions at high press., 4.2 to 800K *(Russian)* 77−31774

heat of transformation continued
$CuCr_2O_4$, heat capacity, entropy, polymorphic transition, 298-1000K 78−10196
Cu_2S, $Cu_{1.8}S$, $\alpha \rightarrow \beta$ transition, thermographic investigation of heats, entropies and activation energies 80−88314
$Cu_xZn_{1-x}SiF_6.6H_2O$, heat capacities and thermodynamic props., 14 to 300K, cooperative Jahn-Teller transition 80−21314
Cu(100), adsorption of Xe monolayers, thermodynamics and kinetics, LEED and AES obs. 79−99423
n-D_2, triple point determ. 79−95124
Fe-C, lamellar eutectoid, calorimetric determ. of interfacial enthalpy 78−60668
Fe-Ni, enthalpy of transform. of γ to α′ and α′ to γ transforms. *(French)* 79−47683
γ-Fe_2O_3, heats of transition by quantitative thermography 77−9110
γ-Fe_2O_3, struct. vacancy distrib., effect on $\gamma \rightarrow \alpha$ transform. heat 78−6051
Ga_2O_3, α to β monotropic transition heat determ. 80−54370
$Ga_xV_{1-x}O_2$, resistivity, EPR, enthalpy and entropy meas., rel. to semicond.-metal transition 78−88004
$GeS(Se)_x$, x=1 or 2, ht. of transition determ. by thermography 78−22847
γ-GeTe, investigation by elec. resist., latent heat of phase transform. and plasma refl. of light 79−99317
HfV_2, latent heat of structural transform. 80−24589
IF_5, vapour press., phase transform. enthalpy *(German)* 78−51654
IF_7, vapour press., phase transform. enthalpy *(German)* 78−51654
In-Tl alloy, FCC→FCT martensitic transformation, on cooling, enthalpy meas. and X-ray exam. 78−39773
InSb, heats of transformation for high pressure, orthorhombic modification, exam. 78−56627
InSe, $InSe_{1.2}$, In_2Se_3, molar heat capacity and enthalpy of transition, 129 to 920K range 77−29030
KDP-type crystals, polarisation, dielec. const. thermodyn. props. 77−59527
$KH_3(SeO_3)_2$, thermal anomalies rel. to acoustic phonon instability 77−76545
KNO_2, polymorphism, calorimetric investigation 78−75827
$LaMnO_3$, ferromag.-paramag. phase transition, neutron diffr., calorimetric investigs. 78−31072
$LaNi_{5-x}Al_x$ ternary alloys, Al addition effects on structural and H_2 absorpt. props. 79−52761
Li soaps, $n.C_{13}$-$n.C_{20}$, phase transition temps. and enthalpies, DSC obs. 80−45544
$LiMSO_4$, M=Li, Na, K, Li_2SO_4-$ZnSO_4$, ht. capacity and ht. of transform. 78−26690
Li_2SO_4 based solid electrolytes, FCC phase transport mechanism studies and uses 80−107525
Li_2SO_4:$Na^+(K^+)(Mg^{2+})(Zn^{2+})(Cd^{2+})(Al^{3+})$, monoclinic-cubic transform., effect of impurities 79−52744
Mn_3GaN, sp. ht., 6 to 350K, mag. and crystallographic phase transitions 80−71060
Mn_3ZnN, sp. ht., 6 to 350K, mag. and crystallographic phase transitions 80−71060
MoF_6, vapour press., phase transform. enthalpy *(German)* 78−51654
$NaNO_2$, enthalpy of soln. and dilution, obs. 78−80781
Ni-Co-Cr system, heats of formation and of transformation 80−50599
$(Ni_{1-x}Cu_x)Ti$, martensitic, shape memory effect kinetics and thermodynamics 80−3021
$Ni_{1-x}Rh_xS$, nonvolume effect of Rh substitution on paramag. metal-antiferromag. nonmetal transition 79−28277
$Ni_{1-x}S$, metal-semimetal transition, lattice dynamics and thermodynamic props. 80−29324
NiTi, martensitic, shape memory effect kinetics and thermodynamics 80−3021
P, crystalline to amorphous transition, thermodynamic functions 80−54354
PLZT ceramics, diffuse phase transitions and thermodynamics 80−29694
$PbNb_2O_6$-$NaNbO_3$, DTA *(French)* 77−44234
$Rb_2Hg(CN)_4$, spinel, ferroelasticity and phase transformation 79−7646
S, orthorhombic-monoclinic heat of transition, by mass spectral determination of sublimation heat 79−73302
Sb, liquid-quenched, stabilisation and transformation kinetics of metastable phases 80−3022
Sc_2O_3, fission and phase transition enthalpies 79−99299
Sc_2O_3, solid and liq. phases, thermophysical and electrophysical props. 80−103495
Se, glass transition temp., enthalpy rel. to annealing, DSC 77−15561
α-Se, monoclinic, heat capacities and thermodynamic properties, 3-300K 78−95162
Sn-Ni electrodeposit, metastable, transform. kinetics, X-ray and SEM meas. 78−38979
$SrAl_2O_4$-$BaAl_2O_4$ system, solid solubility, α-β transition 78−63860
$SrSi_2$, dimorphic, transform. of three-dimens. three-connected Si nets 78−42944
$SrTiO_3$, thermodynamic props. 77−39680
Ti-Ag(Au)(Si), thermodynamics and kinetics of β to α_m transformation 78−84795
$TlMnCl_3$, sp. ht. and latent heat, under press. 79−7694
$TlNO_3$, boiling and melting pts., heats of transformation, solid-solid transformation 78−91441
α-U, pseudo-single cryst. and polycryst., low temp. sp. ht. 78−83972
UF_6, vapour press., phase transform. enthalpy *(German)* 78−51654
V_3O_5, heat capacity anomaly near 425K, and enthalpy change 77−47576
V_3O_5, latent heat of phase transition obs., X-ray diffr. and DTA meas. 77−28001
V_6O_{11} single crystals, heat capacity anomaly at 172K 78−10197
V_3Si, neutron irrad., sound velocity, magnetic susceptibility and upper critical field 78−88074
V_3Si, neutron-irrad., ht. capacity and resistivity 78−88075
WF_6, vapour press., phase transform. enthalpy *(German)* 78−51654
Y_2O_3, fission and phase transition enthalpies 79−99299
$Y_2[Pt(CN)_4]_3.21H_2O$, first order phase transform., spectroscopic and thermodynamic anal. 78−38829
ZnP_2, Zn_3P_2, polymorphic transitions 78−23699
ZrV_2, latent heat of structural transform. 80−24589

heat of vaporisation
alkali halides, heat and entropy of evaporation, Trouton's rule generalisation 79−77735
alkanes, latent heat of vaporisation calc. at normal boiling pt. by group contrib. method 79−77737
1-alkanols, liq., H-bond order temp. depend. from Hildebrand rule 80−7838
anthracene, chemical thermodynamic props. 80−21312
atoms as structural components in metallurgy *(Dutch)* 80−96465
Barker parameters, determ. using enthalpies of vaporisation *(German)* 80−59641
benzene, tables of thermodynamic props. 77−24419
benzene, vapour-flow calorimetry 78−91058
binary mixtures, latent heat of vaporisation, prediction 78−83930
dimethylsulphoxide, density up to 257°C, vap. press. up to 189°C, crit. density 79−90768
ethane, use of high press. recycle-flow calorimeter 80−42228
group contribution mol. model of liqs. and solns., thermodynamic props. 77−58932
halomethanes, vap. press. and boiling point data tables 79−77736
heat of evaporation and liq.-vapour equilib., appl. to real substances 79−4409
hydrocarbons, heavy liq., vapour press. and enthalpies of vaporisation by group-contrib. method 80−40726
hydrocarbons, thermodynamic props. correls., third parameters 79−95184
II-VI compounds, heat and entropy of evaporation, Trouton's rule generalisation 79−77735
latent heat of vaporisation prediction at normal boiling pt., correl. 79−86881
liquid, viscosity temp. var., ratio of viscous flow energy to vaporisation energy 77−31793
liquid metal, pure, surface tension and electron density 78−51803
liquid theories, validity, agreement with pertinent experimental fact 80−38881
liquid-vapour equilibrium, Van der Waals' eqn. of state, heat of evaporation 78−51640
low-temperature heat pipe wick evaporation *(Ukrainian)* 78−90639
metal tip profile change meas. for evaporation rate determ. 77−24403
metals, atomic binding energy and surface energy rel. to prediction of physical props. 80−59434
monoalkylcyclohexanes, heats of vaporisation by gas chromatography-calorimetry method 79−34344
2(4)-monooxopyrimidines, gaseous, matrix, soln., tautomeric equilib., IR and UV absorpt. spectra 80−58256
organic liquids, acentric factor and heats of vaporisation 80−19928
organic liquids, polar and nonpolar, entropies of vaporisation 78−26676
petroleum fractions from USSR fields, isobaric integral heats of condensation *(Russian)* 79−65181
phenanthrene, chemical thermodynamic props. 80−21312
polar compounds, liq. props. representation, by modified Redlich-Kwong eqn. of state 78−34590
rare earth metals, theor. determ. from valence band model 78−91431
rare earth mononitrides, heat of vaporisation and standard heat of form. 77−52664
rare earth nitrides, Knudsen cell vaporization, vaporization enthalpies 79−10936
reactive gas flow through porous barrier, exit flux, composition depend. 77−31383
square-well fluid, eqn. of state and thermodynamic props. 77−7834
steel, stainless, multilayer desorption meas. using heat of vaporisation spectrometer 79−82453
Stefanian cell diffusion coefficients, effect of heat of vaporisation *(Japanese)* 79−86882
toluene, tables of thermodynamic props. 77−24419
transition metal, 3d, liq., density of states of d-band, heat of vaporisation 78−95253
transition metals, 3d, effect of d-band on heat of vaporisation and sp. ht. 77−76539
transition metals, 3d, liquid, Percus-Yevick eqn. soln. *(Japanese)* 77−76579
vapour pressure, prediction using equation of state 80−103443
water, student expt. 80−27081
water, student lab. meas. method 79−30175
Ag, vaporization, thermodynamic props. determ. by mass spectroscopy 78−22841
Al_4C_3, vaporis. thermodynamics, 1321-1607K 80−66859
Am, vap. press., 1200-1600K, heats of vap. and La mixing 80−15232
B_2O_3-GeO_2 system melts evaporation coeffs. 79−65180
BeO, heated on W, thermal anal. using mass spectrometric, technique, vaporisation behaviour 80−79932
Bi, vapour pressure calc. from transpiration expts. on Mg-Bi and Pb-Bi alloys 77−76571
CaO, heated on W, thermal anal. using mass spectrometric, technique, vaporisation behaviour 80−79932
CdSe, film, vacuum condensation thermodynamics, starting powder comp. effects 77−81220
Co, liq., density of states of d-band, heat of vaporisation 78−95253
Cs, liq., vapour press., thermodynamic functions determ., Knudsen-effusion radiotracer method 78−26678
Cu, vaporization, thermodynamic props. determ. by mass spectroscopy 78−22841
Gd on W in field ion microscope *(Russian)* 77−47662
GeO_2-SiO_2, glass, evaporation by high temp. mass spectrometry 80−79927
GeTe, high temp. mass spectrometric obs. 77−76542
^{3}He film adsorbed on graphite 78−87842
^{4}He-^{3}He mixture, surface pot., heats of vaporisation, ^{3}He bound state 77−1274
Hg, condensation, two-dimensional, on W 80−107666
In_2Se_3, vapour press. temp. depend., heat of evap. and form. 80−59642
K_2SO_4, mass spectrum obs. of vaporisation, vapour comp. and press., transition and form. heats 80−19933
Mg-Bi, thermodynamic study vapour pressure measurement by transpiration 78−44395
MgO, heated on W, thermal anal. using mass spectrometric, technique, vaporisation behaviour 80−79932
MgO-Al_2O_3-Cr_2O_3, vacuum vaporisation, Langmuir method 78−95149
MgO-Cr_2O_3, vacuum vaporisation 78−91434
MoF_5, vapour, thermodynamic props. calc. 78−38826
N_2, meas., Dewar for student expt. 77−9840

heat of vaporisation continued
Na_2O-SiO_2 glass, evaporation by high temp. mass spectrometry 80−79927
Pu, liq., hard-sphere model, phys. prop. meas. interpret., adjacent solid phase implications 77−19866
Pu, pure, vap. press. at high temp. 79−55880
RbI, vaporisation thermodynamics, mass-loss Knudsen effusion, mass spectrometry 79−28093
Sc_xS, high temp. vaporisation, enthalpy, atomisation, dissoc. energies 77−1223
SmF, vaporisation, sublimation, Knudsen effusion method 80−6508
$SnSe_2$, rel. to p-T projection of phase diag. of SnSe-Se 78−27485
Sr, vapour pressure below 660K, heat of vaporisation 79−37825
$ThCl_4$, thermodynamics of vaporisation and melting 79−60492
Ti, liq., density of states of d-band, heat of vaporisation 78−95253
(U,Pu)N, self-consistent normal fluid eqn. of state, press., density, and enthalpy of vaporisation calc. 78−8909
$(U,Pu)O_2$, liq., v.p. up to 5000K 77−1239
U, liq., hard-sphere model, phys., prop. meas. interpret., adjacent solid phase implications 77−19866
UCl_4, vaporisation thermodynamics 78−44394
UF_4, vaporisation behaviour 80−84283
UO_2, and (U, Pu)O_2 nuclear oxide fuels, vapour pressure meas. for fast reactor safety anal. by laser techniques to 5000K 80−13591

heat of wetting *see wetting*

heat pipes
3.5 m heat pipe for solar collector, charact. *(Japanese)* 79−79378
adiabatic, performance deterioration with excess wetting fluid 77−5831
artery and header system, for single or two-phase operation 78−90981
CANDU reactor, heat exchanger tubing materials 78−29583
capillary struct., amount of coolant effect on operation 78−75037
centrifugal, cylindrical, heat transfer, heat flux density and vap. press. effects 78−79188
coloration apparatus for laser-quality alkali halide crystals 78−74917
composite annular wick heat pipe analysis and performance 79−62153
compound parabolic concentrator heat transport to storage 79−62102
counter-flow heat exchanger, charact. 78−33993
cryogenic, heat and mass transfer 77−13758
cryogenic, with metal-fibre wick, thermophys. charact. investig. 80−4725
cryogenic heat pipe/radiator dynamic testing 78−94532
cryosurgical heat tube instrument design 77−78031
Czochralski growth, appl. of heat pipe 79−61511
effects of various working fluids on operational characteristics of heat pipes *(Japanese)* 79−37320
EHD heat pipe designs, performance charact. 78−87241
electric field effects on charact. 80−83728
ethane, flow continuity in arterial capillary systems in cryogenic heat pipes 80−64536
evacuated heat pipe solar collector, rectangular performance charact., trap mechanism 80−3531
evaporation zone, heat exchange mechanism and vapour formation laws 80−24023
evaporator section, evap. and vap. flow between parallel planes 80−10115
finned heat pipe latent thermal energy storage system performance 79−57487
fluid circulation control in conventional and heat pipe planar solar collectors 80−66994
frequency domain dynamics 79−14216
gas flow regime choice in pipes with max. temp. at outlet 80−19396
gas-controlled, for meas. thermophysical props. 80−23878
gas-controlled cryogenic heat pipe, performance anal. 78−75034
gas-loaded, near ideal, analytical model 80−53615
gas-regulated heat pipe, anal. of operating temp. regimes 78−194
glycol-water solution saturating active porous material, solar energy applics. 80−66986
gravity-assist heat pipes with capillary flow, dry-out phenomena 80−79398
header and artery systems, theory and design 78−94679
heat exchange intensification, fission reactor tubular fuel elements 77−61497
heat transfer charact., application to waste heat recovery 79−49223
high temperature, subsonic vapour flux, heat exchange and friction 77−75779
laminar vapor flow calculations in a flat-plate heat pipe 80−23869
liquid metal, for central solar receiver gas turbine plant 79−48096
liquid metal heat carrier, low temp. region, effect of compressibility, friction and evaporation 77−47066
liquid trap thermal diode, development for space applications 80−27292
low temp. heat pipe, metal-fibre wick thermal cond., heat transfer coeffs. 78−83217
low temperature, heat transfer in heating zone for capillary structs. 80−38226
low temperature, with metal fibre wicks, thermophysical charact. 78−4611
low temperature pipes with vapour injection 79−14217
low-temp. heat pipes, vapour-gas bubbles removal in arteries 80−19490
low-temperature, efficiency calcs. 77−10030
low-temperature heat pipe wick evaporation *(Ukrainian)* 78−90639
low-temperature wickless heat pipe, crit. heat/mass transfer 78−42517
metal-screen wick low temp. heat pipe, internal heat transfer visualisation 78−94533
metallic heat carrier in loops, phase transition process, temp. field 79−55867
operating characteristics, efficiency, of heat pipe with active porous medium filling, for solar appl. *(French)* 77−42725
operating limits 80−92028
operating principles, construction, and appl. *(French)* 79−3896
osmotic, problems and promises 78−16790
pipe with extended temp. range 80−38231
porous wick, heat transfer agent flowrate, conformal mapping approx. calc. method 78−75197
principles, charact. props., design and performance *(German)* 80−52198
process heat recovery utilising heat pipe exchangers, design and performance 80−61398
review, operation and instrument applications 77−10010
rock melting drills, thermal analysis 77−17258
rotating, temp. distrib. and heat load charact. noncondensable gas effects 78−33992

heat pipes continued
rotating, temperature and heat load distrib. 80−64341
rotating heat pipes, condensation heat transfer, noncondensable gas effects 78−51167
screen wick, heat transfer, Freon-113, ethyl alcohol and H_2O 80−48548
solar collector heat pipe array with common heat exchanger 79−62038
solar energy earth storage and utilisation, technical and economic aspects 79−57475
solar heating equipment, for building, community and agricultural appl. 79−57412
solar receiver gas turbine plant, 10 MWe, conceptual design 79−52910
solar thermoelectric generator using tubular heat-pipe with concentrator 80−89658
space nuclear propulsion, out-of-core thermionic power conversion system 79−48160
space vehicle radioisotope thermoelectric generator, heat pipes design and testing, Cu/H_2O, axially-grooved 79−48144
spacecraft radiator elements, NEP thermionic system design 80−40887
spacecraft thermal control heat pipes, commercially available, evaluation 80−8984
spectroscopic, operation 80−106708
supersonic flow and shock waves 79−32568
surfaces covered with capillary-porous structures, heat transfer with boiling, approximate theory 78−94537
theory of operation, comparison of theoretical and expt. data *(Japanese)* 78−29106
thermal resistance, low-temp. pipe, evaporator-condenser interrelation effect 77−89003
thermal resistance of low-temp. heat pipes with metal fibre wicks 80−43601
thermionic convertor appl., using Li and K working fluids 79−48153
thermionic technology development, for space nuclear propulsion, NASA's program 1978 status, objectives and plans 79−48159
thin film evaporator grooves, fluid evaporation and boiling heat transfer 80−38227
transport-opposing body forces field effect, mathematical model 79−41552
turbulent vapour stream gasdyanmics 79−90335
two-phase thermosyphon feasibility for solar energy transport and storage 79−57491
water, exptl. obs. *(Chinese)* 78−30171
water heat pipe, evaporator heat transfer, obs. 78−83216
wick, liq. evaporation, drop carry-over phenomena in capillary struct., obs. 79−18948
wickless tank, gas-controlled, steady-state and starting characts. 78−79187
Ar loaded K heat pipe performance characteristics 78−89934
Cs, H atom anal. appl. for plasma 80−70043
Cs vapour heat pipe discharge tube pumping for 823 cm^{-1} tunable IR laser 78−63069
Cu/H_2O axially-grooved heat pipes, fabrication and performance testing for space vehicle appls. 80−37028
Hg gravity fed heat pipe for production of high purity fixed density of Hg atoms 80−69627
K heat pipe, heat transport characteristics, transverse mag. field effects 79−37127
Li/He heat pipe, start-up power, heat transport, thermal regulation 80−53615
Na heat pipes, evap. process, sonic limits to power transfer 79−18672
Na vapour heat pipe performance rel. to nozzle discharge theory 78−75033
Na vapour laminar flow during non-uniform heating of evaporator *(Russian)* 77−80166
Na-filled stainless steel heat pipes, with long adiabatic sctions, performance limits 80−38236

heat pumps
see also heat sinks
air to water heat pump and solar installation for single family house *(German)* 79−87968
air to water heat pump and solar water heating, dual purpose installations for family house *(German)* 79−87969
air-to-air, heating and drying appls. *(German)* 80−50995
chemical, H_2SO_4-H_2O chemical heat pump energy storage system 80−30515
chemical heat pumps for solar energy conversion using $LaNi_5$ hydrides 80−89667
classification according to source and working substance *(German)* 80−94099
development possibilities of energy resources *(German)* 80−21355
domestic, gas versus electric *(German)* 79−57438
domestic heating applications *(French)* 80−30518
domestic space and water heating, appraisal of solar power appl. 79−74494
domestic space heating appls. *(German)* 80−94099
dwellings appl., single family computer-aided analysis 79−43784
economic analysis, optimised heat utilisation *(German)* 79−96483
with electric drives and gas drives, comparison *(German)* '80−7952
energy and environmental considerations in extending appls. 77−17976
energy recovery 79−43782
energy roof, solar energy utilisation and heat recovery *(German)* 80−61285
exergetic balance sheet of premises heating installations using a heat pump *(French)* 77−46901
finite speed, coeff. of performance 80−79131
fluidyne heat engine, pump op. low operating temp. 79−85206
fossil fuel heat pumps for domestic, commercial and industrial space heating 80−89666
gas-fired heat pump systems, energy performance anal. by computer 80−35728
geothermal heating installation *(French)* 77−46902
geothermal power for heating purposes *(Slovak)* 79−87963
heat recovery/heat pump combination for sports centre heating system, operating experience *(German)* 80−16830
house energy conservation measures obs. and evaluation, using minicomputer, Philips expt. house (West German project) 79−61951
hydride absorption chemical heat pump for steam recycling *(French)* 80−55881
hydride conversion and storage system, chemical heat pump, space heating or cooling 80−72077

heat pumps continued
ice-maker, two plate-type, Remcor and 'no-penalty' harvest schemes comparison 79−48165
indoor sports centre heating appl. *(German)* 80−16829
injection laser system, temp. control 77−19324
with internal combustion engine drives, economic advantages *(German)* 79−74535
large scale use in Austria, expenditures and savings, first assessment *(German)* 79−87981
laser/component cooling appl., development trends 78−22136
magnetic refrigerator for operation near 2K 78−37012
metal hydride chemical heat pumps, materials and performance characts. 80−40927
metal hydride heat pump as topping cycle for power generation 80−40928
metal hydride solar heat pump and power system, design and costs for space heating appls. 80−30521
metal hydrides use as energy conversion media, review *(Japanese)* 80−55934
methanol based heat pumps for storage of solar thermal energy 80−30587
office complex design, with solar power utilisation, up to 70% energy savings 80−40831
operating principles and performance 78−71274
operation, efficiency and economics *(Italian)* 80−45722
Peltier, improvement of process separation availability, thermodynamic anal. 80−35734
rational use of energy in houses *(Dutch)* 80−40836
recreation centre, all-electric, open-air swimming pool heating appl. *(German)* 80−16828
rectangular monolithic infinite cascade thermojunctions 78−57944
single-stage thermoelectric heat pumps, design, characterisation and optimisation 80−35735
solar, combined, performance evaluation, for residential space and water heating 79−88000
solar air heating systems, heat pump assisted, performance anal. 80−66996
solar ammoniated salt heat pump for energy storage 80−81484
solar assisted, operation 80−61395
solar chemical heat pump/storage system for air conditioning 80−55886
solar energy, recovery from soil, deep ground coil evaporators for heat pumps 79−87967
solar energy model anal. to 2010 *(German)* 80−26109
solar energy system with dual-source heat pump and long-term storage 79−57453
solar ground coupled heat transfer, expt. and GROCS computer model of heat pump system 80−66987
solar heat pump, series, flat-plate collectors, vapour compression, energy conservation 80−72078
solar heat pump and thermal storage system based on $CaCl_2$ and methanol vapour reaction for space heating 80−85307
solar heat pump evaporator, thermal performance 80−30520
solar heat pump house heating system with low quality thermal flow 80−76617
solar heat pump plant for space heating in winter, air conditioning in summer 80−76615
solar heating, of houses with swimming pool, Austrian development 79−57413
solar heating system, heat accumulator utilisation, calc. procedure 80−40825
solar house heating system, possibilities of integrating heat pump *(Rumanian)* 80−97804
solar pump systems using submersible motors 80−61401
solar space heating and cooling, Dunham-Bush development 80−40830
solar thermal energy storage by chemically driven heat pumps 79−57476
solar water pump for lift irrigation, thermodynamic anal. and simulation 80−61397
solar-boosted, computer simulation 79−57414
solar-boosted, performance improvement, design problems 79−57439
solar-electric heat pump for houses, design and tests *(German)* 80−7951
solar-powered absorption cycle with energy storage, theoretical anal. 80−55885
solar-powered opencycle chemical heat pump/energy storage system 80−30512
solar-powered solid-state heat transfer device based on photovolt. and Peltier effects 80−217
space heating, experimental installation, using solar absorbers, heat pumps, heat exchangers and measurement and control gear *(German)* 80−35741
space heating, solar collectors combined with ground heat pumps, economic advantages *(German)* 80−76605
sports centre all-electric, heating requirements, appl. *(German)* 80−16827
sports facilities and indoor swimming pools, heating, two heat pump appls. *(German)* 80−16832
steam generation from industrial waste heat, technology impact study of a high efficiency industrial heat pump 80−35732
steam heat pump system for process steam generation 80−35729
steam power plants, energy conversion by alternative working fluids, book contrib. 79−43783
Stirling engine powered, heat activated, system level performance 79−48164
Stirling engine powered heat activated heat pump development 80−35725
Stirling engine powered heat activated heat pumps, system performance 80−35727
Stirling engine-driven gas heat pump system, energy efficiency 80−35740
Stirling free piston engine, development of a heat activated heat pump 80−30541
storage assisted heat pumps using phase change materials 80−35733
storage of thermal energy, annual cycle, ice storage and three-coil heat pump 80−55917
swimming baths and associated buildings, heating appls. *(German)* 79−92088
swimming pool outdoor, heating, appl. *(German)* 80−16781
thermal energy storage, SO_4/H_2O vapour mixture in heat pump mode 80−26169
thermochemical heat pump/refrigerator thermodynamic analysis 80−35716
thermodynamic cycle of fluid *(French)* 77−46900

heat pumps continued
thermoelectric, cross flow, anal. of operation and performance using mathematical model 80−107836
thermoelectric, single-stage, simplified method for optimization 80−108811
thermoelectric, two-stage, design criteria anal. for cool-down speed maximisation 80−108812
thermoelectric 80−35713
thermoelectric coolers, electrical analogue simulation of transient behaviour 78−21140
thermoelectric coolers, fast transient response of novel Peltier junctions 78−21141
thermogravimetric reversible total energy system 80−55884
trithermal absorption cycle process for upgrading waste heat 80−35731
valveless low temp. heat pump, performance 77−17991
vapour compression heat pumps, thermodynamic eval. of high temp. operation 80−35730
water pumping solar systems using photovoltaic convertor arrays 80−61402
water-to-water, school with gymnasium, heating appl. *(German)* 80−16831
wind heat system utilising wind turbine driven heat pump 80−66926
Si solar cells with concentrators and heat pump for solar energy conversion 80−61371

heat radiation
absorbing and anisotropically scattering slab with reflecting boundary, radiative transfer 80−79122
absorbing and anisotropically scattering slab with reflecting boundary, radiative transfer, rigorous approach 80−79123
aqueous suspensions, three flux method for predicting radiative transfer 80−6052
arc, DC low voltage, anode energy balance investig. at reduced press. 80−19637
atmosphere, model transmission function rel. to remote sensing 77−9498
atmosphere outgoing thermal radiation, meas. rel. to O_3 profile determ. 78−92945
atmosphere thermal radiation, particulate pollution effects rel. to climatology 78−85678
atmospheric, fluctuations, influence on radiotelescope sensitivity, expt. *(Russian)* 77−21832
atmospheric IR properties relevant to building envelope heat losses 80−58895
axisymmetric cavities, radiation heat transfer 77−11118
black body monochomatic emissive power, fast calc. by nomograph 78−22257
black body sources, in band flux density calcs. 79−37135
black-body radiation and thermal equilibrium in static gravitational field 79−67238
blackbody cavities, directional emissivity calc., Monte Carlo method 80−83729
blackbody radiant flux calc. simplification 80−106710
blackbody radiation interaction with LF atomic transitions, Zeeman, Stark and stimulated emission 79−41127
blackness of cylindrical cavity containing gas, calcs. using Monte Carlo method 80−106711
building envelope heat radiation losses and countermeasures 80−58894
ceramics, brittle, partially absorbing, thermal stress anal. subjected to symmetric radiation heating 80−59570
Chandrasekhar H-equation, soln. by Newtons method 80−87710
channel laminar flow, thermal entrance zone, heat transfer, optically thin gas layer effects 80−74861
channels, radiant heat transfer problems commonly encountered in convective heat transfer analysis 80−48562
characteristics expression, effective temperature *(Japanese)* 80−43602
closed cylindrical radiating systems with specular surfaces, zonal anal. 80−79120
coatings with variable degree of blackness, heat-radiating, efficiency 77−28027
coaxial radiative and convective heat transfer in gray and nongray gases 80−102963
combined heat transfer, state of the art review 80−79119
condensed medium, semitransparent, plane layer radiative-conductive heat transfer 80−43590
contact interface temp., internal thermal radiation effect 78−18151
convective radiative heat transfer of thermally thin body 80−79110
coupled radiative plus conductive heat transfer, absorption coeff. temp. depend. allowance 80−74698
cryogenic vessel, thermal load by radiation from the neck *(German)* 78−86276
cryopumps, influence on H_2 v.p. meas., 2 to 4.5K 77−5848
crystal, internal radiation spectral composition at high temp., energy transfer and thermionic emission 77−43359
crystal growth, one-dimensional Stefan problem, expansions in time 80−64354
cylinder, diffusion of heat, with radiation boundary conditions 78−45577
cylinder, perforated, radiated energy anal. 80−19228
cylindrical electric arc, radiant energy transfer, temp. profiles with boundary reflection corrections 80−79600
cylindrical ingot, shrinkage effects on solidification rate under radiative heat transfer 80−66493
cylindrical radiating systems of various configurations, temp. field anal. 80−74720
diethylphtalate layer, heated by radiant heat source, heat and mass transfer 80−74717
differential formulation for radiative transfer, successive approx. approach 80−74721
direct differential methods, review 80−64352
early universe, thermal radiation during quantum era rel. to relic radiation origin *(Russian)* 78−81717
Earth IR emission, Lambertian, of spherical surface, radiation press. on satellite *(French)* 78−81529
Earth surface radiation balance, influence of irrigation 79−29863
education, blackbody radiation and Planck function, derivative spectroscopy expt. 80−77563
emission line shapes from a rotating ring radiator 80−83998
emissivities for halfspace geometry, variational procedure 78−87245
emissivity meas. by thermoreceiver/gas heat exchange 77−22552
emissivity measurement of partially transparent materials to thermal radiation, high speed spectrometric method 79−7280

heat radiation continued
emitter, radiant heat exchange with heated body, appl. to vapour deposition *(Russian)* 78−95701
energy absorption distrib. in material with spatially varying optical props. 77−75419
ethyl acetate, gas, radiatively heated by CO_2 laser, cooling mechanism investig. 80−75021
film boiling, conduction and radiation from flat plate *(German)* 79−72789
fins, nonlinear problems, 1-D conduction, initial value problem 80−83726
flash tube radiation, interaction with cooling liq., nonlinear hydrodynamics 77−11121
flat bodies, nonsymmetrical, ordered thermal mode relationship 77−74332
flow metrology, appls. of heat waves 79−68879
fluid thermal cond. meas. by transient line source method, radiation effects 78−94889
fluidised bed, high-temperature, radiant, conductive-convective components of external heat exchange 80−43709
fluidised beds, combustion facility, radiation heat transfer, particle size and flow parameter effects 80−69641
furnace radiation flux model 78−93689
gas, propagation of initial disturbances, velocity dispersion and exponential decay *(Russian)* 80−48834
gas flow past surface, interaction of radiation with convection *(Russian)* 80−99994
gas layer, heat cond., radiation interaction in presence of band spectrum 79−55307
gases, radiatively heated by CO_2 laser, cooling mechanism investig. 80−75021
geometric-optics coefficient, determ. by Monte Carlo method 77−50867
glass fibre drawing process, extensional instabilities 80−89258
glass plane layer, thermal radiation spatial distrib. rel. to temp. field, internal reflect. 79−59913
glass system, layered, thermal radiative props. for solar diffuse radiation flux 79−94473
glassy material, destruction at critical point in radiative gas stream *(Russian)* 79−32910
gray, planar, absorbing-emitting-scatt. medium bounded by nonisothermal walls, radiative heat transfer 80−1413
grey medium between concentric cylinders, 2 dimens. radiative equilib. 78−42523
harmonic function with radiation type boundary conditions, Acker conjecture 1-dimens. auxiliary problems *(French)* 79−98600
heat eqn., general free boundary problems 77−68375
heat exchanger, heat transfer coefficient, iteration-free calculation 78−1655
heating, using paraboloidal reflectors 79−97392
high rate local heat flux meas. probe 80−47050
high temp. heat exchangers, heat transfer improvements, radiation between walls, effects *(Japanese)* 78−87244
high temp. radiative props., expt. determ., spectral emissivities for Mo, Ta, Nb, ash 80−74718
high temperature measurement of small specimens of metals, alloys, structural materials appl. 79−7281
high temperature radiation, absorption in matter 80−64353
high vacuum chamber for thermokinetic studies of solid surface thermal shock 80−73373
HTGR radiative gas heat exchangers, radiation effects at high temps. 80−95338
HTR pebble bed heat transport, particularly radiation, in hypothetical accidents *(German)* 79−49791
human body heat load, effect of radiant environment 77−48761
hydrocarbons, saturated, thermal cond., rad. effect interferometry method 77−11745
hypersonic flow past disintegrating blunt bodies, radiative heating in H_2-He atms. 80−69865
hypersonic shock layer, screening of selective heat radiation in boundary layer *(Russian)* 79−32497
infinite cylinder, two-dimensional radiative heat transfer, with allowance for shading 77−53839
initial disturbances, exponential decay and dispersion vels., thermal radiation influence *(Russian)* 80−69640
intensity of radiation, rigorous constructive solns. in radiative heat transfer 78−9553
IR emission spectra, during crystn., distinguishing features 80−1952
irradiated semitransparent surface, simultaneous radiative and conductive heat transfer, boundary conditions 80−74719
isothermal isotropically scattering medium 77−80056
isotropic scattering, gaseous absorpt., optical path length calcs. 80−79125
isotropically scattering semiinfinite medium, two-dimens. radiative transfer expansions 78−42522
laser fusion reactor, cylindrical shell, thermal vibrs., general soln. 80−95433
layer with high particle concentration, radiant component of heat cond. 79−86318
layered systems, heat conduction eqn. including radiation across gap, numerical soln. *(German)* 80−1407
liquid He dewar, heat anal., reduction of evaporation rate 79−75533
LMFBR deck insulation, thermal radiation transfer, through non opaque insulator 79−59147
luminous flares, heat of radiation calcs. *(German)* 80−68154
massive spherical particle, heating by radiation and convection 77−50866
melting semitransparent material, approx. temp. profile calc. emthod 77−75787
metal surface, rough, hemispherical emittance 80−70434
metal-dielectric inhomogeneous selective absorpt. of solar energy 79−48181
Mie highly anisotropic scattering, influence and treatment 80−74722
molecular gas radiation in the thermal entrance region of a duct 80−6051
moving boundary problems, weak soln. 80−179
multicomponent medium, heat radiation attenuation factor calc. model 79−94472
multidimensional body, radiative-convective heating, unsteady temp. calc. method 78−90640
multilayer building struct. subject to periodic surface heating *(German)* 77−42724

heat radiation continued
multilayer insulation, simple struct. insulating material props. for low temp. appl. 80−57307
multilayer scatt., absorb. materials, radiant energy transport 77−7297
multiple-plate glass systems, spectral directional radiation characts. prediction 78−74956
nearly layered randomly inhomogeneous medium, thermal radiation 80−18968
night sky as heat sink for heat engine, for teaching 80−27082
non-gray gases, radiative transfer, simple differential approx. 80−38240
nongrey, nondiffuse surfaces, 3-dimens. radiative exchange factors, Monte Carlo method 80−10128
nonisothermal cavity radiator, spectral radiant exitance 79−50569
nontransparent medium, bounded flat layer effective temp. determ. 80−69638
nuclear reactor, fuel rod arrays, radiative heat transfer, Monte Carlo method 78−78447
nuclear reactor, radiation heat transfer in a 19-pin sodium-voided bundle 79−85596
ocean thermal radiation, critical phenomena for periodically rough water surface *(Russian)* 78−81188
optical cavity, one-dimens., with output coupling, thermal radiation, fluctuation-dissipation theorem 79−978
organic liquids, radiant heat exchange effect 80−19996
packed solids, radiation studies *(German)* 80−19226
parabolic boundary value problem optimal control, heating process 78−67021
parabolic reflectors, diffuse-specular axisymmetric surfaces, radiative anal. 80−33438
paraffin latent heat storage system theory and expt. 79−57484
parallel plate channel, convective-radiative interaction, air-operated solar collectors appl. 80−96259
parity violating currents in rotating thermal radiation 79−17633
phase changes subject to convection and radiation, perturbation solns. 79−76962
photon bunching in thermal radiation, temp. depend., photodetector thermal fluctuation 78−24748
photon-scalar boson scatt., impact on Planck's radiation law and Hubble effect 78−54212
pipe flow, laminar with nonlinear wall heat fluxes, axial cond. 79−27636
piston, magnetic field effect, self-similar magnetogasdynamic problem with radiative heat transfer 80−64578
Planck's radiation laws, scalar photons and Hubble effect *(German)* 77−45305
plate, flat, transparent, non-absorbing, natural convection due to solar radiation, buoyancy-driven flow 80−69826
polarisation, permanent snow fields from meas. obtained from the 'Meteor' satellite 78−88870
polarisation effects on surface due to radiative transfer *(French)* 80−79127
polarised radiation, Draper and Kirchhoff laws *(French)* 80−79126
pressure shock in gases at high temp. 79−18910
PWR rod bundles, radiative heat transfer calc. method 80−33602
pyrometry, principles and practical instruments *(German)* 77−5844
radial heat transfer, conduction, convection and heat of phase change 78−90700
radiant exchange for a fin and tube solar collector 79−76955
radiant flux density measurement, 1 to 40 W/cm^2, using calorimeter with 90° aperture angle 79−71452
radiant heat exchange calc. in absorptive and scattering medium 77−14885
radiant heat transfer at cryogenic temperatures 79−76950
radiant plate, diametrical Ar gas flow *(Russian)* 78−94565
radiant-flux detectors, comparison 79−35831
radiative gas dynamics, radiation transfer eqn. *(Russian)* 80−64653
radiative heat exchange in black body system, conduction, radiation, scatt. and absorpt. 80−38239
radiative heat transfer, integral eqn. finite element soln. 80−10127
radiative heat transfer between isothermal parallel plates, flow models, numerical analysis 80−14547
radiative heat transfer problem solvability, radiation, scatt., absorpt. 80−33436
radiative melting of ice layer adhering to a vertical surface *(German)* 79−76956
radiative plus conductive heat transfer, differential anal. method 80−74699
radiative transfer in planar medium, anisotropic scatt. and directional boundaries 78−90679
radiative-conductive heat transfer in temperature-wave conditions 80−24020
radio brightness temp. of Earth from Kosmos 243 and Nimbus 5, SHF obs. 80−72521
randomly inhomogeneous stratified media, thermal radiation calc., appl. to Earth surface *(Russian)* 78−96312
recording by two-stage freq. conversion detects., $AgGaS_2$, α-HIO_3 79−46002
rectangular waveguide, blackbody radiation, EM fluctuations 79−41309
relativistic free particle, in thermal radiation within classical electrodynamics, equilib. distrib. 80−8935
scattering, two-dimens. isotropic, in semiinfinite medium 78−42521
selective radiative heat exchange screening in shock boundary layer 79−90283
semi-infinite adjoint strips radiative interchange 80−69639
semi-transparent irradiated plate, combined conduction-radiation heat transfer, anal. soln. 78−75051
semitransparent material strip, radiation transfer *(Russian)* 79−98597
shape factors between rings and inverted cones 79−81705
shape factors in space thermodynamics, determ. using shape factormeter *(German)* 78−73610
shield, for cryogenic apparatus, thermodynamic optimisation 78−81982
shield, heat-absorbing, thermal vac. chamber, natural thermal radiation calc. 77−65666
sky radiator, effect of surface characteristics and atmospheric conditions on radiative heat loss to a clear sky 80−79121
slab, anisotropic radiative transfer, iterative soln. 80−33439
snow, frost, heat transfer, cond., radiation and water vapour diffusion model 78−94563
soil, radiothermal radiation rel. to stored productive moisture remote determ. 79−29795
solar panel, equilibrium temp. in real conditions *(French)* 77−19514
solid body radiation problem, soln. 80−77734

heat radiation continued
solidifying semitransparent cylindrical medium, thermal stresses, radiation and conduction 79−46200
space probe or meteorite reentry, mass loss and shape change with radiative heating 80−31198
specimen in spectrophotometer, effect of radiation heating on meas. accuracy 79−30589
spherical particles, thermal radiation emission 80−14556
spherical particles, thermal radiation emission 80−14557
stagnation point boundary layer flow with radiation 80−79258
steam generator, radiant heat flux distrib., light model simulation 78−94567
steel, sheet, type 08Kp, blackness degree rel. to heat treatment in controlled atms. 79−57165
Stefan problems with nonlinear boundary conditions, polygonal method soln. 79−26010
Stephan's constant determ., student expt. 78−69948
stochastically macro-inhomogeneous medium, integral equation of mean radiation intensity *(Russian)* 78−5639
thermal conductivity prediction of heterogeneous mixture, digital simulation technique 78−87247
thermal emission, doubling and superposition methods 80−1414
thermal radiation of nonlinear material, generalised Kirchhoff law, fluctuation-dissipation theorem 80−4679
thermal radiation property meas. of materials 80−96181
thermal-radiation absorption factor, temp. behaviour 77−51526
thermoelectric coolers, heat load estimation curves 78−45613
thermostatic control, rot. conical (spherical) jacket radiatively heated from side 77−42710
transfer effects in annular passages of heat exchangers *(Japanese)* 77−23239
transfer model, nongrey semiinfinite media with boundary 79−32204
transient combined laminar free convection and radiation in rectangular enclosure 77−7388
transient heat exchange between a radiating plate and a high-temperature gas flow 79−94609
transient temp. of body, surface radiation and convection, quasilinearisation approach 77−80054
transition of radiation field in a radiation layer 80−106712
trench with radiative wall conditions, free convection 80−79324
two-phase Stefan problem when latent heat of fusion →0 *(French)* 79−71382
US appl. in solar and IR heat transfer 80−74723
vector field, electroconductive, analogy 78−90681
vitreous material at critical point, disintegration by radiating gas 79−94740
volumetrically heated fluid layer, combined natural turbulent convection and radiation 80−74871
walls, permeable, cooling characts., heat exchange, rad. emitter design 80−64535
water, thermally-stratified, cooled from above, free convection 79−46315
water covered with foam, thermal radio emission from foam structures 79−29497
water layer, heated by radiant heat source, heat and mass transfer 80−74717
weakly absorbing material calorimetric meas., theory 79−76773
CO_2 gas flow impinging on heating surface, heat transfer radiation 80−43710
Ge, low-temperature bolometer, heat transfer coeff. 79−30561
H_2-He gas mixtures, 1000-25000K, transport property correlations 80−75029
Na, Rydberg atoms, selective field ionisation, 300K blackbody radiation detect. 79−58787
SO_2, radiation, emissivity and absorption coeff. calc. 77−55126
SiO_2, high temp. plasma, emissivity and opacity, photon group means 77−7573

heat sinks
Candu reactor moderator effectiveness as LOCA heat sink 79−81021
cooling element for radiation detector, shape effect on heat removal efficiency 78−12691
fusion reactor, TFTR, high energy heat sink, ion beam dump and calorimeter 80−99394
fusion reactor thermosyphon energy removal system design 77−34465
plate, heated, semiinfinite, vertical, with heat sources and sinks natural convection 80−59035
selective covers for natural cooling devices 79−43750
temperature sensor with temp. sink chip on flexible dielectric cable 78−86264
Nd:YAG laser pumping system, heterostructure spectrum convertor, opaque and sapphire heat sink 79−27272
$Si_{1-x}C_x$ protective coating for GaAs laser 80−5753
Zn hot galvanisation coatings, production components, installation and power supply *(French)* 80−66686

heat systems
see also boilers; heating
centralised, energy distribution and storage 79−48184
domestic space heating using low-temp. solar thermal systems *(Czech)* 79−83566
evacuated heat pipe solar collector, rectangular performance characts., trap mechanism 80−3531
hot water supply systems using solar collectors, technical problems *(German)* 80−94106
preheater operation control, in MHD/steam combined-cycle plant, computer simulation appl. 79−52943
solar energy applications, hot water systems, dyeing, in textile industry, commercial aspects 79−83576
solar energy management system 80−66951
solar energy system installation suggestions for space heating and water heating *(German)* 80−94102
solar energy systems, modern control theory appl. reviews 80−66949
solar energy thermal processes, digital simulation 79−24890
solar plant for hot water supply *(Rumanian)* 80−97766
solar power water-heating systems, design method 79−83629
solar water heater, natural circulation, with linear and nonlinear temp. distribs. 77−75778
solar water heating systems, economic assessment based on measured performance 80−97807
solar water heating systems, temperature and flow of entering water control, by thermal operated mechanical device 79−62138

heat systems continued
space heating, experimental installation, using solar absorbers, heat pumps, heat exchangers and measurement and control gear *(German)* 80−35741
space heating, water heating system using solar collectors *(German)* 80−94105
spectral characteristics for improving solar collector performance 80−35650
temperature regulator for heating units 77−37880
wind furnace systems, advanced, for residential and agricultural heating and power supply 79−48070

heat transfer
see also condensation; convection; cooling; evaporation; heat conduction; heat radiation; radiative transfer; thermal diffusivity
^{4}He, superfluid, heat transfer at wall, healing and relax. 78−75899
ablating blunt body, heat transfer near stagnation point 78−94736
ablating bodies, heat transfer coeff. area rule, angle of attack depend. flow 80−92135
ablating body shape, numerical soln. method *(Russian)* 78−75134
ablation of elastic solid, variational principle 78−90698
absorption measurements by laser calorimetry 79−55308
AC conductor, cooled by cryogenic liq., heat transfer models 80−5926
accelerated flow, at permeable graphite burning surface, turbulent heat/mass transfer 78−38417
acetone, heat emission in crit. region, press. and heating surface temp. effects *(Russian)* 80−69634
acetone, transient heat transfer during natural convection *(Russian)* 77−68367
acoustic turbulence, heat transfer in gas 79−86425
acoustic wave 78−5599
adjoint space in heat transport theory 80−58887
adsorbent fixed bed, temp. profiles 79−23359
adsorption, nonisothermal one-component sorption in adsorbent particle, interparticle heat transfer 80−70523
aerodynamic ablation of spinning steel shells, side force 79−37347
aerodynamic heat transfer meas. using transient techniques 77−80258
aerodynamic heating of bodies with deep cavity 79−86454
aerodynamic heating problems with 1st order shape change, reentry vehicle, review 78−94735
aerodynamic heating test, use of melting liq. crysts. 79−77299
aerodynamically heated body, stable shape during ablation *(Russian)* 78−75162
aerosol pipe flow, heat transfer 78−9684
agitated vessel, flow behaviour and transport phenomena, correlation eqns. *(Japanese)* 78−38300
agitated vessels, heat transfer models, thermal boundary layer 80−79288
agitated vessels with bare and finned vertical tube baffles, heat transfer, power expenditure 79−1052
AGR, heat transfer to accel. gas flows, expt. and calcs. 78−54823
AGR fuel elements, heat transfer characteristics with rough surfaces 77−54283
air, dissociated, hypersonic flow over blunt axisymmetric body, nonsteady heat exchange 79−37319
air, flowing, heat transfer efficiency from rough plate 80−48704
air, turbulent flow in circular pipe, temp., velocity profiles, heat transfer, flow resist. 79−55370
air cooled heat exchanger, characteristics of corrugated straight fin surfaces 78−18287
air cooling and dehumidifying coil, heat, mass and momentum transfer 79−192
air flow in vertical annular channel with rot. inner cylinder, heat transfer 77−58679
air fluidised beds and horizontal Cu tubes, heat transfer coeff. 80−79317
air in heated channel, turbulent flow, velocity and temp. pulsation characteristics 80−14820
air jet, heat transfer coeff. for quenching of hot plate 77−47053
air plasma flow in channel inlet zone, local heat transfer 80−64687
air preheaters, converse-type, heat transfer improvements influenced by geometrical characteristics *(Russian)* 80−96177
air turbulent flow in heated channel, effect of gravitational field 80−64533
air water downflow through packed beds, apparent wall heat transfer coeff. 80−74953
air water downflow through packed beds, effective thermal conductivity 80−74952
air-atomised water mixture, high temp. surface impact, heat transfer *(French)* 79−4015
air-cooled, cross-flow heat exchangers, mean temp. difference calcs. 80−6054
air-sea heat flux during AMTEX 75 mesoscale cellular convection 77−78322
air-sea sensible and latent heat transfer coeffs., meas. 200 km from land 80−72552
air-steam mixtures, heat transfer to moving droplets 78−90997
air-stream mixture, direct contact dondensation on single droplet 77−68370
air-water film flow, transport phenomena, wary interface motion 77−35213
air-water fogs, mass, momentum and energy transfer rel. to audible sound propag. 78−1473
air-water interface, combined heat and mass transfer coeff. 78−30166
air-water interface, energy transfers at high wind speeds, effect of spray 78−85574
air-water interface, turbulent heat and mass transfer 79−68551
air-water mist flows, uniform heat flux wedge 79−23352
air-water mixture, vertical flow, temp. influence on boundary lines between flow regimes 80−43764
air-water stream, heat transfer, expt. meas. unit 77−42941
air-water two-phase flow in concentric annulus, heat transfer 78−91002
air-water two-phase flow in vertical pipe, heat transfer *(Japanese)* 77−24011
Alad'ev wall superheat correl., expt. validity test 78−83393
alkali metal vapour condensation from gas flow (He,Ar,N_2) heat and mass transfer 78−75192
alloy, laser surface melted, heat transfer props. and microstructs. 79−70085
alloy, vapour bubble growth dynamics, electron-beam vol. heat source 77−47565
alumina sphere packed bed thermal storage analysis 79−57486

heat transfer continued
amonium alginate, aq. solns., laminar flow heat transfer in helical coils 80−59030
analogies between electric and temperature fields, engineering calc. appl. *(Czech)* 79−68343
annular channels in turbulent flow of gases with variable props. *(Russian)* 79−90256
annular channels with turbulent gas flow, bilateral heating *(Russian)* 79−7375
annular channels with turbulent gas flow, unilateral heating *(Russian)* 79−10559
annular flow condensation, of steam inside tubes, heat transfer 78−14003
annular flow of gases with varying physical props., turbulent, two-sided heating 80−48702
annular gap between concentric inclined cylinders 79−23322
annular pipe, heat transfer for turbulent flow of liq. with const. thermophysical props. 78−1657
annular pipe heat exchanger, laminar flow heat transfer coeffs. 79−72779
annular spaces inner surface, heat transfer in turbulent flow 80−14686
annular turbulent flows with heat transfer 78−94718
annuli, (non)-uniformly heated, pressure drop during boiling, expt. results 79−81971
annuli, heat transfer crisis, inlet flow parameters data correlation 77−62251
annuli, laminar flow, pressure drop and heat transfer with dissipation allowance 80−74858
annuli carrying turbulent flows of gases with variable physical props., one-sided heating 80−48701
annuli heated from both sides, critical heat flux density and turbulence 80−48694
annuli with turbulence promotors, heated, lengthwise-uniform and non-uniform heat release, boiling crisis 80−48703
annulus, rot. inner cylinder, outer cylinder heat transfer to enclosed flowing liq. 78−83478
annulus turbulent air flow heat transfer, physical prop. variability depend., expt. 78−83482
approximation method for solution of nonlinear integral equation with error estimation for problems in heat or mass transfer *(Russian)* 78−57879
aqueous solution boiling, heat transfer coeff. calc. *(Rumanian)* 79−81693
Arctic ice pack heat and mass balance 79−39750
Ariane launch vehicle, model firing tests, acoustic field, heat flux, press. distrib. 78−4062
aromatic hydrocarbons, heat transfer to ascending (descending) streams, near-crit. press. 77−65742
artificially disturbed strata, temp. distrib. during air filtration *(Russian)* 77−25667
artificially fractured rock, heat transfer agents flow patterns 80−17239
artificially intelligent problem solver, system design outline 80−99916
asymmetrical heated tube, turbulent airflow heat transfer charact. 80−38402
N.Atlantic central water, vertical mixing due to salt fingers 78−85571
N.Atlantic Ocean, advection rel. to sea surface temp. year to year changes, (1948 to 1974) 80−67367
atmosphere, bulk transfer velocity to and from natural and artificial surfaces 79−25302
atmosphere, heat and moisture balance in Baltic Sea region from aerological climatology 77−87057
atmosphere, heat flux and turbulence meas. in unstable surface layer over land 77−66962
atmosphere, influnece of sensible and latent heat fluxes over land on four-day forecast 79−96805
atmosphere, meridional heat transfer and equatorial energy budget *(Russian)* 80−81988
atmosphere, middle, heat flux rel. to damped planetary wave interaction with zonally averaged circulation 80−109217
atmosphere, N.hemispheric distribs. of Earth surface vertical heat fluxes 79−96804
atmosphere, non-linear small-scale sea-air interaction parameterisation, effects of ice cover *(Russian)* 77−53068
atmosphere, observational study of upward sensible heat flux by synoptic-scale transients 80−94591
atmosphere, planetary wave heat and momentum fluxes rel. to stratosphere and mesosphere meridional circulations 80−109219
atmosphere, radiative heat exchange in tropics *(Russian)* 79−84476
atmosphere, results and prospects of Complex Atmospheric Energetics Experiment (CAENEX) 78−3904
atmosphere, sensible heat advection, local and regional components 79−20942
atmosphere, vertical heat flux determ. on basis of semiempirical turbulence theory 78−3907
atmosphere baroclinic planetary boundary layer above sea, heat and moisture fluxes parameterisation *(Russian)* 79−16576
atmosphere during 1976 hot spells, heat flux micrometeorological charcts. 79−79961
atmosphere global scale transport processes *(Dutch)* 78−3889
atmosphere heat and momentum transfers under strong stability in boundary layer 79−16584
atmosphere heat transfer, charcts. of nonstationary processes 80−41481
atmosphere large-scale eddy transports, linear parameterisation 80−17361
atmosphere/land surface heat exchange, force-restore method for ground surface temp. prediction 80−98469
atmospheric boundar layer, turbulent flow through vegetation canopy 80−26570
atmospheric boundary layer, heat and humidity exchange laws, model approach 77−66948
atmospheric boundary layer, heat transfer with ocean, reef effects, AMTEX 1975 obs. 80−26567
atmospheric boundary layer, pine forest affecting turbulence and heat transfer 80−26569
atomised liquid dropwise evaporation, mist cooling 80−6506
augmentation techniques, impact on entropy generation 80−79118
average Nusselt numbers for external flows 80−38412
axial air flows, heat transfer from wire 80−48700
axially grooved heat pipes, Marangoni effect and capacity degradation 80−14551

heat transfer continued
axisymmetric bodies, super- and hypersonic freestream turbulence effects 77−75916
axisymmetric cavities, radiation heat transfer 77−11118
axisymmetric channels of different configuration, heat transfer, gradient method appl. 80−24098
axisymmetric drawing through curved dies, heat transport anal. 77−52432
axisymmetric field flow around obstacle, effect of turbulence *(Russian)* 78−83385
axisymmetric laminar boundary layer, swirling flow through conical hydrocyclone, heat transfer 79−98733
axisymmetric rotating round nosed bodies, flow and heat transfer, buoyancy effects 80−79306
axisymmetric starting plume cap, transition from laminar flow 79−18872
axisymmetry jet, inblow parameter effect on separation, boundary layers and heat transfer *(Russian)* 80−24064
Barber boundary conditions for thermoelastic contact, heat flows 80−69745
BCC lattice, second sound, mol. dynamics study 77−24453
bed to surface heat transfer, fluidised bed of large particles 78−63269
Beloyarskaya Atomic Electric Power Plant, channel reactors, permissible power operating calculations 79−80984
benzene, nucleate boiling heat transfer, press. factor 77−69080
benzene aqueous hetero-azeotrope mixture, condensation heat transfer coeff. *(German)* 80−33425
bibliography, 1975-76 77−27526
bibliography, 1975-76 77−84250
bibliography, heat and mass transfer, Polish works (1977-78) 80−57020
bibliography, heat and mass transfer, Soviet works 78−22343
bibliography, Japanese works 78−22344
bibliography, Japanese works 79−23317
bibliography, Japanese works 80−31442
bibliography, Japanese works 1974-76 77−15012
bibliography, Polish works, (1975-1976) 78−38320
bibliography, Soviet work on heat and mass transfer 79−86430
bibliography, Soviet works, 1976 78−34126
bibliography, Soviet works 77−58672
bibliography, Soviet works 79−32180
bibliography, Soviet works 80−94938
bibliography 77−58671
bibliography 78−63425
bibliography 78−75141
bibliography 79−32503
bibliography 79−68700
bibliography 80−51978
bibliography 1976-77 78−34127
bibliography of Soviet work 77−39288
bibliography of Soviet works on heat and mass transfer 78−75027
bibliography of Soviet works on heat and mass transfer 80−41972
binary boundary layer with press. pulsations, friction and heat and mass transfer 80−14653
binary gaseous mixtures, transient heat conduction 80−64670
binary mist flow, heat and mass transfer anal. *(Japanese)* 79−14467
binary mixture, nucleate boiling, bubble growth, saturation press.-temp. relation 77−46892
binary mixture, thin shear flow layer, momentum, heat and mass transfer *(German)* 77−39293
binary vapour mixture, condensation in presence of inert gas 77−80051
binary vapour mixture condensation into immiscible liquids *(German)* 78−18760
binary vapour mixtures, simulation of unsteady state behaviour of dephlegmation 79−7285
Bingham fluid, forced convection of polymeric and disperse systems in ultradeep boreholes 79−68762
biological tissue, perfusion rate meas. by dynamic thermal dilution 77−40883
biological tissue Pennes model vs. Wulff model 77−40635
black liquid solar collector analysis and expt. 79−62097
Blasius flow, horizontal, heated from below, longitudinal vortices onset 78−71342
blast waves with heat transfer 77−35166
blocked annular channel in turbulent flow of air with variable props. *(Russian)* 79−94620
blood, rheological characts., heat transfer rel. to myocardial infarcts 79−79573
blood vessel heat transfer 80−108851
blunt body, in hyperthermal flow, near free mol. heating 79−94671
blunt body moving in atmosphere, heat protective coating destruction *(Russian)* 78−87251
blunt circ. cylinder, separated, reattached, redeveloped air flow, heat transfer characts. 77−58692
blunt flat plates, air flow, 2-D, thermal boundary layer characteristics, nose shape effects 80−92121
blunt-body boundary layers, three dimensional, surface curvature effects 80−1520
bodies in contact, heat transmission, optimal control thermoelastic stress constraint 80−19223
bodies in gas-filled contact, integral equation numerical solution 79−37130
bodies in granular bed, heat and mass transfer 78−9701
body of revolution with heating and cooling, boundary layer transition and separation 80−64518
body submerged in granular layer, heat and mass transfer 78−94536
body-plethysmograph systems, time const. 77−40875
boiler tube, serpentine geometry at high press., two phase heat transfer 78−94077
boilers, superheaters, flue-gas temp. difference influencing pressure loss calculation programme *(German)* 80−38225
boiling, bubble departure frequency, effect of superheat and cavity size 77−80610
boiling, convective, of refrigerants in horiz. tube, statistical anal. of heat transfer data 79−7283
boiling, critical heat flux for liquids in free motion conditions *(Russian)* 77−24400
boiling, critical heat flux variation, very nonuniform annular heat release 78−51043
boiling, from porous coated surface 79−76946
boiling, heat transfer enhancement 78−9530

heat transfer continued
boiling, in circuit system, effect of intense electric field *(Russian)* 78−46887
boiling, maximum heat fluxes under special conditions 78−9547
boiling, non-stationary heat transfer crisis *(Russian)* 77−24401
boiling, nucleate, heat transfer model 78−75056
boiling, nucleate, subcooled, latent heat transport contrib. 78−75046
boiling, nucleate, superheating, heterogeneous nucleation theory calc. 79−46170
boiling, nucleation centres interaction, obs. technique 78−14065
boiling, pool saturated, subcooled, in narrow spaces, interferometry obs. 78−94527
boiling, pool-type, heat transfer stability prediction, finite disturbances 78−75044
boiling, solid quenching in subcooled water, propag. of wetting front *(French)* 79−77108
boiling, under increased gravitation, heat exchange mechanism, bubble form., review 77−46895
boiling and evaporating liq. heat transfer, on capillary and porous surfaces 78−94526
boiling at surface near peak heat flux, mechanism 77−75780
boiling crisis at concentric (eccentric) annuli with turbulence promoters 78−55639
boiling crisis in swirled flow of water in pipes 79−90241
boiling curve, water in cylindrical cavity in copper block, quenching data and heat loss 77−84119
boiling delay, unsteady heat transfer with phase transition 80−48690
boiling heat transfer, heating surface material effect 77−42704
boiling heat transfer, surface roughness effect 78−9534
boiling heat transfer coefficients, heater plate thickness effects 78−34124
boiling heat transfer crisis in annular channel containing unheated sections 77−23945
boiling heat transfer in two-phase thermosyphons 78−90686
boiling heat transfer rates, Rohsenow's pool boiling correlation eqn. 77−80052
boiling in capillary gaps, heat and mass transfer 78−46885
boiling in narrow channels and capillaries 78−9543
boiling in steam generating pipe with Fe oxide deposits on wall, steam bubble growth 79−76947
boiling layer, laser radiation probe of bed space 77−15115
boiling liquid in granular bed, heat transfer enhancement 78−9533
boiling liquid thin film rupture, heat-transfer surface state effect 78−55552
boiling loop in low-pressure operation of BWR at PNC Japan, stability anal. 78−8894
boiling of binary mixtures 78−9538
boiling of liquid at finned wall, heat transfer simulation 77−42817
boiling on circumferential fins 78−59272
boiling on surface coated with porous structure, transport mechanism of nonvolatile impurities 78−2365
boiling point drying by volumetric abs. of RF and MW EM energy, heat and mass transfer characts. 80−79130
boiling surface, in closed containers, similarity approach *(German)* 77−11684
boiling under reduced gravity conditions 77−4192
Boltzmann equation, boundary conditions, and heat transfer between parallel plates 77−67390
Boltzmann gas, heat transfer between parallel plates 77−87688
boundary control of heat eqn., time depend. reachable states 79−44886
boundary layer, calc. on spinning and curved surfaces 77−65737
boundary layer, compressible stagnation point, discontinuous solns. for three-dimens. flow 77−42856
boundary layer, conservation relations with heat/mass transfer and vel. slip 77−62246
boundary layer, dimensionless temp. profiles downstream from heat line source *(French)* 77−15008
boundary layer, improvement of heat transfer coeffs. using turbulence promoter 77−72297
boundary layer, laminar, small temp. factor, high Mach no. 78−34156
boundary layer, laminar to turbulent transition, wall heating effect 78−38334
boundary layer, nonstationary, with self-induced press. 78−34164
boundary layer flow, laminar, thermal response behaviour 78−75136
boundary layer flow, unsteady, compressible, 3-D, near axisymmetric stagnation point 80−103011
boundary layer flows, large Prandtl numbers, second order effects 77−35140
boundary layer heat transmission, dimensional analysis *(Spanish)* 79−59906
boundary layer on conical body with gas injection *(Japanese)* 78−59417
boundary layer on cylinder drawn from aperture in presence of heat transfer *(Russian)* 79−77062
boundary layer on heated plate 79−4004
boundary layer on rough surface, temp. distrib. 78−30279
boundary layer turbulence, heat transfer coeff. meas. by dilatometry 78−83388
boundary layer turbulence, integral method soln. 79−72890
boundary layers, laminar, compressible, Prandtl=0.72, sharp pressure rise effect 80−83782
boundary layers, thermal, second-order layer on blunted wedge 77−7379
boundary layers in gradient flow around nonisothermal surfaces, temp. depend. of fluid thermophys. props. influence *(Ukrainian)* 77−51054
boundary layers with flow reversal 79−37313
breeder reactor spent fuel shipping cask design, heat transfer tests 79−85640
bubble, of vap., with microlayer, universal growth relations 78−71266
bubble and liquid during exponential compression of bubble *(Russian)* 77−35224
bubble collapse, heat transfer controlled, in isothermal tube 78−90979
bubble growth, inertia and diffusion controlled, implosion, pure and binary systems 78−1552
bubble growth, noncondensing gas-vap. injected into liquid 78−55553
bubble growth in superheated water at reduced pressures, finite difference anal. *(Japanese)* 80−92150
bubble nonequilibrium collapse, heat transfer effects 79−98794
bubble Reynolds number effect on heat transfer of forced convection subcooled boiling *(Japanese)* 80−19365
bubble separation mechanism on horiz. heater face 77−51104
bubble thermal migration, internal heat transport effects in weightless liquids 80−24075
bubbling electrofluidised bed, heat transfer rates 78−87242

heat transfer continued
building, fundamentals in reln. to heating and cooling load calcs. 78−90628
buoyancy boundary layer, supercritical solns. 79−55384
buoyancy driven flows originating from heated cylinders submerged in a finite water layer 80−59024
buoyancy induced flow over inclined heated porous surface, vortex instability 80−33601
buoyant atmospheric plumes, critical thermal power during atmosphere penetration *(French)* 80−33585
buoyant flow, thermally driven, equations of motion 79−23334
buried convective heat source, in semiinfinite solid, steady temp. distrib., surface temp. 77−58534
buried cylindrical heat source, transient temp. distrib., upper and lower bounds 78−75048
burnt skin heat and water losses, thermal modelling 78−31790
BWR, dryout/post-dryout heat transfer, low flow, single tube 77−61498
BWR fuel assembly, radiant heat transfer 78−17287
BWR pressure-suppression system, steam chugging anal., heat transfer and fluid mechanics characts. 80−95339
BWR vertical separator superheater tube bundles, condensation heat transfer, noncondensing gas effects 80−47535
BWRs, natural circulation of water by hydrodynamic models 79−93684
CAI source for final year B.Sc. students 77−60877
canal, converging, unsteady 2-D compressible boundary layer flow 79−20885
CANDU cooling with supercritical fluids, feasibility study 79−76064
capillary porous bodies, boiling heat transfer to liquid N_2 or He 80−1575
capillary porous materials, product quality under heat processing, heat flux direction influence *(Russian)* 79−32203
capillary porous media with variable parameters 78−83471
capillary-porous bodies, heat and moisture transfer, analytical formulae 78−67013
capillary-porous body, nonlinear heat/mass transfer problem, soln. using invariant groups 78−55688
capillary-porous structs., heat transfer and max. heat flux with boiling 80−33600
capillary-porous submerged coating, boiling model 77−65792
carbon tetrachloride aqueous hetero-azeotrope mixture, condensation heat transfer coeff. *(German)* 80−33425
carbon tetrachloride-I_2-water system, mass transfer in pulsed perforated plate column 78−71385
casting, continuous, heat transfer anal. by finite element anal. 78−30167
casting process, direct chill, semi-continuous, numerical heat transfer model 80−43592
catalytic beds, effect of granulometry and nature of catalyser on heat transfer *(French)* 77−68689
catalytic reactors, runaway inhibition 79−47983
cathode arc spot temp., Joule heat liberation effect 78−26361
Cauchy problem, classical mechanics of diffusion and Schrodinger eqn. 78−28985
cavity flow motion and heat transfer, fixed and floating boundaries *(Russian)* 77−35144
cavity packed with fibrous glass, effective thermal cond. 79−55317
ceramics, brittle, heat-transfer variables effect as thermal stress resist., meas. by quenching expts. 80−79871
ceramics, brittle, partially absorbing, thermal stress anal. subjected to symmetric radiation heating 80−59570
ceramics, thermal stress resistance, figures of merit, review 79−83290
channel, annular, with vortex generators, and uniform (nonuniform) heat injection length, crit. heat flux *(Russian)* 78−83397
channel, corrugated wall, heat/mass transfer characteristics 77−80157
channel, heat-insulated, laminar flow with nonuniform vel. and heat input distribs. *(Russian)* 79−64662
channel, local heat transfer coeffs. in initial heated section during laminar flow *(Russian)* 77−54862
channel, packed with spherical elements, hydrodynamics heat exchange 79−94712
channel, radiused corners, smooth entry, heat transfer in entry section *(Russian)* 77−23955
channel, rectangular, forced flow boiling and burnout 78−94530
channel array with interconnections, finite-difference scheme 79−4012
channel flow, heat transfer dynamics, anal., impulse function method 79−37317
channel flow, variable viscosity, with high heat generation 78−9717
channel flow of reacting gas, momentum change due to heat injection 79−94741
channel flow of viscous gas, heat exchange 77−80218
channel flow of viscous media, heat transfer 78−1662
channel flow wall heat transfer, thick wall, difference method 79−37129
channel flows of high temp. gases, heat transfer 78−94722
channel laminar flow, thermal entrance zone, heat transfer, optically thin gas layer effects 80−74861
channel thermal inlet zone, heat transfer in laminar boundary layer 79−1178
channel turbulent gas flow with HF press. fluctuations, heat transfer rate depend. 78−83487
channel two phase flows, threshold steam qualities and cutoff heat fluxes 79−90242
channel variable-viscosity flow, temp. effects 78−9716
channel with falling liq. film and two-phase flow, heat transfer 78−30337
channel with nonuniform heat emission, crit. heat flux density determ. *(Russian)* 79−64489
channels, internal radiative transfer *(Russian)* 78−38330
channels with lengthwise nonuniform heat release, critical heat flux density 80−69824
channels with rough surfaces, heat exchange intensification *(Russian)* 80−53779
channels with single- or two-phase heat transfer fluid, computer simulation of transients 78−90969
channels with unequal wall temps., low Peclet no. heat transfer 77−42813
checkerboard pipes in rarefied gas stream, coefficients determ. and obs. 79−23325
chemically reacting multicomponent systems, Langevin forces and noise correls. 77−16823
chemically reacting system, coupled heat and mass transfer, finite element soln. 80−68153
chemically reactive flow, aerodynamic heating of blunt bodies 80−74998
heat transfer continued
chemically reactive flow, heat and mass transfer, approximate theory 79−68821
chemically reactive flow characts., simultaneous heat-mass transfer *(Japanese)* 78−22431
chemically reactive flow in porous catalyst, conc. and temp. profiles, computation method 79−86523
chemically reactive metals, heat exchange in gas flow *(Russian)* 78−47068
chladone 21 film condensation on vertical tubes, heat exchange 80−24577
chromosphere, thermal shock waves rel. to pulsed microwave bursts with quasithermal spectrum 77−78762
circular channel with laminar flow, convective heat transfer *(French)* 78−63424
circular cylinder, local heat transfer by turbulence of free-stream flow of viscous liquid, theoretical determ. of influence *(Russian)* 80−96252
circular cylinder in liquid Na crossflow, local heat transfer, numerical study 80−64539
circular cylinder in stabilised twisted flow 77−72309
circular cylinder moving in stationary fluid, skin friction and heat transfer 79−50701
circular cylinder with circumferential edge crack under uniform heat flow, thermal stresses 80−48641
circular cylinder with tripping wires, heat transfer, flow and wakes *(German)* 80−1589
circular impinging jet, heat transfer characts., stagnation point, boundary layers 80−79303
circular jet staggered array with crossflow, heat transfer characteristics 80−6057
circular jets with crossflow, inline and staggered arrays, heat transfer coeff. variations 80−74873
circular pipes, heat transfer with corona discharge 80−64342
circular plate, optical hot spot, thermal stresses 77−11044
circular rods with regular polygonal concentric inner bore, heat flow shape factors 78−51048
circular tube, heat transfer crisis and development for cosinusoidal thermal flux distrib. 77−35206
circular tube, non-Newtonian fluid linear flow, heat transfer 79−98810
circular tube laminar flow, heat transfer with temp. depend. heat generation 77−68582
circular tube under centrifugal accel. field, condensation heat transfer 80−74713
civil AGR multistart helically ribbed fuel pin development 80−23111
coal gasification, demands made on materials used in process *(German)* 80−45438
coal liquefaction preheaters and reactors, modelling of heat transfer characts. 80−30337
coal pyrolysis, in entrained bed flow reactor, theoretical exam. with aid of physical models 79−48062
coastal inlet water temp. change due to artificial heat input 79−16506
coated cement stone heat and mass transfer obs. *(Russian)* 79−14219
coaxial cyclone flow, heat transfer from a cylinder 80−48698
coefficient, local and overall, meas. by Pt film thermoprobe *(French)* 77−74393
coefficient determination use of simplex direct search and finite element methods 77−3712
coefficient prediction, in drag reducing turbulent pipe flow 77−51052
coefficients of heat transfer between hot gas and thermally thick wall 77−42702
coiled tubes, laminar flow and heat transfer, efficient numerical procedure 80−64633
cold finger, for cryosurgery, internal surface cooled by boiling liq. N_2 *(Russian)* 77−22556
collapse of massive star cores, supernova explosion from shock heating 80−56863
combination, theory and analysis methods, review 79−81703
combined heat and mass exchange processes, model eqns. and techniques *(German)* 80−27236
combined Taylor vortex and axial flows, heat transfer characts., Reynolds analogy soln. 79−59974
compact heat exchanger evaluation *(German)* 80−53614
compact heat transfer surface development, for heat exchanges with gaseous carriers 78−30296
complex heat exchange in scatt. laminar flow in cylindrical channel 78−83490
composite annular wick heat pipe analysis and performance 79−62153
composite cylinder, nonstationary temp. field 78−67014
composite materials, constant temperature front advancement 77−14884
composite solids with heat generation 79−76949
composites transient hygrothermal stresses, coupled diffusion of heat and moisture 80−33451
compound parabolic concentrator heat transport to storage 79−62102
compound unbounded cones, temp. fields *(Ukrainian)* 78−54317
compressible gas, heat exchange in free convection condition *(Russian)* 80−28502
compressible gas, turbulent boundary layer, surface roughness 78−90931
compressible laminar boundary layer, development and separation with adverse press. gradient 78−26144
compressible laminar boundary layer with large acceleration and cooling 77−11213
compressible laminar boundary layers, stagnation point flow with continuous moving surfaces 77−15054
compressible laminar boundary-layer, 2D eqn., near separation, numerical soln. 77−46989
compressible liquid flow with heat transfer, acoustic vel. 79−14131
compressible nonadiabatic gas flow in tube, eqns. system numerical integration *(Russian)* 78−83427
compressible stagnation pt. boundary layers for laser heated flows 77−89141
compressible turbulent flow, kinetic theory, comparison with classical theory 77−3814
compressible turbulent tube flow, heat transfer 78−71314
computer aided calc., programming 77−7289
computer aided calc., programming 77−7292
concave surface, with single jet in crossflow 80−1661
concentrator-receiver system with selective absorbing surface, heating characts. 80−91874
concentric cylinders, horizontal, outer cylinder rotating, inner cylinder at rest 77−84116

heat transfer continued
concentric domains, two dimensional heat equation general solution *(German)* 80−99918
concrete, effect of liner on heat and mass transfer characts. 78−17388
concrete block with double hollow, thermal performance, appl. for wall/roof insulation 80−19222
condensable mixture, high temp., heat transfer 80−33588
condensable rarefied gas flow through porous media, heat and mass transfer 78−59473
condensate film flow on finned surfaces, heat transfer, heat exchanger design 78−75038
condensate pattern for condensation of immiscible liquid binary vapour 78−94558
condensation, filmwise, onto vertical fluted plate, numerical anal. 78−94552
condensation, flow of vap. over cylinder, two-phase boundary layer eqns. 79−46306
condensation, gas-vap. mixture, in high-press. pipe 78−94589
condensation, laminar, intermittent charact. 78−94555
condensation, superheated vapour in vertical tube 78−87783
condensation and evaporation, contact angle and solid surface prop. effect 79−77867
condensation augmentation, horizontal tube, using twisted tape inserts and internal fins 78−71265
condensation between two parallel plates, emperical correlation predicting Nusselt number *(Japanese)* 80−92153
condensation dropwise theory, further developments 80−38245
condensation heat transfer, effect of surface thermal conductivity 78−22252
condensation heat transfer, nonequilib. temp. profiles, mass transfer engineering calc. 80−63227
condensation heat transfer in horizontal tube, effect of in-line static mixer 77−41626
condensation in channel, local (total) heat transfer coeffs., friction factors 78−51045
condensation in tubes with in-line static mixers, surface renewal model 78−75060
condensation of binary vapour in inert gas, heat and mass transfer 79−59916
condensation of laminar film on helical elliptical cylinders, governing eqns. soln. 78−9689
condensation of steam in tubes, augmented internal geom., and press. drop 78−94556
condensation of water vapour in rectangular channel, partially cooled perimeter 78−94557
condensation on rotating disc in presence of const. axial suction 77−42839
condensation over vertical flat plate, generalised soln. 80−59028
condensed film, flow down vertical surface, effect cooling conditions on heat exchange *(Russian)* 78−46934
condenser efficiency and performance enhancement, evaporative cooling *(German)* 79−72781
condensing mixed vapors, suction effects heat and mass transfer *(German)* 80−33609
condensing turbulent annular-mist flow, wall and interfacial shear stress 78−94812
conducting fluid, flow and heat transfer in channel in mag. field *(Russian)* 78−75218
conducting plate with temp. depend. resistivity and surface heat loss, temp., current and elec. field distribs. 77−42696
cone, rotating, flow and heat transfer obs., disc theories applicability 77−58673
cone in transition Reynolds no. domain, tangential injection effect on heat transfer 79−64654
conference, Aug. 78, Toronto, Canada 78−90624
conference, Davis, Calif., USA, Jun 1976 77−39295
confined perfect gas, thermal disturbance response, slow transients 79−81976
conical body laminar boundary layer with heat transfer *(Japanese)* 78−30257
conical nozzle and diffuser, laminar compressible boundary layer swirling flow 80−48768
conical tube, heat transfer with internal cooling by swirling air jet 77−55063
conjugate, numerical method calcs. 78−94522
conjugate heat exchange problems, soln. method *(Russian)* 79−64483
conjugated heat transfer in plate in flow, integral eqn. 78−87345
conjugated nonstationary heat exchange with pulsating fluid flow in circular tube *(Russian)* 79−68817
constitutive equations, for materials with memory 78−33986
contact angle hysteresis, dropwise condensation heat transfer 78−71273
contact conductance theory, effect of multiple sources 79−76942
contact heat transfer between heat-liberating element and surface of subliming solid cryoagent 78−81987
contact interface temp., internal thermal radiation effect 78−18151
contact of internally heated bodies, in fluid, temperature increase obs. *(German)* 77−35019
convective component in complex heat exchange in model of direct heating furnace 78−5631
convective heat exchange in fibrous materials, at elevated press. in gaseous medium 80−19217
convective heat transfer intensification and comparative heat transfer surface evaluation 78−30151
convective heat transfer with diffusion, finite element anal. 79−4011
convective heat transfer with phase change, finite element anal. 79−3887
converging shock and thermal waves, numerical study 77−62282
conveyors, vibrating, for bulk materials *(German)* 79−55314
cooled porous wall, temp. state, numerical soln. 80−14693
cooling, in oscillating liquid-filled cylinders 80−10117
cooling efficiency in flow around wall, initial turbulence effects 80−79315
cooling pond, heat transfer processes evaluation 78−61458
cooling pond with waves, heat transfer through thermal skin 79−100878
cooling ponds, atm. effects, numerical model study 80−8380
core-retention bed, horizontal heat transfer from molten fuel 77−46317
Cosserat fluid with heat transfer, universal stability and uniqueness of unsteady motions 79−50705
Couette flow, permeable wall layer, heat transfer and temp. distrib. 78−51165
Couette flow and heat transfer in rot. system 77−75878

heat transfer continued
countercurrently flowing fluids separated by thin wall, heat transfer 77−23949
coupled heat and mass transfer, stability, inertial wave effects calcs. 80−105593
crack, insulated line in semiinfinite medium under uniform heat flow, thermal stress near tip 77−72242
critical boiling heat fluxes to liquids at subatmospheric pressures 80−64345
critical energy in heat transfer channels of complex shape, fuel rod assembly 78−78453
critical heat flux for forced convection boiling in heated round tubes, generalised correlation 79−68697
critical heat flux in annuli, general correlation 80−43705
critical heat flux in vertical tubes, small length to diameter ratio, analytical study *(German)* 80−99922
critical heat flux of saturated natural convection boiling with heating from below 80−10114
critical heat transfer to flowing cooling water 77−74910
cross-current-flow past circular cylinders, surface roughness influence on heat transfer *(German)* 77−35134
cross-flow heat exchanger, performance where overall heat transfer coefficient is variable 78−8401
crossflow heat exchanger, approximate dynamic anal. by method of weighted residuals 80−92021
crossflow heat transfer efficiency for in-line tube bundles, one design factor effects 80−1573
cryogenic and ordinary liquids on vertical surface, film boiling heat transfer 80−48555
cryogenic conduit, calc. of stationary heat transfer zone under cooldown 80−10129
cryogenic container, cylindrical estimation of steady state heat link 79−35750
cryogenic electrical cables, heat influx problem, calc. 78−81988
cryogenic fluid, boiling, vapour bubble growth rate 77−24397
cryogenic fluid, boiling, vapour bubble growth rate 77−24398
cryogenic fluids, nucleate boiling, heat transfer rate 77−39199
cryogenic heat exchanger, transient performance of extended surfaces 77−30168
cryogenic heat pipe, heat and mass transfer 77−13758
cryogenic heat pipe, with metal-fibre wick, thermophys. characts. investig. 80−4725
cryogenic insulation, porous gas-filled, configurational effects on heat transfer 79−58734
cryogenic liquid, boiling, heat transfer coeffs. 78−9539
cryogenic liquid, heat transfer during transition boiling 77−35017
cryogenic liquid, pool boiling heat transfer, vapour bubble dynamics 77−31765
cryogenic liquid pool boiling, crises and heat transfer 80−1576
cryogenic liquids, boiling, crit. heat flux, heating surface props. effects 78−90662
cryogenic liquids, boiling in capillary-porous bodies, heat transfer 80−48552
cryogenic liquids, nucleate boiling, influence of thermal props. of heating surface material 77−46888
cryogenic liquids on flat horizontal surfaces, film boiling heat transfer 80−48553
cryogens, porous solids, gradientless heat transfer, cryogenic liq. crystn. 79−59903
cryogens, porous solids, gradientless heat transfer, metallic thermal cond. theory 79−59902
cryostat throat, with coaxial extension elements, heat exchange efficiency 80−77769
cryosurgical probe, heat transfer coeff. within cavity formed by tip 80−36188
crystal growth, macroscopic equilib. and transport concepts, book 80−27054
crystal growth by vertical directional crystallisation device, heat transfer, analytical investig. *(Russian)* 78−52654
crystal growth from melt, thermal conditions effect on stability 77−76343
crystallisation, plane front stability in single component system 77−31616
crystallisation front interaction with turbulent alloy melt stream, heat exchange *(Russian)* 80−74708
crystallisation on cooled wall with forced convection in melt 78−26022
crystallisation on vertical wall with thermal convection in melt 78−26021
cuboid, freezing, heat-balance integral calcs. 77−27981
current transformers, oil insulated, parameters influencing heating assessment using sensibility matrix *(Hungarian)* 80−87708
curved duct laminar flow and heat transfer 78−75144
curved pipe laminar flow anal., heat transfer 79−32674
curved semicircular sectors, fully developed viscous flow and heat transfer, Navier-Stokes soln. 80−14814
curved surfaces, turbulent boundary layer heat transfer 80−6056
curved tubes, fully developed laminar flow and heat transfer 80−79308
cyclohexane aqueous hetero-azeotrope mixture, condensation heat transfer coeff. *(German)* 80−33425
cyclonic, solar gas-solid chemical reactor, flash pyrolysis of wood sawdust *(French)* 80−61296
cylinder, and rising two-phase flow, electrochem. method 77−55076
cylinder, axisymmetric stagnation flow, steady state heat transfer, boundary layer solns. 77−31296
cylinder, circ., impulsively started from rest, heat transfer, numerical anal. 80−10248
cylinder, circular, three-dimensional transient thermal stresses under nonaxisymmetric temp. distrib. 80−92054
cylinder, heated, melting around it, photographic appl. 79−23195
cylinder, heated, turbulent temp. and thermal flux characts. using four-wire probe 80−19541
cylinder, hollow, heated on outer surface, cooled on inner surface, temp. and thermal stresses *(Russian)* 80−74712
cylinder, hollow, with finite width ring heat source, temp. distrib. exact soln. 77−84124
cylinder, rotating, non-steady temp. distrib. *(Polish)* 78−13885
cylinder heat transfer to turbulent cross-flow of water at critical Re *(Russian)* 78−34132
cylinder immersed in packed bed, heat transfer to gas flowing through bed 80−69823

heat transfer continued
cylinder immersed in porous medium, unsteady heat transfer, Darcy flow 80−83794
cylinder in cross flow, turbulence effect on heat transfer 79−1075
cylinder in cross flow in turbulent pipe flow, heat transfer 78−90874
cylinder in longitudinal flow, artificial boundary layer turbulence effect *(Russian)* 78−14008
cylinder in stabilised swirl flow having aerodynamic axis parallel to flow, calc. 80−79321
cylinder in turbulent or pulsed flow, heat transfer improvement *(French)* 77−42824
cylinder oscillating in cross flow, heat transfer 79−55386
to cylinders, between continuum and free mol. flow limits 79−98756
cylinders, one dimens. Stephan problems, direct and inverse, solns. 80−14552
cylinders in turbulent flow, heat transfer 79−1198
cylindrical and plane parallel layered materials, thermographic determination of heat transfer coeff. 80−19221
cylindrical annulus phase-change energy storage simulation 79−57478
cylindrical cavity wall, surface temp., periodic flux heating effects 77−46880
cylindrical heated pipe, suction effects on time derivs. of vel. fluctuations and temp. *(French)* 77−51116
cylindrical pipe, heat flow inequalities, appl. optimisation problem involving free boundaries 78−13889
cylindrical shrouded cavities, with rot. and coolant through flow 77−72294
cylindrical specimens in underheated media, calc. of heat transfer during quenching *(Russian)* 78−39821
cylindrical surface, aerosol particle capture, thermophoresis forces 80−103060
cylindrical thermocouple with plane frontal area, recovery factor in turbulent subsonic flow *(German)* 80−74882
Darcy flow, chilled pipe freezing zone, finite difference method 78−94734
data, book 78−154
n-decane, liq., thermal cond., meas. by transient hot-wire technique 80−103522
deconvolution of heat pulse transients 77−72403
desalination evaporator, falling-film, with vertically finned surfaces 80−58891
detached flows past a cylinder with a flat end, subsonic and transonic vels. 80−92187
deteriorated, in vertical steam generating tube at low pressures and moderate mass velocities of flow 78−67257
detonation wave front, heating of contained particles, residual cryst. defects anal. *(Russian)* 79−68749
Devon Island ice cap, Canada, heat transfer eqn. rel. to temp. profiles 79−16524
diamond type IIb, soft X-ray source for high resolution X-ray lithography 79−97481
dielectric drop in electric field, low Peclet number heat and mass transfer 80−6050
dielectric fluid, boiling on porous coating *(Russian)* 79−72788
dielectric fluid, flow and heat transfer in annular channel, electric field effect 80−103077
dielectric fluids vapours condensation, freon-113 and diethyl ether *(Russian)* 79−1055
dielectric layer, heat transfer coeff. meas., dilatometer method 78−45616
dielectric liquid, film condensation, heat transfer enhancement in elec. field 78−55551
diesel engine composite pistons, heat transfer calc. method *(French)* 78−63424
differential eqns. of heat and mass transfer, chessboard difference soln. method 77−82471
differential equations solution, using finite element method *(French)* 77−78965
diffusion boundary layers, with surface reactions, laminar or turbulent regimes, thermal simulation method 77−75912
diffusion equation, sols. by Picard's method 79−7273
dilute alloys solidification, numerical soln. model 79−69228
dimensionless equations for heat transfer in laminar flow with variable physical properties 78−83384
dimers, dissociating, in nonisothermal ideal gas phase, stationary state anal. 78−76848
in direction of gravitational force *(German)* 77−80049
disc rotating in air, partially enclosed, uniform wall heat flux 78−42601
disc rotating in jacket in presence of transitional boundary layer, local heat transfer 79−94608
disc with cut-out opening, temp. gradient 78−83222
disperse annular flow, crit. heat transfer, liq. distrib. 79−32209
disperse powder interaction in high temp. gas flow *(Russian)* 80−106830
disperse reactive system, nonsteady heat exchange 80−26061
dispersed drop-vap. flow, heat transfer, wall deposition and boiling 77−75965
dispersed droplet past-dryout regime, nonequilib. heat transfer model 80−64548
dispersed flow, heat and mass transfer, phase transition effect 78−67252
dispersed flow, heat and mass transport eqns. derivation, closure problem 77−89188
dispersed phase flow, heat transfer 78−90996
dispersed system in contact with vertical heating (cooling) surface 79−1069
dissociated high enthalpy hypersonic laminar air flow, heat transfer to flat plate 80−69828
dissociating gas in pipe flow, heat transfer crisis, flow laminarisation 79−1265
dissociating turbulent gas flow around triangular rod bundle, heat and mass transfer *(Russian)* 79−68822
domain perturbation and Green kernels in heat eqn., variational formula 79−97321
domains with sources having variable power, soln. 79−72891
double pipe heat exchangers, calc. of overall heat transfer coeff. 79−77109
downward-facing flat plate, stable film boiling heat transfer 77−23954
drag reducing viscoelastic fluid, heat transfer to turbulent flow 77−84249
drag reduction with surfactants at elevated temp. 77−68579
drop, drying of solute skin-covered soln. drop *(Russian)* 79−68561
drop, heat transfer, electric field effect 78−59276

heat transfer continued
drop, in electric field, transient heat and mass transfer 77−80226
drop condensate heat transfer, differential inequalities anal. 78−18293
droplet combustion, unsteady temp. modelling criteria 78−38179
droplet evaporation, modelled by wet porous sphere, heat-transfer meas. 78−59268
droplet evaporation on heated surfaces, theory 78−87785
droplet vaporisation in two-phase, gas+solid particle, flow 78−55677
droplets, saturated, impinging on heated vertical surface, expts. *(Japanese)* 80−10271
droplets, saturated, impinging on heated vertical surface, heat transfer characteristics and dynamic behaviour 80−14688
droplets in gas, heat and mass transfer rel. to high-intensity sound attenuation 77−62082
droplets in turbulent flow, heat and mass transfer 78−22410
droplets of soln. dispersed in gas flow, heat and mass transfer during evaporation 78−90998
drops, direct contact heat transfer with intermittent electric field 80−74869
drops and films, heat and mass transfer during vapour absorpt. 78−63427
drops in continuous fluid, effect of pulsation on mass and heat transfer *(French)* 78−55686
drops in immiscible liquid, intermittent elec. field heat transfer augmentation 78−94872
drops in liquid, diffusional interaction 79−81947
dropwise condensation, heat flux and drop size distrib. 79−50573
dropwise condensation, max. drop size rel. to heat transfer coeff. 78−94559
dropwise condensation of Hg, heat transfer meas. 78−94560
dry cooling, feasibility study, for industrial applications 80−87705
drying, heat and mass transfer, optimal control 78−67006
drying, heat transfer between plate and fluidised bed 77−11243
drying, temperature coeff. depend. on heat and mass transfer similarity criteria 78−83214
drying, various conditions, heat and mass transfer formulae 77−84123
drying intensification, thermolabile porous material in contact with sorbent, in vac. 77−89641
dryout in an SGHWR rod bundle, exptl. and calc. comparison 79−3192
DTA, thermal curve interpretation 80−45599
dual extremum principles for heat eqn. 78−70077
dual extremum principles for heat transfer problems with variable thermal props. 78−66999
dual jet discharged into rectangular duct, flow and heat transfer 80−43751
duct, narrow, plane, temp. distrib., heat flow to dense blown layer *(Russian)* 78−83402
duct, variable density fluids, vel. profile axial development due to heat transfer 80−74987
duct entrance region, laminar heat transfer, finite element method 80−69836
duct entrance region, numerical prediction of turbulent flow and heat transfer 77−80164
duct flow, with transverse plate blockage, surface heat and mass transfer coeffs. 78−75138
duct of arbitrary cross section, const. rate heat transfer 77−62304
duct rotating around perpendicular axis, flow and heat transfer, finite difference method 78−94752
duct with heated parallel plates, turbulent flow and heat transfer in entrance region, num. prediction 77−42830
ducts, one-dimensional models for transient gas-liquid flows 80−64614
ducts, spanwise-periodic and corrrugated, heat transfer and laminar flow 80−64547
Duluth-Superior Harbour, turbulent heat transport rel. to ice growth 79−2299
dust laden gas flow over plate, combined heat transfer, thermal fluxes 80−79289
dust particles and liquid in circular pipe, two-phase flow heat transfer 80−64607
dust-gas flows, steady and oscill., mean heat transfer 80−89536
dust-laden gas flow, heat transfer 78−14067
dusty gas flow in horiz. and vertical tubes, heat transfer 78−22409
dynamic heat transfer meas. at Mach 8, digital Fourier anal., boundary layer transition 80−14682
dynamic two-phase layer, heat exchange and mass transfer coeffs. of flat element 77−7439
Earth crust, heat and mass transfer from ascending magma 79−34768
Earth crust, heat transfer anisotropy assoc. with metamorphism rel. to heat-flow distrib. temporal changes 80−101347
Earth crust, heat transfer rel. to geothermal survey and search for fracture waters in Ukrainian Shield *(Russian)* 80−104935
Earth global heat balance, annual var. 78−73300
Earth global heat heat transport, rel. to ocean temperature-salinity curve 80−72534
Earth mantle, parametrised convection model rel. to Earth thermal history 79−16429
EBR II primary heat transport cct., steady state natural circulation performance 77−38326
EBR-II, whole core thermal-hydraulic phenomena, experimental study, 77−88206
eccentric spherical fluid shell, heat and mass transfer at large Peclet number 77−27520
eddy diffusivity, near open channel free surface, heat transfer expt. 78−5798
eddy turbulent heat transfer in stabilised pipe flow, calc. 78−83474
Eells-Sampson heat eqn., lifetime *(French)* 78−86227
effects of various working fluids on operational characteristics of heat pipes *(Japanese)* 79−37320
EHV transmission cable, in backfill, heat and mass transfer, physical props. effects 78−94543
elastic viscoplastic body, differential rheological eqn. *(Ukrainian)* 78−55617
elastic wave excitation by laser beam, through thermoelastic effect 80−103503
elastico-viscous MHD fluctuating flow past porous plate, heat transfer 79−90342
electric arc deformation by narrow insulating slot *(Russian)* 80−28861
electric motors, ribbed frames with external fans, heat transfer coefficient measurements *(Hungarian)* 80−87709
electrically conducting media with nonlinear heat release, turbulence props. 80−103024

heat transfer continued
electro-optic reflector, controlled, temp. fields, thermal distortions 80−96021
electrolyte aq. soln., boiling, heat transfer coeff. 78−9532
electrolytic cell, nonaqueous medium, heat transfer through diaphragm 78−73049
electrolytic method of mass transfer meas., advantages and disadvantages 79−68827
electron bombardment heater for heat transfer studies 77−30146
electronic components cooling tube, calc. method *(Russian)* 78−59271
electroslag refining, mathematical formulation for EMF, fluid flow, and heat transfer 78−52722
electroslag remelting, steady state segregation and heat flow 79−11629
ellipsoidal concentrators, shaping errors, effects on radiant energy characteristics 79−96418
emission of a rough-surfaced tube in turbulent water flow *(Russian)* 80−74837
energy balance in leaves, crops, hot and cold blooded animals 77−32875
engine, internal-combustion, heat exchange, b.c.s of 1st kind determ. from b.c.s of 2nd kind, numerical method *(Russian)* 79−68554
SW.England heat flow anomaly 77−49041
entrainment from body surface under convective aerodynamic heating, numerical soln. 79−81949
entrance region heat transfer in tube 78−26119
entrance region heat transfer in tube 78−26120
entrance region of straight channel with uniform heat flux, heat transfer 77−58688
entropy prod. of extended irreversible thermodynamics, invariant transforms. 80−73293
epitaxy of monocrystalline films, from gaseous phase *(Russian)* 80−55301
ethane, flow continuity in arterial capillary systems in cryogenic heat pipes 80−64536
ethane, heat transfer during boiling in tube *(Russian)* 77−68589
ethanol, aq. subcooled soln., acoustic phenomena during nucleate boiling 78−10181
ethanol, boiling, crit. heat flux in low press. region 78−90663
ethanol, boiling heat transfer coefficients, heater plate thickness effects 78−34124
ethanol, evaporating meniscus profile, evaporative heat flux 79−77868
ethanol, nucleate boiling heat transfer, press. factor 77−69080
ethanol evaporating meniscus, capillary flow heat transfer model anal. 79−82416
ethanol-water mixture, saturated, min. film boiling temp. on horiz. stainless steel and Cu surfaces 78−90692
ethylene, heat transfer during boiling in tube *(Russian)* 77−68589
ethylene glycol solution, flow boiling and pool boiling critical heat flux, effect of flow passage geometry 77−62250
ethylene-ethane mixtures, boiling heat transfer 78−9535
evacuated heat pipe solar collector, rectangular performance characts., trap mechanism 80−3531
evacuated multilayer insulation, method for evaluation of normal heat flux 80−53610
evaporating droplets, radiative absorption 80−33426
evaporating interline region, const. heat flux model 78−38178
evaporating surfaces, boiling heat transfer aspects 77−89011
evaporation from cooled surfaces, nonlinear eqns. numerical soln. *(German)* 80−58893
evaporation of drop, in EM field, theory 79−72787
evaporation of organic solvents, internal heating by IR irrad. 78−87237
evaporation with natural convection, simultaneous heat and mass transfer in laminar boundary layer, numerical anal. *(French)* 80−53778
evaporation zone of heat pipes, heat exchange mechanism and vapour formation laws 80−24023
evaporative, spray evaporator for spacecraft thermal control systems 80−29160
evaporative cooling, porous heat-producing element 79−32213
exchange monitoring between flame ang glass surface in furnace 77−26298
exchanger, wiped-film type, local heat transfer coeffs. 79−1051
exchanger design optimisation, w.r.t. transfer efficiency *(Russian)* 78−16789
experimental data acquisition system operational analysis models *(Russian)* 79−80588
experimental heat transfer data processing, automatic unit 79−93110
explosions, heat balance and reactant consumption 77−90601
explosive flashing in pools of liquids 80−92024
extended Graetz problem, approx. soln. by orthogonal collocation 77−89118
extended Graetz problem at low Peclet numbers 80−74850
extended Graetz problem with Dirichlet wall boundary conditions 80−74706
extended liquid masses, film boiling heat transfer, partial evaporation method 78−90668
extended surface heat transfer with condensation on to fin 78−94551
extended surfaces, total efficiency, uniform fouling deposit effects 79−1091
eye movements, caloric nystagmus, mathematical model 77−73525
falling film gas-liquid reactor anal. 79−86526
falling film vaporising surfaces, heat transfer coeff. 78−9542
fast nonstationary processes, characteristic method calcs. 80−83796
fast reactor transfer functions determ. 77−3082
FBR, attenuation of HCDA work potential by heat transfer 79−93773
FBR, HCDA, 2Z 79−49669
FBR HCDA, convective heat transfer correlations for molten core debris pools growing in concrete 80−83196
FBR meltdown, post accident heat removal anal., turbulent convection and interfacial freezing 79−49670
FBR meltdown, post-accident heat removal, heat transfer mechanism associated with immersed melting surfaces 79−49671
ferrofluid, transverse heat transport in mag. field 80−59031
ferromagnetic fluidized bed in mag. field, interphase heat exchange *(Russian)* 79−18675
ferromagnetic suspension, heat transfer for shear flow conditions 79−46394
ferromagnetic suspension, mag. field effect on heat transfer, thermal cond. 78−59500
ferrosuspension, MHD flow, heat transfer *(Russian)* 78−26203
film, condensation of moving vapour on horizontal cylinder, exptl. dependences 80−58892

heat transfer continued
film, liq., flowing down inclined plane with heat transfer, interfacial shear, stability 79−37290
film boiling, contact heat transfer meas. 77−42037
film boiling, effect of adsorption characts. on minimum temp. 80−79114
film boiling, heat-exchange intensification, nitrogen in pipes 79−81876
film boiling, hot sphere in subcooled liq. press. excursion of vap. film 79−14231
film boiling, minimum heat flux anal. 78−90665
film boiling crisis, surface material thermophys. props. influence, data correl. 80−5923
film boiling from cylindrical surfaces 79−23194
film boiling on sphere, in forced convection 79−32211
film condensation enhanced by surface forces, optimum condenser tube fin geometry 78−75039
film condensation inside pipes, heat transfer, general correlation 79−46312
film condensation of steam in vertical Cu tube, heat transfer coeff. 78−94553
film condensation of vapour in elec. field, heat exchange intensification 79−86331
film cooling with density difference between mainstream and secondary fluid, heat-mass transfer analogy 78−30293
film flow down rough surface, kinematic features *(Russian)* 80−79277
film heating in axisymmetric flow around cylinder, bulk flow twist effect on efficiency 77−23952
film- and transition-boiling heat transfer to cryogenic fluids 80−92026
film-type condensation, data correlation using method of thermodynamic similitude 79−90250
fin and tube heat exchanger, heat transfer, water spray effects 79−193
finite difference schemes for heat eqns. 79−37109
finite double layer body, one-dimens. heating problem *(German)* 80−38235
finite element analysis, heat transfer calcs., HEATRAN, diffusion eqn. soln. 77−3710
finite element method of calculation *(Japanese)* 78−89414
finite element nonlinear analysis, using an explicit stable method 77−89004
finned assemblies, dimensions effects on heat flowrate, free convection to condensation 80−74714
finned steam generating tubes, heat transfer enhancement, optimum geometry 80−48551
finned tube bundles in crossflow, heat transfer 80−1574
finned tube heat exchangers, improved design methods 80−95097
finned tubes bundle heat exchanger air flow heat transfer characts. investigation 78−21133
finned tubes with longitudinal flow 78−94731
finned-pipe solar energy collector optimal profile 79−62065
fins, extended surface array, heat flow evaluation, efficient algorithm 78−90635
first-order Cosserat fluid kinetic energy decay with heat and mass transfer 78−94524
fission reactor, effect of radiative heat transfer on thermal fluid behaviour of molten UO_2 79−93783
fission reactor, nuclear heating in B_4C control rod 77−42115
fission reactor, safety rel. to heat transfer problems 77−65276
fission reactor containment heat removal by passive heat solns. following LOCA 77−42019
fission reactor containment heat transfer following LOCA, anal. 77−54314
fission reactor fuel can temp. and thermoelastic stress perturbations, conjugate heat transfer effects 77−54284
fission reactor fuel test rods, directly heated, influence of thermocouples in wall 79−93706
fission reactor fuel thermal behaviour, relocated gap width estimation for gap conductance calcs. 80−589
fission reactor fuel-coolant interaction, UO_2 fragmentation by thermal stress and pressurisation 77−88226
fission reactor fuel-coolant interactions, temperature noise in one-phase heat transfer: stochastic models 80−68726
fission reactor LOCA, gravity-driven reflood hydrodynamics, EFLOD code 79−89426
fission reactor LOCA, reflood heat transfer and entrainment expts. 79−31060
fission reactor LOCA, thermal hydraulic phenomena resulting in early critical heat flux 79−81005
fission reactor rod bundle blowdown heat transfer instrumentation, transient two-phase flow meas. 80−685
fission reactors, flow boiling dynamics in film region 80−83142
fixed and fluidised beds, heat transfer from particle to fluid, stochastic model 78−51234
flame, atm. press., heat and mass transfer meas. using Ir/Ir-Rh alloy thermocouple 77−86314
flame, counterflow diffusion, struct. in elec. field, interferometric obs. 80−16685
flame, premixed, propag. in supersonic airstream 77−84339
flame, premixed, turbulent, interaction effects 77−11279
flame, turbulent mixed gases, thermal exchange effect on reaction rate 78−7205
flame front, distorted, hydrodynamic discontinuity model 77−58802
flame gases, effect of EHD boundary layer on heat transfer 77−80228
flame jet, premixed, impinging on plane surface, turbulent heat transfer 79−4054
flat bodies, thermal stress with absorption under local heat source *(Russian)* 79−64485
flat duct, inlet turbulence, local heat transfer, expt. 78−83480
flat duct, inlet zone turbulence under differing boundary layers, heat transfer, expt. 78−83481
flat duct thermal entrance region, anal. 77−54993
flat plate, gradual acceleration in variable viscosity fluid 78−30281
flat plate in electrostatic field, flow pattern, induction curtains, heat dissipation *(Korean)* 77−27619
flat plate solar collector with selective transparent and absorbing plates, thermal anal. 80−61427
flat plate solar collectors, insulation damage if fluid flow stops 80−3519
flat porous plate with suction, unsteady heat transfer, boundary layers 79−77105
float glass, heat transfer and temp. control in annealing, computer appl. 78−27543
flow, annulus entrance, finite-difference method 79−4013
flow, fully-developed, in non-circ. passages, prediction method 79−1254

heat transfer continued
flow, in tube, of air, local heat exchange meas. using heat flux transducers *(Russian)* 78−83509
flow, in two-dimens. channel, turbulent, with separation 80−19356
flow, nonequilib., two-phase, relation between thermal and flow characts. 78−55694
flow, over blunt nosed body, laminar or turbulent, heat transfer and curvature effects, numerical soln. 79−1173
flow, periodic thermally developed regime in ducts with streamwise periodic wall temperature or heat flux 78−59484
flow, steam-generating tubes, rough (smooth), post-dryout, heat transfer 78−55678
flow and heat transfer in the thermogravitational generation mode 78−94684
flow around rotating cones and discs, momentum, heat and mass transfer 79−1203
flow around smooth and rough surfaces, calc. of ht. transfer coeff. *(Russian)* 77−54992
flow boiling crisis in horizontal tubes, fluid-to-fluid modelling, water and Freon-12 80−48785
flow film boiling, void fraction meas. 80−92207
flow in base region of body, surface thermal conditions effect 78−42603
flow in circular tube, laminar and turbulent heat transfer calc. *(Russian)* 78−38175
flow in narrow annular channel, heat exchange, hydraulic resistance *(Russian)* 77−72299
flow inside rot. cavity 79−81899
flow measurement, hot-wire calib., for vel. and temp. meas., low-freq. effects 79−50825
flow normal to perforated plates, heat transfer and friction loss 78−94733
flow of compressible, viscous, heat-conducting gas, numerical simulation methods 80−38449
flow over 79−46308
flow over blunt body, wall accommodation at stagnation region 79−41708
flow over blunt plate, separated and reattached 79−32500
flow past nonuniformly heated plate, construction of upper and lower solns. 77−75915
flow past roughened surface, slope and intercept of dimensionless velocity profile 80−43701
flow section of elbow, overall heat transfer coeff. *(Russian)* 77−23958
flow-through reservoir, vel. and temp. fields, num. simulation 77−17152
flowing liquid, heat transfer and flow stabilisation problems *(Russian)* 77−80165
flows with heat addition, review 77−916
fluctuating flow past an infinite plate with suction and constant heat flux, analysis 79−50724
fluctuating free convection flow on horizontally magnetised plate 80−33683
fluid, cold, displacement by hot fluid in porous medium, stability 79−27691
fluid, combustion, vaporisation and heat transfer under elec. field 80−7798
fluid, electric field induced promotion of combustion, vaporisation, and heat transfer 79−20370
fluid film, laminar, convective coupled heat transfer, Nusselt no. computation 78−59398
fluid flow and heat transfer around two circular cylinders of different diameters in cross flow 80−14687
fluid flow in packed beds, effective heat transfer parameters, theoretical predictions 80−14802
fluid interfaces, isothermal and deformable, mass transfer and surface tension, review 80−33564
fluid interfaces, Marangoni instability, dissipative structures and nonlinear kinetics 80−33565
fluid interfaces dynamics and instability, conf., Lyngby, Denmark (May 1978) 80−31423
fluidic oscillator channels, heat transfer 77−58677
fluidised bed, axial heat transport and solid phase displacement 79−14473
fluidised bed, external heat transfer rate 78−9707
fluidised bed, free-space and external heat transfer fluctuations 77−84319
fluidised bed, heat and mass transfer, flow anal., separated flow model 78−9700
fluidised bed, heat and mass transfer, jet channelling theory 78−9702
fluidised bed, heat exchange intensification using bubble motion control 79−86508
fluidised bed, heat exchange with surface within bed, physical model 77−42918
fluidised bed, heat transfer depend. on packing *(Russian)* 79−68556
fluidised bed, heat transfer enhanced by turbulent jet 79−72940
fluidised bed, heat transfer from surface of fixed body 78−79368
fluidised bed, heat transfer from transverse streamlined cylinder during surface boiling 80−43708
fluidised bed, heat transfer in horizontal direction, thermal conduction coefficients determ. 79−60058
fluidised bed, heat transfer to staggered tube bundle 78−9708
fluidised bed, modified packet theory 77−35230
fluidised bed, plasma jet cooling mechanism 78−79371
fluidised bed, radiative contribution to total heat transfer 80−19384
fluidised bed, steady-state heat transfer 78−9704
fluidised bed, surface to bed heat transfer intensification at controlled gas distrib. 79−1246
fluidised bed, temperature pulsations of immersed body, heat transfer problem 77−47086
fluidised bed, to horizontal tube surface, adaptability for air cooled heat exchanger *(Japanese)* 77−58785
fluidised bed, vibrated, heat transfer coeffs. from tube bundles 78−9711
fluidised bed, vibrated, heat transfer from hot surface 78−9710
fluidised bed, wall to heat transfer 77−31380
fluidised bed, with immersed bank of smooth tubes 79−77241
fluidised bed 78−9703
fluidised bed in oscill. mode, heat and mass transfer 78−22417
fluidised bed two-level coolers, heat transfer 78−9705
fluidised bed with immersed horizontal tubes, local heat transfer coeffs. *(Russian)* 80−74880
fluidised bed with vibro-rotational motion, heat and mass transfer 78−9709
heat transfer continued
fluidised beds, heat exchange rate control, using magnetic field *(Russian)* 77−55083
fluidised beds, heat transfer coeff. between bed and vertically inserted tube wall 80−74971
fluidised beds, heat transfer to horizontal tube *(German)* 78−59387
fluidised beds, packed or quiescent, heat transfer from immersed heater 78−71391
fluidised beds, three-phase, heat transfer 79−60056
fluidised glass ballotini-packed fixed bed, at low/intermediate Reynolds nos. 79−1244
fluidized bed heat storage, baffled heat transfer anal. 80−30592
fluids, self organisation mechs., synergetics, analogy with laser process 77−34867
fluids, transport processes, space environment 79−46825
fluted tube, condensation heat transfer, Gregorig model 78−87236
fluted tubes, condensation heat transfer coeffs., valley flow and gravitation effects 80−19368
forced and free convective heat and mass transfer *(French)* 80−48689
forced convection heat propagation eqn., singularity theory *(Italian)* 79−18670
forced convection heat transfer enhancement by d.c. high voltage electric fields *(Japanese)* 79−98593
Fourier-Bessel series summation *(Polish)* 78−77818
fractured medium, transient 2-D diffusion 80−106841
free and forced convection, heat and momentum transfer with opposing flow 80−6061
free boundary problems for heat eqn. 77−54866
free convection and heat transfer from inclined isothermal plate, local nonsimilarity soln. 80−38403
free convection boundary layer flow and heat transfer, variational technique 80−106796
free convection effects in flow past accelerated plate in dissipative liquid 80−10246
free interface film hydrodynamic and heat transfer characteristics 80−92140
free molecular flow, recovery factor, accommodation coeffs. 77−15065
free molecule heating of micron size particles at hypersonic speeds 80−19442
free stream turbulence, effect on flow and heat transfer in annulus inlet 77−58647
free stream turbulence effect on skin friction and heat transfer from bluff body 79−86413
free stream turbulence effect on transfer to axisymmetric bodies 77−11216
freely flowing liquid film, cooling, heat transfer, turbulent transport model calcs. 80−64560
freezing, multidimensional problems in arbitrary domains, numerical method 78−90693
freezing in finite domains not initially at fusion temp., singular perturbation theory 77−66014
freezing in steady state turbulent flow between parallel plates 77−58680
Freon 22, boiling in internally finned tubes, heat transfer and hydraulics 79−81694
Freon F-113, boiling on porous Cu coating *(Russian)* 79−72788
Freon-113, boiling and heat transfer on horizontal pipes with annular fins 80−74855
Freon-114, Leidenfrost phenomena, crit. press. obs. 78−90667
freon-114 boundary layer, stability, press. gradient and heating effects 79−18891
Freon-11, pool-boiling, heat transfer from inclined plate 78−51046
frost, snow, heat transfer, cond., radiation and water vapour diffusion model 78−94563
frost formation, under forced convection, heat transfer and mass transfer *(Japanese)* 77−58533
frozen crust in forced flow on insulated wall, thermal stability 80−24011
frozen layer over convecting liq., frozen upper layer cooled by atoms 78−26118
fuel, liq. droplet, combustion, quasi-steady analytical model predictions 78−35681
fuel element modeling rod bundle in longit. air flow, heat transfer expt. 78−82415
fuel-to-cladding heat transfer coefficient in a reactor fuel element *(German)* 80−610
fully developed free convection flow in a circular pipe 79−64766
fully developed turbulent flow, between parallel plates, heat transfer in entrance region 78−1658
fundamental convective heat transfer, entropy generation 80−38411
fundamentals of momentum, heat and mass transfer, book 77−39294
fundamentals of transport props. of flows, book contrib. 77−84345
furnace heat transfer, 3-dimens, computer model predictions test 78−59504
furnaces, heat transfer and pollution *(French)* 79−16001
furnaces, industrial, heat recovery from exhaust gases *(German)* 80−38224
furnaces, walking-beam, numerical soln. of two-dimens. temp. field, boundary condition modification *(Polish)* 80−87706
fusion reactor, Doublet III beamline calorimeter, three dimens. heat transfer anal. 80−99381
fusion reactor blanket first wall time-depend. thermal stress model 78−787
fusion reactor blankets, MHD coolant flows, 3-D model 80−23119
fusion reactor thermosyphon energy removal system design 77−34465
gamma, teletherapy unit, radiation head, temp. distrib. 79−72790
gas, between parallel plates, higher kinetic moments, differential eqns., boundary conditions 77−75921
gas, in presence of acoustic turbulence, mean internal energy and oscill. absorpt. *(Russian)* 78−46962
gas, reson. oscills. in channel, local heat transfer coeffs. 78−1659
gas, thermally conducting radiative, propagation of initial disturbances, velocity dispersion and exponential decay *(Russian)* 80−48834
gas, turbulent heat transport meas., second order effects *(German)* 77−15030
gas, visco-magnetic heat flux, boundary and bulk regimes 79−98844
gas, with variable physical props., pipe flow, turbulent momentum and heat transfer calc. 78−90869
gas blast circuit breaking arcs, radiative energy transfer 80−1416
gas bubble, rise and cooling in viscous fluid *(Russian)* 80−74949
gas bubbles, flow and temp. fields, global collocation calcs. 77−47067
gas bubbles in liquids, thermal effects in forced radial oscills. 77−31375

heat transfer continued
gas carrying ducts in plate type heat exchanges, heat transfer and pressure drop 80−79291
gas centrifuge with insulated end walls, Stewartson layer struct., temp. distrib. 78−46973
gas centrifuge with insulated side wall, Stewartson layer struct., linearised eqns. 78−46974
gas cooled fast breeder reactor, roughened fuel rod bundle, expts. 77−18651
gas cooled fast breeder reactor thermohydraulic design codes, expt. verification 77−14221
gas cooled rough rod bundles, thermofluid dynamic expts., evaluation with code SAGAPO 80−24002
gas dispersion turbulent flow in tubes, nonisothermicity rel. to deposit form., heat transfer 79−55409
gas equilibrium temperature, heat transfer near Hartmann-Sprenger tube end plate *(French)* 77−62247
gas evolving electrodes, heat transfer concept 79−34314
gas flow, transient heat transfer in presence of time depend. temp. 77−84252
gas flow in duct with fin, heat transfer, drag 77−62253
gas flow in rectangular channel with single fin, heat exchange and pressure drop *(Russian)* 77−23957
gas flow in smooth and rough channels, heat transfer efficiency comparison 78−51243
gas flow instability, nonlinear stabilization of unstabel acoustical vibrations in a bounded heat-evolving medium 80−6028
gas flow over semiinfinite plate with heat sources, unsteady conjugate heat exchange 77−75918
gas flow regime choice in pipes with max. temp. at outlet 80−19396
gas fluidised bed, bubble induced heat transfer 77−7435
gas fluidised bed, heat transfer assisted by alternating electric field 78−9697
gas injection into liquid stream, heat transfer rates 78−14075
gas jet, heat transfer to porous baffle 79−98776
gas jet, wall impact model, subsonic 78−34176
gas kinetic boundary value problem, non-equilibrium thermodynamics 80−19544
gas mixture, binary, condensation in boundary layer flow, numerical method 79−1236
gas mixtures, removal of condensing component by suction through porous walls 79−98787
gas separation in vortex tube, theory and expts. *(Japanese)* 79−4021
gas suspension flow in long horizontal pipe, heat exchange investig. 80−19388
gas system entropy waves dissipation, power plant appl. 80−19395
gas temperature in Hartmann-Sprenger tube calc., using Lagrange equations *(Japanese)* 79−4041
gas turbine, temperature gradient along cooling channel surface, heat transfer in initial hydrodynamic section, effects 79−18892
gas turbine combustion chamber, isothermal model, bluff body, recirculation phenomena in primary zone 79−47925
gas turbine holes rows, anal. 79−7376
gas turbine stator, meas. method 79−98731
gas-cooled annuli, turbulent heat transfer 78−94723
gas-film cooling efficiency in supersonic axisymmetric nozzles 79−98715
gas-liquid cocurrent flow through packed beds, radial effective thermal conductivity 78−1723
gas-liquid dispersion, mechanically agitated, heat transfer to helical cooling coil 79−4063
gas-liquid flow in vertical tubes, Graetz problem 78−91001
gas-liquid mixture, bubble mode of flow in vertical pipe 80−24081
gas-particle heat transfer in shallow fluidised beds 77−35227
gas-radiating particle mixture, shock wave struct. numerical investigation 80−10298
gas-regulated heat pipe, anal. of operating temp. regimes 78−194
gas-solid flow, nonreacting, heat and mass transfer, thermodynamic approach 78−51223
gas-solid flow local heat transfer, particles distrib. 78−9686
gas-solid flowing mixtures, heat transfer 77−58773
gas-solid fluidised bed, particle temp. meas. 78−83464
gas-solid interactions, rel. to reduction of aerodynamic friction and aerothermal heating 79−95896
gas-solid layer, mech. agitated, fully- (partly-) fluidised, thermal evolution *(French)* 78−34193
gas-solid mixture, pulsating flow, hydraulic resistance, heat transfer 78−38392
gas-solid packed bed systems, conduction mode 79−68705
gas-solid packed bed systems, heat transfer, review 79−68704
gas-solid packed bed systems, overall heat transfer rates in adiabatic beds 79−68706
gas-solid particle suspension, turbulent flow in curvilinear channel, local heat exchange 78−63484
gas-solid reactive flow near stagnation point, transient heat and mass exchange 79−77104
gas-solid suspension, free turbulence influence on heat transfer 77−42898
gas-solid suspension, turbulent heat transfer during motion in tubes *(Russian)* 77−24020
gas-solid turbulent flow, heat transfer, model 79−1232
gas-vapour droplets, nonuniform mixture, acoustic wave attenuation 78−83154
gasdynamic stand for heat transfer and combustion product testing 79−39085
gaseous screen with longitudinal press. gradient 80−23998
gases, heat flow birefringence, improved meas. apparatus 80−10355
gases, theory for wide press. variations 78−30402
gauge, thin film type for shock tube *(Japanese)* 77−19654
GCFR cores, heat transfer with He and Na coolants, review 79−45331
general, anal. using CSMP package 78−75145
generalised thermomechanics, principle of least constraint *(Russian)* 78−59295
geothermal, conduction-limited wells, energy output estimation 79−87964
geothermal energy, heat extraction from hot dry rock masses 78−61378
geothermal energy extraction, through hydraulically induced fracturesin hot dry rock 79−34424
geothermal energy resources of Kamchatka, unsteady heat and mass transfer model 77−64234
geothermal heat, extraction by water circulation through crack in dry hot rock mass 79−57355
heat transfer continued
geothermal reservoirs, mathematical modelling of heat and mass transfer 80−55802
geothermal saturated strata maintained by linear, ring batteries of wells, heat exchange 80−45630
geothermal steam power plants, using fossil superheating, thermodynamic analysis 79−48088
glass container formation, glass-metal boundary heat flow 80−79117
glass melting, review 78−3084
glass melting process model, for flameheated tank furnace melting *(Polish)* 80−70380
glass to mould heat transfer during pressing 78−80500
glass workability rel. to melting history, microstruct., apparent liquidus temp., mechanical props. 80−11633
glow discharge heat transfer, stabilisation method for diffusion bonding 80−38221
glow discharge infinite, dense gas homogeneity, theory 77−51253
granular material pneumatic conveying, gas-to-particle heat transfer 79−18927
granular materials, flow around heated cylinder, thermal wake and separation point 77−31302
granular materials, heat and mass transfer with low Peclet number flow *(German)* 78−42656
granular materials pneumatically transported, heat transfer and lateral mixing 78−87378
granulate-fluid heat exchange, analogy with calorimetry problem 78−90644
graphite, thermal shock on a finite orthotropic thin shell 79−68587
graphite-air mixture steady and oscill., mean heat transfer 80−89536
gravitational field influence on turbulent flow and heat exchange, review 79−86427
gravity-assist heat pipes with capillary flow, dry-out phenomena 80−79398
Greens kernels, domain perturbation in heat eqn. 80−48546
grid generated turbulence, uniform strain effect on thermal fluctuations 80−103026
grid-generated turbulence, temp. fluctuation decay obs. 79−32506
ground to atmosphere *(French)* 79−84403
Hall and ion slip currents effect on heat transfer in MHD fluid in channel 79−27702
Hartmann-Sprenger tube, thermal effects, finite difference method for analysis 80−14771
heat and mass transfer, book contrib. 77−58693
heat and mass transfer bibliography−Soviet works 79−23318
heat and mass transfer bibliograpphy−Soviet works 80−90618
heat and mass transfer development in USSR 79−14201
heat and mass transfer in a suspension of matter in gas with capillary-porous particles 79−87885
heat and mass transfer in capillary-porous body, kinetic eqns. 78−5796
heat and mass transfer in domains with variable and fixed boundaries 78−33995
heat and mass transfer in porous media subject to fires 79−86507
heat and salt transfer across diffusive interface, grid generated turbulence 77−7381
heat collectors, with direct and concentrated radiation, maximum equilibrium temp. determ. 80−92031
heat conducting simple fluid with memory, nonsteady helical flow 79−81900
heat conductors with randomly varying boundaries, Green's functions *(German)* 79−32188
heat diffusion as source of aerodynamic sound 77−7382
heat diffusion in solid sphere, Fourier theory 80−31456
heat engines, minimum entropy prod. and optimisation 80−85297
heat eqn., general free boundary problems 77−68375
heat eqn., general free boundary problems 77−68378
heat eqn., solvability of boundary value problem *(Ukrainian)* 77−67204
heat eqn. with u.s.c. obstacle, soln. existence *(French)* 79−26001
heat equations, Green kernels and domain perturbation 79−68563
heat exchange between two-phase flow and nozzle wall with condensate film 79−46357
heat exchange intensification, fission reactor tubular fuel elements 77−61497
heat exchanger, air-water greater operational efficiency of P-67 boiler 79−68710
heat exchanger, circulation loop, heat transfer 78−33994
heat exchanger, linear heat transfer in wall *(Russian)* 79−98594
heat exchanger, porous cylindrical board temp. field, heat transfer efficiency 78−5793
heat exchanger for divided solids 79−59912
heat exchangers, countercurrent, dynamic response to temp. disturbance and step flow variations 79−1084
heat exchangers, heat flow calcs., algorithm *(German)* 80−1418
heat exchangers, heat transfer augmentaion techniques for conservation of available work 80−103021
heat exchangers, multitube type, operation, influence of deposits *(Rumanian)* 79−94467
heat exchangers, surface scale formation anal., heat transfer surface utilisation 80−48550
heat flux equation, turbulent boundary layer, local similarity model 78−75142
heat flux rectifiers 79−58751
heat flux-flow coupling effects in the stability of vapour generators *(German)* 80−74967
heat generating and transmitting elements, thermal dynamics anal. 78−9548
heat generating fluids, one-dimens. flow, thermal unsteady regimes, nuclear reactor appl. 79−1179
heat instability in thermoviscoelastic coupled dynamic problems *(Russian)* 79−10489
heat pipe, 2-component, heat and mass transfer 80−24021
heat pipe, centrifugal, cylindrical, heat transfer, heat flux density and vap. press. effects 78−79188
heat pipe, gas-loaded, near ideal, analytical model 80−53615
heat pipe, high temp., subsonic vapour flux, heat exchange and friction 77−75779
heat pipe, low-temp., evaporator-condenser interrelation effect on thermal resistance 77−89003
heat pipe, performance deterioration with excess wetting fluid 77−5831
heat pipe, theory of operation, comparison of theoretical and expt. data *(Japanese)* 78−29106
heat pipe, wickless, low-temp., crit. heat/mass transfer 78−42517

heat transfer continued
heat pipe entrainment limit, max. operating heat transfer rates 80−14683
heat pipe with active porous medium filling, for solar appl., operating characts., efficiency *(French)* 77−42725
heat pipe with capillary struct., thermal characts. 80−14558
heat pipe with extended temp. range 80−38231
heat pipes, flow with injection 79−1065
heat pipes, heat and mass transfer, one-dimens. model 79−1064
heat pipes, heat transfer characts., application to waste heat recovery 79−49223
heat pipes, operating limits 80−92028
heat pipes, rotating, temperature and heat load distrib. 80−64341
heat regenerator, approx. soln. of regenerator eqn. 79−59918
heat resistant monocrystal growth apparatus, heat regimes, crystallisation *(Russian)* 80−107071
heat storage unit, finite conductivity effect 79−55316
heat storage unit, transient response 79−55313
heat transfer and drag on moving bodies 78−9706
heat tube, hydrodynamic characts. *(Russian)* 78−30280
heat-emitted pipe, with surface boiling, temp. fluctuations *(Russian)* 80−102962
heated cone, heat transfer and shear stress 79−46168
heated flat plate in water, critical Reynolds number, heat transfer 80−69766
heated pounds, turbulent boundary layer of stratified airflow, surface waves 80−92133
heated spherical particle motion, reduction of temp. and mass influences 79−46320
heated tubes, alternate dry and rewet, flow boiling, obstruction effects 79−1181
heated wire and doped insulating liquid, influence of elec. field on heat transfer *(French)* 80−28409
heating element, heat exchange, effects of nonstationary liberation of power *(Russian)* 80−69636
helical channel flow, heat transfer 80−6150
n-heptane, boiling heat transfer coefficients, heater plate thickness effects 78−34124
n-heptane, pseudoboiling mechanism, improved heat transfer 78−6152
n-heptane, self-excited thermoacoustic oscills. in heat transfer 78−79186
n-hexane, heat transfer from horizontal wire, AC and DC-electric field effect 77−31202
n-hexane and mixtures with n-pentane, nucleate boiling from tube arrays 78−22251
high intensity local, meas. errors anal. *(Russian)* 80−74865
high-speed rotating anode disc, spot motion and erosion calc. 78−71498
high-vacuum insulation, calc. method 77−89123
holographic interferometry methods and applications *(French)* 79−7099
horizontal coiled tube banks, two-phase flow boiling heat transfer and hydrodynamics 80−48708
horizontal cylinder, local boiling heat flux density, saturated, subcooled conditions 78−90659
horizontal flat plate, heat transfer in natural convection flow *(Japanese)* 79−64658
horizontal gas filled current conductor, calc. 78−1656
horizontal heated surface, heat transfer to water spray *(Japanese)* 80−99917
horizontal heated surface, post-nucleate boiling and crit. heat flux models 78−90664
horizontal immersed tubes in fluidised bed, heat transfer, surface roughness effects 80−6044
horizontal multitube bundles, boiling heat transfer 80−10122
horizontal tube, heat transfer with filmwise condensation, vapour vel. influence 80−33598
horizontal tube transition and flow boiling heat transfer, bubble flow 78−18292
horizontal tubes, saturated flow boiling, non-uniform heat flux effects *(German)* 80−74716
horizontal tubes in fluidised beds, local heat transfer coeffs. 80−74875
horizontal wavy channels, heat transfer and flow 80−69921
hot film in reversing shear flow, heat transfer 77−15014
hot film probe, heat transfer to substrate *(French)* 79−23381
hot film transmitter, simulation, Beuken method *(German)* 78−55546
hot wall with impinging liq. droplet, transient temp. profile 78−75050
hot water storage tank, heat loss rel. to thermal insulation *(Japanese)* 80−5918
hot wire in liquid, heat transfer, transverse oscills. effects, holographic interferometry 77−15013
hot wire readings, wall proximity effects heat transfer, laminar and turbulent boundary layers 80−48822
HTGR, passage walls heat transfer performance study *(Japanese)* 77−18687
HTGR piping, heat transfer characts. of horizontal annular insulation layer *(Japanese)* 79−26520
HTR core, radiant heat transfer following failure of afterheat removal system 80−773
Hugoniot eqn. corollaries, impact heat transfer and shock waves 80−92132
human skin and subcutaneous tissue, unsteady state heat transfer, similarity transformations 78−95990
humid materials, diffusivity and specific heat, transient temp. changes *(French)* 80−64355
hybrid thermal energy storage system, transient simulation 80−30588
hybrid thermal energy storage with water systems, eval. using analytical models 80−30589
hydraulic resistance of annular heat transfer channels rel. to boiling *(Russian)* 77−80143
hydrocarbons, boiling heat transfer 78−9535
hydrocarbons, pool boiling, heat transfer, surface roughness effect 80−48705
hydrodynamic resistance and heat exchange from flow past rotating cylinder *(Russian)* 80−1586
hydrodynamic thermal breakdown in viscous fluid, Couette flow between cylinders 78−83391
hydrophobic and hydrophilous surfaces, effect on transfer at crit. temp. *(Russian)* 80−23871
hydroresistor thermoanemometer, empirical heat exchange eqn. 80−21852
hydrothermal systems, transport phenomena assoc. with cooling plutons 78−36206
hyperbolic heat eqn., equilibrium soln., asymptotic stability 78−13887

heat transfer continued
hypersonic boundary layer over slender sharp cone, turbulent shear stresses, heat transfer 77−23989
hypersonic flow, body form for minimum heat transmission *(Russian)* 79−37131
hypersonic flow about yawed blunted cone, similar boundary layer anal. for lee-surface heating 77−27553
hypersonic flow over blunt body, viscous shock-layer eqns. 79−60002
hypersonic flow past disintegrating blunt bodies, radiative heating in H_2-He atms. 80−69865
hypersonic free-molecular heating of micron size particulate 79−4058
hypersonic laminar heat transfer to cones at angle of attack 79−1211
hypersonic shock tunnel, development for aerospace simulation 79−41777
hypersonic turbulent compression corner flow, numerical simulation 77−62276
hypersonic viscous shock layer, leeward vortex-induced heat transfer 77−80179
hypersonic viscous shock layer, three-dimens., numerical calc. on sharp cone at incidence 77−47041
hyperthermia in dogs, rel. to post surgical rewarming by thoracic flush 78−80834
hypoelliptic degenerated operator heat eqn. behaviour for short times *(French)* 79−93077
ice, heat and mass transfer during sublimation, thermal shock method 77−50864
ice, heated water jet impingement melting, cavity formation, expt. and simulation 78−95133
ice, thermal fracture 79−65141
ice layer profile on const. temp. plate in forced laminar convection flow 80−24006
ice-water interface, wave formation, heat transfer in presence of turbulent flow 80−103015
Icelandic subglacial volcanism, magma/ice heat transfer rel. to eruption character 80−101350
immiscible liquids, direct-contact heat exchange 78−30155
impinging jets, heat transfer, appl. to compact heat exchangers 79−1071
impringement flow, skin friction and heat transfer meas., hot and cold-film sensors 77−27629
impulse chamber for intensifying heat exchange *(Russian)* 80−43597
impulsive stagnation flow, unsteady thermal boundary layer 77−75914
in-reactor fuel-to-sheath heat transfer meas. 79−13408
incipient fluidisation, particle to gas heat transfer, axial gas thermal dispersion coeffs. 80−10238
inclined air layers, heat transfer, secondary instability 80−38397
inclined flat plate with isothermally heated surface downwards, natural convection heat transfer investigation 79−10563
inclined rectangular plate, heat transfer and fluid flow, finite width effects 79−81884
inclusion flaws, and delaminations, heat transfer formulation 80−71820
inclusions in gas-liquid mixture, effect on interphase heat and mass exchange 80−103059
incompressible flow including heat and mass transfer, vel.-press. coupling treatment 80−69832
incompressible laminar limit layer, heat transfer with phase transition *(French)* 78−94561
incompressible liquid, gradient turbulent flow, heat transfer of nonisothermic surfaces in wide range of Pr and Re numbers 77−35135
incompressible liquids, laminar heat transport anal. using nonlinear temp. transform. *(Spanish)* 79−68693
incompressible MHD flow with heat transfer between inclined walls 79−68819
incompressible temp. boundary layer, von Mises variables, explicit finite difference method 79−80448
incompressible viscous fluid, entrance region heat transfer in plane Couette flow, num. procedure 77−15020
indirect heating systems, heat-carrying molten salt eutectic mixture *(German)* 80−38233
induction gas heater discharge channel heat exchange *(Russian)* 79−18677
industrial plants, heat exchanger installations, heater min. furnace diameter determ. *(German)* 80−38234
infinite plate, thin liquid film evaporation, surface temp. and heat transfer 80−64346
infinite porous plate, heat and mass transfer 78−30352
ingot, heat exchange between melt stream and crystn. *(Russian)* 79−69043
inhomogeneous heat eqn., uniqueness and representation theorems 79−71383
inhomogeneous heat equation with right side supported in strip, fundamental soln. 78−22253
inhomogeneous rod in complex heat exchange conditions, temp. calcs., film sputtering evaporators *(Russian)* 80−38230
inhomogeneous thermal system, thermal cond. and boundary resistance at low temp., heat flow model calc. 80−10120
initial boundary value problem for three dimensional heat equation, Rothe's line method *(German)* 78−30147
injection bubbling and boiling in liqs., heat transfer 77−68672
injection of heat into liquid, new technique 78−5637
injector with distrib. multijet liquid supply, efficiency and performance 80−74939
inorganic hydrate, solidification, heat transfer processes *(Japanese)* 80−6372
inorganic solid, interfacial endothermic reaction, abnormal thermal decomp. rate 78−76852
insulated plate thermometer, incompressible boundary layer flow 78−55626
insulated water layer, combined heat transfer, stratified layer, energy eqn., boundary value problem 80−79290
insulating element, laminated, vac. drying in inert heat-transfer vap. 78−56875
insulating oil, Senftleben effect, under uniform DC elec. stress 77−31395
integral eqn. kernel approx. in axially symmetric temp. problem 79−35643
interfacial stability with heat and mass transfer, appl. to Rayleigh-Taylor and Kelvin-Helmholtz cases 78−67253
interferometry, high fringe density technique, appl. to heat transfer *(German)* 78−21212
interline region heat transfer, London-Van der Waals dispersion force effect 78−71276

heat transfer continued
intermittency in free turbulent shear flows 80−19348
internal boiling and superheating in vaporizing multicomponent droplets 79−3906
internal flows with initial swirl, generated heat and mass transfer law 80−24025
internally energised flat shaped porous element, non-Darcy flow with phase change 79−94709
internally finned helical coil, fluid flow and heat transfer 77−62249
internally finned tube and annuli, turbulent flow and heat transfer 79−81979
internally finned tubes, refrigerant 22, evaporative heat transfer and pressure drop 80−5919
interphase mass flux and mass fluxes within phases 80−48561
interrupted wall channels heat transfer and flow anal., appl. to heat exchangers 79−81883
intratumour temperature in heated superficial tumour 77−32876
inverse problem for the heat equation, Neumann and Dirichlet data correl. 79−23184
ionosphere, diffusion and heat flow eqns. with large temp. differences between interacting species 79−66857
ionosphere, electrons collision freq. and transport props. 79−80079
ionosphere, topside, protonospheric heat flux rel. to electron temp. models 80−67460
irreversible chemical process, in elec. field, heat and mass transfer 78−11545
irreversible transport processes, noncoupled, nonstationary, classical variational principles 78−4567
irrotational flow, heating by rigid walls 79−98730
isobutane-air, in packed bed, heat and mass transfer, axial mass dispersion 78−75200
isoperimetric lower bound for one sided linear radiation condition 79−32195
isotherm migration method along orthogonal flow lines, implicit scheme 80−24000
isothermal continuous cylinder, thermal laminar boundary layer 78−22321
isothermal flat plate, boundary layer flow with transpiration, heat and mass transfer 79−94613
isotropic porous media, heat and mass transfer, physical props. effects 78−94543
isotropic semiinfinite plate heated by moving point source of heat, temperature stresses 80−43628
Japanese literature (1975-1976) 78−79314
jet, axially symmetric, impingement on plate, heat transfer characts., inner peak in heat flux 80−28540
jet, axisymmetric, turbulent bulge struct. 78−90955
jet, free, heated, turbulent, high temp., eddy diffusion, methane combustion obs. 78−30329
jet, heat transfer during impingement on sphere or cylinder rel. to turbulence *(Russian)* 78−38327
jet, impinging, eddy struct. effect on heat transfer 79−1227
jet, laminar axisymmetric impinging, heat transfer 77−42888
jet, laminar rectangular, mass transfer due to impinging on flat surface 77−68651
jet, laminar slot type, flow field and impingement heat transfer, num. prediction 77−42891
jet, nonisothermal axisymmetric turbulent transfer, vel. and temp. fluctuations, correl. coeffs. 78−83445
jet, subsonic, flow and heat near blunt body stagnation point 77−65774
jet, turbulent and heated, temp. and vel. meas. 78−94784
jet, turbulent mixing layer, conditional meas. 79−32598
jet entrainment at density interface in thermally stratified vessel 80−6119
jet flow from round impinging array, heat transfer and hydrodynamics 80−79374
jet flow with vectored surface mass transfer, heat transfer 78−26174
jet heat transfer, impact model, hydrodynamic conditions 78−83447
jet impact system with unilateral outlet, air flow, heat exchange *(Russian)* 78−83449
jet impinging on rotating disc, heat transfer 78−30334
jet impinging wall, heat and momentum transfer, approx. solns. 79−60041
jet row impinging on concave semi-cylinder surface, heat transfer, theory and expt. 78−94794
jet stagnation point heat transfer on plate, turbulence effects, liquid crystal meas. 78−18327
jets, axisymmetric and flat, heat transfer in vicinity of stagnation point, turbulence effect 80−48697
jets, impact system, with unilateral flow outlet, local heat exchange *(Russian)* 79−64730
jets, micropolar fluid, impinging normally on flat plate, thermal boundary layer 80−28536
jets and wakes, intermittency determ. from probability density function of passive scalar 77−3827
Joule heat concentrators, metal foil expts. max. heat release, cracks in conductors 80−92022
Joule heat engine and pump, demonstration 80−105480
Jupiter, solar heating and internal heat flow 78−85888
Jupiter atmosphere heat transports, role of zonal flow baroclinic instabilities 80−31245
Kilauea 1977 lava flow, heat transfer meas. 80−85632
Knudsen gas, heat transfer between two plates at unequal temp. 79−86469
kohlestein thermal insulation, temp. and heat flux distribs. meas. *(German)* 78−26023
lake ice cover, dissipation, effect of surface meltwater accumulation, heat flow 80−8364
lake vertical temp. profile determ. by one-dimensional heat transfer eqn. soln. 78−77290
lakes, latent and sensible heat fluxes prediction from surface water temps. 80−72562
lakes, stagnant, thermal stratification 80−36340
Lambertian cavity with dielectric window, effective absorptivity 80−38237
lamina, porous, generalised boundary conditions, heat and moisture transfer Prudnikov problem soln. 78−1551
laminar airflow through heat exchanges, heat transfer and press. drop results 80−19379
laminar boundary alyer flow, heat transfer, rel. to vel. fluctuations 78−94710
heat transfer continued
laminar boundary layer, finite amplitude high frequency oscillations 80−6024
laminar boundary layer, heat transfer, mass transfer and friction coeffs. *(German)* 80−74881
laminar boundary layer, heated, stability 78−9626
laminar boundary layer, heated, with nonuniform surface temp. distrib., stability 78−67175
laminar boundary layer, with press. fluctuations heat transfer, friction *(Russian)* 77−89114
laminar boundary layer behaviour on continuous, accelerating surfaces 78−22320
laminar boundary layer flow along vaporising liq. layer *(German)* 78−83403
laminar boundary layer heat transfer along static and moving cylinders 80−79316
laminar boundary layer heat transfer over rot. bodies 79−32517
laminar boundary layer swirling flow with heat and mass transfer in conical nozzles and diffusers 79−81842
laminar boundary layer with press. fluctuations, friction and heat transfer 79−64652
laminar boundary layers, nonsimilar incompressible heat transfer analysis using method of strained coords. 77−42811
laminar boundary layers, separation in water, heating and suction, comments 79−14378
laminar boundary layers on concave curved walls, heating effect on stability 77−65745
laminar boundary on surface of circular cylinder moving in fluid, flow pattern and heat transfer 80−28487
laminar channel flow, heat transfer in entrance region 79−32518
laminar channel flow, heat transfer internal conjugate problem 79−90254
laminar chemically nonequilibrium mixture flow, characts. of combined heat and mass transfer *(Russian)* 79−59965
laminar compressible boundary layer, with vectored mass transfer 77−23974
laminar compressible boundary layer on rot. sphere with heat transfer, buoyancy and viscous dissipation effects 77−15053
laminar compressible boundary layer swirling flow in nozzle, flow and heat tranfer 78−94795
laminar compressible boundary layers for laser heated swirling nozzle and diffuser flow 80−53831
laminar compressible MHD boundary layer flow, effect on heat transfer 79−14489
laminar condensation heat and mass transfer at stagnation point of droplet in ternary mixture 79−14227
laminar Couette flow between parallel plates, heat transfer 77−31299
laminar cyclone, free and forced convection 78−55548
laminar falling liquid films, mass transfer with heat transfer and interfacial shear 80−80033
laminar film boiling heat transfer, thermal conductivity and convection effects 80−74864
laminar film condensation, non-condensing gas in tube 78−94554
laminar film condensation on vertical surface with heat generation 79−72786
laminar flow, circular channel with rod clusters, heat transfer characts. 78−75140
laminar flow, constricted parallel duct, numerical anal. 77−80155
laminar flow, coupled heat and mass transfer, around flat plate with uniform heat flux 78−1631
laminar flow, steady heat transfer between parallel plates, with conduction in wall 77−47003
laminar flow around plate containing heat sources 77−23948
laminar flow at supercritical pressure 79−81872
laminar flow between parallel plates with suction, heat transfer characts. 80−79301
laminar flow between porous plates, heat transfer 79−68708
laminar flow in curved annulus 77−42820
laminar flow in duct with one moving wall 77−7456
laminar flow in internally finned tubes 78−94725
laminar flow in planar (quasiplanar) channel with variable cross section, heat transfer 78−1661
laminar flow in straight horizontal elliptical tubes, heat transfer to Newtonian liquids 79−94584
laminar flow instability in multiple channels 79−90217
laminar flow through finned tube, friction factors 78−94730
laminar fluid film, heat transfer, variable viscosity influence 80−64561
laminar free convection past heated vertical plate, leading and trailing edge and discontinuous temp. effects 77−15028
laminar gas jets, heat exchange *(Russian)* 80−53829
laminar heat exchange in thermally initial portion of tube with variable wall temp., asymptotic soln. 77−58675
laminar heat transfer, downstream of sudden duct enlargement 78−67196
laminar heat transfer for boundary layers with mass injection and chemical reactions *(Chinese)* 80−59020
laminar heat transfer in circular tubes and annular passages 77−72133
laminar heat transfer in tube, liq. solidification in thermal entrance region 78−18346
laminar impinging jets, heat and mass transfer 78−94777
laminar jet, dynamic and heat problems 78−67241
laminar jet impingement heat transfer to melting ice surface 78−22394
laminar liquid films, dependence of temp. variation of film substance viscosity 79−41686
laminar longitudinal flow over cylinder, numerical investig. 80−19389
laminar MHD pipe flow with heat transfer 79−14482
laminar periodic flow regime in channel, appl. heat exchanger 77−58678
laminar plane wall jet, temp. distrib. due to variably heated wall 80−19463
laminar steady free surface flow past a permeable bed, buoyancy effects *(German)* 79−41665
laminar swirling impinging jet, heat transfer, numerical calc. 79−1228
laminar tube flow with varying wall temp., heat transfer anal. 78−38318
laminar unsteady viscous plane stagnation flows, incompressible boundary layer, heat transfer 80−1584
laminar vapor flow calculations in a flat-plate heat pipe 80−23869
laminar wall plume in transverse mag. field 79−86398
laminar water boundary layer on heated cones, variable viscosity effect, heat transfer, shear stress 79−32520
laminar-vacuum insulation, nonstationary heat and mass transfer 78−59279

heat transfer continued
laminar-vacuum insulation, nonstationary heat and mass transfer 78−59280
land basin with snow, radiative cooling 78−88872
large deflections of heated orthotropic plates 79−32262
laser beam hygroscopic aerosol interaction 77−79888
laser beam materials processing, thermophys. and hydrodynamic effects 78−19957
laser CW material processing, heat transfer model 80−64336
laser flash method, error evaluation in heating disc 77−6552
laser heated nozzle flow with swirl, axisymmetric comp. boundary layer 80−14775
laser surface transformation hardening, heat flow model for cylinder 80−93700
laser-fusion reactor, surface heating of 1st wall by pulsed photon and ion irrad. 78−89979
latent heat solar energy storage system, heat transfer eqns., numerical soln. 80−55926
Laval nozzles, flows with heat addition, book contrib. 80−1671
law of metastability, appl. to effect of mag. field on boiling liqs. 78−79199
layered porous medium transient 2-D diffusion 80−106841
Lewis number, heat and mass transfer coeff. derivation 80−14698
Lighthill nonlinear integral equation, soln. 79−6061
limiting relative law of heat and mass transfer and friction, permeability parameter effect 80−23999
limiting vapour qualities in second boiling crisis 79−81970
linear heat equation from kinetic theory of gases 78−94877
liquid, dielectrophoretic heat transfer 78−94874
liquid, forced channel flow with surface boiling, analogies between heat and momentum transfer 77−47014
liquid, with temp.-depend. thermophysical props., flow over nonisothermal surface *(Russian)* 79−64661
liquid acceleration in channel by intermittent vaporisation, pulsed transfer of energy 79−94701
liquid axisymmetric jet on baffle, heat and mass transfer 79−98775
liquid boundary layer flow on plate, heat transfer rel. to external flow *(Russian)* 78−38329
liquid drop deposition in two phase dispersed flow heat transfer 79−81959
liquid droplet, direct contact with high temp. surface, Leidenfrost temp. model 78−90666
liquid drops moving in single file in liquid continuum, heat transfer 79−46367
liquid filead porous medium, linear thermoconsolidation eqns. 79−98601
liquid film, evaporating heat transfer model 78−30154
liquid film, falling, laminar, evaporation model 79−46305
liquid film, falling, laminar, transport augmentation by surface waves 78−71343
liquid film, in vertical tube with turbulent gas flow, friction coeff., press. losses 77−89189
liquid film, subcooled, heat transfer and film breakdown 78−34121
liquid film, turbulent, heat transfer predictions for nonsheared and sheared films 77−15024
liquid film, with nucleate boiling, heat transfer and film breakdown 78−34122
liquid film crossflow around cylinder, local heat transfer 79−98711
liquid film flowing down polymer surface, heat transfer 78−30278
liquid film hydrodynamics and heat transfer expts. *(German)* 78−18305
liquid film on rotating surface, hydrodynamics and heat exchange, entrance section influence, interface frictional forces 79−86433
liquid film turbulent flow, heat transfer, friction factor 77−42819
liquid film vapour absorption, combined heat and mass transfer 79−19430
liquid films, boiling, heat transfer peculiarities 78−90656
liquid films, heated horizontal channel, heat transfer and dry patch formation 80−64554
liquid films on horizontal tubes, combined boiling and evaporation 79−81882
liquid flow around cylinder, thermophys. characts. rel. to friction and heat transfer *(Russian)* 78−38328
liquid flow blockage in circular tube below freezing point, theory and expt. 78−94830
liquid flow in rot. pipe, fully developed heat transfer 77−58689
liquid fuel droplets, transient heat flow in combustion gases, models 78−63507
liquid fuel film, combustion behind shock wave, heat and mass transfer in turbulent boundary layer *(Russian)* 78−71401
liquid fuel fluidised bed combustion, heat transfer to horizontal steam generator surfaces 80−48549
liquid He, pool heat transfer, in high centrifugal accel. field 77−15034
liquid in closed rot. annular cavity, heat exchange, flow regimes 78−5753
liquid in rot. system, Hall effects on MHD Couette flow and heat transfer 79−41681
liquid jet, burnout in nucleate boiling 78−90991
liquid layer flowing down inclined plane, heating and cooling effects on stability 80−79254
liquid layer on rot. Archimedes spiral, heat transfer 79−14410
liquid layer on rot. surface, heat transfer, gas flow interaction 78−22347
liquid layers, superposed, boiling, convection heat transfer 78−30159
liquid metal boiling, mag. field effect on bubble growth 79−32217
liquid metal film, turbulent flow down vertical wall under gravity, heat transfer 78−59396
liquid metal flow in heat pipe, low temp. region, effect of compressibility, friction and evaporation 77−47066
liquid metal flowing in closed cylindrical cavity *(Russian)* 77−67799
liquid metal heat transfer in closed conduits 77−47016
liquid metal heat transfer in regular fuel element arrays, Nusselt no. calc. 78−89932
liquid metal second-order thermal boundary layer 79−77106
liquid metal tube flow, turbulence, heat transfer, thermogravitation effect 78−71315
liquid metals, flow in tube in mag. field, turbulent transfer coeff. *(Russian)* 78−75220
liquid metals, heat transfer criterial eqns. anal. 79−68707
liquid metals, heat transfer with gas bubbled through *(Russian)* 80−38395
liquid metals, turbulent heat transfer, Nusselt no. calcs. 77−31304
liquid metals, turbulent heat transfer characts. 78−42602
heat transfer continued
liquid metals, turbulent temp. fluctuations, in heated pipe flow, theory 77−84246
liquid metals in metallic containers, thermoelectric MHD 79−64787
liquid Na crossflow, heat transfer round circular cylinder 79−86429
liquid phase crater profile calc., formed by conc. heat source *(Russian)* 77−72131
liquid pipe flow, heat exchange and resistance calc. 78−94819
liquid refrigerants, heat transfer enhancement during boiling at low heat fluxes 78−9529
liquid solidification about cold cylindrical pipe 80−19383
liquid-filled closed volumes, temp. stratification at const. heat flux density 79−81871
liquid-gas interface, heat and mass transfer 78−30338
liquid-metal-H_2O stratified flow, horizontal co-current, interface heat transfer, turbulence model 80−92131
liquid-solid evaporator, wall to liq. heat transfer, distillation plant 79−1245
liquid-vapour flow, heat transfer crisis, wall shear stress 78−90986
liquid-vapour flow, wave pattern and liq. film burnout 78−90985
liquid-vapour flow in heat transfer crisis, liq. film limiting flow rate 78−90987
liquid-vapour interface stability and eqn. of motion, heat flux 80−92023
liquid-vapour transformations, statistical kinetic theory 77−20044
liquids, critical heat flux density in annular channels *(Russian)* 78−37407
liquids and gases, measurement using transient hot-wire technique 79−200
liquids in longwave limit, static and dynamic stability, heat diffusion 80−92138
LMFBR, coolant thermodynamics and fluid dynamics *(Spanish)* 79−6726
LMFBR, effects of Na entrainment and heat transfer with UO_2 vapour during HCDA 79−93775
LMFBR, HCDA, dryout in porous bed of nuclear fuel debris, heat transfer regimes 77−46316
LMFBR, intersubassembly heat transfer effects during natural circulation 80−584
LMFBR, Na-H_2O steam generator, calc. local heat fluxes in circular channels 79−36312
LMFBR, radiative heat transfer in horizontal molten fuel layer with volumetric heating 79−93786
LMFBR, red. of two-phase thermal cond. and heat transfer by entrained inert gases 79−30897
LMFBR, temp. distrib. of subassembly including intersubassembly heat transfer 77−83014
LMFBR, thermal-hydraulic core anal., interassembly heat transfer, TRITON computer code 79−59153
LMFBR core assemblies, interassembly heat transfer, using CORTEMP code 79−59154
LMFBR evaporator tube, critical heat flux meas. 80−591
LMFBR evaporator tubes, corrosion and heat transfer 79−1088
LMFBR finite hexagonal bundles, three-dimensional coupled coolant cell heat transfer anal. 80−586
LMFBR HCDA radiological consequences, attenuation by thermal radiation 77−46321
LMFBR heat exchangers, liquid metal temps. in pipes with wall fast flow discontinuities *(Spanish)* 77−74907
LMFBR hypothetical core disruptive accident, simplified multicomponent phase transition model 79−31016
LMFBR plant, modelling thermal hydraulic transients 77−88207
LMFBR wire wrapped rods, 3-D thermal-hydraulic anal. 77−79425
local, cross flow, free convection and free stream turbulence effects 77−15009
local equilibrium theory for steady states with heat flow near critical points 80−105599
local heat exchange during axisymmetric air jet interaction with cylinder lateral surface *(Russian)* 79−60043
local heat flux distributions, highly inhomogeneous, auxiliary-wall meas. method 80−5917
local heat transfer between plate and immobile and boiling layers 79−14218
local heat transfer coeffs. for flow around sphere, semi-empirical method 80−24026
local heat transfer from inline tube bank to air crossflow *(Russian)* 78−5746
local heat transfer in tubes with heat flux constant over length and variable over perimeter 78−30163
local mass/heat transfer distribution on surfaces roughened with small square ribs 80−19506
longitudinal and cross flow around heat exchanger tube bundles comparison, heat transfer efficiency aspects 78−94687
longitudinal gas flow in cylindrical channel, heat transfer with elec. arc 77−11189
longitudinally ribbed surfaces, turbulent boundary layer drag and heat transfer characts. 80−14684
low temp. heat pipe, internal heat transfer visualisation 78−94533
low temp. heat pipe, metal-fibre wick thermal cond., heat transfer coeffs. 78−83217
low temperature heat pipes, heat transfer in heating zone for capillary structs. 80−38226
low velocity vertical steam-water flow, void fraction in pipes 80−74964
low-flow vessels, temp. gradients, appl. to blood temp. distrib. 78−27990
low-temp. heat pipes, vapour-gas bubbles removal in arteries 80−19490
low-temp. solar water heaters, tubular heat receptacles screen parameters optimisation 80−92030
lumped mass approximation of heat eqn., uniform convergence 79−18669
LWR, effect of pellet cracking on fuel temp. 77−3085
LWR, heat transfer model of quenching in reflooding phase *(Japanese)* 78−8874
LWR safety, condensation heat transfer in stably stratified systems 80−63311
MacCormack's scheme, acceleration, appl. to heat eqn. 78−36808
magmatic diapir folds, heat exchange with crustal materials rel. to evolution *(Russian)* 80−104957
magnetic fluids, heat and mass transfer 80−59123
magnetisable liquid, thermomagnetic convection between coaxial cylinders with distributed heat source 79−94622
magnetofluid, self-gravitating, local behaviour of congruences 78−89384

heat transfer continued
magnetohydrodynamic generator, semi-hot, heat transfer between duct wall element and holder *(Japanese)* 79−72791
magnetorheological systems, heat transfer 79−81988
mainstream acceleration effect on heat transfer and wall temp. downstream of gas injection 79−1251
major satellites of outer planets, internal structs. 79−62770
Manicouagan impact melt sheet, Quebec, clast-melt heat transfer rel. to thermal history 78−81167
Mare Serenitatis, heat transfer during mare flooding rel. to elec. cond. anomaly 80−56730
marine two stroke compression ignition engines, computer modelling 80−30529
Mars, thermal history and evolution and surface heat flux 78−65533
Mars atmosphere, baroclinic eddies and topographically forced long waves 78−45255
mass and heat transfer between turbulent flowing fluid and solid wavy surface 80−14681
mass force field boiling crisis, critical heat flux for swirling tube flow 79−90248
mass transfer and friction under complex thermogasdynamic conditions 79−1209
massive bodies, optimum heating given restriction of heating control and rate *(Russian)* 79−68546
mathematical model, stochastic perturbation effect 78−94546
Maxwellian molecule gas, heat transfer between parallel plates, Navier-Stokes eqns. 80−87839
mean heat of emission and hydraulic resist. of banks of tubes *(Russian)* 80−96262
mean zonal wind in upper troposphere, determ. with allowance for turbulent heat fluxes *(German)* 78−32137
measurement, light fibre-photomultiplier combination 77−2658
Mediterranean Sea, heat and water budgets, dependence on climate and Atlantic waters 79−84291
melt reacting with gas jet, heat and mass transfer, mathematical modeling 80−87819
melt solidification, heat and mass transfer 79−14236
melting, closed form solution to problem with heat generation by viscous friction *(Japanese)* 80−19225
melting, Landau problem, numerical soln. of bedding eqns. 79−14233
melting, of substrate into different miscible liq. layer, hydrodynamic instability, heat transfer 78−90695
melting and evaporation simultaneously due to area heat source *(German)* 78−59282
melting and freezing problems, heat balance integral method, refinement 79−14229
melting behaviour induced by horizontal row of heating cylinders 80−33442
melting heat transfer in steady laminar flow over flat plate 77−15027
melting in finite domains not initially at fusion temp., singular perturbation theory 77−66014
melting problem of slab with heat generation by friction, approx. anal. *(Japanese)* 80−14555
melting process, with convective boundary condition, surface temp. rel. to time 79−76960
melting solid, role of natural convection 78−71275
melting/freezing interface, annular region, perturbation soln. 78−59286
meniscus thin film transition region, heat transfer 80−6058
l-menthol, vap., homogeneous nucleation, high-temp. Becker-Doering theory predictions 78−67820
metal, freezing at mean heat exchange intensity in irregular mode stage *(Russian)* 79−52193
metal, mathematical model for unidirectional solidification, massive moulds 79−56971
metal fibre wicks, max. heat flux 80−19390
metal surface crater form., by laser pulse, frontal method, approx. soln. 77−77327
metal-liquid He interface, electron-phonon interaction, thermal boundary resistance 78−67899
metallic heat carrier in loops, phase transition process, temp. field 79−55867
metals, heating by concentrated energy sources, simple analytical expressions *(Russian)* 80−38215
metals, thermal instabilities due to recomb. of radiation-induced Frenkel pairs 79−23597
meter dynamic properties *(Russian)* 78−86265
methane(-ethane)(-N_2), heat transfer in nucleate boiling of liquified gases and binary mixtures *(German)* 79−18687
methane-hydrogen mixture, flow through glass bead bed, axial dispersion coefficients 79−46378
MHD, gas boundary layer swirling nozzle and diffuser flows with mag. field 80−1693
MHD, heat transfer between porous discs, one rotating one at rest 80−28561
MHD, nonsimilar incompressible laminar boundary layers, finite-difference scheme 78−79386
MHD, two-dimens., parallel plane channel flow, heat transfer 80−14833
MHD air heater, directly fired, using cored brick matrix, materials and design concepts testing 79−52949
MHD channel, ion slippage 78−75431
MHD channel flow heat transfer, Hall effect and ion slip 77−80220
MHD channel flow heat transfer, third-kind temp. boundary conditions 77−47095
MHD channel flow of rarefied gas, external circuit effects on heat transfer 80−83860
MHD channel with uniform wall heat flux, heat transfer, Hall and ion-slip current effects 80−92230
MHD Couette flow, Hall and ion-slip effects, heat transfer 79−94726
MHD Couette flow, with variable wall temp., heat transfer 79−27640
MHD Couette flow and heat transfer in rotating system 77−35246
MHD Couette flow with porous boundary 80−53876
MHD Ekman layer on porous flat plate, heat transfer, steady asymptotic soln. 78−79385
MHD flow, between coaxial cylinders with wall temp. discontinuity, temp. distrib. 80−1690
MHD flow, effects of pressure gradient, suction, injection 80−53872
MHD flow, past porous flat plate, Hall effects 78−14093
MHD flow and heat transfer over semi-infinite plate under transverse mag. field 77−80225
MHD flow between parallel plates, temp. field, vel. field, skin friction, heat transfer 77−68700

heat transfer continued
MHD flow in rot. channel, wall conductances effect on heat transfer 78−51245
MHD flow over stretching sheet 79−72956
mHD flow past a semi-infinite flat plate with heat transfer, exact numerical solns. of boundary layer similarity eqns. 80−83861
MHD free convection about semi-infinite plate in strong cross field, skin friction, heat transfer 77−15134
MHD generators, liquid-metal, two-phase, power generation cycle, interfacial heat and mechanical energy transfers 80−1409
MHD laminar flow in parallel-plate channel with unequal wall temperature, thermal entry heat transfer 77−42927
MHD plant, coal-fired, thermal modelling of components 79−52946
MHD power generation problems, overview 78−87503
MHD rotating channel of parallel plates, Hall effects on heat transfer 77−42926
MHD shock waves with heat addition 79−55427
MHD slip flow regime over porous plate, skin friction and heat transfer 77−31392
MHD turbulent heat and momentum transfer in 2-dimens. channel with transverse mag. field 78−94848
MHD unsteady thermal boundary layer flow 77−7460
microcalorimeters, conductive type 77−10025
microemulsions, heat transfer meas. by laser-induced thermal blooming 80−91833
micropolar fluid, heat transfer in boundary layer flow, past curved surface 79−46316
micropolar fluid, heat transfer in stagnation point flow 80−79356
micropolar fluid, thermal boundary layer at stagnation point 80−53820
micropolar fluid layer subject to magnetic field, thermal instability 80−64585
micropolar fluid on circular cylinder, thermal boundary layer 78−75174
micropolar laminar radial channel flow, heat transfer 78−30328
microstructural fluid, heat exchange under boundary conditions of the third kind 80−87771
microwave thermography: principles, methods and clinical applications 79−100691
Mirror Fusion Test Facility supercond. coil development 79−31202
miscible non-isothermal vertical displacement stability through homogeneous porous medium *(French)* 80−43771
mist flow, evaporation of droplets 77−55350
mist flow over heated cylinder, particle size and temp. difference effects 80−38409
mixing vessel wall, heat transfer coeff. correlation 80−10123
mixing vessels, unsteady heat transport *(German)* 80−33608
mixture, binary, nucleate boiling heat transfer, conc. depend. 78−87249
modelling of eigenvalues and eigenfunctions of heat and mass transfer systems 77−14872
moist material, external heat transfer, calc. methods, drying kinetics 78−59467
moist materials, drying kinetics calc. method, heat (moisture) transfer 78−55555
moist porous material subject to sudden heating, mass transfer, press. rise 77−58787
moisture transfer, multiphase, in porous media with temp. gradient 80−19497
molecular Prandtl number, influence on turbulence in shear flow, book contrib. 80−1541
molecular-kinetic generalisation of the heat-transfer equation 78−67219
molten salt, thermal cond., heat storage, review *(Japanese)* 80−6573
momentum, heat and mass transfer during flow around a sphere, free stream turbulence effects, mathematical model *(German)* 79−41678
momentum, heat and mass transfer during flow around a sphere, free stream turbulence effects *(German)* 79−41677
momentum balance of continuous media, correction based on Ott's transformation 78−41249
moving boundary domains, heat and mass transfer with phase transition 79−81695
moving boundary problems, weak soln. 80−179
moving layer, heat exchange, numerical-anal. soln. 77−7291
moving surface and flowing medium, penetration model predictions 77−42835
multicomponent flow through porous media from underground nuclear explosion, flow stability 80−53857
multicomponent fluid systems, symmetry of transport matrix for diffusion and heat flow 80−99997
multicomponent gas mixtures, effect of thermodiffusive separation on heat transfer 79−81696
multicomponent system, heat transfer rates effect on diffusion 77−7393
multijet mixing chamber of plasma heating unit, heat exchange calcs. *(Russian)* 77−68813
multilayer antisolar glazing heat throughput calc. 78−94415
multilayer insulation, heat and mass transfer during evacuation 77−30167
multilayer insulation, heat flux, residual gas press. distrib. 77−30163
multilayer insulation, heat transfer model 79−94465
multiphase flow, spherical particles, thermal conductivity determ. 78−71390
multiphase processes, density-wave oscillations, linear stability anal. 80−48775
multiple scatt. in semi-infinite spatially inhomogeneous medium *(Russian)* 77−75786
multiple-jet thermal mixing in a piping tee 79−81938
multistage countercurrent fluidized-bed heat exchanger, optimal heating surface 77−89200
multistage flash evaporation phenomena 78−2246
muscle contraction, simulation of thermophysical processes 78−96063
narrow ducts and circular tubes, laminar flow-heat transfer, series solutions 79−72946
narrow zone heating of bodies *(Russian)* 77−72132
natural convection boundary layer turbulence next to heated vertical surfaces 79−68684
natural convection in liquid layer in flat inclined solar energy panel *(French)* 79−18894
natural fluid circulation, horizontal pipe, closed at one end 77−47091
near-critical fluids in turbulent flow through tubes, heat transfer num. prediction method 77−42832
nematic liquid crystal flow in flat channel, heat transfer anal. *(Russian)* 77−72397
neutron and photon, heat deposition, rate in nuclear reactor 78−29565

heat transfer continued
Newtonian and non-Newtonian fluid, laminar heat transfer, in tubes 78−9624
nomogram for heat transfer coefficient determ., water flowing in pipes or tubes 78−9641
non-flowing boiling water films, critical breakup thicknesses 79−94468
non-isothermal disc rot. in quiescent compressible gas, heat transfer 80−14704
non-isothermal liquid flow and heat transfer in sintered metallic porous media 79−86506
non-linear transport equations: Properties deduced through transformation groups 80−4680
non-Newtonian flow, in coiled tubes, anal. and exptl. verification 77−55052
non-Newtonian flow through pipes, heat transfer 79−32592
non-Newtonian fluid, free convection, heat and mass transfer 79−68765
non-Newtonian fluid, heat transfer by fluctuating flow past porous plate 78−38309
non-Newtonian fluid, laminar boundary layer, surface heat transfer rate 80−24055
non-Newtonian fluid, laminar pipe flow, nonisothermal, heat transfer, with internal heat sources 79−68763
non-Newtonian fluid, pipe flow, heat and mass transfer 79−46309
non-Newtonian fluid, unsteady laminar incompressible boundary layer eqns., flow, heat and mass transfer, similarity solns. 79−32590
non-Newtonian fluid duct flow, heat transfer 79−1219
non-Newtonian fluids, heat transfer in plane Couette flow with additional pressure gradient including entrance effects 79−50760
non-Newtonian fluids, literature review 77−23999
non-Newtonian fluids in jacketed agitated vessel, heat transfer, viscosity correl. 78−75143
non-Newtonian laminar falling film, with smooth wave free gas-liq. interface 79−7389
non-Newtonian liquid, heat flux from nonisothermal surfaces to gradient flows *(Russian)* 79−68767
non-Newtonian nonisothermal flow, in slowly converging channel 77−89168
non-Newtonian solid-filled systems, transfer phenomena, interface-adjoining phase struct. effects 79−77099
non-Newtonian turbulent transport in circular tube 77−39313
non-Newtonian unsteady flow between parallel walls, velocity and temp. fields 77−39314
nonequilibrium isobaric chemically reactive flow, parameters for heating (cooling) *(Russian)* 80−59131
nonequilibrium reactive flow over solid body, conjugate heat and mass exchange 77−42931
nongrey radiation, IR band model correls. 77−57286
nonhomogeneous medium, backwards heat eqn. soln. approx., partial differential eqn. 80−53611
nonideal thermal contact, heat exchange between thin walled bodies *(Russian)* 80−14553
nonisothermal fixed bed adsorpt. column with nonlinear equilib., heat and mass transfer 77−80209
nonisothermal flow of viscous or non-Newtonian fluids over rotors of centrifugal heat exchangers 79−77097
nonisothermal heat transfer equations, hyperbolic, derivation from variational principle *(Russian)* 79−68543
nonisothermal laminar flow in pipes 77−58741
nonisothermal mixture motion through porous media, sorption dynamics and heat exchange kinetics 77−7447
nonisothermal sorption within adsorbent particle, heat and mass balance 79−19452
nonisothermal turbulent suction-controlled boundary layer, heat and mass transfer coeffs. at chemically-reactive surface 79−77102
nonlinear, finite element anal. 79−23189
nonlinear, iterative-variational method 78−94511
nonlinear, soln. by variational imbedding 77−65669
nonlinear anisotropic simultaneous transport processes, variational principle *(Russian)* 79−88893
nonlinear boundary condition problems 77−72127
nonlinear direct and inverse heat and mass transfer, analogue and hybrid simulation 77−53767
nonlinear heat and mass transfer in porous media 80−1577
nonlinear interdependent heat and mass transfer, variational solution *(Russian)* 79−88894
nonlinear Rayleigh-Taylor stability with mass and heat transfer 79−90224
nonlinear simultaneous transport processes, complimentary form of variational principle *(Russian)* 79−54076
nonlinear simultaneous transport processes, variational principle *(Russian)* 79−58653
nonlinear thermal conductivity boundary-values qualitative anal. 77−14879
nonlinear Volterra integro-differential equation, heat flow appl. 79−18668
nonlinearity viscoplastic liquid, convective dissipative heat exchange 80−87772
nonNewtonian duct flow, wall heat transfer in entrance region 79−4049
nonparallel stability of two-dimensional nonuniformly heated boundary-layer flows 80−38401
nonstationary, finite element calcs. 80−83795
nonstationary flow between rotating coaxial porous discs, porosity effects 79−32657
nonstationary heat exchange in a plane slot *(Russian)* 80−1578
nonstationary heat exchange with phase transformations, delayed boiling influence *(Russian)* 78−83235
nonstationary heat flux measurement by auxiliary wall sensors 80−86287
nonstationary heat fluxes meas. by heat meters using auxiliary wall method 78−59275
nonstationary heat processes in spent nuclear fuel element containers *(Bulgarian)* 80−69637
nonuniform fluidised bed, external heat exchange mechanism 77−47085
North Sea, heat exchange with atmosphere rel. to sea surface temp. changes, (1948 to 1974) 80−67367
novel Monte Carlo binning technique 79−160
nozzle, convergent-divergent, compressible turbulent boundary-layer heat transfer *(German)* 78−22399
nozzle, critical air flow, heat transfer, numerical study 79−98778
nozzle, heat flux determ. using computer 77−42894
nozzle, heat transfer of transonic air flow 79−1230
heat transfer continued
nozzle, subsonic and supersonic, turbulent boundary layer heat transfer 79−1229
nozzle, two phase, efficiency at high rates of heat and mass transfer 80−48767
nozzle boundary layer equations for laser heated flow, similarity soln. 77−31355
nozzle expansion in turbulent flow, downstream heat and mass transfer 80−1669
nozzle gas blast flows with arc heating 79−46502
nozzle of rocket, compressible turbulent boundary layers, heat transfer and skin-friction 79−14451
nozzles with turbulent high temp. gas flow 80−24068
nuclear electric plants, vertical steam generator tubes, forced convection heat transfer *(French)* 79−98729
nuclear fuel element cladding, corrosion product deposition, heat transfer model *(Bulgarian)* 80−71818
nuclear fuel pins, eccentrically placed pellets, finite difference method for heat transfer 78−82419
nuclear fuel rod, computer code for calc. effect of asymmetric geometries 79−49743
nuclear fuel-cladding interaction between cracked surfaces, mechanical and temp. contact 78−66341
nuclear heat exchanger, shell-and-tube, flow distrib. anal., rel. to CRBRP-IHX 77−42052
nuclear materials interfaces, thermal radiation props. 79−80980
nuclear power plant heat exchange problems 80−18372
nuclear power station spray cooling, heat and mass atmospheric transfer 78−94078
nuclear reactor, fuel element array, temp. distrib. for turbulent liq. metal flow 78−13203
nuclear reactor, fuel rod arrays, radiative heat transfer, Monte Carlo method 78−78447
nuclear reactor, GCFR, thermohydraulic performance of ribbed surfaces 77−50200
nuclear reactor, heat transfer between hot metal spheres and subcooled heat 77−26832
nuclear reactor accidents, molten fuel-coolant interaction modelling, INTER and CEFRA *(Czech)* 78−66352
nuclear reactor flow boiling anal., numerical standards 77−79448
nuclear reactor fuel, Leidenfrost temperature for spherical fuel particles, rel. to FCI anal. 78−17371
nuclear reactor fuel element, turbulent flows in tubes, Nu-number determ. *(German)* 77−38432
nuclear reactor fuel element gap conductance, heat transfer over range of Knudsen number 78−13213
nuclear reactor fuel rod bowing effect on critical heat flux 77−46253
nuclear reactor LOCA, anal. of containment heat transfer 77−46248
nuclear reactor reflood heat transfer mechanisms 77−46241
nuclear reactor thermal channel gap, calc. by numerical methods 78−21630
nuclear reactor thermal-hydraulic calcs., effect of variable thermal conductivity 77−3084
nuclear reactor transient thermal hydraulic analysis, RELAP4 transform. into fully implicit iterative code 77−65257
nuclear reactors, critical heat transfer in Freon-12 cooled 3-rod bundle, orientation effects, meas. 79−93709
nucleate boiling, conservative nature of heat transfer laws 77−24395
nucleate boiling, mechanism 77−75785
nucleate boiling, self-similarity region boundary in terms of heating wall thickness 79−90245
nucleate boiling heat transfer, bubble population density correl. 77−27525
nucleate boiling heat transfer, nucleation factor 77−69079
nucleate boiling in horizontal tube, heat-transfer correl. for refrigerants 79−59911
nucleate boiling of liq. Ar, N_2, in centrifugal accel. field, heat transfer and flux 78−94538
nucleate pool boiling, meas. of void frequency distribs. and profiles using neutron beams 80−27691
nucleate pool boiling, Mikic-Rohsenow correlation for heat flux 79−55324
nucleate pool boiling heat transfer including microlayer evap., model development 77−42833
nucleate to film boiling transition collective phenomena, Nukiyama curve 78−9531
nucleation, liquid superheat and vapour subcooling, corresponding states correlation 79−32218
numerical solution of transfer theory problems by the direct reduction method 80−22309
ocean, diffusion parameterisation of mesoscale eddy effects from numerical expt. 79−48508
ocean, heat conservation calculations in natural coordinates with example from Baltic Sea 80−51433
ocean, low-freq. momentum, heat, salt and nutrients fluxes at Scotian Shelf edge 79−2242
ocean gyre, poleward heat flux 80−85668
ocean heat and salt mixing, double-diffusive intrusions into density gradient 78−85569
ocean surface, heat flow conditioned by wind pulsations *(Russian)* 77−60414
ocean surface heat loss in cyclone regions 80−77009
ocean surface layers, heat exchange model and appl. to study of climate 78−20433
ocean surface mixed layer, heat transport during catastrophic mixing events 79−16503
ocean thermal energy conversion, OTEC power modules optimisation 79−83615
ocean-atmosphere boundary layer, heat transfer meas. using radio thermal microwave systems 79−84546
ocean-atmosphere interface, coupled energy transfer, turbulent and radiative 79−2290
oceanic heat flow meas. over E Canada continental margins 77−5144
oceanic warm front propagation, theory with appl. to Sagami Bay Kyucho phenomenon 80−94538
oceans, Southern Hemisphere, poleward heat fluxes 79−48496
oceans in Southern Hemisphere, mean annual poleward energy transports 80−51406
n-octane, liq., thermal cond., meas. by transient hot-wire technique 80−103522

heat transfer continued
n-octane, low-press. boiling on Cu surface, accel. heat transfer due to porous Ni layer 77−85056
oil, transformer, heat transfer efficiency from rough plate 80−48704
oil film transient heat exchange in transverse electric field *(Russian)* 79−94607
oil shale, transient temp. distrib. due to combustion flame in retort 79−37110
oil-cooling baffled shell-and-tube heat exchanger expt. 78−83395
once through steam generator, Na-heated, stability anal. nuclear reactor systems model 80−91218
one dimensional heat and mass transfer, Stefan flow and Lewis number influence *(German)* 80−1590
one-dimensional model, inverse soln. *(German)* 77−11115
one-dimensional turbulent flow at rough wall, heat transfer and hydraulic resist., effect of viscosity variation 77−42816
one-dimensonal heat equation with nonlinear time-dependent boundary conditions, global attraction 78−16754
open cavity, modelling 78−55640
open solar regenerator, heat and mass transfer coefficients, moisture evaporation 80−38238
optical fibres, cooling rates during drawing 80−66538
optical fibres, heat transfer in laser drawing 79−94377
optical pulsed radiation on absorbing plate, heating effect 77−14658
optical radiation heating of matter, sound generation 77−34977
optically thick horizontal fluid layer heated below, heat transfer 80−99993
optimal control problem, finite element and conjugate grad. methods 80−19220
organic heat carriers, charact. *(German)* 78−79198
organic liquids, radiant heat exchange effect 80−19996
oscillating flow past flat plate, heat transfer, viscous dissipation effect 77−80151
oscillatory flow of electrically conducting fluid past porous plate, free convection currents 79−55428
oscillatory turbulent subcooled flow, transient radial heat transport effects 77−42834
OTEC system performance study 80−104514
overheated water reactor pin rewetting, effect of thermal diffusion from fuel pellets 77−46212
overpressure conditions in isolated piping section 77−74955
packed bed, optimal control of heat and mass transfer *(Ukrainian)* 79−32655
packed bed flow, particle-to-fluid heat transfer rel. to fluid dispersion 79−68795
packed bed heat recuperator, film coefficient for dry sorbent solids 78−5742
packed bed heat recuperators, precision numerical anal. 77−75974
packed bed of spheres, heat transfer coeff. determ. by quasistationary cyclic method 77−15116
packed bed thermal storage systems, single- and two-phase models 78−91009
packed bed thermocline, anharmonic analysis 79−27494
packed beds, estimation of parameters from radial temp. profiles 78−83467
packed beds, gas-liquid concurrent, wall heat transfer 79−50790
packed beds, heat transfer, length effect 78−9695
packed beds, low Peclet number particle-to-fluid heat and mass transfer 78−94799
packed beds, thermal response at low Reynolds number 78−87386
packed fluidised bed with horizontal flow, lateral heat transfer 79−50788
packed-bed particle-to-fluid heat transfer coefficient, determination from radial heat transfer measurements 78−9699
parabolic capacity and heat equation with irregular obstacle *(French)* 79−26002
parabolic free boundary problem, numerical soln. via Newton's method 80−69632
parabolic partial differential equatn. TEDDY2 program package 79−2613
paraffin wax, solar energy storage heat transfer characts. 80−55921
parallel channels with short flow constriction, laminar transport phenomena 79−81886
parallel flow between concentric cylinders, stability, heat transfer 77−11190
parallel plates, isothermal heat flux, and Knudsen layer 78−5638
parallel porous discs of different permeability, laminar flow heat transfer 80−14810
parallel tube banks in transverse viscous flow, heat transfer and hydraulic drag *(Russian)* 79−10450
parallel-flow and counter-flow condensation on an internally cooled vertical tube 80−64555
partial nucleate boiling, eval. of Kutateladze's eqn. 80−79298
partially buried buildings, heat flux through soil, calc. *(German)* 78−55554
particle in fluid with steady linear ambient vel. distrib., mass and heat transfer 80−19385
particle shape, in laminar flow, by optical mixing *(Russian)* 79−10619
particle-fluid heat transfer in fixed and fluidized beds 79−68552
particles, spherical, interacting, different sizes and compositions transfer rate calc. by method of images 80−77729
particles of disperse material, and plasma fluxes, heat exchange calcs. *(Russian)* 80−23997
passive solar heating systems, calc. of heat-transport-medium flow rate in heat receivers 80−99913
PBHTR, afterheat removal system failure, radiant heat transfer anal. 80−95364
PDX neutral beam injector, multi-aperture ion accel. electrodes thermal anal. 80−102371
peak heat flux in pool boiling, hydrodynamic and surface effects 78−90661
penetration gas cooling, porous wall with external heat appl., stability determ. 79−64761
n-pentane, liquid, containing suspended particles, superheating expt. 78−90642
n-pentane and mixtures with n-hexane, nucleate boiling from tube arrays 78−22251
pentane/chloroform mixture, liquid, containing suspended particles, superheating expt. 78−90642
perforated plane, thermoelastic-plastic problem *(Russian)* 78−55571
perforated plate composite cooling in turbulent gas flow 79−98716

heat transfer continued
perforated surfaces, heat exchanger cores, three forms of heat transfer augmentation 78−38402
periodic heat flux through a three layered slab exposed to solar radiation 80−43598
periodic heat transfer with temperature dependent thermal conductivity 79−59980
periodic thermal storage, regenerator 80−35760
periodically interrupted surface, developing and fully developed heat transfer coeffs. 79−81885
periodically varying heat transfer coeff., 1D boundary-value problem, steady-state soln. 77−84125
peripheral flow cooling internally heated body, oblique derivative boundary conditions 79−72778
permafrost, active layer heat transfer medium *(Russian)* 80−81943
permeable bed boundary layer flow, temp. distrib. and Nusselt no. 78−51166
permeable plate gas screen region, heat transfer and friction laws 79−1250
permeable surface, injection, laminar to turbulent transition, heat and mass transfer 78−83361
permeable tube with wall injection, transient turbulent boundary layer 78−83486
phase boundary, moving, analytic heat eqn. soln. 78−90694
phase change materials elemeat, thermal behaviour *(French)* 79−68550
phase change problem, with temp. dependent thermal conductivity, noniterative soln. 79−27493
3-phase ESR slab production, heat flow 80−10241
phase transformation-involving one-dimens. thermal problems, efficient numerical technique 78−59270
phase transition boundary displacement on pulse heating *(Russian)* 79−68557
photoacoustic effect, one dimensional theory for solids 80−65168
photoacoustic effect, three-dimens. heat flow 80−48840
photoacoustic spectroscopy of solids, heat flow effects 79−89007
photosphere, radiative equilib. rel. to upper bound on energy transport by solar global oscills. 78−32430
pipe, asymmetrically heated, turbulent transport and thermal diffusivities 80−64636
pipe, energy dissipation with flow effect on heat transfer rate 77−75905
pipe, entrance region, meas. and prediction 78−42666
pipe, heated, horizontal flow, temp. and vel. fluctuations obs. 77−75894
pipe, heated, vertical, gas buoyancy effect on downward flow and heat transfer 78−74427
pipe, horizontal, straight, heated, entry flow 79−32675
pipe, laminar friction factor and heat transfer, finite-element technique 80−10247
pipe, laminar pulsating flow, heat transfer 79−94621
pipe, local heat transfer to turbulent flow, superposition principle, expt. 78−83479
pipe, turbulent aerosol flows at high wall temps., heat transfer 80−74862
pipe entrance region, turbulence and heat transfer meas. and prediction 77−65734
pipe flow, fully developed, turbulent velocity and temp. fluctuation struct. 79−77254
pipe flow, laminar with nonlinear wall heat fluxes, axial cond. 79−27636
pipe flow, thermal entry length problem, numerical soln. *(German)* 78−83494
pipe flow, turbulent, in rough circular pipe, vel. and heat transfer calc. 79−60065
pipe flow of anomalously viscous liqs. 78−59485
pipe flow with coolant temp. depend. thermophysical props., heat transfer 78−94821
pipe flow with high viscosity, acoustical streaming and thermal effects 77−15122
pipe flow with thermal load variation, heat transfer 78−94820
pipe flow with uniform internal heat generation, turbulent heat transfer *(German)* 79−72893
pipe inlets, turbulent local mass and heat transfer, swirling effects 80−64542
pipe outflow, turbulent, with wall suction, dynamic and thermal fields *(French)* 79−4082
pipe subjected to circumferentially varying external heat transfer coeff., laminar heat transfer 80−10242
pipe with changing thermal power 80−23866
pipe with laminar flow in boundary layer and const. wall temp., initial section heat exchange 79−86432
pipeline compressible flow and heat transfer simulation program 77−19638
pipes, header and artery systems, theory and design 78−94679
pipes, heat transfer to low Prandtl number turbulent fluids, numerical prediction 80−69833
pipes, laminar heat transfer data with step-varying wall heat flux 77−50210
pipes, local heat transfer using heat flux sensors 80−48709
pipes, turbulence and heat exchange 80−24094
pipes with buoyancy effects, turbulent flow and heat transfer 79−90253
planar melting front stability in two-phase thermal Stefan prob. 80−43600
planar thermoelastic contact problems, Green's function for exterior contact 80−38350
plane channel of arbitrary shape, occupied by grid, heat and mass transfer, comput. method 77−7453
plane collector, equilibration temp. in real conditions *(French)* 77−123
plane jet, heated, ventilated, heat transfer to plane wall 80−59025
plane laminar gas jet in infinite space, thermal characts. *(Russian)* 79−18926
plane membrane in way of a flowing stream, temp. change effects *(German)* 79−41557
plane non-Newtonian Couette flow, heat transfer 79−86471
plane steady temp. field, effect of biperiodic system of plane inclusions 80−19224
plane thermal boundary layer, temp. distrib. determ. by var. formulation 77−23947
plane two-layer plate, numerical analysis in thermal steady-state of heat transfer *(Polish)* 80−87703
plane walls of variable thermal cond., transient temp. fields *(Polish)* 78−18155
planetary surface layers, validity of radiative-conductivity, theory 77−17354

heat transfer continued
plasma jet, heat exchange with obstacle 78−47130
plasma jet mixing chamber, heat transfer *(Russian)* 77−84534
plasma jet on baffle, flow behaviour and heat exchange 79−98774
plasma jet or electric arc to rotating water-cooled cylindrical wall *(French)* 80−28850
plasma jet-blunt body heat exchange near stagnation point 79−77103
plasmatron gas average enthalpy, forced heat exchange calcs. *(Russian)* 80−38724
plasmotron, thermal and elec. characts., depend. on channel radius and flow 78−1910
plastic injection moulding, heat transfer problem 80−38242
plastics, thermolabile, drying, heat and mass exchange in vibro-rotational bed *(Russian)* 77−68377
plate, downward-facing, flat, heat transfer augmentation by nonuniform elec. field corona 78−94873
plate, flat, with uniformly distributed vectored surface mass transfer, flow and heat transfer analysis 77−42838
plate, heat transfer from high enthalpy hypersonic air boundary layer 78−34210
plate, permeable, turbulent boundary layer with injection, heat transfer 79−1247
plate, radiant, heating by high temp. gas flow *(Russian)* 78−18154
plate, simultaneous heat and mass transfer to flat plate in humid air stream under frosting conditions 79−7284
plate, thin, in gradient current flow, coupled heat exchange *(Russian)* 78−83398
plate, thin semiinfinite, mobile normally-distributed heat source on lateral surface *(Russian)* 80−23870
plate, vertical, with time depend. temp. or heat flux, unsteady natural convection 77−75777
plate, with discrete energy source, stationary temp. field, approx. soln. 77−46879
plate, with suction, three-dimens. fluctuating flow, heat transfer, skin friction 78−87389
plate, with temp. and vel. profile nonuniformities, laminar flow and heat transfer 77−75913
plate at angle to flow, heat loss meas. for boundary turbulence and separation 78−90846
plate condenser with grid pattern slotlike channels, low-press. steam condensation, heat transfer 78−75040
plate heat exchange systems, expt. frequency anal. *(Japanese)* 78−9642
plate heat transfer rel. to external liquid flow turbulence *(Russian)* 79−81873
plate heat transfer to highly turbulent air stream, expt. *(Russian)* 79−46318
plate heating, optimal fast response control under temp. field gradient constraints 80−38232
plate heating by localised volume heat source with power-time depend. *(Russian)* 80−53608
plate in accelerated liquid flow *(Russian)* 78−18299
plate surface with mass blowing and suction, heat transfer in turbulent boundary layer 80−64559
plate to high turbulence air flow heat transfer 80−79292
plate type heat exchangers, with hemispherical projections, heat transfer and drag 80−48560
plate with crack or ribbon like inclusion subjected to uniform heat flow, thermoelasticity 80−48578
plate with cylindrical heat generating inclusion, temp. field *(Ukrainian)* 78−55549
plate with nonsteady temp. on lower surface, laminar flow, conjugate heat transfer 80−74879
plate with steady state thermal boundary layer flow, appl. of governing principle of dissipative processes 79−50722
plate-fin heat-exchange surfaces, convective heat exchange intensification 79−81691
plate-semi-infinite space, heat exchange process control, thermoelastic stresses *(Russian)* 80−53606
plates, collinear, interrupted, flow-aligned, heat transfer and press. drop 78−87232
plates, piecewise-constant coeff. of heat transfer, thermoelasticity, method of integral charact. *(Russian)* 78−38188
plates floating on air cushion, heat transfer 78−83220
plume, buoyant, turbulent, issuing vertically into stratified or uniform ambients 77−58756
plume, turbulent, thermal, along vert. wall, struct. and heat transfer 78−90880
PMMA, spreading of two-phase film of melt, heat and mass exchange, ignition and combustion *(Russian)* 78−76861
pneumatic gauging appl. to mass and heat transfer coeff. meas. 78−58329
pneumatic transmission line transient response anal. by characteristic curve method 79−77244
PNP-3000, prototype nuclear process heat reactor, core temp. transients, heat transfer calc. *(German)* 80−83180
polyatomic gases, turbulent tube flow, heat transfer 79−14395
polydisperse filter bed, immobile, heat and mass transfer eqns. soln. 77−7446
polydisperse gaseous suspension, heat transfer between subsonic nozzle walls, rel. to particle motion parameters 77−24019
polyethylene, extended chain, prep. and study of separated single crystals 78−42924
polyethylene oxide, dilute aqueous solution, effect of chemical additives on flow 80−83823
polymer, flammability, heat transfer meas., moving wire technique 80−3347
polymer, heat transfer processes relax. 79−90122
polymer containing liquid, turbulent pipe wall flows, friction and heat transfer 79−98802
polymer extrusion flow and heat transfer relationships, numerical anal. 79−77188
polymer melt, viscoelastic, 2-dimens. nonisothermal processing between calender rolls, mathematical model 79−68670
polymer melt flowing through duct, heat transfer 80−103049
polymer melting, during extrusion, integral energy-balance model 77−46899
polymer sheet, stretching, with suction and blowing, heat and mass transfer 78−34033
polymeric liquid, viscoelastic, gas bubble pulsations and assoc. dissipation effects 80−59079

heat transfer continued
polymers, high-temp. pyrolysis, heat transfer processes at gas/solid surface *(Russian)* 80−61152
polymethylphenylsiloxane liquid, pumped, improved heat transfer near crit. press. 77−7421
polymorphous material, Stefan problem, melting or freezing, interfacial boundaries 80−64350
polynary mixtures, natural convection boiling, heat transfer 78−90658
polystyrene suspension, laminar flow, augmentation of heat and mass transfer, correl. of data 80−53840
polyurethane foam, cylindrical cryogenic containers 79−35750
pool barbotage, heat transfer coeffs., high-speed cine-photography and oscillography 78−90982
pool boiling, Rohsenow eqn. 79−59910
pool flames, heat and mass transfer *(German)* 78−94677
pool water, flash evaporation phenomena 78−2245
pool-boiling and bubbling heat transfer, freely convecting liq. 79−32212
pool-boiling of horizontal cylinders, effect of heater diameter on critical heat flux 77−39281
porous bed, heat waves, heat transfer coeffs. determ. 77−42914
porous bodies, stresses induced by drying, elastoviscoplastic model, finite element anal. 80−23904
porous body, heat and mass transfer, two-dimensional isoparametric finite element method 77−42708
porous body, sublimation, heat, mass transfer from parallel capillaries 79−37395
porous ceramics, frost action under one dimens. heat flow *(Japanese)* 79−79140
porous cermet, heat transfer and stability for moving evaporating coolant 80−64563
porous cylinder with intense injection, heat transfer 78−79370
porous cylindrical bodies, heat and mass transfer, boundary layer method 77−2625
porous element under phase conversion and vap. superheat, steady and transient operation 77−7442
porous fibrous metallic material, flow and internal heat transfer 77−35228
porous material, environment effects *(Polish)* 79−18674
porous media, heat and mass transfer, numerical soln. 77−7441
porous media, heat and mass transfer during phase and chemical transformations 77−42917
porous media, saturated, natural convection with heat generation 77−51114
porous media, simultaneous heat and mass transfer governing eqns., soil heating appl. 78−94562
porous media, thermomigration, capillary diffusion coeffs. *(French)* 77−89006
porous medium being dried, generalised model *(Hungarian)* 80−83839
porous medium during gas blow through, exothermal reaction wave propagation 79−79222
porous medium with circulating heat transfer fluid, thermal storage *(French)* 80−40916
porous metal, coeff. determ. method 77−66738
porous moist body, contact heating moulding, temp. distrib. heat/mass transfer 77−75784
porous pipe in a pipe heat exchanger, laminar flow, vel. changes 80−64512
porous plate, turbulent boundary layers 79−98714
porous reactors, with temp. depend. heat generation rate, element geom. effects 78−94738
porous sintered materials, expt. data correlation 77−42915
porous sphere in low Reynolds number flow, heat transfer 78−59482
porous sphere in stream of small Reynolds no., heat transfer 78−42608
porous structures for cooling laser reflectors, theoretical study 80−91809
porous surface, heat exchange optimal control 79−32661
porous tube entrance segment, heat transfer anal. with initial flow swirl and transverse injection 77−24025
positive thermic majorization of temperatures on infinite strips 79−76936
post-dryout heat transfer, review 79−1094
powder grains, melting, in plasma flame 79−60200
power law fluid, laminar flow heat transfer in helical coils 80−59030
power law fluid Couette flow, entrance region heat transfer 79−32587
power law fluid flow in pipes, entrance region heat transfer 79−1218
power law fluid in pipes and channels, extended Leveque solns. 80−24095
power law fluids laminar pipe flow, heat transfer 78−59425
power law pseudoplastic laminar tube flow, heat transfer 77−80184
power overhead lines, current carrying capacity determ. 77−84126
power reactor, water cooled and moderated, tube film boiling heat transfer coeffs. 80−73877
power-law fluid, nonsteady heat exchange during steady flow in initial thermal section of tube 77−47046
power-law fluids flowing between two rot. coaxial circular cylinders, heat transfer rates 77−58742
power-plant heat rejection, regional climatic effects 77−25768
premixed turbulent flame combustion, heat transfer obs. and calc. *(French)* 78−94688
pressure fluctuations in heat transfer channels with surface boiling *(Russian)* 78−14088
pressure gradients generated during the drying of porous shapes 79−68801
pressure transducer measurements, thermal transient effects 80−31700
pressure tube-type reactors, moderator temp. coeffs. of reactivity meas. 80−57893
pressure-induced diversion cross flow for rod bundle subchannel interconnection geometry 78−13215
primary fluid heated by solar energy in linear collector, thermal regimes and appl. 78−75061
propagation, finite vel. problem, kinetic theory anal. 77−46881
propagation speed of heat disturbances in memoryless materials 77−5774
pseudo-similarity solutions of heat equation in presence of moving boundaries 80−27240
pseudoplastic fluid, flowing upward in vert. heated tube, variable physical props. 78−90945
pseudoplastic fluid crossflow around circular cylinder, heat and mass transfer 80−19370
pseudoplastic fluids, heating in laminar flow 78−34128
pseudoplastic fluids in agitated vessel 77−35174

heat transfer continued
pseudoplastic non-Newtonian liquid, laminar natural convection heat transfer 79−64713
pulsatile flow in porous channel 77−19604
pulsatile laminar flow in tubes, heat tranfer 78−30289
pulsating laminar-boundary layer, heat transfer and skin friction 78−94711
pulsation bed of disperse material, heat exchange with horizontal tube bundle *(Russian)* 77−72137
pulsation effects on laminar heat transfer between two parallel plates *(German)* 80−33681
pulsed air flow in pipes, heat transfer coeff. 77−62252
punch contact with elastic half-space, effect of heat flow on contact area 77−7294
PWR, heat transfer equations for boiler tubes *(Rumanian)* 79−3189
PWR, superheated containment atmosphere heat/mass transfer to passive heat sinks, analytical model 79−49658
PWR containments following LOCA, heat transfer coefficient 80−86958
PWR fuel assembly, lumped subchannel model anal. of enthalpy transfer 79−76063
PWR fuel assembly, thermohydrodynamic process, obs. 79−30902
PWR LOCA reflooding phase, two-phase flow and heat transfer at and near quench front 80−757
pyrolysis, of single solid particle accompanied by consecutive reactions, vol. reaction model 79−47896
pyrolysis of solid particle, cyclic dynamics 79−47897
qualitative analysis of unsteady heat and mass transfer modes in a boundary layer with chemical reactions and intensive injections 80−69819
quantum theory, jump processes, Cauchy problem for Schrodinger eqn. *(French)* 80−31596
α-quartz, heat transfer at low temps., lattice thermal cond. 80−92729
quasi-one dimensional steady compressible flow, time marching finite area calc. 79−81912
quasi-stationary Stefan problem for a hot pipeline in a frozen mass 79−23324
quench front motion, heat transfer coeff., surface approx. using boundary layer anal. 79−45342
quenching, heat transfer between high temp. solid and boiling water *(French)* 77−62136
quenching temperature, 0.03-1.3 MPa, base material thermal props. depend. 78−94587
R & D on advanced heat exchangers in Japan, review 80−35737
rabbit, influence of hypercapnia on aspects of heat exchange 80−97863
radially rotating pipe, heat transfer coeffs. in various flow regimes 78−1668
radiant heat exchange calc. in absorptive and scattering medium 77−14885
radiant heat transfer, to dilute cloud of drops or particles 77−58537
radiant in absorptive and scattering medium, calc. by iterative zonal method 77−72138
radiation absorbing bodies, temp. fields, Julich reactor expts., finite element calcs. *(German, English)* 77−82998
radiation dose rate evaluation from radiation heating of sample during irrad. 77−50311
radiation heat exchanger, temp. distribution, model, boiler appl. 77−39210
radiation-conduction problem soln. method, LMFBR meltdown accident anal. 80−19381
radiative, integral theory with anisotropic scatt. and general boundary conditions 78−32339
radiative, iterative soln. of difference eqn. system *(Russian)* 77−58540
radiative heat exchange, calculation methods, for inhomogeneous absorbing and dispersive media 79−81698
radiative heat transfer in horizontal magnetohydrodynamic channel flow with buoyancy effects and an axial temperature gradient 79−60069
radiative heat transfer problem solvability, radiation, scatt., absorpt. 80−33436
radiative transfer from plate to non-conducting flow 80−14692
radioactive waste disposal in bedded salt, thermally induced movement of canisters 79−26573
radiometer optical head thermostabilisation structure 78−86316
random heat transfer, flat channels, timewsie var. of ambient temp. 79−23313
Rankine-Hugoniot jump conditions, viscous and thermal effects 78−59418
rarefied flow, low-speed flow over sphere, convergence of integral methods 78−22375
rarefied gas, heat transfer between coaxial circular cylinders, with large temp. difference 79−94664
rarefied gas, heat transfer in plane Couette flow, ellipsoidal model 77−72330
rarefied gas, temp. jump problem in BGK model 77−53841
rarefied gas, thermal transpiration, thermal and friction forces 77−35171
rarefied gas between parallel plates, heat transfer *(Russian)* 78−46961
rarefied gas between parallel surfaces, collisional models 79−86464
rarefied MHD laminar channel flow, heat transfer 80−48687
re-entry vehicle heat transfer meas. in separated laminar base flow 78−61708
reacting binary mixture, turbulent flow, Reynolds eqns. and heat and mass transfer *(German)* 77−11281
reactor fuel element to sheath, heat transfer coefficients 78−29580
reactor fuel elements, temperature field, generalised Duhamel integral 80−22943
reactor LOCA, critical heat flux expts. on blowdown heat transfer 80−23005
reactor molten core-vessel system, heat transfer steady state anal. 77−83023
reactor thermal-hydraulics, quality influence on the departure from nucleate boiling in cross flows through bundles 80−95340
reactors, chem., relaxation oscills. 79−39120
reattaching laminar and turbulent separated flow, three-dimens. heat and mass transfer 77−65759
recovery temperature data for cylinders in compressible flow 77−47036
rectangular channel, heat transfer downstream of blockage with discrete permeability 80−69915
rectangular curved channel hydrodynamics and heat transfer expt. 80−19398
rectangular ducts, localised heat transfer systems *(Chinese)* 79−37126
recuperative heat exchange, source/sink even model *(Hungarian)* 79−14226
heat transfer continued
reference theta pinch reactor, first wall thermal-mechanical anal. 77−57750
refrigerant R-113 upflow in heated tube, liq. film dryout 78−90989
refrigerator finned tube, experimental charcts. *(Japanese)* 77−23861
regenerative heat exchange, calcs. with realistic boundary conditions 79−189
regenerative heat exchanger high temp. behaviour, numerical model 77−62140
regenerative heater, high-temp., refined math. model 80−22365
regenerative refrigeration, generalised ideal reference cycle, isothermal systems 80−38228
regenerative refrigerators, closed-cycle, for cooling small supercond. devices, concept 78−93698
regenerative solar still, inclined-stepped design, productivity and efficiency calc. 79−83622
regenerators with hygrostatic materials, combined heat and mass transfer 79−81689
regime of combined buoyancy mode driven flow, stability 78−18302
regular thermal regime method for heat transfer meas., nonideal sensor thermal simulation 77−57323
relativistic equilibrium thermodynamics, heat flow 80−52017
relativistic gas, one-component, transport eqns. 77−966
relativistic hydrodynamics, thermal waves and growth eqn. *(French)* 80−28579
residual resistivity specimens, heat transfer coeff. to He gas in electron irradiation facility 77−54016
resonance tube, jet flow and heating, unsteady complex shock struct. 80−6115
respiratory, under environmental conditions of deep diving, modelling and analysis 78−15856
restoration, evaporation and melting of materials in high temp. gas flow *(Russian)* 80−39271
retina, light-induced transient thermal response 78−7340
review of 1976 literature 78−5740
review of 1977 literature 79−14392
review of 1978 literature 80−23860
Reynolds analogy for boiling, heat transfer 78−59277
rheogoniometry, viscous heating and heat transfer 79−82013
rib-roughened surface, friction factor and heat transfer correlations with rib charcts. 78−87233
ribbed plate, local heat transfer charcts. in flow 78−83381
rigid wall-hot gas stream interaction, heat cond. eqns. soln. 78−79194
river to atmosphere heat and mass transfer data 78−96253
rocks, hot, dry, hydraulically fractured linearly expanding cracks, eqns. *(Japanese)* 79−34809
rod bundles, boiling crisis and press. drop, heat transfer enhancement devices 78−55638
rod bundles, three dimensional coolant flow calcs. 80−48699
rod bundles longitudinally bathed by gas, heat exchange intensification 78−79191
rod cluster, recirculating flow due to blockage, finite difference method for temp. 79−3200
rod subject to periodic heating, temp. *(Russian)* 77−19512
rod-type fuel elements in regular lattice, thermal fields for streamline heat exchange 77−42010
roped tubes, helix angle effect on performance 78−94729
rotary kiln, direct fired, exam. of heat flow processes 78−83224
rotary kilns, direct fired, exam. of heat flow processes 78−83225
rotating body, axisymmetric, arbitrary surface temp. distrib., thermal boundary layer, exact solns. 78−75133
rotating bubbling beds, heat and mass transfer 78−30351
rotating channel in porous medium, heat transfer 79−72932
rotating channel with porous walls, heat transfer and temp. distrib. 78−30355
rotating cylindrical body, local heating and cooling on peripheral surface, temp. distrib. 78−67001
rotating cylindrical pipe turbulent nonisothermal flow, temp. fluctuation and pulsatile heat flux calc. 78−83475
rotating disc, heat exchange into unbounded rotating fluid, thermal and hydrodynamic boundary layers 80−59050
rotating disc, laminar boundary layer heat transfer, Prandtl no. effects calcs. 77−31306
rotating disc, local heat transfer, Prandtl's mixing length hypothesis 77−27540
rotating disc, local heat transfer, two-eqn. model of turbulent flow 77−58690
rotating disc with axisymmetric surface heat source distrib., in laminar flow, heat transfer 79−46314
rotating disk with sink flow, heat and mass transfer 80−19402
rotating heat exchanger, frictionless two-phase tube flow, centrifugal accel., choked flow 80−48792
rotating heat pipe, temp. distrib. and heat load charcts. noncondensable gas effects 78−33992
rotating heat pipes, condensation heat transfer, external boundary condition effects 79−94612
rotating heat pipes, condensation heat transfer, noncondensable gas effects 78−51167
rotating heat pipes, condenser heat transfer performance augmentation 80−14550
rotating radial convergent duct, air flow heat transfer boundary conditions, turbulent and transition flow 78−83476
rotating rectangular channels, heat transfer, press. drop calcs. *(German)* 80−1594
rotating short radial blade, laminar and turbulent flow, heat transfer 78−18294
rotating sphere, higher order heat transfer 79−4003
rotating spheres, heat transfer coeffs. for gas-solid two-phase flow 80−19369
rotor blade at high Mach nos. 79−72887
rough cylinder in critical Re water crossflow, heat transfer 80−1571
rough cylinder in transverse water flow *(Russian)* 79−10449
rough pipes, mixing length method 77−7450
rough pipes, variable property turbulent friction and heat transfer 80−6153
rough plate, drag and heat transfer at various Pr numbers 79−94610
rough surface boundary layer calculation methods 80−1595
rough surface heat transfer, turbulent flow in annular channels, result anal. 80−24003
rough surface heat transfer in turbulent boundary layer, mixing length hypothesis 78−83378

heat transfer continued
rough surface turbulent flow heat and mass transfer, Reynolds analogy deviations 78−83380
rough tube, effect of Prandtl number on heat transfer 77−35139
rough wall with blowing and heat transfer, boundary layer struct. 79−81863
roughened surfaces in gas cooled fast breeder reactor heat exchanges, improved transfer 77−18650
round heated jet, heat and momentum transport, intermittency, entrainment 79−32608
round-bottom pool with internal heat generation, expt., LMFBR appl. 79−13470
salt fingers, rot. effects 79−50767
salt solutions, freezing in cells, heat and mass transfer with phase change 80−6493
sapphire, second sound observation by heat pulses method, phonon scatt. processes *(Russian)* 79−99273
sapphire-dilute ^{3}He interface, heat transfer at very low temp. 79−56003
sapphire-Pb interface, heat transfer coeff. meas., 2-80K 80−88419
saturated liquid, boiling onset, film boiling transition, crit. heat flux densities *(Russian)* 78−83234
saturated porous wedge with impermeable boundaries, heat and mass transfer 80−19375
scale prevention, by annular flow of immiscible liquid along heated tube walls 79−1090
scattering medium, nonstationary heat transfer 80−5916
Schrodinger invariant generalised heat eqns., similarity methods and trivial solns. 78−62164
screen wick, heat transfer, Freon-113, ethyl alcohol and H_2O 80−48548
sea ice, air-sea heat flux in dynamic thermodynamic model 80−51432
sea-air small-scale interaction, heat exchange estimates 78−3810
sea-air system, heat exchange rel. to diurnal temp. cycle in boundary layers 78−20434
sea-atmosphere heat-transfer expts. *(Russian)* 78−81206
seawater, optical anisotropy coeff., temp. fluctuation, optical meas. method 78−69488
second order fluid heat transfer for flow around circular cylinder 79−41683
second-order constitutive equations of hydrodynamics, dynamical interpret. 80−36860
secondary cells, heat transfer anal. for thermal management 80−30458
self-oscillatory system with external heating 77−14888
SEM cold stage microscopy, thin frozen hydrated specimens, temp. rise and sublimation of water 78−24198
semi-infinite region with variable physical parameters 79−90116
semi-infinite solid, laser surface melting and subsequent solidification, computer heat flow models 79−69916
semi-transparent slab, temperature fields distrib. under incident radiant flux *(Russian)* 79−76937
semibounded compressible stream, optimal suction at heat-cond. porous surface *(Russian)* 80−79346
semiconducting plate, with temp. depend. absorption coeff., heating kinetics *(Russian)* 77−54867
semiconductor plate, light irradiation, heating and thermoelastic stress 80−25499
semiconductor refrigerating thermojunctions with radial flow of current 79−2766
semiinfinite plate, thermal stresses, heat transfer effect 80−96193
semilinear heat equation, blowing up of finite difference soln. 77−54854
semitransparent material strip, radiation transfer *(Russian)* 79−98597
semitransparent thin cylinder, radiation-conduction heat transfer, light-guide approx. 80−96179
separated air flow, surface orientation effects 79−98709
separated flow, theoretical anal. 78−79315
separated flow behind double step at duct entrance, turbulent fluctuations and heat transfer 77−42829
separated flow over triangular prisms 78−87339
separated flow with laminar mixing region, heat and mass transfer, math. simulation 78−59397
separated supersonic rarefied gas flow at low Reynolds no. 79−98713
sequential estimation of thermal parameters 77−80047
shaft seal, high-speed mag. fluid, heat dissipation 80−59032
shallow fluidised bed heat transfer investigation 79−7404
shape of drop on inclined plane, solar still aspects 78−79856
shattered rock with infiltrating liquid, liquid filtration into shattered rocks 79−81962
shear flow, linear, heat or mass transfer rate from freely suspended particle 80−79313
shear layer, thermally stratified, turbulence structure and stability *(Japanese)* 79−41731
shear turbulence, temp. derivative skewness 77−15002
shear turbulence, temp. fluctuations, struct. functions 78−30274
shear-thinned fluid, laminar heat transfer and drag 79−68764
shearing flow over wavy boundary, heat, mass, momentum transfer, turbulence model 78−87335
shield-hot turbulent jet interaction, nonstationary heat transfer 80−92136
shielding, two-phase porous cooling system, hydrodynamic and thermal characteristics 77−10012
shielding of heat transfer from a boundary 80−5914
shock boiling, liq. discharge through short nozzles, flow blocking 79−86491
shock heat exchange, effect on shock curves *(Russian)* 78−75170
shock interaction with turbulent boundary layer, heat transfer 77−23994
shock layer, hypersonic, vibr. nonequilib., near stagnation streamline, low Reynolds no. flow 78−87417
shock layer blunt body problem, aerodynamic heating, effect of chemical reactions of injected gas *(Japanese)* 79−94739
shock waves, Gyugonio's eqn. rel. to heat exchange *(Russian)* 77−68625
shuttle heat transfer in plastic displacers at low speeds 78−93700
silica gel regeneration by adiabatic desorption mathematical model 79−1967
simulation of quasilinear parabolic equations, by networks of FETs 77−50854
simultaneous eqns. solution by iterative substructuring 79−10564
single and two phase flow, rough surface effects 78−30297
singular parabolic partial differential eqns., impulsive motion appl. 78−38326
skin blood flow, human, modelling of thermal effects 79−24959
heat transfer continued
skin temperature during sweating, estimation by graphical method and thermal cct. model 77−48757
slab, planar radiative transfer with isotropic scatt. 80−23876
slabs, one dimens. Stephan problems, direct and inverse, solns. 80−14552
slip flow, MHD, over porous plate, with variable suction, heat transfer 78−79337
slip flow with suction or injection, Rayleigh problem 77−19627
slip line and band heating in thin crysts. at low temp. 79−69111
slowly moving vapour, film condensation heat transfer 80−19376
snow, heat transfer in vacancy *(Japanese)* 77−86952
snow cover energy budget, energy flux meas. 78−92859
soil, freezing, effect of moisture exchange and heaving 77−25702
soil, heat and mass transfer with phase change 79−1093
soil moisture, heat and salt transport, math. model 80−26563
soil-atmosphere boundary, heat and moisture transport 80−77023
soils, freezing, heat flux, meas. *(Japanese)* 78−88835
solar, thermal power system, open cycle air turbine *(French)* 80−45641
solar, water heater, low-temp., tubular heat receiver, temp. distribution, heat-balance differential equation solution 79−94464
solar absorber-convertor, ideal selective absorbing surface, absorp. and radiation coefficients calc. 80−40900
solar absorber-convertors block unit, thermal characts. experimental investigation 80−97801
solar absorbers, heat transfer by natural convection in an isothermal rectangular cavity open on one side *(French)* 80−61412
solar air heater buoyancy and tube inclination effects 79−62058
solar air heaters, comparative investigation of heat collectors heat-engineering characts. 80−92018
solar air heaters, single and double exposure, heat balance anal. 80−45734
solar air heaters, use of porous flat plate solar collectors 80−35748
solar collector, evacuated cylindrical, analysis 80−21415
solar collector array performances calc., using Hottel-Whillier-Bliss equation and field-derived data 80−45724
solar collector design and construction, flat-plate *(Slovak)* 79−92089
solar collector horizontal coaxial cylinder design optimisation 79−62110
solar collector system, cylindrical, parabolic, transient energy removal calc. 79−52906
solar collector tube, bore heat flux and outside surface temp. variations 78−90629
solar collector/storage system buried in ground, heat transfer anal. 79−7275
solar collectors with multilayer cylinder heat exchangers, heat balance eqn. and thermal stress anal. 80−58977
solar collects, cylindrical black body receiver design, optical and thermal anal. to reduce thermal losses 80−61428
solar compound parabolic concentrator collectors, prediction of thermal performance 80−55905
solar convection zone, heat flow near obstacles 78−28609
solar desaliniation unit with evaporation chamber, test results 80−96178
solar distiller, multistage-inclined type, solar energy distribution determination 79−96423
solar energy absorbers, thermokinetics of glass and semi-transparent materials *(French)* 80−61410
solar energy applications, hot water systems, dyeing, in textile industry, commercial aspects 79−83576
solar energy collector, flat-plate, transient response, efficiency evaluation 79−18676
solar energy collector, performance measurement, tracking system 77−88892
solar energy collector design for low capital costs and least steady-state heat losses 80−104517
solar energy collectors, cylinder-parabolic, with envelope pipe, steam generation efficiency calculation model *(German)* 80−33112
solar energy cooling, operating systems and current developments, review 80−85265
solar energy storage, pebble layer heat exchange investigation 80−21374
solar flares, electrostatically unstable heat flow and its consequences 78−20804
solar flares, heat transfer theory 79−40168
solar flat plate collector transient heat transfer models compared 79−83632
solar greenhouse with soil heat accumulator, temp. conditions anal. 80−40898
solar ground coupled heat transfer, expt. and GROCS computer model of heat pump system 80−66987
solar heating, microclimate of solar greenhouses 80−40902
solar heating equipment, for building, community and agricultural appl., use of heat tube 79−57412
solar heating of buildings, transient thermal flux calc. 79−62144
solar heating system perform. estimation using sinusoidal inputs 80−35648
solar heating/cooling of buildings calc., w.r.t. periodic changes of solar radiation 79−62148
solar installation for refrigeration and water heating, energy characts. 80−101124
solar interior, energy transport by mechanical means rel. to neutrino problem 77−17461
solar pond interaction with ground thermal storage 79−62093
solar ponds, heat transfer model to predict temp. rise 80−55912
solar power plant, transient temp. vars. in primary network 78−75062
solar power water-heating systems, design method 79−83629
solar reflectivity of common building materials, effect on roof heat gain 80−55810
solar regenerator, transient response for varying insolation and flow 79−62025
solar still, thermal losses to atmosphere, determ. 80−87707
solar thermochemical cavity absorber based on NH_3 dissociation, design and cost anal. 80−81489
solar water heater, collector efficiency equation 80−16839
solar water pump, for lift irrigation, modified design analysis 79−70440
solar wind, heat flux regulation by whistler instability 77−45277
solar wind electron heat flux, EM lower hybrid instability 79−88559
solar-thermal conversion, selective surfaces 77−83978
solid+liquid reactions, heat and mass transfer, with gas evolution 79−83443
solid heating by hot air stream, transient heat transfer 77−42705
solid transported by gas in pipe, heat output 78−63486
solid-liquid phase change heat transfer and interface motion 80−53609

heat transfer continued
solid-liquid slug flow, radial heat transfer characts. 78−63495
solidification, heat balance integral method, transformations 77−24380
solidifying melt thermal gravitational convection, impurity distrib. and transfer processes 80−19367
solidifying metal ingots, phase interface motion and variational Biot method 79−83189
solloidal solution droplets, solid, particle form., heat and mass transfer 78−95967
solution droplets vaporisation, in high-temp. gas flow, heat and mass transfer 78−75191
Soviet bibliography, heat and mass transfer 79−68701
Soviet bibliography 80−77557
soyabean oil, heat transfer from horizontal wire, AC and DC electric field effect 77−31202
space above inhomogeneous fluidised bed 77−55085
space heating, energy utilisation improvements using new types of construction *(German)* 80−40903
space heating, heat-loss index incorporating solar, temperature wind and cloud cover effects 80−53605
spacecraft heat rejection improvements using thermoelectric devices 80−108810
spark machining, heat and mass transfer 79−1369
sphere, naturally turbulent outdoor environment 77−80163
sphere in gas slip flow, vel. field, heat exchange, friction dissipation *(German)* 78−34138
sphere in infinite medium, heat transfer problem, temp. profile 77−75783
sphere moving in viscous liq., heat liberation 78−46886
sphere with fluid source at centre, heat transfer to fluid stream 79−18887
sphere-packed beds, limiting Sherwood and Nusselt nos. 78−18339
spheres, almost touching, temp. field or elec. pot. 79−41268
spheres, one dimens. Stephan problems, direct and inverse, solns. 80−14552
spheres in naturally turbulent outdoor environment, heat transfer coeffs. 77−42701
spheres in vertical flow, transient transition boiling heat fluxes 78−90994
spherical bubble growth in uniformly ultraheated liquid 78−1550
spherical cone, generalised temp. fields *(Ukrainian)* 77−72141
spherical drop combustion, asymptotic, drop shrinkage and flame movement, heat and mass transfer 77−81405
spherical droplets in vapour environment, time evolution, physical-mathematical model 79−68789
spherical nozzles of high-temperature heaters, heat transfer calcs. 80−103022
spiral vortex flow characteristics at high Taylor numbers 80−1598
spray drying, of highly viscous conc. solns., heat and mass transport *(Russian)* 78−83230
spray nozzle, transfer processes in droplet plume during counterdirectional atomisation in gas flow 77−24014
spray-cooled cylinder 79−23354
square duct, developing turbulent flow and heat transfer, computational procedure 80−69926
square duct, developing turbulent flow and heat transfer, numerical prediction 80−74986
square plate in oblique airflow, local heat transfer 79−41684
stability of flow between two rotating cylinders, effect of thermal diffusion 78−18308
stably stratified fluid layer under thermal constraint, propagating thermal modes, force Rayleigh scatt. 79−76943
staggered tube bundle, pressure and friction drag, mass transfer effects 80−38388
stagnating thermal turbulent boundary layer mean and fluctuating characts., divergent flow heat transfer 78−83370
stagnation point boundary layers, unsteady, three dimensional, compressible, numerical soln. 79−37335
stagnation point in laminar flow, surface curvature effect 78−38316
stagnation region heat transfer in hypersonic particle environments 77−31325
standard long-range operating stations in shelters with integrated thermal-syphon system 80−53616
stars, rotating, secular instability from thermal cond. 80−21986
static thermal contacts and unsteady cond., thermally equivalent model *(French)* 80−92027
stationary boundary layer flow, plane heat balance eqn. asymptotic soln. *(German)* 78−63430
stationary heat exchange in thermochemical gas analyser *(Russian)* 79−14215
statistical mechanics of nonequilib. steady states, microscopic theory 79−58623
steady and non-steady flow through IC engines inlet valve with heat transfer 78−59390
steady vortex driven by heat line source, math. anal. 79−23329
steady-state heat diffusion equation, alternate general solution 80−79103
steam, condensation inside vertical straight and coiled pipes, heat transfer 79−90244
steam, dropwise condensation, effect of condenser tube material on heat transfer 78−75059
steam, film condensation in tube, heat transfer, vibr. effect 78−51044
steam, horizontal flow on cylinder, condensation 78−94550
steam, superheated, dispersion in saturated water, bubble form., heat transfer 77−47068
steam, superheated, dispersion in saturated water, bubble form., heat transfer 77−47069
steam bubble, nonspherical, collapse in suddenly pressurised water *(French)* 78−33997
with steam condensation, theory, problems of interest 78−30161
steam condensation heat transfer on below-freezing pt. surface 78−75042
steam condensation in annular duct flow, heat transfer to condensate film 78−94709
steam condensation in moving two-phase film, heat transfer, volumetric coefficient 80−48696
steam condensation on bundle of smooth horizontal tubes 78−30164
steam condensation on external entrance length of cooled rot. tube 77−75906
steam condensation on PTFE coated surface 77−89012
steam generating channel, nonuniform heat release, heat transfer crisis location 80−64534
heat transfer continued
steam generating channels, boiling crisis, critical heat loads 79−90247
steam generating channels, heat exchange intensification by surface roughness in transcritical region 79−55371
steam generating tube, with ribbon like dry-out patch, temp. distrib. calcs. 79−1085
steam generating tubes, burnout mechanism 78−90984
steam generator, heat transfer, surface ash and internal pipe deposit resistance calcs. 79−1089
steam generator, Na-heated, local heat exchange characts. 80−23867
steam generator tubes, forced and natural circulation, inception condition correlations 80−74868
steam generators, steady 2-dimens. two-phase flow and heat transfer calc. 79−1237
steam jet condensation, dynamical pressure pulse effects 78−94549
steam jet condensation in turbulent liquid flow, heat transfer 80−33599
steam turbine district heating plant, condensing and regenerating equipment 80−92029
steam turbine heat transfer coeffs. determ. *(German)* 80−53783
steam turbine nozzle cascades, local heat transfer, approach flow turbulence effects 80−38381
steam turbine turbulent flat jet condenser, nozzle hydraulic and heat transfer characts. 78−94793
steam-generating channel, heat exchange in transcritical region 78−42644
steam-generating channel hydraulic characts., two phase flow instability effects 79−90333
steam-generating pipe, containing porous deposits, mass transfer (impurities) 78−38398
steam-generating pipe with internal ribbing, heat exchange 78−4979
steam-inert gas, uncondensable gas content effect on steam condensation heat transfer in vert. tube 78−75041
steam-water, flow characts. at high press. 78−94805
steam-water mixture, with high vap. content, annular flow, heat transfer, press. loss 78−75193
steel, bright strip, light oil annealing, mathematical simulation 77−77512
steel, diffusion melting in Fe-C melts, heat transfer correl. 80−54348
steel, hardening, mathematical model including phase changes 79−4950
steel, Kh18N9T, strengthening by vibrational stirring effect 80−40405
steel, porous, permeability, deform. effects 79−100229
steel, quenched, verification of change of props. in mag. field 78−52985
steel, stainless, cylinder, in thermal aerodynamic tube, nonsteady heat transfer method 79−37147
steel, steady state unidirectionally solidified, dendrite morphology 77−16569
Stefan and dam problems, free boundary convexity 78−83356
Stefan multi-phase problems, similarity solns. 79−12742
Stefan problem, one-dimens., modified variable time step method 80−102960
Stefan problem, one-dimens., third order accurate discontinuous finite element method calc. 79−81701
Stefan problem, soln. analyticity 80−43589
Stefan problem, two dimens., space-time finite element computation of free boundary 78−1556
Stefan problems, semiinverse, soln. using nonlinear thermal conductivity operator 77−72136
Stefan problems, two-dimensional, approx. of integro-differential eqn. 77−80050
stellar surfaces, numerical treatment of unsteady hydromagnetic thermal boundary layer problem 80−92227
Stirling cycle analysis, numerical methods accuracy evaluation 79−48170
stochastic temperature fields in a solid spheric cone *(Ukrainian)* 79−50566
Stokes' problem for vertical infinite plate with variable temp. 79−23301
Stokes problem, for infinite vertical plate with const. heat flux 80−79108
Stokes problem, free convection effects, rarefied gas flow past plate 79−32581
stratified atmosphere, nonadiabatic heat dynamics with mass exchange and water phase transitions 79−58004
stratified gas/liquid flow, local Nusselt number prediction 80−38393
stratified water surface layers, unsteady energy transfer 77−41092
stratospheric balloon trajectory analysis for long-term missions *(Italian)* 77−82055
stream swirling, effect on laminar flow struct., heat exchange in round tube 77−11265
streaming, of vel. and temp., in oscill. boundary layers 78−83358
streamwise-periodic variations of cross-sectional area, flow, heat transfer 77−80156
strip in shear flow, heat and mass transfer 78−51163
structured surfaces to liquid nitrogen, boiling heat transfer *(German)* 80−99919
subcooled boiling flow, flow quality and void fraction for channel 79−90249
subcooled film boiling heat transfer from spheres 78−51047
sublimation-condensation in annular gap, heat and mass transfer 77−35141
submerged steam jet into unbounded space, temp. field 79−72920
subsea permafrost heat and mass transport processes, mol. diffusion and consequences anal. 79−2302
successive cylinders in liquid crossflow, expts. *(Russian)* 78−46967
Sun, dynamo action of mean flow from latitude depend. heat transport 80−90378
sunspots, heat flow in convective downdraught 80−4314
superconducting magnet stability, critical current margin design criterion 80−31807
superconductivity, propagating normal zone (quench), induction, by local energy release 79−38210
superconductor, composite, normal zone propag. calcs. 77−43778
supercooled aqueous solution, freezing, generalised analytical soln. 80−92142
supercritical boiler, algorithm for numerical determ. of transient heat transfer processes 77−23944
supercritical He, pool heat transfer, in high centrifugal accel. field 77−15034
supercritical He I, heat transfer to turbulent flow 80−69631
supercritical HeI, heat transfer to turbulent pipe flow 80−64348
supercritical pressures in heat transfer medium, calc. method 78−9634
supercritical water, transient loads and flow, tube hot spots, nucleate boiling departure 80−64349

heat transfer continued
supercritical water flow in curved channels, heat transfer and drag 79−90246
supercritical water flow in tube under very high press., heat transfer characts. *(Japanese)* 77−42840
superheated binary liquid mixtures, homogeneous nucleation of bubbles 78−67818
superheated droplets, flash boiling, undergraduate student expt. 78−81748
superheated liquid, elec. field induced nucleation, pre-nucleation relax. phenomenon 77−51489
superheated liquid, spinodal, hole thoery 80−19232
superheated liquid, under intense EM irrad., effect of spinodal singularities on evaporation *(Russian)* 77−89533
superheated steam, turbulent flow, local heat transfer during cooling *(Russian)* 79−59985
superheated vapour in horizontal tube, condensation, local convective heat transfer coeff. 80−19927
superheated water, flashing kinetics, γ-radiation effects 80−92025
supersaturated gas mixture-small liquid droplets, energy and mass transfer anal. 77−62135
supersaturation during heat and mass exchange in stationary gas medium 79−94480
supersonic, turbulent boundary-shock wave interaction, aerodynamic heating 78−26155
supersonic boundary layers, highly cooled turbulent flow 78−9652
supersonic boundary layers interacting with cooling wall jets, turbulent and optical characteristics 80−106792
supersonic diffuser with surface cooling, flow and heat transfer meas. in pseudo-shock region 77−42868
supersonic flow, heat transfer on flat porous wall with alternating injection and suction zones 79−98719
supersonic flow, viscous, past corner, energy eqn., asymptotic solns., heat transfer 79−32564
supersonic flow past blunt body, radn. effect on flow field and heat flux 77−47113
supersonic jet, thermogasdynamic interaction with inclined permeable baffle 79−98773
supersonic jet inflow into cavity, press. fluctuations and heating 79−64726
supersonic laminar boundary layer with conjugated heat transfer 79−64687
supersonic turbulent boundary layer of equilib. dissoc. and ionised gas 77−47039
supersonic turbulent compression corner flow, numerical simulation 77−62276
supersonic two-phase flow, nonequilib. condensation, boundary condition numerical anal. 80−64565
surface boiling in tube, heat transfer model 78−9551
surface discharging heated turbulent jet, 3D finite difference model, turbulent diffusivities 80−74845
surface heat flux, rel. to boundary conditions, modified integral method calcs. 79−59978
surface jets, heated, three-dimens., modelling 80−24065
surface roughness effect on heat transfer from cylinder to air cross flow 77−39287
surface roughness influence on boiling heat exchange of light hydrocarbons and N_2 *(Russian)* 79−68562
surface temperature and heat flux, prediction from interior temp. response 77−27460
surface-boiling flow in pipe, high-frequency pressure oscillations 77−35239
surface-mounted beaded thermocouple transient response models 78−8405
surfaces, thermal efficiency determ. 79−27641
surfaces covered with capillary-porous structures, heat transfer with boiling, approximate theory 78−94537
surfactant, aq. subcooled soln., acoustic phenomena during nucleate boiling 78−10181
suspension, solid separation at wall, heat transfer 78−9685
suspension channel flow, particle-wall interactions, heat transfer 78−5787
suspension of asbestos fibres, heat transfer and friction coeffs. for tubular flow 78−22405
suspension of prolate spheroids in shear flow, bulk heat flux 79−46370
suspension of solid in gas, heat transfer rel. to turbulence 79−72928
suspension of solids, transfer process, adiabatic calorimeter problem 79−23353
suspension stream in horizontal pipe, local heat exchange 77−47071
sweat cooled porous hollow cylinder, heat transfer from hot fluid 79−18943
swirled flow, sprayed liquid hydrodynamics 80−79325
swirled flow in pipe entrance, heat transfer law 78−5754
swirled turbulent flow in cylindrical channels, heat and momentum transport, local props. 80−14819
swirling one- and two-phase liq.-gas flow in tube, heat and mass transfer 78−30339
Tasmania, two terrestrial heat flow values 77−33018
Taylor vortex flow, effect on development length in concentric annuli 80−1597
Taylor vortex flow, heat and mass transfer with const. axial flow rates 77−15035
Taylor vortex flow with imposed laminar axial flow and isothermal surface heat transfer, velocity profiles 80−103031
temperature dissipation fluctuations, in turbulent boundary layer, meas. technique and errors 77−84255
temperature distribution of a gas heated in a porous material by concentrated solar radiation, theory 80−53777
temperature drop parameter when testing with const. thermal flux 78−51049
temperature field, heat transfer problems, linear algebraic soln. method 78−59281
temperature field above localised heat source, on vertical adiabatic surface 77−84248
temperature field equations, steady-state and transient case, 2-D, 3-D, finite element anal. 79−23182
temperature field fluctuations in raised temp. turbulent flow *(French)* 80−19371
temperature fluctuation production in airstream, small scale 78−94686
temperature measurement of hot thin plates, heat loss elimination 77−74397
heat transfer continued
temperature pulsation balance in turbulent streams 79−14385
temperature sensitive semiconductors, AC thermal theory 79−11131
temperature waves in nonlinear medium 77−54855
temperature waves in rigid heat conductor 77−14892
ternary gas diffusion, heat transfer rates effect 77−7393
terrestrial heat, transient flux during erosion and uplift with exponential heat source distrib. 79−57887
terrestrial heat flow, erosion effect on palaeoclimatic and topographic corrections 79−34767
terrestrial heat flow, Rumanian tectonic units *(Rumanian)* 80−8268
thermal accommodation coefficients from heat transfer data for low-density gases 77−35167
thermal characteristics of finite element and finite difference calcs. for transient problems, comments 80−69633
thermal creep for gas flow in flat channel, accommodation coeff. 77−11264
thermal curtain efficiency 77−89010
thermal energy storage, short term storage for low temp. solar heating appls. 80−55918
thermal energy storage in a packed bed of iron spheres with liquid sodium coolant, thermocline broadening 80−45762
thermal energy storage material cylinders, heat transfer during melting 79−3894
thermal energy storage tank, thermal stratification during charging 79−3890
thermal energy transport using benzene/cyclohexane reversible chemical reaction systems 80−67009
thermal exchange between sensor and supports, temp. fluctuation meas. in turbulent airflow 78−21135
thermal fluid selection for long-distance heat transmission, theoretical model 80−35761
thermal hydrodynamic instability, heating condition effect 78−18288
thermal inertia mapping by IR imagery, mathematical model 80−109280
thermal instability of an internally heated fluid layer in a magnetic field 80−53875
thermal instability of layer heated from below 78−63476
thermal pipes, sonic restriction on power at high temp. 80−103023
thermal plasma, heat and mass transfer 78−1805
thermal plasma, heat transfer to neighbouring walls or electrodes 78−1804
thermal plasma transport phenomena, conf., Odeillo-Font-Romeu, France (Sept. 1975) 78−1798
thermal plumes development, effect of condensation *(French)* 79−23192
thermal pollution by discharges into waterways, mixing problems 79−8645
thermal quenching, Cu block by liq. N_2, for boiling curve 79−14232
thermal radiation flux distribution from electrodynamic gas heater *(Russian)* 79−18678
thermal regenerator, with variable mass flow rate, computer model 78−75047
thermal regenerator calcs., heat transfer coeff. correlations, transient response 79−68702
thermal regenerator performance, gas heat storage effect 78−5647
thermal sensation evaluation, comfort chart *(Japanese)* 80−81545
thermal storage by sensitive, latent heat,, dynamic model *(French)* 80−40917
thermal storage unit, sensible-heat, solid, transient response 79−3892
thermal stress resistance, effect of spatially varying porosity during steady-state heat flow 80−1488
thermal stresses due to moving heat sources *(Polish)* 78−18184
thermal transpiration, in circular capillary with small temp. difference 79−32191
thermal wave propagation in nonlinear absorbing medium 80−96183
thermal-convective instability through porous medium 80−53769
thermal-ignition analysis in boundary-layer flows 79−64800
thermally developed duct flow, boundary conditions rel. to Nusselt numbers 78−91016
thermoacoustic pressure oscillations in heated channel 79−46319
thermoacoustic vibration generation, in heated channel laminar flow 78−14029
thermoanemometer, influence of probe filament aspect ratio and diameter 80−19532
thermocouple cavity, minimisation of temp. distortion 77−82506
thermodiffusion in elastic cylinder, quasistatic problem *(Polish)* 80−10150
thermodynamics, second law, heat flow direction and Fourier inequality, comparative assessment 79−44896
thermoelasticity theory with appl., book 78−79219
thermoelectric cooling equipment, welded joints, heat emission effects on temp. distrib. *(Russian)* 80−69635
thermoelectric discs, coaxial, radial current flow, heat transport 79−2767
thermoelectric energy conversion, heat losses compensation due to thermal cond. through Peltier heat 80−107773
thermoelectric heat-flow meters, compensated, metrological characts. 79−37144
thermography, medical appls. 77−44737
thermomechanical instability of a heat releasing granular layer, GCR model 80−92134
thermophoretic and diffusiophoretic particle deposition estimation 77−90644
thermophysical coefficients, integral characts. method *(Russian)* 80−69643
thermophysical properties, thermometric method determ., harmonic action of heat flow *(Russian)* 80−69642
thermosiphon, evaporative, heat transfer intensity in boiling section 78−67017
thermosiphon, inverse, thermo-hydraulic design 78−94534
thermosiphons, boiling heat transfer 78−9537
thermosiphons, two-phase heat exchange in supply zone, anal. 80−19387
thermosphere, electrodynamic and particle heating in disturbed polar regions 77−33231
thermosyphon, gas-controlled two-phase, performance 79−1049
thermosyphon, two-phase, heat and mass transfer in evaporation zone 79−1048
thermosyphon steady flow, existence in open curved heated ducts *(French)* 80−43689
thin circular insulating annulus on conducting half-space, steady heat flow 79−59981

heat transfer continued
thin film evaporator grooves, fluid evaporation and boiling heat transfer 80−38227
thin film heat transfer, effects on meniscus profile and capillary pressure 80−14685
thin films, conductor covered with electrolytic deposit, thermoelectric props., thermal flux meas. *(French)* 80−59961
thin liquid films with extensive evaporation, heat transfer *(German)* 80−99920
thin-wall cylinder method for heat transfer studies in tubes and channels 77−24045
three dimensional free convection flow and heat transfer along a porous vertical plate 78−90866
three dimensional separated turbulent flows at supersonic speeds 80−19435
three phase induction motor heat flow model, locked rotor and running-up temp. rise calcs. *(German)* 79−90115
three-component system transport coefficient determ. 78−21082
three-dimensional model of turbulent transfer in rectilinear channel 77−35138
thyristors, high-output, air cooling intensification design method *(Chinese)* 80−19229
time dependent Poisson queue and moving boundary problems for the heat and wave equation 79−63172
tissue, dynamic temp. distribs. in normal and neoplastic tissues during diathermy 78−31776
tissue, surface, two-phase theory for circulatory influence on heat transfer 80−104564
tissue, two-regime model of perfusion meas. heated thermocouple probe 77−5110
Tokamak, time resolved heat flux to wall meas., sheath model with secondary electron emission 78−79468
Tokamak fusion test reactor vacuum vessel, flow-related heating/cooling problems 79−85798
tornado type wind energy system, wind and solar energies effect of line heat source 79−87959
toroidal thermosyphon flow with ang. displacement of heated and cooled sections 80−33680
toroidal vessel partially filled with liquid, heat transfer meas. rel. to leakage 80−5913
total coeff. determ. tests for industrial cooling system of continuous hot rolling mills *(German)* 77−89005
Touchau method for thermal effusivity meas. *(French)* 80−53617
transfer with small accommodation coefficients *(German)* 79−86437
transference function, analytic determ. 79−98590
transformation groups for resolution of partial differential eqns., appl. to gravity, quantum mech. and heat transfer *(French)* 79−49099
transformer, oil-cooled, heat exchange anal., network method *(Russian)* 78−83399
transient (film) boiling on surface of small Cu drop in water 77−1219
transient and steady state, finite difference computer programs 79−14221
transient and unsteady flow past heated circular cylinder 80−24019
transient boiling, bubble nucleation and growth instabilities 78−90649
transient boundary layer on porous plate, coolant injection, laminar flow stability and heat transfer 78−83389
transient effects, leading up to nucleate boiling 78−90650
transient flow boiling in duct, dynamics 78−94528
transient freezing of liquids in turbulent flow inside tubes 80−6494
transient gas flow in channel of cylindrical solid with free movement between end chambers 77−15120
transient heat exchange between a radiating plate and a high-temperature gas flow 79−94609
transient heat flow, two-dimens., method of isotherm migration along orthogonal flow lines 78−46963
transient heat flux, meas. using heat gauges 77−49723
transient heat transfer during natural convection *(Russian)* 77−68367
transient nonlinear diffusion method of differential quadrature 78−16755
transient superheat on vertical surfaces in subcooled boiling 79−7282
transient temperature field approx. in cylindrical and spherical bodies *(Polish)* 79−32192
transient thermal problems, finite difference and finite element calcs., suddenly cooled boundary 80−14554
transient thermal process calculation method, approx. polynomial representation *(Russian)* 78−83211
transient thermal response of two solids in contact over a circular disk 80−79116
transient thermocapillary flow in thin liquid layers 80−92226
transition boiling heat transfer with forced convection, composite test section, steady state method 79−19361
transition flow boiling heat transfer to water in verticle annulus, BWR LOFA appl. 77−23182
transition Knudsen regime, nonstationary heat and mass transfer, book contrib. 80−1649
transition metals electrical transfer of O, N, exam., using heat transfer of interstitial atoms *(Russian)* 79−55931
transparent medium with random absorbing inclusions, laser heating statistics *(Russian)* 77−28666
transparent turbulent gas flow past radiating plate, heat transfer anal. 77−35257
triangular straight fins, periodic heat transfer 80−43599
trichloroethylene aqueous hetero-azeotrope mixture, condensation heat transfer coeff. *(German)* 80−33425
trifluorotrichloroethane, influence of porous coating of heating surface on rate of heat transfer on boiling *(Russian)* 79−10452
trunk pipeline systems, oil and gas, investigation and optimisation of thermal regimes 80−107579
tube, annular high Prandtl no. flow, turbulent heat transfer, surface rejuvenation model 78−71333
tube, circumferential wall heat cond. effect on thermal boundary conditions 79−32200
tube, condensation, appl. to dynamic model of reboiler 77−7298
tube, elliptical, laminar liq. flow, nonsteady heat transfer 78−42598
tube, horizontal, laminar combined convection, circumferentially nonuniform heating effect 78−71331
tube, transversely finned, in air flow, metal thermal cond. effect 78−75043
tube, vert., uniformly-heated, crit. heat flux prediction, generalised graphical method 79−46313
tube, vertical, heat transfer upon steam condensation 80−48547
tube, vertical, laminar and turbulent heat transfer, air and Ar 78−71332
heat transfer continued
tube, vertical, steam generating annular flow, dry-out position prediction, computer model 78−59447
tube bank, heat transfer and flow around second cylinder of three cylinders in cross flow 77−15025
tube bank heat transfer in air crossflow at high Reynolds nos. *(Russian)* 78−14010
tube bank streamlining in critical flow regime with heat transfer *(Russian)* 78−14009
tube banks, heat transfer, viscous flow, numerical anal. 79−55375
tube banks, in-line, with pyramidal roughness, flow and heat transfer 78−18152
tube banks in cross flow, heat transfer 79−1077
tube banks in transverse streamline air flow with high Reynolds numbers *(Russian)* 79−94619
tube banks in turbulent flow, heat transfer prediction 79−1080
tube bundle in compact layer of granular material *(Russian)* 80−43595
tube bundle in crossflow at low Reynolds nos. 79−98712
tube bundle transient heat transfer and hydrodynamics with large flow and heat flux perturbations 78−83484
tube bundles, heat transfer to three dimens. flow 79−1073
tube bundles, viscous fluid crossflow, average heat transfer and pressure drop 80−1572
tube bundles in cross flow at critical Reynolds nos., heat transfer efficiency 79−98708
tube entrance velocity and temp. distrib. with turbulent hot air flow *(Russian)* 78−14087
tube flow, heat transfer problem of flowing liquid solidification onto a melting wall 78−94585
tube flow, with spiral blades, heat transfer, drag resistance 78−1672
tube flow of water, heat transfer in downward flow 78−30288
tube in convergent channel oblique flow heat transfer 78−55643
tube in fin heat exchangers with rippled fins, optimal design for maximum heat transfer 80−6055
tube inlet region, high temp. gas turbulent heat transfer, temp. factor, expt. 78−83483
tube inlet zone, flow and heat transfer with injection into swirled flow 79−98717
tube wall heating during steady state tube drawing *(German)* 78−84899
tube with turbulence promoter 78−94728
tube with variable boundary conditions, heat transfer, Laplace transform appl. 80−74859
tube-in-tube heat exchanger, dynamic analysis, digital algorithm for initial value problem 77−42727
tubes, flattened, in transverse gas flow 79−1067
tubes, heat transfer laws, longitudinal turbulent diffusion influence 80−33597
tubes, horizontal and vertical cooled, boiling crisis and critical heat flux 80−48712
tubes, nonstationary thermal processes, heat transfer coeff. quasistationary value applicability 80−64562
tubes, nucleate pool boiling, critical heat flux, ferric oxide scale effects 80−64343
tubes, straight and coiled, boiling heat transfer with low pressure water flows 80−74856
tubes, temp. and heat transfer coeff. variation upon boiling mode changes 80−69629
tubes in closely spaced in-line bank, heat transfer in cross-flow 80−59026
tubes with nonuniform axial heat distrib., heat transfer burnout 78−94088
tubeside laminar flow heat transfer augmentation 78−94726
tubular casing heat exchanger, effect of transverse baffles on heat exchange in inter-tube area *(Russian)* 78−45618
tubular condenser apparatus *(Russian)* 80−1411
tubular cover solar collectors, performance calcs., transmittance and radiosity 80−61415
tubular reactor, model calc. with longitudinal transfer and heat losses through sides *(Russian)* 78−73043
turbine blade and nozzle guide vane, transient cascade, heat transfer meas., wind tunnel 78−94768
turbine blade cooling, calc. of required level 79−64487
turbogenerator rotor and stator core thermal conductivity solution using integral representation method *(Russian)* 80−100451
turbogenerators, high capacity, heating reduction measures for enhanced reliability and interval between maintenance *(Russian)* 80−96175
turbulence, book 78−90839
turbulence, free-stream, effect on heat transfer and skin friction 78−30276
turbulence, grid-generated, heat transfer 78−59393
turbulence, isotropic, spectral space, comparison between kinematic and scalar fields *(French)* 78−87334
turbulence effects heat transfer from cylinders in crossflow at critical Reynolds no. 79−98707
turbulence effects on heat transfer between jet and obstacle *(Russian)* 80−1579
turbulence generated by grid, temp. fluctuations and heat flux 78−94651
turbulence models for heat transfer, review 79−4017
turbulence structure and mechanisms, conference, Berlin, Germany (Aug. 1977) 78−94647
turbulent, behind hydrodynamic starting length, analytical method *(German)* 79−72892
turbulent, in liq. metal flow near wall 77−35142
turbulent air flow in channel, temp. field 79−4005
turbulent air flow in pipe at high temp. 79−81850
turbulent air stream, local heat transfer from single sphere 78−22342
turbulent airflow in pipe at low Reynolds numbers, effect of flow laminarisation 77−23942
turbulent axisymmetric temperature wake, final decay period modelling 77−3828
turbulent boundary layer, diffusion model and rel. to mass transfer 78−94544
turbulent boundary layer, external flow turbulence effect 78−94713
turbulent boundary layer, free-stream turbulence effects 78−94714
turbulent boundary layer, Hassid-Poreh energy model anal., inc. accel. and surface heat transfer step change 78−51158
turbulent boundary layer, heat transfer, effect of free-stream turbulence 79−55385
turbulent boundary layer, nominally steady, two-dimens., vel. and temp. profile prediction method 80−1624

heat transfer continued
turbulent boundary layer, on heated flat plate, wall suction effects *(French)* 77−58666
turbulent boundary layer, periodic intermittent model for wall region 78−87336
turbulent boundary layer, response to step change in heat flux 77−39291
turbulent boundary layer, supersonic, wall temp. effect 78−94765
turbulent boundary layer, temp. and vel. fluctuations, spectral analogy 77−7376
turbulent boundary layer, temp. dissipation log normality 78−34135
turbulent boundary layer, temp. fluctuations downstream of heat source *(French)* 77−911
turbulent boundary layer, temperature field, dispersion meas. 78−38322
turbulent boundary layer, temperature fluctuations, correlations and probabilities 79−46303
turbulent boundary layer, temperature profile and Reynolds analogy expressions 78−87337
turbulent boundary layer, transport processes model 77−58663
turbulent boundary layer, wall suction and heating *(French)* 77−19595
turbulent boundary layer analysis for air and combustion products *(Russian)* 78−5732
turbulent boundary layer at permeable plate with shock waves, heat transfer 79−81922
turbulent boundary layer downstream of step change in surface temp. 79−81862
turbulent boundary layer flow over flat plate 78−94715
turbulent boundary layer in pipe, temp. distrib. 79−32668
turbulent boundary layer on rough surface with blowing 78−71334
turbulent boundary layer over heated tank of liquid *(Russian)* 77−68577
turbulent boundary layer with suction under nonisothermal conditions, heat and mass transfer 80−92125
turbulent boundary layer with wall heat flux inversion, thermal characts. 80−19350
turbulent boundary layers near separation point, numerical prediction, heat transfer *(French)* 78−94657
turbulent combustions, problems of bias on mean meas. *(French)* 80−53879
turbulent compressible boundary layer on permeable rough surface with heat transfer 79−1176
turbulent compressible boundary layer with heat-transfer effects on conditions at the sublayer 80−14672
turbulent duct flow, heat transfer, mixing length model 78−94720
turbulent entry region of pipe, temp. and vel. fluctuations 78−94717
turbulent filmwise condensation heat transfer coeffs. 78−63429
turbulent flame, interaction of flow pulsation and chem. reaction 77−58801
turbulent flow, coupled transport of heat, momentum, mass, numerical method *(German)* 77−11193
turbulent flow, in tube with circumferentially varying wall heat flux 77−65738
turbulent flow, temperature fluctuations, local isotropy 79−1191
turbulent flow around plate containing heat sources 77−23948
turbulent flow at tube entry region, high Prandtl number 78−94716
turbulent flow in annulus, heat transfer enhancement by fluid injection 79−23319
turbulent flow in channel with permeable wall 78−63426
turbulent flow in circular tube, transient heat transfer 77−47004
turbulent flow in pipes, temp. field struct. 80−69923
turbulent flow in tube, critical heat flux meas. *(Russian)* 79−10558
turbulent flow over isothermal flat plate 77−89121
turbulent flow with subcritical and supercritical press., natural convection effect on heat transfer 78−5739
turbulent fluidised beds, solids circulation and heat transfer to immersed tube banks 80−6141
turbulent fluids, mag. energy transfer in weak mag. fields 78−18350
turbulent forced convection, heat and mass transfer, analogeous relationship *(Japanese)* 79−14396
turbulent gas, heat transfer and heat production *(German)* 78−90867
turbulent gas flow, acoustic oscills. effect 78−59394
turbulent gas flow, heat transfer coefficients using two-zone model 77−89119
turbulent gas flow in annular channels, heat transfer apparatus and technique *(Russian)* 78−34199
turbulent gas flow in tube, temp. fluctuations 78−94721
turbulent gas flows in channels with high freq. press. oscillations, heat transfer 80−24024
turbulent gas streams in channels during resonant vibrs. *(Russian)* 79−50723
turbulent gas suspension, heat transfer and struct. 78−9683
turbulent heat and mass transfer 78−1639
turbulent heat and mass transfer from wall with roughness ridges 77−39286
turbulent heat and mass transfer in abruptly changing wall boundary conditions 78−94545
turbulent heat and mass transfer rates at high Pr, electrochemical modelling 78−83383
turbulent heat flux and temp. fluctuation prediction 80−38400
turbulent heat flux transport eqn. for equilibrium retarded layer 80−19380
turbulent heat transfer, flow between parallel plates, asymptotic expansion calcs. 77−47008
turbulent heat transfer, flow between parallel plates, wall cond. effects 77−47007
turbulent heat transfer, TURF computer schemes 79−4014
turbulent heat transfer across membrane between two liquids *(Russian)* 78−38180
turbulent heat transfer and press. drop in tube, internal solidification effect 79−32512
turbulent heat transfer downstream of a fluid withdrawal branch in a tube 79−77255
turbulent heat transfer from flat plates, facing curved wall effects *(Japanese)* 80−83799
turbulent heat transfer in annulus, transient, heating element, reactor cooling theory 78−86569
turbulent heat transfer in dilute surfactant or polymer solutions 79−77101
turbulent heat transfer in thermal boundary layer 77−42821
turbulent heat transfer measurements in axisymmetric external separated and reattached flows 80−10234
heat transfer continued
turbulent heated flow of He-Ar mixtures in vertical circular tubes 79−59975
turbulent incompressible jas jets, thermodynamic transfer theory *(Russian)* 79−32621
turbulent jet, in coflowing stream, vel. and temp. profiles 77−27569
turbulent jet, joint probability densities and quadrant contribs. 79−32597
turbulent jet, structure functions of temp. fluctuations 78−71380
turbulent jet impinging on cylinder wall *(Japanese)* 80−83800
turbulent jets, heat, mass and momentum transport, into ambient air 78−51210
turbulent liquid flow in heated tube at supercritical press., heat transfer 78−71316
turbulent liquid pipe flow, thermoacoustic oscills. 78−9635
turbulent multiphase flow with phase transitions *(German)* 77−15109
turbulent non-isothermal flow, temp. pulsations 78−94712
turbulent nonuniform boundary layer with condensation, analysis 77−89124
turbulent pipe flow, enlargement, contraction effect on flow characteristics 80−6154
turbulent pipe flow, heat transfer, fluid props., var. calcs. 77−27527
turbulent pipe flow with heat transfer and chem. reaction 78−51257
turbulent pipe flow with heat transfer and chemical reaction 79−1271
turbulent pipe flow with suction or injection, high Prandtl no. heat and mass transfer 80−74857
turbulent Prandtl and Schmidt numbers from modelled transport eqns. 80−19373
turbulent recirculating flow in enclosure 78−38315
turbulent rough-wall heat transfer, variable wall temp. and blowing 78−38308
turbulent shear flow, temperature ramps characterisation by two length scales 79−10560
turbulent shear flow with streamline curvature, algebraic stress-heat flux model 79−27625
turbulent shear layer attachment near Mach 6, peak heating 78−26153
turbulent thermal layers on flat plates 79−23307
turbulent thermal plume rising along isothermal wall, struct. and heat transfer 79−81890
turbulent transfer in a tube, mixing tee effect 79−68812
turbulent transport coefficients, derivation from turbulent parameters in isotropic turbulence 78−46948
turbulent transport to rot. cylinder 77−7402
turbulent tube flow, heat carrier with near-critical parameters 78−42600
turbulent tube flow, of water, with nonuniform heating 79−32513
turbulent viscous incompressible flow in tube, nonsteady convective heat transfer 80−19393
turbulent vortex rings, turbulent motion and heat transfer *(Russian)* 77−55008
turbulent water film, with different initial flow conditions and high temp. gradients, heat transfer 78−90862
twisted air flow in permeable tube, local heat transfer 78−71338
two coaxial cylinders, fluctuating flow and heat transfer for incompressible fluid 80−24013
two coaxial rotating discs, viscous fluid unsteady motion and heat transfer 79−94633
two flat surfaces in contact, thermal conductance with applied load, variation, determination for elastic and plastic surface deformation 79−72782
two infinite parallel plates, non-Newtonian fluid linear flow, heat transfer 79−98810
two moderately rotating porous discs, heat transfer 80−103028
two parallel corotating discs, laminar flow and heat transfer, shear pump appl. *(German)* 80−69840
two phase flow heat transfer in convergent part of nozzle, correl. of expt. data 79−81958
two semi-infinite rods, temp. field in system 77−68373
two solids in friction, thermal contact resistance, relative slipping speed effects *(French)* 79−94469
two-component dense moving layer, heat transfer in cylindrical pipe 77−47074
two-component fluid, laminar boundary layer, temp. and conc. field calcs. *(German)* 78−71386
two-dimensional heat operator, ten-point difference methods, numerical complexity 80−10133
two-dimensional MHD parallel plane channel flow, heat transfer 79−32701
two-dimensional steady state heat transfer with surface heat sources, program *(Italian)* 79−37132
two-phase countercurrent flow in tube, max. heat flux 78−90992
two-phase counterflow with freely-falling dispersed material, heat and mass transfer 78−30340
two-phase flow, annular, crit. heat flux, swirl effect 80−10113
two-phase flow, boundary vapour contents for critical state of heat transfer of second kind 78−1722
two-phase flow, hydrodynamics and heat exchange in film flow 78−91000
two-phase flow, nonstationary velocity tracking by adaptive cross-correl. algorithm 78−14074
two-phase flow, one-dimens., heat and mass transfer, approx. math. model 79−86495
two-phase flow, transient, interfacial heat and mass transfer, surface renewal model 79−27683
two-phase flow in pipe, effect of mass transfer on heat transfer 78−91003
two-phase flow with condensed liq. particles, heat transfer to wall with solid condensate layer 79−86426
two-phase gas-water flow *(Russian)* 80−43761
two-phase laminar flow, in circular pipe, heat transfer, inlet temp. effects 78−67265
two-phase liquid film flow, hydrodynamic and heat transfer in downward annular motion 77−89190
two-phase polydisperse medium with phase transformations and size distrib., thermodhydrodynamic eqns. 79−41743
two-phase rising flow in channels, heat and mass transfer 77−62295
two-phase thermosyphons, max. heat flux, expt. data correlation 80−48559
two-phase two-component heat transfer, review 79−1239
two-phase vapour-liquid mixture in heated channel, integrated momentum model 77−31367
uncooled radial gas turbine, anal. 79−4010

heat transfer continued
undergraduate textbook 79−94623
underground boilers; 3-D heat transfer *(Ukrainian)* 78−55550
underground cable system, convectively cooled, temp. distribs., heat transfer correlations 78−71262
underground channel, cylindrical, fluid flow and heat transfer 77−7455
underground pipeline, unsteady heat loss, analytic expressions 78−83223
underground railway tunnel microclimate, calc. method *(Russian)* 79−68548
underground thermal wells, heat extraction with water 77−44949
underwater plasma weld cooling 79−1932
unequal surface temp. effect on heat transfer in lubrication problems 80−53613
unsaturated porous media, heat and mass transfer, expt. and simulation *(French)* 78−94542
unstable heat transfer conditions, free convection-film boiling transition 78−14006
unsteady critical heat flux during boiling 77−23946
unsteady gas stream temperature determ. using slow-response thermocouple 77−24046
unsteady heat transfer effect on boundary layer growth at forward stagnation point 79−10555
unsteady heat transfer from rotating disc or cone with large suction 77−47025
unsteady heat transfer from suddenly heated infinite plate in rarefied gas 78−34166
unsteady laminar boundary layers at incompressible 3-dimens. stagnation point, heat transfer 79−64659
unsteady state heat transfer through the interface of spherical particles *(German)* 80−1412
upstream adiabatic zone, subsonic, supersonic downstream boundary layer heat transfer effects 78−83379
upward flow, in post-dryout region of heated vertical tube 79−59973
urban-rural canopy analysis, surface heat flux/temp. model 79−20945
US assisted radiant heat transfer into water and air 79−46169
vacuum arc, energy dissipation in cathode 78−5970
vacuum-powder insulation, radiative heat transfer determ. by IR spectroscopy 77−13759
valley ventilation by cross winds 80−48771
vaporisation channels, rough and smooth, heat transfer in post dry-out region 80−96255
vaporisation of particles in high temp. gas, Sherman eqn. calcs. *(Russian)* 80−39270
vaporising liquid layer at nonadiabatic evaporation, binary laminar boundary layer flow *(German)* 80−1588
vapour bubble, in immiscible liquid, collapse 78−94547
vapour bubble collapse, effect of initial radius and subcooling 77−80196
vapour bubble nuclei, stability and nucleation, effect of gases 77−31303
vapour bubble-liquid slug heat transfer, Taylor instability mechanism for LMFBR HCDA 78−8939
vapour bubbles, flow and temp. fields, global collocation calcs. 77−47067
vapour condensation on vertical surface, laminar flow in film condensate 78−75057
vapour dispersion, near surface of evaporation 77−51487
vapour flow in liquid enclosure with temp. distrib. 77−15083
vapour generator for K, heat transfer with drop motion in tube in supercrit. region 80−23880
vapour phase heat transfer in post critical heat flux region 79−9668
vapour-gas bubbles, heat transfer effects associated with oscillations 80−6133
vapour-gas phase, heat and mass transfer during evaporation of fluid 77−55354
variable property heat transfer to single sphere in high temp. surroundings 80−14884
variational irreversible thermodynamics of heat and mass transfer in porous solids 79−4081
velocity field measurements of a laminar thermal 79−68674
vertical annular laminar flow, of immiscible liqs., heat transfer 78−14082
vertical buoyant jets, decay, unified correlation and prediction in turbulence model 80−6118
vertical cavity with saturated porous filling, asymptotic Nusselt number *(French)* 80−43700
vertical cones in laminar free convection, integral method 79−81881
vertical evaporating circuit, heat exchange calc. and optimisation *(Russian)* 77−71321
vertical fin, film condensation on extended surface 80−6505
vertical surface, cooling by liquid spray, heat transfer 80−74711
vertical thermal channels, interferometric simulation of heat transfer 79−17477
view factor, diffuse radiation between the spheres exact and approx. calcs. 77−26252
viscoelastic boundary layer flow, second order, at stagnation point, heat transfer 80−103025
viscoelastic flow in tube, eddy diffusion reduction for heat and momentum transfer 78−22382
viscoelastic fluid, steady flow and heat transfer between two coaxial rot. discs 80−14755
viscoelastic fluid, thermal boundary layer on porous plate 77−84283
viscoelastic fluid flow, heat transfer at low Deborah numbers, rheological effects 80−19445
viscoelastic fluid in channel entrance, hydrodynamic and thermal boundary layers 79−18915
viscoelastic liquid, heat transfer in rot. flow, suction and injection effects 80−33596
viscoelastic reacting fluids flowing over flat plate, boundary layer anal. of surface deposition 78−42675
viscoelastic Rivlin-Ericksen flow past stretching plate, skin friction, heat transfer calc. 77−72272
viscoelastoplastic laminar tube flow, heat transfer 80−10269
viscomagnetic heat flux, in a Burnett regime, gas kinetic theory 78−71400
viscometer, high pressure, non-isothermal flow, thermal boundary conditions *(German)* 78−67292
viscometers, biconical and concentric spherical, heat transfer 79−55318
viscoplastic fluid Couette flow, heat transfer 80−10270
viscosity stratified fluid layer, heated from below, thermal instability 77−58762
viscous dissipation effect on heat transfer, circ. cylinder axisymmetric stagnation flow 78−51164
heat transfer continued
viscous flow, unsteady, around elliptic cylinder, heat transfer, finite difference method *(Japanese)* 80−69831
viscous fluid, flow and heat transfer due to disc small torsional oscills. 79−68691
viscous fluid in pipes, nonisothermal flow, crit. phenomena 80−103074
viscous fluid layer with heat source, stability in presence of inclined mag. field 77−89206
viscous fluid under cyclic deform., self-heating, hydrodynamic thermal explosion 80−58993
viscous fluids in static mixer, heat transfer coeffs. 79−18885
viscous heating at low Reynolds number, stability anal. 77−72280
viscous incompressible liquid between two coaxial cylinders, exponential rate of heat addition, temp. distrib. 77−68586
viscous liquid, transverse flow around cylinder, heat exchange *(Russian)* 78−46971
viscous shock layer, heavy-particle suspension effect on gas flow 80−28554
viscous sublayer turbulent Prandtl no., wall heat cond. influence 79−94616
visualisation, in environmental and technical systems *(German)* 79−86540
wake behind linear heat source, temp. pulsations *(Russian)* 79−14401
wake in steady and pulsed flow *(French)* 79−1188
wake of step, with pulsating jet, thermal convection *(French)* 80−10240
wall, with cylindrical cooling channels, steady-state temp. distrib. 77−65663
wall flux, down-stream from linear heat source in turbulent boundary layer *(French)* 79−32489
wall in electric furnace, plane, temperature dependence on time and spatial coordinates 79−1054
wall jet, radial, temp. field and heat transfer meas. 77−72341
wall region heat and mass transfer in turbulent Newtonian and viscoelastic flow 80−14680
wall with lugs, heat transmission calcs. *(Russian)* 79−50570
water, boiling, heat transfer around single nucleation site 77−24394
water, boiling and heat transfer on horizontal pipes with annular fins 80−74855
water, boiling critical heat flux density, free motion conditions, 1-205 bar *(Russian)* 79−68560
water, boiling curves, subcooled and forced convective conditions 79−14230
water, boiling heat transfer coefficients, heater plate thickness effects 78−34124
water, boiling on finned surface, heat transfer crisis 78−9540
water, layer, semiinfinite, cooled (heated) from below, convection onset, density anomaly influence *(German)* 78−22350
water, MHD free convection flow past infinite porous plate 80−33703
water, nucleate and transient boiling in narrow space between disks 77−84115
water, nucleate boiling heat transfer, press. factor 77−69080
water, pool boiling, produced by distrib. internal heat sources, in homogeneous nucl. reactor 78−90685
water, surface boiling in tubes, heat transfer 78−9541
water, temp. field for surface boiling in round tube 77−42818
water, thermally-stratified, cooled from above, free convection 79−46315
water, transient heat transfer (0-220°C, 1-10 bars) *(Russian)* 78−38183
water, unsteady transient heat transfer with phase transitions 80−48693
water adjacent to vertical uniform flux surface, buoyancy driven flow, transition and transport 79−27631
water at supercritical press., unsteady heat transfer 80−48692
water boiling, vibr. effect on heat transfer crisis 80−33423
water boundary layer along heated cylinder, buoyancy and variable viscosity effects 80−79256
water boundary layers, Tollmien-Schlichting waves and transition 79−81845
water content determ., porous materials, rapid thermal method 77−86258
water droplet evaporation, heat transfer characts., on heated surfaces 78−59269
water droplet initial size effect on evaporation on heated surfaces 79−68558
water droplets, ebullition under steady-state superheated conditions 80−74928
water droplets, ebullition under transient superheated conditions 80−74929
water film flow over cylinder, laminar to turbulent transition, heat transfer rates 77−58691
water film on Teflon surface, boiling heat transfer 79−90124
water films, subcooled, flowing down vertical tube, heat transfer 80−79348
water flow, nondimensional heat transfer law for a slanted hot film 80−74853
water flow in hot pipes, heat removal, wall thermal condtiions 77−68583
water heat pipe, evaporator heat transfer, obs. 78−83216
water in calorimetric vessel and jacket *(Polish)* 77−54996
water jet, round, impinging, heat transfer in interference zone of film flow along wall 77−58750
water jet impinging on horizontal heated surface, single-phase convection and nucleate boiling regions *(Japanese)* 80−48761
water jet impinging on hot surface, boiling heat transfer 78−90993
water pool nucleate boiling heat transfer thermodynamic investigation *(Chinese)* 79−72783
water pulsating flow in heat exchanger effect of pulsations on heat transfer 79−94614
water reactor fuel elements under accident conditions, conf. 77−42159
water subcooled films on horizontal tubes, heat transfer correlation 79−77114
water turbulent heat transfer downstream of unsymmetric blockage in tube 79−55377
water vapour, condensation from moist air in curved channels, mass and heat transfer 79−90251
water vapour, desublimation in vacuum, heat and mass transfer and duration 77−11687
water vapour-N_2, nonstationary rarefaction wave, nonequilib. condensation obs. 77−75937
water-air interface, overall heat transfer coeffs., humidity and density profiles, turbulent pulsations *(Russian)* 78−22349
water-cooled swirl tubes, for neutral beam targets, heat transfer calcs. 78−67018

heat transfer continued
water-in-oil emulsion, boiling, bubble formation, cinemicrophotography 80−74961
wave equation for simultaneous heat and mass transfer in moving media 79−44747
wear frictional heating and oxidational theory 80−44255
wedge-shaped leading edge of plate, local air (water) flow heat transfer 78−1660
welding, thermal stresses and metal movement, computer simulation 78−34002
welding arc constricted by radial gas flow, thermal efficiency, investigation 80−6038
wet bulb thermometer theory and comparison with expt. results *(Dutch)* 77−65039
wet granular material, heating rate during drying 77−89009
wind tunnel test program for determining effect of spin on boundary-layer transition at Mach numbers 5 and 8 on 9-deg. cone configuration 80−14864
wind-induced heat and mass transfer over large bodies of water 77−11186
wire, electrically heated, steady state multiplicity 78−46880
wire, in longitudinal laminar air stream, heat exchange *(Russian)* 78−83401
xerographic toner images, study using electrical analogue networks 80−47139
yawed wedge, local heat transfer 78−18295
Al alloys, 6061, A356, forging of liquid and partially solid alloys 78−80569
Al, heat transfer during cooling with water *(German)* 80−23873
Al ingot, dendrite arm spacing through heat flow control 77−73267
Al plate calorimeter, meas. of local convective heat transfer coefft. by polarisation interferometry 80−82809
Al, rapid melting and solidification of surface layer, exam. using computer heat flow model 78−83228
Al-Si eutectic, pressure effect on metal-die heat transfer coeffs. during solidification 80−7544
Al_2O_3, powder grains, melting, in plasma flame 79−60200
Al_2O_3, temperature drop parameter when testing with const. thermal flux 78−51049
Ar arc heating, high-pressure complex heat exchange expt. *(Russian)* 80−75112
Ar, ionised gas flow, heat transfer to sphere, appl. dimensionless rels. 77−35331
Ar, liquid, superheated, nucleation 79−23741
Ar, porous solid, contact heat transfer of sublimation 77−31767
Au electroplated layer, dropwise steam condensation, thickness depend. 79−46791
Au plasma flame, heat transfer to stationary sphere 80−33824
BF_3, boiling/condensation heat transfer props., cryogenic appls. 78−79192
CMN-^{3}He (^{3}He-^{4}He), heat capacity and heat transfer meas. instrum. *(French)* 79−1097
CO, boiling/condensation heat transfer props., cryogenic appls. 78−79192
CO_2, convection at critical point, heat transmission coeff., holographical method *(German)* 77−35133
CO_2 laser amplifiers, porous tube generated flow field, heat and mass diffusion 80−63969
CO_2, nucleate boiling, heat transfer rate 77−39199
CO_2 supercritical boilers, forced flow, frictional pressure drop 80−14689
CO_2, turbulent cooling tube flow, at supercrit. press. 78−14005
$CaSO_4$ crystallisation, from liq. solns. as heat-transfer surface 80−100772
Co_2 flow in heated tubes, with near critical parameters, turbulent flow, heat transfer 80−59022
Cs, vapour in Ar, fog condensation in MHD generator, heat and mass transfer 80−1410
Cu, continuous casting, heat transfer and surface temp. meas. apparatus *(Russian)* 77−66631
Cu, heat transfer during cooling with water *(German)* 80−23873
Cu, horizontal plate, pool-boiling heat transfer, nucleation centre size, surface roughness 78−90652
Cu ingots, solidification, quality and optimal modes of solidification, prediction from temp. fields 79−83187
Cu plates, gap magnitude effect on their thermal interaction at cryogenic temps. 79−86323
Cu, resistance thermometer, heat shock influence on elec. cond. and thermophysical props. *(Russian)* 80−52210
Cu, sintered, in contact with ^{3}He, thermal conductance, rel. to elec. resist., heat flow model calc. 80−10728
Cu surface roughness, liq. superheat and heterogeneous nucleation 79−37146
Cu wire, transient current pulsed heating, explosive inhomogeneous boiling explosive 78−38562
Cu/H_2O axially-grooved heat pipes, fabrication and performance testing for space vehicle appls. 80−37028
Cu-superfluid ^{4}He interface, exponentially damped surface solutions generated by heat flow 79−55980
Fe, diffusion melting in Fe-C melts, heat transfer correl. 80−54348
Fe, rapid melting and solidification of surface layer, exam. using computer heat flow model 78−83228
Ga, Czochralski growth, heat transfer during drawing *(French)* 78−48309
Ga, liq. particles-He(N_2)(CO_2)(air), nonequilib. Laval nozzle flow calib., numerical soln. 77−75967
GaAs crystal growth, thermal and elastic const. evaluation 80−92586
H, dissociated, heat transfer to catalytic surfaces, shock tube investigation 80−64551
H-O electrochemical matrix-type cells, transport effects study 80−26027
H_2, combustion, heat transfer in furnaces calc. *(French)* 80−19218
H_2 gas launcher, boundary layer closure, heat transfer 79−55387
H_2, liq., bubble growth consts. calc. at various press. and liq. superheats 77−35680
H_2, pool boiling heat transfer coeffs. determ. 78−30165
H_2 storage using hydride beds, thermal transport enhancement using high conductivity materials 80−61466
H_2-N_2-Ar, two-phase flow film boiling, in vap. generator, heat transfer 78−75190
H_2O, boiling, crit. heat flux in low press. region 78−90663
H_2O, condensation onto ice, deposition coeffs. 80−6507
heat transfer continued
H_2O flow in heated tubes, with near critical parameters, turbulent flow, heat transfer 80−59022
H_2O, sessile drop impinging on heated surface, heat and mass transfer mechanism 78−90908
H_2O, supercritical, heat transfer and pressure drop in horizontal tubes *(Japanese)* 79−14399
H_2O, transient heat transfer during natural convection *(Russian)* 77−68367
He, boiling in tubes, heat transfer, cryogenic stabilisation 78−30162
He, boiling on surfaces, heat transfer coeff. 78−9545
He cooling systems, forced flow, numerical anal. of heat-induced transients 80−82773
He I interface with Bi, transient heat transfer 77−85123
He II film boiling, heat transfer prediction 80−33424
He, liq., bubble growth consts. calc. at various press. and liq. superheats 77−35680
to He, liq., in centrifugal acceleration fields, free convection and boiling regimes 77−89604
He, liq., narrow channel flow and heat transfer charact., void fraction in steady and transient states 78−55000
He, liq., Pellam's paradox, quantitative explanation 77−39711
He, liq., sat., nucleate and film pool boiling heat transfer 78−18854
He, liq., transient heat transfer, temp. meas. with μs response time 78−71270
He, liq., transient heat transfer, from bare Cu surfaces 79−72785
He, liquid, heat transfer from heated plate 79−63235
He, liquid, heat transfer in narrow cooling channel below 4.2K 77−30170
He, liquid, heat transfer with solids below 100 mK 80−24701
He liquid, transient heat transfer, static coolant 78−75049
He, liquid film, transient heat transfer, film boiling regime 78−83219
He, nucleate pool boiling, heat transfer 77−31823
He pool boiling, charact. curve 77−46887
He, supercritical, correlation for heat transfer in turbulent flow in small channels 78−18871
He, supercritical, free convection heat transfer 80−79296
He, supercritical, heat transfer in turbulent tube flow 78−30287
He, supercritical, turbulent pipe flow, heat transfer by Melik-Pashayev technique 80−74860
He, thermoacoustic oscillations in nonuniformly heated tubes 80−33441
He vapour column, solid vapour heat transfer, at low temps. 78−83376
He, vapour formation and heat transfer in supercond. magnet cooling channels 79−32197
He-II, critical heat flux for narrow Sn films 79−23795
^{3}He, liq. A-phase, helical textures and anisotropic heat flow 79−23800
^{3}He, superfluid A-phase, anisotropy and flow 79−73367
^{3}He, superfluid A-phase, orbital dynamics in presence of heat flow and mag. field 79−51337
^{4}He, heat transfer and hydraulic drag in tubulent flow in circular tube 80−14821
^{4}He, liq., heat transport and critical slowing down near Rayleigh-Benard instability in cylindrical containers 77−84253
^{4}He, normal liq.-superfluid interface, temp. jumps across phase boundary 79−51334
^{4}He, superfluid, axial heat transport through annular duct with rotating inner cylinder 79−60575
^{4}He, superfluid, cable-in-conduit conductor, heating-induced flows 80−38229
^{4}He, superfluid, combined axial mass and heat transport 78−63894
^{4}He, superfluid, flow, exchange of heat with sintered Cu 77−82526
^{4}He, superfluid, heat transport in long tube 79−60576
^{4}He, superfluid, normal fluid heat-exchange drag 80−49441
^{4}He, superfluid, phonon heat transport and Knudsen's minimum below 0.6K 79−33136
^{4}He, superfluid, properties in zero gravity, appl. as cryogen on spacecraft 77−31822
^{4}He, superfluid, second sound, boundary conditions 79−46857
^{4}He, superfluid, steady state, at atm. press., practical data 79−60565
^{4}He, superfluid, steady-state heat transport at 1 bar 79−60574
^{4}He, superfluid, superheating and bubble formation 78−56000
^{4}He superfluid film, in zero gravity 80−54464
^{4}He, superfluid saturated liq., recovery heat flux from silent and noisy film boiling states 79−72784
Hg, dropwise condensation, at Cu surface, heat-transfer meas. 77−75781
Hg gravity fed heat pipe for production of high purity fixed density of Hg atoms 80−69627
Hg, pool boiling heat transfer in mag. field 80−33584
Hg, turbulent annular flow 77−19602
Hg, turbulent flow on stabilising thermal section, temp. fields and heat transfer 80−19366
hydrocarbon-water, emulsions, superheated, bubble nucleation 78−61056
K heat pipe, heat transport characteristics, transverse mag. field effects 79−37127
Kr, liquid, superheated, nucleation 79−23741
Li, liq. cooled pulsed fusion reactor blanket heat transfer, numerical calc. 78−94141
Li, liquid, transverse flow around tube bundle, heat transfer 80−64537
Li/He heat pipe, start-up power, heat transport, thermal regulation 80−53615
$Li_2B_4O_7$, heat low controlled growth during crystallisation 79−65014
MHD flow and heat transfer, porous disc eccentric rotations at infinity 79−18965
Mo, porous, permeability, deform. effects 79−100229
N_2, boiling in tubes, heat transfer, cryogenic stabilisation 78−30162
N_2, critical heat flux in horizontal tube, up to critical press. *(German)* 80−99921
N_2, flow, cold gas, through porous-tube, heat-transfer, suction effect 78−59474
N_2, heat transfer during boiling in field of centrifugal forces 79−60493
N_2, heat transfer during nucleate boiling, heating wall and metallic coating thicknesses depend. 79−32210
N_2, heat transfer in boiling on surface of vertical cylindrical rod 80−48706
N_2, hypersonic nozzle flow, supercooling and spontaneous condensation 78−1549
N_2, liq., boiling, cryogenic, heat transfer rel. to sinusoidal elec. field 77−72135
N_2, liq., in cryostat dewars, appl. to microwave thermal noise source 79−58700

heat transfer continued
N_2, liq., nucleate boiling heat transfer from PTFE coated surface 78−34000
N_2, liquid, film boiling heat transfer coeff. for vertical surfaces 80−48556
N_2, liquid, heat transfer from heated plate 79−63235
N_2, liquid, nucleate boiling heat transfer at reduced pressures 80−48557
N_2 liquid, pool boiling heat transfer from horizontal plates *(Japanese)* 78−67016
N_2, liquid film boiling heat transfer, orientation effect 80−48554
N_2, pool boiling, heat transfer, surface roughness effect 80−48705
N_2 pool boiling in high centrifugal accel. fields, peak nucleate boiling heat flux 79−59907
N_2, porous solid, contact heat transfer in sublimation 77−31767
N_2, thermomagnetic effect, Knudsen gas between Au surfaces, low temp. 78−30405
N_2, two-phase flow in horizontal tube, heat transfer and pressure drop over extensive pressure range 79−58747
NH_3, flow in steel tubes, wall heat transfer with catalytic dissoc. 78−14099
NO, boiling/condensation heat transfer props., cryogenic appls. 78−79192
N_2O_4 circular channel hydraulic resistance and heat transfer expts. *(Russian)* 79−14213
N_2O_4 corroded annular channels, heat transfer and pressure drop 80−1569
N_2O_4, dissoc. flow in tube, heat transfer and drag 78−71402
N_2O_4, dissoc. laminar gas flow, heat exchange with triangular bundle of rods 77−42930
N_2O_4, dissociating, nonsteady flow in steam-generating channel 79−37422
N_2O_4, dissociating, turbulent pipe flow, heat transfer, resistance 78−91026
N_2O_4, dissociating in vertical tube, boiling heat transfer 80−1568
N_2O_4, fission reactor coolant, heat transfer on condensation *(Russian)* 80−57860
N_2O_4 flow in axisymmetric channels, heat transfer calc. *(Russian)* 79−14214
N_2O_4 flowing in axisymmetric channels, mass and heat transfer calcs. 80−1570
N_2O_4, heat and mass transfer in turbulent stream in axisymmetric channel *(Russian)* 79−18960
N_2O_4, reactive turbulent flow, heat and mass transfer anal. *(Russian)* 77−42932
N_2O_4, turbulent dissoc. flow, along heated tubes, heat transfer 80−63225
N_2O_4-NO mixtures, attainable superheating temp., depend. on NO conc. *(Russian)* 77−72140
$(NO_2)_2 \rightleftarrows 2NO+O_2$, chemically unstable mixture laminar flow in channel, heat and mass transfer *(Russian)* 77−68707
$(NO_2)_2 \rightleftarrows 2NO_2+O_2$, nonequilibrium mixture laminar flow in channel, zone method anal. of heat and mass transfer *(Russian)* 77−72370
$N_2O_4 \rightleftarrows 2NO_2$ equilib. system, condensation heat transfer on horizontal tube bundle *(Russian)* 78−46970
$N_2O_4 \rightleftarrows 2NO_2$, heat transfer meas. *(Russian)* 77−84128
$N_2O_3 \rightleftarrows 2NO_2 \rightleftarrows 2NO+O_2$, heat exchange calc. *(Russian)* 77−84127
Na cooled fast reactor, partly blocked fuel subassembly, heat transfer meas. in air model 77−74964
Na evaporation from slot type capillary structs., crit. heat fluxes 80−74854
Na, incipient boiling in the presence of a mag. field 79−37411
Na, liq., in vert. pipe, hydraulic resistance under boiling conditions 78−90968
Na, liq., incipient superheat meas., expt. and physical parameter effects 78−18289
Na, liquid, evaporation from capillary-porous struct., capillary restriction in initial stages 80−107609
Na, liquid, heat transfer characteristics of flow field *(Japanese)* 78−54815
Na liquid metal boundary layer attenuation of temp. oscillations, appl. to LMFBR 77−83013
Na liquid metal slug flow, transfer function of temp. fluctuations 78−46133
Na, pool boiling heat transfer, liq. head effects 78−89951
Na, superheated, LMFBR safety, formation of critical boiling nuclei 77−88242
Na, vaporisation from capillary-porous structs. (heat tubes, vap. chambers) crit. heat flux 78−90631
Na vapour heat pipe performance rel. to nozzle discharge theory 78−75033
Na-filled stainless steel heat pipes, with long adiabatic sctions, performance limits 80−38236
NaCl gas-droplet counterflow heat exchanger, numerical model *(French)* 80−61396
NaOH fusion for heat storage, heat utilisation for turbo-alternator unit *(French)* 80−40915
NaOH, liq., thermal storage, steel corrosion, appl. in accumulation type steam generator *(French)* 80−40914
$Na_2S_2O_3.5H_2O$, solidification, heat transfer processes *(Japanese)* 80−6372
NbTi solenoid, operating at 9 T in He gas 77−74461
NbTi-Cu, supercond. composite, use in temp. and heat transfer coeff. meas. 80−77780
Ni, heat transfer during cooling with water *(German)* 80−23873
Ni, rapid melting and solidification of surface layer, exam. using computer heat flow model 78−83228
O_2, liquid, pool boiling in inhomogeneous mag. field 77−31766
Pb-acid batteries, for elec. vehicle propulsion, heat transfer, math. anal. 80−3509
Pt, resistance thermometer, heat shock influence on elec. cond. and thermophysical props. *(Russian)* 80−52210
Pt thin wire resistance thermometer dynamic response 77−22549
Sb-Bi, melting kinetics of solid soln. during high heating rates, superheating *(Russian)* 78−15358
Si, amorphous, small dia. laser beam annealed, temp. distrib. and microstructure 79−73098
Si film, electron beam evaporation, for solar cell appl., heat exchanges and columnar growth 79−15609
Si sheet, high speed growth, heat transport analysis 80−107669
Sn-α brass interface, heat flux rectification, rectification coefficient 78−76048

heat transfer continued
Sn-Pb (15 wt.%), forging of liquid and partially solid alloys 78−80569
Ti plate, heat transfer to chemically reacting plate under unsteady state heating 79−81697
UO_2, closed boiling system, effect of condensation on dispersion following LMFBR HCDA 78−8936
UO_2, molten pool, heat transfer to concrete slab following LMFBR HCDA 78−8930
UO_2 molten pool prod. by internal heating, heat transfer meas. 77−88214
UO_2-Na contact interface temp., effect of internal radiation 79−13477
UO_2-PuO_2 fast reactor fuel rods, burnup-dependent heat transfer from fuel to cladding 79−36323
Xe, liquid, superheated, nucleation 79−23741

heat treatment
see also annealing; normalising; quenching (thermal); spheroidizing; tempering; thermomagnetic treatment; thermomechanical treatment
Al alloy blend 6061, isostatically computed powder, effect of heat treatment temp. on tensile strength and hardness 79−61720
alkali silicate glasses, struct. and thermal props. 80−84075
alkali-borosilicate glasses, antireflection film production by heat and chem. treatment 80−66677
allanite, metamict, phase changes on heating, age determ., x-ray fluoresc. anal. 77−51493
alloy, coarsening by temp. cycling 79−29111
alloy, heat-resistant, alloying and heat treatment effects on struct. and strength 78−95758
alloy, high temperature, mechanical, thermal and corrosion props. 78−95763
alloy, memory effects, props., phenomenological theory and appls. *(German)* 77−1864
alloy parts, heat treatment, chem., principles and practical procedures *(Russian)* 79−52260
alloys, rapidly quenched crystalline, struct., and heat treatment effects 80−76292
Alnico, domain struct., variation under influence of heat treatment *(Russian)* 78−23292
aluminophosphate glasses, multicomponent, γ-irrad., EPR study 79−91290
aluminosilicate glasses, Cr_2O_3, TiO_2 and Nb_2O_5 containing, paramagnetic defect formation, ESR study during crystn. 79−65739
amorphous semiconductors, classification into structurally 'soft' and 'hard', thermoelectrical approach 78−42908
analysis and optimisation of heat treatment regimes using simplex proportional designs 80−25734
anodic oxide films on Al, heat treatment effect on photoluminesc. props. 77−28610
ATJ graphite, ultrahigh vac. compatibility, outgassing characts. 79−81080
austenite, hot-worked, struct., post-deform. ht. treatment effects *(Russian)* 77−8859
austenitic stainless steel thermal treatment for spectrally selective surface fabrication 80−35752
austenitizing during continuous heating, qualitative anal. *(French)* 77−81260
automatic induction hardening equipment 78−92284
automatic thermal cycling apparatus, for superconductive thin film devices 78−37014
beryl, channel constituents, electronic absorption spectra of Fe^{2+} 79−69863
bimetal, high-speed steel + machine steel, chem. comp. influence on magnitude of residual stresses in cooling *(Russian)* 79−74183
bone, X-ray and neutron diffr. meas. of apatite cryst. orientation and growth, effect of chem. and heat treatment 79−39431
boride coatings on steel effect of Cu impurities in reaction mixture on brittleness, acoustic emission meas. 80−16581
borosilicate, anisotropic glasses, birefringence and microstruct. 77−8541
brass, Cu-Zn (39(40) wt.%), shape memory effect and martensitic transform. depend. on heating-cooling cycles *(Russian)* 80−97482
brass, heat treatment procedure for interphase boundaries, struct. 80−19813
α-brass, leaded and Pb-free mech. damping 77−63705
brass, recrystallization during induction heating 80−97511
Br.AZhNMts 7-2.5-1.5-9 bronze, Mg-Al, type, fatigue and stress corrosion cracking, welding effects 80−3233
bronze P, heavily cold rolled, yield strength enhancement mech. 77−36539
carbonaceous mesophase, formation at lower temps. 79−90524
carbonaceous mesophase spherules, new mol. arrangement in mag. field, orientation behaviour 79−94869
carbons, artificial, graphitisation shrinkage kinetics 77−48385
carbons, Raman spectra in 2600-3300 cm^{-1} region, heat treatment temp. effect 79−42955
cast steel, effects of explosive loads, radiographic anal. 77−25072
celluloid, mech. props. under proportional load, time lapse, heating and isotropic props. effect *(Japanese)* 79−79043
cellulose nitrate (CN) detectors, effect of pre-irrad. thermal treatment on track revealing props. 78−94168
cellulose nitrate plastics, heating and alpha track revelation characts. 79−49910
cement, hardened paste, transitional thermal creep 80−25785
cement based on $Ca(OH)_2$ and polymethylphenylsiloxane, high-temperature high-strength props. 77−36439
ceramic mould accelerated shell heat treatment models 79−76896
ceramics, development from organosilicon polymers by heat treatment 80−81014
ceramics, tensometric equipment, for determ. of properties, during vacuum pulse drying 80−20965
ceramics treatment methods, drying, cooling, heat treatment, reln. to material props. *(French)* 77−90296
chamotte glazed masses, deformation occurring during heat treatment 78−84747
charcoal, active, heat-treated, spiral growth structs. *(German)* 78−44141
chars, heat treatment, EPR rel. to temp., A-centers 78−43639
chars, heat treatment, EPR rel. to temp., spin centres 78−48036
chemicothermal treatment, mathematical modelling 80−100955
chert artifacts, thermolum. determ. of prehistoric heat treatment 78−24914

heat treatment continued
chinaware, semivitreous, eval. of crazing resistance by stress meas., after autoclaving *(Japanese)* 79−20235
chinaware, vitreous, elimination of crazing by repeating glost firing *(Japanese)* 79−20236
cholesterin ethers, dielec. absorption, heating/cooling and oxidation depth effects *(Russian)* 79−50984
clays, heat treatment, effect on rheological props. of enamel slips 80−60809
coke, shrinkage kinetics during calcination 80−93572
cokes, graphitised, Raman spectra, effective Debye parameter, magnetoresist. 78−44231
cold rolling mills, roll service life, rehardening by heat treatment 80−16347
component checking after heat treatment, steady magnetising field 78−60958
convex beam integrator for laser beam shaping, heat treating appl. 80−53346
cordierite glass ceramics, effect of TiO_2 and ZrO_2 content on phase sequence during heat treatment 78−48381
corrosion resist. depend. on mech. and heat treatments 80−653
corundum, spinel formation during reducing heating 77−36427
corundum single crystal, premetallizing with Mo-Mn-SiO_2 79−47792
corundum-based refractory lining specimen, thermal softening assessment *(Russian)* 79−83237
creep, activation parameters under monotonic heating conditions *(Russian)* 78−23764
creep rupture like improvement mechanism, reheat treatment 78−64666
diacetate-nitrocellulose, long period struct., 180-265°C, X-ray diffr. obs. *(Russian)* 79−24556
diamond, mechanical strength depend. on thermal working parameters, microcracks *(Russian)* 80−55501
diamond, semicond., electron irrad., charge carrier mobility 77−11921
diamond ceramic, elec. cond., temp., freq. depend. 80−54687
diesel nozzle sprayer castings, heat treatment quality inspection 80−35471
E-glass fabric, acid-treated, elec. resistivity studies, effect of post heat-treatment temp. 79−70178
electromagnetic quality inspection with specified intensity of internal field 80−108677
electron beam heating, scattering of beam by target vapour *(Russian)* 77−59825
electron trapping, donor state generation, photo I-V study 80−20210
electropatented wire, austenitizing, supercooling and heating temp. effects 78−23737
electroslag welding, using plate electrodes for Al busbar component parts welding 80−81083
energy flux channel close-up time *(Russian)* 77−55994
epoxy adhesive, A, filled, electrical cond. development by heat treatment 79−73559
epoxy EDT-10, rigid polymer, thermal stress isothermal relaxation 80−71683
epoxy systems, thermoreactive, elasticity modulus, change on curing *(Russian)* 79−64521
epoxysilicon organic tar DFM-135 cement composition, internal friction meas. by composite oscill. method *(Russian)* 80−54312
epoxytitansiilicon organic tar TK-75 cement composition internal friction meas. by composite oscill. method *(Russian)* 80−54312
ethylene, adsorbed on W (100), effect of heat treatment on decomposition 79−66353
ethylene-propylene copolymers, mech., photoelastic props. rel. to chain microstruct. 77−48468
eutectic alloy, yield point analysis 77−8875
eutectic alloys, surface energy considerations 78−44152
FBR oxide fuels, dynamic response of grain boundary cavities to stress and temperature changes under conditions of continuous gas generation 80−66544
ferrite powders, mag. props., explosive shock treatment effects 79−52395
ferrites type 1500 NMZ and 2000 NMI, mag. susceptibility depend. on heating *(Russian)* 80−108603
fibre, high modulus, diffusion barrier appl. 77−77449
fibre lens, plastic focusing, change of ref. index profile during heat treatment process in fabricating 78−83091
fibre reinforced polymer, soaking, wetting and compounding of materials during production *(German)* 80−93535
fibreglass/epoxy laminate curing by microwave heating 77−77457
float glass, commercially produced, thermally toughened and untoughened, surface damage resistances on air and tin side 79−61612
fluidised bed appl., development *(German)* 77−41596
fluorite crystal windows, transmission in vac. UV region, heat treatment effect 77−31137
fluorophlogopite mica, glass-ceramic, thermal diffusivity, crystallisation effects 78−6190
fluoroplastics, mech. props., accumulation of submicrocracks, thermal treatment effects 77−4850
foil, recrystn. during heating in column of electron microscope *(Russian)* 78−48421
foil strain gauges, use on materials with heat constraints during heat treatment 80−25938
fracture, Hertzian, wavy, thermally induced 77−56082
fracture mech. during creep, interference microscopy exam. of 12Kh18N9, 08Kh18N10T 78−56756
furnace, elec. with electrode heating, for electrolytic boriding 80−27309
furnace system for heat treatment, ultrahigh vacuum conditions 80−52222
furnaces, elec. resist., temp. control 80−27307
furnaces, vac. elec. 80−27308
fusion welding of Al alloys, weld susceptibility to hot cracking 80−81143
gelatin film, deuterated, IR absorpt. spectra, heat treatment and ageing *(Russian)* 78−39621
glass, coloured, toughening process, spectral characts. 80−43416
glass, heat treated, thin foil prep. for TEM obs. 78−7154
glass, photochromic, thermo-optic transitions 80−50307
glass, photochromic, thermochemical effects 80−87448
glass, structure, influence of thermal history *(German)* 80−38930
glass, surface flaws, decoration technique 78−14547
glass, surface props. and contact angle after treatment with glow discharge and heating 80−21139
glass, to promote colouring 77−8961
glass, viscous deformation during heating and cooling 80−89314
glass ceramic, bonding thermosprayed Si 78−23848
heat treatment continued
glass devitrification, heat treatment parameters determ. from viscosity changes *(Polish)* 80−40404
glass fabric, effect of phosphate binders on properties 78−44075
E-glass fibre, silane coupling agent deposited on surface, hydrolysis and drying effect on siloxane bonds 80−85072
glass fibre reinforced Al alloy, formed by hot extrusion, heat-treatment 77−24988
glass fibre reinforced composite, thick-walled shell, crack prevention during heat treatment 77−52376
glass fibre reinforced plastic, residual strength, hygrothermal history effect 77−77513
glass fibre reinforced plastic, rolling-in effect on physicomech. props. 78−23658
glass fibre reinforced plastics, heat treatment and heating temp. effect on Young's modulus 80−35233
glass fibres, aluminosilicate, crystn. during heat treatment 79−52258
glass optical waveguide fabrication by effusion 80−5850
glass porous, struct. and texture rel. to heat treatment effects *(German)* 78−44140
glass reinforced polyamide 6, fatigue strength after heat treatment, ageing and coating of Al-containing lacquer *(Polish)* 80−89347
glasses, thermal behaviour during heating or cooling, retardation kinetics 77−4049
grain and phase boundaries between crystals, conf., Konigstein, Germany (Oct. 1977) 78−72762
granite, extraction of fission Xe, anomalous fission yields 78−96216
graphite, EPR, effect of motional averaging, anisotropy, skin effect rel. to heat treatment and neutron irradiation *(French)* 80−34752
graphite fibre, surface anal. by XPS and polar/dispersive free energy anal. 80−65340
graphite surface, adsorbed Cs, dissolution, lamellar cpd. form. *(French)* 80−100399
graphitisation kinetics within first min. of heat treatment 77−66596
graphitisation of bulk mesophases, electron microscope obs. 78−44035
graphitised viscose fibre, fluorination, change in struct. 80−88039
gypsum casts, improvement in impregnation method, exam. of mech. props. 78−48503
Hastealloy X, relations between weld heat affected zone cracking and microstruct., Gleeble test *(Japanese)* 78−52858
Hastelloy X, H permeability using permeation method *(Japanese)* 78−51740
heat resisting, types EhI598, ZhS6KP, and 1, fatigue under mech. and thermal stress 79−66164
hexamethylolmelamine, doped, and condensation resin, room temp. phosphoresc., thermal transforms. 80−45132
n-hexatriacontane film, vacuum deposited on alkali halide crystals, structure and heat treatment 80−103600
ice, floating sheet, viscoelastic response under prolonged loading 78−51093
ilmenite ore, liquid, behaviour above 1500°C, X-ray obs. *(French)* 79−70100
Incaloy IN 738, dispersion hardened superalloy 78−11156
Incoloy 800, creep rupture ductility, 500 to 600°C, hardness and metallurgic exam. 79−43435
Incoloy-800, annealed, mech. behaviour anal. for elevated-temp. LMFBR appl. 80−18428
Inconel 600, thermal treatment, grain boundary microstruct. and SCC resistance 80−71675
Inconel 706 and 718, relations between weld heat affected zone cracking and microstruct., Gleeble test *(Japanese)* 78−52858
Inconel alloy 600 in 10% NaOH soln. at 315°C, influence of thermal treatment 79−91841
Inconel X, X-ray study of stress meas., elastic const. *(Japanese)* 79−66092
induction hardened parts, high frequency, heat treatment quality inspection 78−48598
induction salt baths, automatic temp. control 80−27300
interface study by Auger spectroscopy 80−76587
Invar, X-ray K-absorpt. spectra, depend. on composition and temp. changes *(Russian)* 80−55226
Invar film, superfine mag. struct. *(Russian)* 80−80572
Invar N36 melt, cast metal struct. depend. on heat treatment, subgrain struct. *(Russian)* 80−40343
invariant system with switched element, design and evaluation for heat processes control during extrusion of plastic materials *(Russian)* 80−100854
ion-nitrided steel surface structure and hardness, heat treatment effects *(Japanese)* 79−87718
iron, Armco, effect of low temps. and heat treatment on growth rate of fatigue cracks 79−57027
K-ramic^{R}, ultrahigh vac. compatibility, outgassing characts. 79−81080
kaolin fibres, heat induced changes 79−83244
kaolinite, optical spectroscopy study of structural changes at 700-1000°C 79−65193
Kevlar 49 fibre, poly p-phenylene terephthalate, Raman spectroscopy, heat, stress, radiation effects 79−65871
knife-edge flange, sealing after high temp. vacuum firing 80−77793
laser beam processing, basic physical processes 77−23682
laser spot thermal history, surface heating with laser-coaxial gas jet 77−63494
low C steel, explosive-thermal treatment, sulphide cracking decrease, hydrogen embrittlement *(Russian)* 80−108477
low-aberration focusing fibre, optimum diffusion exchange and heat treatment 78−1378
LPE growth method to reduce thermal degradation of substrates, appl. to LED fabrication 80−104061
lunar regolite, Fe reduction on heating in vacuum, XPES spectra 80−41740
magnesian-spinel materials form. using heat treatment 79−38773
martensite steel, cryst. struct. variation during heating, role of Mn and Al *(Russian)* 79−46600
mesocarbon microbead, heat treatment under high pressure 77−28736
metal, and alloy, strain hardening criteria eval. 77−55982
metal, heating by laser emission, spatial nonlinear problems *(Russian)* 80−7440
metal, oxidizable, laser heating in air by obliquely incident radiation 80−71815
metal, surface properties improvements, using vacuum thermal process techniques 79−100283

heat treatment continued
metal, thin film, heating by light pulse of linear intensity time dependence *(Russian)* 77−59827
metal, US velocity, effects of deform. and high temps. 78−26626
metal bending spring, effects of stress, temp., thermal and mech. treatment on non-elasticity *(German)* 77−77531
metal coating stability, thermoelectric method of assessment *(Russian)* 78−11459
metal heating by laser radiation, calc. allowing for thermal props. temp. depend. 78−30770
metal oxides and binary metal oxides, spinel struct., isoelectric point meas. 80−88609
metal sheet strength improvement by localised thermal shock 78−88483
metal strips, welded, aged, reduction of deformations *(Russian)* 80−97508
metal subjected to intense heat source, plastic deformation 77−86085
metal submicron particle heating in hot gas, plasma metallurgy 80−81092
metal surface, using W-inert gas arc 79−96209
metallic surface, heat treating and melting with scanning laser or electron beam 78−11406
metallurgical industries, vacuum furnace developments, heat treatment, high speed steels *(German)* 79−100174
metallurgical industries, vacuum hardening of high speed steels *(German)* 79−100175
metals, diffusion alloying conditions, deep chemical-heat treatment *(Russian)* 80−40393
metals, electron beam appl. *(French)* 80−66558
metals and alloys, chemicothermal treatment, process kinetics 80−35415
metals and alloys, diffusion layers, effect of chemicothermal treatment on struct., surface energy, and bulk props. 79−96207
MHD refractory materials, arc spot heat impact degradation *(Japanese)* 78−39819
mineral wool fibre composites, mech. props., effects of thermally induced phys. and chem. changes 77−59884
molybdenite ore treatment using 2 kW solar furnace 80−3107
monolithic glass, formation by chem. polymerisation 79−78926
montmorillonite, clay mineral, expanding type, surface props. rel. to heat treatment 79−29406
montmorillonite, Co^{2+} form, optical spectroscopy study of structural changes at 700-1000°C 79−65193
mullite, crystallisation from SiO_2-Al_2O_3 melts 78−47243
mullite ceramic rollers, heat treatment effects 79−61616
multilayer oxide correcting coatings, u.v. transmission cutoff 77−760
natural rubber vulcanizates, vulcanization temp. and systems effect on struct. 78−19705
Ni, adsorption residual C removal by electron beam irrad. and heat treatment *(Chinese)* 80−88421
Ni-Co, H_2 embrittlement, heat treatment and impurities effect 80−76331
Nimonic, ageing, role of quenched-in vacancies 77−52363
Nimonic PE16, neutron irradiated after heat treatment, solute segregation to pt.-defect sinks 79−78976
non-oriented elec., internal oxidation and nitridation effects on mag. props. 79−83336
Nylon 6, pressurized heat treatment effect on fatigue props. 79−87669
optical filter, moisture penetration patterns 77−767
optical waveguides, linear low loss structures of ferroelec. materials, fabrication, heat treatment effect 77−23769
optimisation, simplex method 78−84869
oxidising metal heating by periodically pulsed CO_2 laser 80−7445
PAN fibres, heat treatment, structural changes *(Polish)* 77−28835
PET, crystallised by nonreactive liquids, exam. of mech. props. 79−43338
petroleum pitch, effective ESR conc. as function of heat treatment line 79−96045
phenol formaldehyde resin reinforced with chrysotile asbestos fibres, thermal expansion, specific heat 79−55908
phosphate glass-Al alloy seals, elec. and mech. props., glass transition 80−81018
phthalocyanine polymer, dynamic mech. props. and fracture energy 80−100866
piezoelectric radiators, heat-treatment method for improved resoln. 80−104196
pitch, mesophase form. under reduced press. 77−63571
plastic foil, Li ferrite clad, thermal deform. *(Polish)* 80−30002
plate, volumetric heating and thermal stresses *(Russian)* 77−42714
PMMA, reactor irrad., growth of macroscopic radiolytic gas bubbles, diffusion model 80−65058
PMMA, rigid polymer, thermal stress isothermal relaxation 80−71683
polyacetylene film, heavily doped with AsF_5, degradation by heating and air exposure 79−28353
polyacrylonitrile, prep. of C fibres with large breaking strain 78−44077
polyacrylonitrile, struct. of heat treated fibres, X-ray diffr. 78−83752
polycarbonate, bisphenol A, WAXS pattern, temp. effect and thermal history 80−93583
polyethylene, elec. props. and oxidation after electron beam irradiation and heat treatment 79−87092
polyethylene, fibrillar, high mol. wt., oriented crystallisation, heat treatment effect *(Japanese)* 80−25738
polyethylene, filled, mech. props., cyclic heating effect 80−55526
polyethylene, linear, bulk-crystallised, morphology study 79−32918
polyethylene, low density, α mgch. dispersion in relation to spherulite deform. mech. 80−25781
polyethylene, low density, UV and heat treatment effects, DSC obs. 79−14915
polyethylene, low density foam, two-step heating process *(Japanese)* 77−52369
polyethylene, low-density, temp. changes in large period structure *(Russian)* 77−31603
polyethylene, oxidised, low-temp. dielectric spectrum 79−61304
polyethylene electret, internal pot. topography, Raman and IR spectra 80−7362
polyethylene terephthalate, amorphous state change by heat treatment below glass transition temp. 78−30550
polyethylene terephthalate, effects of preliminary ht. treatment on crystallisation *(German)* 78−75593
polyethylene-metal contact charging, electron transfer mechanism, PES characts. 80−35055
polyethylenes, dielectric γ-dispersion, crystallinity effect *(Japanese)* 79−87384
heat treatment continued
polyethyleneterephthalate, ordering, thermal pretreatment at vitrifying temp. effect *(German)* 79−65006
polyimide film, heat treatment conditions effect on ultimate strength, expt. planning methods 78−6952
polyimide substrate foils for nuclear targets 80−18739
polymer, heat treated, numerical simulation of AC elec. props. 78−43431
polymeric tube, stepwise heat treatment *(Russian)* 77−25082
polymers, thermoreactive, elasticity modulus, change on curing *(Russian)* 79−64521
polymorphic transformations kinetics model, computer modelling *(Russian)* 80−97478
polyphenylene oxides, high temp. ageing effect on struct. and props. *(Japanese)* 77−70078
polypropylene, (Moplen) influence of temp. and mol. wt. on high speed fracture mechanics 80−76341
polypropylene, crystalline, morphological aspects of crack growth 78−76761
polypropylene powder, cold compaction, product strength, heat treatment effects 80−11621
polysiloxane dizwitterionomers, mech., dielec. relax., effect of H_2O sorpt., thermal history 80−50261
polystyrene, nonisothermal rheology 77−32619
polystyrene, plasma polymerised, free radicals, transient elec. current, EPR, heat treatment 80−71178
polystyrene-polypropylene(polyethylene) mixtures, extruded, effect of thermal treatment on elastic moduli *(Polish)* 79−70107
polyurethane, physical and chemical structure mutual effects *(German)* 79−57229
polyvinylidene chloride co-polymer powder, cold compaction, product strength, heat treatment effects 80−11621
porcelain, conventional and rapid fired, comparison of texture and props. *(German)* 78−64510
post weld during power station construction and maintenance 80−93574
powders thermosetting, hot stage microscopic technique for examining curing 79−28979
pressure vessels, heat treated, fracture modelling, acoustic emission 80−35303
PTFE, heat shrinkable tubing, crystallite orientation 77−4795
PVC, different stereoregularities, heat treatment effect on glass transition temp. and c_p changes 79−4985
PVC, influence of thermal history on physical props. 79−4984
PVC, uniaxially stretched, mol. orientation, birefringence, effect of plasticizers, draw ratio 77−48500
PVC film, uniaxially stretched, mol. orientation, polarised fluoresc. investig., deform. mechanism 77−52440
PVC in DMF, THF solns., mol. wt., aggregation, light scatt. investig. *(Polish)* 77−28587
PVC powder, cold compaction, product strength, heat treatment effects 80−11621
PVFD, electret, polarisation process 80−7273
pyrocarbons, EPR, effect of motional averaging, anisotropy, skin effect rel. to heat treatment and neutron irradiation *(French)* 80−34752
pyrographite, Si-containing, high-temp. treatment effects 77−40429
pyrrhotite, Ni recovery by thermal upgrading 77−60034
quartz, heat treatment of dense moving layer, heat exchange development 79−20075
quartz, natural, virgin (γ-irradiated), polarisation effect on thermolum. sensitivity 80−11483
γ-quartz, reaction, with NaCl-kCl melt, exam. of struct., IR absorption spectra 80−55706
quartz, synthetic hydrostatic pressure effect on precip. of structure bound water in microinclusions 78−75838
quartz, thermoluminesc., γ-irrad. sample, heat treatment 78−64418
quartz glass, Si^+O^- defect bands, Raman intensities, thermal treatment effects 79−15444
quartz glass, Ti-doped, acoustic props., thermal stability 77−24356
quartz porcelain fast fired, development of microstruct. *(German)* 78−60625
rapid electrothermal treatment of wire 78−84871
rare earth orthophosphates, high-temp. treatment and formation of oxyphosphates *(French)* 77−44199
rare earth-Co permanent magnets, generation mechanism of high coercive force *(Japanese)* 79−100269
refractories in contact with transformer steel during high-temp. heat treatment, resistance 80−66554
refractory metal, heat treatment and zone melting installation 80−20959
Rene 41, Ni-Cr-Co-Mo-Ti-Al-Fe (18.96, 11.09, 9.65, 3.06, 1.59, 0.89 wt.%) formation of Cr_2O_3 monocrystals on heat treatment 79−52455
resins, thermoplastic, glass-fibre-reinforced, performance at elevated temperatures,obs. 79−95067
resistance furnaces and heat treatment processes, present trends 79−49233
restoration, evaporation and melting of materials in high temp. gas flow *(Russian)* 80−39271
rubber, nitrite, heat ageing, light scatt. method study *(Russian)* 80−40407
rubber toughened plastics, ABS- and AAS-resin, flow props., effect of heating and shearing hysteresis *(Japanese)* 79−94685
shock compression-pulse heating working process, apparatus design 80−16357
silicone, film deposition, glow discharge polymerisation, elec. and thermal characts. 78−6467
simulation, prediction of large component response 78−31435
sitall coatings in Li_2O-Na_2O-CaO-SiO_2 system, heat treatment effects on tech. characts. 78−84853
sitalls, thermal conductivity at various stages of heat treatment 79−60562
Spheron 6, surface group obs. using gaseous reagents, surface acidity evolution during heat treatments *(French)* 77−66767
sputtered particles-substrate, temp. overaging *(Russian)* 80−40385
stainless steel, colouring processes 77−8981
steel, 11YuA, cold worked, heat treated, electromagnetomech. props. NDT 79−4980
steel, 12Cr1MoV, thermal fatigue and creep effect in fracture 80−104297
steel, 18Kh2N4MA, Co effect on struct., and mech. props. 78−44147
steel, 35Kh3MFS, strengthening involving austenite fine grain processing *(Russian)* 77−52358

heat treatment continued
steel, 38KhS, heat treatment quality inspection by magnetic method 79−52574
steel, 3Kh2V8F, brittleness depend. on high temp. deform. at high stress. temp. *(Russian)* 80−50698
steel, 40KhN, austempering effects on H_2 yield *(Russian)* 77−55996
steel, (0.36 wt.% C) Ni-Cr-Mo, electroslag refined, fracture toughness and fatigue behaviour 80−81171
steel, abrasive wear resistance, effects of microstruct. 78−92367
steel, adhesive wear, heat treated load effect 78−11344
steel, age-hardenable, relation between fatigue S-N and P-N charact., definite fatigue limit *(Japanese)* 77−8938
steel, AISI 4340, austenitised at low and high temps., toughness evaluation 77−16621
steel, AISI 4340, sulphide inclusion behaviour during thermomechanical treatment 78−3151
steel, alloy, electroslag remelting effect, an impact-abrasive wear resistance 80−55541
steel, alloy, hardened, electrochem. characts. and stress corrosion cracking, ageing and cold treatment effects 80−108639
steel, alloy, high speed, type R18, hot deformation and recrystn. 80−16391
steel, alloy, HY140, fatigue crack initiation and propag. at notch tip 78−80647
steel, alloy, HY180, fatigue crack initiation and propag. at notch tip 78−80647
steel, alloy, mechanical properties, morphology, transform. kinetics and composition interrelations 77−86146
steel, alloy, Mn-Si-C, exam. of fracture toughness for sheets, using linear elastic fracture mechanics 78−56762
steel, alloy, softening process in deformed type 15GYuT, metallographs *(Russian)* 78−52840
steel, alloy, thermodynamic aspects of gas-metal heat treating reactions 79−24547
steel, alloy, type 11Kh18M, eutectic carbide composition change due to heating 80−16353
steel, alloy, type Kh16N11M3, struct. changes during thermocyclic working, dislocation struct. *(Russian)* 80−54243
steel, alloy, type ST.5, structural and phase changes after high temp. heating *(Russian)* 80−55439
steel, alloy cast, optimal alloying, carburising effect 80−50771
steel, austenite, abnormal decomposition kinetics and mechanism *(Russian)* 80−55344
steel, austenite stabilisation during $\alpha \rightleftarrows \alpha$ transition *(Russian)* 78−44117
steel, austenitic, Cr-Mn-B-N, phase composition and struct. transformations 80−104171
steel, austenitic, explosive-thermal treatment, sulphide cracking decrease, hydrogen embrittlement *(Russian)* 80−108477
steel, austenitic, fracture toughness meas. by Charpy impact testing, welding, heat treatment, neutron irrad. effects 79−5062
steel, austenitic, heavily doped, linear expansion meas. 80−103501
steel, austenitic, intercrystn. corrosion and mech. props., inflence of Cr, N and Nb *(German)* 80−50747
steel, austenitic, KO 34 samples, electron beam welded, Charpy test expts. *(Hungarian)* 80−104252
steel, austenitic, mechanical strength, effect of mech. and heat treatment 77−12659
steel, austenitic, metastable, hardening by cycling of martesitic transform. during rapid heating, in 30N24M4 and 50N21M3 *(Russian)* 79−20074
steel, austenitic, Mn-Al-V-F2, EM characts. after nitriding, aging, austenitizing, NDT of nitrided layer depth 79−11750
steel, austenitic, pearlitic and bainitic transforms., effect of austenitisation conditions *(Russian)* 79−38820
steel, austenitic 30KhGSA, white phases structure after heat treatment 80−76281
steel, austenitic (03KH18N10T), heat treatment for fission reactor appls. 80−66454
steel, austenitic Cr-Mn, $M_{23}C_6$ carbide precipitates comp., heat and thermomech. treatment influence *(Russian)* 80−40361
steel, austenitic stainless, corrosion resistance testing, urea plant applications *(Czech)* 80−61012
steel, austenitic stainless, Cr-Ni-Mo (21,6,9 wt.%), N_2-strengthened, surface segregation of B, Auger and XPS spectra 79−90854
steel, austenitic stainless, creep, performing effect under tensile and compressive load, rel. to Bauschinger effect 79−96103
steel, austenitic stainless, deformation by hydroforming, heat treatment effects *(French)* 78−35450
steel, austenitic stainless, high N, heat treatment effect on struct. and props., N solubility 80−29994
steel, austenitic stainless, microstructural effects on US attenuation 78−11455
steel, austenitic stainless, nitrided, type 03kh17N8G5MFAB, alloying characts. and phase comp. 80−30166
steel, austenitic stainless, thermal cycling, low temp., effect on principal mech. props. 77−81322
steel, austenitic stainless FV548, neutron irradiated, Si-rich phase occurrence of M_6C phase 80−15156
steel, austenitic-martensitic, yield strength rel. to struct. and phase comp. 79−66127
steel, ball bearing, heat treated, fatigue crack propag. 79−20188
steel, Bauschinger effect minimization by dynamic strain ageing 78−48469
steel, BN extraction, and identification, IR anal. 80−85254
steel, brittle fracture resistance, welding and heat treatment effects 80−50723
steel, C, autectic, sintered, isothermal transformation behaviour, porosity effects 80−3031
steel, C, cold strained, effect of rapid heating on strain ageing *(Russian)* 79−11642
steel, C, corrosion carcking by sulphide, effect on props. 80−55587
steel, C, hardened, cold-drawn or shot-peened, residual stresses rel. to temp. *(French)* 77−77494
steel, C, hardened by HF current, mech. testing method 80−61053
steel, C, isoforming and warm rolling, effect of mech. props. 80−11673
steel, C, magnetomechanical acoustic emission for residual stress NDT 80−71149
steel, C, mech. props. rel. to heat treatment, ferrite-pearlite transform. *(French)* 79−20043
steel, C, microstructural inhomogeneity, influence on formability and fracture 80−11682
heat treatment continued
steel, C, quenched, restoration of austenite grains during rapid heating *(Russian)* 80−76272
steel, C, rolling contact fatigue, tufftriding effect on 0.2% C cylindrical specimen 80−100954
steel, C, type 25KhN3MFA, forgings, austenite grain refining 79−38864
steel, C, US exam. of yield and breaking strength 79−15755
steel, C and alloy, restricted durability, subject to pure bending with rotation 77−90431
steel, C content influence on brittle and tough fracture, heat treatment *(Russian)* 80−40500
steel, carburised, microstruct. and fracture 79−24658
steel, case hardening and carbonitriding treatment, mech. props. testing *(French)* 77−59991
steel, case-carburized, low alloy, rolling contact fatigue 78−35518
steel, case-hardened cast, contact endurance rel. to austenizing *(Russian)* 78−56805
steel, cast, effect of non-uniform struct. on props. 78−84850
steel, cast 18OSKhNM, fractographic investigation 77−21266
steel, cast structural, heat treatment and mech. working influence on mech. props. *(Russian)* 80−40392
steel, chemicothermal treatment, diffusional basis 80−104343
steel, constructional, austenite grain shape eval. method 78−35607
steel, constructional, nitriding process in glow discharge *(Russian)* 80−55560
steel, continuously cast, tensile strength and ductility above 800°C 80−55476
steel, corrosion resistant, review of heat treatment, mech. and corrosion resist. characts. *(Korean)* 79−24653
steel, Cr, carburising kinetics, in endothermal atm. 80−76410
steel, Cr, high strength, hot dip galvanized delayed fracture *(Japanese)* 78−15512
steel, Cr, hypereutectic, structural, critical rates of impact, kinetics of failure 80−35325
steel, Cr and Ni-Cr, cyclic re-austenitizing 80−35222
steel, Cr-Mn, effect of composition, plastic deformation, and heat treatment on martensitic transformation 79−100141
steel, Cr-Mn, powder forged, fracture processes and fracture toughness 78−72870
steel, Cr-Mn eutectoid, pearlite growth kinetics and partitioning 80−29963
steel, Cr-Mo:P (2.25, 1 wt.%), stress relief cracking, effect of P segregation 80−89324
steel, Cr-Mo, effect of Mo on high-temp. props. 80−85005
steel, Cr-Mo, martensite to ferrite transform. by fatigue deform. *(French)* 79−66056
steel, Cr-Mo, toughness of heat treated steels of equal tensile strength *(German)* 80−25727
steel, Cr-Mo (1, 0.5 wt.%), heat treated creep failure, role of stress state 79−5047
steel, Cr-Mo (2.25, 1 wt.%), in high temp. Na, heat treatment and metallurgical struct. effects 77−16619
steel, Cr-Mo (9, 1 wt.%) microstructural instability during creep, heat treatment effects 78−48472
steel, Cr-Mo weld metal, reheat cracking, residual elements and microstruct. influence 80−66553
steel, Cr-Mo-Ni-Nb, Nb effect on mech. props. *(German)* 80−30012
steel, Cr-Mo-V, brittle failure influence of cold plastic deform. 78−72858
steel, Cr-Mo-V, notch geometry influence on creep rupture props. *(German)* 80−30055
steel, Cr-Mo-V, steamline bends, restorative heat treatment effects 78−68716
steel, Cr-Mo-V, stress rupture, notch influence, temp. depend. *(German)* 80−60945
steel, Cr-Mo-V, stress rupture strength at high temps. *(German)* 80−40474
steel, Cr-Mo-V (0.5, 0.5, 0.25 wt.%), creep crack growth in notched bend test, microstruct. effect 77−21261
steel, Cr-Mo-V (0.5, 0.5, 0.25 wt.%), heat treated, microstructure effect on threshold region fatigue 78−56757
steel, Cr-Mo-V type X 41 CrMoV 5 1, austenized, carbide detection by etching *(German, English)* 79−91884
steel, Cr-Ni-(Mo), cast, intercritical heat treatment *(Czech)* 80−89268
steel, Cr-Ni-(Mo) (25, 28, 2 wt.%), lattice dilation by N_2 77−16592
steel, Cr-Ni-Cu (14, 5, 2 wt.%), phase transform. and props., preliminary heat treatment effect 79−79011
steel, Cr-Ni-Mn, adiabatic shear band determ. by surface obs. 80−97579
steel, Cr-Ni-Mo-Cu-Nb, martensitic precipitation hardenable, corrosion resistant, structure and props. 79−74169
steel, Cr-Ni-Mo-V, austenite form. during heating, influence of recrystn. during tempering *(Russian)* 80−104188
steel, Cr-V, hardened sping, surface finish effect on fatigue strength *(Japanese)* 79−61708
steel, Cr-W-Mo-Co, high-speed, from atomised powders, mech. and cutting props. 80−66556
steel, creep rate mismatch interaction in stress relief cracking 80−97578
steel, CrMoV, creep resistant, cast, creep rupture and creep *(German)* 77−70098
steel, crystallographic texture perfection in sheet with S,Mn inhibitors *(Russian)* 79−91709
steel, deform. resist., softening effects, analytical depend. calcs. *(Russian)* 80−49293
steel, deformation under modified ausforming *(Japanese)* 79−11673
steel, die, thermal fatigue resistance, high temp. thermomech. treatment effect 80−50715
steel, electric field effect on strength, hardness 80−50714
steel, electric sheet, hot-rolled, recrystallization and texture formation during ht. treatment 77−44271
steel, electroless Ni plated, fatigue strength, effect of P content of Ni film *(Japanese)* 77−52478
steel, En8, surface hardening by 2 kW CW CO_2 laser 79−83396
steel, energy absorption during uniaxial tension and axial compression, geometric and heat treatment effects 77−73312
steel, eutectoid, partitioning of Si during pearlite growth, electron microscopy study 79−83201
steel, eutectoid and hypoeutectoid, time-temp.-austenization diagram *(Japanese)* 78−6900
steel, eutectoid and hypoeutectoid stress relaxation during rapid heating transform. *(Japanese)* 78−11258

heat treatment continued
steel, fatigue crack, decrease in growth rate after thermal treatment and reduced load *(Russian)* 77−25142
steel, Fe-V-C (1, 0.2 wt.%), austenite formation 80−84927
steel, ferrite-pearlite, cyclic behaviour, fatigue, chem. comp. and microstruct. effects 78−60833
steel, ferritic, magnetomechanical acoustic emission for residual stress NDT 80−71149
steel, ferritic, underclad cracking mechanism, effects of residual strain and heat affected zone ductility 77−25158
steel, ferritic-bainitic welded by electron beam, morphology and struct. of heated zone *(French)* 77−73292
steel, first order phase transformations, in non-isothermal conditions, exam. of kinetic parameters *(Russian)* 79−34028
steel, for pressure tanks, yield point influence on brittle fracture, tensile strength *(German)* 80−40539
steel, fracture toughness evaluation using oscillograms, optimum heat treatment 79−57169
steel, free cutting, with MnS inclusions, tensile flow and fracture 78−11290
steel, gas nitrosulphurized, in temp. range 813-903K, wear props., surface and cross-sectional hardness, X-ray diffr. and SEM study *(Japanese)* 79−29224
steel, Hadfield, containing Ni, carbide precipitation, heat and cold work effects *(Korean)* 77−77484
steel, hardening and cyaniding, by heating in electrolytic plasma *(Russian)* 78−11390
steel, heat resistance, thermal stability, stress-rupture strength, and creep 80−81194
steel, heat treated, residual stress calc. with finite element program *(German)* 79−66075
steel, heat treated, test specifications changes *(German)* 77−9019
steel, heat treated rimmed, statistical study on fatigue life distrib. in long life region *(Japanese)* 77−12755
steel, heat treated SCM3, SNCM8 and SUS403, statistical fatigue props. *(Japanese)* 77−48532
steel, heat treatment achievements and prospects in USSR 78−95765
steel, heat treatment specification 79−52247
steel, heat treatment with induction heating, 78−92285
steel, heat-resistant, 12Kh1MF, yield point rel. to dislocation density and cryst. lattice spacing *(Russian)* 77−44291
steel, heat-resistant, martensitic, Kh12NMFB weldability 80−20987
steel, heat-treatment furnace trays, in service embrittlement, microstruct. and props. changes 77−63784
steel, heating effect on phase composition, microstruct. and mech. props. 80−100859
steel, hereditary transfer of lattice defects at γ-α-γ transform. 79−96020
steel, high alloy, strain induced martensite and austenite influence on crack formation *(Russian)* 80−21007
steel, high and low C, wires, electroheated, thermal cycling and corrosion behaviour 80−61006
steel, high C, Burgers vector of dislocations in cementite crystal 77−27891
steel, high C, weld heat affected zone, impact and fatigue props. *(Japanese)* 80−11668
steel, high Mn austenitic, creep rupture, p addition and two-step soln. heat treatment effects *(Korean)* 80−93646
steel, high Si dual-phase, mech. props and microstruct. anal. 80−40444
steel, high speed R6M5, secondary inheritance investigation by austenite recrystallisation 77−90367
steel, high speed YXM62, heat treatment, mech. props., wear, fracture toughness for cutting tool 78−19864
steel, high strength, failure stress, structural relationships 80−81190
steel, high strength, low C, with N_2, yield strength, Mo effects 77−90410
steel, high strength, weld zone resistance to welding induced cold cracking, preliminary heat treatment effects 79−91720
steel, high-C, carburising kinetics, in endothermal atm. 80−76410
steel, high-speed, atomised powders and sintered blanks, particle size effects 77−44188
steel, high-speed, grain size effect on wear characts. 77−59944
steel, high-speed tool, properties, powder metallurgy prep. method *(Czech)* 80−60800
steel, high-strength tool steel D7KhFN, remelting effect on mech. props. 80−76284
steel, hot rolled, low C, low alloy, bainitic alloying addition effects on microstruct. and props. 77−36546
steel, HSLA, HAZ microcrack study in multilayer welding *(Chinese)* 79−100172
steel, inclusions, SiO_2 Al_2O_3, FeS, effect of high temp. heating on size, number and distrib. 78−44145
steel, internal oxidation during carburizing and heat treating 79−24660
steel, Kh15N5AM3, combined heat treatment and mech. working *(Russian)* 77−55997
steel, low alloy, cladded with monolayer austenitic stainless steel, heavy section, residual stresses *(German)* 78−35420
steel, low alloy, exam. of fatigue crack growth, and Paris Law parameter relationship 78−92343
steel, low alloy, exam. of microstructure, in type PZhK-1000 soldered joint by metallography 79−52257
steel, low alloy, low C grain boundary proeutectoid ferrite formation, direct obs. method 80−3074
steel, low alloy, microstruct. effects on fatigue at intermediate and high crack growth rates 79−74247
steel,9low alloy, type 10KhN1M, heat-treated, struct. and resist. to thermal embrittlement 79−15788
steel, low alloy, welded joints, cracking during heat treatment 80−7724
steel, low alloy type 12Kh1MF, effect of thermal cycling on life under creep conds. 79−57075
steel, low C, corrosion, heat treatment and plastic deform. effects 77−63825
steel, low C, dual-phase, law of mixtures, applicability 80−89346
steel, low c, grain size influence on size of brittle transgranular shear facets 80−35327
steel, low C, low alloy, electron beam heat treatment of thin bands 78−3156
steel, low C, low alloy, ferritic-pearlitic, high temp. mech. treatment, cooling effect 80−104193
steel, low C, type 17G2SF, crack critical opening evaluation using plasticity diagram 80−45382
heat treatment continued
steel, low C, type AISI 1018, microstruct. effects on fatigue crack growth 79−61718
steel, low C, V(C,N) precipitation and twinning in $\gamma \rightarrow \alpha$ transform. *(Polish)* 78−52807
steel, low C, with various strain ageing potentials, tension compression fatigue *(Japanese)* 79−20162
steel, low C and medium C, high-temp. heating effect on oxide inclusions 79−96051
steel, low pearlite, Nb microalloyed, ageing at 600°C, mech. props. *(German)* 77−36542
steel, low pearlite, Ti addition effect on transform. behaviour *(German)* 77−90343
steel, low-alloy, bearing, mech. props., carbide behaviour effect *(Korean)* 80−93615
steel, low-C, fracture toughness, electroslag remelting effect 77−63788
steel, low-C-Si, LS1.2, LS1.5, phase transformation 80−45302
steel, low-temperature tempered, shock wave loading with combined treatment *(Russian)* 77−59857
steel, marageing, austenite formation, stability, transformation to martensite *(Russian)* 79−91646
steel, maraging, 18 wt.% Ni, solution heated and aged, surrface damage during machining, unlubricated 78−15599
steel, maraging, effect of thermal cycling (γ to and from α) on props. 80−20986
steel, maraging, heated to high temperatures, γ to δ transformations 80−20930
steel, maraging, heating of thin samples with brief ageing, N6G4M, ON18K9M5T 78−52866
steel, maraging, steady state unidirectionally solidified, austenite reversion and determ. 77−25118
steel, maraging 18%Ni, calorimetric anal. of ageing *(Japanese)* 80−89264
steel, martensite-ferrite combined microstructure, two-phase, tensile fracture strength 78−60783
steel, martensitic, corrosion resistance and mechanical performance in medical instruments 79−39537
steel, martensitic, corrosion resistant type 07Kh16N4B, long time strength and ductility, 340 to 450°C 79−100233
steel, martensitic, heavily doped, linear expansion meas. 80−103501
steel, martensitic grain size effects in H_2 assisted cracking, austenitising 77−28901
steel, martensitic stainless, type 05Kh13N4m, strength and embrittlement, early stages of martensite decomp. effect 80−35227
steel, medium C, 40MnB, dissoln. and precipitation of $M_{23}(C,B)_6$ *(Chinese)* 80−66511
steel, medium C, cast cylinders fragmentation tests 78−35519
steel, medium C, Cr-Mn-Mo, austenising temp. effect on microstruct. and fracture toughness *(Chinese)* 80−66542
steel, medium C, Nb addition, effect on transformation and strength 80−7607
steel, medium C, shell-shaped fracture due to B embrittlement *(Chinese)* 80−55493
steel, metastable alloys, singularities of $\alpha \rightarrow \gamma$ transform. and hardening *(Russian)* 79−52210
steel, microalloyed, precipitation effect on microstruct. and mech. props. *(French)* 80−25708
steel, mild, subject to three point bending and tensile load, acoustic emission 80−3154
steel, mild, surface segregation induced by heat treatment *(French)* 77−59831
steel, mild Cr welding, 550°-850°C heating effects on structure and toughness 79−24540
steel, Mn, plastic deformation, shape recovery during γ to and from ε, ε' transformations *(Russian)* 79−83196
steel, Mn (1.10 to 1.55 wt.%), reactor vessel material, assessment of weld heat affected zone mech. props. 79−29217
steel, Mn-Mo-Nb, high strength, ductile, acicular ferrite struct. 77−21191
steel, Mn-Mo-Ni-Cr, bainitic, microstructures and mechanical properties *(French)* 80−16362
steel, Mn-Si, for springs, metallographic study, present phases rel. to mech. props. *(French)* 80−21090
steel, Mo-V, creep rupture strength, heat treatment effects *(German)* 78−72834
steel, morphology of inclusions obs., influence on ductile fracture *(Spanish)* 80−25744
steel, multicomponent duplex stainless, high temp. precipitation of α' 80−20939
steel, Nb, high and medium C, austenite grain growth 78−11249
steel, Ni, microstruct., plastic zone size and crack propag. 78−60790
steel, Ni-Cr-Mo, Ni effect on fracture toughness, heat treatment effect *(Korean)* 79−91781
steel, Ni-Cr-Mo-U, ferritic, B segregation and high temp. embrittlement 78−7040
steel, Ni-Mn (16, 2 wt.%), 40N16G2, single crystal, stabilisation and destabilisation mechanisms *(Russian)* 78−23732
steel, Ni-Mo, powder forged, fracture processes and fracture toughness 78−72870
steel, Ni-P plated, electroless, fatigue strength and plated layer microstruct. *(Japanese)* 80−93645
steel, oxidation-reduction processes on surface during heating in vacuum *(Russian)* 78−11403
steel, parts, stress calcs. during cooling, program system THEPLA *(German)* 80−35237
steel, pearlitic, creep-induced micropore healing kinetics of 12MKh and 15Kh1M1F, TEM obs. *(Russian)* 80−71690
steel, pearlitic, heat treatment effects on mech. props. and microstruct. *(German)* 77−8857
steel, pearlitic, struct. variations under plastic strain and subsequent heating, cementite decomp. *(Russian)* 80−84954
steel, pearlitic, temp. relationship of failure charact. 78−3158
steel, pearlitic and bainitic transformations in austenite, processes during incubation period 80−40348
steel, pearlitic structural, austenite grains, growth rate during heating 80−100860
steel, plastic, thermally strengthened, not prone to H_2 embrittlement, prod. *(Russian)* 79−52267
steel, powder, prealloyed, struct. formed by atomisation, props. *(French)* 77−70020

heat treatment continued
steel, powder forged for carburizing appl., core props., mech. props. 78−15339
steel, quenched, reheating, to improve plasticity and notch toughness 77−63701
steel, rapid, contrib. to assimilation of new labels *(Rumanian)* 80−35216
steel, reheat cracking in weld zone, method for evaluating sensitivity to cracking 78−72855
steel, restorational carbonisation in one and two phase states *(Russian)* 80−65225
steel, Rheocast, struct. and props. 77−28804
steel, segregation and adsorption of S, influence on carburisation and nitrogenation 80−66701
steel, sheet, type 08Kp, blackness degree rel. to heat treatment in controlled atms. 79−57165
steel, Si, commercial, ordering after heat treatment, Mossbauer meas. 80−7556
steel, Si (6.5 wt.%) Mn, Ni and Al additions influence obs., on mech. and magnetic props. *(Slovak)* 79−5064
steel, Si-Mn-C (1.6-2.0, 0.4-0.6, 1.1-1.4 wt.%), cast graphitised, heat treatment effects on mech. props. and wear resist. 79−96050
steel, sintered, maraging, N14K7M5T, mech. props., effect of Ti additions 77−25081
steel, stainless, 0Kh13N7, 0Kh13AN7, thermocyclic treatment effects, on struct. phase composition and mech. props. 78−44204
steel, stainless, 1Kh16K4N2MVFBA, corrosion-fatigue strength *(Russian)* 79−15856
steel, stainless, 304 and 316, lowering of degassing level *(French)* 79−57159
steel, stainless, AISI 304, dislocation struct., carbides, deform. mech. map 77−16650
steel, stainless, brightness, vacuum heating effect *(Japanese)* 79−61752
steel, stainless, corrosion protection by heat treatment method 78−68836
steel, stainless, Cr-Ni (18, 8 wt.%) average inclusion size and contents exam. measurements using optical microscopy and Br-Methanol methods *(Korean)* 79−66080
steel, stainless, Cr-Ni-Mo (16, 14, 3 wt.%), corrosion resist., vacuum heat treatment effect 79−87754
steel, stainless, Cr-Ni-Mo-N, phase diagrams 80−35161
steel, stainless, electrohydraulic effect and struct. changes *(Russian)* 78−23783
steel, stainless, ferritic, corrosion resistance improvement by Mo and Ti additions 77−90505
steel, stainless, ferritic and duplex, Mossbauer effect study of 475°C embrittlement 78−52933
steel, stainless, fibre reinforced Al alloy, tensile props., cryogenic cooling effect 79−61623
steel, stainless, gas liberation in vac., effect of different methods of surface treatment *(Russian)* 80−45429
steel, stainless, heat treated, oxide comp. and corrosion susceptibility of grades 410 and 430, AES study 80−66692
steel, stainless, intercrystn. corrosion, depletion theory *(Czech)* 80−35408
steel, stainless, maraging, grain growth, temp. effect 79−57019
steel, stainless, maraging, type 03Kh11N10M2T2, exam. of thermal embrittlement 78−84986
steel, stainless, maraging, type 03Kh11N10M2T, exam. of thermal brittleness 78−88526
steel, stainless, martensitic, ageing, strength/structural charact. relationship 77−90426
steel, stainless, martensitic, crack resistance of type VNS-2, heat treatment effects 79−100196
steel, stainless, radiation-thermal treatment, N_2O_4 coolant action, intergranular corrosion *(Russian)* 78−58357
steel, stainless, sensitized, direct evidence of Cr depletion near grain boundaries 77−90358
steel, stainless, stabilised, knife line attack phenomenon, dissoln. of carbides in thermal cycles *(Japanese)* 78−68701
steel, stainless, type 304, effect of cold work as sensitization 79−66071
steel, stainless, Type 304, surface analysis by SXAPS *(Japanese)* 77−70231
steel, stainless 12kh18N9T, wire, mechanical and heat treatment effect on static and cyclical strength *(Russian)* 78−35410
steel, stainless 18N10T, electroplastic drawing, deformation zone current delivery schemes 79−91761
steel, stainless 304, elevated temp. low cycle fatigue, heat treatment effect 78−27626
steel, stainless 304, metallurgical factors on the corrosion and mass transfer in liq. Na *(Japanese)* 80−71804
steel, stainless 304, stress corrosion cracking, chloride effect, constant strain rate testing in high temp. water 78−35568
steel, stainless 304, thermally exposed, tensile props. 77−25083
steel, stainless 316L, heat treatment procedures for obtaining low degassing rates 78−23730
steel, stainless 430, diffusion of H_2, effect of heat treatment 77−47627
steel, stainless martensitic, high alloy, fatigue cracks, effect of chem. comp. and heat treatment *(Russian)* 77−25144
steel, stainless recrystallisation of thin bands, heating time investig. 79−38848
steel, stainless stabilised, knife line attack phenomenon, dissoln. of carbide during isothermal heat treatment *(Japanese)* 78−72784
steel, stainless type 03Kh13AG19, deformation temp. influence on dislocation struct *(Russian)* 80−11698
steel, stainless type 304, evaluating tendency for sensitization using Jominy bar test 80−16337
steel, stainless type 304, fabrication-related sensitisation 80−60887
steel, stainless type 316 welds, post weld heat treatments on struct., composition and ferrite amount 80−29992
steel, stainless type XM-19, influence of recrystn. behaviour on mech. props. 79−83213
steel, strengthening by rapid electrothermal treatment 78−84870
steel, structural, 35KhN1M2F, forgings, struct. inheritance during ht. treatment 78−23735
steel, structural mechanism of recrystallisation during ht. treatment 78−84847
steel, surface Si reinforced type U8, metastable phase, composition, struct. *(Russian)* 80−92599
steel, surface structural changes on exposure to plasma, etch resistance *(Russian)* 79−83234
heat treatment continued
steel, tool, M2, laser surface melted, heat treatment effects on struct. 79−70086
steel, tool, martensite plate size, austenitization 79−24549
steel, tool, thermal treatment effect on abrasive wear resistance 78−92369
steel, tool, type M2, laser melting and heat treatment, microstruct. charact. 79−100188
steel, tool type M2, surface hardening and microstruct. refinement by laser melting, electron beam melting, heat treatment *(Korean)* 79−70093
steel, toughness factor statistics *(Russian)* 77−44418
steel, transformer, formation of perfect cubic texture in thin sheets *(Russian)* 78−80557
steel, transformer, high-temp. heat treatment, resist. of refractories in contact 80−66554
steel, type 12Kh1MF and 15Kh1M1F, damage accumulation during prolonged high-temp. creep 79−57026
steel, type 35L, heat treated, exam. of surface defects using fluorescent liquids 79−15933
steel, type 37KhN3MF, austenite grain growth depend. on structural inheritance *(Russian)* 79−61582
steel, type AC/HT-2, grain diameters, US attenuation 80−89429
steel, type AISI 316, thermal passivation in controlled vacuum 80−76276
steel, ultrahigh C, heat treated, mechanical properties and microstructure 79−57012
steel, US critical angle reflectivity, near-surface metallic prop. gradient effect 80−70516
steel, V strengthened dual phase, deform. and fracture props. 78−48467
steel, VN precipitation after heat treatment 79−29067
steel, VNS-5, damping capacity 77−1849
steel, W-Mo-Cr-V tool, laser surface melted, struct., heat treatment effect 80−76424
steel, wear resistance of broaching bits in relation to boriding and heat treatment 78−85051
steel 40Kh, thermally strengthened, influence of loading rate and sea water on K_{1c} value *(Russian)* 78−56799
steel 45, cracking resistance under impact loading *(Russian)* 77−25138
steel 45, effect of low temps. and heat treatment on growth rate of fatigue cracks 79−57027
steel 45, loading surface parameter, temp. effect 79−66084
steel antioxidation protective glass enamel cladding exam. of development 78−85031
steel austenitic stainless, cold working type, heat treated, tool wear during cutting 79−47782
steel bearing parts, magnetic inspection of heat treatment quality 78−73007
steel boiler tubes, Cr-Ni-Mo, austenisation conditions effect obs., on structure and mechanical props. 80−3151
steel carburisation process, diffusion modelling 80−108632
steel EhI415, US attenuation, heat treatment effects 78−44315
steel fire simulation, determ. method of critical value in case of nonstationary heating *(German)* 77−86268
steel fracture mode, determ. from shear lip width 80−60968
steel hardness and ductility variations and micrographs rel. to heat treatment and phase diagram obs. 79−87609
steel high strength, Cd plated, effect of composition and thermal treatment, on hydrogen embrittlement susceptibility *(Russian)* 79−15769
steel industry heat treatment digital process control systems *(German)* 79−74166
steel pearlite, annealed, hot fatigued, eutectoid, spheroidization 77−52374
steel piping, stainless, type 304, correlation between intergranular cracking and sensitisation 79−67849
steel production, heat treatment, computer based interpretation of heat and cooling *(German)* 79−78995
steel stainless, Ti stabilised, intercrystalline corrosion, repeated cold deform. effect 79−57000
steel tool, martensitic plate arrangement following austenisation 77−40420
steel wire, drawn, age hardening props. obs., mechanical and electrical props. relationship 80−50662
steel wires, pre-strained electroheated, corrosion behaviour, direct resist. heating technique study *(German)* 80−40580
steels, alloy, surface plastic deform., effect of heating conditions, types 45, 40 Kh 78−53033
steels, austenitic stainless, crack propag. rates under high-temp. low cycle fatigue conditions 80−21088
steels, constructional and tool, effects on elec., mag. and mech. props. expt. 77−77719
steels, spring, 60S2A and 50KhFA, heat treatment and mech. working effect on mech. props. *(Russian)* 80−20962
steels, strength reduction by adsorpt., stress corrosion *(Russian)* 79−29265
steels, test for determining reheat cracking susceptibilities of heat affected zones *(French)* 80−16633
steels, with yield pt. of about 420 to 720 N/mm^2, correlation between yield pt./tensile strength ratio and toughness *(German)* 80−66615
steels ShKh15 and 12KhN3A, white phases structure after heat treatment 80−76281
struct. changes, through simulated multiple layer welding, micro-tensile and shearing tests *(German)* 80−35215
sugar carbons, EPR in transition range 80−34751
superalloy, microstructure resulting from alloying and heat treatment, effect on creep, fatigue, fracture strength 78−11246
surface, using plasma torch with rectangular jet 77−27751
surface cleaning techniques review, atomically clean surfaces preparation 80−11804
surface induction hardening universal feeders 79−83243
technological strength and nondestructive methods of testing during heat treatment 78−85090
technology, automobile industry 79−96048
TGS, pyroelec. single cryst., elec. field meas., thermally stimulated charges 80−45012
thermally induced structural changes, specimen surface influence 80−103559
thermobimetal, specific bending, effect of functional parameters and stabilizing heat treatment 77−89555
thermoplastics, post manufacture high temp. heat treatment, controlled geometry loss technique 78−52853

heat treatment continued
Ticonal, domain struct., variation under influence of heat treatment *(Russian)* 78−23292
4-m-toluylene diamine, single crysts., conditions of growth and heat treatment influence in dislocation struct. 79−95020
transform., struct., texture conc. var. depend. on plastic deform. *(Russian)* 79−66050
transition metal dichalcogenides, octahedral intercalate ordering study by electron diffr. 80−15076
triacetate-nitrocellulose, long period struct., 180-265°C, X-ray diffr. obs. *(Russian)* 79−24556
1,3,5-trithiane, single cryst., thermal treatment or ageing, photocond. meas. 77−11959
two-phase nodules, stressed state, connection with nodule size, cooling rate and phase ratio *(Russian)* 80−16334
US crack detection system, automatic recording and monitoring 77−90542
vacuum, efficiency 80−81089
VC-EVAC graft copolymer, mech. props., effect of heat treatment *(German)* 77−63702
vicalloy-2, high heating rate effect on mag. props. *(Russian)* 77−81328
viscose, long period struct., 180-265°C, X-ray diffr. obs. *(Russian)* 79−24556
Vycor glass, manufacture, struct., physical and chem. props. 80−7527
W, field emission tip, microscopic protuberance formation, min. elec. field and temp. 78−6835
welded joint, microstructural and chemical heterogeneity 79−29096
welded joints, flash, fatigue strength obs., microstructures influence 79−15760
welding by grain struct. comparison *(German)* 77−86273
zeolites, type Y, containg catalysts, cryst. struct., IR spectra 79−42958
Zircaloy-2, cold worked, temp. cycling effects on irradiation growth 80−2079
Zircaloy-2, polycrystn., thermal history effect on tensile props. 79−74204
Zircaloy-2, polycrystn., thermal history effect on tensile props., comment 79−74205
Zircaloy-4, accelerated corrosion in high temp., high press. steam, effect of heat treatment 78−44263
Zircaloy-4, heat treatment in SiO_2 capsules, vapour transport of Zr and Si 80−55437
Zircaloy-4/stainless steel, diffusion bonding in presence of Fe intermediate layer 79−10987
Ag and Ag alloys, yield stress temp. variation hysteresis *(Russian)* 78−52905
Ag chemically deposited layer, reflectivity rel. to heat treatment 79−27366
Ag film, optical props. after thermal cycling, thickness and substrate temp. effects *(French)* 77−48263
Ag film, vac. deposited, defect density and activation energy depend. on deposition rate 80−29294
Ag-Cd (45 at.%), morphology and struct. of bainite plates in β' phase 79−52213
Ag-Ni (10 wt.%) wire, plastically deformed, fracture struct. *(German)* 80−71744
Ag-Pd film, thermal treatment and comp. depend. of resist., 273 to 700K *(French)* 77−76963
AgBr, luminescence/wavelength relationship visible and near IR spectra, thermal processing effects *(Russian)* 80−50422
AgCl, luminescence/wavelength relationship visible and near IR spectra, thermal processing effects *(Russian)* 80−50422
AgCl:Pd^{+}, ESR spectrum, quasistatic Jahn-Teller effect 80−71170
Al 2024 alloy, Young's modulus under shock loading, heat treatment effects 77−32611
Al alloy, 2024-T3, adherend surface, chem. comp., effects of chem. and thermal treatments 78−39939
Al alloy, cast, forging and heat treatment effects on diamond planishing treatment 79−43237
Al alloy, forgings, unhealed porosities and crystalline steps *(Chinese)* 79−74178
Al alloy, low-cycle fatigue strength, isothermal hardening effect 79−38863
Al alloy 6061, energy absorption during uniaxial tension and axial compression, geometric and heat treatment effects 77−73312
Al alloy AL22, influence of ultrasonics application on creep during multistage ageing *(Russian)* 79−91708
Al alloys, electric field effect on strength, hardness 80−50714
Al alloys, heat treated, neutron irradiation effects on microstruct., mech. props. and swelling 79−65121
Al and alloys, plasticity variations rel. to heat treatment *(Russian)* 79−57050
Al, anodic oxidation, effect of vacuum and heat treatment *(German)* 79−96225
Al bronze, G, Si additions, corrosion resistance 77−16714
Al, molten, viscous flow, H dissolution temp. depend. X-ray anal. 79−91628
Al, thermal desorption of oxide film, influence of grain boundaries and recrystn. 80−61023
Al-Ag, precipitation study by internal friction *(French)* 80−35190
Al-Ag (15 wt.%), precipitation hardenend cyclic stress-strain response 78−35412
Al-Ag (1.03 at.%) alloy elec. resist. meas. above room temp., Ag atom configuration correlation 78−35534
Al-Ag(10 at.%), supercond., flux pinning, torque meas., decomp. effect 77−1525
Al-Al_3Ni directionally solidified eutectic, microstructural degradation in temp. gradient 78−3145
Al-Al_3Ni eutectic, thermal stability in temp. gradient 79−61611
Al-AlF_3-Al MIM struct., dielec. props. temp. irreversibility *(Czech)* 80−15616
Al-C, dispersion hardened, effect of processing parameters on mech. props. 80−20826
Al-C alloys, dispersion hardened exam. of production method using pressed powders 80−16244
Al-CeF_3-Al(Au) MIM struct., dielec. props. temp. irreversibility *(Czech)* 80−15616
Al-Cu, high temp. internal friction peaks 77−48470
Al-Cu (4 wt.%), aged to contain Guinier Preston zones, crystallographic fatigue crack growth 78−60832
Al-Cu (4 wt.%), single crystal, anisotropy in plane strain compression 77−36599

heat treatment continued
Al-Cu (4 wt.%) alloy, precipitation hardened, single crystal, directional plastic behaviour, exam. 78−39788
Al-Cu (4.8 wt.%), homogenization, temp. gradient driver process 77−52362
Al-Cu-Mg-Mn(-Zn-Cr), low temp. deformed, ageing and mech. props. 79−1881
Al-Cu-Zn system, solid-phase reactions, phase diagram 80−50603
Al-$CuAl_2$ eutectic, heat treatment and interlamellar spacing effect on tensile deformation 80−29979
Al-Cu(Mg), age-hardenable, US cavitation erosion mechanisms, effects of comp. and heat treatment 78−53002
Al-Cu(Si)(Mg) binary and ternary alloys, dimensional changes in heat treatment. 80−89271
Al-Mg, alloy, surface activity of Mg, XPS and AES meas. 79−86975
Al-Mg (5.7 wt.%) alloy, pre-precipitation, elec. resist. investig. 77−32601
Al-Mg alloys, overheating effects on microstruct. and props. 77−63698
Al-Mg-Li alloy, 01420, surface layer props. *(Russian)* 78−80674
Al-Mg-Si, brittleness and heat treatment, statistical design of expts. 77−73349
Al-Mg-Si, DTA exam. after small and medium deform. 80−21002
Al-Mg-Si, dil. alloy, Mn additions and heat treatment effect on $\beta \rightarrow \alpha$ transformation 80−7566
Al-Mg-Si, electron probe microanalysis, depleted zone formation in air and vacuum 79−57013
Al-Mg-Si, Mg loss, mass spectrometry/thermogravimetry 77−16620
Al-Mg-Si alloy, Mg_2Si dispersion hardened US waveguides, concentrators *(Polish)* 80−89237
Al-Mg-Si alloys, DTA meas. of struct. changes in zones after quenching and isothermal heat treatment 79−52248
Al-Mg-Zn, granulated, degassing atm. effect on mech. props. of semifinished products 80−7720
Al-Mg(Zn), electron probe microanalysis, depleted zone formation in air and vacuum 79−57013
Al-Mn, direct chill-cast, struct. changes during heat treating *(German)* 80−40408
Al-Mn, splat cooling and heat treatment effect on struct. and props. *(Russian)* 77−48456
Al-Pd_2Si contacts on Si, elec. and structural characterisation 77−43695
Al-Pr (16 wt.%), resist. depend. on temp. and hot rolling *(Polish)* 80−39555
Al-Si, thermal control of interphase microstresses and mech. props. 77−12654
Al-Si (0.57 at.%), Si precipitate dissolution kinetics 80−84935
Al-Si Schottky barrier solar cell, metallurgical reactions 77−72914
Al-SiO_2-Si MOS structures, charge motion, TSC meas. 80−100534
Al-silicide-Si systems with $CoSi_2$, $Pt_xNi_{1-x}Si$, and $MoSi_2$ as silicide, diffusion, compound form., and microstructure 80−34253
Al-Sn alloys, heat treatment effect on ^{119}Sn Mossbauer spectrum 80−7228
Al-Zn, solid soln., exam. of evolution by thermo EMF meas. *(French)* 78−52862
Al-Zn (10 wt.%), ageing behaviour, calorimetric study 80−45328
Al-Zn (40 at.%), resistance of homogenization in micro-segregation 79−100180
Al-Zn alloy, type 7010, die-forged, tensile props. after heat treatment, stress corrosion 79−66103
Al-Zn-Mg, age-hardenable, precipitation and dissoluton processes, positron annihilation and X-ray small-angle scattering comparison 80−89238
Al-Zn-Mg, decomposition calorimetric study *(German)* 79−74165
Al-Zn-Mg, effect of microstruct. and corrosive environments on stress corrosion cracking *(Japanese)* 79−79159
Al-Zn-Mg, electron probe microanalysis, depleted zone formation in air and vacuum 79−57013
Al-Zn-Mg (4.5, 2 to 3 at.%) solid state reactions by interrupted continuous heating 80−25737
Al-Zn-Mg (4.5, 2 wt.%) alloys, stress corrosion resist., vac. heat treatment effect 79−96203
Al-Zn-Mg (4.5 at.%, 2 or 3 at.%), decomposition behaviour during continuous cooling, XSAS and TEM examination 80−16264
Al-Zn-Mg (4.5 at.%, 2 to 3 at.%), decomp. behaviour during continuous heating 80−29922
Al-Zn-Mg alloy, effect of heat treatment and ageing on elec. resist. of η' precipitates 77−48441
Al-Zn-Mg alloy, elec. resist. study of processes *(Hungarian)* 77−25078
Al-Zn-Mg alloy, thermomech. treatment, precipitation and strengthening 79−24527
Al-Zn-Mg alloy 7075, effect of thermal and mechanical pretreatments, on Guinier-Preston zone 78−39817
Al-Zn-Mg alloys, grain boundary segregation, implications to stress corrosion cracking 80−84936
Al-Zn-Mg-Cu, alloy 7075, effect of purity level, dispersoid type, heat treatment, on fracture toughness 78−80636
Al-Zr, cast, precipitation and solidification *(German)* 77−36519
AlN-Al_2O_3 composites, hot-pressed 77−52275
Al_2O_3 anodised film, surface impregnated by organic phosphors, fluoresc. spectrum *(Japanese)* 80−55170
Al_2O_3, derived from boehmite, phase transformations and microstruct. 80−60857
γ-Al_2O_3, heat treatment rel. to texture 78−72789
γ-Al_2O_3, heat treatment rel. to SO_2 adsorpt. 79−56070
η-Al_2O_3 outgassed at 400, 650°C, heat of adsorpt. of pyridines from soln., surface acidity 80−61154
Al_2O_3, polycrystalline, slip band form. under fatigue stress, Schmid factor effect *(Korean)* 78−44199
Al_2O_3, polymorphic transitions during heat treatment at 900-1500°C 79−11607
Al_2O_3 sintered surfaces, premetallizing with Mo-Mn-SiO_2 79−47792
Al_2O_3, sintering as function of phase comp. 80−66464
Al_2O_3, sputter deposited, struct. and heat treatment charact. 78−15307
Al_2O_3-B_2O_3 system, phase comp. and sorption props., Al salts chem. nature influence 79−51426
Al_2O_3-Mo cermets, effect of processing factors on props. 79−100103
β''-Al_2O_3-Na_2O solid electrolyte, heat treatment effects on ionic cond. and microstruct. 80−65293
Al_2O_3-Na_2O-Li_2O, phase transformations during firing 80−3036
Al_2O_3-SiO_2 glass ceramic, surface streaks and blisters, UV fluoresc. study 80−84347
Al_2O_3-SiO_2 glasses, thermally toughened, residual compressive stresses evaluation 78−31523

heat treatment continued
Al_2O_3-SiO_2-Fe_2O_3-CaO-MgO-TiO_2, refractory, corrosion and mech. behaviour correlations 80−40563
Al_2O_3(Al_2O_3-MgO)-Ag(Au)(Cr)(Cu) cermet selective surfaces for evacuated solar collectors 79−43785
As-Se-Ge(-S), photostructural change in Urbach tail 80−76021
As_2S_3, vitreous, thermal capacity, 300 to 600K 80−103492
AsSe, chalcogenide glass, efficiency of optical recording and erasing, temp. depend. *(Russian)* 77−79908
As_2Se_3, vitreous, thermal capacity, 300 to 600K 80−103492
As_7Se_3 amorphous films, thermal relax. processes determ. by optical props. 77−15716
As_2Te_3, vitreous, thermal capacity, 300 to 600K 80−103492
Au thin films, cryst. ripening rel. to heat treatment *(German)* 80−3109
Au/GaSb (110) interface, heat-treated, struct. and chem. state, angle-resolved XPS 80−97400
Au-Cr bifilm, resistivity and struct. changes under heat treatment, diffusion effects 77−1497
Au-Cu-Zn-Ni (13, 3.4, 8.5 wt.%), white gold, metallographic structure after cold rolling, effect of heat treatment, recrystallisation *(French)* 79−52238
Au-InP, Schottky diodes, behaviour under heat treatment 79−78172
Au-Si thin film double layer, silicide form., electron diffr. study 80−80005
(Au-Ge)-Ni film, for contacts to n-GaAs, metallurgical investigation using inert substrate 77−85313
(Au-Ge)-Pt film, for contacts to n-GaAs, metallurgical investigation using inert substrate 77−85313
Au_3Cd, order-disorder phase transform., X-ray diffr. anal. *(Russian)* 80−45297
Au_4Mn, heat treated, short-range order, diffuse X-ray diffr. study *(German)* 80−88092
B fibre reinforced Al, tensile and compressive strength, prior thermal treatment effect 78−11264
B fibre reinforced Al, thermal degradation of tensile strength, due to fibre strength degradation 78−39861
B fibre reinforced Al, X-ray investigation of internal stresses *(Russian)* 77−73290
B:H amorphous films, optical band gap, thermal treatment effect 80−93415
B_4C fibres, yarn prep. from C fibres, mech., chem. props., struct., book contrib. 78−48365
BN, O content depend. on heat treatment temp., neutron activation analysis 80−16356
BN, polycrystalline cubic, compressive strength and thermal stability 78−44170
B_2O_3-SiO_2 glass, crack growth, phase separation effects 80−89336
B_2O_3-SiO_2 glasses, phase separated, DC cond. and elec. breakdown 78−23400
B_2O_3glass, effect of thermal treatment on low temp. specific heat 80−54401
BaO-SiO_2 glass ceramic, growth and nucleation kinetics 80−7528
BaO-SiO_2-P_2O_5, effect of thermal history on crystallisation of glasses 77−80424
$Ba(PO_3)_2$-MgF_2, vitrification region 77−35676
Be bronze, BrB2 grade, heat treatment quality evaluation, using eddy current device 77−90562
Be, wire, elec. cond., heat treatment and strain effects *(Russian)* 80−24870
Bi_2O_3-WO_3, X-ray diffraction studies 78−38677
$Bi_{1-x}Te_xO_{3/2+x/2}$, solid solutions, phase transformations, dielectric and differential microcalorimetry *(French)* 79−55886
C, activated, interaction with H_2, EPR spectra, alteration of paramag. props. 77−63957
C, amorphous, heat treated, AC cond., 100 to 400K, electron hopping and Mott-Davis models 80−34443
C, anthracene char, density fluctuations effect on physical properties 78−51420
C, char, amorphous, mag. interactions between localised spins 80−34587
C chars, thermally activated paramagnetism, mag. susceptibility meas. 80−75709
C, elec. cond. at low-temp. as function of freq., behaviour of heat treated samples 79−23965
C fibre, graphitisable, prepared by benzene decomp., stepwise heat treatment, TEM expts. 77−85950
C fibre, metal-coated with Cu, Co or Ni, coating struct., SEM study 80−97605
C fibre, morphological charact. rel. to fracture, SEM obs. 77−63791
C fibre, prep. from benzene, struct. changes with stepwise heat treatment up to 3000°C 77−12649
C fibre, supersonic wave propag. and damping as function of thermal treatment temp. 77−89499
C fibre, tensile strength, heat treatment and flaw effects 80−81173
C fibre, thermal treatment temp. effect on struct. and props. 78−23743
C fibre-Mg matrix interaction, strength changes on heating 78−11164
C fibres, durability, elastic props. and struct., heat treatment temp. effect, US meas. methods 80−40446
C fibres, engineering applications, production requirements and mech. props. 80−89168
C fibres, PAN-based type I, II and III, oxidation and heat treatment effect on structural heterogeneity 79−77465
C fibres, pitch and lignite based, exam. of microvoids by X-ray scatt., heat treatment and stretching effects 79−20091
C fibres, production from coal tar pitch, heat treatment *(German)* 78−44033
C fibres struct. and physical props. effects of B additions and heat treatment temp. 78−68715
C film, vac. condensed, graphitisation, electron microscopy 80−40265
C, film, work function, heat treatment 78−64563
C, glassy, graphitisation, density change 78−44142
C, glassy, graphitisation kinetics 79−52246
C, glassy, struct. parameter var. with heat treatment temp. 77−11488
C, graphitisation, cooperative accelerating effect of $CaCO_3$ and N_2 80−55429
C, hard, heat-treated under pressure, characterisation of carbon phase by electron microscope 80−60855
C, heat-treatment and neutron irrad. effects on US atten. and Young's modulus 79−11644
C materials, conf., Baden-Baden, Germany (June 1976) 78−43990
C mixes, extruded, preoxidation treatment effect on transverse breaking strength 77−63767

heat treatment continued
C, modulus of elasticity, interrelationship with crystalline struct., heat and irradiated effects 77−21210
C, phenolic resin-derived, oxidation, ht. treatment effects 78−56790
C, pyrolytic, graphitisation by Ni, activation energy and graphitisation rates 79−57010
C, pyrolytic, oxidation resist. in liq. corrosive medium 77−90471
C reinforced plastic, degraded, study of strain, 20 to 1000°C 80−71680
C, soft and hard, sp. ht. anomalies and spin-spin interactions, review 79−69261
C steel, strain hardening parameters, determination from stress-strain curves 78−80562
C, texture change on ht. treatment under press. 78−60687
C-C composites, existence diagram and properties *(French)* 78−64517
C-fibres, mag. props. after heat treatment 79−69649
C_2S, influence of polymorphic transform. on sinter stability *(Russian)* 80−66503
$CaAl_2O_4$ compounds and cements, quantitative thermogravimetry after hydrothermal treatment 80−16737
CaB_6-SmB_6 system complex borides, prep. and props. 78−52703
CaF_2:Dy sensitivity to UV and ionising radiations, temp. treatment effect 79 26763
CaF_2:U^{5+}, rhombic centre EPR spectrum, heat treatment effects 78−72407
CaF_2-NaF crysts., F_A centres, 385 and 435 nm absorpt. bands of electron irrad. crysts. 78−2889
$CaMg(CO_3)_2$, dolomite, reaction with ZrO_2, mineralisation during roasting 79−43180
CaO:OH^-, room temp. IR spectra, heat treatment and electron irrad. effects 79−51992
CaO-B_2O_3-Fe_2O_3 glasses, effect of heat treatment on electronic props. 78−2480
CaO-SiO_2 glass prep. by gel method 80−100824
CaO-SiO_2 system glasses, IR absorpt. struct. obs. of phases and struct. 80−34918
CaO-V_2O_5-SiO_2 system, compatibility triangles 80−81037
$12CaO.7Al_2O_3$, composition of gases released on heating, crystallisation *(Russian)* 80−93820
$CaSO_4$:Dy thermoluminescence sensitivity and glow curves, 700° to 1300°C 79−85815
Cd, creep, low-temp., thermal heating and quantum mechanisms 80−79868
Cd, single crysts., plasticity study during deformation by twisting *(Russian)* 80−93597
Cd_3As, film, amorphous, crystallisation effects 77−35482
$CdCr_2S_4$, ferromagnetic semiconductor films, prep. and props. *(Japanese)* 79−47308
$CdCr_2Se_4$:In, influence of Se-deficiency on props. 78−30921
$CdCr_2Se_4$:In (Ga)(Ag), and undoped, elec. prop., vac. heat treatment effect 80−15518
CdF_2, conversion into semicond. by heating in H_2 atm., resist. meas. 80−20978
CdF_2:Mn, Y, deconversion due to vacuum heat treatment, elec. resist. and electron probe meas. 79−24025
CdF_2:Mn^{2+},Y^{3+}, thermal stability under vacuum, effect of heat treatment on resist. 79−23969
$CdGeAs_2$ crystals, Bridgman grown, optical props. rel. to O_2 content of starting materials 80−81213
$CdGeAs_2$, p-n junction form. by heat treatment, photosensitivity 77−28247
$Cd_xHg_{1-x}Te$, elec. charcts., impurity effects 80−92890
$Cd_{0.1}Hg_{0.9}Te$, polycrystalline thin film, correlation between structure and 1/f noise 78−39234
$Cd_xHg_{1-x}Te$, dislocation motion, effect of lattice defects on microhardness *(Russian)* 80−70220
CdO film, chromatic changes on heat treatment *(Russian)* 77−55843
CdO films, electrophysical properties *(Russian)* 77−63008
$Cd_3(PS_4)_2$, synthesis by roasting, and exam. of props. 79−4926
CdS films, amorphous and polycrystalline, microinclusion distrib. of high resist. phase and residual cond. 80−7008
CdS layers from CdS+Cr_2O_3 system, effect of heat treatment on spectral distrib. of photosensitivity 78−80017
CdS monocrystalline sputtered X-ray transducer characteristics *(Russian)* 80−47162
CdS polycrystalline film, pot. barrier at grain boundaries from Hall effect *(Russian)* 77−32094
CdS powder layers, surface pot. dark decay, moisture sorption and heat treatment effects 80−18038
CdS, pure and Al doped, vacuum deposited film, heat treatment effect on photoelectric props. 78−60162
CdS single cryst., melt growth, improvement of elec. charcts. 79−38734
CdS sprayed film, heat treatment effect on props. 79−7916
CdS, surface props., photoreflectance spectra in the exciton region 78−95324
CdS:Ag, effect of heat treatment on induced impurity photoconductivity spectrum 77−1447
CdS:Ag, vaccuum deposited film, recrystn. by H_2S heat treatment 80−34328
CdS-Cu_2S, thin film heterojunction, dark I-V charcts. and heat treatment 79−56294
CdS-$CuInSe_2$ solar cell, polycrystalline thin film, high photocurrent, charcts., effect of heat treatment 80−61339
CdSe, effect of heat treatment in Se vapour, photocond. acoustoelec. effect and surface morphology 78−39152
CdSe, heat treatment effect on carrier mobility, role of defect centres 77−72861
$CdSe_xTe_{1-x}$ film, polycrystalline, deposition and physical props. 77−4741
Cd_2SnO_4 film, RF sputtered from powder targets, props. 77−43759
Cd_2SnO_4 film, sputter deposition and characterisation 79−43146
p-CdTe, nondoped, heat treatment in vacuum, dissoc. obs. effects on struct. and props. *(Japanese)* 80−60662
CdTe, photoplastic effect, influence of plastic deform., heat treatment and doping 79−82277
CdTe:Cl, changes in elec. props. and photoluminesc. spectra 77−4685
$Cd_xZn_{1-x}S$ films, chem. sprayed, carrier density and mobility 80−60121
Ce-Pr powder, DHCP⇄FCC transition, X-ray, DTA and resistivity studies 80−50629
Ce_2O_3, hydrated, sorption props. rel. to dehydration conditions 79−66345
Ce_2O_5-P_2O_5 glass, crystallisation 77−51326

heat treatment continued
Co base alloy, creep-fatigue interaction in aligned eutectic and solid soln. 80−108554
Co enamel, vitreous, objective colour evaluation, rel. to firing parameters *(Czech)* 80−42252
Co-Cr-Ni-TaC, directionally solidified eutectic, mech. props. and sruct., thermal cycling effects *(Russian)* 78−92282
Co-Cr-W-C, wear-resistant coating alloy, carbide form. and decomp. 77−32711
Co-Fe (6 wt.%) alloy magnetic properties, 850 to 1000°C range *(Slovak)* 79−4698
Co-Mo-Cr-Si, plasma and detonation coatings, Laves- and carbide-strengthened, comparative props. 78−15562
Co-P, electrodeposited alloys, heat-induced structural changes *(Japanese)* 80−89263
Co-Pt, atomic ordering props. and domain growth in strong pulsed mag. field *(Russian)* 80−54918
Co-Pt, struct. and mag. props. rel. to degree of order 78−72368
Co-Sb-Te ternary system, crystn., heat treatment and phase equilib. 79−52156
Co-W alloy electrolytic coatings, heat treatment effects on coercivity, hysteresis and structure *(Russian)* 80−60381
Co-W(Mo) magnetic alloys for high temp. appl. 77−85503
$CoFe_2O_4$, thermally induced surface chemistry and struct., XPS 78−22939
CoPd, single crysts., domain struct., temp. and field depend. 80−71085
Co_5Sm, coercive field temp. depend. 77−8358
coatings on Cu, effect of pulsed thermal heating 80−23146
Cr spinellide, acid extracted, phase transform. on heating in air *(French)* 79−96003
Cr steel, austenite, abnormal decomposition kinetics and mechanism *(Russian)* 80−55344
Cr, US velocity and damping in Neel temp. range, thermocyclic treatment effect *(Russian)* 79−91282
Cr-Co-Fe, chromindur alloy, field heat treatment, and mag. props. 80−35354
Cr-Co-Fe cold formable mag. alloys for use in telephone receiver 79−52227
Cr-Fe, with Si and Ta additions, metallurgical and mechanical characterisation *(Italian)* 77−66674
Cr-Fe microstructural changes, heating and cooling cycles 79−78956
Cr-Mn-Si steel, heat-treatment quality, higher harmonics of EMF obs. 78−60941
Cr-Mo low C steel forgings, material capabilities 77−42105
Cr-Mo steel types JIS SCMV 2, SCMV 3 and SCMV 4, high-temp. high-cycle fatigue props., press. vessel appls. *(Japanese)* 80−93650
Cr-$NdAlO_3$, dielectric films, phase composition and structure 80−39464
Cr-Ni steel, austenitic, effect of Si on carburising mechanism at 930°C 77−56155
Cr-Ni VKh-4 alloy, deformation and fracture mechanism investigation *(Russian)* 80−11738
Cr-Te system, NMR meas., effect of heat treatment 78−27112
Cr_2O_3 X-ray diffr. studies, crystallite size, phase transformation 77−21138
Cr_2O_3-Al_2O_3, solid soln., effect of Cr on point of zero charge 78−61021
CsCl, twin form. by compressive stress during phase transform. 80−49358
CsI:Tl, crystallophosphor, luminesc. characts., temp. and conc. depend. 80−55175
CsI:Tl X-ray phosphor, spectral characts. 79−8172
Cu clad steel, bond strength through intermediate Zn *(Korean)* 79−66213
Cu, electroplastic drawing, deformation zone current delivery schemes 79−91761
Cu, grain growth rate, 520-970°C *(Russian)* 80−29972
Cu, high-cond., high spt. ht., for cryogenic appl., prep. 78−76670
Cu, high-conductivity, treatment technique for low temp. applics. 78−27650
Cu, plane strain deformed, electron microscope obs. of morphology 78−31424
Cu surfaces, O_2 adsorbed, exam. of structure by LEED, O_2 pressure-temp. diagram *(Japanese)* 78−79884
Cu/Au planar interface, formation of ordered phases CuAu and Cu_3Au 79−82392
Cu-Al (12 wt.%), acoustic emission related to props. 79−34032
Cu-Al-Co liquid alloys, constant Co-content of 5 wt.%, mag. props. *(German)* 80−88720
Cu-Al-Fe, mech. props. rel. to heat treatment 80−50682
Cu-Al-Fe (11, 2 and 1 wt.%), Fe effects on microstruct. and mech. props. *(Korean)* 77−28807
Cu-Al-Mn, Heusler alloy, magnetic prop. investig. of struct. transitions *(German)* 77−8289
Cu-Al-Mn, partial decomp. of β_1 phase, effect on mag. props. and martensitic transform. *(Russian)* 80−45306
Cu-Al-Ni, sintered, internal friction after heat treatment *(Japanese)* 80−11686
Cu-Al-Ni-Fe, (10, 5, 5 wt.%), cast microstruct. 78−80535
Cu-Al-Ni-Fe system, corrosion behaviour in sea water 80−45421
Cu-Be alloy, Young's modulus and yield point obs. *(Czech)* 80−55448
Cu-Be-Ni-Ti-Mg bronze, alloying element influence on minimum thermo EMF, cold working *(Russian)* 80−34426
Cu-Bi-Fe, Fe effects on embrittlement 77−28900
Cu-Cr eutectic, thermal stability in temp. gradient 79−61611
Cu-Cu Zr eutectic composite, struct. and props., heat treatment and crystn. rate influence *(Russian)* 79−38813
Cu-Cu_6Y eutectic alloy, cast and directionally solidified, struct. and props. *(Russian)* 80−104138
Cu-Ga alloy, periodic antiphases obs. *(French)* 77−4772
β-Cu-In, unidirectionally transformed eutectoid, lamellar microstructure, influence of grain boundaries on thermal stability 78−72795
Cu-In eutectoid, coarsening at 829K 79−1885
Cu-Mn alloys, Cu-rich, heat treated, segregation obs. *(Russian)* 78−27517
Cu-Mn-Al, Heusler alloy, single cryst. and polycryst., effect on martensitic transform. *(Russian)* 78−48398
Cu-Nb filamentary composites, powder metallurgy prod., supercond. props. 79−56477
Cu-Ni, evaporation limited segregation 80−70513
Cu-Ni (30-90 wt.%), elect. resist. rel. to cold working and heat treatment 80−71765
heat treatment continued
Cu-Ni dil. paramagnetic alloys, sp. elec. resist., effect of Ni clusters *(German)* 78−95293
Cu-Ni-Co, mag. props. of system of disperse ferromag. particles, 73 to 673K *(Russian)* 80−65968
Cu-Sb, dil., grain growth rate, 520-970°C *(Russian)* 80−29972
Cu-Sn-Al, deform at high temps. *(Polish)* 80−89284
Cu-Sn-Mg, precipitation, effect of thermomechanical treatment *(Japanese)* 79−4970
$CuAl_2$, topological evolution during soln. heat treatment 77−32607
Cu_3Au, elec. resistivity, temp. depend. 79−47078
Cu_3Au-Co, underaged, ordered and disordered single crystal, hardening mechanisms 78−3134
$CuFe_2O_4$, thermally induced surface chemistry and struct., XPS 78−22939
$Cu_{1-x}Fe_{2+x}O_4$, elec. resist., Seebeck coeffs., 20 to 900°C, cation distrib. 79−4575
CuI, photolum., effect of heat treatment temp. 77−52151
$CuInS_2$, cathodolum. spectra, heat treatment and electron irrad. effects 78−10996
$Cu_{0.5}In_{2.5}Se_4$, transition state and domain struct. by electron microscopy and diffr. studies 80−15095
CuNiCr, IN838, heat treatment effect on fatigue and corrosion fatigue behaviour 80−20982
$Cu_{2-x}O$, nonlinear elastic props., nonstoichiometry effects *(French)* 80−34133
$Cu(OH)_2$-α-$Mn(OH)_2$, phase transition during ht. treatment 78−23659
$Cu_{1.8}S$-Cu_2S thin films, phase transforms kinematic electron diffr. study 80−29295
Cu_2S-CdS heterojunctions, role of deep levels in controlling photovoltaic props. 80−92941
Cu_2S-CdS solar cells with interdigitated grid, current-voltage analysis 80−93981
$Cu_{2-x}S$ film, evaporated, ordering process, electron diffr. study 80−39477
$Cu_{2-x}S$/CdS heterostructures, heat treated, capacitance voltage meas. anal. 80−20292
Cu_xS-CdS solar cells, post fabrication treatments 78−39822
(Fe, Ni, Co)-Si-B, amorphous, compositional effect on struct. changes, after heating up to 700°C, exam. *(Japanese)* 78−48433
Fe alloy, oxide dispersed, mech. alloying, microstruct. 77−25063
Fe alloy casting, surface alloy layer on casting by flame spraying technique *(Japanese)* 77−48586
Fe alloy porous powder metallurgical components, gamma nitriding 79−20088
Fe and its alloys, austenite formation kinetics during accelerated heating model, kinetic curves *(Russian)* 79−70058
Fe, Armco, carburising kinetics, in endothermal atm. 80−76410
Fe, atomised powder compacts for mag. cores, oxidation, compressibility, heat treatment *(Japanese)* 78−72752
Fe base superalloy, PHACOMP appl. to σ-phase estimation of various heats *(Chinese)* 79−100109
Fe, cast, effect of heat treatment, on wear resistance, 78−44148
Fe, cast, heated in CO atm., obs. cracks around graphite flakes *(Japanese)* 78−84974
Fe, cast, high Cr, wear resistance improvement 77−70186
Fe, cast, homogenization of property difference due to mass effect by repeated heat treatment *(Japanese)* 79−38857
Fe, cast, increase in yield strength, after phase transformations 78−44125
Fe, cast, interdendritic dispersed graphite, dissolution kinetics on heating, excess time *(Russian)* 77−52360
Fe, cast, mech. props., demodification influence of isothermal holding and Mg additions *(Bulgarian)* 79−15707
Fe, cast, Mg, isothermal dissociation of supercooled austenite, exam. of kinetics *(Russian)* 79−29013
Fe, cast, Mg treated, graphite modularisation by Mg gas bubbles 78−52867
Fe, cast, nodular graphite, welded, struct. exam., heat treatment effects 78−80703
Fe, cast, nodularization efficiency of rare earth alloy treatment, charging effect 79−91714
Fe, cast, spheroidal graphite effects of Si and C on mechanical props. *(Korean)* 79−66114
Fe, cast, thermal treatment influence on mechanical props. *(German)* 80−29980
Fe, cast, white, graphitisation during heat treatment *(Russian)* 80−20971
Fe, cast form. of surface graphitisation centres *(Russian)* 79−11720
Fe, cast H_2 charging effect on nodularizing efficiency of Ce-La additions 78−27544
Fe casting in metal mould, strength before, after heat treatment *(Japanese)* 77−48461
α-Fe, cold rolled, hydrostatic press. effect on microstructural changes during creep 78−39871
Fe, commercially pure, time-temp.-austenization diagram *(Japanese)* 78−6900
Fe, intergranular brittleness, effect of O and S 77−36650
Fe, magnetomechanical acoustic emission for residual stress NDT 80−71149
Fe ore, sintering, agglomeration charge layer shrinkage *(Russian)* 80−16224
Fe, point defect estimation from specific heat and volume in plastically deformed pure metals *(Russian)* 80−54223
Fe powder, ZhGr1.0, optimisation of heat treatment in salt bath 77−28756
Fe, pure, graphite form. *(German)* 77−59818
Fe, pure, tensile deform., sources of acoustic emission 78−19814
Fe rich micas, X-ray absorpt., heat treatment effects, chem. and struct. interpretation 80−84806
Fe, segregation and adsorption of S, influence on carburisation and nitrogenation 80−66701
Fe, volume changes and defect healing due to plastic deform. *(Russian)* 80−81139
Fe, X-ray K-absorpt. spectra, depend. on composition and temp. changes *(Russian)* 80−55226
Fe-Al, domain struct. and magnetostriction, heat treatment effect 80−60398
α-Fe-Al, migration of C, mag. permeability disaccommodation meas. 77−36100

heat treatment continued
Fe-Al, variation in absolute thermoelec. power under heat/treatment *(Ukrainian)* 79−38051
Fe-Al (12 wt.%) alloy 23 kHz US transducer piezomagnetic props. 78−59240
Fe-Al (25 at.%), long-range ordered, compression induced mag. anisotropy 77−69546
Fe-Al alloy, C saturated, at 1873K, activity meas. with Knudsen cell-mass spectrometer 78−39745
Fe-B, amorphous, induced anisotropy by heat treatment in mag. field and under applied mech. stress 80−75758
Fe-B-C amorphous alloys with high saturation induction 80−84617
Fe-base fibres, extruded, heat treatment 78−35414
Fe-C (0.25 wt.%), austenitising temp. effect on proeutectoid ferrite reaction kinetics, scanning Auger microprobe exam. 78−44144
Fe-C (0.8-4.2 wt.%), eutectoid transform., effect of heat treatment in H_2 *(Russian)* 79−4947
Fe-C (30 at.%), production of Fe_7C_3 at high press., morphology and microstruct. *(Russian)* 79−38828
Fe-C (4.3 wt.%), splat cooled, amorphous phase form. and crystn. 77−15323
Fe-C-Mn (0.5, 0.6 wt.%), powder forged, mech. props. 80−21096
Fe-C-Mn-V, austenite microstruct. memory *(German)* 80−84977
Fe-C-(Si)(S) alloys, graphitisation during heat treatment *(Russian)* 80−20971
Fe-Co heterogeneous alloys, fabrication by powder metallurgy, tensile strength 77−63600
Fe-Co-Al-Cu-Ti (40, 14, 7.5, 4.5 wt.%), metastable equilibrium, high coercive state *(Russian)* 80−66476
Fe-Co-C (0.8 wt.%), unidirectional transformation process per struct. relationship, pearlite interlammellar spacing meas. 77−70045
Fe-Co-C(0.8 wt.%), unidirectional transformation, eutectoid reaction kinetics 77−70029
Fe-Co-Cr, magnetic, phase transform. obs. *(French)* 79−47676
Fe-Co-Cr-Si, structural transform. and mag. props. following heat treatment *(Russian)* 77−81274
Fe-Co-Mo-Nb(Ta) semihard mag. alloy, mag. props., thermal expansion, elec. resistivity and hardness *(Japanese)* 80−88789
Fe-Co-Ni-Al (35, 14.5, 7.2 wt.%), high-coercivity, substructure and texture change during bending and upsetting 80−21037
Fe-Co-V, Vicalloy 1, γ-phase morphology and structural inheritance depend. on heating rate *(Russian)* 79−70059
Fe-Co-V alloy, Remendur, heat treatment effects on mech. and struct. props. 77−8846
Fe-Cr, damping capacity *(Japanese)* 79−70104
Fe-Cr, role of C in transform. by heating in (α+γ) phase *(French)* 78−52798
Fe-Cr (25wt.%) alloy, surface comp. rel. to passivation phenomena *(French)* 79−43479
Fe-Cr alloys, damping capacity 79−100206
Fe-Cr-Al-Y, oxidation resistance, heat treatment and Al^+ ion implantation 80−71785
Fe-Cr-C solid solns., ordering and γ to α transforms, effect of heat treatment *(Russian)* 79−24520
Fe-Cr-Co, mag. alloys, Mossbauer spectra 78−19386
Fe-Cr-Co, mechanism of coercive force 80−34674
Fe-Cr-Co alloy, coercive force mechanism 80−71103
Fe-Cr-Co alloys, mag. props., heat treatment effects *(Russian)* 78−39365
Fe-Cr-Co alloys, permanent magnets, magnetic props. and heat treatment *(Russian)* 79−91809
Fe-Cr-Co-Mo high energy permanent magnets, mag. props. 80−97119
Fe-Cr-Mn (11.5, 3 wt.%), microduplex ferritic-martensitic steel, exam. 78−39862
Fe-Cr-Mo alloy castings, thick-section, factors affecting 80−108374
Fe-Cr-Ni austenitic alloys, environment sensitive cracking, metallurgical variables effect 80−35391
Fe-Cr-Ni austenitic alloy, cold deformed, α-γ transition, calorimetric study *(Russian)* 80−55390
Fe-Cr-Ni-Ti-Al, superalloy, Ti, Ni, Al, H_2 variations effect on mech. props. 78−3188
Fe-Cr(W)-M, (M=Si,Mo,Ni,Mn,P,Cr), cellular growth of S-pearlite formed by carburisation 80−108486
Fe-Cu, sintered compacts, cooling effect on strength 77−73293
Fe-Cu (1.77%) alloy, influence of neutron irrad. on electric resist. *(Russian)* 79−38041
Fe-Ga, constitution between 10 and 50 at.% Ga, heat treatment depend., BCC phases *(German)* 77−90325
Fe-Ga, phase constitution depend. on heat treatment, phase diagram *(German)* 78−39748
Fe-M, (M=Cr,W,Mo,V,Ti), morphology and growth kinetics of δ-pearlite formed by carburisation 80−108485
Fe-Mn 8%, type K1525 thermal cycling, effect on impact toughness 80−7608
Fe-Mn-B, B effect on intergranular embrittlement 80−108555
Fe-Ni, α→γ conversion, electron microscope and X-ray spectral microanal. 79−78966
Fe-Ni, α→γ transform., role of grain boundary diffusion, Mossbauer obs., homogenisation effect *(Russian)* 79−52197
Fe-Ni, coercive force depend. on grain struct. and inclusions 77−20635
Fe-Ni (20 to 100 wt.%), exam. of C diffusion coeff., in temp. range 950 to 1100°C 78−51747
Fe-Ni (23 wt.%), struct., composition changes during α to γ transform., martensite plastic deformation influence *(Russian)* 80−11642
Fe-Ni (23 wt.%), α to γ transformation, struct., conc, changes, heating rate, residual austenite influence *(Russian)* 79−83194
Fe-Ni (28 wt.%), martensitic reversion, effect of internal stresses *(French)* 77−21142
Fe-Ni (3 wt.%), grain boundary segregation microanal. using X-ray (STEM) and AES 78−87685
Fe-Ni (32 wt.%), electrohydraulic effect and struct. changes *(Russian)* 78−23783
Fe-Ni (47 to 65 wt.%), soft magnetic alloy with crystallographic texture and field induced anisotropy, pulse permeability and excursion rate *(German)* 79−73779
Fe-Ni alloy, martensitic transform., influence of thermal and electron irrad. treatment of austenite *(Russian)* 80−66509
Fe-Ni alloy, surface decarburisation rate in dry H_2, soft mag. material manufacture 78−60882
Fe-Ni alloys, graim growth texture 79−91687

heat treatment continued
Fe-Ni austenite, α→γ transform and stabilisation, Mossbauer and electron microscopy obs. *(Russian)* 78−23703
Fe-Ni austenitic, effect of Al and Ti on relaxation resist. 80−20993
Fe-Ni system, constant modulus alloys for mech. oscillators 79−61641
Fe-Ni-Al-Co-Cu-Ti alloy YuNDKT, nature of X-phase heat treatment effect on microstruct. 77−90380
Fe-Ni-Al-Co-Ti base alloys, highly coercive, phase comp., Mossbauer meas. 80−39996
Fe-Ni-B-Si, amorphous, mag. props., heat treatment effects 80−89370
Fe-Ni-C, ausformed, ductility of martensite *(Japanese)* 77−48490
Fe-Ni-C, phase diagram determ. 79−24495
Fe-Ni-C (19.5, 0.73 wt.%), banded struct. formed by deform., TEM and optical obs. 78−39869
Fe-Ni-C (24, 0.45 wt.%), martensites, TEM observation of double twinning 78−76651
Fe-Ni-Cr, austenitic, creep strength and ductility, effect of γ′ precipitation 77−36597
Fe-Ni-Cr-Ti-Al, Ti and Al effect on microstruct. and mech. props. *(Chinese)* 79−74130
Fe-Ni-Cr-Ti-Al Elinvar alloys, dispersion-hardened, structural transform. *(Russian)* 79−1872
Fe-Ni-V, austenite, martensite elec. cond. depend. on heating *(Russian)* 79−70177
Fe-Ni-WC hard alloy, struct. and props. 79−79007
Fe-Ni-(C), substruct. of ausformed martensite 77−36548
Fe-Pd (47 at.%) alloy, powders and powder compacts, mag. props. rel. to heat treatment *(Russian)* 79−15816
Fe-Pd crystalline alloy, positive large linear magnetostriction 80−25173
Fe-Pt (22-24 at.%) austenite, long range order parameter, temp. depend. 80−40353
Fe-Si, grain oriented, phosphate coating anal. by IR spectroscopy 80−89570
Fe-Si (3 wt.%), AlN-inhibited, Se effect on primary grain recrystallisation 77−12715
Fe-Si (3 wt.%), effect of heating rate during primary recrystn. on props. after secondary recrystn. 78−84837
Fe-SiO_2-Al_2O_3 Lisakovskii concentrate mixture, sintering process, temp. thermal treatment *(Russian)* 80−55317
Fe-Ti (0.15 wt.%), H trapping obs. by high resolution autoradiography 79−73205
Fe-W system, damping capacity of Gentalloy, internal friction, mech. and mag. props. 79−77679
$FeBO_3$-MBO_3 solid soln., (M=Mn, Cr, Al, Ga, In), synthesis, crystal chem. and mag. props. 78−31058
$Fe_5Co_{70}Si_{15}B_{10}$ amorphous ferromag. ribbons, change of permeability by heat treatment 77−85493
$Fe_{36}Cr_{12}Ti_7Mo_3$, high temp. precipitation kinetics, internal friction study 79−43254
$Fe_{78}Mo_2B_{20}$, Elinvar-type behaviour 79−66091
$Fe_{40}Ni_{38}Mo_4B_{18}$, amorphous, crystallization, heat treatment and irradiation effects *(French)* 79−90558
$Fe_{40}Ni_{38}Mo_4B_{18}$, amorphous, mag. anisotropy, Mossbauer study 80−65864
α-Fe_2O_3, crystalline grain growth during heat treatment 78−11252
Fe_2O_3 haematite platelets, growth and cross-connection in consolidation of haematite pellet *(Chinese)* 80−104186
Fe_2O_3, powder, preparation conditions rel. to morphology 77−8777
γ-Fe_2O_3, prep. from thermal decomp. of $[Fe_3(HCOO)_6(OH)_2]HCOO.4H_2O$ and characterisation 78−80741
Fe_2O_3 thin films, reactively sputtered, mechanical stresses rel. to deposition conditions 80−80146
Fe_2O_3, X-ray diffr. studies, crystallite size, phase transformation 77−21138
Fe_2O_3-Al_2O_3, solid solns., effect on Fe on point of zero charge 78−61021
Fe_2O_3-Cr_2O_3, crystalline size and phase transform. study by X-ray diffr. 77−21138
Fe_3O_4, effect of Al ion on formation and structure *(Japanese)* 77−59727
α-FeOOH decomposition to α-Fe_2O_3 by heat treatment 80−2254
$Fe_{80}P_{13}C_7$ amorphous ferromag. ribbons, change of permeability by heat treatment 77−85493
$Fe(Pd_{1-x}Au_x)_3$ ordering alloys, mag. props., 4.2 to 500K *(Russian)* 79−47301
$Fe_xPd_{82-x}Si_{18}$ metallic glass, mag. phase diagram, weak ferromagnet-spin glass transition 80−54893
Fe_3Pt austenite, long range order parameter, temp. depend. discussion 80−97481
Fe_3Pt austenitising conditions on M_s temp. 80−81088
FeSi, single crysts., domain struct., temp. and field depend. 80−71085
$Fe_{78}Si_{10}B_{12}$ amorphous ferromag. ribbons, change of permeability by heat treatment 77−85493
FeTi, surface and mag. props., heat treatment and hydrogenation effects 80−75447
$Fe_2[As^{III}(As^{V}O_4)_3]$, order-disorder transformation by thermal treatment *(French)* 79−90600
GaAs (001) surface, thermal treatment before MBE growth, RHEED-AES meas. 79−61754
GaAs, deep radiation centres from heat treatment, γ-irrad., deform., probability of nonradiative electronic transitions 80−50408
n-GaAs epitaxial film, undoped, correl. incorporation of donors, photocond. meas. at 4.2K 80−6898
n-GaAs epitaxial layers, alloyed in As_2 beam, metal-Ga contacts 79−95495
GaAs, epitaxially grown (001), (111) and $(\bar{1}\bar{1}\bar{1})$ surfaces, LEED, AES, photoemission 78−38924
GaAs, epitaxy on semiinsulating GaAs, elec. props. of transitional layers rel. to growth conditions 77−15977
n-GaAs, heat treated, origin of 1.41 eV emission band, photolum. expt. 78−72579
GaAs homoepitaxial interface, thermal degradation 77−11988
GaAs oxide, anodic, heat treatment temp. effects, optical props. obs. 78−27658
GaAs oxide, anodised native, influence of temp. on struct. and props. 77−81332
GaAs, photoluminescence intensity rel. to heat treatment in S vapour *(Russian)* 78−48216
GaAs, semi-insulating, effects of heat treatment characterised by SIMS 78−6091

heat treatment continued
GaAs, semi-insulating, surface layer thermal conversion mechanism, Hall effect meas. 80−49772
GaAs, single crystal growth and heat treatment *(Chinese)* 77−73222
GaAs, VPE, hole diffusion lengths, surface prep. and heat treatment effects, etchant evaluation 80−15627
GaAs:Cr, Cr distrib. and heat-treatment migration studies by SIMS 80−107305
GaAs:Cr semi-insulating wafer, heat treatment technique for no thermal conversion 80−100857
GaAs:Cr wafers, semi-insulating, surface degradation by heat treatment at 900°C 77−80820
GaAs:Fe, static magnetis. rel. to doping method and heat treatment conditions 77−36092
GaAs:Fe(Ni) O_2 effects on opt. props. 77−16350
GaAs:Si, stacking fault prod. during heat treatment in As vapour 80−96547
n-GaAs:Te, heavily doped, interband luminesc. intensity, heat treatment effect 78−72593
GaAs:Te, phonon-dislocation interactions, nonstoichiometry effect *(French)* 77−43298
GaAs:Te, solubility and point defect-dopant interactions 79−90687
n-GaAs/Pt/Cr Schottky contact, barrier height change due to heat treatment 79−47165
$GaAs_{0.6}P_{0.4}$, anodic oxide, electronic props., depend. on annealing 79−61771
$GaAs_{0.6}P_{0.4}$, VPE, hole diffusion lengths, surface prep. and heat treatment effects, etchant evaluation 80−15627
$Ga_xIn_{1-x}P$, undoped liquid epitaxial layers, effect of heat treatment on photoluminescence 78−60512
Ga_2O_3 thin films, reactively evaporated, props. *(Japanese)* 79−99648
GaP, IR absorpt. spectra depend. on compensating defects and thermal treatment *(Russian)* 80−71465
GaP:Cu, elec. and optical props., rel. to doping and heat treatment 80−16056
GaP:Fe, heat treated, EPR spectra, struct. defects 80−7158
GaP:N(N,O) epitaxial struct., luminesc. study of degradation during heat treatment 80−45139
Gd-Co, amorphous films, mag. props. ferromag. reson. meas., 20-520°C *(Russian)* 80−97144
GdCu, electrical resistivity and length changes with temp., hysteretic behaviour 80−97600
$Gd_3Ga_5O_{12}$, garnet-perovskite transform 80−15239
Ge, cleaved in liquid He, surface elec. cond. *(Russian)* 80−15588
Ge, compensated by thermal defects, recomb. and optical props. 80−64989
Ge, film, elec. resist. and struct., post-deposition heat treatment effects 79−78229
Ge, high-doped single crysts., impurity atom distrib. changes around growth dislocations in thermocyclic treatment *(Russian)* 80−107307
Ge, impurity cloud form., anal. using heat treatment effects on light scatt. in pure crystals 80−15146
Ge:Cu, degree of Cu contamination in heat treated Ge 80−2359
Ge-As, supersaturated solid soln., dislocation form. during thermocyclic treatment *(Russian)* 80−3057
Ge-As-Se films, light irrad., heat treatment rel. to optical props. *(Russian)* 79−4858
Ge-Si, heat treated, carrier heating by strong microwave elec. field 77−69366
GeO_2, hexagonal and glassy, X and γ-irrad., thermolum. and paramag. centres 77−63472
$GeSe_2$-As_2Se_3-Sb_2Se_3, quenched glass system, elec. cond., low temp. heat treatment effect 80−39586
GeTe-MnTe, heat treatment effect on struct., elec. props. 80−54725
In-Bi (22 at.%), directionally grown eutectic two phase superconductors, magnetisation behaviour 77−28293
In-S system, vac. deposited films, form., reacts. 78−43259
InAs, elec. props. after heating for 300 to 900°C for 1 to 100 hours 78−47793
InAs:Cd,Te interaction between impurities, effect on elec. props., Hall effect. 80−19832
In_2O_3-SnO_2 thin film, effects of heat treatment on resist. and optical absorpt. 78−43495
In_2O_3-SnO_2-InP solar cell junctions, efficiency, InP surface props. 80−85288
In_2O_3+Sb_2O_3(Sb_2O_5.H_2O) reacts., complex oxide form., struct. 77−16516
n-InP, effect on bulk grown and VPE grown material 77−11936
InP substrate, thermal damage suppression by adding Ar in H_2 atmosphere 79−100275
InP-metal ohmic contacts, elec. and metallurgical props., heat treatment effects 80−34514
InP-metal Schottky barriers, effects of heat treatment characterised by SIMS 78−6446
In_2S_3, film struct. and props. 77−80706
InSb films, transverse 1/f noise and S/N ratio of related Hall elements 79−42597
InSb:Cd (Zn) (Ge), ion-irradiated, p-n conversion during heat treatment 80−96558
$In_{2-x}Sn_xO_{3-y}$-ZnS:Mn thin film structure, surface morphology and electro-optical props. *(Russian)* 80−49554
p-InsB, high-resist. compensated, elec. breakdown peculiarities 80−2398
Ir-Ce (0.4 wt.%), field emission characts., crystallography and heat treatment effects 78−2994
Ir-W (0.3 wt.%), grain growth, temp. and time effects 79−100186
$KAlSi_3O_8$-$BaAl_2Si_2O_8$ hyalophane, natural and heat treated, cryst. struct. refinement 78−2072
KCl, cryst., plasma prod. by laser impact, effect on surface 78−1866
KCl, luminesc. of Z_4 centres 79−24355
KCl, undoped and Pb- or NO_3^--doped, colloid centre formation, absorpt. spectra, 300-1000 nm 79−78710
KCl:Eu, flow stress 77−36577
KCl:Pb, impurity distrib., light scatt. and microhardness study, heat treatment 80−96562
KCl:Pb, impurity valence, heat treatment influence, absorpt. spectra obs. 79−38574
KCl:Pb^{2+}, highly doped, state of dispersion of Pb^{2+} 77−1144
KCl:Sr, single crystal, thermally stimulated topochemical reactions 79−28011
KCl:Tl^+, absorpt. spectra, electrolytic coloration, migration in electric field, heat treatment 78−23504
heat treatment continued
KI:Tl, X-ray phosphor, influence of different factors on emission intensity 79−8171
K_2O-Al_2O_3-B_2O_3:Fe_2O_3, glasses, liq.-liq. phase separation, Fe^{3+} ions rel. to mag., optical props. 77−15322
K_2O-Al_2O_3-SiO_2 system, crystallisation of glasses in primary phase field of leucite 78−67658
La_2C_3, solid solution, lattice const. and superconducting transition temp. *(Russian)* 80−92496
$LaMo_6S_8$ thin films, crit. currents and pinning forces 80−34575
La_3NbO_7, synthesis and cryst. growth 80−71590
$LaNi_2H_{4.6}$, effect of synthesis, heat treatment, on comp. stability, chemical props. 80−29985
La_2O_3-B_2O_3-P_2O_5, glasses, struct. changes during heat treatment, NMR obs. 77−7672
La_2O_3-SiO_2, gels, microstruct. and crystallisation, prep. method and thermal treatment effect 79−61913
Li matrix ferrites, coercivity, synthesis, thermostability control 80−80569
$LiAlSiO_4$, β-eucryptite, heating effect on domain struct. 79−66078
LiF dosimeter, thermoluminescence glow curves and light absorption, thermal treatment effect *(Russian)* 77−32954
LiF single crystals, stepwise creep, 300K, in dislocation depletion conditions, thermal cycling effects *(Russian)* 77−15484
LiF:Mg,Ca detectors, variation of parameters of thermally stimulated luminesc. 79−6793
LiF:Mg^{2+}, TLD-100, precipitation reactions and ionic cond. 77−56479
LiF-$Al(PO_3)_3$ glass, phase decomp., X-ray diffr. and IR spectra study 80−30003
$Li_{0.5}Fe_{2.5}O_4$, ht. treatment conditions effect on superlattice formation 77−84922
$Li_{0.5}Mn_{0.15}Fe_{2.35}O_4$ ferrite cores with rectangular hysteresis loops, pulse parameters, effect of Fe_2O_3 heat treatment 80−60370
$LiNbO_3$ optical waveguides, elimination of Li_2O out-diffusion waveguide 77−65641
$LiNbO_3$, reversed polarity layer at positive domain surface, heat-induced, etching investig. 77−63383
$LiNbO_3$:Fe spatial holograms, ageing limitation *(Russian)* 80−74311
LiO_2-Al_2O_3-SiO_2, glass containing ZrO_2, cryst. process 80−103253
LiO_2-Al_2O_3-SiO_2-TiO_2:Sn^{3+}, ESR and X-ray phase anal. 79−99752
LiO_2-Na_2O-MgO-TiO_2-Al_2O_3-SiO_2, exam. of specific heat and thermal conductivity *(Russian)* 79−55898
Li_2O-$3SiO_2$ glass, crystallization 79−74141
Li_2O-Al_2O_3-SiO_2, phase separation of initial stages of sitallisation 80−88053
Li_2O-Al_2O_3-SiO_2-TiO_2 system glasses, Raman spectra obs. of glass-ceramics form. 80−60825
Li_2O-GeO_2 glass, synthesis, Ge coordination state 77−24271
Li_2O-Na_2O-B_2O_3-SiO_3, exam. of metastable phase separation region 78−88450
Li_2O-SiO_2, glass ceramics, phase transformations process 80−3025
Li_2O-SiO_2-P_2O_5 glass ceramic fibres, heat treatment, crystn., tensile strength 80−84995
(Li_2O-Al_2O_3-SiO_2):Fe_2O_3, glass, pyroceramic form., colour centres, magnetochem. investig. 77−16537
$LiTaO_3$ glass-ceramics, transparent fabrication by crystn. of aluminosilicate glasses 77−59734
$LiTaO_3$-SiO_2-Al_2O_3, transparency in relation to microstruct. 78−53005
$LifaO_3$, optical waveguides, elimination of Li_2O out-diffusion waveguide 77−65641
Mg alloy, H_2 evolution during isothermal treatment in vacuum *(Russian)* 77−77625
Mg alloy MA12, thermally strengthened, fatigue cracking in air and vacuum *(Russian)* 78−35481
Mg alloys, heat treated, neutron irradiation effects on microstruct., mech. props. and swelling 79−65121
Mg-Al-Zn (9wt.%Al), sand cast, preferred orientation and mechanical props. *(Japanese)* 80−20979
Mg-Cu-Mn-Ni-Fe-O, UHF ferrites, synthesis, physicochem. state, mag. and dielec. parameters 79−11536
Mg-Ni-S, electroforming, mech. props. rel. to heat treatment 80−35133
$MgCr_2O_4$ spinel, exam. of expansion during synthesis 79−20012
$Mg_xFe_{3-x}O_4$, cation redistrib., lattice const. 79−60338
MgO, (001) film substrates for film growth studies by TEM, O_2 conditioning 79−82489
MgO, dissoc. under heat and electron bombardment 80−7834
MgO, lattice defects., calcination temp. effect 80−15091
MgO, thermally stimulated exoelectron emission *(German)* 80−66404
MgO:OH^-, room temp. IR spectra, heat treatment and electron irrad. effects 79−51992
MgO-Al_2O_3-Fe_2O_3-SiO_2, cordierite, in ceramic, effect of heat treatment on cordierite content 79−20039
MgO-Al_2O_3-P_2O_5 system glass, heat treatment of aluminium metaphosphate influence on thermolum. 80−108285
MgO-Al_2O_3-SiO_2, glass ceramics, phase transformation processes 80−3025
MgO-Al_2O_3-SiO_2, metastable liq. phase separation region, electron microscope exam. 78−88451
MgO-Al_2O_3-SiO_2: ZrO_2, TiO_2, glass, phase separation *(German)* 80−38932
MgO-FeO-P_2O_5 system, glass, ESR spectra, heat treatment conditions effect 79−65722
MgO-NaCl refractory clinkers, Cr containing, densification, thermal treatment and phase composition effect *(French)* 80−76219
(MgO-Fe_2O_3-Cr_2O_3-TiO_2):Na_2O, powder, prep., heat treatment, Na_2O impurity effect on props. 77−16528
$Mg(OH)_2$-α-$Mn(OH)_2$, phase transition during ht. treatment 78−23659
Mn-Cu, alloying addition and heat treatment effects on damping capacity 78−3165
Mn-Cu alloy, local premartensitic instability in FCC phase 80−40355
Mn-V-Al, magnetic props., heat treatment effects 79−29233
Mo and alloys, absorption of N_2 in induction and plasma-arc heating *(Russian)* 77−16732
Mo, deformed, dislocation-free channels prod. by heat pulses, electron microscope obs. and hardness meas. *(Russian)* 79−52251
Mo film, on SiO_2/Si substrate, effect of heat treatment after deposition on internal stress 78−22973
Mo, impurity interactions with C, N, and O, struct., mech. props. and purification 79−52277
Mo, nitriding kinetics 80−35415
Mo, RF sputtered, diffusion barrier props. 78−71887

heat treatment continued
Mo-C-Zr (0.03, 0.17 wt.%), thermal treatment effect on yield drop 77−90382
Mo-Si film-substrate interface, reaction on heat treatment, silicide formation 80−79999
Mo-Ti (up to 5.48 wt.%), internal nitriding, hardness, nitride type, precipitation *(Japanese)* 79−79157
Mo-Zr-C alloys, carburising and annealing effects *(Russian)* 77−59828
Mo_2C coatings, phase and struct. transformations on heating 79−96206
NaCl, cryst., plasma prod. by laser impact, effect on surface 78−1866
NaCl, high-temp. deformed, dislocation grain subboundaries *(Russian)* 80−96534
NaCl-Ca, single crysts., load-microhardness curves, heat treatment, impurity effects obs. 78−30694
NaCl-kCl melt, reaction with LiO_2-$2SiO_2$ X-ray, IR exam. 80−55706
$NaNO_2$, 163°C phase transition, thermal history effects on range of modulated struct. 78−95563
$NaNbO_3$, memory effect, in ferroelec. phase, ESR meas. 79−28696
NaO-B_2O_3-SiO_2, phase separated glass, viscosity and microstruct., heat treatment effect 79−99343
Na_2O-(BaO)-SiO_2 glass, chemical durability of surface, heat treatment effect 79−52405
Na_2O-Al_2O_3-SiO_2-TiO, effect of Cr_2O_3, NiO, and MgO additions on crystallisation 78−87626
Na_2O-Al_2O_3-SiO_2-TiO_2-NiO glass, paramagnetic centres form. during crystn., ESR study 79−65710
Na_2O-B_2O_3-SiO_2, two-phase, stresses arising during leaching 80−81086
Na_2O-B_2O_3-SiO_2 glass, phase separated, HCl leaching rate and microstruct. 79−29242
Na_2O-CaO glass, wettability, effect of cleaning procedures 80−65336
Na_2O-CaO-SiO_2, glass, light scatt. rel. to heat treatment *(German)* 78−84598
Na_2O-CaO-SiO_2-Fe_2O_3 molten glass, optical props., temp. depend. *(French)* 80−100667
$2Na_2O$-CaO-$3SiO_2$ glass, cryst. nucleation rate, viscosity, heat treatment 80−84081
Na_2O-P_2O_5-SiO_2 glass, substitution of Li^+, Mg^{2+}, Sr^{2+}, Ba^{2+}, Zn^{2+} for Na^+ 80−100332
Na_2O-SiO_2, (5.3, 94.7 wt.%) glass, liq.-phase separated, struct., heat treatment effect 80−16359
Na_2O-SiO_2 glass drops, quenched from liq. state, thermally treated, density profile 80−81085
Nb alloys, cold worked, chemicothermal strengthening, internal oxidation 80−35229
Nb, nitriding kinetics 80−35415
Nb spheres, residual resistivity ratio, prep. method effects *(German)* 79−8372
Nb, surface topography formation due to elec. transfer processes *(Russian)* 80−54482
Nb, vacuum heat treatment effects on gas content and elec. and mech. props. *(Russian)* 79−43281
Nb/Cu-Sn-Mg, superconductor, effect of Mg addition to Cu-Sn matrix 80−25028
Nb-Al-(Ge) film, superconductor, high rate sputter deposition and heat treatment 77−36399
Nb-C alloys, alloyed with Mo, Ti, and Zr, phase comp. and precip. after heat treatment 79−57020
Nb-Ga alloy, A15 type, melt produces specimens, supecond., homogeneity, transition temp. *(German)* 78−2608
Nb-Mo(Zr) alloys, vacuum heat treatment effects on gas content and elec. and mech. props. *(Russian)* 79−43281
Nb-Si liquid quenched alloy, metastable A-15 and amorphous phases, interstitials 80−54394
Nb-Ti filamentary superconductor critical current density rel. to thermal treatment 79−33440
Nb-Ti multifilaments, effect of mech. and thermal treatments of supercond. props. 80−104197
Nb-Ti superconducting alloy, critical current density, heat treatment effects *(Japanese)* 78−14909
Nb-W-Zr-Ta (90, 4.5, 3.5, 2 wt.%) creep and creep limit in super vac. at 1100°C, heat treatment effect 80−81133
Nb-Zr-C, strengthening phase struct. and morphology after prolonged high temp. stress in vacuum *(Russian)* 77−25065
Nb-Zr-C (0.1, 0.01 wt.%) plastic deform. influence on electronic state of Nb atoms 80−40463
Nb_3(Al, Ge), effect of thermal treatment on superconducting props. 79−61016
Nb_3Al, and $Nb_3Al_{0.76}Ge_{0.24}$, supercond. props. of cold worked core wires an basis of A15 phases 77−85369
Nb_3Al multifilamentary cable fabrication and props. 79−33438
Nb_3Al superconductors, sputter deposited, BCC to A15 transition, microstruct. investig. 78−27512
Nb_3Al tape, effect of thermal treatment on superconducting props. 79−61016
NbC, and NbC-ZrC solid soln., prep. by impregnation, strength, surface submicrocracks 77−16661
Nb_3(Ge,Si) A15 film, supercond. and structural props. 79−87177
Nb_3Ge, high pressure and temp. treatment effect on supercond. props. *(Russian)* 77−1512
$Nb_3Ge_xAl_{1-x}$, ternary supercond. alloys, comp. variations 80−97022
NbO_x, phase comp. on heating 2000-4000K 80−21267
Nb_2O_5 amorphous film, in Nb-Nb_2O_5-MnO_2 sandwich, elec. cond. variation during heat treatment 79−82593
Nb_3Si, metastable A-15 struct. synthesis by ion implantation, supercond. transition temp. 80−55319
Nb_3Sn, composite wire, boundary resistance and cryogenic stability 79−69629
Nb_3Sn film formation, solubility, precipitating processes *(Russian)* 80−92792
Nb_3Sn, multifilament superconductor, pulsed mag. field losses and critical current densities 80−54853
Nb_3Sn multifilamentary composite supercond. wires, transverse sections prep., ion milling, TEM obs. of grain size 80−101000
Nb_3Sn multifilamentary hollow superconductor and magnet, fabrication and crit. currents 79−38289
Nb_3Sn multifilamentary supercond. composites, crystallographic texturing 80−71669
Nb_3Sn, supercond. props. of cold worked core wires an basis of A15 phases 77−85369
Nb_3Sn, superconducting, formed from Cu-Sn alloy, props. 79−42709
Nb_3Sn superconducting multifilamentary wire, stress effects 79−33431

heat treatment continued
Nb_3Sn, superconducting transition temp., crit. parameters 77−28280
Nb_3Sn superconductors, Kirkendall voids, effects on mech. and supercond. props. 79−33429
Nb_3Sn-Cu multifilamentary composite wire, Nb_3Sn filament morphology and grain size 80−100855
NbTi, composite wire, boundary resistance and cryogenic stability 79−69629
NbTi, supercond., crit. current densities and anisotropy factors, heat treatment effects 79−38285
NbTi, supercond., processing parameter optimisation for high mag. field appls. 79−38290
NbTi supercond. threads in Cu matrix, struct. composition and props. *(French)* 79−73649
$NdAlO_3$, dielectric films, phase composition and structure 80−39464
Ni, 200, high temp. cyclic deformation and hardening 80−21055
Ni alloy, heat resistant, high temp. plasticity at different strain rates 77−21233
Ni alloy EI867, heat resistant, mech. props., effect of prolonged elevated temp. 77−21194
Ni alloys, plasticity, heat treatment effect 80−76277
Ni alloys EhP539L, heat-resist., heat treatment effect on props. and hardening phase morphology 80−29995
Ni base alloy IN792, carbide morphology 77−36508
Ni coating, heat treated, as plated, electrochemical study of corrosive wear 80−16536
Ni, dispersion strengthened, high-temp. cyclic deformation 80−21056
Ni dispersions, semi-amorphous, on Al_2O_3-graphite, mag. characterisation 80−44876
Ni, electrolytic, O, H, N liberation during vacuum heating, Mossbauer spectra *(Russian)* 80−35594
Ni, grain boundary migration during recrystallisation after cold drawing 77−73289
Ni, Ni-Ti (1 wt.%), serrated yielding, 77 to 723K 77−32649
Ni, point defect estimation from specific heat and volume in plastically deformed pure metals *(Russian)* 80−54223
Ni single crystal, stretched, electron microscope exam. of deformation cell structure during polygonization *(German)* 80−7651
Ni, surface decarburisation rate in dry H_2, soft mag. material manufacture 78−60882
Ni ultrafine particles for solar energy photothermal conversion 79−100538
Ni, volume changes and defect healing due to plastic deform. *(Russian)* 80−81139
Ni, X-ray K-absorpt. spectra, depend. on composition and temp. changes *(Russian)* 80−55226
Ni/Pt double layers on Si substrate, silicide formation 78−84010
β_1-Ni-Al, elastic softening and electron diffr. anomalies prior to martensitic transform. 77−8825
Ni-B amorphous films, electronic transport and crystn. activation energies *(French)* 80−6807
Ni-base superalloy, IN-738, microstruct. changes during isochronal heat treatment, 773-1467K 78−27531
Ni-based superalloys, TEM obs. of cellular transformation products 80−3045
Ni-Co electrodeposit, strength, heat treatment and comp. var. effects 77−32660
Ni-Co-Cr-Al-Ti-Mo superalloy IN738, casking porosity removal using hydrostatic press. sintering 80−55322
Ni-Cr, high temp. wire resistance strain gauges 77−53896
Ni-Cr, solid soln., exam. of back stress role in creep behaviour of particle strengthened alloys 78−52889
Ni-Cr (2 wt.%), role of hydrostatic pressure on sintering of creep cavities 79−28980
Ni-Cr alloy KhN70MVYu wire, recrystn., optimum heat treatment 80−76278
Ni-Cr machine steel, austenite grain size effects on mech. props. *(Russian)* 77−44292
Ni-Cr-Al (40, 4 wt.%), γ' and α-Cr duplex precipitation, TEM *(Japanese)* 77−25061
Ni-Cr-Al-TaC, eutectic composite, microstructure, fatigue props. 80−85038
Ni-Cr-Al-Ti (Ti-Co), exam. of back stress role in creep behaviour of particle strengthened alloys 78−52889
Ni-Cr-Al-Ti alloy type ZhS6U, effects of heat treatment in high vel. gas streams on props. 79−57025
Ni-Cr-Al-Y_2O_3 superalloy, recrystn. and texture development 80−16328
Ni-Cr-Co-Mo-Al-Ti (10, 15, 3, 5.5, 4.5 wt.%), superalloy, exam. of creep and fracture behaviour 78−48464
Ni-Cr-Co-Mo-Al-Ti alloys, Waspaloy, Astroloy, exam. of microstruct. effect on crack growth 78−52977
Ni-Cr-Co-Ti-Mo-W-Al (14, 9.8, 5, 4, 3.9, 3 wt.%), low cycle fatigue, prior heat treatment effect 80−60962
Ni-Cr-Fe Alloy 600, acid intergranular corrosion rel. to caustic stress corrosion cracking stress relieving effect 77−66712
Ni-Cr-Fe Alloy 600, stress corrosion cracking in high purity water, effect of microstruct. 77−66713
Ni-Cr-Fe steam generator tubes, stress corrosion susceptibility, heat treatment effect 79−20258
Ni-Cr-Mo steel, corrosion and cavitation-erosion resist. *(Russian)* 78−11395
Ni-Cr-NbC eutectic composite, unidirectional solidification, thermal cycling, temp. range effect on microstructural degradation 80−89272
Ni-Cr-Ta-Ti-Si, EP557 precipitation hardening alloy, mech. props., heat treatment effect 80−60877
Ni-Cr-W-Mo-Ti-Al alloy KhN67MVTYu, heat treatment effect on mech. props. 77−70082
Ni-Cr(Mo), variation in absolute thermoelec. power under heat/treatment *(Ukrainian)* 79−38051
Ni-Fe-Ce superalloy, vacuum melted, Ce effects on microstruct. 77−36552
Ni-Fe-Mo-Cu (79, 16, 4.3, 0.7 wt.%) K-state formation, physical props. exam. 78−47761
Ni-Fe-Nb, hardperm alloy, effect of sheet thickness and heat treatment on magnetic props. *(Japanese)* 78−31095
Ni-Fe-Nb alloys, mag. permeability and struct. *(Chinese)* 78−84450
Ni-Fe-Nb-Al alloys, mag. permeability and struct. *(Chinese)* 78−84450
Ni-Fe-Nb(Ta)-W, high magnetic permeability alloys, Hardperm 77−48012
α-Ni-In, solid solution, lamellar microstructure, influence of grain boundaries on thermal stability 78−72795

heat treatment continued
Ni-maraging weld metal, increasing fracture toughness by heat treatment 78−72871
Ni-Mn alloy film, influence on magnetic properties obs. *(German)* 77−56118
Ni-Mn base polynary alloys, magnetic and elect. props. *(Japanese)* 78−15551
Ni-Mn base polynary alloys, magnetic, and elec. props., composition and heat treatment effects 79−11710
Ni-Mo-Cr-Si, plasma and detonation coatings, Laves- and carbide-strengthened, comparative props. 78−15562
Ni-Nb-Al, unidirectionally solidified γ/γ'-δ eutectic, fatigue crack propag. 79−29184
Ni-P, electroless deposition on Al, X-ray and SEM obs. 79−90907
Ni-P alloy, electrodeposited, heat induced struct. changes *(Japanese)* 78−15433
Ni-S, defect control by heat-treatment in S atmos. 79−43293
Ni-Si, intergranular segregation of Si, electron energy loss spectrometers, X-ray anal. *(French)* 79−8388
Ni-Si interface, NiSi formation from Ni_2Si, Pt marker study 78−87830
Ni-SiC coating, heat treated, as plated, electrochemical study of corrosive wear 80−16536
Ni-SiC coating adhesion to Al alloy, metal interdiffusion *(Russian)* 80−66697
Ni-Ti, heavily doped, linear expansion meas. 80−103501
$Ni_{73}Fe_{27}$, order-disorder transition, Mossbauer study 79−95163
$NiFe_2O_4$, effect of sintering in air in range 1373-1773K on lattice parameter 79−19208
$NiFe_2O_4$ precipitation process from silicate glass, ESR study, effective g value, transition temp. 80−25194
$NiFe_2O_4$, solid state formation, exam. of kinetics for formation at 700 to 1400 degrees C 78−48648
$NiFe_2O_4$, thermally induced surface chemistry and struct., XPS 78−22939
Ni_3Mn, antiphase domain struct. *(Russian)* 78−39814
Ni_3Mn, dislocation struct. after heat treatments, TEM *(Russian)* 77−8848
Ni_4Mo alloy, high temp. oxidation, oxide layer growth, struct., mech. behaviour 78−44269
$Ni(OH_2)$-α-$Mn(OH_2)$ system, precip. and ht. treatment 77−85916
P_2O_5-SiO_2 glass film, thickness and IR spectrum changes on heat treatment in H_2 80−70549
Pa, preparation by Van Arkel method, cryst. struct. 78−39715
Pb creep, low-temp., thermal heating and quantum mechanisms, supercond. transition effects 80−79868
Pb films, hillock growth upon cycling to cryogenic temps. 80−88448
Pb thin films, thermal strain, multiple cycling to 4.2K effects 79−90918
Pb-Ag eutectic alloy, microstruct. coarsening under isothermal and temp. gradient conditions 79−20079
Pb-Bi(Ni), creep, low-temp., thermal heating and quantum mechanisms, supercond. transition effects 80−79868
Pb-Sn, unidirectionally solidified eutectic, lamellar microstructure, influence of grain boundaries on thermal stability 78−72795
Pb(Ag) alloys, effect of Ag content on yield strength 80−76322
Pb_2GaTaO_6, transition from pyrochlore to imperfect fluorite struct. 80−19939
$Pb_5Ge_3O_{11}$, sputtered ferroelec. films, prep. struct. and dielec. props. 80−75452
PbI_2, single cryst., luminesc., photocond. and absorpt. after thermal treatment 79−56855
$Pb_2MnSb_{0.99}Sn_{0.01}$, ^{119}Sn Mossbauer study, compositional and heat treatment effects 79−42875
PbO-B_2O_3-SiO_2-Li_2O-MgO(CaO)(ZnO)(Al_2O_3)(TiO_2)(ZrO_2), glass enamel, heat treated, chemical durability, MgO, CaO, ZnO, Al_2O_3, TiO_2, ZrO_2 addition effects 79−29255
PbO-GeO_2 glass, synthesis, Ge coordination state 77−24271
PbO-SiO_2, glass IR and Raman spectra, heat treatment conditions effect 79−66088
PbS film, appearance of EPR centres in initial form. stage *(Russian)* 77−63283
$Pb(Sb_{1/3}Mn_{2/3})O_3$-$PbTiO_3$-$PbZrO_3$, remanent dielec. polarisation of poled ceramic, heat treatment 79−87390
$Pb(Sc_{0.6}Ta_{0.5})_3$ ceramics, ordering and diffuse phase transitions 80−29699
$PbTiO_3$ glass-ceramics, transparent, fabrication method by crystn. 77−59733
$Pb(Zr,Ti)O_3$, synthesis from cryochem. mixtures, chem. reacts. in sublimation drying 79−11538
$Pb(Zr,Ti)O_3$ thin film, ferroelec., fabrication by RF sputtering *(Japanese)* 80−25560
$Pb(Zr_xTi_{1-x})O_3$ films, deposition by focused ion beam sputtering 80−76177
Pd ribbon, H_2 adsorption, thermal desorption and work function meas. 80−70538
Pd/Al_2O_3, adsorption of CO, IR study 80−108193
Pd-Si amorphous alloy, heat treated, low temp. lattice sp. ht. 80−75368
Pd-W (20 wt.%), permeability, diffusion, and solubility of H_2, elec. resist., heat treatment effects *(Russian)* 79−51307
$Pd_2MnIn_{1-x}Sn$, and $Pd_2MnIn_{1-y}Sb$, Heusler alloys, mag. order, disorder effects 80−88723
Pd_2MnSb, ferromag. Heusler alloy, mechanical and heat treatment effects 79−78582
$Pd_{80}Si_{20}$, plastic flow, fracture, slanted necking and elongation at high temps. 79−57057
Pt-Ir, structural phase transform., ion field emission microscopy obs. *(Russian)* 80−50628
PtSi films, on Si, stress obs. 80−80145
Re, carburised, spectral emissivity at 0.65 μm 80−75374
Rh foil, work function determ. rel. to heat treatment temp., extrinsic photoeffect meas. 77−39918
Rh, resistive film, electron diffr. structure obs., heat treatment effects 77−51620
S, mag. susceptibility meas. rel. to heat treatment 78−34952
Se amorphous film, stabilisation by thermal treatment *(French)* 79−47176
a-Se, hole form. energy, heating time and cooling rate depend. 79−41958
Se, mag. susceptibility meas. rel. to heat treatment 78−34952
Se, vitreous, temp. depend. of sound vel. 77−84855
Se:Ge(Si)(Sn), vitreous, crystn. kinetics study by elec. cond. meas. 79−65526

heat treatment continued
Se:P, vitreous, crystn. kinetics study by elec. cond. meas. 79−64998
Se-As 36.4 at % amorphous alloy, heat treatment effect on acoustic props. 79−86843
Si (111) surface, heating effects on ellipsometric parameters 77−72764
Si, (111) surface structure phase transform, screw dislocations RHEED study 80−88153
Si, amorphous and crystalline, heating by Q-switched laser radiation 80−84963
Si, as-grown Czochralski crystal, appl. of multiple p-n junction structure to solar cells 80−101099
Si, cast polycryst. p-n junction solar cell, hydrogenation effects 80−93916
Si, compensated by thermal defects, recomb. and optical props. 80−64989
Si crystal, Czochralski grown, enhanced Borrmann effect 80−70191
n-Si, deformed, thermal treatment effect on elec. cond. and dislocation mobility 80−107265
Si, dislocation-free, deep centres formed after high temp. treatment 80−96824
Si, dislocation-free, defect formation, high temp. treatment, growth-band influence *(Russian)* 79−4299
Si, dissolved O_2 precipitation, homogeneous nucleation 77−11695
Si, electrical props. affected by heat treatment *(Russian)* 78−11352
Si film, MBE, cryst. defect props., substrate treatment effects 80−70551
Si, floating zone structural perfection changes by high temp. treatment, dendrites, dislocation interactions 80−29049
Si, heat treated, spin-depend. recomb. at dislocations 79−47122
Si, heavily disordered, fast neutron irrad., IR absorption following heat treatment 78−2448
Si, lattice strains induced by localized oxidation, high temp. real-time X-ray topographic studies 80−108489
Si, Li ion implantation, depth distrib. variation after heat treatment 79−86814
Si, light scattering due to microdefects 78−27248
Si, nearly perfect crysts., point defect aggregates, high resolution diffuse X-ray scattering study 80−49211
Si, neutron transmutation doping, photoluminesc. characterisation 80−11453
Si, polycryst., CVD, recrystn. on heating 80−80107
Si, porous layer, struct. and heat-treatment effect 79−1557
Si, precipitation of Au, supersaturated soln., Hall effect meas. 77−89465
n-Si, recomb. parameters of heat treatment defects in diodes 79−56299
Si, surface, etched and heat-treated, optically stimulated ESR investigation 80−11245
Si, thermal donor generation in temp. range 600-800°C 79−11121
Si, thermal oxidation, SiO_2 amorphous film form., struct., mechanism 77−12725
Si, thermally induced donors due to heat treatment and Fe contamination 79−78035
Si, thermally induced microdefect form., C and O role 80−11439
Si, thermally induced microdefects, effect of C, TEM obs. *(Japanese)* 80−54244
Si thin film, polycryst., CVD, elec. props. 80−107934
Si wafer, heat treatment behaviour of microdefects and residual impurities, X-ray diffr. and IR absorpt. study 80−49214
Si:0, electrical activity due to heat treatment, Hall effect meas. 80−15543
Si:Al(B), polycrystn., CVD grown, recryst., influence of dopants on grain growth and size 80−54575
Si:As, segregation and desorption kinetics for evaporation of As 79−99410
Si:B, heat treatment centres changes, EPR obs. 80−29601
Si:B, ion implanted, ellipsometric study for low doses, cryst. damage parameter 79−65105
Si:B, low conc. B diffusion using doped-oxide film 77−76431
Si:B, polycryst., N_2 heat treated, anomalous resist. change due to Bn form. 78−2591
Si:B(P)(As), effect on IR transmittance 77−27325
Si:Fe, EPR and neutron activation anal. of thermal defects 78−91355
Si:H, amorphous, density of states determ. using field effect 80−49937
Si:Ni,O, interaction of Ni with O, influence of heat treatment, IR absorption meas. 77−4667
Si:O, annealing behaviour of O donor, conc. reductions via resistivity meas. 79−51129
Si:O, Czochralski crystal, oxygen striation and thermally induced microdefects 80−100275
Si:O, dislocation-free, Si-O complexes, heat treatment effects 77−62557
Si:O, heat treated, excess carrier recomb. rate, defect levels 80−75579
Si:O, kinetics of donor formation, under heat treatment in 450-900°C range 80−75523
Si:P, metallic, EPR and photoluminesc. changes 77−77262
Si:Te, laser melting, surface Te atom accumulation, profiles 80−100258
Si/Al and Si/Al-Si(Cu), Si regrowth minimisation through overlying Al or Al alloy film 80−70569
Si-Al system, Si regrowth minimisation methods in Al films 80−15384
Si-Al-O-N ceramic, grain boundary desegregation and intergranular cohesion 80−100872
Si-Al-O-N sintered ceramic, microstruct., phase composition and transformation mech., mech. props. 80−40309
Si-SiO_2 interface, bias temp. treatment effect, stability, Cl oxides effect 77−69419
Si-SiO_2 interface, elec. props., rel. to SiO_2 layer struct., 200-600°C heat treatment effects *(Russian)* 77−15967
Si-SiO_2-Mg-Cu powder compact, nitridation to form Si_2ON_2 whiskers *(Japanese)* 80−93674
SiC coated B fibre Al-V-Ti, tensile and compressive strength, prior thermal treatment effect 78−11264
SiC fibre, development from organosilicon polymers by heat treatment 80−81014
SiC fibres obtained from polycarbosilane fibre 80−50582
SiC, reaction sintered, TEM exam. of recrystallisation, phase transformation 78−80567
β-SiC, undoped compact, microstruct. development during heating 80−25746
SiC-coated C fibre, compatibility with Al *(Japanese)* 80−71700
SiC+BaO+$BaCO_3$ react., contact phenomena at SiC grain boundary 79−43193
$Si_{12}Ge_{10}As_{30}Te_{48}$ glass, effect of surface, SEM obs., rel. to switching filament form. 77−47700

heat treatment continued
Si_3N_4, Y_2O_3 doped, hot pressed, improved high temp. strength 79−61613
SiO film and powder, effect of heat treatment on chemical and electronic struct., electron spectroscopy 77−48320
SiO-Al multilayer capacitors and inductors, heat treatment effect on elec. props. 77−32082
SiO_2 concrete, elastic moduli meas. during heating and cooling 80−55451
SiO_2 fibre reinforced Al, thermal degradation kinetics 77−44194
SiO_2 films, dehydroxylation, sintering, IR investig. *(Russian)* 78−75967
SiO_2, fused, refractive index dispersion, thermal history depend. 80−25331
SiO_2 gels, heats of immersion, effects of pore narrowing 79−11833
SiO_2 glass, heat treatment study by positron annihilation 78−55812
SiO_2, on Si, reduction by heating in Ga mol. beam at 800°C 80−50730
SiO_2, optical fibre, phys. behaviour of neck-down region during furnace drawing 78−83127
SiO_2, vitreous, heat treatment effect on viscosity and struct. 80−19714
SiO_2, vitreous, low temp. sp. ht., effect of heat treatment 78−59955
SiO_2, vitreous and neutron irrad., thermal cond., heat treatment effect 79−90837
SiO_2:Na^+, heat treated, heat of immersion in H_2O, organic compds. 80−3396
SiO_2:TiO_2, prep., amorphous struct., effect of roasting, bonds 78−44061
SiO_2/GaAs, interface reaction during high-temp. heat-treatments 80−88439
SiO_2-Al_2O_3, coprecipitated gel, Si-Al spinel formation during transformation on heating 79−78958
SiO_2-Al_2O_3 (8 mol.%) glass, heat treated, devitrified phases 80−66469
SiO_2-Al_2O_3-CaO-MgO-FeO-Fe_2O_3 glasses, struct. transforms during heating 80−15014
SiO_2-Al_2O_3-Cr_2O_3 system, KT-11 type, chromia-containing material production based on high-silica glass fabric 80−45266
SiO_2-Al_2O_3-Fe_2O_3-CaO, basalt glass ceramics, crystallite form. due to heat treatment 80−38917
SiO_2-Al_2O_3-MgO-TiO_2 devitrificates, microstruct. and props. *(Polish)* 80−70141
SiO_2-GeO_2, synthetic, struct, IR spectra 79−42993
SiO_2-Li_2O-K_2O-ZnO-P_2O_5, glass ceramic, phase changes and crystn. processes 80−7562
SiO_2-Li_2O-K_2O-ZnO glass ceramic, prep., phase transformations and physical props. 80−45299
SiO_2-Na_2O-CaO:Fe(As)(Cr) glasses, optical absorpt. changes on heat treatment 78−31224
SiO_2-TiO_2-Al_2O_3-SrO(BaO), glasses, ceramic form. rel. to Al_2O_3 content 77−25005
SiO_3:B, P films doped by pyrolisis and ion implantation, IR absorpt. obs. of impurity conc. 77−72802
SiO_3-Na_2O-CaO-MgO-Al_2O_3 charge, silicate formation during heating 80−55342
SiO_2glass, effect of thermal treatment on low temp. specific heat 80−54401
Si_2Te_3, passivated single cryst., elec. conductivity 78−95299
Sm-Co-Cu-Fe-Zr alloy, reversible changes in coercive force and struct. state during heat treatment 400-800°C *(Russian)* 80−29574
$SmCo_5$ magnets, magnetisation and demagnetisation heating effects 79−38357
$SmCo_5$, sintered, high coercivity, microstruct. and mag. props. 77−69629
$Sm(Co_{0.65}Cu_{0.35})_{5.6}$, cryst. struct. and coercive force, heat treatment effects *(Russian)* 80−44170
$Sm(Co_{0.86-x}Cu_{0.14}Fe_x)_7$, permanent magnet, sintering and heat treatment effects 80−39817
$Sm_2Cu_{1.6}Zr_{0.16}Fe_{3.3}Co_{12}$, enhancement of mag. props. 79−82825
$Sm_3Ga_5O_{12}$, garnet-perovskite transform 80−15239
$Sm_{1-w}MM_w(Co_{1-x-y}Cu_xFe)_z$, (MM-mischmetal), mag. meas. and metallographic exam. 77−56119
$Sm_{0.91}Zr_{0.09}(Co_{0.68}Cu_{0.10}Fe_{0.22})_{6.7}$, alloy permanent magnet, coercive force *(Russian)* 80−65966
Sn, $\alpha \rightarrow \beta$ transform., α-Sn nucleation and growth in β-Sn 78−38838
Sn-Ni, electrodeposited, thermal stability 77−52319
Sn-Ni metastable alloy, surface film comp., time depend., XPS 78−60870
SnO, disproportionation, thermoEMF, Mossbauer spectroscopic, X-ray diffr. anals. 79−11776
SnO_2 CVD coating on glass, elec. resist. rel. to cryst. microstruct. 80−84520
SnO_2, film, effects of Sb and In additions on struct. and resist. 77−20469
SnO_2, heat treated film, electrical conductivity 77−8211
SnO_2:Sb thin films DC sputtered, heat treatment effects, expt. 77−28719
SnO_2-Cu_xS-ZnS:Mn,Cu-Al_2O_3-Al, light-emitting struct., cond. and electrolum., heat treatment 80−97345
SnO_2-ZnS:Mn thin film structure, surface morphology and electro-optical props. *(Russian)* 80−49554
$Sr_2Fe_2O_5$, order-disorder transition from brownmillerite to perovskite under heat treatment in N_2 stream 79−11612
$SrNb_2O_6$-$NaNbO_3$-$LiNbO_3$ pseudo-ternary system, DTA, heat treatment and X-ray diffr. obs. *(Chinese)* 79−52175
$SrTiO_3$, pure and Nb doped, heat treated, Hall effect, electrical cond., optical absorpt., defect states 78−47812
$SrTiO_3$, Sr_2TiO_4, $Sr_3Ti_2O_7$, prep. from coprecipitates of Sr and Ti 77−48374
stainless, carbide precipitation during post heat treatment, knife line attack phenomena 79−20288
Ta carbides, changes in phase structure during prolonged heating in vacuum 78−44095
Ta surface, nonstationary heating and oxidation in low temp. plasma flow, heat and charge transfer obs. *(Russian)* 80−104341
Ta_2O_5, anodic film, thermally stimulated exo-electron emission 80−11546
Ta_2O_5 anodic films, reanodisation effect on exoelectron emission 79−43110
Ta_2O_5 films, Poole-Frenkel effect and cond., effect of heat treatment in oxygen and in vacuum 80−39693
Ta_2O_5, hydrated, heat treatment effect on physicochem. props. 80−20966
Ta_2O_5, plane optical waveguide, fabrication by reactive sputtering 78−71221
heat treatment continued
Ta_2O_5-SiO_2, plane optical waveguide, fabrication by reactive sputtering 78−71221
Tc film, electrodeposited, supercond. transition, AC susceptibility meas. 79−95539
Te, mag. susceptibility meas. rel. to heat treatment 78−34952
α-Ti alloy, crystallographic texture, importance in characterization 77−28821
Ti alloy, cyclical heat treatment *(Russian)* 79−57009
α-β Ti alloy, fracture toughness rel. to microstruct. 77−16673
Ti alloy, heat resistance, thermal stability, stress-rupture strength, and creep 80−81194
Ti alloy, microstruct. and mech. props., room and elevated temps. 77−36554
Ti alloy, microstructure resulting from heat treatment, alloying, effect on creep, fatigue, fracture strength 78−11246
Ti alloy, VT3-1, HTMT effects on struct. and props. 78−23740
Ti alloy, VT3-1 mech. props. and low-temp. creep 77−44314
Ti alloy 679, thermal stability *(Chinese)* 77−73255
Ti alloy VT16, strengthening heat treatment in vacuum 79−79013
Ti alloy VT9L, cast, welded joint mech. props., filler material and heat treatment effects 79−87671
α-βTi alloys, high strength, heat-treated weldments, intergranular fracture 80−21097
α,$\alpha+\beta$ Ti alloys, structural instability during prolonged periods of heating *(Russian)* 78−56664
Ti alloys, texture strengthening 78−23724
Ti alloys VT23 and VT15, etching as a function of struct. *(Russian)* 78−15568
Ti, heating and cooling rate effects on α to β phase transform. and recrystallisation 77−90379
α-Ti, hydride precipitation, resistometric investigation, isothermal ageing effects *(Japanese)* 77−81265
Ti lamellar single cryst. formation by heat treatment *(Russian)* 77−59800
Ti, oxidation behaviour in high temp. steam after heat treatments *(Japanese)* 78−48565
Ti, point defect estimation from specific heat and volume in plastically deformed pure metals *(Russian)* 80−54223
Ti, porous structure, change in presence of liq. phase *(Russian)* 80−16223
Ti, pure, rapid grain growth 80−16343
Ti, volume changes and defect healing due to plastic deform. *(Russian)* 80−81139
Ti-(Al)-Zr-Si (5, 0.5 wt.%), creep 77−36595
Ti-Al-Mo-Cr (4.5, 5, 1.5 wt.%), CORONA-5, effect of microstructure and heat treatment on fracture 78−60805
Ti-Al-Mo-Cr (4.5, 5, 1.5 wt.%), weld metal, α/β interace sliding 80−108512
Ti-Al-Mo-Sn-Si (4,4,2,0.5 wt.%), fracture toughness and crack propagation 78−39892
Ti-Al-Mo-Zr (Cr-Fe), effect of heating on thermal stability of phases, lattice constants and chem. comp. 78−56672
Ti-Al-Mo-(Cr), etching as a function of struct. *(Russian)* 78−15568
Ti-Al-Mo(Cr)(Fe), thermomechanical treatment effect on mech. props., strengthening mechanisms 80−55441
Ti-Al-Sn (5, 2.5 wt.%) alloy, fatigue under combined alternating bending and torsional stresses 77−8923
Ti-Al-Sn-Cu-Zn, (5, 2.5, 3, 1.5 wt.%), embrittlement after high temperature long-time exposure *(Chinese)* 78−95792
Ti-Al-V, plane strain toughness and resistance to crack propagation *(French)* 78−23813
Ti-Al-V (6, 4 wt.%), friction characts. improvement by O_2 dissolution and controlled surface hardening *(French)* 80−45401
Ti-Al-V (6,4 wt.%), α/β interface phase, formation chartacts. 79−52272
Ti-Al-V (6,4 wt.%), improved toughness from prior β-grains 78−15522
Ti-Al-V (6,4 wt.%), microstruct. improvement by cyclic heating *(Japanese)* 79−100185
Ti-Al-V (6.4 wt.%) cast alloy, with improved microstruct., mech. props. *(Japanese)* 80−71701
Ti-Al-V-Sn(Mo-Fe), heavy section extrusion, fabrication and mech. props. 78−6985
Ti-Al-Zr-Mo-Si (6,5,0.5,0.25 wt.%) fracture toughness and crack propag. 78−39892
Ti-alloy, VT16, volume and phase changes during continuous heating *(Russian)* 77−77470
Ti-Fe, H storage material, Mossbauer surface studies, Fe clusters 80−97167
Ti-Hf-O system, $\omega(0)$ phase form. 79−11553
α-β Ti-Mn alloys, etching and electropolishing to reveal α and β-grain size 78−3254
Ti-Mo alloys, elasticity moduli, 80-300°C *(Russian)* 78−80574
β-Ti-Mo-V-Fe-Al (8, 8, 2, 3, wt.%), exam. of stress induced H_2 migration 78−87823
β-Ti-Mo-V-Fe-Al (8,8,2,3 wt.%), metastable, high cycle fatigue crack initation, grain size effect 77−86145
Ti-Mo-Zr-Sn, alloy, βIII, struct. transform. in thermally affected zones after electron beam welding 78−23919
Ti-N system, phase relations, struct. rel. to heat treatment 79−11552
Ti-Ni-Cu (44.5, 10 wt%), opposing stress effect on shape memory and martensitic reversion 78−44185
Ti-Ni-Mo (1.5, 2 wt.%), Mo effect on microstructure 77−36536
Ti-Si_3N_4 system, reactions under heating and plasma conditions 79−95988
Ti-Ti-Co system, phase type after heat treatment in vacuum at 1000°C 79−61580
Ti-W(-Al), mech. props. and heat treatment 80−35274
TiAl, manufacture by extrusion of blended elemental powders 77−28750
η-$Ti_3Be_3(O,N)_x$, formation and struct. 79−73151
TiC base hard metals, N_2-containing surface wear resistant layers, struct. anal. *(German)* 78−92405
TiC coated C fibre, compatibility with Al after heat treatment *(Japanese)* 79−78898
TiC film, CVD, on WC, diffusion processes, ion beam anal. 80−49424
TiC-Kh6V3M steel alloy, reaction during sintering and heat treatment 78−60617
TiC-steel cermet with Cu additions, precip. hardening and ht. treatment temp. 77−40414
TiN, synthesised in SHF discharge plasma, exam. of props. *(Russian)* 80−7524

heat treatment continued
TiO-ZrO_2, pseudo binary system, effect of Ti addition on struct. and props. of zirconia 79−11583
TiO_2, amorphous film, vac. deposited, struct. and crystn., TEM obs. 80−2291
TiO_2, obtained ions $Ti_2OCl(HCOO)_3(OH)_2$, by thermohydrolysis, exam. of crystallisation 80−2173
TiO_2, polycryst., paramag. centres, illumination effects, ESR 77−48041
TiO_2, thermally stimulated exoelectron emission *(German)* 80−66404
α-U, pseudo-single cryst. and polycryst., low temp. sp. ht. 78−83972
α-U, strain rate effect on flow and fracture 80−100887
U-V (0.2 wt.%), mech. and struct. props., effect of internal H *(French)* 77−21253
UO_2 microspheres, prep. from UO_3 $(NH_3)_2$, exam. of mech. and physical preps. 79−6758
V-Al/Cu-Ge composite superconductors, transition temp. and upper crit. field, heat treatment effects 79−38268
V-H rods, twisting effect, anelastic deviations on thermal cycling 80−21043
V-Nb(MO) alloys, effects of welding on mech. props. 77−21176
V_3Ga, multifilament superconductor, pulsed mag. field losses and critical current densities 80−54853
V_2O_5, thermally stimulated exoelectron emission *(German)* 80−66404
V_2O_5-GeO_2 glass, effect of thermal processing on elec. and thermal props. *(Russian)* 77−63814
V_3Si, dislocations, obs. by TEM 77−59012
W alloy wire reinforced stainless steel, fibre/matrix interaction, fabrication and heat treatment effect 79−91607
W, electroplastic drawing, deformation zone current delivery schemes 79−91761
W fibre reinforced Cu composites, correl. between thermal cycling-induced microstructural changes at interphase boundaries and tensile behaviour *(Japanese)* 80−71674
W foil, integral heating by msec laser pulses *(Russian)* 77−59824
W, heat resistant particles in low temp. Ar plasma, heating, melting, vaporisation *(Russian)* 80−40384
W, impurity interactions with C, N, and O, struct., mech. props. and purification 79−52277
W, laser heating in air by obliquely incident radiation 80−71815
W surface layer struct. during milling, plastic deform., failure *(Russian)* 80−40586
W-Re alloys, thermal EMF instability, heat treatment effects 80−75553
W-reinforced Ni and Ni-Fe, fabrication, heat treatment, and mag. and mech. props. 77−40408
WC-Co hardmetals, β-SiC to turbostratic graphite transformation 79−74150
WC-Co hardmetals, heat-treated, single domain obs. 79−73771
WO_3, amorphous film, vac. deposited, struct. and crystn., TEM obs. 80−2291
YAG, interrelationship between mech. props. and elec. relief on surface layer 79−23821
$YAl_3(BO_3)_4$, thermolum. anal. 79−87514
Y_2O_3, cooling rate in melt-growth effect on struct. perfection 77−85925
$Y_2Ti_2O_7$, precipitation from oxalates, carbonates, exam. 80−55641
Zn, creep, low-temp., thermal heating and quantum mechanisms 80−79868
$Zn_xCd_{1-x}S$ films, spray pyrolysis, elec. props. 80−75657
$Zn_{1-x}Ni_xFe_2O_4$, heat treatment and sintering effect on porosity 80−25610
ZnO ceramics, heat treatment effect on cryst. phases, microstruct. and elec. props. 79−100268
ZnO polar surfaces, H and O_2 exposed, ion irrad., and heat treated, cond., EELS study 80−71525
ZnO, thermally stimulated exoelectron emission *(German)* 80−66404
ZnO-Al_2O_3-SiO2, transparent glass ceramics, heat treatment effect on microstruct. 78−56667
ZnO-$Al_2O_3SiO_2$, transparent glass-ceramic, microstruct., physical props., crystallisation ht. treatment depend. 78−80506
ZnO-SnO_2-M_xO_y, M_xO_y=glass-forming additive, I-V characts., heat treatment effects 77−43595
ZnO-TiO_2 system, heat treated, X-ray anal. of phase form. sequence 79−1850
ZnO{10$\bar{1}$0} surface, clean, preparation, XPS meas. 78−39933
$Zn_3(PO_4)_2.4H_2O$, thermal transitions, thermographic investig. 77−9063
ZnS, high-resist., optical transmission thermal processing effects 77−63431
ZnS, polymorphic transition, ($\beta \rightarrow \alpha$) effect of mech. deformation 79−1858
ZnS, vacuum-evaporated conducting films, prep. and props. 79−66007
ZnS:Au, phosphor, 'blue' and 'green' centre form. *(German)* 79−38665
ZnSe, heat-treated in controlled partial press. of Zn or Se, TSC 80−59910
ZnSe MIS diode, blue electrolum., heat treatment effects 78−19569
ZnSe, pure and Cu doped, elec. props. after heat treatment in Zn or Se vapour 79−99505
ZnSe single cryst. for LED, heat treatment effects on elec. props. 80−29406
ZnSe, single crysts., opt. band gap and Mn^{2+} EPR, effects of prep. conditions 77−47730
p-ZnSe:As, ion implantation and heat treatment 78−87700
ZnTe:B^+ native and implant-created defects 77−76446
ZnTe:Cu films, high cond., elec. and optical props. 80−88651
Zr,Nb (2.5 wt.%), interaction of hydride, stress, and crack growth at 600K, metallographic obs. 77−12695
α-Zr-H, volumetric changes, and thermal expansion, dilatometric and X-ray analysis exam. *(Russian)* 79−11665
Zr-Nb (2.5 wt.%), cold-worked, pressure tubing, metallography and mech. props. 80−89269
Zr-Nb (2.5 wt.%), heat treatment effects on slow crack growth, cold working effects 77−28836
Zr-Nb (2.5 wt.%), transforms. during annealing of welded joint, after thermal cycling *(Russian)* 80−29984
Zr-V foil, rapidly quenched and heat treated, supercond. props. 80−54852
ZrC, and ZrC-NbC solid soln., prep. by impregnation, strength, surface submicrocracks 77−16661
$Zr(HPO_4)_2$, cryst., heat treated, acid strength distrib. 78−92377
ZrN, sintering in vacuum and in N_2 77−12586
ZrO_2, cubic single crystal, colour centres 77−15410
ZrO_2-CaO (15 mol.%), precipitation and ordering 80−100837
heat treatment continued
ZrO_2-$CaO(Y_2O_3)$ ceramics with grainy structure, props., effect of heating to 2000°C 80−104194
ZrO_2-P_2O_5, hydrated, heat treatment and coprecipitation, phase transitions 77−90335
ZrO_2-Y_2O_3 (9 mol.%), precipitation and ordering 80−100837
ZrO_2-Zr cermet composite, hot pressed, fracture toughness 78−27604

heated cathodes *see thermionic cathodes*

heating
see also electric heating; induction heating; ovens; plasma heating; refractories; space heating
α-particles, heating and acceleration 79−12376
AC thermometry and DC heating circuitry in thermal props. meas. 78−74000
acoustic heating, sound waves thermal self-action 77−3692
air, heating by flashlamp radiation, ballistic and calorimetric meas. *(Russian)* 78−5843
air warming and cooling rates, urban and rural sites 79−88454
amorphous polymers, specific heat rel. to rate of heating *(Russian)* 77−85986
approx. soln. for damage by pulsed discharge 77−39500
arc cathode spot, ion impact and neutralisation heating 80−38733
artificial kidney construction for solution mixing, heating and degassing *(German)* 79−2161
atmosphere, daily average solar heating or photolysis, exponential approx. 77−5285
atmosphere, forced equiv.-barotropic flow, stationary heating effect 77−86983
atmosphere, inhomogeneous 9.6 μm O_3 band heating, new approx. method 78−88918
atmosphere, middle, heating due to damped planetary wave interaction with zonally averaged circulation 80−109217
atmosphere diabatic heating profile, rel. to preferred mode of Ekman conditional instability of second kind (CISK) 80−72617
atmosphere heating rates, effect of CO_2 80−17376
Atmospheric Explorer, low perigee aerodynamic heating during orbital flight 77−45290
atmospheric temperature, heating effect of Mount Jolmo Lungma on atmosphere from April to July *(Chinese)* 80−8406
auroral ionosphere, heating during aurora 77−21973
baryta crystal gas-liquid inclusion meas. with microscope heating stage 80−76967
borosilicate glass, Simax, internal and surface temp. during heating *(Czech)* 79−42285
chromosphere, heating processes, short period waves 77−74022
chromosphere heating by solar flares, charged particles beam collisional interaction with H target 78−93095
chromospheres of late-type stars, nonradiative heating determ. from chromospheric radiative losses 78−40915
clusters of galaxies, intracluster gas heating by relativistic electrons rel. to X-ray and radio emission 78−57655
clusters of galaxies, viscous heating of intracluster gas 79−9011
clusters of galaxies intracluster gas, heating by relativistic electrons 79−25735
cold early universe, heating by black hole accretion 78−16585
comets, H atmosphere dynamics, dissociative heating effects *(Russian)* 78−20736
composite materials, bearing capacity of designs, subject to intense surface heating 78−67057
cone/plate system in fluid, friction heating and convection 78−87238
container wall, quasistatic stress distrib. due to internal press. and external temp. changing 77−84113
crude oil heating in tube furnaces, anal. 79−18972
cylindrical cavity wall, surface temp., periodic flux heating effects 77−46880
D-region electron heating, appl. to negative ions detect. from Thomson scatt. 79−16739
diffusion pumps, heater problems and solns. 77−41629
dissipative heating of medium during disk rot. in bounded space 78−67012
dye laser, heating effect minimization 80−1198
Earth interior, shear heating as explanation for lithosphere-mantle decoupling 79−20790
Earth surface heating, remote sensing by Heat Capacity Mapping Mission 79−5640
elastomers, repetitively impacted, mech. response and heat buildup 77−54889
electron bombardment heater for heat transfer studies 77−30146
F-region Joule heating events, zonal winds estimation via incoherent scatter technique 78−36344
film heating in axisymmetric flow around cylinder, bulk flow twist effect on efficiency 77−23952
fluorite crystal gas-liquid inclusion meas. with microscope heating stage 80−76967
Fourcault sheet glass, internal and surface temp. during heating *(Czech)* 79−42285
galaxies collisional heating, form. of ellipticals by tidal interactions 77−78865
glass, isobaric thermal behaviour during heating and cooling, rate of recovery, one-parameter model 80−75165
graphite furnace atomic absorpt. spectrometry heated by capacitive discharge, determ. of elements 80−66892
hollow cylinder, internal one sided heating, nomogram construction, for computing temp. state 78−63271
hollow cylinder, temp. and stress fields under action of periodic heat flux to inside surface 77−35013
hollow cylinder heated at inner surface, regular regime anal. 77−46882
hollow sphere, time-optimal control of heating *(Russian)* 79−27491
hypervelocity particle impact, heating and vaporisation, temp. estimation 78−59290
ice, radiative heating 77−84130
incubator, portable, with radiant heating system and fine O_2 control 77−56511
industrial plants, indirect heating systems, heat-carrying molten salt eutectic mixture *(German)* 80−38233
industrial process, gas-cooled graphite-moderated, very high temp. nuclear reactor appl. 77−23245
interstellar dust clouds heating due to molecules desorption from grains 77−9786

heating continued
interstellar dust in type 1 Seyfert galaxies, heating rel. to IR luminosity 78−12357
interstellar dust of galactic extended low-density H II region, heating and diffuse IR emission 79−17047
interstellar gas, heating by galactic UV radiation 80−67839
interstellar grains in compact H II regions, large beam IR obs. 78−16488
interstellar H_2, ionisation, dissociation and heating efficiencies of cosmic rays 78−28454
interstellar H II/OH maser regions, heating by ion streams 80−56912
interstellar medium, heating by photoelectrons from 0^- ions 78−36666
interstellar medium, heating due to weak shock waves dissipation 78−81674
interstellar medium, heating processes rel. to delayed star form. in galaxies 80−105349
interstellar medium mechanical heating, source and rate 80−36682
ionosphere, elect. heating and cooling rates discrepancy, Atmosphere Explorer-C meas. 77−29564
ionosphere, heating by artificially injected 40 keV electron beam 78−40746
ionosphere, heating by strong microwaves from solar power satellite, theoretical anal. *(Japanese)* 80−94634
ionosphere, nighttime, $O(^1D)$ contrib. to heating 79−44288
ionosphere heating expts., effects of HF-induced plasma instabilities on electron temps. 78−40756
Jupiter, solar heating and internal heat flow 78−85888
laminar boundary layer in water, heating and suction effects in separation 78−9625
laser pulse heating, high temp. vapours, phase transitions, equations of state 80−52230
lower thermosphere, heating by acoustic waves dissipation 77−53266
magnetosonic heating of semiinfinite body under periodic loading *(Russian)* 77−50855
Mars, thermal history and evolution model 78−65533
Mars dusty atmosphere, solar heating rates 78−85878
mass-spectrometric leak detector, ion source heating up to 550°C, sensitivity improvement 78−78028
massive bodies, optimum heating given restriction of heating control and rate *(Russian)* 79−68546
massive spherical particle, heating by radiation and convection 77−50866
metal, thin film, heating by light pulse of linear intensity time dependence *(Russian)* 77−59827
metal thin film, preheating as aid to laser recording 80−102753
metals, heating by concentrated energy sources, simple analytical expressions *(Russian)* 80−38215
metals heating kinetics in oxidising medium, exam. using CO_2 continuous laser emission *(Russian)* 79−57135
minor planets, EM heating in early solar system 80−36555
Moon, early collisional heating 80−8563
multilayer thermal-insulation envelope, heat flux calcs. for unsteady heat cond. 77−23853
nanosecond temperature-jump apparatus for high pressures 80−219
neutron stars thermal properties and detectability, cooling and heating processes 80−31323
nuclear and coal heating for industry and home, appl. study 78−37455
nuclear heating, approx. method, direct energy balance calc., γ transport, accuracy 77−6495
nuclear plant heat recovery for agriculture and pisciculture 78−37464
nuclear plants, heat extraction from steam generators 78−37465
ocean, advective mixed-layer model with imposed surface heating and wind stress 80−12395
ocean near-surface mixing layer, microstruct. in stable heating conditions 78−85568
opaque solid slab, laser heating and burnthrough, anal. 77−48284
optimal control of heating of body with thermoelastic stress restrictions *(Ukrainian)* 78−83245
optimal control of heating of cylinder or sphere *(Russian)* 77−54857
optimal heating of solid body and stress relax. role *(Russian)* 78−22258
particle accelerator target heating by ion beam, thermal characts. *(Japanese)* 80−99374
passive solar building thermal performance modelling by passive solar test boxes, expt. 80−3494
passive solar building thermal performance modelling by passive solar test boxes, theory 80−7921
photoelectric heating of interstellar gas 78−77587
planetoids in early solar system, ^{26}Al as heat source 78−65511
planets, internal heating rel. to crustal tectonics, appl. to Moon and Mercury 78−12116
plasma rail accelerator, ambient medium heating expt. 78−75439
plate heating, two-step control *(Ukrainian)* 79−76958
plate optimal heating under constraint on temp. drop 80−102967
polar surface energy budget, stratospheric warming effect 77−66957
powder, polydisperse, heating and vaporisation in plasma stream *(Russian)* 77−59707
power supply regulating system for crystal heater using controlled electron bombardment 78−181
projector having a thermoplastic target and operator's eye, characts. 80−96023
radiant, using paraboloidal reflectors 79−97392
radiation absorbing bodies, temp. fields, Julich reactor expts., finite element calcs. *(German, English)* 77−82998
sample heating apparatus, for laser Raman spectroscopy 80−22439
semiconductors, temp. rise due to nonlinear heat generation 78−87983
soil warming, waste heat from nuclear power station 78−37463
solar, correlation between diffuse and hemispherical and between daily and hourly insolation 79−87975
solar, Czechoslovak agricultural projects *(Czech)* 79−70430
solar, domestic energy units for use in India's rural areas 79−74510
solar, domestic hot water heaters commercialisation in Florida, system sizing and economics 79−57460
solar, evacuated plate-in-tube collector, heat loss characts. evaluation, theory and expt. 79−88004
solar, hot water supply in tropical countries 79−57462
solar, hot water systems analysis and optimisation 79−57461
solar, India's 1978 development trends 79−74509
solar, methods, collector types and insolation data *(Czech)* 79−70431
solar, of mobile home, performance in Kuwait environment obs. 79−62130
solar, of public swimming pools, feasibility 79−87978
solar, of space and water, Indian development 79−62140
solar, of water, flat-plate type domestic heater, heat transfer analysis 79−62141
solar, of water for mine changing house, solar collector plant design 79−74503
solar, residential, evacuated-tube collectors, design 79−88002
solar, water heater, low-temp., tubular heat receiver, temp. distribution, heat-balance differential equation solution 79−94464
solar active region coronal loops, heating mechanism rel. to temp. and density struct. 79−8890
solar air heater, Fresnel lenses concentrator 79−74493
solar air heaters, use of porous flat plate solar collectors 80−35748
solar air heating, direct, theory and practice of heating strategies in Denmark 80−66945
solar atmosphere, electrostatic ion-cyclotron heating 80−51708
solar atmosphere, mechanical heating of outer layers *(Italian)* 78−32431
solar atmosphere, shock heating and chromospheric boundary layer structure 79−53788
solar atmosphere upper layers, heating by convective noise waves dissipation in mag. struct. 78−65600
solar chromosphere, shock heating 77−29745
solar chromosphere heating, acoustic shock waves dissipation and H^- radiation 78−96454
solar chromosphere models, short period acoustic heating theory appl. *(Italian)* 78−85926
solar collectors appl., standards establishment 80−7915
solar collectors for space and water heating systems 80−66943
solar corona, heating by ion acoustic waves 78−4181
solar corona, influence of heating on coronal holes physical struct. 80−46520
solar corona, insufficiency of energy released by mag. fields interaction 77−17482
solar corona, plasma heating by anomalous current dissipation 78−53895
solar corona, rapid heating rel. to collisionless cond. front prod. and hard X-ray bursts 79−44427
solar coronal loops, heating by Alfvenic surface waves reson. absorpt. 79−16905
solar coronal loops, heating processes rel. to thermal instabilities in magnetically confined plasmas 80−36600
solar domestic water heating systems, in Great Britain design and economic aspects 80−40835
solar energy appl., availability, Swiss meas. and collectors efficiencies *(German)* 79−48092
solar energy storage system, ammoniated salt heat pump using $MgCl_2$, $CaCl_2$, NH_4Cl 80−81484
solar energy systems, Conf., San Francisco, CA, USA, (Dec. 1978) 79−83635
solar flares heating, significance of temp. min. region struct. in flares 79−12458
solar heating and cooling systems, computer program validation methodology 80−35742
solar heating system, air-based, sizing phase-change energy storage units 80−7922
solar heating system components, optimal insulation, numerical sensitivity anal. 80−35745
solar heating systems simulation *(French)* 79−92063
solar impulsive flares, adiabatic heating 78−93176
solar powered Rankine cycle system, 18-ton, analysis and design 79−52897
solar powered residential water heating 80−61311
solar quiescent corona, heating and dynamics 78−40885
solar radiation geometric Brownian distribution, implications for economical solar heating system 79−83571
solar radiative heating, in presence of aerosols 79−16665
solar system, for industrial plant, located in Southern Europe 79−62131
solar system optimisation, using continuous flow control 79−62127
solar water, flat plate system with thermosyphonic flow, investigation 79−70464
solar water heater, collector/storage, performance anal. 79−70432
solar water heater, dynamic response prediction 79−62139
solar water heater development, polyethylene, low-cost *(Afrikaans)* 80−7925
solar water heater/steam cooker, design and trials 79−66402
solar water heaters, aluminium alloy rolled-welded heating panels production and use 79−96421
solar water heaters, rural population demand fulfilment 80−89668
solar water heating, freeze-tolerant heater using crosslinked polyethylene 80−66944
solar water heating models comparison 80−30387
solar wind, deposition of momentum and energy by MHD waves 77−37493
solar wind He ions superheating and superacceleration 80−12631
solar wind heating and acceleration, implications of coronal fast waves evanescence 78−89147
solid, by hot air stream, transient heat transfer 77−42705
solid bodies, optimum heating conditions, calc. *(Russian)* 80−14543
space solar furnaces, for materials-science expts. 80−108786
space vehicles, optimum body conformation for radiative heating along a prescribed trajectory 79−80189
spacecraft atmospheric entry, body shape for minimal radiative heat inflow *(Russian)* 78−77457
spectrophotometric research of solutions, in UV and visible range, high-temperature cell and heating block design 80−31899
stellar chromospheres, short period acoustic wave heating mechanism *(German)* 80−109421
stellar chromospheres of late type stars, acoustic wave heating and temp. minima heights 78−20818
stellar cores, heating and mixing by core He flash with two-dimensional convection 80−105230
stellar coronae, heating and mechanisms and energy balance 79−44466
supersonic heat source, sound radiation 78−1688
surface and absorption heating in US field in liquid medium *(Japanese)* 77−72110
surface waves, parametric excitation, heating effect 78−67209
tensile test specimens, furnace for up to 1400°C 80−3265
thermosphere, solar and auroral heating rel. to zonal mean circulation vars. 78−32262
topside ionosphere, electron heating rates during medium solar activity 77−70919

heating continued
universe, dissipative heating by collisional neutrinos in chaotic cosmology 77−57112
upper atmosphere, energy fluxes propagated by diurnal oscills. 77−37473
upper atmosphere, heating by solar wind energy 77−37471
urban heating patterns, satellite temp. meas. appls. 78−65393
USA solar heating and cooling R&D programme 79−57373
vaporisation of plate, thermal pulse shape effects *(Russian)* 77−54858
waste disposal appl., urban, viability assessment *(Spanish)* 79−57419
water heating system, solar, technical and economic anal. 80−50936
X-ray binary stars, X-ray heating effects on absorpt. line vel. curves 77−29878
Zircaloy cladding, internally pressurized, effect of temp. nonuniformity on diametral expansion during transient heating in steam 79−30920
^2H-^2H molten-salt-cooled fusion reactor blankets, nuclear heating and radiation leakage 78−78490
$LiNbO_3$, radiation induced heating by thermal neutrons, meas. of temp. 79−4337
UO_2, LMFBR fuel, mechanical response to transient heating, HCDA conditions 77−14237
W foil, integral heating by msec laser pulses *(Russian)* 77−59824

heating, buildings *see space heating*

heating elements
see also electric heating
Argonne/GA TNS Tokamak reactor supercond. ohmic heating coil design 79−31197
C-CD based control system for Si cryst. growth 78−68623
cermet, sintering, optimum conditions for electric heating elements 77−90287
double helix vacuum resistance heater element design and construction details 78−49839
double-exposure collector system for solar water heating 79−62070
flat plate solar water heater performance comparison 79−62062
forced-circulation solar water heater analysis and expt. 79−62043
implosion heating coil, radially fed, design, fabrication and appl. 78−55006
microwave diathermy, circularly polarised direct contact applicator design and performance 78−7531
nonevacuated compound-parabolic-concentrator solar heating prototypes 79−62105
oxidizing furnace design, for integrated optics processing 78−9461
packed-bed absorbers for solar air heaters 79−62041
parallel connected ohmic heating coil for double Tokamak fusion reactor 78−54930
pipe-and-fin solar water heating plate material economy 79−62050
single crystal diffraction, heating device construction 78−74116
solar air heater buoyancy and tube inclination effects 79−62058
solar air heater cost-effective optimum design 79−62039
solar air heater transient model 79−62042
solar collector-cum-storage water heater transient behaviour model 79−62088
solar flat plate collector heater yields, computation and expt. 79−62101
substrate heater, for sputtering system 79−69983
Tokamak ohmic heating coil design and testing 79−32806
USA demonstration solar heating and cooling collector thermal performances 79−62059
Al_2O_3-$MoSi_2$, for use as heating element, fabrication method and prop. *(Japanese)* 79−95989
Cr, powder, plasma deposition for production of contact portions of cermet electric heating element 78−11364
Fe-Cr, Fe-Cr-Al(Si) film heaters, lifetimes for 800 to 1000°C temp. range 78−215
Fe-Cr-Al, oxide films, SEM obs. 77−16738
$La_{1-x}Ca_xCrO_3$, for high temp. furnaces *(French)* 77−52524
SiC, heater, miniature, for thermo-emf meas. 79−2764
SiC heating elements for elec. furnaces, elec. cond. 79−69510
SiC, high density, development for heating elements using planning method 77−12584
SiC, resistance meas. instrument 77−71349

heavily doped semiconductor materials *see heavily doped semiconductors*

heavily doped semiconductors
see also degenerate semiconductors; superconducting semiconductors
amorphous, switching effect, anomalous temp. depend. 78−26927
antiferromagnetic, stability of canted order 77−12095
antiferromagnetic Faraday light depolarisation in mixed mag. states 80−29726
Auger coefficients 79−19606
band gap narrowing, physical mechanisms 80−15478
bound states in a random potential 77−47762
carrier Debye screening length, temp. depend. 80−88504
cluster model of impurity states 80−20117
compensated, hopping photoconductivity 79−38130
compensated, phonon drag effect in disordered media 77−24576
compensated piezoelectric semiconductor, sound absorpt. coeff. calc. *(Russian)* 79−15194
conductivity electrons and elastic scatt. by static inhomogeneities *(Russian)* 80−29375
degenerate, complex dielec. function 79−90982
density of eigenvalues, localisation, general disordered system 78−56109
density of states at band tail 80−80154
density of states tail in heavily doped closely compensated semicond. 78−47689
disordered semiconductors, recomb. radiation spectrum *(Russian)* 79−4855
Einstein relation for semiconds. with Gaussian band tails 80−80270
electrical conductivity of disordered systems, tight binding approx. in Kubo formalism 79−60778
electron activity coeffs., for electrons with small effective mass 77−39837
electron density dependent ordering parameter and role in elec. prop. anomalies *(Russian)* 77−43582
electronic sp. ht. and transport coeffs., influence of band-tail parameters 79−14941
electroreflectance, electroreflectance and complex interband dielec. function 80−40088
far IR absorption 79−95787
ferromagnetic, degenerate, surface magnetisation 77−8385
ferromagnetic, elec. field response and electrofluctuation instability *(Russian)* 78−56083
ferromagnetic semiconductor with defects, exchange Hamiltonian 79−82777
film, laser irradiation, spontaneously broken gauge symmetry 79−47531
flicker noise in terms of number fluctuation model, surface effects 79−60882
p-GaAs:Zn, diffusional doping, photoluminesc. in mag. field 77−16384
heavily doped, dislocation vel., electronic effects 77−11547
hopping cond. activation energy, percolation method 80−70703
hopping conduction, role of ionic screening 79−65488
III-V semiconductor, pressure volume characts. nonlinearity, intervalley electron redistrib. 77−8012
impurity bands, overlapping electronic orbitals, theory 78−56102
impurity bands, review of expt. results 79−95367
impurity states, optical and transport props. review 79−47039
n-InSb, highly doped, transverse magnetoresistance in strong mag. field 79−56246
interimpurity radiative recomb. 78−31253
laser diode, spontaneous emission linewidth, calcs. 77−10927
lifetime profile measurements in heavily doped emitter structures using electron beams 80−15538
light scattering from single-particle electronic excitation, long range fluctuations in impurity pot. effects 80−93356
magnetoconductivity, effect of resonant phonon-plasmon coupling 80−24954
materials science developments, appl. to thermoelectric heat pumps 80−35713
metal-insulator transition pretransition range anal., screening model 80−6724
n-type, disordered mag. system, hierarchy of exchange interactions 80−80235
n-type, in MOS structs., gate biasing elec. field rel. to charge carriers 78−52092
n-type, Mott transition, dielec. enhancement and conduction electron screening, unified treatment 78−72073
narrow band semiconductor, transport phenomena electron energy spectrum *(Russian)* 79−51616
negative magnetoresistance, appl. to heavily doped superconductors 80−107818
nondegenerate strongly doped compensated semicond., electron props. *(Russian)* 77−11839
paramagnetic, linear response functions and magnetoresist. 77−51770
perturbation potential distrib. and density of states 79−47052
phonon inelastic interband scatt. in transport effects 77−43552
photoemission lineshapes of impurity levels, p-wave resonance 80−76154
piezoelectric, magnetised heavily doped semicond., hybrid mode parametric excitation 80−29427
piezoelectric semiconductor, effect of strong doping on sound attenuation 80−2120
piezoelectric semiconductor, n-type, laser beam modulational instability 79−99570
polyacetylene:AsF_5, heavily doped, transport props., evidence for metallic state 79−87121
polyacetylene, pure and heavily doped, optical and IR studies, electronic struct. calcs. 80−7347
polyacetylene film, heavily doped with AsF_5, conductivity and Hall effect meas. 79−28353
recombination radiation, long wavelength, from heavily doped, compensated semiconductors 80−7403
scattering mechanisms resist. and Hall coeff. maxima 80−75586
Schottky barrier, tunnel effect theory, impurity ion random field contrib. 77−43727
semiconductors, scatt. influence on Auger transition, depend. of impact ionisation on electron energy 80−44608
semiconductors with position-dependent band gap and electron affinity, current densities 77−85210
static conductivity in terms of transport relax. time 79−56213
static electrical conductivity due to many-centre scatt. 80−2374
thin epitaxial layer surface As concentration meas. 79−95037
transparent heat reflectors *(German)* 78−79197
transparent-emitter devices, analytical treatment 79−96444
wafer, influence of discontinuous resist. distrib. on results of four-point probe method meas. 77−39841
n-ZnSe:In, highly compensated, freq. depend. of cond. 79−99548
α-AlB_{12}, heavily doped, elec. props. 78−10446
$Cd_{1-x}Ag_xCr_2Se_4$, Ag acceptor states effect on exchange interaction 80−20397
Cd_3As_2, band struct. from Shubnikov-de Haas and de Haas-van Alphen effects 80−49597
Cd_3As_2, highly doped, Shubnikov-de Haas type oscills. in optical transmission 79−61352
p-$CdCr_2S_4$, single cryst., elec. cond. 79−15148
CdS, amorphous antiferromagnet model, susceptibility and spin-flip Raman scatt. meas. 80−97057
CdS, heavily doped compensated piezoelectric semiconductor, sound absorpt. coeff. calc. *(Russian)* 79−15194
CdS:Cl, heavily doped, fluoresc. spectrum upper threshold calculated 78−52568
CdS:Cu, dye-sensitised, photocond. and photocurrent decay time obs. 80−6893
CdS:Cu, US absorpt. in heavily doped piezoelec. semicond. 79−11189
CdS:Cu(Se)(Zn), heavily doped, defect struct. 78−22756
CdSe, heavily doped compensated piezoelectric semiconductor, sound absorpt. coeff. calc. *(Russian)* 79−15194
p-$CdSnAs_2$, Hall effect, thermo EMF, thermomagnetic effects 80−107822
p-$CdSnAs_2$, heavily doped, elec. transport props. under elastic deformation 80−96915
CdTe:Cl, defect interactions, elec. and photoluminesc. investig. 77−39603
CdTe:In, electron-hole liq. form., luminesc. spectra 80−10884
CdTe:In, lightly- and heavily-doped, cathodoluminesc., temp., injection level and freq. depend. 78−52584
Eu chalcogenides, heavily doped mag. semiconductors, effect of carriers statistics on indirect exchange 77−69280
$EuB_{6-x}C_x$, Mossbauer spectra, cond. electrons effect 80−20545
EuO(S):Gd, indirect exchange 78−23264
$Ga_{1-x}Al_xAs$:Si, Si determ., spectrochem. method, photoluminesc. spectra, Hall effect meas. *(German)* 77−77851
n-GaAs, absorption tails in surface depletion layer and bulk 78−64379
GaAs, ballistic electron motion at room temp. 80−80360

heavily doped semiconductors continued
GaAs, band gap, magnetoabsorpt. oscills. obs. 78−18960
n-GaAs, coupled plasmon-LO phonon modes, Raman scatt. meas. 78−60472
GaAs, density of states, spontaneous emission rate calcs., 120, 160, 200K 77−4292
n-GaAs, density of states tail in heavily doped closely compensated semicond. 78−47689
n-GaAs, epitaxial, ionised donor pair spectrum 77−63477
GaAs, heavily doped, electron effective mass, Kane equation calcs. 79−77989
GaAs, heavily doped, fluctuation-induced tunnelling cond. 80−65516
GaAs, heavily doped electron mobility due to scatt. by pot. fluctuations 80−2387
GaAs heavily doped n-type layers, formation by multiple ion implantation 80−59491
n-GaAs, impurity-band cond., DC cond., Hall mobility, and magnetoresist. meas. 80−49733
n-GaAs, intrinsic luminescence intensity, effect of 0.94, 1.0, 1.2 and 1.3 eV radiative centres 78−23517
GaAs, luminesc. emitted by deep centres, illumination-induced change in internal quantum efficiency 79−91495
n-GaAs, luminescence emitted from deep centres, γ-irrad. induced changes in internal quantum efficiency 80−20701
GaAs, migration of liquid inclusions, effect of DC current and temp. 77−7910
GaAs, n-type layers, heavily doped, formation by multiple ion implantation 80−88187
n-GaAs, non-linear extrinsic luminesc., role of Auger recombination 79−52010
p-GaAs, self energy of phonons 80−44277
GaAs, strongly compensated, hopping cond. 79−47180
n-GaAs, test of cond. band edge random fluctuations by MCD 77−63438
n-GaAs, with Gaussian band tails, modification of Einstein relation 80−80270
GaAs:Fe, static magnetis. rel. to doping method and heat treatment conditions 77−36092
GaAs:Ge film, MBE grown, heavily doped, elec. props. rel. to growth parameters 80−100537
GaAs:Se cathodoluminescence decay obs. with SEM and streak camera, 90 to 300K 80−97348
GaAs:Si, epitaxial layers, photo- and cathodoluminesc. 77−77285
GaAs:Si, hardening by solute-vacancy pairs 77−4794
n-GaAs:Si, ion implanted and/or annealed, As vacancy form., photolum. line 77−27875
GaAs:Si, thick LPE layer growth and characterization 77−12511
GaAs:Si defect density before and after Zn diffusion, SEM and TEM obs. 80−96529
GaAs:Sn, 1.39 eV luminescence, injection level depend., freq. response and thermal quenching 78−19529
n-GaAs:Sn, nonalloyed and in situ Ohmic contacts for FETs 79−56307
n-GaAs:Sn, nonalloyed ohmic contact form. by MBE and metallisation 79−7895
GaAs:Sn, selective LPE, orientation dependent growth, luminesc. 77−12551
GaAs:Te, heavily doped degenerate semicond., Kondo effect 79−61053
GaAs:Te, heavily-doped, annealing-induced prismatic dislocation loops and elec. changes 78−51546
n-GaAs:Te, interband luminesc. intensity, heat treatment effect 78−72593
GaAs:Te influence of fluctuations of impurity pot. on Burstein-Moss effect 78−48240
GaAs:Zn, heavily doped, photolum. obs., above gap 80−29796
p-GaAs:Zn, Raman scatt. by LO phonon-plasmon coupled modes, wave vector non-conservation 80−16033
n-GaAs-$Ga_{1-x}Al_xAs$, heavily doped superlattice, electronic props., perpendicular low temp. mobility 80−65660
GaN:Zn, heavily doped, photocond. spectra 77−72887
p-GaSb, LO phonon-carrier interaction, Raman interf. lineshapes 80−93319
GaSb, migration of liq. inclusions, effect of DC current and temp. 77−7910
n-GaSb, spontaneous radiative recomb., complete vel. and radiative capacity 79−11458
n-GaSb:Te, heavily doped, electron-hole recomb., photoluminesc. spectra 78−84644
p-GaSb:Zn, hole transport props. from 77 to 300K 79−73530
GaSb-InSb solid solns., heavily doped, electronic props. 77−80727
GaSe, space-charge-limited currents at different temps. 77−43607
p-Ge, anomalous magnetoresist. under uniaxial compression *(Russian)* 79−33302
Ge, gamma irrad. above threshold, defect formation impurity ionisation mechanism 80−6433
n- Ge, heavily doped, extrinsic sp. ht. in metallic regime 78−59956
Ge, heavily doped, far IR props. of shallow impurity states 79−95786
Ge, heavily doped, microcreep breakdown 80−97549
Ge, heavily doped, multiplex AC hopping conduction 79−11122
Ge, heavily doped, vacuum hot-pressing thermal and electrical props. 77−40400
Ge, heavily doped, vacuum hot pressing, effect on thermal and elec. props. 80−25594
Ge, heavily doped and compensated, photoluminesc. exam. 78−2902
Ge, heavily-doped single cryst., macroinclusions, annealing in elec. field 77−47474
Ge, lattice disorder influence on optical spectra in interband transition region 79−43006
n-Ge, negative magnetoresistance model, spin-up spin-down electron effective mass variations 79−95423
n-Ge resistance thermometer material for 14 to 300K *(Russian)* 80−49731
p-Ge, self energy of phonons 80−44277
Ge:Al, limiting solubility, rel. to charge carrier conc. 80−24596
Ge:Al, solid solns. decomp. 80−15249
n-Ge:As, heavily doped, luminesc. from electron-hole drops 77−81144
n-Ge:As closely compensated, photolum. of charge carriers localised in trails of density of states 77−77294
Ge:Ba, heavily doped, second phase inclusions on melt growth 78−22751
p-Ge:Ga, elec. resist., 40 mK to 300K 79−38071
Ge:Ga, heavily doped, structure defect evolution during heating *(Russian)* 78−43026

heavily doped semiconductors continued
p-Ge:Ga far IR absorption and photoconductivity obs. 77−39899
Ge:metal, polycrystalline film, electron transport props. 79−99642
Ge:Sb, anomalous magnetoresist., metallic impurity cond., down to 5 mK 79−65502
Ge:Sb, heavily doped, mass anisotropy, and multiple scattering effects 80−107802
Ge:Sb, heavily doped, scatt. of electrons 77−59283
Ge:Sb, heavily doped semicond., scatt. mechanism, resist, and Hall coeff. maxima 80−75586
Ge:Sb, limiting solubility, rel. to charge carrier conc. 80−24596
Ge:Sb, low temp. anomaly of impurity cond. 79−95428
Ge:Sb, solid solns. decomp. 80−15249
Ge:Sb(As), experimental data anal. 77−35933
Ge-Si alloys, n-type, phosphorous doped, precipitation effects due to heat treatment 80−107833
Ge-SiO_2-p^+Si tunnel junctions, for determ. of AC cond. of amorphous Ge 77−24608
H-like impurity wavefunction overlap effect on optical absorpt. spectrum 77−8613
α-HgS, green cathodoluminesc., impurity effects 78−2924
α-HgS, natural, yellow emission 78−68567
InAs, Burstein-Moss effect and near-band-edge luminesc. 79−47525
InAs, migration of liq. inclusions, DC current and temp. effects 77−7910
N-InAs, Moss-Burstein effect, S, Sn, Te dopants 78−64389
InAs:Mn, NMR, magnetoresist., Hall effect and mag. susceptibility meas. 78−26888
n-InAs:Te(Sn), heavily doped, cathodoluminescence, doping effect on luminesc. band position and spectral profile 80−45153
$In_xGa_{1-x}As$, epitaxial solid soln. film, spectral depend. of transparency, absorpt. spectra calcs. 80−45161
InN film, refl. and transmission spectra, band struct. 78−72625
InP:Si, pulse electron annealing, carrier activation and mobility 80−15124
InP:Sn, LPE growth from Sn soln., elec. props., 80 to 300K 79−11250
InP:Te(S), heavily doped, dislocation imaging using transmission cathodoluminesc. 80−29023
InP:Zn heavily doped X-ray topography, cathodolum., and TEM obs. 79−99197
n-InSb, compensated, LF current instabilities 79−7859
InSb, doping depend. of high-field donor spectra 77−90175
n-InSb, high press. effect on electron mobility and conc. 77−4390
p-InSb, LO phonon-carrier interaction, Raman interf. lineshapes 80−93319
InSb, morphological instability under constitutional supercooling during cryst. growth from melt and stabilising thermal gradient 79−4910
InSb:Cd, thermal conductivity down to 0.38K 80−107582
p-InSb:Cu(Zn) film, heavily doped, ionized impurity scatt., Hall effect and DC cond. meas. 79−99643
InSb:Mn, NMR, magnetoresist., Hall effect and mag. susceptibility meas. 78−26888
InSb:S(Se)(Te), reson. states and reson. scatt., elec. props. 80−49738
n-InSb:Se(Te), anomalous press. depend. of thermoelec. power 77−47840
n-InSb:Se(Te), Moss-Burstein effect, optical energy gap depend. on doping conc. 77−8581
InSb:Te, heavily doped degenerate semicond., Kondo effect 79−61053
n-PbTe-p-$Pb_{1-x}Sn_xTe$, heterojunctions, heavily doped, current-flow mechanisms 80−96974
$Se_{1-x1}Te_{x1}$-$Se_{1-x2}Te_{x2}$ heterostructure, amorphous, rectification phenomena and photovoltaic effects 79−99610
Si, 2p core levels and core exciton binding energy, photoemission obs. 78−76583
Si, amorphous, hydrogenated, small angle X-ray scatt., void distrib. 80−15087
Si, bandgap narrowing and diffusion length meas. 79−7781
Si, bandgap narrowing model in moderately to heavily doped material 79−99477
n-Si, carrier conc., comparison of expt. and theory, screening effects 77−85216
Si, carrier mobility calc., 300K 79−56215
p-Si, change of elastic const. due to presence of acceptor impurities 77−84831
n-Si, Debye temp., electronic effect 78−83901
n-Si, degenerate, density of states from elastic consts. 80−6690
Si, electronic characts., electron beam induced current obs. 78−10473
Si, excess intrinsic carrier density, deionisation of impurities as explanation 80−96864
Si, heavily doped, approx. of Einstein relation, carrier diffusivity to mobility ratio 79−65494
Si, heavily doped, bandgap narrowing 80−15479
Si, heavily doped, carrier diffusion coeff. 79−47099
Si, heavily doped, carrier recomb. through shallow donor and acceptor states 80−15535
Si, heavily doped, characts. of distrib. of density of states 79−15072
Si, heavily doped, doping density striation effects in studies of metal-nonmetal transition 79−28383
Si, heavily doped, electronic effects on dislocation velocities 77−62531
Si, heavily doped, electronic effects on dislocation velocity 77−62532
n-Si, heavily doped, extrinsic sp. ht. in metallic regime 78−59956
p-Si, heavily doped, intra- and interband Raman scatt. 79−95788
p-Si, heavily doped, intra- and interband Raman scatt. by free carriers 80−108208
n-Si, heavily doped, intraband Raman scatt. by free carriers 78−19483
n-Si, heavily doped, meas. of minority carrier transport parameters 80−15537
Si, heavily doped, microcreep breakdown 80−97549
n-Si, heavily doped, Raman phonons, interband excitation effects 78−52501
n-Si, heavily doped, self energy of phonons interacting with free electrons, Raman scatt. 78−64366
p-Si, heavily doped contact layers on IR detectors, IR transmissivity 80−108190
Si, heavily doped energy gap 77−43489
Si, heavily doped films, electromigration obs. 80−65295
n-Si, heavily-doped, EPR near metal-nonmetal transition 77−28446
Si, highly doped and highly exerted, Auger coeffs., radiative band to band recomb. lifetime meas. 77−85764
Si, ion implanted, CW laser annealing 80−92550
Si, minority carrier injection, model 77−39874
Si, minority-carrier transport parameters meas. 80−80291

heavily doped semiconductors continued
n-Si, negative magnetoresistance model, spin-up spin-down electron effective mass variations 79−95423
Si, optical constants, heavily doped crystals, Kramers-Kronig analysis 77−85676
Si, polarisation dependent electrorefl. spectra, surface phenomena 78−68479
Si strongly-doped monocrystal Josephson junctions 79−56400
p-Si, thermoelec. coeffs. meas. at semicond. solid-metallic liq. interface 77−39887
Si, transition layer form., band struct., electroreflectance 77−16333
Si:alkali metal, Si amorphous film, heavy doping by alkali ion implantation 80−2045
Si:As, heavily As-diffused, Hall mobility and resist. rel. to carrier conc. 80−107815
Si:As(B), heavy-doping effects and impurity segregation during high-press. oxidation 80−65014
Si:Au, diffusion of Au anal. 79−23786
Si:Au(Pt), heavily doped, gradual p^+-n junctions, trap levels *(French)* 80−34392
Si:B, annealing characteristics obs., Ne^+ ions implantation for damage density control *(Japanese)* 78−18666
Si:B, deep diffusion at solid solubility limits for p-channel MOS IC 78−10070
Si:B, heavily doped, paramagnetic props., anomalous hole spin susceptibility *(Russian)* 80−54861
Si:B, heavily implanted wafers, secondary defect generation suppression by HCl oxidation 78−10069
Si:B, highly-doped polycryst. thin film, growth kinetics and properties 78−44016
Si:B, photolum. of heavily doped p- and n-type 80−20708
p-Si:B-SiO_2 interface in MOS structures, carrier mobility and impurity distrib. 78−34902
Si:B(Ga), heavily doped, form of occurrence of acceptor impurities 77−11581
Si:B(Ga)(Sb), plastic deform. and formation of dislocation loops, effect of Au atoms 79−69184
Si:B(P), heavily diffusion-doped layers, Co diffusion 78−59982
Si:B(P), minority carrier diffusion coeffs. 79−99559
Si:B(P), single crysts., oxidation investigations, 780°-1150°C 79−5068
Si:H,P, amorphous, heavily hydrogenated, high gap state densities 80−49803
Si:H,P amorphous film, elec. cond., thickness and temp. depend. 80−65559
Si:In, neutron irrad. to compensate for residual B, photocond., IR focal plane array 78−67727
Si:Li, strongly doped, piezoresist., gas-liq. type transition 77−43600
Si:P, anomalous wafer bending obs. 78−10074
Si:P, characterisation by IR reflectivity 78−56501
Si:P, degenerate electron gas, Friedman effect, review 77−20242
Si:P, EPR line shift, 0.56 to 4.2K, investig. of interacting donor clusters 77−77084
n-Si:P, elec. cond. and Hall effect meas., impurity effects 78−19032
Si:P, electron-hole droplets, photolum. obs. 1.5 to 80K 77−36289
Si:P, electrostatic field on impurity atoms, heavy doping effects 78−51570
Si:p, film, polycrystalline, low press. CVD, resist. meas. 80−2494
n-Si:P, heavily depend., spin-lattice relax. at high temp. 78−39403
Si:P, heavily doped, 100 GHz ESR of impurity band 79−95631
n-Si:P, heavily doped, carrier conc., Hall coeff. and elec. cond. meas. 77−8094
Si:P, heavily doped, diffusion of Au 77−51550
Si:P, heavily doped, EPR spectra of electron irradiation induced defects 77−81008
Si:P, heavily doped, electronic sp. ht. meas., rel. to metal-nonmetal transition 78−6162
Si:P, heavily doped, electron mobility carrier conc. relationship 79−65470
Si:P, heavily doped, glow-discharge-produced, elec. and optical props 80−2497
Si:P, heavily doped, IR bound-exciton luminesc. spectra 78−15211
Si:P, heavily doped, influence of impurities and crystalline defects on electron mobility 79−78095
Si:P, heavily doped, mag.-field depend. of sp. ht. 80−29183
Si:P, heavily doped, sp. ht., calc. using AMO-MT scheme for impurity bands 79−95182
Si:P, heavily doped, thermal oxidation 78−56793
Si:P, heavily doped semicond., scatt. mechanism, resist, and Hall coeff. maxima 80−75586
Si:P, heavily ion implanted, polycrystalline, grain growth 79−19477
Si:P, high dose implantation, outside dislocation generation 78−87672
Si:P, ion-implanted, carrier conc. reduction caused by wet O_2 oxidation 80−10565
Si:P, metallic region, resist. decrease due to ESR 77−16178
Si:P, origin of photoluminesc. 79−56856
Si:P, paramagnetic spin susceptibility 79−78306
Si:P, polycrystalline, thermal oxidation in wet O_2 78−92376
Si:P, sp. ht. near metal-nonmetal transition, generalized Matsubara-Toyozawa theory 79−73321
Si:P, strongly compensated, temp. depend. cond. meas. down to 1K 77−72865
Si:P, thermal cond., electron-phonon interaction at low temps. 80−92730
Si:P film, polycryst., heavily doped, mobility and carrier conc., optical determ. 80−66314
Si:P heavily-doped, photoluminescence 78−72572
p-Si:P implanted films, piezoresist. stress tensors, ion dose depend., −80 to 120°C 80−100538
Si:P(As)(B)-SiO_2 interface oxidation kinetics, high doping levels, experiment 80−11828
Si:Sb, in solar cell struct., heavily doped, dopant striation, SEM 79−39312
Si:Sb, TEM obs. of impurity effects in dislocation motion 77−43220
p-Si-Ge, heavily doped, hot pressed, high temp. phonon thermal cond. *(French)* 78−43190
Si-Ge, heavily doped vacuum hot-pressing, thermal and electrical props. 77−40400
n-Si-Ge, phonon thermal cond. of hot-pressed alloy, 300-1100K 78−91494
Si-Ge:Al, B, P, hot-pressed alloy, thermoelec. props. 78−91711
Si-Ge:As,P, heavily doped, electron scatt., Hall coeff., Seebeck coeff. and resist. meas., 4-300K 77−4379

heavily doped semiconductors continued
Si-SiO_2 interface oxidation kinetics, high doping levels, theory 80−11827
SiC LEDs prepared by overcompensation method, photon assisted tunnelling 80−97341
SiC:N, conversion factor at high doping levels 78−22744
SnO_2:SB,X, X=Fe,Cu,S, CVD thin film, resist. temp. coeff. 79−38198
Te:Sb, impurity state and impurity cond., press. effect 80−54723
Te:Sb, impurity states and impurity conduction, hydrostatic pressure 80−39521
TiO_2, chemical implantation of 10-keV H^+ and D^+, resist. and optical absorpt. expts. 77−59031
$V_{1-x}Ga_xO_2$, phase transitions, semicond. metal transition, antiferromag. props. 77−11969
ZnS:Mn^{2+}, heavily doped, anomalies in reflectivity 77−20891
ZnSe, donor-acceptor pair emissions charact. *(French)* 80−108249
ZnSe:In, heavily compensated, galvanomag. props. and thermopower 79−51600
ZnSe:In, heavily compensated, negative magnetoresistance 79−91079
ZnSe:In, heavily doped, Hall effect and DC cond. expts., compensating acceptors 78−52013
n-ZnSe:In, heavily doped, high field DC cond. 79−65490
ZnSe:In, impurity band cond., Hall coeff. and cond. expts. 78−72147

Heaviside layer *see E-region*

heavy ion excited X-ray emission *see ion microprobe analysis*

heavy ion-nucleus reactions
for inelastic heavy ion-nucleus scattering, see "heavy ion-nucleus scattering"
^{40}Ar, fragmentation in collisions at 213 MeV/nucleon, energy and isotope distrib. 79−17919
A=70, heavy-ion induced fission-evaporation reactions, magnetic substrate distribs., nuclear alignment 80−73857
absorption effects in low energy heavy ion fusion reactions 78−8851
alpha-transfer reactions, between 1p or 2s-1d shell nuclei, targets with A=10, 12, 14, 16, 20 *(Japanese)* 78−4962
analytic hydrodynamic model for expanding fireballs 78−41745
angular momentum dissipation of fragments, using Fokker-Planck equation 79−36260
barrier-top resonance and heavy ion reactions 77−38291
baryonic inclusive spectra in hadron-, photon- and HI-nucleus collisions, fireball model 80−86892
book, current perspectives 80−27049
cascade evaporation model of high energy nucleus-nucleus reacts. *(Russian)* 78−46107
central asymmetric heavy-ion collisions, moderate energies, hydrodynamical and phenomenological models 80−5164
central high energy heavy ion collisions, possible finite particle number effects, p spectra 80−99181
charge and slope polarisation of nuclei, liquid drop model anal. 79−9543
charge distribution in heavy ion-reactions 78−74304
charge equilibrium and mass transfer, liquid drop model 79−97722
charge equilibrium model using collective high freq. mode and quantal master eqn. 80−27667
charge exchange and knock-out at relativistic energies, Glauber's theory 77−23101
charge exchange reactions, review 77−57690
classical many-body model for heavy ion collisions nuclear binding energy and density 78−66302
classical many-body model incorporating Pauli principle 77−54236
classical microscopic calcs., 117 and 300 MeV/nucleon 77−54250
classical microscopic description of particle cluster collisions 79−9533
cluster correlation, review, book contrib. 80−27670
cluster transfer, shell model investig. 77−14172
clustering aspects of nuclear struct. and nuclear forces, review 79−80887
α-clustering studies, of role of angular correl. anal. 78−634
coherence angle and cross section fluctuations correlation function, resonances 80−57790
coherent and statistical features 78−41771
coherent pion prod. in high energy heavy ion collisions, pion laser 80−73856
coherent rotational states formed in heavy ion collisions, γ-decay 80−27657
cohesion of nuclear matter in heavy ion collisions 78−66314
cold matter at super-nuclear densities including pion condensates 78−17128
collective modes in fission and deep inelastic scatt., ang. momenta equilib. statistical treatment 80−42688
collective paths in adiabatic time dependent Hartree Fock theory 78−525
collective pot. energy surfaces, appl. to Ar+Ag, Kr+Cu, and Xe+Bi 78−41748
collective structure inferred from heavy ion Coulomb excitation 80−5167
collective transition average lifetimes, spin (30-50) region in heavy ion-nucleus reactions 78−89822
colliding ion system, projectile nucleon mean free path, nuclear matter approach, Pauli blocking 80−86920
collision dynamics 79−71868
collision expts. with final state partial resolution, maximal entropy procedure and surprisal anal. 80−18279
collision integral in nuclear matter at zero temperature 79−17928
collisions and microscopic theory, conference 78−563
complete fusion anal. for heavy ion reactions 79−49643
complete fusion cross sections, compound nucleus props. *(French)* 79−577
complete fusion in heavy-ion collisions 80−37400
complex nuclear collisions, quantum description of friction, phenomenological ansatz 80−18340
complex nuclei collisions, scatt. by schematic pot. landscape 77−26782
complex nuclei interaction, generator coordinate method, microscopic treatment 78−66304
composite nucleus scission, fusion and strongly damped collisions, rot. energy, boundary diffuseness 80−102224
composite particle emission in relativistic heavy ion collisions, firestreak, and coalescence model 79−80952
composite particle formation, direct, classical thermodynamic and quantum statistical theories 80−32297
composite-particle interactions, nuclear cluster theory, computational procedures 79−13225
compound nuclei, Z=98, 100, 102, statistical description of (heavy ion, xn) cross section *(Russian)* 78−86549

heavy ion-nucleus reactions continued
compound nuclei prod. in (HI, xn), lifetimes with account of fission process *(Russian)* 78−25233
compound nucleus, relatively cool, with high ang. momentum, production *(Russian)* 78−29519
compound nucleus formation, review 77−14173
compound nucleus formation cross section in heavy ion reactions, shell model calcs. 78−13132
compound reactions, critical ang. momentum effects on high spin selectivity 79−36272
compound reactions, high-spin selectivity, critical ang. momenta determ., spectroscopy 77−54238
compound reactions, spectroscopy, obs. of high-spin states 77−14176
compound-nucleus cross sections from nuclear charge-density distributions 79−9605
compressed zone evolution in high energy nuclear collisions, pion characts. 79−26447
compression and speed of sound in nuclear matter 80−27584
conference, Les Houches, France (July-August 1977) 79−71864
conference, Varenna, Italy (July-August 1974) 77−14169
conference on heavy ion reaction dynamical props., Johannesburg, S.Africa (Aug. 78) 80−17715
conference on nuclear interactions, Canberra, Australia (Aug.-Sep. 1978) 80−4476
conference on nuclear physics, Mikolajki, Poland (2-14 Sept. 1979) 80−101662
conservative force between heavy ions, temp. depend. 77−30624
continuous γ-ray spectra anal. 78−41747
continuum γ rays, multipolarity, enhanced ang. correlation meas., heavy ion-compound nucleus reactions 78−93963
continuum shell model description of resonant structures in nuclear reactions 79−13345
continuum states spectroscopy, narrow resonances 77−54240
conversion electron spectroscopy following (HI,xn) reacts., kinematic Doppler correction method 79−54739
cool compound nucleus formation with oriented heavy ions, ^{258}104 and ^{260}106 prod. 80−99179
cosmic ray nonrelativistic nuclei interactions with emulsion nuclei, fast doubly-charged particles form. 79−80175
cosmic ray nucleus-nucleus interactions, search for hydrodynamic effects 79−80176
cosmic ray reactions, 0.1 to 1.0 GeV/nucleon, characts. of peripheral and central collisions 77−61448
cosmic ray reactions, meson generation 77−61446
cosmic ray reactions, multiplicity distrib. of particles *(Russian)* 79−5719
cosmic ray-nuclear emulsion collisions, ~20 GeV/nucleon, mean meson multiplicity and ang. distribs. 79−58988
cosmic ray-nucleus, complete target fragmentation, shock waves 77−61447
cosmic rays, features of nucleus-nucleus interactions at energies around 10^{12} eV 79−80173
Coulomb energy dissipation in reactions with heavy ions 79−76014
Coulomb excitation, classical limit S-matrix 77−3036
Coulomb fission prompt component, model including rot. states and vibr. motion 79−67783
Coulomb interactions, heaviest nucleon systems, heavy ion experiments at UNILAC *(German)* 78−66435
Coulomb matrix elements, semiclassical approx. including distorting nuclear potentials 77−57640
Coulomb terms in optical model DWBA 77−10431
Coulomb-nuclear interf. in rot. state excitation, ^{40}Ar+^{238}U appl. 77−14151
coupled channel Born approximation code, OUKID, finite range heavy ion direct reactions, appls. 78−89832
coupled rotational bands in even-even nuclei, model 80−27529
Cr ^{130}Te+^{28}Si, diffusion model anal. of onset of friction 78−8848
critical electron state wave function calc. 80−57796
critical scattering and pionic instabilities in heavy ion collisions 78−21586
cross-sections for fusion, quasifission and deep inelastic collisions *(Russian)* 78−54801
damped collisions, interaction times 78−637
damped-heavy-ion collisions, book contrib., review 78−82388
damping, complete 78−21588
damping mechanism approach via elementary excitation modes, polarisation expt. anal. 80−18338
damping of shape oscillations and relative motion 77−3038
Darmstadt heavy ion beam, research and appl. *(German)* 77−67955
deep inelastic, ang. distrib. statistical fluctuation effect 77−14093
deep inelastic and high energy reactions, fragmentation cross section 80−78259
deep inelastic collision, high lying vibrational and incoherent excitations, simultaneous treatment 79−36256
deep inelastic collision cross sections, ang. momentum coherence 79−54451
deep inelastic collision processes, optical model description, statistical considerations 80−68687
deep inelastic collisions, angular momentum dissipation within a classical friction model 79−93644
deep inelastic collisions, classical model with friction and deformation 77−30633
deep inelastic collisions, dispersion around mean classical path, effect on polarization of fragments 79−17891
deep inelastic collisions, dissipative processes, Feynman's influence functional method treatment 80−57789
deep inelastic collisions, dynamic model based on linear response theory *(Russian)* 79−80954
deep inelastic collisions, evolution within ang. distribs. 78−86544
deep inelastic collisions, general form of cross-section 78−13131
deep inelastic collisions, interaction times and transport coeffs. *(Chinese)* 80−42693
deep inelastic collisions, kinetic energy dissipation, nuclear matter density oscillations *(Russian)* 80−37397
deep inelastic collisions, microscopic descript., excitation of surface vibr. modes 78−46085
deep inelastic collisions, reln. to quasi-fission 78−13144
deep inelastic heavy ion collision, shape relaxation and fragment deformation 80−22683
deep inelastic heavy ion collisions, charge and mass distrib. variances, time depend. 79−97651
heavy ion-nucleus reactions continued
deep inelastic heavy ion collisions, light particle emission, dissipation mechanism 78−50191
deep inelastic heavy ion collisions, mass and charge distribs., statistical model 80−18332
deep inelastic heavy ion collisions, quantal theory of Brownian motion, collective vibrs. 79−67774
deep inelastic heavy ion collisions, relax. phenomena anal. 78−13156
deep inelastic heavy ion collisions, statistical fluctuations, quantal effects, l-window 78−89895
deep inelastic heavy ion collisions, unified model, collectivity and statistics, coupled channel eqns. 78−66320
deep inelastic heavy ion reactions, doorway mechanism 78−632
deep inelastic heavy ion reactions, fast light particles and heavy ejectile ang. correlation 80−57791
deep inelastic heavy ion reactions, high multipole isovector modes and charge fluctuations 80−57793
deep inelastic heavy ion scatt., one body dissipation mech. 78−62567
deep inelastic processes, large scale collective motion in nuclear matter 80−5087
deep inelastic reaction, neutron excess degree of freedom relaxation model *(Chinese)* 80−102202
deep inelastic reaction products, rot. energy contribs. to kinetic energies 77−10425
deep inelastic reactions, γ-ray multiplicity, partial ang. momenta *(Russian)* 80−37346
deep inelastic reactions, as probes of nuclear matter, review 78−46083
deep inelastic reactions, charge equilibration 79−49635
deep inelastic reactions, Coulomb and nuclear forces effects on double differential cross section pattern 78−70560
deep inelastic reactions, energy dissipation and angular momentum transfer 78−41679
deep inelastic reactions, particle transfer, excitation of collective surface vibrs., in damping processes 78−70555
deep inelastic reactions well above Coulomb carrier, hydrodynamical and scatt. mechanisms 77−14174
deep inelastic scattering, fragment nuclides distribs., neutron rich nuclei prod., diffusion model 78−58297
deep inelastic transfer, decay of binary nuclear system 80−22848
deep inelastic transfer production high above Coulomb barrier, reaction mechanism 77−14179
deep inelastic transfer reactions, between complex nuclei, review 78−74400
deep-inelastic reactions, zero-point motion of surface vibr. 78−82372
deeply inelastic, random matrix model anal. 78−33213
deeply inelastic, random matrix model based transport theory, 1-dimens. model 79−49633
deeply inelastic collisions, form factors determ. within statistical model 78−50205
deeply inelastic collisions, phenomena, transport theoretical approach 78−46086
deeply inelastic heavy ion collisions, ang. momentum transfer from sequential fission 80−18333
deeply inelastic heavy ion collisions, charge transfer ang. momentum depend., fragment kinetic energies 80−47505
deeply inelastic heavy ion collisions, helicity representation, quantum mechanical cross section 80−47506
deeply inelastic heavy ion collisions, transport eqn. strong coupling effects 80−52693
deexcitation process, fast rotating nuclei, yrast traps 79−71786
deflection function, effect of nuclear vibr. mode and orientation 79−59080
deformations described by density moments 77−41883
deformed and superdeformed nuclei from heavy ion reactions, α-decay amplification 80−102156
delayed fission produced in synthesis induced by heavy-ion beams and neutron currents *(Russian)* 79−89341
dense nuclear matter, construction in lab., book contrib. 80−490
density compression in colliding nuclear slabs 78−642
density isomer formation in high energy heavy ion collisions, 3-dimens. fluid dynamical calcs. 79−49578
density isomers in high energy heavy ion collisions, hydrodynamical model anal. 79−36138
diffractive semi-optical model for nucleus-nucleus collisions *(Russian)* 79−63646
diffuse surface nuclear and Coulomb pot. energies 77−18593
diffusion model, KE, mass, angular distribs. and γ-ray multiplicities 78−54789
direct heavy ion transfer reactions, single and multi-step direct reaction anals. 80−5166
direct reactions and scatt., multi-step processes, asymptotic and peripheral regions 78−50190
direct transfer reactions, DWBA approach review 79−49614
dissipation, mass exchange, microscopic time-scale 78−8853
dissipative collisions, ang. momentum transfer, review 80−13501
dissipative collisions, dynamical description in adiabatic representation, statistical theory 80−5161
dissipative forces, phenomenological determ. of strength 77−71619
dissipative heavy ion collisions, nuclear dynamics 80−42696
dissipative heavy ion collisions, transport equation for microscopic Wigner functions 79−13329
dissipative heavy-ion collisions, doorway concept and relative motion 80−86925
distorted waves method, finite radius of interaction, reaction mechanisms *(Russian)* 80−52647
doorway states, energy dependence of inelastic cross-section, shell model, coupled channel anal. 80−73854
double nuclear cluster system in heavy ion deep inelastic collisions 79−6438
double nuclear intermediate system, deform. by classical model 79−6699
double transfer reaction model, Buttle-Goldfarb approx. 79−6677
double well-cluster shell model, spurious states of cm motion during heavy ion reactions *(Chinese)* 77−14045
DWBA, simplified for heavy ion induced transfer reacts. at high energies 79−93643
DWBA amplitude, strong absorpt. model, effect of ang. momentum depend. pots. 79−85486
DWBA computer program for heavy-ion transfer reactions 78−50145
DWBA form factor for heavy-ion transfer reactions 79−13322
DWBA integrals, evaluating strategies for computation 80−86863
DWBA method for transfer reactions, residual interaction 77−41995

heavy ion-nucleus reactions continued
dynamical properties, field overview 80−18327
dynamical props. from coupled channels calcs. total, direct and fusion cross sections 79−67772
dynamics of heavy-ion reactions 77−41996
dynamics of statistical fluctuations in heavy ion collisions, collective approach 77−14092
effective nucleus-nucleus pot., generator coord. method 78−13139
elastic and quasi-elastic polarised heavy ion collision theory, semi-quantal description 80−18330
emulsion nuclei+^{12}C, 2.1 GeV/nucleon, fragmentation parameters 77−3027
emulsion nuclei+^{14}N, 2.1 GeV/nucleon, fragmentation parameters 77−3027
emulsion nuclei+^{16}O, 2.1 GeV/nucleon, fragmentation parameters 77−3027
energetic heavy ion beam model for radiobiology 80−26293
energetic heavy-ion collisions, noncharact. radiation, prod. mech., differential cross section 78−4963
energetic reactions, relativistic hydrodynamical description 80−37362
energy density formalism of heavy-ion interaction pots. using Fermi type nucleon density distrib. 77−67758
energy dependent structure, review, book contrib. 80−27671
energy dissipation and the stochastic process in heavy-ion collisions 80−106040
energy dissipation in heavy-ion collisions 80−106038
energy loss and ang. distribs., dissipation mechanism, hydrodynamic model 79−3175
entrance-channel coherence in dissipative heavy-ion collisions and compound-nucleus formation 79−49639
equations of motion in Ehrenfest's theorem for heavy-ion collisions 79−17916
equations of motion with nuclear absorption in heavy ion collisions, optical model 79−6684
equilibration in nuclear collisions of high energy, microscopic study 79−93598
exact finite range DWBA form factor for heavy-ion induced nuclear reactions, calc. program adaption 80−9271
exact finite range DWBA overlap integral parametrization 80−68693
exchange effects in nuclar collisions, DWBA calcs. 78−46084
exchange effects in nucleus-nucleus interactions, antisymmetrisation effects 79−36271
excitation function meas. using beam time saving technique 78−70721
excitation functions using Fermi gas model 77−18602
excited nuclear levels, polarisation induced by at. orientation 80−91144
expanding fireball in high energy heavy ion reactions, pion radiation 80−5155
experimental methods of heavy ion physics for radiation detection and meas., review *(Russian)* 79−49900
experimental progress, illustrated by JINR results *(Russian)* 77−50145
fast α-particle emission, anal. of radial friction 77−38296
fast heavy-ion collisions, compressed nuclear matter classical microscopic calc. 77−10432
Fermi Gas model, nuclear response function and dissipation 79−40955
Fermi system particle distrib., nuclear matter, heavy ion collisions and fission 79−36183
Fermidynamics and time dependent Schrodinger-Hartree Fock theory 79−3105
few nucleon transfer reactions, proton pairing and four nucleon correl., reaction kinetics *(French)* 79−557
fireball model, low energy bremsstrahlung cross sections in relativistic heavy-ion collisions 77−54253
fireball model, pion and nucleon total differential cross-sections 78−17241
fireball model for heavy ion collisions, statistical theory 79−6556
fireball model for proton inclusive spectra, heavy-ion collisions 77−6339
fireball model of relativistic heavy ion reactions, chemical equilibrium relations 79−22262
fireballs in high energy heavy ion collisions, hydrodynamical description 78−58294
firestreak model calcs. for relativistic heavy-ion reactions, particle spectra 79−568
fission, saddle point, statistical fluctuations, Suzuki's scaling limit 80−86946
fission fragment angular distrib., shape of saddle point of compound nucleus *(Chinese)* 78−78427
fission induced by heavy ion-collisions, fragment ang. distrib., reaction mech. 78−74412
fluid dynamical and TDHF models, abnormal nuclear matter, density isomers 80−47502
folding calcs. and density depend. interactions 78−8852
form factors for one- and two-nucleon transfer reactions 77−46188
formation and disintegration of high-density nucl. matter 77−10423
fragmentation of relativistic heavy ions 77−82946
fragmentation theory, two body breakup channels in fission, fusion, heavy ion scatt. 78−46037
fragments from heavy ion deep inelastic processes, element identification in ΔE-E telescope, computerised method 77−57839
friction and nucleus-nucleus interaction pot. 78−8850
friction force in heavy ion+nucleus reactions, gas-kinetic model 77−30621
friction model for fusion and deep inelastic reactions, review 78−86546
frictional effects in nuclear reactions with large scale collective motion, review 78−78336
fusion, classical model, empirical nucleus-nucleus potl. 77−74870
fusion, expt. data comparison with classical trajectory models, review 80−9324
fusion, heavy ion induced, yrast lines versus entrance channel limitation 78−89929
fusion, internuclear potential determ. 78−41800
fusion, schematic classification of nuclear processes *(Rumanian)* 78−58313
fusion, sensitivity to friction form factor, dissipative and conservative properties 79−67807
fusion and damped reactions, rolling friction, nuclear pots., classical trajectories 80−78312
fusion and deep inelastic scatt., shape degrees of freedom, classical dynamic model 80−22876
fusion and transfer reactions, resonance effects 80−9283
fusion barrier at sub-Coulomb energies 78−628
fusion barrier of heavy ion collisions, penetrability calc. 78−41798
heavy ion-nucleus reactions continued
fusion barriers calc., microscopic folding estimate 78−25225
fusion channel separation *(Russian)* 77−74880
fusion cross section, energy depend., nuclear matter density distrib., depend. 80−47519
fusion cross section at sub-Coulomb energies, effective pot. barrier 78−58314
fusion cross sections 80−86913
fusion evaporation react., nucl. lifetime meas. using γ-γ coincidence techniques 79−59318
fusion excitation functions, dynamical model, one-body friction 78−50224
fusion reaction excitation function anal., nucleus-nucleus pots. 80−42728
fusion reactions, charge density asymmetry liquid drop model 80−63220
fusion reactions, critical angular momentum phenomenological approach 78−33203
fusion reactions, statistical and liquid drop model anal. 78−66312
fusion reactions, statistical model calcs. 80−42726
fusion reactions, statistical yrast line 80−86948
fusion reactions in fragmentation theory 77−54239
fusion-evaporation, phenomenological restrictions for spin alignment attenuation factors 77−57686
gamma spectroscopy, in heavy ion induced reactions *(Rumanian)* 78−58300
gamma-ray multiplicity in (heavy ion, xn) reactions, higher moments 77−18604
gamma-ray spectra anal., interactive computerised system 79−9509
gamma-ray spectroscopy, nuclear shape and reaction mechanism *(French)* 79−560
generalised master eqn., drift and diffusion coeffs. 80−106075
giant E1 mode, energy broadening in heavy ion reactions 79−30815
Glauber approx. anal. of high energy heavy ion collisions 80−106039
ground-state correlations observable in hard heavy-ion reactions 78−78406
growth points in nuclear physics, book 80−94929
hadron chemistry, heavy ion collisions 78−82389
hadronic mass spectrum from high energy nuclear collisons 78−33049
hadronic matter chemical equilibrium, statistical model for heavy ion collisions, nuclear fireball 79−40948
head on heavy ion collisions, compression and temp. extremes, nuclear matter phase changes *(Russian)* 80−83121
heavy ion national accelerator Ganil, principle and expected performances *(French)* 79−696
heavy ion optical model, surface transparency and resonance phenomena 79−9617
heavy ion transfer reactions 80−5165
heavy ion-light particle angular correlation, forward peaked, light particle emission from l-windows 80−63142
heavy relativistic nuclei, interaction cross section and scatt. phase shift *(Russian)* 78−89908
heavy-ion detector system, low-energy, A≤30, TOF spectrometer and ΔE-E telescope 77−65380
heavy-ion peripheral fragmentation, direct reaction model 78−8847
(HI,πX), 125-400 MeV/N, low energy 0° pion prod., charge ratio 80−95324
(HI,X), inclusive one- and two proton spectra by statistical model 79−93624
(HI,X), rare earths, deeply inelastic transfer reactions, kinematic anal. 80−99186
(HI,xn), cranking model for E1 polarization charge in rotating nuclei 79−85405
high amplitude oscillatory states and external fields, in heavy ion interaction and fission *(Russian)* 79−97650
high density isomeric state in nucleon matter relativistic heavy-ion collisions 79−85390
high density matter, relativisitc quantum many-body problem 78−4909
high density nuclear Mach shock waves, central heavy ion collisions, compressed nuclear matter, meson condensation 78−46089
high energy, current trends *(Hungarian)* 80−57786
high energy collisions, review of four theoretical methods based on classical approx. 79−89326
high energy collisions, theoretical overview 80−42682
high energy collisions of heavy nuclei, Glauber rescatt., Reggeon field theory 78−37369
high energy cosmic nuclei+emulsion nuclei collisions, cross sections, multiplicity distribs. 78−41744
high energy heavy ion collisions, comparison of models, appl. to U+Ne→p+X 78−46088
high energy heavy ion collisions, hydrodynamic and classical microscopic descriptions 78−54791
high energy heavy ion collisions, single nucleon knockout, DWIA formalism 80−99165
high energy interactions of nuclei, review 79−22326
high energy interactions of nuclei, review book contrib. 79−22161
high energy interactions of nuclei, single particle inclusive spectra 78−46087
high energy internuclear reactions, multiple collision theory *(Russian)* 78−94028
high energy nuclear collisions, isobaric-gas model, shock waves, temp., density, pionisation 78−94022
high energy nucleus+nucleus studies at Berkeley Bevalac, expt. data, theoretical predictions 77−50144
high energy reactions, use in nuclear struct. studies 79−45286
high excited nuclear matter, p-wave π absorption, high energy heavy ion appls. 79−93542
high spin state radiative decay in Australian nuclear physics review 77−88021
high spin state studies, (n,γ) complementarity 80−37381
high spin states and band coupling, theory and heavy ion expts. *(Russian)* 80−18160
high-energy collision, cumulative effect anal. *(Russian)* 77−67759
high-energy heavy-ion collision, model 78−33207
high-spin selectivity of heavy-ion compound reactions 80−5048
high-spin states, means and methods of investig. 78−86722
highly dense nuclear matter, formation by relativistic nucleus-nucleus collisions 79−97675
hot compressed zone stability and temp., liquid drop model 80−78316
hot nuclear matter, eqn. of state determ. 79−93538
hot nuclei with high angular momenta, γ-ray emission in heavy ion reactions, rot. bands 78−13133

heavy ion-nucleus reactions continued
hydrodynamic and time-depend. HF calcs. comparison for nuclear matter slab collisions 77−18598
hypernuclei production cross section in relativistic reactions *(Russian)* 79−45298
idealized, one-body dissipation, general classical theory, quantal corrections 78−86494
in-beam spectroscopy, selective population of high-spin states in $1f_{7/2}$-shell 77−18374
inclusive production of hadrons in high energy nucleus+nucleus collisions, scaling laws 78−33204
inclusive production of hadrons in particle-particle collisions at high energies, scaling low 78−54656
inclusive quasielastic d prod. in heavy ion collisions, quasiclassical description 79−6695
inclusive reactions, fragment momentum distrib., from Glauber approx. *(Chinese)* 80−99185
inelastic collisions, heavy ion-light particle angular correlations, sequential three-body reaction 80−42677
inelastic collisions of light nuclei and nucleon-nucleus collisions, dynamical model *(Russian)* 80−37356
inelastic reactions, differential cross section from helicity representation *(Russian)* 80−86924
influence functionals in heavy ion deep inelastic scatt. 78−62565
inner shell excitations, multistep processes, quasimolecular model, coupled channels calc. 80−9303
interaction pot. calc. by Ericson statistical model and ^{252}Cf fission data *(Russian)* 78−41765
interaction potential between magic nuclei, Skyrme interaction energy functional, microscopic and proximity pots. 78−62556
intermediate energy collisions, elastic scatt., Coulomb excitation, nucleon transfer, expt. facilities, models 79−6697
intermediate struct. and nuclear reaction reson. states in continuum shell model 77−54243
intermediate structs. from heavy ion excitation functions 78−13147
ion beam induced reactions for surface anal., UV vacuum sample chamber 77−4970
ion-ion cross section, Pauli principle effects in impulse approx. 80−47500
ion-ion interaction pot., real part energy depend., antisymmetrization effects, Fermi gas model 80−83120
ion-ion interaction pots. and barriers, energy density functionals simple parametrisation 79−93658
ion-ion pot., energy depend. from simplified energy density method, folding model combination 79−6429
ion-ion proximity pot. radial depend. test using fusion excitation functions 80−22859
isobaric distributions in deep inelastic reactions, collective model and independent particle model 80−18270
isospin symmetric nuclear matter, pion condensation, heavy ion collision appl. 80−9252
isovector pairing vibrations, in two nucleon transfer ion-nucleus reactions 78−21487
Israel Physical Society 1980 annual meeting, Rehovot, Israel (April 1980) 80−94909
K-matrix theory, method for compensating for neglected open channels 78−13039
K-shell ionization in heavy-ion collisions, book contrib. 78−82834
large deformations and dissipation in a random-matrix model approach for fission or colliding nuclei 80−18162
large scale collective motion in very heavy ion reactions, macroscopic description 80−5049
large-amplitude collective nuclear motion in fission and heavy ion reactions 80−22675
light heavy ion induced fusion, cross sections and yrast line limitations 80−5192
light heavy ion total reaction cross sections in diffraction model, resonance oscillations 80−13503
light heavy-ion systems, fusion cross section variations, nuclear proximity pot. 80−57815
light nuclei, α-transfer reactions, spectroscopic factors, exact finite range DWBA anal. 80−13372
light nuclei, alpha transfer reactions, review, book contrib. 80−68699
linear response approach to heavy ion deep inelastic collisions, dissipation, quantal fluctuations 78−46043
liquid drop model generalisation *(Rumanian)* 78−58260
long-range heavy-ion potential induced by multiple Coulomb excitation 80−13496
low energy one-neutron transfer reactions between heavy ions, optical model potential 79−45294
magic nuclei, real part of nucl.-nucl. interaction anal. 77−6426
magnetic spectrograph for very heavy ions 79−31315
magnetic spectrometer of Van de Graaff tandem for heavy ion induced reaction study *(French)* 79−707
Markovian and non-Markovian effects in transition probabilities at 10-200 MeV/N 80−102175
mass asymmetry as collective coord. in Hartree-Fock calcs. 79−17914
mass distribution, struct. limitations, time depend. Hartree-Fock calc. 79−30852
mass transfer, kinetic energy, comparison with hydrodynamic and microscopic calcs. 80−57787
mass transfer asymmetry due to valley fragmentation 77−71616
mass transport in nuclear collisions, nucleon exchange, drift and diffusion coeffs. 79−563
mass transport theory, transport coeffs. including ang. momentum 78−58302
massive transfer in heavy ion reactions on rare-earth targets, α-γ coincidence 78−70556
meson condensation and two photon emission in hadron capture by nuclei and heavy-ion collisions 79−3109
microscopic description of nuclei collisions, GCM and RGM framework, appl. to $^4He+^4He$ 77−34272
microscopic theory of collisions between complex nuclei based on generator coord. method 78−13145
microscopic transport theory, fragment shell struct. effects on mass transfer 78−58301
model defining strength function shape, applic. 77−302
moderately deformed nuclei, high-spin states studied in (heavy ion, xnγ) reaction 77−14180
molecular orbital interpretation of $\Delta l=1\hbar$ transfer anomaly in heavy ion collisions 77−82952
molecular reson. in heavy-ion scatt. 78−62561
molecular resonances 78−13148
multi-step amplitudes, variational approach, exact T-matrix and DWBA amplitude differences 79−3167
multichannel direct resonance and heavy ion reactions, exactly solvable model *(Russian)* 79−67732
multifragment decay reactions induced by heavy ions, mica track detector study 78−17234
multipion production, π^- multiplicity distrib. and $\pi^-\pi^-$ correlation function, collective phenomena search 79−85485
multiple angular correlation between many quanta in coincidence, populated by heavy ion reactions 79−36193
multiple collision model anal., at high and relativistic energies 78−86542
multiple Coulomb excitation of deformed heavy nuclei, uniform semiclassical theory 78−8840
multiple Coulomb excitation of heavy ions, semiclassical S-matrix integral representation 78−630
multiplicity distrib. nonlinear phenomena from high energy nucleus-nucleus collisions 79−6685
multiplicity distribution, shape, and low-fold coincidence probabilities 78−54779
multiplicity distributions of charged π in 2 GeV/nucleon ^{12}C, ^{16}O induced reactions in nuclear emulsions 78−66297
multiplicity measurements, statistical algorithm 78−29721
multistep multinucleon transfer, grazing collisions, quantal theory 79−6698
N=50 isotones populated in heavy-ion beam reactions, mag. moments, proton core polarisation 78−21598
narrow structure obs. in continuum, quasi-bound states, shell model anal. 77−14175
nearly head-on heavy ion collision, centrality parameter for intermediate energy 80−22856
neutron ang. distrib., compound nucleus decay, fission fragment anisotropy *(Russian)* 80−5160
nonlocal Hamiltonians, scatt. solns. in terms of generalised Bessel Neumann series 80−57752
nonresonating light systems expts. 79−9622
nuclear dynamics, TDHF and ATDHF, nuclear vibrs., heavy ion collisions and Fermi hydrodynamics 79−67696
nuclear level shifts, generalised relativistic Coulomb problem *(Russian)* 80−52586
nuclear matter, use of heavy ion beams in expts. *(French)* 80−78182
nuclear matter flow, Fermidynamics and commensurability; TDHF restructured into TD-S-HF 79−93539
nuclear matter overlap integral calcs. in diffuse surface model 79−17821
nuclear microprobe, two dimens. scanning, appl. to light element mapping 77−81447
nuclear pion prod. with heavy ions, statistical approach, pion interferometry 79−85487
nuclear pionisation phenomena, collision between relativistic nuclei *(Russian)* 79−6696
nuclear structure, conf. 78−50059
nuclear structure determination in heavy ion collisions 79−54446
nucleon emission from localised hot zone, fireball model 80−42686
nucleon transfer in light+heavy ion reactions, classical statistical model 78−58304
nucleon transfer reactions, effective Q-value model 79−63692
nucleon transfer reactions, symmetry effects 77−54241
nucleon tunnelling model of mass diffusion in deep inelastic heavy ion collisions 78−78409
nucleus+nucleus interaction potential, microscopic approach to real and imaginary parts calcs. 78−37372
nucleus-nucleus collision, new approach to antisymmetrisation and rearrangement 77−2956
nucleus-nucleus collisions, fragmentation velocity, source vel. mass independ. correlation 78−93979
nucleus-nucleus collisions, inelastic, at GeV energies, search for shock waves *(Russian)* 77−338
nucleus-nucleus collisions, Reggeon model for inclusive interaction *(Russian)* 78−45985
nucleus-nucleus interaction pot. using energy dependent delta interaction, Skyrme interaction folding 79−36269
nucleus-nucleus interactions, existence of slowly moving sources, vel. depend. frictional sources 79−6690
nucleus-nucleus pot., static polarisation effects, nuclear shapes 80−5154
nucleus-nucleus total cross section energy depend. 80−106071
odd-A $1f_{7/2}$ nuclei, high spin states, shell model analysis 78−62560
one body dissipation and super viscidity of nuclei, nuclear fission, collisions and deformation 78−86501
one-body dissipation, linear response approach 77−57681
one-dimensional cascade model of interacting nuclei using Glauber theory 78−17233
optical pot. contrib. from coupling to vibrational states 79−67726
optical pot. real part, new effective N-N interaction in folding model 77−18505
optical potential, real part, effective pot. using folding models 78−70499
optical potential, real part, folding technique 80−73830
optical potentials, energy and ang. momentum dependence 77−57692
optical potentials, real part calc. by classical inversion procedure 78−89892
orbiting quasimolecular system, nuclear-surface-wave interpretation 80−86914
p and π inclusive cross sections, non-equilibrium processes 79−40947
parameter free model of strongly damped collisions, mass and charge variance 78−62568
parastatistics with continuous order, possible description 77−71572
parity dependence in heavy ion scatt. 78−4957
particle production, Fermi motion versus collective tube model 79−93659
Pauli blocking on exchange and dissipation mechanism 80−42684
Pauli correlations in collisions at high energies 78−21593
Pauli principle and absorption in heavy ion reacts. 78−50188
peripheral, semiclassical time-independ. formulation in three-dimens with complex trajectories 80−27605
peripheral heavy ion reactions, nucleon exchange model for nuclear alignment 79−89323
peripheral model, single-nucleon transfers due to multiply charged ions 80−22850
perturbation theory of nucl. friction, strong energy damping 77−67766
phase transitions and shock waves in nuclear matter 79−49594
phenomenological nuclear friction mechanism, particle-hole excitation, nucleon exchange *(Chinese)* 80−42694

heavy ion-nucleus reactions continued
pion Bose-Einstein condensation in energetic heavy ion collisions 80−22705
pion interferometry of relativistic nuclear collisions, theory 80−32301
pion prod. and absorption in heavy ion reactions below 500 MeV 79−40952
pion production, Fermi motion effects, multiplicity distribs. and inclusive cross sections 79−93622
pion production cross-section in heavy ion collisions, pion charge depend. 80−37392
pion spectra, Coulomb distortion in final state EM interaction 80−13497
pion spectrum and polariz. operator in nuclear medium in heavy nuclei collisions *(Russian)* 80−68558
polarisation effects in heavy-ion induced reactions, dynamically deformed rot. nucleus calcs. 78−25222
polarisation in heavy ion reactions, Strutinsky model, asymptotic Clebsch-Gordan coeffs. 78−74391
polarizations in quasielastic reactions 78−37368
potential energy surface topography, fusion and deep-inelastic reactions 77−330
potential energy surfaces, binary fission, fusion, liquid drop model *(Rumanian)* 78−86547
potential model, energy dissipation heavy ions reactions 80−22849
potential-energy curves, HF calc. 77−18606
potential-energy surfaces for asymmetric heavy-ion reactions 77−50147
potentials, antisymmetrisation effects 77−18596
precompound emission inference ambiguities from excitation function anal. 79−22319
primary cosmic ray interactions with photoemulsion nuclei using satellite Intercosmos-6 *(Russian)* 78−93063
probabilistic model for deep inelastic reactions 77−71623
projectile fragmentation in nuclear emulsions at 2.1 GeV/nucleon 78−70561
promptly emitted particles in nuclear collisions, fusion nucleon spectra 80−42678
proton-proton correlations in relativistic collisions 77−88170
proximity treatment of the interaction between deformed nuclei 78−78338
QED in strong and supercritical fields 78−74193
QED in strong electric fields, test in heavy ion mol. collisions, pair reaction 78−45829
quadrupole transfer strength, deformed rare-earth nuclei, two-nucleon transfer reactions 77−336
quantum fluctuations and quantum mechanical distribs., heavy ion physics appl. 80−78264
quasi-atom concept and expts. 77−14177
quasi-elastic direct transfer reaction to continuum states, DWBA and diffraction model 80−18277
quasi-fission, focusing effect, large energy loss, classical dynamic model 77−57689
quasi-fission reaction, mass-yield distrib. theory 77−42001
quasiatoms formed in heavy-ion collisions, high energy electron emission spectra 79−3554
quasielastic collisions, time-depend. single particle method 77−34334
quasielastic heavy ion reaction, amplitude for transitions between molecular (two-center) channels 80−18322
quasifree promptly emitted nucleons, prod. mechanism and cross sections 79−71863
R-matrix theory for heavy ion transfer reacts. 78−13150
rare earth nuclei, high spin states from (HI, xn) reactions, discrete γ-transitions 80−5050
rarefaction of oblate shaped nuclear matter, hydrodynamics calcs. of heavy ion collisions 78−89894
reaction mechanism determ. using γ-ray bremsstrahlung spectra 79−76016
reaction products identifier, ΔE-E system 79−746
reaction valleys, two-centre shell model, fission and heavy-ion reactions *(Russian)* 77−82947
recoil effect, kinematics of mol. states approach to heavy ion transfer reactions 78−62557
recoil effects on transfer of one nucleon *(French)* 78−33115
Regge parametrisation of ang. distribs., of heavy ion transfer reactions 78−21592
relativistic, π^- multiplicity distribs., collective tube model 78−89902
relativistic, charged particle emission multiplicities and ang. correlations, firestreak models 80−18328
relativistic, composite particle formation in explosive nucleosynthesis 78−69678
relativistic central heavy ion collisions, spherical and linear fluid dynamical models 80−86926
relativistic collisions, four-channel unitary model 77−41990
relativistic collisions, fragment recoil momenta in double-nova model 77−54255
relativistic collisions, nuclear matter implications 77−26781
relativistic collisions, pion bremsstrahlung and critical phenomena, nuclear matter phases 80−86919
relativistic continuum mechanics for heavy ion high energy collision calcs. 79−45299
relativistic heavy ion accelerator description and applications *(German)* 78−78522
relativistic heavy ion collisions, central and peripheral, p emission patterns 80−73860
relativistic heavy ion collisions, charge multiplicity fireball and statistical model anal. 80−537
relativistic heavy ion collisions, d prod. mechanism, three models, fireball rate eqns. 80−63198
relativistic heavy ion collisions, effective nucleon numbers 80−13499
relativistic heavy ion collisions, exptl. results and theories 79−71871
relativistic heavy ion collisions, fragmentation cross sections, abrasion-ablation model, factorisation 80−78261
relativistic heavy ion collisions, pion sources, discussion 79−59086
relativistic heavy ion collisions, pion volume emission from Δ (1232) decay 79−93651
relativistic heavy ion collisions, projectile fragmentation, two step abrasion-ablation model 79−97724
relativistic heavy ion collisions, reaction mechanism and recent topics, review 80−42683
relativistic heavy ion collisions, viscous hydrodynamical model 80−5163
relativistic heavy ion fragmentation reactions, abrasion-ablation model 79−97695
heavy ion-nucleus reactions continued
relativistic heavy ion peripheral collisions, charge exchange *(Russian)* 80−37398
relativistic heavy ion processes, infinite momentum frame description 79−40944
relativistic heavy ion reaction large fragment yields, abrasion-ablation calcs. 79−45295
relativistic heavy ion reactions, 1.05-7.52 GeV, π prod., statistical interpretation 79−570
relativistic heavy ion reactions, central collisions, review 78−50195
relativistic heavy ion reactions, review of recent expt. and theoretical evidence 79−67765
relativistic heavy ion reactions, target residue mass and charge distribs., calcs. 79−3172
relativistic heavy ion-nucleus reactions, review, book contrib. 80−27672
relativistic heavy-ion collisions, nuclear matter to hot quark matter phase transition 79−3170
relativistic heavy-ion collisions, thermodynamic model for composite particle emission spectra 77−30632
relativistic heavy-ion collisions, two-pion to single-pion inclusive data ratio, pion source parameters 79−3171
relativistic hydrodynamical approach, shock compression effects *(Russian)* 79−30851
relativistic light ion collisions, two-fireball model improvements, p and π spectra 80−5158
relativistic nuclear collisions, π interferometry observation, source space time struct. 79−13324
relativistic nuclear collisions, p, d, and t inclusive energy spectra 80−63199
relativistic nuclear collisions, pulsating blobs of quark matter in hydrodynamical model 80−83122
relativistic nuclear matter, shock waves, heavy ion collision hydrodynamics 80−52602
relativistic nuclear physics, collisions of relativistic ions *(Rumanian)* 78−46104
relativistic nuclear struct. *(Russian)* 77−26788
relativistic nuclei collisions, multi-hadron prod. mechanism 80−57763
relativistic nucleus-nucleus collisions, high density nuclear Mach shock waves 78−633
relativistic nucleus-nucleus collisions, secondary particle multiplicity, multiple scatt. model 80−22847
relativistic scatt., meson and light nucl. prod. 77−71622
resonance reactions as orbiting cluster phenomena 80−47446
resonances, conference, Hvar, Yugoslavia (June 1977) 79−9614
resonances in heavy ion reactions, s-d nuclei with A=24 to 32 79−6403
resonant and non-resonant behaviour of complete fusion cross-sections 79−9625
resonating group method normalisation kernel, eigenvalue asymptotic expression 77−14082
retardation effects, Coulomb gauge calcs. 78−50211
review, book contrib. 80−27668
review of heavy ion physics undertaken with UNILAC 78−50194
review of heavy ion reactions, reaction types, reaction theories 78−74401
rotating nuclei, from heavy ion collision, high spin states instability against fission *(Rumanian)* 78−50150
rotational states, coherent, γ-decay, random quantum meas. 80−73855
rotational states, Coulomb excitation by spherical nucleus, distortion, semiclassical model 79−67620
RPA theory, time dependent, quasi-boson approx. 80−57800
s-d shell nuclei, semiempirical prediction of heavy ion reaction resonances 79−22256
saturation effects in interactive region, microscopic anal. of $^{16}O+^{16}O$ 78−89899
scaling law from ratio of c.m. kinetic energy to Coulomb barrier 77−82962
sd-shell nuclei heavy-ion reaction resonances, low level density regions, shell model 80−57757
second-order excitation in nucleus-nucleus interaction potential 79−36264
semiclassical approxs. for heavy-ion transfer reactions 78−94021
semiclassical Coulomb excitation theory, classical-limit S-matrix, orbital dynamics 78−33205
sensitivity of real part of nucleus-nucleus potential to nuclear densities 78−82291
separable approx. to TDHF calcs. in 3-D 78−74320
several nucleus transfer, nuclear struct. information 77−14171
shell model level densities in evaporation calculations 79−45241
shock wave formation, cascade evaporation model *(Russian)* 78−41766
shock wave formation in high energy reacts., cascade evaporation model 78−33215
shock wave model for heavy ion high energy collisions 79−54402
shock waves in a hydrodynamic model of central heavy ion collisions 79−40946
side peaking, DWBA anal. of ang. distribs. in quasielastic limit 77−57687
single nucleon transfer reactions, optical potential ambiguities, DWBA anal. 77−34341
single-folding models for heavy-ion pots. 77−18597
soft nuclear matter eqn. of state, from heavy nuclei central collision fireballs 80−13395
spectator-participant model 80−73861
spin rotation, high angular velocity, collective aspects of heavy ion collisions 80−78309
spin-zero particle reactions, critical ang. momentum effect on ang. distribs. 77−18607
static adiabatic cluster pots. 77−3033
static model of complete fission 78−86543
statistical γ-rays and ang. momentum alignment 79−67761
statistical fission parameters mass depend. 77−57696
statistical model for nuclei at high excitation and angular momenta 78−86523
statistical model of deeply inelastic heavy-ion reactions 78−50192
statistical thermodynamics of relativistic heavy ion collisions 79−17887
stellar interior, C burning products at const. temp. *(Russian)* 78−61722
streamer chamber study, spatial reconstruction program 79−31348
stripping and pickup reactions on closed shell nuclei, level shifts, DWBA 80−91168
strong compression effects in high energy heavy ion reactions, nuclear fluid dynamics anal. 80−18341
strongly damped collisions, classical phenomenological model 77−34333

heavy ion-nucleus reactions continued
strongly damped collisions, microscopic calc. of kinetic-energy loss in rapid stretching 77−14167
strongly damped or deep inelastic collisions, quasifission, reaction mech. characts. 77−30619
sub-Coulomb transfer reacts., DWBA analytical expressions 77−67760
supercritical fields, charged vac. and pion condensate effects 78−21600
superheavy atoms from heavy ion collisions, electronic binding energy, wave functions 78−46252
superheavy collision system, radiative processes, search for positron emission 80−63752
superheavy collision systems, positron prod., internal conversion 80−5168
superheavy element prod. in compound nucleus reaction, theoretical optimisation method 78−46103
superheavy element synthesis, using ^{48}Ca ion beam, fragmentation 77−74881
superheavy elements, collective motion, stability and prod. in heavy ion collisions 80−18169
superheavy elements, possibility of occurrence in nature 78−20407
superheavy elements, search and synthesis, review 78−50117
superheavy nuclei synthesis and properties, ^{48}Ca induced reactions 77−54242
symmetric, macroscopic potl. energy surfaces 77−14150
symmetric very-heavy-ion reactions, compound nucleus cross-sections 77−74878
tandem accelerators and nuclear phys. conf. 78−13349
target nucleon+^{6}Li potential, microscopic model with antisymmetrisation effects 78−62516
TDHF analysis, spurious centre of mass motion problem 80−102198
theoretical tools, classical analogy, dimensional anal., generator coord. formalism 77−14170
theory, incident nuclei energies up to 20 MeV per nucleon 79−71865
theory of heavy ion collisions, book 77−46189
theory of resonating group method and generator coordinate method, and orthogonality condition model 79−13226
thick targets, radiation transport computer codes 80−39180
Thomas Fermi static and dynamic theory for collective motions 77−18599
three-body breakup reacts., dynamics 78−13040
threshold pion prod., calc. of effective NN collision cross sections 77−46185
time dependent Hartree Fock description, time evolution 77−10424
time dependent Hartree Fock solns. for heavy ion scatt., wave packets to stationary waves 78−62558
time dependent HF calc. comparison with exact soln. in Lipkin model 77−18456
time dependent SCF theory 79−17932
time dependent Schrodinger eqn., alternative approx. soln. for heavy ion reactions 80−32296
time for charge equilibration in heavy-ion reactions, microscopic hydrodynamical model 78−8857
time-dependent variational approach to heavy ion reactions 78−50193
total γ-decay energy meas., selection of high spin nuclear states 79−26391
total pion prod. cross sections in high energy collisions, depend. on nucl. eqn. of state 78−41772
total reaction cross sections and elastic scatt., refractive scatt. or strong absorption 79−567
total reaction cross sections determ., review of methods 79−9624
transfer, classical dynamical theory 78−41769
transfer, fusion and deep inelast. scatt., DWBA anal. 78−13143
transfer reactions, closed form description based on distorted waves theory 80−68691
transfer reactions, DWBA including recoil effects 77−18605
transfer reactions, energy disposal, information theoretic anal., surprisal approach 80−18326
transfer reactions, new methods using particle ang. correls. *(French)* 79−558
transfer reactions, review, book contrib. 80−27669
transfer reactions, study of nuclear structure *(French)* 80−78310
transfer reacts., exact finite-range coupled-channel formalism 77−30620
transfer reacts., nuclear wave function polarisability 78−54785
transport coefficients for deeply inelastic scattering from the Feynman path integral method 79−17922
transport coeffs. for asymmetric fragmentation and generalised Einstein relns. 77−3047
transuranic elements synthesis with stable Pb targets 77−26790
tube models of multiple prod. on nuclei 78−41680
two nucleon transfer, exact finite range microscopic DWBA, FORTRAN program SATTNT 77−61449
two nucleon transfer and scatt. matrix elements from dynamic deformation theory 79−85488
two nucleon transfer reactions, exact four body model 77−10426
two spherical nuclei system, pot. energy calcs. for fission and fusion 79−13326
two-body molecular model for resonances 79−9620
two-centre problem with realistic potentials, single particle energies, wave functions 77−82887
two-centre-oscillator basis, alternative set for heavy ion processes 77−26789
two-cluster transfer reactions, in Coulomb field, classical theory 77−67757
two-nucleon transfer cross sections 77−14155
two-nucleon transfer indirect transitions, coupled channel method 77−50148
two-particle transfer, overlap functions, DWBA anal. 80−73862
two-proton transfer, anal. of direct and indirect processes for reactions on ^{64}Ni and ^{100}Mo 77−34342
unequal fragments, generator coordinate and resonating group methods 77−18490
unified description of fission and nuclear collisions *(Russian)* 78−33163
UNILAC, Darmstadt, heavy-ion research 77−67917
unitary effects in high energy nuclear abrasion 77−6425
universal fragment-momentum distrib. in high-energy collisions 77−71617
very heavy ion-nucleus collisions, struct. effects in dissipative collisions 80−57795
viscosity, quantum phenomenology 78−54298
viscosity, single-particle Schrodinger fluid 77−71577
volatile superheavy elements, synthesis and identification in heavy-ion reactions 79−45288

heavy ion-nucleus reactions continued
X(a,b)Y(c)Z, ang. correlation following sequential decay 79−93645
yrast and statistical cascades, M1 radiation after (MI, XN) reactions 80−42583
yrast isomers from delayed γ cascades in heavy ion reactions 78−8844
yrast region of rapidly rotating nuclei, instability toward nucleon emission 77−88027
yrast traps, obs. in heavy ion collisions 80−37319
Z=103, 105, 107 element prod. from heavy ion fusion, cross sections from statistical model 80−32313
zero-spin particle reactions, angular distrib. anal. 79−13342
α-particle transfer calcs., rot. excitation 77−14168
α-transfer reactions, medium nuclei, calc. of α strength factors 77−18454
α-transfer reacts. between light nuclei 78−54787
α-transfer to α-decaying nuclei 77−79396
(^{12}C,X), 3-12.6 GeV, in-beam nuclear γ-rays from Sr, Na, S, Ca 79−6483
γ-ray multiplicity, reaction mech., ang. momentum and struct. depend. *(Rumanian)* 78−89906
Π multiplicity in central nuclear collisions, standard deviation related to mean π mult. *(Russian)* 80−73864
π prod. and multiplicity at 100-250 MeV/nucleon 77−65234
π production, multiple-collision model in relativistic nucleus-nucleus collisions 78−37365
^{118}Sn+^{6}Li, α and d energy spectra, break up of ^{6}Li d+α clusters in nuclear field 78−46092
^{50}Cr(^{6}Li,pn), ^{54}Fe, mean lifetime of 6.38 MeV 8^{+} state *(French)* 79−45204
^{63}Cu+^{20}Ne, 168 MeV, gamma ray multiplicity distrib. in strongly damped oscills. 79−36266
^{68}2n(^{12}C,2n), ^{78}Kr high spin states, transitions and lifetimes 80−27534
A=12-15, heavy ion induced α-transfer α-clusters, DWBA anal. 79−26454
Ag, A=107, 9, +^{86}Kr, 618 MeV, γ-ray multiplicities and angular momentum fractionation 78−37370
Ag+^{20}Ne, 175 MeV, γ-ray multiplicities and energies, primary fragment angular momenta 78−46093
Ag+^{40}Ar, 340 MeV, binary aspects, particle multiplicities of fragments 78−70554
Ag+^{40}Ar deep inelastic reactions, γ-ray polarisation meas., neg. deflection angles 78−8845
Ag+^{63}Cu, 380 MeV, prod. of new Os and Ir isotopes 77−82961
Ag+^{84,86}Kr, 7.2 MeV/nucleon, nuclear relaxation phenomena, diffusion, orbiting 77−34338
Ag+^{9}Be, breakup of ^{9}Be in Coulomb field 78−50203
Ag+C, rarefaction of oblate shaped nuclear matter, hydrodynamics calcs. 78−89894
Ag+C(O), 0.2-4.2 GeV/N, compression phenomena and Mach shock waves 80−22851
Ag+Ne, 175 MeV, ang. mom. transfer meas. 77−30626
Ag+O, rarefaction of oblate shaped nuclear matter, hydrodynamics calcs. 78−89894
AgBr(^{40}Ar,X), 1.8 GeV, central collisions, Maxwell-Boltzmann distrib. anal. 78−66315
AgBr(^{16}O,X), 2.1 GeV, central collisions, Maxwell-Boltzmann distrib. anal. 78−66315
AgBr(^{16}O,xHeyp), 0.2, 2.0 GeV/nucleon, search for shock-wave effects 77−23102
Ag(^{12}C,X), 4.5 GeV/c, emission of short range particles (R<100 mkm) *(Russian)* 80−63202
Ag(^{12}C, spallation), 25.2 GeV, radionuclide prod. cross sections, charge dispersions and mass yield curves 79−67735
Ag(Fe,f), central collisions, nucleon characteristics, nuclear pionisation in complete fission *(Russian)* 79−80963
^{A}Ag+^{11}B, 86 MeV, A=107, 109 79−67766
^{A}Ag+^{40}Ar, 285 MeV, A=107, 109 79−67766
^{A}Ag(^{63}Cu,X)Y, A=107, 109, new Ir, Os and Re isotopes 78−70563
^{A}Ag(^{86}Kr,X), A=107,109, 620 Mev, deep inelastic scatt., ang. momentum transfer, γ-ray multiplicities 80−27665
^{109}Ag (^{40}Ar, X), α-decay amplification in superdeformed nuclei, high ang. momentum deexcitation 80−22776
^{109}Ag+^{40}Ar, 170-340 MeV, fission barriers at high ang. momenta 77−26786
^{109}Ag+^{40}Ar, 197 MeV, evaporation residue cross section calc. 78−50146
^{109}Ag+^{40}Ar, fusion excitation functions, dynamical model calc. 78−50224
^{109}Ag+^{40}Ar, reaction cross section calc. in boundary condition model 79−9656
^{109}Ag+^{86}Kr, 366-716 MeV, evaporation residue product cross sections 79−17947
Al, reactions induced by ^{12}C and ^{19}F ions, γ-ray spectroscopy of induced activities 77−23107
Al(Ne,X), 400 MeV/N, direct vs. thermal particle emission, inclusive cross sections 80−52688
Al(Ne,X), proton inclusive spectra, direct plus thermal model 80−57799
(^{27}Al,xn) with various targets, continuum γ-ray energy-depend. multiplicities 77−41916
^{27}Al (^{14}N, X), 70, 100 MeV, deep inelastic, charged reaction products ang. correlations, 3-body kinematics 80−5162
^{27}Al+^{12}C, 107, 155, 197 MeV, evaporation residue ^{39}K, prompt γ deexcitation 78−74395
^{27}Al+^{12}C, complete fusion cross sections, excitation functions *(Chinese)* 78−82406
^{27}Al+^{14}N, 100 MeV, α preequilibrium decay 79−6666
^{27}Al+^{14}N, 59 MeV, radiative capture and 1-nucleon emission cross sections 79−93652
^{27}Al+^{14}N or ^{16}O, high spin states prod in ^{35,36,37}Cl and ^{37}Ar, decay schemes 77−2932
^{27}Al+^{16,18}O, 34-81 MeV, total fusion-evaporation cross sections, fusion barrier 80−5190
^{27}Al+^{16}O, 100 MeV, fragment spin orientation meas. 77−30627
^{27}Al+^{16}O, 50-65 MeV, radiative capture cross sections upper limits 79−17923
^{27}Al+^{16}O, 60-80 MeV, fusion cross-sections 77−74898
^{27}Al+^{16}O, fusion excitation functions, dynamical model calc. 78−50224
^{27}Al+^{16}O fusion, 30-70 MeV, statistical model calcs., yrast states and continuum feeding times 79−579
^{27}Al+^{20}Ne, 120 MeV, prompt γ emission, reaction products deexcitation 78−74396
^{27}Al+^{20}Ne, 120 MeV, strongly damped collisions 77−34332

heavy ion-nucleus reactions continued
^{27}Al+^{28}Si, 72 MeV, multinucleon removal 78−41755
^{27}Al+^{32}S, 175 MeV, possible explanation for a second deep inelastic peak 79−63699
^{27}Al(^{12}C,X), 71.5 MeV, deep inelastic cross sections *(Chinese)* 79−59088
^{27}Al(^{12}C,2p), 40 MeV, ^{37}Cl high spin state decay, spin assignments, yrast level lifetime 79−6490
^{27}Al(^{12}C,αn), 27-45 MeV, obs. of ^{34}Cl high spin states 78−82289
^{27}Al(^{12}C,αn), high spin negative parity states in ^{34}Cl, lifetime meas. 78−74327
^{27}Al(^{14}N,2pn), ^{38}Ar high spin states, decay scheme 78−25232
^{27}Al(^{15}N,X), 27-70 MeV, complete fusion, total fusion cross section, entrance channel effects 80−68716
^{27}Al(^{16}O,^{12}Cα)^{27}Al, 65 MeV, pre-equilib. α-decay obs. 77−61390
^{27}Al(^{16}O,^{15}N), ^{15}N$_{3/2}$ (6.33 MeV) state, spin alignment meas. from (^{16}O,^{15}N) using γ-recoil 79−17796
^{27}Al(^{16}O,^{15}N), 36-53 MeV, reaction dynamic depend. of small angle cross sections 77−18600
^{27}Al(^{16}O,^{15}N), 96 MeV, ^{15}N 3/2$^-$ state spin alignment and polarisation, 1/2-spin orbit interaction 80−27622
^{27}Al(^{16}O,X), 88 MeV, inelastic scatt. and multinucleon transfer, Q-value depend. 80−42690
^{27}Al(^{16}O,αα), 50 and 60 MeV, ang. correl. in compound nucleus decay 79−36261
^{27}Al(^{16}O,αp), 50 and 60 MeV, ang. correl. in compound nucleus decay 79−36261
^{27}Al(^{16}O,pp), 50 and 60 MeV, ang. correl. in compound nucleus decay 79−36261
^{27}Al(^{20}Ne,^{12}C), 120 MeV, anal. of continuous spectra by multi-step direct reaction theory 79−45287
^{27}Al(^{20}Ne,^{16}O), 120 MeV, anal. of continuous spectra by multi-step direct reaction theory 79−45287
^{27}Al(^{28}Si,Xγ), 65-81 MeV, fusion evaporation products, reaction cross sections 79−17946
^{27}Al(^{32}S,X), 175 MeV, completely damped process, scissioning systems 79−93647
^{27}Al(^{6}Li,d)^{31}P, 36 MeV, absolute cross sections, ang. distribs. 79−89321
^{243}Am(^{40}Ar,f), product mass distribs., shell effect manifestation 79−93673
^{243}Am(^{49}Ca,xn), production of superheavy elements with A=114-116 78−29493
(Ar,X), in emulsion, nuclear shock wave search 80−22747
(Ar, π$^-$X), 800 MeV/A, π$^-$ energy and ang. distribs., firestreak and hard scatt. model anal. 80−13498
Ar+Au, 285 MeV, ang. distrib. of fission and deep inelastic products 77−82964
Ar+Th, 388 MeV, deep inelastic reactions, double differential cross section calc. 78−8856
Ar(HI,X) 0.2-4.2 GeV/N, nonperipheral collisions, forward-backward asymmetry, compression phenomena 80−18329
^{36}Ar(^{6}Li,d), 17 MeV, ^{40}Ca α-spectroscopic factors, direct α-stripping, zero range DWBA anal. 79−45157
^{36}Ar(^{6}Li,d)^{40}Ca, 0$^+$ levels of ^{40}Ca, DWBA calcs. with optical model parameters 78−62571
^{36}Ar(^{6}Li,d)^{40}Ca, 17 MeV, alpha transfer to 4p-4h states 78−21590
^{38}Ar(^{6}Li,d), location of 0$^+$ 4p-2h and 6p-4h configs. in ^{42}Ca 78−25220
^{38}Ar(^{6}Li,d), wave functions of O$^+$ states in ^{42}Ca 78−74308
(^{40}Ar,X), 160-280 MeV, ^{149g}Tb production in deep inelastic transfer reactions, fragment ang. momentum 79−30854
(^{40}Ar,X), 222-340 MeV, A=116-197, charged particle emission, early collision evolution, fission and evaporation cross sections 80−106072
^{40}Ar+^{12}C 205 MeV/nucleon, ^{28}Ne and ^{35}Al fragment obs. 79−22314
^{40}Ar+^{164}Dy, evaporation residue prod. depend. on excitation energy of compound nucl. 78−21607
^{40}Ar+^{243}Am, 214-300 MeV, fusion-fission reaction, asymm. mass distrib. 77−82963
^{40}Ar+^{27}Al, 340 MeV, energy relaxation and mass transfer *(French)* 80−95327
^{40}Ar+^{40}Ar, 250-1000 MeV/N, intranuclear cascade calcs. for multiplicity and cross sections 80−32300
^{40}Ar+^{58}Ni, 280 MeV, coincidence meas. of deep inelastic collisions 78−33206
^{40}Ar+^{58}Ni, deep inelastic collision at 280 MeV, fragment energy and spin 78−21599
^{40}Ar+^{58}Ni, triple differential cross-section, dynamical model calcs. 78−50212
^{40}Ar+^{58}Ni system, high energy, compound nucleus form. and deep inelastic scatt. *(French)* 79−559
^{40}Ar+Au→^{A}Z+X, 500 MeV/nucleon excited nuclear matter prod. 77−50154
^{40}Ar+various nuclei, negative pion production, 0.4-2.1 GeV/nucleon 78−37364
^{40}Ar(^{9}Be,3n), meas. of ^{46}Ti lifetime by γ-γ coincidence techniques 79−59318
As neutron deficient isotopes (A=68,69,70,71), production in heavy ion reactions 77−38292
Au+^{12}C, 25 GeV, momentum transfer to target fragmentation products 79−6691
Au+^{12}C, 25.2 GeV, target residue mass and charge distribs. 77−74873
Au+^{86}Kr, 724 MeV, coincidence meas., pre-equilibrium α-emission 78−33208
Au(Ar,X), 227 MeV, ang. momentum transfer in deep inelastic collisions 79−45281
Au(^{63}Cu,X), 365 and 443 MeV, ang. momentum transfer in deep inelastic collisions 79−45281
Au(^{86}Kr,X), 724 MeV, deeply inelastic, ^{4}He, ^{1}H emission, fragment spin, semiempirical method 80−47366
^{147}Au(^{40}Ar, f), 340 MeV, H and He emission, rapid energy equilib., to ang. distribs. 80−86936
^{197}Au +^{86}Kr, 618 MeV, γ-ray multiplicities and angular momentum fractionation 78−37370
^{197}Au+^{129,132,136}Xe, near interaction barrier, charge asymm. equilibrium 78−8843
^{197}Au+^{136}Xe, 1064 MeV, fragment spin orientation from continuum γ-ray anisotropy meas. 80−22853
^{197}Au+^{136}Xe, 979 MeV, quasi-fission, charge and ang. distribs., secondary fission of products 77−46193
^{197}Au+^{136}Xe, recoil range distribs. of heavy mass products in deep inelastic reacts. 78−66309

heavy ion-nucleus reactions continued
^{197}Au+^{16}O, 140, 315 and 33600 MeV, isotope yields and cross sections 77−14161
^{197}Au+^{16}O, 140 and 315 MeV, energy depend. of heavy ion peripheral reactions 78−74399
^{197}Au+^{32}S, 373 MeV, in-plane ang. correls. between α and residue heavy ions 78−46101
^{197}Au+^{40}Ar, 217 MeV, fusion and deep inelastic collision, charge and mass anal. 77−82959
^{197}Au+^{40}Ar, 220 MeV, nucleon transfer reactions *(Russian)* 78−33219
^{197}Au+^{40}Ar, deep inelastic reactions, isotopic distribs., n excess degree of freedom relaxation 80−9308
^{197}Au+^{63}Cu, quasifission, strongly damped collisions, 365, 443 MeV, mass and kinetic energy distribs. 77−34337
^{197}Au+^{6}Li, 75 MeV, γ-rays form α and d fragment transfer 78−86545
^{197}Au+^{86}Kr, 620 MeV, diffusion model anal. 77−10427
^{197}Au+^{9}Be, breakup of ^{9}Be in Coulomb field 78−50203
^{197}Au+Ar, 183-248 MeV, fusion and deep inleastic collision, influence of bombarding energy 77−82958
^{197}Au+Kr, recoil range distribs. of heavy mass products in deep inelastic reacts. 78−66309
^{197}Au(^{A}Xe,X), A=129, 132, 136, damped collision, proton and neutron exchange correlations 80−18335
^{197}Au(^{A}Xe,X), A=129, 132, 136, <787 MeV, light and heavy fragment N/Z ratios 80−32292
^{197}Au(^{132}Xe,X), damped collisions, charge distrib. second moments and giant E1 quantal fluctuations 80−27547
^{197}Au(^{132}Xe,X), neutron multiplicities 80−57797
^{197}Au(^{14}N, xn), in flight mass separation of Rn isotopes 78−25381
^{197}Au(^{14}N,X), 85-115 MeV, cross sections, preequilibrium α-particle emission 80−42680
^{197}Au(^{14}N,n), DWBA anal. above Coulomb barrier 80−86917
^{197}Au(^{16}O,Cα), ang. correlations between react. products 78−8849
^{197}Au(^{16}O,X), colliding heavy ion interface, nucleon emission, fusion and strongly damped collisions 80−86922
^{197}Au(^{16}O,p)X, 315 MeV, high energy p emission, fireball and preequilibrium anals. 80−91194
^{197}Au(^{19}F,^{12}B), 186 MeV, deeply inelastic, direct processes and continuum cross sections 79−80951
^{197}Au(^{20}Ne, spallation), 8.0 GeV, cross sections and target residues, model comparison 80−68630
^{197}Au(^{20}Ne,X), 110 MeV, C, N, and O isotopic yields and energy spectra meas. *(Russian)* 79−9612
^{197}Au(^{20}Ne,X), exactly central heavy-ion collisions by nuclear hydrodynamics 80−68690
^{197}Au(^{22}Ne, f), 178 MeV, α-particles and fission fragments, spectra and cross sections *(Russian)* 80−91203
^{197}Au(^{22}Ne,αX), 178 MeV, max. α-particle energy at forward angles 80−68698
^{197}Au(^{32}S,X), 373 MeV, α and heavy ion out-of-plane correlations 79−76021
^{197}Au(^{40}Ar,X), 222, 340 MeV, fusion cross sections, direct and evaporative p and α prod., evaporation, fission 80−13518
^{197}Au(^{40}Ar,X), 240 MeV, fragment shape deformation in deep inelastic collisions 80−47365
^{197}Au(^{40}Ar,X) 259 MeV, differential recoil range distributions, large contrib. of deep inelastic processes 78−70565
^{197}Au(^{63}Cu,X), 400 MeV, neutron multiplicity in deep inelastic collisions 80−18324
^{197}Au(^{63}Cu,X), 9.6 MeV/A, quasi elastic, deep inelastic and fission like ang. distribs. 80−18334
^{197}Au(^{6}Li, X), 75 MeV, Z=1 or 2 fast particle prod. mechanism above Coulomb barrier 80−42687
^{197}Au(^{6}Li, xn+yp), 48-156 MeV, excitation functions 77−18603
^{197}Au(^{6}Li,xn), 75, 85, and 95 MeV, K X-ray multiplicity 79−76019
^{197}Au(^{7}Li,α)^{200}Hg, 12 to 20 MeV excitation, ang. distrib. of evaporation residues, determ. of Γ_n/Γ_f 77−61451
^{197}Au(^{84}Kr,X), 9.6 MeV/A, quasi elastic, deep inelastic and fission like ang. distribs. 80−18334
^{197}Au(^{86}Kr, X), 730 MeV, heavy fragment coincidences, sequential fission probability 79−22316
^{197}Au(^{86}Kr, X), γ-ray multiplicities from diffusion model with one body dissipation 79−6487
^{197}Au(^{86}Kr, Z_3f), 618 MeV, ang. momentum depolarisation, sequential fission 78−62585
^{197}Au(^{86}Kr,X), 620 MeV, independent particle-shell struct. in deep inelastic collisions 79−97726
^{197}Au(^{86}Kr,X), 620 Mev, deep inelastic scatt., ang. momentum transfer, γ-ray multiplicities 80−27665
^{197}Au(^{86}Kr,X) 612 MeV, γ-ray circular polarisation 80−13453
^{197}Au(^{86}Kr,Z) 620 MeV, diffusive relax. along mass asymmetry coord. 77−50149
^{197}Au(HI,X), 60-120 MeV complete fusion cross sections from fission fragment ang. distrib. 80−13516
α-particle transfer spectroscopic factors using interacting boson approx., A=44 to 68 78−78258
^{10}B+^{10}B, fusion below Coulomb barrier, quantum mechanical barrier penetration model anal. 80−18361
^{10}B+^{7}Li, 24 MeV, charged particle reaction channels, reaction mech. 78−8841
^{10}B(^{10}B, α)^{16}O reaction near Coulomb barrier, intermediate structure resonances 79−9450
^{10}B(^{10}B,α)^{16}O, excitation functions, resonance like structures 78−29496
^{10}B(^{10}B,α)^{16}O, intermediate resonance struct. near E$_x$(^{20}Ne)=38 MeV 79−6404
^{10}B(^{14}N,X), 2.9-7.5 MeV, evaporation residue and total fusion cross section 79−22348
^{10}B(^{14}N,α), 8.5-11.6 MeV, ^{20}Ne excitation functions, resonance search 80−27614
^{10}B(^{14}N,α)^{20}Ne, 10 MeV, search for resonances 78−82385
^{10}B(^{14}N,α)^{20}Ne, highly-excited rot. band obs. in Mg 78−33218
^{10}B(^{16}O, d), 60 MeV, ^{24}Mg yrast and high spin states up to 24 MeV, ang. distribs. 80−18175
^{10}B(^{16}O,d), ^{24}Mg high spin selectivity, critical ang. momentum effects 80−13366
^{10}B(^{16}O,d), ^{24}Mg high spin states from selective compound reactions, stat. anal. 80−18180
^{10}B(^{16}O,d), 24 MeV, ^{24}Mg high spin states, high spin particle spectroscopy upper limits for compound reactions 79−36126
^{10}B(^{16}O,d), 60 MeV, ^{24}Mg yrast states up to 24 MeV excitation energy 78−89781

heavy ion-nucleus reactions continued
^{10}B(^{9}Be, X), total reaction cross sections for sub-Coulomb energies, neutron transfer reaction 79−80950
(^{11}B, αX), 116 MeV, heavy ion-alpha in-plane correlations 80−18343
^{11}B+^{13}C, ^{22}Ne backbending, yrast line and rotational motion, Strutinsky method 79−36135
^{11}B+^{10,11}B, fusion below Coulomb barrier, quantum mechanical barrier penetration model anal. 80−18361
^{11}B(^{13}C,αγ), 18.5 MeV, ^{20}F 2.97 MeV doublet γ-decay, J$^{\pi}$ assignment 79−6491
^{11}B(^{14}N, ^{9}Be)^{16}O, 50 MeV, reaction product spectra, non-statistical processes 77−57684
^{11}B(^{16}O,^{15}N)^{12}C, exchange effects on ang. distribs. 78−627
^{11}B(^{18}O,^{14}O)^{15}B, 96, 103 MeV mass of ^{15}B meas. 77−38219
^{11}B(^{6}Li,^{8}B), 80,93 MeV, ^{9}Li energy levels anal. 77−46183
^{11}B(^{7}Li,tγ), 28 MeV, ^{15}N states, cross sections and lifetimes, EM decay strengths 80−9237
^{134}Ba+^{16}O, compound nucleus, ^{150}Gd, deexcitation, evaporation calcs. comparison with exptl. decay data 77−61391
^{134}Ba+^{16}O, formation and decay of ^{150}Gd compound nucleus 77−61453
Be+^{40}Ar, 1.8 GeV/nucleon, central collisions, single particle inclusive spectra, associated multiplicity 79−9607
Be(^{48}Ca,X), 212 MeV/amu, neutron rich nuclide yields from ^{48}Ca fragmentation 80−27660
(^{9}Be,^{8}Be), 50 MeV reacts. on ^{12}C, ^{16}O, ^{26}Mg, ^{28}Si, ^{40}Ca and ^{208}Pb 78−17239
(^{9}Be,^{8}Be) Coulomb break up mechanism 79−36257
^{9}Be elastic scatt., 14-26 MeV, universal optical pot. determ. *(German)* 78−70552
^{9}Be+^{12}C, 2.8-6.3 MeV, fusion and neutron transfer cross-sections 78−41746
^{9}Be+^{12}C, 3.5 to 9.5 MeV, sub barrier, cross sections and optical model calcs. 78−8838
^{9}Be+^{12}C→^{21}Ne*, different decay channels, resonance-like structures obs. 79−13333
^{9}Be+^{16}O, 2 to 5.1 MeV, sub barrier, cross sections and optical model calcs. 78−8838
^{9}Be+^{16}O, 3.2-14.4 MeV, excitation functions from residual nuclei gamma-ray yield 79−49599
^{9}Be+^{19}F, 7 to 16 sub. barrier, cross sections and optical model calcs. 78−8838
^{9}Be+^{7}Li, 2 MeV neutron energy spectrum meas. using nuclear emulsion technique 78−62574
^{9}Be(^{12}C,^{8}Be), 10-15 MeV, excitation functions and resonant enhancements 79−17881
^{9}Be(^{18}O,X), 1.8-6.7 MeV, total fusion and transfer cross sections ^{19}O, ^{21,22,23}Ne, ^{24,25}Na, ^{25}Mg prod. 80−91205
^{9}Be(^{6}Li,^{8}B), 80,93 MeV, ^{7}He energy levels anal. 77−46183
^{9}Be(^{7}Li,^{6}He)^{10}B, spectroscopic factors from DWBA 77−74874
^{9}Be(^{7}Li,^{8}Li)^{10}Be, spectroscopic factors from DWBA 77−74874
^{9}Be(^{9}Be, (p, t, α)), 5 and 12 MeV, absolute differential cross sections 77−67761
^{10}Be+^{14}N, multiparticle nuclear reactions, 9.5 MeV/nucleon, α-particle yield *(Russian)* 79−17927
^{209}Be(^{136}Xe,X), statistical fluctuations in dissipative collisions, multidifferential cross sections 80−37399
Bi+Xe, 1130 MeV, parameter free model of strongly damped collisions 78−62568
Bi+Xe, 1.13 GeV, deep inelastic nuclear reaction, electronic 1sσ vacancy prod., compound nucleus 80−27662
Bi(Kr,X), strongly damped collisions, classical dynamical model with shape deformation 80−27658
Bi(Xe,X), strongly damped collisions, classical dynamical model with shape deformation 80−27658
^{209}Bi+^{12}C, complete fusion cross sections, excitation functions *(Chinese)* 78−82406
^{209}Bi+^{12}C, reaction mechanisms above Coulomb barrier, semi-classical anal. *(Chinese)* 79−22320
^{209}Bi+^{12}C reaction, fission product charge distrib., 40 to 66 MeV 77−79406
^{209}Bi+^{136}Xe, 1130 MeV, differential cross section calc., statistical model 78−50192
^{209}Bi+^{136}Xe, 1130 MeV, statistical model for mass and charge distrib. 79−17929
^{209}Bi+^{136}Xe, damped collision, interaction time 78−637
^{209}Bi+^{136}Xe, deep inelastic collisions, deformation role, cross sections 79−36270
^{209}Bi+^{136}Xe, stochastic model for strongly damped collisions with liquid drop driving forces 78−89834
^{209}Bi+^{14}N, 85 and 95 MeV, preequilibrium α spectra, statistical treatment 78−41750
^{209}Bi+^{14}N, ang. distrib. anal. for quasi-elastic transfer reactions 79−17931
^{209}Bi+^{16}O, ang. distrib. anal. for quasi-elastic transfer reactions 79−17931
^{209}Bi+^{19}F, ang. distrib. anal. for quasi-elastic transfer reactions 79−17931
^{209}Bi+^{40}Ar, ang. distrib. anal. for quasi-elastic transfer reactions 79−17931
^{209}Bi+^{40}Ca, ang. distrib. anal. for quasi-elastic transfer reactions 79−17931
^{209}Bi+^{56}Fe, 8.3 MeV/amu collision, nucleon exchange and A/Z equilibration 79−76020
^{209}Bi+^{84}Kr, 600 MeV, differential cross section calc., statistical model 78−50192
^{209}Bi+^{84}Kr, 600 MeV, strongly damped collisions, time-depend. mean field theory 78−82374
^{209}Bi+^{86}Kr, 610 MeV, ang. momentum transfer in deeply inelastic scatt. 77−79397
^{209}Bi+C^{12}C, 60-72 MeV, excitation functions for Fr and At isotope prod. *(Chinese)* 78−82387
^{209}Bi+heavy ion, A=12-63, 4.5-10 MeV; quasielastic transfer reaction excitation functions 79−3176
^{209}Bi(^{12}C,f), mass distrib. of fission fragments determ. *(Chinese)* 78−86558
^{209}Bi(^{136}Xe,X), 940 MeV bombarding energy depend., fragment deformation, sequential fision 80−86938
^{209}Bi(^{136}Xe,X), deeply inelastic collisions, mass transport, shell effects 80−99188
^{209}Bi(^{14}N,X), 85-115 MeV, cross sections, preequilibrium α-particle emission 80−42680
heavy ion-nucleus reactions continued
^{209}Bi(^{16}O,^{12}C), 93 MeV, α-transfer reactions 79−67762
^{209}Bi(^{16}O,^{12}C)^{213}At, 93 MeV, comparison with α-decay data 77−334
^{209}Bi(^{48}Ca, X), fusion reactions from Cf and Fm integral yields, statistical model anal. *(Russian)* 79−97740
^{209}Bi(^{56}Fe,X), 464 MeV, damped collision, actinide spontaneous fission activities 80−86937
^{209}Bi(^{56}Fe,X), damped collisions, fast A/Z equilibration and correlated nucleon exchange 80−86798
^{209}Bi(^{6}Li,X), 60-156 MeV, break-up fragment transfer, cross sections, recoil ranges 80−13491
^{209}Bi(^{7}Li,5n)^{211}Rn, 38-60 MeV, excitation function 80−95323
^{209}Bi(^{84}Kr, X), TDHF fusion calcs., fusion cross sections 80−37409
^{209}Bi(^{86}Kr, f), 610 MeV, deeply inelastic, Q and Z depend. of ang. momentum transfer 79−67786
^{209}Bi(HI,X), 60-120 MeV complete fusion cross sections from fission fragment ang. distrib. 80−13516
^{209}Bi(HI,X), quasi-elastic transfer, heavy product range and ang. distrib. 80−83119
^{209}Bi(X,Y)^{210}Po, ^{211}At, X=^{14}N, ^{16}O, ^{19}F, ^{40}Ar, ^{40}Ca, ^{56}Fe, ^{63}Cu, 1 and 2 p transfer reactions, determ. transfer prob. 79−36274
^{249}Bk+^{15}N, synthesis of ^{260}104, detection methods 77−23106
^{249}Bk(^{15}N,4n), synthesis of element ^{260}104 79−30850
^{249}Bk(^{18}O,5n), ^{262}105 spontaneous fission half life *(Russian)* 79−59101
Br, isomer ratios in fission fragments at high excitation 80−32261
Br+^{84}Kr, 350 MeV, compound nucleus prompt K X-rays 79−67768
Br+C(O), 0.2-4.2 GeV/N, compression phenomena and Mach shock waves 80−22851
Br(^{12}C,X), 4.5 GeV/c, emission of short range particles (R<100 mkm) *(Russian)* 80−63202
Br(Fe,f), central collisions, nucleon characteristics, nuclear pionisation in complete fission *(Russian)* 79−80963
Br(HI,X), 0.2-4.2 GeV/N, nonperipheral collisions, forward-backward asymmetry, compression phenomena 80−18329
(C,X), light relativistic ion-target interactions, particle emission 80−102193
(C, π$^-$X), 800 MeV/A, π$^-$ energy and ang. distribs., firestreak and hard scatt. model anal. 80−13498
C+C, 800 MeV/A, wide angle inclusive proton spectra 79−40951
C+C 800 MeV/N, p and π inclusive spectra, energy and ang. distribs. 78−54790
C(^{12}C,X), 4.2 GeV/N, multiple π$^-$ prod., mean multiplicity *(Russian)* 80−27647
C(^{12}C,X), 4.5 GeV/c, emission of short range particles (R<100 mkm) *(Russian)* 80−63202
^{A}C(^{16}O,X), A=12, 13 exit channel competition for some residual nucleus 80−47499
(^{12}C,X), A=12-19, total fusion cross sections and fusion barrier parameters 80−9322
(^{12}C,X) on A=144-164, search for high spin isomeric states, shell effects 79−71784
(^{12}C,X) on light nuclei, 1.55, 2.89 GeV/c, total and inelastic cross sections 79−6610
(^{12}C,x) multinucleon transfer reactions on Cr, Zr and Mo isotopes, Q-values 77−3045
^{12}C (^{12}C,X), 4.2 GeV/c, multitudes of secondary negative particles, momentum distrib. ratios *(Russian)* 80−63178
(^{12}C, πX), 4.2, 4.5 GeV/N, pion multiplicities and theoretical models, review 80−42657
^{12}C relativistic ions, Coulomb disintegration into 3 α-particles, total cross section 79−40943
^{12}C to ^{22}Ne induced nucleon transfer reactions 78−41768
(^{12}C, X), in emulsion, 3.6 GeV/N, high energy multiply charged particle emission, nuclear shock waves *(Russian)* 80−86923
^{12}C-^{12}C quasimolecular resonance, coupled channel anal. 78−78402
^{12}C-^{12}C resonances, speculation of nature, excited α-particles 79−13339
^{12}C+^{10,11}B, fusion below Coulomb barrier, quantum mechanical barrier penetration model anal. 80−18361
^{12}C+^{10,11}B, sub Coulomb energy, fusion cross sections, elastic scatt., optical model anal. 77−34335
^{12}C+^{10}B, 100 MeV, 2n and 2p transfer reacts., DWBA anal. 78−50207
^{12}C+^{11}B, 116 MeV, in-plane heavy ion-alpha particle correlations 79−17921
^{12}C+^{11}B, 9.4-17.8 MeV, excitation functions for elastic, inelastic, ^{8}Be, α exit channels, resonances 79−67731
^{12}C+^{12}C, 19.5 MeV, intermediate struct. in continuum shell model, quasi-molecular shape resonance 79−45235
^{12}C+^{12}C, 250-1000 MeV/N, intranuclear cascade calcs. for multiplicity and cross sections 80−32300
^{12}C+^{12}C, 2.8-6.3 MeV, total fusion cross section, S-factor 80−22877
^{12}C+^{12}C, 3.2-64 MeV/nucleon, time-depend. HF calcs. 77−3034
^{12}C+^{12}C, 800 MeV, p and π inclusive cross sections, non-equilibrium processes 79−40947
^{12}C+^{12}C, 800 MeV/nucleon, two-fireball model for p and π inclusive spectra 79−13323
^{12}C+^{12}C, comment on interaction phenomena 79−13315
^{12}C+^{12}C, diffuse surface nuclear and Coulomb pot. energies 77−18593
^{12}C+^{12}C, fusion reactions, Woods Saxon, folding and proximity pot. anals. 79−45316
^{12}C+^{12}C, low energy, HFB and generator coordinate self consistent microscopic approach 80−42679
^{12}C+^{12}C, molecular config., ^{24}Mg high spin props., Strutinsky method 78−50201
^{12}C+^{12}C, multiparticle nuclear reactions, 9.5 MeV/nucleon, α-particle yield *(Russian)* 79−17927
^{12}C+^{12}C, nuclear fragmentation at 2.1 and 1.05 GeV/N, phenomenological anal., diffractive excitation model 77−54247
^{12}C+^{12}C, partial widths of molecular resonances 78−46094
^{12}C+^{12}C, rotation-vibr. model, ^{24}Mg rotational band fragmentation 78−25096
^{12}C+^{12}C, self-consistent heavy-ion potentials 77−6434
^{12}C+^{12}C fusion, 2.5 to 6.2 MeV, γ-ray transitions and cross-section fluctuations 77−30628
^{12}C+^{12}C quasimolecular interactions, recent developments 79−9615
^{12}C+^{12}C reson. at E$_{c.m.}$=19.3 MeV, high spin states in ^{23}Na and ^{23}Mg anal. 77−26579
^{12}C+^{12}C subCoulomb fusion cross-section, 6.5-12 MeV 77−50151
^{12}C+^{12}C system, molecular configuration in ^{24}Mg 79−13193
^{12}C+^{12}C system, quasimolecular states, coupled channel anal. 78−33217
^{12}C+^{12}C(^{16}O), elastic scatt. and fusion cross-section calc. 77−46182

heavy ion-nucleus reactions continued
$^{12}C+^{13}C$, identical core neutron transfer, coupled channel anal., form factors 79−13319
$^{12}C+^{13}C$ resonances, coupled channel anal. with core-exchange model 79−13338
$^{12}C+^{14}N$, 59, 70 MeV, radiative capture and 1-nucleon emission cross sections 79−93652
$^{12}C+^{14}N$ fusion, 248 MeV, cross-section meas. liquid-drop limit for ^{26}Al 78−4959
$^{12}C+^{14}N$ reactions, 53 MeV, ang. distribs., Hauser-Feshbach anal. 77−14166
$^{12}C+^{16}O$, 11 to 27 MeV, structure in gamma-ray yields 77−34250
$^{12}C+^{16}O$, 12.8 to 18.2 MeV, reactions and inelastic scatt., resonance anomaly study by γ ray techniques 78−4955
$^{12}C+^{16}O$, 22 MeV, spins of reson. assigned 78−17236
$^{12}C+^{16}O$, 3.9-12 MeV, total fusion cross section determ. 77−42003
$^{12}C+^{16}O$, 8.5-12.9 MeV, oscills. in excitation function for complete fusion 77−3037
$^{12}C+^{16}O$, light- and heavy-ion emission comparison 78−641
$^{12}C+^{16}O$, nuclear fragmentation at 2.1 and 1.05 GeV/N, phenomenological anal., diffractive excitation model 77−54247
$^{12}C+^{16}O$ complete fusion, partial prod. cross section for nuclides, evaporation model calcs. 79−36294
$^{12}C+^{16}O$ system, coupled channel approx., treatment of resonances 79−9621
($^{12}C+^{16}O$) system, E_{CM}=12.8 MeV resonance, spin parity determ. 79−6405
$^{12}C+^{17,18}O$ one- and many-nucleon transfer reactions at 12.6 to 14 MeV c.m. energies 78−82371
$^{12}C+^{18}O$, excitation functions for dominant fusion channels 7 to 25 MeV, obs. of regular gross struct. 79−36293
$^{12}C+^{20}Ne$, 150-294 MeV, energy depend. of multinucleon transfer reacts. 79−67769
$^{12}C+^{26}Ne$, entrance channel effects coupled channel calc. 77−65235
$^{12}C+^{27}Al$, de-excitation of ^{39}K anal. 77−6293
$^{12}C+^{6}Li\rightarrow^{4}He+^{2}H+^{12}C$, three body phase space distribs. 80−37393
$^{12}C+^{9}Be$, 11.4 MeV cm energy, p, d, t, α production 80−9302
$^{12}C+Ne^{10+}$, in polystyrene, reaction cross-section for ^{11}C prod. 77−3035
$^{12}C+Ni$, de-excitation of ^{70}Se anal. 77−6293
$^{12}C+\alpha\rightarrow 4\alpha$, multiparticle nuclear reactions, 9.5 MeV/nucleon, α-particle yield *(Russian)* 79−17927
$^{12}C+$emulsion, 50 GeV/c, multiple particle prod., cascade evaporation model *(Russian)* 79−22322
$^{12}C+$photoemulsion nucleus, 50 GeV/c, low energy particles in stars produced *(Russian)* 78−89907
$^{12}C+$various nuclei, negative pion production, 0.4-2.1 GeV/nucleon 78−37364
$^{12}C(^{10}B,d)$, 20-20.5 MeV, possible selectivity 78−41764
$^{12}C(^{11}B,^{12}C)^{11}B$, 28 MeV DWBA amplitude, strong absorpt. model, effect of ang. momentum depend. pots. 79−85486
$^{12}C(^{12}C, ^{10,11}B)$, 44-80 MeV, $^{12}C+^{12}C$ gross struct. resonances in excitation functions 80−102167
$^{12}C(^{12}C, ^{10}B)$ 22-42 MeV, resonances in $^{10}B+^{14}N$ and $^{12}C+^{12}C$ channels 79−80910
$^{12}C(^{12}C, ^{16}O)$, 6-11 MeV, $^{12}C+^{12}C$ system resonant structs., J^π assignments, true ^{24}Mg states 80−99163
$^{12}C(^{12}C, \alpha)^{20}Ne$, 6.85-15 MeV, evidence for rotational band and its fragmentation in ^{24}Mg 79−9449
$^{12}C(^{12}C, \alpha\alpha)$, SS-63 MeV, ^{20}Ne continuum states, J^π and branching, ^{16}O states 80−22660
$^{12}C(^{12}C, \alpha\gamma)$, 30 MeV, ^{20}Ne unnatural parity levels at high excitation 77−2933
$^{12}C(^{12}C, \gamma)$, 11.8-20.0 MeV, total cross section resonant and average behaviour 80−106069
$^{12}C(^{12}C,^{12}C^*)^{12}C^*$, 10-15 MeV, excitation function of 4.44 MeV 2^+ ^{12}C states 77−82957
$^{12}C(^{12}C,^{16}O)^{8}Be$, 5.75-8.9 MeV, sub-Coulomb resonances in ^{12}C-^{12}C system 77−57688
$^{12}C(^{12}C,^{8}Be)$, 78 MeV, ^{16}O high spin states, J^π and α-decay branching ratios 80−18166
$^{12}C(^{12}C,^{8}Be)^{16}O^*$, 78 MeV, spectroscopy of high spin states in ^{16}O 78−50066
$^{12}C(^{12}C,^{8}Be)^{16}O(GS)$, excitation functions and Legendre anal. for resonance J^π assignments 78−78347
$^{12}C(^{12}C,X)$, ^{24}Mg intermediate struct. correlations, elastic and reaction channel excitation functions 80−68625
$^{12}C(^{12}C,X)$, 14-20 MeV, ^{20}Ne, ^{23}Na, ^{23}Mg resonances through γ-decay excitation functions 80−63148
$^{12}C(^{12}C,X)$, 14-31 MeV, total and fusion cross sections, ^{24}Mg ground state band 80−42727
$^{12}C(^{12}C,X)$, 27-60 MeV, evaporation residue cross sections from complete fusion, statistical anal. 79−13369
$^{12}C(^{12}C,X)$, collective potentials and inertia parameters, adiabatic time dependent HF calcs. quasimolecular resonances 80−63195
$^{12}C(^{12}C,X)$, optical potential, nuclear matter approach 80−57801
$^{12}C(^{12}C,X)$, two fireball model, pp correlations and inclusive pion spectrum 80−68694
$^{12}C(^{12}C,X)$ 93.8 MeV, X=^{11}C,^{11}B,^{10}B, ang. distribs. and cross sections, DWBA anal. 79−93657
$^{12}C(^{12}C,X)$ fusion cross section oscillations, overlapping compound states availability 80−9321
$^{12}C(^{12}C,X\gamma)$,X=p,d, 14.3,25.2 MeV, p and d exit channel enhancements, $^{22,23}Na$ J^π assignments 79−45154
$^{12}C(^{12}C,\alpha)$, 11-15 MeV, quasimolecular resonances 79−6544
$^{12}C(^{12}C,\alpha)$, 4-8 MeV, ^{20}Ne spin assignments for sub-Coulomb resonances 77−54245
$^{12}C(^{12}C,\alpha)$, 7-15 MeV, excitation function statistical anal., nonstatistical features 80−99167
$^{12}C(^{12}C,\alpha)^{20}Ne$, ^{24}Mg reson. J^π, rot.-vibr. coupling 78−491
$^{12}C(^{12}C,\alpha)^{20}Ne$, 17 to 20 MeV, excitation functions, correl. resonances 77−34344
$^{12}C(^{12}C,\alpha)^{20}Ne$, 45 to 52 MeV, reaction mechanism, ang. momentum effects 77−38295
$^{12}C(^{12}C,\alpha)^{20}Ne$, 6.85-15 MeV, rot. band in ^{24}Mg obs. 78−12951
$^{12}C(^{12}C,\alpha)^{20}Ne$, E_{cm}=6.5-12 MeV, new resonances, J^π determ. 77−54200
$^{12}C(^{12}C,\alpha)^{20}Ne$, evidence for rot. band in ^{24}Mg at 10.5 to 15 MeV 78−13134
$^{12}C(^{12}C,\alpha)^{20}Ne$, populates 8p-4h O^+ level, α-decay 78−50132
$^{12}C(^{12}C,\alpha)^{20}Ne$, resonances, existence of second $J^\pi=0^+$ reson. at high excitation energy in ^{24}Mg 78−25214

heavy ion-nucleus reactions continued
$^{12}C(^{12}C,\alpha)^{20}Ne$, resonance anomaly anal. in fluctuation theory 78−25215
$^{12}C(^{12}C,\alpha)^{20}Ne$, spin-zero particle reactions, critical ang. momentum effect on ang. distribs. 77−18607
$^{12}C(^{12}C,\alpha)^{20}Ne$, statistical methods for resonance detection, nonstatistical struct. 79−45238
$^{12}C(^{12}C,\alpha)^{20}Ne_{g.s.}$, overlapping 10^+ and 12^+ resonances in $^{12}C+^{12}C$ near $E_{c.m.}$=18.5 MeV 77−6432
$^{12}C(^{12}C,d)^{22}Na$, 14.3 MeV, spectra meas., ^{22}Na excitation functions determ. 77−82956
$^{12}C(^{12}C,\gamma)^{24}Mg$, 5 to 11 MeV, γ yields, resonance features 78−54799
$^{12}C(^{12}C,n)^{23}Mg$, 3.54-4.94 MeV, cross section, neutron branching ratio, stellar processes estimates 77−34336
$^{12}C(^{12}C,p)^{23}Na$, schematic model for continuum resonances, shape resonance fragmentation 77−67764
$^{12}C(^{12}C,pX)$, 800 MeV/N, fireball and preequilibrium cross sections, π condensation proximity influence 80−27659
$^{12}C(^{12}C,p\gamma)$, 38.82 MeV, spectroscopy of ^{23}Na high-spin states 77−46131
$^{12}C(^{12}C,t)$ 37-50 MeV, ^{21}Na deduced levels and cross sections 80−469
$^{12}C(^{12}C,x\alpha)$, 12-31.5 MeV, inclusive α-particle yield, resonant like structs. 80−42691
$^{12}C(^{13}C,\alpha)$, 18-32 MeV, ^{25}Mg coherence moment-of-inertia, ^{21}Ne states 79−75815
$^{12}C(^{13}C,\alpha\gamma)^{21}Ne$, 13.9-15 MeV, yield curves near 14.4 MeV reson. 77−54254
$^{12}C(^{13}C,n)$, 13.4-15.3 MeV, nonstatistical population of ^{24}Mg high spin states 78−74385
$^{12}C(^{14}N,\ ^{12}C)^{14}N$, 79 and 155 MeV, DWBA calcs., recoil and sequential transfer effects 78−46090
$^{12}C(^{14}N,\alpha)$, Hauser-Feshbach calcs. and ^{26}Al coherence widths 78−37360
$^{12}C(^{14}N,^{10}B)^{16}O$, DWBA anal., spectroscopic factors 79−6673
$^{12}C(^{14}N,^{13}N)^{13}C$, 100 MeV, exact finite range CCBA anal. 79−17926
$^{12}C(^{14}N,^{13}N)^{13}C$, exchange effects on ang. distrib. 78−627
$^{12}C(^{14}N,^{13}N)^{13}C$ at high energies, simplified DWBA anal. 79−93643
$^{12}C(^{14}N,^{3}He)^{23}Na$, isospin impurity in ^{26}Al compound nucleus 78−33157
$^{12}C(^{14}N,^{6,7}Li)$, ($^{14}N,^{7,9}Be$), E=86.9, 157 MeV, spectra, ang. distribs. meas. 78−33216
$^{12}C(^{14}N,X)$, 27-60 MeV, evaporation residue cross sections from complete fusion, statistical anal. 79−13369
$^{12}C(^{14}N,\alpha)$, 10.1-15.9 MeV, forward angle excitation function structure, nonstatistical struct. 80−86885
$^{12}C(^{14}N,\alpha)$, 30.3-45.5 MeV, ^{22}Na deduced levels 78−93944
$^{12}C(^{14}N,\alpha)^{22}Na$, statistical methods for resonance detection, nonstatistical struct. 79−45238
$^{12}C(^{14}N,t)^{23}Mg$, isospin impurity in ^{26}Al compound nucleus 78−33157
$^{12}C(^{15}N,X)$, 27-60 MeV, evaporation residue cross sections from complete fusion, statistical anal. 79−13369
$^{12}C(^{15}N,\alpha)$, 21-39 MeV, coherence widths in ^{27}Al 78−41619
$^{12}C(^{15}N,\alpha)$, 21.4-39 MeV, ^{23}Na high spin states, excitation functions, nonstatistical effects, Hauser-Feshbach anal. 80−106041
$^{12}C(^{15}N,\alpha)$, 36-39 MeV, population of ^{23}Na levels 78−50070
$^{12}C(^{15}N,\alpha)$ reson. struct. and ^{27}Al yrast levels 77−79348
$^{12}C(^{15}N,\alpha)^{23}Na$, statistical methods for resonance detection, nonstatistical struct. 79−45238
$^{12}C(^{16}O,\ ^{12}C^*)$, 45-53 MeV, $^{12}C^*$ m-substate population, spin alignment and excitation functions 80−42615
$^{12}C(^{16}O,\alpha)$, ^{24}Mg rot. band termination, level lifetimes 80−18174
$^{12}C(^{16}O,\alpha)$, 19.8-23.8 MeV, ^{24}Mg 2_1^+ substate parameters near Coulomb barrier 79−67657
$^{12}C(^{16}O,\alpha)^{24}Mg$, population of resonant $^{12}C+^{12}C$ states 78−62563
$^{12}C(^{16}O,\alpha\alpha)$, 52-58 MeV, ^{24}Mg continuum states, branching ratios ^{20}Ne levels 80−22661
$^{12}C(^{16}O,n)^{27}Si$, 12.8 MeV resonance investig. by time-of-flight spectra and n-γ coincidence 79−9627
$^{12}C(^{16}O,^{12}C,^{12}C)\alpha$, ^{12}C-α-^{12}C chain formation, α emitted at rest search 79−45285
$^{12}C(^{16}O,^{12}C_{2+})^{16}O$, $^{12}C_{2+}$ spin alignment using γ-decay in flight 78−41767
$^{12}C(^{16}O,^{12}C^{12}C)\alpha$, 68-80 MeV, double differential cross section, Hauser-Feshbach anal. 79−63690
$^{12}C(^{16}O,^{12}C)$, 53-88 MeV, ^{16}O level excitation functions, resonances ^{28}Si α-doorway states 80−63146
$^{12}C(^{16}O,^{12}C)^{16}O$, 22.7 to 33.0 MeV, excitation function enhancement for 0^+, 6.049 MeV ^{16}O state 78−58299
$^{12}C(^{16}O,^{16}O)^{12}C^*$ (2^+, 4.44 MeV) mol. reson., band crossing model 78−62562
$^{12}C(^{16}O,^{20}Ne)$, 10-15.5 MeV, cross sections and ang. distribs., resonances, direct and stat. anal. 79−67730
$^{12}C(^{16}O,^{20}Ne)^{8}Be$, 12.25 to 15.07 intermediate struct. effects 78−620
$^{12}C(^{16}O,^{8}Be_{g.s.})^{20}Ne^*$, obs. of α-doorway states 79−6662
$^{12}C(^{16}O,^{8}Be)$, 18.5-22.7 MeV, $^{20}Ne^*$ low lying states and resonances, J^π assignments and energies 79−93592
$^{12}C(^{16}O,^{8}Be)$, 18.8 MeV, ^{20}Ne narrow $J^\pi=10^+$ resonance in strong absorption region, excited states 79−30814
$^{12}C(^{16}O,^{8}Be)$ $E_{c.m.}$=18.5-20.5 MeV, populating ^{28}S 12^+ reson. 77−18508
$^{12}C(^{16}O,^{8}Be)^{20}Ne$, 13.5-23 MeV, excitation functions, ang. distribs. and cross sections 79−13334
$^{12}C(^{16}O,X)$, 128 MeV, X=^{15}O, ^{15}N, ^{14}O, spectroscopic factors, cross sections DWBA anal. optical model parameters 80−13371
$^{12}C(^{16}O,X)$, transparency to l=9 partial wave in 14.7 MeV resonance region 80−78314
$^{12}C(^{16}O,X)$ 10.5-23.3 MeV, low energy fusion cross sections 77−14152
$^{12}C(^{16}O,2p)^{26}Mg$, energy spectra and ang. distribs. meas. 77−38293
$^{12}C(^{16}O,\alpha)$, 145 MeV, ^{24}Mg nuclear molecular resonances in ^{12}C-^{12}C system 80−13430
$^{12}C(^{16}O,\alpha)$, 26.7 MeV, identification of ^{24}Mg 10^+ levels 78−33119
$^{12}C(^{16}O,\alpha)$, 40.6, 46, MeV, ^{24}Mg 6_3^+ level, α and γ decays, branching ratios 79−75901
$^{12}C(^{16}O,\alpha)$, J^π for 12.8 MeV c.m. resonance 79−59045
$^{12}C(^{16}O,\alpha)$, resonance at 12.8 MeV 77−46187
$^{12}C(^{16}O,\alpha)$ 9.4-12.4 MeV, ^{28}Si 10.9 MeV resonance, J^π assignment 79−26414
$^{12}C(^{16}O,\alpha)^{24}Mg$, 10.9 MeV ^{28}Si resonance, spin, parity 78−74384
$^{12}C(^{16}O,\alpha)^{24}Mg$, 13.5-23 MeV, excitation functions, ang. distribs. and cross sections 79−13334
$^{12}C(^{16}O,\alpha)^{24}Mg$, 13.7, 14.2, 14.7 MeV, ang. distribs., intermediate resonance struct. 79−13331
$^{12}C(^{16}O,\alpha)^{24}Mg$, anomaly at 13.7 MeV, optical model anal. 78−21587

heavy ion-nucleus reactions continued
$^{12}C(^{16}O,\alpha)^{24}Mg$, low energy, spin and parity assignments 78−21602
$^{12}C(^{16}O,\alpha\gamma)$, ^{24}Mg, $K^\pi=0^+$, $K^\pi=3^-$ bands, radiative and α-widths 80−18173
$^{12}C(^{16}O,\alpha\gamma)$ 42 MeV, ^{24}Mg, 11.86 MeV level, confirmation of $J^\pi=8^+$ assignment 78−70445
$^{12}C(^{16}O,d)$, resonance at 12.8 MeV 77−46187
$^{12}C(^{16}O,n)$, resonance at 12.8 MeV 77−46187
$^{12}C(^{16}O,p)$, resonance at 12.8 MeV 77−46187
$^{12}C(^{16}O,\alpha)$, ^{24}Mg low spin resonances, excitation functions and ang. distribs. 80−63151
$^{12}C(^{17}O,^{16}O)$, single-n sub-Coulomb transfer reactions, single particle wave function RMS radius, n-excess 79−85355
$^{12}C(^{18}O,^{12}C)$, 125 MeV, ^{18}O 6p-4h states and composite spectra 80−63096
$^{12}C(^{18}O,^{16}O)^{14}C$, two nucleon transfer reactions, one and two step transfer process anal. 78−82370
$^{12}C(^{18}O,^{8}Be)^{22}Ne$, 15-22.5 MeV, resonance strength investig. 79−13336
$^{12}C(^{18}O,\alpha)^{26}Mg$, 15-22.5 MeV, resonance strength investig. 79−13336
$^{12}C(^{20}Ne,X)$, 67.1-157 MeV, ^{32}S compound nucleus formation and deexcitation entrance channel effects 80−549
$^{12}C(^{20}Ne,\alpha)^{28}Si$, energy depend., non-statistical effects 79−13332
$^{12}C(^{24}Mg,X)$, 45-71 MeV, γ-ray yield functions from high spin states, comparison with $^{16}O+^{28}Si$ 79−93492
$^{12}C(^{28}Si,\alpha X)$, 87-91.5 MeV, α-HI angular correlations, excitation functions, statistical anal. 80−86915
$^{12}C(^{40}Ar,X)$, 213 MeV/N, relativistic fragmentation, microscope and macroscopic calcs., np correlation 80−13495
$^{12}C(^{6}Li,{}^{3}He\gamma)$, 34 MeV, ^{15}N 9.155 MeV state, lifetime, cluster nature and parity 79−6424
$^{12}C(^{6}Li,d)^{16}O(\alpha)^{12}C$, ^{16}O 21.8 MeV 6^+ level alpha decay width determ. 77−82880
$^{12}C(^{6}Li,{}^{3}He\gamma)$, 34 MeV, ^{15}N states, cross sections and lifetimes, EM decay strengths 80−9237
$^{12}C(^{6}Li,\alpha)$, polarised ^6Li, ^{14}N residual states, vector anal. power. optical pot. 79−97697
$^{12}C(^{6}Li,\alpha)^{14}N$, 33 MeV, multiple reaction mech., exact finite range DWBA calcs. 78−25231
$^{12}C(^{6}Li,\alpha)^{14}N$, α-particle spectrum sharp lines observation, originating from ^{16}O decay *(Russian)* 78−29495
$^{12}C(^{6}Li,\alpha)^{14}N$, E(^{6}Li)=20 MeV, using polarised ^6Li source, exact finite range DWBA anal. 78−58293
$^{12}C(^{6}Li,\alpha)^{14}N$(2,31 MeV), 9 to 20 MeV, isospin violation 78−41763
$^{12}C(^{6}Li,d)$, $^{12}C(^{6}Li,\alpha)$, 20 MeV, analysing powers 78−46098
$^{12}C(^{6}Li,d)$, ^{16}O 4^+ state nonstatistical population in compound nucleus calcs. 80−102137
$^{12}C(^{6}Li,d)$, ^{16}O highly excited states spin, parity, decay into $A+^{12}C$ 77−79395
$^{12}C(^{6}Li,d)$, ^{16}O level configuration mixing anal., α-spectroscopic strengths 79−6683
$^{12}C(^{6}Li,d)$, 20-34 MeV, ^{16}O levels, Hauser Feshbach and DWBA anal. α-spectroscopic strengths 79−569
$^{12}C(^{6}Li,d)$, polarised ^6Li, 20 MeV, ^{16}O residual states, vector anal. power. optical pot. 79−97697
$^{12}C(^{6}Li,d)^{16}O$, 20 MeV polarised ^6Li, DWBA calc. of analysing powers for ^{14}N 1^+ states 79−6679
$^{12}C(^{6}Li,d)^{16}O$, 20 MeV polarised ^6Li, DWBA calc. of analysing powers, 0^+ g.s. and 2^+ state of ^{16}O 79−6678
$^{12}C(^{6}Li,d)^{16}O$, 42 MeV, α spectroscopic factors, reduced widths, stellar He burning 78−89897
$^{12}C(^{6}Li,d)^{16}O^*$, 18-28 MeV, configuration mixing effect and cross sections, zero range DWBA 80−42692
$^{12}C(^{6}Li,d)^{16}O(\alpha)^{12}C$, 35 MeV, d-$\alpha$ coincidence spectra meas. after ^{16}O break-up, α-cluster state energies 79−63688
$^{12}C(^{6}Li,d)^{16}O\rightarrow{}^{12}C+\alpha$, reaction mechanism from ang. correlations, direct transfer 80−78319
$^{12}C(^{6}Li,d)$90.2 MeV, ^{16}O α-cluster states, widths and resonances, optical model, direct transfer 80−105975
$^{12}C(^{7}Li,{}^{6}He)$, 48 MeV, ^{13}N state transition ang. distrib., optical parameters 79−75904
$^{12}C(^{7}Li,{}^{6}Li)$, 48 MeV, ^{13}C, state transition ang. distrib., optical parameters 79−75904
$^{12}C(^{7}Li,\alpha)$, 48 MeV, ^{15}N three particle states at high excitation energies, J^π, selective population 80−99129
$^{12}C(^{7}Li,\alpha\gamma)$, 28 MeV, ^{15}N states, cross sections and lifetimes, EM decay strengths 80−9237
$^{12}C(^{7}Li,p)$, 16, 18 MeV, ^{18}O deduced levels and ang. distribs., cross sections 79−6686
$^{12}C(^{7}Li,t)^{16}O$, 17 MeV, ^{16}O states, $^{12}C+4$ particles vertex 77−14030
$^{12}C(^{7}Li,t)^{16}O$, 34 MeV, α spectroscopic factors and reduced widths, stellar fusion 78−89896
$^{12}C(^{7}Li,t)^{26}O$, Goldfarb-Buttle method *(Chinese)* 78−8834
$^{12}C(^{9}Be,{}^{8}Be)$, 11.4 MeV to 14.8 MeV (c.m.), search for resonances 79−45290
$^{12}C(^{9}Be,{}^{8}Be)^{13}C$, 20 MeV, α-cluster transfer process contrib. 79−6668
$^{12}C(^{9}Be,{}^{8}Be)^{13}C$, neutron and α-particle transfer processes 79−36255
$^{12}C(^{9}Be,X)$, X=p,d,t,α, 11.4 MeV to 14.8 MeV (c.m.), search for resonances 79−45290
$^{12}C(^{9}Be,\alpha)^{17}O$, 10-15 MeV, excitation functions and resonant enhancements 79−17881
$^{12}C(^{9}Be,\alpha)^{17}O$, ang. distrib. from pick-up model anal. of cluster transfer *(Russian)* 80−37396
$^{12}C(^{9}Be,\alpha)^{17}O$, cluster effects *(German)* 79−76015
$^{12}C\rightarrow{}^{16}O$, measurement of alpha-widths in ^{16}O relevant to astrophysics 79−6682
$^{13}C+^{16}O$, excitation functions for dominant fusion channels 7 to 25 MeV, obs. of regular gross struct. 79−36293
$^{13}C+^{17,18}O$ one- and many-nucleon transfer reactions at 12.6 to 14 MeV c.m. energies 78−82371
$^{13}C+^{60}Ni$, one nucleon transfer, nuclear and Coulomb components 77−34340
$^{13}C+^{94}Mo$, one nucleon transfer, nuclear and Coulomb components 77−34340
$^{13}C(^{13}C,^{24}Mg)$, 3.05-6.88 MeV, fusion cross section energy depend., optical anal. 80−42724
$^{13}C(^{14}N,^{14}C)^{13}N$, sub-Coulomb charge exchange *(Russian)* 78−46106
$^{13}C(^{15}N,^{14}N)^{14}C$, 30 to 45 MeV, ang. distribs., exchange symms. 77−54237
$^{13}C(^{16}O,^{17}O)^{12}C$, non-orthogonality of channel states 80−83115
$^{13}C(^{16}O,^{17}O)^{12}C$, sub-Coulomb, RMS radii of single-particle orbitals, neutron excess 77−333
heavy ion-nucleus reactions continued
$^{13}C(^{18}O,^{19}O)^{12}C$, sub-Coulomb, RMS radii of single-particle orbitals, neutron excess 77−333
$^{13}C(^{6}Li,\alpha)^{15}N$, 32 MeV, ang. distrib. meas., zero-range DWBA calc. 78−13155
$^{13}C(^{6}Li,d)$, 34-36 MeV, ^{17}O high spin 4p-3h strength location from excited peaks 79−3082
$^{13}C(^{6}Li,d)$ 26, 29, 34 MeV, ^{17}O α-cluster states, α-decay orbital momenta and parities *(Russian)* 78−86486
$^{13}C(^{6}Li,t)$, 20-32 MeV, ^{16}O levels and ang. distribs., ^3He spectroscopic strengths, Hauser-Feshbach/DWBA anals. 80−47390
$^{13}C(^{7}Li,p)$, 16 MeV, ^{19}O high spin states 78−21595
$^{13}C(^{7}Li,t)$, 34-36 MeV, ^{17}O high spin 4p-3h strength location from excited peaks 79−3082
$^{13}C(^{9}Be,X)$, 11.6 MeV, p,t,d,α, ^8Be ang. distribs., Hauser-Feshbach and DWBA anals. 80−91193
$^{14}C(^{12}C,X)$, 40-57 MeV, strong resonant behaviour in inelastic and transfer channels, γ-yields 80−52644
$^{14}C(^{12}C,\alpha)^{22}Ne$, 6.1 to 9.7 MeV, excitation functions, statistical fluctuations 77−23103
$^{14}C(^{14}C,{}^{14}B)$, ^{14}B, mass excess and excited states 80−42676
$^{14}C(^{16}O,^{17}O)^{13}C$, exchange effects on ang. distribs. 78−627
$^{14}C(^{16}O,^{18}O)^{12}C$, full recoil one and two step DWBA anal. 78−70564
$^{14}C(^{16}O,^{18}O)^{12}C$, resonance struct. at excitation energies 40-51 MeV in ^{30}Si, comparison with $^{12}C+^{18}O$ 79−13335
$^{14}C(^{18}O,^{18}N)$, ^{18}N mass excess and excited states 80−42676
$^{14}C(^{6}Li,{}^{6}He)$, 62 MeV, Gamow-Teller sum rules and ground state wave function 80−106073
$^{14}C(^{6}Li,{}^{6}He)^{14}N$ and Gamow-Teller strength distrib. 77−6430
$^{14}C(^{7}Li,t)^{18}O$, 20.4 MeV, FRDWBA anal. 78−82381
$^{48}C+^{6,7}Li$, population of $^{51,52}Ti$, ^{52}V yrast states, mean lifetimes meas. 77−2942
$^{65}CU(^{16}O,p2n)$, 48-50 MeV, ^{78}Kr bands, lifetimes and E2 transitions from interacting boson model 80−73771
$Ca+^{40}Ar$, A=42, 48, 236 MeV, fragments mass and charge distribs. in deep inelastic reactions 78−58296
Ca+Ar, 4-17 GeV, search for ultradense nuclei 77−3044
Ca+Ca, classical many-body model for heavy ion collisions 80−536
$Ca(^{12}C,{}^{8}Be)$, 45 MeV, even isotopes A=40-48 77−88172
Ca(Ca,X), 400 MeV, classical eqns. of motion calcs., central collisions, thermal models 80−106070
$^{40,48}Ca(^{18}O,^{17}O)^{41,49}Ca$, 50 MeV, differential cross-sections, direct one-step process 77−74828
$^{A}Ca(^{7}Li,{}^{7}Li)$, A=40, 48, 88 MeV, optical potentials, phenomenological and microscopic 80−52687
$^{A}Ca(^{7}Li,t)$, A=40, 44, 34 MeV, $^{44,48}Ti$ ang. distribs. for transitions, DWBA anal., spectroscopic strengths 80−68584
$^{38}Ca+^{16}O$, 56 MeV, nucleon transfer reactions, effective Q-value model 79−63692
$^{40}Ca+^{14}N$ fusion-evaporation reaction γ-ray spectroscopy study of ^{51}Mn structure 77−18471
$^{40}Ca+^{16}O$, 3-D TDHF calcs. 78−54781
$^{40}Ca+^{16}O$, 45-63 MeV, excitation function determ. 78−82404
$^{40}Ca+^{16}O$, inelastic scatt., exit channel distorting pot., DWBA calc. 78−94025
$^{40}Ca+^{16}O$, single-particle polarisation, two-centre shell model 78−13142
$^{40}Ca+^{16}O$ fusion-evaporation reaction, γ-ray spectroscopy study of ^{51}Mn structure 77−18471
$^{40}Ca+^{40}Ca$, 2- and 3-dimens. time depend. HF calc. comparison 79−17948
$^{40}Ca+^{40}Ca$, 278 MeV, comparison of 2-D and 3-D TDHF 78−82386
$^{40}Ca+^{40}Ca$, 278 MeV, particle transfer width, 3 dimens. TDHF calcs. 78−74389
$^{40}Ca+^{40}Ca$, 284 MeV, energy spectra struct. obs. 78−4958
$^{40}Ca+^{40}Ca$, 3-D TDHF calcs. 78−54781
$^{40}Ca+^{40}Ca$, 3-dimens., time depend. HF calcs. for fusion cross sections 78−66318
$^{40}Ca+^{40}Ca$, 3D TDHF calcs. 78−626
$^{40}Ca+^{40}Ca$, collective modes excitation 79−54448
$^{40}Ca+^{40}Ca$, evaporation-residue cross-sections meas. 78−33211
$^{40}Ca+^{40}Ca$, low impact parameters, energy dependence of fusion cross section 78−41751
$^{40}Ca+^{40}Ca$, self-consistent heavy-ion potentials 77−6434
$^{40}Ca+^{40}Ca$, total fusion cross section, time depend. HF calcs. 79−17945
$^{40}Ca+^{40}Ca$ strongly damped reaction, time scale 77−54244
$^{40}Ca(^{10}B,np)$, 14-36 MeV, ^{48}Cr high spin states, yrast levels and 6^- isomeric state 80−454
$^{40}Ca(^{11}B,{}^{10}B)$, 51.5 MeV, n stripping, DWBA anal. with Woods-Saxon and double folding optical pots. 80−102171
$^{40}Ca(^{11}B,{}^{12}C)$, 32, 68 MeV, single proton pickup, DWBA anal., optical pot. 80−106037
$^{40}Ca(^{11}B,{}^{12}C)$, 51.5 MeV, p pickup, DWBA anal. with Woods-Saxon and double folding optical pots. 80−102171
$^{40}Ca(^{12}C,{}^{8}Be)^{44}Ti$, 45 MeV, semiclassical analysis of α-transfer reactions, partial wave amplitudes 79−45283
$^{40}Ca(^{13}C,{}^{14}N)^{39}K$ and $^{40}Ca\ (^{13}C,{}^{12}C)^{41}Ca$, 60, 68 MeV, spin depend. effects 78−66300
$^{40}Ca(^{13}C,{}^{12}C)$, 18.5, 19.0 MeV, ^{41}Ca $1f_{7/2}$ neutron radial distrib., single particle, orbits, RMS radii 80−42532
$^{40}Ca(^{13}C,{}^{14}N)$, 40, 68 MeV, single proton pickup, DWBA anal., optical pot. 80−106037
$^{40}Ca(^{13}C,{}^{14}N)$, 50 MeV, L=1 proton pickup, ^{39}K $s_{1/2}$ and $d_{3/2}$ states, DWBA anal. 79−67734
$^{40}Ca(^{13}C,{}^{14}N)^{39}K$, sensitivity to $^{39}K+p$ form factor, DWBA anal. 77−34345
$^{40}Ca(^{13}C,{}^{14}N)^{39}K$, helicity flip obs. 77−74872
$^{40}Ca(^{13}C,{}^{14}N)^{39}K$, molecular orbital interpretation of $\Delta l=1\hbar$ transfer anomaly 77−82952
$^{40}Ca(^{13}C,{}^{14}N)^{39}K(3/2^+)$, CCBA fit to anomalous ang. distrib. 77−38297
$^{40}Ca(^{13}C,{}^{9}Be)$, 149 MeV, α-transfer cross sections, direct reaction theory anal. 79−67767
$^{40}Ca(^{14,15}N,^{15,16}O)$, 70 MeV, L=1 proton pickup, ^{39}K $s_{1/2}$ and $d_{3/2}$ states, DWBA anal. 79−67734
$^{40}Ca(^{14}N,np)$, 29-38 MeV, ^{52}Fe yrast state properties, transitions and decays 79−67631
$^{40}Ca(^{14}N,{}^{10}B)$, 153 MeV, α-transfer cross sections, direct reaction theory anal. 79−67767
$^{40}Ca(^{15}N,^{16}O)$, 60 MeV, ^{39}K $9/2^-$ forbidden transition, cross section CCBA anal., L=1 transitions 79−9507

heavy ion-nucleus reactions continued
^{40}Ca(^{16}O, 2p), 45 MeV, ^{54}Fe 8$^+$ and 10$^+$ level spin assignments and lifetimes 80−68531
^{40}Ca(^{16}O, 3pγ), 45 MeV, ^{53}Mn high spin states, decay scheme, J$^\pi$ assignments, mixing ratios *(French)* 79−67627
^{40}Ca(^{16}O, p)^{55}Co, 39 to 89 MeV reaction cross section 80−47496
^{40}Ca(^{16}O,^{15}N)^{41}Sc, effect of polarisation of shell-model states 77−67768
^{40}Ca(^{16}O,^{15}N)^{41}Sc, DWBA anal. including nuclear wave function polarisation 78−629
^{40}Ca(^{16}O,^{16}O), complex heavy ion optical pot., microscopic BHF derivation 80−106067
^{40}Ca(^{16}O,X), 36-75 MeV, absolute and fusion total cross sections, ^{56}Ni excitation functions 80−18362
^{40}Ca(^{16}O,X), 40-214 MeV, fusion and elastic scatt. cross sections, optical anal. 80−32314
^{40}Ca(^{16}O,X), ion-ion interaction pot., imaginary part, effective interaction 80−68692
^{40}Ca(^{16}O,αα), 70 MeV, ang. correl. in compound nucleus decay 79−36261
^{40}Ca(^{16}O,αp), 70 MeV, ang. correl. in compound nucleus decay 79−36261
^{40}Ca(^{16}O,pp) 70 MeV, ang. correl. in compound nucleus decay 79−36261
^{40}Ca(^{20}Ne,^{16}O), 149-262 MeV, breakup cross section, direct mechanism, DWBA anal. 80−18276
^{40}Ca(^{20}Ne,^{16}O), 262 MeV, α-transfer cross sections, direct reaction theory anal. 79−67767
^{40}Ca(^{20}Ne,X), 44.1-70.4 MeV, fusion and elastic scatt. cross sections, evaporation residues 80−550
^{40}Ca(^{28}Si,α2pγ), 93.5, 102 MeV, ^{62}Zn yrast states, possible decay scheme 79−54379
^{40}Ca(^{40}Ar, π$^+$X), 1.05 GeV/nucleon 79−63693
^{40}Ca(^{40}Ar,X), 191, 263, 272 MeV, strongly damped collision cross sections, product energies 80−32291
^{40}Ca(^{40}Ca, X), 10 MeV/N, charged particle emission Q-valve depend. 80−47503
^{40}Ca(^{40}Ca,X), 400 MeV, ^{41}Ca damped reaction fragment, energy spectra struct., evaporation processes 79−93591
^{40}Ca(^{40}Ca,X), 400 MeV, fragment energy spectra struct., giant resonances, direct process 80−47452
^{40}Ca(^{40}Ca,X), deep inelastic, doubly differential cross section, spectra struct. 80−5103
^{40}Ca(^{40}Ca,x), relativistic, compression and pion distrib., Monte Carlo calc. 80−73853
^{40}Ca(^{40}Ca,x) reactions, time dependent HF calcs. 77−54251
^{40}Ca(^{6}Li,d)^{44}Ti, higher-order process, coupled channels calcs. 78−82327
^{40}Ca(^{7}Li,^{7}Be)^{40}K, charge exchange microscopic DWBA anal. 79−26453
^{40}Ca(^{7}Li,^{8}Be), 34 MeV, ^{39}K states and spectroscopic strengths DWBA anal. 80−5069
^{40}Ca(^{9}Be,^{8}Be), DWBA anal., spectroscopic factor determ. 78−17098
^{40}Ca(Li,xn), 10-16 MeV, ^{45}V level scheme, γ-rays, level lifetimes, internal conversion 80−63085
^{48}Ca (^{11}B, pn), 21 MeV 78−70436
^{48}Ca+^{11}B, 25-50 MeV, yrast decay schemes of $^{54-6}$Mn, ^{56}Cr, $^{52-3}$V 77−82854
^{48}Ca+^{15}N(^{18}O) fusion-evaporation reaction, ^{59,60}Fe, ^{59,60}Co yrast decay scheme 78−13154
^{48}Ca+^{16}O 56 MeV, transitions to resolved levels, optical model parameter 78−41758
^{48}Ca+^{9}Be, 25-55 MeV, ^{53}Cr, ^{54}V, yrast levels J$^\pi$ assignments and lifetimes 79−9445
^{48}Ca+heavy ion fusion evaporation reacts., yrast decay schemes 78−66308
^{48}Ca(^{10}B, 5n), 25-50 MeV, ^{53}Mn high spin states, lifetimes, shell model calcs., yrast levels 79−6425
^{48}Ca(^{12,13}C,X), elastic, inelastic and single nucleon transfer excitation functions, ^{49}Ca levels 80−13492
^{48}Ca(^{15}N, ^{14}C)^{49}Sc, 48 MeV, DWBA anal., optical potential ambiguities 77−34341
^{48}Ca(^{16}O, ^{14}C), two nucleon sequential transfer, on-shell anal., cross sections 80−99180
^{48}Ca(^{16}O, ^{15}N), ^{15}N excitation contrib. in optical pot., DWBA grazing peak shift 80−86921
^{48}Ca(^{16}O,^{14}C)^{50}Ti, full recoil one and two step DWBA anal. 78−70564
^{48}Ca(^{16}O,^{14}C)^{50}Ti, two nucleon transfer reactions, one and two step transfer process anal. 78−82370
^{48}Ca(^{16}O,^{15}N)^{49}Sc, 56 MeV, DWBA anal., optical potential ambiguities 77−34341
^{48}Ca(^{18}O, ^{16}O), two nucleon sequential transfer, on-shell anal., cross sections 80−99180
^{48}Ca(^{18}O, ^{17}C), 102 MeV, ^{17}C ions mass excess, low lying level struct. 78−8744
^{48}Ca(^{18}O,^{15}B)^{51}V, mass of ^{15}B determ. 78−70433
^{48}Ca(^{18}O,^{16}C)^{50}Ti, 102 MeV, two-proton transfer reaction 79−63700
^{48}Ca(^{18}O,^{16}O) 50 MeV, cross sections, DWBA multipole expansion calcs., form factors 79−13325
^{48}Ca(^{18}O,^{16}O)^{50}Ca, cross section anal. by DWBA and CCBA 77−3046
^{48}Ca(^{18}O,^{16}O)^{50}Ca, two nucleon transfer reactions, one and two step transfer process anal. 78−82370
^{48}Ca(^{18}O,αpn) 70 MeV, ^{60}Mn, mass and β-decay half life 78−78317
^{48}Ca(^{19}F,^{18}O)^{49}Sc, 56 MeV, DWBA anal., optical potential ambiguities 77−34341
^{48}Ca(^{248}Cm, 2n)^{294}X$_{116}$, super-heavy elements prod. at barrier energies 79−13368
^{48}Ca(^{32}S,^{32}Si)^{48}Ti 125 MeV, double-charge-exchange reaction 79−63701
^{48}Ca(^{7}Li,^{6}He), location of major 2p$_{1/2}$ strength in ^{49}Sc 78−25095
^{48}Ca(^{7}Li,^{7}Be), 52 MeV, ^{48}K mass excess and 0.58 MeV excited state 79−446
^{98}Ca(^{16}O,^{15}C), simple unitary estimate for multistep processes, cross section bounds 79−40922
Cd+^{63}Cu, 380 MeV, prod. of new Os and Ir isotopes 77−82961
Cd(^{10}B,p2n), ^{A}Cs, A=119 , 121, 123, 125, collective props. and level schemes 79−22171
Cd(^{6}Li,3n), ^{A}Sb, A=113,115,117,119, high spin states, J$^\pi$ assignments, decay schemes and lifetimes 79−54381
Cd(^{14}N,3n), ^{A}Cs, A=119 , 121, 123, 125, collective props. and level schemes 79−22171
^{A}Cd(^{63}Cu,X)Y, A=106, 108, 110, new Ir, Os and Re isotopes 78−70563
^{106}Cd(^{12}C, 2n), 52 MeV, ^{116}Xe level scheme and yrast band, in-beam γ-study 80−13360

heavy ion-nucleus reactions continued
^{113}Cd(^{40}Ar,6n), ^{147}Dy charge states and charge distrib. *(Russian)* 79−40840
^{136}Ce (^{18}O, 3n), ^{151}Dy high spin yrast isomers, shell model configs. 79−49573
^{140}Ce(^{16}O, 4n), ^{152}Dy high spin isomers, yrast states and level lifetimes 80−13361
^{140}Ce(^{16}O, 4n), ^{152}Dy high spin struct., in beam γ meas. 80−18179
^{140}Ce(^{16}O, 4n), 89 MeV, ^{152}Dy high spin isomeric states, g-factors 80−13377
^{140}Ce(^{16}O,^{12}C), comparison of reduced widths derived from transfer reactions and α-emitters, DWBA anal. 79−6671
^{140}Ce(^{16}O,4n), 89 MeV, ^{152}Dy continuum γ-ray multipolarity by linear polarisation meas. 79−85408
^{140}Ce(^{16}O,4n), 89 MeV, ^{152}Dy yrast continuum γ-ray multipolarity via polarisation meas. 80−9264
^{249}Cf(^{18}O,4n), ^{263}106, spontaneous fission half life *(Russian)* 79−59101
Cl (Ar, π$^+$X), 250, 400 MeV/A, pion yield near threshold 80−18344
Cl+Ar, 800 MeV/A, wide angle inclusive proton spectra 79−40951
Cl(Ar,X), 0.4-1.8 GeV/u, multipion prod. energy depend. 80−106065
Cl(Ar,X), 800 MeV/N, single particle spectra from high multiplicity events 80−99184
Cl(Ar,X), proton inclusive spectra, direct plus thermal model 80−57799
^{35}Cl induced, targets A=27-124, 70 170 MeV, fusion and interaction barrier parameters, critical angular momenta 77−10428
^{35}Cl, surface anal. using ^{35}Cl ion beams 79−5211
^{35}Cl+^{24,25,20}Mg(^{27}Al)(^{28}Si), 100-70 MeV, mass systematics of evaporation residues 77−38311
^{35}Cl+^{27}Al, 140, 150, 160, 170 MeV, deep inelastic fragment kinetic energies anal. 77−82955
^{35}Cl+^{27}Al, deep inelastic fragment energies, rot. energy contributions 79−63697
Cm(^{48}Ca,xn), production of superheavy elements with A=114-116 78−29493
^{246}Cm+^{18}O, synthesis of ^{260}104, detection methods 77−23106
^{248}Cm, Xe and Kr induced fission at Coulomb energies 77−61467
^{248}Cm+^{16}O, synthesis of ^{260}104, detection methods 77−23106
^{248}Cm+^{48}Ca, 267 MeV, search for superheavy elements 77−74871
^{248}Cm+^{48}Ca, search for volatile superheavy elements 78−94027
^{248}Cm+^{48}Ca superheavy element prod., radiochem. separation 78−74390
^{248}Cm(^{238}U,X), 7.5 MeV/amu, three particle exclusive meas. for exit channels fission fragment ang. distrib. 80−13513
^{59}Co(^{16}O,X), 64 MeV, compound nucleus decay, X-ray identification 80−63196
^{59}Co(^{16}O,2pn)^{72}As, 53-56 MeV, new ^{72}As isomer spin-precession, g-factor 77−54149
^{59}Co(^{19}F,X), 52.5 MeV, compound nucleus decay, X-ray identification 80−63196
^{59}Co(^{6}Li,d), 32 MeV, ^{63}Cu levels, transitions and ang. distribs. from α-transfer 80−73798
^{59}Co(^{7}Li,2n), 18 MeV, ^{64}Zn, J$^\pi$ assignments from γ-ray linear polarisation meas. 79−6383
^{59}Co(^{7}Li,2n), E=18 MeV, high-spin states in ^{64}Zn 78−33145
Cr+^{14}N(^{12}C), single- and multi-nucleon transfer reactions at 60, 70 and 90 MeV 77−14146
Cr(^{14}C,^{16}O), 51 MeV, pickup reaction, ^{48,50}Ti excited states and transition ang. distribs. 80−95308
^{50}Cr+^{22}Ne, energy dissipation as func. of angle data comparison to classical and diffusion models 78−21604
^{50}Cr+^{40}Ar, 236 MeV, fragments mass and charge distribs. in deep inelastic reactions 78−58296
^{50}Cr(^{12}C,α2p), side feeding to ^{56}Fe 6$^+$ doublets 78−13014
^{50}Cr(^{6}Li,pn), 20 MeV, ^{54}Fe 8$^+$ and 10$^+$ level spin assignments and lifetimes 80−68531
^{52}Cr+^{12}C, 56 MeV, heavy ion fusion, evaporation model breakdown, preequilibrium α emission from ^{64}Zn 78−89927
^{52}Cr+^{13}C, 105 MeV, ^{51}V, ^{51}Cr, ^{53}Mn, level scheme, DWBA and optical model anal. 79−36159
^{52}Cr(^{12,13}C,X), elastic, inelastic and single nucleon transfer excitation functions, ^{53}Cr levels 80−13492
^{52}Cr(^{14}N,2p2nγ), 50-75 MeV, ^{62}Cu high spin states, level scheme *(French)* 78−21496
^{53}Cr(^{16}O,pnγ), 35-51 MeV, γ-spectroscopy of ^{67}Ga high spin levels 78−93960
Cu, reactions induced by ^{12}C and ^{19}F ions, γ-ray spectroscopy of induced activities 77−23107
Cu spallation by 25 GeV ^{12}C ions 77−6435
Cu+^{40}Ar spallation, 80 GeV, 35 radioactive nuclide prod. cross sections 78−66260
Cu+Cu system, high energy, compound nucleus form. and deep inelastic scatt. *(French)* 79−559
Cu+Ne, 800 MeV/N, p and π inclusive spectra, energy and ang. distribs. 78−54790
Cu(^{12}C, spallation), 25 GeV, mean kinetic props., momentum transfer, target recoil props. 79−3129
Cu(^{20}Ne,π$^+$), 800 MeV/N, doubly differential cross sections and ang. distribs. 80−9305
Cu(^{16,18}O, xn), 36 to 55 MeV, total neutron yelds, cross sections 77−14163
^{48}Cu(^{7}Li,^{7}Be), ^{48}K mass excess and states 80−9221
(^{63}Cu,X), 280-420 MeV, ^{149g}Tb production in deep inelastic transfer reactions, fragment ang. momentum 79−30854
^{63}Cu+^{147}Au, triple differential cross-section, dynamical model calcs. 78−50212
^{63}Cu+^{197}Au, 365 MeV deep inelastic collisions, neutron multiplicity 78−645
^{63}Cu+^{20}Ne, deep inelastic reaction, evaporation, energy thermalisation 78−94024
^{63}Cu+^{63}Cu, 450 MeV, energy spectra struct. obs. 78−4958
^{65}Cu (^{16}O, 2np), 42-58 MeV, ^{78}Kr band struct., lifetimes and E2 transitions n-p boson model anal. 79−80863
^{65}Cu+^{86}Kr, 366-716 MeV, evaporation residue product cross sections mass-charge distrib. 79−17947
^{65}Cu(^{11}B,2n), 29 MeV, ^{74}Se level scheme, J$^\pi$ assignments, bands and transitions 79−54393
^{65}Cu(^{16}O, 2np), 42-58 MeV, ^{78}Kr band struct., level scheme, from γγ-coincidence 80−18177
^{65}Cu(^{16}O,2n) 50 MeV, ^{A}Rb, A=79, 81, decoupled g$_{9/2}$ bands, level lifetimes and E2 transitons 80−73772
^{65}Cu(^{16}O,2np), ^{78}Kr high spin states, transitions and lifetimes 80−27534

heavy ion-nucleus reactions continued
^{65}Cu(^{16}O,3n), ^{78}Rb β-decay half lives of isomeric and ground state 80−27534
^{65}Cu(^{16}O,p2n), 42-58 MeV, high spin states in ^{78}Kr, band struct. 78−74387
^{65}Cu(^{19}F,2nα), ^{78}Kr high spin states, transitions and lifetimes 80−27534
^{65}Cu(^{19}F,α2n), 48-50 MeV, ^{78}Kr bands, lifetimes and E2 transitions from interacting boson model 80−73771
^{65}Cu(^{19}F,p2n), 50 MeV, ^{A}Rb, A=79, 81, decoupled $g_{9/2}$ bands, level lifetimes and E2 transitons 80−73772
^{65}Cu(^{32}S,2n2p), 120 MeV, ^{93}Tc $^{17}/_{2}$ isomer, parity mixing search, partial γ-decay widths 78−93936
^{65}Cu(^{63}Cu, X) fusion, 55-105 Mev, evaporation residue excitation functions 79−63710
^{65}Cu(^{7}Li,2n), 16-9 MeV, high-spin states in ^{70}Ge anal. 78−33146
Dy(^{40}Ar, xn)Po, 160-270 MeV, excitation functions, statistical model calcs. 77−3042
Dy(^{16}O,xn), ^{A}W, A=172-175, bands and backbending, $i_{13/2}$ neutron decoupling 80−9212
Dy(^{16}O, xn), 70-110 MeV, high spin states in ^{172,174,176}W, decoupled quasiparticle bands, backbending 78−50199
Dy(^{16}O,xn) W, γ-ray spectra, dipole moment in yrast cascade 78−37371
Dy(^{16}O, xnγ), ^{174,175}W quasicontinuum γ-rays yrast cascade dipole component, moment of inertia 80−47424
^{A}Dy(^{16}O,4n), A=161, 163, 83-89 MeV, study of CC ^{A}W, A=173, 175, high-spin states, single-particle structure 78−93922
^{162}Dy(^{13}C,4n), 64 MeV, ^{171}Hf one- and three-quasiparticle states, high spin rot. bands 80−18163
^{164}Dy(^{13}C,4n),^{173}Hf, three quasiparticle isomers and rot. bands 79−26354
^{164}Dy(^{40}AR,5n), ^{199}Po charge states and charge distrib. *(Russian)* 79−40840
^{164}Dy(^{40}Ar,X) 222, 340 MeV, fusion cross sections, direct and evaporative p and α prod., evaporation, fission 80−13518
^{164}Dy(^{40}Ar,Xn) $^{204-x}$Po, $4\leq X\leq 9$, absolute cross sections and excitation function meas. 79−13330
^{166}Er+^{86}Kr, 515 MeV, deep inelastic collisions, angular momentum dissipation within a classical friction model 79−93644
^{166}Er+^{86}Kr, 5.99 MeV/N, are γ-ray multiplicity 78−82375
^{166}Er+^{86}Kr, 5.99 MeV/N, angular-momentum dissipation in heavy-ion collisions 78−82376
^{166}Er+^{86}Kr, 602 MeV, neutron emission in strongly damped collisions 78−82373
^{166}Er+^{86}Kr, deep inelastic strongly damped collision, fragment isobaric distrib, statistical equilib. 79−40949
^{166}Er+^{86}Kr, relaxation times in dissipative collisions, fragment deformation, classical model 79−30853
^{166}Er(^{86}K,X), deep inelastic collision, charge drift and dispersion calc., thermal eqn. model based on shell model 80−57798
^{166}Er(^{86}Kr, X), 600 MeV, deeply inelastic, alignment of transferred ang. momentum, discrete γ-ray ang. correlations 80−47498
^{166}Er(^{86}Kr,X), 12.1 MeV/u, dynamical splitting of projectilelike fragments 80−42685
^{166}Er(^{86}Kr,X), 5.1-7.9 MeV/N, deep inelastic neutron emission, preequilibrium effects search 80−63200
^{166}Er(^{86}Kr,X), 8.18 MeV/amu, energy loss and nucleon exchange 80−18323
^{166}Er(^{86}Kr,X), statistical fluctuations in dissipative collisions, multidifferential cross sections 80−37399
^{166}Er(^{86}Kr,X) 6-8 MeV, dynamic equilib. process observables, energy dissipation, mass, ang. momentum 80−18336
^{166}Er(^{9}Be,4n), ^{171}Hf, three quasiparticle isomers and rot. bands 79−26354
^{168}Er(^{9}Be,4n), ^{173}Hf, three quasiparticle isomers and rot. bands 79−26354
^{170}Er(^{12}C,4n), 66 MeV, ^{178}W high spin states, yrast bands and backbending 80−13352
^{170}Er(^{9}Be, 4n), 44 MeV, ^{175}Hf, three- and five-quasiparticle isomers, rotational bands and residual interactions 80−83022
^{170}Er(^{9}Be,4n), ^{175}Hf multi-quasiparticle states and bands, isomeric states, lifetimes 80−9213
Eu(^{16}O, xn), ^{162,164,165}Lu prod., γ transitions, half-lives determ. 78−62509
F+Ne, 800 MeV/A, wide angle inclusive proton spectra 79−40951
^{19}F, nuclear dealignment of multiply ionised 3 and 6 MeV atoms recoiling in gases 80−78267
^{19}F+^{12}C, 50, 63, 76 MeV, evaporation residue mass distrib. in fusion reactions anal. 77−42004
^{19}F+^{12}C, 92 MeV, fusion and direct reactions anal. 78−21591
^{19}F+^{12}C, fusion reactions, Woods Saxon, folding and proximity pot. anals. 79−45316
^{19}F+^{27}Al, 40, 63, 76, 92 MeV, evaporation residue mass distrib. in fusion reactions anal. 77−42004
^{19}F+^{28}Si spin orbit pot., single folding model and cluster model 80−9196
^{19}F(^{6}Li,d), 16.0 MeV, DWBA anal. of α-spectroscopic factors 78−82383
^{19}F(^{6}Li,d), 36 MeV, ^{23}Na level α-spectroscopic strengths assuming direct cluster transfer 80−27552
^{19}F(^{6}Li,p), 3-15 MeV, cross sections meas. 79−76017
^{19}F(^{6}Li,p)^{24}Na cross-section meas. 79−9611
(Fe,X), 1.9 GeV/N, in emulsion, mean free paths, and fragmentation parameters 80−102197
(Fe,X), in emulsion, nuclear shock wave search 80−22747
Fe group+Ag (Br) relativistic interactions *(Russian)* 77−30634
Fe induced heavy ion reactions, 1.7 A GeV, props. of participants and spectators in non-peripheral reactions 79−49636
Fe+^{32}S, study of neutron deficient Zr isotopes 77−57621
Fe(^{6}Li,d)Ni, A=54,56,58, at 34 MeV, comparison with (t,p) and (^{3}He,n) reactions 77−30631
Fe(^{14}N,X)(^{16}O,X), Ge and Zn negative parity high spin states, spin and lifetimes 80−73768
Fe(^{16}O, ^{12}C), A=54,56, high excitation region of ^{58,60}Ni, two- and four-nucleon transfer spectra 79−6675
^{A}Fe(^{16}O, ^{12}C), 50 MeV, a=54, 56, 58, α-spectroscopic factors, DWBA anal., (^{6}Li, d) comparison 79−63585
^{A}Fe(^{6}Li,X) A=54,56, 10-100 MeV, fusion and nonfusion processes, cross sections 79−45315
^{54}Fe+^{14}N(^{12}C), single- and multi-nucleon transfer reactions at 60, 70 and 90 MeV 77−14146
^{54}Fe(^{11}B, 2pγ), 30 MeV, ^{63}Cu EM decay transitions, level J$^{\pi}$ assignments, level lifetimes 79−85402
heavy ion-nucleus reactions continued
^{54}Fe(^{11}B, npγ), 30 MeV, ^{63}Zn EM decay transitions, level J$^{\pi}$ assignments, level lifetimes 79−85402
^{54}Fe(^{12,13}C,X), elastic, inelastic and single nucleon transfer excitation functions, ^{55}Fe levels 80−13492
^{54}Fe(^{12}C,2pnγ), 50-60 MeV, ^{63}Zn level scheme, spin and parity assignments 79−465
^{54}Fe(^{14}N,X), 42.5 MeV, ^{A}Ga, A=65,67, high spin states and transitions 80−68516
^{54}Fe(^{14}N,npγ), 34-48 MeV, ^{66}Ge levels, lifetimes and mixing ratio, in-beam γ-spectroscopy 80−42541
^{54}Fe(^{18}O, ^{17}O)^{55}Fe, 50 MeV, differential cross-sections, direct one-step process 77−74828
^{54}Fe(^{18}O,2pn), ^{69}As, recoil distance level lifetime meas. 78−78311
^{54}Fe(^{28}Si,3pγ), 88 MeV, ^{79}Rb positive parity decoupled band, levels and J$^{\pi}$ 79−89223
^{54}Fe(^{32}S,X), ^{79}Sr, ^{82}Y and ^{83}Y mass excess values from beta and gamma spectra 80−63137
^{54}Fe(^{58}Ni, X), 290, 320 MeV, ^{A}Sn, A=106-108, yrast levels and transitions 80−105957
^{54}Fe(^{6}Li,t)^{57}Ni, t-energy spectra and reaction mechanism 78−41756
^{55}Fe(^{52}Cr, X), entrance channel mass asymmetry effects on reaction mechanism, fission and fusion 80−106077
(^{56}Fe,X), 0.5-2 GeV/N, on emulsion, secondary mean multiplicities and ang. distribs. *(Russian)* 80−106076
(^{56}Fe,X), 2 GeV/N, anomalous nuclei among relativistic projectile fragments 80−106034
(^{56}Fe,X), X=Al-Mn, relativistic ^{56}Fe fragmentation, charge and mass changing cross sections 79−54453
(^{56}Fe,x), isobaric charge distrib., energy loss depend. in damped collisions 80−99182
^{56}Fe (^{11}B,p2nγ), 30 MeV, ^{64}Zn high spin states, J$^{\pi}$, $T_{1/2}$, γ-decays 80−73767
^{56}Fe+^{12}C, 192 MeV, energy spectra and yields of p,d and t 78−66306
^{56}Fe+^{16}O, energy dissipation as func. of angle data comparison to classical and diffusion models 78−21604
^{56}Fe+^{238}U, 538 MeV, quasifission dominance with projectile A and Z 77−74869
^{56}Fe+^{40}Ar, 236 MeV, fragments mass and charge distribs. in deep inelastic reactions 78−58296
^{56}Fe+^{56}Fe, 8.3 MeV/amu collision, nucleon exchange and A/Z equilibration 79−76020
^{56}Fe(^{13}C, 2np), ^{56}Fe(^{15}N, n2p), ^{66,68}Ga isomeric states, lifetimes, g-factors 78−33147
^{56}Fe(^{16}O, ^{16}O'), Coulomb-nuclear interf., appl. of Austern Blair theory, comparison with DWBA 77−3043
^{56}Fe(^{16}O,^{15}N), 36-53 MeV, reaction dynamic depend. of small angle cross sections 77−18600
^{56}Fe(^{16}O,X), 81 MeV, fragments in incomplete fission 77−14153
^{56}Fe(^{16}O,2pγ), ^{70}Ge level spin and parity assignments 79−3081
^{56}Fe(^{16}O,p2n), ^{69}As, recoil distance level lifetime meas. 78−78311
^{56}Fe(^{6}Li, X), 75 MeV, Z=1 or 2 fast particle prod. mechanism above Coulomb barrier 80−42687
^{56}Fe(^{6}Li,t)^{59}Ni, t-energy spectra and reaction mechanism 78−41756
^{56}Fe(^{7}Li,p2nγ), 14-24 MeV, ^{60}Ni high spin states, J$^{\pi}$, $T_{1/2}$, ang. distribs. and polarisations 80−99116
^{57}Fe(^{12}C,X), 40 MeV, ^{A}Ga, A=65,67, high spin states and transitions 80−68516
^{57}Fe(^{12}C,pnγ)^{67}Ga, high spin states of ^{67}Ga 79−36128
^{58}Fe(^{16}O,^{14}C)^{60}Ni, 50 MeV, ^{60}Ni deduced levels, DWBA anal. 80−47380
^{160}Gα(^{12}C,α), 7.5 to 16.7 MeV/A, incomplete fusion reactions, crit. ang. momentum anal. of excitation functions 79−71862
^{71}Ga(^{7}Li,2n), 15-22 MeV, ^{76}Se high spin states, bands, J$^{\pi}$, transitions and $T_{1/2}$ 80−105951
Gd(^{40}Ar, X), 190 MeV, ^{A}Pb, A=190,192, level scheme, γ-branching, ^{192m}Pb half life 79−75854
Gd(^{13}C,5n), ^{164,166}Yb, high spin yrast states and transitions 80−9208
^{158}Gd+^{12}C, 112-164.7 MeV, fusion pre-equilibrium effects, $^{170-x}$Yb, $^{166-x}$Er, x=4-10, transitions 79−580
^{158}Gd+^{12}C, 152 MeV, fusion, pre-equilibrium particle emission 79−581
^{160}Gd(^{12}C, αxn)$^{168-x}$Er, particle fragmentation accompanied by incomplete fusion, two step model 80−86947
^{160}Gd(^{12}C,2α), 7.5 to 16.7 MeV/A, incomplete fusion reactions, crit. ang. momentum anal. of excitation functions 79−71862
^{160}Gd(^{12}C,xα), 120, 200 MeV, average α-multiplicities, incomplete fusion and breakup 80−27661
^{160}Gd(^{12}C,xαyn), 90-200 MeV, incomplete fusion, fast α prod. absolute cross sections 80−18359
^{160}Gd(^{16}O,4n), ^{172}Hf high spin states, two-quasiparticle struct. 78−25217
^{160}Gd(^{16}O,4n), 87 MeV, ^{172}Hf yrast band and high spin states, $22^{+}\rightarrow 20^{+}$ transition, band crossing 80−42523
^{160}Gd(^{16}O,5n), ^{171}Hf three quasiparticle isomers and rot. bands 79−26354
^{160}Gd(^{16}O,5n), 92 MeV, ^{171}Hf one- and three-quasiparticle states, high spin rot. bands 80−18163
^{160}Gd(^{9}Be,5n), 59 MeV, multiple high spin band struct. in ^{164}Er, backbending 78−70429
Ge+^{84}Kr, 350 MeV, compound nucleus prompt K X-rays 79−67768
Ge(^{10}B,Xγ), 40 MeV, ^{79}Rb positive parity decoupled band, levels and J$^{\pi}$ 79−89223
Ge(^{10,11}B, xγ), 31-40 MeV, ^{A}Kr, A=79, 81, high spin E2 bands, J$^{\pi}$, transitions 80−63061
Ge(^{9}Be,Xγ), 25,35 MeV, ^{79}Rb positive parity decoupled band, levels and J$^{\pi}$ 79−89223
Ge(^{12}C,Xγ), 47 MeV, ^{79}Rb positive parity decoupled band, levels and J$^{\pi}$ 79−89223
^{A}Ge+^{86}Kr, A=70, 74, 76, 50 to 120 MeV, angular momentum limits 78−25224
^{A}Ge(^{16}O,^{16}O'), A=72, 74, 76, coupled channel anal. with double folding potential 79−45282
^{70}Ge+^{32}S, 110, 132 MeV fusion evaporation residues, Monte Carlo simulation 78−41799
^{70}Ge+^{32}S, obs. of γ-cascades in ^{99}Pd and ^{99}Rh 77−30506
^{74}Ge, ^{76}Ge, two-proton transfer reactions induced by 56 MeV ^{16}O beam, spectroscopic anal. 77−14178
^{74}Ge(^{12}C,3n)^{83}Sr, high spin states and spin ordering, γ-ray excitation functions 78−66199
^{74}Ge(^{12}C,p2n), 35-49 MeV, ^{83}Rb high spin states, Jπ and transitions 80−105949

heavy ion-nucleus reactions continued
^{74}Ge(^{18}O,^{16}O), (^{18}O,^{17}O), (^{18}O,^{18}O), 75 MeV, ang. distrib. meas., multistep process 77−82953
^{74}Ge(^{18}O,^{16}O)^{76}Ge, coupled-channel Born approx. anal. 77−82954
^{74}Ge(^{84}Kr,xn), ^{84}Kr excitation function for ^{152,153}Er prod. 79−22315
^{76}Ge(^{12}C,3n)^{85}Sr, high spin states and spin ordering, γ-ray excitation functions 78−66199
^{76}Ge(^{16}O,^{18}O), (^{16}O,^{16}O), 77.6 MeV, ang. distrib. meas., multistep process 77−82953
^{76}Ge(^{16}O,^{18}O)^{74}Ge, coupled-channel Born approx. anal. 77−82954
^{76}Ge(^{86}Kr,xn), 314-376 MeV, γ-multiplicity meas., Er compound nucleus formation 79−89320
H(^{11}B,α)2α used to meas. surface H conc. on ultra cold neutron container materials 80−9446
(HI,X), inclusive pion prod., forward and backward π spectra 79−85484
(HI,π), π radiation from relativistic heavy ion 80−73863
^{1}H(^{11}B,α)αα, H profile distrib. in metals for defect-impurity interaction study 79−5206
^{1}H(^{15}N, αγ)^{12}C, ^{15}N hydrogen profiling method using γ-ray detection 79−5195
^{1}H(^{15}N, αγ)^{12}C, appl. to quantitative H analyses in different materials problems 79−5196
^{1}H(^{15}N,αγ), use for H depth profiling in materials *(French)* 78−91357
^{1}H(^{15}N,αγ)^{12}C, energy loss of ^{15}N in solids, use in ^{1}H profiling 78−59845
^{1}H(^{19}F, αγ)^{16}O, appl. to quantitative H analyses in different materials problems 79−5196
^{2}H(^{13}C,p), 18.9 MeV, ^{14}C first excited 0^+ state, lifetime and E^0 decay 80−102145
^{2}H(^{20}Ne,nγ)^{21}Na, ^{21}Na energy level lifetime 78−41631
^{2}H(^{20}Ne,p)^{21}Ne, mag. moment, g-factor and lifetime meas. of 351 keV $^{5}/_{2}^{+}$ state 78−41631
^{2}H(^{20}Ne,pγ), Doppler shift attenuation lifetime meas. in ^{21}Ne 77−30513
^{2}H(^{40}Ar,nγ)^{41}K, ^{2}H(^{40}Ar,pγ)^{41}Ar, 56 MeV, γ-decays of low-lying states in ^{41}K, ^{41}Ar obs. 77−41986
^{2}H(^{40}Ca, p), 60 MeV, ^{41}Ca, lifetimes of excited $3/2^-$ states 78−70487
^{2}H(^{6}Li,α) 10-31 MeV, ^{8}Be αα* rot. levels search 79−22175
^{3}H(^{13}C,p) 24 MeV, ^{15}C 0.74 MeV $5/2^+$ state g-factor, shell model interpretation 80−32176
^{3}H(^{18}O, pγ), 24.5 MeV, ^{20}O first excited state, g-factor and lifetime 80−102115
^{3}H(^{35}Cl,pγ)^{37}Cl, γ-ray spectroscopy of ^{37}Cl 78−13013
^{4}He+U, relativistic ions, product spectra, statistical models 78−638
^{4}He(^{14}N,α), 8.1-8.3 MeV, ^{18}F $J^{\pi}=3^-$ doublet at 6241 keV, isospin mixing 80−511
^{4}He(^{18}O,n), 20-27 meV, ^{21}Ne 2796, 1747, 2867 keV level mean lifetimes 79−93553
^{4}He(^{19}F,p)^{22}Ne, lifetime of lowest 4^+ state in ^{22}Ne, Doppler shift meas. 78−37307
^{4}He(^{28}Si,p)^{31}P, precision Doppler-shift attenuation lifetime meas. from γ-ray lineshapes 79−36195
^{4}He(^{6}Li,γ)^{10}B, test of weak-interaction models 77−331
^{4}He(^{7}Li,γ)^{11}B, 1.68 MeV, appl. to He concentration profile determ. in materials, meas. technique 79−5200
^Hf(HI,xn), A=170-173, two and three quasiparticle isomers, rot. bands, decays and lifetimes 80−9211
^{171}Hf, hindered electric dipole transitions and lifetimes from (HI,xn) reactions 80−9263
^{176}Hf(^{40}Ar, X), $^{212,\ 213,\ 214}$Th decay energies and half lives 80−47440
^{204}Hg(^{13}C, 5n), ^{212}Rn high spin isomers, excited core states coupled to valence protons 77−74745
^{204}Hg(^{13}C, 5n), ^{212}Rn high spin isomers with core excited neutron configs. 78−54792
^{204}Hg(^{13}C,5nγ)^{212}Rn, high spin yrast states in N=126 isotones 79−45131
^{204}Hg(^{16}O,^{12}C), 88 MeV, ^{208}Pb α-vibr. states 77−38218
^{204}Hg(^{17}O,^{16}O), 85 MeV, 75 MeV, obs. of excited states in ^{206}Hg 77−6242
^{204}Hg(^{18}O,^{16}O), 75 MeV, obs. of excited states in ^{206}Hg 77−6242
^{165}Ho + ^{86}Kr, 618 MeV, γ-ray multiplicities and angular momentum fractionation 78−37370
^{165}Ho+ ^{56}Fe, 8.3 MeV/amu collision, nucleon exchange and A/Z equilibration 79−76020
^{165}Ho+ ^{84}Kr, 714 MeV, statistical model for mass and charge distrib. 79−17929
^{165}Ho+ ^{84}Kr, damped collision, interaction time 78−637
^{165}Ho(^{165}Ho,X), deep inelastic, spin and transferred ang. momentum alignment 80−106043
^{165}Ho(^{24}Mg,4n), collective band struct. in ^{185}Au 79−22166
^{165}Ho(^{40}Ar,X), 192, 297 MeV, ^{205}At mass distribution width for fission and quasifission 79−63707
^{165}Ho(^{56}Fe, xn HI), 8.5 MeV/u, damped collision α- and n-emission, n multiplicities 79−93653
^{165}Ho(^{86}Kr,X), 620 Mev, deep inelastic scatt., ang. momentum transfer, γ-ray multiplicities 80−27665
I-Au system, superheavy quasi-atom with Z=132, X-ray spectra 77−14177
^{127}I(^{19}F,4n), ^{142}Sm ns isomers and yrast isomers, γ-transitions 80−78121
^{115}In (^{12}C,X), 69.0, 83.0, 117.0 MeV, ang. distribs. for target residues 77−50150
^{115}In (^{14}N,X), 130, 97 MeV, ang. distribs. for target residues 77−50150
^{115}In(^{12}C,4n)^{123}Cs, in-beam γ-ray spectroscopy, decoupled band in ^{123}Cs obs. 78−21520
Ir+^{20}Ne, 200 MeV, yields of neutron-deficient isotopes of Fr and Rn *(Russian)* 77−23104
^{191}Ir(^{6}Li, xn+yp), 48-156 MeV, excitation functions 77−18603
^{193}Ir(^{6}Li, xn+yp), 48-156 MeV, excitation functions 77−18603
K (Ar, π^+X), 250, 400 MeV/A, pion yield near threshold 80−18344
K+ ^{84}Kr, 350 MeV, compound nucleus prompt K X-rays 79−67768
K+Ar, 800 MeV/A, wide angle inclusive proton spectra 79−40951
K(Ar,X), 0.4-1.8 GeV/u, multipion prod. energy depend. 80−106065
K(Ar,X), 800 MeV/N, single particle spectra from high multiplicity events 80−99184
K(Ar,X), proton inclusive spectra, direct plus thermal model 80−57799
^{39}K+ ^{14}N fusion-evaporation reaction γ-ray spectroscopy study of ^{51}Mn structure 77−18471
^{39}K(^{39}K,X), π^0 condensation, spin-isospin instabilities, TDHF calcs. 80−83042
Kr induced deeply inelastic collisions, transport eqn. appl. 78−82380
^{84}Kr+ ^{209}Bi, 712 MeV, deform. and transfer in strongly damped collisions 78−21601

heavy ion-nucleus reactions continued
^{84}Kr+ ^{209}Bi, probabilistic model for deep inelastic reactions 77−71623
^{139}La(^{86}Kr, X), TDHF fusion calcs., fusion cross sections 80−37409
^{139}La(^{86}Kr,X), 505, 610, 710 MeV, TDHF calcs., fusion behaviour 80−9323
Li(^{6}Li,^{8}B), 80,93 MeV, ^{4}H, ^{5}H energy levels anal. 77−46183
(^{6}Li,X), 156 MeV, projectile break up in continuous particle spectra, cross section, fragmentation 80−86889
(^{6}Li,d), A=20 to 68, DWBA reduction, ground state α-transfer strengths 80−106068
(^{6}Li,d), A∼60,116, L=0 transitions, cross sections, microscopic anal. 80−78189
(^{6}Li,d), α-clustering and spectroscopic factors, shell effects and deformation correlations 79−6436
(^{6}Li,d), ground state transitions in 1f-2p shell, 34 MeV, spectroscopic factors 79−6670
(^{6}Li,d), pairing vibration model with isospin, α-transfer reactions on A=40-62 nuclei 78−17242
(^{6}Li,d) on odd A, sd shell nuclei, α-cluster spectroscopic strengths, DWBA anal. 79−3104
(^{6}li,d) reaction systematics on doubly even fp shell targets 77−65233
(^{6}Li,d) reactions on even-even fp shell nuclei, review, structure effects 77−67763
^{6}Li induced reactions, depth distrib. of light elements in materials 77−16888
^{6}Li, surface anal. using ^{6}Li ion beams 79−5211
^{6}Li+^{6}Li, effect on reaction rate of fusion reactor with ^{6}Li(p,α)^{3}He cycle 79−22459
^{6}Li+^{6}Li→2α+2d, double spectator poles and quasi-free inelastic scattering 79−93646
^{6}Li+^{6}Li→^{3}He, 0.5-2.75 MeV, meas. of cross sections and fusion parameters 78−50223
^{6}Li(^{14}N, αd)^{14}N, 19.5 MeV, disintegration mechanism *(Russian)* 77−34346
^{6}Li(^{6}Li, 3α), 2 MeV, DWBA anal. of direct prod. of 3 α final states 77−74882
^{6}Li(^{6}Li,^{5}He)^{7}Be, 3-15 MeV, cross sections meas. 79−76017
^{6}Li(^{6}Li,αα)α, 36 to 46 MeV, reaction mechanism 80−83113
^{6}Li(^{6}Li,an)^{7}Be cross section, 1.6 to 5.0 MeV 77−50146
^{6}Li(d,α)α^+, 1.2-12 MeV, $\alpha\alpha^+$ rotational band existence in ^{8}Be 79−13192
^{6}Li→^{3}He+^{2}H+n (^{3}H+^{2}H+p), zero degree fragmentation of relativistic ^{6}Li 79−85438
(^{7}Li,^{7}Li), aligned Li ions, electric quadrupole moment of ^{7}Li 80−78141
^{7}Li+^{7}Li reaction, 2 MeV, neutron energy spectrum meas. using nuclear emulsion technique 78−62573
^{7}Li(p,α)α^+, 4.5-12 MeV, $\alpha\alpha^+$ rotational band existence in ^{8}Be 79−13192
^{175}Lu+^{19}F, 142 MeV fission ^{1}H and ^{4}He emission from ^{194}Hg compound nucleus 78−50220
^{175}Lu(^{12}C,f), fission probability calc., α emission and evaporation effects 78−657
^{175}Lu(^{16}O,6n), collective band struct. in ^{185}Au 79−22166
Mg+^{14}N or ^{16}O, high spin states prod. in ^{35,36,37}Cl and ^{37}Ar, decay schemes 77−2932
^{24}Mg+^{12}C, 42-84 MeV, binary fragmentation, kinematical anal. 78−25223
^{24}Mg+^{16}O system, high spin cluster-like resonances 17-31 MeV 79−6664
^{24}Mg(^{12}C,α), 27.5-35.5 MeV, ^{36}Ar resonances 79−67629
^{24}Mg(^{136}Xe,4n), 595 MeV, ^{156}Dy high spin states lifetimes and feeding times, quadrupole moments 80−32239
^{24}Mg(^{16}O, 2pγ), 38, 45 MeV, ^{38}Ar yrast levels, J^{π} assignments, transitions, branching and mixing ratios 79−67625
^{24}Mg(^{16}O,^{12}C), 17-31 MeV, ^{28}Si backward angle cross section, entrance channel resonance effects 79−30813
^{24}Mg(^{16}O,^{12}C), 24-40 MeV, backward angles, ^{28}Si excitation functions, ang. distribs. and resonant behaviour 80−68622
^{24}Mg(^{16}O,^{12}C), 26.3-32.4 MeV, ^{28}Si excitation functions, ang. distribs., resonance spin assignments 80−68623
^{24}Mg(^{16}O,^{12}C)^{28}Si, excitation functions for O^+ and 2^+ states of ^{28}Si 78−54800
^{24}Mg(^{16}O,^{16}Oγ), 42 MeV, ang. correl. meas. 77−41989
^{24}Mg(^{16}O,2pγ), 38 MeV, model independ. J^{π} assignments in ^{38}Ar 77−18384
^{24}Mg(^{16}O,pαγ), 45 MeV, model independ. J^{π} assignments in ^{35}Cl 77−18384
^{24}Mg(^{18}O, ^{14}C)^{28}Si, ground-state excitation function structure 79−63694
^{24}Mg(^{18}O,p2nγ), ^{39}K high spin states, decay scheme 78−25232
^{24}Mg(^{6}Li,t)^{27}Si, t-energy spectra and reaction mechanism 78−41756
^{25}Mg(^{12}C,^{9}Be), 100, 120 MeV, ^{28}Si 8^+ state, level systematics and energy spectra 80−42528
^{26}Mg+^{18}O, 34 MeV, yrast states in ^{41}K, ^{41}Ca, spins, parities from γ meas. 78−58250
^{26}Mg(^{11}B,^{10}B)^{27}Mg, semiclassical approxs. for heavy-ion transfer reactions 78−94021
^{26}Mg(^{11}B,^{10}B)^{27}Mg, 114 MeV, transfer amplitude and ang. distribs. 79−59081
^{26}Mg(^{11}B,^{10}Be)^{27}Al, semiclassical approxs. for heavy-ion transfer reactions 78−94021
^{26}Mg(^{11}B,^{11}B), (^{11}B,^{10}B), (^{11}B,^{10}Be), 31 MeV, optical model and DWBA anal. 77−26785
^{26}Mg(^{136}Xe, 4n), 4.1 MeV, ^{158}Dy band side feeding pattern and γ-multiplicities, statistical model 79−75821
^{26}Mg(^{136}Xe, 4n), prod. of ^{158}Dy Yrast states, lifetimes 78−54793
^{26}Mg(^{136}Xe, 4n) CC ^{158}Dy high spin states B(E2) values, IBA model test 80−27541
^{26}Mg(^{136}Xe,4n), kinematic correction method for high resolution in-beam conversion electron spectroscopy 79−54739
^{26}Mg(^{13}C, ^{12}C), ^{26}Mg(^{13}C, ^{14}C), 35 MeV, inelastic effects, DWBA, CCBA calcs. 77−3041
^{26}Mg(^{14}N, ^{10,11}B), 60-95 MeV, ^{29,30}Si states, reaction mech., spectroscopic factors 78−66299
^{26}Mg(^{16}O, ^{14}C)^{28}Si, full recoil one and two step DWBA anal. 78−70564
^{26}Mg(^{16}O, ^{16}O'), Coulomb-nuclear interf., appl. of Austern Blair theory, comparison with DWBA 77−3043
^{26}Mg(^{16}O,^{15}N), 36-53 MeV, reaction dynamic depend. of small angle cross sections 77−18600
^{26}Mg(^{16}O,^{18}O), ^{24}Mg ground and γ-bands, direct and multistep processes 80−102094

heavy ion-nucleus reactions continued
^{26}Mg(^{16}O,X), complete fusion, 25-70 MeV evaporation residue cross section, total fusion excitation functions 79−13370
^{26}Mg(^{18}O,^{14}O), 87 MeV, cross section of stripping reaction, ^{30}Mg mass excess 79−3075
^{26}Mg(^{18}O,^{15}O), 85 MeV, ^{29}Mg mass excess 79−3075
^{26}Mg(^{18}O,^{16}O), 50 MeV, ^{28}Mg, differential cross sections for lowest four states 79−67661
^{26}Mg(^{18}O,^{17}F), 87 MeV, ^{27}Na excited states and mass excess 79−3075
^{55}Mn (^{12}C,X), 77 MeV, fragments in incomplete fission 77−14153
^{55}Mn+^{12}C, energy dissipation as func. of angle data comparison to classical and diffusion models 78−21604
^{55}Mn(^{14}N,X), (^{16}O,X), Ge and Zn negative parity high spin states, spin and lifetimes 80−73768
^{55}Mn(^{16}O, pn), 42.5, 47.5 MeV, ^{69}Ge high spin states, EM props., Branching and mixing ratios 80−13347
^{55}Mn(^{16}O,2n), ^{69}As, recoil distance level lifetime meas. 78−78311
^{55}Mn(^{16}O,pn), 37.5-50 MeV, ^{69}Ge high spin states, J assignment, decay scheme 80−68518
^{55}Mn(^{16}O,pnγ), 44 MeV, ^{69}Ge level structure and lifetimes, decay through negative parity band 79−45172
Mo, reactions induced by ^{12}C and ^{19}F ions, γ-ray spectroscopy of induced activities 77−23107
Mo(^{6}Li,^{8}B), 90 MeV, ^{92,96}Zr first excited 0^+ state transition strength 80−78260
^{A}Mo+^{86}Kr, A=92, 98, deep inelastic reactions, fast collective mode, quantal fluctations 79−67636
^{92}Mo(^{16}O,X), entrance channel mass asymmetry effects on reaction mechanism, fission and fusion 80−106077
^{94}Mo(^{12}C, 3nγ), 44-65 MeV, ^{103}Cd levels, J^π and positive parity decoupled band, rotor anal. 80−102096
^{94}Mo(^{12}C,p2nγ), ^{103}Ag collective excitation and J^π, rotor-plus-particle model 80−86782
^{96}Mo(^{13}C,3nγ), 45 MeV, ^{106}Cd collective and yrast levels, γ-transitions, 2 quasiparticle+rotor model 79−22169
^{97}Mo(^{12}C,3nγ), 45 MeV, ^{106}Cd collective and yrast levels, γ-transitions, 2 quasiparticle+rotor model 79−22169
^{98}Mo(^{14}N,4nγ), 50-75 MeV, ^{108}In high spin struct., in-beam spectroscopy, conversion electrons 80−73782
^{100}Mo+^{100}Mo→^{200}Po, two dimensional fusion barrier, penetrability calc. 78−41798
^{100}Mo+^{48}Ca→^{144}Sm, γ-ray multiplicity spectra, nuclear shape at high angular momentum 78−37260
^{100}Mo(^{12}C,^{10}Be)^{102}Ru, 48 MeV, anal. of direct and indirect processes 77−34342
^{100}Mo(^{14}N, ^{12}B)^{102}Ru, 90 MeV, semiclassical analysis of ^{12}B spin polarisation 78−33212
^{100}Mo(^{14}N,^{12}B), ^{12}B polarisation, quantum mechanical explanation 79−17890
^{100}Mo(^{14}N,^{12}B), 200 MeV, ^{12}B spin polarisation meas. 79−3168
^{100}Mo(^{14}N,^{12}B), 200 MeV, ^{12}B spin polarisation in deep inelastic collision 80−63160
^{100}Mo(^{14}N,^{12}B), 90 meV, spin alignment of products, semi-classical model calcs. 80−73859
^{100}Mo(^{14}N,^{12}B)^{102}Ru, 90 MeV, meas. of ^{12}B spin polarisation 77−71562
^{100}Mo(^{14}N,^{12}B)^{102}Ru, 90 and 125 MeV, spin polarisation of ^{12}B 78−50196
N(^{12}C,X), 4.5 GeV/c, emission of short range particles (R<100 mkm) *(Russian)* 80−63202
(^{14}N,x), multinucleon transfer reactions on Cr, Zr and Mo isotopes, Q-values 77−3045
(^{14}N,xnγ), rare earth nuclei, complete fusion process n and γ multiplicity 80−18363
(^{14}N, αX), 156 MeV, heavy ion-alpha in-plane correlations 80−18343
^{14}N-induced reactions energy relax. during fusion determ. by preequilib. α emission 79−26446
^{14}N+^{10}B, 100 MeV, 2n and 2p transfer reacts., DWBA anal. 78−50207
^{14}N+^{10}B, sub Coulomb energy, fusion cross section, optical model anal. 77−34335
^{14}N+^{12}C, 112 MeV, alpha clustering, multiple shape vibrs., TDHFC calcs. 79−3164
^{14}N+^{12}C, 34.1-178.1 MeV, fusion and peripheral reaction cross sections, direct yield 79−67771
^{14}N+^{12}C, fusion reactions, Woods Saxon, folding and proximity pot. anals. 79−45316
^{14}N+^{12}C, TDHF appl. 78−54709
^{14}N+^{12}C, time-depend. Hartree-Fock calcs. 77−46125
^{14}N+^{12}C(^{16}O), 3.6-12.6 MeV, total fusion cross sections meas. 77−42002
^{14}N+^{16}O, 20-60 MeV, compound nucl. form. 78−4954
^{14}N+^{27}Al, 100 MeV, energy relaxation and mass transfer *(French)* 80−95327
^{14}N+emulsion nuclei, 2.1 GeV/nucleon interactions 77−41991
^{14}N(^{12}C,α), 39.3 MeV, ^{22}Na deduced levels 78−93944
^{14}N(^{14}N,X) 9.4-22.0 MeV, low energy fusion cross sections 77−14152
^{14}N(^{14}N,α)^{24}Mg, 10.1 MeV, Hauser-Feshbach calcs. 79−63696
^{14}N(^{7}Li,p), 16 MeV, cross section, ^{20}F energy levels, spin, parity 78−21596
^{14}N(^{7}Li,t)^{18}F, 4p-2H, 1^+ rot. band in ^{18}F anal. 77−79299
^{15}N+X, X=^{11}B, ^{12}C,^{18}O,^{13}C, deduced excited states, shell model wave functions, DWBA anal. 79−45284
^{15}N(^{15}N,X), π^0 condensation, spin-isospin instabilities, TDHF calcs. 80−83042
^{15}N(^{7}Li,t), 40 MeV, ^{19}F final state selective population, triton clustering from band anal. 80−9306
Na+Ne, 800 MeV/A, wide angle inclusive proton spectra 79−40951
NaF+^{20}Ne, 800 MeV nucleon^{-1}, inclusive proton production, classical many-body calc. 79−17918
NaF+Ne, 800 MeV/N, p and π inclusive spectra, energy and ang. distribs. 78−54790
NaF+Ne, evidence for blast wave production in fireball explosions 79−49592
Na(Ne,X), 800 MeV/N, direct vs. thermal particle emission, inclusive cross sections 80−52688
Na(^{20}Ne,π^+), 800 MeV/N, doubly differential cross sections and ang. distribs. 80−9305
^{23}Na α-transfer spectroscopic factors from shell model wave functions of ^{19}F(^{6}Li,d) 79−36149
^{23}Na(^{19}F,X) complete fusion, 25-70 MeV evaporation residue cross section, total fusion excitation functions 79−13370

heavy ion-nucleus reactions continued
Nb+Nb, 67 MeV, Doppler shift and anisotropy of quasimolecular X-rays 77−3048
^{93}Nb+^{16}O, 50-65 MeV, radiative capture cross sections upper limits 79−17923
^{93}Nb(^{14}N,X), 210 MeV, deep inelastic, particle-particle correlations for Li, Be, B, C 80−63206
^{93}Nb(^{63}Cu,F), (^{63}Cu,X), 280 MeV deep inelastic collisions, mass and KE distrib. 77−26783
^{93}Nb(^{84}Kr, αxn)^{A}Re, x=5,6,7, A=168, 167, 166, isotope existance evidence 79−503
^{93}Nb(^{84}Kr, xn)^{A}Ir, x=78, A=170, 169, isotope existance evidence 79−503
Nd+^{12}C, 70.4 MeV, excitation of 3^- states in ^{148,150}Nd deformed nuclei 78−62559
Nd(^{12}C,xn), 65,90 MeV, Dy K-shell internal conversion yields, gamma transition multipolarities 80−78215
Nd(^{12}C, xnγ), 70-100 MeV, ^{A}Dy, A=152, 153, isomeric states and complex band structs. 79−67624
Nd(^{16,18}O,X), 47-116 MeV, Er γ-multiplicities and cross sections, neutron evaporation 80−73824
Nd(^{16,18}O,4n)^{162}Er, γ multiplicities, side feeding pattern, Monte Carlo calcs. 79−578
Nd(^{16,18}O, xnγ), 69-78 MeV, ^{161,162}Er high ang. momentum states, γ decay modes from multiplicity meas. 78−29419
^{A}Nd(^{6}Li,xnypγ), A=142, 146, 150, 54-99 MeV, determ. of cross sections 78−66307
^{142}Nd(^{10}B,3n)^{149}Tb, high spin states obs. 80−18158
^{142}Nd(^{12}C,3nγ), 60, 62 MeV, ^{151}Dy levels, bands and transitions, in-beam γ-rays 80−458
^{142}Nd(^{13}C,^{13}C′), 67.5 MeV, nuclear and Coulomb deform. parameters from DWBA anal. 77−3032
^{142}Nd(^{16}O, ^{14}C), 104 MeV, two proton transfer between pairing rot. states 77−10430
^{142}Nd(^{16}O,4n), 100 MeV, ^{154}Er yrast trap and transitions, decay scheme 80−9206
^{142}Nd(^{6}Li, 3nγ), 25-33 MeV, ^{145}Eu high spin core coupled states and transitions 80−42520
^{142}Nd(^{6}Li,3nγ) 32,34 MeV, ^{145}Eu high spin states, J^π and transitions 80−47350
^{142}Nd(^{7}Li,4nγ) 32,34 MeV, ^{145}Eu high spin states, J^π and transitions 80−47350
^{144}Nd(^{12}C,^{14}C)^{142}Nd, 78 MeV, Coulomb excitation effect 77−46186
^{144}Nd(^{12}C,3n)^{153}Dy, 59 MeV, level lifetimes, instrument testing 78−13375
^{144}Nd(^{12}C,6n)^{150}Dy, 112 MeV, high spin isomers of ^{150}Dy, gamma-ray spectra 78−50075
^{145}Nd(^{14}N,4n), 65-86 MeV, ^{155}Ho high spin states, lifetimes, J^π and rot. parameters 79−85354
^{146}Nd(^{12}C,8n)^{150}Dy, 118 MeV, high spin isomers of ^{150}Dy, gamma-ray spectra 78−50075
^{146}Nd(^{16}O,X), 142 MeV, narrow window for incomplete fusion 80−95325
^{146}Nd(^{20}Ne,4n or 5n), continuum transitions in nuclei at high ang. momenta, are multipolarity 79−17849
^{148}Nd+^{19}F, 166 MeV, massive transfer accompanying proton, dueteron and triton emission 79−93648
^{148}Nd(^{13}C, 5n), 65-84 MeV, ^{156}Dy high spin states, γ-ang. distribs., lifetimes and feeding times 80−13364
^{148}Nd(^{16}O,4n), 85 MeV, ^{160}Er continuum γ-ray multipolarity by linear polarisation meas. 79−85408
^{150}Nd+^{150}Nd→^{300}120, effect of nuclear force finite range on fission and heavy-ion reactions 78−13180
^{150}Nd+^{20}Ne, 128 to 172 MeV, γ-ray multiplicities in evaporation residues 77−14065
^{150}Nd+^{20}Ne, 174.8 MeV, fusion, pre-equilibrium particle emission 79−581
^{150}Nd+^{20}Ne, 175 MeV, cross sections and energy spectra 78−41760
^{150}Nd(^{18}O,4n)^{164}Er, multiple band crossings in ^{164}Er 78−37257
^{150}Nd(^{18}O,4nγ), 69 MeV, ^{164}Er high spin props. in multiple band crossing region 80−83023
^{150}Nd(^{20}Ne, xnγ), multipolarities of yrast and statistical cascades, total γ conversion coeff. 78−70484
^{150}Nd(^{20}Ne,X), 115, 130 MeV, γ-continuum multiplicity distrib., yrast bump 80−9265
^{150}Nd(^{20}Ne,xnαγ), angular momentum effects in pre-equilibrium processes 78−50208
^{150}Nd(^{20}Ne,xnγ), angular momentum effects in pre-equilibrium processes 78−50208
^{180}Nd(^{12}C,xn), deformed Dy quasicontinuum spectrum, M1, E1, E2 components 80−498
(Ne, π^-X), 800 MeV/A, π^- energy and ang. distribs., firestreak and hard scatt. model anal. 80−13498
Ne, 800 MeV interactions, inclusive proton spectra 78−70557
Ne+Ne, classical many-body model for heavy ion collisions 80−536
Ne+W, 340 MeV/nucleon, multiplicities and ang. distrib. 79−93661
Ne(^{6}Li,d)Mg, 32 MeV, Mg α-particle spectroscopic strengths calc. 77−41987
Ne(Ne,X), 117-800 MeV, classical eqns. of motion calcs., central collisions, thermal models 80−106070
(^{20}Ne,X), relativistic collisions, slow and fast fragment correlations, multiplicity association 80−86886
(^{20}Ne, π^+X), 400 MeV/N, pion prod. doubly differential cross sections and ang. distrib. 80−32299
^{20}Ne+^{12}C, 110 MeV, complete identification of products of reaction 77−88165
^{20}Ne+^{12}C, 6.3-13.8 MeV, total fusion cross section, S-factor, γ-yields 80−22877
^{20}Ne+^{20}Ne, 250-1000 MeV/N, intranuclear cascade calcs. for multiplicity and cross sections 80−32300
^{20}Ne+^{238}U, 250 MeV/nucleon and 2.1 GeV/nucleon, relativistic fluid dynamic anal. 77−74877
^{20}Ne+^{27}Al, deep inelastic fragment energies, rot. energy contributions 79−63697
^{20}Ne+^{58}Ni, 164 MeV, alpha clustering, multiple shape vibrs., TDHFC calcs. 79−3164
^{20}Ne+Al, relativistic ions, product spectra, statistical models 78−638
^{20}Ne+U, relativistic ions, product spectra, statisical models 78−638
^{20}Ne+U→^{A}Z+X, 400 MeV/nucleon, excited nuclear matter prod. 77−50154

heavy ion-nucleus reactions continued
^{20}Ne+emulsion nuclei, evidence against copious threshold pion prod. 78−37362
^{20}Ne+emulsion nuclei, Monte Carlo simulation pion and proton multiplicities 78−37363
^{20}Ne(^{12}C,X), 24-42 MeV, complete fusion, total cross section, excitation function 80−68717
^{20}Ne(^{12}C,X), 66.5 MeV, evaporation residue ang. and energy distribs. from statistical model anal. 80−83110
^{20}Ne(^{12}C,X), X=p,d,α, 7-17 MeV, ^{32}S resonances and excitation functions, Hauser Feshbach anal. 80−78249
^{20}Ne(^{20}Ne,X), 132 MeV, TDHFB calc. for total fusion cross section 80−13521
Ni+^{12}C, 107, 155, 197 MeV, evaporation residue Se, prompt γ deexcitation 78−74395
Ni+^{16}O, 100 MeV, deep inelastic, γ-circular polarisation and spin orientation 79−17848
Ni+^{20}Ne, 164 MeV, ang. distribs., total reaction and evaporation residue cross sections 79−565
Ni+^{84}Kr, 350 MeV, compound nucleus prompt K X-rays 79−67768
Ni(^{6}Li,d)^{62,64}Zn, multipole pairing states, correspondence between 2 and 4 particle transfer reactions 78−62569
Ni(^{18}O,^{20}Ne), even Ni isotopes, 63 MeV, energy spectra, ang. distribs., spectroscopic strengths 77−335
Ni(^{16}O,^{18}O), surface transparent pots., and CCBA anal. of diffractive behaviour 78−50206
Ni(^{16,18}O, xn), 36 to 55 MeV, total neutron yields, cross sections 77−14163
^{A}Ni+^{35}Cl, A=58, 62, 155-170 MeV, fission prod. yields, ang. distribs. and mean kinetic energies 78−41790
^{A}Ni(^{40}Ca, fusion), A=58, 60, 62, 113-170 MeV, fusion cross sections and excitation functions 80−32315
^{58}Ni+^{11}B, 116 MeV, in-plane heavy ion-alpha particle correlations 79−17921
^{58}Ni+^{14}N, 148 MeV, 2-particle pre-emission meas. 79−93649
^{58}Ni+^{16}O, ^{74}Kr prod., charged particle evaporation 80−47453
^{58}Ni+^{16}O, 100 MeV, γ-ray circular polarisation meas. 78−54788
^{58}Ni+^{16}O, 96 MeV, particle spectra for hot spot emission 79−22312
^{58}Ni+^{16}O, deep-inelastic collisions, light particle pre-equilibrium emission 78−54786
^{58}Ni+^{16}O deep inelastic collision, hot spot particle emission 78−13152
^{58}Ni+^{16}O fusion, 30-70 MeV, statistical model calcs., yrast states and continuum feeding times 79−579
^{58}Ni+^{208}Pb(^{238}U), 7.5 MeV/amu, ang. momentum transfer in deeply inelastic collisions from exclusive sequential-fission expts. 79−76044
^{58}Ni+^{23}Na, deformed aligned projectile ions, elastic scatt., fusion, polarisation effects 78−58303
^{58}Ni+^{32}S, 110, 132 MeV, fusion evaporation residues, Monte Carlo simulation 78−41799
^{58}Ni+^{32}S, study of neutron deficient Zr and Nb isotopes 77−57621
^{58}Ni+^{58}Ni(^{63}Cu), 290 MeV, prod. of neutron-deficient Te, I, Xe 77−88171
^{58}Ni(^{10}B,pnγ), 28.5 MeV, ^{66}Ge levels, lifetimes, J$^{\pi}$ and transitions 80−73799
^{58}Ni(^{10}B,pnγ), 28.5-30 MeV, ^{66}Ge states and decay scheme, polarisations J$^{\pi}$ and ang. distribs. 80−22692
^{58}Ni(^{12}C, 2p), ^{68}Ge multiple band struct., $g_{9/2}$ orbital, level lifetimes 80−13358
^{58}Ni(^{12}C,2p)^{68}Ge, E=36 MeV, lifetimes of ^{68}Ge excited states 78−13020
^{58}Ni(^{12}C,αp), 39 MeV, ^{65}Ga high spin states, J$^{\pi}$ and transitions, triaxial struct. 80−63062
^{58}Ni(^{16}O, 2pγ), 54.5, 59.5, 64.5 MeV high spin and excitation energy regions in ^{72}Se, γ cascade 78−54795
^{58}Ni(^{16}O, X), 70 MeV, compound nuclei charged particle evaporation, moment of inertia 80−57785
^{58}Ni(^{16}O,^{12}C), 46, 60 MeV, DWBA anal. with optical pot., ^{62}Zn levels 79−6694
^{58}Ni(^{16}O,X), 100 MeV, deep inelastic, fragment spin polarisation and alignment, γ-rays 80−18284
^{58}Ni(^{16}O,2p), ^{72}Se recoil distance level lifetime meas. 78−78311
^{58}Ni(^{16}O,2p), 52.5 MeV, ^{72}Se side band struct., negative parity states and transitions 80−73769
^{58}Ni(^{16}O,2pγ), 40-58 MeV, γ ang. distribs., coincidences, ^{72}Se yrast states, lifetimes 77−54176
^{58}Ni(^{16}O,2pγ)^{72}Se, 54.5-64.5 MeV, high spin and excitation regions anal. 78−25226
^{58}Ni(^{16}O,αα), 70 MeV, ang. correl. in compound nucleus decay 79−36261
^{58}Ni(^{16}O,αp), ^{69}As, recoil distance level lifetime meas. 78−78311
^{58}Ni(^{16}O,αp), 70 MeV, ang. correl. in compound nucleus decay 79−36261
^{58}Ni(^{16}O,pp), 70 MeV, ang. correl. in compound nucleus decay 79−36261
^{58}Ni(^{32}S,X), ^{79}Sr, ^{82}Y and ^{83}Y mass excess values from beta and gamma spectra 80−63137
^{58}Ni(^{40}Ar,X), 280 MeV, deep inelastic, light fragments, thermal equilib., ang. momentum transfer 80−63203
^{58}Ni(^{58}Ni,X), optical potential, nuclear matter approach 80−57801
^{58}Ni(^{58}Ni,xpyn), alpha decay studies of neutron deficient isotopes produced 79−93567
^{58}Ni(^{6}Li,Zn), 25 MeV, ^{62}Ga superallowed Fermi β^{+} decay half life 79−54410
^{58}Ni(^{6}Li,2n), 25 MeV, ^{62}Ga half life of Fermi superallowed β^{+} activities 79−9518
^{58}Ni(^{6}Li,t)^{61}Zn, ^{61}Zn mass, t-energy spectra and reaction mechanism 78−41756
^{58}Ni(^{7}Li, ^{6}Li), pol.^{7}Li, 20.3 MeV, ^{59}Ni levels, cross section and vector anal. power, ang. distribs. 80−106044
^{58}Ni(^{7}Li, pnγ), 20 MeV, ^{63}Zn EM decay transitions, level J$^{\pi}$ assignments, level lifetimes 79−85402
^{58}Ni(^{7}Li,^{7}Li′), 19 MeV, first 2^{+} states Coulomb-nuclear interference, optical and DWBA anal. 80−22852
^{58}Ni(^{7}Li,t), 34 MeV, ^{62}Zn ang. distribs. for transitions, DWBA anal., spectroscopic strengths 80−68584
^{60}Ni (^{12}C,2p), 30-9 MeV, high-spin states in ^{70}Ge anal. 78−33146
^{60}Ni+^{12}C, energy dissipation as func. of angle data comparison to classical and diffusion models 78−21604
^{60}Ni+^{32}S, study of neutron deficient Zr and Nb isotopes 77−57621
^{60}Ni+^{40}Ar, 236 MeV, fragments mass and charge distribs. in deep inelastic reactions 78−58296

heavy ion-nucleus reactions continued
^{60}Ni(^{12}C,X), 77 MeV, fragments in incomplete fission 77−14153
^{60}Ni(^{12}C,np), 30-55 MeV, ^{70}As states, excitation functions, spin and halflifes 79−6414
^{60}Ni(^{16}O, 2n), 45 MeV, ^{74}Kr rot. bands, band crossing and backbending 80−18176
^{60}Ni(^{16}O,2p), 45 MeV, ^{74}Se level scheme, J$^{\pi}$ assignments, bands and transitions 79−54393
^{60}Ni(^{19}F, ^{16}O), 75 MeV, ^{63}Cu levels and transition j-depend., DWBA anal. 80−42542
^{60}Ni(^{7}Li,Zn), 18-21 MeV, ^{65}Ga high spin states, J$^{\pi}$ and transitions, triaxial struct. 80−63062
^{62}Ni+^{35}Cl, fusion excitation functions, dynamical model calc. 78−50224
^{62}Ni(^{12}C, ^{11}B)^{63}Cu, 48 MeV, ang. distribs., exact finite range DWBA and CCBA anal., spectroscopic factors 77−54249
^{62}Ni(^{16}O,^{15}N), 36-53 MeV, reaction dynamic depend. of small angle cross sections 77−18600
^{62}Ni(^{16}O,^{15}N)^{43}Cu, 56 MeV, ang. distribs., exact finite range DWBA and CCBA anal., spectroscopic factors 77−54249
^{62}Ni(^{32}Cl,f), statistical anal. of excitation functions, Bohr-Wheeler and liq. drop model 78−13181
(^{64}Ni, 4n), ^{154}Er yrast cascade to spin 36, side feeding, energy, multipolarity irregularities 79−36191
^{64}Ni, one- and two-proton transfer reactions induced by 56 MeV ^{16}O beam, spectroscopic anal. 77−14178
^{64}Ni+^{40}Ca, 182 MeV, deep inelastic collisions, short lifetime and long lifetime regime 78−21597
^{64}Ni(^{12}C,2n), 39 MeV, ^{74}Se level scheme, J$^{\pi}$ assignments, bands and transitions 79−54393
^{64}Ni(^{16}O, 2np), 60 MeV, ^{77}Br collective bands, lifetimes, spins and E2 transition probabilities 80−13415
^{64}Ni(^{16}O, 2npγ), 60 MeV, ^{77}Br E2 transition probabilities and mean lives 80−13414
^{64}Ni(^{16}O,^{14}C)^{66}Zn, 56 MeV, full recoil one and two-step DWBA anal. 78−46091
^{64}Ni(^{16}O,^{14}C)^{65}Zr, 56 MeV, anal. of direct and indirect processes 77−34342
^{64}Ni(^{16}O,2n), ^{78}Kr high spin states, transitions and lifetimes 80−27534
^{64}Ni(^{16}O,α2n), 80 MeV, ^{74}Se transition energy correlations in γ-continuum 80−95309
^{64}Ni(^{18}O,^{18}O′), coupled channel anal. with double folding potential 79−45282
^{64}Ni(^{18}O,^{20}Ne)^{62}Fe, mass excess of ^{62}Fe 77−41878
^{64}Ni(^{6}Li, d), 28 MeV, ^{68}Zn low lying states, S-values from DWBA anal. 79−36160
^{252}No production, heavy ion complete fusion cross sections 79−67803
O ion induced fission of nuclei from Ag to U, fragment ang. distribs. *(Russian)* 78−17264
O+^{27}Al, total fusion cross section near Coulomb barrier 78−13141
O(^{12}C,X), 4.5 GeV/c, emission of short range particles (R<100 mkm) *(Russian)* 80−63202
O(^{13}C,X), 24 MeV, ^{A}O, A=17, 19, level scheme, two-step transfer contribs., coupled channel anal. 80−32181
^{A}O+^{12}C, A=16,18,22 79−45316
^{A}O(^{12}C,X), A=16,18, fusion cross sections by TDHF calcs. 79−89342
(^{16}O,X), 2 GeV/N, anomalous nuclei among relativistic projectile fragments 80−106034
(^{16}O,X), A=54-208, direct transfer to discrete and continuum states, DWBA diffraction model 80−78262
(^{16}O, 4n), ^{154}Er yrast cascade to spin 36, side feeding, energy, multipolarity irregularities 79−36191
^{16}O induced reactions in nuclear emulsions at 2.1 GeV/nucleon, multiplicity distrib. of white and grey tracks *(Spanish)* 80−47495
(^{16}O, πX), 4.2, 4.5 GeV/N, pion multiplicities and theoretical models, review 80−42657
^{16}O relativistic ions, fragmentation cross-sections in CsI 77−67770
(^{16}O, X), 90, 120 MeV/N, fragmentation reaction mechanism, orbital dispersion, momentum distribs. 79−97723
(^{16}O, xn), population of ^{174,175}W, ^{161}Yb, γ continuum spectra, yrast cascades, dipole component 78−54794
^{16}O+^{10}B, 100 MeV, 2n and 2p transfer reacts., DWBA anal. 78−50207
^{16}O+^{11}B, 115 MeV, α-transfer, DWBA anal., spectroscopic factors 79−22311
^{16}O+^{12}C, 15-72 MeV, gross struct. in γ-ray yields 78−78405
^{16}O+^{12}C, 17-28 MeV, total fusion cross section, γ-ray meas. 77−14162
^{16}O+^{12}C, 45-80 MeV, fusion cross sections using time-of-flight technique, TDMF calcs. 78−94043
^{16}O+^{12}C, fine struct. in fusion cross section 78−89928
^{16}O+^{12}C, isobar total prod. cross-sections, target giant reson. excitation 79−85429
^{16}O+^{12}C elastic scatt. and total reaction cross sections near Coulomb barrier 77−54235
^{16}O+^{12}C system, exptl. survey of resonant structs. below and above Coulomb barrier 79−9616
^{16}O+^{13}C, 105 MeV, α-transfer, DWBA anal., spectroscopic factors 79−22311
^{16}O+^{16,18}O, high spin states of ^{30,32}P, γ-ray meas. 78−74386
^{16}O+^{16}O, 2- and 3-dimens. time depend. HF calc. comparison 79−17948
^{16}O+^{16}O, 3-D TDHF calcs. 78−54781
^{16}O+^{16}O, 3-dimens., time depend. HF calcs. for fusion cross sections 78−66318
^{16}O+^{16}O, 3D TDHF calcs. 78−626
^{16}O+^{16}O, 35-80 MeV, fusion cross sections using time-of-flight technique, TDMF calcs. 78−94043
^{16}O+^{16}O, 384 MeV, alpha clustering, multiple shape vibrs., TDHFC calcs. 79−3164
^{16}O+^{16}O, 64, 80 MeV, fusion events, time dependent HF calcs. 79−36292
^{16}O+^{16}O, diffuse surface nuclear and Coulomb pot. energies 77−18593
^{16}O+^{16}O, entrance channel effects coupled channel calc. 77−65235
^{16}O+^{16}O, fusion cross sections, struct. in γ-ray yields 79−9626
^{16}O+^{16}O, fusion cross section gross struct., excitation functions, coupled channel method 80−52705
^{16}O+^{16}O, microscopic anal. of saturation effects in interactive region 78−89899
^{16}O+^{16}O, mol. config., ^{36}S high spin props., Strutinsky method 78−50201
^{16}O+^{16}O, nucleon-nucleon forces and heavy-ion potentials 79−6657
^{16}O+^{16}O, nucleus-nucleus interaction and nuclear saturation props. 79−6395

heavy ion-nucleus reactions continued
$^{16}O+^{16}O$, self-consistent heavy-ion potentials 77−6434
$^{16}O+^{16}O$, total fusion cross section, time depend. HF calcs. 79−17945
$^{16}O+^{16}O$, total fusion cross section and excitation function, statistical model anal. 79−13371
$^{16}O+^{16}O$ collisions, 105 MeV, appl. of 3-dimens. time-depend. HF calcs. 78−66317
$^{16}O+^{16}O$ collisions, resonating group study, effective two-nucleon forces 79−59044
$^{16}O+^{16}O$ heavy ion folding potential, antisymmetrisation effects 78−94023
$^{16}O+^{16}O$ reaction cross sections, 12.5-30.5 MeV excitation functions 78−643
$^{16}O+^{16}O$ system, strong damping of inner oscills., nuclear saturation props. 78−41749
$^{16}O+^{27}Al$, 30, 40, 60, 80 MeV, evaporation residue mass distrib. in fusion reactions anal. 77−42004
$^{16}O+^{28}Si$, 33-215 MeV, optical pots. anal. 77−41988
$^{16}O+^{58}Ni$, 44.5-76.5 MeV, ^{74}Kr compound nucleus decay 77−88168
$^{16}O+^{58}Ni$, 6 MeV/N, pre-equilib. α-emission 77−82883
$^{16}O+^{7}Li$, 50, 68 MeV, α-transfer, DWBA anal., spectroscopic factors 79−22311
$^{16}O+Au(W)$, fission lifetime distribution and probability estimates 78−659
$^{16}O+Ni(Co)(Cu)$, 42 MeV, unsuccessful isomer search near N=50 80−9223
$^{16}O+X$, X=$^{11}B,^{12}C,^{13}C,^{18}O$, deduced excited states, shell model wave functions, DWBA anal. 79−45284
^{16}O+emulsion nuclei, 150-200 MeV/nucleon interactions 77−41992
^{16}O+emulsion nuclei, 75-100 MeV/N, parallel momentum distrib. 79−9613
^{16}O+emulsion nuclei, 75-200 MeV/nucleon, pion and proton multiplicities 78−37363
$^{16}O(^{12,13}C,\alpha X)$, 140 MeV, fast α prod. and molecular resonance search 80−106066
$^{16}O(^{12}C,\ ^{8}Be)$, 11.5-18.6 MeV, ^{20}Ne low lying levels and intermediate structure J^{π} 80−102166
$^{16}O(^{12}C,^{12}C\alpha)^{12}C$, 68 to 80 MeV, sequential decay via excited states in ^{16}O 78−50189
$^{16}O(^{12}C,^{8}Be)$, 78 MeV, ^{20}Ne high spin states, J^{π} and α-decay branching ratios 80−18166
$^{16}O(^{12}C,^{8}Be)^{20}Ne^{*}$, 78 MeV, spectroscopy of high spin states in ^{20}Ne 78−50066
$^{16}O(^{12}C,^{8}Be)^{20}Ne^{*}$, determ. of resonance struct. in ^{28}Si 79−6663
$^{16}O(^{12}C,X)$, sub-barrier energies, fusion cross section, static and dynamic deformation effects 80−42729
$^{16}O(^{12}C,\alpha)^{24}Mg$, 12.8-14.5 MeV, energy averaged ang. distribs., Hauser-Feshbach calcs. 79−22318
$^{16}O(^{14}N,^{10}B)^{20}Ne$, 155 MeV, direct α-transfer, high spin states in ^{20}Ne 77−14164
$^{16}O(^{16}O,X)$, 9.3 MeV, fusion reaction residue partial prod. cross sections from γ-detection 79−67804
$^{16}O(^{16}O,X)$, fusion limiting ang. momenta, from evaporation, mass distrib. stat. model fit 80−68714
$^{16}O(^{16}O,^{12}C)^{20}Ne$, angular distrib. of ^{20}Ne polarisation at 68 MeV 79−6681
$^{16}O(^{16}O,^{12}C)^{20}Ne$, reaction mechanism by polarisation meas. 80−9301
$^{16}O(^{16}O,^{12}C)^{20}Ne^{*}$, strong polarisation of ^{20}Ne levels obs. 78−25213
$^{16}O(^{16}O,^{16}O)$, quasimolecule dynamical study, L=0 to 30 phase shifts 77−26784
$^{16}O(^{16}O,X)$, 119, 114 MeV, ^{32}S compound nucleus formation and deexcitation entrance channel effects 80−549
$^{16}O(^{16}O,X)$, 30-40 MeV, complete fusion cross section, gross and intermediate width struct. 79−67808
$^{16}O(^{16}O,X)$, 55 MeV 80−83110
$^{16}O(^{16}O,X)$, collective potentials and inertia parameters, adiabatic time dependent HF calcs. quasimolecular resonances 80−63195
$^{16}O(^{16}O,X)$, cross sections, energy dependence, nuclear molecular resonances, band crossing model 80−68686
$^{16}O(^{16}O,X)$, total fusion cross sections and fusion barrier parameters 80−9322
$^{16}O(^{16}O,x)$ reactions, time dependent HF calcs. 77−54251
$^{16}O(^{27}Al,X)$, 105, 145 MeV, backward angle cross sections, evaporation residues, Z=6-9 yields 80−68688
$^{16}O(^{28}Si,X)$, 55-96 MeV, γ-ray yield functions from high spin states, comparison with $^{12}C+^{24}Mg$ 79−93492
$^{16}O(^{40}Ca,\ X)$, ^{56}Ni formation cross section, TDMF calcs. for fusion 79−93676
$^{16}O(^{6}Li,\ d)$, 32 MeV, unnatural parity levels in ^{20}Ne, reaction mechanisms 77−14158
$^{16}O(^{6}Li,^{3}He)$, 46 MeV, ^{19}F final state selective population, triton clustering from band anal. 80−9306
$^{16}O(^{6}Li,\alpha)^{18}F$, 34 MeV, exchange effects, DWBA anal. 77−6431
$^{16}O(^{6}Li,\alpha)^{18}F$, 34 MeV, DWBA anal. of exchange effects 77−46179
$^{16}O(^{6}Li,d)$, 30 MeV, ^{20}Ne high spin states, J^{π} assignments 80−18167
$^{16}O(^{6}Li,d)^{20}Ne$, 19.8 to 32 MeV, reaction mechanism and excitation functions 78−41757
$^{16}O(^{6}Li,d)^{20}Ne$, 20, 32, 38 MeV α-particle spectroscopic strength determ., DWBA anal. 79−26451
$^{16}O(^{6}Li,d)^{20}Ne$, 43 MeV, α spectroscopic factors, reduced widths, stellar He burning 78−89897
$^{16}O(^{6}Li,d)^{20}Ne(\alpha)^{16}O$ at 57.8 MeV, ^{20}Ne α-cluster struct. >3O MeV excit. *(Russian)* 77−74784
$^{16}O(^{6}Li,d)^{20}Ne(\alpha)^{16}O$, ang. correl. anal. in α-clustering studies 78−634
$^{16}O(^{6}Li,d\gamma)^{20}Ne$, dγ ang. correl. reaction strength comparison, DWBA anal. 79−26452
$^{16}O(^{6}Li,t)$, 46 MeV, ^{19}Ne final state selective population, triton clustering from band anal. 80−9306
$^{16}O(^{7}Li,^{3}He)^{20}F$, 24 MeV, ang. distribs. of states below 6.25 MeV, gas target 78−82369
$^{16}O(^{9}Be,^{5}He)^{20}Ne^{*}$, sub-Coulomb alpha transfer cross sections 80−37394
$^{16}O(O,C)^{20}Ne$, 17 MeV, α transfer, cluster transfer process, cross sections 78−25218
$^{16}O(\alpha,\alpha_1)^{16}O^{*}$, resonance observation of 8p-4h state in ^{20}Ne 78−50132
$^{17}O+^{12}C$, 14-33 MeV, max. total fusion cross section 79−22349
$^{17}O+^{13}C$, 12.9, 14 MeV c.m., compound and direct transfer, reaction mechanism 77−88167
$^{17}O(^{11}B,^{8}Li)$, 115 MeV, shell and semiclassical reaction model anal. 80−13494
$^{17}O(^{12}C,^{9}Be)$, 115 MeV, shell and semiclassical reaction model anal. 80−13494
heavy ion-nucleus reactions continued
$^{17}O(^{13}C,^{10}B)$, 105 MeV, shell and semiclassical reaction model anal., ^{20}F spins 80−13494
$^{17}O(^{6}Li,d)$, ang. distrib., cross section, ^{21}Ne low lying states, weak coupling behaviour 78−46100
$^{17}O(^{6}Li,d)$ 32 MeV, α-stripping, ^{21}Ne α-spectroscopic strengths and level J^{π} assignments 79−516
$^{18}O+^{12,13}C$ fusion evaporation reactions, 100 MeV, comparison of residues with statistical calcs. 78−66311
$^{18}O+^{17}O$, one and two neutron transfer reacts., 18.52 MeV 78−54783
$^{18}O+^{18}O$, mol. config., ^{36}S high spin props., Strutinsky method 78−50201
$^{18}O+^{18}O$, neutron transfer excitation levels, recoil DWBA analysis 78−8837
$^{18}O(^{17}O,^{16}O)^{19}O$, sub-Coulomb, RMS radii of single-particle orbitals, neutron excess 77−333
$^{18}O(^{18}O,\ ^{16}O)^{20}O$ 52 MeV, microscopic anal. with DWBA calc. 79−26450
$^{18}O(^{18}O,^{14}O)^{22}O$, 100 MeV, ^{22}O mass meas. 77−22869
$^{18}O(^{18}O,^{15}O)^{21}O$, 91 MeV, determ. of ^{21}O mass 78−50078
$^{18}O(^{18}O,^{19}N)^{17}F$, 91 MeV, exotic nuclei search, ^{19}N mass 77−22868
$^{18}O(^{6}Li,d)^{22}Ne$, 32 MeV, levels, J^{π}, α-particle spectroscopic strengths 77−18594
$^{192}Os(^{12}C,^{14}C)^{190}Os$, 70 MeV, shape transition effect on quadrupole transfer strength 78−644
$^{31}P(^{6}Li,d)^{35}Cl$, 36 MeV, absolute cross sections, ang. distribs. 79−89321
$^{231}Pa(^{48}Ca,3n)_{111}{}^{276}X$ synthesis search *(Russian)* 79−40954
(Pb, xn) reactions, prod. of ^{158}Dy Yrast states, lifetimes 78−54793
Pb, A=193, 5, 7, 9, high-spin states anal. by heavy ion reactions 78−21500
Pb targets, possibilities for producing super-heavy elements Z>102, new projectiles *(Russian)* 78−86548
Pb targets for superheavy element synthesis 77−82960
$Pb+^{12}C$, 25.2 GeV, target residue mass and charge distribs. 77−74873
$Pb+^{14}N$, complete fusion cross sections, excitation functions *(Chinese)* 78−82406
Pb+Ar, 4-17 GeV, search for ultradense nuclei 77−3044
Pb+Ar, 800 MeV/A, wide angle inclusive proton spectra 79−40951
Pb+C, 800 MeV/A, wide angle inclusive proton spectra 79−40951
Pb+C, Pb+Ne, 800 MeV/N, p and π inclusive spectra, energy and ang. distribs. 78−54790
$Pb+C^{12}$, 3.6 GeV, emitted proton vel. spectra max. *(Russian)* 79−9571
Pb+heavy ion hard reaction, ground state correlations from liquid drop model 79−22308
Pb+Ne, 800 MeV/A, wide angle inclusive proton spectra 79−40951
Pb+O, 315 MeV, phenomenological determ. of strength of dissipative forces 77−71619
Pb+Pb, positron emission, evidence for strong field QED processes 78−93833
Pb+U, positron emission, evidence for strong field QED processes 78−93833
Pb(Ar,X), 800 MeV/N, single particle spectra from high multiplicity events 80−99184
$Pb(^{12}C,X)$, 1-2 GeV/n, central collision threshold phenomena, pion prod. 80−95326
$Pb(^{12}C,X)$ 3.6 GeV proton emission invariant cross sections *(Russian)* 80−13500
$Pb(^{20}Ne,\pi^{+})$, 800 MeV/N, doubly differential cross sections and ang. distribs. 80−9305
$Pb(^{16}O,^{12}C)Po$ (A_{Pb}=204,207,208), 93 MeV, comparison with α-decay data 77−334
Pb(Xe,X), deep inelastic, δ-electron emission, reaction time effects 80−32293
$^{A}Pb(^{18}O,X)$, (A=207, 208), (X=$^{17}O,\ ^{19}N,\ ^{21}O,\ ^{22}O$), 93 MeV, light neutron rich nuclei study 79−89322
$^{204}Pb(^{9}Be,3n)$, 40-55 MeV, ^{210}Rn high spin states, decay and lifetimes, spin assignments 80−18168
$^{206}Pb(^{13}C,5n\gamma)^{214}Ra$, high spin yrast states in N=126 isotones 79−45131
$^{206}Pb(^{40}Ar,2n)^{244}Fm$, fusion reactions near Coulomb barrier, optical pot. parameter determ. 79−30874
$^{206}Pb(^{6}Li,\ 3n\gamma)$, 29-34 MeV, ^{209}At high spin states, neutron hole influence 77−2934
$^{207}Pb(^{40}Ar,3n)^{244}Fm$ 79−30874
$^{208}Pb\ (^{16}O,\ X)$, 84, 92 MeV, total reaction cross section fragmentation 79−67775
$^{208}Pb\ (^{208}Pb,f)$ 1539 MeV, exam. of four-pronged double sequential fission events using mica track detectors 80−95328
$^{208}Pb\ (Ar,\ \pi^{+}X)$, 250, 400 MeV/A, pion yield near threshold 80−18344
$^{208}Pb+^{110}Pd$, 1.2 GeV, neutron rich nucleon flow in central heavy ion collisions 79−36268
$^{208}Pb+^{12,13}C$, single-n sub-Coulomb transfer reactions, single particle wave function RMS radius, n-excess 79−85355
$^{208}Pb+^{136}Xe$, 800 MeV, charge and mass transfer near Coulomb barrier 79−22325
$^{208}Pb+^{136}Xe$, double octupole phonon excitation, coupled channel WKB approx. 78−4960
$^{208}Pb+^{16,17,18}O$, single-n sub-Coulomb transfer reactions, single particle wave function RMS radius, n-excess 79−85355
$^{208}Pb+^{16}O$, 140 and 315 MeV, energy depend. of heavy ion peripheral reactions 78−74399
$^{208}Pb+^{16}O$, 20 MeV/A, nucleon motion effect on energy spectra and ang. distribs. 78−4971
$^{208}Pb+^{16}O$, classical, semiclassical and quantum mechanical scatt. and reaction calcs. 79−566
$^{208}Pb+^{16}O$, microscopic model anal. of fragment yields at 20 MeV/A and 2100 MeV/A 78−33214
$^{208}Pb+^{16}O$ peripheral collisions, cross-sections meas. at 315 MeV 77−6428
$^{208}Pb+^{208}Pb$, 14 GeV, nonnuclear positrons creation 79−30847
$^{208}Pb+^{208}Pb$, 1600 MeV, axially symmetric TDHF 78−74398
$^{208}Pb+^{208}Pb$, 7.4 MeV, time depend. Hartree Fock theory test 79−49591
$^{208}Pb+^{208}Pb$, positron form. 78−62873
$^{208}Pb+^{208}Pb$ deep inelastic processes, TDHF and elementary modes of excitation 79−63695
$^{208}Pb+^{20}Ne(^{40}Ar)$, 250-1000 MeV/N, intranuclear cascade calcs. for multiplicity and cross sections 80−32300
$^{208}Pb+^{40}Ar$, 1.8 GeV/nucleon, appl. of multiple-collision model for pion prod. 78−37365

heavy ion-nucleus reactions continued
^{208}Pb+^{40}Ar, deeply inelastic collisions, form factors determ. within statistical model 78−50205
^{208}Pb+^{40}Ca, 255, 300 MeV, lowered fusion cross section 78−41797
^{208}Pb+^{48}Ca mass distribs. of fission fragments meas. 77−71621
^{208}Pb+^{58}Ni(^{90}Zr), fission phenomena in deep inelastic collisions 80−5186
^{208}Pb+^{84}Kr, 494 MeV, strongly damped collisions, time-depend. mean field theory 78−82374
^{208}Pb+^{84}Kr, 500 and 700 MeV, differential cross section calc., statistical model 78−50192
^{208}Pb+^{86}Kr, 469 MeV, search for superheavy nuclei, Z>106, lifetimes >2 ps 78−46102
^{208}Pb+Ar, 1.8 GeV/nucleon, fireball model calc. of π-multiplicity distribs. 78−37366
^{208}Pb(^{12}C,^{11}B), 77 MeV, bound and continuum state excitation, direct and two step processes 80−63205
^{208}Pb(^{12}C,^{11}B), 77-116 MeV, cross-section meas., DWBA anal. 77−6433
^{208}Pb(^{12}C,^{11}B)^{209}Bi, DWBA anal. including nuclear wave function polarisation 78−629
^{208}Pb(^{12}C,^{11}B)^{209}Bi, single-particle polarisation, two-centre shell model 78−13142
^{208}Pb(^{12}C,^{13}C), 77-116 MeV, cross-section meas., DWBA anal. 77−6433
^{208}Pb(^{12}C,^{14}C), 77-116 MeV, cross-section meas., DWBA anal. 77−6433
^{208}Pb(^{136}Xe,X), 1120 MeV, energy, angular, charge distribs. meas. 77−3029
^{208}Pb(^{136}Xe,X), 7 MeV/u, composite system lifetime from δ-electron distrib., sticking times 80−540
^{208}Pb(^{136}Xe,X)Y, 470 MeV, search for delayed fission products from superheavy nuclei 78−70562
^{208}Pb(^{13}C,^{12}C)^{209}Pb near Coulomb barrier, semiclassical description 77−57640
^{208}Pb(^{16}O,^{12}C), 93 MeV, α-transfer reactions 79−67762
^{208}Pb(^{16}O,^{12}C)^{212}Po and α-decay, comparison for α-transfer reaction mechanism 79−6652
^{208}Pb(^{16}O,^{12}C)^{212}Po, semiclassical anal. of α-transfer, calc. of angular distrib. 79−6672
^{208}Pb(^{16}O,^{12}C)^{212}Po, 93 MeV, semiclassical analysis of α-transfer reactions, partial wave amplitudes 79−45283
^{208}Pb(^{16}O,^{14}Nα), ang. correlations between react. products 78−8849
^{208}Pb(^{16}O,^{15}N), 104-312 MeV, fragment emission at high energies, Q value effects 79−6653
^{208}Pb(^{16}O,^{15}N), 312.6 MeV, DWBA anal. of cross-section energy depend. 77−30630
^{208}Pb(^{16}O,^{15}N) 104, 138.5, 216.6 MeV, DWBA and optical model anal., energy dependence 78−82378
^{208}Pb(^{16}O,^{15}N) 312.6 MeV, optical model and DWBA anal., energy depend., lower energy comparison 78−82379
^{208}Pb(^{16}O,^{15}N)^{209}Bi, heavy ion research with cyclotrons 79−54447
^{208}Pb(^{16}O,^{15}O), 312.6 MeV, optical model and DWBA anal., energy depend., lower energy comparison 78−82379
^{208}Pb(^{16}O,^{17}O), (^{16}O,^{15}N), (^{16}O,C), 80-102 MeV, cross sections, optical model parameters 77−54246
^{208}Pb(^{16}O,^{17}O) 104, 138.5, 216.6 MeV, DWBA and optical model anal., energy dependence 78−82378
^{208}Pb(^{16}O,^{18}O)^{206}Pb, 69-73 MeV, 2 neutron transfer mechanism 78−89900
^{208}Pb(^{16}O,Cα), ang. correlations between react. products 78−8849
^{208}Pb(^{16}O,X), 140-315 MeV, projectile fragmentation, ^{15}N, ^{12}C transfer spectra, direct contrib. 80−63155
^{208}Pb(^{16}O,X), 80-313 MeV, optical model anal., dynamic shape or density changes 80−18186
^{208}Pb(^{16}O,f), 80-102 MeV, cross sections, optical model parameters 77−54246
^{208}Pb(^{18}O,^{18}O*)^{208}Pb, quadrupole moment of first excited state of ^{18}O determ. 77−22886
^{208}Pb(^{208}Pb, HI), 7-7.5 MeV/N, product energy and element distrib., fission probab., energy losses 80−86916
^{208}Pb(^{208}Pb, X), giant resonance polarisation pots. from nucleus-nucleus effective pot. 80−78248
^{208}Pb(^{208}Pb,X), exactly central heavy-ion collisions by nuclear hydrodynamics 80−68690
^{208}Pb(^{20}Ne,X), 400 MeV/N, inclusive p, d, t, ^{3}He cross sections from sequential scatt. model 80−57792
^{208}Pb(^{30}Si, ^{30}Si), 106-136 MeV, ^{30}Si first excited state, static quadrupole moment 80−13373
^{208}Pb(^{40}Ar,X), deeply inelastic collisions, form factors, microscopic calcs. 80−18339
^{208}Pb(^{40}Ar,πX), 1.8 GeV/nucleon, appl. of multiple-collision model for pion prod. 78−37365
^{208}Pb(^{48}Ca, X), fusion reactions from Cf and Fm integral yields, statistical model anal. *(Russian)* 79−97740
^{208}Pb(^{48}Ca,γ), nuclear pressure and fission fragment mass distrib. 80−18356
^{208}Pb(^{49}Ca,Xn), excitation functions for compound-nucleus and transfer reactions of magic nuclei 79−22310
^{208}Pb(^{6}Li, αp), 22.2 and 23.0 MeV, break-up near Coulomb barrier 78−636
^{208}Pb(^{6}Li,^{6}Li')^{208}Pb, 156 MeV, giant quadrupole reson. excitation 77−67767
^{208}Pb(^{6}Li,X), 60-156 MeV, break-up fragment transfer, cross sections, recoil ranges 80−13491
^{208}Pb(^{6}Li,αd), 22.2 and 23.0 MeV, break-up near Coulomb barrier 78−636
^{208}Pb(^{6}Li,d), 90 MeV, alpha-cluster transfer from alpha-decaying nuclei 80−91166
^{208}Pb(^{6}Li,xn), 75, 85, and 95 MeV, K X-ray multiplicity 79−76019
^{208}Pb(^{7}Li, ^{4}He 2nγ), ^{209}Bi EM props. of particle vibration coupling states 78−70485
^{208}Pb(^{7}Li, ^{6}He), 52 MeV, ^{209}Bi low lying levels and spectroscopic factors, EFR-DWBA anal. 80−32182
^{208}Pb(^{7}Li,^{6}Me), 52 MeV, ^{209}Bi single particle levels, ang. distribs., spectroscopic factors, DWBA anal. 80−63067
^{208}Pb(^{7}Li,X), 30-34 MeV, ^{213}At, ^{210}Pb, ^{212}Po spectroscopy and levels 80−68542
^{208}Pb(^{7}Li,3n), 32-44 MeV, ^{212}At high spin states, decay, g factor, J$^{\pi}$ assignments, level energies 80−5042
^{208}Pb(^{86}Kr,X), 610 MeV, deep inelastic ang. momentum transfer from sequential fission fragments 80−18325
^{248}Pb+^{16}O, 140, 315 and 33600 MeV, isotope yields and cross sections 77−14161

heavy ion-nucleus reactions continued
^{104}Pd(^{6}Li,xnypγ), 54-99 MeV, breakup, fusion-evaporation and pre-equilib. nucleon emission 78−17238
^{106}Pd(^{6}Li,xnypγ), 54-99 MeV, breakup, fusion-evaporation and pre-equilib. nucleon emission 78−17238
^{110}Pd+^{40}Ar, compound nucleus ^{150}Gd, deexcitation, evaporation calcs., comparison with exptl. decay data 77−61391
^{110}Pd+^{40}Ar, formation and decay of ^{150}Gd compound nucleus 77−61453
^{110}Pd(^{12}C,xnγ), shell effects at high spin in the γ-continuum from Te evaporation residues 79−22165
^{110}Pd(^{208}Pb, X), 1.18-1.28 GeV, charge equilib. time scale, relaxation time 80−18188
^{110}Pd(^{208}Pb, X), equilibrium process time evolution, mass and charge distribs., energy loss 79−97725
^{110}Pd(^{208}Pb,X), 1.2 GeV, central collisions, neutron rich nucleon flow, mass, charge and energy 80−18337
^{110}Pd(^{63}Cu,X)Y, new Ir, Os and Re isotopes 78−70563
^{141}Pr+^{35}Cl, 135-170 MeV, evaporation residue excitation functions 77−88166
^{141}Pr+^{35}Cl, 155-170 MeV, fission prod. yields, ang. distribs. and mean kinetic energies 78−41790
^{141}Pr(^{14}N,4n), 60-101 MeV, ^{151}Dy high spin states, isomers, α-decays and yrast sequence 79−93493
^{141}Pr(^{15}N, 4n), ^{152}Dy high spin isomers, yrast states and level lifetimes 80−13361
^{141}Pr(^{15}N, 4n), ^{152}Dy high spin struct., in beam γ meas. 80−18179
^{141}Pr(^{35}Cl,f), statistical anal. of excitation functions, Bohr-Wheeler and liq. drop model 78−13181
Pt+^{136}Xe, A=192, 194, 196, Coulomb excitation, γ softness from E2 transition strengths 77−82951
^{A}Pt(^{6}Li,xn), A=194, 198, 75, 85, and 95 MeV, K X-ray multiplicity 79−76019
^{192}Pt+^{84}Kr, 370 MeV, Pt transition probabilities determ. 78−62506
^{194}Pt+^{136}Xe, multiple Coulomb excitation, E2 transition probabilities of ^{194}Pt 78−4961
^{194}Pt(^{6}Li,4n), 44 MeV, ^{196}Tl high spin states, γ-decay and rot. structs. 79−440
^{196}Pt (^{20}Ne, ^{20}Ne'), excited states, lifetime meas. using recoil-distance method 80−13413
^{196}Pt (^{58}Ni, ^{58}Ni'), excited states, lifetime meas. using recoil-distance method 80−13413
^{242}Pu(^{48}Ca,xn), production of superheavy elements with A=114-116 78−29493
^{244}Pu, Xe and Kr induced fission at Coulomb barrier energies 77−61467
π production, coherent *(French)* 80−78311
Re(^{20}Ne,X), 124, 206 MeV, ^{205}At mass distribution width for fission and quasifission 79−63707
^{A}Ru+^{32}S, A=96,98, new La and Ce neutron deficient isotopes 79−499
^{104}Ru(^{6}Li,3nγ), ^{107}Ag high spin states, J$^{\pi}$ assignments, polarisations and transitions 80−27536
^{104}Ru(^{7}Li,4nγ), ^{107}Ag high spin states, J$^{\pi}$ assignments, polarisations and transitions 80−27536
(^{32}S,X), 153-184 MeV, fission like processes around A_{CN}=100, mass distrib. strong change 80−9318
(^{32}S,X), A=59-89, double differential cross section, mass asymmetry, transport model 80−102203
^{32}S+^{24,25,26}Mg(^{27}Al)(^{28}Si) fusion reaction, 130 MeV, mass systematics of evaporation residues 77−38311
^{32}S+Mg(^{27}Al), 160 MeV, evaporation residues, isotope and element distribs. meas. 78−13153
Sb, isomer ratios in fission fragments at high excitation 80−32261
^{121}Sb(^{32}S,X), 155-180 MeV, ^{149}Ho low lying yrast states 80−91151
^{45}Sc+^{22}Ne, energy dissipation as func. of angle data comparison to classical and diffusion models 78−21604
Se neutron deficient isotopes (A=68,69,70,71), production in heavy-ion reactions 77−38292
Se+^{12}C, study of neutron deficient Zr isotopes 77−57621
Se(^{86}Kr,xnγ), Yb nuclei at high ang. momentum, moment of inertia from γ spectra 78−13135
^{80}Se(^{6}Li, 3n), 25 MeV, ^{83}Rb high spin states, positive and negative parity bands 80−18178
^{80}Se(^{6}Li,3n), 23-29 MeV, ^{83}Rb band struct., spin assignments and transitions 80−73774
^{80}Se(^{6}Li,3n), 23-29 MeV, ^{83}Rb high spin states, Jπ and transitions 80−105949
^{82}Se+^{40}Ar→^{118}Te, γ-ray multiplicity spectra, nuclear shape at high angular momentum 78−37260
^{82}Se(^{40}Ar,xnγ), shell effects at high spin in the γ-continuum from Te evaporation residues 79−22165
^{82}Se(Li,xnγ), ^{85}Rb high spin states, yrast cascade, J$^{\pi}$, γ-transitions 80−73775
Si+^{16,18}O, 34-81 MeV, total fusion-evaporation cross sections, fusion barrier 80−5190
Si(^{19}F, ^{16}O), 60 MeV, ^{31,33}P levels and transition j-depend., DWBA anal. 80−42542
^{A}Si(^{12}C,X), 20-49 MeV, A=28-30, complete fusion cross sections, excitation function weak struct. 80−5188
^{A}Si(^{16}O,X), 21-61 MeV, A=28-30, complete fusion cross sections, excitation function weak struct. 80−5188
^{28}Si+^{16}O, fusion oscillations, evaporation residue gamma yields, cross section 80−42725
^{28}Si+^{20}Ne, 120 MeV, numerical anal. based on linear response theory 79−36273
^{28}Si+^{20}Ne, frictional coeffs. using linear response theory 79−13327
^{28}Si+^{28}Si fusion reaction, 117.5 MeV, mass systematics of evaporation residues 77−38311
^{28}Si+^{6}Li(^{9}Be)(^{12}C), fusion and strong absorption from elastic scatt. optical pot. 80−102222
^{28}Si(^{10}B,^{9}Be), 59, 75, 132 MeV, l=1 transfer reaction, exact finite range DWBA anal. 79−22317
^{28}Si(^{10}B,^{9}Be), unique l=1 reaction, ang. distrib. wave number depend., 0WBA anal. 80−63204
^{28}Si(^{12}C,^{16}O)^{24}Mg, entrance, exit and reaction channel data at backward angles 79−36254
^{28}Si(^{136}Xe, xn), 630 MeV, ^{159,160}Er energy levels, deexcitation γ-rays, g-factors and hyperfine interaction 80−102114
^{28}Si(^{15}N, ^{14}N), 44 MeV, modified optical pot. from backward elastic scatt. 80−32255
^{28}Si(^{15}N, ^{16}O), 44 MeV, p pickup, DWBA and coupled channel anal., two step processes 79−6552

heavy ion-nucleus reactions continued
^{28}Si(^{15}N,^{16}O), 44 MeV, modified optical pot. from backward elastic scatt. 80−32255
^{28}Si(^{16}O, ^{12}C), resonant like structs., forward α transfer mechanism 79−17876
^{28}Si(^{16}O, ^{12}C)^{32}S, transitions to g.s., meas. of excitation functions 79−17920
^{28}Si(^{16}O,^{12}C), 60 MeV, ^{32}S levels and spectroscopic factors, DWBA anal. 79−22204
^{28}Si(^{16}O,^{12}C), finite-range coupled-channel calcs. 77−10377
^{28}Si(^{16}O,α), 25-45 MeV, ^{44}Ti* band crossing search, Hauser-Feshbach calcs. 79−22174
^{28}Si(^{16}O,$\alpha p\gamma$) or (^{16}O,2pγ), high spin states, in ^{39}K and ^{42}Ca from γ meas. 78−89787
^{28}Si(^{18}O,^{14}C), 60 MeV, ^{32}S levels and spectroscopic factors, DWBA anal. 79−22204
^{28}Si(^{18}O,^{17}O)^{29}Si, 50 MeV, differential cross-sections, direct one-step process 77−74828
^{28}Si(^{18}O,^{18}F), 56 MeV, ^{28}Al ground state doublet ang. distrib., direct charge exchange model anal. 80−9307
^{28}Si(^{18}O,X), 56 MeV, multinucleon transfers, ang. distribs., distorted wave and shell model anal. 80−27663
^{28}Si(^{19}F,^{16}O), 60 MeV, exact finite range DWBA and CCBA calcs. 80−538
^{28}Si(^{20}Ne, X), 120 MeV, linear response theory anal., frictional coeffs. and energy dissipation 80−13502
^{28}Si(^{28}Si, X), ^{56}Ni formation cross section, TDMF calcs. for fusion 79−93676
^{28}Si(^{28}Si,X), 60 MeV, α-α correlations to probe fusion low ang. momentum window 80−106094
^{28}Si(^{28}Si,Xγ), 65-90 MeV, evaporation residues, relative production cross sections 79−45292
^{28}Si(^{32}S,X), 135 MeV, multi-particle prod., two fragment reactions, kinematical anal. 80−83111
^{28}Si(^{6}Li,t)^{31}S, t-energy spectra and reaction mechanism 78−41756
^{28}Si(^{7}Li, ^{7}Be)^{28}Al, 36 MeV, excited states in ^{7}Be+^{28}Al system microscopic DWA anal. 77−14157
^{28}Si(^{8}Be,^{8}Be), DWBA anal., spectroscopic factor determ. 78−17098
^{28}Si(^{9}Be,X), 30-60 MeV, total fusion cross section, evaporation residues, optical model 80−78344
^{28}Si(^{9}Be,X), X=p,d,α, energy dependence, angular distrib. of spectra, optical and statistical model anal. 80−68710
^{28}Si(^{9}Be,α), 20 MeV, localisation of direct reaction processes, fusion and total cross sections 78−78353
^{28}Si(^{9}Be,p), 20 MeV, localisation of direct reaction processes, fusion and total cross sections 78−78353
^{29}Si(^{16}O,^{17}O)^{28}Si, non-orthogonality of channel states 80−83115
^{29}Si(^{16}O,pn), ^{43}Sc, J$^{\pi}$=19/2^{-} isomer, high-spin precursors 80−57656
^{29}Si(^{6}Li,d)^{33}S, 36 MeV, absolute cross sections, ang. distribs. 79−89321
^{30}Si+^{14}N, 59, 70 MeV, radiative capture and 1-nucleon emission cross sections 79−93652
^{30}Si(^{132}Xe,f), 5.4-8.2 MeV/u, ^{162}Er compound nucleus fission at high ang. momentum, fragments 80−99196
^{30}Si(^{16}O,^{15}N)^{31}P, ang. distribs. anal. 77−74875
^{30}Si(^{7}Li,^{3}He)^{34}P, 24 MeV, spectra, ang. distribs., mass excess, cross section 78−25230
^{28,30}Si(^{19}F,^{16}O)^{31,33}P 60 MeV, j depend., spin-orbit effects, optical pot. 77−41993
Sm+^{12}C, population of ^{154}Er, high-spin states 78−29373
Sm+O^{16} fusion, cross sections for spherical and deformed Sm isotopes, shape effects 78−78407
Sm(^{40}Ca,xn), 280 MeV, ^{184}Pb isotope identification 80−32302
Sm(^{16}O, ^{14}C) A=144, 148, 152, 104 MeV, two proton transfer between pairing rot. states 77−10430
Sm(^{16}O,3n), 82 MeV, ^{A}Yb, A=160, 161, backbending, multiple band crossing freq. and alignment 80−47347
Sm(^{16}O,4n), ^{161,162,166}Yb yrast cascade dipole component 80−9266
Sm(^{16}O,xn)^{161}Yb, γ-ray spectra, dipole moment in yrast cascade 78−37371
Sm(^{16}O, x$n\gamma$), ^{161}Yb, quasicontinuum γ-rays yrast cascade dipole component, moment of inertia 80−47424
^{A}Sm(^{16}O,X), 60-75 MeV, A=148, 150, 152, 154 deformation effects on fusion 80−18360
^{A}Sm(^{16}O,X), 60-75 MeV, A=148,150,152,154, fusion cross section, evaporation residues 80−83137
^{A}Sm(^{40}Ar,X) A=144, 148, 154, 3.6-4.5 MeV/A, sub-barrier fusion, evaporation residue cross section, deformation 80−68718
^{A}Sm(^{86}Kr,X), A=144, 154, 490 MeV, transfer reactions and associated γ-multiplicity moments 80−18342
^{148}Sm+^{10}B, 86-96 MeV, ^{148,149}Ho identification and β-decay 79−36166
^{144}Sm+^{86}Kr, 490 MeV, γ-ray multiplicity moments 78−54798
^{144}Sm(^{10}B,4n),^{148}Tb high spin states, γ-ray and electron meas. 79−49582
^{144}Sm(^{12}C,^{9,10}Be), ^{A}Gd, A=146,147, mass and Z=64 shell closure 80−57669
^{144}Sm(^{12}C,3n), 64.5 MeV, ^{153}Er 360 ns yrast trap, γ transitions and lifetimes 80−9205
^{144}Sm(Li,xn) ^{148}Tb high spin states, γ-ray and electron meas. 79−49582
^{148}Sm+^{63}Cu, ^{56}Fe, evolution from deep inelastic transfer to quasi-fission characts. 77−18595
^{148}Sm(^{16}O, 4nγ), yrast state obs. in ^{160}Yb, backbending effect 79−30777
^{148}Sm(^{18}O,^{16}O), interference effects, coupled channels calc. with BCS+RPA wavefunctions 77−26787
^{148}Sm(^{18}O,^{16}O)^{150}Sm, 2_1^+ ang. distributions, shape difference between pickup and stripping reaction 78−33209
^{150}Sm(^{12}C,^{14}C)^{148}Sm, 2_1^+ ang. distributions, shape difference between pickup and stripping reaction 78−33209
^{150}Sm(^{16}O,^{16}Oγ), 46 MeV, Coulomb excitation, ^{150}Sm nucl. struct. *(Japanese)* 77−41890
^{150}Sm(^{16}O,^{18}O), interference effects, coupled channels calc. with BCS+RPA wavefunctions 77−26787
^{150}Sm(^{16}O,^{18}O)^{148}Sm, 2_1^+ ang. distributions, shape difference between pickup and stripping reaction 78−33209
^{150}Sm(^{16}O,x$n\gamma$), Yb nuclei at high ang. momentum, moment of inertia from γ spectra 78−13135
^{150}Sm(^{6}Li,x$np\gamma$), 54-99 MeV, determ. of cross sections 78−66307
^{152}Sm+^{14}N, 135, 165 MeV, massive transfer accompanying proton, deuteron and triton emission 79−93648
^{152}Sm(^{12}C,5n), ^{160}Er, high spin yrast states and transitions 80−9208
^{152}Sm(^{16}O,xn)$^{168-x}$Yb, as test for recoil shadow method in-beam spectroscopy of low energy conversion electrons 78−33372
heavy ion-nucleus reactions continued
^{154}Sm+^{14}N, 135, 165 MeV, massive transfer accompanying proton, deuteron and triton emission 79−93648
^{154}Sm(^{12}C,^{14}C)^{152}Sm, 65 MeV, ground-state rot. band ang. distribs., quadrupole transfer strength 77−336
^{154}Sm(^{16}O,X), 153 MeV, angular momentum transfer in incomplete-fusion reactions 80−9320
^{154}Sm(^{16}O^{18}O), ^{152}Sm ground and γ-bands, direct and multistep processes 80−102094
^{154}Sm(^{40}Ar,X), 222, 340 MeV, fusion cross sections, direct and evaporative p and α prod., evaporation, fission 80−13518
Sn+^{18}O, 100 MeV, quasielastic collisions, time-depend. single particle method 77−34334
Sn(^{40}Ar, 4n), ^{A}Er, A=156, 160, yrast level population, decay, and lifetimes *(Russian)* 79−97648
Sn(^{10}B,3n), ^{A}Cs, A=119 , 121, 123, 125, collective props. and level schemes 79−22171
Sn(^{10}B, 3n), ^{A}Cs A=127, 129, 131, 133, high spin states and collective properties 79−22170
Sn(^{16}O,3n)^{131,129}Ce, band structs., high spin levels, yrast cascades 78−8842
Sn(^{16}O, 4nγ), 76 MeV, lifetimes of yrast states of even Ce nuclei 78−21589
Sn(^{32,34}S, 4n), 150 MeV, ^{152}Dy yrast line single particle nature at high ang. momentum 79−71783
Sn(^{32}S, 4nγ), yrast traps and very high spin yrast states in ^{152}Dy 78−89778
^{A}Sn+^{35}Cl, A=112, 116, 120, 124, 155-170 MeV, fission prod. yields, ang. distribs. and mean kinetic energies 78−41790
^{A}Sn+^{40}Ar, A=122, 124, 50 to 120 MeV, angular momentum limits 78−25224
^{A}Sn(^{40}Ar, xn), (A=116, 120, 122, 124), 161-236 MeV, γ-multiplicity meas., Er compound nucleus formation 79−89320
^{112}Sn+^{32}S fusion, 160 MeV, mass, velocity, angular and charge state distribs. 78−82405
^{112}Sn+^{35}Cl, 135-170 MeV, evaporation residue excitation functions 77−88166
^{114}Sn(^{12}C, 3n), ^{123}Ba high spin levels prod. and anal. 79−45127
^{116}Sn+^{35}Cl, fusion excitation functions, dynamical model calc. 78−50224
^{116}Sn(^{12}C, 3nγ), 45-55 MeV, collective excitations in ^{125}Ba 78−37258
^{116}Sn(^{16}O,^{15}N), (^{16}O,^{14}C), ^{117}Sb, ^{118}Te levels, ang. distrib. anal. of 64 MeV reacts. 78−8836
^{116}Sn(^{20}Ne, 3n), 75-90 MeV, ^{133}Nd, high spin states, negative parity level band based $h_{11/2}$ state 79−75813
^{116}Sn(^{20}Ne, 3n)^{133}Nd, study of high spin states in ^{133}Nd *(French)* 77−61372
^{116}Sn(^{32}Cl,f), statistical anal. of excitation functions, Bohr-Wheeler and liq. drop model 78−13181
^{116}Sn(^{40}Ar,X) 187, 222, 340 MeV, fusion cross sections, direct and evaporative p and α prod., evaporation, fission 80−13518
^{118}Sn (^{6}Li,αd), 22.2 and 23.0 MeV, break-up near Coulomb barrier 78−636
^{118}Sn(^{12}C,3n)^{127}Ba, high spin level structure in ^{127}Ba 77−38226
^{118}Sn(^{18}O,^{16}O)^{120}Sn, 53 to 62 MeV, optimum Q value at the Coulomb barrier 78−78413
^{118}Sn(^{40}Ar,xn), ^{40}Ar excitation function for ^{152,153}Er prod. 79−22315
^{118}Sn(^{6}Li, αp), 22.2 and 23.0 MeV, break-up near Coulomb barrier 78−636
^{118}Sn(^{7}Li,^{6}He), 48 MeV, DWBA anal. with optical model parameters, ^{119}Sb transitions 79−6688
^{120}Sn+^{132}Xe, deeply inelastic, relative motion mass transport and dynamics 79−13320
^{120}Sn+^{35}Cl, 135-170 MeV, evaporation residue excitation functions 77−88166
^{120}Sn+^{40}Ar, deeply inelastic collisions, form factors determ. within statistical model 78−50205
^{120}Sn+^{86}Kr, 5.99 MeV/N, are γ-ray multiplicity 78−82375
^{120}Sn(^{120}Sn,^{118}Sn), semiclassical description of two nucleon transfer in superfluid nuclei, nuclear Josephson effect 79−45296
^{120}Sn(^{12}C,3n), 45-54 MeV, ^{129}Ba triaxial shape and high-spin bands 77−34219
^{120}Sn(^{12}C,3n), 52 MeV, obs. of ^{129}Ba γ-ray linear polarisation 78−50121
^{120}Sn(^{12}C,3nγ)^{129}Ba, E=45-54 MeV, excitation of high-spin levels in ^{129}Ba 78−17104
^{120}Sn(^{40}Ar,X), deeply inelastic collisions, form factors, microscopic calcs. 80−18339
^{122}Sn+^{120}Sn, 630 MeV, multipair transfer calcs. for superfluid ions, coupled channel WKB approx. 78−37373
^{122}Sn(^{16}O,4n), ^{135}Ce yrast cascade dipole component 80−9266
^{122}Sn(^{24}Mg,4n), ^{142}Sm ns isomers and yrast isomers, γ-transitions 80−78121
^{122}Sn(^{32}S,3n), 115-165 MeV, ^{151}Dy high spin states, isomers, α-decays and yrast sequence 79−93493
^{122}Sn(^{40}Ar,4n)^{158}Er, high-spin yrast levels in ^{158}Er, second discontinuity obs. 77−61373
^{124}Sn+^{40}Ar$\rightarrow$^{160}Er, γ-ray multiplicity spectra, nuclear shape at high angular momentum 78−37260
^{124}Sn+^{86}Kr, 440 and 720 MeV, energy division versus mass of strongly damped products 78−54797
^{124}Sn(^{32}S,4n)^{152}Dy, high spin state populations 80−57660
^{124}Sn(^{32}S,xn), continuum γ rays, linear polarisation, feeding high spin yrast states in ^{151,2}Dy 80−497
^{124}Sn(^{40}Ar,xn)Er, 161-236 MeV, pre-equilibrium neutron emission 79−3169
^{124}Sn(^{86}Kr,X), deep inelastic, final and primary yields and dispersions, statistical anal. 79−54452
^{86}Sr(^{18}O,^{17}O), ^{87}Sr 1 $g_{9/2}$ neutron distrib. radial size, states, differential cross sections 80−95301
^{88}Sr(^{12}C,^{10}Be), 60 MeV, coupled channel Born approx. anal., form factors, sequential amplitudes 79−9608
^{88}Sr(^{12}C,3nγ) 45 MeV, ^{97}Ru high spin states, band like structs., transitions 80−73779
^{88}Sr(^{16}O, ^{15}N), 96 MeV, ^{15}N and ^{89}Y excited state ang. distrib., spin alignment and polarisation 79−67709
^{88}Sr(^{16}O,^{15}N), 96 MeV, ^{15}N 3/2^{-} state spin alignment and polarisation, 1/2-spin orbit interaction 80−27622
Ta, reactions induced by ^{12}C and ^{19}F ions, γ-ray spectroscopy of induced activities 77−23107
Ta(^{12}C,X), 4.2 GeV/N, multiple π^- prod., mean multiplicity *(Russian)* 80−27647

heavy ion-nucleus reactions continued
Ta(C,Z), 4.2 GeV.c^{-1}, inelastic cross section meas. and multiplicities obs. *(Russian)* 79−9580
^{181}Ta+^{12}C, 4.2 GeV/N, identical pion$^-$ interference effect, generation range determ. *(Russian)* 80−42695
^{181}Ta+^{20}Ne, 8.0 GeV, target residue mass, charge distrib. determ. 79−17930
^{181}Ta+^{86}Kr, 620 MeV, charge and ang. distribs., kinetic energy spectra, of deeply inelastic fragments 78−25221
^{181}Ta(^{12}C, X), 4.2 GeV/c, multitudes of secondary negative particles, momentum distrib. ratios *(Russian)* 80−63178
^{181}Ta(^{136}Xe,X), 1120 MeV, energy, angular, charge distribs. meas. 77−3029
^{181}Ta(^{14}N,X), 85-115 MeV, cross sections, preequilibrium α-particle emission 80−42680
^{181}Ta(^{16,18}O,xnγ), 95-125 MeV, ^{192}Tl high spin band struct. and transitions, isomeric state 80−47353
^{181}Ta(^{16}N,^{17}O), (^{16}O,^{15}O), (^{16}O,C), 83-96 MeV, cross sections, optical model parameters 77−54246
^{181}Ta(^{16}O,f), 77-102 MeV, cross sections, optical model parameters 77−54246
^{181}Ta(^{18}O,5n), 80-100 MeV, ^{194}Tl high spin states, excitation functions, $I^{\pi}=8^-$ isomeric state 80−32163
^{181}Ta(^{20}Ne, spallation), 8.0 GeV, cross sections and target residues, model comparison 80−68630
^{181}Ta(^{40}Ar,xn), 165-202 MeV, ^{A}Pa, A=215-218, 222, α-decay half life and energies 79−45216
^{181}Ta(^{6}Li,xn), 75, 85, and 95 MeV, K X-ray multiplicity 79−76019
^{153}Tb, fission barrier at 28.5 MeV 80−91202
^{159}Tb+^{86}Kr, 620 MeV, energy spectra, charge and ang. distribs., diffusion model 78−50202
^{159}Tb(^{11}B,X), 51 MeV, fusion and deep inelastic, quantised frictional motion calcs. 80−102223
^{159}Tb(^{14}N,X), 140 MeV, incomplete fusion reactions, sum rule model 80−95332
^{159}Tb(^{14}N,X), 85-115 MeV, cross sections, preequilibrium α-particle emission 80−42680
^{159}Tb(^{14}N,X), 95 MeV, fast α-particle ang. distribs. 80−63207
^{159}Tb(^{14}N,αxn), 22-30 MeV, ^{A}Yb, A=169-x, γ de-excitation and ang. momentum distribs. after fast α-emission 80−18228
^{159}Tb(^{14}N,αxn), 95 MeV, γ-multiplicities following fast α-emission 79−67770
^{159}Tb(^{14}N,αxn)$^{169-x}$Yb, 95 MeV, γ-ray identification 77−57697
^{159}Tb(^{16}O,9n)^{166}Ta, isotope identification, half-life and decay scheme 77−79331
^{159}Tb(^{40}Ar,X), 273 MeV, complete fusion and charge transfer reactions 79−45314
Te(^{40}Ar,xnγ), Yb nuclei at high ang. momentum, moment of inertia from γ spectra 78−13135
Te(^{6}Li, 3n), ^{A}Cs A=127, 129, 131, 133, high spin states and collective properties 79−22170
^{122}Te(^{32}S,X), 155-180 MeV, ^{149}Ho low lying yrast states 80−91151
^{124}Te(^{32}S, 4n), ^{152}Dy yrast traps, isomers and oblate deformations 80−13362
^{128}Te(^{16}O,4n), ^{140}Nd, ns isomers and yrast isomers, γ-transitions 80−78121
^{128}Te(^{16}O,5nγ), prolate-oblate transitions in Nd isotopes 78−70438
^{130}Te+^{16}O, 90 MeV, mechanism of four nucleon transfers in heavy-ion reactions 79−6674
^{130}Te+^{28}Si, 140 MeV, diffusion model 78−82382
^{130}Te(^{32}S,X), 132-163 MeV, Er γ-multiplicities and cross sections, neutron evaporation 80−73824
^{130}Te(^{32}S,xn), continuum γ rays, linear polarisation, feeding high spin yrast states in $^{156-8}$Er 80−497
^{130}Te(^{40}Ar,xnγ), angular momentum effects in pre-equilibrium processes 78−50208
Th+Ar, 388 MeV, phenomenological determ. of strength of dissipative forces 77−71619
Th(^{40,44,48}Ca,f), isotope and mass distribs. of fragments *(Russian)* 77−74897
^{232}Th (^{40}Ar, X), differential cross sections calc. from random matrix model transport theory 79−49634
^{232}Th (^{7}Li,α)^{235}Pa, 12 to 20 MeV excitation, ang. distrib. of evaporation residues, determ. of Γ_n/Γ_f 77−61451
^{232}Th, subCoulomb fission induced by Xe and Kr, excitation functions 77−3061
^{232}Th, Xe and Kr induced fission at Coulomb energies 77−61467
^{232}Th+^{16}O, 140, 315 and 33600 MeV, isotope yields and cross sections 77−14161
^{232}Th+^{16}O, 140 and 315 MeV, energy depend. of heavy ion peripheral reactions 78−74399
^{232}Th+^{16}0, fission following transfer below Coulomb barrier 79−22346
^{232}Th+^{19}F, fission following transfer below Coulomb barrier 79−22346
^{232}Th+^{22}Ne, 172 MeV, energy spectra and isotope prod. with 4≤Z≤9 77−57680
^{232}Th+^{40}Ar, 213 MeV/A, complex fragment emission study 79−6667
^{232}Th+^{40}Ar, 288 MeV phenomenological approach to deeply inelastic collisions 79−54449
^{232}Th+^{40}Ar, 388 MeV, differential cross section calc., statistical model 78−50192
^{232}Th+^{40}Ar, 390 MeV, Z≤38 products energy spectra, reaction mechanism, dynamic deformation *(Russian)* 78−89909
^{232}Th+^{40}Ar(^{63}Cu), deep inelastic reactions, isotopic distribs., n excess degree of freedom relaxation 80−9308
^{232}Th(^{14}B,^{12}B), 129 MeV, ^{12}B spin polarisation 80−63161
^{232}Th(^{16}O,X), (X=^{16}N,^{15}N,^{14}C,^{13}C,^{12}C or ^{11}B), surprisal anal., maximal entropy condition, Q-value depend. 79−9606
^{232}Th(^{16}O,γ), transfer induced fission, excitation functions and cross sections 80−13515
^{232}Th(^{19}F,γ), transfer induced fission, excitation functions and cross sections 80−13515
^{232}Th(N,X), ^{242}Bk electron capture half life and α-branching ratio 79−67716
Ti(^{14}C,^{16}O), 51 MeV, pickup reaction, ^{44,46}Ca excited states and transition ang. distribs. 80−95308
Ti(^{12,13}C,X) 45, 46 MeV, particle-gamma coincidences, isotope assignment for yrast spectroscopy 80−68593
Ti(^{16}O,^{15}N), A=48, 50, 36-53 MeV, reaction dynamic depend. of small angle cross sections 77−18600
Ti(^{16}O,X), 310 MeV, fusion, upper limit to compound nucleus formation 80−78315

heavy ion-nucleus reactions continued
^{A}Ti(^{7}Li,^{7}Li′), A=46,48, 17 MeV, first 2$^+$ states Coulomb-nuclear interference, optical and DWBA anal. 80−22852
^{46}Ti+^{12}C, 5.8 MeV/u, influence of shell effect in nuclear level densities on compound nucleus decay 79−40979
^{48}Ti+^{16}O, 120 MeV, deep inelastic collisions, charged particle+gamma coincidences 78−74388
^{48}Ti+^{16}O, 57.74 MeC, heavy ion fusion, evaporation model breakdown, preequilibrium α emission from ^{64}Zn 78−89927
^{48}Ti+^{16}O, anisotropy of yrast γ-transmissions 79−93650
^{48}Ti(^{12}C,p2n), 26-48 MeV, high spin states in ^{57}Co anal. 77−46115
^{48}Ti(^{16}O,^{12}C), 120 MeV, formation and decay of ^{52}Cr primary fragment 79−45289
^{48}Ti(^{16}O,^{15}N), anomalous ang. distribs., interference effects due to ^{49}V state population 79−17924
^{50}Ti+^{14}N(^{12}C), single- and multi-nucleon transfer reaction at 60, 70 and 90 MeV 77−14146
^{50}Ti+^{32}S, diffusion model anal. of energy depend. of fission like mass distrib. 77−82949
^{50}Ti+^{32}S composite system, fission characts., fragment correls. 77−332
^{50}Ti+^{40}Ar, 236 MeV, fragments mass and charge distribs. in deep inelastic reactions 78−58296
^{50}Ti(^{12,13}C,X), elastic, inelastic and single nucleon transfer excitation functions, ^{49}Ti levels 80−13492
^{50}Ti(^{32}S,f), 121 to 166 MeV, heavy fragments ang. distribs., mass distribs., excitation functions 77−30642
Tl(^{40}Ca,^{40}Ca′γ), 120 MeV, ^{A}Tl, A=203, 205, excited state g-factor 79−22191
^{A}Tl(^{48}Ca, X), A=203, 205, fusion reactions from Cf and Fm integral yields, statistical model anal. *(Russian)* 79−97740
^{205}Tl(^{13}C,5nγ)^{213}Fr, high spin yrast states in N=126 isotones 79−45131
^{167}Tm(HI,xnγ), ang. distrib., multipolarities *(French)* 80−68575
^{169}Tm(^{14}N,X) 85-115 MeV, cross sections, preequilibrium α-particle emission 80−42680
^{169}Tm(^{35}Cl,5n), ^{199}Rn and ^{199}Rn^{m} alpha decay signatures 80−68610
transfer amplitude and ang. distribs. 79−59081
U+^{12}C, 25.2 GeV, large collision residues and fission 77−71618
U+^{136}Xe, 1080 MeV, reaction mechanisms obs. with mica detectors 77−79399
U+^{20}Ne, 250 and 400 MeV nucleon^{-1}, inclusive proton production, classical many-body calc. 79−17918
U+^{20}Ne, nuclear fireballs, break-up densities 78−8790
U+^{20}Ne, quark matter, signature in nuclear fireball model 80−37395
U+^{20}Ne, relativistic nuclear collisions, inclusive ρ spectra, knock-out mech. 77−82950
U+^{238}U, search for superheavy elements 79−6692
U+^{4}He, relativistic nuclear collisions, inclusive ρ spectra, knock-out mech. 77−82950
U+^{84}Kr, 800 MeV, reaction mechanisms obs. with mica detectors 77−79399
U+Ar, 4-17 GeV, search for ultradense nuclei 77−3044
U+Kr$^-$, solid state detector investigs. *(German)* 77−14321
U+Ne→p+X, high energy heavy ion collisions, comparison of models 78−46088
U+Pb, 750 MeV, classical model, kinetic energy, ang. distribs., instantaneous fission fragments 78−13185
U+U high energy nuclear collisions, large baryon densities prod. 78−86540
U(^{40,44,48}Ca,f), isotope and mass distribs. of fragments *(Russian)* 77−74897
U(Ne,X), 250, 400, 800 MeV/N, nuclear matter collective sideward flow, nuclear fluid dynamics 80−57715
U(Ne,X), 250, 400 MeV/N direct vs. thermal particle emission, inclusive cross sections 80−52688
U(Ne,X), proton inclusive spectra, direct plus thermal model 80−57799
U(Ne,n)X, 337 MeV/N inclusive double differential neutron prod. cross sections 80−32294
U(^{208}Pb, f), 1535 MeV, direct evidence for multiple sequential fission 79−30866
U(^{238}U, f), 1785 MeV, direct evidence for multiple sequential fission 79−30866
U(Xe,f), Coulomb fission problem, uniform semi-classical approach to forbidden transitions 79−36287
^{233}U, high-energy spin state obs. using Coulomb excitation 78−17102
^{233}U(^{48}Ca, Zn)$_{112}$^{279}X synthesis search *(Russian)* 79−40954
^{235}U(^{11}B,X), ^{242}Bk electron capture half life and α-branching ratio 79−67716
^{236}U(^{7}Li,α)^{239}Np, 12 to 20 MeV excitation, ang. distrib. of evaporation residues, determ. of Γ_n/Γ_f 77−61451
^{238}U + ^{16}O, 20 MeV/nucleon, peripheral collisions, incomplete momentum transfer 79−30848
^{238}U (^{84}Kr, X), 522 MeV, heavy reaction product ang. distribs. and integral cross sections 79−49638
^{238}U, anal. of Rb and Cs isotopic distrib. in ^{11}B and ^{22}Ne-induced fission 77−18634
^{238}U, meas. of Rb and Cs isotopic distrib. in ^{11}B and ^{22}Ne-induced fission 77−18633
^{238}U, subCoulomb fission induced by Xe and Kr, excitation functions 77−3061
^{238}U, Xe and Kr induced fission at Coulomb barrier energies 77−61467
^{238}U, Xe-induced Coulomb fission, rotation-vibration model for target nucleus 79−13367
^{238}U-^{238}U, mass transfer, quantum mech. anal. within fragmentation theory 77−82948
^{238}U+^{A}Xe, A=129, 132, 136, sub-Coulomb transfer and fission, cross sections 79−67802
^{238}U+^{136}Xe, 4.5-5.9 MeV/N excitation functions and ang. distrib. meas. 77−82965
^{238}U+^{136}Xe, isotope prod. cross-sections *(Russian)* 77−74879
^{238}U+^{16}O, threshold pion prod., calc. of effective NN collision cross sections 77−46185
^{238}U+^{208}Pb, 14 GeV, nonnuclear positrons creation 79−30847
^{238}U+^{20}Ne, 250 MeV/nucleon, comparison of macroscopic and microscopic calcs. 77−50153
^{238}U+^{20}Ne, expt. and relativistic two fluid model energy spectra 78−78298
^{238}U+^{20}Ne(^{40}Ar), 250-1000 MeV/N, intranuclear cascade calcs. for multiplicity and cross sections 80−32300
^{238}U+^{238}U, 14 GeV, nonnuclear positrons creation 79−30847
^{238}U+^{238}U, 1766 MeV, charge, kinetic energy and ang. distrib. of reaction products 79−26455

heavy ion-nucleus reactions continued
$^{238}U+^{238}U$, 1785 MeV, cross sections, charge and mass distribs. of products 78−78408
$^{238}U+^{238}U$, 7.42 MeV/nucleon, charge, energy and ang. distribs. of prods. 78−8846
$^{238}U+^{238}U$, 7.5 MeV/u, theoretical estimates for transuranium element prod. in heavy ion collisions 79−54454
$^{238}U+^{238}U$, deeply inelastic, relative motion mass transport and dynamics 79−13320
$^{238}U+^{238}U$ fragmentation, superheavy element prod. due to collective mass transfer 77−337
$^{238}U+^{32}S(^{40}Ar)$, deep inelastic reactions, isotopic distribs., n excess degree of freedom relaxation 80−9308
$^{238}U+^{40}Ar$, 220 MeV, fissionability of target-like fragments in deep inelastic collisions, reaction mechanism 79−54455
$^{238}U+^{40}Ar$, 263 MeV, ^{37}Si, ^{40}P, ^{41}S, ^{42}S neutron rich nuclide prod. 79−22324
$^{238}U+^{40}Ar$, cross-sections for fusion, quasifission and deep inelastic collisions *(Russian)* 78−54801
$^{238}U+^{58}Ni(^{90}Zr)$, fission phenomena in deep inelastic collisions 80−5186
$^{238}U+^{84}Kr$, 605 MeV, quasi-fission reaction, mass-yield distrib. theory 77−42001
$^{238}U+^{86}Kr$, recoil range distribs. of heavy mass products in deep inelastic reacts. 78−66309
$^{238}U(^{10}B,X)$, ^{242}Bk electron capture half life and α-branching ratio 79−67716
$^{238}U(^{12}C,f)$, $(^{18}O,f)$, $(^{22}Ne,f)$, effective widths of excited state meas. by shadow effect *(Russian)* 77−46196
$^{238}U(^{12}C,f)$, mass distrib. of fission fragments determ. *(Chinese)* 78−86558
$^{238}U(^{16}O,f)$ 20 MeV/N, light particle spectra in central and peripheral collisions 80−5177
$^{238}U(^{16}O,x)$, x=p,d,t, 315 MeV, energy spectra in coalescence model 80−99183
$^{238}U(^{184}W,f)$, Coulomb fission excitation function, cross section 80−5176
$^{238}U(^{238}U,X)$, 7.42 MeV/u, charge, kinetic energy and ang. distribs. of products 80−539
$^{238}U(^{238}U,X)$, 7.42 MeV/N, mass transport, shell effects, anharmonic pots. 80−99187
$^{238}U(^{238}U,X)$, 7.5 MeV/amu, three particle exclusive meas. for exit channels fission fragment ang. distrib. 80−13513
$^{238}U(^{238}U,X)$, 7.5 MeV/A, 3-dimens. TDHF-BCS model calcs., possible fission 80−52694
$^{238}U(^{238}U,X)$, damped collision, proton and neutron exchange correlations 80−18335
$^{238}U(^{238}U,X)$ deeply inelastic collisions, mass transport, shell effects 80−99188
$^{238}U(^{238}U,f)$, 1785 MeV, exam. of multiprong events due to multiple sequential fission using solid state track detectors 80−91199
$^{238}U(^{27}Al,f)$ 169, 190, 227 MeV, Z=105 compound nucleus lifetime using shadow effect *(Russian)* 78−86563
$^{238}U(^{40}Ar,X)$, 237, 250 MeV, differential recoil range distributions, large contrib. of deep inelastic processes 78−70565
$^{238}U(^{40}Ar,X)$, 340 MeV, production of neutron rich nuclides ^{54}Ti, ^{56}V, $^{58,59}Cr$, ^{61}Mn, $^{63,64}Fe$ 80−57802
$^{238}U(^{40}Ar,f)$, 212-340 MeV, I prod. relative thresholds from fusion and transfer induced fission 79−9640
$^{238}U(^{48}Ca,X)$, 276 MeV, differential recoil range distributions, large contrib. of deep inelastic processes 78−70565
$^{238}U(^{48}Ca,\gamma)$, nuclear pressure and fission fragment mass distrib. 80−18356
$^{238}U(^{56}Fe,X)$, 538 MeV, binary coincident fragments, fragment mass and energy, fission following fusion 80−548
$^{238}U(^{63,65}Cu,x)$, 9.6 MeV/nucleon, search for superheavy elements 77−34343
$^{238}U(^{84}Kr,X)$, mass fragmentation, dynamical theory, two centre shell model, binary decay process 80−68628
$^{238}U(^{84}Kr,f)$, 806 MeV, exam. of multiprong events due to multiple sequential fission using solid state track detectors 80−91199
$^{238}U(^{86}Kr,X)$, 730 MeV, transferred ang. momentum for fission and projectile like fragments 79−93675
$^{238}U(HI,f)$, Coulomb fission cross sections from coupled channel calcs. 80−9319
$^{238}U(Xe,f)$, depend. of Coulomb fission on nucl. struct. 78−13173
$^{51}V(^{16}O,X)$, 81 MeV, fragments in incomplete fission 77−14153
$^{51}V+^{16}O$, energy dissipation as func. of angle data comparison to classical and diffusion models 78−21604
$^{51}V(^{12}C,2np)$, 36 MeV, ^{60}Ni yrast state lifetimes and parities 79−45134
$^{51}V(^{16}O,p2n\gamma)$, lifetimes of ^{64}Zn levels 78−13019
$^{51}V(^{16}O,p2n)$, E=36-46 MeV, high-spin states in ^{64}Zn 78−33145
$^{51}V(^{16}O,p2n\gamma)^{64}Zn$, E=50 MeV, lifetimes of quasi-rotational states of ^{64}Zn 78−17140
$^{51}V(^{6}Li,d)$, 32 MeV, ^{55}Mn transitions to low lying levels, α spectroscopic strengths, DWBA anal. 79−45156
^{A}W, A=173, 175, hindered electric dipole transitions and lifetimes from (HI,xn) reactions 80−9263
$^{A}W(^{12}C,f)$, A=182, 183, 184, 186, 80 to 115 MeV, lifetime meas. by crystal-blocking tech. 80−91198
$^{A}W(^{16}O,f)$, A=182, 183, 184, 186, 80 to 115 MeV, lifetime meas. by crystal-blocking tech. 80−91198
$^{A}W(^{19}F,f)$, A=182, 183, 184, 186, 80 to 115 MeV, lifetime meas. by crystal-blocking tech. 80−91198
$^{182}W+^{12}C$, 98 MeV, fission, ^{1}H and ^{4}He emission from ^{194}Hg compound nucleus 78−50220
$^{182}W(^{12}C,^{14}C)^{180}W$, 70 MeV, ground-state rot. band ang. distribs., quadrupole transfer strength 77−336
$^{182}W(^{12}C,X)$ 77-167 MeV, fusion cross sections, direct and evaporative p and α prod., evaporation, fission 80−13518
$^{182}W(^{12}C,f)$, fission probability calc., α emission and evaporation effects 78−657
$^{182}W(^{16}O,6n\gamma)$, 132 MeV, ^{A}Pb, A=190,192, level scheme, γ-branching, ^{192m}Pb half life 79−75854
$^{182}W(^{20}Ne,xn)Po$, neutron deficient isotope prod. 78−8835
$^{184}W(^{20}Ne,Xn)$-$^{204-x}Po$, $4\leq X\leq 9$, absolute cross sections and excitation function meas. 79−13330
$^{184}W(^{40}Ar,pn)$, 165-202 MeV, ^{A}Pa, A=215-218, 222, α-decay half life and energies 79−45216
$^{186}W+^{86}Kr$, cross-sections for fusion, quasifission and deep inelastic collisions *(Russian)* 78−54801

heavy ion-nucleus reactions continued
$^{186}W(^{12}C,^{14}C)^{184}W$, reaction mechanisms, use of accelerators and detection methods *(Norwegian)* 79−13316
$^{186}W(^{12}C,^{14}C)^{184}W$, 70 MeV, ground-state rot. band ang. distribs., quadrupole transfer strength 77−336
$^{186}W(^{16}O,xn)$, ^{A}Pb, A=197, 198, low energy γ-transitions and level lifetimes 80−18221
Xe induced deeply inelastic collisions, transport eqn. appl. 78−82380
$^{130}Xe+^{209}Bi$, 1130 MeV, deform. and transfer in strongly damped collisions 78−21601
$^{132}Xe+^{56}Fe$, 5.73 MeV/u, reaction mechanism, evidence for new type of strongly damped collisions 79−13328
$^{136}Xe+^{209}Bi$, 1130 MeV, very heavy-ion collision mechanisms 78−89905
$^{136}Xe+Th(Au)(Al)$, 624 MeV, internal pair conversion positron spectra 77−67769
$Y+^{84}Kr$, 350 MeV, compound nucleus prompt K X-rays 79−67768
$^{89}Y+^{40}Ar$, 237 meV, γ-ray multiplicities and energies, primary fragment angular momenta 78−46093
$^{89}Y(^{40}Ar,X)$, 237 MeV, ang. momentum transfer in deep inelastic reactions 80−5156
$^{89}Y(^{84}Kr,xn)^{A}Re$, x=5,6,7, A=168, 167, 166, isotope existance evidence 79−503
$Yb(^{16,18}O,xn)$, 77-88 MeV, ^{A}Pt, A=186,188,190, subnanosecond high spin isomers, decay chains and lifetimes 79−45140
$^{170}Yb(^{19}F,4n)$, collective band struct. in ^{185}Au 79−22166
$^{174}Yb(^{12}C,f)$, fission probability calc., α emission and evaporation effects 78−657
$^{174}Yb(^{40}Ar,xn)Ra$ and $^{174}Yb(^{40}Ar,pxn)Fr$, 160-270 MeV, excitation functions, statistical models calcs. 77−3042
$^{176}Yb(^{12}C,8n)^{180}Os$, 120 MeV, continuous γ-ray spectra anal. 78−41747
$Zn(^{12}C,2n)$, 39 MeV, $^{76,78,80}Kr$ yrast states and band struct., backbending 80−13359
$Zn(^{6}Li,d)$, $^{68,70,72,74}Ge$ level excitation, n-p interaction role from α-transfer 80−73821
$Zn(^{16,18}O,xn)$, 36 to 55 MeV, total neutron yields, cross sections 77−14163
$^{64}Zn\ (^{12}C,\ ^{12}C_{2+}{}^{*})\ ^{64}Zn$, spin alignment of $^{12}C_{2+}$state 79−93521
$^{64}Zn(^{12}C,2n)$, 39 MeV, ^{76}Kr rot. bands, band crossing and backbending 80−18176
$^{64}Zn(^{16}O,np)$, 44,52 MeV, ^{78}Rb band struct. and level scheme 79−54380
$^{64}Zn(^{7}Li,^{6}He)^{65}Ga$, 36 MeV, CC ^{65}Ga, spin assignments of levels by forward-angle j dependence 78−93935
$^{64}Zn(^{7}Li,p2n)$ 18 MeV, ^{68}Fe low lying state mean lifetimes and transitions 80−68599
$^{64}Zn(^{7}Li,pn)$, 18 MeV, ^{19}Ge excited state, J, mean lifetimes and transitions 80−68517
$^{64}Zn(\alpha,p\gamma)$, 13-15 MeV, γ-spectroscopy of ^{67}Ga high-spin levels 78−93960
$^{68}Zn(^{12}C,2n)$, 38-38 MeV, ^{78}Kr band structs., in-beam γ-rays 80−22672
$^{68}Zn(^{12}C,Zn)$, 33-38 MeV, ^{78}Kr high spin levels, bands and transitions, level lifetimes 80−42525
$^{68}Zn(^{6}Li,pn)$ in beam gamma-ray spectroscopy of ^{72}Ge levels 80−47343
$^{70}Zn(^{16}O,p2n)$, 52 MeV, ^{83}Rb band struct., spin assignments and transitions 80−73774
$^{70}Zn(^{16}O,p2n)$, 52 MeV, ^{83}Rb high spin states, Jπ and transitions 80−105949
$^{70}Zn(^{18}O,^{20}Ne)^{68}Ni$, mass excess of ^{68}Ni 77−41878
Zr (^{13}C, 3nγ), 45-56 MeV, collective and two-quasiparticle excitation in Pd 77−18601
$Zr(^{16}O,xn\gamma)Cd$, parity assignments of Cd with A=105 to 109 78−41630
$^{45}Zr(^{16}O,4n\gamma)$, 63 MeV, ^{106}Cd collective and yrast levels, γ-transitions, 2 quasiparticle+rotor model 79−22169
$^{90}Zr+^{12}C$, 56 MeV, assignment of γ-ray cascade to ^{99}Rh 78−41762
$^{90}Zr+^{208}Pb(^{238}U)$, 7.5 MeV/amu, ang. momentum transfer in deeply inelastic collisions from exclusive sequential-fission expts. 79−76044
$^{90}Zr+^{86}Kr$, 366-716 MeV, evaporation residue product cross sections 79−17947
$^{90}Zr(^{7}Li,^{6}He)^{91}Nb$, 34 MeV DWBA calcs. 79−26448
$^{90}Zr(^{7}Li,^{6}Li)^{91}Zr$ 34 MeV, 1.21 and 2.03 MeV states, 2.19 MeV doublet in ^{91}Zr, DWBA anal. 79−26448
$^{91}Zr+^{12}C$, obs. of γ-cascades in ^{99}Pd and ^{99}Rh 77−30506
$^{92}Zr+^{10}B$, obs. of γ-cascades in ^{99}Pd and ^{99}Rh 77−30506
$^{92}Zr(^{12}C,3n)$, 48 MeV, ^{101}Pd nonyrast rotational states, transitions, $T_{1/2}$, branching and mixing ratios 80−105950
$^{92}Zr(^{16}O,2np)$, 60 MeV, ^{105}Ag positive parity band, mixing and branching ratios lifetimes 80−9197
$^{94}Zr+^{16}O$, 140, 315 and 33600 MeV, isotope yields and cross sections 77−14161
$^{94}Zr+^{16}O$, 140 and 315 MeV, energy depend. of heavy ion peripheral reactions 78−74399
$^{94}Zr+^{22}Ne$, 174 MeV, energy spectra and prod. cross sections for Be, B, C, N, O *(Russian)* 77−23105
$^{94}Zr(^{64}Ni,4n)$, 275 MeV, ^{154}Er yrast trap and transitions, decay scheme 80−9206
$^{94}Zr(^{6}Li,3n\gamma)$, 23-33 MeV, ^{97}Tc high spin states, spins and transitions 80−73780
$^{96}Zr(^{14}N,3n)$, 49 MeV, ^{107}Ag 80−9197
$^{96}Zr(^{16}O,4n\gamma)$, 56 MeV, γ yields, polarisations, ang. distribs., ^{108}Cd decay scheme 78−66301

heavy ion-nucleus scattering
$^{12}C(^{16}O,^{16}O)$, anomaly at 13.7 MeV, optical model anal. 78−21587
$(^{6}Li,^{6}Li)$ 50.6 MeV elastic scatt. on A=12-208 nuclei, optical model parameters 77−18592
adiabatic approximation for heavy ion scatt. 78−631
angular distribs., nuclear surface diffuseness, diffraction formulae 80−47494
backward glory 79−71866
band crossing model, appl. to $^{12}C+^{16}O$ scatt. 78−89898
band crossing model, resonance and strong absorption phenomena in heavy ion scatt. 79−3165
$C\ ^{152}Sm(^{16}O,^{16}O)$, 72 MeV, coupled-channels anal., nucl. excitation effects 79−26457
cascade-disintegration model, appl. to heavy-ion-nucleus interactions *(Russian)* 79−3177
charged particle scatt., optical pot. in approx. of strong absorption *(Russian)* 78−89839
classical microscopic model of heavy ion reactions 78−66298
closed formalism, elastic and inelastic scatt. 78−37375
clustering aspects and nuclear quasimolecular resonances 79−6439
conference, Les Houches, France (July-August 1977) 79−71864

heavy ion-nucleus scattering continued
Coulomb barrier top energies, WKB calc. 80−86918
Coulomb excitation, effect on reaction cross section determination in heavy ion elastic scattering 79−97720
Coulomb excitation functions, numerical calc. of limiting props. 79−9604
Coulomb excitation of sd shell nuclei, B(E2) values, lifetime meas. 78−25216
Coulomb excitation parameters 78−13149
Coulomb-nuclear interference, implications for reorientation effect meas. 78−70559
coupled eqns. for scatt. problems, iterative method of soln. 77−46148
critical ang. momentum from elastic and inelastic data 77−10421
critical distance for spontaneous positron prod. 77−14159
deep inelastic collisions, characteristic time scales 79−71869
deeply inelastic collisions, mass transport 78−86541
deeply inelastic collisions, shape deformation and viscosity 78−25234
deeply inelastic collisions, simple model calcs. in microscopic transport theory 79−71870
diffraction at backangles 79−17874
direct reactions and scatt., multi-step processes, asymptotic and peripheral regions 78−50190
dynamic polarisation by Coulomb excitation in closed formalism, ^{184}W (^{18}O, ^{18}O) appl. 78−37376
dynamic polarisation pot. for heavy-ion scatt. 78−13136
dynamic polarisation potential for Coulomb excitation effects on heavy-ion scatt. 77−67765
effective internuclear potential, antisymmetrisation effects 79−59085
effective potentials for heavy-ion scattering derived from channel coupling 80−57794
eikonal description 77−41938
eikonal model of hadronic matter distribution of particles and nuclei 79−26317
elastic, Andreev's expansion obtained by generating function method *(Russian)* 79−89327
elastic, interference effects, non nuclear-molecular phenomena 79− 9623
elastic and inelast., DWBA anal. 78−13143
elastic and inelastic scatt., optical pots. and folding model 80−5169
elastic scatt., diffr., refr., interf. effects 77−3031
elastic scatt. pots., spin-orbit terms, appl. to (^6Li,^6Li) 78−66313
elastic scattering, folding model pots. from realistic NN interactions 80−5159
elastic scattering between complex nuclei, barrier penetration effects, semiclassical theory 77−34339
folding model in momentum space, formalism and real potential 77−57682
folding model in momentum space, imaginary potential 77−57683
folding model pots. 79−97728
forward scattering dispersion rels. *(Rumanian)* 80−47501
gasdynamic mechanisms of heavy nuclei inelastic collisions *(Russian)* 77−61452
generalised Fresnel model for very heavy ion elastic scatt., rel. to optical model 78−74393
generalised Fresnel model for very heavy ion elastic scatt., dynamic polarisation effects 78−74394
generalised Fresnel model for very heavy ion elastic scatt. 78−74392
Glauber approx., validity of optical limit, higher order correction effects 77−54252
Glauber multiple scatt. series approx. quasi elastic shadowing 79−17915
Glauber theory, functional integral representation for high energy heavy ion scatt. 79−40945
heavy ion optical model, surface transparency and resonance phenomena 79−9617
heavy ion optical pot., imaginary part 79−97727
heavy ion optical pot., real part energy depend. 79−63691
heavy particle elastic collisions, quantum effects *(Japanese)* 78−21015
high energy collisions, theoretical overview 80−42682
high energy nuclear collective states; existence 77−82804
high spin rotational states population in doubly even nuclei, lifetime meas. 77−30511
high-energy, Glauber's theory, classical transport eqn. 79−6522
high-energy scatt., optical phase shift function 78−639
Hill-Wheeler eqns. direct solns., pot. scatt. and α-α calcs. 78−4956
identical nuclei, collisions, heavy ion real pots. *(German)* 77−57691
impact parameter representation, quantal trajectories 77−14181
inclusive cross sections, collective and statistical effects, fluctuations for complex collisions 79−36258
independent particle model, forces between heavy nuclei 78−635
inelastic, closed form quantal description, DWBA anal. 77−14147
inelastic scatt., coupled channels calcs. for direct reactions, long range Coulomb coupling 80−83117
inelastic scatt., direct reactions, coupled channel calcs., coupled radial eqns. 80−83118
inelastic scatt., with Coulomb interaction, soln. of coupled eqns. 77−65232
inelastic scattering, form factors 79−26458
inelastic scattering, optical pot. deformation 80−13505
interacting composite systems, generalised spectator expansion in multiple scatt. framework 80−27664
intermediate energy collisions, elastic scatt., Coulomb excitation, nucleon transfer, expt. facilities, models 79−6697
internal S-matrix dynamics and internal deflection function 80−78307
ion-ion potls., and Coulomb barrier radius 77−3039
ion-ion scattering, momentum dependence, in microscopic theory 78−41752
ionisation energy losses in ultrarelativistic region, space struct. effects *(Russian)* 78−46105
large-angle scatt., elastic cross-section, excitation functions 80−52689
large-angle scatt., inelastic cross-section and collective state excitation 80−52690
light heavy ions elastic scatt., folding model and optical pots. 80−13424
local optical potential determ., semiclassical derivation 79−59083
local potential models for complex nuclei scatt., appl. to α-α, ^3He-α and ^{16}O-^{16}O 77−34270
local Slater exchange approx. for nucleon and heavy ion scatt. 79−22309
magnetic substate population, inelastic scatt., closed formalism based on DWBA 77−6424
many particle systems, microscopic derivation of classical eqns. of motion 80−102199
mass exchange and ang. distrib., dynamical treatment using Fokker-Planck eqn. 77−61454

heavy ion-nucleus scattering continued
microscopic anal. 78−54780
microscopic nucleus-nucleus optical potential 79−97688
modified perturbed stationary state anal. 79−36262
molecular resonances in heavy ion collisions, review 79−22313
molecular states in heavy ion potentials 79−97730
momentum projection methods in nucleus-nucleus scatt., optical pot. 1-channel problem 78−78403
multiple scattering in thin foils, 1.2 MeV, Ar, Kr, Xe, U ions, ang. distrib. meas. 79−751
multiple scattering in thin foils, 12-40 MeV O, Cl, Fe ions, ang. distrib. meas. 77−61455
N=85 isotones, bands and transitions from α and HI excitation, in-beam study 80−78123
nonlinear Schrodinger eqn. and anomalous backward scatt. 78−17232
nuclear effects in heavy-ion elastic scatt. 78−13137
nuclear isobars elastic scatt., appl. to pion-nucleus interaction *(Russian)* 79−45297
nuclear molecules, two-centre shell model parastatistics 79−9618
nucleon transfer in dynamical two centre shell model, mol. single particle effects 79−89325
nucleus-nucleus interaction pot., transition from light to heavy ions, optical pots 80−63197
nucleus-nucleus pot., folding model, single nucleon knock-out exchange contrib. 77−305
nucleus-nucleus potential from liquid drop model 78−50204
optical model analysis 80−73858
optical model code A-THREE, appl. to heavy ion scatt. 78−89837
optical pot., density depend. interactions and folding model 78−17237
optical pot., long range absorpt., from Coulomb distorted states and Green's functions 78−29494
optical potential elastic scatt., energy depend., Regge pole and Coulomb amplitudes, $^{16}O+^{16}O$ calcs. 78−25228
optical potential resonances, semiclassical method, S-matrix amplitude 79−3120
OPTY, universal optical model code for elastic scatt. 80−73832
partial-wave expansion of amplitude for elastic heavy ion scatt. 77−6423
Pauli-principle resonance effects, analytic representation 79−6659
perturbed stationary state method, low energy collision and mol. resons. 80−78320
phase shifts, angle depend., coupled channel formalism 80−18253
positron prod. in heavy ion collisions 78−50198
potential scatt., multiple reflection expansion 78−41753
potential scattering, single reflection approx. 77−10422
projected proton method for heavy ion energy meas., device for 3-6 MeV beams *(French)* 78−82567
QED in strong and supercritical fields 78−74193
quasi elastic nucleus-nuclear scatt. differential cross section *(Russian)* 80−68696
quasi-classical approximation for heavy ion elastic scattering *(Russian)* 79−63686
quasi-elastic heavy ion scatt., multistep processes and interference phenomena 80−22857
quasi-identical elastic scatt., derivation of local approx. 79−6658
random-matrix model, transport theory of deeply inelastic heavy-ion collisions 77−88163
Rayleigh and whispering gallery waves excited by heavy ion elastic and inelastic scatt. 80−91164
reflected and refracted trajectories in elastic scatt. 78−50200
reflection phenomena, WKB calcs. 80−27656
Regge pole contrib., forward- and backward-angle, Coulomb and nuclear scatt. functions 80−57788
relativistic Coulomb excitation of target and projectile, differential and total cross sections 79−54450
relativistic heavy ion collisions, reaction mechanism and recent topics, review 80−42683
relativistic nuclei, phase shifts and scatt. cross sections *(Russian)* 79−22321
resonance states in two-body breakup channels, theory of fragmentation 79−9619
resonances, conference, Hvar, Yugoslavia (June 1977) 79−9614
review, book contrib. 80−27668
review of heavy ion reactions, reaction types, reaction theories 78−74401
scattering amplitude, using Glauber-Sitenko eikonal approx. *(Russian)* 79−80953
semi-classical description 79−71867
semiclassical description using complex trajectories for very heavy-ion elastic scatt. 79−561
short range correlations in nucleus-nucleus scatt. amplitude, optical phase shift expansion 78−70502
strongly damped heavy ion collisions, nucleon exchange as possible mechanism, semiclassical model 79−6689
sub-Coulomb collisions, e^+-e^- pair creation as probe for strong Coulomb fields 78−12962
subCoulomb elastic heavy ion scatt., influence of low lying collective states 78−78414
supercritical nuclear composites, spontaneous vacuum decay 78−25235
superheavy ion collisions, slow, spontaneous positron creation 79−9603
tidal bore effect, 40-200 MeV/N 77−34331
total reaction cross sections and elastic scatt., refractive scatt. or strong absorption 79−567
two nucleon transfer and scatt. matrix elements from dynamic deformation theory 79−85488
two-proton azimuthal angle correlations, in 2 GeV/N interactions 78−62572
unequal fragments, generator coordinate and resonating group methods 77−18490
unified nuclear pot. for heavy ion elastic scatt., fission, fusion, masses and deformations 80−5189
unified pot. from liquid drop model, description of nuclear props. 79−22213
vacuum polarization potential for two heavy ions, calc. in first order, numerical method 78−21594
very heavy ions with complex trajectories, elastic scatt., semiclassical anal. 80−18331
e^+e^- prod., Dirac eqn. soln. for point nuclei 77−71553
NN interaction, local density dependence, double-folding calcs. 80−83114
Ag(^{12}C,$^{12}C'$), 50 GeV/c, multiplicities and ang. distribs. *(Russian)* 79−22323

heavy ion-nucleus scattering continued
^{27}Al(^{10,11}B,^{10,11}B), 41.6, 50 MeV, ang. distribs., cross sections and deformation parameters, absorption effects 79−67773
^{27}Al(^{12}C,^{12}C), 14-25 MeV, 180° scatt. excitation function and ang. distrib. struct. 80−32253
^{27}Al(^{16}O,X), 88 MeV, inelastic scatt. and multinucleon transfer, Q-value depend. 80−42690
^{27}Al(^{35}Cl,^{35}Cl), 100-170 MeV, elastic scatt. ang. distrib. 78−21605
^{27}Al(^{6,7}Li, ^{6,7}Li), 90 MeV, real optical pot. continuous ambiguity 80−102200
Au(HI,X,), fission fragment backscattering corrections to absolute fission counting rate measurements 80−68685
^{197}Au (^{18}O, ^{18}O) reorientation effect in Coulomb scatt., static quadrupole moment of first excited state in ^{18}O 77−82823
^{197}Au+^{132}Xe, 7.5 MeV/amu ions, neutron multiplicities as func. of total energy loss 78−21606
^{197}Au+^{14}N, 161 MeV, giant resonances in inelastic scatt. 78−62564
^{197}Au+^{63}Cu, mass exchange and ang. distrib., dynamical treatment 77−61454
^{197}Au(^{20}Ne,^{20}Ne), 90 MeV, state lifetimes, weak coupling core excitation model, translation rates 79−63630
^{197}Au(^{35}Cl,^{35}Cl), 120 MeV, state lifetimes, weak coupling core excitation model, translation rates 79−63630
B+^{27}Al, A=10,11, elastic scatt. quadrupole effects at 50 MeV, optical parameters 77−88169
^{10}B(^{14}N,^{14}N), 4.3-9.1 MeV, differential cross sections, incoming wave boundary condition model 79−22348
^{11}B+^{12}C elastic scatt., resonances 78−89901
^{A}Ba(^{16}O,^{16}O′), A=135,137, Coulomb excitation, transition probabilities, γ-rays and level collectivity 80−78201
^{A}Ba(^{32}S,^{32}S′), A=130, 132, 134, 136, 72-80 MeV, 2_1^+ state mag. moments 80−47373
^{134}Ba, reorientation effect and multiple Coulomb excitation meas. 77−61450
(^{9}Be,^{9}Be), optical pot. 79−59087
^{9}Be elastic scattering on heavy target nuclei, 14-26 MeV, universal optical pot. 78−25219
^{9}Be(^{10}B,^{10}B), 9.5-14.2 MeV, ang. distribs., cross sections, elastic p transfer 80−78318
^{9}Be(^{9}Be, ^{9}Be), 5 to 16 MeV, absolute cross sections, optical model parameters 77−67761
^{9}Be(^{9}Be,^{9}Be) 14, 20 and 26 MeV, optical model parameters, 9 to 22 MeV excitation curves 79−26449
^{209}Bi+^{14}N, 161 MeV, giant resonances in inelastic scatt. 78−62564
Br(^{12}C,^{12}C′), 50 GeV/c, multiplicities and ang. distribs. *(Russian)* 79−22323
C (C,C), 800 MeV/N, high momentum nucleons from relativistic nuclear collisions, hard scatt. mechanism 79−40950
C(^{16,17}O,^{16,17}O), two centre shell model, molecular single particle states at level crossings 80−47354
^{A}C(^{9}Be,^{9}Be) A=12, 13, 14, 20 and 26 MeV, optical model parameters 79−26449
^{12}C (^{12}C, ^{12}C), molecular collective excitation theory in two centre model 79−89256
^{12}C (^{16}O, ^{16}O′), 19-23 MeV, intermediate width structs., ang. correlations, spins 80−13431
^{12}C, elastic and inelastic scatt. of ^{10}B, ^{14}N, common optical potential 77−34276
^{12}C, elastic back angle scatt. from α-nuclei 79−6665
^{12}C, vector polarised ^{6}Li elastic scatt., full optical model anal. 78−70553
^{12}C-^{12}C, excit. function struct., momentum space folding model 77−57683
^{12}C-^{12}C excit. function calc. in momentum space folding model 77−57682
^{12}C-^{12}C resonances, speculation of nature, excited α-particles 79−13339
^{12}C-^{12}C scattering, fusion cross-section, folding model study, coupled channel effects 78−89893
^{12}C+^{11}B, 9.4-17.8 MeV, excitation functions for elastic, inelastic, ^{8}Be, α exit channels, resonances 79−67731
^{12}C+^{12}C, 2.1 GeV/n elastic scatt., correlations 78−41761
^{12}C+^{12}C, 6.25 MeV reson., J$^{\pi}$ determ. 77−50099
^{12}C+^{12}C, mol. resonance props. by GCM 79−13321
^{12}C+^{12}C, optical pot. for nucleus-nucleus systems using double folding model 79−45225
^{12}C+^{12}C, partial widths of molecular resonances 78−46094
^{12}C+^{12}C, sub-Coulomb total cross section, simple pot. model of resonances 78−66303
^{12}C+^{12}C elastic scatt., optical model anal. 77−6429
^{12}C+^{12}C elastic scatt., low partial waves 77−71620
^{12}C+^{12}C elastic scatt., induced rot., energy depend. of optical pot. real part 78−89903
^{12}C+^{12}C in elastic scatt., high energy, resonances obs., evidence for band crossing model 78−66305
^{12}C+^{12}C inelastic scatt., gross struct. origin, nonreson. diffr. model calcs. 79−30849
^{12}C+^{12}C quasimolecular interactions, recent developments 79−9615
^{12}C+^{12}C scatt., 10-20 MeV, optical model pot. 79−26456
^{12}C+^{12}C scatt., intermediate molecular resonances, band crossing model anal. 79−6655
^{12}C+^{12}C scatt. and fusion cross sections above Coulomb barrier, folding model, resonances 79−6687
^{12}C+^{12}C system, 7.5 MeV, reson. spin assignment 77−14089
^{12}C+^{12}C system, inelastic scatt. and fusion cross section, folding model, resonances 79−13337
^{12}C+^{12}C system, microscopic nuclear pots., elastic and inelastic channels 79−6654
^{12}C+^{12}C system, nuclear molecule microscopic description, HF and coupled channel calcs. 80−13493
^{12}C+^{12}C(^{16}O), elastic scatt. and fusion cross-section calc. 77−46182
^{12}C+^{12}C→^{12}C(2_1^+)+^{12}C(2_1^+), 15-45 MeV, obs. of molecular resonances 77−74867
^{12}C+^{12}c, rotational band fragmentation rotation-vibr. model 78−54665
^{12}C+^{13}C elastic transfer interaction, intermediate energies, n exchange cross sections 79−13318
^{12}C+^{13}C resonances, coupled channel anal. with core-exchange model 79−13338
^{12}C+^{16}C scatt. reson. and strong absorpt. phenomena, band crossing model 79−3165
^{12}C+^{16}O, 12.8 to 18.2 MeV, reactions and inelastic scatt., resonance anomaly study by γ ray techniques 78−4955

heavy ion-nucleus scattering continued
^{12}C+^{16}O, elastic scatt., simple double folded optical pot. model for resonances 79−6535
^{12}C+^{16}O, resonance behaviour, similarity to that in ^{12}C+^{12} 78−33210
^{12}C+^{16}O elastic scatt., generator coord. calc., reson. spin assignments 77−57685
^{12}C+^{16}O inelastic scatt., microscopic coupled channel calc. 78−625
^{12}C+^{16}O inelastic scatt., microscopic R-matrix method anal. 79−6656
^{12}C+^{16}O multichannel scatt., microscopic calcs. in generator coordinate method, spin assignments 79−564
^{12}C+^{16}O resonances, microscopic double folded model 78−41754
^{12}C+^{16}O resonances, microscopic interpretation 79−13340
^{12}C+^{16}O scatt., band crossing model of resonances 78−89898
^{12}C+^{16}O scatt. reson. and strong absorpt. phenomena, band crossing model 79−3165
^{12}C+^{16}O system, ang. mom. projected microscopic calc. 77−14148
^{12}C+^{17,18}O, 12.6-14.0 MeV elastic scatt., ang. distribs. 78−37361
^{12}C+^{20}Ne elastic scatt., strength of absorpt. 77−3028
^{12}C+^{27}Al, elastic scatt. quadrupole effects at 55 MeV, optical parameters 77−88169
^{12}C+^{28}Si, 17 to 37 MeV, inelastic and elastic backward angle scatt., surface resonances 78−37367
^{12}C+^{28}Si, 17.5 to 33 MeV, resonant backward angle elastic scatt. 78−46096
^{12}C+^{6}Li(^{16}O) scatt., anomalous backscatt. from nonlinear Schrodinger eqn. for nuclear matter 79−6465
^{12}C+^{6}Li(^{7}Li), 9 MeV, isotopic shape effects in elastic scatt. of aligned ions 78−89904
^{12}C(^{12}C, ^{12}C), shape resonance energy and widths, projection operator method 80−78255
^{12}C(^{12}C, ^{12}C) intermediate struct. resonances, ^{24}Mg giant isoscalar quadrupole fission/fusion doorway states 80−37410
^{12}C(^{12}C, ^{12}C)^{12}C*, 0_2^+, 3_1^-, 4_1^+ state excitation functions, resonance structures 80−42616
^{12}C(^{12}C,^{12}C^{1}), 18.5-32.8 MeV, spin alignment and possible molecular resonances 80−86804
^{12}C(^{12}C,^{12}C′), 10-40 MeV, resonance phenomena, band crossing model appl., molecular phenomena 79−54424
^{12}C(^{12}C,^{12}C′), 14.5-32 MeV, gross structure peaks, particle-γ coincidences 79−97693
^{12}C(^{12}C,^{12}C′), gross struct., barrier top resonance model calc. 80−9279
^{12}C(^{12}C,^{12}C′), intermediate resonance, coupled channels calcs. 80−42611
^{12}C(^{12}C,^{12}C′), 50 GeV/c, multiplicities and ang. distribs. *(Russian)* 79−22323
^{12}C(^{12}C,^{12}C), 10-30 MeV, projection operator method, Feshbach doorways, intermediate structure 80−68695
^{12}C(^{12}C,^{12}C), 10-30 MeV, molecular structure, projection operator anal., differential cross sections 80−106033
^{12}C(^{12}C,^{12}C), 13-14.1 MeV, Coulomb barrier resonance parameter direct determ., J$^{\pi}$ assignments 80−513
^{12}C(^{12}C,^{12}C), 35-63 MeV, elastic and inelastic, cross sections, DWBA and optical anal. 79−93656
^{12}C(^{12}C,^{12}C), 6-30 MeV, intermediate struct. from band crossing model, molecular resonances 79−54425
^{12}C(^{12}C,^{12}C), elastic scatt., incoming wave boundary condition model calcs. 80−47504
^{12}C(^{12}C,^{12}C), perturbed stationary state method, low energy collision and mol. resons. 80−78320
^{12}C(^{13}C,^{13}C) 4.8-9.5 MeV, cross-section at Coulomb barrier 77−14154
^{12}C(^{13}C,^{13}C)^{12}C, 12 MeV, accurate determ. of ^{13}C-^{12}C+n spectroscopic factor 77−65194
^{12}C(^{16}O, ^{16}O′), molecular resonances from coupling interactions derived by folding procedure 79−89279
^{12}C(^{16}O, ^{16}O), 35 to 50 MeV, backscatt., dynamic deformation and excitation functions, optical anal. 80−18227
^{12}C(^{16}O,^{16}O′), 315 MeV, giant multipole resonance excitation 79−30812
^{12}C(^{16}O,^{16}O′) 46 to 56 MeV, ^{16}O(0^+,6.05 MeV) intermediate struct. resonances 78−78410
^{12}C(^{16}O,^{16}O*)^{12}C*, 33-54 MeV, intermediate struct. resonances, ang. distribs., statistical anal. 78−82330
^{12}C(^{16}O,^{16}O), elastic and inelastic, 23-32 MeV, strong absorption region resonances, excitation functions 80−86884
^{12}C(^{16}O,^{16}O), resonance at 12.8 MeV 77−46187
^{12}C(^{16}O,^{16}O) 41-65 M-V, ^{16}O $3^-\rightarrow 0^+$ gamma transition, ^{20}Ne $2^+\rightarrow 0^+$ transition 80−63125
^{12}C(^{16}O,^{16}O)^{12}C, 15.4 to 30.9 MeV, correlation between fusion and inelastic scatt. 78−66310
^{12}C(^{16}O,^{16}O)^{12}C, gross struct. features, optical model 77−88164
^{12}C(^{16}O,^{16}O)^{12}C resonant scatt., 15-30 MeV, ang. distribs., interpretation *(French)* 79−3166
^{12}C(^{20}Ne,^{20}Ne), back angle scatt. systematics, structured excitation functions and oscillatory ang. distribs. 80−32295
^{12}C(^{20}Ne,^{20}Ne)^{12}C, elastic, energy depend., non-statistical effects 79−13332
^{12}C(^{24}Mg,^{24}Mg), back angle scatt. systematics, structured excitation functions and oscillatory ang. distribs. 80−32295
^{12}C(^{40}Ca,^{40}Ca), 90° and 180° excitation functions energy depend., DWBA anal. 80−42582
^{12}C(^{6}Li,^{6}Li′), 153 MeV, isoscalar giant quadrupole resonances 80−13440
^{12}C(^{6}Li,^{6}Li′), spin-flip transitions, microscopic α-spectator model 77−79400
^{12}C(^{6}Li,^{6}Li) 5.8, 59.8 MeV, optical pot. inner part, elastic scatt. cross section 79−3173
^{12}C(^{6}Li,^{6}Li)^{12}C, 20 MeV and higher, diffraction model behaviour, anomalies caused by two step-processes 79−13344
^{12}C(^{7}Li, ^{7}Li), 40 MeV, spectroscopic factors, DWBA anal. 79−75904
^{12}C(^{9}Be, ^{9}Be)^{12}C(g.s.), 39.68, 43.75 MeV, back angle cross section enhancement, Hauser Feshbach anal. 79−89324
^{12}C(^{9}Be,^{9}Be), ang. distrib. from pick-up model anal. *(Russian)* 80−37396
^{12}C(^{9}Be,^{9}Be), cluster effects *(German)* 79−76015
^{12}C(^{9}Be,^{9}Be), large angle scatt., optical model and DWBA anal. 79−36259
^{12}C(^{9}Be,^{9}Be), possibility of ^{3}He exchange 79−6669
^{12}C(^{9}Be,^{9}Be) elastic and inelastic 10-15 MeV, excitation functions and resonant enhancements 79−17881
^{12}C(^{9}Be,^{9}Be)^{13}C$_{gs}$, cluster effects *(German)* 79−76015
^{12}C(^{9}Be^{9}Be) 14, 20 and 26 MeV, optical model parameters 79−26449
^{13}C, ^{17,18}O, 12.6-14.0 MeV elastic scatt., ang. distribs. 78−37361
^{13}C+^{13}C, appl. of molecular particle core model 78−82384

heavy ion-nucleus scattering continued
$^{13}C+^{6}Li(^{7}Li)$, 9 MeV, isotopic shape effects in elastic scatt. of aligned ions 78−89904
$^{13}C(^{12}C,^{12}C)$, mixed parity neutron orbits, coupled channel theory with adiabatic assumption 80−9304
$^{13}C(^{12}C,^{12}C)$, molecular neutron orbit formation, $1/2^+$ state excitation, coupled channels calcs. 80−78156
$^{13}C(^{12}C,^{12}C)$ 15, 87 MeV, elastic transfer exchange amplitude, coupled reaction channel and DWBA calcs. 80−32298
$^{13}C(^{17}O,^{17}O)^{13}C$, 12.9, 14 MeV c.m., compound decay reaction mechanism 77−88167
$^{13}C(^{6}Li,^{6}Li)$, 40 MeV, spectroscopic factors, DWBA anal. 79−75904
$^{13}C(^{9}Be,^{9}Be)$, large angle scatt., optical model and DWBA anal. 79−36259
$^{13}C(^{9}Be,X)$, 11.6 MeV, p,t,d,α, ^{8}Be ang. distribs., Hauser-Feshbach and DWBA anals. 80−91193
$^{14}C+^{16}O$ scatt., molecular resonances, generator coordinate study 79−36216
$^{14}C(^{16}O,^{16}O)^{14}C$, resonance struct. at excitation energies 40-51 MeV in ^{30}Si, comparison with $^{12}C+^{18}O$ 79−13335
Ca(Li,Li), (A=40,48), 28 and 34 MeV optical model parameters 77−54248
$Ca(^{32}S,^{32}S)$, 58-130 MeV, elastic scatt., ang. distribs., excitation function, optical model anal. 77−30623
$^{A}Ca(^{12}C,^{12}C)$, A=40,42,48, 47-51 MeV, ang. distribs. optical model anal., surface transparency 79−45291
$^{A}Ca(^{6}Li,^{6}Li')$, A=40, 44, 48, 153 MeV, isoscalar giant quadrupole resonances 80−13440
$^{40}Ca+^{13}C$, 68 MeV, inelastic scatt., anomalous L=1 ang. distrib. anal. 77−65236
$^{40}Ca+^{13}C$, microscopic ion-ion spin-orbit pot. 78−17163
$^{40}Ca+^{14}N$, 161 MeV, giant resonances in inelastic scatt. 78−62564
$^{40}Ca+^{16}O$, polarisation of single particle states, two centre shell model 77−30622
$^{40}Ca+^{20}Ne$, 36-95 MeV, Coulomb-nuclear interference 78−50210
$^{40}Ca+^{40}Ca$, elastic scatt. excitation functions, interf. effects 77−50155
$^{40}Ca(^{A}B,^{A}B)$, A=10,11, angular distrib., Woods-Saxon and double-folding optical models 80−52691
$^{40}Ca(^{12}C,^{12}C)$, 135-150 MeV, elastic excitation function at 180°, resonance like struct. 79−9609
$^{40}Ca(^{12}C,^{12}C)$, 20 to 35 MeV, resonant heavy ion scatt., from s-d shell nuclei 79−67763
$^{40}Ca(^{12}C,^{12}C)$, 20-35 MeV, resonant scatt., ang. distribs., cross sections and excitation functions 79−45237
$^{40}Ca(^{12}C,^{12}C)$, 80-178 MeV, backward angle excitation functions 79−36267
$^{40}Ca(^{13}C,^{13}C')$, 108 MeV, nuclear continuum investigation 80−13506
$^{40}Ca(^{16}O,^{16}O')$, 60 MeV, direct reaction calcs., ang. distribs. 78−58298
$^{40}Ca(^{16}O,^{16}O)$, 60 MeV, long range absorption and optical model effects from strong inelastic coupling 80−535
$^{40}Ca(^{16}O,^{16}O)$, 80-178 MeV, backward angle excitation functions 79−36267
$^{40}Ca(^{16}O,^{16}O)$, optical pot., nuclear matter approach, energy density matter [-] 80−83112
$^{40}Ca(^{16}O,^{16}O)$, rot. band of molecular resonances, generator coordinate model 80−13428
$^{40}Ca(^{16}O,X)$, 40-214 MeV, fusion and elastic scatt. cross sections, optical anal. 80−32314
$^{40}Ca(^{17}O,^{17}O)$, 61 MeV, elastic and inelastic, microscopic single folding model anal. 80−52692
$^{40}Ca(^{20}Ne,X)$, 44.1-70.4 MeV, fusion and elastic scatt. cross sections, evaporation residues 80−550
$^{40}Ca(^{40}Ar,^{40}Ar)$, 191, 236, 272 MeV, cross sections, interaction radius, Fresnel and optical model anal. 79−59084
$^{40}Ca(^{40}Ar,^{40}Ar)$, 191, 236, 272 MeV, elastic cross sections, optical and Fresnel model anals. 80−22858
$^{40}Ca(^{40}Ca,^{40}Ca)$, generator coordinate study, rot. band of molecular resonances 79−75948
$^{40}Ca(^{40}Ca,^{40}Ca)$, 58-130 MeV, elastic scatt., ang. distribs., excitation function, optical model anal. 77−30623
$^{40}Ca(^{40}Ca,^{40}Ca)$, 64-120 MeV, optical model and strong absorpt. model anal. 77−41994
$^{40}Ca(^{40}Ca,^{40}Ca)$, optical pot., nuclear matter approach, energy density matter [-] 80−83112
$^{40}Ca(^{6}Li,^{6}Li)$, velocity of refined model approaches 80−541
$^{40}Ca(^{6}Li,^{6}Li)$, 156 MeV, refined folding model validity 79−509
$^{40}Ca(^{6}Li,^{6}Li)$, 156 MeV, density depend. of N-N interaction 79−6660
$^{40}Ca(^{6}Li,^{6}Li)$ 30 MeV, back-angle anomalies 78−640
$^{40}Ca(^{6}Li,^{6}Li)^{40}Ca$, 30 MeV, ang. distribs. for elastic and inelastic scatt. at backward angles 79−13343
$^{40}Ca(^{9}Be,^{9}Be')$, 45, 60 MeV, low lying collective states, ang. distribs., DWBA double folding pot. anal. 80−78113
$^{40}Ca(^{9}Be,^{9}Be)$, 45, 60 MeV cross sections, ang. distribs., Wegner plot, optical and double folding anal. 80−47497
$^{40}Ca(^{9}Be,^{9}Be')$, 45, 60 MeV, 1^- state excitation Frahn scaling formula for cross section 80−102136
$^{40}Ca(^{9}Be,^{9}Be)$, 20 to 35 MeV, resonant heavy ion scatt., from s-d shell nuclei 79−67763
$^{44}Ca(^{6}Li,^{6}Li)$, 30 MeV, back-angle anomalies 78−640
$^{44}Ca(^{6}Li,^{6}Li)^{44}Ca$, 30 MeV, ang. distribs. for elastic and inelastic scatt. at backward angles 79−13343
$^{44}Ca(^{7}Li,^{7}Li)$, 34 MeV, ang. distribs., cross sections, double folding model anal. 80−78313
$^{48}Ca+^{16}O$ 56 MeV, transitions to resolved levels, optical model parameter 78−41758
$^{48}Ca(^{12,13}C,X)$, elastic, inelastic and single nucleon transfer excitation functions, ^{49}Ca levels 80−13492
$^{48}Ca(^{16}O,^{16}O)$, 56 MeV, ang. distribs., optical potentials 77−34341
$^{48}Ca(^{16}O,^{16}O)$, nuclear and Coulomb components to scatt. amplitude 77−34340
$^{48}Ca(^{6}Li,^{6}Li)$, velocity of refined folding model approaches 80−541
$^{A}Cd(^{16}O,^{16}O')$, 44 MeV, A=112, 114, 0_2^+, 0_3^+ state collectivity, E0 and E2 decay, $T_{1/2}$ 80−73784
$^{A}Cd(^{32}S,^{32}S')$, A=106, 108, 110, 112, 114, 116, 72-80 MeV, 2_1^+ state mag. moments 80−47373
$^{116}Cd(^{16}O,^{16}O'\gamma)$, 33 MeV, quadrupole moments determ. 77−41887
$^{59}Co(^{16}O,^{16}O)$, 142 MeV, optical model anal. of ang. distrib. meas. 78−58295
$^{59}Co(^{16}O,^{16}O)$, 36-56 MeV, cross sections, optical and double-folding model anal. 79−6693
$Cr(^{16}O,^{16}O'\gamma)$, 36 MeV, g-factors of first 2^+ states in ^{50,54}Cr 78−13138

heavy ion-nucleus scattering continued
$^{52}Cr(^{12,13}C,X)$, elastic, inelastic and single nucleon transfer excitation functions, ^{53}Cr levels 80−13492
$^{52}Cr(^{16,18}O,^{16,18}O')$, 30-42 MeV, excitation function differences, optical and DWBA anals. 79−63698
$Cu(^{16}O,^{16}O)$, A=63,65, 40 to 46 MeV, differential cross sections, G-matrix and adiabatic pot. models 78−78411
$^{63}Cu+^{197}Au$, quasi-fission, 443 MeV, γ-ray multiplicity 77−34330
$^{63}Cu(Li,Li)$, 28 and 34 MeV, optical model parameters 77−54248
$^{162}Dy+^{16}O$, Coulomb-nuclear interference for high spin states 78−46097
$^{162}Dy(^{136}Xe,^{136}Xe')$, 547, 612 MeV, high spin state energies and reduced transition probabilities 80−18232
$^{162}Dy(^{40}Ar,^{40}Ar'\gamma)$, 148.6 MeV, ^{162}Dy rotational states lifetime meas. 78−50123
$^{164}Dy(^{32}S,^{32}S'\gamma)$, recoil distance lifetimes of ground state bands 78−8774
$^{164}Er(^{136}Xe,^{136}Xe\gamma)$, 547-620 MeV, high spin props. in multiple band crossing region 80−83023
^{166}Er, Coulomb excitation with ^{4}He and ^{16}O ions 78−8839
$^{170}Er(^{32}S,^{32}\gamma)$, recoil distance lifetimes of ground state bands 78−8774
$^{151}Eu(^{16}O,^{16}O'\gamma)$, 25-42 MeV, energy levels, transitions, spin assignments determ. 77−38294
$^{19}F(^{16}O,^{16}O)^{19}F$, 32.0 MeV, parity-depend. optical model calc. 77−50152
$^{54}Fe(^{12,13}C,X)$, elastic, inelastic and single nucleon transfer excitation functions, ^{55}Fe levels 80−13492
$^{54}Fe(^{16,18}O,^{16,18}O')$, 30-42 MeV, excitation function differences, optical and DWBA anals. 79−63698
$^{54}Fe(^{16}O,^{16}O'\gamma)$, 36 MeV, g-factors of first 2^+ states in ^{54}Fe 78−13138
$^{54}Fe(^{6}Li,^{6}Li)$, 38, 44, 50 MeV, elastic and inelastic scatt., optical model anal. and inelastic scatt. deformation lengths 79−59082
$^{54}Fe(^{7}Li,^{7}Li)$, 36, 42, 48, MeV, elastic and inelastic scatt., optical model anal. and inelastic scatt. deformation lengths 79−59082
$^{56}Fe(^{16}O,^{16}O')^{56}Fe$, magnetic substate population, closed formalism based on DWBA 77−6424
$^{58}Fe(^{7}Li,^{7}Li)$, 34 MeV, ang. distribs., cross sections, double folding model anal. 80−78313
$Gd(^{35}Cl,^{35}Cl'\gamma)$, A=154, 6, 132-43 MeV, lifetime meas. of high spin states 78−13140
$^{A}Gd(^{28}Si,^{28}Si')$, 108-144 MeV, A=144,146,147,148, high spin isomer g-factors yrast traps 80−78146
$^{160}Gd(^{40}Ar,^{40}Ar)$, deformed nuclei surface struct. by radial and ang. localisation 79−85362
$Ge+^{12}C$, 48 MeV, surface transparency of optical pots. 78−13146
$Ge+^{16}O$, 56 MeV, surface transparency of optical pots. 78−13146
$Ge+^{18}O$, 56 MeV, surface transparency of optical pots. 78−13146
$^{A}Ge(^{16}O,^{16}O)$, A=72, 74, 76, coupled channel anal. with double folding potential 79−45282
$^{A}Ge(^{18}O,^{18}O)$, A=72, 74, 76, coupled channel anal. with double folding potential 79−45282
$^{70}Ge(^{16}O,^{16}O'\gamma)$, 36 MeV, g-factors of first 2^+ states in ^{70}Ge 78−13138
$^{4}He(^{12}C,^{4}He)^{12}C$, search for 0^+ level near 8.87 MeV 2^- level of ^{16}O 77−88044
$^{4}He(^{28}Si,\alpha)^{28}Si$, precision Doppler-shift attenuation lifetime meas. from γ-ray lineshapes 79−36195
$^{4}He(^{6}Li,^{6}Li)$, 15.1-22.7 MeV, polarised Li, vector anal. power, spin-orbit pot. 79−67737
$^{201}Hg(^{16}O,^{16}O)$, missing $f_{5/2}$ state Coulomb excitation, level scheme, J^π, transitions 80−47386
$^{139}La(^{86}Kr,X)$, 505, 610 and 710 MeV, elastic and deeply inelastic reactions, optical model anal. 78−66316
(Li,Li) cross sections on $40 \leq A \leq 91$ targets, 28 and 34 MeV, optical model parameters 77−54248
$(^{6}Li,^{6}Li)$, 30, 88 MeV, M3Y folding model eval., model independ. anal. 80−78317
$(^{6}Li,^{6}Li)$ scatt., polarisation and correlation probes of nuclear clustering 79−6437
$(^{6}Li,^{6}Li)$, 22.8 MeV, optical model test from vector anal. power data 79−97729
$(^{6}Li,^{6}Li)$, 99 MeV, A=12-208, ang. distribs. from double folding model pots. 80−106074
$(^{6}Li,^{6}Li)$ elastic scatt., failure of double folded pot. model 78−62566
$(^{6}Li,^{6}Li)$ pol. ^{6}Li, vector and tensor polarisation, closed form description 80−37363
^{6}Li, Coulomb disintegration in field of heavy target nucleus, perturbation theory 78−66319
$^{6}Li(^{14}N,^{14}N)^{6}Li$, 19.5 MeV, optical model anal. *(Russian)* 77−34346
$^{A}Mg(^{16}O,^{16}O)$, A=24, 26, 20-35 MeV cross sections and excitation functions, optical model anal. 79−93655
$^{A}Mg(^{7}Li,^{7}Li)$, A=24, 26, 88 MeV, optical potentials, phenomenological and microscopic 80−52687
$^{24}Mg+^{12}C$, elast. and inelast. scatt. near Coulomb barrier 77−6427
$^{24}Mg+^{12}C(^{16,18}O)$ scatt., ^{24}Mg pot. quadrupole deform. length determ. 78−12963
$^{24}Mg+^{16}O$, 30-81 MeV, fusion cross section, elastic scatt. ang. distrib., optical model anal. 78−78412
$^{24}Mg+^{16}O$, elast. and inelast. scatt. near Coulomb barrier 77−6427
$^{24}Mg+^{16}O$, two step α-transfer reaction 79−76018
$^{24}Mg+^{18}O$, 32-72 MeV, fusion cross section, elastic scatt. ang. distrib., optical model anal. 78−78412
$^{24}Mg+^{7}Li$ inelastic scatt., 34 MeV, microscopic interpretation, double folding model 77−14156
$^{24}Mg(^{12}C,^{12}C)$, 20-36 MeV, ang. distribs., S-matrix elements, optical model parameters 79−93660
$^{24}Mg(^{13}C,^{13}C')$, 35 MeV, γ-rays and spin flip 80−18189
$^{24}Mg(^{13}C,^{13}C')$, 35 MeV, 2^+ population probab., spin-flip and spin orbit pots., coupled channel anal. 80−99125
$^{24}Mg(^{16}O,^{16}O')$, 20-42 MeV, Coulomb-nuclear interf. effects, coupled channel calcs. 77−3040
$^{24}Mg(^{16}O,^{16}O)$, ^{40}Ca composite system, heavy ion resonances 80−86874
$^{24}Mg(^{16}O,^{16}O)$, 17-31 MeV, backward angle cross sections, resonant structure 79−30813
$^{24}Mg(^{16}O,^{16}O)$, 24-40 MeV, backward angles, excitation functions, ang. distribs. and resonant behaviour 80−68622
$^{24}Mg(^{16}O^{16}O)$, entrance, exit and reaction channel data at backward angles 79−36254
$^{24}Mg(^{18}O,^{18}O)$, 29, 35 MeV, coupled channel, first order DWBA, optial pot. calcs. 78−54796
$^{24}Mg(^{32}S,^{32}S\gamma)^{24}Mg$, 67 MeV, ang. correl., ionic charged state preparation 77−67762
$^{26}Mg+^{16}O$, 29-81 MeV 78−78412
$^{26}Mg(^{11}B,^{11}B)$, $(^{11}B,^{10}B)$, $(^{11}B,^{10}Be)$, 31 MeV, optical model and DWBA anal. 77−26785

heavy ion-nucleus scattering continued
^{26}Mg(^{12}C,^{12}C′), 41.3 MeV, ang. distrib. meas. to nucl. shape calcs. 77−65231
Mo(^{16}O, ^{16}O′) A=94-100, 36 MeV, static quadrupole moment determ. 77−6226
^{98}Mo(^{16}O,^{16}O′), 36.5 MeV, static quadrupole moment of first 2^+ state 80−5061
^{100}Mo(^{16}O,^{16}O′γ), 33 MeV, quadrupole moments determ. 77−41887
n+nuclear emulsion, 2.1 GeV/amu, scatt. const. 78−13151
^{14}N+^{12}C, direct inelastic scatt. in 3-dimens. time depend. HF scheme 79−17925
^{14}N(^{6}Li,^{6}Li′), 153 MeV, isoscalar giant quadrupole resonances 80−13440
NaF(Ne,Ne), 800 MeV/N, high momentum nucleons from relativistic nuclear collisions, hard scatt. mechanism 79−40950
Nd(^{12}C,^{12}C), A=143-150 even isotopes, multistep effects in elast. and inelast. scatt. at 70.4 MeV 78−17240
Nd(^{16}O,^{16}O), 40-48 MeV, even nuclei, 2^+ state E2 transition probabilities and quadrupole moments 80−18234
^{A}Nd(^{32}S,^{33}S′), 56 MeV, A=144,146,148, first excited 2^+ state mag. moment meas. 79−17798
^{150}Nd(^{40}Ar,^{40}Ar′γ), 149 MeV, Doppler shift meas. of ground state bands lifetimes 78−50124
^{20}Ne+^{12}C, 17 to 35 MeV, excitation functions, optical model anal. 78−41759
^{20}Ne+^{12}C, elastic scattering, symm., shell effects, absorpt. 79−562
^{20}Ne+^{12}C orbiting dinuclear system, inelastic scatt. cross section 80−22854
^{20}Ne+^{208}Pb, elastic and inelastic, 131 MeV, ^{20}Ne nuclear moments from inelastic data 78−66204
^{20}Ne(^{12}C,^{12}C), symmetry and shell struct. effects on absorption, precompound states 80−27666
Ni+^{12}C, 48 MeV, surface transparency of optical pots. 78−13146
Ni+^{16}O, 56 MeV, surface transparency of optical pots. 78−13146
Ni+^{18}O, 56 MeV, surface transparency of optical pots. 78−13146
Ni(^{35}Cl,^{35}Cl), A=58,62, 100-170 MeV, elastic scatt. ang. distrib. 78−21605
Ni(^{16}O,^{16}O′)N*(2^+), A=58, 60, 62 at 42 and 48 MeV, DWBA anal. 77−74876
^{A}Ni(^{32}S,^{32}S′), 72 MeV, A=58-64 even, magnetic mom. of $2_1{}^+$ states 78−66202
^{A}Ni(^{7}Li, ^{7}Li), A=58, 60, 34 MeV, ang. distribs., cross sections, double folding model anal. 80−78313
^{58}Ni (^{7}Li, ^{7}Li), 14.22 MeV, alignment axis orientation depend. of cross section, mass quadrupole moment alignment 80−68638
^{58}Ni vector polarised ^{6}Li elastic scatt., full optical model anal. 78−70553
^{58}Ni+^{23}Na, deformed aligned projectile ions, elastic scatt., fusion, polarisation effects 78−58303
^{58}Ni+^{6}Li(^{7}Li), 12.7 MeV, isotopic shape effects in elastic scatt. of aligned ions 78−89904
^{58}Ni(^{16}O,^{16}O′), 315 MeV, giant multipole resonance excitation 79−30812
^{58}Ni(^{16}O,^{16}O), 120-215 MeV, backward angle excitation functions 79−36267
^{58}Ni(^{16}O,^{16}O), 60 MeV, cross section ang. distribs., optical model parameters 79−6694
^{58}Ni(^{18}O,^{18}O$_2$*)^{58}Ni, 79−6676
^{58}Ni(^{6}Li,^{6}Li*), 71 MeV, excited states deformation lengths, DWBA and coupled channels anals. 80−68541
^{58}Ni(^{6}Li,^{6}Li), elastic and inelastic, 74 MeV, folding optical model parameters 80−102201
^{58}Ni(^{6}Li,^{6}Li) scatt. of aligned spherical ^{6}Li ion c.f. strongly deformed ^{7}Li ions 79−6680
^{60}Ni(^{13}C,^{13}C), nuclear and Coulomb components to scatt. amplitudes 77−34340
^{60}Ni(^{16}O,^{16}O), 142 MeV, optical model anal. of ang. distrib. meas. 78−58295
^{60}Ni(^{18}O,^{18}O′), stripping-pick-up mechanism, coupled channel theory 78−54784
^{64}Ni(^{18}O,^{18}O), coupled channel anal. with double folding potential 79−45282
O+^{27}Al, total fusion cross section near Coulomb barrier 78−13141
O+nuclear emulsion, 2.1 GeV/amu, scatt. const. 78−13151
O(^{12}C,^{12}C′), 50 GeV/c, multiplicities and ang. distribs. *(Russian)* 79−22323
^{10}O+^{18}O, elastic and inelastic collisions, excitation levels, spectroscopic factors 78−8837
(^{16}O,^{16}O), M3Y folding model eval., model independ. anal. 80−78317
^{16}O, elastic and inelastic scatt. of ^{16}B, ^{14}N, common and optical potential 77−34276
^{16}O, vector polarised ^{6}Li elastic scatt., full optical model anal. 78−70553
^{16}O-^{16}O, excit. function struct., momentum space folding model 77−57683
^{16}O-^{16}O excit. function calc. in momentum space folding model 77−57682
^{16}O+^{12}C, 168 MeV, inelastic scatt., folding model, macroscopic formalism, form factors 78−25227
^{16}O+^{12}C scattering, *l*-depend. absorptive pot., long life pot. resonances 78−62570
^{16}O+^{12}C system, exptl. survey of resonant structs. below and above Coulomb barrier 79−9616
^{16}O+^{16}O, 2.1 GeV/n elastic scatt., correlations 78−41761
^{16}O+^{16}O, direct inelastic scatt. in 3-dimens. time depend. HF scheme 79−17925
^{16}O+^{16}O, eikonal description 77−41938
^{16}O+^{16}O, elastic scatt. and fusion cross-section calc. 77−46182
^{16}O+^{16}O, elastic scatt. excitation functions, interf. effects 77−50155
^{16}O+^{16}O, Z=N nuclei, pot. calc. from α-α interaction 79−6661
^{16}O+^{16}O elastic scattering, GCM calcs., phase shifts, ang. distribs. 77−30625
^{16}O+^{16}O inelastic scatt., gross struct. origin, nonreson. diffr. model calcs. 79−30849
^{16}O+^{16}O scattering, generator coord. method, Kohn-Hulthen variational principle 77−2957
^{16}O+^{20}Ne, elastic and inelastic 50 MeV, contribution of α-cluster exchange 77−10429
^{16}O+^{28}Si, 17 to 37 MeV, inelastic and elastic backward angle scatt., surface resonances 78−37367
^{16}O+CNO, ^{16}O+AgBr, 2 GeV/nucleon, two-proton azimuthal angle correlations 78−62572
^{16}O(^{10,11}B, ^{10,11}B), 33.7-49.5 MeV, mag. distribs., ground state quadrupole moment contrib. 80−42689

heavy ion-nucleus scattering continued
^{16}O(^{12}C, ^{12}C′) quasimolecular resonance, doublet like intermediate structure 79−54421
^{16}O(^{12}C,^{12}C$_{2+}$)^{16}O, ^{12}C$_{2+}$ spin alignment using γ-decay in flight 78−41767
^{16}O(^{12}C, ^{12}C), 18-26 MeV, molecular structure, projection operator anal., differential cross sections 80−106033
^{16}O(^{12}C,^{12}C), perturbed stationary state method, low energy collision and mol. resons. 80−78320
^{16}O(^{16}O,^{16}O′), gross struct., barrier top resonance model calc. 80−9279
^{16}O(^{16}O,^{16}O), 10-41 MeV, molecular resonances γ-yield, band crossing model 80−106032
^{16}O(^{16}O,^{16}O), Coulomb field effects using generalised JWKB method 80−13504
^{16}O(^{16}O,^{16}O), elastic scatt., incoming wave boundary condition model calcs. 80−47504
^{16}O(^{16}O,^{16}O), elastic scatt., l-window formalism 80−68684
^{16}O(^{16}O,^{16}O), optical pot., nuclear matter approach, energy density matter [-] 80−83112
^{16}O(^{16}O,^{16}O), perturbed stationary state method, low energy collision and mol. resons. 80−78320
^{16}O(^{16}O,^{16}O), surface transparent pot. scatt. semiclassical wave propagation matrix method 79−101
^{16}O(^{16}O,^{16}O), symmetry and shell struct. effects on absorption, precompound states 80−27666
^{16}O(^{6}Li,^{6}Li′), 153 MeV, isoscalar giant quadrupole resonances 80−13440
^{16}O(^{9}Be,^{9}Be) 14, 20 and 26 MeV, optical model parameters 79−26449
^{16}O(N,N)^{16}O, resonating group method with generator-coordinate technique 77−10415
^{17}O(^{16}O, ^{16}O), repeated neutron transfer, coupled channels anal. 78−54782
^{18}O, heavy ion excitation, single particle and core polarisation amplitude interference 80−5117
^{18}O+^{12}C, 10-23.6 MeV, periodic structure 78−46095
^{18}O+^{16}O, 10-23.6 MeV, periodic structure 78−46095
^{18}O+^{18}O, elastic scatt. excitation functions, interf. effects 77−50155
^{18}O(^{16}O,^{16}O)^{18}O, 24, 28, 32 MeV, two-particle transfer contrib. 77−3030
^{18}O(^{18}O,^{18}O), symmetry and shell struct. effects on absorption, precompound states 80−27666
^{32}O(^{12}C,^{12}C), finite-range coupled-channel calcs. 77−10377
^{16,18}O+^{16,18}O, elastic scattering, symm., shell effects, absorpt. 79−562
(^{17,18}O,^{17,18}O′), 54-69 MeV, on A=48-92, excited states and ang. distribs., DWBA anal. 79−67705
Pb+Kr, deep inelastic collisions, excitation of nuclear surface modes 78−37374
Pb+Pb(U), positron prod. 78−50197
Pb+Pb(U), positron prod. in heavy ion collisions 78−50198
Pb(C,C), 800 MeV/N, high momentum nucleons from relativistic nuclear collisions, hard scattering mechanism 79−40950
Pb(^{12}C,^{12}C′), A=204,206,208, 60 MeV, quadrupole moment and B(E3) values 79−17797
Pb(^{16}O,^{16}O′), A=204,206,208, 52 MeV, quadrupole moment and B(E3) values 79−17797
^{208}Pb+^{12}C, 96 MeV, inelastic scatt., folding model, macroscopic formalism, form factors 78−25227
^{208}Pb+^{12}C(^{14}N), giant resonances, ang. distrib., inelastic scatt. 78−62564
^{208}Pb+^{6}Li, Coulomb and nucl. excitation in ^{6}Li dissociation 78−41770
^{208}Pb(^{12}C, ^{12}C′), 200 MeV, evidence for giant quadrupole excitation 79−49637
^{208}Pb(^{13}C,^{13}C′), 108 MeV, nuclear continuum investigation 80−13506
^{208}Pb(^{14}N,^{14}N′), 266 MeV, giant resonance excitation 80−78253
^{208}Pb(^{16}O, ^{16}O), elastic scatt., exponential optical pots. 80−42681
^{208}Pb(^{16}O,^{16}O′), 315 MeV, giant multipole resonance excitation 79−30812
^{208}Pb(^{16}O,^{16}O′), 315 MeV, continuous spectrum and giant resonance excitation, coherent state model test 80−32252
^{208}Pb(^{16}O,^{16}O), 312.6 MeV, DWBA anal. of cross-section energy depend. 77−30630
^{208}Pb(^{16}O,^{16}O), 80-102 MeV, cross sections, optical model parameters 77−54246
^{208}Pb(^{16}O,^{16}O), elastic ang. distrib., nuclear contributions, Born approx. validity 79−36252
^{208}Pb(^{16}O,^{16}O) 104, 138.5, 216.6 MeV, DWBA and optical model anal., energy dependence 78−82378
^{208}Pb(^{16}O,^{16}O) 312.6 MeV, optical model and DWBA anal., energy depend., lower energy comparison 78−82379
^{208}Pb(^{16}O,X), 80-313 MeV, optical model anal., dynamic shape or density changes 80−18186
^{208}Pb(^{18}O,^{18}O′), 57-86 MeV, ^{19}O first excited state electric moment, B(E2) transition 79−67651
^{208}Pb(^{24}Mg,^{24}Mg), 80,110 MeV, ^{24}Mg $2_1{}^+$ state quadrupole moment 80−9230
^{208}Pb(^{24}Mg,^{24}Mg), 80-110 MeV, ^{24}Mg first excited state static quadrupole moment, B(E2) value 79−45161
^{208}Pb(^{40,48}Ca, ^{40,48}Ca), dist. of closest approach for classical Rutherford scatt. 78−78404
^{208}Pb(^{40,48}Ca, ^{40,48}Ca), optical model anal., strong absorption radius *(Russian)* 80−68697
^{208}Pb(^{40}Ar, ^{40}Ar), 302 MeV 78−78404
^{208}Pb(^{40}Ar, ^{40}Ar), optical model anal., strong absorption radius *(Russian)* 80−68697
^{208}Pb(^{48}Ti, ^{48}Ti), 252 MeV 78−78404
^{208}Pb(^{48}Ti, ^{48}Ti), optical model anal., strong absorption radius *(Russian)* 80−68697
^{208}Pb(^{6}Li,^{6}Li), elastic and inelastic, 74 MeV, folding optical model parameters 80−102201
^{A}Pd(^{32}S,^{32}S′), A=102, 104, 106, 108, 110, 72-80 MeV, $2_1{}^+$ state mag. moments 80−47373
^{141}Pr(^{35}Cl,^{35}Cl), 100-170 MeV, elastic scatt. ang. distrib. 78−21605
^{192}Pt(Ar,Ar′γ), 149 MeV, lifetimes of ^{192}Pt ground-band states 77−54181
^{194}Pt(^{12}C,^{12}C), 78 MeV, elastic and inelastic differential cross section, triaxial rotor anal. 79−63689
^{194}Pt(^{16}O,^{16}O′), 7-17.5 MeV, Coulomb excitation, low lying collective state reduced matrix elements, triaxiality 78−82269
^{194}Pt(Ar,Ar′γ), 149 MeV, lifetimes of ^{194}Pt ground-band states 77−54181
^{A}Ru(^{16}O,^{16}O′), 36-45 MeV, A=96, 98, 100, 102, 104, first 2^+ excited state quadrupole moment 80−47374

heavy ion-nucleus scattering continued
^{102}Ru(^{16}O,^{16}O), 38-42 MeV, 2^+ state quadrupole moment, reorientation effects and multiple Coulomb excitation 80−5063
^{102}Ru(^{16}O,^{16}O), 38-42 MeV, Coulomb excitation, 2^+ state electric quadrupole moment 80−73793
^{32}S(^{12}C,^{12}C), 20 to 35 MeV, resonant heavy ion scatt., from s-d shell nuclei 79−67763
^{32}S(^{12}C,^{12}C), 20-35 MeV, resonant scatt., ang. distribs., cross sections and excitation functions 79−45237
^{32}S(^{12}C,^{12}C) backward angle scatt., resonant like structs. 79−17876
^{32}S(^{32}S,^{32}S), 58-130 MeV, elastic scatt., ang. distribs., excitation function, optical model anal. 77−30623
^{32}S(^{9}Be,^{9}Be), 20 to 35 MeV, resonant heavy ion scatt., from s-d shell nuclei 79−67763
^{45}Sc(^{15}N,^{15}N), 47.5 MeV, ang. distribs., optical potentials 77−34341
Se(^{16}O,^{16}O′), A=76, 78, 80, 82, 30 to 34 MeV, meas. of static quadrupole moments of first 2^+ excited states 77−65197
^{74}Se(^{16}O,^{16}O′), 33, 34 MeV, first excited state, static quadrupole moment, deformation evidence 79−17802
^{A}Si(^{10,11}B,^{10,11}B), 33.7, 41.6, 50 MeV, A=28,30, ang. distribs., cross sections and deformation parameters, absorption effects 79−67773
^{A}Si(^{16}O,^{16}O), A=28, 30, 20-35 MeV cross sections and excitation functions, optical model anal. 79−93655
^{28}Si, vector polarised ^{6}Li elastic scatt., full optical model anal. 78−70553
^{28}Si+^{12}C elastic scatt. ang. distribs., optical pot. 78−8855
^{28}Si+^{12}C(^{16,18}O) scatt., ^{28}Si pot. quadrupole deform. length determ. 78−12963
^{28}Si+^{16}O, 35 MeV, undamped surface waves 77−74868
^{28}Si+^{16}O, pot. for back-angle enhanced elastic scatt. 79−40953
^{28}Si+^{16}O, smooth cutoff model angular distrib. 77−10376
^{28}Si+^{16}O(^{12}C), elastic scatt., 90° excitation function gross struct. 79−75950
^{28}Si+^{9}Be, ^{12}C, ^{14}N or ^{16,18}O, low energy elastic scatt., global optical model anal. 78−25229
^{28}Si(^{12}C,^{12}C) elastic scatt., 135 MeV, ang. distribs., heavy-ion-like behaviour 77−79398
^{28}Si(^{12}C,^{12}C′), 41.4 MeV, ang. distrib. meas. reorientation effects 77−65231
^{28}Si(^{12}C,^{12}C), ^{40}Ca composite system, heavy ion resonances 80−86874
^{28}Si(^{12}C,^{12}C), 19-48 MeV, ang. distribs., cross sections and optical parameters 80−5157
^{28}Si(^{12}C,^{12}C), 20 to 35 MeV, resonant heavy ion scatt., from s-d shell nuclei 79−67763
^{28}Si(^{12}C,^{12}C), 20-35 MeV, resonant scatt., ang. distribs., cross sections and excitation functions 79−45237
^{28}Si(^{12}C,^{12}C), 24, 29 MeV, coupled channel, first order DWBA, optical pot. calcs. 78−54796
^{28}Si(^{12}C,^{12}C), 27.8-31.5 MeV, elastic and inelastic excitation functions, fine struct., statistical anal. 80−18269
^{28}Si(^{12}C,^{12}C), entrance channel resonances, backward angle scatt., elastic scatt. enhancement 80−27612
^{28}Si(^{12}C,^{12}C), high energy heavy ion scatt., comparison with light-ion data 79−67764
^{28}Si(^{13}C,^{13}C), 20 to 35 MeV, resonant heavy ion scatt., from s-d shell nuclei 79−67763
^{28}Si(^{13}C,^{13}C), 20-35 MeV, resonant scatt., ang. distribs., cross sections and excitation functions 79−45237
^{28}Si(^{16,18}O,^{16,18}O), near Coulomb barrier, coupled channel, first order DWBA, optical pot. calcs. 78−54796
^{28}Si(^{16}O,^{16}O), 55 MeV, Regge pole anal. using optical pots. 79−3174
^{28}Si(^{16}O,^{16}O), 142 MeV, optical model anal. of ang. distrib. meas. 78−58295
^{28}Si(^{16}O,^{16}O), 215 MeV, energy independent Woods-Saxon optical potential 77−14165
^{28}Si(^{16}O,^{16}O), 30-32.7 MeV, elastic and inelastic excitation functions, fine struct., statistical anal. 80−18269
^{28}Si(^{16}O,^{16}O), 45 to 63 MeV, energy depend. surface transparent optical pot. 78−46099
^{28}Si(^{16}O,^{16}O), 50, 55 MeV, backward angle cross section, optical model calc. 79−9610
^{28}Si(^{16}O,^{16}O), 65 MeV, elastic and inelastic, optical and coupled channels model anals. 79−45293
^{28}Si(^{16}O,^{16}O), anomalous large angle scatt., Regge pole contrib. 79−63687
^{28}Si(^{16}O,^{16}O), backward angle elastic excitation function structure 79−36263
^{28}Si(^{16}O,^{16}O), elastic and inelastic, coupled channels calcs., optical pot. energy depend. 79−571
^{28}Si(^{16}O,^{16}O), entrance channel resonances, backward angle scatt., elastic scatt. enhancement 80−27612
^{28}Si(^{16}O,^{16}O), finite-range coupled-channel calcs. 77−10377
^{28}Si(^{16}O,^{16}O), high energy heavy ion scatt., comparison with light-ion data 79−67764
^{28}Si(^{16}O,^{16}O), parity depend. of heavy-ion optical pot. 78−74397
^{28}Si(^{16}O,^{16}O), radial sensitivity of optical pot. 80−86869
^{28}Si(^{16}O,^{16}O) 35 MeV, elastic and inelastic back angle anomalies, nuclear rainbow angle 79−13317
^{28}Si(^{16}O,^{16}O) gross struct. in excitation function elastic transfer amplitudes 79−36215
^{28}Si(^{16}O,^{16}O) optical pot. semiclassical anal. 79−17917
^{28}Si(^{16}O,^{16}O)^{28}Si, 45-64 MeV elastic scatt., quasi-molecular or barrier-top resonance 79−13341
^{28}Si(^{18}O,^{18}O), 60 MeV, optical model parameters 79−22204
^{28}Si(^{18}O,^{18}O), 65 MeV, elastic and inelastic, optical and coupled channels model anals. 79−45293
^{28}Si(^{28}Si, ^{28}Si), 80-150 MeV, elastic and inelastic, energy depend. struct., multistep processes 79−80909
^{28}Si(^{6}Li, ^{6}Li), 154 MeV, differential cross section ang. distrib., optical anal. 80−63201
^{28}Si(^{6}Li,^{6}Li), high energy heavy ion scatt., comparison with light-ion data 79−67764
^{28}Si(^{6}Li,^{6}Li) elastic scatt., 135 MeV, ang. distribs., light-ion-like behaviour 77−79398
^{28}Si(^{9}Be, ^{9}Be′), 45, 60 MeV, low lying collective states, ang. distribs., DWBA double folding pot. anal. 80−78113
^{28}Si(^{9}Be, ^{9}Be), 45, 60 MeV cross sections, ang. distribs., Wegner plot, optical and double folding anal. 80−47497
^{28}Si(^{9}Be,^{9}Be), 121-201.6 MeV, strong absorption dominance, global optical model anal., fusion barrier 80−83116
^{28}Si(^{9}Be,^{9}Be), 20 MeV, localisation of direct reaction processes, fusion and total cross sections 78−78353
heavy ion-nucleus scattering continued
^{28}Si(^{9}Be,^{9}Be), 20 to 35 MeV, resonant heavy ion scatt., from s-d shell nuclei 79−67763
^{28}Si(^{9}Be,^{9}Be), 20-35 MeV, resonant scatt., ang. distribs., cross sections and excitation functions 79−45237
^{28}Si(^{9}Be,^{9}Be), high energy heavy ion scatt., comparison with light-ion data 79−67764
^{30}Si(^{12}C,^{12}C′), 41.3 MeV, ^{30}Si angular distrib., coupled channels calc. 79−97721
^{30}Si(^{16}O,^{16}O), elastic and inelastic, 60 MeV, to 1st excited 2^+ state, coupled channels anal. 78−82377
^{A}Sm+^{20}Ne, A=148, 150, 152, 70 MeV, Coulomb absorpt. obs. 78−70558
^{A}Sm(^{16}O,^{16}O′), A=150, 152, hyperfine dynamic mag. field effects 80−68689
^{A}Sm(^{20}Ne, ^{20}Ne), 70 MeV, A=148, 150, 152, Coulomb polarisation pot., coupled channel calcs. 80−22855
^{A}Sm(^{32}S,^{32}S′), A=150, 152, hyperfine dynamic mag. field effects 80−68689
^{144}Sm(^{13}C,^{13}C′), 108 MeV, nuclear continuum investigation 80−13506
^{152}Sm(^{35}Cl,^{35}Cl′γ), 132-43 MeV, lifetime meas. of high spin states 78−13140
Sn(^{35}Cl,^{35}Cl), A=116,120,124, 100-170 MeV, elastic scatt. ang. distrib. 78−21605
^{A}Sn(^{35}Cl,^{35}Cl′), 108 MeV, A=112-124 even isotopes, $2_1{}^+$ mag. moments and shell model struct. 80−86805
^{116}Sn(^{16}O,^{16}O), (^{16}O,^{16}O′), levels, ang. distrib. anal. of 64 MeV reacts. 78−8836
^{116}Sn(^{16}O,^{16}O) 48 MeV, collective states, E2, E0 transition probabilities, halflife, branching ratios 80−18172
^{118}Sn(^{6}Li,^{6}Li′), 153 MeV, isoscalar giant quadrupole resonances 80−13440
^{118}Sn(^{6}Li,^{6}Li), 42 MeV, optical model parameters for DWBA anal. 79−6688
^{124}Sn(^{6}Li,^{6}Li), elastic and inelastic, 74 MeV, folding optical model parameters 80−102201
^{181}Ta(^{16}O,^{16}O), 83-96 MeV, cross sections, optical model parameters 77−54246
^{181}Ta(^{84}Kr,^{84}Kr′γ), 348 MeV, ground-state rotational band obs. 77−6197
^{122}Te, backscatt. of ^{4}He, ^{14}N, ^{16}O, and ^{18}O, reorientation effect meas. 78−50209
^{124}Te(^{12}C,^{14}C)^{122}Te, 70 MeV, optical model parameters, CCBA anal. 77−18591
^{126}Te(^{22}Ne, ^{22}Ne′), 93.5 MeV, 2^+ state mutual excitation and transitions 79−54404
^{128}Te backscatt. of ^{4}He, ^{14}N, ^{16}O, and ^{18}O, reorientation effect meas. 78−50209
^{232}Th+^{86}Kr, Coulomb-nuclear interference for high spin states 78−46097
^{50}Ti(^{12,13}C,X), elastic, inelastic and single nucleon transfer excitation functions, ^{49}Ti levels 80−13492
^{169}Tm(^{32}S,^{32}S′γ), electromag. props. of ground state rot. band of ^{169}Tm 78−8726
U+U, positron prod. 78−50197
U+U, positron prod. in heavy ion collisions 78−50198
^{235}U+^{235}U, classical microscopic description 77−14160
^{238}U (^{6}Li, ^{6}Li′f), 150 MeV, isoscalar giant resonance struct. 79−89275
^{238}U-^{235}U, 800 MeV, possibility of detecting superheavy quasimolecules 77−14149
^{238}U+^{238}U (^{136}Xe), nuclear Coulomb excitation, inner shell ionisation and internal conversion, quasimol. formation 78−94026
^{238}U+^{40}Ar, Coulomb-nuclear interference for high spin states 78−46097
^{238}U(Kr,Kr′), multiple Coulomb excitation, coupled eqns. soln. by iteration 79−93654
^{238}U(Pb,Pb′), multiple Coulomb excitation, coupled eqns. soln. by iteration 79−93654
W isotopes, A=182, 184, 186, Coulomb excitation with ^{4}He and ^{16}O ions 78−8839
W(^{16}O,^{16}O′), 53, 4 MeV, quadrupole moment determ. 78−12968
^{A}W (^{84}Kr,^{84}Kr′γ) A=183, 184, 186, 340 MeV, Coulomb excitation, energy levels and bands 79−63577
^{184}W(^{12}C,^{12}C′), 70 MeV, 4^+ state excitation ang. distrib., hexadecapole deformation length effects 80−68521
^{184}W(^{12}C,^{12}C)^{184}W, 70 MeV, Coulomb inelastic effects 77−30629
^{184}W(^{18}O,^{18}O)^{184}W, 90 MeV, Coulomb inelastic effects 77−30629
^{136}Xe+^{209}Bi, 1130 MeV, very heavy-ion collision mechanisms 78−89905
^{A}Yb(^{16}O,^{16}O′γ), A=168-176, even nuclei, 58-62 MeV, Coulomb excitation, vibr. and rot. states 80−32162
^{A}Yb(^{40}Ca,^{40}Ca′), A=170,172,174, 168 MeV, rotational g-factor meas. using transient field interactions 80−18193
^{174}Yb(^{32}S,^{32}S′γ), recoil distance lifetimes of ground state bands 78−8774
Zn(Li,Li) (A=64,68), 28 and 34 MeV, optical model parameters 77−54248
Zr(Li,Li) (A=90,91), 28 and 34 MeV, optical model parameters 77−54248
^{A}Zr(^{35}Cl,^{35}Cl′), 90 MeV, A=92, 94, $2_1{}^+$ levels mag. moments 80−105968
^{90}Zr+^{12}C(^{14}N), giant resonances in inelastic scatt. 78−62564
^{90}Zr(^{13}C,^{13}C′), 108 MeV, nuclear continuum investigation 80−13506
^{90}Zr(^{6}Li,^{6}Li′), 153 MeV, isoscalar giant quadrupole resonances 80−13440
^{90}Zr(^{6}Li,^{6}Li′), 2^+(2.18 MeV) and 3^-(2.75 MeV) states in ^{90}Zr, DWBA anal. 79−26448
^{90}Zr(^{6}Li,^{6}Li′), 74 MeV, excitation of giant quadrupole reson. 78−8854
^{90}Zr(^{6}Li,^{6}Li), elastic and inelastic, 74 MeV, folding optical model parameters 80−102201
^{90}Zr(^{6}Li,^{6}Li) 34 MeV, optical model anal. 79−26448
^{90}Zr(^{7}Li,^{7}Li′), 2^+(2.18 MeV) and 3^-(2.75 MeV) states in ^{90}Zr, DWBA anal. 79−26448
^{90}Zr(^{7}Li,^{7}Li) 34 MeV, optical model anal. 79−26448
^{91}Zr(^{6}Li,^{6}Li) 34 MeV, optical model anal. 79−26448

heavy leptons
Bargmann-Wigner and Weyl spin-3/2 fields, spinors, chiral operator 80−31981
Big Bang model, galaxy cluster missing mass from massive leptons, additional ν species 78−81719
bound state pair photoprod. in nuclear Coulomb field 77−6103
cascade, lifetime and branching ratios 78−33108
cascade decay, μ^- induced multimuon prod. 79−17707

heavy leptons continued
cascade decay ν-induced multimuon prod. 79−17707
cascade decay in $\nu N \rightarrow \mu^- \mu^- \mu^+ + X$, gauge model 77−57526
cascade decay in $\nu N \rightarrow \mu^- \mu^- \mu^+ + X$ 77−57524
cascade decay in $\nu N \rightarrow \mu^- \mu^- \mu^+ + X$ 77−57525
cascade decays, lepton prod. anal. 78−33059
charged heavy lepton, SU(2)×U(1) gauge theory 78−45794
charged heavy lepton production by nondiagonal neutral currents *(Chinese)* 79−17668
charm and heavy lepton production by e^+-e^- interactions, recent results, review 79−26337
charmonium photoprod., gluon-exchange model 78−74214
chirality of current from $e^+e^- \rightarrow e^\pm \mu^\mp$ anomalous events 77−74668
chronon in quantum theory of electron, existence of heavy leptons, neutrino spectrum 78−70008
cosmic radiation underground, search using scintillation+Cherenkov detectors 78−65470
cosmological constraints on mass and number of heavy lepton neutrinos 78−45444
CP violation, radiative symm.-breaking, fermion and Higgs boson masses 78−41435
decay, spin $^3/_2$ intermediate vector boson corrections 80−73761
decay into νe+neutral lepton anal. 77−82799
decay into isoscalar vector meson *(Russian)* 79−85349
decay modes, branching ratios 78−8638
decay modes anal., second class currents 78−21352
decay of charged heavy leptons, possibility of new neutrino 77−10237
decay widths, first-order weak interaction theory 78−45899
dilepton and trilepton production in neutrino experiments *(Polish)* 78−89704
dimuon energy asymmetries in neutral heavy lepton decay, ang. momentum constraints 77−38155
dimuon events, heavy lepton decay into massive ν with various spin 78−21412
dimuon events, production by heavy lepton decay, appl. to e^+e^- collisions 77−54093
dimuon events with identical sign, signal of creation of heavy leptons in neutrino expts. *(Russian)* 77−82729
discovery, basic relations and remaining problems *(Czech)* 80−73762
discovery, props., prod. in e^+e^- collision, review 78−89694
Drell ratio and the existence of a second heavy lepton 79−13048
Drell-Yan process, heavy lepton pair prod., non-scaling parton model 77−13928
E7 gauge model, multilepton prod. by ν, heavy leptons 77−74588
E_7 gauge model, lepton assignments and trimuon events in neutrino scatt. 79−17709
elementary particle physics, information from astronomical observations 80−51935
excited-mass states of the electron, chronon 78−21004
existence in quantum theory 78−21363
exotic muon and heavy lepton decays in gauge theories 77−49939
flavour changing neutral currents with b quarks and/or τ leptons 80−73656
four flavour $SU(2)_L \times U(1)$ gauge model with unconfined colour, and heavy leptons, $\Delta I = 1/2$ rule 77−82708
four-element lepton models, non-diagonal neutral currents *(Chinese)* 78−78132
gauge model with heavy lepton, muon number nonconservation 77−61239
grand unification, neutron oscillations and massive neutral Majorana leptons, baryon number 80−91033
hadron constituents 77−30319
hadron leptoproduction, nuclear targets, quark-nucleon inclusive cross section, heavy lepton pairs 80−57607
hadronic decay, production, mass, of heavy leptons from e^+e^- annihilation inclusive hadron spectrum 77−18304
hadronic massive lepton pair prod., theory review, Drell-Yan model 78−89752
hadronic quantum numbers beyond charm as possible source of neutrino induced trimuons 78−12903
heavy fermions in the standard sequential scheme 79−71748
heavy muon in minimal gauge scheme as possible cause of $e\mu$, $\bar{\nu}_\mu$ anomalies 77−61241
heavy neutral strange lepton predicted by mag. quark model 79−75738
heavy neutrino mass, cosmological upper limit from big bang model 80−8728
helicity calculations for prod. in ν interactions and cascade decay 78−93870
Higgs-Kibble mechanism and electron-muon mass ratio 78−66065
inclusive anomalous lepton signals from leptonic and semileptonic decay modes 78−78198
lepton mixing and neutrino oscillations, cosmic neutrinos, heavy leptons, μ decay 78−82193
lepton model, heavy lepton+quark pair 77−49895
lepton-quark correspondence scheme 79−35999
leptonic decay, particle energy angle distrib. 79−71775
leptonic decays of heavy lepton pairs produced in e^+e^- annihilation, computer calcs. 78−21409
mass formula, chronon in electron theory 80−47224
mass formula deriv. 79−58995
mass formula of charged leptons 80−13244
mass spectra similarity with heavy quark masses 79−67508
massive lepton pair hadroproduction, QCD and parton model anal. 80−42421
massive lepton pairs, transverse momentum distrib. from inclusive hadron prod. 78−89760
massive neutrinos, radiative decay rel. to cosmic element abundances 79−92668
massive unstable neutrinos, cosmological implications 78−45437
minimal gauge theory of leptons, new heavy lepton, associated neutrino, muon number nonconservation 77−54096
mixing angle between ordinary and heavy leptons in a (V-A) model, constraints 78−4846
mixing angles of leptons in an extended Weinberg-Salam model 79−71679
muons, heavy, possible existence of 20 GeV muon *(Russian)* 79−6359
neutral effectively stable leptons, test for existence using beam-dump expt. 78−66185
neutral heavy lepton signatures in ν induced dilepton events, SU(2)×U(1) model 78−70353

heavy leptons continued
neutral heavy leptons, search with e^+e^- annihilations at 0.5-1.5 GeV/c^2 78−4848
neutral heavy leptons decay, neutrino induced multilepton events, locality constraints 78−21411
neutral lepton radiative decay, mechanism for supernova shell explosion *(Russian)* 79−8934
neutral right-handed, possible e^+e^- prod. 77−57518
neutrino induced dilepton events, extraction of heavy quark and heavy lepton signals 78−74243
neutrino interactions, SU(3)⊗U(1) gauge model of trimuon prod. 77−74671
neutrino lifetime upper bound in big-bang cosmological model 77−74170
neutrino mass lower bound in big-bang cosmological model 77−78904
neutrino oscills. and heavy lepton mixing review 78−66182
neutrino scattering, trimuon event sources 78−25035
neutrinos, lifetime and mass constraints imposed by big bang nucleosynthesis 79−40308
neutrinos, limits on props. from primordial nucleosynthesis 78−57438
new elementary particles, theoretical predictions, recent expt. results 77−57475
'new particle' searches and discoveries, 'Review of Particle Properties' 1976 supplement 77−57515
number of types, cosmological limits from ^{4}He primordial abundance 77−33716
pair production by cosmic rays 79−36117
photoproduction and decay of L^+L^- pair, energy and ang. distribs. of decay leptons 77−41836
Pontecorvo oscillation and search for τ-leptons in neutrino expts. *(Russian)* 77−87973
prediction in weak interaction theories 80−73657
primoridial stable neutral heavy leptons, annihilation as source of cosmic gamma-ray background 78−93479
production and detection in pp and $p\bar{p}$ collisions 77−54072
production in e^+e^- annihilation, QED background 79−75706
production via decay of heavy vector mesons 77−87974
properties, experimental evidence, theoretical predictions 77−57582
QCD, decays of heavy leptons and intermediate weak bosons 78−8524
QCD, hard semi-inclusive processes 78−93862
QED with internal fermion excitations, $e\mu$ system 80−9130
quark model anal. of τ prod. and decay 78−54605
radiative decay modes, effect on $e\mu$ distrib. anal. 77−18263
selection rule of heavy-lepton decay, $SU_2 \times U_1$ gauge model 79−49500
selections from 1977 Comments on Modern Physics, book 79−30181
semi-hadronic decays, quark model 77−61281
sequential charged lepton, semileptonic branching ratio and lifetime 80−57578
short lived particles search in high energy neutrino interactions 79−49510
Sp(4)×U(1) gauge symm. for weak interaction, $\Delta I = {}^1/_2$ rule 77−34093
spin, decay parameters from e^+e^- anomalous μ prod. 77−61267
spin, possible determ. via $e^+e^- \rightarrow L^+L^-X(X \rightarrow e^+e^-)$ 77−2847
stable heavy neutrinos, dynamical interactions and astrophys. effects 79−5743
stable method heavy leptons, astrophysical mass constraint, condensation in stars and galaxies *(Russian)* 80−72768
stable neutral lepton, astrophysical consequences of existence 78−93091
$SU_L(3) \times SU_R(3)$, leptonic nonet anal. 77−87908
$SU_L(3) \otimes U(1)$ gauge model, exact Cabibbo universality, τ^- and X^- 80−4852
$SU_L(4) \times U(1)$ four-quark model, lepton quartets and W bosons 77−87934
$SU(10)_{flavour} \times SU(10)_{colour}$ unified hadron lepton theory 79−67509
$SU(2)_L \times U(1)$ gauge theory, weak interactions of ultra-heavy fermions 79−75713
SU(2)×U(1) gauge model, right-handed charm current, CP violation 78−45795
SU(2)×U(1) gauge theory of weak and EM interactions, quark model 77−26458
SU(2)×U(1) symmetry group, μe universality breaking in weak interactions, neutron heavy lepton introduction *(Russian)* 79−58918
SU(2)×U(1) vectorlike model: new leptons, quarks, and the axion question 79−40711
SU(3)×U(1) gauge model of weak interactions, quark triplets, charmed hadron decay 77−2789
SU(3)×U(1) model, heavy lepton prod. and decay signature 78−45900
SU(3) gauge theory, leptonic octets and heavy lepton decays 77−34094
SU(n) group, mixing and sequential heavy lepton weak interaction *(Russian)* 79−40720
superheavy, review of exptl. results and theoretical advances *(German)* 78−66184
tau, discovery and antiparticle antitau 78−58222
tauonium: $\tau^+\tau^-$, a bound state of heavy leptons 78−37194
trimuon events, heavy lepton prod. in ν interactions 78−41530
trimuon heavy lepton events in ν interactions, $SU(8)_L \times U(1)$ gauge model 77−79242
trimuon prod., heavy-lepton cascade decay, energy ratios 78−66103
trimuon prod. mechanism, $\nu(\bar{\nu})$ interactions 78−82199
trimuon production by neutrinos, heavy lepton cascade mechanism using SU(2)×U(1) gauge model 78−58180
$U(1) \times SU(4)_L \times SU(4)_R$ based weak-EM synthesis with manifest left-right symm. 78−8571
(V-A) model, mixing between ordinary and heavy leptons, neutral current reactions 78−41472
V-A six lepton model, lepton no. conservation 77−87930
weak doublet of heavy leptons, prod. and decay, lepton mixing, lepton number nonconservation 77−54094
weak gauge boson and neutrino trimuon prod. 78−4851
weak selection rules, inclusive prod. of charmed particles and heavy leptons 78−8679
Weinberg-Salam model of lepton interactions, supersymm. extension, low energy studies 77−49887
$D^- \rightarrow \tau^- \bar{\nu}_\tau$, charmed mesons, heavy lepton decays, ν_τ neutrino mass depend. *(Russian)* 78−62394
e/μ mass ratio, extended Weinberg model with heavy leptons, discrete symm. appls. 77−57482
e-μ universality possible violation in gauge theories with heavy leptons 77−2739
e-μ-τ spontaneous symmetry breaking and rare τ decays 79−9301
E^0, neutral electron-type heavy lepton, and W-boson mass 78−66100

heavy leptons continued
e^-e^+ annihilation, >2 GeV, production of charmed particles and charged τ lepton, review 78−17006
e^+e^-, annihilation, production of new particles, J/ψ, ψ' and τ props. 80−5008
e^+e^-, electron type heavy neutral lepton prod., cross section and coupling const. 80−52485
e^+e^-, electron type neutral heavy lepton, leptonic decays 80−52486
e^+e^-, τ decay modes and mass determ. 78−29325
e^+e^- annihilation, 12-31.6 GeV, τ production and decay branching ratios, lifetime 80−78052
e^+e^- annihilation, 3.1-5.2 GeV, DASP results 80−42483
e^+e^- annihilation, above 6 GeV, inference of τ decay 78−50042
e^+e^- annihilation, anomalous lepton prod., charmed mesons and heavy leptons 78−66134
e^+e^- annihilation, energy bounds for charm and heavy lepton prod. 77−2810
e^+e^- annihilation, form. of forward leptons *(Russian)* 77−2811
e^+e^- annihilation, hadron and lepton prod., τ-lepton decay, $K^\pm$, p, $\bar{p}$ yields, quark flavours 80−73725
e^+e^- annihilation, tests of lepton no. assignments 77−18266
e^+e^- annihilation, triplet heavy leptons, charged energy fraction, anomalous $e\mu$ events 78−45897
e^+e^- collisions, inclusive distribs. from heavy lepton prod. and decay 77−87961
e^+e^- dimuon and other possible heavy-lepton events, short review 77−30473
$e^+e^-\rightarrow e^+e^-$ or $\mu^+\mu^-$, decay products from new charged heavy lepton pair prod. 78−74238
$e^+e^-\rightarrow e^\pm U^\mp$ or $e^\pm$ hadron$^\mp$, anomalous events, heavy lepton pair prod. and decay 78−8676
$e^+e^-\rightarrow e^\pm X^\mp$, 3.1 to 7.4 GeV, threshold behaviour of $\tau^+\tau^-$ prod. 78−70351
$e^+e^-\rightarrow eX$, τ branching ratio and e momentum spectrum, D decay 78−89693
$e^+e^-\rightarrow$hadrons, cross-section struct. in 0-8 GeV range, quark models and heavy leptons 77−30392
$e^+e^-\rightarrow$hadrons, manifestation of heavy leptons, decay props. *(Russian)* 77−26537
$e^+e^-\rightarrow$heavy leptons, coupling of heavy leptons to W^0 anal. 78−33051
e^+e^- inclusive prod. at 4.8 GeV, anomalous muon events, charm and heavy lepton explanations 77−247
e^+e^- interaction, heavy neutral lepton detection 78−21441
e^+e^- interactions, review 79−80833
$e^+e^-\rightarrow L^-L^+\rightarrow$ pions, test for chirality of heavy-lepton current 77−18308
$e^+e^-\rightarrow L^+L^-$, energy spectra of secondary leptons *(Russian)* 77−38156
$e^+e^-\rightarrow L^+L^-$, hadron spectra from heavy lepton decay *(Russian)* 78−12919
$e^+e^-\rightarrow L^+L^-$, heavy lepton decay, energy spectra of secondary e or μ 77−71503
$e^+e^-\rightarrow L^+L^-$, longitudinally polarized beams collisions, energy depend. of parity asymm. 77−38154
$e^+e^-\rightarrow L^+L^-$, scalar model of weak interactions 77−18264
$e^+e^-\rightarrow L^+L^-\rightarrow(e^-\bar{\nu}_e\nu_L)+(\mu^+\nu_\mu\bar{\nu}_L)$, V-A and V+A model anal. 77−18262
$e^+e^-\rightarrow l^+l^-$, l=3, μ, τ, charged lepton universality test 80−32091
$e^+e^-\rightarrow l^+l^-$, polarisation studies at Z^0 pole, expt. feasibility 79−97615
$e^+e^-\rightarrow\mu$+anything, anomalous prod., 3.9 to 7.8 GeV 77−22722
$e^+e^-\rightarrow\mu e$, heavy lepton evidence, new lepton number 77−61268
$e^+e^-\rightarrow\mu e$, intermediate heavy-lepton pairs 77−18265
$e^+e^-\rightarrow\mu e$+anything, longit. polarised beam, asymmetries, props. of heavy leptons 77−10238
$e^+e^-\rightarrow$neutral heavy leptons, prod. and decay mechanisms anal. 78−41524
e^+e^- pair prod., two photon processes at high energy 77−71524
$e^+e^-\rightarrow\tau^+\tau^-$, 3.9-5 GeV, τ lifetime experimental upper limit 79−40826
$e^+e^-\rightarrow\tau^+\tau^-$, neutral-current effects on ψ-like resonance 78−74239
$e^+e^-\rightarrow\tau^+\tau^-$, parity violating effects measurement 79−36057
$e^+e^-\rightarrow\tau^+\tau^-$, τ spin from two body decay energy spectra *(Chinese)* 79−49503
$e^+e^-\rightarrow\tau^+\tau^-$ near Z^0 pole, heavy lepton polarisation and radiative effects 79−22085
$e^+e^-\rightarrow\tau^+\tau^-H^0$, Higgs scalar boson production, Weinberg model calcs. *(Russian)* 80−68442
$e^+e^-\rightarrow\tau^+\tau^-\rightarrow$cascade π and ρ, parity violation from weak and EM interaction interference *(Chinese)* 79−49504
$e^+e^-\rightarrow U^+U^-\rightarrow l^+(p_+)l^-(p_-)$+neutrals, cross section calcs., possible heavy lepton U 78−25029
$e^+e^-\rightarrow U^+U^-\rightarrow\mu^\pm$+hadrons+neutrinos, inclusive and exclusive anal. 77−67663
$e^+e^-\rightarrow U^+U^-\rightarrow\mu^\mp+e^\pm$+neutrinos differential cross-section anal. 77−67640
$e^+e^-\rightarrow U^+e^-$, SU(2)⊗U(1) gauge models 77−71502
e^+e^- transversely polarised annihilation, heavy lepton prod. and decay 77−18261
eN, deep inelastic scatt., heavy lepton mixings, Weinberg-Salam model 80−62992
η_c, production cross sections in e^+e^- colliding beams, two-photon processes 79−36089
$F^-\rightarrow\tau^-\bar{\nu}_\tau$, charmed mesons, heavy lepton decays, ν_τ neutrino mass depend. *(Russian)* 78−62394
$L^0\rightarrow\nu_L\mu^+\mu^-$, heavy lepton spin, massless spin 3/2 ν four fermion interaction 79−13175
L^0 prod. in pN collisions, 400 GeV/c upper limit on cross section 78−37243
$L^+\rightarrow e^+\nu_e\nu_L$, $\mu^+\nu_\mu\nu_L$, radiative corrections to charged heavy leptons decay 78−33050
L_2, second heavy lepton, explanation of Drell ratio 79−13097
$\mu\rightarrow$3e decay heavy neutral lepton mixing 77−65149
$\mu\rightarrow e\gamma$ in Weinberg Salam model, spontaneously broken μ-like charge symm., heavy leptons *(Chinese)* 78−82191
$\mu\rightarrow e\gamma$ or 3e, heavy leptons, CP violation 77−82727
μ magnetic moment, weak coupling contribution, Weinberg-Salam model 80−22607
μ-e events, alternative heavy-lepton model 78−66102
$\mu^+\mu^-$ anomalous prod. from e^+e^- annihilation, heavy lepton prod. and decay 78−82190
$\mu^-\mu^-\mu^+$ events in ν_μ reactions, SU(3) gauge models 77−74674
$\mu^-\mu^-\mu^+$ prod. in neutrino interactions, gauge theory, heavy leptons 77−65085

heavy leptons continued
μN, deep inelastic scatt., heavy lepton mixings, Weinberg-Salam model 80−62992
$\mu N\rightarrow\mu^-\mu^+$+X, new bounds for dilepton prod. from heavy neutral leptons 77−46040
$\mu^\pm N\rightarrow M^0X$, neutral heavy lepton prod., characteristics and possible $M^0\rightarrow\mu^+\mu^-$ search 79−71751
$N_e\rightarrow e^-\mu^+\nu_\mu$, search for at PETRA and PEP energies 78−45903
$N+\nu\rightarrow M^0$, heavy lepton prod. and decay mechanisms cross section and coupling constant *(Russian)* 79−9365
ν associated with heavy leptons, stability, cosmological He production 78−73783
ν high energy experimental physics at Fermilab, review 78−50028
ν interaction, prod. and decay of short-living heavy neutral particle 77−87971
ν interactions, μe prod., heavy lepton decay anal. 78−33057
ν interactions, trimuon prod., heavy lepton cascade decay 78−25038
$\nu(\bar{\nu})$ interactions, heavy-lepton interpretation of multimuon events 78−33058
ν production, prompt sources, and axion decays and interactions, pN beam-dump experiment 80−63028
ν reactions, dilepton events, neutral heavy lepton, rising $\sigma(\bar{\nu})/\sigma(\nu)$ 77−57523
$\nu_\mu(\bar{\nu}_\mu)$N, heavy lepton prod. and decay, differential cross sections *(Russian)* 80−105940
ν_μ+Ne$\rightarrow L^\pm$...., expt. limits on heavy lepton production 78−37197
νN, μ^+ single prod. in inclusive interaction 78−45908
$\nu N\rightarrow\mu^-\mu^-\mu^+$N, 350, 400 GeV, event origin, heavy lepton or quark cascade upper limit 78−89698
νN short-lived heavy neutral particle prod., possible heavy lepton or charmed meson *(Russian)* 77−74677
νN tetramuon prod. sources, heavy quark and lepton cascades, charm prod. 78−70356
$\nu_\mu N\rightarrow\mu^-e^+$, obs. in BEBC 78−78170
$\nu_\mu N\rightarrow\mu^-\mu^+(e^+)$+X, new bounds for dilepton prod. from heavy neutral leptons 77−46040
νp, charged heavy lepton prod. and decay 78−8655
$\nu p\rightarrow p2\pi^0M^0$, neutrino prod. of neutral heavy lepton in E_7 gauge model 79−17710
pN lepton direct prod. via hypothetical hadron and heavy lepton prod. *(Russian)* 77−46074
$\bar{p}p$, heavy lepton prod. and decay, supersymmetrical model of weak and EM interactions *(Russian)* 80−86748
$pp\rightarrow l^+l^-X$, massive lepton pair prod., quark-gluon-parton model, scaling 79−428
$\pi\rightarrow\nu_\tau\rho\pi$, A_1 resonance, $\rho\pi$ mass distrib. 78−45902
τ, charged heavy lepton, mass and leptonic branching ratios determ. 78−4849
τ, decay, weak vector current conservation, neutrino mass depend. *(Russian)* 79−89215
τ, decay calcs. in SU(3)×U(1) theory of weak-electromagnetic interaction with charged-boson mixing 79−35988
τ, decay in six quark-six lepton Weinberg-Salam model 79−35990
τ, decay modes, masses, spin, lifetimes and τ-ν_τ coupling 79−85348
τ, discovery and props., review *(Polish)* 79−89216
τ, identification and characteristics *(Hungarian)* 79−13180
τ, production in e^+e^- annihilation, experimental evidence review 79−75758
τ, properties and searches 80−73763
τ, props. and relation to the other elementary particles *(French)* 79−71776
τ, semileptonic decay, polarisation near Z^0 pole 79−97644
$\tau(1782)$, lifetime estimates, free quark model anal. 79−67544
$\tau(1.8)$, charged lepton anomalous mag. moment, Weinberg-Salam model effects 79−13126
$\tau\rightarrow3\pi$ or 5π, decay rate using current algebra and PCAC 79−3062
$\tau\rightarrow3\pi\nu$ decay, current algebra calcs. 79−30764
$\tau\rightarrow A_2\nu_\tau$, branching ratio calc. for possible A_2 decay mode of a spin 3/2 heavy lepton 79−6357
τ decay, large timelike Q^2, conservation of vector current and current algebra 78−78155
τ decay dynamics, scaling prop. and Michel parameter 78−37195
τ decay involving hadronic vector current 78−66101
τ heavy lepton, possible interactions, quark description 79−45054
$\tau\rightarrow K^*\pi\nu$, in e^+e^- annihilation, T-odd asymmetry in CP violation model *(Russian)* 80−105885
τ lepton, search in neutrino expts., neutrino mixing *(Russian)* 78−54604
τ leptonic decay mode 79−9358
τ mass, from $e^+e^-\rightarrow e^\pm(\mu^\pm)$+1 charged track, cross section energy depend. 78−89695
$\tau\rightarrow\mu\mu e$, flavour changing neutral current search 80−105836
$\tau\rightarrow\mu\nu_\mu\nu_\tau$, branching ratios 79−17703
τ neutrino interactions, signals in beam dump expt. 79−67535
$\tau\rightarrow\nu_\tau$+hadron(s), decay modes and ν_τ-mass 80−63057
$\tau\rightarrow\nu_\tau e\nu_e$, nature of τ-ν_τ-W coupling, ν_τ mass upper limit and lifetime 79−40824
$\tau\rightarrow\nu_\tau n\pi$, T-violation effects, neutrino mass *(Russian)* 80−95294
$\tau\rightarrow\nu_\tau\pi$, suppression by spin of ν_τ 78−21410
$\tau\rightarrow\nu_\tau\rho\pi$, ang. correlations in τ decay 79−63567
$\tau\rightarrow\nu\pi/\tau\rightarrow e\bar{\nu}\nu$ branching ratio anal. for determ. of τ and ν_τ spin values 79−75757
$\tau\rightarrow\nu\pi\omega$, decay width and form factor calc. using vector dominance hypothesis *(Russian)* 80−47271
$\tau\rightarrow\nu\pi\pi$, π invariant mass distrib. predictions, hadronic decay rates 78−70352
$\tau\rightarrow\nu\rho^0\pi$, spin parity anal. 80−105941
$\tau\rightarrow\nu\rho\pi$ decay mode obs. 78−29340
$\tau\rightarrow\nu\rho\pi$ decay parameters from PCAC and current algebra, A_1 charcts. 80−37314
τ particle properties, QCD type gauge theories, absence of $\tau^+\tau^-$ resonance in e^+e^- annihilation 78−37144
τ properties, $e^+e^-\rightarrow$ heavy particle pair $\rightarrow$ secondary particle + X, energy spectrum and angular distrib. 80−62960
$\tau\rightarrow\pi K\nu$, energy and angular correl. meas. 79−89214
$\tau\rightarrow\pi\nu$, decay observation, branching ratio 78−89766
$\tau\rightarrow\pi\nu$, suppression of pionic mode anal. 78−33106
$\tau\rightarrow\pi\nu_\tau$, branching ratios 79−17703
$\tau\rightarrow\pi\nu_\tau$, spin 3/2 heavy leptons, decay suppression, weak current *(Chinese)* 78−82192

heavy leptons continued
$\tau \rightarrow \pi\pi\pi\pi$, π invariant mass distrib. predictions, hadronic decay rates 78−70352
$\tau \rightarrow \rho\nu\pi$, halflife and mass determination from e^+e^- interactions 78−89765
$\tau \rightarrow \rho\pi\nu_\tau$, quark model, current algebra model, divergence of axial vector current 80−57655
τ semihadronic decay rate and branching ratio, QCD calc. 79−36119
τ spin determ. from τ-decay branching ratios 79−75757
τ three particle semileptonic decays, leptonic weak current *(Russian)* 79−97643
τ-neutrinos, in beam dump expts. 78−50004
τ^-, decays, SPEAR, Mark II detectors, recent results 80−74045
$\tau^- \rightarrow \rho^- \nu$, branching fraction meas. 80−13296
τ^+ as a paraelectron, positron and muon decay modes 78−50024
$\tau^\pm$ heavy lepton in e^+e^- annihilation, review 79−49505
$\tau^\pm \rightarrow \nu_\tau A_1{}^\pm (\rightarrow \rho^0 \pi^\pm)$, inclusive distribs. of ρ^0 mesons from cascade decays of τ heavy leptons *(Russian)* 79−9390
$\tau^\pm \rightarrow \nu_\tau(\bar{\nu}_\tau)$+hadrons, beam-dump experiment, observation of ν_τ interactions 80−22601
$\tau^\pm \rightarrow \nu_\tau \rho^0 \pi^\pm$, possibility of observing A_1 meson current algebra anal. 79−13176
$\tau^\pm$ production in e^+e^- annihilation 79−6336
τ', universal lepton mixing and mixing angles in $SU(2)_L \times U(1)$ gauge theory of weak interactions *(Russian)* 79−54298
$\tau^\pm$, implications to lepton physics, review *(Chinese)* 79−13121
$\tau^- \nu_\tau \pi^-$ γ, π form factors, axial-vector and structure dependent, vector meson dominance model 80−62989
$\tau^+\tau^-$, comments on the observability of tauonium 79−63464
$^{56}Fe(\nu_\mu, \mu^- + L^+ + L^0)^{56}Fe$ neutrino-induced heavy-lepton pair production at high energies and multimuon events 79−89298
τ decay as QCD test 80−102006

heavy water
acetylene+acetylene-d_2(D_2O), H-D exchange, equilib. consts. 77−86299
amine process for heavy water, design 79−615
amorphisation by NaOD in solution, collective excitations in liquid and amorphous state, 77 to 300K 80−92636
asymmetric separation process, value function, separative power 77−75001
atom pair correlation functions, X-ray, electron and neutron diffr. data 77−80406
atom-atom and mol. correlation functions, electron diffr. 77−80405
bond length, angle, high momentum transfer liq.-phase neutron scatt. 77−27195
CANDU-PHW reactors, primary and secondary water chemistry, review 79−22382
chemisorption on $SrTiO_3$, oxidation and reduction, isotope exchange study 80−104461
clathrate hydrates prepared from D_2O, identification from NMR line shapes 78−27861
collective excitations in 10^8 cm^{-1} momentum range, neutron scatt. expt. 78−43087
compressed, NMR spin echo obs., self-diffusion coeffs. 77−1250
compressed at low temp., mol. motions, spin-lattice relax., viscosity and self-diffusion 77−76287
concentration meas. by neutron thermalisation method *(Japanese)* 79−93746
density in capillaries, temperature of maximum 78−51801
dielectric constant meas. over temp. range 473K to 643K 80−103912
dielectric effects, high field, Piekara factor meas. 78−68441
dimer, isotopic forms, Ar matrix isolated IR spectra, assignments, config. 77−6780
dioxan-$D_2{}^{16}O$, solns., FP determ., equilib. method 77−20048
dioxane-D_2O mixture, nuclear Overhauser effect factors determ. using dynamic Overhauser enhancement with least square procedure 79−4746
dynamic simulation of the Gentilly-1 reboiler system 78−82439
dynamic viscosity coefficient in supercritical region of parameters of state, experimental investigation 78−67845
dynamic viscosity coeffs. *(Russian)* 78−47550
electrolysis at Hg cathode, $H^+(D^+)$ discharge activation energies in $H_2O(D_2O)$ 80−40707
enrichment using amine process 79−49695
equation of state, up to 380°C and 1000 bar 78−26655
far IR emission, angular correlation with CO_2 pump radiation, Dicke superradiance theory 79−41370
FIR lasers, reststrahlen laser resonator for 66 μm line 78−55385
fission reactor heavy water purification by deuterated ion exchange resins 78−8897
gaseous, viscosity, 200-400°C, up to 300 bar 78−63527
Girdler-Sulphide process, developments 79−22397
glass-transition temperature, crystn. temp., and dielec. const. 80−15229
heat capacity, compressibility and speed of sound 79−82284
heavy and ordinary water dynamic viscosity coeffs. relation in liquid phase 78−21759
heavy stable particles, cosmic ray produced, search in heavy water 79−40048
heavy water, optical consts., absorpt. and refr. index 0.1 Å-1 m 78−48139
HTO, effect on chromosomes of Swiss albino mice 79−2112
ice, cryst., electron traps, electron irrad. effects, EPR 77−1939
ice, crystalline, irrad., temp. depend. of trapped electrons, 77 to 6K 79−83474
ice, hexagonal, i.r. polarisability 77−4639
ice, II and IX, deuterated forms, 10K, OD stretching bands interpretation 78−2836
ice, intramolecular potential from overtone spectrum anal., H-bonding dependence 79−93972
ionisation const., thermodynamic props. determ., 298-523K 77−32821
ionisation process and electron localisation, phase density effect 77−89731
IR spectra, $\nu_2+\nu_3$ band shape 78−62855
IR spectral refl. and complex index of refr. of D_2O 78−68501
IR spectrometric method for meas. of slight heavy water enrichment in natural water *(French)* 80−104718
laser, 385 μm, CO_2 laser pumping, dispersion 80−87375
laser, emission characteristics at 50, 66, 83, 111 and 116 μm 80−58525
laser, far IR, intracavity pumped by TE CO_2 laser 80−87382
laser, far IR, tunable single mode optical pumping 77−42526
laser, far IR superradiant output 77−663
laser, mirrorless, optically pumped, 385 μm emission 79−31871

heavy water continued
laser, optically pumped far IR, candidate transition identification 79−931
laser, phase locking to freq. standard, CO_2-OsO_4 laser freq. meas. 80−95080
laser, pulsed laser-pumped submm amplifier, gain spectrum 78−79000
laser, real-time spectral anal. of far IR pulses 79−45983
laser, superradiant, Raman shifts of 99 μm output, Fabry-Perot freq. meas. 79−55120
laser, synchronous pumping, ultrashort pulse generation at 385, 66 μm 80−102705
laser, synchronously pumped, subnanosec. transients 79−89891
laser, zigzag-pumped, oscillator and superradiance characteristics 79−31873
laser 385 μm transition, laser pumped mol. laser theory 79−36868
laser 385 μm transition pumped by CO_2 laser 80−1192
laser emission, far IR CW, by optical pumping 79−3687
laser induced breakdown, comparison with H_2O 78−68453
laser oscillator, efficient high-power, at 385 μm 80−69422
laser submillimetre with optical pumping energy yield, emission pulse delay time depend. on pumping pulse *(Russian)* 78−71088
laser system, far IR, high power optically pumped 77−54724
leak detection, on-line infrared analyzers, CANDU report 78−82038
liquid, mol. rot., deuteron relax. obs. 77−8432
liquid, single 1.06 μm picosecond pulse superbroadening, concurrence with dielec. breakdown 79−86223
liquid, structural relax. times, model comparison 80−54108
liquid, viscous props. 80−2186
liquid, visible absorpt. meas., pulsed dye laser optoacoustic spectroscopy 80−11426
liquid, volumetric and derived thermal characteristics at low temp. and high pressure 80−107352
liquid structure factor, neutron diffr. meas. 79−46547
low freq. Raman spectra, isotope shifts, ice-like struct. 79−28732
3-methylpyridine-D_2O soln., consolute points, crit. soln. temps., light scatt. obs. 77−77230
moderator, of reactor KS-150, purification from organic impurities by catalysis *(Slovak)* 77−67811
molecule, collisionless multiphoton ionis. energy depend. by TEA-CO_2 laser 78−46405
molecule, cubic anharmonicity constants, normal coord. ab initio calcs. 79−36595
molecule, electroionisation 79−22849
molecule, electron impact dissoc. excitation, Balmer-α emission obs., Doppler profile meas. 79−31706
molecule, electron impact reson. observed in $A^2\Sigma^+ \rightarrow X^2\Pi$ radiation of OD 78−46455
molecule, energy levels and mol. vibr., internal coord. model 79−799
molecule, Feshbach-reson. and dissoc. electron attachment 79−41246
molecule, harmonic vibrations of nine unsymmetrical isotopic forms calc. 77−452
molecule, heterodyne meas. of IR absorpt. freqs. 78−55175
molecule, IR and Raman spectra, bonding, vibr., band shapes 79−6938
molecule, isolated in glassy H_2O, IR spectrum 78−27207
molecule, isotopic species, far IR spectra, assignments, moments 77−6761
molecule, matrix isolation spectra, vibr.-rot. lines, nucl. spin interconversion 78−46336
molecule, multiphoton i.r. absorption, optoacoustic detection 77−507
molecule, NMR in lyotropic systems 79−22732
molecule, O muonic X-ray spectra, H(D) isotope effects 77−75344
molecule, polarised photofluoresc. excitation spectra, VUV photodissoc. excited state lifetimes 78−5261
molecule, spectroscopic consts., rot. energy levels 77−10663
molecule, T_1 and T_2 relax. cross sections meas. 77−34733
molecule, UV and VUV spectra, 180-790 Å, absolute photoabsorpt. cross-section 77−75182
molecule, vibr. freq. shifts in polyatomic solutes 78−58654
molecule, vibrational and rotations meas. by laser spectrosc. 80−43050
molecule+$I(5^2P_{1/2})$, collisional quenching, isotope effects 77−34583
molecule sub mm beam maser spectrum, D hyperfine splitting 77−61874
monomer and dimer, isotopic forms, Ar matrix isolated IR spectra, assignments, config. 77−6779
neutron diffraction by electron LINAC 79−50974
neutron scatt., separation of coherent and spin incoherent scatt. from D_2O by polarisation meas. 77−6655
neutron scatt. cross section determ. by DEUKER computer code 79−54468
neutron thermalisation 77−65253
neutron transport at thermal energies, effect of 1/v absorbers 78−29532
nuclear magnetic relax. of deuterons at identically oriented planar interfaces 77−36148
optical constants, 6-450 cm^{-1}, 19°C 78−6649
optical constants, 70 to 450 cm^{-1}, reflection dispersive Fourier transform spectrometric obs. 77−40203
optical pumping using CO_2 CW capillary waveguide laser 80−48278
partition function ratio, reduced, generalised finite polynomial approx. H_2O rel. to D_2O 78−66529
piezo- and elasto-optic props. under high press. 80−50296
positronium formation, isotope effects 80−93432
process simulation of heavy water prod. plants 79−22396
production, asymmetric process, separative power, resoln. of inconsistencies 78−29622
production, by laser photodesorption 77−54365
production, Girdler-sulphide process phys. props. 78−25300
production, using laser isotope separation 77−83106
production as by-product of electrolytic H 80−30248
production in Fe/S/H_2O system 80−27750
production technology 77−46387
pulsed opto-acoustic spectroscopy 80−62743
PWR with D_2O in primary circuit, preliminary physics design 79−67837
radiolysis, positronium form. inhibition by NO_3^- electron scavenger 79−66325
Raman spectra of O-H and O-A stretching vibrations of ices II and IX 80−66166
seawater distillation, heavy water concentration, numerical model calc. 79−26514
sieve tray froths occurring in heavy water plants, expt. and anal. 78−82438
sieve trays for heavy water plants, development 78−82437
solvated electron, in D_2O, IR and vis. spectra, 292 to 445K 78−74672

heavy water continued
solvated electrons, optical absorpt. spectra. temp., isotope effects 80−55124
sound speed rel. to normal water as function of temp. and press. 78−2201
stimulated Raman scattering excited by CO_2 laser, far IR emission 77−54755
structure, temp. effects, neutron diffr. obs. 77−72544
structure and motion at high pressure 78−87606
structure at pressure, neutron diffr. 79−60253
sum rules for connecting vibr. freq. parameters of H_2O, D_2O and T_2O 79−36615
superbroadening, by self-focused picosec. laser pulses 77−75612
supercooled, polychromatic correlated site percolation 80−22296
supercooled high-pressure D_2O, density max. 77−1162
surface tension from Skeleton table *(German)* 80−75407
thermal conductivity, at 25-350°C, 0.1-245.3 mN/m^2 77−51556
tritiated water, atmospheric condensation-evaporation model 77−29326
tritium water, small samples, radiometry with gas-flow counter 80−17989
US attenuation, for vol. viscosity, 0-60°C 78−63871
US attenuation temp. depend. in associated liq. 77−51441
US excess absorption and compressional viscosity, temp. depend., hole theory 77−4157
US velocities in superheated ordinary and heavy water, thermodynamic props. 80−65156
US velocity experimental determ. 78−21734
vapour, far IR absorpt. coeffs. by H_2O laser meas. 80−9599
vapour, stimulated Raman emission obs. 77−38998
vapour, thermal cond., 375-600°C 79−82026
vapour 9.7 μm radiation absorption rel. to laser design 77−31098
vapour high-power optically-pumped submillimetric laser system 77−38925
vapour laser, tunable, optically pumped with single-mode CO_2 TEA laser 79−55145
vapour laser, zigzag pumped, superradiant 66 μ emisssion 78−33743
water, VUV reflectance, refr. index, absorpt. coeff., isotope effects 78−6695
Zircaloy-2, radiation and isotope effects on corrosion in H_2O/D_2O mixture 77−21314
Ag, and Ag^+, solvation in deuterated-ice matrices, electron spin echo obs. 80−15780
$Cs+D_2O$, ion-pair form., energy, angle and mass anal. of products 78−70970
$CsPFO/H_2O(D_2O)$ system, nuclear mag. relax. of water at identically oriented planar interface 77−36148
D_2O, and T_2O, inertia defects and dipole moments by kinetic consts. method 80−928
D_2O, finite medium age-diffusion kernels in source-sink theory 77−67782
D_2O laser, pulsed, optically-pumped, development for Tokamak plasma diagnostics, review 80−24242
D_2O, local model vibrs. 79−76414
D_2O, mol., Raman scatt. activity and IR intensity, finite field method 79−59462
D_2O, submillimetre laser Thomson scatt. system for plasma diagnostics 77−84526
D_2O thermal column irradiation facility Penn State Breazeale Reactor 80−9339
D_2O, vac. UV absorption spectra, Rydberg series vibr. anal. 78−42093
D_2O, vibr. freqs. from anharmonic ab initio/empirical PE functions 79−76406
$D_2{}^{16}O$, IR spectra, ν_2 band, rot. struct. 78−982
D_2O-H_2O, IR absorption spectra, statistical charact., continuous model of liq. struct. confirmation 78−6671
D_2O-H_2O mixing, diffusion meas. using neutron radiography 77−15605
D_2O-H_2O mixtures, US vel. at 298.15K, adiabatic compressibility 78−10127
D_2O-H_2O-HDO, gaseous mixture, absorpt. meas. by Michelson inclined mirror interferometer, high spectral resolution 80−9023
D_2O-isobutyric acid-d_{10}, coexistence curve, liq. densities 78−18780
D_2O+Ar, energy transfer isotope effect, rate consts. 79−8422
$D_2O+Ar(Kr)$, $(^3P_{0,2})$ state quenching cross sections 78−70912
$D_2O+Cs(K)$, ionising collisions in crossed-beam systems 78−48641
D_2O+D_2O, (010) vibr. relaxation 79−36741
D_2O+H_2, isotope exchange and separation with Pt hydrophobic catalyst *(Japanese)* 80−37901
$D_2O+K(Cs)\rightarrow K^+(Cs^+)+OD^-+D$, 100-200 eV, $D_2O^-(^2A_1)$ state 78−17770
D_2O+methanol-d_0(-d_2)(-d_4), D exchange reaction, thermodynamics 78−94328
$D_2O+NH(ND)$, $(b^1\Sigma^+)$ states quenching, kinetic isotope effects 77−63891
$D_2O+Ne(He)$, Penning ionis. electron spectroscopy, energy peak shifts and shapes 77−42392
$D_2O+Sc(La)(Y)$, O atom abstraction, product internal state distrib., fluoresc. study 78−48643
$(D_2O)_2$, and isotopic species, Ar isolation IR spectra, band assignments, struct. 77−3364
$(D_2O)_2$, and isotopic species, Ar matrix IR spectra, Xe, HCl, $(CH_3)_2$ doping, struct. 77−3365
$D_2O^-(^2A_1)$, obs. in K(Cs) ionis. collisions with D_2O, 100-200 eV 78−17770
$D_2{}^{16}O(HD{}^{16}O)$, isotopic depend. of mol. parameters, contact transformations 77−79550
α-FeOOH+D_2O isotopic exchange surface OH groups, IR investig. 80−2254
$H^+(D^+)$ exchange rates, ^{17}O NMR linewidths, pH depend. 80−91661
H_2O, $(D_2O)(HDO)$, photoelectron spectrum, Franck-Condon, factor calc., geometry and vibrs. *(French)* 77−83652
H_2O/D_2O electrolysis, Pd electrodes, H/D isotope separation factors, and exchange efficiency 79−50149
$H_2O+D_2O\rightleftharpoons 2HDO$, vibr. anharmonicity effect on equilib. 79−74410
$H_2O(D_2O)$, VUV absorption spectra, Rydberg series, rot. line shapes, quantum defect 78−5244
$H_3O^+(H_2O)_{0,1,2}+D_2O$ reactions, SIFT studies, review 80−58435
HTO, atm. vertical distrib. 77−9463
HTO, atmospheric radioactivity data, applicability of Weibull distrib. function 77−2230
^3HOH, effects of chronic ingestion on prenatal brain development, rat expts. 80−36004

heavy water continued
K_2CO_3-D_2O, glass, 4.2K, trapped electron photocond. and optical spectra following radiolysis 79−29378
LiCl-D_2O, aq. 10 M glass, optical absorpt. spectra after X-irrad., electron scavenging efficiency 79−83476
$NaClO_4$-D_2O, glass, 4.2K, trapped electron photocond. and optical spectra following radiolysis 79−29378
NaOD-D_2O, glass, 4.2K, trapped electron photocond. and optical spectra following radiolysis 79−29378
$NiCl_2$-heavy water solution, inelastic neutron scattering 78−91203
O_2, singlet state lifetime in D_2O soln., decay of micellar system 78−46301
OHT, β-decay, ab initio SCF MO calcs. 77−71842
T buildup in D_2O of CANDU reactors, due to $^3He(n,p)^3H$ reaction 79−22389
T storage and monitoring, CANDU heavy water reactors 80−5291

HEED *see high energy electron diffraction*

height measurement
aircraft velocity and altitude measurements using a tunable diode laser 80−13042
ceilometer using low-power laser radar 78−24390
cloud tops, heights from satellite imagery stereographic pairs 78−45017
Geos 3, altimeter data anal. in Tasman and Coral seas 80−3903
Geos 3, altimeter data appl. to sea surface topography obs. 80−3908
Geos 3, altimeter data for determ. of geoid of Kerguelen Islands area 80−3900
Geos 3, altimeter data on coincident orbits rel. to ocean transients 80−72535
Geos 3, altimeter data rel. to Earth gravity model improvement (GEM 9 and 10) 80−3909
Geos 3, altimeter data rel. to geoid heights along Hawaiian-Emperor seamount chain 80−3899
Geos 3, altimetric geoid comparison with gravimetric geoid 80−3898
Geos 3, altimetry data appl. to orbit determ. expt. 80−4226
Geos 3, radar altimeter data rel. to large-scale Gulf Stream frontal study 79−5488
Geos 3 altimeter data, error model for geoid undulations and gravity anomalies recovery 80−3896
Geos 3 altimetry, appl. to ocean gravity anomalies and geoid determ. 80−3905
Geos 3 altimetry data, appl. to ocean geoid investigation 80−3906
Geos 3 satellite, altimeter data rel. to oceanic geoid and tides determ. in NW.Atlantic Ocean 80−3901
Geos 3 satellite, altimetry data for ocean geoid estimation near Blake Escarpment 80−3902
Indian Ocean, GEOS-3 radar altimeter geoid profiles compared with 1×1° gravimetric geoid 79−16365
ionospheric reflection height estimation from Doppler measurements 77−21979
ocean wave height barometric sensor 77−78487
ocean wind wave elevation sensor array system 80−46322
opaque polished surface roughness determ., diffuse reflection method 79−49274
optical pseudo-colour processing of height and flow velocity *(Japanese)* 80−9826
physics field course, for school pupils 77−87612
remote sensing from satellite images using zoom height finder 78−36308
satellite altimetry, algorithm for subsatellite point position vector length determ. 79−29869
satellite altimetry, appl. to ocean geoid spectrum determ. 80−3904
satellite altimetry, refinement of short arc adjustment model 77−60336
snowpile, depth meas. using cosmic-ray snow gauge *(Japanese)* 77−5347
step height determ. by two-wavelength speckle pattern method 80−105614
Venus microrelief irregularites mean height, determination from radio transillumination data 80−72807
water wave probe, parallel wire type 79−18979
wave height meas. using Geos 3 radar altimeter 79−16481
Western Harz test net, height and geoid determ. *(German)* 77−70592
InPb-covered manganin wire, level detector, depth gauge, demonstration of superconductivity 79−35751

Heisenberg model
^3He, solid, two parameter model of mag. and thermal props., spin exchange 80−49461
adsorbed monolayer, classification of continuous order-disorder transitions 80−19910
alkylammonium copper halides, mag. sp. ht., two-dimens. S1/2 Heisenberg ferromag. behaviour 77−32206
alloy, binary random Heisenberg ferromagnet transition temp., crit. conc. RKKY model 78−52266
alloy with two ferromagnetic components, surface excitations 80−25179
amorphisation *(Russian)* 78−80118
amorphous antiferromagnet, spin waves, semiclassical theory 77−36064
amorphous ferromagnet, magnetisation and Curie temp., CPA calc. 80−75703
amorphous ferromagnet, spin disorder resist., force-force correl. function method 80−24918
amorphous ferromagnet, spin waves, effective medium approx. 78−68203
amorphous ferromagnet, variational cluster method 80−39728
amorphous Heisenberg ferromagnet, spin wave excitations and magnetization curve 79−15292
amorphous systems, excitations and critical phenomena within framework of phenomenological models 78−52267
anharmonic Heisenberg ferromagnet, renormalised magnons and phonons 77−59373
anisotropic, existence of phase transitions 77−32202
anisotropic, susceptibility, high-temp. series expansion 78−43546
anisotropic, time depend. correlations in high density limit 79−54071
anisotropic antiferromag., spectrum and correlation functions 79−28499
anisotropic antiferromagnet, phase transition, with external mag. field 79−11316
anisotropic ferromagnet, Bogoliubov inequalities, inhomogeneous dynamic susceptibility, single particle matrix Green's function 79−95564
anisotropic ferromagnet, longit. correl. function, generating Green functions 78−6500
anisotropic ferromagnet, longitudinal correlation function 78−34948
anisotropic Heisenberg chain, nonlinear excitations 80−70927
anisotropic Heisenberg chain with infinite radius of interaction, correl. functions 77−59372

Heisenberg model continued
anisotropic Heisenberg ferromag., inhomogeneous dynamic susceptibility tensor 80−39729
anisotropic Heisenberg ferromagnet, longitudinal correlation function 78−149
anisotropic lattice spin systems, phase transitions 78−73930
anisotropic linear chain, spectral density method 79−47222
anisotropic magnet, low-temperature properties 79−65633
anisotropic magnet mixture, Heisenberg spin system by Monte Carlo simulation 79−78408
anisotropic paramagnet with exchange-bond dilution, sixth freq. moments 80−44789
anisotropic pseudo one-dimensional Heisenberg systems, phase diagrams 78−52289
anisotropic $S=^1/_2$ ferromagnet, reson. susceptibility, statistical mech. theory 77−8413
anisotropic spin system, $S=^1/_2$ frustration effects 80−65763
antiferromagnet, 1-dimens., two-spin IR absorpt., Green's function and classical moments theories 77−40025
antiferromagnet, ABX_3-type, exchange interaction and zero-point spin reduction 77−12080
antiferromagnet, anisotropic, excitations at finite temp., CPA calcs. 79−95562
antiferromagnet, anisotropic, finite cell calcs. 80−60164
antiferromagnet, anisotropic, spectrum and correl. functions in spin-flop phase in generalized HF approx. 78−39283
antiferromagnet, cluster approximation, Neel temp. and specific heat calc. 80−54901
antiferromagnet, dil., CPA calc. 78−68263
antiferromagnet, dil., mag. transitions, MFA-VCA theory 77−63219
antiferromagnet, dil. two dimensional, mean spin per site in linearised spin-wave theory 78−39304
antiferromagnet, dil. with random first- and second-neighbour exchange bonds, CPA theory 78−52187
antiferromagnet, disordered, magnetic atom-conc. near percolation threshold, mag. props. *(Russian)* 78−80171
antiferromagnet, exchange interaction, kinetic, in narrow S-band 77−55655
antiferromagnet, excitations at finite temp. using CPA 79−56554
antiferromagnet, Green function theory 80−107975
antiferromagnet, ground state energy, pair correl. 78−72321
antiferromagnet, impure, impurity banding and mag. reson., theory 80−93181
antiferromagnet, isotropic linear chain, ground state, spectral density method 77−85407
antiferromagnet, light scatt. off surface 78−23475
antiferromagnet, linear chain, biquadratic exchange interaction effects 77−63062
antiferromagnet, low-dimensional, Neel temp. in mag. field 77−32200
antiferromagnet, magnon renormalisation, two-magnon Raman scatt., kinematic interaction 78−23228
antiferromagnet, magnon renormalisation 78−23259
antiferromagnet, one dimens., spin-flop transition 79−73723
antiferromagnet, one-dimens., autocorrelation function, low freq., temp. and field depend. 80−65929
antiferromagnet, one-dimens., impure, mag. susceptibility 80−60168
antiferromagnet, one-dimens. spin 1/2 dimerised, renormalisation group and other calcs. 79−78393
antiferromagnet, one-dimensional, spin waves in spin-flop phase 80−44817
antiferromagnet, phase diagram and multicrit. behaviour 78−56337
antiferromagnet, phase transitions in quantum spin systems 78−84434
antiferromagnet, pseudo-one-dimens., EPR freq. temp. depend. 77−32241
antiferromagnet, quadratic spin 1/2, sp. ht. and susceptibility, comparison with $Cu(C_5H_5NO)_6(BF_4)_2$ data 77−66353
antiferromagnet, randomly dil., excitations 78−23258
antiferromagnet, randomly diluted, field-induced phase transitions 77−36089
antiferromagnet, $s=^1/_2$ linear Heisenberg, zero-temp dynamics in mag. field 80−65764
antiferromagnet, second order Green's function 78−43545
antiferromagnet, short range order effects on EPR frequencies 77−69669
antiferromagnet, spin waves at finite temp., CPA calc. 79−73728
antiferromagnet, two-dimens. S=1/2 model, excitation spectra numerical exam. 77−36044
antiferromagnet, two-dimensional, approx. to susceptibilities 78−47928
antiferromagnet, two-dimensional, expansion for susceptibilities 80−70963
antiferromagnet, two-magnon Raman scatt., temp. effects 77−48178
antiferromagnet, uniaxial, props. by Green's function method 77−85406
antiferromagnet, with two kinds of exchange interactions, surface magnons and surface spin arrangements 77−36043
antiferromagnet, zero temp. props. in 3 dimens. 79−61032
antiferromagnet chain, renormalisation group nearest neighbour interactions 80−60357
antiferromagnet linear chain, spectral density approach decoupling effect 77−80903
antiferromagnetic, second order self-energy 78−56279
antiferromagnetic, triang., spin wave theory 79−7978
antiferromagnetic alloy, critical behaviour *(Russian)* 78−88128
antiferromagnetic alternating spin 1/2 chains, susceptibility calcs., spin-Peierls transition 79−78394
antiferromagnetic chain, alternating Heisenberg, appl. of zero temp. quantum renormalisation group 80−80526
antiferromagnetic chain, nonsinglet excitations 77−4491
antiferromagnetic chain, Peierls distortion energy, exact limit, renormalisation calc. 79−4643
antiferromagnetic chain, random, low temp. thermodynamic props. in zero mag. field 80−34657
antiferromagnetic chain, random, quantum spin-1/2 Heisenberg soln. 80−11148
antiferromagnetic chain, spin dynamics, quantum effects 80−34651
antiferromagnetic classical Heisenberg chain, low temp. dynamics 80−39803
antiferromagnetic exchange-coupled one-dimens. anisotropic chain with S=1/2, comparison with expts. 77−20530
antiferromagnetic Heinsenberg chain, spin 1/2, excitations energy 78−6503
antiferromagnetic Heisenberg chain, first order spin-Peierls transition 78−34986
Heisenberg model continued
antiferromagnetic Heisenberg chains, ground state energies 78−23230
antiferromagnetic insulator, one-dimens., Friedel type oscills. 78−60296
antiferromagnetic insulators, lattice thermal cond. 80−65319
antiferromagnetic lattice, ground-state energy calc., Kadanoff cells renormalisation procedure 77−77015
antiferromagnetic linear chain, ground state energy upper bound from trial functions 79−78293
antiferromagnetic linear chain, spectral density approach 77−40023
antiferromagnetism in amorphous Heisenberg magnet, ground state and frustration, theory 80−65766
antiferromagnets, magnetic susceptibilities in Heisenberg and Ising models 79−24185
antiferromagnets, pseudo-one-dimens., thermodynamic variables 80−65935
antiferromagnets, $S=\infty$ two-dimensional, approx. to susceptibility 77−80905
antiferromgnet, isotropic, hydrodynamic spectrum at low temp. 79−73663
asperomagnetism, short-range order, in Heisenberg magnet 80−65941
asymptotic behaviour of Heisenberg model with long-range interaction 78−56282
atomic system with variable atomic spin value, generalisation of Heisenberg Hamiltonian 78−14669
atomically rough surfaces, mag. excitations 77−69664
Bethe-ansatz excitations, observability in Heisenberg-Ising spin systems 79−82738
bicritical points in antiferromagnets, universality tests 80−84604
biquadratic exchange, Hamiltonian and two-spin eigenstates 77−72968
biquadratic systems, spin 3/2, elementary excitations in antiquadrupolar, ferrimag. and ferromag. phases 79−51763
α-bis (N-methylsalicylaldiminato) copper II, one-dimens. $spin-^1/_2$ Heisenberg antiferromag., high-field spin dynamics 80−71224
Bose expansion, crit. behaviour of Heisenberg model 79−42785
bosonisation, crit. behaviour 77−80948
bosonisation of Heisenberg-Ising chain, spin wave vel. calc. 80−54905
Bravais lattice, ferromagnetic ground state conditions in Ising and Heisenberg models 80−50129
C* algebra of quasilocal observables, Heisenberg eqns., boson and fermion systems 78−57854
chain, classical, higher moments and spectral shape 80−11147
chain, continuous, quantum solitons as magnon bound states 80−60162
chain, explicit Plancherel theorem for ground state representation 77−89921
chains, spin 1/2 Ising and classical Heisenberg models with alternating exhange, static props. 79−82737
CIDN(E)P, in two-dimensional fluid, and Heisenberg spin exchange 80−14157
classical, compressible spin system, zero temperature phase diagram 78−6536
classical, free energy in mag. field 77−4484
classical, with layer structure, mag. phase transitions, anisotropic lattice, theory 80−29557
classical, with three or four spin interactions, linear chain 80−70923
classical 2-D Heisenberg model, low temp. recursion relations, high temp. series expansion 78−10639
classical amorphous chain, thermodynamics 80−108022
classical anisotropic Heisenberg chain, scaling theory 80−80515
classical chain, comparison between continued fraction and computer simulation methods 79−78294
classical compressible model, phase transition exam., anisotropic exchange 77−59414
classical continuous Heisenberg chain, magnon-soliton phase shift 80−107998
classical equivalents of one-dimensional quantum-mechanical systems 79−33448
classical Heisenberg chain, energy fluctuations 80−80472
classical Heisenberg chain, solitons and magnons 80−60161
classical Heisenberg chain with mag. impurities, susceptibility 77−4490
classical Heisenberg chains, low temp. spin dynamics 78−68243
classical Heisenberg model, infinite, nonlinear dynamics, quantum time evolution 80−100576
classical Heisenberg spins on triangular cactus tree, random ordered phase 79−87265
classical impure Heisenberg chain, dynamics near T=0 for low impurity conc. 80−71055
classical nearest-neighbour chain, dynamics, exact perturbative results 78−10700
classical nearest-neighbour Heisenberg chain, low temp. dynamics 80−80524
classical one-dimensional Heisenberg magnet, with biquadratic exchange interaction, correlation functions and susceptibility calc. 77−36048
cluster approximation for dilute Ising and Heisenberg ferromagnets, Curie temp. 77−89916
cluster approximation of random ferromag. 79−82807
cluster expansion of random ferromagnets 78−10637
competing interaction systems, R-S model, series expansion and rigorous results 78−19201
compressible classical Heisenberg chain, phonon dynamics and sound velocity 80−96604
computer simulations of mag. model systems 80−65924
constant coupling approx., derivation 78−76213
continuous Heisenberg spin chain, integration through inverse scatt. method 78−19203
continuous Heisenberg spin chain, solitons 77−55654
continuous spin systems, position-space renormalisation group study 79−38350
continuous symmetry, spontaneous breakdown near two dimens. 77−4489
continuous symmetry breaking in Ising, XY- and Heisenberg model 79−82787
continuum Heisenberg spin system, stationary spherically and axially symm. spin waves 80−34615
continuum spin system, as exactly solvable dynamical system 77−47960
continuum spin system dynamics, spin-wave and solitary wave solns. 77−8263
copper, benzoate, one-dimens. antiferromag., heat capacity, field-induced crossover of spin-dimensionality 80−97099
copper benzoate, low-dimensional Heisenberg antiferromag., high field magnetisation 80−80558

Heisenberg model continued
copper formate.$4D_2O$, field-induced antiferromag. order above T_N 78−84389
copper formate tetrahydrate, two-dimens. spin 1/2 Heisenberg antiferromag., phase transition characts. 77−66352
copper tetraamine sulphate, two-dimensional Heisenberg antiferromag., high field magnetisation 80−80558
copper tetrammine sulphate monohydrate, evidence for exchange coupled quadratic nets 77−24705
correlation inequalities for n-vector spin models 80−54860
correlation theory of static and dynamic properties 80−65765
coupled phonon-linear Heisenberg chain system, phase transition 78−64208
critical amplitudes, universal relations 77−66341
critical behaviour, high temp. susceptibility and internal energy series 78−34987
critical temperature of randomly diluted Heisenberg spin system with anisotropic exchange coupling 79−99702
critical temperatures, random Heisenberg-Ising magnets, binary mixtures, amorphous magnets and spin glasses 80−54911
$CuBr_2$, finite Heisenberg chain effects, temp. depend. 79−47230
di(alkyl ammonium)copper tetrachloride, two-dimens. magnon and phonon thermal cond. in high mag. fields 77−69123
di(propylammonium) copper tetrachloride, mag. suscept. meas. 77−63131
dialkylammonium copper chlorides nearly two dimens. Heisenberg ferromagnet, NMR study of magnetisation 77−85586
dialkylammonium copper tetracholorides, quasi 2-dimens., lattice- and spin-dimens. crossovers 77−59416
diethylammonium copper chloride, Heisenberg ferromag., spin wave theory 77−89922
diethylammonium manganese chloride, Heisenberg magnet, spin diffusion, EPR study 80−66019
diethylammonium manganese chloride, planar Heisenberg magnet, spin diffusion, EPR study 80−15793
diethylammonium-manganese chloride, spin diffusion, quasi-two-dimensional Heisenberg paramagnet 78−88129
dilute antiferromagnet, ground state energy 77−40027
dilute ferromagnet, cluster expansion 80−15734
dilute ferromagnets, with site and bond disorders, Curie temp. 77−59407
dilute Heisenberg antiferromagnet, mean spin on finite clusters 78−68139
dilute Heisenberg magnet excitations near percolation threshold 79−87270
dilute linear Heisenberg chain, partition function and irreducible representation of permutation groups by HLISP 78−34945
dilute magnet, renormalisation group calcs. 79−56550
dilute systems, computer simulation, mag. conc. of clusters, linearised eqns. of motion 79−78409
diluted, spin dynamics at elevated temp. 78−84433
diluted classical Heisenberg ferromagnet, position space treatment 79−87268
diluted Heisenberg magnet, spin diffusion const., conc. depend. 78−88089
diluted Ising and Heisenberg magnets with competing interactions, phase diagrams and mag. props. 80−34672
diluted systems with competing interactions, mag. ordering, appl. to $Eu_xSr_{1-x}S$ 80−65914
dimerised Heisenberg chain, spin dynamics 77−20528
dimethyl ammonium manganese chloride, sp. ht., quasi-one dimens. behaviour 78−52293
dimethylammonium manganese tetrachloride, Heisenberg ferromag., spin wave anal. 79−61237
dimethylammonium manganese trichloride:Cd(Cu), impurities in quasi-one-dimens. Heisenberg systems, anisotropy effect 80−80502
dimethylammonium manganese trichloride, pseudo one-dimens. Heisenberg antiferromag., phase diagrams 79−61148
dipropylammonium copper chloride, nearly 2D ferromag., spin wave theory 77−85436
direct exchange between $3D^N$ ions in transition metals 79−69668
disordered, magnet, collective modes, Heisenberg-Mattis model 80−39797
disordered ferromagnetic states, random exchange integrals 80−80550
disordered Heisenberg binary magnetic alloy with mixed exchange interaction, compensation point *(Russian)* 77−51898
disordered Heisenberg spin model, magnetisation calc. 80−60167
disordered magnetic system, spin waves, Heisenberg model 80−71064
disordered one-dimensional system, Hubbard model 78−10642
disordered spin system, commutator and anticommutator Green's functions 79−51792
disordered spin systems, crit. dynamics 77−43844
disordered substitutional alloy, mag. props., Heisenberg model 79−38342
domain wall type soln., Heisenberg Hamiltonian with local and exchange anisotropy 78−14917
DPPH-benzene complex, ht. capacity, 0.55-20K, mag. susceptibility, 0.4-300K 78−56317
dynamical correlated-effective-field approximation 79−24122
dynamical spin correl. functions at finite temp. 77−69592
Dyson's hierarchical model, Heisenberg models and n-vector 78−31078
education, Heisenberg theory of ferromagnetism, const. coupling approx. 77−78919
effective exchange interactions and magnetic ground state of strongly correlated electrons 79−61036
elastic compliance, cooperative mag. contrib., exchange striction mechanism 77−40108
elastic magnetic system, one-Fermion-one-Boson model 78−43539
equations of state, parametric representation in crit. region 78−79741
equivalence of canonical and grand canonical ensembles 79−30360
exchange coupled spins, in lattice dimens. 1 and 2, 1/n expansion 77−66237
exchange integral, in nonorthogonal basis, for anti- and ferromag. systems 78−2641
exchange interaction Hamiltonian, eigenvalues and eigenvectors 79−78289
FCC ferromagnet, surface spin instabilities 77−69475
α-Fe, mag. ordering affecting homodiffusion coeff., 511-1200°C 79−73711
ferrimagnets, one-magnon light scatt., temp. dependence, two-sublattice systems 78−31061
ferromagnet, 1- and 2-dimens., NMR line breadth 77−48064
Heisenberg model continued
ferromagnet, amorphisation, anisotropically distrib. exchange forces *(Russian)* 77−85408
ferromagnet, and quantum inverse-scattering method 79−61029
ferromagnet, anharmonic, renormalised magnons and phonons 78−91837
ferromagnet, anisotropic, collective Green's function, dynamical RPA 80−70925
ferromagnet, anisotropic, collective Green function, longit. susceptibility *(Russian)* 79−65631
ferromagnet, anisotropic, instantons 80−7066
ferromagnet, anisotropic, quasicollective spin waves in paramag. region 77 43827
ferromagnet, anisotropic, theroy of light scatt. 77−90161
ferromagnet, anisotropic, with biquadratic exchange interaction and uniaxial anisotropy, Curie temp. 80−7118
ferromagnet, anisotropic Landau-Lifshitz, quasiclassical spectra *(Russian)* 80−15678
ferromagnet, appl. of variational method for systems with discrete energy levels 78−31074
ferromagnet, BCC, with $K_2CuCl_4.2H_2O$ struct., ^{17}O transferred hyperfine interactions 78−39439
ferromagnet, biquadratic exchange, Green's function method, Hamiltonian and Curie temp. 80−15675
ferromagnet, classical, magnetisation, Monte Carlo calc. 78−23229
ferromagnet, classical, with dipole-dipole interaction, renormalisation group and crit. exponents 80−60351
ferromagnet, classical spin field model in mag. field, statistical mechanics in one dimens. 78−43544
ferromagnet, containing nonmagnetic impurity, local mean spin deviations 77−66236
ferromagnet, correlation functions in ferromagnetic and paramagnetic regions, RPA 80−71075
ferromagnet, crit. dynamics in $2+\varepsilon$ dimens., low temp. phase 78−76262
ferromagnet, critical dynamics of impurity spin below T_c 80−71076
ferromagnet, critical dynamics spin wave theory, dynamic scaling hypothesis failure 80−97082
ferromagnet, critical points and two-magnon spectrum 79−87274
ferromagnet, cubic, with next nearest neighbour interactions, two-magnon bound states 80−70977
ferromagnet, Curie temp., decoupling of Green functions 77−12133
ferromagnet, density of states and heat capacity near percolation threshold 77−77021
ferromagnet, diagram techniques for Greens functions with spin operators 78−91836
ferromagnet, dil., CPA theory, spin-wave stiffness and Curie temp. 78−31080
ferromagnet, dil., mag. excitations, localisation, wavefunctions 78−60275
ferromagnet, dil. Heisenberg, localisation of excitations near percolation threshold 79−15271
ferromagnet, dil. spin $^1/_2$, renormalisation group treatment 79−69679
ferromagnet, dilute, spin wave localisation near percolation threshold 80−25120
ferromagnet, diluted classical, crit. props. 79−28536
ferromagnet, dipole-dipole interaction, quantisation axis, magnetisation, and critical point effects 78−34946
ferromagnet, disordered, influence of inhomogeneity of effective field on props. 78−10701
ferromagnet, disordered, pair effects in bond model 79−78290
ferromagnet, disordered, phase transitions, mol. field and Landau-Ginzburg theories 80−93118
ferromagnet, disordered, two spin species, spin-wave spectra calc. 77−59375
ferromagnet, disordered two-dimens., CPA theory of bond model 80−60163
ferromagnet, easy-axis, higher order corrections to spectrum 78−80222
ferromagnet, entropy 79−65635
ferromagnet, equation of state, using modified Gell-Mann Low renormalisation group 77−63225
ferromagnet, equivalence of large biquadratic exchange to small uniaxial single ion anisotropy 79−78292
ferromagnet, Faddeev eqns. for three-magnon T-matrix 77−36045
ferromagnet, Gell-Mann and Low renormalisation group, eqn. of state 78−31033
ferromagnet, high frequency, kinetic and thermodynamic props. *(Russian)* 78−19340
ferromagnet, infinite, one-dimens., ground state representation 80−25065
ferromagnet, instanton contrib. to correlation function *(Russian)* 78−95412
ferromagnet, intermediate quadrupolar phase existence 79−51784
ferromagnet, Ising-Heisenberg-XY crossover, bicritical-point, partial differential approximants for susceptibility series 77−85466
ferromagnet, isotropic Heisenberg, with arbitrary spin, correlation functions 78−31075
ferromagnet, isotropic with biquadratic exchange 78−39344
ferromagnet, linear, spin diffusion coeff. and static spin correlators *(Russian)* 77−80942
ferromagnet, linear, with applied mag. field, second-magnon like excitations 80−65837
ferromagnet, linear Ising-Heisenberg, spin waves vs. bound states, exact soln. 78−68202
ferromagnet, local levels arising from spin wave kinematic interactions 77−59374
ferromagnet, localised magnons around impurity 78−39305
ferromagnet, localised magnons around surface impurity *(Russian)* 78−84376
ferromagnet, localized magnons in a spin chain with two 'surface' impurities 79−38310
ferromagnet, longitudinal dynamic susceptibility 78−64181
ferromagnet, low temp. behaviour in spectral density method 80−50028
ferromagnet, low-dimens., crit. temp. *(Russian)* 78−23274
ferromagnet, mag. excitation near surface of high Miller indices 77−51871
ferromagnet, magnetic excitations on ideas and atomically rough surfaces 78−14944
ferromagnet, magnon renormalisation, higher approx. 78−14945
ferromagnet, magnon renormalisation 80−65849
ferromagnet, nearly one- and nearly two-dimensional, long-range order, upper bound for magnetisation 78−34947
ferromagnet, nearly two-dimensional and nearly one-dimensional thermodynamic props., Green's function investigation 79−15275

Heisenberg model continued
ferromagnet, noncond., Green function, contrib. of bubble graphs due to dynamic and kinematic spin wave interactions 77−51894
ferromagnet, nuclear spin quantum mechanical behaviour 77−51872
ferromagnet, one-dimens., symm. crossover 79−87269
ferromagnet, phonon thermal cond., crit. anomalies *(Russian)* 78−80159
ferromagnet, point singularities in micromagnetic systems with radial symmetry 80−107976
ferromagnet, pseudo-one-dimens., EPR freq. temp. depend. 77−32241
ferromagnet, quasi-two-dimensional, EPR at high temp. *(Russian)* 80−11243
ferromagnet, quasi-two-dimensional $S=^1/_2$, expt. susceptibilities compared with high-temp. series expansion analysis 77−4506
ferromagnet, quasiclassical description, soliton solutions 78−39282
ferromagnet, random quenched, crit. behaviour, effective exponents, renormalisation 80−60326
ferromagnet, randomly dil., spin wave excitation exam. 77−24665
ferromagnet, randomly diluted, 2-dimens. dynamics calcs. 77−40024
ferromagnet, randomly noncollinear mag. struct. and spin waves *(Russian)* 79−42764
ferromagnet, S=1/2, two magnon bound states, redefinition 79−42725
ferromagnet, self-consistent renormalisation of spin waves 77−72966
ferromagnet, single site anisotropy, statistical mechanics 78−31034
ferromagnet, spectral density for Green's function after Dembinski's decoupling approx. 80−25064
ferromagnet, spin coherent state representation, spin waves excitation spectrum 78−80117
ferromagnet, spin configurations near singularities in micromagnetism 80−54908
ferromagnet, spin wave excitations at finite temp., CPA calc. 77−32142
ferromagnet, spin wave relaxation due to dipole interactions, damping temp. depend. 79−69664
ferromagnet, spin waves at low temp., method of variational derivatives 79−24152
ferromagnet, spin-one, uni- and biaxial anisotropy, RPA and mol. field approx. 78−34989
ferromagnet, spin-one, with biquadratic and uniaxial anisotropy, Curie temp. 79−61123
ferromagnet, spin-wave renormalisation, consistent linearised Green's function theory 79−4685
ferromagnet, spin-wave renormalisation, S≥1 80−71070
ferromagnet, stepped surface, spin-wave modes calc. 77−73015
ferromagnet, strongly anisotropic, with impurities, in transverse field, one-magnon states 77−69476
ferromagnet, structural disorder effects on Curie temp. 79−78417
ferromagnet, structurally and chemically disordered, critical behaviour 77−43838
ferromagnet, substitutionally disordered, spin dynamics, linear spin-wave approx. 77−40067
ferromagnet, surface magnetisation profile and localised magnons 80−70985
ferromagnet, surface spin instabilities 77−20533
ferromagnet, surface spin waves theory *(Russian)* 77−89939
ferromagnet, three-dimens., two magnon states, effect of next nearest neighbour interactions 78−64178
ferromagnet, three-dimens. solitons 79−82741
ferromagnet, transition temp. calc., depend. on atomic spin and coordination no. *(Russian)* 77−47997
ferromagnet, two-dimens., spin dynamics, renormalisation group calc. 78−47966
ferromagnet, two-dimensional, Heisenberg model, pseudoparticle solns. 79−47223
ferromagnet, two-dimensional dil., density of states near percolation threshold 77−1533
ferromagnet, two-magnon reson. in absence of bound states, calc. 80−60423
ferromagnet, variational method for the cluster model of the structurally disordered Heisenberg ferromagnet 78−91839
ferromagnet, vortex lines, Heisenberg model calc. 80−50026
ferromagnet, with 180° domain walls, quantum mech. treatment 77−48007
ferromagnet, with anisotropic exchange, homogeneous relax., time const. calc. 77−16149
ferromagnet, with biquadratic exchange, first-order quadrupolar transition 77−69571
ferromagnet, with biquadratic exchange 77−63060
ferromagnet, with biquadratic interactions, Green's function approaches 77−55653
ferromagnet, with s-d exchange interactions, Curie temp. 78−19255
ferromagnet, with single-ion anisotropy, correlation functions calc. 78−31076
ferromagnet, with two kinds of exchange interactions, surface magnons and surface spin arrangements 77−36043
ferromagnet, with uniaxial exchange anisotropy, cumulant expansion method 77−12076
ferromagnet, with weakly bound ferromag. impurity, thermodynamic and dynamic props. *(Russian)* 78−27032
ferromagnet eqn. equivalence to nonlinear Schrodinger eqn. 79−95563
ferromagnet in critical region, Bloch renormalised spin wave approx. 79−82784
ferromagnet in mag. field, spin relax., crit. anomalies 78−43669
ferromagnet interface, elastic approximation, vibr. and mag. props. of interface and planar defect *(French)* 77−72767
ferromagnet two-dimensional soln. 80−60166
ferromagnet with antiferromag. impurity with arbitrary spin, ground state calc. *(Russian)* 78−43585
ferromagnet with biquadratic exchange 79−38338
ferromagnet with easy-plane anisotropy, HF magnon energies, kinematic consistency 80−93097
ferromagnet with higher-order exchange interactions, thermodynamic props. 79−42770
ferromagnet with random anisotropy, Curie temp., constant coupling approx. 78−76264
ferromagnet with resonant impurities, Heisenberg model *(Russian)* 79−87280
ferromagnet with single ion anisotropy, collective modes 77−28354
ferromagnetic, anisotropic, Green-function theory 77−16025
ferromagnetic, FCC, two-magnon bound state 77−20575
ferromagnetic, n-layer, effects of dilution and bond randomness 79−78296

Heisenberg model continued
ferromagnetic alloy, critical behaviour *(Russian)* 78−88127
ferromagnetic alloys, surface spin waves, cluster Bethe lattice approach 80−70983
ferromagnetic chain, continuous, finite amplitude spin wave, stability 80−20395
ferromagnetic chain, spin wave theory in lower dimens., failure of dynamic scaling hypothesis 79−78284
ferromagnetic chain with biquadratic exchange, spin correl. length, susceptibility and spin diffusion *(Russian)* 77−69568
ferromagnetic coupling, finite magnetisation 78−43541
ferromagnetic crystal bar, square cross section, magnon excitations 77−77047
ferromagnetic fluid, 1D Ising and 3D Heisenberg solns. 77−85478
ferromagnetic ground state, threshold inequalities 80−7064
ferromagnetic ground state of Heisenberg Hamiltonian, conditions for existence 79−73662
ferromagnetic Heisenberg chain, weakly bound magnon states *(Russian)* 80−100591
ferromagnetic Heisenberg chains with easy plane, validity of classical statistical mechanics 80−44786
ferromagnetic linear chain, Heisenberg Hamiltonian, existence of isolated magnon 79−4666
ferromagnetic one-dimens. chain, solitary magnon solution 77−69473
ferromagnetic phase of three-dimens. quantum Heisenberg models, conditions for $T_c=0K$ 79−38345
ferromagnetic resonance in anisotropic Heisenberg model, magnon-magnon, phonon-magnon interactions *(Russian)* 80−11274
ferromagnetic slab, finite thickness, spin correl. functions 80−80522
ferromagnetic surface, spin behaviour, review 77−20527
ferromagnetic systems, solitary bound states of magnons and lattice deformations, Dyson-Maleev representation 78−91838
ferromagnetism, basic models, classification of theories *(Rumanian)* 78−91840
ferromagnetism, singlet ground state, Heisenberg Hamiltonian model 79−11283
ferromagnets, anisotropic, HF magnon energy renormalisation, kinematic consistency 80−29539
ferromagnets, boson field anal. of crit. temp. region 77−51911
ferromagnets, Heisenberg and planar, exact results for spin-wave renormalisation 79−69660
ferromagnets, surface effect on thermodynamic props. and excitation spectra 79−11282
ferromagnets with biquadratic exchange, uniaxial anisotropy, susceptibility calc. 79−99670
film, mag. structs. 79−38359
film, spin-one isotropic, quadratic interactions, quadrupolar-paramag. T_c 78−64210
film, spin-one isotropic Heisenberg, with biquadratic interactions, phase transition 77−20611
Fokker-Planck equation validity 77−89920
frustration effect in s=1/2 XY and Heisenberg models 80−15677
functional integral method appl. to classical and quantum spin models 80−15676
garnets magnetic excitations 79−99695
Gaussian-to-Heisenberg crossover, specific heat, renormalised perturbation theory 80−60356
generalised, with biquadratic exchange, partially aligned mean-field ground states 78−23227
Ginzburg-Landau-Wilson model, n-component, derivation of nonlinear σ-model, in low temp. limit 80−44787
Green's functions, closing relns. for model with one-ion anisotropy 78−2642
ground state energy, renormalisation calc. 79−61150
ground state energy for linear antiferromagnetic Heisenberg chain, neighbour interactions 80−84606
ground state props. of S=1/2 antiferromagnet 79−15274
ground state representation of infinite 1-D ferromagnet, scatt. theory 78−77807
ground state representation of infinite one-dimens. Heisenberg ferromagnet 77−66234
Hamiltonian, generalisation for crystal with allowance for orbital degrees of freedom 79−4644
heavy rare-earth alloys, mag. ordering temps., Heisenberg exchange 79−61103
Heisenberg ferromagnet, isotropic, second-order Green's function theory 80−2578
Heisenberg ferromagnet, with biquadratic exchange interaction 78−34999
Heisenberg ferromagnetic system with biquadratic exchange interactions, spin wave theory *(Chinese)* 80−88755
Heisenberg multi-quadratic isotropic model, LRO, phase transf., exchange interactions *(Chinese)* 80−88756
Heisenberg-Dzyaloshinsky-Moriya model, high temp. expansions for zero-field susceptibility and specific heat 79−33497
Heisenberg-Ising bonds, randomly mixed three dimens. system, critical props. 78−76249
Heisenberg-Ising chain, correlation functions at T=0 79−24123
Heisenberg-Ising spin chain quantum inverse scatt. method, Jordan-Wigner transformation 80−93068
Heisenberg-Mattis model, long-wavelength dynamic response 80−20409
helical spin chains, static and dynamic props. 79−73661
helimagnetism, isotropic bilinear spin Hamiltonian on Bravais lattice 77−51866
Helmholtz free energy, approx. expressions 77−16024
high temp. self-consistent approach 77−20531
high-temperature representation of anisotropic rotator, XY and Heisenberg models for dimensions D≥2 80−11146
hydrodynamic singularities and the renormalization group 79−54063
ideal Heisenberg ferromagnet, phonon renormalisation and spin waves 80−88754
impure classical chain, dynamic props. using local-moment pair correl. functions 80−15728
impurity band resonance at 0K, theory 80−66041
inequalities for classical spin vector models, X-Y and Heisenberg models 77−91
infinite classical and quantum models, intertwining, Trotter approx., coherent state formalism 79−44713
inhomogeneous mixture of Ising and Heisenberg substances, quenched system, critical temp. 80−88770

Heisenberg model continued
insulating spin glass, obtained from impurity doped antiferromag. insulator 79−51796
insulating systems, magnetic, review of expts. 78−68240
interacting many-level system, thermodynamics, from RPA Green's functions 78−43549
interactions, spirals and phase transitions with and without long range order 80−60350
inverse method for a generalized spin chain 79−99671
isotropic ferromagnet, first-order Green's function theory 77−36046
isotropic Heisenberg ferromagnet, localised spin-wave modes, biquadratic exchange effects 77−51896
isotropic Heisenberg ferromagnet, resistance inequalities, C*-algebra 77−4487
itinerant ferromagnetism, local-band theory, equivalent Heisenberg model 79−82745
itinerant localised systems, dynamic magnetic response 80−34583
lattice diffusion, Heisenberg ferromagnet 78−88090
lattice spin systems, phase transitions from strong coupling expansions 79−6058
layered magnet, phase transition 78−76252
linear chain, alternating spin quantum numbers, mag. and thermodynamic props. 80−34578
linear chain, diffusion coeff. at infinite temp. *(French)* 78−10636
linear chain, disordered, q-depend. mag. susceptibility 78−27010
linear chain, dynamical correl. functions 77−63221
linear chain, spectral density approach to correlation functions 79−24124
linear chain, spin dynamics, theory vs. computer simulation 78−80155
linear chain, with nearest and next-nearest neighbour interactions 77−63059
linear chain magnets with unlike spins, exactly soluble model 77−16030
linear chain of classical spins with randpm Dzyaloshinski-Moriya interactions, exactly soluble model 79−61118
linear chains, dimerisation, variational localised-site cluster expansions 79−60670
linear Heisenberg antiferromagnet, $S=^1/_2$ zero temp. dynamics 79−73741
linear Ising-Heisenberg ferromagnet, excitation spectrum and thermodynamic props. 80−50118
linear Ising-Heisenberg ferromagnet, spectrum of elementary excitations 79−61091
linear spin systems, dynamical spin correlation functions 78−31035
liquid metals and alloys, mag. model 80−88719
longitudinal correlation functions, for system with single-ion anisotropy 78−76214
low temperature Heisenberg ferromagnet dynamical longit. correl. function, hydrodynamic regime 78−31039
mag. excitations, atomically rough surfaces, isolated cluster of overlayer spin 78−31102
magnet, soln. of Bloch eqn. for many-particle lattice systems 77−12078
magnetic crystal, effect of impurity on local density of states 79−33263
magnetisation upper bound, Bogoliubov's inequality 77−43803
magnetization reversal of the two-dimensional Heisenberg ferromagnet with weak Ising anisotropy 80−107977
magnon fields, finite temp. effective pot. methods, loop expansions 78−2640
magnon relaxation, Heisenberg chain, in external field *(Russian)* 78−91854
magnons, in ferromagnetically coupled Heisenberg chain, mag. field 79−65666
manganese acetate tetrahydrate, Heisenberg ferrimag. magnetisation 79−47304
manganese formate dihydrate, 2-D Heisenberg antiferromag., sp. ht. 78−14965
Mattis random magnet, spin waves 77−20572
metamagnet, collinear, mag. phase diagram 80−71035
metamagnetic transition in absence of mag. field, model 80−97092
metamagnetism, spontaneous, four-ion anisotropy as source 79−47277
microcanonical high-temp. expansion 78−2638
migdal renormalization group approach to quantum spin systems 79−38333
Migdal-like approximation, quantum spin systems 80−34649
mixed crystal ferromagnet, mag. props. 80−34579
mixed ferromagnetic Heisenberg and Ising bonds, appl. of effective Hamiltonian method 80−50023
mixed Ising and Heisenberg coupling, crit. props. 78−19256
mixed-spin paramagnet, dynamics 80−60173
Mori continued fraction truncation for spectral function 78−6496
n-component classical model, low temp. renormalisation group and symm. breaking perturbation 79−15315
nearest-neighbour spin-spin correl. functions calc. 80−80537
nitroxide free radical mag. interaction with lanthanides or Cu^{2+} in liqs., ESR 78−68380
nitroxide spin probes, unresolved hyperfine broadening convection in EPR, linewidth and Heisenberg spin exchange freq. determ. 80−71180
noncollinear magnetic order and spin wave spectrum in presence of competing exchange interactions 80−65834
nonlinear excitations in classical ferromagnetic chains 79−78286
nonuniform Heisenberg chain of spins, two-magnon excitation spectrum *(Russian)* 78−23256
O(n) Heisenberg model close to n=d=2 80−98862
O(N) Heisenberg spin systems, N=2,3,4, and Ising model, strong coupling expansions and phase diagrams 79−71378
one dimensional anisotropic Heisenberg model, spin 1/2, Ising like antiferromag., dynamic correlation function 80−75704
one dimensional classical magnet, energy fluctuations 80−70924
one dimensional uniaxial classical Heisenberg ferromagnet, transfer integral, collective coordinate results for free energy 80−93067
one-dimens. spin 1/2 dimerised, spectra excitations, renormalised group calc. 79−78295
one-dimensional, dynamical behaviour 80−29567
one-dimensional, pure and pseudo, temp. depend. of EPR freqs. 78−6563
one-dimensional, single ion anisotropy, magic angle line width in high temp. limit 77−51870
one-dimensional chain of classical spins with weak anisotropy, thermodynamics 77−43805
one-dimensional classical and quantum chains, spin-Peierls transition theory 77−66375
one-dimensional dilute Heisenberg system, mag. props. 78−64179
one-dimensional disordered spin system with isotropic antiferromag. interaction, susceptibility and Knight shift *(Russian)* 78−88202
Heisenberg model continued
one-dimensional disordered systems, magnetism 80−25152
one-dimensional Heisenberg antiferromag., dynamic struct. factor 79−28497
one-dimensional Heisenberg antiferromagnet, spin wave theory 79−91222
one-dimensional infinite model, ground state representation 77−72967
one-dimensional magnet, classical, nonlinear dynamics 80−71056
one-dimensional magnet, in mag. field, dynamic correlations 80−70926
one-dimensional magnetic models, fluctuations in energy-energy correlation function 79−73726
one-dimensional magnetic system, high-temp. dynamics 79−4716
one-dimensional magnetic system, spin anisotropy and exchange alternation 80−34644
one-magnon states in BCC Heisenberg antiferromag., spectral density near stepped surfaces 80−20396
one-spin ferromagnet, high temp. series expansion for mag. susceptibility and sp. ht. 80−25148
open finite chains, spin levels and effective mag. moments as functions of reduced temp. 77−51868
operator equation, nonlinear differential form, auxiliary constraint 80−65762
operator formulation of renormalisation transformation, sp. ht. and free energy calcs. 77−59376
orbital degeneracy, one dimensional two spin models *(Russian)* 80−54899
ordered Heisenberg ferromagnet/liq. ^{3}He system, mag. Kapitza cond. calc. 79−51415
oxovanadium carboxylates, near one-dimensional antiferromagnetism, thermal and mag. props. calc. 77−20602
paramagnet, 2-spin dynamic autocorrels. and energy diffusion 77−47959
paramagnet, approxs. for Mori continued fraction 77−20529
paramagnet, classical, wavelength-depend. fluctuations in mag. field 80−7069
paramagnet, dil., dynamics at high temp. 77−28355
paramagnet, dil. isotropic, freq. moments of spin-correlation function 78−31037
paramagnet, electronic spin dynamics, NMR 78−76266
paramagnet, exchange bond dilution, freq. moments of spin correl. function 80−50030
paramagnet, high temp., dynamical 4-spin 2-time correl. functions 77−40026
paramagnet, randomly diluted, high temp. series expansion 78−56280
paramagnet, relaxation and response functions, Blume Hubbard approach generalisation 77−51867
paramagnet, site- and bond-diluted, correl. function and susceptibility 77−51869
paramagnet, sixth frequency function of relaxation shape function 78−39348
paramagnet, spin-wave spectrum, of systems without long-range mag. order 79−33450
paramagnet, two-spin Raman scatt. 77−85715
paramagnet, two-spin Raman scatt. at high temp. 77−40225
paramagnet, uniaxial anisotropy, frequency moments of spin correlation function 78−84377
paramagnetic with bond dilution, freq. moments of spin correlation function 79−15272
paramagnets, correlation functions long time behaviour 77−89919
paramagnets, low freq. props., nonlinear Langevin eqn. 78−31038
paramagnons and magnons in quantum Heisenberg model 79−82739
phase transition in Heisenberg model, singular bounds on free energy and susceptibility 78−43595
phase transitions, rigorous existence theorems 79−58649
phase transitions in quantum X-Y and Heisenberg models 80−25141
phenyl alkyl ammonium copper chloride, quasi-two-dimens. Heisenberg ferromag., mag. props. 77−66273
planar, two dimens., renormalisation, vortices, and symmetry breaking perturbations 78−10638
planar classical Heisenberg model, quadrupole phase transition 78−95447
planar classical Heisenberg model with biquadratic interactions, theory 77−72970
plane Heisenberg spin lattice, two-magnon excitations 79−42749
pressure analyticity for Heisenberg and plane rotator model 80−2544
pseudo-one-dimensional Heisenberg system, Neel temp. field depend. 78−68277
pseudoparticle configs. in two-dimens. ferromagnet 77−63058
pyridinium manganese trichloride, pseudo one-dimens. Heisenberg antiferromag., phase diagrams 79−61148
quadratic-layer antiferromagnets, short range order, optical birefr. obs. 79−11318
quadrupolar biquadratic systems, S=3/2, spectrum and damping of elementary excitations 77−36047
quadrupolar-coupled quasi-Heisenberg system, Green's function theory of phase transitions 79−38340
quantum anisotropic antiferromag. Heisenberg model, Gibbs state limitation 80−50027
quantum Heisenberg chain near T=0, exact results 79−78291
quantum mechanics, key to understanding magnetism 79−24125
quantum spin systems, S=1/2, manifestation of frustration effect 80−65767
quantum-classical model, high-temp. series 78−80116
quasi one-dimensional spin lattice coupled system, collective modes 80−24896
quasi-low dimensional spin system, 3-D mag. ordering, randomness effects 78−10710
quasi-one-dimensional, reaction field approx. and dipolar interaction 77−36088
quasi-one-dimensional electron gas with strong on site interactions 77−4306
quasi-one-dimensional electron gas with strong on-site interaction 78−67966
quasi-one-dimensional system, first and second order phase transitions, qualitative theory 78−31086
quasi-one-dimensional systems, spin-lattice Peierls instabilities, static and dynamic aspects 80−71052
quasi-two-dimensional magnet, phase transition at marginal dimensionality 79−38332
quasilow dimensional, small dilution perturbation theory at 0K 78−56281

Heisenberg model continued
quinolinium $(TCNQ)_2$, random exchange Neisenberg antiferromag. chain, intermediate field magnetisation meas. 80−103857
radical reactions, local spin symmetry conservations of biradical species 77−32778
random binary magnetic systems, quenched, Neel temp. calc. 77−89963
random binary system, mag. transition temp. and sp. ht. 77−77065
random chain of classical spins, statistical mechanics 78−10630
random classical, exactly solvable model 77−63057
random exchange Heisenberg antiferromagnetic chain, exchange-coupled pair model 80−20423
random ferromagnetic-antiferromagnetic alloy, elementary excitations 79−8001
random ferromagnetics, thermodynamics, cluster approx. 77−16032
random Heisenberg model for mag. alloys, RKKY type interaction 80−44788
random isotropic dipolar magnet, absence of ferromag. long range order 79−28546
random magnetic bonds, phys. props. near crit. point 78−84440
random mixture of Heisenberg and Ising bonds, singularity 77−59411
random one-dimensional classical Heisenberg magnet, spin dynamics, neutron scatt. cross section 80−60312
randomly dilute, renormalisation group calcs. 80−60321
reaction field approximation for ordered phase 79−61030
relaxation function for Heisenberg chain determ. 77−69474
relaxation-shape function, specific heat series 78−31036
renormalisation group approach to phase diag. 80−4847
renormalisation group equations in critical dynamics, scaling far from equilib. 77−28395
renormalisation group transformation for quantum spins 78−47984
renormalization group approach to two-dimensional XY and Heisenberg spin 1/2 models 79−42727
resistance inequalities for KMS states in isotropic model 77−12077
rutile structure Heisenberg paramagnets, two-spin light scatt. 78−80336
semi-infinite Heisenberg ferromagnet, macroscopic theory of response functions and appl. to light scatt. 80−20410
series expansions, low and high temp., for quantum coupled oscillator systems, or quantum fields on lattice 78−29061
short chains of spin-1 atoms with Heisenberg and biquadratic exchange, eigenstates 77−55652
short-range ordered mag. cluster pinning by localised optical excitation 78−68279
site-disordered spin systems, generalised CPA 77−20513
specific heat, high-temp. expansions, numerical investigation *(German)* 77−59420
specific heat, high-temperature *(Russian)* 80−88757
spin 1/2 particles, config. representation, bit patterns appl. 77−43804
spin $^1/_2$ dilute magnet, crit. props. 80−15733
spin $^1/_2$ system, recursion relations, Migdal renormalisation group approach 80−20368
spin anisotropic Ising-Heisenberg chain, appl. of zero temp. quantum renormalisation group 80−80526
spin chain with easy plane type anisotropy, coupled magnon states *(Russian)* 79−33469
spin chain with nearest and next nearest neighbour interactions 77−47955
spin deviation states in spin-1 system with Heisenberg and biquadratic exchange 78−84378
spin echo, cumulant approach 77−85614
spin glass, calc. 80−60301
spin glass, classical, Monte Carlo calc. of internal energy and sp. ht. 77−20612
spin glass, crit. dynamics, renormalisation group approach 79−91237
spin glass, crit. dynamics 78−60295
spin glass, effective field distrib., time dependent order parameters 77−43843
spin glass, excitation spectra, numerical studies 80−60300
spin glass, five-dimensional, Edwards-Anderson ordering possibility 80−60295
spin glass, Heisenberg mode, RPA approx. 80−65904
spin glass, high temp. series, order-parameter susceptibility 79−15312
spin glass, high-temperature series for order-parameter susceptibility 79−28534
spin glass, mean field theory and ε-expansion 78−10705
spin glass, molecular field approx. *(Russian)* 77−80940
spin glass, Monte Carlo exam. 77−24698
spin glass, quantum effects 80−2581
spin glass, random site, phase diagrams and dimensionality shift 78−52282
spin glass, spin dynamics *(French)* 78−39336
spin glass, spin wave stiffness computer simulation 79−78405
spin glass, two-level systems, evidence for existence 80−15736
spin glass, X-Y and Heisenberg, below four dimensions, vanishing of Edwards-Anderson order parameter 80−60347
spin glass freezing temp., conc., Fermi-momentum depend. 78−14970
spin glass model Hamiltonians, zero temp. spin dynamics 77−85467
spin glass order, isotropic, two-dimens. 77−85455
spin glass phase transitions, instability 78−23285
spin glass state, magnetisation of dil. mag. impurities, molecular field approx. 77−20623
spin glasses, quartic operators in Ising, X-Y, and Heisenberg systems 79−33498
spin glasses, recent developments 78−68264
spin glasses, recent progress in numerical simulation 79−69689
spin glasses, susceptibility, time dependent, rel. to spin self-correlation, Monte Carlo model simulations 79−47290
spin glasses and other glasses, symmetry and topology concepts 79−28541
spin one Heisenberg antiferromagnet, with uniaxial anisotropy, thermodynamic props. 79−56539
spin Peierls transition, gap eqns. 80−24801
spin relaxation, Heisenberg exchange interaction between unlike free radicals 78−84490
spin susceptibility, longitudinal, of Heisenberg ferromagnet, at $T<T_c$ 80−50114
spin system one-dimens., relationship between dynamical spherical model and Heisenberg model 79−69683
spin systems, absence of mag. phase transitions, Hubbard identity calcs. 78−34992
spin systems, model, Monte Carlo simulation appl. 80−20421
Heisenberg model continued
spin systems with three-atom exchange, elementary excitations 78−84404
spin Van der Waals systems, time-dependent correls. 79−61130
spin wave dynamics, low temp. 78−6501
spin wave theory, existence of spontaneous magnetization 79−11281
spin waves *(Dutch)* 79−1663
spin-$^1/_2$ ferromagnets, 1st order Green's function theory 78−72323
spin-Peierls transition, first-order, theory 77−20605
spin-Peierls transition in Heisenberg Hubbard models 78−68242
spin-Peierls transition in mag. field, phonon freq., Heisenberg model calcs. 80−25151
spin-S model, mapped onto interacting Bose field 79−47291
spin-wave spectrum in antiferromagnet Heisenberg 1-dimens. chain, external mag. field effect 77−89943
spontaneous magnetisation in d-dimensional models for $d\geq 2$ 78−72319
square lattice, ground state energy 77−80904
surface magnetisation, size effect 78−15008
susceptibility, dipolar and quadrupolar, Heisenberg-biquadratic and Blume-Emery-Griffiths interactions 78−76257
susceptibility, dipolar and quadrupolar, Heisenberg-biquadratic and Blume-Emery-Griffiths interaction 78−76258
TCNQ alkali salt, spin-Peierls transition, 1-D antiferromag. Heisenberg model 80−29395
TCNQ salt, acridinium $(TCNQ)_2$ low temp. heat capacity, Debye temp. 80−2180
TCNQ salt, K-TCNQ, spin-Peierls system, paramag. susceptibility, Heisenberg chains 79−38299
TCNQ salt, $NMP_{0.63}phenazine_{0.37}TCNQ$, mag. susceptibility, 0.03-4.2K 80−25191
TCNQ salt, pyridine $(TCNQ)_2$, phase transition at 80K investig. and interpret. 78−6530
TCNQ salt, Qn$(TCNQ)_2$, Heisenberg antiferromag. chain for low temp. thermometry and cooling, EPR expts. 79−63217
TCNQ salt, quinolinium, electron spin location, elec., mag., and thermal props. 80−25189
TCNQ salt, quinolinium $(TCNQ)_2$, random-exchange Heisenberg antiferromag. chain, sp. ht., 0.07-5K 78−14976
TCNQ salts, n-methylacridium $(TCNQ)_2$, 2,2'bipyridinium $(TCNQ)_2$ and Qn$(TCNQ)_2$, with asymmetric donors, mag. susceptibility, 0.035-4.2K 80−25190
TCNQ-NMP, disordered, paramag. susceptibility 78−10645
tetramethylammonium copper chloride, S=1/2 Heisenberg 1-dimens. ferromag., mag. props. 79−82766
thermal excitations in Heisenberg-xy systems 80−97047
thermodynamic properties, variational calc. 77−85405
three dimensional, crit. exponents and corrections to scaling 80−7117
three-dimens. quantum Heisenberg model, multi-neighbour interactions ferromagnetic Curie temp. 79−42786
three-dimensional, confluent singularities 77−40022
three-dimensional Heisenberg magnet, dil., static behaviour at finite temps., Monte Carlo calc. 79−73752
TMMC:Cu, random one-dimens. Heisenberg antiferromag., spin fluctuations 79−61140
TMMC, classical Heisenberg antiferromagnet, one-dimens., dynamic props., review 80−15737
TMMC, Cu-substituted, spin dynamics, neutron scatt. cross section 80−60312
TMMC, exchange-narrowed EPR linewidth, temp. depend. 78−52292
TMMC, Heisenberg antiferromagnet, magnetism in one dimension, mag. behaviour 79−28495
TMMC, linear Heisenberg antiferromag., effect of mag. field on 3d ordering and spin correlations 78−68229
TMMC, linear Heisenberg antiferromagnet, EPR half-field transitions 80−15792
TMMC, one dimens. Heisenberg system, shift of half-field EPR line 78−23325
TMMC, one-dimens. Heisenberg magnet, EPR sidebands 78−88163
TMMC, one-dimensional Heisenberg mag., EPR, spin diffusion of 4-spin correl. functions 77−4549
TMMC, symmetry crossover in spin dynamics, proton spin lattice relax. calc. 77−40147
transformation methods in anal. of crit. prop. 78−49771
transition metal layer compounds, mag. model, 0K phase diagram, spin wave spectrum 79−87273
transition metal symmetric clusters, Heisenberg exchange system, ferromagnetic and antiferromagnetic ground states 79−7955
triangular antiferroamgnetic lattice, ground state energy, upper bound determ. using renormalisation 78−76212
trimethylammonium manganese trichloride, Heisenberg antiferromag. chain, specific heat and EPR 80−65931
TTF-bisdithiolene metal complexes, spin Peierls transition 77−4523
TTF-$CuS_4C_4(CF_3)_4$, quasi-one-dimens. antiferromag., spin-lattice dimerisation, X-ray scatt. obs. 77−85464
TTF.CuBDt, spin 1/2 Heisenberg chain, spin-Peierls transition 79−61135
TTFCuBDT, spin-Peierls transition in spin 1/2 Heisenberg chains, RPA calcs. 80−25150
two-dimens. isotropic spin system, phase transition 79−42716
two-dimens. XY magnet and Heisenberg antiferromagnet, ground state anal. 79−42728
two-dimensional, crit. temp. 80−71039
two-dimensional, finite, time-depend. spin-correlation functions 77−12079
two-dimensional, thermodynamics taking into account mag. dipole interaction *(Russian)* 77−32144
two-dimensional classical, Monte Carlo evidence for inhomogeneous states 80−44790
two-dimensional classical Heisenberg magnet, mag. props., Monte Carlo calc. 78−23231
two-dimensional ferromagnet, conformal symm. *(Russian)* 78−23232
two-dimensional ferromagnet, second order phase transition 77−16094
two-dimensional heisenberg ferromagnet, open diffusion effects *(Russian)* 77−32201
two-dimensional Ising system, crossing over to two-dimensional Heisenberg system 80−93123
two-dimensional magnet, glasslike ordering Monte Carlo calcs. 79−82740
two-dimensional spin 1/2 anisotropic, quantum renormalisation approach 77−66348
two-dimensional systems, phase transitions 78−68241

Heisenberg model continued
two-magnon bound states in model with anisotropic biquadratic exchange interaction 77−28356
two-spin systems in mag. field, semiclassical approach 79−65634
two-sublattice biquadratic systems, phase transitions 79−99710
two-sublattice isotropic Heisenberg ferromagnet, impurity localised level theory 79−69471
uniaxial ferromagnet, arbitrary spin and single-ion anisotropy of second order, Green's function 78−84379
uniaxial Heisenberg antiferromagnet, phase diagrams 80−15730
variational localised site cluster expansion, wave function higher ansatze, linear Heisenberg model 79−7959
Yang-Lee edge singularities at high temps. 80−20422
zero point effect in ferrimag. and antiquadrupolar biquadratic systems 79−91201
O^{*}, Heisenberg ferromagnet, spin dynamics, neutron scatt. expts. 77−20619
Ba_2NiF_6, specific heat capacity, critical amplitude, cross-over from 2-D Ising to Heisenberg behaviour 80−39791
$CdCr_2S_4$, Heisenberg ferromag., obs. of dynamic dipolar crossover, ESR linewidths meas. 79−24209
Co_4P, amorphous ferromag., mag. excitations calc. in Heisenberg model 77−1546
Cr complex, trimeric clusters, low temp. mag. props. 78−76261
$CrBr_3$, parametric representation of the equation of state of a Heisenberg system in the critical region 78−79741
$(Cr_4(OH)_6(NH_3)_{12})Cl_6.4H_2O$, exchange interactions in Cr^{3+} clusters, inelastic neutron scatt. obs. and Heisenberg Hamiltonian calc. 79−78359
$Cs_2FeCl_5.H_2O$, mag. phase boundaries, susceptibility, 3D Heisenberg antiferromag. behaviour 78−84420
$CsMnBr_3$, quasi-one-dimens. antiferromagnet, inelastic neutron scatt. 78−14929
$CsMnBr_3.2D_2O$, mag. phase diagram near bicrit. point 79−15302
$CsMnCl_3.2H_2O$, Heisenberg antiferromag., linear mag. birefringence meas. 77−16277
$CsMnCl_3.2H_2O$, spin wave anal. 77−8292
$CsMnCl_3.2H_2O$, thermal cond. in mag. field 80−70481
$CsMn_{1-x}Co_xCl_3.2H_2O$, impure Heisenberg linear chain, EPR meas. 78−43634
$CsMn_{1-x}Cu_xCl_3.2H_2O$, impurities in quasi-one-dimens. Heisenberg systems, anisotropy effect 80−80502
$CsMnF_3$, specific heat, crossover from Heisenberg to XY like behaviour 77−85461
$CsMnX_3.2H_2O$ (X=Cl,Br), pseudo one-dimens. Heisenberg antiferromag., phase diagrams 79−61148
$CsNiCl_3$, nearly one-dimens. antiferromag., mag. sp. ht. determ. 77−24702
$CsNiF_3$, anisotropic Heisenberg chain, nonlinear excitations 80−70927
$CsNiF_3$, double-excitonic optical transition intensity, exchange and dimensionality effects 77−69591
$CsNiF_3$, longit. paramag. susceptibility, reaction field approx. 80−97059
$CsNiF_3$, one-dimensional ferromagnet, optical absorpt. and static spin correlation functions 80−71415
$CsNiF_3$, quasi-1D planar Heisenberg ferromag., thermal renormalisation of sine-Gordon soliton mass 79−54036
$CsNiF_3$, quasi-one-dimens. Heisenberg system, reaction field approx. and dipolar interaction 77−36088
$CsVBr_3$, mag. behaviour of V^{2+} in one- and two-dimens. Heisenberg systems 77−66235
$CsVCl_3$, mag. behaviour of V^{2+} in one- and two-dimens. Heisenberg systems 77−66235
$CsVX_3$, X=Br, Cl, I, mag. props. *(French)* 77−16059
Cu complex, α-CuNSal, one-dimensional $S=^1/_2$ Heisenberg system, nucl. relax. at high temp. 77−85610
Cu complex, chloride monodimethylsulfoxide, spin $^1/_2$ ferromag. Heisenberg linear chain, cryst. struct. and mag. susceptibility 80−15706
Cu complex, chloride tetramethylsulfoxide, spin $^1/_2$ ferromag. Heisenberg linear chain, cryst. struct. and mag. susceptibility 80−15706
Cu complex, dichloro-bis-pyridine copper II, one-dimens. antiferromagnet, dynamic props., review 80−15737
Cu complex, halocuprates, ferromagnetic insulator, two-dimens. Heisenberg layers, mag. susceptibility 80−50068
Cu complex, hexa(pyridine-N-oxide)$(BF_4)_2$, Heisenberg antiferromag., mag. props. and sp. ht. 78−23287
Cu triazole complexes 79−47230
Cu-Mn, spin glass, meas. of order parameter 80−34642
$CuCl_2$, anhydrous paramagnetic phase, mag. susceptibility depend. on temp. 79−7965
$CuCl_2$, finite Heisenberg chain effects, temp. depend. 79−47230
$CuCl.2N(C_5D_5)$, one-dimens. antiferromag., mag. excitation line-shape, field depend., neutron study 79−38314
$CuK_2Cl_4.2H_2O$, Heisenberg ferromag., press. effect on Curie temp. and susceptibility 77−28386
$CuK_2Cl_4.2H_2O$, Heisenberg ferromagnet, spontaneous magnetisation under press. *(Russian)* 77−36058
$CuK_2Cl_4.2H_2O$, Heisenberg ferromag., mag. props. at high press. 77−69512
$CuK_2Cl_4.2H_2O$, Heisenberg ferromag., mag. field effect on susceptibility near crit. point 80−39758
$Cu_{0.98}Mn_{0.02}$, spin glass, Heisenberg mode, RPA approx. 80−65904
Cu_2MnAl, Heusler alloy, spin waves, neutron inelastic scatt. meas., Heisenberg Hamiltonian analysis 77−80921
$Cu(NH_4)_2Br_4.2H_2O$, Heisenberg ferromag. press. effect on Curie temp. and susceptibility 77−28386
$Cu(NH_4)_2Br_4.2H_2O$, Heisenberg ferromag., corrections to scaling in sp. ht. 77−66328
$Cu(NH_4)_2Br_4.2H_2O$, Heisenberg ferromag., mag. props. at high press. 77−69512
$Cu(NH_4)_2Br_4.2H_2O$, Heisenberg ferromagnet, phase transition in mag. field 79−7992
$Cu(NH_3)_4(NO_3)_2$, single cryst., low temp. susceptibility and sp. ht., 10 behaviour 77−89929
$Cu(NO_3)_2.2^1/_2H_2O$, singlet ground state system, mag. props. 80−44850
$Cu(NO_3)_2.2.5H_2O$, linear Heisenberg antiferromag., mag. and thermodynamic props. 79−61136
$Cu(NO_3)_2.2.5H_2O$, linear Heisenberg antiferromag., proton spin-lattice relax. times 79−61257
$Cu(NO_3)_2.2.5H_2O$, single cryst., $S=^1/_2$ alternating linear antiferromag. spin dynamics 79−51793
$CuSO_4.5H_2O$ and related linear chain cpds., mag. ordering in external mag. field, NMR obs. 77−66350
Heisenberg model continued
$CuSO_4.5H_2O$, $S=^1/_2$ antiferromag. Heisenberg chain, spin dynamics 80−11285
$CuSeO_4$, $S=^1/_2$ Heisenberg antiferromag. linear chain, proton spin-lattice relax. 78−39433
EuO, Heisenberg ferromagnet, exchange interactions, neutron scatt. expts. 77−20579
EuO, Heisenberg ferromagnet, static crit. props., neutron scatt. expts. 77−20618
EuO, magnetic susceptibility critical exponent, corrections to scaling 80−103846
EuO(S)(Se)(Te), Heisenberg ferromag. semicond., hyperfine and exchange interactions 77−69530
EuS, Heisenberg ferromagnet, exchange interactions, neutron scatt. expts. 77−20579
EuS, Heisenberg ferromagnet, static crit. props., neutron scatt. expts. 77−20618
EuS, three dimens. Heisenberg ferromagnet, crit. relax. spectra mag. susceptibility 79−8000
$Eu_xSr_{1-x}S$, Heisenberg spin glass system, excitations 80−84610
$Eu_xSr_{1-x}S$, paramag. susceptibility, expt. and comparison with high temp. series expansion 80−60176
Fe_3Pt, ordered ferromagnetic alloy, magnetic excitation obs. 80−70978
FeF_2:Mn, Heisenberg antiferromagnet, impurity thermodynamics, NMR meas. 79−61098
FeF_2:Mn, Heisenberg model, impurity band resonance at 0K, theory 80−66041
$Fe_{1-x}O$, low-energy mag. excitation, spin-wave model 79−4665
$GdVO_4$, antiferromag., US attenuation at 9 GHz 77−24728
^3He, BCC lattice, quadruple exchange in Heisenberg antiferromagnet 77−89616
^3He, solid, magnetism *(Japanese)* 79−19425
HoZn, mag. excitations near spin rot. temp., neutron scatt. study 79−19731
$K_2BaCu(NO_2)_6$, antiferromagnetic Heisenberg spin 1/2 simple quadratic lattice, mag. and caloric meas. 79−78397
K_2CoF_4, specific heat capacity, critical amplitude, cross-over from 2-D Ising to Heisenberg behaviour 80−39791
$K_2CuCl_4.2H_2O$ structure compounds, 3-dimens. ferromag., exchange anisotropy by NMR 77−55714
$K_2CuCl_4.2H_2O$ structures, BCC Heisenberg ferromags., transferred hyperfine interactions of ^1H, ^2D and ^{17}O 77−69725
$KCuF_2$, linear chain Heisenberg antiferromag., nearest neighbour correl. function, birefr. expts. 80−71386
$KCuF_3$, one-dimens. antiferromag., spin waves, neutron scatt. study 80−65848
$KCuF_3$, one-dimensional S=1/2 Heisenberg antiferromag., mag. energy, optical birefringence meas. 78−52467
K_2CuF_4, Curie temp. XY-like anisotropy effect, inter-layer exchange 77−59406
K_2CuF_4, layered, mag. sp. ht., two-dimens. $S^1/_2$ Heisenberg ferromag. behaviour 77−32206
K_2CuF_4, nearly two-dimens. Heisenberg ferromag., renormalised spin wave theory 77−66285
K_2CuF_4, quasi two-dimens. Heisenberg ferromag., spin wave spectrum lineshape, neutron scatt. obs. 77−66286
$K_2Cu_xZn_{1-x}F_4$, two-dimens. ferromag., spin correls. near percolation limit 80−44840
$KM_{n_x}Mg_{1-x}F_3$, randomly diluted Heisenberg paramag. nucl. relax. 80−60444
$KMnF_3$, specific heat near Neel temp. *(Russian)* 80−100340
K_2MnF_4, specific heat capacity, critical amplitude, cross-over from 2-D Ising to Heisenberg behaviour 80−39791
K_2MnF_4, two dimens. Heisenberg system, shift of half-field EPR line 78−23325
$K_3Mn_2F_7$, antiferromagnet, two magnon Raman scatt., magnon dispersion nearest neighbour exchange 78−15164
$K_3Mn_2F_7$, double-layer antiferromag., mag. prop. meas. and calc. 77−55666
$K_3Mn_2F_7$, quadratic double-layer Heisenberg antiferromagnet, sublattice magnetis., NMR obs. 77−66270
$K_3Mn_3F_7$, Heisenberg double-layer antiferromag., neutron scatt. 79−61065
$K_2Mn_{1-x}Ni_xF_4$, antiferromagnets, impurity associated and host magnetizations, NMR exam. 78−10800
$KMn_xZn_{1-x}F_4$, three dimens. Heisenberg antiferromag., fluctuations near percolation threshold 79−78390
$KNiF_3$, and K_2NiF_4, double-excitonic optical transition intensity, exchange and dimensionality effects 77−69591
$KNiF_3$, isotropic antiferromag., crossover behaviour of mag. phase boundaries 79−78370
$KNiF_3$:Mn^{2+}, isotropic Heisenberg ferromagnet, localised spin-wave modes, biquadratic exchange effects 77−51896
K_2NiF_4, specific heat capacity, critical amplitude, cross-over from 2-D Ising to Heisenberg behaviour 80−39791
$K_2PbCu(NO_2)_6$, antiferromagnetic Heisenberg linear spin 1/2 chain, mag. and caloric meas. 79−78397
$Li_{0.13}Fe_{2.87}O_4$, acoustic spin wave dispersion branch, exchange const., neutron scatt. study 79−47266
Mn complex, manganese (II)(1,2,4-triazole)$_2$(NCS)$_2$, 2-dimens. Heisenberg antiferromag., mag. props. 78−72336
Mn complex, $Mn(SCN)_2(C_2H_5OH)_2$, two-dimens. Heisenberg magnet, cryst. struct. and mag. props. 79−60337
$MnBr_2.4H_2O$, high-resolution sp. ht. meas. near Neel temp. 77−28393
MnF_2, specific heat, Heisenberg to Ising crossover near Neel temp. 78−47980
MnF_2, uniaxial antiferromag. anisotropy in paramag. susceptibility, cluster variation theory 78−52200
$Mn(Nb_{0.5}Ta_{0.5})_2O_6$, spin flop magnet, four dimens. phase diagram and multicrit. phenomena 79−15304
MnP, ferro-spiral transition, neutron scatt. studies 80−65876
$Mn_{1-c}Zn_cF_2$, Heisenberg antiferromag., linear mag. birefringence meas. 77−16277
$Mn_{1-x}Zn_xF_2$, randomly diluted uniaxial antiferromagnet, CPA theory 79−78388
$Mn_xZn_{1-x}F_2$, three dimens. Heisenberg-Ising antiferromag., fluctuations near percolation threshold 79−78390
$N_2H_6FeF_5$, one-dimens. antiferromagnetism 77−66444
$NdAl_2$, mag. excitations, cubic cryst. field and isotropic Heisenberg exchange models 77−63154
Ni, critical exponent meas. by PAC in Ni-^{100}Rh 77−20774

Heisenberg model continued
O, solid, magnetic props. theory for Heisenberg system *(Russian)* 80−54900
Rb_2CuCl_4, layered, mag. sp. ht., two-dimens. $S^1/_2$ Heisenberg ferromag. behaviour 77−32206
$Rb_2CuCl_4.2H_2O$, BCC Heisenberg ferromag., transferred hyperfine interactions of ^1H, ^1D and ^{17}O 77−69725
$RbMnCl_3$, specific heat near Neel temp. *(Russian)* 80−100340
Rb_2MnCl_4, Heisenberg antiferromag., spin wave anal. 79−61237
$RbMnF_3$, Heisenberg antiferromagnet, paramag. region, NMR, spin pair correl. 78−15032
$RbMnF_3$, Heisenberg antiferromagnet, spin diffusion below T_N 78−34968
$RbMnF_3$, isotropic antiferromag., crossover behaviour of mag. phase boundaries 79−78370
$Rb_3Mn_2F_7$, double-layer antiferromag., mag. prop. meas. and calc. 77−55666
$Rb_2Mn_xMg_{1-x}F_4$, two-dimens. antiferromag., spin fluctuations, neutron diffr. study 80−44846
$Rb_2Mn_xMg_{1-x}F_4$, two dimens. Heisenberg-Ising antiferromag., fluctuations near percolation threshold 79−78390
$RbNiF_3$ spin lattice, susceptibility, Heisenberg model *(Russian)* 80−65893
Rb_2NiF_4, specific heat capacity, critical amplitude, cross-over from 2-D Ising to Heisenberg behaviour 80−39791
$RbVCl_3$, mag. props. *(French)* 77−16059
$Tb_{0.5}Ho_{0.5}$, ferromag. and helical phase, spin wave dispersion relations 79−24149
$TlMnCl_3$, specific heat near Neel temp. *(Russian)* 80−100340
U complex, UCl_4.3DMBA(.3MAA), mag. exchange interaction 79−78303
U_2N_2Te, and related cpds., crit. behaviour 78−43605
UO_2, spin wave spectrum, mag. susceptibility, sp. ht. *(Russian)* 79−33470
V_3O_5, spin order, one-dimensional, Neel transition 80−39799

Heising modulation *see amplitude modulation*

helical dislocations *see screw dislocations*

helicity (elementary particles)
$^3P_0$ generalised model, reln. to Melosh transform. 78−12885
γ^5-invariant eqns. for massive particle 78−29262
chiral invariance for asymptotic momenta, elastic scatt. of hadrons, helicity amplitudes 78−4800
Chou-Yang model and s-channel helicity conservation 79−63449
crossing relations derivation using substitution rule 79−67483
diffractive dissociation kinematic polarisation of large-mass final states, helicity violation 77−82723
Dirac charge Ze particle scatt. by mag. monopole, helicity amplitudes 77−65123
dispersion sum rules for Reggeon-particle scatt. 78−54583
dual models, spin in spectrum of states, helicity partition functions 77−38137
dual strings, functional integrals for partition functions 77−67628
dual-resonance model, M-loop amplitudes for excited states 78−50019
electromagnetic contrib. to NN interaction, one photon exchange helicity amplitudes 78−17040
G_1, spin depend. struct. function, scaling violations 78−93880
gauge model of weak and electromag. interactions, polarised lepton scatt. 78−45901
hadron-hadron high energy collisions, EM-hadronic interference, spin depend. phenomena 79−422
heavy lepton, helicity calculations for prod. in ν interactions and cascade decay 78−93870
inclusive lepton pair prod., invariated helicity struct. funcions anal. 79−13172
isolation of definite naturality exchanges: the general solution 80−101954
Lorentz transform, circular polarised EM evanescent wave 78−32696
meson diffraction dissociation and helicity conservation, Deck model description 77−38153
multiparticle amplitudes, s-channel helicity conservation 78−33004
N resonance electroproduction, helicity structure and quark motion effect 78−398
non-Abelian gauge theories, Born helicity amplitudes and cross-sections 77−2777
nonrelativistic free particle, half integral or integral helicity particles by canonical quantisation 79−6020
partial wave analysis for supersymm. scatt. amplitudes 77−49872
Poincare generators corresponding to lightlike irreducible unitarity representations 77−18193
Poincare group, irreducible unitary representation, velocity operator 78−32713
polarisation theorem for diffractive excitation at large momentum transfer, favoured helicities 77−71497
pomeron flip-non-flip interference term in elastic polarisation, s-channel helicity 78−50021
Pomeron-nucleon-nucleon vertex, helicity struct. using multiperipheral model 77−57511
production processes on nuclei, helicity-flip anal. 77−82797
pseudoscalar transition between spin-J and spin 5/2 baryon 78−50032
QCD of large-p_T hadron prod., helicity of quarks and gluons 78−50057
quark fragmentation in P conserving jet production reactions, spin observables 79−71658
s-channel helicity conservation at $\gamma V,\gamma\gamma$ and NN vertices, vanishing of spin-zero covariant coupling 79−40691
s-channel helicity conservation in multiparticle amplitudes, Pomeron exchange 77−87922
s-channel resonance prod. in πN scatt., amplitude zeros in Mandelstam plane 80−73686
S-matrix amplitude props. in supersymm. theories, helicity conservation law 77−67582
semileptonic decay of charmed particles, formalism using helicity amplitudes 78−4852
spin-1 polarisation, helicity formalism, treatment by extension of spin-$^1/_2$ case 79−63383
SU(2), unification of isospin and hypercharge, electroweak interactions of leptons 80−27439
$SU(3)\times U(1)$ gauge theory, electro-weak interaction, helicity mixed representation 80−78013
supergravity, global supersymmetry transformations of noninteracting massless particles 80−95015

helicity continued
two particle helicity amplitude unitarity for arbitrary spin 77−54058
unitarity restrictions on meson-nucleon helicity-flip amplitudes and slope of the diffraction peak 79−54348
Yang-Mills instanton in Taub-NUT space 79−2691
Zweig suppressed decay of heavy 1^{--} vector mesons, helicity amplitudes 78−54616
d target at high energy, helicity struct. of unstable particle scatt. amplitude 78−45929
$e^+e^-\rightarrow VX$, polarization states of produced vector meson *(Russian)* 78−25058
γ circular polarisation, neutral current effect in bremsstrahlung and pair production 80−73655
$\gamma d\rightarrow pn$, 250 to 800 MeV, model using $\gamma N\rightarrow N\pi$ helicity amplitudes 80−78081
$\gamma\gamma$ collision, deep inelastic, helicity method 80−22606
$\gamma N\rightarrow N\pi$ helicity amplitude, used in model for $\gamma d\rightarrow pn$ 80−78081
$\gamma\rho$-Pomeron-Regge vertex function, spin depend. calc., multiperipheral model 78−82223
Kp meson diffr. dissociation, Deck model and helicity conservation 77−30344
$K^-p\rightarrow\pi^-Y^*(1385)$, 11.5 GeV/c, confirmation of exchange degeneracy predictions in line reversed reacts. 78−82247
Λ helicity meas. in $\Xi^0\rightarrow\Lambda\pi^0$ 78−93878
μ beam, polarised, variable helicity for parity nonconservation studies 77−6598
N-N* EM transition form factors 77−22735
$nd\rightarrow p\pi d$, interference phenomena in coherent production, nucleon diffractive amps., helicity-flip 80−47329
NN I=1 amplitudes struct. at 6 GeV/c 78−70395
$NN\rightarrow NN$, large momentum transfer, spin effects 80−22577
$NN\pi$ amplitudes, parity violating, QCD calc. in Weinberg-Salam model and SU(4) flavour symmetry breaking 79−67520
$N\pi\rightarrow N^*\pi$, Gribov-Morrison rule as kinematic effect 77−49999
ν, massless, left-right symmetric gauge models, $SU_{2,L}\times SU_{2,R}\times U_1$ 80−27461
$\nu(\bar{\nu})$ d, disintegration reactions, helicity flipping neutral currents, tensor coupling 77−49944
$\nu\rightleftharpoons\bar{\nu}$ oscillations, conditions for observation 79−17636
νe elastic scatt., spin correls., allowance for (S,T,P) interactions of neutral and charged currents 78−12901
p-H_2O 6 GeV/c scatt. with polarised protons, helicity-depend. and P-violation 77−30403
$pd\rightarrow p\pi^-\pi^-d$, interference phenomena in coherent production, nucleon diffractive amps., helicity-flip 80−47329
$p\gamma$, Compton scattering, 375 to 1150 MeV, differential cross section 80−57604
pp elastic scatt., ISR energies, spin behaviour of ang. distribs. at large momentum transfer *(Russian)* 79−80849
pp helicity amplitudes at t=0, dispersion theoretic anal. 78−62340
pp inelastic scatt., cross sections for opposite helicities, parity violation 78−62435
pp total cross-section difference of pure helicity states, 2100 to 2500 MeV, obs. of structs. 78−78206
$\pi N\rightarrow(\rho,\Omega)N$, Regge model with derivative relations between S-channel helicity amplitudes 77−74713
$\pi p\rightarrow(\rho\pi)p$, diffr. dissociation, Deck model and helicity conservation 77−30344
$\pi^-p\rightarrow\eta^0n$, 3.3 GeV/c, differential cross section, helicity-flip amplitude *(Russian)* 78−45945
$\pi^-p\rightarrow\pi^0X$, helicity non-flip amplitude in phase modified absorpt. model 77−79288
$\pi^-p\rightarrow\pi^0n$, charge exchange polarisation, Gribov Reggeon calculus, derivative rule, absorpt. model alternative 77−46076
$\pi^-p\rightarrow\pi^0n$, helicity nonflip amplitude in Reggeon calculus 77−22765
$\pi^+p\rightarrow K^+Y^*(1385)$, 11.5 GeV/c confirmation of exchange degeneracy predictions in line reversed reacts. 78−82247
$\pi\pi\rightarrow\bar{N}N$, helicity amplitude, extrapolation of $S^{I=0}$-wave 80−91112
ψ photoprod. and helicity conservation from $\psi\rightarrow l^+l^-$ ang. distrib. 77−18297
τ^+ as a paraelectron, daughter lepton helicities 78−50024

helicons
see also solid-state plasma
electron-hole plasma, strongly degenerate, helical density waves 80−15550
ferromagnetic semicond., spin-helicon wave parametric amplification 79−69665
ferromagnetic semiconductors with hot electrons, instability of coupled spin-helical waves 80−107841
gyrorelaxation damping and excitation 77−72877
LF, excitation and amplification by HF helicoidal wave in medium with degenerate carriers 78−14755
magnetic semiconductor, helicon wave propag., hyperfine interaction effect 80−80307
metal, diamag. domain, helicon attenuation *(Russian)* 78−10721
metal, EM props., general lecture 78−26901
metal, helicon-phonon interaction for parallel wave propagation 78−64054
monopolar crystals, quasi-helicon waves instability 80−70741
narrow band gap semiconductors effects, review 79−95437
narrow-band semiconductors, current-carrier conc. distrib. nonuniformity, contactless meas. 77−76853
narrow-gap semiconductors, microwave effects, review 79−82618
nonlinear interaction with ion-acoustic waves, in turbulent reson. plasma *(Russian)* 79−55488
packet propag. in static mag. field, three-dimens. self-localisation *(Russian)* 79−15176
piezoelectric semiconductor, acoustohelicon waves, parametric excitation 79−38135
piezoelectric semiconductor, stimulated Brillouin scatt. of helicon waves 79−99571
piezoelectric semiconductor-plasma, parametric excitation of helicon and acoustic waves 80−107837
polar semiconductor, TO phonon-helicon coupling 79−73539
semiconductor, excitation and amplification of weak helical waves by strong waves in strong mag. field 78−19077
semiconductor, helicon damping in quantum limit 77−28205
semiconductor, helicon propag., nonlinear effects 77−66180
semiconductor, intrinsic, helicon nonlinear propag. 77−4385

helicons continued
semiconductor, nonlinear propag. of low freq. helical waves, for weak ellipticity of incident wave polarisation 77−62958
semiconductor, surface helicon waves in Faraday geometry, existence 80−44703
semiconductor plasma, surface helicons, theory 80−60019
semiconductor thin film quasistatic and helicon wave propagation 79−56338
semiconductors with negative differential conductance, surface EM wave excitation, helicon and Alfven waves 79−69543
shear waves, rotary activity under helicon-phonon interaction 80−2412
soliton formation in plasma, acoustic wave emission, interactions 77−7537
A, magnetoresistance, field strength function, electrodeless methods 79−91026
Al, nonlinear helicon resonance *(Russian)* 77−28208
Al, with diamag. domains, helicon attenuation below 1K *(Russian)* 77−85254
Bi, Hall effect and helicon reson. at high mag. fields 79−60861
Bi single crystals, helical wave instability, spatial amplification regime 77−24580
$Bi_{1-x}Sb_x$, lattice dielec. const. from helicon wave propag. 77−47756
$Bi_{100-x}Sb_x$, lattice dielec. const. meas. 78−10490
$Bi_{88}Sb_{12}Te_{0.05}$, helicon dispersion, effect of slope of electron ellipsoids 79−28365
$Cd_xHg_{1-x}Te$ solid solns., dimensional resonances of HF helicons, band struct. and electron mobility 77−47846
Cu, with diamag. domains, helicon attenuation below 1K *(Russian)* 77−85254
n-GaAs, two-valley semicond., helicon wave instability 77−47842
Ge, oscillistor effect in strong mag. fields, ambipolar drift and breakdown 78−2511
$Hg_{1-x}Mn_xTe$, microwave helicon propag. and helicon excited EPR 77−43637
In, helicon resonance acoustic satellites, flexural acoustic wave spectrum *(Russian)* 80−2415
In, intermediate state, single cryst., helicon dispersion law and damping *(Russian)* 77−12066
n-In-Sb, polar semicond., TO phonon-helicon coupling, Doppler shifted cyclotron reson. region 79−73539
InSb, helicon beam form. during microwave transmission in mag. field 80−80308
InSb, helicon damping in quantum limit 77−28205
n-InSb, helicon wave propag., quantum mechanical features 79−42571
n-InSb, helicons, parametric decay 80−34472
n-InSb, high power helicon, interaction with semiconductor-free space interface 79−38114
n-InSb, high power helicons, harmonic generation 80−29426
n-InSb, longitudinally magnetized, laser beam modulational instability, phonon-helicon interaction 79−56254
n-InSb, microwave magnetoplasma and heliconlike reson., sample shape effects 77−85252
InSb, periodically doped cryst. prod. by Peltier effect, helicon diagnostics *(German)* 77−48338
n-InSb piezoelectric semiconductors, carrier temp. effect on transverse phonon-helicon interaction 77−15886
n-InSb powder, microwave propag., 90-300K, magnetoplasma and helicon wave excitations 78−72183
n-InSb, propagation of high power helicons 78−19070
n-InSb, quasi-helicon waves instability 80−70741
InSb:Te, periodically laminated plasma, 56.5 GHz transmission, helicon diagrams *(German)* 77−20348
K, bound spin-helicon wave excitation, reson. refl. coeff. 79−95435
K, helicon-phonon interaction 79−4379
K, helicon-phonon interaction, numerical study 79−46758
K, helicon-phonon interaction for oblique propagation, dispersion relation 80−49315
Na, bound spin-helicon wave excitation, reson. refl. coeff. 79−95435
Ni plate, thin, helicon-Doppleron effect on spin wave prop. 77−66394
$Pb_{0.84}Sn_{0.16}Te$ single cryst., anelastic relax., helicon wave dispersion *(Russian)* 77−51437
$Pb_{1-x}Sn_xTe$ solid solution, electron scatt. by charged Te vacancies 77−69328
PbTe, lattice permittivity determ. by magnetoplasma waves method 78−19075
Tl, nonlinear helicon resonance due to open-orbit conduction 80−2324

helicopters
acoustic noise and flight condition investigations 80−19193
aeroelastic stability of complete rotors in forward teetering flight 78−5677
aviation medicine, conf., Fort Rucher, USA (May 1978) 79−79664
blade aerodynamics, lifting line concept appl. to blade computation *(French)* 79−77163
environmental noise impact obs. and evaluation 80−104539
helicopter impulsive acoustic noise signature recording in flight 78−9477
icing problems, role of meteorology 78−85657
interior noise control 80−14519
mobile incubator transport for premature and newborn babies *(German)* 79−16336
multibladed rotor flutter, effect of phase angle 77−7333
noise level meas., development of proposed impulse correction 80−96107
pilot's seat structure, vibrational response 77−31246
rotational noise, wind tunnel meas. 77−19501
rotor, nonlinear mathematical simulation of unsteady flow past rotor 79−86442
rotor blades, radiation characts. of acoustic sources in circular motion 77−23803
rotor noise, Mach number scaling law correction 79−72753
rotor noise, simplified Mach number scaling law 78−83167
rotors, sound radiation props. for free field and near absorptive plane surface 80−102885

heliotron *see plasma devices*

heliports *see airports*

helium
see also nuclei with .....
see also helium atoms; helium films; liquid helium; solid helium
2^1S state, two-photon ionisation, multipole interference 79−22675
2^3S_1 metastable state electron impact excitation differential cross section meas. 79−10210
108-76°1, new halo planetary nebula, He content rel. to primordial He abundance 77−45510
^3He-^{20}Ne stabilised transverse Zeeman laser, tuning characts., freq. fluctuation 80−48273
absorption in neutron irradiated austenitic steel 77−51414
absorption in UO_2 pressurised rods during irradiation 80−37454
abundance, cosmic, influence of time-varying gravit. const. 79−92667
abundance enhancement in planetary nebulae 78−93376
abundance in chaotic Friedmannian Universe 80−67920
abundance in galactic globular star clusters 78−45370
abundance in solar quiescent prominences, theoretical models 78−49405
abundance in stellar atmospheres in O-associations and young clusters *(Russian)* 77−64815
abundance var. in galactic globular clusters 80−56894
adsorbed ^3He layers on Grafoil, interlayer exchange 77−72736
adsorbed ^3He on graphite, sp. ht. 78−87842
adsorbed ^4He on Vycor glass, superfluid transition 77−72737
adsorbed on α-cyclodextrin surface, effects on positron annihilation 79−65952
adsorbed on graphite, band struct. and thermodynamic props. 80−80349
adsorbed on graphite, surface band splitting, theory 80−60058
adsorbed on Ne-plated graphite, single particle and liquid state props. 77−72738
adsorbed on W, accommodation coeffs. calcs. 80−66866
adsorption by NaF, effect on intensity of diffr. atomic beam 77−12480
adsorption on graphite (0001), selective, level crossings 80−71556
adsorption on LiF, band struct. effects 79−73402
adsorption on LiF (001), theory of selective adsorpt., azimuthal and polar dependent intensities 79−60624
adsorption on LiH, ab initio calc. 78−38952
adsorption on metal, interaction energy, quantum mech. density functional formalism calc., comp. with expt. 78−67911
adsorption on metal surface, HF calc. of repulsive pot. contrib. 77−43434
adsorption on metal surfaces, density functional approach 77−85061
adsorption on SiO_2 rel. to EPR relax. time *(German)* 79−95645
adsorption on W, potential of He atom above field adsorbed He or Ne atoms 78−35267
aerodynamic isotope separation technique based on vel. slip in freejet expansions 80−19441
afterglow, electron energy distrib., radial variation 78−71570
afterglow, electron energy distrib. and collisions during decay, peculiarities 78−63621
afterglow, intermediate press., plasma discharge parameter time depend. calc. 79−19102
afterglow, Rydberg states collisional radiative transfer, He^+ electronic recombination 77−62401
afterglow magnetoplasma, low-press, weakly-ionised acoustic wave generation 80−44059
afterglow of low-pressure glow discharge, recombination processes 78−26366
afterglow of pulsed discharge, elec. and optical meas. 78−26329
afterglow plasma, $He(2^3S_1)+e \rightarrow He(1^1S_0)+e+KE$, rate const., electron energy distrib. 78−71571
afterglow plasma, interaction with glass, Cu, steel walls, calorimetric method obs. 78−14177
air-He binary mixtures, flowing, probe for conc. meas. 79−4098
anode sheath, crossed field low press. discharge in magnetron and Penning cell 77−11432
Ap stars He abundance anomalies, role of radiative forces in stellar atmospheres 80−31291
asymptotic interaction with graphite surface 79−99429
atmosphere effect on long-term strength of stainless steel 79−24662
atom, 2^3S_1 metastable state, interactions, optical pumping investig. 80−23377
atom, 4^3D_J, ^3F-2^3P line struct., in low-press. linear discharge 79−14523
atom+H^+, ang. and energy distrib. of ejected electrons 79−31668
atom-atom collision with Rb, disorientation cross-section temp. depend. 77−23546
atoms, low energy positron scattering 79−89786
backscattering from solid surfaces, positive charge fractions 80−66375
beam charge fraction, emerging from solid 80−9716
beam-plasma discharge, optical radiation polarisation 78−67478
blister formation in irrad. Mo, vacancy mutation to divacancies by He trapping 78−51601
blistering at high irradiation doses on austenite steel and Cr-Ni alloys 79−51167
blistering of Nb, large swelling meas., gas press. model 80−88218
boiling in tubes, heat transfer, cryogenic stabilisation 78−30162
bombardment, simultaneous with He, H_2, heavy ions to simulate microstruct. damage from fission or fusion neutrons 79−46723
bubble alignment in α-irrad. Al foils during deform. 80−107345
bubble behaviour in cold worked neutron irrad. Al-Li alloys 77−54359
bubble evolution tracing by positron annihilation in He injected Al 77−19992
bubble formation in V binary and ternary alloys irrad. by 4 MeV Ni^{++} 80−29085
bubble growth in austenitic stainless steel, tensile stress effect 79−87684
bubble growth mech. in α-particle bombarded Al 77−7774
bubbles, and voids, with ringed images in Nb-Zr (1%), TEM and SEM 78−51529
bubbles, embrittlement of austenitic stainless steel irradiated with α-particles 77−69015
bubbles growth in Nb-Zr (1 wt.%), α-particle effects 78−67749
bubbles in Al, behaviour during high plastic deform. 80−29087
bubbles in Al, TEM obs. 77−4132
bubbles in UT_3 produced by triton decay, distribution determ. by NMR 78−19360
cascade ionisation by strong microwave field at low press. *(Russian)* 79−98854
cavity depth distribution in 20 and 500 keV $^4He^+$ irrad. Ni 80−107346
channelling in W, calc. 80−34108
chaotic phenomena and statistical physics, review of the contributions made by J. Schwinger 79−63135
chemisorption on Pd(111) surface, mol. beam scatt. expts. 78−79878
chloroform-He gaseous compressed mixture, mol. reorientation, Raman spectra 80−23422
chloropentafluoroethane-He, multiphoton dissoc., ^{13}C enrichment factor, CO_2 laser wavelength and fluence depend. 80−58331

helium continued
Clausius-Mossotti function, exam. of variation with gas density 78−52418
Clausius-Mossotti second virial coefficient 80−79426
clustering of atoms at $^{1}/_{2}\langle 111\rangle\{110\}$ edge dislocation in α-Fe 78−2154
colar corona, He abundance determ. from He^{+} 304 Å radiation 77−91510
collisional excitation transfer for $3^{1,3}P$ and D states 80−106387
Compton profile asymmetry, high momentum transfer, calc. *(French)* 78−42013
concentration profiles meas., using $^{4}He(^{7}Li,\gamma)^{11}B$ reson. reaction at 1.68 MeV incident energy 79−5200
condensation forevacuum pump 78−86282
condensed spark discharge, integrated luminosity, pulsed longit. mag. field 77−76233
constricted glow discharge, space charge double layer influence obs. 78−67492
continuum radiation emission obs. to near vacuum UV 78−71582
convection, natural, in confined region between two horizontal ducts for variable fluid properties 79−23321
coolant, with graphite suspension, high-temp. power plant efficiency enhancement *(Russian)* 79−68549
cooling system, for fusion reactor molten salt hybrid blanket 78−62614
cooling system large, review of hydrodynamics and heat transfer 79−204
cosmic abundance, enrichment during galactic chemical evolution 77−22208
cosmological abundance, rel. to number of neutrino species and Universe lepton number 80−8730
critical potentials measurements, student expt. 80−12874
cryogenerator cooling appl., system selection and efficiency *(French)* 77−26305
cryogenic discharge, current oscills. 78−67463
cryogenic free-precession ^{3}He magnetometer using a SQUID 79−6153
cryogenic plasma, recombination decay *(Russian)* 79−4104
cryogenic pumping speed of Excalibur CVV2008 liq. He cryosorption pump 79−80633
cryogenic rotating rig for research applied to superconductive alternators with rotating field windings 79−58719
cryopumps, close-loop, design, appl. 79−26062
cryosorption pumping characts. of condensed CO_2 layers, thermal spike effects 79−80635
cryosorption pumping of He by charcoal, cryopump design for fusion reactor 80−105654
cryostat, He cooled closed cycle, for accelerator based radiation damage studies 77−41622
cryostat, rotating, centrifugal field rel. to residual press. in vac. cavity 80−42232
crysorption, pumping at 4.2K by type 5A molecular sieve 78−17422
CTR cryosorption vac. pumping of D, H and He at 4.2K 77−50298
cyclotron resonant laser induced breakdown obs. 77−39499
DC discharge electron free streaming wave propagation obs. 78−75314
deep-sea basalts, He and Xe as measure of magmatic differentiation 80−31040
dense gas, positive ion excess, ion-induced droplets 79−14925
dense gas, semi-empirical eqn. of state and compressibility factors 77−7499
dense gas, transport eqns., shear viscosity and acoustic vel., quasi-particle kinetic eqn. calcs. 80−53906
depolarised light scattering, collision induced 80−14118
depth distribution meas. in Nb 77−30665
desorption by Mo(110) cryst., during stage III annealing, vacancy model 77−1123
desorption from $Co_{56}Ga_{44}$, under electron beam heating 77−31881
desorption from Mo, derivation of Born-Mayer interaction potentials 79−99409
desorption from Mo, Mo-He and He-He interaction pots. 79−19459
dibutyl sebacate diffusivity, from aerosol drop evap. obs. 79−43639
dielectric breakdown across epoxy insulation 78−62658
dielectric constant gas thermometry, 4-27K, and eqn. of state 79−63222
diffusion and solubility in PTFE 80−6561
diffusion in Li_2O-B_2O_3-SiO_2 glass systems, phase separation effect 78−26734
diffusion in RbCl, isotope effects 78−18841
diffusion of methane, coeff. determ., gas chromatography method 77−11298
dimer, electron-beam pumped, anal. of feasibility of stimulated vacuum UV radiation 80−9857
discharge, atmospheric press., for microwave plasma spectrometry 79−16052
discharge, Blumlein-type transverse fast, voltage meas discharges (electric) 80−19642
discharge, cathode spot shape and kinetics, cathode photoeffect from discharge UV irradiation 80−38836
discharge, EM fields near antenna, probe diagnostics 77−24095
discharge, He II resonance radiation intensity, He gas press. depend. 77−84553
discharge, HF asymmetrical, mag. field effect on ionis. freq. *(Russian)* 78−26371
discharge, high-pressure, rapid formation of He_2 a $^{3}\Sigma_u^{+}$ and $b^{3}\pi_g$ molecules 79−37571
discharge, hollow-cathode, partially ionised plasma diagnostics by electron beam scatt. 80−28824
discharge, hollow-cathode, radiation signals in weak mag. field 78−70789
discharge, hollow-cathode type, spectroscopic obs., laser light source appl. 80−59335
discharge, level populations, time resolved spectra 77−80391
discharge, low pressure, line spectrum, mol. transisions effects 79−60212
discharge, luminescent, electrons energy distribution function evaluation, by Monte-Carlo type simulation *(French)* 77−19795
discharge, medium press., contraction mechanism, inhomogeneous heating 80−44024
discharge, modulated positive column, elec. and optical props. 77−27765
discharge, multi-channel, in inhomogeneous field, at 1 to 5 atm *(Russian)* 77−89335
discharge, positive column, axial electric field in transverse mag. field 78−55766
discharge, probe meas. of plasma props. 77−47292
discharge, RF, plasma parameters and volt-ampere characts., two discharge regimes 80−44016
discharge, RF induction breakdown, diffusion theory 77−84562
helium continued
discharge, Tesla coil type, temp. diagnostics from OH A→X intensity meas. 79−64939
discharge, three-body electron attachment to O_2 80−24245
discharge, time-resolved population meas. with N_2-laser-pumped dye lasers 77−80362
discharge, VUV continuum kinetics 79−94827
discharge lamp, low press., reson. line broadening of O I and N I 78−9123
discharge lamp, unbacked Al windows as part of Cu seal between UHV flanges 79−97397
discharge lamp, UV, monochromated, addition to XPS spectrometer 78−89601
discharge plasma, dynamical studies, pulse repetition rates effects 77−62397
discharges, fast electron energy distrib. in positive column and negative glow 80−38764
dishcharge, nanosecond, in weakly ionised plasma, existence of two phases 80−24277
30 Doradus nebular complex, He/H abundance ratio 80−62226
duoplasmatron arc, ionisation meas., line intensity ratios 80−54060
Earth composition, He incorporated from immature Sun *(Russian)* 80−81856
Earth concentration, survey in S.India for structural mapping, water sample obs. 80−8261
earthquake, precursory soil He changes, He diurnal variation limitation 80−94469
electric breakdown, Paschen curve *(French, English)* 77−76221
electric breakdown voltage, 300-2100K *(Russian)* 78−51370
electric discharge, pulsed, high-current, diagnostics and nonequilib. state 79−64942
electric discharge structures in pure He and Ar gas 77−31541
electron distribution function relaxation in high freq. gas breakdown *(Russian)* 80−14957
electron drift velocity, density dependence, high press., quantum mech. theory 79−1285
electron impact excitation, 2nd order pots. method calcs. 78−13608
electron impact excitation of $2^{1}P$ state, eikonal-Born series approx. 78−17799
electron localisation, mobility in dense low temp. gas 80−92247
electron mobility, anomalous density and temp. depend. at low temp. 78−75253
electron radial diff. coeff. to mobility ratio 77−19666
electron scattering, resonance at 19.34 eV at angles of 23, 60 and 90° 80−22481
electron transmission factor numerical determination 80−10350
embrittlement of metals, high temp. embrittlement model 79−83320
energetic radiation belt ions obs. at geomag. equator during quiet conditions 78−88999
enrichment in planetary nebulae 79−21380
enrichment in planetary nebulae 79−35326
equations of state, 3.3 to 14K *(Russian)* 78−83912
evaporation cryostats for expts. in solid-state physics, 5K to 320K 79−58708
exhaled, Schlieren photography of exhaled air, detection of abnormal nasal escape 80−64145
exospheres of Mercury and Venus, He atoms vel. distrib. Monte Carlo simulation 80−67588
F ions recoiling in gases, hyperfine interactions 78−74735
fast electron retardation, ionisation cascade, degradation spectra, anal. *(Russian)* 79−27741
field adsorption on W (111), array model 80−59800
field desorption and field ionisation on metal surface 80−104047
field-theory renormalization and critical dynamics above T_c: helium, antiferromagnets, and liquid-gas systems 78−87767
film, dilute two dimensional interacting quantum fluids 79−1538
fission gas release from UO_2-Zr high burnup nuclear fuel rods 80−57846
flow, alkali metal vap. condensation, heat and mass transfer 78−75192
flow, of liq.-vap. mixture, frictional press. drop, adiabatic and heated conditions 78−90983
flow and heat transfer around in-line tube banks with pyramidal roughness 78−18152
flow of turbulent air boundary layer with slot-injected He, vel. and density profiles meas. 77−42808
flowing discharge, glow/arc transition and cathode-zone wave structure obs. 78−75475
fractionally charged ions, search in He gas 80−8954
free molecule flow and interdiffusion, through porous glass 79−32658
fusion reactor, cryosorption pumping, D_2-He (5 at.%), on mol. sieve, 5A, 4.2K 78−74499
fusion reactor breeders, models for T_2 and ^{4}He transport 78−17424
fusion reactor first wall, prod. of H, D and He by 15 MeV neutrons 79−93831
fusion reactor first wall radiation damage, H and He gas prod. from stainless steel 78−82512
fusion reactor potential materials, He generation by 14.8 MeV neutron 79−67944
galactic abundance determ. from open clusters H-R diagrams anal. 80−56938
galactic He enrichment due to He shell flashes 77−45428
gas, breakdown by alternating electric field near ion cyclotron freq. 78−55765
gas, comparison of 5th and 3rd harmonic conversion 79−18474
gas, compressed, Rayleigh-Brillouin spectrum, hydrodynamic region 80−100063
gas, compressed, Rayleigh-Buillouin spectrum, scaling 80−100062
gas, depolarisation factor *(French)* 79−82034
gas, diffusion of Na vapour, diffusion coeffs. meas. by Stefan method 79−41785
gas, effect on motion of Ag particles supported on graphite 78−34695
gas, elec. breakdown by pulsed high freq. field, electron distrib. function *(Russian)* 80−14876
gas, electron thermalisation, theory 80−53914
gas, heated, elec. breakdown parameters 80−103202
gas, in water, cavitation, gas supersaturation thresholds under high press. 77−16861
gas, ion mobility and longit. diffusion of Ar^{+} and CH_x^{+} *(French)* 79−94766
gas, laser-induced breakdown cyclotron reson. at low press. 79−60100

helium continued
gas, laser-induced breakdown wavelength depend. meas. of threshold 79−41895
gas, low press., relativistic electron beam propag. 79−76569
gas, mobility of H^+ and D^+, 300K 77−11303
gas, partly ionised, viscosity calc., simplified expressions 79−18983
gas, positron and positronium decay rates at high densities 77−54636
gas, positron diffusion, annihilation and scatt. 77−19074
gas, pulsed breakdown at low temp. 80−103216
gas, pulsed electron beam propag., self-focusing polyatomic additives effects 77−68164
gas, second virial coeff., acoustic determ., 1.28-2.13K 80−69965
gas, seventh harmonic conversion of mode-locked laser pulses to 38.0 nm 77−58378
gas, solubility of solid H_2 and Ne at high press. 80−10674
gas, spherical-source expansion, terminal speed ratio prediction, Monte-Carlo calc. 77−84285
gas, temp. fluctuations 79−19414
gas, viscosity, transition regime, density depend., compared with model predictions 79−1280
gas breakdown by pulses from a CO_2 laser 80−6206
gas bubbles in Cu and Ni, superlattice struct. 80−2086
gas bubbles in FCC metals, lattices struct. 79−14858
gas bubbles in neutron irrad. steel, liberation in uniform heating 77−50248
gas discharge, high voltage, low current, anal. of cathode fall 78−51375
gas discharge, low press., emitted photon probe for electron swarm parameters 80−43839
gas discharge flow, contracted strata rel. to turbulence 78−1923
gas flow, in pulsed supersonic jet 77−51093
gas microscopic gas-liquid like phase transition around positron 77−43322
gas re-emission from 20 keV He^+ bombarded Al, critical dose, temp. effects 77−35596
gas thermometer, small, const. vol., sensitivity and linearity at low temps. 79−63223
gas thermometer secondary standard for 0.5 to 40K 80−82762
gaseous, positron mobility edge 80−83880
GCFR claddings, neutron-induced He implantation, calc. of total flux 80−42773
GCFR cores, heat transfer with He and Na coolants, review 79−45331
globular cluster stars, He settling and effect on inferred ages 80−73013
in globular star clusters, He content from RR Lyrae stars evolution 80−51778
glow discharge, 2^3P level population relax., laser absorpt.-perturbation meas. 78−59706
glow discharge, cryogenic, effect of laser radiation (10.6 μm) 80−64803
glow discharge, cryogenic, interferometer meas. of neutral gas temp. 78−1924
glow discharge, electron behaviour in cathode fall, Monte Carlo simulation 78−1941
glow discharge, high press., collision freq. 77−55184
glow discharge, intermediate press., positive column conc. of ions and metastables 80−44017
glow discharge, investigation with cylindrical hollow cathode in Ne and He *(Russian)* 80−28856
glow discharge, laser-induced Raman emission source at 569 and 637 Å 79−46024
glow discharge, negative-luminesc. plasma, electron energy distrib. from line intensities and probe obs. 80−49033
glow discharge, reaction oscills. freq. eqn. derivation, expt. and numerical calc. 77−1027
glow discharge, short, lateral spread 79−46501
glow discharge, spectroscopic element detector for gas chromatography 78−31721
glow discharge and hollow-cathode discharge, negative glow, spectroscopic obs. 77−72516
glow discharge plasma, ionis. waves in positive column 80−1876
glow discharge with constriction, electrokinetic and optical characts., axial distribs. *(Russian)* 77−80393
Hall accelerator, variations in performance when using He gas *(Russian)* 80−103195
He-Ne laser discharge, dynamic characts. 79−98341
He-Ne methane saturated absorpt. stabilised lasers *(Chinese)* 79−59718
HF discharge double-probe meas. 78−67541
HF discharge in inert gas, optical diagnostics, bremsstrahlung 78−9871
high current arc in capillary, dynamic behaviour 77−4002
high-current pulse discharge plasma kinetic and dynamic processes 78−67601
high-current pulse discharge plasma partial LTE disturbances 78−67600
hollow cathode, with plane-parallel geometry, current and radiation mechanisms 78−18474
hollow cathode discharge, slow electron energy distrib., density and temp. 77−55197
hollow-cathode discharge, Ba^+ and Sr^+ formation 78−67527
hydraulic resistance to forced two-phase flow in narrow channels 78−87383
hypersonic flow, Na vapour seed, quantitative flow visualisation 78−47072
hypersonic flow, Na vapour seeded, velocity profile visualisation 78−59530
implantation into Nb, replacement of implanted ^3He by subsequent ^4He bombardment, and vice versa, using $^3He(d, \alpha)$ 79−4325
implanted in pyrolytic graphite, depth profiles 78−95071
implanted tensile specimens of Nb, TEM 77−51398
impurities in metals, electronic struct. 78−10402
impurity in FCC metal, migration energy and binding to vacancy, calc. 80−19798
Incoloy 800, creep and fatigue props. in high temp. gas cooled reactor He environment 79−47776
injection into liquid through porous plate, squeezing out of liq. 80−64622
injection of the He for visualisation of air flow patterns past models 77−58813
intermolecular potential, accurate empirical 79−68291
interstellar neutral gas interaction with solar wind, after gravit. focusing 80−105144
ion, energy and ang. distrib. in passing through C, Cu, Ag films 80−100292
ion, energy straggling in metal foils 80−27905
helium continued
ion beam, magnetic spectrom. meas. using automatic tracking NMR system 80−27869
ion bombardment of Ni, blistering temp. depend. 78−43967
ion damage in Mo, effects on H and D trapping 77−31698
ion implantation in Ni film, effect on domain struct., Lorentz electron microscopy 77−20654
ion irradiation of metals, blister form. and bubble growth 80−65072
ion irradiation of Mo, TEM 77−19994
ion pulse height defect in surface-barrier detector 77−10546
ion source, HF, proton yield increase, influence of various admixtures to H_2 obs. 80−57422
ionisation by relativistic muons, restricted energy loss 77−88355
ionisation path formation by laser beam with retractable focus 79−18992
ions, uniform concentration implantation, simulated neutron irradiation damage 78−79648
irregular bubble growth in Nb-Zr (1 at.%), α-particle effects, TEM study 80−15164
isoelectronic sequence, $\delta(r_1)$ matrix elements using spatially distrib. operators 80−102445
isotopes depth profiling in solids by proton elastic scatt. technique 77−24327
isotopes prod. cross sections in natural Mg, Al, Si, CaF_2 by 12-45 MeV protons 77−17310
isotopes prod. in lunar materials by solar cosmic ray protons, rate calc. 77−17311
isotropic plasma, metastable atoms, equilib. distrib. function 78−91068
jet, calibration of acoustic emission transducers and systems 77−835
jets, axisymmetric, turbulence mixing of gases with different densities 77−58749
Jupiter atmosphere, He conc. from Voyager 1 IR obs. 80−26790
Jupiter atmosphere, He/H_2 and $^3He/^4He$ ratios from cosmic ray albedo neutron fluxes 78−45271
Kilauea fumaroles, He/CO_2 ratios as premonitors of volcanic activity 80−26482
laser, direct nucl. pumped, power density 78−58980
laser, direct nuclear pumped, using $^3He(n,p)^3H$ reaction 77−83851
laser, direct nuclear pumping, kinetic model of plasma generated by fission products 77−23644
laser, nucl. pumping by fission fragments, plasma electron distrib. function 77−23653
laser, nuclear pumped, energy pathways by proton excitation 78−5459
laser action in He I slot cathode discharge 77−61943
laser additive effects on pulsed CO TE and CS_2/O_2 chemical lasers 79−31876
laser heated magnetoplasma, X-ray meas. of electron temp. 77−31493
laser induced tunnelling, avalanche initiating electron prod. 77−39441
laser plasma optically pumped by focusing CO_2 laser beam with axicon 79−32792
laser-induced breakdown 80−96339
lasing on Balmer-α line of shock tube generated plasma ions 77−58317
Lassen Park volcanic gases, He isotope ratios 79−16425
leak detection in large cryogenic vessels 78−93694
leak detector, with RF excited ion source *(Rumanian)* 80−8999
liquid, for cooling rotor of 50 MVA superconducting generator 79−58710
liquid film, transient heat transfer, film boiling regime 78−83219
low press. discharge, electron free streaming waves expansion 80−79595
low-current discharge, metastable atoms, radial density distrib. obs. and calc. 78−67495
low-pressure gas discharges, model 79−37560
low-temp. thermometry reference points 78−206
low-temperature equipment development, valve, tank, pressure gauge and whistle-indicator *(Czech)* 77−61069
lunar dust, inert gas conc., separation methods and methods of treatment *(French)* 80−51674
magnetometer, using pulsed optical pumping 79−67360
mass spectrometry, for microleak detection *(French)* 77−10131
mass spectroscopic chemical anal. using quadrupole mass spectrometer for fissile material accounting 80−63300
Matushiro fault zone, Japan, He spots caused by diapiric magma from upper mantle 79−8618
Mercury, He exosphere model based on Mariner 10 UV spectrometer data 78−77509
metal:He, ion implanted, statistical model of low temp. blister formation 78−67754
microwave discharge, electrodynamic and spectral characts. *(Russian)* 77−11413
microwave discharge, emission processes, steady-state kinetic calcs. 77−68880
microwave gas breakdown, ionisation pot., qualitative theory 80−43837
microwave plasma discharge, electron energy distrib. function *(Russian)* 77−11415
migration in alkali germanate glasses 79−51308
migration in metals, interaction with defects, role in radiation damage processes 77−28041
migration in Na_2O-Al_2O_3-SiO_2 glass 77−7902
mobile, effect on void nucleation 77−51405
mobile He cooling loop system for post-accident heat removal expts. 79−13403
mobility of C^+, S^+, F^-, flow-drift tube meas. 80−43831
mobility of H^+ ions in He, expt. 80−96337
molecular beams, nozzle-formed, energy parameter determ., time-of-flight method 79−64122
molecule, collisional electronic and rot. relax. in afterglow of pulsed discharge 77−61784
molecule, electron impact spectroscopy, high energy, Compton defect 77−88578
multicomponent inhomogeneous plasma, spectroscopic analysis 78−67425
muonium formation by positive muons 79−57272
Mz magnetometer, improving accuracy by reducing intensity of optical pumping 80−62700
naphthalene-He photoionis. plasma, CO_2 additive effect 80−10359
near-critical, friction factors for flow in curved tubes 78−83367
negative glow electron energy distrib., appl. to hollow cathode lasers 77−19790
neutron radiography, contrast enhancement using gaseous ^3He penetrant 80−93707
neutron stars, thermonuclear fusion flashes rel. to X-ray bursts 78−12417

helium continued
noise source, gas jet, absolute calibr. 78−59228
nucleosynthesis in massive stars, effects of stellar mass loss on He yields 80−36614
optical fifth harmonic conversion, 53.2 nm generation 77−10979
optical harmonic generation in gas, fifth harmonic, coherent XUV light 79−46007
origin, differences between Brans-Dicke and relativistic cosmologies *(Polish)* 80−27024
Orion Nebula, He ionisation struct. and abundance, SHF obs. 80−105315
in Orion Nebula peripheral regions, He^+/H^+ ratio and He ionisation 80−36686
orthopositronium decay, 77K, and in solid and liq. phases under press. 77−39713
parametric plasma turbulence, soliton struct. obs. 79−60143
penetration in LiF crystal deformed in liquid ^3He and ^4He 77−20131
permeability, in glasses and Stycasts *(Japanese)* 79−7715
permeability in $2Na_2O$-CaO-$XSiO_2$ glass, interconnectivity, miscibility limits, effect of morphology 78−67864
permeability in hard elastic polypropylene films, extension effects 80−40412
permeability in pyrocarbon coatings for Biso fuel 77−79433
permeation eccentricities of He, Ne, and D-T, from SiO_2-CaO-Na_2O glass microbubbles 78−47598
permeation in glass microsphere laser targets 77−83078
permeation in glass microsphere laser targets 77−83079
permeation through Mo, monocryst. and polycryst. specimens *(Russian)* 79−60554
physisorbed monolayer on graphite, neutron scatt. studies 80−107655
planetary nebulae in Magellanic Clouds, He, N and O abundances, effects of excitation class 80−109519
plasma, 1-4 torr in hollow cathode, population of excited levels, excitation and decay mechanisms 77−80267
plasma, afterglow and inertial expansion, numerical soln. of relax. kinetics 77−27769
plasma, afterglow produced by microwave surfaguide, spectroscopic diagnostic, electron and He_2 rot. temp. 80−44042
plasma, Ar-He mixture, ion-acoustic wave propag. 77−27670
plasma, CO_2 laser prod., ionisation dynamics, spectrosc. obs. 80−43968
plasma, collisional, classical diffusion in large amplitude density fluctuation presence 78−18381
plasma, collisional, vortex diffusion, shear effect 79−32773
plasma, collisional-radiative recombination 77−58841
plasma, continuous emission spectrum *(Russian)* 77−84508
plasma, cooling, nonequilib.-ionised radiating ats. 77−76128
plasma, cryogenic, oscill. excitation by hot electrons 79−55493
plasma, dissipative waves, LF oscills., anomalous diffusion and equilib. 80−33769
plasma, electric field meas., forbidden transition satellites in turbulent plasma 80−38714
plasma, electron beam generated, recomb. decay, Ne addition effects 78−59545
plasma, electron beam-produced supercooled, emission spectrum 77−84501
plasma, electron temp. meas. in JIPP-Ib stellarator, by time history method 77−15241
plasma, electron-impact widths and shifts of neutral He lines 79−27753
plasma, EM waves, parametric decay near upper hybrid freq. 78−59590
plasma, excited atoms, near-reson. Rayleigh scatt. obs. 77−3992
plasma, fission fragment generated, kinetic model 77−31488
plasma, graphite hollow cathode glow discharge C conc. determ. 80−44032
plasma, He I ($3^1P^0-2^1S$) line, Stark broadening parameters, modified adiabatic theory, electron scatt. phase shifts 80−43879
plasma, He I and II radiation enhancement in mag. field, nonlocal thermodynamic equilib. 80−10366
plasma, He II, reson. line Stark broadening and plasma polarisation shift 77−1020
plasma, in θ-pinch with axial current-carrying rod, light scatt. diagnostics *(Russian)* 77−11395
plasma, in rot. steady state centrifuge, rot. rate and temp. diagnostics *(Russian)* 78−5923
plasma, ion state and electron temperature in high-current pulsed discharge *(Russian)* 79−27844
plasma, ionisation wave, effect of electron neutral collisions 80−43846
plasma, laser beam interaction, electron accel. by ponderomotive forces 79−77409
plasma, laser prod., spectroscopic meas. *(French)* 77−62396
plasma, linear Z-pinch, outer 2s-shell electron excitation emission of C-, N-, and O-impurity ions 78−22113
plasma, low-density, electron temp. determ. from He I 3889 Å and 5016 Å line intensities 80−96394
plasma, microwave, induced, excitation source for at. emission anal. 77−56262
plasma, microwave discharge as source 77−35416
plasma, microwave induced, cavity excitation source for optical emission spectrometry 77−44567
plasma, microwave-induced, evaluation as element-selective detector for gas chromatography 77−81450
plasma, moderately dense, electron density and ion temp. meas. using He II lines 78−67407
plasma, neutral beam injection, charge exchange and ionis. rate coeffs., analytical approx. 79−86590
plasma, neutral line broadening meas. 78−18448
plasma, of HF discharge, self-acting field effect on spatial distrib. *(Russian)* 79−99007
plasma, overdense Z-pinch laser-driven hydrodynamic perturbation 79−77385
plasma, partly ionised, strongly inhomogeneous, magnetoacoustic reson. 80−69994
plasma, photon echoes obs., collisional relax. on $2^3S_1-3^3P_{012}$ 79−19089
plasma, plasmon prod. by laser light Raman conversion 78−47125
plasma, power transfer efficiency from microwave field under electron cyclotron reson. condition 78−9789
plasma, primary electron effective MFP meas. in multidipole device 77−24183
plasma, produced by pulsed electron cyclotron reson. discharge in poloidal heliotron type mag. field 77−76127
plasma, relaxation time determ. for establishing quasisteady state population 78−59639
helium continued
plasma, shock-radiative recombination rate in afterglow 79−4205
plasma, stationary recombining, population inversion inferred from intensity meas. 78−9836
plasma, strongly ionised, impact radiative recomb. rate 78−59546
plasma, ultradense reproducible Z-pinch, for laser-pellet interaction simulation, characterisation 78−30463
plasma, weakly ionised, drift-dissipative waves, plasma column steady state 80−38613
plasma, weakly ionised, photon echo relax. obs. in RF discharge 80−43986
plasma, Z-pinch, ionisation and radiation dynamics simulation 78−83606
plasma afterglow, stepwise excitation, electron energy distrib. and density at metastable states 77−84413
plasma beam-transverse mag. barrier interaction, collisionless electrostatic shock 77−80339
plasma chemical device, integrated electron density meas., interferometric method 79−55548
plasma collisional-radiative model, appl. to positive column 79−64836
plasma expansion, supersonic, population inversion 79−27755
plasma from magnetoplasmadynamic source, of supersonic jets 77−35332
plasma heavy ion complex mobility in cool plasma 77−62343
plasma in electron beam-excited discharge, atm. press., relax. obs. and model 79−37569
plasma jet, electrostatic probe meas. of metastable atom conc. *(French)* 79−98972
plasma linear pinch, extreme UV spectra of light impurity ions, appl. of grazing incidence spectrometer 80−59276
plasma non-equilib. diagnostics, PLTE model and true time study 80−38715
plasma satellites, mol. lines in RF discharge 80−44053
plasma supersonic jet, radiation in magnetoplasmadynamic source 77−35329
polarimeter, low temp., 20 to 50 MeV proton polarisation analysing apparatus *(Russian)* 79−76318
polarisability, second and third virial coeffs. meas. 4.2 to 27.1K 80−43825
positive column, axial elec. field in transverse mag. field 78−18472
positive column, in transverse mag. field, plasma parameter diagnostics 79−19103
positive column, magnetised, exptl. study on moving striations 78−83634
positive column, magnetised, temps. of charged particles, nonlinear effect of ionis. waves 80−44023
positive column, moving striations in longitudinal homogeneous mag. field 78−67523
positive column, with diffusion loss to wall, axial elec. field effects *(Japanese)* 78−47196
positive column comp. at intermediate press. 80−19646
positive column ion-acoustic waves, obs. 78−75312
positive column ionisation waves, influence of longitudinal mag. field 78−67522
positive column plasmas, metastable atom density meas. by improved self absorpt. method 80−87968
positron annihilation decay consts., temp., elec., and mag. field depend., computer anal. 78−78809
positron annihilation in rare gases, Doppler broadening meas., electron mom. distribs. 78−55131
positron decay rate nonlinear density depend. 80−71509
positron in condensing He, Monte Carlo lifetime spectra, temp. and elec. field effects 78−55263
positronium annihilation rate in dense gas 78−55258
positronium form. cross sections, diluent gas effect 80−5640
preinjected into V, void swelling on neutron irradiation 77−7765
preinjection into cold worked FV548 steel, 10 ppm, electron irradiation effects 77−19989
pressure, in vacuum chamber in cryogenic environment, meas. technique 78−77925
pressure and temp. oscillations of flowing He near critical states 79−58744
primordial He production within scale covariant cosmology 80−105412
primordial nucleosynthesis, incompatibility with Dirac Large Numbers Hypothesis 79−92900
production and universal anisotropy limits 78−36737
production cross sections for 15 MeV neutrons on 316 and 304 stainless steel 77−50291
production in reactor materials, integral meas. comparison with ENDF/B calcs. 77−23214
production in stainless steel, $^{59}Ni(n,\alpha)$ cross section importance 80−13625
production in stainless steel by neutron effects 79−22282
pulmonary airways, longitudinal mixing, impulse response of He, SF_6 79−20568
pulsed arc, Thomson scatt. diagnostics 80−24297
pulsed discharge, He_2 mol. formation in early afterglow, time-resolved spectra 78−63585
pulsed electrical breakdown at high temps. *(Russian)* 78−34379
pulsed microwave discharge, vac. UV emission characts. 77−35408
pure, preparation and purity meas. 79−20496
purifier, automatic 79−58738
quantum magnetometer, impurities influence on signal parameters *(Russian)* 78−82010
quantum magnetometer with optical pumping, sensitivity in 40-3000 Hz range *(Russian)* 80−90870
quartz, He^+ ion implanted, SAW velocity, influence of annealing 79−14996
quasicontinuous discharge, at high press., spectral obs. *(Russian)* 78−26356
radiation source, VUV He reson. line, for UHV photoelectron spectroscopy 78−89602
in Red Sea brines, evidence for mantle origin 77−25693
refrigerators, use of warm ejectors 79−58725
refrigerators and liquefiers for large superconducting systems, optimization 79−63233
refrigerators for superconduct power transmission lines, optimisation w.r.t. cost and reliability 78−24802
relativistic electron beam on air, He and H_2, charge neutralisation press. depend. *(Russian)* 77−19668
relativistic electron beam transport at low pressures 78−75373
relativistic ion beam laser, continuously IR to X-ray tunable, in negative temp. state *(Chinese)* 80−87373

helium continued
resonance source for photoelectron spectroscopy, impurity lines 77−14787
RF discharge, preionis. power for required electron density 78−9896
RF discharge test obs. with flow 80−44028
rotating plasma device, G-II device *(Japanese)* 80−70042
Sagittarius B2, He abundance problem 78−49496
scintillation detectors appl. *(Czech)* 78−86727
seawater, excess ^{3}He and ^{4}He in Galapagos submarine hydrothermal water 78−40593
second virial coeff., 0-500°C, two-temp. gas-expansion method 78−55711
selective adsorption induced intensity maxima, scattering from LiF surface 78−72667
selective adsorption on LiF(001) during elastic and inelastic scatt. 77−66564
self-oscillating props. of discharge in mag. field 80−64814
shell-burning evolution in accreting neutron stars 80−85968
solar models, He content and convective mixing length 80−26835
solar quiescent prominence spectra, meas. of Ca^+ 8542 and 8498 Å He 4471 Å and Ti^+ 4468 Å 80−90373
solar wind, He abundance long-term vars., Imp 6, 7 and 8 results 78−77452
solar wind, inert gas abundance, 500 Myr ago from lunar dust anal. *(German)* 80−51637
solid surfaces, reflection of slow H^+ and He^+ ions 78−76572
solid-fluid, eqn. of state, melting props. under press. 80−96721
solubility and diffusion in fused SiO_2 above transform. range 80−79965
solubility in metallic H_2, Gibbs energy, fluid state model, He conc. in giant planets 79−60602
solubility in vitreous silica, 100 to 1350 atm., 5 to 80°C 79−4414
sorption, on W, gas-solid interaction dynamics, energy transfer and sticking calcs. 77−51593
spark, cathode spot conversion kinetics 80−44067
spark gap resistance and elec. pulse rise time 77−31538
sparks produced by short laser pulses, spectroscopic meas. of temp. and electron density 77−43086
specific heat of ^{3}He film adsorbed on graphite 78−87842
spectral line shifts produced by electron collisions in He II plasma 80−106879
spectroscopic light source carrier gas glow discharge and hollow cathode types 78−82047
spinal cord seizures elicited by high pressures of He 80−12071
sputtering, physical and chemical of graphite and SiC, 600 to 7500 eV 77−36340
sputtering of ice, MeV ions, erosion rate 78−48268
stars with enhanced He lines 77−37608
steel, austenitic, neutron irrad., He release kinetics 78−79638
steel, austenitic stainless, He implanted 1.4970, high temp. fracture 77−86186
steel, type FV548, 1 MeV electron irradiated, influence of pre-injected He on void nucleation and growth 80−34054
stony meteorites, light noble gases anal. compilation 78−65574
stopping powers and ranges in all elements 78−58565
stratification in model atmospheres of blue horizontal-branch stars 80−90409
in stratosphere particles, detect. of ^{4}He rel. to extraterrestrial origin 77−56878
structural, fast neutron induced H and He producing reaction 80−13841
subdwarfs, He abundance and galactic halo 80−22003
submonolayer physisorbed, rel. to liquid to gas phase transitions in two-dimensional quantum systems 78−77798
Sun, comparison of He II 304 Å and He I 10830 Å spectroheliograms 78−20799
superconducting magnet transfer lines, for cooldown or warmup 79−63234
superconducting power network, He requirements 79−50897
superconducting turbogenerators, heat transfer in rotating excitation winding using He in rotating thermosiphon loops 79−58718
supercritical, correlation for heat transfer in turbulent flow in small channels 78−18871
supersonic radiation waves, excitation by CO_2 laser 79−90433
suprathermal field fluctuations and high energy electrons 80−1847
surface, in contact with atomic H, Bose condensation, adsorption isotherms and stabilty 80−107638
thermal conductivity, 3.3 to 20K, meas. in guarded parallel plate apparatus 77−22553
thermal conductivity, at high press. 80−103099
thermal conductivity, near 300K, density depend., 0.8-35 MPa 78−67304
thermal conductivity, temp. depend. 78−59534
thermal conductivity determ., repulsive wall of interatomic pot. 77−54586
thermal transpiration, theory and expt. comparison, molecular and transition flow 79−32579
thermoacoustic oscillations in nonuniformly heated tubes 80−33441
thermodynamic and thermophysical props. calc. using HEPROP computer program 80−6529
thermodynamic properties and eqn. of state in stellar conditions 79−35241
thermodynamic properties in HTGRs, accident anal. *(German)* 78−25315
thermodynamic properties in range 20 to 1500°C and 1 to 100 bar *(German)* 79−69266
thermosphere, annual var. from Aeros Nims data 80−12578
theta pinch plasma with no bias field, fluctuating fields, spectroscopic obs. 77−11398
third virial coeffs. calcs. using realistic Beck pair potential 78−94880
Tokamak plasma reaction dynamics, corona model, spectroscopic diagnostics *(German)* 79−60103
Tokamak-fusion reactors, He exahust 80−75084
Townsend discharge, macroscopic quantities, Boltzmann eqn. and Monte Carlo calcs. 80−38848
Townsend discharge field emission by higher-order ion clusters 78−67550
trace impurity analyzer for He refrigerator systems 79−70388
tracers for detection of gaseous atmos. pollutant emissions *(French)* 80−7987
transverse HF discharge, electron energy distrib. from spectra *(Russian)* 80−84012
trapping at Xe atoms in W, attachment of mobile particles to non-saturable traps 80−39418
trapping in Nb, temp. depend. 77−31685
turbo-refrigerator with regenerators 79−58723
twin-hollow-cathode interferometer-spectrometer, discharge characts. *(German)* 78−67461
twin-hollow-cathode of interferometer-spectrometer, radial electron temp. *(German)* 78−67462
two dimensional quantum crystal on graphite *(Russian)* 78−60001
two particle radial distrib. function, phase space sampling approach in statistical mech. 78−32753
two-step photoionisation via 4p $^1P_1$ state *(Russian)* 79−59413
underdense gas breakdown by laser pulse, backscatt. and beam refr. 78−5897
unit requirements, for superconductive energy appl. in USA 78−89999
universal abundance 80−62356
in upper atmosphere, electron impact yield spectra 78−28401
upper atmosphere He dynamics, use of Jacchia (1977) empirical model 78−77381
use in groundwater vel. estimation for radioactive waste storage 80−82111
vapour, low-temp. positive ion mobility by absorptive model, WKB calcs. 79−77333
vapour, positive ion mobilities, clustering 77−58837
vapour, thermal cond. as function of density 78−55712
vapour column, solid vapour heat transfer, at low temps. 78−83376
vapour pressure meas. gauge of ^{3}He for use up to 0.3K 80−68207
vapour pressure scale determ. using paramag. salt thermometer and NPL-75 gas thermometer scale 80−95060
venous gas bubble prod. by transient deep isobaric counterdiffusion of He against N_2 78−11790
Venus, thermosphere eddy coeffs. and lower atmosphere He content 79−80255
vibration and electronic excitation results obtained with magnetically collimated electron impact spectrometer 79−49334
vibrational excitation calculation, in gas mixture discharge 79−77442
void form. in self-ion irradiated Ni, He effect 78−6112
void swelling in type 304 stainless steel, 200 keV C^+ bombardment, dose and temp. depend. 77−55309
volume change due to point defects and He bubbles, isotropic elasticity theory 78−47445
Wigner-Kirkwood expansion of second virial coeff., convergence accel. 78−91052
Yellowstone Park volcanic gases, He isotope ratios 79−16425
Ag:He, implanted films, solid solutions radiation induced polymorphism 79−86810
Ag-He CW mW-level laser source at 224 nm 80−43352
Al:He, excited He atom lifetime, optical absorption 79−38578
Al:He, interaction energy of two He atoms, Hohenberg-Kohn-Sham density functional formalism 79−51519
Al:He, pseudopotential calc. of screening of He atom 78−51917
Ar ion laser, He, Ne, impurity effects, ignition enhancement and instability suppression 79−13948
Ar plasma jet, surrounded by Ar, He, N_2, H_2 gases, recombinations in decaying jet 78−9753
Ar^+ mobility in He gas at 82K 80−1733
Ar-He, heat of mixing, low press., theories comparison 78−26230
Ar-He, liq. soln., sound vel., perturbation theory *(Russian)* 77−47512
Ar-He glow discharge with different potential cathodes, expt. *(Russian)* 77−39484
Ar-He ion laser, population inversion radial distrib. and output characts., mag. field depend 80−19019
Ar-He plasma, ion acoustic soliton form., mechanism 78−18457
Ar-He plasma, thermal diffusion factors, binary mixture hypothesis 79−27749
Ar-He plasma, thermal diffusion factor, 2000-4000K, binary mixture hypothesis 79−32743
Ar-He plasma, thermal diffusion of neutral species in plasma jet, 2000-4000K 79−32742
Ar-He rarefied mixture in supersonic nozzle and jet, longit. translational nonequilib. 79−27678
Au-He CW mW-level laser source at 280 nm 80−43352
Be, irradiated with He^+ at 20 keV, surface damage and gas trapping profile meas. *(French)* 80−84218
CO laser output power, active species and buffer He isotope effects *(Russian)* 80−63986
CO-^{3}He nuclear pumped laser, optimisation with 2 MeV protons 80−64000
CO-He, CO-N_2-He glow discharges, CO loss rate 77−19788
CO-He, heat of mixing, low press., theories comparison 78−26230
CO-He, plasma-injection-stabilised discharges at low temp. 78−17959
CO-He glow discharge, positive column, ionisation processes 80−79618
CO-He low press. mixture, CO vibr. distrib. to high level 78−58985
CO-He nuclear pumped laser, high energy beam deposition 80−63999
CO-He-O_2, species concentrations in glow discharge and afterglow, mass spectra, laser conditions 78−14241
CO-He-O_2 gas discharge laser plasma, positive ion generation mechanism *(Russian)* 79−99005
CO-He-O_2-H_2O laser discharge, stability, influence of recombination and ion chem. 78−17915
CO-Xe-N_2-He gas laser power rel. to mixture composition *(Russian)* 79−7114
CO_2:N_2:He plasma, lasing action, gain limiting attainment possibility 79−89884
CO_2-Br_2-He mixture, possible gas lasers with solar excitation 80−99695
CO_2-CO-N_2-He in CO_2 lasers, ionisation wave, slow changes, dispersion curves 80−38822
CO_2-DF-He CW optically reson. pumped transfer laser 77−75471
CO_2-He, species concentrations in glow discharge and afterglow, mass spectra, laser conditions 78−14241
CO_2-He stepwise pulsed photoionisation 77−50479
CO_2-He UV photopreionisation TEA laser, role of He excited atoms 78−17902
CO_2-He-N_2, absorpt. coeff. for 10.6 μm CO_2 laser radiation, 295 to 650 K 80−92252
CO_2-He-N_2, gas dynamic laser, gain coeff. numerical estimates, book contrib. 80−1183
CO_2-N_2-^{3}He, laser, plasma diagnostics of media capable of lasing in nucl. reactor environment 79−10279
CO_2-N_2-H, laser discharge circuit parameters, effect on energy imput mode 77−75476

helium continued
CO_2-N_2-He, coefficient of optical amplification behind an axisymmetric shock wave *(Russian)* 77−89153
CO_2-N_2-He, non-self-sustained plasma discharge instability, electron collisions *(Russian)* 77−76050
CO_2-N_2-He, pulse-periodic operation of electron-beam-controlled discharges, energy characts. changes 80−102695
CO_2-N_2-He, transverse combined discharge laser, 10-20 kW *(Russian)* 77−54703
CO_2-N_2-He, vol. discharge, negative ions effect 80−14956
CO_2-N_2-He (H_2O) gas mixture, method for obtaining vibrational population inversion 79−94210
CO_2-N_2-He CW gasdynamic laser, closed-cycle, construction and operating parameters 80−23717
CO_2-N_2-He discharge, voltage drop, impedance 77−47291
CO_2-N_2-He discharge, electron distrib. relax., numerical study 80−54070
CO_2-N_2-He electroionisation laser, freq. mode, lasing conditions 80−63970
CO_2-N_2-He gas mixtures, fluorescent IR radiation from glow discharge 78−94386
CO_2-N_2-He gas mixtures, time-of-flight meas. of electron transport parameters 78−94387
CO_2-N_2-He gasdynamic laser, effect of weak flow perturbations on gain 80−14316
CO_2-N_2-He laser, civr. temp. approx. for N_2, applicability limit 78−5452
CO_2-N_2-He laser, pulsed microwave discharge pump, skin effect and gain 79−13945
CO_2-N_2-He laser, vibr. population distrib. of N_2, vibr. temp. determ. 77−14688
CO_2-N_2-He laser media excitation by electron beams admitted through gasdynamic windows 80−99694
CO_2-N_2-He laser mixtures, self-sustained glow discharges, low ionisation pot. organic additives effects *(French)* 77−88694
CO_2-N_2-He laser mixtures, electron swarm parameters, Boltzmann eqn. anal. 79−18396
CO_2-N_2-He laser mixture in nonself-sustained discharge, direct heating mechanism 80−28195
CO_2-N_2-He mixture, ionisation and attachment coefficients 78−42706
CO_2-N_2-He mixture in gas-dynamic system with independent thermal excitation, population inversion in two-step mixing 79−89888
CO_2-N_2-He mixture supersonic adiabatic expansion, population inversion and gain 80−19017
CO_2-N_2-He mixture volumetric glow discharge formation at atm. pressure 78−71615
CO_2-N_2-He nozzle flows with boundary layer, gain coefficients 80−14312
CO_2-N_2-He pulsed transverse discharge, investigation of gain 80−9855
CO_2-N_2-He system, CO_2 TEA laser discharge development, high-speed-camera investigation 79−55109
CO_2-N_2-He volume discharge, self-sustained, with UV preionis. 79−60211
CO_2-N_2-He-O_2 discharge mixture, three body electron attachment to O_2 80−64779
CO_2-N_2-He(H_2) laser mixtures, composition effect on excitation efficiency in dicharge 78−5453
CO_2+H+Xe plasma, elec. parameters, Xe effects *(Russian)* 77−84507
CO_2+He(Ar), rot. relax. rates and cross sections 79−848
CO_2+N_2+He, glow discharge positive ion species identification *(Russian)* 80−84014
CO_2(-He) discharge, UV-initiated, electron ion recomb. and CO_2 dissoc. 80−44068
CS_2-He gas binary diffusion coeff. obs. *(Japanese)* 79−10627
Cd-He hollow-cathode laser, small signal gain 79−31881
CdI_2-He, hollow cathode discharge, simultaneous CW lasing by Cd^+ and I^+ 77−10951
Cl, in Ar and He gas, diffusion const. of atom 78−71417
Cl_2+Ar(He)(Cl_2), dissoc. in shock wave, density gradient meas. 77−83682
Cl($3p^5(^2P_{1/2})$)+carbon tetrachloride (Cl_2)(He), VUV metastable state quenching, absolute rate const. 77−79641
Co_2:He:N, glow discharge instability in afterglow 80−6313
Co_2-N_2-He, pulsed discharge with temp. and density gradient in cathode sheath 79−41899
Cs^+ in He and Ne gas, ion mobility and longit. diffusion coeff. 78−67308
Cs-He plasma, steady-state discharge, role of inelastic collisions, spectroscopic diagnostics 78−42709
Cs-Sr(He) mixtures, photocond. at atm. press. 80−87844
Cu, irradiated with 20 keV He^+, surface damage and gas trapping profile meas. *(French)* 80−84219
Cu laser, He buffer gas effect on output parameters 78−9368
Cu, surface tension cct. cavities under Cu^+ ion irradiation, O_2 and He effects *(French)* 77−35611
Cu:He, doubly peaked He depth profile and blistering 78−10078
Cu:In, He, lattice defect struct., PAC meas. 80−70190
Cu_2O:He, ion-implanted, resonance Raman studies of annealing 79−55765
D-^{3}He fusion reactor advanced fuel development and confinement 79−13516
D-^{3}He satellite fusion reactor, field-reversed mirror confinement 78−70643
D_2-^{3}He, filled microspheres, implosion expts. 78−59672
D_2-^{3}He mixture plasma focus, ion temp. 78−5953
D_2-HCl,He gasdynamic lasers, gain 79−64217
desorption from solid Ar(Kr)(Xe) surface, appl. of simplified continuum model 78−87860
ErD_2:He, tailored low Z impurity distribs. in solids, distrib. evaluation by proton backscatt. technique 79−5199
F_2-He, high-press. mixture, neutral atomic F laser lines 79−86167
F_2-He, mixtures, VUV emissions, mol. F_2 laser at 1575 Å 77−75487
Fe:He, BCC, process of interstitial trapping by impurities 79−46697
α-Fe:He, impurity clustering in vacancies bound to edge dislocations 78−91358
α-Fe:He, interaction of He with small self-interstitial platelets 79−60399
H^+, calc. of mobility in He, 10 to 700K 78−66629
H-He, H hyperfine struct. shift, commutator computational method 78−78608
H-He, light source, elec. discharge, Doppler effects *(German)* 79−44946
H-He arc lamp, 60-360 nm, calibration 78−87117
helium continued
H-He fluid planets, dynamics and He distrib. 78−28555
H-He fluid planets, phase diagram and transport props. 78−28554
H-He interface, of neutron star, physical processes in strong gravit. field, electron-positron pair prod., γ-ray emission *(Russian)* 79−80333
H^+-He^{2+}, strongly coupled ionic mixture, density fluctuations, timer depend. 77−80272
H^+-He^{2+} mixture, fully ionised, two-component plasma, mean spherical model 80−87854
H^-+H_2(He)(Li), 50-150 keV, scatt. angle of neutral H 78−5340
H_2 lines emitted from low-press. linear discharge 79−14523
H_2-F_2-He chemical CW laser, flows *(Russian)* 78−74895
H_2-He, nucl. shielding, ab initio coupled HF calc. 79−89690
H_2-He, on W, Mo, Ir and Re surfaces, field depend. of spectral line energy 79−78853
H_2-He, thermal cond. meas., up to 14 MPa 80−64669
H_2-He gas mixtures, 1000-25000K, transport property correlations 80−75029
H_2-He mixture, collision integrals, modelling of spacecraft entry into Jupiter atmosphere 78−71413
H_2-He mixture, pumping speed of Excalibur CVV2008 liq. He cryosorption pump 79−80633
H_2-He mixture, radiant heat transfer coefficient for blunt body in hypersonic flow, similarity law 80−33705
H_2-He negative glow discharge, H Balmer line excitation *(Russian)* 77−46516
H_2-He plasma interface in strong gravit. field, bremsstrahlung, neutron stars and pulsars appl. *(Russian)* 79−67048
H_2^++He, vibr. energy effects on kinetics, phase space model 78−11508
H_3^+, mobility in He gas 78−18371
HCN compact CW laser, output increased by He, Ar, air and O_2 buffer gases 79−10293
HCl-D_2-He mixture, gasdynamic laser theory, gain depend. on parameters 78−50761
HCl-He, discharge, possible laser action on vibr. transitions 80−14332
H_2O-He laser, pulsed oscill., elongation by admixture of He 78−87039
$H_2(^3\Sigma_u^+)$-He(2^3S), discharge ionisation growth, diffusion coeffs. 78−83636
$^3H/^3He$ dating as meas. of O_2 utilisation rates, appl. to Sargasso Sea 77−56654
Hd-Cd hollow cathode laser in mag. field, Cd II stimulated emission 78−79002
He, bubble formation during injection, system pressure and thermophysical effects *(German)* 79−41745
He I, 10830 Å line obs. of HR 1105, cold giant star *(Russian)* 80−17586
He I, expt. investigation of 2-phase flow pressure drop characts. in vertical tubes 79−60052
He I, II excited state population densities in non-LTE plasmas 78−67328
He I, II in interplanetary space, EUV photometer obs. of 58.4, 30.4 nm lines 77−45309
He I 584 Å in quasars and gaseous nebulae, line transfer problem and line strength 80−67550
He I emission lines in T Tauri stars, singlet to triplet ratio 78−28680
He I plasma arc, spectral line profiles, λλ=4471 Å and 4922 Å *(French)* 78−83625
He II, stationary population inversion between low lying levels of He^+ in recombining plasma 77−84494
He II, Z-pinch plasma, Stark broadened profile, 4686 Å, electron density and temp. 77−84495
He II 4686 Å in OB-type stars, line profiles and equivalent widths obs. 79−67006
He II 4686 Å line, Stark profile meas. in high density plasma 80−96390
He II in planetary nebulae, Ly α photons absorpt. rel. to forbidden lines intensities 80−67833
He II resonance discharge lamp, for UV photoelectron spectroscopy 79−58847
He II resonance lamp for UV photoelectron spectroscopy 79−93232
He, microwave breakdown of nanosecond duration, calc. of threshold fields 78−94948
He^- high current source of 70 mA at 10.5 kV 80−95495
He^+ bombardment of stainless steels, effect on stress corrosion cracking and microhardness 80−85087
He^+ flux in solar wind after interplanetary shock, Imp 7 obs. 80−101520
He^+, obs. in driver gas of interplanetary shock wave 80−72735
He^+ shutter controlled microbeam, with scanning system, for 2-dimens. backscatt. images 79−2879
He^{2+}, microdosimetric measurements of pretherapeutic heavy ion beams 80−72337
He^{2+}, terrestrial origin, discovery in outer magnetosphere 78−32295
He/Ar ratio vars. in fault zone groundwater air bubbles for earthquake prediction 78−88803
He/H pregalactic ratio, determ. from obs. of irregular and blue compact galaxies 80−36711
He/H ratio of B-type stars in young clusters and associations 77−29887
He^+/H^+ ratio in H II region G0.7-0.0 (Sagittarius B2) 78−45380
He^3/He^4 high isotope ratio in technical-grade metals and semiconductors 79−86080
He-^{20}Ne-^{22}Ne, orthogonally polarised laser mode interactions *(Russian)* 77−19235
He-air, thermal cond. meas., conc. depend., 315K, 330K *(Russian)* 78−71421
He-Ar, Ar I TEA lasers, energy characteristics 80−63977
He-Ar, collision-induced absorption, exact line shapes 78−66512
He-Ar, corresp. states law and thermal diffusion, two-bulb meas. 77−3910
He-Ar, diffusion coeff., two-bulb meas. 77−11299
He-Ar, gas mixtures, thermal cond. meas. in the range 0.5-15 MPa 80−14874
He-Ar, He-Kr and He-Ne-Xe ion lasers, hollow cathode, CW operation and excitation mechanism 80−69363
He-Ar, solubility in Ar, and related functions, three-body forces 79−10776
He-Ar, spherical expansion into flooded space, separation 79−81948
He-Ar gas mixture, velocity slip in free jet expansions 78−90951
He-Ar high voltage hollow cathode discharge, new Kr II CW laser lines new Ar II CW laser lines 79−13947
He-Ar hollow cathode discharge, CW laser oscill. obs. 78−5454

helium continued
He-Ar hollow cathode discharge, laser generation on Ar II 4765 Å line 80−23671
He-Ar in Cu^+ hollow-cathode laser, IR output depend. on gas press. ratio 80−48223
He-Ar mixture, mass separation with rot. plasma 79−13842
He-Ar mixture, mass separation during molecular beam sampling process 80−31937
He-Ar mixture, thermal conductivity, 400-1500K 77−39394
He-Ar plasma, linear longit. oscill. damping and dispersion, development of turbulence 77−51185
He-Ar-H arc plasma, nonequilib. effects, spectroscopic diagnostics 77−76191
He-Ar(CO_2), natural diffusion coeffs., press. effects 78−26229
He-Ar(Kr)(Ne), thermal diffusion, conc. depend. determ. 77−11300
He-Ar(N_2), heat of mixing, 2-15 bar *(French)* 79−7436
He-Ar(N_2)(O_2)(CO_2), binary diffusion coeffs., press. depend., 300 and 323K, Thorne's eqn. 80−1724
He-Ar(Ne)(N_2)(CO_2) mixtures, thermal diffusion 80−1726
He-Ar(Xe) mixtures, US vel. meas., phase separation 79−27738
He-As CW laser, excitation mechanism 79−3685
He-Au, UV ion laser, dominant transition at 280 nm 79−942
He-Au mixture, Au II ion laser transitions, 253.3 to 763.5 nm 77−7071
He-Au UV laser, spectral range, threshold, power output 78−66809
He-Ba discharge, dipole-dipole pair absorpt. obs. using optogalvanic detect. 80−54064
He-burning in core of massive stars 78−93207
He-CO, pulsed non self sustained discharges, peculiarities 80−38811
He-CO glow discharges, positive ion spectra, ion clusters obs. 80−64807
He-CO_2, nuclear pumped laser, use of fast burst Caliban reactor *(French)* 79−89889
He-CO_2 atomic C nuclear pumped laser collision processes, output delay 80−38002
He-CO_2 pulsed atomic C laser, time and energy characts. in mag. field *(Russian)* 78−22108
He-CO_2-Cs glow discharge, quenching cross section of resonant Cs(6P) state by CO_2 mols. 80−43860
He-CO_2-Cs mixture in rapidly circulating laser, interaction rate of Cs and CO_2, gasdynamic parameters 79−86173
He-CO_2-N_2, vol. discharge with UV preionisation by capillary discharge, ionis. pots. depend. 80−44065
He-CO_2-Xe, supersonic elec. discharge TEA laser, mag. field effects 79−7110
He-CO_2-Xe electrical discharge laser pumped by crossed electric and mag. fields 78−42320
He-CO_2(O_2) volume discharges, electron recombination and attachment 77−19799
He-CO(-O_2), glow discharge, ion cluster in positive column, ion mass spectra diagnostics 80−38752
He-CO(CO_2), C nuclear pumped lasers, energy storage 80−63996
He-Cd, afterglow, Cd^+ excited state prod. by Penning and charge exchange reactions 77−15252
He-Cd, glow discharge, collision rates calcs. 77−68882
He-Cd, hollow cathode discharge tube, voltage, ion spectral line intensities and metastable states 79−46505
He-Cd, hollow cathode laser, output characts. 77−42525
He-Cd, hollow cathode laser oscillations, cathode temp. effects *(Japanese)* 79−50285
He-Cd, hollow cathode long life laser 77−88769
He-Cd, long life hollow cathode laser 78−29968
He-Cd, metal ion laser, noise props. *(Japanese)* 79−64209
He-Cd, usual glow and hollow-cathode discharges, negative glow, spectroscopic obs. 77−72516
He-Cd, whitelight hollow-cathode type laser design based on cathode fall theory 79−27282
He-Cd bipolar hollow-cathode laser, 441.6, 533.7 and 537.8 nm Cd ion lines 79−50319
He-Cd cataphoretic laser discharge tube, He loss meas. rel. to tube life 79−94252
He-Cd DC discharge, excited at. densities, I-V characts. 78−14230
He-Cd discharge, enhancement of rate of charge exchange collisions 77−83862
He-Cd discharge, principal Cd ionis. mechanism, radial profiles meas. 77−27758
He-Cd extended-life laser characts. 78−46586
He-Cd hollow cathode discharge white light laser *(Chinese)* 79−72555
He-Cd hollow cathode laser, 533.7 and 537.8 nm 77−71976
He-Cd hollow cathode laser, He singlet and triplet metastable number densities 78−29938
He-Cd hollow cathode laser, laterally emitted light 78−66810
He-Cd hollow cathode laser, axial mag. field effect on oscills. 79−59681
He-Cd hollow-cathode discharge, external cathode type, morphologic study 79−60207
He-Cd hollow-cathode laser tube, description and performance *(Bulgarian)* 79−27279
He-Cd II hollow-cathode laser, 4416 Å pulse oscillation 79−7122
He-Cd II laser, 05378 μm oscill. spectra meas. using scanning interferometer *(Japanese)* 80−9864
He-Cd II laser, power interaction of laser lines 80−9862
He-Cd II lasers, positive column, hollow cathode types, 4416 Å oscill. characts. *(Japanese)* 78−94392
He-Cd laser, 441.6 nm, low noise, discharge current modulation effects *(German)* 78−22117
He-Cd laser, 442 nm, high order mode crossing signals from Cd II $4d^9 5s^2\ ^2D_{5/2}$ state 79−796
He-Cd laser, 8067 Å, He metastable atoms effect on power 78−33722
He-Cd laser, drift of Cd^+ due to laser field 78−17917
He-Cd laser, freq. self-selection, transverse RF excitation *(Russian)* 77−75490
He-Cd laser, hollow cathode type, quasi-metastable state excitation 78−33721
He-Cd laser, intensity fluctuations meas., comparison with 78−71087
He-Cd laser, intracavity phase modulation, spectral and time characts. 77−61988
He-Cd laser, possible operation using charge-transfer excitation 77−83701
He-Cd low-power low-cost blue lasers 77−19333
He-Cd plasma, in discharge tube, excitation mechanism obs. 78−30479
He-Cd positive column laser power, effect of I_2 additive *(Japanese)* 79−7121
helium continued
He-Cd positive-column laser discharge, excitation mechanisms from radial profiles 77−68205
He-Cd segmental tube laser ageing *(Bulgarian)* 79−18441
He-Cd single-mode laser, linewidth meas. and population calc. 77−14694
He-Cd vapour laser, continuous wave, intensity fluctuations investig. 80−83593
He-Cd^+, cataphoretic laser, 441.6 nm line intensity dip due to vapour separation 77−50659
He-Cd^+, laser, cataphoretic, power noise meas. 79−36885
He-Cd^+, positive column laser, Cd II 441.6 nm line, effect of I_2 77−54697
He-Cd^+ cataphoretic laser, freq. fluctuations of 4416, 3250 Å lines 79−72556
He-Cd^+ hollow cathode laser, He(2^3S) densities and excitation mechanisms 80−48220
He-Cd^+ laser, improved hollow cathode type, design and performance 80−19047
He-Cd^+ laser, output radiation, influence of discharge-current fluctuations 79−10289
He-Cd^+ laser, population densities of He excited states in positive column discharge 78−58989
He-Cd^+ laser, upper and lower laser states population densities, simultaneous determ. 78−87042
He-Cd^+ laser discharge, positive column, non-Maxwellian electron energy distrib., electron density determ. 77−84493
He-Cd^+ laser output, effects of transverse mag. field 79−86169
He-Cd^+ laser plasma, interferometric anal. of spectral lines 77−10892
He-Cd^+ positive column laser discharge, ion density 77−68885
He-Cd^+ positive column laser, power increase mechanisms by I_2 addition *(Japanese)* 79−98346
He-Cd(Zn) hollow cathode laser, upper level decay rate, mag. field tuning dip meas. 78−87043
He-Cl_2-HI chemical laser system, rot. nonequilibrium, kinetic modelling, three model comparison 80−53281
He-Co_2-Xe plasma discharge electron conc. and temp., optical diagnostics method 79−41871
He-Cs discharge plasma, high freq. oscills. in crossed elec. and mag. fields *(Russian)* 77−15189
He-Cs mixture, Cs ion conc. determ. by radn. absorpt. 79−34395
He-Cs mixture discharge, B-invariant transformation theory 78−67503
He-Cs plasma, HF instability in crossed fields, obs. 78−75305
He-Cu discharge, Cu ion laser, at. emission obs. of plasma props. 80−19021
He-Cu hollow cathode discharge, Cu II CW laser oscill. at 8096 Å 79−31878
He-Cu hollow cathode laser, three phase excitation 80−48279
He-CuCl(Br)(I) gas discharges, CW laser oscills. on Cu^+ transitions 79−7116
He-Eu ionic gas discharge laser, increasing energy parameters *(Russian)* 77−58320
He-Eu pulsed laser, pumping rate and electron density meas. 80−9868
He-F, doublet series laser lines near 700 μm, hyperfine splitting and broadening meas. 78−63070
He-F gas mixture, electron drift velocities, laser modelling 78−63061
He-F laser, press. depend. of atomic F laser transition intensities 77−659
He-F_2, dissociative electron attachment, rate coeffs., appl. to lasers 78−46575
He-F^-(Cl^-)(Br^-)(I^-), ion reduced zero field mobilities and free diffusion coeffs. 77−47139
He-F(O)(N)(Ar) mixtures, RF discharge, mass spectroscopy, floating double probe meas. 80−84016
He-H multi-ion plasma, with ion acoustic turbulence, resistivity phenomena 80−48856
He-H_2, H production at 10 torr in pulsed discharge 80−9748
He-H_2, plasma, strongly supercooled quasistationary, prod. by intense electron beam in dense gas *(Russian)* 77−89277
He-H_2 DC discharge, H Balmer-α fine struct. lines, anomalous shifts 79−45677
He-H_2 mixture, conc. depend. of thermodiffusion const. 77−7503
He-H_2 mixtures, isobaric sp. ht. 78−18788
He-H_2 plasma, shock-heated, relax. distance and equilib. electron density diagnostics 77−24180
He-H_2(N_2O)(NH_3), thermal diffusion factors meas. 80−10344
He-Hg afterglow plasma, time resolved double probe study 78−18444
He-Hg direct nuclear pumped laser, optimum conditions for lasing 77−50655
He-Hg laser, Hg II direct nuclear pumped gain at 7945 Å 78−5467
He-Hg nuclear pumped laser, charge exchange pumping 80−63996
He-Hg plasma, prod. by nucl. radiation, charge exchange effects 77−24103
He-Hg RF discharge, atomic ionis. and excitation, spectral line intensities 78−26334
He-I_2 laser, sequential separate multicolour output operation *(Japanese)* 80−28205
He-I^+ laser discharge, positive column, particle densities 80−103215
He-Kr, gas, diffusion coeffs. meas., 350-1200K 80−14869
He-Kr, Kr I TEA lasers, energy characteristics 80−63977
He-Kr gas mixtures, separation using silicone rubber, cellulose acetate membranes, separation factor 77−36791
He-Kr HV hollow cathode laser, gain meas. of Kr II 4694 Å, 4318 Å CW transitions 79−45928
He-Kr high voltage hollow cathode discharge, new Kr II CW laser lines 79−13947
He-Kr hollow cathode CW laser, Kr II 4584 Å generation 80−58510
He-Kr hollow-cathode dischage, CW and pulsed lasing at Kr ion lines 79−3679
He-Kr hollow-cathode discharge, CW laser oscills. on Kr II 4694 Å, 4318 Å lines 79−3680
He-Kr mixture, diffusion coeff. meas. by diffusion in flowing gas 80−83876
He-Kr mixture, diffusion coeff. meas. by diffusion in flowing gas 80−83877
He-Kr^+ ion laser, He metastable atom concentration and time variation 79−55111
He-Kr^+ ion laser, microwave-pulse-excited, spectroscopic expts. 77−71973
He-Kr^+ laser, microwave-pulse-excited, internal plasma parameters, time variation 77−38858

helium continued
He-Kr(Ar)(Xe), ion laser transitions, hollow cathode excitation 80−1184
He-Kr(Xe), scaling parameters for thermal diffusion factors, viscosity, mutual diffusion coeff. calcs. 77−35292
He-like ions, highly charged, electron impact, intermediate-coupling strengths for fine struct. transitions 80−32837
He-like ions, spectral line intensity, density depend., plasma diagnostic appls. 78−83617
He-M, M=CH_4, C_2H_6, C_3H_8, C_4H_{10}, O_2, CF_4, C_2F_6, C_3F_8, SF_6, N_2O binary gas mixture, mutual diffusion press. depend. 77−24047
He-metal vapour lasers, positive column electron densities, experimental study *(Japanese)* 80−69376
He-N_2, discharge ionisation growth, diffusion coeffs. 78−83636
He-N_2, pulsed atomic N laser, time and energy characts. in mag. field *(Russian)* 78−22108
He-N_2 gas mixture, correl. between kinetic theory of thermal cond. and expt., 90 to 300K, 1 bar 79−81707
He-N_2 laser, energy pathways by proton excitation 78−5459
He-N_2 mixture, plasma created by electron beam, spectral composition *(Russian)* 78−30453
He-N_2 mixture, speed of sound, temp. depend. at high press. 77−84388
He-N_2 mixtures, mutual diffusion coeff. meas. depend. on cell geometry 77−3911
He-N_2 plasma, N_2 $B^3\Pi_g$ state excitation, role of long lived states, luminesc. 80−37829
He-N_2-CO_2, discharge ionisation growth, diffusion coeffs. 78−83636
He-N_2-CO_2 mixture, IR laser output from elec. discharge after X-ray preionisation 79−64205
He-N_2-CO_2 mixture in supersonic nozzle, shock activation with overexpansion, jet form. 78−18330
He-NF_3, electron attachment coeffs. using swarm techniques 80−53915
He-NF_3 laser, F^* relax., generating 250 kW at 0.6-0.75 micron, for 2-3ns *(Russian)* 78−1219
He-NF_3(SF_6) hollow-cathode laser using F transitions 80−48289
He-Na mixture, low-pressure discharge, radial cataphoresis obs. 78−67507
He-Ne, 1.15 μm laser line, 260 THz freq. synthesis using $CdGeAs_2$, Ag_3AsS_3 crysts. 79−64263
He-Ne, 3.39 μm laser, actively mode-locked oscill., modulation freq. depend. 77−61983
He-Ne, 3.39 μm laser with no freq. modulation, freq. stabilisation rel. to methane saturated absorpt. 79−76700
He-Ne, 6328 Å, single-mode collapse 78−94404
He-Ne, 632.8 nm laser, energy characteristics, spatial inhomogeneity effect 77−75483
He-Ne, afterglow of low-press. glow discharge, recombination processes 78−26366
He-Ne, anisotropic ring laser cavity, polarisation characts. 79−59726
He-Ne, complex resonator laser, stabilisation by freq. offset-lock 77−31107
He-Ne, gas discharge laser, stimulated emission, vel. to striation 80−37994
He-Ne, generation by hollow cathode discharge excitation, mechanism *(Russian)* 77−10888
He-Ne, glow discharge, striation current conditions 79−55595
He-Ne, glow discharges, AC cataphoresis meas. using light spectrometry 79−60096
He-Ne, HF discharge, electron energy distrib. 77−34874
He-Ne, I_2 stabilised, freq. stability and reproducibility 78−13726
He-Ne, I_2 stabilised lasers, conf., Germany (Feb. 1977) 78−87069
He-Ne, I_2 stabilised laser design, freq. reproducibility 78−87070
He-Ne, I_2 stabilised laser research 78−87071
He-Ne, I_2 stabilised laser with hot wall I_2 cell 78−87073
He-Ne, I_2 stabilised laser, instrumental freq. offsets 78−87084
He-Ne, I_2 stabilised lasers, international intercomparison meas., hyperfine struct. spacings 78−87088
He-Ne, I_2 stabilised lasers, beat frequency, international comparisons *(French)* 78−87090
He-Ne, internal mirror laser, polarisation props. of output beam 77−46744
He-Ne, LG-75-1 laser 79−94256
He-Ne, laser, Ne absorber induced features in AC response 77−3613
He-Ne, laser, scheme for automatic fine frequency tuning along the Lamb depression 80−74385
He-Ne, laser, short pulses, self mode-locking *(Rumanian)* 79−13995
He-Ne, laser frequency measurements: a review, limitations, extension to 197 THz (1.5 μm) 78−81952
He-Ne, laser pumping transition, mol. beam obs. 77−7064
He-Ne, laser revived by running in He atm. 78−46614
He-Ne, laser single frequency generation model and expt. *(Russian)* 77−58314
He-Ne, laser wavelength measurement using digital interferometer 80−37079
He-Ne, lasers, low-power low-cost design and manufacture 77−19329
He-Ne, lasing spectrum, modulation freq. of resonator losses 77−34902
He-Ne, low-ionised plasma, electron kinetics, collision processes influence *(German)* 79−14519
He-Ne, methane and I_2 stabilised lasers, wavelength intercomparison using Michelson interferometer 78−87089
He-Ne, narrow linewidth frequency scannable 3.39 μm laser, appls. 77−88757
He-Ne, oscills. in laser discharge 78−55339
He-Ne, plasma He I 4471 Å line profile obs. at high electron density 78−67472
He-Ne, pulsed atomic Ne laser, time and energy characts. in mag. field *(Russian)* 78−22108
He-Ne, ring laser, difference freq. depend. on active medium gain 77−722
He-Ne, ring laser, rapidly pumped, competition between opposite waves 78−17985
He-Ne, ring laser, Zeeman effect, influence of reson. radiation trapping 77−75574
He-Ne, rotating ring laser, output characts. 78−29982
He-Ne, single mode laser, mode polarisation in transverse mag. fields 78−22107
He-Ne, single mode laser, emission zone nonlinear active lens effect 80−32960
He-Ne, stabilizer two freq. 0.63 μ laser 79−94243
He-Ne, stable laser with methane absorpt. cell, 7 Hz width 3.39 μm line emission 78−17974
He-Ne, thermal diffusion factor, 65 to 300K 78−71418

helium continued
He-Ne, three-mode laser, total intensity under mode locked conditions, freq. stabilisation 77−83853
He-Ne, two-mode ring laser, stimulated emission regimes 77−657
He-Ne, weakly anisotropic resonator laser, natural polarisation fluctuations of emission 77−79801
He-Ne $^{127}I_2$ stabilised laser source for Michelson interferometer, optical feedback obs. 80−106545
He-Ne 3.39 μm laser, FM eliminated CH_4 locked freq. stabilisation in dual feedback control 80−99772
He-Ne 3.39 μm laser mode-locking for ultrashort pulse generation 77−83909
He-Ne ($^{127}I_2$) laser freq. stability, expt. 77−83915
He-Ne CH_4 locked laser, freq. stability meas. 80−87422
He-Ne CW laser nuclear pumping demonstration 79−13949
He-Ne commercial multimode low power laser, conversion to single mode laser 80−53325
He-Ne compact LG-78 laser 79−7148
He-Ne complex resonator laser, stabilisation 78−55374
He-Ne discharge, 3071, 5665 and 10353 nm. laser transitions 77−54692
He-Ne discharge, gain probing by intracavity dye laser spectroscopy 77−7092
He-Ne discharge, striation oscills., spectral width variations 77−62429
He-Ne discharge, striation parameters, discharge current modulation effect 77−84555
He-Ne discharge laser, stimulated reactive oscills., laser-elec. circuit Q 77−58315
He-Ne discharges, striations in narrow discharges 80−38736
He-Ne double mode laser in axial mag. field. *(Russian)* 79−86160
He-Ne dual mode laser, injection modulation in coupled laser oscillators 80−99773
He-Ne gas laser, anisotropic resonator, linear polaris. freq. depend. 77−10961
He-Ne gas laser, behaviour in nonsynchronous frequency modulation regime *(Russian)* 79−7161
He-Ne gas laser, glow discharge electron irrad. rel. to output characts. 79−64198
He-Ne gas laser, modulation method, for relative excitation level, cavity bandwidth and at. temp 80−5771
He-Ne gas lasers, 2 mW and 5 mW, reliability 80−95913
He-Ne gas mixture plasma, role of charge exchange in form. of optical props. 80−28600
He-Ne gas ring laser, unidirectional two-mode lasing, stability region width 79−76721
He-Ne glow discharge, passive freq. charact. 79−50915
He-Ne I_2 stabilised laser, practical approach to design and construction 80−19051
He-Ne IR laser, internal modulation of polarisation 77−19350
He-Ne internal mirror lasers, polarisation in mag. field 78−17907
He-Ne internal mirror laser, degeneration of longitudinal modes and freq. stabilisation *(Japanese)* 78−90426
He-Ne laser, $^{127}I_2$ saturated absorption stabilised, wavelength meas. *(Russian)* 79−22996
He-Ne laser, $^{127}I_2$ stabilised, freq. shifts, limitations 78−90440
He-Ne laser, $^{127}I_2$ stabilised, length or freq. standard 80−106544
He-Ne laser, 0.63 μm emission intensity fluctuations, spectral correl. 78−1212
He-Ne laser, 0.633μm line freq. stabilisation with 3.39μm line locked to CH_4 80−28258
He-Ne laser, 3.39 μm, in-resonator losses, effects on power *(Russian)* 78−5455
He-Ne laser, 60 mW, perturbation spectroscopy *(Rumanian)* 78−50752
He-Ne laser, 6328 Å, output power, using intracavity rot. reflector 79−7113
He-Ne laser, 6328 Å power fluctuations due to striation noise 80−78834
He-Ne laser, anisotropy due to saturating fields 78−55337
He-Ne laser, autodyne effect 79−81404
He-Ne laser, beat freq., high displacement sensitivity meas. 80−95926
He-Ne laser, beat freq. generation between CW dye laser with 80-GHz freq. offset 80−1253
He-Ne laser, cavity losses, phase polarisation method in lasing regime 80−87413
He-Ne laser, compact, transverse microwave discharge, energy characts. 80−64064
He-Ne laser, competitive oscillation mode frequency stabilisation *(Russian)* 79−22962
He-Ne laser, discharge current rel. to optical power, automatic control of radiation level *(Russian)* 77−46716
He-Ne laser, discharge tube design and construction *(Czech)* 79−76702
He-Ne laser, double reson., RF mag. field strength and g-value depend. *(Japanese)* 78−9359
He-Ne laser, doubly resonant intracavity SHG of 1153 nm radiation with stabilization on HFS components of $^{127}I_2$ 80−33077
He-Ne laser, elec. parameters of active element 79−3682
He-Ne laser, field distrib. and spatial coherence of superluminescence at 3.39 μ transition *(Russian)* 78−13682
He-Ne laser, freq. characts. under two-mode generation 80−53264
He-Ne laser, freq. conversion in Na vapour *(Russian)* 78−33776
He-Ne laser, freq. stability improvement with hot wall I cell 77−83914
He-Ne laser, gain, saturation, polarisation and spectral inhomogeneities, relax. consts. 77−50652
He-Ne laser, high stability, single freq., 3.39 μm 78−71121
He-Ne laser, hot wall I cell freq. stabilisation using saturated absorpt. 77−65598
He-Ne laser, I_2 stabilised, wavelength intercomparison 77−19305
He-Ne laser, I_2 stabilised, reproducibility limitations 77−46740
He-Ne laser, I_2 stabilised, freq. shifts 77−50697
He-Ne laser, I_2 stabilised, realisation of length unit 78−87068
He-Ne laser, I_2 stabilised, design construction and performance 79−13978
He-Ne laser, I_2 stabilised, saturated absorpt. lines press. and power broadening 79−76765
He-Ne laser, I_2-stabilised, with long path interferometer, optical feedback effect 77−9544
He-Ne laser, IR lasing lines, anomalous competition effects *(Russian)* 77−68202
He-Ne laser, in axial mag. field, output power dependence of mode locking phenomena 78−71129
He-Ne laser, intensity fluctuations meas., comparison with He-Cd laser 78−71087

helium continued
He-Ne laser, intensity oscillation spectrum obs. for external modulating signal on discharge plasma 77−7066
He-Ne laser, internal pulse-code modulation, 0.6328 μm at 150 Mbits s^{-1} 79−76725
He-Ne laser, intracavity saturable Ne absorber, response enhancement 77−65602
He-Ne laser, kinetics calcs. using electron distrib. function *(Russian)* 77−61941
He-Ne laser, LG-56, radiation power stabilisation 78−17970
He-Ne laser, laser system for 3.39 μm freq. synthesis 78−18001
He-Ne laser, longit. mode locking using Fabry-Perot etalon 79−50318
He-Ne laser, low noise manufacturing 78−79038
He-Ne laser, mag. polarised performance 77−14750
He-Ne laser, manufacturing problems with low noise specification 78−59047
He-Ne laser, methane stabilised, intercomparisons 77−19304
He-Ne laser, methane stabilised, freq. fluctuation analysis 77−31108
He-Ne laser, methane stabilised, 3.39 μm freq. meas. relative to 10.17 μm CO_2 laser 77−31113
He-Ne laser, methane stabilized, low noise laser tube characts. *(Japanese)* 78−25891
He-Ne laser, methane-stabilized at 88 THz 80−73304
He-Ne laser, microwave pumping advantages 78−50754
He-Ne laser, mode coupling, nonlinear effects *(German)* 77−19233
He-Ne laser, mode interaction, transition level degeneration effects *(Russian)* 77−61940
He-Ne laser, mode selection and mode locking, effect on two-photon absorpt. efficiency 78−83023
He-Ne laser, mode stabilisation by axial mag. field, long resonator case 77−7143
He-Ne laser, Ne $3s_2$-$2p_4$ transition, relaxation characts. of degenerate states obs. using polarisation spectroscopy *(Russian)* 80−27348
He-Ne laser, near IR emission characts., coupled transitions 77−27275
He-Ne laser, operating on 0.63, 3.39 μm coupled transitions, intensity modulation 80−69365
He-Ne laser, optical freq. standard, freq. stabilised by warm walled I_2 cell *(French)* 78−42343
He-Ne laser, optical heterodyning of spontaneous emission 78−29995
He-Ne laser, optimal conditions for microwave pumping 80−32961
He-Ne laser, Original Equipment Manufacturer applics. 78−33765
He-Ne laser, output power, unsaturated gain distrib. 78−50751
He-Ne laser, population changes of Ne levels, laser action in intermediate IR 78−29933
He-Ne laser, population inversion radial distrib. in active element, excitation conditions effect 78−71079
He-Ne laser, power characteristics obs., with CH_4 cell, at λ=3.39 μ *(Russian)* 78−1207
He-Ne laser, radial profiles of upper and lower level emission 77−31088
He-Ne laser, radiation field spatial distrib. distortions due to multilayer dielectric mirrors 77−38970
He-Ne laser, refl. anisotropy of 6320 Å mirrors 79−98413
He-Ne laser, rejuvenation methods 77−37687
He-Ne laser, self-locked, pulse velocity, power and mode phase 77−61939
He-Ne laser, simultaneous oscillation at 0.63 and 3.39 μm, output power depend. on loss in mag. fields *(Japanese)* 80−32959
He-Ne laser, six new transitions near 1.49 μm 77−38856
He-Ne laser, spatial anisotropy induced by cascade laser transitions 78−29931
He-Ne laser, stabilised by I_2 saturated absorpt., technological principles *(French)* 78−87075
He-Ne laser, stabilised by I_2 saturated absorpt., performance characts. *(Chinese)* 79−59717
He-Ne laser, stabilised by $^{127}I_2$ saturated absorpt., wavelength international comparisons 80−95872
He-Ne laser, thermal effect of penetrating radiation *(Russian)* 78−22109
He-Ne laser, three mode stimulated emission 77−75485
He-Ne laser, transition probabilities of Ne spectral lines at 352, 363, 345 and 543 nm 78−25851
He-Ne laser, two-mode ring laser power resons. 78−1211
He-Ne laser, two-photon amplification on cascade-transitions, power tuning curve meas. 80−48219
He-Ne laser, type 300.1 TEM_{00} *(Rumanian)* 80−9898
He-Ne laser, unmodulated, stabilizing to $^{127}I_2$ hyperfine component, preliminary expt. 79−50328
He-Ne laser, use at 0.63 μm, intensity fluctuations at quantum level 77−27274
He-Ne laser, wavelength meas. appl., reference standard 77−7124
He-Ne laser, wavelength switching using var. methane press. 77−19312
He-Ne laser, with methane absorpt. cell, reson. freq. shift with methane press. 77−50687
He-Ne laser average output power, resonator losses, freq. modulation 77−34901
He-Ne laser beam, intensity fluctuations, spatial distrib. 79−18458
He-Ne laser discharge tubes, design and technology, review *(Czech)* 79−72586
He-Ne laser energy characteristic control, by discharge current modulation 77−79800
He-Ne laser fluctuation spectra of freq. and amplitude 78−82950
He-Ne laser IR applications 79−94275
He-Ne laser light polarisation in transverse mag. field, Zeeman effect *(Dutch)* 78−29997
He-Ne laser mode locking by three-level reson., Zeeman tuning of intracavity Ne absorber 79−89943
He-Ne laser model LG-10, design *(Rumanian)* 80−87407
He-Ne laser near threshold, intrinsic third-order intensity correlation 77−10887
He-Ne laser photon statistics variation with cavity length 80−53265
He-Ne laser plasma, line profiles meas. by optogalvanic spectroscopy 78−62233
He-Ne laser plasma, metastable at. and electron density diagnostics 77−84499
He-Ne laser pulsed internal modulation 77−61985
He-Ne laser radiation intensity rel. to striations and oscillations 77−83852
He-Ne laser reference IR frequency meas. installation 77−79068
He-Ne laser saturation resonance in static magnetic field 77−54693
He-Ne laser scanning system, for video record player, information identification *(German)* 80−106557

helium continued
He-Ne laser simultaneous oscillation at 0.63 μ and 3.39 μ in mag. field, and with Brewster windows 79−68381
He-Ne laser stabilisation, I_2 absorption cell power densities 80−99767
He-Ne laser stabilisation and performance for dimensional meas. 80−19049
He-Ne laser stabilisation by I_2 612 nm saturated absorption 80−99765
He-Ne laser stabilisation by I_2 611.8 nm saturated absorption 80−99766
He-Ne laser stabilised by saturated absorpt. in I_2 at 612 nm 79−59730
He-Ne laser stabilised by methane E-component saturated absorpt., quantum freq. standard 80−9901
He-Ne laser stabilised by methane E-component, reference source freq. reproducibility 80−106507
He-Ne laser status, I_2 vapour stabilised 78−87072
He-Ne laser tube, laser module LGK 7621, construction 80−53314
He-Ne laser tube construction and cost analysis 77−65599
He-Ne laser tube reconditioning 77−78933
He-Ne laser two-beam interferometer phase errors *(Russian)* 79−6166
He-Ne laser unit, factors affecting service life *(German)* 78−90424
He-Ne laser wavelength drift 80−67978
He-Ne laser wavelength stabilisation on I_2 *(Czech)* 78−87061
He-Ne laser wavelength stability, calibration and traceability 80−19050
He-Ne laser with $^{127}I_2$ saturable absorber, high contrast power reson. 78−29976
He-Ne laser with anisotropic cavity, fluctuations of field polaris. 79−27242
He-Ne laser with external optical resonator, SHG 79−27326
He-Ne laser with I_2 absorpt. cell, nonlinear resonances at 0.63 μm *(Russian)* 79−59672
He-Ne laser with internal mirrors, mode polarisation props. 80−23672
He-Ne laser with methane absorber, reson. obs. in output, freq. stabilisation 77−83854
He-Ne laser with methane absorpt. cell, hyperfine struct. influence on freq. reproducibility 78−50864
He-Ne laser with methane nonlinearly absorbing cell, freq. self-stabilisation effect 79−98420
He-Ne laser with transverse microwave discharge, use of secondary electrons 80−9899
He-Ne laser with waveguide resonator, oscill. modes 77−27311
He-Ne lasers, discharge reson. props. effect on radiation fluctuations, expt. 78−74883
He-Ne lasers, freq. stabilised by ref. to I and methane absorption transitions 77−83913
He-Ne lasers, I_2 stabilised, saturated absorption signal props. 77−75481
He-Ne lasers, I_2 stabilised, 633 nm line, performance improvement 78−90429
He-Ne lasers, I_2 stabilised, with improved performance 79−22964
He-Ne lasers, in hollow Cu cathode, 632.8 nm output characts. 80−63975
He-Ne lasers, iodine- and methane-stabilised, reproducibility comparison 77−7135
He-Ne lasers, life time depend. on impurity gases *(Chinese)* 79−36881
He-Ne lasers, population changes of Ne levels, laser action in intermediate IR 78−29932
He-Ne lasers, stabilised by saturation absorpt. in I_2 78−1270
He-Ne lasers, standard wavelength sources 78−74957
He-Ne lasers, transverse microwave freq. gas-discharge pumping 80−74339
He-Ne lasers levels, modulation spectroscopy 78−46572
He-Ne lasing medium, evaluation of population changes of Ne levels 78−25855
He-Ne low-gain laser amplifier, phase control 80−64059
He-Ne methane system, narrow nonlinear resonances in three level system *(Russian)* 80−78898
He-Ne mixture, cataphoretic gas separation in DC glow discharge with end volumes 80−79428
He-Ne mixture, electron beam prod. plasma decay, appl. to laser pumping 79−41847
He-Ne mixture, primary ionisation relativistic growth 79−86554
He-Ne mixtures, disparate mass, double sound propag., theory 80−33724
He-Ne mixtures, spark channel formation 78−1936
He-Ne mode-locked binary laser oscillator, bistability induced by optical nutation 79−31958
He-Ne modulated positive column, elec. and optical props. 77−27765
He-Ne multimode and single-mode lasers, phase locking to very high coherence degree 79−76710
He-Ne nuclear-pumped CW lasing 80−48216
He-Ne optical waveguide amplifier, operation 80−43363
He-Ne ring laser, 0.6328 μm, self-pulsing conditions 80−87414
He-Ne ring laser, absorbing medium press. influence on power resonance characts. *(Russian)* 80−23725
He-Ne ring laser, freq. shift of 3.39 μm methane transition 79−27298
He-Ne ring laser, influence of pressure on Zeeman effect 80−19056
He-Ne ring laser, methane absorber narrow nonlinear resonances at low press. *(Russian)* 79−76722
He-Ne ring laser, methane stabilised, nonlinear resonance freq. shift due to back scatt. *(Russian)* 80−78874
He-Ne ring laser, Ne isotopic composition changes during prolonged discharge *(Russian)* 78−22110
He-Ne ring laser, nonlinear polarisation interaction of opposite waves 78−50828
He-Ne ring laser, nonlinear Zeeman effect 78−71123
He-Ne ring laser, nonlinear spectroscopic technique 80−91819
He-Ne ring laser, nonreciprocal effects with transverse mag. field applied to active medium 80−91820
He-Ne ring laser, operating well above lasing threshold Zeeman effect 80−33039
He-Ne ring laser, opposing waves competition at lasing line centre of Ne isotope 80−1187
He-Ne ring laser beat frequency deviation rel. to dispersion and modulation 79−68410
He-Ne ring laser placed in longit. mag. field, nonlinear nonreciprocity effects 80−43377
He-Ne ring laser with methane absorpt. cell, power reson. characts. 80−28255
He-Ne ring laser with nonlinear absorber, competition of orthogonally polarised modes 78−17984
He-Ne rotating ring laser, freq. characts., mode composition effects 77−54741

helium continued
He-Ne single mode lasers, meas. of intensity of sources of inherent fluctuations 80−32958
He-Ne stabilised transverse Zeeman laser, light source for optical meas. 80−48272
He-Ne stable gas laser with 0.4 Hz line width 80−48294
He-Ne standing wave laser, two-mode locking *(Russian)* 77−79874
He-Ne travelling wave laser, spontaneous emission spectra, 3.39 μm region 80−37995
He-Ne two mode ring laser for interferometry 78−1260
He-Ne two-mode gas laser, strong, coupling, transient 79−55114
He-Ne two-mode laser with methane absorbing cell, freq. stability and reproducibility 79−89934
He-Ne two-mode travelling-wave laser, Zeeman beats 78−50827
He-Ne waveguide laser, discharge plasma theory, max. output intensity depend. on discharge tube radius 79−55110
He-Ne waveguide lasers, HF discharge stability 79−18401
He-Ne waveguide lasers, props. and current-voltage characts. of discharges 78−1208
He-Ne Zeeman laser, two-transitions with common upper level *(Japanese)* 79−55112
He-Ne/CH_4 FM eliminated laser, freq. stability meas. 80−87423
He-Ne/CH_4 laser, IR freq. absolute meas. *(Russian)* 80−9851
He-Ne-Xe, ion laser transitions, hollow cathode excitation 80−1184
He-Ne-methane ring laser, frequency stabilized, operating charact. 80−14366
He-Ne-methane ring laser, power resonances 80−99761
He-Ne-methane ring laser, freq. synchronisation interval for oppositely directed waves 80−99762
He-Ne-methane stabilised ring laser, freq. stability calcs. *(Russian)* 78−9401
He-Ne(Ar), thermal cond., composition dependence 78−51276
He-Ne(Ar)(N_2)(CO_2), thermal diffusion factors, (m,6,8) pot. calcs. 79−50835
He-O_2, diffusion, search for Senftleben-Beenakker effect 77−15155
He-O_2 breathing, effect on respiratory mechanics 78−27992
He-O_2 corona discharge CV characteristics 78−91168
He-O_2 DC discharge, electron distrib. function 80−92407
He-O_2 diffusion coeff., two-bulb meas. 77−11299
He-O_2-acetylene flame atom cell, for at. spectrometry, characterisation 78−32876
He-SF_6, AC particle initiated breakdown, compressed gas mixture 78−87556
He-SF_6(O_2)(CF_4) mixtures, viscosity and diffusion coeffs. 77−89225
He-Se, metal ion laser, noise props. *(Japanese)* 79−64209
He-Se, vapour laser, continuous wave, intensity fluctuations investig. 80−83593
He-Se laser, cataphoretic effects in power output 77−83863
He-Se laser, noise props. 77−83857
He-Se^+ three-colour laser engineering 78−46644
He-Se^+ white light laser 80−1226
He-Sr, laser plasma, double pulse excitation, singularities *(Russian)* 77−61945
He-Sr laser, possibility of nucl. pumping, 4305 Å Sr II transition 80−58518
He-Sr pulsed laser, pumping rate and electron density meas. 80−9868
He-UF_6 gas mixture, velocity slip in free jet expansions 78−90951
He-vacancy clusters in Cu, computer simulation 77−39583
He-Xe, eqn. of state, Monte Carlo calcs. 80−59158
He-Xe, H_2CO-stabilised laser, freq. stability in axial mag. field 79−22991
He-Xe, high-press. neutral IR laser emission from Xe 79−86159
He-Xe, low-threshold nuclear pumped laser, generation characts. 80−19018
He-Xe, Xe I TEA lasers, energy characteristics 80−63977
He-Xe 3.51 μ laser mode competition in axial mag. field 80−63974
He-Xe laser, 3.51 μm, mode competition in axial mag. field 78−25850
He-Xe laser, freq.-offset-locked at 3.51 μm 79−98400
He-Xe laser, nuclear pumping by vol. source of fission fragments 79−36879
He-Xe laser, Zeeman tuned *(Korean)* 79−7145
He-Xe mixtures, high temp. heat conduction 79−14509
He-Xe optical amplifier, high gain coeff., noise characts. 80−43365
He-Xe optical amplifier, striation form. for DC discharge plasma, noise anal. 80−43366
He-Xe plasma, in mag. field, effect of CO_2 mol. addition on plasma parameters 77−42965
He-Xe recombination lasers, CO%d2 laser-produced plasma-initiated 80−48286
He-Xe-F_2 mixture, pulsed avalanche discharge at high gas press., homogeneous form. conditions 80−49027
He-Xe-I_2(anthracene), gaseous mixture with one low conc. components, thermal diffusion calcs. 77−19661
He-Ze laser, freq. stability at 3.51 μm 79−98401
He-Zh laser, hollow cathode type, oscillation characts. improvement by inert gas additions *(Japanese)* 77−65590
He-Zn, coaxial type hollow cathode laser, oscillation charact. *(Japanese)* 78−13692
He-Zn, hollow cathode laser discharge, selective excitation of 5894, 7479 Å transitions by Ar 77−27280
He-Zn, hollow cathode laser, gain meas. for 7588, 4924, 7479 and 5894 Å Zn^+ transitions 77−88713
He-Zn, hollow cathode laser tube, with direct current excitation *(Japanese)* 79−76704
He-Zn and He-$ZnCl_2$ hollow cathode laser discharges, comparison 80−28203
He-Zn hollow cathode laser, electron density, excited ions radial profiles 78−29937
He-Zn hollow cathode laser, 7588 Å in ZnII, operating characts. and upper level operating mech. 78−63071
He-Zn hollow cathode laser discharge, radiative cascade excitation effect on upper laser levels 80−102697
He-Zn hollow-cathode discharge, excitation processes, rel. to Zn II laser 79−98342
He-Zn II laser, 0.4924 μm oscill. spectra meas. using scanning interferometer *(Japanese)* 80−9864
He-Zn laser, 7588 Å, He metastable atoms effect on power 78−33722
He-Zn laser, negative glow and positive column discharges comparison 78−1217
He+Ar+polyatomic fluorides, VUV spark emission spectra 79−3457

helium continued
He+Be^+ collisions, autoionising core-excited Be II states, alignment prod. 80−14204
He+CO(HCl)(HCN)(HD), press. broadening, rot. energy transfer, infinite order sudden approx. 78−22011
He+Cs, shift, halfwidth, satellite and absorpt line in square-well pot. 80−42993
He+group II metal atoms, gas discharge plasma, Penning ionisation, cross section anal. 80−33735
He+H_2, adiabatic distorted-wave infinite order sudden approx. 80−99558
He+H_2, collision-induced dipole, ab initio VB calc. 78−94202
He+H_2, gas discharge plasma, H_2 dissoc. excitation, cross section anal. 80−33735
He+H_2 microwave plasma, pulsed high current heating at atm. press., MHD instability 78−55728
He+H_2^+, 10 keV dissoc. charge exchange collisions 78−94319
He+H_2^+, endothermic reactive and vibr. inelastic collisions, pot. well effects 79−8430
He+H^+(D^+), runaway mobility obs. 80−38517
He+K($4P_{1/2}$), fine struct. transitions, energy depend. crossed beam determ. 79−86035
He+N_2+N_2^+→N_4^++He, transition state theory 78−27755
He+N^{2+}(O^{2+})(Ne^{2+})(Ar^{2+})(Ar^{3+}), electron transfer cross-section, <100 eV 78−66654
He+Ne^{n+}, (n=1, 2, 3, 4), energy spectra of electrons produced 79−45822
He+OCS, rot. lines, collisional broadening 79−18267
He+SO_2, vibr. relax., shock tube study 80−48062
He+water (cyanomethane), afterglow, excitation and quenching reactions, optical pumping 78−35690
He+Xe^{n0+} depend. of charge transfer on ionisation pot. of atoms 79−64096
He^++Ar(N_2)(He), up to 70 keV, symmetric (antisymmetric) reson. charge transfer cross sections *(Korean)* 78−50636
He_2, formation in afterglow of pulsed discharge 77−15259
He_2, quantum-mechanical calculations 77−14350
He_2, separated electronic pair functions, direct minimisation of energy functional, LCAO-MO SCF, density matrix formalism 79−31392
He_2^+ form. in pulsed afterglow, mass spectroscopic obs. 80−54046
He_2^+, mobility and clustering reaction in He 79−10628
He_2^{2+} $^1\Sigma_g^+$ ground state, hybrid Slater-Gaussian-type 1s orbitals calc. 77−38605
He_2^++O_2 charge exchange laser 78−50759
He_n^+, in afterglow with water (cyanomethane), lasing processes 78−35690
He(-H_2), hollow cathode effect in cylindrical geometry *(French)* 80−33842
He(-Ne), electron pair production cross sections, 2.614 MeV, triplet events 77−57580
HeH^+, mobility in He gas 78−18371
HeI spectral line profile of low-press. afterglow plasma in mag. field 80−6285
^{3}He, adsorbed on solid Ar, desorption heat capacity 80−10735
^{3}He dense vapour, electron surface barrier, density depend. determ. 77−1270
^{3}He, detrapping and release from metal tritide, after ^{3}He decay, strain model 77−60101
^{3}He, distrib. in metal tritides 78−30661
^{3}He excess in Mid-Atlantic Ridge bottom waters, hydrothermal activity 80−101383
^{3}He injection in Gulf of California, meas. in Guaymas Basin 80−85640
^{3}He ion depth profile meas. by deuteron induced reactions 77−19978
^{3}He laser, direct nuclear pumped, power density 78−9362
^{3}He mass spectrometric meas. for environmental ^{3}H anal. 77−9447
^{3}He, outgassing from metal tritide, after ^{3}H decay, ^{3}H conc. effects 77−60100
^{3}He plasma, electron temp. and density, estimation method 80−64785
^{3}He retention characteristics of LiT, NMR study 79−69153
^{3}He, selective adsorption on NaF and LiF, atomic beam scatt. meas., binding energies 78−63935
^{3}He, selective adsorption on basal plane surface of graphite 80−6650
^{3}He, specific heat second layer adsorbed on Grafoil 78−87843
^{3}He, thermal conductivity, quantum effects 79−14510
^{3}He, thermal desorption from $ErT_{1.8}$, comparison of aged and ^{4}He implanted samples 77−60102
^{3}He thermal desorption from Ni, low temp. release 80−34294
^{3}He/^{4}He, high ratios in Hawaii lavas olivine phenocrysts and xenolithic dunites 79−34814
^{3}He/^{4}He ratio in atm. He, mass spectrometric meas. 77−9447
^{3}He-^{20,22}Ne/$^{127}I_2$, 0.63 micron laser generated contrasting power resons. *(Russian)* 77−23651
^{3}He-^{22}Ne 0.63 μm laser stabilised with $^{129}I_2$ nonlinear absorpt. cell, freq. characts. 80−53333
^{3}He-^{22}Ne laser, interaction of orthogonally polarised modes with various transverse distribs. *(Russian)* 77−27276
^{3}He-^{22}Ne laser with I_2 absorption cell 77−79867
^{3}He-^{4}He few atom mixed mols., binding energy, size, particle distrib. 80−32864
^{3}He-^{4}He in liquid ^{4}He, non-additive interaction in solvent effect 79−41120
^{3}He-^{4}He mixture, direct nuclear pumping, fission-induced, heavy particle energy distrib. function 77−23643
^{3}He-Ar (Xe)(Kr)(Cl), volume pumped nuclear laser, survey of lasing 80−63979
^{3}He-Ar nuclear pumped laser, first order model, lasing action depend. on Ar conc. 79−76668
^{3}He-Ar plasma, electron temp. and density, estimation method 80−64785
^{3}He-Ar volumetric nucl. pumped laser, dominating processes and reaction physics 80−63981
^{3}He-Ar(Xe)(Kr)(Cl), nucl. lasing, population inversion mechanism 80−63980
^{3}He-Ar(Xe)(Kr)(Cl) direct nuclear pumped lasers using ^{3}He(n,p)^{3}H reaction 79−31863
^{3}He-Hg (−Kr)+^{3}He(n,p)T, high press. plasma excitation, luminesc. spectra 80−38719
^{3}He-Kr laser, nucl. pumping by volumetric ^{3}He(n,p)^{3}H reaction 77−10886
^{3}He-N_2-CO, nucl. reactor active zone, plasma and sustained discharge props. 80−5729

helium continued
^{3}He-Ne stabilised by saturated absorption ^{127}I, laser wavelength standard development appl. *(German)* 78−79034
^{3}He-Xe, nucl. pumped laser plasma, distrib. functions 79−36880
^{3}He-Xe laser, direct nucl. pumping via ^{3}He(n,p)^{3}H 77−71972
^{3}He-Xe laser, direct nuclear pumping by protons and tritons 78−5458
^{3}He-Xe laser, nucl. pumping by volumetric ^{3}He(n,p)^{3}H reaction 77−10886
^{3}He-Xe nuclear pumped laser, small signal gain coeff. and power output, theory comparison with expt. 80−63983
^{3}He-Xe nuclear pumped laser, electron distrib. function role 80−63984
^{4}He, adsorbed on solid Ne, desorption heat capacity 80−10736
^{4}He charged drops in cryogenic vap., He^+ mobility, 1.3-2.0K 79−32734
^{4}He content of fracture zone water of N.Kirgizia 77−33108
^{4}He dense vapour, electron surface barrier, density depend. determ. 77−1270
^{4}He, desorbing from LiF, comparison with quantum statistical theory of flash desorption 80−44410
^{4}He excess in Teggau Lake, NW.Ontario, rel. to U ore body 78−65353
^{4}He gas lasers, horizontal, heated from below, Nusselt and Rayleigh numbers 80−79311
^{4}He, ion, backscattering anal. 79−96408
^{4}He ion, meas. of W in tissue equiv. gas, dosimetry appl. 80−19550
^{4}He, low temp., momentum distrib., binary cluster term evaluation, 3D Lennard-Jones gas 77−37808
^{4}He primordial abundance, upper limit 78−45444
^{4}He primordial abundance for superweak particle cosmological constrains 79−84667
^{4}He pumping lines, low press. safety value 78−32822
^{4}He, selective adsorption and NaF and LiF, atomic beam scatt. meas., binding energies 78−63935
^{4}He, selective adsorption on basal plane surface of graphite 80−6650
^{4}He stopping cross sections, 1-8.5 MeV 78−58558
^{4}He stopping power, 0.15 to 1 MeV, backscatt. determ. 80−88233
^{4}He, thermal conductivity, quantum effects 79−14510
^{4}He vapour, cryogenic, ion-droplet mobility 79−57308
$^4He_2$ and $^3He_2$ dimers in liquid ^{4}He, non-additive interactions in solvent effect 79−41120
^{4}He-D_2 mixture, binary diffusion coeff. near phase separation line *(Russian)* 80−6191
$(^4He)_3$, interaction through realistic diatomic pots., Faddeev-UPE theory 77−23531
He*-Ne*, Penning ionisation of metastable He* 80−83472
He(1^1S)-He(1^1S, 2^3S, 2^1S), H(1^2S), dispersion energies, charge overlap effects, with freq.-depend. polarisability 79−86025
He(2^3S,2^1S)+H_2, chemiionisation of H_2 77−36739
Hg-He(Ar), modulated discharge, elec. and optical props. 77−7627
Kr^{2+}, mobility in He gas, drift-tube meas. 78−66657
Kr(-He) arc, wall-stabilised, atm. press. 79−46503
Li^+ mobility in He 300K, interaction pot., drift tube meas. 77−76026
Li/He heat pipe, start-up power, heat transport, thermal regulation 80−53615
$LiNbO_3$:He, ion implantation, optical waveguide form., refr. index changes 78−46762
$LiNbO_3$:He^+, ion implanted SAW guides, air-gap Si convolver data 78−42500
Li(2^2S), electron loss in passing through inert gases 79−13805
Mg:He, interaction energy of two He atoms, Hohenberg-Kohn-Sham density functional formalism 79−51519
Mn-He laser, stimulated emission mechanism, energy charact. 77−3571
Mo:^{3}He, trapping of ^{3}He and mutual replacement 80−59493
Mo:H(He), depth profiles of implanted atoms, proton backscatter meas. 79−51136
Mo:He, at. config. of $^1/_2\langle 111\rangle$ screw dislocation 79−65081
Mo:He, interaction of He with edge dislocation, influence of interatomic pot. 79−33014
N_2 laser near-threshold IR enhancement by He additive *(Japanese)* 80−14324
N_2-CO_2(-He) volume discharge, N_2 vibr. levels, stepwise excitation, effect on electron energy balance 80−54071
N_2-He, barrier discharge, struct., spectral anal. *(Russian)* 77−21463
N_2-He ion nuclear pumped lasers feasibility study and quenching 80−64001
N_2-He laser, charge transfer pumping at atm. press., in elec. avalanche discharge 79−10286
N_2-He mixture, film condensation, appls. to condensers for cryogenic installations 78−59941
N_2-He plasma, laser produced, high press. amplified stimulated emission 80−78843
NH_3-He mixture, viscosity, Senftleben-Beenakker effect 80−100054
N_2O-CO-He mixture, radiation amplification factor in supersonic expanding stream of gas 77−10896
N_2O-He, species concentrations in glow discharge and afterglow, mass spectra, laser conditions 78−14241
N_2O-N_2-He, gasdynamic laser, effect of weak flow perturbations on gain 80−14316
N_2O-N_2-He, population inversion of N_2O vibr. levels behind shock wave front 79−31886
N_2O-N_2-He mixture, radiation amplification factor in supersonic expanding stream of gas 77−10896
Nb:He, implant saturation and annealing, effect on struct. and supercond. props. *(Russian)* 78−43538
Nb:He, mech. props. and microstruct. 80−85003
Ne-He and Ne negative afterglows, microwave quenching and recombination processes, Ne spectral emission 77−80307
Ne-He DC glow discharge electron density decay, microwave cavity obs. 78−91167
Ne-He mixture discharges, origin of dark spaces in plasma 78−9881
Ni:He, defect props., quantum-chemical and lattice-defect hybrid approach 79−4528
Ni:He, implanted, profile meas. technique 77−80524
Ni:In, He, lattice defect struct., PAC meas. 80−70190
O_2-He afterglow, $O_2(C^1\Sigma_u^-, C^3\Delta_u, A^3\Sigma_u^+)$ generation from at. recomb. fluoresc. obs. 79−31576
O_2-He mixture, temp. difference of molecular vibr. relaxation freq. from 300 to 675K 80−74238
O_2-He(N_2)(CO_2), O_2 electron attachment coeff. meas., O_2 partial press. depend. *(German)* 79−13821
$O^{7+}(O^{8+})$+He, p-state alignment, X-ray emission polaris. obs. 79−50123
Pb-He discharge, excitation process, Pb^+ emission lines 78−66803
helium continued
S-He discharges, stability, emission spectra 80−107003
SF_6-He, dielec. props., ionisation and attachment coeffs. 80−33726
SF_6-He extracavity saturable absorber, nsec. pulse selection in CO_2 oscillator 79−98382
SF_6-R-He(Ar) ternary mixtures, formation of inert gas fluorides in AC discharge 80−64817
Si:He, B ion implantation 80−96559
Si:He, He impurity props. investigation by EHT calcs. 79−99183
SiC, sputtering, physical and chemical, by H_2 and He, 600 to 7500 eV 77−36340
SiH_4-He, reaction mechanisms of RF glow discharge deposition process 79−95944
Sr+He(Xe), Sr reson. line width, 4607 Å, press. effects, pot. well depths 79−89643
U-He plasma, radiation-induced, electron energy distrib. 77−24054
UF_6-He circulating gas critical expts. 79−13488
UF_6-He fission pumped nucl. laser, power deposition 78−58987
UF_6-He mixture, ballistic piston fissioning plasma 78−5038
W:^{3}He, implanted ion positions, determ. using mol. deuteron beam 80−70240
Xe^{2+}, mobility in He gas, drift-tube meas. 78−66657
Xe:He binary gas mixture convective instabilities in closed vertical cylinder heated from below 79−72880
Xe-He, 3.51 μm laser amplifiers, spectral narrowing and saturation induced rebroadening optical heterodyne obs. 80−63976
Xe-He source, intensity fluctuations of amplified spontaneous emission at 3.51 μm 80−32957
Xe-He(Ne), gas mixture, element and isotope separation in impulse plasma centrifuge *(Russian)* 80−38725
Xe-Ne-He hollow cathode discharge, laser oscill. at 5314 Å Xe II line 79−3679
Xe+Ar(He)(Ne)(Kr), thermal cond., 800 to 2000K from Wassiljewa's expression 79−27736
Zn-He mixture, binary diffusion coefficients, 1 atm., 720-1120K 80−1725
ZnF_2-He positive column discharge cataphoretic distrib. of Zn and F atoms 77−68886
Zr:He, diffusion of He studied by thermal evolution spectrometry 77−69120
Zr-He, implanted, superconductivity enhancement obs. 80−70884

helium, liquid *see liquid helium*

helium, solid *see solid helium*

helium-3 interactions *see helium 3-nucleus reactions*

helium 3-nucleus reactions
for inelastic helium 3-nucleus scattering, see "helium 3-nucleus scattering"
A=170-212 nuclei, 20-60 MeV ^{3}He ion induced fission, effective momenta of inertia *(Russian)* 77−34360
A=21 to 44, spectroscopic factors for single-nucleon transfer, review 77−71563
cross sections in advanced stellar evolution 80−56815
multinucleon removal reactions on ^{24,26}Mg, ^{27}Al, Fe, ^{58}Ni and ^{64}Zn at 80 MeV 77−6421
nucleus-nucleus total cross section energy depend. 80−106071
(^{3}He,n), 25.4 MeV, N=82 nuclei, n ang. distrib., transitions, vibr. band search 79−63574
(^{3}He,n) reactions, ^{206}Pb proton pairing vibr. obs. 78−13128
(τ,t) reactions, two stage processes in direct reactions, (τ,α)(α,t) *(Dutch)* 78−29439
^{27}Al(^{3}He,α), ^{26}Al excited states, isobaric analogues, spins, DWBA anal. 80−105981
^{27}Al(^{3}He,p_6)^{29}Si, coherence energies in pre-equilibrium emission 79−63652
^{27}Al(^{3}He,p) 9-14 MeV, stat. multistep compound emission, residual two-body interaction 80−47493
Ar(^{3}He,n)Ca, A=36, 38, 40, 11.5 MeV, neutron ang. distrib. and energy spectra 77−65227
^{38}Ar(^{3}He,t), 40 MeV, ^{38}K level spectrum and (^{3}He,t) reaction mechanism 79−22229
^{197}Au(^{3}He, 3nγ), level struct. in ^{197}Al anal. 77−46177
^{10}B(^{3}He,pγ), 4.1 MeV, radiative transitions and isospin mixing in ^{12}C 77−38242
^{11}B(^{3}He,n)^{13}N, ang. distrib. at energies below Coulomb barrier 79−40938
^{11}B(^{3}He,n)^{13}N, Coulomb stripping reaction theory 77−54232
^{11}B(^{3}He,np), 7 MeV, ^{12}C negative parity states from ^{13}N isospin forbidden p decays 79−26372
Be(^{3}He,n), 44 MeV, neutron spectra 80−524
Be(^{3}He,n) fast neutron generation in cyclotron 77−88311
^{9}Be(^{3}He, αα)^{4}He, 2.5, 2.7 MeV, energy depend., quasifree reaction near Coulomb barrier 78−74381
^{9}Be(^{3}He, αα)^{4}He, 2.8 MeV, quasi-free and sequential processes 79−67759
^{9}Be(^{3}He,^{3}He), 46.1 MeV, absolute differential cross section, optical model anal. 79−59078
^{9}Be(^{3}He,3α), 29.6-30.5 MeV, ^{12}C excited states 77−18576
^{9}Be(^{3}He,α)^{8}Be, j-depend. of analysing powers, ^{8}Be spectroscopic factor 77−328
^{9}Be(^{3}He,α)^{8}Be(O), reaction mechanism and isoscalar giant resonances in C^{12} *(French)* 78−78341
^{9}Be(^{3}He,αα)α, ^{12}C excited states between 29 and 34 MeV 78−21494
^{9}Be(^{3}He,d), 18 MeV, ^{10}B levels, J^π and ang. distribs. 80−42546
^{9}Be(^{3}He,d)^{10}B, j-depend. of analysing powers, ^{10}B spectroscopic factors 77−328
^{9}Be(^{3}He,n)^{11}C, ang. distrib. at energies below Coulomb barrier 79−40938
^{9}Be(^{3}He,n)^{11}C, Coulomb stripping reaction theory 77−54232
^{9}Be(^{3}He,p), 14 MeV, proton polarisation, ang. distribs., differential cross section 77−82944
^{10}Be(^{3}He,^{3}He), 46.1 MeV, absolute differential cross section, optical model anal. 79−59078
^{11}Be(^{3}He,^{3}He), 46.1 MeV, absolute differential cross section, optical model anal. 79−59078
^{11}Be(^{3}He,n_0)^{13}N, 5-12 MeV, excitation function and ang. distrib. 77−54231
^{209}Bi(^{3}He, 3nγ)^{209}At, gamma-ray spectra of ^{209}At, 26 and 28 MeV 78−74377
^{209}Bi(^{3}He,d), 30 MeV, effective residual interaction matrix elements, spectroscopic factors, cross sections 80−99134

helium 3-nucleus reactions continued
^{81}Br(^{3}He,3n)^{81}Rb-^{81m}Kr production excitation functions and thick target yield curves 80−12253
C(^{3}He,^{4}He)C, A=12, 13, differential cross-sections at 18, 20 and 24.5 MeV *(Russian)* 78−623
^{12}C(^{3}He,^{3}H), (^{3}He,^{3}He′), 44 MeV, study of ^{12}N(2.43 MeV) and ^{12}C(17.77 MeV) analogue states 77−6235
^{12}C(^{3}He,^{3}He), 44.04 MeV, absolute differential cross section, optical model anal. 79−59078
^{12}C(^{3}He,α), 35.6 MeV, ^{11}C energy levels, ang. distribs., DWBA calcs. comparison 78−78396
^{12}C(^{3}He,α)^{11}C, 11 MeV, multistep mechanism, CCBA calcs. 78−41734
^{12}C(^{3}He,α)^{11}C, j-depend. of analysing powers, ^{11}C spectroscopic factors 77−328
^{12}C(^{3}He,d), spectral line shape anal. 78−25203
^{12}C(^{3}He,d)^{13}N, d ang. distrib. anal. in PWBA 77−74863
^{12}C(^{3}He,d)^{13}N, j-depend. of analysing powers, ^{13}N spectroscopic factors 77−328
^{12}C(^{3}He,γ$_0$)^{15}O, differential cross section in giant dipole reson. region 78−78395
^{12}C(^{3}He,n), 12-24 MeV, ^{14}O low lying states, exact finite and zero range DWBA anal. 78−82286
^{12}C(^{3}He,p)^{14}N, 11 to 20 MeV, nuclear alignment 77−57679
^{12}C(^{3}He,p)^{14}N, g-factor, lifetime meas. of 5.106 MeV 2$^-$ state of ^{14}N 78−93965
^{12}C(^{3}He,pd), 90 MeV, angular correlations, elastic break-up of ^{3}He 80−52685
^{12}C(^{3}He,π^0), 180, 200 MeV, inclusive neutral pion prod. cross section 77−6410
^{12}C(τ,d), 36 MeV, ^{12}C+p resonance line shapes 79−59076
^{13}C(^{3}He,αγ)^{12}C, 2 to 12 MeV, radiative capture reaction, ^{16}O energy levels 79−9471
^{13}C(^{3}He,γ$_2$)^{16}O, ang. distrib. and correlation meas. of 26.42 MeV resonance 77−61444
^{13}C(^{3}He,γ)^{16}O, 25 to 300 MeV, struct. in giant resonance region of ^{16}O 79−63650
^{13}C(^{3}He,p), 20 MeV, p ang. distrib., ^{15}N energy levels 78−21581
^{13}C(^{3}He,p), 3.6-6.6 MeV, ^{15}N level excitation functions, resonance, p ang. distribs. 78−93942
^{13}C(τ,d)^{13}N, at 81.4 MeV, ang. distribs., analysis of particle inbound states 77−10418
^{14}C(^{3}He,d), 25.4 MeV, proton shell closure, ^{15}N low-lying positive parity states, Nilsson scheme 79−80871
Ca(^{3}He,n)Ti A=40, 42, 13 MeV, neutron ang. distrib. and energy spectra 77−65227
^{40}Ca(^{3}He, x), pol. ^{3}He, x=d or α, 33 MeV, anal. power and cross sections 80−42628
^{40}Ca(^{3}He,^{3}He′α)^{36}Ar, 70 MeV, GQR J^π 77−50097
^{40}Ca(^{3}He,^{3}He′p)^{39}K 70 MeV, GQR J^π 77−50097
^{41}Ca(^{3}He,d), 20 MeV, ^{42}Sc two particle states, spectroscopic strengths and J^π values 79−63591
^{48}Ca+^{3}He, 82 MeV, cross sections, (^{3}He,t) DWBA anal. 79−13310
^{48}Ca(^{3}He,^{6}He)^{45}Ca, 70 MeV, evidence for $(f_{7/2})^{-3}$ configuration states in ^{45}Ca 77−14034
^{48}Ca(^{3}He,^{8}B)^{43}Cl, 74 MeV, obs. and mass excess of ^{43}Cl 77−10310
^{48}Ca(^{3}He,α), 25 MeV, ^{47}Ca high spin states through double step processes, CCBA calcs. 78−89797
^{48}Ca(^{3}He,d) and (d,t$_0$), comparison with ^{40}Ca data, isotope shifts of $1f_{7/2}$ radii 77−34222
^{48}Ca(^{3}He,t), 66, 70 MeV, reaction mech. and ^{48}Sc Gamow-Teller strength, ang. distribs. 80−42589
^{48}Ca(^{3}He,t), finite-range formalism anal. of (^{3}He,α) (α,t) sequence 78−17229
^{48}Ca(^{3}He,t)^{48}, coupled channel calc., two-step processes, nonorthogonality corrections 77−30615
^{48}Ca(^{3}He,t)^{48}Sc, 23 MeV, finite range effects and nonorthogonality corrections in two-step processes 79−3162
Cd(^{3}He,d), ^{111}In-^{109}In mass difference from Q values 80−63069
^{116}Cd(^{3}He,n), second order processes in DWBA calcs. 78−46076
^{142}Ce(^{3}He,α), 24 MeV, ^{141}Ce levels, single neutron holes, spectroscopic factors, DWBA anal. 79−85353
^{37}Cl(^{3}He,p)^{39}Ar, 17, 19 MeV, DWBA two-particle transfer anal. 77−38288
^{59}Co(^{3}He,α), 34.8±0.3 MeV, α-particle energy spectra distrib., c.f. preequilibrium decay calcs. 79−9598
^{106}Co(^{3}He,3n), ^{106}Sn excited states, coincidence experiments 80−52607
Cr(^{3}He,d), 18 MeV, ^{A}Mn, A=51, 53 small angle cross sections for levels, DWBA anal. 79−22203
^{50}Cr(^{3}He, dγ)^{51}Mn, lifetimes of some low-lying l=1 states in ^{51}Mn 77−79393
^{50}Cr(^{3}He,nγ)^{52}Fe, low-lying states of ^{52}Fe 78−4952
^{50}Cr(τ,α), 16 MeV, ^{49}Cr energy levels, spins, parities, spectroscopic factors 78−33199
^{52}Cr(^{3}He, α), 12, 16 MeV, ^{51}Cr levels, spectroscopic function and analogue states, PWBA anal. 80−68547
^{52}Cr(^{3}He,d)^{53}Mn, 24,25 MeV, ^{53}Mn isobaric analogue states 77−6237
^{52}Cr(^{3}He,dγ), 18 MeV, ^{53}Mn γ decay and splitting of analogue states 78−70505
^{52}Cr(^{3}He,dp)^{52}Cr, 24,25 MeV, ^{53}Mn isobaric analogue states 77−6237
^{133}Cs(^{3}He, 3n)^{133}La, band struct., in-beam γ-ray spectroscopy 78−4951
D(^{3}He, H)^{4}He, radiation induced detrapping of implanted D in Be 80−32482
D(^{3}He, α)H, background reduction in depth profiling expts. using electrostatic deflector 79−14841
D(^{3}He,α)^{1}H, D trapping in fusion reactor materials, temp. dependence 80−37577
D(^{3}He,α)p, D profiles after D_3^+ implantation in Ti, Ti-6Al, Ti-6Al-4V 80−37581
D(^{3}He,p), depth profiling of D by backward proton meas. 80−30309
D(^{3}He,p)^{4}He, appl. to D depth distrib. determ. in 316 austenitic stainless steel 79−4326
D(^{3}He,p)^{4}He, channelling studies on the trapping of deuterium in vanadium by O-interstitials 79−4316
D(^{3}He,p)α, D lattice location in metals for defect-impurity interaction study 79−5206
Dy(^{3}He,d) ^{A}Ho single proton states, A=157, 159, 161, 163 78−489
Dy(^{3}He,d) 46.5 MeV, A=162,164, form factor effects 77−14138
^{164}Er(^{3}He,3n), gamma deexcitation mechanism of rot. levels 79−26442
^{167}Er(^{3}He,α)^{166}Er, 2-quasiparticle states obs. 80−18198
^{254}Es fission coincidence data from d, t, and ^{3}He induced reactions 80−42720

helium 3-nucleus reactions continued
^{151}Eu(^{3}He,3n), 24-32 MeV, ^{151}Tb 11/2 isomer, high spin few-particle states, in beam study 79−17805
^{19}F(^{3}He,^{6}He), 70 MeV, ^{16}F energy levels 78−17231
^{19}F(^{3}He,d)^{20}Ne(4_1^+), 0g orbit mixing and one-step forbidden transition 78−493
^{19}F(^{3}He,dγ), obs. of gamma decays of some T=0, 1 and 2 states above 9.5 MeV in ^{20}Ne 77−34244
Fe+^{3}He, cyclotron prod. of ^{57}Ni and ^{55}Co, bleomycin complex synthesis 77−86629
^{54}Fe(^{3}He, pγ)^{56}Co, 15.15 MeV γ-ray transitions, branching ratios, level lifetimes, spin assignments 79−497
^{54}Fe(^{3}He,dγ), 18 MeV, ^{55}Co γ decay and splitting of analogue states 78−70505
^{54}Fe(^{3}He,p), ^{56}Co particle-hole states, T=1, zero DWBA anal. 80−78308
^{54}Fe(^{3}He,t) 37.7 MeV, ^{54}Co deduced levels, J-depend., two-step processes 79−6412
^{54}Fe(^{3}Hg,pγ)^{56}Co, 11-15 MeV, coincidence, ang. correl. and branching ratio meas. 78−13129
^{54}Fe(τ,α), 18 MeV, populating ^{53}Fe levels to 7.3 MeV excit. 77−74767
^{54}Fe(τ,d), (τ,dp), spectroscopic study of ^{55}Co 77−88029
^{56}Fe(^{3}He,α), 18 MeV, ^{55}Fe levels, J^π, spectroscopic factors, DWBA anal. 80−99127
^{56}Fe(^{3}He,t)^{56}Co, ang. distrib. meas., DWBA calc. 78−29491
^{57}Fe(τ,d)^{57}Co, 18 MeV, level props. study DWBA calcs. 78−93946
^{58}Fe(^{3}He,p), ^{60}Co low lying states, DWBA anal. 78−29478
Ge(^{3}He,d), 21 MeV, ^{A}As, A=71, 73, levels, J^π, transitions, T1/2 80−57684
^{72}Ge (^{3}He,Zn), ^{73}Se production excitation functions 79−39501
^{72}Ge(^{3}He,d), 20 MeV, ^{73}As bound and isobaric analogue states, spectroscopic factors, DWBA anal. 79−54391
^{2}H(^{3}He, p), cross section meas., appl. in ion beam anal. 80−42673
^{2}H(^{3}He,^{4}He)^{1}H, 27 and 33 MeV, polarised ^{3}He beam analysing power and cross sections 79−89316
^{2}H(^{3}He,2pt), 2.2-6 MeV, A=5 levels coupled to nucl.-^{4}He*(0^+) channel 77−2906
^{2}H(^{3}He,p)α, light element profiling of tapered corrosion sections 79−92036
^{3}H(^{3}He, X), 50, 65, 78 MeV, quasifree scattering and quasifree reaction processes 80−13486
^{3}H(^{3}He,^{4}He)^{2}H, excitation functions for incident energy 17 to 33 MeV 79−6640
^{3}H(^{3}He,α)^{4}He, E$_α$=25 MeV, differential cross section, test of Barshay-Temmer theorem 79−80949
(^{3}He,^{3}H), charge exchange reaction, mean energy regions, diffraction model *(Russian)* 78−82352
(^{3}He,^{4}He), microscopic optical pots. to overcome DWBA difficulties 77−54198
(^{3}He,^{6}He), 70 MeV, mass excess and excited states for proton-rich medium nuclei 79−6375
(^{3}He,3n) 60 MeV reactions as search for ^{24}Si delayed-proton emitter 77−22970
(^{3}He,α), 217 (205) MeV, reaction mechanism *(French)* 78−41735
(^{3}He,α), 25 MeV, N=27 nuclei levels and analogue states, DWBA anal. 79−17808
(^{3}He,α), deep hole states observed in particle transfer reactions 80−68511
(^{3}He,d), 70, 90, 110 MeV, projectile break-up and d continuum spectra, reaction mechanism 79−13312
(^{3}He,d), absolute normalisation, comparative DWBA anal. of nucleon-transfer reactions 77−14143
(^{3}He,df) and (^{3}He,tf), extraction of (n,f) cross sections 77−23128
(^{3}He,n) Coulomb stripping reaction theory 77−54232
(^{3}He,p), proton polarisation meas. with Si polarimetry facility 79−31346
(^{3}He,t), Q-value atomic excitation corrections 79−40918
(^{3}He,t) on ^{26}Mg, ^{34}S, ^{42}Ca, ^{46}Ti, ^{50}Cr, ^{54}Fe, precise Q-values, superallowed β decays 77−30618
(^{3}He,t) reactions, gross structure in triton spectra 80−106062
(^{3}He, α), anal. of $1h_{11/2}^{-1}$ neutron strength distrib. in odd Nd and Sm isotopes 77−46100
(^{3}He, d) and (^{3}He, d̄), stripping reactions, zero range normalization factors 79−75956
^{3}He+^{3}He, evidence for high-energy deuterons 77−23099
^{3}He+^{3}He, possible sources of high-energy deuterons, solar neutrino problem 77−18588
^{3}He+^{3}He, quasifree processes, 50-78 MeV, cross-section meas. 77−18586
^{3}He+^{3}He→2p+^{4}He, fusion power feasibility 77−38310
^{3}He(^{3}He, ^{2}H)^{4}He, high energy deuteron prod. 79−93639
^{3}He(^{3}He, dd)pp, 50, 78 MeV, cross sections, two-spectator quasifree process 78−86539
^{3}He(^{3}He,^{2}Hνe$^+$)^{4}He, 11.5 MeV, search for high energy deuterons 79−76012
^{3}He(^{3}He,X) 50, 65, 78 MeV, quasifree scattering and quasifree reaction processes 80−13486
^{3}He(^{3}He,d^{3}He), three body break up reaction energy spectra, computer program 80−27593
^{3}He(^{3}He,dd)pp, 50, 78 MeV, study of four body continuum 77−18587
^{3}He(^{3}He,de$^+$ν)^{4}He, 15, 25 MeV, cross-section and solar neutrino problem 77−50142
^{3}He(^{3}He,p^{3}He), three body break up reaction energy spectra, computer program 80−27593
^{3}He(^{3}He,p)^{4}He, polarisation meas. in final state interactions 77−18589
^{3}He(^{3}He,p)^{5}Li, polarised protons, deuteron transfer obs. 77−329
^{3}He(τ,τp)d, 120 MeV, coincident energy spectra, quasi-free scatt. 79−22303
^{4}He(^{3}He,α), 15.95 MeV (c.m.), phase shift anal., σ$_τ$ determ. 77−88159
^{4}He(^{3}He,n)^{6}Be, 38.61 MeV, ^{6}Be reson. search, solar neutrino flux importance 78−619
^{4}He(^{3}He,p), 15.95 MeV (c.m.), phase shift anal., σ$_τ$ determ. 77−88159
^{174}Hf(^{3}He,3n), gamma deexcitation mechanism of rot. levels 79−26442
^{204}Hg(^{3}He,n) 33.3 MeV, cross sections, DWBA anal. for data near Z=82 79−67733
^{165}Ho(^{3}He,5n)^{163}Tm, high spin rot. levels in ^{163}Tm 78−8722
^{165}Ho(^{3}He,d)^{166}Er, 2-quasiparticle states obs. 80−18198
^{123}I, prep. from gaseous TeF$_6$, nuclear medicine appl. *(French)* 80−98137
^{115}In(^{3}He,3nγ), 25 MeV, ^{115}Sb M2, E3 transition reduced matrix elements, EM core polarisation 79−17847

helium 3-nucleus reactions continued
Kr(^{3}He,n), 25.4 MeV, ^{A}Sr, A=80,82,84-86, levels and transitions 80−18201
^{86}Kr(^{3}He,n), 25.4 MeV, ^{88}Sr 0^+ states struct., subshell closure 78−21582
^{139}La(^{3}He,3n), ^{139}Pr medium spin states, J^π, transitions and shape 80−86779
^{3}Li+^{3}He three-body final states, clustering in ^{7}Li, impulse approx. calcs. 77−3023
^{6}Li(^{3}He, ^{3}He^{3}He)^{3}H, 45 MeV, three trion model 77−88160
^{6}Li(^{3}He, ^{3}He^{3}He)^{3}H, 132 MeV, quasifree scatt., ^{3}He-^{3}He two body cross sections 79−76011
^{6}Li(^{3}He, d), ^{7}Be excitation functions 80−18223
^{6}Li(^{3}He, t^{3}He)^{3}He, 45 MeV, three trion model 77−88160
^{6}Li(^{3}He,^{3}H)^{6}Be, 27 MeV, comparison of experimental data and cluster and distorted wave calcs. 79−76010
^{6}Li(^{3}He,^{3}He^{3}H)^{3}He, Amado model appl., short-range interactions 77−6408
^{6}Li(^{3}He,^{3}He), 44.04 MeV, absolute differential cross section, optical model anal. 79−59078
^{6}Li(^{3}He,α)^{5}Li(GS), ^{9}B 17.637 MeV state form., α-α coincidence meas. 79−475
^{6}Li(^{3}He,$\alpha\alpha$p), 2.5 MeV, ^{5}Li or ^{8}Be formation, direct or compound nucleus mechanism 77−57678
^{6}Li(^{3}He,d), 0.7-2.0 MeV, ^{9}B complex system, excitation functions for 17.19 and 17.64 MeV levels 80−78188
^{6}Li(^{3}He,d)^{7}Be, 2-6 MeV, cross section meas. rel. to fusion reactor first wall 80−13791
^{6}Li(^{3}He,γ), ^{9}B level at 17.11 MeV 79−22193
^{6}Li(^{3}He,p), 14 MeV, proton polarisation, ang. distribs., differential cross section 77−82944
^{6}Li(^{3}He,p), 3-6 MeV, absolute cross sections 77−23297
^{6}Li(^{3}He,p)^{8}Be, 14 MeV, p-^{8}Be optical model parameters 78−25208
^{6}Li(^{3}He,p)^{8}Be$_{16,6}$(2γ), ^{9}B level at 17.11 MeV 79−22193
^{6}Li(^{3}He,p)$\alpha\alpha$, polarisation meas. in final state interactions 77−18589
^{6}Li(^{3}He,pα), 2.9 MeV, quasifree reaction, ^{2}H(^{3}He,pα) contrib., cluster motion 80−13485
^{6}Li(^{3}He,pα)α, 36 MeV, ^{5}Li breakup meas. 77−18590
^{6}Li(^{3}He,π^-), 910 MeV, π^- doubly coherent prod., inclusive π spectra 79−85481
^{6}Li(^{3}He,π^-)^{9}C, 910 MeV, doubly coherent π prod. 80−13487
^{6}Li(^{3}He,t)^{6}Be, α spectra obs. after α+p+p decay 77−74813
^{6}Li(τ,t)^{6}Be, 45 MeV, cross-section calc. by Amado 3-body model 79−6616
^{7}Li(^{3}H,γ)^{10}Be, 0.4-1.1 MeV, excitation curves, ang. distribs. 78−33200
^{7}Li(^{3}He, d_0)^{8}Be, 1.0 to 2.5 MeV, excitation functions, ang. distribs. 77−61438
^{7}Li(^{3}He,^{3}He), 44.04 MeV, absolute differential cross section, optical model anal. 79−59078
^{7}Li(^{3}He,nγ), ^{9}Be first T=3/2 states, γ-decay, branching ratios and total widths 79−6489
^{7}Li(^{3}He,t)^{7}Be, 2-6 MeV, cross section meas. rel. to fusion reactor first wall 80−13791
^{24}Mg(^{3}He,α)^{23}Mg, 10 MeV, ang. distribs., DWBA and CCBA calcs. with inelastic effects 77−61443
^{24}Mg(^{3}He,t), giant dipole reson. excitation 77−6338
^{24}Mg(^{3}He,t)^{25}Al, 38.5 MeV, spin assignments in ^{24}Al 77−18580
^{24}Mg(^{3}He,t)^{24}Al, 44 MeV, 1^+ states in Al anal. 77−79390
^{24}Mg(^{3}He,t)^{24}Al, low-lying 1^+ states of Al anal. 78−29484
^{25}Mg(^{3}He,α)^{24}Mg, 9-13 MeV, excitation functions, and differential cross-sections 77−6409
^{25}Mg(^{3}He,d)^{26}Al, 18 MeV, l-assignments for ang. distrib., level J^π information, spectroscopic strengths 78−62554
^{25}Mg(^{3}He,p)^{27}Al, 13 MeV, statistical multistep compound emission, proton spectrum fluctuations 78−37357
^{26}Mg(^{3}He,pγ)^{28}Al, 11-15 MeV, coincidence, ang. correl. and branching ratio meas. 78−13129
^{55}Mn(^{3}He,3n)^{55}Co, nuclear medicine appl. 80−36132
Mo, activation in cyclotron by p, d, α, ^{3}He 79−30839
Mo(^{3}He,n), 25.4 MeV, ang. distrib. meas. 77−3022
Mo(^{3}He,t)Tc, A=94,98, E=24 MeV, levels of ^{94}Tc, ^{98}Tc determ. 77−26778
Mo(^{3}He, xn)^{97}Ru, in compact cyclotron, ^{97}Ru chem. separation 77−37054
^{92}Mo(^{3}He,^{6}He), 70 MeV, ^{89}Mo mass excess and excited states 80−42531
^{92}Mo(^{3}He,d), 28.5 MeV, ^{93}Tc high spin analogue resonance near N=50 neutron shell, DWBA anal. 80−42613
^{92}Mo(^{3}He,p), 25 MeV, ^{94}Tc levels and J^π, coupled channel and DWBA anal. 79−89239
^{95}Mo(^{3}He,d), 33.6 MeV, proton spectroscopy of ^{96}Tc, shell model anal. 79−63573
^{98}Mo(^{3}He,d), ^{99}Tc level struct., spin-parity assignments 78−8743
^{98}Mo(^{3}He,d)^{99}Tc at 18 MeV populating low-lying states 77−22894
^{14}N(^{3}He,p), 15 MeV, ^{16}O excited states from ang. distrib. meas. 78−89891
^{14}N(^{3}He,p), 15 MeV, ^{16}O T-mixed analogue states, (^{3}He,p)/(t,p) cross section ratio 79−9478
^{14}N(^{3}He,p), 15 MeV, obs. of T=0 pairing vibr. 78−70422
^{14}N(^{3}He,p)^{16}O, 10 MeV proton polarisation ang. distrib. 79−71861
^{23}Na(^{3}He,d), 15 MeV, ^{24}Mg states, Nilsson model spectroscopic factors, collective model rot. bands 79−6421
^{93}Nb(^{3}He,α), 19.5 MeV, ^{92}Nb levels determ. 77−88154
Nd(^{3}He,X), 19-27 MeV, ^{A}Sm, A=148,9, structural connections, levels, bands, J^π, transitions and mixing ratios 79−63576
Nd(^{3}He,α), 24 MeV, ^{A}Nd, A=145, 147, 149, single neutron hole states spectroscopic factors, DWBA anal. 80−78109
Nd(^{3}He,d), ^{A}Pm, A=143-153, odd-A, spectroscopic factors, shell model anal. 80−78137
Nd(^{3}He,d), 24 MeV, ^{143,145}Pm proton states and transitions, stripping strength, shell model anal. 80−68508
Nd(^{3}He,n) 25.4 MeV, Sm even isotopes n ang. distrib., transitions, vibr. band search 79−63574
^{A}Nd(^{3}He,xn), A=146,148, 19 to 27 MeV, ^{146,147}Sm excited states, energy levels, spin, parity, shell and cluster-vibration models 80−57683
^{142}Nd(^{3}He,α), 24 MeV, levels in ^{141}Nd anal., DWBA calc. 77−41979
^{146}Nd(^{3}He,d), 24 MeV, ^{147}Pm proton states and transitions shell model anal. 79−30781
^{150}Nd(^{3}He,d), 24 MeV, ^{151}Pm single proton states, rot. bands, level J^π assignments, spectroscopic strengths 79−67626
Ne(^{3}He,dp), 30.2 MeV, ^{61,63}Cu analogue state decay modes 79−67702

helium 3-nucleus reactions continued
^{20}Ne(^{3}He,^{8}Li), ^{15}F mass excess and T=3/2 levels 78−78264
^{20}Ne(^{3}He,^{8}Li), 88 and 75 MeV, ^{15}F mass excess 78−78245
^{21}Ne(^{3}He,α)^{20}Ne, large angle excitation function fluctuations, DWBA and opt. model calcs. 79−89318
^{21}Ne(^{3}He,p), 18 MeV, ^{23}Na positive parity states ang. distrib., DWBA anal. 78−82284
^{22}Ne(^{3}He,α), 15 MeV, ang. distrib. meas. for levels <10 MeV in ^{21}Ne 79−63684
^{22}Ne(^{3}He,p), 18 MeV ^{24}Na, level struct. and spin assignments, DWBA anal. 78−86477
^{22}Ne(^{3}He,p)^{24}Na 18 MeV, ^{24}Na J^π assignments 77−74760
^{A}Ni(^{3}He, p), 8, 10 MeV, A=58, 60, 62, p spectra compound nucleus contrib., odd-even effect 80−106061
^{58}Ni(^{3}He, α), 25 MeV, ^{57}Ni and ^{57}Co levels and analogue states, J^π from DWBA anal. 79−63592
^{58}Ni(^{3}He,^{8}He), 75.3 MeV, cross-section meas. 77−79394
^{58}Ni(^{3}He,α), 130 MeV, selected transition, DWBA anal., cross sections 80−83086
^{58}Ni(^{3}He,α)^{57}Ni, 15-205 MeV, zero-range DWBA normalisation, energy depend. 77−34280
^{58}Ni(^{3}He,α)^{57}Ni, 70 MeV, mass excess of ^{57}Ni determ. 77−18376
^{58}Ni(^{3}He,d)^{59}Cu, 33.3 MeV, analysing power for polarised ^{3}He 77−67731
^{58}Ni(^{3}He,dγ), 18 MeV, ^{59}Cu γ decay and splitting of analogue states 78−70505
^{58}Ni(^{3}He,pγ)^{60}Cu, 11-15 MeV, coincidence, ang. correl. and branching ratio meas. 78−13129
^{60}Ni(^{3} He,t), 38 MeV, ^{60} Cu energy levels, spectroscopic factors, transition amplitudes 78−46079
^{60}Ni(^{3}He,p)^{62}Cu, 9-11 MeV, gamma transitions from ^{62}Cu excited levels obs. *(French)* 77−26615
^{62}Ni(^{3}He,X), 24.3 MeV, ^{66}Zn* composite particle emission, ang.-distribs., exciton-coalescence model 80−78265
^{62}Ni(^{3}He,X), X=p, d, t, ^{3}He, α, 24.3 MeV, continuous spectra and ang. distribs. meas. 77−3016
^{64}Ni(^{3}He,^{8}B)^{59}Mn, 74 MeV, obs. and mass excess of ^{43}Cl 77−10310
O(^{3}He,n), low spin states populated in ^{18,20}Ne 77−14141
^{16}O(^{3}He, p γ), determ. of O_2 in thin films 80−45610
^{16}O(^{3}He, x), pol. ^{3}He, x=d or α, 33 MeV, anal. power and cross sections 80−42628
^{16}O(^{3}He,^{3}He), 44.04 MeV, absolute differential cross section, optical model anal. 79−59078
^{16}O(^{3}He,γ)^{19}Ne, E_x=11 to 25 MeV, g.s. giant dipole resonance 79−6539
^{16}O(^{3}He,p), 18 MeV, ang. distribs., DWBA anal. 77−34325
^{16}O(^{3}He,p)^{18}F, 19.8 MeV DWBA anal. of exchange effects 77−46179
^{16}O(^{3}He,p)^{18}F and ^{16}O(^{3}He,α)^{15}O prompt reactions, lattice location meas. of O in Nb 79−86813
^{16}O(^{3}He,p)^{18}F in water, ^{18}F prod. and yield 78−28065
^{16}O(^{3}He,t), 35 MeV, ^{16}F energy levels 78−17231
^{17}O(^{3}He, α), 36 MeV, isospin mixing in ^{16}O determ. 78−8832
^{17}O(^{3}He,p), 18 MeV, ^{19}F 5.10 MeV level parity 79−45155
^{17}O(^{3}He,p), 18 MeV, ^{19}F level struct., ang. distribs. anal. using DWBA 80−9232
^{18}O(^{3}He,pγ)^{20}F, 11-15 MeV, coincidence, ang. correl. and branching ratio meas. 78−13129
^{31}P(^{3}He,d), 25 MeV, ^{32}S energy levels and ang. distribs., DWBA anal. 78−78265
Pb(^{3}He,α), 101 MeV, ^{A}Pb, A=205-207, neutron hole states, spectroscopic factors, DWBA anal. 80−47352
^{A}Pb(^{3}He,n), A=204,206,208, 33.3 MeV, cross sections, DWBA anal. for data near Z=82 79−67733
^{208}Pb(^{3}He, π^0), 200 MeV, inclusive neutral pion prod. cross section 77−6410
^{208}Pb(^{3}He,α), 70 MeV, ^{207}Pb inner hole states, spectroscopic strengths DWBA anal. 79−17813
^{208}Pb(^{3}He,α)^{207}Pb, 70 MeV, deephole states, $T_>$=45/2 components 78−82362
^{208}Pb(^{3}He,α)^{207}Pb, T=45/2 isobaric analogue state obs. 78−93928
^{208}Pb(^{3}He,d), 30 MeV, effective residual interaction matrix elements, spectroscopic factors, cross sections 80−99134
^{208}Pb(^{3}He,t)^{208}Bi, 80 MeV, Gamow-Teller M1 state excitation 78−50184
^{110}Pd(^{3}He,d)^{111}Ag, 33.2 MeV, ^{111}Ag level struct. 77−88045
^{141}Pr(^{3}He,3n), ^{141}Pm medium spin states, J^π, transitions and shape 80−86779
Pt(^{3}He,4n), Hg isotopes, level energies, B(E2) values, rot. aligned bands 78−70483
Pt(^{3}He,d), A=194, 196, 198, 41.2 MeV, stripping strength, Au excitation energies, high spin states 78−78398
^{A}Pt(^{3}He,n) A=194,196, 33.3 MeV, cross sections, DWBA anal. for data near Z=82 79−67733
^{241}Pu(^{3}He,αf), ^{240}Pu fission total kinetic energy release, excitation energy depend., scission point anal. 80−18351
^{103}Rh(^{3}He, 3nγ), 28 MeV, ^{103}Ag high spin states, bands transitions, intermediate deformation Coriolis coupling 80−105944
^{102}Ru(^{3}He,n), 25.4 MeV, ang. distrib. meas. 77−3022
^{32}S(^{3}He,p), 18 MeV, spin-parity and transfer L-values for ^{34}Cl states 77−88046
^{32}S(^{3}He,p), cross section meas., verification of ^{34}Cl shell model calcs. 78−13119
^{33}S(^{3}He,α), 15 MeV, ^{32}S levels and spectroscopic factors from pickup DWBA anal. 80−9235
^{45}Sc(^{3}He,α)^{44}Sc, reanalyzed data, sum rule anal. and spectroscopic factors 78−8828
^{76}Se(^{3}He,d), 41 MeV, ^{77}Br level struct., l-transfers, spectroscopic factors, DWBA anal. 78−86479
^{78}Se(^{3}He,d), 41 MeV, ^{79}Br level struct., l-transfers, spectroscopic factors, DWBA anal. 78−86479
^{28}Si(^{3}He, ^{2}He), 52 MeV, ^{29}Si levels, J^π, spectroscopic factor, DWBA anal. 80−86811
^{28}Si(^{3}He,d), 25 MeV, spectroscopic factors 78−66294
^{28}Si(^{3}He,d)^{29}P, stripping to bound and unbound states 77−82934
^{28}Si(^{3}He,t)^{28}P, 38.5 MeV, spin assignments in ^{28}P 77−18580
^{29}Si(^{3}He,d), 14 MeV, ^{30}P positive parity states, transitions and spectroscopic strengths, DWBA anal. 80−102138
^{29}Si(^{3}He,p), 15 MeV, ^{31}P high E_x states, J^π, DWBA anal. 80−68536
^{29}Si(^{3}He,p), 15 MeV, excitation energies and ang. distribs. below 7.2 MeV, in ^{31}P 78−82361

helium 3-nucleus reactions continued
$^{30}Si(^3He,p\gamma)^{32}P$, 11-15 MeV, coincidence, ang. correl. and branching ratio meas. 78−13129
$^{144}Sm(^3He,\alpha p)^{142}Pm$, 39 MeV, proton decay of hole analogue states 78−70451
$^{152}Sm(^3Ne,3n)$, gamma deexcitation mechanism of rot. levels 79−26442
$Sn(^3He, 3n)$, 32 MeV, ^{A}Te, A=117, 119, 121, collective excitations, high spin states and transitions 80−13346
$Sn(^3He,\alpha)$, 81 MeV, deeply bound hole states, isobaric analogue states in $^{115,117,119,123}Sn$ 77−30570
$Sn(^3He,\gamma)$ 39 MeV, $^{111,115,119}Sn$ neutron hole distribs., IAS and spectroscopic factors 80−42519
$Sn(^3He, n)$, 25.4 MeV, ang. distribs., $^{114,118,120,122,126}Te$ deduced levels 78−89890
$Sn(^3He,t)$, 4.9 MeV, IAS, Coulomb displacement energies 77−6337
$^{17}Sn(^3He,\alpha)Sn$, A=114, 116, 118, 120, deeply bound hole state struct. 78−93930
$^{115}Sn(^3He,d)$, 28.4 MeV, ^{116}Sn state excitation energies, and partial half lives, spectroscopic factors 78−66295
$^{116}Sn(^3He, \alpha)$, 39 MeV, ^{115}Sn weak coupling neutron hole states 80−73786
$^{84}Sr(^3He,\alpha)^{83}Sr$, 18 MeV, ^{83}Sr levels, DWBA calcs. using optical model 78−41738
$^{86}Sr(^3He,\alpha)^{85}Sr$, transfer reactions, nucl. struct. obs. 77−46118
$^{88}Sr(^3He,n)$ 25.4 MeV, ang. distrib. meas. 77−3022
$^{88}Sr(^3He,p)^{90}Y$, obs. of ^{90}Y 1^+ and 0^+ states 78−25116
$^{181}Ta(^3He,3n\gamma)$ 24, 28, MeV, ^{181}Re states and transitions, rot. bands and Nilsson states 79−36152
$^{159}Tb(^3He,3n\gamma)^{159}Ho$, use in determ. ^{159}Ho energy levels 77−26556
$Te(^3He,\alpha)$, 20 MeV, A=122, 124, 126, ang. distrib. anal. 77−88153
$Te(^3He,d)$ 35 MeV, ^{A}I, A=121, 123, 125, mass excesses, ^{121}I energy levels 78−78246
$Te(^3He,d)$, A=122, 124, 19.52 MeV, populating I levels 77−34230
$Te(^3He, n)$, 25.4 MeV, ^{A}Xe, A=124,126-8,130,132, levels, transitions and J^π values, DWBA anal. 79−75852
$Te(^3He,t)$, 45.9 MeV, IAS, Coulomb displacement energies 77−6337
$Te(^3He, xn)^{125}Xe$, prod. of ^{125}Xe for medical use using natural Te 78−3604
^{A}Te(^{3}He,d)I, 36 MeV, A=120 to 130, comparative study of $^{121\text{ to }131}I$ proton states 79−63572
$^{120}Te(^3He,d)$, ^{121}I single particle strength distrib. 78−70423
$^{120}Te(^3He,d)$, 36 MeV, ^{121}I mass excess, energy levels and single particle strength distrib. 80−5053
$^{122}Te(^3He,d)$, ^{123}I mass meas. from ground state Q-value 78−4896
$^{125}Te(^3He,3n\gamma)$, ^{125}Xe odd and even parity band structs., level lifetimes 80−27533
$^{126}Te(^3He,\alpha)$, 24 MeV, ^{125}Te low lying negative parity high spin states multistep induced population 80−57657
$^{232}Th(^3He,n)$, 33.3 MeV, cross sections, DWBA anal. for data near Z=82 79−67733
$Ti(^3He, pxn)$, ^{48}V positron source prep. for annihilation radiation line-shapes, positron lifetimes meas. 80−876
$^{nat}Ti(^3He, xn)^{48}Cr$, production of ^{48}Cr for life sciences appls. 80−94367
$^{169}Tm(^3He,5n)$, 42 to 57 MeV, interpretation with level scheme of ^{167}Lu 77−88026
$U(^3He, f)$, 530 MeV, cross section meas. by glass solid state track detectors 78−13179
$^{234}U(^3He,\alpha)$, 30 MeV, states in ^{233}U 78−66208
$^{234}U(^3He,d)$, 30 MeV, ^{235}Np deduced levels and Nilsson band configurations 79−468
$^{238}U(^3He,4n)^{237}Pu$, prep. of gamma-emitting tracer 77−34497
$^{238}U(^3He,f)$, ^{241}Pu compound nucleus lifetime by the shadow effect *(Russian)* 78−86562
$^{51}V(^3He,d)$, $(^3He,^3He)$, 15 MeV, ang. distribs. meas., optical model anal. 78−33192
$^{51}V(^3He,dp)$, ^3He breakup, DWBA calcs. for strongly absorptive projectiles 80−68682
$^{51}V(^3He,n)^{53}Mn$, cyclotron preparation of ^{53}Mn, extraction, anal. 77−61441
$^{51}V(^3He,pd)$, 90 MeV, angular correlations, elastic break-up of ^3He 80−52685
W, activation in cyclotron by p, d, α, ^3He 79−30839
$^{89}Y(^3He, 3n\gamma)$, 20-28 MeV, in-beam γ-ray spectroscopy, ^{89}Nb levels determ. 77−41983
$^{70}Zn(^3He,^8B)^{65}Co$, mass excess of ^{65}Co 78−93931
$Zr(^3He, ^4He)$, A=91-96, E=39 MeV, Zr levels, J^π, ^{95}Zr IAS 78−508
$Zr(^3He,n)$, 25.4 MeV, ang. distrib. meas. 77−3022
^{90}Zr (^{3}He,dp), 30.2 MeV, ^{91}Nb, analogue state decay modes 79−67702
$^{90}Zr(^3He, ^4He)^{89}Zr$, 39 MeV, ^{89}Zr IAS and bound hole states 78−492
$^{90}Zr(^3He,n)$, second order processes in DWBA calcs. 78−46076
$^{90}Zr(^3He,pd)$, 90 MeV, angular correlations, elastic break-up of ^3He 80−52685
$^{90}Zr(^3He,t)$, 80 MeV, ^{90}Nb isovector resonance analogues, Gamow-Teller transition 79−9539
$^{90}Zr(^3He,t)^{90}Nb$, 130 MeV, giant Gamow-Teller resonance, T=4, T=5 components 78−46081
$^{90}Zr(^3He,t)^{90}Nb$, 18.5 MeV resonance, isovector dipole and Gamow-Teller transitions 80−86881
$^{90}Zr(^3He,t)^{90}Nb$, 80 MeV, Gamow-Teller M1 state excitation 78−50184
$^{96}Zr(^3He,\alpha p)$ 39 MeV, ^{94}Y deduced levels spectroscopic factors, spin and parity 78−70451
$^{96}Zr(^3He,d)$, 39 MeV, ^{97}Nb high spin analogue resonance near N=50 neutron shell, DWBA anal. 80−42613

helium 3-nucleus scattering
eikonal approx. and distortions in heavy particle stripping mechanism *(Russian)* 78−78337
elast. scatt. on heavy nuclei, anal. with molecular type pots. 77−18502
elastic scatt., optical spin-orbit pot., spin-orbit strength 79−85480
internal structure influence on elastic scatt. at intermediate energies *(Russian)* 79−30844
light ion scatt., optical pot. and proximity pot. comparison 79−3121
light nuclei, backward scatt. and heavy-particle stripping 78−13107
monopole excitations in heavy nuclei, hadron induced 78−86471
optical model spin-orbit pot. for spin $^1/_2$ particles 79−97686
optical pot. uniqueness of (d, d) and (^{3}He, ^{3}He) 79−97685
optical potentials and volume integrals for targets with A=10 to 58, mass and energy dependence 80−52686
$^{27}Al(^3He,^3He)$, 46 MeV, ang. distribs., optical and DWBA anal., scatt. pots. 79−556
$^{27}Al(^3He,^3He)$ 39.7 MeV, optical pot. mass. depend. 77−34327

helium 3-nucleus scattering continued
$^{197}Au(^3He,^3He)$ 39.7 MeV, optical pot. mass depend. 77−34327
$^{11}B(^3He,^3He)$ 17.5 and 40.0 MeV, elast. and inelast. scatt. from ground state and low excited levels 77−65229
$^{12}C(^3He,^3He')$, 18, 20, 24.5 MeV, differential cross sections, DWBA anal. 79−6647
$^{12}C(^3He,^3He')$, $(^3He,^3H)$, 44 MeV, study of ^{12}C(17.77 MeV) and ^{12}N(2.43 MeV) analogue states 77−6235
$^{12}C(^3He,^3He')$, spin-flip transitions, microscopic α-spectator model 77−79400
$^{12}C(^3He,^3He)$, 20.5-33.0 MeV, energy depend. of analysing power optical model 78−17226
$^{12}C(^3He,^3He)$, E2 strength distrib., giant quadrupole reson. 77−30612
$^{12}C(^3He,^3He)$, incident ion binding energy effects on scatt., qualitative anal. 79−9600
$^{12}C(^3He,^3He)$ 39.7 MeV, optical pot. mass. depend. 77−34327
$^{40}Ca+^3He$ inelastic scatt., isoscalar multipole reson. 78−66190
$^{40}Ca(^3He,^3He')^{40}Ca^*\rightarrow^{36}Ar+^4He$, spin, parity assignments for ^{40}Ca giant resonances 79−93479
$^{40}Ca(^3He,^3He)$, 27-84 MeV, energy depend. of optical model param. 78−41736
$^{40}Ca(^3He,^3He)$, 90-120 MeV, cross sections, deduced unambiguous optical pot. 79−13311
$^{40}Ca(^3He,^3He)$, pol. ^3He, 33.3 MeV, differential cross section and anal. power, optical pots. 80−42627
$^{56}Fe(^3He,^3He)$, 33-83 MeV, details of nuclear surface 77−34324
$H(^3He,^3He)$, 33 MeV, ^3He polarisation anal. power meas. optical model anal. 77−38286
$^3H(^3He,^3He)$, 20-33 MeV, analysing power, differential cross section meas. 78−17227
$He(^3He,^3He)$, 33 MeV, ^3He polarisation anal. power meas. optical model anal. 77−38286
$(^3He,^3He)$, 12-51.3 MeV, ang. distribs., S-matrix formalism frame anal., fission ingoing channel *(Russian)* 80−5152
$(^3He,^3He)$, 18-33 MeV polarised ^3He, ^6Be excitation 78−78400
$(^3He, ^3He)$, 119 MeV, optical pot. parameters energy and mass depend. 80−32289
$(^3He, ^3He)$, coupled reaction channel effects on polarisation 79−85442
$(^3He, ^3He)$, pol. ^3He, vector and tensor polarisation, closed form description 80−37363
$^3He+^3He$, quasifree processes, 50-78 MeV, cross-section meas. 77−18586
$^3He+\alpha$ scatt., exchange Coulomb kernel in resonating group formulation 79−6531
$^3He(^3He, ^3He')$, 120 MeV, continuum energy spectra bump struct., cross sections 80−83108
$^4He(^3He,^3He)$, ^7Be $^4He+^3He$ coupling, dispersion anal. 78−89889
$^4He(^3He,^3He)$, 18 to 70 MeV, differential cross-sections, resonating group method anal. 79−85482
$^4He(^3He,^3He)$, 18-22 MeV, analysing power ang. distrib., differential cross sections, ^7Be excited state 78−46078
$^4He(^3He,^3He)$, 60.2, 113.1 MeV, ang. distrib., optical and coupled channel anal., cross sections 80−47492
$^4He(^3He,^3He)^4He$, four body approach 79−75933
$^6Li(^3He, ^3He)$, 0.7-2.0 MeV, ^9B complex system, excitation functions for 17.19 and 17.64 MeV levels 80−78188
$^6Li(^3He, ^3He)$, excitation functions 80−18223
$^6Li(^3He,^3He)$, 27 MeV, cross sections, three body and optical model calcs. 79−76009
$^6Li(^3He,^3He)$, phase shifts, cross sections, resonating group calcs., odd-even features, resonances 80−68681
$^6Li(^3He,^3He)^6Li^*$, 27 MeV, comparison of experimental data and cluster and distorted wave calcs. 79−76010
$^6Li(\tau,\tau)^6LI^*$, (3.56 MeV), 27 MeV cross-section calc. by Amado 3-body model 79−6617
$^6Li(\tau,\tau)^6Li^*$, 45 MeV, cross-section calc. by Amado 3-body model 79−6616
$^{24}Mg(^3He,^3He')$, 41.2 MeV, isoscalar excitations 78−41616
$^{24}Mg(^3He,^3He')$, giant dipole reson. excitation 77−6338
$^{24}Mg(^3He,^3He)$, 130 MeV, elastic scatt. ang. distribs., optical model anal. 78−94020
$^{24}Mg(^3He,^3He)$, 130 MeV, giant reson. excitation, DWBA anal. 79−89319
$^{26}Mg(^3He,^3He')$, 4^+ states, B(E2) values, and band mixing, rot.-vibr. model 80−83019
^{A}Mo(^{3}He,^{3}He'), A=92,94,96,98,100, 110 MeV, giant quadrupole resonance isotopic depend. 80−9282
$^{58}Ni(^3He,^3He)$, 27-84 MeV, energy depend. of optical model param. 78−41736
$^{58}Ni(^3He,^3He)$, 90-120 MeV, cross sections, deduced unambiguous optical pot. 79−13311
$^{58}Ni(^3He,^3He)^{58}Ni$, 33.3 MeV, analysing power for polarised ^3He 77−67731
$^{61}Ni(^3He,^3He)$ 39.7 MeV, optical pot. mass depend. 77−34327
$^{16}O(^3He,^3He)$, pol. ^3He, 33.3 MeV, differential cross section and anal. power, optical pots. 80−42627
$^{16}O(^3He,^3He)$, E2 strength distrib., giant quadrupole reson. 77−30612
$^{16}O(^3He,^3He)$ 25 MeV, macroscopic description of exchange effects 77−57635
$^{208}Pb(^3He,^3He')$, 108.5 MeV, giant monopole resonance, DWBA anal. 79−71828
$^{208}Pb(^3He,^3He)$, 130 MeV, elastic scatt. ang. distribs., optical model anal. 78−94020
$^{208}Pb(^3He,^3Ne)$, 130 MeV, giant reson. excitation, DWBA anal. 79−89319
$^{105}Pd(^3He,^3He)$ 39.7 MeV, optical pot. mass depend. 77−34327
$^{32}S(^3He,^3He)^{32}S$, ambiguities in ^3He spin-orbit pot. radius, phenomenological optical-model anal. 79−36250
$^{45}Sc(^3He,^3He')$, levels, J^π, transitions and lifetimes 80−63091
^{A}Si(^{3}He,^{3}He), 46 MeV, A=28-30, ang. distribs., optical and DWBA anal., scatt. pots. 79−556
$^{28}Si(^3He,t)^{28}P$, 35 MeV, energy levels and spectroscopic assignments *(French)* 79−45167
$Sm(^3He,^3He')$, 53 MeV, even A=144-154, DWBA anal. of ang. distribs. 78−17230
^{A}Sm(^{3}He, ^{3}He^1), A=144, 148, 152, 154, 150, 40.9 MeV, transition cross sections, deformation parameters, coupled channels anal. 79−67640
$^{116}Sn(^3He,^3He)$, 90-120 MeV, cross sections, deduced unambiguous optical pot. 79−13311
$^{120}Sn(^3He,^3He)$, 130 MeV, elastic scatt. ang. distribs., optical model anal. 78−94020

helium 3-nucleus scattering continued
^{120}Sn(^{3}He,^{3}He), 130 MeV, giant reson. excitation, DWBA anal. 79−89319
^{124}Sn(^{3}He,^{3}He′), ang. distrib. meas. and DWBA anal. 78−13125
^{124}Sn(^{3}He,^{3}He) (elast. and inelast.), 14.35 MeV, Coulomb-nuclear interference calcs. 79−26444
Te(^{3}He,^{3}He), A=122, 124, 19.52 MeV populating I levels 77−34230
Te(^{3}He,^{3}He) A=122-128, 8-18 MeV, optical model and deform. parameters 77−34221
^{A}Te(^{3}He,^{3}He) A=122, 124 (elast. and inelast.), 12.5 to 21 MeV, Coulomb-nuclear interference calcs. 79−26444
^{122}Te(^{3}He,^{3}He′), ang. distrib. meas. and DWBA anal. 78−13125
^{124}Te(^{3}He,^{3}He′), ang. distrib. meas. and DWBA anal. 78−13125
^{46}Ti(^{3}He,^{3}He′), excitation of low-lying 0^+ states, indirect processes 77−6417
^{51}V(^{3}He,d), (^{3}He,^{3}He), 15 MeV, ang. distribs. meas., optical model anal. 78−33192
^{68}Zn(^{3}He,^{3}He), elastic and inelastic scatt. angular distrib. fine struct. 80−106063
^{90}Zr(^{3}He,^{3}He′), 108.5 MeV, giant monopole resonance, DWBA anal. 79−71828
^{90}Zr(^{3}He,^{3}He), 130 MeV, elastic scatt. ang. distribs., optical model anal. 78−94020
^{90}Zr(^{3}He,^{3}He), 130 MeV, giant reson. excitation, DWBA anal. 79−89319
^{90}Zr(^{3}He,^{3}He), 90-120 MeV, cross sections, deduced unambiguous optical pot. 79−13311

helium-3 scattering *see helium 3-nucleus scattering*

helium atoms
1s3d config., Zeeman sublevel energies, anticrossing and degeneracy 77−23417
$1s^2$ ground state piecewise polynomial CI natural radial orbitals wave functions 80−18805
2^1P state excitation, 80 eV electron impact, λ and χ parameters meas. 80−32839
2^1P-state electron impact excitation, 40 to 500 eV, alignment and orientation 80−83499
2^1S_0-1^1S_0 transition, transition matrices higher approx. 78−33458
2^1S and 2^3S states excitation by H and electron impact 77−42412
2^1S state isoelectronic series, Fermi and Coulomb correlations 78−921
2^1S-state, electron impact excitation, intermediate energy calcs. 79−59583
2^3P-3^3D transition, Doppler free intermodulated optogalvanic spectroscopy, obs. 80−52333
2^3S-3^3S electron impact excitation, first Born and Glauber cross sections 78−55243
2^3S-state, electron impact excitation, reson. form. mechanism 80−99463
2(^{1,3}S) excited states, dynamic polarisabilities 77−34772
2(^{1,3}S) excited states and ground state, dynamic polarisabilities, van der Waals force consts. 77−34773
$(2p^2)^3$P doubly excited state, electron impact excitation XUV emission 79−86071
$(2p^2)^3$P state, electron impact excitation, parity unfavoured transition 80−91680
2S metastable states, singlet and triplet; two and three photon ionisation cross section, absolute determ. 80−83329
3^3D_1-2^3P_0 line, press. broadening studies by saturated absorpt. techniques 80−52939
3^3D level, fine struct. changing collisions in glow discharge 80−58346
3^3D levels shift induced by laser radn. 79−98036
3^3P level, excitation and decay study up to high press. pumped by intense relativistic electron beam 80−74250
jK and LS coupling between states, transition probs., depend. on elec. field 80−37782
^{1}S(1s,3s) state excitation by electron impact, Glauber approx. 79−31696
^{1}S ground state, variational perturbation calc., teaching 78−41129
adsorption on and interaction with graphite surface 80−34316
adsorption on carbon black, effects of preadsorbed Xe 77−59172
alkali metal +He(s^3S), Penning ionisation by slow collisions 77−50512
Ap stars atmospheres, nonuniform He distrib. rel. to mag. fields generation *(Russian)* 77−17591
appl. of semiclassical equivalent of Hylleraas var. method appls. 80−58111
approximate relativistic Hartree-Fock eqns., soln. using Slater-type functions 80−58168
atom, photoionisation, relativistic RPA calcs. 77−61719
atom, polarisation transfer collision with Rb, NMR of He 78−33453
atom+Li(Na)(K)(Rb), quenching cross sections of alkali n^2P states, 5-100 eV 79−76505
atom triple-dipole energy calcs. using pseudo spectral theory 78−46418
atomic beam, produced from nozzle flow, high speed ratios 80−5636
atomic beam production, He skimmed from freejet zone of silence 80−5635
atomic electron (positron) elastic scatt., 400 eV, differential cross sections, optical model 77−30990
atomic metastable states, electron and proton impact ionisation, autoionisation 80−102573
atomic spectra, $2^3P_1^0$-1^1S_0 and $2^1P_1^0$-1^1S_0 freqs. and transition rates, relativistic calc. 79−68210
atomic structure, numerical Hartree-Fock calc. of $1s^2$ ground state 79−81155
Auger radiation effect with γ-ray emission 77−50417
autoionisation of highly excited states, config. interaction 78−13445
autoionisation states, electron impact, electron ejection, distribs. 77−50545
autoionising resons., complex rot. method, non- and degenerate perturbation theory 79−72283
autoionising resons., complex-coord. anal. 79−49992
autoionising S states, electron-atom collision resons. theory calcs. 77−58179
backscattering from Au(Cs), fraction reflected 80−60741
beam, scatt. from LiF(001) surface, Lennard-Jones resons. and rel. displacements 77−1773
beam source, high-flux 80−58416
beam-foil spectra, coherence meas. of light polarisation from 60 keV ions 77−71863
bound states in mag. field, binding anal., variational calcs. 80−42940
broadening of 632.8 nm lasing level line width and shift meas. method 80−37066

helium atoms continued
cature of μ^-, effect of alignment of exotic-atom orbital ang. momentum on μ^- depolarisation 80−18946
CI wavefunctions, ang. correl. of electrons 78−62730
classical many-body collision model incorporating Heisenberg and Pauli principles 80−63511
closed shell, Jastrow wave functions, var. calcs. 80−83249
clustering of atoms around positron and positive ions 78−55270
collision with Ag (111) surface, energy transfer, isotropic Debye model 77−16443
collisional ionisation by fast low-charge-state ions 79−86056
collisional radiative model, reson. optical pumping, plasma diagnostics appl. 79−37459
Comet Tago-Sato-Kosaka (1969 IX), H and OH prod. rates 78−28580
Compton defect, high energy electron impact spectroscopy 77−71876
Compton profile determ. by high energy electron impact spectroscopy 77−68083
Compton profiles using Gaussian expansion of at. orbitals 80−945
contact interactions, parity-violating and parity-conserving, new evaluation techniques 79−26872
correlation energy of ground state, pair approx. 78−90065
depolarising collision cross sections, quantum beat obs. 80−87203
diamag. suscept., form factor, variational method 77−18813
dipole polarisability, correl. contribs., coupled HF-perturbation theory 80−106269
dipole polarisability, of 2^3S_1 and 2^1S_0 metastable states 78−1098
discharge lamp in visible region *(German)* 79−59782
dispersion forces between closed shell atoms 77−88522
dispersion interaction between He atoms 77−58114
distribution function in interplanetary corotating energetic particle streams 79−70938
DO white dwarfs, atmospheric He/H ratios and effective temps. 79−35249
Doppler-free two-photon high resolution spectroscopy 80−58197
double excitation wavefunctions, multiconfigurational SCF method 77−10604
double excited states, lifetime meas. by beam-foil technique 78−74590
double photoionisation calculations, variational method 80−37734
doubly excited, supermultiplet energy levels, classification as rot.-vibr. spectrum 80−52900
doubly excited state, 2p3d $^{1,3}L^0$, soln. of Hartree-Fock eqns. 77−75072
doubly excited states classification, for intermediate quantum nos. 79−10046
dynamic multipole polarisability, functional calcs. 78−74595
dynamic polarisability, 2^3S_1 and 2^1S_0 states var. perturbation calcs. 77−54507
dynamic polarisability, CHF method 78−50472
dynamic polarisability, variational calc. 78−22047
dynamic polarisability calc. 77−14599
dynamic Stark effect for elec. field strength meas. in waveguide 80−69103
(e,2e) coplanar symmetry reaction, factorised distorted-wave approx., 200-1200 eV 78−55246
ejected-electron spectra, high resoln. pulsed electron beam time-of-flight 77−3462
elastic electron scatt. phaseshifts, 2s2p ^{3}P autoionisation, 1s2s ^{3}S→1sεp ^{3}P triplet continuum photoionisation 79−31480
elastic form factors, correlated two-electron-core pots., closed form expressions 79−68195
elastic scatt. of electrons in second-order eikonal approximation 80−91667
electron affinity of $(1s2s)^3$S state, CI calc. 79−59591
electron and neutral collisions, Rydberg level transitions 79−45821
electron and positron elastic scatt., DWBA 77−30995
electron and positron elastic scatt. 77−19075
electron and positron elastic scattering, 100 and 200 eV, differential cross section 79−98221
electron and positron scatt., elastic, 500 eV, differential cross sections, perturbation theory 77−30997
electron and positron total scatt. cross sections, positronium form. 78−62916
electron angular correlations, CI and Hylleraas wave functions 77−26985
electron Compton profiles from energy loss spectra 79−7013
electron correl. effects, ang. and radial, in momentum space 77−88399
electron correlation and Coulomb hole in momentum space 78−86793
electron correlation effects on one-electron distribs. in He isoelectronic sequence 77−10598
electron correlations, combined CI and Hylleraas calc. for four lowest ^{1}S and ^{1}P states 77−38617
electron elastic and inelastic scatt., Glauber eikonal series 80−43183
electron elastic cross sections, 0.04-1.5 eV 78−42214
electron elastic scatt., 50-500 eV, optical model semiclassical wavefunction approx. 78−22030
electron elastic scatt., 5 to 200 eV, cross-sections meas., calibration 80−63822
electron elastic scatt., angle depend. resonance profile parameter 77−88563
electron elastic scatt., Born approx. 77−57217
electron elastic scatt., differential cross sections, eikonal approx. 80−53138
electron elastic scatt., p-wave reson., Breit-Wigner formula calc., perturbation method 77−38731
electron elastic scatt., phaseshift anal. of ang. distribs. 79−22833
electron elastic scatt., resonance struct. 77−50532
electron elastic scatt., two-pot. eikonal approx. calcs. 80−99573
electron elastic scatt. at low energy, exchange effects, natural boundary conditions methods 79−22831
electron elastic scatt. local optical pot., second order partial wave amplitude 78−25703
electron elastic scattering, 100-500 eV, optical model, two-pot. approx., ang. depend 78−25701
electron elastic scattering, differential cross sections, variational calc. 79−89785
electron elastic scattering, improved second Born calc. at intermediate energies 79−36770
electron elastic scattering, intermediate energy 78−22032
electron elastic scattering, intermediate energy plane wave approx. calcs. 77−10758
electron elastic scattering, modified Glauber approx. 78−74764
electron elastic scattering, total cross-section calcs. 78−42220

helium atoms continued
electron energy loss function in range 50 eV to 1 keV 77−61859
electron excit. in n=3 states, polarisation and excitation functions 77−6934
electron excitation, electron-photon coincidence meas., quantum mech. excitation amplitudes phases determ. 77−10762
electron excitation functions for 2^3S, 2^1S, 2^3P and 2^1P states, R-matrix methods 78−25716
electron impact, 2^1S, 2^1P and 2^3P states excitation and ionisation yields 77−31002
electron impact, 7-1000 eV, ionis. cross-section, accuracy of fast at. beam method 79−81283
electron impact, ^3P_g and $^{1,3}D_u$ states excitation, electron correlation influence, Rudge-type approx. 78−74771
electron impact, induced transitions between high Rydberg levels 78−21877
electron impact, ionis. cross-section, accuracy of crossed at. beam method 79−81284
electron impact, n=3 levels excitation, cross sections, angular correlation parameters 77−61855
electron impact calcs. using R-matrix and linear algebraic methods 79−59579
electron impact double excitation, Glauber amplitude 78−1083
electron impact emission, doubly differential cross-sections, 100 and 200 eV electrons 77−83743
electron impact excitation, $1^1S \rightarrow 2^3S$, 2^3P, R-matrix method extension 79−64107
electron impact excitation, ^3P_g and $^{1,3}D_u$ states, electron correlation influence, Born-Oppenheimer approx. 78−74770
electron impact excitation, Bethe approx. modifications, impact radiation polarisation 79−31695
electron impact excitation, Born-Oppenheimer exchange amplitude and local exchange pot. 78−29854
electron impact excitation, correl. effects near ionisation threshold 77−10764
electron impact excitation, cross section calc., Crothers and McCarroll method 78−25715
electron impact excitation, cross-sections, modified Oppenheimer approx. 78−82843
electron impact excitation, distorted wave theory of electron interaction 80−23554
electron impact excitation, electron-photon ang. correl. meas., 80 eV 78−42229
electron impact excitation, electron-photon angular correlation meas. 80−63826
electron impact excitation, exchange polarisation effects 77−42417
electron impact excitation, ground$\rightarrow 3^1S,4^1S$, intermediate energy calc. with exchange 80−53143
electron impact excitation, high Rydberg state, dipole transitions, impact parameter method 78−62922
electron impact excitation, in autoionisation region, parametrised close-coupling calcs. 77−54612
electron impact excitation, intermediate energies calcs. 79−76517
electron impact excitation, low energy, high Rydberg states, cross-sections and distrib. of quantum states 77−83744
electron impact excitation, near threshold, UV emitting levels obs. 78−5170
electron impact excitation, photon emission, ang. correl. 77−14584
electron impact excitation, radiation decay obs. 80−43188
electron impact excitation, resons., near n=3 threshold 79−36773
electron impact excitation, sensitivity of cross-section and ang. correl. to scatt. parameters 80−5596
electron impact excitation cross sections, rel. to photon interactions 80−27985
electron impact excitation cross-section, Born-Ochkur approx. calcs. 77−19088
electron impact excitation of $1^1S \rightarrow 2^1P(3^1P)$, excitation cross section and polarisation fractions, XUV emission 79−22841
electron impact excitation of $1^1S \rightarrow 2^1S$ and $1^1S \rightarrow 2^1P$ 80−91679
electron impact excitation of 2^1P state, first-order many-body theory 78−42223
electron impact excitation of 2^3S level, differential cross section in second Born approx. *(Russian)* 78−1087
electron impact excitation of $^3P(2p)^2$ state, integral form of close-coupling approx. 77−539
electron impact excitation of (1^1S-2^1P), coincidence meas. 77−46641
electron impact excitation to n^3S states (n=2, 3, 4), 200 and 300 eV, calc. 80−14235
electron impact fluoresc., polarisation of visible and UV lines 77−88568
electron impact fluorescence, polarisation of 5876 line 78−82848
electron impact ionis., post-collision interaction anal. from ejected electron spectra 77−42416
electron impact ionis., triple differential cross section, DWA calc. 77−88574
electron impact ionis., triple differential cross section 78−62924
electron impact ionis., triple-differential three-dimens. cross sections 77−31000
electron impact ionisation, 35 eV, triple differential cross sections 79−36777
electron impact ionisation, 7-1000 eV, cross-section 78−86956
electron impact ionisation, appl. of orthogonality procedure 79−72429
electron impact ionisation, cross section ratios 78−94326
electron impact ionisation, decay modes investig. 79−72422
electron impact ionisation, distorted wave approx., 80-250 eV 78−86955
electron impact ionisation, distorted-wave model, 100-400 eV 79−45824
electron impact ionisation, emitted electron ang. distrib. 78−55241
electron impact ionisation, energy and ang. distrib. calcs. 77−6914
electron impact ionisation, generalised differential oscillator strengths 78−55239
electron impact ionisation, Glauber amplitude 77−83748
electron impact ionisation, reaction mechanism 78−62926
electron impact ionisation, secondary electron doubly differential cross-section, 50-300 eV 79−59585
electron impact ionisation cross sections using RF quadrupole ion trap 79−98224
electron impact ionisation near threshold 79−3578
electron impact metastable excitation, resonance struct. 77−27184
electron impact spectroscopy for Compton profile meas. 78−90299
electron impact threshold excitation of n=2 state 80−83490
electron ionisation, absolute (e,2e) differential cross section, meas. in coplanar conditions 78−25719

helium atoms continued
electron ionisation, autoionising transitions interference 77−42390
electron scatt., 2^1S and 2^3S excitation cross sections, partial wave anal. 78−90301
electron scatt., absolute total scatt. cross sections, 0.5 to 50 eV 78−74765
electron scatt., effective collision freq. calc. 79−3566
electron scatt., effective pot. calcs. 80−53131
electron scatt., He^- resonances in post collision interaction 79−13820
electron scatt., inelastic, cross sections, second Born approx. *(Russian)* 79−36780
electron scatt., ionisation, elastic and inelastic collisions, many body theory appl. 80−48093
electron scatt., large momentum transfer, second Born term 77−538
electron scatt., probability of transitions between metastable 2^3S and 2^1S levels 78−5358
electron scatt., resonances, cusp effects, virtual state 78−25712
electron scatt. at intermediate energy, quantum mechanical treatment 80−91687
electron scatt. at low energies, phaseshift evaluation by pseudopotential method 79−22830
electron scatt. resonances during dilatation transformations, reson. eigenvalues stability 79−18291
electron scattering, 0-16.5 eV, R-matrix calc. 79−36768
electron scattering, $1^1S \rightarrow 2^1S$ excitation differential cross sections, 200 eV, perturbation theory 77−30997
electron scattering, by long-range pots., summation of partial wave expansion 79−41239
electron scattering, coherent excitation of 2^1P state 79−36775
electron scattering, differential cross-sections, eikonal approx. calcs. 79−81278
electron scattering, elastic, 0.00136 to 50.40 eV, adiabatic exchange approx. 77−30991
electron scattering, elastic, at low-energy, polarised orbital calc. 78−82840
electron scattering, elastic, differential cross section, 3-50 eV, 20-130°, rel. to HCN 78−90291
electron scattering, elastic, differential cross-section, 2-19 eV 79−54966
electron scattering, elastic, many-body method, 30-200 eV 80−5620
electron scattering, elastic, many-body method, 30-200 eV 80−5621
electron scattering, excitation of 2^1P and 2^3S states 79−31701
electron scattering, Glauber-Bonham-Ochkur exchange amplitudes 80−69237
electron scattering, interaction with electrons ejected from impact excited autoionis. states 78−42221
electron scattering, intermediate energy, absolute total cross-section meas. 80−18926
electron scattering, low energy, R-matrix calc. 79−59571
electron scattering, momentum transfer cross-section, 4 to 12 eV 77−68115
electron scattering, near 2^1S-state threshold, S-matrix calcs. 77−10761
electron scattering, optical pot. methods 80−102569
electron scattering, Schwinger variational principle, including exchange 79−81277
electron scattering, second-order pot. method calcs. 79−72419
electron scattering, total cross section 80−37881
electron scattering, total cross sections, meas. apparatus 77−54628
electron scattering, zero-energy Born exchange amplitude 77−38732
electron scattering amplitudes for energies less than 19 eV 79−45845
electron scattering length, using effective range theory, 0.009-0.4 eV 78−17793
electron scattering T-matrix eqns., discrete basis function calcs. 80−23551
electron scattering total cross sections, 0-3000 eV 78−25709
electron shadow scattering, cross-sections calcs. 79−59575
electron-photon angular measurements for 2^1P state 80−102575
electronic struct., dilute gas, double excitation CI anal., coupled electron pair approx. 78−21856
electronic struct., universal STO basis sets 79−10021
energy analysis, 200 eV-10 keV range 77−83763
energy density functional, gradient corrections 78−25428
energy eigenvalues and eigenfunctions, CI method 77−50371
energy levels, classical first order perturbation theory 80−58118
energy levels, doubly excited states, three particle Coulomb problem, hyperspherical coords. framework 80−52875
energy levels in magnetic fields, review 77−50383
energy of S states, appl. of modified interelectronic pot. 78−29736
exchange and correlation pots., density functional theory 80−52848
exchange energies, Born-Oppenheimer exchange amplitude, Bonham series calcs. 78−29854
excitation, primary, specific, by fast pions (protons) (electrons) from accelerator 80−23559
excitation and ionisation, by instationary shock fronts 78−59540
excitation energy calc., improved virtual orbitals in extended basis function space 77−46491
excitation of simple atomic and mol. systems, long-range force effects 79−10170
excitation transfer between excited states, neutral atoms in transient plasma 78−70914
excitation transfer in n=4 levels after laser pumping 77−3324
excited, optically-allowed, long-range interaction pots. with electrons, protons and atoms 77−14520
excited S, D and F state radiative lifetimes, electron impact method 78−94325
excited state formation from He_2^+ in afterglow, theory 79−22802
excited states, Galerkin-Petrov method, nonlinear parameters 78−78619
excited states, relativistic corrections 78−62734
factorized wave function 79−3355
field-ion appearance pot., theory 77−545
fine structure, 2nd order contribs. from all intermediate states 79−3354
fine structure, triplet P state splittings, higher order corrections of theoretical calc., book contrib. 78−82632
fine structure interval 2^3P_0-2^3P_2, optical microwave atomic beam mag. resonance meas. 80−102585
fine structure intervals, elec. field-induced anticrossing meas. 78−42031
fine structure intervals in 3^3P and n^3D states, level crossing meas. 77−14396
fine structure of triplet term of 1s3d configuration 79−3595
forbidden radio lines, 2^3P state fine struct. 77−23447
formaldehyde+He(H_2), collisional relax. times and lineshape distortion, Stark absorpt. linewidth obs. 78−74744

helium atoms continued
frequency depend. multipole polarisability and dispersion energy between interacting pairs 79−18306
g_J-factor, isotopic ratio, 2^3S_1 state 77−10608
Galaxy, increasing He content rel. to chemical enrichment of disc dwarfs 79−88733
generalised oscillator strength, variational determ., extremum principle appls. 78−94213
generator coordinate method 78−29731
glow discharge, low press., excitation transfer and quenching of n=3 excited states 80−38743
glow discharge, n=3 sublevel quenching and energy transfer, laser perturbation method 80−44060
ground and first excited states, electron Hamiltonian, effective one-body, with correct asymptotic behaviour 79−45619
ground state, dispersion relations and AC Stark shifts 78−945
ground state, electron impact excitation, alignment and orientation parameters calcs. 79−36772
ground state, explicitly correlated wave functions 78−17566
ground state, Galerkin-Petrov method calc. 77−46485
ground state, Hylleraas six parameter wave function, minimisation method 80−27925
ground state, model for Singer geminals tempering methods comparison 80−52845
ground state, oscill. strength distribs., Stieltjes imaging determ. 77−6731
ground state radial limit, config. interaction and many-body perturbation theory 78−37560
ground state s^2 correlation, Hartree-Fock calcs. 80−83281
ground state static polarisability and hyperpolarisability, numerical SCF method 79−36567
ground state wavefunction, SCF HF calc. 78−90070
hadronic, bound quark, atomic spectral lines calc. 79−86092
Hanle effect 77−23474
Hartree equation, variational method 79−49941
Hartree operator, upper and lower bounds to critical values 77−23426
Hartree-Fock density matrix equation, soln. 77−14339
Hartree-Fock electron density, kinetic energy functional 79−26879
Hartree-Fock energy, perturbative corrections, incomplete basis set problem 78−70744
He^+, bombardment of second row element target, K-shell X-ray prod. 79−47550
$^4He+H_2(v=0,j=0) \rightarrow {}^4He+H_2(v'=1,j')$, fully converged sudden rotation total integral cross sections 77−58135
He II 304 Å line redshifted to 1450 Å in far UV background 80−41893
HF calcs. using piecewise polynomial electronic wavefunctions 78−5115
HFS, using Doppler-free intermodulated optogalvanic spectrosc. 79−50169
high-flux fast neutral beam source 78−54507
high-L states, laser driven forbidden transitions, line shapes 79−22638
imaginary frequency mutipole polarisability and long-range dispersion consts, functional calcs. 78−74596
impact on Ag surface, generalised Langevin theory 77−8700
impact on W surface, tangential momentum accommodation coeff. meas. by acoustic vel. and absorpt. obs. 80−66867
interaction with graphite surface, anisotropic He-C pair interaction 80−96738
intermolecular force, scaled electron gas approximation 79−98181
interplanetary He, dynamical effects in 584 Å reson. scatt. 80−8509
interstellar He I, obs. with gas absorpt. cell, implications for local interstellar medium struct. 80−62234
interstellar medium, local He density correction 79−92834
ion, backscattering from solid Pb, emitted radiation intensity rel. to incident energy 79−89762
ion recombination and level populations, resolution of ang. momentum states 77−45529
ionisation, electron wavefunctions for (γ,2e) and (e,3e) processes at high energy, double Fourier transform 78−17628
ionisation, primary, by ~2 MeV relativistic electrons *(Russian)* 77−75309
ionisation by UV radiation from CO_2 laser produced Cu plasma 78−17624
ions, beam-foil excitation, relative initial populations, lifetime curves 80−14210
ions, electron impact excitation 80−78712
ions backscatt. from solids, charge state distribs., target temp. depend. 79−95887
ions in radiation belt, equatorial α/p ratio near 1 MeV 80−4205
irradiation of O_2 with ^3He and ^4He particles, recoil ranges of ^{18}F in Au determ. 80−71931
isoelectronic sequence, 2^1S states, analytic wave function 80−9525
isoelectronic sequence, correlated and HF electron density differences 78−46275
isoelectronic sequence, dielectronic recomb. coeffs. 77−27172
isoelectronic sequence, E1 and E2 oscillator strengths, MCHF calcs. 80−106292
isoelectronic sequence, pot. energy relationships 79−22584
isoelectronic sequence, Schrodinger eqn. finite difference soln. 79−31373
isoelectronic sequence up to Z=10, D and F states fine struct. 77−544
isoelectronic sequences, screening constants, ground and excited states 78−62701
isoelectronic series, (H^- to C^{4+}), correl. energy calcs. 79−36543
isoelectronic series, dipole matrix elements derivation 77−83519
isoelectronic series, dipole oscillator strength distrib. moments, systematics 78−86821
isoelectronic series, dipole transitions, transition integral cancellation 80−69052
isoelectronic series, electric field variant orbitals, STO field gradient depend., atomic quadrupole polarisability 80−23295
isoelectronic series, energy level and classifications of doubly-excited states 78−62736
isoelectronic series, excitation regimes, nucl. orientation due to hyperfine interaction 78−70928
isoelectronic series, ground state specific mass shift, HF variation perturbation calc. 80−47889
isoelectronic series, Koopmans' ionis. pot., virial scaling corrections 79−45655
isoelectronic series, time depend. Hartree Fock theory, reduced Green's function anal., multipole polarisability 79−3358
isoelectronic series, transition moments, exchange and core polarisation effects 77−54531

helium atoms continued
isoelectronic series, var. energy functionals involving 1-electron operators 77−83484
isoelectronic series 79−85894
isoelectronic spectra autoionisation states n=3 hydrogenic threshold, complex rot. method 79−31477
isoelectronic systems, ground state, Coulomb holes and correl. pots. 79−89594
isotopic shift, $1s2s\ ^1S_0$, meas. using tunable vacuum UV anti-Stokes light source 79−18149
kinetic energy functional, gradient expsn. 77−6665
Koopmans' ionisation potential relax. correction 79−18308
l-limit energies for ground state atoms using hyperspherical basis sets 80−14076
Lande g-factor determ. from free radn. beats 77−18880
laser induced level shift 78−58627
laser magnetic resonance spectroscopy 79−72445
laser spectroscopy in intense magnetic fields 80−62738
level crossing signals in inhomogeneous mag. field *(German)* 77−27037
lifetimes of doubly excited states, autoionisation and radiative decay 79−18146
light scattering spectra of gas, collision-induced scatt. 79−18137
light shift of 4^3S-2^3P line by CW CO_2 laser beam 77−30829
line profiles in RY Persei spectra, visible obs. 80−67795
local interstellar medium, He component anal., UV obs. 79−30100
long-lived states population decay 79−54954
magnetic hypersusceptibility *(Russian)* 77−14598
magnetic interactions of electrons *(German)* 78−82610
many electron system, photoionisation and photoexcitation, at. transition strong config. interaction effect 80−47909
matrix effective potential for electronic response in 30-400 eV electron scatt. 80−58388
mesic, X-ray radiation anisotropy, suppression coeffs. *(Russian)* 78−22058
mesic and muonic mol. ion formation in liq. He, X-ray intensities, Auger and Stark transitions 78−94338
mesoatoms, π^-, μ^-, K^-, p^- atoms, energy spectra, wave functions *(Russian)* 78−55264
mesonic atoms, formation in mixtures of lightest elements 80−87252
metastable, (2^3S), bi- and ter-mol. deexcitation reaction rate coeffs. meas. in afterglow 79−36748
metastable, electron impact ionisation cross-section meas. 77−6931
metastable, impact on Mo[110] surface 78−95642
metastable, in He-Kr^+ ion laser, conc. and time variation 79−55111
metastable, multiphoton transition detection, n^3S-n^3D splitting meas. 80−58231
metastable, photoionisation rel. to laser development 78−13476
metastable, two-photon ionisation, multipole interference effects 80−23466
metastable, two-photon ionisation calc. for linearly and circularly polarised laser light 79−797
metastable $1s2s^1S$ state, photoionisation, perturbation theory calcs. 78−78759
metastable 2^1S, 2^3S, elastic electron scatt., 7-500 eV Glauber cross sections 77−19077
metastable 2^3S state, electron impact excitation cross-sections calc. *(Russian)* 80−53149
metastable atoms high intensity beam with good vel. resolution 77−14609
metastable beam source for surface spectroscopy 77−36334
metastable state, two- and three-photon ionisation 80−91518
metastable states, high resolution study via electron scatt. 77−6935
metastable states, props., energy transfer mechanisms, exptl. techniques 80−27921
metastable thermal, interaction with solid surface, obs. of He^+ ions creation *(French)* 77−79684
methane+methane (He)(Ne)(Ar), dispersion forces 78−13565
molecular beam diffraction from Ag (111) surface 77−85880
multiconfiguration Hartree Fock problem, finite-difference Newton-Raphson soln., He $1s2s^1S$ state appl. 77−6663
multiphoton ionis. pot. in intense circ. polarised laser beam 80−43010
multiphoton ionisation potential, circularly polarized light 79−27101
muonic, $2S_{1/2}$-$2P_{3/2}$ level splitting, test of QED predictions on electronic vacuum polarisation 77−3494
muonic, 3p-3d transitions calcs., energy splittings 80−87253
muonic, atomic spectra, QED, strong and supercritical fields, book contrib. 78−74193
muonic, hyperfine struct., relativistic, radiative and recoil corrections, QED test 80−14256
muonic, three-particle system with Coulomb interaction, correl. wavefunction calcs. 77−68144
muonic atoms, hyperfine structures 80−69273
muonic D+He, μ^- transfer rate 77−42447
n=4 resonances, complex rot. meas. calcs. 79−97995
N-body excited states, Hartree-Fock eqns. derivation 79−93934
neutral muonic atoms, ground state hyperfine splitting 79−68334
one-dimensional atom, bound states, for teachers 79−40317
optical escape factor, 3^1P-1^1S transition, laser perturbation method 78−37586
optical excitation function of 5876Å line near threshold 78−70797
optical harmonic coeffs., third-order, R-matrix calc. 77−57955
optogalvanic spectroscopy, Doppler-free two-photon 80−52960
orbitals calculations, using extended STO basis sets 79−6844
ortho-positronium self-trapping in dense fluid He 77−10793
oscillator strength, sums, one-term approx. 78−66509
oscillator strength and first derivative, optical limit 77−3305
oscillator strength calc., allowed np-n'd and nd-n'f transitions 79−31467
oscillator strength determ. from resonance radn. self-absorpt. 77−18847
outer 1s, 2s and 2p electron loss cross sections by multicharged ions 78−42185
Pade type variational functions, appln. to ground state 80−87025
parity violation in atomic electrons and electron-electron interaction effects 79−54788
parity-violating elec. dipole transitions 80−69094
path integral formalism of perturbation theory, simple mols. and atoms 79−6841
Penning collisions, orientation transfer for ion excited state lifetime meas. *(French)* 78−50621
Penning ionisation electron spectroscopy, metastable He impact, electron energy distrib. 79−52060

helium atoms continued
Penning ionisation of di/triatomic mols., electron spectra, vibr. transfer 77−14555
photoabsorption, modified RPA calcs. with exchange 78−13477
photoionis. cross-section, hyperspherical coord. method calcs. 80−102496
photoionisation, correl. satellites and subshell cross-sections, electron spectrosc. obs. 79−31485
photoionisation, expt. techniques, processes, theory, review 77−14402
photoionisation, frozen-core HF perturbation theory, oscillator strength, dipole length and vel. calc. 78−78672
photoionisation, two-electron, threshold law and photoelectron spectra 78−29767
photoionisation above n=2 photoionis. threshold 80−102497
photoionisation and photoabsorption cross sections for aeronomic calcs., data tables 80−41599
photoionisation cross section from excited state $^4p^1P_1$ *(Russian)* 77−61722
photoionisation cross sections for VUV region 77−46547
photoionisation cross sections of excited states 78−66523
photoionisation cross sections up to n=2 excited state, evidence of autoionisation 80−91520
photoionisation cross-section using UV laser plasma light source 79−19096
photoionisation cross-sections, ground state inversion pot. method 78−33481
pionic, isotope effects, 1s state energy shift and line broadening for ^{3}He-^{4}He pair *(German)* 80−48107
planetary atmospheres He thermal escape, assoc. non-Maxwellian effects 79−80264
plasma, non-equilib., of strong current pulse discharge, diagnostics *(Russian)* 78−75271
plasma, of theta pinch, $N^{+,2+,3+}$ lines Stark broadening, He(II) line diagnostics 80−24249
polarisabilities, static and dynamic dipole, dynamic quadrupole 77−18810
polarisabilities and shielding factors, coupled HF approx. 78−22048
polarisability, effective potential approximation method 77−88587
polarisability, freq. depend. polarizability, LCAO SCF perturbation theory 79−31387
polarisability, quadrupole, using elec. field variant GTO basis set 79−76359
polarisability and Verdet consts., freq.-depend., calcs. 78−62781
polarisation potential, quasiadiabatic, for elastic electron-atom scatt. 77−6929
polarised light emission after HeH^+ impact on C foil 80−58361
positive column discharge, IR optogalvanic spectrosc. using F-centre laser 80−78563
positive ions, completely stripped, charge-transfer eqns. 77−75294
positron elastic S-wave collisions, optical pot. formulation 77−14576
positron elastic scatt., polarised orbital approx. 77−30996
positron elastic scattering, phase shifts, simplified RPA calcs. 77−10759
positron induced droplet form. in gas 77−68148
positron inelastic scatt. at intermediate energies, time of flight spectra 80−18932
positron s-wave scatt., total cross sections 77−42406
positron scatt., low energy elastic cross-sections 78−5343
positron scatt., total cross section 78−70933
positron scatt., total cross section meas., with positron TOF spectrometer 79−3568
positron scatt., total cross sections 79−86065
positron scatt. cross sections 79−3569
positron scattering, elastic, intermediate energy, total cross sections, modified Glauber amplitude 80−23549
positron scattering, positronium formation 79−89772
positron scattering, second-order pot. method calcs. 79−72419
positron scattering polarisation effects, orbitals calcs. 77−3457
positron total scatt. cross sections 77−14573
positron total scatt. cross sections 77−83729
potential energy curves, dispersion damping functions, Hartree Fock interaction energy 79−98176
pseudospectral dipole oscillator strength distribs. 78−50503
quantum defects rel. to angular momentum, nuclear charge, Coulomb-Born approx. method *(Japanese)* 77−50534
quantum mechanical energy spectra calc. using trajectory integrals 78−21838
quantum static multipole polarisabilities 78−82859
radiation trapping in electron beam, spatial distrib. of line intensity 77−79572
resonance photoabsorption in (3s3p) ^{1}P reson. region 79−45659
resonant states, high resolution study via electron excitation 77−6936
RPA eigenvalue eqns., excitation frequencies and oscillator strengths 78−17570
Rydberg atom, electron collisions 80−63833
Rydberg series transitions, opto-galvanic spectrosc. 79−54779
Rydberg states, mag. and elec. fine struct. calcs. 79−76333
Rydberg states transitions, IR mag. reson., subDoppler lineshape obs., using motional Stark effect 78−947
S autoionising states, appl. of at. reson. theory 80−23329
S resonant state, improved line width expression appl. 80−5505
S state electron correlation 79−49952
S-state eignefunctions, Kinoshita's expansion 78−16674
scattering by crossed at. and mol. beams, elastic differential cross section 79−10171
scattering by graphite (0001) surface, bound state reson., interaction pot., band struct. effects 80−29840
scattering from and interaction with graphite 80−60732
scattering from Cu (117) ordered stepped surface 78−15277
scattering from hydrocarbons at high velocities, short-range pots. determ. 77−27142
scattering from hydrocarbons at high velocities, short-range pot. determ. 77−27143
scattering from LiF (001), hard corrugated surface model, GR method 77−85863
scattering of 63 meV He atoms from LiF, single Rayleigh phonon interaction 78−80447
SCF electron-gas local-spin-density model including correlation 80−9488
SCF ion improved virtual orbitals excited configs. calcs. 77−10585
Schrodinger equation, nonseparable, series solns. and variational principle 79−36504
Schrodinger equation in symmetric coords. 79−21589
Schrodinger equation solns., existence criterion 78−41117

helium atoms continued
seawater ^{3}He distrib. in deep water over Mid Atlantic Ridge 77−5242
second order correlation energies, variational-perturbation method, radial basis saturation errors 79−97985
self-consistent electron pairs with higher order effects, effect of quadruples 78−46276
self-consistent perturbation theory, generalisation for perturbation-dependent nonorthogonal basis set 78−17563
short range interactions between two rare gas atoms 79−26888
singlet-triplet anticrossing, elec. field induced 77−14404
Slater-transform-Preuss functions, min. basis sets 79−59343
solar quiescent prominences, H and He spectra 77−13295
solar wind, H and He ions vel. differences rel. to Alfven instabilities 77 -49259
solar wind He ions, temps. and vels. rel. to plasma microinstability 77−87222
spectral broadening, of (2^1P-2^1S) line, 0.3-20 torr. 79−13673
spectral density, photoabsorpt. and dispersion profiles, moment theory 77−6709
spectral line profile, hollow cathode source 77−23469
spectral line profile at 504.7 nm excited in discharge 77−18848
spectral line width, use of hollow cathode discharge for determ. *(Russian)* 77−46529
spectral lines, singlet, self-broadening, resonant interaction 80−63574
spectrogram using moderate-resolution spectrometer with interf. selective amplitude modulation 79−30588
spontaneous decay probability of 3^3P level, expt. and theoretical values 78−50501
Stark broadened 4121 Å and 4437 Å lines in plasma, electron impact effects 77−27025
Stark broadening, satellite transitions, in turbulent plasma 77−61759
Stark broadening in plasma, close electron collisions effect 77−23459
Stark effect, high-freq., mol. lines effects on meas. 80−9544
Stark effect in 3-D stochastic elec. fields and static mag. field 78−5855
Stark effect on optically excited plasma atoms in static mag. field 78−66505
Stark profile in arc plasma, heavy-particle temp. 79−46484
Stark shift and line broadening in 3-D stochastic laser field, He plasma 78−50502
static multipole polarisabilities, integral equation approach to scaled 1/Z expansion 80−63846
structure, channel coupling array calcs. 79−31362
Sun, He diffusion theory 77−56888
surface scattering pot., surface electron density depend. 80−104027
synchrotron radiation scattering cross sections 78−55213
tetrafluoromethane+He gas mixture, collision induced for IR translational spectra 80−83353
three-body problem, eigenvalue calc. *(German)* 77−33881
three-particle atomic system, binding energy, Faddeev method calcs. 77−57858
three-photon ionisation from metastable states, cross-sections 77−42296
three-photon transitions, dichromatic laser field 78−17643
tight bounds on multipole dispersion coefficient calcs. for interaction of the atoms 80−83320
total scattering cross sections for low-energy electrons 80−58417
transition probabilities in constant electric field, general perturbation theory 78−13466
triplet principal series, Stark effect at high field strengths *(German)* 77−83537
triplet state, excitation energy transfer among upper levels 79−26901
triplet states, doubly excited, spectrum and polarisation 80−99472
two-electron excited states 78−58605
two-electron systems, ground-state energy, var. calcs. 77−61679
two-electron wavefunctions, few-parameter, ground state 77−75051
two-photon ionisation cross-section calcs. 78−21888
two-photon ionisation for 2^3S and 2^1S states 80−37791
two-photon light shift and two-photon Lamb dips, cross-saturation method appl. 79−36591
in upper atmosphere, electron impact cross-section 78−28398
van der Waals interaction with Al I, line broadening and shifts 79−6912
variational energies for highly excited states 78−62737
variational perturbation theory, Hyleraas type base *(Russian)* 77−37775
Voigt profile, absorpt. line calcs. for the 396.5, 361.4, 318.7, 492.2, 587.6 and 447.1 nm lines 80−99471
Voigt profile, line absorpt. calcs. of 388.9 nm triplet, 501.6 nm singlet lines 78−90123
VUV source, laser induced two photon blackbody radiation from He atoms in glow discharge 78−58102
X-ray scatt., total, two-electron density functions 78−70889
(e,2e), absolute double- and triple-differential cross sections, 0.2-2.8 keV 80−5623
$(\mu^-{}^4He)^+$ ion, meas. of $2S_{1/2}$-$2P_{3/2}$ splitting, QED vacuum polarisation 77−34785
^{4}He(3^3P), fine struct., level crossing obs. 78−82686
Al+He^+(H^+), 1.9 MeV, Kα X-ray polaris. and line strengths 77−30983
Ar+$^4He^{2+}$, ionis. cross section, Z^2 effect 78−33595
Ar+He, Penning ionis., ejected electrons energy and ang. distrib. 79−81266
Ar+He* Penning ionisation, semiclassical descretisation procedure 78−90275
Ar+He*(1s2s,^{3}S), coupled channel calcs. of chemi-ionisation 77−27166
Ar+OH, colisional relax., laser mag. reson. study of press. broadening 79−94020
Ar^++He, $X^2\Sigma$ and $A^2\Pi$ states, CI pots. 78−74727
Ar^{n+}+He, 3≤n≤8, single and double electron transfer cross-sections 77−6924
Au+$^4He^{2+}$, L-shell ionis. probability, X-ray prod. 79−18276
Au+He^{2+}, high energy ionis. probability, semiclassical approx. with relativistic Hartree-Fock function 79−6998
B+He(Ne)(Ar), ground and excited states interaction, B spectral line breadth 77−68092
B^{3+}+He, charge-exchange total cross-sections 77−79691
B^{q+}+Ar(He)(H_2), keV electron capture cross section 80−14229
Be, correlation energies, Hartree-Fock Hamiltonian 78−41965
Be^++He, Be Auger spectra 77−57951
C^{4+}+He, charge-exchange total cross-sections 77−79691
C_3, ($^1\Pi_u$) radical excited state radiative lifetimes and the collisional deactivation 79−27018

helium atoms continued
$CH_4+H^+(He^+)(O^+)$, 1 MeV dissociation, kinetic energy spectra 78−94302
CO^+, vibr.-excited $A^2\Pi$ state, radiative and radiationless vibronic deactivation rates with He 79−10134
CO+He, press. broadening, rot. energy transfer, infinite order sudden approx. 78−22011
CO+He, rot. excitation, infinite order sudden approx. 78−74740
CO_2-Cs-He discharge, CO_2+Cs reaction rate meas. by IR absorption, press. depend. 78−44367
CO_2+He, rot. inelastic collision, ab initio SCF, electron gas and pot. energy surfaces 80−83468
CO_2+He, rot. transition classical integral cross section, surprisal predictions 77−54594
$CO_2+He^+(H_2^+)$, charge transfer, energy transfer, product ion excitation and fluoresc. 77−75288
CO_2+He(Ar), dipole and Raman line press. broadening temp. depend. 79−68265
$CO(\nu=1)$+He, vibr. relax., collinear and 3D rate consts., temp. depend. 77−38717
$CO(\nu=1)$+He, vibr. relax., collinear and 3D rate consts., temp. depend. 77−38718
$CS_2+He(Ar)(N_2)$, perturbed rot. diffusion of CS_2, IR spectra 78−75245
Cd II+He, relax. consts. for depolarising collisions 77−19239
^{114}Cd+He, collisional effects on 326.1 nm line rel. to temp. and conc. 78−5336
Cl+He(C)(O)(Ne), K-shell ionising collisions, average L-shell ionisation probability, K_α spectra 79−72408
$Co^+ + e^- + He \rightarrow Cs + He$, rate coeff., pulsed discharge at 625K 78−17789
Cs-He, new absorption/emission bands perturbed Cs transitions assignment, pot. energy curves 78−66486
Cs-He afterglow, spectral emission from excited Cs ions, 380-750 nm 79−82116
Cs+He, interaction pot. and oscill. strength 80−91645
Cs+He, optical pumping, spectral line shape *(Spanish)* 79−22662
Cs+He^+, spin dependent charge transfer in low-energy collisions 77−75293
$Cs_2+He(Ne)(Ar)(Kr)(N_2)(CH_4)$, collision-induced dissoc., atom-mol.-exchange optical pumping 78−22008
CsI+He, elastic and inelastic scatt. 77−58119
$Cs(6^2P_{3/2})$+He(Ne)(Ar)(Xe), collisional depolaris., nucl. spin depend., by Zeeman scanning 77−19012
$Cs(8^2P)$+He(Ar)(Xe), fine-struct. transition cross sections, semiclassical calcs. 77−30972
D-^{3}He, clean fusion reactor feasibility study 78−33288
D_2+He, vibr. relax., 400-80K 77−10736
$F^{7+,8+}+H_2$(He), 20-56 MeV, F K X-ray cross sections, inner shell Coulomb excitation 77−19025
F^{8+}+He, X-ray prod. cross sections resulting from electron capture and electron excitation of F^{8+} ions 79−3557
H, population inversion obs. in FM-1 spherator 77−7048
H:He, 15 to 150 keV ionising collision, electron ang. and energy distrib. 80−53121
$H+{}^4He^{2+}$, electron capture and charge exchange cross sections 77−68108
$H+C^{6+}(He^{2+})$, ionis. cross sections 79−22805
H+He, D+He, low energy elastic scatt., pot. well depth determ. 77−6884
H+He, H Balmer-α fine-struct. line shift and broadening 80−37783
H+He, H hyperfine press. shift, MCSCF-variational procedure 77−6735
H+He, H hyperfine shift, exchange perturbation theory 77−6736
H+He, long and intermediate range interaction, model pot. calc. 79−22789
H+He (2^3S), pot. energy surfaces and autoionisation lifetimes calcs. 77−34740
H+He(Ar), press. effects on H_α and H_β Balmer series 77−18845
H+inert gas atom, interaction pot. from electron gas model 79−31637
H^-+H_2(He)(Ar), electron detachment, Born cross sections, Pade approximants 78−17742
H^-+H(He), electron detachment cross sections 78−90265
H^-+He(Ar), electron detachment cross sections 78−58810
H^++He, double electron capture, close-coupling approx. calcs. 77−71868
H^++He, proton energy degradation, approx. yield spectrum 79−31643
$H^+ + He^+$, charge transfer and ionis. cross sections, coincidence meas. 78−50634
$H^+ + He^+$, fast collision, ionisation and charge transfer, cross section meas. 78−25698
$H^+ + He^+$, He^{2+} form. by charge exchange and ionis., cross sections 77−83708
$H^+ + He^+$, ionis. and charge transfer cross sections 78−42186
$H^+ + He^+$, ionisation and charge transfer using intersecting beams 77−68104
H^++He(Ar), charge exchange, differential cross sections 79−7006
H^++He(Ar) electron transfer cross sections 78−58809
H^++He(Ar)(Kr)$(O_2)(H_2)(N_2)$, 2.2-8.2 keV, H(n=3) form., absolute cross sections 77−34755
H^++He(Ne)(Ar), K-shell ionisation cross-sections, Glauber approx. calcs. 77−46629
$H^++He(1s^2)$, K-shell electron capture collision, static pot. effect 80−91660
$H^+ + He(1s^2) \rightarrow H^* + He^+(1s)$, continuum distorted wave approx., total cross section 77−68109
H_2^{2+}, two-electron bond, energy expectation values from density matrix partitionings 77−75059
H_2-He, mixed-pole terms in anisotropy of long-range interaction coeffs. 77−30950
H_2-He mixtures, isotopic anal. using high resolution mass spectrometer 77−77844
H_2-He(Ne), NMR longit. relax., mole fraction depend. 77−61767
p-$H_2+{}^4$He, vibr. relax., 50-2000K, coupled channel, coupled states and effective pot. methods comparison 79−6995
H_2+He, far IR absorpt., collision-induced at 77.4, 195 and 292K 78−13495
H_2+He, gas phase NMR, kinetic theory, single relax. time approx. 77−14451
H_2+He, inelastic collisions, statistical decoupling 77−517
helium atoms continued
H_2+He, nucl. mag. relax., DWBA cross sections from S-matrix formalism 77−27151
o-H_2+He, relax. and kinetic cross sections, DWBA calc. 78−25655
H_2+He, rot. relax. time, <300K, classical trajectory method invalidity 77−10739
H_2+He, rot.-vibr. energy transfer collisions, distorted wave infinite order sudden approx. method 77−75265
H_2+He, vibr. relax., pot. surface depend. 77−75266
H_2+He, vibr. relax. cross section 80−99494
H_2+He potential surfaces, SCF and MRD-CI calcs. 79−10172
H_2+He^+, 0.5-3.0 keV, direct and charge-exchange scatt. 77−75263
H_2+He*, Penning ionisation, singlet interaction pot. anomalous struct. 77−75274
$H_2+He(2^3S_1)$ mol. ionis., optical atom orientation method *(Russian)* 78−13591
$H_2+He(2^3S)$, Penning ionisation, quantum mech. scatt. calcs. rigid rotor approx. 77−34741
$H_2+He(2^3S)$, pot. energy surfaces and autoionisation lifetimes calcs. 77−34740
H_2^++He, 10 keV, dissoc. excitation, ionis., energy distrib. 77−61849
H_2^++He(Kr)(Xe), collisional dissociation, ion-pair prod., negative ion prod., cross sections 77−14529
$H_2^+ + He \rightarrow H + HeH^+$, endoergic exchange, DWBA calcs. 77−9055
$H_2^+ + He \rightarrow H + HeH^+$, reaction dynamics, vibr. state channels, beam expt., trajectory calcs. 77−77739
$H_2^+ + He \rightarrow H + HeH^+$, total cross sections, quasiclassical trajectory results compared with mol. beam data 77−60051
HBr_2+He, classically forbidden vibr. excitation, S-matrix 77−516
HCN+He, press. broadening, rot. energy transfer, infinite order sudden approx. 78−22011
HCN+He, rot. excitation, infinite order sudden approx. 78−74740
HCl+Ar(He), rot. excitation, infinite order sudden approx. 78−74740
HCl+He(Ar), press. broadening, rot. energy transfer, infinite order sudden approx. 78−22011
HD+He, press. broadening, rot. energy transfer, infinite order sudden approx. 78−22011
HD^++He collisions, rotational transitions 78−70909
$H^-(D^-)$+He, collisionally induced electron detachment, 0.5 MeV, target effect 80−37858
$HD(^1\Sigma_u^+)$+He, fluoresc. quenching and energy transfer processes 79−86032
$H_2(E,F^1\Sigma_g^+)$, +He(H_2), quenching rates, IR fluoresc. obs. 78−37698
$H_2^+(H_3^+)$+He, Hadamard mass spectroscopy, mass spectra 79−30601
$H_2(^3\Sigma_u^+)$-He(2^3S), discharge ionisation growth, diffusion coeffs. 78−83636
He + H_2, vibr. inelastic integral cross-sections calcs. 79−31660
He, 2^1S and 3^1S, CI expsn., convergence patterns 77−50378
He 2S metastable state, three-photon ionis. 79−18167
He (1^1S) and (2^3S), electron loss in passing through inert gases 79−13805
He (2^3P)+Ca(Sr), collisional quenching of metastable states, excitation transfer cross sections 78−66653
He, (2^3S_1) state excitation by electron impact, at. time of flight meas. 77−19083
He (2^3S_1)+H_2, ionis., interaction pot. at thermal energies *(Russian)* 79−94077
He (2^3S), resons. below n=3 doubly excited states, electron impact excitation 77−50543
He, absolute photoionisation cross section curve 78−37612
He beam, fast, formed by 25-90 keV He^+ beam neutralisation, 2^3S population 79−31740
He, electron elastic scatt., minimum variance method, discrete-basis-set approach 77−83734
He, electron impact, low energy, post collision interaction, ejected electron energy distrib. 79−72423
He, electron scatt., inelastic Feshbach resons., quasi projection operator calc. 80−58395
He, ground state electron correlation visualisation 79−3367
He, He^--positron bound states, CI-Hylleraas calcs. 77−10603
He I, $2s^1S$-$3p^1P$ excitation, linear polarisation fraction, foil material effects 78−21893
He I, $3p^3P$ level decay, zero field quantum beats 78−961
He I, 4^1F and 5^1F lifetimes 78−37599
He I, 4471 Å line profile in various plasmas, ion perturbation effects 78−94214
He I, beam-foil excitation, temp. depend., linear polarisation of transitions 80−14213
He I, beam-foil excited, 70-400 keV, relative initial populations 80−14211
He I, exeited states decay, lifetime meas., lab. mag. field effects 77−10640
He I, exptl. line profiles near 4471.5 Å 77−6725
He I, He II, population densities in TPD plasma machine, collisional-radiative model 77−47160
He I, heavy ion impact excitation, alignment relax. of nonresonant levels *(French)* 77−61842
He I, heavy ion impact excitation, relax. of 3 ^{1}P level *(French)* 77−61843
He I, heavy ion impact excitation, orientation by anisotropic relax. of 4 ^{1}D level *(French)* 77−61844
He I, in shock tube plasma, electron density from Stark widths 77−80374
He I, in solar flare, levels populations calc. 77−53538
He I, interf. beat period determ. of nondegenerate states 78−70807
He I, lifetime meas. by beam-foil spectra 77−75104
He I, saturated absorpt. on 587.5 nm line, pressure effects 77−23448
He I, spectral line shift and Stark broadening in plasma 77−18843
He I, Stark broadened 4471 Å line struct. in dense plasma 77−6722
He I, Stark broadening of 3965 Å line in plasma jet 79−98023
He I, transfer excitation energy between n=5 levels 78−70942
He I 10830 Å triplet in sunspot umbral spectra *(Russian)* 80−36604
He I 1s3d levels, cascade-free lifetime meas., using He^++He 35 keV collisions 78−58607
He I 2^3P-3^1D intercombination line, collision-induced, obs. by laser absorpt. spectroscopy 80−58194
He I $2^3S \rightarrow 2^3P$ transition, rate coeff. for electron impact excitation 79−48664
He I 4026 Å narrow-band index for B-type stars in young clusters and associations 77−29887

helium atoms continued
He I 447.1 and 492.2 nm lines, ion motion effects on Stark profiles 80−69105
He I 584 Å, solar line profile modification in propag. through interplanetary medium 79−66973
He I 584 Å, solar reson. line profile and intensity meas. 79−40153
He I 584 Å dayglow emission and exospheric He seasonal-latitudinal var. 79−75007
He I 584 Å dayglow meas., contrib. of O II 537 and 581 Å lines 77−41253
He I 584 Å dayglow obs. by rocket-borne reson. absorpt. cell 77−64503
He I 5876 Å radial vel. var. in nova HR Delphini 77−82249
He I 58.43340 nm geocoronal and interplanetary emission obs. 80−4155
He I and He II emission lines in 2A 0526−328 optical counterpart 80−73075
He I beam-foil excitation, 60-180 keV, alignment production, foil temp. depend. 79−54956
He I D_3 line, Stokes parameters for quiescent prominences, Hanle effect quantum theory 78−85924
He I D_3-line in solar prominences, emission line intensities rel. to model calcs. 79−44447
He I D_3-line polarization in solar prominences, level-crossings effect 80−94772
He I envelope in Hd 151932, single WN 7 type star 79−44493
He I glow discharge, low-press., quenching of singlet states by N_2 80−49030
He I in solar flare, levels populations calc. 79−62809
He I line profiles, ion motion effect in low electron density plasma 80−43877
He I line profiles with forbidden components induced by fluctuating fields in small theta pinch plasma 77−80353
He I lines in B-type stars spectra, wavelengths 77−25999
He I lines in early-type stars, Copernicus UV obs. 80−41825
He I lines in spectra of QSOs and Seyfert galaxies 78−36717
He I overlapping lines, model microfield method Stark profiles, ion dynamics effect 79−82049
He I plasma lines, Stark broadening, quantum mechanical calcs. 80−43880
He I radiation, polarised, appl. in valence electron spectroscopy 77−492
He I satellite line shape in plasma, stochastic theory 78−38460
He I singlet transitions, polarisation meas. following beam-foil excitation 79−13665
He I transitions, polarisation meas. using beam-foil excitation, foil tilt angle depend. 80−14212
He II, 4686 Å line, Stark broadening, meas. and calcs. 80−91504
He II, 4686 Å Stark broadened profile 77−23460
He II, electron ionisation cross sections of excited atoms and ions 80−43186
He II, excitation spectrum and second virial coefficient calc. 80−102549
He II, Paschen lines, red shift in plasma 80−103128
He II, plasma polaris. red shift, Stark profile, temp. depend. 77−18842
He II, radiative level widths in low electric fields 78−37589
He II, spectral lines branching ratios 77−46518
He II, Stark broadening of VUV transitions at 304, 1215, 1640 Å 78−66506
He II, Zeeman splitting of high-n recomb. lines 80−58210
He II 10124 Å line obs. of O-type stars 79−67003
He II 304 Å, solar line profiles 79−12452
He II 4686 Å, laser action in stellar envelopes 77−13354
He II 4686 Å emission in spectrum of HDE 226868 (Cygnus X-1) 79−21328
He II 4686 Å line phase shift from spectrophotometry of DQ Herculis 79−21296
He II abundance and IR excess in H II regions 78−86000
He II excited states in optically thin plasmas, role of direct ionisation-excitation 80−102579
He II recombination lines, calc. intensities in UV 78−94212
He III acceleration in solar wind, interactions with transverse waves, comments and reply 79−80184
He I+He, excitation energy transfer 77−50514
He ion isoelectronic series, X-ray line excitation 79−44453
He ions +Ti(Fe)(Cu), K-shell ionisation cross-section, 85 to 790 keV 80−106390
He, isoelectronic series, charge densities and 2-electron intracule functions calcs. 77−88382
He isoelectronic series, static dipole polarisability, reduced Green's functions, HF calcs. 77−71750
He isoelectronic series, Z=2-10, hyperfine struct. calcs. 77−31018
He pair, dispersion interaction, independent particle model, polarisabilities 80−37732
He photofragments angular distribution, parity favoured electric dipole transitions 80−58330
He, polarised state electron excitation, electron photon coincidence 77−6930
He, positron and electron elastic scatt., 100-700 eV, optical model calcs. 77−34761
He, positron annihilation, average energy, lifetime spectrum, Monte-Carlo calcs. 77−88558
He, positron elastic scattering, total cross-section calcs. 78−42220
He, purely L^2 method for calculating resonance widths 78−46283
He, scatt. from LiF (001) surface, sudden decoupling approxs. 78−64437
He sequence, 2p3d $^{1,3}L^0$ doubly excited state, soln. of Hartree-Fock eqns. 77−75072
He to Xe, radial density functions, HF calcs. 77−42238
He^-, 1s2s2p config., nonrelativistic energy *(Russian)* 77−75048
He^-, $(1s2s2p)^4P^0$ metastable state, CI calc. 79−59591
He^-, binding energy of metastable $1s2s2p\ ^4P^0$ state 80−9524
He^-, electron impact, post-collision interaction, reson. states 77−10767
He^-, electron loss in passing through inert gases 79−13805
He^-, existence in strong mag. field, binding energy, isoelectronic semicond. impurity trapping 78−9097
He^-, form. by $He^{2+}+H_2$ collisions 78−58811
He^-, highly excited states, electronic struct., oscillator strengths and resons., HF calcs. 77−46506
He^-, inelastic Feshbach resons., quasi projection operator calc. 80−58395
He^-, ion source, K charge exchange vapour, Pelletron accelerator injector 78−5085
He^- ions fractional yield from $Rb+He^+$, 3-20 keV, vapour target 77−1919
He , isoelectronic sequence, triply excited bound state, variational calc. 80−9526
He^-, metastable, electron affinity calc. 79−31439
He , reson. calcs. with correlated target state wave functions, complex coord. method 79−26939
He resons. in 56 to 64 eV electron collisions, autoionising states and spectral line polarisation 80−53145
He , resons. near doubly excited states thresholds, close coupling calcs. 77−54612
He^-, wave function structure, complex coord. method 78−94190
He^+, 180° scatt. from amorphous and polycryst. surfaces, anomalous yield enhancement 79−100008
He^+, 195 keV, light emission after focusing and channelling interactions with Ni (101) 78−35240
He^+ abundance in galactic H II regions, recombination line obs. 80−98703
He^+ abundance in H II regions in Galaxy 79−21389
He^+, Auger deexcitation spectrosc., impact on Ni(100) with adsorbed K^+ 79−100010
He^+, beam-foil excitation, alignment, 50 to 500 keV 78−22022
He^+, bombardment of $^{31}Ga(^{33}As)(^{34}Se)(^{35}Br)(^{55}Cs)$ L-shell X-ray prod. 79−47548
He^+, bombardment of Mo, accumulation and distrib., monolayer conc. by sputtering quantitative anal. 80−49253
He^+, channelled in Au thin single cryst., coherent electronic excitation 78−22778
He^+, conversion to mol. ions, three body association coeffs. determ. using drift-tube mass spectrometer 80−108699
He^+, $\chi\alpha$ statistical exchange calcs. 77−30766
He^+, detection of $6D_{5/2}$-$6S_{1/2}$ double quantum transition 77−61858
He^+, dielectronic recomb. in a mag. field 80−91662
He^+, dynamic multipole polarisability, functional calcs. 78−74595
He^+, electron impact excitation, Coulomb-Born-Oppenheimer calcs. 77−6938
He^+, electron impact excitation, five-state model calcs. 77−10770
He^+, electron impact excitation, n=2 level, generalised two-pot. distorted wave model calcs. 78−37748
He^+, electron impact excitation to S states exchange effects 78−58835
He^+, electron impact excitation cross-sections, reson. parameters calcs. 80−91686
He^+, electron impact ionisation, in threshold region, three body theory 77−19087
He^+, electron impact ionisation, electron ang. momentum exchange 78−78820
He^+, electron inelastic scatt., effective exchange potentials 78−90300
He^+, electron scatt., 1s-2s transition, Coulomb-Born and Coulomb-Born Oppenheimer calcs. 77−50539
He^+, electron scatt., elastic, ^1P continuum phaseshift, autoionis. state 77−88561
He^+, electron scatt., elastic, modified Coulomb-Glauber approx. 78−86949
He^+, electron scatt., Glauber exchange amplitudes 78−74772
He^+, electron scatt., reson. state assoc., incomplete spectrum of Hamiltonian matrix 80−99568
He^+, electron scatt. ^1S reson., restricted perturbation scheme calcs. 77−83736
He^+, electron scatt. near ionis. threshold, ang. momenta 79−31698
He^+, electronic recombination in afterglow 77−62401
He^+ escape fluxes from polar ionospheres, calcs. 79−35037
He^+ excess in dense He gas, ion-induced droplets 79−14925
He^+, excitation in hollow cathode discharge, rel. to plasma electron density and temp. 77−7589
He^+, expt. results on $\bar{W}$-values for heavy particles 79−7000
He^+, fine struct. obs. by beam-gas spectroscopy, level crossing resonances 80−9719
He^+, He_2^+, and metastable He and He_2 densities in afterglow, mass spectroscopy 77−24221
He^+, He^{2+}, nonadiabatic behaviour in quiet time radiation belts, theory and obs. 78−45158
He^+, imaginary frequency mutipole polarisability and long-range dispersion consts, functional calcs. 78−74596
He^+ impact on C foil, quantum beat pattern depend. on foil thickness 80−58343
He^+, in afterglow with water (cyanomethane), lasing processes 78−35690
He^+, in galactic centre source G 0.7−0.0, interpretation of recomb. line emission 77−17651
He^+ in thermosphere, Atmosphere Explorer-C abundances rel. to solar EUV flux 79−16919
He^+ ion bombardment of Cu, origin of autoionisation electron emission 77−20973
He^+, ion+electron scatt., static exchange approx. Schwinger variational principle, photoionisation cross section 80−43192
He^+ ions, electron impact ionisation 78−66666
He^+, isoelectronic series, Lamb shift, Bethe mean excitation energy, variational approach 78−9092
He^+ Lamb-shift measurement by the quenching-radiation anisotropy method 80−18824
He^+, lifetime of metastable state, ion beam meas. 78−55141
He^+, local diagnostics in H-D plasma after at. beam scatt. *(Russian)* 77−19774
He^+, low energy ion scatt. from clean Ni (110) surface 80−104026
He^+, mobility in He gas, calc. 79−55447
He^+, multiphoton RF reson. meas. 77−448
He^+, n=2, 3, electron impact excitation, Coulomb-Glauber-Ochkur approx. appl. 80−69238
He^+, n=2 state electron impact excitation, hybrid algebraic close coupling approx. 80−18930
He^+, n=4 level, fine struct., level-crossing and anti-crossing reson. obs. *(French)* 78−25488
He^+, neutralisation, reionisation in O_2, ion pair form., differential cross sections determ. 80−53120
He^+, outflow from terrestrial ionosphere 78−49221
He^+, pulse height defect in Si, meas. via field ionisation device 77−50330
He^+, reflection, from metal surface, atomic excitation calcs. 79−87541
He^+, reson. line regularities in plasma Stark widths and shifts 80−43881
He^+, Stark broadening, line shape calcs. 77−10636

helium atoms continued
He^+, Xα statistical exchange method, orbital energies, HF method comparison 78−9071
He^{++} enriched plasma in driving piston of solar flare-generated shock wave 80−72740
He^{++} in dawnside magnetosheath, bulk flows and energy anals. 80−4204
He^{2+} 650 MeV ions study for possible radiation therapy applications *(French)* 77−66835
He^{2+} acceleration in solar wind, effects of interactions with transverse waves 78−40788
He^{2+}, mobility in He gas 79−7440
He^{2+}, mobility in parent gas 79−7439
^4He, muonic, formation and hyperfine struct. 80−91707
$^4He^+$, stopping power in Au at 50-500 eV 77−76478
He^{x+}, energy loss straggling in N_2, Ne and Kr, ion energies of 50-500 keV per nucleon 77−46620
He^+/H^+ in M8, ratio from radio recomb. line obs. at 5 and 10 GHz 79−84832
He-alkali dimer anisotropic interaction pot., influence on transport cross sections 80−9677
He-Ar, van der Waals pot. determ. 79−10167
He-Ar mixture, collision induced far IR absorption at high press. 78−5161
He-Ar mixture, translational IR spectrum at 165K, binary and ternary absorptances 77−68042
He-Ar mixture HP collision-induced translational far IR absorption obs. 77−38628
He-Ar(Kr)(Xe), 208 and 707K, intermol. forces, virial, diffusion, and viscosity coeffs. 77−75256
He-Ar(Kr)(Xe), intermol. forces, combining rules 78−66622
He-CH_3^+ interaction energy, nonempirical calc. 78−86799
He-Cd mixture, Penning ionis. and nonreson. charge exchange in afterglow 79−72414
He-Cd vapour excitation in hollow cathode discharge 80−64815
He-Cs, turbulent plasma, charact., electron energy balance *(Russian)* 79−27779
He-H, low-density gas, H-atom diffusion, 4.2-77K 79−50053
He-H_2, rot. relax and spectral line shapes, coupled states calcs. 77−50500
He-H_2, thermal dissociation, vibrational relaxation at high temps., ab initio calcs. 79−74367
He-H_2^+, classical trajectories, on 3D cardinal spline fitted surfaces 77−90584
He-He, Born Oppenheimer pot. using Hylleraas-type electronic wave functions 80−91442
He-He, Born-Oppenheimer pot. using Hylleraas-type electronic wave functions 79−31438
He-He, energy and interaction potential of two ground-state atoms 80−63740
He-He, exchange dispersion energy, multiple expansion, rate of convergence 77−46614
He-LiH, rot. inelastic collisions, ab initio pot. energy surface calcs. 80−87208
He-like atoms, 2^3S_1-state nonexponential decay profile 77−88407
He-like atoms, n=2 states radiative transition rates, oscill. strengths, RRPA extension 77−34584
He-like atoms and ions, gradient expansion of atomic kinetic energy functional 80−95530
He-like ions, effects impeding obs. of parity nonconservation *(Russian)* 77−75078
He-like ions, electron impact, collision strengths for fine-struct. transitions 78−62925
He-like ions, line intensities results 78−89051
He-like ions, multiple charged, reson. photoionis. 79−54818
He-like ions, multiply charged, laser plasmas, 1.5-15 Å 78−13462
He-like ions, P_1^0-1^1S_0 and $^3P_1^0$-1^1S_0 intercombination-line transitions 78−70771
He-like ions, photoionisation, 2-channel relativistic random phase approx. calcs. 79−59407
He-like ions, radiative 2^3S_1-1^1S_0 transition, correlation effects 79−97989
He-like ions, spectral broadening in plasma, theory, high-Z 80−6223
He-like ions, triplet-state, electron impact excitation cross sections obtained by Coulomb Ochkur Rudge approx. 80−102576
He-like ions, X-ray form factors and total scatt. X-ray intensities 79−10063
He-like ions in laser prod. plasma, anomalous intensity ratios of reson. to intercombination lines 79−23454
He-like multiply charged ion, superdense plasmas, line intensity ratio 78−63538
He-like positive ions, electron impact excitation, electron exchange, CBO approx. calcs. 79−36771
He-like target+fast projectile, electron capture cross-sections 80−69231
He-like three-electron atoms and ions, inelastic-reson. quasiprojection operators 79−3581
He-like two electron atoms, three-body problem 79−3372
He-N_2, de excitation rate consts., energy transfer, pulse radiolysis obs. 80−30303
He-Ne, 632.8 nm line broadening, perturbation energies additivity 79−54941
He-O_2(NO), thermal cond. Senftleben effect meas. 79−18985
He-proton diffusion coeff. in stars 79−16811
He^{2+}-H^+, ionised mixture, dense, binary, dynamical props., statistical mechs. 80−43895
He^3-He^4 mixture, relax. of 2^3S_1 metastable atoms 80−102469
He+ $CO^+(CS)(C_2)$, vibr. relax. 80−53106
He+^{16}O, hyperfine interactions of highly stripped ions recoiling into He 77−22932
He+$^3He^{2+}$, many-electron systems OEDM orbitals 80−48081
He+2I→I_2+He, energy transfer mechanisms studied using trajectory calcs. and Monte Carlo method 80−66785
He+$(C^-)(O^-)(F^-)(Cl^-)$, electron stripping, at. beam form. 77−6926
He+Al(Sn), inner-shell multiple ionisation systematics, X-ray obs. 80−63790
He+Ar, interatomic pot. well depth, SPFD pot., diffusion, viscosity and second virial coeff. 80−5599
He+Ar, scatt. pot., He in (2^3S) state, 0.02-0.12 eV 79−54938
He+Ar, van der Waals pot., from crossed at.-mol. thermal beams scatt. 79−27053
He+Ar mixture, collision induced absorpt. calcs. 77−6777
He+Ar^+, 100-550 keV, 3s vacancy production 79−13809

helium atoms continued
He+Ar^{+Z} (Z=3 to 7), electron capture into different electron states by multiply charged ions *(Russian)* 78−17788
He+Ar^+(Ne^+), integral elastic scatt., repulsive potentials derivation 80−63744
He+Ar^{2+}, charge transfer, energy defect and sealing laws 80−48083
He+Ar^{6+}, collisional excitation, excitation cross sections 79−98209
He+Ar^{n+}, electron capture into different excited states in plasma 80−64679
He+ArH^+, ab initio pot. energy data, SCF-LCAO calcs. 80−63530
He+Ar(Kr), translation band spectral moments, induced dipole moments 78−55218
He+Ar(Kr)(Xe), 2^1S and 2^3S assoc. and Penning ionisation cross sections vel. depend. 79−3551
He+Ar(Kr)(Xe), He*(2^1S) scatt., low energy repulsion systematic struct. 78−22000
He+Ar(N_2)(NO)(O_2)(N_2O)(CO_2), Penning ionisation of target mol., for He(2^3S) 79−41228
He+atom, He upper states, excitation energy transfer mechanisms 80−28102
He+atom, K_α/K_β ratio for at. X-ray transitions 80−27972
He+atom (ion), ionis. by one or two electron at. particles, Born approx. 79−54960
He+B^{3+}(C^{4+})(N^{5+})(O^{6+}), electron transfer 78−13598
He+B^{5+}(Li^{3+})(H^+), K-shell charge transfer cross sections, Bates-Born formalisms 79−45834
He+B(Be)(C), target atom K-shell binding energy by Auger spectra 78−50525
He+B(C)(N)(O)(F) bare nuclei, electron capture to excited states, X-ray cross-sections 77−71814
He+BaCl, intermultiplet energy transfer 79−27063
He+BaCl($C^2\Pi$), collisional quenching, laser induced fluoresc. decay meas. 79−27075
He+Be^+, Be II 2^2P excitation, alignment and orientation 80−91647
He+Be^+, charge transfer and excitation, differential cross sections, 2-5 keV 79−36764
He+Be^+(Mg^+), ns-np excitation, alignment and orientation, impact, parameter theory 80−91648
He+Be^+(Mg^+) high energy, excitation cross sections, impact radiation polaris., models comparison 78−1069
He+Br^-, electron detachment, SCF calcs., BrHe$^-$ and BrHe pots. 80−23503
He+Br^-(Cl^-)(I^-)(Sb^-), term parameters, electron spectra-scatt. cross sections 77−27148
He+C^{x+}(N^{x+})(O^{x+})(F^{x+}) electron capture, K X-ray emission ang. distrib. 77−57919
He+CF_2, vibr. deactivation of CF_2 first excited single state 79−94061
He+CH(OH), collisional pumping of Λ-doublet transitions, pot. energy surface 80−23516
He+CO, intermol. pot. energy surfaces from electron gas model, ang., distance, and vibr. depend. 79−3520
He+CO, nuclear mag. shielding consts., interaction geometry depend., chemical shift, gauge invariant method 78−62866
He+CO, polarised mol., differential scatt. cross-sections calcs. 79−89733
He+CO, rot. inelastic scatt., coupled eqns. for single initial state, variation-iteration method 79−68301
He+CO, unitary approx. for inelastic collisions 78−13569
He+CO, vibr.-rot. energy transfer, stochastic theory 79−54944
He+CO_2, anisotropic intermol. pot. for differential scatt. cross-section 79−13788
He+CO_2, collinear atom-triatom transition probabilities for anharmonic triatom pots., quantum mech. calcs. 80−83455
He+CO_2, IOS opacities and integral cross sections, partial wave parameter identification effects 77−38719
He+CO_2, repulsive pot. energy surface, approx. calc. and differential scatt. expt., comparison 79−22788
He+CO_2, rot. and vibr. inelastic scatt., rot. IOS approx. calcs. 78−46433
He+CO_2, translational-vibrational energy transfer, quantum dynamical study 80−63746
He+CO(HCl), effective pot. and coupled states approx., differential and gas kinetic cross sections 77−61827
He+CO(HCl), rot. excitation, classical and quantum calcs. 78−1059
He+CO(HCl)(HCN)(HD), press. broadening cross-section, ang. momentum approx. calcs. 77−34696
He+CO(HCl)(HCN)(N_2H^+), scattering cross-sections, factorisation and fitting, IOS approx. 78−33575
He+CO(HF), vibr. relax., unitary distorted-wave approach 79−36738
He+CO(N_2), differential scatt. 0 to 5×10^{-2} rad. detector angle, 800 eV He *(Russian)* 77−79674
He+CS, Penning ionisation, $CS^+(B^2\Sigma^+\rightarrow A^2\Pi_i)$ fluoresc., flowing afterglow 80−14197
He+CS_2, metastable atoms, energy transfer processes 80−83466
He+Ca, Ca, $^1P_1$ level lifetime, Hanle measurement 80−23365
He+Ca*(Mg*), model pot. curves, including CI 78−42154
He+Ca(Li), press. broadening, line shifts 78−5290
He+Ca(Sr), nonstatistical excitation of mag. substates of $^1P_1$ level 78−42194
He+Cd, Penning ionisation cross section of target atom, for He(2^3S_1) 80−63777
He+charged particle, Glauber scatt. amplitude, numerical method in Lommel function 79−22795
He+Cl^-(Br^-), total electron detachment cross sections, near threshold energies 79−3555
He+Cl^+, highly charged low vel. recoil ion time of flight spectra, cross section energy depend. 80−14222
He+Cs(Rb), interatomic pots., hyperfine shifts, diffusion coeffs., perturbation exchange theory 79−41220
He+Cs→He+Cs^++e, reaction rate const., meas. in afterglow plasma 79−82116
He+F_2(H_2)(D_2), vibr. relax. times, 3D semiclassical theory 78−25667
He+F^{6+}, 10 to 40 MeV, F^{6+} K-vacancy production, role of excitation 80−37859
He+F^{q+}, (q=1-9), X-ray prod. by electron excitation, ionisation and capture 79−76379
He+formaldehyde, rot. excitation, coupled-channel calcs., microwave doublets cooling 77−3436
He+H, associative and Penning ionis. cross-sections, pot. energy curve study 79−87836

helium atoms continued
He+H, collisional coherent excitation, meas. of Lyman α-photons 80−99552
He+H, elastic scatt. cross-section, using model pot. 79−13786
He+H, excitation cross-section, Born-Ochkur approx. calcs. 77−19088
He+H, low energy elastic scatt. cross section MCSCF calc., van der Waals forces 78−70897
He+H, simultaneous ionisation investig. 80−32815
He+H, stripping cross-section, 0.3 to 3 keV 78−78807
He+H (inert gas atom), long range interactions for (2^1S) and (2^3S) states 78−70895
He+H_2, (2^3S_1) at. state, isotope effects, 77 to 300K 79−36752
He+H_2, anisotropic interaction pot., total cross-section calcs. 78−29835
He+H_2, anisotropic intermol. repulsion, pot. energy models 77−46610
He+H_2, anisotropy of long-range interaction 79−36734
He+H_2, CI pot. energy surface, small distances 77−38708
He+H_2, close coupling calcs., averaged definite parity j_z approx. with Clebsch-Gordan weights 77−58111
He+H_2, collinear collision, first order nonlinear matrix differential eqn. 80−37853
He+H_2, collision dynamics, generalised Langevin eqn. approach 78−70900
He+H_2, collision induced dipole IR spectra, ab initio SCF LCAO calc. 79−89737
He+H_2, collisional dissoc., quasiclassical trajectory calcs. 78−42172
He+H_2, collisional energy transfer, stochastic reductions, generalised cumulant expansion calcs. 77−71847
He+H_2, exchange forces, Hellmann-Feynman theorem calc. 77−54589
He+H_2, exponential gap relation, rot. inelasticity 80−78693
He+H_2, final quantum state assignment, improved quasiclassical histogram method 78−66617
He+H_2, formation of polarised H-atoms in ionising collisions *(Russian)* 79−7002
He+H_2, inelastic scatt., vibr. effects, classical mech. calcs. 77−34735
He+H_2, inelastic scatt., vibr. adiabatic basis functions calcs. 80−102551
He+H_2, inelastic scatt. exponential perturbation theories 80−74217
He+H_2, intermol. forces, generalised electron gas-Drude model 79−98182
He+H_2, mag. transitions, close coupling calcs. in uncoupled space frame 78−17769
He+H_2, mol. energy transfer by quasiclassical trajectory methods, vibr. relax. and dissoc., rot. effect 80−99557
He+H_2, orbital angular momentum quantum numbers in definite parity j_z CCS approx. 77−14511
He+H_2, Penning ionisation by metastable atom *(French)* 80−1060
He+H_2, pot. energy surface, analytical expressions from constrained optimisation 77−6698
He+H_2, pot. energy surface, ab initio calcs., van der Waals const. determ. 80−106372
He+H_2, rot. and vibr. inelastic cross-sections, distorted wave integral approx. 78−42175
He+H_2, rot. and vibr. inelastic mol. collision cross section calc. 79−59542
He+H_2, rot. excitation, 0.403-1.900 eV total energy, classical trajectory method 77−30962
He+H_2, rot. excitation, effective pot. and classical trajectory calcs. 77−88539
He+H_2, rot. transitions, quantum mech. and semiclassical cross-sections calcs. 77−83690
He+H_2, scatt., opacity functions, j_z-conserving approx. calcs. 77−6878
He+H_2, simultaneous rot. and vibr. transitions, cross-sections calc. 77−68098
He+H_2, stochastic theory, master or Fokker Planck eqn. numerical solns. 77−30965
He+H_2, sudden rot. approx., rot. and vibr. cross sections 77−30966
He+H_2, T-matrix element approx., j_z-CCS calcs. 77−19003
He+H_2, V→T rate constants, deconvolution 77−27152
He+H_2, Van der Waals pot., ab inito SCF model 78−74728
He+H_2, vibr. excitation, classical trajectory problem, Fourier transform method 79−98189
He+H_2, vibr. inelastic cross-section, para-H_2, threshold behav. 79−45804
He+H_2, vibr. inelastic integral cross-sections, transitions to $v=2$ level 80−99559
He+H_2, vibr.-rot. inelastic cross section adiabatic distorted wave IOS calcs. 79−94066
He+H_2, vibr.-rot. relax., high temp., exponential distorted wave technique 78−37721
He+H_2, vibrationally inelastic collision, rot. energy sudden approx. 79−68303
He+H_2 (CO_2), rot. inelastic, moments of final state distrib., direct method 78−33562
He+H_2 (O_2), rot. cross-section, exponential distorted wave and effective Hamiltonian 78−37709
He+H_2 rot. and vibr. distorted wave integrals, stationary pt. struct. 78−46436
He+$H_{2-4}{}^+$, 200-850 eV, attenuation and fragmentation 78−62968
He+$H_2{}^+$, collinear trajectories, pattern recognition 80−45481
He+$H_2{}^+$, collision in laser field, vibr. excitation 78−86937
He+$H_2{}^+$, collisional dissoc., expt. and quasiclassical trajectory calcs., eV region 78−42201
He+$H_2{}^+$, form of selected vibr. state $H_2{}^+$ beam at high press. by electron impact 77−65547
He+$H_2{}^+$, reactive and dissociative scatt., crossed-beam and trajectory obs. 78−64833
He+$H_2{}^+$, vibr. and rot. transitions, trajectory calcs. 79−13793
He+$H_2{}^+(H^+)(H_3{}^+)$, interaction pots. from ion mobility data 77−14518
He+$H_2{}^+$→H+HeH product ion ang. distrib., quantum mech. impulse approx. calcs. 79−24727
He+$H_2{}^+$→HeH^++H, diatomics-in-mols. and spline fitted ab initio surface, vibr. effects 78−20010
He+$H_2{}^+$→HeH^++H, spline-fitted ab initio surface, quantum mech. scatt. calcs. 77−63898
He+$H_2{}^+$→HeH^++H, vibr. state distrib. prod. by H_2 vibr. autoionisation cross-section depend. 77−48628
He+H_2O, collisional excitation of interstellar molecules, rate consts. 80−67816
He+$H_2O(D_2O)$, chemi-ionisation and secondary ion reactions, ^{3,1}S He metastables 77−40531
He+$H_2O(D_2O)(H_2S)(SO_2)$, Penning ionis. electron spectroscopy, energy peak shifts and shapes 77−42392
He+$H_2(D_2)$, vibr. deexcitation, cross sections, rate consts., vibr. rot. model 78−62879
He+$H_2(D_2)(T_2)$, vibr.-rot. transitions, optical potential approach 78−62885
He+H_2(HCl)(CO)$(HN_2{}^+)(H_2O)$(formaldehyde), rot.-translational energy transfer, nonlinear vs. linear rotors, surprisal anal. 79−76492
He+H_2(HD) potential, asymmetric, isotope substitution effect, Legendre expansion coord. transformation 78−70894
He+H_2(HD)(HT), interaction second virial coeff. nonspherical pot. terms effects 77−3432
He+H_2(He)(Ar)(N_2), fast metastable at. collisional destruction cross section 78−74760
He+H_2(He)(N_2)(Ne)(Ar), 25-450 keV, metastable ion beam electron loss and deexcitation cross section 77−34745
He+$H_2(\mu H)$, interaction pots. and rot. scatt. calcs. 80−43158
He+$H_3{}^+$, collision-induced dissoc. 77−42383
He+H , 1 to 5 keV, production cross sections for 3d,3s,4s,5s states of H 78−33603
He+H^-, differential scatt. cross-sections, time of flight spectra 78−42161
He+H^-, electron detachment cross-sections, 100 keV-10 MeV 79−59561
He+H^-, electron detachment cross-section, target distortion calcs., 100 keV-100 MeV 79−59562
He+H^-, electron detachment collision 80−23536
He+H^-, electron detachment in adiabatic regime, mechanisms 80−63800
He+H^-, electron-loss cross-section, double closure calcs. 77−50518
He+H^-, low-energy total electron detachment cross-sections, approximation 79−72405
He+H^-(He)$^-$, collisional detachment cross-sections, high-energy obs. 77−3442
He+H^-electron detachment, theoretical obs. 80−63799
He+H^+, 25-1000 keV, $1^1S \rightarrow n^1S$ excitation cross sections, Glauber approx. calc. 79−54959
He+H^+, 25-3000 keV, electron-capture, continuum distorted wave approx., correl. energy 77−83727
He+H^+, 293 keV, electron capture differential cross sections 77−88552
He+H^+, charge transfer, approx. close-coupling calcs. 77−23560
He+H^+, charge transfer to H(n=2), mixed parity elec.-dipole oscillations 79−31678
He+H^+, collisional excitation, 2nd order pots. method calcs. 78−13608
He+H^+, determ. of He excited state populations by two-photon reson. ionisation spectroscopy 78−82707
He+H^+, differential scatt., 1-12 eV, high resolution beam meas. 80−58348
He+H^+, double He ionis., polarised electron vel. distrib. effect 80−53109
He+H^+, double ionis. of He, binary-encounter theory 78−1066
He+H^+, double K-shell electron capture, theory 79−68315
He+H^+, elastic scatt. and 2^1s and 2^4p excitation cross-sections 79−36747
He+H^+, electron capture, 4-20 keV, production of highly excited H atom 79−54963
He+H^+, electron capture, charge-state distrib. 80−32814
He+H^+, electron capture cross sections, electron correlations 77−34758
He+H^+, electron capture coherent electron density distrib. oscillations 79−10200
He+H^+, electron capture into ground and 2s states, cross sections 77−27177
He+H^+, electron capture total cross sections 78−5322
He+H^+, electron ejection, energy and ang. distrib. calcs. 77−6914
He+H^+, electron ejection differential cross sections 77−46625
He+H^+, excitation, ang. differential cross-sections for 25, 50 and 100 keV protons 78−82832
He+H^+, excitation process *(Japanese)* 78−42193
He+H^+, H(n=4) s-d coherence, zero-field quantum beats obs. 80−32676
He+H^+, ionisation, projectile energy depend., secondary electron energy distrib. 78−42211
He+H^+, ionising collision, first-order Faddeev approx. 79−22827
He+H^+($^4He^{2+}$), $1^1S \rightarrow 4^1S$ excitation cross-section calcs., 10 to 5000 keV 78−25689
He+$H^+(H_2{}^+)$, emitted electron's energy and angular distrib. support for charge transfer to continuum theory 78−37740
He+$H^+(H_2{}^+)(H_3{}^+)(He^+)$ collisions, polarisation degree of prominent He lines 78−70916
He+$H^+(He^{2+})$, K-electron capture, cross section scaling, high energy 79−41236
He+$H^+(He^{2+})(N^{x+})$, multiply ionised ats. prod. 80−28098
He+HCN, translational-vibrational energy transfer, quantum dynamical study 80−63746
He+HCl, mag. transitions, initial-l labelled CS approx. computations 79−3552
He+HCl, rot. energy transfer, quasiclassical trajectory calcs. 78−42173
He+HCl, state-selected collision cross-sections calcs. 78−22001
He+HCl(CO), energy sudden approx., beam-scatt. meas. mol. anisotropy effects 78−78802
He+HCl(HF)(DCl)(DF), slow collisions, rot. excitation cross-sections, quantum mech. calcs. 77−12795
He+HD, relax. and kinetic cross-sections, DWBA calcs. 79−41782
He+HD, rot. excitation, classical trajectory study 78−25666
He+HD, thermal energy scatt., distorted-wave and close coupling calcs. 78−86938
He+HD, vibr.-rot. relax. from high vibr. states 79−54945
He+HD collisions, single quantum rot. excitation by pulsed molecular beams 78−29840
He+HF, rot. excitation cross sections, use of rot. and orbitally adiabatic basis functions 79−59543
He+H(2S), excitation and ionisation contributions to sum-rule Born cross sections 80−99551
He+H(2s), 5-25 keV, H(n=3) excitation, Balmer α emission obs. 80−53113
He+H(2s), collisional de-excitation, 5-26 keV 79−59546
He+He, (Ne), (Ar), optical emission spectra 77−14551
He+He, (2^3S) and (2^1S) metastable states, direct and assoc. ionisation rate consts. in afterglow, electron energy spectra 79−13812
He+He, He^- decay cross section oscills. *(Russian)* 77−19038
He+He, interatomic force calcs., zeroth-order exchange energy for optimised atomic basis set 80−43131

helium atoms continued
He+He, ionisation mechanism, theory 77−14550
He+He, isotropic intermolecular forces evaluation using semi-empirical approach 79−36726
He+He, low-energy interactions with phenomenological pots. 77−34714
He+He, metastable atoms, collisional ionisation cross-sections 78−70911
He+He, Rydberg states ang. momentum transfer, singlet-triplet anticrossing 77−88543
He+He, weak intermol. interactions, intramol. correl. effects, perturbation anal. 79−86038
He+He (2^1S, 2^3S), differential cross sections, rel. to He_2 excimer long range pots. 79−81167
He+He ion, He I fluoresc. excitation, mag. field depend. *(German)* 77−27037
$He+He_2^{**}$ collisional deactivation 79−100338
$He+He^+$, 0.7-2 MeV, charge-changing collisions, electron capture 80−58372
$He+He^+$, 2 and 3 keV, one and two electron excitations in He, quantal treatment 78−37730
$He+He^+$, (Ne)(Li), gas-phase collisions, intermediate and high velocities, excitation 80−32822
$He+He^+$, autoionisation electrons and scatt. ions, ang. correl. determ. 80−63792
$He+He^+$, autoionising transitions interference 77−42390
$He+He^+$, coherent excitation and decay of autoionising states 79−45789
$He+He^+$, double collision spectroscopy 80−58378
$He+He^+$, elastic and inelastic collision 79−45785
$He+He^+$, excitation cross-section calcs. 78−90273
$He+He^+$, low energy collisions, excitation of 2 ^1S, 2 ^1P and 3 ^1P, 3 ^3P levels 80−58342
$He+He^+$, resonant charge transfer cross sections, 2 to 100 eV 78−66655
$He+He^+$, scattered ion-autoionisation electron ang. correl. determ. 80−9725
$He+He^+$, triplet excitation cross-section, Ochkur-Rudge approx. calcs. 80−28101
$He+He^+$ interactions, electronic forces 79−22790
$2He+He^+(Ne^+)$, three body reaction, rate coeffs., temp. depend., 100 to 300K 80−108703
$He+He^+(Ne)$, tensor polarisabilities of 1snd ^1D level, fluoresc. depolarisation obs. 80−69099
$He+He^{2+}$, double K-shell electron capture, theory 79−68315
$He+He^{2+}$, electron capture collisions, spin conservation 78−82837
$He+He^{2+}$, single and double electron capture, high vels., independent electron approx. calc. 80−18923
He+He(Li), intermol. forces, ab initio VB calc. using nonorthogonal basis set 80−23490
He+He(Ne)(Ar), dispersion interaction, series coeffs., variation method 79−3518
He+Hg, metastable He, collision rate consts. in pulsed discharge afterflow 78−50627
He+highly stripped ion, multiple-ionis. cross sections, Monte Carlo calcs. 79−64091
$He+I_2$, collisional relax. of vibr. excited mol., reson. enhanced 79−64081
$He+I_2$, energy transfer, centrifugal sudden approx., classical infinite order sudden approx. 80−27933
$He+I_2^*$, energy depend. of collision induced intramolecular energy transfer 80−83470
$He+I_2^*$, sudden rot. approx., rot. and vibr. cross sections 77−30966
$He+I_2^*$, sudden rot. total rot. inelastic cross section 77−30967
He+I*, low energy collisions, energy redistrib. 80−63765
He+K, 93 eV, excitation of K atom, photon-scatt.-atom coincidence study 78−82829
He+K, K 5^2P level broadening and collisional relax., quantal, semiclassical and expt. comparison 80−18903
He+K, photon emission polarisation anal., coincidence studies 80−5614
$He+K(Zn^+)$, 0.7-500 keV, $K(Zn^+)$ excitation, reson.-line emission and polaris. 80−18911
He+Li, fine-structure transition probability, semiclassical multichannel scatt. matrix 80−37854
$He+Li_2(A^1\Sigma_u^+)$, rot. inelastic collisions, subsequent state multipoles transfer 80−5608
$He+Li^+$, 2 to 5 keV, ejected electron profile variation with impact angle 78−37729
$He+Li^+$, <5 keV, autoionised electron spectra 80−32823
$He+Li^+$, excitation, optical emission line shapes 80−18820
$He+Li^+$ autoionisation, electron spectra 80−91653
$He+Li^+(C^+)(N^+)(Ne^+)(Na^+)(Mg^+)$, slow collision, ionis. obs. 79−10194
$He+Li^+(Co^+)(Au^+)$, cross-section, closure-Born approx. 78−66630
$He+Li^+(Mg^+)(Mg^{2+})(Na^+)(Ne^+)$, relative level excitation, orbital ang. momentum quantum number depend. 78−25688
$He+Li^+(Na^+)(F^-)$, electron gas model, polarisation inclusion 78−37699
He+LiH, rot. inelastic collisions, dynamics 80−87209
He+LiH, rot. inelastic collisions, state-to-state cross sections determ. 80−87210
He+Li*, Li principal series line broadening and shift, interat. pot. consts. 78−42165
$He+Li^*(2^2P_J)$, collision induced fine struct. transition 80−74220
$He+Li(Be^+)(Na)(Mg^+)(K)(Zn^+)$, collision-induced alignment, reson.-line emission polaris. obs. 80−18912
He+Li(Be)(B)(C), collisional excitation, prompt decay line energy, projectile Auger spectrosc. 79−85941
He+Li(Na), excitation cross sections, Li I and Na I resonance line emission and polarisation 77−61846
He+Li(Na) excitation cross sections, model pot. calcs. 77−58152
He+methane, ^1H and ^{13}C mag. shielding, intermol. effects 78−37571
He+methane $(NH_3)(H_2O)(SF_6)$, differential scatt. cross-section, intermol. pot. 79−36728
He+methyl ion, ternary association reaction in energy range 0.04-0.1 eV 80−71896
$He+Mg^+$, 3^2P differential excitation, alignment and orientation 79−86053
$He+Mg^+(Ne^+)$, charge exchange, Rydberg state excitations 77−58159
He+multiply charged ions, electron capture and impact-ionis. cross sections, Monte Carlo calcs. 79−27083
$He+N_2$, intermolecular pots. from Thomas-Fermi-Dirac functional 77−19009

helium atoms continued
$He+N_2$, rot. inelastic scatt., appl. of sudden approx. 80−95705
$He+N_2^+$, $(A^2\Pi_u)$ Meinel band deactivation cross sections above thermal energies 78−66635
$He+N_2^+$, ion loss cross-section, 2.4-24.3 keV 80−58373
$He+N_2^+$, N_2^+ selectively excited, collisional deactivation 80−83338
$He+N_2^+$ collisions, vibronic excitation, curve-crossing trajectories 80−23520
$He+N_2(CO)(CO_2)(N_2O)$, collisionally excited neutral and ionic emission, flowing afterglow 77−51248
$He+N_2(CO)(O_2)$, vibr. state distrib., charge exchange 150-2400 eV 78−42195
$He+N_2(O_2)$, $He(2^3S)$ quenching reactions 78−22014
$He+N_2(O_2)(CO)(NO)$, anisotropic intermol. pots., crossed beam expts. 79−31639
$He+N_2(O_2)(HCl)$, Pennin ionis. electron spectra, new differential retarding field analyser characts. 77−41735
$He+N^{2+}$, electron capture, product ion energy loss spectra 79−36762
$He+N^{2+}$, electron capture, 0.2-2.4 keV, kinetic energy change 79−59558
$He+NH_3$, pure rot. line, press. broadening calcs. 80−78656
$He+NH_3$, rot. excitation rate consts., semiclassical method 79−3538
$He+NH_3$, rot. relax., double and triple reson. obs. 78−90196
$He+NH_3$, rot. relax. double and triple reson. obs. 78−66570
$He+NH_3$ 79−94057
$He+NH_3$(formaldehyde), rot. excitation, IOS approx. calcs. 79−45801
He+NO, multiphoton ionisation spectra in supersonic expansion, laser entranced collisional effects 80−83459
He+Na, 3^2P differential excitation, mechanism 79−86052
He+Na, collision induced dissoc. rate, vibr. distrib. depend. 79−22791
He+Na, D2 reson. linewidth 79−31647
He+Na, excited state, collisional depopulation cross-sections meas. 79−86057
He+Na, Na ($3S_{1/2}$-$3P_{1/2}$) photon echo, collision vel. changes and dissimilar electronic states superposition 80−32803
He+Na, non-Lorentzian spectral line shape 80−106297
$He+Na_2$, elastic scatt. and rot. excitation, model pot. energy surface 77−6895
$He+Na_2$, optically pumped state to state differential cross sections for rot. transitions, rainbow phenomena 80−5609
$He+Na_2$, rot. excitation, rainbow oscills., coupled states and IOS approx. calcs. 80−23518
$He+Na_2$, rot. transitions, state-resolved differential cross-sections 78−62887
$He+Na_2$, rot. transitions differential cross sections, laser fluoresc. meas. 80−63771
$He+Na_2$, rotational inelastic scatt., uniform semiclassical sudden approx. 80−99544
$He+Na_2$, rotationally inelastic scatt., state-to-state differential cross sections 80−74234
$He+Na_2^*(A\Sigma)$, rot. energy transfer, power law scaling 79−98204
He+NaK collisions studied using circularly polarised laser fluorescence, molecular reorientation obs. 80−69215
He+Na($3P_{1/2}$), vel.-changing collisions, effect on 2 photon and stepwise absorpt. line shape 80−87221
He+Na($3S_{1/2}$,$3P_{1/2}$), total cross section, stimulated photon echo obs. 79−76503
He+Na(nd), l-changing Rydberg at. collisions, rel. to low-energy electron scatt. 79−50112
He+Ne, 2^1s_0-level excitation, rate const., temp. depend. 80−87218
He+Ne, 2p-levels, excitation obs. 80−9712
He+Ne, afterglow, metastable state energy transfer, spectra 80−43167
He+Ne, fluoresc. spectra, mol. bands, 0.1 to 6 atm., 3000-8200 Å 79−3394
He+Ne, low pressure broadening and shift of Ne line, Lennard-Jones pot. 80−102554
He+Ne, multiple ionisation of Ne 2s and 2p electrons 80−18918
He+Ne, Ne emission lines press. broadening, rel. to repulsive forces 80−9692
He+Ne, scatt., orbiting reson. total cross-sections 78−5320
He+Ne pot., differential cross section, quantum mechanical inversion 78−70896
$He+Ne_2^+$, pot. energy surface, reaction cross sections, ab initio calcs. 80−11881
$He+Ne^+$, impact excitation, cascade-fluorescence spectroscopy, level-crossing techniques 80−23357
$He+Ne^{n+}$, slow ion and electron prod., VUV radiation 78−5321
$He+Ne^{n+}$ (n=1,2,3,4), excitations, emission cross-sections 77−57914
He+Ne(Ar)(Kr)(Xe), absolute total elastic cross sections 77−30953
He+Ne(Ar)(Kr)(Xe), energy transfer, time-resolved VUV spectra 77−19028
He+negative ion, electron-loss cross sections 80−37877
$He+O_2$, dissoc. ionisation, kinetic energy spectra 78−25684
$He+O_2$, long lived collision complexes, exact classical and quantum mech. calcs. 78−33576
$He+O_2$, vibr. energy transfer, exact classical and quantal calcs. 77−19014
$He+O_3$, collisional energy transfer in unimol. reaction, classical trajectory calcs. 78−62882
$He+o\text{-}H_2$, NMR, spin-spin and spin-rot. relax., IOS calcs. 79−18209
$He+O^{q+}$, electron capture to continuum states, forward ejected electron spectra 79−45831
He+OCS, emission spectra in He afterglow 80−87139
He+OCS, gas, EPR of rot. transitions, T_1 press. depend. 80−9621
He+OCS, rot. spectral line shift and widths, collision induced phase shifts 77−75222
He+OCS, translational-vibrational energy transfer, quantum dynamical study 80−63746
He+OH, colisional relax., laser mag. reson. study of press. broadening 79−94020
He+OH, mean collision cross sections from microwave spectroscopy 80−1046
He+OH, rot. inelastic collision, microwave spectra 79−45806
He+one electron ion 79−22812
$He+p\text{-}H_2$, vibr.-rot. inelasticity, stochastic theory 77−71848
He+PH, collisional deactivation of $PH(b^1\Sigma^+)$, time resolved quenching 79−54948
He+positron, second-order nonadiabatic polaris. pot. for elastic scatt. 79−22836
He+Rb, quasielastic and inelastic collisions in S and D Rydberg states 80−83462

helium atoms continued
He+S, collision-induced emission of S(^{1}S), 232 and 425K 79−81264
He+S_2, fluoresc. quenching and lifetimes of S_2 78−46386
He+S^{q+}, (q=6-16), K X-ray prod., charge-state depend. 80−106391
He+SF_6, mol. vibrational-translational energy transfer, mass spectrometric meas. 79−36739
He+SO_2, Penning ionis. due to He(2^3S), SO_2^+ fluoresc. 79−13758
He+Si*, collisional quenching, reson. line absorpt. expt. 78−46297
He+Sr, $^1P_1$ level lifetime, Hanle measurement 80−23365
He+Xe, electron-loss cross section struct., 0.05-4 MeV 78−9236
He+XeF*, quenching rates for XeF in (B) state 78−58730
He+Xe(Ar), collision induced microwave absorpt. spectra 80−74216
He^-+Ar(H_2)(He)(N_2)(Ne), collisional detachment cross-sections, high-energy obs. 77−3442
He^++1,3-butadienes, singlet-triplet transitions, energies, relative cross sections 78−86942
$He^{+,2+}$+Ar, 2 MeV, ejected electron spectra, 20-450 eV, 0-10° 77−34746
He^++acetylene-d_0(-d_2), CH^+(CD^+), A-X luminesc., in near-thermal charge exchange 78−50632
He^++alkali metal, charge exchange, He metastable beam form., composition 79−89775
He^++alkali metal atom, ionisation cross sections, binary encounter approx. with HF electron vel. distrib. 78−55225
He^++Ar, charge exchange, quasimolecule model, four-state calcs. 77−14571
He^++Ar, charge transfer reaction rate coefficient 79−91932
He^++Ar, direct excitation and charge exchange processes 77−75279
He^++Ar, ionisation, differential cross-sections, 0.3 to 2 MeV 79−81271
He^++Ar, ionisation double differential cross sections 80−18913
He^++Ar, low energy charge transfer collisions, kinetic energy depend. 78−86947
He^++Ar(H_2)(He)(Kr)(N_2)(O_2), metastable ion electron capture, loss and de-excitation 77−6904
He^++atom, metastable state deexcitation, 2S- and 2P-state mixing and Penning ionisation 77−42394
He^++Be(B)(O), double K-shell ionis. of Be, B, O 78−25680
He^++C, beam-foil spectra, He atom orientation, ang. variation 78−86944
He^++C, K-shell ionisation, impact parameter depend. 78−62891
He^++CO, dissoc. charge transfer, energy transfer processes 78−74759
He^++CO_2, CO_2^+ electronically excited states prod. 77−3454
He^++CO_2, dissociative charge exchange kinematics 80−3318
He^++CO(NO), dissociative ionis. 79−10188
He^++CS_2, dissoc. charge-transfer, CS^+($B^2\Sigma^+$-$A^2\Pi_i$) emission prod., Morse pot. Franck-Condon factors calc., vibr. anal. 80−99539
He^++Ca(Ba), 2-1000 eV, spontaneous ionis. mechanisms 79−64090
He^++Cd collisions, slow, Cd II excitation 77−83701
He^++Cd(Hg)(Zn), thermal energy charge transfer reaction, ion states, relative yields 79−45840
He^++Cs, total charge-transfer cross-section meas. 77−50527
He^++Cu(Ag), K-shell X-ray prod. cross sections 78−5337
He^++e system, complex quantum defects 79−13622
He^++H, excitation of H to n=2 state, cross-section calc. 79−41229
He^++H, unpolarised and spin-change collision, low energy 78−86943
He^++H_2, charge transfer at 1.5 and 3 keV, He(^{3}P) excitation 78−66658
He^++H_2, DIM approx. pot. energy surfaces and nonadiabatic coupling 80−23330
He^++H_2, dissoc. charge transfer, vibr. enhancement 78−33597
He^++H_2, H^+ prod., from H_2^+ dissoc. states or H_2^{2+} 78−20015
He^++H_2O, 50 to 250 keV, OH radical form. 78−56890
He^++H_2(D_2), dissociative ionisation, H^+ and D^+ energy spectra 77−58154
He^++H_2(D_2), dissociative charge transfer, 78-330K 80−61079
He^++H_2(D_2)(N_2), small angle charge exchange, 0.5 to 1.0 keV, time of flight spectra 78−33604
He^++H_2(He), charge transfer, appl. of atom-photon coincidence meas. 79−45829
He^++H^+, ground-state electron capture cross-sections, Coulomb-Born calcs. 78−42166
He^++H(H_2), H(2p) and H(2s) excitation cross sections, 5-26 keV 77−58150
He^++H(1s)→He^++H(2p), ion excitation cross section calc., effective Feynman diagram approach 80−23531
He^++He, 150 eV, one-electron excitations, quantal treatment 77−71854
He^++He, 2^1P level, direct and charge-exchange excitation, 150-1000 keV 78−70913
He^++He, 2^3S and 2^1S excitations, differential cross sections 77−3444
He^++He, autoionisation electrons and scatt. ions, ang. correl. determ. 80−63792
He^++He, autoionising state excitation, ion-electron coincidence, electron azimuthal depend. 78−37734
He^++He, charge exchange cross section, drift-vel. meas., 0.3-8 eV 78−25694
He^++He, charge exchange cross section meas. 78−25697
He^++He, charge transfer collision, approx. diabatic mol. representation 80−9728
He^++He, elastic scatt. and charge exchange, differential cross-section, 0.4-30 eV 78−66659
He^++He, electron loss cross section 79−27080
He^++He, He_2^+ mol. collision complex, pot. energy curve spectrum 77−19008
He^++He, He^+(2s) destruction, He^+(2s/2p) form. 77−30977
He^++He, He(2^3S) formation, elastic and resonance charge exchange perturbations 77−42386
He^++He, high-energy collisions, experimental device for study of elastic and inelastic diffusion *(French)* 78−22053
He^++He, interference struct., optical emission interpretation 79−45816
He^++He, low energy cross section, calc. 79−55447
He^++He, multicurve-crossing problem, numerical test of semiclassical approx. 78−13590
He^++He, reson. charge transfer, merging-beam technique 79−41235
He^++He, scattered ion-autoionisation electron ang. correl. determ. 80−9725
He^++He, symmetric reson change transfer, 0.1-3 keV, 3-state close-coupled calcs. 77−50524
He^++He, triplet excitation cross-section, Ochkur-Rudge approx. calcs. 80−28101
He^++He^+(Li^{2+})(H), two-body dispersion interaction, freq. depend. multipole polarisability, variational calc. 80−37758

helium atoms continued
He^++He^{2+}→He^{2+}+He^+, 10-1700 eV, absolute. cross-sections meas. 79−3560
He^++He(Ne), coherent excitation and decay of autoionising states 79−45789
He^++He(Ne), model pot. for law energy scatt. 78−66642
He^++He($2p^2$ ^{1}D), collisionally excited, autoionisation electron ang. distrib., interference struct. 80−32819
He^++Hf(Ta)(W), L-subshell ionisation cross section, branching ratios, fluoresc. yield, Coster-Kronig factors 80−43166
He^++Hg_0→He_0+(Hg^+)*+ΔE, cross sections, rate consts. 78−17785
He^++inert gas, binary encounter calc., cross section calc. 79−72413
He^++inert gas, collisional quenching cross sections, two-state theory calcs. 80−69217
He^++Li, excited state form. obs. 80−9686
He^++Li, Li excitation mechanisms, Auger and autoionisation spectra 77−19042
He^++metal, fast ion scatt. by surface plasmons, theory 80−45190
He^++methanol, dissoc. charge transfer reaction studied at rel. translational energies from 600 eV to 5000 eV 80−104432
He^++Mg, inner-shell ionisation by H^+, He^+ impact, target atom ionic alignment, Born approx. 78−78789
He^++Mg(Zn), inelastic collisions, 2-800 eV, excited state form. 78−94312
He^++N_2, ≲0.1 eV, charge exchange, UV and visible luminesc. spectra 77−83722
He^++N_2, charge exchange, time-resolved emission probe 78−86946
He^++N_2, collisional excitation processes, visible emission, cross-sections 80−99571
He^++N_2, K-shell ionisation, total cross-sections calcs. 79−31663
He^++N_2, low energy collisions, vibronic excitation model 77−83689
He^++N_2, N_2^+ 3914 Å emission cross sections, 0.5-34 keV 77−54598
He^++N_2O, rate coeffs. meas. at 300 and 100K in flowing afterglow 79−20346
He^++Na, crossed beams, l-changing collisions, n-depend. 80−58345
He^++Na, Na $2p^5 3s^2$ $^2P_{3/2}$ state alignment by 5-30 keV excitation 80−14200
He^++Na(K), excited state form. by inelastic processes, energy partitioning 78−82833
He^++Na(K) single-electron capture cross-sections 78−37737
He^++Na(K)(Cs), 5-100 keV, electron capture form. of fast metastable He 78−74760
He^++Ne, 10-150 keV, Rydberg-state total cross section, oscillatory behaviour 77−83716
He^++Ne, He(3^1P) level excitation, total emission cross section, fast oscills. obs. 80−58362
He^++Ne, inelastic scattering data inversion, interaction function recovery 79−89741
He^++Ne, Ne($2p^5 3s$, $2p^5 3p$) excitation 80−43185
He^++Ne*→He*+Ne^+, cross sections 79−22821
He^++Ne(Ar), attenuation and single electron charge exchange cross sections, 500-5000 eV 77−34752
He^++Ne(N_2)(SF_6), K-shell ionisation, AES meas. 77−10749
He^++Ne→HeI+Ne^+, HeI 3^3P polarisation 79−13813
He^++O_2, (N_2), charge transfer reactions, product ion distribs. 77−73445
He^++O_2, charge transfer product state distribs., time of flight obs. 80−87223
He^++O_2, metastable O^{+*} ion production 79−91933
He^++O_2, thermal energy charge transfer, O^+ product ion obs. 79−64100
He^++OCS, dissoc. charge-transfer, CS^+($B^2\Sigma^+$-$A^2\Pi_i$) emission prod., Morse pot. Franck-Condon factors calc., vibr. anal. 80−99539
He^++Pb, at. beam and surface interaction, scatt. ion yield oscills. 78−55221
He^++SO_2, dissoc. charge transfer reaction, SO^+ ($A^2\Pi$-$X^2\Pi_r$) emission 80−95659
He^++Si(Al), X-ray spectra, two-electron one-photon transition in solid target, 2 MeV 78−94209
He^++Xe, internal energy distrib. at 100 eV 80−99564
He^++Xe charge transfer, optical emission cross sections 77−61853
He^++fluoromethanes, thermal energy charge transfer reactions mechanism 77−63889
He^{2+}+Ar, ionisation, differential cross-sections, 0.3 to 2 MeV 79−81271
He^{2+}+atom, 10 MeV, binary encounter stopping cross sections, straggling and screening 78−17754
He^{2+}+atom, excitation functions rel. to ionisation *(French)* 79−31669
He^{2+}+atom collisions, inner shell excitation, impact parameter dependence 77−19047
He^{2+}+C foil collisions, electron emission, energy distribs., solid state effects 77−19062
He^{2+}+C(N)(O)(Ne), K-shell Auger electrons ang. distrib. 79−89756
He^{2+}+H, charge transfer cross sections, molecular bases calcs. 79−98217
He^{2+}+H, electron capture, impact parameter calc. 78−33591
He^{2+}+H, electron capture into n, l levels, 100 keV/amu 79−22826
He^{2+}+H, electron capture in 3s level, distortion approx. 80−37876
He^{2+}+H, electron transfer, 0.1-20 keV, mol. orbital calc., convergence 78−42210
He^{2+}+H, electron transfer, plane-wave factor, mol. state treatment 80−63807
He^{2+}+H, excitation, asymptotic cross-sections calcs. 79−18279
He^{2+}+H, mol. treatment, cross sections and charge exchange probabilities 77−58128
He^{2+}+H_2(O_2), electron capture collisions, spin conservation 78−82837
He^{2+}+H_2→He^+H$^+$+H$^+$, two-electron capture 78−58811
He^{2+}+H(1s), charge transfer, 0.025-200 keV/amu 79−22823
He^{2+}+H(1s), charge transfer, Coulomb-Born approx. calc. 80−43175
He^{2+}+He, 2 MeV, non-occurrence of Fadeev interference struct. in 245 eV electron spectrum peak 77−58155
He^{2+}+He, 5 to 100 keV, elastic and double charge exchange, mol. treatment 78−82813
He^{2+}+He, diabatic correl. diagrams for quasi-mol. description 79−3525
He^{2+}+He, diatom. quasimolecule form., shielded-orbital model 79−10165
He^{2+}+He, electron capture and impact-ionis. cross sections, Monte Carlo calcs. 79−27083
He^{2+}+He, He^+ form. in various electron states *(Russian)* 78−58815
He^{2+}+He, high-energy, electron capture cross-sections, continuum distorted-wave approx. 77−83724

helium atoms continued
He^{2+}+He, radiative charge transfer coeffs. 79−7010
He^{2+}+He, radiative single charge transfer cross section 79−7011
He^{2+}+He, single charge exchange, reson. contrib., thermal 79−76511
He^{2+}+He, thermal energy collisions, quantum mech. calcs. 80−23507
He^{2+}+He, two-electron excitation of quasimol. states 79−18274
He^{2+}+He^{+}, ionis. and charge transfer cross sections 78−42186
He^{2+}+He(Ne), electron capture collisions, spin conservation 78−82837
He^{2+}+He(Ne), multiply ionised ats. prod. 80−28098
He^{2+}+He($1s^2$), differential and total cross-sections 80−23506
He^{2+}+He($1s^2$)→He^{+}(Σ)+He^{+}(1s), continuum distorted-wave approx., cross-section 77−68109
He^{2+}+Hg, autoionisation, 5-20 eV, electron and ion ang. distrib. 78−78795
He^{2+}+inert gas atom, electron capture into different excited states in plasma 80−64679
He^{2+}+Li, electron capture, ionis. cross section, low-vel. He^{+}(3l) production, X-ray production 79−22822
He^{2+}+Li, excited state form. obs. 80−9686
He^{2+}+Li collisions, soft X-ray emission obs. 80−83591
He^{2+}+methane, (Ne), (Ar), inner shell electron capture cross-sections 79−76510
He^{2+}+N_2, 200-600 eV, 0-20°, comparison with He^{2+}+Ne(Ar) 78−74732
He^{2+}+Ne(He), electron transfer cross-section, <100 eV 78−66654
He^{2+}+Ti, ratio of single K-shell ionisation cross section to double K-shell ionisation cross section 80−53119
He^{2+}+Zn(Cd), L- and M-shell Auger electrons 79−27076
$^4He^{2+}$+He, 1^1S→4^1S excitation cross-section calcs., 10 to 5000 keV 78−25689
He_2, $^1\Sigma_g^+$ states, pot. curves, ab initio multiconfig. SCF calcs. 77−46632
He_2, 600 Å emission continuum 80−1012
He_2, 600 Å emission continuum struct., in 700-900 Å region in glow discharge 80−95641
He_2, $a^3\Sigma_u^+$ metastable state, fine struct., mol. beam mag. reson. obs. 78−78720
He_2, collision induced Raman spectrum, polarisability anisotropy 79−72320
He_2, dissoc., high-order replacements inclusion in CI calc. 80−63504
He_2, electronic and rot. energy relax., reactive collisions by isotope selective excitation 78−33541
He_2, energy and interaction potential of two ground-state atoms 80−63740
He_2, exchange forces, Hellmann-Feynman theorem calc. 77−54589
He_2 excimer potentials, long range, from He+He differential cross-sections 79−81167
He_2, ground state, generalised dipole polarisability, bivariational calcs. 78−58611
He_2, ground state, interaction energy, many-body perturbation theory calcs. 80−69210
He_2, He_2^+, MO correlation diagrams 77−61689
He_2, high freq. Stark effect, interference with meas. in He 80−9544
He_2, high mag. field spectroscopy 79−72445
He_2 high press. afterglows, reviews 80−64823
He_2, interaction polarisabilities, comparison with H_2, ab initio SCF calcs. 80−27943
He_2, intermol. forces, Gaussian basis function calcs. 78−21993
He_2, intermol. interactions, supermol. density, statistical methods calcs. 79−6983
He_2, laser-driven transitions to high Rydberg states 80−106360
He_2, metastable states, laser excitation spectra 80−5578
He_2, molecular spectrum and structure, singlet Π states 4pπ-9pπ 78−42080
He_2 optical absorpt. spectra and kinetic behaviour 80−95635
He_2, pair polarisability correl. effects, SCF-CI-GTO-SO calc. 78−82651
He_2, photoionis. cross sections of excited states 78−66523
He_2, polarisability, generalised London formula for dispersion coeff. 78−82662
He_2, polarisability and collrision induced Raman spectra 80−48005
He_2, possibility of existence, Lennard-Jones pair potential 80−52869
He_2, pot. curve using CEPA-PNO correl. wavefunction 79−63932
He_2, pot. surface well depth calc. 77−79667
He_2 potentials, configuration interaction calculations, superposition corrections 79−72382
He_2, Raman spectra, collision-induced, diatom polarisability 79−64011
He_2, spectra, struct., triplet states, 4pπ, 5pπ UAO's 77−34647
He_2, vibr.-rot. interaction factor 78−42036
He_2^+, bond strength ab initio LCAO MO CI calcs. 80−87046
He_2^+, dissoc. energy calc. 79−55447
He_2^+, ion beam prod. by coaxial electron impact ion source 80−62795
He_2^+, rate coeffs. for bimol. and termol. ion-mol. reactions 78−53188
He_2^+ recombination, high-temp., in plasma jet *(French)* 80−43861
He_2^{2+}, autoionising states, adiabatic pot. energy curves calcs. 78−42140
He_2^{2+}, bound excited states, potential energy curves and rovibronic energy, dissociation 80−23327
He_2^{2+}, electronic energies, James-Coolidge method calcs. 78−17564
He_2^{2+} quasimolecular states, radial and rot. coupling terms 79−26896
He_2^{2+}, static polarisability determ. by optimised rot. method 79−54990
$^4He_2$, bound state at small and large separations, variational calcs. 78−50609
He_2+$N_2(O_2)$, $He_2(2^3\Sigma)$ quenching reactions 78−22014
He_2^++Cd collisions, slow, Cd II excitation 77−83701
He_2^++Li, excited state form. obs. 80−9686
He_2^++Mg(Zn), inelastic collisions, 2-800 eV, excited state form. 78−94312
He_2^++Ne, surface-hopping trajectory calc. 79−52637
He_2^++Ne(Ar)(N_2)(CO)$(CO_2)$$(Ch_4)$, bimol. and termol. charge transfer reactions, rate coeffs. 77−1910
He_3, 3-body nonadditive interaction, nodal struct. 78−1049
He_3, dipole moment, large separation, perturbation theory 78−62946
He_3 three-body interatomic forces, electron gas model and SCF calcs. 78−33564
$^4He_3$, gas, Efimov effect 77−30042
HeH, neutral and negative ion states SCF pot. energy curves 78−62745
HeH^+, collisional formation, SCF calcs. 77−6893
HeH^+, spectroscopic characts. in ground and first excited triplet states, Dunham pot. approach 77−42234
HeH^{2+}, lowest 20 states, eigenvalues, electronic wavefunctions, w.r.t. internuclear separation 77−18811

helium atoms continued
$^4HeH^+$, ro-vibr. quasi-bound levels of $X^1\Sigma^+$ state, eigenenergies, dissoc. 77−26997
$He^{2+}(H^+)$+X, (X=Nb to Gd), K-shell X-ray prod. cross-sections 77−71865
$^4HeH^+$+He, 1 keV, collision-induced dissoc., ro-vibr. assignments, proton spectra obs. 79−3556
$He^+(He^{2+})$+H, charge transfer and direct excitation processes 78−25696
$He^+(He^{2+})$+He(Ar)(C), ionisation processes viewed in forward direction 77−71866
He(He_2)+Ar, metastable destruction rates 78−37728
$He^+(He_2^+)$+N_2(CO)$(CO_2)$$(H_2S)$, charge transfer Penning ionis. 78−17784
$He_2(He_2^+)$, variational electronic struct. calcs. using Hylleraas type wavefunctions 77−88375
HeI, 3^3D-2^3P transition, light polarisation depend. on time and exciting electrons energy 80−37891
HeI, beam-foil mean life meas. of 1s 3p ^1P level 77−3320
He(I), XPS relative intensity and photoionisation cross-section 80−63599
HeI+Na^+, anisotropic collisions, direct meas. method 80−23498
He(II), XPS relative intensity and photoionisation cross-section 80−63599
HeNe, detection in nozzle beam, total collision cross section determ. 77−61826
$HeNe^+$, collisional form., excitation, pot. energy curves calcs. 77−6697
He(^1S), correlation energy calc. of at. in spherical box 79−97984
He(^1S) excitation energy, eqn. of motion method calcs., approxs. and error anal. 79−36501
He(^3S) metastable state g_J factor, TOF at. beam mag. reson obs., rel. to O($^5S_2$) 79−3593
He($^1S_0$)+Na(Li) radiative Penning ionis., photoionis. cross section depend. of continuum radiation 77−19034
$He_2(^3\Sigma)$+Ar, press. depend. reactions, rate coeffs. 78−64823
$He_2(\Sigma_g^+)$, general-model-space diagrammatic perturbation theory appl. 80−47844
$He_2(^3\Sigma_u)$+Ne(Ar)(N_2)(CO)$(C_2)$$(CH_4)$, excitation transfer reaction rates 78−5332
$He_2^+X^2\Sigma_u^+$ state, ab initio CI calc., pot. energy curve, vibr. and rot. levels 77−3263
^{3}He, 1^1S_0 ground state, NMR obs. by transverse modulation of mag. field 78−82671
^{3}He activation analysis, for determ. of elements with Z=12-47 78−11575
^{3}He and ^{4}He superimposed spectra, isotope shift, mass and vol. effect, Fe arc spectrum calibration, teaching 80−46763
^{3}He atom, near surface of liq. ^{4}He, binding energy calc. 79−77853
^{3}He atom forbidden singlet-triplet anticrossings, D levels 80−99491
^{3}He, dynamical Hanle effect, line halfwidth, sensitivity threshold, signal to noise ratio *(Russian)* 77−54541
^{3}He, hyperfine-induced singlet-triplet mixing obs. 80−106399
^{3}He in atmosphere of primary component of 68=μ Herculis 77−57045
^{3}He in lunar rocks, method for solar flare cosmic ray proton flux determ. 80−98576
^{3}He in solar flares, 8666 MHz superfine structure line detection 80−109417
^{3}He ion+Al(Si) collisions, K-shell ionisation cross sections 77−23555
^{3}He, metastable electronic states, electron impact excitation, time of flight spectra 80−106411
^{3}He, nucl. relax. in gas discharge at liq. N_2 temp. 80−100114
^{3}He, opt. pumped maser, saturation polaris. intensity depend. *(Russian)* 77−7046
^{3}He, optical pumping signal, special features 78−82700
^{3}He, optically oriented nuclei, in two-chamber cell, NMR linewidth obs. 78−17591
^{3}He, optically oriented nuclei, maser excitation and characts., appls. 78−17891
^{3}He, optically oriented nuclei, in two-chamber cell, spin maser appls. 78−17892
^{3}He, pionic, X-ray transitions obs. 77−65549
^{3}He, reactions inducing plasmas, neutron irrad. UV and visible spectra obs. 80−64784
^{3}He/^{4}He ratio in josephinite 78−65313
$^3He_2$, variational calc. of binding energy 77−54503
$^3He^4$He, ground state binding energy, Faddeev-UPE method 79−72377
$^3He_3$, ground state binding energy, Faddeev-UPE method 79−72377
^{3}He-^{3}He interatomic potls., nonlocality, Brueckner calcs. 77−26593
^{3}He-^{4}He isotope mixtures, mag. resonance line widths of 2^3S_1 states, metastability exchange cross sections *(Russian)* 77−10614
^{3}He-^{4}He mixture, optical pumping, transients theory 80−91509
$^3He^+$, 2s state, HFS, improved electrostatic device and microwave state selection 77−83757
$^3He^+$, interstellar, probable detect. and significance 79−25689
$^3He^+$ beam, appl. to evaluating Faraday cups for laser plasmas diagnostics 78−5941
$^3He^+$ polarised ion sources for a CN Van de Graaff accelerator 79−68106
$^3He^{++}$, solar wind spectrum, ion frequencies and velocities *(German)* 80−51636
$^3He^+$+Ho(Sm), X-ray intensity ratios, projectile energy depend. 80−23535
$^3He^+$(2S) state ion beam with nuclear polarisation, RF source 79−59602
$^3He^{2+}$, impact on C foil, nonexistence of wake bound states 78−13571
$^3He^{2+}$+$^4He^+$, charge exchange, cross section meas. 80−32827
$^3He^{2+}$+H*→$^3He^+$+H^+, merged beams, cross section 77−75292
$^3He^{2+}$+H(H_2), electron loss, capture cross-sections 78−22026
$^3He^{2+}$+H(H_2), electron capture at impact energies below 10 keV 78−50633
^{3}He-rich solar flares, plasma mechanism 79−5795
^{3}He+^{3}He, collision cross-sections, Ramsauer-Townsend effect 77−6892
^{3}He+^{4}He, metastability exchange, coherency transfer *(Russian)* 78−13594
^{3}He+^{4}He, metastability exchange cross-sections, coherent transfer in 2^3S_1-state 79−89743
^{3}He+Au, L-subshell ionisation, Coulomb deflection effects 78−22020
^{3}He+CO, vibr. relax., deactivation rates, pulsed fluoresc. meas. 79−89698
^{3}He+π^-, strong interaction shift, multiple scatt. and absorptive effects, calc. 78−62958
$(^3He)_3$, quantum exchange effects in Lennard-Jones 12-6 pot. 78−1117

helium atoms continued
^{3}HeI^{4}He ratio in interstellar cloud assoc. with open cluster (NGC 6530) 77−45504
^{4}He +X, (X=Nb through to Gd), X-ray production, 0.6 to 2.4 MeV 78−13586
^{4}He, 3^3P-state fine struct. 80−23568
^{4}He, 3p ^{3}P state alignment and orientation as function of foil tilt angle, quantum beat spectra 79−94071
^{4}He (2^3S_1) to H ($1^2S_{1/2}$) electronic g-factor ratio from Zeeman resonance meas. 78−13467
^{4}He atoms, scattering from superfluid ^{4}He surface, quantum interference 79−99382
^{4}He, beam foil and quantum beat spectra *(Chinese)* 80−32638
^{4}He, beam velocity regulation and meas., using Doppler tuning 77−19110
^{4}He, electronic g_J-value of 2^3S_1 state, by atomic beam mag. reson. method 77−23446
^{4}He ground state binding energy, near threshold behaviour in 2 and 3 dimens. 80−91716
^{4}He II, widths of Stark components calc., beam-foil data comparison *(French)* 80−9545
^{4}He, kaonic and pionic X-rays, strong interaction widths and shifts 79−98253
^{4}He, laser mag. reson., 7^1S-9^1P energy separation, motional Stark effect, Zeeman tuning parameters 79−6911
^{4}He, metastable electronic states, electron impact excitation, time of flight spectra 80−106411
^{4}He, muonic, Lamb shift calcs. 78−94199
^{4}He, Rydberg states, fine struct., D, F and G states meas. 77−50418
^{4}He, Rydberg states, fine struct. obs. 80−23350
^{4}He, singlet-triplet anticrossings, ^{1}D and ^{3}D state separation, mixing 77−6738
^{4}He, threshold condition for forming atomic trimer 80−63741
^{4}He trimer and tetramer, ATMS appl., bounding and ground state energies 79−86026
^{4}He trimer and tetramer, binding energy, appl. of ATMS 78−94349
$^4He_2{}^3$He, ground state binding energy, Faddeev-UPE method 79−72377
$^4He_2$+^{4}He, zero-energy, Faddeev-unitary pole expansion theory 78−37572
$^4He_3$, bound states, Faddeev-unitary pole expansion theory 78−37572
$^4He_3$, Efimov states and binding energies, Faddeev coord. momentum approach 78−46259
$^4He_4$, tetramer bound state binding energy, pot. model 80−63883
^{4}He$^+$, beam, heavy element ionisation cross-section ratio determ., X-ray method 77−6920
^{4}He$^+$, g_J-factor determ., optical pumping method 80−87085
^{4}He$^+$, impact on C foil, nonexistence of wake bound states 78−13571
^{4}He$^+$, quantum beats in C foil interaction *(French)* 79−59544
^{4}He$^+$ II, H-like, fine struct. Stark effect *(French)* 78−943
^{4}He^{++}, solar wind spectrum, ion frequencies and velocities *(German)* 80−51636
^{4}He$^+$+^{3}He^{2+}, charge exchange, cross section meas. 80−32827
^{4}He$^+$+H(H_2), electron loss cross section 78−22018
^{4}He$^+$+H(H_2), electron loss, capture cross-sections 78−22026
^{4}He$^+$+He, electron vel. distrib., nonexistence of wake bound states 78−13571
^{4}He^{2+}, slowing down in solids, 0.4 to 4 MeV range, calcs. 77−7776
^{4}He^{2+}+Xe(Ne), optical transition excitation function and cross sections 80−63787
^{4}He^{2+}+heavy atom, 2-5 MeV, inner shell ionisation cross section 79−45825
^{4}He-$\bar{p}$, X-ray spectrum, energies and relative intensities for 3d and 2p levels 78−70979
^{4}He+^{3}He, metastability exchange cross-sections, coherent transfer in 2^3S_1-state 79−89743
^{4}He+^{4}He, collision cross-sections, Ramsauer-Townsend effect 77−6892
^{4}He+Au, L-subshell ionisation, Coulomb deflection effects 78−22020
^{4}He+CO, vibr. relax., deactivation rates, pulsed fluoresc. meas. 79−89698
^{4}He+H_2, inelastic collision, R-matrix study 80−87204
^{4}He+HD, vibr. relax., 80 to 400K 80−5607
$(^4He+\mu^-)^+$ muonic ion, $2S_{1/2}$-$2P_{1/2}$ energy transition meas. 78−33641
^{4}He+p-H_2, vibr. relax., analytical approx. 80−63761
$(^4He)_3$, Faddeev theory, binding energy 77−26995
^{3,4}He+U, collisional relax. of highly excited states, laser-induced fluoresc. obs. 80−58205
$(^{3,4}He)_3$ molecular bound state, variational and exact studies 77−27214
He*, collisional transfer rates between excited levels 79−22793
He*, impact on Mo surface, clean and gas covered, deexcitation, pot. energy transfer mechanism 80−60743
He* impact on Pd (111) surface, clean and CO covered, electron emission, energy and ang. distrib. 80−60744
He*, Rydberg state charge transfer reactions, time of flight mass spectrometric obs. 77−71867
He*+Ar, complex potential from elastic differential cross sections 77−23534
He*+Ar, Penning ionis., multichannel calcs. 80−53111
He*+Ar, Penning ionisation, laser modified collisional effects in electron energy spectrum 78−90278
He*+Ar, Penning ionisation, angular distrib. of electrons 79−89763
He*+Ar(Kr)(Xe), elastic scatt., repulsive rainbows and optical pots. 79−840
He*+CO, Penning ionisation of CO adsorbed on Pd, theory 80−60735
He*+D, Penning and assoc. ionis. with metastable He, 0.01 to 10 eV beams 79−27074
He*+D_2(Ar)(Kr) interaction pots. 77−83674
He*+H(H_2)(Ar), metastable state, ionis. processes 78−62907
He*+He, (*=excitation or charge), differential scatt. inversion procedure, symmetric exchange, classical, semiclassical theory 79−13802
He*+He, collisional ionisation, cross-section meas. 77−46631
He*+He, collisional ionisation, He_2 $^1\Sigma_g^+$ state pot. curve calcs. 77−46632
He*+He, excitation exchange and collisional relax. 80−69226
He*+He, inelastic collision, 1-5 keV, autoionising states 78−13581
He*+N_2, Penning ionisation, ejected electron spectra obs. 80−48074
He*+Ne, (1^1S, 3^3S, 3^1P, 3^3P) de-excitation cross section temp. depend., time resolved spectra 80−28100
He*+Ne*→He+Ne$^+$+e, Penning ionisation, merging beams obs. 78−33585
He*Ar(Kr)(Hg), Penning and assoc. ionisation, correl. diagrams calcs. 77−50521
helium atoms continued
He*N_2, sensitised fluoresc., vel. depend. 77−10744
He*(^{3}S)+Ar+ħω→He+Ar$^+$(^{2}P)+e$^-$, intense laser radiation assisted collisional ionis. 79−76497
He**, doubly excited, spatial correl. of at. electrons 78−70760
He**($2p^2$ ^{1}D), collisionally excited, autoionisation electron ang. distrib., interference struct. 80−32819
He*(1s2s,^{3}S)+Ar, Penning ionis., discrete-continuum states coupling 79−10193
He*(2^1P)+Ar→He+Ar$^+$+e$^-$, anisotropic interaction potential, impact parameter method 77−68102
He*(2^3S), (2^1S)+O_2, ion pair form., ion beam neutralisation reionisation spectroscopy 80−53120
He*(2^1S)+Ne, elastic and reactive scatt., ang. distribs. 77−6919
He*(2^3S)+F, Penning ionisation and excitation transfer, unified treatment 78−25672
He(1^1S)+H$^+$, He(n^1P) excitation cross sections computation 79−94070
He$^+$(1s)+H^{2+} symmetric resonance charge transfer 80−32826
He$^+$(1s)+H(1s), excitation and ionis. processes 78−42189
He($1s^2$)+O^{8+}, electron capture into n,l excited states 80−23543
He(1s2p)^{1}P, eigenvalues and eigenfunctions, time-depend. HF calcs. 77−42241
$He_2(1\sigma_g)^2(1\sigma_u)$npλ triplet levels, multichannel quantum defect anal. 80−91542
He(2^1P), high-momentum transfer electron excitation amplitudes form, Faddeev-Watson approx. 80−23555
He(2^1S, 2^3S), threshold to 0.10 eV, energy-integrated total cross section ratio 80−37885
He(2^1S, 2^3S)+Ne(e$^-$), transition probs., pots. 80−58371
He(2^3S, 2^1S)+Ba(Y)(Ce), Penning process, double ionisation 77−3439
He(2^3S,2^1S)+H, Penning ions. 79−64089
He($2S)^2$, autoionising reson., appl. of complex-rotated Hamiltonians 79−31427
He($2^{1,3}$S), electron impact excitation and ionis., cross sections 77−31001
He($2^{1,3}$S), inelastic scatt., RPA and 1st Born approx. calcs. 80−53148
He(2^3S) bubble in liq. He, phenomenological model 77−20147
He(2^3S) collisions, elastic scatt., Penning ionisation, polarisations *(Russian)* 78−70922
He(2^3S), electron impact ionis. to 1s, 2s, and 2p state, autoionis. 80−1068
He(2^3S), quenching rates meas., in pure afterglow 77−75206
He($2^{1,3}$S)+H, autoionising system, Siegert eigenvalues, variational calcs. 79−50106
He(2^1S)+Ar, optical interaction pots. from differential cross sections 77−30956
He(2^1S)+H(D), associative and Penning ionisation, autoionisation, calcs. 78−25674
He(2^1S)+H(1^2S) 78−33586
He(2^1S)+He, long-range excimer pot. determ., high resolution at. beam expt. 77−42371
He(2^3S)+Ar, differential cross-section meas., optical interaction pots. 77−3443
He(2^3S)+CS_2, CS^+ and CS fluoresc. spectra assignments, vibr. populations, transition moments 77−14473
He(2^3S)+H_2O(H_2S), energy transfer processes, reaction products, UV and visible obs. in flowing afterglow 78−85138
He(2^3S)+HF(HCl)(HBr)(HI), Penning ionis. electron spectra 77−79687
He(2^3S)+H(D), associative and Penning ionisation, autoionisation, calcs. 78−25674
He(2^3S)+H(D), Penning and assoc. ionis. cross sections, vel. depend. 79−22815
He(2^3S)+molecule collisions, exit channels rate consts. 79−13800
He(2^3S)+Ne(Ar)(N_2)(CO)(CO_2)(CH_4), high press. afterglow, bi- and termolecular de-excitation rates 77−27168
He(2^3S_1) in alkali-He quantum magnetometer 80−17965
He(2^3S_1)+Ca(Sr)(Ba), coherent $^2P_{3/2}$ levels excitation by Penning ionis., Hanle effect 80−5520
He(2^3S_1)+e→He(1^1S_0)+e+KE, in afterglow, rate const., electron energy distrib. 78−71571
He(2^3S_1)+Hg_0→He_0+Hg^++e, in afterglow, rate const. meas. 78−17785
He(2^3S_1)+Na(K)(Rb)(Cs), Penning ionis. in stationary afterglow 78−42184
He(2^3S and 2^1S)+H_2(D_2), Penning, rearrangement and total ionis. cross sections, vel. depend. 79−22816
$He_2(2^3\Sigma_u^+)$+He_2(Ne), reaction rate consts. meas. in afterglow 78−7173
He($2p^2$ ^{3}P), electron impact parity unfavoured excitation, trapped electron data reinterpretation 77−58180
He(2s-3p transitions), beam foil spectra, emitted light polarisation, depend. on foil tilt angle 80−63786
He($2s^1$S,2^3S)+Ne(Ar)(Kr)(Xe), Van der Waals forces, one-electron model pot. calcs. 80−14094
He($2s^3S_1$)+Sr, alignment of ions in Penning collisions, polarised emission obs. 80−23533
He(2s2p)^{1}P autoionised transition, ang. correl. function (e,2e) fast coincidence technique 77−83738
He(3^3S) decay rates in high-press. afterglow 79−41898
He(3^3S)(3^3P)(3^3D)+He(1^1S), deactivation rate, 300-600K, time-resolved spectra 77−19037
He(5^3D)+He, collisional quenching probability, 2-250 mtorr 78−25679
He(metastable)+dichloroethylene (dichlorobenzene), mol. ionis., collisional energy depend. 79−54950
Hg+He, afterglow, Hg^+($7^2P_{1/2}$, $7^2P_{3/2}$), excitation processes, rate consts. *(Russian)* 78−29848
Hg+He, laser excitation of Hg $6s6d^3D_1$ level, transition probabilities and collisional excitation transfer 78−55146
Hg+He(Xe), collisionally induced coherence, orientation and alignment, transfer among 6s6d levels 78−74747
I_2+He, vibr. relax. cross section, in I_2He_n photodissoc. expt. 79−100410
In+He^+, chem. effects on oscillatory cross sections in low energy scatt. 77−6889
K-He(Ne)(Ar)(Kr)(Xe), oscill. strengths, for induced dipole transitions, pot. energy curves 77−75100
K+He, 4^2P state j_1m_1→j_2m_2 Zeeman transition, total cross section energy depend. 80−83475
K(4p)+He, fine struct. transitions, vel. depend., interatomic pots. 77−42388
KrF+He(Ne)(Xe)(NF_3), quenching rate consts. meas. 79−24718
Kr*+He, $^3P_2$ metastable state, disorientation cross-sections 77−71853
Kr*+He, persistence of velocity following elastic collisions 78−78779

helium atoms continued
Kr*+He(Ar), vel. changing collisions studied by saturated absorpt. 78−62892
lHe+HCN, HCN excited vibr. state, T_2 meas. 80−102498
Li-He, oscill. strength, for induced dipole transitions, pot. energy curves 77−75100
Li+H(He) 78−9127
Li+He, direct excitation of Li I (nl) levels in keV collisions 78−90280
Li+He, elastic scatt., fine-struct. transition cross sections, eigenphase formulation 78−25651
Li+He(Ne), inelastic collisions, Baylis-Gombas pseudopot. appl. 77−58151
Li^++He, 10-50 keV, mol. promotion, many-electron aspects 79−50124
Li^++He, interaction pot., direct determ. from gaseous ion mobility 77−10720
Li^++He, Li excitation mechanisms, Auger and autoionisation spectra 77−19042
Li^++He, quasimol. study of collisions in 0.3-50 keV range 77−88529
Li^++He collisions, K-shell vacancy sharing, ab initio LCAO-SCF, CI calcs. 77−19054
Li^++He collisions, Li-K shell excitation, autoionisation spectra meas., total cross sections 77−19053
LiH+He, rot. inelastic collisions, rigid shell models 80−99545
Li*+He(Ne)(Ar), thermal, high-Rydberg Li behaving as ion core 78−22004
Mg+H^+(He^+) and electron impact ionis., Auger study of collisionally induced alignment 78−90279
N_2+H^+(He^+), 1 MeV, dissoc. ionis., time-energy spectra 77−34744
N_2+He($2^{1,3}S$,$2^{1,3}P$), Penning ionis., N_2^+, $B^2\Sigma_u^+$ state effective cross sections 77−79688
N_2^++He, low energy collisions, vibronic excitation model 77−83689
NH_3+H_2^+(He^+), dissociative charge transfer reactions, energy transfer depend. 77−25258
NH_3+He(Ar), ammonia inversion spectrum press. broadening 78−86915
NH_3+NH_3(He)(Ar)(N_2)(O_2), ν_2 state vibr. relax., laser induced vibr. fluoresc. obs. 79−18269
N_2O+He(He^+), in afterglow, N_2^+(N_2O^+) optical emission obs. 79−68251
Na-(Ne)(He)(Ar)(Kr)(Xe), oscill. strengths, for induced dipole transitions, pot. energy curves 77−75100
Na-He model pot. calcs., fluoresc. line profile 79−36723
Na-He-N_2 dense vapour system, optical pumping, RF spectrum analyser appl. 79−76393
Na+He, collisional freq. redistrib. of scatt. laser light 77−30815
Na+He, total elastic cross sections meas. 77−30954
Na+He, two-photon optical free induction decay meas. by broad-band excitation in unidirectional beams 79−76489
Na+He(Ar)(Ne), press. broadening coeffs. of Na 3S-4D transition 78−25481
Na+He(Ne), Rydberg states, cross sections for collisional ang. momentum transfer 79−6997
Na+He(Ne)(Ar), Rydberg states, collisional angular momentum mixing meas. 77−68093
Na+He(Ne)(Ar), Rydberg S and D state relax., trilevel echo effect 79−72409
Na+He(Ne)(Ar), Rydberg transitions, excitation transfer cross-section calcs. 77−50520
Na^++He (Kr) thermal, two trajectory model from meas. cross-sections 77−75257
Na*(nd,nf)+He, ang. momentum mixing 79−10175
Ne+^{3}He(^{4}He), $2p_4$ state alignment destroying cross sections 79−89757
Ne+He, population transfer between Ne 2p levels *(French)* 77−30975
Ne+He^+, $2s^02p^6$-$2s^12p^5$ radiative transition in Ne III, UV spectra 79−6900
Ne+He^+(Li^+)(Mg^+)(Na^+)(Ne^+), autoionising level excitation, electron spectra 77−14554
Ne+Ne(He), 7d′ states, isotope shift, press. shift, press. broadening, two-photon spectra obs. 78−55155
Ne+Ne(He), population transfer from 2p levels *(French)* 79−851
Ne^++He, 10-150 keV, Rydberg-state total cross section, oscillatory behaviour 77−83716
Ne^{2+}+He, charge transfer rate coeff. and astrophysical appls. 80−56701
Ne^{2+}+He(Ne)(Ar)(Xe)(Kr), cross sections for electron capture, 60 to 200 keV 78−46442
Ne^{z+}+He(H_2)(Ar), (z=1-4), electron capture into excited projectile states 77−75291
Ni+H^+($^4He^{2+}$)(O)(Li), K-shell ionis., impact parameter depend. 77−83707
O+NO+M→NO_2+M, (M=He, Ne, Ar, Kr), 217-500K, absolute rate consts. 77−16787
O_2+He, 118750 GHz transition, press. broadening 77−75136
O_3+He(D_2)(H_2), vibr. relax. rate consts. 80−74231
O_3^-+X→O^-+O_2+X, X=He, Ar, CO_2, long-lived excited (or isomeric) state of O_3^- 78−5318
OCS+He, rot. energy transfer, microwave-microwave double resonance 77−19016
OCS+He, rot. energy collisional transfer, M-depend., microwave double reson. 78−46435
Pb+He^{2+}, 25- 40- 74-MeV, K-shell ionis. probability 77−528
Rb*+He(Xe), thermal, 5p $^2P_{1/2}$ state depolarisation cross-sections 77−71852
Rb(6^2P)+He(Ar)(Xe), fine-struct. transition cross sections, semiclassical calcs. 77−30972
S_2($B^3\Sigma_u^-$,v=4)+He(Ar)(Xe), collision-induced transfer rates 79−94062
SF_6^-+He, decomposition, SF_5^- form. 78−29833
Si+H_2(O_2)(He)($SiCl_4$), $3p^2$($^1D_2$) state behaviour, at. absorpt. spectra 78−29846
Si^{12+}+He, K X-rays for population in $^3S_1$ metastable state, Si^{12+} from C, Au foils 78−17776
Si^{q+}+He, q=2-11, K-shell fluoresc. yields, charge-state depend. 78−55231
SiH_4+He, vibr. energy transfer 77−524
Si($3p^2$($^1S_0$))+He($SiCl_4$)(O_2)(N_2O), attenuation of reson. radiation, time-resolved kinetic obs. 78−5329
U+H^+(He^+), 2-18 MeV, L-subshell ionis. cross section, projectile energy depend. 77−19031
Xe-^{3}He plasma, plasma parameters determ. 80−54047
Xe+He, saturated absorpt. of 3.51 μm line, vel. changing collisions by line width 78−86819
helium atoms continued
Xe_2(−Kr,He), time-resolved excitation spectra, 1500 Å region, fluoresc. lifetime 77−75195
Zn^+-He, positive column laser discharge, upper and lower state densities, Penning collision 80−32964

helium compounds
HeH^{2+}, photodissoc., rel. to UV flux deficiency of stellar spectra 80−9654
H_2^+He, total energy, interat. dist., geometric configurations, LCAO MO SCF calcs., stability, binding energy 77−42236
He H^+, formation and destruction in gaseous nebulae, assoc. IR emission line spectrum 79−44589
He^++Ar, charge transfer cross section, kinetic energy dependence in low energy region *(Japanese)* 78−90100
$HeCN^+$, SCF calcs., dissoc. energies, rot. and hyperfine const. determ. 80−95531
$HeCl^+$, interaction potential, HF dissociation energies, LCAO SCF calcs. 77−6880
$HeCrCl_2O_2$, vibr. predissoc., spectroscopic origin identification appl. 78−5239
HeH, bond strength ab initio LCAO MO CI calcs. 80−87046
HeH, HeH^+, variable screening model calcs. 78−74587
HeH, neutral and negative ion states SCF pot. energy curves 78−62745
HeH^+, (HeD^+), rot. predissoc., nucl. motion effects on rovibr. energies and widths 78−70885
HeH^+, bond energy calcs., using density matrix partitioning 78−46417
HeH^+, collisional dissoc., excited electronic states effects 80−9687
HeH^+ dissoc. on impact at C foil, emitted light polarisation meas. 80−58361
HeH^+, dynamic dipole polarisabilities calcs. 80−74110
HeH^+, electron impact excitation, rot. transitions 79−41244
HeH^+, electronic momentum distribution, Coulomb shift and correl. coeffs. 80−83266
HeH^+, electronic states, variable-screening method 78−25410
HeH^+, energy loss in C foil, moving ion pot. determ. 78−33572
HeH^+, excitation energy, pot. curves, oscill. strength, Hartree-Fock calcs. 77−6685
HeH^+, excited states, variable screening models, natural spin orbital analysis of wave functions 80−37747
HeH^+, fast ion dissoc. in thin foil, theory 77−19998
HeH^+ impact on C foil, quantum beat pattern depend. on foil thickness 80−58343
HeH^+ in planetary nebula NGC 7027, search for near IR emission lines 78−73748
HeH^+, ion beam prod. by coaxial electron impact ion source 80−62795
HeH^+, mobility in He gas 78−18371
HeH^+, photodissoc. by electronic and vibr. transitions 78−90244
HeH^+, radiative recombination rates 78−37708
HeH^+, static polarisability determ. by optimised rot. method 79−54990
HeH^+, struct., channel coupling array calcs. 79−31362
HeH^+, Temple lower bound mol. orbitals, GTO calcs. 78−41935
HeH^+, triplet Σ, Π and Δ states, config. interactions 78−78633
HeH^+, vibrational self-ionisation of mol. and recomb. processes *(Russian)* 77−79700
HeH^+, $X^1\Sigma^+$ electronic ground state, pot. curve, rovibronic and dissoc. energies 79−72254
HeH^{++}, partial wave treatment, convergence 79−10017
HeH^{2+}, LCAO MO calcs. using reduced Bessel functions 79−31361
HeH^{2+}, LCAO method, improvement by directed variation of exponential parameters 79−41101
HeH^{2+}, pot. energy curves for 2pπ and 3dδ excited states 78−29756
$^4HeH^+$, IR rot.-vibr. spectrum obs. 80−23420
HeH^++C thin solid target, 50-300 keV, collisional at. physics using mol. projectiles 79−45813
HeH^++H, reaction, ion cyclotron reson. mass spectrometric obs. 79−64098
HeH^++H_2→H_3^++He, reaction rate. coeff. 78−18371
HeH^++Ne, collinear reaction, pot. energy surface SCF-LCAO-MO and DIM calc. 78−92467
$^4HeH^+$+He, 1 keV, collision-induced dissoc., ro-vibr. assignments, proton spectra obs. 79−3556
HeH_2^+, CI calc. extrapolation, using perturbation theory natural orbitals 79−85907
HeH_2^+, electronic struct. 79−31414
He_2H^+, ground state pot. energy surface for form. by collinear collision, DIM calcs. 79−97996
He_2H^+, quantum-mechanical calculations 78−33424
$HeHe_2^+$, doublet, ab initio pot. energy surface calcs. for ground and lower excited state 79−63898
HeI_2, rot. fluoresc. spectra, nonlinear equilib. struct. 78−37672
HeI_2, van der Waals mol., vibr. predissoc. lifetimes 79−68278
HeI_2, Van der Waals mol. vibr. predissoc. anharmonicity effects 80−52971
HeI_2, vibr. excited mol., dissoc., predissoc., quasiclassical trajectory obs. 79−87839
$HeLi^{4+}$, pot. energy curves for 2pπ and 3dδ excited states 78−29756
$HeNO_2$, molecular geometry and stability, ab initio calcs. 78−90075
$HeNO_2$ van der Waals complex, fluoresc. spectrum 77−46591
$HeNO_2$, vibr. predissoc., rel. to van der Waals triatomic mol. theory 78−55208
$HeNO_2$, vibr. predissoc. rel. to van der Waals mol. theory, anharmonicity effects 78−55209
$HeNe^+$, visible spectrum obs. in discharge 79−13729
HeO_2, breathing, dogs, mechanisms of increased max. expiratory flow 80−56083

helium films
adsorbed, NMR measurements 80−107605
adsorbed monolayer struct., neutron scatt. 77−7942
adsorbed monolayers, dipolar anisotropy effects in spin relax 77−7940
adsorbed on graphite, band struct. effects in heat capacity 80−59788
adsorbed on graphite, nucl. mag. susceptibility below 4.2K 77−20155
inhomogeneities 77−76641
interaction with graphite surface, anisotropic He-C pair interaction 80−96738
monolayer, phase diagram, order-disorder transition 80−107604
monolayer, quantum tunnelling, NMR linewidth 77−39720
monolayer, solidification, theory 77−20158
monolayer adsorbed on Grafoil, phase determ. by sp. ht. meas. 77−11764
monolayer films, on graphite, ordering 79−65287

helium films continued
monolayer systems, book contrib. 79−99390
multicritical behaviour from triangular lattice gas model 77−74328
multilayer adsorbed, in restricted geometries, book contrib. 79−99391
ordered, finite size effect, crit. parameters and three-state Potts model 77−31836
physisorbed low-density submonolayer thermodynamics, potential scatt. theory calcs. 79−95243
sound modes of two-dimensional electron gas 77−69145
specific heat, low-density phase modification produced by substrate changes 77−76642
superfluid, current flow effects *(Dutch)* 79−1534
superfluid, excitation spectrum, neutron scatt. 77−7942
superfluid, nonequilibrium statistical mechanics 79−33137
superfluid density, jump 80−44387
superfluid density in two-dimens., XY model 79−95242
superfluid film, excitation spectrum, neutron scatt. 77−7942
superfluid film, very thick, electrohydrodynamic instability 79−51382
superfluid film near λ point 77−66070
superfluid properties 80−34270
superfluidity suppression, effect of substrate 79−69314
surface backscatt. phonon pulse time delay, heat-sensitive detector obs. 78−22927
thermodynamic theory of clustering and percolation transitions 77−47697
transfer, effect of solidified gases *(Russian)* 77−69143
transient heat transfer, film boiling regime 78−83219
two to three dimens. 78−47633
^{4}He films, vortices and superfluid decay 80−96710
^{4}He, superfluid, sp. ht. of confined sample, near superfluid transition 79−46859
^{3}He-^{4}He mixture film, 2-D interface excitation spectrum 80−96718
^{3}He, adsorbed, on MgO, nucl. mag. relax. props. 80−49457
^{3}He, adsorbed, with triangular lattice, exchange and mag. order 80−107606
^{3}He, adsorbed film on Grafoil, NMR, intermediate and near-monolayer coverages 79−46878
^{3}He adsorbed layers, antiferromag. indirect exchange 79−99389
^{3}He adsorbed layers, NMR studies 79−65286
^{3}He, adsorbed monolayers, nuclear magnetic relaxation for two dimensional systems 80−103534
^{3}He, adsorbed monolayers on Grafoil, NMR, low coverage 78−91503
^{3}He, adsorbed monolayers on solid Ne, desorption heat capacity 79−51383
^{3}He adsorbed on Grafoil, nuclear spin relax. and atomic motion 79−51369
^{3}He, adsorbed on graphite, NMR relax, times 79−51374
^{3}He adsorbed on superfluid ^{4}He surface, ripplons and heat conduction meas. 80−49459
^{3}He, adsorbed on Vycor glass under press., nature of phases, entropy and magnetisation expts. 80−49458
^{3}He film, submonolayer and multilayer, adsorbed on Grafoil, pulsed NMR study 80−49456
^{3}He, film on metal surface, superfluidity mechanism *(Russian)* 78−30809
^{3}He, in Grafoil, NMR obs. of magnetisation 79−51370
^{3}He, liq., reinforcement of low temp. surface ferromag. instability due to ^{3}He-wall attraction 79−51373
^{3}He, liq. confined in Al_2O_3 and Pt powders and Grafoil, NMR expts. 79−51371
^{3}He, monolayer film, adsorbed on Grafoil, pulsed NMR meas. 79−33152
^{3}He, normal, nuclear spin relax. in confined geometries 79−51372
^{3}He, solid, magnetic polarisation around vacancies, on two-dimens. lattice 79−51368
^{3}He, superfluid, behaviour in zero gravity 79−55987
^{3}He, superfluid, surface magnetism 79−51361
^{3}He, superfluid, two-dimensional, phase transitions 79−33143
^{3}He, theory of motional inhibition of interlayer quantum tunnelling 80−54466
^{3}He, two-dimensional, in ^{4}He film, sp. ht. meas. 80−39382
^{3}He-^{4}He, many body approaches to liquid-vapour transition 78−51783
^{3}He-^{4}He, mixture film, superfluidity precipitous onset 79−23802
^{3}He-^{4}He, third sound meas. using TOF techniques 79−51381
^{3}He-^{4}He film, adsorbed on graphite, nucl. mag. susceptibility below 4.2K 77−20155
^{3}He-^{4}He film, many body approaches to liquid-vapour transition 78−51783
^{3}He-^{4}He liquid solution films, thickness calc. from dielec. const. data *(Russian)* 79−11003
^{3}He-^{4}He mixture, adsorbed on Vycor glass, superfluid mass and transition temp. 79−51385
^{3}He-^{4}He mixture, adsorbed film, systematic exptl. study 80−107603
^{3}He-^{4}He mixture, film, superfluidity and phase separation 79−77857
^{3}He-^{4}He mixture films, unsaturated, third sound and decay of persistent currents obs. 80−75402
^{3}He-^{4}He mixture superfluid thin film, third sound vel. calc. 80−107602
^{3}He-^{4}He mixtures, tricritical behaviour in vicinity of walls 79−51387
^{3}He-^{4}He solution, thermodynamic theory 77−4238
^{4}He, adsorbed on disordered substrate, heat capacity meas. 0.08-1.3K 80−2239
^{4}He, adsorbed on graphite substrate, layering and thermal cond., heat capacity and vapour press. meas. 79−51386
^{4}He, adsorbed on Vycor glass, superfluid mass and transition temp. 79−51385
^{4}He, Bose-Einstein condensation, thermodynamic functions 79−82399
^{4}He, Brownian motion, boundary layers and quantised vortex prod. 80−6579
^{4}He, confined film near T_λ, sp. ht. scaling 78−38894
^{4}He, energy spectrum and specific heat of 2-dimens. interacting Bose gas 77−15656
^{4}He film, adsorbed, few atomic layers, excitations, two-dimensional roton. 80−39381
^{4}He film, specific heat near Tλ 77−80664
^{4}He film, vortex pair prod., boundary layer problem 79−99378
^{4}He, film adsorbed on Grafoil, onset and third sound vel. meas. 80−44388
^{4}He film growth on graphite, MgO, and Mylar substrates, vap. press. meas. 80−70499
^{4}He films adsorbed on graphite, transition temp., entropies, internal energies and heats of desorption, vapour press. meas. 80−2238

helium films continued
^{4}He, heat cond. by ripplons 79−51375
^{4}He, hypernetted chain generalised eqn. optimal solns. 80−75396
^{4}He, in Vycor glass, finite size scaling of sp. ht. 79−56015
^{4}He, influence of substrates on superfluid density at T=0 77−69144
^{4}He layered films on ZYX graphite, thermal resist. below 2K 80−70500
^{4}He, liq., free surface, crit. behaviour near λ point 80−2228
^{4}He, monolayer adsorbed on Kr-plated graphite, possible Ising transition 80−34298
^{4}He monolayer superfluid films, third sound modes, superfluid solitons 79−10998
^{4}He on solid H, film transfer velocity, Van der Waals interaction *(Russian)* 80−54465
^{4}He, saturated superfluid, on rough surfaces, persistent currents in presence of third-sound reson. 77−20156
^{4}He submonolayer film adsorbed on Grafoil coated with monolayer Ar, sp. ht. 0.4-4.0K 79−51379
^{4}He, superflow onset, 2-dimens. XY model 78−47623
^{4}He, superfluid, adsorbed on Al_2O_3 powder, surface tension sound 80−24691
^{4}He, superfluid, behaviour in zero gravity 79−55987
^{4}He, superfluid, complete decay of persistent currents, pulsed third sound TOF expts. 79−51378
^{4}He, superfluid, dissipation below 1K 79−51376
^{4}He, superfluid, dynamics 80−59748
^{4}He, superfluid, dynamics of vortex pairs using Fokker-Planck equation 79−69313
^{4}He, superfluid, film thinning during persistent flow 79−73360
^{4}He, superfluid, film thinning during crit. and subcrit. flow 80−20002
^{4}He, superfluid, finite size effects, effect of boundary conditions, below 0.5K 78−47616
^{4}He, superfluid, kinetic thinning 77−35793
^{4}He, superfluid, microscopic theory, excitation spectrum and thermodynamics props. 80−24709
^{4}He, superfluid, modified eqn. of state, mech. reson. meas. 80−24692
^{4}He, superfluid, on oscillating planar substrate, energy dissipation 78−47620
^{4}He, superfluid, persistent current stability 77−7923
^{4}He, superfluid, rate of energy dissipation 79−51377
^{4}He, superfluid, saturated, oscills. induced by persistent circulation 77−47637
^{4}He, superfluid, solitons at low temps., Korteweg-de Vries eqn. 80−96717
^{4}He superfluid, strong decay of persistent currents, thickness depend. 79−33133
^{4}He, superfluid, subcooled, heat transport, Kapitza resistance of Al 79−23794
^{4}He, superfluid, superflow, healing and relax. in He II flows, film thinning 79−14976
^{4}He, superfluid, superflow in very long glass-capillaries 79−65273
^{4}He, superfluid, superflow decay, vortex pinning effects 80−84332
^{4}He superfluid, surface wave, small amplitude long wave propag., linearised theory 78−56002
^{4}He, superfluid, thinning in persistent flow 77−35792
^{4}He, superfluid, third sound long pulse propag. 77−20148
^{4}He, superfluid, third sound attenuation, 0.1-200 Hz 77−20159
^{4}He, superfluid, third sound propag. and attenuation *(Russian)* 80−92733
^{4}He, superfluid, two dimens. systems, phase transitions, review 80−52149
^{4}He, superfluid, two-dimensional, critical temp. gap and phase condensation 78−95201
^{4}He, superfluid, wave process propag. in flow, new related phenomenon 79−51330
^{4}He, superfluid film, crit. vel. 77−7941
^{4}He superfluid film, fifth sound 79−60570
^{4}He superfluid film, in zero gravity 80−54464
^{4}He, superfluid film, long wavelength excitations, ripplon dispersion 79−73356
^{4}He superfluid film, superfluid density and dissipation in transition region 79−51384
^{4}He superfluid film, surface electrons, quantum oscill. effects *(Russian)* 79−11105
^{4}He superfluid film, two-reservoir, oscills. below 1K, damping 78−14535
^{4}He superfluid film, unsaturated, direct obs. of third-sound mass displacement waves 78−30804
^{4}He, superfluid film third sound meas. as capillary condensation probe in probe material 80−20005
^{4}He, superfluid rot. film, melting of two-dimensional vortex lattices 80−2539
^{4}He superlattices on graphite, ground-state energy, variational calc. 80−24710
^{4}He thin film, superfluidity 80−107594
^{4}He, third sound, two-dimens. hydrodynamics and elementary excitations 79−7721
^{4}He, two-dimens., excitation spectrum and thermodynamic props. 79−86959
^{4}He, two-dimensional film, superfluid transition 78−67877
^{4}He, universal jump in superfluid density 78−18856
^{4}He-^{3}He film, low temp. heat capacity, ^{3}He surface states 79−51380
unsaturated films, decay of persistent currents obs. ^{4}He superfluid, 80−75397

helium nuclei *see nuclei with mass number 1 to 5; nuclei with mass number 6 to 19*

Hellman-Feynman theorem *see quantum theory*

Helmholtz free energy *see free energy*

Hertzsprung-Russell diagram *see stellar evolution*

heterodyne detection *see demodulation*

heterodyne wavemeters *see wavemeters*

heuristic programming
see also artificial intelligence
BWR control rod programming, heuristic and mathematical approaches 79−9779
chemical structure determ., automatic rule formation in mass spectroscopy, meta-DENDRAL 77−18775
ECG analysis automation, advantages 78−7493
gated cardiac scintigram anal., digital boundary detect. techniques 80−98106
image edge enhancement 80−43273

heuristic programming continued
medical imaging techniques implemented on pipeline minis and array processor, nerve fibre counting appl. 80−98165
metal-composite shell, three-layer, stochastic formulation of optimisation using heuristic methods 80−38268
nuclear facility, optimisation of radiation detector position and number 78−55043
nuclear reactor, point-model, heuristic approach to reinforcement learning control 78−46144
prosthetic arm decentralised control hierarchical approach 77−40924
spatial reactor control methods 77−83056
ventricular hypertrophy diagnosis, three-orthogonal-lead ECG criteria 79−44034

h.f. amplifiers *see high-frequency amplifiers*

HF calculations
see also Xalpha calculations
1p-shell nuclei, HF charge distribs. 77−14024
σ-model appl. to nuclear physics in one dimension, fission, Hartree approx. 79−80890
$\langle J^2 \rangle$ quantum number calcs. 78−90059
A=12-208, adiabatic TDHF approx. isoscalar quadrupole collective motion, cranking mass 80−68507
A=2, 4, 16, photonuclear sum rule enhancement factor, Hartree Fock, Bethe-Goldstone eqns. 79−3137
A=42 nuclei, T=1, J=0 states, Coulomb displacement energies, Hartree-Fock wave functions, charge depend. 78−89773
A=90 region, core pol. effects and giant quadrupole resonances, HF and macroscopic calcs. 80−57756
ab initio effective core pots., reduction of all electron to valence electron calcs. 77−14361
ab initio LCAO-HF-concentrated GO crystal-orbital program 77−55471
ab initio-LCAO-Xα-SCF, atoms in mols., theory and appl. 77−57869
acetylene, chemisorbed on metal surfaces, geometric and electronic struct., UPS obs. and HF LCAO calc. 79−86988
acetylene, effective core potential calcs. 79−31437
acetylene, electron density distrib., electron correl. effects, approx. HF-CI calcs. *(German)* 78−33439
acetylene, near HF dipole polarizability, using EFV GTOs 79−31395
acetylene dimer, ab initio HF calc. for 64 conforms. 80−23333
acridine C-radical, polarised absorpt. and ESR spectra, dichroism and HF-CI calc. 78−50563
actinide configurations, isotope shifts rel. to $|\psi(0)|^2$ 78−17580
actinide ions, tetrapositive, nucl. hexadecapole antishielding factors 79−26909
actinides, and positive ions, non-relativistic Hartree-Fock X-ray scatt. factors 78−37602
actinides, electronic excitation energies calcs. 80−54592
adenine, tautomeric forms protonation, ab initio HF Roothaan SCF calcs. 80−78534
adenine tautomers, relative stabilities, nonempirical MO calcs. 80−21442
adiabatic TDHF approx., mass parameters, single collective variable, theoretical aspects 80−73765
adiabatic time-depend. description of nucl. collective motion 77−74786
adiabatic time-depend. HF method, large amplitude collective motion 77−88061
adiabatic time-depend. theory of collective motion in finite systems 79−486
adsorbate relaxation energies in XPS 78−15283
adsorbed layer, nonuniform charge distribution, phase transitions, Hartree-Fock calcs. 80−54525
advances in nuclear physics, clustering and self-consistent field theory, book 79−75879
Aitken δ^2 transformation, geometric approx. 77−10595
alkali fluoride crysts., modified electronic charge density 77−62502
alkali halides, U-centre, electronic struct., self-consistent model 79−65406
alkali metal, excited state lifetime var. along isoelectronic series *(French)* 77−46538
alkali metal atoms, ground state correl., photoelectron spectra, multiconfig. Hartree-Fock calcs. 77−50471
alkali metal hydride, variational time-dependent H-F calcs. in pseudopot. framework 77−10588
alkali metals, outer p shells multiplet and satellite struct., photoelectron spectra 80−87039
alkanes, solvent effects, quantum mech., macroscopic electrostatic contribs. 77−30801
allene, transition state for internal rot., HF/STO-3G calcs. with correlation energy corrections 78−25430
allyl-radical, pi-electron system, appl. of UHF Green's function method 77−61684
alternant hydrocarbons, approx. calc. by spin-extended HF method 79−26889
amino acid protonation ab initio Hartree-Fock-Roothaan SCF calcs. 80−9503
Anderson model coupled to boson field, HF approx. and RPA 77−40033
angular momentum depend. cranked HFB inertia parameter, high spin states 80−42524
anharmonic collective motion, adiabatic TDHF as consistent theory 78−78291
anharmonic Heisenberg ferromagnet, renormalised magnons and phonons 77−59373
anions, struct. and energetic predictions, modified HF procedure evaluation 78−62720
anthracene, excited states calc., unrestricted HF theory in PPP approx. 77−50377
antiferromagnetic exchange-coupled one-dimens. anisotropic chain with S=1/2, comparison with expts. 77−20530
antiferromagnetism itinerant electron theory, spin susceptibilities 78−6504
approximate method using density approximations and Coulomb field corrections 80−91421
approximate methods using density approximations and Coulomb field corrections, testing 80−91422
approximate relativistic Hartree-Fock eqns., soln. using Slater-type functions 80−58168
approximation with pseudowavefunctions 79−3357
aromatic substitution mechanisms 77−9056
asymmetric semi-infinite nuclear matter, HF calcs., surface symmetry props., finite range forces 80−57713
ATDHF theory 78−54710

HF calculations continued
atom, As to Yb, Compton profiles from HF wavefunctions 77−14393
atom, binding and kinetic energies, Thomas-Fermi-Dirac-Weizsacker calcs. 77−6680
atom, bound state quantum fluctuations and variational method, relativistic HF calc. with radiative effects 80−42918
atom, electron exchange pot. simplification 77−75054
atom, Hartree-Fock energies, scaled 1/Z expansion, integral eqns. 80−47886
atom, $K\alpha\alpha^h$ emission, method for L-shell config. calc. 77−42269
atom, kinetic energy functional, gradient expsn. using HF density 77−6665
atom, neutral, with Z up to 54, coherent scatt. factors *(Japanese)* 77−43103
atom, nonradiative low-energy transitions, exchange and relax. effects, appl. to Zn 79−3396
atom, orbital rel. to total SCF energies, HF SCF approx. formula 78−21837
atom, Slater transition-state calculations of multi-electron X-ray transition energies 78−90110
atom, Sturm expansions in the Hartree-Fock method 78−25409
atom Breit interaction between electrons, calc. angular coeffs., computer program 80−18779
atom total energies, RHF calc., GTO basis sets for heavier elements 77−61686
atom-ion core level shifts, ΔSCF calcs. 80−87176
atomic, HF function determ. in case of term mixing 79−63911
atomic and molecular electronic energies, homogeneity prop. 80−63539
atomic anions positron complexes, ground and excited states theoretical studies 80−42934
atomic collision processes, distorted-wave amplitudes 80−5596
atomic data handbook 77−23398
atomic effective charge distrib. in cpds., chem. shift of electron levels 78−86785
atomic electron binding energies, determ. from relaxed-orbital relativistic Hartree-Fock-Slater calcs. 77−42255
atomic electron elastic scatt., perturbation theory calc., computer program 78−50637
atomic electron excitation probabilities during orbital electron capture by the nucleus 79−45211
atomic excited terms generator program 79−54759
atomic field isotope shift off-diagonal parameter in $(5d+6s)^N$, ab initio evaluation 80−47912
atomic form factors, relativistic Hartree-Fock, tables for Z=1-100 79−59381
atomic independent particle pots. comparison 80−52846
atomic ionisation potential, X_α eigenvalues and Slater transition state 79−31394
atomic multiconfigurational eqns., numerical soln., computer program 77−42226
atomic multiplet struct. obtained from HF, statistical exchange and local spin density approx. 80−32619
atomic neutral systems, total binding energy, virial theorem appl. 80−47840
atomic $np^2(n+1)s$ excited-state config. quadrupole moments, Sternheimer shielding factor, of N(P)(As)(Sb) 80−37755
atomic orbitals, approximation by Gauss functions 77−67985
atomic oscill. strength, gauge props. of HF and RPA approx. 78−950
atomic quadrupole shielding factors calc. using elec. field variant orbitals 80−106276
atomic shell rearrangement during electron capture 79−75921
atomic struct., numerical HF radial function during SCF iteration, convergence 78−58574
atomic structure, relativistic HF eqn. from QED bound states 79−21992
atomic system, isoelectronic energy changes 79−76340
atomic systems, expectation values, correlation effects 79−6821
atomic systems, pair electron distrib. func. calc. for He to Ne, Li^+, Be^{2+} 79−81150
atoms, 70≤Z≤82, Kα X-ray linewidths and relative intensities, energy dispersive meas. 80−99483
atoms, electron gas exchange and Fermi hole density, HF calcs. 78−17565
atoms, electrostatic electron interactions, relativistic calcs. 77−57894
atoms, exchange potential simulation 80−9505
atoms, HF model, intrinsic props. 80−106252
atoms, HF model, nucl. charge rel. to orbital contribution to values $\langle r_{12}^n \rangle^{-1/n}$ 80−58115
atoms, hyperfine structure, UHF and PHF methods calcs. 79−36517
atoms, mag. hypersusceptibility *(Russian)* 77−14598
atoms, one-photon decay of two-hole states *(Russian)* 77−79592
atoms and molecules, second-order properties, coupled perturbed Hartree-Fock method improvement 80−58148
atoms in first three rows, UHF calcs., spin densities 78−41951
atoms on semi-infinite linear chain, chemisorption theory and superoperator formalism 80−93800
atoms total Hartree-Fock energy-eigenvalue sum relationship 79−59338
Auger decay theory at. orbital non-orthogonality, Wentzel Ansatz 77−18871
Auger electron transition energies calcs., contributions from beyond relativistic HF limit 77−18874
Auger kinetic and relax. energies in atoms and solids 78−15297
axially symmetric rare earths, mag. moments, current densities in projected HF approach 79−89236
azacyclobutadienes, conjugated mols. electronic struct. and geometry, Hartree-Fock instability 80−69055
back bending, Hartree-Fock Bogolyubov approach, cranking method 78−58228
back bending effect, Hartree-Fock-Bogolyubov treatment of cranking method, yrast states 78−82264
band calculations, validity of two-centre approx. 77−76726
band structure calculations, relationship between semiempirical and HF methods 80−75495
band structures, generalised HFB approach in intrinsic frame of reference, equilib. deformation 80−22664
band structures, generalised HFB approach in SU(3) framework 80−22663
band theory, Mott-Hubbard condition for electron localisation 79−73417
basis states generation by variational methods 78−78295
benzene, dynamic polarisabilities, calcs., superposition method of excited config., nonstationary perturbation theory eqns. 80−69257

HF calculations continued
benzenes, substituted, C-C coupling consts., coupled Hartree-Fock calcs. 77−27091
benzynes, geometry optimisation by generalised Hartree-Fock 78−25427
Bethe-Goldstone time-depend. first-order theory, short range correl., transition moments 78−25449
bonding energies, Hartree Fock Slater method, transition state method 78−9075
bonds, AH and AB (A, B=Li-F), linear momentum operator expectation values calcs. in molecules 79−7566
Born-Oppenheimer adiabatic pot. energy hypersurface gradient, exact formula 79−9992
Bose fluids, normal, conserving evaluation of dynamic struct. factor, HF approx. 79−14975
boson condensation, solvable quantum field theoretic model 77−57447
boson system, 1-D, with δ-function interactions, time-depend. Hartree approx. 79−9184
bound neutral polyneutron systems, existence anal. 78−70475
Brueckner's theory of nuclear matter, external field 78−33137
Brueckner theory, unification with HFB theory 80−105995
t-butyl radicals, ab initio geometry calc., ^{13}C hyperfine coupling 77−10580
caffeine, semi-empirical excited state Morokuma's EHP calc., geometry and order of states 78−46256
carbenes, unrestricted HF calcs. of electronic structure 77−6683
carbonyl oxide, config. interaction calc., using DODS natural orbit approach 78−66476
carbonyl to oxacarbene rearrangement, conformation, ab initio SCF MO calcs. 77−32780
CDW instability of electron gas in a strong magnetic field 78−79950
CDW of two-dimensional electrons, in strong mag. fields 78−43316
chalcogens, photoionisation cross sections and ang. distribs., outer p subshell 80−9572
chemisorption, electronic and ionic motion, exact unidimensional model 80−15369
chemisorption, embedding problem, SCFMO formalism 78−71977
chloromethane, mol., valence and core ionis. energy, RHF-SCF and PNO-CEPA calc. 79−85890
Choquard nonlinear eqn. minimising soln. existence and uniqueness 78−67315
chromium formate, mol., Hartree-Fock instability of SCF wavefunctions 80−9492
CI methods for improving unrestricted Hartree-Fock spin densities 80−32617
closed shell Hartree theory with orthonormal orbitals 80−69051
closed shell nuclei, elementary excitations unified model 77−67712
closed shell system, Hartree-Fock-Roothaan equations, program for soln. by Roothaan's method 77−88395
closed shell systems, ionis. pot., Koopman's theorem 78−906
closed-shell atoms, approximate relativistic Hartree-Fock eqns., soln. using Slater-type functions 80−58168
closed-shell atoms, Jastrow wave functions, var. calcs. 80−83249
cluster calculations, unrestricted HF approach, cluster-environment interaction 78−84117
collective excitations from high-q electron scatt., RPA AND ATDMF calcs. 80−22673
collective inertiae, in variational frameworks, canonical approach for auxiliary Hamiltonian *(French)* 77−87657
collective motion, independent-particle description 77−14021
compressed atom model, energy level shifts for changed boundary conditions 77−43473
conductivity electrons-localized d(f) electrons, exchange interaction, energy within Hartree-Fock theory *(Russian)* 78−43580
conjugated molecules, triplet-triplet excitation, atomic localisation calcs. 79−54830
conjugated polymers, effect of long-range coulombic repulsion of electrons on ground state 77−68147
constrained Hartree-Fock and quasi-spin projection 80−99141
constrained Hartree-Fock Hamiltonian, simple cure to breakdown 78−536
convergence problem, restricted and unrestricted wavefunctions 77−418
coordinate space representation and gradient iteration, spherical Hartree-Fock 80−18216
copper (II) complex, bis(dithiocarbamate), HF-Slater-LCAO calcs., mag. coupling parameters and optical spectrum 80−99447
coreless pseudopots. for atoms K through Zn 78−55121
correlation energy calculation, from CHF method 78−90087
Coulomb barriers, thermal Hartree-Fock approx. excitation-energy depend. 77−10346
Coulomb displacement energies, isobaric analogue resonances, TDHF calcs. 80−42518
Coulomb ionisation of inner shell electrons, screening effects 78−74749
Coulomb systems HF eqn. solns. 77−46479
coupled HF-perturbation theory of atomic and mol. props., correl. corrections 80−106269
cranked harmonic oscillator pot., self-consistent condition 78−17122
cranked Hartree-Fock-Bogoliubov wave functions, ang. momentum distribs. at band crossings 78−93956
cranked HFB treatment of pairing force, back-bending model 77−278
crystal Hartree-Fock theory, ab initio effective potentials 80−103290
crystal orbital calculations, deformation density method, transferable integrals, neutral atom pots. 80−38993
cummulene type infinite chain cryst., energy bands, ab initio Hartree-Fock orbital calc. 78−60066
cyclopentadienyl cation, geometry optimisation by generalised Hartree-Fock 78−25427
d-electron collapse, influence on np^5nd to np^6 transitions 80−47887
deformable jellium model, long-range order HF-type orbitals 80−2349
deformable-jellium model, self-consistent long-range order in terms of non-plane-wave HF states 79−19533
deformation energy dissipation, linear response function HF and HFB approx. 79−26366
deformation energy of nuclei, one particle spectrum, self consistent calcs., Hartree Fock variational method 78−12957
deformations of rare earth nuclei, Skyrme-HF calcs. 78−62480
deformed nuclei, collective props., HF calcs., review 78−50064
deformed nuclei calc. by HF method with Skyrme's interaction *(Russian)* 79−456
degenerate narrow bands, intraatomic Coulomb and exchange energies 80−84452
delta function fermion gas, solitons and HF solns. 78−49755
HF calculations continued
dense plasma, atomic energy level deform. and eqn. of state 78−71435
density compression in colliding nuclear slabs 78−642
density functionals in unrestricted Hartree-Fock theory 79−89583
density matrix equation, soln. 77−14339
density-dependent Hartree-Fock and Brueckner-Hartree-Fock theories, nuclear forces, nuclear struct. *(German)* 77−82842
diamond, five-atom clusters, unrestricted Hartree-Fock calcs. 77−11866
diamond clusters and corresponding saturated hydrocarbon ab-initio HF and PCILO calcs. 78−42951
diatomic molecules, electric polarisabilities, EFV GTO basis set 78−50661
diatomic molecules, LCAO Hartree-Fock-Slater method calcs. 79−31374
diatomic molecules, polarisabilities and dipole moment derivatives, virial theorem calcs. 77−57865
diatomic mols., 2nd row, STO and HF calcs., bond length, dipole moment 77−23431
diatomic radicals, wavefunctions, populations and orbital energies, Roothaan calcs. 78−86773
diatomic systems, nonadiabatic coupling matrix elements by Hellmann-Feynman theory and HF 80−83263
dielectric function, time-dependent Hartree-Fock formalism 79−69448
diethylcyanine, vibrational Raman bands, excitation profiles *(French)* 80−83380
1,2-difluoroethylenes, ab initio HF comparison of cis and trans energies 77−18786
dihydroquinoxalinediones, conjugated mols. electronic struct. and geometry, Hartree-Fock instability 80−69055
dilute Fermi gas, self energy, momentum distrib., and effective mass, nuclear matter 80−63119
dimethyl ether, low-lying excited states, improved virtual orbitals calcs. 77−14372
direct CI method, generalised to Hartree-Fock interacting space for doublets, quartets etc. 79−85908
direct CI method, Hartree-Fock interacting space for doublets, quartets and open-shell singlets 80−52889
direct energy minimisation methods in self-consistent nuclear fields, ground state props. 80−22702
dissipation in 1-dimens., time depend. HF calc. for slow neutron capture 79−63613
doubly closed shell nuclei, isovector giant monopole resonances, sum rule approach 80−78244
doubly magic nuclei, giant monopole resonances calcs. using adiabatic HF theory 79−22260
dynamic polarisability, TDHF theory and RPA sum rules 78−78292
effective convergence to complete orbital bases and at HF limit through systematic Gaussian primitive sequences 80−14065
effective interaction constraints imposed by antisymm. and charge independ. 78−86500
effective interactions, HF self-consistent potl. and linked valence expansions 77−6273
EHF theory in chem. reactions, wave functions symmetry props. 78−92447
eigenfunctions and eigenvalues evaluation, time-depend. HF calcs. 77−42241
elastic scattering, reson. width, stabilisation method, variational calc. 77−19011
elecronic excitation properties, RPA-CI calcs. using hypervirial relations as constraints 79−76413
electron affinity, variation-perturbation approach 77−54513
electron charge ordering, Peierls distortion, quasi one-dimensional spinless fermion model 79−87050
electron correl., second-order perturbation energy, modified HF operator, virtual MOs perturbation anal. 77−18797
electron correl. in extended systems, restricted HF calc., gap eqn. minimisation 80−54627
electron density, bulk and surface atoms, from ab initio model calcs. 79−4590
electron gas, interacting, local-field correction to dielectric constant, review 80−107731
electron gas, optical props. in generalised HF approx. 80−24825
electron gas, relativistic, spin-polarised, Bloch theory 80−15465
electron gas, spin polarised, model for conduction electrons of simple metal in mag. field and ferromag. Gd 77−8034
electron gas, two-dimensional, in strong mag. field, phase diagram properties 79−78024
electron gas, two-dimensional, pair correlation function 77−35877
electron-electron interactions, radiative effects, canonical transformation calcs. 77−3275
energy band calc. using OPW method 80−10856
energy functionals, difference in props. based on density matrices 80−907
energy-weighted moments, relations between nucl. collective theories 78−33130
ESCA photoionisation cross section, relative intensities calcs., comparisons 78−50464
ethane, effective core potential calcs. 79−31437
ethane cation, relative stability of $^2A_{1g}$, ^2E_g states 80−58140
ethenoxy, config. interaction calc., using DODS natural orbit approach 78−66476
ethyl radical, geom. struct., Hartree-Fock calcs. 78−62722
ethylene, chemisorbed on metal surfaces, geometric and electronic struct., UPS obs. and HF LCAO calc. 79−86988
ethylene, effective core potential calcs. 79−31437
ethylene, Hartree-Fock energy and Moller-Plesset perturbation energy, harmonic vibr. freq. 80−52852
ethylene, near HF dipole polarizability, using EFV GTOs 79−31395
ethylene, photoelectron spectrum, vibronic coupling effects 79−10090
ethylene, reaction heat, HF limit energies, correlation energy 79−8447
ethylene cation, state geometries, electronic vibr. coupling consts., HF calcs., comparison with Xalpha calcs. 80−27946
ethylenes, substituted, unstable twisted forms, excited states, DODS-NO CI calcs. 79−13643
even parity states in ^{19}F, ^{21}Ne, ^{23}Na, generator coord. method, projected Hartree-Fock, and complete diagonalisation calcs. comparison 78−89796
even-even nuclei, excited states, angular momentum projection method, appl. to ^{162}Er 0^- band 79−3069
even-even nuclei in 2p1f shell, HF calcs. using velocity depend. effective interaction 79−71792

HF calculations continued
even-even nuclei in 2p-1f shell, binding energy, quadrupole moment, by HF calc. 79−17843
exchange energy density functional, gradient expansion, rel. to at. energy functional 80−99441
exchange interactions of atoms in paired orbital approx. 77−88521
excitation during collective deformation, time depend. Hartree Fock Bogolyubov method, fission process 78−58229
excitation energy, validity of excited minus ground state calcs. using HF/pair correlation 77−38620
expansion of MO wave functions into VB work functions 78−74580
expectation value variation as linear functions of nuclear charge 79−44776
expectation values, systematic behaviour 79−3365
extended even-tempered orbital bases for atomic and mol. calcs., systematic approach 80−32591
extended Numerov method for the numerical solution of the Hartree-Fock equations 80−83245
extended systems, Hartree-Fock orbital and total energies 79−4498
extended systems, HF density of states, appl. to thin films and polymers 80−6689
$f_{7/2}$ shell nuclei, odd-A, collective bands of positive parity states 78−54677
Fermi surface in double magic nuclei, self consistent description *(Russian)* 78−33120
fermion system, Hartree-Fock states in thermodynamic limit, low-density clustering 78−54296
fermion systems, Hartree Fock soln. existence 80−98852
fermion systems, long-range order Hartree-Fock states with different magnetic properties 79−42476
ferrihaemoglobin hydroxide, nucl. hyperfine interaction, HF LCAO calc. 79−2002
ferromagnet, tight binding model, surface magnetisation 80−103807
ferromagnet with easy-plane anisotropy, HF magnon energies, kinematic consistency 80−93097
ferromagnetic alloy, binary ordered, dynamic mag. susceptibility, spin wave stiffness constant 79−38307
ferromagnets, anisotropic, HF magnon energy renormalisation, kinematic consistency 80−29539
Feynman diagrammatic calculation of HF energies 77−26981
film, HF formalism for calc. of total energies and charge densities 80−49850
finite nuclei, saturation props. of infinite nuclear matter 79−45198
finite temperature shape transitions, stability conditions, level density, HF and HFB calcs. 79−67644
first-order Hartree-Fock perturbation theory, symmetry calcs. 79−6854
first-row atoms, atomic X_α calcs. 80−83280
first-row elements, s-shell spin polarisation calcs. 77−75318
first-row hydrides, correl. energy difference models 77−10600
fission, ATDHF validity 78−50149
fluoromethane, LCAO-Xα-SCF, atoms in mols. theory and appl. 77−57869
force constant, Hartree-Fock-Roothaan calcs. with differentiated integral estimation 77−23573
formaldehyde, first hyperpolarisability, Hartree-Fock-Slater calc. *(French)* 78−78625
formaldehyde, orbital contribs. to relax. energies accompanying core ionis., ΔSCF HF calcs. 78−82642
formaldehyde, semi-empirical excited state Morokuma's EHP calc., geometry and order of states 78−46256
C_{2v}-formaldehyde, Tamm-Dancoff approx., relativistic correction, vertical excitation energy, radiative lifetimes 78−9090
formaldehyde-water, heuristic intermol. pot. function, ab initio MO calcs. 78−33566
formic acid, monomer, cyclic dimer, charge transfer through H bonds, Hartree-Fock calcs. 77−58157
formic acid, valence and Rydberg state empirically adjusted ab initio calcs. 77−10609
fractional occupation, local Xα pot. calcs. 80−95538
fragmentation of actinides, neutron multiplicities and fragment energies 77−30635
free ions, electron density near nucleus, isoelectronic change, nonrelativistic calcs. 79−54768
free lattice electron gas with nearest and second nearest neighbour hopping 78−51873
free radical reactions, selection rules 78−7181
free radicals, RHF CI INDO spin density calc. 80−919
frozen core, Lagrangian multipliers in terms of Slater integrals 78−17554
frozen core Hartree-Fock program for atomic discrete and continuous states 80−9509
furan, ionisation pots., transition operator calcs. 77−30771
g-shell nuclei, charge distrib., self consistent calc. *(Russian)* 77−38234
gamma-ray internal conversion coeffs. for all at. shells, $30 \leq Z \leq 104$ 79−45206
gas atom, photoionisation cross-section, multiconfig. Hartree-Fock calc. 78−17630
gauge invariance in second quantisation, Hartree-Fock and random phase approximations 79−75395
Gaussian basis sets, Ga, Ge, As, Se, Br, and Kr, HF calcs. 77−38611
generalised Brillouin theorem and generalised forces in SCF and MC SCF theories, and H-F limits 77−14366
generalised Fermi sea for plane wave HF theory, 3-dimens. semi-realistic interactions 80−105999
generalized Fermi sea for plane-wave Hartree-Fock theory: one dimensional model calculation 79−45196
generator coordinate method with conjugate parameters, adiabatic time depend. HF relation 78−86498
giant isoscalar and isovector resonances, TDHF calc. 79−85433
giant multipole resonances, light deformed nuclei via radiative capture, microscopic study 77−54139
giant resonance description, RPA, GCM, and semiclassical theories unification 78−54671
giant resonances, electric monopole and dipole vibrations, TDHF equations, fluid dynamical Lagrangian 80−47447
graphite, Compton profiles, momentum densities, comparison with glassy C 80−2895
graphite, electronic struct. exact exchange HF calcs. 80−65438
graphite, H chemisorption, cryst. orbital NDO calcs. 77−7965
Group IVA elements, excited states, quadrupole moments, Sternheimer shielding factors 78−82630

HF calculations continued
guanine, tautomeric forms protonation, ab initio HF Roothaan SCF calcs. 80−78534
guanine tautomers, relative stabilities, nonempirical MO calcs. 80−21442
hadrons, extended, second-quantisation of strongly interacting fields 80−13270
half-projected Hartree-Fock model, basis effects, appls. to mol. dissoc. *(Spanish)* 77−67983
half-projected HF scheme, stability conditions 77−61676
halogens, photoionisation cross sections and ang. distribs., outer p subshell 80−9572
Hamiltonian, zero-order, for many-body perturbation theory 80−9483
hard X-ray lines, chemical shifts, applicability of Koopmans' theorem, HF calcs. 80−74145
hard-core interactions, Hartree-Fock calcs. possibility due to overlapping orbitals 78−89811
Hartree Fock Bogoliubov method, high nuclear spins, quadrupole pairing, moment of inertia, yrast traps 78−54712
Hartree Fock Bologiubov theory, appl. to light/heavy nuclei, book contrib. 79−75881
Hartree iterative solution of general SCF eqns., convergence criteria 77−61675
Hartree-Fock states, thermodynamic limit, generalised Overhauser orbitals 77−54504
Hartree-Fock wave functions, convergence in Roothaan's SCF eqns., 'level-shifting' method 78−41920
Hartree-Fock-Bogolubov eqns., exact soln. 80−27582
Hartree-Fock-Bogolyubov approach to nuclear band description *(Russian)* 79−3107
Hartree-Fock-Slater method, calc. of multiplet energies 77−61685
He, Hartree-Fock energy, perturbative corrections, incomplete basis set problem 78−70744
heavy ion+atom collisions, K X-ray transition energies, two electron-one photon mechanism 77−18828
heavy ion+atom collisions, mol. M-X-rays, self-consistent relativistic HF-Slater many electron correl. diagrams 77−14567
heavy ion+nucleus, RPA theory, time dependent, quasi-boson approx. 80−57800
heavy ion collisions, collective potentials and inertia parameters, adiabatic time dependent HF calcs. quasimolecular resonances 80−63195
heavy ion collisions, comparison of time depend. HF with exact soln. in Lipkin model 77−18456
heavy ion collisions, fluid dynamical and TDHF models, abnormal nuclear matter, density isomers 80−47502
heavy ion collisions, mass asymmetry as collective coord. in Hartree-Fock calcs. 79−17914
heavy ion collisions, radiative electron capture, line profiles 77−14565
heavy ion collisions, TDHF analysis, spurious centre of mass motion problem 80−102198
heavy ion potential-energy curves 77−18606
heavy ion reactions, Hartree-Fock approx., statistical aspects 78−50193
heavy-ion collisions, struct. limitations of mass distrib., TDHF calc. 79−30852
heavy-ion react., separable approx. to TDHF calcs. in 3-D 78−74320
Heine-Abarenkov optimised potential for 27 elements, radial Schrodinger eqn. soln. 77−11833
Heisenberg anisotropic antiferromag., spectrum and correlation functions 79−28499
Heisenberg antiferromagnet, anisotropic, spectrum and correl. functions in spin-flop phase in generalized HF approx. 78−39283
helical systems, energy band calcs. using Hartree-Fock SCF-LCAO formulae 78−10329
heteronuclear molecules, alternant mol. orbitals energies, generalised formula 79−6867
HF subsystems, long range induction and dispersion interactions 80−53092
high order partial wave contrib. to nuclear matter binding energy for model interactions 79−45144
high spin rot. motion, TDHF cranking model and RPA descript. 80−102091
highly charged ion, $1s^2 2s^2 2p^5 3d$ configuration, energy spectra in relativistic approx. 80−14082
highly ionised atoms, relativistic effects, book contrib. 78−74588
highly-charged ions, spectral characts., relativistic effects, theory 79−10061
hole states in nuclear matter, single-particle potential 80−32150
Hubbard antiferromag. semiconductor, electron correlations, weak coupling 78−67969
Hubbard model, local moments 78−95414
Hubbard model, magnetic instabilities, influence of short-range correlation effects 79−7963
Hubbard model, one-dimensional, with nearest and second nearest neighbour hopping in Hartree-Fock approx. 77−32149
Hubbard model, two band, mag., orbital and charge ordered states 78−27012
Hubbard model with nearest and next nearest neighbour hopping in Hartree Fock approx. 78−52189
hybridization effect on phase transitions in the Falicov-Kimball model 78−91617
hydrides, MH^+, MH_2, M=alkaline earths: Zn, Cd, Hg, Yb, No, relativistic (non-relativistic) HF one-centre expansion calcs. 80−52908
hydrocarbon radicals, ab initio calc. of spin densities 79−93938
hydrocarbons, α-substituent effects in ^{13}C NMR, quantum chem. calcs. 78−74680
hydrocarbons, conjugated, ^1H chem. shifts calc. 79−98121
hydrocarbons, cyclic, non alternant, nonsingle instabilities of HF solns. 80−58164
hypernuclei, ΛN effective force, binding energy, excitation spectra, self consistent calcs. 77−6283
hypernuclei, ΛN interaction and spin-orbit coupling 77−71580
hypernuclei, interdisciplinary viewpoint of theories and developments *(Czech)* 80−22749
hyperpolarizability, freq. depend., time depend. HF eqn., second order LCAO SCF pertubation theory 79−31388
III-V semiconductors, deep centres, many-electron effects 79−15117
improved uncoupled Hartree-Fock perturbation methods, 2nd-order energy bounds in UCHF perturbation theory 79−85884
incomplete basis set problem, perturbative corrections to coupled Hartree-Fock theory 79−18100
incomplete basis set problem, virtual orbitals and CIBS expansion of HF energies 80−52844

HF calculations continued
induction energy, coupled Hartree-Fock calcs. 80−43139
inert gas atoms, He to Xe, electron density, kinetic energy functional 79−26879
inert gas isoelectronic sequences, positive ion p-subhsell photoionisation cross-sections calcs. 77−50374
inert gases, initial state wave functions for photoionisation cross-sections, multiconfigurational HF calcs. 80−47908
inert gases, photoabsorption to bound state and photoabsorption to continuum state (ionisation), comparison, HF calcs. 80−47910
inert gases, photoionisation cross-sections, multiconfig. Hartree-Fock calcs. 77−50373
infinite nuclear matter, response function, quantum field theory of fermion systems 78−70480
inhomogeneous electron gas at jellium surface, exchange energy 80−10901
inner electron shell, change in atomic quantities when vacancy occurs 79−63909
instability threshold and peculiar solutions of Hartree-Fock equations 79−85881
intermediate valence, theory, electronic sp. ht. calc. 80−79956
intermediate valence compounds, mag. susceptibility and sp. ht., mean-field theory of periodic Anderson model 78−47937
internal conversion calc., Hartree-Fock-Slater and Hartree-Fock models 80−18238
internal conversion coefficients, $30 \leq Z \leq 104$, Hartree-Fock-Slater model calcs. 79−36199
interorbital pair correl. energies and absolute overlap integrals, 1s and 2s HF orbitals 77−46501
ion elastic stopping cross-section, target atom Z depend., Hartree-Fock calcs. 77−10725
ionic crystal, quadrupole antishielding factors and polarisabilities 77−51346
ionic crystal, Sternheimer antishielding factors of F^-, Cl^-, Br^- and I^-, approx. free- and cryst.-ion pot. influence 80−39544
ionisation, Xalpha transition state and transition operator method calcs. 78−70743
ions, closed-shell cryst. field and self-consistency effects on dipole and quadrupole polarisabilities 79−87072
ions, positive and negative, Hartree-Fock-Roothan wavefunctions with 3d and 4d electrons 78−17569
ions, radial density functions, expectation values 78−62718
ions with partly filled L-shells, relativistic Hartree-Fock energy calcs. 78−82656
isocyanoacetylene theoretical study and rot. const. 78−33633
isocyanoethynyl radical, theoretical study and rot. const. 78−33633
isoelectronic sequence, correlated and HF electron density differences 78−46275
isoelectronic series, Politzer's energy rel. determ. using HF data 80−91425
isopropyl radical, pot. energy surfaces, ab initio UHF calcs. 80−106258
itinerant ferromagnet, effect of planar defects on electronic struct. and mag. ordering 79−99672
itinerant-electron ferromagnetic film on nonmagnetic metallic substrate, mag. props. 80−20371
k-particle generalisation and new generalisation of SCF type theories 80−102432
ketene, UHF-INDO perturbation calc., localised spin orbitals, spin anomaly and second order substituent effect 79−68191
Koopmans atomic valence electron ionisation energy, 1/Z expansion method, reorganisation corrections 78−78623
Kramers restricted Hartree-Fock approach 80−102435
lanthanide ions, tripositive nucl. hexadecapole antishielding factors 79−26909
large scale collective motion in very heavy ion reactions, macroscopic description 80−5049
lattice density waves in nuclear matter 79−71815
LCAO Hartree-Fock-Slater method, evaluation 79−31374
light atoms (up to Ni), contact term, use of local spin density functional method 80−58158
light deformed nuclei, Skyrme interaction spin components, spectra, projected HF theory 80−73820
light deformed nuclei, stability, shape, Hartree-Fock calcs. *(Russian)* 80−52568
light nuclei, Hartree-Fock calc. accuracy 79−45195
LiH, correlated potential energy curve, correlation hole concept *(Spanish)* 80−14081
linearised Hartree Fock model, effective charge, isoscalar nuclear shifts, rms radius ^{208}Pb, ^{90}Zr 78−25138
Lipkin model special case for Hartree-Fock and many-body problem solns. 79−13229
local density kinetic energy expressions for electronic struct. calc. 80−65473
local electronic structure in molecules, Hartree-Fock theory 77−79541
local mixed valence model, exact limit 77−51705
localised HF orbitals for mol. clusters, layers and solids 78−9076
localised spin orbitals, spin anomaly and second order substituent effect 79−68191
localised Wannier functions, numerical calc. from ab-initio Hartree-Fock wave functions 79−60671
long-range behaviour, uniform, resulting from self-consistent orbitals 80−9485
low density α clustering effects of Skyrme N+N interactions in nuclear matter 78−29398
m-scheme configuration interaction calcs., interaction integrals 79−45645
magnetic alloy, highly concentrated Kondo effect 79−24134
magnetic order coexistence with charge density waves 80−97096
magnetic solutions of Hubbard model, Hartree-Fock approx. 78−52195
magnetisation equation, HF-calculations *(Russian)* 78−27016
many body systems, low lying excited states, extension of ground state variational methods 79−36177
many-body perturbation theory, modified pots., 3- and 4-body contribs. 77−88376
many-body problem, classical hydrodynamics and collective motion approx. 80−83027
many-body system, effect of increasing N *(French)* 78−37539
many-body system, Hartree and Hartree-Fock solns., large momentum behaviour 78−17555
many-electron atoms, foundations of relativistic theory, Hamiltonian H_+ and h_+ and related relativistic HF eqn. derivation 80−99458

HF calculations continued
many-electron atoms, self-consistent theory of induction and dispersion forces, HF approx. 79−36725
many-electron atoms, spectra calcs. 80−23347
many-electron molecule, self-consistent theory of induction and dispersion forces, HF approx. 79−36725
maximum overlap mol. orbitals versus ab initio HF-SCF-MO calc. dipole energy 78−9070
MC-SCF equations, restricted, open- and closed-shell, soln. algorithm 79−63891
MCSCF procedures, 2nd- and approx. 2nd-order, convergency, appl. to Be and O_2 79−93907
metal, adsorption of He, HF calc. of repulsive pot. contrib. 77−43434
metal, quasi one dimens., plasmon dispersion relations, RPA and HF calcs. 78−34789
metal surface bonding, book contrib. 80−24990
metal-metal bonds, unstable, singlet unrestricted HFS model 80−902
metallic elements, core elections, Sternheimer antishielding factors calcs. 78−21862
metals, electron-deformation interaction, lattice contraction, Hubbard model calcs. *(Russian)* 80−59592
metals, ground state energy, structural expansion, HF approx. 80−65420
metals, press. eqn., Hartree-Fock approx. 78−72103
metals, simple, electron-electron interaction, self-consistent perturbation theory based on Hartree-Fock theory 79−95357
methane, effective core potential calcs. 79−31437
methane, elastic and inelastic electron scatt. differential cross section, obs. and calc., struct., binding energy 80−28110
methane, elec. dipole polarisability, coupled and uncoupled Hartree-Fock calcs. 77−34539
methane, first hyperpolarisability, Hartree-Fock-Slater calc. *(French)* 78−78625
methane, force consts., equilib. geom., Hartree-Fock and CEPA calcs. 78−70753
methane, large angle elastic and inelastic electron scatt. differential cross section, exchange corrections 80−28111
methane, localised molecular orbitals, HF theory 79−97980
methane, mag. shielding consts., coupled HF perturbation theory 79−6863
methane, mag. susceptibility, HF perturbation method 77−79702
methane, nucl. elec. shielding tensor calcs. 80−83296
methane, proton mag. shielding const., HF perturbation theory 78−46258
methane cation, photodissoc., ab initio RHF and MRD CI calcs. 80−95695
methane derivatives, stabilisation of planar tetracoordinate C, substituent effects, RHF/STO-3G calcs. 77−6671
methanol, low-lying excited states, improved virtual orbital calcs. 77−14372
methanol, mol., nucl. spin-spin coupling const., Hartree-Fock calc. 80−9618
method of moments extended HF wave functions, mol. props. determ. 77−50357
methyl ion, electrostatic force theory appl. to mol. geometry ab initio verification 79−98002
s-methyl nitrite, methyl group rot. barriers in cis and trans forms, ab initio calcs. 80−74111
methyl radical, ab initio projected unrestricted Hartree-Fock calcs. 78−58582
methyl radical, hyperfine coupling, in ground and excited states, Green's function calcs. 77−6692
methylene, singlet-triplet excitation energy, relativistic correction 80−69059
methylene peroxide, struct., energy levels, ab. initio UHF and MRUHF NO CI calcs. 80−83287
microscopic binding energy calcs., modified Strutinsky correction 79−67638
mirror nuclei, configuration mixing, Coulomb energy anomaly 78−25099
mixed valence compounds, structural phase transitions, effect of electron-phonon coupling 79−33265
mixed valence cpds., elec. cond., periodic Anderson model, memory function approach 80−84458
modified virtual orbitals, HF calcs. of second order perturbation energy 80−102437
molecular, electronic spectra, projected-unrestricted Hartree-Fock theory 78−46313
molecular aggregates, nonvalidity of SCF vibronic spectra calcs. 77−10655
molecular electron density contour diagram, polarisability anisotropy 78−66681
molecular electronic struct., UHF Green's function method, appl. to allyl-radical 77−61684
molecular electronic structures, orbitals calcs., omega like techniques 80−18792
molecular energy gradient, ab initio HF program 79−89606
molecular excited states, SCF calcs. using Binkley-Pople-Dobosh formalism 77−6694
molecular extra correlation energy, calc. by CHF method 79−76350
molecular Hartree-Fock calcs., symmetry adapted Fock matrices construction algorithm 77−23424
molecular Hartree-Fock integral eqns., soln. 79−76325
molecular hyperpolarisabilities, HF calc. with correlation method, appl. to HF mol. 80−23342
molecular ionisation energies, self-consistent-charge Hartree-Fock-Slater calcs. 77−6687
molecular open shells, RHF treatment without Lagrange multipliers 80−32589
molecular polarisabilities calcs., superposition method of excited config., nonstationary perturbation theory eqn. 80−69257
molecular systems with spatial point symmetry, unrestricted Hartree-Fock group theoretical struct. 80−37741
molecular total energy and orbital energy, semiempirical calcs. 78−78614
molecular transition energies, oscill. strengths, time-depend. model *(Spanish)* 77−6684
molecule, incomplete basis set correction, HF approx., differential eqn. formulation 79−63890
molecule, orbital energies and total energy 78−25433
molecule, orbital rel. to total SCF energies, HF SCF approx. formula 78−21837

HF calculations continued
molecule, polar, anion ab initio ground state pot. energy surfaces calc. 80−47923
molecules, diamagnetic susceptibilties and NMR chemical shifts in terms of localised MO's 80−106256
molecules, interacting, rigid, HF, self-consistent nonorthogonal group function approx. 79−31430
molecules, magnetic susceptibilities, anisotropies, CNDO/2 calc. *(French)* 78−37559
molecules, monochromatic wave perturbation, time depend. HF calcs. *(French)* 80−63516
molecules, pair energy, perturbative corrections, incomplete basis set problem 80−78507
molecules, relations between matrix elements in relativistic Hartree-Fock-Roothaan theory 79−36521
molecules, two criteria for labelling approx. treatments as fully quantal ones 80−23289
molecules in applied elec. field, virial relations 80−53087
molybdenum formate, mol., Hartree-Fock instability of SCF wavefunctions 80−9492
momentum eigenfunctions in complex momentum plane, Hartree Fock functions 80−63517
mono-energy pair conversion of nuclear multipoles, form factors, Hartree-Fock-Slater wave functions *(Russian)* 79−93555
monofluoromethane, X-ray photoelectron spectral linewidth of F core, ab initio HF calc. 78−62841
multi-configuration Hartree-Fock program 78−50471
multicentre multielectron system, wave function construction 78−893
multiconfiguration Hartree Fock method, appl. to at. energy levels and transition probabilities calcs. 80−23318
multiconfiguration Hartree Fock problem, finite-difference Newton-Raphson soln., He $1s2s\,^1S$ state appl. 77−6663
multiconfiguration Hartree-Fock procedures, 2nd and approx. 2nd. order, convergency 80−47901
multiconfigurational Hartree-Fock calcs., radial orbitals anal. approxs. 79−54760
multiconfigurational Hartree-Fock procedure, second-order, 2-electron integral transformations 80−87045
multiconfigurational HF calculations, quadratically convergent reference state optimisation procedure 79−97966
multiconfigurational time-dependent Hartree-Fock approach 79−85889
multiply charged ions, spectra calcs. 80−23347
multiply charged ions, superposition of quasidegenerate configurations 80−42956
N=82 region, high spin isomers, deformation energy surface, shape constrained cranked HF theory 80−57666
N=Z even-even nuclei, 2s-1d shell Hartree-Fock calcs. s-wave interaction 79−26385
N-body excited states, Hartree-Fock eqns. derivation 79−93934
N-electron atomic Hamiltonian first eigenvalue, Hartree-Fock approx. method 78−90062
naphthacene, excited states calc., unrestricted HF theory in PPP approx. 77−50377
naphthalene, excited states calc., unrestricted HF theory in PPP approx. 77−50377
naphthalenes, methyl substituted radical cations, UHF spin densities, additivity model calcs. 80−58139
narrow-band solids, real and imaginary-time Green's functions for HF and narrow-band limits 79−56112
neutron and nuclear matter, non-plane wave HF states, nuclear homework pot. 80−32224
neutron matter, spin zero sound and spin diffusion coeff. 77−57278
neutron rich nuclei stability, HF calcs. *(Russian)* 80−78181
neutronrich nuclei, analogue energy splitting, isoinvariant linearisation 77−65205
Newton-Raphson algorithm, soln. of HF eqn. *(Russian)* 77−49584
nitrone, config. interaction calc., using DODS natural orbit approach 78−66476
non-closed shell many-electron-theory at. charge wavefunctions, Be through Ne and Si 77−57849
nonbonded interactions, density response theory, appl. to rot. barriers 78−41913
nonlinear dynamics reaction theory, S-matrix TDHF theory 80−86834
nonperturbative open shell theory, mol. ionisation pot. and excitation energies, HF multiple cluster expansion 79−22599
nuclear adiabatic time-depend. theory, classical Hamiltonian quantisation for collective phenomena 78−526
nuclear average effective-interaction calcs. in HF and harmonic oscill. basis 77−57605
nuclear calcs. with effective interaction, self-consistency *(Russian)* 77−18458
nuclear collective excitations, macroscopic eqns. of motion and dynamic polarisability 77−41903
nuclear collective model for light nuclei, HF calc. shape anal. 77−41882
nuclear collective motion, consistent microscopic theory in an ATDHF approach framework 78−70472
nuclear collective motion, damping, time depend. Hartree model study 78−54711
nuclear collective motion, gauge invariant periodic TDHF eigenstates 80−27532
nuclear collective motion, generalised Schwinger representation, time depend. Hartree Bogoliubov theory quantisation, anharmonic vibr. 78−54673
nuclear collective paths in adiabatic time dependent Hartree Fock theory 78−525
nuclear collective rot., microscopic theory, SDHFB and HFBP methods test 79−67619
nuclear collisions, conf. 78−50136
nuclear collisions, TDHF calcs. using separable three dimens. wavefunctions, $^4He+\alpha$ appl. 78−50111
nuclear cranking model, HF calcs. of gyromagnetic ratio and moment of inertia 79−93482
nuclear dipole polarisability sum rule, HF calc.,, ^{16}O, ^{40}Ca appl. 78−21504
nuclear drop model, mass formula, higher-order vol. symm. terms, Hartree-Fock effective interactions 78−89808
nuclear dynamics, adiabatic TDHF limit versus TDHF, in soluble model 78−50113
nuclear dynamics, TDHF and ATDHF, nuclear vibrs., heavy ion collisions and Fermi hydrodynamics 79−67696
nuclear dynamics of heavy-ion reactions 77−41996

HF calculations continued
nuclear Fermidynamics and time dependent Schrodinger-Hartree Fock theory 79−3105
nuclear fluid dynamical model, spin-, isospin-, spin-isospin-, and normal sound 77−54167
nuclear fluid dynamics, extended TDHF for approach to thermal equilibrium 80−13448
nuclear forces, constrained HF calc. 78−8758
nuclear Hartree Fock theory, ambiguities, auxiliary pot. 78−25137
nuclear hydrodynamic and time-depend. HF calcs. comparison for nuclear matter slab collisions 77−18598
nuclear internal dynamics and collective rot., double variational method 77−50071
nuclear intrashell quartet states, ang. momentum projection 77−10348
nuclear isoscalar effective charges with scaling and HF wavefunctions 77−26559
nuclear large deformations, single particle levels, self-consistent field rearrangement, HF method 80−78107
nuclear mag. moments, variational approach 78−12967
nuclear many-body problems, energy of nuclear system 80−47414
nuclear many-body problems, finite density Hartree-Fock anal. 77−18457
nuclear mass and BE calcs. 77−22862
nuclear mass and neutron distribs., HF calcs. for ^{28}Si, $^{32,34}S$, $^{40,48}Ca$ *(Russian)* 77−82815
nuclear matter, abnormal occupation, two body correlations and plane wave HF energy 80−86844
nuclear matter, comparison of Brueckner and λ_{00} approx. 77−2929
nuclear matter, correl. between Brueckner-HF and correlated basis functions approaches 79−40869
nuclear matter, dispersion relations, HF method for hard core interactions *(German)* 78−54713
nuclear matter, hard core pots., crystalline struct. binding energy, HF calcs. 79−93543
nuclear matter, mean field near Fermi surface, energy dependence, single-particle quantities, Brueckner-Hartree-Fock calcs. 80−68572
nuclear matter, N-N separable non-local interaction, single particle potential 78−58245
nuclear matter, Overhauser's model, Skyrme force 78−12997
nuclear matter, self consistent periodic quartet formation 77−14052
nuclear matter, single-particle response and ground-state properties 80−105997
nuclear matter and surface, relativistic calc. 78−25142
nuclear matter density determ., HF versus droplet model 80−68574
nuclear matter flow, Fermidynamics and commensurability; TDHF restructured into TD-*S*-HF 79−93539
nuclear matter props., charge dependent N-N potential, HF calcs. 78−50115
nuclear meson dynamics in many-body problem, HF approx. 77−22917
nuclear one-body density matrix determ. by iterative steepest descent approach, appl. to ^{20}Ne 78−17125
nuclear proton and neutron densities, HF calc. 77−18380
nuclear proximity interaction from HF functional with Skyrme interactions 80−83043
nuclear rate states, Hartree-Fock-Bogoliubov approx. 77−10347
nuclear rotational states in HF calc. with Skyrme interactions 77−34212
nuclear scatt. formalism, nonsymmetric nonlocal pots. 78−17126
nuclear shell model, core and single particle props. 77−26596
nuclear single determinantal states, HF and energy variance minimisation methods 77−6204
nuclear single particle states, systematics in a Woods-Saxon potential *(Rumanian)* 79−59003
nuclear single-particle energy levels, shell-model anal. 78−17071
nuclear Skyrme tensor interaction, HF spin-orbit effects in spherical nuclei 77−61350
nuclear spin-spin coupling consts., finite perturbation-CI calcs. 80−5563
nuclear stability limits, HF calc. with Skyrme interaction 77−18377
nuclear struct., pairing motion, large amplitude, time-dependent Hartree-Fock method 78−4908
nuclear struct., soln. of constrained Hartree-Fock-Bogolyubov eqn. 77−18459
nuclear struct. calcs. *(Rumanian)* 77−26602
nuclear structure, droplet-model theory of the neutron skin 80−47416
nuclear two-quasi particle excitations, high-spin rot. state, ang. momentum projection 78−41615
nuclei, A=4n, densities, form factors, transitions, multipole moments in s-d shell, HFC 80−37321
nuclei, axially symm., soln. of HF eqns. in coord. space 77−88060
nuclei, backbending, HFB cranking wave functions 80−83049
nuclei, constraints in 2s-1d layer *(French)* 78−33115
nuclei, deformed, constrained HF energies, two-step iterative method 80−83053
nuclei, props. far from stability *(Russian)* 77−41908
nuclei, rotating, current distribs., cranked HF model 80−63059
nuclei, self-consistent wave functions, oscillatory parameters *(Russian)* 78−21596
nuclei in rare earth and Ni regions, density dependent HF description 77−54170
nuclei with A=4n, energy levels, BE(2) transition rates, HF approx. using Skyrme force 78−82315
nucler matter flow, fluid dynamics of small finite systems, energetic collisions 78−46018
odd A shell nuclei, positive parity states, collective bands, Hartree-Fock calcs. 79−30778
odd p-shell nuclei, lowest positive parity state from projected HF theory 79−463
one-body dissipation and nuclear dynamics, TDHF calcs. 80−52597
one-dimensional homonuclear molecular systems, nature of energy gap 79−11063
one-dimensional TDHF eqn. numerical soln. with and without collision term 80−5083
open shell excited states, perturbation effects, restricted Hartree-Fock calcs. 78−86770
open shell restricted HF eqns., role of coupling operators 79−758
open shell RPA unitary group formulation, Hartree Fock stability eqns. 80−52860
open shell SCF MO LCAO method in unrestricted Hartree Fock formalism 79−31389
open shell states, operators for cases not fitting Roothaan-like model 78−21848

HF calculations continued
open shell system, Hartree-Fock-Roothaan equations, program for soln. by Roothaan's method 77−88395
open-shell ions, coupled HF calc., static dipole polarisabilities and shielding factors 79−6862
open-shell restricted Hartree-Fock density matrix direct calculations 80−102434
optical HF pot., particle vibration coupling effects 79−93578
optical model complex pots. determ. from Reid's hard core interaction 77−88092
optimal plane-wave Hartree-Fock states for many-fermion systems 80−27587
orbital amplitudes of nuclei, extrapolation procedure, gaussian basis set and nucl. cusp eqn. 78−74560
orbital calculations, deformation density method, transferable integrals 80−38992
organic molecules, relax. phenomena, following core ionis., LCAO MO SCF calc. 79−10030
organic mols., relative Raman intensities, CNDO/2 INDO param. effect 80−95633
organic radicals, HFS coupling const. calcs., RHF+CI method in INDO approx. 79−770
organic reaction mechanisms, generalised mol. orbital theories, review 78−44366
orthogonality, radial orbitals, energy invariance 78−84
outer atomic electrons, corrected by statistical correl. pots. *(German)* 78−90083
oxalic acid, theoretical deformation density, ab initio Hartree-Fock calcs. 79−32982
p-f shell nuclei, HF calcs., vel. depend. effective pot., binding energy, quadrupole moment 80−461
particle collision inclusion in extended time dependent HF approx. 78−49780
particle energy loss, individual atomic orbital contrib., Hartree-Fock-Slater orbital 78−43060
particle transfer during nuclear deformation, Hartree-Fock calcs. *(Russian)* 79−3079
path integral approach to many-nucleon systems and time-dependent Hartree-Fock 80−78180
path integrals and time-dependent mean-field theories, many-body problem, Hartree-Fock eqns., Slater determinants 80−37342
path-integral approach to time-dependent self-consistent field theories 79−59023
Pauli principle imposed on Hartree product wave function 79−97968
Peierls-Hubbard model, quasione dimens., antiferromagnetism and Peierls distortion 78−67931
pentacene, excited states calc., unrestricted HF theory in PPP approx. 77−50377
periodic systems electronic struct., LCAO SCF ab initio HF calcs. method 80−65419
perturbation theory, many-body, algebraic approx. 77−18776
perturbation theory, many-body, arbitrary point group symmetry, wave operator matrix elements 80−23311
perturbed 1st-order HF theory, use of symmetry in mol. props. calcs. 79−85916
perturbed boundary conditions, for differential equations in theory of atoms 78−33432
perturbed energies, 2nd order, coupled HF iterative procedure, geometric approx. 79−9991
perturbed Hartree-Fock calculations, with reduced Green's functions, theory 77−14338
perturbed Hartree-Fock theory 80−91440
phase transition, 1st order, Landau-type theory 77−55339
phenyl cation, singlet, triplet state mol. geometries, energies, ab initio UHF STO calcs. 77−6672
photoemission relaxation energies, non-relativistic ΔSCF-optimised HFS calcs. *(French)* 77−36357
photoionisation, one-electron excitations, local pots., many-electron effects 79−54817
polarisability of atoms and molecules, freq. depend. 79−45652
polarisation propagator calculations of frequency-dependent polarisabilities, Verdet constants, and energy weighted sum rules 78−58647
polaron gas, interacting, ground state energy 77−76758
Politzer-Parr partitioning, electron correl., isoelectronic, isonuclear, spin and excitation aspects 80−78522
polyacenes, linear, open-shell ground state wave functions 79−762
polyacetylene, metallic, mixed Peierls phase, Hartree-Fock calcs. 80−70689
polyacetylene type infinite chain cryst., energy bands, ab initio Hartree-Fock orbital calc. 78−60066
polyatomic closed-shell systems, ab initio Hartree-Fock instabilities 78−78628
polyatomic system, large, ALGOL-60 program for MO LCAO calcs. in Mulliken-Rudenberg approx. 77−88388
polycyclic aromatic hydrocarbons, diamagnetic susceptibility NCHF (SCF-PPP) calcs. 77−6686
polycytosine, ab initio energy band struct. 77−70415
polydiacetylene backbone sequence, electronic structs., unrestricted HF approach 78−63975
polydiacetylenes, ab initio 'exact' exchange Hartree-Fock cryst. orbital method 78−26811
polyene, energy bands, ab initio Hartree-Fock cryst. orbital calcs. 77−89717
polyene band struct. calc., excitons in polyene chain 78−26816
polyenes, DODS methods with HF variations 77−23425
polyethylene, deformation, Hartree-Fock SCF calcs. 80−18949
polyglycine chain, electronic struct. and transport props., ab initio Hartree-Fock crystal orbital calc. 79−42448
polymer chains, Coulombic contributions, LCAO-SCF-CO method, Fourier representations 80−32862
polymers, electron problems by SCF method, HF matrix 77−79718
polymethineimine, cryst. orbital studies by HF methods 80−44148
polyyne, linear infinite chain, ground-state props., ab initio studies 79−95306
positive atomic ions, orbital SCF energies, rel. to total SCF energies 79−3350
positron+H(He), second-order nonadiabatic polaris. pot. for elastic scatt. 79−22836
positron annihilation in heavy at. shells, nuclear orientation *(Russian)* 79−49602
HF calculations continued
positronium halides, [X^-; e^+], electronic struct., annihilation characts., HF calc. 77−50567
positronium halides, [X^-; e^+], electronic struct., annihilation characts., HF calc. 77−50568
positronium nitrate, [NO_3^-;e^+], existence, Hartree-Fock-Roothaan calcs. 80−83254
positronium nitrite, [NO_2^-;e^+], existence, Hartree-Fock-Roothaan calcs. 80−83254
potential energy first derivative, open-shell restricted HF and MC SCF calcs. 79−98004
projected, appl. to rotational motion in 1-p shell odd-A nuclei 77−6207
prop-1, 2-dienyl radical, ab initio SCF HF MO calc., electronic struct. and one electron props. 77−42231
pseudopotential form factor determ., exchange interaction and correlation effects 80−49639
pseudopotential method, nonparametrised, for Hartree-Fock-Slater calcs. 77−57859
pseudopotentials, ang. momentum projector, 1st principles HF and local density functional schemes comparison 78−62702
pyridinium salts, hydrogen-bonded systems, deuteron quadrupole coupling 79−78563
quadrupole pairing forces influence on backbending, cranked Hartree Fock Bogoliubov approach 78−29401
quantization of time dependent self-consistent fields and finite boson representations for many-fermion system 79−6048
quark-mass generation by pseudoparticles, spontaneous breaking of chiral symm. 77−74646
quasi-spin projection in an exactly soluble model 79−71812
quasiparticle theory of large-scale configuration on mixing calcs. 78−13437
radical, small, isotropic hyperfine coupling consts., MINDO/3 calcs. 80−52894
radical+radical reactions, reaction path calc. using perturbation expansion *(German)* 79−34300
rapidly rotating nuclei, semiclassical HF description, smooth quantal corrections, density and total energy 80−32171
rare earth deformed nuclei, high spin region excited rot. bands, RPA calcs. 80−78108
rare earth orthovanadates, covalency, chemical bonding and opt. spectra 77−80442
rare earths, electronic excitation energies calcs. 80−54592
Rayleigh-Ritz principle in generator coordinate method, optimal TDHF solns. 80−42569
reality conditions for classical motions along collective paths 78−66234
reciprocal lattice expansion, Hartree-Fock exchange term, LCAO calcs. 78−47691
relativistic atomic wave functions, Hartree-Fock calcs. 79−10009
relativistic degenerate electron plasma, dielectric response in mag. field, plasma oscillations 80−54022
relativistic effects in oscillator strength calculations, ab initio methods 80−9519
relativistic pseudopotential theories and corrections to Hartree-Fock method 80−63523
restricted Hartree-Fock method, external instability, theory 79−10001
RHF energy values calcs., influence of mol. integral errors 77−50354
RHF molecular potential eqns., interactions of open-shell systems 77−30949
rotating nuclei, selfconsistency conditions in cranked harmonic oscillator model, HF calcs. 78−58239
rotational and intrinsic nuclear motions, semimicroscopic derivation of coupling 77−30498
rotational nuclei, A=159-181, transverse form factors from projected HF approach 80−105965
rotational spectra calc. using ang. momentum constraint, HF method 79−85403
RPA and pairing vibration approximations, multiple basis set calcs. 77−5755
S and ground band interaction in cranked HFB model 80−95299
s-d shell nuclei, HF calcs., vel. depend. effective pot., binding energy, quadrupole moment 80−461
s-d shell nuclei, HF two-determinantal deformed approx. 77−18461
SCF methods, constraints, stability 77−57870
Schwinger boson representation, quantised rotator 80−18164
sd-shell levels, fixed-JT averaging method rel. to projected HF method 77−10345
second-row atoms, atomic X_α calcs. 80−83280
second-row elements, s-shell spin polarisation calcs. 77−75318
second-row hydrides, correl. energy difference models 77−10600
self consistent long range order in nuclear matter Hartree Fock Overhauser orbitals 78−17127
self consistent pseudopots. in thermodynamic limit, state depend. one body field, HF calcs. 80−83054
self-consistency accel. procedure 80−78529
self-consistent calculations of nuclear properties with phenomenological effective forces, review 79−22218
self-consistent field calcs., HF calcs., NN interactions, and results of appl., book contrib. 79−75880
self-consistent field rearrangement in large nuclear deformations, HF calcs. 80−18184
self-consistent perturbation theory, generalisation for perturbation-dependent nonorthogonal basis set 78−17563
self-consistent pseudopots. in thermodynamic limit, correlation field, nuclear matter single particle orbitals 80−9253
semi-infinite nuclear matter with complete forces (finite range and spin-orbit term) 78−86499
semi-infinite nuclear slab dynamics of TDHF 79−75888
semiconductor, saturated, dielectric response 78−10384
semiconductor, two-dimensional electron-hole systems in high mag. fields, phase transitions 80−49608
semiconductors, doped, shallow impurity states, Hubbard bands and donor excitonic states, HF calc. 80−100443
semiempirical all-valency MO methods, derivation using restricted HFR theory *(German)* 78−21853
semimetal, phase transitions in strong mag. field, HF approx. 78−23028
semimetals, two-dimensional, electron-hole rearrangements in high mag. fields 79−87028
shell model, self consistency and many body monopole forces 79−67685
shell occupation number, rel. to coeff. for radial integrals of energy of electrostatic interaction of atomic electrons 79−63906

HF calculations continued
shifted Hartree-Fock eigenvalues and Slater's transition-state concept 80−83261
short-range correlations and pseudopotentials, even-even isotopes, Hartree Fock Bogoliubov method 78−535
silaethylene, singlet-triplet energy separations 77−57866
silaethylene, triplet carbenoid isomers, thermodynamic stability 78−90076
single particle nuclear density struct., Hartree-Fock and model independent anal. *(Russian)* 79−80941
single particle width in nuclei, deviations of mass operator from HF values 78−62477
single-particle models, relation between average kinetic energy and mean-square radius 80−52567
singlet biradical species, correl. effects, spin density wave calcs. 77−18796
singlet-triplet energy difference and singlet generalised oscillator strength, Lassettre-Dillon relation 80−63508
Skyrme interaction, mag. moments, polarisability, gyromag. factors 78−21501
Skyrme-type interactions, spectroscopy of light nuclei, density dependent Hartree-Fock 80−22717
Slater determinants, energy functional, extremum problem, Hartree-Fock equations, gradient method 80−62573
$(Sn)_x$ chain, energy band struct., Hartree-Fock and CDW solns. 79−23885
solid, appl. to nearly free electron gas 78−30857
solid, cond. band calcs., use of electron atom scatt., phase shifts 77−85139
solid, new Hartree-Fock energy band struct. determ. using LCAO basis, appl. to diamond 77−35848
solid electrolyte, mobility paths for MI_4^{-3} clusters, ab initio electronic struct. calcs. 80−70458
soliton solution of Hartree eqn., Newtonian interaction with screening 80−68569
soliton stability, 3-D nonrelativistic *(Russian)* 80−4583
solvent effects, virtual charge model representation of solvent polaris. 78−74593
spherical Gaussian basis sets, for relativistic Hartree-Fock calcs. 80−32595
spherical nuclei, Hartree-Fock-Bogolyubov calcs., D1 effective interaction, nuclear matter, binding energies 80−63105
spherical nuclei, small amplitude vibrs., giant resonances, TDHF, fluid dynamics comparison 78−66233
spherical shell model, collective features, review 78−50098
spherical shell model, renormalisation for collective model within truncated space 78−54697
spin density waves, nearly commensurate, effect of harmonics, Hartree-Fock calcs. 78−88104
spin exchange and polarisation changes, RPA breakdown from HF connection 80−99142
spin glasses, magnetisation relaxation time near freezing temp., HF calc. 80−34665
spin systems, coupled itinerant localised systems, dynamic magnetic response 80−34583
spin-degenerate system, Martin-Schwinger functional differentiation method 77−30765
spin-extended Hartree-Fock INDO calcs. 77−30781
spin-extended Hartree-Fock method, approx. variant 77−79531
spin-free quantum chemistry, Hartree-Fock theory, unitary group-formulation 79−85885
spin-orbit coupling, charge and spin density wave effects 79−91009
spin-orbit formalism of Hartree-Fock energy and Moller-Plesset perturbation energy 80−52852
spinless fermion systems, Coulomb repulsion, bond alternation, Peierls distortion, HF approx. 80−44524
static eqns., rapidly convergent direct density method 79−97674
static Hartree Fock problem, imaginary time step method 80−86832
static self-consistent HF problems, alternative methods 80−68568
stationary nonlinear Hartree eqn., asymptotic soln. 78−49723
Sternheimer valence shielding and antishielding factors for 2p and 3p ats. and ions 80−18807
strongly interacting systems, energy decomp. scheme 79−31431
sum rule, cubic inverse energy-weighted and adiabatic inertial parameters in HF calcs. 77−79316
superheavy nuclei, HF calcs. using Skyrme and finite range forces 77−46101
superheavy nuclei HF calcs. for magic numbers Z=126 and 138 77−88062
surface, narrow-band, self consistent model calcs. of electronic states 77−85295
syndnone, semi-empirical excited state Morokuma's EHP calc., geometry and order of states 78−46256
TCNQ alkali salt spin-Peierls transition 80−29395
TDHF, particles+core reduction 78−33135
TDHF and functional approaches, Lipkin model 78−93957
TDHF approximation and exact Schrodinger dynamics, Taylor series comparison 80−42568
TDHF eqns. for quantum mechanical many body systems 78−78296
TDHF equations of motion for algebraic Hamiltonians in a coherent state representation 80−57709
TDHF Hamiltonian, variational derivation 79−93536
TDHF time depend. phases, TDHF variational principle 79−93535
TDHF with two-body dissipation 80−91140
TDMF phase, unique implication of variational principle 80−27583
tempered orbital energies, SCF calc., relation to Mulliken-Walsh ordinate and extended Huckel orbital energies 79−763
tetracyanoquinodiamine, LCAO-Xα-SCF atoms in mols., theory and appl. 77−57869
tetrafluoromethane, elastic and inelastic electron scatt. differential cross section, obs. and calc., struct., binding energy 80−28110
tetrafluoromethane, valence electron binding energies, molecular symmetry restrictions effect 80−63528
tetrafluoromethane, X-ray photoelectron spectral linewidth of F core, ab initio HF calc. 78−62841
tetrathiofulvalene, LCAO-Xα-SCF atoms in mols., theory and appl. 77−57869
thermodynamic Fermi systems 80−4642
Thomas-Fermi method modification 79−85899
three-dimensional crystal, Hartree-Fock theory of surface states 80−44468
HF calculations continued
three-electron model system, unrestricted and projected Hartree-Fock calcs. 79−6850
time depend. Hartree eqn. quantisation, boson expansion, particle hole excitations 79−13230
time depend. Hartree-Fock and functional approaches, anal. using Lipkin model 79−36178
time dependent, evolution, implications for heavy ion reaction calcs. 77−10424
time dependent Hartree eqn. quantisation, finite and infinite boson expansions 79−13231
time dependent Hartree Fock solns., adiabaticity of collective motion 79−9498
time dependent Hartree Fock solns. for heavy ion scatt., wave packets to stationary waves 78−62558
time dependent HF polarisability and RPA sum rules, collective model restoring force 79−6461
time dependent HF polarisability and RPA sum rules, isovector giant resonances 79−6462
time dependent HF theory, collective path concept, validity range 79−17844
time dependent theory for nuclear collective motion *(German)* 77−67714
time-dependent Hartree equations, global solutions, and nonlinear Schrodinger eqn. 80−73193
time-dependent Hartree-Fock dynamics and phase transition in Lipkin-Meshkov-Glick model 80−52598
time-dependent mean-field approximation for nuclear dynamical problems 80−63113
time-dependent mean-field theory and quantized bound states, Lipkin model 80−63114
time-dependent multiconfigurational Hartree-Fock theory 80−58117
time-dependent variational principle and effective action 79−63359
time-dependent-S-matrix Hartree-Fock theory of complex reactions 80−63112
TiO, local density of states, X-ray spectra, Hartree-Fock and Xα calcs. discrepancies 79−77980
total HF SCF energy, of ats. and ions, approximation methods comparison 79−31366
transition elements, higher types, electronic config. and nucl. quadrupole interaction, atomic SCF Hartree-Fock calcs. 79−60777
transition metal, atom and ions, mixing of $3d^n4s^k$ configurations 79−63910
transition metal, chem. shifts of X-ray emission K-lines, free-atom approx. applic. 80−11513
transition metal, chemisorption of ordered atomic layers, HF Green's function formalism and phase shift technique 80−24733
transition metal, nonmag., possibility of mag. monolayer formation 78−15009
transition metal alloy, electronic structure, mag. props. 78−95254
transition metal atom, many-config. approx. in X-ray and electronic spectra interpret. 80−32615
transition metal atoms interactions with PF_3 and CO ligands, MO calcs., boundary props. of adsorption systems 79−85896
transition metal complex, LCAO-HFS-STO calc., basis set effects 80−52882
transition metal complexes, LCAO Hartree-Fock-Slater method calcs. 79−31374
transition metal compounds, localisation of electrons, review 80−49650
transition metal nitrosyls, ab initio HF calcs. 78−90082
transition metal nitrosyls, appl. of HF and CI calcs. 80−9513
transition metal surface, chemisorbed H_2, Hartree-Fock-Slater model cluster calc. 78−26929
transition metal surface atom interaction with ethylene and acetylene, MO calc. 80−6623
transition metal surface clusters, Hartree-Fock-Slater model calcs. 77−72899
transition metal trifluorides, mol. and electronic structs., ab initio restricted Hartree-Fock calcs. 79−63900
transition metals, 1st period, at. correlation energies, perturbation calc. 79−36508
transition metals, 3d, core electrons, Sternheimer shielding-antishielding factor 80−39534
transition metals, electronic structure and ordering of sp defects 78−91639
transition mtals, hydrocarbon catalysis 78−11550
translationally invariant self-consistent field theories 77−74788
transverse dynamic susceptibility and spin waves in itinerant electron SPW states 80−97076
triatomic dihydride molecules, Walsh's rules and small bond angle states 80−106255
triaxial nuclei, Hartree Bogoliubov predictions 78−33116
triaxial shapes in nuclei, projected HF and Hartree-Fock-Bogoliubov overlap integrals 78−78293
trimethylene diradical, generalised Hartree-Fock natural orbital config. interaction approach 77−75062
trimethylene diradical, geometry optimisation by generalised Hartree-Fock 78−25427
trioxolane, methyl substituted, stability, pseudorotation, electronic effects in final ozonide 79−45654
trioxolanes, methyl substituted, stability, pseudorotation, electronic effects in primary ozonide 79−49961
truncated space calcs. of exact bound state energies 79−3090
two identical molecules, level shifts due to overlap of MO's 77−46494
two-band alloy model, self-consistent cluster Bethe lattice study 80−29303
two-body collisions and time dependent Hartree-Fock theory 79−36208
two-dimensional, Hartree-Fock soln. of CDW in mag. field 79−28302
two-dimensional electron system in strong mag. field, crystallisation 78−30966
two-electron atoms, nucl. charge correl. with $(r_{12}^n)^{-1/n}$ function 79−68178
two-electron systems, pair function calcs. 80−32590
two-electron systems, RPA eigenvalue eqns., excitation frequencies and oscillator strengths 78−17570
UHF orbitals, ionisation energy calcs. appls. 80−58141
UHF wavefunctions, spin densities improvement 78−62688
UHFS model, CI, CC, and MBPT approaches, appl. to weak δ-δ bonds and δ-δ^* excitation 80−32585
unitary group decomposition of Hamiltonian operators 79−80889
unitary group formulation of Hartree-Fock theory 80−4589

HF calculations continued
universal atomic basis sets, light atom HF ground state energies 78−78605
universal basis set, for Hartree-Fock total energy 79−36502
unrestricted Hartree Fock equation, in mol. systems, group theoretical classification of solns. 79−36522
unrestricted Hartree Fock wave function, spatial symmetry recovery by spin projection 80−58150
valence electron methods, effective core pot. valence electron UHF method 77−30786
variation-iteraction soln. of Hartree Fock eqns., Green's integral operator, SCF formalism 79−6842
vector perturbation series based upon a representation in a finite Banach space 79−63893
velocity parameters of atomic HF wavefunctions 77−71744
virtual orbitals calc. method, in extended basis function space 77−46491
virtual orbitals modification, computational implementation 79−85880
water, liq., structure and props., minimal basis set description 80−6347
wavefunctions, piecewise polynomial 78−5115
work function theory, comparison of Hartree Fock and X_α formalism 77−76900
X-ray elastic scatt., electron density and ionisation pots., Thomas-Fermi and Hartree Fock anal. 79−52041
X-ray K emission lines, chem. shifts, free-at. approximation interpretation 77−50395
X-ray photoionisation cross section calcs., at. and mol. levels, HF rel. to OPW method 77−42353
x-ray scattering factors of ions in crystals 80−49046
yrast traps at very high angular momenta, microscopic description 78−70426
yrast wave function, variational principle used to solve Hartree Fock problem 79−93537
yrast-yrare interaction in $i_{13/2}$ shell, oscillating behaviour 79−93481
Z=11 to 103, theoretical, L-shell Coster-Kronig energies 77−83524
α-α scatt., 75.2 MeV, TDHF calcs. in 2 and 3 dimensions 78−78401
e^+A^-, positron-containing ground-state negative ions, self-consistent Fock field 80−47888
e^+Br^-, positron-containing ground-state negative ions, self-consistent Fock field 80−47888
e^+I^-, positron-containing ground-state negative ion, self-consistent Fock field 80−47888
N and Δ resonances in nuclei, coupled channel eqns. soln. for nuclear matter 79−17845
np interaction and nucl. deformation 78−8748
π condensation in nuclear matter, Hartree-Fock and generator coord. methods 78−17129
acetylene, electrostatic terms in lattice energy calcs., based on HF mol. change distribs. 79−51040
Ag, 4d-subshell absorpt. spectra, ab initio Hartree-Fock calcs. 79−18139
Ag, ionisation energies and oscill. strengths calcs. 80−5488
Ag isoelectronic series, excitation energies and oscillator strengths 79−54918
Ag, oscillator strengths, relativistic HF, core-polarisation model pot. 78−86818
Ag, valence-core electron exchange interactions, local approx. 80−91416
AgCl, electronic contact charge density of ^{107}Ag, core and overlap contrib. 79−78064
AgF, -Z 79−78064
AgI isoelectronic series, oscill. strengths, relativistic HF calcs. 79−98034
α-AgI, superionic, anal. of Ag K-EXAFS data 80−97377
Al, atom, photoelectron ang. distrib. of 3s subshell 79−76397
Al, collective properties of degenerate electron gas, (e, 2e) technique *(Russian)* 79−56149
Al, electron scatt., transitions, oscill. strengths, config. superposition calcs. 77−6732
Al II, $^3F^0$ Rydberg series, energy levels, multiconfigurational HF procedure 80−47882
Al, ion-induced Auger electron emission, depend. on ion energy 79−78814
Al, optimised model potential parameters Hartree-Fock-Slater procedure for calc. 77−69214
Al, static quadrupole polarisability and shielding factor, Hartree-Fock calc. 78−41950
^{27}Al, shape mixing using ang. momentum projection from Hartree-Fock intrinsic states 78−86472
Ar, 40 keV electron scatt. 7-200 mrad, relativistic and electron correlation effects 77−34760
Ar, and isoelectronic sequence, E1 transitions, relativistic oscill. strengths 78−949
Ar atom, Raman scatt. of light, HF approx. *(Russian)* 77−30808
Ar, atomic polarisabilities and shielding factors, coupled HF approx. 78−22048
Ar, electron impact ionis., calc. for $3s^2$ subshell 79−31700
Ar, electron scattering, elastic, low-energy, polarised-orbital calcs. 80−37882
Ar, first order density matrix, effective core pot. valence electron UHF method 77−30786
Ar IX, Ne I like reson. and Na I-like satellite lines, relativistic HF calc., beam-foil spectra 78−94210
Ar, inner electron energy characteristics, validity of Hartree-Fock-Pauli approx. 80−42957
Ar, momentum eigenfunctions in complex momentum plane, Hartree Fock functions 80−63517
Ar, Raman scatt., single particle HF approx. and RPA many-electron correlations calcs. 80−23374
Ar, shake-up energies, Slater transition-state calcs. 79−89651
Ar, total state energies, L-, M-electron processes, ab initio CI investig. 77−18801
Ar, two and three-electron Auger transition, with vacancies in 2p-shell 79−63972
Ar^-, free-free radiative absorpt. coeff. calcs. 77−423
Ar^{2+}, levels of $2p^53p^5$ 78−74574
Ar^{2+}, multiple open shell configs. calcs., modified HF method 77−50356
Ar-like atoms, gradient expansion of atomic kinetic energy functional 80−95530
Ar+Ar(Ar^+) collisions, multielectron excitation energy calcs. 78−1071
Ar_2, short range interactions between two rare gas atoms 79−26888
Ar_2^+, bound-free absorpt. cross section for Π and Σ states 78−5140
ArHF, van der Waals complex, ab initio RHF calc., struct. 79−76339
ArHO, van der Waals complex, ab initio RHF calc., struct. 79−76339

HF calculations continued
^{36}Ar, cranked Hartree-Fock-Bogolyubov calcs., p,n pairing correlations 79−6460
^{37}Ar, M/L capture ratio, multiconfig. Hartree-Fock calc. atomic electron correlations 78−62510
Au, ab initio effective core pot., Dirac-Hartree-Fock and Hartree-Fock calcs. 78−33426
Au complexes, electronic config. and elec. field gradient, relativistic HF method 80−54664
Au, oscillator strengths, relativistic HF, core-polarisation model pot. 78−86818
Au, relativistic 1s wavefunctions test, using exptl. Compton profiles 80−32600
Au, valence orbitals, Dirac-Fock scheme, direct and indirect relativistic effects 78−41969
Au+He^{2+}, high energy ionis. probability, semiclassical approx. with relativistic Hartree-Fock function 79−6998
AuI isoelectronic series, oscill. strengths, relativistic HF calcs. 79−98034
B, ground state energy, HF calc., second-order correction 78−86784
B, ground state wavefunction, SCF HF calc. 78−90070
B isoelectronic series, dipole oscill. strengths, multiconfigurational Hartree-Fock calcs. 77−83540
B^+, dynamic multipole polarisability, coupled Hartree-Fock 78−82858
B^{5+}+He(C)(Ne), K-shell charge transfer cross sections, Bates-Born formalisms 79−45834
BF, matrix HF calcs. using universal basis sets 79−59354
BF, $X^1\Sigma^+$ state, many-body effects, HF STO calcs., diagrammatic perturbation theory 77−50355
BF_3, dissoc. pathways and mol. vibr., compliance consts. and min. energy coords. 78−35661
BH, ab initio spin-projected EHF method pot. curve calcs. 79−10054
BH, electron density, basis set, electron correl. effects 78−74581
BH, mag. susceptibility calc. 79−868
BH^+, spin-extended Hartree-Fock ab initio calculations for small radicals 78−70746
BH_2, Walsh's rules and small bond angle states 80−106255
BH_3, electronic wave function determ., genealogical technique using Clebsch-Gordan coeff. 80−95529
B(I) hydrides, ab initio calcs., proton and hydride affinities 79−10029
BN, electronic struct., exact exchange HF calcs. 80−65438
^{10}B, triaxial deformation in shell model non-central forces, projected HF calc. 80−13367
^{11}B, projected HF calc. in intermediate coupling 77−18460
Ba II, ab initio calc. of isotope shifts 78−37555
Ba, term dependence of position of 4f electron in $4d^94f$ configuration 77−26973
B(e,e), A=10, 11, form factors, Hartree Fock calcs. 78−58263
Be, and isoelectronic sequence, correlated and HF electron density differences 78−46275
Be, atom, HF polarisability, second order correlation correction 78−25429
Be, BCC, high-temp. resist. and band struct. 79−51551
Be, correlation energies, Hartree-Fock Hamiltonian 78−41965
Be, dynamic multipole polarisability, coupled Hartree-Fock 78−82858
Be, electric field variant orbitals, STO field gradient depend., atomic quadrupole polarisability 80−23295
Be, excitation energies and transition moments in a second order polarization propagator approach 79−10051
Be, freq.-depend. polarisabilities and Verdet consts., calcs. 78−62781
Be, ground state wavefunction, SCF HF calc. 78−90070
Be, Hartree-Fock density matrix equation, soln. 77−14339
Be, highly excited states, electronic struct., oscillator strengths and resons., HF calcs. 77−46506
Be, ionisation energies and oscillator strengths, polarised frozen core approx. 79−36524
Be, isoelectronic sequence, transition probabilities, relativistic effects calcs. 77−27028
Be, isoelectronic sequence, relativistic transition probability calcs. 77−54533
Be isoelectronic sequence, multiconfig. calc. of mag. quadrupole transitions 78−33420
Be isoelectronic sequence, mag. dipole transition contrib. 79−81153
Be, isoelectronic series, Coulomb holes and correl. coeffs. 77−88398
Be, multiconfig. Hartree-Fock calcs. convergency 80−47901
Be, multiconfigurational time-dependent Hartree-Fock approach 79−85889
Be, SCF ion improved virtual orbitals, excited configs. calc. 77−10585
Be, second order correlation energies, variational-perturbation method, radial basis saturation errors 79−97985
Be^{2+}, ion compexes with HF, H_2O, and NH_3 solvent molecules, structural and electronic props. calc. 77−57873
Be^{2+}, numerical Hartree-Fock calc. of $1s^2$ ground state 79−81155
Be-type atoms in $1s^22s^2\ ^1S$ state, soln. of Hartree-Fock eqns. with nonorthogonal radial orbitals 77−46493
Be_4 (Be_4^-), atomic clusters, electronic struct., LCAO-MO-SCF and HF calcs. 80−63880
BeF_2^-, ground state, conform., electron affinity, extended basis SCF calcs. 79−72253
BeH radical, hyperfine splitting const., electronic energy, UHF-type, CCI calcs. 80−52909
BeH, spin-extended Hartree-Fock ab initio calculations for small radicals 78−70746
BeO(BeO^-), electron affinity and dipole moment, ab initio calc. 78−41938
^{7}Be, electron capture radioactive decay probabilities in atoms and ions 79−59556
^{7}Be, L/K capture ratio, multiconfig. Hartree-Fock calc. atomic electron correlations 78−62510
^{8}Be fission mode, large amplitude collective motion, adiabatic TDHF calcs. 80−86786
^{9}Be, molecular model, ground state props. via HF and GCM calcs. 77−54137
^{12}Be, Hartree-Fock calculations of nuclear bulk properties with density- and starting-energy dependent effective interaction 80−9246
Be(2^3P)+methane, reaction, ab initio MO calcs. 79−8431
Bi, electron config. mixing and parity nonconservation 78−13439
Bi, neutral current-induced parity nonconserving optical rot., Dirac-HF calcs. 80−47948
^{209}Bi(^{84}Kr, X), TDHF fusion calcs., fusion cross sections 80−37409
Br I, isoelectronic sequence, multiconfiguration HF calc. of sp^6-s^2p^6d interaction 78−9072

HF calculations continued
BrF_3, electronic struct. and ionisation pot., SCF DV Xalpha method 80−69057
BrF_5, electronic struct. and ionisation pot., SCF DV Xalpha method 80−69057
C, $^3P \rightarrow {}^1D$ electron impact excitation, distorted wave approx., exchange and polaris. effects 77−34764
C allotropes, diamond, graphite, gas-solid interface, electronic struct. HFR calc. 80−54745
C, glassy, Compton profiles, momentum densities, comparison with graphite 80−2895
C, ground state energy, HF calc., second-order correction 78−86784
C, ground state wavefunction, SCF HF calc. 78−90070
C, theoretical ionis. energies and oscill. strengths, excited s-, p- and d-levels 78−86823
C^{2+}, dynamic multipole polarisability, coupled Hartree-Fock 78−82858
C-C bond length electron difference density depend., approx. HF calc. *(German)* 78−5127
$C_2(C_2^-)$ pot. energy curves calc. using SCF, MCSCF and CI methods, dissoc. energies, bond lengths, electron affinity 80−95523
CF, electronic Rydberg states, dissoc. energy, multiconfig. HF calcs. 79−59360
CF, low-lying electronic valence states, dissoc. energy, multiconfig. HF calcs. 79−59359
CF_2 dimerisation reaction, UHF and MINDO/2′ calcs. 77−12793
CH^+, $a^3\Pi$-$b^3\Sigma^-$ transition moment, ab initio calcs. 80−87047
CH^+ indirect nucl. spin-spin coupling const., Hartree-Fock and polarisation propag. calcs. 78−9170
CH_2, dimerisation reaction, UHF and MINDO/2′ calcs. 77−12793
CH_2^+, Walsh's rules and small bond angle states 80−106255
$CH_3(CH_3^+)(CH_3^-)$, HF, GVB and CI calcs. 77−75063
CHF dimerisation reaction, UHF and MINDO/2′ calcs. 77−12793
CN, CN^-, HF electron affinity, SCF calcs. 77−67979
CN^-, electron density distrib., theoretical and expt. determ. 77−61683
CN^-, first hyperpolarisability, Hartree-Fock-Slater calc. *(French)* 78−78625
C_2N_2, and $C_2N_2^+$, electronic struct. UV and PE spectra 80−23304
C_2N_2, electrostatic terms in lattice energy calcs. 79−51040
C_3N, Hartree-Fock calcs. rel. to poss. detect. in IRC+10216 77−26041
CO chemisorption on Ni, Pd, Pt, Ir, mol. cluster calc. 80−100407
CO, core ionisation single orbital relax. energy, LCAO-SCF basis set depend. 79−89604
CO, first hyperpolarisability, Hartree-Fock-Slater calc. *(French)* 78−78625
CO, freq.-depend. polarisabilities and Verdet consts., calcs. 78−62781
CO, HF calcs., compared with optimised LCAO results 78−5139
CO, Hartree-Fock-Slater calcs., using pseudopot. method 77−57859
CO, indirect nucl. spin-spin coupling const., Hartree-Fock and polarisation propag. calcs. 78−9170
CO, matrix HF calcs. using universal basis sets 79−59354
CO, nucl. elec. shielding tensor calcs. 80−83296
CO, numerical coupled Hartree-Fock parallel polarisability, partial wave SCF calc. 78−9079
CO, orbital contribs. to relax. energies accompanying core ionis., ΔSCF HF calcs. 78−82642
CO, photoabsorption, photoionisation cross section, separated channel static exchange Stieltjes-Tchebycheff calc. 79−3502
CO, vibr. struct., core and valence ESCA spectra, Frank-Condon and HF anal. 80−32602
CO, X-ray K-absorpt. spectra, vibr. fine struct., ab initio restricted HF calc. 78−86883
CO, X-ray K-absorpt. spectra, reson. obs., near fine struct. 80−37817
CO^+, electronic struct., CO(e, 2e) reaction meas., CI calcs. 77−34769
CO_2, elastic and inelastic electron scatt. differential cross section, obs. and calc., struct., binding energy 80−28110
CO_2, electrostatic terms in lattice energy calcs., based on HF mol. change distribs. 79−51040
CO_2, ionised states, core and valence, ab initio HF calcs. 77−79597
CO_2, large angle elastic and inelastic electron scatt. differential cross section, exchange corrections 80−28111
CO_2, static polarisabilities, ab initio SCF HF calcs., internucl. separation depend. 78−9073
$(CO_2)_2^-$, struct., stability, electron affinity of neutral dimer, Hartree Fock calc. 79−63912
COH^+, orbital contribs. to relax. energies accompanying core ionis., ΔSCF HF calcs. 78−82642
CSiH, matrix Hartree-Fock calcs. 79−5874
^{12}C, adiabatic mass parameters, isoscalar quadrupole modes 77−14049
^{12}C, alpha cluster in Hartree Fock calcs. 80−63110
^{12}C, pion-exchange contribs. to charge densities, HF calcs. 78−46001
^{12}C spin-orbit force and deformation, self-consistent HF calc. 79−455
$^{12}C+{}^{12}C$, 3.2-64 MeV/nucleon, time-depend. HF calcs. 77−3034
$^{12}C+{}^{12}C$, low energy, HFB and generator coordinate self consistent microscopic approach 80−42679
$^{12}C+{}^{12}C$ system, nuclear molecule microscopic description, HF and coupled channel calcs. 80−13493
$^{12}C(e,e'p)^{11}B$, recoil momentum distribs., optical potential variation effects, HF calcs. 77−41955
$^{12}C(\mu^-,\nu_\mu)^{12}B$, Hartree Fock wavefunction, correlations, pseudoscalar coupling constant, capture rates, recoil nuclear polarisation 80−22774
$^{12}C(\pi^-, NN)$, bound π absorpt., HF wave functions, branching ratios, ang. distrib. 78−54803
^{13}C III, $1s^22s3p\ {}^3P^0$ state,, HFS, beamfoil expt., CI and Hartree-Fock calcs. 77−75276
^{13}C-^{15}N spin-spin coupling consts. calcs., lone pair contribs. 77−480
Ca I excitation series, potential barrier effects, single configuration HFC 80−78558
Ca isotopes, nuclear rms radii using Skyrme interaction with state depend. effective mass 79−45147
Ca, isotopes 40, 42, 44, 48, charge distrib., Hartree-Fock anal. *(Russian)* 78−70747
Ca XV, transition probabilities, energy spectra calcs. 78−70791
^{A}Ca, A=40,48, nuclear radii, energy density and HF-BCS methods 80−47363
^{A}Ca(e,e), A=40,42,44,48, elastic and inelastic scatt. cross-sections from Hartree-Fock densities *(Russian)* 79−13287
^{A}Ca(p,p), A=40,42,44,48, elastic and inelastic scatt. cross-sections from Hartree-Fock densities *(Russian)* 79−13287
^{A}Ca= A=40, 48, Hartree-Fock calculations of nuclear bulk properties with density- and starting-energy dependent effective interaction 80−9246

HF calculations continued
^{40}Ca, adiabatic mass parameters, isoscalar quadrupole modes 77−14049
^{40}Ca, charge form factors of doubly closed shell nuclei 77−6274
^{40}Ca, monopole vibration damping, TDHF calcs. 80−22667
^{40}Ca, nucleon-nucleon scatt., correlations, short-range, with pseudopotentials 78−37225
^{40}Ca, pion-exchange contribs. to charge densities, HF calcs. 78−46001
^{40}Ca, relativistic Hartree-Fock eqns., 1 boson exchange pot., spin orbit splitting 79−3106
^{40}Ca structure, supersoft-core pot., HF approx., ground state props. 78−533
^{40}Ca, vibrating nucleus, adiabatic anal. of time-dependent HF solns. 79−40863
$^{40}Ca+{}^{16}O$, 3-D TDHF calcs. 78−54781
$^{40}Ca+{}^{40}Ca$, 2- and 3-dimens. time depend. HF calc. comparison 79−17948
$^{40}Ca+{}^{40}Ca$, 278 MeV, comparison of 2-D and 3-D TDHF 78−82386
$^{40}Ca+{}^{40}Ca$, 278 MeV, particle transfer width, 3 dimens. TDHF calcs. 78−74389
$^{40}Ca+{}^{40}Ca$, 3-D TDHF calcs. 78−54781
$^{40}Ca+{}^{40}Ca$, 3-dimens., time depend. HF calcs. for fusion cross sections 78−66318
$^{40}Ca+{}^{40}Ca$, 3D TDHF calcs. 78−626
$^{40}Ca+{}^{40}Ca$, total fusion cross section time depend. HF calcs. 79−17945
$^{40}Ca(^{16}O,{}^{16}O)$, complex heavy ion optical pot., microscopic BHF derivation 80−106067
$^{40}Ca(^{40}Ca,x)$ reactions, time dependent HF calcs. 77−54251
$^{40}Ca(\mu,\gamma)$, photon asymmetry, $O(1/m^2)$ and nuclear effects 80−78219
$^{40}Ca(\pi,\pi)$, nuclear matter distribs., density depend. HF anal. 79−487
^{42}Ca, collective states, quasi-degenerate intrinsic Hamiltonian, variational methods 80−68505
^{48}Ca, nuclear incompressibility, Hartree-Fock calc. *(Russian)* 79−49577
^{48}Ca, pion-exchange contribs. to charge densities, HF calcs. 78−46001
$^{48}Ca(\pi,\pi)$, nuclear matter distribs., density depend. HF anal. 79−487
^{208}Ca, nuclear incompressibility, Hartree-Fock calc. *(Russian)* 79−49577
Cd, electron binding energy and shift, core level XPS 80−87088
Cd, ground state correl., photoelectron spectra, multiconfig. Hartree-Fock calcs. 77−50471
Cd, inner core neutral atom binding energy, relaxed-orbital relativistic Hartree-Fock-Slater calc. 78−13433
Cd, quadrupole antishielding factors, Hartree-Fock perturbation theory 78−62723
Cd UV subshell photoionisation cross section, expt. and GIPM theory 78−21887
$CdCl_2$, deformation densities, relativistic effect 80−42928
^{A}Cd, A=105,107,109,111, odd neutron deficient, rotor+particle model anal. 79−36127
Ce II, isotope shift and screening, pseudo-relativistic HF calc. 78−90096
Cl I, isoelectronic sequence, multiconfiguration HF calc. of sp^6-s^2p^4d interaction 78−9072
Cl, initial state wave functions for photoionisation cross-sections, multiconfigurational HF calcs. 80−47908
Cl, static quadrupole polarisability and shielding factor, Hartree-Fock calc. 78−41950
Cl, two and three-electron Auger transition, with vacancies in 2p-shell 79−63972
Cl VIII, Ne I like reson. and Na I-like satellite lines, relativistic HF calc., beam-foil spectra 78−94210
Cl^-, atomic core states, antishielding effects calcs. 80−83299
Cl-containing systems, core Auger and core electron binding energy shifts, ab initio LCAO SCF MO UHF calcs. 77−30777
Cl_2, ground and ionised states, Koopman's theorem and Mo relax. in ab initio calcs. 78−1035
Cl_2, Hartree-Fock-Slater calcs., using pseudopot. method 77−57859
Cl_2, inner shell excited states, X-ray absorpt. spectra, HF calcs. 80−78536
$(ClF)^+$, structure, theoretical investigation 80−904
$ClF(ClF_2^-)(ClF_3)$, ground and ionised states, Koopman's theorem and Mo relax. in ab initio calcs. 78−1035
$ClFH^+$, structure, theoretical investigation 80−904
Co (VII), semiempirical investigation of spectra 78−33434
Co complex, O_2CoCl_4 and $O_2CoCl_4NH_3^{2-}$, struct. and bonding model, CNDO-UHF calcs. 80−95541
Co, ferromag., HCP, electronic struct. calcs., band props. 78−39012
$CoCl_n$, electronic struct., INDO theory 80−42948
CoO, self consistent energy band calc. 78−23022
CoO, unrestricted Hartree-Fock calc. for cluster model 80−2320
^{59}Co, electron elast. scatt. cross sections, phase shift anal. and HF calcs. *(Russian)* 78−41707
Cr, A=48-52, effective charges and E2 transitions in 1f-2p shell nuclei 78−544
$Cr(CO)_{6,2}$ LCAO-HFS-STO calc., basis set effects 80−52882
Cs, $5p^6 6s^2$ level, Hartree-Fock calcs. 79−59349
Cs, deformed nuclei, low-lying positive parity states 77−6240
Cs, discrete level raising into far continuum, oscillator strength to shape reson. transfer 78−78624
Cs, excited np states, fine struct., core electrons effect 77−18807
Cs I, atomic wavefunctions collapse 78−70733
Cs, inner core neutral atom binding energy, relaxed-orbital relativistic Hartree-Fock-Slater calc. 78−13433
Cs, photoionis. of 6s electron, spin-orbit interaction, ab initio calc. 79−81191
Cs, term dependence of position of 4f electron in $4d^94f$ configuration 77−26973
Cs^+ and Cs, analytic SCF HF ground state wave function, ionis. pot., mag. props. 77−18785
CsI, isoelectronic series, oscill. strengths, relativistic HF calcs. 79−98035
Cu, A=63, 65, electron elast. scatt. cross sections, phase shift anal. and HF calcs. *(Russian)* 78−41707
Cu, chemisorption of H, density of states and chemisorption energy calc. 80−34315
Cu complex, $Cu(NH_3)_2(NCX)_2$, X=O, S, electronic struct., stereochem. 80−58156
Cu IV, wavelength region 700-1200 Å, extended analysis 80−99473
Cu isoelectronic series, core polarisation influence on oscillator strengths 79−45672
Cu isoelectronic series, Hartree-Fock line strengths 78−9122
Cu, oscillator strengths, relativistic HF, core-polarisation model pot. 78−86818
Cu sequence, ^2S-^2P transitions, oscill. strengths calc. 77−50406

HF calculations continued
Cu^+, electron exchange pot. simplification 77−75054
Cu^+, reson. transition, effect of correl. in $3d^n$ core, HF calcs. 80−47911
Cu-like ions, E1 transitions, wavelengths, oscillator strengths and transition probabilities, data tables 80−37780
CuCl, defect and impurity bands, lattice consts. 80−54638
CuCl, electronic struct., ab initio HF SCF MO calcs of $CuCl_4^{3-}$ cluster 78−95262
CuCl, self-consistent energy-band study 79−69408
$CuCl_4^{2-}$, charge distrib. and ligand field splitting calc. 77−62879
$CuCl_4^{2-}$, core ionisation in 3d, 4f and 5f series, rearrangement effects 80−53065
$CuCl_n$, electronic struct., INDO theory 80−42948
$CuCl_2(Cl_4^{2-})(Cl_6^{4-})$, electronic struct. studies by SCF, MSXα and INDO method 80−74119
$Cu^{2+}F^-$ and $Cu^{2+}F^-Cu^{2+}$, transferred hyperfine interactions 80−70659
$CuF_2(F_6^{4-})$, electronic struct. studies by SCF, MSXα and INDO methods 80−74119
CuO, ab initio HF-MC-SCF with GTO basis set, dissoc. energy and bond length 80−47890
^{40}Cu, nuclear incompressibility, Hartree-Fock calc. *(Russian)* 79−49577
Dy, quadrupole moment calc. using HF method *(Russian)* 80−13375
^{A}Dy, A=156-164, deformation hexadecapole moments, Hartree-Fock calcs. *(Russian)* 80−63081
Er *(Russian)* 80−13375
^{A}Er, A=162-170, deformation hexadecapole moments, Hartree-Fock calcs. *(Russian)* 80−63081
^{158}Er, moment of inertia anomaly at ang. momentum of 26 to 30 78−62496
^{158}Er, second backbending using cranked Hartree-Fock-Bogoliubov method 79−13188
^{158}Er, var. calc. and HFB calc. of back-bending 77−57584
^{162}Er energy spectrum anomalies, rot. bands, cranking model with Hartree-Fock-Bogolubov theory 79−3064
^{164}Er deformed nucleus, excited rot. bands, selfconsistent HFB treatment 80−42515
^{164}Er rot. states, HF and HFB self consistent calc. with Skyrme interaction 80−22662
^{166}Er, Skyrme-HF calcs., deformation, electric moments, spin-orbit potentials 78−62480
^{166}Er(^{86}K,X), deep inelastic collision, charge drift and dispersion calc., thermal eqn. model based on shell model 80−57798
F, ground state energy, HF calc., second-order correction 78−86784
F I, Fe XVIII, Zn XXII, Ge XXIV, Se XXVI, spectral line identification 79−72230
F^{q+}+Ne, radiative electron capture X-ray profiles from fast collisions, calcs. 79−49975
F_2, ground and ionised states, Koopman's theorem and Mo relax. in ab initio calcs. 78−1035
FBO, electronic struct. calcs. 77−30772
$FClO^+$, radical cation, struct. and electronic props., ab initio RHF SCF MO calc. 80−52883
FH, freq.-depend. polarisabilities and Verdet consts., calcs. 78−62781
FH, indirect nucl. spin-spin coupling const., Hartree-Fock and polarisation propag. calcs. 78−9170
FH, numerical coupled HF hyperpolarisabilities, basis set depend. 79−76357
FH, one-electron props., review of expt. and theoretical data, Hartree-Fock calcs. 77−67980
^{19}F, even parity state, EM props., collective struct., generator coord. method, HF method anal. 79−89220
Fe, A=52, 4, effective charges and E2 transitions in 1f-2p shell nuclei 78−544
Fe group ions, spectra, calcs., allowance for d^n shell pair excitations 77−42261
Fe, hyperfine interaction parameters, effect of local exchange, Xα and HF calcs. 78−78622
Fe, intercell exchange energy, Hartree-Fock approx. 80−60239
Fe, martensite, molecular cluster theory for electronic struct. 77−55497
Fe rich binary alloys, effect of transition impurities on structural stabilisation 77−76552
Fe, structural stabilisation, influence of C interstitials 79−11611
Fe XXI, transition probabilities, energy spectra calcs. 78−70791
Fe^{2+} and Fe^{3+} hydrate clusters, aq. electron exchange reaction, ab initio RHF MO calc. of inner shell reorganisations, vibr. freq. 80−102564
Fe^{3+}, quadrupole antishielding factors, Hartree-Fock perturbation theory 78−62723
α-Fe:C, electronic struct. 78−14692
Fe-V alloys, BCC, ferromag., polarised neutron diffr., appl. of multiband CPA theory 77−77033
$FeCl_n$, electronic struct., INDO theory 80−42948
$Fe_xCo_{1-x}S_2$, ferromagnetic solid soln., electronic sp. ht. coeff., calc. by CPA and Hartree-Fock approx. 79−7990
FeO, self consistent energy band calc. 78−23022
$Fe_4S_4(SH)_4^{0,2-,3-}$, HFS-LCAO calcs., 4-Fe active site model in high pot. Fe protein and ferredoxin 80−42929
^{54}Fe(p,p'), testing self consistent models of collective and single particle struct. 78−82300
^{57}Fe, hyperfine fields in Xe matrix, Mossbauer spectroscopy, Hartree-Fock calcs. 78−43749
^{57}Fe, rot. band mixing microscopic theory using modified Kuo-Brown interaction 80−68513
Ga I, oscillator strengths for $np^2P_{1/2,3/2}\rightarrow(n+1)^2S_{1/2}$ and $np^2P_{1/2,3/2}\rightarrow nd^2D_{3/2,5/2}$ transitions, relativistic calculation 79−89609
Ga I, Rydberg series, discrete levels and continua of finite bandwidth 78−74603
GaAs (110), electronic states and initial steps in oxidation 78−91534
GaAs, electron-hole drop transition to metallic condensed state, Hartree-Fock theory 79−56136
GaAs, nucl. spin levels, elec. induced shifts 80−34408
Gd, quadrupole moment calc. using HF method *(Russian)* 80−13375
^{A}Gd, A=152-160, deformation hexadecapole moments, Hartree-Fock calcs. *(Russian)* 80−63081
^{146}Gd, spherical HFB calcs. for Z=64 shell closure 80−22716
^{150}Gd, high spin states, pairing correlations and nuclear shape, HFB approach 80−42517
Ge, electron-hole drop transition to metallic condensed state, Hartree-Fock theory 79−56136
Ge isotopes, shape transition and quadrupole softness, Hartree Bogoliubov calc. 80−68527
GeH_2, struct. determ., restricted HF calcs. 80−87030

HF calculations continued
H atom finite chains, HF solns. stability and symmetry breaking, independent particle model calcs. 80−87035
H, electron elastic scatt. phaseshifts H continuum, frozen-core Hartree-Fock approx. perturbation theory 77−75295
H linear chain, near Hartree-Fock limit study 79−32938
H, metallic, Hartree-Fock and correlation energies 78−34674
H^-, and isoelectronic sequence, correlated and HF electron density differences 78−46275
H^-, numerical Hartree-Fock calc. of $1s^2$ ground state 79−81155
$H+C^{2+}(C^{3+})(N^{2+})$, radiative charge transfer, rate coeffs., pot. energy curves 77−88554
$H+CH_4\rightarrow H_2+CH_3$, transition state, UHF method in INDO approx, 79−43578
H+methane, abstraction and exchange reactions, energy barriers, UHF-CI calcs. 78−11512
H^++He(C)(Ne), K-shell charge transfer cross sections, Bates-Born formalisms 79−45834
H^++Kr, mol. orbit approach, spin-orbit interaction, adiabatic pot. and projected valence band treatments 77−533
H_2, $^1\pi_u$ and $^3\pi_u$ states, singlet-triplet energy difference, Hund's rule, inequality formulation 78−66482
H_2, excitation energy, pot. curves, oscill. strength, Hartree-Fock calcs. 77−6685
H_2, mag. field depend. orbitals for mag. screening and susceptibility of mol. 78−78611
H_2, metallic and mol. crysts., X-ray scatt. factors, Hartree-Fock calc. 79−60219
H_2, nucl. mag. shielding, elec. field, accurate coupled Hartree-Fock 78−25434
H_2, semiempirical model for polarisation of s-type AOs, pot. curve and surfaces determ. 77−88400
H_2, solid, HF calc. using plane wave basis 79−7772
H_2, total energy, HF SCF approx. formula, internucl. distance depend. 78−21837
H_2^+, semiempirical model for polarisation of s-type AOs, pot. curve and surfaces determ. 77−88400
H_2-He, nucl. shielding, ab initio coupled HF calc. 79−89690
$H_2+C(O)(N)$, pot. surfaces, HF calc. 80−16669
$H_2+D_2\rightleftharpoons 2HD$ catalysis, MgO surface, SCF UHF calc. 77−9120
H_3, interrelationships between effective hamiltonians 77−30767
H_3, semiempirical model for polarisation of s-type AOs, pot. curve and surfaces determ. 77−88400
H_3^-, dissociating states, lowest singlet and triplet PE surfaces, HF calcs. 79−81160
H_4, triplet state, instability of restricted Hartree-Fock, orbital degeneracy 78−25457
HCN, dipole moment derivative, sign anomaly, CGTO ab initio calc. 78−74795
HCN, semi-empirical excited state Morokuma's EHP calc., geometry and order of states 78−46256
HCO^+, orbital contribs. to relax. energies accompanying core ionis., ΔSCF HF calcs. 78−82642
HCl, bond dependence of dipole polarisabilities 78−74573
HCl, electrostatically interacting mols., CI multipole function calcs. convergency 80−91458
HCl, second order mag. props., coupled Hartree-Fock perturbation theory 80−87042
HD, Hartree-Fock calc., paramagnetic orbital contrib. to spin-spin coupling const. 79−89689
HD, indirect nucl. spin-spin coupling const., Hartree-Fock and polarisation propag. calcs. 78−9170
HD, spin-dipolar term, spin-spin coupling const. corrections, Fermi contact terms calcs. 80−99448
HF, ab initio HF-STO perturbation Auger transition rate calc. 79−72368
HF, bond dependence of dipole polarisabilities 78−74573
HF, electrostatically interacting mols., CI multipole function calcs. convergency 80−91458
HF, HF calcs., compared with optimised LCAO results 78−5139
HF, mag. field depend. orbitals for mag. screening and susceptibility of mol. 78−78611
HF, mol. hyperpolarisability, second-order SCF perturbation method, coupled Hartree-Fock calc. 78−33422
HF molecules, infinite linear chain, equilibrium structure and stabilisation energy 80−63856
HF, NMR shielding consts. and mag. susceptibilities, coupled HF with extended GTO basis 80−5480
HF, numerical coupled Hartree-Fock parallel polarisability, partial wave SCF calc. 78−9079
HF, $X^1\Sigma^+$ state, many-body effects, HF STO calcs., diagrammatic perturbation theory 77−50355
HF, $X^2\Sigma^+$ state, 3- and 4-body perturbation theory modified pots. 77−88376
$(HF)_n$, n=1-∞, ab initio hydrogen bond and electronic parameters, phonons 77−14342
HNF_2, force consts., geometry, ab initio Hartree-Fock calcs. 77−57864
H_2NF, force consts., geometry, ab initio Hartree-Fock calcs. 77−57864
HNOO, singlet and triplet diradicals, unrestricted 79−97975
H_2O, ab initio VB and localised HF MO hybridisation 77−57852
H_2O, elec. and mag. props. in static fields, perturbed Hartree-Fock calcs. 78−50462
H_2O, elec. dipole polarisability, coupled and uncoupled Hartree-Fock calcs. 77−34539
H_2O, electron density, basis set, electron correl. effects 78−74581
H_2O, electronic ground state, SCF HF and CI calcs, pot. energy hypersurface, spectroscopic consts. 78−50473
H_2O, low-lying excited states, improved virtual orbital calcs. 77−14372
H_2O, mag. susceptibility, HF perturbation method 77−79702
H_2O, nucl. elec. shielding tensor calcs. 80−83296
H_2O, one-electron props., review of expt. and theoretical data, Hartree-Fock calcs. 77−67980
H_2O, photoabsorption, Stieltjes-Tchebycheff calculations, Hartree-Fock calcs. 79−18238
H_2O, polarisabilities, finite-field calc., perturbation correlation 79−72249
H_2O, proton mag. shielding const., HF perturbation theory 78−46258
H_2O, valence shell electron pair interactions, VSEPR theory test 79−31393
H_2O, vertical valence ionis. pot. calc. by perturbation, CI and CPA techniques 80−69263

HF calculations continued
H_2O^+, states geometries, electronic vibr. coupling consts. HF calcs., comparison with Xalpha calcs. 80−27946
H_2O_2, struct. and barrier to internal rot., HF and Rayleigh-Schrodinger perturbation calcs. 79−13636
H_2O_3, struct., barrier to int. rot., HF and RS-MP perturb. calcs. 79−13637
H_3O radical, stability, ab initio UHF-CI calcs. 78−5137
$HOO(H_2O)$, electronic struct., and config., semiempirical UHF INDOC calc. 79−59356
$HO_2.H_2O(NH_3)$ complex form., ab initio calcs., min. energy configs. 77−14340
HS_n^-, n=1-4, electronic struct., ab initio Hartree-Fock-Slater calcs. 80−74107
HS_n^{2-}, n=1-4, electronic struct., ab initio Hartree-Fock-Slater calcs. 80−74107
H_2S, electron density, basis set, electron correl. effects 78−74581
H_2S, second order mag. props., coupled Hartree-Fock perturbation theory 80−87042
H_2S, valence shell electron pair interactions, VSEPR theory test 79−31393
H_2S_n, n=1-4, electronic struct., ab initio Hartree-Fock-Slater calcs. 80−74107
H_3SiCl, mol., valence and core ionis. energy, RHF-SCF and PNO-CEPA calc. 79−85890
$HSiO^+$, $HOSi^+$, quantum mechanical study 78−37541
He, 2p3d $^{1,3}L^0$ doubly excited state, soln. of Hartree-Fock eqns. 77−75072
He, and isoelectronic sequence, correlated and HF electron density differences 78−46275
He, atomic polarisabilities and shielding factors, coupled HF approx. 78−22048
He, correlation energies, Hartree-Fock Hamiltonian 78−41965
He, dynamic polarisability, CHF method 78−50472
He, electronic struct., universal STO basis sets 79−10021
He, energy density functional, gradient corrections 78−25428
He, freq.-depend. polarisabilities and Verdet consts., calcs. 78−62781
He, ground state s^2 correlation, Hartree-Fock calcs. 80−83281
He, ground state wavefunction, SCF HF calc. 78−90070
He, HF calcs. using piecewise polynomial electronic wavefunctions 78−5115
He, Hartree-Fock density matrix equation, soln. 77−14339
He isoelectronic sequence, electron correlation effects on one-electron distribs. 77−10598
He isoelectronic sequence, $\delta(r_1)$ matrix elements using spatially distrib. operators 80−102445
He, isoelectronic sequence, E1 and E2 oscillator strengths, MCHF calcs. 80−106292
He isoelectronic series, ground state, Coulomb holes and correl. pots. 79−89594
He, isoelectronic series, ground state specific mass shift, HF variation perturbation calc. 80−47889
He isoelectronic series, static dipole polarisability, reduced Green's functions, HF calcs. 77−71750
He, isoelectronic series 79−3358
He like atoms, dipole transitions, transition integral cancellation 80−69052
He, numerical Hartree-Fock calc. of $1s^2$ ground state 79−81155
He, photoionisation, frozen-core HF perturbation theory, oscillator strength, dipole length and vel. calc. 78−78672
He, quantum-mechanical calculations 77−14350
He, RPA eigenvalue eqns., excitation frequencies and oscillator strengths 78−17570
He, SCF ion improved virtual orbitals, excited configs. calc. 77−10585
He, second order correlation energies, variational-perturbation method, radial basis saturation errors 79−97985
He sequence, 2p3d $^{1,3}L^0$ doubly excited state, soln. of Hartree-Fock eqns. 77−75072
He, static multipole polarisabilities, integral equation approach to scaled 1/Z expansion 80−63846
He to Xe, radial density functions, HF calcs. 77−42238
He, two-step photoionisation via 4p $^1P_1$ state *(Russian)* 79−59413
He^-, highly excited states, electronic struct., oscillator strengths and resons., HF calcs. 77−46506
He^+, Xα statistical exchange method, orbital energies, HF method comparison 78−9071
$He\text{-}CH_3^+$ interaction energy, nonempirical calc. 78−86799
He-He, Born-Oppenheimer pot. using Hylleraas-type electronic wave functions 79−31438
He-He, potential energy curves, dispersion damping functions, Hartree Fock interaction energy 79−98176
He-like atoms, oscillator strength calc., allowed np-n'd and nd-n'f transitions 79−31467
He-like atoms and ions, gradient expansion of atomic kinetic energy functional 80−95530
He-like target+fast projectile, electron capture cross-sections 80−69231
He+CO, nuclear mag. shielding consts., interaction geometry depend., chemical shift, gauge invariant method 78−62866
He^++alkali metal atom, ionisation cross sections, binary encounter approx. with HF electron vel. distrib. 78−55225
He_2 potentials, configuration interaction calculations, superposition corrections 79−72382
He_2, short range interactions between two rare gas atoms 79−26888
$HeCl^+$, interaction potential, HF dissociation energies, LCAO SCF calcs. 77−6880
HeH^+, excitation energy, pot. curves, oscill. strength, Hartree-Fock calcs. 77−6685
$HeNe^+$, collisional form., excitation, pot. energy curves calcs. 77−6697
^4He, charge form factors of doubly closed shell nuclei 77−6274
$^4He(\alpha,\alpha)$, large amplitude collective motion, adiabatic TDHF calcs. 80−86786
$^4He(\alpha,\alpha)$, time dependent HF calcs. reaction cross sections 79−26443
He(1s2p) ^1P, eigenvalues and eigenfunctions, time-depend. HF calcs. 77−42241
He(2^3S), electron impact ionis. to 1s, 2s, and 2p state, autoionis. 80−1068
Hf IV, 6s $^2S_{1/2}$-6p $^2P^\circ_{1/2,3/2}$ transition, relativistic oscillator strengths, influence of core polarisation 80−58132
Hf, quadrupole moment calc. using HF method *(Russian)* 80−13375
^{A}Hf, A=176-180, deformation hexadecapole moments, Hartree-Fock calcs. *(Russian)* 80−63081

HF calculations continued
^{174}Hf, angular momentum fluctuation energy in the cranking model 79−89254
^{174}Hf, approximate ang. momentum projection from cranked HFB wave functions, yrast energies 79−30776
Hg atoms, elastic electron scatt., relativistic effects 80−102568
Hg, electron binding energy and shift, core level XPS 80−87088
Hg, ground state correl., photoelectron spectra, multiconfig. Hartree-Fock calcs. 77−50471
Hg, photoionisation cross sections, Hartree-Slater and Hartree-Fock calc. 79−89653
Hg, positron scatt. at low energy 80−91670
Hg_2-Pt, ^{199}Hg Mossbauer meas., isomer shift and quadrupole splitting calcs. 80−28039
$HgCl_2$, deformation densities, relativistic effect 80−42928
Hg_2F_2, ^{199}Hg Mossbauer meas., isomer shift and quadrupole splitting calcs. 80−28039
$Hg_2(X^1\Sigma_g^+)$ potential, intra-atomic correl. in HF calcs. 78−5314
^{188}Hg, HF calc., shape and lowest band struct., B(E2) values 80−32148
^{199}Hg, internal conversion coeffs., HF calcs. and expts. 77−57628
I I, isoelectronic sequence, multiconfiguration HF calc. of sp^6-s^2p^4d interaction 78−9072
$I_2(I_2^+)(I_2^-)$, HF and SCF calcs., pot. curves, electron affinity and quadrupole moment determ. 80−95527
In I, oscillator strengths for $np^2P_{1/2,3/2}\rightarrow(n+1)^2S_{1/2}$ and $np^2P_{1/2,3/2}\rightarrow nd^2D_{3/2,5/2}$ transitions, relativistic calc. 79−89609
In I, Rydberg series, disctete levels and continua of finite bandwidth 78−74603
In ions, analytical HF solns. for ground and excited states 77−72835
In, quadrupole antishielding factors, Hartree-Fock perturbation theory 78−62723
In($^2P_{3/2}$), at. quadrupole shielding factor 79−10222
Ir, hyperfine interaction parameters, effect of local exchange, Xα and HF calcs. 78−78622
K, ^2P fine struct. splittings, Hartree-Fock calcs. 77−10606
K, excited np states, fine struct., core electrons effect 77−18807
K, inner core neutral atom binding energy, relaxed-orbital relativistic Hartree-Fock-Slater calc. 78−13433
KCl, charge transfer and pair polarisability anisotropy 80−43173
KCl, polarisability, near-Hartree-Fock limit SCF MO calc., bond length 78−42239
KCl:$In^+(Tl^+)$, HF calc. for ground and excited states of impurity centre 77−72835
KCl(Br)(I), U_2 and U_1 centres, optical excitations 80−2803
KOH, MHD plasma mol., pot. energy curves and dipole moment, bond lengths 78−71462
$^{39}K(^{39}K,X)$, π^0 condensation, spin-isospin instabilities, TDHF calcs. 80−83042
Kr, elastic positron scatt., phaseshifts and elastic, diffusion and annihilation cross section 80−53134
Kr, electron scattering, elastic, low-energy, polarised-orbital calcs. 80−37882
Kr, inner electron energy characteristics, validity of Hartree-Fock-Pauli approx. 80−42957
Kr, large angle elastic and inelastic electron scatt. differential cross section, exchange corrections 80−28111
Kr, shake-up energies, Slater transition-state calcs. 79−89651
Kr VIII, excited state energies and lifetimes, beam foil spectra 80−63591
La, ground state, two band Hubbard model, for almost mixed valence system 78−84171
La, term dependence of position of 4f electton in $4d^94f$ configuration 77−26973
$^{139}La(^{86}Kr, X)$, TDHF fusion calcs., fusion cross sections 80−37409
$^{139}La(^{86}Kr,X)$, 505, 610, 710 MeV, TDHF calcs., fusion behaviour 80−9323
Li, ^2P-state, hyperfine structure, UHF and PHF methods calcs. 79−36517
Li (100), O adsorption, cluster models, ab initio HF LCAO theory 78−71978
Li Al, electronic struct., mol. cluster calc. 78−14649
Li, and isoelectronic sequence, correlated and HF electron density differences 78−46275
Li, and isoelectronic series, photoionisation resons. characts., Z depend. 77−50412
Li, at. HFS, unrestricted and projected Hartree-Fock methods 79−63924
Li, autoionisation spectrum, theory *(Spanish)* 79−89647
Li cluster, chemisorption of H, ab initio HF calcs. 77−76670
Li, core charge polarisation 79−45627
Li, correlation energies, Hartree-Fock Hamiltonian 78−41965
Li, cryst. and electronic props., Hartree-Fock calcs. 79−60698
Li H^-, mol. orbital calcs., diffuse functions for basis sets, electron affinity 78−25436
Li, highly excited states, electronic struct., oscillator strengths and resons., HF calcs. 77−46506
Li, hyperfine coupling, in ground and excited states, Green's function calcs. 77−6692
Li, isoelectronic sequence, transition probabilities, relativistic effects calcs. 77−27028
Li isoelectronic sequence, theoretical oscillator strengths *(French)* 77−34586
Li isoelectronic sequence, quartet states hyperfine consts., Hartree-Fock and CI calcs. 78−919
Li isoelectronic sequence, 1s2s3p $^4P^0$ state, nuclear charge expansion 78−37569
Li isoelectronic sequence, Hartree-Fock eqns., perturbation calcs. 79−6846
Li isoelectronic sequence, doubly-excited states, relative ordering 79−31424
Li, isoelectronic series, doubly excited states, Hartree-Fock energy 79−22613
Li, isoelectronic series, Hartree-Fock line strengths 78−9122
Li isoelectronic series, quartet states, HF and CI calcs. 78−17582
Li isoelectronic series, relativistic pseudopot. appl. in HF calcs. 80−27960
Li, local orbital energy bands using Kohn-Sham and near Hartree-Fock exchange 78−30866
Li, perturbed Hartree-Fock wavefunctions for ^2S and ^2P states 79−10033
Li, SCF ion improved virtual orbitals, excited configs. calcs. 77−10585
Li to Ne, coreless Hartree-Fock pseudopotential method 79−68188

HF calculations continued
Li^+ 2p3d $^{1,3}L^0$ doubly excited state, soln. of Hartree-Fock eqns. 77−75072
Li^+ ion complexes with HF, H_2O, and NH_3 solvent molecules, structural and electronic props. calc. 77−57873
Li^+, numerical Hartree-Fock calc. of $1s^2$ ground state 79−81155
Li-like atoms, $^4S^e$ doubly excited states, orbital config. assignment 79−41118
Li-like ions, fine struct. in $1s2p^2\ ^4P$ and $1s2s2p\ ^4P^0$ states 78−66471
$Li+H_2$, inelastic collision, ab initio pot. energy surface 79−10055
$Li+H_2$, rot. and vibr. transitions, close-coupling calcs. 77−58136
Li+He, direct excitation of Li I (nl) levels in keV collisions 78−90280
Li^{3+}+He(C)(Ne), K-shell charge transfer cross sections, Bates-Born formalisms 79−45834
Li_2, and anion, electronic struct., spin-unrestricted, spin-restricted SCF HF calc. 78−90331
Li_2, floating spherical Gaussian orbital, Hartree-Fock-Roothaan and pseudopot. calcs., comparison 78−46262
Li_2, lowest $^1\Pi_g$, $^1\Pi_u$, $^3\Pi_g$, $^3\Pi_u$ states 77−54517
Li_2, pot. energy surface, half-projected HF model 79−36564
Li_2, $X^1\Sigma_g^+$ and $A^1\Sigma_u^+$ states, electronic struct. and spectra 79−89615
Li_3, potential energy surface and config., RHF CI calc. 77−34562
Li_3, spin density, Gaussian basis set 78−33427
Li_3, spin populations, restricted Hartree-Fock calcs. 77−57906
$LiBeF_3$, pot. energy surface, struct., stability and internuclear distances, ab initio calc. 80−58147
$LiBeH_3$, ab initio calc. of pot. surfaces and geometry 79−10024
LiCl, aqueous soln., self consistent wavefunctions, HFS Xα pot. in cluster model, Compton profile calc. 79−78783
LiCl, charge transfer and pair polarisability anisotropy 80−43173
LiCl, polarisability bond length depend. 77−23422
LiF, elastic electron scatt. intensity, rel. to electron density distrib. 78−1079
LiF, F-centres, defect electron struct., extended-ion model calcs. 80−59907
LiF, $X^1\Sigma^+$ state, many-body effects, HF STO calcs., diagrammatic perturbation theory 77−50355
LiF(LiF^-), electron affinity and dipole moment, ab initio calc. 78−41938
LiH, half-projected HF scheme, stability conditions 77−61676
LiH, Hartree-Fock density matrix equation, soln. 77−14339
LiH, layers and solid, localised HF orbitals 78−9076
LiH, NMR shielding consts. and mag. susceptibilities, coupled HF with extended GTO basis 80−5480
LiH, one electron props., Xα multiple scattering wave functions 80−42945
LiH, polarisabilities and dipole moment derivatives, virial theorem calcs. 77−57865
LiH, solid. Hartree-Fock energy band calc. using OPW method 80−10856
LiH^+, spin-extended Hartree-Fock ab initio calculations for small radicals 78−70746
LiI, Mossbauer charge density of $^{129}I^-$ 79−61275
LiNa, and anion, electronic struct., spin-unrestricted, spin-restricted SCF HF calc. 78−90331
Li_2O, elastic electron scatt. intensity, rel. to electron density distrib. 78−1079
Lu III, 6s $^2S_{1/2}$-6p $^2P^\circ_{1/2,3/2}$ transition, relativistic oscillator strengths, influence of core polarisation 80−58132
Lu, valence orbitals, Dirac-Fock scheme, direct and indirect relativistic effects 78−41969
Mg I, $^3F^0$ Rydberg series, energy levels, multiconfigurational HF procedure 80−47882
Mg, intercombination line oscill. strength, including core-polaris. and relativistic effects 78−25475
Mg, ion-induced Auger electron emission, depend. on ion energy 79−78814
Mg, isoelectronic sequence, excitation energies and line strengths, MC Hartree-Fock calcs. 77−83658
Mg isoelectronic sequence, static dipole quadrupole polarisabilities and shielding factors calc. using HF scheme 80−99450
Mg, isoelectronic series, D-F transitions, Mg sequence, D-F transitions oscillator strengths 79−54809
Mg^{2+} atomic core states, antishielding effects calcs. 80−83299
Mg^{2+} ion complexes with HF, H_2O, and NH_3 solvent molecules, structural and electronic props. calc. 77−57873
MgF_2^-, ground state, conform., electron affinity, extended basis SCF calcs. 79−72253
$Mg_4(Mg_4^-)$, atomic clusters, electronic struct., LCAO-MO-SCF and HF calcs. 80−63880
$MgO(MgO^-)$, electron affinity and dipole moment, ab initio calc. 78−41938
^{23}Mg, even parity state, EM props., collective struct., generator coord. method, HF method anal. 79−89220
^{24}Mg, HF microscopic anal. of core struct. for deformed nucleus 78−78294
^{24}Mg(p,p'), 49.5 MeV, consistent folding model, HF calc. for E2, E4 transitions 79−22288
^{24}Mg(p,p') 17.5 MeV 79−22288
^{26}Mg, 2_1^+ state quadrupole moment in band mixed HF model 80−52578
Mn I inner shell absorpt. spectrum, 3d wavefunction collapse 77−23455
Mn^{2+}, electron exchange pot. simplification 77−75054
$Mn^{2+}F^-$ and $Mn^{2+}F^-Mn^{2+}$ systems, transferred hyperfine interaction at F^- site 80−70657
MnO_4^-, valence mol. orbital energy, nonempirical pseudopot. 79−22592
Mo even isotopes, HFB calc. of deform. due to isoscalar n-p interaction 78−74302
Mo ions, X-ray emission spectra, from laser produced plasma, line identification via HF calcs. 78−33459
Mo, X-ray spectra, Kα hypersatellites 80−63576
Mo XIV, spectrum and energy levels, ionisation energy 79−49954
^{A}Mo, A=98-110, deformation and shape transition, HFB calcs. 79−93502
N, ground state energy, HF calc., second-order correction 78−86784
N_2, core ionisation, single orbital relax. energy contrib. calcs. 78−82637
N_2, core photoelectron line shape, localisation role 79−59512
N_2, correlated electron density using AHF GTO wavefunctions 80−23313
N_2, elastic and inelastic electron scatt. differential cross section, obs. and calc., struct., binding energy 80−28109
HF calculations continued
N_2, electron density distrib., electron correl. effects, approx. HF-CI calcs. *(German)* 78−33439
N_2, HF calcs., compared with optimised LCAO results 78−5139
N_2, large angle elastic and inelastic electron scatt. differential cross section, exchange corrections 80−28111
N_2, matrix HF calcs. using universal basis sets 79−59354
N_2, Raman intensities calcs., ab initio method 80−52993
N_2, Raman intensity, ab initio calc. 80−1028
N_2, static polarisabilities, ab initio SCF HF calcs., internucl. separation depend. 78−9073
N_2, vertical valence ionis. pot. calc., by perturbation, CI and CPA techniques 80−69263
N_2, vibr. struct., core and valence ESCA spectra, Franck-Condon and HF anal. 80−32602
N_2, X-ray K-absorpt. spectra, vibr. fine struct., ab initio restricted HF calc. 78−86883
N_2, X-ray K-absorpt. spectra, reson. obs., near fine struct. 80−37817
N_2+He^+, K-shell ionisation, total cross-sections calcs. 79−31663
NCNO⇌NC+NO, ground state pot. energy surface, ab initio calcs. 77−90593
NH_2^+, quintet states, pot. energy surfaces, ab initio SCF MO calc. 78−25419
NH_3, elec. dipole polarisability, coupled and uncoupled Hartree-Fock calcs. 77−34539
NH_3, first triplet state, photodissoc. and Rydbergisation investig. 80−53067
NH_3, freq. depend. hyperpolarisability, time-depend. Hartree-Fock calcs. 79−36559
NH_3, HF geometry calcs. and SCF calcs. 80−47877
NH_3, lone pair contributions to the IR intensities 80−63630
NH_3, mag. susceptibility, HF perturbation method 77−79702
NH_3, NH_3^+ ion, electrostatic force theory appl. to mol. geometry ab initio verification 79−98002
NH_3, nucl. elec. shielding tensor calcs. 80−83296
NH_3, proton mag. shielding const., HF perturbation theory 78−46258
NH_3^+, ionisation pot. of ^2E state, Jahn-Teller effect 78−62948
$^{15}NH_3$, nucl. spin-spin coupling consts. calc., vibr. averaging effects 78−33521
NH_3+2H_2, triplet n3S Rydberg state, ab initio UHF CI SCF calc. 80−53095
$NH_2(F_2)(Cl_2)$, SCF-MO-HF calc., struct. and one-electron props., population anal. indices 79−76338
NO, core photoelectron line shape, localisation role 79−59512
NO_3, mag. hyperfine interactions, MO LCAO UHF calcs. 77−14369
NO_3^{2-}, coupling consts., geometry, LCAO UHF and ENDOR data calcs. 77−14369
$^{14}N+^{12}C$, 112 MeV, alpha clustering, multiple shape vibrs., TDHFC calcs. 79−3164
$^{14}N+^{12}C$, direct inelastic scatt. in 3-dimens. time depend. HF scheme 79−17925
$^{14}N+^{12}C$, TDHF appl. 78−54709
$^{14}N+^{12}C$, time-depend. Hartree-Fock calcs. 77−46125
$^{15}N(^{15}N,X)$, π^0 condensation, spin-isospin instabilities, TDHF calcs. 80−83042
Na, ^2P fine struct. splittings, Hartree-Fock calcs. 77−10606
Na core polarisation effect on oscillator strengths and energy level locations 78−82688
Na, excited np states, fine struct., core electrons effect 77−18807
Na, inner core neutral atom binding energy, relaxed-orbital relativistic Hartree-Fock-Slater calc. 78−13433
Na isoelectronic sequence, theoretical f-values 78−37593
Na isoelectronic series, Hartree-Fock line strengths 78−9122
Na, photoionis. cross section resons., time-dependent HF theory 80−32684
Na^+, atomic core states, antishielding effects calcs. 80−83299
Na^+ ion complexes with HF, H_2O, and NH_3 solvent molecules, structural and electronic props. calc. 77−57873
Na-like ions, transition probabilities for reson. transitions 78−66494
Na_2, and anion, electronic struct., spin-unrestricted, spin-restricted SCF HF calc. 78−90331
NaCl, interatomic Auger processes 77−85892
$NaCl^-$, mol. orbital calcs., diffuse functions for basis sets, electron affinity 78−25436
NaCl(Br)(I), U_2 and U_1 centres, optical excitations 80−2803
NaF, ab-initio calc. of cohesion energy, compressibility and density 78−71782
NaF(NaF^-), electron affinity and dipole moment, ab initio calc. 78−41938
NaH^-, mol. orbital calcs., diffuse functions for basis sets, electron affinity 78−25436
^{A}Na, (A=21, 23), even parity state, EM props., collective struct., generator coord. method, HF method anal. 79−89220
^{23}Na high spin positive parity state, approx. microscopic methods, shell model comparison 79−85352
^{23}Na, S states, HFS, many body perturbation technique 77−68023
Ne, 40 keV electron scatt., 7-200 mrad, relativistic and electron correlation effects 77−34760
Ne, at. struct. by many-body perturbation method, algebraic approx. 77−18776
Ne, atomic polarisabilities and shielding factors, coupled HF approx. 78−22048
Ne, atomic struct. calc., symmetry adapted pair functions, Rayleigh Schrodinger HF variational perturbation theory 80−42944
Ne, Auger energies, intensities, for initial K vacancy, many body calc. 77−18869
Ne, converged $E^{(2)}$ values 78−66479
Ne, energy density functional, gradient corrections 78−25428
Ne, ground state wavefunction, SCF HF calc. 78−90070
Ne, momentum eigenfunctions in complex momentum plane, Hartree Fock functions 80−63517
Ne, second-order correl. energy calcs. 78−33436
Ne, shake-up energies, Slater transition-state calcs. 79−89651
Ne, temp. perturbed Thomas Fermi eqn., variational principle 80−69074
Ne, total muon capture rates using HF wave functions 80−63135
Ne, vertical valence ionis. pot. calc. by perturbation, CI and CPA techniques 80−69263
Ne^+, converged $E^{(2)}$ values 78−66479
Ne-like atoms and ions, gradient expansion of atomic kinetic energy functional 80−95530
Ne-like ions, E1 and M2 transitions, HF calcs. 79−59401

HF calculations continued
Ne_2, pair polarisability tensor, extended Gaussian basis set, perturbation coupled HF calc. 77−75058
Ne_2, short range interactions between two rare gas atoms 79−26888
^{A}Ne, (A=19,21) , even parity state, EM props., collective struct., generator coord. method, HF method anal. 79−89220
^{20}Ne, basis states generation by variational methods 78−78295
^{20}Ne, deformed nucleus, quadrupole moment, HF calc. exponential convergence and acceleration 79−85367
^{20}Ne, HF microscopic anal. of core struct. for deformed nucleus 78−78294
^{20}Ne, moment of inertia from cranked HF method 80−102098
^{20}Ne, nuclear current from cranked HF solns. 80−9241
^{20}Ne, rotational moment of inertia, cranked HF formalism with Skyrme force 77−30477
$^{20}Ne+^{58}Ni$, 164 MeV, alpha clustering, multiple shape vibrs., TDHFC calcs. 79−3164
$^{20}Ne(^{20}Ne,X)$, 132 MeV, TDHFB calc. for total fusion cross section 80−13521
$^{20}Ne(p,p')$ 24.5 MeV, consistent folding model, HF calc. for E2, E4 transitions 79−22288
Ni (VIII), semiempirical investigation of spectra 78−33434
Ni (100), chemisorption of first row atoms, molecular cluster theory 77−1309
Ni (100), chemisorption of CO, Hartree-Fock-Slater mol. cluster calcs. 79−51650
Ni, adsorbed CO, core level spectrum, satellite struct., ab initio HF-LCAO calc. 80−40233
Ni, adsorption of CO, binding and energy level shifts, NiCO and Ni_2CO electronic struct. 78−34882
Ni, chemisorption of H, Xα cluster calcs. *(Japanese)* 78−72002
Ni I isotope shift for stable isotopes, nuclear charge radii 80−99484
Ni:He, defect props., quantum-chemical and lattice-defect hybrid approach 79−4528
Ni-Cr(V)(Co)(Mn)(Mo)(Ru)(Fe), spin wave stiffness consts., RPA CPA band model 79−61088
Ni-Cu, ferromag., mag. moment, local environment effects, HF CPA cluster calc. 80−65817
Ni-Mn alloys, ferromagnetism-to-spin glass phase transition and strong mag. field effect 80−75773
Ni-Pd(Pt) mag. props., average and local density of states, CPA calc. 77−59242
Ni+Ni, beam-foil collisions, X-ray transitions between correl. many electron quantum states 77−79689
Ni+Ni, exchange interactions and exchange integrals 80−37849
Ni_2, Hartree-Fock-Slater calcs., using pseudopot. method 77−57859
β'-NiAl, self consistent embedded cluster model for Fe, Co, Ni mag. impurities 80−2549
NiCO, and core ionised, binding and relax. energy ab initio LCAO MO SCF calc. 78−62712
$Ni(CO_4)$, ionisation energies, approx. SCF Hartree-Fock-Slater calcs. 77−75334
$NiCl_4^{2-}$, charge distrib. and ligand field splitting calc. 77−62879
NiCu molecule, electronic states determ. by ab initio HF and CI methods 80−69087
NiH, pot. energy curves, Hartree-Fock and valence bond methods 78−41958
NiH_2, pot. energy curves, Hartree-Fock and valence bond methods 78−41958
NiNO, ground and core hole states, config. depend. HF LCAO SCF calc., relax. and binding energy 80−29453
NiO (001) surface, chemisorption of H, surface and second-layer defect effects 80−65369
NiO, cluster model, unrestricted Hartree-Fock calcs. 77−85125
NiO, H chemisorption, cluster model, bonding 78−38939
NiO, H chemisorption, perfect surfaces, cation vacancies, self-consistent HF-VB calcs. 79−69351
NiO, self consistent energy band calc. 78−23022
NiVI, sixth spectrum analysis 220-335 and 890-1325 Å regions 80−95565
^{56}Ni formation cross section, TDMF calcs. for fusion in $^{16}O+^{40}Ca$ and $^{28}Si+^{28}Si$ 79−93676
^{58}Ni, charge density, HF calcs. from (e,e) data 79−89260
^{58}Ni, HFB and dynamic anal., collective motion, zero point energy correction 80−18161
^{58}Ni, nuclear radii, energy density and HF-BCS methods 80−47363
^{60}Ni, electron elast. scatt. cross sections, phase shift anal. and HF calcs. *(Russian)* 78−41707
O, ground state energy, HF calc., second-order correction 78−86784
O Hartree Fock pot., truncated space calcs. of exact bound state energies 79−3090
O_2, core photoelectron line shape, localisation role 79−59512
O_2 molecule, UHF description of ground and lowest singlet states 78−90056
O_2, multiconfig. Hartree-Fock calcs. convergency 80−47901
O_2, photoexcitation and photoionisation cross sections, HF Gaussian method 80−53064
O_2, RH-GTO-MCSCF calc., 1s photoelectron spectra, multiplet intensity ratio 78−5134
O_3, ab initio projected unrestricted Hartree-Fock calcs. 78−58582
O_3, ab initio UHF and UHF-natural orbital CI studies 80−102452
O_3, approximate spin extended HF calcs., singlet and triplet states 78−78621
O_3, conformation, ab initio HFS method calc. 79−36526
OCl_2^+, radical cation, struct. and electronic props., ab initio RHF SCF MO calc. 80−52883
OH, spin-extended Hartree-Fock ab initio calculations for small radicals 78−70746
$^{A}O(^{12}C,X)$, A=16,18, fusion cross sections by TDHF calcs. 79−89342
^{16}O, adiabatic mass parameters, isoscalar quadrupole modes 77−14049
^{16}O, Brueckner-Hartree-Fock calcs. with Δ resonance inclusion in one-boson-exchange potential 77−54155
^{16}O, Brueckner-Hartree-Fock approach, variational definition of single particle pot. 80−32170
^{16}O, charge form factors, of doubly closed shell nuclei 77−6274
^{16}O energy states, HF calcs. using cartesian basis wave functions 78−74319
^{16}O, Hartree-Fock calculations of nuclear bulk properties with density- and starting-energy dependent effective interaction 80−9246
^{16}O, isoscalar giant monopole vibrs., time-depend. HF calc. 77−22986

HF calculations continued
^{16}O, mesonic and isobar degrees of freedom, Brueckner Hartree Fock calc., binding energy 79−63600
^{16}O, monopole vibration damping, TDHF calcs. 80−22667
^{16}O, nuclear incompressibility, Hartree-Fock calc. *(Russian)* 79−49577
^{16}O, nucleon-nucleon scatt., correlations, short-range, with pseudopotentials 78−37225
^{16}O, pion-exchange contribs. to charge densities, HF calcs. 78−46001
^{16}O, relativistic Hartree-Fock eqns., 1 boson exchange pot., spin orbit splitting 79−3106
^{16}O, vibrating nucleus, adiabatic anal. of time-dependent HF solns. 79−40863
$^{16}O+^{12}C$, 45-80 MeV, fusion cross sections using time-of-flight technique, TDMF calcs. 78−94043
$^{16}O+^{16}O$, 2- and 3-dimens. time depend. HF calc. comparison 79−17948
$^{16}O+^{16}O$, 3-d TDHF calcs. 78−54781
$^{16}O+^{16}O$, 3-dimens., time depend. HF calcs. for fusion cross sections 78−66318
$^{16}O+^{16}O$, 3D TDHF calcs. 78−626
$^{16}O+^{16}O$, 35-80 MeV, fusion cross sections using time-of-flight technique, TDMF calcs. 78−94043
$^{16}O+^{16}O$, 384 MeV, alpha clustering, multiple shape vibrs., TDHFC calcs. 79−3164
$^{16}O+^{16}O$, 64, 80 MeV, fusion events, time dependent HF calcs. 79−36292
$^{16}O+^{16}O$, direct inelastic scatt. in 3-dimens. time depend. HF scheme 79−17925
$^{16}O+^{16}O$, total fusion cross section, time depend. HF calcs. 79−17945
$^{16}O+^{16}O$ collisions, 105 MeV, appl. of 3-dimens. time-depend. HF calcs. 78−66317
$^{16}O+^{4}He$, 3-D TDHF calcs. 78−54781
$^{16}O(^{16}O,x)$ reactions, time dependent HF calcs. 77−54251
^{17}O, M3 suppression in HF theory 78−33134
$^{17}O(e,e)$, mag scatt., form factors, HF calcs., core polarisation effects 80−42579
^{18}O, effective interaction, Hartree-Fock effects 78−534
^{18}O, modified HF calcs. for low-lying collective states 77−22916
^{22}O, Hartree-Fock calculations of nuclear bulk properties with density- and starting-energy dependent effective interaction 80−9246
P, two and three-electron Auger transition, with vacancies in 2p-shell 79−63972
PH_3, NMR shielding consts. and mag. susceptibilities, coupled HF with extended GTO basis 80−5480
PH_3, second order mag. props., coupled Hartree-Fock perturbation theory 80−87042
P_2H_4, conformation, ab initio, HF, PNO-CI and CEPA calcs. 77−46495
$PH_2(F_2)(Cl_2)$, SCF-MO-HF calc., struct. and one-electron props., population anal. indices 79−76338
PN, valence state interactions, ab initio and semiempirical estimates 78−74567
$P(P^+)(P^{2+})$, static quadrupole polarisability and shielding factor, Hartree-Fock calc. 78−41950
Pb, relativistic 1s wavefunctions test, using exptl. Compton profiles 80−32600
PbO, appl. of effective pots. to relativistic HF calcs. of mol. props. 78−74559
^{208}Pb, neutron and proton surface thickness, HF calcs. 77−71557
^{208}Pb, nuclear radii, energy density and HF-BCS methods 80−47363
^{208}Pb, pion-exchange contribs. to charge densities, HF calcs. 78−46001
$^{208}Pb+^{208}Pb$, 1600 MeV, axially symmetric TDHF 78−74398
$^{208}Pb+^{208}Pb$, 7.4 MeV, time depend. Hartree Fock theory test 79−49591
$^{208}Pb+^{208}Pb$ deep inelastic processes, TDHF and elementary modes of excitation 79−63695
$^{208}Pb(N,N)$, <30 MeV, microscopic optical pot. in nuclear struct. approach, HF field 80−527
$^{208}Pb(e,e')$, 50 to 335 MeV, mag. spin state excitation cross section 78−50155
Pd clusters, density of states profiles, Hartree-Fock-Slater model 77−31930
Pd-Pt alloys, mag. props., average and local density of states, CPA calc. 77−59242
$Pd(CO_4)_4$, valence mol. orbital energy, nonempirical pseudopot. 79−22592
$^{118}Pd+^{118}Pd$, 637 MeV time depend. Hartree-Fock-Bogoliubov calc. for fusion and subsequent ^{236}U fission 79−36265
Pr^{3+}, correlation contributions to nuclear antiscreening factor, many-body calc. 79−56153
PsO, stability and dissoc. energy, restricted HF and correlation correction calcs. 77−54634
PsS, stability and dissoc. energy, restricted HF and correlation correction calcs. 77−54634
Pt, ground state configs., ab initio HF calcs. 80−42987
Rb, excited np states, fine struct., core electrons effect 77−18807
Rb I, 4p subshell excitation spectra, 15 to 19 eV, a new interpretation 79−779
Rb, inner core neutral atom binding energy, relaxed-orbital relativistic Hartree-Fock-Slater calc. 78−13433
Rb, ionisation energies and oscill. strengths calcs. 80−5488
Rb, valence-core electron exchange interactions, local approx. 80−91416
RbI isoelectronic series, oscill. strengths, relativistic HF calcs. 79−98035
Re_3Cl_9 metal cluster complexes, He(I) photoelectron spectrum, SCC DV Xα calcs., $Re_2Cl_8^{2-}$ comparison 80−28063
Ru complex, HF calc., electron densities and Mossbauer isomer shift, chemical binding 78−50470
Ru, hyperfine interaction parameters, effect of local exchange, Xα and HF calcs. 78−78622
S, two and three-electron Auger transition, with vacancies in 2p-shell 79−63972
S_3, conformation, ab initio HFS method calc. 79−36526
SBr_2, transient species, He(I) photoelectron spectroscopy, discrete variational HFS calc. 79−31594
SCN^-, electron density distrib., theoretical and expt. determ. 77−61683
SF_6, ionisation pot., discrete variational Xα calc., Slater-type orbitals in Hartree-Fock basis 78−78837
SH_3^+, struct., ab initio HF calcs. 79−31371
$(SN)_x$, 1-D chain, ab initio treatment, HF LCAO calc. 77−1349
$(SN)_x$, electronic props., ab initio LCAO HF orbital calc. 77−51635
$(SN)_x$, quantum chem. calcs. of electronic struct. 78−6257

HF calculations continued
S_2N_2, $(SN)_x$, (x=2 or 3), minimal STO-3G basis HF ab initio LCAO SCF MOC, geometry 78−903
SO_3, dissoc. pathways and mol. vibr., compliance consts. and min. energy coords. 78−35661
^{32}S, nuclear radii, energy density and HF-BCS methods 80−47363
Sb VII, $4d^9$, $4d^85p$ configurations, spectra analysis 79−54794
Sc I, hyperfine struct., far-config.-mixing effects 77−42240
ScH_3, valence mol. orbital energy, nonempirical pseudopot. 79−22592
^{A}Sc A=44,46,48, HF projection formalism, energy levels, static moments, EM transition probabilities 79−3083
^{A}Sc, A=45, 47, HF projection formalism, energy levels, EM moments, transition probabilities 79−22199
^{41}Sc-^{41}Ca Coulomb displacement energy, HF calcs. 80−42527
Si $^3P\rightarrow{}^1D$ electron impact excitation, distorted wave approx., exchange and polaris. effects 77−34764
Si (111), chemisorption of H, localised model, ab initio HF-LCAO calc. 80−6930
Si (111), electronic states and initial steps in oxidation 78−91534
Si (111) inversion layers, CDWs, effect of four valley interaction terms 79−33324
Si (111) surface, relax. of surface atoms, Si_4H_9 clusters 77−35980
Si, (111) surface, 2×1 reconstruction mechanism 77−66079
Si, ab initio effective pots. 77−69222
Si, electron-hole drop transition to metallic condensed state, Hartree-Fock theory 79−56136
Si, first order density matrix, effective core pot. valence electron UHF method 77−30786
Si III, $^3F^0$ Rydberg series, energy levels, multiconfigurational HF procedure 80−47882
Si, ion-induced Auger electron emission, depend. on ion energy 79−78814
Si, Rydberg series electronic struct. 79−22614
Si, two and three-electron Auger transition, with vacancies in 2p-shell 79−63972
Si_2, charge density and pseudo charge density, pseudopot. and SCF calcs. 78−70740
SiCH, matrix Hartree-Fock calcs. 79−5874
SiF_3, low-lying electronic states, ab initio HF calcs. 77−54512
SiH_4, ab initio Hartree-Fock SCF-LCAO-MO method 78−94195
SiH_4, mol., valence and core ionis. energy, RHF-SCF and PNO-CEPA calc. 79−85890
SiH_4, second order mag. props., coupled Hartree-Fock perturbation theory 80−87042
SiH_4, SiH_3F, SiH_2F_2, CH_3SiH_3, core Auger shifts, ab initio LCAO MO SCF calcs. 78−904
Si_2H_6, barrier to internal rotation 78−66680
SiH_2F_2, ab initio Hartree-Fock SCF-LCAO-MO method 78−94195
SiH_3F, ab initio Hartree-Fock SCF-LCAO-MO method 78−94195
SiO_x, chem. shift of Si 2p core level, relax. contrib. 79−47141
$Si(Si^+)$, static quadrupole polarisability and shielding factor, Hartree-Fock calc. 78−41950
^{27}Si, shape mixing using ang. momentum projection from Hartree-Fock intrinsic states 78−86472
^{28}Si, appl. of theory of bi-determinantal intrinsic states 79−9484
^{28}Si, deformed nucleus, quadrupole moment, HF calc. exponential convergence and acceleration 79−85367
^{28}Si, generator coord. calc. 77−50073
^{28}Si HF microscopic anal. of core struct. for deformed nucleus 78−78294
^{30}Si, 2_1^+ state quadrupole moment in band mixed HF model 80−52578
Sm I ^{144}Sm-^{152}Sm isotope shift J depend., in ground term. 77−75101
^{150}Sm deformation, collective spectra and moments of inertia starting from nuclear force 79−17790
^{152}Sm, HF one body density for core and valence nucleons 78−78294
^{154}Sm, Skyrme-HF calcs., deformation, electric moments, spin-orbit potentials 78−62480
Sn ions, analytical HF solns. for ground and excited states 77−72835
SnH_2, struct. determ., restricted HF calcs. 80−87030
Sr I, strong configuration interaction, multiconfiguration Hartree-Fock calcs. 77−67987
Sr I excitation series, potential barrier effects, single configuration HFC 80−78558
Tc I, atomic spectra, mag. HFS splitting of ground level explained by spin-core polarisation 77−68002
Te VIII, $4d^9$, $4d^85p$ configurations, spectra analysis 79−54794
ThO_2, electronic struct. and bonding, molecular cluster approx. 77−51657
Ti, $4s3d^3$ and $3d^4$ states, HF descriptions, alternative orbital config. 80−63534
Ti, A=44-50, effective charges and E2 transitions in 1f-2p shell nuclei 78−544
Ti I, hyperfine struct., far-config.-mixing effects 77−42240
Ti:C, molecular cluster approach to electronic struct. and bonding mech. for impurity C 77−20270
$TiCl_4$.trimethylaluminium+ethylene, Zeigler-Natta reaction mechanism, restricted Hartree-Fock calcs. 77−73441
TiH_3F, valence mol. orbital energy, nonempirical pseudopot. 79−22592
TiO, Hartree-Fock and local exchange energy bands, disagreement of results 77−76724
TiO, soft X-ray spectra and XPS, Xα and Hartree-Fock calcs. discrepancies 79−77979
^{48}Ti(e,e), elastic and inelastic scatt. cross-sections from Hartree-Fock densities *(Russian)* 79−13287
^{48}Ti(p,p), elastic and inelastic scatt. cross-sections from Hartree-Fock densities *(Russian)* 79−13287
Tl I, oscillator strengths for $np^2P_{1/2,3/2}\rightarrow(n+1)^2S_{1/2}$ and $np^2P_{1/2,3/2}\rightarrow nd^2D_{3/2,5/2}$ transitions, relativistic calc. 79−89609
Tl I, Rydberg series, disctete levels and continua of finite bandwidth 78−74603
Tl ions, analytical HF solns. for ground and excited states 77−72835
Tl, valence orbitals, Dirac-Fock scheme, direct and indirect relativistic effects 78−41969
U I, electronic configs., HF relativistic calc., spin-orbit const.-Slater integral relation 77−18793
U, relativistic Dirac-Slater calcs. *(Japanese)* 77−42252
U^++U^+, critical two-centre distance, HFS relativistic calc. 79−22801
UF_5, electronic struct., Hartree-Fock-Slater and Dirac-Slater calcs. 79−31370
UF_5, electronic struct. calc. 80−6716

HF calculations continued
UF_6, electronic struct., non-relativistic Hartree-Fock-Slater method 78−50469
UI plasma, absolute emission coeff. 80−64693
UO_2, electronic struct. and bonding, molecular cluster approx. 77−51657
$^{238}U(^{238}U,X)$, 7.5 MeV/A, 3-dimens. TDHF-BCS model calcs., possible fission 80−52694
$^{238}U(e,e')$, scatt. from octupole band, HF calc. of intrinsic equilib. density 78−37333
V, A=47-51, effective charges and E2 transitions in 1f-2p shell nuclei 78−544
V, electron distribution 78−75979
V isotopes, A=47-51 78−25114
$V^{2+}F^-$, $V^{2+}F^-V^{2+}$ π-electron systems, transferred hyperfine interaction, HF calc. 80−24859
VO_4^{3-}, charge transfer transition, bond length effects calcs. 77−83721
V_2O_3 insulating phase, realistic Hartree-Fock calc. 79−38306
W (001), chemisorption of H, HF Green's function formalism and phase shift technique 80−24733
W, chemisorption of H_2, HFS model cluster calcs. 77−51795
W, quadrupole moment calc. using HF method *(Russian)* 80−13375
^{A}W, A=182-186, deformation hexadecapole moments, Hartree-Fock calcs. *(Russian)* 80−63081
Xe, $5p^5ns$, $5p^5np$, $5p^5nd$ and $5p^54f$ config., HF calc. 77−23468
Xe, $5s^2$ subshell, discrete excitations, generalised oscill. strength calcs. 77−65441
Xe, ab initio effective core pot., Dirac-Hartree-Fock and Hartree-Fock calcs. 78−33426
Xe, elastic positron scatt., phaseshifts and elastic, diffusion and annihilation cross section 80−53134
Xe, electron scattering, elastic, low-energy, polarised-orbital calcs. 80−37882
Xe II $5s5p^6\ ^2S_{1/2}$ state, lifetime meas. 79−13670
Xe, inner electron energy characteristics, validity of Hartree-Fock-Pauli approx. 80−42957
Xe like ions (I^-, Cs^+, Ba^{2+}, La^{3+}) $3d^94f$ config., collapse of 4f electron, X-ray spectral obs. *(Russian)* 80−58204
Xe, photoelectron branching ratio in 4d subshell 79−18164
Xe, relativistic Hartree-Fock calcs. using spherical Gaussian basis sets 80−32595
Xe subshell photoionisation, multichannel k-matrix calc., spin orbit interactions 80−63600
Xe, term dependence of position of 4f electron in $4d^94f$ configuration 77−26973
Xe_2, effective core pot., Hartree-Fock calc., relativistic and nonrelativistic effects 78−46281
Xe_2^+, effective core pot., Hartree-Fock calc., relativistic and nonrelativistic effects 78−46281
XeF, effective core pot., Hartree-Fock calc., relativistic and nonrelativistic effects 78−46281
Yb II, 6s $^2S_{1/2}$-6p $^2P^\circ_{1/2,3/2}$ transition, relativistic oscillator strengths, influence of core polarisation 80−58132
Yb, quadrupole moment calc. using HF method *(Russian)* 80−13375
^{A}Yb, (A=168, 170), angular momentum fluctuation energy in the cranking model 79−89254
^{A}Yb, A=166, 168, 170, backbending and moment of inertia in HFB cranking method 80−42521
^{A}Yb, A=168, 170, approximate ang. momentum projection from cranked HFB wave functions, yrast energies 79−30776
^{A}Yb, A=168-176, deformation hexadecapole moments, Hartree-Fock calcs. *(Russian)* 80−63081
^{160}Yb double backbending and rot. states, HFB cranking model anal. 80−32155
^{160}Yb yrast levels, 2nd and 3rd backbending, cranked HFB calcs. 80−63064
^{162}Yb high spin states, HF self consistent calc. with Skyrme interaction, cranking approach 80−9210
^{162}Yb high spin states with Skyrme interaction, cranked Hartree-Fock calcs. 79−13189
^{162}Yb rot. states, HF and HFB self consistent calc. with Skyrme interaction 80−22662
^{298}Z, triple clustering at fission barrier, Hartree-Fock calc. 77−10454
Zn, electron binding energy and shift, core level XPS 80−87088
Zn, ground state correl., photoelectron spectra, multiconfig. Hartree-Fock calcs. 77−50471
Zn I isoelectronic series, theoretical oscillator strengths for resonance transitions 78−74616
Zn I isoelectronic series, $4s4d^1D$-$4p^21D$ interaction, multiconfig. Hartree-Fock calcs. 79−76351
Zn, inner core neutral atom binding energy, relaxed-orbital relativistic Hartree-Fock-Slater calc. 78−13433
Zn, isoelectronic sequence, oscill. strength and MCHF wavefunctions, outer correl. 80−91505
Zn, UV subshell photoionisation cross section, expt. and GIPM theory 78−21887
Zn, Zn^{2+}, quadrupole antishielding factors, Hartree-Fock perturbation theory 78−62723
Zn-Mn(Cr), dil, mag. anisotropy, Hartree-Fock calcs. 80−11162
$Zn(CH_3)_2$, valence mol. orbital energy, nonempirical pseudopot. 79−22592
$ZnCl_2$, deformation densities, relativistic effect 80−42928
^{62}Zn, band mixing HF model, struct. and electromag. transitions 78−54676
^{90}Zr, nuclear radii, energy density and HF-BCS methods 80−47363
^{90}Zr, pion-exchange contribs. to charge densities, HF calcs. 78−46001

h.f. transformers *see high-frequency transformers*

h.f. transmission lines *see high-frequency transmission lines*

hierarchical systems
see also multivariable systems
ambulatory neuromuscular activation control model 79−57638
biocybernetic multilevel system, nervous regulation of internal organs *(Russian)* 78−48779
biomedical engineering component quality control system 77−48884
calibration errors influence on end item performance 80−98788
dissipative systems, dynamical field theory, hierarchical struct. of field thermodynamics 78−73132
distributed microcomputer control system for high-energy gas-laser facility 77−61975
eye movement hierarchical control model 77−25429
optical/digital pattern recognition automated system 80−48175

hierarchical systems continued
parametric linear systems, time delays, optimality, control coordination and entropy *(French)* 77−9161
photodiode array integration with optical power spectral analysis 80−99645
physiology system models, breathing control example 80−41058
prosthetic arm decentralised control hierarchical approach 77−40924

high-energy cosmic ray interactions
0.4 to 10 TeV cosmic rays, research via Tskhra-Tskaro system 79−84626
γ-ray spectra at 30-500 TeV 77−64574
γ-ray spectra recorded in X-ray emulsion chambers, decascading 77−64578
γ-rays from hadron interactions above 2.5 TeV 77−64573
γ-rays recorded by nucl. emulsion and X-ray film 77−64572
γ-rays ultra-high energy, emulsion chamber anal. *(Chinese)* 78−89028
air, electron-photon cascade curves 79−44322
air showers, >10 TeV, acoustic detection 79−62691
atmosphere prompt neutrinos, W-bosons prod. 79−3014
atmospheric nuclear cascade characts., calc. for Pamir expt. 79−80157
baryon pair production with large decay Q-value. Brasil-Japan emulsion chamber collaboration 79−58992
cascade showers generated by muons in ionisation calorimeter, fluctuations anal. 79−84618
cascade showers in Pb and Fe, hadron-induced 77−60561
cascade showers prod. by muons in Fe at 0.3-3 TeV 77−64570
centauro, Geminion and multipion events, quark matter hadronisation, prod. cross sections 80−47331
Centauro event, high density nuclear matter, and quark model interpretation 79−63565
Centauro event(s), quark hotspot scenario 79−67618
Centauro type events, new type of nuclear interaction in the total $E_\gamma > 10^{14}$ eV region 79−63561
cluster prod. in 1 TeV interactions, comparison with multiperipheral mechanism 77−50036
cluster size, multiplicity correlation strength depend. 79−101038
clustering in multiparticle production in (2 to 1000) GeV/$\hbar$ hadron interactions 79−101037
clusters of particle prod. at high energies 77−64579
coherent hadron radiation at TeV energies *(Russian)* 79−92641
coherent hadron radiation interpretation of cosmic ray anomalous events *(Russian)* 79−92642
conference, Yakutsk, USSR (Jun. 1977) 79−80110
conference on cosmic rays and particle physics, Newark, USA, Oct. 1976 79−58987
dense target interactions, determ. of cluster mass released as gamma quanta 79−80171
deuterons and antiprotons production mechanisms 79−29955
discrete cluster mass spectrum, cosmic ray data anal. 78−33104
Earth, background rate rel. to nucleon stability tests limits 79−22093
EAS, 10^{15}-10^{18} eV, experimental data, implications for particle accelerators, review 79−8786
EAS, conflict with scaling, 10^{15} to 10^{17} eV 77−61336
EAS, hadron interaction model and mass spectrum *(Russian)* 79−96873
EAS, high p_T cross section from multiple core rates 79−62703
EAS, high transverse momentum of γ-ray bundles, $>10^{12}$ eV 79−62701
EAS, obs. of energetic delayed hadrons, correl. with massive long lived particles 79−66897
EAS, scaling incompatibility from pulse profile studies 79−25421
EAS, simultaneous detection of γ-ray bundles and air showers 79−62700
EAS, upper troposphere, balloon obs., nuclear reactions, 10^{15} eV energy particles 79−80161
EAS, validity of Feynman scaling 78−28469
EAS and energy deposition 79−66898
EAS data relation to high-energy particle prod. models, simulation 77−70962
EAS growth, significance of fragmentation and pionisation ranges in inclusive spectra 79−84614
EAS research, primary cosmic ray energy $>10^{17}$ eV, equipment system parameters, capabilities 77−64569
electron showers, Cherenkov radiation from electron ang. distrib. function *(Russian)* 79−80861
electron spectra in Earth's radiation belts during mag. storms 77−53314
electron-photon cascade energy determ., effects of optical density and energy spectrum meas. errors 79−84613
electrons, relativistic, inverse Compton interactions rel. to astrophysical gamma-ray prod. 80−17448
electrons, ultrahigh energy, traversing cosmic blackbody photon gas, effective penetration distance 79−5742
EM cascades in air, caused by 10-100 GeV electrons and photons 79−21120
emulsion chamber C-jets, computer simulation using conventional particle physics 79−58990
emulsion stack combined with ionisation calorimeter 78−49263
emulsion stack connected with ionis. calorimeter for high energy cosmic ray obs. 78−25386
energy estimates of incident particles in cosmic-ray collisions 80−22647
event analysis at Yunnan Cosmic Ray Station *(Chinese)* 79−96872
expected and observed rates for high energy interactions above 10 TeV, summary 79−62706
explosive quark matter, hypothesis for Centauro event 80−22648
fireball coplanar decay, 24 GeV/c proton-nucleus interaction 78−50157
fluxes meas. at 4370 and 4880 m above sea level 77−64551
for interaction in graphite 79−29959
forward hard scattering in hadron-hadron collisions in the energy region $\sim 10^{14}$ eV 80−86773
gamma quanta produced by cosmic-ray hadrons of tens of TeV energies, energy characts. 79−80148
gamma ray-charged particle correlations in nuclear interactions, 20 TeV 78−45170
gamma-quantum families prod., Monte Carlo studies 79−80158
gamma-quantum families with $\Sigma E_\gamma > 30$ TeV, energy characts. in Pamir expt. 79−80156
gamma-ray air family, lateral structure function 77−41274
gamma-ray lines observed in balloon flights at high rigidity, extraterrestrial line flux upper limit 80−21882
gamma-ray spectra, high energy, near top of atmos. detection+meas. by emulsion chamber 79−29958
hadron+nuclei interactions, 400 GeV, secondary particle ang. distrib. and multiplicity meas. 77−64571
hadron and γ-ray spectra with $\Sigma E_\gamma > 500$ TeV 77−64575
hadron energy spectra produced by primary cosmic ray particles, $E > 10^{14}$ eV 80−21880
hadron families prod., Monte Carlo studies 79−80158
hadron families production, characts. calc. rel. to elementary act model depend. 79−80160
hadron high-energy spectra obs. with Fe emulsion chamber 77−60556
hadron interactions, transverse momenta at 10^{14} to 10^{15} eV in Pamir expt. 79−80170
hadron multiple prod., cosmic-ray-nucleus reactions, muon time-correl. meas. *(Russian)* 77−14133
hadron spectrum depend. on hadron inelastic cross-section increase *(Russian)* 77−46093
hadron-nucleus, pseudorapidity distribs., 24 GeV/c-4 TeV, energy and target depend. 80−91115
hadron-nucleus interactions, slow particles characts. rel. to high-energy interaction models 79−80177
hadronic collisions, models rel. to computer simulation of large cosmic ray showers 78−57415
hadronic component lateral struct. function, atmospheric shower phenomena 77−56804
hadronic interactions, 10^{12} to 10^{15}eV, and cosmic ray components in atmosphere 79−62708
hadrons, cascade curves in Fe between 20 and 8000 GeV 80−36464
hadrons with E>2 TeV, integral flux, attenuation in air, NN cross section *(Russian)* 77−78589
heavy-lepton pair production by cosmic rays 79−36117
heavy nuclei+emulsion nuclei, meson generation 77−61446
high energy γ-ray family events, large emulsion chamber expt. on Mt. Fuji 79−63562
high energy interactions and cosmic ray components in the atmosphere 79−62707
highest-energy cosmic rays, detected by EAS obs. 79−2450
Homestake neutrino detector, mass composition of cosmic ray primaries, muon multiplicities meas. 79−66903
induced fission of heavy nuclides, influence on apparent ^{238}U fission track ages 79−40047
magnetic monopoles prod. in atmospheric high-energy collisions 78−49262
model for 10^6 GeV cosmic rays in atm., Feynman scaling, e/μ ratio 77−45271
Monte Carlo simulation of high-energy EM air showers 77−64577
multiple meson production, total $E_\gamma > 2\times10^{13}$eV 79−58989
multiple meson production by 10^{13}-10^{16} eV cosmic rays, longitudinal behaviour of γ air family 77−33309
multiplicity distrib. of particles *(Russian)* 79−5719
multiplicity distributions, cross sections, cosmic nuclei+emulsion nuclei collisions, ~19 GeV/nucleon 78−41744
muon ground level spectra and generation processes 77−25898
muon sea level charge ratio, energy depend. 80−94665
muons, inelastic interaction with Fe nuclei 79−84616
muons, parent nucleons, energy distrib., at sea level and underground, phenomenological model 80−61974
muons, radiative energy losses in ground 79−84619
muons and muon pairs, EM interactions, 5-1200 GeV *(Russian)* 78−73598
muons in EAS at mountain altitudes, comparison with numerical calcs. 77−87218
muons penetrating large depths in rock and water 77−29612
negative pions, multiple charged-particle generation in inclusive reactions with nuclei 79−76022
neutrino production at ultrahigh energies, fluxes and detect. techniques 78−49264
neutrinos, detection and neutrino-nucleon interactions, 1-100 TeV 78−36413
new physics from experiments above 100 TeV, appl. to QCD, weak interaction, and gauge theory 79−63564
nonstationary convection and high-energy particle prod. 77−53312
nuclear emulsion, ~20 GeV/nucleon, mean meson multiplicity and ang. distribs. 79−58988
nuclear event, ~42 TeV, high multiplicity, large transverse momenta, giant fireball 78−33105
nuclear interactions around 20 TeV, characts., comparison with Monte Carlo simulation 79−58991
nuclear primary air showers, phenomenological model 77−22028
nuclei, ultrahigh-energy, metagalactic, spectrum calc. 77−53342
nucleon-photoemulsion hadron interaction, high multiplicity events at >1 TeV *(Russian)* 79−45124
nucleus-nucleus interactions, search for hydrodynamic effects 79−80176
nucleus-nucleus interactions at energies around 10^{12} eV, features 79−80173
particle production in cosmic ray collisions, multiplicities and rapidity distrib., collective tube model 80−8507
penetrating-particle beams, local generation at air equivalent depth 200 m 79−84603
photomultiplier, cosmic ray induced noise from Cherenkov radiation 77−33308
photons, ultrahigh energy, traversing cosmic blackbody photon gas, effective penetration distance 79−5742
pion photoproduction in large cosmic-ray showers, theory 80−4214
pion production spectrum derivation from primary cosmic ray spectrum and scaling consts. 77−25897
primary cosmic ray interactions with photoemulsion nuclei using satellite Intercosmos-6 *(Russian)* 78−93063
primary cosmic rays, energy 10^{14}-10^{16} eV, comp. and interactions, Tien-Shan data 79−80149
proton-emulsion collisions, 67 to 400 GeV/c, energy independence, pseudorapidity distribs. for shower particles 79−75808
rapidity distribs. of secondary particles, multiperipheral model 77−22821
scaling and charge ratio at 1-10 TeV, γ-ray, electron, muon spectra 77−64576
scaling features of high-energy cosmic-ray components in atmosphere 78−93062
scaling violation and momentum transfer increase above 100 TeV, and exotic phenomena 79−63563
sea-level expt., analytical and Monte Carlo interpretations 77−67016
sea-level expt., hadronic and muonic fluxes obs. 77−67015
secondary particle correl., N-nucleus interactions, 10^{12} eV 78−66178

high-energy cosmic ray interactions continued
secondary particle production in cosmic ray interaction at 10^{12} eV 80−5032
short lived particle production, cosmic ray evidences 79−58993
soft-photon emission effects and radiative corrections for electromagnetic processes at very high energies 79−71752
source composition, energy depend. at high energies 77−67013
space radiation, high-energy astronomy expt. 78−85780
spectrum and interaction characteristics in 10^{13}-10^{16} eV range, scaling model implications 77−56803
stratospheric superfamily with $\Sigma E_\gamma \sim 2.10^{15}$ eV 79−2451
time correlation of muon pairs and multiple hadron production 79−80178
ultra-high energy nuclear interaction event with large transverse momentum at 445 TeV *(Chinese)* 80−105140
ultrahigh energy interactions, scaling deviations and modified models 79−80172
ultrarelativistic particles interaction, multiparticle effects detect. via cavitation 79−84617
unstable and energetic particle production, anal. of 10 to 100 TeV emulsion chamber events 79−62705
very high energy cosmic ray-nuclear interactions, new particle search, X particles 80−8508
XTR-detector, Monte-Carlo simulation, 0.5-5 TeV cosmic ray hadron interactions *(Russian)* 79−49564
αN, 0.1-1.21 TeV, multiple pion production, role of clusters 77−34199
D, mass and mean life from high energy cosmic ray data *(Chinese)* 80−102045
γ-ray cascades prod. at 10^{13} eV 77−61322
γ-ray families and high-energy interactions 77−87221
γ-ray high-energy spectra obs. with Fe emulsion chamber 77−60556
γ-ray lateral distrib. from fireball prod. behaviour, multiple meson prod. 77−53381
μN inelastic scatt., four-momentum depend. determ. 77−61337
NN, 0.25-42.3 TeV, multiple pion production, role of clusters 77−34199
NN, 10^{12} eV, rapidity gap distrib., Snider multiperipheral cluster model 80−73757
NN collision events, modified Duller-Walker approach, 100-10000 GeV 78−49261
NN collisions around 10 TeV, nucleon fragmentation by diffr. rel. to high-energy γ-quantum prod. 79−80174
NN inelastic interactions, $\sim 10^{12}$ eV, depend. of cluster size and clustering on inelasticity 79−63566
$\nu e \rightarrow W^{\pm} Z^0(\gamma) X$, high energy behaviour and hard photon prod., cosmic rays 80−5028
p-air inelastic cross section and hadron energy spectrum, scaling model of energy depend. 79−44325
p-atmospheric interactions, direct lepton prod. *(Russian)* 80−12627
p-nucleus collisions around 20 TeV, momentum and energy spectra 77−22029
pN in emulsion, 200, 400 GeV/c, multiparticle prod., azimuthal and rapidity effects 80−63035
pp interactions, cosmic γ-ray spectrum, fireball model 77−18364
pp total cross section at cosmic ray energies up to 100 TeV 79−96868
πp interaction characteristics at 40 and 10^4 GeV, comparison 77−61335
Σ_c^+, mass and mean life from high energy cosmic ray data *(Chinese)* 80−102045
^{36}Cl prod. in proton induced high-energy spallation, cosmic ray effects 77−61421
Fe+cosmic ray photon, prod. of 300-1000 GeV muons, cross section, shadowing 77−64580
Fe+μ, 2 to 800 GeV, EM interactions of cosmic ray muons, e^+e^- prod. and knock-on e^- prod. 79−66902
Fe(μ,μ'), small Q^2 and >200 GeV, implications for photonuclear process 77−23001
Ge detectors in space, computer spectral anal. of cosmic ray proton induced radioactivity 79−12413
He, Ne, Ar isotopes and ^{236}U prod. by solar cosmic ray protons in lunar materials 77−17311
NaCl+cosmic ray muons, photonuclear cross section, nuclear muon losses 77−64581
^{16}O relativistic ions, fragmentation cross-sections in CsI 77−67770
Pb, electron-photon cascade curves 79−44322

high energy electron diffraction
see also reflection high energy electron diffraction
A15-superconductor, surface characterisation by energy loss spectra, AES and HEED 77−24635
alkali and halide ionised atoms, elastic scattering amplitudes, numerical calcs. 80−49057
anomalous transmission, effect of Bloch waves *(Japanese)* 77−43117
atomic string approximation, in cross-grating HEED, dispersion surface and Bloch waves 80−49056
atomic string approximation use in obtaining dispersion surfaces 80−100143
band theory, zone axis crit. voltage effect 78−83659
Bloch functions rel. to at. or mol. orbitals 78−83662
Bloch wave absorpt. 80−10466
Bloch waves, corresponding atomic and mol. orbitals 79−27880
branch points, critical voltage effect, band theory models 78−1961
convergent beam diffraction in HV electron microscope 78−83674
Convergent beam diffraction of 300 keV electrons *(German)* 78−63646
critical voltage effect, zone axis, interpret. using atomic string approx. 80−96421
decahedral particles, high symmetry orientations, HEED and TEM study 79−86732
epitaxy, growth modes, exp. techniques, book contrib. 80−49558
HCP metals, critical voltages, using n-beam dynamical theory 78−71644
high stability constant current source, diffraction appl. *(Chinese)* 79−44991
imperfect crystal, semiclassical anal. of HEED, stacking faults 79−1373
isocahedral particles, high symmetry orientations, HEED and TEM study 79−86732
many beam problem, use of Gauss-type orbitals and plane waves 78−83661
metal, electron wave flux distrib. fine struct. near Bragg refl. 78−83670
Monte Carlo calculations of electron scatt. in solids 80−96422
optical potential use, thermal averaging and dynamical diffr. 80−75121
quartz, single crysts., Ar and O_2 interaction at high temp., surface struct. changes *(German)* 80−96725
scattering approximation, Feynman path-integral formulation 78−26391

high energy electron diffraction continued
SEM, ultra-high, vac., diffr. unit 78−83699
theory 79−68985
virtual inelastic scattering 78−26390
zone axis patterns, depend. on string integrals or number of bound states, HEED 77−84598
zone axis patterns rel. to projected cryst. pot, HEED 77−84597
Ag, vacuum deposited film, surface struct., HEED meas. 78−6234
Al film, room temp. oxidation, scanning HEED expts. 78−91567
Au, Bloch waves, corresponding atomic and mol. orbitals 79−27880
Au, vacuum deposited film, surface struct., HEED meas. 78−6234
CdS(Se)(Te) films, vac. condensed, growth and struct., HEED obs. 80−29292
Cu, cryst. pot. in electron diffr. and band theory 78−83677
Cu, HEED, virtual inelastic scattering estimated 78−26390
Cu, vacuum deposited film, surface struct., HEED meas. 78−6234
$Cu_{2-x}S$-CdS p-n heterojunction, optical energy convertor, struct. and recomb. props. 80−72065
Ge film, amorphous, ^{74}Ge ion implanted, defect struct. obs. 78−51848
Ge, HEED, virtual inelastic scattering estimated 78−26390
$In_{1-x}Ga_xAs$-$GaSb_{1-y}As_y$ superfine heterostruct., MBE 78−95348
Mo, Bloch waves, corresponding atomic and mol. orbitals 79−27880
Ni-Nb (5, 10 at.%), oxidized specimen study using SEM, HEED X-ray diffr. and ion backscattering anal. *(Japanese)* 79−24651
PbS, film condensation on amorphous substrate, struct. and growth 78−38981
PbTe(Se) vacuum deposited thin films, struct. and growth 79−19482
Si, Bloch waves, corresponding atomic and mol. orbitals 79−27880
Si, electron transmission at 15 MeV 78−83671
Si, HEED, virtual inelastic scattering estimated 78−26390
Si sputter-machined surface, Ar^+ ion, lattice disordering obs. *(Japanese)* 80−3228
SiO_2-Si interface, interaction of point defects, electron microscope exam. 77−7979
Xe, adsorbed monolayer, THEED intensity meas. 78−84075
ZnO film, sputtering using Zn target, technique and characterisation 78−3040

high-energy nuclear reactions and scattering *see nuclear reactions and scattering*

high fidelity amplifiers *see audio-frequency amplifiers*

high field effects
see also Gunn effect; hot carriers; impact ionisation; limited space charge accumulation; Poole-Frenkel effect; Schottky effect; Zener effect
alkali halide thin films, high-field electron injection, ionic cond., photocond. 80−75665
alkali halides, high field transients, three-level model 79−91055
alkali halides, high-field transients, three-level model 77−59289
alkanes, electron mobilities through liq. and critical regions 78−2536
amorphous semiconductors, DC and AC cond., high field effects, magnetoresist., EPR, carrier transport, review *(Japanese)* 77−35943
amorphous semiconductor, computer simulation 78−88002
amorphous semiconductor, elec. cond. at strong elec. field and high hydrostatic press. *(Czech)* 77−24560
amorphous semiconductors props., principles and appl., w.r.t. electronic band state *(Japanese)* 79−23979
amorphous solid, anomalous transient-time dispersion 78−31155
anthracene, mol. cryst., elec. field independent electron drift mobility 79−51645
anthracene, photo-oxidised, current oscills. due to recomb. instability in high field domain 77−4353
anthracene, trapping effects on emission-limited current flow 80−29413
anthracene thin films, high field effects and switching, local centres importance 79−73548
argon liq., expt. results 79−4587
bipolar conductivity equations, approx. solns. 77−69336
bisphenol-A-diglycidyl epoxy, light emission under high elec. field, compared with photolum. 80−25465
calcium behenate monomolecular layers between Al electrodes, nonlinear dielec. props. 80−80405
carrier distribution function, high energy asymptote *(Russian)* 78−72163
chalcogenide glass, charged dangling bond model reassessment 77−72813
chalcogenide glass, localised states role in cond. in high elec. fields 77−76841
chalcogenide glass films, high field, short pulse cond. expt. 80−49751
chemical relaxation spectrometry, new electric field methods 79−8586
collision-ionisation space charge effect on high-field conduction in solids, simple dielec. model 80−84469
corona charged insulating film high-field conduction and breakdown 80−15975
crystal without inversion centre, current quadratic in field and photogalvanic effect 78−10505
current density under high elec. field 79−28352
current fluctuations in strong elec. field, interelectron collisions, drifted Maxwellian distribs. *(Russian)* 80−2436
degenerate semiconductors, transverse magnetoresistance in strong mag. fields 79−99565
diamond, natural, anisotropy and saturation of hot carrier drift velocity 80−6867
diamond, natural, lattice scattering and effective mass of holes 79−60842
dielectric, dynamic charge injection unidimensional numerical simulation of carrier and field distrib. *(French)* 77−32079
dielectric, solid, high field conduction and breakdown, review 80−84691
dielectric breakdown of solids, gaseous model, macroscopic channel development in strong elec. field, tree growth and return streamer 80−84696
dielectric liquid, bubble creation in high elec. fields, explained in terms of struct. 79−91370
dielectric liquid, high field cond. and breakdown 79−91355
dielectric liquid high field carrier transport, electron multiplication and breakdown, mol. struct. depend. 80−84694
dielectric liquids, cond. and breakdown, conf., Mont-Saint-Aignan, France (July 1978) 79−91354
dielectric liquids, high-field cond. and breakdown, anal. 77−8506
dielectric liquids, high-field electron transport *(Japanese)* 78−2495
dielectric liquids electric conduction, thermal activation energy, anal. 78−43399
dielectrics, electric field enhanced conductivity 77−35951

high field effects continued
N,N′-diphenyl-p-phenylenediamine, current carrier traps, space-charge-limited currents 78−47799
disordered electronic system, scaling theory of localization and non-ohmic effects in two dimensions 80−44539
disordered semiconductor, high-field cond. in random field 79−65489
displaced Maxwellian distribution, correction 78−10454
electrolytes, stepwise-dissociating acids, bases, salts, high field conductance 77−40551
electron-hole pairing, collective modes, current states 77−39838
energy-focused atom probe design and performance 78−85276
films, amorphous, prep., struct., props., review, book contrib. 78−48321
free and trap modulated mobility transition 79−82598
fused salt, simulation of high field cond. 80−54421
galvanomagnetic phenomena, difficulties in nonlinear theory 79−11151
glass, ionic conductivity, weak electrolyte theory 80−84322
graphite, high-field galvanomagnetic props. 77−62941
Gunn diode, anode domain disappearance dynamics, computer simulation calcs. 80−6859
n-hexane, impurity particle behaviour and cond. pulses 79−91059
hexatriacontane, single crystal, elec. props. *(Japanese)* 79−51592
history of hot electron physics 78−26869
hot photoexcited electrons, time evolution of electron temp. in high mag. field 80−54709
hydrocarbons liq., geminate pair of charges, neutralisation escape with field depend. electron mobility 78−26865
II-VI semiconductors, SHG efficiency at 77K under high field condition 80−84470
III-V semiconductors, negative resistance and peak velocity in central (000) valley 79−73522
III-V semiconductors, noise calc. using Monte-Carlo method 80−75575
III-V semiconductors, quaternary and ternary, alloy scatt., high field transport 78−30929
impurity breakdown in mag. field 77−24564
insulating films, hot electron energy distribs., Monte Carlo study 77−51832
insulator, high field electronic cond. 78−30931
insulators, transient radiation induced ionisation effects 77−80788
ionic transport in solids, high field nonsimultaneous place exchange mech. 80−70456
Josephson junction, high-frequency, high-voltage effects on useful limit 77−1521
krypton liq., expt. results 79−4587
low temp. plasma in mag. field, periodic signal generation, I/V charact. *(Russian)* 77−20352
many-valley semiconductor, current-voltage characteristics, with multivalued depend. of current on elec. field 78−26876
many-valley semiconductors, ellipsoidal energy surface, high field magnetoresist. and magnetothermal EMF 77−43621
MOS capacitors, establishment of inversion layer in Si substrate under high oxide field conditions 77−66202
MOS structure, negative bias stress at high elec. field, rel. to MNOS device degradation 77−62996
Multiphonon effects in the theory of electron tunelling between deep impurity levels and the conduction band in strong electric fields 78−2447
naphthalene, mol. cryst., elec. field independent electron drift mobility 79−51645
narrow band gap semiconductor, high elec. field conduction in space and time superlattices 80−49756
narrow gap semiconductor, modification of Einstein relation for inversion layers in strong elec. field 80−96959
negative electron diffusivity in high fields 78−30935
non-linear transport theory, field depend. of carrier screening 80−29415
noncentrosymmetric crystals, subjected to strong elec. field, theory of transport phenomena 79−11136
nondegenerate semiconductor electrons in strong elec. and quantizing mag. fields 78−10457
noninteracting electrons, in strong elec. field, distrib. function, mean values *(Russian)* 78−87984
nonlinear dielectric relaxation 78−60389
organic liquids, expt. results 79−4587
p-n junction injection charact. in strong elec. fields 77−76913
p-n-p-n structures, turn-on at high voltages and high currents 77−1475
paraffin wax, elec. cond., 33-55°C and 1-2 kV cm^{-1} 79−99555
piezoelectric semiconductor, acoustohelicon waves, parametric excitation 79−38135
polar crystal, hot electron transport, eikonal approx. for energy loss 77−1426
polar crystal, hot electron transport, loss to single phonon modes 77−1427
polar semiconductor, high elec. field, electron momentum distrib. 77−1428
polar semiconductor, high field collision rates 78−30932
polar semiconductor, nonlinear transport, field-dependent relaxation time 80−6866
polar semiconductor, transient high-field conductivity, theory 78−79998
polycrystalline semiconductors, electrical conductivity theories *(Czech)* 79−42537
polyethylene, DC partial discharge and current 78−43790
polyethylene, electrical capacitance under high DC elec. field 80−54705
polyethylene, high field cond. current and elec. breakdown 77−76835
polyethylene, low density, absorption currents exam. 78−43785
polyethylene, relation between electrostatic capacity and electronic space charges induced by high field 79−15154
polyethylene film, 1/f noise, 10^{-4}-1 Hz, 20-80°C 79−51643
polyethylene film, uniaxially drawn low-density, pre-exponential factor in elec. cond. 77−21224
polyethylene films, low density, γ-irrad., elec. cond., effect of elongation 79−4564
polyethylene terephthalate, high field transient cond., 50 μs-1 ms 78−43402
polyethylene terephthalate, Mylar C film, high field relaxation currents 79−11259
polyethylene terephthalate film, 1/f noise, 10^{-4}-1 Hz, 20-80°C 79−51643
polyethylene terephthalate films, gamma radiation induced cond. under high elec. field 78−47798
polyethylene terephthalate films, high-temp. elec. conduction 79−51588
polyethylene terephthalate under high elec. fields, γ-ray induced cond. 79−60840
high field effects continued
polyethylenenaphthalate, elec. cond., appl. of model 80−24940
polymer, amorphous, excess charges, band gap levels and elec. props. 78−23053
polymeric double layer system, high field cond., xerographic charact. 79−95448
polymonochloro-p-xylylene, γ-ray-induced cond., hole injection effects 80−34452
polystyrene, γ-ray-induced cond., hole injection effects 80−34452
polystyrene film, 1/f noise, 10^{-4}-1 Hz, 20-80°C 79−51643
proton semiconductors, with H-bonds, quantum theory of proton cond. 80−65641
PVC films, soln. grown, DC cond. mechanisms, field and temp. depend. 80−97021
runaway electron-heating dynamics 80−39597
semi insulating layer with conductivity gradient, charge storage 77−80784
semiconducting photocathodes, carrier transport simulation, Monte Carlo method 80−71575
semiconductor, absorpt. and amplification of US at moderate freq. 78−19102
semiconductor, amorphous or disordered, cond. mechanisms, model of medium-range comp. disorder 78−79994
semiconductor, bounded samples, phonon heating influence on volt-ampere charact. 77−39863
semiconductor, bounded samples, volt-ampere charact., nonequil. phonons influence on thermal dimensional effects 77−43611
semiconductor, carrier capture by attractive centres in strong elec. fields 79−11144
semiconductor, diffusivity of charge carriers, in strong elec. fields 77−35950
semiconductor, disordered, constrained cond. in powerful field *(Russian)* 77−55536
semiconductor, doped photoemission, calc. of escape probability of electrons *(Russian)* 79−24408
semiconductor, double injection characteristics under high voltages 79−51590
semiconductor, electron drift vel. and phonon multiplication 80−6848
semiconductor, electron heating by strong static and HF elec. fields 77−8112
semiconductor, electron transport phenomena, high-field transport and quantum transport in strong mag. fields *(Japanese)* 77−55526
semiconductor, electron-runaway and quasi-stationary states in electric field 77−4359
semiconductor, HF EM effects, nonquadratic dispersion law of carriers 78−19078
semiconductor, HF field energy absorpt. in strong parallel mag. and elec. fields 79−73801
semiconductor, high field longitudinal magnetoresist and bound states 78−23113
semiconductor, high field transport, balance eqns., in finite collision duration regime 79−60843
semiconductor, high field transport, inter-valley scatt., intra-collisional field effect 80−34455
semiconductor, hopping transport theory for strong elec. field 77−8106
semiconductor, hot electron distrib. in strong electric and quantised mag. fields 79−95417
semiconductor, hot-electron energy distrib. in strong mag. field 78−43400
semiconductor, IR transmission, cond. variations effects 79−15158
semiconductor, magnetoresist. in strong UHF electric fields 77−1437
semiconductor, method for determ. of cond. mechanism in strong elec. field 77−1430
semiconductor, Nernst-Ettingshausen effect, thermopower, strong elec. field 78−23122
semiconductor, nonlinear conductivity, vortex waves, carrier mobility and lifetime 80−96893
semiconductor, nonlinear current density, theory 78−56149
semiconductor, nonohmic hopping conduction, theory 77−20328
semiconductor, optically stimulated negative conductivity 77−4357
semiconductor, phonon induced hopping between Stark levels 80−92900
semiconductor, plasma self-oscillations within submillimetre freq. range 80−84473
semiconductor, quantum transport theory under high elec. field 78−23099
semiconductor, strong EM wave interaction 80−6852
semiconductor, two-valley, carrier vel.-field charact. under high elec. field 80−70713
semiconductor, UHF heating of charge carriers using lumped-capacitance resonators 80−20203
semiconductor, unipolar, n-type, field-effect mobility, energy spectrum of surface states 80−39657
semiconductor, zero-gap, magnetophonon oscills. of transverse magnetoresist. in strong elec. fields 80−96916
semiconductor electron-hole-plasma, instability in heating elec. field 80−15552
semiconductor film, electric-field-induced anisotropy, differential carrier mobility tensor derivation 77−39973
semiconductor modelling, bulk, negative-cond., transverse spreading of high-field domain, two-dimens. simulation and equivalent cct. model 79−1602
semiconductor of simple geometries, field penetration and band bending in high elec. fields 79−87106
semiconductor plasma, oscillatory overheating instability 77−76855
semiconductor plasma, unstable EM wave propagation, hot carriers, Hall effect, calc. 80−39620
semiconductor spectral noise meas. between 30 and 400 MHz, pulse technique device *(German)* 79−47134
semiconductor superlattice, plasma oscills. in strong elec. field 80−44637
semiconductor transport, quantum kinetics eqns. for finite collision duration regime 79−73519
semiconductor with quasirelativistic band struct., hot electron kinetic equation 78−84222
semiconductor with superlattice, EM oscillations in electric field, transport theory 79−69521
semiconductor with superlattice, EM wave propag., mag. field effect 80−70745
semiconductor-metal contact, minority carrier injection in strong elec. field 77−55609
semiconductors, dopant distrib. from carrier drift distrib. in high elec. field 79−51140

high field effects continued
semiconductors, electrical conduction in strong elec. fields, percolation mechanism 80−20206
semiconductors, free carrier density in strong electric and quantised mag. fields 80−6860
semiconductors, hot electron transverse escape galvanomagnetic effects *(Russian)* 80−80289
semiconductors, quasi monopolar, integrally weak diffusion effect of I-V characts. 78−2491
semiconductors with superlattice, absolute negative resist. *(Russian)* 78−34838
silicon oil, behaviour under HV stress 79−91368
silicone liquid film, cond. currents obs. 79−91062
solids, instabilities during high-field elec. cond. 77−24562
SOS structures, high-field electron transport, drift vel. meas. 80−80387
Stark-Ladder current theory 78−68035
strong elec. field, pulsed V-I characteristics *(Russian)* 78−64156
superlattice semiconductors, cond. in strong elec. fields 77−55539
TCNQ, salt, $Me\phi_3As(TCNQ)_2$, nonOhmic elec. cond., tunnelling model and expt. 79−99558
temperature sensitive semiconductors, AC thermal theory 79−11131
tetra-n-butylammonium picrate, soln. in benzene, field dissoc. effect on ion pairs 79−91061
tetracene, trapping effects on emission-limited current flow 80−29413
thermomagnetic effects in strong magnetic fields 77−62954
uniaxial conducting crystals, excitation and amplification of EM waves 77−69335
weakly conducting layer, elec. field transient penetration 78−84525
xenon liq., expt. results 79−4587
$Al/Al_2O_3/Al$ structures with organic monomolecular layer, cond. at high elec. fields 80−80402
$Al\text{-}SiO_2\text{-}Si$ capacitor, current and C-V instabilities at high fields 77−80841
$Al\text{-}SiO_x\text{-}Al$ evaporated film anomalous dielectric dispersion under high DC field 80−15620
AlB_{12}, α- and β-forms, elec. props. at high temps. and in strong elec. fields, thermistor appls. 80−92903
a-As, opt. and elec. props. 77−39894
$(As_2S_3)_{2-x}(PbS)_x$ 79−42553
$AsSe_x$ amorphous films, high field behaviour 79−87172
As_2Se_3, glassy, elec. cond. meas. in high elec. field 77−4355
$As_2Se_3\text{-}As_2Te_3$, vitreous, localised states role in cond. in high elec. fields 77−76841
$As_2Se_xTe_{3-x}$ chalcogenide glasses, cond. meas., field strength and temp. depend. 78−84225
As_2Te_3, glassy, field depend. elec. cond. and localised states role 77−76829
B, β-rhombohedral, elec. props. at high temps. and in strong elec. fields, thermistor appls. 80−92903
β-B, rhombohedral, localised states charact., review, book contrib. 78−47728
$B_{14}Si$, switching and high field effects, cond. mechanism 78−64048
BaF_2, barrier instability in strong elec. fields 79−69522
BaF_2, current oscills. in elec. field of $\sim 10^6$ Vm^{-1} *(Russian)* 77−20334
$BaTiO_3$ ceramic, degradation under high AC elec. field 80−60499
Bi, electron gas heating at low temp. 78−60133
Bi, nonlinear properties under sound generation conditions 79−60845
$Bi_{1-x}Sb_x$, semiconductor, anomalous conductance in strong electric and longit. quantised mag. field *(Russian)* 78−76084
$Bi_2Te_3\text{-}Sb_2Te_3$ film, residual cond. 78−52110
$Bi_2(Te_{1-x}S_x)_3$, quasi 2-D cryst., I-V and magnetocond. meas. 77−85360
CaF_2, barrier instability in strong elec. fields 79−69522
Caf_2 current oscills. in elec. fields of $\sim 10^6$ Vm^{-1} *(Russian)* 77−20334
$Cd_{1-x}Ag_xCr_2Se_4$, ferromag. semicond., influence of strong elec. field on microwave absorption 77−28207
$CdCr_2Se$, ferromag. semicond., high field effects, magnon carrier scatt. 78−87981
$CdCr_2Se_4$, velocity-field characts., above T_c 78−64049
$CdGaS_2$, single crysts., peculiarities of photocond. in strong elec. field 80−54736
$Cd_xHg_{1-x}Te$, current-voltage characts., pinch effect, mag. field effects 80−6858
$Cd_xHg_{1-x}Te$, graded gap epitaxial layers, elec. and photoelec. props. 77−85362
$Cd_xHg_{1-x}Te$, resistivity, Hall effect and magnetoresist. in strong elec. field 77−28199
$Cd_xHg_{1-x}Te$, strong elec. field effect on galvanomagnetic effects 79−11159
$CdInGaS_4$:Au, single crystal, thermostimulated conductivity *(Russian)* 79−11142
$CdO\text{-}P_2O_5$ glass, thin film, elec. cond., high and low fields 80−80427
CdS, electron drift vel. and phonon multiplication 80−6848
CdS, epitaxial film, conductivity control by S vacancy form., light modulation appls. 77−4455
CdS, film, residual conductivity, effect of transverse electric field 77−4458
CdS, parametric action of strong radiation field 78−14752
CdS, phase memory effect and vel. of trap-controlled high-field domains 77−47855
CdS, photocond. cryst., stationary and non-stationary temperature-electric instabilities 79−7833
$CdS\text{-}Cu_2S$ solar cell, minority carrier generation and transport in emitter 77−43649
CdSe film, current noise due to thermal field ionisation 79−91110
CdTe, microwave cond. and dielec. permittivity using reson. cavity method 79−51620
p-CdTe:Cl, mech. of electron recomb. 79−11176
Cu, discontinuous film, ageing effect on elec. cond. 79−24084
CuB_{24}, elec. props. at high temps. and in strong elec. fields, thermistor appls. 80−92903
Cu_2O, hole mobility, scatt. mechanisms, elec. field effect 77−80786
EuO, excitation of spin waves by current carriers, magnetisation and elec. cond. reduction *(Russian)* 79−7981
EuSe, dynamical conductivity in high mag. fields 79−78118
GaAs, DC biased, filamentation of laser radiation 80−74428
GaAs, deep trap study by free exciton refl. spectra 79−60761
GaAs, diffusion and power spectral density and correl. function of vel. fluctuation for electrons 80−65576
GaAs, dynamical response of electron distrib. to high elec. field fluctuations 77−51758
n-GaAs, electron drift vel. meas. at high elec. fields 77−39861

high field effects continued
GaAs, electron dynamic properties in strong elec. field, anal. *(German)* 78−43404
GaAs, electron transient vel. charact., Γ-L-X cond. band ordering 78−79997
GaAs epitaxial layers, photocond. high field effects on carrier capture and recomb. 77−43646
n-GaAs film, cond. mechanism in strong elec. field determ. 77−1430
GaAs, $\Gamma_6^c\text{-}L_6^c\text{-}X_6^c$ cond. band ordering, velocity field characts., Monte Carlo calcs. 78−18957
GaAs hot electrons drift rate/field strength characteristic in microwave fields *(German)* 78−43430
n- GaAs, hybrid-hybrid mode interaction in crossed elec. and mag. fields 78−51997
n-GaAs, IR transmission, cond. variations effects 79−15158
GaAs, transient dynamic response calculation by Monte Carlo techniques 80−107796
n-GaAs, two stream instability 78−2509
GaAs, UHF heating of charge carriers using lumped-capacitance resonators 80−20203
GaAs:Cr, high resist., anomalously strong elec. field induced release of carriers from traps 78−6397
GaAs:Cr, single cryst., optical quenching spectrum, disappearance of stationary high-field domain 78−47830
GaAs:Cr, strong quenching of thermally stimulated conductivity by elec. field *(Russian)* 77−1434
GaAs:H amorphous sputtered films, high field cond. props. 80−44607
GaAs:O, impurity photocond. in high elec. field, 90K 78−19095
n-GaAs:S, Zn VPE film, LF current oscill., negative photocond. 77−80858
$Ga_xIn_{1-x}Sb$, electron transport props. calc. by Monte Carlo method 77−76834
GaSe film, amorphous, I-V characts. in strong elec. fields, 173-373K 78−56248
GaSe, thin film, photoelectrical props. at high electric field *(Russian)* 79−11247
Ge amorphous films, high elec. field cond. and magnetoresist. at 4.2K 80−49748
n-Ge, anisotropy of thermal and convective noise, in magnetic field 78−34873
p-Ge, diffusion coeff. for hot holes in mag. field 80−39614
n-Ge, doped, dopant distrib. from carrier drift distrib. in high elec. field 79−51140
p-Ge, double injection characteristics under high voltages 79−51590
Ge, drift velocity of plasma cloud 80−6887
n-Ge EM wave interaction with hot electrons, in strong mag. field with Voigt config. 77−69367
Ge, electron heating by nonuniform elec. field, I-V characteristics 77−47825
Ge, electron heating in inhomogeneous elec. field 78−2494
Ge film, amorphous, 100-300K 77−24563
Ge, hole diffusion 78−6372
p-Ge, hole drift vel. in high field 79−95415
Ge, hole drift velocity, time-of-flight meas. 78−10444
Ge, hot-electron diffusion coefficient 78−87982
Ge, impurity breakdown field increase due to strong compensation 80−20204
Ge, lightly doped, heavily compensated by fast neutrons, electrical props. 77−89766
p-Ge, linear magnetoresist. in strong elec. fields 77−43632
n-Ge, longit. piezoresist., in strong elec. field 78−56147
n-Ge, noise, small signal conductivity and diffusion in strong elec. fields 79−11192
p-Ge, noise calc. in strong elec. field using Monte Carlo method 80−15578
n-Ge, noise spectra of hot carriers 78−76083
p-Ge, odd magnetoresist. in strong elec. and mag. fields 79−51612
Ge, p-type, hole conductivity anisotropy 77−4360
p-Ge, stretched along ⟨111⟩ axis, bulk negative differential cond. and current oscills., 78K 79−19601
Ge surface, field penetration and band bending in high elec. fields 79−42613
Ge, transmutation doped, high field magnetoresist. of hopping transport 78−10474
Ge, UHF heating of charge carriers using lumped-capacitance resonators 80−20203
Ge, voltage-current curves, specimens of variable cross-section 77−8113
Ge:Au, moving elec. domain, impedance 77−1429
Ge:Cu photodetector, high field domains, rel. to I-V characts. 78−19141
Ge:Mn, Sb, recombination waves, convective instability development 80−70721
n-Ge:Ni, recomb. waves, current instabilities obs. 77−1431
n-Ge:Ni, recombination of hot electrons on Ni impurity centres 80−44612
Ge-As-Te, thin chalcogenide glass film, high-field switching effects 77−32052
$Ge_{33}As_{27}S_{15}Te_{25}$, chalcogenide thin films, coupled carrier theory test, high field conditions 80−100466
$Ge_7Si_9As_{39}Te_{35}Ga_{10}$, chalcogenide thin films, coupled carrier theory test, high field conditions 80−100466
He, solid, charge carrier mobility in strong electric fields *(Russian)* 77−62706
^3He, liq., positive ion nonlinear behaviour, expt. and parameterless theoretical prediction comparison 79−14978
InAs, transient dynamic response calculation by Monte Carlo techniques 80−107796
InAs-oxide-$Pb_{50}Bi_{20}$ junction, hot electron temp. in InAs meas. by tunnelling 77−4352
$In_xGa_{1-x}As$, electron drift vel. in high elec. fields 78−30928
InP avalanche photodiodes, microplasmas, investigation 80−60018
InP, deep trap study by free exciton refl. spectra 79−60761
n-InP, high field props. under high press. 78−26872
InP, high-field transport 77−8107
InP, transferred electron effects under high press. 80−34453
n-InSb, coherent microwave emission in high mag. field 79−60863
n-InSb, cond. electron cooling induced by CO laser and non-ohmic DC field 80−96941
n-InSb, convective instability in crossed mag. and elec. fields 77−62939
InSb, high field polaron transport 78−30932
n-InSb, hot electron noise temp., Monte Carlo calc. 80−107877
n-InSb, magnetoresist. in strong elec. field *(Russian)* 78−19056

high field effects continued
InSb, mobility from soln. of Boltzmann eqn. for electron-LO phonon scatt. 79−19586
InSb, surface carrier accumulation in crossed elec. and mag. fields 80−20205
InSb-NiSb, 8 mm band noise generation *(Russian)* 78−39175
InSe, current induced by impurity-absorbed IR radiation 78−10511
KBr, barrier instability in strong elec. fields 79−69522
KBr, current oscills. in elec. fields of $\sim 10^6$ Vm^{-1} *(Russian)* 77−20334
MgO, defect aggregation and thermal-electric breakdown, TEM obs. 79−42069
MgO, elec. field effects on cond. above 1300K, elec. breakdown 79−42551
MoS_2(2H), electro-absorpt. edge spectra, cryst. thermal modulation, exciton state field ionisation 79−61395
Na, highly excited d states, elec. field ionisation 77−6658
NaCl, barrier instability in strong elec. fields 79−69522
NaCl, current oscills. in elec. fields of $\sim 10^6$ Vm^{-1} *(Russian)* 77−20334
Na_2O-TiO_2-SiO_2 glass, elec. props. and energy gap 78−26921
Nb-Al_2O_3 composite, semicond. films, cond. on localised states 77−24628
Pb chalcogenides, elec. cond. anisotropy in strong electric fields *(Russian)* 79−38082
Pb, high-field thermal and elec. magnetoconductivities meas. 77−59279
PbS, microwave incremental conductivity, high-field, 77K 80−11026
$Pb_{0.8}Sn_{0.2}Te$:Cd, influence of Cd doping on high field magnetoresist. and Hall effect 80−75590
n-PbTe film, epitaxial, hot electron transport effects 77−12035
PbTe, high field drift vel. and Hall coeff. 78−26875
S, high-field injection currents 78−47801
S_n, liq., mobility variations of photoinjected charge carriers 79−91065
p-Sb_2S_3, bistable switching 79−73553
Sb_2S_3, hopping cond. in cryst. subjected to strong elec. fields 79−95456
SbSe, amorphous thin film high field charge transport and quasi-Fermi level location 80−70863
Si, amorphous, electrical transport and photocond. 77−85355
n-Si, appearance of high-field domain in pinch channel 78−26900
n-Si, bulk, high field characts. *(Japanese)* 78−34837
Si, charge transport properties, review 77−39851
n-Si, cond. in warm electron region, temp. depend. of anisotropy of nonlinearity coeff. 77−43610
Si, conductivity of holes at low temp., electric field depend. 77−28179
n-Si, current instability due to temp.-elec. domain pulsations 77−43608
n-Si, current-voltage characts., static high field domains 78−84223
Si, diffusion and power spectral density and correl. function of vel. fluctuation for electrons 80−65576
n-Si, elec. cond. control by hot electron intervalley transfer 80−59993
Si, electron drift in high elec. fields, long-time tail of autocorrelation function 80−103702
n-Si, electron heating by static elec. field 80−96894
Si, electron transport and ionisation at high fields 78−30933
n-Si, electron-phonon scatt. and high-field transport 79−42552
n-Si, electron-two phonon scatt. 77−47527
n-Si, field and current domains, at low temp. 80−6868
Si, high field electron transport, effect of ionised impurities 77−28186
Si, hole diffusivity, time-of-flight and noise meas. 79−56233
p-Si, hole drift vel. in high field 79−95415
n-Si intervalley electron-phonon deform. pot. consts. from high-field transport props. 77−62938
Si inversion layer, high field drift vel., Monte Carlo calc. 77−32087
Si inversion layer, negative differential resist. 78−60225
Si inversion layers, high field magnetocond. 77−32020
Si MOSFET, electron and hole drift velocities in high elec. field, Monte Carlo calc. 78−60224
n-Si, neutron or γ-irrad., elec. props., in strong elec. fields 79−95416
Si pin diode, current filament temp. and Au acceptor level capture cross section temp. depend. 78−95351
Si resistors, polycryst., elec. props. in nonlinear regime, grain boundary trapping model 79−38204
n-Si, size-induced magnetoresist. in strong elec. fields 80−65582
Si surface, field penetration and band bending in high elec. fields 79−42613
Si, UHF heating of charge carriers using lumped-capacitance resonators 80−20203
Si, voltage-current curves, specimens of variable cross-section 77−8113
Si:B, photoconductivity, impact neutralisation of H^--like centres 77−69377
n-Si:P(B), elec. cond. oscills., electron instability effects due to dislocations 80−103704
Si-SiO_2 boundary, relaxation of nonequilibrium capacitance in electrolyte in intense elec. fields 80−70845
Si-thermal SiO_2-electrolyte system, cond. in superhigh elec. field 78−52080
n-Si-V_2O_5 system, carrier transport mechanisms 77−62999
$Si_{6-z}Al_zO_zN_{8-z}$, hot pressed, DC elec. props., 18-500°C, fields up to 1.1×10^4 V cm^{-1} 78−26860
n-SiC, 6H, epitaxial layer, saturated electron drift velocity meas. 78−19168
SiC, point contact, stable elec. oscill. generation by high field strength *(Russian)* 77−62989
SiC, semi-insulating in struct. with injecting contacts, cond. in strong elec. field 78−19160
$Si_{12}Ge_{10}As_{30}Te_{48}$ glass, nonlinear I-V characts. 79−99557
$Si_{12}Ge_{10}As_{30}Te_{48}$, vitreous, localised states role in cond. in high elec. fields 77−76841
Si_3N_4, amorphous, in MIS struct., high field conductivity 78−23101
Si_3N_4, and Si_3N_4-MgO, hot pressed, DC elec. props., 18-500°C, fields up to 1.1×10^4 V cm^{-1} 78−26860
Si_3N_4, unsteady cond. in high elec. fields 78−76152
SiO_2, amorphous, high-field transport of excess electrons and holes 77−89767
SiO_2, amorphous electron transport and breakdown at high elec. fields 79−78108
SiO_2 film, spin-on oxide, phys. and cond. meas. 77−43762
SiO_2, high field electronic props. 78−30930
SiO_2, high field electron capture by screened Coulomb attractive centre 79−56237
SiO_2, in MOS struct., location of positive charged generated by high-field stressing 77−51820
SiO_2, thermal, elec. stressed film, dielec. breakdown 78−64322

high field effects continued
SiO_2, transport of electrons at high electric fields 80−20208
$Si_{12}Te_{48}As_{30}Ge_{10}$ amorphous film, high-field transient conduction 78−43500
$SnCl_2.2H_2O$ layered single cryst., protonic cond. and crit. behaviour 79−28136
SnO_2, glaze, high field cond., 4.2-470K 78−23100
SnTe, structural phase transition threshold instability in strong EM field 80−103477
TaS_2 (1T), nonlinear cond. in two-dimens. CDW system 80−10997
Te, electron mobility, elec. field depend., 77K 77−85233
Te film, field effect meas. 77−43757
p-Te Hall effect meas. at high elec. fields 77−66175
$Tl_2Se.As_2Te_3$, vitreous, thermal switching process in high electric fields 80−2432
V_2O_5, elec. cond. in strong fields, tunnelling mechanism 78−91699
ZnO, ceramic, nonohmic props. 77−85229
ZnO, elec. cond. at high fields 80−80287
ZnO, high-field cond. characts. calcs. 79−91056
ZnO, hot-electron microwave conductivity, hot-electron, high DC field 79−38113
ZnO, surface phenomena, interpretation by compensation model 78−95323
ZnO-based ceramic varistors, current-voltage characts., leakage and breakdown regions, 100 to 1300°C 79−56231
ZnS, current and refractive index oscills. in electric fields due to barrier instability 79−91372
ZnS, refr. index oscills, in strong. elec. field 79−28720
ZnS, single crystal, effect of elec. field on cond. 78−84228
ZnS:Cu, current pulses stimulated by elec. field at low temp. 78−39121
ZnS:Mn film, current conduction and light emission, physical mechanism 78−14840
$ZnS_{1-x}Se_x$:Cu,Br ceramic, current oscills. and electrolum. under high elec. fields 79−38677
ZnSe, cryst., elec. cond., dislocation motion effects 80−54710
n-ZnSe:In, heavily doped, high field DC cond. 79−65490

high-frequency amplifiers
see also microwave amplifiers; radiofrequency amplifiers; ultra-high-frequency amplifiers
50 MHz passband, stellar electrophotometer appl. 77−74434
bridge RF spectrometer, high freq. preamplifier 80−22380
pulse generator, HF oscillator with single coil transducer, for NMR spectrometer 79−2802
RF preamplifier, tunable, low-dissipation, for low temp. NMR appls. 79−17458
two-cascade cooled amplifier appl. to UHF quasi-zero double-comparison spectrometer, 21 cm *(Russian)* 77−29658
US amplifier for directly driving solid-dielectric capacitance speakers 80−19186

high-frequency discharges
AF glow discharge positive column, stratification obs. 78−67509
air, low-press. discharge characts. between polymer dielecs. 80−10448
air, microwave breakdown field calc., resonator and rectangular waveguide expt. 79−41789
air, reduced-press., bipolar elec. macroparameter diagnostics 80−1854
air, RF discharge, electron temp. and density 78−51371
air, unipolar HF discharge, determ. of gas and rotational temperature *(German)* 77−1033
air breakdown in superimposed DC and HF electric fields 78−67571
air HF corona discharge ignition characteristics 78−67589
arc, high current, burning in channel 78−63614
arc column helical instability in axial mag. field, damping and RF-DC discharge 78−71595
arcing voltage, two-valued discharge mode depend., geometric reson. *(Russian)* 77−47283
atomiser for at. absorpt. spectroscopy *(Russian)* 77−86426
beam-plasma discharge, microwave field spatial distrib., visible emission polaris. 78−67372
biological objects electrographic obs. *(German)* 80−17216
n-butane, decomposition in RF discharges, 10-40 torr 78−3318
collisional HF-discharge in RF range, ion distribution *(Russian)* 80−106986
combined RF and LF discharges 79−23477
corona, alternating, with superimposed DC field, at threshold voltage 80−1860
crossed-field discharge plasma instabilities, obs., 10 kHz to 2 GHz 78−75306
DC and UHF field energy transfer to glow discharge plasma electrons 78−67539
degree of nonequilib., freq. depend. 80−24275
density perturbations following pulsed discharge, laser beam obs. method 79−7498
diagnostics with Fabry-Perot interferometer, apparatus function 78−9872
dicyclopentadiene, liq., CO_2 laser breakdown plasma ignition, chem. reactions 80−66821
drift-dissipative instability, excitation suppression by weak transverse mag. field *(Russian)* 80−33829
dynamic plasma discharge microwave oscillation expt. 77−84433
electrodeless discharges, second stage with external magnetic field applied to plasma, investigation 80−24296
electrodeless in air, count rate emission with time of exposure to discharge 79−64936
electrodynamic properties, near-electrode layers of space charge effect 78−30510
electron energy distribution in a low-pressure RF discharge 80−87979
electron heating, nonlinear kinetic theory 80−44041
EM wave ionisation instability model 78−67512
ethane, decomposition in RF discharges, 10-40 torr 78−3318
ethylene, chemistry in RF discharge, mass spectrometric obs. 77−9084
ethylene, decomposition in RF discharges, 10-40 torr 78−3318
ethylene polymerisation and dissociation 77−70299
field visualisation technique applied to sub-mm diagnostics of axisymmetric plasma 80−43980
fluoromethane, RF discharge chemistry, added H_2 effect 80−33832
free plasma column, afterglow on switching off UHF power *(Russian)* 77−15265
free plasma column in gas at high pressure 78−75477
gas discharge source, nanosecond light pulses 78−22183
gasdynamic parameters meas. and calc. 78−94934

high-frequency discharges continued
H-pinch discharge, quasistationary, EM characts. and energy balance, erosion plasma generator 80−19630
hexafluoroethane, RF discharge chem., added acetylene effect, mechanistic model for fluorocarbon plasmas 80−84017
hexafluoroethane, RF discharge chemistry, added H_2 effect 80−33832
in inductor of finite size, EM field distrib. calc. *(Russian)* 77−19783
inert gas, continuous bremsstrahlung emission, radiation standard 80−1856
inert gas, optical diagnostics, bremsstrahlung 78−9871
inert gas high-current discharges, Z-pinch dynamic and radiative characts. 80−19631
inert gas plasma, weakly ionised, photon echo relax. obs. in RF discharge 80−43986
inert gas-SF_6 mixture, formation of inert gas fluorides in AC discharge 80−64817
ion source using HF glow discharge, temp. and electron density profile meas. *(German)* 78−70221
ionisational instabilities of EM wave in homogeneous high-freq. discharge *(Russian)* 78−34382
ionosphere, discharge around rocket following injection of electron beam 77−78570
isotope separation, HF stationary discharge, travelling mag. field, barodiffusion separation 80−44049
lamp with hollow electrode, for atomic spectroscopy 80−26090
laser spark, electron conc. limitation, electrodynamic mechanism *(Russian)* 80−59333
linear wave props., parametric decay, heating 78−42758
low pressure HF discharge, anomalous cond. mag. field effects 80−44047
low-pressure discharge in mag. field, alternating voltage distrib. obs. 78−67546
low-pressure discharge rectifying props., expt. 78−67545
low-pressure RF discharge electron temp. probes 78−67542
magnetic field, effect on alternating elec. field of HF discharge plasma *(Russian)* 79−37559
methane, decomposition in RF discharges, 10-40 torr 78−3318
methane-N_2-H_2 gas mixtures, RF discharge, vibr. and rot. anal. of CN, N_2 and C_2 78−5241
microwave, Langmuir probe meas. of electron energy distrib. 77−47293
microwave breakdown in gases, Schwinger variational principle 79−41788
microwave cavity discharge, behaviour at various press. and flow rates 79−23467
microwave discharge, breakdown and maintenance electric fields meas. 78−22587
microwave discharge, fast wave emission diagnostics 80−92391
microwave discharge, off-reson. technique appl. in ion source 78−327
microwave discharge, plasma probe characts. affected by microwaves 79−10733
microwave gas discharge problems in lasers *(Russian)* 80−14345
microwave induced plasma, mixed-gas low-pressure, excitation conditions 77−62422
microwave induced plasma discharge, emission source appls. 78−32880
microwave plasma, electron density determ. at atm. press. by hot wave method 77−35420
microwave plasma discharge, appl. to passivation of metals by polymerisation 78−64762
microwave plasma discharge, electron energy distrib. function *(Russian)* 77−11415
microwave plasma generation at atm. pressure, departure from LTE 78−67597
molecular-gas discharge in a rotating electric field 79−77444
multicomponent inhomogeneous plasma, spectroscopic analysis 78−67425
multipactor microwave discharge, electron vel. distrib., homogeneous polyphase reson. anal. 77−7628
near electrode region, spectra 80−38833
non-equilibrium HF discharge in quasi-stationary fields, stationary structs. *(Russian)* 80−84015
nonequilibrium discharge in converging wave beam, dynamics 80−44051
nonequilibrium microwave discharge, laser diagnostics 77−62405
ns surface discharge study in low press. 80−19640
optical discharges by laser radiation, continuous equilib. plasma maintenance 80−59259
with oscillating electrons in strong mag. field, optimum parameters *(Russian)* 78−26370
parametric decay instabilities in UHF discharge due to inhomogeneity parallel to pump field 80−19644
parametric instabilities excitation 78−34285
partially ionised inert gases in travelling HF mag. field 78−75474
photoelectron spectroscopy for investigation of excited molecules formed by HF gas discharge 79−36455
plasma, of corona and HF discharge, technological process appls. 80−1855
plasma, resonantly sustained, by Tonks-Dattner resonance 79−4142
plasma anomalous skin effect conditions 78−67544
plasma polymerisation on solid substrates, thin film form in RF discharge 80−2963
plasmatron, high freq. torch discharge calcs., burning regimes *(Russian)* 80−38723
plasmotron, capacitative, optimisation 79−55568
point discharge formation, photoelectric obs. 78−67581
polymer breakdown plasma analysis, mass-spectrometric installation 78−88670
pulsed capillary discharge, wall charge effects *(German)* 77−58908
pulsed high-pressure microwave discharge, electron density and elec. field calcs. 77−76238
pulsed high-pressure microwave discharge, electron temp. and distrib. calcs. 77−76239
pulsed microwave inert gas discharge, ion composition, mass spectra 79−14616
pulsed Xe discharges, in quartz chamber, elec. cond. meas. 79−55605
quiet plasma, in mag. field, produced by transverse diffusion from RF discharge 78−79448
reactive ion etching RF discharge plasma deceleration filter 78−41370
resonant HF radiation, from stationary discharge in Hg vapour *(Russian)* 79−55580
resonators for lower hybrid plasma heating, RF breakdown, 0.8-0.9 GHz 77−84564
RF, for sputter deposition and sputter etching, RFI/EM 78−71566
RF, gamma regime, ionis. balance and plasma characts., model 80−44022
high-frequency discharges continued
RF, oxidation of methane and n-butane with CO_2 78−15670
RF discharge, effective electron collision freq., energy dissipation, press. depend. *(Russian)* 77−19784
RF discharge, electrode sheath 80−44052
RF discharge, electron heating and ionisation, rate eqns. 77−24237
RF discharge, frequency characts. investig., in Ar-Hg mixtures 80−38761
RF discharge, neutral gas entrainment, rot. mag. field 79−10737
RF discharge, quiescent plasma prod. 77−7568
RF discharge in air, refined theory 77−76240
RF discharge in mag. field, plasma rate equation 78−67455
RF discharge plasma skin effect counteraction by external mag. field 78−67543
RF discharge plasmas, mag. field effects, probe and microwave meas. 77−7594
RF discharge-plasma interaction, energy exchanges, magnetoacoustic wave generation 78−30485
RF ion source 15 cm stable working region determ. 78−75381
RF plasma, press. depend. of electron temp. using RF-floated electrostatic probes 77−47253
RF sheath in self-sustained plasmoids, size and disappearance analysis 80−44026
RF spark ion source, multiply-charged species rel. abundance distribs. 77−61151
second-step discharge meas. and equivalent cct. 79−7505
self-acting field effect on spatial distrib., appl. to He *(Russian)* 79−99007
spectral determ. of excited atoms concentration, in Ne and Ar *(German)* 80−70053
spectral line widths in HF plasma diagnostics 79−10708
spectroscopic light source, for anal. of semicond. film on dielec. backing 80−66904
stability under conditions of strong skin effect *(Russian)* 78−14242
stationary stratified HF discharge in plane wave fields 78−67513
stellarator plasma, drift instability, stabilisation by AC elec. field *(Russian)* 79−7459
streamers, primary-secondary sequence in short point to plane air gaps 78−87569
surfatron low-pressure RF plasma source 78−67548
Tesla coil, effect on plastic track detectors 78−86742
tesla discharge, effect on soda glass, influence of ageing 78−39138
Tokamak microwave discharges, refraction losses, from measured plasma density profiles 78−22549
torch discharge, 2450 MHz, effect of water vapour in spectrochem. anal. *(Japanese)* 77−44554
transverse HF discharge, electron energy distrib. from spectra *(Russian)* 80−84012
trifluoromethane, RF discharge chemistry, added H_2 effect 80−33832
UHF and DC electrodeless discharges, charact. comparison 80−38762
UHF discharge plasma, parametrically excited relaxation oscills. 80−53978
UHF discharge plasma parameter meas., three-probe method 78−63630
UHF discharge with preliminary locally ionised gaseous medium 80−38851
UHF nonequilibrium plasma diagnostics by atomic bremsstrahlung continuum 78−67483
UHF plasma use as atomiser in atomic absorpt. spectrometry 79−92027
unipolar and electrodeless capacitively-coupled, excited at atm. press., appls. 80−1861
vacuum discharge, cathode spot, models analysis 80−19636
vacuum discharge, cathode spot parameters, existence diagram method applic. 80−24276
water, vapour RF discharge, low press., afterglow, spherical plasmoid, optical diagnostics 78−38568
waveguide, reduced press., UHF discharge propag. *(Russian)* 79−99008
Ar, arc type, spectral parameters 80−1873
Ar breakdown in superimposed DC and HF electric fields 78−67571
Ar, DC magnetron discharge, spectroscopic obs. 80−44010
Ar, excited atoms and metastable state densities meas. 79−14606
Ar HF torch discharge, spectral diagnostics 79−14607
Ar, high-frequency discharge, spectral parameters meas. *(Russian)* 79−10742
Ar induction HF discharge plasma in crossed fields, with Cs seeding, Hall parameter 79−55465
Ar inductively coupled RF plasma, spatial distrib. of temp. and number densities of electrons, atoms and ions 77−68873
Ar, low press. discharge afterglow, dissoc. recombination, microwave diagnostics 78−9876
Ar, optical gas breakdown, reduced threshold in two-freq. field 80−64819
Ar RF discharge plasma, magnetically stabilised, electron temp. using optical spectroscopy *(German)* 78−63582
Ar UHF discharge, spectral meas., Ar II lasing lines 79−99016
Ar, UHF discharge theory *(Russian)* 77−62430
Ar-Cs plasma, HF induction discharge, Hall effect *(Russian)* 77−43101
Ar-N_2 mixture, electrodeless RF discharge, discharge current harmonics obs., conc. depend. 80−44029
CF_2 radical, UV emission in microwave discharge, assignments 77−50461
CO-He-O_2 gas discharge laser plasma, positive ion generation mechanism *(Russian)* 79−99005
CO_2, capacitative discharge, high-freq. gas overheating suppression 80−38856
CO_2 cross-flow CW laser output and gain rel. to discharge instability 78−46563
CO_2 laser, continuous, fast flowing, thermal discharge contraction *(Russian)* 79−99009
CO_2, laser excitation by RF discharge with rot. elec. field, linear and circular polarisation 80−37991
CO_2, laser generation by pulsed microwave excitation 78−74879
CO_2 laser irrad. of air, breakdown plasma prod., elec. field meas. by probes *(Russian)* 80−59334
CO_2, plasma-chemical dissoc. in nonequilib. UHF and high freq. discharges 79−15990
CO_2-N_2-He, transverse combined discharge laser, 10-20 kW *(Russian)* 77−54703
CO_2-N_2-He laser, pulsed microwave discharge pump, skin effect and gain 79−13945
Cd vapour, RF discharge, isotope separation 80−79619

high-frequency discharges continued
GaN, deposition from plasma reactor, organo-metallic and donor-acceptor complex exchange in HF plasma 80−38839
H, HF discharge, gas breakdown, electron diffusion eqn. exact soln. 80−19658
H, RF induction discharge breakdown, diffusion theory 77−84562
H_2 dissociation in microwave discharge 78−23935
H_2, microwave discharge in atmospheric gas flow 78−42847
H_2-Ne, hollow-cathode discharge, electron energy distrib. 78−71573
H_2(-He), H production at 10 torr in pulsed discharge 80−9748
HCN+acetylene, cyanodiacetylene form. in RF discharge 79−5156
$H(^2S)+Ar(^3P_{0,2})$, energy transfer collisions, Lyman-α emission profile obs., in microwave discharge and reaction cell 80−58359
He, asymmetrical, mag. field effect on ionis. freq. *(Russian)* 78−26371
He, electron distribution function relaxation in high freq. gas breakdown *(Russian)* 80−14957
He flow, RF discharge test obs. 80−44028
He HF discharge double-probe meas. 78−67541
He I beam-plasma discharge, optical radiation polarisation 78−67478
He, microwave discharge, electrodynamic and spectral charact. *(Russian)* 77−11413
He, microwave discharge, emission processes, steady-state kinetic calcs. 77−68880
He, microwave discharge as source of atmospheric pressure plasma 77−35416
He, plasma, microwave-induced, evaluation as element-selective detector for gas chromatography 77−81450
He, preionis. power for required electron density 78−9896
He pulsed arc, Thomson scatt. diagnostics 80−24297
He, pulsed microwave discharge, vac. UV emission charact. 77−35408
He, quasicontinuous discharge, at high press., spectral obs. *(Russian)* 78−26356
He, RF, plasma parameters and volt-ampere charact., two discharge regimes 80−44016
He, RF induction discharge breakdown, diffusion theory 77−84562
He-F(O)(N)(Ar) mixtures, RF discharge, mass spectroscopy, floating double probe meas. 80−84016
He-Hg RF discharge, atomic ionis. and excitation, spectral line intensities 78−26334
He-Ne, electron energy distrib., laser appl. 77−34874
He-Ne laser radiation intensity rel. to striations and oscillations 77−83852
He-Ne laser with transverse microwave discharge, use of secondary electrons 80−9899
He-Ne waveguide lasers, HF discharge stability 79−18401
He-Zn hollow-cathode discharge, excitation processes, rel. to Zn II laser 79−98342
He_2 lines role in RF discharge plasma satellites 80−44053
^3He, nucl. relax. in gas discharge at liq. N_2 temp. 80−100114
Hg 40.8 MHz discharge electrode space-charge sheath thickness obs. 78−67547
Hg, HF discharge mode two-valued depend. on arcing voltage, geometric reson. *(Russian)* 77−47283
Hg-Ar, HF discharge, electron energy distrib. and atom ionisation processes 80−44048
Kr, high-frequency discharges, at sub. atm. press. 78−67460
Kr microwave afterglow, Kr_2^+ dissoc. recombination coeff., electron temp. depend. 78−30501
Kr-Xe, isotopic mixtures, separation in high-freq. discharge in mag. field *(Russian)* 77−75317
Mg nitridation in HF discharge, temp. effect 80−3399
N_2 breakdown in superimposed DC and HF electric fields 78−67571
N_2, DC glowing discharge rel. to microwave discharge, electron energy distrib., probe meas. *(Russian)* 77−47280
N_2, microwave discharge at high press., vibr. excitation *(French)* 78−14239
N_2 plasma heating in electrodeless RF capacitative discharge, mechanism, impurity effect 80−59312
N_2^+, excitation in RF discharges *(French)* 77−61868
N_2-O_2 mixture transient discharges, RF techniques 80−70067
N_2-O_2 nonselfsustaining discharge plasma, current establishment/relax. processes, rel. to CO_2 laser *(Russian)* 79−99011
N_2(N_2+Ar) pulse excited microwave discharge diagnostics at moderate press. 78−9873
NO, high frequency discharge 79−82105
NaH, $A^1\Sigma^+$ states radiative lifetime in HF discharge 77−6841
Ne, 4 MHz discharge, electron energy distrib., probe diagnostics 78−38566
Ne HF discharge plasma electron energy distrib. 78−67540
Ne, laser fluoresc. spectroscopy in microwave discharge 79−36578
Ne, low press. discharge afterglow, dissoc. recombination, microwave diagnostics 78−9876
Ne microwave breakdown field calc., Monte Carlo method 78−67551
Ne, RF discharge, emission modulation due to fast electron distrib. time variation 79−41900
Ne, with and without electrodes excited atoms concentration determ., comparison with glow discharges *(Russian)* 80−70050
Ne-Ar mixtures, glazed electrode AC discharge mode transition obs. 78−67558
Ne-H_2 h.f. pulsed discharge, atomic excitation of H *(French)* 77−433
Ne-Hg RF discharge, atomic ionis. and excitation, spectral line intensities 78−26334
O, RF capacitively coupled low press., spatial and temporal emission spectroscopy 79−27847
O_2 (inert gas), surface modification of polymer, ESCA obs. 78−3438
O_2 capacitative discharge, high-freq. gas overheating suppression 80−38856
O_2, prod. of cold plasma rich in metastable species *(French)* 78−14238
O_2, RF discharge, moderate press., O production kinetics 79−64934
SF_6-R-He(Ar) ternary mixtures, formation of inert gas fluorides in AC discharge 80−64817
Xe, arc, wall-stabilised, dynamic analysis, radiation transport 80−44066
Xe discharge, HF, with propag. EM wave, isotope distrib. *(Russian)* 77−76235
Xe, high power pulse gas dischargees development, photographic obs. 80−14954
Xe isotope separation in HF discharge, thermodiffusion *(Russian)* 77−46649
Xe, isotope separation in RF discharge light inert gas admixture effects 79−41250
high-frequency discharges continued
Xe, microwave discharge, energy charact. 78−5979
Xe, pulsed high frequency discharge, energy spectrum and electron density meas. *(Russian)* 78−26354

high-frequency effects
see also helicons; hot carriers; skin effect; solid-state plasma
alkali metal-ammonia solns., metal-insulator transition, h.f. and u.s. props. 77−1369
amorphous semiconductor, cond. tensor, freq. depend. in presence of mag. field 80−44631
chalcogenide glasses, elec. cond. at room temp., contact effects 77−20354
chalcogenide semiconductors, glassy and liq. states, elec. cond. freq. depend. 77−76856
charge density wave condensate high freq. cond. at low temps. 79−95392
charged-particle stream, wave interaction, nonlinear effect 80−80310
compensated semiconductors, HF impedance 79−15212
conducting medium in const. mag. field, two EM waves secondary field generation 79−36828
conductor, EM wave penetration, effect of impurities and spatial dispersion 79−7813
conductor, high-frequency props., electron relax. time and impurity scatt. amplitude *(Russian)* 77−32033
crystals, dipole-impurities, HF elec. cond., dielec. losses and light absorption 77−63363
degenerate free electron metal, cyclotron wave propag., finite $\omega\tau$ effect 77−20228
degenerate semiconductor, EM wave absorption 78−95308
degenerate semiconductors, EM absorpt. theory 79−33307
diamond:Li, ion implantation, Hall effect and elec. cond. meas. 80−15526
dimensional quantisation effect, HF characteristics at low temps., multiphoton absorpt., tunnelling *(Russian)* 78−68073
disordered gyrotropic systems, cond. tensor, freq. depend. in presence of mag. field 80−44631
disordered semiconductor, photon-phonon-assisted hopping, theory 80−44642
disordered system, zero-phonon high-freq. cond. 78−47824
disordered system of two level atoms, high-freq. phononless conductivity *(Russian)* 78−43432
disordered system with two level atom, low temp. zero photon high freq. conductivity 78−91718
disordered systems, phononless HF cond. 77−89789
Eccosorb HF-2050, AC resistivity meas., 100-320K, 500-2000 MHz, von Hippel's method 77−32314
electrical conductivity freq. depend. in disordered system two site model *(Russian)* 80−54666
electrolyte solution, HF elec. cond. and dielec. const., determ. in RF region 77−21396
electron gas, conductivity of interacting electrons 77−20351
EM wave excitation and amplification under negative differential cond. conditions 77−15865
excitonic and optical insulators with nonequilibrium distrib. of quasiparticles 77−15888
ferrite-semiconductor structure, resonance galvanometric phenomena in semicond. 78−87989
ferromagnetic conductor, plasma effects, selective transparency near antiresonance region 80−100476
ferromagnetic metal, freq. depend. elec. cond. 77−66181
ferromagnetic metal slab, transmission of 24 GHz radiation, effect of diffuse surface scatt. of carriers, calc. 80−34780
ferromagnetic semiconductor, LF magnetostatic waves with discrete spectrum 77−89792
n-GaAs, intrinsic avalanche response time, orientation depend. 79−51587
p-GaSe, relaxational oscillations of photoconductivity and dark conductivity 77−69379
p-Ge, 2 mm wave radiation, interaction with charge carriers *(Russian)* 78−87991
granular material, HF conductivity, theory *(Russian)* 78−23124
graphite, intercalation compound with AsF_5, high elec. cond. 78−26838
graphite, intercalation compounds with AsF_5, elec. cond. meas. with high anisotropy 78−26837
Hall mobility, microwave meas. method 79−54154
helicons, LF, excitation and amplification by HF helicoidal wave in medium with degenerate carriers 78−14755
HMTSF-TNAP, microwave cond. at 35 GHz 80−24963
ice VI, polymorphic transition at high-press., 123.1K, HF permittivity study 79−55883
inhomogeneous semiconductor with nonequilibrium carriers, EM wave propag. 78−52024
insulator, modulation oscills. of travelling EM wave 80−24962
intercalation compounds 78−26836
intermediate conducting solid, microwave eddy currents and EPR 77−80996
intrinsic semiconductor, nonlinear theory of EM wave propagation *(Russian)* 78−60150
Josephson effect, electronic analogue prototype 80−100560
Josephson junction, high-frequency, high-voltage effects on useful limit 77−1521
Josephson tunnel junctions, high frequency losses 78−88083
liquid semiconductors, resistivity temperature dependence, meas. apparatus for 10^{10} Hz freq. region 78−21169
many-valley semiconductor, longitudinal bulk EMG due to inhomogeneities 78−19045
many-valley semiconductors, conduct. in heating electromag. wave 80−84483
MBBA, HF electrohydrodynamic instability in NLC *(Russian)* 80−54130
metal, EM generation of ultrasound in static mag. field 78−14768
metal, RF size effect, line shape, exactly solvable models 78−43429
metal, RF size effect, small-angle scatt., exactly solvable models 78−47821
metal, surface charges waves *(Russian)* 78−64077
metal, surface impedance in mag. field, cyclotron waves 77−89787
metal, wave excitation, with mirror surface, near cyclotron resonance *(Russian)* 78−35040
metal conductivity, plasma model 80−80311
metal film, EM energy transformation into acoustic energy, temp. depend. 77−55619

high-frequency effects continued
metal film, surface impedance oscillation effects due to one sided RF excitation *(Russian)* 80−11106
metal film, transverse E-type quantum waves *(Russian)* 78−91785
metal plate, radioelectric effect 80−70744
metal surface, semiclassical infinite barrier model 78−64079
metal surface problems in microwave region, theory and meas. *(Chinese)* 80−44704
metallic crystal, RF size effect, electron scatt. by impurities diffuse layer boundary *(Russian)* 78−91717
metallic plate, electron refl. effect on EM field transmission *(Russian)* 77−11952
metallic thin film, EM wave transmission under resonance conditions *(Russian)* 80−54805
metals, microwave transmission, time-of-flight effects in Fermi vel. determ., calc. 80−20238
metals and semimetals in strong mag. fields, EM excitations, review 77−8130
microwave conductivity determ. from eddy current losses in planar specimens of high cond. 80−47077
MIS, HF capacitance, minimum value and position 77−85338
MIS structure, EMF origin in pulsed UHF field 77−4448
MIS structure, optical phonon-electron gas interaction, high freq. cond. 80−6888
narrow band gap semiconductors effects, review 79−95437
narrow gap semiconductor, sound absorpt. in strong EM field 77−55590
narrow-gap semiconductor, carrier quasienergy spectrum in strong EM wave field 80−92922
narrow-gap semiconductors, microwave effects, review 79−82618
negative conductivity of media with inhomogeneous distrib. of mobility in crossed E- and H-fields *(Russian)* 79−1606
negative high-frequency conductivity of media having a nonuniform distribution of mobility in crossed E and H fields 79−82619
NLC, high frequency electrohydrodynamic instability, permittivity, elec. cond. *(Russian)* 80−49099
nondegenerate semiconductor, quantum correction of Einstein reln. at high freqs. 78−19072
nonlinear absorption of EM waves by band charge carriers in laser field 77−14767
parametric excitation in solids, quantum calcs. 80−103714
piezoelectric semiconductor, acoustohelicon waves, parametric excitation 79−38135
piezoelectric semiconductor, resonant microwave absorption by electrons in strong piezoacoustic wave 77−85270
polar liquids, HF conductivity and relaxation time 80−96929
polar semiconductors, HF mobility in longitudinal quantising mag. field 79−51619
polar semiconductors, peak electron velocity, simple method for estimation 77−8129
polar semiconductors HF conductivity at low temperatures, anal. *(Russian)* 77−8128
polyacene quinone radical copolymer, reversal of usual electric field effect and nomadic polarisation 77−12304
polyacetylene:I, dc microwave cond., permittivity 80−107843
polyacetylene:I, electric props. in semicond. and metallic regions 80−29432
polymer, heat treated, numerical simulation of AC elec. props. 78−43431
powder semiconductors, HF conductivity depend. on surface energy band bending *(Russian)* 77−15890
quantised inversion layer, hot carrier transport 78−30993
quasi one dimensional charge transfer salts, soliton model for dielectric permeability 80−40036
quasi one dimensional organic materials, microwave cond., dielectric const. *(Hungarian)* 78−26850
rare earth arsenides, microwave resist. meas. 77−4383
SCLC diode, influence of carrier transit time on small-signal admittance 77−85305
Seebeck effect, volume component determination 80−49788
self-oscillatory semiconductor medium, coupled temp. and carrier density self-oscills., photoelectron heating, microwave field 79−11166
semiconductor, absorption of strong EM waves, weak electric field effects 79−95400
semiconductor, amorphous or disordered, cond. mechanisms, model of medium-range comp. disorder 78−79994
semiconductor, carrier relax. time and effective masses determ. by microwave photocond. meas. *(Russian)* 78−19071
semiconductor, carrier relaxation time anisotropy effect on free carrier dispersion studies 80−84474
semiconductor, dislocation cond. process at low temp. 79−99551
semiconductor, electrical instability, negative differential cond., electron heating by static and alternating elec. fields 79−11165
semiconductor, electron distrib. function in alternating fields, single particle Monte Carlo method 77−89791
semiconductor, electron heating by strong static and HF elec. fields 77−8112
semiconductor, exciton condensation, microwave cond., book contrib. 80−11043
semiconductor, HF EM effects, nonquadratic dispersion law of carriers 78−19078
semiconductor, HF field energy absorpt. in strong parallel mag. and elec. fields 79−73801
semiconductor, hopping conduction influence of HF elec. field 78−52025
semiconductor, inertia of Benedicks effect in carrier heating by microwave field 79−15173
semiconductor, inhomogeneous, EM waves under elec. and mag. field 80−20237
semiconductor, inverted hot electron states and negative cond. *(Russian)* 77−43612
semiconductor, IR transmission, cond. variations effects 79−15158
semiconductor, Kane, thermoelec. power and thermomag. effects of hot electrons 78−56174
semiconductor, magnetoresistance in strong UHF electric fields 77−1437
semiconductor, many-valley, conductivity in RF heating field *(Russian)* 78−76085
semiconductor, microwave absorpt. near optical phonon creation threshold 78−47823
semiconductor, microwave magnetoconductivity in large quantising mag. field, effect of band non-parabolicity 79−47112
semiconductor, n-type, mag. and elec. dimens. reson., gyrotropic sphere problem 79−42570
high-frequency effects continued
semiconductor, n-type, surface wave SHG 79−60860
semiconductor, nonhomogeneous hot solid state plasma, transverse EM instabilities 77−66177
semiconductor, nonlinear intense EM wave absorpt. *(Russian)* 80−29425
semiconductor, normal transverse waves in longitudinal mag. field 80−80309
semiconductor, odd magnetoresist. in Hf elec. field 77−28198
semiconductor, optoelectric effect and oscillations near surface 77−8172
semiconductor, piezoelec. and nonpiezoelec. cyclotron-phonon resonance due to polarisation scatt. from phonons 79−95649
semiconductor, possible apperance of negative differential conductance at microwave freq. 79−11164
semiconductor, quantum electron-phonon system, theory of parametric excitation 78−10489
semiconductor, size quantised, superlattice state 78−39142
semiconductor, waveguide method of measuring elec. parameters at microwave freq., review 79−93170
semiconductor, weak heating of electrons, cyclotron reson. conditions, quantising mag. field 78−39141
semiconductor diodes, minority and majority mobilities, transit time effect determ. 78−14753
semiconductor electron plasma, EM wave propag. in external alternating mag. field 77−20350
semiconductor film, quantised, indirect interband absorption rel. to surface irregularity 78−39618
semiconductor film with macroscopic surface defects, size depend. of HF cond. 77−89888
semiconductor in inhomogeneous EM field, nonlinear HF cond. 77−51773
semiconductor microwave conductivity meas. by eddy current loss method 78−8417
semiconductor plasma in electric field EM wave propag. 77−43636
semiconductor quantised inversion layers, hot electron microwave cond. calc. 77−43734
semiconductor subjected to mag. and US fields, EM radiation gain 80−48201
semiconductor superlattice, nonlinear HF conductivity 77−15889
semiconductor surface-state props., using field effect anal. 79−24053
semiconductor with negative differential conductance, amplification of HF waves 79−15177
semiconductor with quasirelativistic band struct., hot electron kinetic equation 78−84222
semiconductor with superlattice, EM wave absorpt. by free carriers, high freq. quantum transport eqn. 78−60148
semiconductor with superlattice, EM wave propag., mag. field effect 80−70745
semiconductor with superlattice, high freq. cond. 79−69542
semiconductor with superlattice, nonlinear interaction of two waves 78−10494
semiconductor-dielec. superlattice, high freq. electromagnetic response 78−19073
semiconductor-insulator boundary, space charge layers, HF magnetoconductivity 78−60231
semiconductors, ballistic electron transport, AC impedance meas. 80−80306
semiconductors, cyclotron resonance, high frequency differential cond., needle shaped distribution model 79−65509
semiconductors, elementary excitations in disordered systems with localised electrons, polarons *(Russian)* 80−49632
semiconductors, freq. breakdown 80−75592
semiconductors, surface magnetoplasma wave spectrum in HF mag. field 80−24995
semiconductors with superlattice, absolute negative resist. *(Russian)* 78−34838
semiconductors with superlattice, nonlinear amplification of EM oscillations 79−51623
semiconductors with superlattice, third harmonic generation *(Russian)* 77−27315
semimetal-exciton phase transition, microwave cond. 80−29430
soda glass, ageing effect of HF discharge on conductivity and dielec. const. 78−39138
solid electrolytes, microwave conductivity 79−55929
static conductivity change under quantum cyclotron reson. 78−39143
stearic acid film, in MIM struct., AC cond. and dielec. props., freq. depend. 80−55030
superconducting contact, crit. current, effect of UHF field *(Russian)* 78−72313
superconducting short bridges, critical current depend. on high. freq. field 80−44774
superconductivity theory, HF cut offs of Coulomb interaction, real freq. Coulomb pseudopotential derivation 80−49980
superionic conductor, microwave cond. theory, hopping model 80−59710
superionic conductors, freq. depend. cond., correl. effect, Scher-Lax model 80−34238
superlattice, nonlinear plasma oscillations in high freq. elec. field 79−19612
superlattice semiconductors, negative absorption in strong HF fields 77−55539
surface impedance in mag. field 77−89786
TCNQ salt, TMTSF-TCNQ, microwave cond. at 35 GHz 80−24963
TCNQ salts with asymmetric donors, transport props. 79−23953
tetraselenotetracene bromide, positive microwave dielectric const. 78−47771
tetrathiotetracene iodide, positive microwave dielectric const. 78−47771
thin conductors, SHG and size cyclotron reson. 78−72186
thin metal conductors, surface impedance oscills. in RF range *(Russian)* 79−91090
thin metal disks, anomalous microwave transmission 79−60864
$(TMTSF)_2X$, ($X=PF_6^-$, AsF_6^-, SbF_6^-, BF_4^-, NO_3^-) highly conducting salts, props. 80−59969
transition metal oxides, 3d-, microwave cond. at high temp. *(Japanese)* 78−91715
TSeF-TCNQ, nonlinear electronic transport, microwave harmonic mixing obs. 80−20168
TTF-TCNQ, anal. of harmonic microwave mixing 80−44635
TTF-TCNQ, and Se analogues, microwave conductivity meas. by coaxial resonator technique 77−4384
TTF-TCNQ, controlled defects effect on microwave cond. and dielec. function 80−24885

high-frequency effects continued
TTF-TCNQ, Hall mobility using Faraday rot. method at 9.3 GHz 77−47801
TTF-TCNQ, microwave eddy currents and EPR 77−80996
TTF-TCNQ, nonlinear electronic transport, microwave harmonic mixing obs. 80−20168
TTF-TCNQ, positive microwave dielectric const. 78−47771
TTF-TCNQ, semicond., driven oscills. of carrier conc. 80−15551
two-level system resonant processes in presence of nonresonant fields *(Russian)* 80−14308
type I superconductor, order parameter, influence of HF fields 79−28486
uniaxial semiconductor with hot carriers, EM instability 77−32021
n-ZnSe:In, highly compensated, freq. depend. of cond. 79−99548
Ag, anisotropy of electron-phonon collision frequency on Fermi surface, RF size effect 77−15750
Ag, size effect, ballistic-type field penetration at 45 GHz, 3 MHz 80−44634
Ag-Cu eutectic composite wire, HF conductivity and skin effect 79−33305
Al, bicrystalline, RF size effect at intercryst. boundary *(Russian)* 80−29431
Al, electron-phonon collision frequencies, RF size effect, Fermi surface study 79−90945
Al, film, surface resist. freq. depend. in range 7.7 to 37 GHz 77−20468
Al film in microwave radiation field, resistive state transition *(Russian)* 80−93038
Al, point contact Josephson junction, microwave-enhanced critical currents 77−8242
Al rod, US amplitude distrib. generated by direct EM method 78−2526
β-Al_2O_3, Na, K and Ag substitued, lattice vibrs., ion transport spectra 77−20121
As-Se-Te system glasses, AC cond. and permittivity, freq. and temp. depend. 77−76857
As-Te-Cu system glasses, DC and AC cond., thermo-EMF, freq. depend., 100 to 370K 77−76827
As_2S_3, amorphous, shear wave attenuation and high freq. elec. cond. 80−11027
As_2Se_3 glass, microwave elec. cond. and struct. 80−49793
As_2Se_3, molten chalcogenide semicond., temp. depend. of 10^{10} Hz elec. cond. 77−4388
$Ba_{0.4}Sr_{0.6}TiO_3$ films, DC conductivity, strong microwave field effect 80−65727
$BaTiO_3$ a-domain crystals, domain struct. influence on physical consts. 79−69798
Bi, dielectric anomalies, electronic relax. times at far IR frequencies 77−24513
Bi, EM wave dispersion and damping, Voigt configuration, non-local calcs. 80−100475
Bi, EM wave excitation *(Russian)* 77−32093
Bi, instability induced by microwave field, carrier overheating 78−19076
Bi, magnetoplasma waves in strong mag. fields at 300 GHz 79−38116
Bi, microwave magneto-absorption, NENP Cohen model 77−39766
Bi, surface impedance change, reflected RF EM wave interaction *(Russian)* 80−49867
Bi-Sb, magnetoplasma waves in strong mag. fields at 300 GHz 79−38116
Bi-Sb narrow gap semiconductor, EM wave propagation in direction parallel to mag. field 78−80014
$Bi_{0.89}Sb_{0.11}$, effect of band structure on the dispersion of magnetoplasma waves 77−47845
$Bi_{0.9}Sb_{0.1}$, magnetophonon effect on hot electrons *(Russian)* 80−107814
$Bi_{0.924}Sb_{0.076}$, doped, optical, oscillation and galvanometric effects *(Russian)* 77−85247
$Bi_{100-x}Sb_x$, lattice dielec. const. meas. 78−10490
Cd, surface impedance, in mag. field *(Russian)* 78−19079
$Cd_{1-x}Ag_xCr_2Se_4$, ferromag. semicond., influence of strong elec. field on microwave absorption 77−28207
$CdAs_2$ based glasses, cond. and permittivity, freq. depend. 77−76859
$CdCr_2Se_4$:Ag, ferromag. linewidth and eddy current losses 79−33541
$Cd_xHg_{1-x}Te$, photomag. and photothermomag. effects *(Russian)* 79−78137
CdS, parametric action of strong radiation field 78−14752
CeP(As)(Sb), microwave resist. meas. 77−4383
$Co_{0.83}(Pt(C_2O_4)_2).6H_2O$, cond., dielec. const., microwave obs. 80−44636
Cr_2O_3, dielectric const. and loss, cond., 10^2-10^7 Hz, 30-450°C 77−59504
Cr_2S_3, rhombohedral single cryst., AC cond., freq. and temp. depends. 77−76810
Cu, open orbit microwave transmission peaks 78−10491
EuO, HF conductivity meas. 79−33304
EuO, microwave and DC cond., dielec. const., 1.7 to 300K 77−20347
EuO, microwave cond., influence of mag. ordering 79−69544
EuO:Gd, critical specific heat depend. on doping, microwave cond. 79−95602
EuSe, annealed, AC conductivity and dielectric anomaly 80−34445
EuSe, HF conductivity meas. 79−33304
EuSe, microwave and DC cond., dielec. const., 1.7 to 300K 77−20347
Fe-Al (45%), ordered and disordered states, optical and elec. props. 77−85826
Fe_3BO_6, spin-reorientation, elec. resist. and microwave absorption 78−14751
α-Fe_2O_3, electrical conductivity 77−69365
Fe_3O_4, dielec. props. of low temp. phase, at microwave freq. 78−64309
n-GaAs, conductivity relax. times in warm electron range, intervalley transitions 77−55537
GaAs, diffusion and power spectral density and correl. function of vel. fluctuation for electrons 80−65576
GaAs, electron dynamic properties in strong elec. field, anal. *(German)* 78−43404
n-GaAs, epitaxial, thermoelec. power, temp. depend. in mm wavelength range 79−23996
GaAs, Gunn diode, velocity-field characts. at 35 GHz, impurity conc. var. 77−85306
GaAs Gunn diodes, microwave oscill. generation at two freqs. 80−65614
GaAs hot electrons drift rate/field strength characteristic in microwave fields *(German)* 78−43430
n- GaAs, hybrid-hybrid mode interaction in crossed elec. and mag. fields 78−51997
n-GaAs, IR transmission, cond. variations effects 79−15158
GaAs, inertia of intervalley redistribution of electrons, meas. of V(E) relationships by microwave method 79−82621

high-frequency effects continued
n-GaAs, inverted hot electron states and negative cond. *(Russian)* 77−43612
GaAs ion implantation parameter determ. by microwave contactless mobility meas. 78−10527
n-GaAs, limiting freq. of Gunn effect in polyharmonic LSA mode 80−6856
n-GaAs, parametric interaction of HF waves, anal. 80−15554
n-GaAs, subject to crossed static elec. and mag. fields, microwave amplification 77−1440
n-GaAs, submillimetre cond. and carrier heating, two-electron-temp. model 77−20349
GaAs:S(Se), ion implanted, evaluation by contactless mobility meas. 79−1448
$Ga_{0.47}In_{0.53}As$, HF carrier mobility, temp. depend., theory 80−75593
$Ga_xIn_{1-x}Sb$, electron transport in RF field, Monte Carlo simulation 80−96932
Ge, amorphous film, high freq. cond., AC loss 80−49792
n-Ge, anisotropy of thermal and convective noise, in magnetic field 78−34873
n-Ge, current carrier-dislocation interactions, resistance in UHF range *(Russian)* 80−54732
Ge, determ. of nonradiative decay rate in electron-hole drops at 1.6K 77−8143
Ge, diffusion coeff. of hot holes meas. 78−6387
p-Ge, dislocation microwave cond. and Hall effect meas. *(Russian)* 77−47848
n-Ge, dislocational microwave conductance anisotropy *(Russian)* 79−91092
Ge, drift velocity of plasma cloud, at high elec. field 80−6887
n-Ge EM wave interaction with hot electrons, in strong mag. field with Voigt config. 77−69367
Ge, electron-hole drop motion recorded by microwave probe meas. 77−76755
p-Ge, energy spectrum of impurities and effect of mag. field *(Russian)* 77−47770
Ge, exciton condensate and electron-hole droplet, metastable state, effect of illumination and high-frequency heating 79−15097
Ge, exciton condensation, microwave cond. below 1K, book contrib. 80−8997
Ge, exciton condensation, microwave cond., book contrib. 80−11040
Ge, exciton condensation, microwave breakdown, luminesc., book contrib. 80−11471
Ge, exciton microwave breakdown, electron-hole drops, book contrib. 80−11041
Ge, excitons, influence of temp. on high freq. breakdown in presence of electron-hole drops 78−26820
Ge, explosive instabilities in electron-hole drops under microwave radiation 77−31951
Ge, Foucault currents in electron-hole drops *(Russian)* 77−8030
Ge, HF field effect meas. 77−55556
n-Ge, homogeneous, avalanche ionisation and current oscills. 77−15864
Ge, magnetic field effects on hot-hole noise 77−4415
p-Ge, magneto-microwave Kerr effect, expt., scatt. mechanisms 78−39139
Ge, magnetoconductivity meas. at 9.3 GHz, using three-wave interferometer *(French)* 77−47844
Ge, microwave absorption by nonequilibrium carriers, carrier density determ. method 77−8148
Ge, microwave absorption by nonequilib. current carriers, book contrib. 80−11042
Ge, microwave exciton breakdown and luminesc., under one- and two-photon excitation 77−31955
Ge, microwave exciton discharge, collision frequency, hot carrier temp. determ. *(Russian)* 79−65507
Ge, near intrinsic, negative differential cond., ambipolar size effect due to hot carriers 78−72185
Ge, nonuniformly deformed, electron-hole drop density depend. on size *(Russian)* 80−20092
Ge, oscillatory exciton breakdown, microwave cond. 80−103716
Ge oscillistor, hysteresis effects and N-shaped V-I characts. 79−33306
Ge, periodic explosions of electron-hole drops 77−11950
n-Ge, single cryst. with dislocations, UHF cond. *(Russian)* 79−78128
Ge slab in waveguide, microwave absorpt. due to geometric reson. of longitudinal-section elec. surface waves 80−39874
Ge, strong microwave field effect on electron-hole drops, luminescence kinetics 79−87047
Ge, surface, high freq. cond. and cyclotron reson. 80−11273
Ge surface microwave cond. observations *(Russian)* 80−2447
n-Ge, vel. component of hot charge carriers' thermoelectromotive force 80−44630*
Ge waveguide, nonlinear third harmonic generation of submillemetre waves 80−44632
Ge:Au, unipolar injection influence on high frequency conductance 80−34474
n-Ge:P,Ga, compensated, uniaxially compressed, anisotropy of mm. and submm. wave absorpt. 78−19074
Ge-Si, heat treated, carrier heating by strong microwave elec. field 77−69366
He, liq., surface, 2D electron plasma, RF absorpt., parallel pumping *(Russian)* 78−22911
He, liq. surface, electron liq., high freq. cond. electron correlation effects 80−107589
He, liquid, surface electron high freq. cond., electron system heating, I-V characts. *(Russian)* 80−29244
HgTe, and ternary compounds, mag. field induced microwave transparency 80−49797
n-InP, submillimetre cond. and carrier heating, two-electron-temp. model 77−20349
n-InSb, 2 mm wave radiation interaction with charge carriers *(Russian)* 78−87991
n-InSb, degenerate plasma, Coulomb collision photon absorpt. dynamic screening *(Russian)* 80−92924
p-InSb, elec. instability and oscills. of transparency in transverse mag. field 78−6407
InSb, electron drift velocity in fields up to 800 V/cm in presence of impact ionisation 78−39120
InSb, HF props. of hot electrons at 77K, calc. using Monte Carlo method 80−15553
n-InSb, helicon wave propag., quantum mechanical features 79−42571

high-frequency effects continued
p-InSb, high resist. compensated, generation of microwave radiation 80−34476
InSb, hot electron energy relax. time 77−80783
InSb, impact ionisation and magneto-transport, high crossed elec. and mag. fields 80−107797
InSb magnetoresistive elements, fundamental effects *(Japanese)* 80−11013
n-InSb, microwave displacement effect in longit. elec. and transverse mag. fields 78−87992
InSb, microwave magnetoplasma matching effect 78−14750
n-InSb, millimetre rare modulation in semicond. plasma, use of effects of high elec. field. 78−60149
InSb n-type, heavily doped, effects of hydrostatic pressure on electron mobility and conc. 77−4390
p-InSb, oscills. of microwave photocond. and cyclotron reson. of photoelectrons 79−28377
n-InSb powder, microwave propag., 90-300K, magnetoplasma and helicon wave excitations 78−72183
p-InSb, radioelec. effect, 100-300K 79−56255
n-InSb, subjected to mag. field normal to current, coherent HF oscills. 78−52026
InSb waveguide, nonlinear third harmonic generation of submillemetre waves 80−44632
$LiAlSi0_4$, β-eucryptite, superionic conductor, order-disorder transition, microwave impedance obs. 79−14966
$MgSO_4$, aq. soln., electrolytic conduct. affected by US waves 79−23997
$Mn_{0.7}Zn_{0.1}Fe_{2.2}O_4$, temp. depend. of microwave resistivity 79−69540
$Na_{0.33}V_2O_5$, dielec. const. and microwave cond. 78−60378
Nb wire interaction with stationary gases in high vacuum, HF fields effects *(Polish)* 79−34394
$NbSe_3$, freq. depend. conductivity 80−107838
$Ni_xFe_{3-x}O_4$, $x<1$, anomalous microwave loss 79−69540
NiO, microwave cond. and DC cond. meas., 803-1873K 77−43638
Pb, superconducting thin film resonator, high-freq. characts. in mag. field *(Russian)* 78−31014
Pb-PbO_x-Pb small supercond. tunnel junctions, effect of capacitance in I-V characts., high-freq. obs. 80−80448
$PbCo_{1/2}Te_{1/2}O_3$, antiferroelec., high-frequency permittivity, temp. depend. 80−71325
PbS, microwave incremental conductivity, high-field, 77K 80−11026
$PbSc_{2/3}Te_{1/3}O_3$, ferroelec., high-frequency permittivity, temp. depend. 80−71325
n-PbSe, polar semicond., mag. field influence on high-freq. relaxation time 79−95438
PbTe, asymm. strip line wall, EM wave propag. in mag. field 77−76854
PrP(Sb)(Bi), singlet ground state paramag. system, microwave resist. meas. 77−20353
Pr_3Tl, microwave resist. meas., rel. to singlet ground state paramag. systems 77−20353
Se, amorphous film, AC conductivity at radio and microwave frequencies 79−11248
Se-Ge amorphous system, AC elec. cond., near T_g, temp. depend. 80−49791
Se-Ge system, amorphous, press. depend. of AC cond. 77−76858
Si, complex permittivity and cond., microwave meas. 79−65784
n-Si, current carrier-dislocation interactions, resistance in UHF range *(Russian)* 80−54732
Si, diffusion and power spectral density and correl. function of vel. fluctuation for electrons 80−65576
Si, dislocation energy spectrum, appl. of EPR and elec. meas. 79−82547
Si, HF field effect meas. 77−55556
Si inversion layer, high freq. cond., Drude relax., 2D plasmons and minigaps in surface lattice 78−60230
n-Si, microwave and far IR hot carrier mobility, Monte Carlo calc. appl. to mm. transit time oscill. efficiency 78−72184
p-Si, millimetric and far IR cond., evidence for interband transitions 78−52022
p-Si, millimetric and far-IR cond., freq.-depend. carrier relax time 80−34460
n-Si, nonlinear birefr. and dichroism at microwave freqs. and intervalley scatt. 79−19602
Si powder semicond., microwave propagation, Rayleigh limit 79−78126
Si, powdered, microwave propag. 78−56175
n-Si, rod, in rectangular waveguide, microwave field distribution 80−39622
Si, two-dimensional electrons in superlattice, HF cond. 78−64055
Si wafer, nondestructive method for meas. of spatial distrib. of minority carrier lifetime 80−13098
Si:B(P), dislocated crystals, microwave cond., localised electron energy spectrum 78−14694
Si:P, heavily doped, metallic region, resist. decrease due to ESR 77−16178
Si:Zn, recombination waves threshold parameters in microwave field 77−28206
Sn, surface impedance change, reflected RF EM wave interaction *(Russian)* 80−49867
Sn-SnO-Sn Josephson tunnel junction, temp. depend. of cosϕ conductance, plasma reson. expt. 79−33405
TCNQ salt, TSeF-TCNQ, anal. of harmonic microwave mixing 80−44635
$Tb_eY_{1-e}As(P)(Sb)$, singlet ground state systems, microwave resist. data 77−47843
Te, breakdown in high microwave impulse field, by impact ionisation 77−62957
$TlGaS_2$, mechanism of cond., AC cond. and permittivity meas. 78−14754
$TlGaSe_2$, mechanism of cond., AC cond. and permittivity meas. 78−14754
$Tl_2SeAs_2Te_3$, molten chalcogenide semicond., temp. depend. of 10^{10} Hz elec. cond. 77−4388
$Tm_y(La,Y)_{1-y}S$, microwave resistivity 77−11949
$Tm_y(La,Y)_{1-y}Te$, microwave resistivity 77−11949
TmN(P)(As)(Sb), singlet ground state paramag. system, microwave resist. meas. 77−20353
VO_2 film, optical and elec. props., 0.8 to 4.2 mm, near metal-semicond. transition 77−32473
W plate, impedance oscillations in mag. field 78−39140
W, RF size effect signal, anomalous behaviour 77−89788
W thin plate, oscillations of surface impedance in circularly polarised RF fields *(Russian)* 78−39144

high-frequency effects continued
Y-Er, surface, high-freq. elec. cond. dispersion function, effects of polishing and annealing 78−19506
ZnO, hot-electron microwave conductivity, hot-electron, high DC field 79−38113

high-frequency electronic transport *see high-frequency effects*

high-frequency heating *see radiofrequency heating*

high-frequency transformers
concert hall sound system for touring quartet 80−92013

high-frequency transmission line measurement
1-butanol, permitt. meas. by transmission time domain spectroscopy 77−67462
chlorobenzene, permitt. meas. by transmission time domain spectroscopy 77−67462
current intensity unit, USSR state standard 78−36979
dielectric time domain spectroscopy, transmission methods 77−67462

high-frequency transmission lines
linear accelerators, HF struct. with standing waves *(German)* 78−50420
pulse generator, nanosecond, high-power, wave processes 77−18730
quarter-wave spark source, 323MHz, appl. stable spark discharge production 77−80394
slotted tube resonator for high freq. NMR, transmission line geometrical dimensions 77−30192

high-pass filters
atmospheric precipitation optical array probe, small-particle response as high-pass filter charact. 80−51577
numerical digital filter for on-line processing of wind tunnel data *(French)* 80−19537
real time phaseless filter with delay circuit, ECG appl. *(Japanese)* 80−56253
US Doppler shift signal processing, maximum frequency follower 79−62320

high power amplifiers *see power amplifiers*

high-pressure effects in solids
see also high-pressure solid-state phase transformations; piezo-optical effects
AB-type compounds, high-press. and high-temp. behaviour, review 78−22850
action potentials in single axons, effects of hyperbaric air and hydrostatic press. 80−56007
adamantane, elastic props., press. depend. rel. to intermol. forces 80−54297
adamantane, thermal cond. and heat capacity under press. 80−80008
2-adamantanone, absorption and fluoresc., high-press. 77−52113
Adirondack anorthosite, deform. characts. 78−61399
alkali feldspar, deformation, plastic defects, TEM investig. 78−32066
alkali halide crystals, Szigeti effective charge parameter, strain derivative 79−7571
alkali halides, exchange charge shell model analysis of strain derivatives of static polarisability, effective charge parameter 78−91296
alkali halides, off to on centre defect transitions under hydrostatic press. 78−15199
alkali halides, props. under hydrostatic press. 79−38436
alkali halides, vol. depend. of dielec. consts. and effective charge parameter, under hydrostatic press. 78−14689
alkali metal tungsten bronzes, superconductivity at press. up to 20 kbar 79−38226
alkali metals, bulk modulus and eqns. of state under press. 80−88293
alkali metals, heavy, supercond. and high temp. resist. at high press. 77−47917
alkaline earth oxides, analysis of press. derivatives of second order elastic consts. 77−35618
alkali halide, optic mode Gruneisen parameters and strain derivatives, Born-Mayer and Sziegti model 78−55929
almandine, synthetic, hydrostatic compression, isothermal bulk modulus 78−40545
aluminates with perovskite struct., elasticity meas. to 6 kbar 77−51428
aluminium methylammonium selenate alum, effect of hydrostatic pressure on dielec. props., near transition pt. 79−56712
amorphous semiconductor, electrical conductivity at strong elec. fields and high hydrostatic press. *(Czech)* 77−24560
anils, cryst., high-press. optical effects 78−31170
anils, polystyrene soln., high-press. optical effects 78−31171
anion exchange, in tablet pressure for IR spectroscopy *(Russian)* 78−95927
anorthite, thermal eqn. of state up to 120 GPa, appl. to Earth mantle 80−109136
anthracene, Davydov splitting of lowest singlet exciton under high press. 77−72823
anthracene, lattice parameters press. depend., elastic consts. 78−38686
Araldite AW106/Hardener HV953U epoxy resin, thermal props. at high press., glass transition 77−59160
Armenian basic and ultrabasic rocks, elastic wave vels. at high pressures 77−44972
bacteriorhodopsin, effect of high press. on absorpt. spectrum and isomeric composition 80−67041
basalts from Faeroe Islands, compressional and shear wave vels. at high temp. and press. 79−84244
benzene, mol. reorientationally disordered phases, thermodynamics 79−46782
benzene, thermal cond., heat capacity, 105-375K, up to 2.4 GPa 79−90839
benzene, thermal expansion at high press., near melting 79−77777
Bridgeman anvils, optimal distrib. of stresses 79−23679
brittle metal, ductility under tension or compression *(Japanese)* 78−35617
butadiene-nitrile elastomers, high temp., and press. chem. transformations *(Russian)* 79−52659
$CaO-SiO_2-CO_2$, subsolidus and liquidus phase relationships to 30 kbar 80−85643
chalcogenide glasses, elec. cond., press. effects 78−56142
chemostress effect in ionic crysts. and metals 79−28193
trans-1,4-chlorobromocyclohexane, liquid, crystalline and amorphous state, conformation and vibr. spectra, IR obs. 80−60568
trans-1,4-chloroiodocyclohexane, liquid, crystalline and amorphous state, conformation and vibr. spectra, IR obs. 80−60568
cokes, acicular and spherulitic, high pressure effects on graphitisation 77−36414
comminution of solids under hydrostatic pressure, technique 78−52702

high-pressure effects in solids continued
component hydropressing, residual stress distribs. *(Russian)* 80−93567
compressed atom model, energy level shifts for changed boundary conditions 77−43473
conference, Moscow, USSR (May 1975) 77−43279
copper formate tetrahydrate, dielec. props. under hydrostatic press. 77−20789
corundum, hydrostatic compression, X-ray diffr. meas. 79−99269
Crazing under applied compression 78−19875
crystal defects, elastic interaction under high hydrostatic press. 80−96512
crystal under high pressure, dislocation theory 78−55870
crystal under hydrostatic press., electronic polarisability and ion size var. 78−26487
crystalline body, dislocation interaction between pores while being healed by external pressure *(Russian)* 77−19963
cubic and non-cubic solids, Gruneisen parameters, vol. depend. 80−29145
cubic antiferromagnetic, first to second order transition crossover 78−10709
cubic metals, press.-vol. relations calc., pseudopotential method 77−11662
cupric formate tetrahydrate, pressure effect on dielectric props. *(Japanese)* 79−65787
cyclohexane, thermal cond. and sp. ht. under press. 78−22906
cyclopentanone, solid, phase behaviour, at press. up to 3 kbar, DTA 78−43108
deep struct. changes, NQR obs., high-press. and temp. effects 80−54139
diamond, brittle failure due to liq. Si., 60 to 70 kbar pressure 77−15720
diamond, N aggregates, partial dissoc. by high press.-high temp. treatment, IR spectra obs. 78−43904
diamond, polycryst. with Ni additives, sintering under ultrahigh pressure 80−84870
diamond, research aimed at production of metallic form 79−42146
diamond, sintered compact, stress-strain curves using ultrahigh-pressure apparatus 79−43322
diamond, synthesis, shock loading from graphite-metal mixtures *(Russian)* 77−90298
diamond, synthesis *(Japanese)* 80−80994
diamond, transformation of type IB dispersed N into type IA aggregate N 78−6089
diamond against diamond, high press. generation, thin film effect 79−55821
diamond indentor-anvil system, resist.-vs-press. relations 79−77681
diamond polycrystal, sintering under high press., binary inclusion-diamond interaction *(Chinese)* 78−80484
diamond synthesis by graphitisation of carbon materials at high press. and temp., Ni influence 80−60795
diamond-graphite equilib. line, from synthesis and graphitisation of diamond 78−24811
dicalcium barium propionate, ferroelec. in press. induced phase VI 79−91393
p-dichlorobenzene, expansivity, determ. by calorimetric compression from 0 to 400 MPa 80−44339
trans-1,2-dichloroethane, solid, NQR at high press., hindered rot. 79−95672
dislocation configuraiton form. on pore healing under press. *(Russian)* 78−10050
dislocation mobility at high hydrostatic pressure 78−55869
dislocation structure, high press. effects, plastic deform. *(Russian)* 80−88159
dislocations and point defects in hydrostatically compressed crystals *(Russian)* 78−75666
ductile-brittle transition pressure, grain size effect *(Japanese)* 78−60745
dunite, elec. cond during shock compression from 12.5 to 45 GPa 78−85536
dynamic stress/strain measurements under superimposed high press., torsion bomb machine 80−85130
effect of pressurisation on acoustic emission characts. during tensile testing 78−92304
elastic wave transit time meas., 100 kbar apparatus 78−79176
elastically nonlinear media, expressions for forces acting on dislocations *(Russian)* 79−51106
elastically nonlinear medium, self action force of dislocation loops *(Russian)* 79−27979
epoxy polymers, high temp./press. materials test for undersea environment 78−3213
equations of state, shock wave expts. *(German)* 78−59858
equations of state at finite strain, evaluation using lattice model 80−96620
equations of state of solids, comparison of theories using high-compression exptl. data 79−20779
ethylene, solid, phase diagram and NMR at high press. 80−11279
f-band metals, mode softening and lattice instability under press. 77−51833
ferroelectric phases, rel. to Earth and planetary interiors 78−69334
ferroelectric with H bonds, exchange integral press. depend. *(Russian)* 78−35097
ferroelectrics, sp. ht. meas. by dynamic method at high hydrostatic press. 80−47059
fibre reinforced composites 77−36602
film, sputtered, high press. induced shifts in supercond. transition temp. 77−85374
fluorenone fluoresc. in plastic, high press. effects., quantum yield 78−25601
formate crystal, dehydration, influence of hydrostatic press., ^{7}Li NMR 78−2758
frozen food, hydrostatic press. effect on phys. props. 78−26706
furan, crystalline, P-V-T relations, 210 to 260K, up to 1000 MPz 79−95122
furan, mol. reorientationally disordered phases, thermodynamics 79−46782
n-GaAs:O, press. depend. of deep level associated with O, transient capacitance meas. 78−64000
glass, inorganic, cylindrical shell, with initial geometric imperfections, precritical deform. under external hydrostatic press. 77−81306
glass, K-8, dynamic compression and unloading 77−9029
glass, thermal conductivity effect of strain at 0.1K 77−89602
glass fibre reinforced plastic tube under cyclic pressurisation 78−68761
glass inorganic, shell, stress/strain state investigation under external hydrostatic press. 77−81370

high-pressure effects in solids continued
grain boundary migration under influence of high hydrostatic press. 77−68981
graphite, pressure-depend. conducting calcs. using band model 77−28171
graphite melting point rel. to press. 78−24811
Gruneisen coeff. press. depend. meas. method and apparatus 77−35714
guanidinium aluminium sulphate hexahydrate:Cr^{3+}, press. meas. from ESR 79−38375
guanidinium gallium sulphate hexahydrate:Cr^{3+}, press. meas. from ESR 79−38375
heart rate changes associated with high-pressure convolutions in rodents 80−67124
heterophase systems, pressure-induced elastic fields, effective inclusion method 79−10502
hexagonal crystals, elastic consts., finite strain theory *(French)* 79−1475
hexamethylenetetramine, thermal cond. and heat capacity under press. 80−80008
high-density quantum statistical model 79−55824
homogeneous isotropic material, high press. eqn. of state and sound vels. to fourth order elastic consts. 79−37806
hydrostatically compressed crystals, crack nucleation mechanism 79−10893
Hypalon 40, chlorosulphonated polyethylene, mech. props., press. effects 77−32618
hyperbaric air, modification of synaptic facilitation and bursting patterns in Aplysia californica 80−56008
hyperbaric hyperreflexia, tendon-jerk and Hoffman reflexes in Man, soleus muscle 80−61530
ice, Antarctic deep core, mech. tests under hydrostatic pressure *(Japanese)* 79−79890
ice, thermal conductivity of nine solid phases 78−30801
ice VI, high-pressure Raman spectra, bending and librational bands 78−68499
ice VII, melting curve up to 150 kbar 78−67812
III-V semiconductor, heavily doped, pressure volume characts. nonlinearity, intervalley electron redistrib. 77−8012
impact welding, wavy interface characts. and formation 80−97680
impact welding process, fundamental parameters 80−97679
Indiana limestone fracture toughness, confining pressure effect 78−57197
insulating mechanical supports, appl. to meas. thermal conductance 80−82772
Invar, Mossbauer effect at high press. 80−15858
ionic crystals, nonstoichiometric, equilib. with gas phase in mech. vibr. field 78−43388
isentrope extrapolation in high pressure region, isotropic compression case 80−24532
lanthanum ethyl sulphate nonahydrate: Tb^{3+}, ESR spectrum, spin lattice relax., effect of hydrostatic compression 78−88185
layered semiconductors, effects on electronic structure and vibr. props. 77−51654
leucite rocks under water vapour pressures up to 25 kb., expt. investigation 77−70648
limestone, high press. effects on plastic state 79−74889
longitudinal wave vel. and absorpt. in rocks and minerals at high press. and temp. 79−39704
magnetic alloys, dil., press. effects 79−99676
material stability under high press., eqns. of state *(Chinese)* 80−6461
metal, Arrhenius plot of diffusion, curvature, disappearance under press. with single-vacancy model 79−10975
metal, BCC, dislocation (100) stability, field stress effects *(Russian)* 80−10558
metal, containing dislocations, quantum oscillations of thermodynamic props. *(Russian)* 79−86899
metal, FCC, deformation mechanism under high hydrostatic pressure *(Ukrainian)* 80−25758
metal, Gruneisen coeff. rel. to press. depend. of Poisson ratio 77−47504
metal, kinetic effects at high anisotropic strains, elec. transport props. meas. 78−54384
metal, non-cubic, electric field gradient, press. and temp. depend. 77−8057
metal, plasticity under hydrostatic pressure *(Russian)* 78−68726
metal, specific volume meas., for ruby R_1 fluoresc. press. gauge calibration, 0.06-1 Mbar 78−70150
metal failure, due to hydrostatic pressure, exam. of kinetics 78−52944
metal polyphosphinates, bulk compressibility meas. to 30 kbar 80−76306
metal-H systems at high H press., physicochemical props., book contrib. 80−24535
metal-semiconductor contact, axial pressure effects on surface-state density redistrib. *(Russian)* 77−89847
metallic glass, Fe Mossbauer effect at high press. 80−15858
metallic solid soln., diffusion by press. *(Russian)* 78−18833
metals, constitutive model at high strain-rate, shear modulus, yield strength 80−75292
metals, effect of hydrostatic pressure and stress on plasticity 78−52907
metals, electrical conductivity, high pressure effects 80−92879
metals, high press. expts., review *(Japanese)* 78−71790
metals, sp, elec. field gradient at ^{111}Cd, effects of high press., TDPAC meas. 80−25266
metals, specific heat meas. method at low temperatures and high pressures 80−52246
Metglas 2826A, Invar related system, high press. Mossbauer spectra 79−56642
methane, phase III, Raman spectra 79−65849
methane, solid, high press. NMR obs. 80−50214
methanol, solid, phase behaviour up to 3 kbar by DTA 77−76528
mica, pulse electric breakdown under pressure, lamination effects 80−66110
microorganisms, lack of intracellular bubble formation at very high gas supersaturations 80−81562
minerals, bulk modulus-volume relationship, for cation-anion polyhedra 80−41434
minerals, post-shock temps. meas. 79−92527
minerals pressure-density path, effect of viscosity on release adiabat meas. 80−51388
minerals relevant to Earth interior geophysics, Hildebrand equation of state 80−56464
molecular crystals NQR freq. press. depend. 80−54971
molecular polycrystals, effect of high hydrostatic press., EPR meas. 78−19307
molybdenum chalcogenides, multicomponent, physical props. 80−84577

high-pressure effects in solids continued
montmorillonite, mech. props. at high press., rel. to fault behaviour 79−84234
Mossbauer apparatus for resonance studies at high press. and low temps. 78−49943
Mossbauer effect, second order Doppler shift, press. depend. 80−66088
Mossbauer isomer shifts, press. effects, book contrib. 79−87353
naphthalene, lattice parameters, elastic consts., press. depend., neutron diffr. obs. 78−26558
naphthalene anthracene doped, decay times and diffusion coeffs. of singlet excitons, under press. 77−20911
naphthalene-d, press. depend. of lattice freqs. at 100K 79−46768
Neoprene WB, polychloroprene rubber, mech. props., press. effects 77−32618
nepheline-kalsilite system, subsolidus phase relations at 0.5, 2.0, and 5.0 kbar 79−66041
noble metal complexes, hexafluoro, review of struct. obs., pseudorot., press. effects 78−6045
NQR, spectral parameters, baric dependences 79−78559
NQR pressure sensitivity, vol. depend. of elec. field gradient and lattice vibrs. 77−12225
Nylon 6, pressurized heat treatment effect on fatigue props. 79−87669
Nylon 6 film, prior high-press. treatment effects, weight swelling, density, IR crystallinity, X-ray and viscosity obs. 80−81025
nylon II, high-press. X-ray structural study 78−14296
nylon-6, chain extension mechanism during crystallisation under press. 77−56008
olivine to spinel transition kinetics, rel. to deep-focus earthquake genesis 77−5190
omphacite, Mossbauer spectra study 79−65771
organic impurity crystals, press. effect on shift of zero-phonon lines 79−95824
organometallic semiconductors, activation energy of elec. cond. rel. to press. 78−24811
oxides, semi-sintered, as press. transmitting media 80−52259
paramagnetic substance, electron spin-lattice relax. at high press. *(Russian)* 77−43868
parametrisation for solids under hydrostatic press. 78−72120
perovskite-like oxides, high-pressure series, rel. between structure and physical properties 78−51493
phase diagrams and struct. under press., index of substances 79−60484
phonon dispersion spectrum and Gruneisen coeff. under press. 77−43287
phonon spectra under press., neutron scatt. obs., book contrib. 77−89504
PMMA, amorphous, thermophysical props. depend. on hydrostatic press. 78−47612
PMMA, thermophysical props. at high hydrostatic press. 78−2317
PMMA, X-ray absorption, shock wave compression meas. *(German)* 78−95618
poly(alkyl methacrylate), vitreous state, thermal cond., hole theory of liqs., press. 78−84013
poly(vinylidene fluoride) film, strong piezoelec. under high press. annealing 80−11344
poly-N-vinylcarbazole, in polymer film, excimer fluoresc., high press. effects 80−34966
polyacetylene, pristine and doped, press. effects on resist. 80−103698
polyalkylmethacrylates, vitreous, thermal cond., press. and temp. depend. 78−2315
6-polyamide films, cond. and relax. under very high press. 77−35748
polycarbonate, amorphous, thermophysical props. depend. on hydrostatic press. 78−47612
polycarbonate, yielding and crazing behaviour in torsion under superimposed hydrostatic press. 78−52898
polycrystals of anisotropic substances under hydrostatic press., microstresses 79−25231
polydiacetylene, single cryst., polymerisation under hydrostatic press. 79−20367
polydiacetylene-bis(toluenesulphonate), refl. spectra, 0-15 kbar, doublet press. shift 78−43891
polyester polymer-C black composition, elec. cond. under press. 77−28224
polyethylene, dynamic modulus under high press., nature of high press. phase *(Japanese)* 80−3120
polyethylene, hexagonal, high press. crystn., review 79−23529
polyethylene, high molecular weight, effect of density on properties 77−90403
polyethylene, meas. of high chain extensions by gel permeation chromatography 77−88611
polyethylene, mol. conformations after recrystallisation or annealing at high press. 77−88612
polyethylene, polyethylene-D_4, migration and copolymerisation at high press. with shearing stress 78−51678
polyethylene, specific vol. under high press., appl. of novel dilatometer 77−37844
polyethylene, X-ray diffr. at press. up to 14000 kg cm^{-2}, 298K 77−35492
polyethylene cryst., unit cell variations with temp. and high press. 78−47250
polyethylene high press. phase, struct., phase diagram and compressibility 78−9961
polyethylene terephthalate, press. effects on compressibility and crystn., thermodynamic interpret. 80−84102
polymer, air permeability subject to high press., testing apparatus 78−27823
polymer, amorphous, under press., glass transition phenomena, model 79−23706
polymer, light and Raman scattering obs. of high press. phases *(Japanese)* 80−2773
polymer, partially crystalline, sp. vol. press. depend. *(German)* 78−75852
polymer, thermal conductivity-pressure relationship *(German)* 77−20139
polymers, amorphous, press. effect on thermal cond. *(German)* 79−95225
polymethylpentene, press. effects on melting 78−56625
polyolefins, plastic flow, yield limit rel. to press. *(Russian)* 80−7657
polypropylene, isotactic, diffusion const., increased hydrostatic press. effect 78−22898
polypropylene, mech. behaviour rel. to combined press.-temp. effects 77−16648
polystyrene, amorphous, press. effect on glass transition and glassy state 78−26674
high-pressure effects in solids continued
polystyrene, amorphous, thermophysical props. depend. on hydrostatic press. 78−47612
polystyrene, high impact, under press., mech. behaviour 79−52305
polyurethane, high temp./press. materials test for undersea environment 78−3213
polyurethane foam, press. wave propag. and refl. characts. 77−35634
polyvinylidene fluoride, X-ray high press. study 80−6369
prefluorinated polymer, DuPont Krytox 143-AB, viscoelastic and dielectric props. 80−1503
press. depend. of effective mag. fields on ^{57}Fe nuclei 78−52383
PTFE, relaxational props. effect of temp. and hydrostatic press. *(Russian)* 77−44325
PVC, X-ray absorption shock wave compression meas. *(German)* 78−95618
pyrene, perylene doped, decay times and diffusion coeffs. of singlet excitons, under press. 77−20911
Pyrex glass, isothermal compressibility to 20 kbar, inductance coil method 80−49302
pyrope, synthetic, hydrostatic compression, isothermal bulk modulus 78−40545
α-quartz, compression to 120 kbar 77−15493
α-quartz, Gruneisen constants for optical modes, neutron irrad. and press. effects *(Russian)* 78−22815
quartz, Gruneisen parameter at high press. 80−8299
quartz, porous, Hugoniot synthesis at high pressures 79−95080
quartz, synthetic hydrostatic pressure effect on precip. of structure bound water in microinclusions 78−75838
α-quartz 80−72490
quartzite, Gruneisen parameter at high press. 80−8299
radiative electronic transitions of impurities, effects of hydrostatic press. 80−11446
radioactive materials, high press. X-ray diffr. studies 80−3450
rare earth alloys, RM_x (R=La, Ce, Pr, Er, M=Co, Ni), H(D) sorption at press. up to 1500 atm. 80−97819
rare earth compounds, pressure effect on mag. ordering temp. 80−100584
rare earth heavy binary alloys, press. effect on mag. props. *(Japanese)* 77−43835
rare earth intermetallics, neutron scatt., induced moment magnetism, high press. 80−15699
rare earth systems, high pressure studies, review 79−69193
review 77−43278
Rochelle salt, dielectric props. near upper Curie pt. under hydrostatic press. 79−82935
(Rochelle salt)$_{1-x}$(ammonium Rochelle salt)$_x$, phase transitions, hydrostatic press. effects 80−93246
rock, apparent resistivity changes under uniaxial compression *(Chinese)* 80−3995
rock, thermal expansion expts. at high-press. 80−21719
rocks, compressional and shear wave velocities under high press., effect of high-low quartz transition 80−12380
rocks, compressional wave vels. at high temps. and press. rel. to crustal low-vel. zones 80−41435
rocks, elastic props. experimental studies rel. to Earth crust press.-temp. conditions modelling *(Russian)* 78−96207
rocks, longit. waves vel. press. depend. rel. to rocks mineral comp. prediction at great depths *(Russian)* 80−104956
rocks, NRM stress sensitivity meas. using cryogenic magnetometer 80−26506
rocks, P-V meas., 5 to 45 kb *(Chinese)* 79−23676
rocks, quartz-bearing and quartz-free, high temp. and press. effects on compress. wave vel. 78−32081
rocks, seismic anisotropy meas. under high-press., high-type conditions 77−49059
rocks, subsolidus attenuation at simultaneous high temp. and press. 78−3764
rocks and minerals, conf., Newcastle, England (April 1974) 77−37194
rocks physical props. under mantle conditions, conf., Durham, England (Aug. 77) 78−69333
rubber, natural, thermal properties depend. on temp. and press. 79−95223
ruby:Cr^{3+}, exchange integral, pressure depend., test of theory 78−87741
ruby, cryst. struct. and compression up to 46 kbar 79−37682
ruby, single cryst. struct. determ. for press. up to 90 kbar 78−83875
sandstone, porosity destruction through press. soln. 77−91110
Schottky diode, effect on V-I curve and barrier height *(Russian)* 77−39934
seismic effective velocities of minerals, var. with press. and use in vel. prediction 79−44179
semiconducting glass, elastic props., US vel. meas. 78−26628
semiconductor, donor levels, anomalous press. effects, Hall const. meas. 77−51693
semiconductors, energy states under high press. *(Chinese)* 79−56128
semiconductors, kinetic effects at high anisotropic strains, elec. transport props. meas. 78−54384
semimetal, pressure induced transition to state with strongly anisotropic electron-hole pairing 77−47735
shaped charge jet formation, Pugh-Eichelberger-Rostoker solution representation 79−94692
shock adiabatics at ultrahigh press. *(Russian)* 77−27941
shock wave generation and application in solids *(Japanese)* 79−68475
shock wave interactions, dimensionless Hugoniot eqn. of state 79−69191
sodium acetate trihydrate, press. depend. of methyl tunnelling motion 80−10603
solid state physics at high pressures, general review 79−90729
spin glasses under high press., resist. meas. 78−52277
spinal cord seizures elicited by high pressures of He 80−12071
stability under shear stress, hydrostatic press. 80−59462
stannates with perovskite struct., elasticity meas. to 6 kbar 77−51428
steel, alloy, ductility, hydrostatic press. effects 78−80615
steel, C, quenched and tempered, ductility, effect of hydrostatic press. 78−44190
steel, deformation anisotropy in yield point, precompression effects *(Russian)* 78−11268
steel, eutectoid, U8, cold hydraulic press. forging effect on transform. and heat treatment *(Russian)* 79−52235
steel, high C, quenched and tempered, hydrostatic press. effect on brittle fracture stress 79−61727
steel, high speed, powder, cold isostatic compaction effect on thermophysical props. 78−52717

high-pressure effects in solids continued
steel, high-strength low alloy, H_2 attack, 350-510°C 80−97636
steel, low C, pressurised, strain rate sensitivity prior to serrated yielding onset 78−48482
steel, maraging, and HY-80, deform., hydrostatic pressure effect 77−36596
steel, microhardness changes under high-press. and laser irrad. *(Russian)* 77−59903
steel, plasticity depend. on hydrostatic press. in low-angle fatigue, Manson-Coffin coeff. *(Russian)* 79−61651
steel, rotating bending fatigue tests in hydrostatic environment 77−21343
steel, stainless, cylindrical shell reinforced with longitudinal separate ribs under external pressure pulse, critical pulse estimate 79−14884
steel, stainless, Invar related system, high press. Mossbauer spectra 79−56642
steel, stainless, Mossbauer effect at high press. 80−15858
steel, stainless, type 310, antiferromag. ordering, press. depend., Mossbauer meas. 79−73861
steel, surface structural changes on exposure to plasma, etch resistance *(Russian)* 79−83234
steel, TRIP, hydrostatic extrusion shock treatment rel. to strength and plasticity 77−44281
stishovite, compression to 100 kbar, eqn. of state from bulk modulus 77−17085
strong-coupling superconductors, press. coeffs. of critical field, Ginzburg-Landau parameter, penetration depth 80−54833
superconducting film, Pauli paramagnetism and Fermi surface topology changes under press. 78−2612
superionic conductor, with fluorite struct., activation vol. 80−107557
TCNQ salt, TMTSF-DMTCNQ, metallic state at low temp. under pressure 79−91033
TEA$(TCNQ)_2$, elec. cond. and thermoelec. power under hydrostatic press. 80−11024
Teflon, creep in shear, hydrostatic pressure effect 79−57065
TGFB, ferroelec. Curie point press. coeff. tensor 79−33635
TGS, ferroelec. Curie point press. coeff. tensor 79−33635
TGSe, ferroelec. Curie point press. coeff. tensor 79−33635
TGSe, hydrostatic pressure and deuteration effects on order of phase transition 77−12334
thermal energy relaxation in shock compressed solids, anal. of Cu, Al, Pb, Au, NaCl, Fe 77−69043
thiourea, polycryst., mol. dynamics under hydrostatic press., NMR study 80−80619
titanates with perovskite struct., elasticity meas. to 6 kbar 77−51428
TMMC phase behaviour, DTA using Ge-Ag thermocouple 79−65186
$(TMTSF)_2PF_6$, one dimens. conductor, superconds., resist. meas. and mag. field effects *(French)* 80−44753
transition metal, BCC isothermal compression to 100 kbar 78−43069
transition metal alloys, magnetically ordered, effect of magnetic field on P-T diagram 78−52246
transition metal mixed valence complexes, quasi-one-dimens., elec. props. at ultrahigh press. 78−2470
transition metal oxides, pressure-induced high-spin-low-spin transitions 78−85549
transition metals, BCC, supercond. transition temp. and press. effects 77−4461
transparent dielectric, optical stimulation of compression pulses, absorbing layer effects *(Russian)* 77−1174
1,3,5-trichlorobenzene, ^{35}Cl NQR, high press. behaviour 79−33560
TTF-TCNQ, const. vol. resist., linear temp. depend. 78−51977
TTF-TCNQ, deuterated, compressibility under hydrostatic press., neutron diffr. meas. 78−2197
TTF-TCNQ, one-dimensional conductor, fluctuation conductivity in high press. phase 79−91034
TTF-TCNQ and related cpds., magnetic props., press. effects 77−47981
TTF-TCNQ phase transition, press. depend., longitudinal lockin, stacking axis resistivity meas. 78−47520
twinning and linear compressibility anisotropy under hydrostatic press. 78−51553
type II superconductors, high field expts. on press. effects up to 15 kbar 79−61006
uniaxial stress component, effect on eqns. of state determ. with opposed-anvil X-ray apparatus 80−49301
US propagation in cryst. under quasihydrostatic compression, elastic characts. 77−51445
viscoplastic medium, formation of contact with solid surface under pressure 79−69320
viscoplastic medium, optimum control of transient process under press. *(Russian)* 79−72821
Viton B, vinylidene fluoride-hexafluoropropylene copolymer, press. effects on mech. props. 77−32618
X-ray diffraction, diamond anvil cell, high press., pseudo-Kossel lines 80−79623
X-ray diffraction patterns, high-press., nonuniform line broadening 80−79629
Ag, elec. resist., press. variation 78−84193
Ag, isothermal compression curves to 120 kbar, X-ray diffr. study 78−83876
Ag, pressure effect on shear modules and internal friction, EM reson. technique 77−31709
Ag, thermal conductivity at high press. meas. 78−95283
AgBr-AgCl mixed crystal, elastic consts., temp. and press. derivatives 77−11620
$AgClO_3$, ^{35}Cl NQR spectrum under press. at 311K 80−11291
Ag_2HgI_4, polycryst., Raman spectra, press. depend. 77−73137
AgI, BI phase, high press. elastic props., thermally activated rel. anomaly 80−44261
Ag_4I_5, ionic cond., effect of press. 78−51733
Ag_8MSe_6, (M=Si, Ge, Sn), forbidden energy gap changes under high press., polymorphic transitions 77−51649
Ag_8MSe_6, M=Ge,Sn,Si, absorpt. edge under hydrostatic press. 77−85740
$AgNa(NO_2)_2$, order-disorder ferroelec., influence of hydrostatic press. on polarisation dynamics 80−103913
γ-Ag_5Zn_8, high pressure effect on brass struct. 80−107108
Al, cast, strength and plasticity under hydrostatic pressure 78−56694
Al, compression, effect of press. on lattice defects up to 90 kbar *(Japanese)* 77−72654
Al, constitutive equation for porous materials with strength, press. effects 80−79875

high-pressure effects in solids continued
Al, electronic Gruneisen parameter in shock Hugoniot eqn. of state 80−10635
Al, Gruneisen coeff. depend. on specific volume, phonon spectra calcs. 79−65165
Al, Gruneisen parameter behaviour at high press. 78−83899
Al, internal friction, strain amplitude dependent, hydrostatic press. effect 77−77520
Al, isothermal compression curves to 120 kbar, X-ray diffr. study 78−83876
Al, melting curve and Gruneisen coeff. at high press. 80−65200
Al, microhardness under high hydrostatic press., meas. by microindentation 80−3182
Al, porous, Hugoniot synthesis at high pressures 79−95080
Al, pressure effect on diffusion, theoretical study 78−47566
Al, pressure effect on shear modulus and internal friction, EM reson. technique 77−31709
Al, resistivity, press. depend., calc. 80−20151
Al, shear constants, press. effect up to 2500 atm., −196 to 25°C 77−31710
Al, shock compression at high press. *(Russian)* 80−92608
Al, shock-waves, ultrahigh-press., laser-driven 79−55823
Al single crystal, polygonisation at high press. kinetic regularities, dislocation struct. at 140°C 79−66070
Al, singularities of effect of pressure on stages of creep *(Russian)* 79−29134
Al, sp. ht., 0-100 kbar 77−51512
Al, thermal cond. form diffusivity, press. depend. up to 2.5 GPa 77−85195
Al, US velocity, temp. depend., stress effects 80−75307
Al, X-ray absorption, shock wave compression meas. *(German)* 78−95618
Al-Cu (4.5 wt.%) cast alloy, press. effect during solidification on struct. and mech. props. *(Korean)* 77−77469
Al-Ge alloy, effect of high press. on phase equilibrium *(Russian)* 79−1844
Al-Mg, ageing process, effects of Ag additions and pressure *(Russian)* 80−45321
Al-Si alloy, compression, effect of press. on lattice defects up to 90 kbar *(Japanese)* 77−72654
Al-Zn, X-ray diffr. after omnidirectional compression *(Russian)* 80−88262
$Al_xGa_{1-x}As$, press. coeff. of direct band gap from optical absorpt. meas. 80−11430
Al_2O_3, elec. props. under isentropic compression up to 500 GPa 78−71789
Al_2O_3 films, static compression to 1.2 Mbars, elec. resist. 79−55822
α-Al_2O_3, impurity energy levels, uniaxial stress effects 80−54642
Al_2O_3, semisintered, shear strength at high press. 80−76308
β-Al_2O_3-H_3O^+, high press. thermal stability 79−23678
β-Al_2O_3-NH_4^+, high press. thermal stability 79−23678
Ar, solid, thermodynamic props. under press., multiparametric pairwise and Lennard Jones potential calcs. 80−39316
Ar:NO_2, Raman spectra, high press., low temp. effects 78−52479
As, amorphous, effect of high press. on elec. props. 77−59309
As, electrical resist. and anisotropy at press. up to 80 kbar 77−43554
As metal, electric field gradient, temp. and press. variation 80−93205
a-As, second and third order elastic consts., ultrasonic velocity meas. 80−103408
As, zone centre phonons and elastic consts., hydrostatic press. depend. 78−59905
As_2S_3, chalcogenide glass, effect of press. on elastic props. 80−10590
As_2S_3, glassy, deep struct. changes, NQR obs., high-press. and temp. effects 80−54139
As_4S_4, effects of pressure and temp. on phonons, Raman scattering study 80−7360
$As_2S_3(Se_3)$ glasses, elastic moduli, hydrostatic press. effect, US wave vel. meas. 80−34115
As_2Se_3, and As_4Se_5Ge glasses, struct. changes, Mn^{2+} EPR expts. 78−79534
$As_{40}Se_xTe_{60-x}$ amorphous system, resistivity press. depend. 79−82592
As_2Te_3, amorphous, press.-induced semicond.-metal and supercond. transitions 77−43671
$As_4Te_5Ge(Si)$ glass, struct. changes, Mn^{2+} EPR expts. 78−79534
$As_{50}Te_{45}I_5$, glass, semicond., elec. switching, high press. effects 78−72212
Au, elec. resist., press. variation 78−84193
Au, polycrystalline, dislocation relaxation under high pressure 79−77605
Au-Cd (47.5 at.%), temp. and press. derivatives of elastic consts. near martensitic transform. 77−63667
Au-Cr, dil., spin glass, elec. resist., press. and conc. effects 78−52278
$AuGa_2$ film, supercond., mag. susceptibility and Knight shift press. depend. 77−43777
$(Ba,Sr)TiO_3$, ferroelec. props., press. depend., anharmonic oscillator model 80−80716
Ba, BCC, superconductivity under press. 78−14858
Ba, superconductivity, pressure dependence, ion core 78−91805
$Ba_{0.92}Ca_{0.08}TiO_3$ ceramic, uniaxial stress effects, US dilatometric and dielec. meas. 78−52454
BaF_2, ionic cond., activation vols., freq. depend. cond., press. effects 80−100354
BaF_2, powder, elec. cond. transition under high press. *(Russian)* 77−20370
Be, Fermi surface, stress-induced changes 80−96770
Bi, Bi-Pb and Bi-Sn, elec. cond. and thermal EMF at press. up to 12 kbar 77−47806
Bi, electron isoenergic surface coherence var. under press. *(Russian)* 77−55476
Bi, energy spectrum changes under strong uniaxial compression, Shubnikov-de Haas effect 77−28098
Bi, low-temp. phase diagram, using diamond anvil pressure cell and X-ray diffr. 78−1951
Bi, magnetoreflectance, L-pt. band parameters 80−25344
Bi, Shubnikov-de Haas effect and Fermi surface under strong uniaxial deform. 77−43474
Bi, superconducting modification obtained by impact compression *(Russian)* 80−93020
Bi, US attenuation, annealed sample, 0.6 kbar, 25-120°C 78−47474
Bi, US propagation anomalies, under hydrostatic press. *(Russian)* 78−83884

high-pressure effects in solids continued
Bi, zone centre phonons and elastic consts., hydrostatic press. depend. 78−59905
Bi-Pb alloy, supercond. crit. temp., effects of press. up to 30 kbar *(Russian)* 77−20484
Bi-Tl film, superconductivity and phonon spectrum *(Russian)* 79−91190
Bi(-Sn), hydrostatic press. effect on band struct., thermoelec. power meas. 79−69406
n-BiSb, cyclotron mass meas., high hydrostatic press. 79−77991
p-$Bi_{0.9}Sb_{0.1}$, Fermi surface anisotropy var. on press. induced transition to gapless state *(Russian)* 77−43483
$Bi_{1-x}Sb_x$, band inversion under press., Fermi surface anisotropy, galvanomag. meas. 77−51637
$Bi_{1-x}Sb_x$, semicond.-semimetal transition, temp. and press. depend. of transport props. 78−76120
$Bi_{1-x}Sb_x$, supercond. transition temp., press. depend., 30-80 kbar 77−8223
Bi_2Te_3, galvanothermomag. props. up to 14 kbar 77−47829
Bi_2Te_3, Shubnikov-de Haas effect, high press. effect on band struct. 77−51767
Bi_2Te_3-Sb_2Te_3 film, cond., galvanomag. Seebeck and Nernst-Ettingshausen effects under press., band model 77−47907
C, glassy, migration into steel during shock compression 80−24679
CO, press. depend. of melting and α-β phase transition temp. 77−69075
CO_2, solid, Fermi reson. press. tuning, Raman spectra 80−93293
CO_2, solid, high press. mol. libration calc. with Kihara core pots., Gruneisen parameter and lattice 80−65173
CaF_2, ^{19}F NMR chemical shift, press. depend. 0-4 kbar 77−20733
CaF_2 (fluorite), Gruneisen parameter at high press. 80−8299
CaF_2, ionic cond., activation vols., freq. depend. cond., press. effects 80−100354
CaF_2, powder, elec. cond. transition under high press. *(Russian)* 77−20370
CaF_2:Gd^{3+}, S-state splitting, investigation by ESR and ENDOR at high pressure 78−52345
$CaGeO_3$ perovskite, elasticity meas. to 6 kbar 77−51428
$CaMoO_4$, luminesc. efficiency, temp. and high-press. 78−23507
$CaWO_4$, luminesc. efficiency, temp. and high-press. 78−23507
$CaWO_4$:Nd^{3+} $4f^3$ configuration, ground level energy state variation rel. to press. *(Russian)* 77−16358
Cd and Cd-Mg, Fermi surface press. derivatives, de Haas-van Alphen effect meas. 77−43477
Cd, de Haas-van Alphen effect under press., Fermi surface and pseudopot. form factors 77−43475
Cd, elastic consts., finite strain theory *(French)* 79−1475
Cd, electrical resist. and anisotropy at press. up to 80 kbar 77−43554
Cd, Fermi surface, stress-induced changes 80−96770
Cd-Pb, high pressure effects, eutectic temp. 80−55361
Cd-Sb diffusion couple, layer growth of CdSb phase at high press. 80−2217
Cd-Sb diffusion couple, layer growth of CdSb phase at high press., elec. meas. 80−2218
Cd_3As_2, band structure, pressure dependence of galvano- and thermomagnetic effects 80−6722
CdF_2, ionic cond., activation vols., freq. depend. cond., press. effects 80−100354
CdF_2:Eu^{2+}, EPR spectra, hydrostatic press. and temp. effects 80−84648
CdF_2:Gd^{3+}, hydrostatic press. and temp. effects on EPR spectrum 78−76304
n-$CdGeAs_2$:In(Te), resist. and Hall coeff. meas., influence of press. 77−47810
$Cd_xHg_{1-x}Te$, photoconductivity under uniaxial compression, band gap 77−43657
$CdMoO_4$, luminesc. efficiency, temp. and high-press. 78−23507
CdS, rock-salt type high-press. phase synthesis using metal sulphide additives 80−104084
CdS-CaS, solid soln., rock salt struct., high press. phase equilibrium study 78−52777
CdS-MgS, solid soln., rock salt struct., high press. phase equilibrium study 78−52777
CdS-SrS, solid soln., rock salt struct., high press. phase equilibrium study 78−52777
p-CdSb, elastic moduli depend. on hydrostatic press. up to 17 kbar 79−37755
p-$CdSnAs_2$, heavily doped, elec. transport props. under elastic deformation 80−96915
$CdSnAs_2$, hydrostatic press. effect on resist. and Hall coeff., band struct. 77−47808
$CdWO_4$, luminesc. efficiency, temp. and high-press. 78−23507
Ce, determ. of specific heat at 300K, up to 20 kbar *(French)* 79−95177
Ce, elastic properties up to 84 kbar, US vel. meas. *(Russian)* 79−60434
Ce, electronic structure vol. depend., rigorous cellular method, γ- and α-forms 77−20233
α'-Ce, high press. phase, struct., X-ray diffr. data, reappraisal 77−55260
Ce, high press. superconductivity, phonon softening 78−14852
γ-Ce, Kondo-like anomaly 80−96857
Ce, sp. ht., 0-16 kbar 77−51512
Ce, sp. ht. and temp. coeff. of resist., 20 kbar at 300K 78−83973
Ce, thermo-EMF up to 75 kbars 80−24882
$CeAl_2$, Anderson lattice system, mag. moment reduction, press. effects 80−7093
$CeAl_2$, electronic transition under pressure, resist. meas., rel. to mag. to nonmag. transition 79−33311
$CeAl_2$, magnetisation curves under high mag. field and hydrostatic press. 77−63233
$CeAl_2$, press.-induced electronic transition 80−20147
$CeAl_2$, resistivity and volumetric meas., phase diagrams, comparison with CeS 80−107789
$CeH_{1.98}$, $CeH_{2.98}$, elastic props. at high press. 77−84825
CeO_2, conductivity at high O press. 77−20367
CeP(As)(Sb), compressibility, room temp., from neutron diffr. meas. of lattice parameter variation up to 41 kbar 77−27940
CeS, resistivity and volumetric meas., phase diagrams, comparison with $CeAl_2$ 80−107789
$CeSn_3$, low temp. mag. behaviour, press. induced valence change 77−63078
Co, ferromag., spin subband level position determ. by de Haas-van Alphen meas. under press. *(Russian)* 79−90947
Co, lattice dynamics and compression curves 78−38793
Co-Sn, dil., hyperfine field, press. depend., Mossbauer spectra meas. 79−95375

high-pressure effects in solids continued
$CoCl_2$, antiferromagnetic resonance, effect of hydrostatic pressure *(Russian)* 78−35042
Cr, anomalous US damping under hydrostatic press. 79−14890
Cr, spin density wave, stress and impurity conc. depend. 77−73029
Cr-Al, disordered alloy, effect of high press. on resistivity 78−95286
Cr-Co, dil., antiferromag., elec. resist. min., press. and impurity effects 80−59970
Cr-Fe, antiferromagnetic, effect of press. on hyperfine mag. fields at Fe nuclei *(Russian)* 80−15936
Cr-Fe, dil,, antiferromag., elec. resist. min., press. and impurity effects 80−59970
CrAs, mag. transition under press., volume striction mechanism 77−24696
Cr_2O_3, hydrostatic compression, X-ray diffr. meas. 79−99269
CrS, X-ray diffr. obs., high press., diamond anvil camera method 77−4082
CrTe, effect of high pressures on magnetic properties 78−52238
CrTe, mag. ordering under high-press., ferromag. transition, ESR and neutron diffr. *(French)* 78−31053
Cr_5Te_6, high press. effects on magnetisation and mag. transitions, 77 to 360K 77−77057
$CrTe_{1-x}Se_x$ (Sb_x), Curie temp., high press. and doping effects *(Russian)* 77−12125
$Cs_2Au_2Cl_6$, ^{197}Au Mossbauer high press. study of mixed valence compound 78−52387
$Cs_2Au_2Cl_6$, electronic state of Au at high press., Mossbauer spectra 80−60467
$CsCdF_3$, nonlinear elastic behaviour, US velocity, 1 bar-3 kbar 78−59851
CsCl, thermal expansivity determ. at high press. 78−79787
CsH_2AsO_4, pres. depend., LF dielec. response, ferroelec. props. 78−15120
CsH_2PO_4, ferroelec. transition, deuteration and press. effects 78−35101
CsH_2PO_4, ferroelec., press. induced antiferroelectricity 79−4774
$Cs_2[ZnCl_4]$, Raman-active phonons, $[ZnCl_4]^{2-}$ distortion, press. effects 77−52073
Cu, compressed powder, thermal cond. meas. *(German)* 80−70669
Cu, elastic constants, up to 2500 bar, −196-25°C, US pulse echo obs. 79−87680
Cu, elastic moduli second press. derivatives 79−96058
Cu, elec. resist., press. variation 78−84193
Cu, Gruneisen parameter behaviour at high press. 78−83899
Cu, interdiffusion with sintered Al powder, struct. effect at high press. 78−60606
Cu powder under press., elec. cond. *(German)* 79−69485
Cu, pressure effect on shear modulus and internal friction, EM reson. technique 77−31709
Cu, residual temperature, meas. during quasi-isentropic compression *(Russian)* 77−89495
Cu, sp. ht., 0-100 kbar 77−51512
Cu, thermal conductivity under high pressure 78−30901
Cu, US velocity, temp. depend., stress effects 80−75307
Cu-Cr, dil., spin glass, elec. resist., press. and conc. effects 78−52278
Cu-mild steel explosively welded interface, SEM examination *(German, English)* 80−96746
Cu-Mn-Ni alloy, Manganin, elec. resist. under static pressures up to 110 kbar, pressure gauge appl. 79−1594
CuCl, anomalous diamagnetism, high temp. Meissner effect *(Russian)* 78−34955
CuCl, behaviour under press., possibility of superconductivity 79−38239
CuCl, interface superconductivity? 80−39696
CuCl, optical absorption under press. 80−34949
CuCl, possibility of excitonic dielectric-supercond. phase transition 77−43797
CuCl, possibility of high temp. superconductivity 79−38238
CuCl, zincblende struct., high press. Raman scatt., 77K 78−60463
$CuCl_2.2H_2O$, antiferromag. reson., HF, press. depend. *(Russian)* 77−36137
$CuCl_2.2H_2O$, effect of press. on mag. phase transition, NMR meas. 78−19253
$CuCl_2.2H_2O$, flop of sublattice moments and Neel temp., press. effects, NMR obs. 77−40058
Cu_2HgI_4, polycryst., Raman spectra, press. depend. 77−73137
$CuK_2Cl_4.2H_2O$, Heisenberg ferromagnet, spontaneous magnetisation under press. *(Russian)* 77−36058
$CuK_2Cl_4.2H_2O$, Heisenberg ferromag., mag. props. at high press. 77−69512
$Cu_xMo_3S_4$, superconductivity, lattice transforms., electronic instabilities 77−39990
$Cu(NH_4)_2Br_4.2H_2O$, Heisenberg ferromag., mag. props. at high press. 77−69512
Cu_2O polycrystalline and single cryst. mech. behaviour 78−95777
$CuRhS_4(Se_4)$, press. depend. of supercond. transition temp. meas. 77−12050
γ-Cu_5Zn_8, high pressure effect on brass struct. 80−107108
$Cu_{40}Zr_{60}$, amorphous alloys, supercond. transition temp., press. depend. 80−84524
D_2, solid, equation of state 79−46781
o-D_2, solid, up to 150 kbar, 5K, Raman spectrum 80−50332
Dy, hexagonal-orthorhombic transition temp., effects of press. and crystallinity 80−24585
$DyPO_4$, mag. transitions under hydrostatic press., neutron diffr. study 80−71030
$ErFeO_3$, sound velocity meas. at high press., spin-reorientation transition 78−76254
$Er_{1-x}Gd_xRh_4B_4$, supercond. and mag. transitions at press. up to 19 kbar 79−38236
$(Er_{1-x}Ho_x)Rh_4B_4$, superconductive and mag. interactions, hydrostatic press. effect 80−49973
Eu complex, benzoylacetonate, energy transfer at high pressures 78−52541
Eu intermetallic compounds, hyperfine interactions, high press. Mossbuaer expts. 78−43714
Eu, Mossbauer isomer shift and magnetic hyperfine field, press. effect 78−52386
Eu^{2+} activated phosphors, luminesc. efficiency, temp. and high pressure 78−23508
Eu+t_2, high press. Mossbauer spectra, interconfig. charge fluctuations 77−63341
EuB_6, resistivity press. variation, lattice consts. 80−100456

high-pressure effects in solids continued
EuB_6, valence state of Eu, X-ray line displacement meas. 80−70633
$Eu_{0.95}Ba_{0.05}Pt_2$, Mossbauer studies on ^{151}Eu at high press. 80−39923
$Eu_{0.25}La_{0.75}Rh_2$, high press. Mossbauer spectra, interconfig. charge fluctuations 77−63341
EuO, anomalies in transport props. under hydrostatic press. due to bound mag. polaron 77−20372
EuO, hydrostatic press. effects on elec. resist. in temp. range 3 to 300K 79−23968
$EuPt_2$, ^{151}Eu Mossbauer studies at high press. 80−39923
$Eu_{0.98}Sm_{0.02}O$, ferromag. semicond., elec. cond. meas. 80 to 370K, press. effect to 20 kbar 77−51751
$(Eu_{1-x}Sn_x)S$, high press. Mossbauer exam. of Curie temp. and transferred hyperfine field 79−56643
$(Eu_{1-x}Sn_x)Se$, high press. Mossbauer exam. of Curie temp. and transferred hyperfine field 79−56643
EuTe, Neel temp. and hyperfine interactions, press. depend. up to 60 kbar, ^{151}Eu Mossbauer obs. 77−63181
Fe based porous metals, exam. of volume change under high pressure 78−52906
Fe, carbonyl powder, specific elec. conductivity, 5 to 200 MPa *(German)* 80−70664
Fe, cast strength and plasticity under hydrostatic pressure 78−56694
Fe close-packed phases, eqns. of state and implications for Earth core 79−20780
Fe effect of repressing and double sintering on impact strength *(Japanese)* 78−92217
Fe, equation of state determ., high temp. and pressure, computer expt. 78−75800
Fe, FCC, electronic struct. at Earth core press. 77−1356
Fe, Gruneisen parameter behaviour at high press. 78−83899
α-Fe, hydrostatic pressure effect on creep rate and failure time 78−92306
Fe melting temps. in Earth core, depend. on interatomic pots. choice 79−74863
Fe, Mossbauer effect at high press. in α-, ε- and γ-phases 80−15858
Fe, positive muon diffusion, press. depend. 80−75907
γ-Fe precipitates, antiferromag. ordering, press. depend., Mossbauer meas. 79−73861
γ-Fe precipitates in Cu, Invar related system, high press. Mossbauer spectra 79−56642
Fe, single crysts., effect of hydrostatic pressure on plastic flow props., dislocation distribs. 79−38887
α-Fe, solubility of H_2 at press. up to 67 kbar *(Russian)* 79−51260
Fe, thermal props. at high-press. (150 GPa), from shock-wave expts., Earth core struct. 80−21683
Fe: ^{119}Sn, pressure dependence of effective magnetic fields 78−52382
Fe-Al-Si, bending test, mech. props. under high press. and temp. *(Japanese)* 78−76711
Fe-C (30 at.%), production of Fe_7C_3 at high press., morphology and microstruct. *(Russian)* 79−38828
Fe-H system, influence of H press. on Fe crit. points and H solubility 78−52758
Fe-Mn (15(24)(30)wt.%), high hydrostatic pressure influence on stress-strain curve 80−25805
Fe-Pt alloys, solubility of H_2 at press. up to 67 kbar *(Russian)* 79−51260
Fe-Si (3 wt.%), exam. of plastic deformation, slip band dislocation, under hydrostatic pressure 78−56695
$Fe_{80}B_{20}$, amorphous, crystn. temp. under press. 79−23523
$FeBO_3$, Curie temp. displacement under press. up to 3 kbar 77−20603
$FeBO_3$, magnetisation near crit. temp., up to 3 kbar hydrostatic press., scaling theory 77−8316
$FeCl_2.4H_2O$, pressure effects on hyperfine interaction in single crysts. in mag. field 77−16211
$Fe_xCo_{1-x}Si$ alloys, disordered, hydrostatic pressure effects on mag. props. 77−32175
$Fe_xCo_{1-x}Si$, mag. props. 79−56532
$Fe_xCo_{1-x}Ti$, high press. mag. props. 78−23271
$Fe_xCo_{1-x}Ti$, mag. props. 79−56532
FeF_2, EXAFS at high press., bond compressibility, at. spacings 78−39628
FeF_2, Mossbauer effect at high press. 80−15858
$FeGe_2$, Fermi surface press. depend., de Haas-van Alphen method 77−43478
$Fe_{32}Ni_{36}Cr_{14}P_{12}B_6$, Metglass 2826A, mag. props. under high press., Mossbauer meas. 79−73860
α-Fe_2O_3, hydrostatic compression, X-ray diffr. meas. 79−99269
Fe_2O_3, semisintered, shear strength at high press. 80−76308
Fe_3O_4 (magnetite), mag. susceptibility under hydrostatic press. and implications for tectonomagnetism 80−26504
Fe_3O_4, magnetite, isothermal compression up to 70 kbar under hydrostatic conditions 78−30698
$Fe_{1-x}Rh_x$, press. effects on mag. phase transition, resist. meas. 77−4516
FeS, pressure effect on elec. resist. and thermoelec. power 80−70308
FeS_2, EXAFS at high press., bond compressibility, at. spacings 78−39628
FeS_2, mag. susceptibility press. depend., bandstruct. calcs. 78−19212
Fe_2SiO_4 (fayalite), shear strength and press. distrib. in diamond anvil press 78−12710
Fe_2SiO_4 in solid media apparatus, high press. and temp., controlled O_2 fugacities, buffer techniques *(German)* 79−93162
Fe_2SiO_4, spinel, isothermal compression up to 75 kbar hydrostatic press. 77−43280
$FeSn_2$, hyperfine mag. fields at ^{57}Fe, ^{119}Sn nuclei, under press. *(Russian)* 78−39486
Ga, electronic struct. under pressure, Fermi surface meas. using magnetoacoustic technique *(Russian)* 77−47716
$Ga_{1-x}Al_xAs$, deep levels, pressure effects 80−49651
$Ga_{1-x}Al_xAs$, velocity saturation and cond. band struct. under press. 78−26863
GaAs, deep levels, photocapacitance meas. under hydrostatic press. 77−85259
GaAs, direct energy gap, press. depend. up to 180 kbar 77−8020
GaAs, electron heating under hydrostatic pressure, Monte Carlo calcs. 77−69334
GaAs, electron irrad. induced defect levels, hydrostatic press. effect 80−92858
GaAs, hole effective mass, press. depend., theory and tunnelling expts. 78−75986

high-pressure effects in solids continued
n-GaAs, strain sensitivity of specimens obtained from pressed powders 77−36177
n-GaAs, transferred electron effects under hydrostatic pressure 77−32018
n-GaAs, transferred electron effects under hydrostatic press. 78−26871
GaAs-$Ge_{1-x}(GaAs)_x$ n-p heterojunctions, hydrostatic press. effect on elect. and photoelectric props. 80−20304
GaAs-Pb junctions, electron tunnelling under high press., transition temp., energy gap, phonon energies 79−15257
$GaAs_{1-x}P_x$:N, LED, external quantum efficiency, press. effect 77−8655
$GaMo_3S_6$, mag. and struct. transition temps., press. effects, 0-6 kbar *(Russian)* 77−89956
GaN:Zn, temp. and press. depends., electrolum. 78−19567
GaP:Co, deep levels, IR photoluminesc., stress effects 80−55163
GaS(Se), absorpt. edge, exciton levels and Raman scatt., press. effects above 40 kbar 77−48187
p-GaSb, cond. mechanisms, uniaxial compression effects 77−20312
GaSe, press. induced metallic and supercond. state 80−75666
GaTe, transport properties under hydrostatic pressure 80−75589
Gd complex, benzoylacetonate, energy transfer at high pressures 78−52541
Gd, ferromag. Fermi surface and band struct., press. effects, dHvA expts. 78−14656
Gd, magnetocrystalline anisotropy, temp. and press. depend. 77−20586
GdB_2, high press. synthesis 78−18608
$GdH_{2.92}$, electrical resistance anomalies at high pressures 80−29381
$Gd_2(MoO_4)_3$, uniaxial stress effect on ferroelec. transition, Raman scatt. 78−80360
$Gd_xY_{1-x}Fe_2$, s-d exchange interaction integral, change due to hydrostatic compression 78−88199
Ge, acceptor ground state, stress effects 80−34385
Ge, dislocation electron states, from press. depend. of photocond. 80−96819
Ge, EXAFS at high press. 80−97376
Ge, effect of pressure on the Raman shift 78−92064
Ge, electron hole drop, surface energy calcs. 77−47741
Ge, electron-hole droplet shape under uniaxial stress 77−43518
Ge, electronic struct. of fast donor defect, stress effects, calc. 80−54641
Ge, eqn. of state, under press. 78−75801
Ge, lattice dynamics under press 80−92627
p-Ge, negative magnetoresist. and Hall effect, press. and field depend. 80−70733
Ge, phonon energy variation under high press. band struct. changes, tunnel spectroscopy study *(Russian)* 80−2134
Ge, pressure tuning of picosecond pulse transmission, enhanced transparency 77−88871
Ge, supercond. at high press., crit. temp. 80−60130
Ge transparent IR window design for uniform pressure loading 79−23088
Ge:As(P)(Sb), impurity photocond. spectra under uniaxial compression 80−44656
Ge-Se glass, elastic props. under press., US interferometry 78−79658
Ge_2N_2O, pressure induced tetrahedral tilting and deform. 80−24415
GeO_2, α-quartz structure, compression mechanism 79−23673
GeTe, high pressure effects on hole conc. and thermoelec. props. 78−26894
H, metallic, cubic structure, mechanical stability 77−4242
H, metallic, struct. and stability 78−14305
H-He metallic, solid alloys, phase separation and thermodynamic functions calc., 0-19000K, 15-90 Mbar 77−43333
H_2, eqn. of state of megabar press. using z-pinch method *(Russian)* 79−33071
H_2, FCC solid, first-order shifts in electronic states 79−82510
H_2, isentropically compressed, elec. cond. at Mbar press. 78−95315
H_2, melting curve up to 10 kbar *(Russian)* 77−27987
n-H_2, molar volume press. depend. at 77K *(Russian)* 79−86832
p-H_2, rotation-libration transition under press., Monte Carlo study 80−49460
p-H_2, solid, induced near IR absorption spectrum, freq. shift, intensity, up to 10 kbar 78−6658
H_2, solid, installation for isothermal compression up to 25 kbar, 60 to 130K 79−35769
H_2, solid equation of state 79−46781
HBr, far IR Ar matrix isolated spectra, 4.2K, press. and conc. effects 78−62801
HCl, far IR Ar matrix isolated spectra, 4.2K, press. and conc. effects 78−62801
He, FCC, lattice dynamics 78−10255
He, melting at room temp. and high-press. 80−80025
^4He, melting, at ambient temp. under high pressure *(French)* 79−73373
Hg_2Br_2, powder, Raman spectra, press. effects 78−2837
$Hg_{1-x}Cd_xTe$, zero-bandgap state induced by press., galvanomag. props. 77−47725
Hg_2Cl_2, powder, Raman spectra, press. effects 78−2837
$HgMoO_4$, luminesc. efficiency, temp. and high-press. 78−23507
I_2, FCC metallic, self-consistent APW Xα electron-band calc., up to 22000K 77−39762
I_2, solid, metallic, insulating-metal transition at high-press., exptl. and theoretical shock-compression curves 77−39781
In, Gruneisen parameter behaviour at high press. 78−83899
In, Lifshits transition, electron-phonon interaction 80−29502
In, superconducting energy gap and phonon frequencies under press., tunnelling meas. 77−32112
In-Sn alloy, Lifshits transition, electron-phonon interaction 80−29502
n-InAs, magnetophonon resonance under hydrostatic press. 77−47832
$InAs_{1-x}P_x$, deep levels and semicond.-semimetal transition at high press. 80−11056
n-InP, high field props. under high press. 78−26872
InP, photoluminescence meas. using diamond-anvil press. cell 80−108256
n-InP, transferred electron effects under hydrostatic press. 78−26871
n-InP, transferred electron instabilities, hydroststic press. effect 80−6869
InP, transferred electron effects under high press. 80−34453
n-InSb, heavily doped, high press. effect on electron mobility and conc. 77−4390
p-InSb, high press. effect on elec. props., 50-300K 77−47807
n-InSb, hydrostatically compressed, instabilities of current, Gunn effect meas. 77−1432
InSb, hydrostatically pressed, negative differential cond. at room temp. 79−19600

high-pressure effects in solids continued
InSb, thermal cond., elec. cond., and thermoelec. power, press. depend. 80−59744
InSb, thermoelec. power and relative resist. at press. up to 35 kbar 79−65505
n-InSb, undoped, press. induced slow relax. of free electron conc., Hall coeff. meas. 77−47833
p-InSb, uniaxially stressed, elec. cond., Hall coeff. and photocond. at 15K 77−47828
p-InSb:Ge, photocond. in quantising mag. field, uniaxial press. influence 77−15907
n-InSb:Se(Te), heavily doped, anomalous press. depend. of thermoelec. power 77−47840
InSb:Te, anomalous anisotropy of magnetoresist. and g-factor 77−47831
K, device for press. variation of yield stress, elastic constants 78−53047
K, mode Gruneisen parameters, neutron scatt. obs., 4.5K, 0.001-4.1 kbar 77−4179
K, pressure dependence of Fermi surface, de Haas-van Alphen meas. 78−26807
K, thermodynamic props. at high press. *(Russian)* 78−47536
KCN, Raman spectra, at very high press. 79−1759
KCl absorption and emission of F_A(Li) centres under hydrostatic pressure 78−92117
KCl, cryst. isolated pore healing under press., dislocation struct. evolution *(Russian)* 80−100245
KCl, press. shifts of F-centre hyperfine interaction parameters 78−79957
KCl single crystal, healing of isolated pore under pressure due to isostatic compression 77−21046
KCl, thermal cond. under press. meas. 78−30802
KCl:Ag,Tl, cryst. high-press. energy transfer, sensitised luminesc. 77−36281
KCl:KNO_2(KNO_3), anion exchange during tablet pressing, IR spectroscopy appl. 80−2764
KH_2AsO_4, pres. depend., LF dielec. response, ferroelec. props. 78−15120
KH_2PO_4, ferroelectric transition, press. induced tricrit. point 78−80301
KH_2PO_4, KD_2PO_4, high-press. struct. rel. to dynamical models 78−80307
KH_2PO_4, press. and deuteration effects on static ferroelec. props., four-particle cluster approx. 80−34861
KH_2PO_4, single crystal neutron diffraction study at high pressure 80−92497
$KHSO_4$, phase diagram of 3.2 GPa, 450°C 80−76237
KI, thermal cond. under press. meas. 78−30802
KI:NO_2^-, Raman spectra, high press., low temp. effects 78−52479
KI:Tl^+ type phosphor, press. effects on triplet relaxed excited states, quadratic Jahn-Teller interaction 78−23510
$K_{0.75}Li_{0.25}TaO_3$, press. depend. of impurity soft modes, low energy Raman scatt. meas. 78−2852
$K_xNa_{1-x}TaO_3$, press. depend. of impurity soft modes, low energy Raman scatt. meas. 78−2852
$K_2PbCu(NO_2)_6$, uniaxial stress, EPR meas. 80−20455
$K_2Pt(CN)_4Br_{0.3}.2.7D_2O$, under hydrostatic press., compressibility, neutron diffr. 79−46742
$KTa_{0.7}Nb_{0.3}O_3$, pressure-induced resistance and colour change obs. 80−75608
(La, Ce)Sn_3, dil. alloys, supercond. and normal state props. 78−76184
La, electronic structure vol. depend., rigorous cellular method 77−20233
La, low temp. P-T diagram 77−47550
La-Ce, Kondo system, intermediate temp. supercond. under hydrostatic press. 79−24097
$La_{78}Au_{22}$, amorphous supercond., T_c and fluctuation cond. under high press. 79−7935
LaB_6, elec. cond. under hydrostatic press. 79−7832
$LaCuO_3$, struct. rel. to phys. props., high-pressure series of perovskite-like oxides 78−51493
LaF_3:Nd^{3+}, cryst., $4f^3$ config., ground level energy state var. rel. to press. *(Russian)* 77−16358
$LaH_{2.96}$, elastic props. at high press. 77−84825
$LaH_{2.98}$, electrical resistance anomalies at high pressures 80−29381
$LaMg(NO_3)$:Ni^{2+}, pressure depend. of zero-field splitting of two mag. centres *(Russian)* 77−32249
$La_2Mg_3(NO_3)_{12}.24H_2O$:$Ce^{3+}$, electron spin-lattice relax. under uniform compression 77−90028
$La_2(MnO_3)_3$, hydrostatic press. effect on mag. struct., neutron diffr. 77−51886
$LaSn_3$, dilute alloy containing light rare earth impurities, press. depend. of supercond. transition temp. 79−47184
Li halides, F-band energies press. effect 78−60086
Li, thermodynamic props. at high press. *(Russian)* 78−47536
LiCl, press. shifts of F-centre hyperfine interaction parameters 78−79957
LiF TLD, press. deform. and recovery 77−8668
LiF, thermal cond. under press. meas. 78−30802
LiF, thermal expansivity determ. at high press. 78−79787
LiH, electronic struct. and equation of state up to 100 Mbar 77−1361
LiH, insulator-metal transition press. calc. 78−34769
LiH, zero temp. phases, high density props. 78−75725
Li_2O-Al_2O_3-SiO_2, glass ceramic, elastic props. at high press., US meas. 78−83863
$LiTi_2O_4$, press. depend. of supercond. transition temp. meas. 77−12050
Lu, electric field gradient, at ^{181}Ta substitutional atoms, pressure dependence 78−52385
Lu, supercond. T_c meas. up to 200 kbar 77−47916
$(Mg,Fe)_2SiO_4$, dislocation recovery rate affected by high-press. 80−94515
$(Mg,Fe)_2SiO_4$, shock deform. expts., Hugoniot data implications 80−94497
Mg, elastic consts., finite strain theory *(French)* 79−1475
Mg, heating by shock compression, of porous material, vap. form. *(Russian)* 78−2195
Mg, melting temp. under shock loading 77−47553
$Mg(Cu_{1-x}Zn_x)_2$, crystal struct. and lattice spacing under high press. comp. depend. 77−72581
MgIn, X-ray diffr. exam. of compressibility 78−51610
MgO, bonding, pressure effects in lower mantle 80−72491
MgO, compression to 8 GPa, meas. with WC-anvil X-ray apparatus and epoxy press. medium 77−89496
MgO, F centre luminesc., effects of uniaxial stress and ODMR 80−20690
MgO, semisintered, shear strength at high press. 80−76308

high-pressure effects in solids continued
MgO, strength under confining press. of 250 kbar, brittle-ductile transition 77−47510
MgO, thermal cond. up to 40 kbar 79−1533
Mg_2SiO_4, forsterite, single-cryst., shock wave compression 79−84242
$MgWO_4$, luminesc. efficiency, temp. and high-press. 78−23507
$Mg[Pt(CN)_4].7H_2O$, high press. tuning of optical transitions 79−28813
Mn-Ni-C system, pressure effect on melting diagram *(Russian)* 77−55943
MnAs, orthorhombic, low temp. magnetic transitions *(Russian)* 80−11193
$Mn_{1-x}Co_xSb$, press. effect on saturation magnetisation *(Russian)* 77−80919
$Mn_{1-x}Fe_xAs$, high-pressure phase, magnetic properties 78−52247
$MnFe_2O_4$:Sn, hyperfine mag. fields at ^{119}Sn and ^{57}Fe nuclei, influence of press. 79−99811
$Mn_{1.77}Sn$, 170K transitions temp. in ferrimag. state, pressure and γ-irrad. effects 77−51902
$Mn_{1-x}Ti_xAs$, ferro- to paramag. transition, press. effect up to 7 kbar 77−89954
MnZn ferrites, mag. susceptibility freq. spectrum, effect of pressure 78−95420
Mo, anomalous US damping under hydrostatic press. 79−14890
Mo, dislocation (100) density variation, deformation effects, dislocation stability *(Russian)* 80−15108
Mo dislocation a ⟨100⟩ stability, plastic deform. at high-press. 78−43030
Mo, Fermi surface press. depend., surface impedance and US attenuation oscills. in mag. field 77−43476
Mo, polycrystalline, fracture and ductile-brittle transition, hydrostatic press. effects 78−60735
Mo, powder, cold isostatic compaction effect on thermophysical props. 78−52717
Mo, solid solubility of N_2 determ. using high-pressure autoclaves 77−15592
Mo-Ti-La-C, influence of high pressure on mech. preps. after nitriding *(Russian)* 79−57137
$MoCr_2O_6$, hydrothermal cryst. growth, 40 kbar, 873K, cryst. struct. *(French)* 78−35342
MoS_2(2H), Raman spectra, phonon modes, high press. effects 80−40111
N_2, solid, far IR 4.2K absorption apparatus 79−30583
ND_4Br, neutron diffr. exam. of P-T phase diagram 77−7861
ND_4Cl, sp. ht. at high press. meas., near order-disorder transition 77−84944
ND_4Cl:Cu^{2+}, high-press. EPR, order-disorder transitions 78−19310
NH_3-H_2 mixture, rel. to possible existence of metallic ammonium 80−24567
NH_4Br, neutron diffr., exam. of P-T phase diagram 77−7861
NH_4Cl, ordered phase, press. depend. of Raman scatt. meas. 77−12388
NH_4Cl, sp. ht. at high press. meas., near order-disorder transition 77−84944
$NH_4Cl(Br)(I)$, NMR under high press. 78−84485
$(NH_4)_3H(SO_4)_2$, press.-induced ferroelectricity, dielec. const. meas. 77−12328
Na, thermodynamic props. at high press. *(Russian)* 78−47536
NaBr, EXAFS at high press. 80−97376
NaBr:Cu^+, absorpt. spectra, pressure effects up to 6 kbar, comparison with NaCl:Cu^+ 79−4826
NaCN, Raman spectra, at very high press. 79−1759
NaCN, Raman spectrum, hydrostatic press. effects 78−6663
NaCl, dislocation mobility under high press., temp. depend. 80−75235
NaCl, dislocation struct. of slip bands, hydrostatic press. effect 80−54249
NaCl, elastic props. at press. up to 9 GPa, ultrasonic wave velocities 79−95073
NaCl, eqn. of state to 32 kbar and 500°C, length change meas. 80−70361
NaCl, Gruneisen coeff. press. depend. up to 33 kbar 77−35714
NaCl, high hydrostatic press. effects on dislocation mobility 78−14358
NaCl, high press. eqn. of state and sound vels. to fourth order elastic consts., 270 kbar 79−37806
NaCl, high press. metallic modification, superconduction obs. *(Russian)* 79−65576
NaCl, polycrystalline, acoustic vels. at 300K from 2.5 to 270 kbar 77−27945
NaCl, press. effect on ionic cond. at 300K 77−7895
NaCl, press. shifts of F-centre hyperfine interaction parameters 78−79957
NaCl, screw dislocation mobility under high hydrostatic press. 79−69109
NaCl, strength under confining press. of 250 kbar, brittle-ductile transition 77−47510
NaCl, thermal cond. under press. meas. 78−30802
NaCl, thermal cond. up to 40 kbar 79−1533
NaCl, US vel., Poisson's ratio and shear modulus meas., 9 GPa 77−4140
NaF, isothermal compression at 673K, up to 10 GPa, X-ray diffr. study 80−59565
NaF, thermal cond. meas. at high press. 80−75392
NaF, thermal expansivity determ. at high press. 78−79787
NaF, US vel., Poisson's ratio and shear modulus meas., 9 GPa 77−4140
β-Na_2O-Al_2O_3, thermal dissoc. at high press. 77−36435
Na_2O-SiO_2 glass, stability at high press., X-ray diffraction obs. *(German)* 78−92251
Na_xWO_3, $0.22<x<0.84$, low temp. struct., press. effects, NMR study 80−59443
Na_xWO_3, Knight shift, spin-lattice and spin-spin relax., high press. NMR obs. 80−50211
$Na_{1-x}Zr_2Si_xP_{3-x}O_{12}$, press. and comp. effect on fast Na^+ ion transport 80−107516
Nb, plastically deformed, hydrostatic pressure effect on dislocation relaxation, US exam. 78−76696
$NbD_{0.04}$, neutron scatt. exam., press. depend. of superstruct. reflection 78−22696
Nb_3Ga, critical data, under hydrostatic pressure to 15 kbar 79−47217
Nb_3Ge, high pressure and temp. treatment effect on supercond. props. *(Russian)* 77−1512
NbI_4, metallic state, resistivity anomaly 79−15136
NbI_4, quasi-one dimens., press.-induced metal-insulator transition 78−43447
NbN, critical data, under hydrostatic pressure to 15 kbar 79−47217

high-pressure effects in solids continued
NbN diffusion wires, crit. currents and supercond. crit. field under high press. 79−38287
NbO_2, semiconducting, elastic const., press. depend. at 296K 79−23672
NbS, supercond. props. at press. up to 20 kbar 79−24111
$NbSe_3$, superconductivity under press. 77−76995
$NbSe_2$(2H), CDW onset temp. and supercond. crit. temp., press. effects up to 20 kbar 77−39987
Nb_3Si A15 phase from amorphous Nb-Si alloys, high-press. synthesis 80−93516
Nb_3Sn, critical data, under hydrostatic pressure to 15 kbar 79−47217
NdP_5O_{14}, ferroelastic, hydrostatic press. effect on phase transition temp. 80−70293
Ne, P-V-T data for Morse pot., computer expt. 78−75800
Ne, phonon dispersion relation, Gruneisen parameters at high press. 79−42179
Ne, solid, elec. cond. obs., insulating up to 500 GPa 78−95315
Ni based porous metals, exam. of volume change under high pressure 78−52906
Ni Curie temp., press. depend., using press. cell developed for meas. with cubic-anvil press 80−13109
Ni, electrical resistance and H solubility at high press. *(Russian)* 79−91018
Ni, hydrostatic press. effect on magnetisation Procopiu effect and hysteresis meas. 77−48023
Ni, polycryst., recrystn. kinetics *(Russian)* 77−48453
Ni, polygonisation, high press. grain growth, dislocation struct., electron microscopic obs. 77−16613
Ni, positive muon diffusion, press. depend. 80−75907
Ni, sp. ht., 0-100 kbar 77−51512
Ni:^{119}Sn, 78−52382
Ni-Co, electrical resistance and H solubility at high press. *(Russian)* 79−91018
Ni-H, in high press. H conditions, published results anal., atomic ratio calcs. 79−69254
Ni-Mn (up to 32 at.%), Curie temp., press. depend., using press. cell developed for meas. with cubic-anvil press 80−13109
NiAs crystal lattice alloys and cpds., mag. transitions, mag. field and high press. effects 79−82780
NiF_2, press. depend. of elastic moduli to 10 kbar 77−35619
NiS, metal-nonmetal transition under press. 77−69228
NiS, X-ray diffr. obs., high press., diamond anvil camera method 77−4082
$NiS_{2-x}Se_x$, elec. resistivity temp. depend., pressure depend., paramagnetic-antiferromagnetic transition 78−10690
$NiSiF_6.6H_2O$, ESR spectra at low temperatures and high pressures 78−52339
NiZn ferrites, mag. susceptibility freq. spectrum, effect of pressure 78−95420
NiZn ferrites under high press., grain growth *(Chinese)* 78−52825
$NpCo_2Si_2$, mag. props., high press. studies with ^{237}Np(60)-resonance 80−39924
P, black allotrope, orthorhombic bonding, up to 26.6 kbar, neutron diffr. obs. 79−99106
PCl_5, ^{31}P NMR of three solid phases, ionis. of PCl_6^- at high-press. 79−82882
PCl_5 III, Raman spectra of phase formed by high-press., PCl_6^- ionising dissoc. 79−82968
PCl_5, phase diagram, PCl_6^- ionising to PCl_4 and $2Cl^-$ under press. 79−82314
(Pb,Sr)TiO_3, ferroelec. props., press. depend., anharmonic oscillator model 80−80716
Pb, diffusion of Sn up to 30 kbar 78−10224
Pb, Fermi electron vel. change under press., Tomasch tunnelling *(Russian)* 77−72950
Pb, Gruneisen parameter behaviour at high press. 78−83899
Pb, P-V meas., 5 to 45 kb *(Chinese)* 79−23676
Pb, phonon softening, neutron scatt. at high press. 78−80091
Pb, shock compression at high press. *(Russian)* 80−92608
Pb, superconducting, press. depend. of supercond. transition temp. 78−84340
Pb, thermal conductivity in supercond. and normal states, press. effects 77−43779
Pb-In, superconductive, electron tunnelling under hydrostatic press. 77−51850
Pb-Sb, crystal struct., supercond. after subjection to high press. 78−88064
Pb-Si superconducting solutions, effect of hydrostatic compression on tunnelling *(Russian)* 80−65746
Pb-Zn, pressure effect on solubility and diffusion of Zn 77−43385
$PbBr_2(Cl_2)(I_2)$, ionic cond. and activation volumes, high press. effects 80−100353
PbF_2, cubic and orthorhombic, press. and temp. depends. of ionic cond. 79−95207
$PbHAsO_4$, hydrostatic press. effect on ferroelec. transition 78−35102
$PbHPO_4$, crystals, ferroelec. phase transition, hydrostatic press. influence, dielec. meas. 80−88936
$PbHPO_4$, hydrostatic press. effect on ferroelec. transition 78−35102
PbS, epitaxial layer on rock salt substrate, stresses, hydrostatic press. effects 78−51831
n-PbSe, pressure induced transition to gapless state 78−2533
PbSe, pressure tunable CW injection laser, emission spectra 79−18419
$Pb_{1-x}Sn_xGe$:In, press.-induced transition to gapless state, galvanomag. effects 78−19108
$Pb_{1-x}Sn_xSe$, (x=0.125), pressure induced band inversion, effect on energy spectrum *(Russian)* 78−39007
n-$Pb_{1-x}Sn_xSe$, single crysts. and diodes, elec. props. under high press. 77−47809
p-$Pb_{1-x}Sn_xTE$, pressure-induced transition to zero-gap state, changes in energy band parameters 79−69413
$Pb_{1-x}Sn_xTe$, energy spectrum under hydrostatic pressure 79−65381
$Pb_{1-x}Sn_xTe$, Mossbauer investig. of phonon softening at semicond.-semimetal transition 77−43908
p-$Pb_{1-x}Sn_xTe$, single crysts. and diodes, elec. props. under high press. 77−47809
$Pb_{1-x}Sn_xTe$:Ge, anomalous behaviour of impurity centres under press. *(Russian)* 80−65491
$Pb_{1-x}Sn_xTe$:In, energy spectra modifications due to comp. changes and press. appl. 80−10915
PbTe-based cpds., thermoelec. power and Hall effect under hydrostatic press. 79−23990

high-pressure effects in solids continued
Pb(Zr,Ti)O_3, dielectric response in solid-medium high-pressure device 78−43766
Pb(Zr,Ti)O_3:Nb ceramic, stress effects on ferroelec. hysteresis, macroscopic strain, US vel. 79−4778
Pd, electrical resistance and H solubility at high press. *(Russian)* 79−91018
Pd, electronic states, effect of hydrostatic press. 79−11055
Pd-Co, pressure effect on Curie point, Debye temp. in ferromag. state *(Russian)* 77−32194
Pd-Fe-Mn, dil. alloy, high press. study 80−34600
Pd-H, in high press. H conditions, published results anal., atomic ratio calcs. 79−69254
Pd-H system, thermodynamic props., 245-352°C, up to 34 atm. 79−23749
Pd-Rh-Ag, mag. susceptibility, pressure effect up to 4000 atms. 77−16142
Pd-Rh-Ag, magnetic susceptibility press. depend., d-band deform. and exchange var. 77−47967
Pd_xSn_y (x=0.95, y=0.05; x=3, y=1), Mossbauer spectra, high press. effects, force consts. 80−84669
$Pd_{30}Zr_{70}$, amorphous alloys, supercond. transition temp., press. depend. 80−84524
Pr pnictides and chalcogenides, press. depend. of cryst. field splitting 78−68392
Pr, resistance anomalies under pressure up to 40 kbar 79−65430
PrSb, neutron scatt., press. induced antiferromag. 80−15699
Pr_3Se_4, induced ferromagnet, effect of press. on magnetisation 78−95422
Pt, electrical resistance and H solubility at high press. *(Russian)* 79−91018
Pt, electron irradiated, interstitials activation vol. 79−51154
Pt, solubility of H_2 at press. up to 67 kbar *(Russian)* 79−51260
Rb, search for supercond. at high press., elec. resist. meas. 79−56359
$RbAg_4I_5$, ionic cond., effect of press. 78−51733
RbBr, thermal cond. under press. meas. 78−30802
$RbCaF_3$, nonlinear elastic behaviour, US velocity, 1 bar-3 kbar 78−59851
$RbCdF_3$, nonlinear elastic behaviour, US velocity, 1 bar-3 kbar 78−59851
RbCl:Li^+, new off-centre defect system, studied with dielec. techniques under hydrostatic press. 79−19834
RbH_2AsO_4, pres. depend., LF dielec. response, ferroelec. props. 78−15120
RbI, non-linear press. depend. of phonon freq. 77−35650
$Rb_2PbCu(NO_2)_6$, uniaxial stress, EPR meas. 80−20455
Re, Anderson-Gruneisen parameter, bulk modulus and compression curves 78−30690
Re, Fermi surface hydrostatic press. depend., de Haas-van Alphen phase shift meas. 80−54593
Re single crystal, Hall effect, 4.2K, under 12 kbar press. *(Russian)* 77−80762
ReO_3, mag. breakdown above compressibility collapse transition 80−103617
Rh_2CoSn, hyperfine mag. fields at ^{119}Sn, under press., Mossbauer expts. 79−99812
Rh_2FeSn, hyperfine mag. fields at ^{119}Sn and ^{57}Fe, under press., Mossbauer expts. 79−99812
Ru, Fermi surface, influence of press. *(Russian)* 79−4501
Ru, lattice dynamics, thermal expansion and bulk modulus, lattice parameter press. variation 77−59079
S, metallic state, elec. resist., press. effects up to 600 kbar 78−26920
S, new form from decomposition of S_4N_4 79−10911
S, transition to conducting phase 77−35972
S, transition to supercond. state at high press. *(Russian)* 79−7923
S, transition to supercond. state obs. at high press. *(Russian)* 79−7922
α-S, under hydrostatic press., deformable mol. lattice statics 80−49175
α-S, zone-centre lattice vibrs., including hydrostatic press. effects 80−49314
S-Ni-Fe system containing monosulphide solid soln., elec. and struct. relations 80−90038
$(SN)_x$ and S_4N_4, high press. study 78−52782
$(SN)_x$, electrical cond. at high press., scatt., evidence for semimetallic band struct. 77−43573
$(SN)_x$, supercond. at high press. 78−23194
$(SN)_x$, supercond. props., press. depend., up to 9.5 kbar 78−68106
S_4N_4, effects of pressure and temp. on phonons, Raman scattering study 80−7360
Sb, carrier energy spectrum, effect of hydrostatic pressure 78−87903
Sb, cryst. struct. to 26 kbar via diamond anvil cell and X-ray diffractometer 77−31560
Sb, electrical resist. and anisotropy at press. up to 80 kbar 77−43554
Sb, electronic structure change with press., pseudopot. calcs. *(Russian)* 79−47006
Sb, partial Fermi levels of electrons and holes, press. depend. 77−43490
Sb, thermoelectric figure of merit, 1-12 kbar, 100K 78−80013
Sb, zone centre phonons and elastic consts., hydrostatic press. depend. 78−59905
Sb_2S_5, deep struct. changes, NQR obs., high-press. and temp. effects 80−54139
SbSI, tricrit. point, NQR under press. 79−38469
Sc, electric field gradient of ^{181}Ta substitutional atoms, press. depend. 78−52385
Sc, superconducting high-pressure phase 79−33378
Sc_2O_3-ScF_3 system, phase ratios at 100 kbar press. 78−19729
ScS, supercond. props. at press. up to 20 kbar 79−24111
Se, amorphous, elastic props. at high press. 79−37753
Se and Se-Ge system, amorphous, press. depend. of AC cond. 77−76858
Se, elec. cond., 0-500 kbar 79−99589
Se, electronic struct. of cryst. phases and hydrostatic press. effects 80−59865
Se, metallic state, press. induced, elec. cond. meas. 80−96949
Si, compression, effect of press. on lattice defects up to 90 kbar *(Japanese)* 77−72654
Si, compression to 8 GPa, meas. with WC/anvil X-ray apparatus and epoxy press. medium 77−89496
Si, dislocation formation, under high stress, low temp. 78−47386
p-Si, elec. resist., shock wave compression effects 80−80265
Si, electronic structure at high press. near semicond.-metal transition 80−49586
Si eqn. of state, under press. 78−75801

high-pressure effects in solids continued
Si, generalised Gruneisen parameter elements determ. using uniaxial press. for inelastic neutron scatt. 77−35442
Si, Gruneisen coeff. from stress-induced phonon energy meas., inelastic neutron scatt. 79−82298
n-Si, impurity-assoc. magnetophonon reson. 80−20221
Si, lattice constant, press. depend., X-ray diffr. meas. effect of nonhydrostaticness of press. 77−35439
Si, lattice dynamics under press 80−92627
Si, metallic state, press. induced, elec. cond. meas. 80−96949
Si, p-n junction, current-voltage charact., misfit dislocations, high press. effects 80−65671
Si:Re, diode, barrier capacitance and photocapacitance, uniaxial press. effect 77−20416
n-SiC, cubic, piezoresistance meas. under hydrostatic compression 77−4344
α-Si_3N_4, lattice and atomic position parameters, neutron diffr. study 79−42040
SiO_2, α-quartz structure, compression mechanism 79−23673
SiO_2, coesite, crystn. from soln. at high press. and temp. *(Japanese)* 77−72556
SiO_2, coesite, thermal cond. up to 40 kbar 79−1533
SiO_2, fused, isothermal compressibility to 20 kbar, inductance coil method 80−49302
SiO_2, shock compression at high press. *(Russian)* 80−92608
SiO_2 stishovite, thermal cond. up to 40 kbar 79−1533
Sm monochalcogenides, semicond.-metal phase transition 79−47017
SmB_2, high press. synthesis 78−18608
SmB_6, resistivity press. variation, lattice consts. 80−100456
$Sm_{1-x}Gd_xS$, press. induced electronic transitions 78−68058
$Sm_{1-x}Gd_xS$, resistivity investig. of metal-semicond. transition, press. effects 77−62829
SmH_x [x=2.78, 2.85, 2.91], electrical resistance anomalies at high pressures 80−29381
$Sm_{1-x}M_xS$, M=Eu,Ca,Yb, valence transition under high press. 79−73551
$Sm_{1-x}R_x^{3+}S$, (R is rare earth metal), semicond.-metal phase transition 79−47017
SmS, first-order transition from semiconducting to metallic state 78−52040
SmS, Hall effect near semicond.-metal transition 77−62968
SmS, high-pressure mixed-valence phase, diagram and electronic entropy, neutron diffr. obs. 79−33267
SmS, press. effect on lattice parameter, mag. susceptibility, and reflectivity 79−56272
SmS, valence transition, positron annihilation study 80−15454
SmSe, pressure-induced reflectivity changes and semiconductor-metal transition 79−56763
Sn, elec. field gradient on Cd, press. depend., TDPAC expts. 78−48092
Sn, electrical resist. and anisotropy at press. up to 80 kbar 77−43554
Sn, Fermi surface press. depend., surface impedance quantum oscills. in mag. field 77−47717
β-Sn, Fermi surface press. depend., de Haas-van Alphen meas. 79−73422
$SnCl_2.2H_2O$, effect of hydrostatic press. on isomorphous phase transition, complex dielec. const. meas. 77−76551
SnO, under hydrostatic press. up to 41 kbar, Mossbauer study 79−51892
$Sn_2P_2S_6$, investigation of p-T diagram near a singular point *(Russian)* 80−88937
Sn_2S_3, resistivity, Mossbauer spectra, press. effects 79−73862
SrF_2, ionic cond., activation vols., freq. depend. cond., press. effects 80−100354
SrF_2, powder, elec. cond. transition under high press. *(Russian)* 77−20370
$SrTiO_3$ under [111] uniaxial stress, neutron scatt. 78−67798
$SrTiO_3$, uniaxial stress induced ferroelectricity *(Japanese)* 79−65814
TGS, ferroelec. cryst., complex permittivity at microwave freq. and high press. 80−2685
TGSe, ferroelec. cryst., complex permittivity at microwave freq. and high press. 80−2685
TTF-TCNQ, DC Hall effect meas. 77−89753
Ta, polycrystalline, dislocation relaxation under high pressure 79−77605
Ta-Ga, crystal struct. at high press., polymorphism 80−88112
TaC_xN_y, supercond. and normal props. under hydrostatic press. 77−12049
Ta_2N film, high temp. nitriding kinetics depend. on press. *(Russian)* 80−50838
TaS_2 ($4H_b$), press. effects on CDW transitions 77−51680
TaS_2-NH_3 intercalation complex, press. induced diffusion effects, NMR study 79−19797
TaS_2(1T)(2H), nucl. quadrupole interactions, high press. effects 78−35072
TaS_2($4H_b$), electrical cond. and CDW transitions under press., rel. to supercond. 77−43574
$TaSe_3$, effect of press. on supercond. transition temp. 79−91182
$Tb_2(MoO_4)_3$, hydrostatic press. effect on phase transition 78−27166
Te, elec. cond., 0-500 kbar 79−99589
Te, electronic struct. of cryst. phases and hydrostatic press. effects 80−59865
Te, energy gap meas. under press., photocond. and transmission spectra 77−85267
Te, energy gap under press., elec. resist. and Hall effect meas. 78−30926
Te, high-press. metallic, supercond. transition temp. press. depend. 80−80435
Te, interband photocond. at up to 10 kbar, 1.6-200K 77−47850
Te, intervalence band absorption, press. and defects influence 80−55149
Te, mag. inversion of Hall effect *(Russian)* 77−4376
Te, metallic state, press. induced, elec. cond. meas. 80−96949
Te, opt. props. under high press., band struct. transform. 80−55112
Te, pure and Sb doped, impurity state and impurity cond., press. effect 80−54723
Te, trigonal, ^{129}I Mossbauer obs. of electronic changes 80−55005
Te, undoped, elec. cond., magnetoresist. and Hall meas., hydrostatic press. effect 77−47830
Te, valence band struct., hydrostatic press. effect 77−47724
Te, valence band struct. under press., spin-orbit splitting, intraband absorpt. spectra 80−2330
Th, electronic states under press. 80−54600
Th-Cr, supercond., press. meas. to 20 kbar 80−88667

high-pressure effects in solids continued
Ti alloys, hydrogenation at 200-600°C and up to 10000 kPa 80−107435
Ti-Mo (3 to 35 wt.%), high pressure influence on transition temp. to supercond. 80−107952
$TiFe_{1-x}Co_x$, mag. props., under high press. and in high mag. fields 78−95423
TiN single crysts., supercond. T_c at high press. 79−38228
TiO_2, rutile, isothermal compression under hydrostatic press. to 106 kbar 80−31035
TiO_2, rutile, vol. depend. of refr. indices under hydrostatic press. 77−52036
TiO_2, uniaxial stress depend. of direct-forbidden and indirect-allowed transitions, absorpt. edge obs. 79−42990
Ti_2O_3, press. depend. of elastic consts. at 296K. 79−42134
$TlCdF_3$, nonlinear elastic behaviour, US velocity, 1 bar-3 kbar 78−59851
U, electric field gradient, of ^{181}Ta substitutional atoms, press. depend. 78−52385
U, Hugoniot data, ultrahigh press. (TPa) shockwave from underground nuclear explosion 80−59580
UAl_2, high field, high press. mag. props. 80−11172
UCr_2O_6, hydrothermal cryst. growth, 40 kbar, 873K, cryst. struct. *(French)* 78−35342
UFe_2O_6, hydrothermal cryst. growth, 40 kbar, 873K, cryst. struct. *(French)* 78−35342
$UMnNiO_6$, hydrothermal cryst. growth, 40 kbar, 873K, cryst. struct. *(French)* 78−35342
UMn_2O_6, hydrothermal cryst. growth, 40 kbar, 873K, cryst. struct. *(French)* 78−35342
UN, mag. susceptibility under press. 80−7086
$UNi_{5-5x}Cu_{5x}$, NMR and press. effects 80−25230
UO_2, elastic props. at high press., US meas. 77−4141
U_3P_4, press. effects on elec. resist. and Curie temp. 80−75559
US, ferromag., AC mag. susceptibility at high press. 80−7085
V_2O_3, hydrostatic compression, X-ray diffr. meas. 79−99269
V_2O_5, splat-cooled, crystallisation, high-press. effects 78−9956
V_4O_7, metal-insulator phase transition temp. depend. on hydrostatic press., DTA meas. 79−73438
V_3Si film, sputtered, high press. induced shifts in supercond. transition temp. 77−85374
V_3Si, press. depend. of positron lifetimes 78−11015
V_3Si, static compressibility, up to 20 kbar 77−43281
W, Fermi surface press. depend., surface impedance and US attenuation oscills. in mag. field 77−43476
W, grain boundary migration initiated by high hydrostatic press. 78−51554
W, P-V meas., 5 to 45 kb *(Chinese)* 79−23676
W, powder, cold isostatic compaction effect on thermophysical props. 78−52717
W powder, hydrostatic pressing 78−11161
W, stacking faults, microstress relax. effects, field ion images 77−89453
WC, MP depend. on press. up to 80 kbar, optical meas. *(Russian)* 77−80604
WC-Co, elastic moduli and their press. derivatives 79−83248
WC-Co cemented carbide, stress-strain curves using ultrahigh-pressure apparatus 79−43322
WF_6, effect of high hydrostatic press. in reorientation and internal motion, ^{19}F NMR spectra 79−15364
Xe, metallic state at static press., elec. cond. meas. 79−33313
Xe, metallic state transition under high press., supercond. *(Russian)* 79−60713
Xe, solid, high press. equation of state 79−37809
YIG, ferromag. reson., press. up to 6.5 kbar 77−51956
YIG, press. depend. of effective mag. fields on ^{57}Fe nuclei 78−52383
YIG:Fe^{2+}, magnetocrystalline anisotropy, effect of high hydrostatic press. 77−43831
Yb, FCC, Fermi surface parameters, de Haas-van Alphen effect, press. depend. 77−28092
Yb, FCC phase, low temp. mag. props., impurity effects 80−20387
Yb, resistivity meas., semimetal-semiconductor transition 78−14727
Yb, shock compressed, elec. cond. behaviour and transitions, up to 220 kbar *(Russian)* 77−80761
YbB_6, resistivity press. variation, lattice consts. 80−100456
YbO, Yb_3O_4, form. at high press. from Yb+Yb_2O_3 78−85192
ZN, anomalous US damping under hydrostatic press. 79−14890
Zn, de Haas-van Alphen effect under press., Fermi surface and pseudopot. form factors 77−43475
Zn, elec. field gradient on Cd, press. depend., TDPAC expts. 78−48092
Zn, electrical resist. and anisotropy at press. up to 80 kbar 77−43554
Zn, hydrostatically compressed single crystal, work hardening studied by stress relax. method 79−20069
Zn, plastic deform., effect of hydrostatic press. stress relax. meas. *(Russian)* 79−96102
Zn, singularities of effect of pressure on stages of creep *(Russian)* 79−29134
Zn, US attenuation under high hydrostatic press., dislocation mechanism 77−43284
Zn-Sb diffusion couple, layer growth of ZnSb phase at high press., elec. meas. 80−2218
Zn-Sb diffusion couple, ZnSb phase layer growth kinetics, 240-320°C, up to 30 kbar 78−10229
$Zn_xCd_{1-x}S$:Cl, $Cu^+(Ag^+)$, high pressure luminesc. 78−19533
$Zn_{1-x}Cu_xGeF_6.6H_2O$, depression of dynamic Jahn-Teller effect 77−16164
ZnF_2, elastic moduli, press. depend., 0-10 kbar 78−10117
ZnS, cubic, compression 80−107358
ZnS, interimpurity high press. luminesc. 78−19532
ZnS:Cl^-, $Cu^+(Ag^+)$, phosphor, thermoluminesc. 78−64419
ZnS:Cu, Co, deep traps and stationary luminescence *(Russian)* 78−48227
ZnS:Pb^{2+} (Mn^{2+}), high press. luminesc., localised excitations 78−19534
ZnS(Se)(Te), thermal expansion and lattice dynamics under press. 80−100316
ZnSe cold pressing 77−52258
ZnSe:Cu, Cl, high press. luminesc. 78−19532
$ZnSiF_6.6H_2O$:Mn^{2+}, ESR spectrum, effect of uniaxial compression 80−29609
$ZnSiF_6.6H_2O$:Co, influence of hydrostatic press. on Co^{2+} EPR spectrum 78−27084
$ZnSiF_6.6H_2O$:Ni^{2+}, cryst. field, uniaxial compression method *(Russian)* 78−35027

high-pressure effects in solids continued
$ZnSiF_6.6H_2O:Ni^{2+}$, spin-lattice relax. at press. up to 6.5 kbar 78−48033
$ZnSiF_6.6H_2O:V^{2+}$, paramagnetic impurity ion spin multiplet initial splitting parameter, immediate environments distortion influence on sign 79−65720
$ZnSiF_6.6H_2O:V^{2+}$, spin-lattice relax. at normal and high press. 80−2632
ω-Zr, electric field gradients at substitutional Ta atoms, TDPAC high-pressure study 78−52384
ZrO_2, semisintered, shear strength at high press. 80−76308
$ZrSiO_4$, compression to 8 GPa, meas. with WC-anvil X-ray apparatus and epoxy press. medium 77−89496

high-pressure phenomena and effects
see also high-pressure effects in solids
acetonitrile, soln., high press., mol. reorientation, correl. times, depolarised Rayleigh scatt. obs. 80−29748
AGR boiler tube, serpentine geometry at high press., two phase heat transfer 78−94077
alcohols, H-bond system, liq., high-press. effect 80−49080
alkali iodides in acetone, press. effects on Walden products, ion-solvent interactions 80−3398
alkali metal nitrates, melting pressure curves up to 5 kbar 77−15547
alkali metals, liq., density, enthalpy, up to 1500 bars 77−84821
alkanes, ethane-, hexane-polar component binary mixtures, up to 1000 bar, phase separation, critical phenomena 77−35695
alkanes, liquid, press. induced changes in mol. conform. 78−9269
alkenes, ethene-, 1-hexene-polar component binary mixtures up to 1000 bar, phase separation, critical phenomena 77−35695
alkoxybenzylidenaminobenzonitriles, elec. field and press. induced transitions, transparency and texture 77−43317
4′-n-alkyl-4-cyanobiphenyls, press. effect on liq. cryst. phase transitions 79−95138
p-n-alkyl-p′-n-alkoxytolanes, hydrostatic pressure effects, phase transitions *(French)* 78−14448
amorphous state form. under high press. *(Chinese)* 80−28917
andesite melt, viscosity at high press. 77−29291
anthracene, mesophase formation during carbonisation under pressure 77−44182
aqueous nonelectrolyte solutions, thermodynamic excess functions at high press. 78−18793
asymmetric mixture vapour-liquid equilibrium calc. 79−4408
auramine O, fluoresc. efficiency, solvent viscosity effects at high press. 78−9188
basalt melt, viscosity at high press. 77−29291
basalt-seawater alteration reactions, studies via dynamic hydrothermal experimental system 79−5686
benzene, high press. Brillouin scatt., hypersonic speed 77−48182
benzene, liq., mol. motion at high press. 80−103509
benzene-d_6, liq., Raman spectra vibr. relax. and band widths 78−23440
benzene-toluene and benzene-o-xylene mixtures, US vels., compressibility, expsn. coeff. 79−33038
bis-(4,4′-n-alkoxybenzylidene)-1,4-phenylenediamines, smectic polymorphism up to 3 kbars, differential thermal anal. 79−55873
n-butanol, phonon MFP formula, H bond collisions, low temp. 77−35655
carbon tetrachloride, emulsion dispersed, high pressure phases *(French)* 77−56253
carbon tetrachloride, thermal cond. and phase diagram under pressure 78−75893
carbonisation under pressure, mesophase formation 77−44182
carboxylic acids+urea, γ-irradiated reactions under high pressure *(Japanese)* 79−52707
cardiovascular system, haemodynamic obs. in awake rabbits during hyperbaric He-O_2 exposure 80−101200
cast Fe, spheroidal graphite, hydrostatic pressure effects on ductile fracture 78−60779
CBNA, nematic-isotropic transition at high press., turbidity meas. 80−92655
CBOOA, liq. cryst.-isotropic transition at high press., P-V-T eqn. of state 79−95135
CBOOA, smectic-A reentrant nematic transition under press., X-ray obs. 80−59637
cell membranes, effects of hydrostatic pressure, review 78−15790
chloroform and -d, Raman spectra study of mol. reorientation 79−24303
chloroform-He(Ar)(N_2) gaseous compressed mixture, mol. reorientation, Raman spectra 80−23422
chlorotrifluoromethane, compressibility, 298 to 348K, Burnett expansion obs. 79−27733
cholesteryl esters, liq. crysts., P-T diagrams up to 5000 kg/cm^2 78−2003
cholesteryl nonanoate, liq. cryst.-isotropic transition at high press. 79−95135
coal tar and petroleum pitches, pyrolysis, press. effects on coke yield and microstruct. form. 77−70289
conference, Darmstadt, Germany (Mar. 1977) 79−23677
conference on high pressure physics and technology, Moscow, Russia (May 1975) 78−51611
crystal violet, fluoresc. efficiency, solvent viscosity effects at high press. 78−9188
cyano Schiff bases, high press. reentrant nematic bilayer smectic-*A* transition 79−28087
cyanobiphenyls, high press. reentrant nematic bilayer smectic-*A* transition 79−28087
cyclohexane+n-hexane, effect of pressure on excess enthalpies at 298.15K 78−48689
cyclopropane, liq., mol. dynamics, Raman and NMR studies of orientational motion 80−93296
cylindrical shells, dynamic behaviour under transient inner pressures 79−23215
decahydronaphthalene-H_2O, liq.-liq. phase equilib., crit. phenomena 78−18764
trans-decahydronaphthalene-polystyrene system, press. and mol. wt. depend. of polymer solubility 79−23734
dense plasma ionisation and cohesion, critical density and press., approx. formulas 80−59253
diamond formation from hydrocarbon dissociation, Hugoniot data, high temp. and press. 79−47927
diamond with garnet inclusion, expt. crystallisation conditions study 80−46172
dichloromethane, high press. and temp. IR absorpt. spectra, stretching fundamentals *(German)* 80−47999
1,1-difluoroethane, nucl. recoil ^{18}F chemistry at high press. 80−89510

high-pressure phenomena and effects continued
2,6,dimethylpyrazine, PMMA soln., fluoresc. and phosphoresc. quantum yield and lifetime, 20-120 kbar 79−54902
1,8diphenyl-1,3,5,7-octatetraene, high press. fluoresc. studies of radiative and nonradiative processes 80−1011
1,6-diphenyl-1,3,5-hexatriene, high press. fluoresc. studies of radiative and nonradiative processes 80−1011
discharge, in H_2 (D_2)(inert gas), props., electrode influence, spectroscopic obs. 80−38806
dyes, substituted methane, press. effs. on viscosity-depend. fluoresc. 77−34672
dynamic and static high-pressure event differences 79−21557
Earth interior, high-press. phenomena rel. to thermal model 78−15982
Earth mantle elements compounds and modifications, high press. and temp. thermodynamics 80−81874
Earth upper mantle, rare earths partitioning between silicate melt, amphibole and garnet peridotite 79−20775
EBBA, nematic-isotropic transition at high press., turbidity meas. 80−92655
EBBA, pVT data and viscosity-press. behaviour 78−94989
equations of state, Thomas-Fermi shell model, and high temps. 78−79738
ethane, fluid, saturated, compressed, sound velocity meas., compressibility, sp. ht. determ. 77−76488
ethane, gas, up to 50 atm, refr. index, 328, 3103 MHz *(French)* 78−14129
ethanol, phonon MFP formula, H bond collisions, low temp. 77−35655
ethanol-water mixtures, specific volume, compressibility, viscosity, up to 3200 bar, 15, 25°C 78−10113
ethylbenzole, thermal cond., 30-400°C, 1-10^3 kg cm^{-2} 78−26739
ethylene, high pressure polymerisation investig. using near IR spectroscopy *(German)* 77−21384
ethylene, pure, IR absorption obs. of C-H stretching fundamentals up to 2 kbar and 200°C 79−22701
ethylene-polyethylene mixtures, phase behaviour under high-press., polymer mean mol. wt. influence 79−24745
feldspar/water O isotope exchange, effect of fluid press. 78−57204
flexible chain polymer, topomorphism and phase dualism 78−14265
fluid binary mixtures, phase equilibria and critical phenomena at high press. 78−51648
fluid binary mixtures at high press., phase equilibria, critical phenomena calcs. 77−35664
fluorides of alkaline earths and transition metals, high-press. melting systematics 77−51475
free radical copolymerisation kinetics, monomer reactivity ratios under high press. conditions, meas. methods 79−91950
Freon, F-13V1 and F-23, thermal cond., −168 to 160°C, up to 6.10^7 Pa 77−47628
freon 12, gas, up to 50 atm, refr. index, 328, 3103 MHz *(French)* 78−14129
fuel droplet evaporation at elevated press. and temp., math. model investig. 77−52675
furan, liquid, P-V-T relations, 210 to 260K, up to 1000 MPz 79−95122
gas, high press. breakdown in strong static elec. field, plasma mechanism 80−79614
gas discharge prebreakdown processes, electrode surface inhomogeneity effects 79−14628
gas-gas equilibrium, thermodynamics at high press. 78−18734
heptane, liq., Raman scatt. at high-press., chain kinking 79−87429
heptanol isomers, static permittivity and density, press. and temp. depend. 78−35078
4-4′-di-heptyloxyazoxybenzene, liq. cryst.-isotropic transition at high press. 79−95135
hexadecane, liq., Raman scatt. at high-press., chain kinking 79−87429
hexane, liq., Raman scatt. at high-press., chain kinking 79−87429
n-hexane, refr. index meas. to 14 kilobars by optical interferometry 77−49764
HF discharges and DC arcs in H_2(D_2)(inert gas), instability obs. 80−38807
hydrocarbons, shock compression, dynamic high press. eqns. of state 80−6450
hydrostatic pressure effects on fracture, exam. 78−60779
ice, press. effects on Raman spectrum 78−95582
ice, pressure melting within glacier, indicated by regelation ice chem. comp. 78−61447
ion-ion recombination rates, calcs., rel to excimer laser kinetics 78−31621
iron, pure, tensile deformation behaviour under high pressure *(Japanese)* 80−16381
kerosene, combustion in air rel. to press. 3-15 kgf.cm^{-2} 79−66297
light scattering, appl. to biological substances *(Dutch)* 78−27901
liquid, under high press., refr. index vs. density 79−28712
liquid, under high press., refr. index vs. press. and strain 79−33668
liquid crystal, high press. mesomorphic and polymesomorphic transitions 78−18750
liquid crystal, viscosity-pressure behaviour rel. to transition pts. 79−23707
liquid crystals, phase transitions up to 3 kbar, transition enthalpy, entropy 77−20051
liquid interfacial instability, mass transfer under high press. 79−94601
liquid solidification press. meas., dielectric loss method 77−45868
macromolecular conformation under press., optical rotatory dispersion meas. method 77−48984
magnetosonic heating of semiinfinite body under periodic loading *(Russian)* 77−50855
malic acid+formamide, γ-irradiated reactions under high pressure *(Japanese)* 79−52707
matter under very high pressure, 10^3 to 10^6 kbars, high pressure meas. and phenomena *(French)* 80−90811
MBBA, liq. cryst.-isotropic transition at high press., P-V-T eqn. of state 79−95135
MBBA, nematic-isotropic transition at high press., turbidity meas. 80−92655
MBBA, pVT data and viscosity-press. behaviour 78−94989
MBBA, volume meas. and phase transitions at high press. 79−90764
melting-pressure curves, press.-temp. analysis 79−23697
mesocarbon microbead, heat treatment under high pressure 77−28736
metal-H_2 systems, determ. of absorption/desorption isotherms, high press. 78−51679
metal-vapour/inert-gas mixture discharge peculiarities 78−71620

high-pressure phenomena and effects continued
metals, contact melting, state of cryst.-liq. boundaries, influence of impurities and hydrostatic pressure *(Russian)* 79−37812
methane, dense gaseous and liq., thermal cond.-viscosity correlation, up to 500 atm., 95-500 K 77−80657
methane, gas, up to 50 atm, refr. index, 328, 3103 MHz *(French)* 78−14129
methane-trifluoromethane, liq.-liq. phase equilib., crit. phenomena 78−18764
methanol, phonon MFP formula, H bond collisions, low temp. 77−35655
mineral oils, viscoelastic behaviour at high press., relax. spectrum 77−65727
minerals, effects of stress on soln. rates 77−86865
mixtures, high-press. vap.-liq. equilib., phenomenological description, review 78−30737
molecular electronic spectra, high press. effects 78−78754
molecular electronic spectra, high pressure effects, Morse potential formulation 80−63617
β-N_2, cryst. struct. at 25 kbar and 296K 80−10528
naphtha tar pitch, mesophase formation during carbonisation under pressure 77−44182
neurological syndrome, comparative physiology, compression rate effects 79−88070
nitrobenzene-aniline, US vel., sp. ht. and compressibility 79−33037
4-nitrophenyl-4′-alkoxybenzoates, incommensurate smectic A phase 80−10647
nucleation kinetics for non-spherical nuclei, and high pressure effects 80−19730
octane, liq., Raman scatt. at high-press., chain kinking 79−87429
4′-n-octyl-4-cyanobiphenyl, smectic bilayers, press. effects, phase diagrams *(French)* 78−10177
4′-n-octyloxy-4-cyanobiphenyl, smectic bilayers, press. effects, phase diagrams *(French)* 78−10177
oil, density change meas. at high pressure, using impact viscometer 79−14872
oil-water interface, fatty alcohol adsorbed layer phase transition, high-press. effect 79−99395
oils, viscosity and solidification press., 0-10^4 Pa, 20-180°C 77−43266
OOBPD, smectic, DTA obs. of phase transitions to 3 kbar 79−23708
optical fibre, multimode, optical loss changes caused by hydraulic pressure 79−41440
organic compounds, high-press. expansivity determ. by piezo-thermal anal. 77−72705
organic compounds, high-press. thermodynamics, review 79−24500
organic liquids, thermodynamical Gruneisen parameter, press. depend. 78−14479
organic molecules, long-chain, diffusion through polymer matrix, hydrostatic press. effect on diffusion coeff. 80−92697
oxidation-reduction reactions, thermal effects, appl. to undifferentiated earth 79−25218
n-pentane, refr. index meas. to 14 kbar by optical interferometry 77−49764
perfluorocyclobutane, dense fluid, self-diffusion, shear viscosity, density, and temp. depend., NMR 77−36152
phase diagrams of specimens at high temp. and under tensile used for shear stress, theoretical exam. 79−7674
phase equilibria, computational methods 80−75329
phase equilibria in mixtures, computational effects 80−75330
phenanthrene, mesophase formation during carbonisation under pressure 77−44182
pipe guides, pressurised, nonstationary discharge of boiling liq. in thermodynamic equil. approx. 79−81711
plasma, thermodynamic inconsistency of modified Saha eqn. at high press. 78−36450
polyacrylamide-fluorescein conjugates, fluoresc. polarisation, high press. obs. 80−20683
polyethyl siloxane, liqs., thermal cond. at high press., 20-200°C 78−79825
polyethylene, effect of pressure and environment on fracture and yield 78−76757
polyethylene, extended-chain cryst., high-press. crystallisation and melting obs. 77−27985
polyethylene, hydrostatically compensated, SRO in precrystallisation phase 79−69033
polyethylene terephthalate, molten, press. effects on compressibility and crystn., thermodynamic interpret. 80−84102
trans-1,4-polyisoprene crystals, press. effect on growth rate 80−88064
trans-1,4-polyisoprene crystals, press. effect on melting temp. and lamellar thickness, press. crystn. 80−88302
polymer solutions, thermodynamic props. under high press., light scatt. obs. *(German)* 78−20049
polymer systems, phase dualism, gas-, liq.-like, appl. to compression effects 79−1388
polymethylsiloxane-2, liq., thermodynamic props. at high press., US propag. meas. *(Russian)* 80−65157
polyoxymethylene, effect of pressure and environment on fracture and yield 78−76757
polypropylene, effect of pressure and environment on fracture and yield 78−76757
polystyrene, effect of pressure and environment on fracture and yield 78−76757
polystyrene, soln. in trans.-decalin, viscosity and thermodynamic props., press. depend. 79−69275
polyvinylidene fluoride, high-press. melting and crystallisation 78−91422
porous glass:In, effect of press. on transition temp. 80−97027
porous material, press. soln. thermodynamics, chem. and mech. forces interaction 77−60369
pressed powder bed, determ. of side pressure distrib. 78−84734
PWR pressure vessel vibration excitation, noise correlation and modelling 79−13442
pyrazine, PMMA soln., fluoresc. and phosphoresc. quantum yield and lifetime, 20-120 kbar 79−54902
quartz sand, press. soln. expt. 77−60370
quinoline, liq., depolarised light scatt., 1-1800 bar 79−24327
retinyl acetate, high press. fluoresc. studies of radiative and nonradiative processes 80−1011
reverse-buckling safety discs, release pressure 78−89489
saturation dive, 17-day 18.6 ATA exposure effects 79−92256
seawater, eqn. of state at high press. 80−101369
seawater, press. effects on sound absorpt. 78−1481
seawater, sound speed meas. at high press. 78−13837

high-pressure phenomena and effects continued
serpentine, solubility of inert gases, meteoritic abundance 80−12712
silica, fused, temp. in high-press. shock state 80−72490
silicone liquids, viscosity and solidification press., 0-10^4 Pa, 20-180°C 77−43266
smectic C* liquid crystal under press. *(French)* 79−99061
space charge limited current in N_2 and air, high pressure effect 79−32735
steam bubbles direct contact condensation in water at high press. 77−39202
steel, high-strength low alloy, H_2 attack, 350-510°C 80−97636
steel, mild, tensile deformation, behaviour under high pressure *(Japanese)* 80−16381
steel corrosion in NH_3 and NH_3-N_2-H_2 mixture at high press. and temp., testing unit 77−56174
supersonic air flow through high press. gas valves into atm., noise and flow pattern obs. 80−59067
surface viscosities at high pressure gas-liquid interfaces 78−75907
Teflon, creep under joint action of tension, hydrostatic pressure 78−68750
1,2,3,4-tetrahydronaphthalene-H_2O, liq.-liq. phase equilib., crit. phenomena 78−18764
tetramethylpyrazine, PMMA soln., fluoresc. and phosphoresc. quantum yield and lifetime, 20-120 kbar 79−54902
thermometer, Pt resistance, up to 100 MPa, 294 to 1095K 79−6124
thulium ethyl sulphate, Van Vleck paramag., mag. reson. on uniaxial and uniform compression *(Russian)* 79−61243
TMTSF-DMTCNQ, metallic state at low temp. under press. *(French)* 79−82579
triethylenediamine aq. soln., dielectric relaxation rate 79−78619
trithiane, Raman spectrum, press. effect on internal rot. angle 78−37642
ultra-high pressure studies and the earth sciences *(Chinese)* 79−71479
urea+acrylic acid (acrylamide), γ-irradiated reactions under high pressure *(Japanese)* 79−52707
vapour-liquid equilibria, generalised method for calc. and prediction at high press. 78−87780
vapour-liquid equilibrium, high press., quantitative description 79−14923
vapour-liquid equilibrium, high pressure experimental technique 79−42227
vapour-liquid equilibrium, high-pressure, isothermal, meas. and correl. 78−18755
vapour-liquid equilibrium, phenomenological description 78−91415
vapour-liquid equilibrium, quantitative description 79−1486
viscosity of fluids at evaluated pressures 80−2191
water, anomalous compressibility to 1-9 kbar, correl. with supercoding 79−65134
water, cavitation, gas supersaturation thresholds under high press. 77−16861
water, dielectric relaxation rate 79−78619
water, high-pressure Raman spectra, bending and librational bands 78−68499
water, liq., solubility in compressed air 78−34631
water, liq., thermal conductivity at high pressures, meas. with Ag co-axial cylinder cell *(Japanese)* 80−80007
water, molar heat capacity under high press. near solidification point 78−51695
water, self diffusion, high-press., low-temp. spin-echo NMR obs. 77−8446
water, self-diffusion coeff., pressure and temp. depend. meas. by proton spin echo 80−39328
water, shock compression at press. approaching 1 Mbar *(Russian)* 80−79851
water, thermodynamic props. at high pressures from US vel. 79−94474
water, thermodynamical Gruneisen parameter, press. depend. 78−14479
water, viscosity, 10-150°C, press. effects 78−51715
water(-d), high-press. supercooled, density max. 77−1162
water and steam, thermal cond. equation, 0 to 800°C, triple pt. press. to 1000 bars, crit. region 80−39364
water structure and motion at high pressure 78−87606
water vapour, thermal cond., 375-600°C, 250 mPa 79−90367
Ag, adsorption of O, surface species identification by XPS, high press. 79−28191
Ag, melting curve to 60 kbar press., reinvestigation 80−39260
Al, solidification, high press. effects 80−66499
Al-Si (25.4 wt.%), solidification, high press. effects 80−66499
Al-Zn-Mg-Cu, alloy 7075, hydrostatic pressure effects on ductile fracture 78−60779
Ar and Ar-NH_3 mixtures, viscosity under press., density depend. and mol. assoc. 80−1727
Ar arc heating, high-pressure complex heat exchange expt. *(Russian)* 80−75112
Ar, dense gas, thermal cond. and viscosity coeffs., irreversibility and Kirkwood superposition hypothesis *(French)* 78−94881
Ar, ionised gas, high press. elec. cond. meas. 78−26233
Ar, liq., shock wave compression, 400 to 910 kbar 80−29101
Ar, thermal cond. 80−103099
Ar, viscosity meas. at very high press. 80−59155
Ar-H_2(Ne) liquid solution, dielectric props., intermolecular interactions *(Russian)* 80−88904
As, elec. cond. and density meas., crit. parameters 77−47562
As, liq., Anderson transition, cond., at high temp. and supercrit. press. 78−34869
Au, melting curve to 60 kbar press., reinvestigation 80−39260
BeF_2, melting curves at high press., rel. to SiO_2 extended phase diagram 77−11672
$BeSO_4$ soln., high press. conductance meas., transfer mechanism 77−76586
Bi-BiI_3($BiBr_3$) liquid binary mixtures, phase separation under press. 80−34183
Br_2, photolytic cage effect in high-press. gases, laser wavelength depend. 80−11925
CO, liq., ^{13}C NMR for mol. diffusion and spin-rot. interaction, 0-1.73 kbar 79−99777
CO_2, fugacity at high temps. and press. from exptl. decarbonation reactions 79−16439
CO_2, in N_2, 20-140 bar, dipolar correlation function meas., IR band shape anal. 77−61743
CO_2, liq., 100 to 3000 atm., depolarised Rayleigh spectra, orientation dynamics, wings 78−92084
CO_2, turbulent cooling tube flow, at supercrit. press. 78−14005

high-pressure phenomena and effects continued
CO_2-polar component binary mixtures, up to 1000 bar, phase separation, critical phenomena 77−35695
$CaO-Al_2O_3-H_2O$ system, chemical degradation under high gaseous pressure and temp. 79−20464
$CaO-SiO_2-CO_2$, subsolidus and liquidus phase relationships to 30 kbar 80−85643
$CaO.6Al_2O_3$, thermodynamic stability, reaction with Ti, Cr and Zr oxides 80−92687
Cd_3P_2, high press. phase relns. and cryst. structs. 78−59792
CoO, high temperature physico-chemical interactions with oxygen under pressure *(French)* 78−31549
Cs, high press. melting curve maximum 80−75337
Cs, liq., specific heat meas., at temp. up to 1700K under pressure 78−51696
Cs, plasma, eqn. of state, 30-140 atm, 3000-4000K, by adiabatic compression 78−14132
Cs, saturation effect on thermo-EMF up to 1950°C and 140 atm. 77−51727
CsCl, aq. soln., density, isothermal compressibility, 293.15K, up to 200 MPa 80−44243
Cu, in seawater, hydrostatic pressure effects on corrosion 79−52420
Cu, melting curve to 60 kbar press., reinvestigation 80−39260
$CuCl_2.2H_2O$, NMR, high press. effect on existence domain width of intermediate state 79−87255
$CuFe_2S_3$, cubanite polymorph, synthesis above 200°C and 1 GPa, lattice constants 80−108367
n-D_2, fluid, eqn. of state from P-V-T and US vel. meas. up to 20 kbar 78−63837
D_2O, compressed at low temp., mol. motions, spin-lattice relax., viscosity and self-diffusion 77−76287
D_2O, gaseous, viscosity, 200-400°C, up to 300 bar 78−63527
D_2O, sound speed rel. to normal water as a function of temp. and press. 78−2201
D_2O, struct. at press. 79−60253
Fe, positive muon spin precession, effect of press. 80−40030
Fe-C system, liq.-solid equilib. at high press., influence of graphitising elements *(Russian)* 78−56613
Ga metastable phases, melting curve under atm. and high press. by microcalorimetry *(French)* 77−43314
Ga-Bi liquid binary mixtures, phase separation under press. 80−34183
GeO_2, melting curves at high press., rel. to SiO_2 extended phase diagram 77−11672
GeO_2 melts, density, viscosity, struct., at high and low press. 79−87431
H-He fluid planets, phase diagram and transport props. 78−28554
H_2, diffusion through Pt membranes at high press. and temps. 78−55984
n-H_2, equation of state from PVT and sound vel. meas., 75-307K, 2-20 kbar 77−62609
H_2, fluid, Raman meas., 0.2-630 kbar, at room temp. 80−58269
H_2, solid, high pressure phase, 57 kbar, 25°C, transparent crystalline mass 79−55870
H_2, viscosity meas., 25-100°C, up to 120×10^5 Pa 79−32731
H_2-NH_3 mixture, viscosity meas., 25-100°C, up to 120×10^5 Pa 79−32731
HCl aqueous soln., H^+ mobility, 15, 25, 40°C, up to 5000 atm 78−10207
$HNO_2+OH\rightarrow H_2O+NO_2$ react. kinetics, at high temps. behind shock waves 77−44477
H_2O, high-press. props. and struct., mixture model 77−84612
H_2O, liq., proton NMR chem. shift, press. depend. 77−8428
H_2O, shock compression at high press. *(Russian)* 80−92608
H_2O, supercooled, longit. proton relax. times, press. and temp. depend. 77−85598
H_3PO_4, aq. soln., elec. cond. and Raman spectra at high-press., 25°C 79−56220
He, 3^3P level, excitation and decay study up to high press. pumped by intense relativistic electron beam 80−74250
He, thermal cond. 80−103099
^{3}He, first sound attenuation under press. *(Russian)* 80−10730
^{3}He-^{4}He, mixture, isotropic phase separation temp. press. depend. 80−92751
^{3}He-Hg (−Kr)+^{3}He(n,p)T, high press. plasma excitation, luminesc. spectra 80−38719
^{3}He-superfluid ^{4}He mixture, dispersion law of ^{3}He quasi-particles under press. *(Russian)* 79−42336
^{4}He, solidification at room temp. under high press. 79−82413
^{4}He, superfluid, phonon dispersion at long wavelengths and low temps. 77−11752
^{4}He, superfluid, polarisation pots. and elementary excitations at low temps. 77−15643
Hg, electrical and thermodynamic props. in metal-semicond. transition range 80−20144
Hg, liq., sound vel. near metal-nonmetal transition, up to 1600°C and 2000 kg/cm^2 80−39222
Hg melting line, pressures up to 1200 MPa 80−84281
Hg, supercritical, elec. cond., four electrode method 80−62685
Hg, temp. and press. depend. of Debye temp. 77−1202
Hg, thermodynamical Gruneisen parameter, press. depend. 78−14479
I_2, photolytic cage effect in high-press. gases, laser wavelength depend. 80−11925
InCl disproportionation under influence of high pressure 80−16660
K, liq., density meas. up to 1800K and up to 100 atm. 77−43264
K solubility in Fe-S liq., silicate-K-(Fe-S liq.) equilibria and planetary implications 78−11843
K, thermodynamics of melting at high pressures 78−91426
KH_2PO_4, aq. soln., elec. cond. and Raman spectra at high-press., 25°C 79−56220
KNO_2, melting pressure curves up to 5 kbar 77−15547
KNO_2, molten electrolytic cond., pressures up to 6 kbar 77−15609
^{40}K, pressure-induced changes in electron-capture decay const., theory 80−22771
Kr, thermal cond. 80−103099
Kr, viscosity, 130-1300K, up to 10^9 dyne cm^{-2} 79−60536
Li, thermodynamics of melting at high pressures 78−91426
Li-Na liquid binary mixtures, phase separation under press. 80−34183
Li_2BeF_4, melting systematics at high press. 77−51475
LiCl, aq. soln., density, isothermal compressibility, 293.15K, up to 200 MPa 80−44243
LiCl, concentrated aqueous soln., IR absorpt. to high press. and temps. 80−80803
LiCl, heavy water soln., anionic hydration, 1 bar and 1 kbar, neutron diffr. obs. 80−30212
$LiTmF_4$, Van Vleck paramag., mag. reson. on uniaxial and uniform compression *(Russian)* 79−61243
Mg particles, combustion in air, pressure effects *(Russian)* 77−70302
Mg SiO_3 melt, instantaneous struct. under high press., simulation by mol. dynamics 80−84049
Mg-AgCl seawater battery, performance and EMF at great ocean depths 80−76623
N_2, density up to 2000K and 6 kbar by displacement method 78−51266
N_2, dielectric strength, bubble-phase equilib., high press., low temp. *(Russian)* 77−20798
N_2 gas, up to 50 atm, refr. index, 328, 3103 MHz *(French)* 78−14129
N_2, NO, N_2O, dry air, chemisorbed on transition metals at high pressures, XPS 77−20990
N_2, non-self-maintained discharge, high press., ionisation instability, pulse discharge train *(Russian)* 77−47282
N_2, press.-density depend. at high density, functional depend. using osculating curves 79−93109
N_2-CO_2, N_2 non-self-maintained discharge, high press., ionisation instability, pulse discharge train *(Russian)* 77−47282
N_2-methane mixture, US propag. vel. up to 40 kbar, additivity deviation 77−42959
N_2+methane, liquid mixture, press. effect on excess thermodynamic functions 78−47494
N_3^-, high press. IR vibr. spectroscopy *(German)* 80−74170
NH_3, pure, Raman scatt., high press., high temp. 77−27077
NH_3-ethylene (propylene) mixtures, crit. curves at high-press. 79−23715
NH_4Cl soln., crystal growth under press. *(Korean)* 77−73266
$NH_3(D_3)$; liq., longitudinal proton and deuteron relaxation rates, press. and temp. depend. 80−44941
NO_2^-, high press. IR vibr. spectroscopy *(German)* 80−74170
N_2O, gas, up to 50 atm, refr. index, 328, 3103 MHz *(French)* 78−14129
N_2O_4, evaporation in enclosed containers, N_2 medium, 1.12-4.96 gauge atm. 77−47564
$NaAlSi_2O_6$, jadeite, melt, changes in viscosity and struct. at high press. 77−29290
$NaAlSi_2O_6$ melts quenched at high press., struct. from IR and Al K-radiation data 79−32907
$NaAlSi_3O_8$, albite, melt, viscosity and struct. changes at high press. 79−29754
Na_2BeF_4, melting systematics at high press. 77−51475
NaCl, aq. soln., isothermal compressibility, hydration parameters, up to 350°C and 10^3 kg cm^{-2} 78−10112
NaCl, aqueous soln., direct calorimetric meas. of enthalpies, at high temp. and pressure 79−57286
$NaClO_3$, molten electrolytic cond. pressures up to 6 kbar 77−15609
$NaNO_2$, melting curve maximum 77−43311
$NaNO_2$, molten, electrolytic cond., pressures up to 6 kbar 77−15609
$NaNo_3$, aq. soln., Raman spectra, vibr., orient. relaxation *(French)* 78−62808
Na_3PO_4, aq. soln., elec. cond. and Raman spectra at high-press., 25°C 79−56220
$Na_3R(XO_4)_2$ (R=rare earth; X=P, As, V), pressure synthesis *(French)* 80−93509
$Na_2Si_3O_7$ melt, changes in viscosity at high press. 77−29290
Ne, thermal cond. 80−103099
Ne-H_2 mixture, liquid vapour phase equilib., sound vel., compressibility, thermodynamic perturbation theory obs. *(Russian)* 80−39306
Ne-Kr, partially miscible mixture, high press. mol. dynamics using Lennard-Jones pot. 79−41929
Ne-Kr, time-dependent props. near crit. mixing point, 2000 bar, mol. dynamics calcs. 80−24580
Ni, positive muon spin precession, effect of press. 80−40030
$NiCl_2$, heavy water soln., anionic hydration, 1 bar and 1 kbar, neutron diffr. obs. 80−30212
O_2, phase equilibria near 298K, Raman spectral study of solid and fluid 80−19937
Pb, evaporation in shock compression release waves *(Russian)* 78−18761
Pb, melting curve, elec. resist. determ. at high pressure 80−49337
PbI_2, high press. phase diagram to 3.5 GPa 80−104126
Rb, liq., simultaneous meas. of density, elec. cond., absolute thermopower up to 1400°C and 400 bar 77−1402
Rb, thermodynamics of melting at high pressures 78−91426
S, effect of system configuration on polymorphism and melting curve 78−43104
S, liq., eqn. of state determ., crit. props. and mol. comp. 80−49336
S, liq., optical absorption spectrum, up to supercrit. conditions 78−88320
SCN^-, associated with metallic cations in aq. soln., press. effect, Raman spectra *(French)* 78−80333
SF_6 thermal cond., 230-350K, up to 50 MPa 79−33123
SO_2 ($^3B_1$), phosphorescent lifetimes, press. saturation effect on quenching by CO_2, CO, N_2 78−1017
$SbCl_5$, phase diagram to 43 kbar 80−2144
Sc-H, p-T phase diagram and influence of H pressure, on decomposition temp., DTA exam. 80−29929
Se, liq., Anderson transition, cond., at high temp. and supercrit. press. 78−34869
Se, liq., electronic transport props., equation of state, to 1900K and 1800 bars 80−65574
Se, liq., eqn. of state determ., crit. props. and mol. comp. 80−49336
SiO_2, high press. supercooled liq., density max. 77−1162
SiO_2, melting curves at high press. 77−11672
Te-Se liq. semicond., resist. meas. under high press. 77−51791
Te-Se mixtures, liquid, electrical conductivity and thermoelectric power, high temps. and pressures 80−39639
Tl-Se, liquid mixtures, press. effect on two-phase region 80−75347
Tl-Se liquid binary mixtures, phase separation under press. 80−34183
Tl-Te liq. semicond., resist. meas. under high press. 77−51791
WC-Co(TiC-Co), powder compacts, effect of additional pressing at hydrostatic pressures on props. 78−56596
Xe, thermal cond., 170-1300K and press. to 200 Mpa 79−82025
Xe, thermal cond. 80−103099
Xe, viscosity meas., 170-1300K, up to 1000 bar 78−42698

high-pressure solid-state phase transformations
AB-type compounds, high-press. and high-temp. behaviour, review 78−22850

high-pressure solid-state phase transformations continued
actinides, struct. props. rel. to F electrons 78−83951
adamantane, NMR, spin-lattice relax., plastic-brittle phase transform. 79−95665
adamantane, plastic cryst. lattice vibr. study of phase transition 80−7355
albite, phase behaviour between 100 and 280 kbar at 1000°C 78−53644
alkali halides, FCC→SC pressure phase transitions 80−44315
alkali halides, structures in compressible ions theory 80−33971
alkali halides, sudden jump transitions, transformed fraction and reaction rate meas. 78−51667
alkali hydrides, structural transition from NaCl to CsCl type under high press. 80−96458
alkali metal halides, ionic crysts., impulse compression temps. 80−100307
alkali metals, pressure influence on absolute zero isotherms, polymorphic transform., phonon spectra *(Russian)* 80−49363
alloy steels N30 and N29T, press. effect on reverse martensitic transform. and mech. props. *(Russian)* 79−38824
aromatic hydrocarbons, IR spectra and high-pressure phase transitions 80−10659
benzene, cryst., press. depend. of nuclear spin-lattice relax. time 79−28635
benzene, Raman and IR spectra at high press. 78−35127
benzene, thermal cond., heat capacity, 105-375K, up to 2.4 GPa 79−90839
benzene derivatives, solid, phase transition under press., IR spectra 79−38531
benzene derivatives, symmetrically substituted, IR spectra, high press. solid-state phase transform. 77−43984
Bi, polymorphic transition up to 30 kbar, neutron diffr. investigation 79−14723
bis (methylammonium) tetrachlorometallates (II), IR spectra and phase transitions of 10-25 kbar at 25°C 80−10658
calcite rock, phase transitions rel. to compression wave studies 78−81151
carbonate rock, interrelation of flow or fracture and phase transition during deform. 80−51389
coesite-stishovite transition determ. by in-situ X-ray meas. 77−17092
coke, pressure effects on structure, polymorphic transitions X-ray diffr. anal. 79−1859
condensed gases, solid phase transition, optical meas. in diamond-anvil cells 80−73381
conference on high pressure physics and technology, Moscow, Russia (May 1975) 78−51611
crystal classification by transition mechanisms *(Russian)* 78−60401
crystal lattice stability and deform. phase transitions under press. 80−59624
cubic crystal under hydrostatic loading, Born and classical stability criteria divergences 80−10595
cyclohexane, differential thermal anal. under high press. 78−51669
cyclohexane, plastic cryst., NMR determ. of phase diagram 77−12210
cyclohexanone, solid, phase behaviour, at press. up to 3 kbar, DTA 78−43108
cyclopentanol, solid, phase behaviour, at press. up to 3 kbar, DTA 78−43108
diamond, 'melting' to solid metallic C phase above graphite triple point 80−15236
diamond, crystallisation under high press. with catalyst and solvent *(Polish)* 79−87592
diamond, form. by shock compression of graphite, cryst., surface struct. 78−44060
diamond, with rhombic dodecahedral faces, growth using catalyst metal 77−48339
dicalcium barium propionate, press. induced ferroelectricity, dielectric meas. 79−51920
p-dichlorobenzene, expansivity, determ. by calorimetric compression from 0 to 400 MPa 80−44339
dielectric crystal, optical studies of phase transitions, use of diamond anvil devices *(Japanese)* 80−49362
2,2′-dimethylbutane, differential thermal anal. under high press. 78−51669
displacive phase transitions, pressure effect on transition temps. *(Japanese)* 79−65814
Earth crust, phase transition rel. to nature of Ukrainian Shield M discontinuity *(Russian)* 77−44948
Earth mantle, stresses due to phase changes in subduction zones 77−73718
enstatite-pyrope system, high press./temp. phase behaviour rel. to Earth mantle 78−11882
enstatite-wollastonite system, phase transforms at high press. and temps. with emphasis on diopside 79−79825
ethylene-d_4, phases I and II, struct. determ. by neutron diffr. 77−27870
f-band metals, mode softening and lattice instability under press. 77−51833
FCC to BCC transition, under [100] tensile loading, theory 80−39279
ferroelectric phase formation energy in inhomogeneous inclusion under press. 77−12338
ferroelectrics, hydrostatic press. effect on phase transitions 79−15413
fluorite-type dioxides 80−101363
garnet lherzolite, high-press. phase equilibria and Mg^{2+}-Fe^{2+} partitioning among constituent minerals 79−66687
germanates, $MGeO_3$, (M=Ni, Mg, Co, Zn, Fe, Mn), HP phase transform. 80−19941
glycine silver nitrate, and deuterated analogue, ferroelec. transition, hydrostatic press. effects 77−36185
graphite, pressure effects on structure, polymorphic transitions, X-ray diffr. anal. 79−1859
graphite⇄diamond equilib. transition press. 78−34617
graphite to diamond, probability under high temp. and press. *(Chinese)* 80−65220
graphite to diamond under shock wave loading *(Chinese)* 79−82337
graphite-diamond, shock induced transform. anal., post shock graphitisation 80−79933
graphite-diamond equilibrium, thermodynamic stability 79−65184
Gruneisen parameter, influence of press.-induced phase transitions 79−1497
Gruneisen parameter and eqn. of state determ. 80−90031
Gruneisen parameter in Landau theory for pressure-induced phase transitions 79−34807
n-heptacosane, differential thermal anal. under high press. 78−51669
hexafluorobenzene, cryst., press. depend. of nuclear spin-lattice relax. time 79−28635
high-pressure solid-state phase transformations continued
hexamethyl benzene, high press., variable temp. Raman spectra 78−56488
hexamethyldisilane, plastic cryst., NMR determ. of phase diagram 77−12210
high press. transforms., kinetics and hysteresis 78−51668
ice VI, polymorphic transition at high-press., 123.1K, HF permittivity study 79−55883
ice VI, shock compression expts. for Hugoniot function 80−84248
ice VI, VII and VIII, press. up to 35 kbar 77−87839
II-V semiconductor, electronic theory, covalent-metallic or covalent-ionic phase transition under pressure 78−72105
II-VI semiconductors, high press. transition, expt. results 78−22854
III-V semiconductor, electronic theory, covalent-metallic or covalent-ionic phase transition under pressure 78−72105
III-V semiconductors, high press. transition, expt. results 78−22854
inorganic compounds, polymorphic phase transform. rel. to temp. and press. 79−8289
intermetallic compounds, press. depend. of martensitic and supercond. transition temp. 79−19681
isobaric specific heat of solids, for pressures up to 250 MPa and 150-350K temps., measuring installation 77−76572
jadeite, phase behaviour between 100 and 280 kbar at 1000°C 78−53644
lanthanum ethyl sulphate:Pr, phase transition under pressure, absorpt. spectra *(Russian)* 80−92667
malononitrile, ^{14}N PNQR obs. of phase transition press. depend., line splitting 77−77120
methane, crystalline, struct. and compression at high press., room temp. 80−107199
methane, solid, high press. PMR, second moment 79−8059
methane, solid, phase II, theory of phase transitions 77−51494
methane, solid, Raman spectra and II-III phase transition 80−2745
methane, solid-state phase transitions, 5-80K, PMR spin-lattice relax. up to 3 kbar 77−40137
$(Mg_{0.88}Fe_{0.12})_2SiO_4$, natural peridot, shock-prod. olivine glass, TEM 78−10178
minerals and Earth's deep interior materials, review *(Japanese)* 78−28225
molecular crystal, structural instability under influence of axial stress *(Russian)* 80−10669
nematic-isotropic phase transition at high press., thermodynamics *(Russian)* 78−87778
nepheline, phase behaviour between 100 and 280 kbar at 1000°C 78−53644
NQR and stationary NMR studies 80−19934
octafluoronaphthalene, high press. struct., neutron powder diffr. 78−63743
octafluoronaphthalene, phase transitions at elevated press., Raman and mid-IR spectroscopy obs. 80−45062
n-octatriacontane 78−51669
olivine, partial phase transition from 12.5 to 45 GPa, evidence from dunite elec. cond. 78−85536
olivine, shock induced high-pressure transformation 78−11883
omphacite, P2/n to C2/c transform. study 79−65183
organic compounds, high-press. expansivity determ. by piezo-thermal anal. 77−72705
organic solids under pressure, IR spectra and phase transitions 79−95743
oxides, ABO_4 type, high press. phase transforms. and struct. types, cryst. chem. aspects 80−79940
phenol I and II, permittivity and molar polarisation at pressures between 140-2000 bar 77−77136
piston-rotation technique for piston-cylinder devices 78−41324
plastic crystal, DTA obs. 79−23540
poly(vinylidene fluoride), melting and crystn. temps., press. depend., DTA meas. 79−90568
polydiacetylene cryst., electronic struct. change at phase transition, Raman spectra 78−2833
polyethylene, crystallisation at high-pressure, obs. using new dilatometer *(Russian)* 77−17950
polyethylene, high press. phase, US, DTA, and X-ray diffr. study 80−75188
polyethylene, high-press. phase transforms., X-ray diffr. obs. 77−80617
polyethylene, pressure phase transition, function of pressure and temp. 79−77745
polymer, glass transition under high-press., dielec. loss method obs. *(Russian)* 78−71841
polymorphism at high press. and temp., thortveitite struct. stability *(French)* 80−10657
polyvinylidene fluoride, direct obs. of cryst. transform. process under high press. 78−38630
praseodymium ethyl sulphate, phase transition under pressure, absorpt. spectra *(Russian)* 80−92667
PTFE, NMR and X-ray diffr. investig. of press. induced III-I transition and mol. motion 77−51969
PTFE, Raman spectra obs. of high press. phase conformal deform. 79−1757
pyrophillite, phase transform. promoted by water under ultra-high press., high temp., technical appls. *(Chinese)* 79−1499
pyrophyllite, phase transitions, importance in diamond synthesis *(Chinese)* 77−70049
pyroxene-garnet solid-soln. equilibria in $Mg_4Si_4O_{12}$-$Mg_3Al_2Si_3O_{12}$ and $Fe_4Si_4O_{12}$-$Fe_3Al_2Si_3O_{12}$ systems 77−81895
quartz, high-low transition, effect on compressional and shear wave vel. in rocks under high press. 80−12380
quartz, hydrothermal crystallization at 250°C and 15 kbar, mechanisms 78−49014
quartz, isentropic compression by ultrastrong mag. field *(Russian)* 78−47468
quartz, shock compressed, phase equilib. and kinetics 77−62584
quartz, shock-loaded, IR spectroscopic studies, solid-state glass prod. 79−19157
quartz, synthetic hydrolytically-weakened α-β phase transform. effects on creep props. 77−43274
quartz-coesite equilibrium curve for high-temp. calibration of solid-phase cell 80−105669
rare earth formate, IR spectra and phase transitions, under pressure 78−31179
rare earth sulphides, polymorphic transforms. on impact compression 77−47575

high-pressure solid-state phase transformations continued
rare earths, struct. props. rel. to F electrons 78−83951
RbBr, structural phase transition, Born-model and effects of hydrostatic and non-hydrostatic stresses 79−23721
review of developments 77−43278
review of solid state physics at high pressures 79−90729
rocks, on island of Naxos, Greece, metamorphsim 77−44985
sanidine, $(K,Na)AlSi_3O_8$, monoclinic-to-triclinic reversible transformation at high press. 77−17090
semiconductor, homologous series, semicond.-metal transitions, homeomorphous, polymorphous and morphotropic transitions 79−37988
silicate glasses, struct. and phase transform. 78−64538
Solenhofen limestone, II-III transition rel. to high press. US propag. 79−29756
squaric acid, hydrostatic press. effect on phase transition, dielec. and dilatometric meas. 78−55941
squaric acid-d_0,-d_2, 2-dimens. antiferroelec., dielec. props. and phase transitions, press. effects 79−95700
stacking faults, plasticity and transform. kinetics under high press. 78−51560
steel, high-strength, dynamic yield strengths, phase transition press. and Hugoniot parameters 80−75331
structural and electronic changes under 200 kbar press. and above 80−24588
superconductor under pressure, $2^1/_2$ order transitions, Kohn anomalies *(Russian)* 77−47914
tetracene:pentacene, pressure-induced phase transition, mag. field effect on guest fluoresc. 79−33083
tetracene, press.-induced phase transition, fluoresc. mag. field depend. 77−1728
tetracene single crystals, Davydov splitting, press. depend., phase transition obs. 78−27250
tetramethylammonium tetrachlorocobaltate, ferroelec., effects of hydrostatic press. on successive phase transitions 79−47402
tetramethylammonium tetrachlorocobaltate, ferroelec., pressure-temp. phase diagrams 80−97205
tetramethylammonium tetrachloroferrate, press. induced ferroelectricity, dielec. and DTA meas. 80−80722
tetramethylammonium tetrachlorozincate, ferroelec., effects of hydrostatic press. on successive phase transitions 79−47402
tetramethylammonium tetrachlorozincate, ferroelec., pressure-temp. phase diagrams 80−97205
tetramethylsilane, phase rels. under press., DTA obs. 78−71850
TGFB, high press. influence on anomalous specific heat, tricritical point 80−25322
TGS family, change of order of phase transition under hydrostatic pressure 78−52452
TGS-TGSe solid soln., phase transitions under hydrostatic press. 79−99840
TGSe, behaviour under press. near tricritical point 79−95716
TGSe, deuterated, thermal and dielectric props. at high hydrostatic press. 80−34864
titanates, $MTiO_3$, (M=Ni, Mg, Co, Zn, Fe, Mn), HP phase transform. 80−19941
transition metal tetrametaphosphates, cryst. struct., high press. effects *(French)* 77−15373
1,1,2-trichloroethane, phase diagram, 0-10 kbar 77−72679
1,1,1-trichloroethane, polymorphism under high pressure *(French)* 80−96644
tris-sarcosine calcium chloride, phase transition, hydrostatic press. effect, dielec. const. meas. 80−71327
TTF-TCNQ, elastic neutron scatt. evidence for charge transfer change at high power 80−2163
α-Zr, ω phase proportion during high press. deform. *(Russian)* 79−74147
Ag, grain boundary energy misorientation, hydrostatic press. effect, press. induced struct. phase transformations 80−54257
Ag_3AsS_3; NQR study of phase transitions, high press., tricrit. pt. determ. 79−77746
Ag_2CO_3, high press. phase relations, DTA 77−43329
AgF_2, high press. modification, cryst. and mag. props. 80−38988
$AgGaS_2$, press. depend. of energy gap, absorption edge, induced phase transform. obs. 77−12401
$Ag_8GeS_6(Se_6)(Te_6)$, Ag_8SiSe_6, $Ag_8SnS_6(Se_6)$, absorpt. edge investigs. at phase transitions 78−35149
Ag_8GeSe_6, polymorphic transition, absorpt. coeff. meas. 78−2257
AgI, elastic behaviour near phase transitions with negative dP/dT 78−83885
$AgInSe_2$, $AgInTe_2$, $AgGaSe_2$, pressure-induced phase transformations 78−30748
n-$AgInSe_2$, rel. to press.-induced compensation, resist. expts. 78−30919
Ag_8MSe_6, (M=Si, Ge, Sn), forbidden energy gap changes under high press., polymorphic transitions 77−51649
$AgNO_2$, high-pressure phase behaviour, crystal chemistry of univalent nitrites 78−30749
$AgNa(NO_2)_2$, crit. dynamics, hydrostatic press. effect, dielec. props. meas. 80−71328
Ag_2O, phase transitions at press. up to 39 kbar 77−31770
Al_2O_3-SiO_2 system, andalusite and kyanite powders, shock induced transformations 80−45301
Al_2O_3-ZrO_2 mixture, stress induced transformation of tetragonal ZrO_2, exam. 78−48392
$AlPO_4$, high-low cristobalite transitions, DTA meas. 79−82335
Am, high press. form, cryst. struct., X-ray diffr. obs. up to 14 GPa 80−24399
Am, X-ray diffr. obs. 80−107422
As, cryst. struct. calc., pseudopot. expansion method 77−27848
As_2Se_3 glass, mech. props. var. due to high press. phase change 77−76481
BN, conversion of wurtzite into cubic form, stress state effect 80−64943
BN, cubic, form. using H_2O, H_3BO_3 and urea catalysts 79−83160
BN, cubic, press. and temp. stability region in presence of ammonium borate 77−85922
BN, martensitic character of transition from wurtzite-type to graphitelike modification 79−43248
BN, polymorphic modifications form. under low and high press. 79−15597
BN, shock-compressed pyrolytic and hot-pressed, phase transitions to 120 GPa 77−70048
BN, sphalerite transform., simple direct mechanism *(Russian)* 77−21135

high-pressure solid-state phase transformations continued
BN, structural changes at high pressures and temps. 80−40345
BN structure after high temp. shock compression 80−39220
BN, toughening by stress-induced phase transforms. 78−80635
BN, wurtzite type, effect of TiB_2 and B additions, on transformation to zinc blende type 78−80542
BN wurtzite-sphalerite phase transition, stacking fault role 80−6418
Ba, elastic properties, Debye temp., 20°C, 20 to 70 kbar, US wave velocity meas. 78−87735
Ba I-Ba II phase boundary, Ba I fusion curve peak at high press. *(Russian)* 80−2165
Ba, phase transformation in high-press. chamber *(Russian)* 77−76544
Ba, phase transitions under high press. 80−96641
β-BaF_2, (111) single cryst., behaviour under room temp. shock compression 77−62585
β-BaF_2, stress wave profiles 80−96593
$BaGeF_6$, Raman spectra at press. up to 25 kbar 78−6670
$Ba_2NaNb_5O_{15}$, high press. phase transitions, Raman scatt. studies 80−71402
$Ba_2NaNb_5O_{15}$, high-pressure phase transitions, ferroelastic phase 79−7687
$Ba_2NaNb_5O_{15}$, phase transition at high press., Raman scatt. obs. 79−55884
BaS, press. induced phase transform., X-ray diffr. study 80−39283
$BaSi_2$, semicond.-metal transition, high-press. and temp. 78−43299
$BaSi_2$, trimorphic, transform. of three-connected Si nets, press.-temp. phase diagram, 40 kbar and 1000°C 80−75198
$BaSi_{2-y}Ge_y$, solid solution with type $SrSi_2$ struct., lattice parameters at high press. 80−54203
Bi, Gruneisen parameter, high press. phase transitions 79−60467
Bi, phase transformation due to high press. and shear stress 80−75357
Bi, phase transformation in high-press. chamber *(Russian)* 77−76544
Bi, phase transitions under high press. 80−96641
Bi, shock loading and unloading, 293 and 473K 77−84840
Bi-Pb alloy, rel. to press. effects on supercond. crit. temp. *(Russian)* 77−20484
$BiVO_4$, ferroelastic phase transition, birefringence meas. at simultaneous high pressure and temp. 80−80743
Bn, cubic, formation from hexagonal BN using Cao and Li_3N catalysts *(Japanese)* 80−54374
C, film, work function, heat treatment 78−64563
C, hard, heat-treated under pressure, characterisation of carbon phase by electron microscope 80−60855
C, nature of metastable phases 77−89404
C, noncrystalline conversion to diamond, diffusion conversion enhanced rate due to shock compression 80−39221
C, polymorphic modifications form. under low and high press. 79−15597
C, texture change on ht. treatment under press. 78−60687
CF, cryst. struct. from X-ray diffr. 78−83766
CU_2O high press. phase transforms, optical and X-ray studies 80−44313
$CaAl_2O_4$, high pressure modifications 80−104149
$Ca_2Al_2SiO_7$, gehlenite, new high-press. phase, rel. to Earth interior 79−29753
$Ca_{1-x}Eu_xSi_2$, solid solns., α-$ThSi_2$ struct. type, comp. and press depend. 78−91322
CaF_2, fluorite, phase relations, to 60 kbar and 1800°C 78−84785
CaF_2-ScF_3, phase relationships at 100 kbar and 1200°C 77−43335
$CaGa_2O_4$, high pressure modifications 80−104149
Ca_2GeO_4, with K_2NiF_4-type struct., high press. decomp. 79−1507
$CaMgSiO_4$ (monticellite), high-press. phase transforms. and implications for upper mantle mineralogy 80−17255
Ca_2MnO_4, with K_2NiF_4-type struct., high press. decomp. 79−1507
$Ca(NO_3)_2.4H_2O$, high press. phase behaviour, dehydration and congruent melting 79−78947
CaO, B1-B2 transition, Earth mantle implications 80−79876
CaO, eqn. of state at high press., appl. to Earth core and mantle 80−109122
CaO high pressure metallisation, tentative evidence 80−84427
CaO, modified electron gas theory, high press. effect 77−19899
$Ca_3(PO_4)_2$, new cryst. phase prep. and struct. *(French)* 78−83789
$Ca_3(PO_4)_2$:Cu^{2+}, ESR, high press. struct. transition 80−97134
$CaSi_2$, high press. transform. of three-connected Si nets 79−77744
$CaSi_2$, high-pressure phase transform., cryst. struct. 77−35693
$CaSiO_3$, wollastonite, exptly. deformed, polytype transforms. 79−65021
Ca_2SiO_4, K_2NiF_4-type structure, high pressure synthesis, crystal chemical and geophysical implications 79−69089
$Ca_{1-x}Sr_xSi_2$, solid solns., α-$ThSi_2$ struct. type, comp. and press depend. 78−91322
Cd-Sn binary system, high press. study 80−93539
Cd-Tl binary alloy system at high press. 80−97461
CdHg alloy, ω phase, mag. susceptibility anisotropy w.r.t. uniform compression *(Russian)* 80−71143
$Cd_{1-x}Mg_x$, magnetic susceptibility anisotropy, press. effects, electronic phase transitions *(Russian)* 80−54869
$Cd(NO_3)_2.4H_2O$, high press. phase behaviour, dehydration and congruent melting 79−78947
CdS, high pressure effects on electrical resistivity and structure 77−15574
CdS, porous, dynamic phase transition at high press. 79−23723
CdS, X-ray diffr. investig. of high-press. polymorphism 77−43324
CdS(Se)(Te), determ. of wurtzite, zincblende and rocksalt phases 80−100219
CdTe, relations pressure-volume under high pressure 80−39219
Ce, α″ high pressure phase cryst. struct. 79−23565
Ce, α⟶α′ high press. transition, volumetric study 78−83940
Ce, cryst. structs. at high press. 77−19890
Ce, elastic properties up to 84 kbar, US vel. meas. *(Russian)* 79−60434
Ce, electrical resist. behaviour at press. induced α′-tetragonal phase transform. 77−35916
Ce, high pressure phase transition, anomalous Gruneisen parameter behaviour 80−79934
Ce, inelastic neutron scatt. under press. near first order γ-α phase transition 77−63102
Ce, new allotropic phase above 121 kbar, X-ray diffr. obs. 77−35509
Ce, polymorphic γ⇄α transform. and volume anomalies under press. 80−34189
Ce, sp. ht. and temp. coeff. of resist., 20 kbar at 300K 78−83973
Ce, TCR up to 15 kbar in α and γ phases *(French)* 79−95383
Ce, thermoelec. power up to 6 GPa 79−51556
Ce, thermopower behaviour under press. up to 7500 MPa γ-α and α-α′ transitions 79−47083

high-pressure solid-state phase transformations continued
CeAg, mag. and structural phase transition at hydrostatic press., elec. resist. meas. 79−61102
$Ce_{1-x}La_x$, dil., $\gamma-\alpha$ transition temp. and press., elec. resist. meas. up to 10 kbar 80−59643
CoO-SiO_2 systems high press. phases stability and MO-SiO_2 systems phase diagrams code 79−90779
Cr-Os, magnetic transition T-P-C diagram, triple points *(Russian)* 80−54895
CrAs, high press. paramag. antiferromag. transitions, elec. props., band model development *(Russian)* 80−60277
$CrAs_{0.42}Sb_{0.58}$, mag. and struct. transitions under press., elec. resist. meas. 78−27038
CrS(Sc), high press. semiconductor to metal transitions 78−26924
Cs, absolute zero isotherms and polymorphic transition 79−73310
Cs, electronic transition from self consistent APW Xα calcs. 78−51884
Cs, supercond., elec. resist. and phase transforms. under high press. *(German)* 80−107763
$Cs_2Au^{I}Au^{III}Cl_6$, influence of high hydrostatic pressure on cryst. struct. in pressure range up to 52×10^8 Pa 79−51249
$CsCdCl_3$ and $CsPbCl_3$, NQR investig. of press. induced phase transition 77−12224
$CsCdCl_3$, phase transition under pressure 78−51664
$CsCrO_4$, solid-to-solid transition temperature under hydrostatic pressures to 0.6 GPa 80−24586
CsH_2PO_4, high press. phase diagram 78−52457
CsH_2PO_4, press.-induced antiferroelectricity *(Japanese)* 80−15992
CsH_2PO_4-d, antiferroelec. under hydrostatic press. 79−91384
$Cs_2NaMO_xF_{6-x}$, M=Ti, V, Nb, Mo, W, high press. transforms. *(German)* 77−89400
$CsPbCl_3$, phase transition under pressure 78−51664
Cs_2SO_4, solid-to-solid transition temperature under hydrostatic pressures to 0.6 GPa 80−24586
$CsSbF_6$, high press. phase relations, vibr. spectra, and cryst. chemistry 80−108200
Cs_2SeO_4, solid-to-solid transition temperature under hydrostatic pressures to 0.6 GPa 80−24586
Cu I, press.-induced phase transitions, Raman scatt. obs. 77−43995
Cu-Pd alloy, pressure effect on β-phase transition by elec. resist. meas. 79−15660
Cu_3Au, metastable states domain existence, phase transition ordering energy, press. effect *(Russian)* 80−45303
CuCl, high press. phases and anomalous props. 79−7689
CuCl, ismorphic transitions at high press., 4.2 to 800K *(Russian)* 77−31774
CuCl, optical microscopic, X-ray diffr. and elec. resist. studies at high press. 80−11051
CuCl, pressure depend. of structural, chemical, elec. and mag. props. 80−96596
CuCl, struct. types in phase diagram, DTA and dilatometry meas. up to 35 kbar 78−18770
$CuGaS_2$, press. depend. of energy gap, absorption edge, induced phase transform. obs. 77−12401
$CuInTe_2$, pressure-induced phase transformations 78−30748
$CuK_2Cl_4.2H_2O$, Heisenberg ferromag., press. effect on Curie temp. and susceptibility 77−28386
$Cu(NH_4)_2Br_4.2H_2O$, Heisenberg ferromag. press. effect on Curie temp. and susceptibility 77−28386
Dy, conversion of metastable high-press. phase into stable phase 77−55357
$EuSi_2$, high-pressure phase transform., cryst. struct. 77−35693
$Eu_{1-x}Sr_xSi_2$, solid solns., α-$ThSi_2$ struct. type, comp. and press depend. 78−91322
Fe, Armco, dyuamic $\alpha\rightleftarrows\varepsilon$ transform., stress gauge meas. 80−96594
Fe, Armco, shock front phase transition kinetics 78−10122
Fe, cast, structural changes, due to pulsed action of high temps. and pressures *(Russian)* 80−7554
Fe, Curie point and A-γ transition to 53 kbar 79−56529
α-Fe, struct. after polymorphic transform. under press. *(Russian)* 80−29946
Fe-Co alloy, isothermal compression and BCC→HCP phase transition, up to 300 kbar, at room temp. 77−90346
Fe-Mn, γ to ε phase transform. induced by high press. and plastic deform. 78−68686
Fe-Mn (22 wt.%), $\varepsilon\rightarrow\gamma$ transformation, effect of H_2 pressure up to 23 kbar on transition temp. *(Russian)* 79−24517
α-Fe-Ni, struct. after polymorphic transform. under press. *(Russian)* 80−29946
Fe-Ni alloys, influence of hydrostatic press. on γ to α' transform. during plastic deform. *(Russian)* 79−15663
Fe-Ni-Ti alloys, high pressure effect on martensite crystal nucleation and growth *(Russian)* 78−39769
FeF_2 (rutile), high press. phase transform. 78−79761
$Fe(H_2O)_6.SiF_6$, pressure-induced orbital ground state inversion, Mossbauer study 80−39979
$(Fe_{0.5}Mg_{0.5})Ti_2O_5$, armalcolite, stability as function of press. and O_2 fugacity 77−64275
FeO, eqn. of state at high press., appl. to Earth core and mantle 80−109122
FeO-SiO_2 system, high press. phases stability and MO-SiO_2 systems phase diagrams code 79−90779
α-Fe_2O_3, elec. resist. and phase transition under shock compression 80−72496
FeOOH, high-pressure phase, neutron diffraction study 78−52212
$FeSiO_3$, high pressure and temp. phases rel. to Earth's mantle 77−9403
Ga II, superconducting high pressure phase, sp. ht. 80−70894
Ga, polymorphism at high press. *(French)* 78−47279
GaAs(P), semiconductor-metal transition, press. calibration above 100 kbars fixed points 80−77808
$Ga_{1-x}In_xSb$, press.-induced structural phase transition 78−30751
$GaMo_5S_6$, mag. and struct. transition temps., press. effects, 0-6 kbar *(Russian)* 77−89956
$GaNbO_4$, polymorphic transition under high press. 80−100835
n-GaP:S, elastic moduli and mode gammas 79−73242
$GaPO_4$, high-low cristobalite transitions, DTA meas. 79−82335
GaSb, relations pressure-volume under high pressure 80−39219
GaSb, single crystal, stress-induced phase change 79−23720
GaSe, pressure-induced polytypic transforms. and edge absorpt., exciton lines 77−28595
Gd, conversion of metastable high-press. phase into stable phase 77−55357
high-pressure solid-state phase transformations continued
$Gd_2Ge_2O_7$, polymorphism under pressure *(French)* 78−95150
Ge, metallic, eqns. of state under high press. 79−60475
Ge, mode Gruneisen coeff. at point X, effect of lattice softening 78−38804
Ge, non-cryst., high-press. expts., quenchable products 77−19874
Ge, semiconductor-metal transition and indentation hardness 78−35499
Ge, single crystal, stress-induced phase change 79−23720
GeO_2, new high-pressure modification 78−75825
H, metallic, transition press. and physical props. *(Chinese)* 80−54467
H_2, eqn. of state of solid and liq. phases, metallic state *(Russian)* 79−19354
H_2, metallic and molecular, transition press. and eqns. of state calc. 78−26685
H_2, solid, HCP to FCC transition at 80 to 100 atm. *(Russian)* 77−55259
^{4}He, extension of HCP-FCC phase diagram to about 9 kbar 80−39383
^{4}He, solid-fluid, eqn. of state, melting props. under press. 80−96721
HfO_2, high pressure polymorphism 80−59429
HfO_2-R_2O_3 solid solns., prep., crystn., R=Nd,Sm,Dy,Yb 78−42909
Hg chalcogenides, electrical charact. of pressure-induced transition 77−84921
Hg_2Cl_2, calomel, press. depend. optical soft mode 79−55859
Hg_2Cl_2, high press. induced phase transitions, X-ray study 79−69242
Hg_2Cl_2, p-T phase diagram, pressure effect on phase transition 80−107370
HgI_2, cryst. growth from soln., doping rel. to elec. cond., phase transitions 77−55880
HgSe, elec. resist., high press. phase transform., band gap 80−70707
HgSe, press. induced phase transitions, nucleation, resistance discontinuity 77−27996
HgTe, pressure-induced polymorphic transition 80−10667
Ho, conversion of metastable high-press. phase into stable phase 77−55357
I, metallic solid, high press. struct., phase transition, X-ray diffr. study 78−87647
I_2, press.-induced struct. phase transition, X-ray obs. 79−65192
In, superconducting energy gap and phonon frequencies under press., tunnelling meas. 77−32112
In-Bi alloy system at high press. and temp. 78−92238
In-Sb, cryst. struct. after appl. of high press., supercond. transition temp. 80−70169
InAs, single crystal, stress-induced phase change 79−23720
In_2Bi, press.-induced supercond. phase transform. 79−24099
InP, depend. of phonon spectrum on hydrostatic press., Raman spectra 80−93315
InP, press. depend. of direct absorption edge, up to high press. phase transition 80−93365
InSb, amorphous, pressure induced struct. transform., X-ray diffr. obs. 77−11690
InSb, polymorphism and cryst. struct. at high temp. and press. 78−95026
InSb, relations pressure-volume under high pressure 80−39219
InSb, single crystal, stress induced phase change 79−23719
InSb, sputtered NaCl-type compression 79−46751
K, absolute zero isotherms and polymorphic transition 79−73310
K, electronic phase collapse rel. to Earth thermal model 78−15982
KAg_4I_5, superionic cond., pressure effect on phase transitions 80−70405
KBr, Gruneisen parameter, high press. phase transitions 79−60467
KC_{24}, press. induced staging transition 80−79938
KCN, cryst. phases at press. up to 55 kbar, Raman spectra obs. 79−82975
KCN, disordered ordinary and metastable phases, light scatt., press. depend. 78−95151
KCN, order-disorder transition, high-press. Brillouin scatt. exam. 77−44009
KCN, polymorphism, high pressure, Raman spectra 78−88302
KCl, polymorphic transition press. at high temp., elec. resist. meas. 78−38837
KCl(Br)(I):Tl, emission spectra, press. effects 78−23509
KDP monocrystal, expansion and contraction coeffs., tricritical point, Landau theory explanation *(Russian)* 80−44340
KD_2PO_4, high press. phase diagram 78−52457
KD_2PO_4, struct. at high press. in rel. to effect of press. on T_c 79−42915
KF, high press. B1 to B2 phase transition, X-ray diffr. obs. 79−23722
$K_3Fe(CN)_6$-KCl, press. induced reduction, IR spectra after pressurization 80−66776
KH_2AsO_4, ferroelec. phase transition under hydrostatic press., NQR spectra obs. 79−69785
KH_2AsO_4, ferroelectric phase transition under high hydrostatic press., mol. dynamics, NQR study 80−75880
KH_2PO_4, and isomorphs, IC spectra and phase transitions, under pressure 78−31180
KH_2PO_4, pressure effect on ferroelec. transitions *(Japanese)* 79−65814
KH_2PO_4, struct. at high press. in rel. to effect of press. on T_c 79−42915
KH_2PO_4, tricrit. point, γ-ray and neutron diffr. 78−39516
KH_2PO_4, tricrit. point, neutron diffr. study under high press. 79−33624
KH_2PO_4-type crystals, H bond in ferroelectricity, role of high pressure research 79−15414
KI:Tl, emission and excitation spectra, press. effects 79−83028
$KMnF_3$, exciton line and magnon satellite in UV spectrum at high press. *(Russian)* 79−4517
$KMnF_3$, stress-induced phase transition, optical props. meas. 77−20067
$K_2Mn_2(SO_4)_3$, phase transition press. effect, dielectric const. meas. 79−37834
KNO_2, high-pressure phase behaviour 78−30749
KNO_2 polymorphs, high press. Raman spectra 77−85725
KNO_3, antiferroelec., press. induced II to IV phase transition, Raman scatt. 78−15161
KNO_3 in alkali halides tablets, phase transition and ion exchange, IR spectra 80−79937
$K_2PbCu(NO_2)_6$, effect of hydrostatic press. on successive Jahn-Teller phase transitions 78−43120
K_2SeO_4, incommensurate phase transition, stress depend. of T_c 79−4391
K_2SeO_4, incommensurate to ferroelec. transition, hydrostatic press. effects, neutron scatt. study 80−108166
K_3SmF_6, press.-temp. phase diagram to 35 kbar and 900°C 77−15575
$KTaO_3$, stress-induced ferroelectricity, Raman scatt. obs. 77−40190
K_3YF_6, press.-temp. phase diagram to 35 kbar and 900°C 77−15575
$K[Ag(CN)_2]$, Raman scatt., press.-induced phase transitions and phonons 79−33698

high-pressure solid-state phase transformations continued
$K_2[Pt(CN)_4]Br_{0.3}.3H_2O$, high press. structs. and phase transitions 80−107423
La, low temp. P-T diagram 77−47550
La, supercond. transition temp., press. depend., mode softening 78−14847
La, superconducting, electron-phonon coupling, hydrostatic press. depend. 78−80087
LaAg, under hydrostatic press., supercond. and phase transform, elec. resist., 1-300K 78−10595
La_2CuO_4, small polaron cond. to semicond. phase transformation 78−6156
LaF_3-$La(OH)_3$, high pressure phases, X-ray diffr. and IR spectroscopic anal. 79−47679
LaOF-LaF_3, high pressure phase transitions 80−55368
Li_2BeF_4, high-press. polymorph and melting systematics 77−51475
LiF-MgF_2, high-pressure phase relations rel. to mixed oxide zone of Earth mantle 77−37193
$LiND_4SO_4$, ^7Li and ^2D NMR exam. of high-pressure phase 79−11396
$LiNH_4SO_4$, ferroelect. and press. induced phase transitions 79−38473
$LiNbO_3$, shock-wave compression, 2.4-44 GPa 80−34139
$LiTmF_4$, Van Vleck paramag., mag. reson. on uniaxial and uniform compression *(Russian)* 79−61243
Li_2WO_4, high press. modifications, IR spectra *(German)* 78−23459
$Lu_2Si_2O_7$, crystal struct. of X form, polymorphism under press. *(French)* 77−47430
$Lu_2Si_2O_7$, polymorphism under press., cryst. struct. 77−35692
$M_{1-x}Sr_xSi_2$ (M=Ca, Eu, Ba), solid solution with type $SrSi_2$ struct., lattice parameters at high press. 80−54203
β-$(Mg, Fe)_2SiO_4$, high-press. spinel phase identification in Tenham chondritic meteorite 79−80284
$Mg_3Al_2Si_3O_{12}$, pyrope garnet-ilmenite transition 77−49063
MgF_2 (rutile), high-pressure phase transformations 79−44181
Mg_2Ge, polymorphism under high press., radiographic data 77−20068
Mg_2GeO_4, determ. of olivine-spinel transition up to 20 kbar and 1300°C 77−53044
MgO, compressed, SCF electronic struct. calcs., necy. press. for conversion to metallic state 78−43300
MgO, modified electron gas theory, high press. effect 77−19899
MgO-SiO_2 system, high-press. phase transistions calcs. rel. to mantle discontinuities 79−90780
Mg_2Si, polymorphism under high press., radiographic data 77−20068
$MgSiO_3$, enstatite, high-press. phase relations, absence of oxide mixture 77−37185
$MgSiO_3$, HP phase transform. 80−19941
Mg_2SiO_4, forsterite, high-press. phase relations, absence of oxide mixture 77−37185
Mg_2SiO_4, temp. in high-press. shock state 80−72490
Mg_2Sn, Mossbauer effect exam. under press. up to 75 kbar 79−69759
Mg_2Sn, phase transition under hydrostatic pressure, Mossbauer effect and electric resistance 78−51665
Mg_2Sn, phase transitions under high hydrostatic press., Mossbauer spectra 79−87628
$MgVO_3$, high-pressure modification, struct. and mag. props. 79−23727
Mn-Bi mictomagnetic alloy, mag., elec. and elastic props. *(Russian)* 80−108028
MnAs, generalised P-T phase diagram, mag. and structural phase transition 80−39780
MnF_2, rutile type, polymorphism at high press., distorted fluorite phase 79−69050
MnF_2, X-ray diffr. investig. of high-press. polymorphism 77−43324
$Mn_{1-x}Fe_xAs$, magnetic transition under high press., exchange striction model calcs. *(Russian)* 80−50096
MnNiGe, coupled nature of mag. and struct. transition under press. 79−8033
ND_4Br, neutron diffr. exam. of P-T phase diagram 77−7861
ND_4Cl, order-disorder transformation, elasticity and heat capacity temp. depend., US obs. 78−71851
$(ND_4)_3D(SO_4)_2$, press.-temp. phase diagram 78−38834
ND_4I, Raman spectra at high press. 79−47459
ND_4I, Raman spectrum, press. effects 80−97261
$NH_4Ag_4I_5$, superionic cond., pressure effect on phase transitions 80−70405
NH_4Br and NH_4I, Raman scatt., 1 bar-7 kbar, 86-295 K 80−34909
NH_4Br, neutron diffr., exam. of P-T phase diagram 77−7861
NH_4Br, order-disorder phenomena, high press. US investigation 79−37835
NH_4Br, phase diagrams, from Raman meas. under high press. 78−52776
NH_4Br, proton spin-lattice relax. time up to 2200 bar, phase transitions 77−63307
NH_4Cl, molar heat capacity near order-disorder transform. under high press. 78−51697
NH_4Cl, order parameter, electro-optic measurement 78−88280
NH_4Cl Raman spectra, pressure effects 80−97268
NH_4Cl, thermal cond. and heat capacity of solid phases under press. 80−2225
$(NH_4)_3H(SO_4)_2$, pressure-induced ferroelectricity, dielec. const. meas. 78−23412
$(NH_4)_3H(SeO_4)$, ferroelec. transition, press. and temp. effects on dielec. props. 78−23413
NH_4I, phase diagram from Raman meas. under high press. 78−52776
NH_4I, Raman spectrum, press. effects 80−97261
NH_4IO_3, effect of hydrostatic press. on ferroelec. phase transition 79−51917
NH_4LiSO_4, ferroelec., phase transition points, hydrostatic press. effect 77−77155
NH_4LiSO_4, ferroelec., hydrostatic press. effect on I-II phase transition, dielec. meas. 79−38496
NH_4LiSO_4, high press. phase, point group symmetry 79−51039
NH_4LiSO_4, I-II phase transition in improper ferroelec., hydrostatic press. effects 78−84533
NH_4LiSO_4, point group symm. at high press. phase 80−70150
NH_4NO_3, shear-stress-induced transitions, IR study 77−32368
$(NH_4)_2SO_4$, ferroelec., ion group reorientation temp. and press. depend., PMR obs. 78−72470
$(NH_4)_2SO_4$, solid-to-solid transition temperature under hydrostatic pressures to 0.6 GPa 80−24586
$NaAlSiO_4$ (nepheline), high-press. to transform. to first silicate Ca ferrite isotype 77−64270

high-pressure solid-state phase transformations continued
$(NaAl)_xSi_{2-x}O_6.H_2O$, analcite, polyhedral tilt transitions obs. at high press. 80−6515
NaCN, cryst. phases at press. up to 55 kbar, Raman spectra obs. 79−82975
NaCl, phase transformation due to high press. and shear stress 80−75357
NaCl primary press. gauge, failure of central force model 77−15492
NaCl(Br) (F) (I), lattice dynamics and statics, three-body-force shell model 80−49323
NaCl(Br):Tl, emission spectra, press. effects 78−23509
$NaClO_3$, Raman spectroscopy exam. of high-pressure phase transform. 78−10186
$NaH_3(SeO_3)_2$, β to δ ferroelec. transition under press. Raman spectra study 80−80725
$NaH_3(SeO_3)_2$, high-pressure phase transform., ^{23}Na NMR obs. 77−63380
$Na_3M_2Li_3F_{12}$, M=Al, Fe, fluoride garnets, high press. form 77−76554
$NaNH_4SeO_4.2H_2O$, ferroelectric crystal, effect of hydrostatic pressure on phase transition 78−52453
$NaNO_2$, high-pressure phase behaviour 78−30749
$NaNO_3$, shear-stress-induced transitions, IR study 77−32368
$NaNO_3$, soft mode dynamics at ferroelec. transition 78−80308
$NaNbO_3$, hydrostatic press. effect on permittivity, phase transition, hysteresis 80−80670
$NaPF_6$, high press. phase diagram, vibr. spectra 78−60446
$Na_3R(XO_4)_2$ (R=rare earth; X=P, As, V), pressure synthesis *(French)* 80−93509
NbS_2, high pressure polymorphs 78−51459
$NbS(Se)_2$, polymorphism at high press. and temps., T_c and band struct. 78−26528
$NbSe_2$, high pressure polymorphs 78−51459
Nb_3Si, high press. phase, prod. by recrystn. of metastable sputter deposits, struct. and supercond. props. 78−60571
$NbTe_2$, high pressure polymorphs 78−51459
$NdH_{2.82}$, high-pressure structural phase transforms. 78−10185
Ni complex, $Ni(NH_3)_6(ClO_4)_2$, high-press. phase, EPR meas. 78−38842
Ni-C. exam. of metastable phase diagrams, at high temp. and pressure *(Russian)* 79−56955
Ni-Co-H system, phase transform. under high H_2 press., Co additive effects *(Russian)* 78−60645
NiF_2, press. induced strain transition obs., neutron powder diffr. meas. 78−55948
NiF_2, tetragonal to orthorhombic transition at high press., possible mag. ordering 78−18765
$Ni(NH_3)_6(ClO_4)_2$, EPR determ. of phase transition temp., line shape anal. 77−20063
$Ni(NH_3)_6(NO_3)_2$, jumpwise vol. change in structural phase transition 79−42233
O_2, phase equilibria near 298K, Raman spectral study of solid and fluid 80−19937
P, black, pseudopotential crystal-struct. stability calcs. as function of press. 79−60503
P, red to black conversion in quasiisentropic compression 79−33036
P-Se, phase diag. and crystallisation of glasses at high press. 77−52297
PCl_5, phase diagram, PCl_6^- ionising to PCl_4 and $2Cl^-$ under press. 79−82314
Pb, superconducting transitions at liquid He temps., determ. via X-ray diffr. 77−11442
Pb-Sb, phase transform. at high press., DTA, eta, beta thermodynamic stable phases *(Russian)* 79−66051
PbF_2, cubic, dielec. const., ionic cond., soft modes 78−14427
PbF_2, ionic cond., activation volumes and high press. phase transitions 80−70461
PbF_2, polymorphic transition temps. under hydrostatic press., DTA study 80−2156
PbF_2, sp. ht. anomalies, phase transition 79−86901
PbF_2, US vel. near press. induced cubic-to-orthorhombic transform. 80−103476
PbI_2, cubic, elastic consts., hydrostatic press. effect, US vel. meas. 80−49292
PbI_2, high-pressure phase transition, optical props. meas., 300K and 78K 77−51495
PbI_2, ionic cond. and activation volumes, high press. effects 80−100353
$Pb_{0.97}La_{0.02}(Zr_{0.92}Ti_{0.08})O_3$, ferroelec. ceramic, stress effects 80−2119
$Pb_3(NO_4)_2$, press. induced ferroelastic phase transition, neutron diffr. study 79−73308
$Pb_{0.99}Nb_{0.02}(Zr_{0.95}Ti_{0.05})_{0.98}O_3$, ferroelec. ceramic, stress effects 80−2119
PbS, phase transitions under action of high press., elec. cond. meas. 77−4196
$Pb_{0.59}Sn_{0.41}Se$, struct. phase transition, temp and hydrostatic press. influence, Hall effect, resistivity *(Russian)* 78−51675
$Pb_{1-x}Sn_xSe$, displacive transition, temp. and press. depend., elec. meas. 80−10672
$(Pb_{0.97}Sr_{0.03})Zr_{0.51}Ti_{0.49}O_3$, ferroelec. phase transition under high press. 77−36188
$PbTiO_3$-$Pb(Ni_{1/2}W_{1/2})O_3$ system, solid soln. form., struct., dielec. props. and thermal expansion *(Japanese)* 78−27501
$Pb(Zr, Ti)O_3$, ferroelectric ceramics in solid matrix, high pressure effect on dielectric props. 77−16259
$Pb(Zr,Ti)O_3$ piezoceramic, phase transition under shock loading *(Russian)* 77−69041
$Pb(Zr,Ti)O_3$, temp. and hydrostatic press. depend of vibr. modes, rel. to phase transforms 77−89510
$PbZrO_3$ based ceramic, press. induced ferroelec. to antiferroelec. transition 79−24273
$PbZr_xTi_{1-x}O_3$, ferroelec. phase transition under high press. 79−99833
PdF_2 flourite-type form, mag. props., structure studies *(French)* 80−34187
PdF_2, high press. modification, cryst. and mag. props. 80−38988
$Pd_{1-x}Rh_xTe_2$, high-press. phase transform. obs. 77−15584
$PdS_2(Se_2)(Te_2)$, polymorphism at 75 kbars, 400-1350°C 79−82173
$Pd_{80}Si_{20}$, amorphous alloy crystn., high press. effect 78−95001
Pr, localised 4f shell breakdown under press. 80−70411
Rb, absolute zero isotherms and polymorphic transition 79−73310
Rb, elec. resist. and phase transforms. under high press. *(German)* 80−107763
RbBr, thermal cond., press. depend., up to 10 kbar, jump at phase transition 77−62694
RbBr, thermal cond. under press. meas. 78−30802
Rb_2CO_3, high press. phase relations, DTA 77−43329

high-pressure solid-state phase transformations continued
$RbCaF_3$, shift of first order transition under hydrostatic press. 80−59649
RbCl, Gruneisen parameter, high press. phase transitions 79−60467
RbCl, sp. ht., at phase transition 79−7701
RbCl, structural phase transition, Born-model and effects of hydrostatic and non-hydrostatic stresses 79−23721
RbCl:Li^+, new off-centre defect system, studied with dielec. techniques under hydrostatic press. 79−19834
RbF, high press. B1 to B2 phase transition, X-ray diffr. obs. 79−23722
RbH_2PO_4, high press. phase diagram 78−52457
RbI, mosaic struct. in metastable press. region, gamma-ray diffr. meas. 77−20065
RbI, NaCl to CsCl phase transition by elastic diffuse and inelastic neutron scatt. 80−2162
RbI, phase transition, diffuse neutron scatt. in metastable press. region 78−67825
RbI, phase transition NaCl→CsCl type, preferred orientation of CsCl type 80−49160
RbI, press. depend. of I nucl. relax. press. induced polymorophic transform. study 79−1720
RbI, single cryst., press.-induced B1-B2 phase transition, X-ray diffr. meas. 78−63852
RbI, single crysts., mosaic struct. changes, press. induced 77−51507
RbI:Tl, emission and excitation spectra, press. effects 79−83028
$RbICl_4$, NQR of ^{35}Cl, press. and temp. depend., phase transform. obs. 80−15820
$Rb_2LiMO_xF_{6-x}$, M=Nb or Mo, high press. transforms. *(German)* 77−89400
$RbMnCl_3$, high-pressure cubic phase, mag. props. 79−47260
$RbNH_4SO_4$, ferroelec., ion group reorientation temp. and press. depend., PMR obs. 78−72470
$RbNO_3$, permittivity and dielec. cond. press. up to 5 kbar, antiferroelec. transition obs. 77−36183
Rb_2SO_4, solid-to-solid transition temperature under hydrostatic pressures to 0.6 GPa 80−24586
ReO_3, compressibility collapse phase transition, NQR study 80−39282
ReO_3, phase transition at high press., Fermi surface and X-ray studies 79−65188
S_4N_4, Raman scatt. and opt. absorpt., press. and temp. depend. 77−36227
Sb and Sb-Bi, X-ray diffr. investig. of high-press. polymorphism 77−43324
Sb, carrier density at press. up to 80 kbar, magnetoresist. and Hall effect obs. 79−73534
Sb, phase transformation due to high press. and shear stress 80−75357
Sb, polymorphism at high press., temp. hysteresis, DTA *(Russian)* 79−82328
$SbCl_5$, phase diagram to 43 kbar 80−2144
SbSI, Raman scatt., near tricritical point 78−15159
Sb_2Te_3, thermoelectric properties and phase transition, under hydrostatic pressure up to 9 GPa 80−65609
Sc-H system 78−63853
Sc_4C_3, superconducting phase synthesis at high press. and temp., critical field *(Russian)* 80−65732
ScF_3, metastable high press. phases, X-ray diffr. and IR absorpt. expts. 77−11499
ScO(OH), ScOF, and $Sc(OH)_3$, metastable high press. phases, X-ray diffr. and IR absorpt. expts. 77−11499
$Sc_2Si_2O_7$, polymorphism at high press. and temp., thortveitite struct. stability *(French)* 80−10657
Se, amorphous, struct. and elec. cond. transitions under high press. 79−42237
Se, atom positions, effect of press. 78−34465
Se, cubic modification prepared by shock compression 78−34494
Se, trigonal, Raman scatt. at very high press. 80−60566
Si, metallic, eqns. of state under high press. 79−60475
Si, metallic, superconducting transition temp., press. effects, elec. cond. 80−103777
Si, polymorphism under high press. *(Russian)* 78−59947
Si semiconductor-metal transition and indentation hardness 78−35499
Si, static compression in [100] and [111] directions, elec. resist. obs. 80−65637
Si-H, amorphous, struct. and press. induced transition 80−44131
Si-O bonds, cryst. chem. at high press., rel. to Earth mantle mineralogy 79−48470
SiC, phase transition under isostatic press., microhardness meas., −196 to 1700°C 79−19318
SiO_2, high-low cristobalite transitions, DTA meas. 79−82335
SiO_2, new high-pressure modification 78−75825
SiO_2, temp. in high-press. shock state 80−72490
Sm_4Bi_3, press. induced valence instability, elec. resist. transition 78−95317
Sm_4Bi_3, press.-induced valence instability 80−20261
$Sm_{1-x}La_xS$, press.-induced semicond.-metal transition, refl. and lattice compression meas. 77−62826
SmS, metallic phase, compressibility anomalous behaviour 80−29114
SmS, vol. changes at press. up to 20 kbar 78−71791
SmS-GdS system, crit. effects and phase equilibria 79−7692
$Sm_{1-x}Y_xS$, press.-induced semicond.-metal transition, refl. and lattice compression meas. 77−62826
Sn-Bi, crystal struct. and superconductivity after appl. of high press. and quenching 80−10531
SnO, under hydrostatic press. up to 41 kbar, Mossbauer study 79−51892
SnTe, phase transition at high hydrostatic pressure, Mossbauer study 79−95162
SnTe, polymorphism, high press. and temp., X-ray diffr. study 80−54375
$SrB_2O_4:Eu^{2+}$, luminesc. of high-press. phases 80−100680
$Sr_xBa_{1-x}Nb_2O_6$, high press. phase transitions, Raman scatt. studies 80−71402
$SrCl_2$, ionic cond., activation volumes and high press. phase transitions 80−70461
$Sr_2Nb_2O_7$, high press. phase transitions, Raman scatt. studies 80−71402
$SrSi_2$, high-pressure phase transform., cryst. struct. 77−35693
$SrTiO_3$, stressed, trigonal-to-tetragonal transition, EPR data, realisation of 3-state Potts model 77−28525
TGSe, anomalous sound velocity near ferroelec. phase transition at high pressure 78−52456
TGSe, deuterated, NMR investig. of ferroelec. and press. induced transition mechanisms 77−16189

high-pressure solid-state phase transformations continued
$(TSeT)_2Cl$ complex, phase transform. under press., cond. *(Russian)* 80−92674
TTF-TCNQ, high press. structural transitions, neutron scatt. study 80−96647
$TTT_2I_{3+\delta}$ complex, influence of press. on metal-dielectric phase transition *(Russian)* 80−92818
$TaSe_2$, (2H) CDW, reentrant lock in transition at high press. 80−88320
Tb, conversion of metastable high-press. phase into stable phase 77−55357
Tb, high-pressure phase, mag. field effects *(Russian)* 77−66021
Tb, press. induced polymorphic transition, X-ray obs. 77−59113
Te, atom positions, effect of press. 78−34465
Te, high pressure metallic phase, cryst. struct. 80−49161
Te, monoclinic, electronic states above high-press. phase transition 79−99476
Te, Mossbauer spectra under press. up to 8000 MPa 80−80647
Te, trigonal, ^{129}I Mossbauer obs. 80−55005
Te, trigonal, Raman scatt. at very high press. 80−60566
TeO_2, paratellurite, phase transition at high-press., Raman and far IR spectra 78−80328
TeO_2, paratellurite, stress induced changes in Raman spectrum 78−39540
TeO_2, zone centre optical phonons under uniaxial stress 78−79700
Ti, $\alpha\rightarrow\omega$ transform., pressure-induced, impurity effects and reaction kinetics 78−11220
Ti-Mo alloys, structural stability under high-pressure soaking 80−104151
Ti-Mo-Fe (3, 0.13 at.%), metastable phases, Mossbauer study 80−7243
Ti-Mo(V), metastable diffusionless equilibria, high press. conditions 80−71627
Ti-V (10 at.%), $\alpha\rightarrow\omega$ transformation, electron diffr. evidence of intermediate BCC phase 80−81051
TiO_2, Raman spectra and struct. at high press. 79−87442
TiO_2, rutile, Raman study at high press. 80−89002
TiO_2, rutile phase, shock induced phase transition anisotropic behaviour 80−103475
TiO_x, (x=0.88, 1.27), effect of heating at high press. on struct. 78−10190
Tl, phase diagram and high press. phase transforms., DTA study *(Russian)* 80−66474
Tl, phase transformation in high-press. chamber *(Russian)* 77−76544
Tl, time of flight neutron diffraction meas. of c/a ratio and vol. change at transition 77−15335
$TlAsS_4$, struct. and soft mode behaviour 78−91327
Tl_2CO_3, phase diagram to 80 kbar 77−15576
$TlGaS_2(Se_2)$, phase transforms. under hydrostatic press., Raman scatt. study 80−25366
$TlMnCl_3$, sp. ht. and latent heat, under press. 79−7694
TlN_3, press. induced transition dynamics, light scatt. 78−80362
Tl_3PSe_4, struct. and soft mode behaviour 78−91327
Tl_2SO_4, solid-solid transition temp. to 34 kbar *(French)* 77−20064
$TlSbS_2$, phase transitions under action of high press., elec. cond. meas. 77−4196
TmSe and its mixed crysts., valence instabilities, phase diagram 80−70651
$TmSe_{1-x}Te_x$, phase relationships and press. induced transitions 80−19771
$Tm_2Si_2O_7$, crystal struct. of X form, polymorphism under press. *(French)* 77−47430
$Tm_2Si_2O_7$, polymorphism under press., cryst. struct. 77−35692
$UC_{1.5}$, creep behaviour and phase change under compression stress 78−35432
$V_{0.986}Fe_{0.014}O_2$, metal-insulator phase transition, effect of hydrostatic press. 80−6725
V_3O_5, phase transition temp., hydrostatic press. depend. 77−62827
V_5O_9, metal-insulator phase transition temp. depend. on press. 80−29327
V_6O_{11}, metal-insulator phase transition temp. depend. on press. 80−29327
V_3Si, nontransforming, press.-induced phase transformation 78−80084
V_3Si, supercond. transition temp. and phase transform. at press. up to 45 kbar 79−56352
WF_6, effect of high hydrostatic press. in reorientation and internal motion, ^{19}F NMR spectra 79−15364
YOF-YF_3, high pressure phase transitions 80−55368
Yb, semimetal-semicond. transition at high press., Seebeck coeff. meas. 77−62956
Yb, structural and electronic changes under 200 kbar press. and above 80−24588
Yb-H system 78−63853
$Yb_2Si_2O_7$, crystal struct. of X form, polymorphism under press. *(French)* 77−47430
$Yb_2Si_2O_7$, polymorphic transforms. and phase diagram under press. *(French)* 77−15573
$Yb_2Si_2O_7$, polymorphism under press., cryst. struct. 77−35692
ZnF_2, X-ray diffr. investig. of high-press. polymorphism 77−43324
$Zn(NO_3)_2.6H_2O$, high press. phase behaviour, dehydration and congruent melting 79−78947
Zn_3P_2, high press. phase relns. and cryst. structs. 78−59792
ZnS, phonon dispersion under extreme press. and metallic transform., Raman spectra meas. 78−10895
ZnSe, phonon dispersion under extreme press. and metallic transform., Raman spectra meas. 78−10895
$ZnSiO_3$, HP phase transform. 80−19941
ZnTe, phonon dispersion under extreme press. and metallic transform., Raman spectra meas. 78−10895
ZnTe, polymorphism at elevated temp., elec. resist. and X-ray diffr. under press. 80−49359
ZnTe(S), semiconductor-metal transition, press. calibration above 100 kbars fixed points 80−77808
Zr-C, exam. of metastable phase diagrams, at high temp. and pressure *(Russian)* 79−56955
ZrO_2, baddeleyite, high-press. phase transform., Earth mantle appl. 80−8296
ZrO_2, containing metastable tetragonal phase, stress induced phase transform. effect on props. 78−68683
ZrO_2, high pressure polymorphism 80−59429
ZrO_2, polymorphism at high press., X-ray diffr. obs. 79−73311
ZrO_2-R_2O_3 solid solns., prep., crystn., R=Nd,Sm,Dy,Yb 78−42909

high-pressure solid-state phase transformations continued
$ZrSiO_4$, zircon, cryst. struct. and compressibilty at high press. 79−82184
$ZrSiO_4$, zircon, high-press. phase transform., Earth mantle appl. 80−8296

high-pressure techniques
10 kbar hydrothermal installation with internal heater 79−67333
20 kbar pressure system using reciprocating hand pump, for magnetic resonance studies 79−67335
AC calorimetry for press. up to 3 kbar 77−41616
acoustic microscopy in high-pressure gases 80−43561
ampoule for NMR meas. of self-diffusion coeffs. of liquid molecules under pressure 79−35773
analogue experimental techniques for high pressure and temp. *(Chinese)* 79−80638
anvil, truncated, compressive strength, high press. apparatus appl. 78−84906
anvil device with lune toroid, effectiveness of monolithic materials for creating high pressures 80−73377
apparatus and research at very high press. and high temp. 78−24811
apparatus for low-temp./high pressure Mossbauer absorber study, modified 79−17591
apparatus for magneto-transport and far IR magneto-optical expts. 79−35708
apparatus with shaped Bridgman anvils, calibration 78−49856
autoclave process for high-press. polymerisation of ethylene 79−24744
autonomous high pressure chamber for diode laser tuning 77−46742
bending test apparatus for high press., high temp. 80−85126
bending test apparatus under high press. and high temp. *(Japanese)* 78−76795
biaxial stress production at low temp. 78−45609
Boyd-England apparatus at NPL, design and construction 80−101804
calibration, using ruby fluoresc. R-lines at ambient and low temps. 77−18106
calibration curves for devices with profiled anvils 77−82540
calibration scale based on Au, Ag and Cu melting curves, revision 80−39260
capillary piezometer with opticomech. readout, for compressibility meas. 77−39264
cell, for Curie temp. meas. with cubic-anvil press 80−13109
cell design for hydrostatic pressure up to 25 kbar 80−52260
cell for depolarised light scatt. from liquids *(German)* 79−21799
cell for gas-mixture expts. at low temperatures 80−86334
cell for Raman spectroscopy, appl. to hexamethyl benzene 78−56488
cell for solid-phase 'anvil-toroid' apparatus, for electrical conductivity measurements up to 8 GPa 80−31794
cell for X-ray diffuse scattering studies up to 5 kbar and down to 77K 80−86336
chamber calibration, phase transitions in standard materials *(Russian)* 77−76544
chamber calibration using ruby R_1 luminescence line shift, 80 to 550K 78−86284
chamber for neutron diffraction up to 30 kbar 79−93158
chamber for pulsed NQR spectrometer 78−86308
chamber for research in 2-300K range and to 25 kbar 78−21158
chamber of Mossbauer spectra investig. at 50 kbar 77−41634
chamber thermocouple lead-ins for highly compressible media 78−86285
chaoite, a new allotropic form of carbon, produced by shock compression 80−80997
chemical kinetics, high pressure pressure-jump apparatus 80−62681
clamp cell for elec. conductivity measurements up to 8 GPa 80−37047
coal dissolution at short reaction times, fast-dump reactor apparatus 77−44575
coaxial DTA cell for study of liquid crystalline transitions at elevated pressures 77−22564
coaxial suction jet, pneumatic gauging system 80−9001
comminution of solids under hydrostatic pressure, technique 78−52702
complex apparatus for viscous and elastic prop. meas. at high press. of liquids 78−9734
compression device for high-pressure production in elastoplastic media 6-piston 100 kbar 79−35774
compression installation, isothermal, for solid H_2 up to 25 kbar, 60 to 130K 79−35769
compressors, for low-density polyethylene process, design 77−13764
conductivity meas. for high press. chem. kinetics in soln. 79−93161
conference, Darmstadt, Germany (Mar. 1977) 79−23677
conference on high pressure physics and technology, Moscow, Russia (May 1975) 78−51611
conical plug seals, plastic flow under pressure, tightness mechanism 78−54386
contacting surfaces, optimisation of elastic strain distrib., anvil shape 78−49847
continuous flow helium cryostat for optical studies at fixed high pressure 78−81984
critical flow venturi nozzle, calibration in high pressure gas 79−68844
cryogenics, appl. of sintered diamond tipped, opposed piston apparatus 80−86322
cryostat with optical high-pressure chamber 80−31767
crystal growth system, high compression 80−66415
crystal structure research, using Philips PW 1100 diffractometer 80−38873
crystallisation, fractional, applying very high pressure 80−100775
cubic-anvil type pressure apparatus, resistance meas. of Manganin wire 79−44919
deep-sea animals trapping, pressure vessel with simply actuated closure 78−3821
deep-sea instrument float, evaluation of Isopar-M, press.-vol. isotherms 77−25786
depressurisation of high-pressure systems with liq. heat carrier, thermodynamic equil. approach 80−17957
diamond, nucleation and growth, 55 kbar and 1450K 79−99087
diamond against diamond, high press. generation, thin film effect 79−55821
diamond anvil cell, calibration, 0-15 kbar, for X-ray diffr. expts. on polymers 77−41635
diamond anvil cell, for high press. far IR obs. 79−12874
diamond anvil cell, Raman spectroscopy on ultrasmall samples 77−87839
diamond anvil cell, variable temp., for polycrystalline X-ray studies to 2K 78−1951

high-pressure techniques continued
diamond anvil cell adaption to automatic for circle X-ray diffractometer 78−75501
diamond anvil cell as sampling device in IR expts. 79−93157
diamond anvil cell for high pressure measurement, with uniform internal stresses at 200 kbar 79−67334
diamond anvil cell for high-press. generation *(Japanese)* 78−29124
diamond anvil cell for IR study of shear-stress-induced transitions 77−32368
diamond anvil cell for X-ray diffr. expts. on polymers, high press-temp. variation 77−74418
diamond anvil cell up to 50 kilobar for single cryst. X-ray diffractometer use 77−31560
diamond anvil device for X-ray diffraction on single crystals to 100 kbar 77−68896
diamond anvil for X-ray diffr. up to 100 kb and down to 1.5K 79−73070
diamond anvil press, press. distrib. and shear strength of fayalite 78−12710
diamond anvil press for high temp. and press. studies 77−10037
diamond anvil pressure cell falling sphere viscometer, wall effects 79−82023
diamond cell, melting of inert gases between 4 and 500K up to 1 Mbar *(French)* 79−73373
diamond cell, single cryst., revised operating method, NaCl struct. refinement at 32 kbar 78−67610
diamond selection for anvils in high-press. devices for IR and Raman spectroscopy 77−57413
diamond-anvil cells, optical meas. of condensed gas solid phase transitions 80−73381
diamond-anvil high pressure cell used in automatic diffractometer up to 90-kilobars 78−54387
diamond-anvil high-pressure cell, for X-ray diffraction studies 78−30514
diamond-anvil press. cell for photoluminescence meas. 80−108256
diamond-anvil press. cell for X-ray diffr. obs. with solid-state or proportional counter 80−75119
diamond-window pressure cell, sustained static generation at 1.36 to 1.72 megabars 79−17438
die for powder pressing for refr. index meas. 77−156
dielectric meas. apparatus at high pressures and freqs. 79−67346
differential scanning calorimeter 80−86311
dilatometer, high press. and high temp., construction and appl. 77−37844
dilatometer for PVT meas. of liquids and plastic crystals at low temperature 80−68208
ductility meas. under tension or compression at high press., apparatus *(Japanese)* 78−35617
dynamic hydrothermal experimental system, for seawater-basalt reactions study 79−5686
dynamic stress/strain measurements under superimposed high press., torsion bomb machine 80−85130
electric drive, vacuum-tight, with gear pump for corrosive liqs. pumped circulation 77−74376
electric lead-ins with composite seal for high pressure chambers 80−105665
electrical conductivity meas. of crystalline materials, high press. and temp. using buffer techniques *(German)* 79−93162
electrical conductivity of conducting liqs., gases, at high temp., press. meas. 80−62685
electrical feedthrough for gas pressures up to 10 kbar and low temps. 80−31787
electrolytic heating use in high-pressure chamber 80−17958
electromechanical high-press. torsion apparatus, for polymer testing 77−51005
epoxy resin as pressure transmitting medium, appl. to compression expts. on Si, MgO, and $ZrSiO_4$ 77−89496
EPR cavity sensitivity improvement 78−54419
EPR spectrometer attachment for studying materials in 120 to 350K. $1\text{-}10^4$ atm. range 80−105686
equipment for reaction kinetic meas. *(German)* 79−49244
ESR meas. at hydrostatic pressures to 60 kilobars 78−54418
ethylene polymerisation plant, high-press. equipment design 79−24746
extrusion, adaptation of conventional press, for hot and cold hydrostatic extrusion *(French)* 77−57344
far IR gas cell, high press., low temp. 77−30207
ferromagnetic resonance apparatus 77−51956
filling of dischargers with mixture of SF_6 and N_2 80−105668
fixed points for pressure calibration above 10 GPa 77−13765
flat-anvil chamber designed according to opposed anvil principle, thermoelectric force meas. *(German)* 80−90863
flow calorimeter for condensable gases, low temp. and high press., design and eval. 80−37033
flow calorimeter for condensable gases, low temp. and high press., computer program prediction and exptl. data comparison 80−37034
fluid pressure generation and measurement equipment, up to 2700 MPa 79−21763
fluids, simultaneous investigation of eqn. of state and elec. cond. to 0.2 Gpa 77−55337
free piston gauge 78−54385
fusion reactor tritium high press. equipment 77−50294
gas equation-of-state meas. interferometry 80−77810
gas flow test facilities, EEC intercomparison campaign, transfer standards 79−72979
gas high pressure cell for optical studies at low temp. and hydrostatic pressure 78−82016
gas thermal compressor, piston free, optimum characts. calcs. 79−54152
gas-discharge tubes, device for filling and sealing 79−35772
gas-operated pressure balance, rotational freq. dependence 79−54151
gaskets, anal. of pressure distrib. 80−86337
gauges, zeranin resist. for secondary meas. of high press., expt. *(Polish)* 77−65042
generation in large volume, up to 77 kbar and 2000°C 78−57972
glass capillary for high resolution NMR measurements at pressures up to 400 MPa 78−65950
glass-PTFE stopcocks for use at elevated temps. and pressures 77−10000
Hall effect measurements to 40 kbar under hydrostatic pressure in piston-cylinder device, 150 to 300K 79−67337
heat capacity measurement, low temp., of metals under press. 78−81979
high pressure cell construction with carbonado anvils *(Russian)* 80−4731

high-pressure techniques continued
high-pressure anvils, relationship of yield stress to press. attained at yielding and ultimate attainable press. 79−54150
high-pressure laser cell with a transverse excitation scheme 80−78859
hydraulic press. for developing 500 tons 80−105636
hydraulic pump for laboratory high pressure installations 79−93159
hydrostatic compression chamber, for galvanomagnetic effects meas. 80−47069
hydrostatic forming, novel industrial appls. 77−44191
hydrostatic liquids for obs. of NMR of ^1H at high press. and low temp. 79−2801
hydrostatic pressure cell, up to 90 kbars, elec.- and mag.- meas. appls. 79−17436
hydrostatic pressure testing device, tensile, upsetting tests 80−25959
hydrothermal solutions experimentation, new reaction cell 80−41555
inlet for elec. conductor into high-pressure chamber 78−74016
ion-molecule reactions, gas-phase, and high-press. mass spectrometer, review *(Japanese)* 78−64830
ionization chamber for spatial growth meas. in CO_2 77−46657
IR interferometer diamond anvil cell interface with beam condenser 80−86384
IR spectroscopy, gas cells, for high press. and temp. 77−38033
IR spectroscopy at very high press., refr. beam condenser for use with diamond anvil cell 77−71389
isobaric specific heat of solids, for pressures up to 250 MPa and 150-350K temps., measuring installation 77−76572
K-band cell for EPR-ENDOR studies 79−67336
laboratory for chem. engng. development 79−21507
laser system, with electron beam controlled discharge 78−5496
liquid compressibility meas. over wide temp. range 77−43265
liquid metal, simultaneous meas. of density, elec. cond., abs. thermopower at high temp. and high press. 77−1402
liquid MP determ. centrifuge cell 80−31783
liquid press. meas., up to 75 kb, from spectra of immersed ruby crystals 77−26321
liquid-solid interface transmission IR spectroscopy 80−98985
liquids, high-press. optical interferometry to 14 kilobars 77−49764
loading diamond-anvil cells with high-pressure gases 80−86338
low temperature, press. cells and hydraulic press working down to 10 mk 79−63229
low-temperature single crystal strong uniaxial compression apparatus 78−57973
manganin resistance gauge for high pressure meas. 77−10036
materials development by high press. technology *(Japanese)* 80−84863
materials synthesis at high press. 79−47645
mechanical press for Mossbauer spectroscopy at low temps. 78−21803
mechanical pressure generators, anal. 78−86287
metals, high press. expts., review *(Japanese)* 78−71790
metals, specific heat meas. method of low temperatures and high pressures 80−52246
micron-thick specimen preparation 79−17408
microwave cavity for EPR at high hydrostatic pressures 78−89518
miniature diamond anvil high pressure cell 80−237
miniature toroid high press. cell with superhard pistons 78−49858
mixture calorimeter, high press. *(German)* 78−16797
molecular beam mass spectrometric sampling, high temp. mols., review 80−52355
molecular fluorescence polarisation meas. at high press. 78−66576
molecular vibrational spectroscopy and conformational analysis 80−9758
Mossbauer apparatus for resonance studies at high press. and low temps. 78−49943
Mossbauer effect measurement apparatus for use at high press. and low temps. 77−67548
Mossbauer effect measuring installation for pressure at low temp. 77−77129
multichannel surface spark gaps 79−18436
nanosecond temperature-jump apparatus for high pressures 80−219
neutron diffraction meas. on liq. metal up to 1400K and 200 bar, technique and exptl. set-up 77−1064
neutron spectrometer appls. 78−49852
NMR high-pressure probe, high-resolution proton NMR 78−89517
NMR probe for high-pressure and high-temp. expts. 80−22403
NMR spectrometer modification for high pressures 78−45664
NMR spin-echo high-pressure system 78−58002
nonferrous metal, semi-brittle, high-speed backward extrusion using superimposed hydrostatic press. 80−84865
NQR, apparatus for study under high hydrostatic pressure 78−74038
opposed anvil type apparatus, using WC balls 77−5856
opposed anvils, yield stress calc. 77−57343
opposed-anvil high-press. devices, material strength effect 80−47068
optical cell for Raman scattering at low temps. 79−49247
optical cell for Raman studies of gases, liquids and molecular solids 78−12767
optical chamber with fixed pressure up to 16 kbar, single-window, 1.5-300K 79−35770
optical low-temperature chamber with fixed pressure, use of liquid N_2 80−57358
orifice metering installations for natural gas 77−84372
orifice plate meters, appl. to gas flow under high press. 79−68884
oxidation process development *(Japanese)* 79−29249
oxides, semi-sintered, as press. transmitting media 80−52259
phase equilibrium study cell, 220-300K and up to 6.7 MPs 80−62821
photopreionisation-stabilised discharge scheme for nanosecond excitation of dye vapour and metal halide plasmas 79−98982
photoresistor IR detectors for optical investigations at high pressures 78−21267
physical measurements under ultrahigh press., review *(Japanese)* 77−67457
piezoelectric transducer appl., for variable pressures up to 6×10^8 N/m^2 80−31785
piston-cylinder device for determination of melting curves of In, Bi, effects of asymmetrical friction 80−86292
piston-cylinder device for H_2 compression to 30 kbar 78−49853
piston-rotation technique for piston-cylinder devices 78−41324
plasma cutting at elevated press., underwater appl. 78−87507
polycrystalline cubic BN plunger chamber for high-pressure Mossbauer meas. 80−31786
polymers, deformation under combined action of shear stress and hydrostatic pressure, testing equipment 77−56184
porosimetry technique for up to 6 kbar, Hg porosimeters design 79−21761

high-pressure techniques continued
pressure apparatus, split-octahedron type, for X-ray diffraction studies at high pressure 79−49246
pressure balance standards, international comparison over 1 to 10 MPa range 80−105671
pressure balance standards of NPL and PTB, intercomparison expts. 79−21764
pressure calibration by resistance-jump transitions up to 500 kilobars 78−54388
pressure cell for neutron scatt. from liq. ^3He 78−14246
pressure reducer, piston type, for continuous pressure meas. up to 1 MPa 78−4602
pressure transmitting fluid, thermophysical props. *(Japanese)* 77−49739
pressure vessel for tensile testing in high-pressure gases at high temps. 78−44303
pressure vessel optical windows, testing up to 45 kbar 79−90016
pressure-jump apparatus suitable for repetitive experiments 79−17437
primary high-pressure standard, USSR 78−49855
proportional counter at low temperatures 80−23250
pulsed wire probe measurements, appl. to heat capacity and thermal cond. determ. 77−41613
pumps, piston and diaphragm type, for high press. use *(German)* 79−21762
quasihydrostatic apparatus, methods and results, high temp. *(Chinese)* 77−74417
quasihydrostatic pressures, up to 300 kbar at 0.1 to 200K, production method 78−49848
radiospectroscopy studies of phase transitions at high press., apparatus 80−19934
Raman matrix isolation spectroscopy 78−45721
Raman spectroscopy, diamond anvil cell method, weak Raman signals obs. 77−71383
Raman spectroscopy, matrix-isolation, high press. cell 80−272
recycle-flow calorimeter, 2 to 20 MPa 90 to 400K 80−42228
reflectance spectra, meas. press. to 70 kbar by micro-optic system 77−61133
registering superconducting transitions under high pressure by contactless methods 78−23191
resistivity meas. method for up to 50 kbar and 1000°C 78−57978
resistivity measurements using high-pressure cell, 13 GPa, 1.2K 79−80637
reverse-buckling safety discs, release pressure 78−89489
review of techniques for low temp. use 78−12709
rocks and minerals physical props. meas. *(Russian)* 77−70850
rocks elasticity and density simultaneous meas. *(Russian)* 77−70851
sample preparation lock for surface analysis in ultrahigh vacuum chamber *(German)* 80−52261
sampling interface employing stroboscopic extraction of atmospheric press. species into vac. 77−77858
seal, electrically-insulating high-pressure seal for use at cryogenic temps. 77−41633
seal for high press. and low temps., simple closure 78−4626
seals elastoplastic behaviour obs., for chemical apparatus appl. *(German)* 78−21160
secondary standard gauges for measurement up to 1 GPa 80−27289
shear press apparatus with roller bearing 77−41592
shear strength measurement installation 80−50787
shock tube for synthesis of diamond at high temp. and press. *(Russian)* 77−90298
sintering of metal powders, at 1 to 10 MPa, melting mechanism *(German)* 80−35122
sliding anvil device for high press. and large volumes *(French)* 80−47067
sliding anvil device for high press. generation 78−49849
sliding anvils apparatus for high temperature-high pressure studies 80−86317
solid-phase cell for 40 kbar, 1500°C operation, pressure and temp. distribs. 80−105669
solid-press. cell, generation of uniform press. and temp. distrib. 78−49857
solid-state research apparatus for pressures up to 200 kbar and temp. 2 to 1500K 77−71337
solidified gas constant-volume thermal conductivity meas. cell 80−31739
specific heat meas., at temp. up to 1700K under pressure, expt. on liq. Cs 78−51696
specimen cross section during low temp. compression, apparatus design 78−57940
spectrophotometer cell, UV, for meas. of liquids at high press. and temp. 77−53992
spectroscopic cell for quantitative IR absorption meas. *(German)* 78−12769
spectroscopy, high-pressure techniques and lab. equipment availability 77−57399
Speer carbon resistors as pressure gauges 80−95108
split Hopkinson pressure bar use in obtaining dynamic stress/strain data at const. strain rates *(Japanese)* 80−16630
spring-piston differential manometer 77−67456
standard gas mixture preparation at high pressures certification 78−93718
stopped flow apparatus up to 3 kbar 80−3350
stopped-flow apparatus for rapid mixing and study of two fluids under high hydrostatic pressures 80−98929
stopped-flow apparatus for study of fast reactions in soln. under high pressure 80−86335
strain gauge manometer for pressures up to 14 kbar *(German)* 77−26322
supercond. A15 cpds., high-press. synthesis 77−70022
supersonic flow electronic transition lasers, low-temp. and high-pressure, pulsed blowdown and electron gun facility 79−59723
surface structure analysis, at high press. by electron spectroscopy 78−73103
tapered anvil apparatus for achieving higher press., design 77−74419
temperature field distrib. determ. for high press. chamber 78−82001
temperature meas. in liquid He region 80−31748
tetrahedral type high press. apparatus, effect of intensification plate on press. *(Japanese)* 79−40590
thermal conductivity of low-temperature fluids, meas. using guarded parallel plate apparatus 77−22553
thermal neutron high press. sample container for diffr. and spectroscopy on fluids 79−46513
thermal neutron scatt. of condensed matter under high press. 79−37592

high-pressure techniques continued
thermophysical properties meas. of metals, submicrosecond-pulse-heating method 80−52220
torque magnetometer for vacuum-to-high-pressure H_2 environments 80−4746
transpiration mass spectrometry, of high temp. vapours 80−52356
triaxial loading apparatus, for determ. of time-depend. behaviour of rock 77−9538
triaxial testing cell for powders 79−74329
triple-stage opposed anvil type apparatus, with sintered diamond as last-stage piston 77−71336
turbine flowmeter for high press. 79−55431
turbine meters, appl. to gas flow under high press. 79−68884
ultimate shear stress meas. by modified impact viscometer at high pressures 79−18980
ultra-high pressure studies and the earth sciences *(Chinese)* 79−71479
ultramicrospectroscopy, mid IR, using gasketed diamond anvil cell 79−44955
undersea hot water storage system 80−45763
uniaxial press, for inelastic neutron scattering 77−35442
US measurements up to 9 GPa, press. cell 77−4140
US velocity measurement, liqs., pulsed exptl. arrangement, press. to 2000 atm. *(Russian)* 79−94427
vapour-liquid equilibrium, high pressure experimental technique 79−42227
very high pressure appl. *(Japanese)* 78−45644
very high pressure generation and meas. technical limits *(Japanese)* 78−45643
viscometer, applic. up to 4 kbar and 300°C 78−59515
viscosity measurement, using small volume inclined falling ball viscometer 78−1772
viscosity measurement method at high press. 80−69955
volumetric technique for water compressibility to 1.9 kbar 79−65134
wide-band optical-mechanical system for acoustic emissions meas. at high temp. and press. 78−1525
X-ray diamond-anvil cell, improved beryllium diamond support 78−30515
X-ray diffraction, at high pressure *(Chinese)* 78−26385
X-ray diffraction, energy dispersive miniature piston-cylinder apparatus 80−38870
X-ray diffraction, oscillating diamond anvils for high press. work 79−4209
X-ray diffraction at liquid He temps., high-press. apparatus 77−11442
X-ray diffraction examination of materials, B pellets preparation from powder 80−50569
X-ray diffraction multi-anvil apparatus for press. up to 150 kbar 78−1950
X-ray diffraction study, high temp.-high press., appl. to press. calibration above 100 kbar *(Japanese)* 78−24809
X-ray diffractometer, automatic four-circle, for high-press. struct. investig. 79−23495
X-ray diffractometer, high-pressure-low-temp. type, appl. 78−82089
X-ray diffractometer with high pressure cell, data collection measuring procedure 78−75495
X-ray stopping power, cavity theory verification by ionisation chamber 80−9476
Ar, compressed gas, PVT meas. at high press. 80−98927
BeCu pressure clamp cell, for low temp. specific heat and magnetisation meas. 80−17956
Bi foil pressure transducer, determ. normal stress components in solid state high pressure test cell 80−73378
CO_2, compression to 34 kbar, apparatus and technique, diamond anvil cell 78−74017
CO_2 high-pressure reinjection oscillator design and performance 80−78867
D_2 gas, thermal cond. meas., 2-36 MPa 80−64668
GaP high-pressure reaction synthesis 77−77372
H_2 gas, thermal cond. meas., 2-36 MPa 80−64668
H_2 sorption kinetic studies using high-accuracy volumetric device 79−56071
H_2-D_2 gas, thermal cond. meas., 2-36 MPa 80−64668
H_2-He, thermal cond. meas., up to 14 MPa 80−64669
He containment cell, melting expts. at room temp. 80−80025
He, liq., appl. of gas oscillation to pressurisation in storage vessel 80−57305
He purifier, automatic 79−58738
Hg melting line determ., latent heat method, high press. 77−37903
N solubility in liquid metals under pressure by droplet weighing method 79−86889
N_2, density measurement up to 1800K and 8 kbar, procedure 78−81947
N6d2-Ne discharge lamp, meas. method for partial H_2 press., selective gettering action 77−87775
NaCl primary press. gauge, failure of central force model 77−15492
Ni-Cr thin-film resistor pressure transducer for quickly varying pressure, expt. *(Polish)* 77−65041
O_2, isotopically enriched, prep. and storage under press. 79−29620
$Pb(Zn_{1/3}Nb_{2/3})O_3$, perovskite type, high-press. high temp. synthesis *(Chinese)* 78−68654
Si dry pressure-oxidation for low-temp. IC processing 78−7068
TiO_2, rutile, single cryst., high temp. compression in O_2 atmosphere *(French)* 79−51194
Xe hydrostatic medium for diamond anvil cells to 300 kbar press. 79−97402

high-temperature phenomena and effects
see also refractories
AB-type compounds, high-press. and high-temp. behaviour, review 78−22850
ablation, statistical characteristics of mass lost in thermal destruction, zero gas dynamic press. 78−83429
accommodation coefficients, of Na, Rb and Cs on Ni, 658-1095K 77−47666
acoustic noise from unflanged duct exit, high temp. effects on radiation impedance 77−84069
atom, UV photoelectron spectra at high temp., interpretation 78−17718
baddeleyite-corundum refractories, fused, elec. resist., 1300-2300°C 79−28345
basalts from Faeroe Islands, compressional and shear wave vels. at high temp. and press. 79−84244
biotite, temp. transformations, spinel formation 77−78163

high-temperature phenomena and effects continued
butadiene-nitrile elastomers, high temp., and press. chem. transformations *(Russian)* 79−52659
charcoal, catalytic graphitisation by gaseous species from Ca 80−11872
chemical processes, review, book contrib. 77−40545
chemical states at surfaces exposed to high-temp. vapours 78−11559
corrosion at high temp., review *(Japanese)* 78−72911
α-Corundum, enthalpy, 800-2300K 77−47592
crack growth at high-temp., fracture mech. appl., review 79−41628
diamond formation from hydrocarbon dissociation, Hugoniot data, high temp. and press. 79−47927
diamond-graphite equilib. line, from synthesis and graphitisation of diamond 78−24811
dichloromethane, high press. and temp. IR absorpt. spectra, stretching fundamentals *(German)* 80−47999
3,5- dimethylphenol formaldehyde resin carbon, catalytic graphitisation from various metals 80−11871
Drucker postulate verification at high temp. 80−30025
Earth mantle elements compounds and modifications, high press. and temp. thermodynamics 80−81874
Earth upper mantle, rare earths partitioning between silicate melt, amphibole and garnet peridotite 79−20775
enstatite, wet polycrystalline, high temp. flow 78−32082
fatigue, low cycle expt. at elevated temps., frequency effect 77−48553
fluorite-structure compounds, high-temp. elasticity of CaF_2, SrF_2 and BaF_2 77−81878
fuel droplet evaporation at elevated press. and temp., math. model investig. 77−52675
glass tank furnace, physical models, selection criteria for liquids to simulate melted glass 79−8263
graphite fibre epoxy composites, exposed to high temp., degradation of tensile and shear props. 80−81113
graphite melting point rel. to press. 78−24811
hard sphere gas, 2nd virial coeff., high temp. quantum corrections 77−76012
Inconel 625, creep rupture strength and corrosion in HTC in He *(German)* 77−77557
industrial gaseous environment characterisation, Brinkley method 80−93817
Ising model, high-temperature low field expansions extension 79−93045
JANAF thermochemical tables, thermodynamic properties evaluation and compilation 80−41959
LMFBR, post-accident containment, high-temp. behaviour of concrete 79−31000
longitudinal wave vel. and absorpt. in rocks and minerals at high press. and temp. 79−39704
metal matrix fibre reinforced composite, high tem. appl., creep, dislocation processes 77−48369
metal oxides, high temperature interactions with Re 80−16665
metallurgy, conf., Helsinki, Finland, June 1975 77−52295
metals, high temp. stress anal. by finite element method 80−96203
meteorites, primitive, thermal metamorphism, trace element loss from Allende heated to 1400°C 80−109401
meteorites, primitive, thermal metamorphism, trace element loss from Allende (C3V) heated to 1400°C 80−109402
microcreep, meas. device for high-temp. thin samples *(French)* 77−73388
minerals relevant to Earth interior geophysics, Hildebrand equation of state 80−56464
Mt. Burnet Dunite, high-temp. creep meas. 78−7624
Ni-base alloy 713LC, creep rupture strength and corrosion in HTR in He *(German)* 77−77557
Nimonic 80A, creep rupture strength and corrosion in HTR in He *(German)* 77−77557
olivine, hardness var. with temp., rel. to polycryst. yield stress 80−26500
olivine, optical absorpt. spectra and radiative heat transport at high temp. 79−79818
optical fibre high-temperature fatigue strength and OH^- stress-induced corrosion 78−1387
oxide crystal, IR spectra at high temps. 77−48155
peridotite, high-temp. anelasticity and elasticity 80−17256
phenol formaldehyde resin carbon, catalytic graphitisation from various metals 80−11871
primitive meteorites thermal metamorphism, trace elements loss from Tieschitz H3 chondrite 78−20765
PVC, rheology, viscoelasticity, panel discussion 79−3984
pyrographite, IR spectral emissivity at high temperatures 80−103505
pyrophillite, phase transform. promoted by water under ultra-high press., high temp., technical appls. *(Chinese)* 79−1499
pyroxene-garnet solid-soln. equilibria in $Mg_4Si_4O_{12}$-$Mg_3Al_2Si_3O_{12}$ and $Fe_4Si_4O_{12}$-$Fe_3Al_2Si_3O_{12}$ systems 77−81895
quartz, single crysts., Ar and O_2 interaction at high temp., surface struct. changes *(German)* 80−96725
quartz, synthetic hydrolytically-weakened α-β phase transform. effects on creep props. 77−43274
quartz sand, press. soln. expt. 77−60370
radiation pressure, Thomas-Fermi eqn. of state, high temp., coupling to high-density electron plasma 77−3925
regenerative heat exchanger high temp. behaviour, numerical model 77−62140
rocks, compressional wave vels. at high temps. and press. rel. to crustal low-vel. zones 80−41435
rocks, elastic props. experimental studies rel. to Earth crust press.-temp. conditions modelling *(Russian)* 78−96207
rocks, quartz-bearing and quartz-free, high temp. and press. effects on compress. wave vel. 78−32081
rocks, seismic anisotropy meas. under high-press., high-type conditions 77−49059
rocks, subsolidus attenuation at simultaneous high temp. and press. 78−3764
single laser diode CW output power limitation *(German)* 78−37886
solid-state reactions at elevated temps., X-ray diffr. study 77−47303
steel, C, EM excitation of US 80−33412
steel, Kh2G2P, high-temp. plastic strain influence on austenite transformation kinetics *(Russian)* 80−21004
steel, low alloy, coarsening at high temp. of small carbide particles dispersed in ferrite 77−52335
steel corrosion in NH_3 and NH_3-N_2-H_2 mixture at high press. and temp., testing unit 77−56174
steels, austenitic stainless, crack propag. rates under high-temp. low cycle fatigue conditions 80−21088

high-temperature phenomena and effects continued
thermal transport props., work of CODATA task group 77−45818
thermoelectric material, thermal cond. meas., 1100-2000K 78−24798
Ukrainian shield rocks, correls. of electrical parameters at high temps. *(Russian)* 79−8628
UV photoelectron spectra at high temp., interpretation 78−17718
Westerly granite, permeability changes during water flow at 100-400°C 78−40546
Ag_2Te, liq., elec. cond. at high temps. and pressures 79−11119
Al, atomistic images of field ion microscopy at high temps. 78−55792
Al, high-purity, high temp. creep, approx. determ. of parameters *(German)* 80−50688
Al, validity of Nernst-Lindemann eqn. over temp. range 293 to 925K 77−72695
Al_2O_3, high temp. gas phase equilib. formation enthalpy, dissoc., mass spectra 78−23925
Al_2O_3-Dy_2O_3, phase diagram at high temps. *(Japanese)* 80−50619
Al_2O_3-SiO_2 (3 wt.%), J-integral meas. at high temps. *(German)* 80−93624
$Al_2O_3+W(WO_2)$ reacts. in H_2, vacuum, high temps., reduction, oxidation conditions 77−16518
$AlPO_4$, high temp. behaviour up to liq. state, phase relations, X-ray diffr. and therm. anal. study *(French)* 80−10660
Ar, positron annihilation decay rates, high temp. behaviour 80−58389
As_2S_3, glassy, deep struct. changes, NQR obs., high-press. and temp. effects 80−54139
As_2S_5, glassy, deep struct. changes, NQR obs., high-press. and temp. effects 80−54139
Au, atomistic images of field ion microscopy at high temps. 78−55792
BN in contact with W, barrier layers for good high-temp. stability 79−70194
Bn, cubic, formation from hexagonal BN using Cao and Li_3N catalysts *(Japanese)* 80−54374
C_3, linear, high temp., rot.-vibr., anharmonicity, thermodynamic function calcs. 80−43830
CO_2, fugacity at high temps. and press. from exptl. decarbonation reactions 79−16439
CO_2, linear, high temp., rot.-vibr., anharmonicity, thermodynamic function calcs. 80−43830
CO_2-water vapour mixtures, 2.7 micron band absorption, 1000 to 2200K, 0.25 to 3 atm. 77−58006
CaF_2, fluorite, phase relations, to 60 kbar and 1800°C 78−84785
Ca_3SiO_5-Cr_2O_3(Al_2O_3)(Fe_2O_3) solid solns., elec. cond., 800-1000°C, hydration 80−54683
Co, impure, thermal cond., resistivity, total and spectral emissivity, linear expansion coeff., 300-1700K 77−47790
Co-Mn (0 to 45 wt.%), high temp. oxidation 80−35371
Co-superalloy, cast, high temperature fatigue behaviour 80−40485
Cr-Mo steel types JIS SCMV 2, SCMV 3 and SCMV 4, high-temp. high-cycle fatigue props., press. vessel appls. *(Japanese)* 80−93650
CrF_2, thermodynamic props. meas., electrochem. method 77−7874
Cu, atomistic images of field ion microscopy at high temps. 78−55792
$Cu_xMo_6S_8$, constitution diagram, 11-2000K 80−108407
EuTe, evaporation and reactivity 80−103469
Fe, cast, structural changes, due to pulsed action of high temps. and pressures *(Russian)* 80−7554
Fe close-packed phases, eqns. of state and implications for Earth core 79−20780
Fe-Cr-Al, kinetics and mechanism of high temp. S corrosion 80−25911
$(Fe_{0.5}Mg_{0.5})Ti_2O_5$, armalcolite, stability as function of press. and O_2 fugacity 77−64275
Fe_3O_4-Co_3O_4 spinels, phase diagram anal., thermodynamic props. 80−3009
β-$FeSO_4$, high-temp. polymorph, stability, mag. struct., mag. props. 77−43815
FeV_2O_4, free energies of form., 1400-1750K, electrochem. method determ. 79−43613
GaAs-$Al_xGa_{1-x}As$ DH laser, high-temp. degradation *(German)* 78−37884
H-He metallic, solid alloys, phase separation and thermodynamic functions calc., 0-19000K, 15-90 Mbar 77−43333
$HNO_2+OH \rightarrow H_2O+NO_2$ react. kinetics, at high temps. behind shock waves 77−44477
Hg, supercritical, elec. cond., four electrode method 80−62685
I_2, FCC metallic, self-consistent APW Xα electron-band calc., up to 22000K 77−39762
K_2CO_3 melt in combustion prods. medium, vaporisation of drops 79−57290
$KO_{0.5}$-$AlO_{1.5}$-SiO_2 system, activities calc. from vapour press. meas. and known data 79−91985
$La_xEu_{1-x}B_6$ solid soln., thermal cond., 300 to 2000K 80−59741
LiF, high-temp. behaviour of elastic moduli, comparison with MgO and CaO 77−11621
LiH, liq., density and surface tension, 982-1280K 80−59548
LuS_n, high-temp. vaporisation and thermodynamics 79−73325
Lu_3S_4, high-temp. vaporisation and thermodynamics 79−73325
Mg_2GeO_4, determ. of olivine-spinel transition up to 20 kbar and 1300°C 77−53044
MgO:CaO(SiO_2)(B_2O_3)(Cr_2O_3), effective of impurities on high temp. creep 80−40455
Mg_2SiO_4, ^{18}O self-diffusion expts., high-temp. creep implications 80−81870
Mn, corrosion, at high temp. in pure SO_4 80−50774
Mn_3O_4-Co_3O_4 spinels, phase diagram anal., thermodynamic props. 80−3009
NaCl, aqueous soln., direct calorimetric meas. of enthalpies, at high temp. and pressure 79−57286
NaCl:Sr, Cottrell effect and thermal decomposition 79−20351
NaF, high-temp. behaviour of elastic moduli, comparison with MgO and CaO 77−11621
$NaTaO_3$, high temp. structs. neutron powder diffr., comparison with $SrZrO_3$ and $NaNbO_3$ 80−88094
Nb, thermal expansion, 1200-2000K 79−55905
NbO_x, phase comp. on heating 2000-4000K 80−21267
Nb_2O_5, carbothermal reduction in N_2 intermediate phases 79−11773
Ni, 200, high temp. cyclic deformation and hardening 80−21055
Ni, dispersion strengthened, high-temp. cyclic deformation 80−21056
Ni, pure and alloyed, and fibre reinforced, at elevated temps. 77−52353
Ni-Al-Cr_3C_2, eutectic, directionally solidified, high-temp. oxidation 80−50775
high-temperature phenomena and effects continued
Ni-Cr-Nb-Al eutectic alloys, sulphidation/oxidation at high temps., corrosion mechanism 78−72934
Ni-Ti (1.6, 7.64 wt.%), monophase high temp. scaling, metallography study 80−21159
Ni_3Al-Ni_3Nb eutectic, directionally solidified, high-temp. oxidation mechanism 80−16544
NiO, physicochem. props. at high temps. *(French)* 80−39582
$PbSO_4$-PbO.$PbSO_4$(PbS)(SO_2), solid, EMF determ. of O_2 equilib. press., 1000-1100K 78−48683
Pt, emissivity, integral, meas., modulation technique 80−62672
Pt, wire, thermal cond., 900-1800K, elec. cond., 800-1800K 78−26845
$^{239}PuO_2$, stoichiometric, high-temp. deformation 80−81111
Rb, liquid, expanded, eqn. of state, transport up to 1700°C, 400 bar 80−2136
Rb_2ZnCl_4, ^{35}Cl NQR, incommensurate struct. phase transition 79−47401
SF_6 high-temp. electrical breakdown parameters 78−67567
Sb_2S_5, deep struct. changes, NQR obs., high-press. and temp. effects 80−54139
ScP, thermodynamics and high temp. vaporisation 80−88310
SiC, fracture toughness and high-temp. slow crack growth 80−81153
SiO_2-base cores, for superalloys, high temp. characterisation 80−10640
Ta, electrical resistance temp. depend. in solid and liq. states, 2200-4200K 78−10415
Te-In alloys, direct reaction calorimetric study, 737 to 1340K *(French)* 80−49382
ThO_x:Y_2O_3 solid electrolyte high-temp. vaporisation obs. 78−14456
Ti corrosion by a hot perfluoropolyether 80−93684
TiO_2, IR spectra, up to 1635K 77−48155
TmSe, nonstoichiometry, high temp. chem. and valence instability *(German)* 79−23743
UO_2, crystn., specific heat anomaly 80−84299
W fibre reinforced Ni, high temp. stability 77−48372
W fibre reinforced Ni alloy, high temp. composite development 77−48370
W fibre reinforced Ni composite, study at high temp. in O_2 and combustion gases 77−48567
W, surface, self-diffusion coeff., determ. from van der Mast's expt. data between 3000-3600K 79−11011
W wire, incandescent, motion and growth of K bubbles *(Hungarian)* 77−48460
Xe, thermal cond., 170-1300K and press. to 200 Mpa 79−82025
YbTe, evaporation and reactivity 80−103469
ZrC-TaC solid solns., high-temp. creep 79−11661
ZrN-NiO, solid-phase reactions 79−11774
ZrO_2 stabilised with lime, electrical conductivity *(Rumanian)* 80−65575

high-temperature techniques
see also pyrometers; refractories
abrasion test machine for refractories testing at high temp. 79−52505
abrasive and impact abrasive wear testing equipment for materials at elevated temps. 78−7136
absorption spectroscopy for temp. meas., principle 78−54375
acoustic thermometers with W resonators 79−32153
adsorbed molecule spectra meas. using high-temp. spectral vessel 77−41690
adsorbed species, catalytic reaction, high temp. IR obs. 78−88655
alkali metal alloy specimen preparation, for thermal analysis up to 1500°C 77−28948
alloy structure determ. by Mossbauer effect in high-temp. chamber 77−17982
analogue experimental techniques for high pressure and temp. *(Chinese)* 79−80638
apparatus and research at very high press. and high temp. 78−24811
arc heating of gas, plasmatron design *(Czech)* 79−68958
atomic beam source, employing radiant heating 78−330
Auger electron spectroscopy blanking resistive heating cct. 77−29078
autoclave, demountable, gas-balanced autoclave with chemically inert reaction vessel 80−86316
bellows valve of all-metal construction 77−49715
bending test apparatus for high press., high temp. 80−85126
bending test apparatus under high press. and high temp. *(Japanese)* 78−76795
bimetallic plates, deflection meas. during high-temp. heating 78−7134
black-body model for energy photometry 77−26300
Boyd-England high-pressure apparatus at NPL, design and construction 80−101804
calibration and temperature scales, based on Au melting point *(Rumanian)* 80−47061
calorimeter, for meas. of enthalpies of solids and liquids in 1200-3000K range *(French)* 77−13754
centrifuge construction 78−57938
ceramic minerals, exam. by X-ray diffr. *(French)* 79−96234
coal analysis, Cl_2 content determ. using British Standard high temp. method 80−85252
coal dissolution at short reaction times, fast-dump reactor apparatus 77−44575
composite materials, universal chamber for high temp. strength testing up to 2000°C 77−63858
contactless testing by EM acoustics 78−85095
α-corundum, enthalpy, 800-2300K, empirical eqn. 78−14478
creep testing of refractories, at different loadings, laboratory equipment *(Russian)* 78−19970
crystal growth from high-temp. melt, reaction cell for microscopic obs. 78−64457
crystal maximum temperature measuring system using irradiated diamond powder, engineering applications 77−33991
diamond, nucleation and growth, 55 kbar and 1450K 79−99087
diamond anvil press for high temp. and press. studies 77−10037
diatomic molecule production, using matrix isolation spectroscopy, optimisation 78−46462
dilatometer, high press. and high temp., construction and appl. 77−37844
dilatometer for measuring length changes in thin wires 79−97380
dilatometric measurements, high temp. method accuracy 80−73308
dilatometric measurements, high-temp., systematic and fiducial error estimation 80−101796
displacement meas. using capacitive transducers 78−172
DTA analysis, quantitative, curve-fitting, appl. to basalt 80−77144
dynamic testing of metals, alloys over wide temp. range, unit 78−60908

high-temperature techniques continued
education, positron annihilation in solids, high temp. vacuum chamber for source protection, crystal defect obs. 79−9068
effusive beam source, heterogeneous reaction type, chem. equilib. 80−52362
electrical conductivity meas. of crystalline materials, high press. and temp. using buffer techniques *(German)* 79−93162
electrical conductivity of conducting liqs., gases, at high temp., press. meas. 80−62685
electrolytic heating use in high-pressure chamber 80−17958
electron bombardment heater for heat transfer studies 77−30146
electron diffraction, by gases, review 80−52237
electron microscope, ultrahigh temperature, functional features 77−45923
electroplating method for high-temp. stress meas., fundamentals *(Japanese)* 78−15616
emissivity meas., apparatus 77−45844
EPR cavity for easily oxidised fluorides 80−77831
EPR multipurpose cavities, 1.6-1300K appl. 78−8430
EPR spectroscopy using CO_2 laser-heated sample holder 80−68233
exchange monitoring between flame and glass surface in furnace 77−26298
film heaters using sputtered Fe-Cr, Fe-Cr-Al(Si), lifetimes for 800 to 1000°C temp. range 78−215
film strain resistor for temp. up to 1000°C 77−37920
flame, atm. press., temp. meas. using thermocouple of Ir/Ir-Rh alloy 77−86314
flames, diagnostic techniques, ion-molecule thermochemistry 80−55664
flow tube, IR spectral meas. of gas phase species 80−52235
fluids, simultaneous investigation of eqn. of state and elec. cond. to 1350°C 77−55337
free radical reactions, photolytically initiated, high temp. kinetics meas. technique 80−61085
fuel cell pellet sample holder 79−88928
furnace, electric with RF coil, for NMR measurements up to 2000K 79−63214
furnace interior temperature meas., by means of radio transmission *(Czech)* 77−2659
furnace temp. distrib. measurement using thermocouples and wire bridge cct. 80−31758
furnaces, gas temp. meas. by multiple-thermocouple method 77−49728
gamma attenuation technique for thermal expansion meas. of solids. 80−31960
gas and vapour characterisation, conf., Gaithersburg, USA (Sept. 1978) 80−53910
gas diagnostics by spectral remote sensing 78−74002
gas temperature meas., stationary, thermal probe 80−95101
gaseous mixtures, equilib. at high temp., Raman scatt. obs. 80−45619
gases, characterisation, reactive flow in shock tubes, laser absorpt. spectroscopy 80−45618
gases and vapours, thermal conduct. coeff. meas. up to 2500K by differential technique 77−33989
geothermal well logging using 300°C hybrid IC 77−73895
glass-PTFE stopcocks for use at elevated temps. and pressures 77−10000
heat capacity, true, of high-melting cpds. pulse method and meas. unit 80−19953
heat capacity measurement, modulation method, thermal losses compensation 79−85144
heat treatment under ultrahigh vacuum conditions, apparatus design 80−52222
hemispherical integral emissivity meas., modulation method 80−62672
high pressure chamber, temp. field distrib. determ. 78−82001
high response fluctuating pressure meas. probe 78−13855
high-melting metal multicrystal hollow ingot growth 79−69978
high-pressure high-temp. methods and results with quasihydrostatic apparatus *(Chinese)* 77−74417
hot gases, convective heat transfer coeffs. to solid surface, moving thermocouple meas. 80−42230
HTGR fuel and graphite structure stress analysis methods and programs *(Japanese)* 78−74434
hydrocarbons, reactions, rate consts., temp. depend., photolysis, high temp. fast flow reactor technique 80−42231
impact fatigue test equipment for use at high-temp. 79−52492
instrument operation in adverse environments, conference, London (1976) 78−189
instrumental complexes developed as metrological guarantee 78−212
internal friction apparatus for freqs. up to 200 Hz, automated control 78−22308
internal friction meas. instrument for use at high temps. 78−13977
IPTS-68 values of secondary ref. pts. above 2000K 77−45819
IR pyrometry for measuring target temps. in solar furnace 77−41603
IR spectroscopic measuring cell, appl. to benzene adsorption on γ-alumina *(German)* 79−28757
IR spectroscopy, gas cells, for high press. and temp. 77−38033
IR transmission spectrophotometry of solid sorption systems, via cell with Si windows 78−299
IR tunable diode laser technique, temp. meas. of high-temp. gases 78−86268
laser Doppler anemometry of high-temp. industrial gas flow *(German)* 79−10618
laser Doppler velocimetry, high-temp., improved seeding method 78−9730
laser microscope, design details 80−90891
laser pulse heating, high speed pyrometry and spectroscopy, review of techniques 80−52225
liquid chromatography, automatic, Waters GPC 150C equipment, polymers appl. 79−10806
liquid metal, simultaneous meas. of density, elec. cond., abs. thermopower at high temp. and high press. 77−1402
liquids, opaque and diathermanous, total normal emissivity meas. at high temp. 80−102965
LMFBR high-temp. neutron detector test results 77−74909
LMFBR safety application of US thermometry 79−45400
low-cycle testing unit for use in vacuum and at high temp. 79−52503
manometer, glass membrane, usable up to 820°C 80−86329
mass spectrometer effusion for thermodynamic props. determ., surface evaporation effects and elimination 77−184
mass spectrometry, angular distribution, charact. of high temp. vapours 80−55769
mass spectroscopy, Knudsen effusion cells, thermodynamic and physicochemical bahaviour, review 80−52354

high-temperature techniques continued
measuring chamber for high-temp. investigations of opt. charact. of materials 79−21798
mechanical testing devices for high and cryogenic temps. 78−7137
melt dynamic viscosity meas., vibr. method 77−90519
melting point standards, secondary, for temp. range 2000-3000°C, chemical aspects of choice 80−52226
metal, group V, thermophys. props. determ. at high temp. using deform. vibrs. of plates 79−85143
metal, refractory, water vapour attack, immersion heater appl. in vacuum radiation furnace *(German)* 80−21184
metal foil seal production using seam welding 79−80597
metallic species, absorpt. and fluoresc., high temp. fast flow reactor technique 80−42231
metallography, high temp., attachment, appl. to graphite form. on supersaturated solid soln. surfaces 79−29306
metals, thermal props. at high temps. meas., acoustic method 79−14222
metrological cooperation between USSR and GDR *(German)* 78−4622
microcalorimeter, differential with thermoresistive elements for high temps. *(Russian)* 77−79098
microcreep, meas. device for thin samples at high temps. *(French)* 77−73388
microsamples, high-temp. mech. testing, unit 78−60904
microwave rotational spectroscopy 80−52236
minifurnace, 25 to 1600°C, for NMR measurements 79−49235
modulated heating-beam technique for thermal diffusivity meas. of solids 80−52221
moire gratings strain meas., long time high temperature appl. 80−38361
molecular beam mass spectrometric sampling, high press., high temp. mols., review 80−52355
molecular beam mass spectrometry, in situ anal. in crystal growth ambients 80−52357
molecular beam mass spetrometric sampling system, ion concs. in coal-fired MHD plasmas 80−52358
molecular shape determination, of high temp. species 80−52233
molecule, matrix isolation studies, high temp. 80−57399
MOSFET charact. for geothermal instrumentation, up to 300°C 78−73553
mould material deformation meas. at high temp., apparatus 78−3266
multimirror radiation furnace, optical-energy charact. investigation 80−17945
neutron diffraction meas. on liq. metal up to 1400K and 200 bar, technique and exptl. set-up 77−1064
neutron scattering expts. on liquid metals up to 1900K using sapphire container 79−63215
Nichrome, Kh20N80, varying porosity, effective thermal cond., 373-1400K, meas. method 78−75053
NMR probe for high-pressure and high-temp. expts. 80−22403
optical constants, high-temperature determination method 77−85680
optical cuvette, high temp., for transmission spectra meas. over 2-13 μm, 300-1600K ranges 79−2839
photoelectron spectroscopy, charact. of vapours oven heated inorganic solids 80−52239
photoelectron spectroscopy, of high temp. vapours 80−52238
photoionisation mass spectrometry, of high temp. vapours 80−52238
plasma spraying utilisation in research work 79−83117
platinorhodium-Pt thermocouples, 1000-1300°C range, cold junction electrode compensation 78−216
porous cylindrical specimens, effective thermal cond. meas. method, 373-1400K 78−75053
pressmold materials, stand for high-temp. mech.-props. test 77−56183
pressure generation in large volume, up to 77 kbar and 2000°C 78−57972
pressure vessel for tensile testing in high-pressure gases at high temps. 78−44303
processes and applications, high-temp., technological requirements, R and D, report 80−45222
properties of materials, meas. over wide press. range using laser heating system 77−77699
proton storage ring, NAP-M, for use to 300°C, mag. and vacuum system 77−65362
pulse heating method, 1500 to 1900K, Ti, heat capacity and electric resistivity 78−43139
pulsed plasma source temperature calibration spectropyrometer 77−7590
pyrometallurgy, industrial methods and research, review, book contrib. 77−40407
pyrometer, photon counting, 1400K to above 2200K within 0.5K and 1.0K 80−52232
pyrometer, radiation, for molten cast Fe, design and field test *(Japanese)* 80−98917
radiant heating, using paraboloidal reflectors 79−97392
radiating power, integral normal, high-temp. meas. technique, appl. to Nb 77−65667
radioactive waste conversion to glass, exptl. joule-heated ceramic melter 80−18471
Raman spectroscopy, review 80−52234
rapid pulse heating method for sp. heat of refractory metals near melting point 77−35704
reactor structural displacement and strain analysis by picture processing *(Japanese)* 80−78352
reference standards for radiation pyrometry, silver and copper freezing points 78−57888
reflectivity measurement of specular sample, Fourier transform spectrometer alignment 79−17498
refractories, integral radiant capacity, calorimetric meas. method 80−65259
refractory ceramic, deform. test apparatus and method *(Russian)* 78−35613
refractory metals, internal friction meas. from 20 to 2000°C in superhigh vac. 77−86249
regenerative heater, refined math. model 80−22365
research activity, thermonuclear fusion control, Hungary *(Hungarian)* 77−67443
resistance thermometry, review 80−52206
resistivity meas. method for up to 50 kbar and 1000°C 78−57978
rheogoniometer, Weissenberg-type, sample temp. meas. procedure 78−75113
sample cell for extended X-ray absorption fine structure meas. up to 1000°C 80−57454
sealed oscillating crucible viscometer for corrosive volatile liquids 77−15140

high-temperature techniques continued
secondary ref. stand., MP of Y_2O_3 77−45821
semiautomated torsion pendulum for high temp. damping studies 77−11153
semiconducting ceramic, meas. cell and setup for elec. resist. meas. 300-1400°C 79−30488
semiconductors, high temp. conductivity and Hall effect meas. 77−87786
sensing element comprising GaAs thermionic diode (1 to 400 °C) 77−37886
shock tube for synthesis of diamond at high temp. and press. *(Russian)* 77−90298
sliding anvils apparatus for high temperature-high pressure studies 80−86317
solar compound parabolic concentrator requiring monthly tilt adjustments 79−62104
solar concentrator, paraboloidal, flat receiver melting temp. calc. 77−45843
solar furnace, high temperature *(Japanese)* 78−45631
solar furnace temp. meas. using digital pyrometry system 77−37896
solar receiver radiative loss and eye hazard evaluation by Net-Radiometer 80−89673
solid electrolytic cell, meas. at 700K and higher 80−31760
solid-phase cell for 40 kbar, 1500°C operation, pressure and temp. distribs. 80−105669
solid-state phase transformation detect. by AC induction at high temp. 77−39674
solution calorimetry, appl. to enthalpy of formation of B_4C at 1320K 79−11814
space-shuttle thermal-protection coating, testing techniques at 870°C 78−35604
specific heat meas., at temp. up to 1700K under pressure, expt. on liq. Cs 78−51696
spectral emittance, meas. system at temp. up to 3000°C 77−22550
spectrophotometer cell, UV, for meas. of liquids at high press. and temp. 77−53992
spectroscopic techniques, achievement of high-temp. and material selection *(Japanese)* 78−45726
standard temperature lamps, with W ribbon filaments 80−95102
steel high-temperature ultrasonic testing *(Italian)* 79−96242
strain gauge, resistance type, appl. in study of thermal stresses 77−44442
stress measurement, temporary and residual stresses, high-temps. 80−64498
surface temperature meas. through radiance temp. and emissivity, algorithm for calc. 80−52209
surface temperature meas. using radioactive kryptonates *(Czech)* 77−45842
surface temperature measurement using infrared photoresistors *(Russian)* 80−82763
system characterisation, models, phys. and chem. reference data sources 80−41958
target exposed to intense pulsed electron beam, kinetic temp. meas. method 77−82524
TEM, tilting high temperature gas reaction chamber 80−101894
temperature measurement via pyrometry, effect of scattered light 77−26301
tensile testing, prolonged high temp. testing method with subseqeunt microscopic exam. 77−52581
tensile testing at high temp., self-locating grips design 79−52507
tension-compression fatigue testing machines, characterisation of materials under cyclic loading at high temperature *(French)* 78−15628
thermal conductivity meas. by heated filament method 77−33990
thermal conductivity meas. of refractories above 1000°C 79−202
thermal diffusivity meas. of molten salts, accuracy anal. 77−82525
thermal expansion at high temps., meas. via laser interferometry of two fibres 77−26270
thermal radiation sources for calibrating radiometers 80−17946
thermoelectrode emissivity, test method 77−89556
thermogravimetric method for recording mass transport of materials under action of radiant fluxes 80−17944
thermogravimetric system for investigating gas-metal reactions at elevated temps. 80−229
thermometer, high-temp., based on elec. cond. charges in ionic crystals 80−52203
thermometers, unconventional, Mossbauer, noise and US types 80−52202
thermometric characteristics of double-layer As_2Se_3-HgSe detector system 79−88952
thermophysical meas. above 2500K, apparatus 77−45845
thermophysical properties, conf., Dubrovnik, Yugoslavia (June 1978) 80−51944
thermophysical properties, temp. measurement methods at high temp. 80−52208
thermophysical properties dynamic meas. techniques 80−52219
thermophysical properties meas. of metals, submicrosecond-pulse-heating method 80−52220
thermostat system, automatic, for high temps. 79−6112
torsion deformation test apparatus for 0-1150°C range in different gaseous atms. 78−7123
transpiration apparatus, viscous, incongruently vapourising melts 80−52231
transpiration mass spectrometry, of high temp. vapours 80−52356
two-phase flow, high-temperature optical void probe 79−93705
ultra high vacuum, HT facility for heavy ion simulation of neutron radiation damage 77−57786
US apparatus for elasticity characts. and thermal cond. of materials 78−5705
US thermometers, nuclear fuel temp. profile meas., TRESON expts. 78−57955
vacuum chamber target, two-axes sample positioning mechanism 77−61076
vacuum furnace, regulated particle-delivery system 78−21139
vapour pressure meas. up to 5000K, pyrometric-laser heating technique 77−1239
vapour pressure measurement, phase transitions, equations of state, appl. of laser pulse heating 80−52230
vapour properties determ. above 3000K, by pulsed-electron-beam heating, appl. to Au 77−15567
vapours and gases, high-temp. characterisation, conf., Gaithersburg, USA (Sept. 1978) 79−40579

high-temperature techniques continued
variable-temperature apparatus for detect levels in Si semiconductor wafers 79−88951
vibratory magnetometer, for high temp. anal. of low stability carbon steel 77−28946
viscosity measurement, using small volume inclined falling ball viscometer 78−1772
viscosity mesurements at high-temperature by gas percolation through porous medium 78−1781
wide-band optical-mechanical system for acoustic emissions meas. at high temp. and press. 78−1525
X-ray diffraction apparatus, for in-situ high temp. water corrosion 80−90936
X-ray diffraction study, high temp.-high press., appl. to press. calibration above 100 kbar *(Japanese)* 78−24809
X-ray diffraction unit, for polycrystalline materials 77−39503
X-ray diffractometer furnace, temp. calibration using eutectic transitions of alloys *(Japanese)* 79−6128
X-ray diffractometers, high-temp. attachment 79−49355
X-ray small-angle scattering expts., temp. stabilisation of sample cell 77−13830
X-ray thermographic installation, for temp. recording up to 1500°C 78−74003
X-ray topography system, for investigation of semiconductor single crysts. 77−76261
Al_2O_3, optical consts., high temp. determ. 77−85680
Au-Si, liq. alloy, thermodynamic activity meas. by Knudsen-cell mass spectrometry *(French)* 80−10684
C fibres in tension, testing equipment 77−40497
CO_2 4.3 μ band radiance meas. of internal combustion engine gas temp. *(Japanese)* 78−29119
Co, viscosity, up to 2100K, vibr. method 78−38866
Cs vapour source, thermionic energy convertor with Cs-He gas controlled heat pipe 80−64791
Cu-Ge, liq. alloy, thermodynamic activity meas. by Knudsen-cell mass spectrometry *(French)* 80−10684
Cu-Ni-Sn, liq. alloy, mixing enthalpies determ. using a SETARAM high temp. calorimeter *(German)* 80−44324
Fe, viscosity, up to 2100K, vibr. method 78−38866
FeO-Fe_2O_3-SiO_2 system, molten, struct. by high temp. X-ray diffr. 80−49084
Ga and alloy high-temp. couplants for acoustic transducers 79−14195
Ga, gaseous reduction and extraction from mica 78−92216
$Ga_xAl_{1-x}P$ high-temp. solar cell with 0.3 eV band gap 80−21400
H high-temp. probe for proton magnetic resonance expts. 79−49234
Hf, 0.3 wt.% Zr, melting pt. and radiance temp. meas. by pulse heating method 77−53914
Ir, empirical thermal expansion formula for 440-2220°C 77−11709
$LaAlO_3$ perovskite electrolytes for high-temp. fuel cells 79−29467
Mo, fusion reactor appl., quick heating thermal fatigue test, ultra-high vac. environment *(Japanese)* 80−93716
N_2, arc jet enthalpy meas. by fast miniature total calorimetric probe 78−67486
N_2, density measurement up to 1800K and 8 kbar, procedure 78−81947
Na_3PO_4-$Ni_3(PO_4)_2$ system, phase equilibrium diagrams, crystallographic study, double orthophosphates *(French)* 80−93546
Ni *(Japanese)* 78−15617
Ni, viscosity, up to 2100K, vibr. method 78−38866
Ni-Ni_2B eutectic, high temp. X-ray anal. 80−71639
O+methane→OH+methyl reaction, photolytically initiated, high temp. kinetics meas. technique 80−61085
O_2 flow regulator, solid-state 80−57301
$Pb(Zn_{1/3}Nb_{2/3})O_3$, perovskite type, high-press. high temp. synthesis *(Chinese)* 78−68654
Pt, resistance thermometers for high temperatures *(Russian)* 78−57958
SF_6, arc, temp. determ. accounting for demixing 80−70057
SiN powder formation, in high-temp. N flow *(Russian)* 80−100818
Ta treated, graphite atomiser tubes, for high temp. AAS 78−73093
Te-In alloys, direct reaction calorimetric study, 737 to 1340K *(French)* 80−49382
$(U,Pu)O_2$ fuels, eqn. of state up to 5000K, high-temp. laser technique 77−27971
W, stand. ref. mat., thermal. cond. and elec. resist., 4-3000K 77−45820
Y_2O_3, laser heated pellet, melting point determ., secondary melting point standard 78−37011
ZrO_2, cell electrolysis of H_2O at 800° to 1000°C *(French)* 80−26024

high vacuum gauges *see vacuum gauges*

high-voltage engineering
see also high-voltage techniques
80 kV accelerating voltage transmission electron microscopes 80−27380
air insulation, predischarge-stabilised breakdown voltage *(German)* 78−63608
Antares laser fusion project, 300 kJ, 200 kA Marx energy storage module 80−68954
arc quenching system for transient and statistical flashover, fusion reactor systems 78−75455
four-electrode field emission pre-ionised triggered spark-gap switches, 10 to 30 kV, parallel operation 80−70075
fusion reactor implosion heating coil, radially fed, design, fabrication 78−55006
fusion reactors, Wendelstein VII and ASDEX, neutral beam injectors, HV power supply system, thyristor control 80−99332
high-density Z-pinch experiment pulse power supply, design and operation 80−70028
HV standard, principle and appl. 78−240
laboratory ion density due to repetitive impulse generation 78−65913
laser fusion, eight-beam system, high-voltage engineering 78−58492
long spark-gaps, breakdown voltage *(French)* 80−33828
low-pressure wire-cylinder corona discharge with wire at positive potential, and mag. field effect 79−94831
measurement devices, needle gaps, spark voltage charact. appl. *(Korean)* 78−1931
neutral beam accelerator electrodes, spark discharge protection, for fusion reactor 78−62609
ohmic heating system for TFTR Tokamak 78−55017
plasma valve design with liq. metal cathodes, high-power conversion/switching appls. 78−9865
polyethylene, elec. trees free radical ESR study 78−60393
protection of HV devices, parylene (vacuum deposited polymeric coating) appl. 80−108607

high-voltage engineering continued
pulse transformer-based HV system of streamer chamber 78−5095
rod-to-plate system, initial corona voltage calculated according to Townsend's Theory *(Czech)* 80−87961
Shiva laser, 25 MJ energy storage and delivery system 78−55015
spectrometer, high voltage power module and charge amplifier design 78−40826
superconducting magnet HV insulation problems 79−30512
switch, 100 kA, explosively actuated, 70 μs opening time 78−8984
transistor nanosecond amplifier for unipolar pulse signals amplification 78−12720
transmission line elec. and mag. field exposure effects and hazards 78−77083
UHV transmission line, biological effects obs., on plants and animals 80−17003
vacuum electric breakdown initiation 78−30509
SF_6 insulated switching installations and devices, gas chromatography appl. *(German)* 78−88668
SF_6 insulation, predischarge-stabilised breakdown voltage *(German)* 78−63608
SF_6-gas mixtures electric breakdown 79−37438

high-voltage techniques
1 kV SCR pulse generator for US pulse echo excitation 79−70290
600 kV repetitive stacked line transformer pulse generator 78−77935
AC Penning discharge, vacuum pumping characts. 78−93713
air gap corona pulse delay obs. and HV insulation design 79−19117
analogue safety data link, for Princeton Large Torus control room 78−54938
arc snubber using transformer core, theory 80−59315
capacitance meter operation with 10 kV Bias Isolation Unit 77−57364
clearing electrode control system for CERN ISR 77−38514
combined discharge in average press. gas using two HV pulse sources, gas laser development 80−44027
corona gaps, asymmetrical, as high-voltage rectifiers 77−57352
corona inception study on three-electrode systems, test *(German)* 77−7611
current meas. using capacitor type electro-optic voltage dividers *(Italian)* 77−26339
DC voltage meas., transducers using solid-state sensors 79−44916
double pulse production for pulsed elec. discharge prod. *(Russian)* 78−1946
dust deflection from optical components by 20 kV negative potential 79−76888
EHV choke coil measuring bridge *(German)* 77−18047
EHV synchronous generation for US pulse-echo systems 77−78011
electrical parameters meas. at HV levels by optical methods 78−24822
electron gun power supply protection 79−44989
electron microscope in situ deformation expt. limitations 79−60238
electron microscopes with supercond. microwave lenses, development prospects w.r.t. mol. imaging 77−10147
electron microscopy, total scatt. cross-section obs. 79−21859
electrostatic inflector and extractor for cyclic accelerators, HV expts. 78−50421
electrostatic kilovoltmeter errors in unearthed circuits 77−13773
electrostatic separator with built in HV generators 78−29693
equipment temperature meas. by IR instrument 77−10039
exploding wire voltage pulse rel. to conductor inhomogeneities 77−19798
fusion reactor, fibre optic telemetering for high voltage test stand 78−54939
fusion reactor, JET, high voltage network to load AC/DC pulse power conversion 78−58497
fusion reactor, pulser system, air-driven fibre-optic coupled for Los Alamos ZT-40 expt. 78−54943
fusion reactor, use of homopolar generator for inductive energy storage 78−54948
gap breakdown initiation by microparticle impact 80−96413
generation using chemically enhanced opening switch 77−49744
glow discharge theory 80−19629
heavy-current arc gap 78−87514
HF high voltage meas. by electro-optical effect 78−86301
high-voltage pulse generator, controlled spark gaps 78−5965
high-voltage subnanosecond electron beam generator 78−4733
HV nanosecond transient meas. from pulsed low inductance gas discharge, Kerr effect 78−51380
HV pulse controller and temp. monitor microcomputer-based, Kerr effect study appl. 79−6103
ion beam accelerator, multimegawatt, high-voltage power system, design philosophy, for fusion reactor 78−62613
ion beam generation increase through moving plasma boundary 80−63439
LEED apparatus, using high-tension source, construction 78−38591
liquid variable resistance, high-voltage technology appl. 77−37918
measurement using quartz electrogyration effect 77−41656
neutral beam high-voltage test stand, for fusion reactor 78−70632
neutral beam source 8 MW voltage series regulator, for fusion reactor 78−70631
particle physics DC separator design optimisation rel. to vacuum breakdown 77−26921
particle radiation therapy constraints and requirements 79−20622
petrol surface tension and flow, high-voltage effects *(Russian)* 79−83464
power supplies, voltage testing techniques 77−74422
power supply cct. for parallel feeding of multigap spark chambers 80−63456
power supply to EMIS isotope separator 77−14268
power supply to MEIRA isotope separator 77−13778
probe with subnanosec. rise time 77−10061
pulse forming transmission line charging 80−63419
pulse generator for modulation spectroscopy 78−77995
pulse power supplies development 78−8990
pulsed corona meas. in coaxial electrode structures 79−19114
pulsed electron accelerator, hydraulic surge damping with high-power water-filled shaping line 80−27837
pulsed field meas. using electro-optical device 78−4644
spark chamber pulse generator, with efficient irradiation of spark gap 77−34511
streamer chambers, HV circuit for two-pulse supply 77−6619
Tonus 2M accelerator, high-voltage pulse generator of stored energy 135Kj 78−5067

high-voltage techniques continued
trigger system, optically isolated, for pulsed high voltage plasma expt. 77−41650
vacuum beam diodes, repetitively pulsed 80−63386
vacuum feedthrough, description 77−26315
vacuum feedthrough, noise pick-up screening 78−24814
Van de Graaf generators, voltage grading improvement using resistor chain 77−54377
vertical single-pole earthed sphere gap, voltage measurement influence of neighbouring surfaces *(German)* 78−29880
water switches, streamer model 80−107002
X-ray tube supply, constant potential supplies 77−38068
Al ingot solidification by HV pulses, impurity distrib. and conc. region formation *(Russian)* 80−20919
Kr, hollow-cathode glow discharge with gas flow 78−67532
SF_6 breakdown distributions, low-value fractile determ. 78−67578
ZnS:Cu,Cl, electrolum. voltmeter design, accurate high-voltage meas. 78−24813

history
1178, June 18, interpretation of eye witnesses account of lunar crater form., meteor crossing Moon explanation 77−71174
1950s, philosophy and history of science 78−4452
acoustic microscopy *(Russian)* 77−75763
acoustic microscopy review, historical development 78−46877
acoustical measurements and instrumentation, historical review 77−45666
acoustics, golden age of 19th century 78−12526
acoustics, Kircher's 'Phonurgia nova' *(German)* 78−81788
acoustics, notebooks of Wallace C. Sabine 77−49545
ad hoc auxiliary hypotheses and falsificationism 77−33817
Adams, Roger, his role in American chem. education and research 80−4497
adaptive optics technology, historical review and prospects 79−59793
aerolites from Moon, translation of 1808 dissertation 77−87622
Age of Newton workshops in optics, mechanics and mathematics 77−87586
agriculture, expansion in late 19th century rel. to CO_2 levels in atmosphere 78−53717
air pollution events (up to 1970) 80−7975
air pollution levels in London, 1500-1900 period 78−44982
airline meteorology, early days 77−49544
Albert Einstein, physicist (1879-1955), review of his life and work 79−67132
albumen paper, manufacture and use 79−35515
alpha particles, 1903-1977, discovery, props., alpha decay 77−78942
American acoustics, conference, Washington, DC (Apr 1976) 77−45660
American acoustics, introductory comments 77−45661
Amici, G.B., contrib. to optical microscopy 77−57138
ancient Mesopotamia, barley harvest dates rel. to temp. 79−5597
Andulasian earthquake, 1884 December, 25, focal parameters, aftershock sequence 79−84178
Anger, Hal O., work at the Donner Lab., nuclear medicine appl. 80−42027
angle-resolved photoemission, expt., Adelaide Univ., 1908 79−30187
Ann Arbor school of astronomers, foundation, 1852-63 80−86062
Ansei earthquake, Japan, 1854 December 23, tsunami and crustal deform. *(Japanese)* 77−41001
Archimedes' mirrors, siege of Syracuse, feasibility *(French)* 79−62988
architectural acoustics to 1930 in America 77−45662
archives, use as generators of personal notes 77−87618
Argentine National Observatory and Charles Dillon Perrine 77−37702
Aristotelian philosophy, J.B. van Helmont's attack 80−31474
Aristotle's theory of falling bodies, pre-sixteenth century objections, for teachers 78−62026
Aristotle's theory of time, Renaissance critiques 77−82355
Aryabhata, 5th century Indian astronomer and mathematician, life and works 78−65741
Askesian Society of London, 1796-1807, social and institutional context 77−41450
astrolabes, Settala collection in Ambrosian picture gallery, Milan *(Italian)* 79−35132
astronomical archives, in Southern Africa 78−36473
astronomical compound eyepiece development, late 17th century 77−37704
astronomical ephemerides of the early seventeenth century 78−77659
astronomical events and Gospel records rel. to Christ's birth date 78−93127
astronomical observatory, Ole Romer, Vridslosemagle, Denmark *(Danish)* 80−8765
astronomical orbarium of 1582 made by Hieronymus Vulparius 77−37705
astronomical records from the Orient 77−45326
astronomical telescope, 152 cm reflector at Boyden Observatory, Orange Free State 80−12665
astronomy, ancient and mediaeval observational accuracy and theory 77−37703
astronomy, Fredericton, New Brunswick, mid-19th century 77−25955
astronomy, low light ground based techniques development 77−29657
astronomy, mechanical displays, early visual aids 78−36787
astronomy, observational, contrib. of Tobias Mayer 80−62438
astronomy, observational effects of defence science 78−36471
astronomy, the dark night sky, 'Olbers' paradox', history and resolution 77−33758
astronomy, William Herschel's 20 ft. telescope, discovery of original copperplate engraving 77−2340
astronomy and civilisation in time of Aryabhata I, 5th century AD 78−89289
astronomy history, Latin terminology relating to aurorae, comets, meteors and novae 80−62437
astrophotometric scale definition by N.R. Pogson 77−49306
astrophysics, America, E.C. Pickering and Henry Draper Memorial 78−86102
asymmetric C atom, case history for independent discovery, inductivist model 79−25821
atmospheric O profiles, early balloon borne obs. 78−16617
atomic physics, in USSR, development 79−9069
atomic theory, quantum theory, Einstein and Planck *(Russian)* 79−84933
aurora borealis, origin of metaphor 79−58512

history continued
auroral changes during 18th and 19th centuries, implications for solar wind and sunspot activity long-term vars. 80−98498
auroral research, the less known contributors 80−73157
auroras, catalogue from European sources, 450-1466 AD period 79−75010
aviation, work of Christiaan Huygens 80−31475
Bacon, Francis 77−13562
Ball, Sir Robert Stawell, Victorian astronomer and mathematician 79−88783
Basel earthquake, 1356 October 18, review, basic data 79−84181
Bavarian land survey, historical and modern outline maps *(German)* 77−2081
Beclere, Antoine, pioneer of radiation therapy techniques, biography 79−62982
Belgium, meteorological events in 17th century in Namurois *(French)* 77−64391
Benjamin Franklin, expts., theories and background 77−9845
Bergers, W.G., and J.M., work on dislocation theory 80−62440
Berthelot's first publication, 1850, subjection of liqs. to tension 78−32639
Bhabha first order relativistic wave eqns., historical development 78−14
biological effects of microwaves, research, medical appls. and hazards, 1940-60 80−86066
biomedical engineering education in Sweden and other Nordic countries 77−71169
biomedical equipment review *(German)* 77−77994
biomedical measurement *(Japanese)* 80−12288
biomedical radioassays, development 80−42034
biophysics in USSR 78−93506
Birmingham, England 1917/18-1976/7 winters, snow depth records 78−44890
Bjork-Shiley tilting disc heart valve 77−56525
Bohr's 1913 atomic theory, chem. aspects 77−67170
Boll, Franz, (1849 to 1879), investigator of retinal pigments, biography 78−20927
Boltzmann's H-theorem, was it capital η? 77−33812
Born's discovery of the quantum-mechanical matrix calculus 80−82615
Bose's second paper, conflict with Einstein, history of science 77−33813
boundary layer theory, history, book contrib. 77−46992
Brahe, Tycho, instruments and observational techniques *(Swedish)* 77−57139
Brecht's Galileo, changing perceptions of Galileo Galilei as scientific exemplar 80−51996
Bremmer, H., scientific work 79−62984
British Isles, systematic rainfall recording since 1677, tercentenary 78−44950
Brownian motion, account of discovery, for teachers 78−86090
Brownian motion, theoretical development *(German)* 77−49684
Brumberg, Y.E., biographical note 79−75309
Brunnow, Franz, role in training of astronomers at Ann Arbor, MI, USA 80−86062
building acoustics in America (1920-1940) 77−45663
CAI historical development outline 78−12502
California, great earthquake, 1857 January 9, felt effects, isoseismal map 79−84128
California, great earthquake, 1857 January 9, foreshocks 79−84129
calotypist-photographer correspondence (1841-7) 79−21515
Canadian radioastronomy, beginnings 80−8542
α Canis Majoris (Sirius) B, story of its discovery 79−84932
cardiovascular dynamics instrumentation evolution (1940-80) 79−83983
Carnot's contributions to classical thermodynamics *(Czech)* 77−32
Cassiopeia A supernova remnant, historical records 80−77430
Cassiopeiae A, supernova remnant, historical records 80−72792
Castle Frederick, eighteenth-century Nova Scotia observatory, history 78−40843
CERN, 25 years history and equipment *(French)* 80−98778
CERN, 25 years of physics, review 80−82626
CERN, international scientific cooperation *(Dutch)* 77−45669
Chamberlin-Moulton cosmogony, rise and fall 78−32641
Chamberlin-Moulton cosmogony 78−86104
charged cosmic ray particles, fiftieth anniversary of discovery, review 79−2448
charged particle counters in the pre-modern period, historical perspective 79−72190
chemical analysis, achievements of Joseph Louis Gay-Lussac (1778-1850) 79−49001
chemical bonding in inorganic complexes, quantum mech. ideas development and use 80−12878
chemical bonding in inorganic complexes, quantum mech. ideas development and use 80−12879
chemical compound structure, historical review *(Danish)* 79−9071
chemical formulae, historical development, review 78−73822
chemical rotation evolution, changing role of symbol 77−87621
chemisorption on metals, historical review 79−46920
China, earthquakes correl. with heliocentric planetary alignments 77−5136
China, Zhang Sui and first astronomical geodetic survey *(Chinese)* 77−64911
Chinese cosmology 77−33816
Christmas Star, identification as supernova in Aquila 78−81781
chronology of historical, scientific and technological events for teaching 77−41444
chronometers for maritime use, 1770-1920 79−39
cinematography, colour film processes and cameras, review, 1894 to date *(German)* 78−93773
climate correl. with wheat prices and wages 78−81346
climatic changes, role of anthropogenic changes in Earth albedo 80−81893
climatology, historical data on Hudson Bay rivers, content anal. 77−2224
climatology, review 79−16641
clinical physics, the lessons of history, review 80−62447
closed universe, S^3 topology, rel. to Dante's Divine Comedy 80−41980
Colombian alluvial platina, processing historical account 80−86060
colour centre physics, last fifty years 80−105487
colour vision perception in Greek literature 80−22184
comet discovering machine hoax, hydrocarbon bond detection 80−13
comets, ancient and naked-eye objects (2314 BC-AD 1970) 80−105181
comets, obs. in Greek and Roman sources before 410 AD 78−77658
communication satellites 77−64602

history continued
Compton currents, historical aspects and recollections 78−80018
computer development, review 80−4503
computer technology developments in relation to nuclear research 77−13566
concept acceptance in scientific research phlogiston theory example 80−27102
continental drift, Arthur Holmes' convection hypothesis 79−12559
continental drift debate, historical review 77−29277
continuity of scientific ideas, problems rel. to evaluation and assessment, review 79−44694
continuum mechanics and field theory, role of Thomson and Maxwell 79−17179
cosmic rays, first high-altitude meas. on balloons 79−80141
cosmogony, origin of planetesimal theory 77−87623
cosmological velocity-distance relation 80−12880
cosmologies of Lemaitre and Freidman in the modern context *(French)* 79−2581
cosmology, origin of Universe *(French)* 79−84931
cosmology, review 77−53715
course in liberal arts technology 78−86061
covariance principles, Einstein study, 1912 to 1916 79−40343
Crab supernova explosion of 1054, sighting in Near East 78−62028
Crussard, C., work on dislocation theory and slip of Al single crysts. 80−62443
crystal imperfections, early work, and forerunners of dislocation theory 80−62450
Dahlgren, amateur astronomer, reminiscences *(Swedish)* 78−36469
Dancer microphotographic emulsion identification 79−17177
Darwinian revolution, applicability of Planck's principle 79−62991
de Broglie's thesis, critical retrospective 77−13520
de Saussure, H.-B., first mountain meteorologist 79−21513
definitions of the science of metrology 80−52153
developments at the Cavendish Laboratory 80−37948
diffusion pumps 80−57321
dilution refrigeration 79−41
discovery and progress, role of scientific literature since ancient times 78−8209
discovery of cosmic microwave background radiation 80−57074
dislocation behaviour of Ag halide crysts., survey of post-war research 80−62449
dislocation theory for metals, research of A.H. Cottrell and colleagues, (1945-55) 80−62444
dislocations, TEM, work of Hirsch et al., (1946-56) 80−62445
Doppler effect, historical evidence for discovery by Friedrich von Hahn *(German)* 77−53727
Doppler research in the nineteenth century 80−86070
Draper, Henry, 'discovery' of O emission lines in solar spectrum 77−37706
DTA development in US, (1887 to 1976) 77−33815
Duane, William (1872-1935), life and work 79−30183
Earth's core discovery 80−105486
Earth bow shock, first evidence and early studies, historical introduction 80−85816
Earth density structure, Bouguer formula of 1749 rel. to gravity corrections 79−29692
Earth rotation, periodical fluctuations due to lunar tides, calc. by Einstein *(German)* 77−67169
earthquake in Kandalaksh Gulf region, White Sea in 1542 79−74854
earthquake in Odawara City, Japan, 1853 March 11, intensity, damage and magnitude from old documents *(Japanese)* 78−96146
earthquakes, Japanese, records in 'Diary of Librarians of Edo Bakufu (Feudal Government)' 78−65200
earthquakes in China, people's struggle against them *(Chinese)* 77−67171
East Anglia, England 1646 meteorite fall record 79−96978
East Anglian 'meteorite' of 1646, meteorological interpretation 80−68009
economic growth and energy consumption, in Britain, 1700-1975 79−79364
Edison the scientist 80−22179
Edo, Tokyo, history of disastrous earthquakes *(Japanese)* 78−11815
Edo earthquakes, Tokyo, 1855 November 11, study of historical documents *(Japanese)* 78−11814
educational course in physics, history and society 77−41429
educational courses, physics, for non-science students, rel. to history and arts 77−71165
Einstein, Albert, a correspondence with Adolf Schmidt, an archive discovery *(German)* 79−84924
Einstein, Albert, life and scientific work 79−71211
Einstein, character rel. to scientific contributions 80−36828
Einstein, early paper, ether in magnetic field *(Russian)* 79−84925
Einstein, light quanta, radiation, relativity in 1905 77−31
Einstein, quantum mechanics, conceptual problems 80−46783
Einstein's 1907 essay-translation 77−87619
Einstein's contribution to cosmology 80−77530
Einstein's contribution to twentieth century physics *(Chinese)* 80−17
Einstein's cosmological works *(Czech)* 80−27097
Einstein's General Theory of Relativity and press reaction 80−57075
Einstein's nonrelativistic work *(Czech)* 80−27095
Einstein's part in the development of quantum concepts 80−98781
Einstein's relativity paper (1905) and the electromagnetic world picture 78−16616
Einstein's route to general relativity theory *(Czech)* 80−27096
Einstein's second postulate 77−2
Einstein's sources of theoretical awareness *(German)* 80−90642
Einstein's theory of relativity and Lorentz's theory compared 77−3
Einstein's thinking in science 79−75315
Einstein's work and effect on atomic physics at the turn of the century *(German)* 80−90648
Einstein and Berlin physicists, 1927 to 1930 *(Russian)* 79−84927
Einstein and general relativity, historical perspectives 79−40316
Einstein centenary 80−46782
Einstein-de Haas effect, expt. works by Einstein 80−98783
elasticity, its development during the 17th and 18th centuries 79−17167
electric lamps, historical review of development 80−9977
electro-optics (1665-1979) *(German)* 80−15
electroacoustics (history to 1940) 77−45665
electrocardiological work of W. Einthoven (1861-1927) 79−35514
electrodialysis and its applications 80−55702

history continued
electrodynamics, classical, field, conservation principle, history, review *(Russian)* 78−36849
electromagnetic induction, history of Arago's, Babbage and Herschel's and Faraday's experiment 80−68013
electromagnets, high field, development review, mech. strength, performance limits 77−10073
electromotive force: Volta's forgotten concept 80−73143
electron cyclotron maser, historical review 77−38843
electron diffraction, 50 years 78−18505
electron diffraction, 50 years ago, lives, work of Davisson and Germer 78−30519
electron microscope historical development 80−68320
electron-dipole system, min. dipole moment for binding, historical development 77−78926
electronic distance meas. technology, surveying appl. 77−67410
electrostatics, quest for charging mechanism to end of 19th century 78−12525
elementary particles discovered during 1974-7 *(Czech)* 78−86103
elliptical orbits and inverse square law of gravity 80−46755
EM field theory development 80−16
EM induction discovery, teaching 79−44682
energy science and technology in Belorussian SSR, historical review *(Russian)* 79−35516
England, annual rainfall totals for 1725-1973 period 77−17207
SE.England, summer weather in 54 BC 77−49149
equivalence principle, evolution to general relativity 80−98779
Esintein's theory of relativity, acceptance in Canada 80−68012
Europe, climatic and human history rel. to Latin American comparison 79−2590
Evans, Thomas Simpson, 1777-1818, mathematician and astronomer 78−89287
Ewalds theory, X-ray crystal optics historical review *(German)* 79−50932
exponential law, concepts prior to 1900, review 78−86052
extraterrestrial radio emission detection, Jansky's original 1932 data 79−17144
far IR interferometry, (1950-76) 78−4456
far IR research, grating era (1925-60) 78−4455
far IR research, Rubens era (1892-1925) 78−4454
Faraday's denial of electrostatic action at a distance, conceptual and expt. bases 79−17180
Faraday and the concept of force 80−57048
Fermi and molecular min. dipole moment for binding electron 78−12
ferroelectricity 78−8208
fibre optics development 77−7194
Flamsteed, probable observation of Cassiopeia A supernova 80−62436
fluid dynamics, turbulence, statistical mechanics, progress in last thirty years 78−89290
fluid mechanics at Cambridge, book contrib. 78−57726
fluorescence spectrometry, anal. appls., historical review 78−93507
francesco Patrizi da Cherso's concept of space and its later influence 80−31478
Frank, F.C., development of theory of Frank-Read sources 80−62442
Franklin, Benjamin, exptl. philosopher, theory of electricity, for teaching 78−24630
Fraunhofer, Joseph, contributions to astronomy *(German)* 77−57142
Frederick Soddy and the practical significance of radioactive matter 80−86068
free electron devices for light prod., history, book contrib. 79−27147
French Revolution, du Ponts, Lavoisiers 80−57051
Fresnel's classical papers, history and present appls. *(French)* 78−37800
fuel cells, development 79−70448
Fulton's orrery, 19th century instrument to demonstrate planetary system motions 78−69695
fundamental physics research in India in last three decades 79−17178
Galileo, first telescopic obs. of Moon (December 1609) 77−29978
Galileo, satellite predictions for Jupiter 79−88784
Galileo's theory of motion, conceptual changes in period 1604-1610 77−82356
Galileo's tidal theory, reassessment 77−29980
Galileo's two bodies falling through air, numerical anal. for teaching 80−17755
Galileo and Aristotle re-assessed 77−49541
Galileo and Tower of Pisa expt., discussion 78−49582
gas transport, in synthetic polymer membranes, history 78−76912
gaseous nebulae, riddle of spectra, history 80−8676
Gassiot's cascade, 19th century discharge tube demonstration 80−77586
Gauss, Carl Friederich, correspondence on heliotrope and geomag. meas. *(German)* 77−67168
Gauss, C.F. Contrib. to astronomy 78−19
Gay-Lussac, biography 79−25815
general relativity, events leading up to 1919 eclipse test, book contrib. 80−22249
general relativity historical development *(Hungarian)* 77−26224
Genroku earthquake, Japan, 1703, tsunami inundation heights on South-Kanto coast *(Japanese)* 77−2121
geology, methodologies of Gilbert and Chamberlin 79−17182
geothermal technology, development into an exact science 80−61781
Gibbs phase rule, history and development *(German)* 77−78943
Gilbert, Grove Karl, 1843-1918, life and contribs. to geomorphology 78−45451
glaciers structure, obs. by Forbes and Agassiz and dispute over priority 79−17181
gravitation, as Newton saw it, historical background for teachers 78−4436
gravitational radiation, Albert Einstein's papers *(Polish)* 79−75313
Gray, Stephen (1666-1736), astronomer 80−77601
Great Debate of galactic astronomy, actual proceedings 77−29979
great year in Greek, Persian and Hindu astronomy 78−81790
Grigg, Emanuel Radu Newman, (1916-1976) radiologist and historian, biography 80−42026
group theory, historical development and appl. *(French)* 80−25
group velocity, W.R. Hamilton's investigation 80−17815
growth of science, review of measurement indicators 79−58519
guest star of AD 1408, Japanese record 80−90641
Hall effect, discovery and applications 80−31477
Hall effect discovery 80−27099
Hamiltonian dynamics, integrable and nearly integrable systems historical review 78−93521
history continued
hardness, attempts to define, measure and use (1390 BC to AD 1925) 79−92916
Harriot, Thomas, 1560-1621, biography, astronomical instruments and obs. 79−35512
Harriot's lunar maps drawn in 1609 and 1610 78−81783
Hawking, Stephen and black hole studies 78−8042
heart valve bioprosthesis, devel. from xenograft (1965-77) 77−56528
heat, Rumford's theory reassessment 77−57292
heat capacity of crystals and the vibrational spectrum, historical review 80−57071
Heisenberg's work on anomalous Zeeman effect and multiple spectra of atoms 78−70784
Helmholtz, H. von, evolution of empiricism, study of a universalist 78−8212
Henry Norris Russell, and Hertzsprung-Russell (H-R) diagram 78−69957
Herschel-Talbot photographic pioneering correspondence 79−97168
Hertzsprung-Russell diagram, discovery, meaning, development appl. 78−45322
historical accounts, solar and lunar 79−80411
history of industrial meteorology and weather modification 77−49542
Holden, Edward S., founder of Astronomical Society of Pacific, California-Wisconsin astron. connection 79−75310
Hopi Indians astronomy, social and theological aspects 78−36472
hot electron physics 78−26869
Hungarian development in the use of radioisotopes *(Hungarian)* 80−90646
Idrija earthquake, Yugoslavia, 1511 March 26, seismological parameters reconstruction 79−84180
image formation theory, work of D.S. Rozhdestvenskii 80−18999
Inca people (Peru), evidence of astronomical knowledge *(Swedish)* 78−32640
Indian epicyclic astronomy, history and chronology of treatises 80−62448
Indian observatories and 'instruments' built by Jai Singh 80−17490
industrial meteorolgoy and American Meteorological Society 77−49543
industrial weather service, starting difficulties 77−53099
inelastic electron tunnelling spectroscopy, past and future 78−90255
inert gas solids, research history, book contrib. 77−49547
inertia, concept development from Aristotle to Newton 78−81786
inorganic micro and trace analysis, historical perspectives 78−81784
Institute of Optics, Univ. or Rochester, 1929-79, brief commemorative 80−4501
instrumentation, History of Sciences Collections, Royal Swedish Academy of Sciences, catalogue 78−81789
internal cohesion of liquids, Reynolds' work 79−58511
International Union of Crystallography, early history 77−17738
interstellar molecules, pioneering investigations 1935-42 period 78−69855
ion selective electrodes, review 78−85165
ionospheric pulsed sounding, historical review 77−5395
Japan, historical earthquake records 77−25659
Japan, map of historical earthquake disaster areas 77−41003
Japanese old dates, first day of disputed lunar months, discussions *(Japanese)* 78−16620
Japanese photographic education history and status 79−92910
Johann Georg Soldner (1776-1834), forgotten bicentenary 78−81787
Johann Georg von Soldner and the gravitational bending of light, with an english translation of his essay on it published in 1801 79−17176
Johannes Hevelius (1611-1687), Polish astronomer 77−26120
John Goodricke and variable stars 79−49005
John Tyndall's demonstrations on sound (1854-82) 77−22362
joint replacement development 77−90960
Joseph Everett, and King's College Observatory, Nova Scotia 79−34
Joseph Henry (1797-1878) *(Czech)* 79−44689
Kelvin, background, teaching motivation, demonstrations 80−42025
Kepler, rejection of solid celestial spheres 80−36830
Kepler's celestial mechanics, dynamical theory 79−88787
Kepler's star of 1604, translation of original description 77−33536
Kepler and Galileo, correspondence during late 16th and early 17th centuries 78−20934
Kepler and Mars, construction and rejection of first oval orbit 78−62027
Kerr magneto-optical effect, historical background, and modern appls. 77−69806
Kilmartin Stones, lunar observatory hypothesis reassessment 79−96927
kinetic theory of gases, early development 80−17782
King's Observatory at Richmond 77−67033
Kropotkin, Pyotr Alekseevich (1842-1921), meteorologist *(Russian)* 79−97167
Kuhne, Friedrich Wilhelm, (1837 to 1900), chem. processes in retina, biography 78−20928
Lambert, J.H., self-taught scientist, life and work on cosmology 77−82354
Lambert, Johann Heinrich, 1728-1777, contribs. to philosophy, mathematics, astronomy and cartography *(German)* 79−17174
Laplace, P.S., chronology and citations of early work, 1770-1773 period 78−93505
Laplace (Runge-Lenz) vector, origins 77−13565
laser development, recollection by Townes 79−21517
laser spectroscopy, historical perspective 80−52331
lasers, historical evolution 80−91807
lasers, influence in biological and medical research, review 80−26318
Latin America, climatic and human history rel. to European comparison 79−2590
lens design without a computer 79−86235
Levi ben Gerson on instrumental errors and transversal scale 78−21
liberal arts physics, history and philosophy, relevance 77−22348
Lichtenberg figures 79−44693
Liege, Meteorological events in the 15th century *(French)* 79−2328
liquefaction of air, from Cailletet and Pictet to microkelvin 79−40
liquidons and gasons, continuity of state historical controversies 80−12882
Lisbon earthquake, 1755, isoseismal map from Spanish data 79−84179
Louis de Broglie's thesis, conceptual background, comment 77−87620
Louis de Broglie's thesis, conceptual background, reply 78−13
lunar crescent first visibility prediction 78−24442
lunar megalithic site in Kintyre, survey 79−96929
lunar megalithic sites in Britain, reconsideration 79−8854
lunar obs. of crater Linne, possible var. rejected 77−78680
lunar rotation, development of understanding 80−57064

history continued
lunar transient phenomena, catalogue of observations, 1178-1977 period 79−21208
lung imaging with radionuclides, history 80−42035
Lyapunov, M.V. (1820-68), work as third Kazan astronomer (1840-55) *(Russian)* 79−88789
magnetism, developments during past 25 years, personal reminiscences 80−36829
magnetism from Maxwell to discovery of electron spin *(German)* 79−25816
magnetopause, development of understanding 78−61667
mammographic imaging, historical review in terms of image quality and reduced radiation dose 80−41229
Mandel'shtam and sound propagation in microscopically inhomogeneous media 80−101704
Marat, Jean Paul, medical use of electricity 80−17781
Marconi's scientific activity, role of his discoveries in radio research 79−17172
Marquis de Charbert (1724-1805), biography and link with Louisbourg Observatory 80−68010
Mars, surface markings, change in opinion on nature, 1877 to 1914 period 79−80406
Mars satellites, history of discovery 78−89099
Martian atmosphere, W.W. Campbell's spectroscopic study 77−71047
Martian satellites, history of discovery and positional obs. (1877 to 1977) 78−89101
mass spectroscopy, history of development 78−56928
mathematical manuscripts of Nathaniel Torporley and Thomas Harriot 77−82357
mathematical physics, success and failure viz. Kolmogorov-Arnold-Moser theorem, gravit. collapse, singularities, matter stability *(German)* 78−65744
of mathematics, causal and formal logic unification 78−77639
mathematics, renaissance of empiricism 77−1
mathesis universalis, philosophers conception from Descartes for Leibniz 80−31479
Maunder sunspot minimum, 1645-1715 period 77−71103
Max Born, biography, review of contributions to physics 78−86100
Maxwell, development of ideas 80−27087
Maxwell, discoveries relevant to wireless and colour reconstruction 80−27093
Maxwell, diversity of interest across phys. sciences 80−27092
Maxwell, James Clerk, (1831-79) 80−27090
Maxwell, J.C., scientific contribs. and upbringing role 80−27091
Maxwell's inaugural lecture at King's College (1860) 80−27088
Maxwellian electrodynamic theory, history from eqn. discovery to mag. monopoles *(German)* 78−65791
Mayan astronomy, depth of knowledge and archaeological evidence 80−27098
Mayan astronomy, Venus studies 79−88782
Mayer waves, history and methodology 79−29537
measurement systems, ancient to SI *(Norwegian)* 77−33972
medical applications of nucl. physics *(French)* 78−45453
medical external counting procedures 80−42033
medical use of Ga radionuclides 79−53955
medicine, early 2D reconstruction and recent topics stemming from it 80−86029
megalithic astronomical alignments, significance tests 79−96928
megalithic astronomy, statistical significance of astronomical orientations 78−36475
megalithic astronomy 77−33759
megalithic sites in Shetland, surveys 78−36474
Mercury craters, discovery from Earth (in 1901) 78−53847
Mesoamerican calendrical systems chronology reconstruction 78−81782
Mesopotamia, city wall and street orientation rel. to winds 78−49074
metals, electron theory, work at Univeristy of Bristol, 1930-37 80−57068
metals, quantum mechanical electron theory develop., 1900-28 80−57065
meteor astronomy in 18th century terrestrial comets and theories of Thomas Clap 77−74017
meteorite falls, science and social intelligence about anomalies 79−40346
meteoritics, early chemical and mineralogical work 77−71175
meteorological events between 1574 and 1609 from journals of Pierre de l'Estoile *(French)* 79−58510
meteorological notes from Charles Darwin's voyage on the Beagle 79−17173
meteorology, 350 years of development 78−44970
meteorology, chronology of development 78−45452
meteors, meteor showers and meteorites in Middle Ages, from European mediaeval sources 78−86105
MHD power generation, closed cycle 80−45717
Michelson, Nobel Prize winner, work including Michelson-Morley expt. 77−13563
Michelson experiment seen 90 years after first execution *(Italian)* 79−17175
microchemistry *(German)* 78−81785
micromagnetics and domain theory, developments from 1930 78−68288
Miksa Hell, Hungarian astronomer *(Danish)* 80−8766
modulation meter development, special features, calibration *(French)* 77−53948
molecular biology, origins, autobiographical review 80−57052
Moon, radar contact in 1946 80−85866
Moon surface features nomenclature, reason for name Aristarchus for brightest crater 79−49004
Moseley's expts.: Kα line freqs., rel. to at. number, reinterpretation 80−82616
multipurpose radiometer, development for thermal-vacuum testing at Johnson Space Center 80−90894
N-particle problem, reduced density operators, theory, historical review 79−5945
N-ray affair 80−86069
N-rays, 1903-1906, expt. investigation of spurious radiation, for teachers 77−33814
N-rays, work of Blondlot and assistant (1903) 78−49626
Nabarro, F.R.N., dislocation physics research 80−62441
N.American astronomy, seventeenth century 78−28907
nature, unity of, as an incentive to research *(German)* 80−77533
nebulae, William Herschel's early investigations 80−12876
Neptune, obs. by Galileo, (1612 and 1613) 80−105485
Neptune, ring, observational evidence in 1846-7 from Lassell and Challis 80−67652
Neptune ring, history of obs. 78−69745
history continued
Netherlands National Institute for Nuclear and High Energy Physics, exptl. programme *(Dutch)* 77−46475
neutrinos, early experiments 79−80408
neutrinos, historical review 78−89288
neutron dosimetry by thermoluminescence dosimeter 77−60262
neutron scattering research, early developments 79−44696
neutron transport theory, historical review 79−58659
New England, 1816, snow and frost in year without summer rel. to Tambora volcano eruption 80−4089
New Madrid earthquakes, 1811-1812, archaeoseismology 79−84130
Newcomb, Simon, American astronomer, 1835-1909, life and works 78−93504
Newton, particles and concepts of force, discussion for teachers 78−4437
Newton, Sir Isaac (1642-1727), symposium (Cagliari, Italy, 3-5 October 1977) 79−62986
Newton's telescope, review of design for teachers 78−8187
Newton's views about space and time 79−38
nineteenth century British atomism, A.W. Williamson and atomic theory 78−32637
non-Euclidean geometry and physical basis, Galilean geometry and relativity, book 79−62989
nonverbal thought in technology, review 78−8210
Nova Tauri 396 AD, identification with V471 Tauri *(Russian)* 79−101162
nuclear energy, historical review of peaceful use in Belorussia *(Russian)* 79−35517
nuclear fission, discovery 80−57063
nuclear instrumentation, historical perspective of early detectors and counters 79−72189
nuclear medicine, computer appls. 80−42037
nuclear medicine, tumour-localising radionuclides in retrospect and prospect 80−42036
nuclear medicine in the UK 80−42039
nuclear power plants development *(Croatian)* 77−34479
nuclear pulse propulsion, historical review of advanced consent 80−36475
nuclear reactor development, secrecy and simultaneous discovery, 1938-45 78−12523
nuclear reactor pressure vessels, pre-stressed concrete, historical review 79−601
occultations of planets by eclipsed Moon, 100 BC to 3000 AD period 77−49319
H.C. Oersted, first spark of electrotechnology, biography *(French)* 78−69955
Oklo natural nuclear reactor, discovery and reactor parameters, geological formation 79−2240
'On the theory of the Schrodinger equation', Leontovich and Mandel'shtam, 50th anniversary 79−49090
online isotope separation, ISOLDE-0 facility 77−22364
operational arguments, occurrence in history of physics *(German)* 78−12527
optical fibre information transmission, development since 1966, review *(German)* 77−50760
optical instrument manufacturing, cyclical growth characteristics and prediction 79−76862
optics, contributions of Isaac Newton and Carl Friedrich Gauss *(German)* 78−4453
origin of the elements, review 79−97118
Oxford, England, private records of rainfall in 1767-1814 period 78−44948
palaeoclimatology, overview, and European air temp. trends *(German)* 79−16639
Paris Observatory 80−77288
parity nonconservation, discovery and nondiscovery, history 80−370
partons, ancient Greek theory 77−64910
partons, similar concepts in ancient Greek, Hindu and Chinese philosophy, for teaching 78−54143
pecked cross symbol in ancient Mesoamerica, possible significance 79−53954
Pecs University Biophsyics Unit, Hungary, 25 years of radioisotope appls. *(Hungarian)* 80−90647
Peierls and theoretical physics, symposium, Oxford, UK, (July 1974) 77−64909
Peirce's theory of the geometrical structure of physical space 78−28906
pendular motion theory, pre-Galilean era 79−37
Periodic Comet Halley, historical records rel. to orbital evolution tendency *(Chinese)* 79−16886
phase transitions, theory 79−44695
philosophy of science, theories as historical entities 77−67172
phoenix of nature, fire and evolutionary cosmology in Wright and Kant 79−5764
photographic nucleonics history, record of lost opportunities 78−65986
photographic researches of Hurter and Driffield 80−22181
photographic science, 1928 to 1978 79−58513
photography, contribution of W.H. Fox Talbot 78−17
physical acoustics, history and future, review 77−49548
physics, high school course, slide/transparency presentation 77−41442
physics, quantum mech. appls., history 77−18773
physics education, history and quasi-history 79−97130
physics teaching methods, of Joseph Henry, biographical review 79−44692
physiological acoustics, Ohm-Seebeck dispute and work of Helmholtz 77−57141
picosecond light pulse techniques, historical overview of rapid phenomena meas., book contrib. 77−65026
Pierre Gassendi, 17th century, early mechanics and philosophy 78−62025
Planck's law and the light quantum hypothesis 77−13564
plethysmography over past 30 years 78−31933
Pluto, discovery and known data (book) 80−82591
Poincare's conventionalism, origin and significance 78−86109
Poincare's conventionalism of applied geometry 78−86110
Poincare and cosmic evolution 80−57073
Poland, teaching of history of science and technology in Polish higher education 78−32638
Polish mechanics, history before 1918 *(Polish)* 78−20930
Polish Physical Society, 1920 to 1939 *(Polish)* 78−54145
ponderomotive forces, past controversies, discussion 79−41263
powder metallurgy, applications, history and development 80−68014

history continued
Prague, Czechoslovakia, meteorological obs. since 1775 at Clementinum 78−49075
Priestley's mind, synoptic nature, electrical thought 79−84930
probability theory, Jeu de Rencontre, critical elaboration of de Moivre's resolution *(Italian)* 80−4499
probability theory, Jeu de Rencontre, work by Euler 1751 *(Italian)* 80−4500
probability theory, Jeu du Treize, demonstration of Nicolas Bernoulli's formula *(Italian)* 80−4498
projection microradiography, historical development and applications 80−37138
psi meson, history and significance 79−80409
psychological and physiological acoustics, history (1920 to 1942) 77−45664
Ptolemaic system, success as kinematic predictor of planetary positions 77−78941
Ptolemy, Galileo, and scientific method 79−25819
Ptolemy (2nd century astronomer), reassessment 79−67131
Pulkovo Observatory, astronomical activities 78−81538
pulsilogium of Sanctorius for pulse rate meas. 79−71215
PWR development 79−93811
quadrupole mass spectroscopy, book contrib. 77−22363
quantitative analysis techniques appl. to elementary particle weak interaction theory 79−53953
quantum electronics and Einstein's theory of radiation 80−98782
quantum field theory, notes for history 78−28904
quantum logic, props. of states 80−12947
quantum mechanical tunnelling, historical survey 78−54141
quantum mechanics, development and Heisenberg's role *(Polish)* 78−89291
quantum mechanics, meas. problem 80−12948
quantum mechanics development, work of Heisenberg 77−9844
quantum theory, hidden variables controversy 79−62975
quantum theory, wave-corpuscle duality *(German)* 80−68016
Quetelet, A.L.J., life and spread of science in Belgium during 19th century *(French)* 78−65742
radiation chemistry in Czechoslovakia, past history and present status *(Czech)* 79−21516
radiation damage research, (1950-60) 80−62446
radiation protection, development in use of radioisotopes in Hungary *(Hungarian)* 80−90644
radiation protection and meas., USA 77−37708
radiation research, lab. contamination in the early period 80−42031
radiation therapy, history of the use of radioactive iodine 80−42032
radioactivity, aggregate recoil theory 80−57062
radioactivity and quantum mechanics unification, probabilistic conceptions 80−12946
radioactivity warning symbol, design history 79−67135
radioastronomy, pioneering work by Jansky, and Penzias and Wilson 79−44655
radioastronomy evolution and Cygnus A *(French)* 79−40287
radiochemistry, early research 80−86067
radiointerferometry, Mandel'shtam's research 80−105488
radioisotope scanning of bone, historical survey 80−42029
radioisotope tomographic imaging, historical review 80−42038
radioisotopes, artificial, initial stages of use in Hungary *(Hungarian)* 80−90643
radioisotopes, review of development in use *(Hungarian)* 80−90645
radiological physics, early history 79−80410
radiometry, development trends 77−61105
radiotherapy in oncology 80−81708
rainbow, physics, historical review 77−73854
rainfall in Norwich, homogeneous records of monthly totals for years (1836 to 1976) 78−3886
rainfall recording at Oxford, England, since 18th century 79−29810
Raman effect, 50th anniversary of discovery *(Polish)* 79−75314
Raman effect, combinational scatt. of light, discovery and history 80−27101
Raman effect, combinational scatt. of light, history 80−27100
Raman effect, its discovery 78−73819
Raman effect discovery 78−49627
Raman spectra, recent developments and historical review 78−73821
Raman spectroscopy, fiftieth anniversary, review 79−49003
random walk problem, history, in consideration of interdisciplinarity 78−16618
rare earth research developments since 1950 78−84116
realism and instrumentalism in 19th-century atomism 79−97172
records of supernovae 77−2448
reference coordinate system concept, in astronomy, development *(German)* 77−13642
reflecting telescope technology, Third Earl of Rosse expts. 78−18
Regiomontan, Johannes, astronomer, life and work *(German)* 77−53726
Regiomontanus, Johannes, 15th century astronomer, life and works 78−20929
relativistic electron wave equation 80−101702
relativity, 1907 to 1915 *(Russian)* 79−84934
relativity, creation and gnosiological lessons 80−98780
relativity, Einstein's 1907 paper, retranslation 77−71173
relativity, Einstein's first paper, retranslation, comments 77−33811
relativity, physicists' reactions and popular attitudes, historical account 80−77602
relativity theory, influence of Mach's philosophy 78−8211
retinal anatomy and physiology, reprint of 1877 paper 78−20932
retinal chemical processes, reprint of 1879 paper 78−20933
retinal stimulation by Ra 79−71213
rockets, early stages in theory of propulsion and dynamics 78−16
Romer, Ole, determ. of hesitation (velocity) of light *(Danish)* 77−57140
Rontgen, second 'original' first page of manuscript 79−71214
Rontgen's discovery of X-rays, accidents role in scientific enterprise 80−4502
Royal Astronomical Society, catalogue of archives and manuscripts 78−69705
Royal Astronomical Society, manuscript archives 78−32636
Royal Meteorological Society 79−2376
Royal Observatory, Greenwich, 1675-1975, conf., Greenwich, England (July 1975) 77−29646
Royal Society in 17th century 77−26121
ruby maser, research and development 80−27094
history continued
Rutehrford, life and work, swift rotation, appl. in beam choppers, turbine drives etc. 78−32643
sand clock, historical development 80−22185
Santorini, soil conditions during Minoan times around 1500 BC 78−40552
Schrodinger's contribution to relativity 77−45659
Schrodinger's route to wave mechanics 80−17783
Schwinger and nuclear physics 79−62987
science, in undergraduate education 80−12864
scientific collaboration, French scientific elite (1799 to 1830) 79−75317
scientific collaboration, professional origins of co-authorship 79−58522
scientific controversies, J phenomenon of Barkla 79−62983
scientific instrument makers contrib. to physics knowledge 77−49546
scientific revolutions, Einstein and Lorentz examples 80−82594
E.-central Scotland, snow and sleet freq. var. in 1708-1975 period 78−44951
Seasat artificial oceanographic satellite, microwave instrums. 80−94678
seawater, history of standards development 79−79871
seismic activity and large earthquakes, Sanriku district, Japan *(Japanese)* 79−70749
SEM and electron microprobe *(German)* 78−41381
semiconductor electronics 80−68015
semiconductor physics and technology, history and development in USSR, brief survey 78−54142
sensing apparatus and techniques, source guide 78−4457
ship magnetism, rel. to mag. compass, history, Airy-Scoresby controversy 78−4451
Shroud of Turin, blood presence identification, spectroscopic and chem. tests 80−102875
Shroud of Turin, IR reflectance spectrosc. and thermographic investigations 80−87578
Shroud of Turin, scientific investigation 80−87576
Shroud of Turin, spectral props. 80−87577
Shroud of Turin, UV-visible reflectance and fluoresc. spectra 80−87579
'Sidereus nuncius' composition, dating from Galileo's lunar observations 79−8853
simple fluids, dynamics, history of inelastic neutron scatt. determ. 79−46539
sintered permanent magnets, development history, magnetic and physical props., appl. 80−29901
Sir John Herschel 20 feet reflector, description 79−88788
SN 1181 (3C 58), absolute magnitude and type classification 80−56862
Soddy at Oxford 80−86064
solar activity, long-period vars. from historical records *(French)* 78−73695
solar constant, Smithsonian Astrophysical Observatory program, (1902 to 1962) 80−36606
solar cycles during 1540-1700 period, from solar and auroral obs. 79−21267
solar eclipses, ancient Chinese obs. 80−72916
solar energy concentrators, design methods, historical aspects 78−83063
solar granulation, discovery and history 77−2382
solar power harnessing, biography of A.B. Mouchot *(French)* 80−105484
solar rotation, determ. from Thomas Harriot's sunspot obs., (1611 to 1613) 79−75182
solid state physics, 1925-33 80−57066
solid state physics, contrib. of Gottingen school, 1920-40 80−57070
solid state physics, historical aspects, symposium, London, England (Apr.-May 1979) 80−56999
solid state physics, history since first appls. of quantum mechanics 80−57072
solid state physics, schools of thought, 1930 to mid 1960s 80−57069
solid state theory, 1926-33 80−57067
solid-state research at Bell Laboratories 77−41449
soliton history in mathematics of solns. to nonlinear evolution eqns. 79−75365
soliton physics development, anal. based on INSPEC tapes 79−62990
solitons, numerical studies, historical review 79−75367
sound propagation in atmosphere, historical review 78−15
South African radiation control, historical growth and development 79−67134
space and time, concept, historical development *(Hungarian)* 80−46784
space exploration, American and Soviet space programs, book 77−57149
Space Telescope 79−84928
Spanish America, early history of science before 1820 77−17746
special relativity, background *(Hungarian)* 77−22407
special relativity, ether drift, historical review 80−49
special relativity, secondary-school course not relying on historical approach 78−86096
special relativity and Michelson-Morley experiment, history of physics, role in education 80−8759
spectrophotometer, prism instruments, Beckman Instrument Inc., historical review 77−61125
star catalogue in Ptolemy's Syntaxis, position meas. method 80−67586
Star of Bethlehem, astronomical hypotheses *(French)* 79−84923
Star of Bethlehem, Far East record searches 80−17507
Star of Bethlehem, identifications rel. to Nativity chronology 79−67136
Star of Bethlehem, possible nova in 5 BC 78−32365
Steiner surface, piecewise surface approx., finite element calcs., isoparametric method 80−12881
stellar convection theory (1930-1945) 78−89177
stellar parallax meas. of pole Star by Flamsteed 79−88786
Stephen Gray, astronomer (1666-1736) 80−22182
stochastic reasoning, history in philosophy 77−82361
Struves of Pulkovo, family of astronomers 78−24632
sunspot cycle before Maunder minimum, evidence for 11-year periodicity 78−61825
sunspot cycle irregularity, historical evidence 79−58307
sunspot Maunder Minimum, rel. to Andrew Marvell's poetry 80−12877
sunspot pretelescopic records from Orient, catalogue, 28 BC-AD 1604, activity excursions 79−66975
sunspot records in 'The Book of Changes' *(Chinese)* 80−77366
sunspot research, past and present, review *(Norwegian)* 79−75312
sunspot turning points and aurorae since (AD 1510) 80−21980
superconductivity *(French)* 79−7931
supernovae, historical and theoretical review *(Norwegian)* 79−80329
supernovae, historical records, book 79−17002
Tappan, Henry, role in training of astronomers at Ann Arbor, MI, USA 80−86062

history continued
teaching, physics, history and society 77−33726
teaching natural philosophy, Patrick Copland in 1800 A.D. 78−12452
terrestrial magnetism, research, international collaboration in early 19th century 78−4450
tesla (T) unit acceptance in SI system for magnetic induction *(Slovenian)* 79−40526
thermodynamics and natural philosophy, William Thomson's heat theories 77−26122
Thomson and Bohr atomic models 77−45668
Tien-Kuan guest star of 1054, Crab supernova, historical records *(Chinese)* 78−65743
time measurement rel. to angle meas. 78−20931
Tokyo, winter temps., spectral anal. of data for 1443-1970 period 77−45128
topology and physics, historical review *(Russian)* 80−8770
transistors, development, decisions and attitudes 78−12524
tree-ring evidence of past climatic variability 79−16642
tsunami magnitude and wave source regions, N.E.Japan, 1611-1901 period *(Japanese)* 77−2122
tsunamis, in Japan Sea, behaviour and source areas 78−65198
tsunamis, Nankaido, Japan, historical monuments, inundation heights rel. to 1946 tsunami *(Japanese)* 79−70751
tsunamis of 1707 and 1854 along Shizuoko coast, Japan, field surveys *(Japanese)* 78−96149
tsunamis propag. from sources off N.E.Japan Pacific coast *(Japanese)* 78−11813
twelfth century science, conceptual revolution 78−28905
Tycho Brahe's astronomical instruments, errors 78−32642
Tycho Brahe's solar observations 79−88785
ultrasonics, historical aspects 79−46105
Ulugh Beg observatory, meridian instrument axis azimuth rel. to continental blocks rot. 78−53613
undersea acoustics to 1950, review 77−45667
UNESCO solar energy programme 79−57358
United Kingdom Climatological Network, history and role of co-operating observers 79−5618
unusual weather frequency variability over last century 78−73479
v=gt expression, origins of derivation 80−77593
vapour pressure measurement, effusion method, review 80−51995
Venus 1151 year period discovery, Babylonian or Persian? *(German)* 79−35166
virus negative staining technique, applications in electron microscopy 80−41348
vision, physiology and psychology, development, contrib. of Joseph LeConte 80−86063
vision at threshold, light quanta 77−25443
vision paper by Jean Mery written in 1704 80−57050
VUV photochemistry 79−49006
Waller, I., early work on lattice dynamics and X-ray diffr. 80−62439
water pollution control in United States 77−33818
wave mechanics, invention, Schrodinger-Einstein correspondence 79−84898
wave-particle duality and quantum theory, attitudes, 1900-1920 80−57061
weather forecasting on radio and TV, development in America 77−49549
weather prediction, development and status 77−82358
weather prediction with computers, 1950 ENIAC computations 80−42030
wet printing systems development and future 79−21826
winter of 1657-58, Denmark's frozen sea areas, invasion by Swedish army 79−88791
winter weather in W.Fife in 18th century 77−29981
wireless transmission, 1900-1935, early ionospheric research 79−9070
Wolf's astronomical observatory in Gdansk, Poland, in 18th century *(Polish)* 79−88591
Wollaston, W.H., processing of Colombian alluvial platina 80−86060
X-ray crystal optics, diffraction topography and interferometry *(German)* 79−46508
X-ray engineering, development in the operating theatre 80−101703
X-ray photoelectron spectroscopy, development (1900-1960) 79−12560
X-ray photoelectron spectroscopy 1900 to 1960, review 77−82359
X-rays, history of discovery *(Danish)* 77−64912
Young Avestan and Babylonian calendars and the antecedents of precession 79−48693
Yuan Dynasty, latitude determ. in China *(Chinese)* 78−24631
Zemplen's studies on shock waves *(Hungarian)* 80−31476
ZGS, history, conference, Argonne, IL, USA (Sept. 1979) 80−90600
ZGS history, the early stages 80−91297
ψ meson, e^+e^- expts. (1975 and 1976) 77−87991
ψ/J discovery, expt. details, charm particles, review 77−54113
ψ/J particle discovery, experimental details, personal recollection 77−54112
^{3}He, superfluid phase discovery *(Polish)* 79−37894
O I and N I forbidden lines emission in nightglow, historical review 79−5699
Pd, discovery and elemental nature, Wollaston/Chenevix controversy 79−30185
Se, semiconducting, and related materials, historical study, 1833-1919 78−57727
^{236}U, as extinct natural parent of Th, premature falsification of correct theory 79−30186

HIXE *see ion microprobe analysis*

HMO calculations
π-binding energy and bond orders relation *(German)* 79−76346
σ−pi consistency method, appl. to furan, pyrole and pyridene 77−67957
alkanes, electron density, bond order, hydrogen suppressed graphs, extended Huckel theory 78−90088
alternant hydrocarbons, polarisabilities rel. to bond orders using Huckel's method *(French)* 79−31405
anthracene, excited states calc., unrestricted HF theory in PPP approx. 77−50377
benzenes chemisorpt. on α-Fe, π complex form., MO LCAO calcs., thermodynamics 77−52674
bond orders, lengths, MO calc. methods, correl. with experimental values, teaching appl. 77−29974
carotenoid pigments, radical ions, radiolysis generation, absorpt. spectra, MO calcs. 77−65488
characterising indices for Huckel parameters *(German)* 80−47896
HMO calculations continued
characteristic polynomial construction, group-theoretical rules 77−23432
conjugate molecules, Huckel rule, proof 77−30748
conjugated molecules, excited state, mol. geometry, vibr. and optical spectra *(Japanese)* 77−42253
covalent elements, cohesion in condensed phases, corrections to simple Huckel approx. 78−59779
covalent elements, cohesion of σ and π bonds in condensed phases, simple Huckel approx. 78−59778
crystallites, finite SC and FCC, with (100) surfaces, tight binding eigenvalues 78−34745
cyclopenta[h]cycl[4.2.2]azine, electronic struct., photoelectron data 78−5286
cyclophanes, double and triple-layered, triplet state zero field splitting parameters, HMO calc. 77−50366
diatomic alkaline earth halides, multiplet splitting, extended Huckel approach 80−74127
1,2-dicyanocyclopropane, stereomutations, isomerizations, reaction rate consts., extended Huckel calcs. *(Italian)* 79−20348
education, minicourse in HMO theory using small computers 78−25444
graph theory, atom self-polarisability, electrophilic substitution reactions 77−9076
graphical method of reduction of Huckel matrix 80−14085
graphite, heteroatom doped, electronic struct., energy spectrum, HMO LCAO calcs. 77−43539
homologous linearity for energy of mol. orbitals and physicochemical props., quantum chemical basis 80−78541
Huckel matrix, degenerate eigenvalues investigated under insertion of additional bond or centre 80−78542
hydrocarbons, small, electron momentum distribs. in π orbitals from (e,2e) expts. 80−14239
large molecular systems, local pot. surface and charges, parametrisation scheme for quantum mechanical computation *(German)* 80−18793
mapping properties of Huckel parameters *(German)* 78−13434
metal clusters, distortions induced by finite size in regular clusters 77−35507
molecular geometry, iterative EHT calcs. 78−46271
naphthacene, excited states calc., unrestricted HF theory in PPP approx. 77−50377
naphthalene, excited states calc., unrestricted HF theory in PPP approx. 77−50377
nickel oxalate, electronic struct. from Huckel calcs., optical props. and reactivity 77−89741
organic hypohalites, electron structure, stability and reactivity 80−14086
pentacene, excited states calc., unrestricted HF theory in PPP approx. 77−50377
polycyclic conjugated molecules, π-electron energy contrib. of ring, rel. to linear analogue 77−30787
polyene, infinite, electronic states under local perturbation 77−57878
polyenes, highly branched, large networks, abnormal bond orders 79−59610
quantum chemistry, simple approximation method *(Hungarian)* 79−3341
quantum chemistry, spin-free, particle-hole and pairing symmetries 79−6812
small molecules, HMO-CI, HMO-AO-CI methods, quantum chemistry model studies *(German)* 78−29753
stilbene derivatives, electronic struct., frontier electron density, chem. reactivity *(Rumanian)* 79−72242
student use, computerised visual aids 78−77649
three-centre systems, charge transfer effects and Huckel parameters, mapping concept *(German)* 79−22604
TMMC, antiferromag. coupling in linear chains, molecular orbital approach 78−52239
transition metal compounds, XPS, anal., approx. mol. orbital theories 77−18975
tricycloquinazoline, excited states, fluoresc., phosphoresc. 77−61789
unsaturated P-containing peroxides, electron structure, stability and reactivity 80−14086
virtual charge model of polarisable medium as basis for Huckel calcs. with ω-technique 80−69083
visual excitation, mol. mechanism for initial process, optical activity in rhodopsin and bathorhodopsin 77−52783
Ag, cluster and microcrystal, matrix isolated, optical absorpt. spectra, photolysis and plasmon absorpt. 79−89820
$CsNiCl_3$, antiferromag. coupling in linear chains, molecular orbital approach 78−52239
$CsVCl_3$, antiferromag. coupling in linear chains, molecular orbital approach 78−52239
Cu surface, H and H_2 adsorption, appl. of extended HMO theory 77−15682
Fe crystallites, vacancy diffusion and vacancy lattices semi-empirical mol. orbital calcs. 77−1121
Ge(111), chemisorption of Cl, threefold co-ordinated site chemisorption, cluster model calc., extended Huckel theory 78−39178
Ge(111), dangling-bond surface states 78−43452
Li, cluster and microcrystal, matrix isolated, optical absorpt. spectra, photolysis and plasmon absorpt. 79−89820
LiH, cluster cryst., extended HMO calc. of defects 79−51521
$MnO_3F(Cl)$, He (I) photoelectron spectra, metal-ligand bonding, EHMO calc. 78−9193
$Mo_2Cl_8^{3-}(Mo_2Cl_9^{3-})$, electronic struct. and metal-metal bonding, HMO calcs. *(Russian)* 78−1118
Na, cluster and microcrystal, matrix isolated, optical absorpt. spectra, photolysis and plasmon absorpt. 79−89820
Na particle, consisting of ats., metallic Na, model, electronic levels 78−50673
$Nb_2Cl_9^{3-}$, electronic struct. and metal-metal bonding, HMO calcs. *(Russian)* 78−1118
Ni crystallites, vacancy diffusion and vacancy lattices, semi-empirical mol. orbital calcs. 77−1121
Ni surface, H and H_2 adsorption, appl. of extended HMO theory 77−15682
$Re_3Cl_9^-$, electronic struct. and metal-metal bonding, HMO calcs. *(Russian)* 78−1118
S_2N_2, semiempirical electronic struct. calcs., applicability testing, and for $(SN)_x$ 77−6681
Si compounds, free mol. chemical shift, binding energy and Auger spectra 80−32782
Si:Li, defect electronic struct. and config., semi-empirical calc. 80−107739

HMO calculations continued
Si_xO_y structures, $Si(OA)_4$ clusters, A=H,Li,K, HMO calcs., energy stability, charge distrib. *(German)* 79−89822
Si(111), dangling-bond surface states 78−43452
H_3O^+ *see hydroxonium ion*
hobby computing *see personal computing*
hodoscopes *see cosmic ray apparatus*
hole mobility *see carrier mobility*
hole theory of liquids *see liquid theory*
hole traps
see also electron traps
alkali halide, dynamics of nonrelaxed and self-trapped holes *(Russian)* 80−80607
alkali metal halides, hole self-localization and capture, temp. depend. 80−92526
amorphous material, trap-controlled transient current injection, models of trapping level 79−23984
amorphous semiconductor, size and field variation of activation energy for drift mobility 80−49769
amorphous solid, photoconduction, model involving capture and escape from multiple traps 77−76863
anthracene:perylene crystal, trapping factors anisotropy 77−59291
anthracene, cryst., photocurrent induced by detrapping of charge carriers trapped by radicals 79−82643
anthracene, electron and hole generation under electron bombardment 79−73524
anthracene, prep. and growth of single cryst. 78−64463
anthracene, surface states and persistent internal polarisation via photocurrent transients 77−89825
anthracene, trapping effects on emission-limited current flow 80−29413
anthracene single crystals, hole trapping by photo-oxidation products, injection currents *(Russian)* 80−92904
bipolymer, charge carriers origin and mobility, adsorbed water effects 79−92461
capacitance methods for minority and majority carrier trap characterisation 77−51692
capacitance transient spectroscopy, book contrib. 78−10548
chalcogenide glass, charged dangling bond model reassessment 77−72813
chalcogenide glasses, electronic gap states, origin, structural relax., electronic transport and trapping 80−54648
chalcogenide glasses, trap controlled transient photocond. 80−44641
chalcogenide semiconductors, optical and elec. props., comparison with SiO_2 78−6721
charged dislocation, hole capture cross section *(Russian)* 78−23108
covalent semiconductors, low temp. galvanomag. effects, shallow attractive traps 80−88575
deep level capture, two stage model 78−10396
degenerate semiconductor, recombination-generation currents derivation 78−52007
diamond, natural, hole trapping levels 79−76278
dielectric, SCL cond., field ionisation and annihilation of traps of different elec. nature *(Russian)* 77−69330
2,3-dimethylnaphthalene, transient photocurrents, hole trapping *(German)* 77−59303
N,N′-diphenyl-p-phenylenediamine, current carrier traps, space-charge-limited currents 78−47799
disordered semiconductor, hopping mechanism of dispersive transport 80−10971
dispersive transport by hopping and transport, theory 78−14726
DLTS, photo-excited, minority carrier trap meas. 80−96816
equilibrium carrier trapping by centres localised in disordered regions 77−43618
finite systems containing traps, Hall effect, two-carrier one-dimens. transport anal. 80−44614
GaAs MBE growth, deep levels effect on electron and hole trap densities 80−49652
Gaussian trap distribution in solids, theory of single and double injection 77−11935
graded and stepped energy band-gap MIS structures 80−2473
graphite, neutron irradiation, electron transport, annealing study 80−39165
hydrocarbon, long chain single cryst., carrier transport meas. 80−6874
II-VI compounds with three deep trapping levels, theory of transient photocond. processes 77−76865
III-V semiconductors, point defects and deep traps, thermodynamic history, model 80−59908
indandione-1,3 derivative, layer, electrooptical effect *(Russian)* 79−73900
insulated crystal, primary photocurrent kinetics for simultaneous trapping and recomb. 80−6899
insulator, extension of theoretical description of space-charge-limited currents 78−39128
ionic crystal, intrinsic electronic excitations and defects, review *(Russian)* 80−10881
LED, deep trapping levels energy and conc. meas. *(Polish)* 78−34797
Lexan polycarbonate, N-isopropylcarbazole and triphenylamine doped, trap-controlled dispersive hopping transport 77−15850
MIS structure, thermal generation of carriers through surface centres 79−69603
MNOS devices, small-signal response of bulk traps 77−39959
MNOS structure, trap parameters determ., review of expt. techniques 77−55612
MOS, charge build-up due to radiation, mathematical model 79−19667
MOS capacitor, threshold voltage instability due to defect states produced during e-beam metallisation 78−72264
MOS capacitors, irradiated and avalanche injected, trapping effects 79−19669
MOS device, nonequilibrium response to linear voltage ramp, bulk discrete traps 78−6450
MOS structure, hole emission from interface states, transient capacitance meas. 78−14830
MOS structure, quench-in defects and interface states exam. by transient capacitance techniques 78−39225
MOS structure, slow-trapping instability, effect of high temp. H_2 annealing 78−47880
MOS structure under strong inversion conditions, freq. response of bulk traps. 77−39958
MOS structures, inversion layer near electrode edge, pot. and charge density distribution 80−88642
hole traps continued
MOS structures, irradiated SiO_2 film, electron and hole trapping 80−11098
MOS structures, quasistatic and nonequilibrium phenomena with constant gate-current bias 80−80385
MOS structures, thickness dependence of radiation charging, hole trapping model 77−20442
multilevel trapping fluctuation processes spectral props. of physical processes of Markov-correlated events 79−21665
multiple trapping theory 77−55542
multiple-trapping model and time-dependent random walk 78−34842
naphthalene, cryst., photocurrent induced by detrapping of charge carriers trapped by radicals 79−82643
naphthalene, deep exponential distrib. of traps, long-time decay of surface pot. 79−47041
one-dimensional, semiconducting polymer, demonstration of high mobility 80−20212
organic molecular crysts., charge carrier generation by exciton-exciton collisions 80−88568
organic semiconductor films, relax. currents, polarisation and depolarisation currents obs. 80−49764
p-n junctions, TSC, impurity centre parameter determ. 78−47857
PbI_2, trapping levels, TSC meas. 78−23107
pentacene, evaporated film elec. cond. meas. for various temps., SCL 78−10584
photochromic glasses, electron-hole separation, influence on recombination probability 80−11445
photographic emulsion sensitisation during latent image formation, nature of sensitivity specks 77−82637
phthalocyanine thin layers, metal-free, mobility and thermally stimulated polarisation meas. 79−73527
poly(n-vinylcarbazole)-trinitrofluorenone films, charge carrier trapping 78−14846
poly-N-vinyl carbazole, hole hopping mobility, transit pulse dispersion 80−65565
poly-N-vinyl carbazole, trap-free lifetime, neutral traps, hopping systems 80−65566
polyethylene, γ-irradiated, effect of elec. field on TSC 79−65790
polyethylene, oxidised and gamma-irradiated, carrier traps, thermally stimulated currents 78−19050
polyethylene films, corona charged, charge trapping 80−88571
polyethylene TSC resulting from trapped carriers 78−6393
polymer, carrier trap study by X-ray induced TSC and thermoluminescence *(Japanese)* 80−54713
polymer film, carrier transport meas. 80−6874
polymer film electret, charge distrib., generalized model 80−6873
polymers powders, corona-charging props. 80−6946
polystyrene, pure and doped, metal contact effect on persistent internal polarisation 79−78617
polyvinylcarbazole, fast hole transport 79−51628
polyvinylidene fluoride, TSC and thermoluminescence, reln. to molecular motion *(Japanese)* 80−55200
quartz, comparison of different radiation effects 78−26596
quartz, crystalline, thermolum. sensitivity, proton and gamma induced 77−90205
α-quartz, hydrogenic trapped hole species, EPR studies 80−44915
α-quartz, X-irrad., paramag. Ag_2^+/AlO_4 centre, EPR obs. 79−28612
relaxation semiconductor, theory of carrier transport in p^+-ν junction 79−60914
rhodamine B surface state hole traps, surface photovoltage meas. 80−39654
sapphire, Czochralski-grown, excess charge carriers, generation, transport and trapping 79−82646
Schiff's base, thin layer samples, mechanism of change carrier photogeneration *(Russian)* 77−32045
Schottky diode, effect of thin oxide layer between metal and semicond. 77−20432
semiconductor, deep bound states, temp. depend. of ionisation energies 77−31975
semiconductor, Faraday rotation in presence of attractive traps 78−76081
semiconductor, nonradiative multiphonon carrier capture and ejection props. of deep traps 78−35190
semiconductor, nonradiative multiphonon carrier capture props. of deep charged and neutral centres 77−15866
semiconductor, p-type, field emission theory, surface states and recomb. processes 77−85901
semiconductor, photo-EMF during charge carrier trapping *(Russian)* 79−42574
semiconductor, recombination and generation mechanisms, band-type models exhibiting phase transitions 79−47049
semiconductor, recombination at deep traps, review 79−38100
semiconductor, spatial distrib. of traps obs. with SEM *(Russian)* 77−32449
semiconductor, techniques for detecting electrons and holes trapped at bulk and interface imperfections 77−11934
semiconductor, transient injection currents, charge transport allowing for trapping 78−26884
semiconductor containing traps, minority, carrier lifetime 78−60137
semiconductor film, trap-limited model for dispersive transport 78−6378
semiconductor models for non-equilibrium phase transitions due to impact ionisation from traps 79−51520
semiconductor under illumination, simple model of generation and recombination processes 79−69523
semiconductor with arbitrary energy spectrum of trapped states, surface region of space charge 80−107811
semiconductor with position depend. composition, carrier generation, recomb., trapping and transport 77−43613
semiconductor with traps, ambipolar photoelec. current 79−91101
semiconductors, Auger recombination processes 79−38091
semiconductors, Auger recombination with traps 80−49763
semiconductors, capture of carriers by attractive centres 79−7836
semiconductors, recombination processes, review 79−38088
semiinsulator, minority carrier injection effect on TSC 78−10466
sisal wax, electronic conduction and persistent internal polarisation 78−80277
smoky quartz, thermal props. at very low temp. 80−24610
surface avalanched p-n junctions, localised charge injection and trapping 77−76907
TCNE, hole drift mobility, temp. depend. and anisotropy, photocond. meas. 80−80314

hole traps continued
Teflon films, hole transit, trap modulated mobility and dispersive hopping discussion 79−69616
tetracene, noncryst., localised valence states in forbidden gap 78−72113
tetracene, trapping effects on emission-limited current flow 80−29413
thermoluminescence method for trap depth determ. 80−80211
transport via extended states with traps, space-charge hopping equivalence 79−95399
triphenylamine in 3-methylpentane and ethanol glasses, γ-radiolysis, IR spectra, trapped electron 77−16842
TSC technique, trap modulated electron and hole mobility meas. in insulators 78−10441
TSCD meas. method and applic. 77−43615
TTT, dark cond. and photocond. effect of strong mag. field, at charge carrier injection *(Russian)* 79−69607
TTT, dark injection current, sign inversion of low mag. field *(Russian)* 79−73602
wave hierarchy interpretation of multiple trapping model 80−6894
wide-gap semiconductor, recomb.-trap barriers 77−8119
Ag halide emulsion grains, photographic effects of electron and positive hole traps 77−82635
Ag halide photochromic glass:Cu^{2+}, characterisation of Cu ions 78−5530
Ag halide photochromic glass, darkening mechanisms under pulsed laser excitation 78−25938
AgBr, doped, neutralisation of trapped photoholes 78−76108
AgBr, Stark effect on I-bound exciton 79−28719
AgBr:Pd(II), photolysis-induced trapping behaviour, EPR study 80−54949
$AgBr_{1-x}Cl_x$, Jahn-Teller type self-trapping of holes 79−65709
AgBr(I) microcrystals, photohole motion 78−26903
AgBr(I) microcrystals, photocond. and luminesc. 78−26904
AgCl:Pd^{2+}, EPR, role of vacancies in impurity based trapping 77−28439
β-AgI, drift mobility of holes 77−47814
β-AgI:Cu, pure and doped, photoconductivity, band struct., trap nature 79−95449
(Al,Ga)As double-heterostructure lasers degraded, deep-level changes during accelerated ageing at high temps. 80−74356
AlGaAs semiconductor lasers, single-mode stabilisation by traps 80−95893
Al_2O_3 film, MOS gate insulator, photoconductive processes 77−8216
Al_2O_3, X-irrad., electron and hole traps, TSC and optical bleaching meas. 79−28356
As_2S_3-Sb_2S_3, vitreous, dispersive charge transport analysis 79−95418
As_xS_{100-x}, chalcogenide glass, hole trap levels, TSC *(Russian)* 79−91074
$(As_2S_3)_{0.55}(Sb_2S_3)_{0.45}$ vitreous film, dispersive charge transport, time-of-flight meas. 79−19594
As_2Se_3, amorphous, defect states, exptl. study. 80−54645
As_2Se_3, amorphous, transient hole transport props., trap controlled hopping model 77−47820
As_2Se_3, localised gap states estimated by dielec. relax. 78−35087
As_2Se_3:Ag, amorphous, doping effect of gap states and elec. cond., dielec. relax. and DC cond. meas. 79−47098
As_xSe_{100-x}, chalcogenide glass, TSC *(Russian)* 79−91074
As_2Te_3, charge screening length 79−23974
$As_{40}Te_{48}Si_{12}Ge_{10}$, charge screening length 79−23974
Au-tetrathiotetracene-Al systems, dark cond., photocond. mechanisms rel. to contact phenomena *(Russian)* 78−52103
$Ba_3(PO_4)_2$, recomb. luminesc. mechanisms 80−2874
$BaSO_4$, X-ray irrad., electron and holes traps, g-factors, ESR obs. 80−50183
$BaWO_4$:Mo, P, thermoluminesc. traps, EPR meas. 77−90032
CaF_2:Dy^{3+}, thermolum., associated luminesc. centres and traps 77−28638
$CaWO_4$:Mo, P, thermoluminesc. traps, EPR meas. 77−90032
CdS, electron and hole trapped centres, EPR, photoluminescence, photoconductivity study 80−108071
CdS, hole-capture coeff. of deep charged centres, temp. depend., photocurrent meas. 79−7804
CdS, phase memory effect and vel. of trap-controlled high-field domains 77−47855
CdS, polycrystalline evaporated layers, donor and trap densities 80−20213
CdS, trapping level parameter determ., limiting current injection *(Russian)* 78−39129
CdS:Li, photocond. characts., electron and hole traps obs. 77−8140
CdS-Cu_2S junctions, carrier trap density, deep level defects 80−107801
CdTe detectors, gamma and electron irradiation effects 78−41893
CdTe, film, theoretical models of impurity levels 79−82557
CdTe, high-resistivity, carrier transport and trapping processes, growth parameter effects 77−39871
CdTe, thermostimulated capacitor discharge, trapping levels obs. *(Russian)* 78−10842
CdTe:Cl(In), photoelectronic investig. of trap depths, TSC and SCL cond. 77−39893
$Cd_{1-x}Zn_xS$ heteroepitaxial single-cryst. layers, photoluminesc. props. 80−100692
n-$CuInS_2$, mag. props., obs. 80−70939
9,10-dichloroanthracene, mag. field effect on exciton processes and photodetrapping 77−4668
$Ga_{1-x}Al_xAs$, epitaxial, radiative deep states 80−76061
GaAs, bulk and epitaxial crysts., hole traps characterisation 78−6392
GaAs, deep bound states, temp. depend. of ionisation energies 77−31975
GaAs, deep centres, electron and hole capture cross sections 79−99510
n-GaAs, deform. produced deep levels, DLTS meas. 80−54634
GaAs, epitaxial layers, grain boundaries, deep level transient spectroscopy study 80−49234
GaAs, epitaxy by metallorganic and chloride depositions, defect characterisation at growth interface 80−59817
p-GaAs, Fe-compensated, photocond. under strong excitation 77−15904
GaAs, LPE, deep levels rel. to growth conditions 79−28314
GaAs LPE layers, deep levels by photocapacitance and related techniques 78−6334
GaAs MESFET, deep trapping effects at GaAs-GaAs:Cr interface 78−72245
GaAs p^+-n junction, deep levels obs. 77−89834
GaAs, proton irradiated, low energy, deep level defects and hole diffusion length meas. 80−60000
hole traps continued
GaAs Schottky-contact, influence of surface states and hole traps *(Bulgarian)* 80−25006
GaAs type FET with buffer, bias effects due to deep centres in struct. *(French)* 80−107917
GaAs, VPE, incorporation of deep levels, effects of growth conditions 80−20111
GaAs, VPE layers, growth conditions effect on deep levels 79−95360
GaAs:Be, deep levels 80−29358
GaAs:Cr, carrier transport in p^+-ν junction based on relaxation semiconductors 79−65543
GaAs:Cr, deep acceptor level, DLTS and optical DLTS study 80−92852
GaAs:Cr, hole traps, ESR studies 80−75843
GaAs:Cr, optically induced transient EPR phenomena 80−50168
p-GaAs:Cr, semi-insulating photoelectronic analysis 77−80804
n-GaAs:Cr, semi-insulating, contact effects, trapping levels 78−10465
GaAs:O, semi-insulating, excitation temp. effect on TSC 80−70717
GaAs-insulator interface, processes of electron emission from traps 79−73598
$GaAs_{0.6}P_{0.4}$, anodic oxide, negative flat-band shift related to photo-holes trapped in interface states 79−61771
$GaAs_{1-x}P_x$, bound exciton, luminesc. reson. excitation 79−95840
GaP crystals, radiation defects, TSC obs. 80−65588
n-GaP, deep state controlled minority carrier lifetime 80−20211
GaP, electron irrad., radiation defects annealing 80−29059
GaP, hole traps, rel. to two stage model for deep level capture 78−10396
GaP, p^+-n diode junction, admittance meas. and carrier traps 78−91757
GaP, VPE, background deep level defects, transient capacitance obs. 77−62854
GaP:Bi,N, photoluminesc., electroluminesc., 4.2 to 300K, excitons and hole traps 80−108275
p-GaP:Cr, hole traps, ESR studies 80−75843
GaP:N, bound excitons, low temp. photoluminesc. thermal quenching 77−48228
GaP:N VPE layers, thermal emission energies, trapping, and carrier lifetimes, deep level capacitance spectroscopy 79−42487
n-GaS, Bridgman crysts., hole traps, photocond. and thermal quenching study 80−75580
n-GaSe, photoconductivity and TSC investig. of trapping centres 77−20359
Ge, adsorption of N_2 and CO, adsorption potentials and trapped electrons role 79−90872
Ge, donor-acceptor electron transfer at low temps., photocond. tail 78−84249
n-Ge, electron irradiated, energy levels 79−28316
Ge FET, fabrication on high purity substrate 79−45579
Ge, high purity, carrier trapping 79−47104
p-Ge, Li-compensated, carrier capture 77−15792
Ge, light scattering, by pure single cryst., influence of photoexcitation 79−28780
Ge p-i-n diodes, deep level transient spectroscopy 79−47105
p-Ge:Hg(Cu)(Cd)(Zn), deep levels, optical-phonon-assisted capture of carriers 79−51597
Ge-Si_3N_4 system, potential barriers determ. from photoinjection carriers trapping 80−103756
Ge_xSe_{1-x} chalcogenide glasses, trap-controlled carrier mobility, time of flight meas. 79−4557
Ge_xSe_{1-x} chalcogenide glasses, drift mobility of optically injected carriers 79−19627
HgI_2, and photomagnetoelectric and photocond. meas., carrier lifetimes 77−55562
HgI_2 crystals, native defect compensation, doping, mobility-lifetime and TSC meas. 77−55492
HgI_2 detectors, recent improvements 78−37507
HgI_2, photo-EM effect and photocond., trapping effects 77−32042
HgI_2, photoelectronic props. 78−41897
HgI_2:Ag, trapping effects, TSC, photocond. and photolum. meas. 77−32023
n-InP, hole traps by deep level transient spectroscopy and transient capacitance methods 79−51514
n-InP-SiO_2 capacitor, carrier generation and trapping 80−49929
KBr:NO_2, Na effect of Na^+ impurity on self-trapped hole *(Japanese)* 78−67982
KCl:Eu^{2+}, γ-irrad., photostimulated low temp. recomb. luminesc. 80−11435
KCl:Tl, effective cross sections ratio of charged and neutral centres for holes and electrons *(Russian)* 79−28319
KCl:Tl, low-temp. ionisation of activator, photoexcitation, in region of interzone transitions *(Russian)* 79−28320
$KClO_4$, ClO_3^- detection by EPR of ClO_3 radicals created by X-irrad. 78−76311
LiF TLD phosphor, residual thermoluminescence effect on sensitisation 80−108287
$LiNbO_3$, X-ray photovoltaic effect and its correl. with ESR 79−82639
MOS, photocurrent-voltage characts., insulator bulk trapped charge 78−30991
$MgAl_2O_4$, γ-irradiated crystal, TSC, thermoelec. power, thermolum. and afterglow 80−75583
MgF_2:Fe^{2+}, γ-irrad., F-centres, Fe^{2+} ion hole traps, absorpt. and EPR meas. 79−7598
MgO doped powder phosphors, photo- and thermostimulated luminesc. obs. *(Russian)* 80−66263
MgO, electron irradiated, luminescence, radiative recombination kinetics 80−7421
MgO:Al, and nominally pure single crystal, thermally stimulated luminesc. rel. to temp., and EPR *(Russian)* 80−84789
MgO-P_2O_5-Al_2O_3-$3P_2O_5$ glass, absorpt. shift, electron and hole traps, thermolum. meas. 79−65897
NaCl, irradiated, at 80K, thermolum. processes 80−34990
NaCl, migration of nonrelaxed holes, self-trapping, ESR and luminesc. obs. *(Russian)* 80−66033
Na_2O-SiO_2 glass, tunnelling recomb. luminesc. 80−2875
PbS oxide, optical excitation meas. of trap charging surface film *(Russian)* 78−76180
Sb_2S_3, defect drift in elec. fields and bistable switching 80−92947
Se electrophotographic films, ageing effects on structure and properties 77−47699
Se, modulated photocurrent, analysed for trap-limited case *(Japanese)* 80−60030

hole traps continued
α-Se, multiple-trapping model of anomalous transit time dispersion, transient photocurrent data 78−34860
Se-binding agent electrophotographic film characteristics and sensitivity *(German)* 80−4789
$Se_{12}Te_{49}As_{29}Ge_{10}$ semiconductor amorphous films, field effect, trapping 80−84472
Si, amorphous, Schottky barrier solar cells, deep hole traps, spectral response and TSC meas. 80−50962
Si, deep level transient spectroscopy *(French)* 79−11079
Si, electron emission coeffs. for electron and hole traps 79−91075
p-Si, electron irrad. induced defects, thermally stimulated capacitance 77−11933
Si, MOS device, subject to linear voltage ramp, non-steady-state studies 79−78189
Si MOS struct., space-charge generation props. of Au 80−2475
Si MOSFET n-channel, Hall meas. on trap states at 77K 80−44732
Si n^+-p solar cells, degradation mechanisms associated with Ti impurities 80−81465
Si, neutron-produced defects, deep level transient spectroscopy 79−47047
Si p-n junction I-V reln. calc. 77−43704
Si p-n junctions, spin depend. surface recomb., electron irradiation effect 80−88627
Si pin diode, current filament temp. and Au acceptor level capture cross section temp. depend. 78−95351
Si, temporary trap characteristic after heat treatment *(German)* 80−34459
Si thin film, polycryst., CVD, elec. props. 80−107934
Si:Al, P-diffused, recomb. centres, thermally stimulated capacitance meas. 77−72834
Si:Al, thermally induced deep levels, TSC meas. 77−31974
Si:Au p^+-i-n^+ diode, double injection switching, effect of trapped space charge 77−1473
p-Si:B, defect energy levels with 1 MeV electron irrad. and annealing, transient capacitance spectra 77−62860
p-Si:B, Fe, 0.45 eV majority carrier trapping level after quenching 78−18990
Si:B, hole trapping by B atoms at low temps. 79−7837
Si:B effect of elec. field on carrier capture by attractive centres. 79−11145
Si:C, electron irrad., C interstitial, photo EPR 77−16175
Si:Co, study of impurity states 78−76020
Si:H amorphous, plasma-deposited, luminesc. decay 79−73989
p-Si:Mn, defect levels, transient capacitance spectroscopy 78−6322
Si:Os, P, photoelec. props., depend. on P conc. 79−91099
Si:Pt, elec. props., deep-level transient spectroscopy and thermal emission meas. 79−82542
Si:Pt, hole capture cross-section at E_v+0.34 eV, capacitance meas. *(French)* 80−65493
Si:Ti, deep level impurity, Hall meas. 80−6768
Si:V p-n junctions, thermal emission rates and capture cross sections of majority carriers at V centres 80−96980
p-Si:Zn^-, deep levels, optical-phonon-assisted capture of carriers 79−51597
Si/SiO_2 interface, slow-trapping instability, kinetics 78−76151
p-Si-As_2S_3 isotype crystalline-amorphous heterojunctions, electrophysical props. 79−24063
Si-SiO_2 interface, inversion layer transport, radiation hardness effects, review 79−19673
Si-SiO_2 interface, props. 78−23170
Si-SiO_2 interface, rad. hardness, carrier localisation in inversion layer 77−85332
Si-SiO_2 interface in MOS solar cells, operational characts. and struct. 80−93901
Si_3N_4, film, cond. mechanism, double injection, trap SCL current 77−32099
Si_3N_4, low press CVD film, steady-state electron and hole space charge distrib. 80−29493
SiO_2, amorphous, defect-controlled carrier transport 79−91049
SiO_2, amorphous, high-field transport of excess electrons and holes 77−89767
SiO_2, amorphous, optical and elec. props., comparison with chalcogenide semiconds. 78−6721
SiO_2, avalanche injection of holes 78−26959
SiO_2 film, in Al-SiO_2-Si struct., positive trapped charge location by internal photoemission 77−51820
SiO_2 film, thermally stimulated depolaris. current, model *(Russian)* 79−56342
SiO_2 film on Si, negative bias instability 78−91773
SiO_2 in MOS struct., exciton transport rel. to surface states 78−34901
SiO_2 layers, in MOS struct., hole trapping induced by ion implantation and annealing at room temp. 80−54792
SiO_2, multiple trapping model and hole transport 78−6394
SiO_2 thermal films, hole and electron trapping density reduction 80−2400
SiO_2, vitreous, exam. of electron excitations and intrinsic defects 78−87905
SiO_2, vitreous, paramag. centres associated with bonding defects 80−80609
SiO_2:B, ion implanted, props. 79−65106
p-Si_2Te_3, photoelectric props., luminesc., hole lifetime and trapping 77−39892
Te_xSe_{1-x}, localised gap states estimated by dielec. relax. 78−35087
TlCl-TlBr mixed cryst., impurity-induced self-trapping of holes and minority-ion percolation 78−64398
p-$Zn_xCd_{1-x}Te$, negative photocond. excited by fundamental absorpt. region light 77−15905
ZnO, single crysts., photocond. lifetimes, Zn^+ hole traps 80−75581
ZnP_2, trapping levels, TSC and thermolum. meas. 79−15115
Zn_3P_2, thermoluminescence glow curve method for radiation induced traps 80−60689
$Zn_3(PO)_2$, thermoluminescence glow curve method for radiation induced traps 80−60689
ZnS:Cu,Al phosphor, shallow hole traps 78−31237
ZnS-CdS:Ag(Cu), phospors, nature of fluorescent centres and traps 79−91484
ZnSe, laser induced modulation of opt. absorpt. 78−88324
n-$ZnSiP_2$, deep impurity levels, Schottky TSC meas. 79−95419
ZnTe:O, deep centres, photocapacitance detection 79−95362

hollow cathodes *see cathodes*

holmium
see also nuclei with .....
adsorption and absorption of $H_2(D_2)$ 77−4257
adsorption on W, field emission electron study 80−100393
APS, soft X-ray, of 4f states 77−24911
atom, α-particle impact K-shell ionisation, 40 to 110 MeV 78−17752
atom, incoherent γ-ray scatt. by K-shell electrons 77−83560
atom, IR emission spectra and hyperfine struct. *(French)* 78−13452
atom, keV electron impact, L X-ray prod. cross section 79−18293
atom, nuclear K-X-ray satellites, Z=50-83, by α-bombard., 17.5-22.5 MeV 80−42984
atom, photoabsorpt. spectra 77−88417
atom, spectra, energy levels and hyperfine struct., parametric calcs. *(French)* 78−41984
atom, X-ray emission, K shell, energy shifts, role of atomic struct. 78−70777
bulk modulus, thermal expansion, third order elastic constants 77−84875
calibo glass:Eu^{3+}, Ho^{3+}, energy transfer 78−76510
elastic constants, 80-140K, 95K anomaly and annealing 79−46734
elastic constants, in paramag. temp. range, magnetoelastic contrib. 77−4538
electrical resistivity, high-precision meas., 1-4K 77−15817
electron and positron multiple scatt. 80−15171
electron energy loss spectrum and surface electron states 77−85860
electron irradiated, defect annealing, recovery spectra 79−23648
EXAFS, white lines, interatomic distances 77−40302
film, elec. resist., thickness depend., effect of presence of dihydride 77−51829
film, helimag. order, surface deform., exchange and single-ion magnetocrystalline anisotropy energy 77−66390
film, O_2 and H_2 contamination effect on elec. resist. 77−80856
fluoride, MF_2:Ho^{3+}, (M=Ba,Ca,Cd), far IR Stark and Zeeman splitting 77−48190
gamma-ray emission from oriented nuclei in multiaxis nucl. spin system, ^{165}Ho:^{166}Ho^m 79−82905
germanate glass:Ho^{3+}, absorpt. and emission 79−11439
Hall constant and elec. resist., 80-700K *(Russian)* 78−60110
Hall effect, field and temp. depend., 4.2-150K, singularities *(Russian)* 80−29387
lattice dynamics, microscopic theory 77−43292
lattice dynamics, phonon freqs., calc. 80−15206
lattice dynamics of rare-earth HCP metals 77−7805
liquid, mag. susceptibility, elec. resistivity 80−20377
liquid, struct. factors, high temp. X-ray diffr. obs. 79−7544
low field susceptibility and helical-ferromag. field induced phase transition 78−47975
magnetic aftereffect obs. 77−8364
magnetic phase diagrams, helicoid-ferromag. transform. *(Russian)* 80−50089
magnetic phase transition, second order, order parameter in mag. field, neutron diffr. 79−61104
magnetoelastic coupling, meas. in paramag. region 77−80984
magnetoelastic interactions 78−64252
metastable high-pressure phase, conversion into stable phase 77−55357
microcontact magnon spectra, electron-magnon interaction *(Russian)* 80−54768
particles, effect of size on paramag. Curie temp. 78−60317
phase transition along mag. field, X-ray obs., 77-292K *(Russian)* 77−4504
pionic atom, quadrupole hyperfine interactions, nucl. moment 78−37772
plastic deformation, substructural changes, stress-strain diagrams and microhardness meas. *(Russian)* 79−52296
point defect production during electron irrad. at low temp. 80−49273
preparation from oxide, vac. thermal reduction with Th *(Russian)* 80−16226
rare earth compound:Ho^{3+}, phosphors, active layer effective thickness calc. *(Russian)* 79−43039
rare earth oxysulphide, R_2O_2S:Yb^{3+},Ho^{3+}, anti-Stokes emission band assignments, energy transfer mechanism 77−40277
specific heat, using lattice dynamical model for HCP metals 79−51273
spin fluctuation resistivity near T_N, theory 77−40071
SXAPS, N_5 and M_5 levels, anomalous structure 77−73191
tellurite glasses: Ho^{3+}, nonradiative relax. 77−24881
thermal expansion in magnetically ordered phases, single crystal 78−2269
thermophysical properties at high temps., exam. *(Russian)* 79−28105
transverse magnetoresistance in single cryst. 77−66154
X-ray L_{III} absorption discontinuity, bidirectional orbital interpretation 77−16423
X-ray L_{III} absorption edge, white line struct. 79−15560
X-ray production by 9.5 to 41.8 MeV Fl ions, total L-shell cross-sections 77−85847
X-ray production surface impact of F^{n+} and Si^{n+}, Lα X-rays 79−69907
$3Al_2S_3$.La_2S_3:Ho^{3+}, radiative and multiphonon relax. 79−33794
BaY_2F_8:Ho^{3+}, ESR spectra and spin-lattice relax. 80−11263
$Bi_{12}GeO_{20}$:Ho, luminesc., emission and excitation spectra 80−103975
$Bi_4Ge_3O_{12}$:Ho^{3+} crystal growth, spectral and laser props. 80−45115
CaF_2:Ho, V_k-centre recomb. kinetics, phosphoresc. 77−55817
CaF_2:Ho^{3+}, ^{19}F NMR studies 80−60429
CaF_2:Ho^{3+}, fluoresc., relative intensities, lifetimes 78−27296
CaF_2:Ho^{3+}, site-selective spectroscopy 80−29791
CaF_3:Ho^{3+}, laser excited fluoresc, rise and decay meas., expt. 80−22448
CaO-Li_2O-B_2O_3, calibo glass, Dy^{3+}→Ho^{3+} non-radiative energy transfer, diffusion limited relaxation 79−65925
CaO-Li_2O-B_2O_3 calibo glass, diffusion limited energy transfer from Tb^{3+}→Ho^{3+} 78−31235
^{111}Cd impurity electric quadrupole interaction temp. depend. 80−39900
Er_2SiO_5:Ho^{3+}, single cryst., luminesc. and stimulated emission 77−69895
$3Ga_2S_3$.La_2S_3:Ho^{3+}, radiative and multiphonon relax. 79−33794
$Gd_3Ga_5O_{12}$:Ho^{3+}, stimulated emission and cascade laser action 79−91466
$GdVO_4$:Ho^{3+}, optically excited doublet splitting in magnetically ordered state 78−19238
H_3 and He, stopping powers meas. 80−42904
H^{3+} amino acid complexes, supersensitive transition intensities, spectra *(Russian)* 77−88461
^{165}H muonic X-rays, K- and L-transitions energies meas. 77−79711

holmium continued
Ho I, Ho II, excited level lifetimes and oscillator strengths, visible spectra 80−63573
Ho I, II spectra in photographic IR region 77−14382
Ho III, energy levels, parametric anal. of spectrum 77−46519
Ho^{3+} in molten $LiNO_3$-KNO_3, transition probabilities in absorpt. and fluoresc. spectra 79−50085
Ho^{3+} in oxygen-containing crysts., stimulated emission at low temps. 80−106526
Ho^{3+}, intermediate coupling props., relativistic average of config. wavefunctions applicability 78−17574
Ho^{3+} rare-earth ions, charge transfer and crystal field theory 80−70654
Ho:^{119}Sn, mag. hysteresis of hyperfine field, compensation in mag. field *(Russian)* 77−81039
Ho:$LiYF_4$, 750 nm laser oscill., flashlamp and dye laser pumping 78−9386
Ho:$LiYF_4$ laser, TEM_{00} mode and Q-switched operation 80−74395
Ho^{3+}:$BaYb_2F_8$ 80−95902
Ho^{3+}:$ErVO_4$, CW and pulsed laser emission at 2.0416 μm 77−19254
Ho^{3+}:$KGd(WO_4)_2$, stimulated emission by subsidiary transitions 79−3696
Ho^{3+}:$LiEr_{0.945}Tm_{0.05}Ho_{0.005}F_4$ laser, tuning at 2.06 μm 80−83611
Ho^{3+}:$LiYF_4$, 1.392, 1.673 and 3.914 μm stimulated emission, laser cascades 80−9886
Ho^{3+}:$LiYbF_4$, active medium for Nd laser freq. convertor, cascade stimulated emission 80−102727
Ho^{3+}:$LiYbF_4$. laser converter for 2.06 μm radiation, ND primary laser 79−18427
Ho^{3+}:YAG, 2.09 μm stimulated emission, resonant pumping by Nd laser 78−17944
Ho^{3+}:YVO_4, CW and pulsed laser emission at 2.0412 μm 77−19254
$Ho+H^+$, relativistic K-shell ionisation cross-section meas. 78−33593
$Ho+H^+(^3He^+)$, X-ray intensity ratios, projectile energy depend. 80−23535
$Ho+N_2O \rightarrow HoO^*+N_2$ chemiluminesc. reaction, cross-section 78−76847
$Ho_3Ga_5O_{12}$:Ho^{3+}, stimulated emission 77−52135
HoI, relative oscill. strengths 79−98038
$Ho_3Sc_2Al_3O_{12}$:Ho^{3+}, stimulated emission 77−52135
^{67}Ho-^{19}F(^{28}Si), target Lα X-ray prod., projectile charge state depend. 79−47549
^{155}Ho $L_{2,3}$ subshell X-ray fluorescence and Coster-Kronig yields from ^{165}Er decay 80−69102
^{165}Ho, calibration of isomer shifts by conversion electron spectroscopy 80−39918
^{166}Ho, calibration of isomer shifts by conversion electron spectroscopy 80−39918
^{166}Ho, electrosorption on anodically polarised Pt surface 79−52684
$KY(WO_4)_2$:Ho^{3+}, 3 μ stimulated emission at 300K 80−20667
$LaCl_3$:Ho^{3+} parametric energy level anal. 78−18991
LaF_3:Ho, cryst. field anal. of triply ionised ion spectra 80−2796
LaF_3:Ho^{3+}, laser excited fluorescence absorption spectra, symmetry groups 78−60514
LaF_3:Ho^{3+} single crysts., multiphonon relax., fluoresc. obs. 79−47495
LaF_3:Ho^{3+}(Dy^{3+}), laser excited fluoresc. rise and decay meas., expt. 80−22448
$LaNbO_4$:Ho^{3+}, EPR and spin-lattice relax., Stark levels *(Russian)* 77−85563
$LaNbO_4$:Ho^{3+} crystal, 3 μm stimulated emission by Ho^{3+} ions 79−99910
$La_2S.3GaS_3$:Ho^{3+}, fluoresc., visible and IR spectra assignments 77−52150
$LiYF_4$:Ho^{3+}, optical absorpt. and luminesc. spectra 79−4844
$LiYF_4$:Yb^{3+}, Ho^{3+}, sensitised anti-Stokes luminesc., theory 77−66537
$Lu_3Al_5O_{12}$:Er^{3+}(Ho^{3+}), stimulated radn., electron-phonon interaction *(Russian)* 77−8605
$Lu_3Al_5O_{12}$:Ho^{3+}, sensitized stimulated emission at 3 microns 80−53302
$LuYScO_3$:Ho^{3+}, thermolum. meas. 80−97354
NaBr:Eu^{2+},Ho^{3+}, single cryst., cluster luminesc. centres *(Russian)* 77−20922
NaBr:Ho^{3+},Eu^{2+}, single cryst. synthesis, rel. to purification methods 77−8744
Na_2O-TeO_2:Ho^{3+}(Er^{3+})(Yb^{3+}) glass, luminesc. quenching by OH and OD *(Russian)* 79−28839
$NaYF_4$:Ho, Yb, two photon anti-Stokes effect, excited by 2 μm radiation 78−50852
Si:Ho, impurities behaviour 79−78568
SnO_2:Ho^{3+}, luminesc. and charge compensation 78−76532
SrF_2:Ho, far IR spectra 79−33736
SrF_2:Ho, V_k-centre recomb. kinetics, phosphoresc. 77−55817
SrS:Ho phosphor, prep. methods, X-ray diffr. appraisal 77−51350
$Tb^{3+} \rightarrow Ho^{3+}$, diffusion limited energy transfer in DMSO soln., fluoresc. obs. 79−61428
YAG:Er^{3+}(Ho^{3+}), stimulated radn., electron-phonon interaction *(Russian)* 77−8605
YAG:Ho^{3+}, low-lying cryst. field levels 79−91007
YAG:Ho^{3+}, oscillator strengths of impurities, 5000 to 30000 cm^{-1} 79−4830
YAG:Ho^{3+}, spectroscopy, stimulated emission 80−93374
$Y_3Ga_5O_{12}$:Ho^{3+}, low-lying cryst. field levels 79−91007
$Y_{1-x}Gd_xAl(Sc)O_3$:Ho^{3+} and $Y_{1-x}La_xAl(Sc)O_3$:Ho^{3+}, stimulated emission of Ho^{3+} ions 77−81126
Y_2O_2S:Ho, Yb, two photon anti-Stokes effect excited by 2 μm radiation 78−50852
Y_2SiO_5:Ho^{3+}, single cryst luminesc. and stimulated emission 77−69895
$(Y_{0.80}Yb_{0.19}Ho_{0.01})F_3$, IR to visible conversion 78−48210
Zn tellurite: Ho^{3+} glass, visible green emission 79−15523

holmium alloys
hexagonal anisotropy effect on thermal expansion 79−51283
Mo Co_2, single crystal, polarised neutron diffraction, various temp. and applied fields 78−2650
Ag-Ho, dil., high field magnetoresist. 80−15503
Au-Ho, dil., conduction electron-local moment interactions using dHvA waveshape anal. 79−77981
Au-Ho nuclear orientation thermometer for use from 1-30 mK 79−17419
$Ce_{0.73}Ho_{0.27}Ru_2$, spontaneous mag. order below superconducting transition temp., Mossbauer study 80−39701
$Ce_{0.73}Ho_{0.27}Ru_2$, superconductors, mag. correlations and crystal-field levels 80−34547

holmium alloys continued
$(Ce_{1-c}Ho_c)Ru_2$, superconducting, mag. props., neutron scatt. study 80−44808
Co-Ho film, amorphous, stripe domains and mag. anisotropy by Lorentz microscopy 77−63243
Co-Ho-Sm magnet, prep. and characterisation 77−8351
Dy-Ho, Kaufman approach to calc. of intra-rare earth phase diagrams 80−25657
$Dy_{1-x}Ho_xNi_2$, cryst. field quenching of Dy^{3+} 4f shell, Mossbauer effect meas. 78−39480
$Er_{1-x}Ho_xRh_4B_4$, mag. and supercond. transitions, cryst. field effects 80−107950
$Fe_2(Tb_{0.2}Dy_{0.22}Ho_{0.58})$, highly magnetostrictive alloy, vibrating-reed meas. of ΔE effect and internal friction 79−42819
Ga-Ni-R, (R=Dy, Ho, Er, Tm, Lu), struct. determ. by X-ray powder method *(Ukrainian)* 80−39001
Gd-Ho, mag. anisotropy, magnetisation meas. 77−12115
$Gd_{0.99}Ho_{0.01}(Rh_{1-x}Fe_x)_2$, spin echo meas. on ^{165}Ho, quenching effect of Fe substitution 78−48079
$(Ho,Y)Co_2$, first order phase transitions 78−84426
$(Ho,Y)Co_2$, mag. props., elec. resist. and thermal expansion 78−76246
Ho-Ag, crystal field parameters from neutron spectra, rel. to mag. props. in ordered state 77−43546
Ho-Al_2, cubic Laves phase compounds, exchange striction determ. 80−44895
Ho-Au, dil., hyperfine interaction of Ho^{3+}, nuclear orientation expts. 78−43717
Ho-Au, dil., Mossbauer exam. of mag. hyperfine field at ^{197}Au impurity 78−88244
Ho-Cd, dil., elec. field gradient, at ^{111}Cd impurities, temp. depend. 79−28642
Ho-Co, amorphous film, Kerr and Hall effect meas. 77−24722
Ho-Co alloy amorphous thin films, anisotropic mag. and microstruct. props. 78−95487
Ho-Co amorphous film, anomalous Hall hysteresis loops near compensation point 78−19286
Ho-Co amorphous film, prep. by dual-source evaporation, mag. props. 77−89988
Ho-Co film, amorphous, microstruct. and magnetism 78−64230
Ho-Co film, evaporated, struct. and mag. anistoropy, electron microscopy 79−56578
Ho-Co film, vapour quenched, amorphous, struct., electron diffr. meas. 77−28086
Ho-Cu, crystal field parameters from neutron spectra, rel. to mag. props. in ordered state 77−43546
Ho-Cu intermetallics, resist. and magnetoresist., mag. ordering obs. 80−70677
Ho-Dy-Sm, magnetic moment growth due to Sm addition *(Russian)* 80−34608
Ho-Fe-O system, O-stabilised intermetallic $Ho_{12}Fe_{32}O_2$, prep. and characterisation 77−8956
Ho-Ga, exam. of phase diagram, using differential thermal and X-ray phase anal. *(Russian)* 79−11555
Ho-Ga-Ni (60, 30 wt.%) cryst. struct., isostructural compound structural study 80−33930
Ho-La, HCP, mag. phase diagram, neutron diffr. meas. 80−70950
Ho-Mg, crystal field parameters from neutron spectra, rel. to mag. props. in ordered state 77−43546
Ho-Sm, Hall effect, field and temp. depend., 4.2-150K, singularities *(Russian)* 80−29387
Ho-Sm, magnetic moment growth due to Sm addition *(Russian)* 80−34608
Ho-Sm, magnetic phase diagrams, helicoid-ferromag. transform. *(Russian)* 80−50089
Ho-Sm(Eu), mag. props. at low temp. in high mag. fields 79−56570
Ho-Sn, dil. alloy, hyperfine interaction of ^{119}Sn, Mossbauer meas. 78−91998
Ho-Ta, dil., elec. field gradient at ^{181}Ta, temp. depend., TDPAC meas. 79−95689
Ho-Ta, dil., mag. hyperfine field determ., TOPAC meas. 79−91330
Ho-Tb (50 wt.%) alloy, mag. phase diag. from anomalous US propag. 78−6526
Ho-Zn, crystal field parameters from neutron spectra, rel. to mag. props. in ordered state 77−43546
HoAg, amorphous, bulk mag. props., field, time and temp. depends. 77−89932
$HoAl_2$, anisotropic magnetostriction, temp. depend. 80−39841
$HoAl_2$, biquadratic pair coupling from mag. anisotropy 77−28383
$HoAl_2$, cryst. field volume magnetostriction calc. 79−8029
$HoAl_2$, heat capacity, 1.5-12K, magnetocryst. anisotropy effects 78−68236
$HoAl_2$, Ho moment reorientation, polarized neutron diffr. study 79−42761
$HoAl_2$, magnetisation and neutron diffr. meas., cryst. field and exchange 77−63163
$HoAl_2$, magnetisation reorientation 79−87291
$HoAl_2$, magnetoelastic effects on elastic consts., 4.2-280K 78−72385
$HoAl_2$, orbital and spin polarisations of cond. electrons 80−65791
$HoAl_2$, single cryst., redeterm. of Ho neutron scattering length 79−99032
$HoAl_2$, spin reorientation, sp. ht. meas. 79−73724
HoAlGa, mag. props. and struct. 78−39302
$HoAl_xGa_{2-x}$, mag. props. and phase transitions 80−25133
$HoAu_3$, mag. phase diagram 80−75761
$HoAu_3$, mag. props. *(German)* 79−51761
$HoAu_{3.6}$, ordering temps. and effective moments 78−60283
Ho_2Au, mag. props., 4.2-300K 79−7972
HoAuNi$_4$, mag. props. 77−20595
$Ho_3Au_3Sb_4$, mag. suscept. meas., 4 to 300K 79−51742
HoBi, electronic struct., LCAO calc. *(Russian)* 77−39777
HoCo film, amorphous, sputtered, in-plane anisotropy induced by rare gas annealing 78−84458
$HoCo_2$, cryst. field induced spin rot., Mossbauer meas. 77−16227
$HoCo_2$, easy direction of magnetisation, Mossbauer data, 4.2K 78−43584
$HoCo_2$, elec. resistivity, thermopower, X-ray struct. meas. 80−24874
$HoCo_2$, field induced vol. magnetostriction 78−91920
$HoCo_2$, ground state spin excitations, inelastic nneutron scatt. study 80−50077
$HoCo_2$, mag.excitations, neutron inelastic scatt. meas. 80−60231
$HoCo_2$, magnetisation reorientation 78−23300

holmium alloys continued
$HoCo_2$, paramag. and ordered phases, Pauli type Co susceptibility, polarised neutron diffr. obs. 77−63077
$HoCo_2$, spontaneous vol. magnetostriction and thermal expansion meas. 77−12183
$HoCo_2$, sublattice magnetisation, powder neutron diffr. meas. 79−19725
$HoCo_2$, vol. magnetostriction, point charge cryst. field model 77−63254
$HoCo_2$:^{57}Fe, easy magnetisation directions, spin rotation like transitions 77−63168
$HoCo_3$, effect of absorbed H_2 on mag. behaviour 79−33483
$HoCo_3$, Ho_2Co_7, $HoCo_{5.5}$ and Ho_2Co_{17}, Kerr effect determ. of domain structure, Bloch wall energy 80−39806
$HoCo_5$, mag. moment orientation, anisotropic mol. field model 77−89950
Ho_2Co_{17}, magnetisation, magnetocryst. anisotropy and magnetostriction 77−8303
Ho_2Co_{17}, single cryst., magnetostriction const. temp. depend., 78 to 300K 79−51836
Ho_2Co_{17}, spin wave excitations, 4.8 and 78K 80−60230
Ho_4Co_3, cryst. field effect on mag. moment direction, neutron diffr. meas. 78−80132
Ho_xCo_{1-x} amorphous films, microstruct. and mag. anisotropy 79−82838
HoCoAl, mag. props. 78−2659
$HoCo_{5.5-x}Mn_x(Fe_x)(Ni_x)(Cu_x)$, cryst. struct. and mag. props. 80−75800
$HoCo_{5-x}Ni_x(Cu_x)$, lattice parameters and mag. props. 79−82817
$HoCu_2$, mag. struct. and elec. resist., neutron diffr. obs. 80−60206
Ho_xCu_{1-x}, amorphous film, magnetisation meas., local anisotropy effects 78−68309
$HoCu_4Ag$, mag. props. and cryst. struct. 77−20562
$Ho_xDy_yTb_{1-x-y}Fe_2$, Laves phase cpds., anisotropy and magnetostriction 77−63167
$HoFe_2$, amorphous, small angle neutron scatt. study of mag. order and mag. microstruct. 79−15283
$HoFe_2$, amorphous, struct. determ., EXAFS exam. 78−51421
$HoFe_2$, amorphous, ultrasonic exam. below T_c 79−73793
$HoFe_2$, crit. phenomena, Mossbauer effect 78−52403
$HoFe_2$, crystal field interaction contribution to specific heat 80−39788
$HoFe_2$, Czochralski growth, and cryst. quality determ. 77−8742
$HoFe_2$, effect of H on sublattice magnetization, elastic neutron scatt. obs. 79−78327
$HoFe_2$, electronic heat capacity coeffs. 80−39787
$HoFe_2$, mag. struct., polarized neutron diffr. study 79−78326
$HoFe_2$, magnetostriction and magnetisation temp. depend. 79−73795
$HoFe_2$, magnetostrictive material, changes in vibr. modes near mag. phase transition 79−90736
$HoFe_2$, spin wave and cryst. field excitations, neutron scatt. 78−68196
$HoFe_2$, spontaneous magnetoelastic distortion, X-ray diffr. expts. 77−63253
$HoFe_3$ and Ho_6Fe_{23}, magnetostriction, room temp. to 80K 80−65993
$HoFe_3$, effect of adsorbed H on mag. props. 77−63129
$Ho_{1-x}Fe_x$, amorphous film, cosputtered, struct. and mag. props. 78−60323
Ho_6Fe_{23}, magnetostriction, temp. depend., 20 to 350K 80−65994
Ho_xFe_{1-x} amorphous film, crystn., TEM obs. 79−87019
HoFeAl, scatter order cpd., mag. props. 77−51891
$HoFe_4Al_8$, mag. props. 78−52250
$Ho_2Fe_3Co_{14}$, Kerr effect determ. of domain structure, Bloch wall energy 80−39806
$HoFe_2H_{4.5}$, mag. props. and lattice consts., effect of hydrogen absorpt. 77−20561
HoFeMn, Laves phase, mag. moment on Ho, neutron diffr. obs. 77−63107
$Ho(Fe_{1-x}Mn_x)_2$, phase struct., mag. and Mossbauer meas. 77−20563
$Ho(Fe_xNi_{1-x})$, mag. interactions, mol. field model 77−73010
$Ho(Fe_xNi_{1-x})_2$, mag. behaviour, susceptibility and Mossbauer expts., 4.2-1300K 78−52235
$Ho(Fe_xRh_{1-x})_2$, mag. props., Mossbauer spectra 80−25108
$HoFe_2Si_2$, mag. props. 4.2 to 950K 77−20544
$Ho_2Fe_4Si_9$ and $HoFeSi_3$, cryst. struct. and mag. suscept., temp. depend. *(Russian)* 78−34957
HoGa, ferromag., mag. props., 4.2 to 350K 77−63230
$HoGa_2$, mag susceptibility, 1.5-300K and Neel temp. 78−68184
$Ho_{0.01}Gd_{1-x}Y_xNi_2$, spin echo meas. on ^{165}Ho, limited quenching of Ho moment by cryst. field 79−73851
Ho_5Ge_4, mag. struct., neutron diffr. study 80−25093
Ho_2In, mag. props., 4.2 to 270K 79−56512
Ho_3In, mag. props. 80−108009
Ho_5Ir_2, cryst. struct. 80−96473
$HoMn_{12}$, mag. interactions, mag. meas. and neutron diffr. 77−63103
$HoMn_2$, Laves phase, mag. moment on Ho, neutron diffr. obs. 77−63107
$Ho_{30}Nd_{70}$, mag. struct. and ordered moments, neutron diffr. data 77−66252
$HoNi_2$, Mossbauer effect of ^{57}Fe 77−69743
$HoNi_3$, amorphous, resist. meas., 1.2-290K 78−19015
$HoNi_5$, ferromag., magnetisation and paramag. susceptibility 80−25082
Ho_2Ni_{17}, ferrimag. struct., neutron diffr. expt., cryst. field calcs. 77−73001
$HoNi_{0.5}Cu_{0.5}$, sp. ht. and modulated mag. struct. 77−32167
$HoNi_{0.7}Cu_{0.3}$, mag. behaviour 79−99688
$HoNiSi_3$, mag. susceptibility, 80-1200K *(Russian)* 77−66281
Ho_3Os, cryst. struct. 80−96474
Ho_5Pd_2, mag. props. 77−20547
$Ho_{40}Pr_{60}$, mag. struct. and ordered moments, neutron diffr. data 77−66252
$HoPt_5$, low temp. mag. susceptibility 80−93075
Ho_2Pt, mag. susceptibility meas., mag. transitions obs. 80−60222
Ho_3Pt_4, mag. props., 4.2 to 160K 79−78343
Ho_5Pt_4, isotypic with Pu_5Rh_4, X-ray cryst. struct. refinement anal. 79−4271
HoSb, mag. phase diagram, quadrupolar interactions 80−65820
HoSb, quadrupole scatt. anisotropy, magnetically ordered material 78−64034
HoSm elec. props. in temp. range near zero to 150K *(Russian)* 79−11098
$Ho_xTb_{1-x}Co_2$ lave phase compounds, elastic props., temp. and magnetic field dependence 80−60393
$Ho_{0.58}Tb_{0.20}Dy_{0.22}Fe_2$, magnetoelastic surface wave propagation, mag. field depend. 77−85535
$(Ho_{0.58}Tb_{0.2}Dy_{0.22})Fe_2$, microwave mag. props. 80−65860

holmium alloys continued
$Ho_xTb_{1-x}Fe_2$, and $Ho_xTb_yDy_{1-x-y}Fe_2$, high magnetostriction cpd., mag. anisotropy origins 78−68217
$Ho_xTb_{1-x}Fe_2$, Laves phase, mag. anisotropy meas., cubic harmonic anal. 78−84410
$Ho_xTb_{1-x}Fe_2$, single cryst., spin orientations 78−84425
$Ho_xTb_{1-x}Fe_2$, single crystals, continuous spin orientations, magnetisation easy direction 78−84453
$Ho_xY_{1-x}(Fe_{0.1}Co_{0.9})_2$, ^{57}Fe hyperfine interaction, mag. props., Mossbauer study 80−39951
$Ho_{1-x}Y_xNi$, ferromag. behaviour, struct., Curie temp. 79−99677
$Ho_xY_{1-c}Sb$ system, magnetisation, elec. resist., and sp. ht. meas. 80−60213
HoZn, mag. excitations near spin rot. temp., neutron scatt. study 79−19731
HoZn, magnetic excitations 80−25115
HoZn, magnetoelastic and quadrupolar couplings 78−52328
HoZn, magnetoelastic consts. 78−15005
HoZn, spin wave spectrum, Green function analysis 78−2666
^{181}Ho-^{181}Ta, dil., elec. field gradient at impurity, anomalous temp. depend., host 4f levels, γ-γ correls. 78−95272
La-Ho/AlO_x/Al tunnel junctions, cond. meas., cryst. field effects 80−88694
Mg-Ho, dil., macroscopic shape effect due to quadrupole orientation, magnetostriction and thermal expansion meas. 80−60396
Mg-Ho, dil., magnetoresist., anomalous Hall effect 80−15502
Mg-Ho, phase diagrams and transformations, Ho solubility *(Russian)* 79−52162
Nd-Ho, HCP struct., mag. props. 77−63177
Ni-Fe-Ho film strips, domain struct. and new rot. processes 77−85533
NiFe-Ho film strips, curling-type mag. domains 77−48020
Pr-Ho, HCP struct., mag. props. 77−63177
rare earth-Ho dil. alloy, nucl. spin-lattice relax. of ^{165}Ho 78−48069
Tb-Dy-Ho, phase diagram, alloy struct. *(Russian)* 77−25016
Tb-Ho, influence of internal strain on Neel temp., thermal expansion and elastic const. meas. 77−63176
Tb-Ho, Kaufman approach to calc. of intra-rare earth phase diagrams 80−25657
Tb-Ho, paramag., anomalous thermal expansion, up to 273K 79−7967
Tb-Ho, single cryst., annealed, thermal expansion 78−47541
Tb-Ho, thermal expansion in vicinity of Curie temp. 79−28524
Tb-Ho, US attenuation and elastic consts. in 3 mag. phases, 4.2 to 300K 77−72645
Tb-Ho (50%), antiferromagnetic, thermal expansion, US attenuation anomalies 79−47319
Tb-Ho film, helimag. order, surface deform., exchange and single-ion magnetocrystalline anisotropy energy 77−66390
$Tb_{0.20}Dy_{0.22}Ho_{0.58}Fe_{1.95}$, grain-oriented, permeability, magnetomechanical coupling and magnetostriction 79−78491
$Tb_xDy_yHo_zFe_2$, temp. depend. of magnetomechanical coupling factor 77−90002
$Tb_{0.5}Ho_{0.5}$, ferromag. and helical phase, spin wave dispersion relations 79−24149
Th-Ho (1 at.%), Heisenberg exchange, residual resist. meas. 80−75558
Y-Ho, mag. susceptibility, 4.2 to 300K, Neel temps. 79−19735
$Y_{1-x}Ho_xCo_5$, NMR meas. of ^{59}Co 77−85585

holmium compounds
see also holmium alloys
ethylsulphate, pseudomagnetic moment of ^{165}Ho and spin-lattice relax. times 77−63306
formate, IR spectra and phase transitions, under pressure 78−31179
phthalocyanine solutions, bleaching by ruby laser beam 78−30030
vac. thermal reduction with Th, for Ho prod. *(Russian)* 80−16226
Al_2O_3-Ho_2O_3 system, high temp. phase diagrams 80−40340
$(Al_2O_3)_{0.2}(Ho_2O_3)_{0.2}(SiO_2)_{0.6}$, amorphous low temp., AC susceptibility, freq. depend. of spin freezing temp. 79−82808
CdF_2:HoF_3 films, electroluminesc. meas. *(French)* 79−11471
$CsHo(MoO_4)$, permittivity temp. depend., polymorphic transition 80−92670
$CsMHoF_6$, (M=Na, K, Rb), mag. behaviour *(German)* 80−65774
$Dy_{0.5}Ho_{0.5}FeO_3$, mag. transitions, influence of Dy^{3+}, Ho^{3+} ground states 77−89955
$Dy_{0.5}Ho_{0.5}FeO_3$ orthoferrite, domain struct., temp. depend. 80−71086
$Er_{0.3}Ho_{0.7}FeO_3$, mixed orthoferrite crystals, ^{57}Fe NMR in spin reorientation range 78−15039
$(Er_{0.6}Ho_{0.4})Rh_4B_4$, reentrant supercond., magnetisation meas. near lower crit. temp. 80−25043
$Er_{1-x}Ho_xRh_4B_4$, ferromagnet, sp. ht anomaly at lower superconducting transition temp. 79−47194
$Er_{1-x}Ho_xRh_4B_4$, re-entrant supercond. and mag. ordering 78−60240
$Er_{1-x}Ho_xRh_4B_4$, supercond., phase diagrams and upper crit. fields 80−2531
$(Er_{1-x}Ho_x)Rh_4B_4$, superconducting ferromag., Josephson effect, point contact junction meas. 80−7043
$(Er_{1-x}Ho_x)Rh_4B_4$, superconductive and mag. interactions, hydrostatic press. effect 80−49973
$Er_{1-x}Ho_xRh_4B_4$, ternary superconductor, mag. interactions 79−73613
$Er_{1-x}Ho_xRh_4B_4$ type cpds., supercond., phase stratification *(Russian)* 79−42685
GdF_3-HoF_3, stabilisation of rhombic β-YF_3 type struct. 78−67700
HaIG, spontaneous Faraday rot. rel. to sublattice magnetisation 80−66159
Ho-YIG, magnetic props. in strong fields at low temp., Ising approx. calcs. *(Russian)* 80−54920
$HoAlO_3$, Czochralski growth and props. 77−48335
$HoAlO_3$, electronic and nucl. mag. ordering, mol. field approx. 80−60157
$HoAlO_3$, neutron diffr. at 0.04K, mag. ordering *(French)* 78−10653
$HoAlO_3$:Yb^{3+}, Mossbauer relax. 80−15875
$HoAl_3[BO_3]_4$, thermal stability, X-ray struct. anal., refractive indices 79−4297
HoB_{12}, nature of magnetism *(Russian)* 78−31049
HoB_4, antiferromag. props. *(French)* 77−20566
HoB_4, mag. and elec. props., metallic character 80−20386
$Ho_4Ba_6(BO_3)_9$, flux growth and chem. characts. 78−23595
HoBi, thermal expansion, thermal cond., 300-900K 78−91453
$HoBiTe_3$, prep., elec. props., and crystallographic date 80−59981
$HoCO_3Y^{3-}$, (Y=ethylenediaminetetracetate ion), formation constants *(French)* 80−104458
$HoCl_3$, white line struct. in X-ray L_{III} absorption edge 79−15560

holmium compounds continued
$Ho(ClO_4)_3$, osmotic coeffs. 80−45556
$HoCl_3.6H_2O:Gd^{3+}$, spin Hamiltonian parameters EPR meas. 77−36128
$HoCl_3.6H_2O$-$EuCl_3.6H_2O$, in DMSO soln., $Eu^{3+}\rightarrow Ho^{3+}$ radiationless energy transfer 80−5499
$HoCoGa_5$, X-ray cryst. struct. determ. 80−1993
Ho_2CoGa_8, X-ray cryst. struct. determ. 80−1993
$HoCo_2Ge_2$, crystal and magnetic structure obs. 80−64976
$HoCoO_3$, ^{59}Co NMR, quadrupolar and hyperfine interactions 79−15366
$HoCoO_3$, spin state of Co^{3+} ion, X-ray photoemission line broadening 79−82751
$HoCo_2Si_2$, mag. props. 80−107988
$HoCrO_3$, cryst. field levels and mag. interactions, inelastic neutron scatt. study 77−69277
$HoCrO_3$, Ho^{3+} mag. form factor meas. by inelastic neutron scatt. 78−52221
$HoCrO_3$, mag. form factor of Ho^{3+}, inelastic neutron scatt. meas. 77−16050
$HoCrO_3$, magneto-optical investig. of Ho-Cr and Ho-Ho interactions 77−52055
$Ho_{0.5}Dy_{0.5}FeO_3$ orthoferrite, domain wall struct., stability conditions, Morin transition, anisotropy const. 80−34684
$Ho_{0.7}Er_{0.3}FeO_3$, crystn. on seeds, layer morphology 78−72041
HoF_3, ^{19}F NMR, ligand hyperfine interaction, shift tensor determ. 78−48056
HoF_3, bomb calorimetric determ. of enthalpy of formation 80−50879
HoF_3, crystal growth by Bridgman-Stockbarger method and Czochralski method 78−52660
HoF_3, crystal structure by powder neutron diffr. study 80−15077
HoF_3, enthalpy of formation by calorimetry 80−7843
HoF_3, mol. force, compliance and Coriolis consts. 79−31726
HoF_3, monocrystal, thermal cond., temp. dependence 77−55402
HoF_3, single cryst., Ho^{3+} energy level spectrum calc. 79−1586
HoF_3, thermodynamic props., galvanic cell meas. 80−21316
$HoFe_2B_2$, compounds with $CeAl_2Ga_2$ structure type *(Ukrainian)* 79−32970
$HoFe(CN)_6.5H_2O$, powder, elec. transport props. obs. 80−70701
$HoFe_2H_x$, mag. props. 80−25095
$HoFeO_3$, field induced spin reorientation, Mossbauer spectroscopy 80−65878
$HoFeO_3$ orthoferrite, rare earth-Fe interactions 79−56525
$HoFeO_3$, Raman scatt. from magnons, anisotropy consts. determ. 80−66178
$HoFe_2O_4$, magnetic props., 77-300K 80−11225
$Ho_{12}Fe_{32}O_2$, struct. and ferrimag. props., neutron diffr. obs. 79−78319
$Ho_3Fe_5O_{12}$:Pb film, grown from fluxed metals by LPE 77−24972
HoGa garnet, mag. ordering induced by hyperfine interaction, neutron diffr. meas. 77−66265
$Ho_3Ga_5O_{12}$, hyperfine interac. induced antiferromag. order *(French)* 77−59392
$Ho_3Ga_5O_{12}:Ho^{3+}$, stimulated emission 77−52135
$HoH_2(D_2)$, mag. props., 1.5 to 10K, Mossbauer meas. 79−78578
HoIG, anomalous Faraday behaviour, mag. props. 79−82955
HoIG, Faraday rotation, mag. field depend., 4.2 to 300K, magneto-optical coeffs. 78−95577
HoIG, mag. permeability, Faraday rotation expts. 77−16287
HoIG, mol. field coeffs., magnetisation and mag. susceptibility anal. 78−95406
HoIG, spin reorientation from Faraday effect meas. 79−51780
$Ho(Ir_xRh_{1-x})_4B_4$ pseudoternary system, supercond. and mag. ordering 80−70876
$Ho_{1.15}Lu_{0.05}Mo_6S_8$, long range mag. order in supercond. state 79−65653
$Ho_2(MoO_4)_3$, DC electrical cond., 650 to 1150K 79−60831
$Ho_2(MoO_4)_3$, mag. susceptibility, ferromagnetism, mol. field theory 78−34966
Ho_2MoO_5, cryst. struct., IR spectra, elec. and mag. props. 80−33954
$HoMo_6S_8$, long range mag. order in supercond. state 79−65653
$HoMo_6S_8$, reentrant supercond., direct. obs. of long range ferromag. order 78−76190
$HoMo_6S_8$, superconductor, neutron scatt. exam. of mag. phase 79−73680
$Ho_{1.2}Mo_6S_8$, low temp. magnetisation meas., and supercond. props. 79−8018
$Ho_{1.2}Mo_6S_8$, re-entrant ferromag. supercond., heat capacity and AC mag. susceptibility 79−60948
$Ho_{1.2}Mo_6S_8$, supercond. destruction by mag. ordering 77−69449
$Ho_{1.2}Mo_6S_8$, supercond. transition temp., upper critical field, local spin fluctuations 79−38250
$HoMo_6S_8(Se_8)$, mag. supercond., neutron scatt. obs. 80−70952
$Ho_{1.2}Mo_6Se_8$, crystal field excitations, inelastic neutron scatt. obs. 79−78321
HoN, vaporization enthalpy, Knudsen cell vaporization of rare earth nitrides 79−10936
$Ho(NO_3)_3$ solns., f-f transitions, intensity anal., correl. with cond. and US absorpt. 80−97292
$HoNbO_4$-$CaWO_4$, phase transitions of fergusonite-scheelite *(French)* 80−19942
$HoNi_2Si_2$, mag. props., 4.2-200K 80−84602
Ho_2O, Ho_2O_2, HoO_2, atomisation energies and stand. ht. of formation 77−54622
Ho_2O_3, 300 to 900K, mag. susceptibility and Curie temp. meas. 78−56288
Ho_2O_3, EXAFS and chemical shift 77−81176
Ho_2O_3, photoacoustic spectra using Helmholtz reson. cells 80−9048
Ho_2O_3 powder, redeterm. of Ho neutron scattering length 79−99032
Ho_2O_3, powdered cryst., high resolution optoacoustic spectroscopy 80−31898
Ho_2O_3, solid, photoacoustic spectra 78−58044
Ho_2O_3, white line struct. in X-ray L_{III} absorption edge 79−15560
Ho_2O_3, XPS, charging effects on core-level binding energies 79−24409
Ho_2O_3-GeO_2-NaOH-H_2O, hydrothermal crystallisation 77−40344
$(Ho_2O_3)_{0.194}(Al_2O_3)_{0.227}(SiO_2)_{0.579}$, amorphous, low temp. spin glass behaviour 80−60297
$Ho(OH)_3$, Mossbauer spectra, cryst. field and mag. props. 80−15873
Ho_2O_2S powder, redeterm. of Ho neutron scattering length 79−99032
$Ho_2O_2SO_4$, antiferromag., mag. props. and Zeeman effect meas. 79−33464
$Ho_2O_2SO_4$, antiferromag., specific heat, 0.6 to 30K 79−33487
$Ho_2O_2SO_4$, mag. ordering, magnetisation, AC susceptibility and Zeeman effect meas. 80−60205

holmium compounds continued
$Ho_2O_2SO_4$, magnetic phase diagram, magnetisation and mag. susceptibility meas. 80−15720
$Ho_2O_2SO_4$, magnetic struct. in antiferromag. and ferrimag. states 80−15695
HoP, flopside mag. struct. to ferromag. transition, elastic neutron scatt. obs. 80−50058
$HoPO_4$, cryst., IR spectra, complex anions internal vibrs. resonance splitting 80−34907
$HoPO_4$, IR and Raman spectra 80−34904
$HoPO_4$, metamagnet, mag. phase transitions, elastic neutron scatt. study 79−78371
$HoPO_4$-$Pb_2P_2O_7$, solubility curves for high temp.-melts for growth of single crysts. 78−95687
$HoPo_4$, single crystal, conditions for transfer and formation 77−12507
$HoRh_4B_4$, cryst. struct., X-ray diffr. 77−89423
$HoRh_4B_4$, electronic struct. and reentrant magnetism 78−10340
$HoRh_4B_4$, ferromag., mag. struct., neutron diffr. obs. 79−78323
$HoRh_4B_4$, ferromag. Curie temp. 77−89893
$HoRh_4B_4$, low temperature magnetic properties 80−88728
$HoRh_4B_4$, NMR and sp. ht. in supercond. and mag. ordered phases 80−7037
$HoRh_4B_4$, supercond., re-entrant magnetism, energy band calcs. 78−52140
Ho_2S_3, polymorphic transforms. on impact compression 77−47575
$Ho_3Sc_3Al_3O_{12}:Ho^{3+}$, stimulated emission 77−52135
$HoScO_3$, synthesis and lattice const. 78−30593
Ho_2Se_3, elec. resist., thermoelectromotive force, temp. depend., 300 to 1400K *(Russian)* 78−84243
Ho_2Se_3, mag. susceptibility 77−40032
$Ho_2(SeO_4)_3.SH_2O$, thermal decomp. and IR spectra 80−3319
C-,D-$Ho_2Si_2O_7$, single cryst. flux growth 79−52097
$Ho_xSn_xMo_6S_8$, supercond. props. 80−97023
$HoTaO_4$, heat of form. 79−83494
$Ho_{0.58}Tb_{0.2}Dy_{0.22}Fe_2$ magnetoelastic surface wave dispersion obs. 79−47321
Ho_xTe, mag. ordering, neutron diffr. meas. 78−2649
$HoTiO_3$, bulk mag. and struct. props., ferrimag. order 80−107993
$HoTiO_3$, magnetic structure determination, neutron scatt. study 80−65809
$HoVO_3$, antiferromag., at. and mag. struct., neutron diffr. meas. 79−24142
$HoVO_4$, below 1K, nuclear orientation study of Van Vleck enhanced nuclear antiferromagnet 80−88899
$HoVO_4$, enhanced nuclear cooling and antiferromagnetism 79−61070
$HoVO_4$, first excited doublet, zero field splitting 77−20870
$HoVO_4$, NMR, parameters in nuclear Hamiltonian 78−72422
$HoVO_4$, NMR predictions of properties, dipolar interactions and antiferromagnetic exchange 80−50203
$HoVO_4$, RF susceptibility below 1K, mag. sp. ht. 80−84585
$HoVO_4$:Gd, indirect superhyperfine interaction, EPR line width meas. 80−2633
$Ho_2(WO_4)_3$, mag. props., 300 to 900K 79−28510
Ho_2WO_6, growth from soln. in melt 77−1806
$Ho_xY_{1-x}F_3$, calc. of $Ho^{3+}\rightarrow Ho^{3+}$ energy transfer rates *(French)* 78−79966
HoYIG, level intersection and instability of mag. struct. *(Russian)* 77−43816
$Ho_xY_{1-x}Sb$, mag. props. 80−34634
$Ho_2Zr_2O_7$ dielectric thin films from vaporisation by cathode ray and HF ion-plasma methods 77−77380
$KHo(PO_3)_4$, cryst. struct. 77−43188
$LiHoF_4$, NMR shift tensors, temp. and field depend. 79−38391
$LiHoF_4$, uniaxial dipolar ferromag. crit. behaviour 79−61149
$LiHoF_4$, uniaxial dipolar ferromag., critical behaviour, mag. susceptibility meas. 80−80528
$LiY_{0.416}Er_{0.5}Tm_{0.067}Ho_{0.017}F_4$, Stockbarger single cryst., charact. of solidification behaviour 77−24948
$(Lu_{1-x}Ho_x)Rh_4B_4$, interaction between superconductivity and magnetism 79−38248
$Lu_{1-x}Ho_xRh_4B_4$, supercond., phase diagrams and upper crit. fields 80−2531
Na_2O-SiO_2-Ho_2O_3 glass, magneto-optical props. 79−65894
RbF-HoF_3, cpd. formation 77−44226
Sc_2O_3-Ho_2O_3, solid solution, use of segregation phenomena to exam. solidification phase diagrams *(French)* 79−8293
$(Y,Ho)VO_4$:^{165}Ho, enhanced NMR meas. 77−66428
$Y_{1-x-y}Ho_xEr_yAlO_3$, $Y_{1-x-y}Ho_xEr_yScO_3$, stimulated emission of Er^{3+} ions 78−6705
YHoIG, magnetisation anomalies in strong mag. fields *(Russian)* 77−43854

holographic gratings
aberration balancing for grating mountings with large aberrations 78−66906
aberration theory, geometrical 79−55068
aberrations, chromatic and spherical, of single glass lenses, holographic correction 79−86226
ACCOS V, commercially available optical design and anal. program 79−86230
achromatic holographic optical elements 79−22917
aspherical, for improved Wadsworth mounting 80−99824
astigmatism compensation, concave and plane holographic diffr. gratings 80−48428
asymmetrical groove profile grating prod. 78−37857
attenuated sinusoidally modulated, in volume holograms, diffraction efficiency 77−10868
attenuated thick gratings, anomalous absorption 78−1188
attenuated thick gratings, diffr. efficiency 78−1187
beam expansion with diffr. grating in dye laser cavity 78−66858
binary information image reconstruction, aberrations, shrinkage effects 78−78967
blaze properties, first, second and third order 77−79945
blazed, spectral performance, numerical anal. 77−42617
blazed holographic gratings, suitable for use on synchrotrons 78−63187
blazed ion-etched holographic grating, prod. methods, optical props. *(Japanese)* 80−10021
blazed ion-etched holographic grating prod., high spectroscopic qualities 79−76847
blazing techniques comparison 80−53438
Borrmann-like anomalous effects in volume holography 80−102664

holographic gratings continued
boundary conditions for diffracted EM fields 79−3660
Bragg and Raman-Nath diffr. regimes rel. to grating thickness 78−71028
Bragg device anal., 4-port 80−83564
Bragg effect waveguide coupler analysis 78−33827
chalcogenide glass semiconductors, holographic recording with IR readout, diffr. efficiency 78−46548
'Chirped' grating coupler: a holographic approach 79−76854
chirped grating lenses anal. 80−87563
chirped gratings, improved holography 80−102667
colour separation phase gratings 78−83072
computer-generated, prod. of two-dimens. laser beam deflections 78−58956
computer-generated holograms, techniques and appls., book contrib. 79−76645
concave, imaging properties *(Japanese)* 78−37971
concave and plane gratings, achromatic imaging of distant objects, in selective wavelength bands 78−94372
concave diffr. grating, fabrication by holographic method, astigmatism compensation 79−32067
concave grating design 80−1153
concave holographic grating, automatic design, for Seya-Namioka monochromators 79−10390
concave holographic grating, for slitless optical fibre laser Raman spectrometer 77−71380
concave holographic grating *(Chinese)* 79−72539
concentric spectrograph using holographic grating 78−32896
contour mapping of 1st and 2nd derivatives of plate deflection using modulated diffr. gratings 79−6086
coupled wave analysis of volume holograms, effect of second order derivatives 80−53232
coupled wave diffraction, holographic grating-fringe pattern phase mismatch determ. 79−50250
coupled wave theory, arbitrary attenuation 77−46707
coupler, using hologram recorded with guided wave evanescent field 77−10869
crossed Gaussian volume grating, Bragg diffr. of Gaussian beam 77−65569
crossed-beam diffraction gratings theory 79−23071
crossed-beam volume gratings, three dimens., diffr. characts. 80−78975
dephasing measure in plane wave diffraction by hologram grating 79−3659
design considerations *(Japanese)* 79−45914
design techniques advancement 79−7202
diazo salt sensitised gelatin for holographic recording, grating form. 80−78798
dichromated colloid layer holographic diffraction grating characteristics 79−27424
diffraction efficiencies of holographic transmission gratings in the region 80-1300 eV 80−90963
diffraction efficiency of amplitude binary discrete holograms 77−23633
diffraction efficiency theory 78−13790
diffraction efficiency with modulation changing through the thickness 77−3553
dispersive device linear in wave-numbers, space-time optics appls. 77−72071
dual toroidal grating XUV monochromator, performance 80 to 1280 Å 80−90941
dye CW laser, spectral narrowing and continuous tuning by grating beam-expansion 79−59720
dye CW laser, tunable by holographic grating 79−27288
dye CW laser, tuning and spectral narrowing using low-loss diffr. grating 78−71109
dye laser, narrow linewidth short pulse operation, using dual prism beam expander and grating 79−971
efficiency calculation model 80−1149
electro-optic crystals, beam coupling and light amplification 79−86137
electro-optic crystals, hologram formation arbitrary transport length anal., photovoltaic effects 80−78802
electro-optic crystals, nonlinear theory, steady state case 79−86136
electromagnetic theory as it applies to X-ray and XUV gratings under grazing incidence 80−90962
equivalence of ruled, holographic, and lamellar gratings in constant deviation mountings 80−87474
evanescent wave holograms, diffraction efficiency 79−18375
evanescent-wave holograms, diffr. efficiency, angular and polarisation depend. 80−48189
fine, made of positive photoresist AZ2400, anal. of two-dimensional etching effect on profile 78−82928
flat-field spectrograph design, holographic grating appl. 80−68264
focused light ATR method, appl. to guided waves on grating 78−74992
focusing diffraction grating, for integrated optics, holographic production *(Russian)* 77−84009
Fourier hologram machine synthesis *(Czech)* 78−66784
Fraunhofer diffr. of partially coherent light by amplitude, phase gratings 77−46681
GaAs holographic grating transduction from bulk to surface acoustic waves 77−31199
gelatin, dichromated, for holographic optical element fabrication 79−89865
gelatin, hologram filter telescope for use in dispersive laser cavity 80−9839
grazing incidence for UV monochromators using toroidal holographic gratings 80−90946
grazing incidence monochromators with holographic toroidal gratings, 10 to 150 eV 80−90947
high flux grazing incidence monochromator based on holographic grating for synchrotron radiation 78−62271
high-resolution holographic aplanatic objective *(French)* 77−83837
holographic grid production modelling, using photographic material charact. curves *(Russian)* 77−631
image correction for electron microscope aberrations 77−18139
image-forming reflection system testing by grazing-incidence Linnik interferometry 79−76891
imaging properties, aberrations 78−5563
impurity doped solid, electronic excitation spatial diffusion meas. by degenerate four-wave mixing 79−64274
in-plane strain meas. by holographic modulated diffr. grating 79−90202
incoherently superimposed gratings, optical propagation in thick holographic material 79−76634

holographic gratings continued
integrated optical functional elements based on holographic gratings in As_2S_3 film waveguides 77−79972
integrated optics, grating lens fabrication 78−75004
integrated optics light deflector using chalcogenide amorphous film on graded index $LiNbO_3$ waveguide 80−48463
interference diffraction gratings, holographic hallmarkings 79−911
interference fringe bending analysis and expt. 80−106494
interference fringe bending due to pre-stress in photographic emulsion 79−98318
interferograms of lens elements 77−72045
interferometric fabrication of diffraction grating and optical waveguide coupler 78−1440
invariant processing using combined geometrical and optical transforms 77−71935
ion-etched grating, optical props. *(Japanese)* 78−46542
laminar holographic gratings, efficiency, synchrotron radiation monochromisation 78−63189
laser damage resistances compared 77−19283
laser produced gratings, review *(Rumanian)* 80−87542
lateral shearing interferometer using gratings, high efficiency 77−26391
lens analog for holographic optical element, mathematical equivalence 79−59653
lens design techniques, 488 nm construction, 633 nm read out 79−89866
light beam transformation, by dynamic phase holograms, efficiency 77−7034
lossy idelectric attenuated hologram grating, diffraction efficiency calc. *(Japanese)* 77−38826
magnetic hologram recording, using MnBi film, diffraction efficiency anal. *(Russian)* 77−1573
matched filtering system adjustment by diffraction gratings 78−87027
mechanically ruled and holographic concave diffr. grating parameter relationships 80−87543
metal with dielec. coating, polarisation anomalies 77−62058
modal theory, thick holographic gratings with sharp boundaries, EM wave propag. 80−83672
modal theory, unslanted holographic transmission and refl. gratings, EM wave propag. 80−83673
modulated grating hologram synthesis 77−58291
moire topography, historical review 80−9024
moire topography using grating hologram, appl. to human body 77−5893
monochromator for 5 to 1000 eV synchrotron radiation 78−18049
monochromator for holographic concave grating, design *(Chinese)* 80−58676
monochromator using concave holographic grating and plane mirror, imaging props. 80−99856
multiple grating flame spectrometer, for simultaneous determ. of five elements 77−21455
multiple imaging by lensless Fourier transform holography 79−81389
multislit spectrometer for the night airglow observation 78−73542
nonlinear holographic gratings for high energy laser beam sampling 80−14476
normal incidence monochromator for synchrotron radiation, charact. modification using holographic concave gratings 78−62236
object deformation, determ. of components from 1 double-exposure hologram 79−94193
object-plane Fourier processing with volume-hologram filters 79−94172
one-dimensional kinoform preparation using photographic template *(Russian)* 79−22914
optical element generation, modification, expt. 77−83966
optical elements anamorphotic props. with astigmatism 79−98319
over-pumping energy effect, two interfering beams in nonlinear medium *(Russian)* 77−7161
overlap gratings, beam expanders diffr. efficiency 79−72680
pentacene doped p-terphenyl mol. cryst., laser induced photoacoustic grating effects 79−55215
periodic surface corrugation generation by holography 78−55469
phase control hologram grating for hologram fringe stabilisation 77−38823
phase profiles generation, recent advances, book contrib. 79−76644
phase-hologram material, using four-centre-type photopolymerisation in cryst. state 78−37832
photopolymer imaging systems, for laser recording 78−71173
photorefractive crystals with arbitrary electron transport lengths, holographic grating form. 80−1151
photosensitivity anal. of organic media *(Russian)* 77−179
plane grating, stigmatic mounting 78−25817
plane gratings, self-focusing, aberrations 77−58450
plasma-optical emission spectrometer, inductively coupled, light scatt. effect 80−86455
polarisation characteristics, concave gratings mounted in Seya-Namioka monochromator 79−18526
polarisation effects on thin transmittance grating fabrication and diffr. efficiency *(Korean)* 78−50731
polarisation orientation influence on TIR hologram diffr. efficiency 78−37836
polarizing properties 80−69342
polymeric waveguide medium, Bragg grating form. by self-fixing process 77−7215
production and basic principles, book contrib. 77−31081
production by laser irradiation of photoresist *(German)* 80−33254
production methods, characteristics, quality *(Korean)* 80−43289
pyroelectric mechanism for recording 78−42300
Raman-Nath diffr. as manifestation of two-ray Bragg diffr., holographic gratings 80−48147
ray path calculation algorithm for arbitrarily oriented holographic diffr. gratings 80−99677
reflection volume hologram, sequentially stored phase gratings, diffr. efficiency determ. 78−33704
research and development of Soviet State Optical Institute 79−94199
review of Japanese research 80−10018
ruling with stepped profile 79−76898
scanner with aberration corrections 77−61924
scattered light, specification and meas. from diffr. gratings 78−78905
self-diffraction of light by excitons 80−53389
semiconductor, dynamic conversion of light beams, by phase shifted free-carrier holograms 78−46547
semiconductor, nonequilibrium processes exam. by method of transient holograms 78−23105
semiconductor, photochemical etching mechanism 77−16709

holographic gratings continued
semiconductor film, two-photon absorpt., optically induced diffr. 77−7154
semiconductor hologram recording, photochem. etching control 80−28179
semiconductor-metal light sensitive systems for holographic gratings, charcts. 78−13810
semiconductors to record pulse holograms 79−55091
sequentially stored gratings in transmission vol. holograms, beam-coupler and splitter appls. 78−25821
sinusoidal, optimal linear transfer function determ. 80−23635
solar selective thin film absorbers, interf. films deposited on diffr. gratings 79−14103
spatial filtering of 2-D periodic structures, inspection 77−38819
spatial filtering properties of volume holograms 79−27211
spectrograph, astronomical, with holographic and ruled diffr. gratings 78−40831
spectrophotometer, high-energy, 0.25-2.4 μm, for rapid food constituent anal. 79−17508
spectrophotometer, single-beam, holographically recorded concave diffraction grating appl. 78−54468
spectrophotometer, UV-visible, high throughput, optical and optomechanical design 80−95155
specular multiplexed holograms recorded on Kodak 649F plates, diffr. efficiency 80−23638
stigmatic imaging with pair of concave gratings 79−72670
stigmatically focusing grating coupler formation 79−59842
thick grating, multiwave diffr. anal. 78−9445
thick grating, recorded in absorptive medium, charcts. 79−18372
three-dimensional phase holograms, diffraction efficiency, dynamic approx. theory 77−31080
torical grating calc. for very wide field camera *(French)* 78−81547
toroidal gratings, aberration correction for grazing incidence regime 80−91911
toroidal holographic gratings, design and performance *(Japanese)* 79−27412
toroidal substrate, astigmatism 80−58482
total internal reflection selector for tunable lasers 77−79840
total-internal-reflection hologram grating, diffr. efficiency 79−64347
transient undisplaced grating, light beam intensity and phase transform. 77−75452
transmission, appl. to UV and X-ray synchrotron radiation monochromators 78−63186
transmission diffraction gratings for soft X-rays 80−90965
transparent, in spectrograph 80−57395
two-layer mag. structures, thermomag. recording 80−100588
UV region, 300 to 2000 Å, simple selection rules 78−55435
visor helmet-mounted display, optical design 79−86149
volume amplitude holograms in photodichroic materials 78−17871
volume hologram using spherical wavefronts, props. 80−78805
volume holograms as frequency-selective elements 79−27212
volume holograms for image restoration 80−83566
volume holograms in electrooptic crysts., dynamically produced refr. index variations 77−19195
volume holograms with strong coupling, scatt. phenomena 78−33700
volume phase grating, angular depend. of width of Bragg peak 80−78811
volume phase grating, reflection, Mathieu functions theory 79−14113
volume phase grating, TM and TE mode diffr. efficiency, comparison 80−74507
volume phase gratings at higher Bragg angle incidence, coupled wave differential eqns. 80−102666
volume phase holograms, non-sinusoidal high order modes 80−102665
volume phase holograms, two dimens. theory of higher order modes 80−14300
VUV monochromators with toroidal holographic gratings, Strehl criterion 80−90949
wavefront inversion mechanism 78−9350
wavefront reconstruction method, plane waveguide hologram coupled system 80−5708
waveguide interferometer using modular holographic elements 77−61116
wavelength selector in external resonator, for semiconductor laser 79−98406
wax film, hologram recording at 10.6 μm, image reconstruction 78−17868
X-ray microscope, using holographically made zone plates and gratings 78−37855
X-ray reflection gratings, stigmatic 77−54034
Ag holographic gratings, polystyrene coated, Raman spectra enhancement by plasmon surface polaritons 80−80885
Al surface, light diffr., photon excitation of compound plasmon resonances 79−28307
As_2S_3 focusing diffraction grating with const. spacing 79−23096
As_2Se_3-Cu (10-20%) film, glassy, darkening kinetics, and hologram diffr. efficiency 77−62027
$As2S_3$ amorphous chalcogenide film inorganic photoresists, holographic resolution evaluation 79−76629
CdS, laser induced transient gratings 78−38020
CdS, single cryst. surfaces, diffr. gratings, electrochem. recording of holograms 80−32934
CdSe, dynamic holographic gratings based on excitons 77−3556
CdTe, dynamic holograms, diffr. charcts. using laser beam 79−46048
GaAs, interference grating blazed by ion-beam erosion 80−1302
Ge surface, self diffraction of light, mechanism, rel. to nonequilib. carrier behaviour 79−72685
KCl, hologram recording by photodichroic F_A centres at room temp. 77−34846
KCl:Ca, vol. holographic grating, modulation charcts. 79−94197
KCl:Na and pure, hologram recording through F→X conversion 80−48190
$KNbO_3$ reduced, phase hologram recording sensitivity, energy transfer, photovoltaic effects 80−78799
$KTa_{1-x}Nb_xO_3$, holographic storage using photorefractive effect, dielectric const. 80−78800
$LiNbO_3$, beam coupling and light amplification, expt. compared with theory for electro-optic crysts. 79−86137
$LiNbO_3$ electrooptic crystal, dynamic holographic light beam conversion, geometric factors 79−13928
$LiNbO_3$, expt. confirmation of theory for electro-optic crysts. in steady-state case 79−86136
holographic gratings continued
$LiNbO_3$, $LiNbO_3$:Fe, amplification of laser beams by ferroelectrics 78−90393
$LiNbO_3$, $LiNbO_3$:Fe, holography in ferroelectrics 78−90394
$LiNbO_3$ volume holographic grating as spatial-freq. selector for tunable dye laser 80−53240
$LiNbO_3$, wave front convolution in 4-wave interaction with nonlocal nonlinear media *(Russian)* 79−86205
$LiNbO_3$:Cu, for electro-optical laser beam modulation 77−3672
$LiNbO_3$:Fe crystal, transient optical storage 80−9838
$LiTaO_3$, wave front convolution in 4-wave interaction with nonlocal nonlinear media *(Russian)* 79−86205
Na atomic vapour, Doppler-broadened system, degenerate four-wave mixing, line shape and strength angular depend. 80−43391
NaCl, amplitude phase hologram recording on colloid type centres *(Russian)* 80−69347
NaCl:O, hologram recording, colloidal type centre transformation *(Russian)* 80−55147
Nd:glass ring laser, holographic dispersion element *(Russian)* 78−59051
Si blazed holographic grating fabrication by selective etching 80−74320
Si, recording of free-carrier holograms by ultrashort pulses *(Russian)* 77−14680
α-SiC crystals, dynamic holographic grating recording 77−79785
SiC, for vac. UV, fabrication 77−79920
$Si0_2$ blazed holographic gratings, fabrication by reactive ion etching 80−53484

holographic instruments
see also holography
achromatic interferometers for white light optical processing and holography 80−53234
achromatic lens system, design using ray tautochronism principle 79−3759
applications and theory review, background and current status 78−74866
beam scanner using auxiliary reflector 77−83951
beam splitter, optical problems 77−68182
Bragg diffraction imaging, aspect ratio restoration by holographic lenses 79−46122
camera, automated thermoplastic for two-wavlength contouring 80−74318
camera for use in normal room lighting conditions 79−89867
coherence meter for spatial coherence of ruby laser determ. 80−9837
compact real-time matched-filter optical processor 78−74869
contours generation by dye laser 77−14671
corneal wound holographic stress testing in postoperative patients, specular illum. arrangement 78−65102
correlator with matched filtering using band-limited illumination 80−69531
correlometer with phase modulation, viscous, superviscous light scatt. media study 80−74321
electronic speckle pattern interferometry of surface shapes 78−94380
errors in measuring the dimensions of drops by holographic methods 79−67252
flexible holographic disc for laser scanner 79−94188
gas discharge track chamber 77−10551
head-up display 79−50266
holocamera, clinically useful, for 3-D microscopy of unanaesthetised eye 78−48863
holocamera, lens assisted, motion pictures of microscopic plankton 78−48946
holocamera for 3-D micrography of the alert human eye 80−98057
holocamera for particulate studies 79−22919
hologrammetric plotter for three-dimensional meas. 79−7103
interferometer, for optical glass homogeneity determ. 78−90401
interferometer, lateral shear, using twin three-beam holograms 80−99673
interferometer, three-dimens. optical inhomogeneity quantitative evaluation 78−87030
interferometer with computer generated holograms for optical testing 77−42632
ionising radiation dosimetry, by holographic interferometric method 80−852
IR, using scanning image convertor 79−76636
IR tracking receiver with holographic information processing 78−78970
large-aperture interferometer with low-resolution holographic corrector plate 80−74315
laser beam deflector quality factor N/τ, comparison of holographic and acousto-optical deflectors *(French)* 78−55318
laser coherence length meas. 77−7100
laser diode lensless MSF holographic optical element correlator, optical pattern recognition 80−102663
laser light deflector, operational holographic, document scanner appl. 79−10268
longwave holography, double circular scan format generation 80−43555
microinterferometer to meas. plasma electron densities and other transparent objects 80−43964
microscope, interferometric, for dynamic systems obs. 78−45685
microscope, lens assisted system, resolution tests 78−46539
microscope, real time, using holographic illuminating system, rotary shearing interferometer 79−81388
microscope, theory and appls., review 78−45690
microscope attachment for making holograms 77−23631
microscopic equipment, methods, appls. and related topics, bibliography 80−73124
one-tube goggle system engineering 80−78988
optical path stabilisation of holographic platform 80−99678
Pancake Window reflective system 80−1165
point-of-sale hologram scanner for bar-code reader 80−48182
production planning problems, system of indices 77−31145
pulse holography, appl. of active Q-modulators *(Russian)* 79−68371
radiography, holographic 3-D synthesis of X-ray pictures 80−67245
sandbox system for seed studies 80−67325
scanner, computer produced hologram, with auxiliary reflector 78−71054
scanner, computer-generated hologram, for laser materials processing 79−18367
scanner, interferometric zone plate, for point-of-sale systems, aberration corrections 79−81383
scanner, two-dimens., design considerations 78−46535
scanner for bar code reader, lattice scan pattern generation 78−42309
scanner from opaque documents, holograms as beam deflection elements, projection and collection lenses 77−88672

holographic instruments continued
scanner imaging systems, active and passive, 8 to 13 μm, charact. 80−91755
scanners for UPC symbols 78−42308
scanning system, lens design for hologram generation 78−50742
schlieren system, holographic interim recording 79−76641
shearing interferometer, description of new instrument 78−37847
shearing interferometer for recording of pulsed gasdynamic processes 77−47117
shearing interferometer with narrow ref. beam for flow investig. in reflecting nozzle of shock wave 77−47118
spectrograph, hologram Fourier transform parameters 78−37858
strain gauge 80−52182
stroboscopic interferometer, dynamic optical component evaluation, remote-site operation 79−85164
thick, holographic optical element design and construction 78−55315
US field meas. by optical holography 80−14532
UV holographic microinterferometer and probe beam design for plasma probing 80−59270
vibration dissipation using springs and viscoelastic substances *(German)* 80−17986
viewers for synthetic aperture radar imagery 79−31843
visor helmet-mounted display, optical design 79−86149
X-ray microscope, using holographically made zone plates and gratings 78−37855

holographic interferometry
1 MHz crystal anharmonic AT modes, holographic displacement amplitude meas. 79−54097
3D phase objects, multifreq. hologram element appl. 80−9835
absolute retardation accurate meas. 79−27201
achromatic interferometers for white light optical processing and holography 80−53234
acoustic field holograms, moire processing 78−55539
acoustic field visualisation by optical holography 78−59216
aerodynamic flow study appl. *(French)* 78−5833
aerospace component testing 77−7039
aortic valve study, by holographic interferometry and shadow Moire methods 80−104613
applications and theory review, background and current status 78−74866
applications of holography 77−38837
aspherical surface testing appl. 79−85116
aspherical surfaces, holographic methods of testing, review 80−33257
astrophotography, isoplanicity meas., speckle holography 80−56717
automatic pattern processor for simple and complex interference patterns 80−13129
axisymmetric optical inhomogeneities, strong refraction, calcs. 77−7009
b-scan Fourier transform holography 79−83421
beam-plasma system enhanced energy deposition, interferometric obs., simulation 77−31490
biological specimen 3-dimens. imaging using vibro-interference and holography 78−53584
birefringent object, isopachics meas. using immersion method polarisation holography 80−99672
blade, rotating, vibr. analysis using holographic interferometry 78−32807
bolted joints in wood, photomech. stress determ. 79−32406
boundary diffr. wave, holographic anal. *(German)* 78−63041
boundary layer transition, detection using holography 78−14101
brass plate, corrosion by HNO_3 vap., holographic interferometry 79−3658
broad light source-displacement interferometer holograms, supersonic flow visualisation appl. 80−19008
camera for use in normal room lighting conditions 79−89867
cantilever plate, deflection meas. 79−94568
chest motion due to heart action, imaging by holographic interferometry 79−20699
cine recording of real-time holographic interference fringes 80−23642
cineholographic method for interferometry of fast processes 77−71958
cineholography, investigation of high-speed events 78−37842
circuit board, high density, identification of hot spots 77−71950
circular hole, normal surface displacement, reflection holographic interferometry 78−57893
circular surface trueness testing, simple holographic method 79−50245
coal particle combustion, holographic meas. 79−76630
coating swelling meas. by real-time holographic interferometry 79−98316
cochlear model vibration mode visualisation 79−2083
coherence length adapted hologram interferometer 77−22590
coherence of ruby laser, rel. to pumping energy 77−75440
compensation for rigid body motions *(German)* 79−98317
composite pressure vessel, holographic exam. 77−28957
computer analysis of holographic interferograms for nondestructive testing 80−9836
computer-aided interferograms evaluation, of thermal boundary layers *(Czech)* 78−62220
computer-generated holograms, techniques and appls., book contrib. 79−76645
concrete, stress determ. by holographic and speckle techniques *(French)* 79−27603
concrete to steel rod chemical bond 78−88593
conference, Bad Harzburg, Germany (June 1979) 80−51951
confidential data storage in sandwich holograms 79−76631
continuously scanning reconstruction beam, fringe evaluation 77−88664
continuously scanning reconstruction beam, strain and displacement determ. 78−71055
contour fringe computer-aided analysis 77−49766
contour fringe generation by dual-index immersion 77−49765
contour mapping of 1st and 2nd derivatives of plate deflection using modulated diffr. gratings from double exposure holography 79−6086
contouring by Moire holography 78−1183
contouring method by parallel light Moire holography 78−33702
corrosion analysis by holographic interferometry 80−71853
corrosion process, holographic interferometry 79−3658
crack initiation determ. 78−60933
crystal growth from soln., diffusion coeffs., exam. by transmission holographic interferometry 78−39680
crystal growth from solution, convection effects, holographic interferometic obs. 80−77565
curved surface contouring, two-wavelength speckle imaging methods 79−85121
cylinder distortion measurement *(German)* 79−34273

holographic interferometry continued
cylindrical surface shape meas., artificial holograms by photographic method 79−7095
deflection measurement from moire fringes and holograms 80−32936
deformation anal. with additional degrees of freedom during reconstruction 79−32411
deformation analysis, one fixed and one movable reconstruction source 77−38829
deformation analysis of opaque bodies, book 80−27050
deformation and vibration of objects investigation 77−46976
deformation behaviour of human vertebrae *(German)* 77−77924
deformation field measurement *(German)* 77−22594
deformation measurement, in-plane, by video-electronic hologram interferometry 80−106488
deformation measurement, out-of-plane, using holographic interferometry and speckle photography, comparative accuracy 80−78804
deformation of mech. struct., accuracy and reproducibility of heterodyne holographic interferometry 78−37843
deformation zone form. and development study at edge of notch 79−50687
deformations of diffusive-reflective objects, methods for evaluation *(Czech)* 79−72534
dental moulding volumetric variation meas. appl. 79−88214
dentistry, methods and appls. 80−67203
dentistry applications, review 78−48859
depolarising diffusers, autocorrelation by holography *(French)* 79−31801
diamond laser beam use *(Russian)* 78−31595
differentiation of holographic-moire patterns 79−59951
diffuse object, equal inclination fringe loci and visibility 77−79143
diffuse objects, autocorrel. of transmittance of holograms 78−1185
diffuse objects, fringe loci and visibility in holographic interferometry 78−58951
diffusely reflecting objects, deformation meas. by lasers, appl. of holography and speckle, review *(Japanese)* 80−9832
diffusely reflecting objects with time-varying surface microrelief, holographic interf. deform. recording 80−74322
diffusing object surface state study by double speckle photography 79−85120
dipropylammonium manganese chloride, layer perovskite, step bunching obs. by compound holographic microscopy 78−63682
direct visualisation of thermal distributions around hot wire probe 77−61114
direction-sensitive displacement analysis by multiple freq. holographic interferometry 78−54338
disc memory recording heads, investigation of dynamic mechanical props. that appear as stresses during small motions 80−22422
displacement, deformation and vibration meas. *(Italian)* 78−54337
displacement anal., three-dimensional from image plane hologram 79−17385
displacement component determ., holographic method using image plane techniques 79−44901
displacement components and derivatives, holographic-moire technique 78−51140
displacement determination in special alloys by holographic and speckle interferometric methods 78−27688
displacement distribution meas., of twisted belt *(Japanese)* 77−7029
displacement distribution measurement, on twisted belt 78−13673
displacement evaluation, general formulation 77−38830
displacement field eval., 3 dimensional, exact general theory *(German)* 79−32409
displacement field inside stressed sample, double exposure recording 77−57299
displacement meas., derived holographic interferometric methods *(German)* 80−91758
displacement meas. by combined holographic and double-aperture speckle interferometry *(Japanese)* 79−80670
displacement measurement, 3-dimens., from single image hologram, combined holographic and speckle interferometry 77−83831
displacement measurement, appl. to membrane flexing 80−8962
displacement measurement, motion direction and fringe order determ. 77−18077
displacement measurement, using double exposure holograms 79−40537
displacement measurement techniques, expt. comparison 78−71057
dosimetry, interferometry and holographic interferometry appls. 80−42871
double exposure, appl. to vibr. amplitude and phase determ. 77−58292
double exposure, automatic meas. of 3D displacements by scanning technique 78−37844
double exposure, NDT and breaking point mech. appls. 79−6175
double exposure, using common-path reference waves 77−71947
double exposure holography, many-component motion anal. 79−7329
double exposure interferometry through speckle photography *(French)* 80−83568
double exposure method, partial coherence and interference pattern visibility *(German)* 78−82932
double exposure method for quadratic motion analysis 77−61927
double exposure technique, appl. to crazing on polystyrene 77−12680
double exposure/double direction illumination, nondestructive testing 79−27206
double impulse method, nondestructive testing of cracks in metals 77−9033
double pulsed time differential method 77−22591
double-exposure, interference anal. by analogue/digital video technique 79−86139
dual computer-generated holograms, interferometric testing of aspherical surfaces 80−9830
dye laser, rhodamine 6G in aq. and alcohol solns., thermooptical inhomogeneities, μ second pumping 77−75501
ear drum, human, vibr. meas. using electronic speckle pattern interferometry 79−53205
education, holographic double exposure interferometry for small rot. meas. 78−36758
elastic and plastic deform. study 77−62223
elastoplastic strain meas., elastic and residual components, single plate hologram interferometry 80−32932
electrolysis, solid-liquid mass transfer meas. appl. 79−87852
electron beam controlled discharge, cathode density waves 80−38798
electron irradiated solid, dynamic and dosimetric characts., laser and holographic interferometry obs. *(Rumanian)* 80−90886

holographic interferometry continued
electronic equipment, components, vibration charact. determ. by holographic interferography 78−29916
electronic speckle pattern interferometric system based on a speckle reference beam 80−58472
electronic speckle pattern interferometry, phase modulated, principle 79−85167
electronic speckle pattern interferometry of surface shapes 78−94380
electronic speckle pattern interferometry used to meas. eardrum vibrs. and other biol. movements 80−67209
embedded interacting defects in transparent model, holographic meas. of magnification factor 79−32413
emulsion monobath and reversal processing techniques 80−102668
epoxy resin, stresses arising during high-speed droplet impact 80−71764
errors in small vector displacements meas., statistical anal. 78−78953
evaluation with weighted orders *(German)* 80−63950
extrapolation of strain and stress from holographically measured surface displacement 79−32410
eye deformation due to intraocular press. changes, holographic interferometry meas. 79−20720
facial skeleton strain distrib. arising from orthodontic appliance activity 80−67143
fibre reinforced composite, fatigue damage, early detection by NDT 77−28951
film, stress measurement method using real-time holographic interferometry 78−84099
film adhesion testing, simple real-time holographic interferometry method 78−92411
flame, singing, struct. investig. *(Russian)* 79−29361
flame structure determ. method *(Russian)* 78−94851
flat surface vibration meas. appl. *(Polish)* 79−183
flaw detection, using He in test chamber 80−93723
flow, local mass-transfer coeffs. meas. method 78−75234
flow, transonic, from square nozzle, 3-dimens. density field meas., holographic technique 78−47080
flow measurement, 3D, separate reference and scene holograms 77−89210
flow over cone, dual-plate holographic interferometry 78−63512
flow velocity distribution, double exposure technique 78−5831
flow visualisation 77−55117
flow visualisation holography, appl. of generalised phase control during reconstruction 79−94742
flow visualisation holography, generalised phase control during reconstruction 79−50246
flywheels, filament wound composite materials, characterisation 80−81097
four-point bending machine assessment by meas. of steel bar deform. 79−34266
Fourier lensless technique, hologram recording and reconstruction, using materials with low resolving power *(Czech)* 78−90399
fracture toughness tests, plastic zone obs. 77−9034
free convection mass transfer from horizontal surface, electrochemical and holographic interferometric obs. 78−87344
fringe assessment by semi-quantitative method, surface displacement obs. 77−75444
fringe contrasts appl. to holographic interferometry of diffuse surfaces *(French)* 77−61928
fringe dynamics in quantitative evaluation of interferograms *(German)* 77−10097
fringe evaluation, using a continuously scanning reconstruction beam 78−37845
fringe formation analysis, for displacement or flow velocity distrib. meas. 78−25820
fringe multiplication, appl. to crack detection 79−41357
fringe order number and sign determ. method 77−164
fringe visibility and optimum experimental procedure for holographic interferometry using a swirl type shutter *(Japanese)* 80−95844
frozen-fringe method, using thermoplastic recording media 78−90402
gas flows, low density, multipass hologram interferometry 79−32724
gas laser medium, large-bore CW high-energy, holographic interferometry during power extraction 80−28172
general displacement field measurement 79−17397
ghost image interferometer, anal. 78−32863
glass fibre reinforced epoxy, multilayer circuit board, holographic interferometry appl. to real-time studies of heat effects 79−91873
hearing mechanism, vibr. characts. obs. by holographic interferometry with optical fibres 80−76879
heart valves, crescent-shaped aorta, deform. props. by holographic interferometry 80−61616
heat transfer at critical point of CO_2, heat transmission coeff. determ. *(German)* 77−35133
hemispherical shells partially filled with liquid, expts. on vibration 79−81792
heterodyne, electronic instrumentation employing accurate phase measurement 80−87352
heterodyne, props. and appls., review 79−86141
heterodyne holographic strain and stress determ., accuracy 79−94562
n-hexane, tank flame, turbulence, holographic interferometric synchronous photography *(German)* 78−51255
high-energy laser mirror thermal distortion test facility 80−14348
high-speed photography combined with real-time holographic interferometry 78−37839
highly sensitive plates for short exposure times *(Russian)* 80−1164
hip joint prosthetic component deformation meas. *(German)* 80−12302
hologram reconstruction, fringe modification 79−86140
holographic interferometry for vibrations investigation, beam modulation methods *(Polish)* 79−3649
holographic length comparator using phase heterodynage, appl. to gauge blocks 78−58953
holographic photoelasticity, Faradays effect appl. *(Chinese)* 80−5998
holography table effective size increase 79−35694
Homalite, stress intensity factor measurement, dynamic fracture toughness determination from isopachics of a running crack [holographic interferometry] 79−34257
honeycomb panels, inspection by non-destructive method 77−34843
hot wire in liquid, heat transfer, transverse oscills. effects, holographic interferometry 77−15013
hydrostatic stress and deformation meas. appl. 79−7353
image motions due to reconstruction light source movements, deform. analysis applic. 77−10866

holographic interferometry continued
in-plane motion measurements with Fourier lensless holography 80−77746
in-plane strain meas. by holographic modulated diffr. grating 79−90202
information content enhancement by controlled rotation during lighting *(German)* 79−31838
inhomogeneous acoustic wave visualisation 80−102943
injection moulded GFRP distortion meas. 79−79020
instrument errors for narrow reference beam 77−640
interference electron microscopy using electron holography 80−32929
interference fringes, of equal inclination and thickness *(Rumanian)* 79−13926
interference fringes produced by hologram displacement, anal. *(Japanese)* 77−27265
interference pattern parameters adjustment, aberrations effect 78−17875
interferogram quantitative evaluation procedures *(German)* 80−87344
interferogram quantitative interpretation 79−86138
ionising radiation dosimetry, by holographic interferometric method 80−852
IR impulse holography and interferometry, appls. *(Russian)* 77−14678
isopaches, of integral order *(French)* 80−32931
isopachi fringe patterns using immersion method polarisation holography 77−19196
isopachic fringe compensation, using two reference beam interferometry 79−41356
Kodak 649-F plate 5-min. processing monobath 77−633
large size in real image 77−68188
large-aperture interferometer with low-resolution holographic corrector plate 80−74315
laser beam external self-modulation for double pulse prod. 77−83902
laser measurement of optical, thermal and mech. props. of materials 77−74513
laser produced plasma, ultraviolet probing with picosecond pulses 78−42827
laser speckles, bibliography (1976 to 1978) 80−82593
laser-produced shock wave optical diagnostic system 80−79421
lasers in industrial metrology, review *(German)* 77−14734
lateral shear interferometer, appl. to testing 77−7023
lateral shear interferometer for differential interference contrast method 80−63947
lateral shear interferometer using twin three-beam holograms 80−99673
layergram iterative method for 3D ref. index distrib. reconstruction 79−54172
length meas. device appl. *(Rumanian)* 78−49796
length standards, by holographic interferometry with phase heterodynage 79−6095
lens aberrations determination by speckle interferometry *(French)* 79−72653
light beam deflection angle determ. from holographic shear interference patterns 80−95848
light beam optical distortions in disc amplifier, double-exposure holographic interferometry meas. 79−10338
light pencil and interferometer for amplitude and phase profiles 80−102680
liquid crystal electro-optic valve testing using laser light *(French)* 80−28311
liquid diffusion, double exposed hologram meas. 79−37861
liquid irradiated, dosimetry by holographic interferometry *(Rumanian)* 80−9412
lithography for integrated optics 79−14116
localisation geometry of interf. fringes in classical and holographic interferometry 79−30536
locomotor system analysis in humans *(Croatian)* 78−44519
low density flow visualisation, capability of holographic phase-shift interferometric technique *(Chinese)* 79−72964
machine part displacement meas. method 78−9348
machine tool framework, rigidity meas., stiffening depend. *(German)* 77−7040
magnetic domain walls, off-axis electron microholography 78−82080
magnetic field distrib. mapping of thin mag. foils by holographic processing 79−89868
material properties from single view by use of particular optical config. 77−31073
materials testing, defect detection by holographic interferometry 79−15935
MBBA, nematic liq. crys., refractive index distrib. and mol. alignment in electro-optical effect *(Japanese)* 80−20613
measurement, control and testing, coherent light appl. *(French)* 80−23641
measurement and testing appl., development trends *(German)* 78−39975
measurements by optically generated patterns 79−3648
measuring techniques, significance of holography *(German)* 78−90395
mechanical measurement, holographic system for interferogram form., processing and interpretation 77−75449
mechanical testing, review 79−87788
medical and biological applications 79−8528
medical implant device evaluation 80−40659
memointerference or vibrointerference phenomenon and application 78−55313
metal removal rate obs. during electropolishing 77−8985
metal surfaces, shape and deformations, holographic contour immersion method *(Polish)* 80−62630
metallic coatings, nondestructive testing, appl. *(German)* 79−79186
methods and applications *(French)* 79−7099
metrology and testing by lasers, review 77−5817
MHD flow parameter determ. appl. *(Hungarian)* 78−22433
microinterferometer to meas. plasma electron densities and other transparent objects 80−43964
microprocessor-controlled hologram interferometry analysis using intelligent TV system 79−76648
microscope, MGI-1 80−5706
microscope technique, appls. 77−34015
microscopy methods, for dynamic systems obs. 78−45685
milling machine, sandwich hologram interferometry 77−88662
mineral dispersed macromolecular matrix, holographic interferometric meas. of displacement vectors on boundaries 79−79015
mining applications, subsidence and ground movement meas. 78−57343
mirror surface curvature and local distortion meas. 79−76796
model interferogram construction for object geometrical shape, deform. and motion 77−82592

holographic interferometry continued
modulation error effects, linearised subfringe holographic interferometry 80−78803
moire fringes, multiple beam interferometry 79−18371
Moire technique for microwave field recording 77−34841
moire topograms, real-time, video electronic generation 80−67198
moire topography, devel. and present status 80−63960
moire topography for 3-D shape meas., opto-electronic processing technique 79−86146
monochromatic light interference meas. 78−32867
motion picture apparatus vibration meas. *(Russian)* 80−37112
MTF and wavefront aberration meas., Francon's method meas. of MTF, wavefront aberration 79−3647
multichannel data processor using holography and integrated optics 79−36853
multiframe ps holography appl. to high power laser effects in dielectrics 78−26328
multiple exposure holographic interferometry, fringe form. anal., appl. to flow vel. distrib. meas. 80−9831
multiplexing by optical beam coding *(French)* 77−159
multislit one-step rainbow holographic interferometry 79−31835
NDT, holomoire interferometry appl. 79−20294
NDT, method for fringe control 80−31851
NDT 79−43497
NDT appl. 78−53164
NDT application 78−35628
NDT fringe control techniques 80−45450
NDT of structures and materials holographic interferometry 79−8420
NDT system application of laser speckles 77−75457
non-vibration protection objects, stroboscopic illumination and phase ref. mirror methods *(German)* 78−33710
noncoherent source utilisation for recording intensity of phased objects *(Russian)* 77−50643
nondestructive evaluation, kevlar-epoxy composites pressure vessels 80−81275
nondestructive evaluation by laser beam 77−21345
nondestructive test system, composite mobile, quantitative fringe interpretation 77−75454
nondestructive testing appls., quality testing and micrometry *(French)* 78−42305
nondestructive testing at Fourier plane 78−46536
nondestructive testing of brazed, and epoxy bonded honeycomb panels 78−40017
nondestructive testing of materials and components *(German)* 78−48576
nonlinear effects, appl. to unconventional displays 77−61925
nonlinear effects for double exposure data 78−33714
nonlinear recording, fringe location errors 79−76633
nonlinear two-exposure system, fringe sharpening and diffr. effects 77−31074
object deformation, determ. of components from 1 double-exposure hologram 79−94193
object geometries comparison, speckle pattern interferometry, holographic illum. elements 78−66785
object movement generated fringe localisation analysis *(Japanese)* 78−22096
one-step rainbow holographic interferometry 80−74317
optical glass homogeneity determ. using holographic interferometer 78−90401
optical holographic microscopy, for investigation of polymers 79−17474
optical material absorpt. meas., real time holographic interferometry 80−83569
optical separation, of displacement components by holographic-moire technique, extension to 3D 79−35661
optical spatial filtering *(Russian)* 80−95128
optical windows at high-press. chamber, strain determ. by holographic interferometry and finite element anal. 77−26323
organic photochromic materials, holographic recording *(Russian)* 80−1161
orthopaedics, exptl., quantitative eval. of holographic deform. investigations 80−67197
orthopaedics, grating−TV method, image evaluation using moire figures 80−67199
osteosynthesis appl. 79−88213
particle vel. distrib. meas. *(Japanese)* 78−95873
particle velocity distrib. meas. by holography 80−5705
particle velocity measurement in Fraunhofer plane using double exposure holograms 79−44904
phase objects, refractive index distrib., holographic interferometry meas. 78−37846
phase objects, using diffuse scatterer in reference beam 77−27266
phase objects with scatterer, fringe visibility and localisation 78−50736
phase variation testing in large transparent objects 79−3654
phase-hologram material, using four-centre-type photopolymerisation in cryst. state 78−37832
phased objects, diffusely illuminated, holographic interferometry using 3 dimens. recording media *(Russian)* 77−50642
photoelastic material, holographic method for matching and measuring refractive index 79−17466
photoelasticity, holographic determination of absolute retardation fringes by vectorial reconstruction 78−87315
photoelasticity, interferometric and holographic fringe patterns, unified interpretation 79−18844
photoelasticity, investigation of 2-D models *(Polish)* 78−18263
photoelasticity, technique for calibration of isochromatic and isopachic fringe pattern *(Rumanian)* 79−86388
photoelasticity, using dual-hologram method 77−19198
photoelasticity measurement, separation of constraints, frozen deform. *(French)* 77−68187
photometric standard lamp gas flow visualisation 79−12835
photorefractive effect, appl. to optical memories, holographic interferometry, and integrated optics 79−3756
photothermoplastic recording material 77−7038
piezoceramic radiators defects visualisation *(Russian)* 78−1530
pipe under internal press., lens holographic moire technique for displacement component determ. 79−44900
planar deformation analysis, speckle correlation method *(Dutch)* 80−32930
plasma, gas discharge holographic time-differential cine interferometry 80−38716
plasma, laser prod., holographic study at 10.6 μm 80−38685
plasma diagnostic technique, for laser spark diagnostics 79−64921
holographic interferometry continued
plasma diagnostics, MHD, using Fourier filter correlation, Hungarian progress report 80−48965
plasma flow phenomena, Ba II ion density meas. 78−55751
plastic parts, nondestructive testing 77−7037
plate, cantilever, strain meas. from holographic data 79−20303
plate, rib stiffened, studies on vibrations 78−83297
plates, uniform circular, holographic interferometry study of flexural vibrs. 77−68504
PMMA, methanol crazes, craze-strain profile from holographic interferometry meas. 78−72844
polarised light impulse response matrix formalism, appl. to holography 78−63045
polarised light in holography and optical information processing 77−46708
pressure vessel, defect detection, strain evaluation laser holographic and speckle photography methods 77−81365
principles and appl. to strain meas. *(German)* 80−78815
projection matrices use 80−37965
prosthetic deformation measurements using holographic interferometry *(German)* 78−35911
pulsed, for nondestructive evaluation and anal. of structs. 78−60977
pulsed holography for interferometric anal. of superposition of three sinusoidal vibrs., theory 77−71955
pulsed laser real-time holographic interferometry 80−74319
Pulsed lasers in electronic speckle pattern interferometry 78−65961
pulsed sandwich holography, exam. of electric drill vibrs. 78−33701
pulsed sandwich holography 77−75435
quantitative evaluation, modified dynamic method *(German)* 77−18085
radiation pressure effects, double exposure holographic interferometric demonstration 79−5943
rainbow interferometry, one-step multiwavelength technique and appls. 79−31836
rainbow process, double exposure and time-average interferograms 78−55320
real time obs. of HF temp. fluctuations, vortical plasmatron stream 77−43068
real-time, with photoconductive electro-optic crystal $Bi_{12}SiO_{20}$ 79−86142
real-time double-exposure interferometry using $Bi_{12}SiO_{20}$ 77−71951
real-time fringe obs., interferometry without reference beam 78−71063
relative numbers of bands, determ. method *(Russian)* 78−46549
relative numbers of bands determ. 79−55083
repositioning of hologram by interferometric technique 80−23640
residual strains in components, determ. by holographic interferometry 80−99980
residual stress measurement using holographic interferometry and etching 77−52577
reversible mirror design, for real time holographic interferometry 78−33705
review of interferometry, including holographic interferometry 78−37050
rigid body displacement evaluation by differential holographic interferometry 80−105610
rigid body motion compensation, in biomedical meas. 80−67213
rigid body motion compensation, Moire technique 77−26387
rigid-body motions determ., appl. to orthodontics 79−72527
rigid-body movement induced speckle motion 79−76590
rocks, wave propag. study by holographic interferometry 78−20536
rotating object, vibration anal., image detector in hologram interferometry and speckle photography 78−59351
S/N ratio improvement, image subtraction method 79−86144
sandwich holography, meas. of in-plane displacement and compensation for rigid body motion 79−98312
sandwich technique, theory of images and fringes *(French)* 78−17872
schlieren investigation of laser-induced plasma density 77−72503
schlieren photography and interferometry, coloured patterns appl. *(Russian)* 77−34852
seed studies, simple set-up 80−67325
seminar, San Diego, CA, USA (Aug. 1979) 80−73096
sensitivity increase by deform. of diffusely reflecting objects 77−58289
sensitivity vector determination in hologram interferometry, two known object rots. 80−95840
sensitivity vectors, direct determ. 78−13672
shearing interferometer for recording of pulsed gasdynamic processes 77−47117
shearing interferometer with narrow ref. beam for flow investig. in reflecting nozzle of shock wave 77−47118
shearing interferometers with a wide light source 80−43293
shearing interferometry for plane stress state determ. in models *(German)* 79−32426
shell of revolution, resonant oscillation obs. by holographic interferometry *(Russian)* 78−22297
shock wave visualisation, at few torr 77−55038
silicone elastomers, dental impression materials, dimens. stability, holographic and interferometric study 80−67204
silicone elastomers, for teeth impressions, holographic interferometric meas. of dimens. variations 79−94195
skull, holographic interferometric NDT 80−41162
skull and auditory ossicle vibr. anal., human preps., using holographic interferometry 80−67210
solid deformable body, residual stresses by creating holes, holographic interferometry appl. *(German)* 80−79243
sound reduction in small elec. appliances, investigation using time average holography *(German)* 79−37086
space-time optics in shape and surface metrology 79−6093
Spacelab, holographic interferometry feasibility study *(German)* 78−33711
speckle, astronomical, isoplanicity and temporal correlation meas. *(German)* 79−75116
speckle hologram, strain meas. near stress conc. in life size specimen 77−119
speckle holography measurements of stars ζ Cancri and ADS 3358 78−93120
speckle patterns, holographic projection appl. to remote metrology 80−14299
speckle photography and holographic interferometry, scatt. geometry, topology, vector fields, theory 80−87347
speckle photography rel. to holography 77−18083
speckle shearing interferometer for studying aberration of optical system *(French)* 77−65616
spinning disc, vibration anal., using image derotated holographic interferometry 79−81822

holographic interferometry continued
steam turbine flow holographic interferogram processing by minicomputer 77−19656
steel, case hardened gas carbonitrided, holographic interferometry study of plastic flow *(German)* 77−77723
steel bar deformation meas. by holographic interferometry using four point bending machine 78−60721
steep aspheric surface measurement, holographic comparison test 78−42402
stellar observations, mutual coherence function 78−53838
stellar spectra recording by interferometric method in thick photographic emulsions 78−73651
strain analysis, expt. implementation of fringe-vector theory 79−18839
strain components from fringe contrast 77−88665
strain meas. by combined two-beam and holographic interferometry 79−3650
strain measurement, quantitative 78−32794
strain studies on flat metal plates, holographic interferometry, high-freq. moire technique, and speckle correlation 79−32421
stratified flows, holographic interferometry obs., isopycnic contours 78−1713
stress, variable, residual, meas. by holographic interferometry 79−29312
stress analysis, expt., conf., Munich, Germany (Sept. 1978) 79−34256
stress analysis using holographic interferometry and speckle photography 78−70095
stress measurement of electroplated metallic thin films 80−20806
stress measurement of plate vibrating in water 79−3653
strobe-hologram method, interference effect, linear approx. 78−1192
stroboscopic, for mech. vibrs. anal. in industrial environment 79−32422
stroboscopic, survey *(Czech)* 77−19197
stroboscopic, vibr. anal. with space-variant phase 77−58296
stroboscopic analysis of asymmetric membrane vibrs. 78−66786
structural deformation meas. by holographic speckle interferometry *(French)* 78−30249
surface contour and inhomogeneity testing, interf. fringe distortion with imprecise focusing 78−89531
surface contouring by displacing object and illum. beam 78−74864
surface deformation measurement, double-exposure and fringe projection techniques comparison *(Polish)* 78−32788
surface deformations of transparent fluids 79−7094
surface displacement meas., stress determ. in components *(German)* 79−32425
surface displacement sign identification 77−75438
surface topography, holographic contouring, and study of contact rigidity of rough surfaces 80−64494
synthetic modal interferometric laser imaging 77−83829
system path length difference controller *(Russian)* 79−22916
Takiwax films for pulsed IR holography 79−18363
teeth and mandibles, deforms. due to occlusal forces 80−67205
temperature field meas. by holographic interferometry 78−37009
testing method with computer-generated holograms, aberration balancing 78−46845
thermal deformation, prod. of interference fringes 80−78806
thermoplastic film, photoconducting, double exposure holographic interferometry using memory effect *(Chinese)* 80−37967
thermoplastic moulding quality assurance using holography and speckle photography 78−27720
thermoplastic recording with homogeneous mixture of thermoplastic and organic photoconductors 78−63161
theta-pinch, fast, double-frame hologram interferometer meas. of density 79−19097
theta-pinch plasma, multiple pass CO_2 laser heating, density profile, diagnostics 79−60160
thin plate plastic deformation determ. *(German)* 77−77653
three beam technique *(Rumanian)* 78−46544
three-beam technique, appl. to study of thermal turbulent wake *(French)* 77−62316
three-dimensional optical inhomogeneity quantitative evaluation 78−87030
tightness inspection, sensitivity determ. 79−36862
time average, using photocond. electrooptic $Bi_{12}SiO_{20}$ crysts. 78−25813
time-average electronic speckle pattern interferometry system for measurements of HF vibrations of piezoelec. transducer 80−37966
time-average hologram fringe pattern interpretation 77−38838
time-averaged hologram interferometry, vibration anal. 80−63953
time-averaged holography theory, for three dimens. vibrs. at single freq. 78−90397
tissue change detection in rabbit urinary bladder *(German)* 79−34625
trabecular bone from human vertebral body, elastomech. props. 80−67141
transient jet of propelling gas during diaphragm rupture in shock tube, holographic images 79−77181
transient wave motion obs. from single doubly-exposed hologram 78−25825
transmission holographic bench, for qualitative and quantitative analysis *(Rumanian)* 78−46545
transonic flow meas. *(French)* 77−65826
transonic gas flow meas. appl. 79−86542
triple exposure, for displacement vector meas. 79−75498
turbine blades, crack detect., holographic interferometric method 78−35625
turbine blades, fatigue crack detect., strobed hologram method 78−35624
turbine blades, vibr. anal., time average holography 77−5901
turbine-engine component, photoelastic and holographic anal. 79−37257
turbulence diagnostics 79−60078
turbulence effects on optical wavefront, holographic appl. 78−82936
TV picture system for holographic interferogram anal. 80−106489
two reference beam, for aerodynamic flow meas. 78−34226
two wavelength holographic interferometer, metrological charact. 77−26393
two-reference-beam, nonlinear cross talk 77−14675
two-wavelength contour holography, fringe form. 77−19194
tympanic membrane investigations in living man using holographic interferometry 80−67207
tympanic membrane vibr. studies in living man using holographic interferometry 80−67208
uniform illumination, selection of working point on amplitude-exposure curve *(Russian)* 80−1162
universal interference and polarisation apparatus 78−19986

holographic interferometry continued
urinary bladder interferometry, holography of bladder deforms. in vitro, rabbit expt. 80−67201
urinary bladder interferometry, tumour and lesion detect. by holography 80−67202
US field investigations, theoretical analysis of light intensity distrib. 80−32903
US field visualisation in optically transparent media 79−18643
US fields investigation, appl. of holographic interferometry 78−1519
US wavefront visualisation using holographic interferometry 80−48526
UV holographic microinterferometer and probe beam design for plasma probing 80−59270
velocimetry of submicron particles 77−19203
vibrating plate like struct., displacement and strain meas. using time average holography 79−46272
vibration anal. by combined holographic interferometry and finite element anal. *(German)* 78−90806
vibration analysis, 3D, from time-averaged holograms 79−18840
vibration analysis, computer-aided, for vectorial displacements of bladed discs 78−71056
vibration analysis by multiplied moire fringes holography, expansion of meas. limitation 80−64505
vibration analysis using moire fringes holography, facilitation of fringes counting 80−64504
vibration detection of living bodyparts *(Swedish)* 79−43981
vibration meas., stroboscopic and time-average methods using swirl type shutter *(Japanese)* 80−69748
vibration measurement, accurate interpretation of fringes 77−2651
vibration measurement, review *(German)* 78−33709
vibration measurement application, review *(French)* 77−2646
vibration measurement by general shifted reference holography 80−1150
vibration measurement methods *(German)* 80−91759
vibration study in 3 dim. using time averaged holographic interferometry 77−79837
vibration superposed on random motion recording, short exposure and biasing holography 77−58288
vibration waveform measurement using temporally modulated holography, in biomedical appl. 80−67212
vibrational modes in compression blades, exam. of holographic technique 79−41355
vibrations, phase mapping using bright fringes 77−65582
vibrations, strobohолographic method of investigations 77−54681
vibrations real-time obs. using finite fringe field of background *(Czech)* 80−58989
visualisation of US travelling waves, by linearised subfringe interferometric holography 79−1036
volume reflecting Fourier holograms *(Russian)* 80−95127
wavefront shearing technique 80−43294
wear of articulating surfaces in protheses, holographic interferometry exam. 78−40415
weighted order difference evaluation *(German)* 80−69340
welded joint strain concentration zone detection appl., expt. 77−40512
white light interferometric microscopes 79−223
wide field angle of view, appl. to refr. index field reconstruction 79−76637
Z-pinch, overdense, He plasma, laser-driven hydrodynamic perturbation, shock density struct. 79−77385
Z-pinch high density plasma, EM radiation transmission intensity depend. 79−60145
Z-pinch ultradense plasma, density dynamics, interferometric meas. 79−77413
zero order fringe identification, direction of motion detection, in holographic displacement meas. 78−63044
Al alloy, type 2024-T3, fatigue deformation and crack growth, holographic study 80−25836
Al bicrystal, tensile and creep deform. obs. *(Japanese)* 77−56197
$Bi_{12}SiO_{20}$ crystal, real-time holographic recording 79−72540
C fibre reinforced resin, optimisation of thermally stable structures using holographic interferometry *(German)* 79−90804
CO_2, thermal diffusivity and cond. in crit. region *(German)* 78−59942
Fe heterogeneous plate vibration meas., up to 21.5 kHz *(German)* 77−74388
^{3}He-^{4}He liquid mixtures, holographic obs. of diffusion waves 79−60595
^{3}He-^{4}He mixture, near absolute zero, holographic interferometry exam. of phase changes 78−38905
^{3}He-^{4}He mixtures, dynamic behaviour, appl. of holographic interferometry technique 78−51781
I, iodoseptofluoropropane photodissoc. laser, refr. index distrib. fields, double exposure holography 80−9873
KBr, additively dyed, amplitude-phase holograms *(Russian)* 80−1152
Li wire high energy density exploding plasma, linear charge density 79−77436
$LiNbO_3$:Fe(Cu), photorefractive centres, optical absorption, EPR and Mossbauer spectra meas. 77−32403
N_2+H_2O 78−66631
VO_2 film as holographic recording medium, diffr. efficiency 80−28180
Zr-Nb (2.5 wt.%), meas. of crack growth at elevated temp. by holographic interferometry 79−38933

holographic storage
aperture synthesis for increased capacity 77−58297
applications, interferometry, data storage and processing 77−38837
archival memory, optical channel design 80−14301
associative access to data, memory with controlled transparency 79−31841
associative holographic memory, pseudorandom signals as key words 80−74306
associative parallel-search memory, correlation search using coded key words 79−10265
automated test using BASIC M-400 interpreter *(Russian)* 79−94180
beam addressed memory, lens aberrations effect on storage capacity 77−19202
binary data recording with multichannel acousto-optical modulator *(Russian)* 79−94178
binary information image reconstruction, aberrations, shrinkage effects 78−78967
birefringent crystals, use for holographic storage of information 79−98322
bleached holograms with binary data, parameters under physical development 78−50735
boracites, spontaneous birefr., meas. and appl., light gates 79−15434

holographic storage continued
brain model for associative memory chains 77−90753
bulk holographic store controller *(Russian)* 79−22915
capacity, photochromic and photorefractive media 79−27203
coherent noise reduction by freq.-modulated zone plate fabricated by holographic techniques 79−86134
colour image archival storage using Fourier multicolour holograms 80−102674
colour video memories, recording and playback technique 80−9833
computer polarisation holography, phase recording by polarisation effect of photodichroic materials 78−42299
computer-generated holograms, techniques and appls., book contrib. 79−76645
confidential data storage in sandwich holograms 79−76631
control system and software *(Russian)* 77−58262
crosstalk noise from multiple thick phase holograms 77−38827
DATA pattern construct. 77−79771
data readout reliability by optoelectronic channel 79−27216
data recording phase-random mask production by multichannel acousto-optical modulator *(Russian)* 79−94179
data search functions *(Russian)* 78−37823
data storage and processing, photosensitive electro-optical materials *(French)* 77−31077
data storage using holographic memories 78−25818
design, large block-organised *(German)* 77−3548
deterministic phase shifter 77−14676
deterministic phase shifters for hologram memory 77−46787
device based on injection lasers *(Russian)* 78−37824
devices, laser appls. 77−88673
dichromated gelatin as holographic storage medium 80−43303
diffuser for Fourier transform hologram recording 80−43285
digital holograms, optimum quantisation 78−33699
digital recording, LF micro-holograms on photographic film 77−34845
digital recording. optical A/D conversion and page composition 78−5436
digital storage of TV signals 80−87353
disc with high data transfer rate, audio response memory appl. 80−58477
document reduction system design *(Russian)* 79−98309
document retrieval and conversion to photographic microforms 79−76643
electro-optic crystal, holographically recorded data pages, digital processing 77−42511
electro-optic crystals *(German)* 79−27198
electrophotographic recording media, high resolution, expt. characts. 78−70208
equipment and techniques 77−3554
ferroelectric devices for optical systems 78−90473
Fourier beam system, double, data recording and processing appl. *(Russian)* 80−28165
Fourier high-data-density hologram recording, using glass fibres 79−10271
Fourier hologram recording in optical system with synthetic aperture 80−95852
Fourier hologram recording of paraphase-coded binary data 79−76639
Fourier hologram recording using Selfoc-type optical fibres 80−95850
Fourier holograms, stacked, reconstruction 80−87348
Fourier transform hologram, alignment and design conditions 78−29901
Fourier transform image hologram for ROM 78−87032
Fraunhofer hologram recorded near transforming lens focal plane, reconstruction 79−72526
Fraunhofer subhologram array, simple permanent memory system 79−18366
frequency-domain nonvolatile optical storage scheme 80−43282
Fresnel copies of holograms, aberration props. 80−99676
high resolution holographic recorders, using transparent electrophotographic film 80−102671
holographic information storage 79−50265
image reconstruction, distortion effect of Gaussian reference beam 79−76638
index memory system *(Russian)* 77−58259
information retrieval in presence of speckle and quantum noise 79−76606
information retrieval using associative holographic memory *(German)* 77−3549
information storage, seminar, Washington, USA (Apr. 1979) 80−41942
integrated waveguide-hologram memory design approach 80−32940
interfaces between optics and electronics 77−7042
Kanji character generation by holographic memory system 78−37854
Kanji-character memory system 78−9351
laser apparatus for recording transparencies of ROM 80−28177
liquid crystal controlled transparency of 128×128 element capacity, for hologram recording 79−50254
mass memories using vol. holograms 77−7041
mass storage systems, digital optical data storage and retrieval 80−78790
matched filter correlator memory techniques and storage capacity 80−102643
materials and methods, conf., San Diego, USA (Aug. 1977) 78−71171
matrix-addressable controlled transparency, spatial modulation in holographic memory recording 79−10401
medium specification and performance trends, review 80−43415
memory devices, optoelectronic ROM memory, injection laser appls. in construction *(Polish)* 80−19007
microfilms, expts. to improve recording density 78−82931
mosaic liquid crystal controlled transparency for holographic store data input *(Russian)* 79−94182
multichannel acousto-optical modulator control system *(Russian)* 79−72525
multiple exposure hologram generation from controlled transparencies *(Russian)* 79−94177
one-dimensional Fourier hologram line data recording scheme *(Russian)* 79−22912
optical arrangements, generalised design method 79−7098
optimum quantization and relative information content of holographic magnitude and phase 80−43286
optoelectronic devices, digital data processing, review 80−19106
optoelectronic memories, data storage density enhancement 77−58298
optoelectronic memory system, holographic beam splitter form. 78−17882
parameter optimisation of memory allowing for aberration 79−55085
phase mask fabrication and testing 79−27195
holographic storage continued
photo-thermoplastics for fast optical recording *(German)* 79−72530
photoconductor thermoplastic devices for high density storage, expt. 77−3546
photodiode matrix readout system *(Russian)* 77−58266
photorefractive materials for optical data storage 78−79086
photorefractive materials for optical storage and display, phase hologram form. 77−75445
photorefractive materials for optical storage and display 77−71961
photorefractive memory materials, elec. field and photocurrent meas. 78−71066
principles and application prospects 79−89860
principles and descriptions *(German)* 78−29910
prototype systems and appl., using photographic or optically reversible materials 79−27208
readin system parameter optimisation *(Russian)* 78−13670
recording and replay, review 80−58478
redundancy evaluation by spatial and defect permittance 78−1197
redundant information storage, hologram optimal size *(Hungarian)* 80−43287
reflection phase hologram storage system 78−78966
reversible media development, 1978 state of art 79−18377
review of recording media 78−71172
ROM recording with stationary reference beam 79−81396
spread-spectrum signal optical processing 79−72518
structure for holographic information search 78−29920
structures and technical feasibility of holographic information search *(Japanese)* 78−37829
thermoplastic photoconductor tape performance 80−43305
thermoplastic photoconductor technology for optical recording and storage 78−71175
thermoplastic recording, IR laser heating 78−71065
truth-table look-up optical processing utilizing binary and residue arithmetic 80−69334
volume amplitude holograms in photodichroic materials 78−17871
volume hologram memory, capacity limitations 77−7028
volume phase holographic storage in ferroelec. crysts. 78−82929
writing and reading at various wavelengths, expt. *(Russian)* 78−37825
As-S chalcogenide glass holographic recording efficiency, photocond. and annealing effects *(Russian)* 80−15556
AsGe chalcogenides, amorphous semicond. layers for recording information *(German)* 78−42395
$Bi_{12}GeO_{20}$, high sensitivity read write vol. holographic storage 77−7026
$Bi_{12}SiO_{20}$, electrooptic photorefractive crysts. for optical information processing 80−74313
$Bi_{12}SiO_{20}$, high sensitivity read write vol. holographic storage 77−7026
Co-Pt films, mag. and magneto-optic props., appl. to holographic and bit-by-bit storage 79−33512
EuO film, thermomag. effects for reversible holographic storage 77−34851
EuO, resolution as hologram recording material 77−83834
Fe-Pt films, mag. and magneto-optic props., appl. to holographic and bit-by-bit storage 79−33512
$KTa_{1-x}Nb_xO_3$, holographic storage using photorefractive effect, dielectric const. 80−78800
$LiNbO_3$, electrooptic photorefractive crysts. for optical information processing 80−74313
$LiNbO_3$, hologram indexing with tunable pulsed laser source 79−94186
$LiNbO_3$, hologram storage depend. on envelope field, space charge field 80−78801
$LiNbO_3$, holographic storage and retrieval 80−99669
$LiNbO_3$, phase hologram, dynamic holography 78−95572
$LiNbO_3$ photorefractive crystals for computer interfaced optical memory system, hologram characterisation 80−58475
$LiNbO_3$, vol. holograms, photorefr. recording dynamics, multiple storage 77−38834
$LiNbO_3$:Fe, dynamic hologram recording, high speed memory appl. 77−83835
$LiNbO_3$:Fe, electrically accessible Lippmann hologram memory 77−88663
$LiNbO_3$:Fe, hologram nondestructive readout using different recording and readout wavelengths 80−14302
$LiNbO_3$:Fe, phase hologram storage and fixing, review 77−19210
$LiNbO_3$:Fe, pulsed photorefr. process for hologram recording 80−53235
$LiNbO_3$:Fe, two different phase holographic recording processes, expt. 77−19211
$LiNbO_3$:Fe crystal, transient optical storage 80−9838
$LiNbO_3$:Fe electro-optic crystal holographic storage data error probability 80−43304
$LiNbO_3$:Fe holographic information storage material 78−55321
$LiNbO_3$:Fe photosensitive electro-optical crystals for image storage display and processing 77−19215
$LiTaO_3$:Fe crystal, holographic storage process 80−32942
MnBi magnetic film, method for recording holograms of diffusely scattering objects 78−74862
PLZT ceramics, optical recording *(French)* 77−31078
PLZT spatial light modulator for a 1-D hologram memory 80−37963

holography
see also acoustic holography; computer-generated holography; holographic gratings; holographic instruments; holographic interferometry; holographic storage; microwave holography
2-dimensional volume holograms, power conservation theorem 77−3550
aberration coefficient estimation 80−63949
aberration compensation of optical system, computer modelling 77−50640
aberration elimination, holographic microscopy 78−74861
aberrations, chromatic and spherical, of single glass lenses, holographic correction 79−86226
achromatic coherent system, noise performance 79−98295
achromatic triplet using holographic elements 77−58415
achromatism of optical wedge of holographic elements *(Russian)* 78−13787
acousto-optic deflector, holographic distortion correction *(Russian)* 77−75690
acousto-optical image and hologram convertor using nematic liq. crysts. 80−76002
adaptive holographic matched spatial filter for pattern recognition 77−7011
aerial reconnaissance film interrogation by optical matched filtering 77−78484

holography continued
aerial survey image interactive hybrid optical/video processing system 77−53254
aerosol hologram, automatic assessment with new reconstruction config. 77−7031
aerosol spectrometer using two-pulse Fraunhofer holography, fibrous particle motion anal. 80−58476
alkali halide hologram, high-efficiency recording by selective colloidal centre destruction 80−63955
alkali halide photodichroic crystals use for coherent opt. data processing 77−68248
alkali halides, photodichroic, as optical processing elements 78−83056
ambiguity processing by joint Fourier transform holography 80−58468
amplifying dynamic holograms 79−94191
amplitude 3-dimensional hologram, in amplifying media, light field transformation theory 78−1186
amplitude hologram efficiencies, photographic film model 78−9345
amplitude hologram intermodulation noise, effect of hologram thickness 79−50249
amplitude phase reocrding/reading efficiency in chalcogenide glasses *(Russian)* 80−43299
amplitude transmittance expansion in Taylor series *(Spanish)* 78−50732
amplitude-phase holograms, optical parameter dispersion 80−58481
amplitude-reflective, diffusibility influence by emulsion layer thickness *(Russian)* 77−54683
anomalous dispersion methods, for anal. of spatially inhomogeneous objects 79−63303
applications, interferometry, data storage and processing 77−38837
and applications 80−63959
applications and theory review, background and current status 78−74866
applications in measurement and testing 78−46551
artistic applications, using 3-dimens. recording and Lippman photography 79−55089
aspectogram, spectral props., image multiplication appls. 79−55090
aspectograms and composite holograms, Lippmann method anal. 77−10874
aspectrogram filtering, multiplying mask prod., photographic method 79−27196
aspheric surface quality assurance 78−50962
aspherical lenses, side band Ronchi test, hologram appl. 78−33798
astronomical negative information processing using thick-film holograms 79−48690
astronomical speckle interferogram masking, holography and phase flipping 80−109373
atmospheric aerosols, flash holography investigation 78−16217
atmospheric sciences, electro-optic and holographic meas. techniques 78−49184
atomic system, transient four-wave mixing and real time holography 79−55171
autocorrelation of diatoms as a function of depth of focus [holography in biology] 80−67324
automation of real-time optical meas. of small structures 79−85115
axial hologram lens with remote entrance pupil, cancellation of aberration 80−32933
axial holographic lenses, monochromatic aberrations 79−98321
axial lens, aberration compensating method 77−23634
bar code reader, using optically generated holograms 77−14673
basic principles, book contrib. 78−25831
basic principles and electronics industrial applications 77−68184
beam splitter, variable-ratio, reflection prism, use in holography *(Spanish)* 77−88945
beat wave imaging props., in stimulated Raman scatt. medium, holographic appl. 80−5709
binary input hologram recording with single acoust-optical modulator *(Russian)* 77−58287
binary seismic holography, kinematic principle *(Russian)* 78−92795
binary transparancy recording *(Russian)* 77−58294
biohologhraphic models of neural structs., optical system *(Russian)* 80−76878
biological volume reproduction by foreshortening roentgenograms, compound hologram method 79−57748
biomedical, conf., Munster, Germany (Mar. 1979) 80−62390
biomedical holography using pulsed lasers 77−25540
biomedical research, laser appls. 77−9298
biostereometrics, automatic iconics meas. system 80−67214
bleached holograms with binary data, parameters under physical development 78−50735
bleached single (multiple) exposure holograms, diffr. efficiency, SNR and resolution 78−71059
book, holography and coherent optics, information theory 80−98764
book, optics and lasers 78−22079
Borrmann-like anomalous effects in volume holography 80−102664
boundary layer transition, detection using holography 78−14101
broad-band coherent imaging 78−5424
bubble chamber event recognition by optical correl. *(German)* 78−70704
cavitation and flow research, in-line Fraunhofer holography 78−38436
chalcogenide film, effectiveness for optical holographic recording *(Russian)* 77−71960
chalcogenide glass film as master for PVC copied holograms 77−23632
chalcogenide glass films, opt. inform. recording uses 77−75633
character identification, use of holographic filter *(German)* 77−88668
Chinese character recognition with real time optical correlator 78−29904
chromate gelatin props. for holographic recording 79−18381
chromatic Fourier hologram as matched filter, for spatially coherent white light correlator 79−3642
chromogen developed photography emulsions 78−55319
cine film, three min, ruby laser appl. *(Russian)* 78−29917
cinematograph systems for three-dimens. colour images *(Russian)* 79−26169
cinematography, shooting parallax panoramogram and apparatus for stereo images *(Russian)* 80−22466
cinematography appl., principles 79−85192
cinematography in USSR 78−78976
cinematography system, based on integral photography with large aperture lens *(Russian)* 80−43296
cinematography using holography *(Russian)* 80−43295
circular cylinder with variable thickness free flexural vibrations 79−68620
coal particle combustion, holographic meas. 79−76630

holography continued
coaxial jet drop generator for holographic flow visualisation in water tunnels 78−5836
coded aperture imaging, analogical deconvolution appl. to nucl. medicine *(French)* 78−35943
coded reference beam use, theory 78−50739
coded-aperture image deconvolution, single-emulsion-layer holographic inverse filters 79−76647
coding of spatial and chromatic information by Fourier holography 77−3555
coherence function meas., spatial, modulus and phase *(Russian)* 80−5703
coherence implications for laser appls. 77−75599
coherence properties modification of light beam, optical processing appls. 80−78769
coherence relaxation methods 78−78977
coherent imaging, speckle power spectrum, effect of moving diffuser 79−31811
coherent noise reduction by freq.-modulated zone plate fabricated by holographic techniques 79−86134
color motion picture preservation with holographic process of 3 lasers 79−17530
colour, determining exact characts. of photographic recording materials 77−634
colour, synthesized, using single He-Ne laser 78−46552
colour blur of rainbow hologram 79−13922
colour film archival storage by rainbow holographic technique 79−18373
colour holograms, Lippmann, recorded in methylene blue sensitised dichromated gelatin 79−94196
colour holograms, plane, information colour coding methods 78−33703
colour holograms of a focused image, recording and interference copying with freq. and angular colour coding *(Russian)* 80−48191
colour holography using single wavelength laser and monochromatic holographic plate *(Chinese)* 79−50247
colour image generation with one-step rainbow holograms 78−66781
colour TV digital signal recording on photographic film *(German)* 78−22101
commercial appl. to photography *(Czech)* 78−37838
compact recording of information by the holographic method 80−63951
compensation for inclined beam aberrations in lens-hologram system *(Russian)* 77−19381
cone shaped cover for 360° holography 77−75436
conference, Jerusalem, Israel (Aug. 1976) 78−33712
contact printing method utilising heated photoresist adhesive prop. for hologram copying 80−5704
contemporary optics, book 79−81353
continuous random phase mask 78−66788
contour generation by rainbow holography 80−63948
contour mapping application *(Japanese)* 77−88674
contour mapping of moving object, using injection locked flash pumped dye laser 78−50737
control of optical gauges, expt. set-ups *(Rumanian)* 80−48185
convex spherical mirror appl. *(Russian)* 79−18379
copying of holograms, review 79−45915
copying using amorphous film as master 78−29912
correlation filtering for increasing diffr. efficiency 80−96028
correlator, noise sources, accuracy improvement 77−23636
correlators, expts. to improve accuracy 77−65583
corrugated waveguide boundary, TM-polarized light diffraction, zero diffraction effect 79−64339
coupler for optical fibre bundles using holographic lens 78−25839
current sheet formation, in Ar plasma, cineholographic obs. *(Russian)* 78−38529
data processing using volume holograms in far field zone 78−17867
data storage and processing, photosensitive electro-optical materials *(French)* 77−31077
deep-image rainbow holograms 78−71061
deformation meas., real-time hologram observation with photothermoplastic film *(German)* 78−1182
demonstration, comparison of real and virtual lens 78−16599
depolarising diffusers, autocorrelation by holography *(French)* 79−31801
diazo salt sensitised gelatin for holographic recording, grating form. 80−78798
dichromate gelatin, information recording *(German)* 79−27207
dichromated gelatin as holographic material, book contrib. 78−25833
dichromated gelatin as holographic storage medium 80−43303
diffraction, edge parameter effects, holographic method 77−34807
diffraction efficiency, depend. on size of developed Ag particles 78−78965
diffraction efficiency of recordings on high resolution photographic plates *(Rumanian)* 80−48188
diffraction efficiency of thin holograms with multiple internal refl. 79−55086
diffraction patterns, third and fifth order aberrations, holographic display 80−9829
diffuse light recording method using holographic beam splitter 77−68186
diffuse noise in holographic images, statistical characts. calc. 80−28176
diffuser with pseudorandom phase sequence [hologram recording] 80−14298
diffusing surface optical autocorrelation 80−99646
digital, joint meas. of ang. coords. and range on basis of optical phase fronts 78−78933
digital, what is it *(Chinese)* 80−63957
digitally simulated and optically produced holograms compared 77−75456
3,4-dimethyl-1,2,5-thiadiazol plasma polymerised film for holographic recording 80−106490
direct picture transmission in single optical fibre, restoration with holographic filters 79−89871
directional filtering two-dimensional patterns, hybrid character recognition system *(German)* 77−83819
disc brakes, location of squeaking noise, using laser holography *(German)* 78−37834
discharge, hollow-cathode, holographic meas. of radn. coherence props. 79−76784
discrete carrier holograms, diffr. efficiency 77−58299
discrete phase binary holograms, diffr. efficiency 79−3656
disdrometry for disperse system particle size determ. 79−7104
dispersion photorefraction due to triplet state processes in prod. 3D phase holograms 79−27210

holography continued
dispersions, particle size and velocity distribution, in flowing media, meas. methods *(German)* 78−34213
display systems and devices *(Japanese)* 79−68368
displays, colloquium, London (1978) 79−50258
document miniaturisation system automation 79−72538
drop size in dense fuel sprays, in-line holography meas. 78−37827
droplet image analysis by TV camera and table calculator via IEC-Bus 78−36337
drying procedure effect on diffraction efficiency, optical density *(Russian)* 79−59657
dye solution amplifying dynamic holograms, wavefront reversal 80−48331
dynamic, rel. to wavefront reproduction in stimulated scatt. 79−10361
dynamic correction scheme for disturbed laser wavefront *(Russian)* 78−55326
dynamic echo holograms, particle motion effect on transient optical phenomena 80−1283
dynamic holograms, amplification *(Russian)* 78−82934
dynamic holograms for light stimulated scatt. 79−89964
dynamic holograms on superposition states of atoms 78−37837
dynamic holography and optical image processing 79−94194
dynamic photoelastic constant meas., time averaged holography technique *(Japanese)* 79−64610
dynamic spatial filtration of coded optical image signals from noise 80−95826
dynamic three-dimens. phase holograms for light beam parameter correction 77−10876
ear, stapes footplate movement 77−44690
edge enhancement, real-time, using photorefr. effect 80−99642
education, one beam transmission holography, practical hints 80−57046
education hyperbolic mirrors, holography and Fermat's principle, geometrical anal. 77−45647
educational course, liberal arts-physics 78−73798
electro-optic crystals, photo-induced electron and hole transport holographic method for determ. 79−28375
electro-optical crystal recording medium, set-up for hologram parameters meas. 78−87031
electro-optical medium, kinetics of recording and erasing *(Russian)* 77−10872
electro-optics/laser international conference, Brighton (1976) 77−38800
electrochemical, at semicond. electrodes, diffr. grating recording 80−32934
electron, advantages of TEM field emission gun for in-line Fraunhofer holography *(French)* 77−34057
electron, optical spatial domain filter theory in gas molecule images 80−10016
electron beam spatial modulator using KH_2PO_4 77−72077
electron holography, high resolution, with field emission electron microscope 79−30614
electron holography, off-axis by field emission electron microscope 80−101905
electron holography, review of progress *(Japanese)* 80−52369
electron holography appl. to micro-area electron diffr. 80−49055
electron lens spherical aberration correction by holography 79−85203
electron microscopy, and holography 80−33862
electron microscopy, image reconstruction and holographic methods 77−65062
electron-wave holography, molecular image reconstruction 77−79705
electronic heterodyne recording and processing using phase modulated reference waves 78−46537
electronic heterodyne recording and self-interference term rejection 80−91756
electrooptic crystals, holographic recording, photogalvanic effect mechanism of nonlinear wave interaction 80−102672
electrophotographic transparent film for optical data storage 77−71946
emulsion monobath and reversal processing techniques 80−102668
emulsion thickness change effects, in 3-dimens. holograms 78−78968
evanescent wave holography using Gaussian beam, recording geometry and colour sensitivity 80−58473
evanescent wave holography with reference Gaussian beam, diffr. efficiency theory 80−43290
evanescent waves, diffr. efficiency, TE polarisation 78−66782
evanescent waves, diffr. efficiency, TM polarisation 78−66783
evanescent-wave hologram recording 80−63954
expanded laser beam use in correlation expts. 77−23629
eye, holography application *(Japanese)* 79−79515
eye, human, holographic diagnosis 80−12209
fatigue failure prediction by dynamic correlation intensity 78−11483
ferroelectric crystal., optically induced refr. index changes, holography appls. 77−50742
ferroelectric crystals for hologram storage, book contrib. 78−25834
ferroelectrics, photogalvanic current detection by optical recording holographic lattice 80−70748
fibre bundle coupling by holographic elements 78−46550
fibre optic illuminators for hologram recording and reconstruction 79−41353
fibre tape for image and hologram transmission, using chromatic encoding *(French)* 79−3785
film-grain noise in holography 79−55082
filter for three dimens. object recognition *(French)* 79−18359
filter holograms, method to determine plane of spatial frequencies 79−94189
filtering unwanted reference beams 79−89869
filters, for electron micrography image improvement 80−99680
fine-grained bleached emulsion scatt. model and expt. 80−102670
fingerprint identification, matched filtering on basis of thick holograms 77−79781
flat field holographic lens with no first order astigmatism 77−10995
flow visualisation, use of photopolymer 80−6176
flow visualization of cavitation in water jets and nuclei distribution measurement by holography 80−106862
focused image holograms, diffr. efficiency for multimode laser radiation 77−75450
fog, coherence requirements for light source 78−58949
fog, improved visibility using holography, new technique 79−912
four counterpropagating wave interaction in medium with cubic nonlinearity, dynamic holography concepts 80−91839
Fourier colour holograms, archival characts. 78−55314
Fourier complex one-dimensional radio-hologram processing method *(Russian)* 77−19207

holography continued
Fourier hologram, transmission freq. charact. of photothermal plastic layer at latent image stage *(Russian)* 80−43300
Fourier hologram optimisation, computational method 77−50639
Fourier hologram optimisation 77−19209
Fourier hologram recording in optical system with synthetic aperture 80−95852
Fourier hologram recording of paraphase-coded binary data 79−76639
Fourier hologram recording using pulse semiconductor laser radiation 78−50738
Fourier hologram recording using Selfoc-type optical fibres 80−95850
Fourier holograms, enhancement of diffraction efficiency *(German)* 78−78954
Fourier holograms, long-wavelength, recording and reconstructing schemes 78−87029
Fourier holograms recorded and decoded in polychromatic light 80−37970
Fourier holograms transmission over TV channel, image distortion anal. 77−54684
Fourier holography, double exposure method, intermodulation noise *(German)* 78−82932
Fourier holography, two-point resolution *(German)* 78−82933
Fourier holography in white light, optical processing using extended incoherent source 80−37960
Fourier multiple-imaging system, compensation of distortion 79−76640
Fourier spectrometer for recording holograms 79−68369
Fourier spectroscopy, nonlinear processing of interferogram 78−89553
Fourier transform analysis, reference and illuminating sources size effect 79−72531
Fourier transform hologram, resolving power characts. *(Korean)* 77−50638
Fraunhofer, appl. in high resolution electron microscopy 80−99016
Fraunhofer hologram recorded near transforming lens focal plane, reconstruction 79−72526
Fraunhofer holography using N_2 laser as light source 79−76635
frequency swept imaging, computer simulation 77−75446
frequency swept imaging, computer simulation 77−75447
frequency swept imaging principle 78−78964
frequency translated holography, S/N, smallest detectable vibr. 77−7022
frequency-shift, for obs. of US bulk waves in liquid wedge 80−79089
frequency-shift, for observation of surface waves and bulk waves in SAW devices 79−81600
Fresnel amplitude and phase holograms, reconstructed second-order image props. 80−63952
Fresnel copies of holograms, aberration props. 80−99676
Fresnel hologram recording, quasi-Fourier transform reconstruction of object 79−59652
Fresnel zone plate used as aperture for shadow holograms prod., min. acceptable no. of zones determ. 77−68193
FTIROS, pulsed hologram storage medium, imaging spectrum polaris. state *(Russian)* 77−75448
full view rainbow holograms 78−5439
Gabor holography, twin image and quadratic term error correction *(French)* 77−42510
gain saturation of Nd:YAG laser for phase conjugation 79−64272
gas molecules, image reconstruction by electron holography 79−68367
gas molecules, image reconstruction by electron holography 79−68366
gated viewing by holographic range-gating 78−71060
gelatin, dichromated, for holographic optical element fabrication 79−89865
gelatin, dichromated, methylene blue sensitised, methods of increasing sensitivity 79−94184
generalised holographic form. of lensless Fourier transform, different geometries 80−19003
geometrical analysis of holographic imaging 80−43291
Girard grille, holographic simulation 80−69337
grainless focusing screen for light scatter reduction 80−101836
grating equation, Hilbert's independence integral 79−899
guided optical wave holograms, diffr. efficiencies, theory 80−83563
heterodyne LF holograms, detect., transmission, recording and reconstruction 77−88669
HF, with ruby lasers, appl. to laser-prod. cavitation bubbles *(German)* 77−75437
high frequency, using ruby laser *(German)* 77−79779
high-contrast point-image holography in turbulent atmosphere *(Russian)* 80−63943
high-energy laser cavity diagnostics, holographic subtraction technique 77−19285
high-speed holocinematography of cavitation bubbles 78−37841
highlights, on diffuse surface, simulation using programmed diffuser, for hologram synthesis 78−46546
holocinematography, high speed, acousto-optic beam deflection for spatial freq. multiplexing 78−74860
holocinematography, high speed, spatial multiplexing for image separation 77−46704
hologram copying, contact printing method, optimum conditions 77−88678
holographic brain model for associative memory 79−74640
holographic images, 360°, a simple procedure teaching 78−28892
holographically stored X-ray images, grey-tone reproduction 78−65120
hydrocarbons, heavy, self-holograms of laser-induced surface depressions 78−82927
hyperbolic mirror virtual image, for teachers 79−35476
hypersonic target material, subject to impact with water droplet, holographic investigation 78−42306
hypervelocity particle measurement method 78−36978
IAE films for pulse holography, effect of wavelength on photosensitivity *(Russian)* 79−68372
ice crystals, holographic meas. of shapes, sizes and concs. 79−25364
image and plate substrate quality relationship 80−48193
image coding with far-field holograms 78−90389
image contrast changes during recording in nonlinear media with local response 80−69346
image contrast degradation with partially coherent light reconstruction 80−102678
image correlation, real-time high-resolvance, by Bragg diffr. in saturable absorbers 80−48159
image deblurring by convolution with impulse response operator 77−65580
image deformation at reconstruction 80−83567
image degradation due to reflected light depolarisation 78−90398

holography continued
image digital reconstruction with limited-length arithmetic register *(Russian)* 79−22910
image discretisation using holographic filter, spectral analysis *(Russian)* 78−37809
image enlarging by composite holograms 77−10875
image formation, coherent transfer functions and resolution 80−43292
image formation, role of organically accelerated bleaches 77−14672
image formation modes, progress 79−50259
image from inline hologram, interfering output suppression using digital processing technique 79−50248
image luminance, depend. on hologram recording geometry 78−63042
image magnification, new methodology 80−95851
image motions due to reconstruction light source movements, deform. analysis applic. 77−10866
image phase compensation and real-time holography by four-wave mixing in optical fibres 78−63039
image plane hologram reconstruction, multiple object beam methods *(Japanese)* 77−10865
image plane holograms, for students 78−77647
image plane holograms for holographic microscopy 78−58944
image processing resolution improvement and three-dimens. reconstruction 77−10862
image quality, recording process statistics effect 77−50641
image reconstruction, distortion effect of Gaussian reference beam 79−76638
image reconstruction, unconditionally stable algorithms *(Russian)* 79−22909
image reconstruction from hologram without using reference beam, brightness characts. *(Russian)* 80−69348
image reconstruction from kinoforms and distorted holograms *(Russian)* 78−13664
image reconstruction from large holograms 80−1156
image reconstruction in reflected light, ray inversion method appls. 78−25828
image reconstruction using propag. law of mutual intensity 77−624
image scanning by SAW on monolithic MIS structure 77−23771
image subtraction via processing simultaneously recorded holographic images 77−46700
image-plane hologram with non-image-plane motion parallax 80−48186
imaging of atoms three dimensional molecular structure reconstruction, opto-digital computing 77−39510
imaging through phase-distorting media without alignment 80−99679
in-line absorption holograms, improved microimages, particle size analysis appl. 79−36857
in-line Fraunhofer hologram field, partially coherent illumination 77−19200
in-line hologram processing, comparison of phase and absorpt. modes 79−81384
in-line holograms, elimination of DC in reconstructed wavefronts 78−55323
in-line holograms, FT analysis 77−88637
incoherent diffraction correlator with a holographic filter 80−37955
incoherent imagery system, introduction of partial coherence by holographic components 80−95853
incoherent polychromatic imaging with holographic optical elements 80−69349
industrial, principles, applications *(German)* 80−95841
industrial applications, review *(Japanese)* 78−78958
information processing experiment set for undergraduates 78−28885
integrated optical multichannel data preprocessor, using holographic subtraction 79−3813
intensity ratio setting method 80−77588
interference correlators, theory 78−78969
interference electron microscopy using electron holography and Mach-Zehnder interferometry 79−54231
interference fringe bending due to pre-stress in photographic emulsion 79−98318
interference pattern electronic heterodyne recording 80−74316
inverse radon transform by optical convolution 78−66777
invisible information imaging techniques 77−5819
IR, reconstruction and replica prod. *(French)* 79−98314
IR holographic elements, laser materials processing appl. 80−37964
IR holography at 10.6 μm, use of TEM_{10} laser mode 79−27199
IR impulse holography and interferometry, appls. *(Russian)* 77−14678
IR-to-visible image conversion with a thick-layer hologram 80−87355
irregular phase objects, dynamic interferometry, differential holography using phase conjugate refl. 80−37969
joint Fourier transform processing with thermoplastic device 79−72512
joint-Fourier-transform correlator, dual-axis, hologram recording 79−59649
Kodak 649-F plate 5-min. processing monobath 77−633
Kodak 649F plates, intermittent characteristic curves at 514.5 nm 80−23637
Laplacian formation by holographic zone plate moire patterns 79−13917
large scale holographic display, in photographic emulsion, image reconstruction 78−78974
large volume holography using holographic scatter plates 79−98323
large-aperture holographic visual simulator 80−102679
large-scale reflection and transmission, for displays 78−78975
laser application to optical data processing 77−88832
laser beam, diverging, conversion into plane wave by dynamic vol. hologram 79−18376
laser beam applications, survey *(German)* 77−698
laser beam coherence and divergence *(Spanish)* 80−87424
laser beam deflection using moving holographic elements *(Russian)* 80−63956
laser beam deflector design, development *(Russian)* 80−1158
laser beam deflector performance characteristics 77−19287
laser beam machining appl., single versus multiple exposure, investigation 77−77645
laser beam profile measurement using spatial sampling, Fourier optics and holography 79−86201
laser engineering and appls., conf., Washington, USA (May-June 1979) 80−1216
laser holocinematography, for cavitation bubble dynamics recording 79−86147
laser induced breakdown in liquids, high speed holography 78−18360
laser nonstationary generation induced interference pattern phase distortion, holographic meas. 78−58945
laser power and coherence requirements 79−50260
holography continued
laser radiation divergence reduction, holographic method *(Russian)* 78−63147
laser speckle reduction by US modulation 79−3638
laser technology appl. *(German)* 78−5522
lasers and applications, conf., Dresden, Germany (Mar.-Apr. 1977) 77−83881
lasers and applications, conference Erice, Italy (May-Jun. 1970) 77−38906
leg-foot, complex, in conditions of lesion and reconstruction 80−67142
lens, axial, on spherical substrate with remote pupil, aberrations 80−95849
lens, image quality estimation criteria 78−25824
lens design techniques, 488 nm construction, 633 nm read out 79−89866
lens element, astigmatism free 77−46784
lens element, s and t formulae 77−46785
lens recording techniques for IR wavelengths 80−95847
lens system, astigmatism and coma reduction 80−53238
lens system, method for wave aberrations calc. 80−28175
lens system design 78−9425
lens-hologram optical system, monochromatic aberrations 79−3760
lenses, coherent transfer functions anal. 77−68190
lensless Fourier transform, generalised holographic form., spherical wave illum. 80−74312
lensless Fourier transform, wavelength difference between recording and reconstructing wavefronts 80−58471
lensless matched filter, operating principle, third order holographic aberration 77−7013
lensless reconstruction of Fourier holograms by injection laser radiation 78−17881
light diffraction, in 3-dimens. holograms, vector eqns., Kogelnik theory *(Russian)* 78−22100
light energy transfer by semiconductor in crossed elec. and mag. fields *(Russian)* 77−75453
light source, low intensity, holographic determ. of spatial coherence 78−25823
light sources, conventional, for holographic displays 79−50261
light wave transformation by reflection 3D holograms 79−3657
light-in-flight recording 78−94379
$LiNbO_3$:Fe(Cu), photorefractive recording of volume holograms 78−37849
linear coherent processing by input scanning technique 79−76622
linear optical transfer, three-dimensional, by holographic depth selection 77−10867
Lippmann hologram recording technique 79−31840
liquid crystal controlled transparency, information optical recording in microholograms 79−10406
liquid crystal incoherent-coherent image convertor, hologram recording 80−28342
liquid crystal polarization rotator for intermodulation spatial-bandwidth reduction holography 80−53439
long-wave hologram point-object reconstructed image field intensity distrb. 79−55093
long-wave imaging with super-resolution by wavelength diversity 80−102675
long-wavelength hologram focusing parameters, estimation method using focused pattern 80−14304
longwave holography, double circular scan format generation 80−43555
luminance determination of holographic image 79−81394
macromolecules in liq. cryst., optical changes obs. method 79−64135
magnetic domain walls, off-axis electron microholography 78−82080
magnification of object image, dynamic holograms in nonlinear media 79−913
magnified dark-field image holographic recording 77−19214
maleic anhydride-styrene copolymer, photochromic, recording material for holograph 79−72537
matched filter, increasing information capacity 78−25815
matched filtering with multichannel US modulators *(Russian)* 77−58426
matched holographic filters with Pockels readout optical modulators 80−53456
matched-filter optical processor using holographic Fourier transform lenses 79−45913
materials for optical storage and reproduction 80−33109
maximum recordable number of particles 78−58946
measurement of fan vibration using double pulse holography 79−30462
measuring techniques, significance of holography *(German)* 78−90395
medical and biological applications 79−8528
medical diagnosis, holographic techniques as aids *(German)* 79−96645
medical images, 3-dimens. display 77−29193
micro-optoelectronic parallel processors *(Russian)* 78−46517
microscopic plankton, holographic motion pictures 78−48946
microscopy, real time holographic, using holographic illuminating system, rotary shearing interferometer 79−81388
microvelocimeter, ocean particle dynamics meas. 80−12567
mirror fabrication based on holographic simulation 80−87351
mirror simulation by reflection holograms 77−71945
modified Michelson interferometer for hologram prod., undergraduate expt. 80−105473
moire for flexible coupling flange geometry stress distribution optimisation *(Italian)* 77−42508
moire-fringes, differentiation by wavefront reconstruction with white light sources 79−86145
molecular spectroscopy, holographic recording 78−62954
motion paths display, speckle photography, holographic reconstruction 77−18084
motion picture sound recording and reproduction using a holographic method *(Russian)* 79−10273
movie camera and projection system 80−78808
moving object, using Q-switched ruby laser freq. chirp 79−7093
multicolour image from superposition of rainbow holograms 78−58957
multicolour imaging with white-light source 77−83833
multicolour reflection holograms, improved image techniques 80−48184
multicomponent hologram, spatially multiplexed, arranger for unordered fibre bundle image transmission 80−78957
multifrequency hologram elements, 3D phase objects interferometry 80−9835
multifrequency hologram matrix, appl. to two-dimens. imaging, computer simulation 79−22921
multifrequency synthetic detecting holography, geophysics appls. *(Chinese)* 77−64444

holography continued
multiple Fourier holography for processing optical data matrices 79−13910
multiple hologram appl. to variable size 3-D object recognition *(French)* 77−46705
multiple point hologram lens array generation, appl. to micro-electronic mask making 80−95842
multiple recording, dynamic range limits of photographic layer 79−7097
multiple recording with coded reference wave 77−75451
multiple-beam hologram, resolution 79−13927
multiple-grating interferometers for hologram-forming process, MTF first-order theory 79−76632
multiple-reference-beam nonlinear holography, intermodulation background noise suppression appl. 80−99674
multiplex holographic representations of space-variant optical processors 80−48192
multiplex holography with chirp-modulated binary phase-coded reference-beam masks 79−27202
multiplexing technique 79−18369
multiplexing technique 79−13925
multislit spatial filtered pseudocolour holographic imaging 80−53236
NDT, using holographic techniques, book contrib. 79−18380
neutron holography, using Fresnel zone plate encoding 80−48131
NMR determination of phys. and biological struct. *(Rumanian)* 78−49874
noncoherent illumination, elimination using amplitude mask *(Russian)* 79−45917
noncoherent optical projection system input holograms *(Russian)* 80−14297
nonlinear effects with two reference point sources 78−13671
nonlinear optical four-wave mixing as real time holography 78−50853
nonlinear source, incoherent holographic record 77−38828
nonlinearity recorded matched filter, false alarm rate reduction 77−62037
nonoptimally exposed holograms, reprocessing techniques 80−58474
nosetip ablation holography in 10 MW plasma arc facility 78−20621
numerical optical processor configurations 80−48194
numerical reconstruction, two dimens. Fourier transforms, monochromatic, multifrequency 78−1180
object's wave state of polarisation recording and reconstruction by vol. hologram 80−23636
object beam depolarisation effect on holographic image light flux *(Spanish)* 78−50733
object scanning holography, resolving power 78−17870
objective, hemispherical, concentric, in holographic memory, spherical aberration calc. method *(Russian)* 78−71184
objective for holographic recording devices 79−32028
objectives' two-dimensional transfer functions, holographic meas. test 79−50253
off-axis image electron holography, proposal 77−10151
oil films for dynamic IR holographic recording *(French)* 79−18364
oligourethaneacrylate photopolymerised layers, production of holograms *(Russian)* 79−7102
on-axis hologram, student experiment 78−86084
one-dimensional amplitude-phase holograms, diffraction efficiency calcs. 77−68189
one-step multicolour rainbow holograms with wide angle of view 79−72535
one-step rainbow holography with field lens 79−13923
ophthalmology and vision research, appl. of lasers, holography 80−12210
ophthalmology appl. 78−7342
ophthalmology applications 80−67200
optical branching elements 77−10870
optical coherence applications, seminar, San Diego, CA, USA (Aug. 1979) 80−77542
optical computing, conference, London (1978) 79−72511
optical data processing, appls., book 78−90388
optical data processor using holographic reflective lenses 77−34829
optical element design using analogous lens model 78−58955
optical element fabrication using dye-sensitised dichromated gelatin 78−63043
optical element generation, modification, expt. 77−83966
optical elements, axisymmetrical, third order aberrations 80−69341
optical elements, third-order aberration theory and generalised aplanatic condition 80−74314
optical elements anamorphotic props. with astigmatism 79−98319
optical fibre radiation, from exit end as reference and/or illuminating wave 78−17884
optical image and signal processing, United States Air Force programmes 78−74854
optical image charact. processing methods 77−625
optical image phase recording using sensitised photooxidation reactions 80−87350
optical information storage, seminar, Washington, USA (Apr. 1979) 80−41942
optical material inspection procedure using holographic filter technique *(German)* 77−31142
optical preprocessor, use in Earth-resources satellites 80−67430
optical processor with variable operators, operation of hologram recording, readout units 79−13920
optical reconstructions from projections via deconvolution 80−63962
optical sectioning for three-dimensional image information reduction 77−88679
optical signal and image processing, conference, San Diego (1977) 78−74853
optical storage materials and methods, conf., San Diego, USA (Aug. 1977) 78−71171
optical volume holography, features and appls. 80−32937
optical-fibre-bundle holographic coupler, expt. 78−42419
optics applied to metrology, conf., Strasbourg, France (1977) 79−6159
optimisation of 3D hologram recording conditions 79−72536
optimum colour rendering of holographic images *(Russian)* 77−7035
optoelectronic devices and optical imaging techniques, book 80−27059
organic photochromic materials, holographic recording *(Russian)* 80−1161
orthopaedic applications 80−67196
otology applications 80−67206
page-composer technique for 1-D hologram using acousto-optic deflector 79−81397
parallel matched filtering, vol. effect minimisation 77−7012

holography continued
partially coherent light holography, using Michelson interferometer 80−58480
particle field holograms, Fraunhofer plane analysis 80−73306
particle sizing high-resolution system 79−81392
particle track holograms, 2 laser techniques *(Russian)* 78−25827
pattern recognition appl., using optical spatial filter *(Japanese)* 80−5699
pattern recognition for 'simple' objects 80−53230
pattern recognition of Korean alphabet using matched spatial filters *(Korean)* 79−22920
pattern recognition of Korean alphabets, discrimination enhancement using phase modulated matched filters 80−95854
perforated screen, hologram on layers of photoresist 80−28178
periodic multiple imaging structures 77−627
phase characteristics of PL-3 type holographic plates for optimal exposure and development *(Russian)* 80−91763
phase conjugate optics and real-time holography 78−83034
phase control hologram grating for hologram fringe stabilisation 77−38823
phase determination of amplitude modulated complex wavefront 78−55305
phase distributions, linear and nonlinear, determ. using electro-optical system 78−58954
phase hologram recording materials, photopolymers and organo-metallic semicond. 79−86143
phase holograms, action of bleaching, comments 77−71949
phase holograms, action of bleaching 77−71948
phase inhomogeneities, 3-dimens., shadow method obs. 77−10094
phase microscopy, holographic approach 78−45684
phase plate consisting of bleached holographic lens, for noise-free coherent imaging systems 79−31817
phase relief hologram recording on semiconductor films *(Russian)* 78−50741
phase retrieval and polarisation identity 78−71042
phase shifter in hologram recording, deterministic phase code synthesis 78−37835
phase-hologram material, using four-centre-type photopolymerisation in cryst. state 78−37832
phase-reflective Fourier hologram transparency images restoration *(Russian)* 79−27204
phase-transformation interference reversible light reflector, stable memory 77−54680
phosphenes in the light of bioholographic models 79−74632
photoanisotropy in yellow mordant azo dyes *(Russian)* 80−42290
photochemical reaction kinetics use 79−29383
photochromic glass, holographic data recording optimisation, diffr. efficiency 78−25829
photochromic glasses, anisotropic recording of optical data *(Russian)* 77−1651
photochromic inorganic materials for hologram storage, book contrib. 78−25835
photochromic recording medium, exponential transfer curve appl. 80−78796
photoconductive-thermoplastic devices appl. 79−31837
photodetector matrices and scanistors for hologram information processing, switching transients 78−45703
photodichroic materials as coherent optical computing elements 77−71962
photodichroic spatial light modulator for joint Fourier transform correlation 80−106617
photoelastic applications, simultaneous determ. of isoclinic and isochromatic lines 80−63946
photoelastic birefringent material stress determ. in single hologram exposure 80−106770
photoelasticity, holographic, matrix theory, book 79−64612
photoelasticity determ. *(Chinese)* 79−81828
photoelectric detector, 1-D data recording 78−1195
photoelectric recording, correl. methods 77−79784
photographic emulsion requirements 79−50262
photographic emulsion response relationship for holography 80−1148
photographic emulsions used in optical correlators, laser damage 79−27303
photographic materials, determ. of freq.-contrast charact. by multibeam method *(Russian)* 79−27219
photographic materials, diffraction, transmission, sensitivity at 442, 633 nm for holographic appls. *(Russian)* 80−43301
photographic noise in data processing by coherent light *(Italian)* 78−22088
photomaterials with mirror layer for newly developed holographic process *(Russian)* 78−55325
photopolymer imaging systems, for laser recording 78−71173
photopolymer laser recording materials development 77−54678
photopolymer latent imaging system, for vol. phase hologram recording 78−42298
photopolymer recording material, sensitised by redox system *(Japanese)* 77−7030
photorefractive effect, Gaussian beam at const. voltage 77−3552
photorefractive medium, hologram recording sensitivity 78−5438
photoresist, Shipley AZ-1375, sensitivity and nonlinearity at 441.6 and 457.9 nm 78−90475
photoresist recording material, beamsplitter choice for minimum exposure time 79−59655
photoresists for hologram recording *(Russian)* 79−98324
photoresists for relief phase hologram recording, book contrib. 78−25837
photothermoplastic devices, conventional and self-developing, sensitivity and development 79−44958
photothermoplastic devices, performance and limitations 77−38832
photothermoplastic film, high resolution, meas. of sensitivity and transmissivity *(Russian)* 79−46022
photothermoplastic film, measurement and nondestructive testing appl. *(German)* 78−22097
photothermoplastic film on flexible terylene backing, heating to record optical information *(Russian)* 77−71959
photothermoplastic films, effect of latent image formation on band-pass transfer charact. 79−18382
photothermoplastic layer, diffraction effectiveness, registration of discrete holograms *(Russian)* 79−7100
photothermoplastic layers, optical transmission function, charge carrier drift effects *(Russian)* 79−3661
photothermoplastic recording with rapid switching 80−32941

holography continued
physical structure meas. and recording, advantages 80−95843
picture scrambling for confidential picture taking technology, method 77−19208
plane to spherical wave conversion by volume holograms, vector effects 80−106496
plasma imaging, appl. of submillimetre waves in plasma physics 78−47182
plastic recording media, 10.6 μm 77−71952
PMMA, photodielectric media for holographic recording, photochem. response 78−7219
polarisation form reconstruction using diffuse reference beam *(French)* 77−71954
polarisation of object and reference waves, influence on hologram quality 80−23643
polarisation orientation influence on TIR hologram diffr. efficiency 78−37836
polarisation state reconstruction 78−25822
polarisational holographic recording on practical photoanisotropic materials 77−75443
polarised light, spectral analysis, polychromatic and coherent optics *(French)* 79−50209
polarised light in holography and optical information processing 77−46708
police investigations appl., footprint obs. *(French)* 78−9347
poly (alkyl cyano acrylate), sensitised with parabenzoquinone, holographic storage mechanism exam. 78−37850
polymer, photodielectric, for phase hologram recording 77−34842
polymethyl-α-cyanoacrylate, photodielectric media for holographic recording, photochem. response 78−7219
porous ceramic, eval. of frost resistance by holography *(Japanese)* 78−19987
positive photoresists, FP-383, prod. of holograms *(Russian)* 80−74323
principles, materials, applications, review *(Italian)* 77−42507
principles developed on Fresnel eqn. basis, Jones vector representation of images 78−90400
principles for electronic engineers *(Japanese)* 80−19005
printing of discrete stereograms of group portraiture *(Russian)* 80−23644
processing, space-frequency equivalence 79−76646
projection-type holographic displays 78−78972
projector unit, small formal hologram to large-screen projection appl. *(Russian)* 78−29918
prosthesis mechanical efficacy determ. by holographic strain meas. *(German)* 79−8573
prosthesis wear, holographic studies using optical contouring 80−67288
pseudocolor encoding, spatial filtered imaging technique 79−18370
pseudocolour encoding, of holographic imaging, new technique 78−78963
pseudocolour encoding of holographic images using single wavelength 78−87025
pseudoscopic image restored by a hologram, peculiarities of visual perception *(Russian)* 79−50255
pulse holography, appl. of active Q-modulators *(Russian)* 79−68371
pulsed holographic recording, in Fe-doped $LiNbO_3$ monocrystal *(Russian)* 77−629
radio hologram recording using linear Hall detector multipliers in mm range 77−639
radioastronomical aperture synthesis imagery data optical reconstruction 78−69702
radiography, flashing tomosynthesis 80−67243
radiography, holographic methods of 3-D representation from no. of plane images 80−67244
radiography applications 80−67242
radiotelescope data, digital hologram reconstruction 77−64653
radiotelescope optical modelling using coherent optics and holographic methods, expt. *(Russian)* 77−22096
rainbow hologram by one-step process 78−71062
rainbow hologram formation, image blur 78−25826
rainbow holograms, demonstration of diffraction and interference of light *(Polish)* 80−68001
rainbow holograms, recording techniques for specularly and diffusely reflecting objects *(Russian)* 79−59659
rainbow holograms using large-aperture condensing lenses 78−78962
rainbow holography, astigmatic one-step process 80−23639
rainbow holography using full object beam aperture, one-step method 80−63945
reader-copier development and speckle suppression 79−81395
real image of point source in idealised holographic system 78−63040
real-time, mechanical vibrations testing appl., in precision units *(German)* 80−38366
real-time coherent object edge reconstruction with $Bi_{12}SiO_{20}$ crystals 78−90372
real-time holographic viewing in moving fog 80−102676
real-time holography and phase conjugate optics 79−81476
real-time optical processing using the liquid crystal light valve 80−63936
rear reflections in plates, elimination technique 80−73145
recent trends 78−33713
reconstructed images intensity distrib. 80−9834
reconstruction, near region, fast algorithm based on fast convolution *(Chinese)* 79−18368
reconstruction of image, field diffracted by transparent object identity 78−37826
reconstruction of two stacked Fourier holograms 79−18374
recording, and reconstruction in spatially incoherent white light 78−78955
recording, determ. of holographic transmission characts. *(Russian)* 80−91760
recording, effects of photographic emulsion speed and contrast nonlinearity 80−106497
recording, in amorphous semiconductor films 77−88677
recording, processing of chromatised gelatin layers *(Russian)* 80−91762
recording, using acrylamide photopolymerisation, Fe^{3+} sensitised 77−54677
recording and read-out with evanescent field of guided waves 77−10869
recording and read-out with evanescent field of guided waves 78−37862
recording in nonideal conditions, techniques *(Czech)* 79−31839
recording materials, book 78−25830
recording materials, reversible *(Japanese)* 79−3651
recording materials and devices, book contrib. 78−25838
recording media comparative indices, optimal linear transfer function 79−89870
holography continued
recording medium, optimal linear transfer function determ. 80−23635
recording of optical data in absorbing materials, effective depth determ. *(Russian)* 78−29908
recording process, using photopolymer material, redox sensitized 78−13674
recording source beam allowable angular displacement 78−17879
recording with local reference beam obtained by spatial freq. separation 77−38825
reference wave diffraction effects *(Russian)* 79−50256
reflected-light holograms, photoinduced anisotropic recording media 79−41354
reflection, 360°, method of construction 77−26
reflection hologram, real image reconstruction, resolving power and diffr. efficiency 80−53237
reflection hologram of triangular shape, anal. 80−32928
reflection hologram preparation by interf. copying of transmission holograms 79−45916
reflection holograms, reduction of resolving power requirements of photographic. materials *(Russian)* 79−59658
reflection holograms in dichromated gelatin 80−19006
reflection holograms of diffusely reflecting objects, improved efficiency 80−32939
reflection holographic portraits, diffraction efficiency and safety 80−37968
reflection-transmission holograms obtained using mirror photolayers 77 58300
reflector phased array aberration effects, optical modelling *(Russian)* 78−16290
refractive index changes, holographic meas. 78−74865
refractometer for refractive index increments for macromolecules in soln. 79−27205
relief hologram recording on semiconductor surfaces *(Russian)* 77−19199
remote sensing multichannel data sets, integrated optical comparator 80−64213
repositioning of hologram by interferometric technique 80−23640
research and development of Soviet State Optical Institute 79−94199
reversal of path of ray through nonuniform phase medium, S/N ratio 77−31075
review *(Japanese)* 78−78957
review of 1948-78 development *(Czech)* 79−98315
review of work at Ukrainian SSR Acad. of Sci. *(Russian)* 79−45950
ruby, phase modulated conjugate wave generation, hologram model 80−83643
ruby laser, Q-switched, power dependent freq. sweep 77−19256
S-parameter representation of lossy volume-holograms 79−36858
salicylideneaniline, photochromic, optically induced changes in refr. index 79−81497
α_1-salicylideneaniline, photochromic props., appl. as holographic recording 77−68183
salicylideneaniline hologram, image reconstruction, reading beam not satisfying Bragg condition 78−37828
sampled Fourier transform hologram, interpretation, simplification techniques 78−1181
sandwich holography and applicability biomedical investigations 80−67211
sapphire disc impact obs. by back reference holography *(French)* 78−42307
SAW holographic visualisation, improved S/N ratio *(French)* 78−75023
SAW observable amplitude limitation in freq. shift holography 78−71058
SAW propagation patterns obs. by freq. translated holography method *(Japanese)* 78−22222
SAW visualisation, using acousto-optical holography *(German)* 80−70515
scalar diffusor autocorrelation *(French)* 78−90369
scan aberration correction 77−83828
screen aberrations, effect on a 3 dimensional image *(Russian)* 79−18378
screens for colour flat image, projection *(Russian)* 80−9066
screens production with third order spheric aberration compensation *(Russian)* 78−90404
seams, welded and soldered, Fourier hologram appl. for flaw detection in ICs 79−52580
seismic holography, integral representations of space time functions *(Russian)* 78−85483
seismic imaging 80−46130
self diffraction of laser beam by liquid crystal struct. 80−5803
semiconductor, photosensitive etching in nonoxidising etchants 80−78813
semiconductor photosensitive etching for hologram recording, attainable spatial freqs. 80−69343
semiconductor-electrolyte interface, photoelectrochem. processes, hologram recording utilisation 77−88667
semiconductors to record pulse holograms 79−55091
sensitised film preparation methods *(Italian)* 78−50730
sequential coherent optical reconstruction from projections using a ROACH filter 80−63961
sequential information retrieval, tape recording of audio signals 77−7024
shifted reference, advantage of freq. translation error 78−42304
signal and image processing, US Air Force research programme 80−78791
simulation of non-circular zone plates 79−50252
single beam, demonstrations 80−41983
single beam 360° hologram, recording and display expt. 77−60872
single side band, in bright- and dark-field microscopy, iterative algorithms 77−7640
single sideband image holography 77−38831
sinusoidal phase modulated stroboscopic holography, for vibration anal. 78−29919
small particle analysis 79−13924
small particles, brightness and contrast of holographic images 80−99675
sodium-alumoborosilicate photochromic glasses, Weigert effect *(Russian)* 77−68250
solid rocket propellant combustion, holographic recording 78−82935
sonar Doppler phased array coherent imaging and processing by metaxial optics 79−72521
sound and TV recording appls., general principles 77−34844
space and time variables in optics and holography, expt. aspects 77−34830

holography continued
space variant systems, holography using phase coded reference beams 78−33698
space-time random speckle pattern optical analysis 80−102682
space-variant holographic systems using phase-coded reference beams 78−74868
spatial electric filters, 2-D image formation book contrib. 77−79772
spatial filtering properties of volume holograms 79−27211
spatial inverse filters, simplified holographic fabrication 79−23077
spatially incoherent imagery process 77−46706
spatially incoherent object, illumination, reverse beam imaging *(Russian)* 77−14679
spatially periodic media, second-order coupled-mode eqns. 78−13655
speckle averaging, imaging step, subchannel holography 79−22918
Speckle noise of redundant Fourier holograms for one class of diffusers 78−50734
speckle pattern holographic projection, metrological applications 80−106493
speckle reduction by complementary spatial sampling 77−58290
spectral analysis, log-freq. variable resolution system using holographic mapping 77−638
spectral selectivity of 3D holograms 79−27209
spectrum-hologram, prod. and practical possibilities 80−37098
specular multiplexed holograms recorded on Kodak 649F plates, diffr. efficiency 80−23638
spherical aberration compensation in hologram lenses for short-wave shift in reconstructing radn. 77−19206
STEM object wave reconstruction, off-axis holograms 79−54230
stereogram imagery 78−78978
stimulated light scatt., wavefront reconstruction 80−64107
student laboratory apparatus, holographic animation apparatus 79−97134
sucrose benzoate host for recording volume phase holograms 77−632
summation using thermoplastic photographic plate *(Russian)* 79−22911
super resolution technique in Fresnel transform holography 80−9840
super-resolution derivation by analytical continuation methods 78−29915
superorthicon television system, for hologram reception and transmission 77−641
surface displacement meas., coherent optical correlation technique 79−75499
surface profile meas. of electrically regulated information recording carriers for holographic storage *(Russian)* 80−63958
synthesized hologram accuracy testing 77−31079
synthesized holograms, information visualisation 78−82930
T-E curve classification, appl. in spectrum analysis and holography 78−82916
Takiwax films for pulsed IR holography 79−18363
teaching, holographic experiments on optical imaging 80−12872
teaching, holographic road show 79−58503
teaching demonstration using Hg vapour street light 78−24628
TEM, holographic method for recording electron image 79−6224
temporal, image transmission through monomode 80−69512
temporal holography for 2D coherent space-variant processing, theory 80−23624
terrain displays in 3D 78−78979
theory, rel. to phase problem in electron microscopy 80−99681
theory, wave eqns. and photographic process 77−38836
thermochromic materials, IR hologram recording 79−86135
thermoplastic film for holographic display and recording 79−50263
thermoplastic films, quasistatic theory of frost deform. 79−56052
thermoplastic media for hologram recording *(Russian)* 78−58948
thermoplastic photoconductor media, review *(Japanese)* 78−78956
thermoplastic photoconductor tape development for holographic recording 77−88671
thermoplastic photoconductor technology for optical recording and storage 78−71175
thermoplastic recording, book contrib. 78−25836
thermoplastic recording, IR laser heating 78−71065
thermoplastic recording 77−75455
thermoplastic recording 78−78961
thermoplastic recording media, dynamic range, noise effect *(Russian)* 77−88675
thermoplastic-photocond. device for holographic recording, diffr. efficiencies 80−5707
thermoplastic-photoconductor, holographic recording technique 78−9346
thermoplastic-photoconductor films for optical data processing 78−50875
thermoplastic-photoconductor hologram recording media, frost suppression 78−17869
thermoplastic-photoconductor media, charge carrier behaviour, microscopic response 79−28370
thermoplastic-photoconductor plate, exam. of microsocpic response in holographic recording 78−58947
thermoplastic-photoconductor tape for holographic recording, spatial filter prod. 78−90391
thick, holographic optical element design and construction 78−55315
thick film phase holograms recorded using coded reference waves 78−50740
thin holograms recorded with oppositely directed beams 79−13930
thin unbleached holograms, diffraction efficiency, relief phase modulation 78−66789
three dimensional display using stereograms and composite holograms 77−79921
three dimensional hologram copying method 77−71957
three dimensional imaging, conf., San Diego, USA (Aug. 1977) 78−78971
three dimensional phase holograms, diffraction efficiency 77−34849
three dimensional stress analysis holophotoelastic method appl. *(Chinese)* 79−72866
three-beam polarisation holography, influence of photographic material nonlinearity 78−58952
three-dimensional, optical charact., acoustic field effects 77−10877
three-dimensional image prod., reversal method using reflective and lenticular screens 78−90403
three-dimensional image recording on Lippman photographic plates, techniques 79−86148
three-dimensional information 78−78973
three-dimensional measurement on image reconstructed by holographic process 78−58958
three-dimensional measurement technique combining streak camera with modelocked laser 77−83832
time resolution improvement in high-speed holography 78−37840

holography continued
time-dependent reference wave for hologram recording, S/N ratio, energy characts. 80−32935
topogram sensitivity, wavefront correl. effect 80−69345
translator-hologram recording with spatially modulated reference waves, optimisation 80−37971
translucent three-dimensional holograms, mode theory taking account of the absorption 80−91757
transmission and reflection props. of holograms recorded with backward and accompanying beams *(Russian)* 77−68194
transmission holography limitations in particle analysis 77−19213
transmission type vol. holograms, 2D, amplitudes of transmitted and diffr. beams 77−79783
transparencies, 2-D, hologram synthesis 80−95845
travelling interference pattern recording, freq. shift 77−34850
tribromomethane-propyl alcohol conc. fluctuation kinetics, holographic study *(Russian)* 78−19508
trihedral reflectors, for holography with local reference beam 78−37853
TV, appl. of CRT with electro-optic crystal *(Russian)* 80−37974
TV appl., minimum frequency band evaluation *(Russian)* 77−54682
TV holographic system signal frequency spectrum 77−7036
TV transmission of Fresnel holograms 80−19009
twin-image holography, chromatic lens system, astron. appls. 80−87346
two-dimensional volume, coupled wave differential eqns. derivation 78 55317
two-dimensional volume holograms, general soln. 78−1189
two-phase nozzle flow, liq. film size at mouth, holographic meas. 79−86537
Two-stage holographic rejector filter *(Russian)* 77−75675
two-wavelength contouring with automated thermoplastic holographic camera 80−74318
tympanic membrane vibration study, phase sensitive technique *(German)* 78−3513
tympanic membrane vibrs. in human temporal bones, double pulsed holographic anal. 78−40289
Vander Lugt holographic filters, optical correlation for pattern recognition 77−79765
vector shadow method for colour images 80−1155
vibrating plate sound radiation study using optical holography 77−836
vibration analysis by wavefront modulated holography 79−3652
vibrations of square plate with parabolic thickness variation 79−68628
viewing techniques and engineering display applications 79−50264
N-vinylcarbazole containing polymers, sensitization to Ar laser for single laser photothermoplastic devices 80−83651
virtual holography, method of source and channel encoding, decoding of information 79−94185
viscosity measurement by holographic method, appl. to amorphous Se 79−37263
visualization of light propagation, hologram construction 79−81391
volume, large, two-dimensional case with overlapping inscribing beams 77−42509
volume dynamic holography, image conversion *(Russian)* 80−1160
volume hologram, arbitrary attenuation, coupled wave theory 77−46707
volume hologram, finite beam reflection-type, properties 79−10269
volume hologram power conservation theorem 79−81390
volume hologram reading-out, transient self-enhancement *(Russian)* 79−27217
volume hologram representation of space-variant systems 78−33696
volume hologram superimposed information display 80−78807
volume hologram two-dimens. theory, incl. varying average dielec. const. effect 78−78960
volume holograms, functional properties and appls. 79−94187
volume holograms, general two-dimens. theory 78−25816
volume holograms, mode theory allowing for photographic process nonlinearity 80−102673
volume holograms, reconstruct. fidelity for finite width and variable index modulation 79−72533
volume holograms, two-dimensional N-coupled wave theory 78−17873
volume holograms as colour-sensitive spatial filters 78−87150
volume holograms constructed from computer-generated masks 78−87026
volume holograms in electrooptic birefr. crysts., light diffr. 79−55084
volume holograms with elec. polarisation in grating plane, 2D theory 79−72532
volume holographic multiple recording on photographic plates *(German)* 80−43288
volume holography, associativity 77−19201
volume holography, coupled-wave theory generalisations 80−106495
volume holography using Gaussian beams, kinematic theory 77−626
volume light source, spatial coherence of spontaneous radn., holographic meas. 79−98455
volume phase hologram reconstructing properties, reference beam relative intensity effect 79−50251
volume phase holograms, 3-D vectorial theory 79−81385
volume phase holograms, signal distortion noise 77−79782
volume phase holograms, two dimens. theory of higher order modes 80−14300
volume phase holograms operation, model 78−55316
volume phase holographic recording media, organic materials 79−3755
volume phase holography, crystal two light wave interaction, photoexcited, photogalvanic effects 79−27214
volume phase holography, vector differential equations solns. 79−81386
volume reflection hologram, conjugate image appearance 80−28181
volume-phase reflection hologram, recording medium thickness effect on image luminance 80−58479
volume-surface wave interference for hologram formation 80−37973
VR-M fine grained photographic films for holography with opposing beams *(Russian)* 79−68370
wave aberrations caused by misalignments of aspherics, and their elimination 80−33127
wavefront conversion by volume holograms between cylindrical and plane waves 78−90396
wavefront reconstruction method, plane waveguide hologram coupled system 80−5708
wavefront registration and volume object image reconstruction by stimulated Raman scatt. *(German)* 80−53367
waveguide hologram recording with guided reference and readout waves 80−106492
waveguide hologram using optical thin films high-efficiency relief-type hologram 78−66958

holography continued
waveguide holograms, recording and reconstruction, integration 77−14674
waveguide holography, expt. techniques and results 80−28173
waveguide holography with guided reference and/or reconstructing wave 78−1198
wax film, hologram recording at 10.6 μm, image reconstruction 78−17868
wear meas. using contour fringe images 80−87345
white light, coherent method, wavelength compensation 77−83817
white light, methods of production and associated problems 79−50257
white light, principles, techniques, difficulties and applications *(Italian)* 80−53233
white light hologram technique 79−10267
white light holographic portraits, still or animated 79−18365
white light multiplexed holograms of 3D objects 79−81387
white light reflection holography, developer compositions compared 80−102669
white-light holograms, reduction of coherent light requirement for viewing 77−7033
white-light transmission/reflection holographic imaging 78−37852
wide-angle holography, step by step multi-sided recording technique *(Chinese)* 78−90392
wind tunnel particle and droplet field holography 79−76642
workpiece quality control by optical correlation 77−50644
X-ray, intensity requirements at 1 Å, unfeasibility 77−42504
X-ray crystallography, holographic computing step for image display 78−91199
X-ray hologram recording, optimal conditions *(Russian)* 79−93266
X-ray holographic microscopy *(Russian)* 78−12799
X-ray imaging using holography or electronics, tomosynthesis 77−40847
X-ray incoherent holography *(Korean)* 79−6250
X-ray laser holography, pumping by synchrotron radiation from storage rings 78−55322
X-ray microscopy, possibility of utilizing holographic schemes 79−36861
X-ray synchrotron radiation, coherence props. and power 77−75442
X-ray tomogram reconstruction by holographic methods 80−67246
Young's experiment with n holes, appls. *(French)* 78−42274
zone-plate coded imaging of laser-produced plasmas 77−55167
zone-plate coded imaging on microscopic scale 77−54673
Ag halide high resolution materials, 3-D hologram recording, exposure characts. 78−17880
Ag halide photographic layers, 3D holograms recorded with short exposures, diffr. efficiency 79−55087
Ag halide photographic materials for holography, book contrib. 78−25832
Ag halide sensitised gelatin processing, phase volume hologram form. 80−78797
Ag-As_2S_3 sandwich structure, holographic characts., recording kinetics 78−29913
AgBr polydispersed particles in unsensitised holographic emulsion, bulk attenuation and absorpt. *(Russian)* 79−2865
AgBr(Cl)-CuBr(Cl), photochromic film for hologram recording 79−64184
Al alloy 2024, fatigue damage detection by optical correlation 78−27717
Al film, wave front reversal, holography applications *(Russian)* 80−58483
Al-Cu, high strength, type 2024-T3, crack growth, fatigue induced surface deform., holographic detect. 80−85120
As-S, glassy film optical props., photostimulated effects and hologram recording 79−27215
As-S chalcogenide glassy semiconductors, induced anisotropy 79−32013
As-S glass media, temp. control of hologram props. 78−17883
As-S semiconducting glass film holographic recording media *(Russian)* 77−10864
As-S system glasses, photostruct. transforms. under laser radiation, use in holographic recording 77−76316
As-Se-Ge, amorphous film, relief-type hologram mode, hologram replication *(Japanese)* 78−78959
As_2S_3, amorphous film, light enhanced vaporisation, photolithographic process, photographic appls. 77−5949
As_2S_3 chalcogenide film surface relief hologram selective etching *(Russian)* 79−94181
As_2S_3 film, hologram recording using total-internal-refl., polarisation depend. 80−106491
As_2S_3-Ag light sensitive material, development of non-interchangeability under continuous laser radiation *(Russian)* 80−50870
As_2S_3-Ag photosensitive film systems, hologram recording 78−1194
$As_2S_3(Se_3)$ films, vitreous, photodecomp. and photostruct. changes 77−76318
As_2Se_3 chalcogenide film surface relief hologram selective etching *(Russian)* 79−94181
As_2Se_3, vitreous, hologram recording light sensitivity spectral distrib. *(Russian)* 78−1191
As_3Se_2 chalcogenide film surface relief hologram selective etching *(Russian)* 79−94181
$As2S_3$ amorphous chalcogenide film inorganic photoresists, holographic resolution evaluation 79−76629
Au-Si_3N_4-GaAs-GaP structures, as elec. controlled optical transparencies, optical processing use 77−85339
$(Ba_{1-x}Sr_x)_{1-y}(Nb_2O_6)_y$:$CeO_2$ crystals, photoelectric and photorefractive props., hologram recording 80−53239
$BaTiO_3$, holographic storage props. 80−87354
$Bi_{12}GeO_{20}$, high sensitivity read write vol. holographic storage 77−7026
$Bi_{12}GeO_{20}$, holographic recording and photoinduced refractive index change exam. 78−37851
$Bi_{12}GeO_{20}$, vol. hologram recording, charge transfer process 78−5437
$Bi_{12}SiO_{20}$ crystal, real-time holographic recording 79−72540
$Bi_{12}SiO_{20}$ crystals, phase-conjugate wavefront generation via real-time holography 79−27213
$Bi_{12}SiO_{20}$ electrooptic crystals, vol. phase holograms, light diffr. and nonlinear image processing 80−37972
$Bi_{12}SiO_{20}$, high sensitivity read write vol. holographic storage 77−7026
$Bi_{12}SiO_{20}$, holographic recording and photoinduced refractive index change exam. 78−37851
$Bi_{12}SiO_{20}$, optically active photorefractive cryst., light diffr. by vol. holograms 79−64185
$Bi_{12}SiO_{20}$, phase-conjugate wavefront refl. depend. on dynamic hologram spatial freq. 80−53358
$Bi_{12}SiO_{20}$ photoelectret, in optical processing and X, γ ray imaging 80−23764
holography continued
$Bi_{12}SiO_{20}$, photorefractive, vibr. struct. mode pattern visualisation, phase conjugation and dynamic holography 80−95938
$Bi_{12}SiO_{20}$, vol. hologram recording, charge transfer process 78−5437
$Bi_{12}SiO_{20}$, volume hologram polarisation props. and appls. 78−74859
CdS:Cu, Cd, data storage, optical and photoelec. reading 78−1193
CdS:Cu, recording holographic medium, exposure characts. *(Russian)* 77−635
Co film, mag. domain wall obs. by electron holography 80−80582
$Co_xFe_{3-x}O_4$, single cryst. mag. films, holograms recording and thermomagnetic writing 78−55324
Cu-As-Se glasses, recording and erasure by laser beam *(Russian)* 78−71170
Cu-PbI_2, thin sprayed layer, glass substrate, hologram recording *(Russian)* 77−71956
Cu_2HgI_4, thermochromic material, IR hologram recording 79−86135
EuO film, thermomag. effects for reversible holographic storage 77−34851
EuO film for thermomagnetic recording, anisotropy of resolving power 80−20404
EuO film threshold characteristics in holographic and bit recording *(Russian)* 80−63944
EuO, resolution as hologram recording material 77−83834
GaAlAs visible diode laser for hologram recording of three-dimens. object 80−95839
GeO amorphous film, hologram recording, photochem. props. 79−64186
H_2 laser, stimulated Raman scatt., appl. to holography 80−91782
HF laser beam spectral anal. using near field holography 77−23680
HgI_2, low temp. luminesc. spectra by holographic spectroscopy 79−33820
$Hg_3Se_2I_2$ film, holographic characts. *(Russian)* 77−79786
InSe film, photochem. production of holograms on surface *(Russian)* 79 7101
KBr, additively coloured crystal, depend. of bleaching kinetics on F-light intensities, holographic storage *(Russian)* 79−27351
KBr, additively coloured crystal, amplitude-phase holograms *(Russian)* 79−59654
KBr, additively coloured, self-enhancement of amplitude hologram *(Russian)* 80−9828
KBr, gamma-irrad., hologram recording by F-centre bleaching 80−78814
KBr, with F-centres, vol. holograms diffr. efficiency 77−19205
KBr:Ca, $F \rightarrow Z_1$ colour centre conversion, hologram recording appls. 78−17877
KCl, cryst. γ-irrad., holographic information recording appls. *(Russian)* 79−27218
KCl, diffr. by M-centres, thick plane wave hologram recording 77−7021
KCl, hologram recording by photodichroic F_A centres at room temp. 77−34846
KCl, photo-induced F-centres, hologram recording 80−28174
KCl, with F-centres, vol. holograms diffr. efficiency 77−19205
KCl:Ca, $F \rightarrow Z_1$ colour centre conversion, hologram recording appls. 78−17877
KCl:Cu, additively-coloured crysts., for hologram recording plates *(Russian)* 78−29914
KCl:K, F-centre coloured, for highly efficient holographic storage 78−37833
KCl:K^+ crystal, highly efficient phase holograms 78−33707
KCl:Na, photodichroic holographic recording, polarisation sensitivity 78−29911
KCl:Na, photoinduced reorientation of A-centres near room temp. 78−64344
KCl:Na and pure, hologram recording through $F \rightarrow X$ conversion 80−48190
$KNbO_3$ crystals, reduced, hologram recording and erasure sensitivity *(Russian)* 80−78795
$KNbO_3$, reduced, diffr. efficiency and energy transfer during hologram form. 79−72528
$KNbO_3$, reduced, phase hologram recording, energy transfer and sensitivity 80−69338
$KNbO_3$:Fe, optically induced refractive index changes 77−4612
$KNbO_3$:Fe, photorefr. effects and photocurrents 78−43434
$KNbO_3$:Fe photorefraction and photocurrent effects *(Russian)* 79−7091
$LiNbO_3$ birefringent crysts., holographic writing, image polarisation characts. storage 77−61926
$LiNbO_3$, doped, photorefr. and photovoltaic effects 77−38835
$LiNbO_3$, hologram, light diffr. with electro-optical rot. *(Russian)* 78−1190
$LiNbO_3$, hologram form. in external elec. field, transient energy transfer 78−22098
$LiNbO_3$, hologram indexing with tunable pulsed laser source 79−94186
$LiNbO_3$, hologram recording by photorefr. effect 77−83830
$LiNbO_3$, hologram recording, γ radiation effect 80−78812
$LiNbO_3$, holograms stored by photorefractive effect, reading and optical erasure 78−90390
$LiNbO_3$, holographic storage at high temp., optical damage relax. 77−14677
$LiNbO_3$, holographic storage, effects of nonstoichiometry and Fe-doping 80−69344
$LiNbO_3$, $LiNbO_3$:Fe, dynamic holography and optical image processing 79−94194
$LiNbO_3$, light diffr., elec. field effects, spatial hologram appls. *(Russian)* 77−23635
$LiNbO_3$, light diffraction from volume phase holograms 79−36860
$LiNbO_3$, mechanism of hologram writing, expt. 77−19212
$LiNbO_3$, phase holograms fixation kinetics 79−81393
$LiNbO_3$, photorefractive medium, hologram form. theory 77−68185
$LiNbO_3$, photorefractive, optical information storage 78−33708
$LiNbO_3$ photorefractive reversible optical memory *(Russian)* 78−58943
$LiNbO_3$, pure, two-photon photorefractive recording 78−31220
$LiNbO_3$, pure and Fe doped, photorefraction kinetics under irradiation and heating 79−42934
$LiNbO_3$, reduced, photovoltaic effect and holographic recording mechanisms 79−69556
$LiNbO_3$, reduced cryst., photovoltaic effect, appl. to holographic recording *(Russian)* 79−51635
$LiNbO_3$ SAW device, holographic obs. of bulk waves and surface waves through side planes of several cuts 78−71238
$LiNbO_3$, surface acoustic wave device, obs. of bulk waves by freq. shifted holography 77−19505
$LiNbO_3$, vol. holograms, photorefr. recording dynamics, multiple storage 77−38834

holography continued
$LiNbO_3$, vol. hologram recording and reconstruction 78−9349
$LiNbO_3$, vol. phase hologram for coherent beam structural conversion 79−59656
$LiNbO_3$, volume phase hologram erasure 78−42301
$LiNbO_3$, wave front convolution in 4-wave interaction with nonlocal nonlinear media *(Russian)* 79−86205
$LiNbO_3$ waveguide, holographic writing technique based on multiphoton photorefractive processes 77−38824
$LiNbO_3$ Z-cut crystals, bit and holographic recording, electric field control *(Russian)* 77−42512
$LiNbO_3$:Fe, characts. for holographic storage appls. 77−23630
$LiNbO_3$:Fe, dynamic hologram recording, high speed memory appl. 77−83835
$LiNbO_3$:Fe, dynamic optical storage 78−33706
$LiNbO_3$:Fe, efficient hologram recording using Nd:YAG laser pulses 79−55081
$LiNbO_3$:Fe, electro-optic cryst., light induced charge transport, holographic obs. 80−70747
$LiNbO_3$:Fe, electron irrad., photoinduced charge transfer and hologram recording 79−36859
$LiNbO_3$:Fe, hologram recording, photorefr. effect time depend. *(Russian)* 77−7032
$LiNbO_3$:Fe, hologram writing, beam coupling and transport length in bulk photovoltaic effect 79−94190
$LiNbO_3$:Fe, hologram nondestructive readout using different recording and readout wavelengths 80−14302
$LiNbO_3$:Fe, holographic recording and thermal fixing, invest. of mechanisms 80−78810
$LiNbO_3$:Fe, nonlinear image processing in 3-dimens. hologram 80−14303
$LiNbO_3$:Fe, phase hologram storage and fixing, review 77−19210
$LiNbO_3$:Fe, photorefractive recording of vol. holograms 77−637
$LiNbO_3$:Fe, photorefractive effects under external elec. field 77−23723
$LiNbO_3$:Fe, photorefraction, γ-irrad. influence, polarisation-optic and holographic obs. 80−11359
$LiNbO_3$:Fe, recording dynamical holograms in crystals with photovoltaic effect, nonstationary energy exchange *(Russian)* 79−31842
$LiNbO_3$:Fe, temp. depend., electron cond., holography appl. 78−14731
$LiNbO_3$:Fe (0.05%), hologram recording γ radiation effect 80−78812
$LiNbO_3$:Fe crystals, volume hologram storage; exam. of material 78−37848
$LiNbO_3$:Fe crystals, reflection hologram recording 79−10272
$LiNbO_3$:Fe photosensitive electro-optical crystals for image storage display and processing 77−19215
$LiNbO_3$:Fe spatial holograms, ageing mechanism and thermal fixing *(Russian)* 80−74311
$LiNbO_3$:Fe; photorefraction for holographic recording, thin hologram diffr. efficiency 79−55086
$LiNbO_3$:Mn, photorefractive sensitivity, holographic and photocurrent investig. 77−24581
$LiTaO_3$, characterisation as holographic storage materials 78−29909
$LiTaO_3$, photorefractive sensitivity, holographic and photocurrent investig. 77−24581
$LiTaO_3$, wave front convolution in 4-wave interaction with nonlocal nonlinear media *(Russian)* 79−86205
$LiTaO_3$:Fe, electro-optic cryst., light induced charge transport, holographic obs. 80−70747
$LiTaO_3$:Fe crystal, holographic storage process 80−32942
MnBi film, ferromag., diffr. efficiency of mag. holograms, Faraday effect 77−32355
MnBi film, hologram form. at 2.76 μm, using $CaF_2:Er^{3+}$ crystal laser 79−10270
MnBi film for recording optical information, analogue characts. *(Russian)* 78−50716
MnBi holographic film, reduction of thermomag. recording energy threshold *(Russian)* 80−43302
MnBi, problems for holographic recording *(Russian)* 80−91761
$Mn_{0.75}Ti_{0.25}Bi$ films as magnetooptic storage medium, mag. interferogram recording 78−19288
NaCl, amplitude phase hologram recording on colloid type centres *(Russian)* 80−69347
NaCl crystal, radiation coloured by electron beam, holographic lattice recorded by He-Ne laser 78−58950
NaCl crystals with dipole O colour centres, radiation colouring and holographic recording 80−48187
NaCl, hologram recording, F-centre bleaching by 633 nm light 79−22922
NaCl plates, γ-irrad., hologram recording, He-Cd laser radiation 78−17878
NaCl:Ca, hologram recording on R-centres 80−1157
NaCl:Ca, holographic appls., diffr. efficiency 77−54679
NaCl:Ca, reflection holograms recording 79−98320
NaCl:Ca crystals, optimum temp. for holographic recording *(Russian)* 80−1163
NaCl:Na, diffr. efficiency and self-amplification 79−7096
NaCl:O, hologram recording, colloidal type centre transformation *(Russian)* 80−55147
NaCl(:Ca) cryst., radiation colouring, amplitude-phase hologram appls., diffraction efficiency 77−68191
NaF photodichroic crystals, hologram synthesis in in-line scheme 77−88670
Si single crystal hologram recording time and diffraction efficiency *(Russian)* 77−58286
α-SiC (6H), dynamic hologram high-speed recording and erasure mechanism 80−5710
SmS film amplitude-phase hologram recording *(Russian)* 79−94192
SmS film for holographic storage, laser-induced semicond.-metal transition 77−88676
$(Sr,Ba)Nb_2O_6$:Ce, high sensitivity holographic storage 77−71953
VO_2 film, dynamic hologram recording *(Russian)* 77−10873
VO_2 film, dynamic holography, coherent props. of Cu vapour laser 79−13929
VO_2 film as holographic recording medium, diffr. efficiency 80−28180
VO_2 film based recording medium, holographic characteristics calc. *(Russian)* 79−7092

homopolar generators
500 V for Tokamak device power supply 78−5957
design for fusion reactor energy storage 80−68953

homopolar generators continued
electrical contacts, for homopolar generators, tests at high surface vels. and current densities 78−54964
fast discharging 10 MJ machine design, for fusion reactor 78−54950
fast discharging homopolar demonstration model as fusion reactor pulsed power supply 77−23283
fusion reactor, fast discharge machine, design, fabrication, testing 78−54952
fusion reactor, Shiva Faraday rot. coils, circuit and mag. anal. 78−54951
fusion reactor, TEXT, pulsed homopolar generator power supply, engineering and design 78−55016
fusion reactor, Tokamak, commercial, plasma driving system requirements 78−54954
fusion reactor, use of homopolar generator for inductive energy storage 78−54948
Lorenz model, periodic solns. and bifurcation struct. at high R 79−81692
motor-generator system for fusion power reactor energy storage 78−5044
pulse power machine current collection system, for fusion research 78−54949
pulsed homopolar power supply, misalignment and eccentricity anal. 77−23287
pulsed homopolar power supply for experimental Tokamak device 77−23286
radially stacked drum type, for Tokamak Ohmic heating 78−13337
superconducting field coils, design and appl. 78−54927
Tokamak, Texas exptl., homopolar generator, eddy currents, EM forces (torques), due to misalignment 78−54953
Tokamak device power supply appl. 78−5958
for Tokamak toroidal field coil-system 77−23257

homopolar machines
see also homopolar generators; homopolar motors
10 MJ fast discharging model, for fusion device 78−13335
electric and magnetic fields calc., Green and influence functions appl. *(Russian)* 77−53745
fast discharge, for fusion expt., mag. fields calc. 77−23288
fusion reactor, inductive and rotating machinery energy storage and transfer 79−85782
fusion reactor, ohmic heating energy storage for power reactor, costing 78−58495
glow discharge, rotation, Doppler shift of spectral lines 80−33838
inertial and inductive energy storage programs at LASL fusion reactor 77−23284
load coil, 1.5 MA, 10 MJ, for pulsed homopolar machine 78−13336
magnetic wheel unipolar machine, for teachers 78−12499
rotary machines as I/O system for superconducting magnetic energy storage system, appl. *(Japanese)* 80−85306

homopolar motors
motor-generator system for fusion power reactor energy storage 78−5044

homopolymers *see polymers*

hopping conduction
1/f current noise, random walk model 77−8162
AC conductivity due to intimate pairs of charged defect centres 79−4563
AC conductivity in random structs., renewal theory 78−141
AC hopping conductivity, percolative approach, time dependent cluster approx. 80−39577
actinide, transport props. and sp. ht., role of optical and acoustic phonons 77−15821
actinides, lattice vibrs. role in phys. props. determ. 77−28158
alkali metal-ammonia solns., metal-insulator transition, h.f. and u.s. props. 77−1369
alloys, substitutional, disordered, with strong electron correl. 77−62885
amorphous film, thickness depend. 77−89887
amorphous material, continuous time random walk, simple approx. solns. 77−43584
amorphous materials, dispersive transport, computer simulation, time of flight signals 80−70696
amorphous semiconductor, DC conductivity using quasiclassical approx. 78−23080
amorphous semiconductor, DC hopping cond., pre-exponential factor 78−76074
amorphous semiconductor, electrical conductivity, super-linear freq. depend. 79−28348
amorphous semiconductor, hopping conductivity, rate eqn. formulations, quantum transport approach 77−15841
amorphous semiconductor, local elec. field character, and electron transport mechanism 78−23088
amorphous semiconductor, localised gap states, hopping cond. and chem. bonding 78−23052
amorphous semiconductor, localised gap states, variable range hopping, susceptibility and EPR 77−72866
amorphous semiconductor, macroscopic theory of carrier pulse propagation 78−72154
amorphous semiconductor film, ion bombardment effect on electronic props. 79−65125
amorphous semiconductors, AC and DC conductivity theory in disordered hopping systems 80−54698
amorphous semiconductors, AC hopping cond., Kirchhoff equations, computer calc. 80−39579
amorphous semiconductors, conductivities, drift and diffusion 79−95413
amorphous semiconductors, doped, electronic props. 78−19030
amorphous semiconductors, hopping carriers, AC cond. and DC Hall mobility 80−44585
amorphous semiconductors, localised gap states, chemical trends 78−39067
amorphous semiconductors, mobility gap, phononless hopping 77−55527
amorphous semiconductors, thermopower, conductivity, statistical shift, doping effects 79−69537
amorphous substances, charge transfer mechanism, two-centre model *(Russian)* 78−30918
analytical formulae for DC hopping rate 77−72859
Anderson localisation, mean field theory and ε-expansion 80−80203
Anderson localised states, negative magnetoresistance 79−28357
anisotropy of hopping conduction, percolation theory 78−72156
anthracene, electron drift mobility, temp. depend., transient photocond. 77−66164
anthracene, temp.-independent mobilities, phonon-induced electron hopping 79−28347

hopping conduction continued
benzene-deuterate benzene cryst., triplet migration, cluster method 79−73510
Brownian motion in periodic potential, hopping to free conduction transition 79−44860
cadmium behenate in Langmuir multilayer assembly system, single layer conductance 79−51701
cadmium stearate, multilayer Langmuir films, DC cond., $T^{-1/2}$ law 77−12022
chalcogenide glass, AC conduction, theory 78−23077
chalcogenide glass, AC conductivity, temp. depend. 78−72153
chalcogenide glasses, AC conduction mechanism, electronic versus atomic 80−29409
chalcogenide glasses, elec. cond. at room temp., contact effects 77−20354
chalcogenide semiconductors, glassy and liq. states, elec. cond. freq. depend. 77−76856
chalcogenide semiconductors, optical and elec. props., comparison with SiO_2 78−6721
charge-transfer solid, quasitone dimens., Hall effect and transverse mobility 77−4326
chlorophyll-a, microcryst., trapped-electron doping in photovoltaic sandwich cells 78−53334
compensated semicond. film, jump-over cond., control by external field 78−80080
computer simulation in quasi one-dimens. disordered system 77−4334
computer simulation in three-dimens. disordered system 77−4336
computer simulation in two-dimens. disordered system 77−4335
conductivity and thermopower, percolation and effective medium theory 79−78103
coronene thin films, elec. cond. mechanism 77−28189
correlation effects, DC and AC cond. 79−65480
correlation effects, rate eqn. 77−89762
correlation effects 77−47818
correlation effects in hopping transport theory, applic. to cond. and thermal EMF *(Russian)* 78−23079
correlation effects in hopping transport theory, general relns. *(Russian)* 78−14734
covalent semiconductor, Hall effect sign in hopping cond. 77−72872
cupferron and complexes, amorphous, hopping cond., 0 to 150°C 79−60828
DC and AC cond. in hopping electronic systems 79−65478
DC conduction, numerical calcs. 79−60832
DC hopping conductivity, r-percolation in 3D 78−51958
degenerate hopping in wide bands 77−89761
diamond:B, variable-range hopping cond., effect of electron irrad. induced compensating centres 77−43599
diamond:B hopping conductivity in range 12 to 1300K 78−51994
diamond, synthetic, elec. cond. 78−56144
dielectric loss, charge carrier contrib. 79−56718
dielectric matrix calculation, Clausius-Mosotti relations 80−59898
disordered chains, electronic props. 80−2363
disordered insulator, continuous-time random walk model 80−96863
disordered materials, electronic hopping transport 80−39580
disordered one-dimensional lattice systems, diffusion and hopping conductivity 80−59991
disordered quasi-one-dimensional materials, review 78−6361
disordered semiconductor, DC hopping cond., photon- and US-induced, microscopic theory 77−76872
disordered semiconductor, DC phonon assisted hopping conduction, in mobility gap, theory, rate eqns. 79−60826
disordered semiconductor, hopping mechanism of dispersive transport 80−10971
disordered semiconductor, photon-phonon-assisted hopping, theory 80−44642
disordered solids, dispersive transient transport, expt. and theory 79−28342
disordered solids, electron-electron interaction effects on low temp. hopping 80−44584
disordered structure, deviations of polaron hopping mobility from Mott law 77−8095
disordered system, DC Hall effect in hopping region 77−66174
disordered system, freq. depend. of hopping cond. 77−28174
disordered system, Hall mobility due to hopping-type cond. 79−15167
disordered system, low-freq. cond. due to variable range hopping, cluster approx. 80−92886
disordered systems, AC hopping cond., cluster approx., one-dimens. systems 79−95379
disordered systems, cluster approx. in theory of AC hopping cond. 80−2372
disordered systems, dispersive hopping transport, Monte Carlo calcs., variable range percolation 80−44587
disordered systems, elec. cond. and Hall mobility, theory 80−54697
disordered systems, elec. transport mechanisms 79−69483
disordered systems, freq. depend. of cond. due to repeated jumps 80−15528
disordered systems, freq. depend. two-site model 77−76825
disordered systems, hopping Hall mobility 77−72846
disordered systems, random walk 80−75534
disordered systems, random walks and AC cond. 80−70661
disordered systems, theory of Hall effect in hopping region 77−47836
disordered systems, theory of Hall effect in hopping region 77−51713
dispersive transport by hopping and transport, theory 78−14726
effective medium theory in high elec. fields 80−20192
excess electrons in condensed media, migration in dilute mol. solns. 77−81457
exponential band tail, calc. method 79−87100
FEP polymer foil, charge transport, injected carrier hopping model 78−19171
ferrites, electronic cond. mechanisms, review 77−20314
frequency dependent, scaling approach 77−15861
generalised hopping system, with internal dynamics 80−39348
glass systems, electronic props. 79−42495
glasses, elec. props. 78−2479
granular metal film, thermally activated hopping, carrier-carrier interaction 77−15972
Hall effect in disordered and ordered systems, theoretical view 79−51605
heavily doped semiconductor, compensated, hopping photoconductivity 79−38130
hopping conduction continued
hopping model, semi-classical, effective mass and carrier mobility calc. 80−96872
Hubbard model, Ward identities, particle number conservation, analytical structure of self energy 78−79913
II-IV p-n amorphous heterojunction, phenomenological model 80−54769
ilvaite, Fe temp. depend. oxidation states, electron hopping, Mossbauer spectra, X-ray diffr. obs. 78−2779
impurity band, hopping promoted by electron-electron coupling 80−59987
impurity bands, in inversion layers 79−47171
impurity conduction phenomena, review of exptl. work *(Japanese)* 80−49737
p-InSb:Cu, Ag, deep impurity centres, acceptor conc. effect on conduction type 80−44602
insulator-semicond. interface, impurity-band hopping conduction in surface layers 80−75649
ionic, freq. depend., model calcs. 80−107507
ionic compounds, hopon mechanism for ion transport 79−14957
ionic conductor, elec. dipolar coupling between intracell dielec. response and intercell hopping response 79−55918
ionic conductor, frequency-dependent dielec. response, separation of vibr. and hopping contrib. 79−60538
Kapton, pyrolysed, cond. polymer, transport and mag. props. 80−96887
kinetic equations, effect of strong EM wave 78−76107
kinetic theory, localised state separation, Pauli master eqn. 80−80276
Langmuir films, dye-sensitized, anisotropic photocond. 80−80327
Langmuir multilayer films, structure-dependent carrier transport obs. *(Japanese)* 80−20339
Langmuir multilayer films with and without dye-sensitisers, elec. props. 80−97006
lattice of randomly placed sites, diffusion, appl. to AC conductivity 77−8097
Lexan:triphenylamine, molecularly doped, hole transport by hopping 78−34831
Lexan polycarbonate, N-isopropylcarbazole and triphenylamine doped, trap-controlled dispersive hopping transport 77−15850
linear chain, two-sublattice, hopping particle occupancy correlation function normal modes 80−49402
localised electron states, establishment of transport eqn. *(French)* 78−56141
magnetic semiconductors, small polaron form. and motion 80−96882
master eqn. approach in presence of mag. field 80−103697
master equation approach *(German)* 80−27237
metal powder, thermally activated hopping, carrier-carrier interaction 77−15972
metal-insulator-metal junction, hopping model of zero-bias tunnelling anomalies, mag. field effect 79−60936
methane-ethane liquid mixture, field-depend. excess electron mobility 77−89822
methylglyoxal-protein complexes, hopping conduction, theory 79−24935
MIM structure, zero-bias anomalies due to Kondo scatt., hopping model, mag. field effect 77−59334
MIM tunnel junction, magnetically doped, hopping model of zero-bias tunnelling anomalies, comparison with expt. 80−65703
molecular crystal, mixing between Frenkel excitons, and charge transfer states, effect on charge carrier transfer 77−89707
molecular crystals, electron mobility, temp. depend., hopping model 79−19588
naphthalene, electron band hopping transition 78−39155
naphthalene, mol. cryst., elec. field independent electron drift mobility 79−51645
naphthalene, pure and deuterated, band-hopping mobility transition 80−6833
naphthalene, temp.-independent mobilities, phonon-induced electron hopping 79−28347
noncrystalline materials, optical props., lecture 78−27263
noncrystalline system, Kubo eqn. for AC cond. 77−15853
one dimensional periodic model, boundary condition, limiting processes 79−60825
one-dimensional bond percolation model 80−103655
one-dimensional hopping, moment expansions and occupancy (site) correlation functions 78−55972
one-dimensional hopping conduction and diffusion, theory 78−6355
one-dimensional hopping conductivity, effect of impurities, current saturation 77−72856
one-dimensional hopping conductivity of interacting particles 78−10214
ordered and disordered solid, DC hopping cond. using correl. function method 80−10972
ordered and disordered solids, review 77−1420
ordered and disordered solids, review 77−15851
organic molecular crystal, electron mobility, temp. independent, theory 79−69509
oxide glasses, elec. cond., polaronic hopping model 79−65479
phonon assisted DC hopping conductivity, Anderson localised electronic states 77−32010
phonon-assisted DC hopping cond., exact asymptotic formula 77−62920
phonon-assisted hopping due to both acoustic and optical phonon interactions 77−66146
polar semiconductor, nonlinear transport, field-dependent relaxation time 80−6866
polaron, small hopping, reaction rate treatment, role of vibrational relaxation 78−72092
polaronic hopping conduction at low temp. 78−51906
poly(γ-methyl L-glutamate), electric conduction mechanism *(Japanese)* 80−54696
poly-2-vinylpyridine-iodine, semicond. film, elec. cond., depend. on I conc. and temp. 79−73606
poly-N-vinyl carbazole, and Br-substituted derivative, transient hole hopping transport, 150-500K 78−39108
poly-N-vinyl carbazole, hole hopping mobility, transit pulse dispersion 80−65565
poly-N-vinyl carbazole, trap-free lifetime, neutral traps, hopping systems 80−65566
poly-N-vinylcarbazole thin amorphous film, hole drift mobility, mol. mass. depend. 80−75663
polyacene quinone radical polymers, elec. props. described by variable range hopping model 80−44588
polyacene quinone radical polymers, two-dimens. variable range hopping 79−51608
polyacetylene:AsF_5, Hall effect meas. 80−24955

hopping conduction continued
polyacetylene, doped, elec. cond. and thermopower 80−96951
polyacrylonitrile, AC conduction mechanism, freq. and temp. depend. *(Japanese)* 80−54706
polyacrylonitrile, pyrolyzed, elec. cond. and dielec. const. in AC regime 78−60173
polyethylene, carrier mobility determ. by current oscillation method 79−28344
polyethylene, elec. cond. of high and low density samples, oxidation effects 80−107784
polyethylene, oxidised, charge carrier, transport phenomena 80−15515
polyethylene 2,6-naphthalate, AC conduction mechanism, freq. and temp. depend. *(Japanese)* 80−54706
polymer, molecularly doped, carrier drift, percolation approach 80−2390
polymer electret, charge dissipation, transport mechanisms 80−7268
polyolefins, elec. cond., review 78−26867
polyphenylacetylene films, phys. struct., AC and DC cond. 80−44750
polytetrahydrofuran film, electrochemically prepared between Pt and Au electrodes, AC elec. props. 80−40062
polytetrahydrofuran films, electrochemically prepared between metal electrodes, DC elec. props. 80−39695
polyvinylcarbazole, amorphous, hopping transport, reinterpretation of mobility meas. 79−42563
polyvinylcarbazole, Coloumb trap controlled hopping mobility model tests, mobility and permittivity meas. 79−56226
polyvinylcarbazole, fast hole transport 79−51628
power dissipation as function of equivalent cond. magnitude 79−82591
power law frequency dependent dielectric function and nonanalyticity properties 78−60387
protein model chain, aperiodic, electronic spectra, hopping cond. 80−5641
proteins, hopping conduction, theory 79−24935
PTFE films, plasma-polymerized, cond. mechanism, AC cond. and capacitance meas. 79−24093
PVC:Cu films, electron transport and dielec. props. 79−82700
quantum mechanical and semi-classical theory 77−15855
quantum mechanical theory 78−30925
quasi-one-dimensional disordered compounds 78−10425
quasi-one-dimensional lattice gas with three-dimensional ordering, hopping conductivity 78−91473
quasi-one-dimensional model with long range interaction, coupled Tomonaga chain, exact soln. 80−96856
p-quaterphenyl oriented layers, charge carrier transport, hopping model 80−2506
random media, hopping transport simulation, cluster method 79−73510
random one-dimensional system, asymptotic behaviour, theory 80−80279
random one-dimensional system, Monte Carlo computer simulation 80−80278
rare earth chalcogenides, cond. mechanism and thermoelec. efficiency 79−38110
rare earth pyrochlores, $R_2(V_{4/3}W_{3/3})O_7$, (R=Gd, Tb, Dy, Ho, Er, Tm, Xb, Lu), synthesis and elec. props. 80−29914
rate equations, theory 77−43590
semiclassical theory 79−91052
semiconductor, disordered, hopping thermoelec. power, temp. depend. 79−23995
semiconductor, disordered, theory of photon-induced DC hopping cond. 78−30952
semiconductor, hopping conduction influence of HF elec. field 78−52025
semiconductor, hopping transport theory for strong elec. field 77−8106
semiconductor, layered, DC hopping cond. due to stacking disorder and electron localisation 77−47819
semiconductor, moderately compensated, correl. effects 80−49711
semiconductor, n-type, lightly doped, hopping acoustoconductivity mechanism 80−65635
semiconductor, quantum transport theory under high elec. field 78−23099
semiconductor nonohmic hopping conduction, theory 77−20328
semiconductors, amorphous, electronic transport mechanisms and coeffs. 80−80282
semiconductors, compensated and amorphous, hopping cond. and density of localised states 77−89763
semiconductors, disordered, carrier mobility and transient pulse dispersion for hopping mechanisms 80−44586
semiconductors, doped, variable range hopping, computer simulation 80−24929
semiconductors, heavily doped, hopping cond. activation energy, percolation method 80−70703
semiconductors, heavily doped, role of ionic screening 79−65488
semiconductors, lightly doped, 1/f noise for hopping conduction, theory 80−44683
semiconductors, multicharged defects, screening of electrostatic fields 78−79959
semiconductors, weakly doped compensated, hopping photoconductivity in disordered systems *(Russian)* 80−65573
shellac platina, elec. cond., temp. and thickness depends., mechanism 79−99645
simulation of hopping transport for random spatial distrib. of localised sites 79−23971
solid, dielectric polarisation, many body model 78−10840
solid electrolytes, microwave conductivity 79−55929
space-charge hopping and its equivalence with transport via extended states 79−95399
spinel ferrites, thermoelectric power, effect of exchange interactions 78−43422
superionic conductor, 3-D hopping model 78−26719
superionic conductor, hopping model 79−37869
superionic conductor, microwave cond. theory, hopping model 80−59710
superionic conductor, thermoelec. power calc., nature of hopping process 78−51727
TCNQ bipyridine salt, anisotropic semicond. state for symm. donor mols. 77−32003
TCNQ salt, N,N′-di(n-propyl)-4,4′-bipyridylium^{2+}(7,7,8,8,-TCNQ)$_4^{2-}$, cryst. struct., elec. props. 79−27971
TCNQ salt, Qn(TCNQ)$_2$, non-ohmic elec. cond. 79−4553
TCNQ salts, complex, with aromatic donors, interchain coupling and disorder 78−6314
TCNQ salts, complex, with symmetric and asymmetric donors, transport and mag. props. 78−6315
TCNQ salts 78−6356
hopping conduction continued
TCNQ salts organic semiconducting polymers, electron transfer mechanisms 79−42544
Teflon films, hole transit, trap modulated mobility and dispersive hopping discussion 79−69616
p-terphenyl, hopping cond. among localised states 80−70861
p-terphenyl, polycrystalline thin film, elec. cond., temp., thickness and elec. field depend. 79−65572
p-terphenyl film, polycryst., charge carrier transport and DC cond. 80−70858
p-terphenyl polycrystalline layers, AC cond. 80−44746
tetracene, hopping cond. among localised states 80−70861
tetracene, polycrystalline layer, hopping transport in localised states 79−65569
tetramethylammonium manganese chloride, energy migration rel. to impurity trap behaviour 77−55811
theory, semiclassical and quantum-mechanical formulation 77−20316
TMTTF-TCNQ, quasi one-dimens. conductor, diffusive hopping, theory 80−54677
transient hopping process, numerical simulation 80−75570
transition metal oxide films, dielec. dispersion and polarization 78−2803
transition metal vanadates, elec. and mag. props., stoichiometry 78−51991
transition metal vanadates, elec. and mag. props. 79−78094
trap filling differential equation, tunnel hopping current in insulating layers 79−65555
trinitrofluorenone, amorphous, hopping transport, reinterpretation of mobility meas. 79−42563
trinitrofluorenone-polyvinylcarbazole, freq. depend. photocond. 77−8141
triphenylamine-bisphenol-A-polycarbonate solid soln., pot. discharge technique for hole transport meas. 78−43438
TTT film, hopping cond. AC and DC meas. and EPR 80−11111
two sublattice structure 78−56140
two-dimensional impurity bands, carrier-density dependence of activation energies 80−88561
vanadium phosphate glass, comp. depend. of elec. cond. 77−62922
variable range, freq. depend. 77−32008
Wigner instability, Mott's $T^{1/4}$ law as evidence 77−80751
ALF_3, evaporated layers DC props. and α-particle scatt. 78−14845
ALF_3 film, amorphous, AC elec. props. 78−2804
Ag^+ superionic conductors, US attenuation due to hopping of Ag^+ ions 78−22890
AgI, conductivity, hopping system, master equation 80−39348
β-AgI, low temp. electronic hopping 78−39111
Al, granular, hopping cond., supercond., magnetoresist., Zeeman splitting 78−60243
Al-Si_xNyO_z-Al systems, mechanism of current transfer *(Russian)* 77−69427
α-AlB_{12}, heavily doped, elec. props. 78−10446
α-AlB_{12}, hopping cond., book contrib. 78−47797
β-Al_2O_3, Na, K and Ag substitued, lattice vibrs., ion transport spectra 77−20121
β-Al_2O_3-$(Na,Li)_2O$, ionic motion obs. using NMR and internal friction 80−108099
β-Al_2O_3-$(Na,Li)_2O$ solid electrolyte, Li motion and activation obs. using ^{7}Li NMR 80−108100
amorphous film, thickness depend. 77−89887
As, amorphous, effect of high press. on elec. props. 77−59309
As-Te-Cu system glasses, DC and AC cond., thermo-EMF, freq. depend., 100 to 370K 77−76827
As-Te-Cu system glasses, elec. cond. and thermo-EMF 79−42540
As_2S_3, amorphous, shear wave attenuation and high freq. elec. cond. 80−11027
As_2S_3, electron drift mobility temp. depend., transient photocond. obs. 77−66164
As_2S_3 glasses, DC elec. cond. and thermo-elec. power 80−96865
As_2S_3, temp.-independent mobilities, phonon-induced electron hopping 79−28347
As_2S_3, vapour-deposited, pure and doped, hole mobility 80−49728
As_2S_3 vitreous, Ag, Cu, Sn and Ge impurities influence on electrophys. props. 77−76826
As_2S_3:Te glasses, doping influence on AC conductivity, electron transport by hopping 79−78106
As_2Se_3, amorphous, field-depend. dispersive hole transport 78−14728
As_2Se_3, amorphous, transient hole transport props., trap controlled hopping model 77−47820
As_2Se_3, amorphous, transient electrical transport, general and unified treatment 80−59977
As_2Se_3 glass, microwave elec. cond. and struct. 80−49793
a-As_2Se_3:Ga(Tn)(Il), hopping transport channel modifications due to impurity concs. 79−60846
As_2Se_3:I, hole drift velocity enhancement by I doping 77−39883
As_2Se_3-As_2Te_3 glass thermoelec. power, and transport mechanism 80−2408
As_2Te_3, amorphous, defect and impurity states, hopping cond. obs. 80−54650
As_2Te_3 and As_2Te_3Ge, amorphous, AC cond. at low temps. 80−80269
Au-SiO-Au structure AC conductivity, bulk and interface effects 80−54798
B, amorphous, and β-rhombohedral, hopping cond., book contrib. 78−47797
B, β-rhombohedral, field effect on hopping cond. 79−82589
B, residual photoconductivity in single crysts. 80−20241
β-B, rhombohedral, AC cond. meas., 150 to 300K, hopping cond. mechanisms 80−15521
β-B, rhombohedral, high field elec. cond., single voltage pulse meas. 80−20201
β-B, rhombohedral, influence of impurities on elec. cond. 77−4345
β-B, rhombohedral, localised states charact., review, book contrib. 78−47728
β-B, rhombohedral, thermally activated hopping, 140-300K 80−20189
B_xCy, metal-insulator transition, elec. cond. and thermoelec. power, 80 to 700K 80−44673
B_2O_3-CaO-Fe_2O_3 glasses, semicond., cond. models, electronic props., 77-800K 80−54688
$BaFe_{12}O_{19}$, ferrite, DC cond., dielec. props., lattice consts. 80−80272
BaO-Al_2O_3-B_2O_3-V_2O_5 glass, spectra, oxidation-reduction behaviour, DC cond. 77−76814
BaO-B_2O_3-SiO_2 system glass, electronic cond. of Ti ions 78−23095
BaO-B_2O_3-SiO_2:Ti^{3+}, elec. cond., struct. 78−72148

hopping conduction continued
$BaO-B_2O_3-V_2O_5$ glasses, polaron hopping cond., optical absorpt. and ESR spectra 79−23966
$BaO-B_2O_3-V_2O_5(Fe_2O_3)(Cu_2O)$, glass, resist. and activation energy, reduced valency 77−51749
$BaO-K_2O-VO_2-SiO_2$, glass, elec. cond. rel. to ion polarisability, polarons 80−49729
$BaO-La_{0.6}O-VO_2-SiO_2$, glass, elec. cond. rel. to ion polarisability, polarons 80−49729
$Bi_{12}GeO_{20}$, carrier mobility and density 78−19040
C, amorphous, heat treated, AC cond., 100 to 400K, electron hopping and Mott-Davis models 80−34443
C, amorphous, prepared by glow discharge method, elec. and optical props. 77−21036
C disordered, variable-range hopping cond. and negative magnetoresist. 80−34436
C, elec. cond. at low-temp. as function of freq., hopping cond. between localised states 79−23965
C film, amorphous, planar and transverse resist. 77−20474
C, film, amorphous, two-dimensional variable range hopping cond. 80−10977
C, glassy, negative magnetoresist. 78−23118
$(CH_4)NMnCl_3$, nearly-one-dimensional cpd., energy migration rel. to impurity trap behaviour 77−55811
$Ca_2MnO_{4-x}F_x$, antiferromagnetic props. and elec. cond. *(French)* 80−29526
$CaO-B_2O_3-Fe_2O_3$ glass, electronic and dielec. props. meas. 77−24574
Cd-palmitate (arachidate) multilayer struct., hopping rate, direct evaluation 78−88045
Cd_3As_2 films, amorphous, elec. resist., Hall mobility, temp. depend., cond. mechanism 77−76982
$CdCr_2Se_4$:In, influence of Se-deficiency on props. 78−30921
$CdO-P_2O_5$ glass, thin film, elec. cond., high and low fields 80−80427
CdSe, electrical cond. near metal-insulator transition 79−73550
CdTe, nearest-neighbour hopping cond., effect of electron irrad. induced compensating centres 77−43599
CdTe, photoconductivity, extrinsic, contrib. by hopping through excited states of donors 78−6411
p-CdTe-Cl, compensated, hopping cond. 77−76818
CeO_{2-x}, conductivity and Seebeck coeff., small polaron and hopping mechanisms 77−76812
CeO_{2-x}, small polaron mobility, elec. cond. and nonstoichiometry meas. 78−47785
$Ce_{3-x}S_4$, $Ce_{3-x}Sm_xS_4$, elec. cond. mechanism, thermoelec. power, Hall and absorpt. coeffs. 77−24559
CoO, electronic cond., rel. to basic processes of Co corrosion 77−25198
$Co_xZn_{1-x}Fe_2O_4$, ferrite, DC cond., dielec. props., lattice consts. 80−80272
Cr_2S_3, rhombohedral single cryst., AC cond., freq. and temp. depends. 77−76810
$CuO-CaO-P_2O_5$ system glasses, DC cond., hopping transport, 300 to 620K 78−23096
DyIG, thermoelectric power, elec. cond. charge carrier conduction mechanism 80−34441
Dy_2S_3, semimetallic, elec. and thermal transport meas. 78−10442
Er_2O_3, mag. susceptibility, elec. cond. and dielectric const., hopping cond. 77−12083
$EuGd_2S_4$, nonstoichiometric, elec. transport props., semicond. and metallic cond. 80−107786
EuO(Se), complex elec. cond. anomalies 80−107812
EuSe, annealed, AC conductivity and dielectric anomaly 80−34445
EuSe, dynamical conductivity in high mag. fields 79−78118
$Eu_2(WO_4)_3$, mag. susceptibility, elec. cond. and dielec. const. meas. 77−11916
$FeAl_{2-x}Cr_xO_4$, spinel, elec. cond. behaviour during oxidation 79−19593
γ-$(Fe_{1/3}Al_{2/3-y}Cr_y)_2O_3$, lacunar spinels, elec. cond. behaviour during oxidation 79−19593
$FeCoCrO_4$ spinel, elec. resistivity, temp. var. 79−38065
FeF_3 film, elec. cond. mechanisms 79−99649
FeF_3 film, localised electronic states effect on elec. cond., MIM struct. meas. 80−20328
$FeO-P_2O_5$ glass, elec. props. effect of high energy γ-radiation 79−11173
$FeO-P_2O_5$ glasses, electrical and mechanical losses 78−80283
$Fe_2O_3-V_2O_5$ system, elec. transport 79−51576
Fe_3O_4, Coulomb gap and hopping cond., effects on thermopower and Verwey ordering 80−44583
Fe_3O_4, hopping conduction and the Coulomb gap 80−44605
Fe_3O_4, magnetite, charge carriers, optical props. 80−34874
Fe_3O_4, magnetite, electronic cond. mechanisms, review 77−20314
Fe_3O_4, selective excitation double Mossbauer exam. of electron hopping 77−69750
$Fe_3O_{4-x}F_x$ substituted magnetite, low temp. resistivity, Seebeck coeff., thermopower 80−20234
$20Fe_2O_3.80[3B_2O_3.(1-x)PbO.xGeO_2]$ glass, phys. props. 80−49119
1T-$Fe_xTa_{1-x}S_2$, Anderson localisation, elec. resist. and magnetoresist. meas. 80−44596
$Fe_{1+x}V_{2-x}O_4$ spinels, prep. and negative resist. charact. *(Korean)* 78−39119
GaAs anodic oxide film, direct current-voltage charact. 78−23186
GaAs, compensated, magnetoresist. and magnetothermoelec. power, band to hopping cond. transition 77−43627
GaAs, H^+ irradiation, effect on electrical props. 80−65567
GaAs, heavy doped, strongly compensated 79−47180
GaAs, low temp. gamma irrad., donor-acceptor pair formation 79−69158
GaAs:Te, Ge, compensated, activated cond. 77−76968
Ga_2O_3:Mg(Zr) single crystals, quenched, ionic and elec. props. 78−30922
GaP film, deposited by RF sputtering *(Czech)* 78−52667
n-GaS(Se), hopping and impurity cond. anomalies 77−59287
p-GaSb, cond. mechanisms, uniaxial compression effects 77−20312
GaSe film, amorphous, I-V charact. in strong elec. fields, 173-373K 78−56248
GaSe, layered, DC hopping cond. due to stacking disorder and electron localisation 77−47819
Gd_2S_3, semimetallic, elec. and thermal transport meas. 78−10442
P- Ge, acceptor wavefunctions in spherical approx. and piezoresist. 80−29405
Ge, amorphous, anomalous magnetoresist., hopping model 78−23117
Ge, amorphous, Mott's parameters for hopping cond., effect of annealing 77−69324
Ge, amorphous, thermoelec. power in phonon-assisted hopping regime, Coulomb effects 78−76097
Ge, amorphous and polycryst. layers, sputtered, elec. cond. and thermoelec. power 78−2586
Ge, amorphous film, freq. response charact. 79−56334
Ge, amorphous film, high freq. cond., AC loss 80−49792
Ge, amorphous film, thickness depend. 77−89887
Ge, amorphous film, variable range hopping 78−76176
Ge amorphous films, self-ion bombard., electronic props. 79−28422
Ge, DC hopping, analytical formulae, degenerate hopping in wide bands 77−89761
a-Ge, elastoresistive effects 79−60838
Ge, evidence for correlated hopping in impurity cond. at moderate impurity conc. 77−20317
Ge film, amorphous, two-dimensional variable range hopping cond. 80−10977
Ge film, amorphous evap., structural aspects in electronic transport data interpret. 77−76977
Ge, heavily doped, multiplex AC hopping conduction 79−11122
Ge, hopping cond. at intermediate impurity concs. 80−6840
n-Ge, hopping magnetoresistance percolation analysis 79−38106
p-Ge, hopping transport at high mag. field at uniaxial stress 79−95412
Ge, lightly doped, nonohmic impurity cond. 78−14738
Ge, low-temp. dislocation cond. mechanism in plastically-deformed pure samples 80−15527
Ge, sputtered hydrogenated amorphous, steady-state and transient photocond. meas. 78−10506
Ge, transmutation doped, high field magnetoresist. of hopping transport 78−10474
Ge:Mn, amorphous, cond. increase by Mn doping 78−72155
n-Ge:Sb, exciton absorption 78−6688
n-Ge:Sb, fast neutron irrad. effects on donor conc., and annealing 78−56107
n-Ge:Sb, γ-irrad. effects on donor conc. and compensation by acceptors 78−56106
Ge:Sb, neutron irradiated, hopping cond. between shallow defect levels 77−4347
Ge:Sb(As)(Ga), fast-neutron irradiated, shallow radiation defect levels, electronic props. 78−23049
Ge:transition metal, amorphous, impurity effects on hopping conductivity 79−65485
N-Ge-Bi-Se glass, elec. and optical props. 80−65550
Ge-Sb-Se glass, elec. props, comp. depend. 80−70697
Ge-Se-Fe films, metallic and semicond., amorphous, mag. and elec. props. 78−52319
Ge-Se-Fe phase system, amorphous films, mag. and elec. props. 79−51695
$Ge_{100-x}As_x$ glass, elec. props. 77−76966
$Ge_{33}As_{27}S_{15}Te_{25}$, chalcogenide thin films, coupled carrier theory test, high field conditions 80−100466
$Ge_xNi_{1-x}O$, crystallographic and elec. props. 77−32011
GeSe amorphous films in Al-GeSe-Al structs., AC cond. and capacity, thickness depend. 79−65566
$Ge_{0.8}Si_{0.2}$, elec. cond., density of states, impurity and temp. depend 80−65568
p-$Ge_{1-x}Si_x$, $0.004 \leq x \leq 0.08$, hole mobility and hopping cond. rel. to composition fluctuations 77−76819
$Ge_7Si_9As_{39}Te_{35}Ga_{10}$, chalcogenide thin films, coupled carrier theory test, high field conditions 80−100466
GeTe film, amorphous, evaporated and annealed, variable range hopping cond. 78−80077
H_xWO_3, amorphous film, electronic transport meas., insulator-metal transition 77−72923
n-InP, hopping cond., nonohmic nature 79−23976
InSb, elec. cond. in intense mag. field, freeze out, hopping 77−20338
n-InSb, Hall coeff. and magnetocond. in mag. freeze-out regime 79−60849
n-InSb, heavily compensated, hopping cond. in mag. field 79−7842
n-InSb, hopping photoconductivity *(Russian)* 77−89801
n-InSb, photoconductivity mechanism, 4.2 to 77K 80−70766
n-InSb, sub mm photocond. *(Russian)* 79−38134
p-InSb, uniaxially deformed, mag. field induced semicond.-metal transition 79−95457
n-InSb, variable range hopping cond., percolation theory *(Japanese)* 78−14733
InSb:Cr,Zn, transport props. meas. 77−1424
InSb:Cr:Zn, nonparabolicity of band and p-type contrib. from hopping cond. 79−15169
$K_{1+x}Fe_yGa_{11-y}O_{17}$, electron hopping and excitation at room temp., ^{51}Fe Mossbauer spectra 80−25257
$KNbO_3$, elec. and thermoelec. singularities due to small polaron hopping motion cond. transition 79−42565
$La_{1-x}Sr_xCrO_3$ $(0 \leq x \leq 0.4)$, localised level hopping transport 80−10974
$La_{1-x}Sr_xCrO_3$, x=0-0.2, AC and DC cond., 77-1300K, hopping of polarons 78−2477
Li ferrite, carrier transport phenomena 78−19039
$Li_2Ti_3O_7$, NMR data for new ionic hopping rate prefactor expression, superionic conductor 78−47559
$Li_2Ti_3O_7$, NMR data for new ionic hopping rate prefactor expression, superionic conductor 78−47560
MgF_2 film, crystn., AC glec. props. 78−2804
MgMn ferrite, carrier transport phenomena 78−19039
5 wt.% $MgO-Si_3N_4$, hot-pressed, dielec. props. 78−10822
$Mg_{0.25}Zn_{0.75}Fe_2O_4$, ferrite, DC cond., dielec. props., lattice consts. 80−80272
Mn ferrites, Fe-excess, charge carriers, optical props. 80−34874
MnO, electronic cond., rel. to basic processes of Mn corrosion 77−25198
MnZn ferrite, combined Sn-Ti substitutions, improved props. *(German)* 77−20644
MnZn ferrites, elec. cond. mechanism in paramag. and ferrimag. phases 80−15524
MoO_3, film and cryst., long range potential centres 78−30920
$MoO_3-P_2O_5$, glass, polaron hopping DC conduction mechanism 78−6376
$MoTe_2$, elec. cond. and thermoelec. power 79−91047
$Na_2O-B_2O_3-SiO_2-As_2O_3(As_2O_5)$ glasses, DC and AC resist., bipolaronic hopping cond. 80−88558
Nb-Al_2O_3 composite, semicond. films, cond. on localised states 77−24628
Nb-N system, disordered, expt. evidence for electron correl. effects, low temp. 78−14729

hopping conduction continued
Nd_2S_3, semimetallic, elec. and thermal transport meas. 78−10442
Ni-SiO_2, granular film, hopping cond., magnetoresist. 78−56240
NiO, dipole orientation from bound polaron hopping 80−84437
NiO, electronic cond., rel. to basic processes of Ni corrosion 77−25198
NiO, localised charge carrier transport, Seebeck, resistivity meas. 78−72152
P_2O_5-FeO glass, electrical cond., nonadiabatic hopping of small polaron 77−1417
Pb-Si:Sb Schottky tunnel junction, variable range hopping assisted tunnelling 80−39670
$Pb_{1-x}In_xTe$, impurity-state conduction and temp. depend. of transport coeffs. 78−47795
$Pb_2Nb_2O_7$, electric cond. and dielect. props. of cathodic-sputtered films *(French)* 79−33371
PbO-SiO_2 glass, reduced channel-plate, variable range hopping conductivity 80−107466
PbO-SiO_2-Fe_2O_3(0,2,10 wt.%), conduction process 77−8096
$Pb_{1.8}Zn_{0.15}Na_{0.05}Nb_2O_{6.95}F_{0.05}$, electric cond. and dielect. props. of cathodic-sputtered films *(French)* 79−33371
Pr_6O_{11}, mag. and transport props., multiphonon hopping conduction 78−19211
Sb amorphous film, elect. resist. 78−95390
Sb-Au amorphous film, elec. resist. 78−95390
Sb_2O_3-Na_2O-B_2O_3-SiO_2 glass, elec. cond. meas., −160 to 200°C 80−20190
p-Sb_2S_3, bistable switching 79−73553
Sb_2S_3, elec. and mag. props., carrier transport mechanism 78−47792
Sb_2S_3, hopping cond. in cryst. subjected to strong elec. fields 79−95456
Sb_2Se_3 crystals, mag. and elec. props. 80−96873
$Sb_{35}Se_{65}$, polycrystalline, elec. cond. mech. 80−49705
$(Sb_2Se_3)_{0.7}(Bi_2Se_3)_{0.3}$, solid soln., prep. and elec. properties of layered crystals 80−70762
Se, amorphous, carrier lifetime and drift mobilities 78−87985
Se, amorphous, theory of anomalous dispersion of photocurrent transients 78−6412
Se, amorphous, transient electrical transport, general and unified treatment 80−59977
Se, amorphous film, AC conductivity at radio and microwave frequencies 79−11248
$Se_{60}Te_{30}Ge_{10}$, amorphous, neg. magnetoresist. 79−51603
Si, amorphous, AC cond., bipolaron hopping 79−23928
Si, amorphous, anomalous magnetoresist., hopping model 78−23117
Si, amorphous, Coulomb gap and hopping cond. 80−44583
Si, amorphous, doping effects on cond. in hopping transport regime 79−28424
Si, amorphous, hopping model for activated charge transport 79−87099
Si, amorphous, hydrogenated pure and B doped, annealing effect on cond. *(Korean)* 79−15142
Si, amorphous, hydrogenation and density of defect states, hopping cond. 79−60757
Si, amorphous, ion-implanted, hopping parameter at natural phonon freqs. 79−15152
Si, amorphous, thermoelec. power in phonon-assisted hopping regime, Coulomb effects 78−76097
Si, amorphous, transient electrical transport, general and unified treatment 80−59977
Si, amorphous, undoped and B doped, ESR-linewidth temp. depend. meas. 80−20459
Si amorphous film, EPR rel. to elec. cond. 77−69692
Si, amorphous film, electron beam evaporated, freq.-depend. dielec. behaviour 79−99549
Si, amorphous film, in Ti-Si-Ti struct., elec. cond. processes and threshold switching 79−78207
Si, amorphous film, thickness depend. 77−89887
Si, amorphous film, variable range hopping 78−76176
Si, amorphous films, hopping conduction, dangling bond generation by high temp. annealing 80−60115
Si amorphous films, self-ion bombard., electronic props. 79−28422
Si, amorphous ultrahigh vacuum evaporated films, ESR obs., deposition effects 79−33534
Si, CVD films, polycryst., elec. and optical props., electronic density of states model 79−56332
Si, electron irrad. damage, capacitance meas. 80−24935
Si, electron-beam-evaporated amorphous thin films, noise meas. 79−24091
Si film, amorphous, hopping cond. control by ion bombard. induced struct. modification 80−92898
Si, film, amorphous, two-dimensional variable range hopping cond. 80−10977
Si film, amorphous evap., structural aspects in electronic data interpret. 77−76977
Si film, sputtered amorphous, P and B doped, elec. cond. and thermopower meas. *(French)* 78−47403
Si, inversion layer, 1/f noise and percolation in impurity bands 79−24029
Si, photoconductivity, extrinsic, contrib. by hopping through excited states of donors 78−6411
a-Si:B(P), Hall effect and impurity cond. 77−72871
a-Si:H, spin defect and recombination influence on electronic transport 80−50409
Si:Mn, amorphous, cond. increase by Mn doping 78−72155
Si:Mn(Fe)(Ni) amorphous films, ESR and elec. cond. 80−50171
Si:Ne, amorphous, implanted, cond. change 78−23097
Si:O, semi-insulating polycryst. film, cond. through localised and extended states 77−28268
Si:P, impurity cond., hopping conduction and the Coulomb gap 80−44605
Si:P, impurity doped, electron lifetime and transport in upper Hubbard band 79−95452
Si:P, ion implanted low temp. elec. cond. 79−56225
Si:P, variable range hopping conduction, in lowest temp. region 79−73511
Si:P, variable range hopping at very low temp. 80−49736
Si:transition metal, amorphous, impurity effects on hopping conductivity 79−65485
Si-Au amorphous film, metal-nonmetal transition, elec. cond., thermoelectric power meas. 79−47132
Si-Ge film, amorphous, ESR line intensity anal., rel. to cond. mechanism 78−43645
hopping conduction continued
Si-SiO_2, interface, hopping conduction, anal. in impurity bands in inversion layers 79−47171
$Si_{(6-z)}Al_zO_zN_{(8-z)}$, sialons, hot-pressed, dielec. props. 78−10822
SiC amorphous film, elec. props. and hopping transp. 77−66211
SiC_x, amorphous, prepared by glow discharge method, elec. and optical props. 77−21035
$Si_{1-x}Co_x$ film, metastable impurity band, conductivity meas., semiconductor-metal transition 77−76884
Si_3N_4, hot-pressed, dielec. props. 78−10822
$Si_{1-x}Ni_x$ film, metastable impurity band, conductivity meas., semiconductor-metal transition 77−76884
SiO_2, amorphous, high-field transport of excess electrons and holes 77−89767
SiO_2, amorphous, optical and elec. props., comparison with chalcogenide semiconds. 78−6721
SiO_2, amorphous, transient electrical transport, general and unified treatment 80−59977
SiO_2 gate insulator MOS capacitors, hole transport, recovery characts. following electron beam irrad. 77−20439
SiO_2 layers, DC current-voltage behaviour 77−85333
SiO_2, thermally grown films, LF conductance 78−80081
SiO_x, amorphous, ESR and hopping cond., He^+ irrad. effects 79−61213
SiO_x film, Cole-Cole diagrams of ionic hopping systems 77−66217
SiO_x film, MIM struct., DC bias dependent dielectric dispersion props. 78−76178
SmB_6, valence fluctuating state, sp. ht. 80−20127
SmS (001) surface, mixed valency and phase transitions 80−39658
SnTe film, amorphous, evaporated and annealed, variable range hopping cond. 78−80077
Ta_2O_5, amorphous and cryst., elec. cond. mechanism, admittance meas. 80−70705
1T-TaS_2, and 1T-$TaS_{2-x}Se_x$, Anderson localisation, elec. resist. and magnetoresist. meas. 80−44596
1T-TaS_2, pure and cation-doped, charge carrier localisation 80−44597
1T-$TaS_{2-x}Se_x$, electronic cond. process, resist. meas., 1.3-240K 80−44595
TaS_2(1T) pure and doped, Mott and Anderson localisation, commensurate phase transition 80−39641
TbF_3 thin films, AC conduction obs. 80−70868
Te, amorphous film, vac. deposited, phonon-assisted hopping cond. 80−2392
Te film, thermally evaporated, elec. cond., Hall voltage and thermoelec. power 77−47913
Te:Cu films, elec. transport props. 80−60120
TiO_2-SiO_2, semicond. glass, small polaron hopping cond. 78−60126
TiO_2-Ti_2O_3-P_2O_5, glass form., struct. and elec. props. 80−44592
Ti_4O_7, hopping conduction and the Coulomb gap 80−44605
$TlGaS_2$, mechanism of cond., AC cond. and permittivity meas. 78−14754
$TlGaSe_2$, mechanism of cond., AC cond. and permittivity meas. 78−14754
U_3O_8-Y_2O_3(Sc_2O_3), solid soln. electrode, high temp. electrochem. appl. 80−6828
$V_{1-x}Fe_xO_{2-x}F_x$, $0<x<0.20$, magnetic susceptibility and electron cond. *(German)* 80−39754
$V_{1-x}Fe_xO_{2-x}F_x$, mag. susceptibility *(German)* 79−78305
V_2O_5, amorphous hopping small polarons, effect of random glass struct. 79−23972
V_2O_5 amorphous layers, gel deposited, semicond. props. 80−92887
V_2O_5-BaO-K_2O-ZnO glasses, elect. props. and struct. 80−15547
V_2O_5-GeO_2-PbO glasses, memory and threshold switching 78−23142
V_2O_5-P_2O_5 glasses, anomalous cond. mechanism 77−76832
V_2O_5-V_2O_4-$BaZnO_2$ glass, V ion states, mag. and elec. props. 80−88556
$V_{1+x}P_{1-x}O_{5-c/2}$ glasses, structure, adiabatic hopping conduction model 77−43588
WO_3 amoprhous film, sublimed under different conditions, elec. transport props. 80−7015
WO_3 amorphous film, elec. cond. and dielec. const. 78−60238
WO_3 powders, hopping mechanism and Poole-Frenkel effect, elec. props. determ. 80−49734
WO_3-P_2O_5 glass, DC elec. cond., 100-400K 78−39106
YIG, elec. props. 79−99552
YIG, elec. props. meas., 600-1500K 77−8098
Y_2O_3-AlN-SiO_2 oxynitride glasses, elec. props. 80−80267
$Y_2(V_{4/3}W_{2/3})O_7$ pyrochlore, synthesis and elec. props. 80−29914
ZnO film, high-resist., band and hopping cond., AC cond. and capacitance meas. 77−72928
ZnSe, amorphous thin film, prep. and electronic props. 77−85350
ZnSe, film, hopping cond. 80−2499

horology *see time measurement*

hospital administration *see medical administrative data processing*

hot carrier conduction *see hot carriers*

hot carriers
alkali halide, dynamics of nonrelaxed and self-trapped holes *(Russian)* 80−80607
anthracene, time-resolved transient photocond. obs. 80−6892
buried channel MOS structures, charge-handling capacity under hot electron conditions 80−80381
calculations, review 78−26870
chalcogenide glass film, switching phenomena 77−39976
n-channel MOSFET, Si inversion layer, negative differential resistance 78−30996
conference, Denton, USA (July 1977) 78−26868
covalent semiconductor, heating of charge carriers, energy dissipation 80−49755
cubic many-valley type semiconductor, cond. in warm electron region, phenomenological theory 77−43586
cubic semiconductors, bulk hot-electron props., review 79−99553
current instability, hydrodynamic modes, soft modes and fluctuation spectra 79−65491
current instability due to Bragg scatt., travelling dipole domains, fluctuations 78−26874
degenerate quasi-two-dimensional semiconductor, warm electrons 78−60222
degenerate semiconductor, p-type, hot carrier distrib. function and cond. 77−28190
degenerate semiconductors, hot electron transport in parabolic energy bands, kinetic theory, transport coeffs. 80−29412

hot carriers continued
diamond, natural, anisotropy and saturation of hot carrier drift velocity 80−6867
dielectric liquids, high-field electron transport *(Japanese)* 78−2495
distribution function, warm electron range 78−26856
distribution functions, expts., review 78−27231
doped semiconductor plasma, inelastic light scatt., spin diffusion 77−36241
drift solutions, discontinuities, hot carriers injection and accumulation 78−51999
drifting hot carriers, EM wave amplification, linear theory *(Russian)* 79−69539
electron heating, electron conc. analysis near special Van Hove pts. *(Russian)* 78−26835
electron temperature superlattice appearance in stationary elec. field *(Russian)* 77−11931
electron-hole plasma stratification on heating by light or elec. field *(Russian)* 77−11951
energy relaxation of photoexcited hot electrons at very low temperatures 78−91724
ferroelectric semiconductor, electron theory 78−43801
ferromagnetic semiconductor, hot electron relax. *(Russian)* 79−51593
ferromagnetic semiconductors, conduction electron heating, critical scatt. effects 79−91040
ferromagnetic semiconductors with hot electrons, instability of coupled spin-helical waves 80−107841
fluctuation spectra near the threshold of a current instability 79−24037
history of hot electron physics 78−26869
hybrid mode instability 77−80800
III-V semiconductor, low temperature, high mobility transistor materials 78−87970
III-V semiconductors, optical heating of electrons at 78K 79−15185
inhomogeneous semiconductor with nonequilibrium carriers, EM wave propag. 78−52024
insulating films, hot electron energy distribs., Monte Carlo study 77−51832
insulator, high field electronic cond. 78−30931
IR hot carrier diode mixer 78−29161
isotropic semiconductor, differential relax. times and diffusivities of hot carriers 77−62936
laser plasmas, hot electron energy relaxation and transport *(Japanese)* 80−96347
layered struct., interaction of spin waves with hot carriers 79−15291
many-valley cubic semiconductor, elec. conductivity tensor, warm electron range 78−39123
many-valley semiconductor, conductivity in RF heating field *(Russian)* 78−76085
many-valley semiconductor, new type of galvanomag. effect for hot electrons 77−32028
measurement equipment, for monocrystalline, polycrystalline and amorphous materials, using RC surge generator *(Czech)* 77−61078
metal, low temp., hot electron distrib. *(Russian)* 77−12056
metallic thin films, hot electron distribution function, nonlinear elec. resistance *(Russian)* 80−65717
MIM, thin film, use as non-heated source of electrons 80−84516
Monte Carlo calc., book contrib. 80−100458
MOS inversion layer, hot electron effects in Landau levels 80−6998
MOS inversion layer, hot electron effects in Landau levels 80−20315
MOS structure hot electron transport, review 78−60221
MOS structures, hot electron transport, expt. review 78−30994
n-n^+ point contacts, current-voltage characts. 78−26940
narrow gap semiconductor with symmetrical carrier spectra, hot electrons 79−23982
negative differential cond. of hot electrons in mag. field due to carrier density nonlinearity 77−55540
noise, exptl. and theoretical aspect, survey 79−28389
nondegenerate semiconductor electrons in strong elec. and quantizing mag. fields 78−10457
ohmic contact, hot minority carrier effects on thermoEMF and photovoltage 77−15956
p-n function, instability of EMF 78−26941
p-n junction, anomalous hot carrier-voltaic effect, electron emitter and light detector appls. 77−76861
p-n junction, CdTe-based, photoeffect quantum efficiency depend. on photon energy *(Russian)* 79−78168
p-n junction, planar, junction breakdown walkout exam. 78−60199
p-n junction as a contact with negative differential capacitance and conductance 79−69590
p-n junction with hot carriers, thermophotoelectric effects 79−73576
p-n junctions, current-voltage characts., effect of space charge defects 80−25001
p-type semiconductor, effective mechanism of hot electron energy relax. 78−26878
photoexcitation, high intensity, hot electrons and phonons 78−26905
photoexcitation phenomena, low density 78−27319
photoexcited hot electrons in high mag. field, mean energy 78−30955
piezoelectric semiconductor film, mobility of hot electrons 78−56247
polar crystal, hot electron transport, eikonal approx. for energy loss 77−1426
polar crystal, hot electron transport, loss to single phonon modes 77−1427
polar semiconductor, high field collision rates 78−30932
polar semiconductor, high field quantum magnetotransport theory 78−30941
polar semiconductor, surface inversion layers, energy loss of warm and hot carriers 77−11981
quantised inversion layer, hot carrier transport 78−30993
quantum energy distribution function in crossed elec. and mag. fields 77−32019
quantum magnetotransport, review 78−30940
quasi-two-dimensional semiconductor, warm carrier relax. via acoustic phonons 77−43694
radiative spectra from hot photocarriers 78−31249
reliability physics, conference, Las Vegas (1977) 77−79086
ruby, nonequilibrium luminesc. of hot electrons, nonradiative transition probability 77−32436
runaway electron-heating dynamics 80−39597
semiconducting thermoelement as a medium containing hot electrons 80−107829
semiconductor, ambipolar hot-carrier size effect kinetics 80−107799
hot carriers continued
semiconductor, Auger recombination rate, nonequilib. carrier distrib. 80−65578
semiconductor, capture of charge carriers rel. to I-V curves, phonon heating 79−51589
semiconductor, compensated, influence of carrier heating on exclusion 77−8110
semiconductor, current instability, bifurcation and stability of dynamical structs. 79−91071
semiconductor, current-voltage characts. of hot electrons under phonon heating and recomb. conditions 79−51591
semiconductor, displaced Maxwellian distribution function and warm electrons problem 78−26864
semiconductor, doped photoemission, calc. of escape probability of electrons *(Russian)* 79−24408
semiconductor, double injection characteristics under high voltages 79−51590
semiconductor, elec. cond. in quantising mag. field, and electron heating, mutual electron-phonon drag 77−69355
semiconductor, electro-optic effects anisotropy and hot electron cond., free carrier-impurity scatt. 77−4626
semiconductor, electron heating by strong static and HF elec. fields 77−8112
semiconductor, electron temperature superlattice, nonlinear theory *(Russian)* 79−78112
semiconductor, electron trap, positively charged, hot electron capture coeff. 78−52003
semiconductor, energy relaxation of photoexcited hot electrons in near-surface region 80−92928
semiconductor, Faraday rotation in presence of attractive traps 78−76081
semiconductor, Faraday rotation in the presence of deep repulsive traps 80−29724
semiconductor, galvanomagnetic-effects in strong elec. field 78−56163
semiconductor, gapless, bottleneck effect at low temp., hole heating 78−10470
semiconductor, gapless, magnetophonon reson. for hot electrons and holes *(Russian)* 79−4565
semiconductor, hot carrier oscillatory magnetoresistance phenomena studies, mag. field modulation technique 78−4657
semiconductor, hot electron current voltage curves, transverse mag. field, phonon heating 78−6384
semiconductor, hot electron distrib. in strong electric and quantised mag. fields 79−95417
semiconductor, hot electron energy tails, Monte-Carlo calcs. 77−62931
semiconductor, hot electron fluctuations with displaced Maxwellian distrib. 80−29418
semiconductor, hot electron waves in transverse mag. field 77−4387
semiconductor, hot electrons, photoexcited in quantizing mag. field, energy distrib. calcs. 79−42586
semiconductor, hot electrons in quantizing mag. field and impact ionisation of impurities 78−6386
semiconductor, hot plasma, wave instability 78−84245
semiconductor, hot-electron energy distrib. in strong mag. field 78−43400
semiconductor, inertia of Benedicks effect in carrier heating by microwave field 79−15173
semiconductor, inhomogeneous, EM waves under elec. and mag. field 80−20237
semiconductor, inhomogenous, eigenoscills, of hot electrons in classically strong mag. field 79−73520
semiconductor, inverted hot electron states and negative cond. *(Russian)* 77−43612
semiconductor, Kane, thermoelec. power and thermomag. effects of hot electrons 78−56174
semiconductor, magnetic susceptibility of hot electrons 78−10648
semiconductor, mobility of hot electrons in mag. field 77−4368
semiconductor, n-type, microwave induced emission of hot electrons, secondary emission study 79−69964
semiconductor, Nernst-Ettingshausen effect, thermopower, strong elec. field 78−23122
semiconductor, nondegenerate, magnetophonon reson. in acoustic relax. of hot electron energy 78−26892
semiconductor, nonparabolic, Monte Carlo transport calcs., acoustic scatt. inelasticity effects 77−51754
semiconductor, nonradiative multiphonon carrier capture by deep neutral traps 80−6871
semiconductor, optical props. under intense laser fields 78−72513
semiconductor, optical spectroscopy 79−95845
semiconductor, quasi-two-dimens., transient response under hot electron conditions 78−60223
semiconductor, quasi-two-dimensional, crit. conc. of hot carriers 77−35977
semiconductor, second harmonic generation by hot-electron and electron transfer effects, optimum conditions 79−41491
semiconductor, spatially inhomogeneous, effect of heating field on reflection of EM waves 79−15157
semiconductor, spreading and noise diffusion coeffs., identity 78−64047
semiconductor, temperature superlattice with hot electrons 80−20202
semiconductor, with hot electrons, temp. superlattice, transport props. effects *(Russian)* 78−34839
semiconductor, zero-gap, magnetophonon oscills. of transverse magnetoresist. in strong elec. fields 80−96916
semiconductor hot electron physics, review *(Japanese)* 80−49754
semiconductor in nonlinear region, spectral noise meas. between 30 and 400 MHz, pulse technique device *(German)* 79−47134
semiconductor negative conductivity due to hot electrons transfer in geometric space *(German)* 78−56150
semiconductor plasma, EM wave instability, effect of density gradient 79−1607
semiconductor plasma, unstable EM wave propagation, hot carriers, Hall effect, calc. 80−39620
semiconductor quantised inversion layers, hot electron microwave cond. calc. 77−43734
semiconductor with charged defects, elec. cond. and magnetoresist. 80−20225
semiconductor with electron heating by constant electric field, magneto-plasma wave instabilities 77−43639
semiconductor with quasirelativistic band struct., hot electron kinetic equation 78−84222

hot carriers continued
semiconductor with two types of hot carriers, under overheating instability conditions, current-voltage characts. 77−62943
semiconductor-electrolyte boundary, hot carrier injection, tunnelling from semiconductor states in depletion region 80−75637
semiconductors, carrier heating, optical temp. waves 77−89770
semiconductors, electrostrictive effect of hot electrons spherical energy band model 79−69778
semiconductors, energy-balance eqn. for hot electrons 79−73521
semiconductors, ferromag., hot electron relax. time 80−59996
semiconductors, galvanomagnetic effects in high mag. fields, for electron scatt. by optical phonons 80−2405
semiconductors, hot electron distrib. function, response to step changes in elec. field 80−24937
semiconductors, hot electron maximum mobility in longitudinal quantising mag. fields 79−69519
semiconductors, hot electron recombination at impurity centres 80−10995
semiconductors, hot electron transverse escape galvanomagnetic effects *(Russian)* 80−80289
semiconductors, hot electrons in longitudinal quantising mag. fields 80−39593
semiconductors, hot-electron diffusion, Boltzmann eqn. 77−51757
semiconductors, narrow gap, hot electron phenomena, I-V curve calc. 80−34457
semiconductors, p-type, mag. oscills. of momentum distribution of hot photoexcited electrons *(Russian)* 80−2854
semiconductors, photocond., photoelec. effects, book contrib. 80−84488
semiconductors, quasi elastic hot electron impurity scatt. in quantising mag. field 80−24938
semiconductors, semimetals, electron heating by phonons, acoustic absorpt. and acoustoelectric current quantum oscills. *(Russian)* 79−19639
semiconductors, two-dimens., transient response of hot electrons, calc. 80−49747
single-injection solid-state diodes with exponential trap distrib., elec. cond. of hot carriers 79−99556
single-valley semiconductor, current instability and domain propag. due to Bragg scatt. 77−28187
SOS structures, high-field electron transport, drift vel. meas. 80−80387
static conductivity change under quantum cyclotron reson. 78−39143
thermal noise, effects in p-Si and SCLC diodes 79−24036
time resolved reflectivity of ps pulses 78−31217
TTF-TCNQ, pure and irrad. crystal, nonlinear transport at low temp. 79−4552
two-valley semiconductor, hot electron instability, intervalley scatt. *(Russian)* 80−92921
uniaxial semiconductor, EM instability in strong elec. field 77−32021
Ag film, inertialess glow induced by picosecond laser pulses *(Russian)* 80−100714
AgBr, streaming cyclotron motion of hot electrons, at intense microwave fields 80−6703
AgBr(Cl), evidence for population inversion of hot electrons 79−91085
AgCl(Br), crossed elec. and mag. fields, hot electrons, streaming motion, population inversion 80−44649
AgCl(Br), hot electron population inversion, in crossed elec.-mag. fields, 4.2K 79−38128
$Al_xGa_{1-x}As$, graded-gap crystal, voltage-current characteristics 79−69613
$Al_xGa_{1-x}As$, p-n homojunction, hot carrier recomb., overheating luminesc. 78−92122
$Al_xGa_{1-x}As$-GaAs heterostructure, quantum-well, hot electrons and phonons 80−84505
α-Al_2O_3 recombination luminescence excitation by synchrotron radiation 79−95841
Ar, liq., α-irrad., geminate recomb. of charges, hot electron thermalization length 80−20266
Au film, inertialess glow induced by picosecond laser pulses *(Russian)* 80−100714
Au-Si internal photoemission struct., spatial distrib. of excited electrons *(French)* 78−23166
Bi, electron gas heating at low temp. 78−60133
Bi, instability induced by microwave field, carrier overheating 78−19076
Bi type semimetals, electron heating due to acoustic phonon scatt. *(Russian)* 80−10991
$Bi_{0.9}Sb_{0.1}$, magnetophonon effect on hot electrons *(Russian)* 80−107814
n-$Cd_xHg_{1-x}Te$ alloys, x=0.19 to 0.21, electron optical heating influence on photoelec. effects 79−11183
$Cd_xHg_{1-x}Te$, effects of electron heating at low temps. 80−49823
n-$Cd_xHg_{1-x}Te$, semicond. current carrier recombination heating in photoelectric effects *(Russian)* 79−78138
CdSe, collisions between hot excitons and hot electrons 80−7415
CdSe, direct gap, picosec. time resolved reflectivity obs. 78−76495
CdTe, excitation spectra, resonant Raman scatt. versus hot electron effects 79−38645
CdTe negative dielectric relax. of hot electrons 78−52001
Cu film, inertialess glow induced by picosecond laser pulses *(Russian)* 80−100714
Eu chalcogenides, multiphonon inelastic light scatt., hot recomb. 77−8559
Eu, monochalcogenides, multiphonon inelastic light scatt. 77−90144
$Ga_{1-x}Al_xAs$, hot electron distrib. meas. and calc. 78−27318
GaAs, compensated, influence of electron gas heating on negative magnetoresist. 77−89778
n-GaAs, conductivity relax. times in warm electron range, intervalley transitions 77−55537
GaAs, diffusion coeff. of hot electrons 79−15156
GaAs, direct gap, picosec. time resolved reflectivity obs. 78−76495
GaAs, electron dynamic properties in strong elec. field, anal. *(German)* 78−43404
GaAs, electron heating under hydrostatic pressure, Monte Carlo calcs. 77−69334
n-GaAs, epitaxial, thermoelec. power, temp. depend. in mm wavelength range 79−23996
n-GaAs, freq. depend. of effective temp. of hot carriers 79−11135
GaAs, hot carrier impact ionisation, band struct. depend. 78−30934
n-GaAs, hot electron distrib. function with LO phonon kink, photoluminesc. 79−19925
GaAs, hot electron distrib. function, inter-carrier scatt. effect 80−2395
n-GaAs, hot electron magnetophonon resonance, Fourier anal. 80−54718
GaAs, hot electrons and exciton-electron collision under external elec. field 78−43928

hot carriers continued
GaAs hot electrons drift rate/field strength characteristic in microwave fields *(German)* 78−43430
GaAs, hot photoluminescence depolarisation in mag. field, 0.4 eV energy state electron lifetime *(Russian)* 80−16086
GaAs, hot photoluminescence spectrum on pumping across the L-valley *(Russian)* 80−103984
GaAs, IR field induced Gunn oscills. 78−30956
GaAs, intervalley electron transfer, drift velocity and diffusion coefficient 80−39594
n-GaAs, inverted hot electron states and negative cond. *(Russian)* 77−43612
GaAs, light scatt. spectra, interference effects 79−82977
p-GaAs, linear polarisation of hot photoluminescence 79−38661
GaAs, lower conduction band minima, ordering and props. 77−28114
GaAs luminesc. emitted as a result of carrier heating 77−52185
n-GaAs, magneto-impurity effect, review 79−91081
GaAs microwave devices and their use for generation and freq. conversion of microwave oscillations 80−15534
GaAs, negative differential mobility and geometrical magnetoresist. calc. 77−43624
n-GaAs, non-Maxwellian electron distribution function, from electric field-depend. photolum. spectrum 79−11450
n-GaAs, non-equilibrium acoustic phonon generation by hot electrons 80−6477
GaAs, optically pumped, absorption spectrum, band filling, hot electron effects 78−31199
GaAs p^+-n diode, radiative hot carrier recomb., photoluminesc. and electroluminesc. meas. 79−38676
GaAs, photocarrier thermalisation by laser excitation spectroscopy 78−31250
GaAs, photoexcitation phenomena, low density 78−27319
GaAs, photoexcited, carrier relaxation determ. from time resolved transmission spectrum changes 79−99583
GaAs, polar semiconductor, collisions between hot excitons and hot electrons 80−7415
n-GaAs, submillimetre cond. and carrier heating, two-electron-temp. model 77−20349
GaAs, two photon absorpt., hot electron-hole plasma, relax. time depend., picosecond spectra 79−51979
n-GaAs, two-valleyed semicond., hot electron diffusion coeff., random walk calc. 78−68033
GaAs:Cr, hot electron relax. process and ionization of traps *(Russian)* 79−28354
GaAs:Cr, strong quenching of thermally stimulated conductivity by elec. field *(Russian)* 77−1434
GaAs-$Al_xGa_{1-x}As$, negative differential resist., real-space electron transfer 80−6958
GaAs-$Al_xGa_{1-x}As$ heterostructures, real-space electron transfer by thermionic emission, analytical model 80−100512
GaInSb, intervalley electron transfer, drift velocity and diffusion coefficient 80−39594
$Ga_{0.3}In_{0.7}Sb$, negative differential mobility and geometrical magnetoresist. calc. 77−43624
GaP, Cs(Cs-O) activated, with negative electron affinity, thermalised electron emission 78−11073
GaP, Cs(Cs-O) activated, with negative electron affinity, near UV photoemission and secondary emission 78−11074
Ge, ambipolar hot-carrier size effect kinetics 80−107799
n-Ge, anisotropy of thermal and convective noise, in magnetic field 78−34873
p-Ge, carrier heating by weak electric field 77−11927
n-Ge, compensated, switching effect, injection mechanism of hot holes 77−69387
p-Ge, diffusion coeff. for hot holes in mag. field 80−39614
Ge, diffusion coeff. of hot holes meas. 78−6387
p-Ge, double injection characteristics under high voltages 79−51590
n-Ge EM wave interaction with hot electrons, in strong mag. field with Voigt config. 77−69367
Ge, electron heating by nonuniform elec. field, I-V characteristics 77−47825
Ge, electron heating in inhomogeneous elec. field 78−2494
Ge, electron-hole droplet cloud kinetics, thermalisation phonons 80−88483
Ge, electron-hole two component liq. phase diagrams under stress 80−29332
Ge, electronic subsystem heating by Dember field for ambipolar diffusion *(Russian)* 77−39898
Ge, far IR radiation amplification on hot hole population inversion *(Russian)* 80−16060
Ge graded p-n junction, volume EMF of hot carriers 77−47895
n-Ge, H-linear planar Hall effects of hot electrons 78−76082
Ge, HF breakdown of excitons effect on kinetic of electron hole droplets *(Russian)* 77−59260
Ge, hot electron diffusion coefficient anisotropy 77−76838
Ge, hot hole distribution function, effect of impurity and hole hole scatt. 79−11139
Ge, hot hole distribution function at low densities 79−11138
p-Ge, hot hole relax., IR saturated absorption, LO phonon emission 77−28569
Ge, hot light hole distrib. function and light absorpt. 79−60844
Ge, hot-electron diffusion coefficient 78−87982
n-Ge, IR absorption by hot carrier 80−40087
p-Ge injecting contact, sign of developed hot-carrier thermo-EMF 77−55606
Ge, injection current in presence of electron and hole mobility, gradients 77−69326
Ge, intervalley diffusion of hot electrons 78−84227
Ge, magnetic field effects on hot-hole noise 77−4415
Ge microwave exciton discharge, collision frequency, temp. determ. *(Russian)* 79−65507
n-Ge, microwave Faraday effect in strong mag. field 77−1662
Ge, n- and p-type, magneto-impurity effect, review 79−91081
Ge, near intrinsic, negative differential cond., ambipolar size effect due to hot carriers 78−72185
p-Ge, noise, energy relax. time and diffusion of hot holes 77−76839
n-Ge, noise, small signal conductivity and diffusion in strong elec. fields 79−11192
n-Ge, noise spectra of hot carriers 78−76083
n-Ge, nonlinear absorption of CO_2 laser radiation by nonequilib. carriers 79−32000

hot carriers continued
p-Ge, odd magnetoresist. of warm holes 77−43628
p-Ge, odd magnetoresist. under weak carrier heating conditions 80−96917
p-Ge, optical cooling and carrier heating, intraband photocond. meas. 79−11174
Ge, p-n junction, hot photocarrier and hot electron effects 78−30980
p-Ge, p-n junction with hot carriers in charge accumulation regime, influence of light on operation 79−51661
Ge, p-n junction with hot carriers, current-voltage characts. 79−91135
Ge p-n junctions with hot carriers, current amplification, elec. domain form. 80−6966
Ge, photomag. EMF, reson. struct., energy relax. mechanisms 78−2515
Ge, plasma excitation, ultrafast optical props. 78−31248
Ge, stressed, recombination luminescence from hot carriers in electron-hole droplets 78−6754
n-Ge, subjected to high voltages, distrib. of injected carriers 79−56239
p-Ge, temp. depend. of noise and diffusion of hot holes 78−39174
p-Ge, uniaxial compression influence on carrier heating by weak electric field 80−10978
n-Ge, uniaxially stretched along [111] axis, negative differential conductance 77−51759
n-Ge, vel. component of hot charge carriers' thermoelectromotive force 80−44630
n-Ge:Au, electron capture by negatively charged traps, effect on hot electron enrgy energy distrib. 78−43398
Ge:Cu, hot photoexcited holes at low temp. 78−30954
p-Ge:Ga, carrier heating by weak elec. field, hole-hole collision influence 78−72161
n-Ge:Ni, recombination of hot electrons on Ni impurity centres 80−44612
Ge:Ni compensated, hot electron recomb. anisotropy 78−39125
p-Ge-In injecting contact, sign of developed hot-carrier thermo-EMF 77−55606
Ge-Si, heat treated, carrier heating by strong microwave elec. field 77−69366
Ge-Si single crystals, heat treated, hot carrier thermo-EMF 77−24575
He, liq., hot electrons on surface *(Russian)* 78−87832
He, liquid, short-wave surface excitation study using electron gas nonlinear I-V characts. *(Russian)* 80−10717
^{4}He liquid surface, hot carrier mobility 78−59988
^{4}He liquid surface, theory of hot electrons 78−22915
n-$Hg_{0.8}Cd_{0.2}Te$, microwave bolometer heterodyne receiver based on magnetic field induced phase transition 80−13735
$Hg_{1-x}Cd_xTe$, avalanche formation, high intensity IR transmission limit 79−78684
$Hg_{1-x}Cd_xTe$ hot-electron photoconductive detection of near mm wave radiation 80−57377
$Hg_{1-x}Cd_xTe$, zero-gap semicond. with nonparabolic band struct., hot electron mobility and conc. 78−76080
n-InAs, avalanche formation, high intensity IR transmission limit 79−78684
n-InAs, cathodoluminescence, radiative recomb. of hot carriers 77−8667
n-InAs, hot electron temp. determ. by interference modulation of radiation 80−44610
InAs-oxide-$Pb_{50}Bi_{20}$ junction, hot electron temp. in InAs meas. by tunnelling 77−4352
InAsP, intervalley electron transfer, drift velocity and diffusion coefficient 80−39594
$InAs_{1-x}P_x$, high field instabilities, press. and comp. depends. 78−26873
$In_{1-x}Ga_xP_{1-y}As_y$ LPE films, hot electron and magnetotransport props. 78−26977
In_2O_3-SnO_2-Si SIS solar cells, reverse current-voltage characts. under illumination 80−89622
InP, hot carrier noise, Monte Carlo simulation 77−51792
InP, intervalley electron transfer, drift velocity and diffusion coefficient 80−39594
InP, luminesc. emitted as a result of carrier heating 77−52185
InP, luminescence, hot electron effects 80−66277
n-InP, magneto-impurity effect, review 79−91081
InP, negative differential mobility and geometrical magnetoresist. calc. 77−43624
InP, polar semiconductor, collisions between hot excitons and hot electrons 80−7415
n-InP, submillimetre cond. and carrier heating, two-electron-temp. model 77−20349
InP-Ag Schottky barrier, hot electron attenuation length 80−49904
InP-$In_{1-x}Ga_xP_{1-z}As_z$ heterostructure laser, single and multiple quantum-well, liquid-phase epitaxial growth 80−38031
InSb, avalanche formation, high intensity IR transmission limit 79−78684
InSb, carrier heating by microwave field, inertia effects 80−65580
n-InSb, convective instability in crossed mag. and elec. fields 77−62939
n-InSb, cyclotron emission intensities, description using hot electron distrib. functions 79−61226
n-InSb, cyclotron reson. of conduction electrons, strong mag. field, hot electrons 80−2640
n-InSb, directional temp. of hot electrons under elec. and mag. fields 78−84135
n-InSb electron heating and energy relaxation time in quantising mag. field 80−10996
n-InSb, electron heating dynamics in longitudinal electric and quantising magnetic fields 79−69520
n-InSb electronic bolometer using hot-electron effects. millimetre and submillimetre wave detection 78−24860
InSb, HF props. of hot electrons at 77K, calc. using Monte Carlo method 80−15553
n-InSb, high field electron diffusion, Monte-Carlo calc. 78−10455
InSb, high field quantum magnetotransport theory 78−30941
n-InSb, high power helicon, interaction with semiconductor-free space interface 79−38114
InSb, hot electron energy relax. time 77−80783
n- InSb, hot electron energy relax. in quantizing mag. fields 78−31259
n-InSb, hot electron magnetophonon effect, 77K, mag. field modulation method 78−60140
n-InSb, hot electron noise temp., Monte Carlo calc. 80−107877
InSb, hot electrons, Monte Carlo calc. of transport characts. and distrib. functions of hot electrons 80−6853
n-InSb, hot electrons relax. in quantising mag. field *(Russian)* 80−6876
InSb, hot photoexcited electrons, time evolution of electron temp. in high mag. field 80−54709

hot carriers continued
InSb, impact ionisation and magneto-transport, high crossed elec. and mag. fields 80−107797
n-InSb, influence of mag. field on hot electron effects 78−2493
InSb, intrinsic and n-type, elec. cond., carrier wave instability in elect. and mag. fields 79−82617
n-InSb, magnetophonon reson. under hot electron conditions 77−24568
n- InSb, mangetophonon structure in magnetoresist., elec. field depend. 78−30943
p-InSb, mobility, diffusion and thermoelectric power of hot holes 80−39595
InSb, nonlinear optical properties, hot electron effects 78−71139
InSb, overheating luminescence, carrier generation-recomb. equilib. shift in elec. field 77−44068
n-InSb, phonon heating by hot electrons in quantising mag. field 77−4354
n-InSb, photo-induced magnetophonon reson., 4.2K, peak shifts 78−84250
n-InSb, photoconductivity, 1.8K, hot-carrier and free-carrier absorption. effects 78−84254
n-InSb, photoconductivity of laser excited hot electrons 80−11045
n-InSb piezoelectric semiconductors, carrier temp. effect on transverse phonon-helicon interaction 77−15886
InSb plasma, EM wave instability, effect of density gradient 79−1607
n-InSb, propagation of high power helicons 78−19070
n-InSb Raman spin-flip laser, hot electron effect distrib. calc. 80−23743
n-InSb, recomb. of hot electrons, photoelectromag. and dynamic photocond. meas. 79−38081
n- InSb, Shubnikov-de Haas effect, CO_2 laser induced hot electron effects 78−30957
n-InSb, Shubnikov-de Haas effect expts. on optically heated electrons 79−73529
InSb, warm electron coeff. 78−10452
KBr:Tl, electroluminescence, spectra and quantum yield activator conc. depend., cond. changes 80−89070
KCl:Tl, electroluminescence, spectra and quantum yield activator conc. depend., cond. changes 80−89070
NaCl, thin single-crystal film, hot electron emission 79−15244
NaCl:Ag, diffusion parameters of hot holes created by ionising radiation 78−47800
NaCl:Ag, thermolum. light sum storage by ultrasoft X-rays 77−20939
Ne, dense, electron injection, comparison with H_2 and He 79−73567
Pb chalcogenides, spectral depend. of internal quantum efficiency 77−4402
Pb chalcogenides, warm electron cond. 79−91066
n-PbTe film, epitaxial, hot electron transport effects 77−12035
n-PbTe, Hall effect of hot electrons 77−55547
PbTe, high field drift vel. and Hall coeff. 78−26875
n-Si, 77K hot electron repopulation and anisotropy *(Japanese)* 79−82600
Si (100) inversion layer, hot electron drift velocity, Monte Carlo calcs. inc. 3 subbands 78−91752
n-Si, anisotropy of differential conductivity and transverse diffusion coefficient 78−76078
n-Si, bulk, high field characts. *(Japanese)* 78−34837
n-Si, cond. in warm electron region, temp. depend. of anisotropy of nonlinearity coeff. 77−43610
Si, electrical conductivity, inertia of electron heating, expt. and theory 80−65613
n-Si, electron heating by static elec. field 80−96894
Si, electron transport and ionisation at high fields 78−30933
n-Si, electron-phonon scatt. and high-field transport 79−42552
n-Si, hot carrier noise and generation-recomb. noise 79−38140
Si, hot electron diffusivity, theory 77−62940
n-Si, hot electron repopulation at 77K, electron-electron scatt. effect 78−10456
Si, hot hole diffusion and white noise, microscopic Monte Carlo model 78−30937
Si, hot holes, drift and diffusion 79−78110
Si, hot holes negative Hall effect 79−87118
n-Si, hot-electron diffusion, effect of ionised impurity scatt. 78−56151
n-Si, hot-electron diffusion noise, meas. using radiometric method in X-band region 77−39905
n-Si, impurity-assoc. magnetophonon reson. 80−20221
Si inversion layer, photoconductivity meas. 78−10498
Si inversion layer, transient response of hot electrons, calc. 80−49747
Si, inversion layers, far IR emission from hot electrons 78−30995
Si inversion layers, harmonic generation due to hot electrons 80−65694
p-Si inversion layers, hot carrier effects in high mag. field, 1.25-20K 78−34908
n-Si, ionisation of low donor levels and recomb. of hot electrons at low temp. 79−51596
Si, luminesc. emitted as a result of carrier heating 77−52185
p-Si MOSFET, intersubband reson. photoresponse, mechanism 79−82677
Si, many-valley semiconductor, linear galvanomag. effects of hot electrons 79−11154
n-Si, microwave and far IR hot carrier mobility, Monte Carlo calc. appl. to mm. transit time oscill. efficiency 78−72184
n-Si, multivalued Sasaki effect 80−107795
Si, n-n^+ point junctions 80−44719
Si, n-type, V-I response in epithermal electron range 77−4361
Si, negative differential mobility and geometrical magnetoresist. calc. 77−43624
n-Si, noise and hot carrier diffusion in mag. fields 79−11193
p-Si, odd magnetoresist. under weak carrier heating conditions 80−96917
Si p-n junction, breakdown voltage drift, walk-out phenomenon, model 77−80834
Si, p-n junction, with hot carriers, amplification 78−39203
n^+nn^+Si planar device, hot electron flicker noise at 78K 80−103732
Si quantised inversion layers, hot electron effects 77−28188
Si, shallow p-n junction, energy loss and escape depth of hot electrons 79−78159
Si, surface emission of hot electrons 78−30998
Si, transport phenomena in strong elec. fields, intervalley electron scatt. 79−56240
n-Si, warm-electron magnetoresist. 79−65503
Si:Au, influence of carrier heating on exclusion 77−8110
Si:B, hot-carrier scatt. and recomb. characts. 79−91069
Si-SiO_2, emission probability of hot electrons into oxide 77−32084

hot carriers continued
Si-SiO_2, hot electron emission from Si under low level avalanche multiplication 77−80851
Si-SiO_2, hot electron emission into SiO_2 78−30997
Si-SiO_2 interface, avalanche injection of charge carriers, oxide current decay 77−43728
Si-SiO_2 interface, effect of hot electron injection on interface charge density 80−49921
n-Si-SiO_2 interface, hot carrier surface thermo EMF depend. on surface band bending 80−44734
Si-SiO_2 MOS interface, surface-state density and minority carrier generation rate, meas. by DLTS, hot hole effect 80−100527
SiC reverse biased p-n junctions, prebreakdown violet luminesc. 80−7420
SiO_2-Si interface, hot electron capture process, expt. method for study 79−38180
Ta-Ta_2O_5-ZnS:TbF_3-Au thin films, MIS struct., DC electrolum. obs., Poole-Frenkel effect 78−88038
Te, acoustoelectric domain induced transparency near 11 micron 77−85727
p-Te, magneto-impurity effect, review 79−91081
Te, warm hole conductivity 78−72160
Te, weakly doped, impurity spectroscopy, magnetoresist. meas. under nonohmic conditions 78−30942
Yb chalcogenides, multiphonon inelastic light scatt., hot recomb. 77−8559
Yb monochalcogenides, multiphonon inelastic light scatt. 77−90144
ZnO, hot-electron microwave conductivity, hot-electron, high DC field 79−38113
ZnS sputtered film, interband photocond. edge *(French)* 77−8212
ZnS:Mn, electrolum. film, direct impact excitation of Mn centres 77−24900
ZnS:Mn Schottky diodes, reverse-biased, electroluminescence, hot electron impact excitations 80−25005
ZnSe, photoexcited hot electrons at 2K, photolum. meas. 79−78741

hot cathode tubes *see thermionic tubes*

hot cathodes *see thermionic cathodes*

hot electrons *see hot carriers*

hot pressing
alumina, role of $\alpha \rightarrow \gamma$ polymorphic transform. in hot pressing 77−63612
apparatus for laboratory investigation 77−10038
automated sintering and hot pressing system 79−33961
borsic fibre reinforced Al, hot pressed forged, plasma sputtered *(Russian)* 78−35330
carbide fuels, vibro-compacted, initial stages of sintering and hot-pressing 80−16254
cement, hot pressed, type III, role of admixtures on pastes and H_2O cured cement, exam. 78−44073
cement, hot-pressed paste, strength, X-ray diffr., DTA, Ir spectra, microstruct. exam. 77−8864
ceramic, fine powder, compaction during pressing and green strength, absorbed layer effect *(German)* 77−77450
ceramic fuels, vibro-compacted, initial stages of sintering and hot-pressing 80−16254
ceramics, non-oxide hot pressing review 80−25641
ceramics, technique for studying internal and external gas pressure within pores 80−11606
ceramics, transparent, continuous vacuum hot pressing and press. design criteria 78−23643
chamber, with US activation facility 77−59709
coke, effect of addition of borides on hot-pressing 80−40282
consolidation study by absolute thermoelectromotor force 77−73246
continuous hot press, design and construction *(Chinese)* 79−33963
crystal growth by solid state techniques review 77−85935
densification mapping multimechanism model, for intermediate and final stages 78−44040
densification of porous body during hot extrusion, theoretical analysis 77−44189
densification of porous solids in hot rolling 77−63583
disperse materials, pressing pressure effect on consolidation 79−74116
dynamic, process parameters for parts of varying complexity 80−100799
dynamic hot densification of porous blanks, degree of deformation 77−63585
FCC metal, hot pressing diagram 79−70027
ferrite, coprecipitated, for appl. to mag. heads 77−85968
ferrite, hot pressing, charge:oxidizer ratio 77−48379
ferrite and ceramic joining, bulk interaction *(Russian)* 80−40277
fibre reinforced porous matrix materials, densification kinetics in free hot pressing 80−25618
fibre reinforced powder, densification during hot pressing 77−12566
fibre-reinforced hard alloy, effect of microstruct. on impact strength 77−56099
glass ceramic prep. by hot pressing and crystallisation of glass powder, mech. props. 78−15351
glass to mould heat transfer during pressing 78−80500
glasses, refractory, obtained by hot pressing of gels, crystallisation *(French)* 78−11193
granular materials, hot isostatic pressing in sheaths, process parameters calc. 80−84874
graphite based composite material, with ZrB_2 and SiC additions, prep., props., struct. 77−28775
graphite-BC body, hot pressing, props. *(Japanese)* 79−78923
graphite-Si powder mixture, reaction hot pressing 78−60592
green bodies, isostatically pressed, extruded and slip cast, binder distrib. 78−27448
hardening press for discs 79−57022
high level radioactive waste disposal, incorporation of $3CaO\text{-}Al_2O_3$ cement 78−78485
hot-pressed with crystn. grain boundary phases 78−95716
hydrostatic extrusion, adaptation of conventional press *(French)* 77−57344
Incaloy IN 738, dispersion hardened superalloy 78−11156
indentation hardness and hot pressing, calc. methods 80−58981
installation, GPV-4, for large blanks and parts 80−60799
isostatic, hard metals, characteristics, applications *(German)* 77−52351
isostatic, of rare earth magnetic materials, permanent magnets flux stability enhancement, gyroscope-based guidance systems performance improvement 80−50144
isostatic, review 78−19681
isostatic hot compaction, review 79−33960

hot pressing continued
metal, porous, densification during volume plastic deform. without work hardening 77−40402
metal powder, milling conditions effect on densification during pressing and sintering 78−11149
metal systems, high-temp., conf., Helsinki, Finland, June 1975 77−52295
metals and alloys, sintered, hot pressing, effect on formation of struct. and props. during sintering 79−100088
MgO-ZrO_2 ceramic reinforced with filamentary crystals, mech. and thermal props. 80−45262
Nichrome/steel, porous metal-thread sheet materials, filteration, permeability and strength props. *(Russian)* 79−78915
piezoceramic SAW propagation loss reduction 78−2356
PMMA-PVC mixtures, dielec. relax. and struct. rel. to formation *(Russian)* 77−20073
polyethylene, direct ram extrusion, correl. between chain folding and tensile modulus 77−44209
polymer, coorientation with low molecular organic substances *(Russian)* 77−21089
porous body in rigid sheath, energy expenditure in densification 80−16216
porous materials, densification kinetics in hot pressing, under quasi-isostatic conditions 80−11585
porous materials, densification kinetics in hot pressing under quasi-isostatic conditions 80−25592
porous materials, production method using stainless steel gauzes, exam. of hydraulic characteristics 80−16243
porous solid, densification during gasostatic hot pressing 77−12567
powder, homogenization by dynamic hot pressing 77−73244
powder, pressing in vacuum with adsorbed layers, boundary surface adhesion *(German)* 77−32540
powder consisting of anisotropic grains, effective thermal and elec. cond. 77−89601
powder layer on steel backing plate, joint form. kinetics 80−100961
powders, dynamic, laboratory unit 79−100071
prealloyed powder blending, composite materials fatigue and tensile props. *(French)* 80−20850
pressure sintering, inhomogeneous flow and effective press. 80−93512
PVC-Cu composites with chemically deposited ultrafine copper particles 80−93534
reactive, identification of stages 79−11542
refractory, dense, sintered, role of isostatic pressing 79−28995
reinforced magnetically hard material, fibre-reinforced, porosity and impact strength 77−55916
review 79−74113
S glass-Ni sphere composite, exam. of crack shape and fracture toughness 78−72886
shrinkage measurement during hot pressing strain gauge device 78−11146
β'-Sialon, sintering kinetics and rates of microstructural changes 79−100102
steel, alloy, maraging, 250-grade, ductility and toughness of hot isostatically pressed powder 78−52925
steel, austenitic, hot isostatically pressed superalloy A286, fracture path 78−23824
steel, Cr-W-Mo-Co, high-speed, from atomised powders, mech. and cutting props. 80−66556
steel, high speed, atomised powder, defects in parts produced by hot isotactic pressing 78−60612
steel, high speed, W-Mo-Co-Cr-V, production from atomized powder 80−20837
steel, high-speed, 30Kh2N2SMKt, deform. effects on physicomech. props. 78−23741
steel, low-C, bond form. between powder layer and dense basis during hot pressing 79−24669
steel, maraging, inert gas atomised, hot isostatic pressing temp. effect 79−24460
steel, stainless, fibre reinforced porous coating, isostatically compressed for bone ingrowth 80−35134
steel fibre reinforced Al, vacuum hot pressing, strength *(Czechoslovakian)* 77−32543
steel welded joint impact strength, preheating and tempering effects 79−24542
superalloy, hot consolidation of rapidly solidified powders, review 79−33965
surface-relief phase gratings for image recording and display 77−19429
thermoelectric materials, B_4C_x and $(B,Si)_4C_x$ P-type LaS_x N-type alloys, fabrication and thermoelectric props. 80−107771
thermoelectric pressed powder specimens, elec. characts. anisotropy rel. to textural anisotropy 77−52515
transition metal carbides, elastic moduli, scratch geometry, micromech. tests 78−35416
uniaxially reinforced powder, densification by dynamic hot pressing in rigid sheath 77−12568
Zircaloy-2, hot-pressed, influence of diffused C on structure and oxidation 80−61016
Ag-polystyrene powder mixture, hot-pressed, elec. resist. 77−32556
Al disc porous electrode, prep. by powder metallurgy, performance in LiAl/FeS_x cell 80−26130
Al-C, dispersion hardened, effect of processing parameters on mech. props. 80−20826
Al-C alloys, dispersion hardened exam. of production method using pressed powders 80−16244
Al-Cu (33 wt.%) eutectic, superplasticity, in-situ obs. by TEM 77−28876
Al-Cu-Mg alloy, extruded, press forming in liquid/solid coexisting state, mech. props., Mg effects 78−11151
Al-Si (35 wt.%), Cr, Co, Si addition effects on strength of powder 77−24983
Al-Si-N-O system, comps. corresponding to β'-sialon phase reaction hot-pressing 80−84891
Al-Zn-Mg plasma sputtered, mech. props. rel. to heat treatment *(Russian)* 80−40387
α-AlB_{12}, prep. and electrothermal props. 80−20863
$AlMgB_{14}$, prep. and electrothermal props. 80−20863
AlN, creep during hot pressing 78−23650
AlN, hot pressed, effect of O_2 content on flexural strength and compact density 79−11668
AlN powder, effect of O impurity on sintering and thermal cond. *(Japanese)* 79−20017

hot pressing continued
AlN-Al_2O_3, phys. and mech. props. 77−52275
AlN-Al_2O_3, powders, crystalline phase obs. 78−95720
α-Al_2O polycrystalline grain orientation, permeable pressing effect *(Japanese)* 78−15349
Al_2O_3 78−27456
Al_2O_3, composite base ceramic coating, hot pressed, H_2 permeability 77−56164
β-Al_2O_3, hot isostatic press. 80−108377
Al_2O_3, hot pressed, fracture stress-reflecting spot relations 80−71731
Al_2O_3 hot pressed, high density, effect of grain size on grinding 78−39723
Al_2O_3, hot pressing, microstruct., texture 80−40299
β''-Al_2O_3, Li_2O-stabilised, hot-pressing 80−40298
β-Al_2O_3, polycryst. with preferred grain orientation, hot pressing of gibbsite and Na_2CO_3 *(Japanese)* 79−56948
Al_2O_3, pressing method, for the telecommunication industry *(Hungarian)* 78−52728
Al_2O_3, reactive hot pressing, exam. of pressing characteristics 78−80499
α-Al_2O_3, sintered or hot-pressed, porosity effect on positron mean lifetime 78−27463
Al_2O_3, sintering under press., survey *(Polish)* 78−31368
Al_2O_3, transparent ceramic manuf., characts. of powder and process 77−48383
Al_2O_3, transparent hot-pressed, transparent and translucent properties 80−60533
β-Al_2O_3-K_2O/K ferrite, interfaces and solid soln., thermal expansion and lattice parameter variations 78−55959
Al_2O_3-Mo (20 wt.%) cermet, ZrO_2 crystal addition effect on thermal fatigue resistance 80−40528
Al_2O_3-Mo cermets, effect of processing factors on props. 79−100103
β-Al_2O_3-Na_2O, hot pressing and phys. props. 79−4940
β-Al_2O_3-Na_2O, preferable orientation for Na^+ cond. 80−35144
β-Al_2O_3-Na_2O, vacuum hot pressed, densification kinetics 78−72758
Al_2O_3-Si_3N_4 preparation, compressive strength 80−25634
Al_2O_3-SiO_2 glass powder, mullite crystallisation during hot pressing 78−60639
Al_2O_3-$ZrSiO_4$ mixture, reaction sintering, correlation between densification and reaction 80−29911
β-Al_2O_3.Na_2O, ceramic tube fabrication, crystallite preferred orientation, ionic cond. 77−8781
B fibre reinforced H, hot pressed forged, plasma sputtered *(Russian)* 78−35330
B-B_4C materials, hot-pressed, elastic modulus and flexural strength rel. to grain size and porosity 79−79018
BC, sintered and hot pressed, friction and wear, 20 to 1500°C 78−60844
$B_{12}C_3$, sintering and subsequent high temp. annealing, struct. and props. 80−20858
B_4C, densification kinetics during hot pressing, 1800-2200°C 80−60817
B_4C rings, Al bonded, exam. of fabrication techniques 78−72748
BN, shock-compressed pyrolytic and hot-pressed, phase transitions to 120 GPa 77−70048
BN, turbostatic, hot pressing, struct. rearrangement, temp., residence time effects 77−8789
BN/BN composites, prep., mech. props. 77−21080
B_2O_3-SiO_2, glass synthesis by hot pressing of gels 79−15637
BaF_2, optical ceramic, hot pressing in vacuum, rel. to spectral transmission 78−52730
$BaHfO_3$, $BaSnO_3$ and $BaZrO_3$, high-density ceramics prep. and elec. props. 80−60812
Be, low oxide, isostatically pressed block, factors affecting tensile strength, elongation, impact resistance 77−16610
$Bi_{12}GeO_{20}$, X-ray sensitive ceramic, sintering 80−25621
$Bi_2Te_{3-x}Se_x$, thermoelec. mat., prep. effects on inhomogeneities 78−51576
C fibre reinforced Al, formed by ion plating and vacuum hot pressing, mech. strength 78−11165
C fibre reinforced glass, SiC fibre coating, hot pressing production method *(German)* 78−95724
C fibre reinforced Ni, hot pressed and electrodeposited, strength 79−38898
C-fibre reinforced SiO_2-glass, prep. for high temp. appl. 80−45267
CaB_6-SmB_6 system complex borides, prep. and props. 78−52703
CaF_2, hot pressed, dielectric, optical props. 79−56720
CaO-CaF, effects of CaF_2 addition, sintering behaviours and microstructs. investig. *(Japanese)* 78−95721
CaO-MgO-Al_2O_3-SiO_2, glass-ceramic prep. by hot pressing and crystallisation of powder 78−11192
CaO-MgO-Al_2O_3-SiO_2, glass ceramic, prep. by hot pressing and crystallisation, mech. props. 78−15351
$CaSnO_3$ and $CaZrO_3$, high-density ceramics prep. and elec. props. 80−60812
Co, powder, hot pressing on steel substrate, densification kinetics 80−40290
CoO, pressure sintering densification model, computer program 78−44040
CrC-Ni alloys, exam. of activated sintering 80−16241
Cu, powder, hot pressing on steel substrate, densification kinetics 80−40290
Cu, pressing pressure effect on consolidation 79−74116
Cu-BN composite electromachining tools, dynamic hot pressing 80−84889
Cu-Ni, powder, sintered, effect of cold and hot dynamic pressing, upon structure and props. 79−33970
Cu-Sn warm pressed compact prep. 80−35136
EuB_6, synthesis and hot pressing fabrication for appl. to neutron absorbing core control material 78−8904
Eu_2O_3/metal cermet prep., in situ deposition of metal coating and hot pressing 77−32713
Fe, carburised sintered and pressed specimens, wear resistance 77−77590
Fe compacts, porous, dynamic hot pressing, press. rel. to density, time 78−60599
Fe, dynamic hot densification, degree of deformation 77−63585
Fe effect of repressing and double sintering on impact strength *(Japanese)* 78−92217
Fe, powder, hot pressing on steel substrate, densification kinetics 80−40290
Fe powder, sintered and hot pressed, effect of porosity, grain size on magnetic props. 79−96159
hot pressing continued
Fe powder layers, sinter-bonded, hot-pressed, on steel, struct. and props 79−95976
Fe, sintered, produced by dynamic hot pressing, recrystn. diagram 79−70017
Fe, sintered and pressed, props., effect of atomised Fe powder particle size distrib. 80−11601
Fe-B_4C sintered material, mech. props. and struct. characts. 79−100084
Fe-C-Ni-Cr(Cu), dynamically hot pressed, mech. props., additives effect 78−60620
Fe-Ni heterogeneous alloys, ferrite, martensite and austenite phase distrib., effect on mech. props. 80−45363
Fe-Ni-Al(Ti)(V)(Nb), cryogenic toughness, strength, rel. to reactive metal addition 78−39885
Fe-Ni-Cr-Ti, superalloy A286, powder, exam. of microstruct. and mech. properties 78−52979
Fe_2O_3, powder, compression in moulds, meas. apparatus *(Dutch)* 77−44205
γFe_2O_3, transform. to α-phase, effect of preliminary pressing or vibromilling 78−84798
β-Ga_2O_3-K_2O/K ferrite, interfaces and solid soln., thermal expansion and lattice parameter variations 78−55959
Gd_2O_2S, compact specimen prep. 77−85951
Ge, heavily doped, vacuum hot-pressing thermal and electrical props. 77−40400
Ge, heavily doped, vacuum hot pressing, effect on thermal and elec. props. 80−25594
Ge-Si alloy, vacuum hot pressing, effect on thermal, electrical props. 80−25594
$Ge_{30}Si_{70}$, hot press sintering 80−50572
HfC, pressing regime influence on high-temp. creep *(Russian)* 80−100852
(K,Na)NbO_3 ceramic, hot pressed, dielec. props. 79−87375
K(Ta,Nb)O_3 ceramic, prep. and electro-optical props. 80−25620
La-Si-O-N system, new compound form. with fluorapatite struct. 79−4941
La_2O_3-SiO_2, glass synthesis by hot pressing of gels 79−15637
La_2O_2S, compact specimen prep. 77−85951
La_xS_y, stoichiometry and opt. props. during hot pressing 78−23653
LiF, ceramic, characts. on pressing in vacuum and in air 78−52734
LiF compact, particle size rel. to pore characts. 78−60631
LiF tile and sheet for thermal neutron shielding *(Japanese)* 78−74510
$LiTi_2O_4$, prep., characterisation and supercond. props. 77−40010
Mg-Al spinel, hot pressed ceramic, annealing effect on transparency and microstruct. *(Japanese)* 79−74188
MgF_2, hot pressing in vacuum, compaction kinetics, selective recryst. 77−16517
MgO, hot-pressed, elasticity props. of polycrystals and single crystals 80−54301
MgO polycrystals, ultrafine grained, compressive creep 77−32639
MgO, pore distrib. and grain size in intermediated sintering stage *(Japanese)* 79−74124
MgO powders, hot pressing, mechanisms 80−40300
MgO, stresses on hot pressing 77−36425
MgO:LiF, accretive recrystallisation during hot pressing 77−36421
MgO-Al_2O_3 transparent spinel ceramic, fabrication by reactive hot pressing *(Japanese)* 77−77454
Mn_2SiO_3, effect of vibration during sintering, on electrical resistivity 80−16258
MnZn ferrites, hot pressed, mechanism of protective action of Zn0 coating *(Russian)* 79−15822
MnZn, pressing powders, spray dried, pressing behaviour and props. 80−11617
Mo-Cr, powder mixture, activating effect of Group VIII metals on alloy form. during sintering 77−59728
Mo_3C_2, pressing regime influence on high-temp. creep *(Russian)* 80−100852
(Na,Li)NbO_3 ceramic, optimum prep. conditions and characterisation 78−3079
$Na_{0.5}Bi_{4.5}Ti_4O_{15}$, hot-forged ferroelec. ceramic with layer struct. 79−43175
β-Na_2O-Al_2O_3, thermal dissoc. at high press. 77−36435
β''-Na_2O-MgO-Al_2O_3, thermal dissoc. at high press. 77−36435
$Na_2O.11Al_2O_3$, polycrystalline with preferably orientated grains, preparation *(Japanese)* 80−81012
NbB_2, hot pressing 80−25635
NbC, pressing regime influence on high-temp. creep *(Russian)* 80−100852
Nb_3Sn, hot isostatically pressed, plastic deform. 80−108510
Nb_3Sn, powder metallurgically produced, microstruct. characts. 80−89233
Ni alloy powders hot hydrostatic pressing of disk, capsule design 80−20839
Ni, powder, hot pressing on steel substrate, densification kinetics 80−40290
Ni powder, positron annihilation, interaction with defects in grain and pores *(Russian)* 77−16520
Ni-Al_2O_3 cermet, fabrication and mech. characts. 79−38781
Ni-based-Ta(Cn,N) hard metals, isostatic hot pressing influence on mechanical properties 78−92219
Ni-Cr (20 wt.%), powdered, prod. of Mo fibre reinforced composite by hot pressing exam. of strength 78−56710
Ni-Cr-Al sintered alloy, hot vac. pressure, fracture and mech. characts. 80−66667
Ni-Cr-Co base superalloy APK1, hot isostatically pressed, heat treatment, fracture props. 77−73251
Ni-Cr-W-Co granules type ZhS6U, EP741, hot hydrostatic pressing 80−60796
Ni-Fe powder, effect of vibration and current pulses on shaping 79−95973
Ni-Zn ferrites, hot-pressed, key props. 78−15348
Ni-ZrB_2 powders, densification by hot pressing 80−25604
NiZnCo ferrites, temp. stability, effect of Fe content and processing conditions 79−28993
PLZT, exam. of grain growth in hot pressing, and liquid phase sintering 79−33981
PLZT porosity and transparency affected by vacuum hot pressing 77−12556
PLZT powders, chemical prep. and hot pressing 78−44059
PLZT slugs, powder hot pressing technique 80−81007

hot pressing continued
PLZT, transparent ferroelectric, ceramics obtained by hot pressing, optimum conditions *(German)* 79−43176
$(Pb,Sr)(Zr,Ti)O_3$, piezoceramic, effect of glass additions on props. during hot pressing 79−24475
$PbBi_2Nb_2O_9$, hot-forged ferroelec. ceramic with layer struct. 79−43175
$PbBi_4Ti_4O_{15}$, hot-forged ferroelec. ceramic with layer struct. 79−43175
$Pb_2Bi_4Ti_5O_{13}$, hot-forged ferroelec. ceramic with layer struct. 79−43175
PbS, hot-pressed compact, elec. behaviour, adsorbed atmos. gas effects 77−66601
PbTe, effect of pressing and sintering, study of induced defects by SEM 80−59983
$Pb(Zr,Ti)O_3$-$Pb_3Ge_5O_{11}$ ceramic, sintering conditions rel. to piezoelec., dielec. props., microstruct. 77−16252
$Pb(Zr_{0.42}Ti_{0.58})O_3$, hot-pressed piezoelec. ceramic, effect of nonferroelectric phase 77−43936
PuN, fabrication, high-temp. thermodynamic and transport props. 77−28774
PuO_2 fuel, reproducible fabrication 77−77452
PuO_2, fuel prod. by powder techniques 79−9846
Sc_2O_3 78−27456
Si-Al-O-N ceramic, single-phase, prep. by hot-pressing, microstruct. investig. 77−8792
Si-Al-O-N ceramic, single phase form. using hot pressing *(Japanese)* 79−70031
Si-Al-O-N composites, dense direct prep. from naturally occurring SiO_2 and Al powder 78−11187
Si-Al-O-N polytypes, hot-pressed, microstruct. 80−3023
Si-Al-O-N system, TEM exam. of X phase structure 78−56606
Si-Al(Ti)C, sintered, exam. of props. 80−25644
Si-Ge, heavily doped vacuum hot-pressing, thermal and electrical props. 77−40400
n-Si-Ge, phonon thermal cond. of hot-pressed alloy, 300-1100K 78−91494
Si-Ge alloy, hot-pressed, thermal cond., effect of grain size 77−31813
Si-Ge:Al, B, P, hot-pressed alloy, thermoelec. props. 78−91711
SiAlON, prepared from siliceous sand and Al powder, hot pressing, steatite contamination effects *(Japanese)* 80−93528
$Si_{6-z}Al_zO_zN_{8-z}$, β-Sialon, form. from Si_3N_4-SiO_2-AlN system *(Japanese)* 80−45261
$Si_{6-z}Al_zO_zN_{8-z}$, hot pressed, DC elec. props., 18-500°C, fields up to 1.1×10^4 V cm^{-1} 78−26860
SiC and Si_3N_4, hot pressed, comparison of high-temp. thermal fatigue resistance 77−36623
SiC, dense, joining by hot pressing, and bond strength 80−66458
SiC fibre reinforced Ni-Cr alumina coated fibres, hot pressed, annealed, IR study 78−60623
SiC fibres reinforced Ni complex alloy, influence of TiN coating on fibre matrix interaction *(Russian)* 78−95820
SiC, hot pressed, brittle fracture and subcritical crack growth 78−72885
SiC, hot pressed, K_{Ic} and delayed fracture meas. 79−61701
SiC, meas. of critical stress intensity factor and subcritical crack propag. rates 78−72880
SiC, polytypic transform. during hot pressing 78−52739
SiC, role of grain boundaries, addition of B, B_4C and Al_2O_3 77−24999
SiC-AlB_2 (0.61 to 1.2 wt.%), hot pressed, microstruct. 80−93563
Si_3N_4, and Si_3N_4-MgO, hot pressed, DC elec. props., 18-500°C, fields up to 1.1×10^4 V cm^{-1} 78−26860
Si_3N_4, consolidation by hot isostatic pressing 80−11605
Si_3N_4, high-speed rolling bearings, fatigue strength 80−93655
Si_3N_4, hot pressed, effect of powder composition and sintering temp., on phase transformation kinetics, microstructure and mech. strength *(German)* 79−4939
Si_3N_4, hot pressed, flawed plate under combined stresses, failure prediction 78−72884
Si_3N_4, hot pressed, fracture phenomenology, fracture surface energy, crack propagation 79−57090
Si_3N_4, hot pressed, high temp. compressive cracking, optical and electron microscopy exam. 78−76733
Si_3N_4, hot pressed, slow crack growth from controlled surface flaws 78−80632
Si_3N_4, hot pressed, surface wave scatt. from elliptical cracks for failure prediction 80−55608
Si_3N_4, hot pressed, Y_2O_3 fluxed, microstruct. 78−64512
Si_3N_4, hot pressed with different grain struct., mech. props. 79−61700
Si_3N_4, hot pressing, effect of ZrO_2 *(Japanese)* 77−55929
Si_3N_4, hot pressing with Mg-Si-N-O system additives *(Japanese)* 77−36437
Si_3N_4, hot pressing with Y_2O_3 and Li_2O additives 78−92220
Si_3N_4, hot-pressed, creep and strain recovery 80−100874
Si_3N_4, hot-pressed, fracture in bending *(Japanese)* 79−79113
Si_3N_4, hot-pressed, strength anisotropy origins 80−89330
Si_3N_4, hot-pressed with crystn. grain boundary phases, prep. 78−95715
Si_3N_4, impurity phases, TEM obs. 79−8260
Si_3N_4, meas. of critical stress intensity factor and subcritical crack propag. rates 78−72880
Si_3N_4, MgO-fluxed, hot pressed, grain boundary phases 78−27464
Si_3N_4, optimization of props. as tool material, for high fracture toughness and hot pressing prod. 79−95987
Si_3N_4, oxidised, with Y_2O_3 densification aid, temp. and compositional stability of $Y_6Si_6O_{21}$ 78−27664
Si_3N_4 powder, high press. hot pressing 79−38772
α-Si_3N_4 powder, hot pressing, kinetics 77−55925
Si_3N_4, reaction bonded and hot pressed. exam. of thermal shock behaviour *(German)* 78−64561
Si_3N_4, recrystallisation during hot pressing 77−12587
Si_3N_4, starting powder requirements, review 79−33987
Si_3N_4 with Y_2O_3 and Al_2O_3 additions, hot pressed, exam. of mech. props., grain boundary crystallization 79−20009
Si_3N_4, Y_2O_3 doped, hot pressed, improved high temp. strength 79−61613
Si_3N_4, Zr-based hot pressing aids effect on oxidation resist. 77−8971
Si_3N_4-Al_2O_3, hot-pressed with crystn. grain boundary phases, prep. 78−95715
Si_3N_4-Al_2O_3, hot-pressed with crystn. grain boundary phases 78−95716
β-Si_3N_4-AlN-Al_2O_3-MgO, insolubility of Mg in β-Si_3N_4 79−10953
Si_3N_4-CeO_2 additive, hot-pressing and oxidation behaviour 80−71618
Si_3N_4-MgO, hot pressing and α-β phase transform. 78−27461
Si_3N_4-MgO (2-5 wt.%) hot pressed, tensile creep testing 80−40423
α-Si_3N_4-MgO (5 wt.%), hot-pressed, mech. strength development 78−44195
hot pressing continued
Si_3N_4-Y_2O_3, hot-pressed, oxidation kinetics 80−16520
Si_3N_4-Y_2O_3(CeO_2), hot pressed, sintered, microstruct., flexural strength and fractographic anal. 80−40293
Si_3N_4-ZrO_2, sintered and hot pressed, exam. of mech. props. 78−48509
Si_3N_4+MgO, hot pressing and effects 77−63614
Si_3N_4+MgO, reaction during hot pressing 78−68658
Si_2N_2O-Al_2O_3, solid soln., prep., effect of Si_3N_4 powder reactivity 80−45256
Si_3N_4.Y_2O_3 prepared by hot press, cryst. struct. 80−10534
Si_3Ni_4, hot pressed, subcritical crack growth boundaries at internal fracture origins 80−11748
Si_3Ni_4, hot pressed MgO fluxed grain boundary impurity phases, lattice fringe imaging obs. 79−11540
SiO_2, glass synthesis by hot pressing of gels 79−15637
SiO_2-B_2O_3 glass system, gel hot pressing synthesis and characterisation *(French)* 80−66468
$Sr_x(Na_{0.5}Bi_{0.5})_{1-x}TiO_3$ ferroelec. ceramic, hot pressing, numerical simulation *(French)* 80−76220
$SrSnO_3$ and $SrZrO_3$, high-density ceramics prep. and elec. props. 80−60812
TaC, pressing regime influence on high-temp. creep *(Russian)* 80−100852
TaC, ultrafine grain, high pressure hot pressing 79−70024
(Ti, Cr)B_2-based alloys, densification of powder mixtures by hot-pressing, elec. and mech. props. 80−20812
(Ti,V)C carbides, prep. and mech. props. 78−64518
Ti, fatigue strength, oxidation effect 79−96137
Ti-Al-V (6,4 wt.%), porous compacts, determ. of effective stress in hot pressing 80−100807
TiB_2, electrode, hot pressed, erosion resistance, struct. and porosity effects 78−3228
TiB_2, low temp. radiation damage, calorimetric investigation 77−27916
TiB_2-TiC powder mixtures, hydrostatic pressing 79−100098
TiC-C composites, hot pressed, thermophys. props. at high temps. 80−59675
TiC-Cr_3C_2(Cr_3C_2-WC), powder mixture, steel bonded, exam. of sintering behaviour 78−52712
TiC-TiB_2, preparation and high temp. antifriction props. 79−1918
TiO_2 based construction ceramics, fibre-like cryst. reinforced, mech. props. 80−55341
W fibre reinforced Ni composite, prep. by hot isotactic pressing, mech. props. *(Slovak)* 78−19694
W fibre reinforced Ni-Cr (20 wt.%), hot pressing kinetics 78−35334
W-Re(Mo)(Cr), powder mixture, activating effect of Group VIII metals on alloy form. during sintering 77−59728
WC-Co alloys, P additions, effect on hot pressing, hardness and wear resist. 78−11162
WC-Co hard alloys, hot pressed, mech. props. 79−100260
WC-Co hard alloys, hot-pressed, wear resist. under abrasive friction, heat treatment effect 80−66555
WC-Co-C based hard alloy VK6, densification kinetics in hot pressing 80−11600
WC-TaC-Co, cemented carbide, strength improvement by hot isostatic pressing 78−84969
YIG, open die hot pressing, spin wave and FMR line width 80−89170
YIG, permeability, domain rot. and wall displacement contrib. 80−80564
Y_2O_3 78−27456
Y_2O_2S, compact specimen prep. 77−85951
ZnO, fully dense, grain growth 80−93526
ZnO, segregation of Li_2O at grain boundaries 78−64513
ZnS, hot pressed, water drop impact damage, SEM exam., IR transmission 78−88543
ZnS phosphors, synthesis under unidirectional pressure and roasting in vacuum 77−32547
ZnSe, hot-pressed powder LED fabrication and characts. 78−23639
ZnSe, recrystallisation during hot pressing 77−85952
ZrB_2, hot pressing, applied press. effect *(Japanese)* 79−38780
ZrB_2-SiC-C(-V)(-Nb), refractory cermet, hot pressing and oxidation resist. 80−3231
ZrC-C composites, hot pressed, thermophys. props. at high temps. 80−59675
ZrC-ZrB_2, preparation and high temp. antifriction props. 79−1918
ZrO_2, cubic, nitride stabilised 78−92223
ZrO_2, partially stabilized, processing defects 80−97558
ZrO_2-Y_2O_3/metal cermet prep., in situ deposition of metal coating and hot pressing 77−32713
ZrO_2-Zr cermet composite, hot pressed, fracture toughness 78−27604
$ZrSiO_4$-Al_2O_3 mixture, reaction hot pressing 79−38775

hot shortness *see brittleness*

hot strength *see tensile strength*

hot working
alloy, vacuum rolling at high temp. *(Russian)* 79−15708
alloys, hot plastic strain, stress- strain-time dependences *(Russian)* 80−40430
Alnico alloys, properties *(German)* 77−52352
austenite, hot-worked, struct., post-deform. ht. treatment effects *(Russian)* 77−8859
austenite, hot-worked, subgrain struct., X-ray diffr. and electron microscope obs. *(Russian)* 79−15698
austenitic steel, 17G1S struct. and austenite transformation kinetics variation on deform. *(Russian)* 79−70060
bimetal rolling, calc. of strains by variational method *(Polish)* 80−45323
brass, crystal structure and morphology of thin needle-like martensite 78−31425
α-βbrass, exam. of creep fracture by tensile tests 78−88531
brass, hot stamping type, resistant to dezincification 79−70208
α-brass sheet, shear bands and recrystallisation 79−91680
cordierite, dense ceramic prep. with sintered condition over 300°C interval 79−33983
deformation resistance, depend. on hot press. working speed *(Russian)* 80−65126
die filling and densification in hot extrusion forging of porous preforms 78−23645
helical shape extrusion from round billets 79−29102
hot plastic deform., relation between formability and deform. stress *(Czechoslovakian)* 77−32604

hot working continued
hot rolled T-section finite element anal. of temp. field *(Russian)* 79−29101
hot rolling, simplified load calcs. incorporating material strain rates 77−52359
hot rolling exam. of empirical relations for plastic flow strength 79−61630
hot strip rolling simulation, by hot torsion technique 80−29990
hot twisting, shearing stresses, anal. determ. 78−60900
Inconel 617, microstruct., mech. props., thermal ageing effect 77−36557
Lawsonite end plates for working spaces of liq. H_2 targets, prep. technique 77−67926
material nonhomogeneity due to existing temp. field *(Polish)* 79−52242
metal, bulk deform. process 78−31459
metal, hot deformability test methods, comparative evaluation *(German)* 77−36713
metal, recovered dislocation substructure, prod. and utility, review 77−84749
metal, vacuum rolling at high temp. *(Russian)* 79−15708
metal deformability, flow curves mathematical description, thermal dependence *(German)* 78−15484
metals, fracture during laser working, depend. on physico-chem. props., heat cond. *(Russian)* 80−55432
metals, hot plastic deform., stress/strain/time relations *(Russian)* 80−20968
metals, recrystallisation during hot deform. 78−68714
metals, thermal conductivity models, during hot deseaming *(Russian)* 80−24869
multilayer materials, vacuum rolling at high temp. *(Russian)* 79−15708
Ni-Cr-Mo and Ni-Cr, impact strength, effect of modified ausforming *(Japanese)* 79−11692
nucleation, criterion for dynamic recrystallisation during hot working 78−52852
pipes, hot-rolled, automatic mag. quality control on prod. line 80−108661
polyethylene, high mol. wt., porous, hot drawing 80−60894
polyethylene, struct. changes on hot-rolling 77−86051
polyethylene, structural changes on hot-rolling 77−86052
polyethylene fibre, high-strength high-modulus, morphology and tensile prop. relations 80−103264
polyethylene surface-growth fibres, hot drawing 80−97517
polypropylene monofilaments, draw rate effect on long period 79−47726
porous materials, contact stresses in hot rolling 77−77515
porous solids, hot rolling, rheology, stressed state determ. 79−100194
profile measurement of hot rolled strip during hot rolling *(German)* 80−25929
PVC, reaction with maleic anhydride in heated roll mill *(Japanese)* 79−38856
recrystallisation, conf., Leeds, England (April 1978) 79−47706
rolling, hot longitudinal, periodically charging sections with flash, pressures calc. *(Polish)* 80−89257
rolling, torque calc., mechanical model 79−20078
servocontrolled hydraulic hot-torsion machine for hot working studies 78−27698
shock compression-pulse heating working process, apparatus design 80−16357
steel; low alloy, high strength, hot compression dynamic precip. and coarsening of Nb(CN) 80−97514
steel, 18H2N4WA, hot-worked, kinetics of austenite grain growth, rel. to deformation degree *(Polish)* 80−45322
steel, 45G17Yu3, deformed, influence of hot rolling on struct. *(Russian)* 77−25073
steel, Al-stabilised, texture formation in continuous annealing, effect of coiling temp. of hot strip 79−91688
steel, alloy, cluster formation susceptibility in 40 KhN, influence of isothermal working in H_2 *(Russian)* 78−56643
steel, alloy, high speed, type R18, hot deformation and recrystn. 80−16391
steel, alloy 4340, fracture and high temp. props., 533K to 1255K 78−60821
steel, austenite hot deformation influence on phase transformations 80−7606
steel, austenitic, 30KhGSA, heat treatment, preliminary, cold deform., elec. heating rel. to mech. props. 79−24554
steel, austenitic, 45Kh2N12GS, post deformation holding at deform. temp. effect on struct. and strength of austenite and martensite *(Russian)* 79−1880
steel, austenitic, Cr-Ni-Mo, Mo effect on lattice parameters and chem. comp. of σ-phase and $M_{23}C_6$ carbides 77−70072
steel, austenitic, deform., struct., transform. kinetics hot working effects *(Russian)* 77−52361
steel, austenitic, dislocation structural changes on hot rolling *(Russian)* 77−59805
steel, austenitic, hot-worked, formation of high-C martensite, struct. *(Russian)* 78−6950
steel, austenitic, metastable, 0Kh14AG12M, Cr-Mn and Cr-Mn-Ni, phase transform. kinetic effect on mech. props. *(Russian)* 79−34024
steel, austenitic, microalloyed with V and N, hot rolling 77−52364
steel, austenitic, Nb modified, HSLA, interaction between recrystallisation and precipitation during high temp. determ. 79−100187
steel, austenitic, substructure change in hot deform. process *(Russian)* 77−16617
steel, austenitic stainless, 08Kh18N10T, hot-worked precipitation kinetics and struct. of dispersed phases, Ti effect 80−29964
steel, austenitic stainless, 12Kh18N10T, deformed, phase comp. and props. after prolonged heating 80−30040
steel, austenitic stainless, 12Kh18N10T, intercrystalline corrosion, hot rolling effect 79−79010
steel, austenitic stainless, AISI 316 L, viscoplastic deformation under hot working conditions, struct. model 79−83278
steel, austenitic stainless, cavitation erosion resistance, martensitic transform. effect *(Russian)* 78−35524
steel, austenitic stainless, Cu-Mo substituted 18/8 type, austenitic stability 79−91716
steel, austenitic stainless, recrystallization after hot rolling 79−47734
steel, austenitic stainless, viscoplatic constitutive eqns. under hot working conditions 79−57024
steel, B-Si, grain-oriented, high induction, Cu impurity effects 80−89366
steel, C, crack propag. and sealing, effect of thermal working *(Russian)* 79−34078
steel, C, hot plastic deform., vac. colour etching investigation 80−61036
hot working continued
steel, C, isoforming and warm rolling, effect of mech. props. 80−11673
steel, C, pearlite grade ShKh15, struct. transformations, hot plastic strain influence *(Russian)* 80−20927
steel, C-Mn and C-Mn-Nb, weldable, high temp. thermomechanical treatment 79−15709
steel, C-Mn-Nb, Nb microalloying, weldable, structural, recrystallization and precipitation induced by high temp. deform. *(French)* 79−61632
steel, continuously cast, optimum conditions for annealing castings during dynamic working *(Russian)* 78−44134
steel, continuously cast billets, influence of hot working on internal cracks 79−83242
steel, Cr-Ni(-Mo) austenitic, strengthening by modified ausforming 78−76665
steel, Cr-Ni-C (3, 1, 0.6 wt.%), grain boundary sulphide precip. and hot ductility *(Japanese)* 80−71654
steel, Cr-Ni-Mo, dynamic and static softening behaviour at hot forming temp. *(German)* 80−25728
steel, deep drawing, texture control as affected by processing variables 79−91689
steel, effects on products props. *(German)* 80−3108
steel, hereditary transfer of lattice defects at γ-α-γ transform. 79−96020
steel, high C, Burgers vector of dislocations in cementite crystal 77−27891
steel, high C, tensile strength, working and heat treatment effects *(Japanese)* 80−104209
steel, high strength, low alloy, response to cyclic plastic deform. 78−7035
steel, high strength, Nb(C, N) precipitation in austenite, effect on mech. props. *(Japanese)* 77−21186
steel, high strength, thermally strengthened by rolling heat, H_2 embrittlement *(Russian)* 77−77562
steel, high-speed, 30Kh2N2SMKt, deform. effects on physicomech. props. 78−23741
steel, high-speed, cast, mech. props. at high temps. 79−20135
steel, high-temperature thermomechanical treatment, holding after deform. effect on strengthening 79−38868
steel, hot deformed austenite, transition from discontinuous to continuous formation of pearlite *(German)* 80−35214
steel, hot rolled, low C, low alloy, bainitic alloying addition effects on microstruct. and props. 77−36546
steel, hot rolled, M1 tool type, microparticle distributions and mech. response 77−44279
steel, hot rolled Al killed sheet, strain ageing control 79−61628
steel, hot rolled strip and plate shape meas. device 80−35498
steel, hot rolled strip formability, mech. testing and mech. props. *(German)* 79−66089
steel, hot rolling, simulation while preserving criteria of similarity *(Russian)* 79−52266
steel, hot-rolled high quality sheet use of stat. maths. for NDT determ. of mech. props. 79−11749
steel, HSLA, V and N effect on recovery and recrystn. during and after hot working 80−84973
steel, impact and tensile props., Si effects 79−24614
steel, Kh15N5AM3, combined heat treatment and mech. working *(Russian)* 77−55997
steel, large forging, mech. props. 77−4797
steel, law-C, hot deform., austenite strengthening and weakening 80−76282
steel, low alloy, high strength, residual stresses during low cycle fatigue 79−29201
steel, low alloy, hot deform. behaviour and modified ausforming *(Japanese)* 78−11244
steel, low alloy composite, ferrite-carbide struct., cold plastic deform. 77−90408
steel, low C, carburizing, hot plastic deform. effects 77−90377
steel, low C, crack propagation energy rel. to temp., time factors 79−29179
steel, low C, effect of heat treatment on resistance to fatigue crack propag. 80−11675
steel, low C, hot rolled and cold deep drawn, nonmetallic inclusion distrib. in microcavities *(Russian)* 79−52265
steel, low C, hot rolling effects on struct. *(Russian)* 78−19793
steel, low C, low alloy, ferritic-pearlitic, high temp. mech. treatment, cooling effect 80−104193
steel, low C, Mn, recrystallisation and grain growth in hot rolling 79−47714
steel, low C, Mn, strain hardening parameters, electron microscope obs. 77−63690
steel, low C, Mn effect on recrystallisation and texture *(French)* 80−3110
steel, low C hot rolled sheet, drawability improvement by Al addition *(Ukrainian)* 79−78996
steel, machining, 12L14, effect of Pb and Te on hot-shortness mechanism 80−104190
steel, maraging, effect of deformation on props. 80−21032
steel, maraging, hot work die use, mech. props., heat resistance 77−70081
steel, martensitic, low C wire, strain tempering by rapid heating *(Japanese)* 78−31428
steel, medium C, Mn, type 42Mn2 cylinders, flake immunisation by hot working *(Chinese)* 80−66540
steel, medium C, Nb addition, effect on transformation and strength 80−7607
steel, medium C 80−11752
steel, microalloyed, hot-rolled, Nb(C,N) precip. and austenite recrystn. 80−97513
steel, microalloyed, types V1599, V1600, V1286, NbCN precipitation in undeformed austenite 80−89230
steel, microhole working by laser irrad., accuracy increase *(Russian)* 80−55434
steel, Mn-V reinforcing type, strain ageing characts. rel. to mech. props. 80−84969
steel, Nb,(V),(Al), hot-rolling, laboratory simulation, recrystn. of austenite 80−97512
steel, Nb, controlled-rolled into ferrite temp. range, soln. temp. and rolling effects 80−11678
steel, Ni-Co-Mo-Ti, hot formed, recrystallization and grain boundary precipitation effect on mech. props. *(German)* 79−66073
steel, nonmetallic inclusion, effect on hot ductility 80−29999

hot working continued
steel, plastic, thermally strengthened, not prone to H_2 embrittlement, prod. *(Russian)* 79−52267
steel, plastic deform. resist. during continuous hot rolling *(Russian)* 80−55462
steel, plastically deformed, force and speed criteria interactions during hot rolling *(Russian)* 80−55463
steel, plasticity of grooved specimens at high temp., rel. to hot forming 78−23902
steel, plate, thickness and rolling ratio influence on inclusion behaviour 80−16340
steel, process induced matrix inclusion separation 77−28818
steel, rare earth additions, effect on physicomechanical props. 77−12639
steel, ShKh15, carbide particle size and pearlite grain size changes *(Russian)* 78−6946
steel, Si, nonoriented sheet prod. with texture of {100} (ovw) 80−89246
steel, Si (3 wt.%), hot rolled, effect of initial texture on secondary recrystallisation *(Czech)* 79−91711
steel, stainless, 304, deformed in torsion, annealed, static recrystallization and restoration after hot deform. 79−47735
steel, stainless, Cr (17 wt.%), recrystallisation texture, effect of N *(Japanese)* 79−4978
steel, stainless, duplex, hot ductility and fracture mechanism 78−60731
steel, stainless, hot rolled texture, effect on cold rolled and annealed textures *(Japanese)* 78−48425
steel, stainless, hot rolling resist., multistage mode of deform. effects *(Russian)* 78−80583
steel, stainless, Kh18N10T, struct. and mechanical props., effect of previous deform. in rolling *(Russian)* 79−29099
steel, stainless, martensitic, crack resistance of type VNS-2, heat treatment effects 79−100196
steel, stainless, tempering after air hardening from rolling heat *(German)* 80−93571
steel, stainless austenitic, low alloy 316, high temp. plasticity, B addition effects *(Russian)* 77−28852
steel, stainless Cr (17 wt.%), hot rolled sheets, martensite distrib. effect on ridging phenomena 79−1887
steel, structural, 35KhN1M2F, forgings, struct. inheritance during ht. treatment 78−23735
steel, thermally and thermomechanically treated, struct. and decomposition of martensite 78−19784
steel, thermomechanical treatment effect on mech. props. and microstruct. *(French, German)* 79−66090
steel, transformer, texture formation tendency *(Russian)* 77−59803
steel, two-phase austenitic-ferritic, plastic deformation under hot working conditions 77−48466
steel, type 34Cr4, post-hotforming recrystallisation condition, use of NEOPHOT 2 and EPIQUANT 80−84949
steel, types 15Kh2NMFA and 45, fatigue tests, low cycle, material variance distrib. law 79−91799
steel, V, high C, faceted Mn sulphide formation on crystn., thermomech. treatment effect on dendritic struct. *(Russian)* 80−50621
steel, W-Mo, high speed, hot deform. and heat treatment effect on props. 77−90372
steel alloy, austenite transformation in hot rolled strips 80−55407
steel plates, hot rolled, anisotropic texture, exam. of elastic deformation behaviour *(Japanese)* 78−64586
steel spheroidised type AISI 1090, hot rolled H_2 promotion of plastic instability 78−60725
steels, hot forming property and struct. *(German)* 80−25730
steels, hot plastic strain, stress- strain-time dependences *(Russian)* 80−40430
steels 45, 17G2AF, 55S2, 60S2, faceted Mn sulphide formation on crystn., dendrites *(Russian)* 80−50621
steels 4Kh4VMFSSh and 45Kh3V3MFSSh, grain size, hot deform. and austenitising effects 80−76286
β-III Ti alloy, powder compacted by hot swaging, tensile and toughness prop. 79−38764
Ag-Ga (27 at.%), cooling rate depend. of thermal arrest, transform. temp. 79−29053
Al alloy, AK4-1, hot-worked, struct. states and recrystn. *(Russian)* 78−19778
Al alloy, dil., recrystallisation during hot rolling 79−47732
Al alloy, ductility effects during plastic deform., rel. to struct. changes and hot forming 78−23770
Al alloy, recrystallisation during hot deform. and after cold working 79−47715
Al alloy 7050, fatigue, effect of intermediate thermomech. treatments 79−8352
Al alloys, preliminary forging effects on struct. and mech. props. of extruded sections *(Russian)* 78−80564
Al alloys, thermomech. treatments, effects on microstruct. 80−100858
Al and Al alloy granules, hot rolling, angle parameters and forward slip 80−25601
Al, atomized powder, metallic contact for hot rolling in air 77−73294
Al billet, hot extrusion, nonsteady state temp. distrib., numerical method 80−60886
Al, orientation distribution function determ. using one pole figure *(German)* 77−25242
γ'-Al-Ag (15 wt.%), dislocation splitting mechanism, cessation above critical temp. 78−26572
Al-alloy plates, type VAD23, thermomech. parameters effect on struct. and props. 80−20988
Al-$CuAl_2$ eutectic, deformed, thermal stability 77−52348
Al-Cu(Si)(Zn)(Mg)(Cr), recrystallization texture 79−91679
Al-Mg (4 wt.%), struct. and strengthening in hot working 80−84968
Al-Mg-Si, effect of quenching on recrystn. after hot working 79−43289
Al-Mn(Cu)-Zr, particle stabilized structures, hot deform. 79−47733
Al-rare earth alloys, granules, rolling to form foil, exam. 80−20825
B fibre reinforced Al alloys, hot compression moulding, optimum parameter calc. by pipe piercing *(Russian)* 79−66027
B fibre reinforced Al-Zn-Mg, packet rolling, thermodeform. process parameters *(Russian)* 80−55433
n-$Bi_2(Te,Se)_3$ semiconducting solid solns., plastic deform. during hot extrusion 79−20143
p-Bi_2Te_3-Sb_2Te_3 semiconducting solid solns., plastic deform. during hot extrusion 79−20143
Cd-Zn (1.5 wt.%), warm worked, effect of grain size, texture, on mech. props. 79−4988
Cr-Sm-Pr, Sm and Pr additions and plastic deform. effects on texture *(Russian)* 77−55983

hot working continued
Cu, grain refinement of dynamic recrystallisation during hot working *(Japanese)* 77−52345
Cu, polycrystalline, recovery and recrystallization after hot working 79−91661
Cu, polycrystn., strain localisation during hot deform. 80−104195
Cu, rolled at room temp. and 200°C, variation in props., hardness and X-ray meas. *(Russian)* 77−73285
Cu wire rod, rolling temp. effects 77−70084
Cu, wires, effect of heat treatment during drawing 78−56659
Cu-Al (4.5 at.%), alloy, dislocation recovery anomalies *(Russian)* 77−21163
Fe and Fe-C, (0.8 wt.%), sintered, hot forging ahd chemicothermal treatment, effect on wear resistance 80−25606
Fe, Armco, dislocation struct. after hot and cold rolling *(Russian)* 77−8847
Fe, cast, white, graphitisation, effect of hot impact deform. 78−19780
Fe, powder preforms., hot consolidated rolled strip, mech. props. 78−15338
Fe-Al, hot- and cold-rolled, texture form., pole figures method *(Russian)* 80−45317
Fe-C (0.64 wt.%), quasicleavage during fatigue crack propag., pearlitic microstruct. effect 79−11702
Fe-Co-Ni-Al-Nb (15-20, 14, 9, 0.1-5.5 at.%), Nb effect on magnetic props., lattice parameter *(Russian)* 77−55689
Fe-Co-Si (4,1.5 wt.%), textured, mag. props. 80−35200
Fe-Mn, warm rolled, rel. contribs. of texture and grain shape to props. 79−91705
Fe-Nb-C (0.04, 0.02 wt.%), strengthening, hot rolling *(Chinese)* 79−100154
Fe-Ni (15, 25 at.%), longitudinal forces in the hot torsion test *(German)* 79−38889
Fe-Ni heterogeneous alloys, ferrite, martensite and austenite phase distrib., effect on mech. props. 80−45363
Fe-Ni-C (19.5, 0.73 wt.%), banded struct. formed by deform., TEM and optical obs. 78−39869
Fe-Ni-Cr-Mo superalloy, mech. props., η-phase form. effect *(Chinese)* 80−20925
Fe-Si (3 wt.%), chemical comp. and hot rolling effect on brittleness *(Czech)* 80−50712
Fe-Si (3 wt.%), cube-on-edge oriented, high permeability, mill processing and mag. props. 77−86045
Fe-Si (3 wt.%), hot rolled sheet steel, ductile-brittle transition temp. *(Chinese)* 78−31498
Fe-Si (3 wt.%), orientation development during secondary recrystallisation, primary matrix effect, magnetic props. *(Czech)* 78−60679
Fe-Si (3 wt.%), texture form., plastic strain effect, hot rolled 79−79002
Fe-Si (3.1 wt.%), solubility product of BN 79−10955
Fe-Si (6.5%) alloy, struct. and rolling texture 79−79006
Fe-Si-B, high induction, hot rolling treatment 80−89266
Fe-Si-MnS-Al, Al effect on hot rolling struct., recrystallization, texture magnetic props. *(Chinese)* 78−11237
FeAl-Pr (16 wt.%), tape recorder mag. heads, resist. depend. on temp. and hot rolling *(Polish)* 80−39555
$Fe_{40}Ni_{40}P_{14}B_6$, Metglas 2826, hot forming 80−84980
MO-B, B effects, rolled, segregation of implanted elements, Auger spectroscopy exam. *(Russian)* 78−35389
Mg, recrystallisation after straining by rolling, −25 to 100°C *(French)* 77−59815
Mn-Al-C alloy, anisotropic, permanent magnet appl., properties and production *(German)* 79−8309
Mo, microhole working by laser irrad., accuracy increase *(Russian)* 80−55434
Mo sheet, 45° brittleness due to partial recrystallisation, 45° crack formation and propagation *(Russian)* 79−100238
Mo-V-C, hot-worked, substructural hardening and high-temp. strength *(Russian)* 80−25731
$Nb_3(Al, Ge)$, effect of thermal treatment on superconducting props. 79−61016
Nb_3Al tape, effect of thermal treatment on superconducting props. 79−61016
Ni alloy, KhN55VMTFKYu, produced by powder metallurgy, hot worked, short- and long-time strength 77−28752
Ni alloy, recryst. after hot deform. *(German)* 80−25716
Ni, Ni-Ti (1 wt.%), serrated yielding, 77 to 723K 77−32649
Ni, sintered carbonyl type and with dispersed ZrO_2 inclusions, struct. effect on high-temp. ductility 77−63757
Ni-based alloys, binary, ternary, complex, TiC additions, effects 78−92305
Ni-based superalloys, hot workability, effect of S, Ca, Mg, Y and Zr minor elements 80−66552
Ni-containing alloys, hot workability after reheating using S-containing fuel 80−108483
Ni-Cr-Co superalloy IN-792, crack growth resistance, metallurgical effects 77−36655
Ni-Cr-HfO_2, dispersion-strengthened, hot rolling effects on props. *(Russian)* 77−59797
Ni-Cu (30 wt.%), cast cold- and warm-worked, recrystallization 79−29092
Ni-HfO_2 (3 wt.%), dispersion hardened alloy VDU-2, thermal and mech. treatment 77−90376
Ni-Nb(-Cu)-C, NbC dispersed supercond. tapes, fabrication and characts. 78−19773
steel, C, eutectic, YU8, effect of segregating structurally free ferrite *(Russian)* 79−15677
steel, Nb, deform., recrystn. and precip. interaction 80−97515
Ti alloy, hot deform. *(French)* 77−52371
Ti alloy, VT22, thermomechanical treatment, effects on struct. and props. *(Russian)* 78−19785
Ti, crystalline orientation distribution analysis of texture development 79−91669
Ti, hot-rolled, anisotropy of Young's modulus calc. *(Russian)* 78−23749
Ti-Al (6.1 wt.%), hot rolled sheet, ductile fracture nuclei, SEM obs. 78−64654
Ti-Al-V-Sn(Mo-Fe), heavy section extrusion, fabrication and mech. props. 78−6985
β-Ti-Mo-V-Fe-Al (8,8,2,3 wt.%), metastable, high cycle fatigue crack initation, grain size effect 77−86145
Ti-Nb-Zr-Fe-Mo-V, cold worked, struct. and phase transform. during ageing 78−3153

hot working continued
Ti-Ni-Cu (44.5, 10 wt%), opposing stress effect on shape memory and martensitic reversion 78−44185
W fibres, dependence of fine struct., on processing parameters 79−34082
W sintered rods, hot rolling with four roll passes, effect on struct. and mech. props. 79−100195
Y_2O_3-TiB_2, ceramic, production by sintering in vacuo, or hot moulding at 1500°C 78−60629
Zn, hot rolled, grain boundary fine structures, TEM exam. 78−76680
Zn, plasticity under hot deform. conditions, temp. depend. *(Russian)* 79−29133

household appliances *see domestic appliances*

hovercraft
acoustic noise, design problems 80−74598
ship hydrodynamics, drag on displacement ships, hydrofoils, hovercrafts 78−63423
tracked high speed traffic, levitation methods 79−49011

Hubbard model
actinide compounds, electronic configurations correlation 80−6385
actinides, electronic struct., Hubbard's alloy approx. 79−73665
alloys, magnetisation calc. method based on moments of density of states 80−65770
alloys, substitutional, disordered, with strong electron correl., elec. cond. 77−62885
amorphous semiconductors, covalent, localised electronic states, Hubbard model calcs. 77−89732
amorphous system, theory of electron localisation 77−1391
Anderson model, orbitally degenerate, exchange coupling in atomic limit, rel. to two-site Hubbard model 80−108000
anfiferromagnet, superexchange, charge transfer light absorpt. 78−34975
antiferromagnet, electron struct. in mag. field *(Russian)* 78−60287
antiferromagnetic extended Hubbard chain, excitonic effects on optical absorption 79−61323
antiferromagnetic ground state 79−82742
antiferromagnetic Hubbard chain, interband absorpt., Peierls dimerisation, excitonic effects 80−25072
antiferromagnetic ordering onset, alloy, analogy approx. 77−36049
antiferromagnetic semiconductor, collective excitations, weak coupling limit 78−19210
antiferromagnetic semiconductor, electron correlations, weak coupling 78−67969
antiferromagnetic structure, effects of four spin interactions 77−51885
antiferromagnetism in half-filled s-band 77−63070
antiferromagnetism itinerant electron theory, spin susceptibilities 78−6504
antiferromagnetism onset 78−19206
arbitrary electron density case, functional integral approach 78−76219
benzene, noncrossing and degeneracy in Hubbard models 80−14096
binary alloys, disordered, electron-electron correl, T-matrix approx. 79−78026
binary ferromagnetic alloys, with itinerant electrons, magnon lifetime, theory 78−34949
t-butyl derivatives, liq., reorientational correlation times, Hubbard model 79−61353
canonical perturbation expansion 79−38296
chain, modified Hubbard, solitary solns. derived step-by-step 80−10849
charge and orbital ordering in crystals 78−34738
charge density waves *(Russian)* 79−65395
charge density waves *(Russian)* 79−65396
charge ordering in generalised model 80−39513
charge ordering in localised state, critical temp. 79−69456
charge-ordered ground state in half-filled Hubbard model 80−39487
charge-ordered solution within alloy analogy approx. 77−39759
charge-transfer organic salts, strongly correlated, interband absorpt., long-range Coulomb interaction 79−4525
chemical potential of Hubbard model, T=0 80−107685
cluster-variation method in two-site approximation to Hubbard model at high temp. 80−7071
computer renormalisation-group technique 79−19716
conductivity and characteristic temp. 77−32150
conductivity at low temp. in narrow half-filled Hubbard chain 78−47755
correlation effects in hopping transport theory, general relns. *(Russian)* 78−14734
CPA treatment, degenerate d-band, two sublattice alloy analogy method 78−19208
cyclobutadiene, noncrossing and degeneracy in Hubbard models 80−14096
degenerate, charge-ordered soln. 78−39284
degenerate in mag. field, appl. to Jahn Teller systems 77−28358
density of states and damping calc., applic. to disordered alloys 77−51874
diatomic molecule, electron correlations, cryst. field interactions, Hubbard calc. 80−75530
dielectric function, strong correlation limit 78−87929
dielectric function of 1-dimens. Hubbard model 79−60740
disordered alloy, electron correl. in Hubbard model, and spin susceptibility 77−76762
disordered alloy, electron correls. and ferromagnetism 78−43548
disordered linear chain, exchange probability distrib. 78−10641
disordered local moment state 78−95414
disordered one-dimensional system 78−10642
disordered quasi-one-dimensional materials, review 78−6361
disordered quasi-one-dimensional systems with electron correlation, electronic properties 78−87966
disordered system, elec. cond. Coulomb interaction influence and calcs. 79−60778
doubly degenerate, CPA alloy analogy 77−32151
doubly degenerate, functional integral approach 79−99711
doubly degenerate, long range order 80−50029
doubly-degenerate Hubbard model, elec. cond. calc. 77−20284
dynamic electric and magnetic susceptibilities near metal-insulator transition, functional-integral method 77−28119
electrical conduction in single narrow energy band 77−1400
electrical conductivity calc. including electron-phonon interactions 77−47804
electrical conductivity calculation, dielectric function and plasma oscillations 78−64020
electrical conductivity in strong-coupling non-half-filled band Hubbard model 78−43348
electron correlation, self consistent theory in Hubbard model 79−60673
Hubbard model continued
electron gas, Hubbard model at low temp., mag. props. *(Russian)* 78−43550
electron transfer, intramol., electron propagator method 77−34560
electron-hole pair, Nagaoka's theorem, appl. to excitonic spin polarons in Mott insulators 80−107978
electrostatic interaction Hamiltonian, tensor struct. *(Russian)* 78−76216
equivalence of d-dimens. Hubbard model to (d+1)-dimens. classical problem 77−47706
equivalent spin Hamiltonian, for phase transition studies 80−80474
exchange interaction, kinetic, in narrow S-band 77−55655
extended Hubbard model, ferromag. solns. 80−80473
extended model Hamiltonian, phase transitions 78−6531
extrinsic semiconductors, impurity interaction and metal-nonmetal transition 80−29325
extrinsic semiconductors, negative magnetoresist., Hubbard model *(Russian)* 78−47816
Falicov-Kimball model, intermediate soln. 79−47015
FCC antiferromagnet, fourth order interaction effects 78−23235
FCC lattice, mag. and elec. props. 78−56334
Fermi liquid theory of effect of spin fluctuations 77−62853
ferromagnet, disordered itinerant-electron, spin waves 78−95427
ferromagnet, itinerant, spin waves, surface effects, RPA calc. 80−60226
ferromagnet, itinerant electron, surface spin waves, tight-binding Hubbard model 80−39763
ferromagnet, tight binding model, surface magnetisation 80−103807
ferromagnetic binary alloys, narrow-band with random hopping, spin wave stiffness const. 79−56524
ferromagnetic instability in two-band Hubbard model 79−1653
ferromagnetic metal, exciton condensation effects on props., Hubbard model 80−60171
ferromagnetic phase transition 77−77062
ferromagnetism, basic models, classification of theories *(Rumanian)* 78−91840
ferromagnetism, Hubbard model, mag. susceptibility, modified Stoner criterion 79−51736
ferromagnetism in degenerate Hubbard model 77−69479
ferromagnetism in narrow S-band with inclusion of intersite correlations 77−63066
finite disordered Hubbard cluster, thermodynamic and mag. props. 77−85409
free lattice electron gas with nearest and second nearest neighbour hopping 78−51873
functional derivative study, perturbation method and first-order approx. 77−43465
functional derivative study, self-energy correction, self-consistent eqn. and complete soln. 77−43466
functional Fourier transform 80−84416
Green's function, functional-derivative study 80−75483
Green's function determ. using group theoretical diagram method 77−62791
ground state energy, using degenerate perturbation theory 78−18938
ground state energy and total spin on 2×2×2 lattice 80−29518
half-filled, ground-state energy and momentum distrib. 77−47961
half-filled, mag. couplings 78−52192
half-filled band, local field correction to plasmon freq. 80−24823
half-filled-band Hubbard dimer, dimerized, and uniform Hubbard chains, thermodynamic and correlation functions 78−6249
Hall and Verdet coeffs., conc. depend., Green function method 80−80240
hamiltonian, correlated motions 77−72982
Hamiltonian, coupled spin and charge fields 77−32147
hamiltonian, functional formulation, symmetry props. 79−47225
Hartree-Fock band theory, Mott-Hubbard condition for electron localisation 79−73417
Heisenberg spin systems, absence of mag. phase transitions, Hubbard identity calcs. 78−34992
Holstein-Frolich modified one-dimens. half-filled band Hubbard model, transport props. 78−23237
hopping conduction, correl. effects 77−89762
Hubbard model, half-filled, charge ordered solution local mag. moments, repulsion energy renormalisation 79−61034
hybridised model, absence of ferromagnetism 80−39731
indirect exchange interaction through narrow conduction zones *(Russian)* 79−4538
insulator-to-metal transition for half-filled Hubbard band in paramagnetic state 80−92817
interacting many-level system, thermodynamics, from RPA Green's functions 78−43549
intermediate valence, mag. susceptibility and mag. instabilities 80−39532
intra-site vibration effects on elec. cond. in disordered Hubbard model 80−107775
intraband absorption in low-density Hubbard chain 77−24809
intramolecular electron transfer rate, purely electronic effects, simple model Hamiltonian 77−10592
Ising model, random, in transverse field, CPA approach 77−36040
itinerant antiferromagnetism, antiferromag. instability and energy gap 78−31044
itinerant antiferromagnetism, s-band Hubbard model, zero temp. props. 77−4493
itinerant antiferromagnetism 78−91841
itinerant electron paramagnets, coupled charge and spin fields 77−72991
itinerant ferromagnet, effect of planar defects on electronic struct. and mag. ordering 79−99672
itinerant ferromagnet, spin wave stiffness const., electron correl. effects 79−19733
itinerant magnet with unmag. electron bands, phase diagram 79−91202
itinerant magnetic-systems, general alloy analogues 77−85410
itinerant-electron ferromagnetic film on nonmagnetic metallic substrate, mag. props. 80−20371
kinetic exchange interaction, doubly degenerate narrow bands 78−23263
lattice gas, thermoelectric power in half-filled bands 79−60859
linear chain, disordered, arbitrary filling cases 78−31043
liquid metals, theory combining lattice gas model and Hubbard model 77−69220
magnetic instabilities, influence of short-range correlation effects 79−7963
magnetic insulators with Jahn-Teller ions, temp. depend. of exchange integrals 80−103827
magnetic material, conduction electron-localised electron interaction mechanism 77−59377

Hubbard model continued
magnetic phase diagram 78−80119
magnetic phases, nearest and next nearest neighbour hopping in Hartree Fock approx. 78−52189
magnetic solutions of Hubbard model, Hartree-Fock approx. 78−52195
magnetic susceptibility of strongly correlated electrons, calc. 80−25069
metal, one-dimens., electron interaction effect on Peierls instability *(Russian)* 79−51490
metal-insulator interface, Hubbard model, possibility of insulator-metal transition 78−52084
metal-insulator interface region, band gap closure in insulator 80−11086
metal-insulator transition, anharmonism effects 78−56072
metal-insulator transition, Hubbard model, Poisson approx. to functional approach 80−96790
metal-insulator transition, model Hamiltonian 80−34361
metal-insulator transition based on generalised Hubbard model, appl. to TCNQ-NMP 78−18966
metal-insulator transition due to electron correl. 77−11854
metallic phase transitions, interaction between two Hubbard bands as mechanism 77−85148
metals, cubic, intra-atomic correl. energies with canonical d bands, Hubbard interaction calc. 80−39518
metals, electron-deformation interaction, lattice contraction, Hubbard model calcs. *(Russian)* 80−59592
metamagnetic dielectrics, at finite temp. *(Russian)* 78−88118
mixed valence state, electronic structure, spin-orbit interaction effects, mag. susceptibility 80−54657
mixed valence systems, Hubbard regime, at. and nearly free state hybridisation 80−44546
Mott insulator, magnetism and charge ordering 79−60751
Mott magnetic semiconductor, freq. depend. elec. cond. 77−11907
Mott metal-insulator transition, ten-fold spin-orbital degeneracy 78−52285
Mott transition, mag. field effect 78−34748
Mott transition criterion within Hubbard model, mag. field effect *(Russian)* 77−28120
Mott transition in Hubbard long range model, isostructural instability, thermodynamic props. *(Russian)* 80−65454
Mott transition in the multidimensional Hubbard model *(Russian)* 79−28282
Mott transition in the presence of impurities, Hubbard model and SCF anal. 80−10878
Mott transitions, temperature induced, Hubbard model theory 80−29326
Mott-Hubbard insulator, one-dimens., charge transfer absorpt. 79−37958
narrow band systems, momentum distrib., cluster var. method 78−72060
narrow-band region, quasiparticles, electron relax. and transport props. 80−80151
narrow-band solids, Hubbard Hamiltonian, derivation from many-body Hamiltonian 79−56112
Nesbet equation for molecular calculations, appl. to Hubbard model 80−87029
neutral, appl. of information theoretical model to metal-insulator transition 79−47014
neutral, strong-coupling props. 77−24667
NMP-TCNQ, magnetic susceptibility and chem. pot. of two-site Hubbard Hamiltonian 77−47963
NMP-TCNQ, partial charge transfer effect, one dimensional disordered Hubbard model study 80−70687
off-diagonal long-range order 77−28118
one dimensional conductors, Fermi gas model, reviews 79−78083
one dimensional Hubbard chain, optical spectrum 78−10920
one-dimensional, correl. functions *(Russian)* 77−31929
one-dimensional, elementary excitation with complex wave vector 80−75783
one-dimensional, extended, $2k_F$ and $4k_F$ correl. functions, computer renormalisation group calcs., appl. to one-dimens. conductors 80−54625
one-dimensional, half-filled, ground-state energy calc. 80−39488
one-dimensional, with nearest and second nearest neighbour hopping in Hartree-Fock approx. 77−32149
one-dimensional $2k_F$ and $4k_F$ correl. functions, computer renormalisation-group calcs. 79−78029
one-dimensional charge transfer conductors, press. effects on mag. props., review 78−6505
one-dimensional conductivity, theory 78−10422
one-dimensional Fermi gas, energy gap, boundary conditions for renormalisation-group eqns. 78−10317
one-dimensional Friedel oscills. around a nonmagnetic impurity 80−25073
one-dimensional homonuclear molecular systems, nature of energy gap 79−11063
one-dimensional Hubbard model, antiferromag. and Peierls instability 78−23233
one-dimensional system, correl. functions, limiting relationships 77−62790
one-particle spectrum, correlated electrons, free-electron limit 78−23005
optical absorpt., half-filled Hubbard band, strong coupling 77−59546
optical absorption spectra of extended Hubbard model with two-lattice-site Coulomb interaction 77−20812
optical conductivity, strongly attractive chain model 78−79915
paramagnet, electron state density for narrow-band model with Coulomb interaction 80−10852
paramagnet, narrow-band with strong Coulomb correlations, electron. sp. ht. *(Russian)* 80−103487
partly filled narrow band, electron correlation and mag. props. 78−67968
Peierls transition, electron-spin coupling, relative importance 79−28280
Peierls-Hubbard model, antiferromag. and lattice-distortion 77−47964
Peierls-Hubbard model, antiferromagnetism and lattice distortion 77−55656
periodic Anderson Hamiltonian, alloy analogy treatment for mixed valence states 80−75527
phase transition due to CDW *(Russian)* 79−4526
phase transitions, low-temp. 78−72359
phase transitions in Hubbard Hamiltonian 77−85462
photoemission spectrum, effect of electron correlation 79−78828
quantal spin system, classical representation and scaling props. of spin Hamiltonians 78−14919
quasi-one-dimensional system, first and second order phase transitions, qualitative theory 78−31086
quasi-particle energy in weak correlation regime 79−28305
Hubbard model continued
quasione dimensional Peierls-Hubbard model, antiferromagnetism and Peierls distortion 78−67931
random, coherent ladder approx. 77−62799
random Hubbard alloys, paramag. susceptibility singularities, derived from Fermi liquid approach 78−43547
random one-body approx., higher dimens. lattices 79−37945
random one-body approx., one-dimens. case 79−37944
random one-body approximation, formalism 79−37943
random one-body approximation, mag. interactions 78−23236
rare earth metals, electronic struct., Hubbard's alloy approx. 79−73665
rare earth-transition metal alloys, amorphous, Hubbard hamiltonian, mag. props. 77−72985
self consistent many-body theory, appl. to spin waves in itinerant ferromagnets 79−73702
self-consistent approximation 77−28357
semiconductor, doped, Coulomb repulsion term in Hubbard model for impurities 79−42492
semiconductor, doped, impurity band density in atomic limit 80−107735
semiconductor, doped, metal-insulator transition, anal. 80−88478
semiconductor, magnetic phase transitions in impurity band *(Russian)* 80−50097
semiconductor, magnetoresist. in narrow energy bands, Hubbard model 77−32029
semiconductor, three-impurity clusters, ionisation energies and electron affinities 80−65496
semiconductors, doped, shallow impurity states, Hubbard bands and donor excitonic states, HF calc. 80−100443
single band, magnetic phase diagram, cluster variational calc. 80−60340
single band with infinite repulsion on 2×2×2 lattice, thermodynamic props. 79−87225
single site approximation 78−2643
small extended Hubbard rings, thermodynamic props. 80−2546
solid solution, vol., electron correl. effect 77−28133
solitons in a one-dimensional modified Hubbard model 78−87895
spin susceptibility for itinerant electrons with energy dependent effective interactions 78−19209
spin-Peierls dimerised Hubbard chain, optical absorption spectrum 79−60677
spin-Peierls transition in Heisenberg Hubbard models 78−68242
spin-wave excitations in narrow s-band, including intersite exchange interactions 77−16033
split-band solution and energy gap, narrow-band region 80−75484
strong correlated system, single particle Green's function calc. of elec. cond. 80−20142
strong coupling, electron dynamics 78−39342
strong coupling limit, molecular field theory, asymptotically exact variational approach 77−11836
strong ferromagnetic 3d alloys, electron correls. 77−40030
strongly correlated system, electronic transport 77−1401
susceptibility, high temp. series expansion 78−23239
symmetric Wolff model theory, weak coupling time low temp. limit 78−43318
system with two parameters, Mott and ferromagnetic transitions, phase diagram of the extended Caron Pratt model 79−15083
TCNQ, dimer gas model 78−87926
TCNQ complexes, elec. resist. and thermoelec. power meas. 80−107777
TCNQ salt, NMP-TCNQ, realisation of disordered Hubbard model, dielec. props. 78−79917
TCNQ salts, complex, with symmetric and asymmetric donors, transport and mag. props. 78−6315
TCNQ salts, sp. ht. meas., 0.2-300K, extended Hubbard model *(French)* 77−35710
TCNQ-K, dielectric function of 1-dimens. Hubbard model 79−60740
TCNQ-NMP, disordered, paramag. susceptibility 78−10645
TCNQ-NMP, metal-insulator transition theory based on generalised Hubbard model 78−18966
temperature induced antiferromagnetic-ferromagnetic phase transition, s-f two-band Hubbard model 80−60253
thermodynamic and correl. functions, field and temp. depend. 79−73666
thermoelectric power near atomic line 79−47086
transformations 77−72972
transition metal, chemisorpt. of H, Hubbard-type surface mol. model binding energy calcs. 78−71990
transition metal alloys, disordered, density of states, elec. cond., extended Hubbard model 79−37948
transition metal alloys, disordered ferromag., spin wave stability 80−70994
transition metal alloys, spin glass behaviour, simple itinerant model 78−84436
transition metal alloys, temp. depend. of asphericity of mag. moment distrib. 77−20538
transition metal borides, narrow band types, electronic density of states, many-electron Hubbard model calcs. 80−20064
transition metal oxides, sulphides, and selenides, Mott transition electronic and mag. phase diagrams 78−51894
transition metal surface, spin fluctuations 78−95451
transition metals, band struct., parametrisation via Hubbard's scheme 77−31938
transition metals, correlation effects, perturb. treatment within Hubbard model 80−70582
transition metals, correlation effects, perturbation treatment 80−59897
transition metals, energy of cohesion calc., Hubbard Hamiltonian with exchange interaction 77−69261
transition metals, partial resonance, Hubbard's theory of phase shifts 79−28264
3d-transition-metal dichalcogenides, mag. props. rel. to Hubbard model 79−78373
TTF-TCNQ, enhancement of mag. susceptibility by Coulomb correlations 77−77023
TTF-TCNQ, spin waves, scatt. at $4k_F$, spin-Peierls fluctuations 78−72093
TTF-TCNQ and related cpds., magnetic props., press. effects 77−47981
TTF-TCNQ electronic props., PMR 78−2763
TTT-$(I_3)_{0.5}$, one-dimens. metal, mag. susceptibility, elec. resist., thermopower meas. 78−87967
two band extended model, mag., orbital and charge ordered states 78−27012
two dimensional periodic lattice, electron ordering, CDW-disordered state transition, Hubbard model *(Russian)* 80−6754
two-dimensional systems, phase transitions 78−68241

Hubbard model continued
two-point doubly degenerate, in half-filled case, thermodynamics 77−4492
two-site extended Hubbard Hamiltonian with arbitrary electron density, mag. susceptibility 79−38297
two-site Hubbard Hamiltonian, half-filled band, thermodynamic props. 77−24505
two-site model with orbital degeneracy, thermodynamic props. 80−2545
valence bond theory of narrow band conductors 80−24777
variational method for ground state energy calc. 77−62788
Ward identities, particle number conservation, analytical structure of self energy 78−79913
Co, ferromag., HCP, electronic struct. calcs., band props. 78−39012
Co, ferromag., HCP, electronic struct. calcs., mag. hyperfine field 78−39080
Co, ferromag. HCP, electronic struct. calcs., cohesive energy and exchange splitting 78−34791
$DyCo_{3.4}$, amorphous, mag. props., Hubbard Hamiltonian 77−32177
Fe, theory of magnetism 79−78299
Fe-V alloys, BCC, ferromag., polarised neutron diffr., appl. of multiband CPA theory 77−77033
Fe_3 magnetism, randomised exchange field theory 80−39733
hexamethylphosphoramide:Li glass, metallic condensation of Wannier-Mott impurity states 78−2420
La, ground state, two band Hubbard model, for almost mixed valence system 78−84171
$La_{1-x}Sr_xVO_3$, high-temp. transport meas., band model 77−11917
Ni complex, (1,4,5,8,9,12,13,16-octamethyltetradbenzporphinato nickel)$^{+\gamma}$ $(I_3^-)_\gamma$, atomic limit of Hubbard model and polarons 80−39860
Ni, correlation effects, perturbation treatment 80−59897
Ni, correlation effects, perturb. treatment within Hubbard model 80−70582
Ni, ferromag., exchange integral maximisation, neutron scatt. obs. and ten-fold degenerate Hubbard model comparison 80−71004
Ni, ferromagnetic state, energy bands, self-consistent calcs. 79−19509
Ni-Pd alloys, mag. props., average and local density of states, CPA calc. 77−59242
Ni-Pt disordered alloy, off-diagonal, T-matrix itinerant electron ferromagnetism calcs. 80−25067
Pd-Pt alloys, mag. props., average and local density of states, CPA calc. 77−59242
Rh, band structure calc., ground state and effects of change of volume 79−77994
Si:B(P), dislocated crystals, electron energy spectrum 78−14694
Si:P, heavily doped, degenerate electron gas, Friedman effect, review 77−20242
Si:P, impurity band states calc. in Hubbard model 77−8046
Si:P, impurity doped, electron lifetime and transport in upper Hubbard band 79−95452
Sm compounds, mixed valence, metals or small gap insulators, two-band Hubbard Hamiltonian 80−34399
VO_2, discontinuous metal insulator and spin dimerisation transition, Hubbard model 78−51893
VO_2, first principles calc. of intra-atomic correlation energy 79−23920
V_2O_3, 500 to 530K, magnetic susceptibility meas., high temp. transition, interacting Hubbard bands 78−39325
V_3Si, intra-atomic Coulomb interaction effect on band type of Jahn-Teller effect 79−78057
$ZrZn_2$, phonon contrib. to Stoner enhancement factor, ferromag. and possible superconductivity 80−25070

Hubble model *see cosmology*

Huckel molecular orbital calculations *see HMO calculations*

hue *see colour*

Hugoniot diagrams *see equations of state*

human engineering *see ergonomics*

human factors
see also biocybernetics; ergonomics; man-machine systems
acceleration tolerance, objective ultrasonic determ. method 78−3619
Australian climate, classified by thermal stress 80−31115
Chinese firemen, responses to noise 77−39157
climate trends in four cities of New York State, possible anthropogenic causes 80−105044
climatic stress on man, parameter recording and processing, math. method *(German)* 80−82047
clothing of Bedouins in hot deserts, why black robes? 80−40969
education, risk of dehumanisation 79−17155
experimental design and statistical analysis of data, measurement of period of simple pendulum 80−42017
head protective devices design, bioengineering considerations 78−11793
image transformations, picture processing algorithm 78−58939
land use, study via remote sensing 77−5349
lighting, physiology response of human eye *(German)* 78−8434
loss of contrast in visual tasks using a visual and physical photometer, aspects 79−9234
LWR power plant human errors 79−13459
man's influence on climate, conference, Manlo Park, California (1979 February 21 to 22) 80−62381
mental activity evoking pupil dilation, link with intelligence 80−61532
nuclear accident phenomena, human elements *(French)* 78−57084
nuclear material safeguard systems efficiency evaluation 79−85741
nuclear power, human factors, safety system problems and risk assessment 80−22968
nuclear power plants, human factors engineering 78−21711
nuclear power plants, operator performance and response time, stress degradation, Poisson model 80−63415
nuclear power stations, control rooms, human factors design approaches, improvement of man-machine interface, error reduction 80−63327
nuclear power stations, HTGR risk assessment, operator actions, event and fault tree anal. 80−63330
nuclear power stations, human operator errors, analytical model 80−63329
nuclear power stations, normal operation and emergency procedures, errors, safety, maintenance, working conditions 80−63328
O'Neill space colonies, motivation rel. to realisation prospects 77−87230
picture distortion ratings compared with objective error measures 78−44510
plant information measures selection criteria nuclear reactor monitoring appl. 79−41006
population exposure to air pollution, satellite-aided evaluation 79−92116

human factors continued
reliability and maintainability symposium, Los Angeles (1978) 78−50250
retinal image processing, two-channel model 80−94215
site selected variables effect on human responses to traffic noise 80−61491
site selected variables effect on human responses to traffic noise 80−61492
study methods, conf., San Francisco, USA (Oct. 1977) 78−48742
university entrants, cognitive level by Piagetian tasks 79−4
urbanisation effects on annual rainfall, stochastic anal. 80−98407
visual prosthesis design, human factors and electrophysiological considerations 78−53583
visual simulation and image realism, seminar, San Diego, USA (Aug. 1978) 80−3639
weather station operation, management practices on USAF stations 80−46215
windchill maps of lowland Britain, calc. from instantaneous data 80−61893

human-machine systems *see man-machine systems*

human relations *see social and behavioural sciences*

humanities
see also archaeology; art; history; language translation; linguistics; literature; music
astronomy of Hopi Indians, social and theological aspects 78−36472
Brecht's Galileo, changing perceptions of Galileo Galilei as scientific exemplar 80−51996
creativity model, alternating intuitive and rational critical phases *(French)* 77−9159
science and the humanities, The Two Cultures gap, teaching 80−41979
star of Bethlehem, possible triple conjunction of Saturn and Jupiter 77−13256

humidity
see also atmospheric humidity; hygrometers
aerosol centrifuge, calibration at unmatched relative humidities between stream and aerosol air 79−41775
aerosol particle growth and size distrib., humidity effects, effects on visibility 77−25321
air-condenser microphone, effects of humidity 77−84091
air-intake flowmeter using corona discharge principle for automobile engines, humidity compensation 80−33716
alkaline cell, creepage rate of electrolytes, effect of external relative humidity and moisture 79−61967
anemometry, hot-wire, influence of humidity changes 80−75007
ceramic bars, fired, high Al_2O_3, modulus of rupture, relative humidity depend. 80−40473
coating swelling meas. by real-time holographic interferometry 79−98316
composite insulating materials, fatigue behaviour, influence of superposition of elec., mech. and environmental stresses 80−97590
dielectric materials, complex, effect on elec. characts. *(Russian)* 79−42881
epoxy-graphite laminate creep behaviour humidity effects 77−66682
filters, humidity effect in flow resistance of loaded fibres 77−29451
glass on rubber rolling friction, humidity effect 79−79118
hexamethylolmelamine, doped, and condensation resin, room temp. phosphoresc., thermal transforms. 80−45132
hygroscopic particle size, air humidity depend., applic. to lung dynamics 77−90841
LMFBR, Clinch River, humidity effect on burning rate of Na droplets, Fick's eqn. anal. 78−13297
metallisation corrosion, IR microscopy failure anal. 80−98976
metals, indoor corrosion rates meas. 80−76404
mixed salt aerosols, phase transform. and droplet growth in moist atmosphere 79−52783
optical fibres, UV curable epoxy acrylate coated, long-term mech. behaviour effect on stress-free ageing 78−95802
organic solute evap. phase conc. estimation, from rel. humidity meas. 78−34614
polyamide fibre, chain-segment orientation, US vel. meas., humidity effects *(German)* 78−75590
polyester-E glass composites, types SMC-25, SMC-65 and SMC-30EA, moisture absorpt. 80−93799
polymer film, relax. mechanism of electret charge at high humidity *(Russian)* 77−63360
rubber glass-interface, propag. of cracks, effect of humidity 77−86133
sandpaper, standardised, for Taber abraser, influence of relative humidity an abrasive quality *(Japanese)* 79−8369
spark gaps, HV switching surges, influencing factors *(German)* 80−87958
stratification, effect on conditions for free convection *(Russian)* 79−10562
water-air interface, overall heat transfer coeffs., humidity and density profiles, turbulent pulsations *(Russian)* 78−22349
Al-As_2Se_3-Al, photographic process based on electrochem. reactions *(Russian)* 79−6213
BN films, elec. resist., depend. on relative humidity 79−4609
GaAlAs-GaAs DH laser diodes, long-life diodes for optical fibre communication 80−48246
HNO_3-water, homogeneous nucleation, relative humidity depend. 78−71846
H_2SO_4-water, homogeneous nucleation, relative humidity depend. 78−71846
$MgCr_2O_4$-TiO_2, porous ceramics, humidity-sensitive electrical conduction 80−107782
N_2, relaxation freq. depend. on water content 78−1058
NO_x, surface reaction on Cu, relative humidity depend. 79−5176
PbI_2, film, reflectance meas., optical consts., humidity effects 80−34994
^{220}Rn unattached decay products, diffusion coeff. depend. on ventilation and rel. humidity 77−9279

humidity control
air, air, relative humidity control, error comparison for various sensors, accuracy 77−10034
aspirator saturator, performance, dew point data of air *(Japanese)* 79−40580
ceramic humidity sensitive resistor device characts. and appls. *(Japanese)* 77−71332
creep testing, at const. temp., humidity, appl. to nylon-6,6 78−95883
fuel cell, H-O, with self-control of external humidity exchange, operation analysis 79−34429

humidity control continued
heat pumps, energy and environmental considerations in extending appls. 77−17976
semiconductor thermocamera, thermojunction method appl. *(Russian)* 78−45693
solar air conditioning with solid absorbents, earth and underground water cooling 80−72018
solar regenerator buoyancy effects, study 79−68709
system using saturated aqueous solution and gas mixture 80−4730
test chamber, convectively mixed, calibration appl. 78−54379

humidity measurement
see also hygrometers
air, above 100°C 78−226
air, air, relative humidity control, error comparison for various sensors, accuracy 77−10034
air, microwave refractometer using Fabry-Perot interferometer 77−18073
air and gas, metrological aspects *(Hungarian)* 78−37024
air enthalpy meas. by LiCl humidity sensors 80−90858
atmosphere, from effects on IR and microwave propag., optimization of conditions *(Russian)* 79−34898
atmosphere, mixing ratio meas. via two-balance direct method 77−73866
atmosphere remotely sensed from Earth orbit using microwaves 80−41573
atmospheric, integral, by means of passive radar 79−74991
atmospheric humidity profile, passive microwave profiling technique 80−21856
atmospheric meas. with standard hygrometer *(German)* 78−16194
biological exposure chambers, automatic system for monitoring temp. and humidity, microprocessor controlled 79−49239
boundary layer, eddy flux meas. made by powered glider 80−51509
capacitance humidity-sensing transducer 80−4729
capacitive dew-point sensor 78−81421
capacitive sensor Panahume *(Japanese)* 80−105658
ceramic humidity sensitive resistor device charcts. and appls. *(Japanese)* 77−71332
chamber, Oblako universal gas-water vapour generator, humidity test facility 80−62653
dew point hygrometer design 77−74410
dew-point hygrometers, automatic, condensate phase state determ. 78−8408
digital ventilated psychrometer, direct reading relative humidity meter using thermistors 79−2777
digital ventilated psychrometer for direct reading 79−35763
electro chemical hygrometer, direct reading *(Spanish)* 78−32254
electron microscopy, indirect meas. of relative humidity in side entry environmental stage 78−8480
electronic thermometer appl., dual 78−65925
environment protection when siting power station, temp. and humidity meas. methods *(French)* 79−12318
evaporative water loss meas. from small animals by dew-point hygrometry 78−20326
evapotranspiration meas., Bowen ratio precision 77−33122
fluidic frequency-analogue measurement system for extreme conditions *(German)* 79−97396
forests, Ge diodes for temp. and humidity profile meas. 77−64463
gases, noncorrosive, measurement using automatic microclimate testing and control system 79−67318
hair hygrometer, technique to linearise hair extension *(German)* 80−46284
high frequency hygrometry, modulated and unmodulated schemes, sensitivity analysis *(Russian)* 77−67444
Humiceram-III, ceramic sensor, multifunctional sensor to detect humidity and gases *(Japanese)* 80−105659
hygroscopic materials for humidity sensors, extension charcts. 78−41320
IC circuit meter 80−90857
industrial processes using hygroscopic materials *(German)* 80−101798
microwave moisture content-attenuation-voltage convertor with time-domain attenuation comparisons *(Polish)* 78−70131
multiple atmospheric parameter meas. laser radar system 78−4009
optical fibres, coated *(Japanese)* 79−59822
porcelain, neutron-retardation behaviour for continual moisture determ. *(German)* 80−105660
psychrometer, bimetallic, bulb wetting by saturated $MgCl_2$ soln. *(Japanese)* 77−87772
psychrometer, direct indication, of temp. difference and temp. type *(Japanese)* 79−40581
psychrometer, with grafted thermometer *(Japanese)* 80−31771
psychrometers, principles and improvement techniques *(French)* 77−78451
psychrometric determ. of relative humidity and dew point using microprocessor-based instrument *(German)* 79−29875
psychrometrics and industrial processes 78−41321
psychrometry, Lewis factor effect on accuracy *(German)* 79−12808
radioisotope instrumentation, industrial appl. *(German)* 77−70245
sensor based on thin film capacitor, Finnish development of meteorological instruments 79−12310
skin, using bridge cct. and digitally steered logic cct. 77−13018
soil, microwaves non-conventional appl. survey *(Italian)* 80−13093
sorption-gravimetric hygrometer, standard, description 77−87770
standards and calibration 79−49240
variable-path Lyman α hygrometer, operating charcts. 77−33194
wet-bulb temp. and moist air heat content meas. 80−52211
wood chippings, neutron technique for moisture meas. *(German)* 80−105661
BN films, humidity sensitive elec. props. and switching charcts. 80−107938
CO laser driven spectrophone, humidity trace detection in H_2 and air 79−20477
CO_2-N_2 mixture, shock tube, operating channel humidity determ., apparatus *(Russian)* 77−7057
LiCl heated electrical hygrometer, modified instrum. 80−95104
$LiNbO_3$ sensor for elec. hygrometer *(Japanese)* 80−95103
$MgCr_2O_4$-TiO_2 porous ceramic humidity sensors 80−86325

h.v. engineering *see high-voltage engineering*

hybrid computer methods *see hybrid simulation*

hybrid computers
analogue recursive computer 77−43321
ECG and EEG analysis 77−40842

hybrid computers continued
filtration simulation, use of electrically conducting paper with discretely distributed capacitance *(Russian)* 78−88850
hybrid computer for dye-dilution curves 78−40365
multidither adaptive optical system, 69-channel hybrid controller 80−33136
optical/digital processing systems, assessment 77−10853
optoelectronic devices, digital data processing, review 80−19106
real-time processing cardiological data 77−86677

hybrid integrated circuits
see also flip-chip devices; microwave integrated circuits
cardiac pacemaker, high-reliability hybrid IC procurement 80−30942
charge to time convertor, gated seven channel 78−13388
cm-wave radiometer, with enhanced long-term stability, for solar radio emission obs. 80−109361
cochlear implantable prosthesis realisation, hybrid technology 80−46099
digital NMR gaussmeter using hybrid IC 79−71501
dual registration channel cct. for proportional counters 80−23266
geothermal well logging instrumentation appls. for 300°C operation 78−3976
implantable 8-channel stimulation system for labyrinthine deafness *(German)* 79−16347
implantable systems for animal expts. 80−76887
IR/CCD focal planes, performance, appls. 79−3798
manufacture using natural and halocarbon waxes, thermoxidative stability 79−100271
microcircuit design, performance, geothermal well logging instrumentation appl., 79 96845
monolithic crystal filter 77−39171
optoelectronic modules for OEM fibre-optic data systems 79−86259
p-i-n/FET hybrid optical receiver for communication systems 80−33158
preamplifier, linear read out electronics for multiwire proportional counter 80−58091
quasimonolithic and hybrid integrated optical circuits on Si substrates 80−64218
rotatable microscope stage, used for hybrid microcircuits inspection 80−90889
soldered thick-film conductor, adhesion meas. technique 80−50811
thermal resistance calc. 77−84104
thick film, 300°C hybrid IC for geothermal well logging 77−73895
Al_2O_3 moisture sensor for sealed hybrid packages 77−87754
Au conductor bonding performance and failure mechanisms 79−71436
LiI hybrid IC pacemaker, reliability, experience 77−81736

hybrid reactors
14 MeV neutron interactions with ^{232}Th, $^{238,235}U$, and ^{239}Pu, neutron and γ-ray spectra 79−93612
analysis, separation technique for transport eqn. and sensitivity theory 80−57823
applications, role in US energy economy 80−57956
balanced approach to excess fuel from breeder reactors 79−59248
beam driven deuterium fuelled fusion-fission system 79−81081
blanket, optimum designs and heat flow diagrams for gas-cooled blanket 79−76130
blanket cooling under LOCA conditions 78−775
blanket data and development, review, simulation test facilities 80−106170
blanket design, accidental criticality 80−32497
blanket design, Th based, nucleonic performance aspects 80−47714
blanket designs, accidental criticality 78−778
blanket performance for hybrid reactor based on HTR fuel 79−85792
catalysed D fusion-fusion hybrid reactors 78−58436
commercial fusion reactors, small Tokamak hybrid design 80−13797
commercial Tokamak hybrid reactor, blanket and shield design 80−106179
commercial Tokamak hybrid reactor, fissile fuel and power prod. 80−13808
commercial Tokamak Hybrid Reactor, reference design 80−106171
conference on fusion reactor materials [Miami Beach, Florida, Jan. 1979] 80−31407
CTR fusion-fission blanket calcs. ^{238}U pulsed sphere meas. 77−23298
Demonstration Tokamak Hybrid Reactor, design of advanced bundle divertor 80−13834
design 78−802
design concept for optimal U resource use 80−95404
development of fusion power, pure and hybrid reactor options, review 80−63389
direct enrichment and self-protected fissile fuel prod. 80−95390
using divertored Tokamak, optimisation 78−798
driven magnetic fusion reactors, conf., Erice-Trapani, Italy (Sept. 1978) 80−41948
economics and performance 79−9872
electric energy supply system modelling 78−740
electricity costs for fusion breeder-fission convertor reactor systems 80−13804
electron beam heated solenoid reactors for fusion power and fissile fuel breeding 78−8992
energetics assessment 78−797
energy research program 79−22471
energy storage system, economic feasability 78−796
FFHR, tailoring the breeding-fission ratio by neutron moderation with iron 78−21677
FFHR power systems, performance parameters 79−81084
FFMR, mass-energy anals., fuel and power prod. 79−81085
fissile and fusion fuel exchange between fusion hybrid reactor, tritium producer reactor, and fission reactors 80−13811
fissile fuel prod. using fusion neutrons 80−47706
fissile fuel prod. using hybrid reactors 79−76123
fission neutron energy recirculation using nuclear pumped lasers 80−95408
fission product decay heat removal with fusion-fission hybrid mobile blanket 80−99282
fission reactor fuel breeding using fusion-fission hybrid reactors 79−71950
fuel breeding, development 78−5047
fuel cycle considerations 79−22474
fuel factory, replacement of LWR 80−42867
fuel production for fission reactors, fuel cycle options 80−27812
fusion, fission blanket, ^{238}U fueled, data deficiencies, weighting functions, neutron source effects 77−23295

hybrid reactors continued
fusion driven fissile fuel breeder systems, review of design, performance and costs 80−57954
fusion-driven symbiotic energy systems, economic anal. of fuel cycle and power costs 80−23141
fusion-fission fuel factory concept 80−47707
fusion-fission hybrid concept 79−85787
fusion-fission hybrid facility, multipurpose 79−85788
fusion-fission reactors, performance parameters, design and fuel cycle anal. 79−17973
fusion-supported decentralized nuclear energy system with 10 to 300 MW PWR 80−32515
fusion/fission reactors, inertial confinement systems, review 79−13519
hybrid shielding, radiation heating rates, two-dimens. transport anal. 80−106178
imploding liner blankets for fission product transmutation, neutronics 78−17420
inertial confinement fusion, anal. of fissionable pellets 80−13803
inertial confinement fusion reactor, appl. PWR fuel rod reenriching 80−106174
inertial confinement hybrid reactor design with flowing Li/molten salt 80−95405
integrated fusion-fission nuclear energy system with fuel self-sufficiency, thermal-electric conversion efficiency decrement 80−57907
ion ring compressor, power generation in combination with subcritical fission blanket 77−23276
laser driven, fuel breeding and power prod. 79−22473
laser fusion breeder, impact on nuclear economy 78−50336
laser fusion breeder-fission converter system economics 79−85790
laser fusion driven actinide waste burner, neutronics anal. 78−58459
laser fusion driven for actinide waste disposal 79−22421
laser fusion fissile-enrichment fuel factory, three-dimensional neutronics anal. 79−85794
laser fusion hybrid SOLASE-H, LWR fuel bundles, direct enrichment 79−85793
laser fusion-fission reactor, lattice calcs. and three dimens. effects 79−81088
laser-driven fission-fusion microexplosions, nuclear and thermohydrodynamic calcs. 80−47696
laser-fission-fusion systems, coupled nuclear-thermohydrodynamic anal. 79−13520
laser-induced thermonuclear fusion 79−9874
light water hybrid reactor blankets, constant power, Li control 79−85791
long-term nuclear energy strategies, role of fission and fusion 80−78354
magnetic mirror blankets and drivers 79−13517
magnetically confined reactors, review 80−74019
materials, neutron spectra meas. and calcs. for Cu, Nb, ^{232}Th, ^{238}U 80−23142
materials implications for reactor design 80−32430
mirror, conversion of ^{232}Th and ^{238}U 80−42860
mirror confinement, fuel design consideration 79−22472
mirror fusion hybrid reactor, T handling systems 78−62617
mirror fusion reactor design, hybrid fusion-fission reactor, surface bombardment rates 77−30662
mirror fusion-fission reactor, safety 79−22461
mirror hybrid reactor power plant, mechanical struct. 78−58449
mirror hybrid reactors, reference design 79−76124
mirror reactors, economic significance of Q 80−47722
mirror-torus hybrid, two-energy-component plasma 77−15223
molten salt fusion-fission symbiotic systems, nuclear performance calcs. of catalysed D-D and D-T reactors 80−57948
molten salt hybrid blanket, He-cooled, theory 78−62614
neutron transport eqn. separation technique and sensitivity theory 80−37632
non-electric fusion energy applications 80−42866
nuclear energy options, for future, fusion-fission concepts, accelerator breeding 80−13838
nuclear energy strategy, Japan, possibility of FFHR 80−42868
nuclear fuel trajectories of fusion-fission symbionts 80−68947
plasma models for standard mirror reactors 80−6273
power plant economics 78−789
reaction rate calcs. in ^{238}U and ^{232}Th blankets around D-T neutron source 80−52782
reaction rate sensitivity to fission spectrum changes 80−47712
reference mirror design 78−801
relativistic electron beam hybrid reactor, economic model 78−58412
relativistic electron beam hybrid reactor, parametric anal. of conceptual design 79−76121
scoping studies for power generation 78−5026
secondary neutron streaming in plasma vacuum cavities surrounded by hybrid blankets 80−95416
SOLASE-H, blanket neutronics calc. for blanket design 80−13805
SOLASE-H, error estimation of fissile fuel and T prod. 80−95409
superconducting poloidal field coil design 78−70640
symbiotic, fusion-driven energy systems, neutronic and economic anal. of CTR blanket using XSDRNPM code 80−57955
symbiotic design, simple fuel reprocessing 78−66365
symbiotic energy system, U fuelled, economic anal. using SYMECON code 80−106172
symbiotic system, managing fusion burn, economic analysis 80−106173
symbiotic system economic evaluation using SYMECON 80−106177
tandem mirror fusion-fission system studies 80−37607
tandem mirror hybrid; ^{233}U prod. 80−47708
tandem mirror hybrid reactor, gas cooled blanket 80−37608
tandem mirror hybrid reactor, nucl. performance sensitivity of Be/molten salt blanket 80−37606
tandem mirror hybrid reactor design study 80−13799
tandem mirror reactors, design, fissile fuel production 80−27811
tandem mirror reactors 80−42856
tFTR blanket module experiments 80−37609
TFTR breeding modules, neutronics 80−37611
TFTR electric power module, conceptual design 80−32508
TFTR exptl. blanket modules, mechanical design 80−37610
THR−a commercial Tokamak hybrid reactor 80−13798
Tokamak, comparative anal. with hybrid reactors 79−18043
Tokamak, driven, plasma parametric studies and appl. 80−42865
Tokamak, T breeding, optimisation with geom. program 78−74477
Tokamak demonstration hybrid reactor, blanket neutronics analysis 79−22469
hybrid reactors continued
Tokamak demonstration hybrid reactor, fissile fuel breeding and blanket power prod. 79−22470
tokamak demonstration hybrid reactor 78−58418
Tokamak fusion-fission hybrid reactor, beam-driven, design parameters 77−34459
Tokamak hybrid blanket, neutronics and thermal hydraulics 78−66406
Tokamak hybrid blanket design, breeding and power capabilities 78−62615
Tokamak hybrid breeder blanket, liq. metal coolant, MHD effects 78−74481
Tokamak hybrid demonstration reactor, eval. of steam and boiling-water cooled blanket concepts 79−85789
Tokamak hybrid reactor, for prod. of Pu fuel and elec. energy, preliminary design 79−76122
Tokamak type, with fissioning matter, blanket parameters 77−34446
Tokamak-type thermonuclear hybrid reactor for the production of fission fuel and electric energy preliminary evaluation 79−71954
two-component torus hybrid reactor, double wall for first wall, struct. anal. 78−66409
two-component Torus hybrid system, pressure tube convertor for hybrid blanket 78−74478
US energy strategy, role of hybrid nuclear reactors 80−42743
wetted-wall ICF fissile fuel factory studies 80−13806
D-D fusion-fission hybrid reactor, energy multiplication and fissile prod. 79−36409
D-D fusion-fission hybrid blankets, neutronics anal. 80−13809
DT-Pu plasma, neutron induced fission, fission fragment slowing down 79−26749
DT-Pu plasma, neutron induced fission, enhancement of neutron prod. and fusion rate 79−26750
^{3}H and Pu reproduction problems 77−38403
^{239}Pu direct enrichment of LWR assemblies in a fusion hybrid 80−37604
^{239}Pu seeded DT plasma, neutron induced fission 79−71946
^{90}Si transmutation in fusion reactors 79−26559
^{90}Sr fission reactor waste management, by fusion reactor transmutation 78−70642
T and fissile fuel exchange between hybrids, fission power reactor and T prod. reactors 80−47703
Th blanket reaction rate calc., central DT neutron source, ENDF/B-IV cross sections 80−13792
Th-Li hybrid reactor blanket, enhanced fuel prod. using UO_2 multipliers 80−13810
U/Pu systems, trade-offs between fuel and power prod. 80−37605
^{A}U, A=235, 238, fission and activation by fusion plasma neutrons 79−13521
^{233}U factories based on D-T and D-D cycles 80−37630

hybrid simulation
aquifer permeability and storage identification by artificial recharge hybrid simulation 77−45043
axisymmetric transonic flow around slender bodies 77−42861
Beuken model thermal conductivity nonlinear changes 77−42700
biological model parameter reliability range determ. 77−44581
body fluid distribution, flowing-mixing compartmental hybrid model 77−44582
brain O_2 transport, nonlinear Monte Carlo simulation, hybrid computer implementation 78−40131
cardiac catheterisation data analysis via remotely located hybrid computer system 77−40869
cardiac catheterisation data on-line analysis by remote access computer system 77−40870
cardiovascular simulation of infants with transposition of great arteries after surgical correction 77−44713
controllability studies for CANDU advanced BLWR with enriched fuel 77−71683
diffusion nonlinear parameter identification by hybrid computation 77−53766
digestive tract electrical rhythms simulation 78−64970
EM scattering, hybrid computation by Unimoment/Monte Carlo technique 77−14646
filtration, dynamic, use of electrically conducting paper with discretely distributed capacitance *(Russian)* 78−88850
gas dynamics, Prandtl-Meyer function soln. 77−11164
haemodynamics, coronary, analysis by circulation model *(Japanese)* 77−5021
HWR reboiler dynamic simulation 78−8949
hydrodynamic forces on cylinders, Morison eqn. coefficient determ. 77−54962
indoor natural radiation environment and dose distribution in man, multi-compartment models 79−12015
material fatigue under random complex state of stress 77−42786
mathematical physics equation soln. by variable-structure environment simulation 77−41470
multidimensional quasineutral plasma simulation model 79−7481
myelinated axon impulse cond. simulation, sensitivity to nodal and internodal parameters 78−35831
nerve cell kinetics simulation using Interactive Simulation Language 77−21507
neuron, stochastic electronic model 77−48775
neuron electric potential field evaluation, with time-dependent surface potential 77−86478
nonlinear direct and inverse heat and mass transfer, analogue and hybrid simulation 77−53767
nonlinear heat conduction simulation by analogue and hybrid computers 77−53768
nonlinear recursive estimation procedure, convergence and hybrid simulation 77−53850
nuclear reactor dynamics, LWR *(Czech)* 77−54309
nuclear station, with water-cooled water-moderated reactor cooling system faults, hybrid simulation *(Russian)* 78−5008
opto-digital, three dimensional molecular structure reconstruction, imaging of atoms 77−39510
pattern recognition, hybrid method, suboptimal statistical transform *(French)* 77−46703
pulmonary oedema fluid transport 78−27915
PWR power plant self-tuning control and simulation 79−9827
reactor spatial dynamics, hybrid computer simulation 78−29567
respiration rhythmogenesis model, Lotka-Volterra equations *(German)* 77−48772

hybrid simulation continued
saccadic eye movement control system, digital analogue simulation 77−44654
semiconductor structures modelling, MOS, Poisson partial differential equation solution *(Slovak)* 80−75643
ship structure, stress fields hybrid simulation 79−41637
stationary discrete and adjoint continuous iteration processes, hybrid computation appl. 78−45472
stationary magnetic field iterative modelling with hybrid analyser 77−42463
tension determination in elastic element on motionless sheave, hybrid calculator appl. *(Bulgarian)* 80−23894
tomographic system error propagation, hybrid anal. 78−40327
transient field initial-boundary value problems 77−41469
transient groundwater flow simulation by hybrid computer 77−45044
vocal tract real-time hybrid simulation 77−44692

hydrated electrons *see solvated electrons*

hydraulic amplifiers
vortex amplifiers, two-stage shear-modulated hydraulic 77−53237

hydraulic control equipment
see also hydraulic amplifiers; hydraulic motors
arm prosthesis, hydraulically actuated, performance criterion 77−48951
artificial heart control, using miniature Stirling engine 79−53287
component fatigue crack acoustic emission inspection 77−40513
electrohydraulic knee-torque controller, electrohydraulic, for prosthesis simulator 78−11779
fatigue servo-hydraulic testing machines 80−108649
heart power supply and control modules, implantable 78−31978
impact absorption with two-stage variable area orifice hydraulic damper 77−50953
liquid oscillations in cavity in solid body, effect on solid body control device motion *(Russian)* 78−14031
micromanipulator for biological experiments, versatile remote control, economic construction 79−25163
noise analysis and control, PDP 11/40 minicomputer dynamic analysis system, graphical presentation of results 80−64327
pion⁻ radiotherapy, dynamic rangeshifter for modifying depth-dose distribs. 78−3595
pion range shifter for clinical therapy hydraulic servomechanism 77−32953
pipeline under hydraulic impact noise level calc. 80−102927
pressure regulator device, behaviour anal. 78−93668
pumps, speeds control for motors, Conf. on Earth resources electronics Rome, Italy (Mar.77) *(Italian)* 77−82056
PWR, control systems for selectively inhibiting protection system functions 78−37418
semiautomatic Sun-tracking system for concentrated solar cells 79−62012
solar collector tracking device design and evaluation 79−62123
urethral occlusive techniques for restoration of urinary continence, development 78−7543

hydraulic motors
liquid and dry friction power losses calc. method 78−85009
paraplegic human leg orthosis, hydraulic power control system 78−53577
servo actuator for prosthetic arm, with seven degrees of freedom 78−40404
servocontrolled hydraulic hot-torsion machine for hot working studies 78−27698

hydraulic systems
algae aqueous suspension, fragile nonspherical solid particle hydraulic transport investigation 77−73618
artificial heart designs compared 79−48367
branching pipeline system pressure pulsation calc. and expt. *(Japanese)* 79−90337
compound parabolic concentrator heat transport to storage 79−62102
fatigue servo-hydraulic testing machines 80−108649
fatigue testing, low-cycle, adapted hydraulic machine 79−57175
hydraulic lines, wave phenomena, coupled vibrations in bending and branching lines 80−14778
lifting system, for domeless solar telescope *(Japanese)* 79−96914
linear hyperbolic mixed boundary value problem, soln. existence, uniqueness, hydraulics appl. *(German)* 78−93514
materials-testing system with 10 nm positional accuracy 78−85065
noise control 80−53561
press for developing 500 tons 80−105636
prosthesis simulator, knee control scheme for level walking 77−48955
pump for laboratory high pressure installations 79−93159
resonant hydraulic circuit pulsatile water flow meas. using laser Doppler velocimeter 80−103091
solid transport, use of inductive flowmeter *(German)* 79−77318
universal testing machine, K value determ. *(German)* 80−90836
volumetrically controlled hydraulic drive dynamics calc. 79−35571
weight handler, electromechanical, for piston gauge 78−8399
Pb-Bi eutectic alloy flow rate meas. apparatus 77−79412

hydraulic turbines
characteristic parameters, measurement errors, using laboratory models 79−63186
Coriolis ocean turbine energy system status 80−45628
hydroelectric storage plants, underground pumped, high-band turbomachinery, cost anal. 80−61432
liquid flowmeter calibration automated secondary standard 77−37841
ocean current power plant, vertical axis turbine, design and anal. 80−61272
ocean hydropower systems for electrolytic H energy prod. 80−30374
ocean thermal energy conversion systems (OTEC) turbine parameters w.r.t. working fluids 79−83617
Osmo-Hydro power, salinity gradient energy conversion feasibility and system design 80−45721
reversible pump-turbine, axial, for tidal power plants 79−43735
wave power generation, Mauritius 'passive' project, electro-mechanical aspects 79−43724

hydroacoustics *see underwater sound*

hydrodynamics
see also jets; liquid oscillations; liquid waves; viscosity of liquids
10-day Cepheid variables, theoretical models using dynamic zoning method 78−49449
ablating material surface, hydrodynamic boundary conditions 79−10939
accretion, spherical, buoyancy effect 80−109349
accretion disc, selfgravitating, model 79−25466

hydrodynamics continued
accretion discs in close binary systems, tidal torques 78−12296
accretion disks, optically thick, pulsational instability to axially symm. oscills. 80−82190
accretion onto binary stars, numerical simulation 79−21358
accretion onto compact gravitating object, hydrodynamic calcs. 80−67551
accretion onto rapidly moving gravitating centre, self-similar soln. 80−17609
adsorbed polymer layers, hydrodynamic thickness, Navier-Stokes eqn. calcs. 77−65726
advection eqn., anal. of local second moment conserving quasi-Lagrangian scheme 79−72871
Aegean basin, hydrodynamic eqns., numerical solns. 78−65317
aerosol induced breakdown in air, two-dimensional modelling 79−90368
Agulhas Current, topographically induced changes in struct. of inertial coastal jet 80−72545
n-alkanes, oligomers, hydrodynamic behaviour, viscosity 77−559
annular gap turbulent flow calcs. 79−55417
aquatic animals swimming in scombroidal way, hydrodynamic theory *(Ukrainian)* 77−32928
aquifers, hydraulic characts. 77−9450
Archaean peridotitic komatiites in La Motte Township, Quebec, emplacement hydrodynamics 78−77234
artificial viscosity, nine-point, for two-dimens. hydrodynamics 79−3989
asthenosphere, flow rel. to plate motions 78−96180
asthenosphere, thermal stability or instability of shear flow 78−20370
astrophysical gas flow, isothermal accretion, stability 78−49303
N.Atlantic, fluid-parcel vels. and paths calc. with aid of diagnostic models 79−29780
N.Atlantic Ocean, advection rel. to sea surface temp. year to year changes, (1948 to 1974) 80−67367
E Atlantic Ocean, equatorial adjustment 78−88836
N.Atlantic Ocean waters integral circulation, numerical realisation of hydrodynamic model 78−3811
atmosphere, hydrodynamical model of inner struct. of planetary jet stream *(Russian)* 77−64371
atmosphere, internal waves, hydrodynamic instability *(Russian)* 80−61852
atmosphere dynamics in quasistatic approximation, characterisation of approximation *(German)* 80−98383
atmosphere flow, kinetic energy three power law kinematic props. 80−77087
atmospheric circulation and pollution analysis using hydrodynamic models *(Italian)* 79−100892
atmospheric thermohydrodynamic eqns., vertical derivatives approx. rel. to short-range weather forecast *(Russian)* 77−60450
axisymmetric bodies at free surface, zero-freq. hydrodynamic coeffs. 77−89219
axisymmetric potential flow in ducts 79−14480
Baltic Sea horizontal mixing, Lagrangian and Eulerian meas. 80−17290
barotropic vorticity equation, new class of steady solns. 80−85667
Basset-Langevin equation, impulse waveform and duration effects on solution 79−41653
Bay of Fundy, Canada, tidal flow vels. rel. to bedforms hydraulic stability relationships 78−88814
Beatton River, British Columbia, regional trend to meander migration 80−101391
Bernoulli's principle apparatus for student expt. 77−41448
bifurcation in steady flows of viscous fluid, expt. 78−30267
bifurcation in steady flows of viscous fluid, theory 78−30266
binary mixture, pretransitional effects near convective instability 77−41536
biomacromolecules, rigid, modelling approaches of hydrodynamic props. 80−61613
black hole accretion discs, boundary-layer behaviour of flow at disc inner edge 80−46598
black hole accretion discs, Lightman-Eardley instabilities rel. to disc thickening 80−31324
black holes, primordial, self-similar growth for general sound speed case 79−5856
Black Sea, H_2S and O_2 zone boundaries rel. to water mass dynamics *(Russian)* 80−12435
bodies in non-planar stream, 3D motion, finite difference method soln. *(Russian)* 78−75116
body moving in liquid, dynamic density measurement and viscosity effects 79−6097
body moving in liquid, stability problems *(Russian)* 77−54972
Boltzmann eqn., reduction to fluctuating hydrodynamics 78−8245
Bondi accretion, linear stability problem 79−44359
book, liquids and their props., mol. and macroscopic treatise 78−87604
Bose-Einstein condensate dynamics, two-fluid hydrodynamics, Mori theory 77−28061
boundary conditions, generalised surface, including kinematic and general slip 78−9926
boundary layer for even symmetrical channels, numerical solution *(Bulgarian)* 77−80131
boundary-layer flows from fixed to moving surfaces, gap effects 79−14377
Boussinesq fluids, viscosity, conductivity and power spectrum of turbulent convection 80−98543
branch-to-trunk area ratio, effect on transition to turbulent flow, cardiovascular system appls. 80−67108
Brownian motion, fluctuating hydrodynamics, slip coeff. fluctuation-dissipation theorem 78−8348
Brownian particles, rotating, angular velocity autocorrelation function 77−27932
BWRs, natural circulation of water by hydrodynamic models 79−93684
canyon rivers, rapids characts. 80−72564
capacitor discharge, current increments, using arc channel hydrodynamic model *(Russian)* 79−82109
capillary jets, flow and instability of jets interacting with surrounding medium 80−6110
carbon tetrachloride, generalised transport coeffs., hydrodynamic eqn. 78−87803
cassini oval, with line source in front, 2-dimens. fluid flow 79−94755
cavitation at a circular cylinder, characts. 78−1701
cavitation zone, shock wave theory and hydrodynamic drag 77−27567
cell analysis in flow systems, geometry for orienting flat cells 78−77161
cell hydrodynamics, information-conserving theory 78−55623

hydrodynamics continued
cell membrane nuclear hydrodynamic shear, non-equil. Ising model, master eqn. 78−61146
cellodextrin alditols, alkali solns., hydrodynamic props., frictional envelope form. 77−28031
cellular motion in liquid heated below rel. to surface deformation and active agents *(Russian)* 77−54973
cellulose acetate butyrate, in soln., hydrodynamic behaviour 80−64876
Cepheid variables, double-mode and bump, rot. and convection effects on period ratios 78−93249
cholesteric liquid crystal, acceleration wave propag., theory 80−75154
cholesteric liquid crystal, statistical hydrodynamics, microscopic theory 77−39540
circumferentially ground rough disc, elastohydrodynamic lubrication 78−64708
circumstellar gas flow, hydrodynamics rel. to stars interaction with dense interstellar gas clouds *(German)* 80−109500
classical fluid, linear transport equations 79−77054
classical two fluid process, relationship with Schrodinger quantum theory 79−40385
closed torus, virtual mass in axisymmetric motion 79−32437
clusters of galaxies, cluster wind driven by viscous heating 79−9011
clusters of galaxies, intracluster gas dynamics rel. to X-ray source evolution 79−17133
coaxial circular discs, hydrodynamical problem 80−24032
cochlear fluid mechanics, kinetic theory 78−53440
cochlear hydrodynamics model, digital simulation 78−31821
collapsing isothermal spheres, predictability limit, rel. to star form. 79−75088
collisionless spherical stellar system in steady state 79−5865
collisionless subsonic accretion, stellar appl. 80−46380
colloids, sedimentation hydrodynamic interaction between spherical particles, effect of repulsive interparticle forces 80−45577
Comet West (1976 VI), H syndynamic model 80−46485
comets, hydrodynamic forces in splitting icy nucleus 80−46491
compressibility, added to incompressible hydrodynamics computer codes 80−53803
contact angle of fluid with hard surface, interface motion, drop spreading, solns. *(Russian)* 77−27640
contained water bodies, wind-induced drift 79−48512
continental drift 79−44386
continuity equation solutions 79−61
convective motion in a porous medium near equilibrium instability threshold 79−14398
convectively unstable atmospheres in shear flow, hydrodynamic instability 77−87253
Coriolis ocean turbine energy system status 80−45628
counter-current system with capillary-size vessels, fluid movements due to hydrodynamic forces 77−5024
coupled solid/fluid/surface wave dynamic interaction problem, improved fluid superelement 78−81108
Crab Nebula filaments, shock waves hydrodynamics effects on spectra 78−85997
cratering explosion, pulsed hydrodynamic model 78−51180
critical point hydrodynamics 78−59361
crystal growth from melts, hydrodynamic behaviour under large intertial accelerations 80−66421
crystal growth rate studies 80−100188
CVD, two-component gas mixture with axisymm. stagnation flow geom. 77−40384
cylinder, circular, half-immersed, long-wave behaviour of virtual mass 80−83810
cylinder, half-immersed, virtual mass, integral equation method 80−87783
cylinder, two-dimensional, oscillating in shallow water, hydrodynamic forces and moments 78−38269
cylinders heaving in water, added mass, damping coeff. 77−58828
cytometry, hydrodynamic orientation of sperm heads in flow systems 78−77162
debris dent effect on elastohydrodynamic lubrication 78−64709
deep ocean, bottom boundary layer short-term variability 79−2269
deep ocean, currents fine struct. rel. to internal gravity waves and wave breaking 78−85578
defect hydrodynamics in nonplanar magnetic media *(Russian)* 80−49445
deformable body moving in pot. flow, hydrodynamic moment 79−64626
deforming ellipsoid in liquid, motion *(Russian)* 77−55121
degenerate accretion disc model 79−25467
dense fluid, collective modes and neutron scatt. 80−92442
dense fluid, high freq., small wavelength 77−19860
descending turbulent flow of liquid film and gas 77−7437
dielectric phonon gas nonlocal hydrodynamics, second sound attenuation, thermal cond. *(Russian)* 78−47478
disc accretion in soft potential well, excess surface density ring form. 80−8532
disc motion in presence of collapsing cavity *(Russian)* 77−31342
discharge, pulsed, hydrodynamic processes 77−47290
discrete hydrodynamics, dynamic renormalisation prescription 79−86395
disk galaxy, hydrodynamical model *(Chinese)* 80−85996
dispersion-free limit, roots of hydrodynamic matrices 77−7364
dispersive magnetisable media, hydrodynamics including Brownian motion 80−59120
dolphins and pinnipeds, echolocation system acoustics and hydrodynamics 77−36963
downdraught in rotating environment, vortex form., appl. to cloud mech. 80−8399
duct, noncircular, with sharp corners, friction factors 79−81968
Dufour's effect and hydrodynamic stability *(French)* 78−30284
dynamical fluctuations in simple fluids, kinetic theory 77−7652
Earth core, effect of boundary irregularities on fluid speed and geomag. field 78−73333
Earth mantle, shallow global flow due to lithospheric plates accretion and subduction 79−44163
Earth mantle flow, one-dimensional modelling 79−39698
East River tidal strait, New York, hydrodynamic characts. 77−37222
eddy viscosity in truncated and averaged hydrodynamical eqns. 78−44936
elastic rectangular plate interaction with ideal incompressible fluid, classical boundary value problems *(Russian)* 77−68556
elastic sphere, interaction with weak shock waves, hydrodynamic forces 77−58595
hydrodynamics continued
elastohydrodynamic contact optimisation 78−79288
elastohydrodynamic lubrication, low elastic moduli material, elliptical contact 79−90198
elastohydrodynamic lubrication, non-Newtonian effects of volume relaxation 80−103009
elastohydrodynamic lubrication of elliptical contacts for materials of low elastic modulus 79−20214
elastohydrodynamic problems for rough bodies with non-Newtonian lubrications *(Ukrainian)* 80−24054
elastohydrodynamics, solns. to steady-state problems 77−35107
electrochemiluminescence cell 80−45506
electrolytes, complete conductance eqn., hydrodynamic terms 79−23755
ellipsoidal aerosol particles in binar binary gas mixture, diffusophoresis under hydrodynamic conditions 80−66888
elliptic problem solution, hydrodynamics appl. 79−90210
emulsion, films, thinning vel. and lifetime, surfactant in continuous and dispersion phases 77−84306
emulsion films, thinning vel., surfactant in continuous and disperse phases 77−84305
energy estimates analogous to Saint-Venant's principle 80−36856
entropy production deceleration 78−93094
equations of motion and transport coefficients, using discrete formulation 79−90504
estuaries, hydrodynamic model using smooth elements, accuracy 80−98356
estuarine flow, nonlinear partial differential eqn., finite element anal. *(Japanese)* 78−8233
Eulerian and Lagrangian computer codes, pressure iteration, multigrid method 80−53738
evaporation and condensation, kinetic theory, hydrodhnamic eqn. and slip boundary condition 78−63903
extragalactic double radio sources, gas dynamical calcs. 79−67107
eye, hydrodynamic model of aqueous flow in posterior chamber 78−69122
FBR containment response to HCDA, effect of struct. components, Eulerian hydrodynamic anal. 80−23014
FBR safety analysis, multicomponent hydrodynamics, implicit Eulerian technique 79−634
Fermi superfluid hydrodynamics, time-depend. BCS formalism, compared with He II, finite nuclear systems 78−22920
fermion systems, superfluid, microscopic derivation of hydrodynamic equations, appl. to ^{3}He-B 79−46865
fibre lightguide form., from tubular blank, optimisation 77−75719
film on rotating surface, hydrodynamics and heat exchange, entrance section influence, interface frictional forces 79−86433
fission of self gravitating rotating elongated gaseous disc 77−87546
fixed-bed electrodes, three-dimensional, mass and charge transfer *(French)* 80−71920
fjords, hydrodynamics rel. to fronts in surface waters 79−57953
flagellated microorganisms, hydrodynamic theory of swimming 77−90820
flame front, distorted, hydrodynamic discontinuity model 77−58802
flames, ignition and propagation, self-consistent 2-dimens. hydrocode 78−47066
flat plate streaming potential investigations: hydroynamics and electrokinetic equivalency 80−106777
floating body, oscillations damping by liq., inertial effects *(Russian)* 78−22295
floating zone melting using reduced gravity environment, floating zone structure 79−28909
flow birefringence and hydrodynamic boundary conditions for ellipsoid particles and Rytov dip 80−45030
flow induced vibrations design considerations rel. to fluid/struct. coupling 77−84190
flow modelling by AC induced electric fields *(German)* 77−57200
fluctuating Boltzmann gas, stochastic theory of hydrodynamic systems 79−75476
fluctuation theories 78−87327
fluctuations as Mori variables in generalised Langevin scheme 77−72279
fluctuations near threshold of Benard convection 78−26099
fluid, classical, transport coeffs. computation by cell hydrodynamics 78−38600
fluid, continuous, modified Alder-Wainwright model for vel. autocorrelation functions 77−51293
fluid fluctuations about hydrodynamic nonequilibrium steady states, Langevin method calcs. 80−53761
fluid force on oscillating disc in a still fluid 80−14724
fluid interface problems, simple line interface calculation method 77−58777
fluid-structure coupling problem soln. using boundary-integral eqn. method 77−54920
fluidised bed, heat exchange intensification using bubble motion control 79−86508
fluidised bed, vibrofluidised, shallow, vibr. grid gas flow influence on hydrodynamics 79−86509
fluidised bed at high Archimedes numbers, variational formulation 77−11257
fluids, corrections to linear hydrodynamics eqns., low-freq. sound dispersion *(Russian)* 79−3990
fluids, noncanonical Hamiltonian density formulation 80−103010
fluids, one and two dimensional, hydrodynamics, viscosity, heat conductivity, kinetics *(Russian)* 80−79972
flux-corrected transport algorithm, rezoning technique 80−31516
Fokker-Planck approach to Brownian rotation 78−62160
force transmission through incompressible viscous fluid-isotropic elastic solid interface 78−43252
forced waves in baroclinic shear flow, forced waves, evolution near instability threshhold 80−8393
forces and moments acting on body emerging from infinite plane into inviscid fluid 77−3802
forces on cylinders, Morison eqn. coefficient determ. 77−54962
form drag of in-line tube banks in water cross-tlow *(Russian)* 79−7412
frontal solution method, finite element anal. 80−74825
g- and p-modes of non-adiabatic self-gravitating fluid, perturbational-variational expansion 78−32337
galactic bulge wind, interaction with gas disc, hydrodynamic model 80−77476
galactic corona, origin and dynamics 79−25709
galactic winds, supernovae-driven, rel. to Hubble sequence 79−8989
galaxies, bar-driven spiral density waves in disk 80−8684

hydrodynamics continued
galaxies, corrugation waves in differentially rotating gas layer 77−5571
galaxies, density waves energy and lifetime rel. to galaxies classification and spiral struct. 80−98715
galaxies, dispersion of local disturbances and spiral waves in disk-halo systems 80−56934
galaxies, global instability of polytropic gaseous discs with Toomre density distrib. 80−98725
galaxies, spiral arm development, sufficiency conditions 80−77483
galaxies discs, second-harmonic oscills. of Maclaurin spheroids in halos 79−8993
galaxies formation by gravit. instability, role of ang. momentum 80−98722
galaxies spiral structures origin, magnetotidal and hydromagnetic models 79−25714
galaxies with discs, bar-driven spiral waves, hydrodynamic calcs. 78−49523
galaxy coronae, hot gas dynamics simulation 80−82481
galaxy formation, adiabatic cosmological perturbations propag. through matter-radiation decoupling era 80−62337
gas, dilute, kinetic-hydrodynamic transition obs., Brillouin scatt. 77−7508
gas clouds, inhomogeneous, one-dimensional collapse, role of small perturbations *(Russian)* 80−36497
gas clouds in Seyfert galaxies and quasars, containment by particle flux 79−8820
gas clouds spherical gravitational collapse, unsteady hydrodynamics 78−45212
gas dynamics in barred spiral galaxies, gaseous density waves and galactic shocks 80−12819
gas flow in barred spiral galaxies 80−90521
gas flow instability, nonlinear stabilization of unstabel acoustical vibrations in a bounded heat-evolving medium 80−6028
gas isothermal movement in pipe of spherical packing, hydrodynamic resistance determ. 77−75941
gas phase transport, definition of hydrodynamic regime acquired during crystn. 79−51029
gas-liquid flow in channels, hydrodynamics 79−81951
gas-liquid flow in granular layer, hydrodynamic modes 78−9712
gas-liquid upward flow in granular layer, hydrodynamic conditions 78−34188
gas-solid mixture, use of relative velocity of gas to solids *(Croatian)* 80−14799
gases, high velocity flows, nonequilib. homogeneous condensation, determ. of maximal supercooling 80−6086
general relativistic fluid spheres, physical solns. 79−21169
general relativistic hydrodynamics of stellar cores, adiabatic collapse 79−96903
generalised, extension to molecular dimensions 79−25864
generalised hydrodynamics construction by nonequilibrium statistical operator method 77−30116
geostrophic ocean currents determ. independently of reference level, inverse technique 80−51574
Gironde estuary vertical circulation, real time two-dimensional model *(French)* 79−62519
glaciers, hydraulic transients as seismic source 79−100816
glass tank furnace, physical models, selection criteria for liquids to simulate melted glass 79−8263
globular star clusters, gas outflow models including photoionisation 78−93338
glyceraldehyde 3-phosphate dehydrogenase, EPR, saturation transfer EPR 79−98124
gravitating gas cloud, rotating, wave-wave interactions 80−105154
gravitating systems, spherical stellar models, stability and normal modes 79−29983
gravitational collapse of rot. gas cloud, binary systems form. 78−65494
gravitational cylinder, hydrodynamic instabilities 77−78628
gravitational field influence on turbulent flow and heat exchange, review 79−86427
groundwater flow systems, oxidation-reduction sequences 79−84303
N.Gulf of Alaska, coastal flow from dynamic topography and satellite-tracked drogued drift buoys 80−51431
NE Gulf of Alaska, processes affecting suspended matter distrib. and transport 80−12398
Gulf of Genova, effect of low freq. winds on sea level and currents 80−8322
Gulf of Guinea, simple upwelling model 78−88837
W.Gulf of Maine winter circulation current and press. obs. 80−51430
Gulf Stream, fronts and wave disturbances compared with atmospheric jet stream 79−2268
Gulf stream ring frontal zone, asymmetric disturbances obs. 79−2267
Hamiltons principle appl. to flow problems 80−48600
harmonic lattice, impurity motion, generalised hydrodynamics and microscopic theory of long time tail *(Korean)* 77−49683
heart valve prostheses, rel. to vol. flow rate 77−25597
heat exchangers, multitube type, operation, influence of deposits *(Rumanian)* 79−94467
heat transfer equation, mol.-kinetic generalisation 78−67219
heat tube, hydrodynamic charact. *(Russian)* 78−30280
heaving cylinders, added mass and damping coeffs. 79−3988
helical flagella, hydrodynamic props., Oseen-Burgers' theory *(Japanese)* 78−11685
heterogeneous mixture, variational hydrodynamic model in Eulerian and Euler-Lagrangian formulations *(Russian)* 79−90211
heterogeneous mixtures, variational hydrodynamic model in Euler- and Euler-Lagrange formulations 80−92100
homogeneous vapour nucleation, in carrier gas, hydrodynamic theory 79−69236
horizontal heated surface, post-nucleate boiling and crit. heat flux models 78−90664
hydraulic electronic instrumentation, rain models, sediment transport *(Italian)* 77−91334
hydraulic equivalent of generalized one-dimensional flow 78−94627
hydraulic meas. devices, electronic instrumentation, rain models, sediment transport *(Italian)* 77−91334
hydraulic resistance of channel during rot. about axis perp. to channel axis 77−58698
hydraulic shock during tube filling by liquid *(Russian)* 80−24053
hydrocode convergence 78−36834
hydrodynamic oscillations in Gentilly-1 reactor steam mains, GISMO program 78−54824

hydrodynamics continued
hydrodynamics, drag on displacement ships, hydrofoils, hovercrafts 78−63423
hydroelastic shell opening in fluid flow numerical soln. *(Ukrainian)* 79−50592
hydroelasticity and aerodynamics, unsteady, modelling, for arbitrary motions 78−14033
hydroextrusion under hydrodynamic lubrication conditions *(Russian)* 79−38852
hydrofoil characteristics, in supercavitating flow, press. gradient effect *(Japanese)* 77−68649
hydrofoils, tail-loaded, fully cavitating, avoidance of turbulent separation 78−94659
hydroplane impact, ricochet rel. to angle of attack *(Russian)* 77−55123
hydroplaning of a rotating cylinder on water 78−63522
hydroplaning plate, lift, drag 78−63523
hypersonic accretion flow from an inhomogeneous medium 80−67552
ideal liquid, equations of motion *(Russian)* 79−90362
impactor performance, effect of boundary layers 77−60133
imperfect borehole, hydromechanics and stationary filtration *(Russian)* 79−88375
inclined sinkage element on rigid surface, elastohydrodynamic squeeze film action 77−15144
incompressible flow influenced by gravitation, hydrodynamic soln. 79−41648
incompressible irrotational axisymmetric flow about body of revolution and the inverse problem 78−94630
Indian Ocean, deep current meas. rel. to continuous spectrum of equatorial waves 80−98331
Indian Ocean, wave-induced longshore currents in Krishnapatnam nearshore zone 80−41447
inhomogeneous Boltzmann gas, lumped phase space, non-linear diffusion approx., stochastic hydrodynamic theory 80−64666
inhomogeneous spherical gravitating systems dynamics, simplest hydrodynamic models 80−17620
initial, periodic and travelling disturbances, unsteady waves development, asymptotic anal. *(Russian)* 78−77254
instabilities in heated channel, identification using appl. of vibration signals 80−28500
instability in isotropic fluids, review, book contrib. 77−89098
interaction between two spheres in viscous fluid, hydrodynamic interaction tensors 78−30253
interface between immiscible liquids, convection induced by chem. react.-hydrodynamic coupling *(French)* 79−41682
internal resonances 78−1627
interplanetary He, dynamical effects in 584 Å reson. scatt. 80−8509
interstellar clouds, rotating, nonaxisymmetric collapse theory rel. to protostar form. 80−85927
interstellar clouds, rotation, axially symmetric collapse and protostellar form. 80−77380
interstellar clouds fragmentation, three-dimensional hydrodynamical calcs. 80−62236
interstellar contracting CO clouds, fragmentation 80−67838
interstellar cylindrical clouds, two-dimensional collapse calcs. 79−40247
interstellar gas flow stability in disk-halo galaxies 80−56933
interstellar medium, effect of OB-type stars on struct. and cloud form., effect of eqns. of state 80−109506
interstellar medium, influence of initial vel. fields upon star form. 80−21985
interstellar rotating clouds, protostellar formation, numerical methods and tests 80−56902
interstellar turbulent 80−56910
inviscid fluid, accelerating flow horizontal divergence, turning vorticity eqn. anal. 80−77013
ionic solution, light scatt., hydrodynamic theory 78−6692
ionization front propag. in inhomogeneous medium 80−46379
irrotational waves and convergence of Levi-Civita's series 77−58711
jet, plane turbulent, in incompressible liquid *(Russian)* 77−55060
jet flow from round impinging array, heat transfer and hydrodynamics 80−79374
jet flow model, three-dimensional 80−79369
Jupiter, Great Red Spot, atmosphere baroclinic model, solitary waves on unsymmetric shear flow 80−82266
Kolmogorov turbulent spectrum, direct interaction model 78−18275
Kuroshio jet current system region, density field calc. 78−92843
Laccadive Sea, water movements rel. to chemical oceanography and biological productivity 80−104995
Lagrangian and Hamiltonian formulations of compressible hydrodynamics 79−94581
Lagrangian hydrodynamics meshes, discrete rezoning algorithm, hot interacting bubbles calcs. 78−42628
Lake Ontario, geostrophic adjustment theory for intermittent full upwelling 77−33110
laminar boundary layer on porous surface with suction, triparametric calc. *(Russian)* 77−54967
Langmuir circulations, controlled laboratory expts. 79−23330
large Reynolds number, 2-D hydrodynamic lubricating theory *(Russian)* 78−59368
large-scale hydrodynamic system simulation programs 77−21799
laser beam penetration hydrodynamic limit 77−40313
laser fusion, electron thermal cond., plasma hydrodynamic calcs. 77−68750
laser radiation action on condensed medium, hydrodynamic effects 80−93439
light scattering from fluid with stationary temp. gradient 80−45097
Ligurian Sea continental shelf, wind and current autumnal data series anal. 80−85675
linear block copolymers, hydrodynamics 79−69273
linear hydrodynamics exterior problems, variational formulation 79−32434
liquid, coupling of vel. gradients to molecular orientation, light scatt. and flow birefringence anal. 80−25398
liquid, laser breakdown, photoacoustic and photohydrodynamic parameters 78−52597
liquid cross flow, dynamic response of circular cylinder 79−81838
liquid crystals, instabilities generated by US field, review 78−91235
liquid crystals, nonlinear reversible hydrodynamics, external mag. field influence 80−75156
liquid film flow regimes, on rot. disc 78−1671
liquid jet hydrodynamic development, surface active materials effect 79−46883

hydrodynamics continued
liquid layer on rot. surface, heat transfer, gas flow interaction 78−22347
liquid local order theory characterisation by vectors and tensors, internal energy density multipolar expansion 80−49070
liquid spreading on liquid surface, hydrodynamics 78−30814
liquid surface response to intense laser pulse, hydrodynamic anal. 77−24468
liquid with deformable and interacting particles, rel. to rot. and microdeform. rates 77−54950
liquids, hydrodynamic interactions and pair correl. functions on reaction kinetics, dynamic effect 80−97684
liquids, momentum transfer, cooperative effects 80−68160
liquids, rotational relaxation, molecular hydrodynamics, long time tails 80−59357
LMFBR, hydrodynamics of large-scale fuel-coolant interactions 80−78409
Lorentz model, hydrodynamic kinetic stages asymptotic equivalence 79−55438
lubricant, glass transition rel. to elastohydrodynamic lubrication 79−29227
lubrication, free boundary problem, variational inequalities 80−62475
lubrications, roughness effect 79−20207
2,6-lutidine-H_2O, phase separation, hydrodynamic effects 78−83960
LWR, neutronic thermohydrodynamic interaction model *(French)* 79−89349
RR Lyrae, UV light curve rel. to hydrodynamic atmospheric models 77−45435
main-sequence stars envelopes, hydrodynamical instabilities constraints from Li, Be and B obs. 78−93202
marine circulation and dispersion of pollutants in shallow sea 77−37241
Markovian processes and irreversibility, hydrodynamic equations, stress tensor and local eqn. 80−82720
Markovian processes and irreversibility, hydrodynamic equations from constitutive equations 80−82721
mass exchange in filter medium, hydrodynamics *(Russian)* 79−37292
MBBA, nematic liq. cryst., ultrasound produced rolls, spatial coherence props. of scatt. light 78−75534
meteorology, vertical eqn. of motion and wind eqns. 78−69428
meteorology dynamical topics, vorticity and divergence 79−12226
methane, gas, Rayleigh-Brillouin scatt., hydrodynamic effects calcs. 77−470
Mezen' Bay (White Sea), marine tides EM fields, rel. to hydrodynamics 78−73378
microcontinuum theory for elastohydrodynamic inlet zone of line contact, lubricant film 77−50998
microhydrodynamics, characteristic effects, developments 77−68681
mixture, force between components 79−55439
mixtures, motion of, generalized diffusion theory 79−17233
mode crossing stability, Lagrangian nondegenerate fluid or Vlasov plasma 78−42735
model of upper ocean frontal dynamics, development and anal. 80−4028
model of upper ocean frontal dynamics 80−4029
molecular dynamics, fluctuation driven reson., hydrodynamic and kinetic theory simulation 77−55124
molecular fluids, binary mixtures, hydrodynamics eqns., VH light scatt. 78−35158
molecular hydrodynamics of inhomogeneous systems, slip boundary conditions 77−89165
molten salt, binary, charge and mass fluctuations in hydrodynamic limit *(French)* 77−31573
molten salt, hydrodynamic correlation functions 77−31577
moments of multiple distrib. functions 78−49750
mooring cable in nonuniform stream, equilib. shape and tension *(French)* 78−63277
multi-inflow reservoirs, flow dynamics 78−20452
nebulae ionisation-shock fronts hydrodynamic linear theory 80−17625
nematic liquid crystal, extensible, micropolar continuum theory 79−4244
nematic liquid crystal, hydrodynamic instability phenomena and mechanisms, book contrib. *(French)* 77−84229
nematic liquid crystals, hydrodynamic correlation functions, propagating modes 78−94988
nematic liquid crystals, Marangoni effect 78−6009
nematic planar liquid crystal, nonlinearities close to thermal threshold 79−99058
nematics, molecular form and hydrodynamics connection, reactive coeff. *(Russian)* 80−64894
Neptune atmosphere, equatorial flow model rel. to rot. 80−67653
neurons, numerical methods for creeping flow 77−5019
neutron stars, supercritical time-dependent accretion 80−85967
neutron stars plasma accretion, interaction with mag. field and accretion flow hydrodynamics 80−109452
non-Newtonian lubricant hydrodynamic theory *(German)* 78−79341
nonlinear acoustics, exact solns. of Zabolotskaya-Khokhlov eqn. 77−805
nonlinear fluctuation theories 79−77055
nonlinear free surface flow problems, divergent low Froude number series expansion 78−51146
nonlinear hydrodynamical eqns., external fields, Einstein relations for kinetic coeffs. *(Russian)* 78−50
nonlinear oscillatory modes in systems of the hydrodynamic type 77−87652
nonlinear periodic waves in self-gravitating fluid rel. to galaxy formation 79−70946
nonlinear problems, discrete vortex element methods 78−30302
nonlinear wave propagation in relativistic continuum mechanics, limiting case of relativistic hydrodynamics 80−22203
nonstationary gas flow, two dimens., variational approach to finite difference scheme 78−51147
normal modes of self-gravitating fluids in perturbed configurations, perturbational-variation procedure 78−32336
North Sea, mathematical and numerical hydrodynamic models 77−37216
nuclear power plant heat exchange problems 80−18372
nuclear viscosity, single-particle Schrodinger fluid 77−71577
ocean, 'Marrubbio' phenomenon rel. to S.Sicily Basin oscills. eigenperiods 77−53062
ocean, advective mixed-layer model with imposed surface heating and wind stress 80−12395
ocean, artificial upwelling induced by ocean currents theory and expt. 78−81217
ocean, current variability and mid-ocean boundary-forced planetary waves response model 80−72541
hydrodynamics continued
ocean, currents rel. to computed and observed surface topography 78−77250
ocean, development of spatial internal waves generated by moving disturbances *(Russian)* 78−77251
ocean, equatorial undercurrent dynamics 80−72558
ocean, frontal circulation due to cabbeling and double diffusion 79−2263
ocean, hydrodynamic friction layer instability rel. to Langmuir circulation 78−92840
ocean, Langmuir circulations and wind drift currents, Langmuir vortices, struct. 77−49074
ocean, low-freq. momentum, heat, salt and nutrients fluxes at Scotian Shelf edge 79−2242
ocean, mobile sand grains underwater detect. 78−96192
ocean, normal Rossby modes of closed basin with topography 78−73385
ocean, realistically stratified, nonlinear energy and enstrophy transfers 80−101370
ocean, rel. shear microstructure and energy dissipation meas. adjacent to island 78−85573
ocean, sea level transients obs. by Geos 3 coincident orbits 80−72535
ocean, slope/shelf water intrusions obs. via remote acoustic monitoring 79−2241
ocean, trace metal enhancements in estuarine tidal front rel. to advective transport 79−2265
ocean, upwelling circulation meas. during Hurricane Eloise (1975) 78−77302
ocean, upwelling over shelf break 80−72550
ocean, vertical and cross-shelf flow meas. in coastal upwelling region off Oregon 80−12397
ocean continental shelf circulation, diagnostic model 78−85581
ocean continental shelf circulation, effects of buoyancy flux 80−72540
ocean deep-water channel flow, rotating hydraulics theory 80−94539
ocean dynamics, equilib. Langmuir circulation model 80−101381
ocean dynamics investigation, realisation of four dimensional topographic reference system 78−77176
ocean free surface vibrations caused by internal waves, experimental investigation *(Russian)* 79−16478
ocean frontal zones, light scatt. obs. 79−2266
ocean hydrodynamics, 7th Liege Colloquium (1975, May 5-9) 77−37211
ocean large-scale density anomalies, non-linear evolution *(Russian)* 79−16479
ocean mesoscale eddies, influence on sea surface temp. *(Russian)* 78−81191
ocean mixed layer evolution, laboratory investigation in homogeneous fluid *(Russian)* 80−94529
ocean near-surface mixing layer, microstruct. in stable heating conditions 78−85568
ocean oil spill trajectory modelling, wind and current forcing functions 79−5509
ocean surf zone, hydrodynamic instability as mechanism for horizontal gyres form. 79−2244
ocean surface intrusions, fronts and internal waves, numerical study 79−2262
ocean synoptical eddies, numerical scheme *(Russian)* 78−81190
ocean tidal currents, interaction with wind-generated sea waves 80−51428
ocean water masses advection, radioactivity and salinity changes *(Russian)* 78−77275
ocean waters mixing, effects of eddies and islands 78−85572
ocean waves energy absorption 79−43726
oceanic circulation around New Zealand, numerical model 80−72538
oceanic warm front propagation, theory with appl. to Sagami Bay Kyucho phenomenon 80−94538
oceans, vel. meas. rel. to kinetic energy dissipation field struct. *(Russian)* 77−13082
Okhotsk Sea, currents, rel. to pack ice drift radar meas. *(Japanese)* 78−96224
Okhotsk Sea coast of Hokkaido currents rel. to ice field divergence and rot. meas. *(Japanese)* 78−96223
open channel flows, junction losses, frow anal. 80−6156
open disk theorem, hydrodynamic stability, upper bound of eigenvalues 78−59370
open sea, strongly nonlinear internal motion obs. using range-gated Doppler sonar 80−51422
ordered media containing defects, gauge-like variables 79−88889
Pacific Ocean waters, circulation rel. to nitrate N distrib. 80−31065
packed beds with gas-liquid concurrent upflow mass transport phenomena and hydrodynamics 79−50784
paramagnetic liquid, mag. field effect on depolarised light scatt. *(Russian)* 80−108221
partial differential eqns., hydrodynamic type, lowering of order of system of eqns. 79−17234
particle acceleration in supernovae and extragalactic radiosources 80−31313
pattern selection in non-equilib. processes, marginal stability theory, eutectic solidification model 80−60852
pipeline hydrodynamical resistance reduction by dynamical effects *(Ukrainian)* 79−32670
planar magnetic media, defect hydrodynamics *(Russian)* 80−49445
plane channel of arbitrary shape, occupied by grid, heat and mass transfer, comput. method 77−7453
plane Couette flow hydrodynamic stability rel. to finite amplitude perturb. *(Russian)* 79−37291
plane harmonic Dirichlet problems, soln. for canonical domains 79−21548
planetary atmosphere banding 79−44386
planning plate with high speed in regular waves, pitching and heaving *(Chinese)* 80−43721
plasma, hydrodynamic Cherenkov instability, electron flow-surface wave interaction *(Russian)* 77−72440
plate, in flowing water, loss factor rel. to fluid vel. *(German)* 77−820
plate, simply supported, shear and bending moments by hydrodynamic analogy, results 79−64524
Poiseulle flow, thermally stratified plane, linear differential eqn., asymptotic fundamental system construct. *(German)* 77−902
polar liquid, IR absorpt. spectra and hydrodynamic model *(Russian)* 79−78689
polyatomic chemically reacting gases, hydrodynamic eqns. 79−32711
polyatomic fluids, generalised hydrodynamics 77−1055
polycaprolactam, after polycondensation, falling film evaporator system *(Japanese)* 79−70325

hydrodynamics continued
polyethylene, uncrosslinked amorphous matrix embedded cryst. orientation distrib., strain energy and hydrodynamic pot. effects 78−9968
polymer liq. flow, hydrodynamic eqns., centre of mass model, friction approx. 78−55664
polymer mols., struct. depend., theoretical description 77−50575
polymer solution, mean field theory 78−67227
polymer solutions, concentrated, transport properties, hydrodynamic mean field theory of voscisity of sphere suspension 79−4422
polymer solutions, dil., coherent scattering law, continued fraction formalism 80−103234
polymer solutions, dynamics and hydrodynamics, book contrib. 79−60261
polymerisation in flow-through reactor, low-temp. conditions 80−61092
polymers, flexible rings, nondraining, intrinsic viscosity, translational friction coeff. 79−18855
polymethylene, short-chain molecules, hydrodynamic behaviour, extended Rouse-Zimm theory 77−558
polyphenyl ether fluid operating in elastohydrodynamic contacts, IR emission spectra 79−91807
polystyrene-cyclohexane system, temp. depend. of hydrodynamic lengths 80−92449
polytropic fluid flow in central gravitational field, time depend. eqns. of motion 77−45301
porous media, moving boundary problems, theory and numerical analysis 78−81252
potential fields, nonstationary, nonlinear distrib. function, hydrodynamic eqns. *(Russian)* 80−52033
potential flow of an ideal liquid past a periodic system of bodies 80−6018
prestellar gas clouds, hydrodynamics rel. to relic radiation spectral lines *(Russian)* 78−77628
primary production model including circulation influences in Lake Superior 78−49041
primordial black holes formation, hydrodynamics 79−21324
profile contour closures solution, singularity method appl. *(Bulgarian)* 77−80132
prosthetic heart valve models, effect of channel diffusion, cut-off element on hydrodynamic resistance *(Russian)* 79−44053
protosolar nebula, dust grain motion time evolution 80−82234
protostar, rotating, fragmentation, comparison of two three-dimensional computer codes 80−26850
protostellar cloud, rotating, collapse and stability, turbulent viscosity effect 80−109510
protostellar clouds, rotating, ring form. during dynamic collapse 80−56820
protostellar clouds evolution, three dimens. dynamics 79−16929
protostellar envelopes of masses 3 M⊙ and 10 M⊙, struct. and hydrodynamic evolution 80−36616
pseudofluidised layer, hydrodynamical eqns. *(Russian)* 77−35233
pure harmonic tide in canal, eqns. of motion quadratic resistance term linearisation 78−69369
PWR, MULTIFLEX code, anal. of hydraulic force with hydro-structural interactions during LOCA 78−58373
quadratic friction effect in multi-storeyed nonlinear systems *(Russian)* 77−91213
quantum fluid, hydrodynamics equations in presence of vortices *(Russian)* 79−33141
quantum hydrodynamics, vel. operator 77−82449
quantum liquids, hydrodynamics, canonical eqns. 78−91497
quantum theory, rel. to structural information theory of sound 77−14822
quartz, dynamic wetting angle of dry lyophilic surface 80−88405
quasars, radiatively driven gas clouds dynamics and stability, plane-parallel slabs theory 80−22107
radiation effects, basic eqn. soln. with large and small Bouguer number 77−68708
radiative hydrodynamics, opacity enhancement by Doppler shift 77−75991
radio sources, extragalactic, pinching and fluting modes rel. to jets configuration and propag. 80−31374
radioactive waste migration, groundwater environment, hydrodynamic dispersion in transport models 80−17146
random velocity field perturbations, 3-dimens. characteristic functional eqns. 80−12909
rarefied fluid, ang. vel. correlation function with slip boundary conditions 77−47043
rarefied gas, acoustic dispersion, hydrodynamic soln. 77−68630
rarefied gas, thermal transpiration, thermal and friction forces 77−35171
Rayleigh-Taylor instabilities, reproducible, generating device 80−6178
rectangular curved channel hydrodynamics and heat transfer expt. 80−19398
reduced model theory, hydrodynamical approach for vel. autocorrelation functions 80−27135
Reiner effect, hydrodynamics of viscous fluid in A.S. Predvoditelev's form 77−55046
relative diffusion, meas. at small scales and oceanic appls. 78−88838
reversal phenomena in simple hydrodynamical systems *(Russian)* 77−11161
Reynolds equation at very low spacing, compressible, numerical soln., factored implicit scheme, mag. recording appl. 80−92183
rheology of suspension of deformable particles, elastohydrodynamic theory 77−35104
River Tiber, physical processes related to discharge into sea, aerospatial obs. 80−108831
Rockall Trough, hydrographic and geological inferences from near-bottom traverse 79−62483
Rossby waves in rotating annulus, laboratory and theoretical study *(Russian)* 80−19509
rotating body in Ostwald fluid, rate distrib. near wall, electrochem. methods *(French)* 77−42847
rotating gas cloud collapse, equatorial ring formation, Lagrangian method 78−12628
rotating gaseous masses, secular stability and points of bifurcation 77−42843
Rouse-Zimm theory of hydrodynamic props. 77−559
sea model, hydrodynamic, 3-D, variable vertical eddy viscosity, finite element anal. 80−85661
sea surface layer, dynamically passive impurity propag. by currents and turbulent pulsations 80−31063

hydrodynamics continued
second-order constitutive equations of hydrodynamics, dynamical interpret. 80−36860
Sedov-Taylor blast wave solns. stability 79−35104
self-consistent analysis for two-dimensional hydrodynamics 80−4533
self-gravitating disc, density waves accretion-induced overstability 78−73752
self-gravitating fluids, definition of g-modes and p-modes 77−41291
self-propelled body, surrounding liq. flow 79−86399
self-similar spherical expansion, Rayleigh-Taylor instability., astrophysical appls. 79−8823
Severn estuary, seasonal and spring neap tidal depend. of axial dispersion coeffs. 80−94534
shallow sound, energy balance and wind effects 79−2243
shallow-water slender-ship flow past slowly varying bottom 78−1742
shell-fluid system, steady periodic motions appearance *(Ukrainian)* 77−31240
ship, flat, low-aspect-ratio, planing at infinite Froude number 78−32684
ship, heave and pitch motions in shallow water, forward speed effects 77−47126
ship, slender body potential flow between closely spaced walls 77−89095
ship model, hydrodynamic resistance, analytic calc. *(Russian)* 78−75123
ship planing hulls, model tests using recirculating water channel, resistance characts. 79−18978
ships, drag on displacement ships, hydrofoils, hovercrafts 78−63423
shock propagation, nonlinear hydrodynamic field equations, finite element anal. and method of weighted residuals 80−53813
shock wave decay, Maxwell-like relations in condensed materials 79−41702
shock waves, astrophysical, post-collisional propag. and amplification *(Russian)* 79−44360
shock waves, metagalactic, thermal processes 80−46678
short-chain molecules, hydrodynamic behaviour, extended Rouse-Zimm theory 77−558
short-chain molecules, hydrodynamic behaviour, viscosity 77−559
slide journal bearing, stationary oil flow, estimation of soln. of Navier-Stokes and energy eqns. 79−55353
sliding interfaces and impact, numerical treatment 79−41631
slip boundary condition, rough sphere ang. vel. correlations, hydrodynamic anal. 77−51286
slip boundary condition for rough sphere rotation 77−31335
slow nova, hydrodynamic study of outburst 78−40954
sluice gate exchange flow for stratified liquids *(Russian)* 77−55053
smoothed particle hydrodynamics, theory and appl. to non-spherical stars 78−12203
SOLA-VOF computer code for finite difference solns. of Navier-Stokes eqns. 79−49659
solar coronal expansion, hydrodynamic blast wave theory with radiation heat flux 80−90377
solar coronal hole flows, models 79−58313
solar faculae, mag., vel. and brightness struct. 79−25557
solar granulation, physical model 79−30026
solar nebula, nebula, primitive, interaction with giant gaseous protoplanets, computer anal. 80−56727
solar nebulae, mass transport processes in rotating dust cloud 80−8556
solar photosphere, downdraught development at sunspot origin 80−72908
solar photosphere, hydrodynamic motions rel. to mag. fields fine struct. 80−98646
solar photosphere, vel. field spatially averaged props. and hydrodynamics 79−16912
solar wind, 3-D model of corotating hydrodynamic streams 80−72737
solar wind, corotating streams, three-dimens. model, theory 79−35086
Soret driven instability, transient and steady state behaviour, analogy with laser instability 79−55413
sound generation mechanism 79−32172
Southern Ocean, large-scale relative dynamic topography and current flow 78−85580
sphere approaching permeable wall, hydrodynamic force 79−46383
sphere in channel with variable cross section, hydrodynamic balancing 79−77246
sphere in viscous incompressible fluid, surface force density calc. 77−7368
sphere moving in incompressible fluid, surface force density 77−7369
spheres, deformable contiguous, in incompressible inviscid fluid, hydrodynamics 78−1727
spherical accretion onto compact X-ray sources, luminosity thermal limit 80−82546
spherical Brownian particle in flow, hydrodynamic model for attractive pot. self-diffusion 77−11293
spherically symmetric accretion flows, stability anal., X-ray sources appl. 80−46387
spherically symmetric accretion of gas with self-gravitation 79−8834
spherically symmetric polymers, in soln., Faxen theorems 78−94342
spherically symmetric polymers, in soln., hydrodynamic interaction 78−94343
spheroids, in streaming suspension, dynamics, dielectric consts. 78−76374
spiral galaxies, interstellar gas hydrodynamic flows in regions of Lindblad resons. 78−96527
spiral galaxies, normal, post-explosion gas depletion in central regions 80−62272
stability, non-linear, unipolar injection of insulating liquid, Galerkin method 80−74835
stability of liquid films and jets, effect of soluble surface-active substances 80−6027
stability problems, computer program for testing linear stability of vel. profiles 77−54975
stars, self-gravitating systems, fluctuating hydrodynamics and thermodynamics 78−77485
statistical hydrodynamics for the Burgers turbulence *(Japanese)* 80−14667
statistical mechanics, response theory for systems nonlinearly displaced from equilibrium, graphical approach 80−22285
steam mains, Gentilly-I generating station, inertial analysis of hydrodynamic oscills. 78−89944
steel, molten, heat loss during solidification hydrodynamic eqns., hardening front kinetics *(Russian)* 80−55385
stellar atm. with gravity stratification, perturbation propag. *(Chinese)* 80−85934

hydrodynamics continued
stellar collapse, adiabatic hydrodynamics and shock wave propag. 80−56861
stellar collapse, hydrodynamics 78−45318
stellar collapse and explosion, massive star core hydrodynamics 79−16995
stellar collapsing core, shape instability pressure stabilisation 80−8537
stellar convection, hydrodynamics rel. to solar obs. 78−89182
stellar convection, value of mixing length 80−77379
stellar convective envelopes, non-local convection, statistical theory *(Chinese)* 80−85933
stellar core collapse, effects of eqn. of state on outcome of collapse 80−85928
stellar dynamics in thin disk galaxies, hydrodynamic eqns. 79−92809
stellar formation hydrodynamic model reviews *(Polish)* 80−67709
stellar hydrodynamic equations, rel. to radius depend. of elliptical galaxies vel. dispersion 80−51876
stellar line accretion theory, gas press. effect 78−32525
stellar models, complete viscous polytropes, linearized theory validity 79−35244
stellar penetrative atmosphere, instabilities 79−84783
stellar systems, prolate, instability 80−101642
stellar wind flow past compact object, hydrodynamic eqns. and X-ray intensities 80−22116
sticking and slipping boundary conditions, friction of rot. bumpy cylinder 78−63410
stochastic properties of complex nonlinear oscillation regimes 80−8919
stochastic self-oscillations and turbulence, review 80−4537
stochastic treatment, instability at onset of convection 77−19590
Stokes equations, Galerkin-type representations 78−51143
Stokes flow ellipsoid of min. drag, limited by cylindrical front *(French)* 79−53982
Stokes problem, effects of free convection on oscillatory flow past infinite porous vertical limiting surface 80−109348
Stokes problem for a suspension of spheres at finite concentrations 78−55967
Stokes problem for suspension of spheres, effective medium theory 79−81836
strain-dependent eddy viscosity, spectral characts. 78−44937
stratified water circulation, forecasting for water quality management planning in coastal zone 79−5543
structural relaxing fluids, hydrodynamics theory *(Russian)* 80−19453
submarines, aero/hydrodynamic forces and moments 77−89094
submerged cylinders, forced oscills. test in water 78−5728
submerged tube surrounded by rigid tubes, hydrodynamic inertia coeffs. 77−7335
Sun, loop prominence knots, motions, Hα line filtergram obs. 80−67693
superconductors below T_c, dynamics 80−44760
superfluid, Vortex formation near protuberances on a solid surface and the structure of the Ginzburg-Pitaevski equations 79−86947
superfluid degenerate fermi gas, hydrodynamic eqns. allowing for finite coherence length *(Russian)* 80−12989
superfluid Fermi system, Bose spectrum, hydrodynamic action functional *(Russian)* 78−14534
superfluid systems, hydrodynamics with account for ponderomotive forces *(Russian)* 79−19409
superfluid viscous liq., hydrodynamics and transport coeffs. 77−69134
supernova remnants, evolution and struct. of interacting remnants 80−4423
supernovae, explosive core overturn and mass ejection 80−72988
supernovae, self-similar oscillations of gas *(Russian)* 79−17001
suspension, hydrodynamic screening and viscous drag at finite conc. 78−35725
swirled flow, sprayed liquid hydrodynamics 80−79325
Taylor vortices above higher instability points 78−75150
theory, review 77−14973
thermal breakdown in viscous fluid, Couette flow between cylinders 78−83391
thermohydrodynamics equations, derivation from Boltzmann eqns. 77−75875
thin disc galaxies, stellar hydrodynamics 79−25706
thin films, role of disjoining pressure in equilib. and flow 79−14984
thin films with nondeformable surfaces, generalized equations of hydrodynamics 80−10224
tidally distorted configurations, external form and potential, third-order approx. 80−41714
toroidal reactor primary containment vessels, consistent mass matrix anal. of hydrodynamic effects 79−76066
torus, floating, analysis of oscillations due to incident waves 78−22356
traction prediction in elastohydrodynamic contacts 78−63394
transport processes, nonlinear 80−22310
transport processes, relativistic generalisation in continuum *(Hungarian)* 78−89383
transport relaxation equations, reciprocity, boundary conditions 77−13719
travelling wave, hydrodynamic effects *(Russian)* 80−38423
tsunami accompanying Tonankai earthquake of 1944, source model *(Japanese)* 80−67344
tsunamis, transform. in coastal zone 78−77192
tube bundle transient heat transfer and hydrodynamics with large flow and heat flux perturbations 78−83484
turbogenerator, with hybrid hydrostatic hydrodynamic lubrication, behaviour in laminar and turbulent conditions *(Italian)* 80−81208
turbojet noise suppression investigations using hydrodynamic press. meas. and cross-correlation techniques 78−79157
turbulence, onset, effect of nonequilib. fluctuations 78−18272
turbulence formation during flow around elastic membrane *(Russian)* 79−41666
turbulent flow, numerical methods in statistical hydrodynamics 77−35121
two-dimensional, transport modes, exponential decay 78−5721
two-dimensional hydrodynamics and water quality by finite element method 78−92877
two-phase flow, compressibility effect on hydrodynamics, resistance coeff. 78−55684
two-phase flow, hydrodynamics and heat exchange in film flow 78−91000
two-phase porous cooling system, hydrodynamic and thermal characteristics 77−10012
tyre tread on wet surface, elastohydrodynamic squeeze film action 77−15144

hydrodynamics continued
underwater spark induced axisymmetry unsteady motion betweeen shock wave front and contact surface *(Russian)* 79−77323
Universe, hydrodynamics, book contrib. 77−49516
unstable wave excitation at tangential discontinuity by high-intensity US beams 80−58851
unsteady flow in open channels, num. analysis method, teaching aid paper 77−29972
upper atmosphere hydrodynamical accelerator, numerical modelling *(Russian)* 78−16225
Uranus atmosphere, equatorial flow model rel. to rot. 80−67653
vaporisation, hydrodynamic effects, in thermal model of condensed media under action of intense EM radiation *(Russian)* 79−69922
variable quasars as pulsating accretion discs 80−46693
variational inequality finite element approx. 77−13613
variational principle generalisation in Euler represent. *(Ukrainian)* 77−30011
velocity, double use in hydrodynamics *(French)* 79−75349
Venice, sea-lagoon exchange in modified tide regime 80−12431
ventricular pumping model, source impedance and internal reactive power 77−37007
Venus thermosphere, H global circulation and distrib. 78−89093
vestibular apparatus, transform. of angular accels. by system of semicircular canals 77−16943
vibrational relaxation in liqs., hydrodynamic theory 77−35734
vibratory liquid-gas mixture, nonlinear resonance expt. *(Ukrainian)* 78−90811
viscosity, soft-sphere, numerical calc. using discrete hydrodynamics 79−90505
viscous drop, almost spherical, Brownian motion and fluctuating hydrodynamics 80−87787
viscous fluid in pipes, nonisothermal flow, crit. phenomena 80−103074
viscous impressible fluid bounded by cylindrical boundaries, slow motion of small sphere 77−14978
viscous liquid flow through annular clearance over rotating inner cylinder 80−64626
viscous or perfect incompressible fluids, gravity waves with surface tension and capillarity strain *(French)* 77−65749
void fractions in the phase flow, hydrodynamic and hydraulic studies for reactors 79−55411
volcanoes, hydraulic transients as seismic source 79−100816
vortex flow on contour, hydrodynamic effect 79−86438
vortex motion, integrals of hydrodynamic equations, Helmholtz 1858 paper 79−9072
vortices on sphere *(Russian)* 79−32529
water bodies, wind effects on surface to bottom fronts 79−2261
water film flow behaviour and effect on cocurrent air flow, press. distrib. along rigid wavy structures 77−55029
water tunnel turbulence measurements behind a honeycomb 79−18874
water waves, oscillatory boundary layer meas. using laser Doppler anemometry 79−27719
wave and force measurement system 79−41780
wave diffraction theory appl. to free floating and moored rigid structs. 79−7321
wave/mean flow interaction, introduction to generalised Lagrangian-mean distribution 80−109214
wave/mean flow interaction, mean motion induced by transient inertio-gravity waves 80−105029
waves, small amplitude, scale selection in phys. modelling *(Ukrainian)* 77−51069
waves development from periodic disturbances in non-uniform fluid, surface tension effect *(Russian)* 78−77253
Weddell Sea, bottom water outflow variability and dynamics 80−67366
wing in limit of small elongation above uneven surface (underwater) *(Russian)* 77−55122
zonal model for general atmosphere circulation, development, climatology data comparison *(Russian)* 80−12479
H II regions gas dynamics, two-dimensional axisymmetric calcs. 80−12791
H_2, compressed, Rayleigh-Brillouin spectrum rel. to translational hydrodynamics 77−24856
H_2O, cavitation nuclei conc., holographic and hydrodynamic obs. 78−83440
He cooling systems, large, review of hydrodynamics and heat transfer 79−204
He, flowing superfluid, hydrodynamics of vortex generation 77−1272
He II, pressure-modulated flow in narrow channels, nonlinear friction force effect on vel. *(Russian)* 78−22914
He II, superfluid, rotating with vortices, defect hydrodynamics *(Russian)* 80−49445
He II, superfluid flow hydrodynamics, normal density component velocity depend. *(Russian)* 80−65326
^{3}He, A-phase, Lagrange and Hamilton hydrodynamic eqns. *(Russian)* 78−10248
^{3}He, rotating superfluid, equilibrium order parameters, chemical potentials 80−96713
^{3}He, superfluid, A-phase, arbitrary textures, hydrodynamics 77−31833
^{3}He, superfluid, A-phase, equilibrium textures, hydrodynamic and mag. effects in cylindrical pore 77−72734
^{3}He, superfluid, A-phase, Hamiltonian equations of hydrodynamics 77−69138
^{3}He, superfluid, A-phase, hydrodynamics and macroscopic dynamics in high mag. field 77−72733
^{3}He, superfluid, anisotropic A phase, orbital hydrodynamics, large angles of rotation of orbital momentum 77−80669
^{3}He, superfluid, B-phase, appl. of two-fluid hydrodynamic equations 79−46865
^{3}He, superfluid, Barnett effect 80−88388
^{3}He, superfluid, chiral fields, in Ginzburg-Landau region 79−55991
A-^{3}He, superfluid, hydrodynamic eqns. *(Russian)* 77−4237
^{3}He, superfluid, hydrodynamic modes interaction, sound propag. and spin waves *(Russian)* 79−37897
^{3}He superfluid, hydrodynamics and inhomogeneous states 80−49453
^{3}He, superfluid, order parameter, sp. ht., mag. props., sound propag., hydrodynamic props., book contrib. 79−99388
^{3}He, superfluid A phase, theory of orbital dynamics, hydrodynamic eqns. 80−54461
^{3}He, superfluid A-phase, entropy production and non-linear hydrodynamic eqns. 77−80668
^{3}He, superfluid A-phase, helical textures, hydrodynamic stability study 79−55990

hydrodynamics continued
^{3}He, superfluid A-phase, hydrodynamics in Lagrange formalism *(Russian)* 77−55413
^{3}He, superfluid A-phase, intrinsic angular momentum, and its hydrodynamics with unclamped normal fluid 78−22922
^{3}He, superfluid A-phase, microscopic theory for orbital hydrodynamics 80−70494
^{3}He, superfluid A-phase, textures, hydrodynamic and mag. effects in slab 77−1273
^{3}He, superfluid B-phase, microscopic evaluation of transport parameters 79−51354
^{3}He, superfluid B-phase, nonlinear hydrodynamics 80−59750
^{3}He-A, superfluid, gauge wheel, rot. symmetry and phase of order parameter 79−82409
^{3}He-A, superfluid, helical texture stability, hydrodynamic free energy 79−95238
^{3}He-He II degenerate soln., kinetic coefficients, thermodynamic props., hydrodynamic, acoustic and spin wave propag. *(Russian)* 78−18867
^{3}He-superfluid ^{4}He mixture, density matrix, hydrodynamic eqns. 77−35790
^{4}He, dynamic structure factor near λ temp. 77−66049
^{4}He film, superfluid, dynamics 80−59748
^{4}He film, third sound, two-dimens. hydrodynamics and elementary excitations 79−7721
^{4}He, liq., hydrodynamic theory, variational methods 79−42331
^{4}He, rotating superfluid, equilibrium order parameters, chemical potentials 80−96713
^{4}He, superfluid, appl. of hydrodynamic eqns. accounting for ponderomotive forces for superfluid systems *(Russian)* 79−19409
^{4}He, superfluid, canonical hydrodynamic equations *(Russian)* 78−79835
^{4}He, superfluid, hydrodynamics, Zilsel's variational principle derived from Lin's principle 80−24695
^{4}He, superfluid, three particle condensate model 78−22919
^{4}He superfluid films, geometry induced third sound splitting 80−96712
InSb melt, hydrodynamic behaviour in cryst. growth under large inertial accelerations 80−66421
Lu_5Pt_4, isotypic with Pu_5Rh_4, X-ray cryst. struct. refinement anal. 79−4421
Rb, liquid, longitudinal modes, transverse modes and velocity correlations 78−94954

hydroelectric power stations
see also dams; hydraulic turbines; pumped-storage power stations; tidal power stations; water supply; wave power generation
acoustic emission of turbine spiral during pressure testing 80−28391
Austrian development on river Danube *(Czech)* 79−66401
Campotosto reservoir, seismic recording network *(Italian)* 80−101446
Dnieper navigable lock, geological and civil engineering problems *(Russian)* 77−86883
electric power generation technology, reviews 79−24883
evaluation of alternative energy sources for the Guyana energy crisis 80−61270
flood gate of Spilja plant, water routes hydro-chemical analysis *(Croatian)* 80−12443
hydro-photovoltaic plants, peak power generation economics and reliability 80−45706
hydroelectric generation in Austria, short term and long term fluctuations *(German)* 79−87961
hydropower potential in Austria, current assessment *(German)* 79−87962
hydropower potential in Burundi 80−81417
hydropower reservoir lakes and dams construction, environment protection aspects *(German)* 80−30373
Italy's electric power requirements, nuclear programme, pumped storage hydroelectric integration 79−26733
James Bay hydroelectric complex, developments 80−21369
Maneri Bhali Hydel scheme, stage I, hydraulic model, India 77−9452
nonlinear estuarine response to tidal action for potential hydroelectric power generation 77−70692
promotion in Austria, economic aspects *(German)* 79−87981
Scottish Highlands hydroelectric potential assessment 80−7911
steel penstock, large diameter, embedded in rock, strain measurements, using strain gauges 79−43544
surplus water discharged over spillway during heavy flow, electricity generation source 79−100481
thermoclines, solar thermal energy resource for enhanced hydroelectric power production 79−92060
Tornio River plans, review 78−57236
water run off at Syr Darya, recording aspects *(Russian)* 77−86942
wave energy conversion, in random sea, using half-plane and omni-directional convertors 79−52875
Zaire River hydroelectric pot., specifications and cost estimates of proposed plants 80−30375

hydrogen
see also nuclei with .....
see also deuterium; hydrogen ions; hydrogen neutral atoms; hydrogen neutral molecules; protons; solid hydrogen; tritium
absorbed by Th_6Mn_{23} and Y_6Mn_{23}, influence on mag. behaviour 77−85423
absorbed by Th_7Co_3 and Th_7Ni_3 effect on mag. behaviour 80−60184
absorption, by $CeRu_2$, change of valence of Ce ions 79−47185
absorption, by $LaRu_2$, supercond. disappearance 79−47185
absorption, by rare earth-transition metal alloy 77−35812
absorption, in Nb-V system 80−59808
absorption, in Pd, electronic band struct., comparative study of electric and mag. props. 78−95259
absorption, on $LaNi_5$, kinetics, diffusion consts. 78−14508
absorption, on reduced Ni oxide 80−76529
absorption (desorption) by activated $LaNi_5$, slow step 78−18894
absorption and desorption by $LaNi_4$ 77−81400
absorption and desorption by $LaNi_{5-x}Al_x$ alloys, metal hydride appls. 77−86308
absorption and desorption kinetics in $LaNi_5$-type ternary alloys 80−55932
absorption by austenitic stainless steel, H_2 induced transform. *(Japanese)* 80−11640
absorption by discontinuous Pd film, effect on elec. cond. 77−47905
absorption by $EuRh_2$, degradation by cycling 78−34628
absorption by FeTi, catalytic effect of surface segregation 79−11626
absorption by $GdNi_2$, and its effect on struct. and mag. behaviour 78−10685
absorption by $GdNi_2$, effect on struct. and mag. behaviour 78−2682
absorption by $LaNi_5$, $NdCo_5$, and $ErCo_3$, 77-300K 79−23737
absorption by $LaNi_5$ for storage appls., effect of Ni, Ce, Co alloying additions 80−45790
absorption by rare earth intermetallic RNi_4Al, and cryst. struct. of hydride 78−34487
absorption by rare earth-Fe_2, effect on mag. props. 77−63178
absorption by ReO_3, electron diffr. obs. of H_xReO_3 phase 79−60513
absorption by $ThNi_{5-x}Al_x$ 77−84932
absorption by $Ti_{1-x}Zr_xMn_2$, hydriding characts. 78−44402
absorption by $Ti(Al_xB_{1-x})_2$, (B=Cr, Mn, Fe, Co) 79−28198
absorption by Ti-Co, Ti-Ni alloys, press.-composition-temp. relationships, enthalpy, entropy 80−2267
absorption by Ti-Co, Ti-Ni alloys, thermodynamic parameters calc. 80−2268
absorption by TiCu intermetallic compounds, decomposition reaction *(Japanese)* 78−23668
absorption by V-Cr alloys, thermodynamic parameters 78−87862
absorption by Zircaloy, Sn(Fe)(Cr)(Ni) effect 80−49527
absorption by Zircaloy-4/stainless steel type 304 diffusion bonded junction 79−65200
absorption by Zr-3d Laves phase binary and pseudobinary intermetallics, effect on mag. props. 80−88821
absorption by $ZrS_2C_{80.37}$ lamellar cpd. 80−44418
absorption capacity in pseudobinary Laves phase cpds., phenomenological model 77−84935
absorption capacity in $Zr(A_xB_{1-x})_2$ (A=V, Cr, Mn; B=Fe, Co) 80−88433
absorption in ε-FeTi, effect of Ce 79−73315
absorption in AB_2 Friauf-Laves phases 80−24406
absorption in EuPd and $EuRh_2$, mech. 78−38846
absorption in Fe and Cu single crysts., stress-strain analysis 78−15463
absorption in FeTi, surface segregation and catalytic effect on hydrogenation 78−84819
absorption in Invar, mag. struct. depend., Stoner's band model calcs., Mossbauer spectra 80−65787
absorption in La_2Co_7 and $LuFe_2$, mag. props. changes 80−71270
absorption in $LaNi_{4.4}B_{0.6}$ 80−88432
absorption in $LaNi_5$, Fe-Ti and Mg_2Ni, effect on magnetism 80−70941
absorption in $LaNi_5$, kinetics *(Chinese)* 80−103561
absorption in metal, determ. by mag. sound technique *(Russian)* 77−60009
absorption in Ni single cryst. foils, H_2-induced deform., electron optical obs. 79−57059
absorption in $ScFe_2$, effect on Mossbauer isomer shift 80−75903
absorption in Zr and Hf based intermetallic cpds. 79−77754
absorption kinetics in Ta, 77-700K, effect of O_2 sorption layers 79−95169
absorption kinetics on Ta wire, 500 to 700K 80−49528
absorption on FeTi, effect on mag. props. 80−75447
absorption on Ni surface, demagnetisation of surface due to absorption 77−80990
absorption on rare earth metals 77−4257
absorption on Re, within wide temp. range 80−10778
absorption on steel, aniline surfactants effectiveness, HCl conc. effect 80−108638
absorption on transition metal intermetallic cpds., effect on mag. props. 80−60224
absorption on YMn_2 and Y_6Mn_{23}, lattice consts. and mag. props. 77−36061
absorption rate in Nb(Ta), metallic film effect 80−49525
absorption-desorption characts. for Mischmetall-Co_5 cpds. 77−89640
absorption-desorption characts. of mischmetal-Ni-Al alloys 79−95168
absorption-desorption characts. on $TiCo_{1-x}Mn_x$ 80−96735
absorption/desorption isotherms, metal-H_2 system at high press. 78−51679
ACT-1 toroidal plasma, externally launched ion Bernstein wave 80−106967
activated C+H_2, react. rel. to C paramag. props. 77−63957
addition to α-Fe, effect on shear modulus 77−36561
addition to Si, effect on nitridation 79−57129
addition to Ti-Al-V (6,4 wt.%), effect on sustained loading cracking 78−48515
adsorbed H on W (001), atomic nature of β-states, electron energy loss spectra 77−76664
adsorbed layer, inelastic low energy electron scatt. 78−72653
adsorbed layer on Mo (001) surface, band structure self-consistent calc. 80−15585
adsorbed layer on Ni surface, laser induced desorption 79−1548
adsorbed layer on Si {100}(1×1) surface, LEED study 78−67910
adsorbed layers on Ta and Pt, energy loss spectra *(French)* 79−83069
adsorbed monolayer on Cu surface, UV-visible polarised modulation spectra obs. 78−72619
adsorbed on α-cyclodextrin surface, effects on positron annihilation 79−65952
adsorbed on Be, secondary ion emission, coverage dependence 80−35043
adsorbed on Cu, adsorbate induced photoemission 78−95668
adsorbed on $GdFe_3$, $DyFe_3$ and $HoFe_3$, effect on mag. props. 77−63129
adsorbed on jellium surfaces, charge density oscills. and adatom-adatom interaction 79−42389
adsorbed on microcrystalline WC, mol. dynamics 78−71941
adsorbed on Mo(100), photoemission rel. to surface resonances and surface reconstruction 80−44417
adsorbed on Nb, distrib., electron-stimulated desorption ion imaging 80−103572
adsorbed on Ni, inelastic neutron scatt. 78−18898
adsorbed on Ni(111), proposed struct. 79−60628
adsorbed on Ni (100)(110)(111) surface, insert model 80−50889
adsorbed on Ni (110), adatom configuration, He diffr. study 80−103569
adsorbed on Ni (111) surface, Raman spectra 79−28769
adsorbed on Ni surface, effect on single ion self-diffusion 80−103548
adsorbed on Pd(111)(110) surface, inert model 80−50889
adsorbed on Pd black, vibr. spectrum assignments, inelastic neutron scatt. obs. 78−71942
adsorbed on Pt (111) surface, inert model 80−50889
adsorbed on Ru(110), UPS and work function meas. 79−99424
adsorbed on Ru (110), UPS and work function change meas. 79−78834
adsorbed on Si (100) surface, LEED and AES meas. 78−60016
adsorbed on stepped Pt surface, adsorption sites study by EELS 80−49521

hydrogen continued
adsorbed on W, electron stimulated H^+ desorption, (100) face 77−66091
adsorbed on W (001), LCAO calc. of band struct. 77−8168
adsorbed on W (011) face, bidimensional lattice *(Russian)* 79−7744
adsorbed on W (100) and Ni (111), angle-resolved and variable impact energy electron vibr. excitation spectroscopy 80−76119
adsorbed on W (100) face, fluctuation, thermal impurity depinning and commensurate-incommensurate transition of CDWs 79−42611
adsorbed on W (100) surface, induced lattice reconstruction, surface vibr. obs. 79−19445
adsorbed on W (111), vibr. states, EELS 77−66090
adsorbed on W surface, Cl_2 scatt. 80−20743
adsorbed on W surface, energy spectra for electron stimulated desorption of H^+ calc. 78−79892
adsorbed submonolayer, ortho-para separation coeff., mol. alignment and rot. levels 77−7971
adsorption, and chemisorption on Ni surfaces, semi-empirical CNDO MO calcs. *(German)* 79−95465
adsorption, and dissolution, on ZrC-W eutectic alloy 79−69951
adsorption, dissociative, on Cu stepped and unstepped surfaces, theory 77−89636
adsorption, O_2-induced and reaction with other adsorbates on Ag(110) 80−55714
adsorption, on metal surfaces, adsorption mechanisms 79−69368
adsorption, on Ni (100), LEED, work function meas. and thermal desorpt. obs. 79−23843
adsorption, on Pt, electrolyte environment and crystallite size effects 78−27774
adsorption, on Pt (110) clean and oxidised surfaces, binding states and sticking coeffs. 77−28078
adsorption, on Pt (111), and desorption, obs. by dynamic meas. of work function 79−77915
adsorption, on Pt electrode, dynamic impedance meas. 79−74393
adsorption, on Pt-graphite catalyst, ESR obs. 79−24818
adsorption, on Sc (0001) and Ti (0001), geometric vs. electronic factor in surface electronic structure 80−70788
adsorption, on Ta surface, mass spectra and field-emission obs. 77−76673
adsorption and absorption by Pd thin layers, kinetic analysis of models 77−47679
adsorption and catalytic reactions with CO and O_2 on Pt 80−81362
adsorption and desorption, on Mischmetal-Ni alloy *(Japanese)* 77−47668
adsorption and desorption charact. in $LaNi_5$, $CeCo_5$, $SmCo_5$ *(Japanese)* 77−47667
adsorption and desorption kinetics of H_2 from clean and S covered Ru 80−6644
adsorption and desorption on Fe(100), C, O, S and K adlayer effects 80−71573
adsorption by $CeNi_4Al$, effect on mag. susceptibility 80−107990
adsorption by FeTi, hydrogenation-dehydrogenation cycling, positronium form. 80−18947
adsorption during Te electrodeposition on Sn in Sn/Te/electrolyte system 77−63923
adsorption in Si vacuum-crushed surface, EPR meas. 79−46957
adsorption into Hf_2Fe, mag. moment form. 79−87343
adsorption isotherms on Ni single cryst. surfaces 77−11776
adsorption of atmospheric gases on mol. sieves 13X and 4A at low press. and temp. *(German)* 80−88423
adsorption of CO on Al_2O_3-Ni catalyst in H_2-He, effect of H_2S on IR spectrum 78−71945
adsorption of H_2 onto W surface in presence of adsorbed H 77−51594
adsorption of HCl and water vapour 79−73398
adsorption of W, FEM study of binding states *(Japanese)* 78−2370
adsorption on γ-irrad. SiO_2 gel, rel. to colour centres 79−69156
adsorption on and desorption from TiH_x films, kinetics 80−6620
adsorption on $BaTiO_3$, effect on work function and spontaneous polarisation *(Russian)* 78−6211
adsorption on BeO, effect on thermally stimulated exoelectron max. 79−43109
adsorption on clean and oxidised Pt (111), binding states and sticking coeffs. 77−72787
adsorption on CO covered Ni films, resist., work function changes, isotherms 78−75926
adsorption on Cu-Ni (110), UPS, thermal desorption, AES,and LEED study 80−80087
adsorption on $ErFe_2$ surface, effect studied by spin polarised photoemission 80−29854
adsorption on evaporated Co film, surface pot. meas. 77−31890
adsorption on GaAs (110), surface photovolt. spectroscopy 80−49499
adsorption on graphite, 63 to 90K *(French)* 77−11791
adsorption on graphite, dynamics, neutron scatt. study 79−60641
adsorption on graphite, effect of non-orthogonality between localised orbitals of adsorbed atom 77−43435
adsorption on graphite of o-H_2, NMR, orientational behaviour, weak crystal field 78−75935
adsorption on Ir, effect on Ir work function 77−66094
adsorption on Ir, field emission energy distrib. spectra 80−25535
adsorption on Ir, influence of surface steps and clusters, field emission investig. 77−28698
adsorption on Ir (110) surface 78−38961
adsorption on Ir and surface reaction with O_2, thermal desorption and FEM obs. 79−52774
adsorption on LiF (001) surface, molecular orbital calc. 78−87878
adsorption on LiH (100) surface, FSGO calcs. *(German)* 79−33196
adsorption on metal, interaction between gas atoms on approach to surface 78−14609
adsorption on MgO during α-irrad., thermostimulated surface cond. obs. 80−34499
adsorption on NaCl, electrostatic interaction energies 79−23831
adsorption on Nb, sticking coeff. calc. 80−59803
adsorption on Ni, activation mechanism, extended Huckel calc. *(French)* 79−42379
adsorption on Ni, extended Huckel theory 78−10286
adsorption on Ni(111) surface at low temps., LEED meas. 78−56045
adsorption on Ni (001) surface, mol. dissoc., calc. 80−101036
adsorption on Ni (100), combined XPS/LEED/SIMS exam. 79−83075
adsorption on Ni (100)-p(2×2)C surface 79−91995
adsorption on Ni (110), substrate reconstruction, LEED constant momentum transfer averaging study 80−39445
hydrogen continued
adsorption on Ni (110) effect on electron spin polarisation 78−14933
adsorption on Ni (111), LEED intensity spectra, 173K 79−28192
adsorption on Ni and Cu surfaces, HMO studies 77−15682
adsorption on Ni film, ferromag. reson. 78−15028
adsorption on Pd and PdAg wires, heat of adsorpt., sticking probabilities 78−43240
adsorption on Pd film, reciprocal titration with O_2, film surface area determ. 77−1318
adsorption on Pd ribbon, thermal desorption and work function meas. 80−70538
adsorption on polar ZnO surfaces, cond., EELS study 80−71525
adsorption on polycryst. Re, work function *(French)* 77−28075
adsorption on Pt, face specificity, field emission probe-hole microscope obs. 77−11783
adsorption on Pt, Pd blacks, effect of PtO, PdO irrad. 77−11796
adsorption on Pt, reaction with adsorbed O 80−49514
adsorption on Pt, rel. to electrocatalysis 78−38935
adsorption on Pt, thermal desorpt. spectra 78−14607
adsorption on Pt, UV photoemission spectra 78−14608
adsorption on Pt (100) (5×20) and (1×1) surface 80−75434
adsorption on Pt (111), kinetics of interaction with O_2 77−55461
adsorption on Pt (111), role of at. steps 77−15690
adsorption on Pt electrode surface, struct. and comp. exam. by LEED and AES 79−70342
adsorption on Pt/MgO catalyst, 300-873K *(French)* 78−38967
adsorption on rare earth metals 77−4257
adsorption on Re, temp. controller for filament heating appl. *(Japanese)* 77−51603
adsorption on reconstructed GaAs (100) surfaces, ang. resolved photoemission from surface states 80−16143
adsorption on Rh, mass spectra 78−38970
adsorption on Ru (0001) surface, AES, LEED and thermal flash desorption meas. 78−38954
adsorption on Ru ($11\bar{2}0$), ellipsometry-LEED study 80−103570
adsorption on Ru field emitter, field-induced redistrib. processes 79−78854
adsorption on SbSI, effect on work function and spontaneous polarisation *(Russian)* 78−6211
adsorption on Si(100) surface, effect on struct., LEED meas. 78−14602
adsorption on Si (100), MeV ion scatt. study 80−80071
adsorption on Si (110), kinetics of H generation and adsorption, UPS 77−55450
adsorption on SiO_2 rel. to EPR relax. time *(German)* 79−95645
adsorption on SnO_2, desorpt. and cond. meas. 80−10790
adsorption on W, field emission current instability, freq. spectrum 77−32509
adsorption on W, PMR meas. of adsorption state, surface migration 78−10275
adsorption on W, surface reflectance spectroscopy on low index planes 78−71965
adsorption on W, thermal desorption and pulsed time of flight mass spectra anal. 80−30285
adsorption on W(100), nondipole electron impact vibr. excitations obs. 78−63922
adsorption on W(100) surface, adsorbate density determ. 77−1320
adsorption on W (001), effect on displacive transition, theoretical model 80−65352
adsorption on W (001), surface reconstruction and reordering 79−23835
adsorption on W (001), surface reconstruction and reordering, MeV ion scatt. studies 79−82443
adsorption on W (100), displacement by CO, photoemission and thermal desorpt. investig. 77−28079
adsorption on W (100) and (110) surfaces, chemical effects in N_7 VV Auger spectra 77−32474
adsorption on W (110) surface, band struct. and adsorbate geometry, surface-reflectance-spectroscopy 80−44416
adsorption on ZnO polar surface (0001) ($000\bar{1}$), specificity, field emission meas. 77−21009
adsorption on ZnO powder, C impurity effects 77−89638
adsorption on ZnO powder, light irrad. effects *(Japanese)* 78−95230
adsorption on ZnTe, manometric and mass-spectroscopic obs. 77−35808
adsorption on ZrC, effect on work function, thermionic emission expts. 78−2970
adsorption on ZrC and ZrC-Re alloys 79−19467
adsorption on ZrS_2Cs_x, mol. sieving effect *(French)* 79−65305
adsorption Si(100), (1×1)H struct., averaged LEED 77−62720
adsorption softening, kinetics, of solid interface of Al/Sn *(Russian)* 79−61619
adsorption-desorption kinetics on Si and Ge surfaces 77−47684
air and surface water composition, of N.Atlantic 80−77057
air streams, H_2 selective oxidation before CO anal. 77−63978
air-H_2 flame, temp. profile, two-line at. fluoresc. method meas. 77−71328
alkali halide:H^-, local modes and colour centre absorpt. bands, analogy 80−60632
alkali metal:H(0), impurity investigation using residual resist. and optical absorpt. meas. 79−95816
alkali metal vapour-H plasma, charge exchange role in optical props. 80−59284
analysis in different materials problems, using $^1H(^{15}N, \alpha\gamma)$ and $^1H(^{19}F, \alpha\gamma)$ reactions 79−5196
arc, at. and mol. no. densities meas. by VUV spectroscopy 79−94828
arc, contracted low-press., electron energy distrib. 78−18477
arc, contracted low-press., electron energy distrib. 78−18478
arc, high power, 53-92 nm continuum radiation source standard 80−44054
arc, high press., electron density, interferometric determ., refr. index calc. 80−24284
arc, high-power, as continuum radiation standard source, 53 to 92 nm, VUV radiometry 79−94311
arc, pulsed, dense plasma, Balmer spectrum near photorecombination threshold, press. depend. 80−38569
arc axial ground state population meas. 78−67598
arc plasma, forward scatt. at 10 μm using light mixing to meas. ion temp. 77−89313
arc plasma, isotope separation, mass spectrometric anal. 79−90457
arc plasma Balmer spectrum decay and two-fluid model 78−67603
atmosphere, effect on elec. cond. of MgO with paramag. surface defects, 20-250°C 77−20313

hydrogen continued
atom recombination at Ge surface, elec. cond. and chemomag. effect *(Russian)* 79−91125
atomic, chemical reduction of refractory oxides 79−93830
atomic, spin-polarised, mag. eqn. of state 80−100374
atomic, superfluid, spin-aligned, elementary excitation 77−72729
atomic beam, low tem., direct determ. of temp. and density 80−14875
atomic beam, optical diagnostics of high-power neutral beam 79−17556
atomic interactions with dislocations in Fe of varying purity 77−52377
atoms, in crysts., X-ray high-order refinements, theoretical approach 79−19121
automobile propulsion using H_2-gas-fueled internal combustion engine 80−16769
automotive fuel, technico-economic feasibility of storage, transportation, distrib. 80−16766
backscattering from solid surfaces, positive charge fractions 80−66375
beam discharge, electron kinetics in collisionless non-equilibrium plasma 80−92402
beam-foil spectroscopy, stray electric field due to high C foil resistance 80−42978
bibliography of H_2 energy 80−12863
biological photoprod. using sunlight, review 80−45777
biological prod. by solar energy conversion, coupling of hydrogenase and chloroplast photosystems 80−45778
biologically-assisted production, use of polymeric viologen mediators in a bioreactor based on hydrogenase-catalysed $Na_2S_2O_4$ decomposition 80−61460
biophotolytic production from H_2 using solar energy 80−61457
blister formation on Al during annealing in moist atm. *(German)* 80−25923
boiling, internal characts. 77−89529
bombardment, simultaneous with He, H_2, heavy ions to simulate microstruct. damage from fission or fusion neutrons 79−46723
bond dynamics in soln. 78−84573
breakdown in crossed elec. and mag. fields, modified Paschen's law 80−24121
breakdown potential 6.2 MHz elec. field, perpendicular mag. field, 350 G, 500 G, 0.5-8 torr 77−35422
bubble chamber, two-meter type, Ludmila, for particle interaction investigs. *(Czech)* 77−42215
bubble form. in Al-Zn-Mg at grain boundaries after water vapour embrittlement 78−15564
bubbles, submicron particle collection 78−11560
BWR, H_2 and O_2 monitoring in containment and off-gas systems 80−32414
catalytic interaction with CO on Ni (100), temp. programmed desorption study 80−66876
catalytic oxidation on Fe and Cr carbides 80−104462
catalytic production, highly concentrated, using Clusius separation column 79−24832
catalytic surface activity, $LaNi_5$ surface segregation *(German)* 80−51008
cathodic impregnation in stainless steel, austenite stabilisation *(German)* 79−47680
charging of Fe, effect on yield 78−15474
charging of Fe, lattice distortions, X-ray diffr. obs. 78−79629
charging of Fe, resist. recovery at low temp. 78−26729
charging of steel (type 304), twinning and martensitic phases, TEM 77−21222
chemical feedstock, supply and demand in USA (conf. Houston, Texas (Dec. 1977)) 80−16765
chemical industry, electrolytic hydrogen production, raw material of the future *(French)* 79−96328
chemical trapping in cryst. Si, vacancies, SiH_1-like centre form. 79−99916
chemically trapped, in Si_3N_4 CVD films, reflection spectrometry 78−10081
chemisorbed, on Ni foil, surface states and thermo EMF 78−91674
chemisorbed on graphite, regular phases 78−38965
chemisorbed on metal substrate, vibr., freq. shifts due to adatom interactions 80−39407
chemisorbed on metal surface, electron correl., friction coeff. 78−60026
chemisorbed on Mo(001), self-consistent electron struct. 80−44693
chemisorbed on Ni, desorption kinetics, rate equations 79−82448
chemisorbed on Ni, photoemission spectrum, Anderson model parameterisation 77−40334
chemisorbed on Ni(001), reaction with CO, extended muffin-tin orbital theory 80−76557
chemisorbed on Ni(111) face, geometry, LEED anal. 79−28200
chemisorbed on Ni (111), electronic struct. using angle-resolved photoemission 79−69573
chemisorbed on Si, relation of Si-H vibr. freq. to surface bonding geometry 80−49502
chemisorbed on Si (111) surface, electronic struct. 78−39182
chemisorbed on Si and Ge surface, cluster model approach for electronic struct. 78−56205
chemisorbed on transition metals, effect of surface spin fluctuations 80−75613
chemisorbed on W, surface cond. and intrinsic surface states, surface refl. spectra 80−15378
chemisorbed on W, vibr. spectra characts., adsorption sites 80−70535
chemisorbed on W, vibr. states, electron energy loss spectra 77−31877
chemisorbed on W(100), vibr. excitation of hydrogenic modes, angle dependent electron energy loss meas. 79−46914
chemisorbed on W (100), ν, vibrational mode, IR study 80−60582
chemisorbed on W (100), isotope effects obs. by SIMS 79−5234
chemisorbed on W (100), struct. determ. by surface vibr. modes anal., EELS obs. 80−39435
chemisorption, effect of metal surface on atomic H levels 77−35979
chemisorption, on Au(Pt) electrode, volume of adsorbed species, temp. and press. effects 78−84060
chemisorption, on defect MgO surface, quantum mechanical approach 77−62761
chemisorption, on Fe, small particles, magnetisation-pressure isotherms 78−39949
chemisorption, on graphite, cryst. orbital NDO calcs. 77−7965
chemisorption, on Ir (110), adsorption and desorption kinetics, struct. of overlayer 80−84367
chemisorption, on jellium surface, self-consistent calc. 79−95260
chemisorption, on Ni(111), geometry, order and disorder 79−65311
hydrogen continued
chemisorption, on Ni catalysts, dynamics, neutron spectrosc. obs. 80−59778
chemisorption, on Pd(111), bonding, photoemission spectra, SCF electron struct. 79−33320
chemisorption, on Pt electrode, entropy, temp. and press. effects 78−84059
chemisorption, on Rh and W perfect surfaces 79−86979
chemisorption, on transition metals, chemisorpt. energy trends 80−107631
chemisorption, on transition metals, Hubbard-type surface mol. model binding energy calcs. 78−71990
chemisorption, on W(100), adsorbate-induced surface reconstruction 79−4472
chemisorption, on ZnO, effect on ESR and NMR *(Japanese)* 80−50186
chemisorption, pot. energy function of two H atoms around Pt atom protruding from metallic Pt surface 80−10781
chemisorption bonding on Ni, Pd and Pt (111) surfaces, UPS obs. 77−76671
chemisorption by Ni (110) surface, demagnetisation, positive spin polarisation in electron field emission 78−52646
chemisorption geometry on Ni (111), LEED, thermal desorption, and work function meas. 80−39433
chemisorption in jellium, simple model 77−69171
chemisorption in KC_8 intercalation compound *(French)* 79−43624
chemisorption in $KC_{8}H_{2/3}$ intercalation compound *(French)* 78−27432
chemisorption of $H_2(D_2)$(HD) on Ni (100), vibr. excitation and struct., electron energy loss spectra 78−47660
chemisorption of H on 'cubium' clusters, size effects, embedding 77−59202
chemisorption of jellium, simple model 79−60625
chemisorption of Ni, surface magnetism 78−95510
chemisorption on AgNa mordenite 80−2752
chemisorption on Al, adatom geometry and binding energy 77−66093
chemisorption on Al, Mg, Na, calc. of adsorption sites and binding energy 79−46953
chemisorption on CeO_2, kinetics and characts. 78−51821
chemisorption on clean Fe (100) and (111) surfaces, LEED and thermal desorption 78−71996
chemisorption on Cu, density of states and chemisorption energy calc. 80−34315
chemisorption on Fe, equilibration and replacement reactions between H_2 and D_2, anisotropies 77−24482
chemisorption on Fe, LEED, UPS, thermal desorption spectroscopy, work function meas. 78−14566
chemisorption on Fe(111) clean single crystal surface, of N_2, NH_3, H_2, photoelectron spectroscopy, LEED studies 77−66087
chemisorption on Fe and Ni films, surface demagnetisation, ferromagnetic reson. study 80−80616
chemisorption on Fe fine particles, Mossbauer study 80−39415
chemisorption on ferromag. substrates, spin-spin interactions, UPS spectra calc. 80−6630
chemisorption on flat and stepped Pt surfaces, calcs. 79−28208
chemisorption on Ge (111), calc. using Anderson Hamiltonian 77−55463
chemisorption on Ge single cryst., highly efficient electron accommodation *(Russian)* 79−78818
chemisorption on graphite, regular phase, CO-NDO approx. 77−15681
chemisorption on graphite, substrate relax. effects 77−7962
chemisorption on Ir, photoemission, multiplets 77−15694
chemisorption on Ir surface, LEED, AES and thermal desorption meas. 77−1297
chemisorption on jellium, interpreted by one-parameter analytic model 77−39735
chemisorption on jellium surface, contraction of mol. band 79−28202
chemisorption on LaB_6, time of flight atom-probe FIM study 80−6652
chemisorption on Li cluster, ab initio HF calcs. 77−76670
chemisorption on metal substrate, model including image charge effects 79−73405
chemisorption on metal surfaces, linear response theory 78−91543
chemisorption on metal surfaces, relax. energies in UPS 78−91544
chemisorption on metals, surface sp-conduction electrons, spin-density functional formalism 79−33321
chemisorption on Mo(001), atomic displacements, LEED obs. 80−70514
chemisorption on narrow d-band metals, semiempirical theory 78−75927
chemisorption on Nb, photoemission studies 80−76145
chemisorption on Nb, two-state model kinetics 80−75438
chemisorption on Ni, interaction between adsorbates, model Hamiltonian calc. 79−46964
chemisorption on Ni, isothermal desorption near Curie temp., rate meas. 80−29268
chemisorption on Ni, order-disorder transitions on (111) surface, LEED observation 78−47668
chemisorption on Ni, Pd, and Pt, bond nature 80−34297
chemisorption on Ni, Pd, and Pt, embedded cluster model 80−39427
chemisorption on Ni, Pd, and Pt, model, comparison with UPS data 79−46932
chemisorption on Ni, Pt and W (001) surface, localised orbital approach 78−14587
chemisorption on Ni, Raman spectra, vibr. bands 79−61368
chemisorption on Ni(100), periodic surface model calc. 78−30822
chemisorption on Ni (001), surface and second-layer defect effects 80−65369
chemisorption on Ni (100), molecular cluster theory 77−1309
chemisorption on Ni (110), LEED 77−24470
chemisorption on Ni (111) or Pd (111), UPS obs. 77−1786
chemisorption on Ni and Pt (001), localised orbital approach 77−69166
chemisorption on Ni cluster surface, bond energy, HF calc. 79−39204
chemisorption on Ni clusters, macroscopic props. 79−82445
chemisorption on Ni film, effect on ferromag. reson. 78−72375
chemisorption on Ni film, influence on magnetism, ferromag. reson. spectroscopy 77−66395
chemisorption on Ni surface, molecular complex model 77−1314
chemisorption on Ni surfaces, Xα cluster calcs. *(Japanese)* 78−72002
chemisorption on Ni-SiO_2 supported catalysts, Mossbauer study 80−7219
chemisorption on NiO, cluster model, bonding 78−38939
chemisorption on NiO, theory, perfect surfaces and cation vacancies 79−69351
chemisorption on Pt, LEED, AES obs. of surface struct. and states 77−1300

hydrogen continued
chemisorption on Pt, Pt-Au and Ni (100) surfaces, interaction with O_2 77−51600
chemisorption on Pt(100), (111), polycryst. electrode surfaces, electrochem. activity, comparison 78−61015
chemisorption on Pt (100), (1×1) and (5×20) configs. 77−51599
chemisorption on Pt black, incoherent inelastic neutron scatt. study 79−60642
chemisorption on Pt electrodes, anion effects on multiple states, reflection spectra obs. 79−43634
chemisorption on Pt surfaces, field emission study 77−24477
chemisorption on Pt-Au, effect of surface segregation 77−51601
chemisorption on Raney Ni, neutron inelastic spectroscopy investig. 77−48686
chemisorption on reduced and stoichiometric $SrTiO_3$(111), UPS and XPS studies, illum. effects 80−71572
chemisorption on Rh (111), thermal desorption spectra and LEED obs. 79−86989
chemisorption on Rh (111) and (100) surfaces, LEED, AES and thermal desorption meas. 78−38951
chemisorption on semiconductor, effect of surface states 78−51823
chemisorption on Si, atom-probe FIM obs. 78−71968
chemisorption on Si, electronic struct. calc. 78−14784
chemisorption on Si, magnetic-sector atom-probe field ion microscopy exam. of hydride form. 77−80699
chemisorption on Si(111), conduction-band surface resonance 78−52051
chemisorption on Si(111) surfaces, formation of monohydride and trihydride phases, LCAO model appl. 79−15004
chemisorption on Si (100), new type of chemisorptive bond, theory 78−26930
chemisorption on Si (100) and Ge (100), pairing model calcs. and expt. 78−34719
chemisorption on Si (110) surface, UPS spectra meas. 77−20186
chemisorption on Si (111), Auger surface spectroscopy 80−50472
chemisorption on Si (111) 77−62743
chemisorption on Si surface, local density of states method and bond orbital model calc. 77−8165
chemisorption on Ti, flash desorpt. mass spectrometry 77−89646
chemisorption on TiO_2 (100), electron spectroscopy, evidence for Ti^{3+} photogeneration 78−38940
chemisorption on transition d-metals, heat of chemisorption calc. 78−38959
chemisorption on transition metals 78−2378
chemisorption on transition metals and semiconductors, Anderson model, including correlation and overlap effects 77−76662
chemisorption on W, angled resolved UPS exam. 77−55865
chemisorption on W, HFS model cluster calcs. 77−51795
chemisorption on W(100), localised orbital approach 77−69165
chemisorption on W(110) surface, effects on dielec. function, refl. spectra 80−75616
chemisorption on W {001}, displacive surface phases, LEED study 80−49520
chemisorption on W (001), angle-resolved photoemission, symmetry-related polarisation effects 78−56566
chemisorption on W (001), HF Green's function formalism and phase shift technique 80−24733
chemisorption on W (100) and Mo (100) surface, phase changes, LEED obs. 79−77911
chemisorption on W (100) substrate, adatom charge and binding energy, self-consistent calc. 77−62734
chemisorption on W (110), work function, Fowler-Nordheim studies 80−34501
chemisorption on ZnO, electrical cond. exam. adsorption centres 78−67913
chemisorption props. and catalytic activities of Pt surfaces with variable kink concs. 80−35576
chemisorption Rh (755), (331), desorpt. temp. and decomp. characts. 79−65318
cluster approach to single H atom in single crystal of Ni 78−47334
co-adsorption with CO on Rh (111), segregation of co-adsorbed species 80−65361
coadsorption with CO on Fe, effect of preadsorption of one on adsorption of other 79−19451
coadsorption with CO on Ni(111), surface carbide influence, vibr. electron energy loss obs. 79−52772
coadsorption with CO on polycrystalline Pt 77−59220
coadsorption with CO on Rh, thermal desorption mass spectroscopy meas. 79−46948
coadsorption with CO on Rh (111) surface, 2-dimens. phase separation 80−107634
coadsorption with CO on W (100), CO/H surface complex obs. 79−4478
coadsorption with O_2 on Rh (111) below 140K 80−29276
coadsorption with Th on W surface 79−90869
coherent transient Raman pulse propag., 30 atm., self-induced gain/loss modulation 77−10980
combustion, heat transfer in furnaces calc. *(French)* 80−19218
compressed, Rayleigh-Brillouin spectrum rel. to translational hydrodynamics 77−24856
concentration determ., based on contact potential meas. *(Czech)* 79−70386
concentration in Nb and V, neutron scatt. meas. 78−67735
concentration profile, in Si_3N_4, chem. bonding 79−33205
condensed gas films, thermal radiation absorpt. 78−32824
condensed on surfaces, spin aligned, obs. 78−63929
cryogenic data relevant to mag. fusion energy 80−8746
cryogenic isotope distillation for fusion power reactors 79−93833
cryogenic pumping, large-capacity, for nucl. fusion 78−21151
cryogenic pumping speed of Excalibur CVV2008 liq. He cryosorption pump 79−80633
cryogenic storage, liquefaction processes, storage and distrib. equipt. 80−45784
cryogenic storage and refuelling for automobiles 80−30604
CTR cryosorption vac. pumping of D, H and He at 4.2K 77−50298
cyclotron resonant laser induced breakdown obs. 77−39499
degassing metals for extreme low pressures 80−98924
dense gas, electron drift velocity 78−1785
dense gas, self-diffusion, quasielastic incoherent neutron scatt. obs. 78−22451
dense plasma, H_β line red shift expt. 78−67473
dense plasma, ionisation, master eqn. analytical soln. 78−59544

hydrogen continued
deorption, from Cu surface, production and meas. of atomically clean surface environment 80−52250
depth profiling in materials, use of $^1H(^{15}N,\alpha\gamma)$ resonant reaction *(French)* 78−91357
depth profiling in solids, using neutron TOF from H(t, n) 79−5198
desorption, electron stimulated, of H from W 79−86999
desorption, formation of Ni particles in $LaNi_5$ hydrides, 4.2K paramag. susceptibility 80−70934
desorption, from Ni(100), Ni(111), Pd(111) and Pt(111), preexponential factors 79−46918
desorption, Ni surface, activation barrier with holes model 77−80697
desorption, pulsed laser atom-probe FIM expts. 80−66402
desorption from Fe into ultrahigh vac. system, using permeation cell 80−86326
desorption from Ir (110), thermal desorption mass spectrometry, order plots 80−44409
desorption from metals by light ion bombardment, cross sections 78−95096
desorption from Ni, H_2, HD and D_2 mol. vel. distribs. 77−43431
desorption from TiH_x film at room temp., anomalous behaviour 80−29261
desorption isotherms of $DyFe_3$ hydrides 80−103565
desorption on Cu-Ni alloy, long and short range electronic effects in bonding 77−7974
detection, using Pd gate MOS transistor, fabrication and elec. characts. *(French)* 78−2569
detection by MOS structures 78−2578
detection in metals by $^1H(^{15}N,\alpha\gamma)$ reaction 80−55767
detection using Pd-MOS structure 77−73470
detection using SnO_2:ThO_2, effect of H_2 exposure on elec. resist. 79−56219
detector, based on H_2-sensitivity of Pd-ZnO Schottky barrier diode 80−11085
determination, combustion-gas chromatographic method, data processing 80−40762
determination, in coal, neutron activation techniques 79−52852
determination, in H_2O after photolysis, gas chromotography 78−61089
determination, in metals, spectrochemical method *(Russian)* 78−31748
determination, in molten Al and Al alloys, electrochem. probe method 79−11843
determination by nuclear reactions *(Czech)* 80−3430
determination by simultaneous heavy-ion induced nuclear reacts. and at X-ray emission 78−85240
determination in metals, plasma-ion analyser 78−15746
diamond, natural gem, H impurity conc., ion beam spectrochemical anal. 78−14374
diffusion, and solubility in solid metals 80−49422
diffusion, in BCC metals phonon-assisted quantum-mechanical tunnelling of interstitials 80−59730
diffusion, in Mo electrodes of glow discharge 77−7629
diffusion, in Nb, Ta and V single crystals, Debye-Waller factor, neutron spectroscopy 79−37881
diffusion, in V, Nb, and Ta, isotope effects, crystal field stabilisation 80−59728
diffusion and NMR in inert gas liquids 79−61249
diffusion and permeability in Fe at 49 to 506°C 78−59977
diffusion and solubility in β-Zr, above 1000°C and below 1×10^{-4} mm Hg *(Russian)* 80−24671
diffusion and solubility in Al *(Japanese)* 79−99370
diffusion and solubility in molten LiF-NaF-KF 78−34640
diffusion and solubility in PTFE, activation enthalpy 78−79775
diffusion and trapping in BCC and FCC metals 80−70447
diffusion and trapping in bead-on-plate welds 80−96697
diffusion coefficient in metal with low adsorption activity, steady-state flow method 80−10795
diffusion coefficient in Ti_2Ni, quasielastic neutron scatt. 78−30781
diffusion coefficients calc. for H isotopes in FCC metals *(Russian)* 78−91483
diffusion coefficients in metals *(Japanese)* 80−7604
diffusion constant in Nb, anomalous temp. depend., quasielastic neutron scatt. 77−43381
diffusion flame, Rayleigh temp. profiles meas. 80−16692
diffusion in α-Nb-H, thermal neutron scatt., general multisublattice jump diffusion model 77−66046
diffusion in α-NbH_xD_y, NMR spin echo obs. 80−34228
diffusion in α-Pd, by galvanostatic charging 78−84001
diffusion in α-Pd, next-neighbour jumps of H in quasi-elastic neutron scattering 78−91487
diffusion in α-Ti-Al *(Korean)* 78−30794
diffusion in β Ti-Fe alloys *(Korean)* 79−42312
diffusion in β-$LaNi_{5-y}Al_y$ hydrides, NMR studies 80−15298
diffusion in β-$LaNi_5H_x$, NMR meas. 79−82378
diffusion in β-Ti, V, Nb and Ta, neutron radiography meas. 77−39696
diffusion in β-Ti and β-Ti-Fe alloys *(Korean)* 78−18838
diffusion in β-$TiFeH_{1.03}$ 80−10707
diffusion in Ag, using membrane permeability method 79−37879
diffusion in alkali cryst., activation energy calcs. 77−51546
diffusion in alloy steels *(Japanese)* 78−52857
diffusion in annealed and cold worked Ni *(Japanese)* 78−51739
diffusion in BCC metals, quantum model 80−2212
diffusion in BCC transition metals, neutron spectroscopy 80−59731
diffusion in Co_5Sm, mag. aftereffect meas. 79−56573
diffusion in electrodeposited Fe-Co alloys and evolution overpot. 77−43377
diffusion in FCC metals, anomalous isotope effect 77−24444
diffusion in FCC metals and Cu, isotope depend. 80−59727
diffusion in Fe, 230-300K *(Japanese)* 78−84004
diffusion in glassy and rubbery polymer films, isotope effect 80−84327
diffusion in high strength alloy steel, effect of quenching and tempering 77−90384
diffusion in high strength steels HT80, HY130, effect of quenching and tempering *(Japanese)* 78−64565
diffusion in liquid Fe and Ni *(Russian)* 77−55369
diffusion in Lu, hopping process 80−24673
diffusion in metals, complex jump diffusion model rel. to quasi-elastic neutron scatt. by H 80−24638
diffusion in metals, correlated jump diffusion model, nonlinear eqns. 79−82386
diffusion in metals, localisation, rel. to μ^+ SR 80−50248
diffusion in metals, neutron radiography meas. 77−24438

hydrogen continued
diffusion in metals, neutron scatt., studies 79−42316
diffusion in metals, nonclassical processes 78−47591
diffusion in metals, random walk model with correlated jumps 80−24639
diffusion in metals, slow neutron scatt. obs., review 80−34248
diffusion in metals, theory, book contrib. 79−82389
diffusion in metals at low temps. 79−55941
diffusion in Mg quenched to 4.2K 77−28042
diffusion in Mo, 900-1100°C *(Russian)* 78−79811
diffusion in Mo enhanced by self-interstitial atoms, surface reaction const. determ. 80−75386
diffusion in molten Cu, stationary method determ. *(German)* 79−10974
diffusion in Nb, influence of H-H pairing, jump model 78−75878
diffusion in Nb, Ta, low temp., from quenching and annealing study 80−6555
diffusion in Nb, theory of Gorsky effect for low interstitial H conc. 79−10896
diffusion in Nb(V)(Pd), role of tunnelling, reson./nonreson. approaches 80−59718
diffusion in Nb and Mo, trapping at ion implantation induced defects 77−47622
diffusion in Nb-N, incoherent neutron scatt., interstitial effects 79−60558
diffusion in $NbH_{0.04}N_{0.07}$, interstitial trapping by quasielastic neutron scatt. 79−42298
diffusion in NbN_xHy, PMR obs. 79−69287
diffusion in Ni, trapping and mobility near vacancies, dislocations and cracks 80−49426
diffusion in Ni impure lattice 80−49425
diffusion in Ni single- and polycrystals at 60°C, grain boundary effects *(German)* 80−2211
diffusion in niobium 78−6182
diffusion in No, Pd, Va, quantum rate theory for symmetric double well pot. 78−55970
diffusion in Pd, effect on mechanical props. 79−65138
diffusion in Pd, induced elec. pot. investig. *(French)* 77−43379
diffusion in Pd, model 79−73338
diffusion in Pd, Ni, Fe, Nb, Ta, V, book contrib. 79−82390
diffusion in Pd alloys, alloying effect on activation energy 80−107571
diffusion in PdH_x, influence on nucl. spin-spin relax. *(Russian)* 77−51977
diffusion in Pt, diffusivity and diffusion-elastic phenomenon 79−51310
diffusion in pure Fe, 230 to 300K 79−95220
diffusion in stainless steel, effect of heat treatment 77−47627
diffusion in stainless steels, induced tip deflection of steel beam 80−39360
diffusion in Ta, Zr and Ti, effect on thermo EMF 79−23950
diffusion in Ta and Nb, expt. compared with theory for light interstitial diffusion *(Russian)* 77−15632
diffusion in TaH_x, and electronic struct., pulsed NMR obs. 80−54967
diffusion in Ti_2, nonisothermal, in temp. field of instantaneous plane heat source *(Russian)* 77−20123
diffusion in $Ti_3NiH_2(FeTiH)(LaNi_5H_6)$ storage materials, neutron diffr. obs. 80−51013
diffusion in Ti and Zr alloys at room temp. 79−51312
diffusion in Ti-Al, Ti-Cr and Ti-Ni alloys at room temp. *(Japanese)* 80−19987
diffusion in Ti-Fe, Mossbauer study 80−34838
diffusion in TiH_x, NMR obs. 80−34813
diffusion in transition metals 78−47596
diffusion in transition metals 80−29219
diffusion in V, effect of impurities 78−47604
diffusion in V, Nb, Ta, V-Cr, V-Fe, V-Nb, V-Ti alloys *(Japanese)* 78−10221
diffusion in V, Nb and Ta foils, thin Pd coating effect 79−52467
diffusion in water, laser interferometric study 77−76584
diffusion in Y, neutron scatt. and absorpt. study 79−60556
diffusion in Zircaloy, neutron scatt. and absorpt. study 79−60556
diffusion in Zircaloy-2, numerical soln. *(Korean)* 80−19989
diffusion in zone melted Fe, reversible dilation of lattice 77−11732
diffusion in Zr-Ni, 900 to 1080°C *(Korean)* 80−19988
diffusion into solid Al, desorption meas. 78−30797
diffusion mechanisms in TiO_2 79−73341
diffusion of H_2 towards crack in stressed solid, eigensoln. 77−24446
diffusion of protons in noble metals, config. and activation energies 79−37878
diffusion rate in Au thin layers 80−100359
diffusion through graphite powder compacts, time-lag analysis 78−2301
diffusion through metal junctions, behaviour of interstitial H 80−44368
diffusion through Pd membrane, diffusion-cell for separation H_2 containing mixtures, solar furnace appl. 80−92245
diffusion through Pt membranes at high press. and temps. 78−55984
diffusion traps for divalent ions, dielectric loss and ionic thermocurrent techniques 80−6566
diffusivity, in Ni_3Fe, Ni_3Pt and Ni_3Mn, change with order-disorder transformation 80−59729
diffusivity in Pd, 496 to 946°C 79−77815
diffusivity permeability and solubility of H_2 in Pt 79−95170
dilute impurities in rare gas liquids, nucl. spin relax. 79−56623
direct observations of H entrapment 78−48585
discharge, filled with H plasma, intense electron current and secondary plasma formation 79−64929
discharge, ohmic heating, ionis. 78−38511
discharge, RF induction breakdown, diffusion theory 77−84562
discharge cleaning of PLT vac. vessel, residual gas and surface comp. changes 79−80631
discharge lamp, integration with monochromator into vacuum UV source 77−42582
discharge plasma, resonant multiphoton optogalvanic spectroscopy, diagnostics appls. 79−23448
dissociated, heat transfer to catalytic surfaces, shock tube investigation 80−64551
dissociated gas, viscosity, thermal cond., 1-1000 bars, 2000-10000K 77−39391
dissociation on Cu (100) surface, classical trajectory calcs. 77−1947
dissociation poison and H_2 embrittlement 77−9079
dissociative adsorption of H_2-D_2 mixture on stepped Pt surface, reactant ang. of incidence effects 77−47670
dissociative chemisorption on Li clusters, ab initio SCF-MO calcs. 79−77918
dissolution in Mg, resistometric study under press. 80−70417

hydrogen continued
dissolution of interstitial atoms in metals, diffusion coeffs., reverse isotope effect *(Russian)* 80−88368
dissolved in Pd-Ag alloy, dil. soln., H-H interaction 78−71862
distribution in Cr-plated steel, laser-mass spectrometer investig. 78−61113
distribution in natural gas equipment, operating, safety and material problems 80−61468
distribution in plate subjected to external stresses, kinetics *(Russian)* 79−14836
distribution kinetics in vicinity of crack *(Russian)* 77−25132
distribution using contemporary natural gas distrib. equipment 80−97818
dry H_2 method used to remove C, N, O from Fe *(Japanese)* 78−11234
ductile fracture topography, geometrical contribs. and H_2 effects 79−83310
Earth core, H contrib. to density deficit 77−66895
effect on steel 12 MKh strength, ductility at 1000 kg/cm^2 press., 450°C *(Russian)* 79−15723
electric breakdown, Paschen's law violations 78−87570
electric breakdown, Paschen curve *(French, English)* 77−76221
electric discharge, non-equilib. ionisation rate calcs. 80−59319
electrical breakdown condition in JFT-2 Tokamak 79−14569
electrical energy and hydrogen production from fission product decay heat 79−18005
electro- and thermotransport in metals, book contrib. 80−24644
electro-/thermochemical prod. from H_2O by Westinghouse sulphur cycle 80−55940
electrochemical adsorption in Pt, adsorpt. states, tensiodynamic meas. 77−20196
electrochemical behaviour and solubility, in molten alkali acetates, fuel cells technology appl. 79−57244
electrochemical electrode impedance, relationship with structure and flow *(French)* 78−27766
electrochemical oxidation in fused alkali metal carbonates 80−72040
electrochemical prod., development of high efficiency alkaline electrolysis technology 80−30601
electrochemical prod., solid polymer electrolyte water electrolysis status for large scale hydrogen production 80−30605
electrochemical storage, of H in $LaNi_5$ alloys, nature of H bond 79−24917
electrochemical/thermochem. prod. using S cycle, laboratory prod. model and electrolyser development 80−30602
electrode, construction 77−25329
electrolyser, low cost hydrogen production *(French)* 80−7803
electrolytic prod. by H_2O, decomposition in acid molten electrolytes at 220 to 320°C 80−45769
electrolytic prod. by inorganic-membrane-electrolyte H_2O electrolysis 80−45804
electrolytic prod. by ocean thermal energy conversion 80−30546
electrolytic prod. using mobile generator 80−45805
electrolytic production, design and operation of advanced H_2O electrolysers, review 80−61449
electrolytic production, development and operation of advanced electrolysis cell 80−61441
electrolytic production, development of advanced electrolysis cell 80−45654
electrolytic production, development of solid-polymer-electrolyte electrolyser 80−30437
electrolytic production, exam. of reaction kinetics with Pd electrodes 80−30434
electrolytic production, high temp. electrolysis of H_2O vapour 80−30439
electrolytic production, O_2 evolution reaction kinetics on $NiLa_2O_4$ electrochem. electrodes 80−30430
electrolytic production, solid polymer electrolyte water electrolysis development status 80−30438
electrolytic production, storage, and utilisation for domestic appls., Hydrogen Homestead project 80−40921
electrolytic production, unipolar water electrolysers 80−30436
electrolytic production *(Spanish)* 80−35766
electrolytic production by H_2O dissociation, review 80−30429
electrolytic production by high temp. steam electrolysis 80−61440
electrolytic production from seawater, utilisation of ocean hydropower systems 80−30374
electromigration effective charge for ^3H in Zr and Ti, H conc. depend. 77−51545
electromigration in Ni, effective valency effects *(French)* 79−23781
electromigration in Ta, temp. depend. *(Russian)* 77−84986
electromigration in Ta, temp. depend. of mobility, 20-250°C *(Russian)* 78−47587
electromigration in Ti 80−34247
electromigration measured by resistance method in Nb and V 79−23783
electron avalanche, Monte Carlo simulation 80−38521
electron beam sustained discharge, electron neutral inverse bremsstrahlung '78−63604
electron cyclotron resonance plasma, for metal surface cleaning 79−47821
electron cyclotron resonance plasma, for metal surface cleaning of Cu 79−47822
electron drift velocity, density dependence, high press., quantum mech. theory 79−1285
electron drift velocity and longit. diffusion coeff. time-of-flight meas. 77−80264
electron stimulated desorption from W (100) and (110), threshold behaviour 77−47678
electron surface barriers for dense phases 78−91754
electron swarm motion simulation for high E/N 77−19667
electron-stimulated desorption from TiO_2, species characterisation 80−34305
electrosorption on Pt surfaces, oxidation, effect of soluble prods. *(German)* 80−55717
electrotransport in V(Nb)(Ta) at high H concs. 80−34246
energy, demand and supply of hydrogen as chemical feedstock in the USA 80−45817
energy, industrial appls. of liquid and gaseous H 80−45801
energy, production, storage, transmission, [Conf. Zurich, Switzerland. (Aug. 1978)] 80−22144
energy, R and D programs, review 80−45802
energy bibliography (1974-79) 80−26173
energy economy, R&D programmes 80−26171
energy prospects 80−45799

hydrogen continued
energy research programs in Japan, review 80−61435
energy resources 80−45798
energy storage, absorption by $NdNi_5$ and $LaNi_4Cu$ intermetallics, cell volumes and desorption pressures correlation 78−22860
energy storage, kinetics of hydrogen absorption and desorption by ternary $LaNi_5$ type intermetallic compounds 80−45813
energy storage, social implications 80−67001
energy storage, using metallic hydrides 79−43792
energy storage, wind energy conversion schemes, South African feasibility study 79−43714
energy storage in FeTi, surface segregation, catalytic effect on hydrogenation 80−45814
energy storage in metal hydrides 80−61445
energy storage systems, prospects 79−66418
energy storage using atomic H_2 at 1K *(German)* 80−89681
energy storage using electrochem. reduction of CO_2 80−7934
energy system for H-fuelled passenger bus, design 80−40924
enthalpy of solution in Mo-Nb solid solutions meas. 80−2166
equation of state from PVT and sound vel. meas., 75-307K, 2-20 kbar 77−62609
ethylene, surface reaction on Pt (111), EELS of radical vibrs. 78−71947
evacuation at 25 m^3/sec by electric arc unit 78−21144
evolution, H_2O electrolysis, nucleate boiling, vapour bubble behaviour, heat and mass diffusion 80−67013
evolution effect on current distrib. during vertical electrode electrodeposition 80−35543
evolution from $La_xNi_yH_z$, thermokinetics 80−30593
evolution from Mg alloys during isothermal treatment in vacuum *(Russian)* 77−77625
exotic superheavy, search in terrestrial substances *(Chinese)* 79−59605
extraction from LiF-LiCl-LiBr melt, appls. to fusion reactor blanket processing 78−53217
FBR mixed oxide fuels, determ. of total H_2 content *(German)* 79−49809
field desorption and field ionisation on metal surface 80−104047
fission research reactors, high-temperature nuclear heat source for hydrogen production 79−93686
flame, Na-seeded H_2-O_2-Ar, population inversion, two-photon laser excitation 79−34307
flame gas, electron-neutral energy exchange in AC field 77−42519
flame in air, laminar diffusion, Raman spectra diagnostics 79−47928
flashlamp light pulse shape calibration, using synchrotron radiation excitation standard 79−72642
fluid, Raman meas., 0.2-630 kbar, at room temp. 80−58269
freezing on inner surface of spherical polymer shell, cryogenic targets for laser-driven fusion 78−86688
fuel, electronic fuel injection techniques for H_2-powered internal combustion engines 80−45622
fuel, gaseous H_2-fuelled internal combustion engines 80−45819
fuel, health benefits derived from a planned hydrogen community 80−55947
fuel, produced by photolysis of H_2O *(French)* 80−55776
fuel, safety aspects of a future hydrogen technology 79−74551
fuel, storage in form of metal hydrides 80−72096
fuel for single cylinder diesel engines 80−61228
fuel source potential 80−108816
fuel storage and distrib. for automotive vehicles, techno-economic feasibility study 80−45820
fuelled vehicles, design and engine modifications with Fe-Ti hydride storage 80−40925
fusion reactor first wall, prod. of H, D and He by 15 MeV neutrons 79−93831
fusion reactor first wall radiation damage, H and He gas prod. from stainless steel 78−82512
fusion reactor-high temperature electrolysis system for H_2 prod. 79−18041
fusion Tokamak experiments, H(D) recycling model, influence on discharge behaviour 80−10393
galvanostatic desorption from PdH_x layer, quantitative theory 80−40694
gas, 16 μm, generation by CO_2, pumped rot. Raman scatt. 78−94410
gas, 97.2 nm generation by reson. freq. mixing *(Russian)* 78−46723
gas, ^{208}Pb stopping cross-section meas. with TOF spectroscopy 77−23569
gas, coherent Raman scattering with three lasers 79−23016
gas, compressed, Raman laser, axial mode self-locking 79−94223
gas, effect on field emission current stability of glassy C tip 80−11544
gas, effect on motion of Ag particles supported on graphite 78−34695
gas, efficient higher-Stokes-order Raman conversion 80−33082
gas, electron swarms, anisotropic scatt. model 78−91059
gas, flow through aperture into vacuum 78−9621
gas, influence on field emission of glassy C tips 80−11543
gas, IR generation, tunable, by coherent Raman mixing 77−42561
gas, laser-induced breakdown wavelength depend. meas. of threshold 79−41895
gas, lateral diffusion to electron mobility ratio 79−1284
gas, light scattering, approx. line shapes 78−90221
gas, monitoring by Pd gate MOSFET 78−44645
gas, para-, generation of 15 μm radiation by four-wave mixing 77−50720
gas, partially ionised, thermal cond. 79−86562
gas, partly ionised, viscosity calc., simplified expressions 79−18983
gas, powerful tunable IR and far IR Raman sources 80−5787
gas, prebreakdown current growth, ionis. coeffs. 77−80385
gas, Raman gain dependence on pump laser bandwidth 79−81483
gas, Rayleigh-Brillouin spectrum at high densities 78−90189
gas, stimulated Raman scatt., creation of laser source, near IR to submillimetric waves *(French)* 79−31993
gas, stimulated Raman scatt. gain of Nd laser radiation by rot. levels 80−69464
gas, stimulated Raman scatt. of excimer laser wavelengths for new lines in UV 79−59755
gas, stimulated Raman scattering, tunable coherent radiation source, 185 to 880 nm 79−31980
gas, stimulated rot. Raman scatt. pumped by CO_2 TEA laser 78−94411
gas, thermal cond., thermistor detector, ortho/para H_2 comp., temp.-jump region, 1-30 Torr 78−86263
gas, thermal cond. meas., 2-36 MPa 80−64668
gas, tunable efficient VUV generation using ArF pumped stimulated Raman scatt. 80−38072
gas bubble struct. in proton irradiated Cu at 300K 80−92569
gas coherent anti-Stokes Raman scatt. due to rot. transition 77−10971
hydrogen continued
gas discharge, low press., emitted photon probe for electron swarm parameters 80−43839
gas launcher, boundary layer closure, heat transfer 79−55387
gas puffing in JIPP T-II plasma, Mo impurity diffusion 80−28602
gas temperature meas., 300-1200K, choice of informative parts of rot. spontaneous Raman spectrum *(Russian)* 77−31416
generation, photoelectrolysis of water in sunlight 78−19143
generation by water solar photolysis, large-scale impracticability 80−26172
generation for automotive appls. utilising gas permeation and steam-on-iron processes 80−55778
glow discharge, diffusion in stratified positive column, impurity effects 77−11320
glow discharge, electron macroscopic props. *(Russian)* 80−92403
glow discharge, H penetration of Mo cathode, point defect depend. 79−41903
glow discharge, ion flow mass-energy relations, near hollow cathode 77−84563
glow discharge, Mo cathode surface layer form., electron diffr. obs. 77−55311
glow discharge, stationary and moving layer relationships *(German)* 80−24289
glow discharge with variable degrees of dissoc., diffusion theory of positive column 80−44018
p- and n-H_2, viscomag. effect, temp. depend. 78−9745
hardening of Fe, effect on struct., anodic behaviour *(Russian)* 79−15855
Haynes alloy 188, H_2 permeability 77−46399
heat of adsorption on polycryst. Fe film 78−91530
heat of soln. in Al, electron charge distrib. calc. 78−51689
heat of soln. in Mg, electron charge distrib. calc. 78−51689
heat of solution in Al, spherical model 80−96656
heliosphere H atom ionisation, near Sun trajectories 80−105145
HF discharge, gas breakdown, electron diffusion eqn. exact soln. 80−19658
high-pressure environments, measurements using automatic torque magnetometer 80−4746
hollow cathode discharge, ion mass composition 79−68969
human, body, in vivo N meas., by prompt neutron capture γ-ray analysis, body H use as internal standard 79−92441
hybrid solar/H fuel system producing high energy 80−45809
hydride storage, development of low cost Ni-rare earth hydrides 80−45791
hydride storage, high temp. hydrides for vehicular appls. 80−45793
hydride storage, technological aspects and characteristics of industrial hydride reservoirs 80−45792
hydride storage using $CeMg_{11}V(Cr)(Mn)(Fe)(Co)$ alloys 80−51009
hydride storage using rare earth alloy hydrides, props., book contrib. 80−45291
hydrogen permeation characts. 79−67948
hydrogenation of steel, influence of conc. depend. of anilines *(Russian)* 79−15854
hydrogenation of Zr-N system, phases form. 79−43200
hypersensitisation of AgBr(I) emulsion coating, to diminish recomb. and increase quantum efficiency 77−5942
hypersensitisation of photographic emulsions *(Russian)* 80−73511
implanted in solid, depth distribution meas. by reson. nuclear reactions 77−81435
impregnated p-GaP electrode, with metal adatoms, surface states form. 80−54778
impregnated vitreous SiO_2, γ radiation effects, hydride, hydroxyl formation 79−87874
impurities, atomic in solid H_2 dynamic local field approx. 79−69316
impurities in ferromag. Ni, μSR, self-consistent calc. 80−84447
impurities in metals, electronic struct. 78−10402
impurities in transition metals, screening and lattice deform. 79−77611
impurity effect on IR spectra of quartz, amethyst and citrine 78−43910
impurity electron struct. in free-electron-like metals 79−95365
impurity in CoGd, H_2 and N_2 contaminated amorphous films, mag. props. 79−1690
impurity in Fe, influence on martensitic transform. *(Russian)* 77−66643
impurity in FeGd, H_2 and N_2 contaminated amorphous films, mag. props. 79−1690
impurity in simple metal, electronic struct. 78−67978
impurity profiling with 2.5 MeV van de Graaff accelerators 79−77626
industrial scale, production from natural gas, naphtha, coal, review 80−35791
inert gas:H, quasifree electron energy, inference from ESR studies 79−69459
internal combustion engines, electronic fuel injection techniques 80−72094
internal friction, influence of H_2 on Ti *(French)* 78−75723
internal friction of deformed V, H effect 80−76300
interstital, in Zr-Rh, energy calc. 79−82198
interstital, in Na, thermodynamics, rel. to delocalised particles 79−46653
interstital impurities, localised vibration in FCC γ-Ce 80−75322
interstital position in Pd, Nb and Ta from entropy of solution 77−65989
interstitials, random walk diffusion models, generalisation to correlations over two jumps 78−79794
interstitials in metal, rel. to μ^+ trapping in Cu(V)(Nb)(Ta) expt. 80−50247
interstitital, ordering in α-Fe 79−7597
Invar, magnetic structure, absorbed H_2 effect 80−20534
inverted, optical gain at Lyman-α spectral line 80−95880
ion implanted in metal, interstitial positions and vibr. amplitudes, fast ion channelling study, review 80−79848
ion source, HF, proton yield increase, influence of He, Na, Ar, Kr, Xe and N_2 obs. 80−57422
ion-ion hybrid damping in D_2-H_2 plasma 79−77361
ionisation path formation by laser beam with retractable focus 79−18992
ionised gas, H_α-, H_β-line Stark broadening, space charge field 77−39409
isotope abundances in lunar samples 77−60676
isotope diffusion in BCC metals, self-capture effect and activation energy *(Russian)* 78−75879
isotope enrichment using low-temp. glow discharge technique 78−66675
isotope ratio, determ. in microwave induced plasma 79−41868

hydrogen continued
isotope separation by H_2-Pd system, effect of isotopic conc. on separation coeff. of H-T, H-D and D-T mixtures 79−71979
isotope separation in H-Pd system 77−50551
isotope separation using focused DF laser in formaldehyde 79−94094
isotopes, nuclear reaction anal. techniques, implantation studies, appls. 78−3422
isotopes depth profiling in solids by proton elastic scatt. technique 77−24327
isotopic exchange equilibrium with Li fusion blanket 79−49845
jet, axisymmetric, turbulence mixing of gases with different densities 77−58749
kaonic, strong interaction effects, K^-p scatt. length Coulomb corrections 80−14257
KERMA values, consistent set for H, C, N, and O for neutrons from 10 to 80 MeV 80−68967
lamp using hollow lightguides, optical and operational characts. 80−53395
lamp window, radiation coloration removal methods 79−72698
laser, compact high repetition rate VUV, for scientific appl. 78−37899
laser, efficient tunable Raman type 80−28245
laser, high power tunable IR compressed type, for spectroscopy 80−48277
laser, high-power, vac. UV emission at high pulse repetition freq. 78−29977
laser, Raman, use of waveguide for improved conversion efficiency 77−658
laser, recombination dynamic H plasma, freely expanding, from supersonic nozzle 77−19240
laser, stimulated Raman scatt., appl. to holography 80−91782
laser, transversely excited, oscill. characts. in vacuum UV region *(Japanese)* 78−22148
laser, tunable IR waveguide Raman type pumped by dye laser, 0.7-7 μm range 79−45959
laser, vac. UV, appl. to mol. photoionisation in mass spectrometer 77−88606
laser, vac. UV discharge, elementary processes 78−9370
laser, vacuum UV, high power, excited by longit. elec. discharges *(German)* 78−37896
laser, VUV, with sealed gas-discharge tube 80−74399
laser fusion microsphere targets, nondestructive anal. using rot. Raman spectroscopy 80−50896
laser-fusion prod. by radiolytic-thermochem. cycles 80−45811
laser-heated H_2 rocket, analysis of nozzle flow 80−10283
liberation from aqueous solns. irradiated in nuclear reactors 79−100416
liberation from electrolytic Ni during vacuum heating, Mossbauer spectra *(Russian)* 80−35594
liberation on austempering of 40KhN steel *(Russian)* 77−55996
liquefier with He refrigeration cycle 79−58740
liquid, bubble chamber, Ne-H_2 mixture, H_2 track sensitive target 77−396
liquid, bubble growth consts. calc. 77−35680
liquid, corresponding states, quantum, mech. law 79−55945
liquid, eqn. of state of solid and liq. phases, metallic state *(Russian)* 79−19354
liquid, investigations on heat transfer during pool boiling 79−60494
liquid, isotopic fermion-boson mixture, ground state configuration, theory 80−107601
liquid, localisation of electrons on surface *(Russian)* 79−33322
liquid, normal and para-, dielectric props. *(Russian)* 79−87374
liquid, perturbation theory and quantum effects, thermodynamic props. and quantum stat. corrections *(Russian)* 78−22867
liquid, photoelectric determ. of conduction state energies and electron ranges 77−89487
liquid, polarimeter for recoil proton polarisation meas. in $\gamma p \rightarrow \pi^\circ p$ reaction 79−93898
liquid, self-diffusion 77−35746
liquid, shock compression obs., various geometries 77−58732
liquid, shock wave vel. meas. 77−75999
liquid, slow neutron scatt. rel. to intermol. excitations, analyt. model 77−58941
liquid, submerged centrifugal pump 77−22560
liquid, thermodynamic properties, effect of ortho-para composition *(Russian)* 78−34419
liquid, thermodynamics below Debye temp., thermal capacity temp. depend. *(Russian)* 79−10999
liquid, US vel., 18.25-32.38K *(Russian)* 78−75731
liquid, US vel. and intermol. interactions *(Russian)* 79−65144
liquid, velocity-autocorrelation function from neutron scatt. 77−1058
liquid, vibr. energy transfer, isotopic impurities, relax. 79−6993
liquid, vibr. population relax. in gas and fluid 80−29775
liquid automobile fuel, cryogenic storage, and semiautomatic refueling station 80−40926
liquid H_2 fuel for commercial aircraft, production and liquefaction facilities 80−45818
liquid metal, electron kinetic eqn. with exchange, elec. resist. 79−15131
LMFBR, H burden from steam side corrosion in Na heated steam generators 78−58355
low pressure gas, electron energy distribution meas. 80−96412
low-temp. thermometry reference points 78−206
LWR fuel-cladding gap, Cs-U-Zr-H-I-O system, chemical thermodynamics 78−82440
LWR mixed oxide fuels, determ. of H_2O, Hz content by hot extraction methods *(German)* 79−49808
Lyman alpha radiation source with high spectral purity 78−13775
Lyman-α, 4-wave sum mixing in Be 80−23747
Lyman-α line core, effect of emitter ion dynamics 77−47161
magnetic relaxation study in Fe 78−64228
magnetic susceptibility and anisotropy calc. *(French)* 78−37559
maser, atomic resonance effects on long-term freq. stability 77−75465
maser, field-operable design improvements 79−55099
maser, for use in spacecraft, operating development model 79−54105
maser, passive, as freq. standard 79−55100
maser, temp. dependence of wall and spin exchange effects, expt. 77−79792
maser, time-dependent freq. shift obs. 78−89457
maser, time-dependent freq. shifts obs. 79−21713
maser, VLG-11, performance evaluation 79−55098
maser, wall shift, comparison between TFE 42, FEP 120 Teflon coatings 78−78984
maser autotuning system analysis 79−55101
hydrogen continued
maser autotuning systems, theoretical anal. based on freq. or phase method 80−83575
maser cavity, tuning using variable capacitance diode 79−72545
maser design for NAVSTAR Global Positioning System satellite clock 78−58969
maser dissociator, H beam production performance characts. 78−87034
maser improvements at Smithsonian Astrophysical Observatory 78−58971
maser microwave resonator, miniature design 79−55097
maser response to coherent Zeeman perturbations 78−58972
maser with double configuration bulb for wall shift meas. 78−58970
metal, H-impurity, energy and electron density of states 80−34398
metal, superconductivity and crystal struct. *(Hungarian)* 78−38659
metal hydride chemical heat pumps, materials and performance characts. 80−40927
metal hydride heat pump as topping cycle for power generation 80−40928
metal-H system, basic props., book 79−82349
metal-H system, bond energy calcs. 78−51940
metal-H system, elastic interaction and phase transition, book contrib. 79−83178
metal-H system, inelastic neutron scattering meas. of optical vibr. freq. distribs. 80−59605
metal-H system, lattice strains, expt. methods, book contrib. 79−82202
metal-H system, multiplateau absorpt. isotherms, theory 80−103564
metal-H system, NMR depend. on struct., H diffusion and electronic struct., book contrib. 79−82887
metal-H system, permeation technique for electron transport studies 77−7904
metal-H system, permeation technique for electrotransport studies 77−7903
metal-H system, solubility, mobility, and phase transitions, book contrib. 79−82350
metal-H system, thermal neutron scatt., general multisublattice jump diffusion model 77−66045
metal-H system, thermal neutron scatt., general multisublattice jump diffusion model 77−66046
metal-H systems, appl. oriented props., book 80−22154
metal-H systems, heat transformer for energy cascading, book contrib. 80−26151
metal-H systems 79−82906
metallic, appl. of dynamics of crystallised one-component plasma 80−107384
metallic, Coulomb crystal energy, analysis of the tail of the density series 78−91300
metallic, electron-phonon interact., comparison with metallic hydrogen 77−66125
metallic, ground-state energies of liq. and solid phases, variational and Monte Carlo methods 80−70502
metallic, liquid state, ground state energy at zero temp. 79−38006
metallic, solubility of He, Gibbs energy, fluid state model, He conc. in giant planets 79−60602
metallic H in giant planets interiors, condensed matter physics 80−77307
metallic liquid, struct. and forces 78−22636
metals, FCC, H implantation, lattice location and trapping, ion beam anal. 79−55769
methane-H_2, in packed bed, heat and mass transfer, axial mass dispersion 78−75200
methane-hydrogen mixture, flow through glass bead bed, axial dispersion coefficients 79−46378
microbial production from replenishable resources 80−16768
microwave discharge in atmospheric gas flow 78−42847
mobility in MgO, electron irradiation induced 77−55390
mobility in Pd and Pd alloys, book contrib. 80−24605
molecular, cryst. field theory for interact. with solid matrix. 80−80229
monolayer, on triangular lattice, orientational phases 78−75934
monolayer, on W (001), surface phonons, lattice dynamical model 80−39405
monolayer (1×1), adsorbed on Ti (0001) film, electronic struct., surface geometry 80−54750
monolayer on Si(100) 1×1 surface, electronic props., self-consistent calc. 77−43690
monolayers adsorbed on charcoal, graphite, H_2 dynamics 79−66341
motion in Pd and $Pd_{0.9}Ag_{0.1}$ alloy, thermodynamic data 79−65254
motor fuel, technico economic study of the use of hydrogen and methanol for road transport 79−74512
neutral, behaviour calc. in wall region of high temp. plasma, wall interaction 77−35377
neutron energy transfer, 30 to 100 MeV 77−52890
neutron kerma factors for H, C, N, O and tissue, 20-70 MeV 77−73584
neutron scattering, 0.1 to 14 MeV, slowing down times and distances calcs. 77−65409
nuclear bombardment, thin liquid target for low energy nuclear physics expts. 80−78471
nuclear bombardment target, liq., for neutron scatt. 79−706
nuclear power stations, fusion, combined heat and power, production possibilities *(German)* 79−67935
nuclear reactor, LWR hydrogen formation during core melt accident 78−50267
optimal development strategies for a whole energy system based on hydrogen 80−45795
ortho to para conversion on paramag. and antiferromag. surfaces 79−34362
ortho-para conversion on atomically rough surfaces, mag. excitations 77−69664
oscillator, wall induced frequency shift measurement, F-10 polymer flexible accumulator vessel 79−2749
overbarrier states in metals, subsystem heat capacity, equilibrium props. *(Russian)* 80−79998
oxidation, reaction kinetics calc. using thermodynamic model *(German)* 79−5130
oxidation on Pt, matrix isolation and laser fluoresc. obs. of prods. 80−66865
para-ortho conversion, action of TiP catalyst 80−55316
partial monolayers on Si(111), UV photoemission, disordering effect 77−1308
pellet injection system, pneumatic, for ISX Tokamak 79−60202
penetrability of C-coated Pd membrane *(Russian)* 77−77808
penetration, into Ni-Cu alloy, reversed kinetic isotope effects 77−43387

hydrogen continued
permeability, diffusion, and solubility in Pd-W alloy, 300 to 800°C *(Russian)* 79−51307
permeability, diffusion and solubility in Ni-Mn 80−107573
permeability, diffusivity and solubility in pure Fe at 10 to 60°C 78−75887
permeability and diffusivity in nickel *(Japanese)* 78−66345
permeability and solubility in Pd-Ag, Pd-Ce, and Pd-Y alloys, comparative study 79−23738
permeability in α-brass 77−62675
permeability in alloy steel-austenitic stainless steel bimetal 80−107572
permeability in Fe-V alloys, 300-700°C *(Russian)* 77−15627
permeability in steel Kh18N10T, effect of surface treatment *(Russian)* 79−15853
permeability of Al_2O_3 sintered tubes 80−24675
permeability of Fe, influence of microstruct. changes induced by cold working *(Russian)* 77−20182
permeability of Fe membranes with electrodeposited metal coatings, proposed catalytic mechanism 78−53252
permeability of heat exchange material, oxide protective layer formation meas. 78−8895
permeation, in Pd, comparison to D_2 *(Russian)* 78−75881
permeation, radiation enhanced, in stainless steel 4301 80−59732
permeation and diffusion in 310 stainless steel, 472 to 779K 79−55937
permeation and diffusion in Inconel 718 and Incoloy 903 78−26730
permeation characteristics of 316-SS, 321-SS, Inconel-625 79−69295
permeation in Fe in fusion reactor 80−34242
permeation in glass microsphere laser targets 77−83078
permeation in glass microsphere laser targets 77−83079
permeation in high temp. nuclear reactors *(German)* 79−3204
permeation reduction using Pd foil in liquid metal *(Japanese)* 80−68770
permeation through Cu membrane, kinetics 79−99371
permeation through He heated tube walls in HTR 77−50250
permeation through HTGR heat exchanger tubes, reduction using calorising method *(Japanese)* 80−100360
permeation through Incoloy-800 reactor material 79−77822
permeation through metal barrier, adsorpt. processes 78−63879
permeation through Mo, monocryst. and polycryst. specimens *(Russian)* 79−60554
permeation through Ni and Hastelloy X *(Japanese)* 78−51740
photoassisted production, reactions of H_2O with C and ethylene over Pt/TiO_2 80−55703
photobiological prod., key enzymes and biochem. systems, tech. problems of H_2 prod., review 80−61446
photocatalytic prod. using TiO_2 electrodes, solar energy 77−1932
photocatalytic production by carbohydrate conversion using $RuO_2/TiO_2/Pt$ photocatalyst powder 80−94120
photocatalytic production from H_2O on TiO_2 using solid C 80−26150
photochemical prod., H_2O photolysis using fission pumped gas lasers 80−45810
photochemical prod. by H_2O photolysis using sunlight 80−45776
photochemical production by H_2O dissociation utilising solar energy, review 80−61452
photochemical production using visible light on aqueous solns. of a Ru complex 80−85192
photoelectrochem. prod., semiconductor-liquid junction systems, review 80−61453
photoelectrochemical generation at p-semiconds. 77−89844
photoelectrochemical prod., solar beam-assisted electrolyser applied to Yokohama marks 5 and 6 [system for hydrogen production] systems 80−45768
photoelectrochemical prod. using TiO_2-Si solar cell hybrid electrodes 80−45775
photoelectrochemical production, ZnTe and CdTe as electrodes 77−70311
photoelectrochemical production using solar energy, TiO_2 electrode 77−11956
photoelectrochemical production using solar energy and Zn(Mg)(Cr)(Ni) phthalocyanine dyes *(French)* 80−55936
photoelectrode kinetics of evolution at semicond. electrode 78−44388
photoelectrolytic prod. from H_2O, storage efficiency estimate 80−51016
photoelectrolytic production by H_2O decomposition using sunlight, review 80−45774
photoelectrolytic production of H_2 and electricity, $LaCrO_3$-TiO_2 photoactive anode 80−12024
photolytic prod. by H_2O solar photolysis by engineering methods using biological materials *(Japanese)* 80−45765
photolytic prod. using biological and artificial catalysts 80−61444
photolytic production using chlorophyll-catalysed H_2O photolysis and solar energy storage 80−61458
photolytic productionby H_2O solar photolysis using Pt/(chlorophyll a.$2H_2O$) reaction 80−89663
photomachining type 410, evidence for lack of H_2 embrittlement in failure 79−74246
photosynthetic unit of H_2 evolution 77−77875
physisorbed monolayer on graphite, neutron scatt. studies 80−107655
plasma, anisotropic, cyclotron and electrostatic instabilities criteria 80−38627
plasma, at. fluoresc., collisional depopulation rate of n=2 level 78−79463
plasma, Balmer lines, plasma-broadening in wall-stabilised arc, low electron density 80−43891
plasma, consequences of electron energy distrib. departure from Maxwellian 77−80274
plasma, dense, produced by conic electrode source, mag. field effect on flow 77−58873
plasma, dense, TEA-CO_2 laser pulse interaction 80−38683
plasma, dense, two-particle effective pot., near 10^4K 80−38533
plasma, dense thermal, radiation emission 80−103120
plasma, departures of electron energy distrib. from Maxwellian, electron kinetic eqn. 77−80266
plasma, diagnostics using reson. multiphoton ionis. 80−58640
plasma, discharge, laser-induced transient striations obs. 79−27785
plasma, electron kinetic coeffs. interpolation calcs. *(Russian)* 78−71429
plasma, electron transport coeffs. at high E/N values 79−94835
plasma, endothermic reduction of BCl_3 in thermal plasma and nonequil. plasma discharge 78−15671
plasma, Fe-H mixture, confined atom-, and Debye Huckel-, Thomas-Fermi-Dirac models 77−24053
plasma, freely expanding, population inversion obs. 80−95877

hydrogen continued
plasma, H_β line profile for plasma microfield distrib. function reconstruction 78−71539
plasma, H conc. by reson. fluoresc. from Kr 3rd harmonic generation *(Russian)* 77−79895
plasma, H line curvilinear trajectories and Stark broadening 78−67324
plasma, H local population diagnostics, reson. laser scatt. *(Russian)* 77−19763
plasma, HF, electron temp. meas. by spectroscopic and double probe methods 77−65910
plasma, high-temp., proton neutralisation cross-section by impurity ions *(Russian)* 77−11310
plasma, in θ-pinch with axial current-carrying rod, light scatt. diagnostics *(Russian)* 77−11395
plasma, in DIVA Tokamak, Au impurity X-ray emission 79−32820
plasma, in FT-1 Tokamak, reson.-fluoresc. meas. of atomic radial profile 79−90467
plasma, in mirror trap, drift loss-cone instability stabilisation by cold ions addition 79−32800
plasma, in monoplasmatron arc, electrokinetic parameters space distrib. *(Russian)* 80−53925
plasma, in Tokamak, Pfirsch-Schluter friction on H^+ 78−34272
plasma, inertial confinement, reaction gains, reheat calcs., collective model 78−59664
plasma, instantaneous population densities of excited levels 77−47149
plasma, ion temp. and electron density depend. studied by laser light scatt. and emission spectroscopy 80−96342
plasma, ionisation in uniform elec. field *(Russian)* 80−53923
plasma, K impurities, optical props. 80−103119
plasma, large θ-discharge, n-α line Stark profiles 77−24084
plasma, laser amplitude calibration from Raman spectra, for diagnostics *(Russian)* 80−38702
plasma, laser heated, heat flux limitation and ion-acoustic turbulence 78−18453
plasma, laser radiation propagation, mag. field effects *(Russian)* 77−7552
plasma, laser-produced, laser light propag., 2D-simulation 78−5921
plasma, line broadening theory, screening process dynamics *(Russian)* 80−69988
plasma, Lyman system nonsaturated laser line intensity obs. 78−71089
plasma, Lyman-α Stark broadening, dynamic screening effects 78−18386
plasma, mag. mirror confined, turbulent heating, rel. to Buneman instability 77−24106
plasma, magnetic piston study in theta-pinch *(Russian)* 80−83971
plasma, MHD and transverse ionising shock waves, jump conditions, ionis. effects 79−32775
plasma, neutral beam injection, charge exchange and ionis. rate coeffs., analytical approx. 79−86590
plasma, neutral H ats. penetration, kinetic theory 79−32782
plasma, nonequilib., radiative props., computer program 79−90388
plasma, nonequilib., stopping power for incident α-particles 80−64742
plasma, nonisothermal and rarefied, transport processes and Lenard-Balescu eqn. 80−6222
plasma, $O^+ + H$ charge exchange, Monte Carlo simulation 78−34260
plasma, optically thin, UV spectral emission coeff., quantum statistics of recomb. continuum *(Russian)* 79−77348
plasma, pair correlations down to r=0 80−14883
plasma, parametric instability depend. on laser line-width, time-depend. theory 79−60138
plasma, permeation through Ti, reduced by layer of interstitially built ϵ-Ti_2N 80−16566
plasma, photon escape probabilities for Stark-broadened Lyman series lines 80−24143
plasma, pulse discharge, electron conc. *(Russian)* 77−27753
plasma, quasi-nonideal, comp. analysis 77−72411
plasma, quasistationary thermonuclear, H radiative recomb. *(Russian)* 77−39465
plasma, radial density and temp. profiles, using magnetoacoustic oscills. 79−19082
plasma, recombining, weakly ionised, population inversion 80−87849
plasma, resonance fluorescence diagnostics 80−48971
plasma, resonant Balmer line irrad. 80−75099
plasma, spectral intensity near series limit, taking into account sub-barrier ionisation *(Russian)* 77−31436
plasma, thermal cond. and diffusion, ionised collisions effect *(Russian)* 78−47093
plasma, thermal emission and Debye shielding 80−64692
plasma, thermally anisotropic, cyclotron instabilities 78−1814
plasma, thermodynamic functions, composition, and elec. cond., calc. method 79−32738
plasma, turbulent resistivity at high drift vels., particle diagnostics 78−38541
plasma, underdense, CP_2-laser radiation filamentation 80−14941
plasma, underdense, stimulated Brillouin scatt., press. depend. 78−42764
plasma, UV spectral radiance calibration *(French)* 78−12774
plasma, viscosity calcs. *(Russian)* 80−53953
plasma, Z-pinch, strong optical attenuation, shadowgraph meas. 78−26294
plasma anisotropic noise, HF, in turbulent plasma, H Stark profiles 78−1896
plasma beam, electron macroscopic props. *(Russian)* 80−92403
plasma collision-dominated electron distrib. function with turbulent heating 78−71509
plasma development in 2kJ focus discharge accelerator, optical image structs. 79−82076
plasma diagnostics, laser-induced parametric instabilities 78−51345
plasma distribution function inference from optical spectra 78−67406
plasma focus heating by TEA CO_2 laser and anomalous absorpt. obs. *(Japanese)* 77−43013
plasma formation, in arc discharge, dissoc. excitation role 77−84398
plasma impurity, flux on wall of DITE Tokamak 80−28688
plasma ion temperature determ. in mag. field, gridded probe method 80−70033
plasma satellites, mol. lines, in afterglow 80−44053
plasma target investig. *(Russian)* 80−106981
plasma transport functions by precision arc expts., H Balmer spectrum 80−103187
plasma transport theory, H_2 transport in toroidal plasma using multigroup discrete ordinates methodology 80−69978
plasmatron, 2 MW, for generation of high-press. high-temp. hydrogen flows 77−58904

hydrogen continued
plasmochemical prod. by H_2O decomposition in non-equilib. plasma 80−45773
polyamides, carborane-containing, H_2 production during friction *(Russian)* 79−57123
pool boiling, heat transfer coeffs. determ. 78−30165
porosity, secondary, in Al, development and pore growth *(Russian)* 80−19946
positive corona discharge, current oscills. 77−11431
pressure, in vacuum chamber in cryogenic environment, meas. technique 78−77925
prod. by H_2O pyrolysis using solar thermal energy 80−45770
production, by thermolysis of water in solar reactor, thermal calculations 79−39319
production, comparison of thermochem. and electrochem. methods 80−16826
production, electrolysis of steam, high temperature, in fusion reactors, synfuel production 80−72099
production, EPRI R and D program for electric utility industry, review 80−30610
production, exergetic/energetic/economic anal. of electrolytic, thermochem. and hybrid processes 80−55938
production, from high temperature electrolysis and fusion reactor 79−52915
production, H_2O electrolysis, module design, geometry, capacity, operating temps., pressures, electrode types 80−72098
production, high temperature fusion blanket design for synthetic fuel plant 80−99275
production, on-site, electrolysis of H_2O, for generator cooling 80−72097
production, techno-economic evaluation using OPTIMO code 80−45797
production, theoretical design of solar engine 80−30598
production, thermochemical or hybrid cycles of hydrogen production techno-economical comparison with water electrolysis 80−45796
production, use, storage and transportation of H_2 as energy vector (conf. Brussels, Belgium. Oct 1978) 79−74511
production, utilising nuclear energy, global energetic system, mathematical model *(Rumanian)* 80−35623
production and distrib., US safety regulations and standards, bibliography 80−41976
production and storage utilising solar energy conversion, book 80−57017
production and utilisation, EEC R&D program progress and results 80−16767
production and utilisation, EEC R and D program review 80−45821
production by alkaline electrolysis using inorganic-membrane-electrolyte 80−72092
production by biological and biochemical solar energy conversion, review 80−61454
production by direct solar energy conversion at sea, review 80−61456
production by direct thermal decomposition of H_2O utilising solar energy, thermodynamics review 80−61450
production by electrolysis of water using solar energy *(Czech)* 77−29014
production by H_2O decomposition, using solar energy conversion 80−97813
production by H_2O dissociation using solar energy 80−30597
production by H_2O electrolysis in fused NaOH 80−76660
production by H_2O photolysis using solar radiation, feasibility of large scale generation 80−72095
production by H_2O radiolysis, thermoradiation dehydrogenation using nuclear power, kinetic anal. 80−67010
production by KOH electrolysis, materials, geometry and characts. of electrolyser cell 79−74397
production by medium temp. high press. water electrolysis 79−74398
production by photobiological energy conversion 79−70456
production by polynaphthoquinone-SO_2-I_2 system for H_2O decomposition 80−16825
production by pressurised coal gasification 80−30609
production by solar energy, homogeneous photoredox system 80−3387
production by solar energy conversion 80−30608
production by solar energy conversion utilising synthetic chloroplasts 80−30508
production by solar photochemical decomposition of H_2O 80−16822
production by solid polymer electrolyte H_2O electrolysis 80−61442
production by solid polymer electrolyte H_2O electrolysis 80−67012
production by steam reforming of natural gas, chemical kinetics 80−97815
production by water decomposition by thermochemical and thermoelectrochemical cycles 80−26029
production by water electrolysis, economics and technology *(French)* 79−100543
production by Westinghouse electrochem./thermochem. S-cycle process 80−45808
production cross sections for 15 MeV neutrons on 316 and 304 stainless steel 77−50291
production for solar energy utilisation 80−51014
production from coal by centrifugal separation from gasification products 80−76643
production from coal using steam-Fe process, development status 80−55942
production from falling water, 1978 overview and prospects in USA 79−52958
production from fusion reactors coupled with high temp. electrolysis 80−45771
production from H_2O by two-stage plasmochemical cycle 80−45772
production from H_2O using solar energy, eval. of a hybrid process 80−104519
production from natural gas, naphtha and coal on industrial scale 80−61438
production from radioactive waste heat and utilisation in gas turbines 80−30326
production from water, corrosion stability of steel and alloys to double iodate-iodide salt melt *(Russian)* 80−55593
production from water using biomass feedstock and bromination process 80−61459
production from water using solar energy, one-step effusional process 78−15672
production in decomp. of water by fusion energy, synthetic fuel 78−50335
production in fusion-synfuel blanket, thermal hydraulics 80−106176
production on illuminated transition metal surfaces, tight binding model 80−45812
hydrogen continued
production using fusion reactor heat, from $2CO_2 \rightarrow 2CO+O_2$, $CO+$-steam$\rightarrow CO_2+H_2$ 80−67014
production using fusion reactor heat and gas dynamic compression heating 80−35793
production using HBr electrolysis 80−35777
production using high temp. nuclear reactors 80−97814
production using HTGR nuclear heat source 80−45803
production using hybrid cycles with HBr electrolysis 80−97816
production using hybrid electrochem./thermochem. cycles, search for electrochem. reactions 80−45807
production using nuclear process heat from HTRs 80−30595
production using thermoelectrochem. cycles 80−16820
production using thiazine dye-Fe photoelectrochem. cells, instabilities 80−16814
production utilising HTGR 80−42742
profiling using ^{15}N bombardment, method and appl. 79−5195
pulse discharge regime, time-depend. of radiation *(Russian)* 77−84548
pumping by Ti film, pumping speed comparison between H_2 and D_2 78−51819
pure gas, enthalpy, Carlson-Thodos van der Waals eqn. calcs. 80−83878
purity effects on steel Kh18N10T fatigue characts. *(Russian)* 79−15764
quartz:H, impurity concentration profiles by nuclear reaction method 79−60396
quasars, H line and continuum emission calcs. 80−27003
radiolytic/thermal cycles for production 80−51011
railway motive power systems using H-fuelled locomotives 80−40923
Raman amplifier with broadband pumping, gain enhancement 80−43398
Raman laser, compressed, tunable i.r. emission 77−668
Raman laser, for efficient coherent summation of Nd laser nanosecond pulses 80−23718
Raman laser, improvement using up to 10 m path length 77−72033
Raman laser, multiple-pass-cell, controllable pulse compression 80−91825
Raman laser, tunable high power systems and appls. 77−27302
Raman scattering, cooperative effect observations *(Russian)* 80−5553
rare earth alloy-hydrogen system, $R^1_xR^2_{1-x}H_2$-H_3, phase transitions 78−18767
rare earth-transition metal alloy thin films vapour deposition, influence of gaseous phase on mag. props. *(Polish)* 80−39820
reaction with Al, influence of surface reactions on rate *(Russian)* 80−66863
reaction with CO, C_8FeCl_3 behaviour, effect of activation 79−43623
reaction with vitreous hydroxyl free SiO_2, diffusion absorpt. spectra 80−85210
recombination on semiconductor surface, nonequilib. charge carrier generation *(Russian)* 79−91126
recombining atomic plasmas, population inversion 80−32679
recombining plasma, population inversion using collisional-radiative model 79−46423
reduction, of PtO_2 sputtered film, optical props. 80−20728
reduction of β-Sb_2O_3 to Sb powder, atomic H effect 80−2978
reduction of graphite intercalation compound with $AuCl_3$ *(French)* 78−27820
reduction of MoF_6, chem. kinetics eqn., adsorbed component interactions *(Russian)* 80−35569
reduction of MoF_6 in the presence of HF *(Russian)* 80−61076
reduction of MoO_2 powder bed, reaction kinetics 80−16230
reduction of WO_3, starting specific surface effect on kinetics 80−11599
refractivity and dispersion in visible and IR regions 78−34258
regional myocardial perfusion determ. from H_2 washout curve 79−92459
relativistic electron beam on air, He and H_2, charge neutralisation press. depend. *(Russian)* 77−19668
release from fusion reactor first wall materials 80−37579
release of hydrogen isotopes co-dissolved in Ti, Nb 80−37580
release rate from clean metal surface 78−95187
removal from flowing Ar, U and Ce as hydriding materials 78−17438
residual gas effect on thermionic emission of ZrC and ZrC-Re 78−48269
retention and release from TiB_2 and B_4C first-wall coatings for Tokamaks 80−18620
RF breakdown in longit. mag. field, diffusion theory validity 77−39491
rotational energy, specific heat, temp. depend. determ., demonstration 78−12465
safety analysis of H_2 fuel 79−74552
Saturn, Lyman α emission from disc and ring system 78−12150
scattering, adsorption, and absorpt. on Pd (111), mol. beam study 80−29277
scattering from and selective adsorption on graphite (0001) surface 80−71553
segregation kinetics in Fe alloys *(Russian)* 78−18832
self-diffusion in V-H system, NMR, and phase transition 77−16571
separation from HI-H_2-I_2 mixture in thermogravitational column 80−45561
solar energy conversion, photoreduction of methylviologen adsorbed in cellulose 80−81491
solar energy direct conversion to H_2 fuel by water photoelectrolysis 79−62014
solar energy storage as hydrogen from bromine from hydrogen bromide 79−57470
solar energy storage by H_2 prod. using Mg(Al)(Fe)(Co)(Ni)(Cu)(Zn) sulphates *(French)* 80−55935
solar energy storage by metal hydride, review 80−61455
solar H_2O photoelectrolysis, H_2/hydrocarbon fuel prod. via biomass conversion wastes 80−89653
solar-H_2 energy systems, H_2 production and utilisation 80−61447
solar-H_2 systems using metal hydrides 80−61464
solar-thermochemical prod. of H_2O, appl. of fixed mirror solar concentrators 80−45767
solid, ablation by magnetised plasma, semi-empirical calc. 80−38666
solid, equation of state for α-N_2 and HCP type lattices, at 0K 77−47537
solid, secondary electron emission, electron and ion induced 79−1803
solid, stimulated Raman scatt. and CARS 78−13752
solid p-H_2, very low O-H_2 conc., order-disorder transition, NMR 78−56384
solid pellet ablation in rotating plasma, density meas. by laser interferometry 79−4188
solid pellet ablation rate in plasma 77−65878

hydrogen continued
solid solution with Pd-Cu(Ag)(Au) alloys, superconducting transition temp. behaviour *(Russian)* 80−70879
solid- liquid mixture, nonstationary diffusion of neutrons 79−4212
solubility, in nonstoichiometric Pd_3P_{1-x} 80−59662
solubility and bulk modulus in transition metals, exam. 78−55950
solubility and mobility in Pd-Ag(V), appearance pot. spectra obs. 80−55231
solubility in α-Fe, Pt, and Fe-Pt alloys at press. up to 67 kbar *(Russian)* 79−51260
solubility in α-Mg 77−25024
solubility in α-Ti, neutron diffr. study 80−15254
solubility in Al, kinematic viscosity temp. depend. porosity, supercooling *(Russian)* 80−54425
solubility in binary alloys conc. depend., 850-1150°C *(Russian)* 77−59120
solubility in CuTi, $CuTi_2$, $PdTi_2$, $Cu_{0.5}Pd_{0.5}Ti_2$ alloys, decomp. reacts. 79−65197
solubility in dil. Pd-Fe alloys 79−33091
solubility in dilute alloys, isotope effect 78−14470
solubility in Er-Co-Ni 77−89543
solubility in Er-Fe-Al(Mn)(Co) 77−89543
solubility in Fe in 600-1500°C temp. and 0.1000 atm. pressure ranges *(Russian)* 78−59948
solubility in Fe-Co-Ni liquid binary and tertiary alloys, 1400 to 1800°C 77−1231
solubility in $LaNi_4Al$, effect of Al 80−103482
solubility in $LaNi_5$, trapping thermodynamics 80−107444
solubility in liq. metals rel. to that in solid phase *(Russian)* 80−65222
solubility in liquid Al, kinematic viscosity temp. depend. porosity, supercooling *(Russian)* 80−54425
solubility in liquid Fe-NI-Ge *(Russian)* 78−11202
solubility in metal, deviations from Sievert law 77−76567
solubility in Nb-H(D) system, enthalpy and entropy, isotope effects 77−20069
solubility in Nb-Mo 77−89542
solubility in Nb-Ta allo-s and characts. of solid solns. 79−86894
solubility in NbO, NbO_2, $Nb_2C_xO_y$ and NbC_xO_y 80−34191
solubility in Ni, Ni-Cr, Ni-Mo, 500-1000°C *(Japanese)* 78−38845
solubility in Ni, Pd, Pt and Ni-Co, and effect on elec. resist. *(Russian)* 79−91018
solubility in Pd, lattice defects influence, extended core model 80−88326
solubility in Pd-Cu, effect on elec. cond. 77−35699
solubility in Pd-H and Ni-H systems, phase diagram and thermodynamic properties calcs. 80−66480
solubility in superpure Pt, temp. depend. 79−77756
solubility in Ta at higher temp. 77−84934
solubility in TaC_x, Ta_2C_x and $Ta_2C_xO_y$ 80−44318
solubility in TiO_2 powder 77−11698
solubility in transition metals rel. to electron density 79−51266
solubility in U BCC alloys 79−96302
solubility in YCo_5 and YNi_5 *(Russian)* 78−15356
solubility in Zr, optical metallography, internal friction meas. 78−83962
solubility in ZrC_xO_y, ZrN_zO_y, $ZrC_xN_zO_y$ 77−84930
solubility of H_2 and D_2 in Y *(Japanese)* 78−18784
solution in Pd, isotope effect model 77−66026
solution in Pd-Rh(Pt) alloys, partial thermodynamic parameters determ. 77−66027
solution in $TiCr_{1.8}$, enthalpy, solubility and mol. vibr. determ., comparison with soln. in metals and binary alloys 80−79951
sorption, on Pd membrane, adhesion and penetration probabilities, extreme values 80−101040
sorption at press. up to 1500 atm. on rare earth alloys, RM_x (M=Co, Ni) 80−97819
sorption by Laves phase AB_2 intermetallic compounds, capacity and preferred location 79−43791
sorption by PdAu wires 78−43239
sorption by rare earth-transition metal alloys, effect on mag. props. 78−68231
sorption by Ti, gas-discharge device appl. 80−10796
sorption capacity of Fe-Ti and Mg alloys for H storage appls. 80−45792
sorption effect on mech. strength of steel *(Russian)* 78−31570
sorption in amorphous Ni(Zr,Ti) alloys 80−49526
sorption in La_2Mg_{17} 77−84933
sorption in $LaNi_5$, rel. partial absorption (desorption) enthalpies 80−50881
sorption in Pt-Pd system during cathodic charging, deflection technique meas. 79−51427
sorption kinetic studies using high accuracy volumetric device 79−56071
sorption on Ce-3d and Y-3d intermetallic cpds., structural charges 80−88429
sorption on Os cryst. in H_2SO_4 soln. 79−61873
sorption on Pd, piezoelectric quartz microbalance meas. 79−60626
sorption on polar ZnO surfaces, EELS 78−64434
sotrage, sorption props. of Al-containing Laves phase intermetallics 80−45794
spark, laser-triggered, electron densities meas. 80−106975
spark arc discharges, laser-triggered, electron density meas. 80−64822
spherical shells for inertial confinement targets, prod. by acoustic excitation of superheated liq. H_2 jet 79−85766
spin aligned, rel. to liquid to gas phase transitions in two-dimensional quantum systems 78−77798
spin-aligned, ground-state energy and finite temp. props. 77−61014
spin-polarised atom, binding to free surface of liq. ^4He 80−34277
stabilised arc as vacuum UV radiation standard for 600 to 900 Å 78−66879
stability effects on Ti-Mn base beta alloys, solid solns., hardness *(Japanese)* 77−81261
steel, austenitic stainless, internal friction due to H_2 gas molecules 80−71682
steel, carbide phase determ. by annealing in moist H_2 *(German)* 79−39231
steel, Cr (13 wt.%), abnormal behaviour of H_2 at low temps. *(Russian)* 77−24434
steel, H_2 permeability in inhibited H_2SO_4 corrosion, stress level effects *(Russian)* 77−52530
steel, H discharging phenomena effect of ε-Cu precipitates *(Japanese)* 80−7583
steel, martensitic, ageing, effect of H_2 on stresses in process of $\gamma \rightarrow \alpha$ transformation *(Russian)* 80−76252
steel, type 1045, hydrogen enhanced nucleation of microvoid as function of local plastic strain 79−79053
steel (0.45 and 0.8 wt.%), strength, fracture, effect of H_2 *(Russian)* 77−25129
steel welding, in Ar, resistance to cold cracking obs., C and H_2 content influence 77−21283
sticking coefficient, initial, on polycryst., O_2 and S covered Ni surface 78−63937
stimulated Raman scatt. in multiple-pass Raman gain cell filled with H_2 gas 80−48334
stimulated Raman scattering, refractive props. *(Russian)* 77−88865
stimulated Raman scattering, tunable IR source 78−1301
stimulated Raman scattering, tunable UV radiation obs. 78−55408
stopping powers and ranges in all elements, book 78−26607
storable conc. of atomic H in T-impregnated crystalline solid H_2 80−30594
storage, comparison of technologies and economics for fixed site storage 80−67011
storage, diffusion-rate-limited hydriding and dehydriding kinetics 80−35764
storage, effect of the interstitial hole size and electron concentration on complex metal hydride formation [for H storage] 80−45789
storage, electrolysis-based technology R and D at BNL, review 80−40920
storage, high pressure gas storage using microcavity structures 80−61462
storage, HYCSOS chemical heat pump, low grade heat enhancement using $LaNi_{5-x}Al_x$ 80−61467
storage, in La-Ni, Ce-Ni, hydriding characts. 78−83955
storage, in $LaNi_5H_y$ system, neutron scatt. obs. of static and dynamic props. 78−14323
storage, isotope effect in dissociation of UH_3 80−26174
storage, $LaNi_{5-y}Al_y$ alloys and their hydrides, metallurgical, structural and thermodynamic props. 80−45816
storage, prep. of FeTi for TEM *(German, English)* 80−30197
storage, props. and characts. of rare earth compounds 80−21416
storage, reversible alloys, hydrogenation *(French)* 79−74549
storage, $SmCo_5$ and $LaNi_5$ thin film alloys, H_2 absorption 80−65238
storage, $SmCo_5$ hydriding kinetics, inverse over pressure effect 80−55944
storage, survey of liquid hydrogen container technology for highway vehicle fuel system applications 80−30607
storage, thermal efficiency of H_2 compression using hydrides 80−61465
storage, thermodynamic and structural properties of $LaNi_{5-y}Al_y$ compounds and their related hydrides 80−16847
storage, TiFe-based hydrides for bulk storage 80−61463
storage, transmission and distrib., review 80−61439
storage, transmission and distribution 80−30596
storage, use of Ti binary alloys for solid metal hydride storage 80−45786
storage, using Ti-Mn alloy systems *(Japanese)* 80−61443
storage and distrib., potential for pipeline transmission in Switzerland 80−45780
storage and distribution, problem rel. to use of natural gas distrib. eqpt. 80−45779
storage and transport, effect on steel 79−74259
storage and utilisation using metal hydrides 80−45785
storage as metal hydrides, props. and appls. 80−76661
storage at fixed sites for distribution 80−61461
storage by alloys hydrogenation, alloy bonding theory approach 78−18786
storage by metal hydrides for automotive propulsion 80−40922
storage by use of cryoadsorbents 80−45783
storage efficiency of rare-earth and Th-transition metal intermetallics calc., desorption isotherms depend. on d-bandfilling 78−18912
storage in amorphous plasma-sprayed Sm-Co, effect of H_2 atm. on crystn. and mag. props. 80−64898
storage in Fe-Ti hydrides, specific heat meas. at room temp. 80−65248
storage in interstitial alloys, review 79−10956
storage in metals, book contrib. 80−26175
storage in metals, electronic struct., many electron theory 80−49667
storage in Mg rich-rare earth alloys *(French)* 79−66419
storage in $TiFe_{0.8}Be_{0.2}$ alloys 80−97817
storage materials, design criteria; thermodynamics, absorpt. kinetics, economics and materials science 80−55943
storage properties of $Zr(V_{1-x}Co_x)_2$, rel. to electronic struct. 80−76662
storage using cryoadsorbents, 65 to 150K, comparative evaluation 79−74548
storage using cubic metal binary alloys 80−45787
storage using FeTi hydrides, struct., heat of soln., diffusion and hydriding kinetics 80−40930
storage using hydride beds, thermal transport enhancement using high conductivity materials 80−61466
storage using intermetallic Ni_5La *(Russian)* 80−55937
storage using $LaNi_5$, effect of Ni, Ce, Co alloying additions on H_2 absorption 80−45790
storage using $LaNi_5$, fundamentals and appl. 78−18785
storage using $LaNi_5$, self restoring of active surface 80−45815
storage using metal hydrides, numerical physical property data 80−40929
storage using Mg-La(Ce)(mischmetal) alloys 80−72093
storage using reversible Mg alloys 79−74547
storage using small scale NH_3 prod. 80−45782
storage using Ti-Zr-Cr-Mn/$LaNi_5$ hydriding alloy mixtures 80−45788
storage using VH and VD, expt. exam. of isotope effects 80−45281
structural, fast neutron induced H and He producing reaction 80−13841
submonolayer-covered Ni (111), surface phonons obs. by EELS 80−39403
superdense cold, nuclear reaction energy output in mag. field *(Russian)* 77−29801
superpure, storage and production, use of FeTi crystals *(German)* 78−53184
supersonic combustion in vitiated airstream, using transverse injection 78−14095
supersonic flames, chemical kinetics and unmixedness effects on burning 80−64649
surface contamination of ultracold neutron storage bottles 78−17461
surface H-H interactions on Pt(111), heats of adsorption and desorption 78−18899
surface layer anal., influence of ion beam bombardment 79−37731
synfuel prod. by high temp. electrolysis using fusion energy 80−35792

hydrogen continued
synfuel prod. from fusion power using hybrid thermochem. $Bi_2O_3.SO_3$ cycle 80−40931
synthetic fuel prod. and transportation for solar energy utilisation 80−51015
synthetic fuel production, Tokamak high-temp. blanket 78−74479
thermal conductivity, quantum effects 79−14510
thermal diffusion apparatus 80−100358
thermal release from amorphous $Gd_{0.27}Co_{0.64}Kr_{0.09}$ UHV mass spectrometric technique 80−3439
thermo-electro-chemical production by Westinghouse H_2SO_4 process, heat penalty and economic anal. 80−61437
thermo-electrochemical prod. using solar energy *(French)* 79−24918
thermochemical compression for hydride thermosorption, theory *(Ukrainian)* 80−76657
thermochemical cycle, adaption of fusion reactor process heat concept 80−37614
thermochemical prep. by H_2O dissoc. using S-I cycle 80−16823
thermochemical prod., engineering impact on the validity of the Mark-16 thermochem. cycle 80−45806
thermochemical prod. by H_2O decomposition, equilibrium effects in high press. prod. 80−35775
thermochemical prod. by H_2O decomposition, impact of thermal burdens and kinetics 80−35787
thermochemical prod. by H_2O decomposition, review 80−45800
thermochemical prod. by H_2O decomposition using Mg-I cycle 80−35786
thermochemical prod. by H_2O decomposition using solar energy 80−40919
thermochemical prod. by H_2O decomposition utilising solar heat 80−61451
thermochemical prod. by H_2O dissoc. using Sb-I-Ca process 80−16824
thermochemical prod. by H_2O pyrolysis, computer thermodynamic anal. and optimisation 80−45766
thermochemical prod. by H_2O pyrolysis, solar-H_2 energy systems 80−61448
thermochemical prod. by high temp. H_2O decomposition using solar energy 80−45822
thermochemical prod. from H_2O, noncorrosive two-reaction low temp. cycles based on mordenite-hosted redox reactions 80−55939
thermochemical prod. using $Bi_2(SO_4)_3$ cycle, process engng. design 80−30599
thermochemical prod. using Br-Ca-Fe H_2O-decomposition cycles 80−35784
thermochemical prod. using General Atomic S-I cycle for H_2O decomposition 80−55941
thermochemical prod. using S-Br cycle, development of lab.-scale plant 80−35774
thermochemical prod. using SO_2-I_2 water splitting cycle 80−30600
thermochemical prod. using the Mark-13 process, status report 80−30606
thermochemical production, based on reactions of $CeTiO_2$ for water-splitting 80−55929
thermochemical production, by HBr pyrolysis 80−35772
thermochemical production, engineering impact on the validity of the mark-16 thermochemical cycle 80−55931
thermochemical production, H_2O decomposition using S compounds, feasibility anal. 80−35768
thermochemical production, H_2O decomposition using S cycles, thermochem. anal. of energy balance 80−35779
thermochemical production, H_2O decomposition using S-I cycle 80−35769
thermochemical production, H_2O decomposition using S-I cycle, process eng. and bench-scale studies 80−35770
thermochemical production, H_2O pyrolysis using Fe-Cl cycle, chem. engineering anal. 80−97811
thermochemical production, HBr decomposition using $FeBr_2$ and Fe_3O_4 80−35778
thermochemical production, HI decomposition and H separation 80−35771
thermochemical production, irreversibility anal. of separation schemes from binary gas mixtures 80−35767
thermochemical production, plasmochemical H_2O decomposition using nuclear energy source 80−61436
thermochemical production, process assessment and economics *(French, English)* 77−86309
thermochemical production, $SO_2/H_2O/X_2$ reactions (X_2=Br_2, I_2) 80−35773
thermochemical production by coal gasification using steam 80−35789
thermochemical production by H_2O decomp., optimum temp. conditions utilizing HTGR nuclear heat 80−35781
thermochemical production by H_2O pyrolysis 80−55928
thermochemical production by Mark-13 cycle, development of laboratory-scale plant 80−76659
thermochemical production by steam reforming of methane, kinetic anal. 80−35788
thermochemical production from H_2O, development of two new thermochem. cycles at ORNL 80−35780
thermochemical production using air blown coal gasification, economics 80−35790
thermochemical production using Ce-Cl cycle 80−35783
thermochemical production using fusion energy source 80−51010
thermochemical production using fusion energy using metal oxide thermochem. cycles 80−76658
thermochemical production using H_2SO_4-SO_2 cycle, electrochem. aspects 80−97812
thermochemical production using Hg-I ANL-4 cycle 80−35785
thermochemical production using open-loop cycles 80−55930
thermochemical production using ZnSe cycle, chemical and process design studies 80−35782
thermochemical water-splitting cycles based on Ce and alkaline earth phosphates 80−55945
thermodynamic properties and eqn. of state in stellar conditions 79−35241
thermoelectrochemical prod. using H_2SO_4-SO_2 cycle, electrochem. aspects 80−35776
thermoelectrochemical prod. using NaCl 80−55946
thermoelectrochemical prod. utilising electrolyzer and fuel cell 80−45718
thermometric fixed points determ. 77−82511
thin surface layers, nondestructive anal. by alpha-particle scatt. 77−56297

hydrogen continued
threshold for pore form. during solidification in Al-Si (8 wt.%) alloys 78−52794
Tokamak fusion reactor first walls, hydrogen profiles 80−37578
Tokamak plasma, Doppler temp. and particle confinement time from H_α-line meas. 78−55737
Tokamak plasma reaction dynamics, corona model, spectroscopic diagnostics *(German)* 79−60103
Townsend discharge, transverse diffusion and ionis. coeffs. 79−1367
transition metal alloy, ferromag., H-impurity complex obs. by mag. aftereffect 78−72373
transport by dislocations 77−21263
transport in various liquids and metals, neutron radiography study, results review 78−59961
transportation, conversion of gas transmission networks to hydrogen 79−74550
transportation, suitability of contemporary gas distrib. equipment 80−30603
trapping and re-emission in TiB_2 coatings for Tokamaks, annealing effects 80−37582
trapping and replacement of 1 to 14 keV H and D in stainless steel 78−95070
trapping enhancement after He ion damage in Mo 77−31698
trapping in Fe alloys, electrical analogue model 79−46841
trapping in metals, book contrib. 80−24491
trapping mechanisms, by permeation techniques 79−37880
trapping of H isotopes, materials exposed to high power discharges in PLT 80−37576
triple, boiling and 17K equilib. points realization, cryostat and method 80−27314
tunable coherent Raman mixing, 4.3-13 μm 77−88850
tunnelling in surface diffusion on W (110) plane 80−75416
turbo molecular pump, performance for H_2 *(Japanese)* 80−13085
two-photon enhanced third harmonic generation and Raman scatt. 77−88843
underground storage in aquifers, physical, chemical, energy aspects 80−55933
uptake kinetics and energetics by Mn vacuum evaporated films 80−88430
UV light source for plasma diagnostics, 121.5-121.6 nm *(Russian)* 78−25942
vapour pressures, 4 to 30K, isotope effects 77−72674
very high temp. nuclear reactor, graphite moderated He cooled for H_2 production 77−23247
volcanic hydrothermal vents from E.Pacific rise, H_2 and CH_4 content 80−41422
water thermolysis, solar furnace, thermodynamic analysis 79−83625
X-ray attenuation coefficients, 6 to 25 keV 77−75233
Z-pinch dense plasma, emission spectrum, thermal equilibrium departure 79−82094
Zircalloy in thermal gradient, calc. of supercharging effect of H_2 and hydride distrib. 78−21639
a-Si:H, effect of H conc. on photovoltaic props. 79−99577
Ag-H_2 electrochemical cell design using rolled stack configuration 80−101084
Al alloys, H impurities, improving productivity and detection threshold, by removing moisture with light pulse 80−26076
Al:H, impurity energies and geometrics, self-consistent jellium calc. 79−99507
Al:H, interaction energy of two H atoms, Hohenberg-Kohn-Sham density functional formalism 79−51519
α-Al_2O_3:Co,H, Co and proton ENDOR, IR and optical spectra charge compensator nature and defect struct. 80−44956
$Al_2O_3+W+H_2$ react., high temp., reduction, oxidation conditions 77−16518
Ar, ionising shock waves, stability, H impurities effect 78−22371
Ar plasma, H impurity, equilib. state of highly ionised plasma 78−83597
Ar plasma jet, surrounded by Ar, He, N_2, H_2 gases, recombinations in decaying jet 78−9753
Ar:H, solid, struct., pair pot. calcs. 78−2215
Ar:H crystalline matrix, Xα scattered wave cluster model 79−73468
Ar:H_2, nuclear spin relax. of H_2, crystal field meas. 79−51875
Ar-H_2, elec. breakdown, time and space resolved spectra 78−18470
Ar-H_2, liquid solution, dielectric props., intermolecular interactions *(Russian)* 80−88904
Ar-H_2 plasma, thermodynamic properties 78−63542
Ar-N_2-H_2 plasma equilibrium compositions and thermodynamic props. 78−71433
Ar+H_2, atmosphere for thermal damage suppression of InP 79−100275
Ar+H_2, plasma, transport coeff. calcs., 2000-25000K 77−11314
B:C,H amorphous film, IR absorpt. spectra 77−77312
B:H amorphous CVD films, IR, visible, and near UV optical props. 80−50442
B:H amorphous films, optical band gap, thermal treatment effect 80−93415
B-H, possibility of thermonuclear fuel in relativistic plasma *(Russian)* 80−37573
BBr_3-H_2 mixtures, B CVD, thermodynamic anal. 79−47634
BBr_3-PCl_3-H_2, gas phase equilib. comp. 80−35166
in C polymer chars 78−11551
C:H amorphous films, elec. cond. and optical absorpt. 80−49723
C:H films, amorphous, elec. props., chem. modifications 80−84523
C-H plasma, laser prod., spectral line emission 80−43969
CO+H_2, adsorpt. on Rh, reflection-absorption IR and thermal desorpt. obs. 78−6226
CO+H_2, kinetics, methane formation using polycryst. Ni ribbon catalyst 78−40078
CO+H_2 combustion in air, gasdynamic laser operating on combustion products, construction, amplification coeff. *(Russian)* 77−7075
CO_2-N_2-H_2 electron beam controlled laser, efficiency and output energy depend. on H_2 78−58978
CO_2-N_2-He(H_2) laser mixtures, composition effect on excitation efficiency in dicharge 78−5453
Ca-H_2, single freq. laser, 5.54 μm emission, mag. field tuning 78−46634
CaF_2:H^-, mechanism of resonant absorption by impurities 78−6715
CdTe:H^+, ion-implanted, optical waveguiding and electrooptic modulation 77−7197
Cl_2-O_3-H_2 dilute mixtures, photolysis products, Fourier Transform IR kinetic obs. 80−26033
ClF-H_2 chemical laser, electron-beam initiation, energy parameters, stimulated emission from HF, HCl 79−89903

hydrogen continued
ClF+H_2, reaction rate const. for H+ClF→HCl*+F 77−71980
$ClF_3(F_5)+H_2$ chemical laser, stimulated emission rel. to reaction mechanism 77−50667
Cr_2O_3, reduction by H_2, reaction kinetics 80−11950
Cs halides:H, luminesc. of interstitial atomic H 80−103986
CsI:H^-, U-centres, force consts. using Green's functions 79−46775
Cu:H, interaction of H and vacancies, positron annihilation, Doppler broadening 78−80434
CuH dilute alloy, Hall coefficient, relaxation times, Fermi surface 80−84460
D-H plasma, HF heating by magnetoacoustic waves *(Russian)* 77−3960
F+H_2 chemical laser, vib. populations in V→V, V→R,T energy transfer corrections 77−32794
F_2-H_2 mixture, parameters influence on flame propag. velocity, rej to HF chem. laser 80−50855
α-Fe, Armco, determ. of H solubility 80−54390
Fe, Armco, strength, fracture, effect of H_2 *(Russian)* 77−25129
in Fe, average trapping depth and trapping sites density 80−84297
Fe, H diffusion coeff. meas. at low temps. by electrochem. alternating method *(Japanese)* 80−39354
in Fe, H martensite production *(Ukrainian)* 77−52321
Fe, pure, effect of H_2 on relaxation 77−52391
Fe, softening vs. hardening effects produced by high fugacity H charging 79−74172
Fe:H, deformed, deep trapping states for H 80−29045
Fe/H abundances of extreme Population II stars in globular and dwarf galaxies 78−40939
Fe-Cr alloys, cold worked, internal friction due to H *(Japanese)* 80−70305
Fe-H, recovery of hydrogenated and quenched alloy, solute diffusion 77−77510
Fe-H system, effect of H on struct. during creep 77−16652
Fe-Pd, magnetic after-effect of H isotopes 80−75817
$Fe_{65}(Ni_{1-x}Mn_x)_{35}$, H solid solutions magnetisation behaviour in pulsed mag. fields 79−65674
Fe_2O_3, direct reduction by H_2 reaction kinetics 80−40689
FeTi, hydrogen storage, annealing effects *(Japanese)* 79−100542
n-GaAs:H, ion implanted, carrier removal, capacitance-voltage profiling 80−84195
GaAs:H amorphous sputtered films, high field cond. props. 80−44607
GaP:H/GaAs, amorphous film/crystal junction, optical and elec. props. 79−99611
GdF_3:H films, H, F profiles meas. by sputter-induced optical emission 78−47407
Ge, impurity levels of H and muons 79−56162
Ge:H, amorphous, H content determ. by IR absorpt., gas evolution and nuclear reaction methods 80−44130
Ge:H, amorphous, H-states exam. 78−39059
Ge:H, amorphous, voids, atom probe FIM 80−49107
Ge:H, interstitial impurity levels, pseudopot. calc. 80−44533
Ge:H, photoelec. spectra, acceptor and donor behaviour 80−29443
Ge:H amorphous films, photoemission spectra 80−50517
H adsorption and desorption, self-consistent model calc. 79−46943
H atom gas with unsaturated electron shells, third virial coeff. calcs. 79−90752
H containing mixture extraction from D compounds, ionis. radiation effects *(Russian)* 77−6961
H, discharge lamp light source, Doppler effects *(German)* 79−44946
H II region, H137β/109α intensity ratio interpretation 80−31344
H, spin-polarised, density, magnetisation, compression and thermal leakage 80−44391
H, stabilisation at low temp. 80−44390
H^- polarised ion sources, recent advances 79−45498
H^+, coupled transport in a liposome suspension 79−53069
H^+, mobility in polyester, from ionic injection current at strong diffusion 80−2210
H/D, abundance ratio, mass spectrometric method 78−8462
H/D isotope separation factors, and exchange efficiency at Pd electrodes 79−50149
H/D ratio in planetary atmospheres, determ. from CH_3D 9613 Å band 78−86861
H-^{2}H, rotating plasmas, balance and separation processes 78−1911
H-air, laminar diffusion flames, chem. nonequilib. effects model 78−48654
H-Br systems, thermokinetic oscillations in flame propagation, stability diagram 79−79253
H-C, thermal desorption, one-phonon at. scatt., 3-dimens., continuum model 78−87860
H-D discharge, RF, meas. of excitation transfer rate by laser fluoresc. 80−9542
H-D mixture, selective chemisorption by KC_8 intercalation cpd. *(French)* 77−32830
H-D plasma, fast magnetosonic wave mode conversion, in Tokamak 77−72436
H-D plasma, He^+ local diagnostics after at. beam scatt. *(Russian)* 77−19774
H-He, light source, elec. discharge, Doppler effects *(German)* 79−44946
H-He arc lamp, 60-360 nm, calibration 78−87117
H-He fluid planets, dynamics and He distrib. 78−28555
H-He fluid planets, phase diagram and transport props. 78−28554
H-He interface, of neutron star, physical processes in strong gravit. field, electron-positron pair prod., γ-ray emission *(Russian)* 79−80333
H-He multi-ion plasma, with ion acoustic turbulence, resistivity phenomena 80−48856
H-inert gas laser spark, emission spectra 79−82119
H-like ion, relativistic acceleration, quasi-Stark effect *(German)* 78−58621
H-like systems in arbitrary mag. field, excited states, variational approach 79−77973
H-O electrochemical matrix-type cells, transport effects study 80−26027
H-T fusion fuel, liquid-vapour equilib., Raoult's law 79−67947
H^+-He^{2+}, strongly coupled ionic mixture, density fluctuations, timer depend. 77−80272
H+O_3, reaction mechanism studied using photoionisation mass spectrometer, form. of $O_2(a'\Delta g)$ 80−85168
H_2, α-particles stopping cross-section determ. 79−49917
p-H_2 cooled gas, 16 μm source using four-wave mixing and stimulated Raman scatt. 78−1298

hydrogen continued
H_2 electron swarms transport parameters meas., nonuniformities effect 78−83613
H_2 fuelled aircraft, kinetic model anal. of pollution 80−40816
H_2 impurity control in EBR-II sodium systems 79−93696
p-H_2, liq., equil. bulk props., perturbation theory approach and quantum effects *(Russian)* 77−89551
H_2, total scatt. cross sections for intermediate-energy positrons 80−91692
H_2, transverse ionising shock wave, soln. for problem of nonstationary evolution of magnetic struct. 80−70003
n-H_2, vap. press. eqn. between triple and critical pts. 77−55351
H_2^+ molecule energy level splitting, lecture demonstration based on coupled elect. reson. ccts. 79−49949
H_2^+, polarisability, numerical two-centre calc. 79−10232
H_2/CO surface complex, in W (100), flash desorption and AES obs. 78−73083
H_2/D_2 solubility ratios in Pd alloys, meas. 79−99325
H_2/F_2 laser, initiation using surface spark discharge UV light source 80−78923
H_2-air fuel cell with proton conducting solid electrolytes, performance meas. 80−16796
H_2-air mixtures, ignition energy by capacitive discharge *(French)* 80−10446
H_2-air-H_3PO_4 fuel cell performance, effect of NH_3 80−108795
H_2-Ar, liq.-vapor equilib. 83 to 141K, to 52 MPa 79−42226
H_2-Ar hollow cathode discharge, effect of additional gas ionisation by oscillating electrons *(Russian)* 77−31536
H_2-Ar(Kr)(Xe) mixtures, intermol. forces 78−62867
H_2-Br_2 cell for energy storage appls. 80−72029
H_2-CO_2, adsorption on ZnTe, manometric and mass-spectroscopic obs. 77−35808
H_2-CO_2, turbulent flow heat transfer, expt. and numerical anal. 78−94690
H_2-Cl_2 cell, electrochemically regenerative, mass and heat balances 80−3503
H_2-Cl_2 mixture, detonation initiation, nonequilib. physicochem. process simulation 80−38431
H_2-Cs, H^- source for hollow beams 80−23228
H_2-D_2, liq. mixtures, self-diffusion 77−35746
H_2-D_2 gas, thermal cond. meas., 2-36 MPa 80−64668
H_2-D_2 isotope separation by permeation through Pd membrane 80−68959
H_2-D_2 vacuum deposited solid films, struct. study transmission electron diffr. obs. *(Russian)* 79−11035
H_2-D_2-T_2 mixtures, mesic at. and mol. processes 80−23580
H_2-F_2 pulsed laser, flame out 77−27284
H_2-F_2-He chemical CW laser, flows *(Russian)* 78−74895
H_2-F_2-O_2, chem. laser mixture, multiatm., spontaneous explosions 78−73044
H_2-He, nucl. shielding, ab initio coupled HF calc. 79−89690
H_2-He, on W, Mo, Ir and Re surfaces, field depend. of spectral line energy 79−78853
H_2-He, thermal cond. meas., up to 14 MPa 80−64669
H_2-He, thermal diffusion factors meas. 80−10344
H_2-He gas mixtures, 1000-25000K, transport property correlations 80−75029
H_2-He mixture, collision integrals, modelling of spacecraft entry into Jupiter atmosphere 78−71413
H_2-He mixture, conc. depend. of thermodiffusion const. 77−7503
H_2-He mixture, pumping speed of Excalibur CVV2008 liq. He cryosorption pump 79−80633
H_2-He mixture, radiant heat transfer coefficient for blunt body in hypersonic flow, similarity law 80−33705
H_2-He plasma, shock-heated, relax. distance and equilib. electron density diagnostics 77−24180
H_2-He plasma interface in strong gravit. field, bremsstrahlung, neutron stars and pulsars appl. *(Russian)* 79−67048
H_2-He(Ne) glow discharge, H Balmer line excitation by recomb. *(Russian)* 77−46516
H_2-hexafluoroethane mixture, RF discharge chemistry, added H_2 effect 80−33832
H_2-methane mixture, D isotope enrichment by flow discharge exposure 78−13343
H_2-methane mixture properties for hydrogen supplementation of natural gas 80−45781
H_2-methane system in plasma reactor, exptl. and thermodynamic investig. *(French)* 78−15698
H_2-N_2, liquid-vap. equilib., 63-110K and up to 57 MPa 79−55881
H_2-N_2, low-ionised plasma, electron kinetics, collision processes influence *(German)* 79−14519
H_2-N_2 glow discharge, positive column, electron energy-distrib. spatial variation 77−47294
H_2-N_2 mixtures, 300K, proton spin relax., single relax. time approx. 77−61766
H_2-N_2 plasma, transport coeffs. and collision processes *(German)* 79−23395
H_2-N_2-Ar, two-phase flow film boiling, in vap. generator, heat transfer 78−75190
H_2-N_2-Na jet, ignition and extinguishment in simulated LMFBR accident conditions 78−8932
H_2-N_2(Ar) gas mixture, correl. between kinetic theory of thermal cond. and expt., 90 to 300K, 1 bar 79−81707
H_2-NH_3 mixture, viscosity meas., 25-100°C, up to 120×10^5 Pa 79−32731
H_2-NO, thermal cond., mag. field effect 79−94764
H_2-Ne, hollow-cathode discharge, electron energy distrib. 78−71573
H_2-O_2 gas mixture in chem. equilib., elemental diffusional separation in nonisothermal flow 79−55429
H_2-O_2 mixture, explosion limits as stochastic phenomenon 77−21387
H_2-O_2 plasma, electrical conductivity tensor in mag. field *(Russian)* 80−87864
H_2-O_2 reaction boundary layer, numerical anal. *(German)* 77−35253
H_2-O_2 seeded system for MHD generator, elec. cond. 80−76642
H_2-O_2 system with N_2, O_2 diluents, detonation wave instabilities 78−5762
H_2-O_2-N_2 flame, photochem. reactions involving Na*, laser saturated conditions 78−80762
H_2-O_2-N_2 flames, diffusion coeff. meas. for CO, Br, I and Tl 78−51272
H_2-tetrafluoromethane glow discharge, plasma etching of Si and SiO_2 surfaces 79−98922

hydrogen continued
H_2-tetrafluoromethane mixture, RF discharge chemistry, added H_2 effect 80−33832
H_2-thianaphthene mixtures, gas-liq. equilib. 79−65177
H_2-trifluoromethane mixture, RF discharge chemistry, added H_2 effect 80−33832
H_2+Br^-, total electron detachment cross sections for energies around threshold 80−99550
H_2+Cl^-, total electron detachment cross sections for energies around threshold 80−99550
$H_2+D_2(O_2)(N_2O)$, Wassiljewa coeffs., thermal conds., 50 and 100°C 79−37437
H_2+F, in pulsed HF chem. laser, kinetic modelling, rot. nonequilib. 79−36888
H_2+F_2 reaction, coherent emission efficiency 78−17928
H_2+He^+, 25-90 keV, fast beam form, $He(2^3S)$ population 79−31740
$H_2+I(Cl)$, thermal rate constants, quasiclassical trajectory calcs., detailed balance 79−87822
$H_2+NO+CO$ interaction over Pt, Rh, Ru and Os, NH_4OCN formation 78−73082
H_2+O_2 fuel, equilib. compositions, 1000 to 6000K *(Ukrainian)* 79−50571
H_2+O_2 on polycryst. Ni surface, SIMS and thermal desorption meas. 80−40742
$H_2+O^*\rightarrow OH^*+H$, rate const. and vibr. energy distrib. in OH*, for $O(^3P)$ 78−60998
H_2+SF_6 mixture, equilib. composition and transport props., 300 to 15000K 77−24051
$H_2^++H_2\rightarrow H_3^++H$, state-selected ion-molecule reactions threshold electron-secondary ion coincidence technique obs. 80−85166
H_2(-He), H production at 10 torr in pulsed discharge 80−9748
H_2(-He), hollow cathode effect in cylindrical geometry *(French)* 80−33842
HD, isotopic effects in predissociations 78−86924
HD, liq., in He bath, NMR spin-lattice relax., coupled states ang. momentum decoupling 77−77117
HD, viscomagnetic heat flux, in a Burnett regime 78−71400
HD-T_2, liq. and solid, vibr.-rot. IR spectra 80−50313
$H_2(D_2)$-Ne-He(Ar) plasma, combustion driven shock tube, H_β central struct., ion mass effect 78−26327
HI_3O_8, ^{127}I NQR spectra 80−39889
H_2O-H_2 cooling in supersonic nozzle, submillimetre wave generation 80−48229
H_2S^+, $^2B_1$, $^2A_1$ and $^2B_2$ electronic states, pot. energy curves, CI calcs. 80−87048
$H_2SO_4+O,(N),(OH)$, atmos. chemistry, collisional reaction probabilities 80−90168
HT-T_2, liq. and solid, vibr.-rot. IR spectra 80−50313
^1H, ^2H, ^{17}O in muscle water, study of spin-lattice and spin-spin relax. times 80−21443
^3H, continuous monitoring, sensitive method *(German)* 77−372
^3H labelled amino acids, optimisation factors in liquid scintillation counting 80−30951
H83α and H99α recomb. lines in Markarian 668 Seyfert galaxy 80−94864
$H_2\rightleftarrows H+H$ reversible reaction on metal surface, friction coeff. calc. 77−77807
He-Ar-H arc plasma, nonequilib. effects, spectroscopic diagnostics 77−76191
He-H_2, plasma, strongly supercooled quasistationary, prod. by intense electron beam in dense gas *(Russian)* 77−89277
He-H_2 mixtures, isobaric sp. ht. 78−18788
$He+H_2$ microwave plasma, pulsed high current heating at atm. press., MHD instability 78−55728
^4He stopping cross sections, 1-8.5 MeV 78−58558
K-H plasma, low temp. discharge, ion constitution mass spectra *(Russian)* 77−4000
KBr:$H^-(H_2^+)$, absorption bands, V_4- and M-centres 77−48204
KBr:Na,H, U-centres, HFS consts., g-factor, EPR spectra 80−39869
KCN:H^-, U-centre, local mode meas. 77−1199
KCl:Ca,H, ENDOR studies of localised vibrations of substitutional atomic H 78−80248
KCl:H, Ag(Na), UV irrad., anionic H atoms, ESR and optical absorpt. expts. 79−99187
KCl:H, dichroic H- and U-centres by polarised bleaching of interstitial H 80−29766
KCl:H, dynamical superhyperfine interaction 80−2663
KCl:H, ENDOR and ESR study of anion sites 80−108118
KCl:I^-, H, fluorescence of interstitial H-centres 79−73987
KCl:Li,H optical and EPR exam. of H centre, $(LiH)^+$ absorpt. spectra 79−99920
KI:H^-, U-centres, force consts. using Green's functions 79−46775
K_2OsCl_6, single cryst. with H^+ interstitials, protonic cond. from dielec. meas. 80−107515
K_2OsCl_6:H^+, impurity H^+ ion motion, ^{35}Cl NQR obs., 77 and 298K 80−60451
Kr-H_2, ~5 torr, ionisation by Mach 15+shock waves, shock struct. and stability 77−75938
L_β reson. line Stark broadening in dense equilib. plasma 79−32823
$LaNi_5$ storage, effect of O_2, H_2, H_2O, SO_2 on surface segregation *(German)* 80−51008
$LaNi_5H_{\geq 3.0}$, H diffusion coeff., neutron scatt. obs. 80−24643
Li-LiH system, H isotope solubility thermodynamic singularities 80−81356
Li-LiH system, liquid Li, dilute solns., equilib. H press., solubility, heat of soln., CTR materials 77−14266
LiF:H, neutron irrad., ENDOR meas. 79−11356
Li_3N:H, ionic cond., nuclear reaction anal. 80−34454
Li_3N:H, ionic cond. 79−42305
Mg:H, impurity energies and geometrics, self-consistent jellium calc. 79−99507
Mg:H, interaction energy of two H atoms, Hohenberg-Kohn-Sham density functional formalism 79−51519
Mg:H, solid soln. produced by ion implantation 78−67733
Mg-Mg_2Ni storage material 80−30283
MgH_2 storage, reaction with Mg/Mg_2Cu eutectic, hydriding and dehydriding kinetics obs. by press. sweep method 80−35765
MgO:H, electron irrad. induced diffusion of interstitial impurity 77−15452
Mg_2SiO_4:H, forsterite, ionic transport 79−69285

hydrogen continued
Mo:H(He), depth profiles of implanted atoms, proton backscatter meas. 79−51136
N_2-H_2, high-temp. plasma, transport coeff. calcs. 77−62340
N_2-H_2, mixed plasma, elastic collision energy loss *(German)* 79−41793
N_2-H_2 arc, bent and rot., flow mechanism 80−70047
N_2-H_2 mixture, glow discharge, ionisation and excitation obs. 78−67505
N_2-O_2-H_2 nonselfsustaining discharge plasma, current establishment/relax. processes, rel. to CO_2 laser *(Russian)* 79−99011
$N_4^++H_2$, reaction rate determ. 78−60985
N_2O-H_2 flame, appls. to Mn determ. in gasoline by AAS 78−15729
Na-K-H system, H influence on component interactions *(Russian)* 80−54383
NaCl:Li,H, U-centres, HFS consts., g-factor, EPR spectra 80−39869
NaI:H^-, U-centres, force consts. using Green's functions 79−46775
Nb film, H impurity effects on supercond. transition temp. and transition width *(Russian)* 77−66222
Nb, H_2 diffusion, low temp. recovery 79−73342
Nb:N, H, atomic tunnelling of interstitial pair, specific heat meas. 78−47600
Nb:N,H, thermal cond., 0.07 to 1.5K, influence of N interstitials 79−65601
Nb-H, BCC, tetrahedral interstitial site H band modes, neutron scatt. obs. 79−55852
Nb-Ta alloys, H diffusion at 296K 80−84329
$NbH_{0.026}$, nucl. acoustic reson. of interstitial H 79−51867
Ne-H_2 liq. mixtures, phase equilib. effects, thermodynamic perturb. theory *(Russian)* 80−92663
Ne-H_2 mixture, liquid vapour phase equilib., sound vel., compressibility, thermodynamic perturbation theory obs. *(Russian)* 80−39306
Ne-H-H_2 mixture, positive column characts. and comparison with approx. diffusion theory 80−44025
Ni (100), adsorption of O_2 and reduction of surface oxide by H_2 80−108741
Ni, H-charged cold-worked, internal friction peak 80−107368
Ni, slip character, H effect 80−89287
Ni:H, energy and electron density of states 78−51929
Ni:H thin plate, recovery of quenched-in solute H 77−62673
Ni-Cu-H systems, Curie temp. during phase transitions under high press. H_2 80−71029
Ni-Fe-H, Curie points, mag. props. of H solutions FCC metal sublattice parameter behaviour 79−69671
Ni-H_2 sealed storage battery, characts., charging, transient, stationary regimes 77−63930
Ni-thoria dispersed (2 vol.%), meas. and eval. of H_2 trapping by permeation technique 79−60555
O_2-H_2, gas mixture, mag. field effect on thermal conductivity 78−59533
O_2-H_2 mixture, temp. dependence of molecular vibr. relaxation freq. from 300 to 675K 80−74238
O_2-H_2-Ar flame, atm. press., $Na(3^2P)$ lifetime obs. 79−39149
Pd:H, elastic props. of dilute solid solutions 78−75706
Pd:H, electron density of states of interstitial H 77−47766
Pd:H, energy and electron density of states 78−51929
Pd:H, energy of interstitial H 77−47765
Pd-Ag, Fermi energy influence on soln. behaviour of H, B and C *(German)* 80−44323
Pd-Au:H_2, thermodynamic props. at 555 and 700K, vibr. freqs. and excess entropies 80−29186
Pd-H, dil. soln., partial molar props., temp. depend. 78−68910
Pd-H, solid soln., excess entropies, variation of H solubility with pressure 79−46846
Pd-H, vibr. modes, Raman study 77−85713
Pd-H system, solvus hysteresis 80−71659
$Pd_{0.9}Ag_{0.1}$:H(D), free energy, enthalpies of soln. 78−15692
RbCl:Ca,H, ENDOR studies of localised vibrations of substitutional atomic H 78−80248
RbCl:H, dynamical superhyperfine interaction 80−2663
RbCl:H^-, defect pairs of F-centres and U-centres, Raman meas. 79−7599
RbCl:I, H, fluorescence of interstitial H-centres 79−73987
RbCl:Na,H, U-centres, HFS and g-factor, EPR spectra 80−39869
RbI:H^-, U-centres, force consts. using Green's functions 79−46775
Rh:H, energy and electron density of states 78−51929
SF_6-H_2, high-press. radiation-chem. laser, electron beam initiation 77−75562
SF_6-H_2 electric discharge laser pumped by inductive storage unit 79−98409
SF_6-H_2 mixtures, laser irradiated, IR energy deposition and HF fluoresc. 80−23454
Si, H^+ and H_2^+ ion implantation profiles determ. by SIMS 79−4334
Si, impurity levels of H and muons 79−56162
Si:As, H, amorphous system, struct. and defects, Raman and EPR meas. 80−49103
Si:Au, H, film, amorphous, elec. cond. meas. 80−80423
Si:F, H amorphous films, optical props., photoconductivity, photostructural changes 80−11034
Si:F,H, amorphous, elec. and optical props. 80−60031
Si:F,H, amorphous, electronic struct., orthogonalised LCAO calc. 80−44486
Si:F,H, amorphous, glow discharge deposited elec. props. and device aspects 80−44744
Si:F,H, amorphous efficient carrier generation for solar photovoltaic energy conversion 80−92906
Si:H, 50-250 keV H^+ irrad. damage distrib., $^4He^+$ channelling obs. 78−26587
Si:H, amorphous, 2p level shift, XPS obs. 80−97401
Si:H, amorphous, annealing effect on cond. *(Korean)* 79−15142
Si:H, amorphous, Auger electron spectrosc. obs. 80−76112
Si:H, amorphous, band tail absorpt., photocurrent meas. for Schottky barrier solar cell 80−60032
n-Si:H, amorphous, bulk density of deep states, DLTS meas. 80−88518
Si:H, amorphous, control and anal. of deposition, using plasma spectroscopy 80−45230
Si:H, amorphous, controlled hydrogenation at low temps. 79−69119
Si:H, amorphous, defect creation and H evolution 80−50392
Si:H, amorphous, defect photoluminesc. meas. 80−97334
Si:H, amorphous, defect states, luminesc. and ESR obs. 80−76075
Si:H, amorphous, density of states determ. using field effect 80−49937
Si:H, amorphous, discharge prod., optically induced cond. changes 80−96937

hydrogen continued
Si:H, amorphous, dopant conc., glow discharge optical spectroscopy 80−49546
Si:H, amorphous, doped, Fermi level position, photoelectron spectra 79−47592
Si:H, amorphous, effect of gap state density on photocond. and photolum. 79−91096
Si:H, amorphous, electronic states of hydrogenated Si, theory 79−42494
Si:H, amorphous, electronic struct. calc., rel. to UPS data 80−39527
Si:H, amorphous, excess carrier thermalisation and recomb., luminesc. decay and photocond. 80−50397
Si:H, amorphous, exodiffusion of H, EPR expts. 80−49102
Si:H, amorphous, geminate recombination model for photoluminescence decay 80−71481
Si:H, amorphous, glow discharge deposited, thermal dehydrogenation, IR spectra 80−44442
Si:H, amorphous, glow discharge deposited, laser annealing 80−49104
Si:H, amorphous, H content determ. by IR absorpt., gas evolution and nuclear reaction methods 80−44130
Si:H, amorphous, in p^+-i-n^+ struct., hole diffusion length meas. 80−44712
Si:H, amorphous, light-induced ESR and photoluminesc., dangling bonds with positive correl. energy 80−50161
Si:H, amorphous, luminesc., band tail states and thermalization 80−25455
Si:H, amorphous, mobility edge position using continuous random network model for struct. 80−44544
Si:H, amorphous, optical studies of excess carrier recomb., evidence for dispersive diffusion 80−76059
Si:H, amorphous, p^+-i-n^+ struct. solar cells, material parameters and deposition condition optimisation study for higher efficiencies 80−45676
Si:H, amorphous, photoelectrochem. behaviour 80−81480
Si:H, amorphous, plasma deposited, cond. adsorbate and insulating layer effects 80−49749
Si:H, amorphous, plasma-deposited, effect of DC elec. field superimposed during deposition 80−44643
Si:H, amorphous, prod. by high temp. thermal decomp. of SiH_4, and photocond. 79−87585
Si:H, amorphous, ps. relax., optically induced absorpt. 80−48325
Si:H, amorphous, Pt film growth, AES and LEED study 80−88447
Si:H, amorphous, RF sputtered, suitability as solar cell material 80−40864
Si:H, amorphous, RF sputtered, Schottky barrier solar cells, photovoltaic props. and capacitance-voltage charact. 80−45678
Si:H, amorphous, radiative recomb. by diffusion and tunnelling, photocond. quantum efficiency 80−50394
Si:H, amorphous, radiative recomb. and luminescent processes 80−55152
Si:H, amorphous, refr. index, temp. depend., implications for thermoreflectance and electroreflectance 80−50290
Si:H, amorphous, rehydrogenation, photoluminesc. recovery 78−72571
Si:H, amorphous, Schottky diode, spectral response and hole drift mobility 80−39673
Si:H, amorphous, Schottky barrier solar cell, degradation mechanisms affecting stability and operation 80−45680
Si:H, amorphous, Schottky barrier solar cell, deposition parameter effects on elec. props. 80−45681
Si:H, amorphous, Schottky diodes, elec. props., light-induced effects 80−103741
Si:H, amorphous, solar cell struct., photocurrent meas., absorpt. coeff. 80−50960
Si:H, amorphous, solar cells, trap spectroscopy using transient current techniques 80−104508
Si:H, amorphous, solar-cells, charge collection and spectral response 80−85275
Si:H, amorphous, sputter deposited, O_2 incorporation during and after fabrication 80−49541
Si:H, amorphous, sputtered, Auger surface spectroscopy 80−50472
Si:H, amorphous, sputtered on $Gd_2(MoO_4)_3$, ferroelec. domain wall motion, image scanning 80−83663
Si:H, amorphous, sputtered Schottky barrier solar cells, conduction mechanism 80−104506
Si:H, amorphous, stacked solar cells, development 80−94050
Si:H, amorphous, structural model 80−49105
Si:H, amorphous, surface activated, photoemission spectra, minority carrier diffusion length 80−40235
Si:H, amorphous, surface struct., AES and LEED, comparative study *(French)* 80−44398
Si:H, amorphous, surface states distribution using MOS tunnel junctions 80−103735
Si:H, amorphous, temp. depend. of photolum. 80−89063
n-Si:H, amorphous, thickness depend. cond. 80−49724
Si:H, amorphous, vac. evaporated, doping, transport and optical props. 80−49715
Si:H, amorphous and crystalline, hydrogenation and dehydrogenation, luminesc. spectra 80−11477
Si:H, amorphous defect model 80−24363
Si:H, amorphous field induced and quenched-in excess cond. 80−24968
Si:H, amorphous film, anal. of intrinsic photocond. spectrum 79−73541
Si:H, amorphous film, prep. by plasma decomp. of SiH_4 under mag. field, and characterisation 80−45239
Si:H, amorphous film prepared from glow discharge, quantitative H anal. 77−69188
Si:H, amorphous films, plasma-deposited, defect states, IR, ESR, and refractive index meas. 79−65944
Si:H, amorphous Schottky barrier solar cells, depletion region, capacitance study 80−50963
Si:H, amorphous Schottky solar cells, prep. and charact. of diode RF reactive cathodic sputtered films *(French)* 80−61347
Si:H, amorphous sputtered, excitation spectra and photoluminesc. 80−50396
Si:H, amorphous thin film, ion plating, IR absorpt. meas. 80−84857
Si:H, amorphous thin film solar cells 80−81478
Si:H, amorphouse film, optical and elec. props. 79−82694
Si:H, Cl(F), amorphous, photocond., dark cond. and photoluminesc. 80−49802
Si:H, correlations between elastic energy transferred by implanted H ions and H trapping 78−14370
Si:H, defects in monovacancy Si cluster, semi-empirical calc. 78−43329
Si:H, electron states 80−29355
a-Si:H, electronic states and bonding config. 80−64900
hydrogen continued
Si:H, evaporated amorphous film, prep. elec. cond. and photocond. 79−38201
Si:H, glow discharge deposited amorphous film, UV absorpt. spectra 80−25420
Si:H, H^+ sputtered as result of ion bombardment, ionis. mechanism 79−100009
Si:H, implanted, annihilation of free excitons, inelastic scatt. by SiH_4 mols., photolum. obs. 78−19561
a-Si:H, influence of H on optical props., H conc. and H bonds 80−76098
Si:H, interstitial electronic struct., self-consistent pseudopotential calcs. 79−73469
Si:H, ion implanted, anal. of methods used for H profiling in materials using ion beams 79−5197
Si:H, ion implanted Monte Carlo calcs. of profiles of H ions 78−55889
Si:H, ion-implanted, photoluminesc. spectrum 80−45129
Si:H, new IR absorpt. bands 79−87472
Si:H, plasma-deposited amorphous film, proton mag. reson. 80−44931
a-Si:H, spin defect and recombination influence on electronic transport 80−50409
a-Si:H, structural interpretation of vibr. spectra 79−69864
Si:H,B, amorphous, field effect and thermoelec. power 80−96924
Si:H,F,O amorphous, plasma deposited, comp. and optical props. 80−50441
Si:H,Li, amorphous, DC electrical conductivity, absorption edge and IR meas., role of H 80−54694
Si:H,Li, amorphous, photoluminescence obs. 80−66280
Si:H,P, amorphous, heavily hydrogenated, high gap state densities 80−49803
Si:H,P, amorphous, in MOS tunnel junction, electron tunnelling charact. 79−73592
Si:H,P amorphous film, elec. cond., thickness and temp. depend. 80−65559
Si:H alloy, amorphous, dihydride model of vibrational spectra 80−80827
a-Si:H alloys, sputter deposited thin film coatings, property-comp. relationships 80−80975
Si:H amorphous, cooperative charge disproportionation of defects, rel. to photolum. 80−54649
Si:H amorphous, plasma-deposited, luminesc. decay 79−73989
Si:H amorphous, solar cell structure, optical absorption by gap states 80−94052
Si:H amorphous film, H quantitative depth profiling by nuclear reactions and SIMS 78−14373
Si:H amorphous film, plasma-deposited, growth morphology and defects 80−44128
Si:H amorphous film, plasma-deposited, elec. and comp. heterogeneity 80−44745
Si:H amorphous film, prep. by RF glow discharge decomp. of SiH_4, optical props. and H conc. 80−15416
Si:H amorphous film, prop. by glow discharge deposition, and plasma parameter effects on props. 80−45240
Si:H amorphous film, sputtered in Ar-SiH_4 mixtures, props. 79−87023
Si:H amorphous film, sputtered IR vibr. spectra and photolum., effects of partial evolution of H 80−44413
Si:H amorphous films, conductivity and temp. dependence of optical gap 80−100462
Si:H amorphous films, ESR, optical gap and elec. cond. meas. 80−75842
Si:H amorphous films, effects of glow-discharge prep. conditions on H content 79−46969
Si:H amorphous films, IR spectrum and struct. 80−97277
Si:H amorphous films, interference enhanced Raman scatt. 80−50326
Si:H amorphous films, optoelectronic behaviour depend. on impurity incorporation during plasma deposition 80−49804
Si:H amorphous films, photoinduced optical absorpt. and photocond. 80−50361
Si:H amorphous films, porosity and oxidation of evap., sputtered and plasma-deposited films 80−10838
Si:H amorphous films, reactively sputtered, prep. and characterisation 80−100785
Si:H amorphous films, role of Ar in deposition process, IR absorpt. and photocond. meas. 80−50321
Si:H amorphous films for solar cells, optical and elec. props. of RF glow discharge deposited films 80−54576
Si:H amorphous glow discharge film, optical absorpt., near IR region 79−87518
Si:H amorphous layers, ion bombard., AES study, $L_1L_{23}V$ Coster-Kronig transition 79−99992
Si:H amorphous semiconductors, prep. from SiH_4 and charact. 78−48326
Si:H amorphous sputtered film, photoluminesc., photocond. 80−20729
Si:H amorphous sputtered films, optical gap, IR absorpt. meas. 80−50320
Si:H film, amorphous, bombarded, defects, luminesc. and ESR meas. 80−34977
Si:H film, amorphous, elec. cond., effect of adsorbed gases and illumination 78−88048
Si:H film, amorphous, H-associated disorder modes, PMR spin-lattice relax. time meas. 80−93202
Si:H film, amorphous, photocond. imaging 80−1300
Si:H film, amorphous, plasma-deposited, small angle X-ray and neutron scatt. studies 80−59826
Si:H film, amorphous, reactively sputtered, H content effect on props. 80−49714
a-Si:H film, glow discharge deposited, H profiles, doping level 80−84202
a-Si:H highly homogeneous, for low-cost solar cell fabrication 80−72053
a-Si:H MIS junction, electronic struct. study by tunnelling 80−44729
Si:H plasma deposited film, amorphous, microstruct., TEM and SEM obs. 80−10801
a-Si:H Schottky barrier diodes, capacitance studies 80−49908
Si:H solar cells, photovoltage source in photocond. materials due to comp. and doping var. 80−7938
Si:H sputtered amorphous film, luminesc. and non-radiative decay 80−50395
a-Si:H sputtered films, ohmic contacts by H depletion, H diffusion 80−34511
a-Si:H/Pt, Schottky diode, influence of prep. conditions on forward bias currents 79−78171
Si:H(D), amorphous films, CVD, post-hydrogenation 80−54552

hydrogen continued
Si:H(F), amorphous, Schottky barrier profiles, depletion region width 80−49871
Si:O,H amorphous, plasma-deposited, electronic and struct. props. 80−50391
Si-C:H, amorphous film, vibr. spectrum 79−61450
Si-F-H:P, film, dark cond., struct., Raman scatt. 80−88588
Si-Fe-H_2-N_2, combined effect of Fe and H_2 78−95722
Si-H, amorphous, photolum., H content effects 78−15204
Si-H, amorphous, plasma-deposited, H evolution and defect creation 80−44914
Si-H, amorphous film, in situ prepared, photoemission studies 80−35060
Si-H, amorphous plasma deposited film, H content and density 79−82472
Si-H (up to 15 at.%), amorphous, ion implanted, laser annealing obs. 79−69133
a-Si-H sputtered solar cells, temp. depend. of Schottky barrier characts. 80−45669
Si-H:P amorphous film, dark cond., struct., Raman scatt. 80−88588
Si+H, solid surface and low-press. plasma, reactivity 79−47968
Si_xAs_{1-x}:H, amorphous system, struct. and defects, Raman and EPR meas. 80−49103
$Si_{1-x}B_x$:H, amorphous films, thermopower and cond. for mixed band and broad tail state cond. 80−49786
SiC, H_2 effects on epitaxial growth rates 78−22968
α-SiC:H, prepared by reactive sputtering, layer props. *(Japanese)* 80−60695
SiC:H amorphous reactively sputtered film, H content effect on film props. 80−75459
$Si_{1-x}C_x$:H glow discharge films, local atomic struct., XPS and AES study 80−93448
Si_xC_{1-x}:H reactive sputtering deposition, compositional and structural props. 79−99077
$Si_xC_{1-x}H_y$ amorphous films, IR absorpt. bands 80−100705
$SiCl_4$:H_2 binary gas mixture convective instabilities in closed vertical cylinder heated from below 79−72880
Si_xGe_{1-x}:H, amorphous, photoinduced optical absorption 79−82973
$Si_{1-x}H_x$, amorphous, gap states, DLTS 80−49656
a-$Si_{1-x}H_x$, oxygenated thin film, sputtered, elec. cond. and optical props. 79−15239
Si_3N_4:H, amorphous, ion induced H transfer from N to Si, band passivation, elec. props. 78−47439
Si_3N_4:H, film, impurity profile determ. by 1.2 MeV proton-proton scatt. 80−49256
SiO_2:H, vitreous, Raman spectroscopy 77−36230
SiO_2:H(D), γ-irrad., hydroxyls and hydrides form., detect. by Raman scatt. 77−32817
SiO_2+H_2 reactions, rate controlling processes for H_2 transport in vitreous silica 78−26733
$Sm_{0.4}Y_{2.6}Ga_{1.2}Fe_{2.8}O_{12}$, H^+ implanted film, epitaxial, mag. bubbles, walls and fine struct. 77−63241
$SrTiO_3$:H(D), controlled doping, IR spectra 79−28007
T in solid H_2, equilib. stability 77−81396
Ta:H, recovery after cold working at 4.2K, resist. meas. 79−4977
Ta-H, BCC, tetrahedral interstitial site H band modes, neutron scatt. obs. 79−55852
Ta-H system, with mobile H impurities, anomalous nuclear acoustic reson. line shape 77−20730
Ti alloy, crack initiation on planar shear bands, H_2 assisted 80−71749
β-Ti alloys, ductility enhancement by hydrogen *(Russian)* 77−52459
β-Ti, dilute soln. of H and D 79−99322
Ti-Al-H, H effect on mech. props. and lattice constants 80−21036
Ti-Al-V (6,4 wt.%), to H effect on fracture props. and microstruct. 80−40512
Ti-Mn, hydride form. *(Japanese)* 77−52629
Ti-V (40 wt.%), effects of H on anisotropic elastic props. 79−74192
TiO_2:H, IR spectra, 300, 77 and 8K 78−35175
TiO_2:H photoanodes, diffusion and surface chemistry 80−35546
UF_6-H_2/HF nuclear pumped laser, characts. 80−78847
V, internal friction, low temp., H_2 effects 80−40419
V-H, BCC, tetrahedral interstitial site H band modes, neutron scatt. obs. 79−55852
V-H, H effect on tensile props. at moderate temps. *(Japanese)* 78−19831
V-H, H on polycrystalline V, H detection by SIMS, flash-desorption obs. 79−24405
W (100), H adsorbate low energy electron vibrational excitation 80−84375
W:H, correlations between elastic energy transferred by implanted H ions and H trapping 78−14370
WCs, preparation method effects on catalytic activity for H_2 evolution 80−101024
WO_3:H^+, optical and elec. props., suggested band struct. model 77−4654
Zn-H_2 mixture, binary diffusion coefficients, 1 atm., 720-1120K 80−1725
ZnO:Cu, H, and ZnO:Cu, H, D, IR absorpt. line spectra, OH and OD vibr., optical excitation 79−15498
ZnO:Cu,H, motional effects in EPR spectra 78−80207
ZnO:Cu,H, OH and OD centres, IR-active absorpt. line spectra 79−15496
ZnS:Cu, H, double band phosphor, electrolum., −100 to +100°C 78−10987
(ZnS-ZnSe):Cu, H systems, electrolum. 77−4690
α-Zr, H terminal solid solubility, optical metallographic study 80−34195
α-Zr:H, energy of interstitial H calc. 79−23596
Zr-H, implanted, superconductivity enhancement obs. 80−70884
Zr-H system, H location in HCP phase 78−18637
Zr-Ni alloy, H_2 storage in form of capsules *(French)* 79−92091

hydrogen bonds
absorption spectra, interaction between two harmonic oscills. 79−6929
acetate-ferrileghemoglobin, X-ray struct. anal., 3D refinement at resoln. of 2.0 Å 80−104554
acetic acid, cryst., and isotopic species, H-bond, ν_s-ν_o coupling and ν_5 anharmonicity, IR spectra at 10K 79−15450
acetic acid, hypothetical dimer-based cryst. struct. calc. 77−19940
acetic acid, intermolecular O-H bonds weakening by impurities rel. to US relaxation 78−10130
acetic acid, liquid, intermolecular distance 79−7596

hydrogen bonds continued
acetic acid dimer, gas phase, H-bonded complex struct. from elec. dipole moment obs. 78−74791
acetic acid-aliphatic amide intermol. H-bonded systems, charge transfer bands 77−58041
acetic acid-d_0, -d_1, -d_4, cryst., IR spectra, H bonding 77−40217
acetic acid-d_0, -d_1, -d_4, H bonding in solid, IR spectra, vibr. and librational modes 78−43843
acetic acid-d_0(-d_1,-d_3,-d_4), cryst., H bonds, stretching, temp., isotope effects 79−51938
acetic acid-pyridine, H-bonding, proton transfer, isolated system, solvent effect, MO calc. 80−55629
acetone in mixed protic-aprotic solns., C=O stretching, IR spectra 80−45056
acetone vapour, mol. assoc., monomer-dimer equilib., thermal cond. meas., MO calcs. 79−52647
acetonitrile, Raman spectral study of aq. soln. struct., H-bond effects 77−88454
acetonitrile-HCl complex in liq. Xe, IR spectral study 80−95626
acetonitrile-phenol(-d_1), in CCl_4 ($CDCl_4$) solns., H-bonds vibr. relax. bands anal. 78−84560
acetylacetone, H bonding, dielec. dispersion obs. 77−63356
acetylene dimer, ab initio HF calc. for 64 conforms. 80−23333
acetylenic compound, 1,5-hexadiyne, hydrogen bonding effects on Raman line ν(≡C-H) *(French)* 77−75167
acetylenic compounds, 1- and 4-octyne, hydrogen bonding effects on Raman line ν(≡C-H), solvents effects *(French)* 77−71805
acoustic spectroscopy, H bonds investigation, N-butyl acetamide association in solns. 80−5891
acridene-toluene-phenol, luminescence of complexes with hydrogen bonding at 4.2-77K 79−87486
adipic acid, monoclinic crystals, IR absorption and dichroism 78−88293
adipic acid crystals, H bonds, harmonic couplings, IR vibr. modes, isotope effect origin 80−34902
adipic acid crystals, IR spectra, O-H(O-D) stretching bands 79−91422
L-alanine, solid, H bonding, wide line NMR obs. 78−52362
alcohol, dielec. const., hindered mol. rot. influence 78−43767
alcohol H-complexes interactions, H-bond vibr. freq., anharmonic calcs. 80−99453
alcohols, H-bond system, liq., high-press. effect 80−49080
alcohols, OH-stretching vibr. band in overtone region, IR-Fourier spectral investig. *(German)* 80−976
alcohols, self-association in binary mixtures, 2-const. model, vap. press. meas. *(German)* 78−18532
alcohols, vapour and liq. IR spectra, bandwidth, directional mol. rot., H-bonding 79−78661
aliphatic alcohols-2,2,6,6-tetramethylpiperidine nitroxide radical complexes, EPR, PMR, hyperfine coupling consts. 79−65736
alkali metal acid oscalates, neutron inelastic scatt. spectra in 2200-200 cm^{-1} range 80−70327
alkali metal dicarboxylates, H bonding and motion, incoherent inelastic neutron scatt. spectroscopy 80−48095
1-alkanols, liq., H-bond order temp. depend. from Hildebrand rule 80−7838
alkene-halogen compounds, assoc., matrix isolation vibrational spectra, appls. 78−46416
alkoxy primary radical, prod. by X-irrad. of α-methyl-D-glucopyranoside, ESR and ENDOR study 80−45526
amide group in soln., interactions, IR, Raman spectral investigs., peptide, protein struct., review 78−90330
amidinium salts, ^{14}N NQR spectra, H^+ relax. times 80−60448
amines, Raman bands and H bonding in liq. phase *(French)* 77−65479
amines, self-association in binary mixtures, 2-const. model, vap. press. meas. *(German)* 78−18532
aminobenzonitrile, para- and meta-, NQR linewidth, Zeeman effect, mol. config., H bonding, cryst. struct. 77−51986
γ-aminobutyric acid, cryst., film, matrix IR spectra, low temp., neutral and zwitterion forms. 77−18920
4-aminopyridine hemiperchlorate, neutron diffr. and IR spectral obs. of strong asymmetric N-H-N hydrogen bonds 80−92515
ammonium benzoate, IR spectrum, cryst. struct. 78−19455
ammonium halides, cryst., H bonding, order-disorder phenomena 80−6379
ammonium hydrogen bisbenzoate, IR spectrum, cryst. struct. 78−19455
ammonium hydrogen glutarate, H bonding, vibr. spectra 78−43860
anilides of 1-piperidine carboxylic acids, $CDCl_3$,$CHCl_3$ solns., intramol. easily polarisable H-bonds, IR spectra 78−25523
aniline-phenol, liq., US vel., adiabatic compressibility, H-bonded complex form. 77−35635
anilines, free and H-bonded, Hammett freq. factors, effects of non-monotonic ν(XH) function variations *(French)* 79−22690
anilinium halides, and anilinium sulphate, proton mag. relax. obs. 80−34800
anisole, in cyclohexane-ethanol mixtures, UV spectra, solvent effect 79−22770
aqueous mixtures, lower crit. soln. pt. theory 79−4415
L-arginine L-ascorbate, X-ray cryst. struct. determ. 80−35826
aromatic compounds, mol. rearrangement in excited electronic state, fluoresc. with anomalously large Stokes shift 79−85983
L-ascorbic acid, cryst. isolated OH iscillators, IR absorption, temp. and H-bond effects 80−7351
associated solutions, H bonding and anomalous saturation 78−52426
1-azacarbazole, IR spectra, Fermi reson., H-bonding *(German)* 77−12392
7-azaindole, IR spectra, Fermi reson., H-bonding *(German)* 77−12392
1-aziridineethanol, mol. spectrum and hydrogen bonding 78−70820
azo dyes, UV-visible spectrophotometric 80−61207
benzene, monosubstituted, dipole moments, isomerisation and H bonding, INDO calcs. 77−54515
benzoylacetone, H bonding, dielec. dispersion obs. 77−63356
binary complexes, small H-bonded mols. electronic structs., ab initio calcs. 80−74108
bioenergetics, H bonded chain theory 80−76699
biomembranes, proton transport, mol. mechanisms 78−96035
biradical, photogenerated in Norrish type II reaction, solvent effects on lifetime 79−11804
block copolymers, IR spectroscopy for struct.-props. relations 78−91268
bond length and vibr. freq., deuteration effect 79−26911
bond order, maximum principle, LCAO formalism 78−29728
bone powder and ash, PMR and IR spectra, chem. anal., bond lengths 78−3414

hydrogen bonds continued
n-butanol, phonon MFP formula, H bond collisions, low temp. 77−35655
t-butanol and -d_1, deuteration effect on self-assoc., dielectric polaris meas. 79−28672
t-butyl alcohol, struct. determ. from vibr. spectra, H-bonding and heat of mixing *(Russian)* 78−3368
t-butyl cyanide-HF, hydrogen bonded heterodimer, spectroscopic consts. from IR and microwave spectra 80−43039
calcium di-DL-glycerate dihydrate, Ca binding, X-ray cryst. struct. determ. 79−46642
carbamide phosphate, neutron diffr. 77−31652
carbonyl compounds, ^{13}C chem. shifts, approximate SCF perturbation theory 77−6804
carboxyl groups, H_2 bonded, C-O vs. O-H length correlation using neutron diffr. data 79−54987
carboxylic acid dimer, Fermi reson. 79−31501
carboxylic acid-ethanol systems, proton exchange process kinetics, effect of H bond strength in intermediate state *(Russian)* 79−96306
carboxylic acid-fluoride system, H---F bond, ab initio MO study 79−76528
charge transfer theory of H bonds, relation between vibr. spectra and energy 77−3334
chemical reactivity, reliability of quantum mechanical predictions, config. of reaction prod., H-bonded species 80−108691
chemical substitution influence on bond energy 80−37718
α-chloroacetic acid, ^{35}Cl and ^{37}Cl pure NQR, H bonding, isotope effects 78−27111
chloroacetic acid, acid salts, NQR obs. of H-bond pot. energy curves 77−18941
o-chlorobenzoic acid, solid, H bonding, wide line NMR obs. 78−52362
D-chloroform, soln., Raman scattering tensor components 80−99508
D-chloroform-dimethylsulphoxide, soln., Raman scattering tensor components 80−99508
cholesterol, adsorbed monolayer on aerosil, IR spectra 78−15753
cholesterol+water, interaction in organic media, dielec. and NMR spectroscopy 78−76979
choline phosphate calcium chloride tetrahydrate, struct., conformation, metal coordination, model for membrane surface interactions 80−15085
chymotrypsin, charge relay system, H-bond models, IR spectra 78−64935
clusters, small, formation, struct. and props. 80−58437
collagen and muscle elastic moduli, rel. to phonons, Brillouin spectra 77−52824
complex formation, enthalpy change due to electronic excitation, spectroscopic determ. 78−92496
complexes, geometries, CNDO/2 and EHT calcs. 79−36530
complexes, H-bonded, electronic absorpt. spectra calcs., rel. to charge exchange complexes *(Russian)* 78−37628
complexes, H-bonded, microwave spectra, assignments, mol. consts. 78−62794
complexes, H-bonded, PCILO method calcs. 79−10035
complexes with H-bonds, PCILO method 79−10036
crystal, IR absorpt. spectra band shape, X-H stretching vibr. temp. depend., isotope effect 78−76445
α-cyanoacrylate adhesive in first monolayer on bulk Al surface, IR spectra, H-bond form., stretching vibr. 80−87119
cyanomethane-HF, hydrogen bonded heterodimer, spectroscopic consts. from microwave spectrum 80−43038
p-cyanophenol, X-ray obs. 77−24312
cyclohexanal, liq., viscoelastic and structural relax., US rel. and absorption meas. 78−26634
cyclohexanol, polymorphism, Raman spectroscopy 77−73138
decanoic acid, associated vapours, homogeneous nucleation 80−96638
di-t-butyl nitroxide radical, in soln., proton relax., meas. of H-bonding 78−27103
diatomic molecules, shortening of energy relax. time of excited mol. vibr. in dense medium by form. of H-bonds 80−91553
1,4-diazaphenanthrene, zero-field splitting, basic triplet states, H bond effects 78−5366
1,4-diazatriphenylene, zero field splitting, basic triplet states, H bond effects 78−5366
dibenzoyl methane, H bonding, dielec. dispersion obs. 77−63356
dicarboxylic acids, D quadrupole coupling constants, ENDOR study 78−90195
2,6- dichlorophenol, soln., anisotropic reorientation, H-bonding effect, NMR obs. 79−99782
difluoroacetic acid, soln., polarisable H bonds, IR spectrosc. obs. 80−58408
dihydroxy benzenes in ethyl alcohol, dielec. dispersion charact. 80−75932
dihydroxy toluene in ethyl alcohol, dielec. dispersion charact. 80−75932
dimer, partially deuterated, microwave spectra and struct. 80−74212
dimers involving H_2O, HF an and NH_3, PCILO study 79−72238
dimethyl ether, O donor capacity *(Russian)* 77−71741
dimethyl sulphide, S donor capacity *(Russian)* 77−71741
dimethyl sulphoxide, 1:1 and 1:2 complexes with H_2O and D_2O, H-bonding, IR and Raman vibr. spectra 77−34633
dimethylamine-HCl systems, H-bonded complexes studied by ab initio MO method, dipole moments determ. 80−83253
2-dimethylaminoethanol(-d_1), microwave spectrum, hydrogen bonding, rot. consts., struct., dipole moment 77−6764
dimethylammonium manganese tetrachloride, H-bonding, struct. transition, neutron diffr. study 79−42004
dimethylether-HCl(I)(Br) mixture in N_2 matrix, IR induced proton transfer isotope effects, bond strengths 79−29335
2,4-dinitrophenol, cryst. and mol. struct. 77−15394
dioxan(-oxalic acid)(-benzoic acid), solns., compressibility, internal press., US vol., H-bonding 79−82272
dioxan-phenol(-d_1), in CCl_4 solns., H-bonds vibr. relax. bands anal. 78−84560
dioxane, 1:1 and 1:2 complexes with H_2O and D_2O, H-bonding, IR and Raman vibr. spectra 77−34633
dioxane, Raman spectral study of aq. soln. struct., H-bond effects 77−88454
distamycin A, analog cryst. and molecular struct. 79−88051
DNA, double helix, breathing modes and induced resonant melting 79−62180
DNA, molecular electrostatic pots. of complementary base pairs 78−92597
DNA, proton radiationless transitions for hydrogen bonds *(Russian)* 80−97857
DNA conformation, influence of intermol. interactions 80−16900
dye laser, triplet state, rel. to chem. stability and H-bonding 77−75508
dynamical model, Green function method 77−65447
dynamical model, inclusion of proton vibr. 77−65446
elastin, hydrated, dielectric relax. 79−5247
electrochemical storage, of H in $LaNi_5$ alloys, nature of H bond 79−24917
electrolyte, soln. and cryst. *(German)* 80−80804
electrolyte aq. solns., IR librational bands, struct. making and breaking 78−56476
electrostatic molecular potentials for H-bonded systems 79−3356
enolate anion from acetone, gas phase, negative ion chemistry 80−87060
1,2-ethanediol, aq. soln., proton NMR study of H-bonding 79−78545
ethanol, config. and vibr. heat capacities, H-bonds 79−99331
ethanol, effect of hydrogen bonding on Raman spectrum 79−18197
ethanol, H-bonding investigated with supersonic mol. beam using photoionisation quadrupole mass spectrometer 80−102543
ethanol, phonon MFP formula, H bond collisions, low temp. 77−35655
ethanol, US studies of mol. relax. 78−22790
ethanol-water mixtures, specific volume, compressibility, viscosity, up to 3200 bar, 15, 25°C 78−10113
ethylene methacrylic acid polymer and Na salt, ionic aggregation and melt rheology, H_2 bonding effect 78−67159
ethylene oxide deuterohydrate, cryst. struct. at 80K 77−72607
ethylene-vinyl alcohol (<36.3 mol.%) copolymer, elastic moduli of crystalline region *(Japanese)* 79−15715
ethylene-vinyl alcohol (>40 mol.%) copolymer, elastic moduli of crystalline region *(Japanese)* 79−15716
ethylene-vinyl alcohol copolymers, H bonding study by near-IR spectra *(Japanese)* 80−78734
ferroelectric, H-bonded, central peak, thermal cond. 80−93250
ferroelectric, paraelectric reson. of H-bonds and related phenomena 77−28531
ferroelectric materials, H-bonded, coherent crit. neutron scatt. 79−56742
ferroelectric transformation 3-d H-bond model with two critical points *(Chinese)* 79−24268
ferroelectric with H bonds, exchange integral, press. depend. *(Russian)* 78−35097
ferroelectrics, ferroelectric, H-bonded, soft and central modes, mag. reson., review 78−15108
ferroelectrics, H-bonded, NMR and soft modes study 78−88208
ferroelectrics, H-bonded, phonon relax. mechanism 80−79906
ferroelectrics with hydrogen bonds, phase transition into coherent state, two-level proton calcs. *(Russian)* 80−71356
first row hydride H-bonded complexes, ab initio calcs. *(French)* 80−5479
fluids with assoc. mols., van der Waals type eqn. of state 77−967
fluoroform(-d_1)-trimethylamine-Ar(Kr), cryospectroscopic IR study of association 77−468
fluoromethane+HCl, IR spectra, intermol. interactions 80−9605
fluorometh.HF, H-bonded complex, ab initio calcs. *(French)* 80−52866
formaldehyde.$H_2S(H_2O)$ complexes, ab initio SCF MO calcs., binding energy dispersion contrib. 80−27967
formamide, intermol. H bonding, vibr. spectrosc. obs. 79−50018
formamide, partly deuterated, in electrolytic soln., IR spectra, anion-solvent H-bonding 78−84558
formamide dimer, hydrogen bond, ab initio MO calcs. 78−58588
formate ion, hydration, ab initio LCMO calcs. 79−59342
formation constants, effects of neighbouring acidic and electron donor sites 77−67994
formic acid, and dimer, ab initio MO calcs., ground and excited states 77−83492
formic acid, cryst., H bonded, IR spectrum computer simulation 80−97253
formic acid, cryst. struct. at 98K 78−26555
formic acid, H bonding, electronic struct., geometries, moments, dimerisation energies, charge distrib., pseudopotential calcs. 80−27942
formic acid, liq., microdynamic behaviour, struct., nucl. spin-lattice relax. 77−76270
formic acid, monomer, cyclic dimer, charge transfer through H bonds, Hartree-Fock calcs. 77−58157
formic acid, soln., polarisable H bonds, IR spectrosc. obs. 80−58408
formic acid crystals, low temp. IR spectra 77−48153
formic acid crystals $\nu_{O-H...O}$ and $\nu_{O-D...O}$ vib. anharmonicities 77−48154
formic acid dimer, gas phase, H-bonded complex struct. from elec. dipole moment obs. 78−74791
formic acid dimer, hydrogen bond, ab initio MO calcs. 78−58588
formic acid dimer-t_1, H bonding, β^--decay effects, ab initio calcs. 79−54763
formic acid-acetic acid, gas phase, H-bonded complex struct. from elec. dipole moment obs. 78−74791
formic acid-water polymers, gas phase, H-bonded complex struct. from elec. dipole moment obs. 78−74791
$(formyl\text{-}H\text{-}F)^-$, strong H-bond, using recent difinition 79−98240
glasses, oxide type, internal friction 80−92605
L(+)-glutamic acid hydrochloride, deuterium isotope effect, cryst. struct., IR spectra and SHG 77−46755
glycerol, aq. soln., proton NMR study of H-bonding 79−78545
glycerol(-d_3), single cryst., glassy, and supercooled, polarised Raman spectra, anharmonic multiphonon interactions 79−91419
glyoxal-photoreduction-product-radicals, kinetics and intramol. dynamics 77−32808
graphical enumeration of hydrogen-bonded structures 80−106403
graphite-DNO_3, intercalation cpd., mol. dynamics 79−28631
guanidinium uranyl sulphate trihydrate, X-ray diffr., crystal struct. 78−14331
gypsum, struct., vibr. spectroscopic obs. *(Russian)* 78−15175
heptanoic acid, associated vapours, homogeneous nucleation 80−96638
hexamethylolmelamine, doped, and condensation resin, room temp. phosphoresc., thermal transforms. 80−45132
hexamethylolmelamine, doped, phosphoresc., crystallinity, cross-linking and H-bonding effects 79−73984
hydrates, vibrational spectra, H^+ and OH^n aq. soln. 79−73916
hydrazinium hydrogen oxalate, electron and proton distrib. in the short O-H-O bond 79−14789
hydrogen chloride/dimethyl ether complex, temp. depend. of IR spectra of H bond in gaseous state 77−34624

hydrogen bonds continued
hydrophilic side groups, linear H-bonded systems, proton conduction 80−40973
β-hydroxy acrolein, lower excited states, electronic struct. and H-bonding, ab initio SCF and CI calcs., photochemical mechanism 80−83278
p- hydroxy-trans-cinnamic acid, cryst. struct. basis for absence of thermal mesomorphism 80−96509
β-hydroxyacrolein, intramol. H bonds, orbital and transition energies, ab initio SCF and SCF CI calcs. 77−14345
ortho-hydroxybenzophenone, soln., intramol. proton transfer and energy relax. photostability, transient absorption obs. 80−28032
hydroxylapatites, IR spectra, stretching and librational bands of OH groups, and hindered rotation 78−2841
hydroxylic solvents, dielec. consts., effect of non H-bonding solutes 77−48673
hydroxyquinones, H-bonded, zero-phonon photochem., hole burning obs. 79−11802
ice, cryst. binding, H-bonding pot. function 79−32940
ice, crystal structure, CNDO/2 calcs., unit cell polarity effects 78−22683
ice, D_2O, H_2O, intramolecular potential from overtone spectrum anal., H-bonding dependence 79−93972
ice, high-pressure forms, ^2D and ^{17}O NQR from double reson. obs., quad. coupling consts. 77−90069
ice, Ih, polycryst., vibr. spectrum anal., OH stretching region 79−11412
ice, II and IX, deuterated forms, 10K, OD stretching bands interpretation 78−2836
ice, IV, 4000-400 cm^{-1} IR spectra, H-bonding and assignments, orientational disorder 80−16022
ice, press. effects on Raman spectrum 78−95582
ice, rel. to UPS, valence band struct. 79−33890
imidazoline nitroxide radical, H-bonding with H donors, NMR, DNP and spin lattice meas. 79−15971
indigo dye, excited state lifetime, influence of inter- and intramol. H bonding 77−79659
indole, and derivatives, temp. fluoresc. quenching, rel. to H_2O solvent struct. 78−5265
indoles, in glassy hydrocarbons, complexation vs. aggregation, absorption and fluoresc. obs. 79−98132
intermolecular charge transfer, biological implications 80−3572
intermolecular interaction thermodynamic parameters determ. from chem. shifts of functional groups 79−64068
intermolecular interactions, PCILO method for fixed wavefunctions 78−17571
intramolecular bond energy determination, by competing equilibria, IR spectra obs. *(Russian)* 78−29783
intramolecular H-bonds, H, D and T NMR, isotope effects and pot. energy surfaces 79−76447
iodobenzoic acid, NQR of ^{127}I and Mossbauer spectra of ^{125}I, bonding 77−12241
iodohippuric acid, NQR of ^{127}I and Mossbauer spectra of ^{125}I, bonding 77−12241
ion-pair complex, anomalous isotropic freq. ratio of stretching $\nu_{N(+)H}$ vibrs. 77−3366
ionic solutions, in liq. HCl, coord. sphere radius, vibr. spectrosc. investig. 80−50843
ionic solvation, spectroscopic data comparison for methanolic and aqueous solns. 80−26099
IR ν_s absorption band profile of isotopically diluted OH group in crysts. 79−69821
IR absorption of H-bonded species, intramol. interactions effect 78−50595
IR spectra, ν_s band interpretation 78−58653
IR spectra, theoretical interpretation 79−31519
IR spectra of H bonded species, line broadening, kinematic and electronic coupling mechanisms 77−68043
Ising model and config. heat capacity 79−33096
isobutyl alcohol, adsorpt. on Al_2O_3, gravimetry, IR investigs. 79−1546
isopropanol, US studies of mol. relax. 78−22790
isoquinoline, fluoresc., phosphoresc. and H bonding 77−79647
isoquinoline semiperchlorate, H-bonding, strong, stochastic model and IR spectra temp. effects 78−62805
lattice with diamond struct., 3D statistical model of phase transition *(Chinese)* 80−8924
lecithin, adsorbed monolayer on aerosil, IR spectra 78−15753
linear triatomic model, adiabatic approx., freqs. and isotope effects 77−65448
lipid extract from lung surfactant, IR spectra, H-bond lengths 79−24941
liquid mixtures, associating, mol. hyperpolarisability, SHG 77−552
liquid mixtures, binary, US vel. determ., hydrogen bond interactions 80−79881
liquids, HF, H_2O, NH_3, computer simulation, intermolecular potentials 80−38890
lithium formate monohydrate, temp. depend. Raman spectra, H bonds 78−6673
lithium thallium tartrate monohydrate, paraelectric phase structure by neutron diffraction data 79−19238
2,6-lutidine, H bonding to iso- and tert-butyl alcohols, PMR obs. 79−27008
lysozyme, aq., Raman intensities, interac. 78−58704
macromolecular rotational diffusion, ^{13}C spin-lattice relax. data anal., computer program, appls. 79−95664
maleic acid, acid slats, melts, H_2 bonding, IR, NMR investigs. 79−65859
malonic acid, phase transition at 360K, IR study 80−44311
manganese (II) D-gluconate hydrate, X-ray cryst. struct. determ. 79−77587
manganese adipate dihydrate, cryst. struct., H-bonding and O atom coordination 80−96506
matrix isolation vibrational spectra, appls. 78−46416
methanol, aqueous, damped coupled oscillator model used to study Fermi resonance 80−69152
methanol, effect of hydrogen bonding on Raman spectrum 79−18197
methanol, gas thermal conductivity, H-bonds, tetramer form. 77−34776
methanol, H bonding, electronic struct., geometries, moments, dimerisation energies, charge distrib., pseudopotential calcs. 80−27942
methanol, H-bonded struct., IR spectra, assignments 78−62800
methanol, liq., compressed, self-diffusion, NMR spin-echo meas. 77−77122
methanol, phonon MFP formula, H bond collisions, low temp. 77−35655
methanol, US studies of mol. relax. 78−22790

hydrogen bonds continued
methanol (-d), H-bonding investigated with supersonic mol. beam using photoionisation quadrupole mass spectrometer 80−102543
methanol solns., IR spectroscopic detection of free lone-pair groups or terminal methanol mols., PMR 79−19869
methanol-acetonitrile, solns., H bonding, IR and Raman band profiles 77−42320
methanol-d_1, H-bonded in soln., ν_s(OD) band 79−18183
methanol-d_3(d_1) in freon 11, self-associated, OH frequency temp. depend. 80−37809
methanol-proton acceptor binary systems, hydrogen bonded, anharmonicity of OH stretching vibr. 77−6772
methanol-water, assoc. mixture, rot. barrier solvent effect, CNDO/2 calc. 78−29861
methotrexate-dihydrofolate reductase complex form., conform., laser Raman obs. 80−104553
2-methoxyethylomine, microwave spectra, H-bond, torsional motion and mol. vibr. obs., rot. isomerism, mol. moments determ. 80−95603
methyl alcohol, intermol. interaction, thermodynamic parameters determ. from chem. shifts of functional groups 79−64068
methyl methacrylate methacrylic acid copolymer, hydrogen bonding effect on mol. relax., IR obs. of dissoc. process 77−58959
methyl methacrylate-methacrylic acid copolymer, hydrogen bonding effect on dielec. relax., T_g region 77−59512
2-methyl-1-propanol, liq. struct. at 20°C 79−32873
9-methyladenine single crysts., protonic cond. 77−55388
methylamine-HCl systems, H-bonded complexes studied by ab initio MO method, dipole moments determ. 80−83253
methylamine-t_1-NH_3, β^- decay effect on H-bond, ab initio LCAO SCF MO calc. 78−76894
3-methylisoquinoline, semiperchlorate, H-bonding, strong, stochastic model and IR spectra temp. effects 78−62805
1-methylthymine single cryst., cond. determ. using proton-injecting solution electrodes 78−18825
MINDO/3 approximation unsuitability 79−31400
molecular crystals, theory of IR spectra of H-bond 77−40223
molecular electronic absorption spectra, intramolecular hydrogen bond 80−42949
molecules, bridge angle, vibr. behaviour, simplified and accurate calcs. 80−95735
monoadipate-tetraquo-cobalt (II), cryst. struct., H-bonding scheme 80−96504
α-monochloroacetic acid, hydrogen-bond motifs 77−11529
β-monochloroacetic acid, hydrogen-bond motifs 77−15397
2(4)-monooxopyrimidines, gaseous, matrix, soln., tautomeric equilib., IR and UV absorpt. spectra 80−58256
myristic acid, associated vapours, homogeneous nucleation 80−96638
N-substituted amides, liquid, acoustic spectroscopy method for H-bond studies 79−96303
α-naphthol, ν(O-H) k=0 phonon band, width and splitting 77−52066
β-naphthol, IR dichroic ratio, oriented gas and effective charge models calcs. 78−60437
naphthol complexes, H-bonded, form. of ion pairs in presence of crown ethers, proton-transfer photoreactions 80−85199
2-naphthol-toluene-phenol, luminescence of complexes with hydrogen bonding at 4.2-77K 79−87486
near-equilibrium interactions, model 77−30961
NH_4 halides, halides, simple, complex, polycryst., hydrogen bonding, NH_3D^+ probe ion IR spectra 79−82966
nifontovite, cryst. struct., H bonds 79−19232
o-nitrophenol, cryst. and mol. struct., H bond distance 78−51523
n-nitrophenol, H-bonded complexes, IR absorpt. band struct., freqs. and intensities *(Russian)* 77−18928
nitroxide groups in crystals, H bonds and short intermolecular contacts 80−63855
NMR high resolution of solids method, appl. to H-bonded systems 78−76323
nonelectrolytes, aqueous, excess heat capacity, H bonding 78−3362
nucleic acid purine, pyrimidine bases, base pairs, hydration scheme 79−92127
nucleic acids, atom-atom potential parameters, determ. of nonvalent interactions 78−25648
nylon 6, α-form, crystal struct. and molecular packing 80−33905
nylon 6, effect of moisture content on glass transition temp. and Young's modulus 79−4401
nylon-6 dilute soln., gelation and crystallisation, struct. determ. 79−37635
nylons 6, 66, 610, change in cryst. struct. with temp. 77−15324
1-octanol, dielec. consts., solvent struct., effect of H bonding solutes, chain length. 77−48674
1-octanol-H-bonding solute system, chain assoc., dipole correl. theory, dielec. const. anal 77−48675
1-octanol-nonhydroxylic solvent complexes, H bonding, assoc. consts., elec. dipole moments, dielec. consts. 77−48672
order-disorder antiferroelectric, simple model dynamics, diagram method formulation *(Russian)* 80−40070
organic ortho compounds, solid, H bonding, wide line NMR obs. 78−52362
oriented DNA, hydration, neutron scatt. obs. 80−89714
orthocarboranes, IR spectra, CH intra-, intermol. perturbations, hydrogen bonds *(French)* 77−68044
oxalic acid, theoretical deformation density, ab initio Hartree-Fock calcs., emphasis on lone pairs and hydrogen bonds 79−32982
oxalic acid diamide, mol., PMR and IR spectra, easy polarisable H-bonds 79−31516
oxytocin, H bond linking ring and tail β-turns, biofunctional evaluation 80−61511
penninite, one-layer triclinic chlorite, neutron diffraction study 80−84144
peptide linkages, H bonding effects, review 77−10783
phenetole, in cyclohexane-ethanol mixtures, UV spectra, solvent effect 79−22770
phenol, cryst., mol. vibrs., factor group splittings 80−16021
phenol, H bonds to proton acceptors, PCILO calcs. 79−26895
phenol, H-bonded complexes, IR absorpt. band struct., freqs. and intensities *(Russian)* 77−18928
phenol, in cyclohexane ethanol mixtures, UV absorption, solvent effects 79−22767
phenol(d_1)-dioxan(-acetonitrile), in carbon tetrachloride ($CDCl_3$) solns., H-bonds vibr. relax. bands anal. 78−84560
phenol NH_3, intermolecular H-bond, semi-empirical CNDO/2 78−13427

hydrogen bonds continued
phenol-aniline (quinoline) (pyridine), liq., US vel., adiabatic compressibility, H-bonded complex form. 77−35635
phenol-cyclohexane (-ether), UV spectra, solvent effects, matrix rank anal., species determ. 79−22768
phenol-formamide, intermol. H-bond, semiempirical CNDO/2, substituted derivatives 78−13427
phenol-methanol, dimers CNDO/2 calcs.. H-bond energy 78−13428
phenol-phenyl complex, electrostatic mol. pot. contour maps, MODPOT and VRDDO calcs. 80−102463
phenols, orthosubstituted, proton acceptor soln., PMR of H-bonding 78−13517
phenols, substituted, in cyclohexane-ethanol mixtures, UV spectra, solvent effect 79−22770
phthalic acid diamide, mol., PMR and IR spectra, easy polarisable H-bonds 79−31516
phthalimide derivative-tetramethyldiaminodiphenylmethane exciplexes, luminesc. props. 77−68070
1-piperidine carboxylic acids, intramol. H bonds, struct., IR spectra 77−14426
pivalic acid($-d_1$, d_9), liq. and soln., Raman assignments, CH_3 rot. barrier, dimerisation 79−26991
pivalic anhydride, liq. and soln., Raman assignments, CH_3 rot. barrier, dimerisation 79−26991
polar liquid solns., H bonding, dielec. theory, apparent dipole moment, chem. model 77−48671
polar liquids, solns., mol. rot., kinetics 77−51984
poly-n-butylisocyanate, conformation, IR spectra *(Russian)* 77−19123
polyacids, unsaturated carboxylic, in organic solvents, hydrogen bonding, structurisation *(Russian)* 78−71666
polyamide, directionally solidified, X-ray diffr. 79−10809
polyamide, hydrogen bonding rel. to mech. props. 77−4053
polyamide chain, conformational freedom above MP 77−55344
polyamidoimide film, thermomech. props. rel. to mol. struct. *(Russian)* 79−57029
polydiacetylene, urethane substituted, conjugated polymer soln. spectral shift on planar-nonplanar conformational transition 79−64129
polydiacetylenes substituted with urethane, solid and film, visible spectra, refl. and absorpt. 79−87460
polyesteramides, H-bond network disruption and glass transition 79−4402
polyethylene, H bonding effects on skeletal optical and longitudinal acoustical modes 80−34914
polyethylene oxide water complexes in aq. soln. 78−29870
polymer, comb-like, with amide groups in side chains, stabilisation via H bonds *(Russian)* 77−46665
polymer crystal, hydrostatic compressibility, H_2 bonding effect on anisotropy 80−25782
polymers containing main chain heteroatoms, struct., ^{13}C NMR investigs., review 79−55013
polymethacrylic acid-polyethylene oxide polymer complex, H bond form., thermal behaviour *(Japanese)* 79−15454
polyriboxanthylic acid, spatial struct., H bonding 80−53086
polystyrene, glass-like, intermol. interactions temp. depend., IR spectra *(Russian)* 79−51967
polystyrene, intermol. interaction, conform. *(Russian)* 79−23539
polytetrahydrofuran, H bonding effects on skeletal optical and longitudinal acoustical modes 80−34914
polyurethane elastomers, hard segment struct., model 79−64131
polyurethanes based on toluene di-isocyanate, struct.-prop. relns. 78−80509
potassium hydrogen glutarate, H bonding, vibr. spectra 78−43860
potassium hydrogen malonate, carboxylic proton chem. shift tensor 80−58280
potassium hydrogen oxalate, oriented single cryst., Raman spectra with very strong H-bonding 80−25359
1,2-propane diol-dipropylene glycol, dielec. dispersion charact. 80−75932
1,2-propanediol, aq. soln., proton NMR study of H-bonding 79−78545
n-propanol, US studies of mol. relax. 78−22790
propionitriles (-O, NH, S), conformational investig., NMR, IR and semiempirical MO methods 80−95650
p-propoxysalicylidene-p′-butylaniline cryst. and mol. struct., intramolecular bonding 80−44197
propyl acetate-propyl alcohol, dielec. dispersion charact. 80−75932
protein, electron-transport type, H-bonding, ab initio MO 80−51039
protein, structure and bonding, quantum theory, ab initio calcs. 80−61509
proton attractive force at different excitation levels *(Russian)* 80−23493
proton relay model systems, reaction field theory of solvent effects 78−44346
proton semiconductors, with H-bonds, quantum theory of proton cond. 80−65641
protonic conduction in hydrogen-bonded crysts., quantum theory 79−90816
pyrazine.$(H_2O)_n$, n=1,2, ground and n-π^* excited state struct. 79−68241
pyridine, in carboxylic acid soln., stimulated Raman scatt., H-bonded complex effects *(Russian)* 77−3625
pyridine, vibr. reson. lasing threshold, complex form. and solvent effects *(Russian)* 77−75507
pyridine-H_2O, bonding, double quadrupole reson. obs. 80−32749
pyridine-H-bond donors, D spin-lattice relax. meas., mol. interactions anal. *(French)* 80−87151
pyridines, monosubst., H_2O complexes, n-π^* transitions, H bonding, MO theory 80−95550
pyridinium salts, hydrogen-bonded systems, deuteron quadrupole coupling 79−78563
2-pyridone, dimer, vibr. Hamiltonian for IR spectra of H bonding 78−37620
di-α-pyridyl hydroperchlorates, intramol. H bonds, steric conditions and polarisability obs. 80−53160
pyrogallol, PMR, OH group rot., H-bonds 79−47339
pyrrole-acetonitrile, H-bonded complex, ab initio MO calcs. 80−102440
quantum tunnelling of proton and activated complex theory 78−17586
quinine sulphate, acid soln., edge excitation red shift and proton migration 78−1028
quinoline, fluoresc., phosphoresc. and H bonding 77−79647
quinoxaline, zero-field splitting, basic triplet states, H bond effects 78−5366
Raman spectra of liq. phase weak H-bonds, short range order and anharmonicity effects 78−64357
hydrogen bonds continued
retinal Schiff-base, photochem. step of vision, H-bonds, intermol. associations 78−31812
$tRNA^{Phe}$, yeast, in soln., H-bonded protons in tertiary struct., PMR, assignments 77−90728
rubidium hydrogen glutarate, H bonding, vibr. spectra 78−43860
SCF comparative calcs. on H-bonded and H-like bonded systems 78−9068
semiquinones in protic solvents, saturation behaviour, ESR 77−6808
L-serine-L-ascorbic acid, X-ray cryst. struct. determ. 80−35827
sodium acetate trihydrate, cryst. struct. and bonding 77−24309
sodium hydrogen oxalate monohydrate, crystal struct. 78−10032
sodium hydrogen oxalate monohydrate, oriented single cryst., Raman spectra with very strong H-bonding 80−25359
solid, H-bonded, bond failure theory 79−73246
solid, H-bonded, NMR chem. shift tensors *(German)* 78−84489
solute-solute-solvent interaction, dielec. behaviour problems, review 80−25298
solution, aq., hydrophobic hydration around apolar species pair, Monte Carlo simulation 80−6336
solution, H-bonded species, vibr. relax. model 78−84559
solutions with closed loop coexistence curves, directionality depend. of lattice models 78−95158
solvents H-bonded ionic solvation entropy calcs. 79−47959
sorbitol, relax. processes, optical probe obs. 79−47430
squaric acid, cryst., neutron diffr., bond lengths and angles, vibr. modes 77−76384
squaric acid, vibr. props., 2D model 79−90735
stearyl alcohol, H bonding effects on skeletal optical and longitudinal acoustical modes 80−34914
stochastic model, strong H-bonds, IR spectra temp. effects 78−62805
strong H bonded systems, vibr., Raman, IR spectra, biology appls. 78−82735
strontium formate dihydrate, H bonds, deuteron mag. reson. meas. 77−85593
strontium maleate tetrahydrate, cryst. struct., H-bonding scheme 80−96505
styrene-methacrylic acid copolymer, glass-like, intermol. interactions temp. depend., IR spectra *(Russian)* 79−51967
styrene-methacrylic acid copolymer, intermol. interaction, conform., composition depend. *(Russian)* 79−23539
succinic acid diamide, mol., PMR and IR spectra, easy polarisable H-bonds 79−31516
sulphonyl compounds, H-bonding by methyl groups, Raman spectra obs. 79−24320
symmetric $AHA^{(\pm)}$, A-H stretching vibr., liq. IR band shape, strong coupling phonon model 78−64358
tautomeric transform., quantum-statistical model 77−38739
tertiary phosphine oxide+aliphatic alcohol, pπ-dπ conjugation, electronegativity and H-bond energy 78−82863
tetra-isoamyl phosphonium bromide hydrate, clathrate, cryst. struct., X-ray study 80−64987
tetramethylammonium hexachloroplatinate, order-disorder transitions due to weak CH-Cl hydrogen bonds 78−92060
tetramethylammonium hexachlorostannate, order-disorder transitions due to weak CH-Cl hydrogen bonds 78−92060
tetramethylammonium hydrogen bis-trichloracetate ($-d_n$), ^{35}Cl NQR study 80−66064
2,2,6,6-tetramethylpiperidine nitroxide radical.alcohol complex, NMR chem. shift 78−46366
TGS, cryst., vibr. bands, ferroelec. and paraelec. phase H bonds *(Russian)* 78−15172
TGS, deuterated, paraelec. phase, D atom positions 78−14334
2-thiapyridone, dimer, vibr. Hamiltonian for IR spectra of H bonding 78−37620
thiones, N-H-S weak and medium strong H bonds, IR spectra 80−69132
TMNC, phase transition, low temp. far IR spectra 79−24309
o(m)-toluidine+o-chlorophenol, H-bonded mol. complex, microwave absorpt., dipole moment and relax. times 80−14134
2-(2-tosylaminophenyl)-4H-3,1-benzoxazine-4-one, cryst. and mol. struct. 80−84167
tri-i-propygermylamine, and isotopomers, IR and Raman spectra, normal coord. anal. *(German)* 80−32716
tri-t-butylstannylamine, and isotopomers, IR and Raman spectra, normal coord. anal., Mossbauer spectrum *(German)* 80−32716
2,4,6-tribromophenol, Raman and IR spectra, hydrogen bonds 80−84735
trichloroacetic acid-base H bonded complex, ^{35}Cl NQR meas. 78−25555
2,4,6-trichlorophenol, Raman and IR spectra, hydrogen bonds 80−84735
trichlorosilane liquid, Si-H stretching mode vibr. dephasing, Raman study 80−84736
triethanolamine, US relax., intermol. H bonds redistrib. 77−69050
triethylsilylamine, and isotopomers, IR and Raman spectra, normal coord. anal. *(German)* 80−32716
trifluoroacetic acid, soln., polarisable H bonds, IR spectrosc. obs. 80−58408
trifluoroethanol, H-bonding investigated with supersonic mol. beam using photoionisation quadrupole mass spectrometer 80−102543
trimesic acid, L-(or DL-) histidinium trimesate-$^1/_3$ acetone, X-ray cryst. struct. determ. 79−77586
trimethylammonium chloride and deuterated forms, cryst., inelastic neutron scatt. H bond vibr. obs. 77−7796
trimethylcarbinol complexes in soln., weakly H-bonded, IR bandshapes 80−106354
triphenylcarbinol complexes in soln., weakly H-bonded, IR bandshapes 80−106354
tris(ethylenediamine)metal(III), H bonding *(French)* 80−87241
tryptamine:1-thyminylacetic acid (1:1), cryst. and mol. struct. determ. using MULTAN 79−73156
two-dimensional model dynamics, vibrs. freq. rel. to equil. interatomic distances 79−26910
urea, single crystal Compton profiles, H-bonding and dimer config. effects, calc. and meas. 78−80431
van der Waals criterion for H bonding 78−91292
vibrational predissociation in hydrogen bonded complexes 80−61078
water, adsorbed on Pt(100), bonding, electron energy loss spectra 80−34311
water, and ionic dissoc. products, polarisation model 78−91216
water, chemisorbed on Pt (111), EELS spectra, vibr. freqs. 80−80920
water, config. and vibr. heat capacities, H-bonds 79−99331
water, dielectric constant of bonded lattice model 78−23386

hydrogen bonds continued
water, H-bond networks, percolation process 79−69001
water, H-bonded struct. IR spectra, assignments 78−62800
water, hydrogen bond breaking by negative pion capture *(Russian)* 79−94866
water, liq., H bond distrib., Monte Carlo simulation calcs. 80−54106
water, low-density amorphous solid, Raman spectra, OH stretching region 79−11410
water, machine simulation, book contrib. 79−60249
water, Monte Carlo simulation of isothermal-isobaric ensemble 78−30530
water, polymolecular adsorbed layer on quartz surface, IR absorption spectra 80−9595
water, vap., dimerization, from thermal cond. meas., 373K 78−44359
water association, in superheated vap., equilib. consts., H bond vibr. 77−66750
water oligomers, H-bonding, PCILO calcs. 77−83500
water-anion H-bonds, nature, from IR and Raman OH(OD) splittings 78−62811
water-HF(HBr)(HCl) complex, in supersat. soln., Raman spectra assignments 78−70840
water-imidazole, H bond interrupted chain, cooperative effects, STO-3G ab initio calcs. 80−63535
X-H stretching, dynamic theories survey 80−52983
xanthene dye, solute-solvent hydrogen bonding and temp. effects on internal conversion 77−3402
XH_2 molecules 1:2 complexes, H-bonding fluctuation hypothesis, IR and Raman vibr. spectra 77−34632
XH-Y complexes, IR absorpt. spectra, intramol. coupling influence, pot. energy surfaces derivation 80−91624
zinc malonate dihydrate, cryst. struct., X-ray refl. obs. 78−75652
acetone-d_0, d_6, Raman spectral study of aq. soln. struct., H-bond effects 77−88454
$AlCl_3$, aq. solns., order phenomena, X-ray diffr. obs. 80−1915
γ-AlOOD, boehmite, hydrogen bond, neutron profile refinement of struct. 78−71701
γ-AlOOH, boehmite, lattice vibrs., evidence for $C_{2\nu}{}^1{}_2$ space group 79−28756
2-aminoethanol(-d_2)(-d_3), microwave spectra, hydrogen bonding, rot. const. 77−6765
Ar.HBr(DBr), van der Waals complexes, rot. spectra and struct. 80−48055
$(B(OH)_3)_2$, hydrogen bond, ab initio MO calcs. 78−58588
$BaBr_2.2H_2O$, pure and deuterated, low temp. IR and Raman spectra *(German)* 79−19874
$BaCl_2.2H_2O$, polycryst. hydrates, librational motion of H_2O mols., neutron diffr. exam. 80−10604
$Ba(H_2PO_4)_2$, crystal struct. 78−10005
$BeBH_5$, H bridged system, floating spherical Gaussian model 80−78518
C-H-X H bonded systems, ab initio MO calcs. 79−6835
CO-HBr, weakly bound, rot. spectra 80−91544
CO-HCl, weakly bound, rot. spectra 80−91544
CO-HF, weakly bound, rot. spectra 80−91544
^{13}C, NMR of 2,2,6,6-tetramethylpiperidine nitroxide radical.alcohol complex, chem. shift 78−46366
$Ca_2(B_4O_4(OH)_8)$, uralborite, accurate cryst. struct. 78−34492
α-$CaCl_2.4H_2O$, redeterm. of cryst. struct., H bonding and Ca coordination *(French)* 79−37676
$CaHPO_4$, monetite, cryst. struct. refinement, H bonding, neutron diffr. meas. 77−47389
$CaHPO_4$, monetite, low-temp. ordering of H atoms, X-ray and neutron diffr. study at 145K 80−39022
α-$Ca(NO_3)_2.4H_2O$, X-ray cryst. struct. anal. *(French)* 77−58986
$Ca_{10}(PO_4)_6(OH)_2$ halogenated derivatives, IR absorpt. spectra *(Spanish)* 78−52489
$CaSnCl_6$, Cl NQR anomalous temp. depend., crystal struct. and phase transitions 80−54977
$CaZn(SiO_4).H_2O$, clinohedrite, cryst. struct., H bonds 78−79593
$Ca2(NH_4)H_7(PO_4)_4.2H_2O$, X-ray cryst. struct., PO_4 ion with 3 symmetric H bonds 80−64956
$Ca_2[B_8O_{13}(OH)_2]$, refinement of cryst. struct., H-bonding 77−89421
$Ca_2[B_5O_9]C.H_2O$, hilgardite, PMR of water mol. 80−84655
$Ca[Fe(CN)_5(NO)].4H_2O$, X-ray cryst. struct. determ., heavy-atom method 80−92494
$CdBr_2.4H_2O$, cryst. struct. determ. *(French)* 78−26502
$Ce_2(SO_4)_3.9H_2O(D_2O)$, polarised Raman spectra, vibr. props. and role of lattice H_2O 80−66201
ClH-dimethyl ether, H bonded complex, IR and Raman spectra, mech. and elec. anharmonicity 79−89672
ClH-dimethyl ether, vibr.-rot. IR spectra, quantum and classical mechanics 80−91561
Co complex, bisdimethylglyoxime (thiosemicarbazide)-cobalt (III) nitrate, mol. and cryst. struct. of dihydrate 78−83803
Co complex, monofumaratotetraaquocobalt(II) monohydrate, cryst. struct. and cryst. binding 79−37681
Co complexes, $[Co(H_2O)_x(NH_3)_{6-x}][Co(CN)_6]$, x=1,2, hydrogen bonding 77−42437
Co complexes, $Co(en)_2Cl_2.Cl.HCl.2H_2O$, temp. dependence of NQR frequencies 80−66068
$Co(H_2O)_6[SnF_3]_2$, crystal structure *(French)* 80−59441
$Co(NH_3)_6FeF_6$, anomalous Raman intensities, due to interionic coupling by H bonding 78−27230
Cr complexes, $[Cr(H_2O)_x(NH_3)_{6-x}][Co(CN)_6]$, x=1,2, hydrogen bonding 77−42437
Cr-Co complex, $[Cr(OCN_2H_4)_6][Co(NH_3)_2(NO_2)_4]_3.3H_2O$, cryst. struct. 80−6392
$Cr_4H_2(SO_4)_7.24H_2O$, X-ray cryst. struct. determ., H bond study 80−92491
$CrH(SO_4)_2.7H_2O$, X-ray struct. determ., hydrated proton complex and H bonding 77−80449
β-CrOOH, neutron diffr. exam., cryst. and magnetic struct. *(French)* 78−2654
CrOOH(D), barrier to proton or deuteron tunnelling 80−70156
$Cs_2GeF_6.4HF$, cryst., H bond geometry, NMR obs. 79−42844
$CsHCl_2$, H bond bending vibrs., inelastic neutron scatt. obs. 79−89800
CsHClBr, H bond bending vibrs., inelastic neutron scatt. obs. 79−89800
$CsH(NO_3)_2$, inelastic neutron scatt. spectra, H bonds bending vibrs. 79−14893
CsH_2PO_4, ferroelec., X-ray struct. study at room temp. 80−88113
$CsH_3(SeO_3)_2$, paraelec. phase, struct. determ. by neutron diffr. 78−34472
hydrogen bonds continued
$Cs_2SnF_6.4HF$, cryst., H bond geometry, NMR obs. 79−42844
$Cs_2(VOF_4(H_2O))$, neutron and X-ray diffr. struct. determ. 79−90613
$Cs_2[FeCl_5(H_2O)]$, X-ray cryst. struct. determ. 80−107129
Cu^{2+} complex, in water-ethanol soln., struct., EPR 78−50565
(DF) chain, D quadrupole coupling const. calcs. 79−49963
$DF(\nu=1)+DF(\nu=0)$, deexcitation probability, low temp., hindered rot. and H-bond effects 77−88531
$DF(\nu=n)+DF(\nu=0)\rightarrow DF(\nu=n-1)+DF(\nu=1)+\Delta E$, applic. of hydrogen-bond interac. model 77−30961
D_2O, IR and Raman spectra, bonding, vibr., band shapes 79−6938
D_2O, struct., temp. effects, neutron diffr. obs. 77−72544
D_2O-H_2O, IR absorption spectra, statistical charact., continuous model of liq. struct. confirmation 78−6671
$(D_2O)_2$, and isotopic species, Ar matrix IR spectra, Xe, HCl, $(CH_3)_2O$ doping, struct. 77−3365
$(D_2O)_2$, isotopic forms, Ar matrix isolated IR spectra, assignments, config. 77−6780
$D_5O_2{}^+$, isotope effects, easily polarisable H and D bonds 78−94231
F+methane, reaction in Ar matrix, IR spectra obs. 79−96293
$(F\text{-}H\text{-}F)^-$, strong H-bond, using recent difinition 79−98240
FHF ion, H-bond excited electronic states, CI calc., dissoc. and autoionising states 80−5489
FHF^-, H bonds, vibr. dynamics calcs. 80−23397
Fe complex, $[Fe(2\text{-}pic)_3]Cl_2.EtOH$, struct. changes, spin phase transition mechanism 79−78380
FeOOH, H-bonding, strong, stochastic model and IR spectra temp. effects 78−62805
Fe(111), multilayer condensation of hydrazine, strong interaction via H-bonding 79−46956
$GaAs_{1-x}H_x$, amorphous, vib. props., Raman and IR meas. 80−50322
α-D-glucose, struct. refinement, mol. conformation and H bonding 79−42043
H bonded systems, IR spectra, theoretical interpretation 79−31519
H bonding molecules, self assoc., intermolecular interactions, matrix isolation vibr. spectra obs. Raman and IR spectra 80−52995
H-bonded complexes, in polystyrene matrix, mol. relax. processes 79−24259
H-bonded complexes, OH stretching vibr. band, temp. effect 78−90158
H-bonded systems, core and valence ionis., nonempirical LCAO MO SCF calcs. 77−67973
H-bonded systems, cyclic and bifurcated, ab initio MO calcs. 79−41100
H-bonded systems, MINDO/3 geom. optimis. calcs., heats of form. of monomer and dimer 79−31399
H_2+Pt(111) surfaces, interactions, bond breaking activity, model pot. 80−108744
H_n^- (n=5 to 13), ion-induced dipole clusters, binding energies and geometries 79−41261
$HAl_{11}O_{17}$, H β-alumina, IR absorpt. study 80−100655
H_3AsO_4, polarisable acid-acid and acid-water hydrogen bonds 79−76423
HBO_2, cubic, monoclinic and orthorhombic forms, H bonding, IR and Raman spectra 80−76029
H_3BO_3, aq. soln., dielec. props. and struct. 77−89369
HBr, cryst. binding, H-bonding pot. function 79−32940
HCN, self-assoc., matrix isolation vibrational spectra, appls. 78−46416
HCN, self-assoc.; matrix isolation vibr. spectroscopy, complex form. studies 78−62952
HCN, solid state phase transition, bond distance, stretching freq. calc. 78−10183
HCN-HF, dimer, rot. transition intensity, dissoc. energy determ. 78−46323
$(HCN)_2$, IR spectra in Ar matrix, vibr. bands, H-bonds 78−29782
HCN...HF, hydrogen bonded heterodimer, spectroscopic consts. from microwave spectrum 80−43037
HCl and $(HCl)_2$, matrix isolated, pulsed NMR 79−22730
HCl, anhydrous conc. solns. in methanol, Raman and IR spectra 78−82724
HCl aqueous soln., H^+ mobility, 15, 25, 40°C, up to 5000 atm 78−10207
HCl, cryst. binding, H-bonding pot. function 79−32940
HCl, liquid, struct. and mol. dynamics studied using intermolecular force models 80−83445
HCl, mol. cryst., angles of H-bonded mols., ab initio calcs. 78−6037
HCl-dimethylether complex, gaseous, H-bond IR spectra, temp. depend. theory 78−62804
HCl-X, matrix isolation vibr. spectroscopy, complex form. studies 78−62952
HCl(-acetone)(-acetonitrile), soln., IR absorption, H-bonding, solvent effect 78−29778
$HCl.6H_2O$, cryst. struct., H bonds, X-ray determ. 78−83783
$H_3Co(CN)_6$, strong NHN hydrogen bond, vibr. lattice and mol., incoherent inelastic neutron scatt. 80−39232
HDO molecules in solid hydrates, D quadrupole coupling consts., O-H and O-D stretching freqs., H bond distances 78−29773
HF, cluster and chain dipole moments, ab initio calc. 77−26967
HF, cryst., CNDO calcs., struct., binding energy, 4K 77−15338
HF, cryst. binding, H-bonding pot. function 79−32940
HF, H-bonded chains, vibr. modes in liq. and solids 78−59873
HF H-bonded dimers, PCILO calc., energies, geometries 78−37557
HF molecules, infinite linear chain, equilibrium structure and stabilisation energy 80−63856
HF-aliphatic ethers, H-bonded complexes, gas phase, first overtone reconstruction 80−43040
HF-cyclic ethers H-bonded complexes, calorimetry, IR spectra and MO calcs. 79−52738
HF-HCl, H bonding , struct., mol. beam-elec. reson. spectra 78−29777
HF-HCl, SCF energy hypersurface, stationary points, thermodynamics of form. 80−102436
$HF+H_2O$(methanol)(ether), mol. electrostatic pot., H-bonds, CNDO/2 calc. 77−61822
$(HF)_2$, energy decomp. anal. of H-bonding, ab initio SCF MO calcs. 77−57868
$(HF)_2$, H-bonding and indirect exchange ('superexchange') in 79−93912
$(HF)_n$, n=1-∝, ab initio hydrogen bond and electronic parameters, phonons 77−14342
H_2F_2 and H_3F_3 clusters, molecular structures, ab initio calcs. 80−83532
H_3F_3, struct. H bonding, IR spectra obs. 77−54560
$H_3F_4^-$, struct., H bonding, IR spectra obs. 77−54560
$H_4F_5^-$, struct., H bonding, IR spectra obs. 77−54560
$H^+(H_2O)_c$ ion-induced water clusters, mass spectra, IR continuum absorpt. 80−87257

hydrogen bonds continued
α-HIO_3, HI_3O_8, I_2O_5 and deuterated cpds., crystalline, ^{127}I NQR, bonding and mol. dynamics 80−39889
α-HIO_3, vibration level Davydov splitting, adiabatic potential role, dipole-dipole approx. *(Russian)* 80−29365
H_3N-HF, energy decomp. anal. of H-bonding, ab initio SCF MO calcs. 77−57868
HNO_3, aq. soln., H bonds, IR spectra 78−94243
$(HNO_3)_2$, gas phase, H-bonded complex struct. from elec. dipole moment obs. 78−74791
HO-H...OHX, X=H, CH_3, NH_2, OH, F, H-bonds, electron donor substituted, mol. orbital calc. 78−13422
H_2O, $(H_2O)_2$, mag. shielding rel. to hydrogen bonding 77−14348
H_2O, charged clathrates, model for formation and stabilisation 80−91714
H_2O, Compton profile, H-bond contrib., HFS Xα model 78−17726
H_2O, H bonding, electronic struct., geometries, moments, dimerisation energies, charge distrib., pseudopotential calcs. 80−27942
H_2O H-bonded dimers, PCILO calc., energies, geometries 78−37557
H_2O, warm fog and steam clouds, emission spectra variations, evidence for clusters in vapour phase 79−39849
$H_2{}^{16}O$, $H_2{}^{18}O$, isotope fractionation, H-bonds, force consts., liq. water struct. 77−76288
H_2O-formaldehyde complex, IR spectrum in solid Ar, N_2 matrix 80−43042
H_2O-H_2S supersystem, ab initio LCAO MO SCF calcs. of H bonding 79−89607
H_2O-HF heterodimer, H bonding, microwave rot. spectrum, mol. geometry and moment 80−99501
H_2O+H_2O, pair pot. near H bonded equilib. config., amorphous and crystalline solid and liq. 80−64946
H_2O+Li^+, ab initio GTO calc. of vibr. intensity changes of spectroscopic parameters 78−58583
$(H_2O)_2$, and isotopic species, Ar matrix IR spectra, Xe, HCl, $(CH_3)_2O$ doping, struct. 77−3365
$(H_2O)_2$, difference electrostatic mol. pot. contour maps, basis set superposition effect 80−102462
$(H_2O)_2$, electrostatic mol. pot. curves, proton transfer and bridging pot., CNDO/2 calc. 79−94054
$(H_2O)_2$, energy decomp. anal. of H-bonding, ab initio MO calcs. 77−57868
$(H_2O)_2$, H-bonding and indirect exchange ('superexchange') in 79−93912
$(H_2O)_2$, isotopic forms, Ar matrix isolated IR spectra, assignments config. 77−6780
$(H_2O)_2$, struct. from mol. beam elec. reson. spectra 77−54555
$H_5O_2^+$, aq. soln., IR continua with polarisable H-bonds 79−26979
HOD, IR spectra in D_2O, combination vibr. 80−9609
$(H_3O)^+(HSeO_4)^-$, X-ray struct. anal., Patterson technique 80−1975
H_2O.HF, H-bonding and indirect exchange ('superexchange') in 79−93912
$HO_2.H_2O(NH_3)$ complex form., ab initio calcs., min. energy configs. 77−14340
H_2O...HF complex, force field, vibr. freqs., equilib. geometry bond energy, ab initio calc. 77−65450
H_3PO_2, H_3PO_3, H_3PO_4, polarisable acid-acid and acid-water hydrogen bonds 79−76423
H_2S-H_2O complexes, equilib. config., H-bond energies and electron densities, CNDO/2 method 80−14084
$(H_2S)_2$, pot. energy surface, sum of SCF-MO-LCGO energy 77−67977
H_2SeO_3, cryst., vibr. spectra in O-H stretching region 79−51949
$HUO_2AsO_4.4H_2O$ and $HUO_2PO_4.4H_2O$ layered cpds., struct. investigs. below antiferroelec. transition temps., H bond ordered structs. 80−107416
$HUO_2PO_4.4H_2O$, H^+ ion cond., struct. mechanism, X-ray diffr. obs. 78−34651
H.HF, H-bonded complex, ab initio calcs. *(French)* 80−52866
$IN(OH)_3$, cubic, IR spectra comparison with $In(OD)_3$ 79−77568
K salt of β-ketoaldehyde, configurations of anions in solutions studied by IR spectroscopy, H-bond form. 80−87117
$KBO_2.4/3H_2O$, unusual hydrogen bonding 78−2058
$K_2Ca[B_4O_5(OH)_4]_2.8H_2O$, synthetic, X-ray cryst. struct. study, H bond geometry 80−92509
KD_2AsO_4, ferroelec., phase transition and Raman scattering 78−84540
KD_2AsO_4, ferroelectric, high temp. phase transitions, proton dynamics 80−76023
KD_2PO_4, IR and Raman polarised spectra, rel. to crystal struct. 78−56489
KD_2PO_4, polarisation fluctuations, wavevector depend. 80−71295
$KD_3(SeO_3)_2$, D NMR above and below ferroelec. transition, H-bond behaviour 78−52460
$KD_3(SeO_3)_2$, deuteron mag. reson. in ordered and disordered phase 78−39414
$KF(HF)_n$, (n=2,3,4), cryst., anion struct., H bonding, IR spectra 77−54560
KH_2AsO_4, ferroelec., phase transition and Raman scattering 78−84540
KH_2AsO_4, ferroelectric, high temp. phase transitions, proton dynamics 80−76023
$KHCO_3$, inelastic neutron scatt. spectra, H bonds bending vibrs. 79−14893
$KHCO_3$, PMR, proton shielding tensor proton ionis. in H-bond 77−1606
$K_3H(H_2P_2O_7)_2$, single cryst., X-ray cryst. struct. determ., direct methods *(French)* 79−14742
KH_2PO_4, ferroelectric transition, order-disorder character of hydrogen bond 80−93251
KH_2PO_4, single crystal neutron diffraction study at high pressure 80−92497
KH_2PO_4-type crystals, H bond in ferroelectricity, role of high pressure research 79−15414
KH_2PO_4-type ferroelectrics, inelastic neutron scatt. theory 78−48122
KH_2PO_4-type ferroelectrics, IR and Raman spectral interpretation of ferroelectric phases 79−24312
$KHSO_4$, PMR, proton shielding tensor, proton ionis. in H-bond 77−1606
$KHSO_4$:Co^{2+}, conduction and ^3H diffusion 77−15622
$KH_3(SeO_3)_2$, high-resolution PMR 78−35053.
$KHSi_2O_5$, cryst. struct., Patterson function anal., valency balance, hydrogen bonds 80−39051
$K_2HgCl_4.H_2O$, cryst., IR spectra, water mol. struct., H-bonding 77−81089
$K_2InCl_5.H_2O$, crystal structure and H-bonding 80−64978
$KMgCl(ClO_4)_2.nH_2O$, IR spectra and struct. features 79−15452
hydrogen bonds continued
$KMgCl_3.nH_2O$, IR spectra and struct. features 79−15452
$KPbI_3.2H_2O$, X-ray cryst. struct. determ. 80−64958
$K_2SnF_6.4HF$, cryst., H bond geometry, NMR obs. 79−42844
$La_2Mg_3(NO_3)_{12}.24H_2O$, neutron diffr. obs. 78−18598
$La_2(SO_4)_3.9H_2O$, and isotopic forms, water librations, Raman obs. *(French)* 79−28754
$La_2(SO_4)_3.9H_2O(D_2O)$, dynamic disorder of water mols., isotope effect obs. 80−55015
Li salt of β-ketoaldehyde, configurations of anions in solutions studied by IR spectroscopy, H-bond form. 80−87117
$LiBH_4$, H bridged system, floating spherical Gaussian model 80−78518
$LiBeH_3$, H bridged system, floating spherical Gaussian model 80−78518
$LiCH_5$, H bridged system, floating spherical Gaussian model 80−78518
$Li_2Cr_2O_7.2H_2O$, cryst. struct. 79−32980
$LiH_3(SeO_3)_2$, IR and Raman spectra, internal modes, intra- and inter-H-bond tunnelling 78−43853
$LiNO_3.3H_2O$, cryst. struct., X-ray determ. 77−80470
$LiNO_3.3H_2O$, neutron diffr. studies at 120 and 295K, H bond studies 80−88099
$Mg_{9.10}An_{4.04}Mn_{1.89}(SO_4)_2(OH)_{26}.8H_2O$, mooreite, X-ray cryst. struct. determ. and refinement 80−92488
$MgB_{12}O_{19}.5H_2O=Mg[B_3{}^{\Delta}B_3{}^{t}O_7(OH)_5]_2$, cryst. synthesis and struct., bonding, X-ray study 80−33973
$Mg_2CO_3(OH)_2(H_2O)_3$, H bonding 78−18601
$Mg_5(CO_3)_4.(OH)_2(H_2O)_4$, cryst. struct., H bonding, X-ray diffr. meas. 77−47392
$MgCl_2.nH_2O$, IR spectra and struct. features 79−15452
$MgHPO_4.3H_2O$, newberyite, struct. refinement and H bonding 80−15058
ND_3, cryst. struct. between 2-180K, neutron powder profile refinement 79−73134
$(ND_4)_2D_3IO_6$, neutron diffr. study 80−88098
NH_3, adsorbed on amorphous silica, Raman scatt. obs. 80−11948
NH_3, assoc. mols., struct. and dynamics, atom-atom pots., gas, solid and liq., props. 80−23487
NH_3 dimer, inversion, influence of H-bond, SCF calc. 77−50556
NH_3 H-bonded dimers, PCILO calc., energies, geometries 78−37557
NH_3, self-assoc., matrix isolation vibrational spectra, appls. 78−46416
NH_3, solid, rel. to UPS, valence band struct. 79−33890
NH_3-HCl, assoc., matrix isolation vibrational spectra, appls. 78−46416
NH_3-lithium halide complex, ab initio calcs., Li bond rel. to H bond 77−14343
$(NH_3)_n$, (n=1-6), mol. beam elec. deflection obs. 79−72371
NH_4ReO_4, explanation of ^{187}Re NQR freq. anomalous behaviour 78−48075
$(NH_4)_2BeF_4$, ferroelectric, cryst. struct., phase transition, X-ray study 79−28689
$NH_3(D_3)$, liq., longitudinal proton and deuteron relaxation rates, press. and temp. depend. 80−44941
$(NH_4)_2GeF_6$, cryst., highly bent H bonds, IR spectrosc. investig. 80−93292
$(NH_3)_nH^+$, n=1-9, detected in photoionisation of supersonic mol. beam mass spectra, H-bonding 79−74356
$NH_4H_2AsO_4$, H positions, paraelectric phase 79−19210
NH_4HF_2, powder, proton and fluorine 2nd moments meas., 77-395K 80−34803
$(NH_4)_2H_3IO_6$, neutron diffr. study 80−88098
$(NH_4)_2HPO_4$, NH_4^+ motions, PMR relax. times obs., 77-430K, struct. transition 77−85599
NH_4HSeO_4, ferroelec. props. rel. to struct. 80−71345
$NH_4I(ND_4I)$.dioxane complexes, Raman spectra, vibrs., H-bonding 78−25544
$NH_4In(SO_4)_2.4H_2O$, H-bond system, X-ray diffr. obs. 80−6395
$(NH_4)_2M(SO_4)_2.6H_2O$, Tutton's salts, IR spectra, correl. of vibr. freq. and N...O distance for NH_3D^+ 78−92066
NH_4NO_3 conc. aqueous soln., X-ray scatt., NO_3^--H_2O interactions 78−42881
NH_4NO_3 crystals, NH_4^+ ion symmetry in phases II-V, Raman spectra obs. 80−66200
$(NH_4)_2SO_4$, aqueous soln., SO_4^{2-}-H_2O interaction, X-ray scatt. 79−77479
$(NH_4)_2SO_4$, paraelectric, N-quadrupole coupling meas. by proton-N double resonance 80−60459
$(NH_4)_2S_2O_3$, X-ray cryst. struct. determ. 79−77562
$(NH_4)_2SeO_4$, X-ray obs. 77−24299
$(NH_4)_2SiF_6$, cryst., highly bent H bonds, IR spectrosc. investig. 80−93292
$(NH_4)_2SnF_6$, cryst., highly bent H bonds, IR spectrosc. investig. 80−93292
NH_2TNH_3, β^- decay effect on H-bond, ab initio LCAO SCF MO calc. 78−76894
$(NH_4)_2TeO_2(OH)_4$, X-ray cryst. struct. anal. 79−77563
$(NH_4)_2TiF_6$, cryst., highly bent H bonds, IR spectrosc. investig. 80−93292
$(NH_4)_2[Pt(CN)_4]Cl_{0.42}.3H_2O$ quasi one dimensional conductor, physical props., cond. freq. depend. 79−95393
NH_2.HF, H-bonded complex, ab initio calcs. *(French)* 80−52866
NO, hyperfine splitting const., H-bond contrib. 78−74799
Na salt of β-ketoaldehydes, configurations of anions in solutions studied by IR spectroscopy, H-bond form. 80−87117
$Na_8Al_6Ge_6O_{24}(CO_3).3H_2O$, water molecule dynamics 79−90577
$NaBr.2H_2O$, polycryst. hydrates, librational motion of H_2O mols., neutron diffr. exam. 80−10604
$NaCN.2H_2O$, electron density, 150K, X-ray crystallography expts. 77−24295
$NaClO_4.D_2O$, H bonding, D NMR 77−34664
$NaD_2AsO_4.D_2O$, crystal struct. determ. 77−80460
$Na(H_3O)(I(OH)_3O_3)$, pyroelec., cryst. struct. at room temp. 79−10835
β-$Na_2HPO_4.12H_2O$, dosorder of HPO_4^{2-} and H bonds 78−34471
$Na_2HPO_4.2H_2O$, crystal struct., coordination and H bond competition 78−14315
$NaH_2PO_2.4/5H_2O$, X-ray cryst. struct. determ., pseudo-symmetry and H_2 bonding 79−60315
α-$NaHSO_4$, cryst. struct. and hydrogen bonding 79−99128
$Na_3H(SO_4)_2$, cryst. struct. refinement, short asymmetrical H bond, S-OH vs. O-H...O correlation 79−37663
$NaHSO_4.H_2O$ pseudo-symmetric crystal struct., hydrogen bonding 77−55258
$NaHSeO_3$, and $NaDSeO_3$, NMR of ^{23}Na and ^2D, hydrogen bonding 80−44190

hydrogen bonds continued
$NaH_3(SeO_3)_2$, ferroelec., proton motion within H bonds, neutron scatt. study 80−75986
$NaH_3(SeO_3)_2$, IR and Raman spectra, internal modes, intra- and inter-H-bond tunnelling 78−43853
$NaH_3(SeO_3)_2$, proton behaviour in H-bonding, neutron spectroscopy obs. *(German)* 78−22816
$NaIn(SeO_4)_2.6H_2O$, X-ray cryst. struct. determ., H bond system 80−92511
$NaPF_6.H_2O$, IR and Raman spectra 77−61749
$NaSbClF_3.H_2O$, cryst. and mol. struct. *(French)* 77−43200
$Na_3SbS_4.9D_2O$, Schlippe's salt, H bonds and cryst. struct. refinement, by neutron diffr. 79−19191
$Na_3SbS_4.9H_2O$, Schlippe's salt, H bonds and cryst. struct. refinement, by X-ray diffr. 79−19191
$Na_3SbS_4.9H_2O(D_2O)$, vibrational spectra, internal SbS_4 and $H_2O(D_2O)$ vibr. assignments 80−66199
$Na_2ZnCl_4.3H_2O$, NQR of ^{23}Na and ^{35}Cl, single-cryst. study 78−91983
Nb complex, $NH_4[NbO(C_2O_4)_2(H_2O)_2].3H_2O$, neutron diffr. obs. 77−24306
Ni-H interaction, 0.75 Å≤R≤5 Å, NiH form. effect of inner orbitals *(German)* 78−29752
O-H...F H bonds in metal fluoride hydrates, geometry 78−34458
OH, in inert gas matrix, H-bonding and charge transfer, fluoresc. 78−25602
OH-HF, H-bonded complex, ab initio calcs. *(French)* 80−52866
$(OH)_2^{2-}$, electrostatic mol. pot. curves, proton transfer and bridging pot., CNDO/2 calc. 79−94054
OHO H-bond, IR spectra, stochastic model 77−27060
^{17}O, NQR at natural isotope abundance, double reson. new techniques, appl. to H-bonded systems, review 80−53013
$PbHPO_4$, protonic order-disorder transition 78−26478
$RbD_3(SeO_3)_2$, ^2D NMR struct. anal. 80−2661
$RbHSeO_4$, ferroelec. props. rel. to struct. 80−71345
$RbH_3(SeO_3)_2$, paraelec. phase, cryst. struct., neutron diffr. 77−47420
$RbIn(SO_4)_2.4H_2O$, refinement of cryst. struct., interatomic distances, bonds 80−59448
$Rb_2[C_2O_4].D_2O_2$, neutron profile refinement at 5K 80−88103
$SO_2(NHAg)_2$, disilver sulphamide, linkage of Ag-N chains *(German)* 78−10008
Si, amorphous film, IR and Raman spectra of Si-H bonds 78−19482
Si, IR absorption spectra, Si-H bonds, crystal defects *(Chinese)* 80−55073
Si:H, amorphous, discharge prod., optically induced cond. changes 80−96937
a-Si:H, influence of H on optical props., H conc. and H bonds 80−76098
Si:H film, amorphous, reactively sputtered, H content effect on props. 80−49714
Si-C:H, amorphous film, vibr. spectrum 79−61450
SiO_2, g-tensor of interstitial O and broken Si-O bond, MO model calc. 79−78520
SiO_2 layers, room temp. transforms induced by diethyl ether vapour 79−99456
$SnCl_2.2H_2O$, protonic order-disorder transition, H-bond vibr. Raman spectra temp. depend. 78−23437
$SnHPO_4$, hydrogen-bonded dimers 77−15357
TiO_2, H species characterisation by electron-stimulated desorption 80−34305
$VOSO_4 5H_2O$, single cryst. X-ray cryst. struct. determ., H_2 bonding *(French)* 79−73138
Zn_2AsO_4OH, paradamite, X-ray cryst. struct. determ. H bond strengths 79−42016
$Zn_4Si_2O_7(OH)_2.H_2O$, X-ray and neutron diffr. study 79−99159
$Zr_2F_8(H_2O)_6$, cryst. struct. refinement 78−18592

hydrogen compounds
see also deuterium compounds; hydroxonium ion; ice; steam; tritium compounds; water
acetonitrile-HCl complex in liq. Xe, IR spectral study 80−95626
alkylbenzene concentration in atmosphere, study in New South Wales 77−70817
aqua regia, etching of GaP 78−68833
t-butyl cyanide-HF, hydrogen bonded heterodimer, spectroscopic consts. from IR and microwave spectra 80−43039
complexes, H-bonded, frequency shift rel. to IR bandwidth 80−99502
cyanomethane-HF, hydrogen bonded heterodimer, spectroscopic consts. from microwave spectrum 80−43038
diatomic hydrides, variation-perturbation minimal Gaussian geminal basis sets correl. energy calc. 78−78629
diatomic hydrides of first and second row elements, PNO-CI and CEPA calc. 79−768
dimethylether-HCl(I)(Br) mixture in N_2 matrix, IR induced proton transfer isotope effects, bond strengths 79−29335
ESR of H atoms in pure and acidic ices, motional narrowing and spin polarisation 77−20706
first row hydride H-bonded complexes, ab initio calcs. *(French)* 80−5479
fluoromethane+HCl, IR spectra, intermol. interactions 80−9605
gas, proton energy loss distrib. in range 50-150 keV 77−79526
graphite-HNO_3 intercalation compound, in-plane elec. resistivity 80−34435
graphite-Na-N-H intercalation compounds *(French)* 79−52633
group IV hydrides, pseudopot. FSGO calc. 79−22591
H_20, adsorption on Si (111), electron energy loss spectra exam. 77−39736
H_2O:HF ice, single crystal, velocity of individual dislocations by X-ray topography *(French)* 78−87677
H_2O_2, propan-1,3-dioic acid, KIO_3, $MnSO_4$, $HClO_4$, I_2, periodic chem. reactions, bi- and tristability, rel. to biological mech. *(French)* 78−80726
halide, gaseous, powerful tunable IR and far IR Raman sources 80−5787
halide, solid, phase transition 77−15580
halide+unsaturated hydrocarbon, vibr. stimulated addition reaction 79−91928
halides, ab initio SCF calc. of dipole polarisabilities 79−89600
halides, chem. transport media for Cu_2O deposition *(German)* 78−31344
halides, $I^*(5^2P_{1/2})$ quenching, electronic-vibr. energy transfer 78−63114
halides, laser studies of relax. and reaction 80−11918

hydrogen compounds continued
halides, rot. relax. rate consts., information theoretic synthesis 79−86044
halides, rot. relax. with inert buffer gas, comment 80−69221
halides, rot. relax. with inert buffer gas, reply 80−69222
halides, spin-orbit coupling effect on proton mag. shielding 80−23440
halides, thermodynamic properties, phase transitions 78−47518
halides, vibr. transition moments, elec. and mech. anharmonicity influences 80−23459
halides+$I(5^2P_{1/2})$, collisional quenching, isotope effects 77−34583
halides+inert gas, energy transfer as function of collision energy, luminesc. obs. 79−86043
halogen hydride lasers, vibr. energy transfer, from metastable diatomic molecules 79−31882
HCl-inert gas mixtures, van der Waals molecules, far IR spectra 80−95610
HCl-NOCl gas mixture, vibr. relaxation, collisional de-excitation *(French)* 78−86934
HCl-Xe mixtures, low-press. excimer form. and quenching by e-beam excitation 79−50071
HF chemical laser, CW, with unstable telescopic resonator, radiation field structure 80−91786
HF laser nanosecond pulse generation using Ar gas breakdown 79−81465
HNO_3 channel spectral meas., fluorocarbons 11 and 12, contamination effects 77−87054
HX+alkali metal, (X=F,Cl,Br,I), reaction, semiempirical pot. surfaces calcs. 79−74362
hydracids, monatomic matrix-trapped, assoc. forms, struct. and spectral response, intermol. pot. calcs. 79−93996
hydride ions, XH^+, X=first and second row elements, PNO-CI and CEPA studies of electron correlation effects 77−34561
hydride of Z=106, hexavalent, Dirac-Fock one-centre calcs. 79−6837
hydride of Z=114, tetravalent compound, Dirac calcs. 77−34551
hydrides, 10-electron, lone pair localised MOs, energy contribs. and second moments 77−14341
hydrides, aq. dissoc., solvation, MINDO/S calcs. solvation theory 80−97708
hydrides, diatomic, dipole moments, atomic anisotropies effective charges 78−46458
hydrides, first row, $AH_2(H_3)(H_4)$, and positive ions, chemical equilibria, correl., ab initio calc. 78−35714
hydrides, first row, bending pot. calc. using MINDO approx., force const., equilib. geometry 80−95544
hydrides, first row, localised MOs, size-energy relation, at initio LMO GO calcs. 77−50351
hydrides, first-row, pseudopot. calcs. using FSGO 78−9062
hydrides, ionic cryst., cohesive energy calc. 80−6384
hydrides, localised mol. orbital density, spatial distrib., principal lobe description evaluation 78−888
hydrides, near-IR spectra, in Teflon powder matrix 78−3401
hydrides, second row, ab initio calcs. using FSGO basis, mol. parameters correlation 78−901
hydrides, ten electron, localised orbitals, moment analysis 78−41945
hydrides, UV photoelectron spectroscopy, basic concepts, spectra 78−17715
hydrides of 1st three row elements, pseudopotential calcs., PSIBMOL algorithm 77−26963
hydrides of BCC metals, geometric and electronic contribs. to thermodynamic props. 79−46815
hydrocarbon, long chain single cryst., carrier transport meas. 80−6874
hydrocarbon prod. from H_2 and CO, C_8FeCl_3 behaviour, effect of activation 79−43623
inorganic hydrates, applicability to heat storage material of latent heat type *(Japanese)* 78−23606
inorganic hydrides +F, HF IR chemiluminesc., H abstraction rel. rate consts. 77−86319
linear triatomic hydrides, ab initio SCF CI electric dipole moments 79−31410
meson capture, chemical, hydrogen and H isotope effects 80−69277
metal hydride form. for H storage, interstitial hole size and electron conc. effects 80−45789
metal hydrides, appl. to H energy storage 80−45785
metal hydrides, chemical heat pump, hydride conversion and storage system 80−72077
metal hydrides as hydrogen storage media 80−61445
metal hydrides use as energy conversion media, review *(Japanese)* 80−55934
molecule, ground state MNDO calcs. 78−911
molecule+molecule, medium distance interaction, SCF LCAO MO, supermol., perturbation and MCF calc. 79−837
neutral free radicals, in Ar matrix, IR spectrosc. evidence 78−66546
phosphoric acids, glass transition temps. 77−4050
piston engine using $LaNi_5H_x$ as energy conversion medium, prototype 79−70458
polysilicic acid, IR spectra, struct., crystallisation effects *(Russian)* 78−72528
PVC thermal degradation, reinitiation mechanism of HCl catalysis 80−71944
rot. spectra, 714-1667 μm, Fourier interferometric spectrometer 77−83765
silicic acid sol., gel formation, characteristics of light scattering 78−53269
silicic and aluminosilicic acids, effect of increased size of scattering centres in sols 78−53270
steel, mild, descaling by HCl *(French)* 80−108642
steel, mild, electrodes, in H_2SO_4, H evolution reaction kinetics 80−97630
steels, austenitic stainless, Cl and H_2S effect on oxidation resist. 80−45418
struct. and props., SCF calcs. 80−106260
superacids, props. and appls. *(French)* 79−74482
transition metal hydride complexes, struct. geometry bonding, neutron diffr. studies 79−46641
Al anodic oxidation, in H_2SO_4, pH-values effect *(German)* 80−76419
β-Al_2O_3-H_2O, H^+ and H_3O^+ conduction, dehydration effect 78−51726
β-Al_2O_3-H_2O, stability and dehydration 78−51693
β-Al_2O_3-H_3O, with mobile ion species, dielec. relax. 79−91351
Al_2O_3-H_3O^+, β and β″ phases, protonic, conductance and spectroscopy 80−70450
β-Al_2O_3-H_3O^+, high press. thermal stability 79−23678
β-Al_2O_3-H_3O^+, ionic conductivity at 25°C, obs. 78−22893

hydrogen compounds continued
β-Al_2O_3-H_3O^+, pulsed ^1H NMR study, 77 to 440K 79−87329
β''-Al_2O_3-H_3O^+, struct. basis for superionic cond. 80−107498
β-Al_2O_3-H_3O^+ protonic cond., struct. investig. 79−19213
β''- Al_2O_3-$H^+(H_2O)_n$, IR study 80−16037
β''-Al_2O_3-NH_4^+-H_3O^+, single cryst. PMR and proton motion 80−108101
AlOH→HAlO system, intramol. rearrangement, ab initio calc. of pot. surfaces and min. energy paths, geom. parameters 80−32623
Ar-HBr, intermol. pot. energy surfaces calcs. 80−91625
Ar-HCl, liq. density fluctuations, far IR absorpt., neutron scatt. mol. dynamics calc. 78−19461
Ar-HCl, van der Waals mol., far IR spectra 77−79611
Ar-HCl, Van der Waals mol., far IR spectrum, anisotropic intermol. force effects 78−62869
Ar-HI, low electron beam excitation rates 79−86163
Ar+HCl, classical and quantum centrifugal decoupling 77−58127
Ar+HCl, line broadening, short range force effects, semiclassical calcs. 79−98085
ArHCl, mol. interactions, differential scatt. cross-sections meas. 79−89732
Ar.HBr, van der Waals complexes, rot. spectra and struct. 80−48055
BH, correlation energy, many-body Rayleigh-Schrodinger perturbation theory calc. 78−894
BOH→HBO system, heterovalent isomerism, ab initio calc. of pot. surfaces and min. energy paths, geom. parameters 80−32622
Ba+HF→BaF+H, dual mol. beam excitation difference spectroscopy, state-to-state vibr. resolved dynamics 80−89474
BaI_2+Cl_2(HCl)(1,1-dichloroethane)(chloroethene), crossed beam metathesis, total cross sections 77−21354
Br+HCl(v'), Br+DCl(v'), reaction and relax., classical trajectory calcs. 77−48625
C-O-H-N-Si-Ar, computer calculations of heterogeneous equilib. 79−66044
CH_4, triple point, International Practical Temp. Scale, comparisons 79−40566
CaO-P_2O_5-H_2O system, phase diagram at 200°C 80−45286
Ca*+HCl, luminesc. reactive collisions 77−16816
Cl-HBr chemical laser, pulsed, computer simulation, effects of rot. nonequilib. 77−40547
Cl+H_2O_2, absolute rate const., 265-400K 78−15652
Cl+HI→HCl+I, Monte Carlo quasiclassical trajectory anal., product distribs. 77−16783
Cl+HNO(H_2O_2)(HO_2), rate consts., stratospheric appl. 78−85125
Cl^{n+}+Ne(SiH_4)(H_2S)(HCl)(Ar), K X-ray cross section, projectile charge depend. 77−19029
Cl_2+HI, pulsed chem. laser, rot. distrib. time evolution, kinetic master eq. calc. 77−65593
Cl_2+HI reaction pumped flash initiated HCl laser 79−94224
ClH-dimethyl ether, H bonded complex, IR and Raman spectra, mech. and elec. anharmonicity 79−89672
ClH-dimethyl ether, vibr.-rot. IR spectra, quantum and classical mechanics 80−91561
$ClSO_2OH$, superacid, props. and appls. *(French)* 79−74482
Cl'+HCl→Cl'H+Cl, barrier height, PNO-CEPA calculation 77−16795
CoO+H_2S, sulphurisation of {100} face, low-press. *(French)* 79−52754
$CuSO_4$-H_2SO_4, electrodeposition of Cu on plane vertical cathode, distrib. of local current densities 79−70338
D+HCl(HBr), elastic scatt., van der Waals pot. meas. 77−58120
D+HCl(HBr)(HI), abstraction and exchange reactions 78−73025
D+HCl→DCl+H, rate consts., EPR 77−9059
D+HCl→HD+Cl or DCl+H, branching ratios determ. 78−40046
D_2-HCl-Ar(He) gasdynamic lasers, gain 79−64217
DF-HBr CW optical resonance transfer laser 80−64003
DF-HF CW lasers, performance, computer modelling 78−71094
F+H_2 chemical laser, vib. populations in V→V, V→R,T energy transfer corrections 77−32794
F+HBr(HI)→HF+Br(I), electronic and vibr. energy transfer 77−63899
F+HCl(DCl)→HF(DF)+Cl, dynamical props., pot. energy hypersurface computer anal. 77−77735
FH-OH_2(dimethyl ether), H-bonded complexes, cubic force consts. calcs. 80−47868
FHF radical, struct. and stability, ab initio SCF and CI calcs. 77−71887
Fe-Cr (12 wt.%), corrosion in o-phosphoric acid 80−97622
FeO_2 nucleation, kinetics of formation of H_2O and C_2O 79−83449
GaAs/HBr system, heterogeneous reactions, modified entrainment method appls. 79−23551
GaAs-HBr chemical vap. transport system, thermochem. data 78−6854
H halide, CW thermally driven and elec. discharge driven lasers, book contrib. 77−10904
H halide, pulsed chem. lasers, book contrib. 77−10906
H halide-CO_2, pulsed chem. transfer lasers, book contrib. 77−10906
H I, ionisation pot. photoionisation mass spectra 78−25632
H-mordenite, adsorpt. of benzene *(German)* 79−90892
H+HBr, reaction props. dimensionality depend. 77−9050
H+HCO→H_2+CO, classical trajectory study 80−93750
H+HCl, barriers for abstraction and exchange reactions 77−48629
H+HCl, reaction kinetics, ESR and mass spectrometric obs. 77−21357
H+HF (v=2, 3), vib. deactivation 77−58142
H_2 Se, potential function and vibrational spectra 77−68030
H_2/CCl_4, inhomogeneous broadening of Morse oscillator, temp. depend. 77−61803
H_2-air-H_3PO_4 fuel cell performance, effect of NH_3 80−108795
H_2+Hd, vibr. energy transfer rates, IR fluoresc. meas. 79−98145
H_2+Ne*, quenching rate const. for metastable Ne($^3P_2$), flowing afterglow 78−46295
(H-He)$^-$, ab initio calcs. 80−63799
$HAlCl_2$, IR matrix spectrum, vibrs. and force consts. *(German)* 79−11786
$HAl_{11}O_{17}$, H β-alumina, IR absorpt. study 80−100655
H_2Ar, van der Waals complexes, lifetimes calcs. 78−13564
H_3AsO_4, polarisable acid-acid and acid-water hydrogen bonds 79−76423
HB, magnetic susceptibility and anisotropy calc. *(French)* 78−37559
HB rot. relaxation, diffusion theory 80−106313
HBD_2, electronic struct., one-electron props. 80−42935
HBF^+, electronic struct., one-electron props. 80−42935
HBF_2 and DBF_2 harmonic force field and ground-state average struct. determ. 80−83342
HBF_4, corrosion of PbO_2 layer, redox mediator effects 77−90480

hydrogen compounds continued
HBO_2, band strengths, shock tube IR spectrosc. meas. 80−106358
HBO_2, cubic, monoclinic and orthorhombic forms, H bonding, IR and Raman spectra 80−76029
HBO_2, electron attachment, rate coeff. 77−75310
HBO_2, electron attachment, rate coeff., equilib. effects 77−75311
H_3BO_3, aq. soln., dielec. props. and struct. 77−89369
H_3BO_3, chem. bonding, electronic struct., ESCA, Auger, and SIMS spectra 80−50512
H_3BO_3 concentration in primary circuit coolant, method and device for determ. *(Russian)* 77−38331
H_3BO_3 evaporation from seawater, major source of atm. B 79−2293
H_3BO_3, ferroelastic state shift and domain wall angle 78−43063
HBS, and isotopic forms, force consts., coriolis consts., vibr. amplitudes, shrinkage effects 80−43021
HBS, force consts., Coriolis const., vibr. amplitude, shrinkage and isotope effect 79−22863
HBr, absorpt. coeffs. meas. in Nd laser emission band 80−78620
HBr, and DBr, in monatomic matrices, near IR spectra and aggregate structs. 79−89667
HBr, aq. solns., IR spectra, H_3O^+ ion 77−30868
HBr, Balmer radiation production by electron impact 0-2000 eV 79 76521
HBr, CW chemical laser, vibrationally excited molecules *(French)* 77−14699
HBr chemical laser, pulsed, output performance, numerical anal. 80−1197
HBr, chemical shielding temp. depend. 78−5250
HBr, chemical TEA pin laser 79−76711
HBr, cryst. binding, H-bonding pot. function 79−32940
HBr decomposition using $FeBr_2$ and Fe_3O_4 for H prod. 80−35778
HBr, dissociative attachment of electrons 78−62931
HBr, Dunham pot. coeffs., nonlinear least squares fit calcs. *(French)* 78−13561
HBr, Dunham pot. energy coeffs. 78−41979
HBr, electrolysis, appl. to H prod. 80−35777
HBr electrolysis for H_2 production 80−97816
HBr, electron impact ionisation, vibr. excitation spectra threshold peaks, negative ion effects 80−106322
HBr, electron scatt., elastic rot. scatt. and vibr. excitation 78−58822
HBr, electronic to vibr. energy transfer from excited halogen atoms, IR fluoresc. 78−63113
HBr, far IR Ar matrix isolated spectra, 4.2K, press. and conc. effects 78−62801
HBr, fine struct. in dissociative attachment cross sections 80−87248
HBr, fundamental IR band, solvent effect *(Russian)* 78−13501
HBr high-energy laser, parametric and engineering studies 79−41391
HBr, IR matrix isolation spectra, N_2 matrix effects 79−36634
HBr, isotope chem. shift of μ^+ 79−55005
HBr, isotopic struct. and spectral charcts. of vibr. band, using liq. N_2 Raman laser source 78−50859
HBr, laser emission at 4 μm based on chem. generation of Br atoms 80−9878
HBr, laser photodissociation, ^{81}Br isotope enrichment 80−1075
HBr, liq.; transient stimulated vibr. Raman scatt. 78−71144
HBr, liquid, on coexistence line, light scatt., orientational correlation function 80−20632
HBr, mol. consts., rel. to TBr mol. consts. *(French)* 77−57855
HBr, photoelectron angular distrib. 80−58318
HBr, precession magnetic shielding of proton, semiempirical functions 78−82654
HBr, proton affinities calcs. 78−21840
HBr, proton affinity, mol. beam photoionisation method determ. 79−89622
HBr, purely chemical laser 79−10294
HBr, pyrolysis for H prod. 80−35772
HBr, sealed pulsed chem. laser, extended use by Cl_2 activation 78−46622
HBr, spectral intensity, vibr.-rot. bands, dipole-moment expansion 77−75228
HBr, triple-point temp. and pressure, vapour pressure of liquid to 205K 79−7683
HBr, vac. UV absorpt. cross section 80−91574
HBr, vibr. energy transfer, laser selective isotope excitation 78−82790
HBr, vibr. excitation by electron impact, threshold resons. 77−68127
HBr, vibr. excited, photodissoc. cross-section meas. 79−89717
HBr, vibr.-rot. absorpt. spectra at very high foreign gas densities 78−78687
HBr, vibrationally excited, chem. prod. for CW laser using CW supersonic mixing HF chem. laser 80−1196
HBr^-, laser mag. reson. pure rot. transition in far IR 79−89695
HBr^{n+}, highly charged, repulsion energies, nucl. internal conversion, ab initio calcs. 79−76341
HBr-Ar, IR fundamental region, line intensity, line breadth, tunable laser meas. 78−46328
HBr-CO, weakly bound, rot. spectra 80−91544
HBr-HCl, thermodynamics of binary liquid mixtures 78−64876
HBr-nN_2 aggregates, near IR spectra in monatomic matrix 78−21921
HBr-water complex, in supersat. soln., Raman spectra assignments 78−70840
HBr-Xe, thermodynamics of binary liquid mixtures 78−64876
HBr^+-HBr, binding energy, mol. beam photoionisation method determ. 79−89622
HBr+($5^2P_{1/2}$), electronic-vibrational energy transfer, fluoresc. obs. 78−66579
HBr+Ba, laser induced fluoresc. study at different collision energies 80−91632
HBr+Br, vibr. relax. times, laser induced fluoresc. 77−27159
HBr+CO_2, V-V energy transfer, 300-900K 79−59539
HBr+CO(CO_2)(N_2O)(NO)(N_2O)(O_2), rate consts. for vibr. energy transfer meas. using laser. induced fluorescence technique 80−87206
HBr+Cl_2(BrCl), four-centre reaction, quasiclassical trajectory study 79−57213
HBr+Cl^-→HCl+Br^-, vibr. product state distribs., IR chemiluminesc. obs. 80−81309
HBr+Cl→HCl+I, rate const. temp. depend., laser-initiated reaction 78−23929
HBr+D, elastic scatt., van der Waals pot. meas. 77−58120
HBr+D, vibr. energy transfer, phase shift 79−64080
HBr+ethylene, low temp. chain hydrobromination, kinetics and mechanism 80−93735

hydrogen compounds continued
HBr+F, H abstraction reactions, temp. depend., laser photolysis IR fluoresc. obs. 80−93744
HBr+H, elastic scatt., <50 meV, Van der Waals pot. 79−54937
HBr+H, H* prod., IR chemiluminesc. meas. 79−100336
HBr+H_2, collinear collisions, anharmonicity effects, vibr. excitation 79−31656
HBr+H_2, vibr. relax. rate, stimulated Raman scatt. obs. 77−75269
HBr+H^+, rotated Morse curve-spline pot. function 78−80729
HBr+HBr, vibr. energy transfer, dissimilar isotopic species 79−27067
HBr+HCl, single quantum vibr. energy transfer 80−69223
HBr+He, classically forbidden vibr. excitation, S-matrix 77−516
HBr+He(Ne)(Ar), Penning ionis., electron spectra, vibr. transfer 77−14555
HBr+He(2^3S), Penning ionis. electron spectra, 584Å photoelectron spectra 77−79687
HBr+I ($5^2P_{1/2}$), reactive and inelastic channels, rate, temp. depend., AAS obs. 78−35657
HBr+I*($5^2P_{1/2}$), collisional quenching rate const. meas. 77−3299
HBr+K(Ar*), product energy distrib. 80−45509
HBr+N_2O, V-V energy transfer, 300-900K 79−59539
HBr+OH→H_2O+Br, absolute rate const., 249-416K 79−70303
HBr+Xe liquid mixtures, intermol. forces effect on phase diagram and excess props., perturbation theory 80−39287
$(HBr)_2$, IR matrix isolation spectra, N_2 matrix effects 79−36634
$(HBr)_2$, intermol. distances, dipole moments, MINDO/3 and IR intensities and shifts calcs. 78−46335
$HBr^+(A^2\Sigma^+)$ vibrational states, lifetimes, emission cross sections, prod. by electron impact 77−3419
HBr(Cl), adsorption on Si(111), AES, electron energy loss spectra and electron impact desorption exam. 78−43243
HBr(DBr), isotopic forms, Stark hyperfine struct., polarisability anisotropy 77−83645
HBr(HCl), solid, ferroelec. and paraelec. phases, transitions, Raman scatt. 77−43980
HBr*+I, reaction rate, vibr. excitation effect, isotope enrichment 77−90581
HCC^+, equilib. struct., rot. const. 79−98003
HCCF, CW for IR mol. laser, optical pumping with $^{16}CO_2$ and $^{18}CO_2$ lasers 80−74343
HCCl, IR spectra, ν_4 and ν_5 vibr. bands, rot. struct., rot. and vibr. consts. 77−38665
HCL, fluid states, mol. dynamics simulation 80−79671
HCL+HF, HF(v=3) relax. and rate consts. 80−61069
HCN, 337 μm tunable radiation in laser-klystron link through Schottky diode or metal-semicond. point contact 78−46714
HCN ($A^1A''\rightarrow X^1\Sigma^+$), fluoresc. spectrum, using ArF laser excitation 79−36675
HCN (001)+HCN(Ar)(N_2)(CO_2)(CO), relax. rate consts., using Cs vap. IR source 80−9696
HCN, (001)→(000) fluorescence following dye laser photolysis of s-tetrazine 78−88652
HCN, absorption, spectrum calibration, 14-15 μm, using diode laser source 77−18917
HCN, and DCN, electron impact dissoc., product H(n=4) kinetic energy distrib., emission obs. 80−28106
HCN and H_2O vapour mixtures, adsorption by activated and impregnated C 80−39412
HCN and HNC, analytic functions from pot. energy surfaces 78−62743
HCN and HNC, mm wave emission obs. of interstellar clouds 80−90503
HCN, and isotopic derivatives, rot. depend. of Fermi resonance 78−94227
HCN, and isotopic forms, l-type doublet transitions 79−13704
HCN, and stable isotopic species, mol. struct., ground vibr. rot. transitions and consts. 77−10666
HCN, anharmonic pot., determ. of zeroth approx. 77−75255
HCN, CNH, isomer pairs, mol. orbitals calcs., using PLA and LEDO integral approx. methods 78−13418
HCN, CW 337 μm waveguide laser, scaling laws 77−19300
HCN CW compact laser, output characts. expt. 80−38035
HCN CW laser, auxiliary DC discharge effects 79−31925
HCN CW laser, output characts. *(Japanese)* 80−9863
HCN CW laser gain in hollow dielec. rectangular discharge tube 79−72554
HCN compact CW laser optimisation 78−59022
HCN compact CW laser, output increased by He, Ar, air and O_2 buffer gases 79−10293
HCN confirmed in galaxies M82 and NGC 253, 89 GHz obs. 79−44582
HCN crystals, polarition spectra and lattice dynamics 80−49313
HCN dimer, interstellar abundance, upper limit 78−54004
HCN, dimer form., identification 79−10095
HCN, dipole moment, relative sign w.r.t. normal coords. 78−46457
HCN, dipole moment derivatives, MINDO/3 semiempirical calcs. 77−75055
HCN, dipole moment derivative, sign anomaly, CGTO ab initio calc. 78−74795
HCN, dipole moment derivatives and force consts., CI calcs. 78−90091
HCN, dipole moment derivatives of CH and CN, CI method 79−45863
HCN, elastic electron scatt. differential cross section, 3-50 eV, 20-130°, rel. to He 78−90291
HCN, electron elastic scatt., differential cross-sections, effective range theory 80−83485
HCN, electron impact, dissoc. excitation cross-sections, fragment obs. 78−62936
HCN, electron impact excitation of low lying electronic states, assignments 78−25671
HCN, electron impact dissoc., near-threshold CN($B^2\Sigma$) emission 79−54975
HCN, electronic spectra, vibr. struct., ab initio calc. 78−9166
HCN, electronic states, oscill. strengths calcs. 78−9095
HCN electronic struct., one-electron props. 80−42935
HCN, electronically excited states, SCF CI calc. using Slater type orbitals 78−78645
HCN emission detect. in Sagittarius A mol. cloud 78−73750
HCN emission in W3 H II region, LF obs. 80−82446
HCN far IR laser, chem. pumping, 337 μm and 311 μm stimulated emission obs. 79−13958
HCN, Fermi and Coulomb correl. holes, SCF and CI wave functions 80−69085
hydrogen compounds continued
HCN, finite field method calc., moments, polarisability, field-induced shifts in mol. props. 78−74561
HCN formed by laser photolysis of methylamine, mol. fluoresc. obs. 80−97710
HCN, Franck-Condon transition amplitudes for mol. dissoc., semiclassical evaluations 78−62860
HCN, gaseous, radioactivity meas. by internal counting method 79−36483
HCN, ground state pot. surfaces, analytical functions 80−83304
HCN, H-CN dissoc. curves, SCF CI calc. 79−100405
HCN, $H^{13}CN$, far IR laser transition assignments 78−46579
HCN, HNC, electronic reorganisation, with core ionisation 78−94196
HCN, HNC, in Orion Molecular Cloud, J=3-2 lines detect. 79−25669
HCN, HNC, interstellar, form., role of H_2CN^+ isomers 78−81672
HCN, HNC, molecular electronic struct., unlinked cluster effects 78−94185
HCN, harmonic force consts., vibr. freqs., integrated intensities, MINDO/3 method 80−58411
HCN, high speed jets in Comet Kohoutek (1973 XII), origin 77−49332
HCN, IR and Raman vibr. intensity changes due to Li^+ interaction 79−45712
HCN, in interstellar clouds, rot. excitation by electrons 77−22292
HCN in neutral cometary atmospheres, photodissoc. rel. to CN prod. 80−82303
HCN in smoke, tunable diode laser meas. 80−89559
HCN, inner shell electron energy loss obs. 79−45853
HCN, integrated IR intensities of fundamental modes 79−98083
HCN, interstellar, absorpt. lines obs. towards Cassiopeia A 80−101624
HCN, interstellar, distrib. in vicinity of young B-type stars *(Russian)* 80−105321
HCN, interstellar, in $^1\Sigma$ state, collisional excitation by H_2 80−109508
HCN, interstellar, isotopic abundance vars. 77−53657
HCN, interstellar, obs. in AFGL IR sources 80−51856
HCN, intravalence triplet-triplet electronic transition, geometrical struct. and rel. energies determ. 80−99586
HCN, ionis. and photoelectron spectra, inner valence electrons 78−82784
HCN, ionis. by mol. orbital method, many-body calc. 79−36512
HCN, ionisation pot., Koopman's theorem, corrections using energy shifted perturbation theory 79−6845
HCN ionisation potential, Green's function method 77−3260
HCN, isotopic relations, harmonic freq. calc. 77−23486
HCN, J=1-0 transition obs. in southern interstellar mol. clouds 79−8983
HCN, J=4→3, 354 GHz transition in Orion Molecular Cloud 80−101636
HCN, K-shell excitation by electron energy loss spectroscopy 79−31712
HCN, laser, 2m CW, design and characts., brown deposit 77−3605
HCN, laser, CW, 337 μm, spatial coherence meas. 77−3595
HCN, laser, CW power characts., 337 μm, 0.3-0.8 A current 77−3604
HCN laser, plasma effects, radial gain and refractive props. 77−61942
HCN laser, power output, temp. and gas flow *(French)* 78−13686
HCN laser, temporal coherence meas., comparison of TGS pyroelec. detector with W-C point contact diode 80−31871
HCN laser, transversely excited double discharge 80−5749
HCN, laser plasma, microwave spectra of excited vibr. states 78−17656
HCN laser processes, mm. and submm. microwave spectroscopy 78−13685
HCN, laser translator of standard freq. to submm. range 78−17973
HCN, line search in photographic IR spectrum of C stars 77−78786
HCN, linear mol., Compton profile bond additivity, HF calc. 79−68268
HCN, microwave-microwave double resonance 80−53029
HCN, modified virtual orbitals, systematic CI procedure 80−83294
HCN, mol. electron correl., quadrupole excitation in correl. energy theories 79−36538
HCN, multipole expansion of diatomic overlap, MEDO calcs. 78−46264
HCN, nucl. spin-spin coupling, diamag. contrib. 79−36665
HCN, nuclear quadrupole coupling and mol. deformations 78−90191
HCN, $\nu_1+\nu_3$ combination bands, transition moments, integrated intensities 77−79610
HCN ν_2-lines, IR tunable diode laser spectroscopy, techniques and calibration 79−71542
HCN, orbital calculation, SCF+CI method 79−93928
HCN, photodissoc., CN radicals fluoresc. 79−52725
HCN, photodissoc., isotope effects 77−75238
HCN, photodissoc., photoabsorpt., photoemission and CN form. obs. 80−87141
HCN, photodissoc., vibr. energy states population meas. 78−58751
HCN, photodissociation coupled eqns. calcs., final states interactions 78−25637
HCN, photofragmentation vibr. and rot. distrib., quantum anal. 77−14504
HCN, photofragmentation vibr. distribs. 77−18992
HCN, photofragmentation, initial excitation effects calcs. 78−17734
HCN predissoc. Frank-Condon amplitudes 80−95694
HCN, predissoc. in photodissoc., CN radical ($A^2\pi$-$X^2\Sigma$) fluoresc. 77−38691
HCN, predissociation, photofragment excitation spectra measurement 79−45777
HCN, π face bonding of cyclobutadiene 79−98180
HCN, relationships between higher-transition frequencies 80−69119
HCN, relative signs of CH/CN dipole moment derivatives 78−74796
HCN, release from Earth interior rel. to thiocyanate in Red Sea brine, implications 79−57975
HCN, SCF ab initio ground state pot. energy surface, geometry, rel. to HCN 78−78646
HCN, selected fragment vibr. energy distrib. in dissoc. processes 78−1036
HCN, self assoc., intermolecular interactions, matrix isolation vibr. spectra obs. Raman and IR spectra 80−52995
HCN, self-assoc., matrix isolation vibrational spectra, appls. 78−46416
HCN, self-assoc., matrix isolation vibr. spectroscopy, complex form. studies 78−62952
HCN, self-assoc. in matrices, IR vibr. spectra of multimers 78−86858
HCN, self-relax. and energy transfer, laser pumping obs. 80−11918
HCN, semi-empirical excited state Morokuma's EHP calc., geometry and order of states 78−46256
HCN, solid state phase transition, hydrogen bond distance, stretching freq. calc. 78−10183
HCN solns., amino acid formation by ^{60}Co γ-ray irradiation 77−37410

hydrogen compounds continued
HCN Sternheimer shielding, perturbing elec. field and field gradient effects 77−88403
HCN synthesis in HF plasma torch 80−61099
HCN temp. depend. adsorption by activated and impregnated C 80−89522
HCN, transversely excited waveguide laser with UV preionisation 77−54730
HCN, valence excitation energy and UV spectra, HAM/3 calc. 78−25453
HCN, valence shell correl. energies, pair correls., unlinked cluster effects, CPA calc. 79−13648
HCN, vertical ionisation pots., CI calcs. 79−13645
HCN, vibr. energies, wavefunctions, ab initio calc. 78−17652
HCN, vibr. fine struct. accompanying core ionis., STO calcs. 78−62844
HCN wave numbers, intercomparison at 800 to 600 cm^{-1} with diode laser spectrometer 79−98082
HCN waveguide and Fabry-Perot CW laser power scaling laws 79−76715
HCN^-, ab initio calcs., electron affinity, stability 77−42239
HCN^-, SCF ab initio ground state pot. energy surface, geometry, rel. to HCN 78−78646
HCN^+, $^2\Sigma^+$ and $^2\Pi$ states, SCF and CI calcs. for determ. optimum linear geometries, bond angles calc. 80−74114
HCN^+, A and B $^2\Sigma^+$ states, pot. surfaces, ab initio SCF calcs. 80−27959
HCN^+, HNC^+, interstellar, radio search 78−24534
HCN^+, photoelectron spectra of third electronic state, ab initio calc. of pot. energy surface 78−70871
$HC^{14,15}N$ dimer, and $(DCN)_2$, microwave rot. spectrum identification and struct. 77−50427
HCN-CO complex, charge transfer theory, Mulliken population, ab initio calc., multiconfiguration scheme 80−106392
HCN-HF, dimer, rot. transition intensity, dissoc. energy determ. 78−46323
HCN-HF, elect. dipole moment, Stark effect of linear mols. 78−70818
HCN+^{7}LiH, rot. inelastic collision, energy transfer 80−87211
HCN+Ar, electron excitation of Ar* and Ar_2*, fluoresc. and dissoc. energy transfer collisions 77−14580
HCN+Br_2(Ar)(HCN), electronic-vibr. energy transfer, $Br(4^2P_{1/2})$ quenching and HCN (001) deactivation, fluoresc. obs. 77−518
HCN+H_3O^+(H_3S^+)($HCNH^+$)(HCHO.H^+), proton transfer, rate and equilib. consts. 78−48636
HCN+HCN, collisional line broadening of microwave spectra, semiclassical theory, calcs. 78−25516
HCN+HF(DF)(H_2), vib. energy transfer, laser-induced fluoresc. 77−58139
HCN+He, press. broadening cross-section, ang. momentum approx. calcs. 77−34696
HCN+He, press. broadening, rot. energy transfer, infinite order sudden approx. 78−22011
HCN+He, rot. excitation, infinite order sudden approx. 78−74740
HCN+He, scattering cross-sections, factorisation and fitting, IOS approx. 78−33575
HCN+He, translational-vibrational energy transfer, quantum dynamical study 80−63746
HCN+He(H_2)(CH_3F), HCN 80−102498
HCN+Na^+, rotational excitation, Stark shifted level transitions, energy transfer calcs. 79−98059
HCN+OH, reaction rate, press. depend. 78−85135
HCN^++H, reaction, ion cyclotron reson. mass spectrometric obs. 79−64098
$(HCN)_2$, and isotopic forms, microwave spectroscopic investigations of hydrogen-bonded complexes 78−62794
$(HCN)_2$, IR spectra in Ar matrix, vibr. bands, H-bonds 78−29782
$H(CN)_2^-$, IR spectra, rel. to mol. geom. 79−22702
$(HCN)_x$, mol. crystals, quantum theory, mol. tight binding method calcs. 80−49572
HCN(DCN), photodissoc. dynamics, rot. (vibr.) energy disposal 78−48672
$HCNH^+$ + H_2O(H_2S)(HCN)(formaldehyde) proton transfer, rate and equilib. consts. 78−48636
$HCNH^+$+e, dissociative recomb. reaction in interstellar clouds, products, statistical theory 78−57604
HCNO and isomers, interconversion pot. energy surfaces, geometries, electronic structs. 78−35660
HCNO, far IR spectrum, weak vibr. transitions 77−3357
HCNO, IR spectrum, ν_1 and $3\nu_1$ bands 77−3354
HCNO, isomers, geometry, spectra, rot. and force consts., ab initio calcs. 77−34574
HCNO, vertical ionisation pot., Koopmans' theorem, perturbation connections calcs. 80−42966
HCN...HF, hydrogen bonded heterodimer, spectroscopic consts. from microwave spectrum 80−43037
HCO, ground state props., coupled cluster and MBPT methods appl. 80−47881
HCO, HOF, HOCl, HOBr, HOI, force field determ., Redington's method applicability 79−81168
HCO, IR spectra of ν_2 fundamental, laser elec. reson. 78−5226
HCO, ν_2 fundamental band, laser mag. reson. spectra 78−5256
HCO, pot. energy functions for ground state surfaces 79−89620
HCO, prod. by formaldehyde photolysis, vibr. relax., chem. kinetics and spectra 79−11808
HCO, radical formation in acetaldehyde photodissoc., wavelength depend. 79−83490
HCO, vibr.-rot. transitions, IR laser mag. resonance 77−27098
HCO^+ detected toward M82 galaxy, 89 GHz obs. 79−44582
HCO^+, HCN, interstellar, relationship to N_2H^+ and CN 77−33587
HCO^+, in Orion Nebula mol. cloud, distrib. obs. rel. to N_2H^+ and SO_2 77−26034
HCO^+ isotopes, interstellar anomalous line intensities towards dark clouds 79−17054
HCO^+ threshold form. energy in CO_2^++H_2 reaction 80−50844
HCO^++CO, isotopic exchange, interstellar implications 80−61087
HCO^++H_2, J=0-1 transition press. broadening, microwave absorpt. 80−52981
HCO_2^+, geom. struct., ab initio mol. orbital study 78−62939
H_2CO stabilised He-Xe laser, freq. stability in axial mag. field 79−22991
H_2CO^+, geom. struct. optimisation, open-shell restricted HF and MC SCF calcs. 79−98004
H_2CO_3, dissoc. reaction rate meas. using reference electrode liq. junction 77−4906
H_2CO_3, enthalpies of ionis. 79−57284
H_3CO^++H_2S⇄H_3S^++HCHO, chemical equilib. consts., proton affinity of HCHO and H_2S 78−85189
H_3CO^++HCN⇄H_2CN^++HCHO, chemical equilib. consts., proton affinity of HCHO and HCN 78−85189
HCO_3^- (aq), standard enthalpies of solution and formation, standard Gibbs energies of formation and standard entropy 79−57285
HCP, force fields and force consts. of electronically excited states 80−69116
HCP, geometry optimisation, ab initio MO calcs. 77−42232
HCP, ν_1 and $\nu_1+\nu_2-\nu_2$ IR absorpt. bands 78−42060
HCP, ν_3 band, high-resolution IR absorption spectrum 80−47994
HCS^+ formation in interstellar clouds 79−17038
HCS^+-CSH^+ system, pot. surface for H abstraction, internuclear bending for ground and excited states 78−29744
H_2CS, ionis. pot., many-body Green's function method 77−67965
H_2CS, potential energy surfaces and equilibrium geometries for ground and excited states 79−45634
HCSi-HSiC, isomerisation energies, ab initio MRD-CI calcs. 80−106271
HCl, 1-0 absorption bands, absolute wavenumber meas. 77−3361
HCl, 3.8 μm, 10.6 μm CW laser emission based upon Cl atom chem. generation 79−947
HCl, 6,0 band, highly forbidden optical transitions using intracavity laser spectroscopy 77−42331
HCl, absorpt. coeffs. meas. in Nd laser emission band 80−78620
HCl, absorption coeffs. for DF laser radiation, pollution detection appl. 77−27059
HCl, acid vapour, eqn. of state 78−79402
HCl, addition to double-pulse CuCl laser 77−50654
HCl additive effects on ^{27}Al spin-lattice relax. in $AlCl_3$ aq. soln. 80−66058
HCl, adsorpt. on Al_2O_3 79−73398
HCl, air pollutant, remote meas. using chem. laser lidar system 77−21910
HCl and $(HCl)_2$, matrix isolated Raman spectra 78−42063
HCl and $(HCl)_2$, matrix isolated, pulsed NMR 79−22730
HCl, and DCl, in monatomic matrices, near IR spectra and aggregate structs. 79−89667
HCl and HBr, low-lying reson. states in 0.25-1.15 eV electron scatt. 79−45844
HCl and HCl-DCl, ferroelec. transition, ^{35}Cl NQR study 80−71233
HCl, anharmonic molecular vibrations, coherent spectroscopy 79−18187
HCl, anhydrous conc. solns. in methanol, Raman and IR spectra 78−82724
HCl annealing of MNOS capacitor memory oxide, effect on memory window size and location 79−70079
HCl, aq., effect on corrosion and electrochem. props. of Mo_2C 80−11813
HCl, aq. soln., $H_5O_2^+$ and $H_3O_2^-$ IR vibr. freq. assignments 79−73916
HCl, aq. solns., IR spectra, H_3O^+ ion 77−30868
HCl aqueous soln., H^+ mobility, 15, 25, 40°C, up to 5000 atm 78−10207
HCl aqueous solutions, diffusion coeffs. at 298K, conductimetric obs. 80−24628
HCl, Ar-perturbed rot. linewidths, temp. depend. 79−45766
HCl, atmospheric measurements using ground based IR spectroscopy *(French)* 80−81975
HCl automatic control in air by electrochem. methods 79−96491
HCl, Balmer radiation production by electron impact 0-2000 eV 79−76521
HCl, bond dependence of dipole polarisabilities 78−74573
HCl, $C^1\Pi$-$X^1\Sigma^+$ system, (0, 0) and (0, 1) bands, oscillator strength determ. and UV spectra 80−91570
HCl, charge exchange mass spectra 80−43177
HCl chemical laser, initiated by NO+ClO_2 reaction, performance and diagnostics 80−14333
HCl, chemical laser kinetics, book contrib. 77−10903
HCl chemical lasers using ClO_2+NO chain reaction 77−71978
HCl, chemical shielding temp. depend. 78−5250
HCl, chemical TEA pin laser 79−76711
HCl collection using impregnated filters, simulation 79−12257
HCl concentration, effect on H absorpt. of steel, and aniline surfactants effectiveness 80−108638
HCl, controlled electron impact, excited H product translational energy distrib. 80−14238
HCl, corrosion behaviour of Al-Sn alloys 78−85054
HCl cryosorption-pumped CW chemical laser 78−74894
HCl, cryst., internal vibr. electrostatic interactions and IR bandshape 79−91417
HCl crystals, orthorhombic and cubic, CNDO calcs. 80−6383
HCl, del. gas, proton longit. relax. time 77−34720
HCl, detector for environmental monitoring 78−24366
HCl, determ. in ambient air at ppbv level 79−74579
HCl, dipole moment function using wavefunction approx., error calc. 79−98063
HCl, dissoc. electron attachment kinetics in flame, mass spectra obs. 78−68872
HCl, dissoc. excitation in flowing afterglow, Cl form., light emission 78−90115
HCl dissociation for XeCl(B) formation in electron beam assisted Xe/HCl laser discharge 80−63988
HCl, dissociative electron attachment, differential cross section, Feshbach resons. 80−83508
HCl, dissociative-attachment cross sections, fine struct. 77−71884
HCl, dissolved in carbon tetrachloride, far i.r. absorpt. intensity 77−463
HCl, effect on CO_2 gasdynamic laser physical kinetics 78−5451
HCl, effect on oxidation-induced stacking fault growth in Si 80−49241
HCl, effective core potentials, all-electron calcs. 78−62704
HCl elastic electron scatt., short-lived resons., theory 77−14578
HCl, electric field gradient at Cl, two- and one-centre wavefunction expsn. 78−17561
HCl, electron binding energies, one-centre expansion method 77−6677
HCl, electron bombard., rot. excitation, energy dependence of elastic and inelastic cross sections 78−37756
HCl, electron elastic scatt., exchange and polarisation 80−91668
HCl, electron impact, H,D(2s,2p) prod. 78−42230
HCl, electron impact dissoc., H atom sublevel excitation 77−14593
HCl, electron impact dissoc. excitation cross sections 77−61861

hydrogen compounds continued
HCl, electronic spectrum, vac. UV absorpt. 80−9616
HCl, electronic to vibr. energy transfer from excited halogen atoms, IR fluoresc. 78−63113
HCl, electrostatically interacting mols., CI multipole function calcs. convergency 80−91458
HCl, elimination of distributed fixed charge in CVD-oxide 79−42661
HCl, emission K spectra, vibronic and core hole effects, nonempirical orbital defreezing calc. 78−5200
HCl, far IR Ar matrix isolated spectra, 4.2K, press. and conc. effects 78−62801
HCl flash initiated chemical laser, Cl_2-HI reaction pumped 79−94224
HCl, fluid, structure and dynamics 80−38889
HCl formation channels of H+ClF reaction, IR chemilum. obs. 80−26017
HCl, from $H+Cl^-$, vibr. state distrib. 80−66794
HCl, frozen aq. soln., photochem. reactions with H 77−9093
HCl gas, stimulated Raman scatt., creation of laser source, near IR to submillimetric waves *(French)* 79−31993
HCl gas environment effect on at. ion-electron recomb. 80−28601
HCl gas in ambient air, detection using coated piezoelec. quartz cryst. 78−92532
HCl, gas monitoring ion-selective electrode analyser 77−60146
HCl, geometry optimisation, ab initio MO calcs. 77−42232
HCl, helical TE laser, output power enhancement by CO_2 addition 79−98397
HCl, IR matrix isolation spectra, N_2 matrix effects 79−36634
HCl in DMSO-H_2O soln., ion assoc., US absorpt. obs. 79−23513
HCl in diffuse interstellar clouds, abundance and chem. models 80−91570
HCl, in dil. solution IR absorpt. fundamental shape temp. depend., solvent-solute interaction 79−26977
HCl, in nonequilib. plasma, electron energy distrib. function and dissoc. kinetics 80−11882
HCl, in rocket exhaust effluents from space shuttle model, meas. using electrets 79−53548
HCl, in stratosphere, radiometric meas. 77−25745
HCl, in stratosphere, vertical distrib. meas. 78−20470
HCl, in stratosphere, volume mixing ratios meas. 80−72587
HCl, in the bath, NMR spin-lattice relax., coupled states ang. momentum decoupling 77−77117
HCl, infinite chain, ab-initio electronic band struct., MUNICH-CHAIN program 77−8017
HCl, interaction with evaporated metal films, adsorpt. 78−75945
HCl, intermol. partial struct. factors, isotopic substitution and neutron diffr. obs. 80−53157
HCl, isotope exchange reactions, equilib. consts., adiabatic correction, electron correl. effects 78−88626
HCl, isotopic transfer laser, intercavity cold gas isotope filter 78−46590
HCl, K-emission and -absorpt. spectra, vibr. struct., ab initio calcs. 77−79629
HCl laser, using H_2-ClF chain reaction, CW, performance 78−46593
HCl laser, V=3 to V=2 band process, computer simulation 78−71095
HCl, linewidths and shifts in fundamental band broadened by D_2 and H_2 *(French)* 78−972
HCl, liq., IR spectral intensity and Raman cross-section meas. 80−2742
HCl, liq., self-diffusion coeffs., NMR spin-echo meas. 80−50223
HCl liq., time correlation function, computer simulation 80−79670
HCl, liq., transient stimulated vibr. Raman scatt. 78−71144
HCl, liq., vibr. relax., IR double reson. 80−95712
HCl, liq. struct. simulated by a Lennard-Jones pot. 80−1917
HCl, liquid, on coexistence line, light scatt., orientational correlation function 80−20632
HCl, liquid, struct. and mol. dynamics studied using intermolecular force models 80−83445
HCl, matrix isolated, vibr. relax., IR fluoresc. obs. 79−45749
HCl, mol., XPS and KLL Auger effect, line shifts 79−31602
HCl, mol. cryst., angles of H-bonded mols., ab initio calcs. 78−6037
HCl, mol. transition freqs. in resonant optical field, Stark shift 77−14487
HCl molecule, in inert solvents, far IR absorpt., free rotational models 77−450
HCl, nonempirical calc. of X-ray K-absorpt. spectra 77−88465
HCl, nucl. spin-spin coupling consts., ab initio calcs. 80−95647
HCl, nuclear quadrupole coupling and mol. deformations 78−90191
HCl, one electron props. and polarizibility, SCF and CI calcs. 80−58159
HCl, one-centre-expsn. SCF calc., electric field grad., Sternheimer effect 78−37550
HCl, one-electron props., corrections, Moller-Plesset perturbation theory calc. 80−95519
HCl, optical parametric oscillator, resonantly enhanced four-wave, pump intensity 78−9412
HCl, overtone vibr.-rot. bands, intracavity dye laser techniques meas. 80−91532
HCl, oxidation of Si:P, secondary defect generation suppression and diffusivity restraint 79−70191
HCl, photodissoc. cross section, from high vibr. levels, Poschl-Teller oscill. model 78−55210
HCl, polar liqs. models, mol. polarisability effect 80−92444
HCl, polar molecule electron scattering, exam. of models 80−37898
HCl, polymer degradation products, chem. anal. by UV photoelectron spectroscopy 78−53300
HCl, Poschl-Teller oscillator, matrix element of vibr. transitions 78−25510
HCl, precession magnetic shielding of proton, semiempirical functions 78−82654
HCl production mechanism, in cloud, chemical model with trace gases 77−37325
HCl, proton affinities calcs. 78−21840
HCl, proton affinity, mol. beam photoionisation method determ. 79−89622
HCl, proton affinity correl., ab initio SCF calc., MINDO/3, STO and G basis sets 78−33421
HCl, proton spin-lattice relax. time near liq.-vapour critical point 79−73842
HCl, pseudopot. calcs. 80−91446
HCl pulsed chem. laser, plane and helical electrode types, expt. study and modelling 80−32973
HCl, pure rot. lines, press. induced shift perturbed by Ar 77−79652
HCl, purely chem. laser employing transverse flow 78−46591
hydrogen compounds continued
HCl, quasi-energy states and stability in light wave field, width of unsteady zones *(Russian)* 79−94039
HCl, Raman spectra in various solvents, depolaris. ratio and profiles 79−59464
HCl release in coastal atm. 80−90113
HCl, remote conc. meas. using tunable IR laser 77−87118
HCl rot. relaxation, diffusion theory 80−106313
HCl, rot.-vibr. lines collision broadening, in He, Ar, N_2, O_2, CO, temp. depend. 77−58084
HCl, scattering contrib. to internal partition functions for Morse potential 79−81253
HCl, second order mag. props., coupled Hartree-Fock perturbation theory 80−87042
HCl, self assoc., intermolecular interactions, matrix isolation vibr. spectra obs. Raman and IR spectra 80−52995
HCl, semi-empirical INDO calc. of electronic struct. 80−32611
HCl, slow electron impact vibr. excitation wave function, virtual s-state 77−42429
HCl, solid, ferroelec., comparative calcs. 77−8529
HCl, solid, ferroelec. phase, spin-spin interactions, NQR meas. 77−85612
HCl, solid, incoherent neutron scatt. of proton motions 78−75600
HCl, solid, orthorhombic, temp. depend. freq. spectrum 77−15510
HCl solid film, contaminant on cryocooled Ge optical window, IR transmission 79−32007
HCl, spectral data analysis using graphics display terminal 78−54473
HCl, spectral line parameters in IR 79−22766
HCl, Sternheimer shielding, perturbing elec. field and field gradient effects 77−88403
HCl, stimulated emission from $ClF_3(F_5)+H_2$ laser mixture 77−50667
HCl stimulated emission obs., energy parameter of chem. ClF-H_2 laser 79−89903
HCl supersonic chemical laser, visible chemiluminescence flow visualisation 79−76699
HCl titration to determine F atom conc. 77−36830
HCl, tunable far IR generation by stimulated Raman scatt. 79−31983
HCl, tunable far IR Raman generation 78−5525
HCl, vac. UV absorpt. cross section 80−91574
HCl, vapour, etching behaviour of CaF_2 crystals 78−59812
HCl, vib.-rot. wavefunctions and matrix elements, pot. function effects 77−453
HCl, vibr. emission from ClF-H_2 chem. laser 80−97709
HCl, vibr. energy transfer, laser selective isotope excitation 78−82790
HCl, vibr. excitation by electron scatt., virtual state interpretation 78−17808
HCl, vibr. excitation in electric discharge 80−87978
HCl, vibr. state distrib., phase space sampling approach in statistical mech. 78−32753
HCl, vibr.-rot. absorpt. spectra at very high foreign gas densities 78−78687
HCl, vibr.-rot. line broadening by CF_4 and SiF_4 77−27117
HCl, vibr.-rot. lines broadening and shifting by SiF_4 perturber 77−23521
HCl, $X^1\Sigma^+$ states, many body effects, diagrammatic perturbation theory 77−79547
HCl, X-ray scattering, anomalous, Kramers-Heisenberg dispersion calc. 79−89628
HCl^-, reson. states by electron impact, GO and SCF+CI methods, dissociation channels 77−71883
HCl^-, resonance states, CI calcs., pot. energy curves 78−29755
HCl^+, effective Hamiltonian, ab initio calc. 79−45632
HCl^+, emission cross sections for $A^2\Sigma^+,\nu' \rightarrow X^2\Pi_i,\nu''$ on electron impact and lifetime of $A^2\Sigma^+,\nu'$ state 77−38697
HCl^+, PNO-CI and CEPA calcs. of electron correlation effects 77−34561
HCl^+, spin-orbit and spin-rot. coupling calc., isotope depend., pot. energy curves 77−57902
$H^{35}Cl$, collision broadened vibr.-rot. linewidths and shifts in fund. band, low temp. obs. *(French)* 77−68076
$H^{35}Cl$, $H^{37}Cl$, IR Fourier absorption spectra, press. induced shifts 78−74706
HCl:Bi^{3+} solution, characts. of luminesc. spectra, 82 to 130K *(Russian)* 79−28835
HCl:Bi^{3+} solution, kinetics and struct. of luminesc. spectra *(Russian)* 77−77290
HCl:He, state-selected collision cross-sections calcs. 78−22001
HCl/dimethyl ether gaseous complex, temp. depend. of IR spectra of H bond 77−34624
HCl/membrane/NaCl+HCl isotonic osmotic systems, inversion 79−52775
HCl/$SF_5(CCl_4)$, inhomogeneous broadening of Morse oscillator, temp. depend. 77−61803
HCl-Bi^{3+} soln., luminesc., quantum yield and lifetime *(Russian)* 79−33834
HCl-Br_2-Ar, flash photolytically produced Br* to HCl electronic to vibr. and rot. energy transfer 80−48069
HCl-CO, weakly bound, rot. spectra 80−91544
HCl-$CoCl_2$-H_2O, activity coeffs., 298.15K, electrostatic terms effects 79−24812
HCl-D_2, vibr. relax. time meas., by coherent Raman-induced IR fluoresc. 79−7038
HCl-D_2 electric discharge gasdynamic laser, turbulent mixing characts. 78−9366
HCl-D_2-He mixture, gasdynamic laser theory, gain depend. on parameters 78−50761
HCl-DCl mixed crystal, IR spectra, freqs., bandwidths and ν_{01} simultaneous transition 77−28564
HCl-DCl(HBr)(DBr)(HI), absorpt. spectra near 3.5 μm, equilib. config. of complexes *(French)* 78−42046
HCl-dimethylether complex, gaseous, H-bond IR spectra, temp. depend. theory 78−62804
HCl-H_2O, p-V-T relations up to 773K and 1500 bars 78−43096
HCl-He, discharge, possible laser action on vibr. transitions 80−14332
HCl-inert gas rot.-vibr. line pressure broadening and shift calc. 80−69124
HCl-KCl-H_2O mixed electrolyte solns., elec. transport 80−3355
HCl-Kr, rot. for IR spectra, anisotropic density fluctuations 79−54848
HCl-N_2 mixture, electron swarm, Cl^-.HCl cluster formation, dissoc. attachment, drift tube mass spectra 78−68884
HCl-nN_2 aggregates, near IR spectra in monatomic matrix 78−21921

hydrogen compounds continued
HCl-water complex, in supersat. soln., Raman spectra assignments 78−70840
HCl-X, matrix isolation vibr. spectroscopy, complex form. studies 78−62952
HCl-Xe, liq., enthalpy of mixing, calorimetric meas. 80−59661
HCl^+-HCl, binding energy, mol. beam photoionisation method determ. 79−89622
HCl+Ar, differential cross section, quasiclassical close coupling approx. 80−63743
HCl+Ar, elastic and rot. inelastic collisions, quasiclassical and quantum mech. results 77−79679
HCl+Ar, IR line width press. broadening 77−61802
HCl+Ar, inelastic scatt. exponential perturbation theories 80−74217
HCl+Ar, intermol. forces, generalised electron gas-Drude model 79−98182
HCl+Ar, rot. excitation, quasiclassical close coupling approx. 79−27068
HCl+Ar, rot. linewidth calcs., using different pots. 78−66602
HCl+Ar, rotationaly inelastic collision, planar trajectory, classical centrifugal decoupling calcs. 78−58788
HCl+Ar, shock heated steady state dissoc. rate consts. calc. 78−40039
HCl+Ar, shock-heated, collision induced dissoc. 79−34290
HCl+Ar(He), rot. energy transfer, quasiclassical trajectory calcs. 78−42173
HCl+Ar(He), rot. excitation, classical and quantum calcs. 78−1059
HCl+Ar(He), rot. excitation, infinite order sudden approx. 78−74740
HCl+Ar(Xe), infrared line shape, rotational lines, influence of collision duration 80−43110
HCl+Ar(Xe), spectral line shift of vibr.-rot. lines. press. shift 79−18237
HCl+Ba, beam-gas reaction, multiphoton ionisation, product identification 78−23946
HCl+Ba, laser induced fluoresc. study at different collision energies 80−91632
HCl+Br, IR fluoresc. studies of state-selected energy transfer, photochemistry 77−77768
HCl+Br, quenching of $4^2P_{1/2}$ state, vib. excitation, temp. depend. 78−58792
HCl+Br, relax. rates, vibr. photochem. 79−66290
HCl+$CH_3(CF_3)$, H abstraction, energies of activation calc. 78−31632
HCl+CO_2, collisions semi-empirical non-Lorentzian line shape determ. 77−34699
HCl+CO_2, vibr. relax., 300-900K, by laser fluoresc. 79−31658
HCl+CO_2, vibr. relax. rate, chemiluminesc. depletion method meas. 79−72400
HCl+Ca*, (Sr), reaction performed under high resolution, luminescence obs. 80−95662
HCl+Ca(4s3d^{1}D)→CaCl+H, chemiluminescent reaction, state-to-state cross-section, beam-gas expt. 80−45510
HCl+Cl, thermal rate constants, quasiclassical trajectory calcs., detailed balance 79−87822
HCl+Cl, vibr. energy transfer to oscilltory, rstricted rot. and translational motion 78−70908
HCl+Cl_2(DCl)(HCl), vibr. relax., Monte Carlo quasiclassical trajectory calcs. 77−50502
HCl+Cl(Br)(H), vibr. relaxation and reaction rates determ. 80−108698
HCl+D, HCl dissociative ionisation, H^+ signal origin, mol. beam obs. 80−66778
HCl+D(O)(Cl)(Br), relax. and chem. reaction, time resolved IR fluoresc. and mass spectrometry obs. 80−69177
HCl+F, H abstraction reactions, temp. depend., laser photolysis IR fluoresc. obs. 80−93744
HCl+F, reaction rate consts. rel. to stimulated emission 78−3317
HCl+F→HF+cl, time resolved vibr. chemiluminesc. and rate consts. 80−61069
HCl+H, elastic scatt., <50 meV, Van der Waals pot. 79−54937
HCl+H, semi-empirical pot. energy surfaces calc. by diatomics-in-molecules method 80−95556
HCl+H_2, translational and pot. relax., statistical calcs. 77−3435
HCl+H_2, V-V transfer, pulsed fluoresc. obs. 77−14540
HCl+H_2, vibr. energy transfer, collinear and 3-dimens. rate consts. 80−48065
HCl+H_2, vibr. relax. rate, stimulated Raman scatt. obs. 77−75269
HCl+H_2 (o- and p-), press. broadening and alternate ang. momentum coupling, rot. excitation 77−42375
HCl+HBr, single quantum vibr. energy transfer 80−69223
HCl+HCl, rot. transitions, semiclassical strong-coupling method 77−58143
HCl+HCl, rot. transitions, 0.025 eV, semiclassical exponential approx. 78−62883
HCl+HCl, vibr. energy transfer, dissimilar isotopic species 79−27067
HCl+HCl collision, rot. energy transfer, quasiclassical trajectory calc. 80−23524
HCl+HCl-SF_6, nonequilib. rot. distrib. relax., fluoresc. obs. 79−36673
HCl+HCl(Ar), pure rot. Raman lines, press. broadening cross sections 78−74702
HCl+HCl(DCl), vibr.-rot. absorpt. line shift 77−27160
HCl+HCl(HF)(HI)(HBr), supersonic-thermal beam collision, rot. energy transfer, classical trajectory calc. 79−68302
HCl+HF, vibr. relax., laser fluoresc., obs. 77−14484
HCl+HF, vibr. relax. laser induced fluoresc. obs. 79−64037
HCl+He, energy sudden approx., beam scatt. meas. mol. anisotropy effects 78−78802
HCl+He, mag. transitions, initial-l labelled CS approx. computations 79−3552
HCl+He, Penning ionis. electron spectra, new differential retarding field analyser characts. 77−41735
HCl+He, press. broadening cross-section, ang. momentum approx. calcs. 77−34696
HCl+He, scattering cross-sections, factorisation and fitting, IOS approx. 78−33575
HCl+He, slow collisions, rot. excitation cross- sections, quantum mech. calcs. 77−12795
HCl+He(Ar), press. broadening, rot. energy transfer, infinite order sudden approx. 78−22011
HCl+He(Ar), rot.-translational energy transfer, nonlinear vs. linear rotors, surprisal anal. 79−76492
HCl+He(Ne)(Ar), Penning ionis., electron spectra, vibr. transfer 77−14555
HCl+He(2^3S), Penning ionis. electron spectra, 584Å photoelectron spectra 77−79687

hydrogen compounds continued
HCl+I, quenching of $I(5^2P_{1/2})$, temp. depend., time resolved at. absorpt. spectrophotometry 80−32655
HCl+$I^*(5^2P_{1/2})$, collisional quenching rate const. meas. 77−3299
HCl+$I(5^2P_{1/2})$, electronic-vibrational energy transfer, fluoresc. obs. 78−66579
HCl+iert gas, weak collisions, HCl spectral line broadening of IR spectra 80−74161
HCl+inert gas, dissoc. induced by collision, rot. energy depend. 79−100341
HCl+K, ion pair form., energy loss spectra 79−34286
HCl+K, ion pair form. reaction, energy loss spectra meas. 79−61849
HCl+K, mol. beam reaction, rot. state depend. 79−74365
HCl+Kr(Ar), pot. energy surface determ. from rot. line broadening data 79−13784
HCl+methane, pure rot. line broadening obs., transition cross sections 77−75134
HCl+muonium in aq. soln., rate const. 77−38752
HCl+N_2O, vibr. relax., 300-900K, by laser fluoresc. 79−31658
HCl+$N_2(CO)(O_2)$(HCl), HCl linewidth, impact parameter calcs. 79−89714
HCl+$N_2(O_2)(D_2)(H_2)$, HCl ν_0-ν_1 band perturbations, linewidth and shifts calcs., IR spectra obs. *(French)* 80−58251
HCl+NH*, rate const., time resolved chemiluminesc. 78−60982
HCl+Ne, IR induced vibr. transition, Schrodinger eqn. distorted wave calc. 77−23538
HCl+O_3, nonreactive vibr. relax. rate of O_3 (001), 173-419K 79−3545
HCl+$O^-(O_2^-)(NO_2^-)(CO_3^-)(CO_4^-)$, rate consts. at 300K 78−76829
HCl+O(^{1}D), rate consts., temp. depend. 78−27747
HCl+O(OH), reaction rate const. temp. depend., stratospheric implications 78−31616
HCl+O(2^1D_2)→OH+Cl, correl. diagram 77−16798
HCl+pyridine, proton transfer interactions, NMR obs. 78−20007
HCl+$Sr^*(^3P_1)$, laser-excited atom reaction, energy deposition 78−85134
HCl+Xe liquid mixtures, intermol. forces effect on phase diagram and excess props., perturbation theory 80−39287
HCl+XeCl, ground state destruction, quenching rate consts. meas. 80−63758
$H^{35}Cl+H^{37}Cl$, reson. isotopic vibr. energy transfer, temp. depend. 79−72395
$(HCl)_2$, absorpt. spectra near 3.5 μm, equilib. config. of complexes *(French)* 78−42046
$(HCl)_2$, IR matrix isolation spectra, N_2 matrix effects 79−36634
$(HCl)_2$, intermol. distances, dipole moments, MINDO/3 and IR intensities and shifts calcs. 78−46335
$(HCl)_2$, vibr. freqs. in inert gas matrix, force const., MINDO/3 calcs. 78−41952
HCl(-acetone)(-acetonitrile), soln., IR absorption, H-bonding, solvent effect 78−29778
$HCl^+(DCl^+)$, spin-rot. consts., Van Vleck approx., ab initio calcs. 77−34610
HCl(DCl)+Ar potential, asymmetric, isotope substitution effect, Legendre expansion coord. transformation 78−70894
HCl(DCl)+He, cross sectional factorization expressions, close coupling input tested in sudden approximation 79−43571
HCl(DCl)+LiH, rot. inelastic collisions, sudden theories 79−98201
HCl(DCl)+LiH, state-to-state rot. inelastic cross sections, new laser fluoresc. technique 79−98200
HCl(J;υ)+Na→H+NaCl, reaction rate, rot. excitation depend. 78−64818
$HClO_4$, aq. soln., anomalous u.s. props. 77−1176
$HClO_4$, aq. soln., thermal capacity at 25°C 78−83965
$HClO_4$, propan-1,3-dioic acid, H_2O_2, KIO_3, $MnSO_4$, I_2, periodic chem. reactions, bi- and tristability, rel. to biological mech. *(French)* 78−80726
$HClO_4$-H_2O, aq. soln., IR and Raman spectra, conc. depend. *(Russian)* 80−53002
$HClO_4$+muonium in aq. soln., rate const. 77−38752
$HClO_4.H_2O$, wide line PMR spectra, oxonium ion motion *(French)* 79−56616
HCl.H, form. by dissoc. attachment, differential cross section 79−86077
$HCl.2ZnCl_2.2H_2O$, struct. refinement 78−51488
$HCl.6H_2O$, cryst. struct., H bonds, X-ray determ. 78−83783
HCl(ν=1,2)+O(^3P_g), reaction and deactivation, laser-induced fluoresc. obs. 78−35669
HCl(ν=1)+H(D)(Cl)(Br) reactions, selective vibr. excitation effects, kinetics *(German)* 77−21364
$H_3Co(CN)_6$, strong NHN hydrogen bond, vibr. lattice and mol., incoherent inelastic neutron scatt. 80−39232
α-$HCrO_2$, H^+ mobility investig. by nuclear relax. meas. 77−48076
H_2CrO_4, chemical treatment of glass fibre reinforced epoxy laminate *(German)* 80−93670
HD, IR absorpt. spectra, collision induced fundamental band 77−79613
HD, in interstellar diffuse clouds, column densities rel. to temps. determ. 78−93385
HD, spin-spin coupling consts., mol. vibr. contrib., calc. methods comparison 80−23402
HD+$CH_n^+(CD_n^+)$, isotopic exchange, interstellar implications 80−61087
HD+D_2, rot. inelastic differential cross sections, diffr. oscills. in elastic and inelastic scatt. 78−74743
HD+inert gas, isotropic Raman Q branch, vibr. dephasing effects and motional narrowing 78−74738
HD+Kr^+, reactive collision dynamics, isotope effects 78−23930
H(D)I+Cl, exothermic triatomic exchange reactions, prod. energy distrib., statistical dynamic model 78−92455
HDS, CO_2 laser pumped, high power far IR superfluorescent emission 79−27243
HDSe, high resolution IR spectra, anal. of $2\nu_1$ band, rot. ground state const. determ. 80−95616
$H_{2-n}D_nSe$(n=0, 1 and 2) ^{77}Se NMR on XL-100 spectrometer, isotope effects and spin-lattice relax. 80−71211
HD(v=5)+HD(v=0)→H_2+D_2, mol. H_2 exchange, reaction mechanism 80−85167
$HEu(PO_3)_4$, luminesc. props. 80−100675
$HEu(PO_3)_4$, vibr. spectra 80−34905
HF, 1-0, 2-0 absorption bands, absolute wavenumber meas. 77−3361
HF, ab initio HF-STO perturbation Auger transition rate calc. 79−72368
HF acid, presence in stratosphere confirmed by solar spectrum obs. *(French)* 77−53105

hydrogen compounds continued
HF, analytic RKR pot. including higher-order WKB approx. effects 77−57901
HF, aq. solns., IR spectra, H_3O^+ ion 77−30868
HF, atm., pulsed chem. laser, model including rot. nonequilib. effects 79−55127
HF, atmospheric measurements using ground based IR spectroscopy *(French)* 80−81975
HF, Auger spectra, correl. effects, energies and wavefunctions, ab initio CI calc. 80−14125
HF, Auger transition energy calcs. 77−34704
HF, biased laser amplifier concept 77−31087
HF, bond dependence of dipole polarisabilities 78−74573
HF, CW chem. laser, F atom prod. by microwave discharge 77−31099
HF, CW chem. laser, freq. conversion in Ag_3AsS_3, $LiNbO_3$ and $LiIO_3$ 78−30023
HF, CW chem. laser, freq. stabilisation by beat signals and anomalous dispersion 79−86187
HF CW chemical laser, design of multipass telescopic amplifiers 79−27289
HF CW chemical laser, mode competition obs. 80−33040
HF CW chemical laser, longit. and transverse mode competition in stable, unstable resonators 80−95917
HF CW chemical laser, spatial homogeneity of radiation improvement using telescopic resonator 80−106549
HF CW chemical laser amplifier with multiple pass telescope cavity, diffr. 80−19055
HF, CW chemical laser for remote pollution monitoring and process control, HF conc. in Al plant 79−48200
HF CW chemical laser with cylindrical telescopic resonator, flame front model 78−59001
HF CW chemical laser with unstable telescopic resonator, diffr. effects 79−94265
HF CW chemical laser with cylindrical nozzle grid, excitation chain mechanism 80−28227
HF CW optically resonance-pumped laser 80−43356
HF chain, ab initio cryst. orbital calcs., basis set depend. 78−34746
HF chain reaction laser energetics, C_5F_{12} mol. addition and rot. nonequilib. *(Russian)* 77−42530
HF, chain reaction pulsed laser, simple rate eqn. model 77−3572
HF, chem. laser, electron beam initiation, efficiency up to 10% 77−34882
HF, chem. laser, spectral and time characts. 77−75499
HF chemical laser, 10 kW CW arc-driven, diagnostic system for supersonic free jets 77−23667
HF chemical laser, CW, influence of mixing effects on energy characts. 80−9875
HF chemical laser, comparison of two microwave plasma sources for F atom prod. 78−22140
HF, chemical laser, discharge stabilisation using resistive electrodes 78−1251
HF chemical laser, electron beam excited, energy characts. 77−75498
HF chemical laser, emission due to mol. overtone 78−17927
HF chemical laser, F+H_2 threshold times, reaction product rot. distribs., relax. rates 80−28222
HF chemical laser, flame propag. velocity in F_2-H_2 mixture 80−50855
HF chemical laser, flow anal. 79−81420
HF chemical laser, laminar flow pattern *(Russian)* 78−87048
HF chemical laser, modelling, Lorentz broadening 77−79813
HF, chemical laser, optical inhomogeneities in F_2-H_2-CO_2, interferometric meas. 77−674
HF chemical laser, output energy, photoinitiating substances influence 79−89901
HF chemical laser, phase control for coherent optical recomb. 79−72580
HF chemical laser, pulsed, evolution, kinetic model, rot. nonequilib. 79−36888
HF chemical laser, pulsed, evolution, irreversible thermodynamic anal. 79−31887
HF, chemical laser, rot. population transfer effect obs. 78−79013
HF chemical laser, single-line CW, with unstable resonator, temporal stability 77−50690
HF chemical laser, small-scale CW, construction and performance 77−50682
HF chemical laser, spherical telescopic resonator, design 78−71120
HF chemical laser, stable discharges, with large electrode separation 78−55371
HF chemical laser, time-depend. kinetic-thermodynamic description 80−9877
HF chemical laser beam, phase fluctuation meas. 80−48317
HF chemical laser initiation by relativistic electron beam 80−64005
HF, chemical laser kinetics, book contrib. 77−10903
HF chemical laser mixture, H_2-F_2-O_2, spontaneous explosions 78−73044
HF, chemical laser performance *(Japanese)* 77−38876
HF chemical laser phase control servo system 80−33063
HF chemical laser with microwave excitation *(German)* 80−43326
HF chemical lasers, numerical anal. of laser generation conditions 80−9872
HF chemical TE laser, 16 μm emission 80−83600
HF, cluster and chain dipole moments, ab initio calc. 77−26967
HF, colliding system initiated by IR laser absorpt., vibr. inversion generation 77−10707
HF, collisional rot. relax. probability model 77−83697
HF, combustor-driven cold-reaction laser, book contrib. 77−10905
HF, core ionis., single orbital relax., LCAO MO SCF calcs. 78−29739
HF, correl. energy, fourth order diagrammatic, many body Rayleigh Schrodinger perturbation theory 80−63556
HF, correlation energy, many-body Rayleigh-Schrodinger perturbation theory calc. 78−894
HF cryosorption-pumped CW chemical laser 78−74894
HF, cryst., CNDO calcs., struct., binding energy, 4K 77−15338
HF, cryst., Raman spectra 80−55075
HF, cryst. binding, H-bonding pot. function 79−32940
HF, cw chem. diffusion laser, amplifier operation 78−79015
HF, design of compact CW chemical laser using microwave discharge 79−72591
HF dimer, stabilisation energies, harmonic force constants, intermolecular vibrations, SCF and CEPA PNO calcs. 79−98177
HF, dipole moment function, Schrodinger eqn. soln. using Morse pot. 77−79703
HF dissociation with one and two IR lasers, classical mech. treatment 80−23470
hydrogen compounds continued
HF doped ice I_c, anelastic relax. *(French)* 78−6122
HF, double-discharge chem. laser, transitions in SF_6-C_3H_8 mixture, temporal characteristics 80−53282
HF, effect on CO_2 gasdynamic laser physical kinetics 78−5451
HF, effective core potentials, all-electron calcs. 78−62704
HF efficient electron-beam-pumped chem. laser with high specific energy output 79−45963
HF, elastic electron scatt., short-lived resons., theory 77−14578
HF, elec. dipole polaris., near Hartree-Fock value, using EFV GTOs 77−88591
HF electron beam initiated chem. laser 79−13959
HF, electron bombard., rot. excitation, energy dependence of elastic and inelastic cross sections 78−37756
HF, electron impact excitation, dissoc., emission spectrum 78−90305
HF, electron impact rot. excitation 77−42427
HF, electron scatt. cross section, vibr. and rot. excitation, close coupling calc. 80−53154
HF, electron spectroscopy of resonances 79−3583
HF, electronic spectrum, vac. UV absorpt. 80−9616
HF, electrostatically interacting mols., CI multipole function calcs. convergency 80−91458
HF, ellipsoidal Gaussian basis functions, integral formulas and test calcs. 77−23420
HF, emission K spectra, vibronic and core hole effects, nonempirical orbital defreezing calc. 78−5200
HF etchant conditions effect on soda lime glass track registration 80−52815
HF, etchant for fission fragment track visualisation in crysts. 78−66454
HF, etching of quartz 78−27666
HF, far IR line shift, meas. using Michelson spectro-interferometer *(French)* 77−61875
HF, ferroelec. helical system, energy band calc. 78−10329
HF, Feshbach resons., predissoc. investig. 80−83433
HF, fine struct. in dissociative attachment cross sections 80−87248
HF, flowing TE laser using SF_6-H_2 mixture, operation at 10 kHz pulse repetition rates 78−17955
HF, fluoromethanols (mono and tri), decomposition activation of HF, non-statistical energy partitioning, laser emission 79−945
HF, force const. evaluated in first order of perturbation theory 77−34781
HF, force consts., ab initio CI calcs. *(French)* 78−90093
HF formation channels of H+ClF reaction, IR chemilum. obs. 80−26017
HF, fragmentation, enhanced vibr. excitation effect, mass spectra 78−20004
HF gas, self-induced transparency using HF chemical laser 77−88866
HF, geometries, props. and protonation, ab initio mol. orbital study 79−22588
HF, geometry optimisation, using bond function augmented basis sets 78−905
HF ground state, as vac., in many-electron system cluster expansion calcs. 79−26912
HF, ground state props., coupled cluster and MBPT methods appl. 80−47881
HF, H-X bond position, correlation with electronegativity 78−9069
HF, H-bonded chains, vibr. modes in liq. and solids 78−59873
HF H-bonded dimers, PCILO calc., energies, geometries 78−37557
HF, H-bonded dimers involving H_2O and NH_3, PCILO study 79−72238
HF, HF calcs., compared with optimised LCAO results 78−5139
HF, high press. radiation-chem. laser, electron beam initiation 77−75562
HF, high-energy laser, energy extraction, beam quality, for fusion ignition 78−63102
HF, high-power laser for fusion reactor appl. 77−7062
HF, highly excited, ionis. pot., mass spectrometric meas. 78−58603
HF, hyperpolarisabilities, dipole moment, HF calc. with correlation 80−23342
HF, IR absorption in Born-Oppenheimer approx., vibronic gauge function for vibr. intensity 78−966
HF, IR chemiluminesc. quenching, (V-V) and (V-T, R) energy transfer rates 78−20018
HF, IR chemiluminesc. quenching, (V-V) energy transfer rates 78−20019
HF, IR dispersion, refractive index meas., vibr.-rot. fundamental intensities, dipole moment 79−37441
HF, IR Fourier absorption spectra, press. induced shifts 78−74706
HF, IR laser induced collisional pumping 78−25629
HF, IR laser induced collisional pumping 78−25630
HF, IR laser spectra 79−45936
HF in absorption, anomalous dispersion meas. 80−95881
HF, in ClF-H_2 chem. laser, rot. laser emission 79−98349
HF, in stratosphere, volume mixing ratios meas. 80−72587
HF, intermolecular interaction energies calcs. using minimal basis sets 80−78681
HF, ionisation energy, LCAO Xα calcs. 77−50353
HF, K-emission and -absorpt. spectra, vibr. struct., ab initio calcs. 77−79629
HF large-volume laser amplifier, energy extraction 79−86174
HF laser, atmospheric press., initiated by electron beam irradiated discharge 77−7076
HF laser, CW diffusion type amplifier, efficiency 77−34878
HF laser, CW diffusion type, arbitrary degree of F_2 dissoc., numerical anal. 77−34879
HF laser, c.w., longitudinal mode beat intensities, tuning freq. depend. 77−671
HF, laser, electron beam excitation 77−711
HF, laser, H_2F_2 mixture, pulsed, flame out 77−27284
HF laser, H_2+F_2 chain reaction, rotational nonequilibrium mech. vibr.-rotational energy exchange effect 80−48230
HF laser, H_2+F_2 reaction, coherent emission efficiency 78−17928
HF, laser, output spectrum control using selective intracavity loss 77−3607
HF laser, Phoenix oscillator-amplifier system, laser-beam characts., rel. to plasma heating 79−76701
HF laser, photoinitiated pulse H_2-F_2 system, parametric anal. 77−34880
HF, laser, pulsed, rot. relax. rate effect on efficiency *(Russian)* 77−10900
HF laser, pulsed unstable resonator, mode control and performance studies 78−82995
HF laser, rotationa nonequilibrium efficient model 79−22945
HF, laser action by pulsed microwave discharge 78−58998

hydrogen compounds continued
HF laser beam spectral anal. using near field holography 77−23680
HF laser conceptual design for laser fusion 79−86192
HF, laser field interaction, Floquet theory, dynamic Stark shift, broadening 80−63716
HF laser transitions, pure rotational, from exploding-wire metal atom oxidation lasers 77−14701
HF laser with flow-through chem. active medium, pulsed-periodic regime realisation 80−106513
HF laser with resistive Ge electrodes, for optical studies of semiconductors 80−64061
HF, linear response function, diagonal ARPA calcs. 78−74594
HF, liq., computer simulation of struct. and dynamics, assoc. system 79−86667
HF, liquid, computer simulation, intermolecular potentials 80−38890
HF, liquid, Monte Carlo simulations 79−64967
HF, liquid, struct. and props., intermol. pot. function calcs., basis set depend. 79−82134
HF, low lying states, GVB and CI calcs. 77−14362
HF, low-impedance Blumlein discharge initiated laser, efficient operation 79−36919
HF, mag. field depend. orbitals for mag. screening and susceptibility of mol. 78−78611
HF, mag. field depend. susceptibility, gauge invariant GO calc. 78−1100
HF, mag. shielding and susceptibility, ab initio finite perturbation calcs. using GIAOs 77−6670
HF, magnetic susceptibility and anisotropy calc. *(French)* 78−37559
HF master oscillator-amplifier system based on chain H_2+F_2 reaction 79−22947
HF, meas. in upper stratosphere 77−45070
HF, minimal basis set localised orbitals, conjugate gradients method calcs. 79−6849
HF, mol., electronic struct., CI+B_k extrapolation method for ground state 79−97983
HF, mol. hyperpolarisability, second-order SCF perturbation method, coupled Hartree-Fock calc. 78−33422
HF, mol. nucl. spin-spin coupling, diamag. contrib. 79−36665
HF, mol. props. internucl. separation depend., MCSCF calc. 78−70965
HF, molecular energy quantities from localised charge densities, dependence on geometry and basis set 80−63525
HF molecules, infinite linear chain, equilibrium structure and stabilisation energy 80−63856
HF molecules in crystalline solvates, mol. diffusion and spatial symmetry of arrangement 79−42313
HF multiline laser pulses, ns switching, amplification 77−38910
HF, multipole expansion of diatomic overlap, MEDO calcs. 78−46264
HF, NMR shielding consts. and mag. susceptibilities, coupled HF with extended GTO basis 80−5480
HF, nanosecond duration multiline laser pulse generation and amplification 77−38930
HF, near IR absorpt. spectra, collisional broadening, line shapes and half-widths 79−89673
HF, nonempirical calc. of X-ray K-absorpt. spectra 77−88465
HF, nonequilibrium dissociation in electric discharge, vibrational excitation 78−94306
HF, nucl. mag. shielding and susceptibility, elec. field depend., SCF-Hartree Fock method 80−18791
HF, nucl. spin-spin coupling consts., finite perturbation and sum-over-states calcs. 79−85893
HF, nuclear spin-spin coupling, ab initio SCF perturbation theory 78−33525
HF, nuclear spin-spin coupling const., finite perturbation calcs. 78−78616
HF, nuclear spin-spin coupling consts., finite perturbation-CI calcs. 80−5563
HF, numerical coupled Hartree-Fock parallel polarisability, partial wave SCF calc. 78−9079
HF oligomers, Gibbs free energies, gas. equilib., ab initio calc. 79−20456
HF, one-dimens. cryst., ground state energy PCILOCC method 79−10056
HF, orbital relax. energy for single and double ionis. from valence shells 80−106253
HF, orbitals calcs. using modified Adams-Gilbert eqn. 77−34542
HF, photoinitiated chain reaction laser, high elec. efficiency 77−3574
HF, photoionis. cross section calc., for YMζ line, HF vs OPW methods 77−42353
HF, photopreionised atm. press. laser operation 79−967
HF, polar liqs. models, mol. polarisability effect 80−92444
HF, polarisation model representation for chem. reactions 79−39131
HF, Poschl-Teller oscillator, matrix element of vibr. transitions 78−25510
HF, pot. curve, one-config. Hartree-Fock-Roothaam calc. for force consts. 78−82627
HF, pot. curves, diagrammatic perturbation theory, spectrosc. consts. 78−25458
HF, pot. energy curve, minimal basis ab initio VB calcs. 78−50477
HF, pot. energy functions, virial theorem calcs. 77−88519
HF, potential curve calc. using angular momentum depend. of pseudopot. 77−30804
HF, precession magnetic shielding of proton, semiempirical functions 78−82654
HF premixed chain reaction CW laser, spectral output 80−95882
HF, pressure broadened linewidths in 2.5 μm band, influence of polymer form. 80−32777
HF, proton affinity, mol. beam photoionisation method determ. 79−89622
HF, pseudopot. calcs. 80−91446
HF pulsed, chemical laser, with spherical telescopic resonator, energy characts. calcs. 80−14367
HF, pulsed chain and non-chain reaction lasers, book contrib. 77−10906
HF pulsed chain reaction chem. laser, scaling laws 80−32974
HF pulsed chemical laser, operation at high press. of H_2-F_2 working mixture 79−89900
HF pulsed chemical laser of HI-SF_6 system 80−106514
HF pulsed chemical laser of HI-SF_6 system 80−106515
HF, pulsed H_2+F_2 chain reaction laser, rot. nonequilib. mechanisms effect on performance 78−82958
HF pulsed laser, appl. of CW X-ray preioniser 80−64037
HF, pulsed laser, high energy prod. 77−34884
HF pulsed laser, Xe flashlamp efficiency for photoinitiation 80−69403
hydrogen compounds continued
HF pulsed laser initiated with CO_2 laser-produced plasma 80−38009
HF, pulsed laser numerical modelling, rot. relax. 80−87388
HF pulsed photoinitiated chem. laser, characts. rel. to DF-CO_2 laser 79−64219
HF, pulsed-discharge initiated H_2-F_2 chem. laser, comparison with non-chain H_2-SF_6 laser 80−28223
HF recirculating TE-laser, gas consumption characts. 79−68390
HF, relativistic Dirac-Fock multiconfig. SCF calcs. 80−99456
HF repetitively pulsed subsonic chem. laser, flameout using fluidic switching 78−29943
HF resonantly enhanced stimulated Raman scatt. for tunable IR generation 77−54759
HF, restricted and unrestricted HF wavefunctions, convergence problem 77−418
HF, rot. population transfer using IR-laser double-resonance expt. 79−55128
HF, rot. relax., IR double reson. obs. 77−10740
HF rotational line shift, far IR Fourier transform spectrometry improvement 79−30582
HF, SCF theory, multiconfig., direct orbital optimisation 80−87049
HF, STP basis sets, energies calc. 77−3262
HF, short laser pulse generation possibility by cooled H_2-F_2 mixture photolysis 79−22946
HF, simple high-power TEA laser operating in IR 79−94251
HF, solid, ferroelec., comparative calcs. 77−8529
HF, solubility in ice single crysts., 180-270K 77−28007
HF, spectroscopic consts., FSGO calcs. 77−6758
HF, spin-coupled theory of mol. wavefunctions, mol. struct. and props. 77−50337
HF, spin-spin coupling consts., mol. vibr. contrib., calc. methods comparison 80−23402
HF, stimulated emission from $ClF_3(F_5)+H_2$ laser mixture 77−50667
HF stimulated emission obs., energy parameters of chem. ClF-H_2 laser 79−89903
HF, supersonic flow in chemical lasers 77−42528
HF TEA laser, He-free, with MW output 80−64060
HF, threshold photoelectron spectra, photoionis. threshold, resonant autoionis. 77−499
HF, time resolved fluoresc., IR energy deposition in laser irradiated SF_6-H_2 mixture 80−23454
HF, tunable far IR generation using resonantly enhanced stimulated Raman scatt. 79−14031
HF, valence orbitals momentum distribs., (e, 2e) binding energy spectra 80−14237
HF, vertical ionis. pots. calc., CNDO approx. in Green's function method 80−18799
HF, vib.-rot. props. of $X^1\Sigma^+$ and $B^1\Sigma^+$ states, variational calcs. 77−50422
HF, vibr. excited, ang. distrib. of reson. scatt. electrons 77−71881
HF, vibr. excited, chemical laser design 79−31947
HF, vibr. fluoresc. from SF_6H_2 collisionless multiple photon absorpt. photodissoc. 77−58099
HF, vibr. relax., microscopic and macroscopic anal. of non-linear master eqns. 79−36743
HF, vibr. relax. rates, v=3, 4 78−82817
HF, vibr.-rot. band, absorpt. line self-broadening, rot. relax. 80−87213
HF, vibr.-rot. emission, from highly rot. excited states, in ClF_x-H_2 chem. laser 78−17926
HF, $X^1\Sigma^+$ state, many-body effects, HF STO calcs., diagrammatic perturbation theory 77−50355
HF, $X^1\Sigma^+$ states, many body effects, diagrammatic perturbation theory 77−79547
HF, $X^2\Sigma^+$ state, 3- and 4-body perturbation theory modified pots. 77−88376
HF and $(HF)_2^-$, ab initio calcs., electron affinity, stability 77−42239
HF^+, ab initio valence band calcs. 79−6869
HF^+, PNO-CI and CEPA calcs. of electron correlation effects 77−34561
HF^{2+}, singlet state orthogonality constrained SCF calc. 77−26962
HF/HCl, ratio in 14-38 km region of stratosphere 78−20469
HF/HCl ratio in stratosphere, comparison between theory and meas. 79−16568
HF/UF_6-H_2 nuclear pumped laser, characts. 80−78847
HF-aliphatic ethers, H-bonded complexes, gas phase, first overtone reconstruction 80−43040
HF-Ar mixture; HF rotational relax., laser IR fluoresc. 77−83634
HF-CO, weakly bound, rot. spectra 80−91544
HF-CO_2, laser system, interaction between vibr. states, theory 77−23670
HF-ClF complex, and isotopic forms., mol. beam elec. reson. spectra, config., bonding, spectroscopic consts. 77−30860
HF-cyanomethane, microwave spectroscopic investigations of hydrogen-bonded complexes 78−62794
HF-cyclic ethers H-bonded complexes, calorimetry, IR spectra and MO calcs. 79−52738
HF-DF, CW chem. laser, freq. stability and stabilisation 78−22141
HF-DF, pulsed chem. laser, efficient excimer flashlamp initiation 77−88754
HF-DF laser, 10 W repetitively pulsed closed cycle system, elec. excitation 77−88753
HF-DF simultaneous laser excited by ferroelec. ceramic capacitatively coupled discharge 80−69413
HF-H_2O, microwave spectroscopic investigations of hydrogen-bonded complexes 78−62794
HF-H_2O_2-H_2O, chemical polish for opt. microscopy of steels 77−9021
HF-HCN, microwave spectroscopic investigations of hydrogen-bonded complexes 78−62794
HF-HCl, H bonding , struct., mol. beam-elec. reson. spectra 78−29777
HF-HCl, SCF energy hypersurface, stationary points, thermodynamics of form. 80−102436
HF-HCl chemical laser utilising ClF+H_2 chain reaction, kinetic model 80−9874
HF-water complex, in supersat. soln., Raman spectra assignments 78−70840
HF+Ar, IR line width press. broadening 77−61802
HF+Ar, rot. relax. of high rot. levels at 1 torr press. 79−10181
HF+Ar, shock heated steady state dissoc. rate consts. calc. 78−40039
HF+Ar, state-to-state cross sections for rot. to translational energy transfer determ. 80−91644
HF+Ba, product rot. and vibr. distributions and reaction cross sections depend. on reagent translational energy 80−93745

hydrogen compounds continued
HF+$C_2H_3^+$, interaction, struct. and stability, ab initio calcs. 80−58347
HF+CO_2, vibr. relax. rate, chemiluminescence depletion method meas. 79−72399
HF+Ca(Sr), beam reaction, vibr. excitation 78−68877
HF+D, vibr. threshold energies, reagent energy effects 78−85145
HF+DF, DF vibr. deactivation, semiclassical calcs. 80−48061
HF+DF, vibr. relax., laser-induced fluoresc. obs. 79−64028
HF+F^-, proton transfer reaction, polarisation model 79−39131
HF+formyl fluoride, multiple site reactivity, ab initio GO supermol. calc. 78−11498
HF+H, low barrier quantum model, vibr. deactivation 80−69216
HF+H_2O(methanol)(ether), mol. electrostatic pot., H-bonds, CNDO/2 calc. 77−61822
HF+$H_2(D_2)(CO_2)$, vibr. relax. of HF (ν=3,4) 79−50117
HF+$H_2(D_2)(N_2)$, 200K and 295K vibr. relax. rates 80−63766
HF+H_2(HCl)$(N_2)(O_2)(CO_2)$ vibrs. relax., laser fluoresc. obs. 77−14484
HF+$H_2(N_2)(CO_2)(O_2)$(HCl), vibr. relax. laser induced fluoresc. obs. 79−64037
HF+H^-, reaction, ab initio pot. energy surface calcs. 79−39127
HF+HCl$(CO_2)(N_2O)$(CO)$(N_2)(O_2)$, HF(v=3) relax. and rate consts. 80−61069
HF+HF, ab initio pot. surface, ang. depend. fit calcs. 77−19006
HF+HF, classical trajectories, use of perturbation theory in asymptotic region 79−98199
HF+HF, interaction energy, MCF and perturbation calculations 77−27139
HF+HF, interaction energy, multipole anal., charge overlap, orientation and bulk props. 77−34715
HF+HF, momentum exchange rate, Boltzmann eqn. predictions 78−78781
HF+HF, rot. inelastic collisions, partial opacities, integral cross sections, pot. surface 77−38716
HF+HF, rot. line width of vibr. bands 78−33552
HF+HF, rot. relax. collision, scaling theory anal. 80−74232
HF+HF, rotationally inelastic scattering, classical trajectory study 78−82819
HF+HF, vibr. relax., temp. depend. calcs. 78−70906
HF+HF, vibr.-vibr., vibr.-rot., and vibr.-translational energy transfer calcs. 78−70907
HF+HF (methane)(methane-d_4), collision relaxation rate constants and rot. equilibration time meas. 80−69213
HF+HF(DF), vibr.-rot. absorpt. line shift 77−27160
HF+HF$(H_2)(D_2)(CO_2)$(isobutene), vibr. relax. dye laser pumping effects 80−9703
HF+H′→H+H′F, transition state geometry, SCF CI calcs. 78−20009
HF+H(D), kinetic isotope effect and temp. depend. 78−53202
HF+He, rot. excitation cross sections, use of rot. and orbitally adiabatic basis functions 79−59543
HF+He, slow collisions, rot. excitation cross-sections, quantum mech. calcs. 77−12795
HF+He, vibr. relax., unitary distorted-wave approach 79−36738
HF+He(2^3S), Penning ionis. electron spectra, 584Å photoelectron spectra 77−79687
HF+I*($5^2P_{1/2}$), collisional quenching rate const. meas. 77−3299
HF+I*($5^2P_{1/2}$), electronic-vibr. energy transfer fluoresc. decay meas. 77−71846
HF+inert gas, dissoc. induced by collision, rot. energy depend. 79−100341
HF+inert gas, press. broadening and shifting of vibr.-rot. absorpt. lines 77−27161
HF+Li, electron transfer reactions, semiempirical pot. energy surfaces calcs. 78−73022
HF+Li→LiF+H, pot. energy surface, SCF and CI calcs. 80−71904
HF+MgF, V-V energy transfer collisions, 'triple beam' expt. 79−98197
HF+N_2, intermol. forces, multipole results validity, charge overlap effects 79−89730
HF+NaF, V-V energy transfer collisions, 'triple beam' expt. 79−98197
HF+$O_2(a^1\Delta_g)$, E-V energy transfer 77−30960
HF+Sr, endothermic reaction, comparison of effectiveness of vibr. and translational excitation 80−93746
HF+Sr*($^3P_1$), laser-excited atom reaction, energy deposition 78−85134
HF+T hot atoms, energy loss 78−15691
HF^+, Λ-type doubling and spin-doubling 78−74633
HF_2, electric discharge chem. laser, SF_6-H_2 mixture pumped by inductive storage unit 79−98409
$(HF)_2$, energy decomp. anal. of H-bonding, ab initio SCF MO calcs. 77−57868
$(HF)_2$, H-bonding and indirect exchange ('superexchange') in 79−93912
$(HF)_2$, intermol. force model, rel. to liq. struct. 78−78773
$(HF)_2$, intermol. pot. function, ab initio 6-31G calc. 79−18254
HF_2 ion, H-bond excited electronic states, CI calc., dissoc. and autoionising states 80−5489
HF_2, neutral free radicals, in Ar matrix, IR spectrosc. evidence 78−66546
$(HF)_2$, photoionis., HF proton affinity 78−17731
$(HF)_2$, polarisation model representation for chem. reactions 79−39131
HF_2^-, dipole derivatives, rel. to refl. spectra of Na and K salts 78−80324
HF_2^-, four electron three centre bonding units, ab initio valence bond calcs. 80−27949
HF_2^-, IR spectra and mol. struct. 79−63996
HF_2^-, in KBr(RbI), anharmonic interaction of impurity intramol. vibrs. with cryst. phonons 77−77217
HF_2^-, mag. shielding and susceptibility, finite perturbation mol. orbitals calcs. 77−46513
HF_2^-, matrix isolated, IR spectra and struct. 78−74655
$(HF)_3$, 3-body pots., SCF energy partitioning calcs. 80−18953
$HF_{(g)}$+Si, reaction kinetics 77−86288
$(HF)_n$, n=1-∞, ab initio hydrogen bond and electronic parameters, phonons 77−14342
H_2F+F^-, proton transfer reaction, polarisation model 79−39131
H_2F_2 and H_3F_3 clusters, molecular structures, ab initio calcs. 80−83532
H_2F_3, struct. H bonding, IR spectra obs. 77−54560
$H_3F_4^-$, struct., H bonding, IR spectra obs. 77−54560
$H_4F_5^-$, struct., H bonding, IR spectra obs. 77−54560
HFB^+, electronic struct., one-electron props. 80−42935
HFCS, potential energy surfaces and equilibrium geometries for ground and excited states 79−45634
HF(Cl)(Br)(I), ferroelec. and paraelec. phases, elec. multipole interactions 77−59522

hydrogen compounds continued
$HF^+(DF^+)$, spin-rot. consts., Van Vleck approx., ab initio calcs. 77−34610
HF(DF)+He, cross sectional factorization expressions, close coupling input tested in sudden approximation 79−43571
HFF radical, struct. and stability, ab initio SCF and CI calcs. 77−71887
HF(J,υ)+Na→H+NaF, reaction rate, rot. excitation depend. 78−64818
HF($^1\Sigma^+$)+Xe($^1S_0$), expt. and computational study, 0.044 and 0.153 eV 79−89748
HF*, interaction with ClFx, relax. consts., stimulated emission delay 77−7077
HF*-HF, vibrational predissociation in hydrogen bonded complexes 80−61078
HF*+ethylene (fluoroethylenes), vibr. deactivation rate constant 78−50615
HF*+NH*, microscopic vibrotational-electronic energy transfer, IR chemiluminesc. obs. 79−31662
HF(1≤n≤7)+DF(0), vibr. deactivation calc., 300-3000K 79−31655
HFeN_2 complexes, electronic configuration calc. using SCCC-LCAO-MO method *(Chinese)* 80−1082
HF(ν_1,J_1)+HF(ν_2,J_2) collisions, energy transfer, reaction rates 78−29844
HF(ν=1)+F→HF(ν=0)+F, vibr. relax. rate const., 100-3000K 77−3434
HF(v_1=1)+HF(v_2=0), vibrational relaxation temperature dependence, laser-induced fluorescence simulation 79−50069
$H^+(H_2O)_n$, secondary electron emission from charged clusters on 2.4 keV Ar bombarded surfaces 79−15580
HHe^+, N-electron system, Schrodinger eqn. soln. using antisymmetrisation 80−106246
HHe^++Ar, ab initio pot. energy data, SCF-LCAO calcs. 80−63530
H_2^+He, total energy, interat. dist., geometric configurations, LCAO MO SCF calcs., stability, binding energy 77−42236
HI, 1→0 IR absorpt. band 78−86863
HI, 7-0 vibr.-rot. band in near-IR absorpt. spectrum, equilib. mol. consts. 78−21936
HI, anhydrous, reduction of SO_2ClF 79−5150
HI, aq. solns., IR spectra, $H_3O^+_2$ ion 77−30868
HI containing radioactive ^{124}I, ^{126}I, nucl. reson. fluoresc. in ^{124}Te, ^{126}Te obs. 77−2953
HI, crystalline, Raman and IR spectra, mol. vibr., libration and translation 80−2757
HI decomposition and H separation in S-I thermochem. prod. of H 80−35771
HI, dipole moment function, multiconfiguration SCF calc. 77−75330
HI, dissociative adsorption on Pt (111) and (100) superlattice form., LEED, AES, and thermal desorption studies 80−55715
HI, Dunham pot. energy coeffs. 78−41979
HI, H abstraction by thermal H, 10-30K, ESR evidence 78−76839
HI, line strength meas., 0→4 and 0→5 absorpt. bands, dipole moment *(French)* 78−62847
HI nuclear quadrupole HFS in IR spectrum, obs. using tunable diode laser 80−58412
HI, photoelectron angular distrib. 80−58318
HI photolysis, ESR spectrum of ^{127}I atoms in Xe matrices 80−1005
HI, precession magnetic shielding of proton, semiempirical functions 78−82654
HI, proton affinities calcs. 78−21840
HI, relativistically parameterized extended Huckel theory 79−49924
HI, Rydberg states, quantum defect theory applic. 80−32700
HI, solid and liquid thermodynamic properties 78−47517
HI, UV absorpt. spectra, ionis. limit region, assignment 78−21940
HI, vac. UV absorpt. cross section 80−91574
HI-He-Cl_2 chemical laser system, rot. nonequilibrium, kinetic modelling, three model comparison 80−53281
HI-SF_6 system, HF pulsed chemical laser 80−106514
HI-SF_6 system, HF pulsed chemical laser 80−106515
HI+Br→HBr+I, thermal rate const., 220-400K, H/D isotope effect 79−47906
HI+Cl, chem. laser, energy distrib., spectrosc. obs. 78−71096
HI+Cl^-→HCl+I^-, vibr. product state distribs., IR chemiluminesc. obs. 80−81309
HI+Cl→HCl+I, rate const. temp. depend., laser-initiated reaction 78−23929
HI+D, HI dissociative ionisation, H^+ signal, mol. beam obs. 80−66778
HI+D→H+DI, Franck-Condon theory 78−60984
HI+F, H abstraction reactions, temp. depend., laser photolysis IR fluoresc. obs. 80−93744
HI+F $^2P_{1/2}$-state excited I form. 78−23923
HI+H, elastic scatt., <50 meV, Van der Waals pot. 79−54937
HI+He(2^3S), Penning ionis. electron spectra, 584Å photoelectron spectra 77−79687
HI+I*($5^2P_{1/2}$), collisional quenching rate const. meas. 77−3299
HI+O_3, HOI formation, matrix reaction, IR spectra, isotope shifts and band assignments 78−80737
α-HIO_3, ^{127}I NQR spectra 80−39889
HIO_3, $^1H/^2H$ quadrupole reson. freqs. detected by double reson. with level crossing 78−84497
HIO_3, cryst., ^{1}H NMR, −165 to 25°C 79−73828
HIO_3 crystals, anharmonicity effects in Raman spectra 80−25379
α-HIO_3, dispersion anal. of IR reflection spectrum *(Russian)* 78−56493
α-HIO_3, electrogyration coeff. meas. 79−19859
α-HIO_3, near IR absorpt., influence of deuteration 78−27237
α-HIO_3, nonlinear conical refraction, second-harmonic cone 79−27329
α-HIO_3, nonlinear cryst., use for ps reson. spectroscopy, stroboscopic method *(Russian)* 77−83930
α-HIO_3, optically active biaxial crystal, conical diffr. intensity patterns 79−4785
HIO_3, PMR spectra, homonuclear and heteronuclear broadening separation 80−77828
α-HIO_3, parametric superluminesc., picosec. spectroscopy 79−55187
HIO_3, polariton Fermi-resonance and dissociated phonon states *(Russian)* 80−20634
αHIO_3, second harmonic conical refraction 77−46758
HIO_3, single crystal, ang. depend. of Raman spectra 78−72518
α-HIO_3, thermal radiation recording by two-stage freq. conversion detects. 79−46002
α-HIO_3, vibration level Davydov splitting, adiabatic potential role, dipole-dipole approx. *(Russian)* 80−29365

hydrogen compounds continued
HIO_3:Cr(Ni)(Fe)(Mn), growth and struct. perfection, effect of impurity ions 77−12514
HI_3O_8, NQR freqs. of ^{127}I 78−72433
HI_3O_8, XPS, binding energies and bond orders 77−18976
H_5IO_6, XPS, binding energies and bond orders 77−18976
$H_{0.36}MoO_3$ and $H_{1.71}MoO_3$ bronzes, NMR relax. obs. at 77<T<450K, H diffusion 80−108089
$H_{1.6}MoO_3$ bronze, form., kinetic, thermodynamic investig. *(French)* 80−45247
$H_{1.6}MoO_3$ bronze, próton shift tensors PMR meas. 80−71202
$H_{1.6}MoO_3$ bronzes, proton mobility 78−39426
$H_{1.6}MoO_3$, electronic props., mag. susceptibility and spectra 80−80266
H_xMoO_3, ($0<x\leq2.0$), phase relationships, X-ray diffr. exam. of microstruct. 78−76639
H_xMoO_3 ($0.3<x<2.0$), synthesis and phase characterisation 79−1416
H_xMoO_3, structural anal. by neutron diffr. 79−65043
H_xMoO_3, thermochemistry and electrochemical behaviour 79−100427
HN_2^++He, rot.-translational energy transfer, nonlinear vs. linear rotors, surprisal anal. 79−76492
HN_3, and DN_3 pure rot. Raman spectra, rot. consts., K-depend. parameters 78−29791
HN_3, decomposition and ionisation in shock tube *(Russian)* 78−7182
HN_3, flash photolysis leading to NH pure rot. lasing 79−86175
HN_3, ground $^1A'$ state, SCF and CI calcs., conform., geom., vibr. freqs. and dissoc. 80−18806
HN_3 IR multiphonon dissociation with electronic excitation 80−11934
HN_3, IR multiphoton dissoc. 78−80771
HN_3 in ethane or propane solution, photodecomp., NH reactions 79−83471
$HN_3 \rightarrow N_2^* + NH^*$, laser photolysis, primary products, energy distrib., intermediate reactions 78−61037
HN_3, photodissoc., NH photofragment energy distrib. and reaction rates 77−90618
HN_3, photoelectron spectra assignment 80−53043
HN_3, UV photolysis 80−101027
HN_3, vertical ionisation pot., Koopmans' theorem, perturbation connnections calcs. 80−42966
$H^{15}N_3$, rotational-vibrational Raman spectrum of ν_2 band 80−91564
HN_3+F, production of $NF^*(a^1\Delta$ and $b^1\Sigma^+)$ 79−11770
HN_3+F, strong interactions in gas-phase reactions, arrested relax. IR chemilum. obs. 80−7773
$HN_3+NH^* \rightarrow NH_2^* + N_3^*$, rate const., time resolved chemiluminesc. 78−60982
HN_3+$NH(NH_2)$, rate consts. from HN_3 UV photolysis data 80−101027
H_3N-HF, energy decomp. anal. of H-bonding, ab initio SCF MO calcs. 77−57868
$HNB_3(HNBH)$, spectroscopic properties, PNO-CI and CEPA calcs. 78−41961
HNC, and HCN, ^{14}N quadrupole coupling consts., ab initio calcs. 80−58283
HNC and $HN^{13}C$ in interstellar clouds temp. effects and D fractionation producing DNC 79−44578
HNC, and stable isotopic species, mol. struct., ground vibr. rot. transitions and consts. 77−10666
HNC, anharmonic force field, equilib. struct., rot. consts. and bond lengths 78−90147
HNC, electronic struct., one-electron props. 80−42935
HNC, finite field method calc., moments, polarisability, field-induced shifts in mol. props. 78−74561
HNC→HCN, transition state determination and characterisation ab initio calcs. 77−28975
HNC ionisation potential, Green's function method 77−3260
HNC, linear mol., Compton profile bond additivity, HF calc. 79−68268
HNC, millimetre spectrum, rot. consts., force consts., U90.7 interstellar line, struct. parameters 77−57989
HNC, quadrupole coupling constant determ. 78−1101
HNC, valence shell correl. energies, pair correls., unlinked cluster effects, CPA calc. 79−13648
HNC, vibronic coupling and linear to bent transitions 79−45694
HNC^+, $^2\Sigma^+$ and $^2\Pi$ states, SCF and CI calcs. for determ. optimum linear geometries, bond angles calc. 80−74114
HNC^+, radical cation, charge exchange mass spectrometry, HNC^+ ion recombination and ionisation pot. 78−76838
$HN^{13}C$ and HNC, hyperfine structure in dark interstellar clouds 79−101182
$H^{15}NC$, interstellar, J=1→0 emission obs. in DR21(OH) 77−82299
HNCO, 193 nm photolysis, photodissoc. products, $NH(a^1\Delta)$ internal energy distrib. reaction rate with 0_2 79−83489
HNCO, a-type rot. spectrum in excited bending states, rot. consts. 78−21915
HNCO and isomers, interconversion pot. energy surfaces, geometries, electronic structs. 78−35660
HNCO, barrier to linearity, ab initio SCF and CI calcs. 79−3363
HNCO, geometry, spectra, rot. and force consts., ab initio calcs. 77−34574
HNCO, microwave and RF spectra, b-type rot. transitions 78−21914
HNCO, photoelectron spectra assignment 80−53043
HNCO, rot. spectrum, ground and vibr. state reson., centrifugal distortion coupling 80−83364
HNCO, vertical ionisation pot., Koopmans' theorem, perturbation connections calcs. 80−42966
HNCS, a-type rot. spectrum in excited bending vibr. states 79−3437
HNCS, ground state spectroscopic const., microwave, millimeter and IR spectra 80−28010
HNCS, microwave spectrum, K_a=0 and 1 rot. levels inversion 77−38656
HNCS, microwave transitions 78−9143
HNCSe, struct., microwave spectrum 79−18178
HNC⇌HCN, intrinsic reaction coord., ab initio SCF calc. method 77−48626
HNC⇌HCN, isomerisation energy/barrier correlation, rel. to LiNC(BNC) 80−50840
HNF, A^2A'-X^2A'' emission spectrum 79−50033
HNF_2, force consts., geometry, ab initio Hartree-Fock calcs. 77−57864
HNF_2, photoelectron spectra, vibr. struct. obs, ionisation pot. determ., ab initio calcs. of ionic geometry 80−83418
HNF_2, vertical ionisation pot. calc. by perturbation corrections to Koopmans' theorem 80−83520
H_2NF, force consts., geometry, ab initio Hartree-Fock calcs. 77−57864
hydrogen compounds continued
$H^+(NH_3)_n$, secondary electron emission from charged clusters on 2.4 keV Ar bombarded surfaces 79−15580
H_2NNH_2, nuclear fuel processing solutions 78−78487
HNNN, substitution struct., rot. consts. calcs. 80−91534
HNO $\tilde{A}^1A''$ excited state dipole moment, optical-optical double reson. Stark spectrosc. obs. 80−106337
HNO, CI-SCF-MO basis function calc. 77−42246
HNO, four electron three centre bonding units, ab initio valence bond calcs. 80−27949
HNO, fundamental vibr. bands, laser Stark spectra 77−38692
HNO, ground and lowest excited states, SCF ab initio calcs. 78−37544
HNO, HON, electronic reorganisation, with core ionisation 78−94196
HNO interstellar, chem. reactions, form. and destruction rates 78−28764
HNO isomerism, low lying electronic states, ab initio MRD-CI calcs. 80−83291
HNO, low-lying states, pot. energy curves 80−9533
HNO, low-lying states, pot. energy surfaces calcs. 80−102460
HNO, pot. energy functions for ground state surfaces 79−89620
HNO, predissoc., absorpt. spectrum line broadening 77−14503
HNO, vibr. freqs. from anharmonic ab initio/empirical PE functions 79−76406
HNO, vibronic state perturbative and predissoc. mechanisms, fluoresc. excitation spectra obs. 80−9658
HNO^+, ab initio pot. surface, and isomerisation barrier of lowest states 79−22622
HNO^+, ab initio SCF and CI comparison of struct. and spectra, rel. to NOH^+ 77−26972
HNO^+, HON^+, interstellar, candidate mols. formed by NO ion-molecule reactions 78−28739
HNO^+, vertical spectra, heat of form., ab initio MRD-CI calcs. 79−49934
HNO_2, air pollution obs. in W.Europe 80−72106
HNO_2, and protonated forms, electrostatic pot. predictions, basis set depend. 78−74786
HNO_2, isomers, protonation mechanism, electrostatic pot. prediction limits 78−11506
HNO_2, trans and cis, ν_2 fundamental vibrational bands, intracavity CO laser Stark spectroscopy 80−47992
HNO_2+O_3, rate consts. determ. with diode laser 79−70310
HNO_2+O_3 reaction kinetics under stratospheric conditions 78−11499
$HNO_2+OH \rightarrow H_2O+NO_2$ react. kinetics, at high temps. behind shock waves 77−44477
HNO_3 and H_2O_2, photodissociation, solar radiation effects in atmosphere 79−58045
HNO_3, aq., effect on corrosion and electrochem. props. of Mo_2C 80−11813
HNO_3 aq. soln., chem. and electrolytic reaction with LaB_6 rods 79−87850
HNO_3, aq. soln., H bonds, IR spectra 78−94243
HNO_3, aq. soln., heat capacity at 298.15K 78−3364
HNO_3, atmospheric monitoring, chemiluminesc. method 79−16062
HNO_3, CC ^{15}N NMR chem. shift references evaluation 78−24835
HNO_3, centrifugal perturbation in microwave spectrum 77−57981
HNO_3 concentration in stratosphere, NO_2 simultaneous meas. *(French)* 78−16107
HNO_3 concentration in stratosphere, simultaneous inference using inversion algorithm 80−82000
HNO_3, corrosion of Ag-Au and Cu-Au 80−85091
HNO_3 cycle process for ocean thermal energy extraction 78−53660
HNO_3, diffusion coeff. in graphite 79−42310
HNO_3, high resolution spectral meas. of 11.3 μm band, using tunable diode lasers 78−33504
HNO_3, high resolution spectral meas. of 5.9 μm band using tunable diode laser 80−32707
HNO_3, high temp. corrosion of austenitic steels *(German)* 78−44253
HNO_3 IR spectra, 865.5-871.0 and 884.5-887.0 cm^{-1} regions, equiv. width meas., atm. spectrum appl. *(French)* 80−87114
HNO_3, IR spectra rel. to abundance in stratosphere 80−12464
HNO_3 in marine air of equatorial Pacific 80−85702
HNO_3 in rural air, meas. 79−79422
HNO_3, in stratosphere, obs. in N.hemisphere for three seasons 78−81288
HNO_3, in stratospheric in situ obs. 80−105077
HNO_3 intercalated with graphite, Raman scatt. in low stage cpds. 80−20638
HNO_3 intercalation of graphite, chemistry 79−43564
HNO_3 leaching of K_2O-PbO-SiO_2 glass powders, ion exchange during 79−100358
HNO_3, microwave spectra, centrifugal distortion effect 77−34621
HNO_3, ν_5 band rot. struct., anal., band centre and rot. consts. 79−10109
HNO_3, particulate nitrate and acidity measurement in ambient air, filter media 80−104541
HNO_3, source of artifact nitrate, formation on filter media, interference effects 79−83668
HNO_3, spectral linewidth, broadened in air, O_2 and N_2 at 200 and 300K 78−46399
HNO_3, VUV photodissoc., vibr. and rot. distribs. 80−87191
HNO_3, vapour, global tropospheric meas. 78−88904
HNO_3 vapour line parameters meas. by CO laser transmittance 79−26976
HNO_3, vibr.-rot. spectrum, 855-915 cm^{-1} *(French)* 78−50543
HNO_3/NO_2 conc. ratio in daytime stratosphere 78−73460
HNO_3-graphite intercalation cpd., proton relax. meas., two-dimens. system model 77−51968
HNO_3-graphite intercalation compounds, differential scanning calorimetry investigation 79−42234
HNO_3-graphite intercalation compounds, HNO_3 mol. orientation, model 80−24432
HNO_3-H_2O, liq. and glass, mol. assoc., ion pairs, Raman obs. 79−28749
HNO_3-HF mixtures, dissolution of $(Th,U)O_2$ reactor fuel, fuel reprocessing study 78−59951
HNO_3-HNO_2, aq. soln., N isotope exchange in presence of NO 80−16662
HNO_3-water, homogeneous nucleation, relative humidity depend. 78−71846
$HNO_3+NH_3 \rightleftharpoons NH_4NO_3$ equilib. in atmosphere 79−88389
HNO_3+NO, rate consts. determ. with diode laser 79−70310
$(HNO_3)_2$, gas phase, H-bonded complex struct. from elec. dipole moment obs. 78−74791

hydrogen compounds continued
HNO_x-H_2O-NO_x^- clusters, gas phase, thermodynamic quantities, mass spectra obs. 80−50875
H_2NO, hyperfine coupling const. calc., double perturb. theory and CI methods 79−59362
H_3NO^-, ab initio calcs., electron affinity, stability 77−42239
$HNO(A^1A'')$, state-selected fluoresc. lifetimes, collisional quenching rates 79−36674
HNOO, singlet and triplet diradicals, unrestricted 79−97975
$HNO_3.H_2O$, devitrification crystallisation, fast Raman and wide-line NMR obs. *(French)* 79−73915
$HNO_3.H_2O$ glassy form, stochastic rot. motions 79−7551
$HNO_3.H_2O$, wide line PMR spectra, oxonium ion motion *(French)* 79−56616
HNP-HPN, isomerisation energies, ab initio MRD-CI calcs. 80−106271
HNSO, centrifugal distortion anal. 79−59438
H_3NSO_3, sulphamic acid, deformation electron density, X-ray and neutron diffr. 77−19941
$HN(SO_2Cl)_2$, physical props. meas. 79−51293
HNSi, and HSiN, electronically excited states, MRD CI calc. 79−49947
HNSi, structures and microwave freqs. calcs. rel. to interstellar emission lines 78−36648
H_xNbS_2, struct., form. by cathodic reduction, neutron diffr. obs. 79−73150
H_2Ne, mol. interactions, differential scatt. cross-sections meas. 79−89732
HO, detection by laser excited fluoresc., press. depend. of fluoresc. and photolytic interferences 80−95666
HO fluorescence detection, interference suppression by sampling method 80−8431
HO radical form. from H_2+N_2O reaction on Pt surface, laser-induced fluoresc. obs. 80−108738
HO-H...OHX, X=H, CH_3, NH_2, OH, F, H-bonds, electron donor substituted, mol. orbital calc. 78−13422
$HO+HO_2 \rightarrow H_2O+O_2$, rate coeff. meas. by laser mag. reson., atm. chem. appl. 77−52614
HO+methane, H abstraction, rate consts. calcs. 78−95921
HO_2, analytical pot. functions, several surface minima 78−5158
HO_2 and HOCl, struct., vibr. freqs., IR intensities, ab initio calcs. 79−98007
HO_2 free radical, dipole moments and Stark effects from microwave spectra 80−63623
$HO_2 \rightarrow H^+ + O_2^-$ nanosec. pulse radiolysis, react. rate const. meas. 77−16843
HO_2, IR spectra, 1.43-1.51 μm emission bands 79−36635
HO_2, mol., spin-rot. Hamiltonian in reduced form 79−63976
HO_2, pot. energy surface for $H+O_2 \rightarrow HO_2^* \rightarrow OH+O$ reaction, MC SCF CI method 79−74353
HO_2 radical, atmospheric reactions studied by laser mag. reson. spectroscopy 80−12511
HO_2 radical, EPR spectrum, ground state parameters 78−90193
HO_2 radical, microwave spectrum 77−57983
HO_2 radical, near IR emission bands, vibr. and vibronic transitions 78−37633
HO_2 radical, ν_3 fundamental band, laser mag. reson. 78−66566
HO_2, struct. and props., SCF calcs. 80−106260
HO_2, vertical electronic spectrum, MRD-CI calcs. 78−37646
HO_2^+, ab initio calc. of three lowest states 78−62711
HO_2+Cl react. rate const. determ. at 298K *(French)* 78−64817
$HO_2+Cl_2^-$, reaction in pulse irrad. aq. soln. containing Fe^{2+} and Cl^- 78−20036
HO_2+ClO, free radical reaction rate consts. and products at 298K, discharge flow mass spectra 80−67391
HO_2+ClO, reaction product distrib. 80−72586
$HO_2+ClO \rightarrow HOCl+O_2$, reaction rate consts. 79−5140
HO_2+HO_2, gas phase reaction mechanism, FT IR spectrosc. obs. 80−85163
HO_2+HO_2, reaction rate, press. depend. 80−7766
$HO_2+HO \rightarrow H_2O+O_2$, rate coeff. meas. by laser mag. reson., atm. chem. appl. 77−52614
HO_2+NH_2, rate const., in NH_3+O_2, flash photolysis 79−47943
HO_2+NO, reaction kinetics meas. 78−31624
HO_2+NO, reaction kinetics, near IR chemiluminesc. determ. 80−21261
HO_2+NO reaction rate constant effects on O_3 perturbations, model of stratosphere 78−73474
HO_2+NO_2, reaction rate consts. by laser mag. reson. 78−27748
HO_2+NO_2, UV irradiated, kinetics and mechanism, peroxynitric acid form., smog 77−63885
HO_2+NO_2 form. and react. in aq. soln., pulse radiolysis 79−24805
$HO_2+NO \rightarrow OH+NO_2$, kinetics temp. depend. 80−3313
$HO_2+NO \rightarrow OH+NO_2$, rate constant determination in Arrhenius form 79−47904
HO_2+O_3, reaction kinetics, laser mag. reson. obs. 80−102528
$HO_2+O_3 \rightarrow OH+2O_2$, rate coeff., effects on stratospheric O_3 78−96275
$HO_2+OH \rightarrow H_2O+O_2$ gas flow reaction, upper bound and probable value of rate const. 79−24730
$HO_2+O \rightarrow HO+O_2$, rate coeff. meas. by laser mag. reson., atm. chem. appl. 77−52614
H_2O 1.35 cm absorption resonance, atmospheric radio emission features 80−46228
H_2O 22 GHz maser emission from W3(OH), 49N and 51, spatial distrib. 78−93355
H_2O absorption and coolest stellar component of E and S0 galaxies at 2 μ 78−41034
H_2O, bonding electron pairs, size and shape parameters, Gaussian basis set MO calcs. 80−27935
H_2O, complete quartic force field calc., algorithm 80−37736
H_2O emission detection in galaxy NGC 253 at 22.235 GHz 78−16534
H_2O, insolation absorption and thermal excitation of atmospheric tides 79−34890
H_2O interstellar masers, high vel. structures, origin *(Russian)* 79−25697
H_2O maser emission from NGC 4945 galaxy 79−40271
H_2O maser emission from late type stars, catalogue of objects 79−70965
H_2O maser emission from W51 Main 80−8701
H_2O maser sources in galactic plane, southern hemisphere survey 80−73054
H_2O masers, 22 GHz galactic plane survey, 14 new sources 80−77464
H_2O masers assoc. with late-type variable stars, structure 79−71037
H_2O masers near OB associations, 22 GHz obs. 79−25649
H_2O releases in ionosphere and artificially created holes 78−40752

hydrogen compounds continued
H_2O vertical distrib. in stratosphere, UV fluorescence meas. 79−34891
H_2O^-, electron affinity, mol. geom. effects calcs. 78−82618
H_2O^+, mobility in He, flow drift tube obs. 78−34257
H_2O^+, spin and rot. fine struct., orbital angular momentum 80−83247
H_2O^+, vibr. and rot. struct., intensity factors and orbital angular momentum 80−83246
H_2O^+, vibronic A^2A_1 states, lifetimes, delayed coincidence meas. 78−70874
H_2O^+, X^2B_1 and B^2B_2 states, pot. surfaces, SCF and CI calcs. 77−3338
H_2O:HF ice, pulsed NMR 77−28467
H_2O-(HF)(F_2) complexes, CNDO/2 calcs. for electronic struct. and props. 78−25442
H_2O-H_2S supersystem, ab initio LCAO MO SCF calcs. of H bonding 79−89607
H_2O-H_2SO_4, mixtures, transient nucleation, stochastic theory 77−1221
H_2O-H_2SO_4 system, nucleation, aerosol form. 77−70327
H_2O-HCl(HBr)(DBr) complexes, IR matrix isolation spectra, struct. 78−29781
(H_2O)-HF complexes, (x=1 or 2), geometry, CNDO/2 calc. 79−36531
H_2O-HF heterodimer, H bonding, microwave rot. spectrum, mol. geometry and moment 80−99501
$H_2O+Ar(^3P_{2,0})$ crossed mol. beams, ionisation and dissociative fluorescence, energy depend. 79−52669
$H_2O+He(2^3S)$, energy transfer processes, reaction products, UV and visible obs. in flowing afterglow 78−85138
H_2O^++diatomic (polyatomic) molecule, reaction, ICR obs. 79−8429
H_2O_2 80−34826
H_2O_2, ^{17}O pure NQR spectrum 80−9620
H_2O_2 aq. solns., struct. and dielec. props. 78−63659
H_2O_2, behaviour during RBMK reactors startup and shutdown, investigation 79−9822
H_2O_2 decomposition, IO_3^- catalysed, oscillatory Bray-Liebhafsky reaction 79−91931
H_2O_2, electronic states, optical rot. dispersion, oscill. strength calcs. 78−9095
H_2O_2, equilib. geometry, O-H bond length and angle 77−75326
H_2O_2, gas phase XPS, binding energy 77−34689
H_2O_2, geometry, internal rot. barriers, electron correl. calcs. 78−70751
H_2O_2, hindered rot. pot., strongly orthogonal geminal calcs. 77−71751
H_2O_2, hindered rot. pot. recreation, electron pair wavefunction transferability 77−71752
H_2O_2 in rural air, meas. 79−79422
H_2O_2 inactivated papain, optical density, amino acid composition and fluoresc. 78−53344
H_2O_2, internal rot., pot. energy calcs. 79−3521
H_2O_2, internal rotation barriers, exchange energy and orbital orthogonality effects 77−75049
H_2O_2, ionisation energy, LCAO Xα calcs. 77−50353
H_2O_2, lone pair orbital explicit representation, augmented contracted Gaussian basis set 78−25423
H_2O_2, r_0- and r_e-structs. 79−59594
H_2O_2, struct. and barrier to internal rot., HF and Rayleigh-Schrodinger perturbation calcs. 79−13636
H_2O_2, structural parameters of vibr. ground state 80−28116
H_2O_2, sum of states, isometric group, symmetry no., thermodynamic functions 80−58186
H_2O_2, twisted mol., optical rot. strength calcs. 80−95793
H_2O_2, UV absorpt. cross sections 78−42086
H_2O_2, UV prod. of OH radicals, reactions with peptides in aq. soln., EPR 78−68993
H_2O_2, vapour, atmospheric, UV absorpt. cross sections, photodissoc. rate 78−32222
H_2O_2, Zeeman effect and mol. quadrupole moment, beam maser spectrosc. 78−90152
H_2O_2-H_2O, isolation of singular component for heat capacities of supercooled H_2O 80−107437
H_2O_2+acid amide, aq. solns., photolysis, EPR study of spin-trapped radicals 78−68996
H_2O_2+Br, rate constant upper limit 80−30216
H_2O_2+catalase ($[Fe^{3+}(EDTA)]_2$), effect of mag. field on decomposition rate 79−52631
$H_2O_2+Cl(^2P_{3/2})$, reaction kinetics, temp. depend., reson. fluoresc. obs. 77−4903
$H_2O_2+HO_2(O_2^-)$ Haber-Weiss reaction kinetics, chain mechanism 79−83444
H_2O_2+halide coated surface, halide dioxide radical form., EPR obs. 80−7851
H_2O_2+OH, reaction rate const., 298K, flash photolysis-reson. fluoresc. obs. 79−57215
H_2O_3, struct., barrier to int. rot., HF and RS-MP perturb. calcs. 79−13637
H_3O radical, stability, ab initio UHF-CI calcs. 78−5137
H_3O^+ (D_3O^+), plasma dissociative ion electron recomb., rate coeffs. 80−63747
H_3O^+ meas. and water vapour concs. above mesopause 77−73898
H_3O^++2HF, interaction pot., monopole approx., supermol. SCF and perturbation schemes 77−27139
H_3O^++e, dissociative recomb. reaction in interstellar clouds, products, statistical theory 78−57604
H_3O^++$H_2O(H_2S)$(HCN)(formaldehyde), proton transfer, rate and equilib. consts. 78−48636
$H_3O_2^-$, in HCl and KOH aq. solns., vibr. freq. assignments 79−73916
H_4O_2, intermolecular interaction energy, PCILO calc. 77−34572
$H_5O_2^+$, aq. soln., IR continua with polarisable H-bonds 79−26979
$H_3O_{2,2}^-$, in HCl and KOH aq. solns., vibr. freq. assignments 79−73916
$H_6O_4^{2-}$, cluster anion tetrahedral struct. and stability, polarisation model 80−53181
HOB,(HBO), spectroscopic properties, PNO-CI and CEPA calcs. 78−41961
HOB, electronic struct., one-electron props. 80−42935
HOBr, analytical pot. energy functions and surfaces 79−68203
HOCN and isomers, interconversion pot. energy surfaces, geometries, electronic structs. 78−35660
HOCN, geometry, spectra, rot. and force consts., ab initio calcs. 77−34574
HOCN, vertical ionisation pot., Koopmans' theorem, perturbation connections calcs. 80−42966
HOCl, ab initio MRD CI calc., electronic spectrum, dissoc., heat of reaction, formation 78−21857

hydrogen compounds continued
HOCl, ab initio vertical ionis. pot., corrections to Koopmans' theorem 78−25749
HOCl abundance in stratosphere 79−84427
HOCl, analytical pot. energy functions and surfaces 79−68203
HOCl, chloramine, isoelectronic mols., vap. phase UV photoelectron spectra, struct. 78−66600
HOCl, form in Cl_2O+H_2O equilib., UV spectrum 79−79238
HOCl, HOOCl, stratospheric chem., formation and loss reactions 78−16138
HOCl, ν_1 band IR spectrum, rot. anal. 79−98095
HOCl, photodissoc., ab intio SCF CI calcs. 78−50604
HOCl, photodissoc. cross-sections rel. to prospects as atmospheric Cl reservoir 79−12207
HOCl, photodissoc. rot. distrib. 80−95694
HOCl, photolysis product of Cl_2-O_3-H_2 dil. mixtures, absolute integrated IR band intensities 80−26033
HOCl, UV spectrum, stratospheric lifetime rel. to photodissoc. 79−36661
HOCl, vibr. freqs. from anharmonic ab initio/empirical PE functions 79−76406
$2HOCl=H_2O+Cl_2O$, equilib. const., Fourier transform IR determ. 80−7765
$H_2O_2(D_2O_2)$, vibr. consts rot. struct. doubling, Raman spectra assignment 77−54563
HOF, analytical pot. energy functions and surfaces 79−68203
HOF, ground state pot. calc. using orthogonal internal coords. definition 79−76479
HOF, nucl. mag. shielding and susceptibility, SCF calcs. 77−14351
HOF, vibr. freqs. from anharmonic ab initio/empirical PE functions 79−76406
$H_3O^+(H_2O)_{0,1,2}+D_2O$ reactions, SIFT studies, review 80−58435
$H_3O^+(H_2O)_n+D_2O(NH_3)$, binary reactions, rate coeffs. and product ion distributions determ. 80−81305
$(H_3O)^+(HSeO_4)^-$, X-ray struct. anal., Patterson technique 80−1975
HOI, analytical pot. energy functions and surfaces 79−68203
HOI, $O_3(\dot{O})+HI$ matrix reaction, IR spectra, isotope shifts and band assignments 78−80737
HONC and isomers, interconversion pot. energy surfaces, geometries, electronic structs. 78−35660
HONC, geometry, spectra, rot. and force consts., ab initio calcs. 77−34574
HONO (nitrous acid), obs. in urban atmosphere by differential optical absorpt. 80−76677
$HONO+NO+NO_2+CO+$air, UV irradiated, computer simulation, peroxynitric acid form., smog 77−63885
$HO+NO$ reaction, laser-induced fluoresc. of NO_2, quenching rate consts. and lifetimes 80−11930
HO_2NO, UV absorpt., spectra, photodissoc. lifetime meas. 80−83386
HO_2NO, unimol. dissoc., rate consts., temp. depend., atmospheric implications 78−7175
HO_2NO_2, chemistry and abundance in stratosphere 78−20467
HO_2NO_2, form. by reaction of HO_2+NO_2, pulse radiolysis 79−24805
HO_2NO_2, gas phase, UV and IR absorpt. cross sections 79−13733
HO_2NO_2 significance in atmospheric NO_x chemistry 78−11971
HO_2NO_2, thermal decay kinetics 79−5135
HO_2NO_2, unimol. decomp., press. and temp. depend. 78−68887
$HO_2NO_2+N_2 \rightleftarrows HO_2+NO_2+N_2$ react., kinetics, RRKM theory appl. 78−73032
HOO radical, lowest doublet electronic states, rel. to photodissoc. 79−93914
$HOO(H_2O)$, electronic struct., and config., semiempirical UHF INDOC calc. 79−59356
$HOONO_2$, FT IR spectral obs. of $HOO+NO_2 \rightarrow HOONO_2$ 77−28993
$(H_5O_2^+)_3(PW_{12}O_{40}^{3-})$, struct. of Keggin's 'pentahydrate' from X-ray and neutron diffr. data 77−47382
$(H_5O_2^+)_3(PW_{12}O_{40}^{3-})$, struct., X-ray and neutron diffr. study 79−42037
HOS-HSO, isomerisation energies, ab initio MRD-CI calcs. 80−106271
$H_2O.HF$, H-bonding and indirect exchange ('superexchange') in 79−93912
$H_2O.H_2S$, IR spectra of complex in solid nitrogen, 20K 79−10102
β-$H_2O.11Al_2O_3$, conversion from β-$Na_2O.11Al_2O_3$ and characterization 78−3069
H_2O...HF complex, force field, vibr. freqs., equilib. geometry bond energy, ab initio calc. 77−65450
$H_3O^+.nH_2O$ cluster ions, stability, assoc. and dissoc. 77−60055
$H_2Os_3(CO)_{10}$, and $H_4Os_4(CO)_{12}$, polycryst., PMR chem. shift 79−95655
$H_3(PMo_{12}O_{40})$, decomp., in aq. soln., Raman spectra obs. 79−13719
HPN-HNP, isomerisation energies, ab initio MRD-CI calcs. 80−106271
H_2PNH_2, inversion-rot. mechanism, basis set and geometry optimisation effects 80−83273
HPO, emission system, rot. anal. of vibr. bands 80−47957
HPO, in Ar matrix, IR and UV absorpt. spectra 80−47985
HPO, mol. struct. and props., ab initio, calc., Gaussian lobe orbital 78−62713
HPO, vibrational freqs., by rot. anal. of spectra 79−54831
HPO_3^{2-}, in NaH_2PO_2-Na_2HPO_3, quantitative anal. by relative Raman intensities obs. *(Japanese)* 78−23991
HPO_4^{--}, in γ-irrad. $K(H_{1-x}D_x)_2PO_4$, 77K, optical and EPR obs., form. mechanism 78−68379
$H^{32}PO_4^{2-}$, transport into rabbit erythrocyte, high press. effect 77−12900
$H_2PO_2^-$, in NaH_2PO_2-Na_2HPO_3, quantitative anal. by relative Raman intensities obs. *(Japanese)* 78−23991
H_2PO_4, in γ-irrad. $K(H_{1-x}D_x)_2PO_4$, 77K, optical and EPR obs., form mechanism 78−68379
H_3PO_2, H_3PO_3, H_3PO_4, polarisable acid-acid and acid-water hydrogen bonds 79−76423
H_3PO_4, aq. soln., elec. cond. and Raman spectra at high-press., 25°C 79−56220
H_3PO_4, aq. soln., laser Raman spectra, 0.005-15.6 M 78−46348
H_3PO_4, broad-band picosecond light generation by mode-locked ruby laser 79−31989
H_3PO_4, determ. by flame spectroscopy, absorpt. and emission, analogue data processing system 77−36804
H_3PO_4, effect on positve electrode in Pb-acid battery 79−92071
H_3PO_4, etchant for dislocation etch pit production on (001) InP, (GaIn)P, GaP and Ga(AsP) 80−15103
H_3PO_4 fuel cells, technology development for commercial systems, review 80−30464
hydrogen compounds continued
H_3PO_4 reaction with Ga_2O_3 and H_3PO_4, $KGaHP_3O_{10}$, $KGa(PO_3)_4$ and $Ga(PO_3)_3$ crystn. 79−52642
H_3PO_4, solubility of Ga_2O_3, $GaH_2P_3O_{10}$ and $Ga(PO_3)_3$ crystn. 79−52641
H_3PO_4, welding of MgO single crystals, to form bicrystals 78−56796
H_3PO_4, wet process, influence of high-intensity US 79−15993
H_3PO_4-H_2O, superviscous and glass, relax., ^{111}Cd TDPAC obs. 80−15831
H_3PO_4+Ga, interaction in aq. soln., ^{71}Ga and ^{31}P NMR obs. 79−22729
$HPO_4^-(H_2PO_4)$ radicals + organic compounds, reaction rate consts. 78−15669
$H_3PO_4(MoO_3)_{12}.29H_2O$, electrochromic solid-state cells 80−2724
$H_3PO_4(WO_3)_{12}$ electrochemichromic cells 79−15436
$(H_3PO_4)(WO_3)_{12}29H_2O$, electrochromic solid-state cells 80−2724
$H_3PW_{12}O_{40}.21H_2O$, cryst. struct., neutron diffr. 78−42977
$H_2PtCl_6.2H_2O$, wide line PMR spectra, oxonium ion motion *(French)* 79−56616
$H_2Pt(OH)_6$, platinic acid, X-ray cryst. struct. determ. 80−28967
H_xReO_3, formed by H_2 absorpt. in ReO_3, electron diffr. obs. 79−60513
$H_4Ru_4(CO)_{12}$, polycryst., PMR chem. shift 79−95655
HS^-, in KBr, anharmonic interaction of impurity intramol. vibrs. with cryst. phonons 77−77217
HS_2, ground and first excited states, geometry, ab initio SCF calcs. 78−50657
HS_2 radical, ab initio calcs. of geometry and spectra 77−34552
HS_2, rotamers, electronic and geometrical structs., ab initio floating GO basis calcs. 78−74572
HS_n^-, n=1-4, electronic struct., ab initio Hartree-Fock-Slater calcs. 80−74107
HS_n^{2-}, n=1-4, electronic struct., ab initio Hartree-Fock-Slater calcs. 80−74107
H_2S 80−56899
H_2S absorpt. on zeolites with varied Si/Al ratios 78−60029
H_2S, adsorbed on Ru (110), UPS and work function change meas. 79−78834
H_2S, adsorbed on Ru(110), evidence for SH species, UPS and work function meas. 79−99424
H_2S, adsorpt. on ice surface, gas capture by crystallising aq. aerosols investig. 79−39191
H_2S, adsorpt. on Ti(Ta)(Nb) evaporated films, 195 to 473K 79−33197
H_2S, adsorption and dissoc. on Ru (001) 79−79292
H_2S, adsorption on GaAs (110), surface photovolt. spectroscopy 80−49499
H_2S, adsorption on Ni (100) surface, ang. distrib. of S Auger emission 77−32475
H_2S, adsorption on Pt (100), intermolecular forces and kinetics of adsorption 78−75930
H_2S, adsorption on Rh(100), (2×2) surface struct., LEED anal. 79−99426
H_2S, adsorption on Ru (001), LEED, UPS, AES, and thermal desorption meas. 79−99420
H_2S, adsorption on Si (111), electron energy loss spectra exam. 77−39736
H_2S aerosol, possible presence in Uranus clouds 80−31253
H_2S, air pollutant, conc. in remote continental and oceanic areas 79−20983
H_2S, air pollution, new anal. method for remote areas 79−21028
H_2S, and D_2S, inertia defects and dipole moments by kinetic consts. method 80−928
H_2S, aq., Fe corrosion, FeS polymorph form. 80−81231
H_2S atmospheres, formation of contaminating layers on elec. contact materials *(German)* 80−71811
H_2S, atmospheric, determ. using automatic odour analyser *(Japanese)* 80−50924
H_2S, Balmer radiation production by electron impact 0-2000 eV 79−76521
H_2S, bond bending, bond orbitals rel. to nucl. motion 80−95513
H_2S bubbles, coalescence time in water 77−42899
H_2S, centrifugal distortion 77−57974
H_2S, coadsorption with CO on Ni (110), (100) and (111), surface coverage meas. by SIMS 79−90876
H_2S, complete quartic force field calc., algorithm complete quartic force field calc., algorithm 80−37736
H_2S contrib. to atmospheric S cycle 78−73473
H_2S dipole moments, submillimetric Stark cell meas. 77−38694
H_2S, dissociation in seawater 78−3816
H_2S, dissociative chemisorption on H_2S and growth of MoS_2 film 77−1329
H_2S, dissociative electron attachment, H^- energy and ang. distrib. 79−31710
H_2S, distant source sensing by statistical treatment of air quality data 77−70808
H_2S, double hole states POCI calc., Auger spectrum 78−78630
H_2S, effect on IR spectrum of CO adsorbed on Al_2O_3-Ni catalyst in H_2-He 78−71945
H_2S effect on methyl Hg in River Mersey estuary sediments 79−2295
H_2S effect on molten carbonate fuel cell performance, mixed pot. anal. 80−81431
H_2S, electron binding energies, one-centre expansion method 77−6677
H_2S, electron density, basis set, electron correl. effects 78−74581
H_2S, electron impact, vibr. elastic scatt. and vibr. excitation 79−13822
H_2S, electron pair interactions calcs. 80−23298
H_2S, electronic struct., ab initio CI SCF calc., spectra assignments 77−10586
H_2S, emission from open oceans 79−70805
H_2S, energy levels and mol. vibr., internal coord. model 79−799
H_2S, excitation energy, one-centre approx. calcs 78−70737
H_2S frost, near IR reflectance spectra, tetragonal to cubic phase transition 77−81094
H_2S, gas-phase, states in valence photoelectron spectrum 78−94284
H_2S, gaseous 1s binding energy and S $KL_2L_3(^1D_2)$Auger energy, XPS obs. 77−3416
H_2S, gaseous impurity, role in H_2 embrittlement of steel 77−59904
H_2S, geometry optimisation, ab initio MO calcs. 77−42232
H_2S, ground and excited states, SCF and CI calcs. 77−414
H_2S, hydrogen embrittlement of Hastelloy C-276 and C-4, Inconel 625 and MP35N 78−31502
H_2S in air, preconc., determ. by flame photometric detection 78−92535
H_2S in N. eqatorial Atlantic Ocean atmosphere rel. to global S cycle 79−12165

hydrogen compounds continued
H_2S, inner valence electron ionisation calcs., photoelectron spectra obs. 78−82619
H_2S, interaction with Si (111) 7×7 surface, LEED and AES 78−38966
H_2S, ionis, pot., many-body Green's function method 77−67965
H_2S, ionisation energies, self-consistent-charge Hartree-Fock-Slater calcs. 77−6687
H_2S, KLL Auger spectra of S, ab initio LCAO SCF calcs. 77−65515
H_2S, KLL Auger spectrum, obs. and ab initio SCF CI calc. 78−50654
H_2S, $L(S_2)$-MM Auger energies, MC SCF calcs. 78−21977
H_2S, large-scale spatial and temporal distrib. of air pollutant 79−20981
H_2S, liq., optical absorption transients produced by ns pulse radiolysis 79−11803
H_2S, marine pollution in Kuwait 79−5510
H_2S, microwave absorpt. coeff. 77−64378
H_2S, mol., XPS and KLL Auger effect, line shifts 79−31602
H_2S, mol. polarisability and derivatives, ab initio SCF CI calc. 79−59597
H_2S, monitoring by Pd gate MOSFET 78−44645
H_2S, nonlinear optical polarisability meas. 79−54991
H_2S, nucl. spin-spin coupling consts., ab initio calcs. 80−95647
H_2S oxidation by active C, electrochem. model *(German)* 78−35717
H_2S, oxidation in nonurban troposphere 78−32183
H_2S, Penning ionisation and photoelectron spectra 77−83653
H_2S, photoionis., vibr.-excited ions form. in Franck-Condon gaps, threshold photoelectron spectra obs. 79−68262
H_2S, photoionisation cross sections and asymmetry parameters, SCF Xα scatt. wave calcs. 80−63542
H_2S, phys. props., rel. to Girdler-sulphide process for heavy water production 78−25300
H_2S pollutant in troposphere, photochemical sources 80−90112
H_2S, powder, PMR chem. shift anisotropy, nucl. mag. screening tensor 78−17687
H_2S, proton affinity, ab initio HF calcs. 79−31371
H_2S, proton spin-lattice relax. time near liq.-vapour critical point 79−73842
H_2S, pseudopotential calculations, parameter fitting scheme appls. 78−41928
H_2S, pure, use as counting gas in internal-gas radioactivity-counting 78−854
H_2S, reaction with alkaline minerals in coal, pulsed differential reactors appl. 79−20465
H_2S role in tropospheric S cycle 78−49123
H_2S, rot. transitions, press. broadening, microwave spectra 77−50429
H_2S, SCF energy optimisation with regard to Slater's exponents *(French)* 79−49936
H_2S, SS 80−78620
H_2S, second order mag. props., coupled Hartree-Fock perturbation theory 80−87042
H_2S, semi-empirical INDO calc. of electronic struct. 80−32611
H_2S, separated product rules for high and low vibr. freqs. in isotopic mols. 77−34611
H_2S, sextic centrifugal distortion consts., Watson Hamiltonian, perturbation method 77−10785
H_2S, slow electron scatt., rigid mol. model with exchange and polarisation 80−43194
H_2S, solid, low-temp. phase, IR, far IR and Raman spectra 78−27218
H_2S, solubility in water, 10 to 180°C 78−18776
H_2S, stress corrosion cracking of Ni-Cr-Mo-V alloy steel, exam. of overload effects 78−60886
H_2S, sulphiding with metallic Mo and Re 78−3078
H_2S, VB minimal Slater basis set calcs., comparison with H_2O, MO calcs. 79−36536
H_2S, VUV absorption spectrum, Rydberg series assignments 79−64016
H_2S, valence and Rydberg excited states, SCF-Xα-SW mol. oribtal study 79−36550
H_2S, valence electron ionisation and momentum distribs. 80−28107
H_2S, valence momentum distribs., binding energies, binary (e,2e) spectrosc. meas. 79−31713
H_2S, valence shell binding energy spectrum, 8-34 eV, electron scatt. simulation of photoionis. 79−10213
H_2S, valence shell electron pair interactions, VSEPR theory test 79−31393
H_2S, vertical valence ionis. pot., many-body Green's functions 78−22051
H_2S zone in Black Sea, boundary determ. rel. to water mass dynamics *(Russian)* 80−12435
H_2S^+, reaction rate consts., product distrib., ICR obs. 79−8428
H_2S-Ar plasma, spectroscopic study, electron density, ionis. temp. meas. 77−19764
H_2S-H_2O complexes, equilib. config., H-bond energies and electron densities, CNDO/2 method 80−14084
H_2S-hydrocarbon mixtures, phase equilib. calcs., modified Soave eqn. of state 79−19353
H_2S-methane mixture, densities calc., van der Waals model 78−79740
H_2S+Ar^+, emission spectra obs. 78−50622
$H_2S+CH_3^+$, condensation reactions mechanism 80−25996
$H_2S+CH_n^+$, (n=Q-4), reactions at 300K 78−44357
H_2S+Cl_2, laser-initiated chain reactions, rates, mechanisms, chemiluminesc. obs. 80−55651
H_2S+Cl^+, reactions at room temp. 80−93749
$H_2S+Cl \rightarrow HCl+HS$, laser-initiated chain reactions, rate consts., product energy distrib. 78−85144
H_2S+D_2 homogeneous exchange reacts., kinetics 77−48633
$H_2S+H_2S(N_2)(O_2)$, press. broadening of spectral linewidth, calcs. 77−30932
$H_2S+H_3O^+(H_2S^+)(HCNH^+)(HCHO.H^+)$, proton transfer, rate and equilib. consts. 78−48636
H_2S+hydrocarbon mixtures, vapour-liq. equilibrium, crit. locus curve, Soave eqn. 78−83913
H_2S+I^-, endoergic reaction, time-of-flight mass spectral obs. 77−12786
H_2S+K, collisional ionisation, positive and negative ion energy spectra obs. 80−63775
$H_2S+N_2^*$, deactivation, from laser-induced CO_2 fluoresc. obs. 80−63776
H_2S+NO_2, SO chemiluminesc. in Ar matrix 79−5146
H_2S+Ne(He), Penning ionis. electron spectroscopy, energy peak shifts and shapes 77−42392
H_2S+O, ^3P-state, absolute reaction rate, flash photolysis reson. fluoresc. obs. 79−66283
$H_2S+O_2(^3P)$, reaction rate, flash photolysis-reson. fluoresc. obs. 77−4918
hydrogen compounds continued
$H_2S+O^+(Cl^+)$, S highly stripped core ion outer shell rearrangement, Kα X-ray spectra 77−3451
H_2S+O^*, chemiluminesc. matrix reaction, diffusion controlled, 8-20K, $O(^3P)$ 78−61013
H_2S^++Kr, collision-induced dissociation,mass spectra *(Russian)* 77−88549
H_2S_2, electronic struct. and stability of isomers, gaussian SCF MO calc. 79−93921
$(H_2S)_2$, hydrogen bond, proton transfer, pot. energy surface 77−67977
H_2S_2, rot. barriers, internal rot. and electronic struct., valence electron study 80−83344
H_2S_n, n=1-4, electronic struct., ab initio Hartree-Fock-Slater calcs. 80−74107
H_3S^++$H_2O(H_2S)$(HCN)(formaldehyde), proton transfer, rate and equilib. consts. 78−48636
H_3S^++HCN⇌H_2CN^++H_2S, equilib., rate coeffs. and proton affinity, flowing afterglow 78−56885
$H_2S(D_2S)$ photodissoc., SH internal energy distribution 80−95697
HSO, ground and first excited states, geometry, ab initio SCF calcs. 78−50657
HSO radical, Doppler-limited dye laser excitation spectroscopy, rot., distortion and spin-rot. interaction const. determ. 80−83383
HSO, radical, electronic spectrum and struct. 77−75147
HSO radical, ground and excited first states, ab initio SCF and CI calcs. 77−30776
HSO, thermochem. props. 79−5173
HSO-HOS, isomerisation energies, ab initio MRD-CI calcs. 80−106271
HSO_3^-, aerosols form. from SO_2 oxidation by O_3 in cloud droplets 78−44894
H_2SO hypothetical molecule, nonempirical STO calc. of chem. bonds 80−23307
H_2SO_2, S K-LL Auger energies and chemical shifts 80−28069
H_2SO_4 aerosol, filter sampling of air, possible artifacts 80−82079
H_2SO_4, aerosol, form. by flash photolysis of SO_2-gas mixtures 79−66307
H_2SO_4 aerosol growth, kinetic model 77−37340
H_2SO_4 aerosol in coastal atm., form. of particulates 80−90113
H_2SO_4 aerosol medium of Venus clouds, IR optical props. 78−65526
H_2SO_4, aerosol particles props. in subsiding air over Japan 79−20986
H_2SO_4 aerosol particle size measured by impaction method 80−31134
H_2SO_4 aerosols, heterogeneous atmospheric reactions and role as tropospheric sinks 80−72612
H_2SO_4, aerosols characts. in Venus atm. from isophotes, spacecraft obs. 78−81575
H_2SO_4, aerosols form., expt. and theory 78−96256
H_2SO_4, Ag graining, comparison with colour image *(German)* 79−29380
H_2SO_4, air pollutant measurement techniques 80−104542
H_2SO_4, air pollution, new detector, aerosol mobility chromatograph 78−96297
H_2SO_4, air pollution determ. in Netherlands, 1971-76 period 79−21031
H_2SO_4, air pollution emission from chem. plant, precision estimates 79−83682
H_2SO_4 and $(NH_4)_2S_2O_7$ etchant, for NbC, TaC and HfC 80−85097
H_2SO_4 and $SO_3.H_2O$, CNDO/2 calc. of thermal stability 78−76840
H_2SO_4, anhydrous, cryst. struct. refinement 80−19770
H_2SO_4, aq., effect on corrosion and electrochem. props. of Mo_2C 80−11813
H_2SO_4, atm., rel. to ultrafine particle form. and ion mobility 77−25742
H_2SO_4, atm. aerosol, extinction, absorpt., backscattering and mass content relations 80−101403
H_2SO_4 atmosphere-aerosol study of Venus cloud microstructure and optical props. 80−72808
H_2SO_4, conc., diffusion of poly-p-phenyleneterephthalamide *(Russian)* 79−65232
H_2SO_4 decomposition, corrosion tests on possible containment materials 80−45448
H_2SO_4, dissociation and absorpt. consts., ultrahigh resolution obs. of 8.2, 11.3 μm bands 78−70825
H_2SO_4 droplets in CO_2 atm. of Venus, evidence from 17-38 μm emission spectrum 78−40855
H_2SO_4 effect in KBr pellet spectroscopy 79−88034
H_2SO_4, elec. resist. changes of pyrographite during electrochem. insertion *(French)* 80−2437
H_2SO_4 etchant, for revealing struct. inhomogeneities in martensite-ageing steel 80−61035
H_2SO_4 formation in urban atmosphere, flame photometric obs. *(French)* 77−41136
H_2SO_4, frozen soln., EPR of trapped H-atoms produced by UV and X-irrad. 80−3369
H_2SO_4, gaseous, IR absorpt. coeffs., partial press. variations 78−56922
H_2SO_4 glass, γ-irrad., trapped H ESR, vol. relax. effects 79−52703
H_2SO_4, glass, trapped H spin-lattice relax., modulation, saturation ESR 77−9095
H_2SO_4, in automobiles exhaust emissions, particulate anal. technique 77−60173
H_2SO_4 in S hemisphere stratospheric aerosol, impactor and in situ single-particle meas. 78−73437
H_2SO_4, interaction with Cl and Cl_2, surface reactions at low temps. 79−79288
H_2SO_4, meas. in particulate matter from coal and oil combustion 79−74569
H_2SO_4 mist monitor, semicontinuous 80−61495
H_2SO_4, partial vapour press. meas. with tunable diode laser *(German)* 80−43361
H_2SO_4, Pb-acid negative battery plate, form., physicochem. processes 77−4907
H_2SO_4 polydisperse aerosol number and mass conc. meas. by elect. aerosol anal. 80−108753
H_2SO_4, pure, IR and Raman spectra in liq. state, assignments and cryst. spectra comparison *(French)* 79−33699
H_2SO_4, S K-LL Auger energies and chemical shifts 80−28069
H_2SO_4 secondary aerosol form. in urban atmosphere 77−33137
H_2SO_4, secondary particles form. and growth, kinetic aerosol model 79−29492
H_2SO_4, separation processes simulation in H_2SO_4-Br cycle 79−74413
H_2SO_4 soln., opt. consts. in far IR 77−8574
H_2SO_4, solns., static permittivity, kinetic depolarisation, time-domain spectroscopy 78−68440
H_2SO_4, vap. IR absorption coeff., 1190-1260 cm^{-1} 77−68036

hydrogen compounds continued
H_2SO_4, vapour, foreign gas broadening diode laser spectroscopy in IR 78−36261
H_2SO_4 vapour pressure rel. to gas-particle conversion 80−94560
H_2SO_4:Fe^{2+}, frozen aq. soln., photolysis, H form., distrib. and diffusion 78−20044
H_2SO_4:Fe^{2+}, frozen soln., photo- and radiation-produced H-atoms obs. 79−39162
H_2SO_4/H_2O aerosol formation, growth simulation using general dynamic eqn. 79−47990
H_2SO_4-H_2O, aerosol form., nucleation calcs. 78−31709
H_2SO_4-H_2O, vapour mixture, temp. depend. of nucleation, aerosol form. 77−86350
H_2SO_4-H_2O aerosols nucleation rate in presence of ionisation source 80−104464
H_2SO_4-H_2O chemical heat pump energy storage system 80−30515
H_2SO_4-H_2O solution aerosol particles nucleation in stratosphere 77−56678
H_2SO_4-H_2O solution of polyphenylene terephthalamide, phase equilib. 79−73314
H_2SO_4-H_2O_2 cleaning soln. for Si wafers, thermal characts. 80−3225
H_2SO_4-H_2O-ion aerosol particles, ultrafine, stratospheric form., ion-induced nucleation 80−72608
H_2SO_4-$KBrO_3$-KBr-Mn^{2+} system, chem. automat with three steady states 80−7769
H_2SO_4-Mn^{2+}-$KBrO_3$-oxalacetic acid, chaos type reactions anal. 80−85165
H_2SO_4-poly-1,4-phenylene terephthalamide, dilute soln., viscosity 78−75524
H_2SO_4-water, homogeneous nucleation, relative humidity depend. 78−71846
H_2SO_4+gallic acid+BrO_3^- system, uncatalysed oscillatory chemical reactions 78−61004
H_2SO_4+$K_2Cr_2O_7$, in spectrophotometric determ. of reducing agents 79−39234
H_2SO_2, S K-LL Auger energies and chemical shifts 80−28069
HSO_3F, IR and Raman spectra, mol. struct. *(French)* 80−989
HSO_3F-graphite, intercalation compound, Raman spectral study *(French)* 80−60581
HSO_3F-graphite insertion compounds *(French)* 79−52635
$H_2SO_4.H_2O$, wide line PMR spectra, oxonium ion motion *(French)* 79−56616
HSS, struct. and props., SCF calcs. 80−106260
$H_3S^+.H_2O$ cluster ions, stability, assoc. and dissoc. 77−60055
$H_3S^+.nH_2S$ cluster ions, stability, assoc. and dissoc. 77−60055
$HSbCl_6.3H_2O$, cryst. struct., cation $H_{14}O_6^{2+}$ *(German)* 80−107133
H_2Se, and D_2Se, inertia defects and dipole moments by kinetic consts. method 80−928
H_2Se, complete quartic force field calc., algorithm 80−37736
H_2Se decomposition 673 to 748K, appl. to thermochem. H prod. using ZnSe cycle 80−35782
H_2Se, UV absorpt. spectra, 148.3 nm band, rot. contour anal. 77−75179
H_2Se_2, rot. barriers, internal rot. and electronic struct., valence electron study 80−83344
H_2SeO_3, $^1H/^2H$ quadrupole reson. freqs. detected by double reson. with level crossing 78−84497
H_2SeO_3, ^{77}Se Fourier transform NMR 78−95528
H_2SeO_3, and deuterated analog, vibr. spectra 79−24311
H_2SeO_3, cryst., vibr. spectra in O-H stretching region 79−51949
H_2SeO_3, IR overtone spectra and temp. depend. 79−47456
H_2SeO_3, reduction, reaction sequence and CdSe film deposition 80−71603
H_2SeO_4, NMR of ^{77}Se, chemical shift and screening tensors *(Russian)* 78−64285
$H_2SeO_4.H_2O$, wide line PMR spectra, oxonium ion motion *(French)* 79−56616
$HSiBr$, $^1A''$ states, geometry, bending pot. and vibr. freqs. 79−59593
HSiC-HCSi, isomerisation energies, ab initio MRD-CI calcs. 80−106271
$HSiCl$, $^1A''$ states, geometry, bending pot. and vibr. freqs. 79−59593
$HSiCl_3$, Raman and IR spectra, mol. motion 78−64353
H_3SiCl, mol., valence and core ionis. energy, RHF-SCF and PNO-CEPA calc. 79−85890
$H_4(SiMo_{12}O_{40})$, decomp., in aq. soln., Raman spectra obs. 79−13719
HSiN and HNSi, analytic functions from pot. energy surfaces 78−62743
HSiN, structures and microwave freqs. calcs. rel. to interstellar emission lines 78−36648
HSiN-HNSi isomers, MRD-CI calcs. of struct. and stability 78−82635
H_3SiNCO, low freq. bending mode, pot. function 78−82728
H_3SiNCS, far IR and Raman spectra, vibr. mode and quasilinear config. 78−62940
$HSiO^+$, $HOSi^+$, quantum mechanical study 78−37541
H_2SiO, electronic struct., dipole moments, mol. polarisability, force fields, ab initio calcs. 80−78531
HTO, rain scavenging 79−16563
$HTaWO_6$, and $HTaWO_6.H_2O$ defect pyrochlores, NMR study of proton motion 79−82889
H_2Te, mol., submm. rot. microwave spectrum 79−59443
H_2Te, solid, and photodissociated H_2Te in solid Ar, Mossbauer expts. 77−20769
H_2Te_2, rot. barriers, internal rot. and electronic struct., valence electron study 80−83344
$HUO_2AsO_4.4H_2O$ and $HUO_2PO_4.4H_2O$ layered cpds., struct. investigs. below antiferroelec. transition temps., H bond ordered structs. 80−107416
$HUO_2AsO_4.4H_2O$ and $HUO_2PO_4.4H_2O$ layered cpds., single and polycryst., proton cond. behaviour w.r.t. antiferroelec. transition temps. 80−107481
$H_{5n-2}UO_2(IO_6)_n.4H_2O$, n=0.5 to 2.0, high proton cond. 80−107562
$H(UO_2P(As)O_4)4H_2O$, H motion, PMR obs. 78−80239
$H(UO_2PO_4)4H_2O$, solid, fast hydrogen ion diffusion, NMR relax. time meas. 80−2205
$HUO_2PO_4.4H_2O$, rapid H^+ cond. 77−76602
$HUO_2PO_4.4H_2O$, H^+ ion cond., struct. mechanism, X-ray diffr. obs. 78−34651
$HUO_2PO_4.4H_2O$, H^+ ion solid electrolyte, cryst. struct. 79−14759
$HUO_2PO_4.4H_2O$ proton conductor applications 79−29466
$HUO_2PO_4.4H_2O$, high proton cond. 79−77809
$HUO_2PO_4.4H_2O$, film fabrication and appl. as solid electrolyte in electrochromic displays 80−70462
hydrogen compounds continued
$HUO_2PO_4.4H_2O$ solid proton conductor, appl. as electrochromic cell 80−89497
$H_{0.4}WO_3$, inelastic neutron spectra 77−15287
$H_2W_{12}O_{40}^{6-}$, XPS spectra, oxidation states 78−6824
H_xWO_3, amorphous, Anderson transition, disorder depend. and optical detection 78−47840
H_xWO_3, amorphous film, electronic transport meas., insulator-metal transition 77−72923
H_xWO_3, atom motion 78−75874
H_xWO_3 bronzes, Anderson transition, XPS 80−107705
H_xWO_3, crystalline, band struct., XPS meas. 77−59667
H_xWO_3, electrochromic characts. 78−6653
H_xWO_3 films, proton diffusion coeffs. 80−6548
H_xWO_y film, effect of struct. on optical and electrical props. 78−84671
HX (X=Cl,Br,I) dissoc. attachment, negative ion form. and removal kinetics in flame 77−52642
HX, chemical laser performance isotope effects, computer simulation 78−29944
HX+ inert gas atom, (X=halide), rot. excitation 77−10742
HX+F, (X=I, Br, Cl), H abstraction, absolute reaction rate, H/D isotope effect 78−80721
H_2O_2 effect on Ehrlich ascites tumour cell mitotic activity, in combination with gamma-rays 77−52854
^1H, isotropic hyperfine coupling consts. in small radicals 80−52894
H.HF, H-bonded complex, ab initio calcs. *(French)* 80−52866
He+CO(HCl), effective pot. and coupled states approx., differential and gas kinetic cross sections 77−61827
HeH^+, electronic states, variable-screening method 78−25410
HeH^+, mobility in He gas 78−18371
$HeH^+ + H_2 \rightarrow H_3^+ + He$, reaction rate. coeff. 78−18371
$He^+(He_2^+) + N_2(CO)(CO_2)(H_2S)$, charge transfer Penning ionis. 78−17784
$HuO_2P(As)O_4.4H_2O$, water deficiency, enthalpy of dehydration, thermogravimetric anal. 80−65251
$I(5^2P_{1/2}) + HBr(DBr)(methane)(propane)$, collisional deactivation, rate consts. meas. 77−86300
KBr:I^-, OH^-, luminesc. of interstitial atomic H 80−89062
$K_{1-x}Rb_cCl:HF_2^-$, dynamic inhomogeneous broadening of bands of local vibr. 78−92102
$K_xRb_{1-x}Cl:HF_2^-,SO_4^{2-}$, nonuniform broadening of IR vibr. absorpt. bands of impurities *(Russian)* 77−16357
Kr-HCl, intermol. pot. energy surfaces calcs. 80−91625
Kr**+HCl rot. effect on collisional ionis. 77−83702
$Li_{1-x}H_xIO_3$, cryst. growth from soln. and phys. props. 77−31634
$Li_{1-x}H_xIO_3$, dielec. behaviour, Raman and IR spectra 77−32357
$Li_{1-x}H_xIO_3$, piezoelectric props., space charge effects 78−6637
MCN+Ar, CN quartet state production, fluoresc. anal. 78−68888
$MgI_2 + Cl_2(HCl)$, crossed beam metathesis, total cross sections 77−21354
NH_3, GO AO exponents optimisation and scaling effects on mol. props. 77−65424
NH_4Br, dislocation influence on phase transition and light scatt. *(Russian)* 80−59648
$N_2H_6FeF_5$, one-dimensional antiferromagnetism, Mossbauer study 80−65872
$(NHPO_2H)_4.2H_2O$, cryst. struct. determ. 77−24300
$(NH_4)_2S_2O_8$-HCl-H_2O dislocation etchant for β-brass crysts. 80−65004
N_2O_4-HNO_3-H_2O dissociating system, surface tension at liquid-vapour boundary *(Russian)* 78−47643
Ne-HCl mixture breakdown obs. 78−67553
Ne-Xe-HCl, transient optical absorpt. meas. for XeCl laser 79−55115
$Ni_2P_2O_7$-$H_4P_2O_7$-H_2O system, solubility isotherm at 0°C 77−25027
$O + H_2O \rightarrow OH + OH$, energy partitioning 80−101009
$O + H_2S$, matrix reactions, IR spectra of products, chemiluminesc. 77−60057
O+HCl, vibr. excited, laser enhanced reaction rate, OH vibr. distrib. obs. 78−95912
$O_3 + H_2S(OCS)$, SO chemiluminesc. in Ar matrix 79−5146
OH, electron affinity, variation-perturbation approach 77−54513
$OH + H_2O_2 \rightarrow HO_2 + H_2O$, reaction rate consts., laser induced fluoresc. 80−101017
$O(^3P) + HCl(HBr)(HI)$, rate consts. temp. depend. 79−52627
PsH autodissociating Rydberg states 79−76539
Pt-$HClO_4$ electrolyte interface laser speckle movements related to electrode pot., H_2 adsorb. 78−40052
RbBr:I^-, OH^-, luminesc. of interstitial atomic H 80−89062
$S^{n+} + Ne(SiH_4)(H_2S)(HCl)(Ar)$, K X-ray cross section, projectile charge depend. 77−19029
$(SNH)_x$, density of states, CPA calcs., effect of H impurities 79−42431
SOH, ground and first excited states, geometry, ab initio SCF calcs. 78−50657
Si-H, amorphous, energy gap negative-U states, Si-H-Si three centre bond model 78−91606
Si-H amorphous, defect model, light-induced ESR obs. 79−69721
Sr+HF→SrF+H, product state distrib., reagent orientation and rot. effect 79−20361
T+HD, variational transition field theory and unified statistical model 80−97700
$Th_7Fe_3H_{30}$, H induced change from supercond. to mag. ordered state 79−28525
Ti complex, Ti(IV)-H_2O_2, H_2SO_4-aq. soln., reson. Raman spectrum, vibr. assignments, molar absorptivity 77−65469
Xe+$NH_3(H_2S)(SO_2)(HCl)$, ionis. cross sections calc. 77−68103
XeH^+, pot. energy curves, VB calcs. 77−61688

hydrogen embrittlement
adsorption model, and equilibrium crack growth meas. 80−108574
adsorption or decohesion, mechanism 80−97643
alloys, ferrous and nonferrous, failure mechanisms overview 78−11322
brittle fracture in ductile material, model and applic. to H embrittlement 78−23814
cracking and impurity atom migration *(Chinese)* 80−104247
cracking at notches, due to H embrittlement, model, based on stress induced diffusion of H atoms 78−39897
cracking at notches, due to H embrittlement, model 78−84985
critical stress criterion 79−65140
delayed cracking in hydride forming materials 78−27623
diffusion of H_2 towards crack in stressed solid, eigensoln. 77−24446
dissociation poison and H_2 embrittlement 77−9079
enhancement by implanted He 79−28016

hydrogen embrittlement continued
failure, typical examples *(Japanese)* 77−28897
Fe, Armco, long-term strength, H effect 80−55581
Fe, pure, lattice hardening due to H_2 charging, during tensile testing 79−66156
finite element analysis of H_2 delayed cracking by H_2 gathering simulations at plastically deformed notch 78−31539
fracture analysis of failure in service *(Japanese)* 80−104337
fracture of materials, conf., Waterloo, Canada (June 1977) 78−56763
Hastelloy, C-276, H-induced crack growth 80−71747
Hastelloy, H_2 embrittlement in H_2S environments, impurity segregation effects 80−71724
Hastelloy C-276 and C-4 cold worked high alloy material, factors affecting H_2 embrittlement in H_2S environments 78−31502
Hastelloy C-276 and G, accelerated H_2 charging in aq. H_2SO_4 at 0.2% yield stress 80−30144
Incaloy 623, cold worked, factors affecting embrittlement in H_2S 78−31502
inclusion interaction with H 78−30664
Incoloy 903, microstruct. and effect of H_2 charging 77−86143
Inconel 625, accelerated H_2 charging in aq. H_2SO_4 at 0.2% yield stress 80−30144
inorganic materials, acoustic emission meas of H_2 embrittlement 80−11742
internal, failure criterion 77−73322
internal supersaturation produced by dislocation transport 77−36640
lattice hardening due to dissolved H_2 in Fe, and ferritic steel 78−76656
limiter materials, for Doublet III fusion research machine, selection 78−55026
low C steel, explosive-thermal treatment, sulphide cracking decrease, hydrogen embrittlement *(Russian)* 80−108477
metal, hydrogen crack development 79−20189
metal, hydrogenating under continuous static loading, accurate electrolytic method 78−23854
metal lattice decohesion due to H_2 78−15533
metallic cohesion reduction mech., new model for transition metals 80−7679
metals, assessment of techniques for local detection 78−3439
metals, autoradiographic study of H distrib., exptl. difficulties 77−52586
metals, effect of H_2 on mech. prop., methodological approach to study *(Russian)* 78−31507
metals, effect on props. 80−104290
metals, H_2 embrittlement, kinetics, review *(Russian)* 79−15762
metals, H effect on mech. props., review 80−50718
metals, hydrogen brittleness measurement 80−104291
metals, reversible H embrittlement 80−104292
metals and alloys *(Russian)* 77−25128
Mossbauer spectroscopy applics. 77−12749
near surface region of solid, H_2 effect on deform. and fracture, Rebinder-Westwood effect 79−39001
nondestructive measurements, in situ, using Li nuclear microprobe method 78−7299
nuclear reactor materials, PWR, H_2-assisted fatigue-crack growth model 80−71745
Petch-Stables theory, review of objections 78−60738
plasma magnetic confinement system, surface problems 80−57946
plastic fracture processes, exam. of role in hydrogen embrittlement 78−60810
pressure tubes, cracking due to high residual tensile stresses 78−29585
Pyrex glass, near-surface H embrittlement, effect on deform. and fracture props. 79−29180
review, mechanisms 80−50721
simulation appl. to materials, conf., Gaithersburg, USA (April 1976) 78−27387
steel, 12 MKh, creep-respective strength and fracture mode in H_2 *(Russian)* 77−52461
steel, 20, fatigue endurance tests in moist H_2S *(Russian)* 78−31510
steel, 4340, H_2 embrittlement, stress state, thickness and delayed failure in bending 80−71746
steel, 4340, role of gaseous impurities 77−59904
steel, 50 and 1Kh18N9T, strength, effect of H_2 78−3197
steel, AISI 4340, subcrit. crack growth, fracture mech. and surface chemistry obs. 79−8392
steel, Al alloying addition effect on resistance to hydrogen embrittlement 77−59925
steel, alloy, Cr-Mo, alloy SCM3, hydrogen embrittlement, delayed fracture, exam. *(Japanese)* 78−64620
steel, alloy, Fe-Ni, effect of metallurgy on stress corrosion cracking, and hydrogen embrittlement 78−60885
steel, alloy, Fe-Ni-Cr-Mo-V-C, HY130, effect of H_2 and impurities on brittle fracture, review 78−60765
steel, alloy, Fe-Ni-Mn-Si-Cr-Ni-Mo, effect of metallurgy on stress corrosion cracking, and hydrogen embrittlement 78−60885
steel, alloy, forgings, H precipitation kinetics, diffusion to voids, effect on shattercrack formation 80−16344
steel, alloy, JIS SNCM8, crack propagation vel. in delayed failure under cyclic load, temp. and freq. depend. 79−43381
steel, austenitic, ASTM A533B and A542, H_2 embrittlement behavior of unirrad. steels for nuclear reactor press. vessels 79−8340
steel, austenitic, explosive-thermal treatment, sulphide cracking decrease, hydrogen embrittlement *(Russian)* 80−108477
steel, austenitic stainless, acoustic emission during tensile tests, H_2 assisted fracture 79−100257
steel, austenitic stainless, cathodically charged, H_2 embrittlement, α' martensite effect 80−71725
steel, austenitic stainless, dislocation damping, H pinning 78−15501
steel, austenitic stainless, dislocation transport and H_2 embrittlement 80−30087
steel, austenitic stainless, H_2 embrittlement and SCC, austenite stability effect 79−100291
steel, austenitic stainless, H_2 induced strain in single crystal *(Japanese)* 77−48530
steel, austenitic stainless, H plasma effects on fusion device vacuum vessel 80−21111
steel, austenitic stainless, hydride phases rel. to SCC 80−35385
steel, austenitic stainless, type 304, intergranular H_2 assisted fracture, exam. of mechanism 78−80644
steel, austenitic stainless, type 316, hydrogen embrittlement, tensile testing 80−7671
steel, bimetal, alloy with austenitic stainless, H permeability 80−107572
steel, blister-crack array extension 79−24613
steel, book contrib. 79−66172
steel, C, diffusion of H_2, SCC via martensite form. cooling rate changes on Mn and Ni addition *(Russian)* 78−56813
steel, C, ductile fracture, role of hydrogen 79−57103
steel, C, H attack kinetics and service behaviour 78−39951
steel, C, hydrogen attack, steelmaking effects 79−100076
steel, C, hydrogen embrittlement, elastic interaction of H_2 with precipitates 78−92340
steel, C, type 1020, H_2 attack, effect of H_2S 79−96192
steel, C-Mn, accelerated H_2 charging in aq. H_2SO_4 at 0.2% yield stress 80−30144
steel, C-Mo-P, intergranular fracture and grain boundary segregation, P, H, Mo effects *(Japanese)* 79−15775
steel, carbon type, hydrogen press. effect on morphology of hydrogen attack 80−85052
steel, classification of hydrogen traps 80−19792
steel, Co-Cr-Mo HY 180M, SCC in NaCl, temp. effect 80−108633
steel, Cr, high strength, hot dip galvanized delayed fracture *(Japanese)* 78−15512
steel, Cr-Mo, H embrittlement in H_2S environment, Mo effect 80−76415
steel, Cr-Mo, high tension, delayed fracture, fundamental study *(Japanese)* 77−48531
steel, Cr-Mo (2.25,1 wt.%), exposed to H_2-H_2O-H_2S environment, fatigue crack growth 80−40623
steel, Cr-Mo-(Ni), fracture resistance, H_2S in H_2 effect *(French)* 80−16461
steel, Cr-Ni, hydrogen effect on strength, ductile and fracture charcts. 79−38960
steel, crack growth velocity in gaseous H_2 embrittlement, rel. to chemisorption 80−11831
steel, cracking due to H_2S, exam. of fracture surface by SEM *(Japanese)* 78−53024
steel, cracking under wet H_2S environment 77−32721
steel, CrMoNi, cantilever beam method to determ. J_{Icc} and J_{Iscc} *(Chinese)* 78−15488
steel, deformed eutectoid C_2 back stress decrease on annealing and H embrittlement 80−20981
steel, delayed fracture, hydrogen and impurities 78−84988
steel, effect of H_2 on phys. and mech. props. 80−101657
steel, effect on band strength 80−104293
steel, environmental fracture, metallurgical variables effects, review 77−28887
steel, fracture in low-cycle fatigue tests in H_2 *(Russian)* 80−76332
steel, fracture mechanics appl. to H_2 embrittlement under press. *(French)* 78−23821
steel, gas pipe, H_2 press. tests appl. to H_2 transmission 79−74550
steel, H_2 assisted cracking equilibrium and kinetic studies 78−3201
steel, H_2 cracking mechanism *(Russian)* 77−25130
steel, H_2 embrittlement, method of fixing reversible to irreversible transition 80−25840
steel, H_2 embrittlement and selective adsorption 77−36645
steel, H_2 embrittlement prevention, H_2 transport appl. 79−74260
steel, H effect on weldability 80−50720
steel, H embrittlement detection by US velocity 79−52613
steel, H embrittlement mechanism, microcrack formation, dislocation model *(Russian)* 80−65143
steel, high strength, 300-M, slow fatigue crack growth, threshold behaviour, temper embrittlement, impurity segregation effects 77−86152
steel, high strength, alloy, initiation of cracks at delayed fracture, AE study 78−72868
steel, high strength, corrosion fatigue in low press. H_2 gas 79−79172
steel, high strength, dislocation sweeping model for hydrogen assisted subcritical crack growth 80−97577
steel, high strength, environmental effects on initiation and propag. of fatigue cracks 77−86216
steel, high strength, H_2 embrittlement due to cathodic charging during specimen prep. for SEM *(German, English)* 80−11760
steel, high strength, subcritical crack growth, role of time delayed H_2 assisted plastic zone growth 80−97576
steel, high strength, thermally strengthened by rolling heat, H_2 embrittlement *(Russian)* 77−77562
steel, high strength, weld cold cracking, anal. of fracture morphology, using SEM *(Japanese)* 78−52960
steel, high strength AISI 4130, H_2 assisted cracking 78−48522
steel, high tensile, H embrittlement estimation from viscous failure 77−73335
steel, high-strength, criteria for determining struct. strength and reliability 77−60021
steel, high-strength, H distrib. and delayed brittle fracture 80−108577
steel, high-strength, specific energy of fracture, adsorption lowering by H_2, H_2S, HCl and CH_4 gases *(Russian)* 79−52440
steel, high-strength reinforcing, 20GS2, local microstresses on creep strength in hydrogenating media *(Russian)* 77−52462
steel, HSLA type 4340, hydrogen diffusivity and solubility, correl. with embrittlement and SCC phenomena 79−83323
steel, hydrogen embrittlement, standard qualification tests 79−74259
steel, hydrogenation and cracking in H_2S, cathodic polarization and surface layer effects *(Russian)* 77−52528
steel, hydrogenation by cathode polarisation, controlling factors 77−52645
steel, inclusion, grain boundaries and H_2 attack, fracture analysis 77−32695
steel, Kh16N6, fatigue in gaseous H_2 *(Russian)* 78−31509
steel, lath martensite, elastic interaction of H_2 with precipitates 78−3129
steel, lattice hardening and anomalous softening caused by electrolytic H_2 charging *(Japanese)* 79−43398
steel, lattice hardening due to dissolved H_2 77−8952
steel, lattice hardening/softening due to dissolved H_2 77−77581
steel, linepipe, S content influence on H_2 induced fracture 80−30088
steel, long-term strength, H effect 80−55581
steel, low alloy, impurity and strength effect on H_2 induced cracking 78−27625
steel, low-alloy hydrogenation and embrittlement under neutron irrad. in contact with water *(Russian)* 77−52529
steel, low-alloy pipe, low-cycle fatigue in H_2-evolving media, S content and sulphide inclusion effects *(Russian)* 78−11398
steel, maraging, D152, low cycle fatigue in gaseous H_2 *(Russian)* 78−35478
steel, maraging, Hart's model in hydrogen embrittlement 79−24621

hydrogen embrittlement continued
steel, maraging, high strength, gaseous H_2 embrittlement 77−86147
steel, maraging, Ni, H_2 assisted crack growth 77−73346
steel, maraging, Ni, stress corrosion cracking 78−35563
steel, martensitic, quenched, strength variation rel. to H behaviour 77−59924
steel, martensitic grain size effects in H_2 assisted cracking, austenitising 77−28901
steel, mild, and cold-rolled, diffusion, permeation, and accumulation of H_2 *(Japanese)* 77−39692
steel, mild, cathodic protection against corrosion fatigue cracks 79−74281
steel, mild, effect on design requisites for H energy systems 80−30109
steel, mild, electrodes, in H_2SO_4, H evolution reaction kinetics 80−97630
steel, mild, US detect. of H embrittlement 80−71822
steel, Mn, H_2 embrittlement mechanism *(Korean)* 78−68774
steel, Mn(0.9 wt.%), hydrogen embrittlement resist. evaluation *(Czech)* 80−35308
steel, Mn-V and Cr-Mo, for pressure vessels, hydrogen embrittlement evaluation *(Czech)* 79−38950
steel, model including reversible and irreversible processes 77−25155
steel, natural gas environment effects on strength *(Russian)* 78−11401
steel, neutron irradiated 15KhMFA, H_2 induced delayed fracture *(Russian)* 78−35476
steel, Ni (23 wt.%), crack propag. in the presence of H_2 *(French)* 78−15517
steel, Ni-Co-Cr-Mo-C (10,14,2,1,0.16 wt.%), stress corrosion cracking at 22°C in 3.5% NaCl 79−8390
steel, Ni-Cr-Mo-V, corrosion fatigue crack growth in NaOH soln., cathodic pot. effect 80−89403
steel, Ni-Cr-Mo-V, fatigue crack growth, effect of aq. and H_2 environment 79−79173
steel, Ni-Mo-V, fatigue crack growth, H_2 gas environment effect *(Japanese)* 80−104340
steel, pressure vessel type, H_2 effect on corrosion, fatigue strength and embrittlent *(French)* 79−47770
steel, rolled, fisheyes produced by exposure to H_2 at room temp. 77−90455
steel, rolled products, H flaking 80−50719
steel, SAE 1045, permeation meas. of H trapping, rel. to cryst. microstruct. 80−84328
steel, SEM obs. *(German)* 78−19858
steel, spheroidised, H_2 embrittlement, fracture characts., electron probe anal. of inclusions 79−57109
steel, spheroidised AISI 1095, U-notched bend specimens, hydrogen effect on fracture 79−52363
steel, stainless, durability in H_2 up to 500°C 80−30170
steel, stainless, embrittlement by low energy ionic and atomic H particles 78−95809
steel, stainless, ferritic, 18%Cr, stress/strain curve, H_2 charging influence, room temp. *(Japanese)* 78−39884
steel, stainless, hydrogen embrittled, fractography 78−35503
steel, stainless, type 304, exam. of H_2 induced cracking 78−76738
steel, stainless, type 304, hydrogen assisted cracking, martensite formation on deformation effects 79−52362
steel, stainless, type AISI 321, surface damage and mech. changes after H atom irrad. 80−39182
steel, stainless 430, diffusion of H_2, effect of heat treatment 77−47627
steel, struct. type 05KhGM, crack initiation and propagation during H_2 embrittlement 80−35313
steel, structural H_2, embrittlement and H_2S cracking resist., effect of alloying elements and struct. 79−38953
steel, type 4340, effect of H_2 and impurities on brittle fracture, review 78−60765
steel, type AISI 4340, quenched and tempered, U-notched bend specimens, effect of H_2 on fracture 79−61716
steel, types AISI 4340 and A-106, stress state and delayed failure 80−45400
steel, U8, diffusion coating protection for H_2 embrittlement, SCC and tensile tests *(Russian)* 78−31513
steel, ultra-high strength, H induced delayed plasticity and cracking 80−21100
steel, welded-joints, H_2 induced cracking, S content effect 80−97562
steel *(French)* 80−16460
steel *(French)* 80−16462
steel 20, deformability, H_2 absorption effects *(Russian)* 77−77561
steel 20, diffusion coating for protection against H_2 effect on mech. props. 78−31589
steel 35GS and 20GS, thermally strengthened rolled, H_2 embrittlement and cracking resistance *(Russian)* 78−35479
steel 38KhC, medium C, ductility, fracture, effect of H_2 *(Russian)* 77−25131
steel (0.45 and 0.8 wt.%), strength, fracture, effect of H_2 *(Russian)* 77−25129
steel A-106, yield point suppression by H_2 79−8368
steel H_2, embrittlement resist., selection of test conditions *(Russian)* 79−15883
steel H-dislocation interactions rel. to H_2 embrittlement 79−42097
steel high strength, Cd plated, effect of composition and thermal treatment, on hydrogen embrittlement susceptibility *(Russian)* 79−15769
steel susceptibility to H_2 embrittlement, fracture toughness *(Czech)* 77−59915
steel U8, hydrogenation effects on fatigue crack propag. *(Russian)* 78−56800
steel welds, bead-on-plate, H_2 diffusion and trapping 80−96697
steel, C, H_2 embrittlement after patenting and cold deform. *(Russian)* 79−29175
steels, Cr and Cr-Ni-Mo refining effect on low cycle fatigue strength, resistance to hydrogen embrittlement 78−44208
steels, hydrogen cracking under long-term strength tests 77−86243
steels, low alloy, grain boundary anal.,, H_2 embrittlement, scanning AES 79−43256
steels, mechanism of H_2 entry in acid environments 79−39023
stress corrosion cracking, role of H_2, state of art review 80−61017
structural steels and alloys, conf., Kiev, USSR (Sep. 1976) 77−59921
test condition selection for resistance *(Russian)* 79−15883
Tokamak fusion reactor first walls, hydrogen profiles 80−37578
transport by dislocations 77−21263
trap theory, of H embrittlement 80−89325

hydrogen embrittlement continued
Zircaloy, effect of dispersion and spheroidisation treatment of δ ZrH 79−76673
Zircaloy, hydriding reaction kinetics, oxidised specimens 78−26728
Zircaloy-2, pressure tube, fragmentation on failure 78−72863
zircaloy-2 cladding tubes, post neutron irrad. ring-tensile props. pre-hydriding effect 77−42053
Zircaloys, fractographic distinction between hydride cracking and stress corrosion cracking 78−92363
Al alloy, high-strength 7075 78−15523
Al alloy, type 7075, hydrogen induced fracture 79−91837
Al alloy 7075, cyclically deformed, high strength, hydrogen embrittlement 78−31584
Al alloy 7075-T6, embrittlement by cathodic H_2, surface film effect 78−64643
Al alloy OT4-1u, with varying H_2 content, rel. to loading condition *(Russian)* 77−70148
Al-Mg (7 wt.%), corrosion cracking, exam. of slip dissolution and hydrogen embrittlement mechanisms 78−72852
Al-Mg-Zn alloy 7179-T651, reduced ductility under tensile after exposure to water 80−11835
Al-water vapour reaction, stress corrosion susceptibility STEM study, Mg addition effect 80−3247
Al-Zn-Mg, type 7075, strain rate effects on H embrittlement 80−3190
Al-Zn-Mg (6,3 wt.%), hydrogen embrittlement and trapping 80−55490
Al-Zn-Mg (91, 6, 3, wt.%), H embrittlement and trapping, HVEM obs. 80−76364
Al-Zn-Mg alloys, H_2 bubbles in embrittlement 78−19868
Al-Zn-Mg-Cu, type 7075, microstruct. role in hydrogen assisted fracture 80−30091
Cu, disperse Al_2O_3 particles and matrix struct. effect on H-embrittlement *(Russian)* 78−3207
FE, electrolytic, dissolved H precip., effect on flow stress *(Japanese)* 78−39848
Fe alloys, review of hydrogen embrittlement mechanisms 78−72853
Fe, annealed and cold-rolled, diffusion, permeation and accumulation of H_2 *(Japanese)* 77−39692
Fe, Armco, strength, fracture, effect of H_2 *(Russian)* 77−25129
Fe, BCC, atomistic studies of H_2 enhanced crack propag. 78−31538
Fe Based amorphous alloys, delayed fracture in atmosphere, effect of alloying additions *(Japanese)* 79−96212
Fe, commercial, deformability, containing H_2 77−90411
Fe, defect trapping of ion implanted D, depth profile, diffusion eqn. calcs. 80−2047
Fe, effect of H_2 on phys. and mech. props. 80−101657
Fe, embrittlement, fracture mode transition as function of grain boundary sulphur 80−55520
Fe, H_2, induced cracking, crystallographic and fractographic studies 79−5052
Fe, H_2 adsorption at dislocations and cracks 79−20146
Fe, H_2 charged, depend. of softening on specimen size, charging current density and strain rate 80−16455
Fe, H_2 embrittlement and H_2 adsorption 80−89401
Fe, H_2 induced cracking, stress state effect 79−20147
Fe, H_2 permeation, rel. to embrittlement, organic inhibitors, surface treatment 80−108635
Fe, lattice hardening and anomalous softening caused by electrolytic H_2 charging *(Japanese)* 79−43398
Fe, lattice hardening due to dissolved H_2 77−8952
Fe, lattice hardening/softening due to dissolved H_2 77−77581
Fe, plastic deform. and fracture, H_2 effect, studied by electron microscopy and Auger spectrography *(French)* 77−77545
Fe, polycrystalline, H_2 adsorpt. and embrittlement, work function changes 80−96741
Fe polycrystalline whiskers, H_2 embrittlement 79−100259
Fe, pure, cathodic charging effect on creep and tensile deformation 80−76320
Fe, pure, hydrogen-charged, initial cracking obs. 80−108580
Fe, pure, neutron irrad. and H_2 absorption effects on mech. props. 78−34546
Fe, quenched-in hydrogen, yield stress decrease of prestrained specimens 80−16454
Fe, small particles, magnetisation-pressure isotherms for H_2 and SO_2 78−39949
Fe, softening and hardening by H_2 charging during tensile deformation 80−16453
Fe, whiskers, H_2 effect on mech. props. 80−108556
Fe-base amorphous alloys, embrittled by H and heat-treatment 80−55518
Fe-C, effect of H on elastic props., due to internal microcracking *(Russian)* 79−24561
Fe-C alloys, H_2 embrittlement, rel. to metallurgical microstruct. 80−55539
Fe-Cr-Co (28, 10.5 wt.%) ductile magnet alloy, humidity-induced H_2 embrittlement 80−89406
Fe-Cr-Ni austenitic alloys, environment sensitive cracking, metallurgical variables effect 80−35391
Fe-Ni-C, martensitic, H_2 effect on fracture charact. *(Czech)* 78−60746
Fe-Ni-C, mech. and structural props. under cathodic H_2 at elevated temps. *(French)* 77−59920
Fe-Ni-C, quenched martensite, annealing during cathodic hydrogenation, 200°C *(French)* 80−93573
Fe-Si, H_2, induced cracking, crystallographic and fractographic studies 79−5052
Fe-Ti, Ti as H trap for embrittlement control 80−66662
Fe-Ti (0.15 wt.%), H trapping obs. by high resolution autoradiography 79−73205
Fe-Ti alloys, kinetic trapping model for H_2-induced grain boundary cracking 79−29164
H-dislocation, interactions rel. to H_2 embrittlement 79−42097
$LaNi_4Fe$, H_2 absorpt. cracking, acoustic emission characts. *(Japanese)* 80−66631
Mo alloy TsMb, mech. props., effect of gaseous H_2 *(Russian)* 78−31508
Mo, exam. of H_2 embrittlement mechanisms, effect on mech. props. 78−39891
Nb, H_2 embrittlement, macroscopic behaviour at low temps. 77−32665
Nb, H_2 embrittlement, microscopic obs. at low temps. 77−32666
Nb, hydrogen embrittlement, deformation behaviour of Nb-H alloys 79−11687
Nb-H, behaviour of H in Nb, relation to mech. props. 78−80572

hydrogen embrittlement continued
Ni alloy protection, by Cu electroplating, aerospace engine appl. 80−76416
Ni and FCC Ni-Fe *(Japanese)* 77−48526
Ni, cathodic charging of H_2, positron annihilation Doppler broadening obs. 79−83055
Ni, single crysts., H and liq.-Hg embrittlement 80−25862
γ/γ-Ni-Al-Nb, aligned eutectic alloy, H_2 embrittlement 77−8951
Ni-B, hydrogen embrittlement, effect of B additions *(Japanese)* 78−84973
Ni-Co, H_2 embrittlement, heat treatment and impurities effect 80−76331
Ni-Cr-Co-Mo alloy MP35N alloys, cold worked, factors affecting embrittlement in H_2S environments 78−31502
Ni-Cr-Co-Mo alloy MP35N, accelerated H_2 charging in aq. H_2SO_4 at 0.2% yield stress 80−30144
Ni-Nb-Al-(Cr), eutectic, mech. props., high press. H_2 effects 77−63779
Ni-thoria dispersed (2 vol.%), meas. and eval. of H_2 trapping by permeation technique 79−60555
Ni-W (45.5 wt.%), eutectic, mech. props., high press. H_2 effects 77−63779
$Ni_{62}Ti_{29}Zr_9$, amorphous, H-sorption, X-ray and DSC obs. 80−49526
$Ni_{64}Zr_{36}$, amorphous and cryst., H-sorption, X-ray and DSC obs. 80−49526
Pd alloys, controllable hydrogen phase naklep, hardening and phase-strengthening 80−16323
steel, Cr-Mo-V, hydrogen embrittlement resist. evaluation *(Czech)* 80−35308
Ta single crystal, H_2 embrittlement *(Japanese)* 80−66636
Ta-H system, acoustic emission study 80−76257
Ti alloy, H_2 embrittlement, directional diffusion of H_2 *(Russian)* 79−15763
α-β-Ti alloy, stress, H segregation, fracture 77−40450
Ti alloy creep strength rel. to diamond electrochem. cutting conditions *(Russian)* 79−96081
Ti alloy VT30, H_2 effect on low temp. mech. props. *(Russian)* 78−35477
Ti alloys, delayed brittle fracture, H_2 effect 80−100912
Ti alloys, fusion reactor, first wall and blanket structure, impact of H_2, phase stability and solubility 80−32435
Ti alloys, hydrogenation at 200-600°C and up to 10000 kPa 80−107435
α-Ti alloys VT1 and VT5, struct. and phys. props., H_2 effect 80−108576
Ti, hydriding, surface condition and environment influence 80−35380
Ti, uphill diffusion of H and progressive H embrittlement 77−90454
Ti-Al (6.6 wt.%), hydride habit planes, H_2 embrittlement, slip 77−36648
Ti-Al-Mo alloy VT14, fracture anisotropy, with varying H_2 content, rel. to loading condition *(Russian)* 77−70148
Ti-Al-Mo-V (8, 1, 1 wt. %), stress corrosion cracking and slow strain rate H_2 embrittlement 78−48569
Ti-Al-V (6,4 wt.%), H related fatigue fracture 80−76344
Ti-Al-V-Sn (5.5, 5.5, 2 wt%), crack growth, slow, H-induced 80−104272
Ti-Al-V-Sn (6,6,2 wt.%), H_2 induced crack growth, in-situ scanning Auger anal. 79−8355
Ti-alloys, methods of studying effect of H on service behaviour 80−16478
Ti-H, H diffusion and phase consistution, V influence, proton spin-lattice relax. meas. 78−27484
U-Mo (10 wt.%), gaseous O_2 and hydrogen embrittlement, exam. 78−60811
U-Mo (2 wt.%), depleted, effect of microstruct. on mech. props. 80−108497
U-Mo(Nb)-(Zr), gamma stabilised, internal H_2 embrittlement 77−28883
U-V (0.2 wt.%), mech. and struct. props., effect of internal H *(French)* 77−21253
V, hydrogenated, grain size depend. of tensile strength 77−36657
WC-Co, pressure vessels 78−48530
Zr and Zr alloys, cracking, H_2 induced delay, strain energy effect on H_2 solubility 78−92364
Zr-Nb (2.5 wt.%), fractographic aspects of H_2 induced delayed cracking 79−47767
Zr-Nb (2.5 wt.%), H_2 induced subcritical crack growth meas., application of potential drop method 78−27645
Zr-Nb (2.5 wt.%), hydride forming materials, H_2 induced delayed cracking 78−27623
Zr-Nb (2.5 wt.%), hydride TEM obs. in pressure tubing 79−8338
Zr-Nb (2.5 wt.%), hydride induced crack growth, effect of stress, temp. and H_2 content 80−3178
Zr-Nb (2.5 wt.%) pipe, fracture resistance, hydrogenation effect 80−104279
Zr-Nb (97.5, 2.5 wt.%) nuclear reactor pressure tube material, H embrittlement study by TEM 80−76363
ZrNb, pressure tube, fragmentation on failure 78−72863

hydrogen ion activity *see pH*

hydrogen ion concentration *see pH*

hydrogen ions
alcohol+H_x^+, methanol to butanol, x=1-3, charge exchange ionisation *(German)* 77−83700
alcohol+H_x^+, methanol to octanol, x=1-3, charge exchange and ionisation *(German)* 77−83699
atmospheric acid precipitation in N.E. United States, H ion speciation 77−37336
atom+H^+ ion collisions, Z=35 to 56, L X-rays, Coster-Kronig threshold effects 77−18831
atomic energy levels, corrected for fine struct., lamb shift and QED shift, tables 77−79529
backscattering from Au(Cs), fraction reflected 80−60741
beam, heavy element ionisation cross-section ratio determ., X-ray method 77−6920
beam formation by electron beam-plasma discharge 77−6593
charge transfer reactions with N_2, and C_nH_{2n+2}, n=1-4, electron capture and loss cross sections *(French)* 77−38728
chemical sputtering of graphite 77−36341
cluster ions, ioniser for accelerator 77−74551
clusters with odd and even mass number 79−92840
collagen membrane H^+ diffusion-limited binding electromechanics 79−79489
concentration meas., process control by ion-selective electrodes *(German)* 79−16083
cytochrome *a* interaction with mitochondrial matrix H^+ ions 79−43806
duoplasmatron anode plasma, ion temp. 80−6292

hydrogen ions continued
Earth's upper atmosphere, coupled time-dependent diffusion eqns. 80−109285
education, H_2^+ bonding and virial theorem 78−49599
effective ionisation cross section determ. for H, Li, Na, Cu, Ag, Au and Fr, classical theory 77−30998
electric multipole polarisability, relativistic corrections, shielding factors, Dirac eqn. 78−13441
electron excitation of H and hydrogenic ions, cross-sections and rates 78−50649
electron impact excitation cross sections and rates, calc. for H-like ions 77−71873
electron impact ionisation, highly charged hydrogenic ions, Born exchange 77−71875
emission spectrum, last observable line, rel. to solar obs. through Earth atm. 78−77536
field ion source with high angular current 80−68996
fluxes, electrodialysis polarisation, rotating disc studies 79−47933
forest canopy H ion removal, exchange process 77−78392
H_2^+, relativistic corrections, estimation operators 79−54985
H^++Mg collisions double electron capture 78−58777
H radio recombination lines from multiple-component H II regions, press. broadening 80−4419
highly stripped H-like ions, de-excitation cascades, influence on time integrated ang. correl. 78−932
hydrogenic atoms and ions, degenerate state transitions, plasma waves, Stark effect 79−72389
hydrogenic ions, electron capture by charge particles at relativistic energies 80−102565
hydrogenic ions, electron impact, cross section functions meas., hollow beam trapping, dissociation 79−72424
hydrogenic ions, ground state, electron impact excitation, first-order Coulomb exchange approx. calcs. 79−59581
hydrogenic ions, radiative decay of $2S_{1/2}$ metastable state 77−67992
hydrogenlike ions, electron impact excitation, Coulomb-Born-Oppenheimer calcs. 79−10211
impact on Al surface, plasma form., plasma radiative and gasdynamic processes 80−53946
interstellar H II, prod. through Cl chemistry 79−40245
ion+atom, H to Fe^{25+} and H to Fe, single-electron loss, total Born-approx. cross-sections 77−83714
ionisation rates, shock tunnel meas. 80−75022
ionosphere upward flowing energetic H^+ ions latit., diurnal and altitudinal distribs. 78−49199
isoelectronic sequence, electron impact ionisation cross section 80−91688
isoelectronic series, C VI, cylindrical plasma, XUV gain calc. 79−72995
isoelectronic series, excitation regimes, nucl. orientation due to hyperfine interaction 78−70928
isoelectronic series, X-ray line excitation 79−44453
K-shell X-ray production on proton and α-particle impact, 0.6 to 2.4 MeV 78−13586
line broadening and shift due to plasma ions *(Russian)* 80−96350
low energy ion scattering from polycrystalline solids, computer study 77−36338
Lyman-α line wings, contribution of proton perturbers 78−67325
magnetic interactions of electrons *(German)* 78−82610
molecular, Burrau approx., series solns. 77−30763
molecular beams, appl. to prompt nucl. react. anal. 79−36452
photodissoc. cross section, time of flight anal. of reaction products 77−83664
plasma, H lines, electron width and shift *(Russian)* 78−67421
plasma, proton behaviour in JFT-2 Tokamak, charged-exchanged fast ion anal. 78−51341
plasma hemispheric layer total radiation calc. *(Russian)* 78−34278
plasma plane and cylindrical layer emission field calc. *(Russian)* 80−33755
plasma reactors, laminar and turbulent transport model *(German)* 77−11321
plasmapause location and H^+ density decreases, correl. 78−81500
plasmasphere, charge exchange, rel. to H escape rate 77−37469
polarimeter designs for high energy p and d beams, polarised beam spin anal. 78−58516
polarised ion sources and low energy collector rings, H^-, D^- beams 78−58515
proton beam, intense, space charge neutral, trapping in mag. mirror, simulation 78−9825
proton beam, radially convergent, production by cylindrical double diode 78−9856
proton beam characts. control by laser-induced selective multistep processes 80−61122
proton beam formation in electron beam-plasma interaction *(Russian)* 78−29207
proton collective acceleration in intense relativistic electron beams 78−9864
proton escape from metals, use of metal-metal contacts as prevention 80−24595
proton hydrogen bond attractive force at different excitation levels *(Russian)* 80−23493
proton pulse generation, 0.2TW 77−22618
proton transport, in hot BH plasma, moment method calc. 78−22458
protonium formation in flight, $\bar{p}p$, antiproton+neutral and negatively ionised hydrogen atoms 79−85319
protonosphere, induced proton flow into collapsing post-sunset ionosphere 78−49222
pulsed proton source, Penning type, beam parameters 80−87001
quantum oscillations in tunnelling, oscill. freq., tunnelling currents *(Russian)* 80−60065
rainwater chemistry and multiple H ion donor systems, obs. in Minnesota 77−37335
reactive sputtering of low-Z materials by H_n^+, expts. rel. to plasma-wall interactions, review 77−48297
recombination and level populations, resolution of ang. momentum states 77−45529
reflection, from metal surface, atomic excitation calcs. 79−87541
reflection from stainless steel and Nb 77−36336
resonant excitation, H-like and He-like channelled ions in Au and Ag 78−43058
rod outer segments, vertebrate, role of Ca and H ions as transmitters 77−90776
scattering from surfaces, excited state composition and scattered H^+ flux 77−36337

hydrogen ions continued
Seyfert galaxies, broad H lines prod. by suprathermal protons passing through neutral gas *(Russian)* 78−57642
solar chromosphere, H^- radiation and acoustic dissipation 78−96454
solar wind, H and He ions vel. differences rel. to Alfven instabilities 77−49259
solar wind H^+, implantation in interplanetary dust grains rel. to upper atmosphere H chemistry 78−65445
solid surfaces, reflection of slow H^+ and He^+ ions 78−76572
source, duoPIGatron, H^+ fraction enhancement by predissoc. 77−13816
source, magnetic-discharge pump for pulsed H injection 77−23318
sources, high current, ion species comput. 77−42209
sources, plasma reaction cross sections data 77−38538
sputtering, physical and chemical of graphite and SiC, 600 to 7500 eV 77−36340
sputtering by H^+, D^+, T^+ ions 77−36343
sputtering of ice, MeV ions, erosion rate 78−48268
Stark broadening of spectral lines in plasma, review 78−42001
survival probabilities, emerging from Cs coated W and Ni surfaces 80−45187
transport in immobilised protein membranes, assoc.-dissoc. time-scale factor 79−34529
two photon ionisation in presence of one photon ionisation, cross section calc. 80−83327
E United States precipitation, H^+ ions concs. behaviour 78−92962
velocity measurement by Doppler shift of H atoms line spectra after traversing thin C foil 78−16778
$Ag+H^+$, 1 MeV, K-shell ionisation probability, ang. depend. 77−71859
$Ag+H^+$, characteristic X-ray emission polaris. *(Russian)* 79−59394
$Al+H^+$, K-shell ionis., impact parameter depend., 90-200 keV 78−17775
$Al+He^+(H^+)$, 1.9 MeV, Kα X-ray polaris. and line strengths 77−30983
Ar+H collisions, L Auger multiplet excitation 77−14589
$Ar+H^-$, collisional electron detachment, complete ang. distrib. 78−66650
$Ar+H^+$, low energy, L-shell ionisation, binding energy correction 77−54604
$Ar+H^+$ ions, K-Auger spectra, relative satellite line intensities, X-ray spectra 77−19066
$Au+H^+$, L-subshell ionisation cross-sections, X-ray meas. 77−46520
$C+H^+$, absolute C K X-ray production cross sections, 18-26 MeV 77−83719
$C+H^+$, electron capture in foils 78−42203
$C+H^+$, K-shell ionis., impact parameter depend., 90-200 keV 78−17775
$CH_4+H^+(He^+)(O^+)$, 1 MeV dissociation, kinetic energy spectra 78−94302
$CO+H^+$, vibr. excitation, 5-90 eV, forward scatt. differential cross section 78−9228
CO_2+H^+, vibr. excitation in differential scatt. 77−50503
$Ca^{18+}+H^+$, collisional excitation of fine struct. transitions in ground state 77−19017
$Cs+H^+(H_2^+)(H_3^+)$, total charge-transfer cross-sections meas. 77−50527
$Cu+h^+$, Cu K-shell ionis., probability ang. depend. 77−14553
D^+, D_2^+ and D_3^+ fragments traversing thick foils, correls. in motions, integral ang. distribs. 80−16136
$D+H^+(D^+)(He^+)(Ne^+)(Ar^+)(Kr^+)$, reson. charge charge transfer from photoexcited donor state 79−22820
$F+Xe(H)^+(H_2)$, $(^2P_{3/2})$ state quenching, Franck-Condon approach 78−66640
$Fe^{11+}+H^+$, collisional excitation cross-sections for ground configuration 78−33582
$Fe^{20+}+H^+$, collisional excitation of fine struct. transitions in ground state 77−19017
H II, Zeeman splitting of high-n recomb. lines 80−58210
H, ion equilib. density, in low press. system 78−9752
H^- ^1P resonances, pseudostate expansion calcs. 80−32841
H^-, $^1P_0$-reson., DC Stark effect calcs. 78−42000
H^-, $^1p^0(1)$ and $^3p^0(1)$ resonances associated with n=3 hydrogenic threshold 80−78557
H^-, $(2p^2)^3P$-state, CI series convergence 80−27955
H^- affinity radiation, theoretical study of negative absorption 80−38001
H^- and H electron loss in plasma target 78−67371
H^-, and isoelectronic sequence, correlated and HF electron density differences 78−46275
H^-, ang. distribs. from H_2 dissociative electron attachment 77−19099
H^-, autoioniation states, below N=3 hydrogenic threshold, complex-rot. calc. 77−67966
H^-, autoionising states, electric field effect 78−50528
H^- backscatt. from solid surface due to proton bombardment 80−99554
H^-, bakeable hollow cathode duoplasmatron source 77−6602
H^- beam, charge transfer cross sections in gases and vapours, 10 eV to 10 keV, graphs and tables 80−32824
H^- beam, intense, from Penning surface-plasma source, ion-optical charcts. 79−13892
H^- beam source, surface-plasma type, surface Cs loss mechanism *(Russian)* 77−79196
H^-, bound states in mag. field, binding anal., variational calcs. 80−42940
H^-, bound-free photodetachment cross section, rel. to opacity in cool stellar atms. 79−49996
H^-, bound-free photodetachment cross-section calcs. 80−9567
H^-, classical many-body collision model incorporating Heisenberg and Pauli principles 80−63511
H^-, combined CI and Hylleraas calc. for lowest ^1S and ^1P states 77−38617
H^-, DC Stark broadening of $^1P^0$ shape reson. 80−63585
H^-, density meas. by photodetachment 80−48976
H^-, dipole oscillator strength sum, in He isoelectronic series calcs. 78−86821
H^-, direct extraction sources, prod. and destruction in magnetron and duoplasmatrons 77−23340
H^-, double excited states below N=3 threshold, arrangement of resonances in series converging exponentially 80−99462
H^-, dynamic polarisability 79−76526
H^-, dynamic polarisability calc. 77−14599
H^-, elastic form factors, correlated two-electron-core pots., closed form expressions 79−68195
H^-, electron affinity, calc. of ion lifetime in elec. field 79−54986
hydrogen ions continued
H^-, electron correl. effects, ang. and radial, in momentum space 77−88399
H^-, electron detachment by electron impact, 1s state product, Born approx. 78−78816
H^-, electron loss cross sections in gases, using polarised projectiles 80−37872
H^-, electron loss in passing through inert gases 79−13805
H^-, electronic structure, stabilisation calcs. using big mol. Gaussian SCF/CI program 79−18121
H^-, energies and widths of $^1P^0(1)$ and $^1S(2)$ resonant states 79−18130
H^-, energy levels, doubly excited states, three particle Coulomb problem, hyperspherical coords. framework 80−52875
H^-, fluoresc. in γ- and UV-irrad. solvent matrices at 77K 78−70779
H^- form. by surface and vol. processes, neg. ion source appl., review 80−58375
H^-, formation by HCl dissociative electron attachment, differential cross section, Feshbach resons. 80−83508
H^- free-free transitions, target polarisation effects 79−66917
H^-, from H_2^+ ion beam surface interaction, H^- formation by reson. electron capture 80−40691
H^-, from hollow discharge dueoplasmatron, energy spectra 77−79490
H^-, generalised quantum defect, energy and radius depend. 80−14067
H^-, grazing incidence collision with surface, Balmer radiation, elliptical polarisation 78−86804
H^- grazing incidence collision on clean Pb or Ni crystal surface, elliptic polarisation in Balmer radiation 80−35039
H^- ground state, evaluation, failure of local exchange approx. 77−47758
H^-, ground state electron correlation visualisation 79−3367
H^-, ground state energy, post-adiabatic approx. calcs. 78−58827
H^-, H^{2-}, bound states calc. 79−13646
H^-, Hartree-Fock energies, scaled 1/Z expansion, integral eqns. 80−47886
H^-, in solar atmosphere, bound-free electron transitions, review 78−33563
H^-, ion beam bunching with sawtooth voltage 78−4735
H^-, ion beam diagnostics using laser beam 80−95497
H^- ion bound state, extensions to finite nuclear mass 78−29743
H^- ion direct extraction source 77−83393
H^- ion source, 50 mA for accelerator injection, beam quality and reliability 79−72172
H^-, ion source, CW plasma device, current maximisation 79−22521
H^- ion yield from duoplasmatron discharge 78−75382
H^-, magnetron discharge as ion source 77−38528
H^-, many-body perturbation theory with radially restricted basis functions 80−78526
H^-, metastable, electron affinity calcs. 79−31439
H^-, multipole sum rules 77−42257
H^-, n=4 resonances, complex rot. meas. calcs. 79−97995
H^-, numerical Hartree-Fock calc. of $1s^2$ ground state 79−81155
H^-, photoabsorpt. and dispersion profiles, moment theory 77−6709
H^-, photoabsorption spectra, long-range field effect 80−91521
H^-, photodetachment, Feshbach and shape resons. 77−23480
H^- photodetachment, Feshbach resonances 80−37753
H^-, photodetachment cross sections, one and two electrons, multichannel J-matrix calc. 77−18860
H^-, photodetachment cross section, dynamic polarisability calc., sum rules, basis set depend. 78−17635
H^-, photodetachment cross section, Feshbach and shape reson. elec. field depend. 78−37614
H^-, photodetachment cross section, perturbation-variation method 79−6921
H^- photodetachment cross section, narrow resonances near n=3 threshold 80−27988
H^- photofragments angular distribution, parity favoured electric dipole transitions 80−58330
H^- polarised intense beam prod. by atomic beam source 80−37674
H^- polarised ion source, pulse operated, Lamb shift type, for acceleration of polarised protons *(Japanese)* 77−67929
H^-, polarised prod. in ^1H+Cs atomic collision at 40 keV, 2.9 μA 78−55078
H^-, polarised proton sources BNL AGS, polarised proton acceleration 79−72055
H^-, polarised proton sources, 1 to 12 GeV beam transport at ANL ZGSynchrotron 79−72056
H^- positron complex, ground and excited states theoretical studies 80−42934
H^-, prod. by H_2^+ negative surface ionisation on ThO_2, plasma diagnostics appl. 80−6280
H^-, prod. from accel. cluster ions for neutral beam plasma injection heating 77−65376
H^- production, in surface plasma source with unclosed electron drift discharge 80−38846
H^-, production by Hall accelerator in Cs vapour, space-charge effects 78−67375
H^- production by low energy H atom bombardment of Mo surface 79−100006
H^-, production cross section in e^--H_3^+ collision 80−5628
H^- production cross sections in H^0+Cs collisions 80−78698
H^- production in foil breakup of H_2^+, inhibition effect 80−99549
H^-, production in laser-initiated alkali hydride arc 80−32550
H^-, proof of only one bound state, fixed nucleus approx. 77−30805
H^- radiation in acoustic dissipation and solar chromosphere 79−30029
H^- resonances in electric field 80−63607
H^-, S autoionising states, appl. of at. reson. theory 80−23329
H^-, S autoionising states, time stability theory 78−90130
H^-, S reson. state, appl. of improved line width expression 80−5505
H^-, shape reson., Stark effect, complex coords., translation and dilatation transforms 79−18141
H^- short bunch shaping at entrance of linear accelerator, calcs. 79−700
H^- source, pulsed hollow discharge duoplasmatron 77−26432
H^- source development at ANL 77−83394
H^- surface ion source, plasma parameters, diagnostics 78−9849
H^-, surface plasma source, ion form. and secondary electrons *(Russian)* 78−71503
H^-, surface plasma source, prod. by H atom backscatt. from cesiated W 77−3953
H^-, three-particle atomic system, binding energy, Faddeev method calcs. 77−57858

hydrogen ions continued
H^-, two-electon photodetachment threshold, blackbody radiation effects 80−91524
H^- vac. UV spectra, narrow reson. at 1129.5 Å, H-arc spectra 78−66490
H^-, variable energy polarised proton beam for TRIUMF cyclotron 79−72059
H^+ $(H_2^+)(H_3^+)$, impact on metal, backscattered H Balmer-β line intensity 77−23470
H^+ atmospheric daily vars. at mid-latitudes at sunspot max. 79−58167
H^+, backscatt. by Cu or Mo, 4-30 keV, O_2 effect 78−15268
H^+ beam, charge transfer cross sections in gases and vapours, 10 eV to 10 keV, graphs and tables 80−32824
H^+ beam, control using laser radiation 79−27112
H^+ beam, pure, production by four-lens Hall accelerator, focusing 78−66441
H^+, beam impact on C foil, K-shell X-ray yield 77−10624
H^+, beam-tilted C foil interactions, charge-state distrib., photon emission, 100-400 keV 79−22814
H^+, bombardment of $^{31}Ga(^{33}As)(^{34}Se)(^{35}Br)(^{55}Cs)$ L-shell X-ray prod. 79−47548
H^+, bombardment of second row element target, K-shell X-ray prod. 79−47550
H^+, calc. of mobility in He, 10 to 700K 78−66629
H^+, channelling in Au, planar channelling and blocking profile, transfer matrix method 78−22780
H^+ chemical shifts, INDO calcs. 80−32743
H^+ circulation across plasma membrane, role in bacterial growth 77−90751
H^+, collective accel. in vac. diode with sharp tip cathode, by 180 kV pulses 78−37104
H^+, collective accelerator, superconducting solenoids, resonators and cryogenic systems 78−46187
H^+, collective accelerator, superconducting solenoids, resonators, Q-values and field profiles 78−46188
H^+, electron capture from Si foil, cross-section calcs. 78−95623
H^+ electron capture in gas, calc., and s-p coherence quantum beats 79−89773
H^+, energy loss straggling in Kr, ion energies of 50-500 keV per nucleon 77−46620
H^+, expt. results on $\bar{W}$-values for heavy particles 79−7000
H^+ field-aligned downward vels. in mid-latitude ionosphere 79−40015
H^+, grazing incidence collision with surface, Balmer radiation, elliptical polarisation 78−86804
H^+ grazing incidence collision on clean Pb or Ni crystal surface, elliptic polarisation in Balmer radiation 80−35039
H^+, H_2^+ and H_3^+, beam-foil excitation, optical radiation obs. 80−9724
H^+, H_2^+ and H_3^+ interactions with thin foils, electronic polarisation wake effects, dissoc. of mol. ions 80−16135
H^+, impact on Al(Cu)(Mo)(stainless steel) surface, energy refl. coeffs. 78−54969
H^+, impact on C foil, H abundance in emitted beam 78−35236
H^+ in dawnside magnetosheath, bulk flows and energy anals. 80−4204
H^+, in H_2, tensor forces and intermediate particle exchanges 79−64067
H^+, in H_2 gas, energy loss, high-energy calcs. 77−6891
H^+, incident on metallic film, X-ray production, cluster effects 78−43961
H^+, intense beam generation, appl. to controlled fusion 77−76119
H^+, interdiffusion with alkali ions in glass surface, extended Boksay-Doremus theory 80−34254
H^+ ion mobility in He, expt. 80−96337
H^+, ion-surface collision with Mo, optical radiation emission 78−95644
H^+, isoelectronic sequence, quenching radiation anisotropy calcs. 77−27021
H^+, meas. of $\bar{W}$ in tissue equiv. gas, dosimetry appl. 80−19550
H^+ midlatitude trough location from Oreol 2 data 80−8473
H^+ mobility in HCl aq. soln., 15, 25, 40°C, up to 5000 atm 78−10207
H^+, mobility in He and Ne, 300K 77−11303
H^+, prod. by electron impact dissoc. of H_2, kinetic energy, ang. distribs. 80−63838
H^+, RF ion source, RIG 10, intense H^+ beams 80−37671
H^+, removal, using Itaya-zeolite *(Japanese)* 78−95951
H^+, reson. line regularities in plasma Stark widths and shifts 80−43881
H^+, secondary electron acceleration by protons in vacuum, ion bombardment effects 77−52210
H^+ transfer reaction tunnelling probability 80−26032
H^+, tranverse relax. time in H_2 gas at 300K 78−42099
H^{2-}, existence, alternative explanation of results, electron effects 77−19079
H^{2-}, existence, expt. evidence 77−19081
H^{2-}, metastable, electron affinity calcs. 79−31439
H^{2-}, metastable state 77−18805
H^{2-}, Z-Z 80−28104
H^{2+}, existence, alternative explanation of results, ion intensities 77−19080
H-like atom or ion, electron-electron interaction operator, dipole approx. 78−58821
H-like atoms and ions, statistical equilib. among sublevels in non-LTE plasma 77−31426
H-like clusters, DIM pot. energy hypersurfaces, stationary points 78−25763
H-like ion, ground state, Lamb shift, classical theory 79−97992
H-like ion+H charge stripping processes 77−19072
H-like ion+H^+, 1s-2s excitation probabilities, low energy, Coulomb-Born approx. 80−37870
H-like ions, critical ionisation, by electric fields, exact classical method 78−25731
H-like ions, elastic electron (positron) scatt., relativistic Glauber amplitudes 79−31681
H-like ions, electron impact excitation, Coulomb-Born-Oppenheimer calcs. 77−6938
H-like ions, electron impact excitation, distorted-wave approx., accuracy 78−5351
H-like ions, electron impact excitation, resonances, collision strengths 78−33612
H-like ions, electron impact excitation to S states exchange effects 78−58835
H-like ions, electron impact excitation to s state 78−58836
H-like ions, electron impact excitation, Coulomb Born approx. 78−58840
H-like ions, electron impact ionis. from 3s sub-level 78−90297
hydrogen ions continued
H-like ions, fluoresc. polarisation of Stark quenched spin-polarised beam 78−66501
H-like ions, Glauber exchange amplitudes for electron scatt. 78−74772
H-like ions, Lyman α self absorption, effect in quantum 2 and 3 states in recombining plasmas 78−37605
H-like ions, multiply charged, laser plasmas, 1.5-15 Å 78−13462
H-like ions, radiative level widths in low electric fields 78−37589
H-like ions, scaled Coulomb-Born-Oppenheimer collision strengths 79−22839
H-like ions, spectral broadening in plasma 79−46431
H-like ions, spectral line intensity, density depend., plasma diagnostic appls. 78−83617
H-like ions, Stark ionisation threshold electric field and energy calc. 78−25470
H-like ions+H^+, charge transfer cross sections 79−18286
H-like metastable ions, de-excitation in laser plasma *(Russian)* 77−7597
H-like multiply charged ion, superdense plasmas, line intensity ratio 78−63538
H-quark interaction, var. method calcs. 78−37771
H^--H_2 system, pot. energy surfaces 80−74215
H^--like ions, electron correlation and Coulomb hole in momentum space 78−86793
H^--positron bound states, CI-Hylleraas calcs. 77−10603
H^+-affinities of methylamine, ab initio SCF calculations 80−102443
H^+-affinities of NH_3, ab initio SCF calculations 80−102443
H^+-He^{2+}, ionised mixture, dense, binary, dynamical props., statistical mechs. 80−43895
H^+-He^{2+} mixture, fully ionised, two-component plasma, mean spherical model 80−87854
H^+-K^+ exchange and cell enlargement in maize coleoptile segments treated with auxin and fusicoccin 77−86469
$H+H^+$, charge exchange and differential scatt., theoretical calcs. 77−10729
$H+H^+$, charge transfer, Born approx. 79−59552
$H+H^+$, classical 3 body collision, cross section, energy transfer, computer calcs. 78−17783
$H+H^+$, coupled state calc., charge transfer and direct ionis. 79−22810
$H+H^+$, cross section for production of metastable H(2S) state 78−13588
$H+H^+$, differential energy loss cross-sections 77−46630
$H+H^+$, electron capture, 25 to 200 keV 77−88551
$H+H^+$, electron capture in high-energy approx. 77−42400
$H+H^+$, excitation ang. differential cross section, 25, 50 and 100 keV incident 78−66651
$H+H^+$, excited atom collisions, transitions between degenerate states 77−30976
$H+H^+$, fast proton total electron capture cross section, fixed scattered approx. 79−22819
$H+H^+$, interaction energy, perturbation theory, Pade approximants and convergence 79−31635
$H+H^+$, ionis. modified second Born approx. 77−88546
$H+H^+$, n-changing transtions, Glauber approx. 77−79686
$H+H^+$, quantum theory of ionisation in fast collisions 79−3553
$H+H^+$, transitions between degenerate states at low energies 77−79685
$H+H^+$ close capture collision spectroscopy, impact parameter perturbed stationary states 78−22002
$H+H^+$ coupling energy, internuclear separation depend. 77−14523
$H+H^+$ low energy, quantum theory, integrated cross sections, phase shifts 77−30957
$H+H^+(Arq^+)(Kr^{q+})(B^{q+})(C^{q+})(N^{q+})(O^{q+})$ charge transfer and impact ionis. cross sections calcs. 77−88555
$H^-+{}^4He^{2+}$, electron capture cross sections 79−10198
H^-+(He),(Ar),(Xe),(N_2), 1 to 5 keV, production cross sections for 3d,3s,4s,5s states of H 78−33603
H^-+Ar, 0.5 MeV $H(H^-)$ ionisation comparison 79−41230
H^-+Ar, electron detachment, 0.5 to 1.0 MeV 78−22021
$H^-+Ar(H_2)(He)(N_2)(Ne)$, collisional detachment cross-sections, high-energy obs. 77−3442
H^-+atom, electron loss high energy cross sections 78−13597
$H^-+CH_4 \rightleftharpoons CH_4+H^-$ intrinsic reaction coord. ab initio SCF calc. method 77−48626
H^-+Cs, fast atom collisions, charge exchange, equilib. fractions calcs. 78−33601
H^-+e^-, bound state calcs., channel coupling array theory 77−19005
H^-+H, electron detachment cross-sections, 100 keV-10 MeV 79−59561
H^-+H collisions, assoc. detachment process theory 79−44351
H^-+H_2, electron detachment cross-sections, 100 keV-10 MeV 79−59561
$H^-+H_2^+ \rightarrow H_2^*+H$ recombination react., calcs. *(Russian)* 80−55659
H^-+H_2(He)(Ar), electron detachment, Born cross sections, Pade approximants 78−17742
H^-+H_2(He)(Li), 50-150 keV, scatt. angle of neutral H 78−5340
H^-+H_2(He)(O_2)(N_2)(Ar), electron-loss cross sections 80−37877
H^-+H^+, charge exchange, one or two electrons, symmetry effects *(Russian)* 79−3562
H^-+H^+, double charge transfer, 30-200 eV 79−45837
H^-+H^+, electron capture, continuum distorted wave calcs. 78−50635
H^-+H^+, electron detachment cross sections 79−13818
H^-+H^+ charge exchange, quantum transition probabilities calc. 80−9557
$H^-+H^+ \rightarrow H(1S)+H$, level degeneracy effect on charge exchange at term pseudointersection 79−27084
H^-+HF, reaction, ab initio pot. energy surface calcs. 79−39127
$H^-+H(H_2)$, electron loss 80−37857
H^-+H(He), electron detachment cross sections 78−90265
H^-+H(He), electron detachment in adiabatic regime, mechanisms 80−63800
H^-+H(He), electron-loss cross-section, double closure calcs. 77−50518
$H^-+H \rightarrow H+H+e$, electron detachment from H^- 80−37855
H^-+He, electron detachment, theoretical obs. 80−63799
H^-+He, electron detachment cross-sections, 100 keV-10 MeV 79−59561
H^-+He, electron detachment cross-section, target distortion calcs., 100 keV-100 MeV 79−59562
H^-+He, electron detachment collision 80−23536
H^-+He(Ar), electron detachment cross sections 78−58810
H^-+He(Ar) low-energy total electron detachment cross-sections, approximation 79−72405

hydrogen ions continued
H^-+He(Ne)(Ar), differential scatt. cross-sections, time of flight spectra 78−42161
H^-+M^+ (M=alkali metal atom), ion-ion recombination 78−58779
H^-+methane→methane+H^-, nucleophilic substitution, ab initio pot. energy classical trajectory anal. 78−68886
H^-+methane→methane+H^- force decomposition anal. along reaction coord. 78−27741
H^-+N_2 (inert gas), charge transfer, ejected electron spectra 79−45828
H^-+N_2→N_2^-+H, vibr. autodetaching states, excitation and decay 78−33620
H^-+NH_4^+, substitution and abstraction reactions, ab initio calcs. 77−48624
H^++ hydrogenic ion, electron capture in highly excited s-state 79−45839
H^++ Ne, 3p-excitation , spectral analysis of photon emission 80−18916
H^++^{106}Cd, simultaneous nucl. and K-shell excitation, ^{107}In lifetime meas. 80−63130
H^++2HF, interaction pot., monopole approx., supermol. SCF and perturbation schemes 77−27139
H^++Ag, excited X-ray polarisation, Born approx. calcs. *(Russian)* 80−78566
H^++Ag, L-shell ionisation at large scatt. angles 78−90283
H^++Ag(Cu), X-ray emission, optical transition radn. 78−58618
H^++Ag(Cu)(Fe)(Se)(Ti)(Zr), K-shell ionisation cross-section determ. 80−48077
H^++Ag(Gd)(Yb)(Ta)(Au)(Pb)(Th), K-shell ionisation, 7-15 MeV, relativistic effects 78−82830
H^++Ag(Pd)(Sn), L-shell X-ray prod. cross-section determ. 77−6913
H^++Ag(Zr)(Fe)(Cu)(Ti) 80−106390
H^++Al(Cu), K-shell ionisation 0.5 to 40 MeV, meas. and PWBA-BEA calcs. 80−78699
H^++Al(Si) collisions, K-shell ionisation cross sections 77−23555
H^++alkali atom charge exchange, eikonal approx. 80−32830
H^++alkali metal, charge exchange, negative ion form. 79−50128
H^++alkali metal, charge exchange, eikonal approx. calcs. 80−78703
H^++alkali metal, valence and core electron capture collisions 79−94081
H^++Ar, 5-1.5 MeV, ejected-electron energy and ang. distrib., differential cross sections 77−88547
H^++Ar, charge exchange excitation, alignment tensor components, coincidence method 80−63795
H^++Ar, charge transfer and ionisation cross sections 79−89766
H^++Ar, Hα and Hβ emission cross section 80−63783
H^++Ar, importance of d-state couplings in charge transfer, ionisation 79−89760
H^++Ar, inner-shell charge transfer calcs. 77−50528
H^++Ar, ionisation, doubly differential cross sections calcs. 80−9726
H^++Ar, ionisation double differential cross sections 80−18913
H^++Ar, L- and K-shell electron capture, 1-15 MeV 77−54607
H^++Ar, subshell electron capture cross sections 79−89771
H^++atom, Coulomb excitation, proton energy loss depend. on impact parameters *(Russian)* 80−53123
H^++atom, electron capture, two-state atomic expansion 78−62912
H^++atom, emission electron angular and energy distribution 80−87222
H^++atom, excitation functions rel. to ionisation *(French)* 79−31669
H^++atom, inner shell ionis., coincidence exptl. method, theory 80−1066
H^++atom, inner shell ionisation, electronic relativistic effects 77−23552
H^++atom, ionis. cross section, realistic vel. distrib. for target electron 78−46439
H^++atom, ionisation, proton polaris. meas. 80−9482
H^++atom, ionisation cross-sections, thick target technique 78−37726
H^++atom, K_α/K_β ratio for at. X-ray transitions 80−27972
H^++atom, K-shell ionis., plane wave Born approx. model 77−34748
H^++atom, K-shell ionis. cross section for atoms, modified binary encounter model 78−46440
H^++atom, K-shell ionisation, semiclassical approx., projectile trajectory dependence 77−23551
H^++atom, K-shell ionisation, electronic final states description 77−38723
H^++atom collisions, inner shell excitation, impact parameter dependence 77−19047
H^++atoms (Z=27 to 34), K shell ionisation, nuclear Coulomb effect 80−91650
H^++Au(Bi)(u), L X-ray production cross sections, 0.3-1.8 MeV, expt. rel. to PWBA prediction 80−53115
H^++Au(Eu)(Ag)(Rb)(Cu), atomic K-shell ionis., X-ray emission 79−18280
H^++Au(Hg)(Pt), L-subshell X-ray prod., cross-section meas. 77−46575
H^++Au(Ho)(U), relativistic K-shell ionisation cross-section meas. 78−33593
H^++Au(Pb)(Th)(U), L-subshell vacancy production, Coulomb deflection effects 80−9711
H^++Au(Tl)(Pb)(Bi)(Th)(U), L-shell ionis., 0.5-3.5 MeV, X-ray emission obs. 77−54528
H^++Ba, electron capture, single and double, 1-100 keV 79−68313
H^++Be(B)(O), double K-shell ionis. of Be, B, O 78−25680
H^++C, K-shell ionisation, impact parameter depend. 78−62891
H^++C, vel. distribution of convoy electrons, anal. 78−33600
H^++C foil, 0.5-2.5 MeV, forward electron vel. distrib., peak shape 78−78794
H^++CN, perturbed rotational state approach 78−92469
H^++CN, rot. excitation, decoupled l-dominant calcs. 77−6900
H^++CN, scaling of energy and quantum no. for nonreactive collisions 80−9695
H^++CO, computed cross section vibr. threshold effects 80−63759
H^++CO ($^1\Sigma$), ground state pot. energy surface, ab initio SCF calc., protonated equilib. geometry 80−83301
H^++CO_2, vibr. excitation, isotope and time effects 80−63773
H^++CO($^1\Sigma$), vibr. excitation calc., close coupling and sudden approx. 80−78561
H^++CO(CO_2)(N_2O), electron capture into n=3 states, 2.2-8.2 keV 79−50129
H^++CO(NO), dissociative ionis. 79−10188
H^++C(N)(O)(Ne), K-shell Auger electrons ang. distrib. 79−89756
H^++C(N)(O)(Ne)(Ar), electron capture cross sections 78−62912
H^++Ca(Sc)(Ti)(V)(Cr)(Mn)(Fe), K X-ray production, 0.2-0.5 MeV, ionis. cross-section 79−31459
H^++Co(Ni)(Cu)(Zn)(Ge)(Se), K-shell ionisation cross-sections calcs. 80−43165
H^++Cs, charge exchange collision producing H(2s), semiclassical differential cross-section 79−59551

hydrogen ions continued
H^++Cs, elastic and charge exchange collisions, projected valence bond method 78−78804
H^++Cs, elastic scatt., differential cross-section calc., 13.4-24.2 eV 79−59530
H^++Cs, electron capture, H metastable fraction of n=2 population 77−30988
H^++Cs(Rb)(K)(Na), charge exchange, H(2s) form. 79−64101
H^++Cs(Rb)(K)(Na), single-electron capture total cross sections 80−91656
H^++Cs(6s), elastic scatt., pot. determ. from differential cross-sections meas. 78−78778
H^++Cs→H^-+Cs^{2+}, proton conversion, 0.2 to 6.0 keV *(Russian)* 77−1920
H^++Cs→H(2s)+Cs^+, near reson. charge transfer, low energy 79−54964
H^++Cu, K-shell ionis., Coulomb deflection effects, 0.5-2 MeV 78−17779
H^++Cu(Ag), K-shell X-ray prod. cross sections 78−5337
H^++D_2, collisional complex form. 80−58339
H^++D_2, differential inelastic and reactive scatt., low energies 78−62911
H^++D→H+D^+ near threshold rel. to HD molecule formation in interstellar medium 78−89239
H^++Dy(Xe),(Au), ionisation, induced L-shell alignment 80−32813
H^++F($^2P_{1/2}$), nonadiabatic collision processes, electronic degrees of freedom, classical model 79−64062
H^++Fe^{12+}, forbidden lines collisional excitation, importance of short range pot. 77−17457
H^++Ge collisions, charge exchange 77−6922
H^++graphite, 10 keV, chemical sputtering coeff. temp. depend., methane form. *(Russian)* 77−4707
H^++H, 1-7 keV, H(2s) form. and Lyman-α polarisation 80−14221
H^++H, 15-200 keV, excitation and charge transfer cross sections, Sturmian expansion 77−19024
H^++H, 1s charge exchange amplitudes, impact parameter calcs. 77−534
H^++H, 1s→2s excitation at intermediate energy, close coupled and Glauber eikonal theory 78−25643
H^++H, 50-200 keV, excitation and ionis., U-matrix method calcs. 78−17778
H^++H, capture cross sections, Faddeev anal. 77−27178
H^++H, charge exchange probability 79−98216
H^++H, charge transfer, variationally consistent approximation scheme 79−22825
H^++H, charge transfer collisions, angular distribution 78−13599
H^++H, charge transfer cross section calc., up to 100 keV 78−55235
H^++H, electron capture in 3s level, distortion approx. 80−37876
H^++H, electron capture into n, l levels, 100 keV/amu 79−22826
H^++H, excitation, asymptotic cross-sections calcs. 79−18279
H^++H, excitation, differential cross-section 79−59547
H^++H, excitation, distorted wave and coupled-channel calcs. 80−9713
H^++H, excitation, pseudostate expansions and second Born approx. 79−45796
H^++H, excitation and charge transfer to 2s(2p) states, 49-125 keV 80−18910
H^++H, excitation and electron capture, impact parameter calc. 78−33591
H^++H, gas-phase collisions, intermediate and high velocities, excitation 80−32822
H^++H, H excitation, angular differential cross sections 80−63784
H^++H, H(2p) production in slow collisions, peak struct. 80−1057
H^++H, high-Rydberg state high-impact-velocity forward charge transfer as classical process 79−22824
H^++H, in plasma, H line Stark broadening, role of ion dynamics simulation 80−24144
H^++H, inelastic collision, time depend. Schrodinger eqn. for electron motion 79−89774
H^++H, interaction energy, perturbation expansion, symmetry forcing 79−22785
H^++H, ionisation and electron capture to continuum 80−58366
H^++H, low energy, optimised translation factors 80−18813
H^++H, nuclear repulsion, contrib. to charge transfer 80−18922
H^++H, relativistic classical theory of electron capture 80−18920
H^++H, transition probabilities and total cross-sections, high energy behaviour 78−9245
H^++H, vibr. excited H_2^+ form. by stimulated radiative association 79−100346
H^++H collision, eikonal approximation, reson. charge exchange ang. distrib. and atom refl. *(Russian)* 77−34759
H^++H collisions, H(2s), H(2p) production, 1-7 KeV, differential, total cross sections 80−32818
H^++H high energy collision, excitation multipole moments, classical trajectory approx. 80−106389
H^++H_2, charge transfer into continuum 79−89765
H^++H_2, collisions at 3.7 eV, rotational transition probabilities 77−27156
H^++H_2, coupled states calcs. of inelastic collisions at 3.7 eV 77−14538
H^++H_2, elastic of rot. excitation, semiclassical treatment 79−31657
H^++H_2, elastic scatt. and rot. excitation, multistate semiclassical orbital method 79−27058
H^++H_2, electron capture cross-section, anal. evaluation 79−36756
H^++H_2, electron capture into ground and excited s states 79−76509
H^++H_2, H^+ prod., from H_2^+ dissoc. states or H_2^{2+} 78−20015
H^++H_2, inelastic collisions at 3.7 eV, close cou-ing calcs. 77−34734
H^++H_2, rot. and vibr. excitation 78−33579
H^++H_2, rot. and vibr. excitation, energy loss obs. 80−63773
H^++H_2, rot. excitation and vibr. transitions, coupled state approx. 77−61835
H^++H_2, rot. quantum transitions 79−845
H^++H_2, rotated Morse curve-spline pot. function 78−80729
H^++H_2, rotational excitations, close-coupling calcs. 77−27157
H^++H_2, rotational quantum excitation, time of flight spectra 77−27154
H^++H_2, sudden approx. of Cross, computational tests, cross section factorisation, scatt. phenomena 80−58352
H^++H_2, time depend. close coupling, vibr. excitation, impact parameter calcs. 77−88534
H^++H_2, vibr. excitation, ab initio CI pot. energy surface calcs. 80−74228
H^++H_2, vibr. excitation, energy loss spectra, rot. sudden impact calcs. 77−88537

hydrogen ions continued
$H^+ + H_2$, vibr.-rot excitation, ab initio CI pot. energy surface calcs. 80−74229
$H^+ + H_2$, vibrationally inelastic collisions, 3D impact parameter approach 77−75268
$H^+ + H_2O$, inelastic scatt., 4-6 eV energy loss region 78−90277
$H^+ + H_2O(N_2)$, UV and visible band emission cross-sections 77−16847
$H^+ + H_2(CO_2)$, vibr. excitation, 10-30 meV 80−58358
$H^+ + H_2(N_2)$, 5-100 keV, secondary electron energy and ang. distrib. 80−14223
$H^+ + H_2 \rightarrow H_3$, nonadiabatic transitions, comparison of surface hopping and complex-valued time calcs. 77−9049
$H^+ + H^-$, double charge transfer, 30-200 eV 79−45837
$H^+ + H^-$, electron detachment cross-section, crossed beam meas. 77−10728
$H^+ + H^-$, merged beams, double charge transfer cross section 79−22818
$H^+ + H^- \rightarrow H_2^* \rightarrow H_2^+ + e$, 0.001 to 3 eV assoc. ionisation cross-sections meas. 79−3512
$H^+ +$H-like ion, electron capture, Coulomb-Born approx. 79−45838
$H^+ + HNO_2$, mechanism, electrostatic pot. prediction limits 78−11506
$H^+ +$H(D), elastic scatt., rainbow struct. and g-u-interference effects 77−6886
$H^+ +$H(D), elastic scatt. and charge exchange, resonances 78−78777
$H^+ +$H(D), low energy elastic cross sections, impact parameter calc. 77−14526
$H^+ + H(H_2)$, electron capture, H(2s) cross section meas. 79−72386
$H^+ +$H(He)(Ar), K-electron capture, cross section scaling, high energy 79−41236
$H^+ + H(O_2)(N_2)$, energy transfer and ionisation cross-section calcs. 77−50522
$H^+ +$H(O), in upper atm., rel. to H^+ loss during solar cycle 78−93021
$H^+ +$H(1s), charge transfer, 0.025-200 keV/amu 79−22823
$H^+ +$H(1s), radiative charge exchange, 1-50 MeV 78−55234
$H^+ +$H(1s), reson. charge transfer, spin depend. *(Russian)* 78−29850
$H^+ + H(1s) \rightarrow H(1s) + H^+$, electron capture at relativistic energies, scatt. amplitude 80−1061
$H^+ + H(1s) \rightarrow H(nl) + H^+$, cross-sections, continuum distorted-wave approx. 77−68108
$H^+ + H(1s) \rightarrow H(nlm) + H^+$, highly excited states rearrangement collisions 79−59564
$H^+ + H \rightarrow H + H^+$, charge exchange, atomic scattering, many-particle theory 77−10715
$H^+ +$He, $1^1S \rightarrow 4^1S$ excitation cross-section calcs., 10 to 5000 keV 78−25689
$H^+ +$He, 1-1000 keV, electron capture cross-sections, charge-transfer eqns. 77−75294
$H^+ +$He, 25-1000 keV, $1^1S \rightarrow n^1S$ excitation cross sections, Glauber approx. calc. 79−54959
$H^+ +$He, collisional excitation, 2nd order pots. method calcs. 78−13608
$H^+ +$He, determ. of He excited state populations by two-photon reson. ionisation spectroscopy 78−82707
$H^+ +$He, differential scatt., 1-12 eV, high resolution beam meas. 80−58348
$H^+ +$He, double electron capture, close-coupling approx. calcs. 77−71868
$H^+ +$He, double He ionis., polarised electron vel. distrib. effect 80−53109
$H^+ +$He, double K-shell electron capture, theory 79−68315
$H^+ +$He, elastic scatt. and 2^1s and 2^4p excitation cross-sections 79−36747
$H^+ +$He, electron capture and impact-ionis. cross sections, Monte Carlo calcs. 79−27083
$H^+ +$He, electron capture total cross sections 78−5322
$H^+ +$He, excitation, ang. differential cross-sections for 25, 50 and 100 keV protons 78−82832
$H^+ +$He, interaction pot., calculated vs. value from ion mobility data 77−14518
$H^+ +$He, ionising collision, first-order Faddeev approx. 79−22827
$H^+ +$He, mobility and diffusion, runaway effect 80−33727
$H^+ +$He, proton energy degradation, approx. yield spectrum 79−31643
$H^+ +$He, runaway mobility obs. 80−38517
$H^+ + He^+$, charge transfer and ionis. cross sections, coincidence meas. 78−50634
$H^+ + He^+$, fast collision, ionisation and charge transfer, cross section meas. 78−25698
$H^+ + He^+$, ground-state electron capture cross-sections, Coulomb-Born calcs. 78−42166
$H^+ + He^+$, He^{2+} form. by charge exchange and ionis., cross sections 77−83708
$H^+ + He^+$, ionis. and charge transfer cross sections 78−42186
$H^+ + He^+$, ionisation and charge transfer using intersecting beams 77−68104
$H^+ +$He(Ar), charge exchange, differential cross sections 79−7006
$H^+ +$He(Ar), emitted electron's energy and angular distrib. support for charge transfer to continuum theory 78−37740
$H^+ +$He(Ar) electron transfer cross sections 78−58809
$H^+ +$He(Ar)(C), ionisation processes viewed in forward direction 77−71866
$H^+ +$He(Ar)(Kr)$(O_2)(H_2)(N_2)$, 2.2-8.2 keV, H(n=3) form., absolute cross sections 77−34755
$H^+ +$He(Ar)(O_2), charge transfer to H(n=2), mixed parity elec.-dipole oscillations 79−31678
$H^+ +$He(C)(Ne), K-shell charge transfer cross sections, Bates-Born formalisms 79−45834
$H^+ +$He(Ne), multiply ionised ats. prod. 80−28098
$H^+ +$He(Ne)(Ar), ang. and energy distrib. of ejected electrons 79−31668
$H^+ +$He(Ne)(Ar), ionisation, projectile energy depend., secondary electron energy distrib. 78−42211
$H^+ +$He(Ne)(Ar), K-shell ionisation cross-sections, Glauber approx. calcs. 77−46629
$H^+ +$He(Ne)(Ar)(Kr), charge exchange, 80 to 1500 eV, total cross sections 77−61854
$H^+ +$He(Xe)(Kr)(Li)(Na)(K), electron capture cross sections 79−86061
$H^+ +$He(1^1S), He(n^1P) excitation cross sections computation 79−94070
$H^+ + He(1s^2) \rightarrow H^* + He^+(1s)$, continuum distorted wave approx., total cross section 77−68109
$H^+ +$Hf(Ta)(W), L-subshell ionisation cross section, branching ratios, fluoresc. yield, Coster-Kronig factors 80−43166
$H^+ +$Ho(Sm), X-ray intensity ratios, projectile energy depend. 80−23535
hydrogen ions continued
$H^+ +$inert gas, 4s-state electron capture cross-section meas. 78−82836
$H^+ +$inert gas, binary encounter calc., cross section calc. 79−72412
$H^+ +$inert gas, charge transfer into excited states, 10-150 keV, target at. struct. depend. 79−45830
$H^+ +$inert gas, electron capture, charge-state distrib. 80−32814
$H^+ +$inert gas, outer S-shell ionisation cross-section calcs. *(French)* 78−42212
$H^+ +$ion, in solar corona, approximations for fine struct. excitation 77−17463
$H^+ +$Kr, charge exchange cross-sections *(German)* 77−10753
$H^+ +$Kr, mol. orbit approach, spin-orbit interaction, adiabatic pot. and projected valence band treatments 77−533
$H^+ +$Kr(Ar) charge exchange, oscillating cross sections 77−58158
$H^+ +$Kr(Xe), electron capture into 3s state, cross-section meas. 78−42209
$H^+ +$lanthanide atom, L-subshell ionisation cross-section, 150-400 keV 79−45665
$H^+ +$Li, charge exchange, eikonal approx. calcs. 80−78703
$H^+ +$Li, excited state form. obs. 80−9686
$H^+ +$Li, Li excitation mechanisms, Auger and autoionisation spectra 77−19042
$H^+ + Li^+$, charge transfer and ionisation, total cross sections for production of Li^{2+} determ. 80−91657
$H^+ +$Li$\rightarrow$Li(X)+H(nl), (X=1^1S, 2^1S, 2^3S and nl=1s, 2s, 2p) continuum distorted wave method calc. 80−1062
$H^+ +$metal ion, pot. curve, for exchange, Landau-Rosen and Rosen-Zinner model *(Russian)* 77−75287
$H^+ +$methane, (Ne), (Ar), inner shell electron capture cross-sections 79−76510
$H^+ +$methane$\rightarrow H_2^+ +$methyl radical, quantum 80−71911
$H^+ +$Mg, electron capture, single and double, 1-100 keV 79−68313
$H^+ +$Mg, electron capture and impact ionisation cross sections, CI calc. 80−23343
$H^+ +$Mg, inner-shell ionisation by H^+, He^+ impact, target atom ionic alignment, Born approx. 78−78789
$H^+ +$Mg(Ba), metastable H form. by charge exchange 79−81275
$H^+ +$molecule, F K-shell ionisation 77−50515
$H^+ +$molecule (C-, F- or O-containing), K X-ray yields 79−45736
$H^+ +$multielectron atom, fast collision, electron capture, differential cross section calcs. 78−94318
$H^+ + N_2$, N_2^+ 3914 Å emission cross sections, 0.5-34 keV 77−54598
$H^+ + N_2$, vibrational N_2^+ excitation *(Russian)* 80−53156
$H^+ + N_2$ collision, binary encounter calcs. of proton energy deposition 78−74746
$H^+ + N_2$ collision, total ionis. cross section and stopping power for protons 80−69228
$H^+ + N_2^+$, fluoresc. efficiency, 3914 Å band of N_2^+ (1N), 100 eV-10 MeV 78−74697
$H^+ + N_2(CO)(NO)$, vibr. excitation, differential scatt., low energy meas. 79−89749
$H^+ + N^+(O^{2+})(Ne^{4+})(Na^{5+})$ (Mg^{6+}), ^3P_J fine structure transitions 80−37864
$H^+ +$NO, ~10 eV, anomalous excitation of NO Rydberg states 77−14546
$H^+ +$Na, charge transfer cross section and equilibrium fractions, 1-25 keV 80−5616
$H^+ +$Na, Na $2p^5 3s^2\ ^2P_{3/2}$ state alignment by 5-30 keV excitation 80−14200
$H^+ +$Na(Cs), charge transfer processes with plasma gun, Lyman-α radiation exam. 78−46573
$H^+ +$Na(K), excited state form. by inelastic processes, energy partitioning 78−82833
$H^+ +$Na(Mg)(Al)(Si)(Ti), K-shell ionisation cross sections for 15-65 keV protons 78−90284
$H^+ +$Na(k), configuration interaction potentials and rainbow angle scatt. cross section 80−37745
$H^+ +$Ne, multiple ionisation of Ne 2s and 2p electrons 80−18918
$H^+ +$Ne(He), specific primary excitation by fast accelerator particles 80−23559
$H^+ + Ne(N_2)(SF_6)$, K-shell ionisation, AES meas. 77−10749
$H^+ + O_2$, dissoc. ionisation, kinetic energy spectra 78−25684
$H^+ + O_2$, energy transfer, vibronic excitation, emission spectra 78−66578
$H^+ + O_2^-$, nanosec. pulse radiolysis, rate consts. meas. 77−16843
$H^+ + O_2(N_2)$(Ne), K-shell capture cross-section, Auger effect 78−33602
$H^+ +$p-H_2, angular momentum and cross sections, sudden centrifugal pot. calcs. 78−42157
$H^+ +$Pb, (L_α, L_β, L_γ) X-ray emission probability, impact parameter dependence 77−23553
$H^+ +$Pd(Sb)(La), ionisation cross sections for L_1 and L_2 subshells by 250-500 keV protons *(Russian)* 77−6918
$H^+ +$Rb, single photon emission following double K-shell ionisation, contrib. to superheavy element search data 78−50625
$H^+ + SF_6$, mode selective vibr. excitation 80−58351
$H^+ + SF_6(TeF_6)$, mol. ionisation, 0.3-1.8 MeV, ejected electron energy and ang. distrib. 78−22015
$H^+ +$S(K)(Ni)(Cu)(Ga)(Br)(Ag)(Cs)(W), 4 MeV beam-foil X-ray production cross-section 79−7003
$H^+ +$Si collisions, charge exchange 77−6921
$H^+ +$Ti(Fe)(Ni)(Zn), K-shell ionisation calcs. 80−23534
$H^+ +$Ti(V)(Cr)(Mn)(Fe) K-shell ionisation cross sections 77−23556
$H^+ +$U(Ni)(Au)(Sn), 4.88 GeV, K-vacancy production cross sections 77−19036
$H^+ +$Zn(Cd), L- and M-shell Auger electrons 79−27076
H_2^-, autoionising states, complex scaling method calcs. 80−9527
H_2^-, collision induced dissoc., positive and negative ions form. 78−50612
H_2^-, core-excited Σ reson. state, ab initio CI LCAO calcs. 79−31385
H_2^-, free free absorpt. coeffs. dipole length formulation and two centre close coupling calc. 80−83345
H_2^-, free free absorpt. rel. to opacity in stellar atms. 78−81610
H_2^- resonant states, Feshbach projection-operator calc. 78−5153
H_2^-, variational calcs. of resonant states 79−3571
H_2^+, $1\sigma_g$ and $1\sigma_u$, Schrodinger eqn. soln. 77−57854
H_2^+, 400 keV beam dissoc. collisions in air, ang. distribs., vibr. state effects 79−10197
H_2^+, 6 MeV, PIXE anal. of organic materials 80−26087
H_2^+, backscatt. by Cu or Mo, 4-30 keV, O_2 effect 78−15268
H_2^+ beam form., selected vibr. states, by electron impact in high press. Ne 77−65547
H_2^+, binding energy, MINDO/3 calcs. *(German)* 79−3366

hydrogen ions continued
H_2^+ bonding, simplest MO approx. 77−30948
H_2^+, bound state problems, many-body scatt. theory, arrangement channel 77−75044
H_2^+, bound states in strong mag. field 80−99438
H_2^+, calc. of lowest vibr. states where L=0, P=+ 79−31502
H_2^+, collisional dissoc., excited electronic states effects 80−9687
H_2^+, Compton profile and momentum distribution, impulse approx. 78−25626
H_2^+, coupled-channel Schrodinger eqn. bound states, renormalised Numerov method 79−13627
H_2^+, covalent bonding and classical charge density 80−37722
H_2^+ differential cross section rel. to charge exchange cross sections of fragments 80−78704
H_2^+, discontinuous approx. wave function, ab initio LCAO and VB ZDO calcs. 77−50340
H_2^+, dissoc. following beam-foil interaction 78−70920
H_2^+, dissoc. recombination, doubly excited Rydberg states 80−83506
H_2^+, dissociative recombination, projection operator formalism 77−3479
H_2^+, dissociative recombination in low energy electron collisions 79−3563
H_2^+, dissociative recombination cross sections 79−59568
H_2^+, dynamic dipole polarisability, variational perturbation theory 78−94330
H_2^+, dynamic polarisability, electronic states two centre Coulombic Green's function, continuous spectrum exclusion 78−82626
H_2^+, electron cooling through resonant collisions 80−32845
H_2^+, electron elastic scatt., two-centre variational calc. of s-wave phaseshift 79−3570
H_2^+, electron elastic scatt., phaseshifts, quantum defect and two electron excited states 80−91671
H_2^+, electron impact, dissoc. recomb., highly excited atom form. *(Russian)* 78−33621
H_2^+, electron impact, dissociative recombination 79−89796
H_2^+, electron impact dissoc. recomb. cross sections, Rydberg states form., merged-beams expt. 78−25725
H_2^+, electron impact dissociation variationally adjusted LCAO mol. orbitals calcs. 77−3473
H_2^+, electron scatt., Schwinger variational principle appl. 80−48086
H_2^+, electron scatt. eqns. convergence, H_2 continuum states, appl. to photoionis. 78−66663
H_2^+, electronic energy levels calc. 77−57856
H_2^+, electronic stopping power of slow mol. ions in solids 79−10888
H_2^+, energy loss in C foil, moving ion pot. determ. 78−33572
H_2^+, energy spectra of emergent dissoc. and recomb. products from C film 79−45819
H_2^+ energy spectrum, variational cellular method calcs. 78−94192
H_2^+, exchange perturbation theory 80−63518
H_2^+, exponentially small part of wave function *(Russian)* 80−9497
H_2^+, extended LCAO method, 1sσg orbital *(Russian)* 79−93922
H_2^+, floating orbital calc. of elec. field gradient, quadrupole coupling const. 77−12248
H_2^+, grazing incidence collision with surface, Balmer radiation, elliptical polarisation 78−86804
H_2^+ grazing incidence collision on clean Pb or Ni crystal surface, elliptic polarisation in Balmer radiation 80−35039
H_2^+, ground and first excited states in homogeneous magnetic field 78−925
H_2^+, ground state, asymptotic primitive function, symmetry adapted perturbation calcs. 79−6855
H_2^+, ground state, pot. energy curves, 1/R expansion coeff. calcs. 80−91472
H_2^+, ground state energy inverse power expansion of two proton distances 79−97976
H_2^+, HD^+ electron reduced mass use in electronic Schrodinger eqn. 77−10576
H_2^+, high (10^9 G) mag. fields, dissoc. energy, electron binding energy and equilib. separation 80−52910
H_2^+, hyperfine struct., allowed transition freqs. 79−13630
H_2^+, hyperfine struct., refined var. calcs. 77−75067
H_2^+, hyperpolarisabilities, quadrupole and field-gradient quadrupole polarisabilities 80−1086
H_2^+, IR photodissoc. cross sections, calc. and simulation expt. 80−9659
H_2^+, impact on Al(Cu)(Mo)(stainless steel) surface, energy refl. coeffs. 78−54969
H_2^+, impact on C foil, H abundance in emitted beam 78−35236
H_2^+, in H_2 dissociative photoionisation, 19.8-40.8 eV, proton kinetic energy spectra 79−68273
H_2^+, in mag. field, LCAO calcs. 78−82628
H_2^+, incident on metallic film, X-ray production, cluster effects 78−43961
H_2^+, individual orbital contribs. to SCF virial 79−3349
H_2^+, interstellar, role in star form. from hot matter with primordial chemical comp. *(Russian)* 78−40924
H_2^+, intramol. interaction energy, convergence of perturbation expansions 78−17745
H_2^+, ion beam surface interaction, H^- formation by reson. electron capture 80−40691
H_2^+, ion-surface collision with Mo, optical radiation emission 78−95644
H_2^+, ionisation energy, internucl. separation in intense mag. fields, var. calcs. 77−57898
H_2^+, ionisation energy in strong mag. field, variational calcs., equilib. internucl. separation 77−46654
H_2^+, LCAO method, improvement by directed variation of exponential parameters 79−41101
H_2^+, modulated perturbation theory variational calc., ground state second order energy 77−57872
H_2^+, mol. electron density distrib., binding/antibinding anal. 80−95534
H_2^+, mol. energy in strong magnetic field, MO SCF calcs. 79−6858
H_2^+, mol. props. in intense mag. fields 79−81169
H_2^+, moment functions calcs. and radiative corrections 78−90141
H_2^+, multiple scattering technique, space partitioning effects 79−85883
H_2^+, muonic, three-body Coulomb interaction, adiabatic representation 79−31640
H_2^+, natural orbital anal. of nonadiabatic wave functions 79−81151
H_2^+, negative surface ionisation on ThO_2, plasma diagnostics appl. 80−6280
H_2^+, nonadiabatic vibrational energies, ab initio calcs. 78−90142
H_2^+, nonexponential wavefunctions for $1s\sigma_g$ and $2p\sigma_u$ states 77−415
H_2^+, nonexponential wavefunctions for $2p\pi_u$, $3d\pi_g$ and $3d\delta g$, $4f\delta_u$ states 77−416
hydrogen ions continued
H_2^+, nonseparable Schrodinger eqn., series solns. and variational principle 79−36504
H_2^+, one centre partial wave treatment, Coulomb versus electron exchange intermol. forces 79−6839
H_2^+, one-electron wavefunction calcs., expectation values 77−83483
H_2^+, path integral formalism of perturbation theory, simple mols. and atoms 79−6841
H_2^+, photodissoc., H^+ ang. and energy distribs. meas., ion cyclotron reson. cell 77−31026
H_2^+, photodissoc., mass spectra 80−86489
H_2^+, photoionisation calcs., role of dipole operators 77−58091
H_2^+, photoionisation effective cross sections 80−43121
H_2^+, polarisability, internuclear distance depend., excluding continuous spectrum 77−10581
H_2^+, polarised Balmer radiation due to scatt. from Nb surface, adsorbed O_2 effects 80−99569
H_2^+, quantum mechanics *(Hungarian)* 79−757
H_2^+, Raman and Rayleigh scatt. tensors 79−50027
H_2^+, Rayleigh and Raman scatt., diatomic homopolar mol. theory *(Hungarian)* 77−50442
H_2^+, recombination yield on emerging from ultrathin C film below Bohr vel. 79−50108
H_2^+, repulsive states in dissociative ionis. of H_2 at 304 Å 78−82792
H_2^+, reson. states, complex basis functions methods 79−6887
H_2^+, restricted quantum-mechanical three-body problem 80−42083
H_2^+, SCF multiple scatt. calc. 80−916
H_2^+, satellite line shape, classical broadening theory including Doppler effect, pot. effect 79−22764
H_2^+, semiclassical quantisation for low lying electronic states 79−68183
H_2^+, semiempirical model for polarisation of s-type AOs, pot. curve and surfaces determ. 77−88400
H_2^+, semiempirical nonadiabatic pot. energy curves calcs. 78−17744
H_2^+, spontaneous emission lifetimes in ground electronic states 80−32810
H_2^+, spurious avoided-crossings, variationally calc., perturbation theory approach 78−5295
H_2^+, static polarisability determ. by optimised rot. method 79−54990
H_2^+ three lower states, three body problems, separations of variables 80−36903
H_2^+, transmission yield through thin C-foil meas. 80−100732
H_2^+, variational cellular model 78−29726
H_2^+, vibr. eigenenergies representation, functional form 79−68220
H_2^+, vibr. excitation, cooling mechanism for hot protogalactic gas *(Russian)* 79−17149
H_2^+, vibr. Green's function and two-photon dissociation 80−28075
H_2^+, X-ray absorption spectra, method of coupled differential eqns. 77−88466
H_2^+, Xα statistical exchange calcs. 77−30766
H_2^+, Temple lower bound mol. orbitals, GTO calcs. 78−41935
$H_{2\text{-}4)}^+$ + He, 200-850 eV, attentuation and fragmentation 78−62968
H_2+H^+, combined rot. sudden and vibr. exact quantum treatment 78−74739
H_2+H^+, electron capture probability 78−58808
(H_2+H^+, H_2^++H) collinear system, electronically nonadiabatic effects 78−1063
H_2+H^+, inelastic forward scattering, vibr. excitation, glory oscills. 79−22799
H_2+H^+, low energy rot. excitation, ab initio differential inelastic cross section calcs. 77−88542
H_2+H^+ differential inelastic and reactive scatt., low energies 78−62911
H_2^++1,3-butadienes, singlet-triplet transitions energies, relative cross sections 78−86942
H_2^++Ar, endothermic charge transfer reaction, low energy crossed beam study 80−95720
H_2^++Ar, ionisation double differential cross sections 80−18913
H_2^++Ar, low energy proton transfer reactions, crossed beam studies 80−108697
H_2^++Ar(He)(H_2), 10 keV dissoc. charge exchange collisions 78−94319
H_2^++Ar→ArH^++H, electronic transitions, collinear reaction, curve crossing model, DIMZO surface 79−74373
H_2^++C, vel. distribution of convoy electrons, anal. 78−33600
H_2^++C foil, 0.5-2.5 MeV, forward electron vel. distrib., peak shape 78−78794
H_2^++C thin solid target, 50-300 keV, collisional at. physics using mol. projectiles 79−45813
H_2^++CO, dissoc, charge transfer, energy transfer processes 78−74759
H_2^++CO excited products dissoc., proton transfer dynamics, correl. diagram anal., corssed beam obs. 80−48079
H_2^++CO_2, charge transfer, energy transfer, product ion excitation and fluoresc. 77−75288
H_2^++CO→H+HCO^+, 1.89 eV crossed beam study 80−21287
H_2^++D_2→$_2$H++H, product angular and vel. vector distributions meas. by crossed beam expt. 80−101012
H_2^++H, reaction, ion cyclotron reson. mass spectrometric obs. 79−64098
H_2^++H_2, 10 keV H_2^+ dissociation, H-H^+, H^+-H^+ and H-H fragments 77−83688
H_2^++H_2, H^+ prod., from H_2^+ dissoc. states or H_2^{2+} 78−20015
H_2^++H_2, pot. energy surface and nonadiabatic regions, charge exchange and reaction, VB calc. 78−40027
H_2^++H_2, predissociation of $c^3\Pi_u$ state, flight time difference obs. 77−27164
H_2^++H_2, state selected reaction cross sections, coincidence technique obs. 80−66797
H_2^++H_2O, inelastic scatt., 4-6 eV energy loss region 78−90277
H_2^++H_2→H_3^++H, electronically excited products, merged beam apparatus meas. 78−31626
H_2^++H_2→H_3^++H, reaction dynamics, isotopic variations 78−27745
H_2^++H_2→H_3^++H, state selected, threshold electron-secondary ion coincidence method obs. 79−5190
H_2^++H^-→H_2*+H recombination react., calcs. *(Russian)* 80−55659
H_2^++He, 10 keV, dissoc. excitation, ionis., energy distrib. 77−61849
H_2^++He, collinear trajectories, pattern recognition 80−45481
H_2^++He, collision in laser field, vibr. excitation 78−86937
H_2^++He, collisional dissoc., expt. and quasiclassical trajectory calcs., eV region 78−42201
H_2^++He, interaction pot., calculated vs. value from ion mobility data 77−14518
H_2^++He, reactive and dissociative scatt., crossed-beam and trajectory obs. 78−64833

hydrogen ions continued
H_2^++He, vibr. energy effects on kinetics, phase space model 78−11508
H_2^++He(Ar), emitted electron's energy and angular distrib. support for charge transfer to continuum theory 78−37740
H_2^++He(Ar)(C), ionisation processes viewed in forward direction 77−71866
H_2^++He(Kr)(Xe), collisional dissociation, ion-pair prod., negative ion prod., cross sections 77−14529
H_2^++He(Ne)→He(Ne)H^++H, vibr. state distrib. prod. by H_2 vibr. autoionisation cross section depend. 77−48628
H_2^++He→H+HeH^+, endoergic exchange, DWBA calcs. 77−9055
H_2^++He→H+HeH^+, product ion ang. distrib., quantum mech. impulse approx. calcs. 79−24727
H_2^++He→H+HeH^+, reaction dynamics, vibr. state channels, beam expt., trajectory calcs. 77−77739
H_2^++He→H+HeH^+, total cross sections, quasiclassical trajectory results compared with mol. beam data 77−60051
H_2^++Kr, collisional dissoc., 6 to 60 keV *(German)* 77−10733
H_2^++Li, excited state form. obs. 80−9686
H_2^++metal, fast ion scatt. by surface plasmons, theory 80−45190
H_2^++methanol, dissoc. charge transfer reaction studied at rel. translational energies from 600 eV to 5000 eV 80−104432
H_2^++N_2→N_2+H_2, rot. energy distrib., 10 and 25 keV 79−76507
H_2^++Ne, reaction pot. energy surface, LCAO-MO-SCF energies 77−1917
H_2^++Ne, vibr. energy effects on kinetics, phase space model 78−11508
H_{2n+1}^++Ar, n≤7, double differential fragmentation cross section 79−89821
H_3^-, collision induced dissoc., positive and negative ions form. 78−50612
H_3^-, dissociating states, lowest singlet and triplet PE surfaces, HF calcs. 79−81160
H_3^+, $^3\Sigma_u^+$ excited level, GO SCF calcs. 77−46507
H_3^+, ab initio calcs. of vibr. spectrum 77−6753
H_3^+, ab initio vibr. intervals and vibr. freq. refinement 80−47968
H_3^+, backscatt. by Cu or Mo, 4-30 keV, O_2 effect 78−15268
H_3^+, correl., ionis. and attachment operators, diagrammatic method calcs. *(French)* 79−22607
H_3^+, $D_{3h}{}^1A_1'$, Schrodinger eqn. random walk soln., electron spin effects 77−18780
H_3^+, dipole polarisabilities, variational perturbation theory calcs. 78−70765
H_3^+, dissoc. following beam-foil interaction 78−70920
H_3^+ dissoc. recomb., role of H_3 excited electronic states 79−89795
H_3^+, dissociative electron capture, symmetry considerations 77−46646
H_3^+, dissociative recombination in low energy electron collisions 79−3563
H_3^+, electron impact dissoc. recomb. cross sections, Rydberg states form., merged-beams expt. 78−25725
H_3^+, electron impact dissoc., H^- production cross section 80−5628
H_3^+ expt. determ. struct., foil-induced dissoc. fast mol.-ion beam 78−74752
H_3^+ fast molecules, transmission through thin C foils 79−76484
H_3^+, grazing incidence collision with surface, Balmer radiation, elliptical polarisation 78−86804
H_3^+ grazing incidence collision on clean Pb or Ni crystal surface, elliptic polarisation in Balmer radiation 80−35039
H_3^+, IR spectrum, ν_2 band obs. 80−99506
H_3^+, impact on C foil, H abundance in emitted beam 78−35236
H_3^+, ion beam prod. by coaxial electron impact ion source 80−62795
H_3^+, ion density decay in He-H_2 plasma, mass spectral obs. 77−3987
H_3^+, ion-surface collision with Mo, optical radiation emission 78−95644
H_3^+ ions, dissociation, collision induced 77−42383
H_3^+, mobility in He gas 78−18371
H_3^+, Monte Carlo solution of Schrodinger equation 78−46255
H_3^+, photofragmentation, time depend. formulation 79−831
H_3^+, photofragmentation vibr. energy levels and wavefunctions calcs. 78−42143
H_3^+, pot. surface, GTO config. expansion 79−26907
H_3^+ rot.-vibr. spectrum, ab initio calcs. 80−95595
H_3^+, sputtering of 304 stainless steel Tokamak wall, ang. effects 79−46458
H_3^+, struct. props., in mag. fields, var. calcs. 78−21843
H_3^+, two-electron bond, energy expectation values from density matrix partitionings 77−75059
H_3^+, uncoupled symmetric stretching freq. calcs. 78−66532
$H_{3,2}^+$, vibr. excitation, ab initio CI pot. energy surface calcs. 80−74228
$H_{3,2}^+$, Temple lower bound mol. orbitals, GTO calcs. 78−41935
H_3^++Ar(H_2)(air), dissoc., 400-800 keV, product charge state distrib. model 78−82838
H_3^++C foil, 2.2 MeV, ion survival during traversal 79−64103
H_3^++H_2, 10 keV electron capture, electronically excited H_3 form. 79−41204
H_3^++H_2 charge transfer collisions, 10 keV, H_2-H fragmentation 79−853
H_3^++H_2→H_5^+→H_2+H_3^+, ab initio GO pot. surface, C_{2v} symmetry 77−25252
H_3^++He, interaction pot., calculated vs. value from ion mobility data 77−14518
H_3^++Kr, collisional dissoc., 6 to 60 keV *(German)* 77−10733
H_3^++Ne, Petty-Moran ion-impact expt. reinterpretation re vibr. intervals 79−94063
H_3^++XCN, flowing afterglow, rate const. meas. 77−40533
H_4 ions, positive and negative, rectangular configurations, stability, SCF MO LCAO calcs. 77−42235
H_4^+, ground and excited state pot. energy surfaces and geom. struct., SCF and CI calcs. 78−78769
H_{aq}^+, positronium formation, Doppler broadened positron annihilation line shapes 80−45164
H_n^- (n=5 to 13), ion-induced dipole clusters, binding energies and geometries 79−41261
H_n^+, (n=1,2,3), impact on metal surfaces, excited H form. 78−42199
H_n^+ (n=3,5,7,9,11), stability, struct., ab initio MO calcs. 78−74810
H_n^+ multispecies beam, particle species evolution in neutral-beam injection lines 79−85846
H_n^++e, electron-ion dissoc. recomb., rate const., electron beam sustained discharge 78−50652
H_n^++N_2, (n=2 to 27), 250-900 eV collisions, fragmentation 77−88525
H_x^++Al surface, x=1,2,3, relative K X-ray yields 77−75282
H^+Ar(Xe)(Ne)(He)(Kr)(H_2)(N_2), electron capture, 4-20 keV, production of highly excited H atom 79−54963

hydrogen ions continued
HD , collision induced dissoc., positive and negative ions form. 78−50612
HD^+, dissociative recombination cross sections 79−59568
HD^+, ground state vibr.-rot. spectrum, high resolution laser-ion beam reson. expt. 78−82733
HD^+, HT^+, adiabatic relativistic rot.-vibr. energy levels 77−57964
HD^+, HT^+, DT^+, accurate rot.-vibr. energy and transition moment calcs. 77−14412
HD^+, Hellmann-Feynman theorem anomaly 80−63510
HD^+, IR hyperfine struct. of rot.-vibr. transitions calc. 77−42323
HD^+, IR photodissoc. cross sections, calc. and simulation expt. 80−9659
HD^+, laser photodissoc. cross-section calcs. 77−58102
HD^+, nonadiabatic vibrational energies, ab initio calcs. 78−90142
HD^+, radiative recombination rates 78−37708
HD^+, rot. excitation by slow electrons, calc. 78−5360
HD^+, spontaneous emission lifetimes in ground electronic states 80−32810
HD^+, spontaneous IR rot.-vibr. emission probability 78−50535
HD^+, vibr.-rot. transitions, using new two-photon IR photodissoc. technique 80−23405
$H^+(D^+)$ discharge activation energies in $H_2O(D_2O)$ at Hg cathode 80−40707
HD^++HD^+, 0.1-1 eV, rot. transitions and reson. transfer, first-order perturbation theory 77−83698
HD^++He collisions, rotational transitions 78−70909
$H^-(D^-)$+He, collisionally induced electron detachment, 0.5 MeV, target effect 80−37858
HD_2^-, collision induced dissoc., positive and negative ions form. 78−50612
HD_{2v}^+, vibr. spectra, ab initio calcs. 77−83562
H_2D^+, interstellar and circumstellar search, upper limit determ. 79−2562
H_2D^+, vibr. spectra, ab initio calcs. 77−83562
$H_3^+(D_3^+)$+$H_2(D_2)$ collisions, slow ion production, charge transfer cross sections 80−106378
HH ion, hydrogenium ion, metastable states, ground state energy, bound states, lifetimes 79−45868
$H^+(H_2^+)$+C foil, v_i=v_e electron prod., charge transfer to continuum theories 78−13583
$H^+(H_2^+)$+Ne, Ne($2p^53s$, $2p^53p$) excitation 80−43185
$H_2^+(H_3^+)$+He, Hadamard mass spectroscopy, mass spectra 79−30601
$H_2^+(HD^+)$, $1s\sigma_g$ state, pot. energy curves, relativistic corrections 77−57892
$H_2^+(HD^+)$, expectation values, Born-Oppenheimer, adiabatic and non-adiabatic results 78−82624
$H_2^+(HD^+)$, g-factors and related mag. props., calc. theory 79−41124
$H_2^+(HD^+)(HT^+)$, IR transition freqs. calcs. 77−88452
H_2O+H^+, 0.3 to 1.5 MeV, electron ejection, energy and ang. distrib. meas. 77−71851
H_2O+H^+⇌H_3O^+, equilib., H_2O proton affinity calc. 78−92497
H_3O^+, ion mobility in N_2, flow drift tube obs. 77−19663
$H_3O^+(H_2O)_n$ (n=1,2), ion mobility in N_2, flow drift tube obs. 77−19663
H125α recomb. line in M82, SHF obs. 80−82486
H(1s)+p→p+H(1s), 15-200 keV, ang. distrib., differential cross sections calc. 78−82839
He-H_2^+, classical trajectories, on 3D cardinal spline fitted surfaces 77−90584
He+H_2^+, vibr. and rot. transitions, trajectory calcs. 79−13793
He+H_2^+→HeH^++H, diatomics-in-mols. and spline fitted ab initio surface, vibr. effects 78−20010
He+H_2^+→HeH^++H, spline-fitted ab initio surface, quantum mech. scatt. calcs. 77−63898
He+H^+, 25-3000 keV, electron-capture, continuum distorted wave approx., correl. energy 77−83727
He+H^+, 293 keV, electron capture differential cross sections 77−88552
He+H^+, charge transfer, approx. close-coupling calcs. 77−23560
He+H^+, double ionis. of He, binary-encounter theory 78−1066
He+H^+, electron capture cross sections, electron correlations 77−34758
He+H^+, electron capture coherent electron density distrib. oscillations 79−10200
He+H^+, electron ejection differential cross sections 77−46625
He+H^+, excitation process *(Japanese)* 78−42193
He+$H^+(H_2^+)(H_3^+)(He^+)$ collisions, polarisation degree of prominent He lines 78−70916
He_2^++He, endothermic reactive and vibr. inelastic collisions, pot. well effects 79−8430
HeH^+, collisional formation, SCF calcs. 77−6893
HeH^+, spectroscopic characts. in ground and first excited triplet states, Dunham pot. approach 77−42234
HeH^{2+}, lowest 20 states, eigenvalues, electronic wavefunctions, w.r.t. internuclear separation 77−18811
$^4HeH^+$, ro-vibr. quasi-bound levels of $X^1\Sigma^+$ state, eigenenergies, dissoc. 77−26997
$He^{2+}(H^+)$+X, (X=Nb to Gd), K-shell X-ray prod. cross-sections 77−71865
Hg+H^+, L-subshell ionisation cross-sections, X-ray meas. 77−46520
H(muonic)+H^+, elastic scatt., cross section 79−871
H_n^+(n=7, 9, 11, 13), geometry optimisation, ab initio SCF calcs 80−53180
H^+(relativistic)+atom, K-shell ionis., double differential and total cross sections 78−42182
H^+(spin polarised)+atom, inner-shell ionis., subsequent radiation ang. distrib. 80−53114
Li+H^+, Li core excitation cross section, correlation and reorganisation effect 80−87215
M_2^+ ions, dissociative collisions, mol. effects in charge state distribs. 78−17755
Mg+$H^+(He^+)$ and electron impact ionis., Auger study of collisionally induced alignment 78−90279
Mg^++H^+, Mg^{2+} form. by charge exchange and ionis., cross sections 77−83709
N+H_2^+, triplet state ab inito CI pot. energy surfaces 78−74729
N_2+H^+, electron ejection, energy distrib. binary encounter approx. calcs. 77−30971
N_2+H^+, excitation process, N_2 and N_2^+ light emission *(Japanese)* 78−25678
N_2+H^+, spatial distrib. of excited moles. induced by 100 and 150 kev proton beams 78−58793
N_2+$H^+(He^+)$, 1 MeV, dissoc. ionis., time-energy spectra 77−34744

hydrogen ions continued
$NH_3+H_2^+(He^+)$, dissociative charge transfer reactions, energy transfer depend. 77−25258
$Na+H^+$, $2p^5 3s\,^2P_{3/2}$ state alignment, collisionally induced, impact parameter calc. 80−83474
$Na+H^+$ collisions, L-Auger electron emission, autoionising states, line broadening effects 77−14568
$Ne+H^-(D^-)$, electron detachment, dynamical phenomenon 80−106305
$Ni+H^+(^4He^{2+})(O)(Li)$, K-shell ionis., impact parameter depend. 77−83707
$Ni^{14+}+H^+$, collisional excitation of fine struct. transitions in ground state 77−19017
$^{58}Ni+p$, K-shell X-ray photon proton coincidences, nucl. time delay 79−18281
$Pt+H^+$, L-subshell ionisation cross-sections, X-ray meas. 77−46520
$U+H^+(He^+)$, 2-18 MeV, L-subshell ionis. cross section, projectile energy depend. 77−19031
$V+H^+$ ion collisions, K_α satellite intensity meas. 77−23550
$Xe+H^+$, M-subshell ionisation cross section, binary encounter approx. 78−62890
$Xe+H^+$ charge exchange, H spin polarisation 77−61688
Zr-H, inhomogeneous system, time changes of Hall voltage 79−87080

hydrogen neutral atoms
1S Lamb shift and 1S-2S isotope shift 80−91464
1s resonance, stabilisation method calcs., convergence 80−91492
1s-state hyperfine interaction, Blinder operator calcs. 80−14072
$2^2S_{1/2}$ state F=1 hyperfine component, Majorana transitions, LZS model 77−57959
2p state alignment, influence of surface electric fields after beam foil excitation 78−29849
2S level population calc. in turbulent plasma *(Russian)* 78−25451
$3^2S_{1/2}$-$3^2D_{5/2}$ interval, double quantum RF meas. 79−54826
$3^2S_{1/2}$-$3^2D_{5/2}$ interval, two-photon lineshape theory 79−54825
$3P_{3/2}$-$3D_{3/2}$ Lamb shift, double quantum saturation spectrosc. obs. 78−94223
absorption at 21 cm within 3C 178 radiogalaxy 79−5910
absorption in B2 1506+34, peculiar radiogalaxy, 21 cm line obs. 78−54048
abundance in emitted beam from C foil bombarded by $H(H^+)(H_2^+)(H_3^+)$ 78−35236
adbsorbed on He surface, Bose condensation, adsorption isotherms and stabilty 80−107638
adsorbed on Pt (111), vibr. modes, EELS study 80−15377
adsorption, on Cu, potential energy curves, pairwise, additive model calcs. 78−73087
adsorption, on graphite (0001) surface, vibr. spectrum, at. beam scatt. obs. 80−92779
adsorption, on MgO, (α-Al_2O_3), (α-SiO_2), microweighing and X-ray obs. *(German)* 78−51825
adsorption, on Ni (110) surface, structural investig. by He diffraction 79−86984
adsorption on H_2 solid, hyperfine freq. meas. 79−50155
adsorption on perfectly imaging metal, variational calc. 79−33188
adsorption on ZnO, space charge accumulation layers effect on secondary ion yields, H conc. meas. 79−83087
antiprotonic H atoms, first obs. of L X-rays 78−90111
arc-heated high-intensity source 77−3493
asymptotic interaction with graphite surface 79−99429
atom, in diatomic mol., nuclear mag. shielding LCAO MO functions and gaussian expansion calcs. 79−36548
atom triple-dipole energy calcs. using pseudo spectral theory 78−46418
atom-atom pot. parameter in azabenzene, dispersion energy calcs. 80−23489
atomic electron impact excitation, 2s state, differential cross section 78−86953
atomic spectra and radiative transitions, book 80−22159
atomic spectral line shifts for heavy quark atoms 78−62965
atoms produced by IR multiphoton dissoc. of alkenes, IR detection 80−83356
aurorae and sporadic-E ionization 79−62659
auroral H emission oval, temporal variation 77−13145
backscattering from Mo in the presence of O, ion form., line emission 79−3388
Balmer α and β in solar prominences, emission line intensities rel. to model calcs. 79−44447
Balmer α and β line measures rel. to Be-star rotation 77−56983
Balmer α and β line profile rapid vars. in Be-stars *(Russian)* 79−16992
Balmer α and β lines in O6 to G2 stars, equivalent widths and narrow-band photometry 80−8621
Balmer α emission in southern beat Cepheid stars 79−21301
Balmer α emission line var. in M-type dwarf stars 79−21313
Balmer α line fine struct., Stark effect *(German)* 78−82673
Balmer β profile of Markaryan 372 Seyfert galaxy 80−26972
Balmer γ line profiles and masses of DA white dwarf stars 80−77399
Balmer line formation in rotating white dwarfs 79−30059
Balmer lines, formation in bright prominences spectra *(Russian)* 80−77377
Balmer lines produced in sputtering glow discharge *(French)* 77−24229
Balmer series limit, line blurring 80−23351
Balmer spectrum at line merging region, statistically extended recomb. continuum and line dissolution 77−27006
Balmer wavelength calc. with hand calculator, student project 78−12512
Balmer-α fine struct. lines, anomalous shifts, in He-H_2 DC discharge 79−45677
Balmer-α line high resolution spectroscopy techniques 80−52915
Balmer-α line profiles and polarisations in strong mag. field 77−6729
Balmer-β line intensity, excited neutral backscattered from $H^+(H_2^+)(H_3^+)$-metal impact 77−23470
beam, $2^2S_{1/2}$ metastabld ats., nonadiabatic transition in mag. field 78−55157
beam of highly excited atoms, CW source using Doppler-tuned IR radiation 77−27204
beam prod. at. 90 to 500 eV from surface plasma source 80−38729
beam production by cooled microwave discharge source 78−5373
beam-foil excitation, n=2 density operator and prod. probability meas., transition probabilities 80−14219
beam-foil excitation of 2P-state, alignment meas. 80−14215
beam-foil excited, zero-field quantum beats in H_β emission, polarisation energy depend. 80−14218
binding energy, combined algebra for quantum description 78−8271

hydrogen neutral atoms continued
binding energy in strong magnetic field, relativistic correction using perturbation calc. 79−68186
bombardment of graphite surface 80−93665
bound states, so(2,1) algebra 79−10016
bound states in strong mag. field 80−99438
Brackett α line survey of compact IR sources 79−62882
Canes Venatici I galaxy group, neutral H obs. of NGC 4136, 4144, 4190, IC 4182 and (DDO 133) 79−84853
charge exchange involving excited states, Born cross sections 79−45836
charge exchange of nuclei of multicharged ions with allowance for degeneracy of final states *(Russian)* 78−46444
charge transfer cross sections in gases and vapours, 10 eV to 10 keV, graphs and tables 80−32824
charged particle collisions and multiple scatt., Glauber approx. scatt. amplitudes 80−14191
chemisorbed, surface charge fluctuations effect on spectral density 80−65368
chemisorbed on cluster, indirect interactions, Grimley-Pisani model and tight-binding calc. 80−65370
chemisorbed on Ni (111), order-disorder transition, cluster-variation method 80−15372
chemisorption on Be(0001) surface, mol. orbital cluster theory 79−15002
chemisorption on Si (111), localised model, ab initio HF-LCAO calc. 80−6930
Cherenkov line radiation, QSO emission-like spectra *(Chinese)* 80−105378
in clusters of galaxies 79−5896
coherent excitation of n=3 level by electron impact, density matrix anal. 78−78817
collapsing pre-galactic gas cloud, local stability, linear perturbation anal. 80−82513
collisional energy level transition rate, in RF plasma, fluoresc. meas. 77−38726
collisional ionisation by fast low-charge-state ions 79−86056
combustion products, appl. in CO_2 gasdynamic laser 79−27240
Comet Tago-Sato-Kosaka (1969 IX), H and OH prod. rates 78−28580
Compton defect, high energy electron impact spectroscopy 77−71876
Compton profile and X-ray scatt. factors, elec. field and elec. field gradient effects 79−31458
conversion by electron impact, eikonal exchange amplitude in Coulomb break-up processes 80−87232
Coulomb de-excitation of neutral exotic atoms, μ^-p and π^-p H atoms 78−25757
Coulomb Green's function calcs. 77−57907
Coulomb ionisation, Glauber scatt. amplitude, integral representation 77−6915
coupled channels optical model, total reaction cross-sections 80−18929
Debye screening, no evidence for Hγ red shift 79−31369
detection by resonance fluoresc., coherent tunable VUV generation near Ly-β transition 80−99798
detection by resonant three photon ionisation 78−74624
determination, in fast flow discharge systems, titration methods 79−34393
diffusion coeff., in H_2, luminesc. intensity meas. 80−103098
diffusion in amorphous Si films, hydrogenation *(Korean)* 80−45326
diffusion in electrolytic Ni, coeff. determ. *(Russian)* 79−8441
dilute hard-sphere Bose-gas model, low-density atomic H gas property-calc. 80−87194
dipole properties and dispersion energies additivity, using atoms and small mol. models 80−53091
dipole static polarizability for any state, modified Coulombic Green's function Sturm expansion 79−7031
dipole transitions, asymptotic expansion of radial-dipole integral 78−82667
Dirac atom, relativistic, energy level splitting 80−77938
Dirac eqn. approx. soln., Moore's method appl. 80−42926
Dirac equation calcs. 80−46760
Dirac equations, approx. soln. using partitioning technique, 1s, 2s, 2p states 80−23284
Dirac field, self-interacting, charged nonlinear spinor field in Coulomb-like potential, localised solns. 80−68351
direct obs. of the transversal Doppler-shift 79−18151
discharge lamp in visible region *(German)* 79−59782
distribution function in interplanetary corotating energetic particle streams 79−70938
distribution in early type disk galaxies from 21 cm line obs. 79−35357
double-quantum saturation spectroscopy, laser and RF 80−77880
dynamic multipole polarisability, functional calcs. 78−74595
dynamic polarisability, variational calc. 78−22047
effective ionisation cross section determ. for H, Li, Na, Cu, Ag, Au and Fr, classical theory *(Russian)* 77−30998
eigenfunctions and eigenenergies, N-space dimensions calcs. 80−41988
eigenfunctions in spherical and parabolic coords., relationship coeffs. 77−82409
eigenvalue resonances in Stark effect and perturbation theory 78−90118
Einstein's unified field theory, field equations soln. for H-atom space-time struct. 79−21634
elastic electron (positron) scatt., relativistic Glauber amplitudes 79−31681
elastic electron (positron) scatt., S-wave phaseshifts bounds, least norm variational principle tests 80−5619
elastic electron scatt., 20-50 eV, Born calcs. of differential cross section 80−102571
elastic electron scatt., high energy higher order Born approx., differential cross section series approx. 79−72417
elastic electron scatt., modified Glauber theory, intermediate states 80−53139
elastic electron scattering, eikonal Born series calc. 79−36766
elastic electron scattering, pseudostates wave functions determ. in modified close-coupling calcs. 80−99572
elastic electron scattering, static exchange amplitude, dispersion rels. 78−66664
elastic electron scattering amplitude, left-cut contrib. to dispersion relation 79−59574
elastic positron scattering, differential cross sections 79−86028
elastic scattering of electrons, optical model approach, polarisation effects 80−58382
electric field effect on stability of sublevels 79−89634
electric field-induced quantum beats, fringing fields effect 77−42307
electron, forward scatt. dispersion relations, numerical study 77−68113

hydrogen neutral atoms continued
electron and positron bremsstrahlung, differential cross sections 79−18294
electron and positron elastic scatt. 77−19075
electron and positron scattering, elastic, 100 and 500 eV, second-order eikonal approx. 78−78814
electron and proton interaction cross sections 77−50538
electron capture by fast multiply charged ions, q^3 scaling 80−91658
electron capture cross section by ions, charge depend. continuum distorted wave approx. 77−68110
electron coincidence ionisation spectroscopy, rel. to impulse approx. calcs. 79−31715
electron elastic forward scatt., exchange amplitude 78−5342
electron elastic scatt., absolute cross sections 77−50533
electron elastic scatt., differential cross section 78−33605
electron elastic scatt., differential cross sections calc. 78−90293
electron elastic scatt., exchange amplitudes and dispersion relations 77−79693
electron elastic scatt., exchange perturbation theory 80−78709
electron elastic scatt., forward total cross section calc. 78−29852
electron elastic scatt., local pot. method, bound states 77−75296
electron elastic scatt., logarithmic ang. depend. for excited ats. 78−50638
electron elastic scatt., modified Glauber method, Glauber exchange 77−83733
electron elastic scatt., modified Glauber theory with exchange 77−65533
electron elastic scatt., second Born amplitude calcs. 80−32833
electron elastic scatt. at intermediate energies, modified Glauber theory 77−14575
electron elastic scatt. at low intermediate energies 80−106393
electron elastic scatt. below inelastic threshold, finite range problem, effective pots. 78−25704
electron elastic scatt. by 2s state 77−50531
electron elastic scatt. local optical pot., second order partial wave amplitude 78−25703
electron elastic scattering, distorted wave eikonal approx. 77−83731
electron elastic scattering, eikonal-Born series and modified Glauber approach comparison 79−81281
electron elastic scattering, fixed scatterer approx. 79−10204
electron elastic scattering, Fresnel and recoil corrections in Glauber theory 79−50131
electron elastic scattering, two-pot. Glauber-Born approx. calcs. 78−25706
electron exchange scatt., generalised Coulomb-projected Ochkur-Born approx. 77−83730
electron excitation, matrix elements by Faddeev approach 80−78714
electron impact excitation, asymptotic Glauber cross sections 80−9741
electron impact, 1s-2s and 1s-2p excitation, electron-photon coincidence meas. 80−87233
electron impact, coherent excitation in longit. elec. field, Balmer-α flux 78−22035
electron impact, elastic scatt. and n=2 states excitation, fixed-scatterer approx. 77−50544
electron impact, in laser field, Born-Oppenheimer approx. calcs. 79−54973
electron impact, ionisation, angular correls. of outgoing electrons 78−5355
electron impact, transitions between excited states 77−58168
electron impact coincidence, even-odd parity coherence effects, polarisation ang. distrib. 78−9253
electron impact excitation, 1s→2s, exchange corrected eikonal approx. 78−9252
electron impact excitation, 1s→2s transition, exact second Born amplitude 80−102572
electron impact excitation, 1s-2p, ang. correl. parameters, distorted wave approx. calcs. 78−9258
electron impact excitation, Bethe approx. modifications, impact radiation polarisation 79−31695
electron impact excitation, Born and classical cross-sections *(German)* 78−86952
electron impact excitation, coherent state multipole moments, model calcs. 79−76518
electron impact excitation, coherent-state multipole moments, final state interactions 77−83742
electron impact excitation, cross section calc., Crothers and McCarroll method 78−25715
electron impact excitation, cross-sections, multipole moments, quasiclassical calcs. 80−63828
electron impact excitation, differential scatt., semiclassical calcs. 77−14583
electron impact excitation, distorted wave approx. calcs. 77−10771
electron impact excitation, electron-photon ang. correl., for H(2p) 79−31699
electron impact excitation, electron-photon coincidence, large angle expt. 80−83500
electron impact excitation, exchange polarisation effects 77−42417
electron impact excitation, Glauber amplitudes from low to highly excited states 77−68122
electron impact excitation, Glauber exchange effect 78−25720
electron impact excitation, high-momentum transfer, amplitudes form, Faddeev-Watson approx. 80−23555
electron impact excitation, modified Glauber theory calcs. 80−18934
electron impact excitation, n=2 level, generalised two-pot. distorted wave model calcs. 78−37748
electron impact excitation, simplified model, low and medium energy 78−86954
electron impact excitation, two-pot. eikonal approx. 79−22847
electron impact excitation 80−18909
electron impact excitation 2s state, by 100, 300 eV electrons, distorted wave approx. calc. 78−22033
electron impact excitation in circ. polarised laser field 80−18927
electron impact excitation in presence of intense laser beam 78−9261
electron impact excitation modified Glauber method with exchange calc. 78−37751
electron impact excitation of n=2 to n=3 transition, algebraic variational method close coupling calcs. 80−91678
electron impact excitation of resons. below n=3 levels, algebraic variational calc. 78−9254
electron impact ionis., spin exchange effects, 15-197 eV 77−71877
electron impact ionisation, 100 to 250 eV, triple differential cross-section 79−59582
hydrogen neutral atoms continued
electron impact ionisation, cross-section calc. 79−76516
electron impact ionisation, electron-photon coincidence meas. 78−55242
electron impact ionisation, expt. and theoretical 79−22842
electron impact ionisation, in RF ion source, effective cross-sections 78−22034
electron impact ionisation, polarised Coulomb-projected Born approx. 80−106395
electron impact ionisation, spin effects, Born exchange calcs. 78−37749
electron impact ionisation, triple differential cross section 79−36776
electron impact ionisation in intense laser beam 78−46449
electron inelast. scatt. in intense EM field, one photon absorpt., 1s-2s transition 79−36765
electron inelastic scatt., dynamic polaris. pot. 78−78818
electron inelastic scatt., effective exchange potentials 78−90300
electron ionisation cross sections of excited atoms and ions 80−43186
electron low energy elastic scatt., variable phase method, s-, p- and d-wave phase shifts 80−9732
electron scatt., 2p state orientation 77−71874
electron scatt., angular momentum transfer 77−30999
electron scatt., atomic optical potential model 80−99578
electron scatt., complex optical pot. methods 79−22844
electron scatt., dispersion relations, static exchange approx. 77−83735
electron scatt., dispersion relations 78−42216
electron scatt., distorted wave expansion with off diagonal pots., local approx. 79−31694
electron scatt., effective pot. calcs. 80−53131
electron scatt., effective pots. below inelastic thresholds, asymptotic forms 77−83728
electron scatt., elastic, quasi-adiabatic polarisation potential 77−30993
electron scatt., equivalent exchange pots., algebraic variational method, 2p-2p and 2s-2p transitions 80−18931
electron scatt., exchange amplitude, Glauber-Bonham-Ochkur approx., differential cross sections 77−19078
electron scatt., forward elastic exchange amplitudes and forward dispersion relations, anal. props. 78−78812
electron scatt., high-energy, elastic and 2s excitation cross-sections 77−10763
electron scatt., inelastic, cross sections, second Born approx. *(Russian)* 79−36780
electron scatt., large momentum transfer, second Born term 77−538
electron scatt., lowest ^{1}S resonance, Feshbach formalism corrections 77−58178
electron scatt., lowest ^{1}S resonance 77−58177
electron scatt. at intermediate energies, fixed scatter approx. 80−9740
electron scatt. in EM field, reson. emission and absorpt. of photons 79−27087
electron scatt. in presence of a laser field, theory 78−74767
electron scatt. information obtained using symmetrically coupled partial differential eqn. 80−102574
electron scattering, differential cross-section and oscillator strength 79−36774
electron scattering, differential cross-sections, eikonal approx. calcs. 79−81278
electron scattering, elastic, Born amplitude, unitarity sufficiency condition 79−86068
electron scattering, elastic, $E_e \geq 100$ eV, ang. distribs. calc. 80−74248
electron scattering, elastic 5 eV, differential cross sections, perturbation theory 77−30997
electron scattering, inhomogeneous eqn. method 77−27182
electron scattering, L=2, 3 phase shifts 78−37742
electron scattering, low-energy, 1S-approximation channel coupling array 77−10756
electron scattering, modified variational method 78−1081
electron scattering, optical pot. methods 80−102569
electron scattering, partial transition matrix elements, Faddeev approach 77−75297
electron scattering, second-order pot. method calcs. 79−72419
electron scattering, source theory 78−46415
electron scattering, total spin quantum number changes 79−54969
electron scattering length calc. with imprecise target wave function, variation principle 79−72375
electron scattering resonances, coord. rot. method calcs. 77−83736
electron scattering transition amplitude from 1st Landau level, in homogeneous mag. field 79−10218
electron spin density functional gradient expansion, local approx. calcs. 80−44792
electron-photon angular correlation meas. for excitation of 2P state 80−91636
electron-photon excitation, high-energy resonant cross sections 78−70938
electron/positron elastic scatt., least squares calcs. 79−3572
EM field, long wave, H-like atoms behaviour 79−89652
EM vacuum fluctuations, ground state energy in multiply connected universes 80−87050
emission-line spectrum from a slab of hydrogen at moderate to high densities 80−72759
energy, expectation values, by hypervirial relations without perturbed wavefunctions 78−33416
energy analysis, 200 eV-10 keV range 77−83763
energy level calcs. in superstrong mag. field 80−37737
energy levels, 3d,3s,4s,5s, cross sections for production in H^- collisions with He,Ar,Xe,Ne, 1 to 5 keV 78−33603
energy levels, influence of the expanding universe 78−54271
energy levels, nonrelativistic high order perturbation theory corrections, infinite series representation 77−34564
energy levels and bound-bound transitions in strong mag. field 80−58134
energy levels in magnetic fields, review 77−50383
energy levels in strong mag. field 78−90071
energy levels of hydrogenic atoms or excitons near hard walls calc. 79−78014
energy levels of light hydrogen like and muonic atoms, nuclear size corrections 79−36549
energy spectra, angular distrib. from HeH^+ collisions with thin foils 80−66355
energy spectrum in expanding Robertson-Walker universe 78−73869
Europa, H cloud rel. to UV emissions 79−5775
exchange reactions, low temp., tunnelling dynamics 79−29340
excitation by charged particles, differential cross-section, quasiclassical approx. *(Russian)* 77−79676
excitation in Ne-H_2 h.f. pulsed discharge *(French)* 77−433

hydrogen neutral atoms continued
excited, produced by electron impact dissociation of H_2, velocity distrib. *(Russian)* 77−10779
excited atom Lyman-α and Balmer fluoresc. from H_2 photodissoc. 79−86018
excited atoms, charge transfer processes, perturbed stationary state method 79−89770
excited S-states, static dipole polarisabilities, Green's function calcs. 77−6696
excited state, J=3/2-J=5/2 transition, fine struct. interval meas. 77−46542
excited state electron and ion quantum scatt. cross sections, dipole approx. *(Russian)* 79−6996
excited state interaction with photon field, simultaneous eqns. 78−66481
excited states, in elec. field, semi-classical approx. *(Russian)* 78−86797
excited states, pseudopotential calcs., teaching approach 79−84893
excited states, Rayleigh-Schrodinger perturbation theory, Pade approximants calcs. 79−98024
excited states prod. by near threshold photodissoc. 79−86019
excited states relax. in glow discharge *(French)* 79−849
excited states relax. rates in glow discharge 79−7001
exobase, H density and temp. from Lyman alpha absorpt. and polarisation meas. 77−29526
exobase, local perturbations of H density distrib. inferred from Lyman α airglow meas. 78−24400
exobase density distrib. near solar minimum 78−45067
exosphere, H global density distrib. vars., escape fluxes 78−93023
exosphere, H latitude vars., rel. to polar wind, heating and charge exchange processes 78−93024
exponential decay law for $2P_{1/2}\rightarrow 1S_{1/2}$ transition 78−78649
Fermi contact interaction, spin density calcs., Hiller Sucher Feinberg identity 80−69061
fine structure $3^2S_{1/2}$-$3^2D_{5/2}$ interval, separated oscillatory field meas. 80−99482
fine structure levels, Stark component radiative widths 77−3302
finite chains, HF solns. stability and symmetry breaking, independent particle model calcs. 80−87035
first-order wave functions, computer calcs. using Green's functions 78−41934
fluorescence, Balmer series, from H_2 photodissoc. fragments 77−27020
form factor for arbitrary states, dipole moment component matrix element calcs. *(Russian)* 80−58143
form factors and cross sections for nl→n'l' direct collisional transitions 79−31636
formaldehyde, UV photolytic separation of D from H in cryogenic solns. 78−95937
frequency depend. multipole polarisability and dispersion energy between interacting pairs 79−18306
frequency standard and maser development by NASA 77−37861
frequency standard undisturbed transition evaluation 77−79066
fusion reactor neutral beam injection, 24 MW 400 keV H beam 80−91356
g-factor ratio, $g_J(^1H,1^2S_{1/2})/g_s(e)$, spin exchange optical pumping 77−79587
galactic centre region, neutral H survey 79−88722
galactic column densities 79−5875
galactic equator, H I recomb. line emission, 408 MHz obs. 77−13451
galactic H I absorption, obs. of struct. on small ang. scales 80−22051
galactic H I distrib. and diffuse gamma rays 80−41917
galactic H I regions, N.galactic hemisphere, emission spectra profile 80−17643
galactic morphology of H and trace gases, review 77−26070
galaxies, IR magnitude/H I vel. width relation rel. to distance scale and Universe expansion rate outside Local Supercluster 80−105325
galaxies active nuclei, effect of inelastic collisions on H spectrum 77−45599
galaxies active nuclei, H emission-line spectra 78−96557
gas, two-photon absorpt. of ultrashort pulses, reson. intensities 78−59077
gas discharge H atomic source for electron scatt. expts. 78−94332
gas mixture, reacting, atom conc. reson. absorb. meas., microwave discharge lamp calibration 79−92032
gaseous, high-resolution mag. reson. study, 1 to 1.3K 80−95560
gaseous, spin aligned, low-density props. 79−18255
generator, freq. shift due to atomic collisions with storage flask walls 78−77870
generator coordinate method 78−29731
geocorona, Lyman β and Balmer α emissions meas. during Apollo 16 mission 77−37476
geocoronal H, charge exchange with hot plasmasphere ions rel. to H escape rate 77−37469
geocoronal H conc. models, Hα emission rates and solar Lyman β flux 77−25808
ground state, effect of metallic surface 77−35979
ground state energy in interacting system 79−18255
ground state in strong homogeneous mag. field, so(4,2) algebra use in perturbation theory 80−47845
ground state props., polynomial perturbation problem 78−73878
H+FH(FD), low barrier quantum model, vibr. deactivation 80−69216
H(1s)+$e^+\rightarrow$(e^+e^-)(nlm)+H^+, highly excited states rearrangement collisions 79−59564
handedness and parity non-conservation, rel. to unified gauge theories 78−29757
highly excited, H^+ and e collision processes, Glauber approx. and n-changing transitions 77−79686
highly excited, H^+ and e collision processes, transitions between degenerate states at low energies 77−79685
highly excited resonant states, Stark effect, nonperturbative regime 78−70786
highly excited states in static elec. field 77−61707
hot reactions and mechanisms of liq. n-alkanes radiolysis 77−36771
hydrogenic atom in weak mag. field, polarisability, ground-state energy 79−3594
hydrogenic atoms and ions, degenerate state transitions, plasma waves, Stark effect 79−72389
hydrogenic Green's functions, reduced, power moments, and 2nd-kind Green's functions 79−85891
hydrogenic one particle Green's function power moments, 1s-type orbital reduction 78−9051
hydrogenlike atoms, spin-orbit terms derivation 80−73148
hyperfine energy, effect of excited state admixture, H in spherical box 80−906
hydrogen neutral atoms continued
hyperfine frequency and wall shift, 4.2K gas in solid H_2 coated bulb 79−50155
hyperfine frequency meas. of ground state 78−78984
hyperfine quadratic shift in electric field, pressure dependence 78−13442
hyperfine shift, in He buffer exchange perturbation theory 77−6736
hyperfine shift and interatomic pots. in inert buffer gas 80−5491
hyperfine splitting, second-order, with Blinder-type contact operator, ground-state 80−23319
hyperfine splitting inside paraboloidal surfaces 80−99445
hyperfine struct., nonrelativistic calc., delta function contributions 77−14368
hyperfine structure and nuclear size, theory 80−924
hyperfine structure levels excitation and scatt. in reson. line wings *(Russian)* 77−57930
hypervirial relations, giving recurrence relations for radial matrix elements 78−4502
imaginary frequency mutipole polarisability and long-range dispersion consts, functional calcs. 78−74596
in intense mag. fields 77−27137
induced $2s_{1/2}\rightarrow 2p_{1/2}$+one photon transition, rate calcs. 77−50384
inelastic electron scatt., relativistic calcs. *(Russian)* 77−83737
inelastic exchange kernels, semiclassical exchange approximation theory 78−50642
interaction and bound states on liquid He surface 79−18131
interaction with liquid ^{4}He surface, Euler-Lagrange eqn. 79−77850
interatomic retarded dispersion energy, form-factor representation, multipole expansion 77−23532
intergalactic bridge between M81 and NGC 3077, structure and kinematics 79−67093
interplanetary atomic H, parameters from OSO-8 meas. of solar H Lyman-alpha profile 79−2452
interplanetary energetic H, from Earth radiation belts 77−9645
interplanetary H, Lyman α radiation meas. with absorpt. cell spectrophotometer 78−28519
interplanetary H, review 78−49272
interplanetary H I, Lα emission profiles reanal. rel. to local interstellar gas temp. and vel. 80−105141
interplanetary-interstellar H, temp. meas., Prognoz-5 obs. 78−7922
interstellar absorption in galactic centre direction 80−77465
interstellar clouds, H to H_2 transition region 79−25672
interstellar clouds, non-linear relationships between N(Ca II), N(K I) and N(H) 79−92832
interstellar excited H, decametric range radio lines search *(Russian)* 80−12822
interstellar gas, dust and molecules, review 78−54006
interstellar H, adsorpt. on grain surfaces rel. to H_2 form. 79−21367
interstellar H I, new feature discovery in Vulpecula-Delphinus *(Russian)* 80−46654
interstellar H I column densities rel. to galaxy counts, latit. depend. effect interpretation 80−26953
interstellar H I survey from Lyman α absorption meas. towards 100 stars 78−93357
interstellar hot H I between Sun and Earth, solar Lyman α absorpt. 80−31185
interstellar ionisation and expansion, weak R-type ionisation front effects in interstellar gas globule 77−78864
interstellar neutral H, weak R-type ionisation front approaching a contact discontinuity 78−49510
ionisation, by EM wave field, Reiss approx. calcs. 77−10647
ionisation, by microwave-stimulated multiphoton excitation, resons. obs. 77−68019
ionisation, multiple stage cluster beam ionizer 79−67425
ionisation by laser radiation, as polarised proton source 78−78541
ionisation by proton-atom collisions, loss of K-electron calc. *(Russian)* 77−50523
ionisation in AC and DC elec. fields, time depend. 80−63585
ionisation potential and energies in mag. field 80−99585
ionisation threshold for excited states in uniform elec. field 78−37607
isoelectronic sequence, dielectronic recomb. coeffs. 77−27172
isoelectronic series, threshold behaviour of multiphoton ionisation 80−954
isoelectronic series 78−78820
isotope composition of plutonic granitic rocks 78−65221
isotopes, anomalous, including quarks of unit charge, search using cyclotron 77−61879
isotopes, transition radiation from neutral beams, beam foil ionization 79−18299
Jupiter atmosphere, hydrocarbon and H I photochemistry rel. to Lyman alpha albedo 80−105194
Kepler problem for n-dimensional atoms, dynamical symmetries 80−58121
Lα/Hα ratio for solar flares, quasars and prominences 78−61826
Lamb shift, ($2^2S_{1/2}$, F=0)-($2^2P_{1/2}$, F=1) interval RF at. beam meas. 77−6728
Lamb shift, anomalous mag. moment, relativistic Dirac eqn. 80−42954
Lamb shift, temp. depend. 79−787
Lamb shift (n=2), meas. 77−75336
Lamb shift microwave determ. 79−45676
lattice impurity, H atom confined to spherical box with penetrable walls, Schrodinger eqn. 79−84987
level energies and widths in perturbing electric field 77−14378
line profile, Stark broadening, quantum theory, including short-range interactions 78−9114
line profiles in RY Persei spectra, visible obs. 80−67795
line spectrum, relativistic red shift phenomenon 80−32675
local interstellar H and D densities, Copernicus obs. 78−16487
logarithmic perturbation expansions in multipole field 80−37720
longit. excited states in intense mag. fields, rel. to pulsars 80−91469
Lyα radiation reson. scatt. as a neutral density diagnostic for fusion plasmas 78−83612
Lyman α, solar line profile modification in propag. through interplanetary medium 79−66973
Lyman α 1216 Å solar line, temporal var. 78−93186
Lyman α albedo of Jupiter, Copernicus UV obs. 80−94747
Lyman α albedo of Jupiter rel. to solar activity 80−98601
Lyman α and β, interplanetary Voyager UV spectrometer obs. 78−81673
Lyman α and β lines, in solar spectra, exptl. obs. and theoretical profiles 79−8888

hydrogen neutral atoms continued
Lyman α effect on non-LTE model atmospheres of A-type stars 80−90422
Lyman α emission from Jupiter, Voyager 2 EUV obs. 80−77338
Lyman α emission in antisolar direction on Earth's night side 77−87138
Lyman α emission meas. at solar minimum 79−12417
Lyman α formation in expanding spherical nebulae with dust 79−8975
Lyman α in solar chromospheric flares, direct collisional excitation rel. to profile and polarisation 80−41780
Lyman α intensity, in interstellar medium 78−36675
Lyman α line profile of active solar limb filament 79−44446
Lyman α profile in interplanetary space 80−8586
Lyman α profile in solar radiation rel. to interstellar wind dynamics 80−8610
Lyman α/Balmer β intensity ratio interpretation in quasars 79−35418
Lyman alpha coronagraph 79−25486
Lyman-α 1216 Å flux rel. to physics of interstellar medium 77−2459
Lyman-α emission from photodissoc. of H_2O 79−10158
inner M101 galaxy group, H I obs. 80−67885
M33, H I distrib. obs. and spiral struct. 80−56948
magnetic resonance transitions between hyperfine levels, 4.2-77K 79−50053
many-photon excitation spectra, fine structure 79−59419
Mars upper atmosphere, H Lyman α radiation meas. with absorpt. cell spectrophotometer 78−28519
maser, hyperfine transition, affected by coherently excited Zeeman transitions 79−72544
maser failure mode identification 77−37862
mechanical system with second order constraints, quantisation procedure, nonrelativistic H atom appl. 79−75
mesic, atomic X-ray yields 1s and 2p level shifts and widths, cascades, calc. 80−78730
mesonic, primary population, formation cross section by Born approx. 80−43214
mesonic atoms, formation in mixtures of lightest elements 80−87252
mesosphere and thermosphere composition UV dayglow Lyman α and β obs. 80−109290
metastable, form. by charge exchange in $H^+ + Mg(Ba)$ collision 79−81275
metastable 2S state in weak elec. field, radiative decay, bound state QED 80−42959
metastable states, polarised, ion form., charge exchange in ion source *(Rumanian)* 77−46445
migration in meso-tetraphenylporphine, tunnelling rates, quasiclassical calcs. 80−5600
modulated beam of atoms, 3 to 15 keV, produced using voltage pulse generator 79−18315
molecular internal stresses, stress tensor, one electron system 78−62686
in molecular solid, production by T decay 77−29028
monothioformate anion, protonation site, ab initio SCF calc. 79−47894
Monte Carlo solution of Schrodinger equation 78−46255
multilevel atom, excitation and decay 80−9530
multiphoton ionis. pot. in intense circ. polarised laser beam 80−43010
multiphoton ionisation, intense field, via complex dressed states 78−17629
multiphoton ionisation, Pade approx. calcs. 79−98049
multiphoton ionisation, resonant, with intense monochromatic laser 80−32689
multiphoton ionisation of H like atoms, Pade-Sturmian approach 80−87089
multiphoton ionisation of highly excited atoms, rates, perturb. theory calcs. 77−54542
multiphoton ionisation potential, circularly polarized light 79−27101
multiple quantum transitions, excited states in presence of static electric field 78−37618
multiple quantum transitions, two freq. separated oscillatory field technique 77−71892
multiplicative baryon number conservation, $H \rightarrow \bar{H}$ oscill. upper limit, baryon to lepton transform. 79−298
multipole moments, elec. field-induced, polarisability density concept limitations 78−70964
multipole polarisability, dynamic, for S state, closed-form expression 78−82857
multipole polarisability and shielding factors, hydrodynamic analogy to quantum mech. 78−66677
multipole sum rules 77−42257
muonic, collision quenching of 2S-state, distorted waves calc. 77−58211
muonic, formation at extremely low press. 80−74263
muonic atom+Y, muon transfer mechanism from free muonic hydrogen 80−69218
muonic atom formation in low press. targets 78−33639
muonic H, metastable 2s state fraction at 150 and 600 Torr 78−13631
n=2 levels, Lamb shift and fine struct. reson. meas. 80−23321
n=2 state, lamb shift determ., atomic interferometer method 80−23324
n=4 level shift induced by laser radn. 79−98036
negative mesons in H, atomic capture 80−69276
NGC 1023 galaxy group, H I obs. and possible intergalactic H I cloud discovery 80−67886
NGC 1052, elliptical galaxy, field, H I emission mapping and line profiles 80−98719
NGC 4038/39, interacting galaxy pair, H I kinematics and distrib. 79−35365
NGC 5474, peculiar Scd galaxy, H I distrib. and kinematics 80−8683
NGC 7538 and Sherpless 159, H II region/mol. cloud complex, H I aperture synthesis obs. 80−90510
in NGC 925, barred spiral galaxy, high-resolution H I obs. 80−105329
in Nilson dwarf galaxies, H I survey statistical props. 79−92851
nonrelativistic, linear response to external linear polarised EM wave 78−8258
nonresonant two-photon absorption, gauge interaction calcs. 78−37617
one-, two-, three- and four photon absorpt., truncated model semiclassical calcs. 78−17644
one-dimens., $\Psi(x)=\Psi(-x)$ even states, teaching 80−90638
optical harmonic coefficients, third order, at low freqs. 80−78905
optical harmonic coeffs., third-order, R-matrix calc. 77−57955
Orion Nebula, radio obs. of nearby H I distrib. and vels. 80−105322
oscillator, four-dimensional, rot. invariance of coordinate transform., appln. to Stark problem 80−99436
oscillator strength, sums, one-term approx. 78−66509
oscillator strength sums, one term approx. 79−45656
oscillator strengths, 2s-3p transition, Glauber approx. 78−74613

hydrogen neutral atoms continued
parity mixing, relativistic neutral current interactions and nonrelativistic pots. 79−26908
parity mixing of atomic states, spin-depend. weak interaction coupling const. 78−8572
parity nonconservation in emission spectra 79−10086
parity violation as consequences of isoscalar axial-vector current 79−93316
parity-mixing in atomic hydrogen 78−32999
Paschen 7 1005 nm line obs. of O-type stars 79−67003
Paschen decrements and emission line formation in Be-star envelopes 77−56992
passive frequency standard 77−37860
path integral formalism of perturbation theory, simple mols. and atoms 79−6841
Pauli-Lenz vector, extension of SO(3) to SO(4) 80−31550
permeation, through Pd membrane, under different gas and membrane boundary conditions 79−71469
perturbation theory and Pade approx. in electric field 80−91493
photochemical reactions in HCl frozen aq. soln. at 77K 77−9093
photoeffect in H-like atom in super-strong mag. field *(Russian)* 77−75112
photoionisation, absolute cross-sections, expt. meas. techniques 80−63598
photoionisation, two- and three-photon, calc. methods comparison 78−956
photoionisation cross sections elec. field-induced oscills. 80−955
photoionisation in homogeneous elec. field *(Russian)* 80−106309
photon emission, Bohr theory covariant eqns., teaching 80−105482
planetary atmospheres H thermal escape, assoc. non-Maxwellian effects 79−80264
planetary corona, charge exchange effects on H distrib. and escape 77−29674
planetary exospheres, collisionless, satellite atoms depletion by radiation press. 79−96933
plasma, Hα line profile, density meas. 80−43987
plasma, spectral line broadening, ion dynamic effects 79−46432
plasma-immersed, elementary excitation spectrum, exchange and polarisation effects 80−43892
polarisability, multipole, and shielding factors Wiener Askar perturbation treatment 77−34774
polarisability, multipole, freq.-depend., reduced Green's function form 78−1097
polarisability, quadrupole, using elec. field variant GTO basis set 79−76359
polarised atomic H beam intensities, effect of dissociator nozzle cooling 78−16895
polarised beam, possible use as bombardment target 77−34495
polarised beam source, Crypol 2 79−63324
polarised monochromatic laser radiation absorption in electronic transitions, DC mag. field effects 80−9563
polarizability, evaluation of generalised sum rules 77−68132
population inversion obs. in FM-1 spherator 77−7048
population inversion of H levels, in supersonic H-Ar plasma jet 79−3417
positron annihilation rate, p-wave contrib. 78−17790
positron charge exchange, positronium formation, two state approx. 77−79710
positron elastic scatt. lengths and phase shifts, variable phase method 79−22838
positron elastic scattering, low-energy S-wave phase shifts calcs. 78−78813
positron impact ionisation, charge exchange problem 79−50139
positron P-wave scatt., elastic and positronium form. cross sections 77−3468
positron scatt., low energy, semiempirical polarisation pot. calcs. 80−9735
positron scatt., modified Glauber method 78−17797
positron scatt. and annihilation, s and p pseudo-states 78−42217
positron scattering, analytic model, complex scaling 79−18257
positron scattering, elastic, Schwinger variational principle 79−45780
positron scattering, elastic and 1s-2s excitation, two-pot. eikonal approx. 79−31685
positron scattering, Feshbach resonances, close-coupling calc. 77−6940
positron scattering, optical pot. theory 80−43181
positron scattering, positronium formation 79−89772
positron scattering, second-order pot. method calcs. 79−72419
positronium elastic scatt., electronic S=1 state 77−512
production at 10 torr in pulsed discharge 80−9748
productive form factor in inelastic collisions *(Russian)* 77−79675
proton energy loss distrib. in range 50-150 keV 77−79526
proton spreading in strong mag. field 78−70769
protonium formation in flight, $\bar{p}p$, antiproton+neutral and negatively ionised hydrogen atoms 79−85319
pseudospectral dipole oscillator strength distribs. 78−50503
pulsar crust, crust, infinitely magnetised H atom theory 80−77282
quadratic Zeeman effect, perturbative approach 79−22649
quantum mechanical energy spectra calc. using trajectory integrals 78−21838
quantum static multipole polarisabilities 78−82859
quantum yield determination, following laser photodecomp. of formaldehyde 79−96344
quasars, H emission-line spectra 78−96557
quasars, large-red shift, spectra, implications of neutrino rest mass for H I obs. problem *(Russian)* 80−105414
quasars, theory of H line emission from dense plasmas 80−51900
quasars of high redshift, search for 21 cm absorpt. 80−4453
quasi-stationary states in field of strong monochromatic wave, perturbation theory calcs. *(Russian)* 80−58145
quasibound states, Stark effect, variational calcs. 77−3251
quasiequilibrium interaction with Pd membrane, 100-500°C, 10^{-4}-10^{-2} torr 77−29047
radiative magnetic energy shift, H in 2p state 78−58601
radioastronomical spectra 21 cm line, radial vel. contour maps 80−17626
Raman-like two-photon scatt., calc. for metastable hydrogenic atoms 80−47953
Rayleigh scatt. from n=2 states, fusion plasma diagnostics appls. 80−43002
reaction rate constants, for $H+NO_2 \rightarrow NO+OH$ and $H+O_3 \rightarrow O_2+OH$ by atomic resonance fluorescence 77−48618
reactions with MgO and zeolite, EPR anal. via ultrahigh vacuum/flow system 78−7232

hydrogen neutral atoms continued
recombination, heterogeneous, on Ni films, and Pyrex, coeff. calc. 77−48634
recombination, Morse oscillator model 78−20001
recombination excitation of Balmer lines in H_2-Ne(He) glow discharge *(Russian)* 77−46516
recombination on surface of semicond. with p-n junction, photovoltaic chemoelectric effect 77−66185
redshifted H I 21 cm line assoc. with Stephan's Quintet of galaxies 80−67882
relativistic, in strong mag. field 80−9518
relativistic, in superstrong mag. fields 78−90095
relativistic Dirac equation, for teachers 78−62019
relativistic energy levels in strong mag. fields 80−102454
relativistic H atom, Dirac eqn., operator structs. for consts. of motion 78−37124
relativistic model of spin 1/2 particles interacting with external EM field 78−70756
relativistic quantum mech. as weak-field limit of nonlinear theory 79−6878
relativistic spin 1/2 particle dynamics 78−70001
relativistic theory of H atom in superstrong magnetic field 80−23320
resonant oscillating EM field, interacting with highly excited atom 79−76371
resonant pole trajectories in complex scaling, stationarity 79−18126
reversible chemical reactions involving H atoms, formation rates and lifetimes of intermediate complexes 79−15956
in ring galaxies, H I survey 79−5901
Rydberg consts., saturated absorpt., spectroscopy meas. 80−105604
Rydberg levels, selective excitation by three-photon absorpt. 80−5518
Rydberg Stark ionis. threshold scaling laws 77−6721
in Sa spiral galaxies, H I study 80−98714
Saturn rings vicinity, origin of Lyman-alpha emission 79−12430
scalar relativistic approximation 79−26899
SCF calcs. for H in spherical box 77−54508
Schrodinger eqn., Monte Carlo soln. for H atom in mag. field 80−31545
Schrodinger eqn., random walk soln., electron spin effects, ^2P state 77−18780
Schrodinger eqn. appl. *(Hungarian)* 79−3339
Schrodinger eqn. in two-dimens., for teaching 80−31457
Schrodinger equation, trigonometric soln. of polar function 77−67308
Schrodinger equation, two dimens., finite element package MANFEP 78−36870
Schrodinger-Dirac spaces of entire functions, H atom theory 77−54494
Schroedinger equation, influence of constant elec. field on pressurized atom and crystal in box, finite-element method 80−31544
self-interaction of excited at. with radiation field 78−86794
Sharpless 159 and NGC 7538, H II region/mol. cloud complex, H I aperture synthesis obs. 80−90510
simultaneous mag./elec. microwave resonance transition, parity nonconservation, Weinberg-Salam theory test 77−54066
solar atmosphere, evidence for neutral H continuous absorpt. above transition region 79−92738
solar chromosphere, Hα seven components rel. to 9873 MHz line appearance 78−89151
solar photosphere, van der Waals damping rel. to Ca abundance and upper photosphere models 77−33445
solar quiescent prominences, H and He spectra 77−13295
spectra, homogeneous mag. field, variational approach 79−22629
spectra, interaction with external quantised EM field 79−68332
spectra, quasistationary states due to CO_2 laser radiation 77−67997
spectral broadening, by low-freq. elec. field, dense plasma 79−98026
spectral classification, pattern recognition method, H model appls. 78−41982
spectral life time, average, asymptotic expression 79−45671
spectral lines, Lyman series asymm. 77−38639
spectrum, appl. of lasers 79−72267
spectrum in strong mag. field, effect of proton mass 79−59387
spin aligned, condensed on surfaces 78−63929
spin flipping, quantum mech. eqns. of change 78−70003
spin-aligned, condensed, props. from variational calcs. 80−4637
spin-aligned, ground state and elementary excitations 79−54047
spin-aligned, proposed production method 79−55003
spin-aligned, stability at low temp. and high mag. field 77−10723
spin-aligned hydrogen 80−42969
spin-polarised, Bose condensation, phenomenological description 80−77699
spin-polarised, Bose-Einstein condensation 80−77698
Stark and photoabsorption spectrum, density of oscillator strengths, atom c.f. semiconductor spectra 80−83318
Stark and Zeeman effects in parabolic coordinates 79−63957
Stark broadened line shape, unified Franck-Condon-JWKB method 77−10635
Stark broadened profiles, ion motion model microfields 78−13469
Stark broadened profiles, model electronic microfields 78−13468
Stark broadening, effect of reduced mass *(Russian)* 77−79578
Stark broadening, ion dynamics correction to unified classical path theory 79−76382
Stark broadening by ion impact on moving emitter, Doppler H shift, theory 80−47940
Stark broadening of spectral lines, classical and quantum treatment *(Russian)* 77−61708
Stark effect, 1s resonance of perturbed atom, perturbation and variation treatments 80−14105
Stark effect, asymptotic expansion for level width 78−70783
Stark effect, complex coords., translation and dilatation transforms 79−18141
Stark effect, confinement of resons. 79−49982
Stark effect, dispersion relation, asymptotic formulae, ionis. rate, perturbation theory calc. 80−14106
Stark effect, dispersion relations 79−63956
Stark effect, existence and Borel summability of resonances 79−13668
Stark effect, high orders of perturbation theory 79−98025
Stark effect, high orders of perturbation theory for excited states 80−87079
Stark effect, iteration procedure for any field strength 80−69104
Stark effect, perturbation theory 79−22652
Stark effect, second order correction for energy *(Rumanian)* 80−74147
Stark effect, theory, teaching appls. 79−5933
Stark effect and perturbation approxs. 80−52932
Stark effect in Lyman α-line wings 79−22648
hydrogen neutral atoms continued
Stark effect resons., strongly asymptotic approximants 80−52931
Stark effect studied by scattering theory methods 80−63586
Stark energy shifts, dispersion relations 79−93952
Stark line broadening of ionised gas in macroscopic field, direct meas. of current density *(French)* 78−9839
Stark problem, complete separability 79−68209
Stark resonances, calc. from complex-rotation technique applied to variational principle 78−33549
Stark shift, classical adiabatic theory of Stark ionis. threshold 78−82687
Stark spectrum and field ionisation, density of continuum states, normalised wavefunctions 80−83317
Stark-induced anticrossings, $^2P_{3/2}$-$^2D_{3/2}$ Lamb shift meas. 78−33468
Stark-induced anticrossings, Lamb shift meas. 78−33467
Stark-induced quantum beats in H_β 80−9757
Stark-Zeeman effect, dilatation transformation 79−3398
in static multipole field, logarithmic perturbation expansion 80−91431
stellar atmospheres, atomic line broadening by neutral H 79−92665
storage in solid H_2*, rate process theory 77−32770
strongly bound states in intense mag. field 80−37721
strongly magnetised, quantum number assignments, semi-classical approach 78−90055
sublevel excitation cross sections following mol. dissoc., Stark effect determ. 77−14593
submillimetre lines in solar prominences *(Russian)* 79−35228
subnatural linewidth resolution $2^2S_{1/2}$, $2^2P_{1/2}$ level crossing, Lambshift, pulse technique 79−22669
superpermeability, in interaction with Pd membrane 80−81365
surface cleaning, by dissociated H atoms *(Japanese)* 80−16527
surface concentration on ultra cold neutron container materials meas. with $H(^{11}B,\alpha)2\alpha$ reaction 80−9446
symmetry algebra, group theoretical derivation of Hughes-Yadegar algebra 77−17766
terrestrial H escape flux, charge exchange induced, diurnal and solar cycle vars. 78−93022
thermal dissipation in Earth's atmosphere 78−45062
thermosphere H temperature, influence of 63 μm radiation field 79−80066
toroidal plasma, 2-D neutral H transport 78−59661
transition probabilities and expectation values, in intense mag. field 79−10066
trapped atoms and electrons formation on X-irrad. of $NaClO_4$ 80−35559
trapped in inert gas matrix, anisotropic hyperfine interactions 79−65728
trapping and thermal detection using superconducting magnet at low temp. 80−73396
two-photon 1s-2s transition rate and absorption coeff. freq. depend., choice of gauge 78−9132
two-photon radiation, rel. to planetary nebulae continuous UV spectra 79−92843
two-photon resonant absorpt. line profile, quadratic Doppler effect 77−34590
two-photon transition, $3^2S_{1/2}$-$3^2D_{5/2}$, precision meas. 78−17642
two-photon transition matrix elements, group theory calc. 78−62776
two-photon transitions, parity nonconservation effects *(Russian)* 78−21892
uniform mag. field, low lying levels below 10^9 G, adiabatic approx. 79−72235
UV lamp, microwave discharge in H_2-D_2-He, H and D Lyman-α line shapes 79−80698
variations, quantum theory calcs., generator coord. calcs. 80−41987
Venus exosphere, H transport due to temp. day-to-night var. 79−35164
Venus exosphere non-thermal H, ionospheric source and H budget 79−12416
Venus thermosphere, H global circulation and distrib. 78−89093
Virgo cluster spiral galaxies, H I deficiency from 21 cm obs. 80−62277
VUV radiation, narrowband tunable, at Lyman-α wavelength 80−78907
wavefunctions, parabolic, polar, unitary transform. coeffs. *(Russian)* 79−3344
weak interaction effects in transitions 77−13890
Xα statistical exchange calcs. 77−30766
X-ray absorption spectra, method of coupled differential eqns. 77−88466
X-ray spectra, mass absorpt. coeffs. in ultrasoft region, spectral depend. 77−10622
Zeeman effect, dispersion relations 80−27978
Zeeman effect 77−79577
Zeeman levels orientation by reson. radn. in turbulent plasma *(Russian)* 79−98028
K^-p atom and $\Lambda(1405)$, $\bar{K}N$ interaction model 80−68479
$(\mu p)_{2S}$ and $(\mu p)_{1S}$, muon transfer to heavy atom 77−27209
$\mu p+p$, elastic scattering cross section of muonic H atoms 80−69278
$n\rightarrow ep\bar{\nu}$, H atom spectra and metastable state *(Russian)* 80−37262
$\bar{p}$ radiative atomic recombination, antiprotonic atoms 80−83527
$Ar(^3P_{0,2})+H(^2S)$, energy transfer rate const. and mechanism 78−37727
Ar^*+H, collisional quenching rates 80−95548
Br_2+H, classically forbidden vibr. excitation, S-matrix 77−516
$C^{2+}+H$, fine struct. excitation cross section 77−38724
$C^+ + H$, fine structure transition of C^+, collision cross section calc., validity of current approx. 78−25652
$C^{6+}+H(1s)$, low vel. cross-section, adiabatic mol. orbital basis 77−88553
$Cd(^3P_J)(^1P_1)+H_2$ reacts., CdH(CdD) yields, quenching cross sections 79−1948
D, spin-aligned, stability at low temp. and high mag. field 77−10723
D/H for rocks in Tertiary igneous complex of Skye 77−33012
D/H ratio in galactic centre direction, 327 MHz obs. upper limit 80−26949
D/H ratios of natural serpentines, rel. D/H fractionation factors between serpentine and water at 100-500°C 79−34803
DF+H, reaction rate, DF fluoresc., shock tube obs. 77−12784
D_2O+H exchange reacts., water adsorpt. on Pt surfaces investig. 77−80695
$F+H_2$ nonadiabatic effects, scatt. theory, coupled-channel calcs. 78−22010
Fe/H abundance determ., catalogue for 515 stars 77−29815
Fe/H determ. catalogue for stellar atmospheres, comments 77−29806
$Fe^{26+}+H$, electron removal by collision 79−76508
Ge, heterodiffusion due to H atom surface recombination stimulation, Cu, Zn, In coated *(Russian)* 80−59726
H ($1^2S_{1/2}$) to ^4He (2^3S_1) electronic g-factor ratio from Zeeman resonance meas. 78−13467

hydrogen neutral atoms continued
H ($2^1S_{1/2}$), metastable state two-photon decay, Laplace transform method 79−10084
H (2s) elec. field-quenched radiation polaris., Bethe-Lamb theory justification 78−17603
H (2s) metastable state elastic electron scatt. 78−55238
H, degenerate 3s-3d levels, in mag. field, eigenvalues, Bender-Wu formulas 80−83275
H, electron elastic scatt. phaseshifts H continuum, frozen-core Hartree-Fock approx. perturbation theory 77−75295
H, electron impact excitation of n=3 levels, polaris. fractions in Glauber theory 77−34765
H, electron scatt., orthogonality constraints 77−71869
H, electron scatt., polarisation potential 78−42228
H, ground and first excited states in homogeneous magnetic field 78−925
H, He atmosphere, hyperfine press. shift, MCSCF-variational procedure 77−6735
H I, galactic, column density as function of position in southern sky 80−4420
H I, galactic, high angular resolution emission spectra, self absorpt. and other characts. 79−35350
H I, galactic subsystem, 21 cm line profile rel. to galactic rot. curve *(Russian)* 80−36724
H I 21 cm line of NGC 2685 galaxy 80−56943
H I absorption obs. of SS 433, distance 80−56848
H I and D I Lyman α radiation scattering, Venera obs. near Venus 77−78703
H I α observations of Algol type stars 80−109484
H I clouds, high velocity, map 80−26923
H I emission line profiles obs. in o Ceti spectrum *(Russian)* 79−16990
H I emission lines rapid variability in U Orionis spectrum *(Russian)* 79−16989
H I halo round Seyfert galaxy Markarian 348, 21 cm obs. 80−82504
H I halo round Seyfert galaxy Markarian 348, rel. to nucl. activity 80−82505
H I Lyman α line formation in expanding spherical planetary nebula 79−30110
H I radio recombination lines, in interstellar H II regions, quasiclassical anal. 78−28511
H II regions, integrated H I measure rel. to clumping factor 78−20870
H, ionisation by external electrostatic field 78−13622
H isotope exchange between clay minerals and seawater 78−69329
H, metastable quenching, subsequent photoionis., polarised proton prod. *(Russian)* 78−46202
H, positron scatt., forming $(e^+e^-)(1s)+H^+$, first-order approx. 79−55006
H, positron scatt., S-wave reson., generalised scatt. length 78−42226
H, s-p coherence quantum beats, following H^+ electron capture in gas 79−89773
H, spin-aligned Bose gas, Born-Oppenheimer approximation 80−46958
H time and frequency standards with redundancy 77−79065
H^- and H electron loss in plasma target 78−67371
H:He, 15 to 150 keV ionising collision, electron ang. and energy distrib. 80−53121
H-D exchange, catalysis by α-$Cr_xAl_{2-x}O_3$ solid solutions 77−52631
H-He, H hyperfine struct. shift, commutator computational method 78−78608
H-like atom, fine struct. and HFS levels, Zeeman effect, relativistic corrections 80−37776
H-like atom, interacting with EM field, matrix elements and transition probabilities 78−37533
H-like atom, spin-orbit interaction and single electron excitations rel. to mag. dielectrics 79−54780
H-like atom, Stark effect on fine struct. 79−26929
H-like atom near metal surface, quasi-stationary spectrum 79−18132
H-like atom or ion, electron-electron interaction operator, dipole approx. 78−58821
H-like atom+bare ion, electron capture to continuum, cross-section cusp 78−90289
H-like atoms, dipole polarisability of arbitrary hybrid bound states 80−87237
H-like atoms, effects impeding obs. of parity nonconservation *(Russian)* 77−75078
H-like atoms, electron exchange scatt., high impact vels. 79−22846
H-like atoms, quadrupole moments 78−90072
H-like atoms, radiational displacement of energy levels in fields of extended nucleus *(Russian)* 79−10045
H-like atoms, relativistic acceleration, quasi-Stark effect *(German)* 78−58621
H-like atoms and ions, statistical equilib. among sublevels in non-LTE plasma 77−31426
H-like ions, ground-state, elastic electron (positron) scatt., relativistic Glauber amplitudes 80−23550
H-like system, hyperfine interactions, modified delta-function pot. 79−3378
H-quark interaction, var. method calcs. 78−37771
H+ adsorbed H, W(001) surface, pot. model 77−10726
$H+{}^{16}O$, hyperfine interactions of highly stripped ions recoiling into H 77−22932
$H+{}^3He^{2+}$, electron capture at impact energies below 10 keV 78−50633
$H+{}^3He^{2+}({}^4He^+)$, electron loss, capture cross-sections 78−22026
$H+{}^4He^{2+}$, electron capture and charge exchange cross sections 77−68108
$H+A^{z+}$, charge transfer for ground and metastable states 77−42399
H+acetaldehyde, absolute reaction rate consts., 298-500K 77−16788
H+alkali atom, long-range interaction, S-state alkali atom 79−76480
H+alkali metal atom, interaction potentials 80−63736
H+alkali metal atom, S-state, long range interaction 77−50490
H+Ar, 0.5 MeV $H(H^-)$ ionisation comparison 79−41230
H+Ar, collisional charge production, differential scatt. calcs. 77−68107
H+Ar, collisional charge production cross-sections 77−71860
H+Ar, Hα and Hβ emission cross sections 80−63782
$H+Ar^*(Ne^*)$, assoc. ionis., rovibronic struct. in electron energy spectrum 80−106380
H+Ar(Kr)(Xe), ion pair formation, curve crossing model 80−87216
H+Ar(methane), differential collision cross sections, diffraction oscills., data anal. 79−22783
H+atom (ion), ionis. by one or two electron at. particles, Born approx. 79−54960
H+atom collisions, appl. to line broadening in stellar spectra 77−13237
hydrogen neutral atoms continued
H+atom(ion)(electron), general excitation cross section theory 80−37869
$H+B^{3+}(C^{4+})$, charge transfer cross sections, ab initio potential energy curves 78−37741
$H+B^{4+}(C^{5+})(O^{7+})$, excitation distrib. following electron capture 79−36763
$H+B^{n+}(C^{n+})$, one electron capture and loss 80−18921
$H+B^{q+}(C^{q+})(N^{q+})(O^{q+})$, $(2\leq q\leq 4, 5)$, cross sections at keV energies 80−78705
$H+Be^{2+}\rightarrow H^+ + Be^+$, charge transfer total cross-sections 79−3559
$H+Br_2$, H+HBr, reaction props. dimensionality depend. 77−9050
$H+Br_2$ reaction, Br prod., matrix isolated ESR 80−106336
$H+Br_2(Cl_2)$, nonreactive scatt., long range anisotropic pot. determ. 78−66626
$H+Br_2(HBr)$, H* prod., IR chemiluminesc. meas. 79−100336
$H+Br_2\rightarrow HBr+Br$, HBr ang. momentum alignment, scatt. ang. depend. 78−3323
$H+Br_2\rightarrow HBr+Br$, pot. energy surface, ab initio generalised valence bond calc. 78−73026
$H+BrF(IF)\rightarrow HF+Br(I)$, reaction product energy distrib. 80−30219
H+bromotrifluoromethane, reaction rate consts., flash photolysis-reson. fluoresc. obs. 78−3327
H+C, surface chemical reaction of thermal at. H 78−20071
$H+C^+(C^{3+})(N^{2+})(O^{2+})(Ne^{2+})(S^+)(S^{3+})(N^+)$, ionization model for NGC 7027 planetary nebula 78−36671
$H+C^+(N^+)(O^+)$, 0.1-13 keV electron capture cross-sections meas. 79−36761
$H+C^{2+}(C^{3+})(N^{2+})$, radiative charge transfer, rate coeffs., pot. energy curves 77−88554
$H+C^{3+}(N^{3+})$, charge exchange collisions, quantal calcs. 79−94079
$H+C^{6+}$, collisional electron removal, cross-sections, mechanisms 78−25683
$H+C^{6+}$, low velocity charge transfer, two-state approximation calcs. 78−42207
$H+C^{6+}(He^{2+})$, ionis. cross sections 79−22805
$H+CF_2$, IR matrix isolation spectra 80−97706
$H+CF_4(SF_6)$ scattering, obs. of resonance maximum 77−58126
$H+CH_4\rightarrow H_2+CH_3$, transition state, UHF method in INDO approx, 79−43578
H+CN(NC)(NSi), bimolecular exchange reactions, dynamical-statistical method calcs. 80−104435
H+CO, scattering cross-sections, factorisation and fitting, IOS approx. 78−33575
H+CO, total different collision cross section meas., interstellar gas clouds appl. 79−45786
H+chlorotrifluoromethane, reaction kinetics, ESP obs. 77−21358
$H+Cl_2$, collinear nonreactive collision, classical trajectory eqns. calcs. 77−57233
$H+Cl_2$, collinear reaction rate consts., quantum and semiclassical calcs. 77−12782
$H+Cl_2$, collinear reaction, quantal transition probabilities from classical trajectories 77−32773
$H+Cl_2$, Faddeev equations and Franck-Condon models for chemical reactions 80−35507
$H+Cl_2$, Franck-Condon factors for reactive collision processes 77−36741
$H+Cl_2$, Franck-Condon factors in reactive collision dynamics, vib.-rot. distribs. 77−36742
$H+Cl_2$, impulsive triatomic reaction, vibr. state distrib., impulsive energy release model 78−92456
$H+Cl_2$, pot. energy surfaces, inversion calcs. 80−93734
$H+Cl_2$, stochastic-collision complex model theory 80−108696
$H+Cl_2$, uni- and bimodal product energy distribs. 79−57207
$H+Cl_2$ dynamics, Franck-Condon factors rel. to information theory for vib.-rot. distribs. and isotopic branching ratios 77−60041
$H+Cl_2(H_2)$, activation energy and trajectory calcs., temp. and isotope effects 78−76835
$H+Cl_2(SCl_2)(S_2Cl_2)(SOCl_2)(SO_2Cl_2)$, energy disposal, HCl IR chemiluminesc. obs. 78−92484
$H+Cl_2$(organic molecule), rate const., discharge flow-reson. fluoresc. meas. 78−7178
$H+Cl_2\rightarrow HCl+Cl$, quantum mech. reaction coords., point transformation calcs. 77−36730
$H+Cl_2\rightarrow HCl+Cl$, rate consts. meas., Lyman-α fluoresc. technique 77−16780
$H+Cl_2\rightarrow HCl+Cl$, translational and pot. relax., statistical calcs. 77−3435
$H+Cl^-\rightarrow HCl+e$, associative reaction, product vibr. state distrib. 80−66794
$H+ClBr\rightarrow HCl+Br(HBr+Cl)$, product energy distrib., rate const., IR chemilum. obs. 77−81391
H+ClF reaction, IR chemilum., energy disposal and branching ratios 80−26017
$H+ClO_2\rightarrow OH+ClO$, primary energy disposal, laser-induced fluoresc. 79−24726
H+completely stripped positive ions, electron capture 77−23559
H+Cs, fast atom collisions, charge exchange, equilib. fractions calcs. 78−33601
H+Cs(Rb)(K)(Na), single-electron capture total cross sections 80−91656
$H+Cs\rightarrow H^-+Cs^+$, low energy cross sections 79−7009
H+D, close coupling calc., resonant spin-flip process, Ramsauer-Townsend effects 80−99547
H+D, excitation transfer, spectral line broadening and shift 77−46531
H+D, excitation transfer, thermal energy, dipole-dipole interaction 79−31666
H+D, near-resonant excitation transfer cross sections 77−3446
$H+D_2$, collinear motion, energy transfer and dissociation, collision dynamics 80−99563
$H+D_2$, pot. curve, thermal energy absolute integral cross-sections meas. 80−53096
$H+D_2$ reaction, transition state theory calculations, kinetic isotope effect explanation 80−66784
H+DCl→HD+Cl or HCl+D, branching ratios determ. 78−40046
H+e, free-free electron transitions in solar atm., review 78−33563
$H+e^-$ scatt., channel coupling array theory 77−19005
$H+e^-$ scattering at low energy 77−30994
$H+e^-(e^+)$, elastic and inelastic scatt., relativistic spin-dependent amplitude, Glauber approx. 80−63818
$H+e^-(e^+)$, elastic scatt., asymptotic effective pot. 80−14233

hydrogen neutral atoms continued
H+e^+, moment T-matrix approach, ang. distrib., total cross section, below pickup threshold 79−3573
H+e^+, moment T-matrix approach, elastic scatt., total cross section, intermediate energy 79−3582
H+ethane, chemical reaction, 357-544K 78−7198
H+ethylene episulfide→HS+ethylene, absolute rate parameters, flash photolysis reson. fluoresc. 78−3312
H+ethylene→C_2H_5*, rate const., 198-320K, high press. 78−48618
H+ethylene⇌ethyl radical, pot. energy surface, analytic function 79−11779
H+F_2, exothermic triatomic exchange reactions, dynamics, anal. theory 78−3322
H+F_2, impulsive triatomic reaction, vibr. state distrib., impulsive energy release model 78−92456
H+F_2, vibr. prod. distrib., Einstein coeffs. 78−92448
H+$F_2(Cl_2)$, exothermic triatomic exchange reactions, prod. energy distrib., statistical dynamic model 78−92455
H+$F_2(Cl_2)$, reaction probability, information theoretic anal. 77−16799
H+F_2→HF+F, 3-dimens. vibrot. reaction probabilities from collinear results, information theoretic synthesis 79−74354
H+F_2→HF+F, exchange reaction, quasiclassical dynamics calcs. 79−91942
H+F_2→HF+F, isotope effects, quantum mech. and information theoretic calcs. 78−44360
H+F_2→HF+F, vibr. adiabatic and static distorted wave Born approx. calcs. 80−7768
H+Fe^{n+}, 50-1200 keV amu^{-1}, impact ionis. and electron capture cross-sections 78−42204
H+Fe^{n+}, electron transfer cross-section meas. 78−17787
H+fluoromethane, reactions, selective vibr. excitation effects 78−35643
H+formaldehyde, reaction, absolute rate coeffs., 250-500K 79−100349
H+H, cross-section for excitation of high-lying levels, quasiclassical approx. *(Russian)* 77−79676
H+H, diatomic transition operators, numerical calcs., variable phase and amplitude calcs. 78−25653
H+H, dispersion forces between closed shell atoms 77−88522
H+H, dispersion forces calc. 77−14521
H+H, electron loss cross section, four-body trajectory calcs. 80−99566
H+H, electron transfer calc., electron ionization calc., Monte Carlo method, 79−72387
H+H, excitation transfer, thermal energy, dipole-dipole interaction 79−31666
H+H, excited atom ionisation collision, excitation transfer effect 79−81272
H+H, excited states, ionisation collision cross-section energy depend., semiquantal theory 78−42160
H+H, interaction energy, modified perturbation theory calc. 78−9217
H+H, multipole-multipole dispersion interaction, Pade approximants 79−31638
H+H, one electron excited atom ionisation collisions at high energy, improved impulse approx. 79−94072
H+H, pair polarisabilities, continuum electrostatic theory 78−86769
H+H, recombination, orbiting reson. theory, rate consts. meas. 77−83681
H+H, spin-exchange and freq. shift cross sections at low temps. 80−83452
H+H, two body multipole-multipole Pade approximants, second order dispersion energy 80−28081
H+H collisions in laser field, excitation, charge exchange and ionis. *(Russian)* 79−94078
H+H interaction, second order dispersion energy, Borel integral investigation 80−74218
H+H_2, 3-dimens. exchange reaction, surprisal theory, quantum dynamics 79−15964
H+H_2, ang. momentum decoupling approx., quantum mech. reactive and nonreactive scatt. 77−12780
H+H_2, anisotropic interaction pot., total cross-section calcs. 78−29835
H+H_2, atom transfer reactions, reaction rate computing, trajectory calcs. 79−74371
H+H_2, atom transfer reaction in gas phase, reaction rate computing, tunnelling corrections 79−79237
H+H_2, body-fixed coordinates collision theory, asymptotic scatt. matrix solns. 79−64070
H+H_2, CI calc. of three dimens. pot. energy surface 78−56882
H+H_2, collinear, collision-induced dissoc., quantum mech. probabilities calcs. 79−20359
H+H_2, collinear, quantum mech. reactive scatt., exchange kernels calcs. 78−68880
H+H_2, collinear classical dynamics, chemically accurate pot. energy surface 77−48620
H+H_2, collinear exchange reaction, quantum dynamics, surprisal theory 79−6988
H+H_2, collinear exchange reaction, unified statistical model 79−34295
H+H_2, collinear quantum mech. reactive scatt., hyperspherical coords. 80−108694
H+H_2, collinear reaction, isotope depend. transmission coeff., transition state theory 77−36747
H+H_2, collinear reaction, transmission coeff. isotope depend., statistical theory, invariance 77−36748
H+H_2, collinear reaction, Delves radial coord. S-matrix propag. calcs. 80−108695
H+H_2, collinear reactive scatt., Magnus approx. 77−16801
H+H_2, collinear reactive scattering, coupled eqns., soln., R-matrix calcs. 77−16812
H+H_2, coplanar exchange reaction, 0-2 eV, reactivity bands, analytical method 78−35664
H+H_2, elastic differential cross section high resolution meas. 78−50610
H+H_2, exchange reaction, three-dimens., dynamical S matrix method 79−91930
H+H_2, exponential gap relation, rot. inelasticity 80−78693
H+H_2, finite element methods for reactive scattering 78−92453
H+H_2, Franck-Condon factors in reactive collision dynamics, vibr.-rot. distribs. 77−36742
H+H_2, H_3 dynamics, on accurate H_3 pot. surface 79−5139
H+H_2, integral cross section meas. at thermal energy 77−10724
H+H_2, integral total reactive cross section, infinite order sudden approx. 80−30214
H+H_2, interstellar collisions rel. to hot gases cooling by H_2 79−12505
H+H_2, least squares fit to ab initio pot. energy function 78−56883
hydrogen neutral atoms continued
H+H_2, planar reaction, cross section calcs., vibr. and rot. convergences 77−21376
H+H_2, planar reaction, Schrodinger eqn., expansion as partial differential eqns. 77−21375
H+H_2, reaction, quasi-classical trajectory calcs. using new pot. energy surface 80−7767
H+H_2, reaction probability, max. entropy derivation, statistical theories 80−66781
H+H_2, reaction rate constants, modified collision theory expression, comparison with exact expression 79−74370
H+H_2, reactions and collisions in IR laser field, collision-induced absorpt. spectra 80−76499
H+H_2, reactive scatt., sudden approx. calcs. 78−68878
H+H_2, rot. cross-section, linear surprisal plots, theory 77−50498
H+H_2, rot. excitation 79−89746
H+H_2, scatt. wave function modal struct. and global behaviour 80−81307
H+H_2, sudden rot. reactive scatt., 3-dimens., approx. quantum mech. calcs. 80−76498
H+H_2, three dimens. reaction, theory 77−21377
H+H_2, three dimens. reaction, Porter-Karplus pot. energy surface, rot. distribs., rate consts. 77−21378
H+H_2, transition states, trapped trajectories and classical bound states in continuum 78−88630
H+H_2 dynamics, Franck-Condon factors rel. to information theory for vib.-rot. distribs. and isotopic branching ratios 77−60041
H+H_2 reaction, classical trajectories on spline-generated pot. energy surfaces 77−60047
H+H_2^+(HeH^+)(CO_2^+), reaction, ion cyclotron reson. mass spectrometric obs. 79−64098
H+$H_2(Cl_2)$, reaction products ang. distribs., Franck-Condon theory 79−87835
H+$H_2(Cl_2)$, reactivity-selectivity, bounds derivation 80−66763
H+$H_2(D_2)(T_2)$ reactions, accurate pot. energy surface, isotope effects, quasiclassical trajectory study 80−97698
H+H_2(HD)(D_2), exchange reaction rate consts. meas., vibr. effects 79−5134
H+$H_2(O_2)$, quantum reactive scatt. theory, 3-dimens. 80−55637
H+H_2(0,0)→H+H_2, quasiclassical cross sections, pot. surfaces comparison 79−74364
H+$H_2(\nu_i=1)$, exchange reaction, integral and differential cross sections determ. 80−85153
H+$H_2(\nu=1, j=0)$ exchange reaction, 0.9-1.1 eV, sudden rot. calcs. 79−79230
H+$H_2(\nu=1)$→H_2+H, exchange reaction, classical trajectory method, vibr. excitation, partial rate consts. 78−60993
H+$H_2(\nu)$, vibr. relax. in at. exchange reactions, classical trajectory calcs. 77−44467
H+H_2→H_2+H, classical three-body problem. calcs., effective reaction cross section *(Russian)* 79−39144
H+H_2→H_2+H, IR laser induced reaction 78−80761
H+H_2→H_2+H, tunnelling path for reaction 78−11514
H+H_2→H_2+H three dimens. chem. reaction, distorted-wave calcs. 80−81294
H+H_2→H+H+H, two path dissoc. 78−62875
H+H^-, electron detachment cross-sections, 100 keV-10 MeV 79−59561
H+H^-, electron detachment cross-section, target distortion calcs., 100 keV-100 MeV 79−59562
H+H^-, electron detachment in adiabatic regime, mechanisms 80−63800
H+H^-, electron loss by 1-300 keV H^- ions 80−37857
H+H^- collisions, assoc. detachment process theory 79−44351
H+H^-→H+H+e, electron detachment from H^- 80−37855
H+H^+, 1-7 keV, H(2s) form. and Lyman-α polarisation 80−14221
H+H^+, 1s charge exchange amplitudes, impact parameter calcs. 77−534
H+H^+, 1s→2s excitation at intermediate energy, close coupled and Glauber eikonal theory 78−25643
H+H^+, 50-200 keV, excitation and ionis., U-matrix method calcs. 78−17778
H+H^+, charge exchange and differential scatt., theoretical calcs. 77−10729
H+H^+, charge exchange probability 79−98216
H+H^+, charge transfer, Born approx. 79−59552
H+H^+, classical 3 body collision, cross section, energy transfer, computer calcs. 78−17783
H+H^+, coupled state calc., charge transfer and direct ionis. 79−22810
H+H^+, cross section for production of metastable H(2S) state 78−13588
H+H^+, differential energy loss cross-sections 77−46630
H+H^+, electron capture, 25 to 200 keV 77−88551
H+H^+, electron capture, H(2s) cross section meas. 79−72386
H+H^+, electron capture in high-energy approx. 77−42400
H+H^+, electron capture in 3s level, distortion approx. 80−37876
H+H^+, energy transfer and ionisation cross-section calcs 77−50522
H+H^+, excitation, differential cross-section 79−59547
H+H^+, excitation, distorted wave and coupled-channel calcs. 80−9713
H+H^+, excitation, pseudostate expansions and second Born approx. 79−45796
H+H^+, excitation and charge transfer to 2s(2p) states, 49-125 keV 80−18910
H+H^+, excitation ang. differential cross section, 25, 50 and 100 keV incident 78−66651
H+H^+, excited atom collisions, transitions between degenerate states 77−30976
H+H^+, fast proton total electron capture cross section, fixed scattered approx. 79−22819
H+H^+, gas-phase collisions, intermediate and high velocities, excitation 80−32822
H+H^+, H excitation, angular differential cross sections 80−63784
H+H^+, H(2p) production in slow collisions, peak struct. 80−1057
H+H^+, inelastic collision, time depend. Schrodinger eqn. for electron motion 79−89774
H+H^+, interaction energy, perturbation expansion, symmetry forcing 79−22785
H+H^+, interaction energy, perturbation theory, Pade approximants and convergence 79−31635
H+H^+, ionis. modified second Born approx. 77−88546
H+H^+, ionisation and electron capture to continuum 80−58366
H+H^+, K-electron capture, cross section scaling, high energy 79−41236

hydrogen neutral atoms continued
H+H$^+$, low energy, optimised translation factors 80−18813
H+H$^+$, nuclear repulsion, contrib. to charge transfer 80−18922
H+H$^+$, quantum theory of ionisation in fast collisions 79−3553
H+H$^+$, relativistic classical theory of electron capture 80−18920
H+H$^+$, resonant charge transfer in presence of lower field 79−64072
H+H$^+$, transition probabilities and total cross-sections, high energy behaviour 78−9245
H+H$^+$, vibr. excited H_2^+ form. by stimulated radiative association 79−100346
H+H$^+$,(He^{2+}), excitation, asymptotic cross-sections calcs. 79−18279
H+H$^+$ close capture collision spectroscopy, impact parameter perturbed stationary states 78−22002
H+H$^+$ collision, eikonal approximation, reson. charge exchange ang. distrib. and atom refl. *(Russian)* 77−34759
H+H$^+$ coupling energy, internuclear separation depend. 77−14523
H+H$^+$ low energy, quantum theory, integrated cross sections, phase shifts 77−30957
H+H$^+$(Ar^{q+})(Kr^{q+})(B^{q+})(C^{q+})(N^{q+})(O^{q+}) charge transfer and impact ionis. cross sections calcs. 77−88555
H+H$^+$(He^{2+})(Be^{4+})(O^{8+}), electron capture into n, l levels, 100 keV/amu 79−22826
H+H-like ion, charge stripping processes 77−19072
H+HCO→H_2+CO, classical trajectory study 80−93750
H+HCl, barriers for abstraction and exchange reactions 77−48629
H+HCl, reaction kinetics, ESR and mass spectrometric obs. 77−21357
H+HCl, semi-empirical pot. energy surfaces calc. by diatomics-in-molecules method 80−95556
H+HCl, vibr. relaxation and reaction rates determ. 80−108698
H+HCl(HBr)(HI), elastic scatt., <50 meV, Van der Waals pot. 79−54937
H+HF, kinetic isotope effect and temp. depend. 78−53202
H+HF, low barrier quantum model, vibr. deactivation 80−69216
H+HF (v=2, 3), vib. deactivation 77−58142
H+HR→H_2+R, (HR=hydrocarbon), tunnelling reaction, classical S-matrix calc. 77−29007
H+H*, electron loss cross section, four-body trajectory calcs. 80−99566
H+H(H_2), 1s-2s excitation of fast H atoms 79−89764
H+H(H_2), atom-atom pots., Hilbert Schmidt expansion, transition operators 78−66621
H+H(Mu), electron spin exchange cross-sections 80−9685
H+H(inert gas), negative ion form. 77−30988
H+He, associative and Penning ionis. cross-sections, pot. energy curve study 79−87836
H+He, D+He, low energy elastic scatt., pot. well depth determ. 77−6884
H+He, elastic scatt. cross-section, using model pot. 79−13786
H+He, electron capture in 3s level, distortion approx. 80−37876
H+He, H Balmer-α fine-struct. line shift and broadening 80−37783
H+He, long and intermediate range interaction, model pot. calc. 79−22789
H+He (2^3S), pot. energy surfaces and autoionisation lifetimes calcs. 77−34740
H+He$^+$, excitation of H to n=2 state, cross-section calc. 79−41229
H+He$^+$, unpolarised and spin-change collision, low energy 78−86943
H+He$^+$ (Li^{2+}), two-body dispersion interaction, freq. depend. multipole polarisability, variational calc. 80−37758
H+He^{2+}, charge transfer cross sections, molecular bases calcs. 79−98217
H+He^{2+}, electron transfer, plane-wave factor, mol. state treatment 80−63807
H+He-like ion, (of B, C, N and O), electron capture cross-sections 79−59559
H+He(Ar), collisional coherent excitation, meas. of Lyman α-photons 80−99552
H+He(Ar), press. effects on H_α and H_β Balmer series 77−18845
H+He(N_2), stripping cross-section, 0.3 to 3 keV 78−78807
H+He(Ne)(Ar)(Kr)(Xe), low energy elastic scatt. cross section MCSCF calc., van der Waals forces 78−70897
H+He(Xe), simultaneous ionisation investig. 80−32815
H+He($2^{1,3}S$), autoionising system, Siegert eigenvalues, variational calcs. 79−50106
H+He(2^1S)(2^3S), associative and Penning ionisation, autoionisation, calcs. 78−25674
H+He(2^3S,2^1S), Penning ions. 79−64089
H+He(2^3S), Penning and assoc. ionis. cross sections, vel. depend. 79−22815
H+heavy charged ion, total electron capture cross section charge depend. oscill. behaviour 78−66656
H+heavy ion (highly stripped), electron loss, charge state depend. 78−70921
H+Hg, differential cross sections, orbiting contribution 79−41221
H+highly stripped ions, energy gap and couplings at pseudocrossings 79−3526
H+highly stripped ions, S-matrix construction 79−3527
H+ICl, three dimens. collision, exponentiating trajectories and statistical behaviour 80−5595
H+ICl→HCl+I, IR chemiluminesc., product energy distrib. 78−23926
H+ICl→HCl+I, product energy distrib., rate const., IR chemilum. obs. 77−81391
H+inert gas atom, interaction pot. from electron gas model 79−31637
H+ion, charge exchange and ionis. cross sections *(Russian)* 79−50130
H+ketene, reaction rate consts., lab. meas., rel. to interstellar cloud processes 79−74359
H+Li_2, collinear reactions, SCF correl. diagram for Li_2H form. 77−70292
H+Li^+(Co^+)(Au^+), cross-section, closure-Born approx. 78−66630
H+Li^{3+}(Be^{4+})(B^{5+})(C^{6+}), charge transfer cross sections, distorted wave Born approx. 79−72415
H+Li-like ion, (of B, C, N and O), electron capture cross-sections 79−59559
H+LiF, laser-induced nonadiabatic collision process, classical model 80−97701
H+LiH→Li+H_2, LiHH pot. function calc. 77−6699
H+Li(Li_2), superthermal collisions, photon and positive ion prod. 78−78788
H+methane, abstraction and exchange reactions, energy barriers, UHF-CI calcs. 78−11512
H+methane, abstraction and exchange reaction, barrier height calc. using POL-CI wave functions 80−81304
H+methane, H abstraction, rate consts. calcs. 78−95921

hydrogen neutral atoms continued
H+multiply charged ion, electron capture, unitarised distorted wave approx. 80−63814
H+N, stripping cross-sections, binary encounter approx. theory 78−50618
H+N_2, excitation of Hα and Lα emissions, rel. to aurora 79−68309
H+N_2, nitrogen fixation, semiempirical INDO study 80−16898
H+N_2O→N_2+OH, rate const., 2000-2850K, combustion of $H_2/N_2O/CO/Ar$ 78−85162
H+N_2(CO)(O_2), vibr. state distrib., charge exchange 150-2400 eV 78−42195
H+N_2(O_2), charge prod. cross sections and differential scatt. calcs. 78−94313
H+N^+, charge transfer reaction in astrophys. nebulae rel. to ionization struct. 80−46384
H+N^{3+}, charge exchange, assoc. reaction, rel. to interstellar gas 80−7763
H+N^{3+}, multicharged ion thermal charge exchange reaction, rel. to astrophysics 80−63815
H+N^{q+}(O^{q+})(C^{q+}), q=1-5, single electron capture cross sections 78−55233
H+NF, electronically-excited free radical reactions 80−97707
H+NF_2, electronically-excited free radical reactions 80−97707
H+NH_2 rot. energy transfer in vibronic levels, absolute transfer rates 80−9701
H+NH_2→NH_3 react., force, density anal. 78−60997
H+NO_2, population inversion of Λ doublets in microwave spectrum of OH($^2\Pi_{3/2}$, v=1) 80−974
H+NO_2→NO+OH, hydroxyl group internal state distrib., laser-induced fluoresc. crossed mol. beams 77−4905
H+NO_2→NO+OH, rate consts. from at. reson. fluoresc. 77−48618
H+NO_2→OH+NO, energy disposal, information theory appl. 78−15658
H+NO_2→OH+NO, H+NOCl→HCl+NO, rate meas. by Lyman-α fluoresc. 77−21353
H+NO_2→OH+NO, laser induced fluorescence for OH, $^2\pi$ to $^2\Sigma$ region, preferential population of Λ doublets 78−31620
H+NO_2→OH+NO, primary energy disposal, laser-induced fluoresc. 79−24726
H+NO_2→OH+NO, vel. and angular distrib., Fourier transform Doppler spectrosc. obs. 79−80692
H+NO+H_2→HNO+H_2, rate of reaction, temp. depend., third body efficiencies 78−23933
H+NO+M→HNO+M, HgH+NO→HNO+Hg, rate consts. of photosensitised reactions 77−36757
H+Na, D2 reson. linewidth 79−31647
H+Na(K), covalent and ionic states interaction, config. mixing 78−50613
H+Ne^{10+}(Si^{14+})(Ca^{20+}), charge transfer, total and partial cross-sections calcs. 80−23542
H+Ne*, Penning ionisation, electron energy spectrum 79−72406
H+Ne(Ar), electron energy loss 80−87217
H+Ne(Ar)(Kr)(Xe), free electron production, integral cross-sections determ. 79−89754
H+Ne(Ar)(Kr)(Xe), orbiting resons., van der Waals pots., beam scatt. obs. 79−89739
H+Ne(Ar)(Kr)(Xe)(O_2), 20-500 eV, ion pair and free electron production, integral cross sections 78−46437
H+O_2, excitation of Hα and Lα emissions, rel. to aurora 79−68309
H+O_2, singlet state O_2 form., reaction mechanism, mass spectrometric obs. 78−53204
H+O_2 system, production of $O_2(^1\Sigma_g^+)$ 77−63918
H+O_2+Ar, HO_2 free radical prod., rate const. calc. 80−101026
H+O_2(N_2), collisional coherent excitation, meas. of Lyman α-photons 80−99552
H+O_2→OH+O, combustion, quasiclassical trajectory calcs. 78−53201
H+O_2→OH+O, kinetic study, pot. energy surface of HO_2, MO theory 79−74353
H+O_3, absolute reaction rate const., 219-360K 78−80734
H+O_3→HO_2+O(^{3}P), reson. fluoresc. obs. 79−70317
H+O_3→HO_2+O(^{3}P), yields 80−71900
H+O_3→O_2+OH, rate consts. from at. reson. fluoresc. 77−48618
H+O^+ in upper atm., rel. to H^+ loss during solar cycle 78−93021
H+O^{2+}(Ne^{2+}), charge transfer process, astrophys. plasmas appl. 79−59550
H+O^{8+}→H^++O^{7+}*, during neutral beam injection into Tokamak 77−58899
H+O^{n+}(Fe^{n+})(Mo^{n+})(Ta^{n+})(W^{n+})(Au^{n+}), single electron capture cross-section 79−59560
H+O^{n+}(N^{n+})(C^{n+})(B^{n+}), charge transfer cross sections, oscillatory behaviour in low-energy collisions 80−63806
H+OCS→HS+CO, absolute rate parameters, flash photolysis reson. fluoresc. 78−3312
H+OH, interstellar, role in OH 18 cm maser lines pumping 79−48892
H+OH($^2\Pi$), rel. to interstellar OH maser action 79−101186
H+OH→H_2+hν, radiative association reaction for mol. synthesis in interstellar clouds 80−90509
H+PH_3, abstraction rate consts., 209-495K, time-resolved fluoresc. 77−16807
H+Pb($^3P_1^o$), spin-orbit relax., fluoresc. intensity meas. 78−82681
H+positron, charge exchange, excited positronium states form. 78−58873
H+positron, S-wave scatt., lowest reson. calc. 78−37743
H+positron, second-order nonadiabatic polaris. pot. for elastic scatt. 79−22836
H+positronium→H^++positronium$^-$, low energy, field theoretic approach 77−10790
H+proton, charge transfer, variationally consistent approximation scheme 79−22825
H+proton, high-Rydberg state high-impact-velocity forward charge transfer as classical process 79−22824
H+slow doubly charged ions, one-electron capture 80−32828
H+T, excitation transfer, thermal energy, dipole-dipole interaction 79−31666
H+T_2, H-exchange studied by crossed molecular beam experiments 80−93747
H+X^{n+}, sub-barrier charge exchange cross section calc. *(Russian)* 79−7004
H+Xe, electron-loss cross section struct., 0.05-4 MeV 78−9236
H+Xe^{n+}(Ar^{q+})(Fe^{q+}), electron capture by heavy multicharged ions at low velocities total cross sections meas. 80−99548

hydrogen neutral atoms continued
$H+Zn^{2+}(Cd^{2+})(B^{2+})(Mg^{2+})(C^{6+})$, electron capture by slow ions, pseudo-crossing 80−43176
$H^-+H(He)$, electron detachment cross sections 78−90265
$H^-+H(He)$, electron-loss cross-section, double closure calcs. 77−50518
H^0+Cs collisions, H^- production cross sections 80−78698
H^0+N^{3+}, electron loss cross section 80−63805
H^++H, 15-200 keV, excitation and charge transfer cross sections, Sturmian expansion 77−19024
H^++H, capture cross sections, Faddeev anal. 77−27178
H^++H, charge transfer collisions, angular distribution 78−13599
H^++H, charge transfer cross section calc., up to 100 keV 78−55235
H^++H, excitation and electron capture, impact parameter calc. 78−33591
H^++H high energy collision, excitation multipole moments, classical trajectory approx. 80−106389
$H^++H(D)$, elastic scatt., rainbow struct. and g-u-interference effects 77−6886
$H^++H(D)$, elastic scatt. and charge exchange, resonances 78−78777
$H^++H(D)$, low energy elastic cross sections, impact parameter calc. 77−14526
$H^++H(1s)$, radiative charge exchange, 1-50 MeV 78−55234
$H^++H(1s)$, reson. charge transfer, spin depend. *(Russian)* 78−29850
$H^++H(1s)\rightarrow H(nl)+H^+$, cross-sections, continuum distorted-wave approx. 77−68108
$H^++H(1s)\rightarrow H(nlm)+H^+$, highly excited states rearrangement collisions 79−59564
$H^++H\rightarrow H+H^+$, charge exchange, atomic scattering, many-particle theory 77−10715
H_2-H mixture positive column, static electric charact. 78−67500
$H_2+Cl(Br)(I)(F)$, gas phase H-atom transfer reactions, struct.-reactivity correl., pot. energy surfaces 80−104433
$H_2+Cu^{2+}(Ti^{2+})$, electron capture cross-sections, 0.5-14 keV 78−42205
H_2+H, diatomic operator, separable approx., variational approach 78−42150
H_2+H, reactive scatt., 3-dimensional quantum mechanical calcs. 77−30802
(H_2+H^+, H_2^++H) collinear system, electronically nonadiabatic effects 78−1063
H_2+HCD, vibr. excitation cross-sections, rot. averaging calcs. 78−9231
$H_2+H(F)$, minimum energy reaction path, reference coord.-approach 78−40025
$H_2+H(F)(Cl)$, collision induced IR laser absorpt., rate enhancement, theory 79−66275
$H_2+H(He)(OCS)(CS)$, rot.-translational energy transfer, nonlinear vs. linear rotors, surprisal anal. 79−76492
H_2+He, rot. and vibr. inelastic cross-sections, distorted wave integral approx. 78−42175
H_2+NH_3, rot. relax., double and triple reson. obs. 78−90196
H_A line width in at. H atmosphere, shock-tube absorption meas. 79−64834
$H_{\alpha,\beta}$ lines, dense plasma Stark broadened central struct., comment 77−23464
$H_{\alpha,\beta}$ lines, dense plasma Stark broadened central struct., reply 77−23465
$H_{\alpha,\beta}$ lines, Stark broadened, central struct., in dense plasma 77−6722
H_α, 3s, 3p, 3d sublevels populations after dissoc. excitation of alkanes 77−75073
H_α and H_β line profiles in high density plasma *(Japanese)* 77−43065
H_α and H_β spectral profiles from neutral beams and plasmas in high mag. fields 80−83999
H_α and H_β Stark profiles in LF turbulent plasma 77−7593
H_α, H_β, Balmer line intensity ratios following mol. dissoc. of H_2 and benzene 77−10778
H_α line shape, plasma broadened, fine struct. effects at low electron densities 78−62765
H_α, polaris. spectroscopy, Rydberg const. determ. 79−9202
H_β, dynamic Stark effect for elec. field strength meas. in waveguide 80−69103
H_β line Stark broadened spectrum obs. in pulsed relativistic magnetron intense elec. field 79−89635
H_β, Stark broadening, wings calc. 79−31464
$HCl(v=1)+H(D)(Cl)(Br)$ reactions, selective vibr. excitation effects, kinetics *(German)* 77−21364
H(D), ground state Lamb shift, isotope shift and relativistic nuclear recoil correction 78−82696
$H(D)+X_2$, (X=F,Cl,Br,I), exoergic collinear reactions, impulsive energy release model 77−90591
$H_\alpha(D_\alpha)$ Stark broadening in Ar arc plasma 79−36582
$H_2(HD)+He$ potential, asymmetric, isotope substitution effect, Legendre expansion coord. transformation 78−70894
$H(^2S)+AR(^3P_2)$, energy transfer, Lyman-α line obs. 79−64085
$H(^2S)+Ar(^3P_{0,2})$, energy transfer collisions, Lyman-α emission profile obs., in microwave discharge and reaction cell 80−58359
H_2SO_4 glass, γ-irrad., trapped H ESR, vol. relax. effects 79−52703
$H'+BrH\rightarrow H'Br+H$, collinear reaction, barrier height, PNO-CEPA cals. 78−3328
$H'+HF\rightarrow H+H'F$, transition state geometry, SCF CI calcs. 78−20009
$H'+XH\rightarrow H'X+X$, X=H, F, Cl,CH_3, collinear pot. energy barriers, PNO-CEPA calcs. 77−32777
^1H Lamb shift measurement, estimate of proton RMS charge radius 77−50047
^1H, pionic, pion mass high accuracy meas. from transitions 80−106406
H^*, prod. by $H+Br_2$ or $H+HBr$ reaction 79−100336
H^*+chloroform-$d_1\rightarrow HD+CCl_3$, hot atom reaction, threshold energy meas. 78−44356
$H^*+H(1s)$, resonant ionisation, cross section and ionisation probability 80−63785
$H(1^2S)$-$He(1^1S, 2^1S, 2^3S)$, dispersion energies, charge overlap effects, with freq.-depend. polarisability 79−86025
$H(1^2S)+H_2$ (inert gas), electron capture, electron loss and deexcitation cross sections meas. 78−22025
$H(1^2S)+He(2^1S)$, Penning ionisation, semiclassical and Born total cross-sections 78−33586
H110α radio recomb. line in galactic radio sources, SHF obs. 80−77472
$H(1s,2s)+H(H_2)$, electron capture, loss, and collisional destruction, 5-26 keV 80−5611
H(1s) and (2s), electron loss in passing through inert gases 79−13805
H(1s), electron elastic scatt., semiclassical and quantal treatments 77−38733
H(1s), electron impact, elastic phase shift, post-adiabatic approx. calcs. 78−58827
H(1s), electron impact excitation to 2s(2p), Glauber theory modification *(Russian)* 78−29855
H(1s), electron impact excitation to H(2s,2p), appl. of general quasiclassical T-operator approx. 79−50134
H(1s) electron scattering, variable-charge Coulomb-projected Born approximation 80−58392
$H(1s)$-$H(1s)(^3\Sigma_u^+)$ isotropic intermol. force, model for approx. method, crit. test 78−78771
H(1s)+Cs, differential electron attachment and elastic scatt., 30-528 eV 80−63745
$H(1s)+H^+\rightarrow H^+H(1s)$, electron capture at relativistic energies, scatt. amplitude 80−1061
$H(1s)+He^+\rightarrow He^++H(2p)$, ion excitation cross section calc., effective Feynman diagram approach 80−23531
$H(1s)+He^{2+}$, charge transfer, Coulomb-Born approx. calc. 80−43175
$H(1s)+\mu^+\rightleftharpoons Mu(1s)+p$, thermal collision, quantal calc., elastic and transfer cross sections 77−42446
$H(1s)+O^{8+}$, electron capture into n,l excited states 80−23543
$H(1s)+O^{8+}(He^{2+})(H^+)$, charge transfer, 0.025-200 keV/amu 79−22823
$H(1s)+p\rightarrow p+H(1s)$, 15-200 keV, ang. distrib., differential cross sections calc. 78−82839
$H(2S)\rightarrow(2P)$ conversion on photodissociation of H_2, (H_2O), determ. 79−45775
H(2S), form. by electron impact from H_2(HD), time of flight obs. 79−86079
$H(2S)+H_2(N_2)(NH_3)$(acetone)(methanol), collisional quenching, mass spectral obs. 78−25685
H(2S)+He(N)(Ar), excitation and ionisation contributions to sum-rule Born cross sections 80−99551
H(2S)+inert gas, collisional quenching, mass spectral obs. 78−25685
H(2S)+Kr(Ne)(Xe)(H_2), metastable atom total quenching 77−46628
$H(2^2S)+H_2$(inert gas), electron capture, electron loss and deexcitation cross sections meas. 78−22025
H(2s)/H(2p) branching ratio, H_2 photodissoc. near threshold 78−21983
H(2s)+energetic projectile ion, charge exchange, cross-sections calcs. 79−59554
$H(2s)+H_2$(He)(Ne)(Ar)(Kr), collisional de-excitation, 5-26 keV 79−59546
$H(2s)+H_2\rightarrow H_3^++e^-$, fluoresc. of H_2 photodissociating near threshold 78−21983
H(2s)+He (Ne)(Ar)(Kr)(H_2)(N_2), 5-25 keV, H(n=3) excitation, Balmer α emission obs. 80−53113
H(2s)+inert gas, electron capture, H form., 4-25 keV 80−9729
H(3p), excitation in electron impact dissoc. of methane Lyman β and Balmer α obs. 78−46450
H50α, detect. in interstellar mol. clouds 77−60808
H56α radio recomb. line anomalous emission from galactic plane 79−80361
$H=H^+$ collisions, H(2s), H(2p) production, 1-7 KeV, differential, total cross sections 80−32818
$H(ads)+H_2O(ads)\rightarrow OH(ads)+H_2(g)$, H_2 formation mechanism 80−6628
Hα, airglow in upper atmosphere, semi-annual vars. 78−28360
Hα and Hβ, Stark profiles, ion-motion effect 80−63592
Hα emission line asymmetry in solar limb flares *(Russian)* 77−64728
Hα line, fine struct. meas. Rydberg const. determ. 79−54093
Hα(Dα) plasma red shift meas. in Ar arc, ion dynamic depend. 80−10364
He, 2^1S and 2^3S states excitation 77−42412
He/H ratio of B-type stars in young clusters and associations 77−29887
He+H, excitation cross-section, Born-Ochkur approx. calcs. 77−19088
He+H (inert gas atom), long range interactions for (2^1S) and (2^3S) states 78−70895
$He+H^+$, electron capture into ground and 2s states, cross sections 77−27177
$He^++H(H_2)$, H(2p) and H(2s) excitation cross sections, 5-26 keV 77−58150
$He^{2+}+H$, electron capture, impact parameter calc. 78−33591
$He^{2+}+H$, electron transfer, 0.1-20 keV, mol. orbital calc., convergence 78−42210
$He^{2+}+H$, mol. treatment, cross sections and charge exchange probabilities 77−58128
$He^+(He^{2+})+H$, charge transfer and direct excitation processes 78−25696
$^3He^{2+}+H^*\rightarrow{}^3He^++H^+$, merged beams, cross section 77−75292
$^4He^++H$, 35-1000 keV, electron loss cross-section 78−22018
$He^+(1s)+H(1s)$, excitation and ionis. processes 78−42189
$Hg+H(H_2)$, resonance scatt., HgH potential determ. 77−61830
H(muonic)$+H^+$, elastic scatt., cross section 79−871
H(n=2) excitation by ion impact, precision doubly differential cross section meas. 79−45811
$H(n=3)+H_2O$, radiation quenching in pulse radiolytically excited water vap. 79−89738
H(n=4), s-d coherence, quantum beats obs. in $H^++He(Ar)$ 80−32676
Hnα radio recombination lines, profile in static ion field 77−78629
Hnβ radio lines profiles in static ion field 79−62740
Li+H(He) 78−9127
$Li^{i+}+H(H_2)$, (q=1-3), electron capture and loss cross sections 78−42187
$LiH+H\rightarrow Li+H_2$, linear LiH_2 pot. energy surface, MCSCF functions optimisation 77−67960
Lyman α line profile in Ar plasma 79−22658
M+atom, 1 keV to 1 MeV, binary encounter, stopping cross sections, straggling and screening 78−17754
N IV+H charge exchange cross section rel. to intercloud gas 77−45514
$N^{q+}+H$,(q=1 to 7), electron capture and impact ionisation cross sections 77−75290
NH_3+H_2, NH_3 inversion transition, linewidths and T_1/T_2 ratio 80−99499
Ne:H, exciton states and L_α,L_β emission 80−93372
Ni cluster-H, electronic struct. calc., H-metal bonding 77−89823
Ni surface reflecting H atoms after H^+ grazing incidence collision, polarised emission 79−63951
Ni-Mn, hydrogenation kinetics, magnetisation, interstitial H influence 80−35528
$O^{2+}+H$, charge transfer rate coeff. and astrophysical appls. 80−56701
OH+H, rot. excitation in interstellar medium 78−4306
Pd cluster-H, electronic struct. calc., H-metal bonding 77−89823
Pt cluster-H, electronic struct. calc., H-metal bonding 77−89823

hydrogen neutral atoms continued
$Si^{2+}+H$, charge transfer reactions in interstellar medium 77−9789
$^{28}Si+H(H_2)$, single electron capture cross sections 78−58812
T-impregnated solid H_2, storable conc. of atomic H 80−30594
$X+F_2 \rightarrow XF+F$ (X=Mu, H, D, T), quasiclassical smooth sampling study of threshold behaviour 79−61852

hydrogen neutral molecules
3d complex, radiative lifetimes, hyperfine constants 78−70873
3d-triplet complex, Zeeman effect, eigenvectors and g-factors, rovibronic states 79−72353
$3p\pi D^1\Pi_u^+$ state, predissoc., Fano profile anal. 79−68274
3s, 3d: $^3\Sigma$, $^3\Pi$, $^3\Delta$ complex, fine struct., Doppler-free laser spectroscopy 80−1087
$^1\Sigma$ and $^3\Sigma$ state pots., diatomic transition operators, L^2 basis expansions 80−63519
$^3\Sigma_g^+ \rightarrow b\,^3\Sigma_u^+$ light emission meas. by electron impact excitation 78−33618
$^3\Sigma_g^+$ state, improved adiabatic energy, dissoc. energy 79−10011
Λ doubling, $C^1\Pi_u$ states, calc. methods 78−90227
ab initio SCF intermolecular interaction energy calcs. 80−78537
adsorbed layer on Al_2O_3, diffusive motion, neutron scatt. study 79−42394
adsorption, on inert gas solid layer, sorption capacity meas. 79−90865
adsorption, on MgO, (α-Al_2O_3), (α-SiO_2), microweighing and X-ray obs. *(German)* 78−51825
adsorption on graphite, orientational ordering, theory 80−2262
adsorption on Rh-TiO_2 catalyst., surface states, NMR spectrosc. investig. 80−103891
adsorption on W(100), effect on NVV Auger spectra, comp. to band struct. calcs. 78−72643
AMO method at small internucl. distances 79−6838
angular distribution He I (Ne I) photoelectron spectra 79−31606
anharmonic spectral density of librons in o-H_2 and p-D_2 79−14899
anisotropic Compton profile, LCAO calcs. 77−6863
asymptotic interaction with graphite surface 79−99429
atmosphere, H_2 sources and sinks, anthropogenic activity influence 77−64394
atmosphere H_2, production from oxidation of vegetation hydrocarbon emissions 78−88881
atmospheric residence time from interhemispheric HT transport meas. 78−32182
atom+H_2, quasielastic H atom ejection *(Russian)* 78−37712
atom triple-dipole energy calcs. using pseudo spectral theory 78−46418
atoms, electric dipole polarisabilities and hyperpolarisabilities, perturb. theory calcs. 78−17563
atoms-in-molecules theory, non-Hermitian formulation 80−9517
autoionising states, complex scaling method calcs. 80−9527
$B^1\Sigma_u^+$ state, selectively excited continuous vac. UV emission obs. 79−13667
Balmer radiation production by electron impact 0-2000 eV 79−76521
bimolecular reactions with positive ions in interstellar clouds, comets and planetary atmospheres 77−63896
binding energy, MINDO/3 calcs. *(German)* 79−3366
binding type change, and dissoc. for H_2-like mols. in strong mag. field 78−62744
Boltzmann-Langevin eqn., light scatt. and density correlation function 77−11307
$c^3\Pi_u$ metastable state, fine struct. lifetimes 79−64050
catalytic reaction with adsorbed O_2 on Rh (111) 79−83503
chain, infinite, lattice distortions, CNDO/2 calcs. 78−6018
chemiionisation by He(2^3S) and He(2^1S), pot. surfaces, autoionisation widths, cross sections 77−36739
chemisorption on Be clusters, ab initio calcs. 80−3404
chemisorption on metals, quantum chem. model, valence bond calcs. *(German)* 77−31909
chloropentafluoroethane-H_2, multiphoton dissoc., ^{13}C enrichment factor, CO_2 laser wavelength and fluence depend. 80−58331
classical many-body collision model incorporating Heisenberg and Pauli principles 80−63511
cluster beam, nozzle flow formation and detection, high energy beam 80−5638
cluster beam formed from nozzle flow, isotope effect 80−6127
cluster beam source, cryopumping 79−63258
coherent anti-Stokes Raman scatt., linewidth determ. by integrated power meas. 79−3744
coherent anti-Stokes Raman scatt. integrated power, press. depend. 78−59081
collinear reactions, transition state theory generalisations 80−26002
collinear reactions, transition state theory generalisations 80−26003
collisonal excitation of interstellar molecules 78−77586
Compton profile, correl. Gaussian wave function calc. 79−81241
Compton profile, electronic energy calc. 80−37822
Compton profile, impulse approx., electron correl., vibr. and rot. effects 78−17585
Compton profile and momentum distribution, impulse approx. 78−25626
Compton profile determ. by high energy electron impact spectroscopy 77−68083
concentration in near-surface air and dissolved in seawater, tropical N.Atlantic 79−39729
concentration in primitive prebiological atmosphere 78−73514
contamination in He plasma, satellites of He 492.2 nm line, fine struct. interpretation 80−59235
correlation energy, perturbation calc. using Gaussian-type germinals 78−17578
coupled states approximation for scattering of two diatoms 78−62872
covalent bonding and classical charge density 80−37722
cryogenic data rel. to mag. fusion energy 80−8746
density meas. by resonance fluoresc. ($X^1\Sigma_g^+ \rightarrow B^1\Sigma_u^+$ transition) 80−5570
desorption rate, effects of method of return to atm. press. for pressure vessel *(French)* 80−42233
diabatic and reson. states, dissociative photoionisation calcs. 80−47883
diffraction from Ag (111) surface 77−85880
dipole oscill. strength distribs., sums 78−21975
dipole properties and dispersion energies additivity, using atoms and small mol. models 80−53091
dispersion energy consts., dipole oscill. strength, refractivity 77−50492
dissociation, in discharge, as atomic H source for maser 79−86637
dissociation, on Cu surface, effect of surface roughness, classical trajectory calcs. 78−76925

hydrogen neutral molecules continued
dissociation, weak bias and anharmonicity effects 78−82661
dissociation 79−6992
dissociation efficiency, meas. by Wrede-Harteck method 79−72369
dissociation in microwave discharge 78−23935
dissociation on catalyst, surface mag. field effect on mol. dissoc. rate 80−16721
dissociation on Cu(100) and (110) surfaces, classical trajectory calcs. 77−60114
dissociation rates in elec. discharge, calc. 77−46616
dissociative attachment cross sections, interference struct. around 14 eV 79−45856
dissociative chemisorption on Fe(Ni) *(German)* 78−53257
dissociative electron attachment, Faddeev calcs. of cross sections *(Russian)* 78−70945
dissociative electron attachment, H^- ang. distribs. 77−19099
dissociative electron attachment 77−42431
dissociative electron attachment and vibr. excitation, low-energy 80−23565
dissociative photoionisation, 19.8-40.8 eV, proton kinetic energy spectra 79−68273
dissociative photoionisation at 26.9 eV 77−3423
dynamic dipole polarisabilities calcs. 80−74110
$E,F^1\Sigma_g^+$ state, collisional and radiative props. 80−58357
effective vibr.-rot. hamiltonian 77−27052
elastic electron scatt., 30, 50, 100, 200 eV, Glauber cross sections, independ. scatt. centres model calcs. 77−58165
elastic scattering of electrons, 50-400 eV, cross section calc. by potential scatt. formalism *(Japanese)* 77−42404
elastic scattering of electrons, absorption effects calc., 30-200 eV 78−22029
electric dipole polarisability, many-body perturbation theory calcs. 78−21839
electron 1 keV elastic scatt., Glauber model anal. 80−43178
electron attachment dissociative, metastable $c^3\Pi_u$ state, H_2 79−89794
electron Compton profiles from energy loss spectra 79−7013
electron correlation, as rot. polarisation, Heitler-London-Rosen calc. for teachers 80−4492
electron correlation, dynamic description using boson Hamiltonian 79−26897
electron correlation energy and dipole polarisability 79−54775
electron degradation spectrum, statistical anal. of ionisation yield 80−99581
electron diffraction, elastic, differential cross section, intermediate energy range 78−9251
electron dissociative attachment 80−91694
electron dissociative attachment rates, rot. (vibr.) excitation depend., in plasma 80−43848
electron elastic low energy scatt., ab initio pseudostates calc. 78−9247
electron elastic scatt., absolute cross sections 77−50533
electron elastic scatt., free-electron-gas model exchange pot. 78−58824
electron elastic scatt., modified Glauber theory 78−94320
electron elastic scatt., static exchange approx., variational correction 79−7015
electron elastic scattering, intermediate energy, optical eikonal theory calcs. 79−72420
electron energy distribution function, superelastic vibr. collisions and dissoc. effects 79−59589
electron energy loss spectra, $B^2H_u^+$ state cross sections, Franck-Condon factors 78−13616
electron energy-loss spectra in after glow, ground state vibr. conc. 77−31012
electron imact excitation, rot. transitions *(Russian)* 79−76524
electron impact, analytic energy degradation spectrum 77−31008
electron impact, Balmer-α, β, γ radn. emission cross sections 78−1091
electron impact, Balmer-α emission Doppler profile energy depend. 77−42423
electron impact, cross sectional factorization expressions, close coupling input tested in sudden approximation 79−43571
electron impact, degradation, energy apportionment methods calcs. 77−6951
electron impact, dissociative attachment, vibr. and rot. state depend. 79−18298
electron impact, dissociative attachment, vibr. and rot. state depend. 79−13829
electron impact, elastic and rot. excitation, effective pot. theory 80−5627
electron impact, elastic scatt., comparison of local exchange pots. 78−5346
electron impact, elastic scatt. and rot. excitation, close-coupling calcs. 77−6949
electron impact, energy deposition and energy degradation, 2, 10 and 30 keV 79−31709
electron impact, excitation of $G^1\Sigma_g^+$ state, emission cross-section meas. 78−37755
electron impact, H(2S) and D(2S) form., predissoc., time of flight obs. 79−86079
electron impact, rot. excitation, comparison of local exchange pots. 78−5346
electron impact, rot. excitation, low energy, close-coupling calcs. 78−1092
electron impact, threshold excitation and predissoc., electron-photon coincidence meas. 80−18941
electron impact, vibr.-rot. excitation by slow electrons, multiple scatt. calcs. 78−13617
electron impact dissoc., anticrossing signals, Doppler-profile technique 78−33619
electron impact dissoc., cross sections, isotope ratios and polarisation, B H_α and H_β emission 78−25729
electron impact dissoc., excited atom kinetic energy distrib. *(Russian)* 78−22045
electron impact dissoc., vel. distrib. of H(2s), $^1\pi_u$ autoionising state 77−79696
electron impact dissoc. excitation, cross sections, mechanisms 80−37895
electron impact dissoc. excitation, H_α and H_β Balmer line intensities 77−10778
electron impact dissoc. excitation cross sections 77−61861
electron impact dissoc. ionis., 75 eV, emitted H^+ energy spectrum ang. depend. 78−17812
electron impact dissoc. ionisation, energetic protons for autoionising states 78−25728
electron impact dissoc. ionisation 80−83510

hydrogen neutral molecules continued
electron impact dissociation, translational energy distrib. of H* 79−98234
electron impact dissociation, vel. distrib. of produced excited H atoms *(Russian)* 77−10779
electron impact dissociation by vibrational excitation *(Russian)* 78−1096
electron impact dissociative excitation, H 3s prod. cross section 77−58183
electron impact dissociative excitation obs. 78−1090
electron impact dissociative ionisation near $^2\Sigma_g^+$ state dissoc. threshold 80−43197
electron impact excitation, $\nu \leq 4$ vibr. levels, theory 80−18940
electron impact excitation, H_α and H_β lines emission, intensity decay curves meas. 80−83505
electron impact excitation, high vibr. levels of ground state, decay of reson. states 77−88581
electron impact excitation, low energy, distorted wave approx. cross-sections 80−83511
electron impact excitation, of E, F $^1\Sigma^+_g$ states, optical excitation functions 77−61866
electron impact excitation, to high Rydberg states, by threshold energy collision 80−83509
electron impact excitation, transfer of moment impulses, vibration-rotation states *(Russian)* 79−7024
electron impact excitation, two-step, Hanle effect obs. 78−25730
electron impact excitation and dissoc., close-coupling method appl. 78−74778
electron impact excitation total cross sections, oscill. strengths, independent particle model calcs. 77−61856
electron impact excited singlet-g states, optical and time resolved spectra, radiative lifetimes, quenching rates for rovibronic levels 80−23564
electron impact H^+ prod., kinetic energy, ang. distribs. 80−63838
electron impact ionisation cross section 80−78718
electron impact low energy rot. and vibr.-rot. excitation cross sections, static exchange approx. 79−89799
electron impact partial absolute ionis. cross section, 20-350 eV, rel. to H_2O and NH_3 *(French)* 79−861
electron impact rot. excitation, eikonal approx. 77−10777
electron impact spectroscopy, high energy, Compton defect 77−88578
electron impact spectroscopy for Compton profile meas. 78−90299
electron irrad., emission cross-sections for $3p^3\Pi_u \rightarrow 2s^3\Sigma_g^+$ 77−3477
electron momentum distributions from valence-bond wave functions 79−6868
electron repulsion matrix elements, asymptotic form, adiabatic representation 80−87038
electron repulsion potentials calcs. 80−91427
electron scatt., ab initio theory, elastic scatt. and rot. excitation 78−50640
electron scatt., absolute total cross-sections, 0.2-100 eV 80−91674
electron scatt., effective pot. calcs. 80−53131
electron scatt., elastic, incident-energies, 100-2000 eV calcs. 78−55237
electron scatt., elastic and inelastic, Glauber approx. 80−91695
electron scatt., elastic and pure rot. excitation 79−22854
electron scatt., Glauber eikonal approx. calcs. 80−53130
electron scatt., iterative static-exchange calc. 79−18290
electron scatt., low energy, multichannel variational calcs., static exchange approx. 80−83483
electron scatt., Schwinger variational principle, static-exchange approx. 80−63820
electron scatt., vibr. and vibr.-rot. excitation, ab initio calcs. 79−22853
electron scattering, continuum wave functions, discrete basis set method 79−22829
electron scattering, elastic, intermediate and high energies, independ. at. model 80−37884
electron scattering, exchange effects in independ. atom model 79−22837
electron scattering, Gaussian basis Glauber approx., elastic and vibrorotational excitation cross sections 80−58399
electron scattering, isotope effects 77−58188
electron scattering, iterative approach to Schwinger variational principle 80−99580
electron scattering, iterative static exchange method 80−53155
electron scattering, low energy, R-matrix calc. 79−59571
electron scattering, total cross section meas. at very low energies 80−58398
electron scattering elastic, 100-2000 eV, scatt. amplitude and cross-section 80−87228
electron scattering in intense IR field, multiphoton free-free transitions 79−81289
electron swarm transport coeffs. determ. by Boltzmann and Monte Carlo methods 79−90359
electron swarms, motion, Monte Carlo simulation 77−39398
electron total scatt. intensity, first Born approx., SCF CI calc. 77−10755
electron wave function calc. with Weinbaum function supplemented by floating function 79−26882
electronic and vibrational structure, theoretical developments 78−62707
electronic chemical pot., natural orbitals occupation numbers and electronegativity 80−63509
electronic distribution functions and correl. holes, theory 78−17562
electronic energies of $D'\Pi_u$ and $B''\Sigma_u^+$ states, wave functions 77−23438
electronic excitation, mol. thermal strength depend. 77−46595
electronic states, adiabatic energy corrections, CI ab initio calc. 77−83502
electronic struct., valence bond model, pairwise correlation 80−78543
electronic struct. calc., improving Σ perturbation approach, Green's function 79−13642
electronic structure, generator coord. method for wave function 79−26880
electronic structure, SCEP theory calcs. 77−10579
electronic structure calculations, multiple scatt. technique space partitioning effects 79−85883
energy levels, accurate theoretical determ. 77−46503
enhanced self diffusion, incoherent neutron scatt. study 79−46417
Europa, H_2 cloud rel. to UV emissions 79−5775
excitation energy, pot. curves, oscill. strength, Hartree-Fock calcs. 77−6685
excitation energy and transition moment anal. of electronic transitions 78−25620
excited $G+K^1\Sigma_g^+$ double minimum state, Born-Oppenheimer pot. energy curve 77−30847

hydrogen neutral molecules continued
excited levels, lifetimes, measurement by photon-photon delayed coincidence technique 79−89640
excited states, low lying, Rydberg and valence-shell characters, CI calcs. 78−5152
expectation values, Born-Oppenheimer, adiabatic and non-adiabatic results 78−82624
far IR absorption, collision-induced at 77.4, 195 and 292K 78−13495
fast electron retardation, ionisation cascade, degradation spectra, anal. *(Russian)* 79−27741
field ionisation to excited states 77−19002
flame temperature meas. by Raman scattering 77−16822
floating spherical GO calcs. of electron momentum distribs. and Compton profiles 77−30933
force constant evaluated in first order of perturbation theory 77−34781
force constants, SCF method with fixed orbital basis *(French)* 79−94107
formaldehyde+He(H_2), collisional relax. times and lineshape distortion, Stark absorpt. linewidth obs. 78−74744
formation by associative detachment in $H+H^-$ collisions, theory 79−44351
formation in interstellar cloud, reaction rates and chemical kinetics 79−17070
four-body system, adiabatic representation 80−91530
fuel cell development status and prospects *(French)* 79−79389
Fulcher band system, rot. struct. 79−98986
Fulcher system ($3p^3\Pi_u \rightarrow 2s^3\Sigma_g^+$), electronic-rot.-vibr. emission spectra, relative intensities calc. 79−6932
G, K double-minimum excited state, vibr. eigenvalues 78−33442
galaxies, Markarian and Seyfert types, H_2 masses from CO emission search 80−26975
gas phase transverse NMR low density spectrum 78−74681
ground state, bond breaking reaction, MINDO/3 CI calcs. *(German)* 78−21852
ground state, pot. curves, MTXα_R method 80−5482
ground state, vibr. eigenenergies, functional form 80−27998
ground state calcs. 79−22595
ground state correlations meas. by (e,2e) expt. 77−42413
ground state dissociation energy, Born-Oppenheimer pot. calcs. 78−37542
ground state potential energy, non-muffin tin MS Xα calcs. 77−14355
ground state second-order energy lower bound, new variation-perturbation principle 79−10006
H_3 dynamics, on accurate H_3 pot. surface 79−5139
$^4He+H_2(v=0,j=0) \rightarrow {}^4He+H_2(v'=1,j')$, fully converged sudden rotation total integral cross sections 77−58135
$H\bar{H}$ $^1\Sigma_g^+$ state $\bar{H}^1\Sigma_g^+$-$B^1\Sigma_u^+$ transition, $1<R<20$ a.u. 79−98094
high magnetic field spectroscopy 79−72445
high pressure, discharge, in H_2 (D_2)(inert gas), props., electrode influence, spectroscopic obs. 80−38806
hydrocarbon ions+H_2(methane), rate coeffs., ionised product. distribs. 77−44471
infrared spectrum of matrix isolated H_2, mol. rot. and vibr. const. determ. 80−78617
interaction energy, non-additive effects 79−50099
interaction with jellium surface, adsorption curves, independent atom effective pot. study 80−29259
intermolecular force, orientation depend., using charge density and dispersion force data 77−50487
interstellar, densities from CO obs. 79−25687
interstellar, form., catalytic prod. on transition metal grains 78−57616
interstellar, formation on surface of dust grains 77−9790
interstellar, ortho/para abundance ratio 79−40252
interstellar abundances rel. to enhanced metal depletions 77−91605
interstellar clouds, H to H_2 transition region 79−25672
interstellar clouds 78−16491
interstellar dark clouds, CO/H_2 ratio meas. 78−96513
interstellar dark clouds, H_2 densities from CO isotopic fractionation obs. 80−46638
interstellar gas clouds, spherically symm., gravitational collapse, effect of H_2 form. 80−101628
interstellar giant H_2 clouds, collisional growth 79−48877
interstellar H_2, abundance var. in clouds cooled by C atoms and ions *(Russian)* 80−12801
interstellar H_2, collisional excitation of linear mols. CO, OCS, SiO, HCN and HC_3N in $^1\Sigma$ state 80−109508
interstellar H_2, departure from translational equilib. 78−8081
interstellar H_2, form. by catalysis process 78−54005
interstellar H_2, form. on amorphous ice grains and importance for planetary atmospheres 80−26933
interstellar H_2, form. on interstellar grain surfaces 79−21367
interstellar H_2, in sightline to HD 50896, Copernicus UV obs. 77−26036
interstellar H_2, ionisation, dissociation and heating efficiencies of cosmic rays 78−28454
interstellar H_2, OH rot. excitation rel. to maser emission 80−62232
interstellar H_2, rot. excitation rel. to CH^+ prod. by interstellar shocks 80−56898
interstellar H_2, rot. transitions rel. to hot gases cooling 79−12505
interstellar H_2, search for 2.1 μ emission in southern hemisphere IR sources 80−22059
interstellar H_2, vibrationally excited, search for 8150 Å emission line 78−93346
interstellar H_2 clouds, instabilities 80−17629
interstellar H_2 cooling, dissociation and IR emission in shocked clouds 78−41009
interstellar H_2 density and formaldehyde excitation, effects of microwave background radiation observed spectrum 80−36681
interstellar H_2 density rel. to dust and extinction, nearly interstellar cloud interpretation 80−26953
interstellar H_2 emission from Orion Nebula, interstellar extinction meas. 79−25668
interstellar H_2 form. in diffuse clouds, influence of Lyman band absorpt. of UV radiation *(Russian)* 80−73026
interstellar H_2 formation and excitation 78−16514
interstellar H_2 in intercloud medium 77−71136
interstellar H_2 line emission from OH maser regions 80−12800
interstellar H_2 of Cygnus X region, gamma-ray flux prediction rel. to (CG 78+1) 79−92895
ionic-covalent config. mixing, pot. curves 77−34576
ionisation by electron bombard., empirical and semi-empirical calcs. 79−36784

hydrogen neutral molecules continued
ionospheric holes created artificially by H_2 or H_2O releases 78−40752
IR line emission, shock model appl. to Orion Nebula 78−8086
J=1, orientational props. on Grafoil surface, mean field theory 80−15361
Jupiter, H_2 equivalent thickness and polar regions limb darkening and props. 79−62790
Jupiter and Saturn atmospheres H_2 2-O quadrupole spectrum 77−45351
L134 N interstellar dark cloud, NH_3 hyperfine struct. and H_2 density 77−78852
lifetimes from collision induced absorption spectra, IR line broadening 78−33554
lifetimes of $3d^1\Sigma(3D)$ and $3d^1\Pi(3E)$ excited levels *(Spanish)* 77−71833
light scattering, intermol. collision process obs. 80−53001
limited MC SCF calculations 79−36537
liquid, muon capture rate meas. 80−69275
liquid n-H_2, n-D_2, Ne mixtures, deviation from Rao-Wada rule 78−75729
long-range force effects on photon and electron impact excitation 79−10170
lowest singlet and triplet states, interactions, electronic force calcs. 80−63742
Lyman bands, Morse-Franck-Condon factors and R-centroids 77−58088
magnetic interactions of electrons *(German)* 78−82610
magnetic susceptibility, field depend., gauge invariant GO calc. 78−1100
magnetic susceptibility calc. by distinguishable electron method 78−897
magnetic susceptibility calcs. vector pot. variation method, effective selection of gradient transform. functions 80−69258
major planets atmospheres, Raman scatt. 78−28571
many electron systems, chem. binding, local stresses and force densities 80−27920
metastable level electron impact excitation, resonances *(Russian)* 80−43198
metastable state, Doppler-free linear single-photon spectroscopy 78−50487
metastable state, mol. beam reson., vibr. anal., spin-rot. interaction 79−22731
metastable state, spin-rot. coupling, ab initio calcs. 77−18804
methane+H_2, rot. line width of vibr. bands 78−33552
methane(-H_2), long path photoelec. absorpt. spectra 4200-10600 Å, appl. to Uranus 77−83592
methane-N_2-H_2 gas mixtures, RF discharge, vibr. and rot. anal. of CN, N_2 and C_2 78−5241
methylene+H_2⟶methane, ab initio CI calc. on SCF level, insertion reaction min. energy path 80−7774
microwave absorption in atmosphere of giant planets induced by collisions of H molecules 80−90350
microwave absorption of isolated pair of o-H_2 molecules in solid p-H_2, theories 78−2948
MNDO calcs. for ground state 78−911
molecular beam apparatus, appl. as target for storage ring 77−6586
molecular photoionisation cross sections, at. extrapolation, ground state inversion method appl. 80−18787
molecule, electron impact ionis., differential cross sections 78−58839
molecule, master eqn. theory, dissoc. rate consts. 77−77742
molecule+H(2S), collisional quenching, mass spectral obs. 78−25685
MS potential from a set of overlapping densities 80−52850
muonic, pμd, pμt and dμt, ground state energy calc. with correl. wave functions 77−23439
naphthalene anion radical+H_2O, react., H_2 prod. 78−92460
NGC 1068, Seyfert galaxy, nucleus, H_2 existence and form. 80−12816
NGC 7027, planetary nebula, H_2 emission spatial distrib. obs. 80−98698
NMR of gas at 77.5K, proton spin relax. 79−72335
NMR shielding tensor and mag. susceptibility tensor, current density calc. *(German)* 79−76445
NMR study of dilute o-H_2 impurity in rare gas solids and p-H_2 80−25228
nonadiabatic coupling matrix elements by Hellmann-Feynman theory and HF 80−83263
nonadiabatic coupling of EF and GK $^1\Sigma_g^+$ states 79−59431
nonempirical calc. for molecules in electric field 78−25459
nonlinear optical polarisability meas. 79−54991
nuclear magnetic shielding, elec. field, accurate coupled Hartree-Fock 78−25434
nuclear magnetic shielding and susceptibility, elec. field depend., SCF-Hartree Fock method 80−18791
nuclear spin lattice relaxation times, o-H_2 mols. in solid nonmag. host, calc. 80−20483
nuclear spin-spin coupling consts., finite perturbation-CI calcs. 80−5563
octapole magnetisability, multipole SCF perturbation calc. with STO basis set 77−34550
one-electron properties, basis set contraction effects 77−88383
optical susceptibility, dynamical, third-order 79−31724
optogalvanic spectroscopy in discharge, 570 to 620 nm 79−54862
OQ 172, quasar, H_2 lines in absorpt. spectrum 80−36734
orbital calculation, using mag. field depend. orbitals, mag. shielding and mag. susceptibility 78−78611
oriented molecules, vibrationally inelastic electron scatt. 78−67907
Orion Molecular Cloud, H_2 densities from HCN J=3-2 line obs. 79−25669
Orion Nebula, search for H_2 ground state S(2) line 79−8961
ortho, high rot. states, inter- and intramol. effects, mol. beam mag. reson. obs. 78−70852
ortho⇌para conversion, on CoO, MnO mag. surfaces 79−47969
ortho-para conversion, equilibration, appl. in vapour press. thermometry 78−62198
ortho-para conversion, magneto-catalytic reaction, quantum formulation 80−108750
ortho-para conversion on paramagnetic crystal impurity, mag. field effects, theory 78−61050
ortho-para mixtures, 10 to 23K, rot. Raman spectra, quantum calcs. 77−6700
ortho-para ratio in dense interstellar clouds, protoplanets and planetary atmospheres 78−89233
ortho-para transition, catalytic-, radiation-, and self-induced conversion, review 77−90633
ortho-para transition as means of observing weak interaction parity non-conservation *(Russian)* 80−900
oscillator strength, X $^1\Sigma_g^+$-C$^1\Pi_u$ transition, upper and lower bounds 77−83654
oxidation on Pt, OH radical form., laser diagnostics 80−5572

hydrogen neutral molecules continued
pair equations, perturbation contribs. to correl. energy 79−6874
pairwise correlated GVB model, multiconfig. overlap approx. calcs. 79−31408
para, liq.-vap. phase equilib., surface tension *(Russian)* 79−65178
path integral formalism of perturbation theory, simple mols. and atoms 79−6841
PHL 957, quasar, H_2 and CO absorpt. lines obs. *(Russian)* 79−101216
photoabsorpt. spectra, rovibronic interactions 78−992
photoabsorption, photoionisation, predissoc., high resolution obs. 77−477
photodissociation, formation of excited H atoms *(Russian)* 79−3506
photodissociation, fragment Balmer series fluoresc. 77−27020
photodissociation, near threshold, excited atom prod. 79−86019
photodissociation cross section, excited atom form., 620-350 Å 79−86018
photodissociation near threshold, H(2s)/H(2p) branching ratio 78−21983
photoelectron ang. distrib., rot. states anal. 78−33550
photoelectron angular distrib. and intensity, vibr.-rot. struct. 78−46393
photoelectron angular distribs., oriented or rot. resolved unoriented mols., dynamic and struct. data 78−37682
photoelectron angular distribution, 304 Å line, vibr. state depend. 79−45764
photoelectron asymmetry parameters 80−95684
photoelectron spectra, ang. distrib. asymmetry parameter, vibr. state depend. 77−75218
photoelectron spectra, ang. distrib. for He II 79−59511
photoelectron spectra, rot. intensity distrib. 80−91605
photoelectron spectra, threshold region 79−54912
photoionisation, ang. distrib. of photoelectrons 80−37834
photoionisation, body-frame Hund's case b description 78−94295
photoionisation, dissociative, at 304 Å, photoion ang. distribs. photoelectron channels 78−82792
photoionisation, expt. techniques, processes, theory, review 77−14402
photoionisation, resonant, dissociative 79−68272
photoionisation Born-Oppenheimer Hamiltonian, resolvent matrix elements complex coord. calc. 80−52878
photoionisation cross sections, photoelectron ang. distribs. 78−5299
photoionisation cross-section, calc. for vibr. excited mol. 78−17732
photoionisation cross-sections, ang. distrib. and intensity, vibr.-rot. struct. 79−50091
photoionisation cross-sections, involving vibr. states 79−18242
polarisabilities, higher, static, calc., wave-function quality depend. 80−18814
polarisabilities, variation-perturbation calcs. 80−87243
polarisability, CI and Gaussian geminal calcs., using explicitly correlated elec.-field-variant functions 79−36561
polarisability, dipole, coupled perturbed Hartree-Fock method improvement 80−58148
polarisability, finite field MC SCF calcs. 80−14075
polarisability, generalised London formula for dispersion coeff. 78−82662
polarisability anisotropy derivative determ. from relative Raman intensities 78−55177
positron annihilation, positron form. 79−94092
positron annihilation involving low energy positrons, lifetime spectra 79−94091
positron scatt., rot. excitation 78−50653
positron scattering, 50-800 eV, total cross-section meas. 79−31680
potential curves, binding and ionisation energies and config., variational cellular methods 80−32597
potential energy curves, and vibr. levels, Born-Oppenheimer approx. 78−931
precession magnetic shielding of proton, semiempirical functions 78−82654
predissoc., interference effects, lineshape obs. 80−83432
predissoc. linewidths and shapes for $3p\pi D^1\Pi_u^+$ state 80−53066
predissociation, vibr. excited mols., time-of-flight spectra 78−42146
predissociation of $4p\pi\ ^1\Pi_u^+$ state, due to UV radiation 78−37695
predissociation of $^1\Pi_u^\pm$ state vibr. and rot. levels, dissoc. yields meas. 80−32784
predissociation of $c^3\Pi_u$ state, H_2^+ impact, flight time difference obs. 77−27164
predissociation probabilities of $4p\pi^1\Pi_u^+ v' \geq 1$ levels, dissoc. channels interference 80−28074
preionis. and predissoc., rel. to spectral line shape 80−63724
premixed H_2-O_2-N_2 laminar flames, temp. profile, comparison of spectroscopic meas. 80−42227
primordial matter cooling by H_2, rel. to star form. 79−35440
production from coal, water and electrons, reaction rates 79−61962
pseudospectral dipole oscillator strength distribs. 78−50503
quadrupole lines detect. in spectrum of Uranus 78−93149
quadrupole lines in spectra of Jupiter and Saturn 79−70990
quadrupole mass filter sensitivities and β-particle induced exchange kinetics 78−58090
quadrupole moment, adiabatic approx. calcs. 78−62742
quadrupole moments calcs. from line broadening collision with acetaldehyde 80−28065
quadrupole vibration-rotation transition probabilities 78−25512
quantum mechanics *(Hungarian)* 79−757
radiation induced exchange reaction kinetics of H_2, D_2 and T_2, review 78−61005
radiation polarisation, electron-impact excited, Lyman and Werner emissions and Lyman-α 79−36681
Raman spectra, appl. of high resolution CW stimulated Raman technique 78−70973
Raman spectra, vibr. freq. press. shifts 78−78703
Raman spectra of molecules dissolved in vitreous SiO_2 79−33707
reaction with graphite, mol. beam-surface expt., quasi-equilib. treatment 77−86376
recombination on interstellar grains, translational and rot. energy 79−17045
reducing agent in natural U ore deposits 78−36169
relativistic Dirac-Fock multiconfig. SCF calcs. 80−99455
relativistic Dirac-Fock multiconfig. SCF calcs. 80−99456
relativistic yield spectra from electron impact cross sections 78−13614
rotation-translation relax. rates and electron impact. dissoc. in glow discharge *(French)* 79−849
rotational and vib. relax., semiclassical calcs. 77−34723
rotational Raman linewidths, self-broadening calcs. 77−42356
Rydberg state predissoc., Lyman and Balmer emission obs. 77−38702
Rydberg states, nonadiabatic effects, elec. field ionis. 80−9528

hydrogen neutral molecules continued
$S_0(3)$ pure rot. quadrupole transition, obs. using tunable diode laser 78−82723
scattering contrib. to internal partition functions for Morse potential 79−81253
Schrodinger eqn., $^3\Sigma_u^+$ state, random walk soln., electron spin effects 77−18780
Schrodinger eqn. appl. *(Hungarian)* 79−3339
second order properties, dipole polarisability nucl. coupling, fast CI method 80−27950
semiempirical nonadiabatic pot. energy curves calcs. 78−17744
separated electronic pair functions, direct minimisation of energy functional, LCAO-MO SCF, density matrix formalism 79−31392
shielded diatomic orbital method, two-interacting state system 78−5121
shielding const., variable screening method 79−93932
short range intermolecular forces, scattering of molecular beam 79−36727
singlet superexcited levels, radiative emission 80−83415
singlet-triplet anticrossings, doubly excited 3^1K-g$(3d)^3\Sigma_g^+$ states 78−50598
singlet-triplet anticrossings between ungerade states 77−14498
solar flare and sunspots UV spectra, H_2 emission 79−53794
solid, fundamentals, static props., review 80−75403
solubility in water and seawater at 10^{-5} atm partial press., 0-30°C 79−100870
spectral line shapes, for radiative light scatt. in gas 78−90221
spin-rotation parameters calc. 77−88438
Stark effect, resonances, Bender-Wu formula 79−36695
stars, equivalent widths of lines of H_2 Lyman band 77−87368
states velocity auto-correl. function, relax. time, neutron scatt. obs. 80−58401
static polarisability, ab initio SCF wave functions 80−74106
static polarisability determ. by optimised rot. method 79−54990
sticking and accommodation on low-temp. substrate, mol. beam expts. 80−84368
stimulated Raman scatt. obs. between $v=1$ and $v=2$ levels 77−46757
stimulated Raman scattering, coherent source tunable down to 16 μm 77−65605
stimulated Raman scattering, freq. shifting of tunable dye laser radiation 80−9963
STP basis sets, energies calc. 77−3262
structure, channel coupling array calcs. 79−31362
Sun, H_2 EUV emission lines obs. 79−16908
Sun, H_2 lines detect. in EUV spectra 78−12184
sunspots, H_2 reson. fluoresc. with Lyman α 79−8821
superluminescence in surface discharge *(Russian)* 78−37676
synchrotron radiation scattering cross sections 78−55213
T Tauri stars, H_2 emission obs. 78−93230
tempered orbital energies and pot. curve 79−89584
tensor forces and intermediate particle exchanges between protons 79−64067
thermal dissociation at heated filament at low press. 78−85156
Titan atmosphere, non-Maxwellian effects assoc. with H_2 thermal escape 79−80264
total energy, HF SCF approx. formula, internucl. distance depend. 78−21837
Townsend avalanches, gas scintillation counter obs. 80−38805
transcorrelated method, nonlinear parameters optimisation 77−14365
triplet state, pot. curve van der Waals region, MS-MA calcs. 77−79551
triplet state, screening and susceptibility 79−41117
troposphere, H_2 latitudinal and vertical distrib. 78−49089
troposphere and stratosphere, H_2 mixing ratio vertical profiles 78−32181
two-electron bond, energy expectation values from density matrix partitionings 77−75059
two-photon ionis. simultaneously with one-photon ionis. 78−33484
two-photon positron annihilation, ang. correl. 79−81276
two-photon spectroscopy with tunable ArF laser 80−37843
in upper atmosphere, electron impact yield spectra 78−28401
upper atmosphere, H_2 diffusion three-dimensional time-depend. modelling 79−66846
valence bond orbital method for understanding electronic struct. 80−106268
Van der Waals constants, upper and lower limits, analytic eqns. 78−29831
Verdet consts., ab initio calcs. 77−3390
vertical ionis. pot., many-body Green's function calcs. 80−102439
vibration parametric excitation by IR radiation 80−28068
vibrational and rotational transitions, CARS, optical Stark effect 80−99512
vibrational excitation in intense UV interstellar fluxes 78−36647
vibrational force constant, quadratic, from X-ray scatt. factors 79−45864
vibrational population relaxation in gas and liq. 80−29775
vibrational relax. time meas. *(French)* 79−13791
vibrational relaxation, in H_2-Ar mixtures, mechanism, computer simulation 78−46434
vibrational relaxation, optical dispersion *(Spanish)* 79−23394
vibrationally excited state production in charge transfer reactions 77−30968
wave function, discontinuous approx. mol. electronic, ab initio LCAO and VB ZDO calcs. 77−50340
$X^2\Sigma_g^+$ state, vibr. energy levels, radiative corrections calcs. 78−90094
Xα LCAO total energy, rel. to local density models 80−32607
Xα statistical exchange calcs. 77−30766
Xα theory appls. approximations 80−9510
X-ray scatt., total, two-electron density functions 78−70889
Zeeman effect, Bender-Wu formula and SO(4,2) dynamical group, perturbation coeffs. determ. 80−95674
Zeeman effect in 3d singlet states, g-values 78−50571
μ-mesic molecules resonance formation *(Russian)* 78−46471
$AR(^3P_1)+H_2$, energy transfer rate const. expts., reverse reaction effect 77−65520
Ar laminar plasma jet, H_2 diffusion obs. 78−71557
Ar-H_2 solution, far IR spectra, density narrowing of rot. line 79−50086
$Ar+H_2$, 4500K dissoc. collision vibr. selectivity, Monte Carlo trajectory method 79−70307
$Ar+H_2$, vibr. and rot. transfer enhancement of dissoc. cross section 77−34732
Ar^++$(N_2)(H_2)(O_2)$, charge exchange reaction rates 77−86295
$Ar^+ + H_2$, charge transfer cross sections 77−34751

hydrogen neutral molecules continued
$Ar^+ + H_2$, collinear reactions, electronic nonadiabatic transitions 78−7180
$Ar^+ + H_2(O_2)(CO_2)$, reactions in flow-drift tube, rate consts. 78−15664
$Ar^+ + H_2(v_i=0) \rightarrow ArH^+ + H$, electronic nonadiabatic transitions, two-state model calc. 78−73035
$ArH^+ + H_2 \rightarrow Ar + H_3^+$, crossed beam reaction, energy distrib. 77−52626
$Ar^+(^2P_J) + H_2$, Ar^+ two spin orbit state, reaction cross section, direct determ. 80−93748
$B^{q+} + Ar(He)(H_2)$, keV electron capture cross section 80−14229
$BCl_3 + H_2$ laser induced chemistry, theory 78−76884
$Be^+ + H_2(He)(Ne)$(methane), Be Auger spectra 77−57951
$Br + H_2$, laser field interacting with collision dynamics, model system 78−62876
$Br + H_2$, laser radiation field effects, quantum mechanical close coupled expansion 77−50485
$Br + H_2$, proximity induced electric dipole moment effect in laser field 80−83456
$C^+ + H_2$, fine struct. transition excitation 77−42389
$C^+ + H_2 \rightarrow H + CH^+$, energy spectrum and prod. vibr. excitation 77−77745
$C^{3,4,5+} + H_2$, (0.3-1.2) 10^8 cm s^{-1}, single and double electron capture cross sections 77−34756
$CH^+ + H_2$, reaction products translational energies 77−86298
$CO + H_2$, interaction on Ni (100), reaction rate, AES and UPS obs. 79−79290
$CO^+ + H_2$, ion-molecule reaction detection of laser-induced ion spectrum, rot. components 78−74671
$CO_2 + H_2(CO_2)(Ne)(NH_3)(CH_3F)$, rot. transfer collisions, momentum transfer distributions 77−523
$CO_2 + H_2(D_2)$, ab initio LCAO-MO-SCF intermolecular pot. energy surface, V→T transfer 77−50489
$CO_2(00^01) + H_2(D_2)$, intramol. vibr.-vibr. transfer cross sections calc. 100-3000K 78−1053
CS_2-H_2 gas binary diffusion coeff. obs. *(Japanese)* 79−10627
$Cl + H_2$, absolute reaction rate consts., 200-500K 78−15655
$Cl + H_2 \rightarrow HCl + H$, quasiclassical trajectory calcs. 77−60040
Co_3O_4-H_2, interaction with surface, quantum chemical study 80−45549
Cr_2O_3-H_2, interaction with surface, quantum chemical study 80−45549
Cs-H_2 vapour, resonant character of laser induced formation of particles 80−89481
$Cs + H_2$, rot. excitation, infinite order sudden approx. 78−74740
D_2-T_2-H_2, fusion reactor fuel, isotopic exchanges, equilib. consts., 4.2-300K 77−70331
$D_2 + D_2$, collision effect on depolarised light scatt. linewidths 80−53059
$F(^2P_{1/2}) + H_2$, quenching, classical path calcs. 79−22800
$F + H_2$, 3-dimens. electronic nonadiabatic reactive collision theory, electronuclear basis 78−3321
$F + H_2$, electronic-to-rotational energy transfer 77−3431
$F + H_2$, Franck-Condon factors in reactive collision dynamics 77−36741
$F + H_2$, Franck-Condon factors in reactive collisions dynamics, vibr.-rot. distribs. 77−36742
$F + H_2$, quenching, rot. energy transfer, quantum mech. calcs. 77−50499
$F + H_2$, reaction probabilities, information theoretic anal. 77−16799
$F + H_2$, reaction rate consts. rel. to stimulated emission 78−3317
$F + H_2$, reactivity, multiple electronic surface effects 77−21363
$F + H_2$, two electronic pot. energy surfaces, collinear quantum calcs. 80−16646
$F + H_2$ dynamics, Franck-Condon factors rel. to information theory for vib.-rot distribs. and isotopic branching ratios 77−60041
$F + H_2 \rightarrow HF + H$ energy profile, minimal basis ab initio VB calcs. 78−50477
$F + Xe(H)^+(H_2)$, $(^2P_{3/2})$ state quenching, Franck-Condon approach 78−66640
$F^+ + H_2$, empirical and ab initio correlation diagrams, pot. energy surfaces 78−40041
$F^+ + H_2 \rightarrow FH^+ + H$, rot. effects 78−27744
$F^{7+,8+} + H_2(He)$, 20-56 MeV, F K X-ray cross sections, inner shell Coulomb excitation 77−19025
$^{18}F + H_2$, hot atom reaction, nonequilib. time-depend. theory 80−61126
$^{18}F + H_2$, hot-atom reaction, nonequilib. vel. distrib. and reaction rate calcs. 77−63942
$^{18}F + H_2$, nuclear recoil reaction, steady state hot atom kinetic theory calc., rate coeffs. 78−35712
$F^*(^2P_{1/2}) + H_2$, appl. of classical model for electronic degrees of freedom 79−98192
Fe_2O_3-H_2, interaction with surface, quantum chemical study 80−45549
(H,H) quasi-molecular system, 1 s σ orbital, variational calc. 78−37707
$H + H_2$, ang. momentum decoupling approx., quantum mech. reactive and nonreactive scatt. 77−12780
$H + H_2$, body-fixed coordinates collision theory, asymptotic scatt. matrix solns. 79−64070
$H + H_2$, CI calc. of three dimens. pot. energy surface 78−56882
$H + H_2$, collinear classical dynamics, chemically accurate pot. energy surface 77−48620
$H + H_2$, collinear reaction, isotope depend. transmission coeff., transition state theory 77−36747
$H + H_2$, collinear reaction, transmission coeff. isotope depend., statistical theory, invariance 77−36748
$H + H_2$, collinear reactive scatt., Magnus approx. 77−16801
$H + H_2$, elastic differential cross section high resolution meas. 78−50610
$H + H_2$, excited states quenching in glow discharge 79−7001
$H + H_2$, finite element methods for reactive scattering 78−92453
$H + H_2$, Franck-Condon factors in reactive collision dynamics, vibr.-rot. distribs. 77−36742
$H + H_2$, integral cross section meas. at thermal energy 77−10724
$H + H_2$, integral total reactive cross section, infinite order sudden approx. 80−30214
$H + H_2$, least squares fit to ab initio pot. energy function 78−56883
$H + H_2$, planar reaction, cross section calcs., vibr. and rot. convergences 77−21376
$H + H_2$, planar reaction, Schrodinger eqn., expansion as partial differential eqns. 77−21375
$H + H_2$, rot. cross-section, linear surprisal plots, theory 77−50498
$H + H_2$, three dimens. reaction, theory 77−21377
$H + H_2$, three dimens. reaction, Porter-Karplus pot. energy surface, rot. distribs., rate consts. 77−21378
$H + H_2$ dynamics, Franck-Condon factors rel. to information theory for vib.-rot. distribs. and isotopic branching ratios 77−60041
$H + H_2$ reaction, classical trajectories on spline-generated pot. energy surfaces 77−60047

hydrogen neutral molecules continued
H+H_2(HD)(D_2), exchange reaction rate consts. meas., vibr. effects 79−5134
H+H_2(0,0)→H+H_2, quasiclassical cross sections, pot. surfaces comparison 79−74364
H+H_2(ν=1, j=0) exchange reaction, 0.9-1.1 eV, sudden rot. calcs. 79−79230
H+H_2(ν=1)→H_2+H, exchange reaction, classical trajectory method, vibr. excitation, partial rate consts. 78−60993
H+NH_2, spin exchange effects, rot. energy transfer, absolute rate coeff. 79−50119
H^-+H_2(He)(Ar), electron detachment, Born cross sections, Pade approximants 78−17742
H^-+H_2(He)(Li), 50-150 keV, scatt. angle of neutral H 78−5340
H^++H_2, collisions at 3.7 eV, rotational transition probabilities 77−27156
H^++H_2, coupled states calcs. of inelastic collisions at 3.7 eV 77−14538
H^++H_2, inelastic collisions at 3.7 eV, close cou-ing calcs. 77−34734
H^++H_2, rot. and vibr. excitation 78−33579
H^++H_2, rot. quantum transitions 79−845
H^++H_2, rotational excitations, close-coupling calcs. 77−27157
H^++H_2, rotational quantum excitation, time of flight spectra 77−27154
H^++H_2, time depend. close coupling, vibr. excitation, impact parameter calcs. 77−88534
H^++H_2, vibr. excitation, energy loss spectra, rot. sudden impact calcs. 77−88537
H^++H_2→H_3, nonadiabatic transitions, comparison of surface hopping and complex-valued time calcs. 77−9049
H^++He(Ar)(Kr)(O_2)(H_2)(N_2), 2.2-8.2 keV, H(n=3) form., absolute cross sections 77−34755
H^++He($1s^2$), K-shell electron capture collision, static pot. effect 80−91660
H_2 $^1\Sigma_g^+$ ground state, hybrid Slater-Gaussian-type 1s orbitals calc. 77−38605
H_2, $^1\pi_u$ and $^3\pi_u$ states, singlet-triplet energy difference, Hund's rule, inequality formulation 78−66482
H_2 2.1 μm emission line vel. profiles in Orion Molecular Cloud 79−71094
H_2 2.121 μ emission line vel. and width meas. towards Orion Nebula 79−17061
H_2 4-0 S(1) 6368 Å quadrupole line strength and pressure shift 80−43108
H_2 ($^1\Sigma_g^+$), charge density, X-ray scatt. factors, gas phase electron diffr. 78−930
H_2 (D_2) mol. bands, electron impact excitation, rot. transitions, cross sections in plasma 80−37896
H_2 (1-0) s(1) 2.1 μm line detected in IC 443 supernova remnant 80−17630
H_2 (1-0) S(1) 2.12 μm emission from Orion Nebula 80−17631
H_2 (3,0) S1 line search in spectrum of Titan 78−4143
H_2 (4,0) and (3,0) S(1) lines, absorption strengths 79−16852
H_2, (4,0) S(1) quadrupole line intensity and pressure shift 78−90178
H_2, (oriented), scatt., total collision cross-sections, anisotropic pot. parameters calcs. 78−13568
H_2, adiabatic polarisation, ab initio calc., static electric dipole polarisability 79−72229
H_2, approx. wave function accuracy criterion, reduced local energy 77−50348
H_2, biorthogonal VB method, approx. natural orbitals 77−50368
H_2, CI calculations, Waller-Hartree method appls. 77−14363
H_2, channel coupling theory of covalent bonding, dissoc. energy 78−13419
H_2 compressed high-power tunable Raman lasers and applications 77−54709
H_2 density in giant interstellar molecular clouds, formaldehyde obs. 80−51837
H_2 dissociation fronts in circumstellar dense cloud 79−5881
H_2, elastic and inelastic electron scatt., zero-radius pot. appl. *(Russian)* 77−34771
H_2, electric discharge, vibr. excitation, spontaneous Raman scatt. obs. 78−5234
H_2, electron impact dissoc., H atom sublevel excitation 77−14593
H_2, electron impact dissoc. to H^+, from autoionising state 79−54980
H_2, electron impact dissociative excitation 78−13618
H_2, electron scattering, low energy, R-matrix calc. 79−59571
H_2, field ionisation under nonequilibrium conditions 80−74244
H_2 four-wave interactions for tunable IR generation 77−54759
H_2, Fulcher bands, radiative decay consts. 79−22722
H_2 gas, photosynthesis prod. by green algae, turnover times and pool sizes 80−16821
H_2 H_2, intermol. energy, CI ab initio calc. 79−85904
H_2, HD, $^1\Sigma_g^+$ states, adiabatic calc. of vibronic states 78−5198
H_2, HD, dissociative attachment of electrons *(Russian)* 78−13621
H_2, H(2S)→H(2P) conversion, efficiency measurement 79−45775
H_2, harmonic oscillator model, elec. polarisability, mag. susceptibility and chem. shift tensor calcs. 79−81299
H_2 high pressure HF discharges and DC arcs, instability obs. 80−38807
H_2, high resolution electron spectroscopy 80−62740
H_2 in Ar, vibr. energy relax. 80−106384
H_2 in atmosphere, biomass burning as source 80−26586
H_2 in organic solvents, proton chem. shift, Van der Waals solvent effect contrib. 77−68062
o-H_2, in solid p-H_2, interactions 77−68088
H_2, intermolecular pair potential, from solid-state data 79−14727
H_2, isotope exchange reactions, equilib. consts., adiabatic correction, electron correl. effects 78−88626
H_2 matrix shift, CoM freq., in solid Ar, Kr and Xe 79−6969
H_2, metastable $c^3\Pi_u$ state, population densities and quenching times meas. 78−94296
H_2 mol., Green's function Σ perturbation method for mol. calcs. 78−55123
H_2, mol. electronic momentum distrib. functions and correl. holes in p-space 79−97978
H_2, mol. form. in H+H collision, Morse oscill. calcs., dissoc. cross sections *(Russian)* 77−32786
H_2, optical polarisation following electron impact 80−63831
o-H_2 pairs, in solid H_2, microwave absorpt. 77−68034
H_2, pot. energy functions, virial theorem calcs. 77−88519
H_2 quadrupole line reddening determ. for Orion Molecular Cloud 79−71095
H_2, repulsive intermol. pot. 80−32794

hydrogen neutral molecules continued
p-H_2, rotational 0-2 transaction cross-sections *(Russian)* 80−32812
H_2, rotational Raman intensities and polarisability anisotropy change meas. with internuclear distance 80−63641
H_2 S(2) 12.28 μm rotational line in Orion Molecular Cloud 80−41881
H_2, semiempirical model for polarisation of s-type AOs, pot. curve and surfaces determ. 77−88400
H_2, triplet state, molecular polarisability, ab initio calcs. 80−63860
H_2, vibr. autoionisation and H_2^+ vibr. state distrib. depend. 77−48628
H_2 vibrationally excited 2 μm lines toward molecular clouds 80−94853
H_2, $X^1\sigma_g^+$, momentum distrib., electron correl. and mol. vibr. effects, theory 77−88557
H_2-Ar, bound complex form., anisotropic intermol. pot., IR spectra anal. 78−37634
H_2-Ar, relaxation rates, thermal dissociation, decomposition, master equation theory 79−74368
H_2-Ar, states velocity auto-correl. function, relax time, neutron scatt. obs. 80−58401
H_2-Ar, thermal dissoc. of dilute mols., vibr. bias mechanism 79−61854
H_2-BCl_3, photochem. with Ti, Pb catalysts, isotopic excitation by laser 78−64882
H_2-ClF chemical laser, HF rot. laser emission 79−98349
H_2-D_2, exchange on stepped Pt surface 77−1945
H_2-D_2 exchange on Pt surface, mol. beam scatt. data 77−24469
H_2-H, low-density gas, H-atom-diffusion, 4.2-77K 79−50053
H_2-H mixture positive column, static electric charact. 78−67500
H_2-H_2, intermol. pot. surface, ang. depend., nonorthogonal CI calc. 77−46613
H_2-H_2, mixed-pole terms in anisotropy of long-range interaction coeffs. 77−30950
H_2-H_2, overlap parameters from IR spectrum in binary collision-induced H_2 band 77−54561
H_2-H_2 dimers, hyperfine struct. in zero mag. field 80−95700
H_2-H_2 intermol. pair pot., ab initio SCF-CI surface 80−91457
H_2-H_2S, solubility of S in Pd, 600-1000°C, gas mixture composition depend. *(French)* 78−87791
H_2-He, mixed-pole terms in anisotropy of long-range interaction coeffs. 77−30950
H_2-He, thermal dissociation, vibrational relaxation at high temps., ab initio calcs. 79−74367
H_2-He mixtures, isotopic anal. using high resolution mass spectrometer 77−77844
H_2-He(Ne), NMR longit. relax., mole fraction depend. 77−61767
H_2-Kr, bound complex form., anisotropic intermol. pot., IR spectra anal. 78−37634
H_2-NO, flames, OH form., collisional broadening parameter, curve of growth method 80−53052
H_2-Ne, positron annihilation involving low energy positrons, lifetime spectra 79−94091
H_2-Ne, positron annihilation, positron form. 79−94092
H_2-O_2-Ar flame, excitation profiles of Na D-doublet 77−88436
H_2-Xe, bound complex form., anisotropic intermol. pot., IR spectra anal. 78−37634
H_2+ He (metastable), Penning ionisation *(French)* 80−1060
H_2+ ^{38}Cl, reactions, characterisation, effect of ethylene-I_2 scavenger 78−73071
H_2+$^3He^{2+}$, electron capture at impact energies below 10 keV 78−50633
H_2+$^3He^{2+}$($^4He^+$), electron loss, capture cross-sections 78−22026
H_2+^{4}He, inelastic collision, R-matrix study 80−87204
p-H_2+^{4}He, vibr. relax., 50-2000K, coupled channel, coupled states and effective pot. methods comparison 79−6995
p-H_2+^{4}He, vibr. relax., analytical approx. 80−63761
H_2+A, vibr.-vibr. energy transfer, stimulated Raman excitation obs. 79−64086
H_2+alkali metal, exchange reactions and rot. transfer effects on transfer coeffs. 77−66749
H_2+Ar, 4500K shock wave expt. simulation, vibr. state changes and dissoc. 79−61850
H_2+Ar, Arrhenius dissoc. activation energy, vibr. depend., trajectory calc., 4500K 78−35662
H_2+Ar, dissoc., recombination and inelastic scatt. pot. energy surface and cross section Monte Carlo calc. 77−27162
H_2+Ar, H_2 dissoc. rates, nonequilib. vibr. populations, elec. discharge conditions 77−88535
H_2+Ar, induced IR spectrum, overlap dipole moment determ. 77−18924
H_2+Ar, near-reson. energy transfer, fluoresc. excitation 78−9187
o-H_2+Ar, relax. and kinetic cross sections, DWBA calc. 78−25655
H_2+Ar, vibr. energy transfer rate, ab initio calcs. 78−82821
H_2+Ar, vibr. transition rates, thermally averaged, Monte Carlo trajectory calcs. 80−23519
H_2+Ar^+, charge transfer kinematics 78−9242
H_2+Ar^+, charge transfer reactions, excited products, Ar initially metastable 78−68879
H_2+Ar^+(Kr^+)(Xe^+), near-resonant charge transfer, 4-45 keV 77−27176
H_2+Ar^+→ArH^++H, electronic transitions, collinear reaction, curve crossing model, DIMZO surface 79−74373
H_2+Ar^{6+}, collisions, ionisation and excitation resulting from electron capture 80−78683
H_2+Ar^{n+}(Kr^{n+}), charge transfer, collision defects and dynamics, cross section meas. 80−53099
H_2+Ar*(4s), H_2 continuum emission, kinetic studies in Ar-H_2 mixture, e-beam pumped 80−43153
H_2+Ar(Kr)(Xe), orbiting resons., van der Waals pots., beam scatt. obs. 79−89739
H_2+atom (ion), ionis. by one or two electron at. particles, Born approx. 79−54960
H_2+B^{n+}(C^{n+}), one electron capture and loss 80−18921
H_2+Ba, radiation quenching of metastable Ba (5d ^{1}D) in gas 79−85932
H_2+Br($4^2P_{1/2}$), electronic-vibr. energy transfer, fluoresc. meas. 79−72347
H_2+C^-(O^-)(F^-)(Cl^-), negative ion stripping, at. beam form. 77−6926
H_2+C^+, C^+ fine-struct. excitation, interstellar cloud cooling 78−25675
H_2+C^+, CH^+(D^+) $A^1\Pi$ rot.-vibr. population distribs. 80−23396
H_2+C^+*, charge transfer cross-sections, 0.7-2.4 keV, C^+(^{2}P) and C^+(^{4}P) 78−58806
H_2+C^+(^{4}P), reaction, energy and ang. distrib., energy spectra 77−1918
H_2+C^+(N^+)(O^+), 0.1-13 keV electron capture cross-sections meas. 79−36761

hydrogen neutral molecules continued
$H_2+C^+(N^+)(O^+)$, reactant ion electronic states, effect on charge transfer cross sections 80−63809
$H_2+C^+(N^+)(O^+)$, total charge transfer cross section, 5-100 keV 79−3561
$H_2+C^+ \rightarrow CH^+ + H$, classical trajectory anal. 78−53192
H_2+CH, doublet and quartet states, abstraction reactions, pot. energy surfaces calcs. 78−31627
$H_2+CH_2 \rightarrow$methyl radical, SCF calc. involving orbital symm. forbidden reaction pathway 79−98004
$H_2+CH_3(CF_3)$, H abstraction, energies of activation calc. 78−31632
$H_2+CH_n^+$, isotopic exchange, interstellar implications 80−61087
H_2+CHF_3, vibr. relax. times at 298K 77−525
p-H_2+CH(OH), collisional pumping of Λ-doublet transitions, pot. energy surface 80−23516
H_2+CO, coadsorption on Cu-Ni (110) single cryst. surface, TDS and UPS obs. 80−80052
H_2+CO, pot. energy surface anisotropy in nonreactive region, ab initio calcs. 78−29832
H_2+CO, rot. excitation, rel. between tensorial cross sections 80−83454
H_2+CO, thermal energy collision, ab initio pot. energy surface 79−45788
H_2+CO, vibr. deactivation, 250 to 2000K, Morse pot. calcs. 78−46428
H_2+CO_2, exponential gap relation, rot. inelasticity 80−78693
H_2+CO_2, rot. excitation, semiclassical calc. using exponential approx. 77−42379
H_2+CO_2, rot. transfer, ab initio intermol. pot. energy surface 80−58354
H_2+CO_2, vibr. de-excitation of $CO_2^*(\nu_3)$, 200K 79−45802
$H_2+CO_2^+$, HCO^+ form. threshold form. energy 80−50844
H_2+CO(CS)(OCS), rot. excitation, classical and quantum calcs. 78−1059
H_2+CO(CS)(OCS), scattering cross-sections, factorisation and fitting, IOS approx. 78−33575
$H_2+C(^1S_0)$ 80−74241
$H_2+C(O)(N)$, pot. surfaces, HF calc. 80−16669
$H_2+Cd(^1P_1) \rightarrow CdH+H$, product initial rot. state distrib., pump and probe laser obs. 80−85158
$H_2+Cd(5^3P_{0,1})$, absolute quenching cross sections 80−5604
H_2+Cl_2, laser-initiated chain reactions, rates, mechanisms, chemiluminesc. obs. 80−55651
H_2+Cl^-, 4-11 eV, inelastic scatt. 79−98202
H_2+Cl^+, reactions at room temp. 80−93749
H_2+Cl(H)(F)(I), atom transfer reactions, reaction rate computing, trajectory calcs. 79−74371
$H_2+Cu^{2+}(Ti^{2+})$, electron capture cross-sections, 0.5-14 keV 78−42205
H_2+D, pot. surface, isotropic part determ. 79−36729
H_2+D reaction, transition state theory calculations, kinetic isotope effect explanation 80−66784
H_2+D rearrangement collision, vibr. excitation effects 80−71910
H_2+D_2, exchange on Pt stepped surface mol. beam incidence angle depend. 78−31686
H_2+D_2, exchange reaction, at. vs. mol. mechanism, at. absorpt. spectrometry 78−7190
H_2+D_2, exchange reaction, steady-state, surface reaction effects *(French)* 78−85148
H_2+D_2, exchange reaction, gas phase, heterogeneous initiation *(French)* 78−85149
H_2+D_2, reactive and inelastic scatt. using repulsive model pot. energy surface 78−66620
H_2+D_2, reactive and inelastic scatt., semiempirical pot. energy surfaces calcs. 80−74140
H_2+D_2 exchange reaction, on Pt(111) or (332) surface, mol. beam obs. 79−66269
H_2+D_2O, isotope exchange and separation with Pt hydrophobic catalyst *(Japanese)* 80−37901
H_2+D_2(N)(HCl)(CO_2), V-V transfer, pulsed fluoresc. obs. 77−14540
$H_2+D_2 \rightarrow 2HD$, transition state, study of Jahn-Teller instability of H_4 78−60995
$H_2+D_2 \rightarrow 2HD$ on stepped Pt surface, selective adsorption effect 78−20066
H_2+DF, vibr. relax., laser-induced fluoresc. obs. 79−64028
H_2+D(O)(Cl)(Br), relax. and chem. reaction, time resolved IR fluoresc. and mass spectrometry obs. 80−69177
$H_2+D \rightarrow HD+H$, three dimens. ab initio pot. energy surface 80−55646
H_2+ethane, hydrogenolysis mechanism and kinetics on evap. Ir film 79−100436
H_2+F, absolute rate coeffs. at 295 to 765K 80−81303
H_2+F, absolute reaction rate coeffs., time resolved IR emission meas. 79−68258
H_2+F, collinear quasiclassical trajectory study 78−80718
H_2+F, collinear trajectories, reaction dynamics calcs. 79−70311
H_2+F, collinear trajectories, statistical behaviour and detailed dynamics 80−16664
H_2+F, collision in intense laser field, formalism for mag. dipole interaction 79−98190
H_2+F, electronic-rot. energy transfer, for $F(^2P)$ 79−36740
H_2+F, electronic-rot. energy transfer, partial cross-section interweaving 79−59538
H_2+F, hot-atom reactions, Boltzmann eqn. for hot-atom relax. 79−100423
H_2+F, in pulsed HF chem. laser evolution, irreversible thermodynamic anal. 79−31887
H_2+F, rate consts., temp. depend. 80−81302
H_2+F, reaction kinetics, pot. energy surface and Franck-Condon integrals 79−61855
H_2+F, reaction quantum dynamics, reson. model, transition state props. 79−11781
H_2+F, reactive collision, semiclassical dynamics on multiple electronic surfaces, 3-dimens. calcs. 78−27746
H_2+F chemical laser threshold times, reaction product rot. distribs., relax. rates 80−28222
H_2+F_2, branched chain reaction, role of thermally nonequilibrium atoms and molecules 80−76507
H_2+F_2 chain reaction, rotational nonequilibrium mech. vibr.-rotational energy exchange effect 80−48230
$H_2+F+\hbar\omega$, reactive scatt. and inelastic collision, semiclassical calc. 79−47948
H_2+F^*, quenching of excited state, semiclassical studies, comparison between reactive and nonreactive processes 80−106375
H_2+F(Cl)($O(^3P)$), reaction rate constants, Monte Carlo quasi-classical trajectory calcs. 79−74366

hydrogen neutral molecules continued
$H_2+F(H^+)$, rotated Morse curve-spline pot. function 78−80729
H_2+F(H), collinear reactive scattering, coupled eqns., soln., R-matrix calcs. 77−16812
H_2+F(I), collinear trajectories, pattern recognition 80−45481
$H_2+F \rightarrow FH+H$, collinear probability, quantum calc. using pot. energy surface 78−64829
$H_2+F \rightarrow FH+H$, vibr.-rot. energy distrib. of HF, DWBA calc. 78−80722
$H_2+F \rightarrow HF+H$, DWBA transition amplitude kernel 80−81310
$H_2+F \rightarrow HF+H$, reson. struct., quantum scatt. calc. 79−61847
$H_2+F \rightarrow HG+H$, 3-dimens. vibrot. reaction probabilities from collinear results, information theoretic synthesis 79−74354
H_2+Fe^{+q} collisions, 3.4 MeV/nucleon single electron capture and loss cross sections 77−83726
H_2+Fe^{n+}, 262-1100 keV amu^{-1}, electron capture and impact ionis. cross-sections 78−42204
H_2+Fe(001), gas-surface reactions, semiempirical generalised LEPS pot. 78−68923
H_2+H, 1s-2s excitation of fast H atoms 79−89764
H_2+H, 3-dimens. exchange reaction, surprisal theory, quantum dynamics 79−15964
p-H_2+H, angular momentum and cross sections, sudden centrifugal pot. calcs. 78−42157
H_2+H, atom-atom pots., Hilbert Schmidt expansion, transition operators 78−66621
H_2+H, collinear, collision-induced dissoc., quantum mech. probabilities calcs. 79−20359
H_2+H, collinear, quantum mech. reactive scatt., exchange kernels calcs. 78−68880
H_2+H, collinear exchange reaction, quantum dynamics, surprisal theory 79−6988
H_2+H, collinear exchange reaction, unified statistical model 79−34295
H_2+H, collinear quantum mech. reactive scatt., hyperspherical coords. 80−108694
H_2+H, collinear reaction, Delves radial coord. S-matrix propag. calcs. 80−108695
H_2+H, coplanar exchange reaction, 0-2 eV, reactivity bands, analytical method 78−35664
H_2+H, diatomic operator, separable approx., variational approach 78−42150
H_2+H, exchange reaction, three-dimens., dynamical S matrix method 79−91930
H_2+H, exponential gap relation, rot. inelasticity 80−78693
H_2+H, H_3 dynamics, on accurate H_3 pot. surface 79−5139
H_2+H, quantum reactive scatt. theory, 3-dimens. 80−55637
H_2+H, reaction, quasi-classical trajectory calcs. using new pot. energy surface 80−7767
H_2+H, reaction probability, max. entropy derivation, statistical theories 80−66781
H_2+H, reaction rate constants, modified collision theory expression, comparison with exact expression 79−74370
H_2+H, reactions and collisions in IR laser field, collision-induced absorpt. spectra 80−76499
H_2+H, reactive scatt., 3-dimensional quantum mechanical calcs. 77−30802
H_2+H, reactive scatt., sudden approx. calcs. 78−68878
H_2+H, reactivity-selectivity, bounds derivation 80−66763
H_2+H, rot. excitation 79−89746
H_2+H, scatt. wave function modal struct. and global behaviour 80−81307
H_2+H, sudden rot. reactive scatt., 3-dimens., approx. quantum mech. calcs. 80−76498
H_2+H_2, collision effect on depolarised light scatt. linewidths 80−53059
H_2+H_2, dispersion forces calcs. 80−9675
H_2+H_2, elastic scatt., rigid rotor approx. 79−31642
H_2+H_2, exponential gap relation, rot. inelasticity 80−78693
H_2+H_2, isotropic intermolecular forces evaluation using semi-empirical approach 79−36726
H_2+H_2, quadrupolar $S_1(J)+S_0(J)$ double transitions, IR fundamental band, 77K 80−52986
H_2+H_2, rot. cross sections 78−37717
H_2+H_2, rot. energy transfer, classical trajectory calc. 79−31652
H_2+H_2, rot. relax., close coupling calc. 77−58141
H_2+H_2, rot. relax. collision, scaling theory anal. 80−74232
H_2+H_2, total scatt. cross-section, below 10 meV 80−28087
H_2+H_2, V-V and V-T rate coeffs., semiclassical model 77−14535
H_2+H_2, V-V energy transfer, perturbed wave eqn. soln. 80−1051
H_2+H_2, V→T rate constants, deconvolution 77−27152
H_2+H_2, van der Waals pot., electron tunnelling, charge transfer 77−54588
H_2+H_2, vibr.-trans. rate const. and vibr. excitation cross section 79−50116
H_2+H_2, vibrational energy transfer, adiabatic approx. calcs. 77−14532
H_2+H_2 interaction polarisability comparison with He diatom, ab initio SCF calcs. 80−27943
$H_2+H_2^+$, 10 keV dissoc. charge exchange collisions 78−94319
$H_2+H_2^+$, pot. energy surface and nonadiabatic regions, charge exchange and reaction, VB calc. 78−40027
$H_2+H_2^+$, state selected reaction cross section, coincidence technique obs. 80−66797
$H_2+H_2^+ \rightarrow H_3^+ + H$, state selected, threshold electron-secondary ion coincidence method obs. 79−5190
$H_2+H_2^+ \rightarrow H_3^+ + H$, state-selected ion-molecule reactions threshold electron-secondary ion coincidence technique obs. 80−85166
$H_2+H_2^+ \rightarrow H+H_3^+$, reaction dynamics, isotopic variations 78−27745
$H_2+H_2O^+$, rate constants determ. as function of relative kinetic energy 80−81292
$H_2+H_2O^+ \rightarrow H+H_3O^+$, reaction kinematics 78−31625
$H_2+H_2(D_2)$ potentials, isotropic part 78−5311
H_2+H_2(HBr), collinear collisions, anharmonicity effects, vibr. excitation 79−31656
H_2+H_2(He), anisotropic intermol. repulsion, pot. energy models 77−46610
H_2+H_2(He), anisotropy of long-range interaction 79−36734
$H_2+H_2(N_2)$, cross sections for electron stripping of fast H_2 meas. 77−83705
$H_2+H_3^+$, charge transfer collisions, 10 keV, H_2-H fragmentation 79−853
$H_2+H_3^+$, collision-induced dissoc. 77−42383

hydrogen neutral molecules continued
$H_2+H_3^+$, dissoc., 400-800 keV, product charge state distrib. model 78−82838
H_2+H^-, electron detachment cross-sections, 100 keV-10 MeV 79−59561
H_2+H^-, electron loss by 1-300 keV H^- ions 80−37857
$H_2+H^-(He)^-$, collisional detachment cross-sections, high-energy obs. 77−3442
H_2+H^+, 5-100 keV, secondary electron energy and ang. distrib. 80−14223
H_2+H^+, combined rot. sudden and vibr. exact quantum treatment 78−74739
H_2+H^+, electron capture, H(2s) cross section meas. 79−72386
H_2+H^+, electron capture cross-section, anal. evaluation 79−36756
H_2+H^+, electron capture into ground and excited s states 79−76509
H_2+H^+, electron capture probability 78−58808
(H_2+H^+, H_2^++H) collinear system, electronically nonadiabatic effects 78−1063
H_2+H^+, inelastic forward scattering, vibr. excitation, glory oscills. 79−22799
H_2+H^+, low energy rot. excitation, ab initio differential inelastic cross section calcs. 77−88542
H_2+H^+, rot. and vibr. excitation, energy loss obs. 80−63773
H_2+H^+, rot. excitation and vibr. transitions, coupled state approx. 77−61835
H_2+H^+, vibr. excitation, 10-30 meV 80−58358
H_2+H^+, vibr. excitation, ab initio CI pot. energy surface calcs. 80−74228
H_2+H^+, vibr.-rot excitation, ab initio CI pot. energy surface calcs. 80−74229
H_2+H^+, vibrationally inelastic collisions, 3D impact parameter approach 77−75268
H_2+H^+ differential inelastic and reactive scatt., low energies 78−62911
$H_2+H^+(H_2^+)(He^+)(O^+)$, H^+ prod., from H_2^+ dissoc. states or H_2^{2+} 78−20015
$H_2+H^+(Li^+)$, sudden approx. of Cross, computational tests, cross section factorisation, scatt. phenomena 80−58352
H_2+HCD, vibr. excitation cross-sections, rot. averaging calcs. 78−9231
H_2+HCN, HCN excited vibr. state, T_2 meas. 80−102498
H_2+HCN(DCN), rot. excitation in interstellar clouds 77−22292
H_2+HCl, HCl v_0-v_1 band perturbations, linewidth and shifts calcs., IR spectra obs. *(French)* 80−58251
H_2+HCl, translational and pot. relax., statistical calcs. 77−3435
H_2+HCl(DCl)(CO),(NO_2)(HBr)(DBr)(NO)(CO)(^{13}CO), vibr. relax. rate, stimulated Raman scatt. obs. 77−75269
H_2+HF, vibr. relax. dye laser pumping effects 80−9703
H_2+HF, vibr. relax. laser induced fluoresc. obs. 79−64037
H_2+HF, vibr. relax. of HF (v=3,4) 79−50117
$H_2+H+NO \rightarrow HNO+H_2$, rate of reaction, temp. depend., third body efficiencies 78−23933
H_2+H(Cl), atom transfer reaction in gas phase, reaction rate computing, tunnelling corrections 79−79237
H_2+H(D)(T) reactions, accurate pot. energy surface, isotope effects, quasiclassical trajectory study 80−97698
H_2+H(F), minimum energy reaction path, reference coord. approach 78−40025
H_2+H(F), reaction products ang. distribs., Franck-Condon theory 79−87835
H_2+H(F), transition states, trapped trajectories and classical bound states in continuum 78−88630
H_2+H(F)(Cl), collision induced IR laser absorpt., rate enhancement, theory 79−66275
H_2+H(He), anisotropic interaction pot., total cross-section calcs. 78−29835
H_2+H(He)(OCS)(CS), rot.-translational energy transfer, nonlinear vs. linear rotors, surprisal anal. 79−76492
H_2+H(I), activation energy and trajectory calcs., temp. and isotope effects 78−76835
$H_2+H(1^2S)(H(2^2S))$, electron capture, electron loss and deexcitation cross sections meas. 78−22025
H_2+H(1s,2s), electron capture, loss, and collisional destruction, 5-26 keV 80−5611
H_2+H(2S), metastable atom total quenching 77−46628
H_2+H(2s), 5-25 keV, H(n=3) excitation, Balmer α emission obs. 80−53113
H_2+H(2s), collisional de-excitation, 5-26 keV 79−59546
$H_2+H(2s) \rightarrow H_3^+ + e^-$, fluoresc. of H_2 photodissociating near threshold 78−21983
$H_2+H \rightarrow H+H_2$, classical three-body problem. calcs., effective reaction cross section *(Russian)* 79−39144
$H_2+H \rightarrow H+H_2$, IR laser induced reaction 78−80761
$H_2+H \rightarrow H+H_2$, three dimens. chem. reaction, distorted-wave calcs. 80−81294
$H_2+H \rightarrow H+H_2$, tunnelling path for reaction 78−11514
$H_2+H \rightarrow H+H+H$, two path dissoc. 78−62875
H_2+Hd, vibr. energy transfer rates, IR fluoresc. meas. 79−98145
H_2+He, collision dynamics, generalised Langevin eqn. approach 78−70900
H_2+He, collision induced dipole IR spectra, ab initio SCF LCAO calc. 79−89737
H_2+He, collisional dissoc., quasiclassical trajectory calcs. 78−42172
H_2+He, exponential gap relation, rot. inelasticity 80−78693
H_2+He, far IR absorpt., collision-induced at 77.4, 195 and 292K 78−13495
H_2+He, gas phase NMR, kinetic theory, single relax. time approx. 77−14451
H_2+He, inelastic collisions, statistical decoupling 77−517
H_2+He, inelastic scatt., vibr. adiabatic basis functions calcs. 80−102551
H_2+He, inelastic scatt. exponential perturbation theories 80−74217
H_2+He, interaction pots. and rot. scatt. calcs. 80−43158
H_2+He, interaction second virial coeff. nonspherical pot. terms effects 77−3432
H_2+He, mag. transitions, close coupling calcs. in uncoupled space frame 78−17769
H_2+He, mol. energy transfer by quasiclassical trajectory methods, vibr. relax. and dissoc., rot. effect 80−99557
o-H_2+He, NMR, spin-spin and spin-rot. relax., IOS calcs. 79−18209
H_2+He, nucl. mag. relax., DWBA cross sections from S-matrix formalism 77−27151
H_2+He, pot. energy surface, ab initio calcs., van der Waals const. determ. 80−106372

hydrogen neutral molecules continued
o-H_2+He, relax. and kinetic cross sections, DWBA calc. 78−25655
H_2+He, rot. inelastic, moments of final state distrib., direct method 78−33562
H_2+He, rot. relax. time, <300K, classical trajectory method invalidity 77−10739
H_2+He, rot.-vibr. energy transfer collisions, distorted wave infinite order sudden approx. method 77−75265
H_2+He, vibr. deexcitation, cross sections, rate consts., vibr. rot. model 78−62879
H_2+He, vibr. excitation, classical trajectory problem, Fourier transform method 79−98189
H_2+He, vibr. inelastic cross-section, para-H_2, threshold behav. 79−45804
H_2+He, vibr. inelastic integral cross-sections calcs. 79−31660
H_2+He, vibr. relax., pot. surface depend. 77−75266
H_2+He, vibr. relax. cross section 80−99494
H_2+He, vibr. relax. times, 3D semiclassical theory 78−25667
H_2+He, vibr.-rot. inelastic cross section adiabatic distorted wave IOS calcs. 79−94066
H_2+He, vibr.-rot. transition, optical potential approach 78−62885
H_2+He potential surfaces, SCF and MRD-CI calcs. 79−10172
H_2+He^+, 0.5-3.0 keV, direct and charge-exchange scatt. 77−75263
H_2+He^+, 0.7-2 MeV, charge-changing collisions, electron capture 80−58372
H_2+He^+, charge transfer, appl. of atom-photon coincidence meas. 79−45829
H_2+He^+, charge transfer at 1.5 and 3 keV, He(^{3}P) excitation 78−66658
H_2+He^+, DIM approx. pot. energy surfaces and nonadiabatic coupling 80−23330
H_2+He^+, dissociative ionisation, H^+ energy spectra 77−58154
$H_2+He^+(Ar^+)$, small angle charge exchange, 0.5 to 1.0 keV, time of flight spectra 78−33604
H_2+He^+(2s), metastable ion electron capture, loss and de-excitation 77−6904
H_2+He^{2+}, electron capture collisions, spin conservation 78−82837
H_2+He-like ion, (of B, C, N and O), electron capture cross-sections 79−59559
H_2+He*, Penning ionisation, singlet interaction pot. anomalous struct. 77−75274
H_2+He(Ar), intermol. forces, generalised electron gas-Drude model 79−98182
H_2+He(Ne), gas discharge plasma, H_2 dissoc. excitation, cross section anal. 80−33735
H_2+He(Ne), Van der Waals pot., ab inito SCF model 78−74728
$H_2+He(2^3S$ and $2^1S)$, Penning, rearrangement and total ionis. cross sections, vel. depend. 79−22816
$H_2+He(2^3S_1)$, isotope effects, 77 to 300K 79−36752
$H_2+He(2^3S_1)$ mol. ionis., optical atom orientation method *(Russian)* 78−13591
$H_2+He(2^3S)$, Penning ionisation, quantum mech. scatt. calcs. rigid rotor approx. 77−34741
$H_2+He(2^3S)$, pot. energy surfaces and autoionisation lifetimes calcs. 77−34740
H_2+heavy inert gas, small clusters, beam cluster intensity and collision cross section 77−38711
H_2+hexafluoroethane, multiphoton induced chemistry 79−20382
H_2+HgBr, vibr. relax., rate coeffs., fluoresc. obs. 80−63697
$H_2+Hg(^3P_1)$, quenching rate constants determ. with nanosecond light pulser with Hg vapour 80−100111
$H_2+I(5^2P_{1/2})$, electronic to vibrational energy transfer 79−68259
$H_2+I \rightarrow HI+H$, collinear reaction, reson. effects, quantum mech. calcs. 77−52625
H_2+inert gas, cross section meas. with state selected beams 78−62910
H_2+inert gas, intermol. pot. anisotropy determ. from total collision cross sections, expt. 78−21988
H_2+inert gas, intermol. pot. anisotropy determ. from total collision cross sections, theory 78−21989
H_2+inert gas, vibr. relax. mechanism, master eqn. anal., density changes 79−76493
H_2+Kr, differential cross-sections, diffraction undulations, anisotropic pot. calcs. 78−9223
H_2+Kr, elastic total cross section, orbiting effects, Regge theory 78−82814
H_2+Kr^{2+}, charge transfer reactions, rate coeffs. and product-ion distributions meas. 80−104431
$H_2+Kr^{2+}(Xe^{2+})(C^{2+})$, charge transfer reaction rate consts. 80−7779
H_2+Li, exponential gap relation, rot. inelasticity 80−78693
H_2+Li, inelastic collision, ab initio pot. energy surface 79−10055
H_2+Li^+, exponential gap relation, rot. inelasticity 80−78693
H_2+Li^+, ion-molecule forces, generalised electron gas Drude model appl. 79−98183
H_2+Li^+, rot. energy transfer, power scaling law 79−54942
n-H_2+Li^+, rot. excitation, 150-750 eV 79−45805
o-, p-H_2+Li^+, rot. excitation and ang. depend. transition probabilities, time of flight spectra 80−23517
H_2+Li^+, vibr. excitation cross sections, 100-1200 eV 79−27077
H_2+Li^+ rot. inelastic scatt., body frame partitioning approx. calcs. 80−23527
$H_2+Li^+(Co^+)(Au^+)$, cross-section, closure-Born approx. 78−66630
$H_2+Li^+(H^+)$, elastic of rot. excitation, semiclassical treatment 79−31657
$H_2+Li^+(H^+)$, elastic scatt. and rot. excitation, multistate semiclassical orbital method 79−27058
H_2+Li-like ion, (of B, C, N and O), electron capture cross-sections 79−59559
H_2+LiH$(CO_2)(N_2)$, intermol. forces, multipole results validity, charge overlap effects 79−89730
$H_2+Li^*(2^2P_J)$, collision induced quenching and fine struct. transition rate coefficients meas. 80−74221
H_2+Li(Na)(K), excited atom quenching, semi-empirical model 78−1065
H_2+Li(2p), Li(2p) excitation, alignment and orientation obs. 80−63794
$H_2+Li \rightarrow LiH+H$, LiHH pot. function calc. 77−6699
H_2+methane, vibr. energy transfer, fluoresc. 77−519
H_2+methyl cation, ternary assoc. reaction, rate coeffs., 100-300K 79−61845
$H_2+methylene^* \rightarrow CH_3+H$, barrier height, CI with double zeta polarisation basis 78−64812
$H_2+methylene \rightarrow CH_3+H$, triplet methylene abstraction, partial open shell FSGO calc. 78−80719

hydrogen neutral molecules continued
H_2+N_2, nitrogen fixation, semiempirical INDO study 80−16898
H_2+N_2, rot. excitation, fixed nuclei approximation calcs. 79−6990
H_2+N_2, vibr. relax. in liquid phase 79−847
$H_2+N_2^+$, collisional dissoc. cross-section, 2.4-24.3 keV 80−58373
H_2+N_2O, HO radical form. on Pt surface, laser-induced fluoresc. obs. 80−108738
$H_2+N_2+N_2H_4$, mixtures with nonthermal vibr. excitation of mol. N_2, formula for calc. equilib. const. 80−76545
H_2+N^+, charge exchange, 1-3 keV, $N^+(^3P)$ and (^1D) states 79−36760
H_2+N^+, electron capture and ion loss cross-section, 2.4-24.3 keV 80−58373
H_2+N^+, rotational vibrational product excitation 79−47901
$H_2+N^+ \rightarrow NH^+ + H$, classical trajectory calc. 79−100337
$H_2+N^{q+}(O^{q+})(C^{q+})$, q=1-5, single electron capture cross sections 78−55233
$H_2+NH_2^- \rightleftharpoons NH_3+H^-$, chem. equilib., ab initio calcs. 79−34282
H_2+NH_3, rot. relax. double and triple reson. obs. 78−66570
H_2+NH_3 collisions, semi-empirical non-Lorentizan line shape determ. 77−34699
H_2+NO^+, reaction rate consts. meas. 80−7782
H_2+Na, electronic to vibr. energy transfer, close coupling calcs. 79−98203
$H_2+Na_2^*(A\Sigma)$, rot. energy transfer, power law scaling 79−98204
$H_2+Na^*(3^2P)$, electronic to vibr.-rot. energy transfer, differential cross sections 77−38715
H_2+Ne, collision-induced dissociation, Monte Carlo quasiclassical trajectory calcs. 79−74357
H_2+Ne, vibr. excitation effect on dissoc. excitation efficiency 79−76495
H_2+Ne (Ar)(Xe), metastable state breakdown, temp. depend. 79−98211
H_2+Ne^+, energy-loss scaling in 0.5-3.5 keV 80−63768
H_2+Ne^+, thermal energy, reaction rate coeffs. and product distrib. 79−29333
H_2+Ne^{2+}, charge transfer reactions, rate coeffs. and product-ion distributions meas. 80−104431
H_2+Ne^*, quenching rate const. for metastable $Ne(^3P_2)$, flowing afterglow 78−46295
H_2+negative ion, electron-loss cross sections 80−37877
H_2+Ni^+, endothermic reactions, investig. 80−97692
H_2+nitromethane reaction, CO_2 laser initiated, mechanism and yield 80−11912
H_2+O, classical trajectory calcs., ab initio surface, singlet state, rate consts. 80−66786
H_2+O, pot. energy surfaces and reaction rates, ab initio calcs. 80−63531
H_2+O, trajectory calcs., fitted ab initio pot. energy surface 79−74358
H_2+O_2, adsorbed on Pt particles supported on SiO_2 gel, low press. reaction 77−52668
H_2+O_2, combustion, kinetic modeling and sensitivity anal. 80−89490
H_2+O_2, on Pd (111), mol. beam relax. and isotopic exchange meas. 80−35575
H_2+O_2+CO, 500°C, rate consts. involving OH and HO_2 radicals 78−35646
H_2+O_2(HCl), vibr. energy transfer, collinear and 3-dimens. rate consts. 80−48065
n-H_2+O_3, vibr. relax. quenching rate consts. meas. 79−13792
H_2+O^+, linear approach, pot. energy surface for H_2O^+ 80−47922
$H_2+O^+(^4S)(^2D)$, charge transfer reactions, cross-sections meas. 78−92462
$H_2+O^{n+}(Fe^{n+})(Mo^{n+})(Ta^{n+})(W^{n+})(Au^{n+})$, single electron capture cross-section 79−59560
H_2+OCS, collisional line broadening of microwave spectra, semiclassical theory, calcs. 78−25516
H_2+OCS, gas, EPR of rot. transitions, T_1 press. depend. 80−9621
H_2+OH, mean collision cross sections from microwave spectroscopy 80−1046
H_2+OH, rot. inelastic collision, microwave spectra 79−45806
$H_2+OH \rightarrow H_2O+H$, rate constant, ab initio calc. 80−45478
$H_2+OH \rightarrow H_2O+H$, reaction product vibr. distribs, quasiclassical trajectory, calcs. 80−85162
$H_2+O(^1D)$, rate consts., temp. depend. 78−27747
$H_2+O(^3P) \rightarrow OH+H$, potential energy surface, theory 80−45492
$H_2+O \rightarrow OH+H$, product state distrib., laser photolysis-laser induced fluoresc. determ. 79−83446
$H_2+O \rightarrow OH+H$, rot. energy distrib. of $OH(X^2\Pi,v=0)$ 79−87829
$H_2+O \rightarrow OH+H$, vibr. energy effects, classical trajectory calcs. 77−63904
p-H_2+p-H_2, vibr.-rot. relax. 77−34729
H_2+PH, collisional deactivation of $PH(b^1\Sigma^+)$, time resolved quenching 79−54948
$H_2+Pt(111)$ surfaces, interactions, bond breaking activity, model pot. 80−108744
H_2+S, collision-induced emission of $S(^1S)$, 232 and 425K 79−81264
H_2+SF_6 (tetrafluoromethane), collision-induced simultaneous transitions, IR spectra 77−50438
H_2+SiBr_4, SiH_nBr_{4-n} heat of form., mass spectrometric determ. 79−20455
H_2+Si^*, collisional quenching, reson. line absorpt. expt. 78−46297
H_2+slow doubly charged ions, one-electron capture 80−32828
H_2+U, surface reaction, temp. depend. 79−91996
H_2+vinylidene, addition reaction, MINDO/3 study 80−108705
H_2+X^{Z+}, Z≥4, 1-20 keV, electron capture 80−37875
H_2+Xe^{2+}, charge transfer from ground and metastable states 79−31677
$H_2+Xe^{n+}(Ar^{q+})(Fe^{q+})$, electron capture by heavy multicharged ions at low velocities total cross sections meas. 80−99548
H_2+Y, high temp. equilib. meas. 80−66780
$H_2^++H_2$, 10 keV H_2^+ dissociation, H-H^+, H^+-H^+ and H-H fragments 77−83688
$H_2^++H_2 \rightarrow H_3^++H$, electronically excited products, merged beam apparatus meas. 78−31626
$(H_2)_2$, $(D_2)_2$, (HD)$_2$ and H_2-D_2, Van der Waals complexes, mol. symmetry 80−42963
$(H_2)_2$, ab initio calcs., perturbation dispersion energy versus CI treatment 77−26976
H_3, bent, spline-fitted pot. surface 77−57851
H_3, biorthogonal VB method, approx. natural orbitals 77−50368
H_3, CI calc. of three dimens. pot. energy surface 78−56882
H_3, correl., ionis. and attachment operators, diagrammatic method calcs. *(French)* 79−22607
H_3, diatomic state mixing parameter 80−74139

hydrogen neutral molecules continued
H_3, discrete Rydberg spectrum in hollow cathode discharge 79−68239
H_3, elastic and inelastic electron scatt., zero-radius pot. appl. *(Russian)* 77−34771
H_3, electronically excited state obs., vibr. level struct. determ., predissoc. 79−41204
H_3, emission spectra, rot. struct. obs. mol. const. determ., predissociation 80−106331
H_3 excited electronic states rel. to H_3^+ dissoc, recomb. 79−89795
H_3, form. and dissoc., kinetics, historical review, book contrib. 77−40527
H_3, generalised diatomics-in-mols. theory 79−97970
H_3, H_4, pot. energy hypersurfaces, diatomics-in-molecules method extension 77−30780
H_3, interat. pot. energy matrix elements, generalised DIM calc., ZDO approx. 80−52864
H_3, interrelationships between effective hamiltonians 77−30767
H_3, mol. fragmentation energetics of vibr. excited mol., spatial beam profile expts. 79−96292
H_3, pot. energy surfaces, semiempirical calcs. 78−41974
H_3, potential energy surface, LEPS-type 79−63934
H_3, quartet states, diatomics-in-molecules theory, diatomic states mixing and overlap 79−59344
H_3, relative magnitudes of direct and indirect exchange, Heitler-London calcs. 80−69069
H_3, Rydberg spectrum , theory 80−5528
H_3, Rydberg states, Jahn-Teller calcs. 80−9494
H_3, Rydberg states, spectroscopic B_0 consts. 80−74109
H_3, Rydberg states energies and equilib. geometry calcs. 80−9493
H_3, semiempirical model for polarisation of s-type AOs, pot. curve and surfaces determ. 77−88400
H_3, spin-optimised SCF general spin orbitals calcs. 78−5125
H_3, three atom ab initio energy surface calc. 78−82663
H_3, transverse NMR of low-density gas 79−64017
$H_3+Ar \rightarrow H_2+ArH^+$, crossed beam reaction, energy distrib. 77−52626
H_3^++HD, rot. inelastic collision, classical trajectory calc. 79−64078
$H_3^++H_2 \rightarrow H_5^+ \rightarrow H_2+H_3^+$, ab initio GO pot. surface, C_{2v} symmetry 77−25252
H_4, $^1\Sigma_g^+$, Schrodinger eqn. random walk soln., electron spin effects 77−18780
H_4 excimer, electronic and geom. struct., ab initio CI calc. 79−76348
H_4, excited potential energy hypersurfaces, trapezoidal geometry, rel. to photochem. 2s+2s processes 77−30797
H_4, excited potential energy hypersurfaces, 'triply right' (C_{2v}) tetrahedral geometries 77−83501
H_4, FGSO open-shell calcs. 79−10025
H_4, ground and excited states, SCF MO CI calcs. 77−6693
H_4, pot. energy surfaces, valence bond calcs. 80−74129
H_4, rectangular configurations, stability, SCF MO LCAO calcs. 77−42235
H_4 square, $^1B_{1g}$ and $^1B_{2g}$ states, Schrodinger eqn. solved by random walk method 79−63925
H_4, square config., $^1B_{1g}$, $^1B_{2g}$ states, quantum chem. calcs., random walk method 79−36518
H_4, triplet state, instability of restricted Hartree-Fock, orbital degeneracy 78−25457
H_x+H_2, hexadecapolar U-branch transitions in IR fundamental band 80−91631
HCN+H_2 vib. energy transfer, laser-induced fluoresc. 77−58139
HCO^++H_2, J=0-1 transition press. broadening, microwave absorpt. 80−52981
HCl+H_2 (o- and p-), press. broadening and alternate ang. momentum coupling, rot. excitation 77−42375
HD 4-0 and 5-0 bands, absorption strengths 80−43059
HD, 5-0 transition, intracavity photoacoustic detector spectrosc. obs. 80−77877
HD, catalytic activity of Re and W during adsorption 79−69358
HD colling function in primary gas condensation and star birth *(Russian)* 77−33623
HD, detect. in Saturn and Uranus atms., D/H abundance ratio calc. 78−57495
HD detection in Uranus atm. from visible spectra obs. 80−82296
HD, dipole moment and rot. spectrum, perturbation theory calcs. 77−65454
HD, dipole spectrum, influence of intracollisional interference 78−33492
HD, dissociative adsorption on Re surface 79−86987
HD, dissociative electron attachment, Faddeev calcs. of cross sections *(Russian)* 78−70945
HD, elec. dipole vibr.-rot. spectrum, line strengths, ab initio calcs. 78−25514
HD, electric field gradient at deuteron, numerical method 77−10578
HD, electron impact, H,D(2s,2p) prod. 78−42230
HD, electron impact, H(2S) and D(2S) form., predissoc., time of flight obs. 79−86079
HD, electron impact dissociative excitation 78−13618
HD, electron impact dissoc. ionisation 80−83510
HD electron scattering, total cross section meas. at very low energies 80−58398
HD, extremal scattering, from MgO (001) surface 79−95891
HD, formation probability for H_2-D_2 mixed beam impinging on stepped Pt surface, ang. of incidence effects 77−47670
HD, G, K double-minimum excited state, vibr. eigenvalues 78−33442
HD, gas, fundamental band, R and P line shapes 80−23461
HD, ground state props., nonadiabatic var. calcs. 78−58576
HD, Hartree-Fock calc., paramagnetic orbital contrib. to spin-spin coupling const. 79−89689
HD, indirect nucl. spin-spin coupling const., Hartree-Fock and polarisation propag. calcs. 78−9170
HD, intermol. collision process obs. using light scatt. 80−53001
HD, interstellar, IR emissivity *(Russian)* 78−36676
HD, interstellar rotationally excited, towards ζ Ophiuchi, column density 79−25674
HD, ionisation, Franck-Condon factors calcs. 77−58102
HD, isotope exchange reactions, equilib. consts., adiabatic correction, electron correl. effects 78−88626
HD, Lyman bands, Morse Franck-Condon factors and R-centroids 77−58088
HD molecules, rate coeff. for $H^++D \rightarrow H+D^+$ near threshold 78−89239
HD, nonadiabatic effects in the B, C and E, F states, rot. line strengths 78−5148
HD, nucl. spin coupling const., MBPT theory calcs. 80−28035

hydrogen neutral molecules continued
HD, nucl. spin-spin coupling, diamag. contrib. 79−36665
HD, nuclear spin coupling const. calc., using ab initio LCAO MO SCF method 78−25558
HD, nuclear spin-spin coupling const., perturbed at. orbitals calc. *(French)* 77−27095
HD, ν=0 to ν=5 rot.-vibr. band, photoacoustic spectrosc. obs. 80−9589
HD, perturbation var. calc. with contact interaction, effect of approx. zero order wavefunctions 80−58107
HD, predissoc., interference effects, lineshape obs. 80−83432
HD, predissoc. linewidths and shapes for $3p\pi D^1\Pi_u^+$ state 80−53066
HD, Q-branch band shapes, motional narrowing and overlapping effects 78−29785
HD search at 6045 Å, D/H ratio upper limits for Jupiter and Saturn 78−85892
HD, spin-dipolar term, spin-spin coupling const. corrections, Fermi contact terms calcs. 80−99448
HD, spin-spin coupling const., convergence of calc. 80−9506
HD, spin-spin coupling constant convergence, comparative study 80−63536
HD, vibr.-rot. transitions, possible laser appl. 79−55122
HD-inert gas mixtures, $R_1(J)$ and $P_1(J)$ absorpt. spectra, positive intercollisional interference 79−54843
HD-Kr, $R_1(1)$ absorpt. spectra, positive intercollisional interference 79−54843
HD+Br($4^2P_{1/2}$), electronic-vibr. energy transfer, fluoresc. meas. 79−72347
HD+Cl, reactions, branching ratio, energy partitioning and ang. distrib. 79−70312
HD+Cl, thermal rate constants, quasiclassical trajectory calcs., detailed balance 79−87822
HD+D_2, state-resolved Δj=2 rot. transitions 80−63772
HD+F→HF+D(DF+H), branching ratios, information theory test by classical trajectory calcs. 78−64822
HD+H_2, rot. inelastic collision, classical trajectory calc. 79−64078
HD+HD, rot. inelastic collision, classical trajectory calc. 79−64078
HD+HD, state-resolved rot. excitation differential cross sections, crossed pulsed beams techniques 78−17766
HD+HD, total scatt. cross-section, below 10 meV 80−28087
HD+HD(^{4}He)(D_2), vibr. relax., 80 to 400K 80−5607
HD+He, interaction second virial coeff. nonspherical pot. terms effects 77−3432
HD+He, press. broadening cross-section, ang. momentum approx. calcs. 77−34696
HD+He, press. broadening, rot. energy transfer, infinite order sudden approx. 78−22011
HD+He, relax. and kinetic cross-sections, DWBA calcs. 79−41782
HD+He, rot. excitation, classical trajectory study 78−25666
HD+He, thermal energy scatt., distorted-wave and close coupling calcs. 78−86938
HD+He, vibr.-rot. relax. from high vibr. states 79−54945
HD+I($5^2P_{1/2}$), electronic to vibrational energy transfer 79−68259
HD+Kr(Xe), collision-induced fundamental band in room temp. IR absorpt. spectra 77−34627
HD+methane, vibr. energy transfer, fluoresc. 77−519
HD+NH_3⇌H_2+NH_2D, deuterium separation factors, calc. 80−3310
HD+NH(ND), ($b^1\Sigma^+$) states quenching, kinetic isotope effects 77−63891
HD+Ne, j=0 to 1 rot. excitation, differential cross sections, time of flight obs. 80−48104
HD+Ne, j=0 to 1 scatt. differential cross section, interaction pot. anisotropy 77−42382
HD+Ni^+, endothermic reactions, investig. 80−97692
HD+T hot atom exchange reactions, trajectory calcs. 80−26037
$H_2(D_2)$+Ag(111), energy transfer, quantum mech. theory 77−8699
$H_2(D_2)$+Ar*, de-excitation processes, pulse radiolysis, isotope effect 77−65529
$H_3^+(D_3^+)$+$H_2(D_2)$ collisions, slow ion production, charge transfer cross sections 80−106378
HD($^1\Sigma_u^+$)+He, fluoresc. quenching and energy transfer processes 79−86032
H_2(E,F$^1\Sigma_g^+$), two-photon excitation, cross section, radiative lifetime, quenching rate, IR fluoresc. obs. 78−37698
HF+$H_2(D_2)(N_2)$, 200K and 295K vibr. relax. rates 80−63766
HF+H_2(HCl)(N_2)(O_2)(CO_2) vibrs. relax., laser fluoresc. obs. 77−14484
HH, hydrogenium metastable states, ground state energy, bound states, lifetimes 79−45868
H_2(HD), predissoc., Feshbach resons., spin-aligned atom form., stability 77−10723
H_2(HD), rot. levels and consts., nonadiabatic corrections 77−18906
H_2(HD)+Ar, reson. energy transfer cross section, 1st Born approx. appraisal 77−65519
H_2(HD)(D_2), ab initio pot. energy curves and vibr. levels, B″, B̄, B′ states 77−6754
H_2(HD)(D_2), matrix rot. and vibr.-rot. spectra, free and hindered rot. 77−83607
H_2He, rot. and vibr. inelastic mol. collision cross section calc. 79−59542
H_2O maser line evidence for circumstellar ring systems in supergiant stars 78−89195
H_2O^++H_2, ion-molecule reaction detection of laser-induced ion spectrum, rot. components 78−74671
$(H_2O)_n$, n=2 to 8, correlation energies, ab initio and SCF calcs. semiempirically corrected 80−43223
$H_2^+Pe^-$, bound state calcs., channel coupling array theory 77−19005
$H_2(^1\Sigma_g^+)$+$O(^3P,^1D)$→H_2O, potential energy surfaces, extended basis first-order CI study 80−7776
$H_2(^1\Sigma_u^+)$, E and F states, unimolecular decay, nonadiabatic interactions, transition probability as function of Massey parameter 80−35503
$H_2(^1\Sigma_g^+$-$^1\Pi_u)$ excitation, electron-polarised-photon coincidence 79−22852
HT, atm. vertical distrib. 77−9463
HT, atmospheric concs. rel. to water vertical transport in stratosphere 79−2347
HT, dissociation by T beta-decay 77−63941
HT, triton-proton mag. moment ratio determ. by NMR method with 10^{-6}% accuracy *(Russian)* 77−61773
HT+He, interaction second virial coeff. nonspherical pot. terms effects 77−3432
$H_2(X^1\Sigma_g^+)$, semiempirical Morse pot. extension, fitting procedure appl. 79−36560
H_2−D_2, separation by Taylor diffusion 79−18303
$^1H^3H$ and $^2H^3H$, pure rot. and vibr.-rot. Raman spectra 80−14145

hydrogen neutral molecules continued
$^nH_2$, vibr. relax. at low temps., gas, liq. and solid phases 77−83691
H_2*, energy and occupation curves, wave functions, natural spin orbital anal. 77−83493
H_2*+H_2, depolarisation cross-section of (1s 3p) $^3\Pi_u$ (N=1) level 77−61829
H_2*+H_2, van der Waals mols., mol. fluoresc., vibr. predissoc. model 78−42120
H*$_2$+$H_2O(SF_6)$, ionis. collisions 79−64088
H_2**+inert gas, ionising or deactivating collisions 79−100338
$H_2(1)$+$H_2(1)$→$H_2(2)$+$H_2(0)$, V-V energy transfer temp. and rot. depend., semi-empirical pot. calc. 80−28094
$H_2(a^3\Sigma_g^+$→$b^3\Sigma_u^+)$ continuum emission excited by low-energy Ar^+ collisions, UV laser appl. 79−41200
$H_2(c^3\pi_u)$, theoretical radiative lifetime, from mag. dipole, elec. quadrupole interaction 78−33553
He (2^3S_1)+H_2, ionis., interaction pot. at thermal energies *(Russian)* 79−94077
He-H_2, rot. relax and spectral line shapes, coupled states calcs. 77−50500
He+H_2, adiabatic distorted-wave infinite order sudden approx. 80−99558
He+H_2, CI pot. energy surface, small distances 77−38708
He+H_2, close coupling calcs., averaged definite parity j_z approx. with Clebsch-Gordan weights 77−38111
He+H_2, collinear collision, first order nonlinear matrix differential eqn. 80−37853
He+H_2, collision-induced dipole, ab initio VB calc. 78−94202
He+H_2, collisional energy transfer, stochastic reductions, generalised cumulant expansion calcs. 77−71847
He+H_2, exchange forces, Hellmann-Feynman theorem calc. 77−54589
He+H_2, final quantum state assignment, improved quasiclassical histogram method 78−66617
He+H_2, formation of polarised H-atoms in ionising collisions *(Russian)* 79−7002
He+H_2, inelastic scatt., vibr. effects, classical mech. calcs. 77−34735
He+H_2, orbital angular momentum quantum numbers in definite parity j_z CCS approx. 77−14511
He+H_2, pot. energy surface, analytical expressions from constrained optimisation 77−6698
He+H_2, rot. excitation, 0.403-1.900 eV total energy, classical trajectory method 77−30962
He+H_2, rot. excitation, effective pot. and classical trajectory calcs. 77−88539
He+H_2, rot. transitions, quantum mech. and semiclassical cross-sections calcs. 77−83690
He+H_2, scatt., opacity functions, j_z-conserving approx. calcs. 77−6878
He+H_2, simultaneous rot. and vibr. transitions, cross-sections calc. 77−68098
He+H_2, stochastic theory, master or Fokker Planck eqn. numerical solns. 77−30965
He+H_2, sudden rot. approx., rot. and vibr. cross sections 77−30966
He+H_2, T-matrix element approx., j_z-CCS calcs. 77−19003
He+H_2, V→T rate constants, deconvolution 77−27152
He+H_2, vibr.-rot. relax., high temp., exponential distorted wave technique 78−37721
He+H_2, vibrationally inelastic collision, rot. energy sudden approx. 79−68303
He+H_2 (O_2), rot. cross-section, exponential distorted wave and effective Hamiltonian 78−37709
He+H_2 rot. and vibr. distorted wave integrals, stationary pt. struct. 78−46436
He+H_2(He)(Ar)(N_2), fast metastable at. collisional destruction cross section 78−74760
He+H_2(He)(N_2)(Ne)(Ar), 25-450 keV, metastable ion beam electron loss and deexcitation cross section 77−34745
He+HD collisions, single quantum rot. excitation by pulsed molecular beams 78−29840
He+p-H_2, vibr.-rot. inelasticity, stochastic theory 77−71848
He^++H_2, dissoc. charge transfer, vibr. enhancement 78−33597
He^++$H_2(D_2)$, dissociative charge transfer, 78-330K 80−61079
He^++$H(H_2)$, H(2p) and H(2s) excitation cross sections, 5-26 keV 77−58150
He^{2+}+H_2→He^+H^++H^+, two-electron capture 78−58811
HeH^++H_2→H_3^++He, reaction rate. coeff. 78−18371
$^4He^+$+H_2, 35-1000 keV, electron loss cross-section 78−22018
Hg+$H(H_2)$, resonance scatt., HgH potential determ. 77−61830
H_2(j=0)+$F(^2P_{1/2})$ quenching, quantum mech. study, ortho-para mixing role 79−76485
H_2(j=0)+Li^+, rot. alignment, state-selected differential and integral rotationally inelastic cross sections 80−37863
$H_2(\nu_i$=1)+H, exchange reaction, integral and differential cross sections determ. 80−85153
I_2+H_2, vib. relax. in supersonic jet 77−58134
K^++H_2, dissociative collision, H_α, H_β emission prod. 77−75093
Kr^++HD, kinetic isotope effect, cross sections, rot. transfer 77−9041
Kr^+.+$H_2(D_2)$(HD) reactions, temp. depend., isotope effect 78−31630
$LaNi_5$+$3H_2$⇌$LaNi_5H_6$ reaction, absorpt. capacity and reaction kinetics 79−43626
Li+H_2, LiH form. at Mo surface, mass spectroscopic obs. 77−66771
Li+H_2, rot. and vibr. transitions, close-coupling calcs. 77−58136
Li+H_2, vibr. excitation, rotationally sudden calcs. 79−22797
Li^++H_2, dissoc., multiple scatt. theory 78−21999
Li^++H_2, dissociative collision, H_α, H_β emission prod. 77−75093
Li^++H_2, quasiclassical approx. for scatt. amplitude, rot. degrees of freedom *(Russian)* 77−79676
Li^++H_2, rot. excitation dynamics, quasi-classical phase space density functions 77−88532
Li^++H_2, vibr.-rot. excitation at intermediate energies 79−3534
Li^++H_2 78−9234
Li^{1+}+H(H_2), (q=1-3), electron capture and loss cross sections 78−42187
^7Li+H_2, electron capture collisions, 0.2 to 3 keV 77−6925
Li*+$H_2(N_2)$, thermal, high-Rydberg Li behaving as ion core 78−22004
MnO-H_2, interaction with surface, quantum chemical study 80−45549
N^++H_2, reaction dynamics, low energy mol. beam obs. 77−9064
N^++H_2, triplet state ab inito CI pot. energy surfaces 78−74729
N^++H_2(DH), >6 eV reaction dynamics 77−32779
$N^{3,4,5+}$+H_2, (0.3-1.2) 10^8 cm s^{-1}, single and double electron capture cross sections 77−34756

hydrogen neutral molecules continued
N_2+H_2, ($A^3\Sigma_u^+$, ν=0,1) metastable state quenching rate coeffs. 78−90206
N_2+H_2, N_2 dissoc. rates, nonequilib. vibr. populations, elec. discharge conditions 77−88535
N_2+He, rot. inelastic scatt., appl. of sudden approx. 80−95705
$N_2^+ + O_2(H_2)(He)$, ($A^2\Pi_u$) Meinel band deactivation cross sections above thermal energies 78−66635
$NH_2^+ + H_2$, reaction products translational energies 77−86298
NH_3-$N_2(H_2)(Ne)(Ar)(Kr)(Xe)$, as R(1,1) vibr-rot. line parameters, ν_2 band, using CO_2 laser light 79−3444
NH_3+2H_2, triplet n3S Rydberg state, ab initio UHF CI SCF calc. 80−53095
$Na+H_2$, total elastic cross sections meas. 77−30954
$Ne^{z+} + He(H_2)(Ar)$, (z=1-4), electron capture into excited projectile states 77−75291
Ni catalyst, H_2+CO, adsorption, co-adsorption, reaction, neutron inelastic spectroscopy method 79−99408
NiO-H_2, interaction with surface, quantum chemical study 80−45549
o-H_2+p-H_2, ang. momentum decoupling approximations and factorisation 79−72397
$O^{3,4,5+} + H_2$ single and double electron capture cross sections, (0.3-1.2) 10^8 cm s^{-1} 77−34756
$O_3+He(D_2)(H_2)$, vibr. relax. rate consts. 80−74231
$OCS+H_2$, rot. energy transfer, microwave-microwave double resonance 77−19016
$OCS+H_2$, rot. energy collisional transfer, M-depend., microwave double reson. 78−46435
$OCS+H_2$, rot. excitation, infinite order sudden approx. 78−74740
$OCS+H_2(CO_2)$ (fluoromethane), rot. relax. parameters, microwave spectra linewidth parameters 80−28009
OH ($A^2\Sigma^+$)+$H_2(N_2)$(Ar), collisionally induced population change rates, laser-induced fluoresc. obs. 78−5326
$OH+H_2$, pot. energy surface, barrier heights and transition state geometry, POL-CI calc. 80−55649
$OH+H_2$, rot. excitation in interstellar medium 78−4306
OH(ν=0, 1)+H_2(ν=1), rate consts., 298K 79−11768
$O_2(^1\Sigma_g^+)+H_2$, collisional relax. temp. depend. 77−32783
S+inert gas (N_2)(H_2), rare gas sulphide S(^{1}S) emissions 78−82828
$S_2(B\,^3\Sigma_u^-)$+inert gas (H_2)(N_2)(S_2), collision-induced energy transfer 79−3544
SF_6-H_2 mixture photolysis, S atom nucleation particulate formation 78−76836
SF_6-H_e mixtures, collisionless multiple photon absorpt. photodissoc., HF fluoresc. 77−58099
SF_6+H_2 chemical laser, electron beam pumping 80−91784
Si:In, neutron irrad, to compensate for residual B, photocond., IR focal plane array 78−80733
$Si+H_2(O_2)(He)(SiCl_4)$, $3p^2(^1D_2)$ state behaviour, at. absorpt. spectra 78−29846
SiF_4+H_2, SiF_xH_{4-x} heats of form., mass spectrometric determ. 78−7221
SiH_4+H_2, vibr. energy transfer 77−524
$^{28}Si+H(H_2)$, single electron capture cross sections 78−58812
T-impregnated solid H_2, storable conc. of atomic H 80−30594
T+HT→TH+T, collinear reactivity bands 78−85143
Tl+H_2, Tl atomic fluorescence, pressure and Doppler broadening 80−5504
UF_6-H_2, near UV and visible excitation, quantum yield from photodissociation 80−35549
UF_6-H_2 gas dissociation in pulsed IR and UV laser fields 80−91620
UF_6+H_2, laser induced dielectric breakdown obs. 77−28992
V_2O_3-H_2, interaction with surface, quantum chemical study 80−45549

hydrological techniques
alluvial aquifers, hydraulic parameters determ. from resistivity meas. *(Italian)* 77−53079
Amur basin rivers, anal. and forecasting of dates of ice breakup *(Russian)* 77−53088
annual streamflow record extension by correl. methods 80−81950
aquifer permeability and storage identification by artificial recharge hybrid simulation 77−45043
aquifer storage capacity determ., well tide eqn. 80−21785
automatic time-lapse photography, long term, for frost blisters meas. 80−12437
bedload transport measurement, calibration of acoustic device 80−56620
boundary integral eqn. method for two-dimens. steady groundwater problems 79−16718
catchment areas, large, jet flow similitude *(French)* 79−66423
climatology, hydrology, atmospheric research and meteorology from space, conference, Ajaccio, Corsica (1979 November 12 to 16) 80−62397
coastal aquifer water flow analysis 80−26654
contamination-free method of sampling and analysis of thermal waters 77−81844
coring method for lake surface sediments 77−9520
daily river flow, non parametric Markov model, appl. to Cheyenne river 80−81948
data networks, design 79−21022
dialysis of stream water, meas. of dissolved forms of trace elements 80−97851
drainage density prediction techniques, evaluation of surrogate methods 80−8365
EM freq. sounding in groundwater exploration 77−9529
environmental isotope study of Kalamos springs, Greece, recharge area determ. 79−53393
estuarine hydrography and sedimentation, measurement techniques, book 80−36788
evaporation from shallow lakes and ponds, simple determ. method 77−5352
evaporimeters, thermal insulation calc. 79−29803
evapotranspiration estimation, advection-aridity approach 80−8366
fission track registration technique for U conc. determ. in water samples 80−12565
flood forecasting, loss of runoff due to water absorpt. by soil 80−109178
flood forecasting model from rainfall catchment and evaporation data, retention hysteresis 80−81951
flood inundation of agricultural land, LANDSAT digital image anal. 80−61913
flood warning system, on-line, based on adaptive model, desk-top computer appl. 79−34977
flood-plain delineation by multispectral data analysis 77−73885

hydrological techniques continued
flow through heterogeneous earthen dam, problem solvability 80−90110
flow-routing techniques, linear system vs. finite difference models 77−29512
FLUCOMP numerical river flow model 80−26653
fluorescent tracers in hydrology, conc. meas., synchronous excitation method *(French)* 77−77840
forecasts, automatic processing of operational information 78−3842
fresh water, sulphate residue elemental anal., spectrographic technique *(Russian)* 77−12868
freshwater acidification meas. 79−43802
geoelectrical prospecting, resistivity method for geophydrological problems 77−9527
glacier thickness and water content, radar measurement technique 80−98369
glacier thickness meas. from helicopter in W.Spitzbergen *(Russian)* 77−29336
ground surface temperature prediction, force-restore method investigation 80−98469
groundwater contaminant arrival distribs. as general evaluation requirements 79−16533
groundwater contaminant arrival distribs. for steady flow in heterogeneous systems 79−16535
groundwater contaminant arrival distribs. in transient flow systems 79−16536
groundwater contaminant location/arrival time/outflow distribs. for steady flow 79−16534
groundwater contour mapping in Venice, stochastic interpolator method, theory 80−8353
groundwater contour mapping in Venice, stochastic interpolators method, results 80−8354
groundwater filtration characteristics, multiple functions of filters in thermistor meas. *(Polish)* 78−40716
groundwater filtration rates, thermistor-aided meas. *(Polish)* 77−70872
groundwater flow, numerical predictions by method of charact. 77−29342
groundwater flow 2-dimens. eqns. soln., iterative methods 77−64351
groundwater flow calc. by finite element method 78−89320
groundwater flow digital simulation, finite element method 78−93018
groundwater flow parameters, spatial variability and uncertainty, geostatistical technique 80−8352
groundwater flow pathways determ. from satellite altitudes, apparent radiance data appl. 79−16522
groundwater flow simulation with computer-controlled RC network 77−45045
groundwater recharge in Ganges Basin, alternative methods for water supply 80−81952
groundwater recharge mechanism, Los Naranjos area, Mexico, using environmental isotope methods 80−12458
groundwater Rn content, continuous meas. method for earthquake prediction 77−44935
groundwater salinity and ionic strength determination method 80−109176
groundwater searches in Ukrainian Shield fracture zones, appl. of geothermal survey peculiarities *(Russian)* 80−104935
groundwater vel. determ. using organic solute-mineral surface interactions 80−98492
groundwater velocity determ. using natural He 80−82111
groundwater-surface water relationships in Turtz mine, ^{3}H tracer investigation *(Rumanian)* 77−53251
heat flow meas. in small lakes in N.W. Ontario, discussion and reply 77−53016
HF EM induction profiling of boreholes, hydrogeological appl. *(Polish)* 80−51547
hydrometeorological information, optimum conversion to digital form 79−29903
hydrothermal experimentation, noble-metal tubes cold-weld sealing 80−41556
hydrothermal solutions experimentation, new reaction cell 80−41555
hydrothermal system, temp. measurement scale based on chem. comp. of gas fraction 80−98277
ice, dielectric relax. meas. by blocking layer method 80−103914
ice cores age determ. 77−2190
ice sheet radio echo sounding, polarisation of signal 77−56755
ice-cover thickness on rivers and lakes, pulsed radar meas. method 78−92862
inland wetland photointerpretation evaluation, cell analytical method 79−29898
lake hydrographic surveys optimization 79−53378
lake ice, microwave radar and radiometric remote sensing meas. 80−85691
lake quality monitoring, multidate Landsat data extraction progrm 80−17299
lake sediment thermal diffusivity estimation from field obs. 77−2253
lake sediment-water interface sampling with gravity corer 79−88512
lake sediments, E_h meas. reliability conditions 79−48528
lake studies, isotope techniques appl., advisory group meeting, Vienna (1977 August 29 to September 2) 80−41950
lakes, latent and sensible heat fluxes prediction from surface water temps. 80−72562
lakes, suspended solids, anal. using Landsat multispectral data 79−16523
LANDSAT digital data for detect. of moisture stress by Green Index Number method 80−17423
leaky aquifer analysis, finite element method soln. 78−93017
least squares method for statistical tolerance limit computing 78−49179
magnetic meas. for identifying suspended sediment sources 80−4052
map plotting, flow vel. and positional meas. using tachygraph 79−72977
mechanical testing under hydrostatic pressure, of Antarctic deep core ice *(Japanese)* 79−79890
microwave passive remote sensing of snowpacks, theory and expt. 80−26632
microwave remote sensor development and appl. to hydrology 80−105082
mountain rivers, evaluation of max. discharges distrib. parameters 78−3840
multicell aquifer model calibration, iterative method 80−8456
multielement anal. by rotrode direct reading spectrometry, water pollution appl. 77−70355
natural channel flow simulation by computer-controlled RC network 77−45046

hydrological techniques continued
natural fracture water identification by radiological parameters 77−78245
neutrally buoyant capsules, dynamics from experimental drop in Lake Tahoe 80−12438
neutron activation anal. for low level Hg anal. 79−70503
neutron soil moisture meter, design and operation 79−44280
nitrate determ., improved hydrazine reduction method for freshwater samples 79−34467
nitrate determ. in estuarine waters, UV absorption technique 79−16719
nuclear radiation appls. 79−39981
nuclear techniques in hydrology, survey 77−37419
optical methods of water quality determ., turbid waters spectral scatt. props. 80−72560
particulate concs., remote sensing of lakes 80−105056
perched water table detection using EM telemetering systems 80−26655
permafrost, thermal amelioration tests near Schefferville, Quebec 77−33058
permafrost mapping by audiofrequency magnetotellurics 79−58102
permafrost thickness determ. in wells in N. Canada 77−66989
pollution control, tracers appl. *(French)* 80−7995
precipitation measurement, dual-gauge and Wyoming shield systems 80−61928
prediction models, adaptive algorithm 79−53381
prospecting in Africa, geophysical techniques 80−61818
radar meas. of snow drift *(Japanese)* 77−82032
radar subsurface sounding of groundwater in deserts and glaciers 80−67437
radar vertical probing of glaciers, signal depolarisation 77−9557
radio echo sounding of ice sheets, internal props. var. with depth 80−26633
radioactivity meas., very sensitive sampling method 79−39768
radiochemical analysis for Rn in groundwaters appl. to Christchurch artesian wells 77−82039
radiography in hillslope hydrology 79−74910
radionavigation systems appl., available systems survey, modes and accuracy 80−36408
radiotracer methods for speciation study in natural waters 79−88490
radiotracer studies at Mangi for subsoil hydrological investigations 79−34869
rain throughfall under a forest, estimation methods 79−2307
rainfall measurement by weather radar, appl. to hydrology 80−90263
rainfall network analysis, optimal estimation of total areal storm depth 78−49059
rainfall of short duration, runoff calc. method *(French)* 80−77143
rainfall prediction for short response time basins 80−98491
regression models, alternatives, Bayesian study 80−8360
relocation method for lake seston (particulate matter) traps 79−74964
remote level and velocity measurement by random signal anal. from surface waves 79−72976
remote sensing, eqn. for pot. evaporation from soil, water and crop surfaces 77−64334
remote sensing of near-surface soil moisture, theory for passive microwave technique 77−87105
remote sensing of rivers and lakes, spectral response field meas. 77−78469
reservoir surface area from LANDSAT imagery 79−66834
resource system, time variable, recursive estimation techniques appls. 79−5538
river bottom sediments, in situ neutron activation anal., pollution, mapping and prospecting appl. 77−87115
river discharge forecasting using hydrologic model of Mahanadi basin 80−31130
river flow forecasting methods for Bulgarian rivers 80−26562
river flows, transverse mixing coeffs., evaluation from slug tests 77−21806
river ice break-up, satellite monitoring 78−65350
river ice processes, radiohydroacoustic monitoring method 80−26649
river longitudinal slope determ. 80−82108
River Main, County Antrim, sampling freqs. for N and P loads determ. 79−44213
river quality modelling by sequential extended Kalman filters 78−81248
River Tiber, physical processes related to discharge into sea, aerospatial obs. 80−108831
river volumetric flow gauging, electronic methods 77−73891
river water quality modelling and operational control 79−16555
river water temp. forecasting, Fourier series and communication theory techniques 77−25718
rivers, selection of analogues for flood calcs. 78−16073
rivers downstream pollution, one-dimensional transient model for short-term prediction 80−81496
rivers/open channels level and vel. meas. by surface wave signal anal. 78−57328
runoff from steppe zone river, estimation method for spring norm 80−85694
saline seep detection and mapping, IR remote sensing techniques 80−4154
salinity/temperature sensor chain for estuarine meas. 79−5670
seasonal reservoir, optimal releases, deterministic case 80−8362
sediment and nutrient loadings to Lake Ontario calc., methodological arguments 78−77278
sediment lipids, Recent and ancient 80−51583
sediment source identification, mag. meas. techniques 80−8348
sedimentation rates determ. in rapidly accreting salt marsh by ^{137}Cs dating 78−96247
sediments, polymodal, of river-lake system, grain size curves partitioning and interpretation 79−25273
seepage and groundwater flow, numerical analysis, book 79−100884
semipervious stratified aqu. layers, hydrogeological parameter determ. *(Russian)* 78−32236
snow, accuracy of water equivalent meas. with standard densitometer 79−29796
snow, water content meas., calorimetric method *(Japanese)* 80−31142
snow areal extent and water content estimate using LANDSAT imagery 77−78520
snow cover water storage determ. using aircraft-borne gamma-ray surveys 78−16218
snow parameters, investigation by radiometry in 3 to 60 mm wavelength region 80−72561
snow parameters remote sensing, two-stream theory of reflectance 79−88376
hydrological techniques continued
snowfield assessment from Landsat 78−88941
snowgauge measurements, Canada, accuracy 79−70818
soil infiltration, spatial var. of hydrological effects, Monte Carlo anal. 80−8363
soil moisture, basic hydrophys. charact., determ. method 80−85696
soil moisture, determ. in Africa by soil thermal inertia cartography (CITHARE project) 80−76980
soil moisture, microwave remote sensing, sampling techniques for ground truth data 78−65439
soil moisture and geology mapping, thermal intertia method 80−8344
soil moisture calc. methods *(Russian)* 77−29493
soil moisture content, determ. by meas. of reflectance in ultrashort radio wave band 78−16075
soil moisture content, microwave radiometer meas. over bare and vegetated surfaces, comparison 78−88851
soil moisture content meas., quick drying procedure 80−82109
soil moisture meas. with airborne imaging passive microwave radiometer 78−36310
soil moisture measurement, remote sensing simulator 78−49143
soil stored productive moisture, remote determ. technique 79−29795
soil water content, estimation via total solar reflectance and spectral band ratioing 77−60479
soil water flow model with two-dimens. automatic γ-ray attenuation scanner 79−53387
soil water flow modelling, finite difference and Galerkin techniques 78−81249
soil water sampling, water regimes near porous cup samplers 77−66942
solution flow prediction, computer models, appl. to U solution mining 79−88013
space-borne remote sensing *(Italian)* 80−109333
stereometric measurement of streambank erosion 80−17421
storage reservoir analysis, mass-curve techniques, systems and perspective 80−8457
storm runoff, flow component separation, solute conc. and contact time study 80−8358
stream temp. modelling, 'dishonest' method 78−81454
streamflow, empirical data, multivariate gamma distrib. fitting 78−81240
streamflow, multiple monthly series, reconstruction and prediction 78−24373
streamflow changes estimation after reclamation, errors 79−29794
streamflow data, Pearson type 3 distrib. fitting 78−49061
subsurface water detection methods, in Armenia, elec. profiling and sounding 80−85753
sulphate determ. in brines, indirect anals. by atomic absorpt. 80−89556
surface soil moisture remote meas. 79−70896
surface water continuous analysis by NH_4^+-sensitive plastic membrane electrode 80−89701
suspended sediment monitoring by remote sensing, universal multispectral algorithms 79−53558
suspended solids in water, macerated glass fibre filter paper appl. 79−8454
transient groundwater flow simulation by hybrid computer 77−45044
turbid water, instrument ot meas. light absorpt. coeff. 80−82076
turbid waters, remote sensing penetration depth at green wavelengths 79−66832
turbidimetry instrumentation, light scattering techniques appl. 79−12150
underground water mineralisation, reliability anal. of geophys. estimation *(Polish)* 77−73862
underground water movement tracing using halogen tracers and NAA 79−88014
unsaturated water flow within porous materials, obs. by NMR imaging 79−98840
USSR Hydrometeorological Service, automation of data collection and processing 79−34994
volatile organohalogen analysis in water purification processes 79−21080
water levels, obs. via electrooptical distance meas. *(German)* 78−69280
water pollution prediction, finite element method appls. 78−93019
water quality modelling, Kalman filter theory and practice 78−45058
water quality trends, statistical tests for dependent obs. 77−29513
water resource system, Monte Carlo simulation, variance reduction techniques 78−81244
water-data bank compilation, Adour-Goronne river basin *(French)* 79−66720
water-resource development project design, optimal apportionment scheme appl. *(French)* 80−77019
wet soil complex permittivity meas. method at microwave 77−45184
wide rivers, acoustic flow meas. 79−72975
X-ray fluorescence analysis of natural water, preconc. technique 78−61620
B, dissolved, in water, determ. via azomethine H colorimetric method 79−92115
^{36}Cl in environmental water samples, anal. using electrostatic accelerator 79−20895
Fe, determ. in waters, colorimetric-acid digestion method 78−61088
P determination, automated procedure 80−81517
P, reactive, in natural waters, low concs. automated determ. in presence of As, Si and $HgCl_2$ 79−44277
^{226}Ra in public water supplies, conc. determ. *(German)* 80−94138
Rn groundwater monitoring systems for earthquake prediction 80−94467
Rn measurement in groundwater and springs for earthquake prediction 78−88924
Se (−II,0), -(IV) and -(VI) composition of water, by gas chromatography method 80−81928
SiO_2 geothermometer, appl. to warm springs along Jordan-Dead Sea Rift Valley 80−41464
U in natural waters, field meas. technique 78−85705

hydrology
see also groundwater; lakes; rivers
accumulation water of hydroelectric plant, hydro-chemical and hydraulic analysis *(Croatian)* 80−12443
acid mine drainage in impoundments, computer simulation 77−37260
acid precipitation effects, Norwegian SNSF-project on forest and fish 77−37411
acidic rain interacting with rock partially covered by lichen 80−17302
acoustic flowmeter, for use with hydraulic models 79−68878
agricultural land, losses of N_2O dissolved in drainage water 79−43797
agricultural water demand information, remote sensing 79−2315

hydrology continued
alluvial soils and flooding relationship in Piedmont Lowland, SE.Pennsylvania 79−88385
alpha and beta radioactivity meas. *(Rumanian)* 77−49067
S.America, water balance rel. to water vapour transport in atmosphere 79−29820
analysis using simulation of orographic precipitation distrib. 77−53087
annual flow regulation, appl. of probability and statistical methods *(Chinese)* 79−96778
Antarctic dry areas geochemical problems 79−79844
aquatic systems, surface films and foams 79−16549
aquifer inverse problem, statistical method case study 80−98371
Archaean precious-metal hydrothermal systems, Ontario, alteration patterns and metal distrib. 80−12382
Archaean precious-metal hydrothermal systems, Ontario, rare earth element and 0 isotope relations 80−12383
Badlands slope development, moisture budgets rel. to mass movement and piping 80−41468
Box-Jenkins models and rescaled adjusted range 79−16544
Brazil, precipitable water, distrib. maps 80−77075
Britain, water balance, 50000 yr BP to present day 80−72566
catchment model design and parameter estimation using optimisation method 79−5536
channel factors simulation in numerical computations of flow *(Polish)* 79−25280
climate, soil and vegetation, annual evapotranspiration value 79−79895
climate, soil and vegetation, annual precip. distrib. from storm sequences 79−84314
climate, soil and vegetation, annual water balance dynamics 79−79896
climate, soil and vegetation, annual water yield distrib. 79−84316
climate, soil and vegetation, soil moisture movement in liquid phase, model 79−79894
climate, soil and vegetation, storm surface runoff distrib. 79−84315
climate, soil and vegetation, water balance dynamics 79−79893
climatic change detect. and impact on hydrologic design 79−53396
Cobb-Douglas functions in multiobjective optimization 79−53397
Columbia Plateau, E.Washington, age of last major scabland flood 79−66726
computer simulation of hydrological processes, using super-kurtic probability density function 80−26558
computer-supported research into water resources 79−20892
conference, on climatology, hydrology, atmospheric research and meteorology from space, Ajaccio, Corsica (1979 November 12 to 16) 80−62397
curvimeter for meas. of rivers, contours and basins on maps 80−26650
Dakota drainage pattern mapping IR thermal imagery remote sensing 80−81892
Darcy's law generalisation for nonuniform flows 80−10305
Darling River system floods, chronological evolution, Nimbus-5 radiometry obs. 80−94543
deep-sea hydrothermal site on strike-slip fault, discovery 80−21710
deterministic hydrologic models, parameter uncertainty effects, analysis 77−25724
discharge probabilities, empirical formulae 80−26559
dispersion coefficients, longit. and transverse, in unsaturated Plainfield sand 79−53382
distribution functions for hydrologic design 79−53392
drainage basin characteristics, network power model 80−61823
drainage basin charact., flood study, British Isles 79−20878
drainage basin parameters, patterns of variability, India 79−39769
drainage basins, objective criterion for selection of representative basins 80−12457
drainage density and channel network geometry, post-Hortonian studies 79−20874
drainage density and streamflow 79−88384
drainage density changes during rainfall 79−20881
drainage density estimation from topological variables 80−61831
drainage headwater development, modelling 79−20875
drainage network change in Britain 80−81934
drainage network mapping of Pantanal Brazil, Landsat-2 imagery 80−81944
drainage runoff hydrograph calc. for loamy soils in Lithuanian SSR 79−39781
drought definitions 80−105010
drought in California and western Europe, 1976, atm. and oceanographic factors 79−48560
drought in streamflow series, statistical charact. 80−105009
drought in upper Midwest, USA, 1931 to 1969 period 79−70880
droughts, continental, study *(French)* 77−37344
ecological disturbances caused by coastal pollution source, math. model 77−78232
ecological models, time and length scales for one-dimens. assumption 80−12455
ecosystems, acid precipitation effects, review 77−37257
El Tatio geothermal field waters, N.Chile, isotopic comp. rel. to sources 79−16525
entropy concepts reevaluation in fluvial geomorphology 80−12453
erosion cycle and climatic change reversal 77−64338
Europe, hydrogeology rel. to local heat flow patterns from preliminary map 79−70765
evaporation from nonsaturated surfaces, parameterisation 79−53372
evaporation from water surface, scaling theory 80−109179
feature prediction model in synthetic hydrology based on concepts of pattern recognition 79−5527
field data, objective anal. 79−12321
flood flows modelling, use of Wakeby distrib. 79−84330
flood frequency analysis, appl. of incomplete means estimation procedure 79−88378
flood frequency analysis, use of Holocene stratigraphy 79−53390
flood frequency analysis with a generalized skew coefficient 79−5531
flood routing, Muskingum constants evaluation, FORTRAN IV 80−31077
flood statistics comparison in real and log space 79−84319
flood wave propagation in channels with storage areas, diffusion eqn. 79−25277
flooding assoc. with probable maximum hurricane 79−20941
floods, 1975 August, in Orissa, India 79−20886
floods, partial duration series models, Poisson assumption anal. 80−8374
floods, Queensland, Australia, LANDSAT imagery interpretation 79−25283
floods, severe, in River Burhi Gandak, 1974 and 1975 79−20891
floods and their causes, in India 80−101389
hydrology continued
floods in Plynlimon expt. catchments, Wales, geomorphological effectiveness 80−81932
forested watershed Oesling, Luxembourg, chemical erosion 77−81930
fractional Gaussian noise algorithms and rescaled adjusted range 79−16545
free water surface behaviour, porous media, appl. to earth dam seepage 80−8349
freshwater ecosystems in Norway, acid precipitation effects 77−37258
freshwater environment, inorganic As stability and solubility, theoretical aspects 79−16553
frozen soil, prediction using weather records 79−88379
Galerkin finite element procedure for analyzing flow through random media 79−81967
geochemical data processing, agglomerative nonhierarchical Q-mode classification, AGCL (FORTRAN IV) program 77−86941
geologic concept in geophysical research 77−9451
geothermal reservoir simulation, math. models 80−12446
geothermal reservoir simulation, numerical soln. techniques 80−12447
geothermal vapour dominated field, Larderello, Italy, gases and H_2O isotopes content of steam 79−74920
geothermal vapour dominated field, Larderello, Italy, noble gas concs. 79−74919
grazing, hydrologic impact on infiltration 79−2325
Green and Ampt infiltration eqn. parameters depend. on initial water content 79−79899
ground surface temperature prediction, force-restore method investigation 80−98469
Guaymas Basin, Gulf of California, heat flow at spreading centres 80−41411
Gulf of Alaska, coastal circulation, precipitation and runoff effects 80−36312
gypsum hydration water, isotopic comp. 79−20829
heat extraction from hot dry crustal rock via hydraulic fracture 79−74491
heavy metal-organic matter interactions in natural waters 77−60439
hillslope topography role in throughflow generation control 79−48520
hodograph method, use of reference function 79−84323
Holocene climatic change effects on tropical geomorphic processes 77−64418
Hurst phenomenon, evidence for nonstationarity from precipitation records 77−29348
Hurst phenomenon and rescaled adjusted range appl. 79−16543
hydraulic conductivity of unsaturated porous media 79−5526
hydraulic geometry, graphical analysis using BFM diagram 77−33097
hydraulics of water flows, terrestrial equivs. of Martian outflow channels 79−40112
hydrometeorological data for US, autocorrelation charact. 77−66939
hydrometeorological information in USSR, economic effectiveness 79−29909
hydrometeorological time series, spectral analysis for United States 77−64341
hydrometeorology rel. to water resources design engineering 79−70819
hydromorphometric charact. 77−78253
ice sheets, basal temps, and meltwater prod. 77−78250
Iceland, Hg natural conc. 77−64244
independent mixed models, range, drought effects 80−81954
India, effects of drought 77−56707
India, runoff rel. to overall assessment of surface water resources, water balance calc. 77−56662
infiltration during an unsteady rain 79−16538
infiltration model 79−16548
information needs and remote sensing 77−56665
information retrieval publications, comparative study hydrometeorology in USSR 80−36401
inland wetland photointerpretation evaluation, cell analytical method 79−29898
instantaneous unit hydrograph with negative ordinates, appls. 80−12456
instrumentation, review *(French)* 79−39979
interblock hydraulic conductivity values for transient unsaturated flow problems, finite difference soln. 80−12460
internal currents, struct., kineticity effects 77−68570
irrigation, influence on radiation balance of Earth surface and components 79−29863
Jordan-Dead Sea Rift Valley warm springs, correl. between SiO_2 conc. and orifice temp. 80−41464
karst depressions in Jamaica 77−44991
karstic limestone terrain, Texas, USA, drainage history and aquifer 80−56501
Kirishima volcanoes, Japan, heat discharge and H_2O emission rates, hydrothermal survey *(Japanese)* 80−67357
La Porte anomaly, hydrological reanalysis 80−46206
Lake Oroville, reservoir-induced pore pressure and seismic activity 79−2190
land drainage, errors in post reclamation streamflow changes estimates 79−29794
landslip/debris flow, Bilsdale, North York Moors, 1976 September 79−48524
Late Wisconsin flood into Gulf of Mexico 79−29775
limestone cave systems, development in dimensions of length and depth 79−62531
linear model stable estimator development and expt. 77−5259
liquid phase mass transfer coeffs. at natural air-water interfaces 79−20922
loess erosion and redeposition by water, expt., micromorphology 77−81925
log Pearson type 3 distrib., T-year event and asymptotic standard error by max. likelihood theory, comment 80−12461
S.Long Island, New York, salt marsh development rel. to Holocene submergence history 79−74881
lysimeter for W.Australian cereal belt 79−12276
Manic 3 reservoir, Quebec, water percolation rel. to induced seismicity 79−66636
Manning's roughness coeffs. for open estuarial river system 79−79897
mapping discharge conditions in catchment areas *(French)* 77−33105
maximum discharge from basin area, calc. 79−39773
mid-ocean ridges, obs. and implications of ridge crest hot springs 80−98304
mineral, dissolution under Earth surface conditions, rate control 79−20817
models of long-term persistence, skew preservation 77−78273

hydrology continued
moist soil, emissivity in microwave range, temp. effect 79−29797
monthly average water discharge cycles and prediction, spectral anal. 77−78264
mountain watershed, ski basis impact, heavy metals pollution 79−20903
mudslide potential situations, meteorological parameters critical values, Caucasus mountains 79−39782
multiobjective urban drainage and flood control project evaluation 77−37270
multipurpose water projects, efficiency and equity of cost allocation methods 79−88017
Nahal Yael, Israel, arid watershed, climatic variations, hillslope study 80−8342
natural streamflow control coeff., analytical calc. method 79−39777
Nicaraguan geothermal resource utilisation 79−29448
normal distribution approx. by three-parameter log normal distrib. 79−53389
nuclear 'in situ' methods used in hydrology and hydrogeology *(Rumanian)* 79−39982
nuclear techniques in hydrology, survey 77−37419
numerical soln. of transport eqn. 77−64358
open channel flows, junction losses, frow anal. 80−6156
open channels with weirs and flumes, discharge measuring structs. 79−68874
overland flow equations soln., comparison of finite element methods 79−12152
palaeohydrology, continental record of environmental conditions at 18000 yr BP 80−51529
Pearson type III distrib. curves comp., analytical formula 79−29800
Perch Lake Basin, Ontario, hydrological and geochemical studies conference, Chalk River, 1978 April 25 to 26 80−51955
polar desert pond, dynamic chemical equilib., as sensitive index of meteorological cycles 80−12441
pollutants, radioactive tracers appl. *(French)* 80−7995
polluter discriminant analysis using statistics data base 77−5244
pollution, nonpoint source, continuous simulation 79−52967
pollution by ^{239}Pu, ^{241}Am, Ge monitor for in situ assay 77−9546
pollution of surface and underground waters, isotopic tracing *(Italian)* 77−53078
pore fluid effects on seismic wave propag., dynamic poroelasticity fundamental soln. 79−74847
pore water, effect on stress relaxation in sandstone 79−16453
potential evapotranspiration, continental maps based on Penman concept calcs. *(German)* 80−98368
process dynamics investigation using time-varying models 77−41099
radioactive ion concentration using ion exchange resin, field sampling unit 77−9532
rain, heavy, basic characts. determ., max runoff calc. 79−29802
rain mixing with near-surface water 79−53371
rainfall, maximum possible in Great Britain−time limited, determ. methods 80−4091
rainfall, spatial distrib. in small catchment, influence on storm runoff 80−8357
rainfall runoff from multiple watersheds system, computer model 79−29805
rainfall variable infiltration, eqns. 79−53379
Ralston Creek hourly precipitation model 79−16542
records analysis and comparison, statistical program suite 77−21819
remote sensing, spectral response field meas. 77−78469
remote sensing of natural resources using satellite and aircraft scanner data for Finland 79−100988
reservoir design and management, SESLP model 79−2314
reservoir flooding, for oil recovery, shear thinning and shear thickening polymer additives 80−72100
reservoir management for irrigation, chance-constrained linear programming 79−2317
reservoir storage, distrib. of max. deficit of partial sums of variables 80−4651
reservoirs, thermal stratification during winter season 79−5532
resources management, systems anal. and modelling techniques appl. 79−5518
resources planning and management, appropriate model choice 79−83650
river basin management system 79−25288
rivers, winter regime, ice-covered streams, water discharge meas. 79−12160
rock permeability changes due to stress 79−16452
runoff from land receiving animal wastes, pollutant transport, review 80−97831
runoff from rock and shallow soil, tracer study of chem. processes 80−17301
runoff kernel for basin, mathematical derivation 80−61832
Sahel, West Africa drought conditions *(French)* 77−37345
saline environmental waters, IR relative reflectance and complex refr. index 77−45013
saturated-unsaturated flow in deformable porous media, numerical model, appls. 79−81966
sediment graph model based on instantaneous unit sediment graph 79−53394
showers and simultaneous floods in Alps, meteorological study *(French)* 79−66721
simulation procedures for Box-Jenkins models 79−79907
snow accumulation, distribution, melt, and runoff 80−36338
snow areal extent and water content estimate using LANDSAT imagery 77−78520
snow cover in Great Britain 79−12161
snow storage determ. for small high Arctic basins, error anal. 79−70817
soil convective-dispersive solute transport with combined equilib. and kinetic adsorption model 77−64356
soil hydraulic properties, empirical eqns. 79−53385
soil moisture, basic hydrophys. charact., determ. method 80−85696
soil moisture, capillary hysteresis model 79−53386
soil moisture, cartography in Africa by geostationary satellite (CITHARE project) 80−76980
soil moisture vars. under bare conditions rel. to rainfall at Pune and Delhi, India 79−96777
soil physics, book 80−27056
soil water, flow regimes near porous cup water samplers 77−66942
speleothem fluid inclusions, D/H ratio rel. to meteoric precipitation 79−44201

hydrology continued
spring flood hydrograph for marshy lowland basins, math. model 79−62538
spring inflow hydrograph into Tsimlyansk reservoir, long-term forecasting 79−57985
spring-flood forecasting and runoff loss due to water absorpt. by soil 80−109178
stable estimator for linear models 77−5260
steady state shallow water equations, unified treatment, finite element penalty function approach 79−49056
steam reservoirs characts. determ. by ^{222}Rn meas. in geothermal fluid 79−74918
steam-water counterflow in porous media, model, geothermal systems appl. 79−79879
steamflow routing, geomorphic model 80−12452
stochastic models of floods 79−5528
storage-routing model relating drainage basin hydrology and geomorphology 79−79903
storm flow generation, detailed field monitoring of variable source areas 79−88380
storm type effect on precipitation in small mountain watershed, theoretical study 80−8355
stream hydrograph, major base flow components identification and separation 79−79898
streamflow, skewed annual flows generation using fast fractional Gaussian noise generator 79−53395
streamflow calc. from discharge vols. for winter periods 79−25285
streamflow data, empirical, fitting of multivariate gamma distribution 79−34878
streamflow record synthesis, feature prediction model appl. 80−98372
streamflow rel. to precipitation in NE.United States, filtering and intervention anal. 80−8359
streamflow response to differences in transpiration among species of hardwood trees 79−84328
subarctic snowmelt, energy balance computations 77−5262
subarctic snowpacks, runoff generation 77−5261
subsurface hydrology, finite element method using mixed explicit-implicit scheme 79−79900
sulphate residues of fresh waters, elemental, anal., spectrographic technique *(Russian)* 77−12868
SE Sumatra coastal environment, remote sensing appls. 79−53556
summer droughtand autumn rainfall, England, 1976, effects on stream solute levels 79−48523
surface irrigation, kinematic model 79−5529
surface runoff, New Zealand, P transport, effect of fertiliser and grazing cattle 77−53094
surface runoff two dimens. models 79−34874
surface waves on viscous fluid of variable depth 77−11210
suspended sediment monitoring by remote sensing, universal multispectral algorithms 79−53558
Suwannee River sill, effect on Okefenokee Swamp water level 80−8356
Syr Darya hydroelectric power station, recording aspects *(Russian)* 77−86942
thermal IR scanning appls. 79−8723
thermal springs in folded Appalachians, origin from heat flow meas. in western Virginia 80−41414
time series, assessment of long-term persistence models 77−64350
time series, multivariate data synthesis by disaggregation 77−41094
time series, nonstationarity of mean and Hurst phenomenon 78−81253
time-averaged areal mean of precipitation, estimation and network design 79−79901
tracer theory, nonsteady state systems 79−5646
transport phenomena, hydraulic electronic instrumentation *(Italian)* 77−91334
transverse mixing coefficients, evaluation from slug tests 77−21806
trapezoidal profile weirs, 2-dimens., discharge characts. 79−68875
Tsimlyansk Reservoir, hydrometeorological studies 79−39784
turbulent bursting phenomenon, sedimentological implications 77−13093
turbulent current model with sliding on watercourse bottom 79−29801
turbulent flow into homogeneous porous media on inclined bedrock 79−10609
unit hydrographs for Barakar and Yamuna catchments, flood forecasting 79−20887
unit sediment graph 79−79902
United States, floods and their management 77−41073
NE.United States, soil Al leaching by acid precip. in high-elevation watersheds 80−12442
upstream control effect on water supply reservoir 79−57508
urban bulk precipitation and streamflow quality relationships 79−88382
urban flood control programs, ecological and social aspects 79−2316
urban flooding rel. to land use change, stormwater management model 77−37280
urban hydrology and sediment control, symposium, Lexington (1976) 77−37266
urban runoff pollution rel. to land use 79−5530
urban storm water in Sydney, Australia, quality characts. 77−64357
urban storm water management, flood vol. distrib. 80−8361
urbanisation effect on floods, predictive model 77−37276
Vajont rock slide (Italy, 1963) analysis, new approach 79−8633
velocity estimation from hydrographic data 79−21040
wadi flood water sampler 80−98493
S.Wales floods of late December 1979, meteorological anal. 80−98429
water balance of lower Sutlej catchment, estimation by Thornthwaite's method 79−48525
water budget and potential reserves of East Africa source region of Nile 79−100880
water economy, meteorological radar system appls. 79−62543
water quality indices, statistical anal. 80−8368
water quality study, Streeter-Phelps models sensitivity anal. 77−70715
water resource research using Pennsylvania State Univ. reactor 79−12159
water resources policy, scientific and technological considerations 79−8642
watershed models, sensitivity of optimised parameters 79−5523
watershed peak flows size and timing, effects of clearcut logging 80−12451
watershed stream network run-off anal. model, appl. to Nagara River *(Japanese)* 79−16529
watersheds of Eastern USA, ^{137}Cs distrib. 77−25701
watersheds sediment prod. long-term patterns following road construction and logging 79−84322

hydrology continued
weirs, linear, proportional, datum line fixation 79−20898
wetland mapping and classification, high altitude photography of W.Tennessee 80−8340
Wisconsin driftless area, hydrology of small watersheds 77−91169
world water resources, prospects and problems 79−39779
Yellowknife mineralisation, vein geometry and hydrostatics 79−57920
C, mass transfer and isotope evolution in natural water systems 79−20882
^{36}Cl in environmental water samples, anal. using electrostatic accelerator 79−20895
Fe content determination in natural waters 79−84550
NO_3^--N export from drainage basins, Toronto, Ontario 79−66729
O_2 singlet in natural waters 77−56659
Pb in hydrosphere, global and regional distrib. 79−16517
^{222}Rn tracer measurement in aqueous samples by decay product filtration 77−60476

hydromagnetic waves *see magnetohydrodynamic waves*

hydromagnetics *see magnetohydrodynamics*

hydrometers
see also density measurement
crude-oil hydrometers calibration 78−73969
psychrometer, with grafted thermometer *(Japanese)* 80−31771
testing installation for densimeters 79−80582

hydrophones
see also sonar
acoustical tracking, ocean current profiling 80−67427
acousto-optic sensor development 80−14542
acousto-optic transduction used in optical hydrophones 80−14541
acoustooptic hydrophone, coupled waveguide, using intensity modulation 80−14431
active-impedance termination method using travelling-wave equipment, error estimation 79−94429
AF hydrophone calibration intallation 77−75732
array effects on offshore Texas seismic signals 79−53309
array response calc. errors due to two dimensional beam pattern assumption 78−66972
arrays, optimum turbulent boundary layer induced noise suppression with suboptimum realizations 80−19161
arrays, underwater, appl. in passive sonar *(Spanish)* 80−69586
bottom reverberations picked up by hydroacoustic dipoles, spatial correlation functions *(Russian)* 78−53659
C-mode US imaging by electronically scanned coaxial circular spherical receiving array 78−59222
calibration, by modified piezoelectric balancing method 77−11097
calibration, industrial noise meas. appl. *(German)* 77−80039
calibration system using pseudo-Gaussian noise signals 77−84045
calibration using complex exponential signal representation 78−79183
characteristics measurement using, US temperature-depth profile measuring system, expt. *(Japanese)* 77−70864
condenser electret hydrophones 78−38163
CW coherence meas. at low freq. for long underwater paths 80−106654
cylindrical array, analysis of acoustic fill time effects 80−19163
directivity pattern of particle vel. detectors near a baffle 77−50813
fibre optic, improved strain config. and environmental noise protection 79−98471
fibre optic, moving, based on intensity-modulation mech. 80−43455
fibre optic, sensitivity anal. 79−14191
fibre optic hydrophone, using single-mode and multimode fibres, sensitivity 78−13882
fibre-optic, comments on mechanism of transduction 80−58882
fibre-optic, description and advantages 80−58770
fibre-optic, mechanism of transduction 80−10103
fibre-optic, modulation processes 80−58771
fibre-optic, noise-equivalent pressure 80−33387
fibre-optic microphones and hydrophones compared with conventional devices 79−72717
fibre-optic pressure sensor 80−58878
flow noise effect on pressure and pressure gradient hydrophones 79−81605
gain limitations of passive vertical line array in shallow water 80−96117
geometric factors effect on performance 77−50846
geophone and hydrophone recordings in Californian offshore sediment 80−46192
gradient hydrophone flow noise 77−75758
H-58 omnidirectional hydrophone, mounting configuration rel. to infrasonic flow noise 77−47119
HF Lorentz force hydrophone theory and practice 78−42510
hydroacoustic transducers of fixed operating freq., elec. imped. matching *(Croatian)* 79−55287
interferometric fibre optic, static press. sensitivity amplification 80−38094
LF calibration, field nonuniformity effect avoidance 78−42486
line hydrophone array, low-freq. technique for underwater calibration of individual elements 77−79997
linear array, robust formulation of optimum cross-spectral beamformer 79−68495
Lorentz force hydrophone for low MHz frequencies 78−59243
magnetostrictive underwater sound transducers, use of rare earth alloys 80−19204
marine deep seismic sounding system with digital data acquisition 77−87083
membrane hydrophone for 0.5 to 15 MHz range, press. meas. in US fields 80−108987
microballoon reinforced plastics, acoustic and mech. props. rel. to hydrophone applic. *(Japanese)* 77−7793
miniaturised, for biomedical uses, calibration apparatus *(Japanese)* 77−64144
multimode fibre optic, frustrated total internal reflection, testing 80−38096
multipath separation and passive localisation using horizontal wavenumber spectrum 80−91952
noise level meas. using optical fibre interometric hydrophone 80−87673
ocean bottom hydrophone 78−12020
optical, for sonar, using optical fibre, development 79−3832
optical fibre, high-linearity multimode optical fibre sensor 79−68429
optical fibre hydrophone sensitivity, strain configs. 80−23771
optical interferometric, with homodyne detection, signal stabilization by light source tuning 80−87477
optimization of acoustic receiver noise performance 77−84097

hydrophones continued
parametric acoustic receiving array vibration sensitivity anal. 78−66971
parametric hydrophone, compact, using nonlinear interaction within cylindrical rubber waveguide 79−98535
parametric receiving arrays, modulation characts. 80−33393
partially random sonobuoy array directivity index analysis 80−43518
particle velocity hydrophones, LF calibration in liquid layer 79−94443
passive bearing estimation in unequal S/N ratio, optimum element placement 78−87210
passive ranging, errors due to receiving hydrophone position uncertainty 79−41522
piezoelectric, US output assessment 79−23176
piezoelectric polymer, for large receiver arrays 80−14540
piezoelectric polymer flexural disk hydrophone 78−63254
piezoelectric transducers, tangentially polarized cylindrical, for improved sensitivity, intrinsic noise determination 79−94441
pressure-gradient hydrophone, for meas. of particle vel. in fluids *(German)* 77−72118
quartz transducer stability analysis 77−11102
SAW, for use in sonobuoy system 79−94437
SAW sensor using resonator-controlled oscillators 80−74631
SAW transmitting hydrophone development and performance 79−53586
Schlieren multimode fibre-optic hydrophone 80−102938
shadowing by seamounts 80−33308
small-aperture directional, with piezoelec. dipole elements, principle 79−3828
sonar, directional characts. of cylindrical receiving arrays with nonuniform hydrophone response 77−88979
sonobuoy position meas., sound speed adaptive estimation 79−72773
spatial noise spectrum meas. in ocean for small observation baseline 80−102902
spherical multimode hydrophone, improved design 79−14189
stave array, for deep ocean submersions 77−62087
submarine detection system, response to ocean waves 77−72220
Three Array Processor beamforming system 80−43550
towed hydrophone systems tests by high speed research vessel Athena 77−41213
towed hydrophones, location system 79−2401
tracking of slowly sinking floats, meas. vertical profiles of oceanic current and Richardson number 80−67378
undersea acoustic holographic transducer array development 78−59209
underwater signal phase stability, meas. using moving source 80−87623
underwater sound arrival angle estimation by multiple cross-correlation meas. 78−66978
US, cylindrical, theoretical shape of directional pattern 79−81609
$Pb_xSr_{1-x}(Zr,Ti,Nb)O_3$, hydrophone ceramic, effect of one-dimensional uniaxial stress 80−80705
$Pb(Zr,Ti)O_3$, research grade, hydrophone ceramic, effect of one-dimensional uniaxial stress 80−80705
Si rubber as electro-optic material for optical hydrophones 80−43412

hydrophotometers *see photometers*

hydrostatics
celluloid, nonlinear viscoelastic deform. under superimposed hydrostatic pressure 79−34116
cellulose nitrate, nonlinear viscoelastic deform., hydrostatic press. and third invariant of deviatoric stress tensor 80−93587
centrifugal buoyancy forces, particle in rotating fluid 78−12487
damping, internal, in 2 and 3 dimens. continua 78−13970
fatigue, hydrostatic stress-sensitive relationship for biaxial stress conditions 80−74805
ferrofluid, stress theory appl. 78−6116
ferrofluids, Landau and Lifshitz hydrostatic press., thought expts. 80−59111
fluids in steep field gradients and near critical points, hydrostatic density distrib. 77−76523
high-pressure neurological syndrome, comparative physiology, compression rate effects 79−88070
liquid-filled multipole concentric cylinders, stress induced radial press. 77−80565
nematic liquid crystals, universal solns. 79−69007
nematic nonpolar liquid crystals, hydrostatics, universal soln. 78−83722
phospholipid vesicles, hydrostatic press. 80−56000
photoelasticity for stress analysis under hydrostatic press. up to 700 MPa 78−18260
planetary figures, hydrostatic equilib. eqn. numerical soln. 79−62773
pressure effects on Cu corrosion in seawater 79−52420
underwater sound pressure unit, 0.01 to 1 Hz, USSR state standard 78−38160
weighing, treatment of suspension wire *(Japanese)* 79−82006
weighing in immiscible liquids, for porosity determ. of coatings 80−66714

hydrothermal crystal growth *see crystal growth from solution*

hydroxonium ion
aqueous acid solns., IR spectra 77−30868
complexes, produced by collisional dissoc. method, mass spectrometric study, dissoc. energies determ. 80−95707
D-region, positive ion chemical scheme for $H^+.(H_2O)_n$ abundance profile 79−40007
excited states, ab initio CI calcs. 77−30796
inversion barrier, high-order replacements inclusion in CI calc. 80−63504
water cluster ions in mesopause region during winter anomaly, temp. and NO density vars. effect 79−21087
β-Al_2O_3-H_3O^+, ESR of paramag. defects in cond. planes 80−29617
β-Al_2O_3-H_3O^+ protonic cond., struct. investig. 79−19213
$H^+(H_2O)_3$, $H^+(H_2O)_4$, $H^+(H_2O)_5$ in stratosphere, abundance meas. 78−88877
$H(H_2O)_n^+$, macromol. clusters, detect. by SIMS 79−39239
H_3O^+, rot. excitation by slow electrons, calc. 78−5360
$H_3O^+ + NH_3$, bimolecular reactions, product. distrib., rate consts. 78−11513
$H_3O^+(H_2O)_n$ formation in vacuum spark, mass spectrometer expt. 79−32844
$H_3O^+(H_2O)_n$, H^+ motion energetics, ab initio calcs. 78−25413
$H_3O^+(H_2O)_n$, IR spectra, OH stretching vibrs. 78−25529
$H_3O^+(H_2O)_n$ in D-region, implications of laboratory determs. of NO^+ reaction rates 77−53308
$H_3O^+(H_2O)_n$, ion clustering, diffusion, flowing afterglow obs. 77−12799
$H_3O^+(H_2O)_n$, photodissoc. meas. and calc., rel. to atmospheric stability 79−86017

hydroxonium ion continued
$H_3O^+.H_2O$, cluster ion form. mech., rate coeffs. 78−25764
$H_3O^+.H_2O$, mobility in He, flow drift tube obs. 78−34257
$H_3O^+.(H_2O)_n$, electron recomb., electron temp. depend. 78−82854
$H_3O.^+2H_2O$, in 2,5-dichlorobenzenesulphonic acid trihydrate, neutron diffr. obs. 78−58855
$NH_4H_2PO_4:H_3O^+$, inclusions in cryst. growth, pH effect 79−55682

hydroxyl group *see oxygen compounds*

hygiene
see also medicine
industrial atmosphere submicroscopic asbestos fibre evaluation 79−74585
industrial hygiene training at Quinnipiac College, USA 79−84879

hygrometers
see also humidity measurement
air humidity meas. above 100°C 78−226
atmospheric humidity meas. with standard hygrometer *(German)* 78−16194
automatic IR hygrometer, humidity determ. by water vapour absorpt. 78−12707
capacitive, for measuring grain moisture content, analysis of errors 79−75538
capacitor type, for gaseous flow, design and operational principle *(French)* 77−5853
ceramic humidity sensitive resistor device characts. and appls. *(Japanese)* 77−71332
development in Soviet Union 80−22370
dew point type design 77−74410
dew-point hygrometer, fast-response, calibration *(Russian)* 77−13761
dew-point hygrometers, automatic, condensate phase state determ. 78−8408
digital ventilated psychrometer 79−2777
electrical hygrometer with thin layer of LiF *(Czech)* 80−231
electrochemical hygrometer, using AC bridge cct. *(Spanish)* 78−32254
electronic, low inertia, no resistance to gas flow diagnostics appls. *(French)* 77−70564
elongation hygrometer, relative performance of squid skin, egg-shell membrane, bamboo film as hygroscopic body *(Japanese)* 78−57968
fixed hygrometer probe for very dry gases *(French)* 79−54145
frost-point, for horizontal soundings of lower stratosphere 79−21048
gravimetric two-balance hygrometer, for atmospheric humidity direct meas. 77−73866
heated electrolytic sensor 80−109262
HF, modulated and unmodulated schemes, sensitivity analysis *(Russian)* 77−67444
HF capacitive, extension of range of applicability 79−75537
humidity and dew point, standards and calibration 79−49240
humidity sensor, capacitive, Panahume *(Japanese)* 80−105658
hygrometry testing scheme for the Soviet countries 80−57312
hygroscopic materials for humidity sensors, extension characts. 78−41320
injecting water dew point hygrometer, atm. press. type *(Japanese)* 77−33997
IR, meas. of attenuation by atm. H_2O vapour 79−34943
IR fluctuation hygrometer, design, calibration, field trial results 78−77368
Meteorological Office Mk3, frost point meas. systematic error 78−73538
ocean surface meteorological buoy and aircraft VHF link 80−46298
psychrometer, portable differential system construction and operation 80−105072
psychrometer coeff. of wet bulb thermometers used in Met. Office large thermometer screen 77−70879
psychrometrics and industrial processes 78−41321
shipboard meteorological data system 80−46299
sorption-gravimetric, standard, description 77−87770
standard, precision salt, metrological support suite 79−17430
thermocuple psychrometer with rapid auto. scanning and 100 channel digital readout 77−10033
UHF humidity gauges, increasing sensitivity by using travelling wave resonator 80−17950
UV fluorescence hygrometer, stratospheric M_2O vapour meas. *(French)* 78−65401
variable-path Lyman α hygrometer, operating characts. 77−33194
water injection dew point hygrometer, with U-tube water manometer *(Japanese)* 80−8998
wet bulb thermometer theory and comparison with expt. results *(Dutch)* 77−65039
yaRV-2 compact automatic nuclear resonance hygrometer 80−105657
$Li_5Al(Ga)O_4$, ionic cond. depend. on moisture, potential humidity sensors 79−65248
LiCl heated electrical, modified instrum. 80−95104
$LiNbO_3$ sensor for elec. hygrometer *(Japanese)* 80−95103
SiC thin-film thermistors with high thermal response *(Japanese)* 80−105629

hyperfine field interactions (condensed matter)
see also crystal hyperfine field interactions; nuclear screening
4-amino-2,2,6,6-tetramethylpiperidine-N-oxyl and deuterated derivatives, mag. resonance study 80−63686
amorphous materials, Mossbauer spectra anal. of hyperfine interactions 77−20762
ESR spectra, exchange effects and lineshape *(French)* 79−4717
ferromagnet, amorphous and crystalline, evaluation of complex Mossbauer spectra 78−60370
glass:Mn^{2+}, EPR, low-field hyperfine struct. 78−95513
liquid solution, relaxation studies in magnetic resonance spectroscopy 79−73841
Lorentzian lineshapes and isotropic distrib. of molecules, analytical expressions derived for powder samples 80−60401
metallic glass, short-range order, hyperfine field distrib. determ. by Mossbauer spectroscopy 80−39962
metallic glasses, Mossbauer spectra, hyperfine field distrib. determ. 80−39965
Ni-Pd-P, metallic glass, electronic structure, pulsed NMR study 80−75869
nitroxide radical, long range Y-P hyperfine coupling, ESR spectra obs. 80−75858
nitroxide spin probes, unresolved hyperfine broadening convection in EPR, linewidth and Heisenberg spin exchange freq. determ. 80−71180
transition metal based amorphous mag. alloys, elec. field gradient 78−39475

hyperfine field interactions continued
As_2S_3, vitreous local struct., elec. field gradient tensor asymmetry obs. 79−73847
As_2Se_3, and As_4Se_5Ge glasses, struct. changes, Mn^{2+} EPR expts. 78−79534
$As_{25}Te_{75}$, and $As_{45}Te_{55}$, vitreous, local struct., elec. field gradient tensor asymmetry obs. 79−73847
$As_4Te_5Ge(Si)$ glass, struct. changes, Mn^{2+} EPR expts. 78−79534
$As_2Te_{3-x}Se_x$, amorphous and cryst. phases, ^{125}Te Mossbauer expts. 78−88232
$BaO-Fe_2O_3-B_2O_3$ glass, Mossbauer study of struct. and mag. props. 79−47369
Co complex, tris(ethylenediamine)cobalt(III) ion in complex anion solns., ^{59}Co NMR relax. obs. 80−25234
Co_3B, glassy and cryst., hyperfine field distrib., ^{59}Co spin echo spectra 80−80635
$CoO-Al_2O_3-SiO_2$ glass, mag. ordering, Mossbauer exam. 77−24764
$Co_{80}P_{20}$, amorphous, sign and magnitude of ^{60}Co hyperfine field, nucl. orientation 78−48100
Cs-Au liq. alloy, formation of localised electronic states, NMR obs. 80−93201
Cu(II)-DL-proline complex, ESR, magnetic susceptibility and optical absorption 80−93167
DyIG, non-cryst., Mossbauer and magnetisation studies 80−44979
EuIG, non-cryst., Mossbauer and magnetisation studies 80−44979
Fe-B, amorphous paramag. alloys, hyperfine field distrib., Mossbauer study 80−39958
Fe-B (15-25 at.%) glass, quasicryst. struct. Mossbauer expts. 79−4255
Fe-B metallic glasses, short-range orders 79−65002
Fe-B metallic glasses, short range order, meas. and calc. hyperfine fields at Fe sites 79−77528
Fe-B(Si) amorphous alloys, Mossbauer spectra, struct. 80−15840
Fe-Ni-P-B, amorphous paramag. alloys, hyperfine field distrib., Mossbauer study 80−39958
Fe-Ni-Si-B, amorphous paramag. alloys, hyperfine field distrib., Mossbauer study 80−39958
Fe-P-C amorphous alloys, Mossbauer spectra, struct. 80−15840
$Fe_{1-x}B_x$, amorphous, hyperfine fields and local mag. moments, Mossbauer study 80−75895
$Fe_{80}B_{20}$, amorphous, elec. and mag. hyperfine field distribs., Mossbauer study 80−39964
$Fe_{80}B_{20}$, amorphous ferromag., temp. depend. of hyperfine field distrib. 78−43756
$Fe_{80}B_{20}$, amorphous ferromag., hyperfine field distrib., Mossbauer effect 78−60371
$Fe_{80}B_{20}$, amorphous struct., Mossbauer spectroscopy investigation 80−84677
$Fe_{78}B_{12}Si_{10}$, amorphous, continuous versus discrete hyperfine field distrib., Mossbauer spectra 79−33583
$Fe_{78}B_{12}Si_{10}$, amorphous, Mossbauer study of hyperfine interaction and mag. anisotropy 80−40027
$(Fe_{0.5}Co_{0.5})_{1-x}B_x$, amorphous, hyperfine fields and local mag. moments, Mossbauer study 80−75895
$(Fe_{100-x}Co_x)_{79}P_{13}B_8$, amorphous, hyperfine field distrib., ^{59}Co NMR spin-echo meas. 80−34818
FeF_3, amorphous, struct. and mag. props., computer model 80−96446
$Fe(H_2O_6)^{3+}$ ion, amorphous frozen soln., Mossbauer study, hyperfine struct. 80−80644
$(Fe_xMn_{1-x})_{75}P_{16}B_6Al_3$, amorphous, mag. ordering temp., hyperfine field distrib., elec. resist. 80−34633
$Fe_{78}Mo_2B_{20}$, amorphous ferromag., $T^{3/2}$ depend. of hyperfine field 78−39474
$(Fe_{1-x}Ni_x)_{75}B_{25}$, amorphous and cryst., short range order, Mossbauer study 80−39961
$Fe_{40}Ni_{40}B_{20}$, amorphous, hyperfine field distrib., Mossbauer effect meas. 79−4755
$Fe_{40}Ni_{40}B_{20}$, amorphous, hyperfine field distrib., Mossbauer study 79−28657
$Fe_{40}Ni_{40}B_{20}$, amorphous, RF annealing effects 80−108037
$(Fe_xNi_{1-x})_{80}B_{20}$, amorphous, Mossbauer spectra, mag. props. 80−15843
$(Fe_{1-y}Ni_y)_{0.8}B_{0.2-x}P_x$, amorphous, hyperfine fields and local mag. moments, Mossbauer study 80−75895
$Fe_{40}Ni_{40}P_{14}B_6$, amorphous, continuous versus discrete hyperfine field distrib., Mossbauer spectra 79−33583
$Fe_{40}Ni_{40}P_{14}B_6$, glassy, mag. props. and hyperfine interactions, Mossbauer obs., 4.2-1000K 78−10812
$(Fe_xNi_{1-x})_{80}P_{14}B_6$, amorphous, Mossbauer determ. 78−6617
$Fe_2O_3-BaO-B_2O_3$ glass, Mossbauer spectra, ^{57}Fe hyperfine interactions 80−39969
$Fe_{80}P_{20}$, binary amorphous ferromagnet, Mossbauer study 80−34829
$Fe_{75}P_{15}C_{10}$, ferromagnetic, amorphous, spin echo NMR of ^{31}P 78−2770
FeSb solid solution, supersaturated, mag. hyperfine field, Mossbauer study 80−44961
$Fe_{79.5}Si_{1.5}B_{19}$, evaluation of hyperfine parameter distribs. from overlapped Mossbauer spectra at room temp. 79−99804
Fe_xSn_{1-x} amorphous alloy films, magnetisation meas. and Mossbauer spectra 78−95489
Gd-Ni, amorphous, Mossbauer spectra 80−25262
Ge, amorphous, EPR 78−88167
$La_{75}Ga_{25}$, amorphous, local symmetry around glass-former sites, elec. quadrupole effects, NMR 80−80618
$La_{80-x}Pr_xAu_{20}$, amorphous, mag. and supercond. props. 80−75713
$Mo_{70}B_{30}$, amorphous, local symmetry around glass-former sites, elec. quadrupole effects, NMR 80−80618
$Mo_{48}Ru_{32}B_{20}$, amorphous, local symmetry around glass-former sites, elec. quadrupole effects, NMR 80−80618
Na-Fe fluorophosphate glass, EPR and Mossbauer resonance study 80−15838
$Na_2O-Li_2O-B_2O_3:Fe_2O_3$, Mossbauer spectra, isomer shift and quadrupole splitting *(Korean)* 79−51889
$Na_2O-SiO_2-CaO:Fe_2O_3$, Mossbauer spectra, isomer shift and quadrupole splitting *(Korean)* 79−51889
$Na_2O.3B_2O_3.xFe_2O_3$, borate glass, Fe^{3+} spin state and distrib. meas. 80−39966
$(NbCl_nBr_{6-n})^-$ complexes in acetonitrile soln., ^{93}Nb spin relax. and mag. shielding 80−44944
Ni-Pt-P, metallic glass, electronic structure, pulsed NMR study 80−75869
$Ni_{78}P_{14}B_8$, amorphous, local symmetry around glass-former sites, elec. quadrupole effects, NMR 80−80618
$NpBa_6Zr_{12}F_x$ glass, Mossbauer spectrum 80−11304

hyperfine field interactions continued
^{17}O, naturally abundant, nuclear quadrupole resonance spectrum for fine struct. detection 80−75881
$PbO\text{-}2B_2O_3\text{-}Fe_2O_3$ glass, Mossbauer study, struct., crystallite formation, broadened quadrupole doublet 78−59761
Sb-containing glasses, ^{121}Sb Mossbauer spectra 77−20764
Si, amorphous, EPR expts. 78−88167
TlBr melts, Tl doped and pure, stoichiometric, nucl. spin relax. 80−25236
TlCl, melts, stoichiometric, nucl. spin relax. 80−25236
WO_3, single cryst. and amorphous film, ESR of defects 78−10770
YFe_2, amorphous, mag. order, cluster phenomena, hyperfine struct. 77−16079
YIG, amorphous, ionic glass, hard-sphere random-packing model 80−24369
hyperfine field interactions in crystals *see crystal hyperfine field interactions*
hyperfine structure, atomic *see atomic hyperfine structure*
hyperfine structure, molecular *see molecular hyperfine structure*
hyperfragments *see hypernuclei*
hypernuclei
$^{A}Z(K^-,\pi^-)_{\Lambda}{}^{A}Z$, strangeness exchange reaction ang. distribs., Glauber theory 79−75892
Σ, search for dibaryon states with s=−1, −2, review 79−22224
A=3-4 hypernuclei, binding energy anal., Λ-N pot., scatt. length and effective range 80−9256
charmed baryons, binding to single nucleon, finite nuclei, exam. 78−21511
conference on high energy physics and nuclear struct. Vancouver, Canada (Aug. 1979) 80−41936
conference on nuclear spectroscopy and structure, Alma Ata, USSR, (Mar. 78) 79−75809
elementary particle problems, in hypernuclear physics, review 80−47418
EM field inside the nucleus, Salam-Strathdee phase transitions, vanishing Cabibbo angle 78−37296
Friedel sum rule, hadron phys. meaning, nuclear matter density, binding energy 78−82305
ground state prod. and props., present status of experimental research, review 79−30799
hyperon-nucleon low energy interaction, two-channel separable pot. model, hypernuclei 80−47325
impure nuclear matter with Λ, binding energy, functional variational approach 80−22744
interdisciplinary viewpoint of theories and developments *(Czech)* 80−22749
inverse problem in hypernucleus theory 77−14058
light deformed hypernuclei, N=Z even even A≤40, added Λ-hyperon effects 80−27588
meson-nuclear physics, International Topical Conf. 77−6436
mesonic hypernuclei from K^- meson interaction in emulsion nuclei 78−13158
nonmesonic decays of light nuclei with Z=3 to 7 77−22922
nuclear bound states of k−, $\bar{p}$ and Σ 80−13399
nuclear Dirac phenomenology and the Λ-nucleus potential, anomalous mag. moment 80−37344
nuclear emulsion information on ΛN and ΛΛ interactions 77−22923
orbital excitation of the hyperon in hypernuclei 80−106001
P-shell hypernuclei, formation, γ-radiation, and spin values, shell model 79−22223
p-shell hypernuclei, shell model anal. of Λ binding energies 78−78300
p-shell hypernuclei with effective Λ-nucleon potentials, binding energy and well depth 79−36184
production in relativistic ion-nuclei reactions *(Russian)* 79−45298
quasifree formation of and supersymmetry in light hypernuclei 77−14057
recoilless Λ prod. in (K^-,π^-) on light nuclei, hypernuclear spectroscopy 78−50116
review of general properties and experimental methods, book contribs. 79−22161
reviews of forces and nuclear props. 77−14055
stable charmed hyperfragments containing charmed baryon+nucleons, binding energies, lifetimes 78−89815
strangeness analogue states 77−14054
strangeness exchange reactions and hypernuclear spectroscopy 79−67699
strangeness exchange reactions producing hypernuclei, shell model calcs. 78−17130
symmetry classification for excited states, appl. to Be isotopes *(Chinese)* 78−25144
unitary analogue states, (K,K) and $(K^-\pi^-)$ excitation 78−17131
$(\bar{K},\bar{K})$, isobar doorway model, optical pot., Λ-nuclear matter binding energy 80−106079
$(K^-,\bar{\pi}^-)$, 390 MeV/c, formation of hypernuclear excited states in ^{12}C, ^{16}O, ^{27}Al 78−74402
(K^-,π^-), hypernuclei generation, γ-spectroscopy and lifetimes 79−75890
(K^-,π^-), kaons at rest, $^{A}Z_{\Lambda}$, hypernuclear γ-emitters prod. rates 78−46108
(K^-,π^-), strangeness exchange reactions, CERN 79−85561
(K^-,π^-) reactions, 900 MeV/c, sum rule for hypernuclear formation, distorted wave impulse approx. 78−70572
K^-+photonuclear emulsion nuclei, hypernuclei in hammer-like events 78−13162
(Λ,X), Λ as a nuclear probe and hypernuclei 79−85397
Λ(1405) dynamic effect in nuclear matter, implications for kaonic atoms 77−14056
Λ(1405) role in description of kaonic atoms 77−3495
Λ binding energy in nuclear matter with Nijmegen baryon-baryon interaction 80−13400
Λ binding to nuclear matter in Fermi hypernetted chain approx. 79−85396
Λ nucleus, 40≥A≥12, strangeness exchange reactions, anal. 77−292
Λ s-shell hypernuclei, general props. and developments in experimental methods, review 79−22224
Λ- and Σ-hypernuclei, γ-transitions, spin-orbit components of single particle pots. 80−42574
Λ- and Σ-hypernuclei and hyperon-nucleus interactions, review 80−42575
Λ-escape width of excited hypernuclear states 77−61371
Λ-hypernuclei, QCD and spin-orbit splitting, spin-orbit pots. 79−85398
Λ-N interaction and hypernuclei spectroscopy, book contrib. 79−21889
Λ-N two term separable pots., comparison 78−66239
ΛN, Λ well depth with class of equiv. pots., nuclear matter appl. 77−26605
hypernuclei continued
ΛN, reaction-matrix calc. of Λ binding energy in nuclear matter 79−36185
ΛN effective force, binding energy, excitation spectra, self consistent calcs. 77−6283
ΛN effective potentials on p-shell hypernuclei 79−85394
ΛN interaction and spin-orbit coupling 77−71580
ΛN weakly spin depend. pot. in p-shell hypernuclei 79−85395
ΛNN correlations and Λ binding in nuclear matter 80−106000
NN tensor force effect on Λ separation energy 80−86845
Σ hypernuclei, study in (K^-,π) reactions 79−85392
Σ to Λ conversion widths *(Russian)* 80−106003
Σ-hypernuclear state width, model estimation 80−57719
Σ-hypernuclei, QCD and spin-orbit splitting, spin-orbit pots. 79−85398
Σ atoms, meas. of strong interaction effects 78−42251
Σ^0 life time from Λ nucleus→Σ^0 nucleus, Coulomb excitation method *(Russian)* 78−46114
ΣN effective complex pot. from Σ-atoms and scatt. lengths 80−57717
Ξ cascade, decay into two ordinary hypernuclei, $^{13}C\rightarrow{}^{8}Be+{}^{5}He+Q$ by $\Xi^- p\rightarrow {}^{0}\Lambda^{0}$ 80−52603
^{9}B, new decay mode, 1.8 GeV/c K^- nucl. emulsion expt. 79−36186
$^{11}B_{\Lambda}\rightarrow\pi^- + {}^{11}C^*$, produced in p+emulsion nuclei reacts. *(Russian)* 80−9297
$^{9}Be_{\Lambda}$, hypernuclear excited states in 1p shell *(Chinese)* 78−82306
$^{9}Be_{\Lambda}$, in $^{9}Be(K^-,\pi^-)$ strangeness exchange reaction, ang. distribs. PWIA anal. *(Chinese)* 79−80956
$^{9}Be(K^-,\Pi^-)$, 720 MeV/c, Sigma hypernuclei prod., missing mass spectrum 80−57721
$^{9}Be(K^-,\pi)$, narrow Σ-hypernuclear states, estimated widths, quantum number assignments 80−42576
$^{10}Be_{\Lambda\Lambda}$, four body dynamical eqns. in Faddeev-Yakubovsky formalism 80−47419
$_{\Lambda}{}^{9}Be$, binding energy calcs., clustering 79−9501
$_{\Lambda}{}^{9}Be$, excited states and spectra, continuum effects calcs. 80−57720
$_{\Lambda}{}^{9}Be$, Λ separation energy, hyperspherical harmonics method 79−93547
$_{\Lambda}{}^{12}B$ hypernucleus, spin determ. from $_{\Lambda}{}^{12}B\rightarrow{}^{12}C^*+\pi^-$ 80−27589
C_{Λ}, A=12,13, hypernuclear excited states in 1p shell *(Chinese)* 78−82306
^{12}C, coupled channel anal. of Λ′(1405) in kaonic atoms 78−540
$^{12}C_{\Lambda}\rightarrow\pi^- + {}^{12}N$, produced in p+emulsion nuclei reacts. *(Russian)* 80−9297
$^{12}C(K^-,\pi^-)_{\Lambda}{}^{12}C^*$, 800 MeV/c, ang. distribs. from DWIA calcs. 80−32225
$^{12}C(K^-,\pi)$, narrow Σ-hypernuclear states, estimated widths, quantum number assignments 80−42576
$^{12}C(k^-,\pi^-){}^{12}_{\Lambda}C$, strangeness exchange reaction, ground state ang. distrib., 11 MeV excitation 79−85560
$^{12}C(k^-,\pi^-){}^{12}_{\Lambda}C$, Λ-nuclear spin-orbit coupling, ΛN effective interaction 79−85562
^{13}C cascade hypernucleus, decay into two ordinary hypernuclei, $^{13}C\rightarrow{}^{8}Be+{}^{5}He+Q$ by $\Xi^- p\rightarrow\Lambda^0\Lambda^0$ 80−52603
$^{40}Ca_{\Lambda}$, Λ particle full set of nuclear shell orbitals 79−63623
$^{40}Ca(K^-,\pi^-)\,{}^{40}_{\Lambda}Ca$, possible strange giant reson. 77−82969
$^{40}_{\Lambda}Ca(k^-,\pi^-)$, energy excitation spectra, nuclear shell orbitals for Λ 79−85565
$_{\Lambda}{}^{12}C$ hypernucleus detection in p+emulsion nucleus, 250 GeV, Λ binding energy *(Russian)* 78−89816
^{12}C low lying excited states, ang. distribs. from $^{12}C(K^-,\pi^-)$ 80−32226
$^{4}_{\Lambda}H$, binding energy, role of spin forces in Λ-N interactions *(Russian)* 78−54718
$^{3}H_{\Lambda}$, and contrib. of spin forces to Λ-N interaction *(Russian)* 77−79319
$^{3}H_{\Lambda}$, binding energy, Fadeev equation in coord. space, Lambda-nucleon potential 80−63120
$^{3}H_{\Lambda}$, charge symm. breaking, Λ separation energy in hypertriton 78−17132
$^{3}H_{\Lambda}$, charge symm. breaking considerations for hypertriton 78−17133
$^{3}H_{\Lambda}$, decay rates and two-body $(\pi^-{}^{3}He)$ decay mode branching ratio 79−63620
$^{3}H_{\Lambda}$, short range repulsion, separation energy, K-harmonics calcs. 80−86846
$^{4}_{\Lambda}H\rightarrow\alpha\pi^-\gamma$, evidence for γ transitions 79−85393
$_{\Lambda}{}^{3}H$ binding energy using phenomenological ΛN pots. 80−9254
$_{\Lambda}{}^{3}H$, binding energy via rank-2, two-body pots. 77−26604
$_{\Lambda}{}^{3}H$, ground state energy, hyperspherical harmonics method 79−93547
$_{\Lambda}{}^{4}H$, γ-ray spectra of stopped K^- in $^{6,7}Li$ 79−63621
^{4}He, coupled channel anal. of Λ′(1405) in kaonic atoms 78−540
$^{4}He_{\Lambda}$-$^{4}H_{\Lambda}$ binding energy difference, exact 4-body calc. 79−63622
$^{5}He_{\Lambda}$, Λ-N pot. Majorana component on B_{Λ} value, overbinding 80−99144
$^{6}He_{\Lambda\Lambda}$, ΛΛα binding Feddeev's method 77−38238
$^{6}He_{\Lambda\Lambda}$, short range repulsion, separation energy, K-harmonics calcs. 80−86846
$^{6}He_{\Lambda\Lambda}$ hyperfragment, αΛΛ model, Faddeev formalism, two-body local potentials 77−18467
$^{4}_{\Lambda}He\rightarrow\alpha\pi^{\circ}\gamma$, evidence for γ transitions 79−85393
$_{\Lambda}{}^{4}He$, γ-ray spectra of stopped K^- in $^{6,7}Li$ 79−63621
$_{\Lambda}{}^{4}He$-$_{\Lambda}{}^{4}H$ binding energy difference, particle mixing and charge asymmetric ΛN forces 79−75891
$_{\Lambda}{}^{4}He$-$_{\Lambda}{}^{4}H$ binding energy difference, bound states, exact four body calc. 80−9255
$_{\Lambda}{}^{4}He$-$_{\Lambda}{}^{4}H$ bound states using 4-body eqns. and separable pots. 79−75893
$_{\Lambda}{}^{4}He$-$_{\Lambda}{}^{4}H$ mirror pair, separation energy difference, for particle mixing and charge asymmetry in ΛN 79−67596
$_{\Lambda}{}^{4}He$-$_{\Lambda}{}^{4}H$ separation energy difference, Coulomb energy contribution 79−491
$_{\Lambda}{}^{5}He$, Λ-particle induced excitation probability, ang. pot. functions method *(Russian)* 79−26389
$_{\Lambda}{}^{7}He_{g}$ prod. cross section calc., γ decay spectrum, shell model theory 78−62501
$^{6}Li_{\Lambda}$, supermultiplet struct. and decay props. of hypernuclear 1^+ resonances from (K^-,π^-) 80−78186
$^{6}Li(k^-,\pi^-){}^{6}_{\Lambda}Li$, strangeness analogue reson. 79−85566
$^{7}Li(K^-,\pi^-\gamma)$, hypernuclear γ-ray line 78−37377
$^{7}Li(K^-,\pi)$, narrow Σ-hypernuclear states, estimated widths, quantum number assignments 80−42576
$^{8}Li_{\Lambda}$ possible γ-transition from $^{9}Be(K^-,\pi^-p)$ 80−106002
$_{\Lambda}{}^{7}Li$, prod. cross section calc., γ decay spectrum, shell model theory 78−62501
$_{\Lambda}{}^{A}Li$, A=6,7, excited states and spectra, continuum effects calcs. 80−57720

hypernuclei continued
$_{\Lambda\Lambda}{}^{A}$Li, A=10, 11, double hypernuclei, prod. and decay from (K^-,X), emulsion 80−57718
Λ^9Be multiparameter variational calc., clustering in hypernuclei *(Russian)* 77−74791
^{16}O, coupled channel anal. of Λ'(1405) in kaonic atoms 78−540
^{16}O, spin orbit interactions of Λ hyperons, obs. in (K^-,π^-) 79−9628
$^{16}O_\Lambda$, Λ-N residual interactions, Λ spin-orbit splitting and effective mass 80−57722
$^{16}O(k^-,\pi^-)^{16}{}_\Lambda$O, Λ-nuclear spin-orbit coupling, ΛN effective interaction 79−85562
$^{19}O_\Lambda$, pairing correlation effects *(Chinese)* 80−47420
$^{32}S_\Lambda$, Λ particle full set of nuclear shell orbitals 79−63623
$^{32}{}_\Lambda S(k^-,\pi^-)$, energy excitation spectra, nuclear shell orbitals for Λ 79−85565

hyperon absorption
No entries

hyperon capture
see also hypernuclei
No entries

hyperon decay
$\Delta I=1/2$ dominated weak decays of strange hadrons, Weinberg-Salam scheme 80−27499
$\Delta S=1$ nonleptonic weak decays, $\Delta I=1/2$ rule, quark models and current algebra 80−47282
asymptotically nearly-free theories, hadronic weak decays anal. 77−65154
Cabbibo fit, generalised, appl. to quark mixing angs. in sequential Weinberg-Salam model 79−17655
charm changing radiative weak decays in AFS model 80−47285
constituent rearrangement model, nonleptonic hyperon decay 78−62357
extended PCAC hypothesis, soft-meson chiral symm. breaking, nonleptonic hyperon decays 78−21353
flavour changing weak radiative decays, short and long distance effects 80−73712
hadronic, reduction formula in light front formalism 78−12911
hadronic decay, absolute magnitude and EM hyperfine splittings 78−17016
lightlike chiral structure of hadrons, nonleptonic hyperon decays 78−74253
non leptonic hyperon decay amplitudes, calc. without arbitrary parameters 80−13300
non-leptonic decay in (8,8) model of broken chiral symmetry 79−36072
non-leptonic hyperon decays and the baryon spectrum, S- and P-waves, quark model description 79−36073
non-leptonic parity violating decays in SU(8) 77−26523
non-leptonic weak decays in SU(8) 77−49963
non-leptonic weak interactions, book contrib. 78−78163
nonleptonic, absolute magnitude determ. 77−30377
nonleptonic, implications for right handed current 77−67651
nonleptonic, octet enhancement, MIT bag model 77−10249
nonleptonic, renormalisable gauge scheme of weak interactions, asymptotically free theory of strong interactions *(Russian)* 77−46048
nonleptonic, SU(2)⊗U(1) theory of weak interactions, with spiral chromatic currents *(Russian)* 77−221
nonleptonic, SU(3)×U(1) symmetry, gauge theory 78−58153
nonleptonic, violation of $\Delta I=1/2$ rule and Melosh transformation 79−93377
nonleptonic decay, lightlike chiral struct. of hadrons 78−17014
nonleptonic decay, SU_3 symm., second class currents in effective Hamiltonian 77−41842
nonleptonic decay, sum rules for S-wave amplitudes 79−63476
nonleptonic decays, $\Delta I=^1/_2$ rule violation 79−45087
nonleptonic decays, Weinberg-Salam and harmonic oscillator quark model 80−102048
nonleptonic hyperon decay, octet dominance in nonrelativistic quark model 79−388
nonleptonic hyperon decays, CP violation, deviations from $\Delta I=^1/_2$ rule 78−70367
nonleptonic hyperon decays, final state interactions with inelastic effects, comments 80−99099
nonleptonic hyperon decays, QCD corrections 80−91087
nonleptonic hyperon decays and lightlike chiral struct. of hadrons 79−36074
nonleptonic processes, quark sea and $\Delta I=1/2$ rule 77−79255
polarised proton beam production in high energy hyperon decay 78−58517
pseudo-connected line diagrams, ordinary hyperon decay 78−45918
quark quartet model, non-leptonic decay anal. 78−12910
quark rearrangement model unified description 77−54104
quark-diquark model of nonleptonic decays 79−13120
radiative weak decays of uncharmed hyperons, sum rules, branching fractions and asymmetry parameters 80−410
S- and P-wave hyperon decay amplitudes, $\Delta I=^1/_2$ rule deviations, weak current-current interactions 80−9166
semileptonic decay, model with spectrum generating SU(3) symm. 77−38167
semileptonic decay anal., Λ' existence, ninth $I=0\ J^P=1/2^+$ baryon, asymptotic level realisation of SU(3) 77−18245
semileptonic SU(3) spectrum generation, Cabibbo angle 80−9119
SU(3), nonleptonic hyperon decays 79−97624
weak EM decays, 27th Hamiltonian component contribution 79−22101
weak radiative decays in SU(4) and SU(8) 77−87977
$C^+(2.26)$ search in 45 GeV/c neutron beam, C^+ hadronic and semileptonic decay *(Russian)* 79−22145
$\Delta^+\rightarrow p+\gamma$, radiative decay in the MIT bag model 78−66110
$k^-p\rightarrow\Lambda\pi^+\pi^-$, partial wave anal. in Λ(1520) region, Λ partial decay widths *(Russian)* 80−32131
$K^-p\rightarrow\Sigma^+\pi^-$, 460 MeV/c, Σ^+ decay and polarisation props. determ. 77−30432
Λ, polarised, β decay, ang. correl. parameters meas. 78−25044
Λ, quasi-stable, quantum struct. *(French)* 77−57533
Λ(1520)$\rightarrow\Lambda$(1115)+γ, Melosh transform, $[70.1^-]\rightarrow[56.0^+]+\gamma$ *(Russian)* 78−66116
Λ hyperon polarisation, meas. by hybrid Monte Carlo tech. 80−99431
Λ lifetime meas., decay products identified 77−71513
$\Lambda\rightarrow pe^-\bar{\nu}$, meas. of ang. correl. parameters 77−38166
$\Lambda^0\rightarrow pe^-\bar{\nu}$, absolute rate, $\Lambda(\Gamma^0\rightarrow pe^-\bar{\nu})/\Gamma(\Lambda^0\rightarrow p\pi^-)$ precise meas. 80−57593

hyperon decay continued
Λ^+ decay, four body semileptonic decay rates of charmed baryons 78−8665
$\Lambda_c{}^+\rightarrow K^-\Delta^{++}$, observation in pp at ISR energies 79−89150
$\Lambda_c{}^+\rightarrow K^-p\pi^+$ decay mode from pp 63 GeV 79−89204
$\Lambda_c{}^+\rightarrow\bar{K}^{*0}p$, forward K^- trigger, observation in pp at ISR energies 79−89150
$\Lambda_c{}^+$ lifetime, semileptonic branching fractions, nonspectator quark interactions 80−37260
$\Lambda_c{}^+\rightarrow\Lambda\pi(\bar{K}^0p)$, confirmation of $\Sigma_c{}^{++}$, Λ_c baryon and obs. of $\Lambda_c{}^{++}$ two body decay modes 79−75770
$\Lambda_c{}^+\rightarrow pK^0\pi^+\pi^-$, kaonic decay observation, prod. rates 79−26332
$\Lambda_c{}^+\rightarrow p\pi^+k^-$, lifetime of charged charm particles 79−67548
$\nu p\rightarrow\mu^-pk^-\pi^+\pi^+\pi^0$, $\Sigma_c{}^+$ prod. and decay 80−86710
Ω, quasi-stable, quantum struct. *(French)* 77−57533
$\Omega\rightarrow\Lambda K$, QCD and valence quark approx. 80−105893
Ω^- decay branching ratios, $\Delta I=1/2$ rule test 80−22605
Ω^- decays and right-handed currents 78−17015
Ω^- hyperon, spin and lifetime determ. 78−29333
$\Omega^-\rightarrow\Lambda K^-$, current algebra calc. with phenomenological modification of nonleptonic decay amplitude 77−67650
$\Omega^-\rightarrow\Lambda K^-$, Ω^- lifetime, spin from $K^-p\rightarrow\Omega^-+X$, 8.25 GeV/c 78−93877
$\Omega^-\rightarrow\Lambda K^-$, Ω^- lifetime meas. 80−9167
Ω^- nonleptonic decay branching ratios from Weinberg-Salam and MIT bag models 80−37261
Ω^- production in 4.2 GeV/c K^-p reactions, lifetime, mass, decay asymm. parameter 79−3044
$\Omega^-\rightarrow\Theta e(\mu)\bar{\nu}$ or $\Theta^*e(\mu)\bar{\nu}$, branching ratios and lepton energy spectra 80−73701
$\Omega^-\rightarrow\Xi^0\pi^-$, $\Xi^-\pi^0$, or Λ^0k^-, nonleptonic decay rates, $\Delta I=^1/_2$ contrib. 78−62399
$\Omega^-\rightarrow\Xi^*\pi(\Xi^0l^-\nu_l)$, nonleptonic hyperon decays, QCD description, PCAC anal. 80−95269
pp, ISR energies, p fragmentation, D^+ prod. from Λ_c* and Λ_b decay 80−102080
Σ, quasi-stable, quantum struct. *(French)* 77−57533
Σ(2030)$\rightarrow\Sigma\pi$, branching ratio calc. 78−41583
$\Sigma^-\rightarrow\Lambda K$, QCD and valence quark approx. 80−105893
$\Sigma^-\rightarrow\Lambda e^-\nu$, branching ratio meas., Monte Carlo prediction 78−54631
$\Sigma^-\rightarrow\Lambda e^-\nu$, μ 80−42458
$\Sigma^-\rightarrow ne^-\bar{\nu}_e$, g_A/g_V ratio 77−26522
Σ^- production and decay props. in $K^-p\rightarrow\Sigma^-\pi^+$ at 430-493 MeV/c 78−29350
Σ^0 life time by Coulomb excitation method *(Russian)* 78−46114
Σ^0 lifetime measurement using Λ nucleus$\rightarrow\Sigma^0$ nucleus reaction 77−23111
$\Sigma^0\rightarrow\Lambda e^+e^-$, parity violating effects, standard and pure vector Weinberg Salam model 79−36075
$\Sigma^0\rightarrow\Lambda e^+e^-$, parity violation 78−25045
$\Sigma^0\rightarrow\lambda\gamma$, transition moment, SU(6) breaking and strange quark mass 77−18284
$\Sigma^0\rightarrow\Lambda\gamma$, weak effects, small P violating E1 component in M1 EM decay 79−89160
$\Sigma^+\rightarrow\Lambda e^\pm\nu$, isospin violating effects from nonvanishing quark mass difference 79−63385
$\Sigma^+\rightarrow p\gamma$, $1/2^-$ resonance poles to parity-violating amplitude, two-quark weak transitions 80−78062
$\Sigma^+\rightarrow p\gamma$, radiative weak decays of baryons as single-quark transitions 79−40776
$\Sigma^+\rightarrow p\gamma$, sum rules, branching fractions and asymmetry parameters 80−410
$\Sigma^+\rightarrow p\mu e$, flavour changing neutral current search 80−105836
$\Sigma^\pm$, lifetimes and longitudinal accel. 80−86709
$\Sigma^\pm$ lifetimes, decay asymmetry and nonleptonic decay branching ratio, $|\Delta I|=1/2$ rule 80−78061
$\Sigma^\pm\rightarrow\Lambda e\nu$, transverse polarisation anal. 78−45919
$\Sigma_c{}^+$, mass and mean life from high energy cosmic ray data *(Chinese)* 80−102045
$\Sigma_c{}^+$, production and decay obs. 80−105894
Ξ^-, quasi-stable, quantum struct. *(French)* 77−57533
$\Xi^-\rightarrow\Lambda e^-\nu$, μ 80−42458
$\Xi^-\rightarrow\Lambda e^-\nu$ branching ratio meas., Monte Carlo prediction 78−54631
$\Xi^-\rightarrow\Lambda\pi^-$, asymmetry parameter 80−42457
$\Xi^-\rightarrow\Sigma^-\gamma$, decay rate, sum rules, branching fractions and asymmetry parameters 80−410
Ξ^0 lifetime meas., decay products identified 77−71513
$\Xi^0\rightarrow\Lambda^0\pi^0,\Lambda^0$ polarisation meas. 77−30458
$\Xi^0\rightarrow\Lambda\pi^0$, meas. of Λ helicity 78−93878
$Z^-\rightarrow\Sigma^-\gamma$, radiative weak decays of baryons as single-quark transitions 79−40776
$^3H_\Lambda\rightarrow\pi^-{}^3$He branching ratio calc. 79−63620
$\Upsilon\rightarrow 3g$, angular patterns and front-back moments, QCD 80−73702

hyperon detection and measurement
No entries

hyperon-deuteron interactions
see also hyperon-deuteron scattering
No entries

hyperon-deuteron scattering
see also hyperon-deuteron interactions
No entries

hyperon effects
No entries

hyperon interactions *see hyperon-nucleon interactions; hyperon-nucleus reactions; kaon-hyperon interactions; lepton-hadron interactions; photon-hadron interactions; pion-hyperon interactions*

hyperon magnetic moment
broken SU(3) hyperon anomalous magnetic moment sum rules, SU(3) Λ-Λ' mixing explanation 77−18288
charmed hadrons, mag. and transition moments, radiative decay widths 79−71724
Gelfand pattern, charmed hadrons and magnetic moment 80−398
hadron mag. moments, colour mag. moments and transition M1-moments, quark mass parameter 79−97596
SU(3) subalgebras of SU(4), generalised U-spin charmed baryon magnetic moment 79−36078
SU(6) broken summetry model, baryon mag. moment values 79−49417
symmetry breaking mechanism and hyperon magnetic moments 79−63477
topped and bottomed hadrons, mag. moments in additive quark model 80−52478

hyperon magnetic moment continued
truthful hadrons, mag. moments, transition moment, using state vectors and quark additivity principles 79−71723
Λ^0, mag. moment meas. 79−6340
Λ^0 octet baryon mag. moment, MIT bag model 80−47290
$\Lambda_1{}^{/+}$, mag. moment from quark mass difference calcs. 80−37240
Σ^- mag. moment calc. from dispersion relations in t 78−82257
Σ^+ magnetic moment meas. from $K^-p\rightarrow\Sigma^+\pi^-$ 80−22614
Σ^+ magnetic moment meas. in HYBUC using $K^-p\rightarrow\Sigma^+\pi^-$ reaction 77−54119
Σ^+ octet baryon mag. moment, MIT bag model 80−47290
Ξ^0 magnetic moment meas. 80−416
Ξ^0 octet baryon mag. moment, MIT bag model 80−47290

hyperon mass
empirical formula for particles stable against strong decay 77−41833
$K^-d\rightarrow\Xi^-K^0p$, 1.45, 1.65 GeV/c, Ξ^-p invariant mass enhancement 80−57639
K^-p, 8.25 GeV/c, $\Xi^*(2370)$ prod., mass and width determ. 80−47327
Λ, charmed baryon mass in SU(1,4) dynamical group theory 80−62882
Λ, instanton effects on light quark spectroscopy, MIT bag model, hadron mass 78−62372
Λ, quasi-stable, quantum struct. *(French)* 77−57533
$\Lambda_c{}^+$, confirmation of existence from neutrino experiments 79−75770
Ω, quasi-stable, quantum struct. *(French)* 77−57533
Ω^- production in 4.2 GeV/c K^-p reactions, lifetime, mass, decay asymm. parameter 79−3044
Σ, charmed baryon mass in SU(1,4) dynamical group theory 80−62882
Σ, quasi-stable, quantum struct. *(French)* 77−57533
$\Sigma^{\pm}(1385)$, masses and widths from partial wave anal. of $K^-p\rightarrow\pi^+\Sigma^{\pm}(1385)$ 79−6348
$\Sigma_c{}^+$, mass and mean life from high energy cosmic ray data *(Chinese)* 80−102045
$\Sigma_c{}^{++}$, confirmation of existence from neutrino experiments 79−75770
Ξ, quasi-stable, quantum struct. *(French)* 77−57533
$\Delta(1236)$-N(939) mass difference from deep inelastic scatt. quark wave functions, hyperon masses 80−47289

hyperon-nucleon interactions
see also hyperon-nucleon scattering
conference on few body systems and nuclear forces, Graz, Austria (Aug. 1978) 79−67567
hadron interactions, effective radius quantum number depend., quark sum rules *(Russian)* 80−102062
high energy reactions, differential cross sections, inclusive hyperon resonance prod. 77−18331
low energy interaction, two-channel separable pot. model, hypernuclei 80−47325
one boson exchange pot. approach, multichannel Schrodinger eqn. soln. 77−57556
one-boson-exchange-potential model of baryon-baryon scatt., 80−13295
p-shell hypernuclei, shell model anal. of Λ binding energies 78−78300
ΔN, investigation of ΔN interaction in the deuteron 79−67597
ΛN, hypernuclei studies in nuclear emulsions 77−22923
ΛN, particle mixing and charge asymmetry, ${}_{\Lambda}{}^4He$-${}_{\Lambda}{}^4H$ mirror pair separation energy difference anal. 79−67596
ΛN distrib. function, Λ-binding to nuclear matter, Fermi hypernetted chain approx. 80−78131
$\Lambda N\rightarrow\Sigma^0N$ within nucleus Σ^0 life time, Coulomb excitation method *(Russian)* 78−46114
Λp interactions in range 1-10 GeV/c 77−79278
$\Lambda p\rightarrow\Lambda p$, high energy collisions, EM-hadronic interference, spin depend. phenomena 79−422
Σ^- hyperonic atom, nuclear capture rate calcs. using $\Sigma^-p\rightarrow\Gamma n$ amplitude 78−62962
ΣN effective complex pot. from Σ-atoms and scatt. lengths 80−57717
$\Sigma p\rightarrow\Lambda X$, particle exchanges, coupling consts. *(Russian)* 77−50035
Ξ^0p interactions in range 1-10 GeV/c 77−79278
${}^3H_{\Lambda}$, binding energy, Fadeev equation in coord. space, Lambda-nucleon potential 80−63120

hyperon-nucleon scattering
see also hyperon-nucleon interactions
antihyperon-nucleon scatt., total cross section 77−82784
half off-shell t-matrix elements for class of equivalent pots., ΛN scatt. 77−2562
quark model with factorizability assumption, differential cross section for elastic scat t. 78−471
slope parameter, quark model anal. 79−9399
spin dependent EM hadronic interference, pn and Λp elastic scatt. amplitudes 78−12923
total cross section, two-component pomeron 77−82784
Λ well depth with class of equiv. pots., nuclear matter appl. 77−26605
Λ+p elastic scatt., Λ polarisation for momenta 60 to 380 GeV/c 78−37234
Σ^-N scattering amplitudes and Σ^- atoms 79−93452

hyperon-nucleus reactions
for inelastic hyperon-nucleus scattering, see "hyperon-nucleus scattering"
see also hyperon capture; hyperon-nucleon interactions
180-1600 MeV 79−6538
CERN School of Physics, Austerlitz-Zeist, Holland (June 1978) 79−30857
fast particle production on nuclei in quark model *(Russian)* 79−6612
hadron+nucleus cross-section, energy depend., multiplicity, scaling violation model *(Russian)* 79−22350
hadron+nucleus high energy collisions modified cascade model, multiplicities energy depend. 79−59064
hadron-nucleus collisions at high energies, simple collective effects model *(Russian)* 78−89809
hadron-nucleus high energy collisions, two-particle correlations, cluster cascade model 79−49615
hadron-nucleus interactions, existence of slowly moving sources, vel. depend. frictional sources 79−6690
hadron-nucleus reactions, multiple production, expt. results, review *(Russian)* 79−3118
high energy particle-nucleus interactions, discussion 79−30858
momentum space method for hadronic atoms including relativistic hadron-nucleus reactions 79−872
multi-chain model for high energy hadron nucleus collisions 79−59042
relativistic hadron+nucleus reactions, degree of collectivisation 79−40956
(Λ,X), Λ as a nuclear probe and hypernuclei 79−85397
Λ nucleus$\rightarrow\Sigma^0$ nucleus, Σ^0 lifetime meas. 77−23111

hyperon-nucleus reactions continued
Λ nucleus$\rightarrow\Sigma^0$ nucleus, Σ^0 life time, Coulomb excitation method *(Russian)* 78−46114
Λ- and Σ-hypernuclei and hyperon-nucleus interactions, review 80−42575
ΛN, reaction-matrix calc. of Λ binding energy in nuclear matter 79−36185
Σ^- hyperonic atom, nuclear capture rate calcs. using $\Sigma^-p\rightarrow\Gamma n$ amplitude 78−62962
Σ^-+nucleus, treatment used to analyse Σ^- atomic data 79−93452
Σ^-+nucleus low energy reactions in finite range potential model 79−85424

hyperon-nucleus scattering
see also hyperon-nucleon scattering
hadron-nucleus scatt., optical treatment in terms of scatt. amplitudes 78−89838
hadronic atoms, low-energy hadron-nucleus interaction theory 78−70977
inelastic scattering, evidence for giant resonances 79−17883
optical model, for total cross-section, 180-1600 MeV 79−6538
two-channel optical model of high energy hadron-nucleus collisions 79−36210

hyperon production
Λ and $\bar{\Lambda}$ polarisation 79−45122
hyperon-nucleon high energy reactions, differential cross sections, inclusive hyperon resonance prod. 77−18331
neutrino interactions confirmation of $\Sigma_c{}^{++}$, Λ_c baryon and obs. of $\Lambda_c{}^{++}$ two body decay modes 79−75770
nuclear matter with neutrinos retention, hyperon creation order 78−96390
$\bar{p}p$ annihilation, 3.0 GeV/c, differential cross sections and polarisation of $\bar{\Lambda}^0$ and $K_s{}^0$ 78−58197
particle and antiparticle prod. by 200 GeV/c p is CERN SPS charged hyperon beam 79−71768
recoilless Λ prod. in (K^-,π^-) on light nuclei, hypernuclear spectroscopy 78−50116
two-body hypercharge exchange reactions, planar and nonplanar, cross section energy depend. 79−75790
e^+e^- annihilation, 4 and 7 GeV, $\bar{n}$ and $\Sigma^{\pm}$ prod., cross sections 79−63494
e^+e^- annihilation, charmed baryon pair prod., symm. quark model, $c\bar{c}$ pair creation model 77−54111
e^+e^- annihilation, inclusive Λ and p yield 79−9369
$e^+e^-\rightarrow\Delta(1232)X$, struct. functions and nucleon longitudinal polarisation *(Russian)* 79−22121
$e^+e^-\rightarrow\Lambda^0\bar{\Lambda}^0$, neutral current effects in Weinberg model 77−18310
ep deep inelastic inclusive $K_s{}^0$ and Λ electroproduction, quark fragmentation 78−66123
$ep\rightarrow e\Delta^+$ scatt. asymmetry predictions, SU(2) gauge theory 78−58193
$ep\rightarrow eK^+\Lambda^0$, scalar transverse separation 77−71520
$ep\rightarrow eK^+\Sigma^0$, scalar transverse separation 77−71520
$ep\rightarrow e\Lambda X$, electroprod. of forward Λ baryon near/along virtual photon direction 79−22116
$\gamma N\rightarrow K^+\Sigma$, meas. of asymmetries and cross sections using 16 GeV linearly polarised photons 80−13318
$\gamma p\rightarrow K^+\Lambda$, meas. of asymmetries and cross sections using 16 GeV linearly polarised photons 80−13318
$\gamma p\rightarrow K^+\Lambda^0$, resonance region, Λ^0 polarisation 78−66131
$\gamma p\rightarrow\pi\Delta(1236)$, 744 to 1044 MeV, momentum spectra, differential cross sections *(Japanese)* 78−17032
(K^-,π^-) strangeness exchange reactions producing hypernuclei 78−17130
$K^-p\rightarrow\eta\pi$, narrow hyperon state of mass 3.17 GeV 80−37298
$K^-d\rightarrow\Lambda p\pi^-$, 680 to 840 MeV/c, Λp enhancement near ΣN threshold 77−67672
$K^-d\rightarrow\pi^-\Lambda p$, anal. of Λp enhancement at 2.129 GeV in cross section meas. 79−22141
$K^-d\rightarrow\pi^-\Lambda p$, pole in ${}^3S_1$ hyperon-nucleon scattering amplitudes 80−102068
$K^-d\rightarrow\pi^-\Lambda p$, three body Faddeev formalism, unstable dibaryon bound state search 80−32130
$K^-d\rightarrow\pi^-\Lambda p$ breakup process, appl. of Faddeev eqns. 79−75797
$K^-d\rightarrow\pi\Lambda p$, ΣN bound state and Λp enhancement 80−47326
K^-d scatt., effect of hyperon channels, <120 MeV/c 79−9406
$K^-d\rightarrow\Sigma^-p\gamma(\Lambda n\gamma)$, energy spectra, hyperon-nucleon scatt. anal. *(Russian)* 78−29347
$K^-d\rightarrow\Xi^-K^0p$, 1.45, 1.65 GeV/c, Ξ^-p invariant mass enhancement 80−57639
K^+d inclusive reactions, 4.6 GeV/c, topological cross sections, π^-, K^0, Λ prod. 77−50004
$\bar{K}N\rightarrow\Lambda\pi$, 1480 to 2170 MeV, partial wave anal. 77−22782
$\bar{K}N\rightarrow\pi$+hyperon, hypercharge exchange reactions in quasieikonal model *(Russian)* 79−3041
$\bar{K}N\rightarrow\Sigma\pi$, 1480 to 2170 MeV, partial wave anal. 77−22782
$\bar{K}N\rightarrow\Sigma\pi$, 1520-1745 MeV, partial wave anal. 77−18324
$\bar{K}N\rightarrow\Sigma\pi$ around 1660 MeV, partial wave anal. 77−22788
$K^-N\rightarrow K\ \Lambda K$, diffractive excitation at 14.3 GeV/c and 500-1500 GeV/c 77−6175
$K^-n\rightarrow K^0\Xi^-$, formation of cascade hypernucleus in nuclear emulsion 80−52603
$K^-N\rightarrow A\pi(\Sigma\pi)$, review 79−85339
K^-n reactions, quasi two-body final states at 8.25 GeV/c 79−22139
$K^-n\rightarrow\Sigma^-\pi^+\pi^-(\pi^0)$, 2.87 GeV/c, search for exotic I=2 hyperons 78−82234
K^-p, 10, 16 GeV/c, Σ^+, Σ^- inclusive prod. Λ prod. comparison 80−86766
K^-p, 8.25 GeV/c, $\Xi^*(2370)$ prod., mass and width determ. 80−47327
K^-p, inclusive prod. of Ξ^- and $\Xi^*(1530)$, 10 and 16 GeV/c 80−13341
K^-p, inclusive Ξ^- production at 4.2 GeV/c, triple Regge formalism 78−4875
K^-p, neutral channel cross section meas., 1470 to 1560 MeV CM energy 78−82237
$K^-p\rightarrow1^-3/2^+$, 4.2 GeV/c, hypercharge exchange, cross sections, momentum transfer depend. 77−71531
$K^-p\rightarrow(\Sigma\bar{K})^-K^+$, 4.2 GeV/c, $\Xi^{*-}(2030)$ identification 77−61320
$K^-p\rightarrow(\pi^+\pi^-)_{s\text{-wave}}\Sigma^0(1385)$ amplitude anal., additive quark model and duality diagram predictions 77−30430
$K^-p\rightarrow\eta\Lambda$, 4.2 GeV/c, total and differential cross sections, forward production peaks 79−40801
$K^-p\rightarrow\eta'\Lambda$, 4.2 GeV/c, total and differential cross sections, forward production peaks 79−40801

hyperon production continued
K^-p inclusive interactions, 10, 16 GeV/c, polarisation of forward produced Λ 78−62466
k^-p interaction in hydrogen bubble chamber, <300 MeV/c track sensitive target 80−13333
$K^-p \rightarrow K^*(890)\,\Delta(1236)$, 10 GeV/c, multidimens. anal., reaction subchannel separation 80−32127
$K^-p \rightarrow \Lambda^0$+pions, 8.25 GeV/c, resonance prod., fluctuations cluster emission model 78−93904
$K^-p \rightarrow \Lambda^0(\Sigma^0)$+vector mesons, 3.1-3.6 GeV/c, exchange model anal. 77−74718
$K^-p \rightarrow \Lambda^0\pi^0$, strong reaction asymmetry and mass quantisation, particle struct. *(French)* 79−3043
$K^-p \rightarrow \Lambda K^+K^-$, 10 and 16 GeV/c, proton dissociation in 3-body final states 79−85338
$K^-p \rightarrow \Lambda X$, 4.2 GeV/c, polarisation and triple Regge framework 78−45948
$K^-p \rightarrow \Lambda X$, 8.25 GeV/c, off shell $K\bar{K}$ and $p\bar{p}$ interactions, KNO scaling 80−52534
$K^-p \rightarrow \Lambda X$ or Λ(Pions) or $\Lambda p_{slow}X$, multiperipheral model with heavy clusters *(Russian)* 78−485
$K^-p \rightarrow \bar{\Lambda}+X$, 32 GeV/c, total and differential cross sections, energy dependence 80−63048
$K^-p \rightarrow \Lambda$+anything, 4.2 GeV/c, dual anal. of target fragmentation 77−57561
$K^-p \rightarrow \lambda$+pions, 4.2 GeV/c, multiplicities, hadronic temps. and ang. distribs. in $K\bar{K}_1\,\bar{p}p$ annihilations 79−45101
$K^-p \rightarrow \Lambda(\Sigma)K^0,\ K^\pm\pi^\pm$, 4.2 GeV/c, 1550 MeV, I=1 enhancement in $(\Lambda\pi)$ and $(\Sigma\pi)$ systems 78−89735
$K^-p \rightarrow \Lambda\eta$, 6 GeV/c, baryon exchange reactions, ηNN coupling constant, Λ polarisation, nucleon-Regge exchange 80−78098
$K^-p \rightarrow \Lambda\eta$, cross section meas. near reaction threshold 77−82765
$K^-p \rightarrow \Lambda\gamma(\Sigma^0\gamma)$ at rest, photon search using NaI(Tl) detector 80−13332
$K^-p \rightarrow \Lambda\omega$ around 2 GeV/c, resonance parameters 77−22786
$K^-p \rightarrow \Lambda\pi^0$, 6 GeV/c, baryon exchange reactions, ηNN coupling constant, Λ polarisation, nucleon-Regge exchange 80−78098
$K^-p \rightarrow \Lambda\pi^0,\ \Lambda\eta,\ \Lambda\eta'$ at 4.2 GeV/c differential cross sections, polarisations meas. 77−65176
$K^-p \rightarrow \Lambda\pi^+\pi^-$, 4.2 GeV/c, ρ-ω interference 77−30429
$K^-p \rightarrow \Lambda\pi^+\pi^-$, CM energies 1.65 to 1.72 GeV 77−41861
$k^-p \rightarrow \Lambda\pi^+\pi^-$, partial wave anal. in Λ(1520) region, Λ partial decay widths *(Russian)* 80−32131
$K^-p \rightarrow \Lambda\pi\pi$, discussion of new data 77−22782
$K^-p \rightarrow \Lambda\rho(760)$, transversity amplitude analysis 79−80847
$K^-p \rightarrow \Omega^-+X$, 8.25 GeV/c, Ω^- lifetime, spin 78−93877
$K^-p \rightarrow \omega\Lambda$, 1.934-2.516 GeV/c expt. data, threshold to 2.436 GeV partial wave anal. 77−82767
$K^-p \rightarrow \phi\Lambda,\ \omega\Lambda,\ \rho\Lambda,\ \phi\Sigma^0$, or $\rho\Sigma^0$, 4.2 GeV/c, cross sections, density matrix elements, hyperon polarisation 78−41580
$K^-p \rightarrow \pi^-\Sigma^+$ 79−93462
$K^-p \rightarrow \pi^-\Sigma^+$ and $\pi^+p \rightarrow K^+\Sigma^+$, exchange degeneracy 80−57634
$K^-p \rightarrow \pi^-Y^+,\ Y^+=\Sigma^+$ or $Y^{*+}(1385)$, 7 GeV/c, hypercharge exchange in line-reversed π^+p and K^-p 80−82998
$K^-p \rightarrow \pi^-Y^*(1385)$, 11.5 GeV/c, confirmation of exchange degeneracy predictions in line reversed reacts. 78−82247
$K^-p \rightarrow \pi^0\Lambda$, 4.2 GeV/c, total and differential cross sections, forward production peaks 79−40801
$k^-p \rightarrow \pi^0\Lambda$ (1520), 1.71 to 2.17 GeV, partial wave analysis 78−29352
$K^-p \rightarrow \pi^+\Sigma^-$, box diagram calcs. unitarity corrections in strong interactions 80−91110
$K^-p \rightarrow \pi^+\Sigma^-$, cross-sections, 1470-1550 MeV 79−13154
$K^-p \rightarrow \pi^+\Sigma^-(1385)$, 1775-2170 MeV, partial wave anal. 79−6348
$K^-p \rightarrow \pi\Sigma(1385)$, 4.2 GeV/c, total and differential cross sections 77−41860
$K^-p \rightarrow \rho^-Y^+,\ Y^+=\Sigma^+$ or $Y^{*+}(1385)$, 7 and 11.5 GeV/c, hyperon polarisation, vector meson decay angular distribs. 80−82997
$K^-p \rightarrow \rho^-(760)+\Sigma^+(1385)$, amplitude anal. 79−97635
$K^-p \rightarrow \Sigma^-\pi^+$, backward differential cross section 80−63024
$K^-p \rightarrow \Sigma^-\pi^+$ or $\Sigma^+\pi^-$ at rest, interaction ratio for charged Σ prod. 78−78213
$K^-p \rightarrow \Sigma^-\pi^+\omega$, 4.2 GeV/c, B (1235) backward prod., $\pi^+\omega$ mass enhancement 78−89736
$K^-p \rightarrow \Sigma^-\pi^+\pi^-\pi^+$, 4.15 GeV/c, nondiffractive A_1 production, double-Regge model 80−78097
$K^-p \rightarrow \Sigma^0\pi^+\pi^-$, 4.2 GeV/c, ρ-ω interference 77−30429
$K^-p \rightarrow \Sigma^+$+anything, 4.2 GeV/c, dual anal. of target fragmentation 77−57561
$K^-p \rightarrow \Sigma^+\pi^-$, 460 MeV/c, Σ^+ decay and polarisation props. determ. 77−30432
$K^-p \rightarrow \Sigma^+\pi^-$, 460 MeV/c, Σ^+ mag. moment meas. in HYBUC 77−54119
$K^-p \rightarrow \sigma^\pm$ (1385)X, 32 GeV, inclusive and total cross sections 80−105936
$K^-p \rightarrow \Sigma^\pm(1385)+X$, 10, 16 GeV/c, inclusive prod. 77−26552
$K^-p \rightarrow \Sigma^\pm\pi^\mp$, 1.934-2.516 GeV/c, reson. states identification 77−38200
$K^-p \rightarrow \Sigma^\pm\pi^\mp$, around 2 GeV/c, resonance parameters 77−22786
$K^-p \rightarrow \Sigma^\pm\pi^\pm$, threshold and below, ratio of $\Sigma^-\pi^+$ to $\Sigma^+\pi^-$ production 78−70407
$K^0p \rightarrow \Lambda^0\pi^+\pi^+\pi^-$, 1.5 to 2.5 GeV, effective mass distrib. 77−22792
$K^0p \rightarrow \Sigma^0\pi^+\pi^+\pi^-$, 1.5 to 2.5 GeV, effective mass distrib. 77−22792
$K^0p \rightarrow \Sigma^\pm\pi^+\pi^+$, 1.5 to 2.5 GeV, effective mass distrib. 77−22792
K^+p inclusive and semi-inclusive 32 GeV/c interactions, Λ and $\bar{\Lambda}$ prod. 78−21475
$K^+p \rightarrow K^+\bar{p}pp$, 12 GeV/c, $\bar{\Lambda}(1520)$ ang. distribs. and correlations 80−441
$K^+p \rightarrow \bar{\Lambda}X$, 32 GeV/c, $\bar{\Sigma}^{*-}$ and $\bar{\Xi}^{*-}$ antibaryon resonance prod., mass enhancements 80−13340
$K^+p \rightarrow \bar{\Lambda}pn\pi^+$, 12 GeV/c, narrow resonant state in $\bar{\Lambda}\Delta^{++}(1232)$ and $\bar{\Sigma}^+(1385)p$ combinations 78−89744
$K^+p \rightarrow \pi^-\Sigma^+$, 7 and 11.6 GeV/c, Σ^+ polarisation meas. 78−41573
$K^+p \rightarrow \Sigma^+\pi^+$, strong reaction asymmetry and mass quantisation, particle struct. *(French)* 79−3043
$K^\pm p \rightarrow$ hyperon+X, 4-16 GeV/c, unified descript. of $\Lambda,\bar{\Lambda},\ \Sigma^+,\ \Xi^-$ prod., urbaryon model 78−66173
$K^\pm p \rightarrow p\bar{\Lambda}p(\Lambda\bar{p})$, 50 GeV/c, strange bosons decaying into baryon-antibaryon pairs 80−37306
$K_L^0p \rightarrow K_S^0p(\pi^+\Lambda)(\pi^+\Sigma^0)(\pi^+\pi^0\Lambda)$, differential and polarisation cross sections near 550 MeV/c 79−17757
$K_L^0p \rightarrow \Lambda^0\pi^+$, 1605 to 1910 MeV, differential and channel cross section meas. 79−75768
$K_L^0p \rightarrow \Lambda\pi^+$, 1.54 to 1.71 GeV, search for narrow states 78−29354
hyperon production continued
$K_L^0p \rightarrow \Lambda\pi^+\pi^0$, 1.54 to 1.71 GeV, search for narrow states 78−29354
$K_L^0p \rightarrow \Sigma^0\pi^+$, 1.54 to 1.71 GeV, search for narrow states 78−29354
Λ, in K^-p 8.25 GeV/c, study of inclusive Λ, Σ^0 and $\Sigma(1385)$ prod. 79−30749
Λ, inclusive prod. in π^-p 6 GeV/c interactions 79−93454
Λ, $\bar{\Lambda}$ prod. in e^+e^- annihilation 78−17034
Λ hyperon polarisation, meas. by hybrid Monte Carlo tech. 80−99431
Λ inclusive prod., Regge cuts and spin depend. 78−21402
Λ nucleus$\rightarrow\Sigma^0$ nucleus, Σ^0 lifetime meas. 77−23111
Λ prod. cross-section scaling in pp, K^+p, π^+p 80−52539
Λ production in pp interactions, inclusive and exclusive, 6 GeV/c, polarised beam 77−65171
Λ recoilless prod. on nuclei by (K^-,π^-) reaction 77−3053
Λ-hyperon final states of K^- absorption at rest in C nuclei 77−41997
Λ^0, cumulative, production cross section from π^- meson-nucleus reactions *(Russian)* 78−78419
$\Lambda^0,\ \bar{\Lambda}^0$ prod. by p+Be at 400 GeV, polarisation determ. 78−82253
Λ^0, neutral strange-particle prod. by 300 GeV protons in Be, Cu, Pb 79−17905
Λ^0 polarisation in inclusive prod. by 24 GeV protons on Pt 77−67691
Λ_c^+ production total cross section, decay modes from pp interactions 79−89150
$\mu p \rightarrow \Lambda^0(\bar{\Lambda}^0)X$, 225 GeV, deep inelastic scatt., strange neutral particle prod. 80−105902
$n+C \rightarrow (n^* \rightarrow \Lambda k\pi)X$, 45 GeV, production cross section 77−82795
$n+N \rightarrow (n^* \rightarrow \Lambda k\pi)X$, 45 GeV, decay prob. 77−82795
$\nu,\bar{\nu}$ experiments at Gargamelle, strange particle production by neutral currents 78−37200
$\bar{\nu}$ interactions, Λ, Σ^0, K^0 prod. 78−8647
$\nu d \rightarrow \Lambda_c^+X$, high energy charmed baryon prod. obs. 80−105881
$\bar{\nu}_\mu N,\ K^0$ and Λ inclusive prod., fragmentation function and transverse momentum squared 80−32093
$\nu_\mu N \rightarrow {}^-C_0{}^+,\ C_0{}^+ \rightarrow \Lambda^0e^+\nu_e$ Λ polarisation, chiral props. of charmed current 77−61272
$\bar{\nu}p$, strange particle prod. at CERN PS 78−82195
$\nu p \rightarrow \Lambda_c^+X$, evidence for $\Lambda_c^+(2260)$ prod. 80−42442
$\nu p \rightarrow \mu^-pK^+\pi^+\pi^+\pi^0,\ \Sigma_c^{++}$ prod. and decay 80−86710
$\nu p \rightarrow \Sigma_c^{++}X$, evidence for $\Sigma_c^{++}(2424)$ prod. 80−42442
Ω^- production experiment data relevant to spectroscopy 77−22791
Ω^- production in 4.2 GeV/c K^-p reactions, lifetime, mass, decay asymm. parameter 79−3044
(p,Λ^0), inclusive cross section, constituent-constituent multiple scatt. model for dependence on atomic number 80−83101
p+Be(Cu)(Pb), 300 GeV, inclusive prod. of Λ^0 hyperons 78−37253
$p+Be \rightarrow \Lambda^0+X$, 300 GeV/c, Λ^0 polarisation meas. 77−30458
$pd \rightarrow V^0X$, 18 GeV/c, K^0s, γ, Λ, $\bar{\Lambda}$ prod. 77−87993
pN, 29.4 GeV, Σ and Ξ prod. ratios 80−42457
$pN \rightarrow \Lambda^0\bar{\Lambda}^0$, 300 GeV, inclusive prod., triple-Regge behaviour 77−61328
$pN \rightarrow \Lambda^0X$, 28.5 GeV/c, Λ^0 polarisation 80−32137
$pN \rightarrow \Lambda^0X$, inclusive cross section, constituent-constituent multiple scatt. model for dependence on atomic number 80−83101
$\bar{p}p$, 14.75 GeV/c, inclusive and semi-inclusive $K^{*\pm}(890)$ and $\Sigma^\pm(1385)$ prod. 80−5027
$\bar{p}p$, 22.4 GeV/c, γ, K_s^0 and Λ inclusive prod., structure functions *(Russian)* 79−58985
$\bar{p}p$, 22.4 GeV/c, inclusive γ, K_S^0, Λ $\bar{\Lambda}$ production, KNO scaling test *(Russian)* 79−30759
pp, 28 GeV, in H, D, Be, inclusive Λ polarisation 80−47337
pp, 300 GeV/c, inclusive prod. of $K^0,\ \Lambda^0\ K^{*\pm}(890)$ and $\Sigma^{*}\pm(1385)$ 80−95290
pp, 400 GeV/c, inclusive and semiinclusive prod. of $\pi^0,\ K_s^0,\ \Lambda^0,\ \bar{\Lambda}^0,\ \Sigma^0,\ \bar{\Sigma}^0,\ \eta,\ \omega^0$ 79−93472
pp, 53, 62 GeV, forward prod. of $\Lambda^0,\ \bar{\Lambda}^0,\ \Xi^-,\ \Sigma(1385)^\pm,\ \Lambda^0\bar{\Lambda}^0$ simultaneous prod. 79−89206
pp, 63 GeV, Λ_c^+ diffractive prod. at CERN ISR, $\Lambda_c^+ \rightarrow K^-p\pi^+$ decay mode 79−89204
pp, high energies, $\Sigma^\pm(1385)$ inclusive prod., minimised wave function model calcs. *(Russian)* 80−63047
pp, probabilistic quark-model approach to p fragmentation 80−63049
pp, $\bar{\Sigma}^\pm(1385)$ inclusive prod. at 12 and 24 GeV/c 79−6356
$pp \rightarrow (K_s^0,\ \Lambda,\ \text{or}\ \bar{\Lambda})\pi^\pm+X$, 405 GeV/c cross section determ., vector meson dominance 79−89207
$pp \rightarrow (K^-\pi^+p)X$, scalar field with isospin, IR asymptotic behaviour of one-fermion Green's function 79−89205
$pp \rightarrow (\Lambda^0\pi^+\pi^+\pi^-)X$, scalar field with isospin, IR asymptotic behaviour of one-fermion Green's function 79−89205
$\bar{p}p \rightarrow \bar{\Delta}^{++}(1232)X$, 32 GeV, cross sections 80−105937
$pp \rightarrow \delta^{++}(1236),\ \Lambda^0$, 100 GeV/c, one-meson-exchange mechanism anal. 78−8712
$\bar{p}p$ hyperon-antihyperon prod. at 3.6 GeV/c with ≥3 final state particles 77−38187
pp inclusive interactions, 405 GeV/c, inclusive $\Lambda,\ \bar{\Lambda},\ \Sigma^\pm(1385)$ prod. 78−21477
$\bar{p}p$ interactions, 100 GeV/c, inclusive distribs. for $\gamma,\ K_s,\ \Lambda^0,\ \bar{\Lambda}^0$ prod. 77−38213
$\bar{p}p \rightarrow K_S^0X(\Lambda X)\ (\bar{\Lambda}X)$, 3.6 GeV/c, cross section anal. and Λ polarisation 79−45095
$pp \rightarrow K^0(\Lambda)(\Delta^{++})X$, 6 GeV/c, polarised proton 77−30400
$pp \rightarrow \Lambda_c$, 10 to 300 GeV, triple Regge framework 78−21472
$pp \rightarrow \Lambda^0X$, 53 and 62 GeV, Λ^0 polarisation at CERN ISR 79−49550
$pp \rightarrow \Lambda^0X$, high energies, semiclassical model for polarisation 79−89202
$pp \rightarrow \Lambda^0X^{++}$, 69 GeV/c, triple Regge anal. 77−74730
$pp \rightarrow \Lambda K_s^0X$, 19 GeV/c, single particle props. 80−32139
$\bar{p}p \rightarrow \bar{\Lambda}\Lambda$, 1.50-2.06 GeV/c, polarisations, cross sections, spin correl. coeffs. 78−74271
$\bar{p}p \rightarrow \bar{\Lambda}\Lambda$, 6 GeV, cross sections and polarisations 79−407
$\bar{p}p \rightarrow \bar{\Lambda}\Sigma^0$, 6 GeV, cross sections and polarisations 79−407
$pp \rightarrow \Lambda X$, 19 GeV/c, polarisation at high transverse momenta 78−37246
$pp \rightarrow \Lambda X$, Λ polarisation and Regge cuts 77−2876
$pp \rightarrow \Lambda X$, natural and unnatural parity exchange in triple-Regge region 77−65182
$pp \rightarrow \Lambda X$ and Λ polarisation, Mueller Regge model 77−30454
$\bar{p}p \rightarrow \Lambda+X$, 4.6, 9.1 GeV/c, inclusive total, topological and invariant differential cross sections 79−408
$\bar{p}p \rightarrow \bar{\Lambda}+$missing mass, trigger accepted polarisations 79−407
$pp \rightarrow \Lambda(K^0)X$, 12 GeV/c, beam polarisation induced asymmetries 80−42507
$pp \rightarrow \Lambda(\Sigma^0)X$, 69 GeV/c, cross-section 77−22812
$pp \rightarrow n\bar{X}$ or ΛX, 12, 24 GeV/c, n/Λ ratio, cross sections 78−58213
$pp \rightarrow p\Lambda K^+$, 12, 24 GeV/c, diffr. dissoc. 77−82779

hyperon production continued
$\bar{p}p \rightarrow \pi^- X(\Lambda X)$, 22.4 GeV/c, test of factorisation hypothesis for leading Regge trajectories *(Russian)* 79−49561
$pp \rightarrow \Sigma^{\pm}(1385)X$, $\bar{\Sigma}^{\pm}(1385)X$, 12 GeV/c prod. cross sections 78−93911
$\bar{p}p \rightarrow \Sigma(1385)X$, 3.6 GeV, factorisation hypothesis test 80−102055
$p\pi^-$ interaction, K+hyperon prod., mass quantisation anal. *(French)* 78−70401
$\pi^- {}^{12}C$, 40 GeV/c, Λ and $K_1{}^0$ inclusive distribs. *(Russian)* 77−34196
π^-+nucleus, inclusive at 3.9 GeV/c, Λ Feynman scaling obs. *(Russian)* 79−9635
$\pi^+ d$ interactions, strange-particle cross-sections at 4 GeV/c 78−89734
$\pi^+ d \rightarrow K^+ Yp$, E>1 GeV, Glauber correction and final state interaction *(Russian)* 77−6161
$\pi N \rightarrow K$+hyperon, hypercharge exchange reactions in quasieikonal model *(Russian)* 79−3041
$\pi^- n$, 40 GeV/c, cross sections of Λ and K prod. *(Russian)* 77−6184
$\pi^- N$, $\bar{\Lambda}$ hyperon prod. cross section, momentum and ang. distribs. *(Russian)* 80−42497
πp inclusive K and Λ prod. at 19 GeV/c 77−13998
$\pi p \rightarrow \Lambda K$, associated prod. of strange particles at resonance energies 77−22775
$\pi p \rightarrow \Sigma K$, associated prod. of strange particles at resonance energies 77−22775
$\pi^- p$, 100, 200, 360 GeV/c, inclusive prod. of π^0, $K_S{}^0$, Λ^0, $\bar{\Lambda}^0$, cross sections 80−73745
$\pi^- p$, 147 GeV/c, neutral particle prod., K_S, Λ, $\bar{\Lambda}$, γ, multiplicity scaling form 80−22645
$\pi^- p$, 16 GeV/c, Ξ^- and anti-Ξ^+ prod. 79−45113
$\pi^- p$, 16 GeV.c^{-1}, strange particle production, CERN 2m H_2 bubble chamber data *(Russian)* 79−9413
$\pi^- p$, 250 GeV/c, inclusive prod. of neutral strange particles, $K^0{}_s$, Λ, $\bar{\Lambda}$ 78−21479
$\pi^- p$ 5 GeV/c interactions, inclusive distrib. of Γ^0 and $K^0{}_1$ *(Russian)* 78−54652
$\pi^- p$ interactions, 15 GeV/c, $K^0{}_s$, Λ, $\bar{\Lambda}$ prod., Regge anal. 78−45981
$\pi^- p$ interactions, 5 and 40 GeV, inclusive struct. functions of γ, $\pi^{\pm}$, K^0, and Λ *(Russian)* 79−80856
$\pi^- p \rightarrow K_S{}^0$, Λ, $\bar{\Lambda}$, prod. in 16 GeV/c interactions 80−37308
$\pi^- p \rightarrow K^0\Lambda$, 3.5 GeV/c, Λ polarisation, high statistics meas. 80−57637
$\pi^- p \rightarrow K^0\Lambda$, threshold to 2350 MeV, partial wave analysis 78−29349
$\pi^- p \rightarrow K^0\Lambda^0$, 1375 to 2375 MeV, new results and anal. 80−438
$\pi^- p \rightarrow K^0\Lambda^0$, 1400 to 2380 MeV/c, differential cross sections and polarisations, partial wave anal. 78−70405
$\pi^- p \rightarrow K^0\Lambda^0$, up to 1334 MeV/c, cross sections and polarisation, energy depend. phase shift anal. 78−70404
$\pi^- p \rightarrow K^0\Lambda^0$, up to 1334 MeV/c, differential cross sections and polarisation, phase shift anal. 79−412
$\pi^- p \rightarrow K^0\Lambda^0$ up to 2.375 GeV/c, resonance parameters, partial wave anal. 80−32133
$\pi^- p \rightarrow K^0\Sigma^0$, 1395 to 2375 MeV/c, differential cross-section and polarisation meas. 80−9183
$\pi^- p \rightarrow K^0\Sigma^0$, 1395 to 2375 MeV/c, differential cross-section and polarisation 80−57635
$\pi^- p \rightarrow K^0\Sigma^0$, threshold to 1334 MeV/c, differential cross-section and polarisation 78−89733
$\pi^- p \rightarrow K^0\Sigma^0$, threshold to 1334 MeV/c, differential cross section and polarisation data 79−17755
$\pi^- p \rightarrow K^+(K^{*+})\Sigma^{*-}(1385)$, 4.35 and 4.85 GeV/c, backwared prod. of $\Sigma^{*-}(1385)$ *(Russian)* 77−6160
$\pi^- p \rightarrow K^{*0}(890)\ \Lambda^0/\Sigma^0$, 10 GeV/c, K^{*0} polarisation meas. in hypercharge exchange reaction 80−63017
$\pi^- p \rightarrow \Lambda K$, low energy, amplitude anal., Lagrangian model 80−82995
$\pi^- p \rightarrow \Lambda K^0$ or $\Lambda K^*(890)$, 8 GeV/c, differential cross section, Λ polarisation 77−34175
$\pi^- p \rightarrow \Lambda K^0 + X^0$, 4.35, 4.85 GeV/c, mass spectra of N* resonances *(Russian)* 77−6159
$\pi^- p \rightarrow \Lambda K^+ + X^-$, 4.35, 4.85 GeV/c, mass spectra of N* resonances *(Russian)* 77−6159
$\pi^- p \rightarrow \Lambda + X$, 4.9-40 GeV/c inclusive and semi-inclusive distribs. *(Russian)* 78−41610
$\pi^- p \rightarrow \Lambda(\bar{\Lambda})X$, 205 GeV/c cross sections 77−71544
$\pi^- p \rightarrow \Sigma^{\pm}$+anything, 4.35 and 4.85 GeV/c, inclusive spectra *(Russian)* 77−13977
$\pi^+ p$, 32 GeV/c, inclusive strange particle prod., Σ^+, $K_S{}^0$, Λ and $\bar{\Lambda}$ cross sections 80−52541
$\pi^+ p$, strange-particle cross-sections at 10.3 GeV/c 77−87999
$\pi^+ p \rightarrow \Delta^{++}(1236)$, Λ^0, 100 GeV/c, one-meson-exchange mechanism anal. 78−8712
$\pi^+ p \rightarrow K^+\Sigma^+$, 4, 7, 11.5, 70 GeV/c, weak exchange degeneracy, Navelet-Stevens model generalisation 79−93462
$\pi^+ p \rightarrow K^+\Sigma^+$, 7 and 11.6 GeV/c, Σ^+ polarisation meas. 78−41573
$\pi^+ p \rightarrow K^+\Sigma^+$ and $K^- p \rightarrow \pi^-\Sigma^+$, exchange degeneracy 80−57634
$\pi^+ p \rightarrow K^+ Y^+$, $Y^+ = \Sigma^+$ or $Y^{*+}(1385)$, 7 GeV/c, hypercharge exchange in line-reversed $\pi^+ p$ and $K^- p$ 80−82998
$\pi^+ p \rightarrow K^+ Y^*(1385)$, 11.5 GeV/c confirmation of exchange degeneracy predictions in line reversed reacts. 78−82247
$\pi^+ p \rightarrow K^{*+}(890)Y^+$, $Y^+ = \Sigma^+$ or $Y^{*+}(1385)$, 7 and 11.5 GeV/c, hyperon polarisation, vector meson decay angular distribs. 80−82997
$\pi^+ p \rightarrow \Lambda K^+\pi^-$, 10.3 GeV/c, p diffractive dissociation into ΛK^+ and $(\Sigma K)^+$ 78−45966
$\pi^+ p \rightarrow \Lambda K x\pi$, 10.3 GeV/c, threshold enhancements in ΛK mass spectra 78−74284
$\pi^+ p \rightarrow \Sigma^+(1385)K^+(K^{*+}(890))$ 10.3 GeV.c, Y*K and Y*K* prod. 79−49544
$\pi^+ p \rightarrow \Sigma K x\pi$, 10.3 GeV/c, threshold enhancements in ΛK mass spectra 78−74284
$\pi^{\pm} p \rightarrow \Lambda K^+\pi^{\pm}$, proton dissociation in 3-body final states 79−85338
$\Sigma(1385)$, in $K^- p$ 8.25 GeV/c, study of inclusive Λ, Σ^0 and $\Sigma(1385)$ prod. 79−30749
Σ^- production and decay props. in $K^- p \rightarrow \Sigma^-\pi^+$ at 430-493 MeV/c 78−29350
Σ^0, in $K^- p$ 8.25 GeV/c, study of inclusive Λ, Σ^0 and $\Sigma(1385)$ prod. 79−30749
$\Sigma^{\pm}(1385)$, inclusive prod. in $\pi^- p$ 6 GeV/c interactions 79−93454
$\Sigma^{\pm}$ inclusive prod., $K^- p$ interactions at 4.2 GeV/c 77−82773
$\Sigma_c{}^+$, production and decay obs. 80−105894
$\Sigma^- p$ systems, possible resonance existence 80−47340
Ξ^-, inclusive prod. in $K^- p$ interactions 80−13341
$\Xi^0 \rightarrow \Lambda^0\pi^0, \Lambda^0$ polarisation meas. 77−30458
$\Xi^*(1530)$, inclusive prod. in $K^- p$ interactions 80−13341
Ξ^* production experiment data relevant to spectrocopy 77−22791

hyperon production continued
$Y^*(1385)$ prod. in $K^- p \rightarrow \pi\ Y^*$ at 4.25 GeV/c 77−30425
Y^* production experiment data relevant to spectroscopy 77−22791
$Be + p(\bar{p})(K^-)(\pi^-)$, 200 GeV/c, forward inclusive prod. spectra, of K_s, Λ^0, $\bar{\Lambda}^0$, n 78−82393
$^{12}C + \pi^-$, 40 GeV/c, cross sections of Λ and K prod. *(Russian)* 77−6184
$\gamma p \rightarrow K^+\lambda(\Sigma^0)$, $\pi^+ n$, $\pi^- p$, $K^+\Lambda$, $K^+\Sigma^0$ final state comparisons above resonance region 80−105906
$^4He + K^- \rightarrow \Lambda + \pi^- + p + d$, 180 MeV, final state study, double impulse model 79−30855
$K^- n \rightarrow \pi^-\Lambda$, 1750 to 2000 MeV, ang. distrib. and polarisation, comparison with PWA 79−75796
$\bar{p}p \rightarrow \Lambda$, 10 to 300 GeV, triple Regge framework 78−21472
$Pt + K^-$ interactions, 12 GeV/c, Λ^0 prod., search for di-hyperon resonance 77−82970
$Xe + \pi^-$ 3.2 GeV/c, intermediate Δ^- prod. in π^0 and η prod. *(Russian)* 79−36280

hyperon resonances
$S = +1$ and $S = -1$, $K_L{}^0 p$ experiments as probe 77−22793
SU(3) Λ-Λ' mixing explanation of broken SU(3) hyperon anomalous magnetic moment sum rules 77−18288
SU(4) symmetry breaking pattern and baryon masses 78−89690
Δ excitation, contrib. to pp bremsstrahlung field theoretic calc. 78−62451
$\Delta^+ \rightarrow p + \gamma$, radiative decay in the MIT bag model 78−66110
$\Gamma(1405)$, dynamical nature is low energy $\bar{K}N$ interactions 78−70408
$\gamma p \rightarrow \pi\Delta(1236)$, 744 to 1044 MeV, momentum spectra, differential cross sections *(Japanese)* 78−17032
$K^- p \rightarrow \Omega\pi$, narrow hyperon state of mass 3.17 GeV 80−37298
$\bar{K}N$ elastic and charge exchange phase shift anal., 0.44 to 2.0 GeV/c, resonance parameters 77−22784
$\bar{K}N$ interactions, 1480 to 2170 MeV 77−22782
$\bar{K}N$ two body data, energy-depend. multichannel K-matrix anal., amplitudes, resonance parameters 77−22785
$K^- n$ interactions, 1800 to 2200 MeV 77−22787
$K^- n \rightarrow \Sigma^-\pi^+\pi^-(\pi^0)$, 2.87 GeV/c, search for exotic I=2 hyperons 78−82234
$K^- p \rightarrow \Lambda^0$+pions, 8.25 GeV/c, resonance prod., fluctuations cluster emission model 78−93904
$K^- p \rightarrow \Lambda(\Sigma)K^0$, $K^{\pm}\pi^{\pm}$, 4.2 GeV/c, 1550 MeV, I=1 enhancement in $(\Lambda\pi)$ and $(\Sigma\pi)$ systems 78−89735
$K^- p \rightarrow \pi^- Y^{*+}$, 4.25 GeV/c, amplitude anal. 77−18321
$K^- p \rightarrow \rho^-\Sigma^+(1385)$, $\phi\Sigma^0(1385)$, $\omega\Lambda(1520)$ or 0(1520), cross sections, momentum transfer 77−71531
$K^- p \rightarrow \rho^-(760) + \Sigma^+(1385)$, amplitude anal. 79−97635
$K^- p$ two body reactions around 2 GeV/c, resonance parameters 77−22786
$K^+ p \rightarrow \bar{\Lambda}X$, 32 GeV/c, $\bar{\Sigma}^{*-}$ and $\bar{\Xi}^{*-}$ antibaryon resonance prod., mass enhancements 80−13340
Λ, pole of $\bar{K}N$, KN σ-term, uncertainties in determ., K-matrix formalism 80−27522
$\Lambda(1405)$ dynamic effect in nuclear matter, implications for kaonic atoms 77−14056
$\Lambda(1405)$ resonance behavior in nucl. matter 77−18466
$\Lambda_1{}^{1/+}$, mag. moment from quark mass difference calcs. 80−37240
$\Lambda_c{}^+$ lifetime, semileptonic branching fractions, nonspectator quark interactions 80−37260
Λ' existence, ninth $I=0\ J^P = 1/2^+$ baryon, asymptotic level realisation of SU(3), hyperon semileptonic decay anal. 77−18245
$\Lambda 5/2^-(1830)$ inversion relative to $\Lambda 1/2^+(1115)$, symmetry breaking mechanism 78−50013
$\bar{\Lambda}\Lambda$, OBE pot. calc., bound state and reson. energies, widths in 1.6 to 2.7 GeV range 77−49931
NN inelastic processes, SU(3) breaking, N(1688), Λ(1815) and Σ(1915) states 77−71526
$\nu p \rightarrow \Lambda_c{}^+ X$, evidence for $\Lambda_c{}^+(2260)$ prod. 80−42442
$\nu p \rightarrow \Sigma_c{}^{++} X$, evidence for $\Sigma_c{}^{++}(2424)$ prod. 80−42442
Ω^- spin, centrifugal barriers, quantisation of I=0 baryon levels 77−18221
$pp \rightarrow (K_s{}^0, \Lambda, \text{or } \bar{\Lambda})\pi^{\pm} + X$, 405 GeV/c cross section determ., vector meson dominance 79−89207
$pp \rightarrow \Sigma^{\pm}(1385)X$, $\bar{\Sigma}^{\pm}(1385)X$, 12 GeV/c prod. cross sections 78−93911
$\pi^- p \rightarrow K^+(K^{*+})\Sigma^{*-}(1385)$, 4.35 and 4.85 GeV/c, backwared prod. of $\Sigma^{*-}(1385)$ *(Russian)* 77−6160
Σ, pole of $\bar{K}N$, KN σ-term, uncertainties in determ., K-matrix formalism 80−27522
$\Sigma(2030)$ via $K^- n \rightarrow GSS^{-(0)}\pi^{0(-)}$ at CM 1850-2160 MeV 77−67673
$\Sigma^-(1385)$, prod. in $K^- n$ reactions to quasi two body final states 79−22139
$\Sigma^- \rightarrow \Lambda e^- \nu$, branching ratio meas., Monte Carlo prediction 78−54631
Σ^0 life time from Λ nucleus$\rightarrow\Sigma^0$ nucleus, Coulomb excitation method *(Russian)* 78−46114
$\Sigma^+ \rightarrow p\gamma$, $1/2^-$ resonance poles to parity-violating amplitude, two-quark weak transitions 80−78062
$\Sigma_c{}^+$, production and decay obs. 80−105894
$\Sigma 5/2^-(1765)$ inversion relative to $\Sigma 1/2^+(1190)$, symmetry breaking mechanism 78−50013
$\bar{\Sigma}\Sigma$, OBE pot. calc., bound state and reson. energies, widths in 1.6 to 2.7 GeV range 77−49931
$\Theta^*(1820)$ reson., Minnaert spin test 78−89767
$\Xi^- \rightarrow \Lambda e^- \nu$ branching ratio meas., Monte Carlo prediction 78−54631
Ξ^*, enhancement at $\Sigma\bar{K}$ threshold (1680) MeV obs. in $K^- p$ reactions 4.2 GeV.c^{-1} 79−17756
$\Xi^*(1820)$ reson., spin tests 77−30472
Ξ^* production experiment data relevant to spectroscopy 77−22791
$\bar{\Xi}\Xi$, OBE pot. calc., bound state and reson. energies, widths in 1.6 to 2.7 GeV range 77−49931
$Y^*(1385)$ prod., SU(3) symmetry and vector tensor universality 77−18321
$Y^*(1385)$ prod. in $K^- p \rightarrow \pi^- Y^*$ at 4.25 GeV/c 77−30425
Y^* production experiment data relevant to spectroscopy 77−22791
Y^* resonances in $\bar{K}N$ partial wave analyses 77−22790
Y^* states from $K^- p$ reactions, SU_3 classification 78−25077
$Y_0{}^*(1405)$ couplings, K-matrix parametrizations in $\bar{K}N$ and $\pi\Sigma$ two channel systems 78−21452
Y^*s in $K^- p$ elastic and charge exchange scatt. partial wave anal. below 1.2 GeV/c 77−22783
Z^* resonances status from anal. of $K^+ N$ and $K^+ d$ expts. below 2 GeV/c 77−22794

hyperon resonances continued
Z_{20}* and composite resonances in KN scatt. 77−22795
^{32}S, kaonic, Y* resonance nonlocal effects, kaonic shifts and widths 79−7039

hyperon scattering *see hyperon-nucleon scattering; hyperon-nucleus scattering; kaon-hyperon scattering; lepton-hadron scattering; photon-hadron scattering; pion-hyperon scattering*

hyperon spin and parity
Λ polarisation, forward produced particles in K^-p inclusive interactions 78−62466
Λ^0, $\bar{\Lambda}^0$ prod. by p+Be at 400 GeV, polarisation determ. 78−82253
Λ′ existence, ninth $I=0$ $J^P=1/2^+$ baryon, asymptotic level realisation of SU(3), hyperon semileptonic decay anal. 77−18245
Ω^- spin, centrifugal barriers, quantisation of $I=0$ baryon levels 77−18221
$\Sigma^0 \rightarrow \Lambda\gamma$, weak effects, small P violating E1 component in M1 EM decay 79−89160
Θ*(1820) reson., Minnaert spin test 78−89767
Ξ*(1820) reson., spin tests 77−30472

hyperons
see also hyperon resonances
Λ magnetic moments, rel. to quark mass and hadron mass 79−13050
beam physics, review, book contrib. 80−68503
dihyperon, possible stable particle in 6-quark colour gauge theory 77−22691
magnetic moments, implications for quark model 80−13290
magnetic moments, transition moments, SU(3) calcs. 79−13128
nuclear interactions of strange particles and resonances, conf. Warsaw, Poland (Ict. 1976) 78−70406
quark gluon model of hadronic structure functions at $x \rightarrow 1$ *(Russian)* 78−54617
$K^-n \rightarrow \Sigma^-\pi^0(\Sigma^0\pi^-)$, 1.85-2.15 GeV, Σ(2030) prod. and decay 78−41583
Λ, binding energy in nuclear matter, reaction-matrix calculation 79−36185
Λ(1405) and kaonic H atom, $\bar{K}N$ interaction model 80−68479
Λ binding to nuclear matter in Fermi hypernetted chain approx. 79−85396
Λ helicity meas. in $\Xi^0 \rightarrow \Lambda\pi^0$ 78−93878
Λ lifetime meas., decay products identified 77−71513
$\bar{\Lambda}^0$,Λ^0, differential cross section and polarisation from $p\bar{p}$ annihilation 78−58197
Λ_c, structure of hadrons containing heavy quark, MIT bag model 80−86672
Λ=Σ^0, effects of EM mixing on pn mass difference *(Russian)* 78−74255
Ω^- hyperon, spin and lifetime determ. 78−29333
Ω^- lifetime, spin from K $p \rightarrow \Omega^- + X$, 8.25 GeV/c 78−93877
Σ, EM mass differences, quark behaviour 79−58941
Σ, mass shifts 78−45920
$\Sigma^\pm$, lifetimes and longitudinal accel. 80−86709
Σ_c, structure of hadrons containing heavy quark, MIT bag model 80−86672
Σ^{*-}-Σ^{*+}, QCD relation between EM mass differences 79−71750
Ξ, EM mass differences, quark behaviour 79−58941
Ξ^0 lifetime meas., decay products identified 77−71513

hypersonic flow
ablating blunt body, heat transfer near stagnation point 78−94736
ablating graphite nosetips in hypersonic flight, transition front asymmetries 80−19436
ablation, statistical characteristics of mass lost in thermal destruction, zero gas dynamic press. 78−83429
aerodynamic ablation of spinning steel shells, side force 79−37347
aerodynamical anal. of body in hypersonic source flow field *(Chinese)* 80−59066
aerofoil, thin, windward surface shock layer, hypersonic flow 78−34158
air, dissociated, hypersonic flow over blunt axisymmetric body, nonsteady heat exchange 79−37319
air, hypersonic wake, electron recomb. coeff., temp. depend. meas. 79−27834
air, in shock tunnel, mass spectrometric analysis 77−31328
air scoops at supersonic and hypersonic vels., throttling, separation and central body cooling 80−14739
air wake, hypersonic, ionised, free electron attachment coeff. meas. 79−27835
airfoil in supersonic and hypersonic flow, wedge problem 79−41705
airfoils, oscillating, power-law shocks, Newtonian flow theory appl. 79−41706
asymptotic solutions near blunt body *(Russian)* 80−24048
attached shock wave flow over plane delta wings 77−27556
axisymmetric bodies with blowing, gas flow, base region influence 80−43734
axisymmetric body aerodynamics, optimal control solution, with aid of computer 78−4474
axisymmetric flow with const. momentum, shock wave, ideal and laminar regions *(Russian)* 77−55033
axisymmetric hypersonic nozzle. viscous gas flow calc. with departure from vibr. equilib. 80−33649
ballistic device, hypersonic wake, anomalous dispersion meas. 79−82014
ballistics experiment, application of laser light source 78−38433
blunt biconic at incidence, laminar viscous shock layer, supersonic/hypersonic flow 78−30313
blunt bodies, surface friction, physiochemical processes in shock layer 78−46997
blunt body flow, stagnation region, heat transfer and wall accommodation 79−41708
blunt body in flow, viscous shock-layer eqns. 79−60002
blunt cone hypersonic and supersonic flow, near wake Reynolds number effects, interferometric obs. 80−43733
blunt slender cones at high Mach numbers, stability derivatives, nose bluntness effects 80−19438
blunt-slender cones, artificially induced boundary layer transition 80−28496
blunted cones at small angles of attack, shock waves 78−1684
blunted sphere cones, viscous shock layer solns. 78−51186
bodies at high attack angle, shock-layer eqns. 79−4042
body form for minimum heat transmission *(Russian)* 79−37131
body shape for minimal radiative heat inflow, spacecraft atmospheric entry *(Russian)* 78−77457
body shape optimisation, principal approx. methods 78−5765
boundary layer, laminar, nonequil. ionis. problem 80−59129

hypersonic flow continued
boundary layer, laminar, small temp. factor, high Mach no. 78−34156
boundary layer acoustic monitor for hypersonic turbulence transition determ. 78−34237
boundary layer eqns. including chemical reactions, numerical error control, book contrib. 80−1699
boundary layer instabilities, Mach number 7 77−65760
boundary layer over slender sharp cone, turbulent shear stresses, heat transfer 77−23989
bow shock interaction with ice crystal, aerodynamic shattering criterion 77−27558
cavitation of high and low gas mixtures at low density *(German)* 80−1651
channel, converging conical, hypersonic similarity criterion 77−39310
chemical laser, low pressure, line-shape flattening resulting from hypersonic nozzle wedge flow 80−91783
chemically reactive flow, aerodynamic heating of blunt bodies 80−74998
compressible fluid flow past degenerate star-red giant interacting binary stars 80−67779
cone, interference study of hypersonic near wake 79−64665
cone at large attack angle, parabolised Navier-Stokes eqns. 79−1210
conical nozzle, boundary layer separation from compression shock 80−48766
conical wing-body combination, thin shock layer theory appl. 79−46339
corner, three-dimens., Navier-Stokes eqn. soln., numerical code 78−30314
corner flow, viscous-inviscid interaction of laminar boundary 79−32563
cross-sectional shock shape meas. using columnar and plane discharges 79−27666
cylinder surface, pressure distrib. in longitudinal hypersonic flow 80−48744
disintegrating blunt bodies, radiative heating in H_2-He atms. 80−69865
dissociated high enthalpy hypersonic laminar air flow, heat transfer to flat plate 80−69828
drag of three-dimensional body in hypersonic Newtonian flow *(Russian)* 78−22369
dusty gas, hypersonic wedge flow 80−6083
dynamic heat transfer meas. at Mach 8, digital Fourier anal., boundary layer transition 80−14682
entropy layer in two-dimens. flow behind compression shock 78−1691
excitation temperature meas. with spatial resolution, hook method 77−58200
field calc., behind blunt body *(Russian)* 79−86461
flat plate skin friction, between hypersonic continuum and free mol. flow 79−94668
flight, longitudinal stability conditions *(German)* 77−31330
free molecular flow, momentum transport to surfaces 79−64704
free molecular flow, pulse transmission coeffs. for surfaces *(Russian)* 77−89163
free molecular heating of micron size particulate 79−4058
free molecule heating of micron size particles at hypersonic speeds 80−19442
gas, shock wave under continuous energy supply 80−103042
gas blown from cylinder end in hypersonic flow, shocks and blowing parameter 80−33624
gas compression in heavy piston, hypersonic speed, shock waves 80−69869
gas flow, radiant heat and evaporative cooling 78−91028
gun tunnel, two-stage, optimum operating technique 79−41707
gun tunnel flow, Mach 7 jet, anal. of hot wire anemometer signals 78−14054
heat transfer, laminar boundary layer of cone at ang. of attack 79−1211
heat transfer to axisymmetric bodies, freestream turbulence effects 77−75916
holographic shearing interferometer with narrow ref. beam for flow investig. in reflecting nozzle of shock wave 77−47118
hypersonic viscous shock-layer equation, method for successive approximations for integration *(Russian)* 78−59421
ice crystal-shock layer interaction 78−30317
isotope separation techniques based on vel. slip in freejet expansions 80−19441
jet, free, streamlines and local velocities in rarefied atm. 77−42884
jet, hypersonic liq., moving into gas, shock layer anal. 78−26177
jets, hypersonic, high temp., noise rel. to gas parameters *(Russian)* 79−32132
laminar boundary layer, shock wave interactions 77−89151
laminar boundary layer at stagnation pt., slip, mass transfer 77−19625
laminar boundary-layer flow over expansion corner 77−65758
laminar film cooling experiments in hypersonic flow 79−94648
laminar flow over insulated accelerating slender wedge 78−1685
laminar hypersonic wake of a lifting body, Navier-Stokes solns. *(Russian)* 78−87359
laminar near wake of blunted cone, convective heat and mass transfer 79−98752
laminar,unsteady airfoil aerodynamics, viscous and elastic perturbation effects 78−26150
leeside flowfields of planar delta wings, Reynolds number 79−60003
leeward vortex-induced heat transfer, hypersonic viscous shock layer 77−80179
limiting shock layer *(Russian)* 78−30316
liquid jet, interaction with hypersonic gas flow, shape and breakup 80−10277
low-density hypersonic wedge flow, numerical soln. 79−94665
Mach 6 turbulent boundary layer, surface roughness effects 80−19338
magnetic dipole surrounded by infinitely conducting medium appl., exact solutions *(Russian)* 79−77174
magnetoaeroelastic stability of thin panels, space vehicle re-entry *(French)* 77−65702
minimum drag configurations via method of steepest descent 80−10262
Newtonian flow past power-law bodies 77−42863
nonequilibrium free jet expansion, rotational temp. meas for N_2 80−69890
nonequilibrium free jet expansion, translational temp. meas. in N_2 80−64600
nonequilibrium gas mixtures past blunt bodies, Navier-Stokes equation *(Russian)* 79−18909
nonequilibrium ionisation in vicinity of critical point, asymptotic theory 80−14740
nonequilibrium ionised radiating gas flow over blunt bodies 78−9727
nonstationary flow past wedge and cone, thin shock wave method *(Russian)* 77−80180

hypersonic flow continued
nozzle, tunable dye laser meas. 77−68719
nozzle boundary layer, hypersonic, static press. variation and Reynolds stress 77−84294
nozzle flow, vibr. relax. in air 79−68781
nozzles, high enthalpy supersonic flow conversion to hypersonic flow 80−74937
nozzles, viscous flow 79−64733
plasma, nonequilib., two-temp., expanding in disc-shaped channel, hypersonic MHD interactions 80−10368
plasma jet discharge, highly effective radiation sources prod. using freq. doubled pulses 79−93235
plate, heat transfer from high enthalpy hypersonic air boundary layer 78−34210
plate leeside, viscous hypersonic flowfield boundary layer separation 80−48743
radiant heat transfer coefficient for blunt body in hypersonic flow, similarity law 80−33705
radiating laminar boundary flow over flat plate at large free stream Mach no. 79−1270
rapidly rotating gases, thermally-driven axially antisymm. geostrophic flows, flow field calc. 79−90259
rarefied flat plate flow, direct simulation and expt. 79−94667
rarefied flow past forward facing step 77−42872
rarefied gas flow over blunt wedge, cooling 77−35169
rarefied hypersonic flow on wedge, numerical anal. *(Japanese)* 79−32580
rarefied hypersonic flow past flat-plate, numerical simulation 77−19626
secondary shock waves in mag. field *(Russian)* 78−87401
separation, incipient, viscous interaction, laminar and turbulent boundary layers, similitude props. 77−72325
separation behind a lifting plate 77−42864
sharp 5-deg cone at incidence, hypersonic viscous static stability 77−23987
sharp flat plate, drag reduction in rarefied hypersonic flow 79−94669
shock layer, hypersonic, vibr. nonequilib., near stagnation streamline, low Reynolds no. flow 78−87417
shock layer, screening of selective heat radiation in boundary layer *(Russian)* 79−32497
shock layer blunt body problem, aerodynamic heating, effect of chemical reactions of injected gas *(Japanese)* 79−94739
shock layer in flow past blunt axisymmetric body 78−9654
shock layer separation, asymptotic soln. *(Russian)* 80−33625
shock stand-off distance for sphere, formula 77−55030
shock tube flows, unsteady non-equilibrium, discretisation of boundary layer terms, computation at Mach 10 80−14742
shock tunnel development for aerospace simulation 79−41777
shock wave analysis flow through body wall 80−38447
shock wave shape, hypersonic inviscid flow around semicone body, calc. methods 77−89150
shock wave shape found delta wing, mixed boundary value problem solns. *(Russian)* 79−90279
shock-shock interaction in hypersonic flow 79−94673
slender blunt body 77−35164
slender cones, drag meas. in hypersonic flow using mag. suspension and balance 79−4039
slender vehicle dynamics, viscous interaction or support interference 78−71363
slender wing, 3-D flow *(Russian)* 79−10588
slender-body theory, parallel-source correspondence 78−26151
solar wind flow past planets, axisymm. implicit blunt body computation technique 78−96370
space probe or meteorite reentry, mass loss and shape change with radiative heating 80−31198
spherically blunted cone with massive surface blowing, laminar and turbulent flows, shocks 80−38445
stagnation point boundary layers with massive blowing in presence of mag. field 79−94649
stagnation region heat transfer in hypersonic particle environments 77−31325
stagnation temp. meas. in hypersonic flow using fine W wire probe 77−79095
stagnation-point boundary layer with hot wall, mag. field effect 77−72359
strong interaction of boundary layer and hypersonic flow, boundary conditions local perturbation 80−14738
supersonic/hypersonic flow past an oscillating flat plate at high angles of attack 79−14424
surface cooling, multiple slot injection into turbulent boundary layer 78−9653
teflon gas injected into shock layer flow, hypersonic flow past blunt body 80−74998
terrestrial atmosphere, low-density gaseous body motion, rel. to Tunguska catastrophe 79−84554
thin triangular wings, difference method anal. *(Ukrainian)* 78−1686
three-dimensional shapes, optimal surfaces and total drag coeffs. 80−59068
three-dimensional wing 77−19621
transitional/turbulent boundary layer, wall cooling effect 78−26149
turbine blade and nozzle guide vane, transient cascade, heat transfer meas., wind tunnel 78−94768
turbulence model development expts. with numerical simulations 77−27551
turbulent, reson. Doppler velocimeter meas. and direct flow visualisation 77−35285
turbulent boundary layer separation and reattachment on flat plate with ramp 77−23990
turbulent compression corner flow, numerical simulation 77−62276
turbulent flow measurements, electron beam fluoresc. method 77−35282
turbulent shear layer attachment near Mach 6, peak heating 78−26153
unsteady hypersonic flow past a weakly curved profile *(Russian)* 79−32566
unsteady hypersonic gas flow past thin finite-span wing 79−86457
unsteady hypersonic gas-dynamic eqns., approx. solns. *(Russian)* 77−35165
vehicle hypersonic wake, radiation from injected small particles, free molecular regime 80−64650
viscous, iterative methods, convergence rate, comparative study 79−40374
viscous flows over sphere cones at high angles of attack 79−98746
viscous radiating gas, over blunted cones 77−51131
hypersonic flow continued
viscous shock layer, three-dimens., numerical calc. on sharp cone at incidence 77−47041
viscous shock layer equations, num. soln. scheme 79−90280
viscous shock layer flow over highly cooled sphere, coupled eqns. anal. 78−51189
wake, excitation temp. meas. by atomic spectral line relative intensities 80−43732
wake, free electron distrib., RF method 79−27833
wake of blunt body, physicochem. perturbed throat region 79−68743
wake of hypersonic sphere in air, obs. with open microwave resonator 79−77301
wind tunnel, flow core relative area, nozzle similitude ratios 80−48747
wind tunnels, pressure fluctuations, freestream 78−14102
wing aerodynamic charact. at hypersonic speed, slip effect 79−81917
wing-body interference at hypersonic speeds *(Japanese)* 78−30315
yawed blunted cone, similar boundary layer anal. for lee-surface heating 77−27553
CO_2 aerosol/hypersonic air stream interaction, gasdynamic CO_2 laser energy charact. 80−48211
CO_2, in shock tunnel, mass spectrometric analysis 77−31328
CO_2, viscous hypersonic flow over blunted cone, numerical anal. 79−77171
CO_2:Cr I, excitation temp. meas., hook method 77−58200
He high speed flow, Na vapour seed, quantitative flow visualisation 78−47072
He, Na vapour seeded, velocity profile visualisation 78−59530
Kr-H_2, ~5 torr, ionisation by Mach 15+shock waves, shock struct. and stability 77−75938
N_2, hypersonic nozzle flow, supercooling and spontaneous condensation 78−1549
N_2, in shock tunnel, mass spectrometric analysis 77−31328
N_2, oscillatory-dissoc. relax. in hypersonic shock layer at moderate Reynolds number *(Russian)* 77−39311

hypersorption *see sorption*

hypertritons *see hypernuclei; tritons*

hypervirial theorem *see quantum theory*

hypochromism *see light absorption*

hypothesis formation *see heuristic programming*

hypothetical particles
see also charm particles; heavy leptons; intermediate bosons; magnetic monopoles; quarks; tachyons
axion, astrophysical limitations on mass *(Russian)* 78−61835
axion mass in extended SU(2)×U(1) colour gauge theory 78−78080
axion production in νp interactions, 26 GeV, cross sections, decay rate 78−62387
axions, astrophys. constraints on axion mass and number of quark flavours 79−36009
axions, evidence against, from $\bar{\nu}$e and $\bar{\nu}$d scatt. 79−13108
axions, evidence against from ν reactor expts. 78−45904
axions, possible evidence from existing expts. 79−436
axions, review of research 78−66183
axions and Higgs particles, astrophysical mass bounds 79−5745
dyon solns. to classical gauge field theory, stability 77−30261
dyon-dyon nonrelativistic scatt., classical and quantum anal. 77−5985
dyonium model, space reflection operator and boson fermion puzzle 79−36118
dyons, spatial volume integral of Tr F(tilde) F, Yang-Mills theory 80−77943
dyons, supersymmetric Yang-Mills theory 78−62334
dyons in classical Yang-Mills SU(3) gauge theory 77−6014
energy-range relations for heavy protons and heavy quarks, use in detection 78−58566
gauge invariance with massive gauge bosons 80−9107
gauge theory solitons, quantisation, Feynman rules, monopole-dyons 77−2734
gluon properties from eN→e meson baryon reactions, helicity struct. of amplitudes 77−18293
gluons, conserved vector current hypothesis 77−74617
gravitino, supersymmetric theory, mixing of weak and gravit. interactions 78−8578
hadrons as compounds of bradyons and tachyons, ground state and decay anal. 78−58156
heavy particle with single positive charge, search in H_2, D_2 *(Chinese)* 78−876
heavy stable particles, cosmic ray produced, search in heavy water 79−40048
magnetoelectric charge states of matter-energy, magnetoelec. ionisation and magnetoelectrophoresis 80−99114
magnetoelectric dipole structure hypothesis, biological and cosmic appls. 80−91124
magnetoelectric dipoles, appl. to biological effects of mag. fields 80−93157
magnetoelectric monopoles, delocalisation prediction, possibility for detect. 80−99115
monopole-dyon system in nonAbelian gauge theories, Georgi-Glashow model 77−79213
neutral lepton mass, lower limit determ. 77−82799
new particle searches in e^+e^- interactions at LEP energies 79−97617
new particles and weak interactions, models *(Chinese)* 79−93334
non-Abelian dyons, Nambu mechs. descript. 78−41490
orthopositronium decay into axions 78−78125
photino and goldstino, scatt. cross sections on matter 79−97558
Polyakov-'t Hooft monopole and dyon, quantum theory *(Russian)* 78−392
quantum soliton operators for monopoles and Fermionization mechanism of dyons 79−35940
relic θ particle concentration in the Universe *(Russian)* 80−86026
search for massive, long-lived, fractionally charged particles produced by 300-GeV protons 79−89311
soliton, massive elementary particle, maintenance of size and shape 79−71643
spin 3/2 lepton, leptonic decay, secondary lepton distrib. *(Russian)* 80−5034
stable heavy neutrinos, dynamical interactions and astrophys. effects 79−5743
SU(3) gauge theories without scalars, mag. monopoles, dyons, other topologically stable solns. 77−49819
supergravitation, calibration invariance *(Russian)* 78−4548

hypothetical particles continued
superluminal particles motion in gravit. field of nonrot. black hole *(Russian)* 78−93103
supersymmetric new hadronic states, production, decay and detection 78−70302
unconfined colour gluons, possible existence in mass range 1.1 to 1.8 GeV 77−30324
unified field theory, axion, avoidance without massless quarks 79−63403
Universe, very massive unstable particles, prop. bounds 80−82558
X-particles, cosmic ray evidence for short-lived particles 79−58993
L-particles, existance possibility from anomalous cosmic ray events 80−86701
$\nu_\mu N \rightarrow \mu^- e^+ +$hadrons, up to 30 GeV, possible heavy neutral lepton prod. 79−36061
τ particle properties, QCD type gauge theories, absence of $\tau^+\tau^-$ resonance in e^+e^- annihilation 78−37144
θ vector particles, calibration interaction macroscopic confinement radius *(Russian)* 80−47257
Cu+p, 400 GeV, dimuon and trimuon prod., prompt ν source, DD prod., axions 78−89860
Cu+p, 400 GeV, prompt ν prod., axion prod. upper limit 78−89859

hysteresis
see also coercive force; control nonlinearities; dielectric hysteresis; elastic hysteresis; magnetic hysteresis; remanence
body anelastic hysteresis determ. and error formula *(German)* 77−80123
ceramic materials, fine-grained, cyclic plastic deform. as cuase for thermal expansion hysteresis 80−89290
concrete, damping meas., expanded hysteresis loop method 77−12665
contact angle, at homogeneous surfaces 78−51793
deformable metal mirror characterisation techniques 79−59798
degenerate four-wave mixing, hysteresis and optical bistability 80−69446
dislocation behaviour, in fatigue, friction and back stress from hysteresis loops 80−3176
dye CW laser, electrooptically tuned, optical switching and bistability 79−59708
electric breakdown voltage hysteresis, electrode coating effects in air and SF_6 78−87553
electrotechnical steel, hysteresis curves, plotting *(Russian)* 78−76269
Fabry-Perot nonlinear interferometer, beam profile hysteresis variations 80−86393
fatigue, cumulative damage, under random loads algorithm of hysteresis loop counting 80−21064
fatigue, thermal energy losses and steady state temp. field calc. 77−19571
ferrofluid US attenuation anomalies 79−55830
ferromagnetic materials, coercive force determ. *(Russian)* 79−73764
gas laser, linearly polarized waves, interaction with longitudinal mag. field 80−95936
haematite-bearing rocks and concentrates, hysteretic props. rel. to peaked thermomag. curves 79−79824
impact vibrations, steady, of body having hysteresis collision characteristics 80−14602
inhomogeneous systems, hysteresis of phase transitions, general soln. 78−59926
laser, multimode, containing saturable absorbers, bistable operation 80−91862
liquid, meniscus profile, contact angle, differential interference method 79−56039
MBBA, pure and mixed with bezene (chlorobenzene), nematic-isotropic transition, US absorpt., visual hysteresis 80−54355
methane, and $-d_4$, solid-phase transitions, hysteresis effects 79−99316
microcline, maximum, room temp. phase transition, heat capacity meas. 80−54373
microcline, maximum room temp. phase transition, unit cell parameters, thermal expansion 80−54208
microscopic theory 80−80731
MIS structure, elec. parameter meas. of second order equivalent ccts. 80−57332
MOS structure Pt diffused, hysteresis and memory props. 80−96992
optical resonator, containing medium with quadratic susceptibility, props. 80−33074
optical SHG, temperature phase-matching curve hysteresis 80−91852
orientation transitions, stabilising effect of high freq. fields *(Russian)* 77−89972
oscillating conductivity probe, density and density gradient meas., hysteresis effect 78−32796
oscillator with hysteresis, dynamic anal., Fokker-Planck eqn. *(French)* 77−50947
periodic capillary tube, two phase fluid flow and hysteresis 80−107615
periodic capillary tube, two phase fluid flow and hysteresis 80−107616
photomultipliers rate-dependent gain variations, obs. of hysteresis effect 77−54451
piezoelectromechanical transducer, reduction method *(Bulgarian)* 77−62129
polydiacetylene, reflection spectra, thermochromism, temp. hysteresis and phase transformation 78−19452
polymer materials, hysteresis flow model applicability for degree of inelasticity 80−28422
rare earth oxides, phase transition hysteresis, thermodynamic model 77−76570
Rayleigh-Masing model, modification as soln. to second-order differential eqn. *(Russian)* 77−33840
reversible electrodeposition display struct. having dynamic hysteresis characts. 79−49219
ring cavity, dispersive bistability in homogeneously broadened systems, hysteresis cycles 80−14306
Rochelle salt, ferroelectric props., student expt. 79−97162
rotatory hysteresis meas. of ferromagnetic specimen 77−87794
semiconductors electron-photon mechanism of cyclotron absorpt. hysteresis 79−69726
smectic liquid crystal, homeotropic to confocal texture transformation *(Russian)* 78−18548
soil water, hysteretic steady state profiles 77−91172
steel, 11423, cyclic stress anal. within hysteresis loop *(Czech)* 80−30031
steel, high-strength, low cycle fatigue, hysteresis loops, cyclic strain curves, fatigue diagrams *(Polish)* 80−66638
stimulus-response relation, multivalued, in isolated elasmobranch utricles 79−24979

hysteresis continued
superconductor, long thin-film, paradox in crossover of mech. causing hysteresis 80−107971
superconductor longitudinal acoustic wave absorpt., nonlinear effects, hysteresis *(Russian)* 79−19691
systems with hysteresis, linear, and quasilinear self-oscill. *(Russian)* 77−58590
TCNQ salts, crystallisation versus electrical conductivity 80−92885
vibration damping, continuum description 78−67078
Ag-Sn proximity effect bridges, nonequilibrium state, hysteresis of crit. current 79−56411
Al-Cu, precipitation hardened, hysteretic plastic work as failure criterion in Coffin-Manson type relation 77−32657
Cu, single crysts., hysteresis behaviour implications rel. to fatigue, plastic strain cycling 80−3191
Cu-Al, single crysts., hysteresis behaviour implications rel. to fatigue, plastic strain cycling 80−3191
Cu-Mn alloy, manganin, hysteresis-corrected calibration under shock loading 80−74818
Cu-Nb_3Sn superconducting composite, crit. props., AC hysteretic losses 80−50014
Fe, carbonyl powder, specific elec. conductivity, 5 to 200 MPa *(German)* 80−70664
Fe-Mn, Mossbauer spectroscopy of temp. hysteresis of phase transformations *(Czech)* 80−29949
GdCu, electrical resistivity and length changes with temp., hysteretic behaviour 80−97600
$Gd_2(MoO_4)_3$, piezoelectric and electrostriction coeffs. near ferroelastic transition *(French)* 77−40182
H_2O, contact angle on polystyrene, cause of hysteresis 78−95206
In film, crit. current hysteresis prod. by electron overheating 79−56449
In, supercond. and normal states, internal friction hysteresis *(Russian)* 77−36023
KCl, thermal hysteresis in ionic cond., dielec. loss meas. 78−34652
KH_2PO_4, low temp. transition, thermal hysteresis, Cr impurity effect on transition temp. 80−2705
K_2MoO_4, hysteresis of phase transitions and modulated structures 80−29169
K_2WO_4, hysteresis of phase transitions and modulated structures 80−29169
LaB_6, polycrystalline, negative surface ionisation of I atoms, negative ion desorption heat 79−78848
β-$MoTe_2$, metallic in-plane resistivity meas. indicate first-order phase transition 78−30903
$(NH_4)H_2AsO_4$, $(NH_4)H_2PO_4$ and deuterated analogues, low temp. transition, thermal hysteresis, Cr impurity effect on transition temp. 80−2705
Nb, mixed state, hysteresis of US attenuation 80−84549
NbCn, superconducting film, high field critical current densities and resistive transition 79−73648
$NdNbO_4$, ferroelastic domain wall motion, stress-strain hysteresis curve 77−43271
PbF_2, ionic cond., activation volumes and high press. phase transitions 80−70461
Pd alloy-H system, α-β phase transformations, hysteresis of press., elec. resistance, review 80−60859
Pd-H system, α-β phase transformations, hysteresis of press., elec. resistance, review 80−60859
Pd-H system, solvus hysteresis 80−71659
$Rb_2Hg(CN)_4$, spinel, ferroelasticity and phase transformation 79−7646
Sn film, crit. current hysteresis prod. by electron overheating 79−56449
Sn superconducting thin-film bridge, IV curves oscill. instability and quasi-particle recomb. *(Russian)* 80−44769
$SrCl_2$, ionic cond., activation volumes and high press. phase transitions 80−70461
Ti-Ni, effect of alloying on crit. points and martensitic transform. hysteresis 80−20935
VO_2, reactively sputtered film, influence of manufacturing parameters on film struct. and props. *(French)* 77−81218
W (100) surface, electron stimulated desorption of O^+ ion, hysteresis and ion yield minimum 77−59218

I-II-VI_2 semiconductors *see ternary semiconductors*
I-III-VI_2 semiconductors *see ternary semiconductors*
IC *see integrated circuits*
IC engines *see internal combustion engines*
ice
see also glaciology; snow
accretion calc. 79−29799
acoustic wave propag. in frozen random media 77−50814
adsorption of CO_2, H_2S, propane, gas hydrate form. investigs. 79−39191
aerodynamic shattering of ice crystals in hypersonic flight 77−27558
aerosol, thin flat, EM wave scatt. and absorpt. 80−91723
aerosol large particles ingestion by cloud, ice nucleation by freezing 77−37308
AES, chemical-state effects 78−92566
age category differentiation through location and temp. observations using microwaves 80−67380
airborne continuously recording ice nucleus counters, data anal. technique 77−78447
albedo feedback effects on energy-balance climate models 78−7749
albedo of snow- and ice-covered regions, multiple reflections between clouds and surface 77−45131
Alberta, southern and central regions, probable extent of Classical Wisconsin ice 78−36207
alpha-particle stopping cross section, 0.3 to 2.0 MeV 77−55313
amorphous, vac. UV photoelectric threshold 78−48273
amorphous 2500-4000 cm^{-1} Raman and IR spectra, vibr. anal. 77−59562
amorphous ice on Saturn rings and satellites, formation, stability and observability 79−35188
amorphous solid, spontaneous electric polarisation rel. to solid struct., 20 to 100K 79−65791
Amur basin rivers, anal. and forecasting of dates of ice breakup *(Russian)* 77−53088
Antarctic deep core ice, mechanical tests under hydrostatic pressure *(Japanese)* 79−79890
Antarctic deep core ice, X-ray diffr. topographic studies 78−63803
Antarctic ice, 1000 and 5000 yr old, ^{10}Be content meas. 79−2305
Antarctic ice, cryst. size and climatic record down to last ice age 80−94544

ice continued
Antarctic ice as supernovae recorder, NO_3^- produced by Γ- and X-rays 80−31314
Antarctic ice cap, preservation of meteorites 78−36541
W.Antarctic ice sheet, deglaciation threat from CO_2 greenhouse effect 78−28296
W.Antarctic ice sheet, fluctuations in Antarctic Peninsula area 80−94549
Antarctic ice sheet, nonbiogenic fixed N, ecological implications 78−32129
W Antarctic ice sheet, radio-echo layers and recent stability 77−5212
Antarctic ice sheet, thermal radiation calc. from randomly inhomogeneous stratified medium *(Russian)* 78−96312
Antarctic ice sheet thickness mapping by radar *(German)* 77−56770
W.Antarctic ice streams rel. to global climatic stability 77−64321
Antarctic iceberg melting 78−88863
Antarctic topography from balloon obs. 77−78248
anthelion, form. theory, light refl. in ice crysts. in cirrus clouds 79−62583
aqua-acid, UV-radiation illuminated, nuclear-electron effects in EPR, of atomic protium and deuterium *(Russian)* 79−20388
Arctic, effect of Siberian river diversions on ice cover and climate 80−41541
Arctic basin, drifting sea ice, deformation *(Russian)* 78−7652
Arctic Basin, ice movements, external factors 80−26541
Arctic Basin, sea-ice conc. and multiyear ice fraction time depend. 78−81174
Arctic Canada, ice-sheet initiation and climatic influences of expanded snow cover 79−66724
Arctic drift ice, microwave dielec. const. and absorpt. coeff. anisotropy 78−49037
Arctic fjord, ice form. rel. to waters mixing 79−48504
Arctic ice cover, attenuation of 8 and 20 cm EM waves 80−67379
Arctic ice cover evolution rel. to climatic changes 79−29781
Arctic Ice Dynamic Joint Experiment 77−33190
Arctic ice pack heat and mass balance 79−39750
Arctic lakes, L-band imaging radar obs. 77−21816
Arctic leads, atmos. boundary layer turbulence spectra obs. 80−56588
Arctic Ocean, late Wurm ice sheet rel. to N.Hemisphere glaciation 77−45132
Arctic Ocean, sea ice rel. to summertime stratus cloud form. 77−5290
Arctic Ocean ice characteristics meas. by microwave scatterometry 79−84298
Arctic Ocean sea ice, snow and ice cover conditions 80−26547
Arctic oil spillage response techniques 80−46204
Arctic sea ice, 1953-77 period fluctuations 80−36314
Arctic sea ice, compressive strength and stress relax. meas. *(Japanese)* 77−81916
Arctic sea ice, flexural strength meas. *(Japanese)* 77−81915
Arctic sea ice, layered struct. study by radar sounding *(Russian)* 78−16023
Arctic sea ice, surface layer induced thermal stress state meas. *(Japanese)* 77−81917
Arctic sea ice, surface-based radar scatterometer results 79−92544
Arctic sea ice, water drag 77−21781
Arctic sea ice decay following CO_2-induced atmospheric temp. rise 80−61802
Arctic seas, ice forecasts and practical appls. 78−96230
artesian wells drilled in permafrost, temp. field, efficiency of heaters for ice plugging prevention 77−78242
associated liquids, dielec. props. calc. 77−81045
atmosphere, anisotropic light scatt. by artificial ice crystals *(Russian)* 77−29436
atmosphere, biogenic ice nuclei, terrestrial and marine sources 77−5291
atmosphere, hexagonal ice crystals as cause of 46° halo and its arcs 80−82065
atmosphere, ice cryst. props. rel. to halos 79−2373
atmosphere, ice forming nuclei in N. Caucasus 77−78364
atmosphere, ice forming props., effects of impurities and surface state of AgI *(French)* 78−20459
atmosphere, melting ice particles producing rainfall, radar obs. 78−3873
atmosphere, natural and man-made ice forming nuclei 79−48530
atmosphere, solar halo phenomena *(Norwegian)* 79−84475
atmosphere frozen precipitation, corona charging 77−5295
atmosphere ice particles, rapid changes in orientation and alignment along Earth-space radio propag. path 80−17330
atmosphere snow and ice particles, influence on elec. field above Arctic Ocean *(Russian)* 79−48537
atmospheric, AgI surface adsorption, effective pair pot. model 80−100394
atmospheric hydrometeor backscattering cross sections, meas. at 6328 Å 78−49135
atmospheric particles, electric charge meas. by negative-feedback electrometer 79−70895
Azov Sea, USSR, hummocking of floating ice, distrib. 80−26549
Baltic beach sedimentary material stratification (autumn/winter 1976-7) *(Russian)* 80−76962
beach sediments, lower St. Lawrence Estuary, Quebec, frost effects 78−7609
Beaufort Sea ice movements, 1973-1975, determ. by ERTS imagery 77−45011
Bering Sea, medium-scale features obs. along seasonal ice edge 78−3778
bicrystal, anisotropy of migration and faceting of grain boundaries 79−60381
biological sample electron probe microanal., charging effect in electron-irrad. ice 78−57141
Bolivia, evidence for glaciation 3.27 Myr BP 79−34865
brine drainage and convection in young sea ice 79−57963
calorimeter reading unit with water indicator 80−31755
Camp Century core ice, O isotope ratios rel. to late-Wisconsin glaciation in NW.Greenland and N.Ellesmere Island 78−57232
Canadian high Arctic, past glacial activity 78−81236
Caspian Sea ice formation, aircraft radiometry 77−70712
caves of Nahanni River, N.W.Territories, Canada, ice forms *(French)* 77−78238
cirrus cloud, sunpillar form. theory 80−85747
cirrus clouds, falling ice particles survival distance in subsaturated air 77−33151
cirrus clouds, ice content determ. from radiative props. in NOAA 4 VTPR channels 79−39853

ice continued
climate effects of ice cap-albedo feedback, in 2-D energy balance model 80−67407
climate model, sensitivity and role of cloudiness *(Russian)* 78−88902
climate model with ice-sheet dynamics, stable periodic solns. 80−90210
climatic warming effect on W.Antarctic ice sheet 79−34864
cloud, ice nucleation by aerosol particles 80−61864
cloud, ice splinter production during riming, NH_3 addition expts. 80−72585
cloud, microphysical properties from lidar obs. 79−39811
cloud ice nuclei, microstruct. meas. in Kenya high-frequency hail area 79−53484
cloud model, shallow convective, precip. mechanisms 78−81311
cloud particle shape meas. by imaging devices 77−41222
cloud particle size distrib. meas. by optical array probes 77−41220
clouds, crystal habit discrimination using optical backscatt. depolarization technique 77−91309
clouds, directional light scatt. coeffs. in droplet and cryst. clouds *(Russian)* 78−96292
clouds, ice and water content from Nimbus 6 IR sounder data 78−92925
clouds, ice evolution within seeded and nonseeded Florida cumuli 79−100920
clouds, ice nucleus counters 77−41225
clouds, ice particle concs. rel. to Climax and Wolf Creek Pass cloud seeding expts. 80−82094
clouds, ice particle/water droplet discrimination with an optical ice particle counter 79−100973
clouds, ice splinter production during riming 78−85662
clouds, ice-bearing cumulus evolution, numerical simulation and obs. 77−2216
clouds, lidar backscatter from horizontal ice crystal plates 78−92984
clouds, liquid water and ice contents rel. to radiative props. parameterisation 80−56601
clouds, orographic and frontal, over Cascade Mountains, ice particle conc. 77−2210
clouds, phase discrimination with polarisation diversity lidar 78−96269
clouds, possible role of O_3 in ice form. *(Russian)* 77−29367
clouds, thin persistent very high, in stratosphere over Antarctica, nature determ. 78−36247
cloudy layers, back-melting by radiative heating 79−76961
cluster-ion prod. on electron-irrad., lattice and fragmentation energies 77−4911
columnar grained, rheology 79−57044
condensation and phase transitions, electrical effects 78−67821
continental ice sheet, stochastically driven with planetary wave feedback, model 80−77025
continental ice sheet model, spectral response to insolation vars. 79−2300
continental ice sheet model, stability to insolation periodic vars. 78−28251
core samples from Greenland Ice Sheet, atmospheric trace metals and sulphates 78−7667
corona discharges from ice points on metal electrodes 78−67587
creep, high temp., role of grain boundary sliding 80−34128
creep instability analysis, Antarctic and Greenland ice sheets 79−84304
creep rupture at depth in cold ice sheet, obs. 79−2306
Crete, evidence for glacial and nival formations *(German)* 77−64359
crystal, Ic and Ih phases, diffr. patterns and for IR spectra, isotopes, effects 78−6662
crystal, Ih-phase, proton distrib., light scatt. obs. 77−16318
crystal anisotropy, US vel. studies of Antarctic deep ice cores 80−12440
crystal binding and lattice dynamics, H-bonding pot. function 79−32940
crystal collisions, secondary ice particle generation 79−79932
crystal continuous replicator for laboratory cloud chambers 77−78448
crystal growth from vap., diffusion eqn. theory 80−12489
crystal growth from vapour, appearance of non-singular surfaces 79−60297
crystal growth in vapour at high saturation thermodynamic anal. 77−1088
crystal growth on membrane filter, vapour depletion, chamber parameters effects 79−70858
crystal growth rate in subcooled pure water 77−80431
crystal habit change mechanism, ice disc growth from vapour 80−84117
crystal halo form., geometry 79−100942
crystal optics rel. to polarized halos and double refraction 78−36283
crystal size from droplet accretion growth 79−79933
crystal sizes for halo production 79−96798
crystal structure, CNDO/2 calcs., unit cell polarity effects 78−22683
crystal structure of ice accretions rel. to hailstones 78−85668
crystal/water droplet clouds, angular depolarisation and multiple scattering of polarised laser light 80−41549
crystal/water droplet clouds, angular scattering of polarised laser light 80−41548
crystallisation, and melting rate in laminar stream of liquid 80−100770
crystallisation, in capillaries, effect of surface conditions 79−56037
crystallisation front movement, water and gas bubble distrib. 78−22830
crystallisation on CuS aerosol prepared by burning pyrotechnic mixture, freezing temps. 78−96279
crystallisation phenomenon of icicles, growth mechanism, structure and shape 80−59423
crystals, freely falling, produced by two different seeding methods, mass growth meas. 79−87570
crystals, holographic meas. of shapes, sizes and concs. 79−25364
crystals, in clouds, producing concentric solar haloes 1974 April 14 77−2245
crystals, light scatt. expts. *(Russian)* 80−94601
crystals, small sized, freely falling, settling vels. determ. 77−78387
crystals collision with simulated hailstones, lab. study of charge transfer 78−49112
crystals in artificial cloud, anisotropic light scattering *(Russian)* 78−40658
cubes, melting time, water film thickness, interface temp., weight var. 80−29153
cubic, D_2O isolated, H^+ exchange and Bjerrum defect migration, direct spectroscopic obs. 80−88356
cumulus clouds, aircraft meas. if ice, Florida 79−12213
cumulus clouds, ice particle multiplication factors 79−58035
cumulus congestus clouds, NE Colorado, graupel particles characts. 78−81312

ice continued
cumulus glaciation, rime-splintering hypothesis, field-of-flow cloud model 78−20476
Daisetsu Dam, artificial reservoir, Hokkaido, Japan, winter ice cover study *(Japanese)* 77−81945
dangerous weather phenomena prediction, research prospects 79−34932
dendrite formation from vapour phase, morphology, sizes and growth rates 78−10313
dendritic growth in supercooled water, natural convection effect 77−7999
dendritic growth rates, evidence for a universal law 79−4496
dendritic ice form. in pipe, cooling rate effect 78−90690
deposition coefficient meas., appl. to cirrus cloud seeding 77−70779
depositional ice growth, parametrisation 77−70766
detection using surface acoustic waves 78−18129
Devon Island ice cap, arctic Canada, $^{18}O/^{16}O$ climatic record from snow cores 77−41141
Devon Island ice cap, Canada, theoretical and observed temp. profiles comparison 79−16524
Devon Island ice cap, core stratigraphy and palaeoclimate 77−53096
Devon Island ice cap, NWT, artificial radioactivity layers 77−5250
Devon Island ice cap, NWT, Canada, $\delta^{18}O$ vars. rel. to climatic change 80−4050
dielectric anisotropy in Ih phase 78−64310
dielectric const., Onsager-Slater theory and unit model, Bjerrum defects 80−11310
dielectric relaxation in presence of ionic impurities, block layer meas. tech. 80−103914
diffusion cloud chamber, freezing and sublimation expts. with ice forming nuclei *(Spanish)* 77−87046
dislocation creep, creep deform. predictions 78−19815
dislocation form. kinetics, computer simulation 78−30622
dislocation processes and tensile crack formation in glaciers 78−20438
dislocation vel. theory, glide plane influence 80−79805
dislocation velocity, quantum mechanical approach 78−91339
dislocations revealed by etching 78−22725
disordered phase TO-LO splitting 79−91420
dispersed medium freezing, origin of water aspiration 77−60130
drift, numerical modelling *(Russian)* 77−13081
drifting pack ice, surface wind speed from surface weather charts 80−41476
drifting sea ice, inertial period motions *(Japanese)* 80−36327
drops of water, ice or mixed phase, backscatt. at 633 nm 77−64426
droxtals grown from supercooled water droplets, morphology 79−24426
Duluth-Superior Harbour, ice growth meas. 79−2299
Earth ice cover, latit. changes effects on zonal and global albedoes 80−17377
edge dislocation dipole form. by heat treatment, X-ray diffr. topography 79−99203
effect on lake P budget 79−62540
electronic structure investig. by XPS, UPS and UV absorpt. spectra 77−16452
EM properties, at frequencies below 1000 GHz, various Earth surface forms 78−24310
EM scattering and absorption by ice crysts. 78−25795
EM wave scattering and crosspolarisation 78−3853
Enceladus, IR photometry rel. to presence of water frost 78−12146
energy bands in cubic ice, LCMO calc. 77−51656
epitaxial film, on metal (111) substrates, surface struct., LEED obs. 79−86969
epitaxial ice crystals, influence of environmental saturation and elec. field on growth and evaporation 79−42408
ESR of H atoms in pure and acidic ices, motional narrowing and spin polarisation 77−20706
Europa, water ice dissoc. rel. to O and H clouds and UV emissions 79−5775
evaporation in planetary atmospheres rel. to ice-covered rivers on Mars 80−17526
excess electrons in nanosecond pulse ionized ice 78−39176
fast ice, crystal c-axis alignment, Arctic Alaska coast 80−67375
film, low-temp. diffusion of electrons, evidence for polaron bands 77−1380
film, on metal substrate, surface struct. using LEED 79−77879
flexural-gravity wave development, longitudinal tension effects *(Russian)* 79−100855
floating ice layer thickness meas. using nanosecond impulse X-band radar 78−62178
floating ice plate, time depend. deflections, linear viscoelasticity theory 77−17107
floating ice shelves, tidal flexure cracks, fracture mechanics 78−69368
floating sheet, viscoelastic response under prolonged loading 78−51093
folding, experimental, resultant c-axis fabrics 79−57983
folds and gravity tectonics in ice and rocks 77−70658
foreign object motion, liq.-like layer model, wire regelation, particle migration appls. 79−46893
formation in natural and seeded storms 78−61509
forward scatter and cross-polarisation from spheroidal ice particles 77−25733
fossil ice-wedge polygons, Mt. Daisetsu, Japan *(Japanese)* 77−81948
fractured sea ice field in Buzzards Bay, Massachusetts, effect on oil spill dynamics 78−40596
frazil ice conc. meas. system using laser Doppler velocimeter 77−25796
freezing water drops, ice envelope splitting *(Russian)* 77−27982
friction between steel ball and ice single cryst., load, velocity and temp. depend. *(Japanese)* 78−88537
friction between WC ball and ice single cryst., anisotropy *(Japanese)* 78−88539
friction between WC ball and ice single cryst., slider size effect *(Japanese)* 78−88538
frost blisters, growth meas. using long-term automatic time-lapse photography 80−12437
frost depth in soils of Urals and W.Siberia 79−57986
frost heaving in soils, role of disjoining press. 79−29791
frost mounds, Bear Rock, NW Territories, Canada, obs. during 1975-76 period 78−65346
frozen soil, prediction using weather records 79−88379
frozen soil, water and ice envelope pressure potentials 77−78286
Galilean satellites, ice sputtering and water products contrib. to Jupiter magnetosphere 78−45268
Galilean satellites, icy crater model to explain radar scatt. results 78−61789
ice continued
on Galilean satellites, IR spectral reflectance obs. 80−82263
gas content rel. to surface elevation of polar ice sheets 80−4053
in geological conductors, influence on elec. props. *(German)* 79−5472
geophysical timescales from absolute-dated ice cores from Greenland *(Danish)* 79−34776
GL 2591, protostellar source, 3 μm ice absorpt. band, linear polarisation obs. 80−105303
glacial ice, upwelling in stratified ocean due to melting 80−81897
glacial ice free convection melting in saline water 78−3835
glacial ice melting effects on Antarctic surface water 79−34866
glacier ice secondary and tertiary creep meas. by borehole closure rates 77−64339
glacier ice thickness meas., gravity profiling technique 78−32253
glacier structure and flow rel. to elongated air bubbles in ice *(Japanese)* 78−88861
glaze ice and rime deposition, effects of hills relief and geographical location 78−61525
glaze storms and wire icing in Ukraine 78−81329
grain boundaries in ice I_h, internal friction meas. *(French)* 79−55754
grain clusters in wet snow 80−26553
Grand Banks, icebergs drift model 78−81200
granular mass as quartzite model, expts. on grain struct. 80−21718
graupel, freely falling, wind tunnel study of hydrodynamic behaviour 78−49113
graupel development, numerical simulation 79−5573
graupel formation and growth, wind tunnel investigation 80−17324
gravel, ice-thrusting, shear deform. 78−65347
Great Lakes, ice formation, freeze-up, breakup predictions 77−45038
Great Lakes, shore ice rel. to W. Lake Michigan shoreline erosion 79−5542
Great Slave Lake fallout estimation from Cosmos 954 satellite 79−85830
Greenland, ^{26}Al activity compared with N.Pacific deep sea sediments 77−5181
Greenland, NH_4^+, SO_4^{2-}, Cl^-, Ca and Na in snow and ice, natural and anthropogenic origins 79−70815
Greenland and Devon Island ice cores, O isotope profile of last 10^5 years 80−41470
Greenland ice core records, 20 year climatic cycle 79−88470
Greenland ice cores, gas parameters, historical atm. comp. and climate determ. 79−8681
Greenland ice sheet topography from satellite radar altimetry 78−81233
Greenland Sea, LF sound propag. in marginal ice zone 78−85567
ground, perennially frozen, under cold store, struct. *(Japanese)* 78−88834
ground cover remotely sensed by radar, backscatter cross-section 80−46279
growth beneath water film, air bubble precipitation 78−83922
growth in laminar flow through a channel with two parallel flat walls 79−3908
Gulf of Bothnia, sea ice flexural waves meas. *(Japanese)* 78−96225
H_2O:HF ice, single crystal, velocity of individual dislocations by X-ray topography *(French)* 78−87677
hail, correl. with O_3 conc. *(Russian)* 77−29367
hail, crop damage, effect of wind and shelter by trees 77−45097
hail, Doppler radar spectra at vertical incidence 78−65368
hail, dual wavelength Doppler radar obs. at vertical incidence 79−79952
hail, during thunderstorm of 1976 June 27 at Heatree, Devon, England 78−57288
hail, equivalent reflectivity factor rel. to vertical fluxes of mass, kinetic energy 79−84393
hail, form. in axisymmetric cloud model 77−5294
hail, N.America, time and space scales 78−3877
hail, radar detection technique, quasilinear discriminant function 80−21861
hail, radio emission characts. in cm waves 79−96802
hail, review of meas. instruments 77−33196
hail, sampling errors in parameter meas. 78−28279
hail and crop damage, wind effects and hailcube meas. 77−17173
hail development during cumulus cloud seeding by ice particles *(Russian)* 77−81959
hail forecasting, book 77−73821
hail growth and airflow in supercell hailstorms, rel. to hail suppression 77−21856
hail growth simulation, fresh and annealed accretions struct. 79−58034
hail growth simulation, rotation and mixed clouds effects 79−58033
hail identification by radar, ice samples backscatter matrix 79−58046
hail in Colorado hailstorms, radar reflectivity at ground level 79−53470
hail nuclei determ. in clouds by radar and radiometric combined meas. *(Russian)* 79−12195
hail probability rel. to radar echo heights, South African Highveld 79−20925
hail producing clouds, N.E.Colorado, observed and computed microstruct. 78−77?6
hail reports rel. to 45 dBZ contour level 77−56688
hail size sorting in three-dimens. updraught, rel. to hail suppression 79−20926
hail suppression, crop protection, involvement of society 79−8677
hail suppression, current status 77−64363
hail suppression experiment, value assessment 78−7713
hail suppression expts., improvements 77−91218
hail suppression paradox, stratification approach to statistical expt. 77−37312
hail suppression seeding, Ag analysis 78−65367
hail suppression seeding, crop response anal., Nelspruit project, South Africa 78−57257
hail volume model extrapolation from surface meas. 77−21871
hail-prevention operations, cost effectiveness estimation methods anal. 78−93013
hailfall in N.E. Colorado, rel. to convective motion 80−31104
hailfalls kinetic energy, 10 cm radar and hailpad meas. 79−79951
hailfalls kinetic energy, hailstone spectra anal. 78−92924
hailpad calibration for Italian hail damage documentation 77−29488
hailpads calibration 78−93001
hailstone, melting, microwave scatt. 79−64179
hailstone formation, growth and suppression programs *(German)* 80−46243
hailstone growth, mixing processes effect on competition 79−79934
hailstone samples, Project DUSTORM, microprobe anal., element abundances 78−73453

ice continued
hailstone size determ. from dents in cold-rolled Al sheet 79−39890
hailstone trajectories determ. from crystallography, D content and radar backscatt. 78−61614
hailstones, foreign material obs. and derivation 78−96260
hailstones, free-fall kinematics near ground 80−12519
hailstones, from storms in Transvaal, 1972 November 29, D content determ. 78−20483
hailstones, isotopic, crystal and air bubble struct. 77−87008
hailstones, oblate, aerodynamics 78−20485
hailstones, size distribution spectra *(German)* 80−56593
hailstones, water-insoluble particle studies 80−41496
hailstones diameters rel. to entrainment rate in hail clouds *(French)* 77−53151
hailstorms, Switzerland, time-resolved hailstone size distrib. and radar struct. 78−49109
hailstorms in Transvaal, 1972 November 29, radar obs. 78−20482
hailstorms variability on South African plateau 78−92911
hailstripes, aerial photographs of crop damage patterns 78−3848
Hawaiian glaciation chronology, K/Ar and ^{14}C ages 77−33113
heavy, stopping power for low energy deuterons 77−35612
heavy ice Ih (D_2O ice), dielec. props. 80−29671
helicopter icing problems, role of meteorology 78−85657
heterogeneous crystallisation, of supercooled water, role of adsorption 79−95125
heterogeneous nucleation, lattice misfit, hydrophilic sites on hydrophobic surface 79−48530
heterogeneous nucleation of artificially modified ice *(Russian)* 77−29395
hexagonal, i.r. polarisability 77−4639
hexagonal, lattice struct., computer simulation 78−14324
hexagonal, pencil-shaped crystals and origin of anthelion, anthelic arcs and pillar 79−96821
hexagonal, Raman spectra temp. depend., 80 to 250K, translational vibr. modes 77−36221
hexagonal, Raman spectrum of translational lattice vibrs., press. effects 79−24304
hexagonal crystals, solar radiation scatt. 79−94150
hexagonal ice plate with spin, computer simulation of Lowitz arcs 79−96820
hexagonal single crystal, proton anisotropic chemical shift spectra 80−2650
high-pressure forms, ^2D and ^{17}O NQR from double reson. obs., quad. coupling consts. 77−90069
high-pressure Raman spectra, bending and librational bands 78−68499
Holocene retreat of W.Antarctic ice sheet, model 79−66725
Homer City power plant plume, aerosols and ice nuclei meas. 79−74570
Hudson Bay rivers, historical ice break-up dates as climatological data, content anal. 77−2224
hydrogen bond breaking by negative pion capture *(Russian)* 79−94866
hydrometeors, radiative props. at microwave freqs. 79−20940
hydrometeors in clouds, size, conc. and struct. meas. 77−41218
I_h, hexagonal, ferroelec. transition 79−91386
I_h, single crystal Raman intensities, OH bond polarisability, librational modes 78−27208
I_h, water monomer on basal plane, static interaction 78−18891
Iapetus, water ice identification from relative reflectance meas. at 1.6 and 2.2 μm 80−98607
Iapetus light face, ice detect. from near IR reflectivity meas. 80−26800
ice domes, time dependent deformation 79−37152
ice-water interface, dynamic light scatt. during freezing 79−33074
ice-water interface, surface tension meas. by grain boundary groove method 77−24481
ice-water phase boundary, conc. depend. solute redistrib., spontaneous convection, chloride solns. 78−26665
iceberg detection and characterisation, synthetic aperture radar appl. 80−26622
iceberg fluctuations in North Atlantic *(German)* 78−49038
iceberg sounding by impulse radar 78−24388
iceberg underwater shape determ., impulse radar appl. 80−26621
iceberg volume meas. using photogrammetric techniques 77−82048
icebergs, melting in environment with salinity gradient, rel. to fresh water supply 78−24305
icebergs, upwelling prod. in Weddell Sea 77−56647
icebergs from Antarctica for Saudi Arabia water supply 77−81949
icebergs underwater profiling using unmanned submersibles, echo sounder and scanning sonar 79−5673
Icelandic, thermal and physical characts. of subglacial volcanism 80−101350
icicles, examination between crossed polarizers, growth mode determination 79−41995
Ih, dislocations, effect on physical and mechanical props. *(French)* 77−55287
Ih, elastic diffuse neutron scattering due to D-D correlation functions 80−96493
Ih, polycryst., IR spectrum, OH stretching region 79−11411
Ih, polycryst., Raman spectra, OH stretching region 79−11410
Ih, polycryst., vibr. spectrum anal., OH stretching region 79−11412
Ih, thermal resist. near melting point meas. 80−44375
III, dipolar correlation factor and dipole moment of water molecule 79−77548
impact craters in ice and ice-saturated sand, Martian implications 80−67614
impact of rigid body on ice, hydrodynamic model *(Russian)* 77−20002
impurities in Ic struct., divalent ions hydration 79−51122
initiation in cumulus congestus clouds unmixed updraught cores 80−81997
insulating material appls., electrical breakdown at cryogenic temps. 80−45007
interglacial episode termination and Wilson Antarctic surge hypothesis 78−53669
interplanetary and interstellar ice grains, low energy cosmic ray erosion 78−45177
interplanetary ice particles, lifetime 77−29721
interstellar amorphous ice, as source of 3.1 μm absorpt. in mol. clouds 80−26956
interstellar amorphous ice grains, H_2 form. and importance for planetary atmospheres 80−26933
interstellar ice, 45μm signature possible identification in Orion 79−17068
interstellar ice, evidence from refl. nebulae simplified models 78−96526
ice continued
interstellar ice, identification as carrier of 3 μm absorpt. in IR sources questioned 78−49499
intrinsic surface order near melting point 79−14986
ion beam erosion effects, energy depend. 80−65067
IR ν_s absorption band profile of isotopically diluted OH group in crysts. 79−69821
IR absorpt., O-H stretching vibrs., orientation polaris. 78−31177
IR and Raman O-H stretching bands of ice I 78−19454
IR spectra interpretation, OD stretching bands, 10K, ice II and IX 78−2836
Iraq, frost phenomena and damage 77−73795
IV, 4000-400 cm^{-1} IR spectra, H-bonding and assignments, orientational disorder 80−16022
IV, thermal expansion anomaly rel. to order/disorder transition at 115K, 10.54 kbar 79−46819
Jungfraujoch ice-cores, impurity determ. by neutron activation anal. 78−11920
kinematic eddy viscosity of pack ice *(Japanese)* 77−81913
lake ice, microwave radar and radiometric remote sensing meas. 80−85691
lake ice cover, dissipation, effect of surface meltwater accumulation, heat flow 80−8364
lake ice-cover thickness, pulsed radar meas. method 78−92862
Lake Tofutsu, Hokkaido, ice crystallography *(Japanese)* 80−36347
lakes, ice-covered (North Slope, Alaska), radar return differences 79−2298
land-ice slide, glacier-initiated, near Pylon Peak, British Columbia 78−36208
lattice energy, rel. to water struct. theory pot. energy function 79−73125
Laurentian Channel and W Grand Banks, relict iceberg furrows 77−5206
layer formation of given thickness by accumulation on cooled-cylindrical surface 77−7850
lidar scattering from snow and ice crystals in atmosphere, polarization characts. 77−64430
liquid-solid phase transition, photoacoustic detection 78−75810
liquidlike layer on ice surface, thermal expansion meas. 79−19381
Lithuanian lake water temperature rise (spring 1974) *(Russian)* 79−8644
localised excess electrons, semicontinuum models 78−73129
Loch Lomond Stadial in British Isles 79−79887
long-period gravity waves in ice-covered sea 80−67372
lunar polar regions, ice and trapped volatiles existence 80−26759
Mackenzie River, Canada, ice-push features stability 78−28247
major satellites of outer planets, internal structs. 79−62770
marginal ice zone, wave decay, inverted echo sounding from submarine 78−49025
Mars, crust, possible fossil H_2O liquid-ice interfaces 78−65539
Mars, north pole summer temps., dirty water ice 77−56866
Mars, permafrost features 78−20670
Mars, polar ice discovery 77−22130
Mars atmosphere, O_3 layer and two aerosol layers detect. by Mars 5 spacecraft UV obs. 78−49357
Mars atmosphere thermal IR properties, dust and ice clouds detect. from Viking IRTM spectral meas. 79−84712
Mars fretted terrain, rock glaciers flow 78−65537
Mars north polar region, perennial ice margin fluctuations rel. to dust deposits 80−31225
Mars permafrost, implications of atmospheric water vapour global seasonal var. 79−84714
Mars permafrost, melting rel. to explosive volcanic density currents on volcanoes 79−84705
Mars polar areas, volatiles behaviour, model 78−49363
Mars polar landscapes evolution, interplay of perennial ice cover and dust storm intensity vars. 79−84721
Mars surface evidence for H_2O ice from reflectance spectroscopy 80−72834
Martian permafrost, melting rel. to channels form. and ages 78−20669
mechanical properties of sea ice, in-situ meas. using flatjack methods 80−69751
melting, heated water jet impingement melting, cavity formation, expt. and simulation 78−95133
melting, in porous solid, NMR and differential scanning calorimetry obs. 77−62621
melting, one-phase Stefan problem, continuity of soln. in n space dimensions 78−95130
melting in sea water, model, Antarctic ice shelf and iceberg appl. 80−4036
melting layer, heated, free convection onset criterion, density anomaly effect *(German)* 78−22351
melting of ice block with impinging water jet 77−935
melting surface, ablation in impingement region of water jet 80−14766
mesosphere, spherical ice particles, equilibrium temps. rel. to noctilucent cloud formation 77−37302
metal interface, mech. behaviour and crack prod. of single cryst. 78−43230
microcrystal dispersions, dielec. props. *(French)* 78−60374
microcrystals, emulsion, complex dielec. permittivity meas. *(French)* 78−10821
microcrystals, NH_4Cl doped, activation energy of Debye's dipolar relax., influence of salt content *(French)* 78−56424
microwave attenuation at 36.8 GHz in sea ice, freshwater ice and snow, meas. *(Russian)* 77−5209
microwave brightness spectra of layered media 77−81898
microwave meas. of reflectance, at 100, 140 and 180 GHz 79−84552
microwave satellite paths, crosspolarisation phase due to ice crysts. 78−7684
microwave spectroscopic imagery of Earth from Nimbus 6 satellite 78−12026
Milankovitch theory of ice ages, study using simple climate-ice sheet model 78−40644
monolayer ledges on basal surfaces 77−35809
Monte Capellino, ice formation, meteorological conditions statistical analysis *(Italian)* 80−12471
morphology of ice crystals grown from vapour, influence of vapour diffusion and heat diffusion 80−64933
natural clay permafrost, electrical props. 77−44967
natural convection heat transfer from horizontal ice cylinder, anal. and obs. 77−27521
natural nucleation at −1°C using bacteria 77−53221

ice continued
natural nuclei concs. and props. in W. Africa *(French)* 77−9474
neutron elastic diffuse scatt. of Ih struct., series expsn. calc. 78−2027
New England, 1816, snow and frost in year without summer rel. to Tambora volcano eruption 80−4089
noctilucent clouds, circularly polarised light detect. rel. to ice crysts. growth 79−48568
noctilucent clouds, elliptical polarization rel. to ice crystals 78−11946
noctilucent clouds, temp. of aerosol ice particles *(Russian)* 78−16093
North Sea, microwave meas. using SLAR 78−77245
NQR of ^{17}O in ice Ih, double NMR for ^{1}H tunnelling, 1.3 and 4.2K 79−47353
NQR of ^{2}D and ^{17}O in ice II 77−1617
nucleating materials 78−49093
nucleation, effect of rocket effluent 79−88446
nucleation, elemental comp. of natural ice-forming nuclei 78−3881
nucleation, on PbI_2, −10 to −25°C *(French)* 77−78301
nucleation, two-step 78−49094
nucleation by fluid-breaking metaldehyde particles *(Chinese)* 80−12468
nucleation in atmosphere, natural nuclei origin 79−48531
nucleation mechanisms of submicron aerosol particles 79−20947
nucleation on AgI, CNDO calc. 77−4254
nucleation on AgI, exptl. verification of ice-forming activity theory 80−101406
nucleation on AgI, influence of aerosol particle size, struct. 80−61164
nucleation on AgI aerosols at different supercooled fog temps. *(Russian)* 77−27983
nucleation threshold on Cu_2S, Ag_2S, MoS_2 and CdS photosensitive surfaces 77−55343
nuclei, probability of formation in supercooled water 78−3909
nuclei, tropospheric, in summer, background levels in Greenland 80−72609
nuclei and atmospheric aerosols, elemental comp. 78−3882
nuclei conc. meas., filtration theory appl. 79−39887
nuclei generation for weather modification, supersonic expansion method 77−29487
nuclei in seawater and fog off Nova Scotia coast during 1975 Summer 78−16104
ocean, broken ice effects on ship waves *(Russian)* 78−65326
ocean, moored instruments for meas. in permanently ice-covered waters 78−49150
ocean waves attenuated by pack ice 80−36332
ocean wind-driven quasigeostrophic water movements near fast ice edges 78−49026
oceanic ice movement measurement, microwave radiometers *(Danish)* 80−26624
one-dimensional crystal, ground state energy, PCILOCC method 79−10056
ρ Ophiuchi dark cloud, ice mantles and abnormal extinction 79−21376
orientational correlation parameter, water mol. dipole moment for ice VI 80−59407
oscillatory ice states in water internally heated and cooled from above 77−73759
pack ice, drift observed using radar buoys *(Japanese)* 78−96224
pack ice deformation by ridging 79−70807
pack-ice dissipation, atmospheric CO_2 impact on snow and water surfaces cooling 79−92569
particle counting in mixed-phase clouds by optical techniques 77−41221
particle engulfment, theoretical model 80−54351
particle fog, aerodynamic and opt. props. 77−90648
particle types in melting layer vicinity, determ. from Doppler radar meas. 77−78338
particles, interpretation of foil impactor impressions, rel. to hail research 78−57356
passive microwave obs. from Nimbus satellites 80−101422
permafrost, active layer heat transfer medium *(Russian)* 80−81943
permafrost, approx. calc. of thawing zone boundaries under heat sources 77−25706
permafrost, common depth point survey technique appl. *(Russian)* 78−53751
permafrost, computer-assisted interpretation of EM soundings 77−2086
permafrost, dynamics of hummocky microrelief in Canadian north 77−64285
permafrost, effect of seepage flow on thawing and freezing 79−1241
permafrost, elec. props. of active layer, in situ meas. 77−64333
permafrost, icy, in NE.British Columbia, distrib. and thickness 78−77277
permafrost, neutron moisture gauge for water detection *(Chinese)* 79−34997
permafrost, shallow, mapping, EM methods 79−16694
permafrost, struct. changes during freezing and thawing 77−25707
permafrost, thermal amelioration tests near Schefferville, Quebec 77−33058
permafrost, two-dimens. temp. field with arbitrary temp. distrib. on subaerial surface 77−25703
permafrost, US vels. and elec. props. 77−78157
permafrost beneath the Beaufort Sea: near Prudhoe Bay, Alaska 80−94552
permafrost discontinuity geometry and physical props. determ., Schefferville, Canada *(French)* 77−66990
permafrost fossil patterns, S.W. Ontario, resistivity mapping 77−66991
permafrost layer thickness and temp. variations under sedimentation or denudation conditions 77−78241
permafrost mapping by audiofrequency magnetotellurics 79−58102
permafrost near Tuktoyaktuk, NWT, impulse radar obs. 77−17149
permafrost on Mars, thermodynamics 80−67621
permafrost soil, compressional and shear wave vels. using US pulse technique 77−17081
permafrost soil in Yakutia (USSR), long-term studies of thaw dynamics 77−78240
permafrost terrain, EM probing, theory 78−28323
permafrost thickness determ. in wells in N. Canada 77−66989
permittivity at mm wavelengths 80−66098
petroleum industry, Newfoundland, problems rel. to sea ice, icebergs 79−87946
phase transition, ice VII-ice VIII, second-order, Haus-Tanaka model 80−70385
phase transition from disordered VII phase to ordered VIII phase 80−19911
planetary satellites, convection in ice crusts, effect on surface relief 79−84730
ice continued
plastic deformation, ultrasonic wave attenuation by dislocations *(French)* 80−59564
plastic limit analysis with anisotropic parabolic yield function 77−91114
plate crystal oscills. and circumzenithal arc 79−96822
platelets, radiation attenuation effectiveness factor determ., IR absorpt. 80−66141
Pleistocene ice fluctuations rel. to Earth orbit vars. 77−37346
PMR chem. shift anisotropy, nucl. mag. screening tensor 78−17687
polar ice cap, low-level beta counting with an automatic sample changer 80−31147
polarisation processes, in lattice, Kirkwood's theory rel. to thermodynamics of irreversible processes 79−38447
polarisation processes, in lattice, thermodynamics of irreversible processes, universal relation 79−38446
polycrystalline, natural abundance PMR, chem. shift meas. 79−67365
polycrystalline, twinning model with cubic struct. at junctions 77−1136
polycrystalline cores, creep laws for various stress states *(French)* 77−53077
polycrystalline ice I, 2500-4000 cm^{-1} Raman and IR spectra, vibr. anal. 77−59562
polyerystalline matrices, electron spin-lattice relax. of radiation-produced Ag atoms, temp. depend., tunnelling relax. 79−34331
polymorphic transition at high-press., 123.1K, HF permittivity study 79−55883
pre-ice-nucleation conditions in settling cloud chamber, numerical simulation 79−79950
precipitation layers, evaporation effects at base, theory and radar obs. 77−78312
pressure melting within glacier, indicated by regelation ice chem. comp. 78−61447
proton irradiation damage in monocryst. ice, 100 keV proton channelling 80−34102
puddle water, nighttime disappearance with ice needles growth and daytime reappearance 77−29334
Quaternary sediments and stratigraphy, continental shelf, N.Norway, extent of ice-sheet 79−84228
radar returns from sea ice, freq. charcts. *(Japanese)* 80−36328
radiative heating 77−84130
radiative melting of horizontal clear ice layer, rel. to atm. icing *(German)* 79−18679
radiative melting of ice layer adhering to a vertical surface *(German)* 79−76956
radio echo sounding of Greenland ice sheet, polarisation of signal 77−56755
radio echo sounding of ice sheets, internal props. var. with depth 80−26633
radiowave forward/backward scattering from liquid/solid hydrometeors, Rayleigh approx. 79−25321
radiowave propag., scattering amplitudes and crosspolarisation of spheroidal ice particles, calc. 77−70740
Raman spectra of O-H and O-A stretching vibrations of ices II and IX 80−66166
Raman spectra up to 35 kbar, VI, VII and VIII phases 77−87839
Raman spectrum, press. effects 78−95582
random network model, liq. and ice polymorphs, enthalpy and heat content 80−64869
rime deposition, quantitative meas. using fog-gauge 80−56654
rime deposits as indicators of wind direction 80−98428
riming electrification as a charge generation mechanism in thunderstorms 79−34917
riming on thin ice plates 77−78316
riming process, laboratory expts. 80−105037
river channel enlargement, effect on bankfull discharge 80−8369
river ice, book contrib. 78−61476
river ice, influence on behaviour and use of rivers 79−62525
river ice break-up, satellite monitoring 78−65350
river ice jams, physical meas. 79−53398
river ice processes, radiohydroacoustic monitoring method 80−26649
river ice-cover thickness, pulsed radar meas. method 78−92862
rivers, acoustic noise from breaking ice 78−53671
rivers, ice jams form. conditions and forecasts 78−92863
rivers, ice-jam backwater levels cutoff period 79−39778
Ross Ice Shelf, circulation and melting 79−88363
Ross Ice Shelf (Antarctica), basal freezing, confirmed by core drilling 80−101393
Ross Ice Shelf project, results 79−88366
Ross Ice Shelf sea temperatures 79−88362
rupture mechanism exam. *(German)* 78−52976
saltwater drop falling in organic phase, ice growth 80−15218
Saturn B-ring, optical reflectance polarimetry interpretation 80−31248
Saturn ring system, presence of H_2O ice from far UV spectrum obs. 78−53867
scavenging of spherical particles by charged thin ice plates, efficiency 78−44934
sea, ice-covered, flow vel. and ice thickness effects on unsteady waves *(Russian)* 78−65324
sea ice, airborne laser profiles, interactive correction and anal. system 79−25338
sea ice, anisotropic props. in 50-150 MHz range 80−17274
sea ice, CO from arctic surfaces during spring thaw 80−41511
sea ice, complex dielec. const., 0.1-40 GHz 78−61430
sea ice, Danish studies using Landsat and airborne sensor data 80−94527
sea ice, dynamic thermodynamic model 80−51432
sea ice, effect on internal wave development *(Russian)* 77−78193
sea ice, effects on non-linear small-scale sea-air interaction parameterisation *(Russian)* 77−53068
sea ice, EM sounding by Arctic and Antarctic Research Institute, Leningrad 80−4504
sea ice, EM wave scattering from slightly rough boundary 78−77266
sea ice, energy exchange in central Arctic 78−85584
sea ice, failure by compression *(Japanese)* 78−88841
sea ice, haline convection induced by sea water freezing *(Japanese)* 78−88843
sea ice, initial forms, microwave refr. index and absorpt. 78−49036
sea ice, long range forecasting for north coast of Alaska 77−2174
sea ice, low-salinity, radiometer studies 78−81175
sea ice, microwave radiometric obs. appls. 78−81415
sea ice, microwave remote sensing in AIDJEX main expt. 78−81173
sea ice, ocean waves SAR imaging 79−5496

ice continued
sea ice, radar anisotropy due to horizontal c axes preferred aximuthal orientation 79−34836
sea ice, radar wave reflected power intensity reduction with range *(Japanese)* 80−36329
sea ice, relationship between mean stresses and internal forces local values in drifting cover 80−31056
sea ice, remote sensing, appls. 80−77176
sea ice, sea floor scouring 78−92822
sea ice, sidescan sonar imagery, Arctic Ocean 79−25339
sea ice, US vel. meas. 77−33094
sea ice, wind stress meas. *(Japanese)* 78−88842
sea ice and engineering under Arctic conditions, conference (Fairbanks, Alaska, August 1975) 77−37236
sea ice and glacial development in Late Cainozoic N.Hemisphere 80−90098
sea ice and open water in Bering Strait, radar monitoring 77−87100
sea ice and surface temp. meas., enhanced IR satellite imagery 77−37422
sea ice apparent viscosity seasonal vars., drift models 77−33085
sea ice chemistry 79−12128
sea ice cover dynamics averaged eqns., asymm. internal stress tensor *(Russian)* 77−81909
sea ice cover nonuniform thickness effects on navigability 77−78222
sea ice crystal orientation along Arctic Ocean margins 79−16486
sea ice deformation, viscous law as stochastic average of plasticity 78−16028
sea ice distribution determ., appls. of satellite ocean-related imagery programme 79−5681
sea ice drift, oceanic boundary layer effect, model 80−26528
sea ice dynamics in Arctic (May 1975), simulation 78−36192
sea ice field of Okhotsk Sea coast of Hokkaido, divergence and rot. meas. *(Japanese)* 78−96223
sea ice formation, assoc. heat and salt transfer 77−64324
sea ice from glaciers, melting process *(German)* 80−33606
sea ice in Beaufort Sea, August ice cover vars. rel. to mesoscale weather conditions 80−101366
sea ice in polar regions, radio obs. appls. 78−81419
sea ice large-scale numerical model 79−48490
sea ice mapping and drift meas. using aircraft synthetic aperture radar images 79−70809
sea ice meltwater in E.Canadian Arctic, isotope study 80−77002
sea ice near Showa Station, Antarctica, physical props. *(Japanese)* 78−96226
sea ice pressure ridges, statistical distrib. 79−79847
sea ice ridging over Alaskan continental shelf 80−12410
sea ice seasonal change model 77−17128
sea ice shelves tidal flexure, meas. by tiltmeter 80−31050
sea ice structure, effects of artificial inclusion *(Japanese)* 78−88844
sea ice types, radar scatterometer discrimination 77−41198
sea ice underside, geometrical roughness props. 80−98334
sea ice-ocean temp. oscillator model, nonlinear analysis 80−12413
sea-ice, climate feedback systems involving ocean temp. and CO_2 80−98443
secondary crystal prod., rel. to charge separation in atmosphere 80−81998
semi-infinite plate subjected to increasing boundary force, dynamic response, ice sheets 78−83254
shear strength temperature depend. 80−24523
sheet deflection by submerged gas source 77−80120
shorefast sea ice melting study using multispectral LANDSAT data 77−78522
snowcrystals and natural ice nuclei from Colorado winter storms 77−9475
snowflakes rel. to cloud formation and Chinese name for mica 77−91195
soil, frost heave in Tomakomai, Hokkaido, 1976 to 1977 *(Japanese)* 78−92860
soil, seasonal freezing or thawing depth calc., eqns. eval. 77−78243
soil freezing, water migration obs. *(Japanese)* 78−88862
soil freezing velocity meas., recording device design *(Japanese)* 77−82033
soil thawing under polar conditions using synthetic film covers, thermal balance meas. on polymeric film covered surfaces 77−78244
soils, freezing, heat flux, meas. *(Japanese)* 78−88835
solubility of HF in ice single crysts., 180-270K 77−28007
splintering mechanism during rime growth 79−39788
spring break-up of estuaries on Hudson Bay 78−11930
sputtering, MeV light ions, erosion rate study 78−48268
St. Augustine volcano, Alaska, search for atmospheric ice nuclei production 77−13110
static dielectric constant of Debye component in ice Ih, Curie-Weiss behaviour 77−81044
steady flow of viscous nonlinear fluid (Glen body) around perfectly smooth sphere *(French)* 79−7387
steam-water-ice system, two-dimens. triangular lattice model, matrix calc., props. 77−27975
storms, principal component anal., hail index *(French)* 78−96267
strain heating and creep instability in glaciers and ice sheets 77−86954
stratiform ice clouds, precip. development, aircraft and Doppler radar meas. 77−70761
strength meas., in situ tests 77−37423
structure factors, X-ray Pendellosung method 80−1981
subglacial lake, Antarctica, radar sounding 79−29798
sublimation, heat and mass transfer investigation, thermal shock method 77−50864
sublimation, surface process affected by supplied heat 77−46889
sublimation drying in UHF EM field 78−83936
sublimation from frozen salt solns. 77−84918
subsea permafrost heat and mass transport processes, mol. diffusion and consequences anal. 79−2302
supercooled cloud, drop size distrib. influence on secondary ice particles prod. during graupel growth 78−73481
supercooled fog, −20°C, influence of aersol particle size on AgI ice-forming activity 79−53465
supercooled fog, crystn. by means of powdered synthetic zeolite 77−37296
supercooled water droplet surface effect on ice crystal kinetic formation *(Russian)* 77−13099
supercooled water drops, hydrodynamic behaviour, interaction with columnar ice crystals 78−32205
surface, near 0°C, 100 keV proton channelling meas. 78−14549

ice continued
surface, viscosity of nonfreezing thin interlayer between ice column and quartz capillary 80−54475
surface layer, viscosity, from thermal contraction meas., 0 to −50°C 80−49469
surface potential observations, rel. to thunderstorm charge separation 80−51495
surface transition layer, ellipsometric study 80−103545
surface viscosity, activation energy, vacancy migration 80−107458
Swiss randomized hail suppression expt., design of Grossversuch IV 79−84542
tabular iceberg, off Newfoundland Grand Banks, deterioration 77−56646
Tarmanskii Marsh, permanently frozen layers form., influence of human activity 78−92864
terrestrial planetary atmospheres, role of ice clathrate 78−28557
thermal and electrical conductivity, 0 to −20°C 77−24450
thermal conductivity, for 9 phases 78−30801
thermal fracture 79−65141
thermal radio emission from exponential slab, sea ice appl. 78−28244
tidal energy dissipation by Antarctic ice shelf flexing 78−88845
tidal interaction with ice shelves 77−86902
transverse flexure, refined Reissner anal. 80−88247
troposphere ice particles, depolarisation of 19 and 28 GHz Earth-space signals 78−73492
turbulent boundary layer under pack ice 77−17130
two-dimens. square ice, correl. function calcs., approx. methods, Bjerrum fault conc. effects 80−10513
undergraduate experiment on ionic cond., elec. cond. temp. depend. and dielec. props. 79−35503
UPS, valence band struct. 79−33890
UPS study 79−43101
upwelling along edge of Arctic ice pack 79−92547
vacancy concentration calc. from self-diffusion const. 77−35553
vapour pressure formulation using thermodynamic calcs. 78−43117
VI, OH stretching peak freq. press. depend., Raman spectra using diamond anvil cell 80−16023
VI phase, shock compression expts. for Hugoniot function 80−84248
vibrational spectra of ice I, O-H stretching region 77−59563
VII, melting curve up to 150 kbar 78−67812
VII to VIII transition, lattice model 78−10187
viscoelastic behaviour of sea ice, static loading expt. *(Japanese)* 77−81914
viscosity, of thin interlayer of aq. soln., between ice and quartz capillaries 79−55913
vitreous, sp. ht., entropy and 'glass transition' 77−51520
water supercooled droplets, on ice substrate after low speed collision, freezing behaviour, cryst. struct. 80−29152
water transport towards ice front in porous media 77−945
water-acid ices, UV irrad., EPR of H and D, nucl. electron effects 79−83488
water-free crevasses spacing in glaciers 80−21784
water-ice interface, local temp. meas. and convective flow 79−73293
water-ice interface struct., fluctuations during solidification 78−59935
water-water, pair pot. near H bonded equilib. config., amorphous and crystalline solid and liq. 80−64946
Weddell Sea drift ice, pushed north by barrier winds 80−26514
wind interaction with dry snow and bare ice surface 80−109181
X-irradiated, EPR spectra, obs. of thermally reversible radical, g-value 79−5144
X-ray diffraction meas. with DRON or URS-50 spectrometers 78−24910
Ag, and Ag^+, solvation in deuterated-ice matrices, electron spin echo obs. 80−15780
Ag and Pb halide surfaces, ice-forming capabilities, mol. studies 77−31872
Ag solvation, in ice matrix 79−5166
Ag solvation, in ice matrix, ESR and irrad. at 4.2 and 77K 79−8444
Ag solvation in ice matrix, electron spin echo modulation 78−39396
AgI aerosol, ice forming activity, UV irrad. effect 80−71950
AgI aerosol particles, influence of cryst. struct. on their ice-forming activity 79−16048
$Ca(NO_3)_2$-H_2O solns., ice I homogeneous nucleation temp., slow vitrification mechanism 78−26666
D_2D, ^2H quadrupole resonance, double transitions 79−3465
D_2O, H_2O, intramolecular potential from overtone spectrum anal., H-bonding dependence 79−93972
D_2O ice, crystalline, irrad., temp. depend. of trapped electrons, 77 to 6K 79−83474
D_2O, ice cryst., electron traps, electron irrad. effects, EPR 77−1939
D_2O, thermal cond., H and D order effects 78−67871
D_2O-H_2O, intramolecular stretching spectrum, role of Fermi resonance 79−93973
D_2O-H_2O ice, thermal cond., H and D order effects 78−67871
HF doped ice I_8, anelastic relax. *(French)* 78−6122
$H_2{}^{16}O$ and $H_2{}^{18}O$ samples, vap. press. isotope effects, −50 to 0°C 78−18757
H_2O:D_2O, I_c phase cryst., IR spectra, H exchange activation energy 79−99866
H_2O:D_2O, ice Ic, vibr, decoupling, IR spectrum 79−13706
H_2O:HF ice, pulsed NMR 77−28467
N compounds exchange between ocean-atmosphere-continent system 78−3794
Na montmorillonite, water vapour adsorption and ice form. at −5°C 78−65540
Na-ice condensate, EPR lineshape second moment, electron solvation struct. 78−3440
NaOH aqueous glassy systems, 77K, γ-irrad., struct. stabilisation 79−91976
^{17}O, NQR spectrum by double reson. with coupled multiplets, fine struct. 80−54969

iconoscopes · *see television camera tubes*

identification
see also control theory; correlation methods; frequency response; modelling; parameter estimation; simulation; state estimation
beam boundary conditions vibratory identification 77−27480
biological compartmental systems, multi-input and multi-output, controllability, observability and structural identifiability 78−76978
biological compartmental systems analysis, computer program 77−40625

identification continued
biological system, quasi-white random signals optimal use, appl. 77−73528
biological system, quasi-white random signals optimal use 77−73502
biological system, survey 78−31753
biomedical signal modelling and recognition, system identification approach 80−51286
blood pressure control model 77−21557
BWR dynamics, multivariable autoregressive identification 78−94107
cardiovascular system, identification and parameter estimation 80−35947
cardiovascular system, mathematical models and identification problems 80−89780
coeff. in heat conduction equation, inverse Cauchy problem solution *(German)* 80−33419
compartmental system anal., identification method, body tracer kinetics appls. 80−35816
crayfish stretch receptor repetitive firing behaviour nonlinear systems anal. 78−80853
distributed parameter system control, conference, Coventry (1977) 79−3897
distributed parameter system identification using doubly cubic spline, underground aquifer appl. 78−69391
dynamic safeguards accounting and material control via modern estimation methods 77−34417
Earth atmosphere vertical temp. profile estimation method 77−91342
earthquake model, nonstationary, identification, nonlinear filtering approach 79−5458
ECG, multiform ventricular complex identification, 2-dimens. clustering technique 79−66570
ECG ambulatory monitoring, detect. algorithm for multiform premature ventricular contractions 79−66572
ecological system model sampling/identification, input signal anal. 78−69267
EEG isolated events identification, automatic system 79−5400
EEG nonstationary point automatic detect. *(French)* 78−57112
environmental pollution control system methodological approach problems 77−21899
environmental system, conf., Ghent, Belgium (Aug.-Sept. 1977) 79−25250
environmental systems planning, design and control, conf. Kyoto, Japan, (Aug. 1977) 79−52962
external geniculate body receptive field of cat, space-time wt. function 78−64989
external geniculate body receptive fields, neuronal network model 78−64990
fluorescein tracer model, determination of flow rate of aqueous humor in eye 79−43943
hydrological system statistical modelling *(German)* 78−96246
image degradation, methods 78−58941
intervertebral joint, systems identification for material props. 78−69125
neural, state variable approach 78−35825
neural transformations of random signals, Wiener and of functionals of Markov chain 80−76727
nonparametric identification for diffusion processes 79−30374
nuclear facilities vital area, fault tree analysis appl. 79−85691
nuclear industry, nonlinear systems, nonparametric system identification 80−32325
nuclear power plant, PWR, dynamic testing for model validation 77−3087
nuclear power stations 77−88213
nuclear power system and fuel channels stochastic identification and parameter estimation 79−3201
nuclear reactor, dynamic data system methodology 78−25321
nuclear reactor, test inputs review 78−41819
nuclear reactor fuel reprocessing in-process inventory dynamic measurement 77−38371
nuclear reactor system identification technique 77−65266
optical scanning system for 3D objects identification and spatial position meas. *(German)* 79−71405
P wave detection and identification using statistical signal analysis 80−8202
pattern identification, large-spatial, of air pollution by combined model of source-receptor matrix and revised GMDH 79−57543
physiological system, nonlinear, Volterra kernels representation determ. 79−2034
plasma physics problems 78−71532
porous media, miscible or immiscible displacements, identification and modelling 78−69392
probabilistic vector model for identification of intervocalic stop consonants 78−69114
pupillary light reflex system, modelling and identification 80−61554
radioactive tracer kinetics, compartmental system identification by optimum sampling 77−86615
rainfall-runoff process identification, Semois river appl. 79−5537
renal function, identification techniques 79−96658
respiration rate meter, corona discharge identification and ionisation current control *(French)* 79−92411
respiratory system model, identification via mathematical pattern recognition 79−2096
river, dissolved oxygen and biochemical oxygen demand, random signal anal. applic. 77−45047
river water quality monitoring, pollution sources estimation 79−52970
sampling stroboscopic convertor identification by Hammerstein model *(Russian)* 80−74495
semicircular canal afferent response system identification 78−27927
soil automatic identification from digital terrain data 77−73884
speech waveform coders, objective quality meas. equipment and method 80−91981
streamflow, model, identification of seasonal water supply forecasting models using Akaik's information criterion 80−67386
thermokinetics of coupled radiative and conductive transfer, Kalman filtering identification *(French)* 79−41558
3,3′,5′-triiodothyronine plasma to tissue transport rate estimation from 3-compartment model 78−31792
upper extremity prosthesis online control based on EMG signal identification using microprocessor hardware 79−2166
upper limb prostheses multifunctional control via EMG signal identification 78−3683
upper-limb prostheses multifunctional control microprocessor system, myoelectric signal identification method 78−88766
water quality system, biological process models 79−5540

iets *see tunnelling spectra; tunnelling spectroscopy*
IEXE *see ion microprobe analysis*
i.f. amplifiers *see intermediate-frequency amplifiers*
i.g.f.e.t. *see insulated gate field effect transistors*
ignition
see also electric ignition
air-H_2 (methane) mixtures, ignition energy by capacitive discharge *(French)* 80−10446
arc with emitting cathode, ignition, rel. to Cs diode 77−7623
arc with emitting cathode, ignition 77−7622
boundary layer near heated plate, ignition of gas *(Russian)* 78−9725
coal, fluidised bed firing, technological state and economic chances *(German)* 79−92050
coal dust aerocolloids, ignition inhibition, flame extinguishers effects 79−100375
cool flame explosion, during piston compression, time predicted by Livengood-Wu integral method 78−15675
decane-air mixture, spontaneous ignition temp. limits determ. 77−52641
dust clouds, ignition and flame quenching 80−28577
flames, ignition and propagation, self-consistent 2-dimens. hydrocode 78−47066
fuel droplet on hot surface, evap. and ignition 79−96310
fuel droplet on hot surface, evap. and ignition 79−96311
gas mixture, by electric sparks, Kesaev cathode cell formation 80−70066
gas mixtures, ignition energy by capacitive discharge and through discharge of person charged with static elec. *(French)* 80−10446
gas-phase ignition of diffusion flame, in stagnation point fuel boundary layer 77−58803
gasless systems, heat losses effect on ignition by combustion wave 79−100371
internal combustion engine, conc. fluctuation meas. 80−71973
laminar diffusion boundary layers, ignition and extinction 78−64838
metal powder suspension in air, spontaneous ignition temperature *(Russian)* 78−47027
metal-gas system, ignition conditions with account of radiative heat loss *(Russian)* 77−32789
methane, stored energy needed to ignite by discharger from charged person 80−54063
PMMA, spreading of two-phase film of melt, heat and mass exchange, ignition and combustion *(Russian)* 78−76861
propane, ignition by small sparks 79−55587
reactive material ignition by heated surface, asymptotic anal. 78−7206
reactive-diffuse systems with Arrhenius kinetics, multiple solns., ignition and extinction 79−66260
shock wave ignition of metal powders, pre-ignition processes 77−40546
sparks of minimum ignition energy, spark formation 79−10729
stagnation flow at a heated curved wall, ignition condition 80−96242
stagnation-point ignition, premixed combustible 79−16000
thermal explosions, heat balance and reactant consumption 77−90601
thermal-ignition analysis in boundary-layer flows 79−64800
thermionic converter, ignited mode, internal phenomena and output characteristic *(Japanese)* 80−3527
thermionic convertor, ignited mode, electron energy distrib. meas. of Cs plasma *(Japanese)* 80−3528
Al powder, gas suspension, critical spark ignition conditions 79−100373
B ignition and burning *(Russian)* 80−45502
H_2-O_2 mixture, explosion limits as stochastic phenomenon 77−21387
Mg, ignition, critical conditions 79−100372
Mg, powder, gas suspension, critical spark ignition conditions 79−100373
Na arc lamp, light-induced ignition method 80−77599

ignitrons *see mercury arc rectifiers*
II-III$_2$-VI$_4$ semiconductors *see ternary semiconductors*
II-IV-V$_2$ semiconductors *see ternary semiconductors*
II-VI semiconductors
acceptor state model 80−2059
acoustic deformation potential, pseudopot. calc. 77−1363
alignment and orientation of hot excitons, secondary radiation polarisation calcs. 79−65392
amorphous semiconductors, electronic states, sublattice one-band Hamiltonian transform. 80−59861
Anderson-Gruneisen parameter, bulk modulus temp. depend. 78−10154
atomic displacements and enthalpy of vacancy formation 78−38690
band structure trends, isoelectronic series 77−89696
band structures using general model pseudopot. 77−62800
n-$Cd_xHg_{1-x}Te$, current carrier recombination heating in photoelectric effect *(Russian)* 79−78138
$Cd_xHg_{1-x}Te$, vertically grown crysts., effects of growth speed on comp. variations 79−55684
CdS:Cu; V, photoluminescence spectra 79−83027
CdS:Cu,Cl film, photocond., applied voltage freq. effect on props. 80−39635
CdS:N, Mn, ion implanted, anomalous enhancement of EPR signal of Mn^{2+} 78−27080
CdS, green edge luminescence spectrum, temp. depend. 80−108274
CdS, single crystals, laser emission from surface diffraction grating 80−95900
CdS film, polycryst, optical spectra, 0.5-6.5 eV 80−55212
CdS thin films, slow electron mean free path 79−99998
CdSe whiskers, growth in H_2 80−15425
p-CdTe, surface photovoltage spectroscopy in IR and visible range 80−39632
CdTe thin film on ferroelectric TGS, influence of polarisation reversal on elec. cond. 80−65720
CdTe thin polycrystalline film for photoelectrochemical cell 78−23162
charged dislocation motion during plastic deform. 79−82233
Compton line shapes of atoms 77−44080
conference, on cpd. semicond. interfaces, Princeton, USA., (Feb, 1977) 77−85300
core-level photoyield exam. of empty surface states 77−55593
crystal growth, optimal synthesis methods 80−100764
crystal growth from melt, dependence of mass losses upon press. 80−25547
cubic crystals, luminesc. polarisation and hot-exciton orientation and decoupling 78−6733
deep centres, ODMR *(French)* 80−60461
defect structure, electron microscopic investigations 79−32864
direct gap, highly excited, radiative recomb. involving free particle scatt. 79−38648

II-VI semiconductors continued
dislocation motion obs. by SEM in cathodolum. *(Japanese)* 79−46666
displacement energy threshold, from energies of vacancy and interstitial form. and of lattice distortion 77−89430
donor-acceptor recombination emission in cryst. subjected to mag. reson. 79−95684
doping, indirect method *(Czech)* 80−24468
doubly ionisable centre binding energy 79−65405
elastic moduli of close-packed $A^{8-n}B^{n}$ lattices 78−18700
electroless film deposition with variable comp. and polymorphic structs. 79−95952
electron-electron spin-flip scatt. and spin relax. 80−44916
electron-hole liquid, RPA calcs. 80−6743
electron-hole liquid theory, generalised RPA 78−87914
electronic dielectric constant, correlation with interionic separation 79−4758
electronic theory, covalent-metallic or covalent-ionic phase transition under pressure 78−72105
electronic theory, cryst. energy and bulk modulus 78−72104
energy states of semiconductors under high pressure *(Chinese)* 79−56128
epitaxial layer CVD, appl. to Si, II-VI and III-V semiconductor growth 77−32530
exciton spectra, photoreflection *(Russian)* 77−20874
excitonic polarons, Pollmann-Buttner variational method, donor and exciton binding energies 79−42469
exoelectronic emission, mechs., sensitivity meas., surface study appls. 77−52228
film, vacuum deposition *(Polish)* 79−47630
film technology 78−23621
film vacuum deposition methods *(Polish)* 79−56932
Franz-Keldysh effect modulators for laser radiation *(Russian)* 77−88813
fundamental absorpt. spectra, direct interband transitions 78−63972
g-factor examination 78−39393
heat and entropy of evaporation, Trouton's rule generalisation 79−77735
heteroepitaxial, for SAW and electro-optic device appl., prep. and props., book contrib. 79−83134
heteroepitaxial growth and characterisation, book contrib. 79−83133
heterojunction photovoltaic cells, recent results 78−39206
heterojunctions, photovoltaic effects and solar efficiency 78−52076
HgCdTe/CdTe, limited diffusion volume photodiode, characterisation 80−75627
α-HgS, cryst. growth from soln. at low temps. 80−7487
high-pressure phase transform. 78−22854
hollow crystals, morphology, review 77−11494
hydrogen-like impurities interaction 79−82541
II-VI compounds, charged dislocations and plastic deform. 80−107264
II-VI compounds, transition metal ion activated, vibronic struct. in absorption and luminesc. 78−6729
imperfections and photoconductivity, electronic nonequilibrium behaviour 80−44667
impurity and defect centre energy states, luminesc. meas., review 80−55150
injection electroluminescence, review, book contrib. 77−73174
injection lasers appl., with emission in 1.1 to 1.6 μm range *(Czech)* 80−32983
ion implantation, indirect doping method 80−10568
IR luminescence of Co^{2+} impurities, local density of phonon states 79−33778
Jahn-Teller effect, average phonon energy 79−15122
Jahn-Teller interaction calc. for Cr^{2+} doped crysts. 78−2455
laser beam spontaneous action *(Russian)* 77−88820
laser screens, for electron-hole tubes, stimulated emission mechanism 79−94237
lattice defects, electron energy radiation damage thresholds, EPR and luminescence 77−84799
lattice defects, X-ray diffr. and electron microscopic study 80−15088
lattice dynamics, eight-parameter bond-bending forces model 80−70334
LEDs using wide energy gap materials *(Polish)* 79−91501
local force variations due to substitution impurities 78−51633
luminophore, broad fluoresc. bands, spectral distrib. of emission probability 77−8653
magnetic susceptibility, effect of physical parameters 80−44793
magnetoreflectance of exciton-polaritons 79−91410
MBE growth *(Japanese)* 78−15317
mean square atomic displacements, in single crysts., X-ray determ. *(German)* 78−30726
mixed crystal, comp. disorder-induced broadening for free excitons 79−15479
mixed crystals, two photon absorption *(Russian)* 77−20875
multicomponent epitaxial structure synthesis device 77−77414
nonlinear absorption processes, competition between two-photon absorption and two-stage absorption via deep traps 80−29764
optoelectronics appl. *(German)* 77−7745
p-n amorphous heterojunction, phenomenological model 80−54769
p-n heterojunction, photovoltaic props. 77−55600
p-n junction photovoltaic diode, appl. as IR detector 78−86330
performance at large bias currents *(Russian)* 78−76105
phosphors, ODMR, defect excited states 78−80254
piezoelectric semiconductor, piezoresist. of grain boundaries 78−51995
polar semiconductor, impurity levels, influence of electron-phonon coupling 78−64007
quarternary alloys, energy bandgap and lattice constant contours 80−103622
radiation effects, optoelectric props. control 80−25458
reaction with Sn chalcogenides, thermodynamic anal. 80−40728
recombination radiation, ODMR study, detrimental effects of high excitation intensities 80−44958
resonant secondary emission spectra, relax. of energy and polarisation 80−93331
scatterd light intensity variation under secondary illumination 79−33718
Schottky barrier height, $(SN)_x$ and HgSe as contact materials, compared with Au 77−85312
Schottky barrier produced by $(SN)_x$ on III-V and II-VI cpd. semiconds., prep. and evaluation 78−6442
Schottky barrier with Au, correl. of barrier height with anion electronegativity 77−20430
self-interaction dynamcs of Nd laser radiation 79−27342
semiconductor, ionic., ionisation of doubly charged centres 79−11085
SHG efficiency at 77K under high field condition 80−84470

II-VI semiconductors continued
solar cell applic., role of thin film growth morphology and grain size, grain boundaries and lattice mismatch 77−77377
solar cells, CdTe, shallow homojunctions, characteristics and surface resistance influences 80−45690
solar cells, materials aspect, review 80−50971
solar cells, polycrystalline and tandem, for high efficiencies, using compound semiconductors 80−72052
solid solutions, local levels 77−1395
sphalerite, hydrothermal single crysts., feasibility of optical methods for quality control 80−89065
substitutional alloys, band theory, effect of lattice constant variation 80−49596
superhyperfine structure tensor and g-shift of Mn^{2+} impurity 78−39056
surface characterisation by high resolution Rutherford backscatt. 80−25511
surface states and electronic struct. of metal-semicond. interfaces 77−20428
surface structure, chem. and spectroscopy, review 80−59764
surface structure, LEED and AES *(Japanese)* 78−22943
thermal expansion and MP, ionicity and bond length effects 77−47606
thin epitaxial layer, direct synthesis *(German)* 80−104070
transient photoconductive processes in compounds with three deep trapping levels 77−76865
TSCD meas. method and applic. 77−43615
two-photon and two-step absorption of light 80−7389
wurtzite-type, deform. effects on biexcitons 77−52038
zinc blende and wurtzite structure, two photon spectra, quantitative investigation 80−50373
zinc blende structure semiconductors, cyclotron reson. *(German)* 78−10337
zinc blende structure semiconductors, two photon absorption model 79−78679
zinc blende structured semiconductor surface analysis by X-ray photoelectron spectroscopy *(Japanese)* 78−88672
zinc-blende semiconductors, quantum resonances in valence bands under uniaxial stress 79−99480
zincblende (110), surface relaxation 79−38143
zincblende compounds, (111) and $(\bar{1}\bar{1}\bar{1})$ faces, surface electron states 78−80035
zincblende crystals, internal strain and piezoelectric coefficient 78−39505
zincblende structure p-type semiconductors, internal strain on bound hole-phonon interaction 78−91492
ZnS:Mn,Cu, thin-film phosphors, LV DC electroluminescence 79−11472
ZnS:V^{2+}, impurity states by Green's function method 80−92855
ZnS single crystals, O content determ. by fast neutron activation anal. 80−15142
Al-CdSe-Ag dry air stabilised struct., elec. cond. mechanism, breakdown phenomena 80−34527
Al-CdTe-Al thin film VLF dielectric props. *(Slovak)* 79−7907
Al-ZnS-Au structure, coulombic centres, thermal ageing, cond. and photovoltaic characts. *(French)* 77−43741
Au-CdS junction diodes, chemically etched CdS cryst. surfaces effect on barrier layer 80−44722
Au-CdTe-Au structure, current transport props. 80−80408
BeS, electronic energy bands, APW and LCAO calc. 77−20236
BeSe, electronic energy bands, APW and LCAO calc. 77−20236
BeTe, electronic energy bands, APW and LCAO calc. 77−20236
(Cd,Hg)Te epitaxial structures, comp. profile depend. on deposition parameters 80−100795
(Cd,Hg)Te, photoconductive detector, uncooled, for 8-14 μm region 80−31868
Cd chalcogenides, film, on NaCl, preferential epitaxy induced by electron bombard. or elec. field 80−10824
Cd chalcogenides, thin films, VPE, needle-like cryst. growth 80−80148
Cd-Hg-Te, phase diagram, computer estimation 80−20903
Cd_x-Hg_{1-x}Te, cyclotron magneto-optical resons., photoconductivity meas. *(Russian)* 78−23133
Cd_xHg_{1-x} Te, elec. characts., impurity effects 80−92890
Cd_xHg_{1-x} Te, photodetectors, recomb. processes, photoconductive decay obs. 79−38129
Cd_xHg_{1-x}, x=0.2 and 0.26, photomagnetoelectric effect in strongly excited samples 79−47124
$Cd_{0.2}Hg_{0.8}Se$, longitudinal Nernst-Ettingshausen effect, effect of disorder scatt. 78−84240
$Cd_xHg_{1-x}Se$, carrier mobility, 4.2 to 300K, scatt. mechanisms 79−4561
$Cd_xHg_{1-x}Se$, elec. props., 77-400K *(Russian)* 78−2485
$Cd_xHg_{1-x}Se$, Hall coeff. and electron mobility, band parameters 79−73506
$Cd_xHg_{1-x}Se$ mixed cryst., electron mobility and electron scatt. 78−95296
$Cd_xHg_{1-x}Se$, narrow band gap semicond., electron scatt., and transport phenomena 80−49706
$Cd_xHg_{1-x}Se$, phase transition and elastic consts., US vel. study 80−75354
$Cd_xHg_{1-x}Se$ type semiconductor, small-gap, electron scatt. and transport props. 78−95294
$Cd_xHg_{1-x}Se$ type semiconductor, small-gap, electron scatt. and transport props. 78−95295
CdHgTe, anomalous avalanche breakdown 80−80284
CdHgTe detectors, high-performance, for thermal imaging 79−40616
CdHgTe detectors for CO_2 laser appls. 79−40615
CdHgTe, far IR cyclotron emission 79−61226
(CdHg)Te, ion implanted graded gap photodiodes 78−39192
(CdHg)Te photoconductive detector, thermal figure of merit limit 78−89540
(CdHg)Te photoconductive IR detectors, ultimate detectivity 79−58788
CdHgTe photoelectromagnetic detector for 10.6 μm radiation, non-cooled, performance 80−82818
$Cd_{0.1}Hg_{0.9}Te$, polycrystalline thin film, correlation between structure and 1/f noise 78−39234
$Cd_{0.15}Hg_{0.85}Te$, photothermomagnetic effect in mm range 80−92932
$Cd_{0.175}Hg_{0.825}Te$-Au(In) contacts, photo-effect in the 77-300K range, barrier height estimation 80−107850
$Cd_{0.2}Hg_{0.8}Te$, annealing in saturated Hg vapour *(German)* 79−43447
n-$Cd_{0.2}Hg_{0.8}Te$, fundamental absorption edge, influence of temp. 80−20640
$Cd_{0.2}Hg_{0.8}Te$ IR photoresistors/detectors, lateral geometry requirements *(German)* 79−93213

II-VI semiconductors continued
$Cd_{0.2}Hg_{0.8}Te$, ion implantation doping for realisation of IR detectors, responsivity meas., ion range straggling 80−73452
$Cd_{0.2}Hg_{0.8}Te$ recrystallisation for supercooled IR detector production *(German)* 80−86403
$Cd_{0.2}Hg_{0.8}Te$:B, ion implanted, B range and range straggling 80−54273
n-$Cd_{0.21}Hg_{0.79}Te$, excess generation-recombination noise 80−107880
$Cd_{0.24}Hg_{0.76}Te$, mag. quantum oscills. in photovoltaic effect 79−19619
n-$Cd_{0.245}Hg_{0.755}Te$, magnetophonon reson. and quantum oscillations 77−39902
$Cd_{0.25}Hg_{0.75}Te$, p-n homojunction breakdown voltage for onesided abrupt junctions *(German)* 78−56210
n-$Cd_{0.3}Hg_{0.7}Te$, photoelec. props. at 78K, relax. time, minority carrier extraction 80−107864
n-$Cd_{0.3}Hg_{0.7}Te$, recomb. levels 79−91076
$Cd_{1-x}Hg_xTe$, lattice dynamics of low conc. of Hg atoms, perturbation model impurity description 79−55853
$Cd_xHg_{1-x}Te$ film, vacuum departed, struct. and elec. props. 77−59344
n-$Cd_xHg_{1-x}Te$, action of laser pulses, elec. charact. 79−11212
n-$Cd_xHg_{1-x}Te$ alloys, x=0.19 to 0.21, electron optical heating influence on photoelec. effects 79−11183
$Cd_xHg_{1-x}Te$, Auger effect, temp. depend. of Auger lifetime 79−38097
$Cd_xHg_{1-x}Te$, band struct. and optical props. 80−15450
$Cd_xHg_{1-x}Te$, carrier lifetime, effect of comp. fluctuations and second-phase inclusions 80−80294
$Cd_xHg_{1-x}Te$, cast-recrystallise-anneal growth 79−91578
$Cd_xHg_{1-x}Te$, charact. of low temp. transport props. 78−39160
$Cd_xHg_{1-x}Te$, comp. determ. by electroreflection method 77−52708
$Cd_xHg_{1-x}Te$, comp. in successive layers determ. by chem. polishing etching of surface 77−7868
$Cd_xHg_{1-x}Te$ compressed sintered slabs, Hall coeff. and microstructure obs. *(Russian)* 78−10475
n-$Cd_xHg_{1-x}Te$, conduction band struct., IR refl. spectra obs. 80−39502
n-$Cd_xHg_{1-x}Te$, conductivity inversion under laser radiation *(Russian)* 79−15198
$Cd_xHg_{1-x}Te$, correlation between structural and chemical inhomogeneity *(Russian)* 80−49484
n-$Cd_xHg_{1-x}Te$ crystals, carrier recomb. in extrinsic conduction range 80−70722
$Cd_xHg_{1-x}Te$ crystals, donor compensation, low temp. cond. study 80−75571
$Cd_xHg_{1-x}Te$, current-voltage charact., pinch effect, mag. field effects 80−6858
$Cd_xHg_{1-x}Te$, determ. of slip planes by dislocation etching 79−82220
$Cd_xHg_{1-x}Te$, diffusion and struct. of defects 77−84775
$Cd_xHg_{1-x}Te$, dislocation motion, effect of lattice defects on microhardness *(Russian)* 80−70220
$Cd_xHg_{1-x}Te$, disorder scatt. 78−39137
$Cd_xHg_{1-x}Te$, dopants behaviour and p-n junction formation 80−44225
$Cd_xHg_{1-x}Te$, effects of electron heating at low temps. 80−49823
$Cd_xHg_{1-x}Te$, electron irradiated, elec. and recomb. charact. 78−39113
$Cd_xHg_{1-x}Te$, electron mobility and conc. near gapless state, influence of hydrostatic press. 79−65486
$Cd_xHg_{1-x}Te$, epitaxial graded-gap layers, elec. transport props. 77−85358
$Cd_xHg_{1-x}Te$ epitaxial graded gap layers, plasma reflection and magnetoreflection 80−71391
$Cd_xHg_{1-x}Te$, epitaxial growth from stoichiometric melt, crystn. and diffusion 80−75475
$Cd_xHg_{1-x}Te$, epitaxial layer p-n junction, current-voltage characteristics of photovoltaic detectors, 1 to 15 μm 80−86407
$Cd_xHg_{1-x}Te$, film, optical props., struct. depend. 77−1751
$Cd_xHg_{1-x}Te$ films, epitaxial growth, optical, elec., and photoelec. props. 79−11512
$Cd_xHg_{1-x}Te$ films, growth by cathodic sputtering in Hg vapour plasma 80−97431
$Cd_xHg_{1-x}Te$, fine-graded gap struct., electrophysical props. *(Russian)* 78−60144
$Cd_xHg_{1-x}Te$, gap width temp. depend., absorpt. band edge meas. 78−72521
$Cd_xHg_{1-x}Te$, graded gap epitaxial layers, elec. and photoelec. props. 77−85362
$Cd_xHg_{1-x}Te$, graded gap epitaxial layers, spectral charact. of photoelectromagnetic effect 80−60022
$Cd_xHg_{1-x}Te$ graded-gap epitaxial layers, photocond. meas. 0.5 to 6 μm, detector appl. 79−60869
$Cd_xHg_{1-x}Te$, graded-gap layers, galvanomag. props. at low temp. and in weak mag. field 80−75664
p-$Cd_xHg_{1-x}Te$, Hall const. variation with comp. after annealing in Hg vapour 77−15868
$Cd_xHg_{1-x}Te$, homogeneous mixed crysts. with large segregation tendency, Bridgman growth *(German)* 79−33923
$Cd_xHg_{1-x}Te$, IR detector appls., prep., elec. props. *(German)* 78−86332
n-$Cd_xHg_{1-x}Te$, in strong mag. field, current-voltage charact., current instabilities 78−87980
$Cd_xHg_{1-x}Te$, influence of nonparabolicity on transverse magnetoresist. near transition to zero gap 80−20228
$Cd_xHg_{1-x}Te$ inhomogeneous p-n junctions, elec. props. at high hydrostatic press. *(Russian)* 77−80835
$Cd_xHg_{1-x}Te$, inhomogeneous composition effect on carrier lifetime and photosensitivity *(Russian)* 79−73526
$Cd_xHg_{1-x}Te$, intrinsic carriers, Fermi level calc. rel. to conc. 77−55481
$Cd_xHg_{1-x}Te$, isothermal growth of epitaxial layers 78−60577
$Cd_xHg_{1-x}Te$ layers, epitaxial graded-gap, nonlinear elec. effects 80−100468
$Cd_xHg_{1-x}Te$ layers, photoelectromagnetic effect 78−43445
$Cd_xHg_{1-x}Te$, long term stability at 300K, rel. to device appl. 80−59978
$Cd_xHg_{1-x}Te$, low temp. piezoresistance, Hall effect, elec. cond., plastic flow 80−6844
n-$Cd_xHg_{1-x}Te$, magnetophonon oscills. of transverse magnetoresist. 78−72177
$Cd_xHg_{1-x}Te$, magnetoresist. near gapless state, 77-370K 78−2503
$Cd_xHg_{1-x}Te$ magnetoresistor prep. and props. 79−7844
$Cd_xHg_{1-x}Te$, magnetoresistance in range 4.2 to 300K 79−11156
$Cd_xHg_{1-x}Te$ narrow gap semiconductor, charge transfer device for IR detection appl. *(French)* 79−30563
$Cd_xHg_{1-x}Te$, photoconductivity under uniaxial compression, band gap 77−43657
$Cd_xHg_{1-x}Te$ photoconductive detectors, 77 to 300K, normalised thermal figure of merit 80−31878

II-VI semiconductors continued
$Cd_xHg_{1-x}Te$ photodiode, high efficiency, energy level diagram 77−15891
$Cd_xHg_{1-x}Te$ photodiode, IR responsivity and detectivity 78−19139
$Cd_xHg_{1-x}Te$, photoelectric props. at high temp. 77−4403
$Cd_xHg_{1-x}Te$, photomag. and photothermomag. effects *(Russian)* 79−78137
n-$Cd_xHg_{1-x}Te$, photomagnetic effect in the quantum limit under electron heating conditions 79−69553
$Cd_xHg_{1-x}Te$, photomagnetic and galvanomagnetic effects in quantising mag. fields 80−20223
$Cd_xHg_{1-x}Te$, photothermomag. effect and photocond. in millimetre wavelength range 80−44657
$Cd_xHg_{1-x}Te$ polycrystalline films, electrical props., rel. to struct. *(Polish)* 78−31002
$Cd_xHg_{1-x}Te$, precip. 77−90352
n-$Cd_xHg_{1-x}Te$, quantum oscills. of transverse photocond., fields up to 30 kOe, 1.5-4.2K *(Russian)* 77−72885
n-$Cd_xHg_{1-x}Te$, recombination due to surface excitation, photoconductivity, impurity states *(Russian)* 80−60042
$Cd_xHg_{1-x}Te$, resistivity, Hall effect and magnetoresist. in strong elec. field 77−28199
$Cd_xHg_{1-x}Te$, single cryst. homogeneity and molar conc. determ. with electron microprobe *(German)* 78−2109
$Cd_xHg_{1-x}Te$ single crystal, photoconductivity spectral distrib. rel. to surface condition 79−78136
n-$Cd_xHg_{1-x}Te$, single crystal, scattering mechanism on intensity of 1/f noise 80−39642
p-$Cd_xHg_{1-x}Te$ solid soln., thermoelec. effects 79−73538
$Cd_xHg_{1-x}Te$, solid soln., pure and Ag(In) doped, defect struct. model, Hg self-diffusion coeff. 79−95213
$Cd_xHg_{1-x}Te$ solid solns., epitaxial growth under isothermal conditions 77−16504
$Cd_xHg_{1-x}Te$, solid solns., role of stoichiometry defects 77−47813
$Cd_xHg_{1-x}Te$ solid solns., dimensional resonances of HF helicons, band struct. and electron mobility 77−47846
$Cd_xHg_{1-x}Te$, solid solns., solubility in Hg 78−35359
$Cd_xHg_{1-x}Te$, strong elec. field effect on galvanomagnetic effects 79−11159
$Cd_xHg_{1-x}Te$, surface microhardness depend. on surface treatment method 78−15560
$Cd_xHg_{1-x}Te$, temp. shift of energy gap 77−51658
$Cd_xHg_{1-x}Te$, temp. shift of energy gap, contrib. of lattice dilatation 78−51892
$Cd_xHg_{1-x}Te$, thermal cond. in mag. field, thermopower, and Nernst-Ettingshausen effect 77−31814
n-$Cd_xHg_{1-x}Te$, thermal EMF, in transverse quantised EM field *(Russian)* 79−23993
$Cd_xHg_{1-x}Te$, thermally activated slip, microhardness temp. depend. *(Russian)* 78−34567
$Cd_xHg_{1-x}Te$, tunnelling effect in p-n junctions 80−75630
$Cd_xHg_{1-x}Te$, uniaxially compressed, deform. effects, elec. resist. 78−39114
$Cd_xHg_{1-x}Te$, VPE on CdTe *(Russian)* 78−11129
$Cd_xHg_{1-x}Te$, vac. evap. film struct. rel. to carrier scatt. 77−85116
$Cd_xHg_{1-x}Te$, vacancy electron states, acceptor behaviour, electron mobility 80−70193
$Cd_xHg_{1-x}Te$, vacancy mech. of resorption of Hg droplets 80−39070
$Cd_xHg_{1-x}Te$, variable-gap struct., additional p-n junction in epitaxial film, photosensitivity 77−24588
$Cd_xHg_{1-x}Te$, variable-gap structures, galvanomagnetic effects 80−11014
$Cd_xHg_{1-x}Te$, X-ray topographic assessment 79−37716
$Cd_xHg_{1-x}Te$, x=0, x=1, effective mass of heavy holes, 4.2 to 300K 77−1353
$Cd_xHg_{1-x}Te$, zero gap semiconductor, interband optical-phonon scattering 80−6846
p-$Cd_xHg_{1-x}Te$-metal contact, negative resist. effects, impact ionisation 77−4440
$Cd_xHg_{1-x}Te$-metal contact, transport mechanism, thermionic and field emission processes 77−20425
$Cd_xHg_{1-x}Te$-metal contacts, schematic energy band diag., transport props. 77−47897
$Cd_xHg_{x-1}Te$, Auger and radiative recombination of acceptor bound excitons 79−47023
$Cd_{1-x}Hg_xTe$(:Ag), impurity diffusion, gamma-ray effects 80−54441
$Cd_{1-x}Mg_xTe$:Al, donor-acceptor pair and self-activated luminesc. 77−52161
$Cd_{1-x}Mn_xTe$, Faraday rot. meas. up to 150 T 80−29722
$Cd_{1-x}Mn_xTe$, interband Faraday rot., appl. of mixed semicond. calcs. 79−61348
$Cd_{1-x}Mn_xTe$ mixed crystal, fundamental absorption edge 78−10919
$Cd_{1-x}Mn_xTe$ mixed cryst., giant exciton Faraday rotation 78−27260
CdO, aqueous-deposited films, struct. and electronic props. for solar cell appls. 80−100797
CdO, elec. cond. and IR refl. spectra after sintering and compaction 79−56945
CdO, influence of initial compacting press. on elec. resis. Hall coeff. 80−20872
CdO, magnetoresistance, temp. depend. of degenerate, narrow and broad samples 78−95306
n-CdO, polycryst., elec. cond. 78−34830
CdO thin film conductivity, H_2O and CO adsorption effects 79−56340
Cd(S, Se) film grown on InP substrate, mismatch dislocations and lattice distortion, dangling bond density 80−84406
CdS 80−11398
CdS, 200 keV electron induced defects, low temp. annealing 77−80796
CdS, $A_{n=1}$-exciton, reflectance and thermoreflectance spectra, spatial dispersion and angle of incidence effects 80−25409
CdS, A-exciton-polariton, time depend. optical spectrosc. obs. 78−80376
CdS, absorpt. spectra, 400-650 nm, electron irrad. defects and absorpt. edge shift 78−64382
CdS, acoustic noise amplification along c_6 axis, Brillouin scatt. obs. 78−19101
CdS, acoustic phonon intensity fluctuations after strong nonlinear amplification 78−59909
CdS, acoustic wave attenuation, phonon viscosity and dislocation drag 80−70319
CdS, acoustic-wave-induced increase in cond. 77−59307
CdS, acousto-voltaic effect, asymmetric electron ejection from trap levels *(Russian)* 80−65634
CdS, acoustoelec. interaction, influence of surface pot. 77−1455

II-VI semiconductors continued
CdS, acoustoelectric current fluctuations 79−24020
CdS, acoustoelectric fluctuations 79−7866
CdS, acoustoelectric mobility measurement for X-ray excited carriers 77−15916
CdS, acoustoelectronic current SHG 80−6916
CdS active surface, exciton stimulated emission and superradiance refl. spectra, props. 80−25411
CdS, additional waves and polariton dispersion, reflectivity, transmittivity spectra 80−71443
CdS, amorphous antiferromag., mag. props. of dilute neutral donors 79−78367
CdS, anomalous behaviour of transient Langmuir dissociation 79−28092
CdS, anti-Stokes excited crystals, luminescence band at 12K 79−19922
CdS, aq. dispersion, O_2^- generation by photolysis, spin trapping detect. 78−11538
CdS, aqueous-deposited films, struct. and electronic props. for solar cell appls. 80−100797
CdS, attenuation of transmitted light in exciton region, polarisation, coherence, scatt. 77−69852
CdS, Au deposition, Schottky diodes and MIS devices, surface treatment effects, SEM obs. 80−54794
CdS, Auger effects in donor acceptor pair spectra 80−20707
CdS, Auger excitation mech. of 1.6-2.0 micron luminesc. band 79−8184
CdS, Auger interaction between luminescence centres and donor-acceptor pairs 77−63458
CdS, band structure calcs. by modified orthogonalised plane wave (MOPW) method 80−54609
CdS, biexciton, low intensity nonlinear coherent mixing study 80−49619
CdS, biexciton fluoresc. line shape 77−44059
CdS, biexciton levels, luminescence-assisted two-photon spectra 80−29795
CdS, biexciton luminescence, influence of free excitons on profile 77−4684
CdS, biexcitonic luminesc. for allowed and forbidden polarisation 77−44040
CdS, biexcitonic state existence, 2.5 MeV binding energy *(Russian)* 77−39788
n-CdS, bipolar photocond. and acoustoelectric current 79−19636
CdS, Bleustein-Gulyaev wave transmission characts. at corner 77−59197
CdS, Brillouin scatt. of refl. light, surface ripple mechanism 77−73149
CdS, Brillouin scatt. of forbidden polaritons 79−33722
CdS bulk wave-$LiNbO_3$ SAW piezoelectric coupling 77−23845
CdS, calc. deform. effects on biexcitons, compared to piezoemission meas. 77−52038
CdS, carrier density nonlinearity of interacting acoustic fluxes 77−51781
CdS, cathodolum. in red and exciton regions, surface treatment influence 77−77303
CdS, CdS_2Se_{1-x}, single cryst. ingot, laser screen for CRT 77−75561
CdS, characts. of interaction of light with dislocations 78−2137
CdS, charge in energy gap caused by acoustic domains 77−20822
CdS, charged impurity centres, drift during passage of photocurrent 80−70767
CdS, chem. sprayed film, struct. and morphology 78−72020
CdS, chem. sprayed film growth using centrifugal disc atomiser 78−92189
CdS, chemical polish for Cd and S faces 77−73355
CdS, chemically precipitated film, optical spectra, annealing effects *(Russian)* 79−11424
CdS, chemically sprayed film, prod. by centrifugal disk atomizer, struct. 79−65343
CdS, clean surface, AES and LEED exam. 80−10762
CdS cleaved in ultrahigh vac., elec. surface props. determ. 77−15926
CdS, coherent interaction of externally generated 35 GHz of sound with light 77−43964
CdS, collision controlled light scatt. by electrons, influence of elec. field *(Russian)* 78−64375
CdS, compensated, characts. of Auger excitation spectra of photoluminesc. and photocurrent 77−90194
CdS, condensation of optically excited carriers, electron-hole-liquid phase diagram 77−31950
CdS, creation of 2P excitons by two photon magneto-absorption 78−2432
CdS, cryst. grown from melt under press., microstruct. 77−59019
CdS, cryst. growth from vapour by one-dimens. nucleation on (110) singular surface, model 78−2048
CdS, cryst. growth from vapour in sealed silica tubes, emission and mass spectra 79−43117
CdS crystal, SAW amplification, bulk and acoustic noise 80−39637
CdS, crystal growth from vapour phase, model for interface kinetics 77−76335
CdS crystal growth from vapour, preferential deposition, elec. field effects 80−84122
CdS crystal with thin photoproduced semiconducting layer, tests of convolver on transverse surface waves 77−42646
CdS, crystallisation and stability in high-temp. alkaline solns. 77−52240
CdS crystals, doped with groups III and VII elements, self-activated emission, modelling *(Japanese)* 78−31247
CdS crystals, electron-hole plasma, carrier optical orientation 80−100689
CdS crystals, one-photon pumping, active layer structure, light amplification 80−78858
CdS crystals, orientational depend. of photoacoustic effect *(Russian)* 80−65167
CdS crystals, radiative recombination, high excitation rates 80−108269
CdS, cubic, ab initio band struct. calcs. within local density functional formalism 78−87910
CdS cylindrical crystal, transverse SAW obs. 78−84042
CdS, deep level electron trap characts. 79−78036
CdS, deep level IR luminescence, origin 80−20704
CdS, deep level transient spectroscopy *(French)* 79−11079
CdS, defect struct. and config. produced by irrad., elastic scatt. expts. 80−84178
CdS, defects formed by laser radiation of subthreshold intensity, bulk photo-EMF investigation 79−91098
CdS, deform. effects on exciton excitation spectra 78−35191
CdS, deformed, dislocation struct., TEM obs. 80−54250
CdS, deposited anthraquinone, decoration patters 77−1137
CdS, desorption of O_2, photostimulated desorption temp. depend. 80−24737

II-VI semiconductors continued
CdS detector, Voyager Sun sensor, evaluation of radiation interference, simulation 79−23644
CdS, diffusion length determ., resolution limit of EBIC technique 79−21865
CdS, diffusion of In, 729-1411K 78−22895
CdS, dislocation charges determ. 78−2136
CdS, dislocation effects on radiative recombination processes 79−8186
CdS, dislocation emission, photoluminesc. spectra 80−16084
CdS, dislocation motion, TEM obs. 80−79799
CdS, dislocation structural optical absorpt., plastic deformation *(Russian)* 80−34959
CdS, domain elec. instabilities, elec. field and temp. distribs., optical meas. 79−11405
CdS, donors, EPR and spin-lattice relax., Faraday rot. meas. 80−54939
CdS, doped, amorphous antiferromagnet model, susceptibility and spin-flip Raman scatt. meas. 80−97057
CdS, doped laser mechanism and output study 80−43340
CdS, drift mobility in presence of trapping-recomb. centres 78−19054
CdS, EPR of adsorbed oxygen radicals, temp. depend. 80−80612
CdS, edge emission spectra alteration by uniaxial stress *(Russian)* 78−72486
CdS, effect of halide (NaCl, $CdCl_2$, $CdBr_2$, CdI_2) and polysulphide (Na_2S_x, K_2S_x) on recrystn. 78−11171
CdS, efficiency of acousto-electrical effects, meas. by bridge method *(Russian)* 77−76881
CdS, elastic, piezoelec. and dielec. props. 80−108157
CdS, elastic, piezoelectric, and dielec. props., 4.2 to 300K 80−60508
CdS, elastic wave propag. and interaction with charge carriers, appl. of hardened elastic moduli *(Russian)* 78−35095
CdS, elec. cond., plastic deform. and annealing effects 77−55534
CdS, electro-acoustically active, AC impedance meas. 80−103726
CdS, electroacoustic interaction obs. 77−11966
CdS, electrocrystallisation of films on Cd 78−72014
CdS electrode, in aq. soln., flatband potential, effects of dissolved Cd^{2+} and S^{2-} ions 77−51815
n-CdS electrode, photoelectrochemical behaviour in acetonitrile solns. 78−31644
CdS electrode, photoexcited, charge transfer in electrolyte with Na_2S additive 79−99618
CdS, electron and hole trapped centres, EPR, photoluminescence, photoconductivity study 80−108071
CdS, electron beam induced desorption of O_2, AES meas. 79−77921
CdS, electron drift vel. and phonon multiplication 80−6848
CdS, electron traps, admittance spectra on hetero- and Schottky junctions 79−56159
CdS, electron traps, DLTS meas. 80−24949
CdS, electron-beam-pumped laser, basis of scanning optical microscope 80−31864
CdS, electron-exciton elastic scatt. cross sections, central field and exchange approxs. 77−62919
CdS, electron-exciton inelastic collision cross sections 79−90967
CdS, electron-hole condensate, luminesc. obs. *(Russian)* 78−19552
CdS, electron-hole droplet condensation 78−10367
CdS, electron-hole liq., effect of excited electron states lifetime on gain spectra 77−85748
CdS, electron-hole liquid, non-equilib. transmission spectroscopy meas. 77−20883
CdS, electron-hole pairs behaviour in energetic ion tracks 80−65457
CdS, electron-hole plasma, gain and refl. spectra study 80−66227
CdS electronic two- and one-photon Raman scatt. via biexcitons, stimulated config. obs. mag. field shift 80−103963
CdS, emission and transmission spectra, excitonic mols. effect 77−44062
CdS, emission lineshape of excitonic mols., polariton states 77−20918
CdS, energy transfer by normal modes in exciton reson. region 77−89705
CdS, epitaxial film, conductivity control by S vacancy form., light modulation appls. 77−4455
CdS, epitaxial film, structural and electron transport props. 79−82481
CdS epitaxial film, with grain-boundary barriers, field characts. of elec. cond. 77−55626
CdS, epitaxial growth and nucleation, on monocrystn. ZnS, substrate real struct. influence 80−88455
CdS, epitaxial layers on Ge, morphology and six-pointed optic figures obs. 78−2390
CdS, epitaxial layers on (111) Ce, growth and defect struct. 78−18920
CdS, epitaxial layers on Cd single crystal, direct synthesis and struct. 78−68628
CdS epitaxial layers on sapphire, exciton struct. of absorpt., photoluminesc. and photocond. spectra 80−89027
CdS, equivalent gap alteration by light scatt. by acoustic domains 77−85687
CdS, evaporated film, effects of heat treatment on photosensitivity *(Japanese)* 78−39237
CdS evaporated films, growth rate and resist. determ., in situ meas. technique 79−77940
CdS evaporated films, O chemisorpt. kinetics, effects on elec. cond. 78−6464
CdS, even acoustoelec. current due to Lamb waves, freq. depend. 80−20256
CdS, exciton absorpt. at low temps. *(Russian)* 78−48195
CdS, exciton cathodoluminesc. of semicond. with surface pot. barriers 78−88366
CdS, exciton condensation effects on refr. index 77−20818
CdS, exciton condensation, photoluminesc. spectra 80−25448
CdS, exciton droplets, energy condensation *(Russian)* 80−107712
CdS, exciton luminescence, surface recombination, space-charge-layer effects 78−80410
CdS, exciton obs. in thin surface layers, refl. spectrum *(Russian)* 78−2877
CdS, exciton optical and luminescence spectra characts. near dislocation slip bands 80−45111
CdS, exciton polaritons, Brillouin scatt. efficiency, additional boundary conditions 79−73960
CdS, exciton resonant secondary emission spectrum temporal evolution 79−51499
CdS, exciton spectra anomalies, surface state effects 78−18974
CdS, exciton spectrum of high-density gas of nonequilib. carriers 79−38567
CdS, exciton-LO phonon interactions under high excitation and temp. conditions 77−69899

II-VI semiconductors continued
CdS, exciton-contrib. to reflection spectrum at high excitation intensities 78−43900
CdS, exciton-phonon interaction, interpretation of optical absorpt. data 79−14897
CdS, excitonic mol. emission, strain induced splitting 77−44060
CdS, excitonic mol. transitions, optical gain and induced absorpt. spectra 80−11438
CdS, excitonic polariton reflectance, quantitative anal. in spectral range of A-exciton 79−15480
CdS, excitonic polariton reflectance, B-exciton and k-linear term 80−7369
CdS, excitonic region, nonlinear optical meas., 4.2K 78−68531
CdS, explanation for total current spectrum 77−8693
CdS, fast modulator for CO_2 laser, using two-photon magnetoabsorpt. 77−88805
CdS, fast optically controlled modulator using two-photon magnetoabsorpt., for CO_2 laser 78−13736
CdS film, anomalous noise rel. to photomemory effect 77−20374
CdS film, chemical bath deposited, solar energy conversion by photoelectrochem. cells 80−108804
CdS film, chemically deposited, cond. depend. on thickness, grain size, annealing time *(Russian)* 77−8210
CdS film, chemically sprayed, elec. and photocond. props. 78−34913
CdS film, chemically sprayed, carrier conc. and mobility, thermoelec. and photothermoelectric meas. 80−2503
CdS film, cryst. and electronic surface struct., stimulated recrystn. effects 79−78151
CdS film, crystallinity and optical props., effect of cation-anion ratio 77−76689
CdS film, current-field charact. 80−2490
a-CdS film, DC cond. Seebeck data 77−24626
CdS film, dark cond., negative temp. depend. 78−47892
CdS film, doping and recrystn. effect on photocurrent relax. time. 77−4409
CdS film, double-layered polycrystalline, on $LiNbO_3$ substrate, fabrication and props. rel. to SAW appl. 78−64480
CdS film, ellipsometry of natural boundaries *(Russian)* 79−4866
CdS film, exciton exhibiting spatial dispersion, reflectivity, polariton standing-wave struct. 79−4865
CdS film, frozen-in conductivity, nature of recomb. barriers 79−56245
CdS film, growth by chem. bath deposition, photocond. props. 77−59703
CdS film, Hall effect meas. 79−65570
CdS film, high cond., high transmittance, growth by evaporation method, and characterisation 77−77386
CdS film, influence of nonstoichiometric surface layer on props. 78−64148
CdS film, inhomogeneities responsible for residual cond., microinclusions 77−28269
CdS film, non-ohmic elec. cond. 80−2489
CdS film, on Si, structural and transport props. 78−6463
CdS film, polycrystalline, photosensitive, struct., pseudoreplica method, using electron microscopy and microdiffr. 79−15030
CdS film, precipitation from solns., form. charact. 79−11524
CdS film, prep. by hot wall technique, morphology and semicond. props. 79−95292
CdS, film, residual conductivity, effect of transverse electric field 77−4458
CdS film, second harmonic generation by transverse acoustic wave 77−51782
CdS film, spray pyrolysis prep., elec. transport props. 78−2590
CdS film, strain-induced modulation of photoconductivity 79−24009
CdS film, surface energy levels, thermally stimulated contact pot. difference method 79−99601
CdS film, surface states, surface photovoltage spectroscopy meas. 77−1504
CdS film, surface stoichiometry rel. to CdS-Cu_2S cell performance 78−2956
CdS, film, surface struct. and elec. props. 80−34531
CdS film, temp. depend. of dark and residual cond. 77−55625
n-CdS film, transient photoconductivity effects *(French)* 78−87994
CdS, film, X-ray diffr. and elec. cond. 78−64149
CdS film and heterojunctions, grain boundary and interdiffusion studies, AES and SIMS 79−77842
CdS, film electrolytically deposited, surface and bulk photocond. props. 78−60154
CdS, film for solar cells, struct. and elec. props., thickness depend. 78−72289
CdS film growth, with smooth surfaces through boundary layers 79−28244
CdS film preferred orientation, internal stress, and interface characteristics 78−26795
CdS, film prep. from aqueous soln. of thiourea 77−8767
CdS film SAW two-dimensional image processor 77−39164
CdS film solar cell yield rel. to crystallite column statistics 79−62005
CdS film spray fabrication, physical props., Cu_2S-CdS solar cell applications *(French)* 80−60113
CdS, film with high photocond. and good reproducibility, prep. by chemical deposition 79−66019
CdS films, amorphous and polycrystalline, microinclusion distrib. of high resist. phase and residual cond. 80−7008
CdS films, chem. deposited, growth kinetics and polymorphism 80−75463
CdS films, chemically deposited, phase comp. and photoelec. props. 77−40394
CdS films, electrolessly deposited, annealing effect on optical spectra 80−2884
CdS films, from thermal decomp. of organometallics, growth kinetics and struct. 79−78895
CdS films, growth, residual cond., inclusions 78−43492
CdS films, photosensitive, growth by reactive RF sputtering, props. *(French)* 78−35308
CdS, films, photovoltaic effect in wedge shaped film 79−56331
CdS films, precip. from soln., phase comp. change during annealing in air at 200-600°C 80−15393
CdS films, prep. by reactive pulverisation, chemical, crystallographic and electronic props. *(French)* 80−60112
CdS films, pure and Na doped, chemical bath deposited, photothermoelectric effect 80−6906
CdS films, vac. evaporation from CdS.Cr_2O_3 system, photoelec. props. 78−80074

II-VI semiconductors continued
CdS, fine struct. of two-photon absorption, luminesc. meas. 77−24893
CdS, flexural waves in resonator platelets, synchronous amplification and generation 78−84527
CdS, flux exclusion, superconductivity at high temp. 80−97058
CdS, free-exciton multiphonon luminesc. 78−6741
CdS, GaAs excitons, exciton-phonon interactions, review, book contrib. 80−49624
CdS, gain spectroscopy and plasma recomb. 78−88327
CdS, generation of optical radiation in direction of propag. of streamer 80−69401
CdS, granulated films, optical reson. 79−4863
CdS, group velocity of light and polaritons, refl. and luminesc. spectra 77−24863
CdS, grown by vac. evaporation on Si 80−25567
n-CdS, growth from Te soln., photocond. and cryst. perfection 79−99579
CdS, growth rate, sublimation rate and etching behaviour along polar axis 80−24387
CdS γ-ray dosimeters with elevated stability under irradiation 80−86995
CdS, heavily doped compensated piezoelectric semiconductor, sound absorpt. coeff. calc. *(Russian)* 79−15194
CdS heteroepitaxial films on ZnS, surface-wave acoustoelectric domain excitation and probing 79−46904
CdS heterojunction solar cells by CVD method 80−45685
CdS, heterojunctions with InP and GaAs, prep. by CdS CVD and etching 78−52062
CdS, high intensity excited, exciton reflection spectra, reflection struct. 80−20692
CdS, high intensity US amplification *(Russian)* 77−28222
CdS, high pressure effects on electrical resistivity and structure 77−15574
CdS, high-energy electron irrad., photoluminescence spectra, course of annealing 77−90198
CdS, highly excited, stimulated emission process at 80K 80−97307
CdS, highly excited cryst., biexciton, impurity transition and electron-hole plasma 79−15092
CdS, highly excited semicond., linear optical response, electron-hole liq. 79−51980
CdS, highly photoexcited, picosec. luminesc. spectrosc. 79−47517
CdS, hole-capture coeff. of deep charged centres, temp. depend., photocurrent meas. 79−7804
CdS, hydrogenlike donor negative ion, ground and excited states, obs. 80−70645
CdS, hydrothermal crystal growth on seeds of various orientations 77−4730
CdS, IR stimulated edge emission 77−59613
CdS, impact ionisation of excitons, photocond. and photolum. meas. 79−56266
CdS, impurity cond., temp. depend. *(Russian)* 78−47829
CdS, in Al-CdS-Au struct., asymm. Poole-Frenkel effect *(French)* 77−76949
n-CdS in DMF solns., electrochem., photoelectrochem., redox. pot. determ. 79−96322
CdS, indirect doping method *(Czech)* 80−24468
p-CdS, indirect doping technique, using short-life radioactive atoms 77−31688
CdS, induced absorption and gain from high density excitons 78−68533
CdS, induced absorption in energy ranges of exciton and exciton-biexciton transitions 78−72548
CdS, influence of Lamb US waves on exciton spectra *(Russian)* 80−7374
CdS, influence of surface states on absorption edge 77−16344
CdS, influence of surface annihilation of excitons on cathodolum. meas. 77−20937
CdS, intensity fluctuations of nonlinearly amplified phonons, Brillouin scatt. meas. 77−90163
CdS, interaction of excitons with charged impurities 78−43906
CdS, intrinsic exciton fine struct., two-photon absorption 77−12397
CdS, ion implantation effect on luminesc. and cryst. damage 78−6758
CdS, ion irrad. damage, obs. using SEM in cathodolumin. mode 79−7633
CdS, irrad. with high doses of fast reactor neutrons, self-healing of radiation damage 79−73221
CdS, kinetics of recomb. radiation 78−31243
CdS, LO phonons, size effect reson., first order forbidden light scatt. 77−44002
CdS, Lamb US wave induced luminesc., green edge radiation *(Russian)* 79−91509
CdS large- and small-signal lattice attenuation, Brillouin scatt. obs. 79−47130
CdS laser, electron beam pumped, catastrophic and gradual degradation 77−61960
CdS laser; electron-beam pumped, excitation of short cavity rhodamine 6G laser 78−25887
CdS, laser action in dense exciton systems 77−75531
CdS, laser beam spontaneous action *(Russian)* 77−88820
CdS, laser induced transient gratings 78−38020
CdS laser irrad. native defect formation, influence on photoelectric props., IR luminescence *(Russian)* 80−11039
CdS laser radiation under excitation by pulsed bremsstrahlung X-rays 79−91467
CdS, laser thresholds and stimulated emission, intrinsic recomb. processes 79−15489
CdS, lattice attenuation meas. by US injection method 78−76480
CdS, lattice attenuation meas. by acoustic domains 80−49827
CdS layers, by vacuum evaporation, formation mechanism of preferred orientation 79−56094
CdS layers, epitaxial, deposited on InP substrates, vapour growth technique 77−21033
CdS layers from CdS+Cr_2O_3 system, effect of heat treatment on spectral distrib. of photosensitivity 78−80017
CdS, light scatt. by Bleustein-Gulyaev waves on refl. and transmission 79−24288
CdS, light-induced modulation of absorpt., rise kinetics 77−16342
CdS, linear-circular three-photon dichroism 79−51930
CdS, local cathodolum. of single crysts. under colour contrast conditions in SEM 79−8191
CdS, localised level anal. from generation-recomb. noise spectra 78−14777
CdS, long wavelength lattice vibr. modes 80−49318
CdS, low resist. single cryst., photodeform. mechanism 77−89806

II-VI semiconductors continued
CdS, low temp. IR-induced flash of green edge luminescence 77−63457
CdS, luminesc. and gain spectra of two-photon excited excitons 79−33815
CdS, luminesc. data. statistical anal. *(Russian)* 78−68559
CdS, luminesc. from heavy ion tracks 78−88365
CdS, luminesc. of I_2 bound exciton and excitonic mol. 79−91492
CdS, M_1-M_2 luminesc. band, assignment to exciton-impurity complexes 77−8649
CdS MIS devices surface states 78−72267
CdS, magnetic susceptibility, grinding-induced states 79−61040
CdS, magneto-optical effects in field up to 200 T 77−52059
CdS, magnetoabsorption, explained by D^- centres 79−38019
CdS, magnetoreflectance and magnetoluminesc. of A exciton 78−39597
CdS, mode corrected TA phonons, reson. Brillouin scatt. 78−72535
CdS, model $S=^1/_2$ amorphous antiferromagnet, spin polarisation 78−52288
CdS, mol. model for exciton-impurity complexes 77−80740
CdS monocrystal petal lasers, single-photon excitation *(Russian)* 80−99736
CdS monocrystalline sputtered X-ray transducer characteristics *(Russian)* 80−47162
CdS, multiphonon reson. Raman scatt. and exciton-phonon luminesc. 77−16319
CdS, neutron and fast electron irrad., local centre form., TSC and photoluminesc. meas. 78−87719
CdS, neutron irradiated, photoelectric props. 77−35962
CdS, neutron irradiated, intrinsic defects 78−51599
n-CdS, new type photoconduction due to magneto-phonon reson. 77−55565
CdS, nonequilibrium electron-hole plasma, optical orientation of carriers *(Russian)* 78−2904
CdS, nonlinear electronic absorption of US waves 79−15196
CdS nonlinear lens, with variable focal length 79−81511
CdS, nonlinear optical suscept., resonant excitonic contrib. 77−3633
CdS, nonlinear refr. index coeffs. meas. by nonlinear refraction method *(Russian)* 78−79066
CdS, nonlinear refr. index meas. by nonlinear lens method *(Russian)* 79−26111
CdS, nonlinear self-action effect and absolute two-photon absorption coeff. 80−83649
CdS, ODMR, bound excitons 78−80253
CdS, obs. of acoustically induced space charge gratings 77−7203
CdS, obs. of forbidden Brillouin scatt. near exciton reson. 78−15180
CdS, obtained from CdS-Cr_2O_3 system, α-Cr_2O_3 effect on props. *(Russian)* 79−65469
CdS, optical activity in exciton spectra region, reflectance spectra 79−28707
CdS, optical axis inversion *(Russian)* 79−24284
CdS, optical props., spatial dispersion effect *(Russian)* 79−61404
CdS, optical quenching of noise photooscillations, connection with photoconduction *(Russian)* 77−20363
CdS, optical transform. of biexcitons 77−62844
CdS, optically controlled range of refr. index 78−6650
CdS, oriented single cryst. growth method from vapour 77−8734
CdS, parametric action of strong radiation field 78−14752
CdS, parametric interaction of acoustic surface waves *(French)* 77−62083
CdS, phase memory effect and vel. of trap-controlled high-field domains 77−47855
CdS, phonon echoes *(French)* 77−51461
CdS, phonon-coupled photoacoustic spectroscopy 80−54317
CdS phosphor, powdered, in host material, solar cells wavelength shifting 80−85286
CdS, photoanode, flat band pot., depend. on surface ion effects 79−62013
CdS photoanode thin film, for photovoltaic cells, prep. and characts. 78−14818
CdS photoanodes, effect of S substitution, photoelectron spectroscopy obs. 80−2463
CdS, photoanodes in sulphide-polysulphide electrolytes, instability 78−80755
n-CdS, photoanodic behaviour in acetonitrile-iodide solns. 78−47868
CdS, photocond., acoustoelec. fluctuations 79−24022
CdS, photocond., spectral depend. at high excitation intensity, exciton effects 80−65619
CdS, photocond. cryst., stationary and non-stationary temperature-electric instabilities 79−7833
CdS, photocond. cryst. characterisation of electron-trap responsible for acoustic holographic echoes *(French)* 79−19544
n-CdS, photocond. film, phase memory effect and deep levels 79−82556
CdS, photocond. meas. using surface wave acoustoelec. current 77−8131
CdS, photocond. on supplementary X-irrad. *(Russian)* 77−28212
CdS, photoconducting, surface acoustic noise amplification by carrier drift 78−72208
CdS, photoconductive, obs. of high intensity sound self-defocusing 80−24972
CdS, photoconductive, transverse electric current effect on SAW propagation 79−47127
CdS, photoconductivity, luminescence, radiative and radiationless transition mechanisms 78−10948
CdS photoconductivity, spatial homogeneities exam. using DC and microwave techniques 80−93895
CdS, photoemission due to direct transition near L- and M-points in Brillouin zone 77−16451
CdS, photoexcitation, effect of elec. field *(Russian)* 79−1751
CdS, photoexciton waves, restrictions imposed on nature of additional boundary conditions 79−28789
CdS, photoinduced sensitisation process, thermal activity *(Russian)* 80−34477
CdS, photon drag effects 78−23134
CdS, photoplastic effect due to α, β dislocations, spectral depend. 77−90180
CdS, photoplasticity and photocond., excitation energy conc. near dislocations, hardening 77−24346
CdS, photopotential changes due to Ar ion bombardment 77−8174
CdS, photorefl. in exciton region, surface layer influence 78−76489
CdS photoresistor, errors in exposure meter accuracy calc. 77−49773
CdS, photosensitivity degradation mechanism due to photocurrent, phtotcarrier lifetime 80−6903

II-VI semiconductors continued
CdS, piezoelec. frequency mixing of acoustic waves in oscillatory and DC elec. fields 77−35966
CdS, piezoelec. polycryst. film layer struct., acoustic harmonic generation 77−89812
n-CdS, piezoelectric polaron and polaron pinning 77−35872
CdS, piezoelectric semiconductor, space charge distribution at elastic wave propag. *(Russian)* 77−77150
CdS, piezoelectric semicond., acoustoelectric current of Lamb waves *(Russian)* 77−89815
CdS, plastically deformed, optical and electronic transport anisotropies 77−8611
CdS, plastically deformed, photo-EMF rel. to cryst. polarity 77−55581
CdS, plastically deformed, electronic transport and optical props. 79−73508
CdS, plastically deformed cryst. with dislocation slip band, residual cond. 80−6839
CdS plate, amplification of elastic waves by transversely drifting injected carriers 79−7868
CdS platelet laser, emission spectra, optical coupling between partial resonators 80−69400
CdS platelet lasers, optically pumped, spatial and spectral distribution of laser emission 80−64032
CdS plates, noise amplification as function of drift field intensity, conductivity and freq. *(Russian)* 79−73556
CdS, polar semiconductor, electron-hole liquid, electron-phonon interactions 80−6739
CdS, polaritons, two-phonon Brillouin scattering 80−20656
CdS, polaron cyclotron resonance freq. shifts, halfwidths, cumulant expansion method calcs. *(Russian)* 80−88880
n-CdS, polaron effective mass, DC Hall effect meas. 78−39037
CdS, polaron IR cyclotron reson. 80−25347
CdS, polycryst., photoelec. props., pressure time influence *(Russian)* 79−19615
CdS, polycryst. films, microstruct. and X-ray cond. 79−56336
CdS, polycrystalline evaporated layers, donor and trap densities 80−20213
CdS polycrystalline film, pot. barrier at grain boundaries from Hall effect *(Russian)* 77−32094
CdS polycrystalline films, high strain sensitivity 80−93017
CdS polycrystalline layers, electron trapping depend. on preparation conditions 79−78232
CdS polycrystalline thin-film liq. junction photovolt. cell 80−50988
CdS, polycrystn. films, recrystn. accompanying annealing *(Russian)* 80−20948
CdS, polycrystn. layers on CdS substrate, electron microscope study of surface struct. 78−22940
CdS, polytype relative stabilities, entropy contribs. 80−100197
CdS, population-inverted, resonant Brillouin scattering and photoelastic consts. 80−76042
CdS, porous, dynamic phase transition at high press. 79−23723
CdS, powder, mechanically induced localised states in energy gap 80−2354
CdS powder, surface O_2 adsorption, ESR studies 79−65738
CdS powder layers, surface pot. dark decay, moisture sorption and heat treatment effects 80−18038
CdS precipitates from acetate solns., crystal structure and photocond. obs. *(Japanese)* 78−10502
CdS, prepared by ceramic Technol., physical props. 79−60837
CdS, press. quenched, mag. moment, semicond.-conducting transition 80−15683
CdS, props. of shallow acceptors, photocurrent meas. 79−7805
CdS, ps decay kinetics of luminesc., streak camera obs. 79−78752
CdS, ps. spectra, high density exciton system 78−19553
CdS, ps. spectra, high density exciton system 78−19554
CdS, psec time resolved spectroscopy, electron-hole plasma 79−47500
CdS pulsed optically detected resonance, time depend. recomb. processor study 79−38411
CdS, pure and Al doped vacuum deposited film, photoelectric props. and optical absorption 78−60162
CdS, pure and Cl doped, stimulated emission due to indirect band-band transitions 80−7376
CdS, pure spin diffusion without charge transport, spin flip Raman scatt. obs. 80−93329
CdS, quasimonopolar semicond., recombination in near surface space charge region *(Russian)* 80−88574
CdS, Raman shift dispersion near exciton reson., two-phonon cascade processes 80−11405
CdS, recomb. radiation of electron-hole liq., quantum oscills. *(Russian)* 77−36293
CdS, recombination electric domains, production mechanism 80−29433
CdS, reflectance, transmittance and luminesc. spectra, light group vel. near exciton reson. *(Russian)* 77−69857
CdS, reson. Brillouin scatt. near A exciton 77−69846
CdS, reson. Brillouin scatt. by longitudinal acoustic phonons 79−38555
CdS, reson. Brillouin scatt., book contrib. 79−42983
CdS, reson. Brillouin scatt., quasi-static anal. 79−65887
CdS, reson. Brillouin scatt. of exciton polaritons 80−11418
CdS, reson. dispersion of Brillouin shift 78−35160
CdS, reson. forbidden Brillouin scatt. by TA phonon domains 79−56802
n-CdS, reson. obs. in far IR transverse magnetophotoconductivity 78−30949
CdS, reson. Raman scatt., temp. depend. polarisation, A-exciton 77−12386
CdS, reson. Raman scatt., second-order, theory for case of strong excitonic effects 78−76460
CdS, reson. scatt. of exciton-polaritons second emission under monochromatic excitation 77−1717
CdS, resonance hyper-Raman light scatt. on optical photons *(Russian)* 80−14396
CdS, resonant Raman scattering by LO phonons 78−39551
CdS, resonant scatt. of exciton polaritons by LO and acoustic phonons 79−95760
CdS, reversible hardening induced by electron-beam irrad. 77−62580
CdS, reversible threshold modification of luminesc. spectrum by uniaxial compression 79−38662
CdS, richardson-Schottky type photoinjection current from photoconductor into insulating liquid 80−15608
CdS, rock-salt type high-press. phase synthesis using metal sulphide additives 80−104084
CdS, SAW absorpt., effect of transverse electron drift 77−76879

II-VI semiconductors continued
CdS SAW convolver, effect of transverse drift of carriers on operation 80−14529
CdS, SAW meas. of surface elec. props. 77−20387
CdS SAW monolithic convolver with high resistivity surface layer, nonlinear cond. 79−98554
CdS, SAW superheterodyne amplification 77−55589
CdS, scanning semiconductor laser with transverse electron-beam pumping 80−9904
CdS Schottky barrier diode with evaporated Au-Ti blocking contact, rectification props. 77−85319
CdS Schottky barrier solar cells, spectral distrib. and photocapacitance 80−55864
CdS Schottky contact, photovoltage 78−95337
CdS screen, laser electron-beam tube under scanning conditions 79−13983
CdS screen for laser CRT, stimulated emission with TV type operation 78−59028
CdS, second order polaritons associated with van Hove singularities, light scatt. expt. 77−90146
CdS, seeded growth from vapour of large single crystals 78−64449
CdS, semicond., coexistence of surface and bulk acoustic waves in acoustoelec. domains 80−44404
n-CdS, semicond. electrode, electrolum. due to hole injection from electrolytes 77−20926
CdS, semicond. film, contoured anodic photodissolution 79−74277
CdS, semicond. piezoelec. crysts., US investigation of acoustoelectric characts. 77−1456
CdS semiconductor laser, longitudinally pumped, electron beam scanning vel. rel. to output parameters 80−9889
CdS, semiconductor-electrolyte interface, photoelectrochem. processes, hologram recording utilisation 77−88667
CdS, single cryst., band parameters from optical exciton spectra 79−47021
CdS, single cryst., effects of annealing in Cd or S vapour on photoelectric props. 77−16370
CdS, single cryst., laser emission following single-photon excitation *(Russian)* 78−37889
CdS single cryst., lasing action excited by ruby laser picosecond pulses 80−64035
CdS single cryst., melt growth, improvement of elec. characts. 79−38734
CdS, single cryst., polar (0001) and (000$\bar{1}$) surfaces, comparison of AES signals 80−16130
CdS, single cryst., surface treatment effects on photoluminesc., struct. and optical props. *(Russian)* 78−15224
CdS single cryst., vaporization and form. of negative whiskers 80−92659
CdS single cryst. Hall effect, temp. depend., 800-1200K *(Russian)* 77−80797
CdS, single cryst. surfaces, diffr. gratings, electrochem. recording of holograms 80−32934
CdS, single crystal, growth by modified Piper-Polich method, props. *(Japanese)* 79−100036
CdS single crystal, laser emission at one-photon excitation *(Russian)* 77−79835
CdS, single crystal, subnanosecond light pulse generation by laser radiation pumping 79−64234
CdS single crystal growth by sublimation *(Japanese)* 78−11093
CdS single crystal laser screen, photolum., determ. of layer depth disturbed by polishing 78−17977
CdS single crystals, depend. of radiative props. on equilib. carrier density 79−19932
n-CdS single crystals, effect of high-temp. annealing on electrical transport props. 79−78098
CdS single crystals, grown from vapour, analysis of static method 79−52092
CdS single crystals, Roentgenoluminescence, exciton interactions *(Russian)* 80−2853
CdS, single crysts., US luminesc. obs. 80−76092
CdS, single-quantum radiative recomb. of biexcitons due to biexciton-exciton interactions 80−96793
CdS sintered film, photolum. and recomb. photocurrent noise spectra 78−6743
CdS, sintered film, solar cell *(Chinese)* 79−74517
CdS, size effect of dense electron hole systems 80−7413
CdS smoke particle growth, prep. by evaporation in inert gases 77−24938
CdS solar photovoltaic panels, deposited by spray pyrolysis, film and junction structure studies 80−45689
CdS, solution growth, using Te solvent 79−65993
CdS, spatial diffusion of excitons under intense excitation 77−44061
CdS, spatial dispersion and surface layer effects on the phase of reflected light *(Russian)* 78−35182
CdS, spatial dispersion effects, exciton decay const. depend. *(Russian)* 78−72086
CdS, spectra of refl. and transmission coeffs. near exciton absorpt. line 80−88951
CdS, spectral anal. of luminesc. of high density excitons 79−11451
CdS, spectroscopic investigation and electron irradiation using He cryostat 77−37899
CdS, spectroscopic study of local centre interaction, change with external illumination 80−80323
CdS, spin flip Raman scatt. linear k term 78−19475
CdS, spin-flip line shape 78−88307
n-CdS, spin-flip Raman echo obs. 77−19370
CdS, spin-polarised electron-hole liquid, theory 78−43307
CdS, spontaneous and stimulated emission from electron-hole plasmas 77−69241
CdS, spontaneous optical activity in exciton spectrum *(Russian)* 78−35167
CdS spray pyrolysis film prep. and characterisation 78−64492
CdS sprayed film, heat treatment effect on props. 79−7916
CdS sprayed film, prep., optical props., struct. and comp. 79−78875
CdS sprayed films, elect. and optical props. 78−39241
CdS sprayed layers for solar cell prod. *(French)* 79−24901
CdS sprayed thin films for CdS-Cu_2S heterojunction solar cells 79−61988
CdS, sputter-deposited, electrical and optical props. 79−47181
CdS sputtered film, photocond. props. 78−10586
CdS, sputtered film, Rayleigh wave propag. *(French)* 77−62727
CdS, stimulated and spontaneous emission from degenerate electron-hole plasma at 300K 80−29762

II-VI semiconductors continued
CdS, stimulated emission and optical gain in dense exciton system 79−33731
CdS, stimulated Mandelstam-Brillouin scatt. on acoustic phonon amplification *(Russian)* 80−71437
CdS streamer laser, generation of ps. light pulses 80−9908
CdS, streamer luminescence 78−6762
CdS, stress-induced photolum. bands, photocond., rel. to dislocation electron states 80−25447
CdS, study of electron dynamics by spin flip Raman scatt. 79−95789
CdS, subMM radiation excitation by N_2 laser pulse 80−60678
CdS, submillimetre laser emission due to transitions between free exciton level 79−27261
CdS, substitutional Ti^{2+} centres, linear electroabsorpt. 77−66525
CdS substrate, lattice mismatch with ternary chalropyrite films 79−87012
CdS, superluminescence due to pulsed X-rays, 170 and 295K 78−42338
CdS surface, nonequilib. electron effects due to chem. excitation 78−72239
CdS surface, transverse acoustoelec. voltage inversion 77−47885
CdS, surface acoustoelec. current due to Rayleigh wave, ambient medium effects and surface state changes 77−69383
CdS, surface charge and ledge dynamics, point defect annihilation during sublimation 79−90642
CdS, surface electronic struct., slow electron reflection, total current spectroscopy *(Russian)* 80−54759
CdS, surface energy levels, O(C) adsorpt., AES study *(Japanese)* 78−88008
CdS, surface energy struct. changes during ion cleaning and thermal annealing 80−92962
CdS, surface layer, photomechanical and photoplastic effects 79−99264
CdS, surface photovoltage in exciton absorpt. range 78−19119
CdS, surface photovoltage, characterisation 80−60033
CdS, surface props., photoreflectance spectra in the exciton region 78−95324
CdS surface spectroscopy using acoustic surface waves, spectral response 77−69402
CdS, surface state meas. by SAW convolver 79−42617
CdS, surface treated to create accumulation layers, transverse acoustoelectric field meas. 78−10516
CdS surfce, slow electron refl., 0-6 eV 78−11039
CdS, temp. depend. of edge emission band shape 77−20934
CdS, theory of photoelastic effect 77−55769
CdS, thermal decomp. kinetics, in vacuo, free electron density depend. 77−59111
CdS, thermal desorption of O_2, photopot. and surface pot. changes 77−11795
CdS, thermal equilib. phonon populations, acoustic intensity meas. by Brillouin scatt. intensity obs. 80−45098
n-CdS, thermodynamic pot. for anodic dissolution, rel. to photoelectrochem. cell efficiency 78−26948
CdS, thermoelec. and photothermoelec. power meas., inhomogeneity effects 80−54728
CdS, thermoemission of positive ions in simple gas atmos. *(Russian)* 77−28676
CdS, thermoreflectance spectra, additional boundary conditions in terms of optical constants 79−15478
CdS, thick acoustoelec. oscillator, time investig. of parametric interactions 77−47867
CdS, thin film, dark- and photo-currents, annealing time effect 79−38199
CdS, thin film, diffusion of Cu, 20 to 200°C *(French)* 80−15424
CdS thin film solar cell fabrication, HCl etching 80−81474
CdS, thin films, deposition onto hot substances, vapour phase method 78−95694
CdS thin films, growth and evaluation for fabrication of high performance photovoltaic solar cells 80−93501
CdS thin films on brass substrates, nondestructive resistivity meas. tech. 80−93898
CdS thin layers, recryst. from CdS-Cr_2O_3 mixtures, phys. and photoelec. props. 80−96935
CdS, thin plates, piezosemiconductors, second harmonic acoustoelectric current obs. 80−80329
CdS thin-film Lamb wave delay line characteristics and strain effects 77−31185
CdS thin-film optical waveguide polariser 80−33180
CdS thin-film polycrystalline solar cell development 79−61993
CdS, third order nonlinear optical difference frequency generation 78−22176
CdS, three-branch exciton-polariton dispersion, direct meas. by reson. Brillouin scatt. 80−60620
CdS, three-photon absorpt. coeff. determ. by nonlinear luminesc. expt. 80−14384
CdS, time-resolved spectra of spontaneous luminesc. from high density electron-hole plasma 80−40156
CdS, transient phenomena in sublimation 78−30747
CdS, transverse acoustoelec. effect, for SAW optical image scanning 77−11001
CdS, transverse acoustoelec. effect rel. to SAW intensity 78−26917
CdS, trapping level parameter determ., limiting current injection *(Russian)* 78−39129
CdS, two photon absorpt., influence of In and Cu impurities 77−16353
CdS, two photon Raman scatt. at high excitation levels *(Russian)* 80−16032
CdS, two photon reson. Raman scatt. by excitons 77−52086
CdS, two-phonon resonant Brillouin scatt. 78−84597
CdS, two-photon absorpt., excitons *(Russian)* 78−39571
CdS, two-photon absorpt. effect on hyper-Raman scatt. 80−74441
CdS, two-photon absorption coefficient rel. to inverse Raman cross section 78−6678
CdS, two-photon Raman scatt. via biexcitons, angle- and polarisation depend. 79−87446
CdS, two-photon reson. Raman scatt. by excitons via intermediate excitonic mol., polarisation and polariton effects 78−10880
CdS, two-photon-excitation, tunable laser emission, luminesc. processes 80−55127
CdS type, bulk laser damage mechanism, photocond. meas. 80−15567
CdS type direct semiconductor, high excitation 77−48202
CdS, US dispersion of high intensity waves, nonlinear electron absorpt. *(Russian)* 78−26916

II-VI semiconductors continued
CdS, ultrasonic transducer, multilayer systems, amplitude-freqn. characts. *(Russian)* 77−23843
CdS, up-conversion and optical storage, spatially modulated band struct. 78−64397
CdS vacuum evaporated film photoconductivity and In doping effects *(Japanese)* 79−87174
CdS, vap. phase grown cryst., stoichiometry control, elec. cond. 79−100034
CdS, virtually excited biexcitons polaritons dispersion, two photon Raman scatt. 80−45067
CdS, Wannier exciton and Wannier-exciton-ionised-donor complex, binding energies of lowest excited states 80−34363
CdS, Wannier exciton-ionised donor complex, binding energy 80−44509
CdS, wavelength dependence of pressure coefficients of birefringence 77−20820
CdS, wedge shaped film, photovoltaic effect 77−1454
CdS, wide-gap extrinsic semicond., injection currents, theory 78−19052
CdS, with dislocations, optical props. 79−83001
CdS, with electron-hole exchange interaction, energy levels of A and B excitons 79−51494
CdS, with group III or VII dopant, self-activated emission 77−16371
CdS, wurtzite structure, natural optical activity *(Russian)* 79−78647
CdS, X-ray diffr. investig. of high-press. polymorphism 77−43324
CdS, XPS, secondary illumination effects, band bending, level shifts 80−108324
CdS:Ag, induced impurity photocond. spectrum obs. 77−1447
CdS:Ag, Ni thermographic phosphor luminesc. screen, for IR laser pulse recording 79−64342
CdS:Ag, orange luminesc. at 77K and induced impurity photoconductivity 79−43035
CdS:Ag, vaccuum deposited film, recrystn. by H_2S heat treatment 80−34328
CdS:Ag crystals, spectral shifts of induced impurity photocond. bands 80−39633
CdS:Ag phosphor, mechanism of trap ionisation by elec. field, Gudden-Pohl flashes 79−74007
CdS:Bi film, implantation and post annealing, superlinearity 78−52028
CdS:Bi film, spectral response characts. 78−2512
CdS:Cd, Cu, single crysts., IR restoration after optical degradation of photosensitivity 79−60867
CdS:Cd,Cu crystal, formation and bleaching of optically-induced absorption bands 78−31221
CdS:Cd(In), Cu- or defect-compensated, optical ageing rel. to storage cond. 78−84247
CdS:Cl, $Cu^{+}(Cu^{2+})$, photoconductive sensitivity 77−43648
CdS:Cl, extrinsic, exciton absorption 78−72569
CdS:Cl, heaviiy doped, fluoresc. spectrum upper threshold calculated 78−52568
CdS:Cl, resonant Raman scatt. exam. 78−39546
CdS:Cu, C-V curves of MIS diode used to examine trapping levels 80−65697
CdS:Cu, Cd, data storage, optical and photoelec. reading 78−1193
CdS:Cu, Cl films, photocond. growth and decay time 80−60041
CdS:Cu, diffusion doping, photolum. 79−91493
CdS:Cu, dye-sensitised, photocond. and photocurrent decay time obs. 80−6893
CdS:Cu, fast electron irradiated, isochronous annealing of IR photocond. quenching spectra 77−1450
CdS:Cu, Fermi level position, luminesc., and photosensitivity, electron irrad. effects *(Russian)* 78−14652
CdS:Cu, IR photolum. at 10K 79−28824
CdS:Cu, In, Ga, spray deposited, struct., X-ray obs. 78−71713
CdS:Cu, photocond. under high excitation intensity 78−52033
CdS:Cu, photocurrent, elec. field effect on recombination processes *(Russian)* 80−100484
CdS:Cu, photosensitivity degradation mechanism 80−107851
CdS:Cu, recording holographic medium, exposure characts. *(Russian)* 77−635
n-CdS:Cu, Si, photocond., carrier lifetime, X-ray effects 77−59300
CdS:Cu, spectral sensitisation by cyanine dyes 78−64064
CdS:Cu, US absorpt. in heavily doped piezoelec. semicond. 79−11189
CdS:Cu,Cl film, photocond., use in laser-addressed electrolum. display screen 77−51777
CdS:Cu,Pb reflectivity of Ni-salt coated powder, pre-irrad. effect on defect form. 79−27973
CdS:Cu binder layer, photoactive, AC impedance meas. 80−25299
CdS:Cu film, dynamic quenching of photocapacitance, deep levels obs. 77−85175
CdS:Cu films IR quenching of photocapacitance, deep level detection 79−56258
CdS:Cu sintered layers, relaxation photocurrent kinetics *(Russian)* 80−107852
CdS:$CuCl_2$, sintered film, dopant conc. effects on carrier mobility 78−2484
CdS:$CuCl_2$($CdCl_2$) sintered layer, distrib. of energy levels of local centres 80−15568
CdS:Cu(Ag), charge and transport mechanism of impurities, electrodiffusion doping 80−59725
CdS:Cu(Cl), thin layer, electron pulse induced cond. relax. 80−2501
CdS:Cu(Cl) polycrystalline films with residual conduction, kinetic phenomena *(Russian)* 77−15981
CdS:Cu(Cl) thin films, surface and bulk photoconc. 80−88653
CdS:Cu(In), two-photon and two-step absorption of light 80−7389
CdS:Cu(Se)(Zn), heavily doped, defect struct. 78−22756
CdS:D^{-}, binding energy of D^{-} ion 80−92541
CdS:Er^{3+}, spectra of different emission centres *(Russian)* 77−16356
CdS:F(Cl), shallow donors electronic Raman scatt., reson. enhancement 80−45068
CdS:Ga crystal cathodoluminescence, SEM analysis 80−97349
n-CdS:In, containing excess Cd, effects of In on elec. props. 79−56217
CdS:In, impurity resist., Matsubara-Toyozawa theory extension 80−80264
CdS:In, spin flip Raman scatt., electron dynamics 78−80342
CdS:In, two-photon absorpt. spectra exam. of effects of screening of exciton continuum 79−8166
CdS:In film, flash evaporated, prep. and elec. props. 80−20792
CdS:In films, vacuum deposited, growth, elec. and optical props. 79−51460
CdS:In whiskers, prep. by vapour deposition 78−75969

II-VI semiconductors continued
CdS:In(Cl) concentration quenching mechanism of luminescence 80−97336
CdS:In(Ga)(Al), cathodolum. on diffusion front 77−32447
CdS:Li, anisotropy of the absorption by impurity centers in hexagonal crystals 78−88343
CdS:Li, complex luminescence centres, recombination-stimulated conversion 80−108268
CdS:Li, donor-acceptor interactions, photochem. reactions *(Russian)* 77−40285
CdS:Li, luminescence bands, photocurrent spectra *(Russian)* 80−60677
CdS:Li, nature of recombination centres responsible for 0.95 μm luminesc. band 77−69908
CdS:Li, photocond. characts., electron and hole traps obs. 77−8140
CdS:Li, pure and doped, green edge luminesc., complex nature of centres 80−60671
CdS:Li, single crystals, anisotropic luminesc. centres 80−80857
CdS:Li, subjected to elec. fields, drift of defects 80−6558
CdS:Li, TSC and optical photocurrent quenching spectra, Auger excitation of recomb. centres 79−33294
CdS:Li, thermochemical changes in microstructure of anisotropic centres, polarisation modulation method meas. 79−38027
CdS:Li chemically deposited filter, elec. props. 80−11113
CdS:Li film, chemical bath deposited, photocond. and optical props. 80−2426
CdS:Li film, optical props. 80−2886
CdS:Li film, photocond., effects of annealing, S vacancies, and O_2 adsorption 78−34854
CdS:Li lattice, location of implanted Li atoms 80−6428
CdS:$Li^{+}(N^{+})(Ne^{+})(P^{+})$, ion-implanted, edge emissions 77−77274
CdS:Li(Cu), pure and doped, electrodiffusion of shallow donors, photocurrent, TSC, and exciton luminesc. meas. 80−79992
CdS:M, M=Zn, Te, doping and solid soln. prep. during VPE 77−85353
CdS:Mn, vacuum deposited film, Mn migration, EPR and X-ray study 80−65411
CdS:Mn gamma-irradiated ESR meas. 79−11342
CdS:Mn^{2+}, doped, spin-lattice relax. exam. 77−40120
CdS:Mn^{2+}, spin-lattice relax. ang. depend. 79−73807
CdS:Mn^{2+}, temp. depend. of rate of spin-lattice relax. 79−42832
CdS:Mn(Co), intensity and spectral distrib. of luminescence *(Russian)* 77−16392
CdS:N, P, As, Sb, Bi photoluminescence obs. 78−10965
CdS:Na, Hagemark theory, green edge emission line intensity 80−75517
CdS:Na, thin film, dark- and photo-currents, annealing time effect 79−38199
CdS:Na thin film, photoconducting props. 80−39623
CdS:Ni, dark cond. and photoconductivity 78−76110
CdS:Ni, elec., photoelec. and luminesc. props. *(Russian)* 78−84259
CdS:Ni, elec., photoelec. and luminesc. props. 79−95828
CdS:Ni, exciton reflection spectra 78−72557
CdS:Ni, impurity to band electronic transitions, photocond. and dark cond. obs. *(Russian)* 77−8150
CdS:Ni, nonradiative recomb., photocond. spectra 80−70764
CdS:Ni, recomb. parameters, photocond. spectra meas. *(Russian)* 80−49820
CdS:Ni^{2+}, Zeeman effect at Ni impurities 80−60633
CdS:P, implanted, photoluminesc. and electroreflection spectra *(Russian)* 78−52544
n-CdS:Te, grown from Te soln., elec. props. 79−65475
CdS:Te-based photoelectrochem. cell, luminesc., thermal manipulation of deactivation processes 80−81479
CdS:Ti^{2+}, superhyperfine interact., ENDOR study at 4.2K 80−80639
CdS/$Cu_{2-x}S$ heterostructures, heat treated, capacitance voltage meas. anal. 80−20292
CdS/Cu_2S heterojunction solar cells, optimal material props. theory and experimental verification 80−45686
CdS/Cu_2S heterojunction solar cells diffusion length determ. using minority carrier SEM 80−61359
CdS/Cu_2S solar cell, design and fabrication 80−30481
CdS/Cu_2S solar cells, polycryst. thin film photovoltaic materials, photon loss anal., expt. determ. 80−93888
CdS/Cu_2S thin film heterojunctions, photocapacitance meas. of solar cell parameters 80−93897
CdS/Cu_xS, sequential evap. for solar cell applic. 80−93902
CdS/InP epitaxial thin films on NaCl, HEED and TEM study 80−88446
CdS/$LiNbO_3$ system SAW convolution signal photoenhancement obs. 77−27431
n-CdS/n-InP/p-InP heteroface solar cell with ultrathin window layer, computer anal. 80−97788
n-CdS/p-$ZnIn_2Se_4$ thin film solar cell, photovoltaic props. 80−89628
CdS-Al, ohmic contact stability improved by annealing 78−6443
CdS-Al function formation, coupled interface plasmons, low energy electron energy loss spectra 77−24621
CdS-Al_2O_3-Al diodes fabricated by MBE, junction characts. 79−65550
CdS-Al(Au) interfaces, bonding and interdiffusion, XPS obs. 80−80000
CdS-Au, Schottky junction, surface defects, photovoltaic, piezoelectric and V-I characteristics *(French)* 80−49898
CdS-Au contacts, electronic states, vacuum UV photoelectron spectra 80−70827
CdS-Au Schottky barrier, piezoelec. effect due to mech. bending 77−69779
CdS-Au Schottky diode, elec. props. under stress 79−15222
CdS-Au structure, work function of {0001} faces of CdS, effect of piezoelec. props. 78−23164
CdS-based phosphor, microstruct. and luminesc. efficiency 78−10959
CdS-$Bi_{12}GeO_{20}$, air gap coupled system, SAW energy transfer 77−11774
CdS-CdSe, unactivated film, calc. of induced impurity photocond. due to donor-acceptor pairs 77−43749
CdS-CdSe bladed crystal prep. from gas phase 77−16478
n-CdS-CdSe mixed polycryst. electrode for photoelectrochem. cell 78−47867
CdS-CdTe p-n junction screen printed thin film solar cells 80−72055
CdS-CdTe sintered film, prep. and photocond. props. 77−28220
CdS-CdTe solar cell, prep. by VPE, junction struct. and photovoltaic props. 77−73235
CdS-CdTe solar cells fabrication *(Japanese)* 79−87992
CdS-CdTe thin film photoresistors, optimum photoelec. performance *(German)* 79−60941

II-VI semiconductors continued
CdS-Co^{2+}, IR spectrum, 4.2K, electron-phonon interaction effect on emission spectrum 78−27270
CdS-$Cu_{2-x}S$ ceramic solar cells, solar batteries operating characts. 80−93874
CdS-$Cu_{2-x}S$ heterojunction, current flow characts. and energy band struct. 77−43709
CdS-Cu_2S, thin film heterojunction, dark I-V characts. and heat treatment 79−56294
CdS-Cu_2S heterojunction, influence of surface recomb. on photoelec. props. 77−43711
CdS-Cu_2S heterojunctions, photovoltaic mechanism, model 77−43715
CdS-Cu_2S heterojunction model 78−39205
CdS-Cu_2S heterojunction, elec. and photoelec. characts., effect of etching of CdS 78−80048
CdS-Cu_2S heterojunctions, electron trap characterisation by capacitance transient meas. 79−78163
CdS-Cu_2S heterojunction diodes, barrier model estimated from photovoltage and cathodoluminesc. spectra 79−78165
CdS-Cu_2S heterojunction solar cell, interface recomb. vel. determ. by capacitance/collection efficiency variation 80−50959
CdS-Cu_2S heterojunction solar cells, carrier transport, nonmonotonic band profiles 80−61361
CdS-Cu_2S heterojunction, energy-band struct., capacitance-voltage characts., illumination effects 80−96982
CdS-Cu_2S heterophotocells based on CdS films of stoichiometric composition, elec. and photoelec. props. 80−93873
CdS-Cu_2S junctions, carrier trap density, deep level defects 80−107801
CdS-Cu_2S photovoltaic cell, effects of O_2 on efficiency 78−14807
CdS-Cu_2S solar cell fabrication by magnetron reactive sputtering deposition 80−61363
CdS-Cu_2S solar cell photovoltaic effects, self-consistent model 79−61989
CdS-Cu_2S solar cells, preparation and stoichiometric control 78−2560
CdS-Cu_2S solar cells, role of diode exponential factor 79−61990
CdS-Cu_2S solar cells, microstructural study of heterojunction materials 80−93978
CdS-Cu_2S thin film planar junction devices, quantitative photon loss anal. 80−61362
CdS-Cu_2S thin film solar cells, Cu_2S layer separation, struct. 79−95282
CdS-Cu_2S thin-film solar cells, low-cost manufacturing process outline, economic anal. 80−93930
CdS-Cu_2S thin-film solar cells, high open-cct. voltage and low refl. losses 80−94088
CdS-Cu_xS heterojunctions produced by RF sputtering, for thin film solar cells 79−100053
CdS-Cu_xS solar cell, effect on response of thermally induced changes in Cu_xS film 77−8181
CdS-Cu_xS solar cell, minority carrier diffusion length, SEM determ. 77−72911
CdS-Cu_xS solar cell, prep. and characts. *(Croatian)* 80−93876
CdS-Cu_xS solar cells, screen printed, prep. and photovoltaic props. 80−40863
CdS-CuI film heterojunction photocells, prep., photoelec. props. 78−80044
CdS-$CuInS_2(Se_2)(Te_2)$ photovoltaic heterojunctions, growth and characts. 77−39931
CdS-$CuInSe_2$, solar cell, grain boundary effects on performance 79−83603
CdS-$CuInSe_2$ heterojunction, photovoltaic effect, rel. to optimum conditions for solar cell fabrication 77−51810
CdS-$CuInSe_2$ solar cells, grain boundary and interface recomb. effects 79−39311
CdS-$CuInSe_2$ solar cell, polycrystalline thin film, high photocurrent, characts. 80−61339
CdS-electrolyte, boundaries, photo e.m.f. meas., semicond. energy bands 77−1481
CdS-GaAs n-n voltage-enhanced photoanode, solar cell efficiency 78−14810
CdS-Ge heterojunction, grown by chemical transport, props. 77−4422
CdS-HgI_2 photoconducting binder layers, surface charge decay characts. 77−43642
CdS-In, photosensitive granular superconductor 79−78246
CdS-In ohmic contacts, by electrolytic deposition 77−8194
CdS-InP heterostructure formation and elec. evaluation 78−72738
CdS-InP n-p heterodiodes, junction props. using injection electroluminescence 79−82667
CdS-InP photovoltaic heterojunction, growth and characts. 77−39931
CdS-InP solar cell, n-p, fabrication and power conversion efficiency 77−1813
CdS-InP(CdTe)(GaAs)(Ge), solar cell heterojunctions, CVD fabrication, photovoltaic response 80−93878
CdS-Li, hexagonal crystl., orientation degeneracy of anisotropic centres, dichroism of impurity photocond. 79−73981
CdS-$LiNbO_3$, layered structure, acoustoelectric surface current kinetics 78−43232
CdS-$LiNbO_3$ layered structure, transverse acoustoelectric current 80−44669
CdS-$LiNbO_3$ separated medium convolver, illumination effects 77−72766
CdS-$LiNbO_3$ structure, acoustoelectric interaction of surface waves with inhomogeneously distributed free carriers 77−43668
CdS-metal interface, chemical reactions and local charge redistrib. 79−19661
CdS-$NiCl_2$ interface, elec. props. using SAW techniques 79−56302
CdS-$NiCl_2$ interface, transverse acoustoelec. voltage spectroscopy 80−49828
n-CdS-p-CdTe heterojunctions, photovoltaic energy conversion, solar efficiency 77−43700
CdS-PET photoreceptors, air space effects on electrophotographic props. *(Japanese)* 79−44962
CdS-PbS heterojunctions, photoresistive props. 80−6970
CdS-PbTe and CdS-Te heterojunctions, electron irrad. effect on electrophys. props., prep. conditions depend. 79−28421
CdS-resin layer on electrophotographic plate with polyvinylcarbazole overlayer 77−61146
CdS-Si n-p heterojunction photodetector, fabrication and characts. 78−52068
CdS-SiO_2 (glass) layered system, characts. of phase-velocity dispersion and struct. of surface waves 80−59775
CdS-SiO_2-Si solar cell, I-V characteristics 80−89621
CdS-SiO_2-Si structures, elec. props., role of interface states 79−56286

II-VI semiconductors continued
CdS-Te, heterostructure, effect of low cond. CdTe interlayer on charact. 80−44721
CdS-Te-Ge heterojunction, prep. photosensitivity, and negative cond., 77K *(German)* 77−20413
CdS-type semiconds., Dember effect, theory 78−72189
CdS-ZnS(CdSe), film, light transmittance spectra, comparison with Schott GG 495 glass filter 78−33838
CdS-ZnTe, acoustoelectric domain injection across interface, reson. Brillouin scatt. 77−51778
Cd_xS, electrochemical characterisation and comp. modification at 25°C 77−25272
CdS(Se), electrodeposition, using nonaqueous solvents 80−76200
CdS(Se), excitons bound to ionised donors, binding energy calc. 77−28128
CdS(Se) films, electron irrad. effect on electrophys. props., prep. conditions depend. 79−28421
CdS(Se), luminesc. due to exciton-electron scatt., calc. 77−16379
CdS(Se), magnetopolaritons in wurtzite-type crystals 79−78019
CdS(Se), magnetoreflectance spectra of anisotropic II-VI semiconds. by mag. field modulation 77−66519
CdS(Se), optical detection near absorption band edge 77−749
CdS(Se), optical spectroscopy, absorpt. coeff., lattice vibr. modes, band gap, acoustic approach 77−69822
CdS(Se), piezoelec. semicond., sound absorption 80−60051
CdS(Se)-based photoelectrochem. cells, characts. 77−25287
CdS(Se)$_3$ excitons and Landau-levels meas. by magneto-optical spectroscopy apparatus 77−34032
$CdS_{0.4}Se_{0.6}$, reson. excitation of excitons by ultrashort freq.-tunable light pulser 78−46728
$CdS_{0.4}Se_{0.6}$, two-photon absorpt., effect of polarisation of laser radiation 77−69856
$CdS_{0.5}Se_{0.5}$, picosecond optoelectronic switching 80−54734
$CdS_{0.75}Se_{0.25}$, linear electro-optic effect meas., light modulator appl. 78−76434
$CdS_{1-x}Se_x$, chem. comp. and luminescence obs. 80−80869
$CdS_{1-x}Se_x$, comp. disorder-induced broadening for free excitons 79−15479
$CdS_{1-x}Se_x$ film, resonance between Se atom dipole vibr. and interference modes, IR spectra obs. *(Russian)* 80−2888
$CdS_{1-x}Se_x$, graded comp. semicond., tunable narrow-band filter, 5130 to 3700 Å 77−31128
$CdS_{1-x}Se_x$ gradient cryst., pseudointersection of dispersion curves n_o (λ) and n_e (λ) 79−15487
$CdS_{1-x}Se_x$, mixed cryst., electron-hole drops and plasma, luminesc. obs. *(Russian)* 78−92119
$CdS_{1-x}Se_x$ mixed crystals, free excitons, disorder effects 80−34365
$CdS_{1-x}Se_x$, mixed crystals, deformation effects on free excitons 80−76073
$CdS_{1-x}Se_x$ monocrystal petal lasers, single-photon excitation *(Russian)* 80−99736
$CdS_{1-x}Se_x$ single crysts., photocond. and excitonic luminesc. under high laser excitation 78−23127
$CdS_{1-x}Se_x$, spatial distribution and lasing modes under one photon optical excitation *(Russian)* 78−59012
$CdS_{1-x}Se_x$, zone edge phonon, IR absorpt. and Raman scatt. meas. 77−76508
$CdS_{1-x}Se_x$-Cu, electrophotographic props. 77−45910
CdS_xSe_{1-x}, electron traps, DLTS meas. 80−24949
CdS_xSe_{1-x}, laser beam spontaneous action *(Russian)* 77−88820
CdS_xSe_{1-x}, laser damage, self-focusing influence 78−50844
CdS_xSe_{1-x} laser electron-beam tube, possibility of acceleration voltage lowering 79−89929
CdS_xSe_{1-x} mixed crystals, exciton spectra 78−92131
CdS_xSe_{1-x}, photosemiconductor, optically controlled deflector based on thin-film waveguide 80−33206
CdS_xSe_{1-x}, photosensitive layer, in metal-photosemiconductor-insulator multilayered struct., charge pattern form. 80−47129
CdS_xSe_{1-x} photosensitive films, prep., props., and use for photodetectors 80−55298
CdS_xSe_{1-x}, scanning semiconductor laser with transverse electron-beam pumping 80−9904
CdS_xSe_{1-x} solid soln. film by spray pyrolysis 77−81214
CdS_xSe_{1-x}, strongly excited by electron beam, determ. of nonequilibrium carrier lifetime 80−39603
CdS_xSe_{1-x}, thermoelec. and photothermoelec. power meas., inhomogeneity effects 80−54728
CdS_xSe_{1-x} thin-film position-sensitive photoresistor prod. and props. *(Russian)* 78−43503
CdS_xSe_{1-x} triode cathode sputtered films, electrophysical props. *(Russian)* 79−42642
CdS_xSe_{1-x}, triode sputtered films, photoelec. props. *(Russian)* 79−15179
CdS_xSe_{1-x}:In film, flash evaporated, prep. and elec. props. 80−20792
$Cd_{1+y}(S_xSe_{1-x})$ single crysts., vapour phase transport and stoichiometry control 79−28940
CdS(Se)(Te) charged dislocations, flow of charge with plastic deform. 80−85010
CdS(Se)(Te), determ. of wurtzite, zincblende and rocksalt phases 80−100219
CdS(Se)(Te), epitaxial, condensation from gas phase of controlled comp., and props. 80−54562
CdS(Se)(Te), evap. onto electron bombarded NaCl substrates, epitaxial growth and characts. 79−28948
CdS(Se)(Te), excitons detect., precision method 79−19906
CdS(Se)(Te) films, vac. condensed, growth and struct., HEED obs. 80−29292
CdS(Se)(Te), phase diagram of electron-hole liqs. in polar semiconds. 77−89706
CdS(Se)(Te), positron annihilation study 80−60713
n-CdS(Se)(Te) semicond. liq. junction solar cells, photocurrent spectra, carrier recombination 78−76142
CdS(Se)(Te), vacuum deposited film, orientation axis tilt rel. to vapour angle of incidence 80−88456
CdS_xTe_{1-x}, emission spectra at high excitation levels *(Russian)* 79−74004
CdS_xTe_{1-x}, low temp. photoluminesc. *(Russian)* 78−43931
CdS_xTe_{1-x}, recryst. from CdS_xTe_{1-x}-Cr_2O_3 mixtures, photocond. props. 80−96936
CdS_xTe_{1-x}, surface layer conductivity type inversion by ruby laser radiation *(Russian)* 77−15948

II-VI semiconductors continued
n-CdSe, ^{133}Cd and ^{77}Se Knight shifts, impurity carrier wavefunction 78−35049
CdSe 16 μm parametric amplification with HF laser pumping 80−78910
CdSe (11$\bar{2}$0), surface electronic struct. and chem. struct. 78−14788
CdSe, biexcitonic state existence, 1.2 MeV binding energy *(Russian)* 77−39788
n-CdSe, bipolar photocond. and acoustoelectric current 79−19636
CdSe, charge transport 78−84233
CdSe, chemically sprayed thin films as photoanode in photoelectrochem. cells, power charact. meas. 80−85293
CdSe, collisions between hot excitons and hot electrons 80−7415
CdSe, comp. and evap. kinetics on vacuum heating, effects on deposited film charact. 77−85940
CdSe, cryst. struct. and Bijvoet ratios, X-ray diffr. meas. 77−55268
CdSe crystal, stimulated emission from electron-hole plasma, temp. depend. 78−88331
CdSe crystals, photocurrent and electrorefl. spectra, stoichiometry defects revealed by annealing *(Russian)* 77−52134
CdSe, dark current relaxation 80−44613
CdSe, deep dislocation levels, TSC and luminesc. obs. 77−8050
CdSe, defect struct. in Se vapour 78−64043
CdSe, desorption of O_2, photostimulated desorption temp. depend. 80−24737
CdSe, diffusion of Cu, effect of laser radiation on diffusion 79−10983
CdSe, direct gap, picosec. time resolved reflectivity obs. of optically excited hot carrier distrib. 78−76495
CdSe, dynamic holographic gratings based on excitons 77−3556
CdSe, effect of halide ($NaCl$, $CdCl_2$, $CdBr_2$, CdI_2) and polysulphide (Na_2S_x, K_2S_x) on recrystn. 78−11171
CdSe, effect of heat treatment in Se vapour, photocond. acoustoelec. effect and surface morphology 78−39152
CdSe, electrical cond. near metal-insulator transition 79−73550
CdSe electrochem. photovoltaic cells, effect of thin film electrode prep. and conc. on efficiency 80−55847
CdSe, electron irrad., edge emission 80−25461
CdSe, electron-exciton elastic scatt. cross sections, central field and exchange approxs. 77−62919
CdSe, electron-exciton inelastic collision cross sections 79−90967
CdSe, electrorefl. and photocurrent of ground state excitons 79−99905
CdSe, epitaxial film, gas-phase comp. effects on elec. props. 77−85354
CdSe, epitaxial films, carrier scattering temp. depend. *(Russian)* 78−10583
CdSe, epitaxial growth by transport reactions in closed system 77−52232
CdSe, epitaxial growth on ZnTe (111), vacuum evaporated 78−14631
CdSe epitaxial layers, on GaP-CdS substrates, absorption and electroabsorption 80−40178
CdSe evaporated films, struct. and epitaxy, TEM, RHEED, and X-ray diffr. obs. 79−77939
CdSe evaporated films, photoconductivity and effect of deposition conditions 79−95442
CdSe evaporated films, elec. props. 80−2498
CdSe, exciton-phonon luminesc. 77−16319
CdSe, excitonic mol. transitions, optical gain and induced absorpt. spectra 80−11438
CdSe film, as-deposited and recrystallised, struct. and fund. optical absorpt. 77−1753
CdSe film, conductivity instability when exposed to the atmosphere 77−15980
CdSe film, current noise due to thermal field ionisation 79−91110
CdSe film, effect of growth conditions on electrophysical properties 78−44024
CdSe film, Hall voltage meas. 77−69434
CdSe film, laser annealing effects on surface struct. and elec. charact. 79−73605
CdSe film, polycrystalline analogue elec. model 77−36000
CdSe film, polycrystalline, analogue elec. model 77−39974
CdSe film, resistivity rel. to vapour deposition parameters 77−12033
CdSe film, soln. growth 80−66437
CdSe, film, specific resist., deposition conditions, depend. 77−85363
CdSe film, stimulated recrystallisation 77−4272
CdSe film, stimulated recrystn. influence on photocond. 77−43754
CdSe film, struct. props., influence of O_2 partial press. and substrate temp. during vapour deposition 77−39751
CdSe film, thermally stimulated and isothermal discharges of capacitor across film 78−2582
CdSe film, vac. deposited, stabilisation by heat treatment in vac. *(French)* 79−95532
CdSe film, vac. deposited, elec. resist. and surface changes by laser annealing 80−2491
CdSe, film, vacuum condensation thermodynamics, starting powder comp. effects 77−81220
CdSe film, vacuum deposited, struct., resist. and Hall mobility 77−76974
CdSe film, with surface doping, surface parameters determ. 77−15933
CdSe film deposition, and reaction sequence of H_2SeO_3 reduction 80−71603
CdSe film photoanodes for electrochem. photovoltaic cells, fabrication and evaluation 80−76641
CdSe film polycryst., thermal diffusion of Cr, 240-400°C 80−80001
CdSe films, effect of annealing on resistivity and charge carrier mobility 77−8209
CdSe films, growth kinetics and cryst. struct. during vacuum condensation 80−2305
CdSe films, oriented, epitaxial growth by epitaxial nucleation in submicroscopic holes method 80−59834
CdSe films, solar energy conversion using electrodeposited films for photoelectrochemical cell 80−94093
CdSe, free-exciton multiphonon luminesc. 78−6741
CdSe, fundamental absorpt. edge, influence of laser radiation intensity *(Russian)* 80−71445
CdSe, fundamental vibrs., Raman scatt. and IR refl. obs. 78−60451
CdSe, growth rate, sublimation rate and etching behaviour along polar axis 80−24387
p-CdSe, Hall density and mobility, in Se vapour atm., 600-1100K 78−52014
CdSe, heat treatment effect on carrier mobility, role of defect centres 77−72861
CdSe, heavily doped compensated piezoelectric semiconductor, sound absorpt. coeff. calc. *(Russian)* 79−15194

II-VI semiconductors continued
CdSe, hexagonal, anharmonicity, X-ray intensity meas. 77−43286
CdSe, high intensity excited, exciton reflection spectra, reflection struct. 80−20692
CdSe, highly photo-excited, time-resolved luminesc. spectra, 1.8K 78−35197
CdSe, IR quenching and photocond., photon trapping energy depend. 79−56267
CdSe image convertor, liquid-crystal, hybrid optical processors appl. 80−33166
CdSe, kinetics of recomb. radiation 78−31243
CdSe, LPE growth on ZnTe, characterisation of heterojunction 77−4745
n-CdSe, laser excited stimulated emission, optical gain spectrum 80−76050
p-CdSe layers, ion implantation prep., elec. props. 79−51699
CdSe linear photopotentiometers, output charact. 77−1453
CdSe, low resist., mech. for nonradiative recombination of carriers, photoluminesc. and photocurrent charact. 78−19092
CdSe, luminesc. of high density electron-hole plasma at elevated temps. 80−20696
CdSe, MIS thin film capacitance, theory 79−87156
CdSe MIS thin film solar cell 80−45688
CdSe, magnetic susceptibility, grinding-induced states 79−61040
CdSe, magnetoreflectance and magnetoluminesc. of A exciton 78−39597
CdSe, mol. model for exciton-impurity complexes 77−80740
CdSe, monocryst. layers and bulk specimens, spectral comp. of impurity luminesc. 77−16364
CdSe, nonstoichiometry, Cd and Se press. meas., up to 1400K 78−87664
CdSe, optical gain spectra, exciton collision processes and electron-hole plasma 79−28814
CdSe, optical parametric devices, freq. tuning possibility by uniaxial press. 78−59084
CdSe, optical self-diffraction at induced phase lattice 77−3638
CdSe, optically pumped, dynamic polarisation of nucl. moments 78−68411
CdSe, oriented single-crystal films, edge luminescence at high excitation levels 77−1720
CdSe, parametric oscillator, grating-coupled, tunable 15.5 to 16.5 μm 77−58376
CdSe, partial press. meas. by optical absorption 80−15234
n-CdSe, partially illuminated single crystal, current-voltage characteristic and potential distrib. 79−65519
CdSe, phase gratings in semiconductors with one- and two-photon excitation 77−8546
CdSe photoanode improved efficiency by photoelectrochem. etching 80−104512
CdSe photoanodes, effect of Se substitution, photoelectron spectroscopy obs. 80−2463
CdSe photoanodes, S substitution during operation and mech. of surface protection 80−107906
CdSe, photoanodes in sulphide-polysulphide electrolytes, instability 78−80755
CdSe, photocond. film, plasma reson., IR refl. obs. 80−11037
CdSe, photoconductivity, recomb. charact. 77−8118
CdSe, photodetector, limiting sensitivity 79−63309
CdSe photoelectrode, immersed in polysulphide soln., S/Se substitution, XPS obs. 79−19656
CdSe photoelectrode, polycrystalline, for solar energy conversion 78−19147
CdSe, photoionization cross-section temp. depend., deep local levels 79−65408
CdSe photosensitive film production from chelated metallo-organic compounds *(Russian)* 80−49813
CdSe, photosensitivity of elastic properties 78−92049
CdSe, photovoltage transients, expt. and model 77−89802
CdSe, pico-second time depend. of luminesc. line due to exciton-exciton collision 78−39587
CdSe, picosecond time-resolved luminesc. spectra 79−93890
CdSe, plastically deformed, luminescence line 0.96 eV 78−10950
CdSe platelets, determ. of localised level energies by Fermi level statistics 77−31980
CdSe, polar semiconductor, electron-hole liquid, electron-phonon interactions 80−6739
CdSe, polarisation correl. of resonant Raman scatt. or hot luminesc. 80−25384
CdSe, polaron IR cyclotron reson. 80−25347
CdSe, polycryst. film, photocapacitance, inductive effect and US oscills. *(Russian)* 77−8142
CdSe, ps. spectra, high density exciton system 78−19553
CdSe ps. spectra, high density exciton system 78−19554
CdSe, psec time resolved spectroscopy, electron-hole plasma 79−47500
CdSe, pulsed Hall photoeffect, transient processes in scattering of carriers 80−15546
CdSe, radiative recomb. process, P-band, 2-psec time resolution 79−24346
CdSe, recombination mechanism at dislocations, photoluminescence 80−103993
CdSe, reson. absorpt. of coherent IR radn. by acceptors, photocurrent and emission spectra 79−73974
CdSe, resonant Brillouin scatt. via free and bound excitons 79−24330
CdSe, resonant Faraday effect, optical orientation of excitonic polaritons 77−69821
CdSe, resonant Raman and Brillouin spectroscopy, review, book contrib. 80−49624
CdSe, saturation of optical absorpt. and photocond. 79−18487
CdSe, Se-annealed and Cu-diffused, photocond. props. 79−99580
CdSe, signal and idler beam mixing device for optical parametric oscillator 79−14029
CdSe, single cryst., band parameters from optical exciton spectra 79−47021
CdSe, single cryst. elec. props., annealing in Se atm., expt. *(Japanese)* 77−1423
CdSe, single crystal, low-frequency current noise, effect of temperature quenching of photoconductivity 78−34874
CdSe single crystals, effects of impurities on photocond. *(Japanese)* 77−28221
CdSe single crysts., exciton luminesc. and polarisation spectra under one- and two-photon excitation 79−65391
CdSe, single crysts., luminesc. of electron-hole plasma 80−60675
CdSe, temp. depend. phase-matched nonlinear optical devices 80−99794

II-VI semiconductors continued
CdSe, thin film, total current spectrosc. investig. 80−7454
CdSe thin film transistor and MISM struct., effect of annealing on electron mobility and conc. 79−78198
CdSe thin film transistor on Cr substrate, cryst. struct., substrate defect effects 80−70563
CdSe, thin films, exciton piezotransmission 79−24380
CdSe thin-film solar cells 80−93970
CdSe, two-photon absorption, laser calorimetric obs. 80−33076
CdSe, undoped and Cr doped, far IR transmission and reflectance spectra 80−71429
CdSe, wave propag. 79−28042
CdSe, wavelength dependence of pressure coefficients of birefringence 77−20820
CdSe, with dislocations, optical props. 79−83001
n-CdSe, with single deep electron trap, negative photocond. 77−15905
CdSe:Ag, In, cryst., photocurrent and electroreflection, 77 to 300K *(Russian)* 78−23136
CdSe:Ar(N)(P), implanted, electroreflection obs. 80−40089
CdSe:Au impurity light absorpt. for current control in negative resistance region 80−11052
CdSe:Cd, Cu, photo-induced changes in absorpt. spectra 78−80382
CdSe:Cl(In), photoluminesc. props. near fund. absorpt. edge, impurity conc. effects 79−52003
CdSe:Cu, doping profile rel. to photoelec. props. in alloyed surface layers *(Russian)* 77−85268
CdSe:Cu, impurity photocurrent, kinetics and oscills. 80−65624
CdSe:Cu,Cl film, induced impurity photocond., 0.6 to 1.2 eV 79−24012
CdSe:Cu surface layer of CdSe, microstruct., photoelec. props. 78−43221
CdSe:Fe, exciton electroreflectance spectra, impurity effects 77−16335
CdSe:In, epitaxial layers, synthesis and elec. props. 77−47909
CdSe:In, epitaxial layer, effect of activator distribution on conductivity 78−43047
CdSe:Li, pure and doped, reson. Raman and Brillouin scatt., elastic exciton-defect scatt. 80−80788
CdSe:P, effect of P on edge luminesc. 78−64399
CdSe:P(Zn), single crystals, luminesc. 79−87493
CdSe:Ti, optical and elec. investig. of shallow donor levels, reson. states 77−63437
CdSe:V (d^3), absorption and luminesc. spectra 78−15203
CdSe:Zn(Ga), epitaxial film, impurity distrib., current transfer features *(Russian)* 77−47908
CdSe-Al, Schottky barrier diode, I-V and C-V characts. 78−10555
CdSe-Al function formation, coupled interface plasmons, low energy electron energy loss spectra 77−24621
CdSe-As_2S_3($AsSbS_3$) heterostructure, energy bands and interface props., photoelectron spectroscopy 78−2551
CdSe-Au contacts, electronic states, vacuum UV photoelectron spectra 80−70827
CdSe-electrolyte boundaries, photo e.m.f. meas., semicond. energy bands 77−1481
CdSe-Ge (111) heterojunctions, epitaxial, azimuthal rotation 78−84085
CdSe-$LiNbO_3$, semicond.-piezoelec. layer struct., acoustic-wave-induced increase in cond. 77−59307
CdSe-$LiNbO_3$ structure, acoustoelectronic interaction between SAW and transverse drift current 77−69424
CdSe-$LiNbO_3$ structure, electroacoustic effects and signal convolution 80−10098
CdSe-metal interface, chemical reactions and local charge redistrib. 79−19661
CdSe-Mo, Schottky barrier, characts. study 79−51673
CdSe-PbSe heterojunction, elec. props. 77−1478
CdSe-Sb_2Se_3 heterojunction, photoelec. props. 80−70816
CdSe-Si n-n heterojunction, photovoltage sign reversal, energy band profile *(Korean)* 80−29469
CdSe-Si n-p heterojunctions, vacuum deposition, photovoltaic effects *(Korean)* 77−28243
CdSe-SiO_2 (glass) layered system, characts. of phase-velocity dispersion and struct. of surface waves 80−59775
CdSe-SiO_2 thin film transistors, fabrication and electronic characts. 79−33351
CdSe-SiO_2 thin film transistors, slow states, trapping state densities and cross sections 80−15613
CdSe-ZnO thin film n-n heterojunctions, prep. elec. and optical props. *(Korean)* 77−28244
CdSe-ZnTe, and CdSe-CdTe n-p heterojunction, photovoltaic props. 77−55600
CdSe-ZnTe single cryst. film heterojunctions, prep. and props. 79−19652
Cd_xSe_{1-x}, streamer laser 77−79831
CdSe(Te) and solid solns., optimal synthesis conditions for single cryst. growth 80−100776
CdSe(Te), laser calorimetric meas. of two-photon absorpt. coeffs. at 1.06 μm 79−44934
CdSe(Te), NMR, chemical shift and linewidth determ. 79−19792
CdSe(Te)-electrolyte photovoltaic cells, solar cell appls. 77−35990
$CdSe_{0.65}Te_{0.35}$, polysulphide photoelectrochem. solar cell 80−72073
$CdSe_xTe_{1-x}$ crystal, acoustoelec. oscillations affected by surface treatment *(Russian)* 78−10517
$CdSe_xTe_{1-x}$ film, polycrystalline, deposition and physical props. 77−4741
$CdSe_xTe_{1-x}$, solid solns., epitaxial layer prod. 78−23619
$CdSe_xTe_{1-x}$, triode sputtered films, photoelec. props. *(Russian)* 79−15179
$CdSe_yTe_{1-y}$ triode cathode sputtered films, electrophysical props. *(Russian)* 79−42642
CdTe, 10.6 μm absorption meas. using thermal emission 77−1649
CdTe, aB glide dislocations, dissociated into two Shockley partials, stacking fault energy 78−43024
CdTe, absorbing precipitates, catastrophic laser damage threshold estimate 78−25913
CdTe acousto-optic and electro-optic waveguide modulators 77−42624
CdTe, amorphous, photocond., effective density of localised states 77−28210
CdTe, amphoteric behaviour and solubility of Sn 79−33008
CdTe and $Cd_xHg_{1-x}Te$, crystal growth by zone passing techniques 77−40360
CdTe and CdTe:Cl, grown by travelling heater method, EPR defect charact. 77−40125
CdTe and CdTe:Cl, semi-insulating, electroabsorpt. by impurities and defects, dichroism 77−40270

II-VI semiconductors continued
CdTe, anodic oxidation as thin-layer removal technique for impurity distrib. profile determ. 79−34169
CdTe, applications review 77−72894
CdTe, average number of phonons emitted in optical transition 77−8614
CdTe, backward degenerate four-wave mixing obs. 80−53361
p-CdTe, barrier heights of metals on etched surface 80−80378
p-CdTe, bipolar photocond. and acoustoelectric current 79−19636
CdTe, bipolar photoconductivity exam. 78−6410
CdTe, bulk and surface states anal. using synchrotron radiation 77−66574
CdTe cathodic deposition from aqueous electrolytes 78−64484
n-CdTe, cathodoluminescence microscopy obs. of dislocations, compared with etch pit pattern 79−69105
CdTe, charge carrier transport prop. meas. by time of flight technique 77−39850
CdTe, Cl compensated detectors, polarisation suppression methods 77−61661
CdTe, clean and oxidised surfaces, O_2 sticking coeff., ionicity effects, XPS expts. 77−85887
CdTe, clean and oxidised surfaces, surface states, low-energy EELS study 80−11522
CdTe, compensated single cryst., impurity centre parameters, elec. cond. and galvanomag. props. *(Russian)* 77−47811
CdTe, creep activation energy and velocity *(Russian)* 78−56716
CdTe, cryogenic refractive indices and temp. coeffs. meas. 80−7319
CdTe, cryst. growth from vapour 77−24936
CdTe crystal in square waveguide, single sideband generation at 10.6 μm 79−55179
CdTe, crystal size depend. of photoplastic effect 80−92592
CdTe crystals, exciton luminescence spectra rel. to shallow impurity conc. 80−97335
CdTe, crysts., mech. behaviour, yield stress function of temp., stress relaxation 79−60427
n-CdTe, deep trapping levels in high resistivity films 77−72930
CdTe, defect struct., review 77−39581
CdTe, detector grade semi-insulating crystals, determ. of product of mobility and carrier lifetime 80−39601
n-CdTe, detector material, single crysts., activation energy anal. of defect levels 78−6321
CdTe detectors, depletion layer extension 78−41891
CdTe detectors, gamma and electron irradiation effects 78−41893
CdTe detectors, photoscanning, determ. of crystal quality and contact behaviour 77−61664
CdTe, diamond-like semicond., Mossbauer isomer shift meas. 77−16233
CdTe, dielec. const. and loss tangent, temp. depend., 15.95 GHz 77−69763
CdTe, diffusion and solubility of Ge, 630-800°C, prep. conditions depend. 80−103519
CdTe, diffusion of Cu at 250 to 500°C, interstitial process 77−11737
CdTe, diffusion of Sn and intrinsic defects role 79−33116
CdTe diode, generation-recomb. and ionisation processes, temp. depend. *(Russian)* 77−39942
p-CdTe diodes, X-ray escape peak variations 77−71723
CdTe, donor impurity compensation models, impurity-vacancy complexes 77−39601
CdTe, dynamic holograms, diffr. characts. using laser beam 79−46048
p-CdTe, ESR optical detect., Overhauser shift, g-factor 78−80252
CdTe, elec. and photoelec. props. due to double injection, quenching spectra 80−70765
CdTe, electro-optic IR phase modulator, phase and freq. characts. 77−54805
CdTe electrode, redox reaction due to complex $M(CN)_6^{3-/4-}$ *(French)* 80−89482
CdTe, electrodes for photochemical production of H_2, a comparison 77−70311
CdTe, electron induced defect creation rates 78−41892
CdTe, electron mean free path, 350-1450 eV 80−103707
CdTe, electron-beam-controlled transmission of 10 μm radiation 79−81466
CdTe, electron-hole liquid formation in pure and doped crystals, luminesc. study *(Russian)* 80−55184
CdTe, empty surface states and surface order effects on sorption 77−85281
CdTe, energy bands and optical props. calc., tight-binding model with spin-orbit interaction 80−65448
CdTe epitaxial films, on CdS substrate, closed-tube vapour growth 80−55302
CdTe epitaxial films, surface morphology, layer and spiral growth 80−10823
CdTe epitaxial layers on GaAs, cryst. struct. and phys. props. 79−33202
CdTe, equation of state 79−82310
CdTe, excitation spectra, resonant Raman scatt. versus hot electron effects 79−38645
CdTe, exciton magnetoreflectance spectra, multicomponent polaritons, Zeeman splitting 80−88974
CdTe, far IR absorpt., two-phonon density of states 78−15155
CdTe, film, anomalous-photovoltage, current-voltage characts. 79−69549
CdTe film, between Ag electrodes negative differential resist. 78−19161
CdTe film, cathode sputtered, chemical composition and struct. 78−84100
CdTe film, excitation by H of anomalously high voltage *(Russian)* 78−60235
CdTe film, exciton spectra, press. and temp. depend. 80−80886
CdTe film, growth by photostimulated VPE, electrophys. props. 77−40390
CdTe film, low-resist., prep. by multi-source evaporation method, and characterisation 80−25582
CdTe film, photogenerated carrier transport props. 80−88590
CdTe film, photopolarisation 80−25286
CdTe, film, theoretical models of impurity levels 79−82557
CdTe film formation on glass substrates, influence of sublayers of recrystn. stimulators 77−43455
CdTe, film grown by hot wall epitaxy, elec. props. 79−82696
CdTe, film grown in quasi-closed volume, struct. *(Russian)* 78−75952
CdTe films, oriented, epitaxial growth by epitaxial nucleation in submicroscopic holes method 80−59834
CdTe films, structural imperfections depend. on crystn. temp. 79−90661
CdTe films, switching obs. in sandwich structures 77−43752
n-CdTe films, uniform trap distrib., transient photocond. effects 79−28423

II-VI semiconductors continued
CdTe, films grown by hot wall epitaxy, elec. props. 79−28420
CdTe foils preparation, transparent, for TEM, ion sputtering technique appl. *(Czech)* 80−16619
CdTe, grown by chem. transport, morphology, struct. and microhardness *(Russian)* 78−22729
CdTe, growth by travelling heater method, high resistivity charact., γ-ray detector appl. 78−84707
CdTe, growth by vapour phase chem. transport in I_2 77−40342
CdTe, growth from Cd rich soln. by solvent evaporation 77−40355
CdTe, growth from In solvents, self-compensation 77−28144
CdTe, growth from soln. in fused $CdCl_2$ 77−44138
CdTe, growth from Te soln. by slow cooling or travelling heater method, Te inclusions 77−40352
CdTe, growth from Te-rich soln. by travelling heater method, cond. and luminesc. 77−40351
CdTe, growth from Te-rich soln. in vertical Bridgman furnace 77−40354
CdTe, growth of epitaxial layers, activation by UV and IR radiation 80−71598
CdTe, growth on Te substrate by solid-state reaction 79−95287
CdTe, H^+ ion implanted, optical waveguiding and electrooptic modulation 77−75679
n-CdTe, Hall effect and resist., close and distant donor-acceptor pairing effects 77−39881
CdTe, hexagonal film, effective birefringence 80−16004
CdTe, high purity crystal, growth from soln., γ-ray detector appls. 77−14310
CdTe, high-resistivity, carrier transport and trapping processes, growth parameter effects 77−39871
CdTe, high-resistivity, irradiation effects on carrier transport and trapping process 78−2164
CdTe homojunctions from VPE growth, solar cell appl. *(French)* 77−43453
CdTe, IR quenching of photocurrent and switch in type of photoconductivity 77−47862
CdTe, IR transmitting semicond., dn/dT, wavelength depend. 77−77163
CdTe, in metal-semicond.-metal struct., as spectrometric detector of nucl. radiation 77−54460
CdTe, influence of heat treatment on carrier lifetime, photoelectromagnetic effect meas. 77−55576
CdTe, irrad.-induced damage on γ-detector performance 80−23264
CdTe, LPE in CdTe-$CdCl_2$ system 78−35323
CdTe, laser annealing, surface layer temp. distrib. 79−74029
CdTe, laser annealing of ion bombardment damage 80−25502
CdTe, laser window material, vap. deposition 78−27391
CdTe, lattice dynamics and phonon parameters bond bending force model 80−59595
CdTe, lattice mode, dispersive refl. meas. using modular interferometer 78−89568
CdTe layer deposition by ionised cluster beam technique 77−48351
n-CdTe layers, growth and characterisation, heterojunctions and Schottky barriers fabrication *(German)* 80−89151
CdTe layers, on CdS substrate, cryst. perfection and defects, X-ray diffr. obs. 79−56081
CdTe, Li diffusion, 300°C 77−43383
CdTe linear electro-optic translation of IR laser wavelengths 80−78878
CdTe, low temp. luminesc. *(Russian)* 79−91497
CdTe, low temp. themal cond., growth parameter influence 80−92725
CdTe, luminescence and reflect. investig. of excitons, stress and Zeeman splitting 77−40281
CdTe, MIS contacted small portable detector head for X-ray spectrometry 77−61662
CdTe, MSM detectors, charge collection 77−61660
CdTe, mag. susceptibility at 20-1400°C 77−12085
CdTe, melt-growth review, including liquid encapsulation method, defect charact. 77−40350
CdTe metal-semicond.-metal detectors, degradation charact. due to e and γ irradiation 79−45543
CdTe metal-semiconductor-metal γ-ray detector charact. 80−57451
CdTe, microwave cond. and dielec. permittivity using reson. cavity method 79−51620
CdTe, minority carrier diffusion length from photocurrent meas. in semicond.-electrolyte boundary 80−65584
CdTe, n- and p-type, elec. and galvanomag. props. 79−7830
CdTe, NMR, dipole-dipole coupling between ^{111}Cd, ^{113}Cd and ^{125}Te 79−91305
CdTe, near-edge absorpt., effect of light illumination and elec. field 79−38547
CdTe, nearest-neighbour hopping cond., effect of electron irrad. induced compensating centres 77−43599
CdTe, negative and positive photoplastic effect 79−51192
CdTe negative dielectric relax. of hot electrons 78−52001
p-CdTe, nondoped, heat treatment in vacuum, dissoc. obs. effects on struct. and props. *(Japanese)* 80−60662
CdTe, nonlinear magnetoelec. susceptibility, three-dimens. model 80−39845
CdTe, obliquely deposited layers with reduced resist., photovoltaic props. and Cd doping effects 77−43755
p-CdTe ohmic contact with Pd and Pt, I-V charact., temp. depend. of cond., activation energy 78−39211
CdTe, on mica, substrate defects effect on epitaxy 78−26794
CdTe, optical absorpt. coefficient, photovoltaic determ. 77−39890
CdTe optical applications, review 77−42580
CdTe, optical detection of ESR 79−65770
CdTe, optical waveguide, fabrication by LPE using boat-slide technique 77−63570
CdTe, oscillatory magnetoabsorpt. spectra 80−40096
CdTe, P-T diagram, cryst. struct. stability 78−51886
CdTe p-n homojunction, elec. and photovoltaic props. rel. to solar energy conversion 79−51668
CdTe p-n junction, short-circuited, estimation of surface recomb. rates, electron-probe meas. 77−43713
CdTe, partial press. meas. by optical absorption 80−15234
CdTe, phonon conductivity, 2 to 300K, scatt. mechanisms 79−4436
p-CdTe, photocond., photoluminesc., spectral studies 80−88593
CdTe, photoconductivity, extrinsic, contrib. by hopping through excited states of donors 78−6411
CdTe, photoelectron spectra at Schottky barrier *(Korean)* 79−11220
n-CdTe, photolum., plastic deform. effects 79−15509
CdTe, photoplastic effect, influence of plastic deform., heat treatment and doping 79−82277

II-VI semiconductors continued
CdTe, physical props., review 77−39833
CdTe, picosecond absorption spectroscopy 79−47482
CdTe, plastic deformation activation anal. below room temp. 78−84935
CdTe, properties and appls., conf., Strasbourg, France (Jun-Jul 1976) 77−39832
CdTe, purification, efficiency for extraction of Cu and Ag impurities, impurity scatt. meas. 77−8749
CdTe reactive close-spaced vapour transport, simplified theory 80−15396
CdTe, recombination radiation due to high-density excitons 80−93392
CdTe, relations pressure-volume under high pressure 80−39219
CdTe, reson. Brillouin scatt., book contrib. 79−42983
CdTe, reson. Raman scatt. by excitonic polaritons 80−11396
CdTe, Schottky diode, AC small signal capacitance 79−7899
CdTe Schottky solar cell, barrier height, open circuit voltage 77−43721
n-CdTe, semiconductor electrode, electrochem. behaviour in nonaqueous media *(French)* 80−66808
CdTe, semiinsulating, anomalous photocond. and dark cond. 77−62959
CdTe, shallow donors, excited state transitions 78−6710
CdTe, shallow impurity spectral linewidths, 4-10K 77−63443
CdTe single cryst., linear electro-optical props., temp. depend. 80−71376
CdTe, single cryst. IR laser window, low absorption at 10.6 μm 78−79081
CdTe, single cryst. sublimation growth, X-ray topographic characterisation 80−29866
n-CdTe, single crystal, photoreflectance, temp. depend. of exciton spectra *(Russian)* 78−23488
CdTe single crystal IR window for CO_2 laser 77−75566
CdTe, single crystals, plastic deformation and dislocation struct. 79−8321
p-CdTe single crysts., photoreversal of Hall effect 77−43631
CdTe single-crystal film, switching and memory effects 78−76174
CdTe, solubility in Hg 78−35359
CdTe, spatial dispersion rel. to exciton reflection spectra *(Russian)* 80−40126
CdTe, sputter-deposited, electrical and optical props. 79−47181
CdTe, sputtered film, electrode effects in AC charact. from equivalence impedance meas. of metal-CdTe-Al struct. 79−82686
CdTe sputtered films, deposition conditions effects on struct. and props. 77−43452
CdTe sputtered films, struct., photocond., and trap distrib. 80−29489
CdTe surface, nonpolar, electronic struct., tight-binding calc. 77−20383
CdTe surface, sputter cleaning and dry oxidation, XPS and LEED study 80−108618
p-CdTe, surface barrier struct., internal photoelec. emission 77−15958
CdTe, surface characterisation by high resolution Rutherford backscatt. 80−25511
CdTe, surface layers formed by etchants, XPS meas. 78−44240
CdTe, surface photovoltage 78−2540
CdTe surfaces, SIMS, Rutherford scatt. and ellipsometry 79−56046
CdTe, temp.-depend. of root-mean-square dynamic displacements, characteristic temp., X-ray study 78−83895
CdTe, temperature variation in bulk moduli in solids 79−73237
CdTe, thermal cond. and X-ray topography investig. of cryst. defects 77−39706
CdTe, thermostimulated capacitor discharge, trapping levels obs. *(Russian)* 78−10842
CdTe thick films, prep. by sintering and elec. props. 80−29451
CdTe, thin film, stopping power for protons and alpha particles, proton energy straggle values 77−89489
CdTe thin film polycrystalline solar cells prepared by electrodeposition 80−93948
CdTe thin films, oriented, VPE growth, infrared transmission, photovoltaic cells 80−59825
CdTe, time-resolved spectra, carrier relax. time, phonon lifetime 80−11433
CdTe, trace anal. by heavy ion induced X-ray emission and SIMS 80−55755
CdTe, transmission spectrum under uniaxial compression 80−29714
CdTe, tunable high efficiency microwave freq. shifting of IR laser 78−71126
CdTe, two-photon absorption coefficient, 3-band model 79−78679
CdTe two-photon absorption, laser calorimetric obs. 80−33076
CdTe, undoped, high-resist.- characterisation, impurity level investig. 77−39801
CdTe, undoped and donor-compensated, cathodoluminesc. of 1.4 eV bands 77−40291
CdTe, undoped and halogen-compensated, defect conc. calc. 77−39602
CdTe, use in X-ray detectors 78−86745
CdTe, vapour-phase-grown, cathodoluminesc. study 80−76086
CdTe, Yb^{3+} implantation, nonstoichiometry effect 77−15440
CdTe:Ag, with microscopic p-n junction, photopolarisation in anomalous photovoltage 79−11175
CdTe:Ag film, photoelectret effect *(Russian)* 79−28676
CdTe:As^{2+}, photovol. props. of p-n junction prod. by ion implantation 78−43038
CdTe:As(P), ion implanted, elec. props. 80−65021
CdTe:Be, impurity modes and IR absorption 78−76506
CdTe:Cl, anomalous props., molecular centre with charge-state dependent config. 77−89728
CdTe:Cl, capacitance meas. and trapping, mol. centre model *(French)* 77−39872
p-CdTe:Cl, deep level characterisation, gamma-ray detector parameters 77−39802
CdTe:Cl, description of anomalous centres by non-purely electronic model 78−30886
CdTe:Cl, donor levels, anomalous press. effects, Hall const. meas. 77−51693
CdTe:Cl, electron irrad., defects 80−25460
CdTe:Cl, gamma-ray detector growth, travelling heater method improvement 77−40353
CdTe:Cl, grown by travelling heater method, carrier homogeneity investig. 77−39848
CdTe:Cl, heavily doped, elec. and photoluminesc. investig. of defect interactions 77−39603
p-CdTe:Cl, influence of gamma-irradiation on elec. props. 77−62951
CdTe:Cl, influence of lattice defects on electrical behaviour 78−2497
CdTe:Cl, interaction of impurities and lattice defects, changes in elec. props. and photoluminesc. 77−4685
CdTe:Cl, LPE from $CdCl_2$ soln., elec. props., defects 80−39689

II-VI semiconductors continued
CdTe:Cl, localisation of electrons, temp. depend. of cond. and Hall effect 78−14732
p-CdTe:Cl, mech. of electron recomb. 79−11176
CdTe:Cl, semi-insulating, Hall effect and cond. meas., carrier mobility 77−39849
CdTe:Cl, semi-insulating, impurity photocond. spectra, local state distrib. in band gap 80−107865
CdTe:Cl, semiinsulating, Hall effect and elec. cond., impurity levels 77−55532
CdTe:Cl, single cryst., photo Hall effect obs. 78−76094
CdTe:Cl(In), photoelectronic investig. of trap depths, TSC and SCL cond. 77−39893
CdTe:Cr, impurity photoionisation transitions, EPR meas. 80−39857
CdTe:Cr^{2+}, absorpt. and luminesc. of $Cr^{2+}(d^4)$, cryst. field theory interpretation 79−83000
CdTe:Cu, doping effects on evaporation kinetics and electronic props. during high-temp. annealing in vacuum 78−22743
CdTe:Cu films, impurity behaviour, Hall mobility and hole density meas. 80−80420
CdTe:Fe, annealed, magnetically ordered, Hall effect and photocond. 78−19060
CdTe:Fe, dopant solubility 77−90334
CdTe:Fe, Mn, Cr, introduction of elec. active defects 80−103647
CdTe:Fe^{2+}, reson. relax. time for impurity electrons and localised phonons interaction, appl. to thermal cond. 80−59590
CdTe:Fe-group metals, mag. susceptibility *(Russian)* 79−56496
CdTe:Fe(Ni), luminesc. and refl. spectra, high temp. annealing effects 80−24472
CdTe:Ge, dopant behaviour 78−22742
CdTe:Ge, mag. props. 78−56289
CdTe:Ge, negative thermally stimulated cond. 79−19621
CdTe:H^+, ion-implanted, optical waveguiding and electrooptic modulation 77−7197
CdTe:In, lightly- and heavily-doped, cathodoluminesc., temp., injection level and freq. depend. 78−52584
CdTe:In, photoconductivity exam. and IR quenching 79−11181
CdTe:In, pure and heavily doped, electron-hole liq. form., luminesc. spectra 80−10884
CdTe:In, shift optical absorpt. edge with temp. and doping level 79−8165
CdTe:In precipitation and out-diffusion of solute during cooling 80−100840
CdTe:Li, excitation spectrum of Li acceptor and valence band parameters 79−28795
CdTe:Li(Cl), acceptor states study by donar acceptor pair excitation luminesc. 80−100683
CdTe:Mn, photoionisation absorption spectrum 78−23502
CdTe:Mn, spin-lattice coeffs. of Mn^{2+} 80−84646
CdTe:Mn^{2+}, exciton refl. spectra and mag. susceptibility 80−66253
CdTe:Mn^{2+}, luminesc. and magnetooptic reson., mag. field effect 80−93390
CdTe:Mn^{2+}, magneto-optical and microwave-optical double reson. meas. of exciton band *(Russian)* 77−81087
CdTe:Mn(Fe)(Ni), exciton refl., photoluminesc., and mag. suscept. meas., influence of impurities 77−39787
CdTe:P, annealing induced lattice defects, TEM obs. 80−2010
CdTe:p, defect model, from Hall effect meas. 77−43620
CdTe:Si(Cl), force variation due to charged defects 80−92634
CdTe:Ti^{2+}, Jahn-Teller effect on $^3T_1(^3F)$ state, resonance on $^3T_1(^3P)$ state 78−27271
CdTe:V,Cr_2 optical props. meas. 79−73969
CdTe:V (d^3), absorption and luminesc. spectra 78−15203
CdTe:Xe, anomalous Xe^+ ion implantation defect introduction, cathodolum. obs. 77−62554
CdTe:Yb, exciton emission, cathodoluminescence 78−39033
CdTe:Zn, TSC, carrier traps, depth and quenching by IR radiation 78−56420
CdTe/$Hg_{1-x}Cd_xTe$ multilayers, LPE growth 80−80104
CdTe/HgTe superlattice, new IR material 79−72634
CdTe/Langmuir film photovoltaic structures for solar cells 80−49918
CdTe-Ag diode, Schottky type, elec. and photoelec. props. 77−43719
CdTe-AlSb, phase diag. 77−52299
CdTe-Au contacts, electronic states, vacuum UV photoelectron spectra 80−70827
CdTe-Au Schottky barriers, quantum photoelectric yield, theoretical anal. 77−39939
CdTe-Au system, phase diagram rel. to doping 80−16282
CdTe-Au(Al) Schottky barriers, defect effects 79−60921
CdTe-Au(In) contacts, photo-effect in the 77-300K range, barrier height estimation 80−107850
CdTe-based p-n junction, photoeffect quantum efficiency depend. on photon energy *(Russian)* 79−78168
CdTe-CdS heterojunctions, growth by closed-tube chem. transport, elec. props. 80−60070
CdTe-CdS heterojunction, photocapacitance and photocond. 80−96978
CdTe-CdS p-n heterojunction, coordinate sensitive photoelements, longitudinal photovoltage 79−95440
CdTe-CdS thin film p-n solar cells, spectral response temp. depend. 80−93871
CdTe-CdS-CdSe system solid soln. single crysts., forbidden band width determ., comp. depend. 80−55083
CdTe-CdSe, and CdTe-ZnSe p-n heterojunction, photovoltaic props. 77−55600
p-CdTe-Cl, compensated, hopping cond. 77−76818
CdTe-electrolyte boundaries, photo e.m.f. meas., semicond. energy bands 77−1481
n-CdTe-electrolyte solar cells, interface changes during operation, AES, electrolum. and electroreflectance meas. 79−100525
CdTe-HgTe, neutron irrad. rel. to elec. props. 79−15141
CdTe-HgTe, semicond. solid solns., effect of reactor irrad. on electrophys. props. 77−51744
CdTe-HgTe ideal superlattice, electronic props. calc. 80−49885
CdTe-HgTe superlattice on CdTE layers, evanescent states, tight binding calcs. 80−70611
CdTe-In system, equilib. phase diagram and liq. phase epitaxial growth of CdTe from In soln. *(Japanese)* 80−71634
CdTe-In_2Te_3, composition depend. of energy gap, optical absorpt. obs. 77−80728
CdTe-InSb solid solns., electroreflectance spectra, Brillouin zone transitions 80−7330

II-VI semiconductors continued
p-CdTe-Langmuir film interface, prep., characters. and MIS struct. 80−92998
CdTe-metal, diode contact, elec. characts., generation-recombination space charge region *(Russian)* 78−39214
CdTe-metal contact, surface barrier exam. 78−64111
CdTe-PbTe(InSb) superlattices, laser deposition of multilayer heteroepitaxial structs. 80−44450
CdTe-Si heterojunctions, epitaxy and electrical props. *(Japanese)* 77−32074
CdTe-$SnCl_2$ electrolyte heterojunction photoelec. props., feasibility as solar energy convertors 77−76918
CdTe-Te film, prep. by combined hot-wall-flash evaporation method, and characterisation 80−55296
CdTe-ZnS system, phase diagram and solid solubility 80−20909
CdTe-ZnS(Se) solid solns., optimal synthesis conditions for single cryst. growth 80−100776
CdTe-ZnSe pseudobinary system, phase diagram and equil., Bridgman single cryst. growth method 79−43213
CdTe-ZnTe n-p heterojunction, photovoltaic props. 77−55600
CdTe+ZnSe⇄CdSe+ZnTe ternary mutual system, phase equilib. 79−52179
$(CdTe)_{1-x}$-$(ZnSe)_x$ system, mutual solubility and band gap energy *(Japanese)* 77−51501
$(CdTe)_x$-$(CdSe)_{1-x}$, diamond-type semiconductor, Mossbauer spectra, quadrupole interaction of ^{125}Te 80−44992
$CdTe_{1-x}S_x$, long-wavelength optical phonons, composition depend., IR and Raman spectra 78−67788
CdTe(Se):Co, impurity luminescence no phonon line depend. on temp., Debye temp. 80−66273
$CdTe_{1-x}Se_x$, multiband model of impurity complexes 80−65497
$CdTe_{1-x}Se_x$, Raman scatt. spectra, two-mode behaviour 78−60450
$CdTe_{1-x}Se_x$ solid solution films, prep., struct., and photocond. 80−54541
CdZnS thin films, growth and evaluation for fabrication of high performance photovoltaic solar cells 80−93501
CdZnS-CdS bifilm solar photocells, feasibility, study 78−76113
(CdZn)S-Cu_2S solar cell, film form. and characts. 78−68080
$Cd_{1-x}Zn_xS$ 10 μm film optical and electrical characterisation *(French)* 78−64153
$Cd_{1-x}Zn_xS$, electro-optical multilayer film, for data storage and display 78−71176
$Cd_{1-x}Zn_xS$, epitaxial growth of single crystal layers on (111) GaAs substrate, close-space geometry 78−92198
$Cd_{1-x}Zn_xS$, film, technical data, for low cost solar cell 79−48127
$Cd_{1-x}Zn_xS$ films, thermal evaporation prep., phys. props. 80−84410
$Cd_{1-x}Zn_xS$ heteroepitaxial single-cryst. layers, photoluminesc. props. 80−100692
$Cd_{1-x}Zn_xS$, RF sputtered electro-optical film for data storage and display 78−83047
$Cd_{1-x}Zn_xS$ reactively sputtered phtoconductive films for high field applications *(German)* 78−39154
$Cd_{1-x}Zn_xS$ solar cell thin films, microprobe characterisation *(French)* 80−61349
$Cd_{1-x}Zn_xS$ spray deposited film, for low cost solar cells 79−7915
$Cd_{1-x}Zn_xS$, use of parallel and monochromatic beams for comp. determ. by X-ray fluorescence 79−48000
$Cd_{1-x}Zn_xS/Cu_2S$ thin film heterojunction solar cells, operational charact. 80−45687
$Cd_{1-x}Zn_xS$-p-GaAs heterojunctions, elec. and photovolt. props. rel. to growth technique 80−29466
$Cd_{1-x}Zn_xS$-PbS heterojunctions prepared by spray pyrolysis 79−60917
$Cd_xZn_{1-x}S$ film, vacuum evaporated, struct. 78−38985
$Cd_xZn_{1-x}S$ films, chem. sprayed, carrier density and mobility 80−60121
$Cd_xZn_{1-x}S$, vibr. spectra, microscopic theory 79−73949
$Cd_xZn_{1-x}S$-Cu_2S solar cell, interface chemistry modification of current-voltage charact. 79−100523
$Cd_{1-x}Zn_xSe$, epitaxial layer growth with Zn content from doping to solid soln. formation 77−85094
$Cd_{1-x}Zn_xTe$, solid soln., vibr. spectra restructuring anomalies 79−4803
Cds film on metal substrate, resistivity 79−95522
Cds, photoconductive, convolution voltage enhancement due to carrier transverse drift in SAW convolver 80−1381
Cds, reson. Brillouin scatt. by piezoelectrically inactive TA phonon domains 78−84593
CeSe:Fe, long-wavelength fundamental absorpt. edge formation, role of Fe 77−16351
Cr_2O_3 addition to CdS_xSe_{1-x} photoresistors, extension of cutoff freq. *(Russian)* 78−84248
P-Cu_{2-x}-n-CdS, heterojunction, energy band diagram 79−24070
$CuGa_{0.5}In_{0.5}Se_2/Zn_{0.29}Cd_{0.71}S$ heterojunction solar cell, preparation and props. 80−101110
Cu_2S stoichiometric thin films for solar cells 79−61991
Cu_2S-CdS, solar cell, photocurrent, spectral depend. 79−7853
Cu_2S-CdS film junction formation by dry-barrier process 78−64109
Cu_2S-CdS heterojunction interface, depth distribution profiles, Auger spectra 80−88622
Cu_2S-CdS heterojunctions, role of deep levels in controlling photovoltaic props. 80−92941
Cu_2S-CdS solar cells, Cu_2S film growth methods 80−80980
Cu_2S-CdS solar cells, optimised grid patterns 80−108798
Cu_2S-CdS solar cells with interdigitated grid, current-voltage analysis 80−93981
Cu_2S-CdS solar photopiles, tunnel conduction mechanism *(French)* 79−29480
Cu_2S-CdS sprayed solar cells, chemical spray deposition 80−93979
Cu_2S-$Zn_xCd_{1-x}S$ and Cu_2S-CdS thin film solar cells by solid state reaction, comparison 80−101109
$Cu_{2-x}S$-CdS, solns. cell, photo-emf, depend. on degree of doping of CdS 79−52934
$Cu_{2-x}S$-CdS heterojunction V-I characteristic and max. photovoltage, long-term changes *(Russian)* 78−43468
$Cu_{2-x}S$-CdS p-n heterojunction, optical energy convertor, struct. and recomb. props. 80−72065
Cu_xS-CdS solar cell improvement by Cu treatment and front contacting 79−61987
Cu_xS-CdS solar cell junction formation and open-circuit voltage 79−61986
Cu_xS-CdS thin film solar cells, using all film vacuum deposited process 80−93977
$Cu_{2-x}Te$-CdSe heterojunction, elec. and opt. props. *(Korean)* 77−51811

II-VI semiconductors continued
GaAs-ZnSe, X-ray cond. 5.4 to 17.5 keV, spectral and dosimetric charcts. *(Russian)* 77−35964
GaP, two photon absorption relative to Raman cross sections 78−87098
$(GaP)_x(ZnSe)_{1-x}$/GaP, epitaxial heterostructures, chem. microinhomogeneity 77−80831
GaSb-Zn(Cd)Te, quasibinary system, phase equilibrium, intermol. interaction 77−12601
GdTe:P and CdTe:P,In(Ga)(Al), IR absorpt. investig. of localised vibr. modes of impurity centres 77−52136
Ge-ZnSe p-n heterojunctions, effect of interfacial condition on optoelectronic props. 79−24061
GeTe, microstruct. in phase transform. region 79−52177
p-(Hg,Cd)Te, carrier lifetime, dominant Auger transitions comparison 80−49768
(Hg,Cd)Te IR detector array, 72-element, 8-12 micron, performance, FLIR system appl. 79−2829
(Hg,Cd)Te n^+-p photodiodes, 8 to 12 μm IR imaging appls. 80−9044
(Hg,Cd)Te photodiode for 2 μm IR detection 77−82603
(Hg,Cd)Te photodiode IR detectors, planar technology 80−9043
(Hg,Cd)Te photodiodes, wide-bandwidth 10.6 μm IR heterodyne detect. 80−9042
$Hg_{1-x}Cd_xGe$, quantum oscillations of magnetoresistivity *(Russian)* 80−11007
$Hg_{0.985}Cd_{0.015}Se$, interband $\Gamma_6 \rightarrow \Gamma_8$ magnetoabsorption and band parameters 79−82960
$Hg_{1-x}Cd_xSe$, (x=0 to 0.15), Shubnikov-de Haas oscillations, influence of level broadening 79−11155
$Hg_{1-x}Cd_xSe$, IR absorpt. spectra, band struct., refr. index 80−50337
$Hg_{1-x}Cd_xSe$, zinc blende structure, optical and electronic properties 80−6723
HgCdTe, 0.1 eV photodetector performance background dependence 77−32038
HgCdTe, 0.1 eV photodetector performance 77−32039
HgCdTe, 0.1 eV photodetector performance, geometrical enhancement 77−32040
HgCdTe, crystal and photodiode, imperfections and surface conditions using electron induced current technique 79−67385
HgCdTe, electron irradiated, high temp. defects 79−78122
HgCdTe epitaxial material, ion implantation, junction form. 80−100260
HgCdTe IR photovoltaic detectors for 8-14 μm range, review *(Italian)* 78−54451
HgCdTe, interband magnetoabsorption and band struct. 79−82959
HgCdTe MIS structure, modelling and appl. to CCD IR imagery 78−80058
HgCdTe, Magneto transport anomalies at low carrier densities, Wigner crystallisation 80−20222
HgCdTe, narrow band gap semiconductor IR devices, advances 80−48464
n-HgCdTe, photocond., Hall mobility and resist. 80−34478
HgCdTe photodiode IR detector, selection 79−58791
HgCdTe photodiodes formed by double-layer LPE 80−104078
HgCdTe, radiation effects on low-temp. carrier recombination lifetimes, photocond. meas. 78−6400
HgCdTe, recomb. effects, mag. quantum oscills. in Auger transition rate 79−82610
HgCdTe reverse-biased photodiodes for wideband appls., excess noise 80−107876
HgCdTe Schottky barrier diode and n-p diffused junction IR detectors, comparison 80−9039
HgCdTe short-wavelength IR photovoltaic detectors, radiation testing 80−37084
HgCdTe solid solution photodiode for CO_2 laser active medium study 80−95868
HgCdTe, zero gap, unusual high electron mobility and related phenomena 79−82601
HgCdTe-CdTe IR detector arrays, 3 to 11 μm, fabrication techniques 80−9041
HgCdTe-CdTe photodiode, 1.33 μm, grown by LPE, phys. props. 80−107892
$Hg_{0.60}Cd_{0.40}Te$, LPE growth from Te-rich soln. 80−7508
$Hg_{0.6}Cd_{0.4}Te$, annealing temp. effect on carrier conc. 78−72167
$Hg_{0.6}Cd_{0.4}Te$ LPE layer growth from Te-, Hg-, and HgTe-rich solns., comparison 80−76199
$(Hg_{0.6}Cd_{0.4})_{1-x}Te_x$, defect anal., intrinsic material parameters 80−75519
n-$Hg_{0.61}Cd_{0.39}Te$ single crystals, flicker noise due to grain boundaries, meas. 79−1611
$Hg_{0.68}Cd_{0.32}Te$ photodiode, minority carrier lifetime determ. 79−38084
$Hg_{0.7}Cd_{0.3}Te$, 17 to 77K, photo- and cathodoluminesc. 78−52569
$Hg_{0.72}Cd_{0.28}Te$ semiconductor, two-mode reson. polaron 79−15105
$Hg_{0.74}Cd_{0.25}Te$ thin film deposition on Si substrates by RF triode-sputtering, large-area photodetector arrays 80−80965
$Hg_{0.75}Cd_{0.25}Te$, single crystal, reflection spectra 80−40140
$Hg_{0.75}Cd_{0.25}Te$, thermorefl. spectra, effect of excitons on E_1 and $E_1+\Delta_1$ structs. 80−16057
$Hg_{0.77}Cd_{0.23}Te$, near reson. spin-flip Raman scatt. 79−82983
$Hg_{0.77}Cd_{0.23}Te$ nonlinear optical IR generation 80−58642
$Hg_{0.77}Cd_{0.23}Te$, resonant four-photon and higher order mixing 79−41415
$Hg_{0.77}Cd_{0.23}Te$, spin-flip Raman laser, high conversion efficiency 77−79832
n-$Hg_{0.785}Cd_{0.215}Te$, slightly compensated, transport props. of photo-excited carriers 78−47832
$Hg_{0.79}Cd_{0.21}Te$, ion implanted, elec. props. 80−20184
n-$Hg_{0.8}Cd_{0.2}Te$, microwave bolometer heterodyne receiver based on magnetic field induced phase transition 80−13135
$Hg_{0.8}Cd_{0.2}Te$ surface, sputter cleaning and dry oxidation, XPS and LEED study 80−108618
$Hg_{0.8}Cd_{0.2}Te$-ZnS MIS struct., nonparabolic bond semicond., surface state studies, capacitance measurements 79−78190
$Hg_{0.82}Cd_{0.18}Te$, electronic anomalous mass near reson. acceptor level, Shubnikov-de Haas meas. 80−80163
$Hg_{0.85}Cd_{0.15}Te$, acceptor states, galvanomagnetic effects study 79−82560
$Hg_{0.86}Cd_{0.14}Te$, spin-flip electron scatt., longit. magnetoresist. obs. 77−43622
$Hg_{1-x}Cd_xTe$, acceptor bound exciton Auger and radiative transition rates, radiative recomb. 80−6733
$Hg_{1-x}Cd_xTe$, acceptor impurity band form. 80−20119
$Hg_{1-x}Cd_xTe$, acceptor levels due to local impurity potential 79−11084
$Hg_{1-x}Cd_xTe$, anodic oxide films, formation and props. 80−3212
$Hg_{1-x}Cd_xTe$, avalanche formation, high intensity IR transmission limit 79−78684

II-VI semiconductors continued
$Hg_{1-x}Cd_xTe$ breakdown-limited MIS devices, increased charge capacity using ramped gate voltage 80−103751
$Hg_{1-x}Cd_xTe$, CESR *(Russian)* 78−23344
$Hg_{1-x}Cd_xTe$, CESR meas., four-photon mixing via spin-flip Raman scatt. 79−82873
$Hg_{1-x}Cd_xTe$, carrier conc., Hall effect, photocond., IR spectra meas. 80−49771
$Hg_{1-x}Cd_xTe$, cyclotron reson., 337 μm transmission expts., 77 to 150K 78−34750
$Hg_{1-x}Cd_xTe$, degenerate four-wave mixing of 10.6 μm radiation 80−95943
$Hg_{1-x}Cd_xTe$, doping props. of selected impurities, diffusion behaviour 77−72632
$Hg_{1-x}Cd_xTe$, Einstein relation for inversion layers 80−103706
$Hg_{1-x}Cd_xTe$, epitaxial layers, elec. properties in the range 4.2 to 300K *(French)* 80−65721
$Hg_{1-x}Cd_xTe$ epitaxial layers, elec. props. 80−96910
$Hg_{1-x}Cd_xTe$, far IR cyclotron resonance in inversion layer 77−69396
$Hg_{1-x}Cd_xTe$, far IR cyclotron reson., band edge effective mass and relax. time 79−19781
n-$Hg_{1-x}Cd_xTe$, far IR recomb. radiation in elec. field, acceptor states 77−16399
n-$Hg_{1-x}Cd_xTe$, far IR recomb. radiation with applied elec. field 78−27324
$Hg_{1-x}Cd_xTe$, Faraday effect at CO_2 laser freq. 78−64348
$Hg_{1-x}Cd_xTe$ films, Tamm surface states, Kane model 79−28395
$Hg_{1-x}Cd_xTe$, for appl. in IR detector arrays, comp. control 80−31872
$Hg_{1-x}Cd_xTe$, grown from melt, Kirkendall and Frenkel effects 80−100365
$Hg_{1-x}Cd_xTe$, Hall coeff., anomalous temp. depend., 4.2 to 70K 80−65604
$Hg_{1-x}Cd_xTe$, high intensity IR transmission limit 78−79074
$Hg_{1-x}Cd_xTe$, high-pressure reflex growth technique, IR detector appl. 77−40347
$Hg_{1-x}Cd_xTe$, homogeneous single cryst., growth by modified Bridgman technique 78−39682
$Hg_{1-x}Cd_xTe$, Hooge's flicker noise MIS expt. 78−56233
$Hg_{1-x}Cd_xTe$ hot-electron photoconductive detection of near mm wave radiation 80−57377
$Hg_{1-x}Cd_xTe$ IR detector technology 78−77989
$Hg_{1-x}Cd_xTe$ IR focal plane status and performance 78−77987
$Hg_{1-x}Cd_xTe$, IR optical absorpt. and refr. index, 80 to 300K 79−91418
$Hg_{1-x}Cd_xTe$ IR photodetectors for night vision appl. 80−22429
$Hg_{1-x}Cd_xTe$ implanted detector 8 to 14 μm, performance, p-n junction characts. 77−15941
$Hg_{1-x}Cd_xTe$, implanted with Hg, Al, damage and lattice location study 80−103381
$Hg_{1-x}Cd_xTe$, interband magnetoreflectance 78−19448
$Hg_{1-x}Cd_xTe$ interface with native oxide, elec. props. 80−20318
$Hg_{1-x}Cd_xTe$, ionized intrinsic pt. defects, effect on carrier density 77−47835
$Hg_{1-x}Cd_xTe$, LPE current controlled 80−40272
$Hg_{1-x}Cd_xTe$, LPE growth and characterisation 80−50565
$Hg_{1-x}Cd_xTe$, LPE-grown and optically pumped crystal, continuous lasing at 2.79 μm 79−68397
$Hg_{1-x}Cd_xTe$, long-term Hall-type conversion by vacancy diffusion at room temp. 79−65498
$Hg_{1-x}Cd_xTe$, magnetooptical and impurity effects 80−6721
$Hg_{1-x}Cd_xTe$, magnetoreflection studies 79−82963
$Hg_{1-x}Cd_xTe$, material capabilities for 1 to 1.3 μm room temp. photodiodes 78−24859
$Hg_{1-x}Cd_xTe$, mixed crysts., band struct. and optical transitions, distorted atomic orbitals 77−69224
$Hg_{1-x}Cd_xTe$ mixed crysts., magneto-opt. obs., semicond. config., semimetal-semicond. transition 77−73131
$Hg_{1-x}Cd_xTe$, mixed crystals, crystn. by chemical transport 80−20775
$Hg_{1-x}Cd_xTe$, n-surface inversion layers study 80−25017
$Hg_{1-x}Cd_xTe$, narrow-gap semiconductor, high intensity IR transmission limit 80−7361
$Hg_{1-x}Cd_xTe$, near band-gap photoluminesc., bound exciton luminesc. obs. 80−103973
$Hg_{1-x}Cd_xTe$, nonlinear absorption and saturation, 10.6 μm 77−746
$Hg_{1-x}Cd_xTe$, nonlinear optical effects 80−14389
$Hg_{1-x}Cd_xTe$, optical absorpt., quasilocal acceptor level effects, theory 80−92853
n-$Hg_{1-x}Cd_xTe$, optical phase conjugation 80−83644
$Hg_{1-x}Cd_xTe$, p-T diagrams, p=n intrinsic-extrinsic lines 77−36481
n-$Hg_{1-x}Cd_xTe$, photoconductor, contact noise at 77K 78−88028
$Hg_{1-x}Cd_xTe$ photoconductors, gamma ray effects on surface props. and detector props. 79−17489
$Hg_{1-x}Cd_xTe$ photoconductive IR detector, optimum bias attainment with batteries 79−58789
$Hg_{1-x}Cd_xTe$ photodiodes, for IR detection 80−13144
$Hg_{1-x}Cd_xTe$ photodiodes, implanted n^+-p, improved performance using insulated field plates 80−52309
$Hg_{1-x}Cd_xTe$ photodiodes, long cutoff wavelength, effect of trap tunnelling on IR detector performance 80−73451
$Hg_{1-x}Cd_xTe$, photolum. and optical pumping 80−50424
$Hg_{1-x}Cd_xTe$, props. and appls., book contrib. 77−39834
$Hg_{1-x}Cd_xTe$, quasi-local acceptor levels and electron mobility 78−67974
$Hg_{1-x}Cd_xTe$, recombination processes using impact ionization capture cross sections 80−75577
$Hg_{1-x}Cd_xTe$, resonant acceptor level, single and multiple scatt. effect 77−47767
$Hg_{1-x}Cd_xTe$, segregation, compositional characterisation 80−107434
$Hg_{1-x}Cd_xTe$, semiconducting phase, acceptor states and galvanomagnetic effects 80−11017
$Hg_{1-x}Cd_xTe$, semimetallic state, magneto-optical investig. of Landau levels and band parameters 77−63410
$Hg_{1-x}Cd_xTe$, shallow acceptor contribution to near-resonance spin-flip Raman scatt. 79−95754
n$Hg_{1-x}Cd_xTe$, single-phonon and plasmon recomb. lifetime effect, with magnetically tuned bandgap 79−38098
$Hg_{1-x}Cd_xTe$, surface topographic stoichiometry variations, electrolyte electrorefl. obs. 78−27249
$Hg_{1-x}Cd_xTe$, Tamm surface states 77−55595
$Hg_{1-x}Cd_xTe$, theory of optical absorpt., contribution by quasilocal acceptor levels *(Russian)* 80−71451
$Hg_{1-x}Cd_xTe$, transverse magnetoresist. in extreme quantum limit 77−39885

II-VI semiconductors continued
$Hg_{1-x}Cd_xTe$, two-photon absorption coefficient, 3-band model 79−78679
$Hg_{1-x}Cd_xTe$, two-photon absorpt. spectra 80−20660
$Hg_{1-x}Cd_xTe$, vaporisation under Knudsen effusion conditions 80−2154
$Hg_{1-x}Cd_xTe$, zero-bandgap state induced by press., galvanomag. props. 77−47725
$Hg_{1-x}Cd_xTe$, zero-gap semicond. with nonparabolic band struct., hot electron mobility and conc. 78−76080
$Hg_{1-x}Cd_xTe$, zero-gap semicond., reson. states 79−82558
$Hg_{1-x}Cd_xTe$-CdTe photodiodes, backside-illum., LPE growth and thermal noise characts. 79−40610
$Hg_{1-x}Cd_xTe$-In contact, diffusion of In 80−103520
$Hg_{1-x}Cd_xTe$-oxide interfaces, MIS capacitance characts. 80−49926
$Hg_{1-x}Cd_xTe$-type semimetals, kinetic props., local acceptor level effects 80−65557
$Hg_{a-x}Cd_xTe$, (x<0.16), semimetallic phase, acceptor states and galvanomagnetic effects 80−6882
$Hg_{a-x}Cd_xTe$, single-LO-phonon and -plasmon recombination channels narrow-bandgaps 78−91728
$Hg_xCd_{1-x}Te$, Hall effect and elec. cond., carrier density and mobility temp. depend. 77−4341
n-$Hg_xCd_{1-x}Te$, narrow band gap, Auger effect under high mag. fields 79−82609
$Hg_xCd_{1-x}Te$, photodiode, anomalous noise behaviour in heterodyne and background limited operation 79−69568
$Hg_xCd_{1-x}Te$, zero-gap props. correlated to Γ_8 symmetry, review 80−6717
HgCdTe(Se) MIS junction, phonon-assisted tunnelling 79−47170
$Hg_{0.98}Mn_{0.02}Te$, resonance acceptor level 78−23048
α-HgS, band gap shrinkage, cathodolum. under very strong excitation 77−85146
HgS, cathodoluminescence, evidence of donor-acceptor type transition 77−24902
HgS, cinnabar, chem. vapour growth in closed system 78−35283
α-HgS, cinnabar, donor-acceptor transitions, cathodolum. meas. *(French)* 77−48250
α-HgS, cinnabar, reson. Raman effect and luminesc. meas. 80−50338
α-HgS, crystn. in NaHs solutions 77−8740
HgS, electrodeposition, using nonaqueous solvents 80−76200
α-HgS, electronic energy level calcs. 80−6718
HgS film, deposition from colloidal solns. 78−92209
HgS film, RF sputtered, effect of K on cryst. modification 77−62773
α-HgS, gas-phase and solid-state Hg 5d photoionisation processes, direct comparison 80−76149
α-HgS, green cathodoluminesc., impurity effects 78−2924
α-HgS, natural, yellow emission 78−68567
HgS, photo-stable semicond. in electrolyte soln., photo-EMF and photocurrent obs. 79−42637
α-HgS, polarised reflectance spectra, 2-5 eV, 77 and 293K 77−77243
HgS, RF sputtering on NaCl, growth and struct., electron diffr. and TEM obs. 77−90271
α-HgS, trapping parameters determ. by TSC meas. 80−59997
$HgSe_x$, Fermi surface anisotropy parameters, magneto-optical effect 80−25350
HgSe, band struct. and spin splitting Shubnikov de Haas study 80−65445
HgSe, Bridgman growth at hydrostatic press. to 3 kbar, free electron conc. and mobility 77−52245
HgSe, CVD crysts., electrophys. characts. 77−85910
HgSe, elec. resist., high press. phase transform., band gap 80−70707
HgSe, epitaxial growth on CdSe, struct. and electrophysical props. 77−12540
HgSe film, anomalous photocond., electron microscope study 80−65623
HgSe film on Se, dark relax. of anomalous photocond., photofield model 77−51776
HgSe, interband absorpt. and Γ-point band structure parameters 79−47010
HgSe, interband $\Gamma_6 \rightarrow \Gamma_8$ magnetoabsorption and band parameters 79−82960
HgSe, interband $\Gamma_6 \rightarrow \Gamma_8$ magnetoabsorption, temp. study 80−76032
HgSe, magnetooptical and impurity effects 80−6721
HgSe, optical determ. of Γ-point band struct. parameters 79−82523
HgSe, point defect model rel. to elec. props. and phase diagram 77−4339
HgSe, press. induced phase transitions, nucleation, resistance discontinuity 77−27996
HgSe, quantum oscills. in Seebeck effect in high mag. fields 77−72875
HgSe, Shubnikov-de Haas oscills. in pulsed mag. field, Fermi energy var. 77−15873
HgSe, Shubnikov-de Haas oscills., electron conc., g-factor and Dingle temp. 77−69354
HgSe, Shubnikov-de Haas effect 78−6402
HgSe, Shubnikov-de Haas determ. of electron g factors 80−6704
HgSe, thermoelec. power, spin split quantum oscills. 77−11948
HgSe, two-phonon resonant effect, far-infrared reflectivity 80−108203
HgSe, zero-gap props. correlated to Γ_8 symmetry, review 80−6717
HgSe:In, enrichment of doping substances at pseudo phase boundaries *(German)* 80−29036
HgSe/CdSe lattice-matched heterostructs. as Schottky barriers, CVD epitaxial growth and elec. props. 80−49877
HgSe-As_2S_3 structure, anomalous photocond., relax., curves 77−55567
HgSe-As_2Se_3 double-layer system detector for temp. meas. 79−88952
HgSe-CdSe pseudobinary alloy, phase diagram and cryst. growth 78−68620
HgSe-Se, photo-field model, rel. to anomalous photocond. in Se:Hg 77−43658
HgSe(Te), dynamic dielectric function, IR absorpt. meas. 78−68508
HgSe(Te), NMR, chemical shift and linewidth determ. 79−19792
HgSe(Te), narrow band gap semicond., electron scatt., and transport phenomena 80−49706
HgSe(Te), zero-gap semicond., reson. two phonon absorpt. 79−55847
HgSe(Te), zero-gap semicond., impurity states model 79−60758
HgTe, 1.5 to 30K, thermal expansion and heat capacity meas. 80−59681
HgTe, acceptor reson., states in high mag. field 80−49668
HgTe, and ternary compounds, mag. field induced microwave transparency 80−49797
HgTe, conditions for oriented crystn. 79−52124
HgTe, contrib. of resonant states to conductivity 79−51577
HgTe, creep activation energy and velocity *(Russian)* 78−56716
HgTe, diamond-like semicond., Mossbauer isomer shift meas. 77−16233

II-VI semiconductors continued
HgTe, electron conc. temp. depend., 1.6 to 32K, Hall effect and cond. meas. 80−24952
HgTe, energy bands and optical props. calcs., tight-bonding model with spin-orbit interaction 80−65448
n-HgTe, far IR magnetoabsorption involving resonant acceptor states 79−69813
HgTe, freq. tripling and self-interaction of strong EM wave in zero-gap semicond. 79−10355
HgTe, gapless, nonlinear effects in transverse quantising mag. fields 77−69353
HgTe, gapless semicond., magnetophonon conc. oscills. *(Russian)* 77−11943
HgTe, growth of epitaxial layers, activation by UV and IR radiation 80−71598
HgTe, Γ_8 symm. acceptor centre hole mag. props. *(Russian)* 80−88733 *(Japanese)* 77−24967
HgTe, high purity cryst. grown from soln. by travelling heater method 77−52243
p-HgTe, inverted band struct., negative energy gap from IR absorpt. meas. 77−62820
HgTe, long-wavelength magneto-absorptions 80−11397
HgTe, mag. sub-band struct. under uniaxial stress 77−11883
HgTe, magnetooptical study of Γ_8 bands anisotropy 79−82984
HgTe, magnetophonon oscills. of thermoelec. power 80−49789
HgTe, mobility of electrons and holes, 4 to 100K 80−107821
HgTe, optical absorption 77−28572
HgTe, p-T diagrams, p⇌n intrinsic-extrinsic lines 77−36481
HgTe, phonon dispersion relations, neutron study 80−70340
HgTe, photocond. and magnetoabsorption, 1.4-20K 78−34859
HgTe, pressure-induced polymorphic transition 80−10667
HgTe, quantum galvanomag. effects 80−49782
HgTe, resonance states in scatt., variational methods 79−60754
HgTe, self diffusion of Hg and defect struct. 79−23775
HgTe, self-diffusion of Te, layer stripping technique 79−37873
HgTe, single crystal, diffusion of transition metals 79−77818
HgTe single crystals, crystn. from vapour phase, thermodynamical conditions 79−33908
HgTe surface, sputter cleaning and dry oxidation, XPS and LEED study 80−108618
HgTe thin film Hall sensor fabrication 80−2951
HgTe type semiconductor, small-gap, electron scatt. and transport props. 78−95294
HgTe type semiconductor, small-gap, electron scatt. and transport props. 78−95295
HgTe type semiconductors, spin-flip transitions in magneto-optics and magneto-transport 80−50306
HgTe, uniaxial stress effect on magneto-optical props. 77−59558
HgTe, uniaxially compressed, anomalous magnetoresist. and band crossing 79−65501
HgTe, VPE growth control by EM irrad. *(Russian)* 80−34338
HgTe, vacancy doping, effect on elec. characts. 79−82595
HgTe, vacancy doping by off-stoichiometry, influence on transport props. 78−55862
HgTe, vacancy electron states, acceptor behaviour, electron mobility 80−70193
HgTe, vacancy mech. of resorption of Hg droplets 80−39070
HgTe, zero gap semiconductor, review 77−31944
HgTe, zero gap semiconductors, Coulombic resonance states 79−38020
HgTe, zero gap semiconductor, resonant acceptor states 80−6772
HgTe, zero-gap props. correlated to Γ_8 symmetry, review 80−6717
HgTe, zero-gap semicond., reson. states 79−82558
HgTe, zero-gap semicond., absorpt. spectrum in mag. field 80−11370
HgTe, zero-gap semiconductor, variational approach to resonances 79−82559
HgTe:Cu, effect of prep. conditions on impurity distrib., hole conc. 77−8743
HgTe:Cu(In), dopant interactions 77−47834
HgTe:In, enrichment of doping substances at pseudo phase boundaries *(German)* 80−29036
HgTe:Mn, impurity scatt. contrib. to electron mobility and thermoelec. power 77−15852
HgTe-CdTe, distrib. ratios of components during crystn. of melt 77−16485
HgTe-CdTe, epitaxy by evap. and interdiffusion under isothermal conditions book contrib. 77−12549
HgTe-CdTe, high intensity US effects on synthesis and growth 77−819
HgTe-CdTe, mixed semiconductor with comp. fluctuation, kinetics of intraband absorpt. and magnetoabsorption coeff. 79−19865
HgTe-CdTe, mixing energy and short-range order, diffuse X-ray scatt. 77−28006
HgTe-CdTe ideal superlattice, electronic props. calc. 80−49885
HgTe-CdTe(ZnTe) solid solns. form., equil. vacancy conc. changes 77−43208
HgTe-HgSe film, optical spectra in fundamental absorption edge 79−74012
HgTe-InAs, phase diags. 77−52299
HgTe-type crystals, inverted band structure, influence of interband scattering on cond. *(Russian)* 79−51563
$(HgTe)_x$-$(CdTe)_{1-x}$, diamond-type semiconductor, Mossbauer spectra, quadrupole interaction of ^{125}Te 80−44992
HgTe(:Ag), impurity diffusion, gamma-ray effects 80−54441
$HgTe_xSe_{1-x}$, solid soln., intrinsic carrier density and energy band struct. 78−39134
In-CdS-In structure, volt-ampere characts., carrier tunnelling emission *(Russian)* 80−49914
In-ZnSe:Al-In, MSM structure, mechanism of current flow *(Russian)* 79−78208
$(InAs)_x(CdTe)_{1-x}$, band gap and effective mass, IR spectra obs. 78−56491
p-InP:Zn, vapour grown, prep. and props. 80−54268
InP-CdS heterojunction, injection electrolum. 78−23153
InSe, photo-absorption of green exciton 80−80816
$In_{2-x}Sn_xO_{3-y}[SnO_2]$-CdSe-CdS:Cd,Cl sandwich photoconductor injection obs. *(Russian)* 80−54773
$LiNbO_3$-CdSe layer structure, SAW absorpt., elec. field effects 80−65355
$Mg_xZn_{1-x}Te$, high purity, luminesc. and band gap 78−68553
$Mg_xZn_{1-x}Te$, long wavelength optical phonon replica 78−60468
Mn chalcogenides-II-VI compound solid solutions, cryst. growth and physicochem. props. 79−14711

II-VI semiconductors continued
Pb salt DH lasers for IR gas spectroscopy 77−19325
Pb-Al_2O_3-HgSe junction, asymmetry of tunnelling charcts. 79−47169
$Pb_{1-x}Sn_xTe$ film, possible applic. as mechanised stress transducers 77−58621
$Pb_{1-x}Ge_xTe$, Raman scatt. from soft TO-phonon modes 79−95773
$Pb_{1-x}Hg_xS$ film, solution-grown, struct., lattice parameters and optical band gap var. 77−69201
PbS, dispersion relation for magnetoplasma waves 79−51506
PbS oxide, optical excitation meas. of trap charging surface film *(Russian)* 78−76180
PbSe, dispersion relation for magnetoplasma waves 79−51506
PbSe, enthalpy, heat capacity, 300 to 1480K 79−60523
PbSe film, soln. growth 80−66437
PbSe:Tl, high temp. elec. and optical props., impurity states 79−60854
PbSnTe film epitaxial growth on BaF_2 substrates 78−11134
p-$Pb_{0.79}Sn_{0.21}Te$, free-carrier optical absorption 77−52101
n-$Pb_{0.88}Sn_{0.12}Te$ spin flip Raman laser pumped by TE CO_2 laser, charcts. 80−87397
$Pb_{1-x}Sn_xTe$ LPE film IR detector performance 80−86422
$Pb_xSn_{1-x}Te$, oxide and Te monolayer films, Raman backscattering spectra 77−48211
PbTe, dispersion relation for magnetoplasma waves 79−51506
PbTe, effect of pressing and sintering, study of induced defects by SEM 80−59983
p-PbTe, Fermi surface parameters depend. on carrier density, Shubnikov-de Haas oscills. 79−42435
PbTe films, thermal cond. and elec. props., 4.2 to 300K 79−28162
PbTe, undoped, nature of defects, X-ray diffr. and optical absorption meas. 77−43211
n-PbTe:In(Cu) epitaxial films, elec. transport props. 80−75659
p-PbTe-M, M=In, Pb, Zn, Cu, barrier props. 79−7898
PbTe-ZrO_2 (SiO_2), epitaxial MIS struct., fabrication and elec. props. 80−2472
SnO_2-Cu_xS-ZnS:Mn,Cu-Al_2O_3-Al, light-emitting struct., cond. and electrolum., heat treatment 80−97345
SnZ films, from thermal decomp. or organometallics, growth kinetics and struct. 79−78895
p-Te, photocond. and lifetime, surface trapping, spectral distrib. 78−34840
TlSe, vibr. props., Raman and far IR spectra meas. 78−71800
ZNSe, surface, energy-minimisation approach to atomic geometry 78−95213
(Zn,Cd)S:Cu,Al, luminesc. efficiency deterioration due to surface oxidation by $(NH_4)_2Cr_2O_7$ thermal decomp. 80−29810
Zn chalcogenides, film, on NaCl, preferential epitaxy induced by electron bombard. or elec. field 80−10824
Zn chalcogenides, thin films, VPE, needle-like cryst. growth 80−80148
Zn S-CdS:Ag(Cu), cathodoluminesc. investig., appl. to cathode ray tube screening 80−108282
ZnCdS:(Cu+Ag) binder layer for electrophotography 80−4797
(ZnCd)S:Ag phosphor, absolute efficiency under fluoroscopy conditions 78−73203
ZnCdS:Ag screen, electron beam excited, light emission spectra 80−25466
ZnCdS:Cu, binders effect on electrophotographic charcts. 79−80712
ZnCdS:Cu, high field photoconduction in binder layer 79−47121
n-ZnCdS-PTA, photosensitive powder mixed with electrochromic material, photoinduced coloration and electrochem. bleaching 77−81082
$Zn_{0.1}Cd_{0.9}S$, two-photon and two-step absorption of light 80−7389
$Zn_{0.1}Cd_{0.9}S$:Cu, doping effect on two-photon absorpt. spectra, deep levels 77−69870
$Zn_{0.1}Cd_{0.9}S$-CdTe p-n junction, prep. by spray pyrolysis, photovoltaic props. 78−60196
$Zn_{0.35}Cd_{0.65}S$ binder layers, doped and undoped, xerographic charcts. 79−56288
$Zn_{1-x}Cd_xS$ films, polycryst., reactively sputtered, MSM struct. obs. of dielec. props. and cond. mechanism *(French)* 78−14841
$Zn_{1-x}Cd_xS$, graded comp. semicond., tunable narrow-band filter, 4272 to 4584 Å 77−31128
$Zn_{1-x}Cd_xS$ mixed crystals, Raman spectra between frequencies LO(Γ) to TO(Γ) 78−2854
$Zn_{1-x}Cd_xS$, reactively sputtered polycryst. film, cond. mechanism and grain boundary barriers *(French)* 77−76972
$Zn_{30}Cd_{70}S$ ceramic, electroluminesc., stationary thermostimulated cond. 79−87120
$Zn_xCd_{1-x}S$, bound-exciton lines, compositional fluctuation-induced broadening 80−2846
$Zn_xCd_{1-x}S$ epitaxial layers, elec. resist. and luminescence obs. 78−19540
$Zn_xCd_{1-x}S$ film, optimal synthesis conditions for single cryst. growth 80−100776
$Zn_xCd_{1-x}S$ film, prep. by soln. spray method, and struct., optical and elec. props. 78−52666
$Zn_xCd_{1-x}S$ film, prep. and use as heterojunction optical energy converters 79−95488
$Zn_xCd_{1-x}S$, film, single-thermal-source form. 80−2492
$Zn_xCd_{1-x}S$, film for heterojunction solar cell 77−8208
$Zn_xCd_{1-x}S$ films, spray pyrolysis, elec. props. 80−75657
$Zn_xCd_{1-x}S$, forbidden band width, exciton refl. and luminesc. meas. 78−10947
$Zn_xCd_{1-x}S$, graded single crysts., laser or electron beam excited, luminesc. 77−85792
$Zn_xCd_{1-x}S$, granulated films, optical reson. 79−4863
$Zn_xCd_{1-x}S$ laser beam spontaneous action *(Russian)* 77−88820
$Zn_xCd_{1-x}S$, laser damage, self-focusing influence 78−50844
$Zn_xCd_{1-x}S$, lasing modes and spatial distrib. under one-photon excitation, cavity model 78−74913
$Zn_xCd_{1-x}S$ layers on ZnS substrate, VPE growth 77−77420
$Zn_xCd_{1-x}S$ monocrystal, optical and nonlinear optical charcts. *(Russian)* 79−98442
$Zn_xCd_{1-x}S$ monocrystal petal lasers, single-photon excitation *(Russian)* 80−99736
$Zn_xCd_{1-x}S$, platelet single cryst. one-photon optical excitation, spatial distrib. and mode struct. of laser emission 79−31912
$Zn_xCd_{1-x}S$, reflectivity spectrum, excitons and energy band struct. 77−55804
$Zn_xCd_{1-x}S$, resonance Raman scatt. involving exciton complexes 80−16039
$Zn_xCd_{1-x}S$ solid soln. film by spray pyrolysis 77−81214
$Zn_xCd_{1-x}S$ solid soln. films, reactive cosputtering, struct., comp. and opt. absorpt. edge *(French)* 78−6237

II-VI semiconductors continued
$Zn_xCd_{1-x}S$ substrate, rough, lattice mismatch with Cu_2S and InP films 78−43263
$Zn_xCd_{1-x}S$, thin solid soln. films, vapour deposited, elec. and optical charcts. 80−60110
$Zn_xCd_{1-x}S$:Cl, $Cu^+(Ag^+)$, high pressure luminesc. 78−19533
$Zn_xCd_{1-x}S$:Cu, photoluminesc., Birman effect *(Russian)* 79−28837
$Zn_xCd_{1-x}S$:Cu, photoluminescence 80−29783
$Zn_xCd_{1-x}S$:Cu, thermoemission of positive ions in simple gas atmos. *(Russian)* 77−28676
$Zn_xCd_{1-x}S$:In, low resist. film for solar cell window 78−71200
$Zn_xCd_{1-x}S/Cu_2S$ heterojunction solar cells, fabrication and performance 79−79397
$Zn_xCd_{1-x}S/Cu_2S$ heterojunction solar cells, junction anal. 79−92080
$Zn_xCd_{1-x}S$/GaAs heterojunction solar cells, meas. of minority carrier diffusion length 80−26158
$Zn_xCd_{1-x}S$-Cu_2S heterojunction solar cells, props., comp. meas. of interfacial region 80−81472
$Zn_xCd_{1-x}S$(Te), solid soln., broadening of exciton states, depend. on conc. 79−73449
$Zn_{1-x}Cd_xSe$, mixed crystals, antireson. in phonon spectrum, Raman spectroscopy 80−88992
$Zn_xCd_{1-x}Se$, exciton reflection spectra anomalies *(Russian)* 80−97304
$Zn_xCd_{1-x}Se$, vacuum condensates, forbidden band width determ. from transmission spectra 77−8670
$Zn_{1-x}Cd_xTe$ p-n junctions, LPE growth process, elec. props. 77−7981
$Zn_xCd_{1-x}Te$, absorpt. edge luminesc. on high-intensity excitation 78−6745
$Zn_xCd_{1-x}Te$ films, absorpt. spectra in 3.0 to 5.8 eV range 79−52034
p-$Zn_xCd_{1-x}Te$, negative photocond. excited by fundamental absorpt. region light 77−15905
$Zn_xCd_{1-x}Te$, reflection spectra, energy band struct. comp. depend. *(Russian)* 78−56500
$Zn_xCd_{1-x}Te$, relaxation processes, emission spectra *(Russian)* 78−72598
$Zn_xCd_{1-x}Te$, reson. Brillouin scatt. meas. using injected acoustic domains 78−27243
$Zn_xCd_{1-x}Te$, reson. Brillouin scatt., acoustic domain injection 79−38557
$Zn_xCd_{1-x}Te$, reson. Raman scatt. of light by longitudinal optical phonons 77−28577
$Zn_xCd_{1-x}Te$, resonant Brillouin scattering *(Japanese)* 79−15474
$Zn_{0.1}Hg_{0.9}Se$ type alloy, dispersion law of cond. band *(Russian)* 77−1366
$Zn_xHg_{1-x}Se$, band struct. and scattering mechanism, determ. from transport coeffs. 77−59254
$Zn_xHg_{1-x}Se$, band struct. from Shubnikov de Haas effect and hydrostatic press. meas. 80−49599
$Zn_xHg_{1-x}Se$, current carrier scattering mechanism 80−65546
$Zn_xHg_{1-x}Se$, galvanomagnetic effects, Shubnikov-de Haas oscill. determ. of band struct. 80−6884
$Zn_xHg_{1-x}Se$ semimetal-semicond. transition, thermo-EMF in mag. field and Hall expts. *(Russian)* 77−15881
$Zn_xHg_{1-x}Se(Te,S)$ film preparation and props. *(Russian)* 78−11122
$Zn_xHg_{1-x}Te$, impurity influence on thermomagnetic effects and elec. cond. 79−60856
$Zn_xHg_{1-x}Te$, vacancy electron states, acceptor behaviour, electron mobility 80−70193
$Zn_xHg_{1-x}Te$, vacancy mech. of resorption of Hg droplets 80−39070
$Zn_{1-x}Mg_xTe$, cryst. growth conditions and luminesc. *(French)* 77−21019
$Zn_{1-x}Mg_xTe$, growth from melt, luminesc. *(French)* 77−21019
ZnO 10$\bar{1}$0 surface, reaction of O_2, AES, LEED, EPR, desorpt., surface cond. and work function expts. 78−95950
ZnO (0001), (000$\bar{1}$) and (10$\bar{1}$0), UPS rel. to elec. struct. 78−15288
ZnO (000$\bar{1}$), adsorption of alkali metal, anomalous behaviour of Na 78−79883
ZnO (000$\bar{1}$) and (0001), Ar field ion microscopy 79−47601
ZnO (0001) and (000$\bar{1}$) polar surfaces, 6-fold LEED patterns 78−71920
ZnO (000$\bar{1}$) and (10$\bar{1}$0) surfaces, clean and contaminated, reactivity to Cl_2 79−61904
ZnO, (0001) surface, clean and O adsorbed, AES and refl. electron energy loss spectra 79−46927
ZnO (0001) surface, hardness, electrolyte pH and bias voltage effect 78−47654
ZnO (000$\bar{1}$) surface, surface and bulk excitations, reflection electron energy loss spectroscopy 77−20389
ZnO (10$\bar{1}$0), LEED anal. of atomic geometry 77−69149
ZnO (10$\bar{1}$0), surface struct. from LEED anal., matrix inversion method 79−46897
ZnO (10$\bar{1}$0) and (11$\bar{2}$0) surface, atomic geometry from elastic LEED intensities 77−20170
ZnO (10$\bar{1}$0) surface bias voltage effect on hardness, charge exchange near dislocations 78−52078
ZnO, absolute work function determ. 77−28697
ZnO accumulation layers, Hall mobility and work function, correl. 78−60185
ZnO accumulation layers, electrolytic contact quantisation effects, self consistent quantum calcs. 79−60920
ZnO, acoustic phonon intensity fluctuations after strong nonlinear amplification 78−59909
ZnO, adsorbing p- and n-type dyes, surfaces pot., UV light illum. effect 80−75624
ZnO, adsorption of H, space charge accumulation layers effect on secondary ion yields, H conc. meas. 79−83087
ZnO, ang. depend. of reflection spectra and directional dispersion of anisotropic exciton polaritons 78−31216
ZnO, aqueous-deposited films, struct. and electronic props. for solar cell appls. 80−100797
ZnO, attenuation of transmitted light in exciton region, polarisation, coherence, scatt. 77−69852
ZnO, band gap depend. on energy of zero-point vibrs., luminesc. obs. 79−73436
ZnO based varistors, nonlinear cond. theory 79−78192
ZnO, biexciton levels, luminescence-assisted two-photon spectra 80−29795
ZnO, black, possible use as spectrally selective coating for low temp. solar collectors 79−994
ZnO, Bleustein-Gulyaev wave transmission charcts. at corner 77−59197
ZnO, bulk and surface plasmons, single and multiple excitation 77−12474
ZnO, c-direction cryst. growth and crystallographic polarity 79−28902

II-VI semiconductors continued
ZnO CVD epitaxial layer, highly conductive layer, cond. and Hall coeff. obs. 79−51696
ZnO, CVD films on sapphire substrates, use as optical waveguide 78−90500
ZnO, CVD of epitaxial films on sapphire, SAW interdigital transducer fabrication 80−66430
ZnO ceramic, nonohmic, drift phenomena of capacitance and current 80−39587
ZnO ceramic, with additives, nonohmic thermally stimulated current meas. 77−20325
ZnO ceramic containing rare earth metal oxides and Co_3O_4, non-ohmic props. 77−76833
ZnO, ceramic varistor, physical props. of elec. barriers by AES and electron microscopy 77−20326
ZnO ceramic varistors, I-V characts., single grain junction meas. 79−15225
ZnO ceramic varistors, trapping by localized states, effect on dielec. and elec. props. *(Russian)* 79−28671
ZnO ceramics, heat treatment effect on cryst. phases, microstruct. and elec. props. 79−100268
ZnO ceramics, microstructural evaluation 79−55750
ZnO ceramics, non-Ohmic, cond. mech. 78−68034
ZnO ceramics, non-Ohmic transient cond. phenomena, current-voltage overshoots 79−91057
ZnO, change in exciton-phonon mechanism due to defects 78−71804
ZnO, chemisorpt. of water, cond. and ESR meas. 79−56072
ZnO, chemisorption of O_2, charge transfer, obs. by surface piezoelec. effect, contact. pot., and surface photovoltage 77−89824
ZnO crystal, adsorption of merocyanine dye, spectral sensitisation of photocond. 77−47854
ZnO crystalline films, deposition techniques *(Japanese)* 79−74098
ZnO crystals, adsorbed dye laser, charge transfer, field effect and spectrally sensitised photocond. meas. 80−49815
ZnO, defect struct. calc., doping effects 80−107218
ZnO, diffusion of excitons due to scatt. by optical phonons, photoluminesc. 77−24521
ZnO, dislocation loop nucleation on prismatic faults in high voltage electron microscope 77−72620
ZnO, dislocation motion, in situ TEM obs. 77−19961
ZnO, EPR spectra, g∼1.96 signal intensity var. 77−63264
ZnO, elastic, piezoelec. and dielec. props. 80−108157
ZnO, elec. cond. and oxidation kinetics of Zn in O_2-CO_2-SO_2 gas mixture 80−34448
ZnO, elec. cond. at high fields 80−80287
ZnO electrode, in aq. soln., phototransition at 380 nm, anodic photocurrent obs. 78−19145
n-ZnO electrode, photoelectrochemical behaviour in acetonitrile solns. 78−31644
ZnO, electron irrad., vacancies and interstitials, EPR meas. 79−14803
ZnO, electron irrad. damage, orientation depend. 80−2075
ZnO, electron-exciton elastic scatt. cross sections, central field and exchange approx. 77−62919
ZnO, electron-exciton inelastic collision cross sections 79−90967
ZnO, electron-hole liq., optical gain meas. 77−85794
ZnO, electron-hole plasma, gain and refl. spectra study 80−66227
ZnO, electron-hole recombination emission, temp. depend. and phonon repetitions *(Russian)* 79−15521
ZnO, electronic struct. calc., appl. of O nonlocal ionic pseudopot. 77−51659
ZnO, electronic surface and bulk transitions exam. by electron energy loss spectra 78−30964
ZnO, electrophotographic layer, fatigue recovery 79−63321
ZnO epitaxial film, ionized-cluster beam and reactive ionized-cluster beam deposition, cathodolum. characterisation 80−16202
ZnO epitaxial film, nonuniform cond. due to H chemisorption *(Russian)* 80−65723
ZnO epitaxial film, UV luminesc. due to one-, two-photon excitation, laser possibility 79−11468
ZnO epitaxial film electrical props. rel. to substrate orientation and growth conditions 79−56339
ZnO epitaxial film on Al_2O_3 substrate, recombination radiation in intense single photon excitation 80−7410
ZnO epitaxial film with smooth surface from CVD onto a sputtered ZnO film on sapphire, waveguide appl. 78−56588
ZnO, epitaxial layers, influence of deposition conditions on luminescence, electrical props. 79−99924
ZnO epitaxial layers, rel. between elec. and photoluminesc. props. and their deposition conditions 79−95530
ZnO, excited states of bound excitons, photoluminesc. obs. 80−44513
ZnO, exciton luminesc., 16 to 77K 80−97329
ZnO, excitonic mol. emission, strain induced splitting 77−44060
ZnO, excitonic mol. transitions, optical gain and induced absorpt. spectra 80−11438
ZnO, F^+-centre exam., ground and first excited energy level 77−39800
ZnO, F-centre exam., pseudopotential calc. 78−43328
ZnO, fatigue of electrophotographic layers 79−63320
ZnO, field emission energy distrib., surface state emission obs. 78−35258
ZnO, field-effect mobility in accumulation layers on polar surfaces 79−73509
ZnO film, chemisorption of H, electrical cond. exam. adsorption centres 78−67913
ZnO film, etching, for SAW transducers, Al electrode micro-fabrication technique 77−80042
ZnO film, growth rate and defectiveness, rel. to deposition conditions and substrate orientation 78−3057
ZnO film, high-resist., band and hopping cond., AC cond. and capacitance meas. 77−72928
n-ZnO film, highly degenerate, IR absorption by free polarons 77−4697
ZnO film, longit. elastic wave attenuation, 9.4 GHz 78−18888
ZnO film, low energy ion capture, elec. cond. increase *(Russian)* 77−12034
ZnO film, optical waveguide fabrication, CVD on sputtered ZnO film on sapphire 79−86269
ZnO film, prep. by reactive ionized cluster beam deposition, and characterisation 80−10829
ZnO film, sputtering using Zn target, technique and characterisation 78−3040
ZnO, film for solar cell appl. structural, optical and elec. props. 80−2294

II-VI semiconductors continued
ZnO film on glass substrate, high-rate deposition using DC reactive magnetron sputtering 80−80978
ZnO film on ozidised Si, optical measure of acoustic quality 80−80893
ZnO films, amorphous and cryst., CVD growth and elec. props. 77−76973
ZnO films, DC reactive magnetron sputtering technique, quality study 79−78877
ZnO films, RF sputtered single-cryst., on sapphire, struct. and SAW props. 80−80105
ZnO, freq. depend. of TO phonon decay parameter, and phonon-phonon interaction mechanisms 77−59084
ZnO, growth rate, sublimation rate and etching behaviour along polar axis 80−24387
ZnO, heteroepitaxial, for SAW and electro-optic device appl., prep. and props., book contrib. 79−83134
ZnO heteroepitaxial films, grown on Al_2O_3 substrates, X-ray topographic study of struct. 79−15048
ZnO heteroepitaxial film, orientation relations for growth on Al_2O_3 substrates, X-ray diffr. anal. 79−15049
ZnO, hexagonal spot pattern production with light source and electron beam 77−69148
ZnO, high field Faraday rotation, 6.5K 79−38522
ZnO, high rate epitaxy on sapphire by planar magnetron RF sputtering 79−28916
ZnO, high-field cond. characts. calcs. 79−91056
ZnO, highly excited, biexciton states, M-band luminescence 79−78744
ZnO, hollow crystals, growth by oxidation of ZnSe vapour, mechanism 78−34733
ZnO, hot-electron microwave conductivity, hot-electron, high DC field 79−38113
ZnO, IR spectra, surface phonon modes 79−78668
ZnO, influence on frequency-temp. coeff. of SAW devices 80−79066
ZnO, intensity fluctuations of nonlinearly amplified phonons, Brillouin scatt. meas. 77−90163
ZnO interdigital transducer, efficient bulk-wave excitation in layered media 77−69156
ZnO, ion implantation effect on luminesc. and cryst. damage 78−6758
ZnO, laser thresholds and stimulated emission, intrinsic recomb. processes 79−15489
ZnO, low energy cathodolum., surface effects 78−60522
ZnO, low-energy-electron transmission, optical modulation 79−83070
ZnO, luminesc. due to exciton-electron scatt., calc. 77−16379
ZnO, luminescent, phonon detection by shallow electronic trap states 79−14902
ZnO metal-semiconductor electroluminesc. diodes 79−99948
ZnO, microcryst., surface microscopic modes, IR detection 79−38527
ZnO monolithic SAW device, separation of storage effects 79−18611
ZnO, multiparticle exciton complexes, luminesc. spectra *(Russian)* 80−16090
ZnO, near-forward Raman scatt. intensity of E_1(TO) polariton mode 78−23462
ZnO, negative photocond. by excitation of exciton-impurity complexes, recomb. mechanism *(Russian)* 79−28379
ZnO non-ohmic ceramic, degradation props. under AC and DC bias 80−80262
ZnO, nonhomic ceramic, current oscillation phenomena 79−69515
ZnO, nonohmic ceramic, current creep 79−69514
ZnO nonohmic ceramic, formation mechanism 80−60813
ZnO, optical gain and induced absorption from excitonic mols. 78−84609
ZnO, optical gain spectra, direct recording using laser modulation 78−66834
ZnO, optical second-order nonlinear polarisability 78−25919
ZnO, optical surface phonon modes, far IR transmission 77−31863
ZnO, particulate, Dember effect, rel. to electrography 78−95314
ZnO pellets, and ZnO:Li single crysts., photo-induced AC impedance meas., photodielec. effect 78−52034
ZnO phosphor fired with Zn, luminesc. in green and red region 80−66265
ZnO, phosphors, emission spectra, impurity effects 77−32420
ZnO phosphors, origin of UV emission 78−64400
ZnO, photocond., spectral sensitisation mechanism 77−43651
ZnO, photodesorption of CO_2, rel. to surface cond. and AES, band-bending model 77−47671
ZnO, photodesorption of CO_2, pulsed-laser-dynamic-mass-spectrometer study 80−35568
ZnO, photodielectric effect, improved model including effect of traps 77−1445
ZnO, photodielectric effect, space-charge polaris. 79−60872
ZnO, photoelastic consts., absolute sign determ. by Biegelsen method 79−1749
ZnO, photoelectret, nonisothermal relax. 77−12306
ZnO photoelectret, recomb. and trapping kinetics determ. 79−38083
ZnO photoelectret, TSC reversals 77−8493
ZnO piezoelec. film, fabrication and appl. *(Japanese)* 78−23616
ZnO, piezoelec. films produced by gas transport reaction, US excitation efficiency 80−2700
ZnO, polar (000$\bar{1}$) surface, annealing and Ar^+ bombard. effects on conductivity, LEED obs. 79−51653
ZnO, polar faces, space charge layers, anomalous electron mobility 77−62981
ZnO, polar semiconductor, electron-hole liquid, electron-phonon interactions 80−6739
ZnO, polar surface, clean (O_2-H-exposed), reflection energy loss spectra, 2-30 eV 78−64434
ZnO polar surfaces, H and O_2 exposed, ion irrad., and heat treated, cond., EELS study 80−71525
ZnO polar surfaces, specificity, field emissions meas., effect of H adsorption 77−21009
ZnO powder, CO_2 desorption during electron irrad. and interaction with atomic H 77−89638
ZnO powder, Hall effect, O_2 partial press. and illumination effects 79−51607
ZnO, powder, surface cond., effects of O_2 chemisorption and CO_2 photodesorption 77−11980
ZnO, powder layers, conductivity, O_2 chemisorpt. and photodesorpt. effects 78−43441
ZnO powders, electron-beam-induced desorption, phase-sensitive detection 80−54502

II-VI semiconductors continued
ZnO powders, UV luminesc. spectral distrib., comparison with single crysts., excitons role 80−55167
ZnO, prereduced surfaces, room temp. activity for oxygen isotopic exchange 79−91998
ZnO, pure and rare earth doped, photo- and electroluminesc. 79−28803
ZnO, RF sputtered epitaxial film, appl. to integrated optics 77−14821
ZnO RF sputtered films for SAW transducers, X-ray characterisation 80−80138
ZnO RF sputtered films, post deposition annealing behaviour 80−100416
ZnO, rate of deposition and morphology 78−84719
ZnO, red, electronic and opt. props., electrographic props. 77−57419
ZnO, reflection spectra, exciton reflection at high excitation levels 77−69853
ZnO, reson. Raman scatt. 78−35137
ZnO, self-activated phosphor, band width and shift, temp. depend. 77−8623
n-ZnO, semicond. electrode, electrolum. due to hole injection from electrolytes 77−20926
ZnO Sezawa mode pn-diode array memory correlator 79−78178
ZnO, single cryst., photo- and thermoluminescence 80−66311
ZnO single cryst., UV laser, electron beam excited 80−53304
ZnO, single cryst. growth in $ZnO-H_2-H_2O-O_2$ vapour, morphology, electrophys. and opt. props. 78−52649
ZnO, single crystal, excess Zn atom conc. and elec. cond. determ. 78−3435
ZnO, single crysts., photocond. lifetimes, Zn^+ hole traps 80−75581
ZnO single crysts. with stoichiometry deviations, intrinsic defects, thermodynamic analysis 79−42485
ZnO single csytals quantised accumulation layers, Hall mobility of electrons 79−60909
ZnO, slow-electron-stimulated desorption 79−60623
ZnO, small crystal, optical surface phonon modes 78−71940
ZnO, small crystal, surface phonon modes, IR transmission spectra 80−11398
ZnO sputtered films, undoped and Ga doped, props. rel. to deposition conditions 80−107935
ZnO sputtered films, vertical electrode config. to avoid contamination 79−69982
ZnO, stimulated two-photon emission from excitonic molecules 79−28815
ZnO, strong accumulation layers, negative magnetoresistance 78−6428
ZnO substrate, for Ni films, band bending, UPS study 80−7472
ZnO surface, adsorption of O_2 and CO, electron energy loss spectra meas. 78−14601
ZnO surface, photocell, enhancement of photoelec. effect by organic additives 79−57437
ZnO surface, quantised accumulation layer magnetoresistance, spin scattering model 79−69529
ZnO, surface charge transfer in presence of photosensitising dyes 78−68049
ZnO surface electron states, appl. of surface photovoltage spectroscopy 77−69391
ZnO, surface exciton dispersion relations, additional boundary conditions 77−43687
ZnO, surface exciton polariton, nonlinear optical excitation 77−59259
ZnO, surface exciton polaritons, ATR obs., book contrib. 79−42620
ZnO, surface exciton polaritons, nonlinear optical excitation and dispersion relation 79−82657
ZnO surface extreme accumulation layers due to He^+ ions 77−72909
ZnO surface layers, high-field electrolysis during field emission 79−52084
ZnO, surface phenomena, interpretation by compensation model 78−95323
ZnO, surface phonon-plasmon coupling (surface plasmarons) 80−54497
ZnO surfaces, work function, band bending, and electron affinity 79−47145
ZnO, temp. depend. elec. cond. 79−91041
ZnO, theory of photoelastic effect 77−55769
ZnO, thermoemission of positive ions in single gas atmos. *(Russian)* 77−28676
ZnO thin film opt. waveguide, collinear acousto-optic interaction and appl. to tunable opt. filter 80−74509
ZnO thin film SAW device manufacture, sputtering system and film characterisation 78−95692
ZnO thin-film transducer, bulk wave generation due to nonlinear interaction of SAW 79−42359
ZnO, third order nonlinear optical difference frequency generation 78−22176
ZnO transparent films for conductor-insulator-semiconductor (CIS) solar cells 80−93947
ZnO, two photon spectra, quantitative investigation temp. depend. 80−50373
ZnO, two-photon-excitation, tunable laser emission, luminesc. processes 80−55127
ZnO, valence electron states, X-ray Compton profile 79−65955
ZnO, varistor, low temp. AC props. 79−38434
ZnO, varistor action, homojunction breakdown mechanism 78−60193
ZnO varistor ceramics, current-voltage characts., inhomogeneities and single barriers 80−80273
ZnO varistors, barrier voltage determ. 79−56306
ZnO varistors, cond. model 78−14736
ZnO, with chemisorbed neutral red, photocond. meas. *(Japanese)* 79−42572
ZnO, wurtzite type cryst., temp. depend. of one phonon Raman spectra, Gruneisen parameters 77−66500
ZnO, Zeeman splitting of A1-exciton emission lines, k-linear term effects 78−52563
ZnO, Zn 3d core-level transition in electron energy loss spectra, rel. to ZnSe (111) surface 78−68584
ZnO:$^{31}P^+$ implanted nonlinear resistor production and characteristics *(Russian)* 80−49252
ZnO:Bi, Sb, Co, second phase effect on elec. and mag. props. 80−60986
ZnO:Ce(Sm) phosphors, electrolum. 79−99946
ZnO:Ce(Tb) phosphors, electrolum. brightness, voltage and freq. depend. 80−60681
ZnO:Co^{2+}, polarised optical absorpt. spectrum, crystal field transitions 77−48206
ZnO:Cu, excited state, zero phonon lines in emission and Zeeman spectra 79−38026

II-VI semiconductors continued
ZnO:Cu, H(D), IR absorpt. line spectra, OH and OD vibr., optical excitation 79−15498
ZnO:Cu, H(D), OH and OD centres, IR-active absorpt. line spectra 79−15496
ZnO:Cu, O, Fe(Co)(Ni) photocond., electron escape probabilities and trap depths 77−32041
ZnO:Cu^{2+}, electronic struct., optical absorpt. and ESR 79−87312
ZnO:Dy(Nd)(Sm), phosphor, electroluminesc., photoluminesc. spectra 78−80421
ZnO:Dy(Yb)(Nd)(Sm)(Pr)(Gd)(La)(Er), electrolum. brightness, field strength and freq. depend. 80−100696
ZnO:Er,Ag, photoluminescence and electroluminescence 78−27327
ZnO:La phosphor, electrolum. brightness waves, −168 to +85°C 78−52580
ZnO:Li, electron irrad., F^+ centre, photosensitivity of e.p.r. spectrum 77−1594
ZnO:Li, luminesc. donor-acceptor pairs, exchange broadened optically detected EPR spectra 78−23373
ZnO:Li, optically detected ESR, donor-acceptor pairs, line broadening 78−80256
ZnO:Li_2O single crystal, triboelectric charge and photodischarge obs. 79−82663
ZnO:Li(Na), band-edge emission obs. 77−20933
ZnO:Nd, electrolum. brightness waves, 93 to 363K 79−33839
ZnO:Ni^{2+}, Zeeman effect at Ni impurities 80−60633
ZnO:Pr(Gd)(Er), phosphors, photoluminesc. and electroluminesc. spectra 79−11457
ZnO:Yb(Nd)(Pr)(Sm), electro- and photoluminesc. 79−83024
ZnO/CdTe heterojunctions and ZnO films preparation using spray pyrolysis 80−96985
ZnO/quartz for SAW device materials, expt. study of props. 80−80050
ZnO/SOS monolithic SAW amplifier 78−6205
ZnO/Si acoustoelectric devices, magnetron discharge sputtering prep. 80−80332
ZnO/Si SAW structs., anal. of charge injection 80−80049
ZnO-Au-epoxy resin, and ZnO-Au-fused quartz transducers, λ/4-mode operation, theory *(Japanese)* 78−30145
ZnO-based binary semiconductor system nonlinearity prognosis *(Russian)* 78−43406
ZnO-based ceramic microstructure and nonlinear props., B diffusion effects *(Russian)* 80−49423
ZnO-based ceramic varistors, current-voltage characts., leakage and breakdown regions, 100 to 1300°C 79−56231
ZnO-Bi_2O_3, heterojunction, current-voltage characts. 79−56291
ZnO-Bi_2O_3-ZnO structure, injection currents, SCL and TSC obs. *(Russian)* 77−32068
ZnO-binder system, reciprocity failure, photoconductivity 78−39151
ZnO-CdSe thin film n-n heterojunctions, prep. elec. and optical props. *(Korean)* 77−28244
ZnO-Cs, fabrication, UPS meas. 78−15279
ZnO-Cu_2O heterojunction solar cells, prop. by RF sputtering 80−93945
ZnO-electrolyte contact, current-potential characts. 77−1482
ZnO-electrolyte interface, electron transfer sensitisation by salt additions 78−34894
ZnO-glass-ZnO structure, with Bi_2O_3-based glass and granular ZnO layers, current-voltage characts. *(Russian)* 77−69404
ZnO-grainboundary-ZnO junction in ceramic varistor, capacitance-voltage characts. 80−65689
ZnO-NiO:Li_2O n-p heterojunction, contact resist., effects of water vapour 80−34506
ZnO-on-Si SAW convolver development 77−27430
ZnO-Pd Schottky-barrier diode, H_2 sensitivity 80−11085
ZnO-polystyrene photoreceptors sensitised by β-Cu phthalocyanine 79−17552
ZnO-resin photoconductive layers, impedance-freq. characts. meas. *(Japanese)* 79−38120
n-ZnO-rubrene, radical cation reduction, triplet state formation, luminesc. 77−16825
ZnO-SiO_2 (glass) layered system, characts. of phase-velocity dispersion and struct. of surface waves 80−59775
ZnO-ZnS powder mixtures, elec. cond. and Hall effect meas., percolation effects 79−7828
ZnO-ZnS powder mixtures, Hall effect and elec. cond. 79−51607
$Zn_{1+x}O$, nonstoichiometry investig., 400 to 1200°C 77−11543
(ZnO-ZnS)Cu:I, double band electroluminophors, form., props. 78−19568
ZnO(S)(Se)(Te) 79−19906
ZnO(S)(Se)(Te), 93.3 keV Mossbauer transition in ^{67}Zn, isomer shifts 80−39978
ZnO(S)(Se)(Te), charged dislocations, flow of charge with plastic deform. 80−85010
ZnO(S)(Se)(Te), cryst., ionic radii and electronic polarisabilities 77−1091
ZnO{10$\bar{1}$0} surface, clean, preparation, XPS meas. 78−39933
Zn(S,Se), large single crystals, vapour growth and defect characterisation 80−25540
ZnS, ^{57}Co gamma source, time depend. Mossbauer spectra 80−50245
ZnS, ^{67}Zn and ^{33}S nuclear magnetic shielding, chemical shifts and linewidths 80−60434
ZnS, (111) face, flux-grown cryst. dissolution characts. 77−59014
ZnS, additively coloured or neutron irradiated, near IR emission 77−90199
ZnS, appl. of orthogonalised augmented plane wave method, appl. to ZnS 77−66105
ZnS, band structure calcs. by modified orthogonalised plane wave (MOPW) method 80−54609
n-ZnS based heterojunctions, epitaxial, elec. props. *(Russian)* 78−88023
ZnS, Bridgeman growth under pressure, macroscopic inclusions and defects 80−45226
ZnS bulk and surface states anal. using synchrotron radiation 77−66574
ZnS CVD window, IR lattice absorption, phonon assigments and image spoiling 80−33104
ZnS, cathodolum. emission spectra, exciton lines 80−76084
ZnS, chemisorption of O_2 after illumination and in presence of CO and O_2 78−87877
ZnS, clean surface, AES and LEED exam. 80−10762
ZnS, Compton profile, state of valence electrons 78−11018
ZnS, cryst. grown from melt under press., microstruct. 77−59019
ZnS crystal, inhomogeneous, microscopic struct. investig. using synchrotron radiation 77−76424

II-VI semiconductors continued
ZnS crystals, luminescence kinetics, centre discrimination exam. 78−15215
ZnS crystals, structural change under plastic deform., partial dislocation movement 80−79736
ZnS crystals in electrolyte, electrolum. and elec. props. 80−93407
ZnS, crystals with stacking faults, Laue method study 79−94847
ZnS, cubic, compression 80−107358
ZnS, cubic, gel growth, expt. conditions 78−68614
ZnS, cubic, IR-active phonons obs. 80−55084
ZnS, cubic, thermal vibr. temp. depend., anharmonic models 80−92618
ZnS, cubic and hexagonal, lattice coupling with BiOCl, ErOCl and LaOCl for heterojunctions 79−60919
ZnS, current and refractive index oscills. in electric fields due to barrier instability 79−91372
ZnS, current oscills., 300K, 1-6 s period *(Russian)* 77−80819
ZnS, decomposition in H_2 atmosphere, electron-hole mechanism *(Russian)* 77−16409
ZnS, defect form. in single crysts. during implantation of Zn, S, and Ar *(Russian)* 78−14369
ZnS, dependence of hexagonal layer formation on dopant conc. 79−19265
ZnS, deposited anthraquinone, decoration patterns 77−1137
ZnS, diatomic crysts. electron induced X-ray emission, channelling effects 79−56888
ZnS, elastic moduli of polytypic modifications 79−51187
ZnS, elec. struct., piezoelec. consts. *(Chinese)* 79−56122
ZnS, electrolum. phosphors, surface phenomena occurring during ageing *(Russian)* 79−33842
ZnS, electroluminesc. and photoluminesc. spectra, fine struct. *(Russian)* 78−84661
ZnS electroluminescent films, low energy Mn implantation system 78−30658
ZnS, electroluminescent emission, UV excitation after effects 80−45144
ZnS, electroluminophor, ageing rate, voltage effects *(Russian)* 78−84662
ZnS electroluminophors, ageing effects *(Russian)* 78−15231
ZnS, electron irrad., ESR 79−91293
ZnS, energy levels of Mott excitons 78−6282
ZnS, epitaxial film, CVD growth and characterisation *(French)* 77−36403
ZnS, epitaxial growth, appl. to electronic devices, review *(Japanese)* 80−55281
ZnS epitaxial growth, in H_2, mass transport processes and effects of bypass flow 79−23860
ZnS, epitaxial growth by Zn-S-H_2 CVD method 78−27413
ZnS epitaxial layers, growth kinetics on CaF_2 by vapour phase transport *(French)* 80−54572
ZnS, epitaxial layers on Ge and GaAs substrates, exam. of growth 79−1828
ZnS, epitaxy in quasiclosed volume 77−85093
ZnS, equation of state 79−82310
ZnS evaporated film, refl. loss on UV irrad., ZnO form. 80−99813
ZnS evaporated film optical props. 160 to 2000 A 79−15544
ZnS, F-centre exam., pseudopotential calc. 78−43328
ZnS, Fe^{3+}-Cu^{+} complexes and A-centres, g-factor anisotropy *(Russian)* 77−20271
ZnS film, and ZnS-MgF_2 film system, Rayleigh scatt., 441.6 nm, scatt. losses correl. with deposition parameters 79−78782
ZnS film, defect form. and development 80−96759
ZnS film, epitaxial growth on Si in ultrahigh vacuum, source nonstoichiometry effects 77−77387
ZnS film, evaporated amorphous, mechanism of memory phenomena *(Japanese)* 78−23140
ZnS film, ion beam deposition 77−70008
ZnS film, Joule heating, I-V characts. 78−2599
ZnS, film, laser evaporation synthesis, surface struct. 79−28954
ZnS film, on semicond. substrate, early stages of growth, electron microscope obs. *(Russian)* 78−38976
ZnS film, optical inhomogeneity, rel. to struct. 79−83047
ZnS film, photovoltaic effects under illum. from above and below 78−52031
ZnS film, struct. electron microscopy 77−59226
ZnS, film, vac. deposition onto NaCl cryst. in H_2S environment 78−63945
ZnS film, vac.-deposited, origin of mech. stress 79−90925
ZnS film free carrier absorption for laser beam modulation *(Japanese)* 79−7164
ZnS film on Si, fused quartz substrates, H_2O absorpt., IR anal. 80−75446
ZnS films, electrolum., bistable excitation 80−93406
ZnS, four-photon transitions, perturbation theory calc. 80−96786
ZnS, green-blue luminesc. characts., model of luminesc. centres 79−73999
ZnS, ground state of electron subsystem, quasimolecular model 79−69055
ZnS, growth of cubic single crystal by I_2 transport 79−91572
ZnS, growth rate, sublimation rate and etching behaviour along polar axis 80−24387
ZnS, heteroepitaxial growth on GaP by closed space technique 79−28939
ZnS, heterogeneous birefringence 79−95728
ZnS, high field Faraday rotation, 6.5K 79−38522
ZnS, high purity, prep. from ZnO *(Rumanian)* 80−76206
ZnS, high temp. annealing effects on photoluminescence 78−19564
ZnS, high-level photocurrent excitation and carrier recombination expt. *(Russian)* 79−95446
ZnS, high-resist., optical transmission thermal processing effects 77−63431
ZnS, high-voltage photovoltaic effect in polycryst. layers 79−42573
ZnS, highly transparent semicond. crysts., multiphonon IR absorpt. 78−10885
ZnS, horizontal epitaxial growth systems, transport kinetics 79−4920
ZnS, interaction between charged dislocations and luminesc. centres *(Russian)* 79−56860
ZnS, interimpurity high press. luminesc. 78−19532
ZnS ion beam etching, topographic changes, amorphisation, luminescence study 80−76078
ZnS, ion implantation effects on luminesc., thermo-EMF 80−88178
ZnS, large single crystals, vapour growth and defect characterisation 80−25540

II-VI semiconductors continued
ZnS, laser evaporated film, microstruct. TEM obs. 79−82479
ZnS, laser radiation initiated electron emission, evidence for photoelec. mechanism 77−69970
ZnS, lattice dynamics, deformable-ion model 78−91396
ZnS, lattice dynamics, phonon freq., bond bending force model calcs. 80−70335
ZnS, linear electrooptic coeff. dispersion 80−71380
ZnS, low resistivity, ohmic contact noise characts. and contact resistance 78−14827
ZnS, low resistivity, prep. and characterisation for blue LEDs 77−81209
ZnS, low temp. equilibrium compensation limit of intrinsic-defect hole conductivity *(Russian)* 79−1598
ZnS, low voltage cathodoluminescence 78−52585
ZnS, low-temp. trap anal. thermally stimulated luminesc. model extension 80−80877
ZnS, luminesc. data. statistical anal. *(Russian)* 78−68559
ZnS, luminescence of M-centre 80−29779
ZnS, metal-semiconductor LED, injection electroluminescence 77−62992
ZnS, microregions disorientation degree anal. by birefringence, ESK and decoration methods 79−60389
ZnS, natural and stress induced birefringence dispersion 78−6651
ZnS, ODMR of Zn vacancy obs. 80−108121
ZnS, phase diagram of electron-hole liqs. in polar semicond. 77−89706
ZnS, phonon spectra calc. by recursion method 80−59596
ZnS phosphor, exciton struct. in luminesc. excitation spectra 77−52176
ZnS, phosphor, optical flash stimulation, optical absorption, MCD, thermally stimulated luminescence expts. 78−10951
ZnS phosphor, powdered, in host material, solar cells wavelength shifting 80−85286
ZnS, phosphor, voltage and temp. dependence of pre-breakdown electroluminescence 80−45147
ZnS, phosphor, voltage depend. of electrolum. brightness 80−45148
ZnS phosphors, Gudden-Pohl effect, field ionis. of trapping centres 77−73170
ZnS phosphors, synthesis under unidirectional pressure and roasting in vacuum 77−32547
ZnS, photocell, transient photoelec. phenomena 79−82687
ZnS photocells, thickness depend. of interband transition photovoltaic voltage and short circuit photocurrent 77−76871
ZnS, photocond. excited with laser radiation near fundamental absorpt. edge 77−76867
ZnS, photoluminesc. quenching by weak alternating field 77−85778
ZnS, plastic deform. induced luminesc., dislocations role *(Russian)* 78−10985
ZnS, plastically deformed, anisotropic cond. 78−56143
ZnS platelets, cathodolum. analysis using STEM 78−32950
ZnS, polarisation of self-activated luminesc. 77−73159
ZnS, polytype relative stabilities, entropy contribs. 80−100197
ZnS, post field recomb. in pulsed electrolum. 80−71488
ZnS, powder phosphor, IR-induced changes in emission spectra 78−80389
ZnS powder phosphors electroluminescent cells, AC electrolum. characts. *(Japanese)* 80−71489
ZnS, prebreakdown electrolum., domain form. and negative resist. effects 80−84788
ZnS, pulsed optically detected resonance, time depend. recomb. processor study 79−38411
ZnS, RF sputtered film, stoichiometry, chem. comp. 78−34727
ZnS RF sputtered films for SAW transducers, X-ray characterisation 80−80138
ZnS, Raman scatt. by phonon polaritons 80−103959
ZnS, refr. index oscills, in strong. elec. field 79−28720
ZnS, reson. Brillouin scatt., acoustic domain injection 79−38557
ZnS, reson. Brillouin scatt. and piezobirefringence 80−93348
ZnS, S annealed, IR enhancement and quenching of photocond. 78−14763
ZnS Schottky-barrier diodes, blue light emission 79−38671
ZnS, self activated emission, spin depend. donor acceptor pair recombination, ODMR exam. 79−42870
ZnS, self energy effects of valence and conduction electrons 79−37980
ZnS, self-activated, IR sensitivity 78−6742
ZnS, self-activated, orientation of luminesc. centre 78−27307
ZnS, self-activated, trap distrib. and photoelectronic effect due to UV, IR and visible excitation 77−36282
ZnS, shallow traps, thermolum. glow curves obs. 79−91508
ZnS, single cryst., grown from melt distrib. coeffs. of transition metals, Pb and Sn 77−55298
ZnS single cryst., linear electro-optical props., temp. depend. 80−71376
ZnS, single cryst., radiation emission, stimulation by IR light *(Russian)* 77−66542
ZnS single cryst., UV laser, electron beam excited 80−53304
ZnS, single cryst. plate, photovoltaic spectra, intensity depend. 78−14762
ZnS, single cryst. vap. growth by sublimation and chem. transport 78−27390
ZnS, single crystal, effect of elec. field on cond. 78−84228
ZnS, single crysts. excited by laser beam and elec. field, streamer luminesc. and photolum. obs. 80−34986
ZnS, solution growth, using Te solvent 79−65993
ZnS, sphalerite modification, polysynthetic cryst., struct. changes due to uniaxial compression 77−15482
ZnS sputtered film, interband photocond. edge *(French)* 77−8212
ZnS, Stark-Ladder current theory 78−68035
ZnS striated platelets, SEM studies of local variations in cathodolum. 78−15232
ZnS surface, nonpolar, electronic struct., tight-binding calc. 77−20383
ZnS, surface, work function and luminesc. phenomena, effect of H,H_2,O and O_2 adsorpt. 78−10538
ZnS, surface acoustic wave modes 78−2352
ZnS, temp. coeffs. of charact. reflectivity struct. 77−85745
ZnS, temp. depend. of edge emission band shape 77−20934
ZnS, theory of photoelastic effect 77−55769
ZnS, thermoluminescence at different excitation levels 80−93413
ZnS, thermoreflectance spectra, at energies from absorption edges to 9 eV *(Japanese)* 79−11436
ZnS, thin film deposition, by low pressure, high freq. induction plasma *(Russian)* 79−69992
ZnS thin films, effect of fabrication parameters on electroluminescence and related props. *(Japanese)* 80−76083
ZnS, tight binding calc., F-centres, and isoelectronic defects 77−20266

II-VI semiconductors continued
ZnS, tight-binding model of F-centre 77−89729
ZnS, time differentiated Mossbauer spectra from ^{57}Co impurities, relaxation processes *(Russian)* 80−34834
ZnS, time resolved ODMR, electron-hole recombination 79−42872
ZnS, two-photon absorpt. in crossed elec. and mag. fields 77−85693
ZnS type lattices, luminescence, constants, temperature dependence, activation energies 79−99923
ZnS, VPE on GaP in open tube system 79−28938
ZnS, vacuum-evaporated conducting films, prep. and props. 79−66007
ZnS, valence electron states, X-ray Compton profile 79−65955
ZnS, wavelength-modulated refl. spectra, 2.5 to 8 eV 77−20877
ZnS with Au film coating, calc. of defect conc. 78−95052
ZnS, with CdS or Cu_2S addition, phase transform. during crystn., 850 or 1150°C 77−48362
ZnS with substitutional impurity, dipole and weak-dipole vibr. 79−14904
ZnS, wurtzite type cryst., temp. depend. of one phonon Raman spectra, Gruneisen parameters 77−66500
ZnS:^{90}Sr, continuously acting luminous solid for photoelec. meas. over 300-800 nm range 79−3757
ZnS:(Cu, Cl), electroluminesc., voltage effect on ageing rate 79−95848
ZnS:Ag, Al and ZnS:Cu, Al, LV cathodoluminesc. 79−33844
ZnS:Ag, Al(Cu), trap parameters, thermostimulated luminesc. and cond. meas. *(Russian)* 77−72868
ZnS:Ag, cathodoluminesc. investig., appl. to cathode ray tube screening 80−108282
ZnS:Ag, electroluminesc., surface barriers *(Russian)* 78−2919
ZnS:Ag, luminesc. efficiency deterioration due to surface oxidation by $(NH_4)_2Cr_2O_7$ thermal decomp. 80−29810
ZnS:Ag, Ni thermographic phosphor luminesc. screen, for IR laser pulse recording 79−64342
ZnS:Ag, phosphor, luminesc. of surface glow centres 80−29782
ZnS:Ag, photon counting statistics of cathodoluminesc. light emission 79−24371
ZnS:Ag, single crystal, ionisation mechanism of field trapping centres 80−45156
ZnS:Ag, TSC and induced impurity photoconductivity, existence of two electron trapping centres 80−44655
ZnS:Ag,Al, computer calc. of band model for luminesc. and photocond. *(Russian)* 78−52542
ZnS:Ag,Cl, embedded in HBO_3-glass matrix, blue electrolum. 80−55195
ZnS:Ag,Sm, recomb. centre interaction, luminesc. quenching 78−10946
ZnS:Ag film, evaporated, IR quenching of photocapacitance, deep levels obs. 78−56180
ZnS:Ag film, photocapacitance IR quenching, hole photoionisation energy and spectral distrib. 79−87127
ZnS:Ag phosphor prep., physicochemical investigation of processes 78−11170
ZnS:Ag phosphors, luminesc. of glow surface centres *(Russian)* 79−28836
ZnS:Al, IR studies of Al complexes 79−33741
ZnS:Al, signal enhancement by field modulation, ODMR expts. 78−56406
ZnS:Al,Cu(Ag)(Au) phosphors, luminesc. excitation spectra and exciton struct. 80−55164
ZnS:Al(Te) phosphors, luminesc. excitation spectra and exciton struct. 80−55165
ZnS:Au, phosphor, 'blue' and 'green' centre form. *(German)* 79−38665
ZnS:B, new luminesc. centre 79−38635
ZnS:Be, far IR lattice absorpt., Green's function calc. 78−43865
ZnS:Be, impurity modes and IR absorption 78−76506
ZnS:Cl, self-activated, blue emission band 79−38633
ZnS:Cl, shape of self-activated cathodoluminesc. band 80−34987
ZnS:Cl, spectral distrib. of photocond., effect of powerful UV illumination 78−14767
ZnS:Co, Jahn-Teller interaction energy determ., piezospectroscopic expt. *(Russian)* 77−4623
ZnS:Co^{2+}, EPR and spin-lattice relax. of Co^{2+} centres *(Russian)* 79−1706
ZnS:Co(Fe)(Mn)(Ni), impurity-induced Raman scatt., central force const. reduction 77−32379
ZnS:Cr, anomalous temp. depend. of near IR absorption 79−28794
ZnS:Cr^{+}, Fe^{3+}, luminesc., cond. and paramag. centre conc. parameters 78−6724
ZnS:Cr^{2+}, Cr^{2+} $^5T_2$ and ^5E states, Jahn-Teller effect calcs. 80−39539
ZnS:Cr^{2+}, excitation spectrum of IR emission 77−12421
ZnS:Cr^{2+}, Jahn-Teller interaction energy calc. 78−2455
ZnS:Cr^{2+}, photoionisation, lattice relaxation energy 80−6778
ZnS:Cr(Mn)(Fe)(CoXVi), vibr. modes of transition element impurities 78−76472
ZnS:Cu, Al phosphors, mechanism of IR stimulated and quenching 77−69881
ZnS:Cu, Br based electroluminesc. cells, light, const. field effects on electroluminesc. 78−84658
ZnS:Cu, Cl, I, anisotropy of blue Cu luminesc. centres 77−81137
ZnS:Cu, Cl, Mn film, AC electrolum. 80−60680
ZnS:Cu, Cl luminophor, photoluminesc. and struct. props. 77−32414
ZnS:Cu, Co, deep traps and stationary luminescence *(Russian)* 78−48227
ZnS:Cu, current pulses stimulated by elec. field at low temp. 78−39121
ZnS:Cu, deep transition metal impurity states, SCF CNDO cluster calcs. 80−100442
ZnS:Cu, effect of elec. field on photoluminescence, model of luminogen centre 78−76522
ZnS:Cu, electroluminesc. spectra fine struct. 79−95847
ZnS:Cu, Er, Na, phosphor, mechanism of sensitisation effect of Cu and Na ions 77−16369
ZnS:Cu, film effect of Cu valency on cond. 79−11246
ZnS:Cu, Gudden-Pohl effect, flash kinetics 79−24367
ZnS:Cu, halogen, electroluminescent cells, visible light and DC voltage effects on ageing 77−69914
ZnS:Cu, O(Fe,Co,Ni) photoconductors, killer impurities effect on electron escape probabilities and trap depths 77−4392
ZnS:Cu, Pb, phosphors, ruby laser stimulated time delayed emission spectra 77−69874
ZnS:Cu, polycryst. phosphor, excitation storage, recombination barrier participation 78−27316
ZnS:Cu, spectral distrib., rise and decay behaviour *(German)* 80−60625
ZnS:Cu,Al, anisotropy of blue-Cu luminescence centres 78−64390
ZnS:Cu,Al phosphor, shallow hole traps 78−31237

II-VI semiconductors continued
ZnS:Cu,Cl, electrolum. brightness wave, effect of square pulses 77−52184
ZnS:Cu,Cl, electrolum. voltmeter design, accurate high-voltage meas. 78−24813
ZnS:Cu,Cl, exciton refl. spectra, hexagonal struct. 77−44021
ZnS:Cu,Cl phosphor, effect of charged imperfections on electrolum. 77−32443
ZnS:Cu,Cl(Br)(I), green luminesc., interimpurity phototransitions investig. *(Russian)* 77−66541
ZnS:Cu,Co, phosphor luminesc. screen, spectral charact. determ. of IR pulsed lasers 79−10341
ZnS:Cu,Er,Cl film, ageing and forming, DC electroluminesc., impact excitation 79−47522
ZnS:Cu,O, photocurrent spectral distrib., Fe, Co and Ni impurity effects 77−8135
ZnS:Cu,Pb, thermoemission of positive ions in simple gas atmos. *(Russian)* 77−28676
ZnS:Cu,Pb film, sublimated, pulse electrolum. meas. *(Russian)* 77−85806
ZnS:Cu,Pt phosphors, photoluminesc., thermoluminesc. 78−43915
ZnS:Cu 79−24350
ZnS:Cu crystal, powder, epitaxial film, luminescence anomalous thermal 80−76077
ZnS:Cu powder exam. of dielectric constant anomaly, in terms of polarisation catastrophe phenomena 79−51897
ZnS:Cu^{2+}, Jahn-Teller effect, stacking faults and formation of polytypes, absorption and emission spectra 77−4660
ZnS:Cu(Cl), electroluminesc. and photoluminesc. spectra, fine struct. *(Russian)* 78−84661
ZnS:Cu(Pb), phosphor, photocapacitive effect, Gudden-Pohl effect 79−65520
ZnS:Er diodes, electrolum. 79−33840
ZnS:Er^{3+}, ion-implanted, annealing, cathodolum. obs. 80−2868
ZnS:Er^{3+}, luminesc. centres with cubic symmetry 79−38636
ZnS:Eu^{3+}, origin of red fluoresc., occurrence of rare earth oxysulphide inclusions *(French)* 77−69875
ZnS:Fe, luminesc. and ESR investigations 80−2822
ZnS:Fe, piezospectroscopic effect on electron-vibr. lines of Fe^{2+} 78−27269
ZnS:Fe^{2+}, low temp. Mossbauer spectra, in source and absorber expts. 77−28500
ZnS:Fe^{2+}, relax. meas. from Mossb auer absorber and source expts. 80−39956
ZnS:Fe^{2+}, reson. relax. time for impurity electrons and localised phonons interaction, appl. to thermal cond. 80−59590
ZnS:Fe^{2+}, thermal expansion and heat capacity, effect of Fe^{2+} 77−31782
ZnS:Fe^{3+}, spin-lattice relax., expt. evidence for optical phonons 80−20451
ZnS:Ga, self-activated emission, A-centre ODMR 79−95685
ZnS:Ga(Cl), deep traps, impurity electroabsorpt. and photocond. meas. 78−6707
ZnS:In, polarisation of deep centre electroabsorpt., effect of random electric fields 77−48148
ZnS:In, recombination emission by optically detected magnetic resonance 80−66272
ZnS:Mn, AC thin film electroluminesc., filamentary emission and memory effect 79−38672
ZnS:Mn, AC thin-film electrolum. devices, electrolum. efficiency profiles 79−65931
ZnS:Mn, Cu, Cl films, AC electrolum. 80−60679
ZnS:Mn, Cu powder devices, DC electroluminesc. 79−38674
ZnS:Mn, dopant conc. effect on stacking fault energy 80−2041
ZnS:Mn, electrolum. film, direct impact excitation of Mn centres 77−24900
ZnS:Mn, electrolum. films, activating impurity diffusion coeff. *(Russian)* 77−84995
ZnS:Mn, self-activated and Mn^{2+} emission, high press. action 80−16093
ZnS:Mn, spectral distribution and decay times of the luminescence of Mn^{2+} on different lattice sites 79−78743
ZnS:Mn AC thin film devices, domain electrolum. 80−66303
ZnS:Mn AC thin film electrolum. device, filament behaviour 80−20712
ZnS:Mn co-deposited electrolum. thin film device, phys. and elec. characterisation 80−20713
ZnS:Mn electroluminescent films, amplification factor during electric field excitation, population inversion *(Russian)* 79−78757
ZnS:Mn film, AC electrolum., memory effect 78−15228
ZnS:Mn film, AC electrolum., memory effects 79−38673
ZnS:Mn film, current conduction and light emission, physical mechanism 78−14840
ZnS:Mn film, electroluminescence theory 79−11470
ZnS:Mn film, emission centres of DC electrolum. 78−68564
ZnS:Mn film, luminesc. of highly efficient DC diodes 77−8630
ZnS:Mn film, spectral and electro-optical props. 77−1736
ZnS:Mn film device, laser modulation of electrolum. 78−52576
ZnS:Mn films, photoluminesc. and electroluminesc., excitation mechanism of luminesc. centres 79−11459
ZnS:Mn films, surface struct., microrelief rel. to morphology of SnO_2 transparent cond. support 79−56092
ZnS:Mn Schottky diodes, reverse-biased, electroluminescence, hot electron impact excitations 80−25005
ZnS:Mn-H atom systems, surface physiochem. changes, radical recombination luminesc. investig. 79−56863
ZnS:Mn^{2+}, $^4T_1$ excited state, absorpt., MCD, Jahn-Teller model 78−43907
ZnS:Mn^{2+}, $^4T_1$ state, magneto-optical meas. 77−20833
ZnS:Mn^{2+}, $^4T_2$ level, Zeeman splittings, Jahn-Teller effect 80−40141
ZnS:Mn^{2+}, cubic, EPR, ENDOR 77−77093
ZnS:Mn^{2+}, heavily doped, anomalies in reflectivity 77−20891
ZnS:Mn^{2+}, Jahn-Teller effect in fluorescent level 78−52566
ZnS:Mn^{2+}, spin-lattice coupling coeffs. of Mn^{2+} ions in stacking faults 77−20690
ZnS:Mn^{2+}, spin-lattice relax. time, continuous saturation expts., spin diffusion 77−36120
ZnS:Mn^{2+}, spin-lattice relaxation, EPR, optical phonons 80−39852
ZnS:Mn^{2+} phosphors, luminesc. excitation spectra and exciton struct. 80−55164
ZnS:MnF_2 films, effect of Mn conc., XPS obs. 79−33886
ZnS:Mn(Al)(Te), luminesc., exciton struct. 79−33801

II-VI semiconductors continued
ZnS:Na, and undoped, thermoemission of positive ions in simple gas atmos. *(Russian)* 77−28676
ZnS:Ne, implanted single crysts., photolum. and bombardment effect, thermolum. curve obs. 80−55166
ZnS:Ni, IR luminesc. and absorpt. spectroscopy 80−108261
ZnS:Ni^{2+}, Zeeman effect at Ni impurities 80−60633
ZnS:Pb, blue luminesc., photoexcited EPR spectrum 80−108070
ZnS:Pb, luminescence, polaris. emission 79−38634
ZnS:Pb current pulses due to elec. field liberation of electrons from trapping centres by tunnel processes 79−28378
ZnS:Pb phosphor, electrolum. brightness, temp. depend. 77−48249
ZnS:Pb phosphor, ionisation mechanism of field trapping centres 80−45156
ZnS:Pb phosphor mech. of elec. field liberation of electrons from traps 78−72616
ZnS:Pb^{2+}(Mn^{2+}), high press. luminesc., localised excitations 78−19534
ZnS:RF_3 film, AC electrolum., memory effects 79−38673
ZnS:S, photoconductivity and negative differential photo-effect 78−39156
ZnS:Tb, Cu(Ag) phosphors, luminesc. props. 80−100690
ZnS:Tb^{3+}, NdF_3 film, vac. deposited, electrolum. energy transfer 80−2861
ZnS:Tb^{3+}, sputtered film, DC electroluminesc. and host-excited photoluminesc., Tb^{3+} content depend. 77−85807
ZnS:TbF_3, photoelectroluminescence, effect of electron-hole pairs 78−27328
ZnS:TbF_3 film between semicond. Y_2O_3 layers, bright green electrolum. 80−2859
ZnS:Te, single crysts. grown from Te soln., photolum. props. 79−52005
ZnS:Tl(Al)(Zn), UV spectra of donor-doped single crysts. 77−12404
ZnS:Tm^{3+}, charge compensation and polytypism influences on fluorescence 80−89051
ZnS:Tm(Er)(Nd) phosphors, optical scintillation mechanism 79−56867
ZnS:V (d^3), absorption and luminesc. spectra 78−15203
ZnS:Yb^{3+}(Nd^{3+}), spin-lattice relax. times meas. 78−19324
ZnS-Al_2S_3, phase relationships, 720 to 1110°C 79−1852
ZnS-Au electrolum. Schottky barrier diode, S^+-implanted, blue emission 80−76082
ZnS-based phosphor, microstruct. and luminesc. efficiency 78−10959
ZnS-BiOCl, electroluminesc. heterojunction phys. props. 77−66198
ZnS-CdS, equimolar solid soln. formation kinetics 80−39289
ZnS-CdS films, prep. by atomisation 80−16176
ZnS-CdS system, IR luminesc. and absorpt. centres, donor-acceptor pair model 77−44043
ZnS-CdS:Ag, Ni luminophor, temperature-sensitive, biological effect of microwaves determ. 80−36186
ZnS-CdS:Ag(Ni)(Co), electron-irradiated phosphors, void formation mechanism 79−55780
ZnS-CdS:Tm,Ni, recomb. centre interaction, luminesc. quenching 78−10946
ZnS-Cu, comet shaped electroluminesc. lines 78−52578
ZnS-Cu, polycryst., influence of alternating elec. field and UV light on struct. defects, electrolum. expts. 79−43041
ZnS-$CuGaS_2$ heterodiodes, LPE, emission spectra 79−33335
ZnS-$CuGaS_2$ n-p heterojunction, for LED appl., prep. and characterisation 79−1831
ZnS-$CuInS_2$, phase relations, 400 to 1300°C, X-ray and microscopic exam. 79−1853
ZnS-GaAs, n-p heterojunction, struct., multibeam electron microscopy obs. 79−11031
ZnS-GaAs solar cell structs., photolum. props. 80−50958
ZnS-GaP, solid solns., microstruct. investig. 78−2128
ZnS-metal interface, metal-induced chem. reactions and surface states 80−20311
ZnS-metal interface in MIM struct., photoexcitation level assignment *(French)* 80−15622
ZnS-metal Schottky barrier height rel. to chem. reactivity 80−25008
ZnS-Mn crystal, polarisation meas., luminesc. and Raman spectra 79−8138
ZnS-MnS, phase relations, 400 to 1300°C, X-ray and microscopic exam. 79−1853
ZnS-Na_3AlF_6 Fabry-Perot interference filter, neutron irrad. effects on props. 79−76867
ZnS-ZnSe single cryst. grown from melt, anisotropy of mech. props. and struct. 77−24303
(ZnS-ZnSe):Cu, H systems, electrolum. 77−4690
$(ZnS)_{0.2}(CdS)_{0.8}$, elec. props. effect of wurtzite-sphalerite boundary 77−55531
ZnS(Se), highly transparent semicond., multiphonon IR absorpt. 78−60461
ZnS(Se), IR transmitting semicond., dn/dT, wavelength depend. 77−77163
ZnS(Se), ionicity trends in diamagnetism and its temp. depend. 79−19717
ZnS(Se), stress-induced birefringence meas., 1-12 μm 77−24818
ZnSSe:Cu, Br, SCL currents and electrolum. via rad. recomb. 77−44065
ZnS(Se):Mn^{2+}, ^4E levels, orbit-lattice interaction and Jahn Teller effect 80−24860
ZnS(Se):Ni, optical absorpt., impurity ionisation, optical phonon coupling 80−88505
$ZnS_{1-x}Se_x$, electroluminescence with In and Au contacts, comp. depend. 77−59618
$ZnS_{1-x}Se_x$:Cu,Br ceramic, current oscills. and electrolum. under high elec. fields 79−38677
ZnS_xSe_{1-x}, band gap, comp. depend., exciton refl. spectrum obs. 78−56071
ZnS_xSe_{1-x}, electron trap associated with anion vacancy, DLTS study 80−80210
ZnS_xSe_{1-x}, epitaxial film, CVD growth and characterisation *(French)* 77−36403
ZnS_xSe_{1-x}, epitaxial film on CaF_2, comp. and temp. depend. of fund. band gap 80−11115
ZnS_xSe_{1-x}, growth of cubic single crystal by I_2 transport 79−91572
ZnS_xSe_{1-x} laser, electron-beam pumped, end-pumped config., 415-430 nm emission 77K 77−14745
ZnS_xSe_{1-x} layer on ZnS, ZnSe, growth by solid-state diffusion technique 78−56578
ZnS_xSe_{1-x}, phonon spectra calculations by recursion method, mixed crystals 80−103430

II-VI semiconductors continued
ZnS_xSe_{1-x}, VPE, characterisation of defect centres by photoelectronic meas. 80−10914
ZnS_xSe_{1-x}, VPE on CaF_2 substrate, in flowing H_2, growth and characterisation *(French)* 80−107678
ZnS_xSe_{1-x}:Fe, photolum. meas. 79−19921
ZnS_xSe_{1-x}:Mn(Cu), luminesc. obs. 78−60519
ZnS(Se)(Te), clean and oxidised surfaces, O_2 sticking coeff., ionicity effects, XPS expts. 77−85887
ZnS(Se)(Te), relative supersaturation, formula valid for different technological conditions *(Russian)* 78−84081
ZnS(Se)(Te), second order Raman scatt., lattice dynamical calc. and expt. 80−25370
ZnS(Se)(Te), thermal expansion and lattice dynamics under press. 80−100316
ZnS(Se)(Te):Ag^{2+}(Cu^{2+}), absence of EPR spectra due to strong spin-lattice coupling of Kramers doublets 77−85181
ZnS(Se)(Te):Co, impurity luminescence no phonon line depend. on temp., Debye temp. 80−66273
ZnS(Se)(Te):Cr^{2+}, absorpt. and luminesc. of Cr^{2+}(d^4), cryst. field theory interpretation 79−83000
ZnS(Se)(Te):Cr^{2+}, Jahn-Teller coupling 78−67997
$ZnS_{1-x}Te_x$, polytype single cryst. grown from melt 79−14762
ZnS.CdS, flux growth, processes accompanying roasting of CdS+NaCl 78−23590
ZnSe 79−38457
ZnSe, ^{67}Zn nuclear magnetic shielding, chemical shifts and linewidths 80−60434
ZnSe, 10.6 μm absorption meas. using thermal emission 77−1649
ZnSe (100) surface, electronic struct., scattering-theory formulation 79−42607
ZnSe (100) surfaces, surface states meas. by LEED, AES and EELS *(Japanese)* 79−99599
ZnSe (110), LEED intensity anal. and electron spectroscopy 77−43678
ZnSe (110) surfaces, obs., by low-energy-electron loss spectroscopy *(Japanese)* 79−83071
ZnSe (111), low-energy electron loss spectra, bulk and surface transitions 78−11042
ZnSe, absorpt. modulation of light, and its appl. to page composer 77−40258
ZnSe, absorpt. modulation of light, and its appl. to page composer *(Japanese)* 78−83083
ZnSe, amorphous thin film, prep. and electronic props. 77−85350
ZnSe and ZnSe:Sb, photoconduction under Nd laser irrad., local level distrib. 77−55580
ZnSe, attenuated total refl. spectra of surface exciton polariton 77−36262
ZnSe, band-edge photoluminesc., far-below band-gap excitation 80−76063
ZnSe, blende type struct., luminesc. under high excitation 79−19928
ZnSe, blue photoluminesc. excited with strong laser radiation 80−93391
ZnSe, Bridgeman growth under pressure, macroscopic inclusions and defects 80−45226
ZnSe, Bridgman growth under Ar press., temp. distrib. in furnace 78−11100
ZnSe, bulk and surface states anal. using synchrotron radiation 77−66574
ZnSe, CVD, delayed failure 79−99462
ZnSe, CVD, laser window material, impurity absorpt. meas. 78−25909
ZnSe, carrier mobility and deform. pot. const. determ. 79−91051
ZnSe, charged dislocation motion mechanism *(Russian)* 78−79820
ZnSe, clean and oxidised surfaces, surface states, low-energy EELS study 80−11522
ZnSe, cryst., elec. cond., dislocation motion effects 80−54710
ZnSe cryst., IR absorpt., annealing effect 80−80774
ZnSe crystal, difference freq. generation of 2 CO_2 lasers 79−10362
ZnSe crystal, exciton reflection spectra, control of exciton-free surface layer thickness 80−7373
ZnSe crystal, refr. index temp. increments meas. 80−33098
ZnSe, crystallographic polarity and etching behaviour 77−85030
ZnSe crystals, degenerate four-wave interaction, nonlinear optics effects 80−91856
ZnSe crystals, doped and undoped, optical absorption edge 80−60626
n-ZnSe crystals, electron scatt. mechanisms, high mobility 80−34433
ZnSe, cubic, anomalous photovolt. effect in absorpt. tail 79−42583
ZnSe, cubic, magnetoreflectance of Γ_6-Γ_8 exciton ground state 78−23495
ZnSe, cubic, magnetoreflection of s-excitons 78−60426
ZnSe, cubic and hexagonal, lattice coupling with BiOCl, ErOCl and LaOCl for heterojunctions 79−60919
ZnSe, cubic cryst., optical birefringence obs. 77−4616
ZnSe, cubic monocrystal, electron-phonon interaction, low temp. luminesc. *(Russian)* 80−25451
ZnSe, deep centres, photolum., photocapacitance and photocurrent expts. 78−39053
ZnSe, diatomic crysts. electron induced X-ray emission, channelling effects 79−56888
ZnSe, dielec. const. strain depend., spectral behaviour by acousto-optic method 77−48147
ZnSe, direct gap semicond., exciton energy at 300K from reabsorption of luminesc. 79−78728
ZnSe, dislocation motion, influence on elec. cond. 79−15149
ZnSe, donor-acceptor pair emissions charact. *(French)* 80−108249
ZnSe, EXAFS amplitudes, many-body effects 80−97379
ZnSe, elastic moduli, temp. depend., 293-973K, electrostatic reson. determ. 78−59850
a-ZnSe, elec. and optical meas., Mott-type model for amorphous semicond. 78−2414
ZnSe, elec. props. efect of wurtzite-sphalerite boundary 77−55531
ZnSe, electric charge transport by dislocations 80−103709
ZnSe, electroluminesc. exam. high voltage pulses 79−15533
ZnSe electroluminescent diode, ageing effects 77−8660
ZnSe, electroluminescent MIS diodes, surface state density determ. 77−35993
ZnSe, electron beam induced current study of grain boundaries by SEM 80−59479
ZnSe, electron irrad., dislocation climb, TEM obs. 79−1461
ZnSe, electron irrad., short-lived optical absorpt. 79−51989
ZnSe electron irradiation induced displacement defects 77−80543
ZnSe, electron trap associated with anion vacancy, DLTS study 80−80210

II-VI semiconductors continued
ZnSe, electron-beam-controlled transmission of 10 μm radiation 79−81466
ZnSe, electronic struct. of charged Zn vacancy, cluster model 77−47764
ZnSe, electronic structure, self consistent local description 80−20067
ZnSe, empty surface states and surface order effects on sorption 77−85281
ZnSe, energy levels of Mott excitons 78−6282
ZnSe, epitaxial, organometallic CVD, on GaAs, and photolum. 79−8249
ZnSe, epitaxial growth, orienting semiconductive substrate effects 77−47688
ZnSe, epitaxial growth by vapour flow method 78−64482
ZnSe, epitaxial growth on Ge substrate 80−75469
ZnSe, epitaxial layers, close-spaced technique, preparation and optical props. 79−47637
ZnSe epitaxial layers, organometallic CVD prop., growth kinetics and luminescent props. 79−51458
ZnSe epitaxial layers, prep. by chem. transport reactions 80−16192
ZnSe epitaxial layers, growth kinetics on CaF_2 by vapour phase transport *(French)* 80−54572
ZnSe etalon, temp. controlled, multiline oscillation characts. of TEA CO_2 laser 80−74334
ZnSe, evap. onto electron bombarded NaCl substrates, epitaxial growth and characts. 79−28948
ZnSe, exciton emission, halfwidths, thermal and optical activation energies obs. *(French)* 80−66268
ZnSe, exciton energy determ., electron beam excited luminesc. 79−38680
ZnSe, exciton refl. spectra, temp. depend. 80−59886
ZnSe, exciton-impurity complex, electroabsorption meas. 79−15484
ZnSe film, grown on sapphire substrate, stimulated emission 79−78708
ZnSe, film, hopping cond. 80−2499
ZnSe film, MBE and resistivity 79−100059
ZnSe film, on semicond. substrate, early stages of growth, electron microscope obs. *(Russian)* 78−38976
ZnSe film, rare earth fluoride doped, electrolum. meas. 77−16397
ZnSe film, struct., influence of laser beam 79−7761
ZnSe film on GaAs substrate, transition layer form. kinetics 79−87007
ZnSe films, long wavelength IR polariton emission band thermal shift and broadening 80−92833
ZnSe films, reson. Raman spectra 80−80888
ZnSe, grown from Ga soln., near band-edge luminesc. 79−69881
ZnSe, growth centres, crystallographic parameters and etching patterns study *(French)* 79−41998
ZnSe, growth of cubic single crystal by I_2 transport 79−91572
ZnSe, Gudden-Pohl effect, release of electrons from traps 80−45149
ZnSe, heat-treated in controlled partial press. of Zn or Se, TSC 80−59910
ZnSe, high conductivity films appl. to p.n. heterojunctions 78−68100
ZnSe, high field Faraday rotation, 6.5K 79−38522
ZnSe, high-resistance layers, effect of electrode materials on switching 79−65549
ZnSe, highly transparent semicond. crysts., multiphonon IR absorpt. 78−10885
ZnSe, hot-pressed powder LED fabrication and characts. 78−23639
ZnSe, IR absorpt., temp. depend. 78−48155
ZnSe, impact ionisation electroluminesc. 77−44066
n-ZnSe, impurity band, Hall effect, elec. cond., mobility and magnetoresist. expts. 77−35888
ZnSe, impurity effects on two-photon absorpt. spectrum 77−59597
ZnSe in insulator-semicond.-insulator struct., induced birefr., influence of kinetics of transient processes 79−24294
ZnSe, ionisation energy of H-like impurities 80−20120
ZnSe LED, p-n and MOS structs., blue electrolum. 77−32441
ZnSe, LPE from Zn-Ga soln., characts. 79−28965
ZnSe, LPE growth on ZnTe, characterisation of heterojunction 77−4745
ZnSe, laser induced modulation of opt. absorpt. 78−88324
ZnSe, laser window material, multiphonon absorpt. temp. depend., calorimetric meas. 78−25907
ZnSe, laser window material, absorpt. at CO wavelengths, calorimetric meas. 78−25911
ZnSe laser windows, AR coated, photoacoustic chopping freq. studies using CO_2 laser 80−83629
ZnSe laser windows, photoacoustic signal var. with chopping freq. 80−75309
ZnSe, lattice vibration, thermal expansion and pressure effect 80−39233
ZnSe layers, cond. type determ. by pot. profiling 80−73387
ZnSe layers, LPE growth from Zn-Ga soln., photoluminesc. 79−56840
ZnSe, linear electro-optic coeff. dispersion, relation to reson. Raman scatt. 78−56459
n-ZnSe, long persistent cond. relax. and frozen cond. 80−54735
ZnSe, low resist. single crysts., radiative recomb. mechanism, photolum. and electrolum. 78−6744
ZnSe, low resistance ohmic contacts using In-Ga liquid alloy, LED fabrication appl. 80−70823
a-ZnSe, low temp. photocond., increase of activation energy as temp. decreases 78−26902
ZnSe, luminesc., hot electron effects 80−66277
ZnSe, luminesc., reson. Raman scatt. due to excitonic mols. 79−33816
ZnSe, MBE growth, elec. and optical props. 80−75462
ZnSe MBE growth, growth rate and sticking coeff. 77−32532
ZnSe MIS diode, blue electrolum., heat treatment effects 78−19569
ZnSe MIS diode, forward-bias electrolum. 78−23532
ZnSe MIS LED, donor density calc. from C-U meas. 78−47878
ZnSe MOS diodes, injection type electrolum. 77−59614
ZnSe MOS diodes, injection luminesc., edge emission 79−28842
ZnSe, magnetoreflectance of exciton-polaritons, semiclassical treatment 79−99857
ZnSe, mech. of electroplastic effect 79−28035
ZnSe, minority carriers diffusion length by surface photovoltage method 80−60003
ZnSe, moments of phonon spectra from specific heats 80−15203
ZnSe, multiphonon ionisation of deep point centres in a charged dislocation field *(Russian)* 80−100281
ZnSe, nature of large electric charges of moving dislocations *(Russian)* 78−39065
ZnSe, near band edge photoluminescence, electron-hole recombination 80−80835
ZnSe, nonstoichiometry, Zn and Se press. meas., up to 1400K 78−87664
ZnSe, ODMR expts., A and V^--centres, origin of emission bands 78−80255

II-VI semiconductors continued
ZnSe, optical axes for birefringence *(French)* 77−20819
ZnSe, optically detected mag. reson., donor g-factor 77−69732
ZnSe, optically detected mag. reson. of V^- centre and donors 78−10805
ZnSe, optically pumped stimulated emission at 4580 Å, near band edge luminesc. 78−71105
ZnSe, P-T diagram, cryst. struct. stability 78−51886
ZnSe, parasitic birefringence dispersion induced by lattice plane defects 77−4617
ZnSe, phase transition, differential thermal analysis 77−7863
ZnSe, phonon dispersion relations, eight-parameter bond-bending forces model 80−70334
ZnSe, photocurrent, temp. depend. and extinction, elec. inhomogeneity effects *(Russian)* 77−32037
ZnSe, photoelastic and elastic constants determ. using thermal Brillouin scatt. *(Japanese)* 79−51974
ZnSe, photoexcited hot electrons at 2K, photolum. meas. 79−78741
ZnSe, photolum. and blue electrolum. in MIS structs. 77−20928
ZnSe, photoplasticity and photocond., excitation energy conc. near dislocations, hardening 77−24346
ZnSe, piezobirefringence in opaque region 80−60541
ZnSe, polar semicond., radiative recomb., electron-phonon interaction effects, calc. 80−49631
ZnSe, polaritons, reson. Brillouin scatt., heavy and light excitons 79−99898
ZnSe, positron annihilation study 80−60713
ZnSe pulses and single crystals, oxidation in air 77−12724
ZnSe, pure and Cu doped, elec. props. after heat treatment in Zn or Se vapour 79−99505
n-ZnSe, purified by annealing in molten Zn, Hall mobility and polaron coupling 77−85243
ZnSe, reabsorpt. of excitonic luminesc. in direct band gap semiconds. 77−63469
ZnSe, reactor irrad., opt. props. 77−90137
ZnSe, refr. index meas. and nonlinear moment parameters 77−85681
ZnSe, refr. index meas. at 3.8 μm, 10.6 μm, 80 to 300K 79−82938
ZnSe, relaxation processes in Raman scattering and exciton luminescence under resonant excitation 80−25386
ZnSe, residual cond., recomb. of photoexcited carriers, Hall coeff. 80−75605
ZnSe, reson. absorpt. of coherent IR radn. by acceptors, photocurrent and emission spectra 79−73974
ZnSe, reson. Brillouin scatt., lifetime broadening 79−51971
ZnSe, reson. Brillouin scatt., dispersion curves, piezobirefringence anal., electronic state lifetime broadening effects 79−61390
ZnSe, reson. Brillouin scatt., quasi-static anal. 79−65887
ZnSe, reson. Raman scatt. meas. 77−66510
ZnSe, resonance Raman scatt., exciton-polariton luminescence *(Russian)* 80−97287
ZnSe, resonant Brillouin scatt. by injected acoustic waves 77−12394
ZnSe, self-compensation, role of impurities 80−92850
ZnSe, self-consistent localised electronic struct. 79−42445
ZnSe, single cryst., electron-hole drops, boundary luminesc. *(Russian)* 78−80412
ZnSe single cryst., lasing action excited by ruby laser picosecond pulses 80−64035
ZnSe single cryst., linear electro-optical props., temp. depend. 80−71376
ZnSe, single cryst. and film, long wave IR emission by lattice vibrs. 77−51528
ZnSe, single cryst. film, MBE, quality obs. using photoluminesc. 77−77419
ZnSe single cryst. for LED, heat treatment effects on elec. props. 80−29406
ZnSe, single cryst. ingot., laser screen for CRT 77−75561
ZnSe, single cryst. vap. growth by sublimation and chem. transport 78−27390
ZnSe single crystal, exciton photolum. and refl. spectra, 4-90K *(Russian)* 77−66540
ZnSe single crystal, nonlinear optical coeff. and SHG coherence length 77−79893
ZnSe single crystals, birefringence due to native defects and electro-optic effect *(French)* 79−24293
ZnSe, single crysts., grown from melt under Ar pressure, defects form. 79−4312
ZnSe, single crysts., opt. band gap and Mn^{2+} EPR, effects of prep. conditions 77−47730
ZnSe solar spectrum convertor for GaAs solar cells 80−101117
ZnSe, solution growth, using Te solvent 79−65993
ZnSe, streamer laser 77−79831
ZnSe surface, nonpolar, electronic struct., tight-binding calc. 77−20383
ZnSe surface, quantitative XPS meas. 78−56559
ZnSe, surface (110) atomic struct. 79−69331
ZnSe surface barrier diode, hot charge carriers, elec., photoelec., and electroluminesc. props. *(Russian)* 79−33841
ZnSe, surface exciton polaritons, attenuated total reflection spectra 77−24867
ZnSe surface states, electron interaction characterisation, by low energy electron transmission photovoltaic modulation 79−60896
ZnSe, temp. coeffs. of charact. reflectivity struct. 77−85745
ZnSe, thermal expansion, 20 to 1100°C *(Russian)* 79−95188
ZnSe, thermally treated crystals, photoluminesc. 80−60661
ZnSe, thermoelec. power meas. 78−52021
ZnSe, transport props., effect of In-doping and Zn-annealing 78−76075
ZnSe, twinning effect on electro-optical props. 78−68478
ZnSe, twinning on melt-growth under pressure 77−80515
ZnSe, two photon absorpt. by envelope-hole coupled exciton states, polarisation depend. 77−66522
ZnSe, two photon absorption relative to Raman cross sections 78−87098
ZnSe, two-photon absorpt., envelope-hole coupled exciton states 77−52124
ZnSe, two-photon absorpt., effect of polarisation of laser radiation 77−69856
ZnSe, two-photon and two-step absorption of light 80−7389
ZnSe, undoped and doped, pair spectra, edge emission and shallow acceptors 77−28617
ZnSe, VPE on GaAS, role of interaction between gas and solids *(French)* 77−62769
ZnSe, valence-band parameters and g-factors from free-exciton magnets reflectance 79−73905
ZnSe, vapour phase single crystal growth 79−91573
ZnSe, wavelength-modulated refl. spectra, 2.5 to 8 eV 77−20877

II-VI semiconductors continued
ZnSe, with wurtzite-sphalerite boundaries, LF photofluctuations 79−69560
ZnSe, X-ray cond. 5.4 to 17.5 keV, spectral and dosimetric characts. *(Russian)* 77−35964
ZnSe:Ag, low-temp. photolum. meas. 77−20912
ZnSe:Ag(In)(Cu), melt growth, dopant partition coeffs. 79−14837
ZnSe:Al, current switching mechanism *(German)* 79−28385
n-ZnSe:Al, free carrier absorpt., 80-300K 77−63432
ZnSe:Al, thermally stimulated transients, new approach 79−38086
ZnSe:Al, vapour phase doped, thermodynamics 79−90686
ZnSe:Al(As), and pure single cryst., defect struct., Hall effect and Zn self-diffusion meas. 79−1427
ZnSe:Al(As), high temp. electron mobility, lattice scatt. and ionized impurity scatt. 79−91042
ZnSe:Al(Ga)(In), single cryst., doping, blue luminesc. 78−39584
ZnSe:Al(Mn), elec. and luminesc. props. 77−39844
p-ZnSe:As, ion implantation and heat treatment 78−87700
ZnSe:B(F), ion implantation, photocond. and cathodoluminesc. meas. 78−26586
ZnSe:Co, effect of in-band position of states on photoelec. props. 78−23132
ZnSe:Co, optical props. in near IR 78−43924
ZnSe:Cr, piezodichroism due to reorientation of Jahn-Teller centres 80−11363
ZnSe:Cr^{+}, Fe^{3+}, luminesc. cond. and paramag. centre conc. parameters 78−6724
ZnSe:Cr^{2+}, Cr^{2+} $^5T_2$ and ^5E states, Jahn-Teller effect calcs. 80−39539
ZnSe:Cr^{2+}, excitation spectrum of IR emission 77−12421
ZnSe:Cr^{2+}, photoionisation, lattice relaxation energy 80−6778
ZnSe:Cu, Al, single cryst., low-voltage red cathodolum. 78−80423
ZnSe:Cu, Cl, high press. luminesc. 78−19532
ZnSe:Cu, deep energy levels 80−6774
ZnSe:Cu, discovery of bound exciton, electroabsorption 80−45038
ZnSe:Cu, I, ceramic, electroluminesc., electric field induced switching effect under illum. 77−1460
ZnSe:Cu, I ceramic, injection electroluminesc. of p-n microjunctions 80−40163
ZnSe:Cu, luminescence and diffusion behaviour of Cu impurities 78−35188
ZnSe:Cu,Al, LV cathodoluminesc. 79−33844
ZnSe:F, signal enhancement by field modulation, ODMR expts. 78−56406
ZnSe:Ga, defect struct., Hall effect and resist. meas. 79−1428
ZnSe:Ga, P, optically detected mag. reson. of P_{Se}-centre 79−33566
ZnSe:Ga,As, characts. of simultaneous incorporation, by Mn^{2+} ESR and X-ray fluoresc. anal. 80−34017
ZnSe:Ga(As), edge luminesc. 80−20699
ZnSe:I, I vapour transport prep., conductive and photolum. cryst. 79−100035
ZnSe:I/aqueous electrolyte junction, electrochem. behaviour in dark and under illum. 80−25003
ZnSe:In, heavily compensated, galvanomag. props. and thermopower 79−51600
ZnSe:In, heavily compensated, negative magnetoresistance 79−91079
ZnSe:In, heavily doped, Hall effect and DC cond. expts., compensating acceptors 78−52013
ZnSe:In, heavily doped, impurity band cond., Hall coeff. and cond. expts. 78−72147
n-ZnSe:In, heavily doped, high field DC cond. 79−65490
n-ZnSe:In, highly compensated, freq. depend. of cond. 79−99548
ZnSe:In, highly compensated single crystals, thermally initiated current breakdown, current-voltage characts. 80−65579
ZnSe:In, Li, binding energy of excitons bound to donor-acceptor pairs, electron-phonon coupling 77−4689
ZnSe:In, optical absorpt. spectrum, 0.4 to 0.7 μm 77−81136
ZnSe:In, single crysts., new vapour phase growth method, elec. cond. props. and photoluminesc. spectra 79−19982
ZnSe:In films, MBE growth, doping effect on photoluminesc. 80−10818
n-ZnSe:Li, semicond. selective pair luminesc., excited impurity state investigation 79−61439
ZnSe:Li diodes, electroluminescence and fabrication, expt. *(Japanese)* 77−28633
ZnSe:Li(Na), shallow acceptor excited states, luminescence spectra, Rydberg energy 79−78750
ZnSe:Li(Na)(Ga) doped and pure cryst., donor-acceptor bands 80−11465
p-ZnSe:Li(Na)(N)(P), LPE layers, photocapacitance and photocond. meas. 79−99572
ZnSe:Mg, local vibrations of impurities, IR absorpt. spectra exam. 77−7815
ZnSe:Mn thin film, AC electrolum. 79−47519
ZnSe:Mn/n-GaAs low threshold thin film DC electrolum. cell, pulse-excited characts. 80−76081
ZnSe:Mn^{2+}, ligand HFS calcs., EHT-SCCC, scattered-wave, LCAO methods, comparison with expt. 77−55501
ZnSe:Mn^{2+} Schottky barrier diodes, spin depend. cond. and photovoltage 79−91141
ZnSe:Mn^{2+}-n-Ge thin film electrolum. cell with low-threshold voltage 80−84786
ZnSe:Mn^{3+}, Jahn-Teller effect in fluorescent level 78−52566
ZnSe:Mn-n-GaAs, single cryst. substrate low threshold DC electrolum. 77−63465
ZnSe:Mn(Al)(I), Schottky diode, direct impact excitation of luminescent centres 79−7900
ZnSe:N, ion implanted cond. type conversion on annealing *(Korean)* 78−18668
ZnSe:Na, characterisation of edge emission 78−27312
ZnSe:Ni, evidence for exciton binding at Ni impurity sites, photolum. excitation spectrum 80−45135
ZnSe:Ni, photocapacitance meas. of impurity level 77−69372
ZnSe:Ni, photolum. excitation spectroscopy 80−80841
ZnSe:P(Ga), 1.91 eV red emission, optically detected mag. reson. study 79−69750
ZnSe:Pb, luminescence photocond. 79−38634
ZnSe:Ti^{2+}, EPR meas. 80−80594
ZnSe:V (d^3), absorption and luminesc. spectra 78−15203
ZnSe/metal, dielectric phonon-metal electron interaction, effect on optical props. *(Russian)* 79−19663
ZnSe/water, interface, laser-induced damage in ZnSe 80−102746
ZnSe-BiOCl, electroluminesc. heterojunction phys. props. 77−66198

II-VI semiconductors continued
ZnSe-CdTe, and ZnSe-ZnTe n-p heterojunction, photovoltaic props. 77−55600
ZnSe-CdTe heterojunction, radiative recomb., electrolum. obs. 77−32445
ZnSe-CdTe heterojunction, cathodolum. and electrolum. 78−6782
ZnSe-CdTl, epitaxial film, cond. transition, laser switched memory *(Russian)* 77−8182
ZnSe-electrolyte boundaries, photo e.m.f. meas., semicond. energy bands 77−1481
ZnSe-electrolyte junction, current photoresponse 79−82669
ZnSe-GaAs (110) interface, electronic struct., self-consistent calc. 79−95486
ZnSe-GaAs heterojunction, LF noise, I-V and C-V characts., illumination effects *(Russian)* 77−66200
ZnSe-GaAs narrow junction lasers 80−43334
ZnSe-GaAs solid solns., chem. transport cryst. growth, struct. 78−43991
ZnSe-GaAs system, heterovalent substitutionary solid solns., prep. and props. 77−24553
ZnSe-GaAs thin film DE electroluminescent cell with 20 V threshold voltage 78−76141
ZnSe-Ge (100) interface, electronic struct., self-consistent pseudopot. calc. 78−91747
ZnSe-Ge (100) interface, electronic struct. calc., scattering theoretic approach 80−6940
ZnSe-Ge abrupt (110) interface, electronic struct. 78−95339
ZnSe-Ge heterojunction, change in interfacial microstruct. on high temp. annealing 77−28242
ZnSe-Ge(GaAs)(GaP) heterojunctions, elec. and photoelec. props. *(Russian)* 77−32070
ZnSe-Ge(GaAs)(mica) epitaxial heterostructs., growth struct. 78−43257
ZnSe-HgSe, solid soln., defect distrib., elec. props., Hagemark's theory 78−64040
ZnSe-In system, residual conductivity, cathode quenching 79−7902
ZnSe-metal contact, elec. props. 78−14826
ZnSe-metal Schottky barrier height rel. to chem. reactivity 80−25008
ZnSe-Si n-n heterojunction photovoltaic effect, freq. meter in visible wavelength *(Korean)* 79−60915
ZnSe-ZnS semiconductor waveguide laser, electron beam excited, blue emission 79−18447
ZnSe-ZnTe amorphous thin-film p-n heterojunction, fabrication and characts. 79−47154
ZnSe-ZnTe heterojunction, cathodolum. and electrolum. 78−6782
ZnSe-ZnTe heterojunction, epitaxial, photosensitive, photoelec. props. 79−11203
ZnSe-ZnTe heterojunction, prep. and props. 79−95483
ZnSe+CeTe⇄CdSe+ZnTe ternary mutual system, phase equilib. 79−52179
ZnSe+Mn^{2+}, LCAO calc. of d-orbital splitting 77−28148
ZnSe(:Ga)(Al), effect of thermal treatment and doping on elec. props. 77−85223
$(ZnSe)_x(CdTe)_{1-x}$, low temp. photoluminesc. *(Russian)* 78−43931
ZnSeCu, double comet shaped electroluminesc. 78−52577
$(ZnSe)_{1-x}(GaAs)_x$ solid solns., photoluminescence spectra 80−40159
$(ZnSe)_x(GaAs)_{1-x}$, LPE growth, resist., Hall effect and cathodoluminesc. meas. 77−28270
$(ZnSe)_{1-x}(GaP)_x$, reaction of Zn with Se during Czochralski growth and LPE 79−8238
$(ZnSe)_{1-x}(GaP)_x$, two-photon absorpt. at ruby laser freq., clarification *(Russian)* 79−15505
$ZnSe_{1-x}S_x$, luminescence, polaris. emission 79−38634
ZnSe(Te), fine structure of lowest exciton state *(Russian)* 80−96801
ZnSe(Te), NMR, chemical shift and linewidth determ. 79−19792
ZnSe(Te), photolum. excitation spectra of tightly bound holes, valence band contrib. 80−60658
ZnSe(Te), Raman-luminescence problem, interference analogy and expt. discrimination by polarisation correl. 79−95764
ZnSe(Te):Cr^{2+}, spin Hamiltonian parameters and wave function coeffs., LCAO theory 77−39804
$ZnSe_xTe_{1-x}$, MBE, comp. ratio control 79−28947
n-ZnSe−p-GaAs heterojunction high-detectivity threshold photodetectors 79−6181
ZnSe(100) surface, anomalous oxidation props. 78−15558
ZnSe(110), surface struct., kinematical LEED calcs. 77−85034
ZnTE, MBE growth, elec. and optical props. 80−75462
ZnTE, relaxation processes in Raman scattering and exciton luminescence under resonant excitation 80−25386
p-ZnTe 79−43028
ZnTe, ^{67}Zn nuclear magnetic shielding, chemical shifts and linewidths 80−60434
ZnTe, 1.5 to 30K, thermal expansion and Gruneisen parameter meas. 80−59681
ZnTe (110) and (111) surfaces, electron energy loss spectra, bulk and surface losses 79−43080
ZnTe (110) and (111) surfaces, O_2 adsorption, electron energy loss and Auger spectra 79−47568
ZnTe (110) surface, elastic LEED anal. 79−86967
ZnTe (110) surface struct. determ. by LEED, UPS, and EPR 80−49475
ZnTe, anomalous penetration of implanted ^{65}Zn and compensation zone build up 77−19975
ZnTe, band parameters from bound exciton, donor-acceptor pair excitation luminescence 78−92111
ZnTe based metal-semicond. struct., spectral photosensitivity obs. 79−95492
ZnTe, blende type struct., luminesc. under high excitation 79−19928
ZnTe, Brillouin scatt. spectra, elastic and photoelastic consts. 77−59585
ZnTe, bulk and surface states anal. using synchrotron radiation 77−66574
ZnTe, clean and oxidised surfaces, surface states, low-energy EELS study 80−11522
ZnTe, cryst. growth under thermodynamically controlled conditions 77−48327
ZnTe crystals, polariton effects in luminesc. 80−103988
ZnTe crystals, secondary radiation polarization and relaxation of optical excitation 80−11399
p-ZnTe, cyclotron resonance from photoexcited electrons 79−69723
ZnTe, diamond-like semicond., Mossbauer isomer shift meas. 77−16233
ZnTe, dominant acceptors, annealing and quenching 80−24463
ZnTe, donor acceptance pairs, photoluminesc. excitation spectra *(Japanese)* 78−64409
p-ZnTe, doped and pure, photoluminesc. and photocond. spectra 77−55826

II-VI semiconductors continued
ZnTe, doped with group I impurities, fluorescence spectra meas. 78−10949
ZnTe, doping and intrinsic stoichiometric defects, self-compensation 80−59918
ZnTe, edge luminesc. excited by electron bombard. 80−66308
ZnTe, effect of quenching on electrical props. 79−1920
ZnTe, effects of Zn anneals in 400-550°C range on acceptor conc. 80−10571
ZnTe, elec., SEM and TEM studies of impurity segregation during long annealing 80−30001
ZnTe, elec. active intrinsic defects, Hall meas. of carrier conc. 77−51700
ZnTe, elec. field and impurity conc. effects on ionisation energy of impurities, appl. to acceptors 80−88514
ZnTe, electro- and cathodoluminesc., impurity segregation 79−43042
ZnTe, electro-optic suscept. dispersion curve 77−3620
ZnTe electrode, redox reaction due to complex $M(CN)_6^{3-/4-}$ *(French)* 80−89482
ZnTe electrodes for photochemical production of H_2, a comparison 77−70311
ZnTe, electron-phonon coupling, donor-acceptor pairs selective excitation 80−11475
ZnTe, electronic and optical parameters of O related centre 77−24534
ZnTe, energy levels of Mott excitons 78−6282
ZnTe, epitaxial film growth initial stages 77−80707
ZnTe epitaxial growth on NaCl by ion deposition 77−32533
ZnTe, epitaxial growth on GaAs by closed-tube chemical vapour transport method, elec. props. 79−99449
ZnTe, excited acceptor, donor states, luminesc. 78−72604
ZnTe, exciton localisation at impurity pairs 79−37999
ZnTe, excitonic complexes, stress splitting of luminesc. lines 77−4672
ZnTe, excitonic effects at E_0 and E_1 gaps, wavelength modulated reflectivity spectroscopic study 79−61400
ZnTe, extrinsic luminesc., bands, temp. injection level, and freq. depend. 80−20714
ZnTe film, conduction mechanisms in non-ohmic off-state 77−72932
p-ZnTe film, current-voltage characts. 77−66214
ZnTe film, electron irrad. effect on electrophys. props., prep. conditions depend. 79−28421
ZnTe film, exciton spectra, press. and temp. depend. 80−80886
ZnTe film, grown on sapphire substrate, stimulated emission 79−78708
ZnTe film, LF oscills. of dark current obs. 78−19093
ZnTe film, on semicond. substrate, early stages of growth, electron microscope obs. *(Russian)* 78−38976
ZnTe film preparation and props., by single-source vacuum deposition method *(Japanese)* 80−6664
ZnTe films, grown on glass using atomic layer evaporation 80−44453
ZnTe films, internal stress effect on fund. refl. spectra 80−60701
ZnTe films, residual conductivity, Kikuchi lines of electron diffr. pattern 79−91173
ZnTe films, simple and modified Poole-Frenkel cond. 80−97017
ZnTe, free exciton refl., surface layer effects 78−76493
ZnTe, free-exciton emission band under high-intensity photoexcitation 79−73993
ZnTe, growth from In solvents, self-compensation 77−28144
ZnTe growth from vapour, growth interruption 80−97416
ZnTe, high purity acceptor bound and free exciton states 79−99941
ZnTe, high quality p-type cryst., predominant acceptors 78−60504
ZnTe high-purity single cryst. growth by sublimation travelling heater method 79−28901
ZnTe, I_4 bound exciton, magneto-optical meas. 77−20836
p-ZnTe, interface impedance in KOH electrolyte soln. *(French)* 77−51814
ZnTe, ion implantation defect introduction, cathodolum. studies 80−75250
ZnTe ion implanted planar waveguides, refr. index profiles 77−62039
ZnTe, irradiation induced radiative centers obs. 80−66290
ZnTe, LPE growth on ZnSe, characterisation of heterojunction 77−4745
ZnTe, laser thresholds and stimulated emission, intrinsic recomb. processes 79−15489
ZnTe, lattice dynamics and phonon parameters, bond bending force model lattice dynamics and phonon parameters bond bending force model 80−59595
ZnTe, lattice vibration, thermal expansion and pressure effect 80−39233
ZnTe, low temp. vapour growth, closed tube transport technique 77−85914
ZnTe, low voltage green LED, struct. double diffusion procedure 80−100697
ZnTe, luminesc., donor-acceptor-pair excitation spectroscopy 80−25456
ZnTe, luminescence spectra struct. surface and volume polaritons *(Russian)* 80−16089
ZnTe, MBE growth, growth rate and sticking coeff. 77−32532
ZnTe MBE thin film growth, elec. and optical props. 78−47887
ZnTe, magneto-optical effect, I_2 bound exciton 77−12432
ZnTe, magnetoreflectance meas. on Γ_6-Γ_8 exciton 78−6656
ZnTe, moments of phonon spectra from specific heats 80−15203
ZnTe, nonlinear absorpt., temp. depend. *(Russian)* 77−20899
ZnTe, nonlinear magnetoelec. susceptibility, three-dimens. model 80−39845
ZnTe, optical identification of substitutional acceptors by low temp. photoluminescence 79−99940
ZnTe, photoinduced dielec. loss and capacitance changes, rel. to space charge polarisation 80−2417
ZnTe, photoluminesc., donor and acceptor excited states 79−38622
ZnTe, polymorphism at elevated temp., elec. resist. and X-ray diffr. under press. 80−49359
ZnTe, radiative recombination involving free particle scatt. 79−38648
ZnTe, Raman scatt. and exciton luminesc. under reson. excitation 79−38617
ZnTe, real structure effect on luminescence and absorption spectra, dislocations 80−16085
ZnTe, refined, undoped, Cu acceptor, optical absorption and photoluminesc. meas. 80−34970
ZnTe, reflectivity meas., double beam wavelength modulated technique *(Korean)* 80−50365
ZnTe, relax. processes at high excitation levels, Bose-Einstein condensation of excitons 78−48219
ZnTe, relax. times of secondary radiations, circular polarisation correlation 79−28816
ZnTe, relaxation processes, emission spectra *(Russian)* 78−72598

II-VI semiconductors continued
ZnTe, reson. Brillouin scatt., injected acoustic domains obs. 78−19493
ZnTe, reson. Brillouin scatt., acoustic domain injection 79−38557
ZnTe, reson. Brillouin scatt., lifetime broadening 79−51971
ZnTe, reson. Brillouin scatt., quasi-static anal. 79−65887
ZnTe, reson. secondary radiation 79−99886
ZnTe, resonance Raman scatt. of excitonic polaritons by LO and acoustic phonons 79−65879
ZnTe, resonance Raman scatt. at high excitation levels *(Russian)* 80−55109
ZnTe, SEM and luminesc. study of Li segregation 79−38657
ZnTe, secondary emission, transient behaviour under band-to-band excitation 80−108266
ZnTe, self-diffusion profile and trapping of Zn 80−75381
ZnTe, semi-insulating, acoustoelectric domain injection from CdS 77−51778
ZnTe, single cryst., anomalous struct. of exciton refl. spectra 77−44020
ZnTe, single cryst., electron-hole drop conc. *(Russian)* 79−11460
ZnTe single cryst., lasing action excited by ruby laser picosecond pulses 80−64035
ZnTe, single cryst. vap. growth by sublimation and chem. transport 78−27390
ZnTe single crystal, excitonic reflectance 90 to 300K 79−11430
ZnTe single crystal, power depend. of photocurrent on excitation intensity, sublinear behaviour 78−43442
ZnTe single crystal, Schottky-barrier diodes and ohmic contacts props. 80−96987
p-ZnTe, single crystal *(Russian)* 78−23488
ZnTe single crystal electrodes, non-intentionally doped, electrochem. props. *(French)* 79−96326
ZnTe, spin flip scatt. of laser light 77−43976
ZnTe, spin flip scatt. of laser light 77−43977
ZnTe, spin-flip plus phonon scatt., line shape and shift in peak position 79−73907
p-ZnTe, spin-flip Raman scattering, review 80−108209
ZnTe surface, nonpolar, electronic struct., tight-binding calc. 77−20383
ZnTe, surface (110) atomic struct. 79−69331
p-ZnTe surface barrier structures, photo-EMF 77−89851
ZnTe, TEM obs. of precipitates, shape of Te solidus line 80−25703
ZnTe, temp. depend. of Raman scatt. and exciton luminesc. spectra 78−39586
ZnTe thin film, model for off-on transition 80−54742
ZnTe, thin film, stopping power for protons and alpha particles, proton energy straggle values 77−89489
ZnTe, two-photon absorpt. line shape near direct band gap and critical point 79−65898
ZnTe, unalloyed, photoluminesc., mechanism of radiative transitions 80−50405
ZnTe, undoped, electroreflectance of fundamental edge, exciton levels *(Japanese)* 80−20612
ZnTe, valence band parameters and free exciton reduced mass, free exciton magnetoreflectance 80−45046
ZnTe, vapour growth by closed tube method 78−39703
ZnTe, wavelength modulated reflectivity spectra *(Japanese)* 79−11435
ZnTe, wavelength-modulated reflectance spectrum, electron-phonon and exciton-phonon interactions 79−11434
ZnTe: group I element, absorption saturation *(Russian)* 78−35183
ZnTe:Ag, containing dislocation loops, optical absorption-edge fine struct. 78−43905
ZnTe:Ag, dislocation loops creation in region of interface 79−82210
ZnTe:Ag, doped during frowth and by diffusion, defect form. 80−15129
ZnTe:Ag, real structure effect on luminescence and absorption spectra, dislocations 80−16085
ZnTe:Al,Cl, photolum., complex acceptor, ionization energy 80−20693
ZnTe:As(Li), donor-acceptor pair excitation and recomb., photoluminesc. obs. 80−20691
ZnTe:As(P), spin flip acceptor scatt. 78−92072
ZnTe:As(P)(Li), binding energy of shallow acceptors from photoluminesc. excitation spectra for donor-acceptor pairs 79−95809
ZnTe:As(P)(Li), electronic Raman scatt. and IR absorpt. spectra of shallow acceptors 79−73978
ZnTe:Au, impurity identification and characterisation, capacitance, luminescence and IR absorption 80−60639
ZnTe:B^+ native and implant-created defects 77−76446
ZnTe:Bi, laser annealing, channelling, reflectivity spectra 80−66215
ZnTe:Cr^{2+}, Cr^{2+} $^5T_2$ and ^5E states, Jahn-Teller effect calcs. 80−39539
ZnTe:Cr(Mn)(Fe), exciton refl. spectra 80−2806
ZnTe:Cu, doping behaviour, SEM in cathodoluminesc. and photoluminesc. exam. 79−65927
ZnTe:Cu, elec. and optical identification of persistent acceptor 79−60764
ZnTe:Cu, precipitates, electron microscopic investigation 80−45312
ZnTe:Cu, red centre, electric and optical props. 80−20239
ZnTe:Cu, voltage depend. on precip. contrast 79−1433
ZnTe:Cu films, high cond., elec. and optical props. 80−88651
ZnTe:In(Al), pure and doped, Zn vacancy energy levels, elec. and optical props. 79−4827
ZnTe:Li, bleaching by green laser radiation 77−62015
ZnTe:Li, diffusion investigation by SEM and TEM 80−10706
ZnTe:Li, electron-phonon interactions in Raman scatt. 80−60594
ZnTe:Li, impurity segregation during short annealing and quenching, SEM, TEM and elec. meas. 80−10676
ZnTe:Li, Li in Te precipitates, diffusion during thermal anneal 80−39358
ZnTe:Li, O, Hagemark theory, O modification isoelectronic trap 80−75517
ZnTe:Li, Zeeman splitting of ground and excited acceptor states, selective pair luminesc. 80−84780
ZnTe:Li(As), electronic Raman scatt., mag. field depend. 79−73928
ZnTe:Li(Cl)(Al)(In), ion implanted and annealed, photoluminesc. meas. 78−15208
ZnTe:Mn, exciton refl. band, giant mag. splitting *(Russian)* 78−56079
ZnTe:Mn, mag. field splitting α n=2 exciton state *(Russian)* 78−79940
ZnTe:Mn, ordering mechanism 80−2572
ZnTe:Mn, spin-lattice coeffs. of Mn^{2+} 80−84646
ZnTe:Mn^{2+}, forbidden transitions of Mn^{2+} induced by hyperfine interactions 80−60458
ZnTe:Na(Li), spin flip acceptor scatt., transition selection rules, gyromagnetic ratios 79−61380
ZnTe:O, deep centres, photocapacitance detection 79−95362

II-VI semiconductors continued
ZnTe:O, Ne or Al implantation, electronic and optical parameters of O-related centre 78−6399
ZnTe:O,Zn, dual ion implantation, luminesc. spectra obs. 78−87697
ZnTe:P, excitations spectra of donor-acceptor pair photoluminesc. 78−23522
ZnTe:P, pure and doped, electron and exciton excited states of neutral donor 80−34393
p-ZnTe:P, semicond. selective pair luminesc., excited impurity state investigation 79−61439
ZnTe:P, spin flip scatt., shallow acceptor states 77−8587
ZnTe:P(As), g-values, spin temp., determ. from Raman spectra 78−43856
ZnTe:P(As), ion implanted, cathodoluminescence emission spectrum 80−108281
ZnTe:P(Li), luminesc. transitions, quantum efficiency 79−1783
ZnTe:Sb film, electrical props. 78−76172
ZnTe-CdS(Se)(S_xSe_{1-x}) heterojunctions, prep. and electrolum. charcts. 77−24610
ZnTe-CdSe, solid soln. formation and effects 78−27489
ZnTe-CdSe heterojunction, radiative recomb., electrolum. obs. 77−32445
ZnTe-CdSe single cryst. film heterojunctions, prep. and props. 79−19652
ZnTe-CdSe solid solutions phase equilibria *(Russian)* 79−43224
ZnTe-electrolyte boundaries, photo e.m.f. meas., semicond. energy bands 77−1481
ZnTe-electrolyte interface, electrochem. behaviour of single crysts. 79−91138
ZnTe-In Schottky diodes, photocapacitance determ. of electron-hole recomb. *(French)* 79−47119
ZnTe-metal structures, photosensitivity spectrum *(Russian)* 78−76147
ZnTe-MgTe, long wavelength optical phonons, IR refl. and Raman obs. *(French)* 78−60433
ZnTe-ZnSe, and ZnTe-CdSe(Te) p-n heterojunction, photovoltaic props. 77−55600
$(ZnTe)_x$-$(ZnSe)_{1-x}$, diamond-type semiconductor, Mossbauer spectra, quadrupole interaction of ^{125}Te 80−44992
ZnTe(:In), single cryst. film, MBE, quality obs. using photoluminesc. 77−77419
ZnTe(S), semiconductor-metal transition, press. calibration above 100 kbars fixed points 80−77808
ZnTe(Se), optical circular polarisation correl. in secondary radiation, resonant light excitation 77−69885
$ZnTe_xSe_{1-x}$, phonon spectra calculations by recursion method, mixed crystals 80−103430
$ZnTe_xSe_{1-x}$, Raman phonon spectra, resonance interaction effect 80−25375

III-V semiconductors
absorption coefficient of light 79−69803
acceptor levels, anisotropy of Zeeman splitting and polarization of luminesc. in mag. field 79−24365
acoustic deformation potential, pseudopot. calc. 77−1363
acoustoelectric absorption, theory for degenerate nonparabolic semicond. 77−85269
adamantine family of semiconductors, props. and commercial appl. 79−42447
alignment and orientation of hot excitons, secondary radiation polarisation calcs. 79−65392
alloy systems, energy gap variation, CPA calcs. 78−43294
alloys, disorder-enhanced Auger recomb. 79−43014
amorphisation due to ion bombardment, SRO struct. 80−79844
amorphous, electronic local density of states, cluster Bethe lattice method 77−11868
amorphous, local order as determined by electronic and vibrational spectroscopy 79−37627
amorphous semiconductors, electronic states, sublattice one-band Hamiltonian transform. 80−59861
Anderson-Gruneisen parameter, bulk modulus temp. depend. 78−10154
anodic oxidation *(Japanese)* 78−92385
anodic oxidation and applications 77−77598
anodic oxide film formation, current flow mechanism 77−90479
arsenides, chem. transport equilib. with I_2 in gaseous phase *(French)* 77−55876
arsenides, chem. transport equilib. with I_2 in gaseous phase *(French)* 77−55877
atomic diffusion in semiconductors, review 79−4423
atomic displacements and enthalpy of vacancy formation 78−38690
Auger coefficients calculation 79−15160
avalanche breakdown voltage for p-n junction, calc. 78−88020
avalanche photodiode detectors, 1.0 to 1.4 μm region, for high data rate fibre optic systems 79−54188
avalanche photodiodes, high speed response, high quantum efficency 79−80682
average energy gap, calc. *(French)* 79−33228
band structure trends, isoelectronic series 77−89696
band structures using general model pseudopot. 77−62800
bulk crystal growth, LPE and VPE methods *(Czech)* 80−89131
carrier mobility anisotropy due to dislocations 78−60124
CESR, optical detect. by spin orientation techniques, anal. 78−80251
Compton line shapes of atoms 77−44080
conduction band, deform. effects, theory 78−34761
conduction-band struct. from reflectivity meas. when subject to mechanical strain 79−42449
conductivity in quantising mag. field, anharmonicity effect 80−2406
conference, on cpd. semicond. interfaces, Princeton, USA., (Feb, 1977) 77−85300
core-level photoyield exam. of empty surface states 77−55593
covalent bonding effect on mag. susceptibility 80−11153
crystal growth by travelling heater method 80−11553
crystal growth from solution, computer simulation 77−51332
crystal growth of optical device materials for 1.0-1.6 μm region, by LPE and CVD 79−43161
cubic crystals, luminesc. polarisation and hot-exciton orientation and decoupling 78−6733
CVD crystal growth mechanisms *(French)* 79−33939
deep centres, many-electron effects 79−15117
deep centres exam., review 79−11086
deep impurity states and wave functions 78−10404
deep level defects, review 80−24841
deep level studies, growth by time difference method at controlled vapour pressure 80−39522

III-V semiconductors continued
DH photodiodes, diffusion limited transient response 80−70809
dichroism, linear circular, near the two-photon absorpt. edge 79−61334
diffusion of Zn by isoconc. technique, anal. of 'up-hill' region 77−35755
diffusion theory for impurities 79−82246
direct energy gap bowing effect 79−95321
dislocation motion *(Japanese)* 79−42074
dislocations, local temp. distrib., due to Joule heating 78−71734
dislocations, velocities and internal friction 79−82231
disorder potential calc. of alloy scatt. 78−47780
displacement energy threshold, from energies of vacancy and interstitial form. and of lattice distortion 77−89430
doped, zinc blende type, electron-phonon interaction, reson. scatt. theory 78−64036
doping, indirect method *(Czech)* 80−24468
education, Shubnikov-de Haas oscills., InSb degenerate semiconductor, third-year undergraduate expt. 79−9051
electric field gradient-elastic tensor components, acoustic NMR obs. 80−25229
electric field influence on exciton states, Stark effect 80−54617
electroliquid epitaxy, III-V cpds. from molten soln., electrotransport and Peltier effect 79−56095
electroluminescence and related props., state-of-the-art, book contrib. 77−73173
electron transport in quantised inversion and accumulation layers 79 60935
electron-electron spin-flip scatt. and spin relax. 80−44916
electron-hole interaction of d core levels 77−11880
electron-hole liquid, RPA calcs. 80−6743
electron-hole liquid theory, generalised RPA 78−87914
electronic dielec. const., interionic separation d-core effect 78−60046
electronic dielectric const. 79−65398
electronic dielectric constant, correlation with interionic separation 79−4758
electronic structure determ. 77−76751
electronic theory, covalent-metallic or covalent-ionic phase transition under pressure 78−72105
electronic theory, cryst. energy and bulk modulus 78−72104
electronic uses, review 79−65538
emitters and detectors for 1.0-1.6 μ fibre-optic communications 80−10007
energy gap and static dielectric const. 79−11062
energy states of semiconductors under high pressure *(Chinese)* 79−56128
epilayer anodic thinning below avalanche breakdown potential 78−10309
epitaxial films, growth rate in thermoelec. recrystn. 80−100424
epitaxial growth and phase equilib. in vertical rotating LPE reactor *(French)* 77−77430
epitaxial growth by CVD 78−92195
epitaxial layer CVD, appl. to Si, II-VI and III-V semiconductor growth 77−32530
epitaxial layer resistivity meas. using Hg−n-GaAs barrier contact 79−60945
epitaxial layers, determ. of lattice consts. of III-V compounds 79−19479
epitaxial layers, dislocations nature, origin and effects 79−28232
epitaxial layers, electronic and struct. props., correlation 77−89835
epitaxial pseudobinary compounds, lattice deform. determ. by X-ray diffraction 78−6242
epitaxial structures as wide-gap substrates, minority carrier diffusion length determ. by photoluminesc. 80−103992
epitaxial ultra-thin layers, bevel cross sectioning 79−74275
etching, characterizing $A^{III}B^{V}$ compounds, misfit dislocations 80−39099
exciton dispersion law, hyperbolic singularity 79−42466
film, nonintrinsic, magneto-conc. effect *(Russian)* 79−47113
film, sample preparation for TEM studies 78−14258
film, vacuum deposition *(Polish)* 79−47630
film vacuum deposition methods *(Polish)* 79−56932
films, photogalvanic effect calcs., electron mean free path, size effect 80−34487
GaAs holographic grating transduction from bulk to surface acoustic waves 77−31199
galvanomagnetic phenomena, model, transport phenomena in presence of medium range disorder *(French)* 78−56162
growth and doping of films by MBE 77−73239
heat treatment effects on elec. props. 78−43411
heavily doped, pressure volume charcts. nonlinearity, intervalley electron redistrib. 77−8012
heteroepitaxial, for SAW and electro-optic device appl., prep. and props., book contrib. 79−83134
heteroepitaxial growth and characterisation, book contrib. 79−83133
heteroepitaxial interface mech. and crystallographic props. 77−76706
heteroepitaxial structures, appl. in optical electronics, defect form., review 78−23160
heteroepitaxy *(Japanese)* 77−24968
heterojunction, compositionally graded, misfit dislocation energy calc. 77−59237
heterojunctions, misfit dislocation banding, stress-induced birefr. 77−28542
heterojunctions, recomb. vel., appl. to $Al_xGa_{1-x}As$-$GaAs_{1-y}Sb_y$ solar cells *(Korean)* 80−54771
heterostructures, growth and dissolution kinetics by LPE 80−49543
heterostructures for integrated optics 77−39112
high symmetry surface, dispersion law calc. for Tamm states cubic 80−15587
high-pressure phase transform. 78−22854
homojunction solar cell, temp. depend. of photovolt. solar energy conversion 79−43768
hot photoexcited electrons, time evolution of electron temp. in high mag. field 80−54709
hydrogen-like impurities interaction 79−82541
III-V semiconductors, electronic Raman scatt. on donor levels, transition matrix element determ. 79−56792
III-V semiconductors, optical heating of electrons at 78K 79−15185
imperfections and photoconductivity, electronic nonequilibrium behaviour 80−44667
impurities, conc. of C, O, Si 78−59832
injection lasers appl., with emission in 1.1 to 1.6 μm range *(Czech)* 80−32983
integrated optics, appls. of III-V semiconductor technology, overview 80−79010

III-V semiconductors continued
interband electronic Raman scattering, three band semiconductor, resonant EM field 78−23452
interface state of III-V oxide and Schottky barrier form., unified mechanism 80−44724
interfaces in III-V semicond. cpd. structs., TEM analysis 77−89836
interfaces with insulating films, electron states, conferences, Durham, England (July 1979) 80−90612
ion implantation, effect of implantation temp. 78−75683
ion implantation, survey 77−76448
ion implanted layers, amorphisation, recrystallisation 78−63782
ionic, tetrahedral, electrical susceptibility, chemical bond approach 78−87931
IR focal planes in intrinsic semiconductors 78−37994
irradiated, under subthreshold irrad. conditions, defect formation ionisation mechanism possibility 80−6430
k.p perturbation theory 77−43484
laser damage, 10.6 μm CW CO_2 beam 77−63497
lasers, photopumped, book contrib. 80−99732
lattice dynamics, eight-parameter bond-bending forces model 80−70334
lattice thermal conductivity, high temp., role of optical phonons 79−33129
layered multielectronic systems, electronic process investig. survey *(Russian)* 80−107891
local force variations due to substitution impurities 78−51633
localised defects, one-electron pseudopot. 77−24533
low energy ion scattering spectrometry of III-V and related compounds *(French)* 80−71551
low O_2 exposure effects on electronic surface props. 79−47146
low temperature, high mobility transistor materials 78−87970
LPE, book contrib. 77−12553
LPE, Stefan problem, exact soln. describing growth rate with linear cooling 80−59411
LPE doping with groups II and IV *(Russian)* 77−80705
luminescence, electron beam or optically excited, quasi-equilib. approx. 80−84779
magnetic susceptibility calc. using MOLCAO approx. 79−42732
magneto-optical spectra of free excitons, manifestation of electron-hole exchange effects 77−59561
MBE, review and appls. *(German)* 78−68630
MBE, surface reaction steps 79−77941
MBE and applications 78−11135
MBE developments in device fabrication 79−78902
MBE process and problem areas, review 80−10815
mean square atomic displacements, in single crysts., X-ray determ. *(German)* 78−30726
minority carrier recombination at surfaces, dislocations and microdefects, luminesc. evaluation 78−6769
MIS devices, large-amplitude hysteresis, model 79−19665
MIS struct. on III-V narrow bandgap compounds, C-V characts., interface state densities and storage times meas. 77−89861
MIS structures, review 78−95372
mixed, electron mobility theory 78−84210
mixed crystal, energy band calc., using LCBO method, compositional disorder effect determ. 79−42442
MOS processing for III-V semiconductors 78−10570
multilayer structure, as-grown, assessment of defects by differentiated cathodolum. topography 80−59819
multilayer structures, contact resistance profiling method 78−56213
n-channel inversion layers, subband struct. and gate-controlled Gunn effect 77−76929
n-type, new meas. method for compensation and spatial fluctuations of impurities 78−6404
narrow-gap semiconductors, externally induced band population effects on electroreflectance 77−66114
negative electron affinity III-V photocathodes for soft X-ray detection 78−93110
negative resistance and peak velocity in central (000) valley 79−73522
neutron bombarded, optical absorption, struct. defect form. and nuclear alloying *(Russian)* 78−31206
nitrides, physical props. and appls. in integrated optics *(Czech)* 80−28355
ohmic contacts *(Japanese)* 78−47869
optical transitions, effect of perturbed k-selection and gap shrinkage 80−66257
optoelectronic appls., materials characts., review 78−30975
oxidation, water vapour and O_2 excitation effects, XPS obs. 79−100274
oxide coatings by thermal and anodic oxidation 77−32706
oxide film growth, optical props. *(German)* 78−34730
p-n heterostructures, epitaxial growth techniques, appl. to optoelectronics, review 80−54770
p-n junction pressure transducer characteristics *(Polish)* 77−89832
p-type epitaxial layer, thermalisation of electron-hole plasma, photolum. meas. 78−80408
phase diagram and thermodynamic data analysis 78−6913
phonon frequencies, Brout sum rule and trace variable forces 78−59892
phosphide semiconductors, ^{31}P nuclear mag. shielding 79−33549
photo-excited electron momentum distrib., hot luminesc. polarisation 77−16396
photoelectromatnetic effect sign inversion at intense photoexcitation 77−85263
photovoltaic technology, conf., San Diego, CA, USA (Jan. 1980) 80−86041
physical properties and importance *(German)* 79−56127
piezoelectric, US ionisation of shallow impurities 77−43538
piezoelectric coupling and dislocations 79−91377
piezoelectric effect due to dislocations 77−81059
piezoelectric induced polarization charge distribs. around point defects 79−56725
piezoelectric semiconductor, piezoresist. of grain boundaries 78−51995
piezoresistive, local resist. near dislocations, eqns. 78−60123
plates, semicond., scribing marks rel. to sclerometric microhardness 79−15891
point defects, internal friction meas. 78−71787
point defects and deep traps, thermodynamic history, model 80−59908
point defects and dislocation climb 79−82209
point defects near dislocations, thermally enhanced diffusion during device operation 79−90820
positron annihilation 78−72636
preparation technology, nitride powder, thin film and volume crystals *(Czech)* 78−3037

III-V semiconductors continued
properties and optoelectronic device appls. 79−74088
quaternary, $A_xB_yC_zD$ or $AB_xC_yD_z$, energy band gap and lattice constant 79−4296
quaternary, alloy scatt., high field transport 78−30929
quaternary alloys, energy bandgap and lattice consts. 78−67940
quaternary III-V alloys, melt and soln. growth of bulk single crystals 80−35079
quaternary-binary heterojunction, X-ray characterisation of defects 78−95239
radiation-induced defects, review 77−80544
radiative recomb., optical evaluation review 80−60647
radiative recomb. and related phenomena, conference, Prague, Czechoslovakia (Sept. 1979) 80−51940
recombination velocity at III-V compound heterojunctions, $Al_xGa_{1-x}As$-$GaAs_{1-y}Sb_y$ solar cells 80−12010
Schottky barrier formation, Fermi-level pinning, defect mech. 78−95358
Schottky barrier height, $(SN)_x$ and HgSe as contact materials, compared with Au 77−85312
Schottky barrier produced by $(SN)_x$ on III-V and II-VI cpd. semiconds., prep. and evaluation 78−6442
Schottky barrier with Au, correl. of barrier height with anion electronegativity 77−20430
semiconductor, ionic., ionisation of doubly charged centres 79−11085
small-radius scatterers, cyclotron resonance harmonics 80−71183
solar cells, materials aspect, review 80−50971
solar cells, monolithic III-V compound two-junction cascade devices, computer modelling 80−81433
solar cells, polycrystalline and tandem, for high efficiencies, using compound semiconductors 80−72052
solid solutions, interaction parameters 78−51688
solid solutions, local levels 77−1395
solid solutions, optical transitions, review 78−2908
sphalerite-type crystals, effect of effective charges on X_5^v and L_3^v 77−35847
sphaleritic structure, effective mass, forbidden band width and lattice constant relation *(Slovak)* 78−51879
spin depend. wave functions and band parameters 77−72818
stacking fault energy and ionicity 78−30651
stress-induced elec. props. of point defects, piezoresistance effect 79−56726
substitutional alloys, band theory, effect of lattice constant variation 80−49596
substrates for Al_2O_3 films, ion beam etching defect detection 80−89155
superconductor-semicond. device research, future prospects 79−28467
superlattices and related structures *(Slovak)* 80−88620
surface (100), (110), surface electron states, theory, relax. effects 80−6938
surface (110), energy distrib. of dangling-orbital surface states 80−80347
surface and interface anal., secondary ion mass spectrometry technique 80−59763
surface and interface electronic states, Green's function technique, tight binding approx. 80−49855
surface barrier structures with metals, production by chem. precipitation of metals, props. *(Russian)* 78−84298
surface characterisation by high resolution Rutherford backscatt. 80−25511
surface comp., low-energy ion scatt. spectrometry 80−100382
surface microhardness depend. on surface treatment method 78−15560
surface protection, by KCl layer, LEED and Auger spectroscopy obs. 77−89628
surface states and electronic struct. of metal-semicond. interfaces 77−20428
surface structure, chem. and spectroscopy, review 80−59764
surface/adsorbate systems, local density of states calcs. *(German)* 80−60062
surfaces, adatom interactions, photoemission obs. 79−33898
ternary, alloy scatt., high field transport 78−30929
ternary phase diagrams, method for determ. of liquidus surfaces 77−28787
tetrahedrally bonded amorphous III-V semiconds., electronic density of states and optical spectrum 77−62797
thermal expansion and MP, ionicity and bond length effects 77−47606
transferred electron effect 77−39855
transport phenomena, review 79−19587
vapour growth, element incorporation 78−30556
vapour growth, using organometallic sources *(Japanese)* 80−16195
vapour transport reactions and kinetics 79−28931
VPE, by metalorganic CVD *(Japanese)* 80−50562
VPE, recent advances, book contrib. 79−66011
VPE growth, book contrib. 79−69997
VPE growth of $A^{III}B^V$ compounds flow graph model 79−56088
VPE of ternary layers, on-time comp. determ. 78−67915
VPE using organometallics and hydrides *(French)* 79−33936
zinc blende structure semiconductors, cyclotron reson. *(German)* 78−10337
zinc blende structure semiconductors, two photon absorption model 79−78679
zinc blende structured semiconductor surface analysis by X-ray photoelectron spectroscopy *(Japanese)* 78−88672
zinc-blende semiconductors, quantum resonances in valence bands under uniaxial stress 79−99480
zinc-blende structure, plasmon line shape, local field effects 78−76011
zincblende compounds, (111) and ($\bar{1}\bar{1}\bar{1}$) faces, surface electron states 78−80035
zincblende structure p-type semiconductors, internal strain on bound hole-phonon interaction 78−91492
zincblende structure semiconductor in intermediate mag. field, exciton spectra 78−18969
Ag-InP interface, AgP_2 formation during sintering 80−65309
Ag−(100)InP, metal-semicond.cathode contact, metallurgical, physical, chemical processes 80−107911
(Al,Ga)As, CW long-life laser, use of half-wave Al_2O_3 facet coatings 77−23688
(Al,Ga)As, channelled substrate planar struct. injection lasers 77−71996
(Al,Ga)As DH diode laser, double-dovetail constricted, single mode CW operation 79−22949
(Al,Ga)As DH injection lasers, internal quantum efficiency, algorithm for meas. 78−66822

III-V semiconductors continued
(Al,Ga)As DH injection lasers, sustained oscills. depend. on DC current bias 79−68392
(Al,Ga)As DH laser, effect of mounting on pulsed threshold 78−13711
(Al,Ga)As DH laser, pulsations produced by saturable absorber Q-switching, possible model 79−81426
(Al,Ga)As, DH laser, stripe geometry, threshold for amplitude-stabilised oscill. 77−7084
(Al,Ga)As DH laser degradation, facet oxide formation 79−86185
(Al,Ga)As DH lasers, temp. accelerated ageing and degradation charact. 78−22130
(Al, Ga)As DH lasers, water role in gradual degradation 80−74379
(Al,Ga)As DH lasers, superlinear emission charact., negative resist. obs. 80−95895
(Al,Ga)As, DH stripe-geometry CW laser, junction voltage saturation 77−23675
(Al,Ga)As DH wafer, Al distrib. meas. 77−7994
(Al,Ga)As double-heterostructure lasers degraded, deep-level changes during accelerated ageing at high temps. 80−74356
(Al,Ga)As injection lasers, pulsations and adsorbing defects 79−94234
(Al,Ga)As laser, ageing-induced self-pulsation stabilisation and initial degradation elimination by facet coatings 80−43347
(Al,Ga)As, laser, DH, light-current voltage charact. 77−3584
(Al,Ga)As, laser, DH, threshold current var., optical scatt. losses 77−3588
(Al,Ga)As long-lived DH injection lasers for fibre optic communication, degradation exam. 78−50778
(Al,Ga)As proton-bomard. stripe-geometry DH lasers, optical nonliniarities and optical spikes 79−55138
(Al,Ga)As:Zn planar stripe lasers with deep Zn diffusion, guiding mechanisms controlled by impurity concs. 80−78853
(Al,Ga)As/GaAs, LPE grown heterostructures, X-ray diffr. exam. of interfacial elastic strains 78−72019
(Al,Ga)As-GaAs laser, transverse junction stripe, high temp. single mode CW operation 78−74918
Al/GaAlAs, film, epitaxial growth on (100) GaAs by hot vac. deposition and characterisation 79−56085
Al/III-V interfaces, photoemission 80−25526
Al-Ga-As, light emitting heterojunction diode, $\eta_e \approx 40\%$ *(Russian)* 77−81157
Al-Ga-As heterostruct. with confined current flow, fabrication 78−68081
Al-Ga-As heterostructure formation by LPE 77−32517
Al-Ga-As heterostructure photocell with a transition layer 79−19655
Al-Ga-Sb ternary phase diagram, calc., DTA and LPE expts. 80−29931
Al-GaAs-Al sandwich-type sputtered film, elec. props. 78−91780
Al-gelatin-GaAs, capacitance-voltage charact. after and before incorporation of $AgNO_3$ 79−51684
Al-InP Schottky barrier, increase 80−15603
AlAs epilayers, MBE growth on GaAs, self-terminating thermal oxidation 78−92374
AlAs, gas phase dissoc. energy, mass spectrometric determ. 79−81301
p-AlAs, saturation charact. over CO_2 laser spectrum 80−83646
n-AlAs, VPE on GaAs, for heterojunction devices 77−1814
n-AlAs/p-GaAs, VPE growth for solar cells 77−77391
AlAs-GaAs, binary heterostruct. LED, external quantum yield *(Russian)* 77−8661
AlAs-GaAs, heterostructure electroluminesc. charact., active region electron density depend. 77−12446
AlAs-GaAs, strip heterolaser, O^+ implantation optimisation, relative threshold current density *(Russian)* 78−1230
AlAs-GaAs (001) interface and superlattice, electronic props., band struct. 79−95485
AlAs-GaAs (100) interface, tight binding calc. of electronic struct. 78−95342
AlAs-GaAs (100) superlattices, band struct. 78−30868
AlAs-GaAs (110) interface, self-consistent calc. of interface states and electronic struct. 78−52066
AlAs-GaAs abrupt (110) interface, electronic struct. 78−95339
AlAs-GaAs double heterostructure, effective lifetime of nonequilibrium carriers 78−6435
AlAs-GaAs film heterojunction, VPE growth and charact. 78−6439
AlAs-GaAs heterojunctions, on graphite substrate, props., solar cell appls. 78−91760
AlAs-GaAs heterostructure, fabrication by selective liq.-phase epitaxy 79−15618
AlAs-GaAs LEDs, Ge or Zn-doped, mechanism of degradation 77−76911
AlAs-GaAs monolayer crystal, two-photon absorpt. spectrum 78−52589
AlAs-GaAs monolayered periodic cryst., optical props. 77−81079
AlAs-GaAs multipass heterostructure, spectral and ang. charact. of luminesc. 77−20418
AlAs-GaAs multipass heterostructures, external quantum efficiency of luminesc. 77−20419
AlAs-GaAs solid solution, quantitative analysis, use of internal calibration technique developed by AES 77−36834
AlAs-GaAs stripe heterojunction laser, O^+ implantation effect on threshold charact. 79−41383
AlAs-GaAs:Ge double heterojunctions, efficiency of radiative recombination 77−77286
AlAs(Sb), fine structure of lowest exciton state *(Russian)* 80−96801
AlBi, possibility of existence with sphalerite struct. 80−33950
Al_xGa_{1-x}-GaP structure, LPE, double heterostruct. light modulator appl. 79−28963
AlGaAs buried heterostructure lasers, gain and absorpt. spectra meas. 80−91792
AlGaAs CW heterolaser, hysteresis of output radiation power 79−64230
AlGaAs CW injection heterostructure laser, with second order distributed Bragg reflectors, exam. 78−37907
(AlGa)As, CW laser diodes, long-term lifetests at room temp. 79−22963
(AlGa)As CW narrow stripe injection laser with induced waveguide, expt. props. 80−32988
AlGaAs CW oxide defined stripe laser, optical feedback effects 78−79045
(AlGa)As CW oxide-defined stripe laser, reliability statistical study 79−76687
AlGaAs constricted DH diodes, stable single filament laser action obs. 78−55358
AlGaAs constricted DH laser with large optical cavity, CW high-power single-mode operation 80−48276
(AlGa)As DH, proton-striped, proton-induced defects, photoluminesc. study 80−48251

III-V semiconductors continued
AlGaAs DH, temp. depend. of intensities and times of radiative transitions 79−38660
(AlGa)As DH CW laser diodes modulation charact. 77−38965
AlGaAs DH injection phase-locked laser, coherence 80−102726
(AlGa)As, DH junction laser, stripe geometry second derivatives of elec. charact. obs. 77−10923
(AlGa)As DH laser, insulating C film deposition to prevent facet deterioration 78−87049
AlGaAs DH laser, self-pulsations due to proton bombarded region self-annealing during ageing 80−99728
(AlGa)As, DH laser, threshold current temp. depend. 79−81431
(AlGa)As DH laser degradation due to facet oxidation 78−42336
AlGaAs DH laser epilayer struct. optimization for integrated optical circuits 80−99879
AlGaAs DH laser mirror degradation mechanism and lasing charact. changes 80−9919
AlGaAs DH laser preamplifier to improve optical receiver sensitivity 80−53316
AlGaAs DH laser with external grating oscillation properties 80−48247
(AlGa)As DH lasers, catastrophic optical damage generation mechanism, TEM obs. of dark line defects 80−100239
(AlGa)As DH lasers, comparison of 'normal' lasers and lasers exhibiting light jumps 80−106519
(AlGa)As DH narrow stripe injection laser with rigid waveguide, expt. props. 80−32987
AlGaAs DH short wavelength lasers, internal stress and degradation 79−68393
AlGaAs DH stripe geometry lasers, spontaneous radiation, carrier conc., and threshold current, luminesc. meas. 79−36898
AlGaAs DH stripe laser, spontaneous emission factor 77−75514
AlGaAs DH stripe laser, side lobe suppression by Te facet coating 80−5744
AlGaAs double heterostruct. laser, 'window-stripe', high power emission 79−72566
AlGaAs electroluminescent heterostructures, LPE, appl. to LED fabrication 80−55308
AlGaAs, heteroepitaxial waveguides for image transmission *(Russian)* 77−11037
AlGaAs, heteroepitaxial waveguides, far radiation field charact. *(Russian)* 77−11038
AlGaAs heterojunction laser, single transverse and longit. mode operation 78−37887
AlGaAs heterojunction laser diodes for optical analogue link, evaluation 79−68395
AlGaAs heterojunction diode as light source for fibre optical communication 80−58653
AlGaAs heterojunctions, nonradiative recomb. vel. estimate from edge luminesc. props. 80−65668
AlGaAs heterojunction photocell with luminesc. wavelength converter 80−108800
(AlGa)As heterostruct., proton irrad., photoluminesc. 80−29808
AlGaAs heterostructures in integrated optics 77−75713
AlGaAs high-power constricted DH diode laser, for optical recording 80−43351
AlGaAs injection lasers, undoped, estimation of intra-band relax. time 80−43335
AlGaAs injection laser, large optical cavity, with multiple active regions 80−106538
AlGaAs integrated twin guide laser with distributed Bragg reflectors 77−88744
AlGaAs, LPE layers, growth initiation and cathodoluminesc. irregularities 79−87010
(AlGa)As laser, CW, accelerated ageing effect on optical props. 77−38898
AlGaAs laser, monolithic integration with amplifier/detector by twin-guide struct. 78−42466
AlGaAs laser array on Si heat sink, optical power detection 80−74383
AlGaAs laser array with Si detector array for stabilization 80−58817
AlGaAs laser diode, interference and polarisation charact., using single mode fibre cable 79−81535
AlGaAs laser mode, fractional spontaneous emission coupling, power fraction, expt. evaluation 79−959
(AlGa)As laser system, VPE growth and degradation mechanisms 80−99748
AlGaAs lasers, CW high-power single-mode constricted DH lasers with large optical cavity 80−64076
(AlGa)As lasers, facet protection using SiO_2 sputter deposition 79−81444
AlGaAs lasers, relaxation oscillation rel. to carrier diffusion length, spontaneous emission 80−32986
AlGaAs layer, epitaxial, grown from pre-heated Ga soln., photolum. study 78→39591
AlGaAs leaky-mode buried heterostruct. injection lasers 77−68209
AlGaAs mode-locked diode laser, optical pulse generation 80−95907
AlGaAs multimode laser, longitudinal modes intensity fluctuations effect on high bit-rate optical transmission 79−68415
(AlGa)As oxide-defined strip lasers, self-sustained oscillations, ageing effects 80−32991
AlGaAs p-n diodes, I-V charact., tunnelling 80−100510
AlGaAs pulse modulate DH laser, oscillatory longitudinal mode competition 79−81427
AlGaAs resonant laser amplifier, gain and saturation power 80−53315
AlGaAs rib waveguides, charact. 80−33177
(AlGa)As self-pulsing junction laser, saturable absorpt. effects 79−72568
AlGaAs semiconductor lasers, single-mode stabilisation by traps 80−95893
AlGaAs, strip buried heterostruct. laser, linear light-current charact. 78−37908
(AlGa)As strip buried heterostructure lasers, mode locking using external cavity 80−91791
(AlGa)As, stripe geometry DH laser, emission nonlinearities 77−685
(AlGa)As stripe geometry, proton-bombardment delineated DH laser, lifetime 80−106520
AlGaAs stripe-geometry DH laser, filament displacement and refr. losses 80−58536
AlGaAs transverse junction stripe lasers, single longit. and fund. transverse mode oscill. 78−22124
(AlGa)As, transverse junction stripe single mode oscillating laser, gain spectra 78−55356

III-V semiconductors continued
AlGaAs transverse junction stripe laser with distributed Bragg reflector 80−106535
AlGaAs tunnel diode, fabrication and appl. in cascade solar cell struct. 80−35682
AlGaAs twin guide struct., monolithic integration of laser and laser amplifier or detector 78−38082
(AlGa)As, visible CW heterojunction laser diodes, room temp. operation 77−38895
AlGaAs, Zn diffused window structure laser, high optical power density emission 79−98394
p- (AlGa)As:Zn, MBE grown, elec. props., shallow junction solar cell use 79−91175
AlGaAs/GaAs monolithic series-connected solar cell arrays 80−97794
(AlGa)As-GaAS DH lasers prep. by new LPE technique 77−40358
AlGaAs-GaAs, DH laser material, singular instabilities of LPE growth surface 77−24969
AlGaAs-GaAs, DH laser, with bent guide of planar struct. 78−1256
AlGaAs-GaAs, DH semiconductor laser, influence of struct. parameters on lasing characteristics 79−45942
(AlGa)As-GaAs, large area high efficiency solar cell fabrication, LPE process 77−36410
AlGaAs-GaAs, TJS laser, single-mode oscill. with low threshold currents, optical communication appl. 80−14355
AlGaAs-GaAs CW injection heterolaser, single freq., tunable by external dispersive resonator 80−28236
AlGaAs-GaAs cascade solar-cell structure, fabrication and characteristics 79−43758
AlGaAs-GaAs concentrator solar cells of high-efficiency characts. 79−48125
AlGaAs-GaAs DH laser, bent-guide struct. 77−75544
AlGaAs-GaAs DH lasers, accel. life test 77−79828
AlGaAs-GaAs DH laser, impurity effects on relaxation oscillations 78−13710
AlGaAs-GaAs DH lasers, accelerated life test 78−66830
AlGaAs-GaAs DH lasers, coupling efficiency between gain-induced guides 79−23094
AlGaAs-GaAs double heterostructure laser lifetime, point defect generation model calcs. 80−32992
AlGaAs-GaAs heteroepitaxial wafers, Mg doping, surface morphology and photoluminesc. props. laser applics. 77−3591
AlGaAs-GaAs heterostructure, minority carrier lifetime, photon recycling effect *(Japanese)* 79−42556
AlGaAs-GaAs heterostructures, luminescent characts., efficiency and radiative lifetime conc. depend. 80−55151
AlGaAs-GaAs injection laser, spectral band homogeneous broadening and narrow band emission 79−98364
AlGaAs-GaAs lasers, defects and degradation *(Japanese)* 79−31899
AlGaAs-GaAs lasers for optical fibre transmission, defects and degradation 79−41382
AlGaAs-GaAs multimode laser, intensity fluctuations in each longit. mode 77−75512
AlGaAs-GaAs proton irradiated solar cells, deep-level defects, recombination mechanisms, performance characts. 80−81459
AlGaAs-GaAs proton irradiated solar cells, deep level defects and recombination parameters 80−94032
AlGaAs-GaAs remote junction heterostructure laser, recomb. enhanced annealing effect 79−98355
AlGaAs-GaAs ring laser, injection type, laser oscill. 77−75570
(AlGa)As-GaAs solar cells, theoretical perform. of multi-layer grid patterns 80−55846
AlGaAs-GaInAs cascade solar cells, AM 0-AM 5 spectra, anal. 79−79396
$Al_{0.25}Ga_{0.75}As$, optically oriented electron, nuclear spin systems, local anisotropy effects on states, resonances *(Russian)* 78−43679
n-$Al_{0.3}Ga_{0.7}As$, layer of (AlGa)As DH laser, deep levels 78−46605
$Al_{0.3}Ga_{0.7}As$:Te(SN), impurity effects on interface morphology of LPE films on corrugated GaAs substrates 78−88435
$Al_{0.3}Ga_{0.7}As$-GaAs DH mesa stripe laser, metalorganic VPE growth and characterisation 79−98391
$Al_{0.35}Ga_{0.65}As$-GaAs cascade solar cell structs., spectral response and junction characts. 80−93926
$Al_{0.35}Ga_{0.65}As$-GaAs N-p heterojunction diodes, current suppression by cond. band discontinuity 80−80362
$Al_{0.36}Ga_{0.64}As$, LPE films, Te-induced defects 78−43037
$Al_{0.4}Ga_{0.6}As$:Te, saturable optical absorpt. of deep Te-complex centre 79−99917
$(Al_{0.42}Ga_{0.58})As$, LPE grown layer, optical absorpt. coeff. meas. 78−6801
$Al_{0.5}Ga_{0.5}As$, first order phonon spectrum replicas 78−60467
$Al_{0.5}Ga_{0.5}As$:O surface layer, on GaAs p-n junction, surface recomb. current reduction 80−49878
$Al_{0.5}Ga_{0.5}As$-GaAs heterojunction phototransistors, growth by metalorganic vapour deposition 79−67380
$Al_{0.5}Ga_{0.5}As$-GaAs minimum heterojunction width determ. by sputter Auger techniques, interface broadening 79−69586
$Al_{0.7}Ga_{0.3}As$ layers, diffusion of Zn, comparison with GaAs 78−26589
$Al_{0.93}Ga_{0.07}As$-GaAs monolithic series-connected solar cell array 80−7939
$Al_{1-x}Ga_xAs$ laser, transverse junction stripe, with low threshold current and high efficiency 78−82985
$Al_{1-x}Ga_xAs$, transient-mode LPE on GaP 78−72746
$Al_{1-x}Ga_xAs$-GaAs heterophotoconvertors, HV, investigations 80−101097
$Al_xGa_{1-x}As$ CSP laser, analytical waveguide study 79−10302
$Al_xGa_{1-x}As$ heterojunction LED monolithic matrix fabrication 79−56301
$Al_xGa_{1-x}As$, analytic approx. for Fermi energy 78−63973
$Al_xGa_{1-x}As$ and GaAs planar local struct. synthesis by LPE 79−56097
n-$Al_xGa_{1-x}As$, Au-based ohmic contacts TEM obs. 80−34509
$Al_xGa_{1-x}As$ buried heterostruct. laser, fabrication, optical props. and reliability 80−53322
$Al_xGa_{1-x}As$ CW heterolaser, 10000 hr. lifetime tests, degradation of mirror surfaces 80−106542
$Al_xGa_{1-x}As$, CW low threshold, high efficiency injection laser props. 78−22126
$Al_xGa_{1-x}As$ CW multiwavelength TJS laser, MBE, single-longitudinal modes 80−64049
$Al_xGa_{1-x}As$, compensated, electron mobility temp. depend. 80−96868
$Al_xGa_{1-x}As$, cryst. growth by MBE 78−39707
$Al_xGa_{1-x}As$, DH, defect generation in active regions at high optical excitation rates 79−23845

III-V semiconductors continued
$Al_xGa_{1-x}As$ DH, origin of $n \simeq 2$ injection current, photolum. expts. 78−14799
$Al_xGa_{1-x}As$ DH laser, threshold current, stripe width influence 77−61952
$Al_xGa_{1-x}As$ DH laser, linear light output power depend. on effective gain width 77−75553
$Al_xGa_{1-x}As$ DH laser, accelerated ageing and uniform mode of degradation 77−83874
$Al_xGa_{1-x}As$ DH laser, with constricted active region, fabrication and characts. 78−37895
$Al_xGa_{1-x}As$ DH laser, rake-line form. in LPE growth, doping effects 80−2287
$Al_xGa_{1-x}As$ DH laser diodes, temp. rise under transient state conditions 77−68211
$Al_xGa_{1-x}As$ DH laser material, Ar laser induced catastrophic damage 79−86178
$Al_xGa_{1-x}As$ DH lasers, deep-level luminesc. 79−65913
$Al_xGa_{1-x}As$ DH lasers continuously operated, with 70°C lifetimes as long as two years 78−17952
$Al_xGa_{1-x}As$ DH p-n junction, surface recomb. effects on current, luminesc. expts. 78−72246
$Al_xGa_{1-x}As$ DH stripe-geometry lasers, degraded, capacitance spectroscopy 77−14715
$Al_xGa_{1-x}As$ DH superluminesc. diode, with unpumped region, time-delayed laser oscill. 77−54711
p-$Al_xGa_{1-x}As$, DH under optical orientation conditions, diffusion of spin labelled electrons 77−8189
$Al_xGa_{1-x}As$, DX photocond. centres, photocapacitance and DLTS meas. 80−11044
$Al_xGa_{1-x}As$, defect state identification associated with Ga vacancy 77−69269
$Al_xGa_{1-x}As$, dependence of energy spectrum of levels introduced by electron irrad. on composition 79−60766
$Al_xGa_{1-x}As$ double heterostructure laser, CW optical power 77−14716
$Al_xGa_{1-x}As$ double heterostruct. lasers, optical pulsations 79−98354
n-$Al_xGa_{1-x}As$, electrical props. 78−6381
$Al_xGa_{1-x}As$, electron mobility illumination, compensation, space charge regions, carrier scatt. 80−70691
$Al_xGa_{1-x}As$, energy band struct. calc. 78−23019
n-$Al_xGa_{1-x}As$, epitaxial, photolum. emission and excitation spectra 78−76526
$Al_xGa_{1-x}As$ epitaxial diode, neutron and γ-irrad. effects on cathodolum. in SEM 79−11473
$Al_xGa_{1-x}As$ epitaxial film, LPE growth and semi-insulating props. 77−44179
$Al_xGa_{1-x}As$ epitaxial films, microanal. in photoemissive electron microscope 79−16068
n-$Al_xGa_{1-x}As$ epitaxial films, elec. cond. press. depend. 79−56337
$Al_xGa_{1-x}As$ epitaxial film, microstruct., effect on elect. characts. of Schottky diode *(Russian)* 80−107671
$Al_xGa_{1-x}As$, epitaxial growth, orienting substrates effects 77−43444
$Al_xGa_{1-x}As$, epitaxial growth from limited vol. melt 79−70005
$Al_xGa_{1-x}As$, epitaxial layer struct., dislocation etching obs. 77−85095
$Al_xGa_{1-x}As$, epitaxial layer crystn. from soln. in melt, diffusion limited 78−35321
$Al_xGa_{1-x}As$, epitaxial layer, distribution of Te and Ge impurities 78−43046
$Al_xGa_{1-x}As$ epitaxial layers on GaAs, struct. study by scanning Auger electron microscopy 80−80110
$Al_xGa_{1-x}As$, fabrication of mesa-type waveguides by laser irrad. 80−5849
$Al_xGa_{1-x}As$ film, hot photoluminescence spectrum, polarisation depend. 78−31254
p-$Al_xGa_{1-x}As$ film, variable-gap photo-EMF 80−65626
$Al_xGa_{1-x}As$, graded band-gap heterostruct., photo-EMF 79−24072
$Al_xGa_{1-x}As$, graded-gap crystal, voltage-current characteristics 79−69613
$Al_xGa_{1-x}As$ grown by organometallic VPE, luminesc. efficiency 79−78892
$Al_xGa_{1-x}As$, growth of high-resistivity layers by liquid-phase epitaxy 79−70008
$Al_xGa_{1-x}As$, growth of uniform epitaxial layers 77−40393
$Al_xGa_{1-x}As$, Γ-X intervalley junctions 77−4433
$Al_xGa_{1-x}As$, Hall effect measurements to 40 kbar under hydrostatic pressure in piston-cylinder device, 150 to 300K 79−67337
$Al_xGa_{1-x}As$, Hall effect, press. temp. and composition depend. 80−49775
$Al_xGa_{1-x}As$, hetero junction light-emitting diode, construction and performance characts. *(Russian)* 77−85808
$Al_xGa_{1-x}As$ heterojunction laser diode, technology and spectral characts. 77−38885
$Al_xGa_{1-x}As$ heterojunction laser diode, accelerated step-temperature ageing 78−46599
$Al_xGa_{1-x}As$ heterojunction LED, fabrication by negative profiling of substrate and characts. 78−56523
$Al_xGa_{1-x}As$ heterojunction LED 79−28403
$Al_xGa_{1-x}As$ heterostructure laser, improved light-output linearity by antireflective coating 78−17953
$Al_xGa_{1-x}As$ heterostructures, photoelectric convertors of conc. solar radiation 80−12015
$Al_xGa_{1-x}As$, indirect, exciton-phonon coupling, photolum. meas. 79−47511
$Al_xGa_{1-x}As$, indirect-gap, laser oscill. involving N isoelectronic impurities 77−10919
$Al_xGa_{1-x}As$, injection laser, transmitter for fibre optical transmission lines 77−7134
n-$Al_xGa_{1-x}As$, ion implanted films, optical and luminesc. props. 80−60699
p-$Al_xGa_{1-x}As$, LED in red and IR region, multiple-pass heterostruct. 79−19653
$Al_xGa_{1-x}As$, LPE, cathodoluminesc. obs. 78−68565
$Al_xGa_{1-x}As$, LPE, effect of doping on interface morphology 77−81231
$Al_xGa_{1-x}As$, LPE, quantitative analysis by AES 77−89667
$Al_xGa_{1-x}As$, LPE layer, deep levels, photocapacitance obs. 77−15790
n-$Al_xGa_{1-x}As$, large-lattice relax. model for persistent impurity photocond. 77−85261
$Al_xGa_{1-x}As$, laser, spectral, threshold, power and time characts. 77−715
$Al_xGa_{1-x}As$ laser diode, reliability 80−53320
$Al_xGa_{1-x}As$ laser-alloyed stripe-geometry lasers 80−5745

III-V semiconductors continued
$Al_xGa_{1-x}As$ layer, LPE, graded bond gap solar cell, composition profile, Rutherford backscatt. 78−76612
$Al_xGa_{1-x}As$ layers, graded band gap, growth and properties 79−60645
$Al_xGa_{1-x}As$, lower conduction band struct. 78−6270
$Al_xGa_{1-x}As$, MBE grown film, in situ surface characterisation by RHEED, SIMS and AES 77−43410
$Al_xGa_{1-x}As$ MBE layers, ionized beam doping, elec. and optical characts. 79−37721
$Al_xGa_{1-x}As$, metalorganic-CVD, photopumped laser operation meas. GaAs quantum well 79−10303
$Al_xGa_{1-x}As$, mode-stabilised injection laser, longitudinal-mode behaviour 79−962
$Al_xGa_{1-x}As$ native oxide, low leakage, MOS characterisation 78−91795
n-$Al_xGa_{1-x}As$, nonradiative donor related defect centre obs. 78−23497
$Al_xGa_{1-x}As$, optically magnetised, luminescence polarisation anisotropy, hysteresis effect symmetry props. 80−34982
$Al_xGa_{1-x}As$, organometallic VPE growth, and characterisation 79−78899
$Al_xGa_{1-x}As$ oxidised AlAs as multidielectric for GaAs MIS devices 79−65333
$Al_xGa_{1-x}As$, p-n homojunction, hot carrier recomb., overheating luminesc. 78−92122
$Al_xGa_{1-x}As$ p-n junction, photolum. and current, interface recomb. effects 78−95346
$Al_xGa_{1-x}As$, p-n junction solar cells, effect of interface recombination on photoluminescence and current 80−93893
$Al_xGa_{1-x}As$, point defects, recomb. enhanced interactions with dislocation networks 79−60398
$Al_xGa_{1-x}As$, press. coeff. of direct band gap from optical absorpt. meas. 80−11430
$Al_xGa_{1-x}As$ pulsating DH laser, spectral broadening 80−23686
$Al_xGa_{1-x}As$, pure and Ge doped, shallow acceptor photoluminescence 80−76064
$Al_xGa_{1-x}As$, Raman spectroscopy, characterisation of thin films and heterostructures 78−76439
$Al_xGa_{1-x}As$ semitransparent photocathode, LPE, quantum efficiency spectrum 80−76153
$Al_xGa_{1-x}As$ solar cell, intermediate wavelength conversion for operation with concentrators 79−70451
$Al_xGa_{1-x}As$, solid soln., controlled electrochemical and selective etching, integrated optics appl. 77−14814
$Al_xGa_{1-x}As$ solid soln., epitaxial layer growth on GaAs by zone recrystallisation with temp. gradient 77−16510
$Al_xGa_{1-x}As$, solid soln., synthesis by ion implantation Al^+ ions 78−38741
$Al_xGa_{1-x}As$ stripe geometry DH lasers, proton bombarded, intensity pulsations 79−94235
$Al_xGa_{1-x}As$ thick epitaxial layer production, by zone recrystn. in temp. gradient 79−15619
$Al_xGa_{1-x}As$ thin graded band-gap layers, isothermal LPE growth 80−34325
$Al_xGa_{1-x}As$, transverse mode stabilized injection lasers 78−29964
$Al_xGa_{1-x}As$ triggerable semiconductor lasers made by deep proton bombardment 80−69408
$Al_xGa_{1-x}As$, VPE, recent advances, book contrib. 79−66011
$Al_xGa_{1-x}As$, VPE and LPE growth, electron mobility 79−91165
$Al_xGa_{1-x}As$, VPE growth and characterisation 78−35315
$Al_xGa_{1-x}As$, valence and core level photoemission spectra 79−19973
$Al_xGa_{1-x}As$ variable gap junction, photosensitivity 78−39204
$Al_xGa_{1-x}As$ variable gap thin structs., radiative recomb. photoluminesc. spectra 79−43036
n-$Al_xGa_{1-x}As$, variable-gap crystal, magnetoresistance 78−34850
n-$Al_xGa_{1-x}As$, variable-gap solid solns., diffusion length, photolum. meas. 79−38659
$Al_xGa_{1-x}As$, waveguide heterostruct. epitaxial growth with gradual composition change 79−42416
$Al_xGa_{1-x}As$: Sn(Te), persistent photocond., due to donor-related centres, symmetry 80−15558
p-$Al_xGa_{1-x}As$:Be layer, MBE growth, Be doping and diffusion 77−51397
$Al_xGa_{1-x}As$:Cr, deep level props. 79−69465
$Al_xGa_{1-x}As$:Cr, exptl. verification of Cr^{2+} models of photoluminescent transitions 78−27320
$Al_xGa_{1-x}As$:Cr, high resist. film, photolum. and photocond. meas. 78−72596
$Al_xGa_{1-x}As$:Cu, variable-gap semicond., impurity props., carrier recomb. 80−96907
$Al_xGa_{1-x}As$:Cu(Ag)(Au), LPE film, impurity levels, elec. and optical props. meas. 78−26862
p-$Al_xGa_{1-x}As$:Ge layer on GaAs substrate, Hall and elec. cond. meas., Hall mobility 80−2402
$Al_xGa_{1-x}As$:Ge(Te)(Zn), photo- and cathodolum., comp. depend. *(Russian)* 77−48215
$Al_xGa_{1-x}As$:Mg doping characteristics, elec. props., effective hole masses 79−78117
$Al_xGa_{1-x}As$:Mn epitaxial layers, Mn-O association, EPR meas. 77−69677
$Al_xGa_{1-x}As$:N, indirect band-gap, visible laser oscill. at 77K 77−79820
$Al_xGa_{1-x}As$:N, ion implantation, in situ annealing photoluminesc. obs. 80−10567
$Al_xGa_{1-x}As$:N, luminescent material, appl. in optically pumped lasers and electrolum. diodes *(Japanese)* 77−44069
$Al_xGa_{1-x}As$:N, photolum. excitation spectra 77−63451
$Al_xGa_{1-x}As$:N, photoluminesc. and optical absorpt. spectra of N impurity bound-excitons 79−47496
$Al_xGa_{1-x}As$:N^+, (x=0.58), laser annealing of optically active impurities, photolum. charact. 80−20682
$Al_xGa_{1-x}As$:O-n-GaAs heterojunction for MIS device, capacitance voltage meas. 79−87157
$Al_xGa_{1-x}As$:Si, charge state of impurity atoms, positron annihilation meas. 78−39062
$Al_xGa_{1-x}As$:Sn(Te)(Ge), anneal-induced defects, photoluminesc. obs. 79−61422
$Al_xGa_{1-x}As$:Te, epitaxial film, elec. cond. and Hall coeff. rel. to donor levels 77−24630
$Al_xGa_{1-x}As$:Te, persistent photocond. trapping centre, donor complex model, photocapacitance meas. 79−65517
$Al_xGa_{1-x}As$:Zn DH laser, stripe geometry, horizontal transverse mode stabilisation, lasing characts. 77−19313

III-V semiconductors continued
$Al_xGa_{1-x}As$:Zn epitaxial layers, composition and Zn carrier conc. 80−25585
$Al_xGa_{1-x}As/Al_yGa_{1-y}As$ heterostructure lasers, prep. characts., and CW reliability 80−58586
$Al_xGa_{1-x}As/Al_yGa_{1-y}As$ DH lasers grown by metalorganic CVD, CW operation in wavelength range 760-780 nm 80−64053
$Al_xGa_{1-x}As/GaAs$ heterojunction laser, appl. of stress distrib. calc. for multilayer heteroepitaxial struct. 77−72798
$Al_xGa_{1-x}As$-$Al_yGa_{1-y}As$ DH superluminesc. diode, for Nd:YAG laser pumping, room temp. CW operation 77−7122
$Al_xGa_{1-x}As$-Al_yGa_{1-y} DH laser, threshold current temp. depend., potential barrier height influence 80−53296
$Al_xGa_{1-x}As$-$Al_xGa_{1-y}As$ DH IR-visible (0.89-0.72 μm) MBE grown lasers 80−64058
$Al_xGa_{1-x}As$-Au interface, Auger depth profiling 77−89657
$Al_xGa_{1-x}As$-GaAs, CW 300k quantum-well heterojunction laser, optical and injection pumping operation 80−5735
$Al_xGa_{1-x}As$-GaAs, DH integrated optics development 80−33240
$Al_xGa_{1-x}As$-GaAs, diode pump system for YAG:Nd^{3+} laser 79−41396
$Al_xGa_{1-x}As$-GaAs, epitaxial heterostructure, influence of defects on diffusive distrib. of group I impurities 78−43045
$Al_xGa_{1-x}As$-GaAs, heterojunction, interface width, AES obs. 80−20290
$Al_xGa_{1-x}As$-GaAs, quantum-well MO-CVD heterostructure lasers, band-filling props. 79−22954
$Al_xGa_{1-x}As$-GaAs, quantum-well heterostructure laser diode, temp. depend. of threshold current 80−87395
$Al_xGa_{1-x}As$-GaAs abrupt LPE heterojunction, Auger profiling 77−85101
$Al_xGa_{1-x}As$-GaAs DH injection laser, active region internal parameters determ., composite resonator use 80−106548
$Al_xGa_{1-x}As$-GaAs DH laser, short cavity, performance characts. 77−83889
$Al_xGa_{1-x}As$-GaAs DH lasers, metalorganic CVD growth and performance characts. 80−53312
$Al_xGa_{1-x}As$-GaAs DH laser diode, I-V characts., variation of ideality factor 80−64027
$Al_xGa_{1-x}As$-GaAs DH laser operation, phonon contrib. 80−102724
$Al_xGa_{1-x}As$-GaAs DH photodetector, optical power conversion at 8500 Å and I-V characts. 77−87833
$Al_xGa_{1-x}As$-GaAs heterostructure, effect of photon recycling on diffusion length and internal quantum efficiency 77−39929
$Al_xGa_{1-x}As$-GaAs heterostructure photoluminesc., origin of large dark spots 77−85763
$Al_xGa_{1-x}As$-GaAs heterostructure, nonradiative large dark spots rel. to minority carrier transport 78−9378
$Al_xGa_{1-x}As$-GaAs heterostructures, nonradiative large dark spots exam. 78−23149
$Al_xGa_{1-x}As$-GaAs heterojunction photodiodes, high-efficiency fast-response 78−52073
$Al_xGa_{1-x}As$-GaAs heterostructures, MO-CVD, phonon assisted recomb. and stimulated emission 80−1205
$Al_xGa_{1-x}As$-GaAs heterostruct. lasers, metallorganic CVD 80−23692
$Al_xGa_{1-x}As$-GaAs heterostructure, quantum-well, hot electrons and phonons 80−84505
$Al_xGa_{1-x}As$-GaAs heterostruct., varizonal, parameter determ. by photoluminescence method *(Russian)* 80−10829↑
$Al_xGa_{1-x}As$-GaAs interface, Auger depth profiling 77−89657
$Al_xGa_{1-x}As$-GaAs large-quantum-well heterostructures, induced phonon-sideband laser operation 80−95888
$Al_xGa_{1-x}As$-GaAs laser, made by organometallic CVD, continuous room temp. operation 80−1201
$Al_xGa_{1-x}As$-GaAs linear-gradient heterostruct., photoelec. props. 79−11205
$Al_xGa_{1-x}As$-GaAs long life laser, initial degradation, minority carrier lifetime reduction 77−71984
$Al_xGa_{1-x}As$-GaAs multilayer heterostructures, optical birefringence 78−64422
$Al_xGa_{1-x}As$-GaAs multilayers, LPE, using addition of GaCl vapour and new boat struct. 79−33950
$Al_xGa_{1-x}As$-GaAs multiple-quantum-well injection lasers grown by metal-organic CVD, room temp. continuous operation 80−1218
$Al_xGa_{1-x}As$-GaAs n-n heterojunction, LPE, Auger profiling and absence of rectification 78−95349
$Al_xGa_{1-x}As$-GaAs n-n heterojunction, interface width determ. 80−49887
$Al_xGa_{1-x}As$-GaAs phonon-sideband metalorganic-CVD quantum-well heterostructure laser 79−64244
$Al_xGa_{1-x}As$-GaAs photopumped quantum-well heterostructure lasers grown by metalorganic CVD 79−98390
$Al_xGa_{1-x}As$-GaAs quantum-well heterostructure laser, metalorganic CVD growth, CW operation 300 to 337K 79−10304
$Al_xGa_{1-x}As$-GaAs quantum-well heterostructure laser diode, threshold current temp. depend. 80−43331
$Al_xGa_{1-x}As$-GaAs quantum well heterostructure lasers, operation 80−53292
$Al_xGa_{1-x}As$-GaAs quantum-well heterostructures, phonon-assisted recomb. and stimulated emission 80−74358
$Al_xGa_{1-x}As$-GaAs quantum-well heterostruct., exciton in recomb. 80−103990
$Al_xGa_{1-x}As$-GaAs single-quantum-well heterostructure laser diodes grown by metalorganic CVD, continuous 300K operation 79−50309
$Al_xGa_{1-x}As$-$GaAs_{1-y}Sb_y$ solar cells, appl. of recomb. vel. at III-V cpd. heterojunctions *(Korean)* 80−54771
$Al_xGa_{1-x}As$-GaAs-$Al_xGa_{1-x}As$ photopumped quantum-well laser, room temp. CW operation 78−74908
$Al_xGa_{1-x}As$-GaAs-$Al_xGa_{1-x}As$ quantum well, carrier collection 79−15211
p-$Al_xGa_{1-x}As$-n-$Al_yGa_{1-y}As$ junction, electrolum. spectra at high press. 77−48246
p-$Al_xGa_{1-x}As$-n-GaAs heterojunction solar cells, optical characts. study 77−24609
p-$Al_xGa_{1-x}As$-p-GaAs-n-GaAs heterophotocells, optimal parameters for high solar-excitation level 80−93872
$Al_xGa_{(1-x)}As$-$Al_yGa_{(1-y)}As$ DH optically pumped laser, room temp. single pass gain 77−75511
$Al_yGa_{1-y}As$-$Al_xGa_{1-x}As$ laser struct., for integrated optics, MBE 78−13817
$Al_yGa_{1-y}As$-$Al_xGa_{1-x}As$, electrooptic rib waveguide modulators and switches 78−38046
AlGaAsP/GaAs heterojunction, X-ray characterisation of defects 78−95239

III-V semiconductors continued
AlGaAsP(Sb), compositional grading by LPE 80−10844
AlGaAsSb LPE growth, lattice-matched to GaSb, characterisation 80−60794
AlGaAsSb, photodiode, lattice-matched to GaSb 79−71527
n-AlGaAsSb-GaSb-p-AlGaAsSb binary heterostructure injection laser, room temp. operation 78−9381
$Al_yGa_{1-y}As_{1-x}Sb_x$ heterostructure, electroluminesc., appl. to LED's 77−8663
$Al_yGa_{1-y}As_{1-x}Sb_x$ LPE phase diagram 78−11137
$Al_yGa_{1-y}As_{1-x}Sb_x$, LPE, strain effects near miscibility gap, importance 79−7759
$Al_yGa_{1-y}As_{1-x}Sb_x/GaAs_{1-x'}Sb_{x'}$, buried heterojunction electroabsorption modulator, report of operation 78−38044
$Al_yGa_{1-y}As_{1-x}Sb_x$-$Ga_{1-z}Sb_z$ buried heterojunction electroabsorption modulation 78−55439
$Al_xGa_{1-x}As$Zn-GaAs solar cells by LPE, open circuit voltage, fill factor 80−101108
$Al_xGa_{1-x-y}In_yAs$, LPE on InP, solid-liq. equilib. calcs. 78−84083
$Al_xGa_{1-x}N$ epitaxial layers, growth and props. 79−11522
$Al_{1-x}Ga_xP$, IR phonons, lattice reflection spectra 78−51626
$Al_xGa_{1-x}P$, LPE, crystallographic obs. and electrolum. 80−88445
$Al_xGa_{1-x}P$, photoluminescence excitation spectra, bound excitons, Al conc. depend. 80−20687
$Al_xGa_{1-x}P$, proportional ingredient content determ. by X-ray fluoroscopy 80−97747
$Al_xGa_{1-x}P$, Zn diffusion behaviour, device appls. 77−11741
$Al_xGa_{1-x}P$(:Zn), solution-grown single crysts., photo- and electrolum. at 77K 79−52004
AlGaSb, growth and characts. for 1.0-1.8 μm heterojunction devices 78−6870
$Al_xGa_{1-x}Sb$, compositional var. during LPE growth using ternary phase diagram 77−59761
p-$Al_xGa_{1-x}Sb$ epitaxial layers, cathodoluminescence. investig. for varying x *(Russian)* 77−20931
$Al_xGa_{1-x}Sb$, LED, 1.54 μm efficient emission at 300K reproducible fabrication 79−42636
$Al_xGa_{1-x}Sb$ mixed crystal, two-phonon absorption meas., 15-48 μm 77−1682
$Al_xGa_{1-x}Sb$, photolum. intensity increase due to composition variation 79−15528
$Al_xGa_{1-x}Sb$, solid soln., epitaxial layer growth from liq. phase 77−85089
$Al_xGa_{1-x}Sb$, solid soln., depend. of forbidden-band width on composition 78−39602
$Al_xGa_{1-x}Sb$ solid solns., freq. dependences of form of luminesc. spectra 80−40160
$Al_xGa_{1-x}Sb$, soln.-grown, photolum. 80−71476
$Al_xGa_{1-x}Sb$, surface flatness depend. on LPE condition 79−15042
$Al_xGa_{1-x}Sb$, vibr. spectra, Raman light scatt. study 80−45080
$Al_xGa_{1-x}Sb$:Zn, impurity diffusion, p-n junction depth 80−24678
$Al_xGa_{1-x}Sb$:Zn(Si)(Ge)(Sn)(Pb), doping of solid solns. during LPE *(Russian)* 77−85087
$Al_xGa_{1-x}Sb$-Pd contacts, struct., preparation elec. props. 80−65684
$Al_xGa_{1-x}Sb$-Pd contacts, band gap depend. of barrier height 80−65685
AlGaSbAs heterostructures and LED's luminesc. props. in 1-2 micron band 78−10988
$Al_xGe_{1-x}Sb$, photolum. spectra 78−95602
$Al_xIn_{1-x}Sb$, DC sputtering and struct. 78−52674
AlN, absorpt. edge shape interpretation, Wannier excitons absorpt. in charge impurity elec. field 80−66233
AlN, asymmetry in displacement energy for Frenkel-pair prod., n-type to p-type conversion 78−2116
AlN, CVD from $AlCl_3/NH_3$, calc. of equilibrium yields 79−52121
AlN, effect of valence states on X-ray Compton line shapes 77−8682
AlN, epitaxial, refl. spectra, 5-12.5 eV 79−99967
AlN epitaxial films, optical props. in vac. UV region 79−56872
AlN, excitation, luminescence, reflection spectra in fund. absorpt. region 78−10956
AlN film, CVD, characterisation of film props. 78−43496
AlN film, epitaxial growth by reactive evaporation *(Japanese)* 78−23629
AlN film, nonlinear optical susceptibility SHG expts. 78−30012
AlN film, oriented c-axis, low temp. deposition by reactive magnetron sputtering 80−76180
AlN film, thermodynamics and kinetics of CVD 80−108354
AlN film on Si and Ge, growth, struct. and props. 77−55468
AlN films on glass substrate, prep. by reactive DC magnetron sputtering technique, c-axis orientation 80−89146
AlN, heteroepitaxial, for SAW and electro-optic device appl., prep. and props., book contrib. 79−83134
AlN, impurity-doped film, cathodoluminescence spectra 79−83038
AlN, luminesc. excitation spectrum and band struct. 80−84783
AlN, nonlinear susceptibilities 79−27312
AlN, photocond., 6-12 eV, prior UV illum. effect, mechanism 77−89796
AlN, reactive ion beam sputtering deposition, form. and characterisation 80−44452
AlN, single cryst. growth by sublimation-recondensation technique 78−31310
AlN, VPE by closed space vapour process, and optical absorpt. edge 78−88371
AlN:Mn, vol. and surface excited luminesc. 79−38630
AlN:Mn(Eu), luminescence at high excitation levels with and without doping 77−1721
AlN:O, deep impurity states, orbital spectra, CNDO/2 calcs. 78−6319
AlN:O, energy spectrum of deep impurity 79−83035
AlN:O, thermolum. mechanism, 80-420K 79−78761
AlN:O, UV spectra of deep impurity centres, radiative recombination 79−87490
AlP, ground state of electron subsystem, quasimolecular model 79−69055
AlP, multiple pulsed double NMR and nucl. spin dynamics 77−16208
AlP, semicond., ^{31}P nuclear mag. shielding 79−33549
AlP(As)(Sb), APW calc. of electronic structure and optical props. 79−99479
AlP(As)(Sb), avalanche breakdown voltage for p-n junction, calc. 78−88020
AlP(As)(Sb), refractive index dispersion 79−24280
AlSb (110), surface struct., EPR meas. and elastic energy minimisation calcs. 79−51405
AlSb (110), wave functions and surface struct. 78−91519

III-V semiconductors continued
n-AlSb, acoustoelectric effect due to piezoelectrically active wave 80−80331
AlSb, amorphous, localised gap states, hopping cond. and chem. bonding 78−23052
AlSb as high-energy photon detector 77−75026
AlSb film, laser-induced metal-semicond. transition in Al-Sb mixed film 80−6661
AlSb, gravitational influences on liquid-state homogenisation and solidification 79−78864
AlSb, indirect exciton dispersion, 'camel's back' 79−73447
AlSb, laser pulse annealing, induced nucleation, crystal growth 80−84966
n-AlSb, many-valley semicond. anisotropic acoustoelectric effect, thermo-EMF anisotropy fluctuation depend. on ultrasound freq. 79−69562
AlSb, molten, temp. depend. of vel. of sound and adiabatic compressibility 77−27944
p-AlSb, saturation characts. over CO_2 laser spectrum 80−83646
AlSb Schottky barrier solar cells, characteristics and efficiency of Czochralski-grown crystals 80−61366
AlSb solar cell material, epitaxy, ionicity and bond struct. 80−61367
AlSb, thin film growth on insulating substrates, by metal organics CVD 80−60786
AlSb-Bi system, molten, enthalpy change due to mixing *(German)* 79−86892
AlSb-CdTe, phase diag. 77−52299
$Al_{1-x}Sb_x$, amorphous, localised gap states, variable range hopping 77−72866
As_2Te_3-GaAs, amorphous-monocrystalline heterojunctions, space charge limited conduction 78−64099
Au-$Al_{0.5}Ga_{0.5}As$ -GaAs heterojunction Schottky-barrier solar cells, barrier height enhancement 80−85284
Au-AlGaAs-GaAs heterojunction Schottky barrier solar cells, barrier height enhancement 80−94071
Au-$Ga_{1-x}Al_xSb$ Schottky barriers, barrier height 80−96986
Au-GaAs solar cell, practical antireflection coatings 77−763
Au-GaS, Schottky-barrier electroreflectance spectra under uniaxial stress 79−56767
Au-n-AlGaAs-n-GaAs Schottky-barrier solar cells, band readjustment effect 80−81458
Au-n-$Ga_{1-x}Al_xAs$-n-GaP narrow-band variable-gap surface-barrier photoedetector 80−96944
Au-n-GaAs Schottky diodes, interface state density model 77−39937
Au-oxide-n-GaAs MIS structures, reverse bias influence on photocurrent 80−107921
Au-W-GaAs Schottky barrier, elec. and chem. props., AES 80−96973
BN, electronic energy band struct., X-ray spectra, pseudopotential calcs. 79−78008
BN, epitaxial, refl. spectra, 5-12.5 eV 79−99967
BN film, high temp. reactive plasma deposition, struct., resist., and dielec. const. meas. 77−7988
BN films, elec. resist., depend. on relative humidity 79−4609
BN glass transfer process 80−107459
BN, hexagonal, electronic struct. from X-ray emission and XPS 79−47009
BN, semicond. film, chemical deposition 80−71596
BN, wave-vector depend. of electron energy losses 77−51688
BP, cryst. growth from Cu-fluxed melt, and characterisation 77−85920
BP, epitaxial, CVD on Si substrate, cryst. imperfections 78−10294
BP epitaxial film, hardness meas. 77−11629
BP, epitaxial growth on Si substrate, Si impurity profile, ion microanal. 78−87886
BP, epitaxial growth using B_2H_6-PH_3-H_2 system 79−28937
BP, etching by HCl gas, temp. and HCl conc. effects 77−86205
BP film, high temp. thermoelec. power, scattering processes 80−80305
BP, semicond., ^{31}P nuclear mag. shielding 79−33549
BP, VPE, diffused layers formed in Si substrates, device appls. 78−56585
BP:Zn(Se)(Cd), epitaxial layers, ion implantation, defects and lattic locations, channelling obs. 80−88179
BP-BAs, quasi-binary system, X-ray emission and electron spectra of solid soln. *(Russian)* 77−1764
BP_xAs_{1-x} system, electron struct. and interatomic interactions, X-ray spectroscopy 80−20736
CC $Al_xGa_{1-x}As_ySb_{1-y}$, heterostructure composition profile by photoemission microanalysis 80−44717
CC GaAs, n- and p-types, optical consts., 2.5-3.5 eV, normal incidence reflectance meas. 79−15428
CC GaP, improvements in synthesis, solute diffusion (SSD) growth 79−65992
CdS, vacuum epitaxial growth on $CuInSe_2$ 78−92193
n-CdS/n-InP/p-InP heteroface solar cell with ultrathin window layer, computer anal. 80−97788
p-CdSb, elec. props. at low temp. 77−62866
$CdSnAs_2$-InP, n-p heterojunction, elec. props., electroluminesc., band struct. 80−75632
$CdSnP_2$-InP, n-n heterojunctions, growth, elec. characts. 77−11992
Cr-GaAs, Schottky-barrier diode, surface electron states 79−73578
GAP:N LED, acoustic emission study of defects 79−86799
GAs, population inverted semicond., resonant Brillouin scatt., photoelastic consts. 80−89016
(Ga, Al, As) heterostructures and compounds, electronic props., empirical pseudopot. calc. 80−80366
(Ga,Al)As CW diode laser, L(J) charact., external cavity induced nonlinearities 77−79824
(Ga,Al)As DH lasers used for optical recording, hole machining in Te films 79−89954
(Ga,Al)As injection laser parameters, homogeneous degradation calc. from initial rates 79−22951
(Ga,Al)As, LPE growth of multilayered struct., explanation for meniscus lines on surfaces 77−76681
(Ga,Al)As narrow double-current-confinement channelled-substrate planar laser fabrication, double etching technique 80−74371
(Ga,Al)As transverse mode stabilised laser, direct obs. of saturation behaviour of spontaneous emission 78−46600
(Ga,Al)As:Si(Ge), epitaxial layers, radiative recomb., compensation, cathodolum. study 80−66307
(Ga,In)(As,P) DH lasers, 1.55 μm, low-threshold current densities 80−1221
(Ga,In)As, growth of epitaxial layers 77−12542

III-V semiconductors continued
Ga-Al-As(Sb), liquidus surface in ternary phase diagram, simplex lattice method 77−7847
Ga-Al-Sb, liq. phase epitaxy, phase diagram, X-ray microanal. 79−19491
Ga-AlSb-GaSb, phase diagram, LPE of $(AlSb)_x(GaSb)_{1-x}$ solid soln. 77−40392
Ga-As system, phase equilib., Krupkowski model *(German)* 78−95132
Ga-As-Au, alloying behaviour at substrate-film interface, electron microscopy 79−60652
Ga-As-O, equilib. phase diagram, GaAs oxidation 80−104130
Ga-As-P, liquidus surface in ternary phase diagram, simplex lattice method 77−7847
Ga-As-Sb system, two- and three-phase fields obs. 80−55373
Ga-GaAs interface immersed in electrolytic solns., elec. props. 78−95368
Ga-In-As, liquidus surface in ternary phase diagram, simplex lattice mathod 77−7847
Ga-In-As-Sb quaternary system, phase equilib. and heterojunctions 79−34016
Ga-In-As-Sb system LPE layers, pseudoquaternary phase diagram 78−10293
Ga-In-Sb, solidus isotherms and isoconcentration lines 78−56624
Ga-In-Sb system, phase diagram calcs. in Ga+In rich region 80−60842
Ga-In-Sb system, precipitation of solid phase from liq. phase, thermodynamical formulation *(French)* 77−28003
Ga-Sb-Te, props. of ternary solid solution based on GaSb 79−7826
$Ga_x In_{1-x}P$, localised exciton-phonon complex as intermediate state in light scatt. 78−39543
GaA-$Al_{0.27}Ga_{0.73}As$ DH lasers grown by MBE, growth conditions influence on threshold current density 80−32984
GaAS (110), wave functions and surface struct. 78−91519
GaAS, (110) oriented, preferential chemical etching of blazed gratings 79−37067
GaAS, anodic oxide film growth, in situ differential refl. obs. 77−73354
GaAS, binary alloy constituent EDS anal., secondary fluorescence, SEM study *(Chinese)* 80−85231
n-GaAS epitaxial film, radiative recomb. under influence of mech. stresses 80−66291
GaAS, grain boundaries, extended Read model 80−96543
GaAS MIS structure, fabrication by reactive sputtering and props. 78−39686
GaAS, O_2 chemisorption on (110) surface, bonding sites 78−38938
GaAS, oxide, grown in O plasma, physical and elec. props. 79−66189
n-GaAS, plastic deform. effect on elec. props. 77−28178
GaAS, preliminary heated, encapsulation by sputtered deposits of Si_3N_4 and AlN *(French)* 77−32714
GaAS, proton isolation layer, lateral spread, elec. meas. 77−80520
GaAS, semi-insulating and n-type, doping by neutron transmutation 80−96553
GaAS, semiinsulating, heat treatment effects 78−6382
GaAS:Cr, mag. field depend. of single carrier parameters, mixed cond. anal. 79−91043
GaAS-$Al_xGa_{1-x}As$, DH laser and modulation developments *(German)* 78−37903
GaAS-AlGaAs LPE layers, defects formed by oxygen in ambient gas *(Japanese)* 77−70009
GaAS-GaAlAs, DH laser, correlation between optical output characts. and time depend. behaviour 77−68210
(GaAl) As/GaAs five layer heterostructure narrow beam laser, characts. 77−10920
$Ga_{1-x}Al_x As$, metal-gap channel waveguides, intensity modulation 78−66899
GaAlAs actively mode-locked laser, bandwidth limited picosecond pulses 80−95905
GaAlAs based heterojunctions, integrated optics appl., technology advancements *(Slovak)* 80−33226
GaAlAs, buried-heterostructure injection lasers, threshold current reduction 77−10924
(GaAl)As buried-heterostructure laser with buried optical guide, highly efficient operation 80−1219
GaAlAs CW DH diode lasers, 1/f noise behaviour 78−1226
(GaAl)As CW DH lasers with stripe geometry, LF intensity noise obs. 77−38887
GaAlAs CW diode laser, external cavity control, 32 MHz single axial mode 78−1271
GaAlAs DH, optically-pumped, degradation at elevated temps. 79−50295
GaAlAs, DH CW diode laser, picosecond pulse generation 78−83002
(GaAl)As DH diode laser, microscale degradation absorpt. centres 78−13704
GaAlAs DH injection laser, half-ring, room temp. operation 80−58558
(GaAl)As DH laser, gradual degradation accel. as exponent of driving current value 80−32990
GaAlAs DH laser, In solder deterioration, Au diffusion in In 80−33019
(GaAl)As, DH laser, LPE growth, meniscus lines as nucleation sites 77−15706
(GaAl)As DH laser, low-current, proton-bombarded, design and characts. 78−87059
GaAlAs DH laser, narrow stripe geometry, spontaneous carrier lifetime 80−87392
GaAlAs DH laser, optimum p-n junction depth, photoluminesc. method 79−4598
GaAlAs DH laser, stripe geometry, spatially resolved emission 79−27257
(GaAl)As DH laser, threshold current density, growth terraces effect 80−99723
GaAlAs DH laser diode, deep level associated with slow degradation 78−87050
GaAlAs DH laser diodes, catastrophic degradation 79−50290
GaAlAs DH laser diodes, long-lived high-power at 70°C, using Al_2O_3 film coating 79−50321
GaAlAs DH laser diodes, small signal modulation, junction capacitance effect 80−83625
GaAlAs DH laser diode, edge coupling to planar $LiNbO_3$:Ti waveguide 80−87559
(GaAl)As DH laser wafer, photoluminesc. improvement with buffer layer 80−64014
GaAlAs DH laser-diode-to-diffused-waveguide coupling calcs., Gaussian beam model 79−94372
(GaAl)As, DH lasers, degradation mechanisms, temp. depend. 78−66825
GaAlAs DH lasers, electron-hole recomb. effects 79−45944

III-V semiconductors continued
GaAlAs DH lasers, nonlinearity, second and third harmonic distortion 79−31898
GaAlAs DH lasers, proton-bombard., nonradiative recomb., luminesc. time-response meas. 79−98371
GaAlAs DH lasers, SiO_2 insulated, characts. and near field 80−64019
GaAlAs DH lasers, self-sustained pulsation suppression, effect of SiO_2 facet coating films 80−95894
GaAlAs DH p-n junction laser, construction and operating characts. 78−9377
GaAlAs DH photovoltaic detectors, high efficiency 79−11198
(GaAl)As DH stripe contact injection lasers, local attached data fibre link appls. 80−19044
GaAlAs DH stripe geometry lasers, degradation phenomena 80−53290
GaAlAs, diode laser, CW radiation, intensity noise spectra of axial mode groups 77−34890
GaAlAs diode sources for laser-doppler anemometry 79−14499
(GaAl)As heterojunction laser with distributed Bragg refl., mode switching 80−43336
GaAlAs, heterostruct. formed by LPE, growth and dissolution kinetics 79−99439
GaAlAs heterostructure lasers, fine-structure in spectra 80−19033
(GaAl)As high performance diode laser, high-reflectivity cavity mirrors 78−82994
GaAlAs injection DH laser and GaAs Schottky-gate FET, monolithic integration 80−58593
(GaAl)As injection lasers, optimisation of power efficiency 77−42539
(GaAl)As injection lasers, self-pulsations, Q-switching and mode-locking effects 78−66827
GaAlAs injection lasers, AM characts. 79−50330
GaAlAs injection laser, long wavelength radn. spatial distrib. 79−76686
GaAlAs injection lasers, stability in single transverse mode operation 80−38027
GaAlAs injection laser, monolithic integration with Schottky-gate FET 80−48275
(GaAl)As injection lasers operating with optical fibre external resonator, characts. 80−58544
(GaAl)As injection laser operating in external cavity, intensity self-pulsations 80−64013
(GaAl)As injection lasers operating with optical fibre resonators 80−91812
(GaAl)As, LPE, GaAs dissolution kinetic in undersaturated isothermal solns. in Ga-Al-As system 80−80106
GaAlAs laser, coherent pulse generation by active modelocking 79−89941
(GaAl)As laser, stripe struct. for horizontal transverse mode stabilisation 77−79859
GaAlAs laser diode, CW, ps pulse generation 79−50329
GaAlAs laser diode, for heterodyne communication systems, high frequency stability 80−99727
GaAlAs laser nonlinearities, harmonic distortion 80−74357
GaAlAs laser transmitter for optical fibre communication, features 78−90423
GaAlAs laser transmitters using optical tap for feedback control, output power stability 79−64241
(GaAl)As lasers, low threshold proton isolated, spectral and transient response 78−87052
GaAlAs lasers, return-beam-induced noise generation model 80−48244
GaAlAs lateral injection laser, low threshold, single mode operation 77−75545
GaAlAs light intensity modulators using p-n junctions 80−99871
(GaAl)As low threshold current proton isolated DH lasers 78−1258
(GaAl)As low-beam-divergence CW DH laser, grown by low press. metal-lorganic CVD 80−74376
GaAlAs, luminescence circular polarisation, electron optical orientation resonant variation *(Russian)* 80−84782
GaAlAs mode stabilised separated multiclad layer stripe geometry DH laser, optical waveguide 80−64051
GaAlAs mode-stabilised semiconductor lasers 78−46638
GaAlAs, native defects, stoichiometry, doping effect 77−11541
GaAlAs novel DH lasers fabrication 78−50803
GaAlAs on GaAs thin film stacked multiple-bandgap solar cell structs., prep. using CVD techniques 80−94083
GaAlAs oxide, plasma grown, anal. by combined ion beam techniques 79−7760
(GaAl)As oxide-stripe geometry DH laser, cavity length effect on output 79−50323
GaAlAs, p-n and heterojunctions, superinjection coeffs., luminesc. obs. 80−50427
GaAlAs p-n heterostructures, current-flow mechanisms, luminesc. spectra 80−20298
GaAlAs, SEM defect study, transmission cathodoluminescence 79−64964
GaAlAs solar cells, appl. for navigational satellite power systems 80−35694
GaAlAs stripe laser, longit. and transverse mode dynamics on junction plane 77−38890
GaAlAs, surface vacancies, bound state energy levels calc. 80−80340
(GaAl)As system, automated system for growth of multilayered structs. by LPE 79−38752
GaAlAs terraced substrate laser, visible-light-emitting, characts. 80−106523
GaAlAs visible diode laser for hologram recording of three-dimens. object 80−95839
(GaAl)As, Zn diffused DH laser with twin transverse junctions, low threshold current 79−98393
(GaAl)As, Zn diffused proton bombarded stripe laser 79−98392
(GaAl)As:Be implanted DH stripe geometry laser 80−64044
n-GaAlAs:Sn LED DH donor-level analysis, DLTS obs. 79−47040
GaAlAs:Zn recombination radiation drift, charge carrier photon induced drift in varigap semicond. 80−50418
GaAlAs/GaAs, n-p-n heterojunction transistor, elec. props. 79−87149
GaAlAs/GaAs heterostructures, ellipsometric assessment of epitaxial layer during growth in organometallic VPE system 79−37933
GaAlAs/GaAs solar cells, efficiency optimisation at high and low current levels *(French)* 80−61348
GaAlAs/GaAs solar cells, Be and Zn behaviour 80−101111
(GaAl)As/GaAs-heterostructure lasers, degradation studies of sawn cavity lasers under pulsed operation 78−29953
(GaAl)As-GaAs, DH laser, degradation in water due to facet deterioration 79−22970

III-V semiconductors continued
(GaAl)As-GaAs, double heterostructure laser, TEM study of dark line defect growth from dislocation clusters 79−33206
GaAlAs-GaAs, high efficiency heterostruct. solar cell grown by metalorganic CVD 78−11118
(GaAl)As-GaAs, long life lasers, initial degradation mode 77−14712
(GaAl)As-GaAs concentrator solar cells, series resistance effects 79−57427
(GaAl)As-GaAs DH laser, anomalous emission intensity, cavity competition 77−79823
GaAlAs-GaAs DH laser diodes, long-life diodes for optical fibre communication 80−48246
GaAlAs-GaAs DH lasers, degradation caused by growth of dislocation networks 80−53289
(GaAl)As-GaAs deep proton-isolated lasers 79−36923
GaAlAs-GaAs double heterostructure, interfacial recomb. velocity, photolum. meas. 78−68075
GaAlAs-GaAs epitaxial heterostructures for integrated optics functional elements 78−50948
GaAlAs-GaAs heteroface solar cells, 1 MeV electron irrad., analytical and expt. study 79−70450
GaAlAs-GaAs heteroface solar cells, high open-cct. voltage, full-factor and efficiency 80−94081
GaAlAs-GaAs heterojunction prep., Zn conc. effect in epitaxial layer, high-power IR emission *(Spanish)* 77−39932
GaAlAs-GaAs heterojunction solar cells, high temp. props. 25 to 300°C 80−94035
(GaAl)As-GaAs heterostruct. lasers, factors affecting catastrophic degradation 77−75524
GaAlAs-GaAs heterostructures, electronic excitation effects on mobility of point defects and dislocations 78−2561
(GaAl)As-GaAs heterostructure lasers, factors affecting catastrophic degradation 78−17942
GaAlAs-GaAs heterostruct. solar cells, Al, P, Zn incorporation by LPE *(French)* 79−24899
(GaAl)As-GaAs laser, low temp. threshold behaviour 78−46604
GaAlAs-GaAs lasers, channelled substrate, prepared by combination of organometallic pyrolysis and LPE 80−99745
GaAlAs-GaAs n-n heterojunction, rectification 79−28402
(GaAl)As-GaAs narrow stripe laser, improved optical communication system performance 80−102733
GaAlAs-GaAs optoelectronic devices, optical waveguide periodic structures appls. *(Polish)* 78−50947
GaAlAs-GaAs solar cell structs., photolum. props. 80−50958
(GaAl)As-GaAs twin-transverse-junction stripe laser with linear light/current characteristic and low threshold 79−36893
GaAlAs-GaAs-GaAlAs etalon, optical bistability 80−5781
(GaAl)As-heterostruct. stripe lasers, light/current characts. and near field shifts, waveguide self focusing effects 78−29952
$Ga_{0.1}Al_{0.9}As$ LPE layers containing low-cond. regions, charging effects in SIMS anal. 80−66348
$Ga_{0.5}Al_{0.5}As$-GaAs, DH, interfacial recomb., photolum. time decay meas. 78−95347
$Ga_{0.5}Al_{0.5}As$-GaAs(:Ge) DH structure, minority carrier lifetime and internal quantum efficiency of surface-free GaAs 79−43013
$Ga_{0.64}Al_{0.36}As$, plasma grown oxide, phys. and elec. props. 78−48550
$Ga_{0.65}Al_{0.35}As$ epitaxial layer on GaAs, two-dimensional lattice mismatch parallel to interfacial boundary 79−51439
$Ga_{0.65}Al_{0.35}As$, LPE growth, wave morphologies on surface 77−40396
$Ga_{0.7}Al_{0.3}As$ epitaxial film, inclusion-generated dislocation clusters 77−89445
$Ga_{0.7}Al_{0.3}As$-GaAs chemically etched mirror lasers, optical coupling effect 77−72000
$Ga_{0.84}Al_{0.16}As$, surface processing, residual film monitoring by ellipsometry 80−13124
$Ga_{0.9}Al_{0.1}As$, nucleation morphologies on $Ga_{0.65}Al_{0.35}As$ surfaces grown by LPE 78−15323
$Ga_{0.9}Al_{0.1}As$:Ge(Si) epitaxial layers, defect obs. by TEM 77−51618
$Ga_{1-x}Al_xAs$ DH injection laser diode, long-term-degraded, TEM obs. 78−71102
$Ga_{1-x}AlAs$ (110) oxide-free Schottky barriers, surface comp. and characts., AES obs. 79−82661
$Ga_{1-x}AlAs$, LPE layers, electron mobility, scatt. processes 80−84519
$Ga_{1-x}AlAs$:Zn, acceptor energy level and elec. props. 80−65482
$Ga_{1-x}Al_xAs$, alternate monolayer crysts., MBE and props. exam. 78−10289
$Ga_{1-x}Al_xAs$, appl. of theory of electroepitaxy of multicomponent systems 80−65396
$Ga_{1-x}Al_xAs$, band struct. from I-V, C-V meas. on Schottky diodes 80−96989
$Ga_{1-x}Al_xAs$ based layer structures, optimum growth conditions, comp. and struct. perfection 80−104069
$Ga_{1-x}Al_xAs$ buried heterostruct. injection laser, degradation rate, optical flux density depend. 79−50313
$Ga_{1-x}Al_xAs$ buried heterostructure lasers for analogue communication 80−48297
$Ga_{1-x}Al_xAs$, channelled substrate, planar struct. and DFB lasers 78−79032
p-$Ga_{1-x}Al_xAs$ crystals, spectral characts. of photosensitivity, mechanism 80−44735
$Ga_{1-x}Al_xAs$ DH catastrophically degraded laser, TEM obs. of defects 80−32989
$Ga_{1-x}Al_xAs$ DH injection laser, FM at microwave freq. rates 80−58610
$Ga_{1-x}Al_xAs$ DH laser, LPE surface protective coating 78−35320
$Ga_{1-x}Al_xAs$ DH laser, accelerated ageing test 79−76688
$Ga_{1-x}Al_xAs$ DH laser diode, long-lived, high-power, facet coated 80−58564
$Ga_{1-x}Al_xAs$ DH laser hybrid device, reliability 79−27281
$Ga_{1-x}Al_xAs$, DH stripe geometry laser, lasing-induced change in differential resistance 79−45943
$Ga_{1-x}Al_xAs$, deep level-dislocation interactions, DLTS meas. 80−29357
$Ga_{1-x}Al_xAs$, deep levels, pressure effects 80−49651
$Ga_{1-x}Al_xAs$, degraded DH LED, defect struct. by electrolum. topography and TEM obs. 79−60369
$Ga_{1-x}Al_xAs$ double heterostruct. lasers, aging characts. 79−72569
$Ga_{1-x}Al_xAs$ electrodes, interface capacitance meas., flatband pot., conduction and valence band boundaries *(French)* 79−33339
$Ga_{1-x}Al_xAs$, electrolum. study using high-gain image intensifier 80−55193
$Ga_{1-x}Al_xAs$, epitaxial, radiative deep states 80−76061

III-V semiconductors continued
$Ga_{1-x}Al_xAs$, epitaxial layers on GaAs substrate, mismatch stress accommodated by tetrahedral distortion 77−55466
$Ga_{1-x}Al_xAs$, epitaxial layers, reflectivity meas. by wavelength modulation spectroscopy *(French)* 77−59632
$Ga_{1-x}Al_xAs$ epitaxial layers, spectroscopic technique for imaging spatial distrib. of nonradiative defects 78−23498
$Ga_{1-x}Al_xAs$, epitaxial layers, on GaAs substrates, X-ray double-cryst. diffractometry, state of strain 79−19480
$Ga_{1-x}Al_xAs$ epitaxial layer, absorpt. and transmission coeffs. *(French)* 80−2887
$Ga_{1-x}Al_xAs$ epitaxial layer, elec. cond., Hall effect, band struct. 80−49964
$Ga_{1-x}Al_xAs$ feedback-stabilised injection laser for fibre-optic data transmission 77−19343
$Ga_{1-x}Al_xAs$ heterostructure, LPE prep., growth and dissolution kinetics, thermodynamic and kinetic models 80−75456
$Ga_{1-x}Al_xAs$, hot electron distrib. meas. and calc. 78−27318
$Ga_{1-x}Al_xAs$, IR refl. spectra and Raman spectra 80−20623
$Ga_{1-x}Al_xAs$ injection laser automatic bias control cct. 78−5498
$Ga_{1-x}Al_xAs$ integrated optical waveguide LPE 77−75703
$Ga_{1-x}Al_xAs$, intervalley energy gaps, temp. junction, exptl. determ. 80−80179
$Ga_{1-x}Al_xAs$ junction-up TJS laser electron injection efficiency improvement 80−48300
$(Ga_{1-x}Al_x)As$ LOC DBR laser integration with p-n junction detector 78−38066
$Ga_{1-x}Al_xAs$, LPE, growth mechanism and morphology on channelled substrates 79−28960
$Ga_{1-x}Al_xAs$ LPE crystals for DH laser, LEDs, TEM obs. of Ge, Si-doped epitaxial layers 79−1556
$Ga_{1-x}Al_xAs$ LPE film, with x=0.23 and 0.37, grown by linear cooling, thickness comparison with GaAs 78−87892
$Ga_{1-x}Al_xAs$ LPE growth: composition control and growth rate analysis 79−95946
$Ga_{1-x}Al_xAs$, LPE growth and characterisation 80−50566
$Ga_{1-x}Al_xAs$ LPE layer photoluminescence obs. *(Polish)* 77−77268
$Ga_{1-x}Al_xAs$, LPE layer thickness depend. on soln. comp. 78−10295
$Ga_{1-x}Al_xAs$, LPE layers, grown under const. cooling rate conditions, cryst. composition 78−39710
$Ga_{1-x}Al_xAs$ LPE layer on GaAs, lattice mismatch using X-ray source 79−82470
$Ga_{1-x}Al_xAs$ LPE layers, comp. and refr. index, ellipsometry meas. 79−87011
$Ga_{1-x}Al_xAs$ laser, buried heterostruct., stable operation during accelerated ageing at 70°C 79−7125
$Ga_{1-x}Al_xAs$ laser, DH, enhanced localised degradation and anomalous emission spectra 77−680
$Ga_{1-x}Al_xAs$ laser, SHG with $KNbO_3$ 80−74431
$Ga_{1-x}Al_xAs$ laser, stripe-geometry DH, improved light output linearity 77−682
$Ga_{1-x}Al_xAs$, laser, temp. sensitive, enhanced degradation rates 77−79825
$Ga_{1-x}Al_xAs$ laser diode end facet protection by parylene coating 79−36921
$Ga_{1-x}Al_xAs$ lasers, processing stresses effect on residual degradation 79−72567
$Ga_{1-x}Al_xAs$ layer, surface conc. x determ. by rapid localised non-destructive optical method *(French)* 77−62725
$Ga_{1-x}Al_xAs$ layer form. on GaAs during dissolution in Ga-Al-As soln. 80−10799
$Ga_{1-x}Al_xAs$, liquid and solid comp. variations during LPE growth 79−99445
$Ga_{1-x}Al_xAs$ low threshold stripe geometry DH laser, Be implanted, on semi-insulating substrate 80−69409
$Ga_{1-x}Al_xAs$, MBE, state-of-the-art 79−24450
$Ga_{1-x}Al_xAs$ n-p_3-p_2-p_1-p_0 struct., degradation electrolum. 80−50428
$Ga_{1-x}Al_xAs$, non-shallow levels and cond. band struct. from Hall carrier conc. meas. 80−39607
$Ga_{1-x}Al_xAs$, ohmic contacts, metallisation systems 80−25010
$Ga_{1-x}Al_xAs$, optical detection of CESR 77−36155
$Ga_{1-x}Al_xAs$, p^+-n-n^+ heterostructure, distrib. of injected carriers, forward V-I characts. *(Russian)* 80−6973
$Ga_{1-x}Al_xAs$ p-i-n structure photoelectric props. 78−95353
$Ga_{1-x}Al_xAs$ p-n structure, charge-storage diode, variable-gap 80−11076
$Ga_{1-x}Al_xAs$, Peltier LPE, absence of electromigration of As and Al 77−81230
$Ga_{1-x}Al_xAs$, photoluminescence, deep level trap emission capture 80−29805
$Ga_{1-x}Al_xAs$, point defects and dislocation climb, interaction with deep level donor 79−82209
$Ga_{1-x}Al_xAs$, quantum magnetoresist. results, using pulsed fields up to 35 T 79−73528
$Ga_{1-x}Al_xAs$, rapidly degraded LED, defect struct. of ⟨100⟩ dark lines 78−10052
$Ga_{1-x}Al_xAs$, room-temperature CW laser structures and characteristics 77−19323
$Ga_{1-x}Al_xAs$, STEM techniques for simultaneous electronic anal. and obs. of defects 79−14812
$Ga_{1-x}Al_xAs$ Schottky barrier, oxide free, surface composition and fabrication 78−68084
$Ga_{1-x}Al_xAs$ Schottky directional coupler switch, construction and operation 78−25960
$Ga_{1-x}Al_xAs$, Se ion implantation *(French)* 77−68986
$Ga_{1-x}Al_xAs$, self-aligned three dimensional struct. MBE growth 77−59697
$Ga_{1-x}Al_xAs$, semiconductor defects, spectroscopic study of electronic props. 80−84446
$Ga_{1-x}Al_xAs$, Shubnikov-de Haas oscillation, in semiconductor superlattice 77−62947
$Ga_{1-x}Al_xAs$, solar cells appl., technology advancements 79−43776
$Ga_{1-x}Al_xAs$, solid solution, synthesized by ion implantation, Raman scattering 79−42972
$Ga_{1-x}Al_xAs$ stripe laser with stable transverse mode structure 80−48298
$Ga_{1-x}Al_xAs$ structures, STEM and scanning deep level transient spectroscopy in defect centre anal, cathodoluminesc. techniques 80−103642
$Ga_{1-x}Al_xAs$ superlattices, multilayers, periodic and near-periodic, small-angle interferences of reflected X-rays 79−94846
$Ga_{1-x}Al_xAs$, surface phonon polaritons, frustrated total internal refl. expts. 78−47656

III-V semiconductors continued
$Ga_{1-x}Al_xAs$ symmetrised epitaxial variable-gap waveguide, coherent radiation generation 80−38018
$Ga_{1-x}Al_xAs$, topographical stoichiometry determ. using electroreflectance 78−23483
$Ga_{1-x}Al_xAs$ transparent LED, optical wavelength multiplex transmission system appl. 78−30063
$Ga_{1-x}Al_xAs$ transverse mode DH laser with inbuilt plano-convex waveguide 80−48296
$Ga_{1-x}Al_xAs$ VPE layers, X-ray diffr. 80−29296
n-$Ga_{1-x}Al_xAs$, variable gap photodetector, quantum efficiency 79−7903
$Ga_{1-x}Al_xAs$, variation of optical transitions *(French)* 79−60708
$Ga_{1-x}Al_xAs$, velocity saturation and cond. band struct. under press. 78−26863
$Ga_{1-x}Al_xAs$ visible diode lasers, transverse-mode stabilised, nonstigmatic laser beams 79−76694
$Ga_{1-x}Al_xAs$ visible diode lasers, degradation 80−43330
$Ga_{1-x}Al_xAs$ visible diode lasers, degradation mechanisms 80−64026
$Ga_{1-x}Al_xAs$ visible diode lasers, degradation due to macroscopic defects (<730 nm) and facet oxidation (>740 nm), life tests 80−99729
$Ga_{1-x}Al_xAs$, Zn diffusion, depend. on Al content 78−59981
$Ga_{1-x}Al_xAs$:Si, LPE, phase diagram, Hall effect meas., carrier conc., donor ionisation energies 77−72803
$Ga_{1-x}Al_xAs$:Si, linear-gradient p-n junction, barrier capacitance 77−43705
n-$Ga_{1-x}Al_xAs$:Si, room-temp. cond. and band struct. 80−96869
$Ga_{1-x}Al_xAs$:Si, Si determ., spectrochem. method, photoluminesc. spectra, Hall effect meas. *(German)* 77−77851
$Ga_{1-x}Al_xAs$:Si p-n junction, doping in LPE, elec. and luminesc. props. *(Czech)* 78−47851
$Ga_{1-x}Al_xAs$:Si photoelectric convertors, broadband varizone creation 80−40856
$Ga_{1-x}Al_xAs$:Sn, layer Schottky barrier, deep level spectroscopy 80−49666
$Ga_{1-x}Al_xAs$:Te, plasmon-LO-phonon coupling, IR refl. obs. 80−50335
$Ga_{1-x}Al_xAs$/GaAs heterostructure solar cell design for space usage 79−96450
n-$Ga_{1-x}Al_xAs$-Au, Schottky barrier height as function of AlAs content 79−65535
$Ga_{1-x}Al_xAs$-Au variable-gap surface-barrier struct., photoelec. effect 80−39634
$Ga_{1-x}Al_xAs$-$Ga_{1-y}Al_yAs$ DH laser, grown by organometallic CVD, room temp. operation 78−29950
$Ga_{1-x}Al_xAs$-GaAs, abrupt quantum-well heterostruct. grown by metalorganic chemical vapour deposition 79−56933
$Ga_{1-x}Al_xAs$-GaAs, CVD laser diodes, operation and growth processes 78−46598
$Ga_{1-x}Al_xAs$-GaAs, grown by LPE, direct obs. of dislocations 79−65087
$Ga_{1-x}Al_xAs$-GaAs, heteroepitaxial layers on GaAs(001), misfit dislocation asymmetry 77−47694
$Ga_{1-x}Al_xAs$-GaAs, high efficiency solar cell, isothermal etchback-regrowth method 77−59701
$Ga_{1-x}Al_xAs$-GaAs, injection lasers, defects, TEM anal. 79−23866
$Ga_{1-x}Al_xAs$-GaAs, room temp. DH laser, CVD growth 78−37912
$Ga_{1-x}Al_xAs$-GaAs channel guide laser grown by metalorganic CVD 79−10317
$Ga_{1-x}Al_xAs$-GaAs DH injection lasers grown by metalorganic CVD, props. 80−99751
$Ga_{1-x}Al_xAs$-GaAs DH lasers grown by metalorganic CVD, room temp. operation 78−1248
$Ga_{1-x}Al_xAs$-GaAs heterostructure lasers grown by metalorganic CVD, prep. and props. 79−36918
$Ga_{1-x}Al_xAs$-GaAs heterojunctions grown by metallorganic CVD 80−15599
$Ga_{1-x}Al_xAs$-GaAs high-efficiency solar cell 79−29469
$Ga_{1-x}Al_xAs$-GaAs injection laser, branching waveguide coupler fabrication by LPE 78−63202
$Ga_{1-x}Al_xAs$-GaAs LPE multilayer heterostructure photovolt. solar cells, fabrication and performance 79−48128
$Ga_{1-x}Al_xAs$-GaAs laser, degradation, appl. of dislocation climb model 77−1125
$Ga_{1-x}Al_xAs$-GaAs laser, DH, grown by metalorganic CVD, room temp. operation 78−13702
$Ga_{1-x}Al_xAs$-GaAs laser, distributed Bragg confinement, room temp. operation 78−74907
$Ga_{1-x}Al_xAs$-GaAs low threshold room temp. DH lasers grown by metalorganic CVD 78−50804
$Ga_{1-x}Al_xAs$-GaAs narrow stripe laser for improved communication performance 80−48299
$Ga_{1-x}Al_xAs$-GaAs p-n and p-p-n heterojunction solar cells, high efficiency, prep., eval. and characters *(Japanese)* 80−61342
$Ga_{1-x}Al_xAs$-GaAs p-n structures, variable-gap front layer, photoelec. props. 79−7884
$Ga_{1-x}Al_xAs$-GaAs p-n solar cell, with thin variable gap layer, high efficiency 79−24064
$Ga_{1-x}Al_xAs$-GaAs solar cell, deep level obs. 77−89834
$Ga_{1-x}Al_xAs$-GaAs solar cells, photoluminesc. characterisation 80−3512
$Ga_{1-x}Al_xAs$-GaAs solar cell, radiation resist., theoretical evaluation and optimisation 80−35681
$Ga_{1-x}Al_xAs$-GaAs solar cells, computer anal. of cell characts. incl. band gap variation 80−55866
$Ga_{1-x}Al_xAs$-GaAs:Si, momentum distrib. of valence electrons, positron annihilation meas. 79−51530
$Ga_{1-x}Al_xAs$-GaAs-GaAs p-i-n heterojunction, photoelec. props. 78−26938
$Ga_{1-x}Al_xAs$-GaAs-GaAs, p-p-n junctions, variable gap solar photocell with coordinate depend. band gap gradient 79−11213
$Ga_{1-x}Al_xAs$-Ge, MBE of ultra thin film superlattices on GaAs substrates, TEM study 79−37932
p-$Ga_{1-x}Al_xAs$-n-$Ga_{1-y}Al_yAs$, graded band gap, solar cells, theoretical efficiency *(French)* 77−62987
$Ga_xAl_{1-x}As$ channelled-substrate planar struct. injection laser 77−88742
$Ga_xAl_{1-x}As$ DH laser, suppression of output nonlinearities by use of misaligned mirrors 78−17954
$Ga_xAl_{1-x}As$ diode laser, modulation characts. 77−83903
$Ga_xAl_{1-x}As$ embedded stripe DH laser monolithically integrated with strip waveguide 78−59025
$Ga_xAl_{1-x}As$ injection heterojunction distributed output laser, exptl. study 80−43369
$Ga_xAl_{1-x}As$, LPE, charge carrier conc. distrib. *(Russian)* 78−52694
$Ga_xAl_{1-x}As$ layer, optical guiding in Bragg configuration 78−1431

III-V semiconductors continued
$Ga_xAl_{1-x}As$, optically oriented electron, nuclei spin instability *(Russian)* 80−70660
$Ga_xAl_{1-x}As$, Schottky barrier, effect of oxide composition on elec. behaviour, AES meas. 79−87141
$Ga_xAl_{1-x}As$ stripe-geometry laser, current carrier conc. distrib. and threshold props. 77−68212
$Ga_xAl_{1-x}As$:Cu epitaxial layers, spatial distrib. of nonradiative defects, STEM imaging spectroscopic technique 77−89438
$Ga_xAl_{1-x}As$-GaAs DH laser, continuous room temp. operation 78−55363
$Ga_xAl_{1-x}As$-GaAs double heterostructure laser diode, temp. depend. of photolum. 80−5734
$Ga_xAl_{1-x}As$-GaAs heterostructure laser, suppression of internally circulating modes, effect on catastrophic degradation and efficiency 77−83896
$Ga_xAl_{1-x}As$-GaAs heteroepitaxial layer distortion characterisation by X-ray multiple diffr. 80−96754
$Ga_xAl_{1-x}As_x$ photodetector diode on GaAs substrate dark currents, tunnelling, energy gaps, effective masses 80−70805
GaAlAsP-GaAs T-Q DH laser, light induced misfit dislocation motion 77−75518
$Ga_{1-x}Al_xAs_{1-y}P_y$ epitaxial film, nonradiative recomb. at dislocations 80−44213
$Ga_{1-x}Al_xAs_{1-y}P_y$ epitaxial layer heterojunction, nonradiative recombination at misfit dislocations 80−96901
$Ga_{1-x}Al_xAs_{1-y}P_y$ layer of uniform composition grown on GaAs by LPE, temp. diff. method appl. 79−23864
$Ga_{1-x}Al_xAs_{1-y}P_y$-GaAs quaternary heterojunction strains and IR laser diode performance 78−9385
$Ga_{1-x}Al_xAs_{1-y}P_y$-GaAs quaternary heterojunction, misfit dislocation charact. by synchrotron radiation white beam topography 78−63771
$Ga_{1-x}Al_xAs_{1-y}P_y$-GaAs heterojunctions, light-induced misfit dislocation motion, photoluminesc. and X-ray diffr. meas. 79−11200
GaAlAsSb/GaSb alloys, prep. and optoelectronic device appl. 80−25587
GaAlAsSb-GaSb low bandgap solar subcell for high efficiency multibandgap convertors, LPE growth 80−93927
GaAlAsSb-GaSb p-n heterojunction CCD, charge transfer, charge exchange 80−65658
$Ga_{1-x}Al(In)_xAs$, $GaAs_{1-x}P_x$, substit. solid solns., comp. determ. from X-ray integral intensities 77−84584
$Ga_{1-x}Al_xN$ heteroepitaxial films, photoluminesc., cathodoluminesc. 80−66292
$Ga_{1-x}Al_xN$, VPE growth on sapphire, RHEED obs.of orientation rels. 77−20208
$Ga_xAl_{1-x}N$ film, growth and props. 78−39702
$Ga_{1-x}Al_xP$, bending parameters calc. by pseudopot. method 78−26813
$Ga_{1-x}Al_xP$, LPE grown, green electroluminescence 78−19571
$Ga_{1-x}Al_xP$, two-phonon optical absorpt. 78−88341
$Ga_{1-x}Al_xP$ varigap structs., crystallation 80−80993
$Ga_{1-x}Al_xP$:N epitaxial films, ion implanted, cathodoluminescence study 80−60684
$Ga_xAl_{1-x}P$ high-temp. solar cell with 0.3 eV band gap 80−21400
$Ga_{0.5}Al_{0.5}Sb$, surface cleaning by sputter-etch technique 77−48560
$Ga_{0.72}Al_{0.28}Sb$ avalanche photodiodes, ionization coeff. 79−17488
$Ga_{1-x}Al_xSb$, dispersive energy and energy gap calcs. *(French)* 79−99478
$Ga_{1-x}Al_xSb$, LPE growth and phase diagram *(French)* 77−24974
$Ga_{1-x}Al_xSb$, melt growth and elec. props. 79−65999
$Ga_{1-x}Al_xSb$ p-n homojunction LPE and photovoltaic effect obs. *(French)* 78−64108
$Ga_{1-x}Al_xSb$ p-n structure, variable-gap, elec., photoelec. and electrolum. props. 77−11996
$Ga_{1-x}Al_xSb$ p-n structure, variable-gap, electroluminescence 78−52582
$Ga_{1-x}Al_xSb$, second order Raman spectra, photon combinations *(French)* 80−34912
$Ga_{1-x}Al_xSb$, surface oxidation, Raman spectra, residual Sb layers 80−71419
n-$Ga_{1-x}Al_xSb$, transport phenomena in low and high mag. fields 78−80007
$Ga_{1-x}Al_xSb$ variable-gap p-n struct., selective photoelec. effect 77−76912
$Ga_{1-x}Al_xSb$ variable-gap p-n structures, wide-band photoelec. effect 79−42635
$Ga_{1-x}Al_xSb$, variation of optical transitions *(French)* 79−60708
$Ga_xAl_{1-x}Sb$, VPE, closed tube transport technique 79−28935
$Ga_xAl_{1-x}Sb$, VPE with I_2 as transport agent 78−48325
Ga(As,P):N, intermediate range model of N states 79−73467
Ga(As,P):N, isoelectronic impurity states, long-range, short-range model 80−75524
Ga(As,P):N, theory of bound states induced by disorder and isoelectronic pots. 77−35889
Ga(As,P)/(In,Ga)P DH laser, red-emitting, optical and elec. characts. 78−66826
GaAs, 10.6 μm absorption meas. using thermal emission 77−1649
GaAs, 3d core level spectra, electronic polarisation effects 80−6765
GaAs 400 MHz TW laser modulator 80−87541
GaAs (001) surface, thermal treatment before MBE growth, RHEED-AES meas. 79−61754
GaAs (001)-Ag contact, surface stoichiometry and struct., and electronic surface states 78−95361
GaAs (100), angle-resolved photoemission spectra 80−50516
GaAs, (100), comp. and struct. of differently prepared surfaces, LEED and AES 78−91524
GaAs (100), VPE, role of Cl, LEED, RHEED, and AES obs. 77−1327
GaAs (100) and (110), photoelectrons spin polarisation 80−11530
GaAs (100) surface, chemisorption of O_2, electronic struct. theory, oxidation, electron spectra interpretation 79−42376
GaAs, (100) surface, etch pit density meas. using automatic struct. analyser EPIQUANT *(German)* 77−72619
GaAs (100) surface, pot., wave functions, spectrum and charge density calc. 77−20382
GaAs (100) surface struct. determ. by LEED, UPS, and EPR 80−49475
GaAs, (100) surfaces, reconstructed, ang. resolved photoemission from surface states, adsorption and annealing effects 80−16143
GaAs, (100) surfaces, struct. and stoichiometry during molecular beam epitaxy, RHEED anal. 79−4921
GaAs (100)surface, electronic struct., scattering-theory formulation 79−42607
GaAs (110), adsorpt.-desorpt. processes and phase transitions in alkali halide adsorbed layers 78−2361

III-V semiconductors continued
GaAs (110), adsorption of In, N, P, and As, UPS and EELS study, tight-binding calcs. 80−49496
GaAs (110), adsorption of O_2, oxide form., XPS/UPS study 80−49497
GaAs (110), adsorption of O_2, H_2, H_2O and H_2S, surface photovolt. spectroscopy 80−49499
GaAs (110), atomic struct. of clean and As covered surfaces, LEED study 80−49476
GaAs (110), chemisorbed O_2, extrinsic surface states 78−91535
GaAs (110), chemisorption of Cl, photoemission spectra and tight-binding calcs. 80−6629
GaAs (110), chemisorption of Al, electronic struct., tight binding calc. 80−49842
GaAs (110), chemisorption site geometry and interface electronic struct. of Al and Ga, photoelectron spectra 80−49843
GaAs (110), chemisorption of O and Al, ab initio theory 80−75612
GaAs (110), clean, cleaved, surface states, work function meas. 80−49847
GaAs (110), coadsorption of Cs and O_2, initial oxidation, soft XPS obs. 80−10793
GaAs, (110), correl. of short-range order and sputter dose, using vidicon-based LEED system 79−83082
GaAs (110), double-dangling-bond defects and band bending 79−69411
GaAs (110), electron states from transfer matrix method 78−56203
GaAs (110), electronic states and initial steps in oxidation 78−91534
GaAs (110), initial oxidation, XPS and AES study 80−11542
GaAs (110), LEED intensities, dynamical calc. 79−77462
GaAs (110), O chemisorption, surface EXAFS meas. 80−50460
GaAs (110), order-disorder interaction with O_2, LEED anal. 80−75445
GaAs (110), oxidation, 3d core level binding energy, multiple bonds 78−35543
GaAs (110), oxidation, 3d core level binding energy, single bonds 78−35544
GaAs (110), pseudocharge density calcs. 78−84275
GaAs (110), reconstruction and oxidation initial stages, ab initio calc. 80−49473
GaAs (110), self-consistent pseudopotential calcs., electronic struct. and atomic co-ords. 80−49848
GaAs (110), semidynamical renormalised forward scatt. technique for LEED anal. 79−77877
GaAs (110), steps 80−49846
GaAs (110), struct., elec. props., effects of illumination, O_2 absorpt., electron bombard. *(French)* 78−34690
GaAs (110), subsurface atomic displacements, evidence from LEED/CMTA analysis 78−38920
GaAs (110), subsurface atomic displacements, LEDD exam. 78−71912
GaAs (110), surface and near-surface atomic struct., LEED 78−91515
GaAs (110), surface core-level binding-energy shifts 80−103737
GaAs (110), surface electronic struct., ang. resolved photoemission expts. and tight binding calcs. 78−91743
GaAs (110), surface electronic struct. calcs. 80−80343
GaAs (110), surface states and matrix elements in angle-resolved photoemission 78−91741
GaAs (110), surface states symmetry determ. using polarisation-depend. ang. resolved photoemission 78−91742
GaAs (110), surface states, optical techniques 80−6939
GaAs (110), surface struct., EPR meas. and elastic energy minimisation calcs. 79−51405
GaAs (110), surface struct., LEED and AES study, comparison of MBE and ion bombard. surface prep. 80−54496
GaAs (110), unrelaxed, surface states in bond orbital model 78−91749
GaAs (110), valence band Auger spectra 78−35230
GaAs (110), valence band Auger spectra, from Ga and As CCV transitions 78−92149
GaAs (110), with Al or Ga overlayers, interfacial electron states, UPS and LEED obs. 80−80377
GaAs (110), with ultrathin Al and Cs overlayers, O_2 adsorption, comparative studies 80−50740
GaAs (110) clean surface, internal pot., interplanar spacing, LEED 77−89627
GaAs (110) cleaved surface, oxidation, XPS exam. 78−31551
GaAs (110) face, adsorption of one Cs atom, mol. orbital study *(French)* 78−38958
GaAs (110) relaxed surface, electronic states 79−51649
GaAs (110) surface, atomic geometry from elastic LEED intensities 77−20170
GaAs (110) surface, atomic and electronic struct. 78−72223
GaAs, (110) surface, bond angle and lengths of rearranged As and Ga atoms 78−71918
n-GaAs (110) surface, Cs adsorption, work function meas., adsorption site model 79−23839
GaAs, (110) surface, electronic struct. of clean and O_2 covered surface 77−43685
GaAs (110) surface, electronic states near band gap 77−85290
GaAs (110) surface, electronic struct., pseudopot. calc., surface relax. model 80−29456
GaAs (110) surface, exposed to O and O_2 photoemission spectra meas., Space Shuttle expt. 78−35246
GaAs (110) surface, O_2 interaction, order-disorder effects, LEED, UPS anal. 80−6634
GaAs, (110) surface, oxidation, photoemission spectra obs. 77−16460
GaAs (110) surface, relax. effects 77−24601
GaAs (110) surface, surface states, angle-resolved photoemission meas. 77−20984
GaAs, (110) surface, trned in energy distribs. of Ga dangling orbital surface states 79−28397
GaAs (110) surface oxidation process, XPS study 79−15585
GaAs (110) surface states, surface relax. models, tight-binding calcs. 79−4594
GaAs, (110) surface structure, rotational relaxation, cluster model *(Chinese)* 80−107621
GaAs (110) surfaces, ordered and disordered, O_2 adsorption, XPS meas. 80−49498
GaAs (110)/Ge heterojunction, valence band discontinuity in XPS spectra, precise determ. 80−84834
GaAs (110)-Al interface, XPS study of interface interaction, Al proximity effects and replacement reaction 79−100019
GaAs (110)-Al(Ga) interface, interface states, photoemission study 78−95359
GaAs (110)-Al(Ga)(In), Schottky barrier form., defect mechanism 80−49902

III-V semiconductors continued
GaAs (110)-Au Schottky barriers on ordered and disordered GaAs surfaces, props. 78−95360
GaAs ($\bar{1}\bar{1}\bar{1}$), MBE prep., angular resolved UPS of surface states 79−47598
GaAs (111) and ($\bar{1}\bar{1}\bar{1}$) surfaces, XPS study 79−83102
GaAs, (111) epitaxial film, adsorption of Cs, Cs+O, ellipsometric study 80−29282
GaAs (111) substrate, and homoepitaxial layers, characterisation by divergent X-ray beam diffr. 78−31352
GaAs {001} layer, LPE, dislocation etch pits revealed by molten KOH 78−63772
GaAs {100} surface, interaction kinetics of As_2 and Ga 77−60115
GaAs, AB etch reappraisal 78−6065
GaAs, absorption coefficients, method of meas. 78−83048
GaAs, absorption edge broadening by piezoelec. phonon fields 77−16302
n-GaAs, absorption tails in surface depletion layer and bulk 78−64379
GaAs, acceptor bound exciton Auger and radiative transition rates, radiative recomb. 80−6733
GaAs, acoustic plasmons in MOS inversion layers 78−18983
GaAs, active layers produced by high energy Se^{++} implantation, FET appls. 77−39605
GaAs, adsorbed O, (110), surface electronic struct., synchrotron irradiated photoemission 78−43453
GaAs, adsorbed O_2^- EPR spectrum, HFS 77−40118
GaAs, adsorpt.-desorpt. of Zn, thermal desorpt., at. beam adsorpt., AES, SEM, RHEED 78−14591
GaAs, adsorption and field-desorption of O_2 and Au, FEM studies 80−34304
GaAs, adsorption enhancement by electron beam excitation of gas mols. 78−43238
GaAs, adsorption of O_2, adsorption states and Ga depletion, UPS, AES, and thermal desorption meas. 79−46952
GaAs, adsorption of Sb_2, surface state exam. by energy loss spectra 77−15935
GaAs, Al-coated, surface phonon Brillouin spectra 79−78694
GaAs, alloying with Au and Au alloy ohmic contact metallisations, SEM and optical study 80−70820
GaAs, ambient-enhanced photoluminesc. props., mol. adsorption and gas-flow effect 79−99925
GaAs, amorphous, EXAFS, evidence for inequivalent environments of Ga and As 79−15558
GaAs, amorphous, laser crystallisation, for production of large grained sheets for solar cells 80−93570
GaAs, amorphous, localised gap states, variable range hopping, susceptibility and EPR 77−72866
GaAs, amorphous, localised gap states, hopping cond. and chem. bonding 78−23052
GaAs, amorphous, optical absorpt. edge shape, band edge fluctuations 77−20880
GaAs, amorphous, switching obs. 79−11190
GaAs amorphous film, composition, study by nondispersive X-ray anal. *(French)* 79−8457
GaAs amorphous film, EXAFS, optical and elec. props. 80−49547
GaAs amorphous film, effective medium theory and freq. depend of conductivity 79−24090
GaAs amorphous film/cryst. junctions, optical and elec. props. 79−99611
GaAs, amorphous layer formation, ion implantation, IR spectra 78−95063
GaAs, amorphous layers, ion-implanted, low-temp. epitaxial regrowth 80−92790
GaAs, amorphous sputtered films, hydrogenated, photoinduced optical absorpt. 80−50362
GaAs, amorphous state, thermal stability, elec. cond. obs. 80−33888
GaAs and related cpds., conf., Edinburgh, Scotland (Sep 1976) 78−3039
GaAs and related cpds., conference, St. Louis, MO, USA (Sept. 1978) 80−8737
n-GaAs, and Te doped, homogeneity, IR introscopy investig. 79−15446
GaAs, angle-resolved photoemission and valence band dispersions 80−7469
GaAs, annealing rel. to stoichiometry deviation, Hall effect, electron microscope meas. 77−24410
GaAs, annealing with Si_3N_4, Cr profiles meas. 79−90693
GaAs anodic films, XPS study 80−71562
GaAs anodic MIS system, dynamic props. of interface state bands 80−49933
GaAs anodic MOS structs., interface-state band model 80−11093
GaAs, anodic native oxides for MOS devices, quality assessment 79−61767
GaAs, anodic oxidation 77−16710
GaAs, anodic oxidation and MOS devices 77−80845
GaAs, anodic oxidation in nonaqueous electrolyte and MOS characts. 79−38183
GaAs, anodic oxidation in O plasma 79−66188
GaAs, anodic oxidation mechanism, temp. and electrolyte comp. effects 80−3220
GaAs, anodic oxidation under dark and illuminated conditions, behaviour of cell voltage 77−16826
GaAs, anodic oxidation using O plasma, and oxide layer evaluation 78−85015
GaAs anodic oxide, electrical props. 79−38170
GaAs anodic oxide, quantitative chem. depth profiles 77−72799
GaAs anodic oxide, refl. and transmission, 0.01-6 eV 78−95613
GaAs anodic oxide, refr. index meas., Sellmeier eqn. 77−12454
GaAs anodic oxide, states, electrochemical meas. 80−80176
GaAs anodic oxide chem. depth profiles, neutron activation analysis and Auger spectroscopy 77−77619
GaAs anodic oxide film, direct current-voltage characts. 78−23186
GaAs anodic oxide film, optical props. 78−72626
GaAs, anodic oxide film, annealing effect on carrier density profile 78−88040
n-GaAs, anodic oxide film, exam. using SIMS and ellipsometry 79−61770
GaAs, anodic oxide film comp. profile anal., radioactive tracer technique 77−59956
GaAs anodic oxide film prep. by plasma anodisation of O-sputtered surfaces, MOS device characts. 79−66176
GaAs anodic oxide films, composition meas. by ion scatt. spectrometry, influence of current density 80−11802

III-V semiconductors continued
GaAs anodic oxide films, optical studies using rot. light-pipe reflectometer 80−76096
GaAs, anodic oxide for device application, crystallisation dynamics 79−66190
GaAs anodic oxide formation, galvanostatic obs. 77−77620
GaAs anodic oxide growth rate in mixed electrolyte 77−44382
GaAs, anodic oxide layers, chem. depth profiles, XPS determ. 80−3222
GaAs anodic oxide system, multiple angle incidence ellipsometry, meas. at λ=632.8 nm 79−63294
GaAs, anodically oxidised, etch pits, defect characterisation 77−56122
GaAs anodisation, ellipsometric study *(Japanese)* 80−97610
GaAs, anodisation, for MAOS diode with stable charge storage 77−15960
n-GaAs, anodisation, initial film form. in tartaric acid-water-propylene glycol 77−21301
GaAs, anodisation, O incorporation at oxide-electrolyte interface, ion microprobe mass anal. 77−25273
GaAs, anodisation at low substrate temp. by low pressure O_2 plasma 80−104314
GaAs, anodisation ellipsometric and IR spectroscopic studies of oxide film 80−11493
GaAs, anodisation in HF O_2 plasma, oxide film form. mechanism and kinetics *(Japanese)* 80−93667
GaAs, anodisation obs. by in situ differential refl. 80−50732
GaAs, anodised, interfacial reactions, Raman scatt. obs. 80−49544
n-GaAs anodised MOS, electrorefl. spectra 79−99901
GaAs, anomalous avalanche breakdown 80−80284
GaAs, anomalous diffusion of Sn from doped oxides due to dopant depletion effects 77−89461
GaAs antireflecting MOS solar cells, epitaxial and polycryst. using OM-CVD techniques 80−94072
GaAs, atom probe field ion microscopy 78−80460
n-GaAs, Au-SnNi-Au ohmic contacts low temp. alloying electroplated layers, expt. 78−35319
GaAs, Auger recombination, luminesc. meas. 77−85850
GaAs, Auger recombination cross sections associated with deep centres 78−47810
n-GaAs, Auger transitions, nonlinear extrinsic luminesc. study sublinear emission 79−95833
GaAs autoepitaxial structure on heavily Te-doped GaAs substrate *(Russian)* 80−49556
GaAs, automatic electrochemical Hall mobility profiling 79−99615
GaAs, avalanche breakdown field, approx. formula 80−11025
GaAs, back etching and growth by liq. phase epitaxy, surface morphology obs. 80−29287
GaAs, back-wall Schottky barrier solar cell with interfacial layer 77−62993
GaAs, ballistic and near ballistic transport 80−96867
GaAs, band struct., modulation spectroscopy, two-ray methods *(Russian)* 78−54469
GaAs, band structure under high stress, nonperturbative calc. 78−10344
GaAs base laminated epitaxial struct., surface plasmon phonon polaritons *(Russian)* 80−59905
GaAs based laser diodes, comparison with Nd^{3+} based lasers 77−7088
GaAs based MIS structures as possible optical memory elements 79−65556
GaAs based MOS capacitors, scanning photovoltage investigation 80−80396
GaAs, biexciton stability, appl. of theory for polar crysts. 78−76002
GaAs, binding of exciton to neutral acceptor 78−79937
GaAs, birefringence, photoelastic consts. dispersion 80−11361
GaAs, birefringence in presence of electroabsorpt. 77−32351
GaAs, blocking effect, backscatt. method *(Chinese)* 79−90708
GaAs, boat-grown, deep levels *(Japanese)* 79−47043
GaAs, Brillouin scatt. from surface ripples 79−15472
GaAs, Brillouin scatt. of refl. light, surface ripple mechanism 77−73149
GaAs, Brillouin spectra, light scatt. cross section for surface ripples 80−71434
n-GaAs, bulk and epitaxial film, IR reflectance meas. 77−32364
GaAs bulk and epitaxial crysts., electron traps characterisation 77−39865
GaAs, bulk and epitaxial crysts., hole traps characterisation 78−6392
GaAs, bulk hot-electron props. 79−99553
GaAs, CC Ga-3d-excitation, high resolution reflectivity down to 15K 80−25415
GaAs, CESR, optical detect. by spin orientation techniques, anal. 78−80251
GaAs, CVD, S doping behaviour during growth, electron conc. 78−26784
GaAs CVD for solar cell applications 77−77412
GaAs, CVD in Ga-$AsCl_3$-H_2 system with different input supersaturations *(Russian)* 78−68098
GaAs, CVD mechanism, product catalysed reaction of Me_3Ga with AsH_3 77−48345
GaAs, CVD on W coated graphite, characterisation, and Schottky barrier solar cell characts. 79−28930
GaAs, CVD using Ga-As-H-Cl system, theoretical anal. of equilib. adsorption layers 79−23858
GaAs CW DH laser, inherent oscillations and subharmonic resonances obs. in light output 78−74910
GaAs CW injection laser diode specification for integrated optical circuits 80−33034
n-GaAs carrier compensation by O ion implantation, C-V meas. 77−7747
GaAs, carrier conc. and compensation microprofiles 80−80820
GaAs, carrier conc. variations using electrolyte electroreflectance, topographical features 79−99562
GaAs, carrier concentration determ. using electroreflectance 78−23483
GaAs, carrier diffusion in transient response regime 80−103688
GaAs, carrier lifetime, radiation induced changes, edge luminesc. spectra 77−8664
GaAs, carrier mobility profiles meas. at room temp. by Corbino effect 78−60128
GaAs, carrier removal after H_1^+, H_2^+, and H_3^+ implantation 77−8115
GaAs, chem. bond, modulation X-ray diffr. obs. 80−96464
GaAs, chem. etched surface, Auger characterisation 77−25169
GaAs, chem. prep. of surfaces, and AES and XPS characterisation 77−90477
GaAs, chemical etching processes, review 78−95832
GaAs, chemical shift and effective atomic charges 78−88201

III-V semiconductors continued
GaAs, chemisorpt. of O_2 and thin oxide layer form., reviews of synchrotron radiation meas. 79−60637
GaAs, chemisorption and oxidation states of (110) surfaces 79−24049
GaAs, chemisorption of Al, surface barrier formation, localised orbital theory 79−51671
GaAs, chemisorption of Cs, isobars, LEED and loss spectroscopy meas. 77−4262
GaAs, chemisorption of O_2, effect of surface index and atomic disorder AES, LEED and optical ellipsometry 79−60638
GaAs, circuit effects in time-of-flight diffusivity meas., Monte Carlo method 80−88563
p-GaAs, circular polarisation of hot luminesc. 78−52572
GaAs, clean and oxidised surfaces, O_2 sticking coeff., ionicity effects, XPS expts. 77−85887
GaAs, clean or contaminated (001) surface, Au film growth 78−26785
GaAs cleaved (110) face, interaction with O_2, influence of cleavage defects, AES study 80−66684
GaAs, cleaved (110) surface Cl chemisorption geometry 80−6659
GaAs, compensated, electron mobility temp. depend. 80−96868
GaAs, compensated, influence of electron gas heating on negative magnetoresist. 77−89778
n-GaAs, compensated, LF current instabilities 79−7859
GaAs, compensated, magnetoresist. and magnetothermoelec. power meas. 77−43627
GaAs, compensated, magnetoresist. and Hall effect 77−66176
GaAs, compensated, photoabsorption, expt. 78−19521
GaAs, compensated, Shubnikov-de Haas oscills. 77−11941
GaAs compensated VPE thin film, electron Hall mobilities 80−107932
GaAs, complex luminesc. centres at 1.20 and 1.30 eV 77−16386
n-GaAs, conc. calc. using iterative method *(French)* 77−72634
GaAs, concs. of C and O_2 in LEC grown cryst. determ. 77−39612
GaAs conducting MIS structures and metal-semicond. structures, effects of ultrathin oxides 79−1626
GaAs, conduction band, three-level struct., from high-stress and high-field obs. 77−15764
GaAs, conduction band effective mass, influence of high uniaxial stress 80−80162
GaAs, conduction band mapping by angle-resolved photoemission 79−83105
n-GaAs, conduction band nonparabolicity and coupled plasmon-phonon modes, IR refl. spectra 80−55110
GaAs, conductivity of complementary error function n-type diffused layers 77−35944
n-GaAs, conductivity relax. times in warm electron range, intervalley transitions 77−55537
n-GaAs, conversion to p-type after 1 MeV electron irrad. 79−77636
GaAs core exciton binding energies 80−80188
n-GaAs, coupled plasmon-LO phonon modes and Lindhard-Mermin dielec. function 79−82540
GaAs cryst., creep and dislocation vel. at different doping and temps. 78−95783
GaAs, cryst. growth by MBE 78−39707
GaAs, cryst. growth from large Ga:As solns., critical cooling rate 80−64938
GaAs, cryst. prod. in strip and rod form., Stepanov method 78−3017
GaAs, crystal, piezoelectric oscills. meas. by laser interferometry 77−118
GaAs, crystal defect obs. by TEM *(Japanese)* 77−84752
GaAs crystal growth, thermal and elastic const. evaluation 80−92586
n-GaAs, crystal growth by Czochralski method kinetics, total emittance determ. 80−75193
GaAs, crystal pulling of semi-insulating material, liquid encapsulated compounding and Czochralski growth 79−43136
GaAs crysts., IR light scattering and absorpt. microscopy study of dislocations 80−107249
GaAs, current controlled negative resist. at low temps. 78−39133
GaAs current instabilities in semiconductors, theory and expts. *(Hungarian)* 77−39857
n-GaAs, current-voltage characts., dislocation etch pits and perfect cryst. 80−70695
GaAs, cylindrical and spherical localised inhomogeneities in mag. field, anomalous elec. prop. calcs. 80−44621
GaAs, Czochralski grown, pure and doped, elec. props. 80−10989
GaAs, Czochralski growth, melting and regrowth, inclusion density and dislocation generation 77−21016
GaAs, DC biased, filamentation of laser radiation 80−74428
GaAs DH injection laser, modulation behaviour, appl. in high bit-rate fibre optical communications 78−1281
GaAs DH laser, alloying of ohmic contacts, Nd:YAG laser irrad. 80−43357
GaAs DH laser, high speed direct modulation, multimode operation effects 78−13738
GaAs DH laser, life test at room temp. 78−17937
GaAs DH laser, self-induced modulation, noise, instability 80−48250
GaAs DH laser diodes stabilised using self-apertured facet coatings 80−58609
GaAs DH laser/fibre transmission system modulation and injection 77−50764
GaAs DH stripe geometry laser, horizontal mode deform. and anomalous lasing props. 77−19253
GaAs, damage by 1.06 μm laser radn. 79−56890
GaAs, Debye temperature, atomic mean square displacement 78−87757
GaAs, deep bound states, temp. depend. of ionisation energies 77−31975
GaAs, deep centre free energy level determ. by transient capacitance technique 80−103641
GaAs, deep centres, collective thermal emission of electrons 80−10918
GaAs, deep centres, electron and hole capture cross sections 79−99510
n-GaAs, deep electron traps, determ. by time-resolved capacitance meas. 77−39797
GaAs, deep impurity levels, activation energy 80−107742
GaAs, deep level impurities *(Japanese)* 77−89723
GaAs, deep level profile anal., double correlation technique 77−80830
n-GaAs, deep level traps, transient and thermally stimulated capacitance meas. *(Chinese)* 79−91072
GaAs, deep levels, optical and thermal spectroscopy, lattice relaxation *(French)* 80−66248
GaAs, deep levels, photocapacitance meas. under hydrostatic press. 77−85259
GaAs, deep levels investigation 77−76769
GaAs, deep radiation centres from heat treatment, γ-irrad., deform., probability of nonradiative electronic transitions 80−50408

III-V semiconductors continued
GaAs, deep trap characts. by photocapacitance spectroscopy 78−6398
GaAs, deep trap study by free exciton refl. spectra 79−60761
GaAs, deep trapped impurities, photocond. spectra, interpretation 78−52030
GaAs, deep traps exam. by capacitive method 77−11869
GaAs, defect cluster annealing, pot. barrier height determ. 80−84209
GaAs, defect clusters induced by γ-rays and neutrons, effect on elec. props. 80−29408
GaAs, defect revealing etchant, electrochem. process in $NH_4OH:H_2O$ 78−6060
GaAs, defect state identification associated with Ga vacancy 77−69269
n-GaAs, deform. produced deep levels, DLTS meas. 80−54634
GaAs, degenerate, impurity band struct. for dense donors and acceptors 80−29348
GaAs, degenerate, nonequilib. electron distrib. functions 77−63394
GaAs degraded heterojunction lasers, TEM obs. of dark defects 78−14355
GaAs degraded lasers, climb asymmetry, TEM obs. 80−79802
GaAs, degraded layer form. by annealing, photolum. obs. of defects 78−10968
GaAs, density of states, spontaneous emission rate calcs., 120, 160, 200K 77−4292
n-GaAs, density of states tail in heavily doped closely compensated semicond. 78−47689
GaAs, destruction mechanisms by intense IR laser radiation *(Russian)* 78−39633
GaAs device isolation with deuteron bombardment 80−75248
GaAs, device quality, epitaxial growth on Ge/Mo substrates 79−69988
GaAs devices, ion implantation damage, characterisation and appl. 80−92551
GaAs devices, ohmic contacts using epitaxial Ge films 78−88027
GaAs devices ohmic contact fabrication using epitaxial Ge films 78−47871
GaAs, diffraction gratings prod. by interference photoetching 77−46805
GaAs, diffusion and power spectral density and correl. function of vel. fluctuation for electrons 80−65576
n-GaAs, diffusion coeff., Monte Carlo calc., rel. to trapped domain behaviour 78−56152
GaAs, diffusion coeff. of hot electrons 79−15156
GaAs, diffusion in Au-refractory thin film systems obs., by combination of scattering techniques 80−65308
GaAs, diffusion of Cr and Ag, radiotracer profiles 80−24680
GaAs diffusion of ion implanted Be, SIMS and electrical profiling 78−47605
GaAs, diffusion of Se 77−51547
GaAs, diffusion of Sn effect of ambient As vapour press. on surface stability 80−2208
GaAs diode, high temp. and freq. characts., made by gas-transport method 79−19654
GaAs diode, quantum efficiency and nonequilibrium carrier lifetime 77−12442
GaAs diode, reverse-biased, current-controlled negative resist., switching investig. 77−69410
GaAs diode, with Schottky barrier, photoluminesc. *(Russian)* 79−28410
GaAs diode laser, behaviour in optical feedback mode *(Dutch)* 79−76689
GaAs diode lasers coupled to short external resonators, reson. amplifier model 77−31110
GaAs diode temperature sensors, characts. obs. at 4.2 to 393K 80−47054
GaAs, direct energy gap, press. depend. up to 180 kbar 77−8020
GaAs, direct gap, picosec. time resolved reflectivity obs. of optically excited hot carrier distrib. 78−76495
GaAs, direct-gap epitaxial layers, optical compensation profiling 77−76450
GaAs directional couplers and electrooptic switches, wavelength depend. 78−79143
GaAs, directional-coupler switch with stepped Δβ reversal 77−79968
GaAs directional-coupler switch with stepped Δβ reversal 77−88962
GaAs, dislocation density effect on polarisation and intensity of reflected $CuK_{\alpha 1}$ radiation 77−1131
GaAs, dislocation density, ⟨100⟩ cryst., quantitative light microscopy 77−31661
GaAs, dislocation etching of {100} and {111} planes of As 77−43215
GaAs, dislocation free, phonon-defect interaction 77−69061
GaAs, dislocation loops, rel. to dark defects in LEDs 77−80509
GaAs, dislocation states 79−60762
GaAs, dislocation structure 79−82206
GaAs, dislocation-free, point defects and rad. damage 80−88141
GaAs, disorder distrib. extraction, semiempirical method of applying dechannelling correction 78−22781
GaAs, disordered, ion implanted, elec. props. 78−84212
GaAs, dissociated dislocations, statistics of kink formation 79−82207
GaAs, dissociation of dislocations 79−46665
GaAs, distrib. Bragg reflector laser, highly collimated broadside emission 78−13721
GaAs distributed Bragg reflection lasers, large optical cavity, optimal design 80−38028
GaAs, distribution function relax. times 77−55541
GaAs, domain elec. instability in two-valley semiconds. 77−76842
GaAs, donor and acceptor concs. determ. by optical method 78−19525
GaAs donor characterisation by far IR photoconductive techniques 78−43501
GaAs, donor energy spectrum, mag. field effect, submm. photocond. meas. *(Russian)* 77−43666
GaAs, donor van der Waals interactions, spectral lineshapes 80−11450
n-GaAs, donor-acceptor pair recomb., isolated-pair model revisited 79−28825
GaAs, donor-acceptor type complex, mag. field splitting of photolum. line 79−15512
GaAs, donor-acceptor-type complex 80−80837
n-GaAs, dopant conc. determ. using laser IR microscopy 79−86811
GaAs, doped, photoemission, calc. of escape probability of electrons *(Russian)* 79−24408
GaAs, doped, radiative lifetimes, quantum mechanical model 80−55151
GaAs, doped with Group IV elements, etching, electron spectra, cathodoluminesc. study of inhomogeneities 77−11556
GaAs doping structures, production and appl. *(German)* 78−95064
GaAs double and narrow stripe laser structures 80−64062
III-V semiconductors continued
GaAs double cavity laser, with branching output waveguides, exam. 78−37918
GaAs double hetero stripe-geometry laser, two-dim. anal. 78−1231
GaAs double-cavity laser with branching output waveguides 78−63128
GaAs, dual implantation of C^+ and Ga^+, sheet resist. and Hall effect meas. 78−67728
GaAs, during deformation, acoustic emission rel. to cracks, dislocations 80−35441
GaAs, dynamical response of electron distrib. to high elec. field fluctuations 77−51758
GaAs, EHT calcs. of energy bands and pressure dependences *(Japanese)* 78−34747
GaAs, EXAFS amplitudes, many-body effects 80−97379
GaAs, effective dielectric function calc., exchange interaction effects 79−99494
GaAs, effective mass, Raman spectrum determ. 80−24797
GaAs, effects of ion implantation, deep-level transient spectroscopy techniques 80−2046
GaAs, elec. cond., effect of As vapour press. at 200-1000°C 77−15846
GaAs, elec. effects of dislocations 79−82586
GaAs, elec. props. of dislocations review *(Japanese)* 78−6325
GaAs, electrical and optical props. at low temps. 80−39636
GaAs, electrical conductivity and thermoelectric power charge due to melting 80−100490
n-GaAs, electrical instability, negative differential cond., electron heating by static and alternating elec. fields 79−11165
GaAs electro-optic rib waveguide directional-coupler switch with stepped Δβ Schottky electrodes 79−98507
GaAs, electroabsorpt. avalanche photodiode, waveguide detector for 1.06 μm 78−16842
GaAs, electroabsorpt. avalanche photodiode waveguide detectors 78−65965
GaAs, electroabsorpt. avalanche photodiode waveguide detector, freq. demultiplexing 79−17486
GaAs electroabsorption signal, depend. on elec. field 80−103942
GaAs, electrochemical sectioning and surface finishing 80−108611
GaAs electrode, electon injection in liq. NH_3 80−6977
p-GaAs electrode, flatband pot. determ. from differential stress meas. 80−75638
GaAs electrode, interpretation of selective etching, electrochem. props 80−7703
p-GaAs, electrode, photoemission into electrolyte solns. 77−24616
GaAs electrodes, n- and p-type, freq. depend. of impedance 77−12001
GaAs electrodes, photo-induced electrogenerated chemilum. and upconversion 79−91510
GaAs electrodes in acetonitrile solns., photoelectrochem. behaviour 79−4600
GaAs, electrodes in acetonitrile solutions, characterisation and photochemical behaviour 79−70341
n-GaAs electrodes in acetonitrile solns., liq. junction photovolt. cell 79−99617
GaAs electrodes in aqueous electrolytes, localised avalanche breakdown 79−4599
GaAs, electroluminescent study of irrad. induced struct. damage, athermal annealing 80−108280
GaAs electrolyte interface, energetic barrier height hypothesis 79−19657
n-GaAs, electron and gamma ray irradiated, introduction and annealing of defects 78−67736
GaAs, electron and hole impact ionisation coeffs. 78−6389
GaAs, electron and hole ionisation rates meas., elec. field orientation depend. 78−10453
GaAs, electron and neutron irrad., defect clusters 80−2077
GaAs, electron beam induced defect annealing 77−80790
GaAs, electron beam induced current, minority carrier generation distrib. 80−96900
GaAs, electron beam pumped laser, far-field radiation pattern, optical confinement effects 79−86181
GaAs, electron bombardment, absorption of energy 79−14847
GaAs, electron capture by multiphenon emission at B centre 80−24830
GaAs, electron distrib. function in alternating fields, single particle Monte Carlo method 77−89791
n-GaAs, electron drift vel. meas. at high elec. fields 77−39861
GaAs, electron dynamic properties in strong elec. field, anal. *(German)* 78−43404
GaAs, electron effective mass, temp. depend. for various degrees of doping and compensation *(Russian)* 78−79923
GaAs, electron heating under hydrostatic pressure, Monte Carlo calcs. 77−69334
n-GaAs, electron irrad. defects, carrier removal rate, annealing effects 80−75269
GaAs, electron irrad. induced defect levels, hydrostatic press. effect 80−92858
n-GaAs, electron irradiated, defect energy levels, influence of irrad. temp., photocond. meas. 78−2446
n-GaAs, electron mobility, free-carrier absorpt., and compensation ratio 79−56218
GaAs, electron mobility temp. depend. 79−91084
GaAs, electron mobility illumination, compensation, space charge regions, carrier scatt. 80−70691
GaAs, electron scattering interaction with coupled plasmon-polar-phonon modes 79−42536
GaAs, electron states associated with dislocations 79−82544
GaAs, electron transient vel. characts., Γ-L-X cond. band ordering 78−79997
GaAs, electron transport analytical model 79−91039
GaAs, electron trap at E_c-0.75 eV, direct evidence for nonassignment to O 79−90988
GaAs, electron-beam excited, efficient generation of electron-hole plasma 80−76051
GaAs, electron-exciton collision influence on luminescence line profile due to bound excitons 80−29800
GaAs, electron-hole drop transition to metallic condensed state, Hartree-Fock theory 79−56136
GaAs, electron-hole liquid form., luminesc. 79−33804
GaAs, electron-hole plasma, ground state energy 78−84244
GaAs, electron-hole plasma, Coulomb effects on gain and absorption spectra 80−50371
GaAs, electron-irrad., deep-level defect anal. using 2γ positron annihilation and IR absorption spectra 80−16120

III-V semiconductors continued
p-GaAs, electron-nuclear spin coupling, low field, under optical pumping conditions 77−77126
GaAs electron-pumped uncooled laser, degradation rel. to dislocation density 80−14344
GaAs, electron-spin relaxation and recomb. kinetics, time-resolved luminesc. study 80−108074
GaAs, electronic density, multiple scatt. method, muffin-tin approx. 80−27924
p-GaAs, electronic props. 78−68040
GaAs, electronic Raman scatt. of polarised light on donor levels 80−93309
GaAs, electronic states of neutral vacancies 77−11875
GaAs, electronic states associated with 60° dislocations, tight-binding calc. 79−15114
GaAs, electronic struct., mol. cluster model, SCF multiple scatt. method 79−42446
GaAs, electronic structure of (111) and $(\bar{1}\bar{1}\bar{1})$ surfaces 79−87137
GaAs, electronic structure, self consistent local description 80−20067
GaAs, electronic surface props., interaction with Au and O adsorbate layers 77−20385
GaAs, electronic surface structure Cs(Rb)(Na) adsorpt. processes, AES, LEED, EELS, study 78−68068
n-GaAs, electronic transition scheme via radiative centres 77−69905
GaAs, electrooptic effect, birefr. harmonics, permittivity dispersion 77−52044
GaAs electrooptically tuned external-cavity CW injection laser, FM optical communication appl. 80−14351
GaAs, electroreflectance spectroscopy using synchrotron rad. 78−10912
GaAs, ellipsometry of dielectric films on 79−69894
GaAs, empty surface states and surface order effects on sorption 77−85281
GaAs, energy bands and wavefunctions, localised orbital description 78−18942
GaAs epilayer, for FET, hot carrier noise 79−24035
n-GaAs, epilayer, on semi-insulating substrate, elec. field distrib. *(French)* 80−20333
GaAs epilayers, high-quality, sharp-line transitions due to donor-acceptor recomb. 78−6768
GaAs epilayers and p-n junctions, anisotropic phonon generation 79−37784
GaAs, epitaxial, appl. to surface barrier particle detectors 79−72203
n-GaAs, epitaxial, electron mobility calc. 77−69435
n-GaAs, epitaxial, high temp. carrier transport 80−65725
GaAs, epitaxial, impurity gradients caused by surface states and substrate doping 77−84784
n-GaAs, epitaxial, ionised donor pair spectrum 77−63477
GaAs, epitaxial, nonequilibrium carrier relax., recombination radn. 80−7416
GaAs, epitaxial, polycryst., monocryst. layers and whiskers growth by CVD, SEM obs. electron diffr. study *(French)* 79−43150
GaAs, epitaxial, residual donor identification by far IR photocond. 80−60047
GaAs, epitaxial, residual donor identification by far IR photoconductivity meas. 80−103717
GaAs, epitaxial, Si and Ge doping 80−24470
n-GaAs, epitaxial, thermoelec. power, temp. depend. in mm wavelength range 79−23996
GaAs, epitaxial and metallic thin-films, anodic oxidation anal. 78−80673
GaAs, epitaxial deposition from organometallic cpds. 77−47689
GaAs, epitaxial deposition, growth kinetics *(French)* 80−2961
GaAs, epitaxial film, amorphous and polycrystalline, vol. plasmon energy and linewidth, electron scatt. obs. 80−50482
GaAs epitaxial film, chem. transport by water vapour, thermodynamic calcs. 77−12539
GaAs epitaxial film, deep centre reson. charging, photocapacitance meas. on Schottky barrier 78−26908
n-GaAs, epitaxial film, defect clusters, charge-carrier mobility temp. depend. anal. 80−54701
GaAs epitaxial film, enhanced electrodiffusion purification in mag. field 80−66409
GaAs, epitaxial film, field effect struct., elec. breakdown, negative resist. 77−12030
n-GaAs epitaxial film, magnetoresist. at low temp., geometric effect 80−93015
GaAs epitaxial film, microstruct., effect on elect. characts. of Schottky diode *(Russian)* 80−107671
GaAs, epitaxial film, photon transfer of excitation of nonequilibrium carriers, radiative recomb. 77−8639
GaAs epitaxial film, photo-EMF echo at 4.2K 80−60038
n-GaAs epitaxial film, potential barrier height, temp. depend. *(Russian)* 78−68070
GaAs, epitaxial film, positron annihilation, impurity centre study 79−15554
n-GaAs epitaxial film, pure and Cr doped, heavy electron trapping, Gunn oscills. 80−6857
GaAs epitaxial film, surface trap exam. by surface doping and field effect 77−76896
n-GaAs epitaxial film, surface mode phonon amplification, numerical analysis 78−34691
n-GaAs epitaxial film, undoped, correl. incorporation of donors, photocond. meas. at 4.2K 80−6898
GaAs epitaxial film on GaAs substrate, IR characterisation 78−23544
GaAs, epitaxial film on GaAs substrate, two-interface surface polariton modes 78−60180
GaAs epitaxial film recombination props. *(Russian)* 80−49812
GaAs epitaxial films, deep levels, impurity photocond. 80−20247
n-GaAs epitaxial films, residual cond. meas., struct. perfection rel. to photomemory 80−7010
GaAs epitaxial films on strongly doped substrate, basic parameter meas. utilising magnetoresist. and SEM techniques under cathodoluminesc. conditions 80−65728
GaAs, epitaxial growth, gas-phase composition during growth by chloride method 77−12537
GaAs epitaxial growth, molecular beam, uncontrolled doping obs. *(Russian)* 80−2276
GaAs epitaxial growth, in GaAs-$AsCl_3$-H_2 system, elec. field effect 80−2306
GaAs epitaxial growth, CVD-organometallics method, reactional efficiency in solar cell elaboration 80−93498
GaAs, epitaxial growth and etching rate meas. method 77−35829

III-V semiconductors continued
GaAs, epitaxial growth for microwave devices *(French)* 77−48360
GaAs, epitaxial growth in $Ga(CH_3)_3$-AsH_3-H_2 system 78−35312
GaAs, epitaxial growth in Ga-$AsCl_3$-He_2 system, expt.-statistical analysis *(Bulgarian)* 78−60580
GaAs, epitaxial growth under different intake supersaturations in GaAs-$AsCl_3$ gas transport system *(Russian)* 78−26776
GaAs, epitaxial layer, 1.06 μm two-photon absorption coeff., guided wave meas. 78−46707
GaAs epitaxial layer, AuGe ohmic contact production by laser alloying 78−88026
GaAs epitaxial layer, Be, O, Si, S, Zn and Sn impurity concentrations 80−49260
GaAs, epitaxial layer, C distrib., anal. by quasichem. reactions 77−11803
GaAs, epitaxial layer, controlled electrochemical and selective etching, integrated optics appl. 77−14814
GaAs epitaxial layer, comparison of compensation ratios determ. by photolum. and elec. methods 79−28818
GaAs, epitaxial layer, effective doping density, comparison of Hall and magnetoresistance meas. 77−11938
GaAs epitaxial layer, fast electron irrad., impurity distrib. profile obs. 77−76969
GaAs epitaxial layer, free-carrier density determ. by Hall meas., surface and interface depletion corrections 79−91170
GaAs epitaxial layer, laser mag. photoelec. spectra 79−82635
GaAs, epitaxial layer, micron and submicron vap. phase growth, for FET 80−11577
GaAs, epitaxial layer, nondislocation etch pits 80−92535
GaAs, epitaxial layer, partition coefficients of impurities 77−15443
n-GaAs epitaxial layer, planar diode, intervalley carrier transfer, dynamics of capture processes 78−47864
GaAs epitaxial layer, photoluminesc. defect complex 80−29804
GaAs epitaxial layer, strain induced optical waveguiding 79−27388
GaAs, epitaxial layer, surface morphology 79−90852
GaAs epitaxial layer and Sn-doped bulk characterisation 79−82596
GaAs, epitaxial layer growth by chloride process, μ and subμ thickness 78−23624
GaAs epitaxial layer high power Gunn diode developement and fabrication 80−16199
n-GaAs, epitaxial layers, electrical parameter determ. by graphical method *(Russian)* 77−15975
GaAs epitaxial layers, electronic surface props., photoluminesc. exam. 77−20901
GaAs epitaxial layers, photocond. high field effects on carrier capture and recomb. 77−43646
GaAs epitaxial layers, undoped, recomb. of non-equilib. carriers, steady-state photocond. 77−85357
GaAs, epitaxial layers, high density electron-hole plasma luminesc. 78−19537
GaAs epitaxial layers, substrate prep. effect on surface morphology 78−26780
p-GaAs epitaxial layers, electron-hole plasma, quantum effects in magnetoluminesc. 78−72591
GaAs epitaxial layers, characterisation Hall effect and Schottky diode profile meas. 78−91791
GaAs epitaxial layers, growth below 700°C electrophysical props. 79−1827
GaAs epitaxial layers, non-doped, from Ga-$AsCl_3$-H_2 system, TEM and RHEED study of micromorphology and defects 79−65340
GaAs, epitaxial layers, multiexciton complex bound to neutral acceptors, photoluminesc. obs. 79−87503
n-GaAs epitaxial layers, alloyed in As_2 beam, metal-Ga contacts 79−95495
GaAs epitaxial layers, polariton wave packet propag. in exciton reson. 80−2345
GaAs epitaxial layers, from mixed Ga solns., C solubility 80−15392
GaAs epitaxial layers, structural defect and conc. inhomogeneities influence on barrier diode I-V characts. 80−15602
GaAs, epitaxial layers, MBE grown, Hall mobilities, substrate temps. 80−20335
GaAs epitaxial layers, transient processes during doping for large conc. jumps. 80−39134
GaAs, epitaxial layers, grain boundaries, deep level transient spectroscopy study 80−49234
GaAs epitaxial layers, meas. of doping profiles *(Hungarian)* 80−70545
GaAs epitaxial layers, surface impurity gradients, Schottky barrier capacitance meas. 80−70782
GaAs, epitaxial layers, electron irrad. deep level trap energy depend. 80−80205
GaAs epitaxial layers, doping profile degradation due to ion implantation 80−84194
GaAs, epitaxial layers on conductive substrate, elec. characterisation 78−91790
GaAs epitaxial layers on polycryst. GaAs substrates, LPE growth characts. 80−75471
GaAs, epitaxial multilayer, electron irrad. defect study by transient capacitance 79−99241
GaAs epitaxial multilayer photocathode structures, TEM obs. of dislocations generated 80−100241
GaAs, epitaxial struct., nonuniform electroconductivity *(Russian)* 80−70753
GaAs, epitaxial structures, impurity profile 77−39610
GaAs epitaxial thin films with neg. electron affinity, photoelectron energy distrib. 80−100755
GaAs epitaxial tunnel diode pressure sensors 78−57975
n-GaAs epitaxial wafers, IR reflectance and elec. characts. 79−56293
GaAs, epitaxially grown (001), (111) and $(\bar{1}\bar{1}\bar{1})$ surfaces, LEED, AES, photoemission 78−38924
GaAs epitaxy, ultrathin film growth by cracking of organometallic compounds at 40 to 100 torr *(French)* 78−44023
GaAs, epitaxy by metallorganic and chloride depositions, defect characterisation at growth interface 80−59817
GaAs, epitaxy on semiinsulating GaAs, elec. props. of transitional layers rel. to growth conditions 77−15977
GaAs, epitaxy using TMG and AsH_3, chloride etching effect 78−76606
GaAs, equation of state 79−82310
GaAs, etch pit pattern made by light irradiated electrolytic etching 79−95012
GaAs etch solns. containing H_2O_2, correl. between etch and surface film characts. 80−71770

III-V semiconductors continued
GaAs, etchant, universal, multipurpose 78−53008
GaAs, etched, saucer-pit defect identification 78−43021
GaAs, etching by water vapour rate 80−16519
GaAs, etching soln. system H_3PO_4-H_2O_2-H_2O for MESFET fabrication 78−11379
GaAs, exam. as cladding material, for optical waveguides as cutoff polariser 78−55474
GaAs, exam. of magnetic susceptibility and absorption spectra 79−1778
GaAs, exchange interaction, analytical and nonanalytical parts, from polariton spectra in mag. fields 80−50367
GaAs, excitation by 2-4 KeV Ar^+ ions, electron energy spectra 80−11529
GaAs, excited, LO phonon effective temp., Raman meas. 80−20639
GaAs excited by HV pulses, stimulated emission and luminesc. obs. 79−59704
GaAs, excited luminescence, influence of IR illumination 80−76072
GaAs, exciton effects in photocond., photoluminesc. 80−96797
GaAs, exciton ground state and oscillatory absorption spectra in mag. fields, variational calc. 79−11071
n-GaAs, exciton luminescence, excitation intensity depend. 78−52554
GaAs, exciton motion under external electric field 79−56135
GaAs, exciton parameters near absorption edge 79−73448
GaAs, exciton quenching, obs. at room temp. using electrolyte electroreflectance 80−60546
GaAs, exciton-polariton reflectance spectra, exciton impact ionization and illum. intensity effects 79−42943
GaAs, excitonic polariton reson. interaction with LA phonons 78−60481
GaAs, excitonic spectra broadening, influence of phonons and impurities 77−1711
GaAs, excitons, diamond like semiconductor, variational calculation of binding energies 78−79938
GaAs, excitons, exciton-phonon interactions review, book contrib. 80−49624
GaAs, excitons detect., precision method 79−19906
GaAs, excitons in arbitrary mag. fields 80−96798
GaAs extrinsic photoconductor detectors, DC and microwave bias comparison 77−37998
GaAs FET, continuous growth of LPE double layers 78−64487
GaAs FET buffers, high purity LPE growth by sliding boat method *(Japanese)* 79−28955
GaAs FET double layer production, study by sliding boat method *(Japanese)* 79−66014
GaAs FET structure, sharp line photolum. spectra 78−72248
GaAs, facet formation by preferential etching in $1NH_4OH$-$2H_2O_2$ *(Japanese)* 78−44242
n-GaAs, far IR cyclotron emission 79−61226
GaAs, far IR photoconductivity 77−15893
n-GaAs, far IR propag. of surface EM waves 79−42615
GaAs, far IR transmission spectrum 78−4713
GaAs, fast neutron irrad., effect on cryst. lattice period, X-ray diffr. meas. 79−37743
p-GaAs, Fe-compensated, photocond. under strong excitation 77−15904
p-GaAs, field electron emission current-voltage charact. 80−45219
p-GaAs, field emission, role of surface electron states 78−2993
GaAs, field ion microscopy 78−19644
GaAs, field ionisation speed of shallow impurity levels, quantum-mechanical estimates 80−97412
GaAs, field penetration in FIM, band bending 79−87567
n-GaAs film, cond. mechanism in strong elec. field determ. 77−1430
GaAs film, electroreflectance effects 79−43055
GaAs film, epitaxial deposition from gas phase, transient processes, elec. cond. 77−16501
GaAs film, growth kinetics for step-cooling LPE technique 77−40395
GaAs film, MBE, growth and doping kinetics 77−76682
GaAs film, photovoltage anomaly investig., p-n-p microjunction model 77−4398
GaAs film, piezoelec. semicond., cascade capture of carriers by attractive impurity centres, cross sections 78−56157
GaAs film, plasma oxidation and oxide props 78−95825
GaAs film, RF sputtered, ESCA, surface chemistry suitability for photovolt. appl. 80−7476
GaAs, film, radiative relax. time, nonequilibrium carriers 78−84657
GaAs, film, selective anodisation, grain boundary edge passivation 79−11711
GaAs, film, solar cell on large grains 79−100528
GaAs film, vapour-grown, effect of gas-phase stoichiometry on deep levels 78−10393
GaAs, film and solar cell on graphite, struct. and elec. props. 80−2286
GaAs film on recrystallised Ge film, solar cell appl. 78−19671
GaAs film optical components, prep. by MBE using Si shadow masking technique 80−28358
GaAs film plasma oxidation process 77−77614
GaAs film solar cell fabrication, substrate requirements 78−11125
GaAs films for solar cells appl., deposition and characterisation 80−84853
GaAs, final state interactions in gain and absorpt. spectra of electron-hole liq. 78−43305
GaAs, fine struct. in energy derivative reflectance spectra 79−78705
GaAs, fine structure of lowest exciton state *(Russian)* 80−96801
GaAs foils preparation, transparent, for TEM, ion sputtering technique appl. *(Czech)* 80−16619
GaAs for MOSFETs, native oxides, annealing effects and inversion layer mobilities 78−6452
GaAs, forbidden Raman scatt. by LO phonons 78−64367
GaAs forward-biased diode structures, numerical anal. based on direct gap semicond. 79−65542
GaAs, Franz-Keldysh effect modulator parameters for integrated optics systems 80−106624
GaAs, free-carrier impact ionisation, orientation depend. rel. to cond. band 77−76836
n-GaAs, freq. depend. of effective temp. of hot carriers 79−11135
GaAs, fundamental absorption band, influence of phonons on long-wavelength wing 79−69857
GaAs, gain spectrum of electron-hole liquid 80−66279
GaAs, gamma and electron irrad. defect formation depend. on interface, luminescence study 80−34057
GaAs, gamma-irrad., form. of defects, contrib. of inelastic nucl. reactions *(Russian)* 77−27905
GaAs, gas-phase epitaxy, mass exchange during 79−78901
GaAs, gas-phase epitaxy, step stopping centre form. kinetics 80−65407

III-V semiconductors continued
GaAs, grain boundaries investigation using DLTS techniques, photovoltaic material appls. 80−92539
GaAs, ground state of electron subsystem, quasimolecular model 79−69055
GaAs grown by VPE using organometallic method, deep trap levels 80−10923
GaAs, grown-in dislocation density, impurity effect 78−51543
GaAs growth dual-bubbler CVD system, charact., for MESFET applics. 78−6856
GaAs, growth of noncrystalline Si_3N_4 layers by CVD for encapsulation 79−19994
GaAs, Gunn device, planar, domain dissolution for wide range of doping 77−8109
GaAs, Gunn diode, peak electron vel. and threshold field temp. depend. 77−32075
GaAs, Gunn diode, velocity-field charact. at 35 GHz, impurity conc. var. 77−85306
GaAs Gunn diodes, microwave oscill. generation at two freqs. 80−65614
GaAs Gunn diodes, population inversion condition 77−77251
GaAs Gunn diodes, static domain form. 77−8111
GaAs Gunn domain appearance and movement, SEM obs. 77−80785
GaAs, Gunn effect, carrier generation-recomb. processes 79−38080
GaAs, Gunn effect, equal-areas rule 80−107798
GaAs, Gunn oscillator, magnetoresist. meas. of mobility and noise 77−62948
GaAs, Γ_6^c-L_6^c-X_6^c cond. band ordering, velocity field charact., Monte Carlo calcs. 78−18957
GaAs, γ- and electron irradiation, influence on recomb. charact. near surface 80−71478
GaAs, H ion bombard., carrier removal effects 80−92542
GaAs, H^+ irradiation, effect on electrical props. 80−65567
n-GaAs, H-like impurities photocond., mag. field effect 79−82634
GaAs, Hall effect sensor for mag. fields up to 23 T 77−10066
n-GaAs, heat treated, origin of 1.41 eV emission band, photolum. expt. 78−72579
n-GaAs, heat treatment effect on electron traps 78−6396
GaAs, heavily doped, electron effective mass, Kane equation calcs. 79−77989
GaAs, heavily doped, fluctuation-induced tunnelling cond. 80−65516
n-GaAs, heavily doped, impurity-band cond., DC cond., Hall mobility, and magnetoresist. meas. 80−49733
n-GaAs, heavily doped, non-linear extrinsic luminesc., role of Auger recombination 79−52010
p-GaAs, heavily doped, self energy of phonons 80−44277
GaAs, heavily doped, strongly compensated, hopping cond. 79−47180
n-GaAs, heavily doped, test of cond. band edge random fluctuations by MCD 77−63438
GaAs, heavily doped electron mobility due to scatt. by pot. fluctuations 80−2387
GaAs heavily doped n-type layers, formation by multiple ion implantation 80−59491
GaAs, heavily oxidised photoemission escape depth for electrons, energy depend. 77−69969
GaAs, heavily-doped, band gap, magnetoabsorpt. oscills. obs. 78−18960
n-GaAs, heavily-doped, with Gaussian band tails, modification of Einstein relation 80−80270
GaAs, heavy metal migration, ESCA study *(French)* 78−75885
GaAs, heteroepitaxial layers on Si substrates by LPE 79−1832
GaAs, heterogeneous reactions in chemical transport by water vapour, growth kinetics of epitaxial layers 77−16500
GaAs heterojunction diode as light source for fibre optical communication 80−58653
GaAs heterojunction laser, origin of dislocation climb during laser operation 77−51380
GaAs heterolaser, active layer, photoluminesc., temp. depend. *(Russian)* 79−10310
pnpn-GaAs heterostructure laser, barrier controlled low threshold 77−61966
GaAs, high performance refl. NEA photocathode 77−48303
GaAs, high press. electron transport props., three band model 80−15516
GaAs, high resist., linear electroabsorpt., charact., valence band splitting 77−44018
GaAs high speed avalanche photodiode design 78−8446
n-GaAs, high temp. mobility anal. in three-valley (Γ_6^c-L_6^c-X_6^c) model 79−99544
GaAs, high temp. thermodynamic data, quantitative fits to liquidus line 77−63637
GaAs, high-energy ion layer implanted, layer thickness and refr. indices meas. 77−24837
GaAs, high-purity, residual donors, ionisation energies determ. 78−6333
GaAs, highly deformed samples, absence of dislocation-induced luminescence 79−4835
GaAs, highly doped, behaviour of buried O_2 implanted layers 80−59499
GaAs, highly excited, LO phonon Raman lineshape 79−78683
GaAs, highly transparent semicond. crysts., multiphonon IR absorpt. 78−10885
GaAs, highly transparent semicond., multiphonon IR absorpt. 78−60461
GaAs, hole effective mass, press. depend., theory and tunnelling expts. 78−75986
GaAs, holes optical orientation, luminesc. 80−25452
p-GaAs hologram recording, photochem. etching control 80−28179
GaAs homoepitaxial interface, thermal degradation 77−11988
GaAs, homogeneity region calc. 80−92681
GaAs homojunction LED signal source for fibre-optic communication 78−1413
GaAs homojunction LED, mechanical stress induced degradation 80−2860
GaAs homojunction lasers active layer in steady state, thermal conditions *(Polish)* 77−14717
GaAs homojunction laser diodes, in transient state conditions, analysis of junction temp. rise 77−38889
GaAs homojunction rib waveguide directional coupler switch 80−69554
GaAs homojunction solar cells, large-grained, passivation method to improve open-circuit voltage 80−94070
GaAs, hot carrier impact ionisation, band struct. depend. 78−30934
n-GaAs, hot electron distrib. function with LO phonon kink, photoluminesc. 79−19925
GaAs, hot electron distrib. function, inter-carrier scatt. effect 80−2395
n-GaAs, hot electron magnetophonon resonance, Fourier anal. 80−54718

III-V semiconductors continued
GaAs, hot electrons and exciton-electron collision under external elec. field 78−43928
GaAs hot electrons drift rate/field strength characteristic in microwave fields *(German)* 78−43430
p-GaAs, hot luminesc. of semicond. with GaAs band struct. 78−39601
GaAs, hot photoluminescence spectrum, polarisation depend. 78−31254
GaAs, hot photoluminescence depolarisation in mag. field, 0.4 eV energy state electron lifetime *(Russian)* 80−16086
GaAs, hot photoluminescence spectrum on pumping across the L-valley *(Russian)* 80−103984
n-GaAs, hybrid mode instability 77−80800
n- GaAs, hybrid-hybrid mode interaction in crossed elec. and mag. fields 78−51997
GaAs, hydride VPE growth for FETs, and characterisation 78−27407
GaAs hydrothermal oxidation kinetics, exam. 80−40566
GaAs, IR absorption of isolated impurities 77−12407
GaAs, IR field induced Gunn oscills. 78−30956
n-GaAs, IR luminesc. emitted by travelling acoustoelec. domains 78−27329
n-GaAs, IR luminescence from acoustoelectric domains 77−55822
n-GaAs, IR luminescence of acoustoelectric domains 78−31258
p-GaAs IR plasma reflectivity spectra calc., rel. to carrier conc. 78−52511
GaAs, IR thermometry, semiconductor material temperature measurement *(Spanish)* 80−47062
n-GaAs, IR transmission, cond. variations effects 79−15158
GaAs, ideal vacancy, electronic struct., tight-binding calc. 79−4529
GaAs, illuminated, carrier lifetime profile, depth depend. 78−68036
GaAs, image emission platelet laser, for optical information processing 77−58268
GaAs, impact ionisation, electron band struct. effects obs. by temp. tuning 77−85232
n-GaAs, impact ionisation initiated by acoustoelectric effect 78−52038
GaAs, impact ionisation rates for electrons and holes, photocarrier multiplication obs. 78−87995
GaAs, impact ionisation rates, temp. depend. 79−38077
GaAs, impact ionisation of excitons 79−38079
GaAs, implantation disorder, flux and fluence depend., electrorefl. expts. 78−83833
GaAs, implantation of Si, Al, Hf, Ta into InP and GaAs, form. of protective oxide 78−79622
n-GaAs, implanted, IR refl. meas. of free carrier parameters 77−36244
GaAs, implanted p-n junction form. using laser pulse annealing 77−15946
GaAs, impurity anal. by photoelectric spectroscopy, review 77−24584
GaAs, impurity anal. by photoluminescence *(Japanese)* 77−24888
p-GaAs, impurity band Hall mobility 80−70730
GaAs, impurity centres ionis. by Auger electrons, carrier relax. *(Russian)* 79−51594
GaAs, impurity density of states, effect of doping and injections, models and calc. method 79−73466
GaAs, impurity distribs. by chemical methods 77−43237
GaAs, impurity effect on grown-in dislocation density *(Japanese)* 78−6063
GaAs, impurity gettering by ion implantation damage 77−11579
GaAs, impurity scattering of current carriers in quantizing mag. field 78−51954
GaAs, impurity states and core excitons, binding energies, perturb. theory 80−49659
GaAs, impurity-point defect complexes 78−6097
n-GaAs in DMF solns., electrochem., photoelectrochem., redox. pot. determ. 79−96322
GaAs, in MIS system, nature of surface carrier depletion layers 77−1469
GaAs, inertia of intervalley redistribution of electrons, meas. of V(E) relationships by microwave method 79−82621
p-GaAs, influence of light holes on transport props. 77−4367
GaAs, influence of radiation damage on diffusion of implanted P and Kr atoms 78−6082
GaAs, influence of strong transverse mag. field on Gunn effect 80−6854
n-GaAs, influence of uniaxial stress on low field resist. 78−87976
GaAs injection laser, active region effect on single-freq. stimulated emission conditions 80−9884
GaAs injection laser, intensified luminesc. *(Russian)* 78−90416
GaAs injection laser, output instabilities related to optical gain and lasing conditions 80−1203
GaAs injection laser, single heterostruct., mode competition effects, tuning characts. 80−48255
GaAs, injection laser with localisation of injection current, design and characts. 80−106543
GaAs injection lasers, longitudinal mode spectrum, effect of carrier diffusion 78−71099
GaAs injection lasers, spectral output, influence of diffusion and spontaneous emission 79−13965
GaAs injection lasers, amplified luminesc. 80−2824
GaAs injection lasers, direct modulation enhancement effect of HF noise 80−83608
GaAs, injection lasers with filament, junction current and carrier-conc. profiles *(Chinese)* 79−50292
GaAs injection photodiode IR radiometer 79−75597
GaAs, insulating, generation of far IR radiation by freq. mixing 79−50347
GaAs integrated multijunction photodetector with high output voltage 79−6178
GaAs integrated optical circuits by wet chemical etching 79−32092
GaAs integrated optical communication components, overview 80−79012
GaAs, interaction of excitons with charged impurities 78−43906
GaAs, interband Faraday rotation, Roth theory calcs. 77−52046
n-GaAs, interband transition times, luminesc. depolarisation obs. *(Russian)* 79−33831
GaAs, interband tunnel current, influence of press. 77−76910
GaAs interface with anodic and thermal oxides, comparison of AES and ESCA 78−95980
GaAs interface with oxide, photoemission obs. of energy levels induced by adsorpt. 80−93000
GaAs, interference grating blazed by ion-beam erosion 80−1302
GaAs, interimpurity interaction effect on distrib. profiles of impurities diffusing simultaneously 77−76451
p-GaAs, intervalence-band transitions, saturation, theory 80−75997

III-V semiconductors continued
GaAs, intervalley electron transfer, drift velocity and diffusion coefficient 80−39594
GaAs, intervalley electron-electron scattering effect on optical transitions 80−108267
GaAs, intracavity modulation of polarization direction of CO_2 radiation 80−102744
GaAs, intrinsic, on degenerate n-Ge, surface polaritons, hydrodynamical model 80−6752
n-GaAs, intrinsic avalanche response time, orientation depend. 79−51587
n-GaAs, intrinsic emission intensity, role of local centres in determ. of conc. depend. 78−39599
n-GaAs, intrinsic luminescence intensity, effect of 0.94, 1.0, 1.2 and 1.3 eV radiative centres 78−23517
GaAs, intrinsic surface gratings, low-angle X-ray diffr. obs. 77−85035
n-GaAs, inverted hot electron states and negative cond. *(Russian)* 77−43612
GaAs, ion beam induced annealing effects 80−59530
GaAs, ion bombarded, defect distrib., photolum. meas. 77−20920
GaAs, ion bombardment by alkali metal sputter ion source *(Japanese)* 79−54734
GaAs, ion damage, TEM study of laser annealing 80−88215
GaAs, ion etching, effects on optical props. and lattice disorder 78−83122
GaAs, ion implantation, survey 77−76448
GaAs, ion implantation, review 78−6080
GaAs, ion implantation, range distrib. calc. 79−55760
GaAs, ion implantation, disordered layer physical props. 79−77624
GaAs, ion implantation, trends 80−39132
GaAs ion implantation, semiinsulating materials, role of substrate in elec. props. 80−59488
GaAs ion implantation doping, developments 77−59028
GaAs, ion implantation damage, TEM exam. of variation with ion species and stoichiometry 78−59827
GaAs ion implantation parameter determ. by microwave contactless mobility meas. 78−10527
GaAs, ion implantation review 80−88184
GaAs, ion implantation with proximity cap annealing 80−24475
GaAs, ion implanted, capless annealed and dielectrically annealed, comparison of doping profiles 80−100278
GaAs, ion implanted, diffusion of Zn and Ag, profiles 80−24681
GaAs, ion implanted, effect of channelling on elec. props. 77−8114
GaAs, ion implanted, encapsulation surface effects 77−1883
GaAs, ion implanted, laser annealing 79−69124
GaAs, ion implanted, laser induced damage and recrystallisation by freq.-doubled Nd:YAG laser 79−73197
GaAs, ion implanted, laser pulse annealing 80−19825
GaAs, ion implanted, laser induced recrystn. and damage, ion backscatt. and Raman scatt. obs. 80−49248
GaAs, ion implanted, laser annealing 80−107296
GaAs, ion implanted, mode-locked Nd:YAG laser annealing, recrystn. 80−19817
GaAs, ion implanted, ruby laser pulse effects 79−69125
GaAs, ion implanted and laser-annealed, photoacoustic meas. 80−47117
n-GaAs, ion implanted films, optical and luminesc. props. 80−60699
GaAs, ion irradiated, Auger electron spectra struct., possible surface diagnostic methods 79−69946
GaAs, ion-bombarded, energy band struct., electrorefl. obs. 79−19517
GaAs, ion-implantation induced damage profile, ellipsometric study, annealing 80−103400
GaAs, ion-implanted, capless anneal, effect of As partial press. 80−29038
GaAs, ion-implanted, laser pulse annealing of amorphous surface layer, TEM 80−55436
GaAs, ion-implanted, laser pulse annealing, TEM and channelling study 80−100264
GaAs, ion-implanted layers, close contact capless annealing, elec. props. 80−84192
GaAs, ion-implanted semiconductor, annealing, crystallisation, laser pulse energy depend. 78−34528
GaAs ion-irradiated layers switching conduction 78−34868
GaAs, irradiated with fast neutrons, IR vibrational absorpt. 78−75776
GaAs, isolated impurities, local mode sideband IR absorption and second harmonic intensity calc. 77−85707
GaAs, junction laser, spectral hole burning 79−50291
GaAs junction laser long time delays, internal Q-switching 77−79822
GaAs, k-linear coupling, E_1' transitions 78−91583
GaAs, LEC growth using pyrolytic BN crucibles 78−6841
GaAs LED, minority carrier lifetime determ. 79−42560
GaAs LED, optimum p-n junction depth, photoluminesc. method 79−4598
GaAs LED absorption effect on freq. characteristic 79−8189
GaAs, LMTO self consistent band struct. calc. 80−20078
GaAs, LPE, charge carrier conc. distrib. *(Russian)* 78−52694
GaAs, LPE, deep levels rel. to growth conditions 79−28314
n-GaAs, LPE, deep trapping centre characterisation by Hall and photo-Hall meas. 80−88578
GaAs, LPE, dislocations obs. by etching 79−95284
GaAs, LPE, gaseous impurity source and effect on purity 79−28959
GaAs, LPE, growth mechanism and kinetics 78−34726
n-GaAs, LPE, impurity compensation photolum. and free carrier conc. meas. 77−62558
GaAs, LPE, residual impurities and deep levels, FET fabrication 79−28964
GaAs, LPE, smooth, thin layers on nominally oriented substrate 78−44030
GaAs, LPE, temperature instability effect, report 80−66446
GaAs LPE (001) layer, etching by molten KOH 78−34515
GaAs LPE buffer layers for MESFET appls. 80−29887
GaAs LPE film, thickness comparison with $Ga_{1-x}Al_xAs$ for layers grown by linear cooling 78−87892
GaAs LPE from Ga soln., carrier conc., growth condition depend. 80−71584
GaAs, LPE growth, electric current controlled, on n^+ and semi-insulating substrates 77−73240
GaAs, LPE growth, wave morphologies on surface 77−40396
GaAs, LPE growth 78−18924
GaAs, LPE growth from supercooled soln., thickness uniformity 80−54547
GaAs, LPE growth of high purity layers by sliding boat method 78−76610

III-V semiconductors continued
GaAs, LPE growth on O-implanted GaAs substrates, surface morphology 77−28732
GaAs, LPE growth on O-implanted GaAs substrate, elec. props. 78−2592
GaAs, LPE growth rate calc., model of LPE growth 79−19485
GaAs, LPE growth surface, singular instabilities 77−24969
GaAs, LPE in graphite boat, total ionised impurity density 77−12550
GaAs LPE in situ etchback calibration 79−83114
GaAs, LPE layer, deep levels, photocapacitance obs. 77−15790
GaAs, LPE layers, ambient O_2 effect on defects and elec. props. 77−76683
GaAs LPE layers, deep levels by photocapacitance and related techniques 78−6334
GaAs LPE layers, dopant tracing of terrace growth 78−75948
GaAs LPE layers, effect of baking on mobility and doping conc. 79−99641
GaAs, LPE layers, outdiffusion of recomb. centres from substrate during growth 80−39466
GaAs, LPE layers, screw dislocations, optical microscope obs. 77−35561
GaAs, LPE layers, voids and depressions in facet and terrace growth 78−38974
GaAs LPE layers, X-ray topographic studies of defects 77−62772
GaAs, LPE layers, X-ray topographic exam. of defects 78−30844
GaAs LPE on polycrystalline Mo 79−43157
GaAs, LPE with $AsCl_3$-saturated Ga/As solns. 78−63953
n-GaAs, Landau level lifetimes for electrons 79−87112
GaAs, large dislocation-free single crystal growth 80−25550
GaAs large-grained solar cell film recrystallisation 79−38737
GaAs laser, broadening mechanism, limitations to single mode power emission 79−961
GaAs, laser, electron-beam-pumped, transient waveguide effects and lasing time delays 78−37882
GaAs laser, photopumping of quantum well heterostruct. $Al_xGa_{1-x}As$-GaAs-$Al_xGa_{1-x}As$ 79−22956
GaAs laser, refractive-index profile and resonant modes 79−86179
GaAs laser, spectral depend. of gain calc. 77−23677
GaAs laser, spontaneous emission reduction at lasing with long delays 79−64226
GaAs laser, surface temp. distrib. *(Russian)* 78−74909
GaAs, laser, transverse modes, mirror reflectivity dependence 79−68404
GaAs laser, wavelength depend. of gain saturation 78−1229
GaAs, laser alloying of Au-Ge ohmic contacts 79−73583
GaAs, laser annealed, donor implanted, elec. props. 79−4556
GaAs, laser annealed, Ga precipitation, Rutherford backscattering and TEM study 79−79127
GaAs, laser annealing, optical refl. meas. of melted layer 79−78796
GaAs, laser annealing after ion implantation, temp. distrib. 80−54265
GaAs, laser annealing of ion bombardment damage 80−25502
GaAs laser array, integrated, Si substrate package fabrication 79−18555
GaAs laser array source package, with collimating lens and fibre light-guides 77−84007
GaAs laser arrays, Si substrate packaged, thermal performance and limitations 78−46613
n-GaAs, laser beam self-focusing in mag. field, carrier mechanism 78−33788
GaAs laser convex micromirror mode control 79−36920
GaAs, laser damage statistics rel. to structural defect statistics 80−91829
GaAs laser diode, fabrication and characts. *(Korean)* 79−7144
GaAs laser diode, SEM electron beam induced current study, contamination effect 79−43773
GaAs laser diode, spontaneous emission reduction 80−95904
GaAs laser diodes, absorption edge effects on temp. depend. of threshold currents 77−58328
GaAs laser diodes for optical communication transmission *(German)* 80−28252
GaAs laser facsimile printer 80−30207
GaAs, laser heating of lightly damaged material, carrier diffusion effect 80−84809
GaAs, laser irradiated, origin of periodic surface struct. 78−91513
GaAs, laser irradiation effects, capacitance spectra 79−99987
GaAs laser material, secondary dislocation climb during optical excitation 78−75672
GaAs laser reliability, protective facet coatings 79−81452
GaAs, laser reordering of implanted amorphous layers 78−43042
GaAs laser source package for multichannel optical links 78−1266
GaAs laser with integrated interferometric reflectors 77−65642
GaAs, laser-annealed ohmic contacts for microwave devices 79−73584
GaAs laser-annealing behaviour, Si_3N_4 encapsulation effect forming n-type layers 79−79131
GaAs, laser-induced bulk breakdown and free carrier generation, photocond. meas. 80−35018
GaAs, laser-induced microscopic etching 80−76379
GaAs, laser-induced recrystallisation and damage of ion-implanted amorphous samples 79−47557
GaAs lasers, at room temp., modulation at X-band frequencies 78−87079
GaAs lasers, comments on host dispersion in ultra-short pulse generation 80−64024
GaAs, lattice dynamics, phonon freq., bond bending force model calcs. 80−70335
n-GaAs, lattice scatt. identified as cause of 1/f noise 78−64074
GaAs, lattice thermal cond. from three phonon scatt. relax. rate 78−51755
GaAs, lattice thermal cond. at high temp. 79−90838
GaAs, lattice thermal cond., point defect scatt. relax. rate role 80−70478
GaAs, lattice vibration, thermal expansion and pressure effect 80−39233
n-GaAs layer, VPE, influence of growth conditions on incorporation of deep levels 77−4310
GaAs layer grown by MBE, directional coupler switch 79−76878
GaAs, layer growth by electroepitaxy, thickness profiles 79−4486
GaAs, layer structures revealed by decoration method and electron microscopy 77−27902
GaAs layers, electroepitaxy and thermal LPE growth, defect struct. and electronic characts. 80−2290
GaAs layers, from gas phase, impurity influence on growth micromechanism 80−45237
GaAs layers, grown by electroepitaxy and LPE, surface morphology 79−19478

III-V semiconductors continued
GaAs layers, heteroepitaxy, grown on Si and Ge from multiple component solns. *(Russian)* 78−15319
GaAs layers, high resistivity, growth for microwave device appl. 79−100056
GaAs layers, LPE from Au-Ge-Ni melts, elec. props. of Ni/Au-Ge/GaAs contacts obs. 77−77437
GaAs layers, LPE growth, graphite boat construction 78−31348
GaAs layers and p-n junctions grown by current-controlled LPE, elec. characts. 78−6436
n-GaAs layers with SiO_2 overlayer, ohmic props. of Au-Ge contacts 80−2467
GaAs, light scatt. spectra, interference effects 79−82977
GaAs, lightly doped, p-n junctions, forward branches of current-voltage characts. 79−7890
GaAs, lightly doped, p-n structure, parameters of nonequilib. carriers, transient photoeffect method 79−11143
n-GaAs, limiting freq. of Gunn effect in polyharmonic LSA mode 80−6856
p-GaAs, linear polarisation of hot photoluminescence 79−38661
GaAs, liq., semicond.-metal transition at high temp. and press. 77−51784
GaAs, liquid-phase electroepitaxial growth kinetics, Peltier effect and solute electromigration 79−42401
n-GaAs, longitudinal magnetophonon reson. and Fourier anal. 79−4569
n-GaAs, low energy photolum., 77K, deep centre obs. 77−69877
n-GaAs, low temp. field generation of carriers, liberation from surface states 80−92959
GaAs, low temp. gamma irrad., donor-acceptor pair formation 79−69158
GaAs, low temp. plasma oxidation and MIS struct. characts. 78−31546
GaAs, low temp. selective Zn diffusion process using anodic oxides 78−47399
GaAs, low-current-threshold strip-buried-heterostructure lasers with self-aligned current injection stripes 79−72581
GaAs, low-field study of p^+nn^+ or p^+pn^+ structs. on forward direction 80−60072
GaAs, low-temp. absorption spectrum in presence of optical pumping 78−15188
p-GaAs, low-temp. resist. thermometers 78−223
GaAs, lower cond. band struct. 78−6271
GaAs, lower conduction band minima, ordering and props. 77−28114
GaAs luminesc. emitted as a result of carrier heating 77−52185
GaAs, luminesc. emitted by deep centres, illumination-induced change in internal quantum efficiency 79−91495
GaAs, luminescence by laser excitation, photocarrier thermalisation and polariton kinetics 77−66533
GaAs, luminescence due to deep centres, annealing effect on quantum efficiency 77−55825
GaAs, luminescence during streamer discharge *(Russian)* 77−55835
n-GaAs, luminescence emitted from deep centres, γ-irrad. induced changes in internal quantum efficiency 80−20701
GaAs, luminescence emitted from deep centres, plastic deform. effect on internal quantum efficiency 80−60672
n-GaAs, MBE, correl. between electron traps and growth processes 80−65387
GaAs, MBE, growth temp. depend. and characts. 79−28946
GaAs, MBE, process anal. and appl. *(French)* 79−56937
GaAs, MBE, SnTe source of donor impurities 79−95035
GaAs, MBE, surface reaction steps 79−77941
GaAs, MBE, technology and epitaxial layers props. 79−33945
GaAs, MBE, undoped, growth and characterisation 80−10836
GaAs, MBE (001) layers, work function meas. 80−49870
GaAs, MBE and film emission deposition of Al and Au films, comparative study 79−87016
GaAs MBE epilayers, photoluminesc. and elec. characterisation 80−11500
p-GaAs, MBE grown, As_2 and As_4 effects on photolum. 80−103974
GaAs, MBE grown film, in situ surface characterisation by RHEED, SIMS and AES 77−43410
GaAs MBE growth, deep levels effect on electron and hole trap densities 80−49652
GaAs MBE layer, Al_2O_3 film growth 78−39706
GaAs, MBE layers, H_2 effect on residual impurities, photolum. obs. and elec. characts. 79−47636
GaAs, MBE of autoepitaxial films, temp. range for growth, RHEED monitoring 78−44025
GaAs, MBE of doped cryst., thermodynamics and kinetics interplay 80−70144
GaAs MBE physical characteristics and applications *(German)* 79−7618
GaAs, MBE prep., device props. 77−77417
GaAs, MBE with ionised dopant 77−40338
GaAs MESFET, deep trapping effects at GaAs-GaAs:Cr interface 78−72245
GaAs MESFET layers, low temp. VPE growth by halide process 77−90279
GaAs, MESFET structure, buffered, LPE growth 80−40271
GaAs MESFET struct., high-resolution deep level meas., photo-FET method 80−44531
GaAs MIS capacitor, transient capacitance and C-V characts. 78−95374
GaAs MIS devices, diffusion, chemical reactions, contamination, AES and SIMS 80−72066
GaAs MIS devices, multidielectrics using composition-graded $Al_xGa_{1-x}As$ and oxidised AlAs 79−65333
GaAs MIS diodes, interface states determ., by deep-level transient spectroscopy *(Japanese)* 80−49917
GaAs MIS dynamic optically controlled transparencies 78−90523
GaAs MIS Schottky barrier diodes, radiation effects 79−24078
GaAs MIS solar cells, effects of thin oxide layers on characts. 80−89624
GaAs MIS struct., appl. of $Al_xGa_{1-x}As$:O as insulating layer 78−64115
GaAs MIS struct., elec. props., effect of interface As domains 78−88032
GaAs, MIS struct., with natural anodic oxide elec. props. 79−99634
n-GaAs MIS structs., native oxide, effect on interface props. and removal by sputter etching 79−11228
GaAs MIS structs., nitride-based passivation for reduced surface state density 80−16537
GaAs MIS structs., review 78−95372
GaAs MIS structure using LaF_3 insulator 79−78182

III-V semiconductors continued
GaAs, MIS structures, dielec. and interfacial characts. appl. to microwave MISFETs 79−60933
GaAs, MM wave guiding and control by surface plasmons 80−103713
GaAs MOS and Schottky systems, electromodulated reabsorption of luminesc. 79−15524
GaAs MOS capacitor fabrication and transient response for minority carrier lifetime meas. 79−47103
In-GaAs, MOS capacitor struct., elec. props., annealing effects 80−34519
p-GaAs MOS capacitors, anodized, C-V characts., surface pot. 79−11227
GaAs MOS device, new method of fabrication 78−47872
GaAs MOS diodes, interface states, deep-level transient spectroscopy 80−44727
GaAs MOS solar cells by anodisation in active region 80−101107
GaAs, MOS struct. with Al_2O_3 ground by mol. beam reaction under UV excitation 79−60927
GaAs MOS structure, props. of surface carriers 77−20453
GaAs MOS structure, small signal admittance study 80−2478
GaAs MOS structures, props. of capacitance transient 80−25013
GaAs MOS structures, leakage current for anodic oxide layers, space charge trapping effects 80−60091
GaAs MOS structures, native oxide growth by wet anodisation 80−70832
GaAs MOS system, elec. meas. interpretation 78−43484
GaAs MOS system, surface and interface exam. by derivative surface spectroscopy 79−82674
GaAs, magnetic freezeout in ultraquantum limit 78−76017
n-GaAs, magnetised semiconductor, coupled LO phonon-plasmon modes inelastic neutron scatt. 79−73459
n-GaAs, magneto-impurity effect, review 79−91081
GaAs, magnetoelectric susceptibility, nonlinear, three-dimens. model 80−39845
p-GaAs, magnetoluminesc. of cond. band to acceptor transition 77−1716
n-GaAs, magnetophonon resonance, Fourier anal. 79−91080
GaAs, magnetoplasma reflectivity effects, difference method *(German)* 77−12363
GaAs, manifestation of local vibrs. of dislocations in IR spectra 78−88339
GaAs, maximum electric field in high-field domain in Gunn devices 78−79996
n-GaAs, mechanical polishing damage effect on IR refl. and ATR spectra 77−20848
n-GaAs, mechanism of cyclotron reson. induced cond. 78−43396
GaAs, melt grown, improve elec. and luminesc. props. after short time heat treatment 77−63452
n-GaAs, melt-grown, stoichiometry, photolum. obs. 78−72583
GaAs, melted zone displacement by current *(Russian)* 78−26727
n-GaAs, metal filmed photoelectrochemical cell, energy conversion characts. 80−101118
n-GaAs, metal-insulator transition in impurity band induced by loss of dimension 77−47732
n-GaAs, metal-insulator transition in impurity band induced by mag. field and loss of dimens. 78−52042
GaAs microcharacterisation for device appls. 80−10922
GaAs, microscopic mechanism of film growth from non-condensed phases, kinetic anal. 80−54565
n-GaAs, microwave biased, fast rise-time modulation of 337 μm radiation 77−54794
GaAs microwave devices and their use for generation and freq. conversion of microwave oscillations 80−15534
GaAs, migration of liquid inclusions, effect of DC current and temp. 77−7910
GaAs, minority carrier diffusion length, reabsorbed radiation effect 77−28191
GaAs, minority carrier diffusion length, Schottky barriers, electron bombard. investigation 78−68037
GaAs, minority carrier diffusion lengths, contact metal effects 78−72260
GaAs minority carrier diffusion lengths in semicond. SEM meas. interpretation 78−80002
GaAs, minority carrier diffusion length, photon absorption reemission 79−87109
p-GaAs, minority carrier diffusion lengths, photoluminesce meas. 80−29807
GaAs, minority carrier lifetime at high temp., solar cell performance appl. 80−24947
p-GaAs, minority carrier mobility calcs., including screening, scattering mechanisms 79−99545
n-GaAs, minority deep level investig. by new optical method 78−6331
GaAs, mobility of hot electrons in mag. field 77−4368
n-GaAs, model describing removal and scattering of charge carriers by defect clusters 78−76069
GaAs, model relating elec. props. to impurity concs. 77−51697
GaAs, modification of Zn diffusion profiles by proton irrad. 78−43043
GaAs, molecular beam epitaxy for superlattices control 80−2283
GaAs, monocrystalline, lateral definition, prep. by MBE 80−108357
GaAs, multilayer epitaxial growth with Sn doping 77−47690
GaAs, multilayer liquid phase epitaxy, transition to faceting 80−96750
GaAs multilayer with abrupt carrier conc. profile, vapour growth technique 78−11123
GaAs, multiphonon nonradiative transition rate for electrons in semicond. and insulators 78−60503
n^+-GaAs, multiple energy proton bombard. effects on elec. characts. 77−39853
GaAs, multiple insulator layers studied by Auger anal. 79−83345
GaAs, multiple layer LPE growth by controlled supercooling of Ga soln. 77−77429
GaAs, N_2 laser pumped under appl. elec. field, gain anisotropy 77−61958
GaAs, n- and p-type, velocities of α- and β-dislocations, double-etch method 77−51382
GaAs, n^+-n-n^+ and n^+-p^--n^+ structs., ballistic electron motion at room temp. 80−80360
GaAs n^+-p^--n^+ ballistic structure 80−80359
GaAs n^+2n^+ epitaxial multilayers, carrier conc. from Fourier transform anal. of magnetoresist. signal 79−38205
GaAs n-i-n junction, photoelec. props. investig., 77 to 300K 77−28248
GaAs, n-i-n junctions, simulation of long-term relax. of nonequilib. conductivity 79−38156
III-V semiconductors continued
GaAs, n-i-n three layer struct., transmitted phonon effect in strong mag. fields 77−20341
GaAs n-n^+ epitaxial structure for CW microwave electroacoustic amplifier 78−59235
GaAs n-p solar cells, potential for high efficiencies concentrator applications 79−100534
GaAs n-p solar cells, theoretical perform. of multi-layer grid patterns 80−55846
GaAs n-type, computer study of conditions for absolute negative resistance 77−4358
GaAs, n-type layers, heavily doped, formation by multiple ion implantation 80−88187
GaAs, NMR under optical pumping conditions 80−25253
GaAs narrow-channel double-current-confinement CSP lasers, current distrib. effect on performance 80−58539
GaAs, native vacancies study using positron lifetime technique 79−83052
n-GaAs, nature of low temp. field generation of carriers, liberation from surface states 80−92960
GaAs, nearly-cubic, acceptor ground state calc. 77−28113
GaAs, negative differential mobility and geometrical magnetoresist. calc. 77−43624
GaAs, negative electron affinity, optically pumped, depolarization of emitted photoelectrons 79−8223
GaAs negative electron affinity cold cathode 79−87558
n-GaAs, neutron irrad. and thermally induced defects, annealing stages 77−51409
GaAs, neutron irradiated, change in lattice period during annealing 77−55307
GaAs, neutron transmutation doping, shallow donors magneto-optical effects 80−20255
GaAs, nitridation, following oxidation, surface and contact props. of GaN produced 77−20436
GaAs, noise calc. using Monte-Carlo method 80−75575
n-GaAs, non-Maxwellian electron distribution function, from electric field-depend. photolum. spectrum 79−11450
n-GaAs, non-equilibrium acoustic phonon generation by hot electrons 80−6477
n-GaAs nonalloyed ohmic contacts of TiPtAu by pulse-electron-beam annealed Se implants 80−2466
GaAs, noncentrosymmetric cubic cryst., electrooptic effect 79−69812
GaAs, nonlinear electro-optical susceptibility, coupled anharmonic oscill. model 80−2723
GaAs, nonlinear extrinsic luminescence 78−84645
GaAs, nonlinear light absorpt., photoluminesc. meas. 77−66528
GaAs, nonlinear light absorption, effect of deep impurity levels 77−77259
GaAs, nonlinear optical susceptibility and dispersion, electro-optic meas. 77−23707
GaAs, nonlinear refractive index dispersion at helium temp. 78−2820
GaAs, nonradiative capture and recomb. by multiphonon emission 77−43533
GaAs, nonradiative capture, direct obs. of phonons 78−30976
GaAs, nonradiative multiphnon carrier-capture cross sections of deep traps, intermediate-temp. depend. 78−43414
GaAs, nucl. spin levels, elec. induced shifts 80−34408
GaAs, O_2 chemisorption 79−95466
GaAs, O^+ implantation, effect on LPE growth and elec. props. 80−24477
GaAs, O^+ implantation, energy levels, photoluminesc. 80−24838
GaAs, ohmic contact formation with thin film 77−8756
GaAs, ohmic contact form. to n- and p-type samples by MBE, characts. 79−47159
GaAs ohmic contacts wtih Au-Ge, SEM and TEM obs. of struct. 80−100522
n-GaAs ohmic planar contacts formation and elec. props. on basis of Au and Au-Ge alloys 79−15223
GaAs on $Ga_xAl_{1-x}As$, electron scatt., cathodoluminesc., loss spectra 80−104023
GaAs on GaAs and Ge, epitaxy, mechanism, effect of substrate surface struct. 77−51614
GaAs on Ge thin film stacked multiple-bandgap solar cell structs., prep. using CVD techniques 80−94083
GaAs, one-photon absorption coeffs. calcs. 77−20884
GaAs, one-sided heterostructure injection laser, stability of output pulse power 77−83876
GaAs, open tube diffusion of Zn 80−84326
GaAs, operation characteristics *(Rumanian)* 78−87053
GaAs, opt. consts. in 0.6 to 4.2 eV range 79−51928
GaAs, optical absorption spectrum, effect of impurity wavefunction overlap 77−8613
GaAs, optical absorption near fundamental edge due to CO_2 laser pulses 78−39569
GaAs, optical absorption spectrum dynamics using sub-ps. optical pulses 80−11431
GaAs, optical conductivity, constants, refractivity from IR absorption spectra 78−43873
GaAs, optical cross sections associated with deep levels, O centre obs. 80−6777
GaAs, optical detection of CESR 77−36155
GaAs, optical inhomogeneity, physical basis 79−15430
GaAs, optical integrated circuits appl., properties and preparation 77−65644
GaAs, optical meas. of semicond. temps. *(French)* 79−35743
GaAs, optical modulation spectra, proton damage effect 78−76487
GaAs, optical modulation by optical tuning of cavity 79−64314
GaAs optical modulator for coupled waveguides 78−71235
GaAs, optical properties calc., dispersion relations approach, Velicky's method *(Spanish)* 77−90119
GaAs optical waveguides, oxide confined, formed by lateral epitaxial growth 80−58815
GaAs, optically pumped, absorption spectrum, band filling, hot electron effects 78−31199
GaAs, optically pumped DFB laser, with two-dimens. Bragg reflectors 78−1252
GaAs, optically pumped laser, two-dimensional distributed Bragg reflectors, oscillation *(Japanese)* 78−42350
GaAs, optically pumped laser with acoustic distributed feedback 78−82977
GaAs, optoelectronic devices, conf., Berlin, DDR 78−91755

III-V semiconductors continued
GaAs, organometallic VPE, with varying As/Ga ratios, deep states 80−65480
GaAs orientation dependence of ballistic electron transport and impact ionisation 80−49758
GaAs, oscillatory electron drift rel. in non-ohmic regime at low temp. 79−33291
GaAs, oxidation, initial process and oxide/semicond. interface formation 80−50739
GaAs, oxidation, water vapour and O_2 excitation effects, XPS obs. 79−100274
GaAs, oxidation in multipole plasma, MOS elec. props. 80−44737
GaAs oxidation saturation and MOS diode equivalent cct. 78−47875
GaAs, oxidation through Al film, AES and TEM 77−77621
GaAs oxide, anodic, heat treatment temp. effects, optical props. obs. 78−27658
GaAs oxide, anodic, optical props., 1.5-6.0 eV 77−90209
GaAs oxide, anodised native, influence of temp. on struct. and props. 77−81332
GaAs oxide, passivated layers, quantitative in-depth profile, AES-SIMS thermal, anodic and plasma oxidations 78−84087
GaAs oxide, plasma grown, semiquantitative chemical depth profiles Auger spectroscopy and neutron activation anal. 78−53284
GaAs oxide, thermally grown, elec. props. 78−2601
GaAs, oxide film, microscopy with an ellipsometric arrangement 80−17998
GaAs oxide film, plasma-grown, analysis using Rutherford backscatt. and ion-induced X-rays 77−43438
GaAs oxide film, thermal and anodic, in-depth profiles, XPS expts. 78−84086
GaAs oxide film form., ion implantation effects 80−100266
GaAs, oxide film growth, thermal oxidation, optical obs., model 77−56120
GaAs oxide film growth in As_2O_3 vapour, As incorporation 79−77928
GaAs, oxide film influence on adsorption and electrophys. props. 79−42369
GaAs oxide films, anodically and thermally grown, XPS study 80−16141
GaAs oxide films grown by anodization in electrolytes, electron spectroscopy exam. *(German)* 79−15837
GaAs, oxide layers prepared by anodic, thermal and plasma oxidation, in-depth profiles and annealing effects 79−61768
GaAs, oxide-insulated stripe-geometry DH laser, low degradation rate at room temp. 77−23674
GaAs oxides, appl. of selective chemical reaction concept for controlling props. 79−47790
GaAs oxides, plasma-grown, in situ meas. and anal. with spectroscopic ellipsometry 80−76386
GaAs oxidised surface, detection of excess crystalline As by Raman scatt. 78−19453
GaAs, p- and n-type, and Zn-diffused, spreading resist. meas. 79−28343
GaAs, P-T diagram, cryst. struct. stability 78−51886
GaAs p^+-n diode, radiative hot carrier recomb., photoluminesc. and electroluminesc. meas. 79−38676
GaAs p^+-n junction, deep levels obs. 77−89834
GaAs, p^+-η -n^+ electro-optical directional-coupler switch 77−7217
GaAs p^+-n^0 junction, photocurrent, hole diffusion length in lightly doped n-type region 77−28246
GaAs, p^+-n^0-n^+ struct., control of modulation of base resist. 79−91133
GaAs p^+-n-n^+ diode, ns modulation of 10.6 μm radiation by elec. injection 77−34937
GaAs p^+-p(i)-n^+ structures, S-shaped I/V characteristics based on laminated semicond. cryst. structures *(Russian)* 79−42628
GaAs, p-i-n avalanche photodiode, temp. depend. characts. 79−35835
GaAs, p-n homojunction breakdown voltage for onesided abrupt junctions *(German)* 78−56210
GaAs p-n homojunctions, elec. breakdown mechanism 79−87147
GaAs p-n junction, as pressure/temp. transducers *(Polish)* 77−67424
GaAs, p-n junction, conductance oscillations in a two-dimensional impurity band 79−95477
GaAs p-n junction, HV, current induced by electron probe in space charge region 79−24065
GaAs, p-n junction, piezotunnel current *(Russian)* 77−47890
GaAs p-n junction, short-circuited, estimation of surface recomb. rates, electron-probe meas. 77−43713
GaAs p-n junction, surface recomb. current reduction with $Al_{0.5}Ga_{0.5}As$:O surface layer 80−49878
GaAs, p-n junction, Zn^+ implanted, residual radiation defect influence on characts. *(Russian)* 78−84287
GaAs p-n junction formation, laser assisted, TEM and elec. props. 79−69138
GaAs p-n junction pressure transducer characteristics *(Polish)* 77−89832
GaAs p-n junctions, direct biased, temp. depend. of low freq. voltage fluctuations 79−56298
GaAs, p-n junctions, electroepitaxy and thermal LPE growth, elec. characts. 80−2290
GaAs p-n-i-n^+ semi-insulating struct. as integrated optical coupler 80−64212
n-GaAs, parametric interaction of HF waves, anal. 80−15554
GaAs particle detector, semi-insulating, VI characts., γ-ray sensitivity and performance 77−46467
GaAs patterned epilayer structures, MBE writing 78−56590
GaAs, peculiarities of plasma region reflection, effect of surface treatment methods *(Russian)* 79−69827
GaAs, Peltier induced growth kinetics of LPE 78−64485
GaAs, Peltier LPE, absence of electromigration of As and Al 77−81230
GaAs, periodic doping structure, nipi superlattices, HBE growth and characts. 79−95484
GaAs, periodic surface corrugation generation by holography 78−55469
GaAs periodic waveguide, phase-matched SHG obs. 77−19360
GaAs, permittivity at laser transitions freq., excess carriers effect 77−14719
n-GaAs, persistent photocurrents, Hall effect anal. 79−87130
GaAs, phase diagram of electron-hole liqs. in polar semiconds. 77−89706
GaAs, phonon assisted tunnel emission of electrons from deep levels 80−25532
GaAs, phonon surface density, Brillouin elasto-optic cross section 78−72536
GaAs, phonon viscosity tensor 78−34570

III-V semiconductors continued
GaAs photo-FET high speed photoconductive integrated optical receiver 80−58816
n-GaAs, photo-Hall effect meas. of ionised impurity scatt. 78−56182
GaAs, photo-field cathode, ageing and surface state effects *(Russian)* 77−28703
GaAs, photoabsorption and magnetoabsorption effects 77−16332
GaAs photoanode, using n/n^+ struct., power conversion efficiency 80−50990
n-GaAs photoanodes for water photoelectrolysis 77−77789
GaAs, photocapacitive MIS IR detector, spectral response, noise characts. 80−75644
GaAs, photocarrier thermalisation by laser excitation spectroscopy 78−31250
GaAs photocathode, emitted electron transverse energy 77−12489
GaAs photocathode with Cs-O adlayer, negative electron affinity, core-level photoemission of adlayer 79−19965
GaAs, photocathodes, photoelectron emission, energy levels, influence of dimens. quantisation *(Russian)* 78−64447
GaAs, photocathodes exhibiting negative electron affinity *(French)* 77−8724
GaAs, photoconductive carrier lifetime meas. by optoelectronic gating technique 77−47857
GaAs, photoconductivity, impurity induced, low energy edge spectral shift 80−65630
GaAs, photoconductivity and photomagnetic effect spectra 79−11178
GaAs, photoconductivity meas. of cyclotron resonance 79−82638
GaAs photodetector, determ. of theoretical threshold 78−37065
GaAs, photoelectric memory effect, effect of metallic island struct. on surface 77−55570
n-GaAs, photoemission and work function of (111A) and (111B) surfaces, energy states 77−20980
GaAs photoemission characteristics, parameters of emitters with negative electron affinity 79−4898
p-GaAs, photoemission into electrolyte soln., energy diagrams, Volta pots., voltage drop 77−62990
GaAs, photoemission modulation by IR illumination, saturation photocurrents 80−108318
GaAs photoemitter, negative electron affinity, face depend. of emission 77−32496
GaAs, photoexcitation phenomena, low density 78−27319
GaAs, photoexcited, band edge absorpt. dynamics 79−19879
GaAs, photoexcited, carrier relaxation determ. from time resolved transmission spectrum changes 79−99583
GaAs, photoexcited hot electrons energy relaxation in near-surface region of semiconductors 80−92928
GaAs, photoionisation of impurities with deep levels 80−65484
n-GaAs, photolum., rel. to n-InP 77−40272
GaAs, photolum. intensity degradation caused by excitation-enhanced oxidation 78−15205
GaAs, photoluminescence, deep level trap emission capture 80−29805
GaAs, photoluminescence, electron-acceptor, from non-Maxwellian distrib. of photo-excited electrons 80−45138
GaAs, photoluminescence, electron gas coding influence in ion-bombarded layers 80−108272
GaAs, photoluminescence at low temp., free exciton recomb. mechanisms *(Russian)* 77−32438
GaAs, photoluminescence and resonant Raman spectra, press. depend. 78−31251
GaAs, photoluminescence intensity rel. to heat treatment in S vapour *(Russian)* 78−48216
GaAs, photoluminescence intensity of cleaved surface, ambient gas influence 78−88345
GaAs, photomag. effect anomalies and state of surface layer 80−100482
GaAs, photon drag effects 78−23134
p-GaAs photon drag optical rectification detectors, performance in 2 to 33 μm range 79−35834
GaAs, photon transfer of excitation of nonequilib. carriers, conc. profile and relax. time 77−69907
GaAs, photovoltage transients, expt. and model 77−89802
GaAs, photovoltaic conversion characts. *(Czech)* 77−76903
GaAs, picosecond absorption spectroscopy 79−47482
GaAs, picosecond optoelectronic switching 77−23742
n-GaAs, piezo-absorpt. meas. 79−87455
GaAs, piezoelec. coupling and dislocations 79−91377
n-GaAs, piezoelec. film, surface phonon amplification 77−31864
n-GaAs, piezoelec. semicond., nonlinear interaction of acoustic waves with microwave elec. fields 79−42593
GaAs, piezoelectric constant due to bond bending, electron redistribution effect 79−38457
n-GaAs, piezoelectric semiconductor, influence of acoustic phonon disturbances on conductivity 78−91697
p-GaAs, piezoresistance, relax. time for heavy and light holes determ. 79−19599
GaAs, piezoresistance and conduction band minima 78−51993
GaAs, planar diffusion of Sn from doped SiO_2 films, for planar junction fabrication 79−69289
GaAs, planar ion-implanted avalanche photodiodes 80−22431
GaAs planar p-n junction fabrication by Be ion implantation 78−43470
GaAs planar p-n junctions, Be ion implantation, fabrication and characts. 78−88022
GaAs planar stripe geometry and channelled substrate DH laser, lateral current confinement 78−66823
GaAs, plasma anodisation in DC discharge, AES and MIS diode expts. 78−95826
GaAs, plasma-grown oxides, in situ anal. using spectroscopic ellipsometer 79−79138
GaAs, plasma-grown oxides, physical props., Auger and IR spectral anal. 79−91821
GaAs, plasmon-phonon coupling, and IR refl. spectra of impure crysts. 79−56150
GaAs plastic deformation, produced by thermocompression bonding 77−76807
GaAs, plastically deform., photocond., spectral response and decay process 80−29435
GaAs, point defect generation by electron-hole recombination at dislocations 79−37699
GaAs, point defects, laser annealing 80−107224
GaAs, point defects, multiple scatt. Xα model 80−54636
GaAs, polar modes, light scatt. intensities, wave vector depend. 77−77219

III-V semiconductors continued
GaAs, polar semiconductor, collisions between hot excitons and hot electrons 80−7415
GaAs, polarisation anisotropy of hot photolum. *(Russian)* 77−90195
GaAs, polariton fluoresc., spatial and spectral features 79−33760
GaAs, polariton scattering, free carrier effects 78−34783
GaAs, polaritons, surface nonlinear interactions, Green's function theory 78−42379
GaAs, polishing dislocation etch 78−6066
GaAs, polycryst., wet and dry oxides, comparative study by AES, SIMS and XPS 80−80116
GaAs, polycryst. for terrestrial photovoltaic energy conversion 79−15242
GaAs, polycryst. Schottky barrier solar cells, effect of grain size on efficiency 80−50968
GaAs, polycryst. solar cells, thin film growth and grain size, effect on cell efficiency 80−81471
GaAs polycryst. solar cell diagnostics using IR electroluminesc. 80−93885
GaAs, polycrystalline, carrier transport at grain boundaries 80−29411
GaAs, polycrystalline, for solar cells 78−11124
GaAs, polycrystalline, grain boundary resistance meas. effect on solar cell performance 80−93891
GaAs polycrystalline film growth for solar cells 79−33941
GaAs polycrystalline thin film solar cells, fabrication 80−94066
GaAs, population-inverted, resonant Brillouin scattering and photoelastic consts. 80−76042
GaAs, positron annihilation, mag. field effect, positronium states 77−16417
GaAs, positron annihilation rel. to surface treatment *(Russian)* 77−44081
GaAs, positron annihilation in disturbed surface layers 78−6809
GaAs, positron annihilation depend. on doping 80−60710
GaAs, positronium-like states, low temp., ang. correl. of annihilation photons 78−76549
GaAs powder, RF field depend. of memory echoes 79−8095
n-GaAs, preferential photoelectrochemical dissolution in Fe(III) based etches 78−7066
GaAs, prep. of thin films by ionised-cluster beam deposition *(Japanese)* 80−25576
GaAs, primary radiation defect separation by elec. field 80−92522
GaAs, produced by pyrolytic synthesis, photoemission 79−43100
GaAs, produced by VPE using trimethylgallium and arsine, controlled doping 78−6855
GaAs, proton irradiated, low energy, deep level defects and hole diffusion length meas. 80−60000
GaAs, proton-bombarded, lattice strain, precision X-ray meas. 77−27922
GaAs, proton-bombarded, observation of radiation damage using TEM 80−75276
GaAs, psec time resolved spectroscopy, electron-hole plasma 79−47500
GaAs, pulled, dislocation generation, thermoelastic anal. 80−79787
GaAs, pure and N depend, extended Huckel theory appl. 80−59916
GaAs pure and Se-doped, photoluminescence at dislocations, band gap electronic levels 79−99926
GaAs, qualitative anal. of oxygen in thin epitaxial layers by SIMS 79−5233
GaAs, radiation defect obs. using Schottky diode charact: 78−76024
GaAs, radiation detector, characteristics 79−68139
GaAs, radiative yield improvement by laser annealing 80−45128
GaAs, Raman scatt., electron-phonon deformation potential coupling 78−52502
n-GaAs, Raman scatt. by coupled phonon-plasmon mode, nonlocal theory 77−36222
n-GaAs, Raman scatt. by wavevector depend. coupled plasmon-LO phonons 77−40232
GaAs, Raman scattering absolute cross section band struct. model calcs. 80−7349
GaAs, Raman scattering from nonequilibrium LO phonons with picosecond resolution 80−80779
n-GaAs, Raman spectra of coupled LO phonon-plasmon mode, de Haas-Shubnikov like quantum oscills. 78−43863
GaAs, Raman spectroscopy, characterisation of thin films and heterostructures 78−76439
GaAs, reach-through avalanche photodiode, temp. depend. charact. 79−95482
GaAs, reactive ion etching of III-V compounds 80−58813
GaAs, reactor irrad., opt. props. 77−90137
GaAs, reactor-irradiated, anisotropy in diffuse small angle neutron scatt. 78−51598
n-GaAs, real epitaxial surface, photoelec. spectroscopy, mechanisms 78−34858
GaAs, recombination radiation, anomalous temp. depend. 80−2847
n-GaAs, recombination scheme for $h\nu_m \approx 1.0$, 1.2 and 1.3 eV luminesc. bands 77−69906
GaAs, reflection spectra, optical consts. *(Russian)* 79−38571
GaAs, relaxation of photoexcited carriers 78−19080
GaAs, reson. Brillouin scatt., book contrib. 79−42983
GaAs, reson. Brillouin scatt. of exciton polaritons 80−11418
GaAs, reson. polariton fluoresc. obs. 77−85785
GaAs, reson. Raman scatt. at indirect gap 79−73931
n-GaAs, resonance enhancement of Raman scatt. by electron gas excitations 79−65878
GaAs, resonance Raman scattering by 2 TO phonons and cond. band minima ordering 77−20854
GaAs, resonant Brillouin scatt. of excitonic polaritons 77−44010
GaAs, resonant Brillouin scattering 79−78695
GaAs, resonant Brillouin scattering of exciton polaritons 80−93357
GaAs, review of ohmic contacts fabrication 80−49901
GaAs rib-waveguide laser, propag. and radiation charact. 77−79933
GaAs ribbon whiskers, photopumped, laser action 80−91801
GaAs ribbons from Ga-$AsCl_3$-H_2 epitaxy 80−7498
GaAs, S and Se ion implantation 78−55884
GaAs, SAW broadband generation by conversion from acoustoelectrically amplified bulk waves 77−54852
GaAs, SAW meas. of surface elec. props. 77−20387
GaAs, SEM defect study, transmission cathodoluminescence 79−64964
GaAs, SIMS, energy distrib. of sputtered ions 79−38706
GaAs Schottky barrier, Auger de-excitation of metastable state 79−65410
GaAs, Schottky barrier, effect of oxide composition on elec. behaviour, AES meas. 79−87141

III-V semiconductors continued
GaAs, Schottky barrier and semicond./insulator interface states formation 80−49906
GaAs Schottky barrier charge-accumulation detector, photosensitivity spectrum 77−55582
GaAs Schottky barrier diode, detection down to 70.5 μm 77−10103
n-GaAs Schottky barrier diode, electron processes at interface *(Russian)* 78−84301
GaAs Schottky barrier diodes, strain sensitivity mechanism 79−38165
GaAs Schottky barrier diode, under high neutron fluence, current transport 80−65679
GaAs, Schottky barrier electrorefl. under uniaxial stress, band struct. 77−48193
GaAs, Schottky barrier ellipsometric electroreflectance spectra, energy band parameters 79−99853
GaAs, Schottky barrier electrorefl. meas. by sample rotating technique 80−60544
n-GaAs Schottky barrier junction, SEM meas. of hole diffusion length, surface effects 79−87110
GaAs, Schottky barrier solar cells, diffusion length meas. 79−61973
GaAs Schottky barrier structure, defects from proton irradiation, thermal transients and optical capacity *(French)* 80−59534
GaAs Schottky barrier with Au and Au-Ga contacts, high temp. annealing behaviour 77−43725
n-GaAs, Schottky barriers, minority carrier trap meas. 78−26951
p-GaAs, Schottky barriers on polar (111) and $(\bar{1}\bar{1}\bar{1})$ surfaces 80−88631
n-GaAs Schottky diode, impurity photoluminesc. 80−29781
GaAs, Schottky diode, trap levels, admittance spectroscopy 79−51672
GaAs Schottky diode, use in acoustic memory correlator 78−66989
GaAs Schottky gate FET struct., obs. of localisation in two-dimens. systems 78−60213
GaAs Schottky-barrier, linear and quadratic electroreflectance, minicomputer-controlled meas. 80−97241
GaAs Schottky-barrier diode submicron layer LPE reactor 77−77439
GaAs Schottky-contact, influence of surface states and hole traps *(Bulgarian)* 80−25006
GaAs, Se ion-implanted semi-insulating, effects of Cr redistrib. on elec. charact. 80−59982
GaAs secondary ionisation coeffs., interband scatt. effects 78−43408
GaAs, selective etching in nonaqueous bromine and iodine solns. 77−40453
GaAs, selective growth, MBE and self-masking method 77−52256
GaAs, selective in situ vapour etch of substrate and growth 80−2958
GaAs, selective plasma oxidation, interface props. 80−100933
GaAs, self-compensation due to shallow and deep levels 80−24837
GaAs, self-consistent localised electronic struct. 79−42445
GaAs, self-scattering in Monte Carlo calcs. of transient dynamic response 80−103687
GaAs, semi-insulating, cond. mechanism, model explaining temp. depend. of elec. props. 79−51571
GaAs, semi-insulating, conduction model 80−10986
GaAs, semi-insulating, effects of heat treatment characterised by SIMS 78−6091
GaAs, semi-insulating, LPE growth for FET buffer layers 79−66015
GaAs, semi-insulating, magnetophotoconductivity as function of etching time 79−56265
GaAs, semi-insulating, microwave permitt. meas. 80−60479
GaAs, semi-insulating, optical and electron microscopy exam., line dislocation precipitates 80−70205
GaAs, semi-insulating, surface layer thermal conversion mechanism, Hall effect meas. 80−49772
GaAs, semi-insulating, thermal conversion, Hall effect and luminesc. meas. 78−6405
GaAs, semi-insulating, undoped and Cr-doped, compensation mechanisms, Hall effect and optical absorpt. meas. 80−84477
GaAs, semi-insulating substrate, characterisation and modification 77−81215
GaAs, semi-insulating substrates, whispering gallery lasers 80−69405
n-GaAs, semicond. electrode, electrolum. due to hole injection from electrolytes 77−20926
n-GaAs semicond. liq. junction solar cells, photocurrent spectra, carrier recombination 78−76142
GaAs, semiconducting resistance thermometer for low-temp. measurement, 0.3 to 350K range 79−58687
n-GaAs, semidegenerate, acoustoelec. gain and lattice attenuation, X-ray Brillouin scatt. and elec. meas. 79−15193
GaAs, sequential multiple layer VPE, method 77−12545
GaAs, shallow acceptor states exam. by far IR Fourier transform spectroscopy 78−31185
GaAs, shallow core level spectra 80−104037
n-GaAs, shallow donors, elec. cond. and Hall coeff. meas. 77−11942
GaAs, shallow donors, excited state transitions 78−6710
GaAs, shallow donors, screening, energy spectrum of electrons and cond. mech. 79−7831
GaAs, shallow homojunction solar cell, resist. to 1 MeV electron radiation 80−50953
GaAs, shallow impurity spectral linewidths, 4-10K 77−63443
GaAs shallow junction solar cells damaged by electron irrad., recovery of short cct. current 79−29471
GaAs shallow-homojunction solar cells on single crystal GaAs and Ge substrates, CVD fabrication and conversion efficiency 80−61364
GaAs shallow-homojunction solar cells, electron radiation effects 80−97798
GaAs, Shubnikov-de Haas oscillations in semiconductor superlattice 77−62947
GaAs, Si ion implantation and annealing, damage recovery, surface carrier profile 77−4119
GaAs, SiO_2 and Si_3N_4 encapsulants for annealing, photolum. and AES evaluation 78−27657
GaAs signal processing optical electronic devices 80−33242
GaAs single cryst., linear electro-optical props., temp. depend. 80−71376
GaAs, single crystal growth and heat treatment *(Chinese)* 77−73222
GaAs, single crystal growth by liq. encapsulated Czochralski technique using B_2O_3 80−11554
GaAs single-channel injection laser, radiative charact., single longit. mode 79−10309
GaAs single-channel injection laser, polarisation charact. 80−48256
GaAs single-freq. injection laser, CW operation 78−46606
GaAs single-frequency injection laser, coherence of emitted radiation 79−31904

III-V semiconductors continued
GaAs, site selective doping by ion implantation of radioactive nuclei 80−34023
n-GaAs, smooth and continuous ohmic contacts using epitaxial Ge films alloyed with Ni 78−68086
GaAs solar cell, polycryst., grain boundary passivation by oxidation, AES, SIMS and XPS obs. 80−81467
GaAs, solar cell, thin film, prep. by Peeled Film Technology 79−29472
GaAs solar cell arrays, for earth orbital and orbit transfer missions 80−94044
GaAs solar cell polycrystalline conducting substrate, minority carrier diffusion length spatially-resolved meas. 80−94084
GaAs solar cell structs., photolum. props. 80−50958
GaAs solar cells, efficiency improvement using ZnSe solar spectrum convertor 80−101117
GaAs, solar cells, electron-irrad., annealing kinetics 80−7937
GaAs solar cells, electron and proton radiation damage 80−94034
GaAs solar cells, ion-implanted and laser-annealed 79−79390
GaAs solar cells, low-high junction effect, theoretical anal. 80−89626
GaAs solar cells, photoreactance of p-n junction diodes 80−81464
GaAs solar cells, simultaneous radiation damage and annealing 80−94033
GaAs solar cells, thin film growth tech. and characterisation 80−89631
GaAs solar cells on Ge substrates, thin film shallow homojunction struct., quantum efficiencies 80−35677
GaAs solar cells with concentrators, prospects *(Italian)* 80−60025
GaAs solar cells with shallow homojunction on Ge substrates 80−26142
GaAs, solid solubility of Se, SIMS 78−67830
GaAs, solubility in Ga-Al alloys in multilayer LPE of $Ga_xAl_{1-x}As$ 78−52690
n-GaAs, spectra, light induced, electrolyte and Schottky barrier techniques of meas. 80−76046
p-GaAs, spin relaxation of photoelectrons 77−85207
GaAs, spin-depend. recomb., photoluminesc. obs. 80−60666
GaAs spin-polarized electron source 80−69000
GaAs, spontaneous luminesc. due to high density electron-hole plasma under nano- and picosecond pulse excitation 80−40157
GaAs, sputtered layers, EPMA of Kr content 80−3443
GaAs, sputtered-etched surface, Schottky contact characterisation and its recovery by annealing 79−99603
GaAs, sputtering at elevated temps. 80−7456
n-GaAs, stabilisation against photodecomposition, surface damage influence 80−76390
GaAs, stimulated and spontaneous emission from degenerate electron-hole plasma at 300K 80−29762
GaAs, stoichiometry meas. by 15 MeV He^{2+} backscattering 79−99330
n-GaAs, strain sensitivity of specimens obtained from pressed powders 77−36177
p-GaAs, strain sensitivity, piezoresistance *(Russian)* 79−82585
GaAs, stripe geometry laser, optical losses of O^+ and B^+ implanted layers 77−79827
GaAs stripe-geometry laser, nonlinear temp. characteristics *(Chinese)* 80−43337
GaAs, striped DH lasers, anomalous behaviour at low temp. *(Chinese)* 80−87390
GaAs, structural defects in single crysts., first order distribs. eval. *(German)* 78−6049
GaAs, structural defects, detection by electrochemical etching 78−55872
GaAs structures, charge accumulation and transmission, physical modelling *(Bulgarian)* 80−6947
n-GaAs, study of ohmic contacts 80−60083
n-GaAs, subject to crossed static elec. and mag. fields, microwave amplification 77−1440
n-GaAs, submillimetre cond. and carrier heating, two-electron-temp. model 77−20349
GaAs substrate, $CuInTe_2$ epitaxial layer growth and props. 80−108359
GaAs substrate, epitaxial growth of single crystal layers of $Cd_{1-x}Sn_xS$, close-spaced geometry 78−92198
GaAs substrate, MBE growth of insulating oxide films 79−77943
GaAs substrate, Pd/Ge film sintering, Auger spectra, Schottky barrier energy 79−69581
GaAs substrate, Ta_2O_5 and SiO_2 film sputter deposition and MIS struct. characts. 77−89864
GaAs substrate, VPE growth of n-AlAs, for heterojunction devices 77−1814
GaAs substrate, ZnSe film on, transition layer form. kinetics 79−87007
GaAs, substrate for epitaxial growth, backscatt. anal. of surface prep. and anodic oxidation 77−25175
GaAs, substrate for homoepitaxy, vicinal surfaces characterisation 77−20207
GaAs substrate for p-Ge film, cond., Hall effect and transverse magnetoresist., anisotropy 79−51697
GaAs substrate for sputtered GaSb film growth, Hall effect, impurity levels 80−20334
n-GaAs substrates, ion implanted, compensation 78−75680
GaAs substrates, out-diffusion of Cr 80−10708
GaAs, surface, (110), ang.-resolved photoelectron spectra 78−43984
GaAs surface, Ar ion bombardment induced photon emission, rel. to target temp. 78−72612
GaAs surface, chemisorption of Li, charge injection into space charge layers 80−100496
GaAs surface, clean and O_2 covered, work function and photovoltage meas. 77−1446
GaAs surface, cluster model approach for electronic struct. 78−56205
GaAs surface, contact pot. difference meas. 77−20403
GaAs, surface, distrib. of surface states 80−44692
GaAs surface, during vapour phase epitaxial growth, characterisation techniques and meas. *(French)* 77−1817
GaAs, surface, electron struct. and Fermi level pinning by O_2 and metals 80−11066
GaAs surface, energy-minimisation approach to atomic geometry 78−95213
GaAs surface, growth of anodic Al_2O_3 and composite oxides 79−83344
GaAs surface, low temp. thermal nitridation 80−97607
GaAs surface, O_2 sorption and excitonic effects, photoemission expts. 77−85055
GaAs, surface, pulsed electron beam processing, doping, annealing 80−75254
GaAs, surface, vacancies, bound state energy level calcs., tight binding approx. 80−44694
GaAs, surface (110) atomic struct. 79−69331

III-V semiconductors continued
GaAs, surface (111), $(\bar{1}\bar{1}\bar{1})$, (110), XPS, photo-Auger ionisation cross section, electron mean free paths 78−56558
n-GaAs surface barrier diodes for nuclear radiation detection, deep trapping centres 80−92849
GaAs, surface Brillouin scattering from acoustic phonons 80−55113
GaAs, surface characterisation using SAW 80−11069
GaAs, surface characterisation by high resolution Rutherford backscatt. 80−25511
GaAs, surface charge state change during thermodesorpt. 77−80825
GaAs, surface chem. changes on annealing, α-particle Rutherford scattering and channelling study 79−73383
GaAs, surface chemistry and electronic struct., adsorption of O_2, photoemission meas. 77−20985
GaAs surface composition vs. temp., low energy ion scatt. *(French)* 77−59663
GaAs, surface cryst. regularity by X-ray photoelectron diffr. 80−89112
GaAs surface electron states, appl. of surface photovoltage spectroscopy 77−69391
GaAs, surface electron states, (110), photoemission 80−25529
GaAs, surface exciton energy 80−92829
GaAs, surface final-state effects on core electron transition energies 78−91745
GaAs surface grating relief pattern profile altering, oblique shadow deposition technique 79−68451
GaAs surface impurities, struct. and comp. of compounds using IR spectroscopy 78−63918
GaAs surface morphology during etching with H_2O vapour 80−39094
GaAs surface passivation by GaO_xN_y films and multilayer systems 80−11809
GaAs, surface passivation using composite Al_2O_3 and native oxide, MIS characts. 80−93004
GaAs, surface passivation using Si_3N_4, interface characts. 80−93005
GaAs, surface passivation using GaO_xN_y based multiple insulating layers 80−93006
GaAs, surface phonons, scatt. expts. 80−10772
GaAs, surface photogalvanic effect, polarisation depend. photocurrents *(Russian)* 80−80322
GaAs, surface photovoltage due to photo-thermo-ionization of surface states 78−14787
GaAs, surface polaron in mag. field 79−23912
GaAs, surface processing, residual film monitoring by ellipsometry 80−13124
GaAs, surface recomb. velocity, determ. from SEM expts. on p-n junctions 77−55601
n-GaAs, surface recomb. vel. meas., diffr. from transient optical grating 79−1604
GaAs, surface recomb. vel., psec. optical techniques 80−70784
GaAs, surface recombination velocity, diffr. from picosecond transient free carrier gratings 79−47109
GaAs, surface recombination rate reduction by Ru chemisorption 80−49866
GaAs, surface segregation of implanted alkali metals, photoemitter prep. and characts. *(French)* 78−60544
GaAs, surface states, band struct. by discontinuous potential method 80−20276
n-GaAs, surface states, photoemission yield obs. 77−16459
GaAs surface states obs. by XPS 80−50515
GaAs, surface states XPS 80−25528
GaAs, surface structure and orbital symmetries of (110) surface state 78−72229
GaAs, surface studies during MBE growth 79−90899
GaAs, surface wetting with Hg, doping degree influence 80−92762
GaAs surfaces, electronic struct., tight-binding calc. 80−54755
GaAs surfaces (110) and (111)As, UPS and LEED 78−91514
GaAs switch, control of fast Pockel cell for active pulse shaping in ps domain 80−28257
GaAs switch, laser-activated, high-power switching with ps. precision 80−2416
n-GaAs, switching time in low-temp. impurity breakdown 77−15923
GaAs synthesis, Ga+As reaction temp. determ. 77−24978
GaAs, synthesis by molten salt electrolysis 78−64486
GaAs, synthesis in pyrolytic BN boat 78−6840
GaAs, Ta film deposition and oxidation, form. of Ta_2O_5 79−61769
GaAs, technique for doubling electron speed 79−38076
GaAs technology, ion implantation 1978 state of art review 79−42089
GaAs technology, MBE growth, microwave, optoelectronic devices appl. 79−52129
GaAs, temp. coeff. of induced birefringence 80−93277
n-GaAs, temp. depend. density of states, activation energy, screening, chem. pot. calcs. 79−56109
GaAs, temp. depend. of intervalley gap from Schottky diodes meas., thermionic emission theory generalization 79−73586
GaAs, thermal cond. calc. using numerical soln. of Boltzmann eqn. 80−44373
GaAs, thermal equilib. phonon populations, acoustic intensity meas. by Brillouin scatt. intensity obs. 80−45098
GaAs, thermal oxidation, 450 to 760°C, Rutherford back scattering obs. 78−76780
GaAs thermal oxidation rate and activation energy obs., 470° to 830°C *(Japanese)* 77−52517
GaAs, thermal oxidation in wet and dry atm., 470-830°C 77−86204
GaAs, thermal oxidation in As_2O_3 vapour 78−56792
GaAs, thermal oxide film growth and characterisation 80−11808
GaAs, thermalisation of electron-hole plasma 79−95439
GaAs thermally oxidised surface, in-depth comp. profile, Auger analysis 77−89621
GaAs, thermally oxidised, TEM obs. 78−72036
GaAs, thermally stimulated relax. under internal field conditions 80−7279
GaAs thermodiodes and resistance thermometers thermometric characts. approx. 80−31746
n-GaAs, thermoelec. power 79−60857
GaAs, thermomigration of molten Ga 77−69118
GaAs thin film, effect of O on thin film compositions obtained by secondary ion emission 80−26079
GaAs thin film polycrystalline solar cells, props. and prep. 80−81437
GaAs thin film polycrystalline Schottky barrier solar cells, grain boundary chemistry 80−94067
GaAs thin film polycrystalline solar cells, grain boundary edge passivated 80−94069

III-V semiconductors continued
GaAs thin films, differential mobility anisotropy effect on wave propag. 78−88050
GaAs thin films, reactively sputtered, ESCA/XPS study 80−97430
n-GaAs thin films carrier wave amplification, external medium stratification effects *(Russian)* 78−34905
GaAs thin layers, MBE, growth conditions and phys. props. *(German)* 80−55307
GaAs thin Schottky barrier metallisation, thermal reactions 79−78176
GaAs, three level cond. band struct., uniaxial stress effects, resist. and Gunn effect threshold meas. 77−85137
n-GaAs, three valley band struct., high temp. Hall mobility 80−29318
GaAs, time of flight atom-probe mass spectra 78−92584
GaAs, time-resolved spectra, carrier relax. time, phonon lifetime 80−11433
GaAs, trace element conc. meas. by Zeeman atomic absorpt. spectroscopy 80−29046
n-GaAs, transferred electron effects under hydrostatic pressure 77−32018
n-GaAs, transferred electron effects under hydrostatic press. 78−26871
GaAs transferred electron devices, ohmic contacts 78−52082
GaAs, transient and steady-state electron transport props. 77−39812
GaAs, transient dynamic response calculation by Monte Carlo techniques 80−107796
GaAs, transient-mode LPE on InP 78−72746
GaAs, transition element impurities, electron struct. of deep centres 78−39060
GaAs, transmission spectrum under uniaxial compression 80−29714
GaAs, transmutation doped, shallow donors, magneto-optical study, photocond. meas. 78−87996
GaAs, transmutation doping by thermal neutrons 80−10581
GaAs, trapping levels obs. using deep level transient spectroscopy, laser irrad. effects 79−99499
GaAs, travelling heater method growth, dislocation elimination 77−7684
n-GaAs tunable far IR Landau emission with subnanosecond rise time 79−32015
GaAs, tunable stimulated Raman scatt. in far IR, laser feasibility 79−50344
GaAs tunnel diode, electron beam bombard. induced defects, influence on excess current *(Russian)* 77−4424
GaAs, tunnel diode, peak current press. sensitivity *(Russian)* 77−4423
GaAs, tunnel MIS structures, surface states 77−85336
GaAs, two dimensional DFB laser with distributed Bragg and acousto-optic reflectors 77−10946
GaAs, two dimensional impurity bands, Hall mobility 79−95509
GaAs, two photon absorpt., hot electron-hole plasma, relax. time depend., picosecond spectra 79−51979
n-GaAs, two stream instability 78−2509
GaAs, two-hole species plasma, parametric instability 80−2410
GaAs, two-phonon diffuse scatt. of X-rays 78−26374
GaAs, two-phonon Raman scatt. meas. 77−81097
GaAs, two-photon 1.06 μm absorption coeff., absolute meas. 78−19527
GaAs, two-photon absorpt. spectrum, band gap luminesc 78−10888
GaAs, two-photon absorpt. of Nd:glass laser radiation 78−87107
GaAs, two-photon absorption coefficient, 3-band model 79−78679
GaAs, two-photon electroabsorption by excitons 79−42944
GaAs, two-photon interband transitions, carrier drag 79−7858
n-GaAs, two-valley semicond., helicon wave instability 77−47842
n-GaAs, two-valley semiconductor, domain instability *(Russian)* 77−62934
n-GaAs, two-valleyed semicond., hot electron diffusion coeff., random walk calc. 78−68033
GaAs type FET with buffer, bias effects due to deep centres in struct. *(French)* 80−107917
GaAs, UHF heating of charge carriers using lumped-capacitance resonators 80−20203
GaAs, UPS, 5-450 eV, surface states, oxidation behaviour 77−66579
GaAs, UV photoemission, polarisation-depend., angle-resolved spectroscopy 77−66573
n- GaAs, ultra low resistance ohmic contacts 80−20307
n-GaAs, uncompensated, mech. of energy relax. at low temps. 77−62921
n-GaAs, undoped, proton radiation defect detect. by transient capacitance spectroscopy 79−11089
GaAs, undoped epitaxial layer growth from nonstoichiometric solns., O_2 contamination sources 80−108362
GaAs unintentionally doped layer growth using MBE 78−72741
GaAs, unintentionally doped layer grown by MBE, elec. props. 79−91167
GaAs, use of ion induced X-rays for lattice location of S and Mn implanted in single crystals 79−4332
GaAs, VPE, electron Hall mobility meas., attempted correlation with growth parameters 78−43417
GaAs, VPE, fast growth at low temp. and high partial pressure 79−51446
GaAs, VPE, growth method at low H_2 press. 79−28936
GaAs, VPE, growth parameters effect 77−28726
n-GaAs, VPE, hi-lo, carrier conc. profiling by electrochem. methods 80−49958
GaAs, VPE, high purity, residual donors, photocond. expts. 77−85174
GaAs, VPE, hole diffusion lengths, surface prep. and heat treatment effects, etchant evaluation 80−15627
GaAs, VPE, hole diffusion lengths, effect of transition metal diffusional doping 80−15628
GaAs, VPE, incorporation of deep levels, effects of growth conditions 80−20111
GaAs VPE, influence of growth parameters, $AsCl_3$ transport method 80−29881
GaAs, VPE, multi-wafer growth technique using $AsCl_3$-Ga-N_2 system with horizontal reactor 79−28934
GaAs, VPE, partial press. diagrams use for thermodynamic represent. 79−33201
GaAs VPE, residual donor impurities 77−76679
GaAs, VPE, review of growth techniques *(French)* 79−33935
GaAs, VPE, surface defects rel. to technological parameters 78−44015
GaAs, VPE, thermodynamic factor influencing growth rate and layer purity in Ga-$AsCl_3$-H_2 system 79−28933
GaAs, VPE, thermodynamic analysis of Si contamination 79−28932
GaAs, VPE by CVD, vapour-solid interface, expt. anal. *(French)* 79−33940
GaAs, VPE by Ga-$AsCl_3$-H_2 process, role of Si 77−40380
GaAs, VPE by pyrolysis, producing power GaAs MESFETs 78−23623

III-V semiconductors continued
GaAs, VPE by single flat temp. zone method, elec. props. 79−95526
GaAs, VPE film growth in Ga-$AlCl_3$-H_2 system, O_2 injection effect 79−100057
GaAs VPE growth, growth rate anal. 78−52680
GaAs VPE growth, in situ surface anal. 79−95937
GaAs, VPE growth, surface morphology study by optical microscopy 79−60651
p-GaAs, VPE growth and characterisation, doping levels 80−10841
GaAs, VPE growth by single flat temp. zone method, residual doping level 77−48352
GaAs, VPE growth on {110} cryst. plane 80−10840
GaAs, VPE growth rate variation with distance along substrate within const. temp. zone 78−2384
GaAs, VPE in CVD systems, anisotropic phenomena 80−54563
GaAs, VPE in Ga-$AsCl_3$-H_2 system at reduced temp. 79−11519
GaAs, VPE in inert gas-H_2 mixed carrier system, thermodynamic analysis 78−11120
GaAs, VPE layer growth with abrupt doping profile 80−24746
GaAs, VPE layer on Ge, antiphase domain structures 77−69193
GaAs, VPE layer props. control using boundary layer characts. 80−50561
GaAs VPE layers, back surface gettering, Cr out diffusion 80−10802
GaAs VPE layers, elec. props., semi-insulating substrates effect 80−11123
GaAs VPE layers, electron irrad., electron traps 80−25026
GaAs, VPE layers, growth conditions effect on deep levels 79−95360
n-GaAs VPE layers, Hall mobility, effect of Cu contamination, photolum. expts. 80−54810
GaAs VPE layers, role of diffused Ga vacancy in degradation 78−95050
GaAs VPE layers for FET devices, impurity characterisation 80−29491
GaAs, VPE on Ge substrate, and characterisation 78−72736
GaAs, VPE thin layers, thickness uniformity, main factor anal. 80−76197
GaAs, VPE using low press. organometallics 79−100054
GaAs, vacuum deposited Shottky barrier metallisation 79−78153
GaAs, valence band fine struct. from light mod. with nonequilib. opt. phonons 78−39568
GaAs, valence band struct. obtained by magnetophonon effect 77−76748
GaAs, valence band structure, CPA, bond orbital calcs. 78−87909
n-GaAs, valence band studies of clean and O_2 exposed surfaces 78−43298
GaAs, valence-band dispersions, electron and hole lifetimes, angle-resolved photoemission 80−80947
GaAs, vapor-phase etching, mechanisms and kinetics 80−100934
GaAs vaporisation during laser annealing 80−25495
GaAs, vapour phase epitaxy using computer control 79−38744
GaAs, vapour phase epitaxial appl. to hyperabrupt varactor fabrication 80−29288
n-GaAs vapour phase epitaxial film electrophysical props. rel. to growth temp. *(Russian)* 80−49961
GaAs, vapour phase equilibria of As_2O_3 79−66181
GaAs, vapour phase etching and polishing with $AsCl_3$ 78−3243
GaAs, vapour-phase epitaxial growth, transfer mechanism of Si 77−51616
n-GaAs, Verdet const., free carrier density depend. 78−56462
GaAs wafer, defect studies by ASLEEP, SEM and scanning AES 79−19256
GaAs wafer, dissolution kinetics in undersaturated isothermal solns. in Ga-Al-As systems 80−80106
GaAs wafer, double-etching technique for submicron channel fabrication, laser fabrication appl. 80−74387
GaAs wafer, H_3PO_4-H_2O_2-H_2O etching solution system and its kinetics 79−20229
GaAs wafer diagnostics, using computer automated scanning low-energy electron probe 79−4214
GaAs wafers, for semicond. lasers, cleaving process 78−37915
GaAs waisted-rib optical waveguides 80−74487
GaAs, wave functions and optical cross sections associated with deep centres 78−34801
GaAs, weakly excited, luminesc. from exciton polaritons, based on exciton-electron collisions 79−83020
GaAs, whiskers grown on GaAs substrate by thermal decomp. method. 77−55875
GaAs, wide-gap semiconds., HV diodes, current-voltage characts. 79−24068
GaAs, with anodic oxides, leakage currents 79−38169
n-GaAs X-band impact ionisation for 337 μm radiation modulation 77−39069
GaAs, X-ray and Rutherford backscatt. yields from channelled $^4He^+$ ions 79−46730
GaAs, X-ray diffraction, integrated intensity meas. near absorption edge with synchrotron radiation 77−76253
GaAs, X-ray K absorpt. edge, effective ionic charge and bonding schemes 80−29827
GaAs, X-ray structure factors and Debye-Waller factor, from Bragg case diffr. curves 77−62509
GaAs, XPS, secondary illumination effects, band bending, level shifts 80−108324
GaAs, Zeeman split acceptor levels, calc. method 79−28322
GaAs: Cr (O_2), impurity levels charact. using dark capacitance and photocapacitance transient techniques 80−59920
GaAs: Si(Te), radiative recomb. *(Russian)* 79−91499
GaAs:$^{119}Sn^m$, Mossbauer spectra 80−29667
GaAs:^{11}B, physicochem. and resistivity meas. 80−24933
GaAs:$^{56}Fe(^{57}Fe)$, paramag. centres, identification from ESR and ENDOR spectra 80−80600
GaAs:O, effect of displacement upon impurity levels, psuedopotential calc. 77−39803
GaAs:Ag, diffusion of Ag at 1000°C, profiles, Schottky barrier and Hall effect meas. 80−54435
GaAs:Al, optical detection of NQR 79−69752
GaAs:Ar^+-metal, capacitor, capacitance-voltage and current-voltage meas., assuming intermediate dielec. layer 79−56316
GaAs:Au, back surface gettering 80−10758
GaAs:B, deep levels, optically stimulated transient current method *(French)* 80−59919
GaAs:B, electron or neutron irradiated, low symmetry interstitial B centre 78−79605
GaAs:B, incorporation of B during growth 80−93471

III-V semiconductors continued
GaAs:B(Ge)(Mg), impurity conc. profile by glow-discharge optical spectroscopy 80−49258
GaAs:Ba^+, Auger electron and charact. electron energy loss spectra 80−55235
GaAs:Be, annealing effect during MBE 78−79898
GaAs:Be, deep levels 80−29358
GaAs:Be, implantation and annealing, elec. props. 79−99540
GaAs:Be, implanted, determ. of Be concentration profiles by $^9Be(p,\alpha)$ reactions and SIMS anal. 79−4335
GaAs:Be, ion implanted, elec. profiling and optical activation expts. 77−89457
p-GaAs:Be, ion implanted, annealing charact., defect cond. profiling, electron diffr. obs. 79−4318
GaAs:Be, ion-implanted, photolum. spectra, effects of implantant depth distrib. 78−27293
GaAs:Be, ion-implanted, IR refl. and transmission meas. 80−34908
GaAs:Be,Se VPE layers, ion implanted, donor-acceptor pair radiative recomb. 79−91489
p-GaAs:Be layer, MBE growth, Be doping and diffusion 77−51397
GaAs:Be(C)(Ge)(Sn), MBE layers, photoluminesc. 80−29803
p-GaAs:C, ion implantation efficiency, elec. profile and compensation level meas. 77−27880
GaAs:C, Zeeman effect of effective mass acceptor, polarised luminesc. 79−4541
GaAs:C(Sn), diamagnetism quenching 80−6782
p-GaAs:Cd, (110) cleaved surface, defect-induced surface states 80−6925
GaAs:Cd, effect of As vapour press. on etch pit density and junction depth 78−26937
GaAs:Cd, lattice defects caused by quenching, elec. cond. 79−56160
GaAs:Cd, time depend. of Cd diffusion from gaseous phase 79−46844
GaAs:Co, effect of complex formation on impurity diffusion 77−11736
GaAs:Co, epitaxial layers and bulk, diffusion and elec. activity of Co 79−56333
GaAs:Co, neutral state of Co impurities, optical absorption and mag. susceptibility 78−39578
GaAs:Co VPE layers, bound-exciton luminesc., Zeeman anal. 79−95818
GaAs:Co^{2+}, EPR expts., y-factor determ. 78−76301
GaAs:Co^{2+}, piezoabsorption meas. tunnel splitting and Jahn Teller effect in $^4T_1(P)$ state 79−15494
GaAs:Co^{2+}(Ni^{3+}), mag. and optical props. 78−10763
GaAs:Co(Ni), intra d-shell excitations of acceptors 80−84757
GaAs:Cr, 0.84 eV no-phonon luminesc., fine struct. and origin 80−103980
GaAs:Cr, acceptor levels, photocapacitance meas. 79−95443
GaAs:Cr, Be, ion-implanted, semi-insulating, carrier mobility and conc. temp. depend. 77−76808
GaAs:Cr, Be^+ implantation, atomic conc. and defect density profiles after annealing 80−39123
GaAs:Cr, bulk and epitaxial, ion implanted, Cr conc., depth distrib. and diffusion coeff. 80−49243
GaAs:Cr, carrier equilibrium effects, impurity states, elec. resistivity 80−65488
GaAs:Cr, carrier transport in p^+-ν junction based on relaxation semiconductors 79−65543
GaAs:Cr, Cr distrib. and heat-treatment migration studies by SIMS 80−107305
GaAs:Cr, Cr^+ and Cr^{2+} centres, thermal treatment effects, EPR 80−65492
GaAs:Cr, current voltage characterisation, deep levels and Fermi level determ. 79−7823
GaAs:Cr, deep acceptor level, DLTS and optical DLTS study 80−92852
GaAs:Cr, deep levels, wavelength-modulated photocapacitance spectroscopy 80−76055
GaAs:Cr, EPR, annealing and IR excitation effect on Cr^+ signal, Cr content by colorimetry 77−69680
GaAs:Cr, effect of light on EPR centres 78−10767
GaAs:Cr, electroabsorption spectra obs. 80−50301
GaAs:Cr, epitaxial layers, MBE grown, Hall mobilities, substrate temps. 80−20335
GaAs:Cr, exptl. verification of Cr^{2+} models of photoluminescent transitions 78−27320
GaAs:Cr, FET, influence of Cr on mobility of electrons 80−92910
GaAs:Cr, far IR EPR spectroscopy, mag. field-modulation technique 80−15830
GaAs:Cr, fine structure in cathodoluminescence spectrum 78−56524
GaAs:Cr, gettering by back surface mech. damage 80−10759
GaAs:Cr, high resist., anomalously strong elec. field induced release of carriers from traps 78−6397
GaAs:Cr, high resistivity, specific resistance depend. determ. using impedance freq. depend. *(Czech)* 80−15536
GaAs:Cr, hole traps, ESR studies 80−75843
GaAs:Cr, hot electron relax. process and ionization of traps *(Russian)* 79−28354
GaAs:Cr, IR absorpt. determ., emissivity meas. 77−63421
GaAs:Cr, IR spectral detectivity 78−70184
GaAs:Cr, impurity conc. and segregation coeff., optical absorpt. meas. 79−56819
GaAs:Cr, impurity electron states by Xα scattered wave cluster method, electron-electron interactions 80−6767
GaAs:Cr, ion implanted, implantation damage profiles, laser annealing, ellipsometry study 80−79819
GaAs:Cr, local level parameters from thermally stimulated excitation curves, influence of variations of rate of heating 80−6769
GaAs:Cr, low dose n-type ion implantation obs. 77−39608
GaAs:Cr, low temp. gettering 80−96549
GaAs:Cr, luminesc. stress splitting, 4.2K 78−84627
GaAs:Cr, luminescence and absorption spectra, temp. depend. of fine structure 80−6779
GaAs:Cr, Mg, ion implanted, elec. meas. and optical activation studies 79−86806
GaAs:Cr, O, effect of O in photoluminesc. meas. 80−29799
GaAs:Cr, optical charging of paramag. centres, effect of potential relief 77−20694
GaAs:Cr, optical modulation study of proton bombardment 78−6720
GaAs:Cr, optical modulation spectra affected by 150 keV proton beam 78−10871
GaAs:Cr, optically excited, Hall effect meas. 77−20343
GaAs:Cr, optically induced transient EPR phenomena 80−50168
GaAs:Cr, origin of sharp near IR transitions 80−10913

III-V semiconductors continued
GaAs:Cr, p^+-ν-n diode, nonlinear transport phenomena *(Japanese)* 80−6850
GaAs:Cr, parameters determ. using cond., Hall-effect and magnetoresist. meas. *(Slovak)* 78−47802
GaAs:Cr, photoconductivity and photo Hall spectra 78−19091
GaAs:Cr, photoionisation transition $Cr^{3+} \rightarrow Cr^{2+}$, EPR studies 80−60638
GaAs:Cr, photoluminescence, YAG laser or krypton laser 80−60668
GaAs:Cr, photoluminescence in strong electric fields 80−108270
GaAs:Cr, plane-parallel plate subjected to laser illumination, photocond. meas., photodetector for far IR 79−93221
GaAs:Cr, redistrib. of Cr during laser annealing 80−88192
GaAs:Cr, Schottky barrier, effect of trapping processes on photocapacitance 77−76866
GaAs:Cr, Se implantation, carrier conc. and mobility profiles depend. on dose and annealing temp. 77−47479
GaAs:Cr, Se layers, ion implanted, ohmic contact form., contact resist. meas. 79−91158
GaAs:Cr, semi-insulating, i.r. induced modulation of cathodoluminescence, and specimen current 77−1737
GaAs:Cr, semi-insulating, TSC, carrier recomb. and trapping 77−32014
p-GaAs:Cr, semi-insulating, illumination effect on mobilities 77−32043
GaAs:Cr, semi-insulating elec. compensation, Hall and resist. meas. 77−62855
GaAs:Cr, semi-insulating, complex permittivity, 2.5-36 GHz, 300-400K 77−69763
p-GaAs:Cr, semi-insulating photoelectronic analysis 77−80804
GaAs:Cr, semi-insulating, deep impurity level anal. 78−6332
n-GaAs:Cr, semi-insulating, contact effects, trapping levels 78−10465
GaAs:Cr, semi-insulating, characterisation by photoelectronic data 78−68051
GaAs:Cr, semi-insulating, I-V charact. and surface currents 79−56234
GaAs:Cr, semi-insulating, I-V charact. and photocond. spectra dependencies on Fermi level 79−99576
GaAs:Cr, semi-insulating, defect chemistry, EPR study 79−99754
GaAs:Cr, semi-insulating, Cr charge states conc., EPR determ. 80−20450
GaAs:Cr, semi-insulating, thermal conversion suppression by arsine-controlled capless-anneal, ion implantation 80−49245
p-GaAs:Cr, semi-insulating, mobilities and carrier concentrations, temp. depend. 80−70702
GaAs:Cr, semi-insulating, Cr redistrib. during thermal annealing as function of encapsulant and implant fluence 80−84199
GaAs:Cr, semi-insulating, Zeeman studies of 0.839 eV emission 80−103987
GaAs:Cr, semi-insulating, damage gettering of Cr during annealing of Cr and S implants 80−107304
GaAs:Cr, semiinsulating, hole recomb. domains, Hall mobility and photocond. 77−15867
GaAs:Cr, semiinsulating, LPE and elec. props. 77−44178
GaAs:Cr, semiinsulating, I-V charact., photocond., Fermi level, and deep levels 78−39118
GaAs:Cr, semiinsulating solid-state inductance, theory and expt. 78−56138
GaAs:Cr, Si, deep centre photoluminescence spectra 78−95601
GaAs:Cr, single cryst., optical quenching spectrum, disappearance of stationary high-field domain 78−47830
GaAs:Cr, site symmetry of Cr ions, ground-state splitting, ballistic phonon expts. 78−95273
GaAs:Cr, strong quenching of thermally stimulated conductivity by elec. field *(Russian)* 77−1434
GaAs:Cr, surface and bulk recombination parameter determ. from photoluminesc. spectra 77−55820
GaAs:Cr, Te implantation, electron conc. and mobility profiles depend. on dose and annealing temp. 77−39607
GaAs:Cr, thermally grown, DLTS study of Cr trap density 80−96815
GaAs:Cr, VPE grown, exam. of doping GaAs using $Cr(CO)_6$ 78−72737
GaAs:Cr, VPE growth, carrier conc. profiles 79−74099
GaAs:Cr, zero-phonon struct. in Cr^{2+} ($3d^4$) optical absorption 80−60640
GaAs:Cr, Zn(Se) shallow impurity implantation, elec. props. after annealing 80−24465
GaAs:Cr,O, semi-insulating, photocond. anal. of levels 80−20243
GaAs:Cr,O semi-insulating monocrystal development and four-level model 80−88191
GaAs:Cr,Zn, implanted, doping profiles after laser annealing, elec. props. 80−2058
GaAs:Cr (Cr-Te), and undoped, transverse-acoustoelec.-voltage spectroscopy 79−99586
GaAs:Cr capless annealed, under As press., Cr redistrib., SIMS obs. 80−59503
GaAs:Cr diffusion profile meas. 80−6554
GaAs:Cr diode, high magnetosensitivity of negative resist. region 78−26946
GaAs:Cr erosion by laser beams *(Russian)* 78−2950
GaAs:Cr excess electron lifetime determ. by US method *(Czech)* 77−20336
GaAs:Cr photoconductivity, large scale fluctuations of impurity electostatic potential 77−8145
GaAs:Cr photoluminesc. meas. 78−6761
GaAs:Cr plane-parallel photocond. plate, oscills. in current and light intensity in laser irradiation 80−49819
GaAs:Cr plate, illuminated, oscills. in V-I charact. 80−11038
GaAs:Cr pulsed electron beam induced recrystallisation and damage, amorphous layer formation 80−34052
GaAs:Cr semi-insulating substrate, photoluminescence obs. of surface degradation during LPE growth 78−6865
GaAs:Cr semi-insulating wafer, heat treatment technique for no thermal conversion 80−100857
GaAs:Cr substrates and LPE layers, Au film deposition and annealing, Cr redistrib. 80−15312
GaAs:Cr wafers, semi-insulating, surface degradation by heat treatment at 900°C 77−80820
GaAs:Cr^{2+}, cluster calcs. of Cr^2 electronic states 79−87064
GaAs:Cr^{2+}, dynamic Jahn-Teller effect, relaxation time for reorientation 80−6798
GaAs:Cr^{2+}, effect of uniaxial stress and temp. variation on Cr^{2+} centre, EPR expts. 79−95636
GaAs:Cr^{2+}, Jahn-Teller effect for ion impurities 80−107753
GaAs:Cr^{2+}, US attenuation meas. of Jahn-Teller distorted Cr^{2+} centres 79−28048

III-V semiconductors continued
GaAs:$Cr^{2+}(3d^4)$, Jahn-Teller distortion, photoinduced charge conversion, EPR 78−10758
GaAs:Cr^{3+} ($3d^3$), EPR, 5K, evidence for strong Jahn-Teller effects 77−43875
GaAs:Cr(O), deep impurity levels, AC photocond. meas. 78−19082
GaAs:Cr(O), mechanism of thermal quenching of luminesc. and photocurrent stimulation 77−55821
GaAs:Cr(O), photocapacitance of deep levels obs. 79−38021
n-GaAs:Cr(Si), deep-level extrinsic photocond. response, decay at 4.2K 80−2420
GaAs:Cr(Te)(Zn), dopant influence on hardness 77−84777
GaAs:Cr(W), deep trapping centre exam. by thermally stimulated capacitor discharge method and luminesc. 77−55495
GaAs:Cs, oxidation process, UPS obs. 80−50511
n-GaAs:Cu, contaminated single cryst., deep level photoluminesc. model 78−68554
GaAs:Cu, diffused layers, photocond. spectra, hole conc. and mobility *(Russian)* 78−14758
n-GaAs:Cu, electron-phonon interaction in optical transitions between deep impurity level and allowed bands 79−42591
GaAs:Cu, Fe, Cr resistance thermometer expts., 0° to 200°C *(Russian)* 78−45627
p-GaAs:Cu, impurity photocond. and absorpt. coeff., Hall meas. 80−6770
GaAs:Cu, in MSM struct., phototrigger effect 78−56238
GaAs:Cu, LPE, photoelec. meas. of electron density for different Cu introduction methods 78−43437
GaAs:Cu, multiple scatt. Xalpha cluster model, impurity electronic states, dangling bond effect elimination 79−99504
GaAs:Cu, photoionisation spectrum of deep impurities in presence of weak electron-phonon interactions 79−51529
GaAs:Cu, sensitivity of impurity photocond., ordered surface irregularities 79−24018
GaAs:Cu, supersaturated solid solns., decomp., surface impurity content 78−51681
GaAs:Cu, Te, photoelec. props. 80−92936
GaAs:Cu contamination equlib. assessment 79−51134
GaAs:Cu melt grown, 1.36 eV band luminescence studies, edge emission 79−87510
GaAs:Cu(Cr) S-type diodes, thermal quenching of injection currents and current-voltage charact. 78−26942
p-GaAs:Cu(Zn), carrier drag by photons, carrier scatt. mechanisms 79−11185
n−GaAs:Fe, diffusion doped compensated layers 80−15125
p-GaAs:Fe, ESR line width, temp. depend., 4.2-330K 77−12195
GaAs:Fe, exchange-coupled pairs, ESR 79−11343
GaAs:Fe, for FET, VPE and characterisation 78−19672
GaAs:Fe, impurity atom charge exchange, Mossbauer spectroscopy 79−47050
GaAs:Fe, LPE, phase diagram 77−16509
GaAs:Fe, p-π-ν-n struct., photoelec. props. 80−107862
GaAs:Fe, photoionisation cross section meas. of deep levels 77−8042
GaAs:Fe, profile of impurity optical absorption bands 78−56509
GaAs:Fe, static magnetis. rel. to doping method and heat treatment conditions 77−36092
GaAs:Fe, superparamagnetism, spontaneous magnetization 79−11285
GaAs:Fe epitaxial diode, photocapacitance meas. 77−43708
GaAs:Fe LPE layers, negative resist. effects and deep acceptor model 77−72929
GaAs:Fe reverse biased π-ν-n struct., switching effect 80−88628
GaAs:Fe^{3+}, energy spectrum of deep centres, ESR spectrum 77−90023
GaAs:Fe(Co)(Cu)(Ni), substitutional impurity elec. struct. 80−88513
GaAs:Fe(Ni) O_2 effects on opt. props. 77−16350
p-GaAs:Ge, (111) surface, LPE grown, cryst. struct., phys. and chem. props. by Auger obs. 79−73386
GaAs:Ge, cryst. and epitaxial layers, ion-implanted, elec. props. 79−99542
n-GaAs:Ge, film, substrate temp. depend. of Ge incorporation during MBE 80−76196
GaAs:Ge, ion implanted, elec. props., comparison with Sn, Se and Te ion implanted samples 77−39879
GaAs:Ge, ion-implanted, photoluminesc., deep emission centres 80−34965
GaAs:Ge, LPE, on semi-insulating GaAs, film-substrate interface characterisation 78−72017
GaAs:Ge, LPE growth, Ge incorporation 78−27423
GaAs:Ge, MBE layers, complex free-carrier profile synthesis 80−54266
GaAs:Ge, mol. beam epitaxy of n- and p-types 80−10839
GaAs:Ge, solubility and point defect-dopant interactions 79−90689
GaAs:Ge, stress depend. of donor-acceptor recomb. energy 79−15113
GaAs:Ge, VPE, doping, electrophysical charcts. meas. 78−43493
GaAs:Ge, vap. grown, diatomic complex donor and acceptor model 78−80003
GaAs:Ge,Se transmutation shallow donor transition obs. 80−59925
n-GaAs:Ge epitaxial layer, ion-implantation doped, anomalous behaviour of impurities 78−18669
GaAs:Ge film, MBE grown, heavily doped, elec. props. rel. to growth parameters 80−100537
GaAs:Ge MBE power FETs with Sn surface impurities 80−80374
GaAs:Ge p-n junctions by mol. beam epitaxy 79−56289
GaAs:Ge(Sn), LPE layer growth, impurity effect on terrace form. 79−95288
GaAs:H amorphous sputtered films, high field cond. props. 80−44607
n-GaAs:H(D), ion implanted, carrier removal, capacitance-voltage profiling 80−84195
GaAs:Li diffused, lattice imperfections, TEM 77−80521
GaAs:Mg, photoluminesc. temp. depend., 4.2-293K 77−69878
GaAs:Mg ion implanted, photoluminesc. and annealing charcts. 77−16361
GaAs:Mg(Be)(Cd)(Zn), implanted, low temp. photolum. spectra 78−39583
GaAs:Mg(C)(Te)(Ge), ion implanted, laser annealing, ellipsometric and Hall meas. 79−73193
GaAs:Mn, LPE layer, near band edge photoluminescence, 2K, low excitation intensities 78−48218
GaAs:Mn, Mn-O association, EPR meas. 77−69677
GaAs:Mn, photoluminesc., emission props. and radiative mechanism 79−56842
GaAs:Mn epitaxial layers, fabrication and electrical props. 77−80859
GaAs:Mn(Ni), negative magnetoresist. meas. 77−51768

III-V semiconductors continued
GaAs:n, ion implantation, hole conc. and mobility profile meas. 78−23082
GaAs:Na, impurity solubility and diffusion 79−55930
GaAs:Ni, behaviour of Ni impurity in $3d^8$ state, optical absorption and photocond. meas. 78−47737
n-GaAs:Ni, negative photocond. at low temps., impurity levels 80−6900
GaAs:$Ni^{3+}(Co^{2+})(Fe^{+})$, EPR assessment of $3d^7$ transition metal impurity state 78−48031
n-GaAs:Ni(Zn), VPE, deep-level transient spectroscopy 80−34383
GaAs:O, annealing effects, optical absorpt. and I-V charcts. 80−29037
GaAs:O, deep level, Franck-Condon shift, photocond. and Hall effect study 80−70642
GaAs:O, deep traps, photocapacitance meas., complementary transition energy threshold determ. 79−19550
GaAs:O, defect states, IR absorption spectra meas. 77−4666
GaAs:O, electrolum., photolum., negative differential resist. rel. to recomb. processes 80−66304
GaAs:O, electronic struct., multiple-scatt. Xα mol. cluster model 80−15445
GaAs:O, evidence for metastable state of O centre, Schottky barrier photocapacitance meas. *(French)* 78−10556
GaAs:O, Fe, temp. depend. of ionisation energies of O and Fe levels, electroabsorption meas. 78−47736
GaAs:O, field depend. of radiative recomb. 80−20700
GaAs:O, high-resist., extrinsic photocond. meas. 77−85255
GaAs:O, impurity photocond. in high elec. field, 90K 78−19095
GaAs:O, junction barrier depletion region, capture from free-carrier tails 80−70802
GaAs:O, optical characterisation of deep O implants 77−55294
GaAs:O, oxygen-compensated single GaAs cryst., photoelec. memory 79−11184
GaAs:O, photocapacitance quenching effect 78−91727
GaAs:O, photocond., electron traps, level-broadening, 90 to 150K 78−60158
n-GaAs:O, photocond. associated with deep level at 0.4 eV 80−44640
n-GaAs:O, press. depend. of deep level associated with O, transient capacitance meas. 78−64000
GaAs:O, semi-insulating, excitation temp. effect on TSC 80−70717
GaAs:O, slow domains, origin 78−60132
n-GaAs:O carrier removal profiles meas. 78−56154
GaAs:O epitaxial film, impurity states, photocapacitance spectra 80−65625
n-GaAs:O film, influence of O on elec. props. 79−11252
GaAs:O p-ν-n structs., injection current and negative photocond., saturation mechanism 80−92967
GaAs:O(Cr), relax. semicond., Dember effects meas. 79−28372
GaAs:P films, epitaxial growth from melt with components introduced by ion bombardment 77−21044
GaAs:P^{+}, defect form. on P^{+} implantation at various temp., He^{+} backscatt. obs. 78−59828
GaAs:P^{+}, implantation profiles, backscatt. meas. 80−70238
GaAs:P^{+}, ion-implanted, refr. index, IR reflection and transmission meas. 77−1671
GaAs:$p^{+}(N^{+})$, struct. charcts. of radiation damage produced by high energy ion implantation 79−4340
GaAs:S, depth profiling using Cs^{+} bombardment and negative SIMS in UH vac. 79−99232
GaAs:S, implantation depth profiles of S^{+} and S_2^{+} using AES 79−55774
n-GaAs:S, Zn VPE film, LF current oscill., negative photocond. 77−80858
GaAs:S epitaxial layers, dopant conc. control method 77−1807
GaAs:S ion implantation, SiO_2 and Si_3N_4 encapsulants effects, expt. 77−11574
GaAs:S^{+} film, ion implanted carrier characterisation by cyclotron reson. 77−20472
GaAs:S(Se), ion-implanted, evaluation by contactless mobility meas. 79−1448
GaAs:S(Se), MBE grown, surface exchange doping using PbS(Se) captive sources 79−10864
GaAs:S(Si), ion-implanted, capless anneal in As controlled vapour 79−55767
GaAs:S(Te)(Zn), dislocation-free, TEM study of microdefects 79−82213
GaAs:Sb, resonance levels of isoelectronic impurities 80−107740
GaAs:Sb (100) surface, Sb-induced surface states 78−10529
GaAs:Se, and undoped sample, annealed, surface cond. change, n-p double layer 78−64095
GaAs:Se, fast diffusion of elevated temp. ion implantation, SIMS meas. 78−34527
GaAs:Se, Ga, dual species ion implantation, elec. charcts. 80−103377
GaAs:Se, implantation and laser annealing 80−24476
GaAs:Se, implanted, annealing with O-free CVD Si_3N_4 encapsulant 78−83834
GaAs:Se, implanted, depth profile, SIMS obs. 78−30655
GaAs:Se, implanted, multilayered encapsulation using SiO_2:As and Si_3N_4 79−11715
GaAs:Se, ion implanted, surface state study from photoreflectance 79−91465
GaAs:Se, ion implanted, Cr redistrib. during annealing, SIMS anal. 80−10570
GaAs:Se, ion implanted, laser annealing 80−24482
GaAs:Se, LPE growth, Ga-As-Se phase diagram 79−1849
GaAs:Se, multiple scatt. Xalpha cluster model, impurity electronic states, dangling bond effect elimination 79−99504
GaAs:Se, pulsed electron beam annealing, doping profiles 80−6421
GaAs:Se cathodoluminescence decay obs. with SEM and streak camera, 90 to 300K 80−97348
GaAs:Se depth profiles, Cs^{+} SIMS anal. appl. 79−39265
GaAs:Se ion implanted samples, Q-switched ruby laser annealing, improvement in elec. props. 80−100460
GaAs:Se ohmic contacts, pulsed electron beam annealing donor density, mobility 80−65678
GaAs:Se^{+}, Cs^{+}-SIMS and negative ion spectrometry 79−12882
GaAs:Se^{+}, implanted semi-insulating, pulsed electron and laser beam annealing effects on elec. charcts. 79−73196
GaAs:Se^{+}, TEM structural study, surface and interior damage 80−34025
GaAs:Se(Si), ion-implanted, capless annealing by melt-controlled ambient technique 80−75251
GaAs:Se(Sn), annealing kinetics of implanted donor ions 78−6079

III-V semiconductors continued
GaAs:Se(Zn) polycrystalline film, Hall effect, resistivity meas. 80−96911
GaAs:Si, accelerated growth rate effect on MBE, Hall mobility and photolum. meas. 80−104067
GaAs:Si, activation by multiply scanned electron beams 80−75246
n-GaAs:Si, B, IR absorpt. spectra, reson. and localised modes 80−66172
GaAs:Si, charge state of impurity atoms, positron annihilation meas. 78−39062
GaAs:Si, Cr, carrier concs. from Hall effect, microscopy, localised vibrational modes absorption meas. 78−56104
GaAs:Si, current-controlled growth, segregation and amphoteric behaviour 78−31346
GaAs:Si, donor-acceptor pair defects absorpt. bands 80−16064
GaAs:Si, electrical activity of Si 79−15145
GaAs:Si, electron irradiated, LPE layers and Bridgman crysts., IR absorption and Hall meas. 77−16345
GaAs:Si, encapsulated by SiO_2 and Si_3N_4, ion-implanted As profiles 79−4319
GaAs:Si, epitaxial layers, photo- and cathodoluminesc. 77−77285
GaAs:Si, faulted and prismatic loops, TEM obs. 77−51386
GaAs:Si, film, conversion of type of conduction stimulated by ion bombardment 77−4457
GaAs:Si, hardening by solute-vacancy pairs 77−4794
GaAs:Si, heteroface solar cells, diffusion lengths 78−47849
GaAs:Si, IR absorpt. bands, localised modes, Si-related defects 80−76054
GaAs:Si, influence of stoichiometry on recomb. processes 80−93396
GaAs:Si, ion implantation, thermal annealing, Hall meas., SIMS atomic profile meas. 80−75243
GaAs:Si, ion implanted, photoluminesc. 79−69887
n-GaAs:Si, ion implanted and/or annealed, As vacancy form., photolum. line 77−27875
GaAs:Si, ion implanted effect of anneal ambient and occurrence of compensated regions in Si implants 77−51394
GaAs:Si, ion-implanted, depth distrib. profiles of Si ions 77−43230
GaAs:Si, ion-implanted, elec. props. 79−46686
GaAs:Si, ion-implanted, annealing with Nd:glass laser 79−73194
GaAs:Si, LED, effect of struct., defects on quantum efficiency 79−11211
GaAs:Si, Li, IR absorpt., microstruct., charge compensation 80−107565
GaAs:Si, momentum distrib. of valence electrons, positron annihilation meas. 79−51530
GaAs:Si, neutron irrad., strain detection by local mode IR absorpt. meas. 77−69828
n-GaAs:Si, optically enhanced Hall mobility meas. 77−39884
GaAs:Si, positron lifetime temp. depend. 80−29826
GaAs:Si, pulsed laser annealing of implanted layers, defect structure and Hall effect meas. 79−69118
GaAs:Si, quantitative anal. with ion microanalyser *(Japanese)* 78−7292
GaAs:Si, single crysts., asymmetric deform. 79−23616
GaAs:Si, stacking fault prod. during heat treatment in As vapour 80−96547
n-GaAs:Si, thermally treated, photolum., acceptor levels obs. 79−38587
GaAs:Si, thick LPE layer growth and characterization 77−12511
GaAs:Si, transferred-electron devices by low-level ion implantation 80−92543
GaAs:Si,Cr, under layer of SiO_2, effect of annealing, on electron concentration and mobility, and impurity distrib. 79−4323
GaAs:Si defect density before and after Zn diffusion, SEM and TEM obs. 80−96529
GaAs:Si encapsulated with AlN, Si_3N_4 layers, photolum., annealing effects 80−20681
GaAs:Si epitaxial films, elec. and photoelec. props., impurity distrib. 80−7006
n-GaAs:Si LEC crystal, carrier conc., B acceptor centres, Hall meas. and IR spectra 78−6717
GaAs:Si LED, with anti-Stokes phosphor 79−11204
GaAs:Si LED p-n structures, speed *(Russian)* 79−43044
GaAs:Si LEDs grown from restricted soln.-alloy bulk, props. *(Russian)* 79−43043
GaAs:Si LPE layers, surface morphology, substrate misorientation, initial supercooling effects 80−34329
GaAs:Si layers, MBE growth, elec. and optical props., doping characts. 80−10819
GaAs:Si p-n junction, electrolum. power, injection current and temp. depend. *(Russian)* 77−16401
GaAs:Si p-n junction LED, electroluminesc. efficiency 80−71491
GaAs:Si p-n light-emitting structs., soln. of general minority carrier transport eqn. 80−15597
GaAs:Si p-n structs., effect of growing conditions on distrib. of recomb. parameters 80−39668
GaAs:Si p-n structure, radiative recombination region 78−52071
GaAs:Si(Cr), LPE, spiral growth patterns, dopants role 77−72800
GaAs:Si(Ge) LPE layers, luminesc. props. rel. to substrate quality 78−52583
GaAs:Si(Mg), doped and undoped, sputtered epitaxial films, elec. props. 79−78234
GaAs:Si(Se), ion implanted, laser annealing, microwave device appl. 79−69139
GaAs:Si(Sn), ion implanted, laser annealed, high doping levels 80−88181
n-GaAs:Si(Te), radiative transitions induced by modest annealing, photoluminesc. spectra 80−55158
GaAs:Si(Te)(S), vapour phase epitaxial grown layers, photoluminesc. and emission spectra 80−29774
GaAs:Si(s), generation of high mobility n layers, SIMS 80−103375
GaAs:Sn, 1.39 eV luminescence, injection level depend., freq. response and thermal quenching 78−19529
GaAs:Sn, dopant segregation during liq. phase electroepitaxy 80−54384
GaAs:Sn, doping characts. during LPE 79−10866
n-GaAs:Sn, heavily doped, nonalloyed ohmic contact form. by MBE and metallisation 79−7895
GaAs:Sn, implantation, annealing, impurity-defect struct., Mossbauer study 80−54269
GaAs:Sn, influence of growth process in doping profile and mobility profile during LPE 79−70000
GaAs:Sn, LPE, growth rate and temp. depend. of impurity incorporation 78−3063
GaAs:Sn, LPE layers, electronic props., depend. on Sn incorporation 78−87883

III-V semiconductors continued
GaAs:Sn, nature and conc. of point defects over conc. range 10^{17} to 6.10^{18} cm^{-3} 79−14802
n-GaAs:Sn, nonalloyed and in situ Ohmic contacts for FETs 79−56307
n-GaAs:Sn, photoluminesc. spectra 79−43031
GaAs:Sn, proton implantation and annealing behaviour *(Chinese)* 80−44224
GaAs:Sn, selective LPE, orientation dependent growth, luminesc. 77−12551
GaAs:Sn, solubility and point defect-dopant interactions 79−90688
GaAs:Sn, surface segregation of Sn during MBE, SIMS and AES 78−72031
n-GaAs:Sn, Te, compact IR laser source pumped by electron beam from field emission tube 79−59725
GaAs:Sn, Te, luminescence props. 79−52017
n-GaAs:Sn, VPE growth, reactor design 80−2956
GaAs:Sn diode, LPE grown, electron irrad. effect on characts. 80−39667
GaAs:Sn epitaxial layer, electronic props. and epilayer-substrate interface props. 77−89886
n-GaAs:Sn epitaxial layer, free carrier relax. time, transverse magneto-plasma refl. 77−90212
GaAs:Sn films, MBE grown, doping profiles, carrier mobilities, RHEED and AES obs. 79−1447
GaAs:Sn films, MBE power MESFETs 80−50563
GaAs:Sn layers for MESFET, MBE growth 77−15952
GaAs:Sn thermal diffusion from spin-on SnO_2/SiO_2 source 80−96691
GaAs:Sn^+, impurity-defect complex from ^{119}In implantation, Mossbauer study 80−59486
n-GaAs:Sn-p-GaAs:Ge-p-$Al_xGa_{1-x}As$:Ge heterostructure solar cells, LPE growth techniques 80−66977
GaAs:Sn(Be) MBE films, elec. characterization 79−91168
GaAs:Sn(Te), epitaxial film, influence of impurities on stacking fault energy 80−103371
n-GaAs:Sn(Te), pure and doped, diffusion of Sn, radiotracer profiles 79−23782
n-GaAs:Te, 0.93-0.99 eV luminesc. band characts. 78−19560
GaAs:Te, amorphous, ion implanted layers, optical refl., 1.5-7.0 eV 79−8152
n-GaAs:Te, elec. cond. and Hall coeff. temp. depend. meas., three band model 79−33287
n-GaAs:Te, electron-irrad., absorpt. spectra *(Russian)* 78−15200
GaAs:Te, Ge, compensated, activated cond. 77−76968
n-GaAs:Te, heavily doped, interband luminesc. intensity, heat treatment effect 78−72593
GaAs:Te, heavily doped degenerate semicond., Kondo effect 79−61053
GaAs:Te, heavily-doped, annealing-induced prismatic dislocation loops and elec. changes 78−51546
GaAs:Te, implanted and laser annealed, surface crystallinity, refl. and channelling meas. 79−95036
GaAs:Te, impurity cond., microcathode-luminesc. investig. 77−8666
n-GaAs:Te, interaction of positrons with dislocations 79−99974
GaAs:Te, ion implanted, abrupt dopant profile 77−1143
GaAs:Te, ion implanted, laser annealing 79−73192
GaAs:Te, ion implanted, surface crystallinity and stoichiometry of laser annealed samples 79−73198
GaAs:Te, ion implanted, ohmic contacts produced by laser-annealing 79−73585
GaAs:Te, ion implanted optical transitions in modulated reflectivity spectrum 79−73972
GaAs:Te, LPE, Te induced defects, rel. to growth conditions 78−6067
GaAs:Te, laser annealing of implanted Te 78−35400
GaAs:Te, microcathodoluminesc. of effect of struct. defects on radiative recomb. 79−11475
GaAs:Te, phonon-dislocation interactions, nonstoichiometry effect *(French)* 77−43298
GaAs:Te, powder, quadrupole interactions in NMR spectra 79−51880
GaAs:Te, preferential precipitation on dislocation loops 79−7612
GaAs:Te, recombination barrier, dark cond., photocond., and Hall mobility meas. 80−15559
GaAs:Te, solubility and point defect-dopant interactions 79−90687
GaAs:Te, superdilation and defects, lattice parameter meas. and carrier mobility 80−10569
n-GaAs:Te, vibr. props. of 1.0, 1.2 and 1.3 eV luminesc. centres 77−55823
GaAs:Te diffused LED, electron irrad. effect on characts. 80−39667
GaAs:Te influence of fluctuations of impurity pot. on Burstein-Moss effect 78−48240
GaAs:Te Schottky barrier solar cells, diffusion length determ. using minority carrier SEM 80−61359
GaAs:$Te^+(Se^+)(Sn^+)(Ge^+)$, ion implanted, laser annealing effect on elec. characts. 79−73195
GaAs:Te-implanted by laser-annealing, ohmic contacts 79−19658
GaAs:Te(Cd)(Mg)(B), ion implant depth distribs., AES and glow discharge optical spectroscopy meas. 80−65028
GaAs:V, ion implanted, luminesc., level splitting 80−97338
GaAs:W^{2+}, radiative transitions, photoluminesc. obs. 80−108271
GaAs:Zn, diffused, depth profile by photoluminesc., LED applic. 78−72587
GaAs:Zn, diffusion during LPE, impurity gradients and annealing effects 80−29882
GaAs:Zn, diffusion of Zn by two-temp. method, LED fabrication 80−49416
p-GaAs:Zn, diffusional doping, photoluminesc. in mag. field 77−16384
GaAs:Zn, distribution of radiative recombination efficiency 79−78725
GaAs:Zn, heavily doped, photolum. obs., above gap 80−29796
GaAs:Zn, high surface conc. Zn diffusion for good ohmic contact 77−11575
GaAs:Zn, implanted, furnace annealed, electrical, Rutherford backscattering and TEM meas. 80−100272
GaAs:Zn, implanted, hole conc. and mobility profiles meas. 78−23081
GaAs:Zn, implanted, laser annealing, elect., Rutherford backscattering and SEM meas. 80−100273
GaAs:Zn, ion implanted, TEM study after laser and furnace annealing 80−70234
GaAs:Zn, laser annealing of implanted layers 77−55296
p-GaAs:Zn, luminescent, ion doped MBE growth 80−44436
GaAs:Zn, MBE with ionized beam doping 77−77418
p-GaAs:Zn, Mn, degenerate, tunnel p-n junction and semicond.-metal struct., I-V characts. 78−72252
p-GaAs:Zn, optical absorpt. spectra and photocond. after 2 MeV electron irrad. *(Russian)* 77−69859

III-V semiconductors continued
GaAs:Zn, pulsed laser annealing, expt. 78−34828
p-GaAs:Zn, Raman scatt. by LO phonon-plasmon coupled modes, wave vector non-conservation 80−16033
GaAs:Zn, Se, double doping during LPE, exam. of elec. cond. and Hall effect 79−4923
GaAs:Zn, sign inversion of the linear photogalvanic effect *(Russian)* 80−80321
GaAs:Zn, surface conc. control 79−55758
GaAs:Zn (110), spin polarised electron production by photoemission from Cs-O overlayer 79−95903
GaAs:Zn epitaxial layers, composition and Zn carrier conc. 80−25585
GaAs:Zn films, VPE growth and photoluminesc. props. 79−38642
GaAs:Zn ion implanted ionic alloy, electrophysical props., annealing 80−39133
GaAs:Zn MBE layers, ionized beam doping, elec. and optical charact. 79−37721
GaAs:Zn optically pumped ribbon-whisker laser, picosecond pulses 80−99771
n-GaAs:Zn substrate, ion implantation as predeposition process 79−19268
GaAs:Zn-$Al_{0.5}Ga_{0.5}As$ p-n junction, surface layer effect on surface recombination current 79−69585
GaAs:Zn(Cr), As precipitation at dislocations, TEM study 80−79820
GaAs:Zn(S), LPE, and doping charact. 79−33948
GaAs:Zn(Se), recrystn. of implanted amorphous layers, TEM and channelling obs. 77−89459
GaAs:Zn(Si)(Sn), etching rel. to dopant and carrier conc. 77−16704
GaAs/(Ga,Al)As, DH laser diode, electroluminescence near 1 eV 80−60682
GaAs/(GaAl)As channelled substrate narrow stripe lasers, with quarter-wavelength facet coatings 80−99746
GaAs/$Al_xGa_{1-x}As$ heterostruct., anomalous elec. and optical charact. 80−2865
GaAs/Al-Au interfaces, atomic interdiffusion, soft XPS studies 80−65302
GaAs/AlGaAs, DH laser, degradation under Ar laser irrad. 79−98375
GaAs/AlGaAs DH wafers and lasers, defect struct., X-ray topography 79−50312
GaAs/AlGaAs integrated twin guide injection lasers prepared by LPE, coupling coeff. and coupling length meas. 79−81458
GaAs/anodic oxide interface, characterisation of proposed model 80−103754
p-GaAs/Au-Be ohmic contact form. by ionised-cluster beam deposition 77−32528
GaAs/Au-Ge/Au structure, ohmic contact behaviour, alloying time effect 79−19659
GaAs/Au-Ge/Ni, Schottky barrier energy var. with interdiffusion 77−20435
GaAs/Au-Ge/Ni contact system, alloying behaviour, microprobe AES and X-ray diffr. 80−54548
GaAs/Au-Ge-Ni alloy metal-semiconductor thermoelectric coolers, effects of contact resist. and dopant conc. 80−81481
n-GaAs/Au-Ti contacts, interdiffusion and Schottky barrier height variations 77−89849
n-GaAs/Au-W contacts, interdiffusion and Schottky barrier height variations 77−89849
n-GaAs/chalcogenide glass, elec. props. and band diagram 79−99609
GaAs/GaAlAs crowding effect lasers using whispering gallery mode on semi-insulating GaAs substrates 80−58589
GaAs/GaInP DH, MBE grown, optically pumped laser action at 77K 80−95890
GaAs/HBr system, heterogeneous reactions, modified entrainment method appls. 79−23551
p-GaAs/heptyl viologen system, appl. in photoelectrochemical cells and photoelectrochromic displays 80−76640
GaAs/In_2O_3-SnO_2 solar cell, fabrication, charact. and interfacial chemistry 80−21401
GaAs/In-Ge-Ag, semiconductor surface condition, effect on ohmic contact barrier height 77−4435
n-GaAs/K_2Se-K_2Se_2-KOH/C solar cell, Ru (III) chemisorption on photoanode, effect on performance 80−3516
n-GaAs/K_2Se-K_2Se_2-KOH/C liq. junction cell, effect of Ru ion chemisorption on grain boundaries 80−55879
GaAs/metal contacts, recent developments in investigations of preparation and props. *(French)* 80−107909
n-GaAs/N-GaAlAs heterojunctions, microwave detection 79−54186
GaAs/Ni film contact system, alloying reaction 80−96747
GaAs/Ni-Ge-Au cathode struct., with enhanced injection efficiency, contact resist. 77−20431
GaAs/oxide interface, interface states obs. by electrochem. method 79−99626
n-GaAs/Pt/Cr Schottky contact, barrier height change due to heat treatment 79−47165
p-GaAs/rare earth metal contacts, surface pot. barrier 80−60086
GaAs/SiO_2, substrate/film system, Ga content in SiO_2 after annealing at 730-940°C 78−43255
GaAs/SiON substrate/film system, interface formation during CVD, modelling 80−24764
n-GaAs/ZnSe:Mn/Au low threshold thin film DC electrolum. cell, pulse-excited charact. 80−76081
GaAs-(Ga, Al)As heterostructure transmission photocathodes, charact., and epitaxial growth *(French, English)* 78−52616
GaAs-(Ga,Al)As light modulators and distributed Bragg reflector laser, monolithic integration 78−50944
GaAs-(GaAl)As, DH laser, injection enhanced dislocation glide under uniaxial stress 77−27885
GaAs-(GaAl)As channelled substrate buried heterostruct. injection laser, fabrication 77−7087
GaAs-(GaAl)As DH injection laser with pillbox resonator, charact. and fabrication 80−58581
GaAs-(GaAl)As DH lasers, automated LPE growth, CW reliability tests 80−20804
GaAs-(GaAl)As DH stripe lasers, CW life tests 79−98383
GaAs-(GaAl)As epitaxial layers and DH lasers, deep centre 1.02 eV luminesc. 78−80387
GaAs-(GaAl)As injection lasers with circular resonator 80−74377
GaAs-(GaAl)As LOC-DBR laser, high differential quantum efficiency 78−79031
GaAs-(GaAl)As laser, SiO_2 stripe geometry, for wide band optical communication systems 78−42358

III-V semiconductors continued
GaAs-(GaAl)As terraced-substrate injection lasers, fabrication and output charact. 79−50310
GaAs-(GaAl)As terraced substrate laser, fundamental transverse and longit. mode oscill. 79−98357
GaAs-$(SN)_x$, solar cell fabrication and efficiency 80−26143
GaAs-$(SN)_x$ semiconductor-polymer solar cell 79−15219
GaAs-Al (Ni-AuGe) contacts, elec. charact. 80−29476
GaAs-Al interface, ellipsometric anal. methods, correl. between optical props., thickness and surface roughness meas. *(German)* 80−55215
GaAs-Al interface, metal overlayer effect on semicond. (110) surface states 77−4441
p-GaAs-Al interface, produced by diffusion method using heavily doped GaAs, rectifying props. 79−28409
GaAs-Al interface, struct. study by X-ray total-external-refl.-Bragg diffr. 80−34321
GaAs-Al interface, thermal ageing of Al film, optical microscopy and SEM obs. 77−20203
GaAs-Al interfaces, chemically induced charge redistrib. 79−33342
GaAs-Al Schottky barrier diode, prep. by MBE on GaAs, and charact. 78−72257
n-GaAs-Al surface barrier diodes, influence of exciton effects on photo-EMF spectrum 78−10557
GaAs-$Al_{0.27}Ga_{0.7}$ $_3$As Dh lasers grown by MBE, influence of growth conditions on threshold current density 80−58587
GaAs-$Al_{0.2}Ga_{0.8}As$ periodic layered media, optical surface waves 78−43946
p-GaAs-$Al_{0.3}Ga_{0.7}As$, cladded dielec. waveguide, loss meas. using Raman scatt. 79−81539
GaAs-$Al_{0.3}Ga_{0.7}As$ n-N heterojunction, LPE grown, cond. band discontinuity, C-V profiling meas. 80−70801
GaAs-$Al_{0.3}Ga_{0.7}As$ laser diode, spontaneous radiation transfer 80−91796
GaAs-$Al_{0.4}Ga_{0.6}As$, p-n heterojunction, quantum confinement and compositional grading effects on band struct. 79−87151
GaAs-$Al_{0.5}Ga_{0.5}As$-Cr/Au MIS capacitors, charact. meas. 78−95371
GaAs-$Al_{1-x}Ga_xAs$ lar, PbO-SiO_2 glass optical coating 78−71113
GaAs-Al_2O_3 anodic oxide interface, elec. props., rel. to MESFET passivation 80−49934
GaAs-Al_2O_3 interface, fabricated by interactive oxidation, props. 80−49935
GaAs-Al_2O_3 MIS struct., interface props. and MISFET fabrication 79−65557
GaAs-Al_2O_3-Al backwall MIS Schottky barrier solar cell, anal. model 80−85289
GaAs-$Al_xGa_{1-x}As$ transverse junction lasers with low threshold current prep. by MBE on semi-insulating substrates 80−58588
GaAs-$Al_xGa_{1-x}As$, optically pumped multilayer struct. and DH, laser oscillations 77−3589
GaAs-$Al_xGa_{1-x}As$, integrated twin-guide laser with distrib. Bragg reflectors 77−19310
GaAs-$Al_xGa_{1-x}As$, DH laser, lateral current confinement by reverse biased junction 77−58339
GaAs-$Al_xGa_{1-x}As$, single mode optical rib waveguides, MOS control of switches 78−1432
GaAs-$Al_xGa_{1-x}As$, DH LED, self-aligned sphere lens array characteristics *(German)* 78−38014
GaAs-$Al_xGa_{1-x}As$, single-mode rib waveguide switches electro-optical modulation 78−46839
GaAs-$Al_xGa_{1-x}As$, optically pumped taper coupled laser, second order Bragg reflector 78−50788
GaAs-$Al_xGa_{1-x}As$, DH laser, effect of bulk nonradiative recombination 78−82967
GaAs-$Al_xGa_{1-x}As$, monolithic integrated optics, rib waveguide switches with MOS electrooptic control 78−87168
GaAs-$Al_xGa_{1-x}As$, film waveguide, heterojunction lasers with Bragg mirrors, threshold charact. 79−23095
GaAs-$Al_xGa_{1-x}As$, carrier transport across heterojunction interfaces 79−47158
GaAs-$Al_xGa_{1-x}As$, negative differential resist., real-space electron transfer 80−6958
GaAs-$Al_xGa_{1-x}As$, heterojunction and superlattice, magnetophonon reson., polaron mass 80−44715
GaAs-$Al_xGa_{1-x}As$, current transverse junction lasers, low threshold, MBE prep. 80−83614
GaAs-$Al_xGa_{1-x}As$ buried-heterostructure laser, wideband optical sources *(German)* 78−37904
GaAs-$Al_xGa_{1-x}As$ buried-heterostructure lasers, current injection confinement, MBE/LPE hybrid technique 80−74374
GaAs-$Al_xGa_{1-x}As$ CW-diode laser, coupled to freq.-selective external cavity, self-pulsing 77−61982
GaAs-$Al_xGa_{1-x}As$ channelled-substrate-planar-struct. laser with lateral-evanescent-field distributed feedback 79−98398
GaAs-$Al_xGa_{1-x}As$ current injection multi-quantum-well heterostructure lasers, MBE grown 80−19042
GaAs-$Al_xGa_{1-x}As$ DH laser for optical communication 77−50684
GaAs-$Al_xGa_{1-x}As$ DH laser, high-temp. degradation *(German)* 78−37884
GaAs-$Al_xGa_{1-x}As$ DH laser, modulation with coherent light injection *(German)* 78−37922
GaAs-$Al_xGa_{1-x}As$ DH laser structures, high-resolution composition profiling with photolum. 78−71101
GaAs-$Al_xGa_{1-x}As$ DH laser, room temp. threshold current 78−79019
GaAs-$Al_xGa_{1-x}As$ double heterojunctions, dark-line defects and recomb. centres, scanning photocurrent microscopy 79−35822
GaAs-$Al_xGa_{1-x}As$ DH lasers, MBE grown, low current threshold, high lasing uniformity 79−64223
GaAs-$Al_xGa_{1-x}As$ DH broad contact pulse lasers, second-order coherence props. 80−23685
GaAs-$Al_xGa_{1-x}As$ DH lasers, very low current threshold, MBE grown 80−43353
GaAs-$Al_xGa_{1-x}As$ DH lasers, MBE grown, substrate temp. effect on current threshold 80−48243
GaAs-$Al_xGa_{1-x}As$ differentially doped heterojunction interface, two-dimens. electron gas obs. 80−49886
GaAs-$Al_xGa_{1-x}As$ DH laser, MBE grown, CW electro-optical props. 80−102725
GaAs-$Al_xGa_{1-x}As$ epitaxial layer heterointerface, toroidal defect obs. 79−77933
GaAs-$Al_xGa_{1-x}As$ electro-optic frequency- and polarisation-modulated injection laser 80−91810
GaAs-$Al_xGa_{1-x}As$ films for optical devices, masked MBE 78−38100

III-V semiconductors continued
GaAs-$Al_xGa_{1-x}As$ heterostructure superlattice, construction of bound states in continuum 77−32076
GaAs-$Al_xGa_{1-x}As$ heterojunction, MBE, diffusion across interface, optical annealing expts. 78−2305
GaAs-$Al_xGa_{1-x}As$ heterojunction, avalanche phototransistors, detectivity and noise 78−2558
GaAs-$Al_xGa_{1-x}As$ heterojunctions, MBE grown, photocollection efficiency and interface charges 79−11199
GaAs-$Al_xGa_{1-x}As$ heterostruct., photon recycling, diffusion length and lifetime determ. 79−47499
GaAs-$Al_xGa_{1-x}As$ heterojunctions, inelastic light scatt. 79−65867
GaAs-$Al_xGa_{1-x}As$ heterojunctions, LPE grown, 2D electron gas obs. 79−99606
GaAs-$Al_xGa_{1-x}As$ heterojunction interface, two-dimensional hole gas obs., Shubnikov-de Haas meas. 80−80357
GaAs-$Al_xGa_{1-x}As$ heterostructures, real-space electron transfer by thermionic emission, analytical model 80−100512
GaAs-$Al_xGa_{1-x}As$ integrated optics structs., dry processing 77−27383
GaAs-$Al_xGa_{1-x}As$ integrated injection lasers and detectors with etched reflectors 77−62074
GaAs-$Al_xGa_{1-x}As$ integrated lasers and detectors fabricated by wet chemical etching 77−88961
GaAs-$Al_xGa_{1-x}As$ injection laser, direct modulation and spectral props. *(German)* 78−37921
GaAs-$Al_xGa_{1-x}As$ LPE heterojunction, interface states 78−19128
GaAs-$Al_xGa_{1-x}As$ multilayer struct., MBE, selective area growth using Si shadow masks 77−85946
GaAs-$Al_xGa_{1-x}As$ modulation-doped heterojunction superlattices, electron mobilities 79−7877
GaAs-$Al_xGa_{1-x}As$ multilayer, photoluminesc., electron spin orientation 80−25453
GaAs-$Al_xGa_{1-x}As$ MOS rib waveguide polarizers 80−64207
GaAs-$Al_xGa_{1-x}As$ MOS rib waveguide polariser, modulator and isolator 80−64217
GaAs-$Al_xGa_{1-x}As$ multilayers, two-dimens. transport at high mag. fields 80−65724
GaAs-$Al_xGa_{1-x}As$ optical modulator for coupled waveguides 78−71235
GaAs-$Al_xGa_{1-x}As$ proton-isolated DH laser, threshold current optimisation *(German)* 78−37905
GaAs-$Al_xGa_{1-x}As$ single mode rib waveguide COBRA switches, MOS control 77−88970
GaAs-$Al_xGa_{1-x}As$ single heterostructure laser diode, pulse operating, anal. of temp. decrease in active region 78−13706
GaAs-$Al_xGa_{1-x}As$ stripe geometry DH laser, threshold current density, effect of optical mode losses 78−59008
GaAs-$Al_xGa_{1-x}As$ superlattice, mag. field induced dimensionality change 78−64381
GaAs-$Al_xGa_{1-x}As$ structures for DH lasers, LPE *(Polish)* 79−4922
GaAs-$Al_xGa_{1-x}As$ strip buried heterostructure laser densely packed monolithic linear array 79−45956
GaAs-$Al_xGa_{1-x}As$ strip-buried heterostruct. laser with distributed feedback 79−76696
GaAs-$Al_xGa_{1-x}As$ strip buried heterostructure lasers 79−81425
GaAs-$Al_xGa_{1-x}As$ superlattice, electronic props. 80−11080
GaAs-$Al_xGa_{1-x}As$ strip buried heterostructure laser with passive DBR 80−14352
GaAs-$Al_xGa_{1-x}As$ transverse junction stripe laser, single-mode oscillation *(German)* 78−37885
GaAs-$Al_xGa_{1-x}As_x$, heterojunction photodiode, electric and photoelectric characts. 77−55604
GaAs-$Al_xGa_{1-x}As$-GaP photocathodes, minority carrier diffusion length determ. by photoluminesc. 80−103992
GaAs-AlAs, alternate monolayer single cryst., optical waveguides 77−72065
GaAs-AlAs, epitaxial layer, partition coefficients of impurities 77−15443
GaAs-AlAs, epitaxial struct. with alternate layer comp. modulation, fabrication and characterisation 77−1322
GaAs-AlAs, heterolight diodes, mesoconstruction, output *(Russian)* 77−12441
GaAs-AlAs, heterostructure, effects of cation order on energy bands 80−11081
GaAs-AlAs, large area p-n heterojunctions, vapour phase epitaxially grown, elec. characterisation 77−11990
GaAs-AlAs, one-dimensional superlattice, X-ray diffr. 77−27860
GaAs-AlAs, pseudobinary alloy, phase diagram calc. 78−52786
GaAs-AlAs (100) interface, tight binding calc. of electronic struct. 78−95342
GaAs-AlAs alternating epitaxial monolayers, Raman scatt. and zone-folding effects 77−90208
GaAs-AlAs alternating monolayers, zone folding effects on phonons 78−72510
GaAs-AlAs and related monolayer heterostructures, pseudopot. calc. 78−60198
GaAs-AlAs heterojunction, recombination currents 78−14806
GaAs-AlAs layered films, MBE prep., struct., rel. to optical props. 79−77950
GaAs-AlAs layered superlattices, deposited by MBE, exam. of crystal growth kinetics 78−72739
GaAs-AlAs mixed crystal, optical obs. of multiple-photon absorpt. NMR *(Russian)* 77−90073
GaAs-AlAs mixed crystals, valence charge distrib. and elec. field gradients 80−80239
GaAs-AlAs multilayer heterostructure laser, power and photoelectroluminescence characts. 80−53297
GaAs-AlAs superlattice, folded acoustic phonons obs., Raman scatt. 80−88996
GaAs-AlAs system, diffuse scatt. of X-rays by simple crysts. *(German)* 78−30517
GaAs-AlGaAs CW laser coupled to external cavity, multimode operation, output intensity low freq. pulsations 79−68394
GaAs-AlGaAs DH, improved LPE growth, lasing characts. 77−81229
GaAs-AlGaAs DH injection laser, emission energy, wavelength depend. in strong mag. fields 80−48248
GaAs-AlGaAs DH injection laser with stripe contacts, radiation pulse stepped shape 80−91799
GaAs-AlGaAs DH laser, rapid degradation caused by process-induced defects 77−71985
GaAs-AlGaAs DH laser, improved lifetime by defects reduction during LPE 77−75547
GaAs-AlGaAs DH laser, impedance meas. 78−17939

III-V semiconductors continued
GaAs-AlGaAs DH lasers, multipeak freq. response obs. 78−17940
GaAs-AlGaAs DH laser with buried facet 78−55373
GaAs-AlGaAs DH laser, degradation rate rel. to photocurrent 80−28233
GaAs-AlGaAs DH laser structure, defect assessment by differentiated cathodolum. topography 80−59819
GaAs-AlGaAs DH layers, tapered growth by wipingless LPE 77−66594
GaAs-AlGaAs distributed Bragg reflector integrated twin-guide laser, temp. characts. 78−87064
GaAs-AlGaAs double heterostructure, optically induced dislocation glide, cooperative phenomena 78−74911
GaAs-AlGaAs half-ring laser, fabrication by deep Zn diffusion 78−17960
GaAs-AlGaAs heterojunction superlattices, electron mobilities 80−29473
GaAs-AlGaAs heterojunction superlattices, obs. of intersubband excitations in multilayer two dimensional electron gas 80−29753
GaAs-AlGaAs heterostructure thyristors, operation and elec. characts. 79−7891
GaAs-AlGaAs high-radiance LED for optical communication systems, power and modulation bandwidth 78−42416
GaAs-AlGaAs LPE growth, wipinglass method for DH laser *(Japanese)* 78−48304
GaAs-AlGaAs LPE layers, baking effect on surface morphology 78−14625
GaAs-AlGaAs laser array packaged with fibre lightguide array on Si substrate 78−46611
GaAs-AlGaAs multilayer stack, optical surface wave propag. 78−38090
GaAs-AlGaAs photoelectroluminescent diodes, characts., radiant power 80−6972
GaAs-AlGaAs solar cells *(Rumanian)* 80−93877
GaAs-AlGaAs solar cells with valley-transferred electrons for voltage and efficiency enhancement 80−93956
GaAs-AlGaAs superlattice, selective transmission of HF phonons 80−34154
GaAs-AlGaAs transverse junction stripe laser, single mode behaviour after 12000 hr ageing test 78−66831
GaAs-AlGaAs two-junction stacked solar cell, growth and characterisation 80−16811
GaAs-AlGaAs:Si heterojunction interface, two-dimens. electron gas, Hall effect and cyclotron reson. meas. 79−65530
GaAs-Al(Au) Schottky barrier diodes, Richardson consts. 77−20424
GaAs-Al(Ga)(Ge), surface reactions and interdiffusion, photoemission study 80−49532
n-GaAs-anodic oxide interface, C-V and I-V characts. 77−89863
GaAs-anodic oxide interfaces, struct. and chem. props., Raman scatt. obs. 79−47168
n-GaAs-anodic oxide MIS devices, inversion and accumulation layer form. at elevated temps. 79−60934
GaAs-anodic oxide MOS struct. oxide and interface props. 79−60929
GaAs-anodic oxide MOS struct., interface state band 79−60930
n-GaAs-anodic oxide-Al MOS struct., elec. instabilities and annealing effects 79−60928
GaAs-Au, quenching of exciton luminesc. by surface elec. field 80−29801
GaAs-Au, Schottky barrier energy var. with interdiffusion 77−20435
GaAs-Au interface, atomic modulation of interdiffusion, effect of reactive Al monolayers 80−49432
GaAs-Au polycrystalline Schottky barriers, transition with grain size from electrode-limit to bulk-limited cond. 80−65676
n-GaAs-Au Schottky barrier diode, thermally assisted tunnelling currents 77−20412
GaAs-Au Schottky barrier diodes, fabrication using LPE 77−40357
GaAs-Au Schottky barriers, PES and depth profiling obs. 79−42641
GaAs-Au Schottky diode, electroless plating of Au, fast characterisation of epitaxial layers 79−33347
n-GaAs-Au-Mo, RF sputtering, elec. props. of contacts, compensating damage centres form. 80−34507
GaAs-Au(Ag) Schottky barrier solar cells, interface problems, AES, SIMS and XPS study 80−89627
n-GaAs-Au(Al) Schottky diodes, interface state density model 77−80840
GaAs-based mixed cryst. form. by ion beam synthesis, vibr. anal. 80−103376
GaAs-Br_2(-Zn) system, filamentary cryst. prep. 78−52650
GaAs-C, ion implanted, obs. of localised vibrational mode absorption, effects of annealing temp. 80−16068
p-GaAs-$Cd_{1-x}Zn_xS$ heterojunctions, elec. and photovolt. props. rel. to growth technique 80−29466
GaAs-CdS n-n voltage-enhanced photoanode, solar cell efficiency 78−14810
n-GaAs-chalcogenide glass heterojunction, fabrication, characterization, switching 80−49892
GaAs-Cr Schottky diode, I-V characts., inverse branch, effect of dislocation defects *(Russian)* 79−15217
GaAs-Cs-O, negative electron affinity, secondary emission characts. 78−11031
GaAs-Cs-O, negative electron affinity, refl. of slow electrons, 0.4-3 eV 78−11038
GaAs-Cs-O film, polycryst., secondary emission props., activating coating effects 78−2957
GaAs-Cs-O photoemitter, negative electron affinity, fabrication and characts. 78−2979
GaAs-Cu:Tl, cathode luminescence spectra, Hall effect, cryst. defects 80−76087
GaAs-disperse metal film, photoluminesc. at interface 78−26953
n-GaAs-electrolyte interface, surface pretreatment rel. to photocurrent, spectral response 80−3204
GaAs-electrolyte interface, surface barrier electroreflection anisotropy *(Russian)* 80−34895
GaAs-element systems, solidus curves calc. for liq. phase epitaxy technology 77−8768
n-GaAs-ferrite layer struct., boundary spin wave amplification *(Russian)* 77−73016
GaAs-Ga, (110) interface electron states, photoemission study, chemical shift, surface charge redistrib. 78−72259
GaAs-$Ga_{0.7}Al_{0.3}As$ channelled substrate buried heterostructure injection lasers 77−38932
GaAs-$Ga_{0.7}Al_{0.3}As$ (001), (211), threading dislocation in single layer heteroepitaxial struct., bowing 79−65341
GaAs-$Ga_{0.7}Al_{0.3}As$ n-n heterojunction, LPE, rectification 80−49888
GaAs-$Ga_{0.8}Al_{0.2}As$ layered struct., LPE, optical surface waves 78−48244

III-V semiconductors continued
GaAs-$Ga_{1-x}Al_xAl$ superlattice, reson. Raman scatt., 2-D quantum states 77−8577
GaAs-$Ga_{1-x}Al_xAs$, DH, dark line defects induced by mech. bending 77−683
GaAs-$Ga_{1-x}Al_xAs$, monolithically integrated DFB diode laser, freq. multiplexing 77−702
GaAs-$Ga_{1-x}Al_xAs$, DH, improved LPE growth method 77−4746
GaAs-$Ga_{1-x}Al_xAs$, DH distributed Bragg reflector laser, room temp. operation 77−7085
GaAs-$Ga_{1-x}Al_xAs$, optically pumped ring laser fabricated by LPE over chemically etched channels 77−10958
GaAs-$Ga_{1-x}Al_xAs$, LPE growth for solar cells 77−77427
GaAs-$Ga_{1-x}Al_xAs$, DH laser Al_2O_3 facet coating effect on degradation 78−13722
GaAs-$Ga_{1-x}Al_xAs$, DH laser, characts. exam. for communication appl. 78−37891
GaAs-$Ga_{1-x}Al_xAs$, superlattice umklapp processes in resonant Raman scattering 78−64362
GaAs-$Ga_{1-x}Al_xAs$, ultrathin layer heterostruct., pseudopot. calcs. 78−95343
GaAs-$Ga_{1-x}Al_xAs$, single-heterostructure laser diode with short current pulses, heat spreading analysis 79−76690
GaAs-$Ga_{1-x}Al_xAs$, semiconductor superlattices by MBE 79−95939
n-GaAs-$Ga_{1-x}Al_xAs$, superlattice, subband struct. and optical spectra, self-consistent calc. 80−15443
GaAs-$Ga_{1-x}Al_xAs$, variable band gap, photo-EMF 80−20296
n-GaAs-$Ga_{1-x}Al_xAs$, heavily doped superlattice, electronic props., perpendicular low temp. mobility 80−65660
GaAs-$Ga_{1-x}Al_xAs$ buried DH diode laser fabrication 77−75565
GaAs-$Ga_{1-x}Al_xAs$ DH lasers, X-ray topographic obs. of lattice defects rel. to degradation 77−15420
GaAs-$Ga_{1-x}Al_xAs$ DH lasers, long-term degradation due to facet erosion 77−50672
GaAs-$Ga_{1-x}Al_xAs$ DH strip CW laser for optical transmission *(German)* 77−68222
GaAs-$Ga_{1-x}Al_xAs$ double heterostructure LED and injection laser transmitters 77−68282
GaAs-$Ga_{1-x}Al_xAs$ DH crystals, <110> oriented dark line defects 77−80510
GaAs-$Ga_{1-x}Al_xAs$ DH injection laser, curved junction stabilized filament, struct. and characts. 78−33744
GaAs-$Ga_{1-x}Al_xAs$ DH laser, curved stripe, operation and appl. 78−42341
GaAs-$Ga_{1-x}Al_xAs$ DH lasers, electron beam induced current microscopy 80−95899
GaAs-$Ga_{1-x}Al_xAs$ half-ring laser, fabrication by LPE over chemically etched channels 77−684
GaAs-$Ga_{1-x}Al_xAs$ heterostruct. superlattice, props. in high mag. fields 79−73570
GaAs-$Ga_{1-x}Al_xAs$ heterostructures, quantum size effect in superlattices, electronic props. 80−29471
GaAs-$Ga_{1-x}Al_xAs$ laser, low threshold room temp. embedded DH, fabrication and characts. 77−681
GaAs-$Ga_{1-x}Al_xAs$ laser, optically pumped, longit. mode broadening due to transient heating 77−61953
GaAs-$Ga_{1-x}Al_xAs$ LPE wafer stress-free dislocation generation 77−75527
GaAs-$Ga_{1-x}Al_xAs$ multilayer struct., growth over preferentially etched channels, MBE 77−40388
GaAs-$Ga_{1-x}Al_xAs$ n^+-ν-n junction, avalanche carrier multiplication *(Russian)* 78−76140
GaAs-$Ga_{1-x}Al_xAs$ repeated monolayer heterostructure, electronic struct. 77−66197
GaAs-$Ga_{1-x}Al_xAs$ red LED, 4% quantum yield *(Russian)* 77−85809
GaAs-$Ga_{1-x}Al_xAs$ semicond. laser diodes, degradation, lattice defects *(Japanese)* 77−34889
GaAs-$Ga_{1-x}Al_xAs$ single heterostructure laser diode, anal. of temp. rise under transient-state conditions 77−61949
GaAs-$Ga_{1-x}Al_xAs$ superlattices, resonance enhanced Umklapp Raman process 78−39547
GaAs-$Ga_{1-x}Al_xAs$ superlattice, sub-band dimensionality 78−63981
GaAs-$Ga_{1-x}Al_xAs$ stripe geometry lasers 79−94245
GaAs-$Ga_{1-x}Al_xAs$ superlattice, Raman scatt., polar phonon anisotropy 80−45052
GaAs-$Ga_{1-x}Al_xAs$-$Ga_{1-y}Al_yAs$ n^+-i-n heterostructure, electroluminesc. characts., 80 to 330K *(Russian)* 79−28404
GaAs-$Ga_{1-x}Al_xGaAs$ heterostructure, electron tunnelling theory 78−47861
GaAs-$Ga_{2.2}Al_{0.8}As$:Be, LPE, diffusion of Be into GaAs substrate 80−103517
GaAs-$Ga_xAl_{1-x}As$, injection laser with external resonator, mirrors of Michelson interferometer 79−81455
GaAs-$Ga_xAl_{1-x}As$ CW stripe geometry laser fabrication and performance 77−38933
GaAs-$Ga_xAl_{1-x}As$ DH diode lasers, single longitudinal mode operation 78−1243
GaAs-$Ga_xAl_{1-x}As$ double heterojunction laser structures, LPE growth with double source method 79−28962
GaAs-$Ga_xAl_{1-x}As$ DH laser wafers, active layer inhomogeneities 79−74106
GaAs-$Ga_xAl_{1-x}As$ DH lasers, dislocation effects 79−82221
GaAs-$Ga_xAl_{1-x}As$ DH laser material crystal cathodoluminescence, SEM analysis 80−97349
GaAs-$Ga_xAl_{1-x}As$ heterostructure, depend. of efficiency of radiative transitions on composition 78−2909
GaAs-$Ga_xAl_{1-x}As$ injection laser, external resonator, radiative characts. 77−23703
GaAs-$Ga_xAl_{1-x}As$ injection laser, large-optical-cavity, with low-loss distributed Bragg reflectors 78−1244
GaAs-$Ga_xAl_{1-x}As$ laser, degradation, TEM obs. 77−51625
GaAs-$Ga_xAl_{1-x}As$ superlattice, photoconductor with high sensitivity and reduced dark current appl. 79−7881
GaAs-$Ga_xIn_{1-x}P$ heterostructure, elastic stresses and substrate/epitaxial film mismatch, X-ray diffr. method 80−92794
GaAs-$Ga_xIn_{1-x}P$ multilayer epitaxial films MBE technology and epitaxial layers props. 79−33945
GaAs-GaAlAs, DH laser material, rapid optical degradation 77−7083
GaAs-GaAlAs, DH laser material, LPE grown, obs. of melt carryover 78−91553

III-V semiconductors continued
GaAs-GaAlAs, double heterostruct. injection laser, curved junction stabilised filament, exam. 78−37911
GaAs-GaAlAs, heterostructure laser diode, lasing threshold calc. 80−28232
GaAs-GaAlAs, injection laser and MESFET monolithic integration on GaAs substrate 79−64242
GaAs-GaAlAs, inverted-ridge-waveguide DH injection laser with current and lateral optical confinement LPE growth 77−75540
GaAs-GaAlAs, stripe geometry laser, simplified fabrication process, characts. 79−76697
GaAs-GaAlAs, superlattice, subband related anisotropy in negative magnetoresistivity 80−11082
GaAs-GaAlAs, transverse Bragg-reflector injection lasers 78−74926
GaAs-GaAlAs 13 μm wide stripe CW DH lasers linear to more than 10 mW 78−42344
GaAs-GaAlAs (100) abrupt interface, carrier transmission and refl. coeffs. 79−69588
GaAs-GaAlAs (100) interfaces, carrier transport coeffs., tight binding calc. 80−49889
GaAs-GaAlAs bicrystal struct., dislocation half-loops, nucleation and generation 79−95009
GaAs-GaAlAs bipolar transistor and heterostruct. laser, monolithic integration 80−102858
GaAs-GaAlAs CW injection laser, stripe geometry DH, temporal coherence 80−38016
GaAs-GaAlAs channelled-substrate narrow-stripe lasers, low threshold currents 80−23706
GaAs-GaAlAs DFB and distributed Bragg reflector lasers, historical review 77−31102
GaAs-GaAlAs DFB diode lasers with separate carrier and optical confinement, room temp. operation 77−10926
GaAs-GaAlAs DH CW laser, growth by Peltier effect induced LPE 77−48357
GaAs-GaAlAs DH diode lasers with angled pumping stripes, operation 78−46602
GaAs-GaAlAs DH injection laser, integrated optics techniques 80−33033
GaAs-GaAlAs DH injection lasers, external cavity operated angled-stripe geometry, CW operation 80−64078
GaAs-GaAlAs DH internally striped planar laser with flat freq. response up to 2 GHz 78−66829
GaAs-GaAlAs DH LEDs, with thin active layer, Burrus type, internal interference in emission spectrum 78−27325
GaAs-GaAlAs DH LED, transient current trap spectroscopy 78−80049
GaAs-GaAlAs DH laser on semi-insulating substrate using carrier crowding 77−83886
GaAs-GaAlAs DH laser material, secondary dislocation climb in optical degradation 78−17935
GaAs-GaAlAs DH lasers, optical studies of defects and degradation 78−18654
GaAs-GaAlAs DH lasers, single longit. mode operation 78−22125
GaAs-GaAlAs DH laser, unsaturated optical gain spectra above threshold 78−29951
GaAs-GaAlAs DH laser diode, lateral modes 78−59009
GaAs-GaAlAs DH laser, beam scanning with twin-stripe injection lasers 79−10334
GaAs-GaAlAs DH laser with low threshold current, metalorganic CVD 79−50293
GaAs-GaAlAs DH lasers, strain-enhanced luminesc. degradation, photoluminesc. obs. 80−69392
GaAs-GaAlAs DH laser, O^+ isolation compared with SiO_2 isolation 80−74382
GaAs-GaAlAs DH material, dislocation glide and climb, electron diffr. 78−83824
GaAs-GaAlAs double heterostruct., self-absorpt. effects on radiative lifetime 77−39928
GaAs-GaAlAs double heterostructures for CW injection lasers, LPE growth 79−31931
GaAs-GaAlAs embedded stripe DH laser with polycryst. GaAsP, cleaved mirrors 77−75548
GaAs-GaAlAs embedded stripe DH laser with polycryst. GaAsP, etched mirrors 77−75549
GaAs-GaAlAs grating coupled lasers, output power efficiency 77−79858
GaAs-GaAlAs heterostructures, LPE growth, Peltier effect *(Polish)* 78−6861
GaAs-GaAlAs heterostructure, growth by metal-alkyl-hydride process 78−15313
GaAs-GaAlAs heterostructure injection lasers, room temp. operation with curved stripe waveguides 78−37909
GaAs-GaAlAs heterostructure, GaAs preferential etching, using O_2 and CCl_2F_2 mixture 79−8373
GaAs-GaAlAs heterostructure lasers on semi-insulating substrates 79−13977
GaAs-GaAlAs heterostructures, saturation of free exciton absorption 79−61454
GaAs-GaAlAs injection lasers, on semi insulating substrates, using laterally diffused junctions 78−37910
GaAs-GaAlAs injection laser, branching waveguide directional coupler, fabrication and operation 78−38047
GaAs-GaAlAs injection laser sources, for fibre optic communications 78−46637
GaAs-GaAlAs injection lasers on semi-insulating substrates using laterally diffused junctions 78−55364
GaAs-GaAlAs injection laser sources for fibre optic communications, design 79−31923
GaAs-GaAlAs injection laser, radiation divergence reduction by non-waveguide mode excitation 80−91797
GaAs-GaAlAs injection lasers, narrow-stripe proton-implanted, high bit-rate modulation 80−91824
GaAs-GaAlAs LPE layers, laser material, shallow growth pits obs. 77−7985
GaAs-GaAlAs LPE layers, DH material, TEM obs. of crystal defects 78−6241
GaAs-GaAlAs large optical cavity injection layer with low loss DBRs 78−1430
GaAs-GaAlAs laser, degraded, characterisation by selective etching and photoetching 80−48252
GaAs-GaAlAs laser, high-spectral radiance source using integrated optics 79−36931
GaAs-GaAlAs laser, optical repeater using PFM at 1 GHz 79−98395

III-V semiconductors continued
GaAs-GaAlAs laser with integral light intensity detector 79−89917
GaAs-GaAlAs monolithically integrated DFB lasers as freq. multiplexing source 77−34958
GaAs-GaAlAs multilayer struct., Hall mobility enhancement 80−100511
GaAs-GaAlAs multiple-stripe phase-locked laser array, behaviour 79−45955
GaAs-GaAlAs nonplanar large optical cavity laser, pulsed room temp. operation 80−28244
GaAs-GaAlAs optically pumped DFB laser, wavelength tuning effect 78−82979
GaAs-GaAlAs planar stripe DH laser, origin of dark line defects 77−75510
GaAs-GaAlAs room temp. DBR lasers, highly collimated broadside emission 78−1428
GaAs-GaAlAs solar cells, LPE grown, parameters dependence upon impurity concentration and temp. performances for series resistance reduction 80−45692
GaAs-GaAlAs stripe injection laser, CW double heterostruct., technology 79−31933
GaAs-GaAlAs stripe injection laser, high performance, design and charcacts. 79−31932
GaAs-GaAlAs superlattices, metalorganic VPE growth, in sites ellipsometry monitoring 80−70547
GaAs-GaAlAs superluminescent diodes for optical fibre links, modulation bandwidth 79−36993
GaAs-GaAlAs TJS lasers, high power density single mode operation, Si_3N_4 facet coating 79−86186
GaAs-GaAlAs-GaAs rectifying semicond. struct., prep. by MBE and charcacts. 80−65657
GaAs-GaAs oxide interface layer characterisation by spectroscopic ellipsometry 80−50738
n-GaAs-GaAs:Cr, interface elec. props., substrate effects 78−6438
n-GaAs-GaAs:Cr. semiinsulating, low freq. current pulses 77−8176
GaAs-$GaAs_{0.5}P_{0.5}$ almost perfect epitaxial multilayers, TEM obs. 77−89668
GaAs-$GaAs_xSb_{1-x}$, heteroepitaxial structs., mismatch dislocation nets 79−10855
GaAs-GaInAs structure, dislocation struct., TEM anal., appl. as IR LED 80−70206
GaAs-GaP, heterojunction, electronic processes *(Russian)* 79−56312
GaAs-GaP heterostructure, radiative recomb. under influence of mech. stresses 80−66291
GaAs-GaP system, diffuse scatt. of X-rays by simple crysts. *(German)* 78−30517
GaAs-GaP(Sb), pseudobinary alloy, phase diagram calc. 78−52786
GaAs-GaSb, threshold energies for impact ionisation by electrons and holes 78−6390
GaAs-GaSe n-p heterojunction, elec. props., interface states 80−65670
GaAs-Ge, heterostructure, zincblende-on-diamond type systems, MBE growth, (110) orientation as preferred orientation 80−80099
GaAs-Ge, n-n isotype heterojunctions, fixed-interface-charge model 78−56215
GaAs-Ge (100) interface, electronic struct., scattering-theoretic approach 78−95340
GaAs-Ge (110), heterojunction chemistry, photoemission expts. 78−95244
GaAs-Ge abrupt (110) interface, electronic struct. 78−95339
GaAs-Ge abrupt interface, electronic struct., self-consistent wave mechanical calcs. 77−89837
GaAs-Ge abrupt interface, orientation depend. of interface dipole energies, XPS expts. 78−39196
GaAs-Ge heterojunction, band discontinuities, angle-resolved UPS obs. 79−7878
GaAs-Ge heterojunction, electronic structure 79−73572
GaAs-Ge heterojunction, interface geometry, model 80−49879
GaAs-Ge heterojunctions, electronic struct., tight-binding and pseudopot. models 79−42633
GaAs-Ge interface, abrupt, electronic struct., self-consistent calc. 77−24611
GaAs-Ge interface, electronic struct. of Ge overlayers on (100) GaAs 80−49880
GaAs-Ge interface, photoemission 80−25530
GaAs-Ge interface, surface and interface states of (111) surfaces 79−15206
GaAs-Ge interface, XPS obs. of electronic struct. 78−95341
GaAs-Ge interfaces, heteroepitaxial, misfit dislocations, TEM obs. 79−23610
GaAs-Ge junction, interface states and electronic struct. 77−69408
n-GaAs-Ge laser alloying to from ohmic contacts 80−58546
GaAs-Ge n^+-n-p junction, I-V charcts., inverse branch, effect of dislocation defects *(Russian)* 79−15217
GaAs-Ge n-p diode, microplasma breakdown 79−91140
GaAs-Ge structure, electronic struct., ang.-resolved photoemission obs. 80−49881
GaAs-$Ge_{1-x}(GaAs)_x$ n-p heterojunctions, hydrostatic press. effect on elect. and photoelectric props. 80−20304
GaAs-Ge_3N_4-Al structures and MISFETs based on them 79−60932
GaAs-HBr chemical vap. transport system, thermochem. data 78−6854
GaAs-In Schottky barrier interface, covalent bonding of metal atoms 77−20429
GaAs-$In_{2-x}Sn_xO_{3-y}$ SIS heterostructure solar cells, spray-deposited 80−101106
GaAs-$In_yGa_{1-y}P$, CW room temp. DH lasers prep. by VPE 77−10942
GaAs-InAs, pseudobinary alloy, phase diagrams calc. 78−52786
GaAs-InP heterojunction laser output wavelength control 80−74384
GaAs-InSe, heterojunction, electronic processes *(Russian)* 79−56312
GaAs-InSe p-n junctions, 'optical' contacts, elec. props. 78−56222
GaAs-insulator film interface, evidence for growth-induced damage from photolum. expts. 78−75953
GaAs-insulator interface, elec. props. 78−95370
GaAs-insulator interface, processes of electron emission from traps 79−73598
n-GaAs-K_2Se-K_2Se_2-KOH/C thin film solar cell, 7.3% cell efficiency 80−93931
GaAs-metal contacts, excess capacitance, depend. on nonlinear dielectric susceptibility 78−43475
GaAs-metal contacts, intervalley scatt. effect on current-voltage charcts. 77−89845
GaAs-metal contacts, use of Ga to eliminate large As loss peaks 80−80370

III-V semiconductors continued
GaAs-metal diode, surface-barrier, excitons effect on photocurrent 79−82670
GaAs-metal interface, metal-induced chem. reactions and surface states 80−20311
GaAs-metal interface form., chem. and electronic struct. 80−25009
GaAs-metal junction stabilisation by transition metal diffusion barrier 79−38161
GaAs-metal junction stabilisation by intermetallic diffusion barrier 79−38160
GaAs-metal junctions, thermal stability improvement, with and without near noble metals 79−7143
GaAs-metal Schottky barrier, surface states and barrier height, I-V (C-V) charcts. meas. 77−85310
GaAs-metal Schottky barrier diodes, impedance, freq. and voltage depend. 78−64114
GaAs-metal Schottky barrier contacts, interface chemistry 79−74049
GaAs-metal Schottky barrier diodes, elec. props. under mech. stress 80−11087
GaAs-metal Schottky barrier height rel. to chem. reactivity 80−25008
n-GaAs-metal Schottky barrier, ultrathin native oxide, thickness determ. from C-V and photoresponse meas. 80−70821
GaAs-metal struct., photoresponse spectra, electron thermalisation *(Russian)* 79−15221
GaAs-n-$Al_xGa_{1-x}As$ heterojunctions, selectively doped, FET 80−80364
n-GaAs-n-$Al_xGa_{1-x}As$ rectifying heterojunction, cond. props. study 80−88626
n-GaAs-n-GaN, diffusion growth kinetics, morphology and electrical properties 80−20294
n-GaAs-n-GaP, in MIS structures, elec. controlled optical transparencies, optical processing use 77−85339
n-GaAs-n^+-$Al_xGa_{1-x}As$ heterostructure production, by MBE *(German)* 80−44711
p^+-GaAs-n-(Ga,In)As heterostructure, thermally assisted tunnelling currents 77−20412
GaAs-NaOH interface, inversion layer form. and surface states 80−2465
GaAs-native oxide interface, Raman scatt. expts. 77−85709
GaAs-native oxide interface, electronic props. 79−73590
GaAs-on-sapphire spatially distributed thermal light modulator 79−59839
GaAs-oxide, interface layer determ. by spectroscopic ellipsometry 79−95275
n-GaAs-oxide, plasma-grown, surface states, modified DLTS meas. 80−11094
GaAs-oxide interface, field effect 79−87160
GaAs-oxide interface, physical struct. 79−60644
GaAs-oxide interfaces, local atomic and electronic struct., high resolution XPS 80−49927
n-GaAs-oxide-Au structure, influence of reverse bias on photocurrent 80−20323
GaAs-oxide-metal solar cell, field shaping and barrier height 77−20454
GaAs-Pd junction, contact reactions 79−56308
GaAs-plasma grown oxide interface, new resonant ellipsometric technique for characterisation 79−40606
GaAs-polyethylene, for i.r. charcts. rel. to powder band-pass filter design 78−90468
GaAs-Pt interface states energy distrib. and relaxation time 79−33345
n-GaAs-Pt Schottky diode, microplasma breakdown 79−91140
GaAs-Pt-air system, far IR propag. distances of surface EM waves 79−42616
GaAs-S VPE layers, thickness and carrier conc. variations 79−100060
GaAs-Si ion implanted, impurity profiles elec. props. 80−96550
GaAs-Si_3N_4 layer struct., electron-hole liq. at interface 79−69434
GaAs-Si_3N_4 structure, photoluminesc. and collective effects 78−6727
GaAs-Si_xGe_{1-x} n^+-n-p junction, I-V charcts., inverse branch, effect of dislocation defects *(Russian)* 79−15217
n-GaAs-$Si_xO_yN_z$ interface, C-V and I-V charcts. 77−89863
n-GaAs-SiO_2 interface, MOS capacitors, surface states from conductance and capacitance meas. 80−100533
GaAs-SiO_2 MIS structures, fabrication and elec. props. 79−47166
GaAs-SiO_x-Al system, C-V charcts. 79−65553
GaAs-Ta_2O_5 interface, fabricated by interactive oxidation, props. 80−49935
n-GaAs-W contact, Schottky barrier 78−39213
n-GaAs-YIG layered structure, magnetostatic surface wave amplification 78−88107
GaAs-ZnS p-n heterojunction, epitaxial, elec. props. *(Russian)* 78−88023
GaAs-ZnS p-n heterojunction, struct., multibeam electron microscopy obs. 79−11031
GaAs-ZnSe, X-ray cond. 5.4 to 17.5 keV, spectral and dosimetric charcacts. *(Russian)* 77−35964
GaAs-ZnSe (110) interface, electronic struct., self-consistent calc. 79−95486
GaAs-ZnSe heterojunction, elec. and photoelec. props. *(Russian)* 77−32070
GaAs-ZnSe heterojunction, LF noise, I-V and C-V charcts., illumination effects *(Russian)* 77−66200
GaAs-ZnSe system, heterovalent solid solns. of substitution, prep. and investig. 77−24553
n-GaAs-ZnSe:Mn, single cryst. substrate low threshold DC electrolum. 77−63465
$GaAs_{1-x}P_x$, hot photoluminescence spectrum, polarisation depend. 78−31254
GaAs(-GaP) single cryst., defect distrib. near abraded surface 80−92533
$Ga_{1-x}As(Al,In)_x$, heterojunction solar cells, optimum bandgap, computer anal. 79−43767
$(GaAs)_n(AlAs)_m$ multilayers, MBE, interdiffusion, X-ray diffr. study 80−70474
GaAsGaAlAs coated heterostruct. etalon, optical bistability and ns modulation 80−64096
GaAs-$Ga_{1-x}Al_xAs$ DH laser material, rapid optical degradation obs. 77−75528
$GaAs_{1-x}H_x$, amorphous, vib. props., Raman and IR meas. 80−50322
Ga(AsP), dislocation etching of (001) faces with H_3PO_4 etchant 80−15103
GaAsP epitaxial film, TEM obs. of misfit dislocation arrays, nucleation and multiplication 77−39742
GaAsP epitaxial films, planar waveguides for integrated optics appls. 79−10416

III-V semiconductors continued
GaAsP epitaxial film, composition self modulation, defect struct. 80−34331
GaAsP epitaxial waveguide, electro-optic phase modulation of laser radiation 79−10417
GaAs(P), ion irrad. damage, strain effect contrib., channelling meas. 78−67752
GaAs(P), momentum distrib. of electrons, anisotropy, positron annihilation *(Russian)* 78−84676
GaAsP, negative-electron-affinity, photoemission transmission coeff. 78−56560
Ga(AsP) on GaAs, LPE, growth with Ge and Sn solvents, phase diags. 78−88434
GaAsP photocathode, negative electron affinity process obs. by laser beam scanning *(Japanese)* 80−55262
GaAs(P), semiconductor-metal transition, press. calibration above 100 kbars fixed points 80−77808
GaAsP, VPE, lattice forbidden band composition depend. *(Hungarian)* 80−6669
$GaAs_{0.1}P_{0.9}$:Zn, shallow Zn diffusion profile determ. using anodic oxidation and double radioactive tracer method 77−43239
$GaAs_{0.15}P_{0.85}$ ridged waveguide for electrooptic radiation modulator 80−91925
n-$GaAs_{0.6}P_{0.4}$, anodic oxide film, exam. using SIMS and ellipsometry 79−61770
$GaAs_{0.6}P_{0.4}$, anodic oxide, electronic props. 79−61771
$GaAs_{0.6}P_{0.4}$, CVD growth for LEDs 79−19998
$GaAs_{0.6}P_{0.4}$, deep level profile anal., double correlation technique 77−80830
$GaAs_{0.6}P_{0.4}$ LED, deep level radiative defects detection during degradation 77−76770
$GaAs_{0.6}P_{0.4}$ LED, luminesc. investig. of degradation, deep-level form. at dislocations 77−40287
$GaAs_{0.6}P_{0.4}$, low dark-current MOS photodiodes 77−32083
$GaAs_{0.6}P_{0.4}$ p-i-n diode, behaviour of turnover voltage under pulsed conditions 77−20408
n-$GaAs_{0.6}P_{0.4}$, reproducible ohmic contacts 79−73587
$GaAs_{0.6}P_{0.4}$, surface processing, residual film monitoring by ellipsometry 80−13124
$GaAs_{0.6}P_{0.4}$, VPE, hole diffusion lengths, surface prep. and heat treatment effects, etchant evaluation 80−15627
$GaAs_{0.6}P_{0.4}$, VPE, hole diffusion lengths, effect of transition metal diffusional doping 80−15628
$GaAs_{0.6}P_{0.4}$:Be, implanted annealing studies, elec. resist., Hall effect meas. 78−84213
$GaAs_{0.6}P_{0.4}$:N, isoelectronic tape by ion implantation and CO_2 laser annealing 80−24464
$GaAs_{0.6}P_{0.4}$:Zn, control of Zn diffusivity by multiple implantation 78−38877
$GaAs_{0.6}P_{0.4}$:$Zn^+(Ar^+)$, ion-implanted, thermal degradation of mechanical surface perfection and surface photolum. 77−77271
$GaAs_{0.62}P_{0.38}$, negative electron affinity, photoemission of spin polarised electrons 80−2916
n-$GaAs_{0.62}P_{0.38}$, optical absorpt. coeff. and minority-carrier diffusion length, differential photocurrent method of meas. 80−96896
$GaAs_{0.65}P_{0.35}$, gamma irradiated, deep level study using DLTS and photocapacitance methods *(Japanese)* 80−49665
$GaAs_{0.7}P_{0.3}$-$In_{0.34}Ga_{0.66}P$, CW heterojunction laser, visible, laser operation 77−38886
$GaAs_{1-x}P_x$, $0 \leq x \leq 1$, evidence for common nature of certain deep-level radiative centres 78−6767
$GaAs_{1-x}P_x$ based structs., carrier conc., mobility calcs. from Hall effect meas. 78−60138
$GaAs_{1-x}P_x$, bending parameters calc. by pseudopot. method 78−26813
$GaAs_{1-x}P_x$, bound exciton, luminesc. reson. excitation 79−95840
$GaAs_{1-x}P_x$, chemical transport and crystal growth in closed tube *(Japanese)* 78−39673
$GaAs_{1-x}P_x$, continuously tunable electron beam pumped laser 78−50802
$GaAs_{1-x}P_x$, dependence of energy spectrum of levels introduced by electron irrad. on composition 79−60766
$GaAs_{1-x}P_x$, diffusion of implanted Zn ions, ion microbe analysis 78−95190
$Ga(As_{1-x}P_x)$ electrode, equilib. establishment kinetics *(French)* 79−79259
$GaAs_{1-x}P_x$ electrodes, interface capacitance meas., flatband pot., conduction and valence band boundaries *(French)* 79−33339
$GaAs_{1-x}P_x$, electron irrad., radiation defects annealing 80−29059
$GaAs_{1-x}P_x$ epi-wafer, comp. profile of heterogeneous struct., anodisation-electrorefl. meas. 78−26782
$GaAs_{1-x}P_x$ epitaxial films, VPE grown, photolum. spectra 79−73997
$GaAs_{1-x}P_x$ epitaxial layer prep. for electroluminescent diodes *(Czech)* 77−21032
$GaAs_{1-x}P_x$, epitaxial layer, modulation of direct and indirect gaps, piezotransmission meas. 77−24819
$GaAs_{1-x}P_x$ epitaxial layers, charge carrier conc. determ. from low-field electrorefl. spectra 77−85320
$GaAs_{1-x}P_x$ epitaxial layers prep., photoluminesc. and electroluminesc. props. *(Czech)* 78−48233
$GaAs_{1-x}P_x$, heterogeneous struct. obs. by anodisation-electrorefl. technique 78−84088
$GaAs_{1-x}P_x$ heterostructure, LPE prep., growth and dissolution kinetics, thermodynamic and kinetic models 80−75456
$GaAs_{1-x}P_x$, high quantum efficiency photoemission 77−44115
$GaAs_{1-x}P_x$, indirect-gap, evidence for exciton localization by alloy fluctuations, photolum. 80−66276
$GaAs_{1-x}P_x$ LED, effect of band filling on emission spectra shape 78−48236
$GaAs_{1-x}P_x$ layer, growth by isothermal LPE 77−40398
$GaAs_{1-x}P_x$, localised exciton-phonon complex as intermediate state in light scatt. 78−39543
$GaAs_{1-x}P_x$, MBE growth on GaP, and crystallographic evaluation 77−8762
$GaAs_{1-x}P_x$, mol. beam epitaxial growth, cryst. quality, composition investig. *(Japanese)* 77−55895
$GaAs_{1-x}P_x$, molecular beam epitaxial, effect of substrate temp. on composition ratio 77−1811
$GaAs_{1-x}P_x$, N doping using ionised beam in MBE 78−47400
$GaAs_{1-x}P_x$, N implantation, characterisation by photolum. and channelling 80−54262
$GaAs_{1-x}P_x$, N trap bound state, Hall effect determ. 78−19055
$GaAs_{1-x}P_x$, N^+ implantation photoluminesc. props. 77−68987

III-V semiconductors continued
$GaAs_{1-x}P_x$, N^+ implantation, annealing props. 77−68988
$GaAs_{1-x}P_x$, piezomodulation spectra of indirect gap, zero-phonon and phonon-assisted transitions 77−48192
$GaAs_{1-x}P_x$, SIMS, energy distrib. of sputtered ions 79−38706
$GaAs_{1-x}P_x$, solid soln. comp. control during gas-phase heteroepitaxy 77−85091
$GaAs_{1-x}P_x$, solid soln., synthesis by ion implantation P^+ ions 78−38741
$GaAs_{1-x}P_x$ solid solution, disorder scatt. Hall mobility meas. 77−69350
$GaAs_{1-x}P_x$, solid solution, synthesized by ion implantation, Raman scattering 79−42972
$GaAs_{1-x}P_x$, solid state diffused, conc. distrib. obs., electroreflectance and tracer sectioning obs. 80−54389
$GaAs_{1-x}P_x$, structural defects, optical props. effect 80−55208
$GaAs_{1-x}P_x$, thermal oxides, elemental composition and C-V charcts. 79−61772
$GaAs_{1-x}P_x$, VPE on Ge substrate, and LED charcts. 78−72736
$GaAs_{1-x}P_x$:N, $0.6<x<1$, photoluminesc., comp. depend. 78−52546
$GaAs_{1-x}P_x$:N, film, optical absorpt. from photoluminesc. meas. 78−92134
$GaAs_{1-x}P_x$:N, Koster-Slater model and N-states 78−47732
$GaAs_{1-x}P_x$:N, LED, external quantum efficiency, press. effect 77−8655
$GaAs_{1-x}P_x$:N, N isoelectronic trap, model calc. of N_Γ and N_x electronic states 78−10398
$GaAs_{1-x}P_x$:N, photoluminesc. and optical absorpt. spectra of N impurity bound-excitons 79−47496
$GaAs_{1-x}P_x$:N, photolum. and electrolum. study of N isoelectronic traps 80−89061
$GaAs_{1-x}P_x$:N, upper branch of N isoelectronic trap., photo- and electrolum. expts. 77−63462
$GaAs_{1-x}P_x$:N epitaxial layers, absorption and photolum. spectra meas. 77−24894
$GaAs_{1-x}P_x$:N heterojunction, N_x and N_Γ bound states, high-press. effects on electroluminesc. meas. 77−11870
$GaAs_{1-x}P_x$:S, deep level, photoconductivity, carrier nonradiative recombination 80−20112
$GaAs_{1-x}P_x$:Te, thermoelectric figure of merit 79−69538
$GaAs_{1-x}P_x$:Zn, diffusion profile determ., $^{32}P/^{65}Zn$ double tracer technique 78−55888
$GaAs_{1-x}P_x$:Zn implanted, Zn diffusion 77−84993
$GaAs_{1-x}P_x$-Au, surface-barrier struct., photodetectors of visible and UV radiation 77−20437
$GaAs_{1-x}P_x$-GaP heterostructure, photomodulation spectroscopic exam. 77−40257
$GaAs_{1-x}P_x$-SiO_2:N,Zn ion-implanted multiple layers, ion range distribs., secondary ion microprobe meas. 79−42129
$GaAs_{1-y}P_y$-$In_{1-x}Ga_xP_{1-z}As_z$, DH laser, low threshold visible spectrum 78−5471
$GaAs_xP_{1-x}$, surface phonon polaritons, total internal refl. *(Russian)* 79−38688
$GaAs_xP_{1-x}$, band struct., CPA calc. based on linear combination of bond orbitals 79−87035
$GaAs_xP_{1-x}$, elastic consts. and Debye temp. determ. 77−4142
$GaAs_xP_{1-x}$, energy band struct., CPA based on LCBO *(Japanese)* 80−44495
$GaAs_xP_{1-x}$ epitaxial film nonlinear light absorpt., photoluminesc. meas. 77−66528
$GaAs_xP_{1-x}$, liquid phase epitaxial growth on GaP, growth and properties 79−47641
$GaAs_yP_{1-y}$ alloy, composition effects in growth by MBE 80−59816
GaAs(P)(Sb), electronic elementary excitations in far UV and X-ray region 79−95346
$GaAs_{1-x}P_x$(Te), bound exciton stress depend., piezoluminescence, photoluminescence 80−80206
$GaAs_{1-x}Px$, heteroepitaxial solid soln., defects of struct 79−28223
GaAsSb laser, optimum wavelength emission for fibre guides 77−7086
GaAsSb/GaAlAsSb DH lasers, growth and props. 80−69412
$GaAs_{1-x}Sb$, microprocessor controlled MBE growth 78−3058
$GaAs_{1-x}Sb_x$, ($x \leq 0.05$), band gap, temp. depend., from edge photolum. meas. 80−71486
$GaAs_{1-x}Sb_x$, cryst. growth by steady state LPE 78−44032
$GaAs_{1-x}Sb_x$, DH, laser operation between 0.9 and 1.1 μm 77−10922
$GaAs_{1-x}Sb_x$ electron intervalley transfer and drift velocity calc. 77−80778
$GaAs_{1-x}Sb_x$ epitaxial n-n heterostructures, gap energies and interface pots., modulation electroabsorpt. meas. 79−11201
$GaAs_{1-x}Sb_x$, LPE,phase diagram meas. 77−20047
$GaAs_{1-x}Sb_x$ layer on GaAs, dislocation density reduction by improved LPE growth method 80−76202
$GaAs_{1-x}Sb_x$, MBE grown, surface struct. exam. by MEED 78−87847
$GaAs_{1-x}Sb_x$, narrow-gap film on wide-gap GaAs, energy gap grading, optical transmission meas. 77−20943
$GaAs_{1-x}Sb_x$ on GaAs, LPE growth of GaAs 79−61519
$GaAs_{1-x}Sb_x$ photodiode structures, current-voltage charcts., photo-EMF spectra 80−29472
$GaAs_{1-x}Sb_x$ photodiode, speed and sensitivity meas. 80−92937
$GaAs_{1-x}Sb_x$ ternary phase diagram, LPE, band gap and elec. props. 77−55896
$GaAs_{1-x}Sb_x$ undoped epitaxial layers, photoluminesc. meas. 80−20703
$GaAs_{1-x}Sb_x$-$Al_yGa_{1-y}As_{1-z}Sb_z$, DH laser, threshold charcts. and extended wavelength operation 78−9379
$GaAs_{1-x}Sb_x$-$Ga_{1-x}In_xP_{1-y}As_y$ multilayer structure, continuously tunable electron beam pumped laser 78−50802
$GaAs_{1-y}Sb_y$ organometallic VPE, use of trimethyl As and trimethyl Sb 80−45238
$GaAs_{1-y}Sb_y$, organometallic VPE growth using trimethylantimony 80−60788
$GaAs_xSb_{1-x}$, epitaxial layer, struct. defects rel. to luminesc. 78−72040
$GaAs_xSb_{1-x}$, heterostructure composition profile by photoemission microanalysis 80−44717
$GaAs_xSb_{1-x}$, lattice-matched LPE growth in InP substrates 79−42402
$GaAs_xSb_{1-x}$ solid solution epitaxial layer, morphology and defect structure 77−1330
$GaAs_xSb_{1-x}$, spontaneous and stimulated emission, electron beam excitation 77−58333
$GaAs_xSb_{1-x}$-GaAs epitaxial films and multilayer heterostruct., SEM obs. under cathodolum. conditions 79−11023
$GaAs_ySb_{1-y}$, miscibility gap, rel. to LPE 79−33090
$GaAs_{1-x-z}Sb_xP_z$, LPE growth, constant compositional grading 78−6867
$GaAs_{2-x-z}Sb_xP_z$, LPE growth, continuous comp. grading, use as secondary substrate 77−31913

III-V semiconductors continued
$GaAs_xSb_yP_{1-x-y}$, continuously graded comp. layers, LPE 77−24970
$(GaAs)_{1-x}(ZnSe)_x$, LPE growth, resist., Hall effect and cathodoluminesc. meas. 77−28270
p-$(GaAs)_x(ZnSe)_{1-x}$-nn$^+$.GaAs, avalanche heterojunctions, inverse branch of volt ampere characts. *(Russian)* 80−6974
GaAs(110), high resolution photoemission yield, surface states 77−69392
GaAs(110) surface, adsorption of water and methanol, UPS study 80−6632
GaAs(110), surface and interface states, effects of atomic and electronic rearrangements 77−85284
GaAs(110), surface states, photoemission spectroscopy and tight binding calcs. 77−85888
GaAs(110), surface struct., kinematical LEED calcs. 77−85034
GaAs(111), O bonding, thermodesorption and ESCA meas. 77−86206
GaAs($\bar{1}\bar{1}\bar{1}$)As surface, 3 states, comp., struct., surface states and O_2 sticking coeffs. 77−66080
GaAs;Cu, epitaxial and bulk conductivities compared *(Russian)* 78−10585
GaBi, possibility of existence with sphalerite struct. 80−33950
$Ga_yIn_{1-y}As_xP_{1-x}$-InP heterostructure, lattice matching and cryst. perfection 78−6437
GaInAs, efficient photodiode for near IR detection 78−16848
GaInAs, electron-pumped laser, far-field radiation pattern, optical confinement effects 79−86181
GaInAs, photocathode with negative electron affinity, photoemission, influence of strong elec. field 79−8227
GaInAs-InP, growth by low-pressure metalorganic CVD 80−71595
GaInAs-InP injection lasers with longer wavelengths for optical fibre communications, review *(Japanese)* 78−25892
$Ga_{0.47}In_{0.53}As$, electron and hole impact ionisation rates 80−49745
$Ga_{0.47}In_{0.53}As$, HF carrier mobility, temp. depend., theory 80−75593
$Ga_{0.47}In_{0.53}As$, homojunction avalanche photodiode, exam. of props. 78−37072
$Ga_{0.47}In_{0.53}As$ homojunction photodiode, avalanche photodetector for 1.0-1.6 μm region 79−6179
$Ga_{0.47}In_{0.53}As$, LPE growth and characterisation 80−10845
$Ga_{0.47}In_{0.53}As$, MBE, InP/$Ga_{0.47}In_{0.53}As$/InP DH laser fabrication and room temp. operation 78−74906
$Ga_{0.47}In_{0.53}As$ p-n junctions, band-to-band tunnelling current 80−107895
$Ga_{0.47}In_{0.53}As$, photodetector applications 80−95140
$Ga_{0.47}In_{0.53}As$/InP DH lasers double cladded with InP by LPE technique, 1.67 μm operation 79−50314
$Ga_{0.7}In_{0.3}As$ photodiodes, fibre optic appls. 79−40613
$Ga_{1-x}In_xAs$, and $Ga_{1-x}In_xAs_{1-y}P_y$, quantum magnetoresist. results, using pulsed fields up to 35 T 79−73528
$Ga_{1-x}In_xAs$ epitaxial layer growth by organometallic pyrolysis, homojunction LED prep. 80−76194
$Ga_{1-x}In_xAs$, IR reflectivity, cluster effect on optical phonons 80−97259
$Ga_{1-x}In_xAs$, optical detection of CESR 77−36155
$Ga_{1-x}In_xAs$ organometallic VPE, use of trimethyl As and trimethyl Sb 80−45238
$Ga_{1-x}In_xAs$, organometallic VPE growth using trimethylarsenic 80−60788
$Ga_{1-x}In_xAs$ photocathode, negative electron affinity, photoelectron scatt. in Cs-O film 79−28899
$Ga_{1-x}In_xAs$ photodetectors for 1.3 micron PIN-FET receiver 80−13145
$Ga_{1-x}In_xAs$ solid solns., electron scatt. by isoelectronic impurities in covalent crysts. 79−11129
$Ga_{1-x}In_xAs$, VPE grown, refractive index, reflectance meas. 79−4780
$Ga_{1-x}In_xAs$, VPE layers, main electron trap, transient capacitance spectroscopy obs. 78−34800
$Ga_{1-x}In_xAs$:Mn grown by LPE, elect. props. 80−100541
$Ga_{1-x}In_xAs$-GaAs epitaxial interface with small misfits, TEM image contrast 80−2275
$Ga_{1-x}In_xAs$-GaAs low-misfit epitaxial interface, electron microscope contrast 79−73416
$Ga_xIn_{1-x}As$, alloy film surface processes controlling growth by MBE RHEED and AES exam. 78−84084
p-$Ga_xIn_{1-x}As$, Auger recomb., theory and luminesc. expts. 78−56518
$Ga_xIn_{1-x}As$, cryst. growth on (100) InP by LPE 78−56591
$Ga_xIn_{1-x}As$, far IR reflectivity spectrum, damped harmonic oscill. model 77−52070
$Ga_xIn_{1-x}As$, on ⟨111⟩B InP, LPE growth, characterisation of high purity lattice 80−104082
$Ga_xIn_{1-x}As$ on InP, lattice matched LPE film growth and characts. 78−72033
$Ga_xIn_{1-x}As$ p-n junction, growth and electrolum. spectra 77−20420
$Ga_xIn_{1-x}As$, prep. and props. 79−100047
$Ga_xIn_{1-x}As$, spontaneous and stimulated emission, electron beam excitation 77−58333
$Ga_xIn_{1-x}As$, substrate orientation effect on liq.-solid distrib. coeffs., 600-700°C 80−2278
$Ga_xIn_{1-x}As$, VPE growth, thermodynamic anal. 80−2933
$Ga_xIn_{1-x}As$:Ge LED, by LPE, radiation emitted at 1.02 μm 78−48235
$Ga_xIn_{1-x}As$-InP, lattice matched LPE film growth and characts. 78−15320
$Ga_xIn_{1-x}As$-InP, MBE film growth, composition control obs. 80−84399
$Ga_xIn_{1-x}As$-InP heterostructure, growth by MBE 79−8251
GaInAsP alloys, materials and devices for long wavelength optical communication 80−99854
GaInAsP DH laser diode CW modelocking 79−7126
GaInAsP, diffusion-limited growth in LPE 80−10842
GaInAsP diode lasers, self-sustained pulsations in light output 80−64012
GaInAsP, electroabsorption 79−78652
GaInAsP LEDs, 1.3-1.6 μm, appl. in long haul high data rate fibre optic communication systems 80−102854
GaInAsP on InP substrate, epitaxially grown, fabrication of avalanche photodiode 78−37071
GaInAsP quaternary alloys, orientation effects in LPE growth 78−92203
GaInAsP, rectifying and ohmic contacts 80−80376
GaInAsP, VPE growth and props. 80−16194
GaInAsP/InP, DH laser, low threshold current density, 1.3 μm emission 79−94249
GaInAsP/InP 1.5-1.6 micron integrated twin-guide lasers with distributed Bragg reflectors 80−74380
GaInAsP/InP buried heterostruct. laser, 1.6 μm, fabrication and room temp. CW operation 80−58568
GaInAsP/InP DH lasers, with (100) substrate, 1.2-1.5 μm, LPE growth conditions 79−15617

III-V semiconductors continued
GaInAsP/InP DH lasers, direct modulation charact. meas. by sharp pulse method 80−1245
GaInAsP/InP DH lasers, room temp. CW operation at 1.5 to 1.6 micron range, fabrication 80−58585
GaInAsP/InP DH lasers emitting at 1.3 μm, growth and characts. 80−64057
GaInAsP/InP DH stripe geometry lasers emitting at 1.3 μm, growth characterisation 80−69410
GaInAsP/InP DH lasers, 1.3 μm wavelength, LPE growth and characterisation 80−69411
(100)GaInAsP/InP DH lasers, 1.5-1.6 μm wavelength, two phase soln. LPE technique using anti-meltback layer 80−99750
GaInAsP/InP integrated twin-guide lasers with first order distrib. Bragg reflector, room temp. operation at 1.3 μ 80−64077
GaInAsP/InP integrated twin-guide lasers with distributed Bragg reflector, spectral behaviour 80−74381
GaInAsP/InP lasers, 1.5 μm emitting, high temp. CW operation 80−95889
GaInAsP/InP lasers, LPE grown, effect of p-doping on carrier lifetime and threshold current density 80−99726
GaInAsP/InP narrow planar stripe lasers, lasing characts. 80−95897
GaInAsP/InP optical sources for 1.2 to 1.4 μm wavelength region, growth and props. 79−90023
GaInAsP/InP system, chemical etching, fabricating laser diodes and integrated optical circuits 80−38030
GaInAsP/InP terraced substrate DH lasers, fabrication and single transverse mode operation 80−58580
GaInAsP-InP, broad-area and stripe-geom. DH laser, for fibre optic communication 78−42356
GaInAsP-InP, lattice matched, emission spectrum half width rel. to peak wavelength 80−2820
GaInAsP-InP avalanche photodiode, fabrication and characts. 78−54454
GaInAsP-InP buried stripe DH laser, fabrication using meltback method and CW operation 79−3708
GaInAsP-InP buried heterostructure laser with mesa substrate, linear light/current characts. 79−36894
GaInAsP-InP buried heterostructure lasers, 1.6 μm wavelength 80−64055
GaInAsP-InP DH laser, 1.3 μm CW operation at room temp. 77−71986
GaInAsP-InP DH laser grown by newly designed vertical LPE furnace 78−9380
GaInAsP-InP DH laser, relaxation and delay in oscillations 78−13709
GaInAsP-InP DH layers, lattice deform. and misfit dislocations 79−19473
GaInAsP-InP DH lasers with low threshold, narrow-beam divergence 79−36892
GaInAsP-InP DH lasers, for fibre optic communications 79−31924
GaInAsP-InP DH laser, LPE and wet chem. etching techniques for integration 79−98388
GaInAsP-InP DH laser, room temp. CW laser 80−28235
GaInAsP-InP DH lasers made by melt-back method, operating characteristics 80−48287
GaInAsP-InP DH lasers, LPE growth and operational characts. 80−53313
GaInAsP-InP DH injection lasers prep. by LPE, 1.11-1.67 μm operation 80−53321
GaInAsP-InP double heterostructure laser, prep. by LPE growth and laser operation 77−3590
GaInAsP-InP facet lasers with chemically etched end mirrors 80−1228
GaInAsP-InP integrated twin-guide lasers with first-order distributed Bragg reflectors, 1.3 μm 80−58567
GaInAsP-InP lasers and detectors, for fibre optic communications at 1.0-1.6 μm 79−3803
GaInAsP-InP mesa substrate buried heterostruct. injection laser, fabrication and lasing props. 80−53319
GaInAsP-InP planar stripe lasers, sputtered SiO_2 film as Zn-diffusion mask 80−48249
GaInAsP-InP stripe-geometry monolithic laser with etched mirror and monitoring detector 80−64054
GaInAsP-InP stripe laser, etched mirrors fabricated by wet chem. etch 80−99744
GaInAsP-InP surface emitting injection laser, fabrication and lasing props. 80−28234
GaInAsP-InP Zn diffused stripe geometry DH diode laser fabrication 79−98386
$Ga_{0.08}In_{0.92}As_{0.18}P_{0.82}$, band struct., optical studies 79−47013
$Ga_{1-x}In_xAs_{1-x}P_x$, VPE growth and characterisation 78−22970
$Ga_{1-x}In_xAs_{1-y}P_y$-InP DH laser, carrier lifetime meas. 77−61955
$Ga_{1-x}In_xAs_{1-y}P_y$-InP DH lasers, 1000-hour CW operation 78−1265
$Ga_xIn_{1-x}As_yP_{1-y}$, conduction band and phonons, Shubnikov-de Haas effect, magnetophonon resonance, Raman scattering 80−24795
$Ga_xIn_{1-x}As_{1-x}P_x$ film, energy band struct., photolum. meas. 79−7784
n-$Ga_xIn_{1-x}As_{1-y}P_y$, photoluminesc. of epitaxial films, isovalent substitution 80−16097
$Ga_xIn_{1-x}As_{1-y}P_y$, spontaneous and stimulated emission, electron beam excitation 77−58333
$Ga_xIn_{1-x}As_{1-y}P_y$:Ge(Sn)(Te), epitaxial film, elec. and optical props. 79−11251
$Ga_xIn_{1-x}As_{1-y}P_y$-InP, room temp. electron-beam-pumped laser with dielec. waveguide, output characts. 80−5761
$Ga_xIn_{1-x}As_xP_{1-x}$-InP buried-stripe DH diode laser, room temp. CW operation 77−50671
$Ga_xIn_{1-x}As_yP_{1-y}$, CVD by Ga-In-P-H-Cl system, 80−54159
$Ga_xIn_{1-x}As_yP_{1-x}$, epitaxial layers on InP, expt. determ. of effective masses 79−65370
$Ga_xIn_{1-x}As_yP_{1-x}$, thermal expansion coefficients, 25-400°C 79−46817
$Ga_xIn_{1-x}As_yP_{1-y}$, anodisation, effect of pH, current density and illumination 78−95823
$Ga_xIn_{1-x}As_yP_{1-y}$, electron effective mass, cyclotron reson. and magnetophonon effect meas. 80−103618
$Ga_xIn_{1-x}As_yP_{1-y}$, IR refl. spectra 80−60602
$Ga_xIn_{1-x}As_yP_{1-y}$, LPE layers, growth and characterisation 78−38983
$Ga_xIn_{1-x}As_yP_{1-y}$ LPE layers matched to InP, comp. and lasing wavelengths 78−71103
n-$Ga_xIn_{1-x}As_yP_{1-y}$, transferred electron oscill., threshold field 77−85227
$Ga_xIn_{1-x}As_yP_{1-y}$/GaAs structure, LPE growth and lattice consts. matching conditions 80−59822
$Ga_xIn_{1-x}As_yP_{1-y}$/Inp DH laser emitting at 1.15 micron grown by low-pressure CVD 80−64052
$Ga_xIn_{1-x}As_yP_{1-y}$-GaAs substrate, lattice matching 79−90901

III-V semiconductors continued
$Ga_xIn_{1-x}As_yP_{1-y}$-InP, CW stripe-geometry lasers, fabrication and props. 77−10943
$Ga_xIn_{1-x}As_yP_{1-y}$-InP injection laser, partially loaded with distributed Bragg reflector 78−82986
$Ga_xIn_{1-x}As_yP_{1-y}$-InP, rib-waveguide injection lasers made by one-step LPE 79−59710
$Ga_xIn_{1-x}As_yP_{1-y}$-InP injection laser partially loaded with first-order distributed Bragg reflector 79−98387
$Ga_xIn_xAs_yP_{1-y}$-InP substrate, lattice matching 79−90901
$Ga_yIn_{1-y}As_yP_{1-x}$, LPE growth 80−66440
$Ga_xIn_{1-x}As_yP_{1-y}$InP laser, DH, 1500 h continuous CW operation 77−42537
GaInAsSb/GaSb DH lasers, 2 micron CW operation at 80K 80−53291
$Ga_{1-y}In_yAs_xSb_{1-x}$, LPE on GaSb, miscibility gap in liq. phase and lattice mismatch 80−15404
$Ga_xIn_{1-x}As_ySb_{1-y}$, epitaxial film and DH, luminesc. props. 77−686
$Ga_xIn_{1-x}As_ySb_{1-y}$ laser, efficient room temp. stimulated emission, 1.8 to 2.4 μm spectral range 79−10307
$Ga_xIn_{1-x}As_ySb_{1-y}$ tunable electron-beam-pumped laser parameters 80−106524
(GaIn)P, dislocation etching of (001) faces with H_3PO_4 etchant 80−15103
$Ga_{1-x}In_xP$, mixed cryst., IR absorption by zone edge lattice vibrs. 78−19487
$Ga_xIn_{1-x}P$ alloy films, surface processes controlling growth by MBE, RHEED and AES exam. 78−84084
$Ga_xIn_{1-x}P$, band struct. enhancement of indirect transitions, piezoreflectance meas. 77−20823
$Ga_xIn_{1-x}P$, Debye-Waller factors, X-ray diffr. determ. *(German)* 77−27959
$Ga_xIn_{1-x}P$, diffuse X-ray scatt. investig. of cation distrib., segregation 77−24409
$Ga_xIn_{1-x}P$ electrode, in aqueous electrolytes, impedance meas. *(French)* 79−87153
$Ga_xIn_{1-x}P$, epitaxial film, diffusion of Cu(Au)(Zn), intrinsic impurity effects 78−87825
$Ga_xIn_{1-x}P$, flat band pot., impedance meas. and photoelectrochemistry *(French)* 80−49894
$Ga_xIn_{1-x}P$, LPE producing coherent interface, model 77−59229
$Ga_xIn_{1-x}P$ MBE layers, comp., Rutherford scatt. and X-ray diffr. meas. 80−75457
n-$Ga_xIn_{1-x}P$, optical props. and energy spectrum of donors 78−72567
n-$Ga_xIn_{1-x}P$ photoelectrochemical cells, bandgap energy, electronic transition mode, and diffusion length 80−72070
$Ga_xIn_{1-x}P$, real struct. exam. by electron microscopy and channelling 78−2143
$Ga_xIn_{1-x}P$ solid soln. epitaxial layers, stabilisation of composition 78−18933
$Ga_xIn_{1-x}P$ solid solns., isothermal liq. epitaxy 80−60793
$Ga_xIn_{1-x}P$ solid solutions, single cryst prep. and props. 80−16162
$Ga_xIn_{1-x}P$, undoped liquid epitaxial layers, effect of heat treatment on photoluminescence 78−60512
$Ga_xIn_{1-x}P$, VPE, recent advances, book contrib. 79−66011
$Ga_xIn_{1-x}P$, with indirect band struct., radiative recomb. of free excitons, cathodolum. meas. 77−90202
$Ga_xIn_{1-x}P$:Mn, ESR of Mn 79−11341
$Ga_xIn_{1-x}P$:N, Delta lattice parameter model, correl. with electronic props. 78−91560
$Ga_xIn_{1-x}P$:N layers, LPE growth, luminesc. and direct exptl. obs. of band struct. effects 77−52157
$Ga_xIn_{1-x}P$:Si, solid soln., splitting of ground state 79−51527
Ga_xIn_xP, LPE, with GaP saturation source wafer *(Polish)* 78−23633
$Ga_xIn_{1-x}P$, piezomodulation spectra of cond. band struct. 77−48191
GaInPAs, CW strip heterolaser, characts. 78−9382
GaInPAs heterostructures and LED's, luminescent props. in 1-2 micron band 78−10988
GaInPAs laser using multicomponent solid soln., room temp. operation 77−75516
GaInPAs, narrow-band tunable injection laser, 1.06 μm 79−76713
GaInPAs/InP heterostructure DFB laser under optical pumping, lasing characts. 80−87396
GaInPAs-InP, high-efficiency LED 79−65545
$Ga_{1-x}In_xP_{1-y}As_y$, carrier compensation and alloy scatt. 80−29490
$Ga_{1-x}In_xP_{1-y}As_y$, drift vel. elec. field characts., Monte Carlo simulation 77−39839
$Ga_{1-x}In_xP_{1-y}As_y$, electron transient drift vel., influence of effective mass and alloy scatt. 80−2384
$Ga_{1-x}In_xP_yAs_{1-y}$/InP DFB injection laser, one-step LPE 80−58575
$Ga_xIn_{1-x}P_yAs_{1-y}$, 111-A and 111-B faces, defect struct., etching and X-ray diffr. obs. 80−2026
$Ga_xIn_{1-x}P_yAs_{1-y}$, ($0.5<y<0.9$), LPE on InP, Ga, As distrib. coeffs., lattice matching 78−47673
$Ga_xIn_{1-x}P_yAs_{1-y}$-InP(GaAs), DH integrated optics development 80−33240
p-$Ga_xIn_{1-x}PyAs_{1-y}$/Au-Zn, specific contact resist. 80−84509
$Ga_xIn_{4-x}PyAs_{1-y}$, In rich bulk single crysts. growth from melt via gradient freeze method, and characterisation 78−68618
GaInSb, Be ion implantation, device appl. 80−24478
GaInSb, intervalley electron transfer, drift velocity and diffusion coefficient 80−39594
$Ga_{0.3}In_{0.7}Sb$, negative differential mobility and geometrical magnetoresist. calc. 77−43624
$Ga_{0.85}In_{0.15}Sb$, MIS struct., C-V characts., interface state densities and storage times meas. 77−89861
$Ga_{1-x}In_xSb$, effective radiative recombination centre nature, photoluminescence spectra 79−90998
$Ga_{1-x}In_xSb$, epitaxial, vapour-phase growth using open-tube flow system 79−33943
$Ga_{1-x}In_xSb$, inverted diode, electron irradiation effect on props. *(Russian)* 78−14378
$Ga_{1-x}In_xSb$, LPE on GaSb by stepwise grading, and characterisation 78−72745
$Ga_{1-x}In_xSb$, press.-induced structural phase transition 78−30751
$Ga_{1-x}In_xSb$, temp. gradient zone melting 80−50550
$Ga_{1-x}In_xSb$, vapour phase epitaxial growth by open tube method 78−84109
$Ga_{1-x}In_xSb$:Zn(Te), photolum. and stimulated emission obs. 78−72595
$Ga_{1-x}In_xSb$-GaSb, lattice parameter meas. in epitaxic layers 79−11040
$Ga_xIn_{1-x}Sb$ diode, with Au metallisation, interdiffusion effect of heat treatment 78−14820

III-V semiconductors continued
$Ga_xIn_{1-x}Sb$, electron transport props. calc. by Monte Carlo method 77−76834
$Ga_xIn_{1-x}Sb$, electron transport in RF field, Monte Carlo simulation 80−96932
$Ga_xIn_{1-x}Sb$, electron vel. field characts., microwave heating method 79−91058
$Ga_xIn_{1-x}Sb$, Ga-rich, prep. by Czochralski technique 80−60771
$Ga_xIn_{1-x}Sb$, growth by LPE 78−27421
n-$Ga_xIn_{1-x}Sb$ Gunn diode, high field domain characts. 80−59992
$Ga_xIn_{1-x}Sb$ LO phonon obs. using Raman scatt. 78−35152
$Ga_xIn_{1-x}Sb$, LPE, growth by vertical dipping method and elec. props. 77−85949
$Ga_xIn_{1-x}Sb$ p-n junction photodiode fabrication, sensitivity as 1 to 2.5 μm detectors *(Japanese)* 80−52311
$Ga_xIn_{1-x}Sb$, transferred-electron effect, and device performance estimation 78−19049
$Ga_{1-x}In_xSe$ solid solution, IR spectra of static reflectivity 79−69849
GaN and GaN:Zn epitaxial layers, doping effect on cathodoluminesc. 77−20935
GaN CVD layer props. rel. to Ga-GaCl conversion efficiency and HN_3 decompositon 77−77404
GaN, cryst. struct. refinement 77−84731
GaN, deposition from plasma reactor, organo-metallic and donor-acceptor complex exchange in HF plasma 80−38839
p-GaN, doping in nonequilibrium conditions 77−62556
GaN, elastic constant calc., elastic wave propag. vel. 78−87734
n-GaN elec. props., electron mobility calc. 78−30923
GaN, electron struct., ESCA study 80−89116
GaN, epitaxial, cathodolum., 78-300K 78−19575
GaN, epitaxial, refl. spectra, 5-12.5 eV 79−99967
GaN epitaxial films, cathodoluminesc. spectra 80−71496
GaN, epitaxial growth kinetics in Ga-HCl-NH_3 77−80710
GaN, epitaxial growth on sapphire substrates, elec. props., X-ray diffr. anal., photoluminescence spectra 79−4919
GaN, epitaxial layer, characts. from cathodoluminesc. 78−35208
GaN, epitaxial layer, cryst. quality meas. by channelling 78−38986
GaN, epitaxial layer prep. and elec. props. 77−85097
GaN epitaxial layers, exciton cathodolum. *(Russian)* 78−76543
GaN epitaxial layers, exciton cathode luminesc. 79−65933
GaN epitaxial layers for LED, X-ray diffr. topography and cryst. characterisation 79−65336
GaN epitaxy, sapphire substrate prep. 78−39929
GaN film, deposition by pyrolysis of gallium trichloride and triiodide ammoniates 77−36402
GaN film, heteroepitaxial deposition, growth kinetics and catalytic effects 79−4487
GaN film, preparation by pyrolysis of $Ga(CH_3)_3$ in NH_3, cathodoluminesc. 77−4691
GaN, film, secondary ion mass spectrometric qualitative anal. 78−7265
GaN film, thermoelec. power and Hall coeff. meas. 77−55627
GaN, formed from initial oxidation and nitridation of GaAs, surface and contact props. 77−20436
GaN, growth and morphology of crystals *(Japanese)* 80−11548
GaN, high-press. VPE and elec. characts. 78−14627
GaN, indirect doping method *(Czech)* 80−24468
GaN, initial growth, on Al_2O_3 and spinel *(German)* 80−107664
GaN, ion implantation, indirect doping method 80−10568
GaN, luminesc. centres 80−93405
GaN, magnetoplasma reflectivity effects, difference method *(German)* 77−12363
GaN, nonlinear susceptibility and coherence length, SHG meas. 78−25924
GaN on Si, form. with GaCl-NH_3-H_2(He), ESCA and RHEED meas. 79−90909
GaN, photoluminesc. characts. for 35 implanted elements 77−24884
GaN, photoluminesc. spectra, energy distrib. 80−97339
GaN, plasma deposition and elec. cond. 78−60585
GaN, polarised electroluminescence emission, microstructure investigations 80−97344
GaN preparation in sealed fused silica ampoules 80−80982
GaN, preparation variables rel. to dielectric data, GaAs conversion 78−60591
GaN, pure and Zn-doped, epitaxial film lumins. 78−10955
GaN single crystals, growth and morphology *(Japanese)* 79−43112
GaN, stimulated emission under high one and two quantum excitation 78−35171
GaN, thermal conductivity, 25-360K 77−35766
GaN, thermodynamic anal. of prep. methods 80−55328
GaN, VPE, on sapphire, crystallographic aspects 78−2387
GaN VPE for blue LEDs *(French)* 79−28928
GaN, VPE growth rate influence on elec. and luminesc. props. 80−100702
GaN:Al, VPE grown, luminesc. and elec. props. depend. on doping conc., bound excitons 80−20688
GaN:As(P), implanted single cryst. film, cathodolum. 78−60523
GaN:Mg, and undoped, epitaxial growth from vapour, orientation, elec. props. 77−4740
GaN:P, photoluminesc. 79−78730
GaN:Zn, cathodolum. obs., recomb. model 79−11474
GaN:Zn, cathodoluminesc., photocapacitance 79−38679
GaN:Zn, epitaxial layer, effective electroluminesc., blue regime *(Russian)* 77−77302
GaN:Zn, heavily doped, photocond. spectra 77−72887
GaN:Zn, LED, blue, yellow and green emission, temp. depend. 77−8658
GaN:Zn, low voltage LED, epitaxial layer, growth and electrolum. *(Russian)* 77−77297
GaN:Zn, n-i struct., anomalous luminesc. 80−80865
GaN:Zn, polarised electroluminescence, mag. field intensity depend. *(Russian)* 79−91502
GaN:Zn, temp. and press. depends., electrolum. 78−19567
GaN:Zn, VPE grown, optical cross sections, photoluminesc. and optical absorpt. meas. 80−55160
GaN:Zn, VPE growth, photoluminesc. rel. to doping conditions 80−55159
GaN:Zn, violet bipolar LED 79−38190
GaN:Zn epilayers, growth parameters effect on props., device struct. 78−26975
GaN:Zn epitaxial films, luminesc. spectra separation into individual bands by impurity absorpt. region excitation 79−74002

III-V semiconductors continued
GaN:Zn LED, electrolum. centres, rel. to growth morphology, Zn conc. and etch patterns 77−1733
GaN:Zn LED, I-V characts., elec. cond. mechanism 77−55614
GaN:Zn(Fe)(Ni)(Cr), lattice parameters, variation with stoichiometry and doping 79−73153
GaN-AlN, solid solution, epitaxial growth and electrical props. 77−73236
GaP, 1 MeV proton bombardment, lattice deformation investigation by Kossel effect 78−22775
GaP, 3d core level spectra, electronic polarisation effects 80−6765
GaP (III) B surface, negative-electron-affinity, photoemission transmission coeff., comparison with GaAsP 78−56560
GaP (001), dislocation etch pits 78−14351
GaP (100), prep. of negative electron affinity surface by Cs adsorption 80−10768
GaP, (100) surface, thermal desorption props. of Cs and Cs-O adsorbed layers *(Japanese)* 80−15368
GaP (100) thermal and vap. phase etching in H_2-HCl-PH_3, obs. 77−77612
GaP (110), electronic surface states, initial steps of O_2 chemisorption 80−49844
GaP (110), initial oxidation, XPS and AES study 80−11542
GaP (110), surface bands in relaxed cleavage surface, tight binding model 78−91744
GaP (110), surface struct., EPR meas. and elastic energy minimisation calcs. 79−51405
GaP (110), wave functions and surface struct., EPR expts. 78−91519
GaP, (110) surface, trned in energy distribs. of Ga dangling orbital surface states 79−28397
GaP (110) surface oxidation process, XPS study 79−15585
n-GaP, acoustoelectric effect due to piezoelectrically active wave 80−80331
GaP acoustooptic pulse modulator 78−46814
GaP, adsorption and desorption of Cs, LEED, AES, and photoemission meas. 80−70532
GaP, adsorption and field-desorption of O_2 and Au, FEM studies 80−34304
GaP, amorphous, optical absorpt. edge shape, band edge fluctuations 77−20880
GaP amorphous film, EXAFS, optical and elec. props. 80−49547
N-GaP and p-GaP, photon drag-optical rectification detectors, performance in 2 to 33 μm range 79−35834
GaP anodic MOS structs., interface-state band model 80−11093
GaP, anodic oxidation and MOS devices 77−80845
n-GaP, anodic oxide film, exam. using SIMS and ellipsometry 79−61770
GaP, anodic oxide film comp. profile anal., radioactive tracer technique 77−59956
GaP anodic oxide system, multiple angle incidence ellipsometry, meas. at λ=632.8 nm 79−63294
GaP, anodically grown insulating layers, prep. and props. *(German)* 78−64158
GaP, anomalous avalanche breakdown 80−80284
GaP, anomalous photoeffect on connected excitons *(Russian)* 80−92929
GaP, atom probe field ion microscopy 78−80460
n-GaP, Au-coated semicond. electrode, photoelectrochem. behaviour in water 77−21399
GaP, Be-Au and Si-Au ohmic contacts, metallurgical struct. 77−1485
GaP, birefringence, photoelastic consts. dispersion 80−11361
GaP, birefringence observations of strain and plastic deform. 80−50678
GaP, bound excitons in spherical model, low lying excited states 80−10883
n-GaP, CO_2 laser induced photon drag effect 79−42589
GaP, CVD epitaxy, book contrib. 77−12544
GaP, CVD mechanism, product catalysed reaction of Me_3Ga with PH_3 77−48345
GaP, camel's back excitons, rel. to band structure 78−47707
GaP, camel's back induced stabilisation of electron-hole liquids 79−19524
p-GaP, cathode of photoelectrochemical cell 78−10552
GaP, cathodoluminesc. meas. of minority carrier lifetime 78−19572
GaP, chem. vapour growth in closed system 78−35283
GaP, chemical etching processes, review 78−95832
GaP, cleaved (110) surface, electron surface props. 80−11067
GaP, comparison of contact resistances of Au-Zn, Au-Zn-Sb, Au-Ge-Ni and Au-Ge-Ni-Sb alloyed contacts 80−70825
GaP, complex ^{119}Sn impurity-defect, Mossbauer study 80−75898
GaP, complex form of donor energy levels, optical spectra anal. 78−23045
GaP, containing matrix metal inclusions, internal friction study 79−42145
GaP, core exciton binding energies 80−80188
GaP, core levels, chem. shift and relaxation energy, temp. dependence 80−39520
GaP, core levels, temp. depend. of conduction band and core exciton energies 80−24828
GaP, cryst., characterisation by light scatt. *(Japanese)* 77−35498
n-GaP, cryst. growth, synthesis solute diffusion method, elec. characts. *(Korean)* 78−52653
GaP, cryst. growth for green luminesc. diode manuf. 77−40346
GaP, crystal, growth conditions rel. to dislocation struct. 80−88151
GaP crystal, structure defect formation due to annealing and stress, dendrites, slip, dislocations 80−29026
GaP crystals, radiation defects, TSC obs. 80−65588
GaP, Cs(Cs-O) activated, with negative electron affinity, thermalised electron emission 78−11073
GaP, Cs(Cs-O) activated, with negative electron affinity, near UV photoemission and secondary emission 78−11074
GaP, current controlled LPE from finite volume melt 80−20805
GaP, Debye temperature, atomic mean square displacement 78−87757
GaP, deep level impurities *(Japanese)* 77−89723
GaP, deep level profiles at substrate-epitaxial interfaces, photoionisation meas. 79−38025
GaP, deep levels investigation 77−76769
GaP, deep O^- state, model impurity calc. 80−6780
n-GaP, deep state controlled minority carrier lifetime 80−20211
GaP, deformation potentials of direct and indirect absorpt edges 79−69854
GaP, density of states effective mass and cond. band energy minima 77−28101
GaP, diffusivity and solubility of Cu 78−51743
III-V semiconductors continued
GaP diodes, TSCAP and admittance spectroscopy of gamma-ray induced defects 77−89472
GaP, dislocation etching of (001) faces with H_3PO_4 etchant 80−15103
GaP, dislocation loops and bipolar obs. by chemical etching 78−55873
GaP, dislocation obs., SEM EBIC vs SEM CL micrographs 77−80511
GaP, dislocation structure, optical microscopy obs. 80−24458
GaP, dislocations induced by diffusion of Zn with or without P 77−19955
GaP, disorder distrib. extraction, semiempirical method of applying dechannelling correction 78−22781
GaP, dispersion of refr. index and permittivity 77−55765
GaP, dispersion of vibrational excitations, Raman scatt. 78−84588
GaP, donor states theory, camel's back struct. influence 80−59921
GaP donor system, local mode, random force const. change 78−38800
GaP, donor-acceptor pair spectra, electron-phonon interactions 79−38631
GaP, donor-acceptor pair luminesc., excitation spectroscopy 80−25440
GaP, dopant dislocations, scanning electron micrographs, cathodoluminesc. 78−91340
GaP, double reson. in two-phonon Raman scatt. by longitudinal optical phonons 77−24852
GaP, EHT calcs. of energy bands and pressure dependences *(Japanese)* 78−34747
GaP, effective mass anisotropy at X_{1c} and X_{3c} minima of conduction band, optical absorpt. spectra 77−8021
GaP, effective partition coeffs. and elec. behaviour of group IV elements 77−7754
GaP, effects of hydrogen incorporation during deposition by sputtering 79−69981
GaP, elastic moduli, 80-700K, and elastic consts. 79−73245
GaP, elastic moduli and attenuation of elastic waves 77−51429
GaP, electrical and optical props. at low temps. 80−39636
p-GaP electrode, for solar cell, differential capacitance meas. for flatband potential determ. 78−72256
n-GaP electrode, photoanodic dissolution rate, effect on surface electronic band energies 80−103748
n-GaP electrode, photoelectrochemical behaviour in acetonitrile solns. 78−31644
p-GaP electrode, photoelectrochemical effect 80−55673
p-GaP electrode, spectral response extension by metal adatoms 78−34895
p-GaP electrodes with metal adatoms, surface states form. due to impregnated H 80−54778
GaP, electrolum. efficiency degradation and deep level change in red LEDs 77−81155
GaP, electrolum. study using high-gain image intensifier 80−55193
GaP, electroluminescent diode, electron irradiated, negative resistance due to impact ionisation 77−15942
GaP electroluminescent diode struct. prep. by SSD and Czochralski methods, dynamic props. *(Czech)* 80−97425
GaP, electron hole droplet, motion damping, impurity and piezoelec. scatt. 78−67951
GaP, electron irrad., EPR of antisite-impurity defect 80−25211
GaP, electron irrad., radiation defects annealing 80−29059
n-GaP, electron mobility, 77 to 300K, intervalley scatt. of electrons *(Russian)* 79−95407
GaP, electron traps around dislocations in p-n junction and metal-semicond. structs. 80−34388
GaP, electron-hole drop, luminesc. 79−33812
GaP, electron-hole drops, self-consistent surface calculation 80−65464
GaP, electron-hole liq., cathodolum. spectra meas., 4.2-20K 77−63470
GaP, electron-hole liquid obs. by luminesc. spectra 77−51668
GaP, electron-hole liquid exam. 78−2430
GaP, electron-hole liquid, emission band from time-resolved spectra 78−43938
GaP, electron-hole liquid props., luminescence at high excitation intensity 79−69882
GaP, electron-hole plasma photolum. obs. 78−52559
GaP, electron-hole plasma luminesc. 79−38651
GaP, electronic props. of paramag. antisite P(Ga) defect 78−43327
GaP, electronic states of neutral vacancies 77−11875
GaP, electronic structure of neutral phosphorus vacancy, empirical pseudopotential 79−78042
GaP, electroreflectance spectroscopy using synchrotron rad. 78−10912
GaP, epitaxial growth by $GaPO_4$-C system 79−99448
GaP, epitaxial growth from Sb and Bi melts 79−52131
GaP epitaxial growth from solution in melt, crystn. theory 80−16204
GaP, epitaxial layer, carrier recomb. at dislocations 77−20932
GaP epitaxial layer, crystal defects influence on luminesc. obs. 79−87511
GaP, epitaxial layer, thickness and diffusion length, photocurrent meas. 77−32096
GaP, epitaxial layer prep. and elec. props. 77−85096
GaP, epitaxial layers, dislocation recomb., SEM cathodoluminescence studies 79−42558
n-GaP, epitaxial layers, electrical parameter determ. by graphical method *(Russian)* 77−15975
GaP epitaxial layers, stable growth conditions, by molten salt electrodeposition on Si and GaP substrates 79−20000
n-GaP epitaxial layers, transverse magnetoresist. *(Russian)* 77−76964
GaP epitaxial layers for yellow-LEDs, prep. and props. *(Czech)* 78−48234
GaP epitaxial layers grown in Ga-PCl_3-H_2 system, surface defects 77−7993
p-GaP, epitaxial layers grown from liq., overcompensated, doping levels 78−91353
GaP, epitaxial struct., cathodolum. in SEM 78−10991
GaP, etching in aqua regia and bromine-methanol-water solns. 78−68833
GaP, exam. of magnetic susceptibility and absorption spectra 79−1778
GaP, excited 1s-level of S-bound excitons 79−82996
p-GaP, field electron emission current-voltage characts. 80−45219
GaP, field ion microscopy 78−19644
GaP film, deposited by RF sputtering, struct. and elec. props. obs. *(Czech)* 78−52667
GaP film, polycrystalline, with negative affinity, secondary emission *(Czech)* 78−52604
GaP films, RF sputtering on glass and Au film substrates, struct. and elec. props. 80−2311
n-GaP films, reduced work function, energy spectra of secondary electron emission 79−28867

III-V semiconductors continued
GaP films on Si, epitaxial crystallisation by nanosecond laser pulses 80−107674
GaP, fine struct. in energy derivative reflectance spectra 79−78705
GaP, fine struct. of indirect exciton 78−19509
GaP, first order Mott transition of exciton gas 78−76535
GaP, freq. depend. of TO phonon decay parameter; and phonon-phonon interaction mechanisms 77−59084
GaP, frozen-in pt. defects annihilation 79−99949
GaP, GPE layers, nonradiative dark regions along surface ripples 77−59600
GaP, gain in stimulated Raman scatt. by coupled phonon-plasmon modes from spontaneous Raman spectra 79−68418
GaP, green cathodolum. from cryst. defects, SEM, TEM study 80−80870
GaP, green LED, degradation, appl. of dislocation climb model 77−1125
GaP, green luminesc. efficiency, review 77−28636
GaP, grown by SSD method, Zn diffusion for green LED fabrication 77−81208
GaP, growth, LPE method for green LED mass production 77−77422
GaP, growth and props. of LPE layers on Si substrates 78−6864
GaP, growth of dislocation free crysts. from stoichoometric melt. 77−81212
GaP, growth of epitaxial layers from limited of melt-soln. 78−19676
GaP, heteroepitaxial CVD on Si, dual process, film characts. 77−16503
GaP, heteroepitaxial deposition on GaAs, Sn solvent inclusion, surface morphology *(German)* 79−28968
GaP, heteroepitaxial growth on Si, substrate misorientation effects 78−3055
GaP, heteroepitaxial growth on Si substrate by MBE 78−64481
GaP, high-energy ion-implanted, layer thickness and refr. indices meas. 77−24837
GaP, high-order Raman spectra, polariton scatt. 78−56483
GaP high-pressure reaction synthesis 77−77372
GaP, hole traps, rel. to two stage model for deep level capture 78−10396
GaP, hyperbolic singularity of dispersion law of excitons 79−42466
GaP, impurity behaviour during crystallisation from melt 77−84772
GaP, impurity distribution ratios, correl. with covalent and ionic radii 80−54276
GaP, impurity interaction on excited acceptor states, luminesc. excitation spectra 79−15517
GaP, impurity-containing single crysts., refl. spectra 80−80823
n-GaP in DMF solns., electrochem., photoelectrochem., redox. pot. determ. 79−96322
GaP, indirect exciton dispersion, 'camel's back' 79−73447
GaP, indirect exciton fine struct. in absorpt. spectrum, stress effects 79−42986
GaP, indirect exciton fine struct. and effect of uniaxial stress 79−95805
GaP, indirect free exciton, magneto-optical investigation of ground state 77−51670
GaP, influence of shear deform. on interband interaction 78−39116
n-GaP, interface-recomb.-controlled minority carrier lifetime obs. 77−12027
GaP, interimpurity interaction effect on distrib. profiles of impurities diffusing simultaneously 77−76451
GaP, internal friction calc. 80−2116
n-GaP, inversion layers, broken-symmetry ground states 77−47873
GaP, ion implantation, range distrib. calc. 79−55760
GaP, ion implanted, mode-locked Nd:YAG laser annealing, recrystn. 80−19817
n-GaP, ion implanted films, optical and luminesc. props. 80−60699
GaP, ion-bombarded, energy band struct., electrorefl. obs. 79−19517
GaP, ion-implanted, form. and annealing of radiation damage 78−91363
GaP, ion-implanted, radiation damage, ellipsometry expts. 78−38735
GaP, ionised-cluster beam epitaxial growth on GaP and Si, characts. for LED 79−28951
p-GaP, irrad. by visible light, photoelectrolytic decomposition of water 77−77778
GaP, LEC, SSD and CVD samples, Zn tracer diffusion profiles in solids 78−95189
GaP, LEC crystal, cathodolum. and photolum. around dislocations 78−84663
GaP, LEC crystal, etch pit obs. 77−76387
GaP LEC crystal, imperfections obs. by light scatt. 78−6074
GaP, LEC growth of dislocation-free crysts., microdefects and striations 78−9974
GaP, LED, efficiency depend. on O_2 conc. 79−19613
GaP LED, N content by photovoltage meas. 77−11993
GaP LED, negative differential resistance and conductance associated with dielectric losses 77−63468
GaP LED, SEM study of charge collection and cathodoluminesc. 80−65661
GaP LED, surface treatment effect on surface recomb. vel. and leakage current 77−20410
GaP LED with S-shaped characteristic, negative resist. and red electroluminesc., expt. 78−48237
GaP LED's, current/voltage and light/voltage characts. 77−8662
GaP, LPE, cathodo- and electrolum., residual impurity and struct. defect effects 78−19570
GaP, LPE, LED fabrication and electroluminesc. characts. 77−28632
n-GaP, LPE, minority carrier bulk lifetime and diffusion coeff. meas. 77−11932
n-GaP, LPE, non-radiative recombination 78−19565
GaP, LPE at 650°C from In solvent, low Si contamination 78−80480
GaP, LPE growth rate calc., model of LPE growth 79−19485
GaP, LPE layer for LED, photoluminesc. distrib. meas. *(Czech)* 78−48209
GaP, LPE layer perfection, effect of dislocation loops in GaP substrate 78−30843
GaP, LPE layers, comparison of growth rates with theoretical predictions 79−52134
p-GaP, LPE layers, Hall effect 78−91704
GaP LPE layers, low temp. growth from In solvent 79−56924
GaP LPE layers and LEC substrates, correlation between dislocation pits 78−38706
GaP, LPE layers high purity, invest. *(German)* 78−31353
GaP, LPE solvent choice, equilib. in In-Ga-P system 79−87589
GaP lamps, green emitting deep level photocapacitance spectra 77−69409
GaP, large cryst., optical birefr. images of dislocations 78−30627

III-V semiconductors continued
GaP, lattice dynamics, phonon freq. meas., valence-force-field overlap shell model 80−15205
GaP, lattice dynamics and phonon parameters bond bending force model 80−59595
GaP layers, heteroepitaxy, grown on Si and Ge from multiple component solns. *(Russian)* 78−15319
GaP layers, LPE growth, elec. props., residual impurities 79−38202
GaP, light emitting diode structure, effect of neutron irradiation on cathodoluminesc. 79−28843
GaP, light scatt. by LO phonons, high-resolution study 80−80798
GaP, light scatt. spectra of guided wave polaritons 79−15101
GaP, line shape and symmetry analysis of core-level electroreflectance spectra 77−8600
GaP, localised states in presence of P vacancy, pseudopot. calc. 78−18992
n-GaP low absorption monitors for HF laser 79−31964
GaP, low temp. selective Zn diffusion process using anodic oxides 78−47399
GaP, luminesc. emission band, electron-hole liquid 77−69245
GaP, luminesc. from electron-hole drops, 2 to 77K 79−11454
GaP luminophor powders, SAW nonlinear acoustoelectro-luminescence 80−45143
GaP, MBE growth on GaP, and crystallographic evaluation 77−8762
GaP, MCD of phonon-assisted exciton transitions 78−92053
GaP, manifestation of local vibrs. of dislocations in IR spectra 78−88339
n-GaP, many-valley semiconductor, relative displacement of D_1 and D_2', bands under shear deform. influence 79−15080
n-GaP, many-valley semicond. anisotropic acoustoelectric effect, thermo-EMF anisotropy fluctuation depend. on ultrasound freq. 79−69562
GaP meas. of transition press. to conducting phase 79−54150
GaP, mech. props. and photomechanical effect 77−84833
GaP, metallic modification, supercond. transition temp. at high temp. *(Russian)* 77−80867
GaP, microscopic mechanism of film growth from non-condensed phases, kinetic anal. 80−54565
GaP, minority carrier lifetimes at dislocations, SEM meas. using photon counting 78−23109
GaP, minority carrier quasi-Fermi level meas. in illuminated photoelectrolysis cell 77−85308
GaP, minority carrier traps, detection using transient spectroscopy 79−65402
GaP, mol. beam epitaxial growth, cryst. quality composition investig. *(Japanese)* 77−55895
GaP, moments of phonon spectra from specific heats 80−15203
GaP, Mott transition of exciton gas, cathodoluminesc. 79−33845
GaP, multiband and multivalley effective mass theory for impurities 79−65409
GaP, n-, p-type, electrode, impedance in alkaline medium *(French)* 79−43586
GaP, n-type, Zn diffusion, p-n junction depth 77−89841
GaP negative electron affinity cold cathodes, vidicon appls. 78−19133
GaP, non-radiative recombination and structural defects 78−19566
GaP, nonlinear optical susceptibility and dispersion, electro-optic meas. 77−23707
GaP, nonradiative capture and recomb. by multiphonon emission 77−43533
GaP, O_2 adsorpt. monitoring by Auger spectroscopy, electron beam effects 77−72777
GaP, O_2 adsorpt. monitoring by Auger spectroscopy, electron beam effects 78−6218
GaP, obs. of Γ-L indirect transition, phonon struct. 78−48194
GaP, obs. of Raman scatt. by Cu vapour laser 78−95586
GaP on GaAs, LPE, growth with Ge and Sn solvents, phase diags. 78−88434
GaP on GaAs substrate, heteroepitaxial layers, stuct. defects *(German)* 79−23865
GaP, optical absorption and struct. of acceptor centres 78−48205
GaP, optical inhomogeneity, physical basis 79−15430
n-GaP, optical rectification due to free carriers, detector appl. 77−10967
n-GaP, optical rectification and photon drag 77−36224
GaP, optoelectronic devices, conf., Berlin, DDR 78−91755
GaP, overlap integrals and Auger recomb. coeff. direct calc. 79−69524
GaP oxide, anodic, optical props., 1.5-6.0 eV 77−90209
GaP oxide films grown by anodization in electrolytes, electron spectroscopy exam. *(German)* 79−15837
GaP, p^+-n diode junction, admittance meas. and carrier traps 78−91757
GaP, p-i-n LED, I-V characts., electrolum., and photocond. meas. 77−20930
GaP, p-n homojunction breakdown voltage for onesided abrupt junctions *(German)* 78−56210
GaP p-n junction, capacitance-freq. dispersion and electroluminescence efficiency 78−64101
GaP p-n junctions, electron beam excited carrier avalanche multiplication 79−69587
p-GaP photocathode, charge transfer via surface states, water photoelectrolysis anal. 80−75636
GaP photoelectrode, role of Au overlayers 78−14812
GaP photoelectrode, stability 77−20422
GaP, photoelectron spectra at Schottky barrier *(Korean)* 79−11220
n-GaP, photoelement in UV radiation ratemeter 78−285
GaP, photoemission from (111) and $(\bar{1}\bar{1}\bar{1})$ surfaces 79−91562
GaP, photoexcited, Raman scatt. from plasmons 79−38541
GaP, photovoltage transients, intensity and chopping freq. depend. 77−47859
GaP, piezo-modulated spectroscopic investigation of N and N-N pairs, bound exciton 77−66474
GaP, piezobirefringence above direct gap 79−51929
GaP, plasma deposition and elec. cond. 78−60585
GaP, polar semicond., radiative recomb., electron-phonon interaction effects, calc. 80−49631
GaP, polar semiconductor, electron-hole liquid, electron-phonon interactions 80−6739
GaP, polariton dispersion, IR reflection spectroscopy 80−11415
GaP, polariton linewidth in k-space, anharmonicity and permittivity 77−85155
GaP, polished, technique for uniform etching 78−39928
GaP, polishing dislocation etch 78−6066
GaP polycrystals, subgrain boundaries, cathodolum. in SEM 79−1440
GaP, positron annihilation, deep acceptor level props. 79−11485

III-V semiconductors continued
n-GaP, potential of Au overlayer, I-V curves 77−89848
GaP, powder, electroluminesc. excitation by SAW, nonlinear effects 80−16104
GaP, preferential etching of dislocations and stacking faults 77−39589
GaP, proton implanted, thermally stimulated current meas. 80−24943
GaP, pure and N doped, extended Huckel theory appl. 80−59916
n-GaP, quasidirect radiative recombination of free holes at neutral shallow donors 78−64410
GaP, radiation defect accumulation due to ion bombardment, optical absorpt. meas. 77−76438
GaP, radiative and non-radiative recombination around dislocations 78−19576
GaP, Raman scatt. from plasmon-phonon coupled modes 80−93337
GaP, Raman scatt. from surface polaritons, selection rules 77−52083
GaP, Raman scattering selection rules for surface polaritons 78−72091
GaP, Raman spectra, press. depend. optical phonon anharmonicity 77−8586
GaP, rare earth doped, photolum. and elec. props. *(Russian)* 78−52545
GaP, red LED degradation, diffusion model 77−8657
GaP, reevaluation of bandgap and free exciton binding energy 78−60061
GaP, refr. index, 100 to 420K, permittivity calcs. *(Russian)* 77−90156
GaP, reson. Brillouin scatt., near indirect absorpt. edge 80−11423
GaP, reson. photoemission shake-up and Auger processes at 3p photothreshold 80−100748
GaP ribbon waveguide, vapour-grown, phase-matched SHG 80−48339
GaP, S-bound exciton stress depend. 80−29333
GaP, SEM, cathodoluminesc., impurity and defect detect. 78−83695
GaP, scatt. mech., mobility tensor 80−6826
n-GaP, Schottky barrier height data for several contact systems 80−60080
GaP Schottky barriers, voltage fluctuations, meas. 80−15604
p-GaP, Schottky barriers on polar (111) and ($\bar{1}\bar{1}\bar{1}$) surfaces 80−88631
GaP second order Raman spectrum, polarisation meas. 78−64368
GaP, semicond., ^{31}P nuclear mag. shielding 79−33549
n-GaP, semicond. electrode, electrolum. due to hole injection from electrolytes 77−20926
p-GaP semiconducting photoelectrode 80−101119
GaP semiconductor Raman laser 80−78864
p-GaP semiconductor-electrolyte solar cells for photochemical reduction of CO_2 to organic fuel 80−55880
GaP, shallow impurity states, free exciton binding energy 78−79960
n-GaP, shallow trapping centres, electron lifetime from photocond. meas. 79−99563
GaP single cryst., defect distrib. near abraded surface 80−92533
GaP, single cryst., Raman scatt., effective cross-section rel. to nonlinear coeffs. *(Russian)* 78−71152
GaP single cryst., Raman scatt. cross section, nonlinear optical coeffs. 79−56784
GaP, single cryst. electrode, impedance, effect of freq., voltage and electrolyte comp. 78−19146
GaP single crystal, direct obs. of dislocations by birefringence 79−14810
GaP, single-crystal, anodically oxidised layers, AES measurements 78−91556
GaP, site selective doping by ion implantation of radioactive nuclei 80−34023
GaP, soln. growth of bulk crysts., luminesc. and elec. props. 78−92181
GaP, solubility in fused Sb, Bi, thermodynamics, rel. to epitaxial growth 78−34721
GaP, spectral depend. of O photoneutralisation cross-section near threshold, and band gap 79−1788
p-GaP, spin-flip Raman scattering, review 80−108209
GaP, stabilisation of electron-hole liquid by camel's back 80−6740
GaP, Stark effect at H-like impurity centres, forbidden electron transitions *(Russian)* 80−16009
GaP, stress-induced X_{1c}-X_{3c} conduction band mixing 79−19515
GaP, structural etching, characterizing $A^{III}B^{V}$ compounds, misfit dislocations 80−39099
GaP, substoichiometric native oxide layers, $^4He^+$ backscatt. obs. 77−77610
GaP substrate, transient-mode LPE of $Al_{1-x}Ga_xAs$ 78−72746
GaP surface, Ar^+ and e^- excited Ar Auger electron emission 79−47560
GaP, surface, contact pot. difference meas. 77−20403
GaP, surface, energy distrib. of photoemission *(Japanese)* 80−16145
GaP surface, quantitative XPS meas. 78−56559
GaP surface barrier structure, breakdown voltage exam., effect of proton irradiation 79−11225
GaP, surface characterisation using SAW 80−11069
GaP, surface cleaning by oxidation and heating, characterisation for electron emitter appl. 78−35548
GaP, surface layers produced by chemical treatment, comp. and struct. 79−96173
GaP, surface polariton linear photon and two photon absorpt. 80−49863
GaP, surface polaritons, freq. depend. of associated functions 79−78020
GaP, surface polaritons, light scattering studies, effect of surface roughness 80−6753
GaP, surface processing, residual film monitoring by ellipsometry 80−13124
GaP, surface sensitivity, low energy electron transmission optical modulation 78−76567
GaP, surface states, UPS meas. 78−14780
GaP, synthesis by gas chemical transport reactions, exam. of kinetics 79−95933
GaP, temp. coeff. of induced birefringence 80−93277
GaP, temp. depend. of Fermi Level, calc. 80−39491
GaP, thermal etch-pits, morphology 80−34002
GaP, thermal expansion below room temp. 80−79963
GaP, thermoelectric performance of Si-Ge alloy improvement 79−47115
GaP, Thomas-Fermi theory, dielectric functions, screening, dielectric constants 79−99497
GaP, transition metal deep centres, model 79−78045
GaP, transverse acoustoelec. voltage spectroscopy 80−49828
GaP, two-particle states and polariton spectrum 77−59261
GaP, two-photon absorpt., by surface polaritons 77−51676
GaP, two-photon absorption coefficient rel. to inverse Raman cross section 78−6678
GaP, two-stage vapour/liq. epitaxial growth on Si 78−3054
n-GaP, uniaxially deformed, piezoresist. exam. of donor levels 77−4346
GaP, upper polariton branch obs. by ATR 78−68510
GaP, VPE, background deep level defects, transient capacitance obs. 77−62854

III-V semiconductors continued
GaP, VPE cryst., electrolum. characts. 77−28631
GaP, VPE layer on Si or Ge, antiphase domain structures 77−69193
GaP, VPE layer structures for LED's, SEM, and TEM obs. of dislocation density reduction expt. 80−100425
GaP VPE layers, precision lattice parameter meas. by Umweganregung method 79−65047
GaP, VPE Ni contaminant detection, IR photoluminescence of Ni 78−15212
GaP, vac. deposited film, structural, elec. and photoelectric props. 79−82698
GaP, valence band structure, CPA, bond orbital calcs. 78−87909
GaP, vapor-phase etching, mechanisms and kinetics 80−100934
GaP, Zn diffusion into n-LPE layer, for high efficiency green LEDs 77−80519
GaP:^{56}Fe(^{57}Fe)(^{53}Cr), paramag. centres, identification from ESR and ENDOR spectra 80−80600
GaP:0 effect of displacement upon impurity levels, pseudopotential calc. 77−39803
GaP:Au, diffusion, solubility, and electrotransport of Au 78−91489
GaP:Bi,N, photoluminesc., electroluminesc., 4.2 to 300K, excitons and hole traps 80−108275
GaP:Bi(N), luminesc. decay kinetics 79−38646
GaP:C(Mg)(Zn), excited acceptor state investig. by photoluminesc. 77−8632
GaP:Ce(Dy)(Pr) epitaxial films, photoluminesc. spectra 80−66294
GaP:Co, deep levels, IR photoluminesc., stress effects 80−55163
GaP:Co, optical spectra and Zeeman anal. of Co $3d^7$ state 80−66247
GaP:Co(Ni), photolum. excitation spectroscopy 80−80841
GaP:Cr, diffusion parameters and solubility and influence on elec. and optical props. 79−73343
GaP:Cr, ESR of doubly ionised Cr acceptor and IR luminesc. 78−56374
p-GaP:Cr, hole traps, ESR studies 80−75843
GaP:Cr, local level near valence band, photocapacitance 79−11080
GaP:Cr, origin of sharp near IR transitions 80−10913
GaP:Cr epitaxial layers, Cr conc. profile determ. 80−65029
GaP:Cr_2O_3, growth, dopant distribution, elec. resist. 78−34531
GaP:Cs-O simultaneous adsorption, oxidation interface chemical struct. 80−103584
GaP:Cu, deep levels, photoluminesc. and optical cross sections 79−38653
GaP:Cu, elec. and optical props., rel. to doping and heat treatment 80−16056
GaP:Cu, impurity absorpt. bands at 1.05, 0.75 eV 77−44032
GaP:Cu, LPE, photoconductive props. obs. 78−47836
GaP:Cu, Raman scatt. from acceptor state 80−11408
GaP:Cu, thermally and optical excited cond., deep level centres 78−72190
GaP:Cu p^+-n junction, deep level parameters, TSC meas., rel. to photocurrent techniques 78−72249
GaP:Cu-Ni, Schottky barrier, TSC meas., trap levels 78−91709
GaP:Dy, photolumines. spectra 79−52015
GaP:Fe, current-voltage characteristics p-i-n diodes, luminescence, absorpt. double injection methods 79−65407
GaP:Fe, diffusion, solubility, elec. activity and energy levels 77−55395
GaP:Fe, double electron trap state, ESR identification 77−36124
GaP:Fe, double Fe-thermal acceptor centre, energy states 80−96823
GaP:Fe, electron exchange via val. band between Fe acceptor centres, Mossbauer spectra 77−55741
GaP:Fe, heat treated, EPR spectra, struct. defects 80−7158
GaP:Fe, impurity atom charge exchange, Mossbauer spectroscopy 79−47050
GaP:Fe, optical absorption spectrum and Faraday effect 80−108245
GaP:Fe, photo-EPR study Fe($3d^6$) centres and deep electron traps 80−44910
p-GaP:Fe, photoionisation spectrum of acceptor level 77−55810
GaP:Fe, profile of impurity optical absorption bands 78−56509
GaP:Fe n-i-n epitaxial struct., photoconductivity, recombination scheme *(Russian)* 80−15569
GaP:Fe^{2+}, absorpt. and luminesc. spectra 77−16388
GaP:Fe^{2+}(Co^{2+})(Ni^{2+}) d→d luminesc. spectra 80−7414
GaP:Fe^{3+}, deep impurity states investig. 77−15794
GaP:Fe^{3+} ESR spectrum, elec. field, uniaxial compression influence 80−103882
GaP:Fe(Cr), photo-ESR of annealed crysts. 80−15795
GaP:Ge, ENDOR study, superhyperfine interactions 80−93210
n-GaP:Ge, photomemory effect and thermal field impurity breakdown 77−20362
n-GaP:In, LPE from In solvent, dislocation density reduction by doping 78−18919
GaP:Mg, ion implanted, elec. profiles 79−77628
GaP:N, appl. of temp. modulated photolum. induced by photoexcitation technique 78−95605
GaP:N, bound exciton absorpt. line asymmetry, electroabsorption spectra 80−71459
GaP:N, bound excitons, low temp. photoluminesc. thermal quenching 77−48228
GaP:N, Cd(Zn),(C), interimpurity recomb., acceptor binding energies 78−34796
GaP:N, electron binding by N pairs 79−90990
GaP:N, electron charge distrib. in vicinity of substitutional N 77−24531
GaP:N, electron-hole liq., luminesc. obs. 80−25438
GaP:N, electronic energy levels calc., optimisation 79−28315
GaP:N, epitaxial layer, determination of nitrogen concentration from cathodoluminescence spectra 78−38744
GaP:N, epitaxial layer doping 77−51396
GaP:N, epitaxial layers, N concentration determination by two independent methods 80−39142
GaP:N, excited states of excitons bound to NN_i pairs, fluoresc. obs. 77−44039
GaP:N, luminesc. from electron-hole drop 79−33813
GaP:N, N doping profiles in GaP grown by LPE, cathodoluminesc. data 79−23631
GaP:N, phonon satellite intensity distrib. in luminesc. spectrum 77−55832
GaP:N, photoluminesc., temp. depend., exciton recombination mechanism 78−88355
GaP:N, photoluminescence, temp. modulated 79−38623
GaP:N, quenching of luminesc. by charged defects 78−23531
GaP:N, radiative recomb. from electron-hole drops, impurity induced transition 78−19547
GaP:N, radiative recomb. of electron-hole liq. 79−73442

III-V semiconductors continued
GaP:N, spin dependent exciton recombination at N_2 isoelectronic traps 77−69734
GaP:N, temp. modulated photoluminesc. 77−55818
GaP:N, temp.-modulated photoluminesc., phonon assisted tunnelling process 78−23511
n-GaP:N,O,S,C end, dielec. const. from S-C donor acceptor pair spectra 79−65788
GaP:N LED, acoustic emission, NDT of dislocation motion 78−91759
GaP:N LED structures, local dopant conc. determ. using SEM cathodolum. spectra 80−101057
GaP:N p-n structure yellow light emitting source 77−69412
GaP:N VPE LED, deep level centres, DLTS studies 79−42493
GaP:N VPE layers, thermal emission energies, trapping, and carrier lifetimes, deep level capacitance spectroscopy 79−42487
GaP:N(N,O) epitaxial struct., luminesc. study of degradation during heat treatment 80−45139
GaP:N(Te), ion implanted at 40 keV, refl. spectra, 210-2000 nm, annealing *(Russian)* 78−80386
GaP:Ni, absorpt. and luminesc. spectra 79−42996
GaP:Ni, deep traps, near IR luminesc., polarised spectra meas. 80−16077
GaP:Ni, electron-hole recombination via deep state 79−99560
GaP:Ni, Hall effect and absorpt. spectrum investig. of acceptor level 77−44033
GaP:Ni, optical and EPR study of two-electron-trap state 79−73806
GaP:Ni, whisker growth on surface 79−33212
GaP:Ni(Fe), multivalence impurities, EPR and optical absorpt. meas. 80−75844
GaP:O, EPR investig. of deep donor centre, delocalisation 77−28428
GaP:O, impurity concentration determ. by donor-acceptor luminescence 78−6090
GaP:O, multicharged state of O, TSC and photoinduced currents 79−7808
GaP:O, optical transitions via deep levels, phonon interaction 78−87939
GaP:O, optical transitions via deep levels, cross section temp. depend. 78−87940
GaP:O, photoionisation of deep impurity levels 80−34386
GaP:O, wave functions and optical cross sections associated with deep centres 78−34801
GaP:O^-, two electron state, electron capture 78−39054
GaP:O^-, two-electron O^- state evidence, ODMR, IR emission, phonon replicas 80−15828
GaP:rare earth, magnetic susceptibility, impurity states 79−61044
GaP:S, ENDOR meas., symmetries, hyperfine parameters 78−72435
GaP:S, effects of uniaxial stress on luminesc. 79−78739
n-GaP:S, elastic moduli and mode gammas 79−73242
GaP:s, elec. props. following 1.7 MeV electron irradiation 78−80005
GaP:S, ground and excited states of bound exciton complex, stress effects 80−65463
GaP:S, Se, Te, Si, shallow donors, excitation spectra 77−81128
GaP:S, shallow donor states, Stark effect and inversion splitting, electroabsorption spectral obs. 80−50385
n-GaP:S electrical properties investigation, Hall effect and resistivity meas. *(Japanese)* 77−39840
GaP:S LEC grown crystals, HVEM investig. of defects 79−60376
GaP:S(Se), donor bound exciton excited states 80−66284
GaP:S(Se)(Te), pot.-depend. g-values and quenched diamag., props. of donor states 77−62861
GaP:S(Se)(Te), pot.-depend. g-values and quenched diamag., pseudoacceptors D^0, X 77−62862
GaP:S(Se)(Te)(Si)(C)(Zn), IR photocond. response spectra 79−56257
n-GaP:S(Te), IR absorpt. cross-section 79−38582
GaP:S(Te), photostimulation spectra, bound electron phonon interactions *(Russian)* 77−1712
GaP:Sb(Bi), gap vibrs. and impurity conc. determ. 79−69869
GaP:Si p-n struct., on n-$Ga_{1-x}Al_xP$ and n-GaP substrates, electrolum. spectra 79−24368
GaP:Si(s)(O)(Ta), donor centre struct. and conduction band nonparabolicity 78−14695
GaP:Sn, LPE growth from Sn soln., elec. resist. and Hall coeff. meas. 78−2593
GaP:Sn(Sb), lattice location of implanted atoms, ion backscatt. and ion-induced X-ray obs. 77−84785
GaP:Te, defects formed due to precipitation of Te, metallography and TEM exam. 77−84769
n-GaP:Te, doping parameters calc., by means of Hall data analysis 78−51925
GaP:Te, ENDOR meas., hyperfine interactions and elec. field gradient 79−42869
GaP:Te, Hall effect and elec. cond., 80-400K 78−91705
n-GaP:Te, LPE layers, Hall effect 78−91704
GaP:Te, photon drag, optical rectification response meas., anomalous polarisation depend. 78−33769
GaP:Te, struct. imperfections, prep. and doping effects 77−89451
GaP:Te epitaxial layers, dopant distrib. obs. by amalgam polarography 77−39609
GaP:Te on GaAs, LPE growth fron Sn, exam. of impurity band conduction effects 79−11249
GaP:Te(S), nucl. relax. rel. to donor density 80−11284
GaP:Ti(Co)(Ni), positron annihilation meas. rel. to deep levels study 80−60712
GaP:V, ESR exam. 79−11344
GaP:Zn, diffusion profile determ., $^{32}P/^{65}Zn$ double tracer technique 78−55888
GaP:Zn, dopant diffusion profiles at 900°C, radiotracer meas. 77−59147
GaP:Zn, doping from gas phase during LPE 80−55312
GaP:Zn, Hall effect and elec. cond., 80-400K 78−91705
p-GaP:Zn, Hall effect determ. of hole mobility temp. depend., scatt. mechanisms 77−4364
GaP:Zn, implanted, elec. profiling using anodic oxidation in N-methylacetamide 80−54690
GaP:Zn, isolated Ga vacancy due to electron irrad., EPR study 78−95519
GaP:Zn, light attenuation by impurity precipitates 79−11441
GaP:Zn, luminesc., acceptor-bound multiple excitons 80−11476
GaP:Zn, O, influence of impurity-absorbed illumination on luminesc. 80−93395
GaP:Zn, O LED, neutron irrad. effects on capacitance, I-V and electrolum. characts. 77−66543
GaP:Zn, Raman spectra of Zn acceptor 77−77187

III-V semiconductors continued
GaP:Zn, shallow Zn diffusion profile determ. using anodic oxidation and double radioactive tracer method 77−43239
GaP:Zn, Sn doped epitaxial layers, Hall const., hole mobility and conc. 80−15143
GaP:Zn, Te, epitaxial layers, determ. of Zn conc. 79−77614
GaP:Zn, thermodynamics of Zn doping by liquid phase expitaxy 78−83832
GaP:Zn,O, Auger coeff. from luminesc. decay and Hall effect 77−48226
GaP:Zn,O, Auger coeff. from luminesc. efficiency and Hall effect 77−48227
GaP:Zn,O, bulk electrolum. degradation in LEDs 77−81156
GaP:Zn,O, degradation of bulk luminesc. induced by laser excitation 77−1715
GaP:Zn,O, epitaxial p-n junction, IR electroluminesc. exam. *(Russian)* 78−35207
GaP:Zn,O, photodiodes, high temp. emission spectra *(Russian)* 77−66545
GaP:Zn,O, red LED, deep-level changes associated with degradation 77−1472
GaP:Zn,O LED, 76K electrolum, spectrum, γ-irrad, and forward bias effects 79−78756
p-GaP:Zn,S, spin polarisation of donors and acceptors in mag. field, optical and microwave study 80−93393
plGaP:Zn-electrolyte interface, electrochemical LED, luminescence obs. 80−84507
GaP:ZnO, LED, degradation, temp. and current depend. 79−87144
GaP:Zn(Mg)(Cd), multiple bound excitons, photoluminesc. obs. 79−95837
p-GaP/Au-Be ohmic contact form. by ionised-cluster beam deposition 77−32528
GaP/GaAs and GaP:H/GaAs amorphous film/cryst. junctions, optical and elec. props. 79−99611
GaP/$In_xGa_{1-x}P$/GaAs:(Cs-O) high sensitivity transmission photocathodes, photosensitivity, electron diffusion length 79−78832
GaP/Si heterostruct., differential thermal contraction, plastic deform., fracture 80−108494
GaP/Te(S), IR lattice band profile, electron spin reversion in mag. field, Nf-R curve 79−28771
n-GaP-(Ge-Au)/Ni, specific contact resistance calc. 78−43474
GaP-Ag(Au), Schottky barrier, stress effects on elec. props. 80−34512
GaP-$Al_xGa_{1-x}P$, DH electrooptical strip modulator *(Russian)* 78−1344
GaP-AlGaP, stripe-geometry electrooptical modulator 80−23798
GaP-anodic oxide devices, optoelectronic device, processing appl. 78−84304
GaP-anodic oxide MOS struct. oxide and interface props. 79−60929
GaP-Au, Schottky barrier, layer formation, elec. and optical props. 78−91766
GaP-Au Schottky diode, elec. props. under stress 79−15222
GaP-based III-V solid solns., bonding and energy gap, mag. meas. 78−18580
GaP-Cs-O, negative electron affinity, secondary emission characts. 78−11031
GaP-GaAlP, heterojunction cold cathode 79−69965
GaP-GaAlP-GaP, lattice-matched, LPE layer growth under P vapour pressure and reduced O_2 contamination 79−51445
GaP-GaAsP planar heterostructure strip ridged waveguide under mech. load, polarisation modulation 80−96038
GaP-Hg, elec. props. using Schottky barrier capacitance techniques 78−47870
GaP-In LPE layers, carrier diffusion lengths and escape probabilities optical absorpt. and photoemission meas. 79−87559
GaP-InAs solid solns., energy band struct., edge absoprtion spectra 78−39018
GaP-InP, pseudobinary alloy, phase diagram calc. 78−52786
GaP-InP solid solution, quantitative analysis, use of internal calibration technique developed by AES 77−36834
GaP-liq. NH_3 soln. junctions, elec. characts. *(French)* 80−2460
GaP-metal Schottky barrier diodes, elec. props. under mech. stress 80−11087
GaP-metal Schottky barrier height rel. to chem. reactivity 80−25008
n-GaP-n-GaAs, in MIS structures, elec. controlled optical transparencies, optical processing use 77−85339
GaP-NH_3 electrolyte interface, photo-assisted electron injection 79−87152
GaP-$Ni^{3+}(Co^{2+})(Fe^+)$, EPR assessment of $3d^7$ transition metal impurity state 78−48031
GaP-Pd contact system, low temp. alloyed contact formation 80−100519
GaP-Sb, Sb solubility in region of GaP primary crystn. 79−86891
GaP-Si, heteroepitaxial growth, electronic and optical props. 80−104075
GaP-Si, heterostructure, zincblende-on-diamond type systems, MBE growth, (110) orientation as preferred orientation 80−80099
GaP-ZnS, solid solns., microstruct. investig. 78−2128
GaP-ZnSe heterojunction, elec. and photoelec. props. *(Russian)* 77−32070
GaP(As), liquid interaction parameters determ., 580-670°C 80−65197
$GaP_{0.1}As_{0.9}$, gas-transport condensate with superlattice, structural and chemical inhomogeneity 77−85088
$GaP_{0.9}As_{0.1}$/GaP, heteroepitaxial structs., refined formulation of relative orientation criterias 80−44448
GaP_xAs_{1-x} ($0 \le x \le 0.32$) epitaxial film, one-dimens. superlattice, X-ray spectrometer scanning, struct. variations 78−47681
GaP_xAs_{1-x}, exam. of magnetic susceptibility and absorption spectra 79−1778
GaP_xAs_{1-x}, N doped, alloying induced shift between excitation and luminesc. of N bound exciton 79−52013
GaP_xAs_{1-x}, refractive index comp. depend., nonlinearity parameter *(German)* 77−32344
GaP_xAs_{1-x} solid soln., specularly smooth epitaxial layers, superlattice struct. 77−24959
GaP_xAs_{1-x} solid solns., edge absorpt. 77−16334
GaP_xAs_{1-x}, surface defects and comp. inhomogeneity during gas-phase heteroepitaxy 77−85090
GaP_xAs_{1-x}:N, impurity electron states, binding energies and wavefunctions 79−42488
GaP_xAs_{1-x}:N, luminesc. of N bound state excitons, local-environment effects 80−100691
GaP_xAs_{1-x}-GaAs one dimens. superlattice, possibility of X-ray and electron diffr. struct. determ. 80−54560
GaP(As)(Sb), avalanche breakdown voltage for p-n junction, calc. 78−88020

III-V semiconductors continued
GaP(As)(Sb), electronic surface props., contact potential difference and photoemission expts. 77−47884
GaP(As)(Sb), refractive index dispersion 79−24280
GaP(As)(Sb), surface states, contact pot. difference, photoemission, and low energy loss spectra expts. 77−85285
$(GaP)_x(InAs)_{1-x}$ solid solution, IR reflection spectra 77−69830
$(GaP)_x(ZnSe)_{1-x}$, solid solution, reaction of Zn with Se during Czochralski growth and LPE 79−8238
$(GaP)_x(ZnSe)_{1-x}$/GaP, epitaxial heterostructures, chem. microinhomogeneity 77−80831
GaS, absorpt. edge, exciton levels and Raman scatt., press. effects above 40 kbar 77−48187
GaS, Davydov splitting of degenerate lattice modes 79−61382
GaS, indirect exciton exam. 78−39029
GaS_xSe_{1-x}, two photon absorpt. 77−69841
GaSb, 3d core level spectra, electronic polarisation effects 80−6765
GaSb (100) surface, Sb-induced surface states 78−10529
GaSb (110), chemisorption of Cl, photoemission spectra and tight-binding calcs. 80−6629
GaSb (110), oxidation, initial stages, photoemission study 80−16529
GaSb (110), surface core-level binding-energy shifts 80−103737
GaSb (110) surface and InAs-GaSb (110) interface, electronic states, Green's function technique, tight binding approx. 80−49855
GaSb (110)/Au interface, heat-treated, struct. and chem. state, angle-resolved XPS 80−97400
GaSb, accumulation layer localised carriers interaction with LO phonons, Raman interference lineshapes 80−93338
GaSb, acoustic wave attenuation, phonon viscosity and dislocation drag 80−70319
GaSb, adsorption and desorption of Cs, LEED, AES, and photoemission meas. 80−70532
GaSb, amorphous, optical absorpt. edge shape, band edge fluctuations 77−20880
GaSb, amorphous, two-circle SSD diffractometer appl. in angle dispersive mode 79−14641
GaSb amorphous film, elec. props. *(French)* 78−14843
GaSb and alloys, struct. defect, photoluminesc. 80−25459
GaSb, anharmonic force consts. from third order elastic consts. at 300K 77−59074
GaSb, Au overlayer adatom interactions, photoemission obs. 79−33898
GaSb, Auger coeffs. calc. 79−15160
GaSb, Auger recombination, luminesc. meas. 77−85850
GaSb based eutectics, thermal cond. and diffusivity, 300-700K, phonon mechanism 80−103526
GaSb, bound excitons at doubly ionisable acceptors 79−42459
GaSb, bulk and epitaxial, IR reflect. meas., carrier conc. and mobility determ. 80−80769
GaSb, CESR, optical detect. by spin orienation techniques, anal. 78−80251
p-GaSb, CESR, optically detected, giant Overhauser shift 79−4722
GaSb, CVD using organometallics, epitaxial growth 80−29879
GaSb, carrier density depend. on impurity conc., multiple doping effects 77−8047
GaSb, chemical shift and effective atomic charges 78−88201
GaSb, chemisorption and oxidation states of (110) surfaces 79−24049
GaSb, cond. band L-states, i.r. absorption, uniaxial stress 77−1674
p-GaSb, cond. mechanisms, uniaxial compression effects 77−20312
GaSb, core exciton binding energies 80−80188
n-GaSb, coupled LO-phonon-plasmon modes, Raman spectrum 80−11409
GaSb crystal, phonon dispersion curves, valence force field 78−95121
GaSb, crystal growth by travelling heater method 80−11553
GaSb crystals, uniaxial deform., effect on polarised luminesc. 78−10957
GaSb, Debye temperature, atomic mean square displacement 78−87757
GaSb, defect concentration determ. model, Hall effect 80−103385
GaSb, degenerate valence band, diamag. excitons and oscillatory magnetoabsorpt. 77−76754
GaSb, diffusion of In, 520 to 712°C 80−79995
GaSb, dislocation velocities, double etch technique exam. 78−30629
GaSb, E_1 and $E_1+\Delta_1$ edges using electroreflectance, Franz-Keldysh oscills., high mag. fields 77−66518
GaSb, effect of n-doping on Debye temp. 80−2175
GaSb, elastic scatt. of He^+ ions by atomic chains, screening 80−2915
p-GaSb, elec. cond., Hall effect, mobility and carrier concentration *(Russian)* 79−19603
GaSb, electrochemical sectioning and surface finishing 80−108611
GaSb, electroliquid epitaxial growth 80−89160
p-GaSb, electron irrad., annealing 77−51407
GaSb, electron-hole plasma, ground state energy 78−84244
GaSb, electrorefl. spectra from 0.6 to 26 eV 77−20825
GaSb, electroreflectance spectroscopy using synchrotron rad. 78−10912
GaSb film, gamma-irradiated, struct., TEM and SEM obs. 79−15033
GaSb film, ion bombard. effects on elemental Sb incorporation probability during sputter deposition 79−83120
GaSb films, amorphous and cryst. vac. evaporated, Elec. cond. thermoelec. power and optical absorpt. 80−2504
GaSb films, elemental incorporation probability modification by ion bombard. during growth 80−80118
GaSb films, MBE growth and elec. props. 79−23863
GaSb, fine struct. in energy derivative reflectance spectra 79−78705
n-GaSb, fundamental absorpt. and energy relax., elec. field induced changes 77−1688
n-GaSb, galvanomagnetic effects 78−72172
p-GaSb, heavily doped, LO phonon-carrier interaction, Raman interf. lineshapes 80−93319
n-GaSb, heavily doped, spontaneous radiative recomb., complete vel. and radiative capacity 79−11458
p-GaSb, heavy and light holes scattering 78−91692
GaSb, high temp. thermodynamic data, quantitative fits to liquidus line 77−63637
GaSb high-purity and doped layers grown by LPE and VPE methods 78−6863
p-GaSb, hot exciton luminesc., LO phonon Raman scatt. 80−11474
GaSb, interaction of exciton recombination with LO phonons 79−38647
GaSb, interband Faraday rot., Roth theory calcs. 77−52046
GaSb, interband masses of E_1 and $E_1+\Delta_1$ edges 77−32353
p-GaSb, interband optical pumping, optical detection of EPR 77−28483
GaSb interface with oxide, photoemission obs. of energy levels induced by adsorpt. 80−93000

III-V semiconductors continued
GaSb, inversion of Γ and L conduction bands under uniaxial stress, photoluminescence meas. 79−33229
GaSb, inverted diode, electron irradiation effect on props. *(Russian)* 78−14378
GaSb, LEC growth, Hall coeff. 80−89133
GaSb LEC single crystal growth, novel encapsulant material 80−93475
GaSb laser, electron beam excited, spectral and power characts. 77−50676
GaSb, lattice dynamics, phonon freq., bond bending force model calcs. 80−70335
GaSb, lattice vibration, thermal expansion and pressure effect 80−39233
n-GaSb, local resist. near dislocations, eqns. 78−60123
GaSb, MIS struct., C-V characts., interface state densities and storage times meas. 77−89861
GaSb, manifestation of local vibrs. of dislocations in IR spectra 78−88339
GaSb, many-valley semiconductor, space charge, contrib. of different charge carriers *(French)* 80−34458
GaSb mesa photodetectors with very high quantum efficiency between 1.3 and 1.6 μm 80−47102
GaSb, migration of liq. inclusions, effect of DC current and temp. 77−7910
GaSb, molten, temp. depend. of vel. of sound and adiabatic compressibility 77−27944
GaSb, oscillatory magnetoabsorption and excitons 77−55777
GaSb oxide, anodic, optical props., 1.5-6.0 eV 77−90209
GaSb oxide films grown by anodization in electrolytes, electron spectroscopy exam. *(German)* 79−15837
GaSb oxidised surface, detection of excess crystalline Sb by Raman scatt. 78−19453
GaSb, p-n homojunction breakdown voltage for onesided abrupt junctions *(German)* 78−56210
GaSb p-n junction as presssure/temp. transducers *(Polish)* 77−67424
GaSb, p-type, effects of accumulation layer on photocond. *(French)* 77−24582
GaSb, phonon density of states 79−90744
GaSb, photoemission investig. of surface states, effects of O_2 and alkali metals 77−48312
GaSb, photolum., electrolum. meas. in p-n junction, temp. influence 78−72594
GaSb, photolum. spectra under hydrostatic press. 79−19930
GaSb, piezoresistive vibrating circular membrane, reflectance light modulation 80−97232
GaSb, pulled crystal, microfacet obs. near irregularly remelted surfaces 78−91278
GaSb pulled crystal, wavy impurity patterns beside twin boundary 78−18674
GaSb, real surface elec. props., light effects *(French)* 77−72906
GaSb, relations pressure-volume under high pressure 80−39219
GaSb, reson. two phonon Raman scatt. near E_1 and $E_1+\Delta_1$ gaps 78−60470
p-GaSb, saturation characts. over CO_2 laser spectrum 80−83646
GaSb, Schottky barrier and semicond./insulator interface states formation 80−49906
GaSb, second order Raman scatt. meas., comparison with photon density of states calc. 77−8579
GaSb, separate and combined solubilities of donors and acceptors 77−15434
n-GaSb, Shubnikov-de Haas effect, effective mass, Dingle temp., and g-factor 79−51602
GaSb, single crystal, stress-induced phase change 79−23720
GaSb, single crysts., grown by vertical and horizontal travelling heater method, growth parameters and cryst. quality 79−24421
GaSb, site selective doping by ion implantation of radioactive nuclei 80−34023
GaSb, solid solns., impact ionisation, cond. and valence band effects 80−65583
GaSb, sputtered films, on GaAs, growth, Hall effect, impurity levels 80−20334
n-GaSb, stress-induced elec. props. of point defects, piezoresistance effect 79−56726
GaSb, surface, electron struct. and Fermi level pinning by O_2 and metals 80−11066
GaSb surface, quantitative XPS meas. 78−56559
GaSb surface, temp. depend of work function *(French)* 80−6949
GaSb, surface chemistry and electronic struct., adsorption of O_2, photoemission meas. 77−20985
n-GaSb, temp. distrib. around dislocations, due to Joule heating, calc. 78−71734
GaSb, thin film prep. for TEM 77−9027
GaSb thin layers, directed crystn. on sapphire, props. 80−35111
GaSb, two-phonon diffuse scatt. of X-rays 78−26374
GaSb, UPS, 5-450 eV, surface states, oxidation behaviour 77−66579
GaSb, undoped, impurity band parameters calc. 79−51516
GaSb, undoped, intrinsic acceptors, parameters determ. 79−51515
GaSb, valence band structure, CPA, bond orbital calcs. 78−87909
GaSb, vibr. spectra, lattice dynamics ang. force model 80−29127
GaSb:Cd(Zn)(Se)(Te), thermal sensitivity, −170 to +180°C, resist. meas. 77−39906
GaSb:Fe, shallow acceptor level, electrical meas. 79−11087
GaSb:Gd(Yb), elec. props., dopant effects 79−87115
GaSb:Li, dopant behaviour 77−51696
GaSb:Mn(Sm), struct., thermo EMF, galvanomag. props. rel. to dopants, eutectic $Mn_{0.6}Ga_{0.4}Sb$ form. 77−15869
GaSb:S, cond. and Hall coeff. relax., impurity config. model 80−6786
n-GaSb:S, inhomogeneous, temp. depend. of elec. resist. 78−2482
n-GaSb:S, thermal quenching of residual cond. 78−56188
n-GaSb:S-metal surface barrier struct., elec. and photoelec. props. 78−56229
n-GaSb:Se, resonant and bound impurity states, Hall effect and resistivity press. depend. 77−28143
GaSb:Sn, p-n junction, electroluminesc. and photoluminesc. 80−66306
p-GaSb:Te, effective radiative recombination centre nature, photoluminescence spectra 79−90998
n-GaSb:Te, elec. transport mechanism in cond. band from Hall mobility and transverse mangetoresist. meas. 79−73531
n-GaSb:Te, Hall coeff., carrier conc. and mobility, elec. cond., 290 to 550K *(Russian)* 79−19604
n-GaSb:Te, heavily doped, electron-hole recomb., photoluminesc. spectra 78−84644

III-V semiconductors continued
GaSb:Te, indirect gap photolum. 80−29797
GaSb:Te,Zn(Te,Mn), prep. and electrophys. props. 79−87116
n-GaSb:Te(Se), forbidden optical band gap, Moss-Burstein effect 78−88335
p-GaSb:Zn, hole transport props. from 77 to 300K 79−73530
p-GaSb:Zn film, epitaxial, lifetime of nonequilib. carriers, determ. from circular polarisation of luminesc. 77−24898
GaSb-Ag, phase diag. 77−90327
GaSb-anodic oxide MOS struct. oxide and interface props. 79−60929
GaSb-Au contacts, interface struct., technology rel. to elec. props. *(German)* 77−72915
GaSb-Au Schottky barriers, PES and depth profiling obs. 79−42641
GaSb-Au structure, metal-semicond. interaction, soft XPS meas. 78−60203
GaSb-Bi system, molten, enthalpy change due to mixing *(German)* 79−86892
GaSb-$FeGa_{1,3}$, tenso-resistor charact. *(Russian)* 77−55530
GaSb-$Ga_{1-x}In_xSb$ p-n heterojunction, electrolum. spectra and elec. props. 77−12444
GaSb-InAs (001) superlattice, electronic struct., tight binding calcs. 78−95350
GaSb-InAs (001) superlattices, two-dimens. effects and effective masses 80−49883
GaSb-InAs (100) superlattice, electronic struct., self-consistent pseudopot. method 80−49884
GaSb-InAs superlattices, crystallography, Rutherford backscatt. and channelling obs. 80−49533
GaSb-InAs superlattices, semicond.-semimetal transition obs. 80−49882
GaSb-InAs system, (110) surface and interface electronic struct. 80−100494
GaSb-InSb solid solns., heavily doped, electronic props. 77−80727
GaSb-Pb junction, Ar ion bombard. effect on tunnelling props. 80−54783
GaSb-Zn(Cd)Te, quasibinary system, phase equilibrium, intermol. interaction 77−12601
GaSb(As) substrates for Al_2O_3 film, ion beam etching defect detection 80−89155
$GaSb_{1-x}As_x$, disorder-enhanced Auger recomb. 79−43014
$GaSb_{1-x}As_x$, MBE RHEED meas. 78−18916
$GaSb_{1-x}As_x$-$In_{1-x}Ga_xAs$ heterojunction, prep. by MBE, transport props. 77−80827
$GaSb_{1-y}As_y$ alloy surface states obs., using electron energy loss spectra 79−15202
$GaSb_{1-y}As_y$, MBE-grown, substrate effect on lattice consts. 79−77942
$GaSb_xAs_{1-x}$ films, MBE growth and elec. props. 79−23863
GaSe, electron-phonon interaction and optical props. 80−34942
GaSe films, optical props. at lattice vibr. freqs., IR and Raman spectra 80−60696
GaSe, luminescence excited by high-intensity two-photon pumping 77−44038
GaSe, Pockels effect 79−51933
GaI, Brillouin spectra, light scatt. cross section for surface rippies 80−71434
Gap-Ge, compensated, photosensitivity 79−19624
Ge-GaAs, heteroepitaxial systems, misfit dislocations obs. using HV electron microscopy 80−100242
Ge-GaAs, n-n isotype heterojunctions, fixed-interface-charge model 78−56215
Ge-GaAs, p-n heterojunctions, surface electron states 79−73578
Ge-GaAs (110) interface, relax., self-consistent pseudopotentials 78−30981
Ge-GaAs (110) interface, self-consistent calc. of interface states and electronic struct. 78−52066
Ge-GaAs heteroepitaxial system, dislocation struct. in stress measurements 80−29030
Ge-GaAs heterojunction, elec. and recomb. props., interface defect effects 80−80365
Ge-GaAs heterojunctions, electronic struct. 78−19138
Ge-GaAs p-n heterojunction, current fluctuations 79−11209
Ge-GaAs p-n junction, microparameters determ. 79−11216
Ge-GaAs superlattice and interface, electronic struct. 78−52065
Ge-InAs based MIS struct., avalanche carrier multiplication 80−88566
n-Ge-n-GaAs isotype heterojunctions, modelling, charact. 80−103747
n-$Ge_{1-x}Al_xAs$:Te, long-lifetime photocond. effect obs., Hall effect meas. 77−89795
Hg-InP Schottky-barrier diode, contact times, I-V charact. 80−96971
(In,GA)(As,P) binary, ternary and quaternary, hydride vapour phase epitaxy, cryst. growth and props. 80−66434
(In, Ga)Sb, sputter deposited amorphous film, impulse stimulated explosive crystallisation 78−84098
n-In Ar:Te(Sn), heavily doped, cathodoluminescence, doping effect on luminesc. band position and spectral profile 80−45153
In-As system, exam. of thermodynamic consistence of models, and QCE approx. for activity coeffs. *(German)* 80−24615
In-As-P, liquidus surface in ternary phase diagram, simplex lattice method 77−7847
In-Ga-As system, heterophase equilibrium, phase diagram calc. 79−43212
In-Ga-As-P, phase diagram rel. to lattice matched LPE 78−39708
In-Ga-P ternary system, low temp. phase diagram rel. to epitaxial growth 80−84916
In-GaAs:Cu-In S-type diode, role of deep trapping levels in form. of current-volt. charact. 77−76948
In-P system, liquid-vapour equil., VP functional depend., 1023 to 1123K 79−42228
p-In-Sb, effect of static mag. fields on transverse photocurrent spectrum 78−14766
In-Sb-Te, region of In-Sb-based solid solutions 77−36466
In-Te system, IR spectra *(Russian)* 78−84589
p-$In_{0.77}$ $Ga_{0.23}As$/Ag photocathode, field assisted photoemission to 2.1 microns 80−76130
$In_{1-x}Al_xAs$, band gap, IR absorpt. spectra meas. 80−66205
$In_{1-x}Al_xP$:Bi(N)(Zn,O) radiative recombination at isoelectronic centres 79−52027
$In_xAl_{1-x}P$, proportional ingredient content determ. by X-ray fluoroscopy 80−97747
InAs (110) surface and InAs-GaSb (110) interface, electronic states, Green's function technique, tight binding approx. 80−49855
InAs amorphous film, DC sputtered, optical absorpt. 78−19589

III-V semiconductors continued
InAs and solid solutions, recombination mechanisms of excess carriers, luminesc. obs. 80−97337
InAs anodic oxide films prep. and props. 80−55553
InAs, anomalous avalanche breakdown 80−80284
p-InAs, Auger recomb., theory and luminesc. expts. 78−56518
InAs avalanche diode, noise meas. 77−4431
n-InAs, avalanche formation, high intensity IR transmission limit 79−78684
InAs, band gap and effective mass, depend on impurity conc. 79−69412
n-InAs, cathodoluminescence, radiative recomb. of hot carriers 77−8667
p-InAs, charact. of Pb supercond. contact 79−38254
InAs, dislocation velocities, double etch technique exam. 78−30629
n-InAs, EPR, oscillations of transverse magnetoresistance in weak mag. field 79−91086
InAs, elec. props. after heating for 300 to 900°C for 1 to 100 hours 78−47793
InAs, electrical conductivity and thermoelectric power charge due to melting 80−100490
InAs, electron beam excitation, luminesc. and stimulated emission 77−16339
n-InAs, electron irrad., carrier introduction rate, annealing 80−24948
n-InAs, electron irrad., rel. to thermal and electrophysical props. *(Russian)* 80−39154
InAs, electron irrad. at 50 MeV, elec. and optical props. 77−47486
InAs, electron surface props., contact potential difference and photoemission expts. 77−47884
InAs, electroreflectance spectrum 78−19479
InAs, epilayer, MBE growth parameters, relationship with elec. props. 80−2296
InAs epilayers in MOS carrier transport coeffs. determ. by multilayer model 78−2575
InAs, epitaxial, laser action mechanisms with electron beam excitation 80−28240
InAs epitaxial film on GaAs, far IR reflectivity obs. 77−40251
InAs epitaxial layers, on GaAs substrate, electron diffr. and SEM exam., electronic props. 79−1552
InAs, exam. of decomposition of donors 79−1605
InAs, far IR transmission spectrum 78−4713
InAs, film, CVD H_2O transport method, Hall element preparation 77−40377
InAs film, DC sputtering, struct. and elec. props. 77−66567
InAs films, MBE grown on GaAs, electron mobilities, lattice mismatch effect 80−80419
InAs, fine struct. in energy derivative reflectance spectra 79−78705
InAs, fine struct. of diamag. excitons, oscillatory magnetoabsorpt. obs. 78−18971
InAs, gas-phase epitaxy, prep. thermodynamics, use of partial pressure diagrams 79−79279
InAs, Hall effect sensor for mag. fields up to 23 T 77−10066
n-InAs, heated electron gas, longitudinal optical phonon form., IR absorpt. modulation 80−45079
InAs, heavily doped, Burstein-Moss effect and near-band-edge luminesc. 79−47525
InAs, heteroepitaxial, charge transport obs. by gate-voltage-controlled meas. on MOS struct. 77−47912
InAs, heteroepitaxial, far IR refl. and transmission meas., surface and interface effects 80−16044
InAs, heteroepitaxial film, orientation and struct. investigation 79−82480
InAs heteroepitaxial layers, VPE grown, effect of $AsCl_3$ mole fraction on elec. props. 79−11255
InAs, heteroepitaxial layers, $AsCl_3$ mole, fraction and substrate orientation effects on elec. parameters 80−39690
InAs, high temp. thermodynamic data, quantitative fits to liquidus line 77−63637
n-InAs, hot electron temp. determ. by interference modulation of radiation 80−44610
InAs IR filter properties, operational charact. of antireflection coatings 79−14107
InAs, IR hot carrier diode mixer 78−29161
InAs, IR reflectivity, longitudinal optical phonon-plasmon coupling 77−59578
InAs, impact ionisation and Auger recomb. 77−20329
InAs, intensity of 3-phonon diffuse scattering of X-rays 80−84027
InAs, interband Faraday rot., Roth theory calcs. 77−52046
InAs, intrinsic point defects, nature and influence on electrophys. props. 78−79609
InAs laser, electron-beam-pumped 77−50689
InAs, laser excitation, photocond., optical absorpt., electron-hole scatt. 77−43661
InAs, lattice dynamics 79−14895
InAs, longitudinal magnetoresistance in extreme quantum limit *(Russian)* 80−11008
InAs, MBE growth, SEM, RHEED, optical microscopy and elec. meas. 78−18925
InAs, MIS struct., C-V charact., interface state densities and storage times meas. 77−89861
n-InAs, magnetophonon resonance under hydrostatic press. 77−47832
InAs, melt, mutual diffusion of components 80−88345
InAs, migration of liq. inclusions, DC current and temp. effects 77−7910
InAs, narrow-gap semiconductor, high intensity IR transmission limit 80−7361
n-InAs, negative magnetoresist. in extreme quantum limit 78−64051
n-InAs, negative photocond. and photomemory due to pot. barrier on surface 79−19620
InAs, neutron bombarded, optical absorption, struct. defect form. and nuclear alloying *(Russian)* 78−31206
n-InAs, nucl. maser effect 78−19345
InAs, obtained by liquid-seal method, deviation from stoichiometry 77−40345
InAs on GaAs, epitaxial-substrate system, far IR transmission and refl. 78−6802
InAs, on GaAs, heteroepitaxial layers, compositional profile, AES 77−20212
InAs, organometallic VPE growth on InAs and GaSb 80−16193
InAs, oriented single crysts., photoemissive props., photoelec. thresholds 77−59666
n-InAs, oscillations in photocond. and photomag. effects 77−4405
InAs, oxidised surface, detection of excess crystalline As by Raman scatt. 78−19453

III-V semiconductors continued
InAs, p-n homojunction breakdown voltage for onesided abrupt junctions *(German)* 78−56210
InAs p-n junction, carrier multiplication and ionisation coefficients 77−8188
n-InAs phonon propagation, heat pulse obs. 79−46852
n-InAs, photoelectric props., inhomogeneous impurity distrib. 80−107867
InAs, photoluminescence exam. 79−28809
InAs, photovoltaic detector, photoelectric evaluation, for Gaussian incident pulse 79−63306
InAs, plasmon-phonon coupling, and IR refl. spectra of impure crysts. 79−56150
InAs, possibility of local epitaxy in depressions on unmasked substrates 79−42415
InAs, radiation defect formation processes, effect on physical props. 78−2163
InAs, Raman scatt. by LO phonons 77−20852
n-InAs, recomb. of nonequil. charge carriers at high photoexcitation levels 77−44053
InAs, resist. inhomogeneity meas. with single-sonde potential method 80−65549
p-InAs, saturation characts. over CO_2 laser spectrum 80−83646
InAs, second order Raman scatt., electron-two phonon deform. pots. determ. 78−60473
n-InAs, Shubnikov-de Haas oscills., conduction electron density, phonon scatt. 77−15768
n-InAs, Shubnikov-de Haas effect, effective mass, Dingle temp., and g-factor 79−51602
n-InAs, Shubnikov-de Haas transverse kinetic coeffs., quantum oscills. 80−49778
InAs, single crystal, stress-induced phase change 79−23720
InAs, site selective doping by ion implantation of radioactive nuclei 80−34023
InAs, soln. in liq. Sn, vapour phase partial press. meas., rel. to LPE 78−34610
InAs surface, contact pot. difference meas. 77−20403
InAs surface accumulation layers, magneto-transconductance meas. 78−64137
InAs surface accumulation layers, magneto-transconductance study 80−49948
p-InAs, surface conductance of Ar-ion-bombard. samples 79−60910
InAs surface layers, oscillatory transport coeffs. 78−64136
InAs, surface potential and surface states rel. to n-, p-, compensated n-type behaviour 77−15932
InAs, surface space charge investig., reson. enhanced Raman scatt. 77−20849
InAs, temporary diffr. grating form. on surface 79−59801
InAs, thermal oxidation, growth rate and chem. comp., temp. depend. 80−108619
InAs, thin film prep. and elec. props. 79−1633
InAs, three-photon absorption, transition effects *(Russian)* 78−35147
InAs, transient dynamic response calculation by Monte Carlo techniques 80−107796
n-InAs, transport props., influence of higher energy bands, calcs. 79−19598
InAs, transverse acoustoelec. voltage spectroscopy 80−49828
n-InAs, tunnelling spectra in mag. field, dispersion law *(Russian)* 79−60923
InAs, two dimensional accumulation layer, Anderson localisation 80−107871
n-InAs, undoped, electron irrad., Hall coeff., elec. resistivity, optical absorption 77−89479
InAs, undoped n-type single crystals, dislocation velocity 77−11559
n-InAs, VPE layers, on GaAs substrate, electronic profile 79−95525
InAs, valence band structure, CPA, bond orbital calcs. 78−87909
InAs, X-ray thermal diffuse scattering measurements of phonon dispersion curves 79−77701
n-InAs:Cd, p-n junction, photosensitivity spectra depend. on mag. field 79−91137
InAs:Cd, Te, donor-acceptor interaction, elec. cond. and Hall coeff. meas. 80−59988
InAs:Cd,Te interaction between impurities, effect on elec. props., Hall effect. 80−19832
n-InAs:Cr, Czochralski growth of high-resist. single crysts. 77−66587
InAs:Cr, high-resist., energy positions of deep levels, elec. and optical props. 79−7807
InAs:Cu, contamination equilibrium assessment 79−51134
InAs:Mn powder, quadrupole interactions in NMR spectra 79−51880
InAs:Mn^{3+}, Jahn-Teller effect for ion impurities 80−107753
InAs:S(Mg), ion implanted, photocond., photo-EMF, and optical absorpt. spectra 80−70763
InAs:Sb (100) surface, Sb-induced surface states 78−10529
InAs:Sn, single crysts., defect formation 80−88606
InAs:Te(Se)(S), intrinsic pt. struct. defects 80−33998
InAs:Zn, optical absorpt. and refl. spectra 79−91479
InAs:Zn,S,(Se)(Te), exam of microhardness, Hall effect as function of dopant 79−95038
InAs:Zn,S(Se), solubility and donor-acceptor interaction 80−54263
InAs/$LiNbO_3$ structure, SAW generated transverse acoustoelectric voltage, image scanning and signal processing appl. 80−49826
InAs-$Al_xGa_{1-x}Sb$ heterojunctions, elec. and photoelec. props. 79−11206
InAs-AlAs, phase diagram plotting by DTA and thermodynamic calc. 77−86016
p-InAs-Au contacts, influence of free surface on elec. behaviour 78−95362
InAs-FeAs, eutectic, growth from melt, electrical props. 77−11911
InAs-GaSb (001) superlattice, electronic struct., tight binding calc. 78−95350
InAs-GaSb (001) superlattices, two-dimens. effects and effective masses 80−49883
InAs-GaSb (100) superlattice, electronic struct., self-consistent pseudopot. method 80−49884
InAs-GaSb heterojunction, photoelec. props. 77−28245
InAs-GaSb heterostruct. superlattice, props. in high mag. fields 79−73570
InAs-GaSb superlattices, two-dim. electronic structure 78−75995
InAs-GaSb superlattice energy struct. and semiconductor-semimetal transition 79−23893
InAs-GaSb superlattice, cyclotron resonance, energy level quantisation 79−73430

III-V semiconductors continued
InAs-GaSb superlattice, electronic struct., self-consistent pseudopot. calc. 80−29470
InAs-GaSb superlattice, semiconductor-semimetal transition obs. 80−44710
InAs-GaSb superlattices, crystallography, Rutherford backscatt. and channelling obs. 80−49533
InAs-GaSb superlattices, semicond.-semimental transition obs. 80−49882
InAs-GaSb superlattices, mag. field induced semimetal-semicond. transition 80−65656
InAs-HgTe, phase diags. 77−52299
InAs-InP, phase equilib. and dissoc. 80−35170
InAs-oxide-$Pb_{50}Bi_{20}$ junction, hot electron temp. in InAs meas. by tunnelling 77−4352
$InAs_{1-x}P_x$, magnetophonon effect 79−65500
$(InAs)_x(CdTe)_{1-x}$, band gap and effective mass, IR spectra obs. 78−56491
InAsP, intervalley electron transfer, drift velocity and diffusion coefficient 80−39594
$InAs_{1-x}P_x$, deep levels and semicond.-semimetal transition at high press. 80−11056
$InAs_{1-x}P_x$, electron effective mass cyclotron reson. and magnetophonon effect 80−24786
$InAs_{1-x}P_x$ epitaxial layers, sub-threshold velocity-field characts., intervalley separation 77−63010
$InAs_{1-x}P_x$, evidence for reduction in momentum matrix element P^2 due to alloy disorder 79−65853
$InAs_{1-x}P_x$, high field instabilities, press. and comp. depends. 78−26873
$InAs_{1-x}P_x$, quantum magnetoresist. results, using pulsed fields up to 35 T 79−73528
$InAs_xP_{1-x}$, continuously tunable electron beam pumped laser 78−50802
$InAs_yP_{1-y}$ alloy, composition effects in growth by MBE 80−59816
InAs(P)(Sb) MIS structs., review 78−95372
InAsSb, Be ion implantation, device appl. 80−24478
InAs(Sb), in MOS struct., electrorefl., band-population effects under heavy surface accumulation 77−48167
InAsSb/GaSb broad-spectral-band IR detector, backside-illum. heterostructure approach 80−73450
$InAs_{0.85}Sb_{0.15}$, MIS struct., C-V characts., interface state densities and storage times meas. 77−89861
$InAs_{1-x}Sb$, disorder-enhanced Auger recomb. 79−43014
$InAs_{1-x}Sb_x$, epitaxial film, carrier recomb., elec. and optical props. 79−15164
$InAs_{1-x}Sb_x$, LPE on InAs substrate, $InAs_xSb_yP_{1-x-y}$ used as buffer layer 78−3065
$InAs_{1-x}Sb_x$ on GaSb, LPE growth 80−29293
$InAs_{1-x}Sb_x$ p-n junctions, avalanche multiplication 80−6965
$InAs_{1-x}Sb_x$-InAs backside-illum. narrow band photodetectors 77−61118
$InAs_{1-x}Sb_x$-InAs stepwise-graded struct., steady-state LPE, etching, investig. 77−21042
$InAs_xSb_yP_{1-x-y}$, efficient electron-beam-pumped laser at 3.1-3.7 μm 80−5738
$InAs_xSb_yP_{1-x-y}$, LPE on InAs substrate 78−3065
InBi, Fermi surface and band struct., press. effects 77−39779
InBi single crystal, deform. mode under dynamic indentation 80−88163
(InGa)As film, growth kinetics for step-cooling LPE technique 77−40395
InGaAs, LED, 1.06 μm range, neutron and γ-irrad. effects 79−97433
InGaAs, LPE, diffusion-limited step-cooling technique, layer thickness and composition 80−84402
InGaAs, lattice-matched VPE on (100) InP, photodiode appl. 80−35102
InGaAs on (100) InP substrate, VPE 80−40267
InGaAs p-n junction, carrier multiplication and ionisation coefficients 77−8188
InGaAs radiation detector, integrated optics appl. *(Czech)* 80−33227
InGaAs, transferred electron photoemission to 1.65μm 78−68600
(InGaAs)/(InGa)P, DH laser, threshold current temp. depend. 79−81431
InGaAs/InP p-i-n small area photodiodes, fabrication, characts. and performance in 274 Mb/s receivers at 1.31 microns 80−53415
InGaAs-GaAs heterojunction with low misfit, misfit dislocation struct. 77−62783
InGaAs-GaSbAs periodic structures, with controlled emission 79−7880
InGaAs-$In_{1-x}Ga_xAs_yP_{1-y}$ DH laser, LPE fabrication, electroluminesc., lasing characts. 79−3709
InGaAs-InGaP vapour-grown ternary heterojunction laser struct., reliability 79−98385
InGaAs-InP heterojunction detector for 1.0-1.7 μm wavelength range 78−49895
InGaAs-InP punch-through type photodetector fabricated by VPE 80−68253
$In_{0.1}Ga_{0.9}As$, quantitative anal. with SIMS 80−101052
$In_{0.53}Ga_{0.47}As$, growth on (100)-oriented InP, from supercooled solution 79−70001
$In_{0.53}Ga_{0.47}As$, Hall mobility and Hall factor, temp. and donor conc. depend. 80−49773
$In_{0.53}Ga_{0.47}As$, incorporation of Ga during LPE growth on (111)B and (100)InP substrates 78−91557
$In_{0.53}Ga_{0.47}As$, interband magnetoabsorption study, quasi-Ge model application 80−50304
$In_{0.53}Ga_{0.47}As$, LPE growth on (100) InP, for field assisted photocathode appl. 78−15318
$In_{0.53}Ga_{0.47}As$, LPE layer on InP, electron mobility and energy gap 77−24627
$In_{0.53}Ga_{0.47}As$ p-i-n photodiodes, for long-wavelength fibre-optic systems 80−5826
$In_{0.53}Ga_{0.47}As$ p-i-n photodiode-FET photoreceiver for 1.0 to 1.7 μm wavelength optical fibre communications systems 80−58794
$In_{0.53}Ga_{0.47}As$, phase diagram at 650°C and LPE growth of lattice-matched layer 79−96009
$In_{0.53}Ga_{0.47}As$ photodiodes with dark current limited by generation-recombination and tunneling 80−107893
p-$In_{0.53}Ga_{0.47}As$:Zn on InP, elec. and optical props. 80−75662
$In_{0.53}Ga_{0.47}As$/InP avalanche photodetector 80−4764
$In_{0.53}Ga_{0.47}As$-InP, 1.7 μm heterojunction lasers and photodiodes fabrication 78−25880
$In_{0.53}Ga_{0.47}As$-InP avalanche photodiode with guard-ring struct., characts. 80−96939
$In_{0.53}Ga_{0.47}As$-InP avalanche photodiode structure for 1 to 1.6 μm region 80−98978
$In_{0.53}Ga_{0.47}As$-InP heterostructure, LPE growth 80−11582

III-V semiconductors continued
$In_{1-x}Ga_xAs$-$GaSb_{1-y}As_y$ superlattice, optical absorption 79−19887
$In_{1-x}Ga_xAs$ alloy surface states obs., using electron energy loss spectra 79−15202
$In_{1-x}Ga_xAs$, disorder carrier scatt., Green's function calc. 77−11906
$In_{1-x}Ga_xAs$, LPE, electron mobility and max. drift vel., microwave device appls. 77−77431
$In_{1-x}Ga_xAs$, LPE growth on InP substrate, quasi grown layers, photoluminescence meas. 79−23862
$In_{1-x}Ga_xAs$, LPE layer on InP substrate, phys., elec. and optical props. 78−39235
$In_{1-x}Ga_xAs$, LPE on InP substrate, comp. latching phenomenon and lattice mismatching effects 79−28961
$In_{1-x}Ga_xAs$ layer on InP, misfit dislocation free, LPE growth 80−108364
$In_{1-x}Ga_xAs$, MBE-grown, substrate effect on lattice consts. 79−77942
$(In_{1-x}Ga_x)As$, scattering of electrons by potential clusters 77−15842
$In_{1-x}Ga_xAs$-$GaSb_{1-y}As_y$, semiconductor superlattices by MBE 79−95939
$In_{1-x}Ga_xAs$-$GaSb_{1-y}As_y$, superlattice electronic subband struct. 77−72815
$In_{1-x}Ga_xAs$-$GaSb_{1-y}As_y$, new heterostruct. characts. 78−72247
$In_{1-x}Ga_xAs$-$GaSb_{1-y}As_y$ superfine heterostruct., MBE 78−95348
$In_{1-x}Ga_xAs$-$GaSb_{1-y}As_y$ superlattice, with nonlinear energy-wave and energy-momentum relationships 79−7871
$In_{1-x}Ga_xAs$-$GaSb_{1-y}As_y$ heterostructure devices 79−42624
$In_xGa_{1-x}As$ (x=0.03 and 0.05), grown as GaAs substrate, with InGaAsP buffer layer, exam. of dislocation density 80−44447
$In_xGa_{1-x}As$ avalanche diode, noise meas. 77−4431
$In_xGa_{1-x}As$, electron drift vel. in high elec. fields 78−30928
$In_xGa_{1-x}As$ epitaxial layer, waveguiding at 1.06 μm, losses 78−18052
$In_xGa_{1-x}As$, epitaxial solid soln. film, spectral depend. of transparency, absorpt. spectra calcs. 80−45161
n-$In_xGa_{1-x}As$ film, epitaxial growth on GaAs, using CVD system 77−1812
$In_xGa_{1-x}As$, heteroepitaxial, MBE grown, props. 78−84328
$In_xGa_{1-x}As$, heterostructure composition profile by photoemission microanalysis 80−44717
$In_xGa_{1-x}As$, LPE growth on GaAs 79−61519
$In_xGa_{1-x}As$ layers, on GaAs substrate, MBE fabrication and laser operation 80−10820
$In_xGa_{1-x}As$, MBE layers on InP substrates, elec. props., photoluminesc., X-ray and Auger obs. 79−51450
$In_xGa_{1-x}As$ MBE layers on InP substrate, lattice deformation, misorientation 79−90896
$In_xGa_{1-x}As$ multilayer struct., photoluminesc. and X-ray spectroscopic microprobe analysis 77−4687
$In_xGa_{1-x}As$, planar photodiodes made by VPE 79−49286
$In_xGa_{1-x}As$, thick LPE growth, electrolum. obs. 78−60589
$In_xGa_{1-x}As$, VPE on (100), (111)A, and (111)B InP substrates 80−15382
$In_xGa_{1-x}As$, Zn diffusion coeff. and surface conc. 80−39122
$In_xGa_{1-x}As$:Si, p-n junction form. in LPE layers, In content effect on inversion temp. 77−4266
$In_xGa_{1-x}As$:Si p-n structs., electrolum. spectra, 77 to 300K 80−93408
$In_xGa_{1-x}As$:Zn, lattice matching to InP, LPE growth conditions 80−70541
$In_xGa_{1-x}As$-$In_yGa_{1-y}P$ DH laser, CW room temp. operation at 1.06 μm 77−19250
$In_xGa_{1-x}As$-$InAs_xP_{1-x}$ VPE mixed crystal composition rel. to vapour pressure *(Japanese)* 77−55893
InGaAsP, 1.3 μm LED, for high-bit-rate fibre data link 78−46825
InGaAsP, anodic oxidation, refractive indices 80−97601
InGaAsP avalanche photodiodes, leakage current, shot noise, quantum efficiency, gain saturation 79−67381
InGaAsP avalanche photodiode, 1.3 μm, noise performance, −190°C 80−57370
InGaAsP avalanche photodiodes, breakdown mechanism, donor conc. effect 80−70710
InGaAsP, bandgap energy by electroreflectance and photoluminesc. spectra 80−107700
InGaAsP buried stripe laser, modulation characts. 79−98418
InGaAsP DH, luminesc., quantum efficiency determ. 80−108273
InGaAsP DH laser characts., temp. depend. 80−1223
InGaAsP DH lasers with etched reflectors, fabrication, current density 80−64050
InGaAsP, dual-wavelength demultiplexing photodiode 79−63304
InGaAsP, epitaxial layer, defect evaluation by cathodoluminescence 80−2866
InGaAsP heterojunction cathode, transferred electron photoemission 78−48272
InGaAsP, high radiance CW LEDs emitting at 1.30 μm 78−22196
InGaAsP IR heterojunction photodiode detector 79−21813
InGaAsP InP DH lasers, optical power and wavelength stabilisation 80−38036
InGaAsP, injection heterojunction laser at 1.3-1.5 μm 79−89910
InGaAsP LED sources, for near-IR absorpt. meas. 80−77135
InGaAsP, LPE, diffusion-limited step-cooling technique, layer thickness and composition 80−84402
InGaAsP, LPE growth, orientation depend. of incorporation of Ga, As, and Zn 78−6869
InGaAsP, LPE growth on InP, influence of lattice mismatch on surface morphology 79−1553
InGaAsP, LPE growth techniques influence on composition 79−52130
InGaAsP, LPE growth, impurity depend. of distrib. coeff. 80−10843
InGaAsP, LPE grown, impurity effect on surface morphology 80−29291
InGaAsP LPE heterostructs., interface grading, Auger depth profile 80−103585
InGaAsP LPE layers on InP substrate, material selective chemical etching 79−70188
InGaAsP laser, single-mode CW ridge waveguide, emitting at 1.55 micron for optical fibre links 80−9883
(InGa)(AsP) laser system, VPE growth using metal organic sources or halide transports 80−99748
InGaAsP, lattice matched, LPE growth on (100) InP, for 1.15-1.31 μm spectral region 78−64483
InGaAsP low-threshold 1.25-μm vapour grown CW lasers, emission characts. 79−50308
InGaAsP photocathodes for astronomical detectors, UV response 77−57387
InGaAsP photodetector, improved two wavelength demultiplexing 80−58795

III-V semiconductors continued
InGaAsP quaternary alloy IR heterojunction detectors, props. 79−2823
InGaAsP, quaternary alloy, physical props. *(Japanese)* 80−15449
InGaAsP single-mode CW ridge-waveguide laser emitting at 1.55 micron 80−58584
InGaAsP strip-buried-heterostructure high-output power laser 80−58540
InGaAsP strip-buried heterostructure laser, high output power, operation 80−58559
InGaAsP, with and without InP cladding layers, low photolum. regions 79−33754
InGaAsP:Be, avalanche photodetectors annealing temp. effect on photolum. spectra 79−69872
InGaAsP:Be ion-implanted avalanche photodiode, struct. and characts. 79−17487
InGaAsP:Sn(Te)(Zn), LPE growth, influence of growth-solution dopants on distrib. coeffs. 79−47640
InGaAsP/InP, DH laser, 1.5 μm, with optical waveguide structure, fabrication 79−72587
(InGa)(AsP)/InP, DH laser, threshold current temp. depend. 79−81431
InGaAsP/InP, native oxide stripe laser 79−68405
InGaAsP/InP avalanche photodiode, ionisation coeff. 80−15590
InGaAsP/InP DFB injection lasers 80−5746
InGaAsP/InP DH, vapour phase growth by dual-growth-chamber method 80−50559
InGaAsP/InP DH lasers, Zn doping level 79−98373
InGaAsP/InP DH laser, self-aligned struct. 80−9893
InGaAsP/InP DH lasers, temp. depend. characts. 80−58541
InGaAsP/InP DH stabilised 1.3 μm laser diode-isolator module for hybrid optical integrated cct. 80−58583
InGaAsP/InP heterojunction, X-ray characterisation of defects 78−95239
InGaAsP/InP heterostruct. lasers as optical source, CW operation at room temp. 80−1220
InGaAsP/InP injection lasers for long wavelength (1.1 to 1.6 μm) optical communication 80−58582
InGaAsP/InP lasers and detectors for LW optical fibre communication 80−9885
InGaAsP/InP phototransistors, fabrication by LPE, photodetectors 80−95139
p-InGaAsP-Au, Schottky barrier height comp. depend., photoelec. meas. 77−20433
InGaAsP-InP, anomalous luminesc., near heterojunction interface 79−65932
InGaAsP-InP, double heterostructure laser, temp. sensitive threshold current 79−59700
InGaAsP-InP, double heterostructure laser lifetime, point defect generation model calcs. 80−32992
InGaAsP-InP, Zn diffused DH structures, oxide defined transverse junction stripe lasers 79−98389
InGaAsP-InP 1.27 μm CW DH injection lasers, 1.1 Gb/s pseudorandom PCM 78−55390
InGaAsP-InP buried crescent injection laser emitting at 1.3 μm with low threshold current 80−87404
InGaAsP-InP buried heterostructure lasers emitting at 1.3 μm, accelerated ageing characts. 80−95898
InGaAsP-InP CW lasers, 1.5-1.7 μm, VPE 80−78861
InGaAsP-InP DH laser emitting at 1.27 μm, fast pulse behaviour, high speed direct modulation 77−23676
InGaAsP-InP DH laser, room temp. operation, 1.27 μm emission 77−88743
InGaAsP-InP DH lasers, direct modulation 78−42363
InGaAsP-InP DH lasers, carrier lifetimes meas. 78−66828
InGaAsP-InP DH laser, threshold depend. on active layer thickness 79−7127
InGaAsP-InP DH lasers, threshold characteristic 79−81430
InGaAsP-InP DH laser, optical gain meas., low-intensity luminesc. and absorpt. spectra 79−98356
InGaAsP-InP DH lasers, low temp. behaviour of threshold current and carrier lifetime 79−98374
InGaAsP-InP DH lasers, degradation by In solder 79−98402
InGaAsP-InP DH laser with self-aligned struct., oscillation characts. 80−38017
InGaAsP-InP DH laser, 1.55 μm, low temp. LPE growth for room-temp. CW operation 80−64045
InGaAsP-InP DH LED, high temp. aged, dark-spot defects, TEM obs. 80−66300
InGaAsP-InP DH lasers, interfacial recomb., influence on oscill. characts. 80−87393
InGaAsP-InP DH lasers, spatial hole burning, spontaneous emission saturation, direct obs. 80−95892
InGaAsP-InP DH lasers, temp. dependence of threshold and elect. characts. 80−99725
InGaAsP-InP DH lasers, perturbed InP growth, photoluminesc. study 80−106518
InGaAsP-InP DH laser, threshold current, temp. depend. 80−106521
InGaAsP-InP dual wavelength LED 80−15589
InGaAsP-InP embedded mesa strip lasers 80−14350
InGaAsP-InP heterojunction, LPE, lattice mismatch, Auger depth profile 79−87005
InGaAsP-InP high-gain heterojunction phototransistor 80−103745
InGaAsP-InP laser, LPE, 1.5 μm range, effects of double cladding struct. 80−48290
(InGa)(AsP)-InP laser system, 1 μm wavelength, lattice matching techniques 80−99748
InGaAsP-InP lattice-matched heterojunction, LPE growth and characterisation 77−21041
InGaAsP-InP lattice matched DH, growth by two-phase supercooled soln. technique 78−10296
InGaAsP-InP layers, grown by LPE techniques, lattice const., bandgap, thickness and surface morphology meas. 80−59818
InGaAsP-InP photodiodes, microplasma-limited avalanche multiplication at 1 to 1.3 μm 79−26128
InGaAsP-InP photodiodes antireflectively coated with InP native oxide 80−13137
InGaAsP-InP vapour-grown quaternary heterojunction laser struct., reliability 79−98385
InGaAsP-InP:Mg LEDS, for high-bit-rate optical communication systems 80−5823
$In_{0.79}Ga_{0.21}As_{0.54}P_{0.46}$, LPE layer, electroreflectance meas. 79−24290
$In_{0.8}Ga_{0.2}As_{0.5}P_{0.5}$, LPE growth 80−11557

III-V semiconductors continued
$In_{0.83}Ga_{0.17}As_{0.37}P_{0.63}$, reactive ion etching of III-V compounds 80−58813
$In_{0.84}Ga_{0.16}As_{0.46}P_{0.54}$, refractive index, at laser oscillating wavelength of 1.2 μm 79−64224
$In_{0.85}Ga_{0.15}As_{0.39}P_{0.61}$, deep impurity levels 79−87058
$In_{0.9}Ga_{0.1}As_{0.22}P_{0.78}$, effective mass meas. by Shubnikov-de Haas oscills. 78−34754
$In_{1-x}Ga_xAs_{1-y}P_y$ layers on InP substrate, LPE growth, quaternary phase diagram, and band gaps 79−42403
$In_{1-x}Ga_xAs_xP_{1-y}$, p-n junction diodes, fabrication by Be ion implantation 79−47156
n-$In_{1-x}Ga_xAs_yP_{1-y}$, cyclotron reson., cond. band nonparabolicity 80−29311
$In_{1-x}Ga_xAs_yP_{1-y}$, DH laser material, spatially resolved photolum. characterisation and optically induced degradation 79−47486
$In_{1-x}Ga_xAs_yP_{1-y}$ DH laser, low threshold current density, near equilibrium LPE growth 80−19040
$In_{1-x}Ga_xAs_yP_{1-y}$ DH lasers for 1.3 and 1.5 μm optical fibre communications 80−91817
$In_{1-x}Ga_xAs_yP_{1-y}$, electron effective mass from Shubnikov-de Haas meas. 80−80298
$In_{1-x}Ga_xAs_yP_{1-y}$ epitaxial layer, far IR refl. spectra, lattice vibrs. 80−97282
$In_{1-x}Ga_xAs_yP_{1-y}$, evidence for alloy scatt. from press. induced changes of electron mobility 80−88548
$In_{1-x}Ga_xAs_yP_{1-y}$ far IR reflection spectrum 80−60612
$In_{1-x}Ga_xAs_yP_{1-y}$, Hall mobility, comp. depend. 80−75587
$In_{1-x}Ga_xAs_yP_{1-y}$, hole mobility over temp. range 77 to 300K 80−60111
$In_{1-x}Ga_xAs_yP_{1-y}$, LPE growth on InP (100), lattice matched composition 78−87881
$In_{1-x}Ga_xAs_yP_{1-y}$ LPE layers, background carrier conc. and electron mobility. 79−95523
$In_{1-x}Ga_xAs_yP_{1-y}$, lattice vibrs., Raman study 78−91391
$In_{1-x}Ga_xAs_yP_{1-y}$, lattice matched to InP, band gap vs. comp., and Vegard's law demonstration 79−7782
$In_{1-x}Ga_xAs_yP_{1-y}$, oscillatory magneto-transmission, band parameters 79−60707
$In_{1-x}Ga_xAs_yP_{1-y}$ quaternaries VPE 0.75 to 1.35 eV band gap range 79−69987
$In_{1-x}Ga_xAs_yP_{1-y}$, traps in device quality n- and p-type LPE material 80−10999
$In_{1-x}Ga_xAs_yP_{1-y}$, vapour grown, alloy comp., thermodynamic calc. 79−99094
$In_{1-x}Ga_xAs_yP_{1-y}$:Be, ion implantation, hole conc. and mobility, junction depth 79−46685
$In_{1-x}Ga_xAs_yP_{1-y}$/InP 1.5 μm room-temp. CW laser fabrication and operation 80−64070
$In_{1-x}Ga_xAs_yP_{1-y}$-InP DH laser, fabricated on (100)-InP substrate, 500-hr CW operation 77−83890
$In_{1-x}Ga_xAs_yP_{1-y}$-InP DH lasers, fabrication and performance 78−5500
$In_{1-x}Ga_xAs_yP_{1-y}$-InP DH laser on InP (100) substrate 78−29965
$In_{1-x}Ga_xAs_yP_{1-y}$-InP photodetectors, high-efficiency with selective wavelength response, 0.9-1.7 μm 79−21810
$In_{1-x}Ga_xAs_yP_{1-y}$-InP DH laser, 10000 h continuous CW operation, dark-line and dark-spot defects 79−98384
$In_xGa_{1-x}As_{1-y}P_y$ epitaxial layers, characterisation and relation to lattice matching 80−100540
$In_xGa_{1-x}As_xP_{1-x}$-InP photodetectors, construction and performance 78−65966
$In_xGa_{1-x}As_yP_{1-y}$ layers on InP, LPE and opt. props. characteris. 79−28849
$In_xGa_{1-x}As_yP_{1-y}$ photodetector diode on InP substrate dark currents, tunnelling, energy gaps, effective masses 80−70805
$In_xGa_{1-x}As_yP_{1-y}$, surface and dielec.-semicond. interface props. 80−93001
$In_xGa_{1-x}As_yP_{1-y}$, valence band struct., CPA calc. 79−73435
InGaAsSb based injection heterolaser, 1.9 μm stimulated emission 79−18420
InGaAsSb, LPE growth, and appl. in GaSb/AlGaAsSb/InGaAsSb/AlGaAsSb/GaSb DH 80−16205
InGaAsSb-AlGaAsSb DH laser, room temp. operation at 1.8 μm wavelength 80−43358
$In_{1-x}Ga_xAs_{1-y}Sb_y$, LPE growth on (111)B-oriented InAs, growth conditions and lattice matching 77−24973
$In_xGa_{1-x}As_ySb_{1-y}$ laser, nonequilibrium carrier recombination, luminesc. study 80−50431
InGaP/InGaAs struct. for transferred electron photocathodes, VPE growth and characterisation 80−76193
InGaP-GaAs junction, effect of elastic strain on energy band gap and lattice parameters 79−24057
InGaP-InGaAs solar cell, high internal collection efficiency, low bandgap 80−26134
$In_{0.3}Ga_{0.7}P$, N free and implanted, photoluminescence study 80−97322
$In_{0.5}Ga_{0.5}P$-GaAs heterojunction, interfacial recomb. vel. determ. 77−51809
n-$In_{1-x}Ga_xP$, direct-gap semiconductor, cathodoluminesc., electron irrad. effects 80−108283
$In_{1-x}Ga_xP$, epitaxial film, cathodolum. obs., recomb. mechanisms 78−72613
$In_{1-x}Ga_xP$, epitaxial growth from melt, optimisation of growth conditions 79−52132
$In_{1-x}Ga_xP$, epitaxial layers, compositional inhomogeneity 80−88444
$In_{1-x}Ga_xP$, homogeneous bulk, growth from soln. with predetermined cryst. comp. 78−11097
$In_{1-x}Ga_xP$ LEDs and electron-beam-pumped lasers, LPE and VPE growth 80−2281
$In_{1-x}Ga_xP$, LPE, conditions, reacts. in In-Ga-P system 79−11525
$In_{1-x}Ga_xP$, LPE, on $GaAs_{1-y}P_y$, photo- and cathodolum. 78−19559
$In_{1-x}Ga_xP$, non-isodisplacement of P atoms in long-wavelength optical phonons 79−47444
$In_{1-x}Ga_xP$, phonon density of states, cluster Bethe lattice treatment 80−6475
$In_{1-x}Ga_xP$, quantitative characterisation of chemical disorder from wavelength-modulated no-phonon absorpt. 79−15482
$In_{1-x}Ga_xP$, solid soln., evaporation of P during LPE 79−95948
$In_{1-x}Ga_xP$, solid soln. film, photoluminesc. meas. 78−27321
n-$In_{1-x}Ga_xP$ solid solns., electron scatt. mechanisms *(Russian)* 79−4568
$In_{1-x}Ga_xP$, temp. depend. of forbidden band width, photoluminesc. meas. 78−19556
$In_{1-x}Ga_xP$, two-phonon IR absorpt. 78−52493

III-V semiconductors continued
$In_{1-x}Ga_xP$:Bi(N)(Zn,O) radiative recombination at isoelectronic centres 79−52027
$In_{1-x}Ga_xP$:N_2, N-trap bound states, photoluminesc. and absorption data 77−1719
$In_{1-x}Ga_xP$:N(Te), composition depend. of bound state luminesc. transitions 78−39595
$In_{1-x}Ga_xP$:Te,Zn, photolum. and electrolum., direct transition region 77−8659
$In_{1-y}Ga_yP$-GaAs heterojunction, VPE, energy band gap and lattice parameter, lattice mismatch effects 78−95345
$In_xGa_{1-x}P$, proportional ingredient content determ. by X-ray fluoroscopy 80−97747
$In_xGa_{1-x}P$, solid solns., gas phase epitaxy from Ga-In-HCl-PH_3-H_2 systems 78−34722
$In_xGa_{1-x}P$, TEM foil preparation, using polishing set 'Elypovist' *(German)* 79−9264
$In_xGa_{1-x}P$-GaAs heterojunction, interface recomb. velocity determ. 77−89838
$In_xGa_{1-x}P$-GaAs lattice mismatched heterojunction, recomb. props. 78−13707
InGaPAs LPE layers, compositional inhomogeneity, photoluminesc. obs. 80−75451
InGaPAs LPE multilayered DH lasers exhibiting quantum size effects 78−1227
InGaPAs, LPE-grown on (001)-InP, lattice mismatch study using X-ray double-cryst. diffr. 79−99440
InGaPAs-InP DH laser, threshold current temp. depend., potential barrier height influence 80−53296
$In_{1-x}Ga_xP_{1-y}As_y$ LPE films, hot electron and magnetotransport props. 78−26977
$In_{1-x}Ga_xP_{1-y}As_y$ lattice-matched epitaxial layers, LPE growth on GaAs(100), characterisation 80−75465
$In_{1-x}Ga_xP_{1-z}As_z$, DH, operated in external grating cavities, inhomogeneous and homogeneous line broadening 77−10921
$In_{1-x}Ga_xP_{1-z}As_z$, DH, diode and laser performance, limitations of direct-indirect transition 77−39927
$In_{1-x}Ga_xP_{1-z}As_z$ DH lasers, pulsed room temp. operation 77−10941
$In_{1-x}Ga_xP_{1-z}As_z$ DH laser, effective index of refr., wavelength depend. 77−61954
$In_{1-x}Ga_xP_{1-z}As_z$ DH lasers, multiple LPE, lattice matching 77−77421
$In_{1-x}Ga_xP_{1-z}As_z$ DH laser diode, defect and phonon assisted tunnelling 78−13708
$In_{1-x}Ga_xP_{1-z}As_z$ LEDs and electron-beam-pumped lasers, LPE and VPE growth 80−2281
$In_{1-x}Ga_xP_{1-z}As_z$ LPE DH laser with multiple thin layer active region 77−83887
$In_{1-x}Ga_xP_{1-z}As_z$, lattice matched to InP, electroreflectance obs. 80−93416
$In_{1-x}Ga_xP_{1-z}As_z$ near IR DH laser, constant temp. LPE, external grating cavity 77−75550
$In_{1-x}Ga_xP_{1-z}As_z$, room temp. visible heterojunction lasers 78−5501
$In_{1-x}Ga_xP_{1-z}As_z$ single thin active layer visible spectrum heterostruct. lasers 78−63120
$In_{1-x}Ga_xP_{1-z}As_z$ solid solution, radiative transitions 79−11476
$In_{1-x}Ga_xP_{1-z}As_z$, stimulated yellow-green emission under electron excitation, 80K 79−33846
$In_{1-x}Ga_xP_{1-z}As_z$ thin well in InP p-n junction, confined carrier luminesc. and laser modes 78−13703
$In_{1-x}Ga_xP_{1-z}As_z$, visible spectrum laser diode, continuous operation, 6280 Å, 77K 79−960
$In_{1-x}Ga_xP_{1-z}As_z$ well in InP, tunnel injection into confined particle states 78−19130
$In_{1-x}Ga_xP_{1-z}As_z$:Zn, x∼0.12, z∼0.26, LPE, DH lasers, tunnelling involving defects 77−65594
$In_{1-x}Ga_xP_{1-z}As_z$-$In_{1-x}Ga_xP_{1-z}As_z$ visible spectrum multiple-quantum-well heterostruct. lasers 80−106537
$In_{1-x}Ga_xP_{1-z}As_z$-InP, LPE heterojunctions, lattice matching and dislocations 78−23150
$In_{1-x}Ga_xP_{1-z}As_z$-InP, single and multiple layer heterostruct., LEDs and lasers 78−46626
$In_{1-x}Ga_xP_{1-z}As_z$-InP coupled multiple quantum-well heterostructure laser diodes, threshold current temp. depend. 80−78855
$In_uGa_{1-u}P_vAs_{1-v}$-InP, LPE, lattice matching, phase 80−54350
$In_xGa_{1-x}P_yAs_{1-y}$, electron effective mass and Dingle temp., Shubnikov-de Haas oscills. 80−59859
InGaSb, LPE growth characteristics, substrate surface contamination dependence 80−39470
$In_{0.58}Ga_{0.42}Sb$, interband magneto-optical transitions, arbitrary field orientation 79−42948
$In_{1-x}Ga_xSb$ alloy system, interband magnetooptical study using Schottky barrier 79−8124
$In_{1-x}Ga_xSb$, band parameter variations 80−20084
$In_{1-x}Ga_xSb$, drift velocity of electrons 77−20327
$In_{1-x}Ga_xSb$, energy gap, temp. depend. and photovoltaic effect 80−70746
$In_{1-x}Ga_xSb$ film, epitaxial growth by multitarget RF sputtering 77−44157
$In_{1-x}Ga_xSb$ films, elec. props., preparation 80−100473
$In_{1-x}Ga_xSb$, multitarget sputtering using decoupled plasmas 77−12529
$In_{1-x}Ga_xSb$-Au, photovoltaic effect and Schottky barriers 80−49897
$In_xGa_{1-x}Sb$, influence of annealing on microstruct., exam. 78−56669
$In_xGa_{1-x}Sb$, molecular beam epitaxy 79−47638
$In_xGa_{1-x}Sb$, vertical Bridgman Stockbarger growth, magnetic field effect 78−60565
InGaSbAs heterostructures and LED's luminesc. props. in 1-2 micron band 78−10988
$In_{1-x}GaxAs$, MBE, RHEED meas. 78−18916
InN, epitaxial layer prep. using $InCl_3$-NH_3 system 78−3056
InN, epitaxial layer prep. and X-ray analysis 79−38747
InN film, refl. and transmission spectra, band struct. 78−72625
InN film, specular reflection spectra, lattice parameters 80−7428
InN film growth by reactive sputtering in Ar-N_2 discharge, mechanism 80−89107
n-In_2O_3/p-InP heterojunction solar cell, photovolt. effects 80−12014
In_2O_3-InN film growth by reactive sputtering in N_2-O_2 discharge, mechanism 80−89108
In_2O_3-SnO_2-InP solar cell junctions, efficiency, InP surface props. 80−85288
InP (001)-Ag, contact, surface stoichiometry and struct., and electronic surface states 78−95361

III-V semiconductors continued
n-InP (100), photovoltage transients by retarding pot. electron beam techniques 77−24586
InP (100) substrates, for MBE, ion-cleared, contamination, SIMS meas. 78−11353
InP, (100) surface, Auger depth profiling limitations 79−61473
InP (100) surfaces, chem. treatment effects on comp. and nature 79−47794
InP (110), low coverage adsorption, SIMS study 80−49500
InP (110), oxidation, initial stages, photoemission study 80−16529
InP (110) surfaces, cleaved and polished-sputtered-annealed, LEED and AES study 80−103550
n-InP, (110) surfaces, photolum. intensities in vac. and gas ambients 79−61412
InP (111) substrate, and homoepitaxial layers, characterisation by divergent X-ray beam diffr. 78−31352
InP, acceptor excited states, luminesc. spectra 80−16091
InP, ambient-enhanced photoluminesc. props., mol. adsorption and gas-flow effect 79−99925
InP, anal. of anodically oxidised (111) layers by MeV $^4He^+$ channelling effect meas. and AES 79−4492
InP, and InP_xAs_{1-x}, 111-A and 111-B faces, defect struct., etching and X-ray diffr. obs. 80−2026
InP anodically grown native oxide, antirefl. coating for InGaAsP-InP photodiode 80−13137
InP, anodisation, effect of pH, current density and illumination 78−95823
InP avalanche photodiodes, microplasmas, investigation 80−60018
InP, bulk grown, selective spectroscopy, acceptor level studies 80−29778
InP, CESR, optical detect. by spin orientation techniques, anal. 78−80251
InP carrier profiling using liq. barrier contact 78−76087
InP, chemisorption and oxidation states of (110) surfaces 79−24049
InP, cleaved surface, angle resolved photoelectron spectroscopy 80−55258
InP, cleaved surface, metal contact props. and influence of intermediate adsorbed layers 80−49905
InP cleaved surfaces, and interfaces with metal electrodes 78−10554
n-InP, compensated, elec. props., space-charge effects 80−65569
n-InP, compensated impurity conduction and negative magnetoresist. 79−28360
InP, compensation ratio, electron mobility and free-carrier absorpt. 80−80261
InP, concs. of C and O_2 in LEC grown cryst. determ. 77−39612
InP, critical implantation temp. and annealing 79−90691
InP, crystal growth by synthesis solute diffusion method 78−64454
InP, crystal growth by travelling heater method 80−11553
InP, current controlled LPE growth 77−77428
InP, current-controlled LPE growth, Peltier cooling at In-InP interface 77−8770
InP cylindrical magnetron reactive sputtering, for solar cell appl. 78−39693
InP, Czochralski grown, etch pit obs., produced by new etchants HBr/HF or HBr/CH_3COOH 79−60370
InP, damage induced during handling for TEM obs. 80−2024
InP, deep level electron traps, emission and capture props. 80−29806
InP, deep level trap interaction with lowest and upper cond. minima 80−49654
InP, deep trap characts. by photocapacitance spectroscopy 78−6398
InP, deep trap study by free exciton refl. spectra 79−60761
InP, deep-level traps and cond.-band struct. 79−19542
n-InP, defects in homoepitaxial layers, on p-type substrate, accurate lattice parameters 78−47675
InP, depend. of phonon spectrum on hydrostatic press., Raman spectra 80−93315
InP detector, unbiased, using Schottky-barrier diode, operation in submm. wave region 80−105707
InP, diffusion and power spectral density of velocity fluctuations for electrons, Monte Carlo calc. 79−51572
InP, diffusion of Cd acceptors 79−82246
InP, dislocation etching of (001) faces with H_3PO_4 etchant 80−15103
InP, effects of baking time on purity and morphology 78−6862
InP, electrial props. at high temp. and in liquid state 77−11888
InP, electrical and optical props. at low temps. 80−39636
InP, electroabsorption spectra obs., reduced effective mass determ. 80−50301
InP electrode-electrolyte interface, Schottky barrier obs. 78−52079
InP electrodeposition, solvent systems, low melting point comps. in alkali metal metaphosphate/fluoride systems 79−28079
InP electrodes, photo-induced electrogenerated chemilum. and up-conversion 79−91510
InP electrodes in acetonitrile solns., photoelectrochem. behaviour 79−4600
InP, electron irrad. at 50 MeV, elec. and optical props. 77−47486
InP, electron transport props., mag. field and temp. depend. 80−92888
InP, electron-hole plasma, ground state energy 78−84244
InP, electronic struct. of valence and conduct. bands 77−28110
InP, electronic structure of neutral phosphorus vacancy, empirical pseudopotential 79−78042
n-InP, epitaxial, Hall effect, electron mobility and density, temp. depend. 78−72288
InP, epitaxial, kinetics of VPE 80−60790
n-InP, epitaxial, subthreshold velocity-field charact., 77K 78−64038
InP epitaxial films, grown on heavily doped substrates, carrier mobility study, magnetoresist. meas. 80−60116
InP epitaxial growth, in vertical reactor, construction and expt. data *(Slovak)* 77−28081
InP, epitaxial growth, thermodynamic conditions 77−89661
n-InP, epitaxial layer, (100) surface chemistry, ESCA study 80−103552
InP, epitaxial layer, effective doping density, comparison of Hall and magnetoresistance meas. 77−11938
InP epitaxial layers, (100)-orientated, vapour phase deposited in closed-tube system, surface comp. variation 80−24752
InP, exchange interaction, analytical and nonanalytical parts, from polariton spectra in mag. fields 80−50367
InP, excitation by 2-4 KeV Ar^+ ions, electron energy spectra 80−11529
InP, exciton localisation at impurity pairs 79−37999
InP, excitons bound to neutral donors in VPE layers, luminesc. and absorpt. obs. 79−42460
InP, excitons detect., precision method 79−19906
InP, expt. studies on meltback morphology 78−31347

III-V semiconductors continued
InP, far IR LPE photodetector performance 79−30546
InP, Faraday interband effect subjected to quantising mag. fields 80−97246
InP, Fermi level pinning on exposure to O_2 79−60637
p-InP field-assisted photocathodes, quantum efficiency 80−84831
p-InP film, CVD, growth characts. and CdS/InP solar cell efficiency 77−1813
InP film, CVD on preferentially etched Mo, initial growth behaviour 78−51855
InP film, electron-beam annealed, surface conduction 80−84500
InP film, liquid-phase epitaxial growth on (100) and {111} substrates *(Slovak)* 79−15037
InP film, on rough $Zn_xCd_{1-x}S$ substrate, film substrate lattice mismatch calcs. 78−43263
n-InP film, polycryst., deposited on Mo sheets, elec. props. obs., w.r.t. varying deposition conditions 79−4608
n-InP film, polycrystalline, elec. props. 77−76965
InP film, prep. by low press. reactive deposition process 79−24449
p-InP film growth, by close space vapour transport 79−28944
InP films, organometallic VPE grown, props. 80−96753
InP, fine struct. in energy derivative reflectance spectra 79−78705
InP, free carriers, freq. depend. relax. time 80−2385
InP, free excitons in high mag. fields, band struct. 77−52129
InP, fused, SRO structure changes on heating 77−89367
InP grown by LPE, method for free In removal from surface 80−84860
n-InP grown by synthesis solute-diffusion method, electron traps 79−90987
InP, grown-in dislocation density, impurity effect 78−51543
InP, growth and props. 79−1822
InP growth from soln. and LEC, photolum. and elec. meas. 79−87575
InP Gunn diodes, population inversion condition 77−77251
InP, Gunn oscillator magnetoresist. meas. of mobility and noise, contact effects 77−62948
n-InP, γ-ray and electron irrad., annealing of radiation point defects, elec. cond. and Hall coeff. meas. 80−65051
n-InP, Hall effect, 10-300K ,thermal activation energy and influence of compensation 78−72171
n-InP, heat treatment effect on bulk grown and VPE grown material 77−11936
n-InP, heat treatment in controlled P vapour 80−88137
InP, heteroepitaxial deposition on GaAs substrate, using close-spaced method, X-ray analysis *(Czech)* 77−15710
InP, heteroepitaxy on CdS substrates using InI_3 as transport agent 79−56083
n-InP, high field props. under high press. 78−26872
n-InP, high resistivity layers produced by Fe^+ implantation 78−47404
InP, high-field transport 77−8107
InP, high-purity bulk, prep. from soln. 78−6839
InP, high-purity VPE, by $PCl_3/In/H_2$ technique, progress in control 78−6857
n-InP, hole traps by deep level transient spectroscopy and transient capacitance methods 79−51514
InP, homoepitaxial film by MO-CVD process, for heterojunc. solar cell fabrication 79−8250
InP homojunction solar cell, antirefl. coated, high-efficiency 80−104505
n-InP, hopping cond., nonohmic nature 79−23976
InP, hot carrier noise, Monte Carlo simulation 77−51792
InP hydrothermal oxidation kinetics, exam. 80−40566
InP, impact ionis. by electrons and holes 79−99554
InP, impact ionisation by electrons and holes 80−100467
InP, implantation of Si, Al, Hf, Ta into InP and GaAs, form. of protective oxide 78−79622
n-InP, impurity and minimum metallic cond. in mag. field 80−103731
InP, impurity effect on grown-in dislocation density *(Japanese)* 78−6063
InP injection laser, strong mag. field effect on emission 77−58329
InP integrated optical communication components, overview 80−79012
InP, integrated optics appl., heterojunctions preparation and props. *(Slovak)* 80−33225
InP interface with anodic and thermal oxides, comparison of AES and ESCA 78−95980
InP interface with oxide, photoemission obs. of energy levels induced by adsorpt. 80−93000
InP, intervalley electron transfer, drift velocity and diffusion coefficient 80−39594
InP, inversion layers, C-V and surface transport meas. 80−49928
InP inversion-type MISFET with SiO_2 gate insulation interface props., elec. drift 80−93002
InP, ion implantation damage compensation 77−84770
InP, ion implantation used to create n-type, p-type and high resist. layers 78−6076
InP, ion implanted, anodic oxidation and elec. carrier conc. profiles 79−70185
InP, ion-implanted layers, close contact capless annealing, elec. props. 80−84192
InP, ion-implanted n- and p-type layers, characts. 78−6075
InP, ions coeffs. of electrons and holes 80−2394
InP, Kramers-Kronig electroreflection spectra 77−4655
InP, LEC growth of dislocation-free crystals 80−89134
InP, LEC growth using pyrolytic BN crucibles 78−6841
InP, LPE, high purity, use of baking to reduce Si contamination 78−72744
InP, LPE, solvent choice, equilib. in In-Ga-P system 79−87589
InP, LPE grown, impurity effect on surface morphology 80−29291
InP, LPE grown, surface morphology 77−62771
InP, LPE growth 80−11557
InP, LPE growth on GaAs, etching and electron probe anal. 79−11526
InP, large size single crysts., synthesis, solute diffusion technique 79−33917
InP, laser-induced microscopic etching 80−76379
InP, lattice dynamics 79−14895
InP, lattice dynamics and phonon parameters bond bending force model 80−59595
InP, lattice matching to $In_xGa_{1-x}As$:Zn, LPE growth conditions 80−70541
InP layer growth method, model validity evaluation *(Slovak)* 80−54535
InP layers, grown by LPE from supercooled solns., thickness meas. 78−10307
InP layers, LPE growth from undercooled melts, numerical method 80−6665

III-V semiconductors continued
InP, liq.-seal growth, protective props. of B_2O_3 flux 77−12519
InP, liquid encapsulated Czochralski cryst. growth, X-ray study 79−47619
InP, low temp. diffusion of radioactive Ag 78−75884
InP, luminesc. emitted as a result of carrier heating 77−52185
InP, luminescence, hot electron effects 80−66277
InP, MBE, substrate temp. related degradation mechanisms 80−65385
InP, MBE and field emission deposition of Al and Au films, comparative study 79−87016
InP, MBE from In and P_2 beams, substrate temp. limits 80−15385
InP, MBE growth, expt. *(Japanese)* 77−4743
InP, MBE growth on InP substrate, orient.-depend. faceting 77−24966
InP, MBE growth surface, singular instabilities 77−24969
InP, MIS capacitor, transient capacitance and C-V characts. 78−95374
InP MIS capacitor surface states 80−49931
InP MIS devices, diffusion, chemical reactions, contamination, AES and SIMS 80−72066
InP, MIS diode prep. by anodic oxidation 79−74270
InP, MIS structures, dielec. and interfacial characts. appl. to microwave MISFETs 79−60933
n-InP, MOS solar cells, electrical and photovoltaic characteristics 80−85276
InP MOS structure, elec. characts. of InP surface meas. 77−20451
n-InP, magneto-impurity effect, review 79−91081
n-InP, magneto-impurity resonances, obs. of central cell struct. 78−95303
InP, manifestation of local vibrs. of dislocations in IR spectra 78−88339
InP, maximum electric field in high-field domain in Gunn devices 78−79996
InP, model for ~1.10 eV emission band 80−66289
InP, molten stoichiometric, surface tension 78−39684
InP, multiphonon absorpt. bands *(Russian)* 77−85731
InP, n- and p-type, surface recomb. vel. meas., diffr. from transient optical grating 79−1604
InP, N- and p-type electrodes in acetonitrile solns., photoelectrochemical behaviour 79−99616
InP n^+-p-p^+ homojunction solar cells, high efficiency, LPE layer growth, photolithographic fabrication 80−93929
InP, n-type conductive regions produced by ion implantation 78−10067
InP, n-type doping by ion-implantation of S and Si, expt. 78−91351
InP, negative differential mobility and geometrical magnetoresist. calc. 77−43624
InP, noise calc. using Monte-Carlo method 80−75575
p-InP, ohmic contact using Be-Au metallisation, low contact resist. 80−65677
InP ohmic contacts 79−28406
InP, ohmic contacts by thin film epitaxy, Gunn oscill. appl. 79−38159
InP, organometallic growth by cracking of $In(C_2H_5)_3$ and PH_3 80−11575
n-InP, oscill. intrinsic photocond. 79−60871
InP, oscillatory interband magnetoabsorption meas. 79−73909
InP p^+-n abrupt junctions, ionisation coeffs., photomultiplication meas. 80−65655
InP, p-i-ν diode, Franz-Keldysh effect 77−55790
InP p-n junction, grain boundary etching 80−96541
InP p-n junction diodes, fabrication by Be ion implantation 79−47156
n-InP, p-n junction form. by Be ion implantation 80−29474
InP photodiodes, dark current and breakdown characts. 80−70806
n-InP photoelectrode, stabilisation to photoanodic dissolution, in aqueous solutions of Te^{2-}/Te_2^{2-} 78−14814
n-InP photoelectrode, stabilisation to photoanodic dissolution in solns. containing Te^{2-} and Te_2^{2-} 78−19144
InP, photoemission and LEED meas., minority carrier diffusion length 77−69959
n-InP, photolum., evidence for low surface recomb. vel. rel. to n-GaAs 77−40272
InP, photolum. depend on surface treatment 79−78727
InP, photoluminesc. of epitaxial films, isovalent substitution 80−16097
InP, photoluminescence at dislocations, band gap electronic levels 79−99926
InP, photoluminescence intensity of cleaved surface, ambient gas influence 78−88345
InP, photoluminescence meas. using diamond-anvil press. cell 80−108256
InP, photovoltage transients, expt. and model 77−89802
InP, piezobirefringence above direct gap 79−51929
InP planar guarded avalanche diode prod. by ion implantation 79−95473
InP, planar reactive deposition on CdS, heterostruct. formation and elec. evaluation 78−72738
InP, planar Zn diffusion process for p-n junction formation 78−43040
InP, plastic deform. and scratch microhardness meas. 78−27583
InP, polar semiconductor, collisions between hot excitons and hot electrons 80−7415
p-InP, prep. of single and bi-crysts., epitaxial layer and polycryst. films 77−81211
InP, press. depend. of direct absorption edge 80−93365
InP, proton bombard. effects on resist. 77−80552
InP, pure and S doped, VPE, exam. of molar fraction controlled impurity in $In\text{-}PCl_3\text{-}H_2$ 78−56587
p-InP, RF sputtering on CdS and other substrates, and grain size obs. 77−90272
InP, radiation defect formation processes, effect on physical props. 78−2163
InP, reactive ion etching of III-V compounds 80−58813
InP, recoil damage obs. by PAC with ^{111}Cd 77−89484
InP, reflection spectra, optical functions, exciton peaks *(Russian)* 80−50372
InP, relaxation LSA mode obs. 77−8102
InP, reson. Raman scatt., deformation pots. 78−52495
n-InP, room temp. electron irrad., Hall coeff. meas. 77−89478
InP, Schottky barrier and semicond./insulator interface states formation 80−49906
n-InP Schottky barriers, low leakage, near ideal 78−39212
n-InP Schottky barriers, photocapacitance effects of deep traps 78−43325
InP, Schottky diode, barrier height control by S diffusion 77−85309
InP, semicond., ^{31}P nuclear mag. shielding 79−33549
InP single crystals, uniaxial compression deform. characts. 80−84991
InP, site selective doping by ion implantation of radioactive nuclei 80−34023
InP solar cells, thin film growth tech. and characterisation 80−89631

III-V semiconductors continued
InP, soln. in liq. Sn, vapour phase partial press. meas., rel. to LPE 78−34610
n-InP, submillimetre cond. and carrier heating, two-electron-temp. model 77−20349
InP substrate, LEC-grown, defect evaluation by cathodoluminescence 80−2866
InP substrate, thermal damage suppression by adding Ar in H_2 atmosphere 79−100275
InP substrate, transient-mode LPE of GaAs 78−72746
InP substrates, chem. etching by $H_2O_2\text{-}H_2SO_4\text{-}H_2O$ soln. 80−35360
InP substrates, control of thermal degradation in LPE growth with PH_2 partial pressure 79−33949
InP substrates HCl etching speed and polarity obs., with aid of laser beams *(Slovak)* 78−56575
InP substrates preparation, etching and polishing in Br-methyl alcohol solution *(Slovak)* 78−56576
InP, surface, electron struct. and Fermi level pinning by O_2 and metals 80−11066
InP surface, interaction with Cl, electron spectroscopic obs. 78−56036
InP, surface, pulsed electron beam processing, doping, annealing 80−75254
InP, surface (110) atomic struct. 79−69331
InP, surface and dielec.-semicond. interface props. 80−93001
InP, surface chemistry and electronic struct., adsorption of O_2, photoemission meas. 77−20985
InP, surface damage induced during SiO_2 deposition by RF sputtering 79−78879
InP, surface passivation using composite Al_2O_3 and native oxide, MIS characts. 80−93004
InP, surface phonon polariton dispersion and damping, frustrated total internal refl. meas. 80−80792
InP surface preparation for Schottky barrier and ohmic contact formation 80−39671
InP, surface recomb. vel., psec. optical techniques 80−70784
InP, surface recombination velocity, diffr. from picosecond transient free carrier gratings 79−47109
InP, surface space charge layers and Schottky barrier form., Raman scatt. study 80−50319
InP, surface vacancies, bound state energy levels calc. 80−80340
InP, synthesis solute diffusion grown, elec. props., photoluminesc., etch pit profiles 79−4914
InP, temp. depend. of Fermi Level, calc. 80−39491
InP, terracing of LPE growth, doping effects 80−10846
InP, thermal degradation and its control in LPE growth 79−100343
InP, thermal oxidation, growth rate and comp. of oxide 80−55555
InP, transferred electron effect 77−39855
n-InP, transferred electron effects under hydrostatic press. 78−26871
n-InP, transferred electron instabilities, hydroststic press. effect 80−6869
InP, transferred electron effects under high press. 80−34453
InP, transient and steady-state electron transport props. 77−39812
InP, twin-free, prep. using liquid encapsulated Czochralski growth 80−50546
InP VPE, growth kinetics and controlled doping 79−87569
InP VPE, $In\text{-}H_2\text{-}PCl_3$ chemistry 80−11549
InP, VPE, thermodynamics of transfer by water vapour 78−43260
InP, VPE growth for MESFET's 80−103602
InP, VPE layer props. control using boundary layer characts. 80−50561
InP VPE with new metallorganic compound 80−55278
InP, valence band fine struct. from light mod. with nonequilib. opt. phonons 78−39568
InP, valence band structure, CPA, bond orbital calcs. 78−87909
InP, vapour phase epitaxial growth in presence of O_2, elec. props. 79−46971
InP very high purity LPE layer growth 78−3061
InP wafer, defect studies by ASLEEP, SEM and scanning AES 79−19256
InP wafer diagnostics, using computer automated scanning low-energy electron probe 79−4214
InP, weak field Hall mobility and Hall mobility and Hall ratio 78−23116
InP, Zn diffused single-crystal, substitutional dopant and hole conc. meas. 80−75260
InP:Be, ion implantation, hole conc. and mobility, junction depth 79−46685
InP:Be, LPE, Be distrib. coeff., carrier conc. 79−90694
InP:Bi, isoelectronic impurity states, emission and absorpt. obs. 79−42491
InP:Bi, uniaxial stress effect on free and Bi-bound excitons 79−56854
InP:Cd, doping by UV laser photodeposition 80−84191
InP:Cd, p^+-p^--n^- junction form. by diffusion doping 80−84504
InP:Cd(Zn), avalanche photodiode characts., impurity diffusion effects 80−70709
p-InP:Cd(Zn), single cryst. growth by temp. gradient method 79−28907
InP:Co(Cr)(Fe), Hall and resistivity meas. 80−10990
InP:Co(Fe), diffusion solubility and elec. activity of Co and Fe 77−43240
n-InP:Cr, press. depend. of elec. resist. and Cr ionisation energy 80−80281
InP:Cr^{2+}, Jahn-Teller effect for ion impurities 80−107753
InP:Fe, deep acceptor levels, photocond. meas. 80−20116
InP:Fe, deep levels 79−56166
InP:Fe, Fe acceptor charge states, photolum., absorpt. and ESR meas. 77−36123
InP:Fe, photocond., Fe^{2+} intracentre excitation model 80−29436
InP:Fe, precipitate mixture 77−77485
InP:Fe, resonance photocond. 80−44651
InP:Fe shallow trap thermally stimulated cond. spectroscopy, photocond. spectrum under DC conditions 80−65585
InP:Fe^{3+} (Cr^{2+}), EPR, symm., spin Hamiltonian parameters 78−10759
InP:Ni^{3+}(Co^{2+})(Fe^+), EPR assessment of $3d^7$ transition metal impurity state 78−48031
InP:S, SSD growth of low dislocation density crystals 80−89135
InP:S^+(Se^+), ion-implanted VPE layers, laser annealing, elec. and struct. anal. 79−73199
InP:Se, implantation and laser annealing 80−24476
InP:Si, implantation at high temp., elec. mobilities 79−99541
InP:Si, pulse electron annealing, carrier activation and mobility 80−15124
InP:Si, vibr. modes of Si, IR absorpt. bands 78−55922

III-V semiconductors continued
InP:Si(Mg), ion implantation and PH_3 ambient annealing under VPE conditions 79−42085
InP:Sn, LPE growth from Sn soln., elec. props., 80 to 300K 79−11250
InP:Sn film, mol. beam epitaxial growth 77−16505
InP:Te, mag. props. of conduction electrons 78−6510
InP:Te, powder, quadrupole interactions in NMR spectra 79−51880
InP:Te, quadrupole struct. of NMR line 80−20505
InP:Te(S), heavily doped, dislocation imaging using transmission cathodoluminesc. 80−29023
p-InP:Zn, elec. meas., doping levels, hole conc. 78−14745
InP:Zn, isoconcentration diffusion of Zn at 800°C 78−6186
InP:Zn heavily doped X-ray topography, cathodolum., and TEM obs. 79−99197
InP/anodic oxide interface, Auger analysis 77−90478
n-InP/Au-Ti Schottky diode, elec. characts. and barrier height 77−59329
n-InP/Au-Zn Schottky barrier diodes, fabrication and elec. props. 79−33348
InP/CdS epitaxial thin films on NaCl, HEED and TEM study 80−88446
InP/$Ga_{0.47}In_{0.53}As$/InP DH laser, lattice matched, MBE and room temp. operation 78−74906
InP/GaP system, two-layer structs., relaxation of internal stresses 80−34341
InP/$In_{1-x}Ga_xAs_yP_{1-y}$ heterostruct., optically induced degradation 79−86791
InP/In_2O_3-SnO_2, solar cell, fabrication, characts. and interfacial chemistry 80−21401
InP/$In_xGa_{1-x}As_yP_{1-y}$ interfaces, sputter-profiled, depth resolution degradation by cone form. 80−80094
p-InP/In-Zn(Cd) contact evaluation 77−24619
InP/InGaAs heterojunction phototransistor, high-sensitivity 80−100505
InP/InGaAs/InP field assisted photocathode, minority carrier electron transport across p-p heterojunction 78−95651
InP/InGaAsP avalanche photodiodes, with guard ring structure 80−100506
InP/InGaAsP/InP double heterostructure, grown on InP(111)B substrate, threading dislocation multiplication 80−54237
p-type InP/Langmuir film MIS diodes, characts. 80−80384
n-InP/SiO_2 capacitors, minority carrier generation 79−95496
InP/SiO_2 interface formation, thermodynamic considerations 80−100529
InP/SiO_2 substrate/film system, interface formation during CVD, modelling 80−24764
InP-Ag, struct. of Ag contacts, TEM 77−62765
InP-Ag contact system, evaluation of Auger depth profiling technique 79−56893
InP-Ag Schottky barrier, hot electron attenuation length 80−49904
InP-Al interface struct., low temp. interaction, AES study 80−107661
InP-Al_2O_3 MIS struct., interface props. and MISFET fabrication 79−65557
InP-Al_2O_3-Al MIS struct., elec. props. 79−78184
n-InP-Al(Hg), Schottky barrier height and stability characterisation 80−54786
InP-Au boundary, Schottky barrier height, interfacial layer effects 78−14824
InP-Au contacts, conditions of fabrication that control interfacial microstruct. 79−42643
InP-Au Schottky barriers, PES and depth profiling obs. 79−42641
InP-Au Schottky contacts, interfacial oxide layers used to increase effective barrier height 79−7896
InP-Au Schottky diodes, barrier height study 78−52088
InP-Au Schottky diodes, behaviour under heat treatment 79−78172
InP-CdS heterojunction, injection electrolum. 78−23153
InP-CdS p-n heterodiodes, junction props. study by using injection electrolum. 79−82667
InP-CdS photovoltaic heterojunctions, growth and characts. 77−39931
p-InP-Cd(Zn), ohmic contact formation on InP by laser photochemical doping 80−80369
n-InP-chalcogenide glass heterojunction, fabrication, characterization, switching 80−49892
InP-Cu contact system, low temp. alloyed contact formation 80−100519
InP-electrolyte struct., field effect of photoluminesc. 79−99928
InP-$Ga_xIn_{1-x}As_{1-y}P_y$ heterojunctions, energy band diagram 77−16400
InP-$Ga_xIn_{1-x}As_gP_{1-y}$ systems, for optical devices in 1 to 1.6 μm region, LPE growth *(Japanese)* 79−28956
InP-$Ga_xIn_{1-x}As_yP_{1-y}$ DH, LEDs and lasers, fabrication and operation in 1.5 μm region 78−37893
InP-$Ga_xIn_{1-x}As$-InP, DH fabrication, crack form. due to lattice mismatch 77−15704
InP-$Ga_xIn_{1-x}P_yAs_{1-y}$ heterostruct. lasers, growth and characterisation 80−23691
InP-GaInAsP buried heterostructure lasers of 1.5 μm region, fabrication and characts. 80−74388
InP-GaInPAs DH lasers, misplaced p-n junctions due to Zn contamination 78−87051
InP-GaP, solid soln. crystallization from stoichiometric melt, solidus construction 77−85927
InP-$In_{1-x}Ga_xAs_yP_{1-y}$, DH lasers, dielectric-constant step 79−18418
InP-$In_{1-x}Ga_xAs_yP_{1-y}$-InP 1.55 μm DH room-temp. CW laser fabrication and operation 80−64071
InP-$In_{1-x}Ga_xAs_yP_{1-y}$-InP 1.53 μm single-mode CW ridge-waveguide laser 80−64072
InP-$In_{1-x}Ga_xP_{1-z}As_z$ quantum-well LPE heterostructure lasers, band filling and gain 79−22955
InP-$In_{1-x}Ga_xP_{1-z}As_z$ laser, phonon-assisted recombination 79−89906
InP-$In_{1-x}Ga_xP_{1-z}As_z$, valence band discontinuity, quantum well luminesc. 79−91483
InP-$In_{1-x}Ga_xP_{1-y}As_y$, LPE for optoelectronic devices *(German)* 79−95280
InP-$In_{1-x}Ga_xP_{1-z}As_z$ heterostructure laser, single and multiple quantum-well, liquid-phase epitaxial growth 80−38031
InP-$In_xGa_{1-x}As$ alloy photocathodes, semiconductor photoemitters, field-assisted, 1-2 μm range 80−97396
InP-InGaAsP bias assisted photocathodes, photoemission in 1-2 μm range 78−48289
InP-InGaAsP p-n junction avalanche photodiodes, surface passivation techniques 80−100508
InP-InGaAsP-InP, low threshold laser, threshold density temp. depend., LPE method *(Russian)* 78−22133
InP-InGaAsP-InP DH diode lasers, room temp. CW operation 80−1222

III-V semiconductors continued
InP-InGaPAs heterojunction lasers and LEDs, 1.0 to 1.2 μm 80−74362
InP-Langmuir film MIS structures, surface state distrib. obs. 77−89859
InP-metal contacts, intermediate adsorbed layer effect on electronic props. 80−39674
InP-metal contacts, metal beam epitaxy, struct. and elec. props. of films on ion bombarded InP 79−28922
InP-metal ohmic contacts, elec. and metallurgical props., heat treatment effects 80−34514
n-InP-metal Schottky barriers, effective lowering using thin VPE n^+ lasers 77−43717
InP-metal Schottky barriers, effects of heat treatment characterised by SIMS 78−6446
n-InP-metal surface barrier struct., props. 79−11223
InP-S(Te)(Zn), dislocation-free, TEM study of microdefects 79−82213
InP-Si_3N_4 (SiO_2), interface props., plasma deposited dielectrics, n-channel MOSFET action 80−93003
n-InP-SiO_2 capacitor, carrier generation and trapping 80−49929
InP-SiO_2 interface, CVD problems, ESCA profiles 80−93497
InP-SiO_2 MIS struct., with reduced interface state density near cond. band 78−26954
InP-SiO_2 MOS struct., capacitance-voltage and surface photovoltage meas. 79−60931
n-InP-SiO_2 system, interface and dielec. props. 80−49930
InP-SnO_2 heterojunctions, elec. and photovoltaic characts. 80−75628
InP(As), liquid interaction parameters determ., 580-670°C 80−65197
InP(As), surface states, contact pot. difference, photoemission and low energy loss spectra expts. 77−85285
$InP_{1-x}As_x$, long wave and short wave phonons, Raman spectra obs. 80−50317
InP_xAs_{1-x}, absorption edge and band gap comp. depend., bowing effect 77−4653
InP_xAs_{1-x} alloys, thermoelectric characts. 77−11947
InP_xAs_{1-x}, radiation defect formation processes, effect on physical props. 78−2163
InP(As)(Sb), avalanche breakdown voltage for p-n junction, calc. 78−88020
InP(As)(Sb), refractive index dispersion 79−24280
InP(Sb)(As) substrates for Al_2O_3 film, ion beam etching defect detection 80−89155
InP(100) undoped homoepitaxial films grown by MBE, photoluminesc. props. 80−2809
InP(100)-Ag contacts, interface struct. 79−60922
InS, layer single cryst., Raman scatt. meas. 78−76478
InS, Raman scatt. spectra and interpacket interaction 79−8146
InSb, 1/f noise, Hooge's parameter 79−24040
InSb, 100 W average power 10.6 μm isolator based on interband Faraday effect 79−59706
n-InSb, 2 mm wave radiation interaction with charge carriers *(Russian)* 78−87991
InSb (110), chemisorption of Cl, photoemission spectra and tight-binding calcs. 80−6629
InSb (110), clean, O_2 adsorption, AES, LEED, RHEED and field effect meas. 80−49501
InSb (110), cleaved, gap states, field effect meas. 80−84501
InSb (110), initial oxidation, XPS and AES study 80−11542
InSb (110), ion bombard. effect on surface struct. and electronic props. 80−6923
InSb (110), surface struct. by elastic LEED, comparison with GaAs(110) and ZnTe(110) 80−80040
InSb, (110) surface, core level photoionisation spin-orbit branching ratio, initial and final state effects 79−83094
InSb (110) surface, LEED and surface conductivity during gas adsorption 77−62760
InSb (110) surface, LEED intensity dynamical anal. 80−88412
InSb (110) surface, struct. and electronic props., RHEED and field effect meas. 80−11068
InSb (110) surface oxidation process, XPS study 79−15585
InSb (110) surface struct. determ. by LEED, UPS, and EPR 80−49475
InSb, (111) surface, anal. by low energy ion scattering spectroscopy, LEED and AES *(Japanese)* 80−20746
InSb, absorpt. edge, exciton struct. 80−93321
InSb, absorpt. processes near bandgap, laser-induced hot electron and photocond. meas. 79−42584
InSb, absorpt. saturation by nonequilib. electron-hole plasma, luminesc. 78−9418
n-InSb, absorption of millimetre radiation in mag. field 79−11083
n-InSb, acceptor effect of plastic bending 80−6885
InSb, accumulation layer localised carriers interaction with LO phonons, Raman interference lineshapes 80−93338
InSb, acoustic NMR, role of incoherent phonons *(Russian)* 78−80230
n-InSb, acoustoelectric amplification, temp. depend., 77 to 135K 79−51638
InSb, acoustoelectric effect at 77K 78−72209
n-InSb, acoustoelectric gain coeff., nonlinear elec. field depend. 78−76115
n-InSb, acoustoelectric instability, effect of nonparabolic band struct. 79−60875
InSb, acoustoelectric phonon attenuation of X-ray anomalous transmission 77−4160
n-InSb, acoustoelectronic interaction, effect of alternating electric field 79−11188
n-InSb, acoustohelicon waves, parametric excitation 79−38135
n-InSb, acoustomagnetoelec. effect, 20-120K, sign reversal obs., and Hall mobility 77−24592
InSb, amorphous, localised gap states, variable range hopping 77−72866
InSb, amorphous, localised gap states, hopping cond. and chem. bonding 78−23052
InSb, amorphous, optical absorpt. edge shape, band edge fluctuations 77−20880
InSb, amorphous, pressure induced struct. transform., X-ray diffr. obs. 77−11690
InSb amorphous film, AC conductivity, anomalous freq. depend. 77−4456
InSb amorphous film, effective medium theory and freq. depend of conductivity 79−24090
InSb, amplification and vel. change of acoustic waves due to external temp. gradient 78−84260
InSb, anode oxide film coated, ellipsometric and interferential study, optical parameters *(Russian)* 80−50449
InSb, anomalous avalanche breakdown 80−80284

III-V semiconductors continued
n-InSb, anomalous Hall effect at high mag. field 77−15876
n-InSb, anomalous three LO phonon assisted cyclotron resonance 80−108078
InSb, asymmetrical behaviour of 60° dislocation glide 79−7611
InSb, asymmetrical dislocation glide, expt. evidence for 79−82232
InSb, Auger recombination, calc. for diamond-like narrow-gap semicond., compared with expt. 78−63978
InSb, Auger-governed decay of laser-induced plasma, optical probing 80−76105
InSb, avalanche formation, high intensity IR transmission limit 79−78684
InSb based eutectics, thermal cond. and diffusivity, 300-700K, phonon mechanism 80−103526
InSb based MIS structs., charge accumulation in insulator layers 80−6993
n-InSb based MIS struct., carrier generation under nonequilibrium conditions 80−88640
n-InSb, Brillouin instability in magnetostatic field 80−78909
InSb, Brillouin zone spin dependent wave functions calcs. 79−56126
InSb, CESR at high mag. fields, scatt. mechanisms 80−93177
InSb, carrier conc. variations using electrolyte electroreflectance, topographical features 79−99562
InSb, carrier heating, optical temp. waves 77−89770
InSb, carrier heating by microwave field, inertia effects 80−65580
InSb, charact. and phys. props., review *(Japanese)* 80−39576
n-InSb, characts. of Gunn effect 77−55538
InSb charge injection IR imaging array 78−37995
n-InSb, coherent microwave emission in high mag. field 79−60863
n-InSb, compensated, impact ionisation temp. depend. 77−20331
n-InSb, compensated cryst., influence of surface cond. on Hall coeff. and elec. resist. 79−69579
n-InSb, cond. electron cooling induced by CO laser and non-ohmic DC field 80−96941
n-InSb, cond. electron spectra in quantised mag. field, impurity resonance scatt. *(Russian)* 80−93178
InSb, conduction and valence band effective mass parameters 79−60689
n-InSb, conduction band effective mass anisotropy and nonsphericity 79−69414
n-InSb, conduction-band struct. from reflectivity meas. when subject to mechanical strain 79−42450
InSb, conductivity anisotropy in strong electric field 78−19048
InSb, convection in melts, and cryst. growth under large inertial accelerations 80−66421
n-InSb, convective instability in crossed mag. and elec. fields 77−62939
n-InSb Corbino disc, acoustic noise effect on I-V charact. *(Russian)* 80−100492
n-InSb Corbino disc power meter for 3 cm wavelengths 79−71428
InSb, covered with thin oxide protective film, intrinsic photocond. 77−55578
InSb, crystal growth by travelling heater method 80−11553
InSb, crystal growth from melt, facets and twin formation obs. *(Chinese)* 80−59409
InSb, crystal structure stability, P-T diagrams 78−51886
InSb, Cu-coated, surface contamination, ion microprobe mass analyser obs. 77−52729
InSb, current-voltage characteristics at room temperature and high hydrostatic pressure 80−88560
InSb, cyclotron harmonic transitions, warping and inversion asymm. effects 78−68383
p-InSb, cyclotron reson. of nonequilib. photoelectrons, distrib. function and line profile 78−60336
n-InSb, cyclotron reson. of conduction electrons, strong mag. field, hot electrons 80−2640
n-InSb, cyclotron reson. study of conduction electrons, strong mag. field 80−2639
InSb, cyclotron resonance lineshape 80−15801
InSb, Czochralski growth, thermoelec. monitoring of interface temp. 78−31331
n-InSb, damped surface magnetoplasmons, theory 79−7873
InSb, Debye temperature, atomic mean square displacement 78−87757
p-InSb, deformed, giant negative magnetoresistance 78−87990
p-InSb, deformed, Landau levels, photocurrent spectra obs. 78−19097
n-InSb, deformed, spectral oscills. of absorption in quantising mag. field 80−34486
n-InSb, degenerate, acoustomagnetoelec. effect obs. 78−72207
InSb, degenerate electrons, relax. of spin and energy 80−10965
InSb, degenerate four-wave mixing obs. at 5K 80−53355
InSb, degenerate semicond., surface photo-EMF depend. on bulk consts. 79−69580
InSb, depletion layer, plasma and vibr. plasma type guided polaritons *(Russian)* 80−96933
n-InSb, dielec. in solid-plasma waveguide, effect on slow surface wave propag. 79−50862
InSb, dielec. permittivity, electronic contrib. calc. 77−59265
p-InSb diodes, metal-BSG-InSb oxide-p-InSb, C-V charact. 77−80848
n-InSb, directional temp. of hot electrons under elec. and mag. fields 78−84135
InSb, dislocations due to thermal stress, single and composite crysts. 78−2124
n-InSb, dispersion curves for surface polaritons 79−19646
InSb, donor excitation spectra in high mag. field 78−80027
InSb, donor impurities, magnetic freezeout in hyperquantum regime 80−10921
InSb, donor levels, anomalous press. effects, Hall const. meas. 77−51693
InSb, donor spectrum, effect of strong mag. field 79−7806
n-InSb, doping and strain depend. of quantum props. 79−60690
InSb, doping depend. of high-field donor spectra 77−90175
n-InSb, drift induced plasma insolubilities, carrier temp. effects 77−35949
n-InSb, dynamical light scatt. from dielec. bulk waves, appl. of phenomenological theory 79−69829
n-InSb, EM radiation in amplified sounds, theory 77−80812
n-InSb, EM wave resonant absorpt. 78−2757
n-InSb, EPR, oscillations of transverse magnetoresistance in weak mag. field 79−91086
n-InSb, effective g-value of electrons determ. by spin flip Raman scatt. and electric-dipole-excited ESR 78−52494
InSb, Einstein relation for inversion layers 80−103706
n-InSb, elec. cond., press. dependence 80−6830
InSb, elec. cond. in intense mag. field, freeze out, hopping 77−20338

III-V semiconductors continued
p-InSb, elec. instability and oscills. of transparency in transverse mag. field 78−6407
InSb, elec. paramag. reson. and combined reson. of cond. electrons at 24 GHz 77−1596
n-InSb, elec. props. changes during ht. treatment 77−85213
InSb, electrical effects of dislocation, galvanomag. props. 78−23119
InSb, electrodes, anodic and cathodic processes 77−44487
InSb, electron drift velocity in fields up to 800 V/cm in presence of impact ionisation 78−39120
n-InSb, electron gas degeneration in strong mag. field 77−66173
n-InSb, electron heating dynamics in longitudinal electric and quantising magnetic fields 79−69520
InSb, electron irrad. effects on elec. props. and recomb. 79−51584
InSb, electron irradiated, kinetics of changes in carrier density 79−56228
InSb, electron mobility, low-field, Monte Carlo calc. 80−10973
n-InSb, electron mobility at 77K in avalanche regime 79−33295
n-InSb, electron recombination between Landau-levels 79−38096
InSb, electron spin levels resonant excitation, photolum. 80−25454
InSb, electron spin relaxation 80−25187
n-InSb, electron spin-flip relax. time meas., Raman scatt. 77−3631
InSb, electron-electron spin-flip scatt. and spin relax. 80−44916
n-InSb, electron-hole plasma, LF instabilities in crossed fields 78−39146
InSb, electron-hole plasma instabilities, impact ionisation conditions, microwave emission 80−107840
n-InSb, electronic bolometer, appl. in system for millimetre and submillimetre wave detection 78−24860
InSb, electronic interband Raman scatt. 80−11407
InSb, electronic surface struct., Cs(Rb)(Na) absorpt., AES, LEED, EELS study 78−68068
InSb, energy spectra of impurity atoms under 4.2K gamma irradiation 77−89471
InSb, epitaxial film, amorphous and polycrystalline, vol. plasmon energy and linewidth, electron scatt. obs. 80−50482
InSb, equation of state 79−82310
InSb, Ettingshausen and Nernst-Ettingshausen effect meas. *(Russian)* 77−28201
InSb, Ettingshausen effect, influence of surfaces, narrow-gap semicond. characterisation 77−24571
InSb, evaporation kinetics, rel. to film growth 78−3050
p-InSb, excess In, polycryst. thin film, elec. transport props., non-stoichiometric effect 79−95528
InSb, external photoelec. effect 78−27366
InSb, extrinsic and intrinsic, interaction of transverse magnetoresist. effects 80−65596
n-InSb, far IR cyclotron emission 79−61226
n-InSb, Faraday effect in strong EM fields 80−93286
InSb fast response submm. detector 78−89541
n-InSb, ferroelec. semicond., transverse acousto-elec. effect *(Russian)* 78−30958
InSb, film, analysis by attenuation of substrate X-ray fluoresc. 78−27872
n-InSb film, degenerate, electron conc. and resist. temp. depend., band struct. 77−76971
InSb film, degenerate, concs. and ionisation energies of defect levels, Hall effect meas. 79−91087
InSb, film, E_0, E_1 absorption edge size quantisation, optical and electroreflectance spectra 80−34998
p-InSb, film, elec. transport props. 78−72291
InSb film, for monolithic elastic surface wave amplifiers of continuous operation 77−80023
n-InSb film, galvanomagnetic meas. of surface layer carrier conc. and mobility 77−55628
InSb film, gamma-irradiated, struct., TEM and SEM obs. 79−15033
InSb film, grown by MBE, RHEED study 80−100415
InSb film, heteroepitaxial, MBE growth and elec. props. 80−2301
InSb film, ion bombard. effects on elemental Sb incorporation probability during sputter deposition 79−83120
InSb film, light scatt. from surface polaritons 79−8202
n-InSb film, low energy electron irrad. effect on elec. props. 80−7009
InSb film, MBE apparatus and AES 78−47875
InSb film, prep. by rotary type flash method *(Japanese)* 77−40372
InSb film, quantum size effects, transport props. 78−76171
InSb film, synthesis by 2-source mol. beam technique and AES characterisation 78−72729
InSb film, threshold singularity on quantising mag. fields 78−87904
InSb, film, transverse 1/f noise and signal-to-noise ratio of related Hall elements, comment 79−99593
InSb, film, transverse 1/f noise and signal-to-noise ratio of related Hall element 79−99594
InSb film cyclotron-frequency submillimetric oscillation generation model 77−80801
InSb films, elemental incorporation probability modification by ion bombard. during growth 80−80118
InSb films, melt-grown, point defect effect on elec. props., 77-300K 80−2502
InSb films, transverse 1/f noise and S/N ratio of related Hall elements 79−42597
InSb, films, X-ray fluoresc. anal. method, long-term stability 80−61212
InSb films on $LiNbO_3$, prep. and props. 80−35093
InSb, fine struct. in energy derivative reflectance spectra 79−78705
n-InSb, flicker-noise power spectrum, 0.1 Hz to 10 kHz 79−73555
n-InSb, forward biased Schottky barriers on low doped surfaces, current transport 79−24074
n-InSb, freq. depend. cond. tensor in quantising mag. fields *(German)* 80−29419
n-InSb, frequency shift of combined resonance, influence of plasma oscills. of conduction electrons 79−7850
n-InSb, galvanomag. props. at low temp., carrier localisation, metallic impurity cond. 77−28195
n-InSb, galvanomagnetic props. at low temp., mag. field induced metal-nonmetal transition 77−76845
InSb, galvanomagnetic props. of annealed single crystals 80−96909
InSb, gamma irradiated, changes in energy spectrum of impurity spectrum 78−51937
InSb, growth angle determ. from cryst. lateral face shape and solidified separation drops 80−103282
n-InSb, Gunn domains, direct probe meas. 78−26877
n-InSb, Gunn effect, influence of impact ionisation 80−44609
n-InSb, H-like impurities photocond., mag. field effect 79−82634

III-V semiconductors continued
n-InSb, HF EM and acoustic oscill. generation in LF electric field 78−64068
InSb, HF props. of hot electrons at 77K, calc. using Monte Carlo method 80−15553
n-InSb, Hall coeff. and magnetocond. in mag. freeze-out regime 79−60849
n−InSb, Hall effect and magnetoresist. in mag. freeze-out region 79−15165
n-InSb, Hall effect and magnetoresist. in extreme quantum limit, stress depend. 80−11021
InSb, Hall effect sensor for mag. fields up to 23 T 77−10066
n-InSb, Hall mobility of free electrons, determ. using radioelectric effect 77−69327
InSb, Hall plates, temp. and pot. distribs. determ., temp. depend. cond. effect 79−60851
InSb, heats of transformation for high pressure, orthorhombic modification. exam. 78−56627
n-InSb, heavily compensated, hopping cond. in mag. field 79−7842
n-InSb, heavily doped, electron activity coeffs. 77−39837
p-InSb, heavily doped, LO phonon-carrier interaction, Raman interf. lineshapes 80−93319
InSb, helicon beam form. during microwave transmission in mag. field 80−80308
InSb, helicon damping in quantum limit 77−28205
n-InSb, helicon wave propag., quantum mechanical features 79−42571
n-InSb, helicons, parametric decay 80−34472
InSb, heteroepitaxial film, orientation and struct. investigation 79−82480
n-InSb, high field electron diffusion, Monte-Carlo calc. 78−10455
InSb, high field polaron transport 78−30932
InSb, high field quantum magnetotransport theory 78−30941
n-InSb, high power helicon, interaction with semiconductor-free space interface 79−38114
n-InSb, high power helicons, harmonic generation 80−29426
p-InSb, high press. effect on elec. props., 50-300K 77−47807
p-InSb, high resist. compensated, generation of microwave radiation 80−34476
InSb, high temp. thermodynamic data, quantitative fits to liquidus line 77−63637
InSb, high-purity, electron irradiation effects on transport props. 79−23650
InSb, high-purity specimen irradiated at 80K, transport prop. and defect annealing 78−95307
n-InSb, high-resist., prep. using radiation compensation 80−34016
n-InSb, high-resist., recomb. of carriers at 77K 77−51761
InSb, high-resistivity p-type or crystals of n-type, recombination processes, photocond. and photomag. effect meas. *(Russian)* 80−88567
n-InSb, highly doped, transverse magnetoresistance in strong mag. field 79−56246
n-InSb, hole mobility temp. depend. after electron bombardment 79−33290
n-InSb, hopping photoconductivity *(Russian)* 77−89801
InSb, horizontal zone melting in vacuum 79−47624
InSb, hot electron energy relax. time 77−80783
n- InSb, hot electron energy relax. in quantizing mag. fields 78−31259
n-InSb, hot electron magnetophonon effect, 77K, mag. field modulation method 78−60140
n-InSb, hot electron noise temp., Monte Carlo Calc. 80−107877
InSb, hot electrons, Monte Carlo calc. of transport characts. and distrib. functions of hot electrons 80−6853
n-InSb, hot electrons relax. in quantising mag. field *(Russian)* 80−6876
n-InSb, hydrostatically compressed, instabilities of current, Gunn effect meas. 77−1432
InSb, hydrostatically pressed, negative differential cond. at room temp. 79−19600
InSb, IR detector, for pulse radiolysis, reversible component in response time 78−41353
p-InSb IR detector, photovoltaic operation, theoretical anal. 79−224
InSb IR detector array, AES anal. of localised contaminants at interfaces 77−57391
InSb, IR reflectivity, longitudinal optical phonon-plasmon coupling 77−59578
InSb, impact ionisation, influence of external mag. field on recomb. radiation and I-V characts. 79−56864
p-InSb, impact ionisation, electron-hole pair production 80−44611
p-InSb, impact ionisation 78−26879
InSb, impact ionisation at room temp., carrier generation rate 80−20207
InSb, impact ionisation and magneto-transport, high crossed elec. and mag. fields 80−107797
n-InSb, impact ionised plasma, three stream instability 77−55557
InSb, impact-ionisation magnetoelec. effect 78−52016
InSb, impurity distribution, during epitaxial growth from liq. phase 80−88443
InSb, impurity-level assisted two-photon interband absorption of laser radiation 78−23464
n-InSb, in MIS struct., accumulation layer submillimetric cyclotron resonance obs. 77−39912
InSb, in MISIM struct., photovaractor effect and CV characs. obs. 77−8205
n-InSb, influence of electron irradiation intensity on defect formation 79−73216
n-InSb, influence of mag. field on hot electron effects 78−2493
p-InSb, influence of plastic bending on galvanomag. props. 79−28349
p-InSb, influence of plastic deform. on elec. props. 80−103711
n-InSb, instabilities of electron-hole plasma under impact ionization and microwave emission 79−65508
InSb, intensity depend. interband Faraday rot. obs., saturation and reson. enhancement effects 80−108186
InSb, interaction of exciton recombination with LO phonons 79−38647
InSb, interband Faraday rot., Roth theory calcs. 77−52046
InSb, interband magneto-optical transitions, arbitrary field orientation 79−42948
InSb, intraband photocond. in mag. fields 79−47123
n-InSb, intraband processes exam. by stimulated spin-flip Raman scatt. 77−19362
InSb, intrinsic, impact ionisation by elec. fields 77−39864
InSb, intrinsic, photoinjected electron hole pairs, Auger lifetime, photoconductive decay obs. 80−39629
InSb, intrinsic and n-type, elec. cond., carrier wave instability in elect. and mag. fields 79−82617
InSb, intrinsic capacitance in transverse mag. field *(Russian)* 79−91070

III-V semiconductors continued
InSb, intrinsic magnetoresistance 79−69534
InSb, inversion asymm. splitting of cond. band, Shubnikov-de Haas meas. 78−10348
InSb inversion layer, electromagnetic mode 78−60080
p-InSb inversion layer, magnetotransport 78−64138
InSb inversion layer, spectroscopy of electron subband levels 78−10569
InSb inversion layer, spectroscopy of electron subband levels 78−64364
InSb, ion bombard. and defect annealing, n- and p-type cond. layer prod. 78−26606
p-InSb, ion bombardment using 30-80 keV ions, isochronous annealing, elec. props. obs. 79−19295
InSb, ion implantation, dose rate and orientation dependence of radiation damage 77−89482
InSb, ion implantation, anomalous radiation disordering 80−92553
InSb, ion implantation at elevated temps. 79−10870
InSb, ion implanted, efficient void form., TEM obs. 80−44237
InSb, ion implanted, ellipsometric study 80−60537
InSb, ion irrad., isothermal annealing effects 80−6424
n-InSb, ionized impurity scatt. limited mobility, expt. 80−80274
InSb, LPE growth characteristics, substrate surface contamination dependence 80−39470
n-InSb, Landau emission spectra, influence of bakcground radiation 78−43935
InSb, Landau level struct., magneto-electroreflectance 80−25349
n-InSb, Landau-level-electron lifetimes, saturation meas. of magnetoabsorption 78−48150
InSb, laser beam self-focusing, effect of quantising mag. field 77−42578
InSb laser detector, dynamic range increase 78−49899
n-InSb, laser induced magneto-photoconductivity, conduction band transitions 77−55566
InSb, lattic dynamics 79−14895
InSb lattice, static dielec. const. and carrier conc. meas. via gyrotropic sphere reson. 80−97143
InSb, lattice thermal cond. from three phonon scatt. relax. rate 78−51755
InSb, lattice vibration, thermal expansion and pressure effect 80−39233
n-InSb, longitudinal magnetoresistance in extreme quantum limit *(Russian)* 80−11008
n-InSb, longitudinally magnetized, laser beam modulational instability, phonon-helicon interaction 79−56254
InSb, low defect crystal growth by InN doping, IR detector appl. 80−20780
InSb, low intensity nonlinearities, induced by lasers 79−94300
InSb, low temp. electron mobility, theory and expt. 77−89759
n-InSb, low temp. mag. and electric resonances meas., model *(Russian)* 78−56159
InSb, low-power nonlinear refraction effect on laser beam propagation 80−5801
p-InSb, low-resistivity n-type layer form. by laser pulse irrad. 77−69944
InSb, low-temp. annealing effect 77−8091
n-InSb, MCD due to free carriers 78−56462
InSb MIS capacitors, gamma-ray radiation effects at cryogenic temps. 80−34517
InSb MIS device, capacitance measurements, method of separating hysteresis effects, interface state density estimation 77−85324
n-InSb MIS device interfaces, low-temp. CVD of SiO_2, characts. 80−16196
InSb MIS diode, anodised, C-V characts., effect of high elec. field pulse 80−60092
n-InSb, MIS diode, time-dependent photovoltaic effect 80−75601
InSb, MIS struct., C-V characts., interface state densities and storage times meas. 77−89861
p-InSb MIS struct., field effect studies 80−80386
InSb MIS structure, effect of room background on noise props. 80−103755
InSb, MIS thin film capacitance, theory 79−87156
InSb, MISS struct., surface electron and hole mobility and conc. *(Russian)* 80−44701
InSb MOS capacitor, AC behaviour, semicond.-oxide interlayer effect 78−19151
InSb MOS struct., capacitance of n-channel inversion layers, elec. field effects 80−80393
InSb MOS structs., energy spectrum of traps in oxide layer 80−107922
InSb MOS structure, props. 80−49947
InSb, magnetic freeze out *(Japanese)* 78−39130
InSb, magnetic susceptibility of light and heavy holes 79−42734
InSb, magnetically frozen-out, evidence of surface cond. from etching expts. 79−47152
InSb, magneto-optical anomalies of impurity electrons, two-LO-phonon region 78−72415
n-InSb, magneto-optical transitions from deep levels, photocond. obs. 80−55069
n-InSb, magneto-photoconductivity, phonon assisted combined reson. magneto-optical absorpt. reson. 78−47831
InSb, magneto-surface transport props. 77−43693
n-InSb, magnetoacoustic effects using two-band model 78−60170
InSb, magnetoacoustic wave excitation by acoustic wave propagation 80−88597
InSb, magnetoconcentration effect, nonlinear current carrier recomb. 79−33298
p-InSb, magnetoconcentration effect in extrinsic cond. range 80−65593
p-InSb, magnetoconcentration effect, negative differential conductance 80−70729
p-InSb, magnetoconductivity and cyclotron reson. in inversion layers 80−49946
InSb, magnetophonon effect temp. depend., 80 to 190K 77−59293
n-InSb, magnetophonon effect exam. using field modulation technique 78−26918
n-InSb, magnetophonon effect in non parabolic band 79−37962
n-InSb, magnetophonon effect, temp. depend. below 90K 79−56247
n-InSb, magnetophonon oscillations by photomag. effect *(Russian)* 77−43665
n-InSb, magnetophonon reson. under hot electron conditions 77−24568
p-InSb, magnetophonon reson. of holes 79−95424
N-InSb, magnetophonon resonance, damping factor by mag. field modulation technique 80−6878
p-InSb, magnetophonon resonance due to non-equilib. electron injection 80−6881
n-InSb, magnetophonon struct. obs. in transverse magnetoresist. 78−23120

III-V semiconductors continued
n-InSb, magnetoresist. in strong elec. field *(Russian)* 78−19056
n-InSb, magnetoresistance, odd, in HF elec. field 77−28198
InSb, magnetoresistance meas., transverse diffusion currents on source of error 79−7843
InSb magnetoresistive elements, fundamental effects *(Japanese)* 80−11013
n-InSb, magnetotransport experiments, surface treatment induced effects 80−34468
n- InSb, mangetophonon structure in magnetoresist., elec. field depend. 78−30943
InSb, micron size Hall probe for precision mag. field mapping 79−75558
n-InSb, microwave displacement effect in longit. elec. and transverse mag. fields 78−87992
n-InSb, microwave helicon resonances, carrier density, mobility, dielectric const. 80−96930
n-InSb, microwave magnetoplasma and heliconlike reson., sample shape effects 77−85252
InSb, microwave magnetoplasma matching effect 78−14750
n-InSb, millimetre rare modulation in semicond. plasma, use of effects of high elec. field. 78−60149
p-InSb, mobility, diffusion and thermoelectric power of hot holes 80−39595
InSb, mobility from soln. of Boltzmann eqn. for electron-LO phonon scatt. 79−19586
n-InSb, mobility in mag. field, extreme quantum limit, iterative technique 78−2498
InSb, molten, temp. depend. of vel. of sound and adiabatic compressibility 77−27944
InSb, momentum distrib. of electrons, anisotropy, positron annihilation *(Russian)* 78−84676
InSb, morphological and structural changes due to ion bombardment 80−79843
InSb, morphological instability under constitutional supercooling during cryst. growth from melt and stabilising thermal gradient 79−4910
InSb n^+-p and p^+-n photodectors fabrication by S and Be ion implantation 78−49906
InSb n^+-p junctions, photocurrent spectrum near long wavelength edge of fundamental absorption band 80−100483
InSb, n-type, anodic oxide film dielectric, MOS structure *(Russian)* 77−89874
InSb n-type, heavily doped, effects of hydrostatic pressure on electron mobility and conc. 77−4390
n-InSb, n-type, photoconductivity with different surface treatment 78−2517
InSb, narrow band gap semiconductor, optical nonlinearity due to free carriers 79−81491
n-InSb, narrow gap, appl. of effect of pot. fluctuations induced by cryst. inhomogeneities 80−49780
InSb, narrow-gap semiconductor, high intensity IR transmission limit 80−7361
n-InSb, negative longit. magnetoresist., carrier conc. and mobility depend., 77K 80−60007
p-InSb, negative magnetoresist. under press. 80−20224
p-InSb, negative photocond. in strong mag. fields 79−82636
p-InSb, negative piezomagnetoresist. and Hall effect meas., antiferromag. order form. 78−19061
InSb, neutron irrad., defect cluster form., effect on elec. props. 80−65062
n-InSb, noise, round trip acousto-electronic amplification, anodic piezoelectric transducer *(Russian)* 78−23139
InSb, noise calc. using Monte-Carlo method 80−75575
n-InSb, non-degenerate, linear longitudinal elec. cond., US wave effects in DC mag. field 80−88599
n-InSb, non-degenerate semicond., magnetoacoustic effect 80−20257
InSb, nonlinear absorption and pulse shaping for 10.6, 9.6 μm laser radiation 78−79077
InSb, nonlinear optical properties, hot electron effects 78−71139
InSb, nonlinear optical effects obs. using CW CO laser 79−3752
n-InSb, nonlinear optical susceptibility, cyclotron reson. meas. *(Russian)* 79−50341
n-InSb, nonlinear optical susceptibility spin reson. *(Russian)* 79−59749
InSb, nonlinear refraction and absorpt. 80−9939
InSb, nonlinear transmission of picosecond 10.6 μm pulses 80−106559
InSb, one- and two-photon magneto-optical transitions 77−16284
InSb, one-photon absorption coeffs. calc. 77−20884
InSb, optical bistability, signal amplification, low power nonlinear effect applications 80−19066
InSb, optical constants and oxidation with various surface treatment *(Russian)* 80−88955
InSb, optical mixing by mobile carriers 78−25920
n-InSb, optical phonon emission in intraband magneto-optical transitions, photocond. meas. 80−34481
n-InSb, optical SHG in rectang. waveguide 80−43401
InSb optical signal amplification and bistability 80−9937
n-InSb, optical spin resonant four-wave mixing, CW meas. and transient effects 80−48344
n-InSb, optically pumped stimulated recomb. radn. in mag. fields 79−94284
InSb, oscillatory electron drift rel. in non-ohmic regime at low temp. 79−33291
p-InSb, oscills. of microwave photocond. and cyclotron reson. of photoelectrons 79−28377
InSb, overheating luminescence, carrier generation-recomb. equilib. shift in elec. field 77−44068
InSb, oxidation, water vapour and O_2 excitation effects, XPS obs. 79−100274
InSb oxide films grown by anodization in electrolytes, electron spectroscopy exam. *(German)* 79−15837
InSb, oxidised surface, photocond. meas. *(Russian)* 77−43664
InSb oxidised surface, detection of excess crystalline Sb by Raman scatt. 78−19453
InSb, p-n homojunction breakdown voltage for onesided abrupt junctions *(German)* 78−56210
InSb p-n junction, minority carrier injection in mag. field, recomb. radiation obs. 80−11078
InSb p-n junctions, diffused, avalanche multiplication and impact ionisation 80−15595
InSb, parametric amplification of plasma waves 78−43428
n-InSb, parametric excitation of plasma oscills. 77−66179
III-V semiconductors continued
n-InSb, parametric excitation 78−52023
InSb, periodically doped cryst. prod. by Peltier effect, helicon diagnostics *(German)* 77−48338
p-InSb, phonon assisted cyclotron harmonic transitions 78−48046
InSb, phonon assisted cyclotron resonance exact sol. of integral eqn. for Green's function 79−61227
InSb, phonon conductivity, temp. depend., 2-300K 77−31812
InSb, phonon conductivity, 2 to 300K, scatt. mechanisms 79−4436
InSb, phonon dispersion curves, appl. of deformable-ion model 78−59887
InSb, phonon dispersion relations, eight-parameter bond-bending forces model 80−70334
n-InSb, phonon heating by hot electrons in quantising mag. field 77−4354
InSb, phonon viscosity tensor 78−34570
n-InSb, phonon-assisted cyclotron reson. strongly depend. on surface condition 80−70755
n-InSb, photo-induced magnetophonon reson., 4.2K, peak shifts 78−84250
InSb, photocond. under uniaxial deform. 79−82637
InSb, photoconductive and photoelectromag. effect spectral distrib., sample thickness depend. 77−4394
n-InSb, photoconductive lifetime, surface pot. effects 80−11029
n-InSb, photoconductivity, 1.8K, hot-carrier and free-carrier absorption. effects 78−84254
n-InSb, photoconductivity, recombination processes 80−11030
n-InSb, photoconductivity relax. temp. depend., carrier recomb. processes 77−4363
n-InSb, photoconductivity meas. in crossed fields 79−7852
n-InSb, photoconductivity of laser excited hot electrons 80−11045
n-InSb, photoconductivity mechanism, 4.2 to 77K 80−70766
p-InSb, photoexcited exciton spin-flip scatt. 80−74434
n-InSb, photoluminesc. in crossed EM fields *(Russian)* 77−24892
n-InSb, photoluminescence exam. 79−28809
n-InSb, photomagnetic effect anomalies, 90 to 300K *(Russian)* 78−84257
InSb, photoresistor in mag. field, increased responsivity 78−39162
n-InSb photoresistors of Carbino disc shape in mag. field, enhancement of responsivity 78−56186
n-InSb, piezoelectric nondegenerate semicond., magnetoacoustic effects of nonparabolic band struct. 80−96948
n-InSb piezoelectric semiconductors, carrier temp. effect on transverse phonon-helicon interaction 77−15886
InSb, pinch effect at room temp. 80−65615
InSb, pinning struct. of cyclotron-phonon reson., effect of nonequidistant Landau levels 77−11881
InSb planar p-n junction fabrication by Be ion implantation, CCD chip appls. 77−89833
InSb plasma, drift wave instability 79−15175
InSb plasma, EM wave instability, effect of density gradient 79−1607
n-InSb, plasma, nonequilibrium, magnetohydrodynamic instabilities, theory and expt. *(Japanese)* 78−10493
n-InSb, plasma, sausage instability, theory and expt. *(Japanese)* 78−10492
n-InSb, plasma filament form. under impact ionisation conditions 78−60147
InSb, plastically bent single crysts., dislocation struct. obs. 78−59816
p-InSb plate in crossed E and H fields, even magnetoconcentration effect *(Russian)* 77−85244
InSb, polar semicond., longit. magneto-Seebeck coeff. in quantising mag. field 79−56250
InSb, polar semiconductor, impact ionisation in crossed elec. and mag. fields 79−28355
InSb, polycryst. film, Hall and drift mobilities 79−95531
InSb, polymorphism and cryst. struct. at high temp. and press. 78−95026
n-InSb powder, microwave propag., 90-300K, magnetoplasma and helicon wave excitations 78−72183
InSb, prep. of thin films by ionised-cluster beam deposition *(Japanese)* 80−25576
n-InSb, propagation of high power helicons 78−19070
n-InSb, propagation of magnetoplasma waves, Faraday geometry, effect of strong electric field 79−65510
n-InSb, proton irrad. defects energy level scheme, transport props. meas. 80−96576
InSb pulsed spin-flip Raman laser, external cavity, low field operation at 10.6 μm 79−41394
n-InSb, quantum magnetophonon oscills. of piezoresist. 77−15880
p-InSb, quantum oscills. of photocurrent due to relax. of photoelectron energies via acoustic phonons 79−73546
p-InSb, quantum resonances in valence band under uniaxial stress, far IR meas. 79−99481
n-InSb, quasi-helicon waves instability 80−70741
InSb, quasi-static transport characts., expt. and explanation 77−20335
InSb, RF etch sputtering under controlled atmosphere 77−44397
InSb, radiation defect annealing following 50 MeV electron beam irrad. 80−15154
p-InSb, radioelec. effect, 100-300K 79−56255
InSb Raman laser pumping by IR multiline NH_3 laser 79−94216
InSb, Raman scattering study of unoxidised Sb in anodic oxide films 80−88985
n-InSb Raman spin-flip laser, hot electron effect distrib. calc. 80−23743
InSb, reabsorbed radiative recomb. and photon recycling 80−76076
InSb, recoil damage obs. by PAC with ^{111}Cd 77−89484
n-InSb, recomb. of hot electrons, photoelectromag. and dynamic photocond. meas. 79−38081
InSb, recombination processes using impact ionization capture cross sections 80−75577
InSb recrystallised thin films on mica substrate, elec. props. 80−70867
InSb, refractive index and absorpt. coeff., cryst. orientation depend. 80−60536
InSb, relations pressure-volume under high pressure 80−39219
InSb, resist. inhomogeneity meas. with single-sonde potential method 80−65549
InSb, reson. Raman scatt. under uniaxial stress near E_1 gaps 79−42960
InSb, resonance effects in mag. field, effect of additional laser illumination 78−72417
InSb, resonant magneto-Raman scatt. 79−51958
n-InSb, reversal of sign of acoustoconductivity effect 78−2527
InSb, reverse biased diode, negative resist. 78−19129

III-V semiconductors continued
n-InSb, SBS of laser radiation in presence of mag. field, ion acoustic wave nonlinearity 80−45091
InSb, self-diffusion 79−65249
n-InSb, semicond. plasma, Raman scatt. of waves of fluctuations *(Russian)* 79−94299
n-InSb, semiconductors, plasma oscills. within submillimetre freq. range 80−84473
InSb, shallow acceptor contrib. to near-resonance spin-flip Raman scatt. 79−95754
p-InSb, shift of fundamental absorpt. edge in crossed elec. and mag. fields 80−76034
n- InSb, Shubnikov-de Haas effect, CO_2 laser induced hot electron effects 78−30957
n-InSb, Shubnikov-de Haas effect expts. on optically heated electrons 79−73529
n-InSb, Shubnikov-de Haas effect 80−11015
n-InSb, Shubnikov-de Haas transverse kinetic coeffs., quantum oscills. 80−49778
n-InSb, sign change of Hall effect, in quantum limit 77−15875
InSb, single crystal, chem. and ion etching, surface changes *(French)* 80−108614
InSb, single crystal, etching of {111} plane, rates and activation energies 77−12723
InSb, single crystal, stress induced phase change 79−23719
InSb, single crysts., grown by vertical and horizontal travelling heater method, growth parameters and cryst. quality 79−24421
InSb, site selective doping by ion implantation of radioactive nuclei 80−34023
n-InSb, spherical samples, size resonances, magnetoplasma waves 79−11168
n-InSb, spin flip Raman scatt. from electrons in localised donor states 77−3630
InSb, spin flip Raman scattering, gain, linewidth, effective g-value 78−22167
n-InSb, spin polarisation, anisotropic size effect, effect on CESR signal 80−70743
InSb, spin-flip Raman laser, cond. electron T_1 meas. 77−3593
InSb spin-flip Raman laser, pumped by TE CO_2 laser, fund. characts. *(Japanese)* 77−42542
InSb spin-flip Raman laser 77−50674
InSb, spin-flip Raman laser, Stokes output mag. field depend. 77−61959
InSb spin-flip Raman laser characts. *(Japanese)* 78−25883
InSb spin-flip Raman laser, external cavity CO_2-pumped, with intracavity etalon 78−42345
InSb spin-flip Raman laser external-cavity system, oscill. characts. 78−55383
p-InSb, spin-flip Raman scattering, review 80−108209
n-InSb, spin-magnetophonon resonance 80−96918
InSb, sputtered NaCl-type compression 79−46751
n-InSb, stationary energy transport velocity of light scattered from bunched solid-state plasma 79−95720
n-InSb, stimulated Brillouin scattering of helicon waves 79−99571
p-InSb, stimulated magneto-Raman scatt. obs. 77−83924
n-InSb, stimulated recomb. radiation 78−90456
InSb, stimulated spin-flip Raman scatt. and stimulated recomb. radn. 79−72623
p-InSb, stress induced k-linear terms in band struct. 80−49595
n-InSb, strongly compensated, ionized donor mol. optical absorpt. spectra characts., 1.5-2.5 mm 79−11422
n-InSb, sub mm photocond. *(Russian)* 79−38134
n-InSb, subjected to mag. field normal to current, coherent HF oscills. 78−52026
InSb, submillimeter radiation diffr. by electron-density waves 80−7328
n-InSb submillimetric-wave free-carrier Faraday effect in strong longitudinal elec. field 80−66164
InSb substrate, room temp. CVD of Si_3N_4 80−71597
n-InSb substrates, MIS struct. form. by reactive deposition of Si_3N_4, C/V meas. 80−103752
InSb, superconducting phases at high press. 78−88063
InSb surface, Cu deposition, ohmic contact formation, SEM obs. 77−51817
InSb surface, IR spectroscopy of subband levels 80−20277
InSb, surface, reson. excitation of electron subbands 80−49865
InSb, surface (110) atomic struct. 79−69331
n-InSb, surface accumulation layer, sub mm electron cyclotron reson. 78−6576
InSb, surface analysis, X-ray photoelectron spectra, surface oxidation-etchant correlation 78−56029
InSb, surface carrier accumulation in crossed elec. and mag. fields 80−20205
InSb, surface helicons in semiconductor plasma, theory 80−60019
InSb, surface magnetoplasma waves, reson. spectrum and dispersion characts. 79−38148
InSb surface magnetoplasma wave struct. 80−6934
InSb, surface plasmon dispersion 77−1464
n-InSb, surface polaritons, excited by microwave magnetoplasma 79−19530
n-InSb, surface quality improvement by low temp. CVD of SiO_2, and characterisation 80−49932
n-InSb, surface recomb. velocity, temp. and α-bombardment dose effects 77−8173
n-InSb, surface recomb. vel., repeated cyclic surface treatment effects 77−32065
n-InSb, TO phonon-helicon coupling, Doppler shifted cyclotron reson. region 79−73539
InSb, thermal cond., elec. cond., and thermoelec. power, press. depend. 80−59744
n-InSb, thermoelec. power in longit. quantising field, phonon drag component 78−19064
InSb, thermoelec. power and relative resist. at press. up to 35 kbar 79−65505
InSb, thin film, Hall mobility of carriers at room temp. 79−65568
InSb thin film element having non-linear galvanomagnetic effect 80−34534
InSb, thin film prep. with remelting, elec. props. 77−52255
InSb, thin films, electrophysical props. obs. 80−103765
InSb thin films prepared by ion beam epitaxy system *(Japanese)* 78−22976
InSb thin layers, directed crystn. on sapphire, struct. 80−35112
InSb thin layers, interface stability during crystn. 79−65326

III-V semiconductors continued
InSb thin layers, melt grown, mag. field depend. of PEM effect 79−95445
n-InSb, three-phonon assisted cyclotron harmonic transitions in magneto-photoconductivity 80−44652
InSb, threshold energy for displacement of atoms 78−47428
n-InSb, threshold field dependence on sample length, 77K 78−76116
n-InSb, transparency, DC field induced enhancement 79−91407
n-InSb, transverse magnetophonon reson., oscillatory amplitude and damping 78−47813
n-InSb, transverse magnetoresist. in strong mag. fields 79−4571
n-InSb, transversely magnetised, parametric instability of acoustic waves 79−65521
InSb, transversely magnetised plasma, instability of EM waves 80−2411
n-InSb tunable far IR Landau emission with subnanosecond rise time 79−32015
InSb, tunnel diode, V-I characts., hydrostatic press. effects 79−38157
n-InSb, tunnel diode, with high reverse bias, V-I characts. 79−38158
InSb, tunnel diodes, abnormal V-I characts. *(Russian)* 77−8184
InSb, two-circle SSD diffractometer appl. in angle dispersive mode 79−14641
InSb, two-phonon diffuse scatt. of X-rays 78−26374
InSb, two-photon absorption coefficient, 3-band model 79−78679
InSb type semiconductor, small-gap, electron scatt. and transport props. 78−95294
InSb type semiconductor, small-gap, electron scatt. and transport props. 78−95295
InSb type semiconductor, spin-flip transitions in magneto-optics and magneto-transport 80−50306
n-InSb, US absorption in alternating elec. field *(Russian)* 78−30959
InSb, US attenuation and Akhieser loss, temp. depend. 79−86842
InSb ultramicro Hall element for magnetic bubble field distrib. meas. 79−56585
n-InSb, ultrasound modulation in mag. field 79−69196
n-InSb, undoped, press. induced slow relax. of free electron conc., Hall coeff. meas. 77−47833
InSb, undoped and Te-doped, anomalous impurity segregation, Hall and mass spectrum meas. *(Chinese)* 80−59501
p-InSb, uniaxially deformed, mag. field induced semicond.-metal transition 79−95457
p-InSb, uniaxially stressed, elec. cond., Hall coeff. and photocond. at 15K 77−47828
InSb, valence band struct. obtained by magnetophonon effect 77−76748
InSb, valence band structure, CPA, bond orbital calcs. 78−87909
n-InSb, variable range hopping cond., percolation theory *(Japanese)* 78−14733
InSb, volume plasmon dispersion, anisotropy 78−56090
InSb, warm electron coeff. 78−10452
InSb waveguide, nonlinear third harmonic generation of submillemetre waves 80−44632
n-InSb, weakly compensated, sub MM photocond. 80−15565
n-InSb, Wigner cryst., long-wavelength excitations in strong mag. fields 79−82533
InSb, X-ray topographic evidence of asymmetrical pre-yield behaviour 80−75229
InSb, Zener tunnelling in mag. and elec. fields 79−91082
InSb, zincblende and rocksalt type struct., semiempirical LCAO band struct. calc. 77−72816
InSb:Cd, diffusion props. of Cd, modified C-V technique meas. 79−19401
InSb:Cd, thermal conductivity down to 0.38K 80−107582
InSb:Cd (Zn) (Ge), ion-irradiated, p-n conversion during heat treatment 80−96558
n-InSb:Cr, deep impurities, elec. cond. and Hall coeff. meas., 4.2 to 120K 80−107791
InSb:Cr, electron and hole lifetimes, recomb. at trapping and acceptor levels 77−51760
InSb:Cr, press. effects on transport props. 78−56146
InSb:Cr, Zn and InSb:Zn, impurity centre behaviour, impurity conc. and Hall coeff. meas. 80−65490
InSb:Cr,Zn, transport props. meas. 77−1424
InSb:Cr:Zn, magnetic freeze-out electrons at deep Cr level 79−15169
InSb:Cr(Zn)(Mn)(Ge), recombination of nonequilibrium carriers 79−65496
p-InSb:Cu, Ag, deep impurity centres, acceptor conc. effect on conduction type 80−44602
p-InSb:Cu(Ag), ionisation energy of multiply charged impurities, compensation effects 78−18996
p-InSb:Cu(Zn) film, heavily doped, ionized impurity scatt., Hall effect and DC cond. meas. 79−99643
InSb:F, acceptor props. and diffusion coeff. of F 80−70643
p-InSb:Ge, photocond. in quantising mag. field, uniaxial press. influence 77−15907
p-InSb:Ge, proton irrad. defects energy level scheme, transport props. meas. 80−96576
p-InSb:Ge, single cryst. field dependence of Hall effect, cond. and carrier mobility *(Bulgarian)* 78−34848
InSb:Ge, uniaxially compressed, anisotropy of elec. props. 78−19035
InSb:Ge annealing effect on electrical parameters, absorption spectra and photocond. 77−11939
p-InSb:In, two-phase polycryst. films, negative magnetoresist. 80−11011
InSb:Mn_2 powder, quadrupole interactions in NMR spectra 79−51880
InSb:Mn^{2+} nondegenerate semicond., mag. impurity indirect interaction *(Russian)* 80−34591
InSb:NiSb, size reson. scatt. from hard cylindrical pot. obs. in magnetoresist. 79−95421
InSb:S, ion implanted, Hall effect meas. 77−20342
InSb:S(Se)(Te), reson. states and reson. scatt., elec. props. 80−49738
InSb:Se, exam. of defects in crystal 80−6423
InSb:Se p-n tunnel diodes, influence of doping on characts. 79−73575
n-InSb:Se(Te), drift tunnel diode, prod., current ratio meas. *(Russian)* 77−8185
n-InSb:Se(Te), heavily doped, anomalous press. depend. of thermoelec. power 77−47840
n-InSb:Se(Te), Moss-Burstein effect, optical energy gap depend. on doping conc. 77−8581
InSb:Sn, equilibrium distribution coefficient of Sn 79−10872
InSb:Te, anomalous anisotropy of magnetoresist. and g-factor 77−47831
InSb:Te, cryst. growth from melt, pulling method, US effects on facet growth 80−76169

III-V semiconductors continued
InSb:Te, Czochralski cryst. growth, strain configuration study using X-ray anomalous transmission topography 79−23552
InSb:Te, heavily doped degenerate semicond., Kondo effect 79−61053
InSb:Te, periodically laminated plasma, 56.5 GHz transmission, helicon diagrams *(German)* 77−20348
n-InSb:Zn, Zn diffusion out of implanted layers 79−10984
InSb/GaSb superlattice thin films, sputtered, ion-bombardment-enhanced diffusion during growth 78−87882
InSb/$LiNbO_3$ acoustoelectric convolver, gap-coupled, for IR imaging device 78−94492
InSb/$Pb_{0.79}Sn_{0.21}Te$ photodiodes, two-colour sandwich detector 77−82602
InSb-anodic oxide MIS struct., electrophys. props. *(Russian)* 77−39961
p-InSb-Au, surface barrier, structure, photosensitivity spectrum 79−51674
InSb-Au contact system, low temp. alloyed contact formation 80−100519
InSb-Au Schottky barrier, photovoltaic spectra and magneto-optical transitions, Landau levels and excitons 77−47858
InSb-Au Schottky barrier, photovoltage, temp. effects 77−69415
InSb-Bi system, molten, enthalpy change due to mixing *(German)* 79−86892
InSb-CdTe solid solns., electroreflectance spectra, Brillouin zone transitions 80−7330
InSb-Cu non-rectifying contacts by immersion plating 78−30984
InSb-GaAs, interface between two polar semiconds., optic-phonon-magnetoplasmons 78−23146
InSb-GaAs semiconductor plasmas, surface wave instabilities, temp. effects 79−78125
InSb-GaSb, compositionally modulated sputtered superlattice, growth and interlayer diffusion 79−56930
InSb-GaSb alloys, directionally solidified, composition variations, electron probe anal. 79−24513
InSb-GaSb solid solution ingots, orientation, twinning and orientation depend. reflectance 79−28001
InSb-GaSb superlattice, interlayer diffusion 77−85086
InSb-insulator boundary, surface wave resonance in transversely magnetised semicond. plasma 78−30948
InSb-$LiNbO_3$ struct., electroacoustic interaction temp. depend. 79−69336
InSb-MnSb eutectic alloy, temp. depend. of conductivity and Hall effect, field depend. of Hall coeff. 77−24566
InSb-NiSb, longit. thermomag. amplifier 77−47838
InSb-NiSb, photovolt. effects rel. to theory of semicond. with internal elec. short circuits 80−65620
InSb-NiSb system, anisotropic, acoustomagnetoelec. effect, theory 79−24021
InSb-NiSb two-phase system, photomag. effect, orientational depend., 90-300K *(Russian)* 78−2524
InSb-NiSb two-phase system, electron scatt. mechanism *(Russian)* 78−6373
h-InSb-oxide system, interface recombination activity variation on annealing *(Russian)* 79−78199
InSb-oxide-electrolyte interface, electroluminesc. in anodic oxidation *(Russian)* 77−90201
InSb-PbTe(CdTe) superlattices, laser deposition of multilayer heteroepitaxial structs. 80−44450
InSb-Sb eutectic solidification, interface demarcation expts. 79−43228
InSb-type semiconductor, spatial dispersion of permittivity 78−67967
InSb-type semiconductor, inelastic scatt. of electrons by optical phonons 78−76073
InSb-type semiconductors, shallow donor states in magneto-optical props. 80−6785
$InSb_{1-x}As_x$, cryst. struct. and far IR reflectivity 79−56752
$InSb_{1-x}As_xBi_y$, far IR reflectivity 79−56752
$InSb_{1-x}Bi_x$ disordered solid solns, ionisation energy of fluctuation levels 78−72116
$InSb_{1-x}Bi_x$, film, multitarget sputtering growth technique 78−84711
$InSb_{1-x}Bi_x$, metastable epitaxial film, phase diagram 80−76238
$InSb_{1-x}Bi_x$, multitarget RF sputtering, metastable phase, conductivity transition 80−76178
InSb(111) surface, oxidation props., LEED and surface cond. meas. 78−15559
InSe, direct gap exciton exam. by magneto-optics and photoconductivity 79−19527
InSe, molar ht. impurity and enthalpy of transition, 129-920K 77−29030
$In_{2-x}Sn_xO_{3-y}$-$Ga_xIn_{1-x}P(-InP_yAs_{1-y})$ heterojunction solar cells, chemistry and prep. 80−94073
n-Inb, anomalous Hall effect, stress depend. 80−65598
p-InsB, high-resist. compensated, elec. breakdown peculiarities 80−2398
Insb, doped, electron scatt. by deform. pot. 77−72860
n-GaAs, Faraday rotation inhomogeneities anal. and optical transparency visualisation *(Russian)* 77−90123
P_xAs_{1-x}, periodic structs. characts. determ. by means of satellite Bragg reflections 79−46510
Pb/oxide/InAs structure, effective mass determ. by tunnelling spectroscopy *(Russian)* 80−44482
Pt-GaAs contacts, sintered, eval. of W, Ti, Mo and Hf barrier metals 77−8193
$(SNBr_{0.4})_x$-GaAs solar cells, single crystal and polycrystalline, performance 80−16810
Si p-n junction formation, laser assisted, TEM and elec. props. 79−69138
Si:As, epitaxy, lateral autodoping kinetics 78−39699
Si-GaP, heterojunction, photosensitivity spectrum, characts. 79−24071
Si_xGe_{1-x}-GaAs, heterojunction, elec. and recomb. props., interface defect effects 80−80365
SiO_2-InP, MIS struct., prod. by pyrolytic deposition resist., breakdown and interface states 77−15961
SiO_x-GaAs, vacuum evaporated system, acoustoelec. signal, interface props. 80−75646
TLP, possibility of existence with sphalerite struct. 80−33950
ZnSe film, thermostimulated polariton emission 78−2436
ZnSe-GaAs narrow junction lasers 80−43334
ZnSe-GaAs solid solns., chem. transport cryst. growth, struct. 78−43991
ZnSe-GaAs thin film DE electroluminescent cell with 20 V threshold voltage 78−76141
$(ZnSe)_{1-x}(GaAs)_x$ solid solns., photoluminescence spectra 80−40159
n-ZnSe−p-GaAs heterojunction high-detectivity threshold photodetectors 79−6181

III-VI semiconductors
electrical characterisation, review 78−60120
$GaSe_{1-x}Sx$, exciton spectrum nature and anisotropy of electron bands near absorption edge *(Russian)* 79−51483
p-GaSe, relaxational oscillations of photoconductivity and dark conductivity 77−69379
layer compounds, lattice instability, deformation dipole model 80−39249
layered materials, prep. and growth, book contrib. 78−19661
nonlinear absorption processes, competition between two-photon absorption and two-stage absorption via deep traps 80−29764
two-photon absorpt. spectra 80−20660
$Al_xGa_{1-x}As$, modified-strip buried-heterostructure lasers, CW electro-optical properties 80−74359
As-S chalcogenide glass holographic recording efficiency, photocond. and annealing effects *(Russian)* 80−15556
CdS, B exciton-polariton, reson. Brillouin scatt. 79−33717
CdS, granulated films, optical reson. 79−4863
CdS, single cryst., bound excitons in surface layers, luminesc. obs. 79−28294
Ga chalcogenides, energy spectrum of local levels *(Russian)* 79−51517
Ga-Sb-Te, props. of ternary solid solution based on GaSb 79−7826
GaAs, autoepitaxial layer, local impurity inhomogeneities *(Russian)* 79−23854
GaAs, bulk purification by chemical vapour transport 79−24437
GaAs, deep level, strongly anisotropic field ionisation 79−28317
GaAs, device compatible anodic oxidation technique 78−44236
n-GaAs, impurity interaction and donor-acceptor recombination 80−16094
GaAs, point defect equilib., non-stoichiometry 79−90644
GaAs, polycrystalline films, meas. of effective diffusion length by SEM 80−80424
GaAs, refr. index and induced birefringence dispersion 80−2717
GaAs substrate, plasma polymerised polysiloxane film growth, dry etching process 80−25575
GaAs-$Ga_{1-x}Al_xAs$ variable gap p-n junction, variable gap and photo EMFs 80−15596
GaAs-$Ga_xIn_{1-x}P$ heterostruct., MBE layers, photolum. props., assessment as laser struct. 80−20705
GaAs-GaSe n-p heterojunction, elec. props., interface states 80−65670
ε-GaAse, optical consts. for ⊥ and ∥ light polarisation, reflectivity, interf. meas. 77−52077
$Ga_{1-x}In_xSe$, energy bands near absorpt. edge, transmission and photoluminesc. spectra 79−83022
$Ga_{1-x}In_xSe$, energy spectrum and struct., X-ray diffr. and light absorption 79−11437
$Ga_{1-x}In_xSe$, exciton spectrum nature and anisotropy of electron bands near absorption edge *(Russian)* 79−51483
$Ga_{1-x}In_xSe$, layered, luminescence and photocond. obs., two-photon excitation 78−76521
$Ga_{1-x}In_xSe$, magnetic susceptibility anisotropy, chemical bonds, electron density distribution *(Russian)* 80−50073
$Ga_{1-x}In_xSe$, Raman scatt. spectra, optical phonon freq., cryst. vibr. freq. types 80−29744
$Ga_xIn_{1-x}Se$, fabrication, struct., elec. and optical props. 80−44180
GaP complex band semicond. photogalvanic effect mechanism 80−11036
GaP, electrical recomb. behaviour at dislocations 79−82606
GaS, anti-Stokes photon replica emission under two photon excitation 77−52175
n-GaS, Bridgman crysts., hole traps, photocond. and thermal quenching study 80−75580
GaS, Brillouin scatt. by pure transverse phonons 79−78696
GaS, elastic prop. anisotropy, Debye temp. *(Russian)* 80−88244
GaS, electrolum. and electroabsorpt., 77K 77−48247
GaS, factor-group analysis of high-symmetry layer dynamics 79−42160
GaS, indirect excitons *(Russian)* 77−89709
GaS, infrared optical props., polarisation depend., vibr. modes 80−100658
GaS, lattice dynamics parameters, X-ray diffr. study *(Russian)* 80−29146
GaS, layer compound, long-wavelength phonons and elastic consts. 80−65175
GaS, layer cpd., lattice dynamics 79−95105
GaS layer crystal, differential indirect exciton spectra 79−8159
GaS layer semiconductor, IR derivative absorpt. spectra 78−6666
GaS, layered, conduction band photoelectron spectroscopy 77−52217
GaS, luminescence excited by high-intensity two-photon pumping 77−44038
GaS, mag. susceptibility anisotropy, chem. bonding *(Russian)* 79−61045
GaS, optical absorption edge under hydrostatic press. 78−23487
GaS, optical detection of triplet excitons 80−29650
GaS, optimisation of crystal growth conditions by I_2 vapour transport 78−68611
GaS, photoemission props. of III-VI layer compounds 79−65976
GaS, polarisation selection rules for photoemission spectra, test of band struct. calcs. 77−52216
GaS, reflectivity from 4 to 32 eV, Kramers-Kronig anal. 80−34943
GaS, refr. index in far IR, permitt. meas. 78−64360
GaS, refr. index meas. 78−10864
GaS, semiconductor layer cpds., band struct. calc. using tight-binding method 79−65376
GaS, shallow core level spectra 80−104037
GaS, sp. ht., vibr. spectra and Debye temp. 78−87796
GaS, sp.ht., 2-30K, expt. compared wih theory 78−18791
GaS, sputtering conditions effect on film struct. and optical absorption *(Russian)* 77−12525
n-GaS, TSC, electron traps 80−11002
GaS two-photon absorpt., cond. and luminesc. meas. 77−52166
GaS, two-photon photoemission 79−28890
GaS, UPS, polarisation effects 77−12494
GaS, valence and conduction bands, synchrotron radiation photoemission spectra 77−63536
GaS, XPS and valence band density of states, tight binding approx. 78−63974
GaS:Bi_2S_3, photocond. and optical obsorpt. 79−51634
GaS_xGe_{1-x}, valence band states, composition depend., photoemission spectra study 80−100434
GaS(Se), birefringent layer cryst., indices of refraction 77−20815
GaS(Se), $GaS_{0.6}Se_{0.4}$, angle resolved UPS, energy band dispersion curves determ. 79−100022

III-VI semiconductors continued
GaS(Se), growth by I_2 vapour transport using temp. oscill. method 77−77355
n-GaS(Se), hopping and impurity cond. anomalies 77−59287
GaS(Se), layered, optical phonons, IR and Raman scatt. meas. 78−59903
GaS(Se), optical and nonlinear optical props. *(Russian)* 79−51943
GaS(Se), polar optical phonon ang. behaviour, IR refl. meas. 80−20633
$GaS_{1-x}Se_x$, mixed crystals, IR reflectivity spectra 80−66204
GaS_xSe_{1-x}, grown by iodine vapour transport, X-ray struct. studies 79−4411
GaS_xSe_{1-x}, IR reflectivity and transmission spectra, stacking transform. 77−32371
GaS_xSe_{1-x}, indirect exciton spectrum and phase transition, luminesc. and absorption spectra 79−8160
GaS_xSe_{1-x}, recomb. radiation intensity, temp. depend. *(Russian)* 79−33830
GaS_xSe_{1-x} solid solutions, two-mode behaviour of optical phonons, IR reflect spectra 79−78680
GaS_xSe_{1-x}, wavefunction symm. and binding energies, synchrotron radiation photoemission spectroscopy 80−50532
$GaS_xSe_{(1-x)}$ solid solns., electrical props. meas. 78−84216
GaS(Se)(Te), electronic struct., tight-binding calcs. 80−15448
$GaS_{1-x}Te_x$, solid soln., single cryst., crystallography and optical props. 79−55711
GaS(Te)(Se), elastic characteristics, Debye temp., ultrasonic study *(Russian)* 80−79872
GaSb film, polycrystalline, Hall mobility 80−97015
GaSe, ^{110}Ag diffusion, temp. depend. and solution *(Russian)* 80−70467
GaSe, 4 to 12 μm tunable down-conversion from $LiNbO_3$ parametric oscillator 78−66865
GaSe, absorpt. and electroabsorpt. near indirect edge 77−20827
GaSe, absorpt. edge, exciton levels and Raman scatt., press. effects above 40 kbar 77−48187
GaSe, additional IR electrolum. band obs. at 77K 78−72607
GaSe and GaS_xSe_{1-x}, multiphonon reson. Raman scatt., excitonic transition 77−59574
GaSe, anisotropy effects on electroreflectance spectra at oblique incidence 77−52042
GaSe, anodic film form., in situ ellipsometric study 80−104318
GaSe, anodic oxide films, two-dimens. nucleation and growth 80−11807
p-GaSe, back wall Schottky barrier cells, diffusion length, RT spectral response meas. 80−107806
GaSe, band struct., tight-binding calc. 77−80729
GaSe, band struct. and electron density of states in two-dimens. approx. 79−37987
GaSe, band struct. from ang. resolved photoemission 77−59673
GaSe, band structure calc., semi-empirical tight-binding method 77−47726
GaSe based layer crystals, three dimensional electron state nature near absorpt. edge 79−90960
GaSe, Brillouin scatt. by pure transverse phonons 79−78696
GaSe, cascade resonant Raman processes 80−25385
GaSe, cathodolum., 115 and 285K 79−87512
GaSe, constant current anodisation, representation of layer periodicity 80−3218
GaSe, core level excitation effects, synchrotron radiation UPS study 80−40234
GaSe, core-level photoemission anisotropy 78−11076
GaSe, deep free and constrained excitons and biexcitons, collective interactions *(Russian)* 80−66282
GaSe, direct exciton excited state hot luminescence, band struct. props. 80−55183
GaSe, down-conversion of $LiNbO_3$ optical parametric oscillator output, 4 to 18 μm 79−86215
GaSe, electron beam excited free exciton luminesc. 79−19940
GaSe, excitation spectra and structural props., X-ray Laue diagrams and optical transmission *(French)* 80−50358
GaSe, exciton, excitation-induced absorption and luminesc. 78−60516
GaSe exciton absorpt., change under a pulsed dye laser 78−92088
GaSe, exciton absorpt. spectra, additional light wave 77−63445
GaSe, exciton absorption under intense excitation 77−77235
GaSe, exciton absorption spectrum, polariton effects 77−85747
GaSe, exciton luminesc. kinetics, intermediate electron-hole states 80−93389
GaSe, exciton magneto-optical spectra 80−25347
GaSe, exciton spectra at 4.2K rel. to layer struct. 77−16336
GaSe, exciton-phonon bound state, photocond. and visible absorpt. spectra obs. 80−50369
GaSe, exciton-phonon quasibound states, photocond. and luminesc. study 80−96800
GaSe excitonic spectra fine struct., reflection and transmission spectra *(Russian)* 80−55126
GaSe, factor-group analysis of high-symmetry layer dynamics 79−42160
GaSe, Faraday rot. near absorpt. edge, optical dispersion meas. 80−80757
GaSe film, amorphous, I-V characts. in strong elec. fields, 173-373K 78−56248
ε-GaSe films, optical props. in IR region, metal substrate effect 80−71502
GaSe, fine struct. of exciton spectrum 78−39567
GaSe, group theoretical anal. of phonon assisted optical transition 78−39564
GaSe, growth of crysts. with natural facets at large angles to layers 78−15305
GaSe, Hall mobility anisotropy 78−68041
GaSe, high resistivity, electric field stimulated conduction 77−66172
GaSe, highly excited, polarisation of luminesc. spectra and electron-hole plasma radiation 77−52169
GaSe, highly excited photoluminesc. exciton-exciton and exciton-carrier scatt. 77−48244
GaSe, impurity photocond., induced illumination corresponding to fundamental absorption region 80−92933
GaSe, interlayer interaction and exciton spectra study 77−52165
GaSe, isolated layer model, lattice dynamics and elastic props. 80−24547
GaSe, lamellar crystal, exciton translational mass from magneto-Stark effect *(Russian)* 78−48153
GaSe, lattice dynamics, in one-layer approach 79−14900
GaSe, lattice dynamics and elastic props., Born-von Karman model study 80−70337

III-VI semiconductors continued
GaSe, lattice dynamics parameters, X-ray diffr. study *(Russian)* 80−29146
GaSe, layer, upper valence bands using bond-orbital model 79−15078
GaSe, layer compound, long-wavelength phonons and elastic consts. 80−65175
GaSe, layer compounds, lattice instability, deformation dipole model 80−39249
GaSe, layer cryst., elastic props. rel. to zone-centre phonon freqs. 79−46736
GaSe layer semiconductor, IR derivative absorpt. spectra 78−6666
GaSe, layer struct., fine independent elastic const. using Brillouin scatt. 79−19896
GaSe, layered, conduction band, photoelectron spectroscopy 77−52217
GaSe, layered, DC hopping cond. due to stacking disorder and electron localisation 77−47819
GaSe, layered, electronic band struct., direct evaluation by angle resolved photoemission 77−51652
GaSe, layered, photoelectromag. effect meas. of transport parameters 77−59301
GaSe layers, band struct. and state density calc. by empirical tight-binding method 79−42443
GaSe, long wavelength IR refl. spectra 80−11401
ε-GaSe, long-wavelength lattice vibr. 80−92631
GaSe, luminesc. from exciton-electron and exciton-exciton collisions 77−52168
GaSe, luminescence and absorpt. spectrum in region of high-energy resonance 77−44044
GaSe MSM struct., inelastic tunnelling investigation of lattice dynamics, electron-phonon interaction 80−20330
GaSe, mag. susceptibility anisotropy, chem. bonding *(Russian)* 79−61045
GaSe, magnetoluminesc. at 4.2K 79−61345
GaSe, multiple-phonon reson. Raman scatt. processes 77−4634
p-GaSe, negative residual photoconductivity 79−51632
GaSe, nonlinear cryst., IR parametric image conversion from 10 μm to near-IR 79−89970
GaSe, one-carrier SCl currents in solid with two sets of traps distributed in energy 78−72158
GaSe, optical consts. at fundamental absorpt. edge 77−66471
GaSe, optical detection of triplet exciton reson. 79−33567
GaSe, optical excitation, excitonic spectra, stimulated luminesc. 80−40132
GaSe, optical orientation and free exciton alignment on reson. excitation *(Russian)* 77−69812
GaSe, optical orientation and alignment of free excitons, on resonant excitation *(Russian)* 77−90196
GaSe, optimisation of crystal growth conditions by I_2 vapour transport 78−68611
GaSe, photocond. at high excitation rates 78−52036
n-GaSe, photoconductivity and TSC investig. of trapping centres 77−20359
GaSe, photoemission props. of III-VI layer compounds 79−65976
GaSe, photolum. decay 79−15518
GaSe, photolum. under strong optical excitation 79−24364
GaSe, photoluminescence between 4.2 and 40K 78−10974
n-GaSe, photomagnetoelec. and photocond. current spectral distrib. 79−42585
n-GaSe, photomagnetoelectric effect, photocond., in presence of traps 80−39631
GaSe, photosensitivity anisotropy in polarised light, pleochroism coeff., suitability as photoelec. analysers 79−60873
GaSe, photovoltaic spectra 80−20240
GaSe, photoyield reson. enhancement near Se 3d core threshold, photoelectron spectra obs. 80−45207
GaSe plate in elec. field, photostimulated ocills. 79−65799
GaSe, polarisation selection rules for photoemission spectra, test of band struct. calcs. 77−52216
GaSe, polarized exciton luminesc. 78−6734
GaSe polytypes, electronic band struct. calcs. 77−51650
GaSe polytypes, tight binding study of electronic states 79−60705
GaSe, population dynamics and spin relax. of excitons 77−66122
GaSe, press. induced metallic and supercond. state 80−75666
GaSe, pressure-induced polytypic transforms. and edge absorpt., exciton lines 77−28595
GaSe, radiative decay of direct and indirect excitons 78−10975
GaSe, radiative transitions, cathodoluminescence 78−10997
ε-GaSe, Raman scatt., hydrostatic press. effect 80−84745
GaSe, reflectivity from 4 to 32 eV, Kramers-Kronig anal. 80−34943
GaSe, refr. index 0.45 to 330 μm, interf. and refl. meas. methods 77−63387
GaSe, refr. index meas., temp. variation 300 to 75K 80−25328
GaSe, refr. index meas. 78−10864
p-GaSe, resist. and Hall-mobility meas. at 77-850K 77−59295
p-GaSe, resistivity, anisotropy 77 to 750K 79−4559
GaSe, reson. light scatt., luminesc. and Raman spectra 79−38615
GaSe, SHG, absorpt. coeffs. and temp. variation of refr. index difference 80−14390
GaSe, semiconductor layer cpds., band struct. calc. using tight-binding method 79−65376
GaSe, semiconductor-metal contact, photovoltaic props. 77−59330
GaSe, shallow core level spectra 80−104037
GaSe, single cryst., dispersion of refr. indices and exciton absorption 79−73947
p-GaSe, single cryst., negative photocond. induced by elec. field 79−19623
GaSe, sp. ht., vibr. spectra and Debye temp. 78−87796
GaSe, space-charge-limited currents at different temps. 77−43607
GaSe, spatial symm. of valence band struct. by angularly resolved XPS 77−69961
GaSe, spontaneous and stimulated emissions due to exciton-electron and exciton-exciton collisions 77−32421
GaSe, stacking disorder effect on Wannier excitons 77−62834
GaSe, stimulated eimission due to electron-hole plasma recomb. 80−50374
GaSe, thin film, photoelectrical props. at high electric field *(Russian)* 79−11247
GaSe thin films, electroabsorpt. spectra, exciton line splitting 80−107716
GaSe, thin layers, far IR refractive index 80−80799
GaSe, triplet excitons ODMR 80−25252

III-VI semiconductors continued
GaSe, triplet indirect bound exciton, level anticrossing effect on magnetolum. 79−47513
GaSe, tunable medium IR source, difference freq. mixing of Nd^{3+}:YAG and dye lasers 79−55183
GaSe, two and three dimensionality of electron states, normal photoemission obs. 77−32503
GaSe, two-photon absorpt., cond. and luminesc. meas. 77−52166
GaSe, type II crysts., triplet exciton resonances 79−47359
GaSe, UPS, polarisation effects 77−12494
GaSe, valence and conduction bands, synchrotron radiation photoemission spectra 77−63536
GaSe, valence band struct., angle-resolved photoemission spectroscopy 77−1360
GaSe, wave function symmetries of valence band states revealed by polarisation effects in angle-integrated photoemission spectroscopy 79−67395
GaSe, zone-centre optical phonons, Raman scatt. meas. 78−10141
GaSe:Cu(Cd, Sb), photovoltaic spectra 80−20240
n-GaSe:I, SCL currents, expt. test of theory for insulator with two sets of traps distribution in energy 77−89768
GaSe:Sn, ^{113}Sn diffusion, temp. depend. and Sn solubility *(Russian)* 80−70466
p-GaSe:Sn, majority carrier drift mobility meas. 80−92895
GaSe:Sn, single crystal, transient photoconductivity *(Russian)* 79−11171
GaSe:Sn, single crystal, space-charge-limited currents *(Russian)* 80−11001
GaSe-InSe, heterojunction, electronic processes *(Russian)* 79−56312
GaSe-InSe, heterostructure fabrication using laser radiation 79−73580
GaSe-SnO_2 heterojunction, elec. props. and electrolum. spectra 77−59328
GaSe-SnO_2 heterojunction photocell, fine struct. of photo-EMF spectra 80−6967
GaSe-SnO_2 heterojunctions, photoelec. props. 80−96945
GaSe-SnO_2 spray heterojunction, electro-optical props. 78−64102
Ga_2Se_2, sublimation growth, closed tube, mass flow and press. meas. 77−63550
$\alpha(\beta)$-Ga_2Se_3, cryst. growth, optical, X-ray diffr. and SEM study 80−71587
Ga_2Se_3, solid solution, elec. cond. 80−88301
Ga_2Se_3-FeSe, phase diagram, elec. cond., mag. susceptibility 80−88301
GaSe(S), layer dynamics of high-symmetry crystals with atom-atom interactions 78−71799
$GaSe_{1-x}S_x$, magnetic susceptibility anisotropy, chemical bonds, electron density distribution *(Russian)* 80−50073
$GaSe_{1-x}S_x$, polytypes, exciton gap energies, luminesc. study 80−54611
$GaSe_{1-x}S_x$, stimulated photoluminesc. excitons role 77−48201
$GaSe_{1-x}S_x$, struct. transition, Raman scatt. obs. 79−99888
$GaSe_xS_{1-x}$, layered semicond., electroabsorpt. in fundamental absorpt. edge region 77−52043
$GaSe_xS_{1-x}$, X-ray diffr. investig. of stacking sequences 77−43198
GaSe(Te), optical spectra in 2 to 50 eV range 78−10915
$GaSe_{0.9}Te_{0.1}$, undulation spectra associated with acceptor complexes 78−80392
$GaSe_{1-x}Te_x$, energy bands near absorpt. edge, transmission and photoluminesc. spectra 79−83022
$GaSe_{1-x}Te_x$ layered crystal, photoluminesc. meas. 77−1725
$GaSe_{1-x}Te_x$, Raman scatt., optical phonons and phase transition 80−66202
$GaSe_{1-x}Te_x$, Raman spectra, phonon freq. 80−97286
$GaSe_{1-x}Te_x$, room temp. electroreflectance meas. 77−12361
$GaSe_{1-x}Te_x$, zone-centre optical phonons, Raman scatt. meas. 78−10141
$GaSe_xTe_{1-x}$ mixed crystals, near-band-edge optical props., absorption edge spectra 79−61401
$GaSe_xTe_{1-x}$, solid solns., exciton luminesc., cathodoluminescence 78−10992
GaTe, ^{110}Ag diffusion, temp. depend. and solution *(Russian)* 80−70467
GaTe, cryst. struct., TEM and X-ray diffr. study 80−79757
GaTe, exciton polariton effect on absorpt. edge, absorpt. and refl. spectra, 4.2 to 300K 80−20664
GaTe, exciton polariton effect on absorpt. edge, thickness depend. of absorpt. 80−20665
GaTe, excitonic absorpt. edge, transmission and refl. meas. 80−40133
GaTe film, amorphous and polycryst. memory effects 77−20368
GaTe, Hall mobility, resistivity anisotropy 79−11150
GaTe, hexagonal, vacuum deposited, physical parameters and substruct. 78−2393
GaTe, laser modulated reflectance meas. 77−63424
GaTe, layer cryst., polarised IR refl. spectra 80−97279
GaTe layer semiconductor, UV-visible wavelength derivative and thermorefl. spectra 78−6666
GaTe, long wavelength phonons, Raman and far IR spectra obs. 79−69210
GaTe monocrystal, far IR polarised complex reflectivity obs. 80−60609
GaTe, reflectivity, 1-35 eV, electron props. determ. 77−20872
GaTe, resist. anisotropy in layer plane 79−51581
p-GaTe, scatt. by homopolar optical phonons, Hall effect meas. 77−28197
GaTe, Schottky barrier, photovoltaic props. 79−7854
α-GaTe, single cryst., Raman scatt. 80−60599
GaTe, single cryst. prep. and electroabsorpt. spectra investig. 80−103968
α-GaTe single crystals, Raman spectra 79−99883
GaTe, sp. ht., vibr. spectra and Debye temp. 78−87796
GaTe, transport properties under hydrostatic pressure 80−75589
GaTe, vibr. spectrum 77−89513
GaTe, zone-centre optical phonons, Raman scatt. meas. 78−10141
GaTe:Sn, electroabsorption spectra 79−19901
GaTe-SnO_2 heterojunctions, photoelec. props. 80−96945
GaTe-SnO_2 spray heterojunction, electro-optical props. 78−64102
$Ga_{0.25}Te_{0.75}$ amorphous film, nanosecond switching, resist. fluctuations in low-resist. state 80−44676
$Ga_{0.25}Te_{0.75}$, amorphous film, off-state recovery after nonosecond switching 80−44681
$GaTe_{1-x}Se_x$, exciton spectrum nature and anisotropy of electron bands near absorption edge *(Russian)* 79−51483
p-$GaTe_xSe_{1-x}$, resistivity and Hall effect meas. 77−24556
GeS_2, single crystal, far IR transmission 80−80800
HgTe film, vac. deposited, elec. props., 78-420K 80−11119
In-Se(Te), liq., mag. susceptibility meas., electron localisation and chem. bonding 80−60178

III-VI semiconductors continued
n-InAs, edge luminescence band, shape depend. on degree of doping, band gap 80−7405
n-InAs, electron mobility dependence on conc. Hall effect at 300K 78−47794
InGa-GaSe interface, microplasma electrolum. at 300K 79−11469
InGaAsP, expitaxial growth by chloride CVD process, thermodynamic anal. 80−64936
$In_xGa_{1-x}Se$ single crystals, exciton absorption spectra 80−20663
n-In_2O_3/p-InP heterojunction solar cell, photovolt. effects 80−12014
InP, automatic electrochemical carrier conc. profiling 79−99614
InS, IR reflection spectra 80−11389
InS, layer semicond., Raman scatt. meas. 78−35134
InS, prep., and elec. and optical props. 77−77361
InS-Au Schottky-barrier diode, tunnelling current due to thermionic-field emission 79−33340
In_6S_7, single crystal, switching effect and memory *(Russian)* 80−70774
InS(Se), optical and nonlinear optical props. *(Russian)* 79−51943
InS(Se)(Te), fused, charge transfer nature 77−89757
n-InSb, degenerate plasma, Coulomb collision photon absorpt. dynamic screening *(Russian)* 80−92924
n-InSb electron heating and energy relaxation time in quantising mag. field 80−10996
InSb-$LiNbO_3$ layer structures, fabrication and use in SAW amplification 79−41540
InSe, ^{110}Ag diffusion, temp. depend. and solution *(Russian)* 80−70467
γ-InSe, 3R struct. type refinement 80−64962
InSe (hexagonal), X-ray cryst. data redeterm. 80−19767
InSe, ang. depend. of core level photoemission 79−43099
InSe, angle resolved photoemission, 15-29 eV, valence band struct. 77−48319
InSe, anomalous photocond. obs. 77−76869
InSe, band structure, XPS, UPS and tight-binding calc. 77−47727
InSe, band structure calc., semi-empirical tight-binding method 77−47726
InSe based heterojunctions, props. 79−11210
InSe, characts. of photocond. in strong absorption region 77−66184
InSe, core-level photoemission anisotropy 78−11076
InSe, current induced by impurity-absorbed IR radiation 78−10511
InSe, directional dispersion of extraordinary phonons 79−65154
InSe, elastic props. temp. depend. 78−10119
InSe, electronic struct., tight-binding calcs. 80−15448
InSe, energy band structure, chem. bond polarity, photoemission, semiempirical tight binding method 80−44504
InSe, exciton absorpt. spectra, additional light wave 77−63445
InSe, exciton and polaron anisotropies, reson. Raman scatt. study 80−76033
InSe, excitonic absorpt. edge 78−88352
InSe film, photochem. production of holograms on surface *(Russian)* 79−7101
InSe film, structure, influence of laser beam 79−7761
InSe films, residual photocond., field quenching 80−60037
γ-InSe, fundamental absorpt. edge 80−2781
InSe, high field magnetoabsorpt. of hydrogenic excitons at second direct gap 80−6729
n-InSe, influence of elec. fields on anomalous photocond. 77−8147
InSe, LF oscills. of current 78−56187
InSe, large monocrysts., grown from nonstoichiometric melt., comp. and photovoltaic substrate 77−55882
InSe, layer compound, long-wavelength phonons and elastic consts. 80−65175
InSe, layer compounds, lattice instability, deformation dipole model 80−39249
InSe, layer cpd., reson. Raman scatt. at higher Mo exciton edge 79−28764
InSe, layer cryst., Raman and IR refl. spectra meas. 79−95777
InSe, layer semicond., electronic props. 79−28275
InSe, layer semicond., Raman scatt. meas. 78−35134
InSe, layer single cryst., Raman scatt. meas. 78−76478
InSe, layer type, Raman spectrum exam. 78−23461
InSe, layered crystalline slabs, growth by Czochralski method 78−68619
n-InSe, layered semiconductor, current-voltage characts. investig., 130 to 400K 77−4342
InSe luminescent film, production and characterisation *(Russian)* 78−39581
InSe MOS structs. 79−69605
InSe, mag. susceptibility anisotropy, chem. bonding *(Russian)* 79−61045
n-InSe, negative photocond. and photocurrent quenching under impurity excitation conditions 77−4399
InSe, opt. props. new fundamental absorpt. edge 77−16330
InSe, optical const. and interband transitions 77−20816
InSe, optical props. from 2-25 eV 80−29760
InSe, optical props. near fundamental absorption edge 77−12434
n-InSe, optical spectra, photocond. and resistivity 78−88321
InSe, photoconductivity anisotropy at high optical excitation levels *(Russian)* 80−103721
InSe, photoelec. props., generation of elec. pulses 77−55574
InSe, photoelec. props. 79−73543
InSe, photoemission props. of III-VI layer compounds 79−65976
InSe, photosensitivity anisotropy in polarised light, pleochroism coeff., suitability as photoelec. analysers 79−60873
InSe, photovoltaic effect, appl. to solar energy conversion 79−29481
InSe, polar optical phonon ang. behaviour, IR refl. meas. 80−20633
InSe, polarisation selection rules for photoemission spectra, test of band struct. calcs. 77−52216
InSe, Raman scatt. spectra 79−69846
InSe, Raman scatt. spectra, optical phonon freq., cryst. vibr. freq. types 80−29744
InSe, Raman spectra, inter-, intra-layer interaction estimates 78−88313
InSe, reflectivity and low energy absorption 80−34944
InSe, reflectivity from 4 to 32 eV, Kramers-Kronig anal. 80−34943
InSe, SHG 79−81489
InSe, second order Raman spectrum and phase transition 79−38545
InSe, semiconductor layer cpds., band struct. calc. using tight-binding method 79−65376
InSe, semiconductor-metal contact, photovoltaic props. 77−59330
InSe solar cells, photovoltaic conversion efficiency 80−61356
InSe, spin orbit split off valence bands, exciton transitions, Hopfield's quasicubic model, visible absorpt. spectrum 80−50370

III-VI semiconductors continued
InSe thin film, sputter growth and chem. anal. by XPS/ESCA 80−80976
InSe, two and three dimensionality of electron states, normal photoemission obs. 77−32503
InSe, valence and conduction bands, synchrotron radiation photoemission spectra 77−63536
InSe, vibr. energy spectrum *(Russian)* 79−51483
InSe, vibr. spectrum, IR refl. and absorpt. 500-100 cm^{-1} 77−81102
InSe, wavelength modulated optical absorption above fundamental edge 78−27255
InSe, X-ray crystallography, struct. determ. 77−4081
InSe, X-ray photoemission intensity, nearest-neighbour backscatter 79−65977
InSe-GaAs p-n junctions, 'optical' contacts, elec. props. 78−56222
InSe-SnO_2 n-n heterojunctions, photoelec. props. 80−96945
InSe-SnO_2 n-n heterostructures, photoelec. props., 80 to 300K 80−20297
δ-In_2Se_3 (hexagonal), X-ray cryst. data redeterm. 80−19767
In_2Se_3, chem. transport reactions with I, single cryst. growth 77−16480
α-In_2Se_3, rhombohedral and hexagonal, X-ray cryst. data redeterm. 80−19767
In_2Se_3, thermodynamic and optical props. 77−24417
β-In_2Se_3, rhombohedral, X-ray cryst. data redeterm. 80−19767
In_xSe_{1-x}-SnO_2 amorphous film-SnO_2 system, photovoltic spectra, annealing effect *(Japanese)* 80−92926
InTe, In_2Te_3, molten III-VI semiconductors, SRO 77−65945
InTe, Raman spectra, phonon modes 80−40109
InTe thin films, flash evaporation, electrical props. 80−65722
InTe-InSe p-n junctions, 'optical' contacts, elec. props. 78−56222
$In_{0.25}Te_{0.75}$ amorphous film, nanosecond switching, resist. fluctuations in low-resist. state 80−44676
$In_{0.25}Te_{0.75}$, amorphous film, off-state recovery after nonosecond switching 80−44681
In_2Te_3, photoelectric props. 77−8144
In_2Te_3 type semiconductors, basis of ionising radiation detectors 78−86743
$Pb_{1-x}Sn_xTe$ film on BaF_2, electron beam delineation effect on MBE growth, LEED and AES obs. 79−99434
PbTe-Ga_2Te_3, phase interaction, DTA, XPA and microstructural anal. 80−96625
Si-GaSe n-p heterojunction, elec. characts., interface states 80−70812
SiTe-ATe, A=Ga, In, Tl, solid solns., mag. suscept. meas., defects 78−43552
SiTe-GaTe, thermo-EMF, elec. cond. and solubility 77−20346
SnTe-InTe, SnTe-In_2Te_3, solid soln. region, lattice constant variation 77−35697
$TlGaS_2$, IR refl. spectrum., LO phonons *(Russian)* 77−40221
$TlGaS_2$, IR refl. spectrum, Kramer-Kronig analysis, transverse optical phonons 78−19489
$TlGaS_2$, optical and photoelectric exam. 79−11180
$TlGaS_2(Se_2)$, IR reflection spectra, lattice vibrs. *(Russian)* 77−85701
$TlGaSe_2$, electrooptic effect and refr. index anisotropy 77−16281
$TlInS_2$, layered structure crystals, refractive index meas. method 80−98966
$TlInS_2(Se_2)$, electrical cond. of single crysts. with symm. and asymm. Ag-In contacts 80−6835
$TlInS_2(Se_2)$, IR reflection spectra, lattice vibrs. *(Russian)* 77−85701
$TlInS_xSe_{2-x}$ solid solution, optical and photoelectric props. 79−11179
p-TlInSe, piezoresist. effect 77−35942
$Tl_2S(Se)$, molten III-VI semiconductors, SRO 77−65945
TlSe, heat capacity, at low temp. and Debye temp. *(Russian)* 79−10962
p-TlSe, monocrystal, temp. depend. of mechanical strength *(Russian)* 79−10892
TlSe, Raman spectra, phonon modes 80−40109
TlSe, refl. spectrum in 4.2 to 8.0 eV range 79−51984
TlSe, Tl_2Se, Tl_2Se_3, liq., diffusion coeff. of Sn, Ag and Tl *(Russian)* 77−28030
TlSe type crystals, possible second-order phase transitions, group-theoretical anal. 80−92672
TlSe, vibrational spectrum, IR spectra meas. 78−35146
p-Tl_xSe_y, IR bolometer detector performance 78−24856
TlTe, elec. props., cryst. growth *(Japanese)* 79−33907
TlTe, empty lattice band struct. *(Japanese)* 77−51660
TlTe, melt, elec. cond., surface tension, microhardness, influence of impurities 80−88551
TlTe single crystal, resistivity, Hall coeff., magnetoresistance, thermoelec. power 78−43418
Tl_2Te, melt, resistivity, surface tension, microhardness, influence of impurities 80−88552
Y_2O_3, specific elec. cond., m.p. to 3200K, activation energy 78−43383
ZnS, granulated films, optical reson. 79−4863

illumination *see lighting*

image amplifiers *see image intensifiers*

image convertors
see also fluorescent screens; image intensifiers
alkali halides, photodichroic, as optical processing elements 78−83056
alkali metal vapour, IR image upconversion using two-photon resonant optical four-wave mixing 80−58632
bacterial cells, tethered, image conversion for rot. rate and direction detect. 77−73620
biplanar electron-optical image converter as a circuit element 80−78994
biplanar image converter, photocathode switching 80−19105
camera, for laser and laser-plasma diagnostics 78−38550
camera for use with universal astrograting spectrograph 77−67037
cameras, subpicosecond resolution, progress report 77−5951
cholesteric liquid crystal visualisation of microwave fields 78−58031
colour image scanner, using one-colour laser and modified γ-Ruticon image buffer 79−27373
colour imaging multispectral optoelectronic system effectiveness evaluation 79−81553
colour scanner imager for colour picture reproduction 78−42415
crossed grid anode and its image partitioning 78−71217
diagnostic radiology, detector sensitivity and image conversion improvement 77−25546
digitising system for computer input of crystallographic structure models 79−50939
diode array scan convertor, oxide transfer storage 77−75687
display unit for weak luminesc. investig. 78−12763

image convertors continued
distortion evaluation, high-speed photographic recording, of exploding wires 78−41365
dynamic range meas. device 79−68431
earth surface, electron system for image transformation and coding in conventional colours 80−4117
electro-optical deflector streak camera system, for picosecond laser pulse diagnostics 78−33909
electron-optical convertor, multielectron scintillation statistics 79−72695
electron-optical convertor detection characteristics, multielectron scintillation effect 79−72686
electron-optical convertor screen luminance, effect on observer's eye pupil diameter 80−35890
electron-optical photography, pico-femtosecond 78−82064
electrophotographic and electroradiographic image convertors with electronic readout 79−71554
electrostatically focused tubes for nanosecond, subnanosecond photography, dynamic range 78−38034
fibre optic image tube, cooling effect 78−96401
fibre optic sheet prod., appl. for image convertors in facsimile input system 78−42477
fluorescence bronchoscope for lung tumour localisation 77−60277
focusing with strong magnetic field 78−5556
framing camera tube for <100 ps range 78−70207
gas-filled channel convertor for fast coincidence cameras 77−60276
grey-scale to colour convertor for foot pressure distrib. pattern meas. 79−20691
Hall detector convertor applic. to radio hologram recording in mm range 77−639
high speed tubes, laser radiation recording with picosecond, femtosecond resolution 78−33903
high-speed camera, computer treatment of images 78−42295
holography in IR region using scanning image convertor 79−76636
HVEM, for biological specimens 80−104839
hybrid field-effect liquid-crystal light valve, optical data processing performance 80−99860
incoherent to incoherent, liquid crystal, hybrid optical processors app. 80−33166
infrared telescope, 6032 image conversion tube 80−42020
ion beam visual image produced by electron interaction on surface 78−58091
ion imaging for ion implantation and micromachining *(French)* 80−34027
ionography sealed chamber system, optically projected X-ray charge images 78−4748
IR cathodoluminescence topography recording, crystal lattice defects appl. 78−22201
IR image conversion tube, low-cost apparatus for teachers 79−71207
IR image nonlinear conversion allowing for turbulent atm. influence 80−23751
IR photographic methods 79−93243
IR upconvertor for astronomical imaging 78−7883
IR-to-visible image conversion with a thick-layer hologram 80−87355
laser signal, sinusoidally modulated, electron-optical recording with subpicosecond resolution *(Russian)* 77−7105
liquid crystal, for real-time moving object tracking by optical correlation 79−32035
liquid crystal device, with memory effect 79−23711
liquid crystal image convertor, incoherent-coherent, based on semicond.-insulator struct. 80−28342
liquid crystal image transducer, optical props. at normal incidence, off-state behaviour 80−64160
liquid crystal image transducer, spatial frequency spectrum temporal meas. 79−76810
liquid crystal light valve, appl. to real-time optical data processing 78−83102
liquid crystal light valve-image tube hybrid device for data processing 77−72083
liquid crystal transducer, performance effects of liquid crystal thickness 80−102838
liquid-crystal image transducer, normal incidence, on-state optical performance 80−99852
low-temp. plasma diagnosis by laser scatt. method, image convertor and spectral analyser device 79−4180
microchannel plate dark current meas. 79−81555
middle UV low light level imaging devices 77−41319
near IR transparent material, birefringence meas. polarimeter 79−44925
nematic liquid crystal acoustooptical image convertor 78−18062
nonlinear image processing with optical feedback *(Russian)* 77−58258
oil layer, deformable, spatial light modulator as incoherent to coherent image transformer 80−96008
optical/X-ray-framing camera tube 78−37121
optoelectronic scanning device accuracy, raster distortion and instability effects 79−72697
optoelectronic system for detect. and tracking, optimisation in search operation mode 77−50765
parametric, nonlinear optics methods in spatially modulated signal conversion 79−7179
parametric, thickness aberrations investigation rel. to multi-transverse mode pump 78−13765
parametric image convertor with freq. rise, phase aberrations *(Russian)* 78−9455
parametric upconversion, matrix method for anal. 78−46727
PCB, nematic liq. cryst., US imaging, convertor, acousto-optical effect 78−59218
phase shift plate analysis and design *(Russian)* 80−5696
photocathode sensitivity uniformity over surface, distortion of zone charact. by interference in substrate 80−58709
photochronographic device, temporal resolution 78−33908
photoelectric convertors, one-coordinate, signal processing algorithm 80−33199
photoelectric screen convertor, accuracy, reading system ang. aperture effect 77−62066
photoelectronic streak camera tube, magnetically focused 78−33907
photogrammetric automaton 'Zenit' positioning, electromechanical system *(Russian)* 78−21101
photogrammetric system 'Zenit', scanning spot intensity distribution *(Russian)* 78−21104
picosecond exposure scanning camera, and associated recording system *(French)* 78−42429
picosecond image convertor streak cameras, dynamic range 78−38032

image convertors continued
picosecond streak camera, dynamic range and spatial resolution 78−42428
pseudo real-time coded aperture imaging system with intensified vidicon cameras 77−31133
pulsed electron optical convertor, dynamic spatial MTF estimate 80−74502
real time optical sectioning using freq. interleaving, high S/N, 3-D TV 77−72062
ring-rate control system for nanosecond exposures, spatial resolution of images 79−18521
gamma-Ruticon image buffer, imaging props. 78−66915
S/N ratio of electron-optical convertor, rel. to threshold characts. 77−31134
sampling stroboscopic convertor identification by Hammerstein model *(Russian)* 80−74495
satellite microchannel X-ray image convertors *(French)* 78−24436
scanistor, coordinate meas. error, sweep voltage nonlinearity effect 77−14808
scanning optoelectronic systems, optical and electrical filter simultaneous optimisation 79−72696
scanning photoelectric, optical inhomogeneities obs. by spectral modulator 78−59144
scanning radiometer images, electronic conversion to stereographic projection 79−21056
scintillating imaging proportional counter as X-ray to light image convertor 77−65063
self-scanned, anode array UV detector, SSANACON, with microchannel plate multiplier 77−78632
shutter control, transistor pulse generator 78−4653
Skylab ATM television monitors, obs. and recording of instantaneous solar XUV images 77−60605
Sokolov image convertor tubes 77−19494
solid state, with integrated fixed-pattern noise suppression 80−14458
solid state pyroelectric IR image convertor 80−9036
Spatio-temporal resolution of rapid image tubes *(French)* 78−33906
spread function of electron-optical convertor, stroboscopic interpolation 77−7204
state of art, vacuum- and nonvacuum-types survey *(Czech)* 78−63185
streak camera, Nd:YAG laser picosecond pulse meas. 77−19271
streak camera 78−54484
streak camera convertor tubes, picosecond resolution, operating characts. comparison 78−38031
streak camera for subpicosecond chronoscopy 78−38030
streak camera optical measurement, in laser fusion research 78−38549
streak camera synchronisation using picosecond laser pulse activated Si switch, jitter reduction 80−53440
subnanosecond optical detector developments 80−77870
sweep parameters optimisation in systems with storage 77−39059
Synchroscan streak camera, picosecond chronoscopy of repetitive weak light sources 78−38033
thermally induced index gratings Bragg refl., IR optical image conversion, thermal index changes 79−59753
thermo-optical convertor with liq. modulating medium 80−91927
thermoluminescent metal sulphate types, contrast functions conversion efficiency, NDT uses 79−9271
thermoplastic-photoconductor image transducer, input to coherent optical processor 78−83098
three dimensional image transmission, real-time, using vol. scanning spatial modulation 77−72060
time analyzing electron optical convertor with microchannel plate 78−30082
time resolution, contrast-time characts., calcs. 77−7208
time resolution of optical lenses for sub-picosec. processes 77−39012
ultrahigh magnetic field magneto-optical meas. using image convertor camera *(Japanese)* 77−67505
UMI-93ShS, investigation of time frequency-contrast characts. 79−18520
underwater imaging using US image convertor tube 77−19499
underwater US image convertor optimal working frequency estimation *(Russian)* 78−30111
US real-time two-dimensional ECG images, direct conversion 77−60233
vidicon tube for low level X-ray and γ-ray imaging 77−81561
X-ray flaw detection, electroluminescent storage screens, expt. results 77−77722
X-ray imagining system, real-time, for rocket-borne solar coronal obs. 80−41725
X-ray topogram visualisation raster tube with shoot-through target 80−31956
$Bi_{12}GeO_{20}$, spatial-temporal electrooptic modulator, UV image conversion 77−3680
$Bi_{12}SiO_{20}$ photoelectret, in optical processing and X, γ ray imaging 80−23764
$Bi_{12}SiO_{20}$, use in incoherent-to-coherent optical image convertor of transmission type 79−94340
Cs, vapour, IR image up-conversion two-photon reson. pumping by $Nd:La_2Be_2O_5$ laser 77−10968
Cs_2Te, photocathode for proximity focused image convertor, field enhancement of photoemission 78−72677
GaSe, nonlinear cryst., IR parametric image conversion from 10 μm to near-IR 79−89970
LiO_3, up-conversion of signal from thermal source 80−9938
PLZT colour cell for real time two colour incoherent to coherent image convertor 78−38039
PLZT real time 2 colour incoherent to coherent image convertor 79−3805
Pr based, IR quantum counter imaging system, resolution, sensitivity 79−81541

image iconoscopes *see television camera tubes*

image intensifiers
aid for chronic night blindness 77−60288
all-metal autoionisation microscope construction and equipment 79−67433
angiographic universal setups for general hospital with vascular surgery facility 79−92336
astronomical appl. of image convertor-intensifier detector for interference spectroscopy in balloon UV 80−56707
astronomical image-tube systems, effects of phosphor decay on time-modulated meas. 79−88602
astronomical spectrograph appl. of image intensifier 78−73647

image intensifiers continued
astronomical spectrophotometry using intensifier Si vidicon 78−32356
automatic image processing, 'Zenit' photogrammetric system *(Russian)* 78−24466
avalanche transistor pulser for fast-gated operation of microchannel plate image intensifiers 78−37527
biological photoelectron microscopy of surfaces power requirements for high magnification 77−40963
channel plate image intensifier, for high-speed image information preprocessor 80−78982
channel plate image intensifier cameras for low light security and projectile photography 79−40639
channel plate in image tube, MTF 80−19108
channel-plate, single-exposure photography 78−38036
coherent optical image amplification by injection locked dye amplifier 80−19041
computerised scanning device, for 'Zenit' photogrammetric automaton *(Russian)* 78−21102
dynamic data display on large screen by brightness enhancing system 77−58462
dynamic radiography using image intensifier 79−24685
electro-optical, for Al single crystal nonstop uniaxial tensile tests 79−34277
electroluminescent, photoconductive image intensifier parameters *(Russian)* 78−42421
electron image deflection system, crossed elec. and mag. field, intensity modulation 78−89592
electron microdensitometer system for use in TEM 80−95197
electron-optical and X-ray image intensifiers, characts. 79−9270
electronic detectors to enhance optical information from telescopes, image intensifiers and CCDs *(French)* 80−67569
enlarged photofluorography using 12 inch image intensifier *(Japanese)* 78−96087
Fabry-Perot-interferometer imaging system for thermospheric temp. and wind meas. 80−101441
fibre, gradient-index light-focusing, image enhancement 80−69501
fibre laser amplifier output, comparative anal. of image quality under active, passive conditions 79−7225
fibre optics in image intensifier for astronomy *(Russian)* 79−40079
FIM, performance of EMI T2001 intensifier 78−24896
first and second generation image intensifiers compared 77−39105
fluorescence microscopy of living cells, low level, appls. of image intensification 80−94432
fluorescent X-ray intensifying screen, efficiency determ., standard method 80−37140
fluorescent X-ray intensifying screen efficiency determ., standard method 78−69198
fluorography, rapid-sequence, appl. to abdominal surgery 79−92340
fluorography in paediatric radiology 80−41201
fluoroscopic image recording using multiformat camera 80−51234
fluoroscopic spot film system image quality evaluation and optimisation 78−69205
fluoroscopy, automatic brightness control operating protocols and effect on image quality 80−17120
fluoroscopy, surgical treatment of renal and ureteral calculi 79−92342
gamma camera with brightness amplifier *(French)* 77−37036
gamma camera with position sensitive Si strip detector, appl. and description 77−81565
gated image intensifier tubes *(German)* 77−88943
generation 3 wafer tube, image intensification fundamental aspects 79−89988
gradient index fibre image intensifier system 80−14484
high performance image amplifiers, for clinical use *(Japanese)* 77−73579
high speed image intensifier gating circuit 79−37044
high-speed cineradiography, of projectiles 78−41395
holographic one-tube goggle system engineering 80−78988
III-V semiconductors, electrolum. study using high-gain image intensifier 80−55193
image intensifier fluorography with fast exposure technique 78+31900
image isocon, appl. in astrophysical obs. *(Russian)* 80−12671
imaging process efficiency and quality, electrophotographic process, electronographic cameras and image intensifiers 78−78932
incident light microscope image enhancement device 79−85178
industrial hard X-ray channel-plate image intensifier 78−54517
intensified minification camera for low dose radiography 78−20262
intraoperative use of X-ray TV chain with video recorder 79−92334
IR imaging, imaging systems design, operation and performance, applications 80−47111
laser projection microscope, transmitted light, Cu vapour laser as image amplifier 80−73446
laser projection microscope with image-brightness amplifier using Pb and Mn vapour 80−106541
light intensity meas. during elec. breakdown of polyethylene using image intensifier 80−45008
liquid crystal light valve-image tube hybrid device for data processing 77−72083
liquid crystal photoconductor reflective light intensifiers, light sensitivity enhancement 77−42598
low-level imaging, optical signal detection and meas. 79−94350
medical imaging, sensitometry 78−69193
microchannel curved plates picture tube, ARAKS experiment *(French)* 78−40671
microchannel image intensifier quality evaluation *(Spanish)* 79−72681
microchannel intensifier image convertor camera, modular design 78−42427
microchannel intensity amplifier for electron microscope images during X-ray spectral anal. of light elements 77−12848
microchannel plate image invertor performance and applications 77−39094
microchannel plate technology and applications 79−23075
microchannel plate X-ray image intensifier, image resolution 78−35937
microchannel plates, hollow tube fabrication from reducible glasses, characts. 77−50766
microscopy, UV, with image intensification and TV image displays 77−5888
moonlit object real-time optical matched filtering 77−19192
MTF measurement of low light level devices 80−33221
multifunction image intensifier tube for optical image processing 80−99825

image intensifiers continued
neutron radiography with ^{252}Cf, use of TV imaging techniques 78−60922
night vision aid, second-generation intensifier monocular 77−40936
night vision equipment matching to human observer 77−40937
night vision goggles, military low-cost, design and development 80−78990
night vision system with refractive optics, glare charact., surface defect influence 79−32024
optical system design for low light and thermal imaging 79−37041
optical systems with brightness amplifiers *(Russian)* 79−98498
optoelectronics, appl. in measuring gas discharge phenomena 80−107007
phosphor decay and bandwidth measurements in image intensifiers 79−37045
photochron picosec. streak cameras for linear photoelec. recording 80−86365
photoelectron counting with image intensifier tube and photodiode array 77−18090
photofluorographic camera with electro-optical image intensifier 80−36128
Phototitus, image intensifier and convertor for electron microscope 77−45918
protection against damage from high intensity flashes 79−37046
proton, fluorescent intensification screen+photographic film combination, response, radiography appl. 78−20268
pulsed, channel plate and planar diode, exposure time meas. using N_2 laser 77−30205
radiographic $CaWO_4$ intensifying screen, meas. of X-ray induced light photons emitted 80−41218
radiographic imaging, digital video acquisition system for extraction of subvisual information 78−69208
radiographic intensifying screen equivalent blur 78−69197
radiographic intensifying screen information content and contrast, comparison of rare earth with $CaWO_4$ 78−73232
radiographic intensifying screens, sensitivity to scattered radiation 77−77970
radiographic miniaturisation, X-ray image and optically coupled radiographic intensifiers, comparison 77−81560
radiographic proximity X-ray image intensifier tube 78−69206
radiographic screen-film system evaluation, intensity vs. time scale sensitometry 80−41219
radiographic screen-film system evaluation, sensitometric method 80−41220
radiographic tomography in exam. of larynx 78−40312
radiographic X-ray image intensifier video system, design charact. 78−69209
radiographic X-ray image intensifier video system, psychophys. evaluation rel. to system measures 78−73234
radiography, high-resolution low light level video systems 77−40759
radiography, image intensifier with 14 inch input field, clinical experience 78−31899
radiography, integral formulation of total unsharpness 77−16978
radiography, rare earth oxysulphide intensifying screens, resolution and dose 77−21597
radiography screen-film combination selection 80−46047
radiology, medical and industrial *(French)* 77−30223
rapid filming appl., microchannel proximity tubes charact. *(French)* 78−49917
rare earth phosphor intensifying screen speed gain 78−7447
rare earth systems, appl. of fast Fourier digital quantum mottle anal. 77−52868
reactor fuel pin imagery, computer enhancement and mensuration 78−37395
real-time image contrast enhancement, local area histogram equalisation and gain control 77−50636
recent developments for nocturnal remote sensing, review 77−23752
reflective ultra-LV intensifier, using liq. cryst. twisted nematic effect 77−7190
remote sensing imagery, optical and electronic enhancement 77−53253
scintillation camera, large-field, for nucl. medicine appls. 77−5069
scintillation cameras for nuclear medicine 77−40732
SIT camera sensitivity expt. *(Japanese)* 78−89085
Spacelab image intensifying TV camera for airglow and meteor obs. 77−21966
spectroscopic cooled and intensified array detectors 78−65983
state of art, single-stage and multi-stage types *(Czech)* 78−63185
stigmatic spectrograph image intensifier system, appl. to plasma diagnostic work at low light levels 78−93767
streak camera, proximity-focused, for laser fusion obs. 77−5938
subpicosecond proximity-focused visible streak camera, evaluation and appl. 78−59155
TEM image recording and processing TV system 79−58851
thermal band imaging, glare in optical systems 79−32025
time-gated optical imaging system meas. of laser target emitted light angular distrib. 80−79572
time-resolved coded aperture imaging system, for nuclear fuel motion HCDA conditions 78−45764
transmission X-radiographic development trends *(German)* 78−15636
transverse analogue tomography, cross-sectional imaging of X-rays 80−56201
TV, EM image accumulation, digital storage and processing system 80−101901
TV X-ray detector, high sensitivity, biological structure diffr. study appl. 78−89609
Vidicon detector, use in Raman spectroscopy of intact bovine lens proteins 79−29525
vision, problems in matching images to the eye−effects of pictorial noise 80−51113
visual aid for patients with retinitis pigmentosa and night blindness, Generation II 77−21660
visual detection thresholds for electronic imaging systems 79−11936
visual task prediction from image quality data 78−53415
X-ray, 14 in tube 79−16285
X-ray, CCTV viewing system 77−9251
X-ray, closed circuit TV system, patient diagnosis appl. 80−3775
X-ray, design aspects 77−38070
X-ray, dual mode caesium iodide screen 78−21311
X-ray, for digestive tract radiography 78−92694
X-ray, high quality TV-picture transfer 77−5077
X-ray, magnetic interferences *(German)* 80−105761
image intensifiers continued
X-ray, microchannel plate, for TV radioscopic system, 400 kV X-rays *(French)* 77−38071
X-ray, MTF, empirical eqn. 78−65123
X-ray, new generation, charact. *(Czech)* 77−18153
X-ray, noise evaluation, digital method 80−98097
X-ray, Orbiskop, physiological exam. of upper airways in newborn and infants 80−8130
X-ray, phys. principles 79−6247
X-ray, relationship between resolution and speed 78−65124
X-ray camera, photocathodes, charact., for X-ray diagnostics of laser-induced plasmas 77−54031
X-ray diffr. patterns from biological structures 77−66878
X-ray electron-optical convertor and entrance screen, conditions for conversion factor 79−6248
X-ray fibre-optic coupled device, large-area contrast 77−70534
X-ray image amplifier, 14 inch, clinical appls. *(Japanese)* 79−92355
X-ray image convertor with video signal output 80−36125
X-ray image intensifier freq.-contrast charact. curves determ. 78−7427
X-ray image intensifier output screens 78−4755
X-ray image intensifier performance, image quality, and development trends 80−36124
X-ray image intensifiers, biomedical appl. and limitations 79−79644
X-ray image intensifiers, design and future possibilities 79−74756
X-ray image intensifiers, quantum noise meas. 80−46033
X-ray image transmission system response rel. to X-ray diagnosis 78−35941
X-ray imaging, image intensification systems and techniques 80−51236
X-ray intensifying screen, role of reflective layer 80−62816
X-ray microchannel plate image intensifier, noise charact. 78−53483
X-ray screen-film processing sensitometry standard developed by ANSI 78−69196
X-ray streak camera, high time resolution, with X-ray microscope *(French)* 78−42823
X-ray topography camera, high speed, semiconductor lattice defects exam. appl. 77−11443
X-ray TV system, EL-PC type image converting panel *(Japanese)* 77−67551
X-ray using CsI:Tl powdered phosphor screen 79−6246
X-rays, pulsed and continuous, motion picture filming of moving objects 78−57057
BaFCl:Eu X-ray intensifying screen 78−11735
$CaWO_4$ and rare-earth X-ray intensifying screen sensitivity to scattered radiation 78−7450
$CaWO_4$ X-ray intensifying screens, absorbed-energy const. 77−70537
CuCl vapour laser, use for image amplification in projection microscope system 79−98407
GaAs photocathode, emitted electron transverse energy 77−12489
Gd neutron radiographic amplifying screen sensitivity 78−7448
Si intensifier for Isocon low light level TV 79−37042

image orthicons *see television camera tubes*

image processing *see picture processing*

image sensors
see also television camera tubes
acoustoelectric SAW image scanner applications 79−45912
aerial photography reseau mensuration 77−26412
aerospace systems and electronics, IEEE conference, Washington D.C., USA, 26-29 Sept (1976) 77−5420
airborne, reconnaissance, data collection, conf., Washington, DC, USA, March 1978 79−32078
analyser comparative tests 79−14106
area imaging CCD low light level performance 77−39089
astronomical imaging, ground-based, charact. 79−35135
astronomical TV imaging tubes, utilisation *(French)* 78−40829
astronomical ultralow light level imaging by intensified CCD 77−41287
automatic image analysis, variables and errors, definition and quantitative description *(German)* 78−25296
automatic image processing, 'Zenit' photogrammetric system *(Russian)* 78−24466
BLIP systems, effect of f-number and other parameters on FLIR performance 78−77981
body motion computer-aided tracking using CCD image sensor 78−61269
C-CD, charge transfer inefficiency effect on MTF, compensation techniques 80−10026
C-CD, dynamic sampling of object pattern 79−50414
C-CD, modelling and appl. of HgCdTe MIS struct. 78−80058
C-CD based control system for Si cryst. growth 78−68623
C-CD camera, appl. to Einstein X-ray Observatory fields RI photometry 80−62315
C-CD camera on Galileo Jupiter Orbiter Mission 80−85859
C-CD digital image store for Earth resources surveying 79−34964
C-CD imager, edge enhancement using 3×3 pixel neighbourhood operator functions 80−102644
C-CD imagers, evaluation techniques 77−83990
C-CD linear sensor, diameter meas. of Fabry-Perot interf. rings 79−93210
C-CD parallel signal injection using integrated optical channel waveguide array expt. 78−37996
C-CD space-borne Earth imager, high resolution, features 79−35097
C-CD TV line sensors, telecine FDL 60 appl. 80−278
C-CD/SAW devices for signal and image processing, conf., Ottawa, Canada, 1977, Oct. 79−32159
cancer prescreening, automated cell image analysing system *(German)* 79−83892
CCD 800×800 detector arrays on Space Telescope 80−109370
charge injection device as stellar tracking sensor 80−85861
charge injection devices for astronomy 77−41317
charge transfer resistive gate sensor 77−75681
charge-coupled image sensor, direct soft X-ray response 77−74565
charge-coupled image sensor readout organisations 77−39080
coherent image processing photodiode array 79−55076
contactless metrology with image dissector tube and computer *(French)* 77−33975
crossed grid anode and its image partitioning 78−71217
CTEM image recording using CCD 80−68329
diagnostic cytogenetics, automatic system 77−78021
diagnostic radiology, electro-optical imaging 77−21651
digicons, image detection with semicond. array for multichannel photon counting 77−83989

image sensors continued
dissector tube with minicomputer control suitable for IC mask inspection 79−55065
electrical charge injection methods for CCD 77−39082
electrographic image detectors, development, and applications in UV astronomy and scientific research 80−43465
electron spectrometer using new multidetector based on charge-coupled imaging device 80−86502
electronic, conf. Washington, DC, USA, 1978 79−32085
electronic camera for Geneva seven-colour photometry of stars *(French)* 79−84682
electronic imager observer performance rel. to display S/N ratio 77−40679
electronic imaging techniques in EUV spectral region 79−30564
electrophotetic X-ray imager, self-contained instant display erasable 80−22491
fast solid-state camera for high-speed event diagnostics 80−78985
finger length meas. by ferroelectric wedge thermal transducer 77−78001
fixed-frequency laser beam scanning device 78−59135
flexible high-resolution film recorder system 80−102827
flexible high-resolution film recording system design 80−102828
focal planes, electro-optical, performance evaluation for aerial reconnaissance 79−31833
forward-looking IR sensor image segmentation by maximum-likelihood parameter estimation 80−99662
frequency scanning electronic imaging system 77−42589
gamma-ray camera using Compton effect 78−10087
general-purpose meas. microscope with photoelectric readout 79−71524
Hall detector convertor applic. to radio hologram recording in mm range 77−639
high detective quantum efficiency image detectors, review 77−71010
holographic interferometry, real-time, with photo -conductive electro-optic crystal $Bi_{12}SiO_{20}$ 79−86142
hybrid IR/CCD focal planes, performance, appls. 79−3798
image anal., subjective and objective criteria 79−31828
image evaluation methods, project SENTINEL SIGMA for Air Force, resolution meas. 79−31826
image transmission techniques, conference, San Diego, USA (Aug. 1976) 77−79773
Image Understanding Program philosophy and results 80−95818
imaging system shading effects and countermeasures 78−78922
integral colour filter arrays for solid state imagers 77−79960
integrated CCD imaging array, coupled with channel waveguide 78−38077
integrated imaging irradiance sensor for phase conjugate adaptive optics 80−33138
intensified CCD, development 79−32086
intensified CCD test results 77−41318
invisible information imaging techniques 77−5819
IR, CCD appls., book contrib. 78−38026
IR, performance of nearly BLIP detectors 77−61121
IR CCDC image sensors, operation *(German)* 78−63190
IR charge injection and CCD focal plane arrays 77−39088
IR focal planes in intrinsic semiconductors 78−37994
IR sensor figures of merit 80−86419
IR sensor noise reduction algorithms, Monte Carlo evaluation 80−95824
IR staring mosaic sensor background suppression and tracking 80−86415
large imaging CCD array development and test results 77−41316
laser line scanning sensor, spatial filtering design considerations 78−85752
laser radiation image recording, semicond. plate charge distrib. *(Russian)* 77−79951
lecture on optoelectronic devices 78−25990
light characteristics control of PZS image sensor *(Russian)* 79−18361
light source displacement vel. meas. for improving telescope photoguide system *(Russian)* 77−41306
line scan sensor, spatial and temporal coding of GaAs laser 78−83022
linear, minicomputer controlled, fluctuating image time averaging and coherence function detect. 79−41341
liquid velocity measurement and flow trajectory, using image sensor, appl. to stirred vessel 80−69950
low light level device applications, conference, Reston, USA (1976) 77−39091
low light level performance of CCD in electron-bombarded mode 77−39092
low scatter mirror degradation by particle contamination 77−65618
moire pattern detection by solid-state dynamic self-scanned photocell array 79−32084
molecular absorption spectrophotometric detection, using CCD photoarray 79−80689
MOS photosensor charge integration and storage 77−39079
mosaic sensor test and calibration facility for focal plane arrays 80−86425
MTF anal. for post-flight image eval. 79−31827
multichannel photon counting image detector arrays 78−65970
nonlinear, adaptive spatial filter for image classification *(Russian)* 78−42292
one-electron dissector, S/N ratio rel. to image contrast 79−50407
optical image scanning, by electronic control of CdS SAW delay lines, 78−26006
optical sensor array systems for astronomic longitude determ. 77−82023
optical sensor system simulation elements and techniques 79−76851
optoelectronic devices and optical imaging techniques, book 80−27059
optoelectronic instrument, image information content 77−39057
P^2CCD line sensors for slide scanner, photography appl. *(German)* 79−49308
passive image dissector for time-resolved IR spectroscopy 77−41705
pattern recognition by one-dimensional projection recording and processing *(Russian)* 78−42291
patterned optical filters for solid-stage imager spectral encoding 78−66945
photodiode, phototransistor, and CCD imaging 77−37707
photodiode array, simultaneous determination of diameters, velocity of moving solid particles *(Japanese)* 78−95872
photodiode sensor arrays, circuits and performance 77−39077
photographic speed of solid-state image sensor arrays 79−17543
photosensor array aliasing and MTF effects 77−39086
photosensor array XY addressing and organisation schemes 77−39076
photosensor multilayer structure transmittance calc. 77−38008
phototransistor array performance 77−39078
image sensors continued
picture colour component detection in SAW scanning 78−59149
position sensor, light sensitive head and elec. circuit 77−54806
pushbroom CCD time-delay-and-integration mode image sensors 77−39087
pyroelectric target performance improvements 77−39103
pyroelectric vidicon for thermal imaging *(Japanese)* 77−27359
qualitative and quantitative image analyses compared 77−56779
radiography, diagnostic isocon imaging system 77−40760
real time light modulators for incoherent to coherent image conversion 77−72082
real-time adaptive contrast enhancement for imaging sensors 79−32079
resolution through atmospheric turbulence 79−36855
Reticon photodiode array for spectral source profiling 77−63999
satellite image plane scanner for earth observations 79−97436
satellite image sensing and multiplexing system tradeoffs 77−60498
satellite solid-state imaging for meteorology and astronomy 77−39074
satellite thermal imager for Defense Meteorological Satellite Program 79−97435
SAW image scanner, using transverse acoustoelec. effect in photocond. CdS 77−11001
SAW using thin film magnetic garnet oxides *(Japanese)* 77−27429
scanistor, luminous line coord. meas. 80−96019
scanning optical sensor signal peak extraction and multiframe correlation methods 79−81380
scanning optoelectronic device with multielement photodetector, error probabilities 77−58455
scanning photodiode array for nuclear fuel cladding tube deformation monitoring 79−30938
secondary electron conduction image, tube, WX-32193, astronomical appl. 79−35137
signal levels number in presence of additive noise 77−58458
single photon X-ray detection with a CDD image sensor 79−35836
soft X-ray imaging experiments with CCD, astronomical appls. 79−35138
solid state image sensor, utilisation in star tracker *(Japanese)* 79−80227
solid state image sensors, devices and appl. *(Japanese)* 78−59142
solid state imaging devices, comparison with TV camera tubes 77−83986
solid-state, spherical aberrations meas. of photographic lenses 80−23812
solid-state array and camera tube imagers compared 77−39090
solid-state image sensor resolution evaluation by aperture sampling response 78−50939
solid-state image sensors for electro-optical systems 77−39104
solid-state imaging, conference, Louvain-la-Neuve (Sept. 1975) 77−39073
solid-state imaging charge injection devices 77−39083
solid-state imaging devices, conference, San Diego (1977) 78−66944
solid-state photosensor array for electronic imaging 79−21836
Space Telescope, astronomical appl., performance, planning 79−35136
spaceborne astronomy appls. 77−87268
spacecraft remote sensors 77−56813
Spectracon image tubes, operation and results in stellar spectroscopy 77−5451
spectrophotometry, solid state image sensor, photodiode appl. *(Japanese)* 78−4677
spin-scan imaging photopolarimeter for Pioneer Jupiter missions 77−41303
stellar objects monitoring, using TV type photon counter, minicomputer-controlled *(Russian)* 80−31212
step-stare IR sensor design for aerospace vehicle detection 80−86418
stratospheric radiance variation seen by horizon sensors 79−100957
streak camera intensified CCD readout system, sensor props. 79−27825
surface channel CCD image sensors 77−39081
ternary chalcogenide sensors, imaging by photo- and thermal doping 78−1342
thermal, optical-mechanical, electronic and solid-state technologies development *(Czech)* 79−97383
thermal imaging tube, pyroelectric, sensitivity and geometrical resolution improvement *(German)* 80−105715
thermoluminophorous, EM field meas. in open resonators 79−93168
three-terminal charge-injection device image sensor 77−39084
time delay and integration CCD imager, Earth resource thematic mapper appl. 79−35098
TV-microprocessor system, for high speed image counting and sizing 78−94377
US image processing device status and prospects 80−48446
vidicon, Si-intensified-target, low intensities meas., astronomy appl. *(German)* 80−98545
Viking Lander camera design 77−41285
Viking Lander camera performance and data reduction 77−41286
visible imaging CCD and charge injection device arrays 77−19446
water penetration imagery, surface/depth data separation by multispectral scanning 78−69539
wavefront distortion sensing for adaptive optics system control 77−19293
wavefront visualizer for coherent IR beams 78−25986
X-ray imaging scope, low-intensity, principle, appls. 79−30637
X-ray imagining system, real-time, for rocket-borne solar coronal obs. 80−41725
X-ray picture laser scanning system for digital image transmission over telephone channel 78−80953
$Bi_{12}SiO_2$ Pockels readout optical modulator, X-ray response 79−64313
$Gd_2(MoO_4)_3$, ferroelec., amorphous Si:H coating, domain wall motion, image scanning 80−83663
$Gd_2(MoO_4)_3$, one-dimensional ferroelectric image sensor with polymer photoconductor 80−80729
InSb charge injection IR imaging array 78−37995
$LiNbO_3$, acousto-optic interaction with surface waves, for image scanning 77−3673
$LiNbO_3$ acousto-optical SAW interaction multicolour image scanner 77−58483
Si photodetector storage-mode operation 77−39075
Si photodiode imaging array design factors 77−39085

image storage tubes
channel plate in image tube, MTF 80−19108
diode array scan convertor, oxide transfer storage 77−75687
echocardiogram on-line computer anal. 78−80941
electronographic camera, development and use 77−56829
electronographic camera, polarisation maps of nebulae 77−57081
return beam vidicon, high resolution, appls. 77−83988

image storage tubes continued
scintigraphy, medical, digital image processing methods 78−80947
spatial filters from binary computer generated holograms 77−50774
sweep parameters optimisation 77−39059
US real-time two-dimensional ECG images, conversion for video storage 77−60233
X-ray TV chain MTF and image quality determ. factors 80−36126
$NaAlSiO_4$, carnegieite, cathodochromic props., storage CRT applic. 77−8604
SnO_x:Sb,F film CVD for bistable storage CRT 77−77410

images, optical *see optical images*

imaging, acoustic *see acoustic imaging*

imaging, infrared *see infrared imaging*

IMMA *see ion microprobe analysis*

immittance, electric, measurement *see electric immittance measurement*

impact (mechanical)
see also ballistics; impact strength
abrasion, wear, review *(German)* 78−88536
absorber with linear spring and quadratic law damper 77−7332
absorbers, optimum damping ratio 77−72225
absorption with two-stage variable area orifice hydraulic damper 77−50953
acceleration measurement using piezoelectric measuring transducer with mechanical waveguide, anal. of processes 79−30436
accelerations, short, features for reproduction 79−32351
accelerometer, piezoelectric impact, effect of damping on dynamic error 79−30435
acoustic emission simulation by SiC grain brittle fracture and elastic sphere impact, freq. anal. 78−55504
acoustic noise, review and bibliography 79−3848
acoustic radiated noise level calc. of mechanical impact using tapping machine *(French)* 80−87639
aircraft impact, dynamic response of nuclear power station 79−3208
asteroids, collisional disruption rel. to Fe meteorites cosmic ray exposure ages distribs. 79−30015
asteroids, high vel. impact, catastrophic destruction mechanism 80−82257
asteroids, shape distrib. from high-vel. impacts, laboratory expts. 78−45263
astroblemes, shatter cones geometry and description procedure 80−51398
asymmetric, of finite bars, finite element method 77−75847
axial impact buckling of a column with random initial imperfections 79−18762
axisymmetric wave propag. in short length bars 78−5683
bar, elastic and viscoelastic, impact loading model 77−23911
bar, impact excitation, longitudinal vibr. 78−94606
bar, impact vibr., motion and dynamic stability analysis 78−26081
bar, nonuniform elastic, longit. vibr. dynamics of impact excitation 78−75086
bar, phase velocity of longitudinal impact wave, tensor wave theory *(Japanese)* 77−72228
bar, stress meas. in dynamic deform. to plastic range 77−84158
bar carrying concentrated masses, vibr. motion under longitudinal impact *(Russian)* 79−50627
bars with central circular holes, dynamic response to longit. impact 77−65703
basalt, hypervelocity cratering and impact magnetization, lunar surface simulation 77−91115
basalt, shock effects and remanence in hypervel. impact expt. 79−29755
beam, rigid plastic cantilever, in damping medium, motion under transverse impact 77−39243
beam, transverse impact of load, approx. model *(Russian)* 79−37251
beams, dynamic plastic behaviour, rot. inertia and transverse shear influence 80−48601
Bencubbin polymict meteoritic breccia, form. by impact on carbonaceous chondrite regolith 78−96443
borosilicate glass, microparticle impact, high speed photography obs. 78−44223
borosilicate glass surface, damage due to impact of small glass and steel spheres 78−52994
brittle material, dynamic solid particle damage, elastic and elastic-plastic response regimes 77−8910
brittle materials, water drop impacted, damage thresholds 80−81149
buoyant cylinder released underwater, impact motion on a surface body 80−68041
BWR-4 neutron noise analysis spectra, instrument tube flow-induced vibr. 78−94063
Caloris Basin (Mercury), age rel. to global tectonic features 78−85874
Caloris basin on Mercury, comparison with lunar Orientale basin 78−12121
cast iron, white, high Cr-Mo, fracture toughness 80−50726
centrifuge cratering 80−72522
Chenier Crater, on Moon, impacts rel. to lava-like material origin 78−81569
circular rod, controlled impact on isotropic, elastic half-space 79−90167
cloud particles, composition analysis using continuous impactor-replicator 79−53544
collar rocks, shatter cone surface spherules from Vredefort structure, S.Africa 77−53046
colliding cylinders, resulting stress field for linearly elastic material *(Russian)* 80−79237
comet on Earth, as cause of ice ages and ecological disasters 78−53714
cometary impact, rel. to Earth albedo sudden change and ice age onset 79−44241
compact gas gun for materials testing 79−15909
composite, laminate, crack normal to interface, impact response 80−14628
concavity techniques, point mass impact on elastic, viscoelastic or nonlienar elastic rod 79−37172
concentric impact of pointed bodies 79−41604
concrete, impact bending capacity *(Japanese)* 80−89341
cone, floating on incompressible liquid, vel. field after vertical impact *(Russian)* 79−90193
conical punch pressing into elastic layer 77−13612
contact pressure attainable using indentor which is body of revolution 77−11127
contact problem, elastic layer on rigid foundation with cylindrical hole 77−72252
crack response under antiplane shear 78−5691

impact continued
cracked infinite elastic wedge loaded by rigid punch, stress intensity factors 79−77019
crater formation 80−94765
crater shapes formed by high-speed impact 77−33364
crater slumping, role of acoustic fluidisation 80−85653
cratered terrain, thermal regimes and impact melt 77−2125
cratering by meteorite impact 79−21244
craters, coherently overturned flaps produced by hydrodynamic type wave motion 78−57209
craters, modification by fallback ejecta 80−82317
craters, on Earth, Moon and Mars, morphological evolutionary tracks 77−91134
craters formed in viscous-liquid targets, expts. rel. to Martian rampart craters 78−65530
craters in ice and ice-saturated sand, Martian implications 80−67614
cylindrical beam, impact effect on rigid wall *(German)* 80−106763
cylindrical cavity in anisotropic elastic material, impact-initiated wave propag. 78−13943
cylindrical punch, three-dimensional stress field, photoelastic studies 80−93272
Deimos, impact cratering rel. to surface features 80−31224
discs, impact stresses, photoelastic investigation 79−37182
dolomite, strain rate depend. inferred from impact and static compression studies 77−44977
drop impact on hard surface *(Russian)* 78−9688
droplet impact, high-speed, effect of gas medium on dimensions of contact area 77−28942
dynamic analysis of impact attenuation system using plastic deform., effect of strain-rate sensitivity 77−23890
dynamic contract of elastic bodies, direct connection and feedback mechanism *(Russian)* 79−50670
dynamic finite element analysis of cracked bodies subjected to impact loading 80−69742
dynamic finite element and photoelastic analyses, of impacted pretensioned plate 78−67111
dynamic pressures, shock wave parameters, high speed bodies collisions 77−68491
dynamic yield point in multimaterial impact 77−32731
Earth, meteorite impacts rel. to primitive ocean basins form. 79−20770
Earth, ocean basins origin 77−91085
Earth, ring system form. assoc. with Eocene terminal event 80−76890
Earth accretional melting, effect of blanketing by primordial dense atmosphere 79−57935
ejecta parameters depend. on primary vel. 78−59291
elastic conical shell impact anal. *(Russian)* 77−895
elastic cylinder surface impact, numerical soln. 80−38274
elastic disc loading by sudden radial force 79−14298
elastic impact problem, stress wave elementary analysis 79−50628
elastic longitudinal impact, elementary anal. 79−72809
elastic plate, impact load impulse form determination by the displacements and strains of a circular plate *(Russian)* 80−74751
elastic plate indentation by rigid punches 79−72807
elastic sphere torsion by elastic punches 80−99929
elastic-plastic impact problems involving severe distortions 77−17825
elastic-viscoplastic skewed plates, anal. of combined pressure-shear waves 77−65712
elastic-viscoplastic work hardened slab, indentation by rigid punch 80−53721
elastic/viscoelastic bar interface, impact wave behaviour 78−26075
elastically deformable media, liq. drop collisions, simulation of erosion in rainfield 77−56113
elastically deformable striker and solid obstacle, impact phenomena 78−77703
elastohydrodynamic film thickness, meas. of artificially produced dents and grooves 80−36975
elastomers, repetitively impacted, mech. response and heat buildup 77−54889
electrical discharge in vacuum, Fe spherical microparticles impact on polished electrodes, mech. effects *(French)* 78−22595
Elgygytgyn meteorite impact crater, Siberia, probable source of Australasian tektites 77−91135
elliptic infinite bar, impulsive loads, three dimens. elastic stress-strain anal. 78−87259
elliptical punch, elastic contact problems 78−9613
epoxy resin, stresses arising during high-speed droplet impact 80−71764
erosion, book contrib. 78−11350
erosion by impact on moon and planets 78−57476
explosive heating due to projectile impact, numerical anal. 77−72142
extensible string motion in nonviscous fluid *(Russian)* 78−77718
flexible string under transverse impact, dynamic deform. and possible unwinding from drum *(Russian)* 78−22279
floor sound insulation, analysis using L_C and L_A *(Japanese)* 80−79054
floors, elastic coverings, effect of thickness and hardness on impact sound insulation props. *(Japanese)* 80−79053
floors impact testing, impedance problems *(German)* 77−825
force measuring system, instability *(Japanese)* 77−25222
fracture, computational models for one and two dimens. wave propag. 77−11628
fracture mechanics for impact penetration damage, probability approach, appl. to Al panels 78−1606
fracture toughness testing, possibility of diminishing inertial peak under impact loading *(German)* 77−66726
frame, plane, impulsively loaded, large deflections, mode approx. technique extension 80−83757
frictionless indentation by rigid wedge, effect of tangential displacements in contact zone 79−37250
gas gun, short-barrelled, for impact studies 80−64501
glass, annealed and tempered, impact damage, strength 80−85025
glass, surface erosion, produced by meteorite impact 77−90445
glass bead, impact fracture *(Japanese)* 78−92338
glass particles impacting on metal barriers, piercing, stony meteorite simulation 78−89043
glass plates, effect of localized damage on energy losses, during impact by glass spheres 78−52973
glass punch impact on viscoelastic solid *(French)* 78−42535
glasses, partially leached rods, contact-damage resist. 80−50707
granite cylinders, failure under impact loading, brittle fracture process 77−86864
graphite-epoxy hybrid laminates, low level Charpy impact response 78−11333

impact continued
graphite/epoxy laminates, stress wave damage 80−93611
hailpads calibration 78−93001
head impact, tolerance level for bridging vein disruption, math. model 80−16987
head viscoelastic model, impact response 78−40234
head-neck impact response using realistic human model 78−80909
Hertzian impact of two elastic spheres in the presence of surface damping 80−69743
high speed interaction of drop with solid surface, apparatus design *(Russian)* 79−27605
high-velocity, three dimens. finite element calcs. 77−65674
high-velocity impact destruction of basaltic bodies, appl. to Martian satellites 77−64704
hockey ball, collision theory, teaching approach 77−41435
hydrodynamic model for impact of rigid body on ice *(Russian)* 77−20002
hypersonic target material, subject to impact with water droplet, holographic investigation 78−42306
hypervelocity, initial stages finite element analysis 77−41
hypervelocity particle impact, heating and vaporisation, temp. estimation 78−59290
hypervelocity particle-surface impact simulation, using high-power pulsed laser 77−44094
Hysol 8705, mathematical model of impact loading behaviour 77−54890
ideal fibre reinforced, rigid plastic cantilever beam, impulsive loading, subsequent motion 77−80096
ideal fibre reinforced rigid plastic beams, impulsive transverse loading, control impact 77−80094
ideal fibre reinforced rigid plastic beams with end supports, impulsive transverse loading 77−80095
impact ball apparatus, teacher's demonstration 78−8195
impact force meas. by elastic stress wave obs. 79−34215
impact noise reduction by floor coverings, hammer drop expts. *(Japanese)* 80−33331
impactor design for aerosol meas. 77−29448
indentation, dynamic, of elastic half-space by rigid punch, numerical method 78−1612
indentation fracture mechanics, residual stress effects 79−83300
indentation hardness and hot pressing, calc. methods 80−58981
indentation hardness and microhardness test methods for plastic deform. *(Hungarian)* 80−97664
indentation of elastic half space, numerical method *(French)* 79−50673
infinite medium with cavities, response to impact load 77−50945
integrating sound level meters, response to impulsive sounds 79−50547
internal meas. of shear and compression waves, gauge lead effects 80−74817
interplanetary microparticle studies by space-borne instrumentation 78−57460
interplanetary particles, impact collectors on spacecraft 78−57459
jet impinging on liq. pool, submerged biphasic region 77−31350
Joule's constant determination, large scale 19th century expt. method 80−77572
knee joint impact response, comparison of normal and osteoarthritic joints 78−31848
laminated thermoplastics, impact testing machine 78−3272
layered composite containing a crack, impact response 77−50991
linear oscillatory system response to shock impact *(Russian)* 79−9096
linearly elastic rod on thin linearly viscoelastic target 79−81793
long rod penetration of targets at hypervelocity impact, HELP computer code 78−26061
Luna 24 soil samples, meteorite impact rel. to metallic phases comps. 78−32367
lunar crater Giordano Bruno, AD 1778 impact obs. consistent with laser ranging results 78−69717
lunar crustal evolution, major impact processes contrib. 77−60658
lunar far-side ringed impact basins, correl. with magnetised regions 80−36521
lunar highlands, effects of meteorite bombardment on primordial crust 80−109381
lunar impacts by objects in parabolic low inclination order, distrib. 79−2493
lunar maria, absolute time scale of form. and filling 77−60646
lunar regolith, dynamics, rel. to irradiation and accretion of solids in space 77−60562
lunar rocks, microcrater and accretionary grain populations under meteoroid and solar wind bombardment 80−94731
lunar rocks, microcrater and accretionary grain populations from lunar surface and Apollo samples obs. 80−94732
lunar samples, charged particle track anal., thermoluminesc. and microcratering studies 77−60665
lunar surface, chem. changes at impact-induced phase transitions 77−60662
lunar surface impact erosion and solar wind sputter erosion 77−60664
Mach one impact test apparatus utilizing He-driven gas gun 79−75673
machine for impact testing over wide range of deform. rates 78−3271
Manicouagan impact crater, gravity study and upper crust density contrasts 78−81170
Manicouagan impact crater, Quebec, investigation 78−81163
Manicouagan impact melt, Quebec, chemical interrelationships with basement rel. to form. processes 78−81165
Manicouagan impact melt, Quebec, stratigraphy, petrology and chemistry 78−81164
Manicouagan impact melt sheet, Quebec, thermal history 78−81167
Manicouagan impact structure, Quebec, melt rocks petrogenesis 78−81166
Manicouagan melt sheet, Rb-Sr isochron age 78−81168
Manicouagan structure, Quebec, central mag. anomaly 78−81169
Manych meteorite, L-3 chondrite, impact remelting rel. to droplet chondrules comp. and origin 79−30014
Mars, 4 to 10 km dia. craters distrib. and relations to global geologic units 78−65528
Mars, rampart craters morphology 78−53854
Mars impact crater obs., Tharsis region volcanic shield dating 77−5476
Mars impact craters, emplacement of ejecta by surface flow 78−20671
Mars rampart craters, areal distrib. 79−84706
Mercury, endogenic modification of impact craters 78−12129
Mercury, large impact structs., isostasy and average crustal viscosity 78−12120
metal, ductile, jet-impingement solid-particle erosion testing, halo effect 80−76376
impact continued
metal, erosion by high speed particles, temp. effects 80−40556
metal, plastic impact, energy absorbed by elastic waves 80−5972
metal, strong, compressive stress/strain props. meas. at very high strain rates, modified Hopkinson bar system 80−85128
metal erosion by solid particles, high-speed photography 78−39919
metal tube, dynamic lateral compression, strain rate effects 80−83758
metallic plates, oblique perforation by projectiles 77−62141
metallic plates collision, plastic deform., jet form. 79−11669
metals, aspects of impact testing 79−79111
meteorite, craters, internal struct. model 78−44825
meteorite chondrules formation, constraint on impact theories 77−82178
meteorite crater field formation, effects of meteoroid atmospheric breakup 80−94760
meteorite craters, geophysical and geomechanical aspects 80−17265
meteorite craters on Earth, form., props. and catalogue 78−96411
meteorite craters probable number in USSR, calc. 77−66921
meteorite impact and ejecta deposition on airless planetary bodies, topographic effects 78−65523
meteorite impact and impact-explosive craters, destruction asymm. *(Russian)* 77−9726
meteorite impact blast, gasdynamical models and two-dimens. unsteady computs. 77−60565
meteorite impact craters in limestone, calcite microstruct. geological aspects 79−57933
meteorite impact ejecta, depend. of mass and energy lost on planetary escape vel. 78−45295
meteorite parent body, impact melting rel. to origin of Fe meteorites of groups IAB and IIICD 80−109404
meteorites, relative crater prod. rates on different planets 77−60699
meteorites collisions with planets, review 79−8884
meteoritic material at large impact craters, chemistry 78−57208
meteoroid impact effect on spacecraft attitude 78−73608
meteoroid impact on small solar system bodies, seismic effects, rel. to Phobos *(Russian)* 78−69754
meteoroid shield for spacecraft, destructive effect and meteoroid vel. 78−53788
meteoroids on Moon, seismic energy transmission in intensively scatt. environment 77−73685
micrometeoroid impact, laboratory simulation 78−57510
micrometeroid impact on thin film of detector, lab. expts. 80−77292
microparticle impact, strain rate effect 77−80577
microparticles, on brittle solids, high speed photography obs. 78−44223
mineral-fibre composites that resist fracture and cracking 77−8798
minerals, impact abrasion by windblown dust or snow 77−70647
mirror/flaw-size relations, residual contact stresses effect 80−107363
Moon, basis for interpreting ages of Serenitatis, Imbrium and Orientale events 77−60642
Moon, crater dominated chronology for highland stratigraphy 77−60645
Moon, cratering events rel. to Luna 24 drill core soil samples depositional history 79−88608
Moon, early collisional heating 80−8563
Moon, early impact chronology rel. to early collisional history of solar system 77−60640
Moon, impact basins ages from radiometric dating of samples 77−60644
Moon, impact effects on Imbrium stratigraphy, petrological aspects 77−60641
Moon, impacts rel. to elements volatilisation from regolith solid particles 77−9680
Moon, large impact structs., isostasy and average crustal viscosity 78−12120
Moon and Mercury, relative preservation states of secondary craters 78−12118
mortar specimens, repeated impact bending load study *(Japanese)* 80−93622
mushrooming of flat-ended projectile on anvil, numerical meth. 77−72243
nanosecond hydrodynamic diagnostics, streaking camera, fibre optic probes 78−37096
natural glasses and tektites, N concs. 80−41446
noise in buildings, meas. equipment *(Japanese)* 77−88986
noise prediction, acceleration noise 79−72752
non-Newtonian annular film, collapse under axial impact 77−84281
nonlinear elastic half-space, dynamic contact stresses due to axisymmetrical projectile impact 78−42573
nonlinear oscillator and reflectors, periodic vibr. and impact characteristics 80−92089
nuclear plant, impact load for tornado generated missiles 78−51103
nuclear plant equipment response to aircraft impact 78−50416
nuclear power station, full scale tornado-missile impact tests 78−41876
nuclear power station response to aircraft impact 78−41875
numerical treatment of sliding interfaces and impact 79−41631
one-dimensional linear oscillator impacting under harmonic excitation, steady-state response 80−53690
Orientale basin, comparison with Caloris basin on Mercury 78−12121
pendulum impact machines, energy meas. using optical system 80−69746
penny-shaped crack, sudden twisting in a finite elastic cylinder, stress calcs. 78−67110
perforating rods, length reduction at high impact velocities, X-ray studies 78−40016
Phobos, dynamical evolution and time to collision with Mars 78−89104
Phobos, impact cratering rel. to surface features 80−31224
Phobos, Stickney crater impact rel. to groove form. 78−89103
Phobos, Stickney crater impact rel. to grooves distrib., morphology and possible origin 80−72837
Phobos and Deimos, Viking obs. rel. to impact craters 78−20681
planetary bodies, historical size distrib. of impact craters, use of equivalency 78−45250
planetary satellites, effect of proximity to Roche limit on dynamical behaviour of ejecta 80−98592
planetary surfaces, global seismic effects of basin-forming impacts 78−12122
planetesimal impact, hypothesis for form. of chemically peculiar (CP) stars 78−20834
plastic indentation of layer by two rigid punches, interference between deformation zones 77−65693
plastic longitudinal dynamic wave propagation, impact end 79−14294
plastic wave theory, comparison of predictions with impact expts. 80−83742

impact continued
plastics, reinforced, resin selection rel. to impact and fire resist. 80−40322
plate, 2-D high velocity impact problem *(Russian)* 77−50924
plate, bending vibrations and acoustic pressure *(Russian)* 80−23949
plate, elastic deform. due to axisymmetric punch 78−75065
plate, impact force meas. method 80−79242
plate falling upon surface of compressible liq. *(Russian)* 77−929
plate impact experiments, optical alignment of impact faces 77−45876
plate perforation by projectile, comment on paper by Awerbuch et al. 79−27542
plate-impact recovery expt. using star-shaped flyer 78−18262
plug formation in plates, cylindrical projectile impact, nonlocal viscous fluid model 78−49653
PMMA bar, notched and perforated, fracture produced by longitudinal impact 79−43388
polycarbonate blends, yield and deform. behaviour, impact modification 77−36572
polycarbonate of bisphenol bar, notched and perforated, fracture produced by longitudinal impact 79−43388
polyethylene, expanded, dynamic model rel. to drop impact 78−7160
polymer impact resistance, dynamic mech. anal. 80−16626
polystyrene, atactic, indentation recovery, defect struct. produced by deformation 79−43275
polystyrene, atactic, indentation recovery 80−84988
projectile impact on thin flexible struct., dynamic contact *(French)* 77−68408
projectile perforation of multi-layered beams 80−1491
PTFE, impact testing, elastic analysis of conventional test, reassessment of testing 78−60770
pulse phenomena produced by a flat mass on one of its supports *(Italian)* 80−4514
punch-elastic body dynamic contact, superseismic stage, exact soln. 78−55614
PVC rigid plate specimens, Charpy impacted, SEM exam. of fracture surface *(Japanese)* 78−52953
PVC strip, viscoelastic props. from impact studies *(Russian)* 79−32289
Pyrex, impact of small steel spheres 77−73338
Pyrex, indentation recovery, defect struct. produced by deformation 79−43275
PZT ceramics, ferroelec. energy conversion under shock loading 80−108163
quartz, y-cut, impact, appl. of transverse-displacement interferometer 78−12747
rare earth sulphides, polymorphic transforms. on impact compression 77−47575
rebound of elastic bodies in oblique impact 77−50873
rectangular bar, semi-infinite, longitudinal impact, elasticity eqns. anal. 78−90703
regolith reprocessing by cratering, erosion of material layer which loses charact. props. 80−62053
repeated impact tester attachment, for bending impact tests, method of obtaining asymmetric cycles 80−16628
ricochet of dumb-bell shaped projectiles off sand 78−30172
ricochet of high speed long rod projectile, min. target obliquity 80−5994
ricochet of spherical projectile off water and sand 77−17804
Ries crater, nature of C metastable phases 77−89404
rigid body impact on elastic half-space, Fourier synthesis of steady state vibr. 77−80101
rigid punch, flat-ended cylinder with elliptical cross section, Boussinesq problem 79−68663
rigid punch motion at viscoelastic space boundary, dynamic contact problems *(Russian)* 79−81819
rigid punch problem on non-homogeneous elastic half-space 80−53720
rigid punch problems, class involving forces and moments 79−94560
ring subjected to distributed impulsive load, dynamic response 78−13946
ringing noise arising from free vibration, impact noise prediction 80−28377
Rochechouart crater, Massif Central, France, shock zoning study 77−81897
rock half-space, impact of steel cylinder and effects 80−85649
rock penetrator, initial response, elastic rod theory 79−32392
rocks, impact and comminution processes in shale and diorite 78−3763
rocks destruction by meteorite impact 77−66910
rod impact, numerical soln. using Volterra integral eqns. 77−68437
rod penetrating thick target, plastic deform.-jetting flow transition vel. 77−62163
rods, numerical method for analysing elastic wave propag. due to impact 79−32352
rubbing surfaces, impact interaction of microroughnesses *(Russian)* 79−100265
sapphire disc, dynamic deform. by projectile impact back reference holography obs. *(French)* 78−42307
sea ice in Gulf of Bothnia, flexural waves meas. *(Japanese)* 78−96225
semiinfinite elastic cylinder indenting elastic half space 80−53722
shallow spherical shells, stability under axisymmetric loading *(Russian)* 79−14287
shear, and compression wave propag. in impacted solids 80−83755
shell, cylindrical, impact on surface of compressible fluid, numerical method *(Russian)* 80−87746
shell, elastic cylindrical, impact on surface of compressible fluid *(Russian)* 79−37181
shell, rigid-plastic, large deflection under impact of concentrated mass 77−54901
shell, spherical, impact on surface of compressible fluid, numerical method *(Russian)* 80−87747
shock absorbers, fluid-saturated porous solids 80−53726
shock degassing of planetesimal *(Russian)* 79−70973
shock-test stand for repeated impact acceleration effect 79−80611
Signorini's problems, reciprocal variational inequalities soln. 79−41585
single inclined plate impact expt., technique for determ. in-material longitudinal and shear particle velocity histories 78−79289
single mass vibroimpact system, response to white noise random excitation 80−64454
Slate Islands structure, partially submerged meteorite impact crater in Lake Superior 77−78183
soda-lime, impact of small steel spheres 77−73338
soda-lime glass surface, damage due to impact of small glass and steel spheres 78−52994
soldered layer on half-plane, rigid stamp impression 80−38353
solid body accel. sound energy 77−62099
impact continued
solid body-microparticle impact, cratering, viscous effects 79−66255
solid cylinder, annealed, dynamic forming by compression *(Japanese)* 77−70267
spent-fuel rail cask system, high-speed impact and fire test 79−59206
sphere impacting on thin square plate, acoustic generation mechanism 80−74591
sphere with slab, transient sound radiation 79−23128
split Hopkinson pressure bar application to fracture dynamics 80−85140
stability analysis, impact vibration, steady, body with impact hysteresis characts. 78−51099
steady impact vibration of body with quadrilateral hysteresis loop for restitution force 77−23905
steel, alloy, Ni-Co-Mo, fatigue crack growth, during impact tests exam. of kinetics 78−88525
steel, brittle fracture of compressor materials under impact loading 77−25137
steel, C, crack initiation and propagation life under repeated impact tensile loads *(Japanese)* 80−104264
steel, C, failure mechanisms in impact fatigue 80−40493
steel, Cr-Mo, effect of Mo on high-temp. props. 80−85005
steel, Cr-Mo-Ni-V, dynamic stress intensity factor meas., possibilities and limits *(German)* 80−93719
steel, Cr-Ni-Sr (18.15, 17.64, 2.4 wt.%), rare-earth additions effect on impact fracture *(Chinese)* 80−66617
steel, ferritic stainless, embrittlement 80−85041
steel, high Mn-Cr, austenitic struct. stability and low-temp. toughness *(Japanese)* 80−76356
steel, large forging, mech. props. 77−4797
steel, low alloy, fibrous component zones size, depend. in fracture on impact test temp. and notch radius 80−21076
steel, low C, dynamic stress intensity factor meas., possibilities and limits *(German)* 80−93719
steel, low-alloy, testing cracked specimens for impact bending, expt. planning method appl. 80−71831
steel, low-C, fatigue strength and crack propag. behaviour under impact program loading conditions *(Japanese)* 80−66635
steel, low-C, kinetics of void development in fracturing A533B tensile bars 80−76357
steel, maraging, fatigue crack growth, during impact tests, exam. of kinetics 78−88525
steel, medium C, shell-shaped fracture due to B embrittlement *(Chinese)* 80−55493
steel, metastable austenitic, resistance to failure 77−4852
steel, Mn-V reinforcing type, strain ageing characts. rel. to mech. props. 80−84969
steel, Ni-Co-Mo, dynamic stress intensity factor meas., possibilities and limits *(German)* 80−93719
steel, pressing die X45 CrNiWMoVCo 9.9, test results *(German)* 80−50785
steel, pressure tank, heat-treatment effects and mech. props. *(German)* 80−40409
steel, stainless, global bending response analysis of elastic and viscoplastic nuclear shipping cask structures subjected to impact loading 80−76301
steel, types S25C and S45C surface damage produced by pulsating impact contact load *(Japanese)* 80−104263
steel 45G2, fracture resistance, from impact bending tests and oscillograms 80−61047
steel cone, phase velocity of longit. impact wave *(Japanese)* 78−9600
steel rods, longit. impact on plate, contact time meas., student expt. 79−5939
steel shot, cast, impact fracture *(Japanese)* 78−92338
stone meteorite, laboratory simulation of impact *(Russian)* 77−91489
string vibrating against rigid wall, partially elastic or anelastic impact, energy calcs. 78−67028
structural member, dynamic loading and plastic response, review 80−83756
tension-torsion impact testing apparatus, instantaneous plastic property 79−52474
terradynamic penetrators as planetary landers 77−78601
terrestrial cratering history, theory incorporating galactic modulation 80−31043
terrestrial impact craters and astroblemes, morphology and struct. *(Russian)* 77−45000
terrestrial impact structs., so called, non-random geographical distrib., implications 79−34825
terrestrial meteorite impact structures, catalogue of 230 sites 77−73741
terrestrial planets, shock degassing rel. to atmospheres form. during accretion stage *(Russian)* 79−101099
terrestrial rocks, impact shock effects on magnetism 78−85538
testing, deform. meas. accuracy improvement 80−81259
thin elastic bar, impact buckling, Monte Carlo calcs. 79−32317
three point bend testing for notched and precracked specimens, testing and data analysis procedures 78−53053
tibia flexural wave propagation, discontinuous model and in vitro study 77−29169
torsional test by means of dropped bar, appl. to low C steel 79−100304
trace metal aerosol dry deposition, inertial impaction and filtration model 78−73441
transient sound radiated by impact of elastic sphere on thin plate 80−38168
transparent material, small particle impact, high speed photomicrographic recording of shock wave 78−44342
transverse impact force of falling object on horizontal beam *(German)* 79−90200
transverse impact method for studying the viscoelastic properties of materials *(Russian)* 79−32398
transverse impact of fibre-reinforced rigid-plastic plates 78−38211
transversely isotropic half space, elastic strain caused by rigid punch 79−59947
transversely isotropic half-space indented by a flat annular rigid stamp 79−55347
tubes, fluid filled, transients produced by longit. impact 77−72212
Tunguska, 1908, catastrophe, cosmochemical anomaly in silicate microspherules comp. 78−96430
Tunguska cosmic body, chemical comp. and nature 78−61810
Tunguska event, comet collision with Earth 78−49390
two degrees of freedom system, effect of damping on impact response 80−74587
two nonlinearly elastic bodies, impact-contact problem 79−98669
Venus, Mars and Earth, impact ejecta trajectories in atms. 78−40854

impact continued
vibrating string, partically elastic or anelastic impact against wall *(Italian)* 77−72143
vibrations of body with hysteresis collision calcs. 80−14602
viscoelastic, flexible string under transverse impact loading, eqns. of motion *(Russian)* 78−22280
viscoelastic half-space, dynamic indentation and impact by axisymmetric rigid body, iterative method anal. 80−14626
viscoelastic rod, nonlinear waves and finite rod impact on rigid obstacle 79−41606
viscoelastic rod, shock rel. to hard obstacle *(Russian)* 80−23911
viscosity resolution in impacts, using Otani method 79−50657
Vredefort Dome, S.Africa, coesite and stishovite discovery 78−53653
Vredefort structure, S.Africa, comp. of spherules on shatter cone surfaces 79−29773
water drop impact on rigid surface 77−85084
water drops, impaction and electrical effects on collisions with spherical particles 78−28272
wave formation, in metal bodies impacted at high velocity *(Russian)* 77−68478
wear, book 78−48544
weightless plate on liquid surface, central impact 79−90192
Wilkes Land, Antarctica, evidence for possible hypervelocity impact crater 77−17059
wire rope, spiral, normal transverse impact, laws of motion *(Russian)* 77−50877
Wolf Creek crater, Western Australia, gravity investigation 79−100838
Zhamanshin meteor crater, tektites-irgizites form. conditions from Fe ions states 78−61420
Zhamanshin structure, Russia, water content of irgizite tektites 77−87346
Al, 6061-T6, pressure shear impact in transverse displacement interferometer, plastic flow 80−81137
Al, annealed, dynamic testing of rate sensitivity *(Japanese)* 77−70267
Al beam, exam. of elastoplastic contact strength law, using impact bending *(German)* 79−43365
Al, pressure-shear waves due to oblique plate impact 77−65713
Al rod, exponentially varying shape, impact by steel spheres, elastic wave propagation 80−74791
Al, ultimate tensile strength for brief impact 80−70309
Al-Bi(Cd)(Pb)-Ti, containing low-melting pt. inclusions, mech. props. 80−93632
Al-Zn-Mg, type V-95, ultimate tensile strength for brief impact 80−70309
Al_2O_3, biaxially stressed, exam. of localised impact damage 78−72846
C fibre reinforced composite, split Hopkinson press. bar test, opt. and strain gauge methods comparison 80−85132
C fibre reinforced plastics with mixed fibres, exam. of fracture toughness and shear strength 79−20151
CdS, $(10\bar{1}0)$ face, deformed zones around microimprints 78−23812
Cu, annealed, dynamic testing of rate sensitivity *(Japanese)* 77−70267
Cu, impact welding, viscous energy dissipation 77−70058
Cu, polycryst., surface layer hardening by multiple impact 80−108469
Fe microsphere, semi-elastic impact on diamond-polished metal targets 77−11124
Fe microsphere impact on electrode, charge reversal, oxidation effect 77−12042
Fe, soft, annealed, dynamic testing of rate sensitivity *(Japanese)* 77−70267
Fe-C-Mn (0.5, 0.6 wt.%), powder forged, mech. props. 80−21096
Fe-C(0.001 to 0.44 wt.%), C effect on low temp. brittleness *(Japanese)* 80−50711
Fe-Mn (8 wt.%), quenched, exam. of intergranular embrittlement 78−76745
InBi single crystal, deform. mode under dynamic indentation 80−88163
LiF monocrystal, impact damage, influence of particle props. 80−30120
LiF, shock wave, precursor decay, stress threshold 77−4156
MgF, polycryst., quartz particle impacts no. effect on erosion in elastic-plastic response regime 80−81209
MgO short time chemomechanical effects, dislocation generation and motion, drilling simulation 79−87749
MgO single cryst., impact wear characts. 80−76374
MgO single cryst., impact wear damage 80−76375
MgO, spherical particle impact damage, effect of crystallographic orientation 79−79135
Na_2O-CaO glass, shear deform. under pyramidal indentations 80−84989
Na_2O-CaO-SiO_2, plates, exam. of Hertz crack branching 78−72887
Na_2O-CaO-SiO_2 glass, high-vel. liq. impact, oblique impact anomaly 80−89329
Ni-Cr-Fe-Mo-Co (21.41, 19.28, 8.64, 2.16 wt.%), Hastelloy alloy X, exam. of thermal stability 78−84865
Ni-Cr-W-Mo-Al-Ti (15,6,3,2,2, wt.%), wrought, Si effect on transition brittleness *(Chinese)* 80−55491
Pb target, multiple interior impacts, hard target high vel. impact simulation 77−72145
PbO-B_2O_3 phase-separated glass, fracture toughness, Vickers indentation method 80−85023
$PbZr_{0.95}Ti_{0.05}O_3$, impact loading, mech. and elec. response, elec. state effect 78−64317
$Pd_{77.5}Si_{16.5}Cu_6$ amorphous, indentation recovery, defect struct. produced by deformation 79−43275
Si_3N_4, biaxially stressed, exam. of localised impact damage 78−72846
SiO_2, fused, single particle impact damage 80−40508
Ti alloy, brittle fracture of compressor materials under impact loading 77−25137
Ti-Al-V (6, 4 wt.%), targets, metallographic features after ballistic tests 79−79046
Ti-Al-V (6,4 wt.%), effect of air exposure on fracture characts. 80−100890
Ti-Al-V (6.4 wt.%) cast alloy, with improved microstruct., mech. props. *(Japanese)* 80−71701
U, one dimensional spall 77−80579
V, impact deform., influence of previous static loading *(Russian)* 78−6972
Zn, crystalline, wave formation during oblique collision *(Russian)* 77−89494
ZnS, hot pressed, water drop impact damage, SEM exam., IR transmission 78−88543
ZrO_2, transformation toughened, localised impact damage 80−7665

impact avalanche transit-time diodes *see IMPATT diodes*

impact ionisation
alkali halide, avalanche impact ionisation, in optical breakdown 79−42895
alkali halide and other crystals, damage induced by $CaF_2:Er^{3+}$ laser radiation at 2.76 μm 79−91539
alkali halide crystal, laser induced breakdown, avalanche ionisation theory *(Russian)* 77−44095
alkali halides, pulsed-laser-induced damage, role of avalanche multiplication and multiphoton absorpt. 80−48316
amorphous, high field transport, impact ionisation, carrier mobility 80−80286
anomalous avalanche breakdown 80−80284
avalanche breakdown as nonlinear wave of soliton type 77−47824
avalanche noise theory 79−24043
avalanching semiconductors, carrier drift vel. effect on meas. ionisation coeffs. 79−69516
avalanching statistics, strong electric field *(Russian)* 77−66171
bulk semiconductor, I-V characts. based on impact ionisation, model 77−11925
carrier multiplication and noise in avalanche devices 80−15579
chalcogenide glass film, monostable switching obs. 77−8157
crystal with narrow allowed band, elec. field ionisation of deep impurity level 79−15118
current runaway in insulators affected by impact ionisation and drift 78−39501
dielectric, transparent, solid, ionisation threshold development in field of single powerful focused laser pulse *(Russian)* 77−69771
dielectric breakdown by picosecond laser pulses, many-photon and impact ionisation 78−18002
dielectric film, amorphous, covalent, disruption of stationary state and electrical breakdown 77−20332
dielectric film, amorphous, ionic, disruption of stationary state and electrical breakdown 77−20333
dielectric solids, laser damage, conduction-band electron interaction theory 80−35017
donor excited state lifetime, delayed avalanche breakdown 77−85231
donors with excited states, kinetics of electron transitions 80−39600
donors with excited states, non-equilibrium phenomena, theory of kinetics of electron transitions 78−79961
dust particles fast impact on Au or W target, ion plasma comp. rel. to micrometeoroid detect. 77−39438
electron beam propagation in dielectric guide due to space charge neutralisation 80−18716
electron-hole avalanches with constant ionisation coefficient, comment and reply 80−75572
electron-hole avalanches with constant ionization coefficients 79−91054
film, breakdown mechanisms 78−76385
n-GaAs, intrinsic avalanche response time, orientation depend. 79−51587
Gunn diode, impact ionisation of deep levels, effect on time-averaged I-V characteristic *(Russian)* 77−62935
Gunn diodes, population inversion condition 77−77251
heterojunction, avalanche breakdown sensitivit of multiplication layer *(Russian)* 78−34888
heterojunction multilayered structs., effective impact ionisation rates 80−88621
illumination, intense, of optically transparent medium, avalanche ionis., recomb. effect 80−7295
p-InSb, electron-hole pair production 80−44611
n-InSb, impact ionised plasma, three stream instability 77−55557
insulating film, electrical breakdown by impact ionisation, models 79−91373
insulator, current runaway, impact ionisation and recomb. effects 77−4601
insulator current runaway models 78−6630
many-valley semiconductor, anisotropic, kinetic theory of impact ionsation 78−14740
maximum electric field in high-field domain in Gunn devices 78−79996
MNOS struct. with complementary tunnelling emitter bipolar transistors, current transport characterization 79−91146
MOS structure, n-channel, evidence for impact ionised electron injection in substrate 78−88031
n^+-p spherical junction, strong impact ionisation 78−39202
n-n^+ junction point contacts, I-V characts. 77−1480
narrow gap semiconductors, recombination mechanisms, review 80−96905
narrow-gap semiconductor, recomb. instability of electron-hole plasma 80−39621
nonpolar semiconductor, normalised theory of impact ionisation and vel. saturation using Markov chain 79−91067
one-sided abrupt junctions, normalized representation of avalanche breakdown behaviour 80−65666
optical materials, laser induced breakdown, breakdown thresholds and multiphoton absorpt. coeffs. 79−3735
p-n junction, avalanche breakdown voltage and differential resistance *(Russian)* 78−47858
p-n junction, avalanche multiplication 78−84289
plasmon mechanism for secondary breakdown 78−95352
Schottky barrier, avalanche multiplication 78−84289
Schottky diode, effect of thin oxide layer between metal and semicond. 77−20432
Schottky layers, homogeneous avalanche breakdown instability mechanism, microplasma form. 78−72262
semiconducting point cathodes, explosive electron emission 77−59678
semiconductor, adiabatic approx. in transient donor recomb. 80−49761
semiconductor, hot electrons in quantizing mag. field and impact ionisation of impurities 78−6386
semiconductor, impact ionization, review 80−65577
semiconductor, instabilities of electron-hole plasma under impact ionization and microwave emission 79−65508
semiconductor, switching under impact ionisation 78−72215
semiconductor, theory of carrier multiplication and noise due to avalanche processes 80−6865
semiconductor avalanches, intrinsic response time and effective ionisation rate anal. 77−69329
semiconductor heterojunctions, impact ionisation 80−65663
semiconductor models for non-equilibrium phase transitions due to impact ionisation from traps 79−51520
semiconductor particle detector utilizing impact ionisation, resolution 77−6639

impact ionisation continued
semiconductor structures, s-type switching at high current densities 77−20417
semiconductors, Auger recombination processes 79−38091
semiconductors, electron multiplication, phonon scatt., ionisation rate calcs., Markov processes 80−50267
semiconductors, impact ionisation of deep impurity centres 79−73470
semiconductors, impact ionisation theory 80−49752
semiconductors, intervalley electron-electron scattering effect on optical transitions 80−108267
semiconductors, narrow-gap, recomb. instability under crossed elec. and mag. fields 80−70712
semiconductors, phonon assisted electron impact ionisation and Auger recombination, theory 80−39591
semiconductors, scatt. influence on Auger transitions depend. of impact ionisation on electron energy 80−44608
semiconductors nonequilibrium phase transitions, stability and dissipation, teaching 80−105479
solid dielectrics, electric breakdown mechanism, discharge development, electron impact ionisation 80−15961
surface avalanched p-n junctions, localised charge injection and trapping 77−76907
p-Te, impact ionization rate of holes at 77K 80−10993
thresholds, as generalisations of van Hove singularities 77−77295
transparent dielectric, enhanced localised intensities in surface scratches rel. to laser damage 79−22999
transparent dielectric, laser damage probability and avalanche breakdown 77−12471
transparent dielectrics, laser damage, electron avalanche and multiphoton ionisation roles 80−35016
transparent dielectrics, optical break-down in const. elec. fields *(Russian)* 77−8509
transparent solid, laser damage by electron avalanche ionisation 79−19952
Al_2O_3, elec. breakdown during anodic growth 80−55034
CaF_2, damage by UV laser radiation, avalanche ionization mechanism 80−76110
p-$Cd_xHg_{1-x}Te$-metal contact, negative resist. effects, impact ionisation 77−4440
CdS, impact ionisation of excitons, photocond. and photolum. meas. 79−56266
CdS type semiconductors, bulk laser damage mechanism, photocond. meas. 80−15567
CdTe diode, generation-recomb. and ionisation processes, temp. depend. *(Russian)* 77−39942
Cr-Si(GaAs) Schottky barriers, interfacial structural defects effect on avalanche breakdown 79−42644
Cu cathode, electroluminesc. from semicond. impurities on surface 77−90200
GaAs electrodes in aqueous electrolytes, localised avalanche breakdown 79−4599
GaAs, electron and hole impact ionisation coeffs. 78−6389
GaAs, electron and hole ionisation rates meas., elec. field orientation depend. 78−10453
GaAs, epitaxial film, field effect struct., elec. breakdown, negative resist. 77−12030
n-GaAs epitaxial film, magnetoresist. at low temp., geometric effect 80−93015
GaAs, exciton-polariton reflectance spectra, exciton impact ionization and illum. intensity effects 79−42943
GaAs, free-carrier impact ionisation, orientation depend. rel. to cond. band 77−76836
GaAs Gunn diodes, population inversion condition 77−77251
GaAs, hot carrier impact ionisation, band struct. depend. 78−30934
GaAs, impact ionisation, electron band struct. effects obs. by temp. tuning 77−85232
n-GaAs, impact ionisation initiated by acoustoelectric effect 78−52038
GaAs, impact ionisation rates for electrons and holes, photocarrier multiplication obs. 78−87995
GaAs, impact ionisation of excitons 79−38079
GaAs, impact ionisation rates, temp. depend. 79−38077
GaAs, impurity centres ionis. by Auger electrons, carrier relax. *(Russian)* 79−51594
GaAs, luminescence during streamer discharge *(Russian)* 77−55835
n-GaAs, microwave biased, fast rise-time modulation of 337 μm radiation 77−54794
GaAs orientation dependence of ballistic electron transport and impact ionisation 80−49758
GaAs p-n homojunctions, microplasma elec. breakdown mechanism 79−87147
GaAs secondary ionisation coeffs., interband scatt. effects 78−43408
n-GaAs, switching time in low-temp. impurity breakdown 77−15923
n-GaAs X-band impact ionisation for 337 μm radiation modulation 77−39069
GaAs:Fe reverse biased π-ν-n struct., switching effect 80−88628
GaAs-$Ga_{1-x}Al_xAs$ n^+-ν-n junction, avalanche carrier multiplication *(Russian)* 78−76140
GaAs-GaSb, threshold energies for impact ionisation by electrons and holes 78−6390
$Ga_{0.47}In_{0.53}As$, electron and hole impact ionisation rates 80−49745
$Ga_xIn_{1-x}Sb$, electron vel. field characts., microwave heating method 79−91058
GaP, electroluminescent diode, electron irradiated, negative resistance due to impact ionisation 77−15942
GaP p-n junctions, electron beam excited carrier avalanche multiplication 79−69587
GaSb, solid solns., impact ionisation, cond. and valence band effects 80−65583
n-Ge, homogeneous, avalanche ionisation and current oscills. 77−15864
n-Ge, impact ionisation at 4-9.5K 80−10994
Ge, impact ionisation by electrons and holes, threshold energy 79−38078
Ge, impact ionisation of shallow donor states, 4 to 7K 78−30936
Ge, ionisation rates, cryst. orientation depend. 80−103700
Ge Lo-Hi junctions, avalanche injection delay and ionization rate at low electric field 79−95475
Ge, nonequilibrium carrier excitation by CO_2 laser radiation 77−89803
Ge, oscillatory exciton breakdown, microwave cond. 80−103716
Ge-InAs based MIS struct., avalanche carrier multiplication 80−88566
Ge-Sb, far IR emission stimulation by impact ionisation 80−66301
Ge-Si(GaAs) heterodiodes, interfacial structural defects effect on avalanche breakdown 79−42644

impact ionisation continued
$Hg_{1-x}Cd_xTe$, avalanche formation, high intensity IR transmission limit 79−78684
$Hg_{1-x}Cd_xTe$, narrow-gap semiconductor, high intensity IR transmission limit 80−7361
$Hg_{1-x}Cd_xTe$, recombination processes using impact ionization capture cross sections 80−75577
HgTe, gapless semicond., magnetophonon conc. oscills. *(Russian)* 77−11943
n-InAs, avalanche formation, high intensity IR transmission limit 79−78684
InAs, impact ionisation and Auger recomb. 77−20329
InAs, narrow-gap semiconductor, high intensity IR transmission limit 80−7361
InAs p-n junction, carrier multiplication and ionisation coefficients 77−8188
$InAs_{1-x}P_x$ epitaxial layers, sub-threshold velocity-field characts., intervalley separation 77−63010
$InAs_{1-x}P_x$, high field instabilities, press. and comp. depends. 78−26873
$InAs_{1-x}Sb_x$ p-n junctions, avalanche multiplication 80−6965
InGaAs p-n junction, carrier multiplication and ionisation coefficients 77−8188
InGaAsP avalanche photodiodes, breakdown mechanism, donor conc. effect 80−70710
InGaAsP/InP avalanche photodiode, ionisation coeff. 80−15590
InP Gunn diodes, population inversion condition 77−77251
InP, impact ionis. by electrons and holes 79−99554
InP, impact ionisation by electrons and holes 80−100467
InP p^+-n abrupt junctions, ionisation coeffs., photomultiplication meas. 80−65655
InSb, avalanche formation, high intensity IR transmission limit 79−78684
InSb, carrier heating by microwave field, inertia effects 80−65580
n-InSb, compensated, impact ionisation temp. depend. 77−20331
InSb, conductivity anisotropy in strong electric field 78−19048
InSb, electron drift velocity in fields up to 800 V/cm in presence of impact ionisation 78−39120
n-InSb, electron-hole plasma, LF instabilities in crossed fields 78−39146
InSb, electron-hole plasma instabilities, impact ionisation conditions, microwave emission 80−107840
InSb, hot electrons, Monte Carlo calc. of transport characts. and distrib. functions of hot electrons 80−6853
InSb, hydrostatically pressed, negative differential cond. at room temp. 79−19600
p-InSb, impact ionisation 78−26879
InSb, impact ionisation and magneto-transport, high crossed elec. and mag. fields 80−107797
InSb, influence of external mag. field on recomb. radiation and I-V characts. 79−56864
n-InSb, influence of mag. field on hot electron effects 78−2493
InSb, intrinsic, impact ionisation by elec. fields 77−39864
InSb, intrinsic capacitance in transverse mag. field *(Russian)* 79−91070
n-InSb, millimetre rare modulation in semicond. plasma, use of effects of high elec. field. 78−60149
p-InSb, mobility, diffusion and thermoelectric power of hot holes 80−39595
InSb, narrow-gap semiconductor, high intensity IR transmission limit 80−7361
InSb p-n junctions, diffused, avalanche multiplication and impact ionisation 80−15595
n-InSb, plasma, nonequilibrium, magnetohydrodynamic instabilities, theory and expt. *(Japanese)* 78−10493
n-InSb, plasma filament form. under impact ionisation conditions 78−60147
InSb, polar semiconductor, impact ionisation in crossed elec. and mag. fields 79−28355
InSb, recombination processes using impact ionization capture cross sections 80−75577
InSb, room temp., carrier generation rate 80−20207
n-InSb, semiconductors, plasma oscills. within submillimetre freq. range 80−84473
p-InsB, high-resist. compensated, elec. breakdown peculiarities 80−2398
KBr, optical damage threshold anisotropy, polarised laser radiation 77−16433
KNO_3, and KNO_2, fused, electrolum. 79−99945
LiF, damage by UV laser radiation, avalanche ionization mechanism 80−76110
LiF, optical damage threshold anisotropy, polarised laser radiation 77−16433
Mo-chalcogenide glass-Mo-Al struct., strong elec. field effects 80−97004
NaCl, damage induced by CaF_2:Er^{3+} laser radiation at 2.76 μm 79−91539
$NaZnGeO_4$:Mn, electrolum., ionisation domains 80−84787
O^{q+}-He^{2+} collisions, electron capture and impact ionisation cross sections, loss of alpha particle in Tokamak plasmas 79−68936
$Pb_{1-x}Sn_xTe$, epitaxial layers, carrier lifetime meas. 79−42559
$Pb_{1-x}Sn_xTe$:In, dielectric state, avalanche breakdown in strong elec. fields *(Russian)* 80−92901
PbTe, epitaxial layers, carrier lifetime meas. 79−42559
PbTe, high field drift vel. and Hall coeff. 78−26875
$PtSb_2$, high field elec. props., impact ionisation 80−96892
Se, amorphous film, between metal electrodes, switching mechanism 78−39172
Se single crystal, behaviour in strong electric field 77−62942
Si, As-doped, effect of elec. and struct. parameters on avalanche breakdown localisation 77−11926
Si, electron impact ionis., direction depend. of threshold energy 79−42550
Si, electron transport and ionisation at high fields 78−30933
Si, impact ionisation, threshold energies calcs. for electons and holes 77−62933
n-Si, ionisation of low donor levels and recomb. of hot electrons at low temp. 79−51596
Si, laser induced dense plasma, dynamics 80−65612
Si, Lo-Hi junctions, avalanche injection delay and ionization rate at low electric field 79−95475
Si, nonequilib. carrier excitation by CO_2 laser radiation 77−89803
Si p-n junction, avalanche multiplication factor and reverse current 77−11991
Si p-n junction, avalanche multiplication of electron beam generated carriers 77−80833

impact ionisation continued
Si p-n junction, subnanosec. current drops in delayed breakdown 80−75633
Si p-n junction, subnanosec. current drops in delayed breakdown 80−75634
Si p-n junctions, avalanche breakdown anisotropy 80−70811
Si reverse-biased p-n junction DC characteristics interpretation *(Polish)* 78−91761
Si:B, impurity excited state lifetimes 78−60083
Si:P, impact excitation of P at low temps. 78−23098
Si-SiO_2, hot electron emission from Si under low level avalanche multiplication 77−80851
SiC, p-n junction, vapour grown elec. breakdown fields 78−19135
n-SiC, saturation of electron drift velocity in strong electric field 77−76840
Si_xGe_{1-x}-Si(GaAs) heterodiodes, interfacial structural defects effect on avalanche breakdown 79−42644
SiO_2, amorphous charge transport and storage 80−6864
SiO_2, cryst. and amorphous, laser-induced breakdown, electron avalanche damage mechanism 80−100711
SiO_2, dielectric breakdown, impact ionisation-recombination model 78−6633
SiO_2, fused, damage by UV laser radiation, avalanche ionization mechanism 80−76110
SiO_2, high field electronic props. 78−30930
$Si_{12}Te_{48}As_{30}Ge_{10}$ film, temp.-depend. of non-ohmic current and switching characts. 77−8158
Ta_2O_5, elec. breakdown during anodic growth 80−55033
Te, breakdown in high microwave impulse field, by impact ionisation 77−62957
V_2O_5, switching mech. 78−60175
ZnO based varistors, nonlinear cond. theory 79−78192
ZnS:Cu,Cl phosphor, effect of charged imperfections on electrolum. 77−32443
ZnSe, impact ionisation electroluminesc. 77−44066

impact phenomena *see collision processes*

impact strength
see also fracture toughness; notch strength
abrasive and impact abrasive wear testing equipment for materials at elevated temps. 78−7136
alloys, fracture toughness and impact strength, correl, breakdown 80−55523
armour material, selection criterion 78−53063
articular cartilage controlled impact test instrum. and procedure 78−28130
austenitic steel, Cr-Ni alloyed, Ti stabilised, nuclear reactor pipeline appl. *(Hungarian)* 77−18658
beams, impact loading, design curve 78−9579
bone, impact energy absorpt. changes with age 80−3698
bone, impact loading, anisotropy of compact bone tissue 77−25491
boride coating on stainless steel, elec., mech. props., boronising sintering method investig. 78−60594
borides, lightweight ceramic armour appls., ballistic tests, computer simulation, book contrib. 78−48556
brittle circular disc under impact loading, fracture mech. 78−88514
brittle target, impact damage in elastic response regime 78−71785
cemented carbide, simple evaluation method 77−32748
ceramics, impact toughness testing device 80−25941
ceramics, mechanical behaviour, book 79−38983
Charpy impact test instrumentation with capacitative displacement meter *(German)* 77−28959
Charpy tests, instrumented, evaluation of reliability 77−25243
Columbia Resin, CR-39, fracture mirrors, static and impact tests 78−27601
composite materials, fibre-reinforced, impact responses perpendicular to fibres *(Japanese)* 79−43377
concrete, compressive strength and ultimate strain under impact loading 79−70128
concrete, glass or steel fibre reinforced 79−87706
concrete, impact bending capacity *(Japanese)* 80−89341
concrete reinforced walls, local behaviour under missile impact *(French)* 78−44180
concrete reinforced walls, local response to missile impact 78−44181
crown glass, particle impact angle effect on strength degradation 80−50709
crown glass impacted with sharp SiC particles, strength degradation of tempered surfaces 79−66183
cylindrical shells, orthotropic, dynamics under axial impact 79−59936
dynamic fracture toughness determination, by instrumented impact tests 78−68861
dynamic impact test method, new *(German)* 79−11740
elastic bar, longitudinal compressive impact anal. obeying Malvern type constitutive eqn. *(Japanese)* 79−94553
enamel coating on metallic base standardization of estimation 78−23768
epoxy, Al_2O_3-filled, shock-wave compression, 0.4-3.7 GPa 78−59856
epoxy resin, deform. rate depend. of mech. props. at cryogenic temps. 80−55456
epoxy resin, mech. and thermal props., amine hardeners, added softeners and filter effects *(Polish)* 78−68741
epoxy resin composite, powder-filled, of adjustable thermal contraction, mech. props., for construction of superconducting magnets 79−61691
epoxy resin systems, synthesis review, phys. and mech. props. at low temps. 80−25650
epoxy-anhydride-polycaprolactone, cross-linked block copolymer, morphology and impact strength 78−91265
ethylene-base ionomers, impact tensile props. *(Japanese)* 79−96120
ethylene-methyl acrylate, random copolymer, review 80−108330
ethylene-vinyl acetate copolymers, extrusion and heavy duty films, radiation crosslinking, struct. effect 80−66844
ethylene-vinyl acetate-vinyl chloride graft copolymers, rel. between morphology and toughness *(German)* 80−66665
exploding wire cylindrical blast wave high-speed photography for material impact testing 79−79189
fatigue test equipment for use at high-temp. 79−52492
fibre reinforced cement, mech. and rheological props. *(German)* 79−20129
fibre reinforced ceramic, strength and fracture 79−87723
fibre reinforced composite, discontinuous, surface treatment effect analysis and obs. *(Japanese)* 77−77596
fibre reinforced epoxy, laminate, static and impact props. 77−63725

impact strength continued
fibre reinforced unidirectional elastic solid, impact loading, numerical study of fibre orientation effects 79−57094
fibre-reinforced hard alloy, effect of microstruct. on impact strength 77−56099
fracture in elastoplastic regime 78−51133
fracture toughness test by impact-fatigue method *(Chinese)* 80−3258
glass, fracture, by impulse loading, splitting method tests strength properties 79−57118
glass, impact damage, localised 77−44306
glass, strength degradation from impact with spheres 78−27663
glass, tensile and impact strength, effect of surface damaging and annealing *(Czech)* 79−74227
glass fibre reinforced Al alloy, formed by hot extrusion, mech. props. 77−24987
glass fibre reinforced cement, durability in wet and dry conditions, fibre length and content effect 80−71726
glass fibre reinforced composites, impact tensile strength obs. *(Japanese)* 78−23781
glass fibre reinforced plastic, impact tensile fracture energy *(Japanese)* 78−39888
glass fibre reinforced plastic, punching shear tests under static and impact loadings *(Japanese)* 80−55512
glass fibre reinforced plastic, woven-roving type, high-speed punching, failure mechanisms 80−85143
glass fibre reinforced thermoplastic, unidirectional short fibre reinforcement, tensile and impact strength 79−91734
glass plate impacted by glass spheres, localised impact damage 77−56089
glass plates, biaxially stressed, anal. of localised impact damage 78−68772
granite plate, crack propagation by projectile impact load 78−60741
graphite, effective specific work of fracture, evaluation method 79−57170
graphite, reinforced epoxy angle-ply laminate wave propag. during transverse impaction 79−83295
graphite, structural, impact toughness, reln. to compressive strength 78−88605
graphite fibre reinforced epoxy, impact damaged, acoustic emission 79−91875
graphite fibre reinforced glass, impact damage tolerance and reliability 80−81177
graphite fibre reinforced panels, low energy impact testing 78−72845
graphite/epoxy laminate with third phase reinforcement, static and impact behaviour 77−40447
gypsum plaster, plain and glass reinforced, fracture energy 77−36621
hardfacing alloys in impact abrasive loading, wear resistance, temp. effects 79−87737
head response to impact loading, parametric study by finite element modelling 77−48826
heat resistance testing, massive sample for mech. prop. changes obs. 78−7124
high-Si corrosion-resistant steel, 02Kh8N20S6, mech. props. and heat treatment 77−56003
Incoloy 800 and 802, influence of carburisation on mech. props. 79−20254
Inconel 617, microstruct., mech. props., thermal ageing effect 77−36557
instrumentation for impact, erosion and fracture studies 77−81383
instrumented impact testing, critical review 77−36725
Kevlav fibre reinforced cement composites, cement boards, exam. of mech. props. 78−48499
laminated angle ply composite, impact props. 77−56054
laser beam effects on materials with high impact strength review 80−21073
limestone plate, crack propagation by projectile impact load 78−60741
load-time oscillograms used to investig. impact bending 77−63849
long rod penetration of targets at hypervelocity impact, HELP computer code 78−26061
materials under complex stress, with local dynamic loading, strength 79−91768
metal, mech. props. and strain rate, low temperature effects 79−1911
metal, sinter-forging process, powder charact. effects 77−59714
metal-ceramic containing diamond, impact hardening 79−15828
metals, BCC, effect of screw dislocations, on mech. props. *(Russian)* 78−60704
metals, mechanical behaviour under impulse loading, model 79−52332
mineral-fibre composites that resist fracture and cracking 77−8798
mushrooming of flat-ended projectile on anvil, numerical meth. 77−72243
notched specimen, brittle fracture characts. under impact bending 78−23810
nuclear containment vessel response to impact using PISCES finite difference codes 77−3097
nuclear piping, impact loading *(Japanese)* 79−43373
nuclear plant, impact load for tornado generated missiles 78−51103
ophthalmic lenses, thin, chemtempered, strength meas. by drop-ball testing 80−5811
percussive impact wear, development of theory 78−94623
PFFE, impact fracture toughness, rate effect 78−56741
plastic composites 79−29162
plastic deforms ands rupture mechanisms, depend on B additives *(Russian)* 79−61650
plastic material, impact-torsion test machine *(German)* 77−52595
PMMA, effects of notch shapes on Charpy impact values, tensile props., fracture surfaces *(Japanese)* 79−38951
PMMA, impact strength, exam. with pulsed drop impact loading 78−84944
PMMA, impact testing, elastic analysis of conventional test, reassessment of testing 78−60770
polycarbonate, dielec. relax. and ductile brittle transition 78−52438
polycarbonate, notched specimens, impact fracture behaviour 77−28888
polyester cloth reinforced epoxy resin, fatigue strength and reliability under repeated impact tensile load *(Japanese)* 79−61703
polyethylene, filled, linear, struct., strength 79−29149
polyethylene, high density, impact yielding, flow stress rel. to temp. 77−32653
polyethylene, high-density, impact fracture behaviour, adiabatic heating at crack tip 80−85142
polyethylene, impact fracture toughness, rate effect 78−56741
polyethylene, medium density, impact testing, elastic analysis of conventional test, reassessment of testing 78−60770

impact strength continued
polyethylene, ultra-high molecular weight, linear, impact fatigue response 79−100242
polyethylenes, extrusion and heavy duty films struct. parameters influence on cross-linking by radiation 80−66844
polyimide fibre reinforced polyamide-12 80−11754
polymer, failure, book 78−92361
polymer, reciprocating impact wear testing apparatus, results 78−15639
polymer, solid, impact compression crushing at low temps. *(Japanese)* 78−7032
polymer coated graphite fibre-epoxy resin composites, prep., adhesion 79−15644
polymer films and sheets 78−80590
polymers, for denture appl., impact resistance 79−83434
polymers, impact testing, elastic analysis of conventional test, reassessment of testing 78−60770
polyphenylene sulphide, high mol. wt. soluble resin, prep., mech. props. 80−60828
polypropylene, effects of notch shapes on Charpy impact values, tensile props., fracture surfaces *(Japanese)* 79−38951
polypropylene systems, elastomeric impact modifiers rel. to morphology 79−66154
polypropylene/peanut-hull flour composite, strength 79−8365
polystyrene, impact-torsion testing *(German)* 77−52595
polystyrene, improved impact strength by talc and $CaCO_3$ fillers 78−19846
polystyrene, polyisoprene modified, impact strength improvement 78−84993
polystyrene, props. changes upon photooxidation 80−30123
polystyrene, rubber-modified, impact-strength analysis 79−38972
polystyrene-ethylene propylene copolymer, strength and impact props. 78−52899
polystyrene-polyethylene(ethylene-propylene) blends, copolymer modified, mech. props., morphology 79−57088
polysulphone-polydimethylsiloxane, linear block copolymer, morphology and impact strength 78−91265
porcelain, elec., high-strength, development from ceramic raw materials, mech., elec. props. 79−24630
PVC, impact strength, exam. with pulsed drop impact loading 78−84944
PVC, rigid plate, notching method effect on Charpy impact values, fractographic considerations *(Japanese)* 80−108541
PVC, rubber-modified, stress whitening and yield mechanism 79−8324
PVC, slightly plasticised, fracture toughness tests, impact tests 79−5037
PVC cases for Pb-acid batteries, pneumatic shock test *(German)* 78−85093
PVC composite, MBS type multifunctional impact modifier effect on mech. and rheological props. *(Polish)* 78−52751
PVC extruded films, mech. props. *(Polish)* 79−70037
PVC with mineral fillers, mech. props. 80−21042
rare earths, elastic and mechanical properties, review 79−70132
reciprocating impact wear testing apparatus 78−15639
reinforced epoxy angle-ply laminate wave propag. during transverse impaction 79−83295
reinforced magnetically hard material, fibre-reinforced, porosity and impact strength 77−55916
rigid body collisions, spalling, tensile stresses on target, appls. 79−7324
rock plate, loaded by projectile impact, crack propag. 79−83296
sandwich composite beam, impact bending behaviour *(Japanese)* 80−55468
Space Shuttle Orbiter, hypervelocity impact tests on RCC thermal protection material 79−16795
steel, 0.22% C type impact fatigue strength under −100°C low temp. atm. 77−52451
steel, 12X2H4A, nonmetallic inclusion effect on plasticity and impact strength *(Ukrainian)* 78−92296
steel, 35, fracture characteristics, notch sharpness effect in impact tests 79−52536
steel, 35Kh3MFS, strengthening involving austenite fine grain processing *(Russian)* 77−52358
steel, AISI 4340, austenitised at low and high temps., toughness evaluation 77−16621
steel, alloy, corrosion-impact-cyclic strength of boring bars, effective hardening treatment 78−53034
steel, alloy, fracture and fracture energy, subject to static, impact and repeated impact bending 77−63799
steel, alloy, high-temp. combined ht. treatment and mech. working, C content effects *(Russian)* 78−52854
steel, alloy, quenched, high strength, shot blast hardening effect on repeated impact bending 79−1914
steel, austenitic, 30KhGSA, grain size before quenching rel. to mech. props. 79−24553
steel, austenitic, fracture toughness meas. by Charpy impact testing, welding, heat treatment, neutron irrad. effects 79−5062
steel, austenitic, fracture toughness props. of A533B, prior austenite grain size effect 78−60780
steel, austenitic, Mn-base, as LNG storage and transportation system material 79−70133
steel, austenitic, quenched state, influence of austenite stability on impact strength *(Russian)* 80−81146
steel, austenitic stainless, grain boundary segregation studies, intergranular fracturing technique for stress corrosion cracking investigation 79−39057
steel, austenitic stainless JIS type 304, tensile test at elevated temp., high velocity 77−73302
steel, austenitic-martensitic 0Kh15N5M, ductile fracture 78−3226
steel, C, bainitic, microstruct. and cleavage resistance 77−52481
steel, C, fracture criterion determination, using 3-point bending 79−29216
steel, C, wear during impact, effect of C content 79−38986
steel, C (0.21 wt.%), loading wave shape effect on deform., failure, impact tensile strength of smooth specimen *(Japanese)* 79−29146
steel, C and alloy, restricted durability, subject to pure bending with rotation 77−90431
steel, C content influence on brittle and tough fracture, heat treatment *(Russian)* 80−40500
steel, C-Mn, corrosion cracking, role of microstresses and crystal lattice stresses *(Russian)* 77−25190
steel, C-Mn elevated temp. embrittlement under impact loading 77−44366
steel, C-Mn-Cr-Mo (0.4, 0.8, 1.1, 0.25 wt.%) C, Ni, Mo, Cr addition effects on toughness of bainite 78−11327

impact strength continued
steel, carburised, fracture resistance 79−24612
steel, case hardening and carbonitriding treatment, mech. props. testing *(French)* 77−59991
steel, cast, effect of non-uniform struct. on props. 78−84850
steel, cast structural, heat treatment and mech. working influence on mech. props. *(Russian)* 80−40392
steel, constructional, impact strength/brittle fracture relationship in ductile-brittle transition zone 78−56740
steel, correlation links between mech. props. controlled rolling effect 80−35234
steel, Cr, hypereutectic, structural, critical rates of impact, kinetics of failure 80−35325
steel, Cr (40 wt.%), Sn and P segregation effects on impact toughness *(Chinese)* 77−73313
steel, Cr-Mo, cast and forged, difference in mech. props. 77−48465
steel, Cr-Mo, grain size effect on ductile brittle transition 79−24615
steel, Cr-Mo, impact fatigue crack growth at low temps. *(Japanese)* 80−104266
steel, Cr-Mo (10-14, 2-6 wt.%), heat-resist., creep-rupture strengths 80−104271
steel, Cr-Mo (2.25, 1 wt.%) pipe, high temp. fatigue and creep strength 80−85060
steel, Cr-Mo-Ni-WV (6, 4, 3, 2 wt.%), tempering and secondary hardening, TEM obs. *(Chinese)* 80−104245
steel, Cr-Mo-V, 1% Cr, chem. comp. and struct. effect on deform. props. *(German)* 79−1888
steel, Cr-Mo-V, brittle failure, heat treatment and influence of cold plastic deform. 78−72858
steel, Cr-Mo-V, heat treated, mech. props. *(German)* 80−25724
steel, Cr-Mo-V, medium strength, correlation between crack initiation, propag. and microstruct. 78−60787
steel, Cr-Mo-V, press. vessel, fracture, effect of tempering 78−60799
steel, Cr-Ni-(Mo), austenitic, strengthening by modified ausforming 78−76665
steel, Cr-Ni-Mo, combined B and rare earth metal additions effect on microstruct. impact strength and hardness 79−38963
steel, deformability characts. in surface-active medium at decreasing temp., mech. working effect *(Russian)* 77−59851
steel, deformation ageing of 40Kh, effect on impact resistance and tensile strength *(Russian)* 78−31427
steel, ductile structural, crack resistance and cohesive strength 80−50722
steel, dynamic fracture toughness meas. by instrumented impact bend and compact K testing 77−36718
steel, electroslag welded sheet, impact strength and toughness, welding effect *(German)* 77−86139
steel, fatigue, impact loading, friction, wear in surface active media *(Russian)* 79−29268
steel, ferritic, Charpy impact testing criteria 79−47855
steel, ferritic, criteria for Charpy impact testing 80−7752
steel, ferritic, low to intermediate strength, fracture toughness, upper shelf temp. depend. 77−73330
steel, ferritic/austenitic high Cr, development, mech. props. and corrosion resist. 80−45422
steel, fracture toughness, temp. and loading rate effect 77−36663
steel, fracture toughness and impact strength, correl. breakdown 80−55523
steel, fracture toughness dynamic, interlaboratory data, statistical analysis 77−36717
steel, fracture toughness evaluation using oscillograms, optimum heat treatment 79−57169
steel, hardness, rel. to tensile and impact strength 77−90428
steel, hardness, tensile and impact props. correlation, at low temps. *(Japanese)* 77−52413
steel, high C, weld heat affected zone, impact and fatigue props. *(Japanese)* 80−11668
steel, high Ni, medium C, impact fatigue strength 79−79104
steel, high speed, AISI M2 and M7, fracture toughness 77−86141
steel, high speed, sintered, and wrought, type T6 strength and toughness 80−30102
steel, high strength, increasing resistance to cracking, use of overheating before quenching *(Russian)* 77−25135
steel, high strength, low alloy, mech. props. 78−60739
steel, high strength, low alloy, rare earth treated, ductile fracture mech. 78−64658
steel, high strength, low alloy, splitting of tensile and impact specimens 77−63777
steel, hot forging die type, fractography *(Japanese)* 80−108547
steel, hot rolled, low C, low alloy, bainitic alloying addition effects on microstruct. and props. 77−36546
steel, impact and tensile props., Si effects 79−24614
steel, impact strength, effect of surface decarburization and carburization of faces and core struct. 78−23811
steel, impact strength, exam. with pulsed drop impact loading 78−84944
steel, laminar, high hardness, ballistically damaged, fracture mech. approach to residual strength 77−56050
steel, lightly alloyed, S effect on failure following controlled rolling *(Russian)* 79−57086
steel, low, C, rimmed and killed, exam. of impact fatigue behaviour *(Japanese)* 78−88528
steel, low alloy, C-Ni-Cr-Mo (0.36 wt.%), impact toughness rel. to microstruct. *(Korean)* 77−21188
steel, low alloy, quenched and tempered, formation of stony fracture during forging 79−79059
steel, low alloy, radiation embrittlement, heat treatment effects 78−19893
steel, low alloy, softening of heat affected zone under postweld tempering 77−21196
steel, low alloy, toughness, effect of packet size and lath width 77−16677
steel, low alloy, type 3sp, effect of temp. at end of rolling on mech. props., and coercive force 78−72799
steel, low alloy Cr-Mo, heat fatigue, effect of technical factors 79−79058
steel, low alloy type 14Kh2GMR, high strength, welded joint, impact toughness, welding thermal cycle and tempering effects 80−3157
steel, low C, and hardened and tempered, impact specimen fractures, stress concentrator sharpness effect on size of tough component 78−7015
steel, low C, brittle fracture susceptibility, low temp. deform. effects 77−56103

impact strength continued
steel, low C, crack propagation energy rel. to temp., time factors 79−29179
steel, low C, dual phase, impact props., microstruct. element influence 80−40525
steel, low C, impact and tensile props., effect of Si 77−36526
steel, low C, impact strength and crit. brittleness temp., sample thickness and notch radius influence 80−85018
steel, low C, Mn-Nb, quenched and tempered, microstruct. and props. 77−36549
steel, low C, Nb-V microalloyed, Nb, V effect on impact and toughness props. 78−15515
steel, low C, specimens with notch and fatigue crack, fracture surface features 79−43417
steel, low C and low alloy, rolled, nondestructive impact strength testing by coercive force meas. 79−52601
steel, low pearlite, Nb microalloyed, ageing at 600°C, mech. props. *(German)* 77−36542
steel, low S, ESR, overheating effect on toughness 78−52860
steel, low S, ESR and electric arc, notch toughness, interaction between overheating and tempering temp. effects 78−52970
steel, low S, overheating 77−21185
steel, low strength, impact tests with oscillography, exam. of fracture toughness using new method 80−21215
steel, low-C martensitic, Ni addition influence on toughness and ductile-brittle transition 80−30099
steel, maraging, crack resistance, effect of external stress during ageing *(Russian)* 77−59902
steel, maraging, N12K6M5TYu, fracture, influence of high-temp. thermomechanical treatment on charact. *(Russian)* 78−27591
steel, maraging, Ni-Co-Mo (18, 8, 5 wt.%), fatigue strength charact. *(German)* 77−21241
steel, maraging, notch strength 77−56056
steel, maraging 350, produced by powder metallurgy, mech. props. 78−15334
steel, martensitic, as LNG storage and transportation system material 79−70133
steel, martensitic, Cr (12 wt.%), temper embrittlement 79−87722
steel, martensitic, impact bending failure resistance, initial crack length and tempering effects 78−31530
steel, martensitic 12% Cr, temper embrittlement 80−66650
steel, medium C, isothermally quenched, high-temp. deform. effects on struct. and props. *(Russian)* 80−25760
steel, medium strength, fracture toughness eval. of small specimens 78−60762
steel, microalloyed, fine grained, mech. props., effect of hot dip galvanising *(German)* 77−36679
steel, microalloyed, precipitation effect on microstruct. and mech. props. *(French)* 80−25708
steel, mild, impact velocity effect on fracture surface *(Japanese)* 79−96118
steel, mild, notch effect on impact fatigue strength *(Japanese)* 79−43400
steel, mild, plate, effect of striking velocity on perforation energy 78−68818
steel, Mn, as rolled bainitic, tensile, impact and machinability props., transport appl. 78−88503
steel, Mn (1.10 to 1.55 wt.%), reactor vessel material, assessment of weld heat affected zone mech. props. 79−29217
steel, Mn-Mo, castings, mech. props., Cu and Sn trace elements effect 80−66596
steel, Nb, controlled-rolled into ferrite temp. range, soln. temp. and rolling effects 80−11678
steel, Ni(9 wt.%), isothermal bainitic transform., thermomechanical effects on mech. props. *(German)* 80−40383
steel, Ni-Cr-Mo and Ni-Cr, impact strength, effect of modified ausforming *(Japanese)* 79−11692
steel, nonmetallic inclusions effect on ductility 80−30042
steel, nuclear pressure vessel, type A533B-1, three point bending, yield stress, exam., Charpy V-notch and precracked specimens 78−92310
steel, pearlitic, strength, fracture, microstructure effect 77−40449
steel, pearlitic eutectoid, crack initiation and effective grain size for cleavage fracture 80−30085
steel, powder forged, impact strength and fatigue strength, slag inclusion effects 77−21271
steel, powder forged for carburizing appl., core props., mech. props. 78−15339
steel, rail, toughness, effect of Sn, SEM exam. 80−97569
steel, S45C notched specimens, Charpy impact tests, notch angle effects *(Japanese)* 80−85124
steel, SA540, fracture toughness props. for nuclear bolting appl. 78−35514
steel, SHE 4340, tempered martensite embrittlement 80−30084
steel, sheet, 5-7 mm thick, method for assessing susceptibility to ageing 77−63850
steel, shelf energy rel. to fracture surface dimensions *(Czech)* 77−59917
steel, sintered, mech. props. 77−40439
steel, sintered constructional, resistance to cyclic impact loads 77−77583
steel, spall investigations, pressures up to 100 kbar, failure and strength *(Ukrainian)* 77−73317
steel, spalling prod. by sheet charge explosion and collision of plate 78−44198
steel, St.3ps, 18 Gps, 09 G2S, fatigue crack resistance, temp. effect 79−52375
steel, stainless, 316, ductile, prestrained, method of J_Q and δ_i determ. 77−36724
steel, stainless, annealed 310, deform. at erosion sites, TEM and SEM studies 78−64725
steel, stainless, Cr-Mn (21, 14 wt.%), grain boundary precipitation and fracture *(Japanese)* 79−100149
steel, stainless, Cr-Ni, for cryogenic engineering, mech. props. 78−11240
steel, stainless, ferritic, anisotropic lamellar fracture mechanism 78−64639
steel, stainless, ferritic, Cr-Mo-Ni (29,4,2 wt.%) 77−44276
steel, stainless, ferritic, subjected to 475°C embrittlement, exam. of fracture toughness 78−84982
steel, stainless, Kh25T, impact strength and substructure produced by deform. during cold rolling *(Russian)* 79−24535
steel, stainless, shock loading parameter effect on substruct. and mech. props. 79−52360
impact strength continued
steel, stainless, two phase, variation of tensile and impact strength with heat treatment 79−34085
steel, structural, second phase particle effects on impact strength 80−108581
steel, tempered, notched, impact bending tests, cold brittleness curves 80−71758
steel, V strengthened dual phase, deform. and fracture props. 78−48467
steel, very low C, delamination study by impact testing 78−3218
steel, WC reinforced surface layer, serviceability improvement by Ni, Cu-Ni, V alloying additions 77−21290
steel, weldable C and alloy, brittle fracture, metallurgical factor effects, NDT data, impact tests *(French)* 79−5128
steel, welded joints, durability in repeated impact loading, low temp. effects 77−63800
steel, yielded pipeline, fracture resistance changes, impact tests 77−16667
steel 03Kh12N10MT, mech. props. at low temps. 77−16615
steel 12Kh18N10T, struct. and mech. props. after prolonged working at −183°C 77−55988
steel 1Kh18N9T, physico-mech. props. after boring in metallic melts *(Russian)* 78−56736
steel 30khGSNA, low alloy, quenched, grain refinement influence on impact strength *(Russian)* 80−20974
steel 35KhGSA, resist. to fracture after low temp. temperating, P content and grain size effects *(Russian)* 78−48490
steel 40Kh, notch sensitivity under cyclic impact loads 78−3220
steel 45, cracking resistance under impact loading *(Russian)* 77−25138
steel AF1410, wear against stainless steel, repetitive impact, microstruct. effect 79−74263
steel bimetal, low-alloy austenitic ferritic stainless steel, fracture toughness *(Russian)* 78−35482
steel C, types AISI 1008, 1020, 1035, renitrogenized 1010 and 1522, dynamic strain ageing, tensile notch impact and fatigue props. 79−43288
steel cylindrical bar loaded by longitudinal impact, dislocation struct. and plastic deform. *(Czech)* 78−60713
steel fibre reinforced concrete, vibr. compaction, pressure compaction and curing *(Japanese)* 80−89179
steel fibre reinforced porous mat. prod., mat. props. 77−59723
steel high strength X 3 CrNiMoNbN 2317, Bauschinger effect and creep at room temp., effect of heat treatment *(German)* 77−36543
steel Kh12, impact abrasive wear improvement by TiC coating 77−70187
steel SS-41, plastic working with vibr., US hardness tester 78−53044
steel surface deformation by oblique impact of square plates 77−66701
steel U8, struct. and mech. props., effect of hydrostatic extrusion *(Russian)* 77−56022
steel welded joint impact strength, preheating and tempering effects 79−24542
steel-bronze bimetal mech. props., diffusional interlayer effects 79−29169
steels, brittle transition temp. determs. from impact ductility tests, comparative evaluation 79−15888
straight long rod, dynamical buckling under hammering 79−7312
structural steel, microstruct. and brittleness, rel. to austenizing and heat treatments 77−56091
tensile impact tests with rupture diagram recording on pendulum machines, testing procedure 79−29313
test, finite element analysis 78−68806
testing of resilient materials, testing machine and expt. results 77−25223
thermoplastics, structural changes during deformation, rel. to impact resistance 80−25800
thin sheet impact strength study *(Czech)* 80−59571
torsional test accuracy determ. using simulation *(Japanese)* 77−56198
two step program loading involving impact load, fatigue strength and damage accumulation *(Japanese)* 79−66148
V-Nb(Mo) alloys, effect of heat treatment on mech. props. 77−21176
vertical test machine for tension at speeds up to 25 m/sec 78−39968
wear resistance, hardfacing, review 78−72937
weld, heat affected zone extraction and testing of flat, microtensile specimens *(German)* 77−9017
white cast iron, plasticity in impact toughness, bending angle tests 77−56039
wood, thin plate perforated by hard missile, energy dissipation prediction 79−8361
Al alloy, fracture toughness determ., dynamic mode II 77−36720
Al alloy 01205, mech. props. at cryogenic temps. 79−29206
Al alloy 7075, precipitation hardening, toughness and microstruct. *(Japanese)* 78−15509
Al alloy-mica particle composite, cast prep. and mech. props., bearing appl. 80−71613
Al alloys, erosion by ball bearing impact 79−61740
Al alloys, preliminary forging effects on struct. and mech. props. of extruded sections *(Russian)* 78−80564
Al, annealed, subjected to torsional impact loading strain-rate effects 78−92303
Al, dynamic strength and logarithmic modulus of plasticity 77−16655
Al, impact strength, exam. with pulsed drop impact loading 78−84944
Al, longitudinal compressive impact test, comparison of expt. and calc. results *(Japanese)* 79−96119
Al, tension-torsion impact testing, instantaneous plastic property 79−52474
Al tube, thin-walled statically pre-tensioned, torsional impact loading 78−27557
Al-Al_4C_3, dispersion hardened physical props. meas. *(German)* 78−31415
Al-C, dispersion hardened, effect of processing parameters on mech. props. 80−20826
Al-Cu-Mg/mica particulate composite mech. props. 80−100919
Al-Cu(Ag), tensile ductility, effect of ageing and impact velocity *(Japanese)* 78−15465
Al-Mg (7 wt.%), β-phase soln. behaviour and mech. props. *(Korean)* 78−11277
Al-Mg alloy AMg6, mech. props. of welded joints, impurity effects 78−95789
Al-Mg-Li alloy, subboundary brittleness due to horophilic Na *(Russian)* 77−21244
Al-Pb(Bi)(Cd), containing low melting point inclusions, impact props., temp. depend. 78−60792

impact strength continued
AlN-Mo cermets, ZrO_2 and mullite whisker reinforced, strength var. with temp. 80−104232
Al_2O_3, cutting tools, effect of acid etching on cutting performance 79−96169
Al_2O_3, impact fatigue 77−56048
Al_2O_3-Mo cermets, ZrO_2 and mullite whisker reinforced, strength var. with temp. 80−104232
B fibre reinforced Al, impact behaviour under fatigue 80−7661
B fibre reinforced Al, impact damage tolerance and reliability 80−81177
Be, hot-extruded, fracture in impact, static tensile and fatigue tests *(Russian)* 77−52458
Be, low oxide, isostatically pressed block, factors affecting tensile strength, elongation, impact resistance 77−16610
C fibre reinforced polymers, strategic reinforcement of hybrid, impact props. 78−15502
C fibre reinforced polymer, strength props., fibre surface treatment effects 78−27636
C fibre-Kevlar 49 fibre epoxy laminate, impact props. 78−44164
C glass fibre hybrid plastics, review of mech. props 79−20107
C steel, impact-fatigue strength , notch strength, rel. to comp. and ductility of core 77−56093
Cu, dynamic strength and logarithmic modulus of plasticity 77−16655
Cu, fracture criterion, expt. verification 78−64648
Cu, tension-torsion impact testing, instantaneous plastic property 79−52474
Cu-Al (11.6 wt.%), mech. props., tempering temps. effects 78−76669
Cu-Sb, peculiarities in temp. behaviour of internal adsorption *(Russian)* 79−55890
Fe, Armco, impact strength, exam. with pulsed drop impact loading 78−84944
Fe, Armco, struct. and mech. props., effect of hydrostatic extrusion *(Russian)* 77−56022
Fe, cast, white, graphitisation, effect of hot impact deform. 78−19780
Fe, intergranular brittleness, effect of O and S 77−36650
Fe, powder forged, impact and fatigue strengths, slag inclusion effects 77−21271
Fe, sintered, effect of repressing and double sintering on impact strength *(Japanese)* 78−92217
Fe-CaF (6 and 9 wt.%), sintered, elevated temp. mech. props. 77−28878
Fe-Cr alloy, impact strength, rel. to '475°C brittleness' *(Russian)* 78−92323
Fe-Cr-Mn (11.5, 3 wt.%), microduplex ferritic-martensitic steel, exam. 78−39862
Fe-Mn, warm rolled, rel. contribs. of texture and grain shape to props. 79−91705
Fe-Mn 8%, type K1525 thermal cycling, effect on impact toughness 80−7608
Fe-Mn (8.25 wt.%), irreversible temper embrittlement, Mossbauer spectra, impact strength depend. on interstitials *(German)* 79−74235
Fe-Mn (up to 8 wt.%), microstructure, mech. props. and fracture *(Japanese)* 80−35304
Fe-Mn-Ni-V-C (0.5, 3.0, 1.0, 0.2 wt.%), austenite decomp., isothermal transform. characts. 80−97477
Fe-Mn-V-C (0.5, 1.0, 0.2 wt.%), austenite decomp., isothermal transform. characts. 80−97477
Fe-Mo-CaF (15, 9 and 6 wt.%), sintered, elevated temp. mech. props. 77−28878
Fe-Mo-CaF_2 sintered composite, struct. and mech. props., heat treatment effect 80−66526
Fe-Ni (25 wt.%), and single phase, solidified from undercooled melt, mech. props. 77−48540
Fe-Ni-C (9, 0.1 wt.%), effect of intercritical tempering on impact energy, exam. of mech. props. 78−52861
Fe-Ni-C-Mn (3.56, 3.25, 0.6 wt.%), solid soln., quenched, changes during annealing to crystal structure, mech. props. *(Russian)* 79−34076
Fe-Ni-Cr based alloy, KhN35VTYu, temp. depend. of energy of fracture, influence of γ' phase *(Russian)* 80−81147
Fe-Ni-Mo alloy, high-strength ferritic, for cryogenic service, mech. characteris. 77−70143
Fe-Si (3 wt.%), hot rolled sheet steel, ductile-brittle transition temp. *(Chinese)* 78−31498
Fe-Ti(Nb), internally nitrided, mech. props. 77−44307
Ir-W (0.3 wt.%), P segregation to grain boundaries, effect on high temp. ductility 78−95754
Mg-Al-Zn-Mn (8, 0.5, 0.3 wt.%) casting alloy, penetration resistance 80−100901
Mo, fibre, brittle to tough transition, impact strength meas. 80−40527
Mo sheet, shock-induced intergranular cracks 79−57087
Na_2O-CaO glass, impacted with sharp SiC particles, strength degradation of annealed surfaces 79−61760
Na_2O-CaO glass phlogopite mica powders, composite fabrication, cellular struct. 80−84902
Na_2O-CaO-SiO_2 glass, high-vel. liq. impact, oblique impact anomaly 80−89329
Nb bicrystals, impact strength at 20° and −190°C *(Russian)* 80−45379
Ni based alloys, hot hardness and oxidation resistance meas. 78−31588
Ni, dynamic strength and logarithmic modulus of plasticity 77−16655
Ni, shock loading parameter effect on substruct. and mech. props. 79−52360
Ni-Co (10 wt.%), cast single phase, solidified from undercooled melt, mech. props. 77−48540
Ni-Cr-Co superalloy, σ-phase effect on mech. props. *(Chinese)* 79−74229
Ni-Cu (30 wt.%), cast single phase, solidified from undercooled melt, mech. props. 77−48540
Ni-Fe-Cr base superalloy, addition effect on mech. props. *(Chinese)* 80−20998
Ni_3Al-Ni_3Nb composite, long term annealing effect on impact strength and long-term strength *(Russian)* 79−74182
NiO−CaF_2, hot-pressed, mech. props., thermal expansion rel. to CaF_2 additive 79−43321
PVC-Cu, particulate composite, mech. props. effect of particle size 78−95799
$Pb(Zr_xTi_{1-x})O_3$, meas. of Hugoniot curve with commercial manganin stress gauges 80−70362
Si, near (111), fracture by painted indenter, SEM study 80−71734
SiC, impact resistance, instrumented drop weight test 78−11265
SiC, instrumented Charpy impact testing 77−36719
SiC, low blow Charpy impact 79−34122
impact strength continued
Si_3N_4, bending strength, deformability, elastic moduli and brittleness 80−81191
Si_3N_4, hot-pressed, impact resistance, instrumented drop weight test 78−11265
steel, C, castability, in metal mould, mechanical props. *(Japanese)* 80−25681
steels, Cr-C-Mn(Ni), struct. prop. rel., design of struct. steels for high strength and toughness 80−97491
Ti alloy, impact strength, exam. with pulsed drop impact loading 78−84944
Ti alloy VT14, strength in uniaxial dynamic extension, influence of α-ω transform. *(Russian)* 79−52200
Ti alloys, data handbook of low temp. mech. and phys. props. 80−22153
Ti, high purity, data handbook of low temp. mech. and phys. props. 80−22153
Ti-Al(−V)(Mo), impact strength anisotropy, influence of texture *(Russian)* 80−20952
Ti-alloys, methods of studying effect of H on service behaviour 80−16478
TiC-steel composite, effect of method of Cr additions on props. 78−15341
W, fibre, brittle to tough transition, impact strength meas. 80−40527
WC-Co hard alloys, hot pressed, mech. props. 79−100260
Zn, impact strength, exam. with pulsed drop impact loading 78−84944
Zn-Al(Cu), mech. and technological props. *(Polish)* 80−89286
ZrO_2, metastable, tetragonal, erosive damage depth, martensitic transform. effect 79−61738
IMPATT diodes
electron and hole impact ionisation coeffs., influence on performance 78−6389
frequency-stabilised IMPATT source, 115 GHz 80−67573
tunnelling and negative resistance phenomena in negative conductance microwave devices, book 78−26947
GaAs, epitaxial layer uniformity and reproducibility, data 79−38744
GaAs IMPATT diode, maximum efficiency single- and double drift region, 3 to 18 GHz range 79−24058
GaAs, impact ionisation rates, temp. depend., appl. to diode design 79−38077
GaAs, multiple layer epitaxial growth by sequential VPE method 77−12545
GaAs thin Schottky barrier metallisation, thermal reactions 79−78176
GaAs, vacuum deposited Shottky barrier metallisation 79−78153
Ge-GaAs heterojunction, elec. and recomb. props., interface defect effects 80−80365
Si $p^+\pi pn\nu n^+$ structure form. by epitaxial growth 77−76906
Si_xGe_{1-x}-GaAs, heterojunction, elec. and recomb. props., interface defect effects 80−80365
impedance, acoustic *see acoustic impedance*
impedance, electric *see electric impedance*
impedance, electric, measurement *see electric impedance measurement*
impedance, measurement, electric *see electric impedance measurement*
impedance convertors
dielectric loss meas., extended standing wave method, impedance conversion techniques *(Japanese)* 77−45869
ECG surface electrode potential recording apparatus 79−83987
impedance matching
atomic emission spectroscopy, impedance matching network for plasma 79−43678
compensated semiconductors, HF impedance 79−15212
electrostrictive US transducer electroacoustic efficiency and load matching 79−68541
EM transducer dynamic range optimisation 77−19506
grating acoustic scanner for underwater imaging and NDT 79−57198
hydroacoustic transducers of fixed operating freq., elec. imped. matching *(Croatian)* 79−55287
IC nondestructive evaluation by improved reflective scanning acoustic microscope 79−50551
integrated optics multilayer anisotropic structures, impedance matching effects 79−7233
internally lossless transducer conjugate matching, power transfer and backing impedance 79−46158
magnetostrictive transducer, wideband electrical matching 78−5626
microwave radiometer calibration standard with Brewster angle impedance matching 77−5918
microwave reflection coefficients measurement *(French)* 79−67350
monolithic acoustic retina resolution improvement 79−55305
piezoelectric ceramic plates, acoustic array design expt. data 77−84099
piezoelectric transducer matching with shock excited oscillator for US flaw detectors 77−73422
piezoelectric transducers, thickness mode, front face mech. impedance effects 77−31197
radiotelescope transmission lines, antenna arrays and impedance transformation 78−96399
shock wave impedance match at low pressures 78−51264
single-transducer coupler for diagnostic pulsed Doppler or pulse-echo US instrumentation 78−61236
transmitter-receiver matching network for US pulse-echo system 77−78012
tunable variable bandwidth/frequency SAW resonator 78−59247
US transducer lumped wideband equaliser design optimisation 79−46159
wave impedance matching interface layer synthesis *(Russian)* 78−77728
ZnO integrated optical transducer arrays 79−50444
imperfections, crystal *see crystal defects*
impermeability *see permeability*
impulse amplifiers *see pulse amplifiers*
impulse generators *see pulse generators*
impulse testing
artificial kidney, evaluation using systems anal. 78−36074
circular membranes, clamped, charact. method *(Japanese)* 77−28952
elastic/viscoelastic bar interface, impact wave behaviour 78−26075
electrodes, screening, discharge phenomena with UHV positive and negative lightning and switching pulses for dimensioning *(German)* 80−87963
epoxy polymers, unfilled and filled effect of specimen size on elec. strength expt. 77−8505
HV laboratory ion density due to repetitive impulse generation 78−65913
long spark-gaps, breakdown voltage *(French)* 80−33828

impulse testing continued
Marx type fast rise impulse generator using laser triggered gap switches *(Japanese)* 78−94940
metallurgically bonded plates, structural integrity determ. by high energy impulse 79−39111
optical fibre impulse response meas., refined deconvolution technique 79−55242
polyethylene, tree initiation by DC and impulse voltage appl., expt. 77−24790
rod-rod and rod-plane gaps, influence of positive and negative impulses on breakdown voltage, obs. *(German)* 78−5981
tubing, testing and failure localisation by electrodynamic method 77−63847
wood, impulse method of determining moduli of elasticity, shear moduli 77−77661
SF_6 impulse breakdown characteristics for nonuniform field gaps for switchgear design 80−84024
SF_6 insulation, under impulse voltage stress, effects of pressure and vol. on firing delay *(German)* 80−87959
SF_6 insulation breakdown charact. under operating conditions in HV apparatus 80−96414

impulse voltages *see transients*

impulse welding *see resistance welding*

impurities
for impurity vibrations see "lattice localised modes" or "molecular vibrations in solids"
see also chemical analysis; crystal inclusions; crystal purification; diffusion in solids; impurity-defect interactions; impurity distribution; impurity electron states; interstitials; magnetic impurity interactions; phonon-impurity interactions; segregation; semiconductor doping
acenaphthene-α-nitronaphthalene, binary mol. system, phase diagram 77−39664
acetic acid, effect of impurities on US relaxation 78−10130
actinide carbides, lattice defects and rel. to phys. props., review 77−27874
AES, depth profile analysis, influence of impurity gases in UHV systems 78−76958
AES quantitative anal. of impurities *(Japanese)* 78−91356
alkali halide:alkaline-earth cations, defect structs. examined by methods based on Mott-Littleton techniques 80−59487
alkali halide:Eu^{2+} cation vacancy complexes, binding energies 80−96513
alkali halide, electric-dipole ordering of tunnelling impurity centres 80−2215
alkali halide, $OH^-(D^-)$ impurity rot. barrier height and librational modes 77−11491
alkali halide crystals, defect modes due to substitutional anion-pair and cation-pair impurities 80−92540
alkali halide crystals, impurities, monovalent, and impurity pairs, lattice distortions 77−68984
alkali halide crystals, radiation damage review, impurities and colour centers *(German)* 78−10086
alkali halides, doped, impurities effect on nucl. spin-lattice relax. 78−19362
alkali halides, influence of purity of crystals on stability of F-centres and interstitials 78−91336
alkali halides, local and reson. modes due to hydide ions, U-centres and additive cation impurities 79−77710
alkali halides, off to on centre defect transitions under hydrostatic press. 78−15199
alkali halides, strain defects, low temperature props., heuristic model 79−82245
alkali lime germanosilicate glasses, optical absorpt. of transition metal impurities 80−2784
alkali metal alloy, charge-transfer state, from residual resist. of electronegative impurities 79−95372
alkali metal chloride: $F^-(Br^-)(I^-)$, anion impurities substitution, energies of soln., association and migration 78−83831
alkali metal halides, F-colouring role of impurities 80−64995
alkali metal halides, hole self-localization and capture, temp. depend. 80−92526
alkali-halide crystals, two-dimens. nucleation and hole nucleation, mol. beam method *(German)* 80−93499
alkaline earth fluorides, thermodynamics and kinetics of O incorporation 77−84778
alloy, substitutional, low conc., volume change calc. using Morse pot. function 77−15342
alloys, binary, supercond. transition temp. lowering by nonmagnetic impurities 80−100546
alloys, embrittling residuals categorisation by Auger electron spectroscopy 80−66739
alloys, gas solutions in alloys, due to impurity-deoxidising element interactions, thermodynamic analysis *(Russian)* 79−34347
alloys, temper embrittlement, impurities and alloying elements role, review 80−66649
alloys, thermoelectric props., effect of electron-impurity and electron-phonon interactions 79−33282
ammonium oxalate monohydrate:Mn^{2+}, model for defect formation, EPR 80−103880
analytical electron microscopy, reduction of contamination *(Japanese)* 80−11978
anelastic relaxations and magnetic aftereffects in solids, conf., Katowice, Poland (Jan. 1978) *(Polish)* 79−96072
anisotropic crystal, vibr. characteristics at low temp., effect of substitution impurities *(Russian)* 80−103439
anisotropic impurity centres, local relaxational phase transitions *(Russian)* 80−44220
anisotropy, rel. to phase transitions *(Russian)* 80−10907
anodic oxidation, ion implanted impurities effects 77−90502
anthracene: tetracene cryst., triplet-state EPR for isolated mol. orientation 78−26583
atomistic computer experiments of point and extended defects 78−30610
boride coatings on steel effect of Cu impurities in reaction mixture on brittleness, acoustic emission meas. 80−16581
dl-camphene, self-diffusion, effect of impurities, radiotracer and plastic deform. study 78−43177
d-camphor, plastic crysts., impurity size effect on self-diffusion 77−11727
ceramics, recycling, residual and additive elements control by specifications 80−66522

impurities continued
chalcogenide glass, Fe, doped in equil. conditions, impurity cond. and Mossbauer effect 80−49726
chemical impurities, entropy and enthalpy of solution 78−51691
chlorophyll, singlet-triplet optical resonance in solid soln. 77−52741
cholesteric systems, with nonmesogenic additives, Keating-Bottcher theory 80−84057
coke, effect of addition of borides on hot-pressing 80−40282
concentration meas. method for P and B in Si *(Chinese)* 80−65036
critical properties, local near isolated impurity 78−6142
crystal, asymmetrisation in the growth process, sectorial struct. and structural ordering 79−90581
crystal, non-rigid impurity centres, symmetry groups 79−77534
crystal growth, dynamic computer models 80−103284
crystal growth, in pure and impure systems 80−49145
crystal growth from melt, macroparticle capture by growing cryst., influence of particle thermal cond. 78−79543
crystal growth from vapour, kinetics, impurity capture 78−26468
crystal habit, modifications control in growth 80−49150
crystal production and perfection for photodetectors 78−11107
crystal step motion, in the presence of a mobile impurity computer model 79−14713
crystallisation, role of impurities 80−49146
crystals with Jahn-Teller centres, sound absorpt. 79−37765
cubic crystals, growth-layering effect on optical symmetry 80−88072
CVD on quartz substrate from gas mixture of $TaCl_5$-BCl_3-H_2-Ar 80−29880
cyclohexane, plastic-phase, NO-doped, heterogeneous solid soln., mag. reson. evidence 78−34449
dendritic crystal growth, impurity trapping, expt. 78−38993
dendritic crystal growth computer simulation, impurity trapping 78−38992
diamond, B doped, electron irradiated, defects at low temps., elec. resist. meas. 77−11593
diamond, defects and impurities 80−29017
diamond, different types, trace elements conc. 79−14838
diamond, extra-reflections on X-ray diffr. patterns obs. 77−59042
diamond, Fresnel diffraction at platelets, defect struct. anal. by 3 Å phase-contrast microscopy 78−87701
diamond, ion beam analyses rel. to phys. props. 79−5219
diamond, natural, impurity complexes, shape and dimens., diffuse X-ray scatt. obs. 78−47398
diamond, natural gem, H impurity conc., ion beam spectrochemical anal. 78−14374
diamond, synthetic, N impurity effect on strength charact. and thermal stability 80−11726
diamond, transformation of type IB dispersed N into type IA aggregate N 78−6089
diatomics in rare gas matrices, vibr. modulation effects 77−23496
(1,4)-dibromonaphthalene, triplet exciton scatt., absorpt. spectra 78−6696
dielectric, dipolar point defects, studied by ITC 80−6405
dielectric liquid, charge exchange mechanism between impurities and electrodes 79−91356
dielectric liquid, DC cond. due to impurity particles, computer simulation and comparison with expt. 79−91060
dielectrics containing impurities, carrier distribs. and currents, numerical simulation *(French)* 80−70718
diffusion in solid, Kramer's rate formula 78−83992
dilute alloy, electronic config. and vol. of formation 79−90991
dipolar impurity tunnelling model, elastic interaction and const. 78−71826
dislocation motion, lattice resist., effect of impurity interstitials 80−84170
dislocation systems, superconducting states, impurity effects *(Russian)* 80−11131
disordered condensed media, with impurities, energy transfer 80−80217
disordered surfaces, lattice dynamics 79−60616
displacive ferroelectrics, doped, sound vel. change 80−45013
displacive phase transition, second-order, discontinuous freezing-out of local order 79−42204
displacive transformations, single defect behaviour models 78−83904
divalent, NaCl-type crystals, existence of charged aggregates 77−84790
donor fluorescence, t-matrix analysis 80−100679
durene, aldehyde doped cryst., photolysis 10 to 20K, physical and chem. defects 79−52721
electric field distribution, form of inclusions of second phase *(Russian)* 77−55504
electron gas, one-dimens. Tomonaga model, impurity effect, electron localization and delocalization 79−73455
electron transport eqn., with random impurities 78−33654
emulsions, long wave photosensitivity rel. to impurity centres *(Russian)* 78−49925
exciton absorption, linear impurity conc. approx., validity criterion *(Russian)* 80−49620
exotic atoms, conf., Erice, Sicily, (1979) 80−67939
extremely anisotropic crystals, free excitons and exciton-impurity complexes, generation, theory 80−39509
FCC crystal containing substitutional impurities, low temp. heat capacity *(Russian)* 77−84941
ferrite, grade 2000NM1, effect of CaO, MgO and SiO_2 impurities on props. 77−40412
ferrites, manufacture, modified technology development *(German)* 77−21073
ferromagnet, excitonic, zero-sound excitations, Fermi liq. model 80−93101
first-order phase transitions, influence of quenched impurities 79−73289
fluoride film, contamination by 1 MeV proton bombardment, backscatt. obs. 77−11811
fluorophate glasses, containing rare earth ions, magneto-opt. charact. 80−64126
gas, ionis. path form. by laser beam with retractable focus 79−18992
gas purity under measuring conditions, W-value determ. *(German)* 80−104489
gaseous, mass spectroscopic analysis of microconcentrations in nonconducting materials 80−73518
gelatin gels, coloured component addition, struct. form., dynamic shear modulus, viscosity meas. *(Russian)* 80−7871
glass, Libyan Desert Glass, redox form. conditions, EPR obs. of as-received and irrad. samples 78−28228

impurities continued
glasses with rare earth impurities, microwave tunnel echo depend. on external mag. field *(Russian)* 79−65726
grain boundary dislocations, impurity influence on spreading temp. 79−77609
graphite, from reactor, quantitative microanalysis by laser emission spectroscopy 80−81384
graphite, pyrolytic doped with B^{11}, neutron irrad. damage at 60°C 79−90702
graphite, reactor material, laser microemission spectroscopy for local determ. of impurities *(German)* 78−7161
growing crystal face, foreign particle behaviour 78−47264
heterojunction properties analysis and control, cathodolum. appls. *(French)* 79−69892
n-hexane, impurity particle behaviour and cond. pulses 79−91059
homogeneous doped semiconductor, influence of internal elec. field on diffusion of ionised impurity 79−55940
hydrocarbon, in vacuum dependent scientific instruments 79−63259
ice, dielectric relaxation in presence of ionic impurities, block layer meas. tech. 80−103914
ice Ic, divalent ions hydration 79−51122
II-VI compounds, hollow crysts., morphology, review 77−11494
inert gas, liq., electron mobility, role of shallow traps 80−34440
inert gas crystals with imbedded impurities, struct. and diffusion props., review 80−10563
inorganic solids, anal. of H_2 in solids by sputter induced emission spectroscopy 79−5231
insulating oil, breakdown in long gaps, impurity effects 79−91359
insulator, wide-gap, damage by UV laser radiation 80−76110
interface segregation through cooling 79−43294
interfaces, co-segregation of metallic and non-metallic impurities 80−60868
interfacial cohesion, adsorption-induced losses 80−65010
intergranular fracture energy, effects of segregated impurities 79−38928
interstitial diffusion, influence of impurities 78−38879
ionic crystal, continuum model for periodic incorporation of aliovalent impurities 79−33012
ionic crystal, solid soln. hardening by aliovalent cations 77−44265
ionic crystal and liquid, trace element partitioning 78−47255
ionic crystals, lattice defects, conference, Canterbury, England (Sept. 1979) 80−105420
Ising system with quenched impurities, high temp. expansion methods 79−78422
kinetic Ising model with quenched relaxing impurities, crit. dynamics 78−10167
laminate, fibre reinforced composites, moisture diffusion, 3-D Fick's law 78−10218
laser impact on transparent dielectric, shock wave dissipation from imperfections 79−69925
leucosapphire, Cr influence as impurity on thermochem. etching 80−88190
liquid, detection of impurities using moire patterns 78−8440
liquid, migration mechanism of approaching particles, energy transfer, luminesc. quenching study 80−100343
liquid dispersion, suspended impurities effects on wave excitation in sound field 80−81372
liquids, impurity separation, laser thermal method *(Russian)* 77−7859
localised mode in infinite nonlinear lattice 80−10624
LPE, molecular beam mass spectrometry, in situ anal. of minor gaseous species 80−52357
many-valley semiconductor, metal-insulator transition at finite temp., calc. 80−49603
mass spectrometer, sensitivity to microimpurities, algorithm of detection 77−64000
MBBA, doping effect on cond. anisotropy and dynamic scatt. 77−40208
metal, μ^+ SR, localisation and diffusion, rel. to H 80−50248
metal, BCC, strain depend. elastic dipole tensor for interstitial impurities, nonlinear Snoek effect 79−8311
metal, BCC, tensor of deform. of cryst. lattices by impurity atoms *(Russian)* 77−7711
metal, cubic, effect of impurities on electric field gradient 78−23061
metal, impurity atoms, diffusion in region of dislocations *(Russian)* 80−24670
metal, ion implanted H(D), interstitial positions and vibr. amplitudes, fast ion channelling study, review 80−79848
metal, point defects, μSR studies 79−56703
metal, time resolved impurity conc. in DITE Tokamak using RBS anal. 79−1329
metal crystal with and without surfaces, asymptotic displaced charge round impurities 79−95364
metal film, vacuum deposited, grain struct., influence of impurities and alloying elements *(Russian)* 78−56048
metal film mirror prep. by ultraclean DC sputtering, optical props. 77−50748
metal impurity origin in DIVA, ion sputtering, evaporation and arcing 79−656
metal influx in macrotor 79−650
metal surface, interaction between adatom and substitutional impurity atom 79−56076
metal surfaces, clean, AES anal., contamination effects obs. 78−53293
metal-slag interface, interaction under diffusion conditions, impurity oxidation *(Russian)* 80−35390
metals, atomic displacements, three-body interactions around impurity 78−87689
metals, brittle intercrystalline fracture, impurities effect 80−100915
metals, C content determ., isotope-spectral method *(Russian)* 80−55766
metals, defect chemistry, He desorption spectrometry *(Dutch)* 80−96737
metals, dynamical props. of point defects, book contrib. 80−103317
metals, FCC and BCC, grain boundary struct., and segregated impurity sites, computer simulation 79−73173
metals, gas-forming impurities, trends in modern anal. *(Russian)* 80−15123
metals, muon trapping by defects and impurities 80−20573
metals, non-ferrous, recycling, effect on comp. 80−66455
metals, point defect diffusion controlled reaction theory, book contrib. 80−103318
metals, point defect dynamic props. and diffusion controlled reactions, book 80−101674
metals, positive muon interactions 80−71284,
metals, recycling, residual and additive elements control by specifications 80−66522
metals, residuals, impurities and props. 80−66521
methane, effects of impurities and annealing on triple point 78−83919
microbridges, with paramag. impurities, Josephson steady-state effect *(Russian)* 80−93042
Mo, cast, purification of C, O_2 and N_2 using thermal cycling *(Russian)* 79−70114
molecular crystal, energy spectrum, substitutional solid solutions *(Russian)* 79−78720
molecular crystal, struct. disturbance and lattice relax. calc. 79−51099
molecular crystal with impurities, nonequilib. phonon excitation by laser pumping *(Russian)* 79−38664
molecular crystals, impurity effects on positronium formation 77−66554
molecular crystals, neutron scattering and exciton spectrum due to impurities 78−91622
MOS capacitor, filament-metallised, effect of K contamination of W 79−51679
Mott transition in the presence of impurities, Hubbard model and SCF anal. 80−10878
naphthalene:$\beta\beta'$-dinaphthylethylene, stimulated emission suppression in phonon wing 78−2881
nematic phase, induced helical pitch, temp. depend., chiral additives effect *(German)* 79−60277
Ni-Co, H_2 embrittlement, heat treatment and impurities effect, Auger anal. 80−76331
Nimonic 105, creep and stress rupture props., trace elements influence 80−66602
noble gas fluid, press. induced transition in neighbourhood of alkaline earth impurity 78−51770
non-Newtonian fluid, effective diffusion of impurity in laminar flow of liquid 78−67228
nonmetallic crystals, ENDOR of impurity centres 80−25249
nonrigid impurity centres, symmetry groups *(Russian)* 80−65498
p-n-nonyloxybenzoic acid, nematic, cond. anisotropy, dopant effect 77−7667
one-dimensional conductors, disordered, elec. props., coherence length, impurity effects 80−24903
optical fibre, refractive index profile distortion, stress-induced 80−91889
optical fibres, ultratrace impurities determ., and behaviour during production by CVD process *(Japanese)* 80−87505
orbitally degenerate interacting impurity thermodynamics, stress field depend. due to point defects, dislocations 79−69477
organic impurity crystals, press. effect on shift of zero-phonon lines 79−95824
organic surface contaminants, anal. by plasma chromatography-mass spectroscopy, and Raman microprobe technique 80−108773
oscillator ensemble with embedded impurity oscillator, absorption spectrum windows 79−6045
oxidation resistance, effect of P cpds., metal impurities and struct. defects 77−81331
oxide fuel rods, steel-coated, effect of impurities on clad-corrosion *(German)* 79−49693
oxides, impurity diffusion and self-diffusion, review and bibliography 80−59719
oxides, spinel struct., impurity ion pairs, local struct. charact. 78−2146
paramagnetic centres, quadrupole relaxation transitions due to carrier exchange scattering 79−73803
paramagnetic impurity induced nucl. flip-flop transitions 79−47348
paramagnets, ferromagnetic,impurity conc. determ. from Curie-Weiss law deviations *(Russian)* 77−47965
partition coefficients, theoretical calc. of isovalent impurities with due regard for excess entropy of mixing in solid soln. and melt 79−65015
Peierls transition, effect of impurities 79−33237
Permalloy RF sputtered films, O effects in mag. and elec. props. 80−100603
phase transitions, caused by inhomogeneity of transition parameter *(Russian)* 79−23698
phenyl benzoate liq. cryst., doping effect on cond. anisotropy and dynamic scatt. 77−40208
photoemulsions, gels, coloured component addition, struct. form., dynamic shear modulus, viscosity meas. *(Russian)* 80−7871
photovoltaics and absorber/reflectors, diffusion, chemical reactions, contamination, AES and SIMS 80−72066
point defect generation in pulsed impure solid 77−1150
polydimethylsiloxane liquid film, non-pure, dielec. behaviour 80−29672
polymorphic properties, impurity effects, liquid crystalline and solid phases 79−10930
polyoxymethylene diacetate, bulk cryst. and melting, polyoxyethylene additive effects 79−32921
polyphenylene oxide thin films, electrochem. prep., impurity effects on cond., electroforming 80−88655
polypropylene films, dielec. props., impurity effects 80−71304
porphin in host n-alkane crystals, phototautomerism, IR spectral obs. 80−34963
pyrocarbon coatings for Biso fuel, permeability 77−79433
quartz, appl. of cathodolum. microscopy and spectrometry 77−69919
quartz, natural and synthetic, α-β transition, impurities effect, refr. index meas. 80−20928
quartz, single-cryst., Fe^{2+} absorpt. spectra in polarised light and struct. position 79−43007
α-quartz, synthetic, growth, defects induced by seed orientation 80−96454
quartz, synthetic, metallic impurity incorporation 79−19167
quartz, synthetic single crystal, impurity content 77−11583
quartz crystal, impurity content and lattice consts., electrolysis influence 77−35580
quartz crystal, synthetic, dislocations obs. by light scatt. tomography 80−49229
quartz fibre, ESR and IR obs. of microinhomogeneities 77−8401
quartz lattice constants, impurity effects 80−39034
rare earth films, prep., struct., and props., general review 80−54556
rare earth metal film, anomalous crystal structures 79−28222
rare earth oxides, Cu and Fe impurities, at. absorpt. determ. 79−87905
recoil implantation, film thickness optimisation 77−35578
refractory refinement during prep. by self propagating high temp. synthesis 78−60634
ruby, Cr influence as impurity on thermochem. etching 80−88190
ruby colouring due to specific growth, annealing and irrad., exam. of visible, infrared and UV spectra 79−11440

impurities continued
sample contamination, by sputtering, during ion implantation 80−54274
sapphire:Ti^{4+}, plastically deformed, precipitation hardening, TEM study 80−7592
sapphire, vacuum UV spectra, Cr^{3+} impurity and anion vacancy conc. 78−84605
segregation, grain boundary, equilib. impurity conc. *(Russian)* 80−103478
semiconductor, crit. points for electron-hole system 80−44511
semiconductor, defect electronic structure and lattice config., MO approaches 80−65495
semiconductor, dielec. response function, local field effects 79−51505
semiconductor, inhomogenous, eigenoscills, of hot electrons in classically strong mag. field 79−73520
semiconductor, optical and IR characterisation 79−95846
semiconductor DH lasers, effect of impurities on quantum shot noise reson. 78−22132
semiconductor film, laser-induced transmittance oscills. and struct. phase transitions 79−87516
semiconductor impurities, trace element anal. 80−81399
semiconductor impurity anal. by photoelectric spectroscopy, review 77−24584
semiconductor materials, contamination equilibrium assessment 79−51134
semiconductor physics, conf., Edinburgh, Scotland (Sept. 1978) 79−95303
semiconductors, localised transition metal impurities, lattice relaxation in optical transition *(Polish)* 80−70345
semiconductors, Z 80−19799
silica, vitreous, effects on viscosity of impurity alkali oxide, OH, Al_2O_3 and Ga_2O_3 78−64580
SIMS, interfacial impurities, quantitative anal. 80−84396
soft, static and dynamic behaviour 77−72669
solid, impurity atom fluoresc. radiation, intensity correlation, low temp. limit 80−80847
solid solution, heterovalent, use of expt. data to estimate energy of soln. 80−54380
solidification, foreign particle trapping, anomalous influence of body force 78−2045
soliton pinning and central peak theory 79−7668
spin-phonon system, transition to self-trapping 80−10606
steam-generating pipe, containing porous deposits, mass transfer (impurities) 78−38398
steel, alloy, temper embrittlement, comp. influence 80−66658
steel, austenitic, tempering cavity condensation *(French)* 80−55442
steel, austenitic stainless, liquation cracking during welding, comp. influence 80−66645
steel, austenitic stainless, Mn-N interaction, internal friction obs. 78−84883
steel, austenitic type 304, temper embrittlement and impurity segregation, AES and imitation loss spectroscopy study 79−43372
steel, C, plates, residual elements effect on through-thickness props. 80−66660
steel, C, residual elements, effect on props. 80−66643
steel, commercial alloy ferritic, meas. of alloy and impurity elemental distrib. using STEM 80−35601
steel, Cr-C (1, 1 wt.%), hot ductility and S segregation 80−66594
steel, Cr-Mo and Ni-Cr-Mo-V low-alloy, additive remedy for temper brittleness 80−66659
steel, Cr-Mo weld metal, reheat cracking, residual elements and microstruct. influence 80−66553
steel, Cr-Mo weld metal, trace element embrittlement suppression by creep strength effects 80−66656
steel, Cr-Mo-(V) austenitic, creep resist., high-temp. props. residuals effect 80−66600
steel, Cr-Mo-V, strength and ductility in creep, purity influence 80−66598
steel, Cr-Mo-V low-alloy, high-temp. ductility and crack growth, impurities effect 80−66652
steel, Cr-Mo-V low-alloy, mech. props. and stress relief cracking, effects of impurities and deoxidation practice 80−66599
steel, Cr-Mo-V low-alloy, prior austenite grain boundary embrittlement by B 80−66657
steel, Cr-Mo-V low-alloy, stress relief cracking, impurity and alloy content effects 80−66654
steel, Cr-Mo-V low-alloy with high residual element content, cavitation control 80−66663
steel, defective zones in cold rolling, activation analysis method 78−7278
steel, ferritic, creep resist., high-temp. props. residuals effect 80−66600
steel, high strength, 300-M, slow fatigue crack growth, threshold behaviour, temper embrittlement, impurity segregation effects 77−86152
steel, high-strength, 80 kg/mm² class, effects of metallurgical factors on susceptibility of stress relief testing *(Japanese)* 79−43458
steel, high-strength, fatigue, interaction effects between trace impurities and environment 80−66651
steel, hot rolled, M1 tool type, microparticle distributions and mech. response 77−44279
steel, hot shortness, high-temp. embrittlement, residual and trace elements influence 80−66644
steel, impurity element determ. by spark source mass spectrometry using powdered salt 78−7304
steel, impurity spectral lines, intensity, temp. and conc. effects 80−64774
steel, intergranular fracture, impurity effects 77−8842
steel, low alloy, 15Kh2MFA and 15Kh2NMFA, neutron irrad. embrittlement, effect of P, Sb and Sn impurities 80−85055
steel, low alloy, impurity and strength effect on H_2 induced cracking 78−27625
steel, low alloy structural, heat treated, impurities effect on embrittlement susceptibility and temper brittleness 79−38955
steel, low C sheets, effect of N_2 content on recrystn. texture 79−83233
steel, low-alloy, hardened deoxidised, delayed failure, influence of internal adsorpt. of impurities 80−60974
steel, low-alloy, impurities, segregation and creep embrittlement 80−66653
steel, low-alloy, residual elements, effect on props. 80−66643
steel, low-alloy pipe, resist. to fracture, S content and sulphide inclusions effect 79−96128
steel, low-C, structural, grain boundaries, AES 79−24524
steel, Mn-Mo, castings, mech. props., Cu and Sn trace elements effect 80−66596
steel, Mn-Mo-Ni, embrittling effects of residual elements 80−66655
impurities continued
steel, Ni-Cr, cast, tempering embrittlement due to impurities, Auger spectroscopy exam. 80−11683
steel, Ni-Cr, SCC, grain boundary impurity effect 80−30150
steel, Ni-Mo-Cr, embrittling effects of residual elements 80−66655
steel, quenched, tempered, intergranular failure during fatigue crack growth 79−8357
steel, segregation and adsorption of S, influence on carburisation and nitrogenation 80−66701
steel, solubility of W and Mo in $Ti(C,N)_x$ 80−16276
steel, stainless, ferritic, mech. props., impurity effects *(Russian)* 77−52403
steel, stainless AISI 316, Si and Ti effect in phase stability and swelling behaviour 79−78972
steel, structural, addition of solid SiO, effect on ductile fracture 80−16465
steel, structural, impurity effect on crack initiation, dynamical loading *(Czech)* 80−60955
steel, structural 15KhNMFA, resist. to weakening during tempering, high purity effect 80−76279
steel, trace elements 80−84839
STEM, and spectroscopic techniques for electronic props. of defects and impurities in semiconductors 79−14812
Stepanov method, liq. mixing in shaper hole, simulation device 78−3022
substituent impurities in diamond-structure crystals, diffusion equation, complex formation, theory 80−24677
substitutional impurity, driving force for electromigration 77−76618
substitutional impurity, model parameters, determ. from low temp. data *(Russian)* 79−33007
sucrose, crystn. rate in impure solns., influence of non-sugar and colouring substance quantity 80−100767
sucrose crystal formation, and growth, effect of same metallic impurities 80−100768
superconductivity, electron-hole, influence of struct. defects 77−20489
superconductors, strongly anisotropic, nonmag. impurities effect on supercond. transition temp. 80−93035
superconductors with paramag. impurities, NMR theory in singlet state 79−28445
superionic conductor, paramag. impurity contrib. to NMR relax. in one-dimension 80−20477
superradiative transitions, acoustic and EM excitation 78−66872
surface, Auger spectral analysis 77−15671
surface impurities during start up and early operation of ISX-A, surface anal. with sample transfer 79−654
TCNQ salt, $Qn(TCNQ)_2$, decrease of electronic coherence length by impurities 79−69501
TGS, L-α-alanine disordered regions, dielec. prop. changes in transition region 80−108159
TGS, orientation depend. of l-alanine incorporation 78−42938
TNT, creamed, dimensional stability, irreversible thermal expansion, rel. to impurities 79−73316
trace impurities in gasses, IR spectrometric detect., cryogenic method 79−16053
transition metal, BCC, H trapping at impurities in neutron scatt. obs. of fast diffusion 80−59731
transition metal, BCC solubility, heat of solution calcs. 78−6160
transition metal alloy, ferromag., H-impurity complex obs. by mag. aftereffect 78−72373
transition metal film, anomalous crystal structures 79−28222
transition metal-rare earth dil. alloy, hyperfine field of rare earth impurity 79−1588
TTT_2I_3, chem. impurities and neutron irrad. induced defects, effects on DC cond. 80−49699
ultrapure water, trace metal determ. 80−81394
vacuum vessel wall surface conditions, long term changes, PLT appl. 79−653
vapour growth, element incorporation 78−30556
vibrational energy transfer in solids, rot. mode participation 78−63815
vibrations in impure crystals, average local information transfer approx. 79−46774
voids, coated, capture efficiency 80−96515
water impurity concentration in steam-generating channels with capillary-porous structure 80−103071
X-ray intensities, charact., orientations depend. in bi-atomic single cryst., possible impurity atom detection 77−63488
Ag, elec. field gradient generated by nearest-neighbour impurity atoms 79−42510
Ag film on Mo, epitaxial growth, exam. of S impurity segregation at interface 78−84076
Ag host, impurity effect on electric field gradient 78−23061
Ag single cryst., effects of impurities and prestraining on temp. depend. of yield stress *(Russian)* 77−47506
Ag-Cu, highly deformed eutectic composite wire, anomalous props., fibre diameter and foreign atom effects *(German)* 77−36566
AgBr:Li^+, time-depend. infrared absorpt. due to Li-localised mode 79−8133
AgBr:$Na^+(Li^+)$, correlated diffusion of impurities, nuclear spin relax. meas. 80−108094
AgBr:Pt, photochemistry and role of Pt impurity ions 79−24783
AgCl:Pt, photochemistry and role of Pt impurity ions 79−24783
AgCl:Sr, effect of impurity doping on Sr^{2+} diffusion 78−84002
AgCl:X^{2+}, X=Mg, Ca, Sr, Cd, Ba, plasticity, impurity hardening effect 78−47466
AgI, atmospheric ice forming props., impurities and surface state effects *(French)* 78−20459
AgX, X=halide, form. and migration of catalytic nuclei *(Russian)* 79−70378
Al alloy, D16, Fe and Si impurity effects on K_{1c} 78−84990
Al alloys, neutron irradiated, suppression of radiation damage microstruct. by trace impurities 79−77643
Al, anodisation, high voltage barrier, Cl^- ion effects 80−104327
Al castings, grain refinement by gas-generating mold coatings containing hexachloroethane 79−83355
Al film, H incorporation effect on stress and electromigration 80−80139
Al film, vacuum deposited, 7 to 65 μ thick, morphology and purity determ. 77−76699
Al, impurities heat of solution, pseudopot. calc. 77−51393
Al, impurity diffusion 78−47595
Al, impurity influence on superplasticity, elongation decrease at rupture *(Russian)* 79−91735

impurities continued
Al, molten, impurity diffusion of fourth period solutes and homovalent solutes *(Japanese)* 80−70436
Al, μ^+ meson diffusion, impurities effect *(Russian)* 78−35077
Al, positron annihilation, detection of N impurities 79−65777
Al, positron annihilation rel. to thermocyclic treatment 79−52040
Al, quenched, irradiated, and quenched plus irradiated, grain boundary hardening 80−3162
Al, strain rate sensitivity and ductility, trace element conc. effect 80−66597
Al, with dilute pt. defects, thermopower, Hall effect and magnetoresist. 79−65458
Al:Si, film deposition by reactive sputtering 79−66005
Al-Al_2O_3-Al junctions, Dy doped at Al_2O_3-Al interface, electron transport mechanisms and barrier height 78−91778
Al-gelatin-GaAs, capacitance-voltage characts. after and before incorporation of $AgNO_3$ 79−51684
Al-Mg, dil., long-range solute-host interactions 78−95062
Al-Mg alloy AMg6, mech. props. of welded joints, impurity effects 78−95789
Al-Si (9 wt.%), precipitation hardening during isothermal ageing 80−29969
Al-Si alloys, eutectics and hypoeutectics, mech. props. and thermal cond., P impurity effect 79−83271
Al-Zn-Fe-Si, Fe and Si effects on precip., TEM and X-ray diffr. obs., ageing at 90°C 77−48439
AlB_{12}, preparation of single crystal 78−43997
$Al_xGa_{1-x}As$:Mn epitaxial layers, Mn-O association, EPR meas. 77−69677
AlN powder, effect of O impurity on sintering and thermal cond. *(Japanese)* 79−20017
AlN:O, influence of O on luminesc. excitation spectrum in interband transition range 77−8644
AlN:O, thermolum. mechanism, 80-420K 79−78761
Al_2O_3, corundum, impurity striation, light scatt., optical and electron microscopy meas. 78−22757
Al_2O_3, high purity, sintering, impurity effects, analysis *(German)* 78−6881
Al_2O_3, polycrystalline, conditions for formation of anion vacancies 79−10844
Al_2O_3, pure and Fe or Cr doped, polycryst., creep, diffusion mechanisms 78−11272
Al_2O_3:Cr, Mg, stabilisation of Cr^{5+}, thermal cond. meas. 78−22905
Al_2O_3:Cr_2O_3(Ti_2O_3), dopant influence on struct. and mech. props. 80−24471
α-Al_2O_3:Cr(Ti)(V), impurities effect on thermoluminesc. 80−40170
Al_2O_3:Ni^{2+}, corundum, phaser production of transverse phonons by impurity centres *(Russian)* 78−91390
Al_2O_3-Ca_3SiO_5, solid solution, exam. of lattice defects 79−95167
Al_2O_3-Na_2O, β and β'' phases, stability, cond., paramag. impurity effects obs. 77−84976
Al_2O_3-Nb composites, influence of gas impurities on solid-state bonding on annealing 80−11739
As_2S_3, glassy, build-in mechanism of impurities, electronegativity influence 77−76313
$AsSe_{1.2}$:Fe, Fe effect on physiochem. props. of glass 80−24370
As_2Se_3:Pt, glass, effect of impurities on elec. props. 80−103699
$AsSe_{1.1}Te_{0.2}$:Fe, Fe effect on physiochem. props. of glass 80−24370
Au polycrystalline wire, internal oxidation of impurities 78−83842
Au-Ge film, evaporated, for ohmic contacts to GaAs, compositional stratification, effect of source material impurities 79−77951
B, amorphous, microimpurities determ. using hollow cathode discharge 80−85247
B, purity evaluation by elec. meas. 78−59822
β-B, rhombohedral, containing Sc, X-ray diffr. indicating ScB_{28} 78−34464
β-B, rhombohedral, Knoop hardness and room temp. resist., rel to purity 80−21084
B, tetragonal, X-ray diffr. and C doping obs. *(French)* 79−14731
B, zone-refined, Ni doping effects on conductivity type, microhardness, metallographic obs. 77−31682
BN, O content depend. on heat treatment temp., neutron activation analysis 80−16356
BN, wurtzite, impurities, influence on processing props. in prep. of Geksanit-R sinterings 80−25632
B_2O_3 glasses, thermolum., additives effect 78−27337
BP:Ni pillar crystal growth from vapour 80−60758
BaF_2:R^{3+} (R=rare earth) dipole reorientation, ionic thermocurrents obs. 79−95705
BaF_2:Y^{3+},Gd^{3+} production and mech. props. 79−72638
$BaFe_{12}O_{19}$, effect of impurity concentrations, and sintering conditions on grain size *(German)* 79−23630
BaO:Mn^{2+}, impurity pot. well shape calcs. 78−87950
BaO-P_2O_5(SiO_2) glasses, Nd^{3+} luminesc. quenching by transition metal and rare earth ions 80−25449
BaO-V_2O_5-CuO semiconducting glasses, impurity effects, elec. resist. and EPR study 80−103692
$BaTiO_3$, donor doped, exam. of heterogeneous microstructure *(German)* 79−24632
$BaTiO_3$, reduction inhibition by impurity ions 80−101018
$BaTiO_3$:Fe^{3+}, local position determ. by EPR 80−108057
$BaTiO_3$:Mn, polycrystn., annealing effect on transition temps. 80−3100
$BaTiO_3$-based ceramics, impurity atoms chem. state, Mossbauer spectra 80−15902
Be, deformation strengthening, microstruct. and impurity effects 77−4791
Be, low oxide, isostatically pressed block, factors affecting tensile strength, elongation, impact resistance 77−16610
Be, plastic strain mech., effect of impurities *(Russian)* 79−34101
Be, polycryst., yield strength, struct. factors effects 77−63749
Be, RF sputtered film, props. rel. to deposition conditions 77−39965
Be:Os, anomalous displacement of Os atoms from substitutional site 77−59039
Be-Cu, thermal expansion, vibr. characteristics at low temp., effect of substitution impurities *(Russian)* 80−103439
Bi, impurity diffusion, of Rb, Sr, Ba, Cs 79−77819
Bi:Sn(Pb)(Sb)(Te) polycrystal elastic constants for US velocity obs. 79−69180
C fibre, tensile strength, heat treatment and flaw effects 80−81173
C, film with random struct. growth from ion impact damage in butane plasma 79−83139

impurities continued
C in Si, trace anal. by proton activation *(Chinese)* 80−81403
CC GaP, improvements in synthesis, solute diffusion (SSD) growth, Si contamination 79−65992
CO surface contamination of Ti thin film, effect on deuteriding 77−35814
CO_2, pulse laser, UV photoionisation, impurities effect 78−1206
$CaCO_3$, aragonite-calcite transformation, effect of impurities, DTA and IR studies 78−51662
CaF:Eu(Gd)(Dy)(Tb), dimer reorientation activation volume 80−107285
CaF_2 crystals, elec. cond., O^{2-} effect 80−2431
CaF_2, mixed cluster, doubly-doped with rare earths, elec. dipole relax. 79−82924
CaF_2:Ce, Stark struct., phototransitions, g-factors 78−67995
CaF_2:Eu, Mn, cathodoluminescence SEM appl., stroboscopic 80−70088
CaF_2:M, M=Mn, Fe, Co, Ni, X-irrad., impurity effects on defect prod. 80−92525
CaF_2:NaF (YF_3) thermal conductivity of single crysts., 80-300K 77−11747
CaF_2:rare earth, defect model for nonlocally compensated trivalent impurities 77−72629
CaFz crystals, grown from synthetic raw materials, quality, effect of impurities, composition 78−79083
CaO:Cr_2O_3, addition effect on sintering *(Czech)* 80−45258
CaO:Mn^{2+}, impurity pot. well shape calcs. 78−87950
CaO-Al_2O_3:Si(S), effect of addition on reduction of Al_2O_3 by C saturated Fe *(Japanese)* 79−24733
CaO-MgO, doloma, composition effect on creep, impurity effects 79−43318
$Ca_3(PO_4)_2$:Cu^{2+}, ESR, high press. struct. transition 80−97134
CaS:Bi as UV dosimeter 80−34991
CaS:Nd phosphors, X-ray powder diffr. anal. 80−100204
$CaSO_4.2H_2O$, occlusion formation during dendritic crystal growth, expt. 78−38993
$CaWO_4$:Gd, site occupation 79−28608
Cd, vapour grown crystal, morphology and growth mechanism, Bi impurity effects 79−23546
CdS, neutron and fast electron irrad., local centre form., TSC and photoluminesc. meas. 78−87719
CdS sprayed film, prep., optical props., struct. and comp. 79−78875
CdS:D^-, binding energy of D^- ion 80−92541
CdS:I single cryst., I detection by argentometric titration DEP 77−16875
CdTe:Cu films, impurity behaviour, Hall mobility and hole density meas. 80−80420
Ce-Pr powder, DHCP⇄FCC transition, X-ray, DTA and resistivity studies 80−50629
$Ce_2Mg_3(NO_3)_{12}$, heat capacity meas., 0.15 to 0.6K, origin of anomaly 77−35707
CeO_2:CaO(Y_2O_3), oxygen ion cond. and defect struct. 80−107553
$CeO_2La_2O_3$, ceramic, thermal stability, sintering, deform., effect of La_2O_3 79−11532
Co-Mo alloy electrodeposits, codeposited impurities rel. to H_2 permeation, props. 79−19493
Co-W(25 wt.%), cellular decomposition, third element effects *(Russian)* 77−1837
CoGd:H_2(N_2), contaminated amorphous films mag. and elec. props. 79−1690
Cr coatings, electrodeposition, conditions rel. to H_2 conc., internal stresses 77−1933
Cr, Neel temperature and Fermi energy, nonmag. impurity effects 80−65888
Cr, oxidation resist., rare earth impurities effect 80−66703
Cr^{3+} ions, in corundum, comparison of theoretical and experimental values of energy levels 79−54829
$Cr_xFe_{3-x}O_4$, spin and charge density oscillations due to impurities *(Korean)* 80−20565
CsBr(I), single crysts., polarisation of luminesc. and reorientation of NO_2^- centres 79−95823
$CsCdBr_3$:Cr^{3+}(Cr^+), EPR of impurities, charge compensation, X-ray effects 80−60407
$CsDy(MoO_4)_2$, trivalent ion impurity effects on structural phase transition temp., new transition 20-30K *(Russian)* 79−19367
$CsDy(MoO_4)_2$:Eu^{3+}, anomalous effect of impurity on struct. phase transition temp. *(Russian)* 77−69083
CsI:Na^+(K^+)(Cu^{2+})(Tl^{3+})(Eu^{3+}), crysts., influence of impurities on yield stress 79−15748
CsI:Tl, geometrical parameters of impurity centres by scattered-light method 80−2043
CsI:Tl, X-ray phosphor, influence of different factors on emission intensity 79−8171
CsI:Tl single crystal gamma-optical converting screens, factors influencing relative afterglow intensity 79−8173
$CsMgCl_3(Br_3)$:Cr^{3+}(Cr^+), EPR of impurities, charge compensation, X-ray effects 80−60407
Cu, drawability, mech. props., effect of O impurities 79−83272
Cu, effect of impurities 80−50925
Cu, elec. resist. under torsional deform., impurities and tensile strain 78−30898
Cu, Fermi surface orbit integrals, tetrahedron method, Dingle temps. for 3d transition metal impurities 80−44477
Cu film on Mo, epitaxial growth, exam. of S impurity segregation at interface 78−84076
Cu, in rare earth oxides, at. absorpt. determ. 79−87905
Cu, internal friction, impurity effect *(Russian)* 79−87677
Cu, liquid, dissolved O below 0.02 wt.% effect on surface tension 80−107618
Cu, recrystn. centre growth kinetics, impurity effects *(Russian)* 80−89253
Cu, tough pitch wire, rel. between oxygen contents and cupping *(Japanese)* 79−79087
Cu, types MOb and M1, primary recrystallisation kinetics depend. on state of impurities *(Russian)* 79−66069
Cu:Ni, Dingle temps. calcs., tetrahedron method 80−6699
Cu-Ag (Pb)(Bi), evaporation of Ag, Pb, Bi in vacuum induction melting 77−28742
Cu-Ag(Bi)-O, evaporation of Ag, Bi in vacuum induction melting 77−28742
Cu-Ge, dil., point defect props., density functional approach 80−29013
Cu-Ni, cast, strength and hot ductility, alloying and residual elements effect 80−66595

impurities continued
Cu-Ni sulphidised alloys, Ru and Os behaviour during carbonylation *(Russian)* 80−40584
α-Cu-Ni-Zn-Pb, fire cracking, effect of pores and impurities 79−29207
Cu-O, effect of Se, S, Pb impurities on annealability and resistivity 77−28834
Er_2O_3:CaO, elec. cond. and nonstoichiometry 79−11112
EuB_6, simple crystal, prep., floating zone technique 77−85934
Eu_2O_3, monoclinic, growth from molten NaF solvent 78−19653
Fe, BCC containing impurity atoms, Peierls energy of 1/2⟨111⟩{110} edge dislocation, temp. effect 77−84751
Fe based alloys, solute segregation to grain boundaries 78−72780
Fe, bonding of Al, growth of intermediate phases, effect of O and N impurities 78−27680
Fe, cast, Mg, Pb impurity effect on struct. and mech. props. 79−96089
Fe electrode, electrochem. behaviour in liq. NH_4 solns., effects of added impurities 80−50857
Fe film, Hall resist., effect of N impurity codeposition 78−64146
Fe film, thermally evaporated, contamination effects obs. 80−49545
Fe, hot shortness, high-temp. embrittlement, residual and trace elements influence 80−66644
Fe, impure, Snoek peak figures in various strain amplitude ranges 80−66562
Fe, in rare earth oxides, at. absorpt. determ. 79−87905
Fe, lattice distortions due to H, X-ray diffr. exam. 78−79629
Fe, liq., short-range order struct., O impurity influence *(Russian)* 80−38901
Fe, molten, impurities effect on viscosity 78−95172
Fe, muon$^+$ diffusion, spin rotation, effect of impurities 80−7249
Fe, segregation and adsorption of S, influence on carburisation and nitrogenation 80−66701
α-Fe, strengthening kinetics due to deformation ageing, impurity atom sources *(Russian)* 80−55435
Fe surface, adsorbed O_2 effect on chem. reaction kinetics 80−55572
Fe, surface contamination due to polishing, determ. by luminescent-discharge spectrometry *(French)* 79−52839
Fe, thin foil, extrinsic grain boundary dislocations, low C content influence 80−107273
Fe, whisker domain wall interaction with mobile impurities 77−12145
Fe:H, deformed, deep trapping states for H 80−29045
Fe:He, BCC, process of interstitial trapping by impurities 79−46697
Fe:I, ^{131}I NMR, vacancy associated impurity sites 78−91964
Fe:Ti, C induced amorphous surface layers 80−107287
Fe:Yb,O, interaction between impurities, perturbed ang. correlation meas. 77−1628
α-Fe-(Ni,Mn,Cr,Mo,W)-P (1 wt.%). grain boundary segregation, temper brittleness, AES study *(Japanese)* 79−78981
Fe-As melts, influence of Sn, Si, Mn and Cr additions on surface tension and density *(Russian)* 80−15337
Fe-based alloy, effect of sp-3d impurity interactions in resistivity 79−46696
Fe-C-N, BCC, Snoek type reordering during strain ageing *(French)* 79−8312
Fe-Cr (20 wt.%), role of rare earths and reactive elements in high-temp. oxidation 79−79178
Fe-Cr (9 wt.%), extrinsic grain boundary dislocations, low C content influence 80−107273
Fe-Gd film, amorphous, O_2 contamination effects on mag. props. 78−64231
Fe-M-(I) (M≡Ni, Cr, V, Ti, Mo; I≡Sb, P), co-segregation at free surfaces studied by Auger spectroscopy 80−59767
Fe-Ni, crystallization texture, rolling, effect of impurities 78−15425
Fe-Sb system, α-phase, interdiffusion 79−73349
Fe-Si (3 wt.%), tertiary products from deoxidation, electron emission microscope study *(Russian)* 78−11214
Fe-Ti-C, quantitative anal. of H trapping 79−23622
FeGd:H_2(N_2) contaminated amorphous films mag. and elec. props. 79−1690
$Fe(Li_{0.5}Fe_{1.5-x/8}Mn_{x/8})O_4$ $0 \leq x \leq 2$ spinel system, X-ray diffr. anal. of loss of order on Cr substitution 79−73178
γ-Fe_2O_3:Fe_3O_4, magnetite impurity determ. by C_p calorimetry 78−2152
Fe_xO_y film, thermally evaporated, contamination effects obs. 80−49545
Ga, electrode, crystallite interfacial impurities, electrochem. effects, microprobe anal. 77−44569
Ga, small Cu additives effect on cryst. growth from melt 77−32515
Ga, with 100 ppm Ag single cryst. growth by pulling, thermal parameters governing purity *(French)* 78−2046
GaAlAs-GaAs heteroepitaxial devices, interstitial impurities and degradation, Auger obs. 80−99730
GaAlAs-GaAs heterostruc. lasers, interstitial impurities and degradation, Auger obs. 80−99730
GaAs, concs. of C and O_2 in LEC grown cryst. determ. 77−39612
GaAs epitaxial layers, from mixed Ga solns., C solubility 80−15392
GaAs, impurity anal. by photoluminescence *(Japanese)* 77−24888
GaAs, LPE, gaseous impurity source and effect on purity 79−28959
GaAs, LPE, residual impurities and deep levels, FET fabrication 79−28964
GaAs, LPE in graphite boat, total ionised impurity density 77−12550
GaAs, layer structures revealed by decoration method and electron microscopy 77−27902
GaAs layers, from gas phase, impurity influence on growth micromechanism 80−45237
GaAs, MBE layers, H_2 effect on residual impurities, photolum. obs. and elec. characts. 79−47636
GaAs, undoped epitaxial layer growth from nonstoichiometric solns., O_2 contamination sources 80−108362
GaAs, VPE, thermodynamic analysis of Si contamination 79−28932
GaAs, VPE, thermodynamic factor influencing growth rate and layer purity in Ga-$AsCl_3$-H_2 system 79−28933
GaAs:Cr, EPR, annealing and IR excitation effect on Cr^+ signal, Cr content by colorimetry 77−69680
GaAs:Cr^{2+}, US attenuation meas. of Jahn-Teller distorted Cr^{2+} centres 79−28048
GaAs:Mn, Mn-O association, EPR meas. 77−69677
GaAs:Na, impurity solubility and diffusion 79−55930
GaAs:Sn, effect of Sn conc. on point defect generation 79−14802
GaAs:Sn films, MBE power MESFETs 80−50563
GaAs:Sn^+, impurity-defect complex from ^{119}In implantation, Mossbauer study 80−59486
GaAs:Te, powder, quadrupole interactions in NMR spectra 79−51880

impurities continued
GaP, deep level profiles at substrate-epitaxial interfaces, photoionisation meas. 79−38025
GaP-Sb, Sb solubility in region of GaP primary crystn. 79−86891
GaSb pulled crystal, wavy impurity patterns beside twin boundary 78−18674
GaSb:Te,Zn(Te,Mn), prep. and electrophys. props. 79−87116
Gd-Co, sputtered film, growth induced anisotropy 77−16123
Gd-Co film, sputtered, inert gas incorporation effect on uniaxial anisotropy 78−64232
p-Ge, depend. of saturation intensity on impurity conc. and residual absorption at 10.59 microns 80−45125
Ge, donor polarizability, multivalley effective mass calc. 80−96817
n-Ge, doping effects on US velocity and attenuation 80−70325
Ge, light scattering due to microdefects 78−27248
Ge, μ^+ meson polarisation, H impurity behaviour 77−20786
Ge, neutron irrad., substitution of impurity atoms by self-interstitials, Ge(n,γ) reaction 80−39166
Ge:Be(Mg)(Ca)(Ba), positron annihilation ang. distrib 80−45165
Ge:Cu, degree of Cu contamination in heat treated Ge 80−2359
Ge:Fe, amorphous film or ion-implanted, comparison of ^{57}Fe Mossbauer data 77−40159
p-Ge:Ga, cryst. defects due to γ-irrad., annealing 79−55779
Ge:O, Cu, amorphous thin film, impurity effects on struct. 80−107054
Ge:O(Si), effect of impurities on mech. strength in brittle fracture region 79−87682
p-Ge:Sb, cryst. defects due to γ-irrad. 79−55779
GeO_2:V^{4+}(Cr^{3+}), direct mechanism in supertransferred hyperfine interaction 79−23936
GeO_2-P_2O_5-SiO_2 glass fibre, incorporation of OH in modified CVD process 80−50560
$Ge_{42}S_{58}$:Cu(Ag)(I), glass, impurity effect on e.p.r., dangling bonds 77−4553
$Ge_{2.33}SbSe_5$:FE, Fe effect on physiochem. props. of glass 80−24370
H atom lattice impurity, H atom confined to spherical box with penetrable walls, Schrodinger eqn. 79−84987
H_2 embrittlement cracking and impurity atom migration *(Chinese)* 80−104247
H_2, solid dilute atomic H impurities props. calc. 79−60601
He, solid, coherent diffusion of isotropic impurities 80−54468
He, solid, impurities and vacancies 79−65289
He, solid, theory and thermodynamic props., book contrib. 77−47646
^{3}He, HCP solid, with ^{4}He impurities, ^{3}He nucl. mag. relax. behaviours 79−56027
^{3}He, solid, phase separation of dil. ^{4}He impurities 80−88393
^{3}He, superfluid, distortions around small object 77−85012
^{4}He, liq., positive impurity ion struct., modified theory 77−39714
^{4}He, liq., surface, interaction with atomic H, Euler Lagrange eqn. 79−77850
^{4}He, liq., upper limit for conc. of potential dissolved contaminants 80−39373
^{4}He, solid, diffusion coeff. of ^{3}He, detection and study of impuriton-phonon scatt. mech. 79−56029
^{4}He, solid, impurity interaction anisotropy and quantum diffusion of ^{3}He 79−56028
^{4}He, solid, pure and with ^{3}He admixtures, effect of plastic deform. and impurities on internal friction *(Russian)* 79−77860
^{4}He, spin diffusion coeff. of ^{3}He impurities, impuriton model 77−59174
HgI_2, cryst. growth from soln., doping rel. to elec. cond., phase transitions 77−55880
p-Hz, quantum diffusion of O-H_2 impurities 80−96719
I molecular cell, impurity gas detection, He-Ne laser stability appl. *(French)* 77−73496
^{129}I impurities implanted in semiconductors, isomer shift 80−20522
In, intermediate state, doping effect on US attenuation 80−2522
In surface, impurity precipitation and resolution at melting point 78−14553
In, twin boundary movement by creep 80−24460
In-Sn, dil., intermediate state, doping effect on US attenuation 80−2522
InAs:Mn powder, quadrupole interactions in NMR spectra 79−51880
InAs:Te(Se)(S), intrinsic pt. struct. defects 80−33998
In_2O_3, defect chemistry and struct. stability, impurity incorporation 77−35552
In_2O_3:Sn films, elec. and optical props., solar energy conversion appl. 79−65945
InP, concs. of C and O_2 in LEC grown cryst. determ. 77−39612
InP, effects of baking time on purity and morphology 78−6862
InP epitaxial layers, (100)-orientated, vapour phase deposited in closed-tube system, surface comp. variation 80−24752
InP VPE, growth kinetics and controlled doping 79−87569
InP:Te, powder, quadrupole interactions in NMR spectra 79−51880
InP:Zn(S)(Se), liquid encapsulated Czochralski cryst. growth, X-ray study 79−47619
InSb, Cu-coated, surface contamination, ion microprobe mass analyser obs. 77−52729
InSb:Mn, powder, quadrupole interactions in NMR spectra 79−51880
InSb:Se, exam. of defects in crystal 80−6423
Ir, brittle fracture, impurity segregation to grain boundary effects 78−64637
Ir-W (0.3 wt.%): Al(Fe)(Th)(Ni)(Rh), effect of additions on grain boundary composition 79−83309
$KAl(SO_4)_2.12H_2O$, occlusion formation during dendritic crystal growth, expt. 78−38993
KBr bicrystal, grown from melt, interfacial substructure, impurity effects 77−4263
KBr:PbI_2, single crysts. grown from aq. soln., growth striations obs. 77−1089
KBr:Tl excitation in fund. absorpt. region, luminesc. and thermolum. 80−50433
$KCaCl_3$ impurity in NaCl cryst., precipitation and dissolution 79−42259
KCl cryst., Sr and Na impurities radial distrib., influence of form of crystn. front 80−107312
KCl crystals, Eu^{2+} concentration effect on lattice parameter and density of crystals 80−88169
KCl, entropy change associated with substitutional anion defects calc. 78−79782
KCl:Cs^+(I^-), low-temp. heat capacity enhancement due to impurities 80−107442
KCl:Eu, impurity conc. determ. by optical absorpt. meas. 77−32409
KCl:Li, ⟨111⟩ off centre Li^+ under biaxial stress, bistable tunnelling 78−15090

impurities continued
KCl:Li^+, shape of pot. energy well of impurity 79−23692
KCl:Na^+(Rb^+)(Ag^+), entropy changes associated with point defects form. calcs. 77−7741
KCl:Pb, colouring, room temp., influence of conc. and aggregation state of Pb 78−14339
KCl:Pb, geometrical parameters of impurity centres by scattered-light method 80−2043
KCl:Pb, impurity valence, heat treatment influence, absorpt. spectra obs. 79−38574
KCl:Pb exam. of simultaneous effect of heat treatment, Pb concentration on state, phase diagram construction 79−96008
KCl:Pb^{2+}, low temp. sp. ht. 80−2178
KCl:Pb^{2+}(Cu^+) 80−34890
KCl:$SnCl_2$, action of ionising radiation on Sn aggregation processes 78−34543
KCl:Sr^{2+}(SO_4^{2-}), defect parameters, self-consistent set, ionic cond. meas. 80−107487
KCl:TlCl, lattice defects, X-ray line profile obs. 80−24455
KCl_xBr_{1-x}:Sr^{2+}, dielec. loss 77−85646
KF:Li^+(Na^+)(K^+), shape of pot. energy well of impurity 79−23692
KH_2AsO_4, irrad. ferroelec., AsO_3H^- free radical localised near impurity, ENDOR 77−24762
KH_2PO_4, cryst. regeneration of z-cut plates, effect of impurities 79−43120
KH_2PO_4, low temp. transition, thermal hysteresis, Cr impurity effect on transition temp. 80−2705
KH_2PO_4:cation impurities, growth domains 79−99224
KH_2PO_4:CrO_4^{2-}($Cr_2O_7^{2-}$), electrical cond., thermal depolarisation studies 79−95212
$KHSO_4$:Co^{2+}(Fe^{3+}), impurity effect on growth habit from saturated soln. 77−4059
KI-KCl:Cu^+ mixed cryst., off-centre Cu^+ 79−65112
$KLiSO_4$:(Cr), uniaxial crysts., circular dichroism and optical activity 80−45029
KMF_3:Mn^{2+}, (M=Mg,Zn,Mn,Cd), zero-field splitting of Mn^{2+}, superposition model *(French)* 79−15267
$KMgF_3$:V^{2+}, ^{51}V ENDOR meas., spin Hamiltonian parameters 79−28638
$KNbO_3$, layer growth, optical and electron microscopy 77−59021
$KNbO_3$ thick crystals, vol. nucleation of domains by impurities 77−73120
$KNbO_3$:Al^{3+}, dopant effect on domain struct., etching study 79−56749
$KNbO_3$:Ba^{2+}, dopant effect on domain struct., etching study 79−56749
$KZnF_3$:V^{2+}, ^{51}V ENDOR meas., spin Hamiltonian parameters 79−28638
LaB_6, cathode, brightness, cryst. orientation and purity effects 77−12483
LiCl:Na (K,Rb,Cs,Ag), theoretical and experimental study of partition coeffs. of isovalent impurities 79−65111
LiF:Mg, geometrical parameters of impurity centres by scattered-light method 80−2043
LiF:Mg(Eu)(Co)(Si)(O), elec. cond., influence of impurity ion 79−7709
LiI:α-Al_2O_3, model for fast ionic cond. 79−77811
α-$LiIO_3$:Cr^{3+}(Ni^{2+})(Mn^{3+}), absorption spectra, impurity environments 78−27275
$LiNbO_3$ crystal, elec. cond., optical quality, impurity depend., space charge pyroelectric field compensation 79−64295
$LiNbO_3$:Fe(Nb), SHG, phase-matching temp., impurity influence 80−69463
$Li_2O.2SiO_2$ glass, kinetics of crystal nucleation, effect of Pt and other impurities 78−88440
$MgAl_2O_4$ crystals, flux grown, artificial spinel twin form. by $BeAl_2O_4$ addition 80−96542
$MgCu_2$-$MgNi_2$, electronic sp. ht. 1.5 to 4.2K, Fe impurity effects *(German)* 77−59125
MgF_2:Li^+, defect struct., theory 77−47472
MgF_2:LiF crystal, defect struct., anelastic and dielec. relax. meas. 77−27938
MgO, atomic C anal. by $^{12}C(d,p)^{13}C$ method 80−108766
MgO, atomic C anal. by laserflash induced mass spectrometry 80−108767
MgO crystal, yield strength and dislocation mobility 80−93601
MgO, Fe^{2+} and Fe^{3+} conc. and valency, optical density, EPR and MCD obs. 77−89462
MgO, lattice defects., calcination temp. effect 80−15091
MgO single crystals, chem. polishes for {100}, {110} and {111} surfaces, spectrochem. anal. for impurity content 79−29241
MgO single crystals, impurity effects on cationic cond. *(French)* 80−65286
MgO:Al, and nominally pure single crystal, thermally stimulated luminesc. rel. to temp., and EPR *(Russian)* 80−84789
MgO:CaO(SiO_2)(B_2O_3)(Cr_2O_3), effective of impurities on high temp. creep 80−40455
MgO:Cr^{2+}(Fe^{2+}), thermal magnetoresistance 79−10994
MgO:Cr^{3+}, site symmetry of Cr^{3+}, polarised luminesc. meas. 77−12426
MgO:Li, TEM studies 79−29069
MgO:Mn^{2+}(Fe^{2+})(Cr^{2+}), redox behaviour of ions, ESR and X-ray diffr. 78−52341
$MnCO_3$, crysts., Ca^{2+} and Ni^{2+} conc. influence on habit in growth from gel 80−20778
MnZn ferrite, props. rel. to raw materials *(German)* 77−21074
MnZn ferrites, doped; determ. of grain boundary composition, using Auger spectroscopy *(German)* 79−23618
MnZn ferrites, impurity induced exaggerated grain growth 78−92222
Mo alloy, VN-2M, vac.-melted, thermal expansion meas., 971-2153°C, impurity effect 78−26700
Mo, C and Ir impurities in single cryst. growth, effect on fine struct. *(German)* 77−28714
Mo, impurities, interaction mechanism and saturation limit *(Russian)* 77−55358
Mo, impurity interactions with C, N, and O, struct., mech. props. and purification 79−52277
Mo, segregation of impurities and alloy elements at surface *(French)* 79−47697
Mo, surface impurities, depend. on prep. method, ion scatt. spectroscopy 80−40200
Mo, voids, effect of impurities on positron lifetime 77−15453
Mo wire, struct. and high-temp. creep, dopant elements influence 80−66603
$MoSi_2$, oxidation behaviour, Ge additions effect *(German)* 80−71782
N in Si, trace anal. by proton activation *(Chinese)* 80−81403

impurities continued
N_2, liq., impurity separation, laser thermal method *(Russian)* 77−7859
NB-H(D), lattice expansion due to interstitially dissolved impurity 77−39600
NH+CO, vibrational energy transfer in solids, rot. mode participation 78−63815
$(NH_4)H_2AsO_4$, $(NH_4)H_2PO_4$ and deuterated analogues, low temp. transition, thermal hysteresis, Cr impurity effect on transition temp. 80−2705
$NH_4H_2PO_4$:CrO_4^{2-}($Cr_2O_7^{2-}$), electrical cond., thermal depolarisation studies 79−95212
$NH_4H_2PO_4$:Fe^{3+}, mechanism of habit change due to Fe^{3+}, Mossbauer study 79−19821
$(NH_4)_2SO_4$, single crystal growth from aq. soln., effect of impurities on growth *(Japanese)* 78−92182
Na, impurity conc. meas. by automatic plugging indicator 78−17283
Na, thermodynamics of light interstitials, rel. to delocalised particles 79−46653
$NaAl_3(PO_4)_2(OH)_4$, EPR of at. H caused by X-rays 79−28614
NaCl, additively coloured, sensitised with O, photochromic props. 79−28792
NaCl, occlusion formation during dendritic crystal growth, expt. 78−38993
NaCl with divalent impurities, lattice relax. from density meas. 80−70226
NaCl:Bi^{3+}, complex form. in soln., absorpt. spectra 77−28591
NaCl:Ca^{2+} crystals, influence of dipoles and dipole complexes on yield point 80−39208
NaCl:Eu^{2+}, oriented growth and cryst. struct. of precipitated phases 80−24303
NaCl:Mn^{2+} crysts., electrolysis, dendrite form., mechanism 77−1934
NaCl:Pb, colouring, room temp., influence of conc. and aggregation state of Pb 78−14339
NaCl:Pb^{2+} crystals, grown from aq. soln., flotation study 80−39144
NaCl:X (X=Ca, Sr, Ba, Mg, K, Li, Tl, Ag), impurity conc. effect on mech. and elec. props. 78−47469
NaF:Ca^{2+}(K^+)(Li^+), substitutional impurities, defect props. of (001) and (011) surfaces 77−47443
Na_2O-CaO-SiO_2 glass:Fe, Mossbauer spectra of Fe^{2+}, Fe^{3+} impurities *(French)* 79−51893
Na_2O-CaO-SiO_2-Cr_2O_3 glass, redox equilibria of Cr ions, impurity effects 80−89477
Nb alloy, VN2AE, influence of nitriding on heat resist. and brittleness *(Russian)* 79−8380
Nb, electron energy losses due to H, obs. by scanning TEM 80−79850
Nb film, supercond. transition temp. and transition width, impurity effects *(Russian)* 77−66222
Nb, lattice location measurements of O using $^3He/^{16}O$ and $^1H/^{18}O$ prompt nucl. reactions, ion irrad. effects 79−86813
Nb, pure and O doped, muon diffusion and trapping 79−56685
Nb, sputter deposited film, O contamination, Auger anal. 78−52669
Nb, superconductive transition point as reference temp. 80−107943
Nb-Ni amorphous alloys, glass transition and ductility, O additions effect 80−75168
Nb-Y, and Nb, mech. props., neutron irrad. and Y scavenging effects 77−90394
NbC coating, vapour deposition, phys. and chem. props. 77−40456
Nb_3Ge, CVD, impurity doping effect on supercond. crit. props. 78−52174
Nb_3Ge film, nucleation of high-T_c phase in presence of impurities 78−88054
NbH, H impurity screening, lattice deformation, dipole force tensor component calcs. 79−77611
Ne, in solid D_2, effect on sp. ht. 79−33099
Ni alloys, liquation cracking during welding, comp. influence 80−66645
Ni, cold rolled, influence of impurities on recovery and recrystallisation, positron annihilation meas. 79−15696
Ni electrodeposition from alkaline citrate electrolytes, coating impurity quantities and props. *(Russian)* 79−8252
Ni, grain boundaries, mobility, effect of impurities *(Polish)* 79−96073
Ni sputtered films, hexagonal and amorphous, O incorporation, ESCA and electron diffr. meas. 79−11046
Ni superalloy powders, removal of interstitial contaminants 78−84735
Ni:Fe effect on substrate depassivation 79−61777
Ni-Al, liquid, diffusion coeff. differences, rotating-disc determ. 80−39330
Ni-based superalloys, hot workability, effect of S, Ca, Mg, Y and Zr minor elements 80−66552
Ni-Mo alloy electrodeposits, codeposited impurities rel. to H_2 permeation, props. 79−19493
NiH, H impurity screening, lattice deformation, dipole force tensor component calcs. 79−77611
$Ni_{98}M_2$, M=impurity metal, formation of MH(D)-complexes 80−65236
NiO (001) surface, chemisorption of H, surface and second-layer defect effects 80−65369
O in Si, trace anal. by proton activation *(Chinese)* 80−81403
Pb:O, thin film, microstruct. and thermal stress, doping effects 80−88458
Pb-Sn(Bi) alloys, dil., impurity effects on softening at T_c *(Russian)* 78−23220
Pb-Sn(Bi)(Ni), strength loss in supercond. transition, nonmag. and paramag. impurities influence *(Russian)* 80−70875
PbF_2, cubic and orthorhombic, press. and temp. depends. of ionic cond. 79−95207
PbFCl(Br), single crystal ionic cond., deviation from molecularity, effect of O_2 impurities 79−51305
$Pb_5Ge_3O_{11}$:Ba,O, impurities, static central peak 78−92079
PbI_2 crystal, gel-grown AgI impurity effects on struct. transformations during growth 77−76339
PbS, point defects and effect on decopperization of Pb with S 79−47918
$PbTiO_3$-$Pb(Fe_{1/2}Nb_{1/2})O_3$-$PbZrO_3$, with additions, exam. of electrical characteristics 80−2698
$Pb(Zr,Ti,Ge)O_3$, antiferro-ferroelectric transition 78−95565
$PbZr_{1-x}Hf_xO_3$, crystal field distortion by impurities, PAC meas. 80−11306
Pd-Gd (1 at.%), lattice distortion around impurities determ. by polarised neutron method 79−1372
Pt, quenched, coprecipitation of vacancies and C atoms 79−78978
Pt, recovery spectrum after thermal neutron irrad., resist. obs., Au addition effect and defect conc. depend. 80−65057
Pt, sputtered film, Al and Mg contamination, AES, SIMS 77−11822

impurities continued
PtSi surface, and interface with Si, impurity effects 80−80037
$RbAg_4I_5$:AgI,Rb_2AgI_3, polycryst., ionic cond., impurity conc. effects 78−51734
RbBr:Cu^+, off-centre ion position, ionic thermocurrent study 80−7271
RbCl, Pb colloid effect on particularities in vac. evaporated Cr film growth 79−82496
RbCl:$CoCl_2$ system, precipitate form., ionic cond. meas. 80−96653
RbCl:Cu^+, off-centre ion position, ionic thermocurrent study 80−7271
RbCl:Li^+, new off-centre defect system, studied with dielec. techniques under hydrostatic press. 79−19834
Re film, phase comp. depend. on thickness, deposition rate and substrate temp. 77−31915
Sc surface, single cryst., segregation of impurities 79−65299
Se:Te, liq., viscosity, impurity effect, chain length role *(French)* 78−51717
Si, amorphous, epitaxial regrowth, structure and impurities effect 80−84401
Si, and Si:H, amorphous, sputter deposited, O_2 incorporation during and after fabrication 80−49541
Si, annealing, impurity film form., energy loss anal. 77−31916
Si crystal, Czochralski grown, enhanced Borrmann effect 80−70191
Si crystal, impurities determ. and resistivity after reactor neutron irrad. 80−65563
Si crystal growth, for electronic devices 80−66419
Si, crystal growth conditions effect, on microdefect distrib. 80−50549
Si, crystal growth from melt in vac., origin of SiC impurities 80−2940
Si diffused horizontal homojunction solar cells, effects of junction depth and impurity conc. 80−55877
Si, dislocation-free Czochralski-grown, detection of microamounts of O *(German)* 78−26592
Si, donor polarizability, multivalley effective mass calc. 80−96817
n-Si, doping effects on US velocity and attenuation 80−70325
Si epitaxial layers on metallurgical-grade polycryst. substrates, characteris. 79−28967
Si, filamentary, grown by chem. transport reaction method, banded struct. 80−38978
Si film, epitaxial growth on Si, impurities, plasmon energy loss anal. 77−31916
Si, impurities displacement by H^+ or He^+ irrad. 79−86824
Si, impurities of O, N, C, trace anal. by proton activation *(Chinese)* 80−81403
Si, impurity solubility limit after laser induced melting 80−107426
Si impurity-doped cryst. plate, as an X-ray monochromator, strain distribs. for 220 reflection 80−100126
Si ingots, polycrystn., growth and characterisation from metallurgical grade source material 79−87576
Si ion damage critical gettering doses, elec. characts. 78−10085
Si, laser annealing, nonequilib. incorporation of impurities during rapid solidification 80−55286
Si layer, neutron activation analysis, contamination and cross-contamination 78−83837
Si, light scattering due to microdefects 78−27248
Si, luminescence of multiparticle exciton-impurity groups 79−83003
Si, neutron transmutation doping, detect. and identification of potential impurities activated 79−42090
Si, neutron transmutation doping, impurities 80−15134
Si, oxidation at 1000°C, Na contamination and furnace cleaning procedures 77−59955
Si polycrystalline solar cells fabricated from refined metallurgical-grade Si, impurity gettering 80−94011
Si solar cell, transition metal doped Czochralski and web crystals, measurement of impurity effects 78−35297
Si solar cell fabrication, R and D on low-cost processes, effect of impurities on cell performance 80−50978
Si, solar grade, Czochralski growth, solar cell efficiency vs. metallic impurity conc. 78−31330
Si, substrates, review of defects 77−39597
Si, surface, sputter etched, damage, contamination, ion backscatt. obs. 79−33167
Si surfaces, influencing microstruct. deform. process by impurity type *(German)* 79−65107
Si, thermally induced microdefects, effect of C, TEM obs. *(Japanese)* 80−54244
Si wafers, Au contamination during plasma etching 80−19831
Si wafers, Czochralski, gettering of surface and bulk impurities 78−64456
Si:Al ribbon, edge-defined film-fed growth, Al redistrib. 80−29873
Si:Au, method of determining content of impurities with deep levels 80−2056
Si:C, impurity determ. by IR absorpt. spectroscopy, room temp. and low temp. meas. comparison 80−108237
Si:Ga, gettering of Au and Cu during Ga diffusion 78−91350
Si:H amorphous films, optoelectronic behaviour depend. on impurity incorporation during plasma deposition 80−49804
Si:O, dislocation-free, Si-O complexes, heat treatment effects 77−62557
Si:P, determ. of P content in high-purity Si using meas. of Mo in 12-molybdophosphoric acid by NAA and AAS 80−15148
Si:Sb(P) (B) homoepitaxial film, interpretation of temp. depend. of partition and sticking coeffs. 77−7756
Si:Sb(P)(B)(Ga), low angle boundary formation, in single crysts., effect of impurities on cryst. growth conditions 80−11555
Si-B crystal, Bond method, of meas. lattice parameters, asymmetric Bragg reflections appl. 80−38861
Si-SiO_2, recoil implanted O profile after ion implantation through SiO_2 80−88198
SiC, epitaxial film, effect of impurities on polymorphism during growth 80−15414
SiC, epitaxial growth by sublimation sandwich method, effect of impurities 80−25568
B SiC, sintered, effect of Al trace amounts on specimen props. 79−83289
SiC:N, impurity effect on stress gradients and dislocation development 77−4116
Si_3N_4, CVD, chem. bound H, NH_3/SiH_4 ratio and annealing depend. 77−76680
Si_3N_4, containing MgO and Y_2O_3 additives, impurity effect on sintering 79−61543
Si_3N_4, effect of oxide impurities on physicomechanical props. 80−16396
β-Si_3N_4, hot-pressed, containing small amounts of Be and O in solid soln. 80−2985
impurities continued
Si_3N_4, hot-pressed, impurity phases, TEM obs. 79−8260
Si_3N_4, impure, oxidation, phase equilibria 79−70045
Si_3N_4 reaction bonded, iron impurity influences 79−56947
Si_3N_4, reaction-bonded, strength, effect of Si purity in production 80−100902
Si_3N_4-Y_2O_3 ceramic, thermal degradation, C impurity effect 80−50708
Si_3Ni_4, hot pressed MgO fluxed grain boundary impurity phases, lattice fringe imaging obs. 79−11540
SiO_2 films, on Si, role of H_2 79−69376
SiO_2, MOS gate insulator, mobile K ions 77−47623
SiO_2 sputtered layers for semicond. devices, effect of impurities on elec. props. *(German)* 77−16495
SiO_2, surface charge, effect of doping with P+B, differing vacuum deposition conditions *(French)* 77−85286
SiO_2, vitreous, and quartz, impurity C determ. by isotopic spectral method 80−26093
SiO_2, vitreous, Fe^{2+} absorpt. spectra in polarised light and struct. position 79−43007
SiO_2, vitreous, quant. X-ray anal. of cristobalite 80−88049
SiO_2 wafers, Au contamination during plasma etching 80−19831
SiO_2:Al^{3+}, natural quartz, impurity config. effect on thermolum. polaris. sensitivity 80−11483
SiO_2:Fe, vitreous and cryst., with or without Al_2O_3, Na_2O additions, exam. of Fe^{2+} coordination, IR spectroscopy 78−88344
SiO_2:P thin films, plasma deposition in prod. planar reactor and P doping 80−2966
SiO_2-B_2O_3-Na_2O-K_2O system glass, phase separated, loss of oxides during acid leaching, atomic absorpt. anal. 79−11716
SmB_6, specific heat anomalies 80−34199
Sn, crystn., mechanism of influence of soluble impurities 78−71692
Sn film, reactively sputtered, discharge produce evaluation, mass spectrometer obs. 80−6668
Sn, liquid, electron transfer of rare earth impurities *(Russian)* 78−95278
Sn polymorphic transformations ($\beta \rightarrow \alpha$), effect of impurities, exam. 80−7557
Sn-In, dil., supercond., current-induced resistive state 79−51712
SnO_2, cassiterite, appl. of cathodolum. microscopy and spectrometry 77−69919
SnO_2 defective crystals, exciton-impurity complex luminescence spectra *(Russian)* 79−65926
SnO_2, film, diffusion of impurities *(Japanese)* 79−95218
SnO_2:F films, elec. and optical props., solar energy conversion appl. 79−65945
SnO_2:Sb film, DC sputtered, correspondence between Sb content and targets 79−23847
SnO_2:$V^{4+}(Cr^{3+})(Mo^{5+})(Nb^{4+})(Re^{4+})$, direct mechanism in supertransferred hyperfine interaction 79−23936
$SrCO_3$, $NiCO_3$ impurity effect on dissoc. 78−27425
SrCl:Mn^{2+}, shape of potential well, calc. 78−87951
SrF_2:Ce^{3+}, dipole reorientation, Ce^{3+} conc. effect 78−10841
SrO, luminesc. band edge, 4-6.5 eV, optical absorpt., photoluminesc., cathodoluminescence, photocond. obs. 80−50411
SrO:Mn^{2+}, impurity pot. well shape calcs. 78−87950
Sr_2TiO_2:Eu, synthesis, luminesc. of materials 79−11534
Ta, evidence for slow strain-rate embrittlement due to O_2, SEM study 79−79109
Ta film, nucleation of α or β phase, impurity effects 77−24493
Ta, static and dynamic props. of O and H impurities, Mossbauer meas. 80−7246
Ta, superconductive transition point as reference temp. 80−107943
Ta-H(D), lattice expansion due to interstitially dissolved impurity, isotope effect 77−39600
Ti, $\alpha \rightarrow \omega$ transform., pressure-induced, impurity effects and reaction kinetics 78−11220
Ti, commercial, creep behaviour, 25 to 400°C, role of impurities and/or alloying elements *(French)* 80−45354
Ti, sputtered film, energetic neutrals rel. to impurities 79−69980
Ti-Mo (16 at.%), effect of H impurities on lattice spacing, hardness, and plastic strain *(Russian)* 79−11664
Ti-Ni amorphous alloys, glass transition and ductility, O additions effect 80−75168
α-Ti-Zr-W, effect of W impurity on mech. preps. 80−16392
TiC-Mo_2C-Ni cermets, influence of anomalous phases on strength 78−92228
TiD_2, clean and contaminated films, fabrication and AES 78−52600
TiO_2, anatase, influence of Al_2O_3, Ga_2O_3 or In_2O_3 to polymorphic crysts. in vapour 79−78858
TiO_2, sintering, struct., pressing, atm., and doping effects 80−20873
TiO_2:Ta_2O_5(Nb_2O_5), rutile, defect struct. and elec. cond. at 1273K 80−44604
TiO_2-based ceramics, impurity atoms chem. state, Mossbauer spectra 80−15902
Ti_2O_3:Sc_2O_3(Al_2O_3), struct. changes on Sc(Al) substitution 77−55276
Tl_2Se, fused, diffusion of ^{204}Tl, ^{110}Ag, ^{112}Sn impurities 80−54415
TlTe, melt, elec. cond., surface tension, microhardness, influence of impurities 80−88551
Tl_2Te, melt, resistivity, surface tension, microhardness, influence of impurities 80−88552
Tl_2Te_3 melt, impurities effect on surface tension polytherm and adsorption obs. 77−7947
α-U, strain rate effect on flow and fracture 80−100887
UO_2, non-stoichiometric, oxidation reactions and dopants 79−42087
UO_2:Nb_2O_5, additions on elec. cond. 80−49712
V columnar films, crit. field anisotropy, depend. on prep. conditions *(Russian)* 80−93056
V, diffusion of H and D, effect of impurities on coeff. 78−47604
V, electro- and thermo-self-transport, 1480-1822°C, effect of impurities 79−42297
V, electron energy losses due to H, obs. by scanning TEM 80−79850
V, interstitial impurity and substitutional solute interaction, internal friction meas. 78−10082
V, muon diffusion and trapping 79−56686
V, plasticity and strength change in temp. range 20 to 1000°C impurity effects 80−35235
VO_2, doped, morphology, structure and props. *(German)* 78−59823
W, cast, purification of C, O_2 and N_2 using thermal cycling *(Russian)* 79−70114
W, impurity interactions with C, N, and O, struct., mech. props. and purification 79−52277

impurities continued
W, LEED and electron microscopic investigs., review *(Hungarian)* 77−47654
W, self-diffusion parameters, depend. on degree of purity *(Russian)* 79−19391
W wire, struct. and high-temp. creep, dopant elements influence 80−66603
W-Cu (92.8, 7.2 wt.%), liq.-phase sintered, embrittlement and interfacial impurity segregation 80−66647
YAG:Ti, crysts., colour centres, optical absorpt. spectra 79−65080
YAG:Ti, growth conditions from melt 79−95924
$YAl_3(BO_3)_4$-$NdAl_3(BO_3)_4$, substitution of Nd for Y in $YAl_3(BO_3)_4$, exam. 80−11551
$Y_3Al_5O_{12}$, layer structuresrevealed by decoration method and electron microscopy 77−27902
$(YSmLuCa)_3(GeFe)_5O_{12}$, LPE low defect density films, on contaminated substrates 79−87590
$YAl_3[BO_3]_4$, impurity incorp. on growth from soln. 77−52242
Zn-Al (22 wt.%), superplastic, of very high purity, cavitation 79−24586
Zn-Al(Cu), mech. and technological props. *(Polish)* 80−89286
$ZnCl_2$ with $FeCl_3$ impurity, removal by zone melting 79−52111
$Zn_xFe_yMn_zFe_2O_4$, ferrite, production from Fe_2O_3, effect of impurities on props. *(German)* 79−4925
ZnO, negative photocond. by excitation of exciton-impurity complexes, recomb. mechanism *(Russian)* 79−28379
ZnO, sintered, impurity ion effects on crystalline state *(Japanese)* 77−28768
ZnO-CoO_4 (Fe_2O_3), ceramics, impurity at. states, elec. cond. 79−11130
ZnS single crystals, O content determ. by fast neutron activation anal 80−15142
ZnS, sphalerite, appl. of cathodolum. microscopy and spectrometry 77−69919
ZnS with substitutional impurity, dipole and weak-dipole vibr. 79−14904
ZnS:MnF_2 films, effect of Mn conc., XPS obs. 79−33886
ZnS-O, single cryst., fast neutron irrad., optical props. 78−27331
Zr-Cu amorphous alloys, glass transition and ductility, O additions effect 80−75168
Zr-Nb alloy, direct imaging of point defects using TEM 77−35453
Zr-O(2.85 at.%), Pr effect on internal friction of single crystal 77−4155
ZrC coating, vapour deposition, phys. and chem. props. 77−40456
ZrC powders produced by various methods, impurities 80−11615
ZrO_2, doped, ionic cond., theoretical model 80−107552
$ZrSiO_4$, synthesis, influence of rare-earth additives on props. 80−20868

impurity and defect absorption spectra of inorganic solids
actinolite, optical spectra obs. 77−40284
active ions in crystals, spectral thermal line shift mechanism *(Chinese)* 80−7385
adsorption rel. to dopant admixture 78−95596
alkali, borate glass:S, blue and green coloration, absorpt. spectra 79−87470
alkali aluminometaphosphate glass, $MPO_3.Al(PO_3)_3$:U (M=Li,Na,K), vibronic excitation, absorption and emission spectra 78−52524
alkali atom, in inert-gas solid, at level struct. calc. pseudopot. method 80−9532
alkali bromide (chloride):V^{2+}, electron spin transfer 78−87949
alkali bromides and iodides, self-trapped exciton and F-centre form. by picosecond laser pulses 80−10546
alkali halide: $Ge^{2+}(Sn^{2+})(Pb^{2+})$, T-centres, absorpt. spectra, energy level diagram 77−73157
alkali halide: S_2^-, laser-excited spectra and reorientation of S_2^- 77−28563
alkali halide: $Tl^+(In^+)(Sn^{2+})(Pb^{2+})(Cu^-)$, charge transfer absorpt. band 79−73977
alkali halide:$CrO_4^{2-}(MoO_4^{2-})(MnO_4^-)(ReO_4^-)$, frozen solns., absorption spectra, 4.2-300K 79−87467
alkali halide:Cu^+, absorpt., emission and lifetime data, temp. depend. 77−4671
alkali halide:Ga^+,In^+,Tl^+, cryst. field effect on spectral characts. 77−24880
alkali halide:$H^-(D^-)$, local modes and colour centre absorpt. bands, analogy 80−60632
alkali halide:Hg, EPR and optical props. 78−91933
alkali halide:NH_2^-, paraelectric alignment, UV electroabsorpt. and Kerr effect 77−12413
alkali halide:$O_2^-(NO_2^-)$, effect of press. on vibronic spectra 78−52532
alkali halide:Sn^{2+}, V_c-centres, vacancy induced splitting of excited states, Sn^{2+} structure 78−51931
alkali halide:Tl^+, magneto-optical rot. dispersion anomaly near absorpt. bands 77−63400
alkali halide:VO^{2+}, impurity behaviour, elec. cond. and IR absorpt. obs. 77−8607
alkali halide, chalcogen^{2-} vacancy centres, absorpt. and fluoresc. spectra 78−48204
alkali halide, F-centres, vibronic problem in higher excited states 78−10931
alkali halide, far IR props. of lattice resonant modes, hydrostatic press. effects 77−28574
alkali halide, ReO_4^- doped, saturable absorber at 10.6 μm 80−53384
alkali halide, SH^- and SD^- impurities, shift of IR absorption band centre 77−16346
alkali halide, Tl^+-type centres, struct. of Jahn-Teller induced B absorption band 77−12410
alkali halide crystal, containing mol. centres, IR absorpt. spectra, 77-630K 79−99863
alkali halide crystals, activated, physical phenomena and optical data processing appl. *(Russian)* 80−80819
alkali halide phosphors, Tl^+ doped, uniaxial stress effects 78−48202
alkali halides: cation with s^2 ground-state configuration, absorption bands assignment 80−97310
alkali halides, bound polarons, vibronic theory, appl. to F-centre excited states 78−84150
alkali halides, emission band of F-centre 80−76071
alkali halides, F_A-centre optical absorpt., estimate using symmetry-adapted wave functions 80−11448
alkali halides, F_A-centre optical absorption, lattice statics theory 79−43004
alkali halides, F^--centres, thermal and photolytic decay processes 78−95053
alkali halides, F-centre, cluster-Bethe lattice treatment 78−63762
alkali halides, F-centre absorption energy calc. 79−78715

impurity and defect absorption spectra of inorganic solids continued
alkali halides, F-centre photoionisation, semicontinuum model 79−99509
alkali halides, F-centres, first order Raman scatt. *(French)* 78−2828
alkali halides, F-centres, optical pumping, spin-orbit and hyperfine coupling 77−16360
alkali halides, linear dichroism spectra, stress-induced, reorientation of O_2^- and NO_2^- impurity ions *(Russian)* 80−45127
alkali halides, off to on centre defect transitions under hydrostatic press. 78−15199
alkali halides, rare earth ion doped, optical props., review 79−15492
alkali halides, shift and broadening of local vibr. bands, temp. depend. 78−87755
alkali halides, U-centre electronic struct. cluster-Bethe lattice calc. 80−107737
alkali halides with NaCl struct., F-centre absorpt. and ground state 77−62524
alkali metal: rare gas, absorpt. edge, extra-orbital relax. model 79−4825
alkali metal:H(0), impurity investigation using residual resist. and optical absorpt. meas. 79−95816
alkali metal:halogen, charge transfer excitations 79−95815
alkali metal:inert gas, optical absorpt. by impurity, cluster Bethe lattice calc. 77−8612
alkali metal film, inert gas impurities, metal-insulator transition, optical absorption and cond. 77−24598
alkali metal film, inert gas impurities, optical excitation spectra obs. 77−24876
alkali metal film, inert gas impurities, optical spectra, rel. to inert gas solids 77−24878
alkali metal film, inert gas impurities, sharp pair spectra and excited states 77−24877
alkali metal halides, hole self-localization and capture, temp. depend. 80−92526
alkali metal halides, X-ray induced colour centre and halogen aggregate form. 80−96565
alkali phosphate glass:Nd^{3+}, laser material evaluation 77−54715
alkali phosphate glasses, colour and absorption spectra of Fe 77−85752
alkali silicate:Nd_2O_3 glasses, coloured, dichroism *(Polish)* 79−99919
alkali silicate glass: Cu^+/Cu^{2+}, opt. absorpt. rel. to impurity redox equilib. *(Japanese)* 77−12824
alkali silicate glasses, behaviour of VO^{2+} as spectroscopic probe 79−78510
alkaline earth fluorides, hydrogenated mixed cryst., local mode absorpt. 77−81130
alkaline earth halides, rare earth ion doped, optical props., review 79−15492
aluminophosphate glass:Mn:Mg(Sr), optical props. H_2O effects 77−28600
amethyst, Fe^{3+} diffusion, associated phenomena 77−36269
anthracene, irradiated, optical absorption and EPR meas., low temps. 78−68538
As_2S_3, glassy, optical absorption spectra after 4.5 MeV electron bombardment *(Russian)* 77−32408
beryl, channel constituents, electronic absorption spectra of Fe^{2+} 79−69863
borate glass: Ni, absorption spectra, mag. props., coordination behaviour *(German)* 80−40147
borate glass:Er^{3+}, $^4I_{13/2}$ level relax. 79−87476
borate glass:S, (boro-ultramarine), blue chromophore identification 77−20888
borate glass, secondary and tertiary coordination number of Co^{2+} and chem. composition *(Polish)* 78−9960
borate glasses: transition metal ions, electronic spectral bands 78−10347
borate glasses:Cu^{2+}, near IR electronic spectra, effect of alkali contents 78−27267
borate laser glasses, Cl^-coordinated, Tl^+, Mn^{2+} and Nd^{3+} impurities, absorpt. and X-ray obs. 79−38575
borosilicate glass, influence of Ti on absorption spectra of transition metals in glass 77−12403
borosilicate photochromic glasses, photosensitivity rel. to AgCl particle shape 78−31223
calibo glass:Eu^{3+}, Ho^{3+}, energy transfer 78−76510
CaO:OH^-, room temp. IR spectra, heat treatment and electron irrad. effects 79−51992
ceramic translucent systems, absorpt. and scatt. coeffs for visible light, Kubelka-Munk theory 80−60627
chabazite type zeolite, cation substituted, IR spectra 30 to 470 cm^{-1} 78−10933
chalcogenide glasses, optical versus transport processes. 80−84449
chalcogenide semiconductors, optical and elec. props., comparison with SiO_2 78−6721
chlorides, I^- or Br^- doped, optical investigation of atomic hydrogen centres 78−88351
colour centre-phonon many-mode interaction, absorption band shape, adiabatic approx. 78−2883
colour of imperfect crystals, lattice defects and impurities 78−72562
covalent semiconductors, optical absorption by acoustic phonons related to shallow impurity levels 77−4665
crystals, theory of phononless line broadening for impurity center 78−35180
cuprous halide photochromic glasses, spectral props., shell model *(Russian)* 79−27354
D^- centre in strong magnetic fields, optical absorpt. spectrum 80−20670
deep impurities role, book contrib. 78−10403
deep impurity levels, spectroscopic determination by compensation method 80−108229
deep oxide acceptor, intra- versus inter-small-polaron transitions 78−30874
diamond: Sb, ion implanted, defect study using optical absorpt. and EPR 80−24480
diamond:B, B conc. and impurity-to-band activation energy 79−56165
diamond:B, epitaxial layer, charge transfer and acceptor state 78−19169
diamond:N, photocond. in N2 absorpt. band 79−91102
diamond:Ni, synthetic, X-ray absorpt. fine structure study of impurities 80−55133
diamond, dynamic Jahn-Teller distortions at trigonal optical centres 79−87069
diamond, electron irradiation, vacancy charge states, optical absorpt. spectra 77−90177
diamond, GR1 and UV band, fine struct. 80−20678
diamond, GR 2-3 absorpt. line, uniaxial stress effects 78−72563

impurity and defect absorption spectra of inorganic solids continued
diamond, GR defect, high resolution optical spectra after electron irrad. 78−56515
diamond, irradiated, optical spectrum 78−6719
diamond, irradiated, optical study of TR12 and 3H defects 77−85772
diamond, Jahn-Teller coupling at neutral vacancy 80−71453
diamond, N aggregates, partial dissoc. by high press.-high temp. treatment, IR spectra obs. 78−43904
diamond, natural, high conc. of implanted Si ions, He backscatt. and IR absorption 77−89466
diamond, natural, rate of donor defect introduction by 2 MeV electrons, 0.348 eV absorption band 77−89477
diamond, natural, topography of impurity distrib. and neutron-induced colouring 77−39613
diamond, natural type IB, thermal conductivity anomaly, defects obs. 77−85003
diamond, optical absorption and luminesc. spectra, review 80−2848
diamond, optical absorption lines, GR4 and GR8, effect of uniaxial stress 80−34956
diamond, optical transitions between E and T electronic states each coupled to e-modes, GR1 band 80−20677
diamond, pseudo-Jahn-Teller effects in H3 vibronic spectrum 77−90182
diamond, radiation damage tetragonal R2 centre, optical and EPR spectra 78−2888
diamond, semicond., energy band struct., elec. and optical props., review 77−35862
diamond, synthetic, transition metal impurity effect on IR absorpt. 79−82980
diamond, synthetic and natural, neutron irrad., optical and elec. props. *(Russian)* 78−59841
diamond, thermal cond. at low temp., correl. with IR absorpt. features 80−49435
diamond, type Ia, secondary absorpt. edge, optical study 79−19912
diamond, type IB, electron irradiated, 2.367 eV vibronic absorpt. system, optical study 79−73975
diamond, type Ib, electron irradiated, migration of N, optical absorption meas. 78−56505
diamond, uniaxial stress splitting of E to E transitions at trigonal centres in cubic crystals 80−97312
diamond, UV absorpt. produced by substitutional N_2 pairs 80−29770
diamond, vacancy, mol. orbital theory of transitions 77−85757
diamond, vacancy enhanced N aggregation, electron irradiation effects IR spectra 80−70245
diamond, van Hove singularities, absorpt. and luminesc. electronic-vibr. spectra 80−70639
diamond, vibronic bands at 2.498 eV (H4), 2.417 eV and 2.536 eV, absorpt. and luminesc. under stress 77−85758
diamond crystal, deep centres, changes in Van Hove singularities in vibronic spectra 77−8645
diamond electron irradiated, photochromism 80−71454
diamonds, artificially coloured, spectroscopic diagnostic technique 78−65281
diffusion coefficients, determ. from optical absorpt. 79−69294
disordered alloys, optical absorpt. at high temp., CPA calc. *(Russian)* 77−44028
electron irrad., defects, elec. and optical props. 79−19282
F-centre electron levels, temp. depend. shift calcs. 77−28599
F-centre ground state wave function, ENDOR and F-absorpt. data analysis 77−31978
F-centre optical absorption bandshape calc. for transition to state with Jahn-Teller and spin orbit couplings 80−55135
F-centre optical props., dislocation influence 80−108234
F-centres, struct., quantum optics, laser spectra 77−52147
fluorites, natural colour centres and associated rare earth ions 79−61408
fluorochloroapatite, synthetic, defect struct. and colour centres obs. *(Russian)* 78−30612
GaP, reevaluation of bandgap and free exciton binding energy 78−60061
garnet:Nd^{3+}, spectral, structural regularities, anal. 78−51948
garnet:Pb, valence of Pb, spectroscopic data 77−47480
gems and minerals, colour 77−37182
germanate glasses:Cu^{2+}, near IR electronic spectra, effect of alkali contents 78−27267
glass:Cr^{3+}, absorpt. spectra, Fano antireson. and vibronic Lamb shift 80−71458
glass:Eu^{3+}, vibronic spectra, impurity complex model 78−19516
glass:Nd^{3+}, multitype opt. centres 78−68558
glass:Nd, stimulated emission cross section by absorpt. meas. from thermally populated $^4I_{11/2}$ levels 78−71107
glass:Nd, stimulated emission cross sections and absorpt. coeffs. at 1.06 μm, calorimetric meas. 77−71987
glass, alcoholic and aq., 4.2K, trapped electron photocond. and optical spectra following radiolysis 79−29378
glass, electron irrad., colour centre depth distrib. 79−73217
glass, multicomponent Schott, proton-induced colouring 80−9974
glass, opt. anomaly of small particles 77−48209
glass, phase separated, EPR rel. to struct., elec. and opt. props. 78−23333
glass, photochromatic, induced colour by optical/thermal treatment 80−34954
glass, photochromic, spectral characts. control 80−16073
glass, rare-earth activated, polarised luminesc. 78−48224
glass, surfaces joined by optical contact, spectral absorpt. of water layer 78−46852
grains with resonant impurities, optical behaviour model rel. to diffuse interstellar bands 77−53660
H′ colour centre, radiation-tunnel decay 80−103327
halide crystals, 3p→4d transitions of transition metal ions, assignment from expts. on LiCl:Cu^+ 78−27272
halide photochromic centres, isothermal relaxation kinetics 80−16072
II-VI compounds, electron energy radiation damage threshold meas., EPR and luminesc. 77−84799
II-VI compounds, transition metal ion activated, vibronic struct. in absorption and luminesc. 78−6729
II-VI semiconductor, two-photon and two-step absorption of light 80−7389
II-VI semiconductors, radiation effects, optoelectric props. control 80−25458
III-V semiconductor deep impurity states and wave functions 78−10404
impurities, conc. of C, O, Si 78−59832
in Kr matrix, isolation and aggregation 78−45723

impurity and defect absorption spectra of inorganic solids continued
inert gas:Eu(Sm), absorpt. and emission spectra, phonon sidebands 79−43021
inhomogeneous semiconductor, impurity opt. absorpt. and photocond. spectral line profile variation 77−16352
inorganic molecular crystals, metal complexes electronic spectra and intermolecular interactions 80−55137
ionic crystal, anharmonism effect on exciton peak broadening in absorpt. spectra *(Russian)* 80−97317
ionic halide crystals, mol. model for V_k centre 77−85567
IR absorption spectrum, effect of electron-phonon interaction on vibronic peaks and phonon lines 78−43086
IR laser window material extrinsic absorption 79−14049
IR lattice band profile, electron spin reversion in mag. field, Nf-R curve 79−28771
Jahn-Teller centre optical band polarisation dichroism, forbidden transitions 80−55062
kaolinite, optical spectroscopy study of structural changes at 700-1000°C 79−65193
KBr, thermally processed cryst., optical absorption bands *(Russian)* 78−76513
KCl, pure and Ba-doped, γ-irrad., point defect form. and interaction, X-ray and optical studies 79−65078
lanthanide ion fluorescent probes, spectroscopic obs. system 78−11573
lanthanum ethyl sulphate:Pr, phase transition under pressure, absorpt. spectra *(Russian)* 80−92667
librational-rotational motion of impurity mol., strong EM field effect 80−80824
magnetic ordered cryst., with degenerate orbital impurities, one- and two-magnon light absorption 77−63444
magnetic semiconductor, mag. colour centre continuum model 79−28321
metal cavity, lifetime of trapped excited atom, broadening mech. for optical absorption line 79−38578
metal colloids in ionic cryst., preparation, optical, mag. resonance, elec. props. 80−59459
metal oxides, Mollwo-Ivey relation between peak-colour absorption energy and average O ion spacing 77−90179
metals, local excitations, X-ray edge and recoil problems in optical excitation spectra 77−24879
metaphosphate glass: Ag dosimeter, optical absorpt. and radiophotolum., effect of temp. 78−40333
minority deep level investig. by new optical method 78−6331
mixed fluoride crystals, nucl. radiation effects 80−80831
molecular crystals, energy spectrum of impurities, spectral study *(Russian)* 79−78720
montmorillonite, Co^{2+} form, optical spectroscopy study of structural changes at 700-1000°C 79−65193
neutron bombarded, optical absorption, struct. defect form. and nuclear alloying *(Russian)* 78−31206
$NH_4Al(SO_4)_2.12H_2O:MnO_4^-$, visible and UV absorpt. spectra interpretation 80−45116
nonmetal, impurity optical absorption and emission, anharmonic effects 78−56503
optical fibre, neutron and gamma induced transient absorpt. and luminesc. 80−58763
optical glass, radiation coloration due to fast electron irradiation 79−98452
orthovanadates, rare earth activated, spectroscopic props. 77−16363
oscillator strengths of defects, Smakula eqn. generalisation 80−108232
oxide glass:Cr^{3+}, absorption and emission 78−6774
oxide glasses:Sm^{3+}, optical transitions 79−61430
oxide glasses, charact. by magnetic resonance and optical absorption of metallic probe ions *(Japanese)* 79−95640
oxides, excited states of F-centres 78−64006
phase transitions, and impurity centres *(Russian)* 80−10907
phosphate glass: Ni, absorption spectra, mag. props., coordination behaviour *(German)* 80−40147
phosphate glass, secondary and tertiary coordination number of Co^{2+} and chem. composition *(Polish)* 78−9960
phosphate glasses:Cu^{2+}, EPR, optical spectra 78−72399
phosphate glasses:V^{4+}, EPR, optical spectra 78−72399
photochromic glass, γ-ray effects on sensitivity *(Japanese)* 79−38583
photochromic glasses, electron-hole separation, influence on recombination probability 80−11445
photographic emulsions, ultra-fine grained, nature of produced colour centres during photolysis *(Russian)* 80−73517
photoluminescence activation conditions for binary inorganic crystals 78−10394
plagioclase:$Mn^{2+}(Fe^{3+})$, ligand field bands of impurity luminesc. centres and their site occupancy 78−88350
plastically deformed compound semiconductors, electronic transport and opt. props. of dislocations 80−80212
point defects in crystals, book 77−47442
polar crystals, vibrational Raman scatt. induced by Jahn-Teller systems 79−69830
polar semicond., impurity pseudopotential screening, absorption and emission energies 79−15121
polar semiconductors, chemical shift of Zeeman masses 78−10338
polarization dichroism effects in many-phonon optical bands of multiplet-multiplet transitions 79−15125
polyvinyl acetate film, I_2 doped, optical absorpt. band, elec. cond. 77−85234
polyvinyl alcohol films activated, thermochromism *(Russian)* 79−91415
potassium halides, F-centres, optical pumping, spin-orbit and hyperfine coupling 77−16359
pyrene, single cryst., γ-irradiated, EPR and optical absorption meas. 78−72412
quadratic Stark effect, Jahn-Teller effect in electroabsorption 78−68536
quartz:Fe^{3+}, crystalline, absorpt. spectra and structural state 80−16071
quartz, comparison of different radiation effects 78−26596
quartz, electron irradiated, optical and anelastic absorptions and resonator freq. 78−64385
quartz, high-grade low-temp. impurity band IR absorption spectra 79−56825
quartz, IR spectra fine struct., 3400 cm^{-1} 78−43910
quartz, irrad., annealed optical absorpt. power *(Russian)* 77−36273
quartz, irradiated, fused, crystalline, absorpt. spectra, colour centres 80−7384
quartz, OH^- impurity IR absorpt., electron irrad. effects 79−99913
quartz, pleochroic amethyst, optical absorpt. of d^4 ion Fe^{4+} 78−15201

impurity and defect absorption spectra of inorganic solids continued
quartz, rose, charge transfer mechanism for origin of colour, EPR and optical expts. 78−52537
quartz, single cryst., Fe^{2+} absorpt. spectra in polarised light and struct. position 79−43007
quartz, synthetic, characterisation by IR adsorption 79−56824
quartz, synthetic, connection between lattice deform. and coloration pattern 78−10930
quartz, synthetic, deuterisation, EPR and IR absorpt. characterisation 80−92721
quartz, synthetic, electron beam irrad.-induced interstitial ion mobility, ESR centres and IR spectra meas. 80−39153
quartz, synthetic, lattice distortions, optical inhomogeneities by X-ray topography and optical birefringence meas. 78−55887
quartz, transient absorption on pulse electron irrad. 79−1779
quartz fibre, ESR and IR obs. of microinhomogeneities 77−8401
quartz glass, Ge and B dopants, OH impurities, preform material and fibre optic waveguide struct. 80−64173
quartz radiation defects, effect of annealing on absorpt. spectrum *(Russian)* 77−47495
rare earth compound, crystal field and Slater parameters and coordination 78−6771
rare earth ion energy separation, $4f^N$-$4f^{N-1}$ nl, host depend. 80−49676
rare earth ions in cubic field, anal. of absorption spectra $4f^{N+1}\rightarrow 4f^N5d$-6s 80−7382
rare earth orthovanadates:Eu^{3+}, ligand field parameters 78−2453
rare earth oxymolybdates and oxytungstates, R_2MO_6, spectroscopic props. and crystallochem. laws 77−36215
resonance Raman scattering, influence of mass defect disorder 78−35133
resonant far IR absorption by impurities 78−6715
ruby:Cr^{3+}, high mag. field spin-lattice relax. rates in ground state of ion 79−61407
ruby, E, 2A levels, laser excitation, Zeeman spectra 78−43908
ruby, induced absorpt., radioluminesc., thermoluminesc., Cr^{3+} conc. depend. *(Russian)* 77−90206
ruby, optical spectra freq. shifts press. depend., nonperturbative theory 78−23499
ruby, optically-pumped, excited-state Raman processes 79−4798
ruby, radiation-induced optical processes, impurity effects 80−66310
ruby colouring due to specific growth, annealing and irrad., exam. of visible, infrared and UV spectra 79−11440
ruby cryst. R-line absorpt. and dispersion spectra, mag. field effects *(Russian)* 78−92056
sapphire, 14.8 MeV neutron damaged, optical vibronic absorption spectra 80−50384
sapphire, F-type centre induction, 6.1 eV optical absorpt. band 78−88332
sapphire, natural, origin of colour 79−70794
semiconductor, bound excitons, review, book contrib. 80−44519
semiconductor, ferromagnetic, localised states on imperfections and red shift of absorpt. edge 77−66527
semiconductor, impurity band props. 79−23888
semiconductor, many-phonon impurity absorpt. in external elec. field 77−52144
semiconductor, optical absorption by impurities, phonon-electron interaction 78−56502
semiconductor, optical and IR characterisation 79−95846
semiconductor, photoionisation of deep impurity centres in quantising mag. field 78−6330
semiconductor, weakly inhomogeneous, impurity absorpt. and impurity photocond. line profiles 78−19098
semiconductor, with neutral impurities, exciton spectrum, conc. depend. *(Russian)* 78−2894
semiconductor compounds, III-V and II-VI, H-like impurities interaction 79−82541
semiconductor film with impurity centres, light absorpt., quantum size effect 78−27274
semiconductor impurities, photoionisation cross section calcs. 78−2450
semiconductor layer crystals, light absorption by shallow impurity centres 79−15503
semiconductor with dipole impurities, light absorption 79−28796
semiconductors, II-VI and III-VI types, competition between two-photon absorption and two-stage absorption via deep traps 80−29764
semiconductors, n-type, free carrier absorpt., ionized impurity scatt. 79−42999
semiconductors, optical transitions between deep impurity centre levels 79−61410
semiconductors, uniaxial, exciton light absorpt. spectra depend. on crystal anisotropy *(Russian)* 80−50386
semiconductors, weakly doped compensated IR light absorption by small scale fluctuations *(Russian)* 80−66255
Si:P(As)(Sb)(Bi), high resolution study of group V impurities absorption 80−7388
silica glass:Nd^{3+}, laser-spectroscopic method, for studying solids with nonuniform spectral broadening *(Russian)* 79−40630
silicate Fe activated glass, diffraction trating recording by UV laser 80−5842
silicate glass: Cr^{3+}, optical props., 88-273K, energy levels in crossing region 78−6709
silicate glass: Er^{3+}, $^4I_{13/2}$ level relax. 79−87476
silicate glass:Tb^{3+}, photoluminesc. and optical absorption spectra 79−19919
silicate glass, secondary and tertiary coordination number of Co^{2+} and chem. composition *(Polish)* 78−9960
silicate glasses:Cu^{2+}, near IR electronic spectra, effect of alkali contents 78−27267
silicate glasses:Cu^{+}, effect of UV irrad., absorption bands 78−31222
spinel transparent glass ceramics, colour centre form. due to alkali metal vapour and X-ray irradiation 79−87316
strontium tartrate tetrahydrate Co^{2+} electronic absorpt. spectrum 78−92098
sucrose, single cryst., absorption spectrum of electron traps, pulse radiolysis obs. 80−93369
tellurite glass, Cu^{2+}(Ni^{2+}) coloured, band-pass filter characts. 550-616 nm 78−66919
transition metal, impurities, as probes of critical points, in host band structure 78−91645
transition metal ion 3d→4s transitions in crystals, obs. and interpretation 78−6339
transition metal ions, exchange-coupled in ionic crystals, optical spectra *(Rumanian)* 79−87474

impurity and defect absorption spectra of inorganic solids continued
tremolite, optical spectra obs. 77−40284
vibrational spectra crystals with split configuration interstitial *(Russian)* 78−76450
vibronic splitting and Zeeman effect for $^4A_{2g}\rightarrow{}^2E_g$ transition 78−60495
X-irrad., optical absorpt. spectra and dichroism meas. 80−108239
$XY_{1-c}Z$ mixed crystals, impurity centre local oscill. spectral distribution *(Russian)* 80−60643
Ag halide doped photochromic glass absorption spectra *(Russian)* 78−60490
Ag halide photochromic glass:Cu^{2+}, characterisation of Cu ions 78−5530
Ag halide photochromic glasses, colour centres struct. 80−66254
Ag halides, fundamental absorpt., nature and function of A-centres determ. the extra band at the long wave edge *(Russian)* 80−76060
Ag, in Kr matrix, isolation and aggregation 78−45723
AgBr dispersion in gelatin, adsorbed S and Au, transient absorpt. spectra, latent image form. and decay 80−66837
AgBr, pure and doped, identification of shallow electron centres 77−59267
AgBr:Li^+, time-depend. infrared absorpt. due to Li-localised mode 79−8133
AgBr:Li^+(Na^+), impurity induced IR absorpt. 80−7386
AgBr(Cl)(I) ultra fine grained photog. emulsions, impurity obs. spectra *(Russian)* 79−69871
AgCl, colloid centres by heavy ion implantation 78−63780
AgCl, colloid centres induced by reactor neutrons at 20K 78−72560
AgCl, defects induced by energetic ion implantation 78−17518
AgCl photochromic glass, additional absorpt. spectrum, ellipsoidal model of colour centres 80−40142
AgCl, pure and dopded, identification of shallow electron centres 77−59267
AgCl(Br), multivalent impurities 79−19556
$AgGaS_2$, elec. field influence on absorpt. spectrum, exciton parameters and energy of impurity levels *(Russian)* 77−69860
Ag_2SO_4:CrO_4^{2-}, polarised electron spectrum assignments, red colour explained 77−85753
AgX (X=halide) structure and stability of photographic sensitivity centres *(French)* 77−41708
(Al,Ga)As injection lasers, pulsations and adsorbing defects 79−94234
Al ultrafine particles, optical props., 0.3-2.5 μm 80−76020
$Al_2Be_3Si_6O_{18}$:Cu^{2+}, synthetic beryl, ESR, optical spectra and X-ray diffr. meas. 77−16166
AlF_3 film, optical absorption meas., rel. to prep. conditions *(French)* 77−44078
AlF_3 films, electronic transitions near optical absorpt. edge, depend. on prep. conditions *(French)* 77−63429
$Al_{0.4}Ga_{0.6}As$:Te, saturable optical absorpt. of deep Te-complex centre 79−99917
n-$Al_xGa_{1-x}As$, nonradiative donor related defect centre obs. 78−23497
$Al_xGa_{1-x}As$:Cu(Ag)(Au), LPE film, impurity levels, elec. and optical props. meas. 78−26862
$Al_xGa_{1-x}As$:N, photolum. excitation spectra 77−63451
AlH_3, photoelectric effect spectra and kinetics, photochem. mechanism colour centres 78−56506
AlN, absorpt. edge shape interpretation, Wannier excitons absorpt. in charge impurity elec. field 80−66233
AlN, excitation, luminescence, reflection spectra in fund. absorpt. region 78−10956
$AlNH_4(SO_4)_2$:Cr^{3+}, optical spectral, crystal field, spin orbit and exciton interactions 80−34958
$AlNbO_4$, diffuse refl. and luminesc. spectra 78−56516
α-Al_2O_3, additively coloured single crystal, luminescence *(Russian)* 80−55169
α-Al_2O_3, colour centres, AES, electron energy loss, and optical spectroscopy obs. 78−35176
Al_2O_3, corundum, doped, induced absorption spectra, low temp. irrad. effects *(Russian)* 78−72570
α-Al_2O_3, crystal defects from X-ray irradiation, F-centres, X-ray luminesc. obs. 80−55176
α-Al_2O_3, defects in unirradiated cryst., optical absorpt. spectra 79−61409
Al_2O_3, gamma irradiated single crystal, defect centres 79−65117
α-Al_2O_3, IR absorpt. spectra of OH^-, OD^-, and OT^- 80−55145
Al_2O_3, optical props. of F-centre 79−43003
α-Al_2O_3, polarised luminescence in neutron- and proton-irradiated single crystals 80−66271
Al_2O_3:Co, spectra, heat treatment and irrad. effects 77−4659
α-Al_2O_3:Co,H, Co and proton ENDOR, IR and optical spectra charge compensator nature and defect struct. 80−44956
α-Al_2O_3:Co^{3+}, local deform. due to uniaxial stress 80−34140
α-Al_2O_3:Cr^{3+}, local deform. due to uniaxial stress 80−34140
Al_2O_3:Cr^{3+}, radiationless relax., photoacoustic spectra 78−27264
Al_2O_3:Cr^{3+}, shock compression, absorpt. spectra 80−20675
α-Al_2O_3:Er(Cr), crystal defects from X-ray irradiation, F-centres, X-ray luminesc. obs. 80−55176
α-Al_2O_3:Mg, defect. struct., cond. and optical absorptiob 77−55279
β-Al_2O_3:Mn(Co)(Ni), absorpt. and emission spectra, mag. susceptibility 79−87471
β-Al_2O_3:NH_4^+(Nd_4^+), polarised Raman scatt. 80−103947
Al_2O_3:Si, Ti, pure and doped, luminescence, optical absorpt. and colour centres 79−87501
Al_2O_3:Si(Ti)(V)(Fe)(Co)(Ni), gamma-irrad., low temp., induced absorpt. spectra 79−56820
α-Al_2O_3:Ti, defect struct., electronic and ionic cond., optical absorption meas. 78−30603
Al_2O_3:Ti(Si), annealing, electron irrad., absorpt. spectra 77−20890
Al_2O_3:V, valency changes of V ions, γ irradiation, thermal cond. optical absorption and EPR meas. 77−80541
α-Al_2O_3:V^{3+}, local deform. due to uniaxial stress 80−34140
α-Al_2O_3:V^{3+}(Cr^{3+})(Co^{3+}), optical absorption spectra, DC and AC field effects 78−10925
α-Al_2O_3:V^{3+}(V^{4+})(Co^{3+})(Co^{2+}), optically and thermally stimulated reactions, absorpt. spectra 80−80825
Al_2O_3:V^{4+}, dil. solution, stimulated phonon emission 78−63817
Al_2O_3-Na_2O, β and β'' phases, stability, cond., paramag. impurity effects obs. 77−84976
β-Al_2O_3-Na_2O, colour centers, AES, electron energy loss, and optical spectroscopy obs. 78−35176
β-Al_2O_3-Na_2O, EPR and optical absorpt. studies of X-ray produced defects 78−95517

impurity and defect absorption spectra of inorganic solids continued
β-Al_2O_3-Na_2O:Cr, absorpt. and emission spectra, mag. susceptibility 79−15495
β-Al_2O_3-Na_2O:Fe, coordination site, oxidation state, Mossbauer, absorpt., emission spectra, mag. susceptibility meas. 78−68431
Al_2O_3-P_2O_5:Nd^{3+} glass, high Nd conc., spectroscopy and lasing obs. 78−46609
Al_2O_3-SiO_2, struct., localised radiation centres, spectroscopic investig. *(Russian)* 77−69844
$AlPO_4$, synthetic berlinite, electron irrad. effects, ESR, ENDOR, optical spectral study 80−80608
$AlPO_4$:Fe^{3+}, luminesc. emission and excitation spectra 79−69873
Ar:S_2, absorption spectra of matrix-isolated S_2 molecules 77−52139
^{40}Ar:^{40}K, matrix isolation model system 78−45722
As, amorphous, bonding coordination defects, Raman scatt. and IR absorption meas. 78−60498
As:Ni(Ge)(S)(Se)(Te) film, amorphous, chemical modification of props. 80−49250
As-Se:^{197}Au, glassy, Au impurity influence, elec. cond., optical absorpt. and Mossbauer meas. 77−24558
$As_{2-x}S_{3+x}$, hydrogenated chalcogenide glasses, prep. by plasma decomposition 80−49735
As_2S_3, glassy, diffusion, elec. transport and first group impurities effect on elec. and opt. props. 77−76623
As_2S_3, glassy, photoinduced defects, EPR and absorpt. spectra 80−59398
As_2S_3, glassy, X-ray induced paramag. colour centres 78−19327
As_2S_3:Ag film, Ag photodoping rate, localised struct. transform. effect, absorpt. meas. 77−31914
As_2S_3-Tl_2S and As_2Se_3-Tl_2Se system glasses, comp. depend. of IR absorpt. props. 77−16292
$As_2S_3(Se_3)$, X-ray induced paramag. states and luminesc. 78−95520
$As_{2-x}Se_{3+x}$, hydrogenated chalcogenide glasses, prep. by plasma decomposition 80−49735
As_2Se_3, amorphous, photocond. and photoinduced optical absorpt. 79−82645
As_2Se_3, glassy, optical absorption spectra after 4.5 MeV electron bombardment *(Russian)* 77−32408
As_2Se_3, glassy, X-ray induced paramag. colour centres 78−19327
As_2Se_3, glossy, Cu, Ag and 0 impurities influence on electronic energy spectrum and mol. vibr. spectrum 77−90181
As_2Se_3, lone-pair semiconductor, defect chemistry 80−25421
As_2Se_3:Mn^{2+} film, reversible photostructural change, ESR obs. 77−32411
As_2Se_3-$GeSe_2$ glass, bulk and impurity IR absorpt. 80−71455
Au-Ti, dil., virtual bound states, optical absorption meas. 78−2891
Au-ZnSe:Ga(Al), Schottky diode, wavelength modulated photoresponse spectra 78−6714
B:H amorphous CVD films, IR, visible, and near UV optical props. 80−50442
B_2O_3 glass, absorption spectrum of Nd^{3+} ion, chem. composition effects, group IV element effects *(Polish)* 78−10932
B_2O_3-M_2O:S_2 glass, (M=Li, K, Na), absorpt. spectra of S_2 mols. 79−24337
B_2O_3-SiO_2:Ce glasses, radiation resistance mechanism, optical absorpt. and luminesc. obs. *(Polish)* 79−86825
$BaBr_2$:K^+, X-irradiated, perturbed F-centre, EPR and optical absorption 77−68966
$BaBr_2$:Sm^{2+}, fluoresc., and vibr. and electronic absorpt. spectra 77−8627
$BaCl_2$:Pb, absorption and emission spectra *(Russian)* 78−23527
$BaCl_2$:Sm^{2+}, fluoresc., and vibr. and electronic absorpt. spectra 77−8627
$BaCl_2(Br_2)$, F-centre localisation, absorpt. spectra calc. and EPR spectra analysis 77−48203
BaF_2, F^- interstitial and substitutional trivalent cations, phonon reson. and IR absorpt. 80−84752
BaF_2, U-centre, electronic struct. and optical transition energies, SCF MS Xα calc. 79−4532
BaF_2, undoped, H-centre prod. by reactor neutron irrad., optical absorpt. meas. 77−59010
BaF_2, undoped and U-doped, neutron irrad., absorpt. band attributed to F_2- centres 80−7380
BaF_2:Co^{2+}(Mn^{2+})(Ni^{2+}), far IR absorpt. spectra peaks 78−27265
BaF_2:Dy^{3+}, far IR absorption 80−40143
BaF_2:Mn^{2+}, far IR absorption spectra 78−76507
BaF_2:Pb^{2+}, band struct., Jahn-Teller effect, UV luminesc. and optical absorpt. spectra 80−66243
BaF_2:Pr^{3+}, wavelength and temp.-modulated UV absorpt. 80−2799
BaF_2:RF_3, cryst., absorpt. spectra, γ-ray effects 77−12409
BaF_2:Sm^{2+}(Tm^{2+}), vibronic spectra and dynamics of impurity-contaiing lattice 79−1787
BaF_2:U, absorption band spectra following neutron irrad. 80−29763
BaFBr, X- and γ-irrad., thermolum. and optical absorpt. spectra 79−95857
BaFCl crystals, F-centres, X- and γ-irradiation, thermoluminescence and optical absorption spectra 80−45155
BaO, electronic struct. of V^- and related centres 80−2355
BaO-B_2O_3:UO_2^{2+}→Er^{3+} glass, energy transfer 78−2895
BaO-B_2O_3-SiO_2:Ti^{3+}, optical absorpt. spectra 78−72564
$Ba_3(PO_4)_2$ transition metal ion, optical and magnetic props. 78−64196
$BaTiO_3$, OH^- impurity IR spectra meas. 80−20679
$BaTiO_3$:Cr^{3+} crystal, radiationless relax., photoacoustic spectra 78−27264
$BaTiO_3$:Eu(Sm), absorption spectra, Ti^{3+} ion and Z-centre formation 77−24871
$BaTiO_3$:Nb, ferroelec. and paraelec. phases, props. 79−42919
$BeAl_2O_4$:Cr^{3+}, alexandrite, potential laser material, stimulated emission and absorpt. spectrum 79−33734
BeF_2 glass, IR and UV transmission spectra 80−89019
BeF_2:Eu^{3+} glass, struct. and optical props. 80−84067
BeF_2:Eu^{3+} glass, struct., Monte Carlo simulations 80−96448
$Bi_{12}GeO_{20}$:Mn, Cr, reversible photochromic effects, absorpt. spectra before and after illum. 79−91471
$Bi_4Ge_3O_{12}$ crystals, doped with Dy^{3+}, Ho^{3+}, Er^{3+}, Tm^{3+}, Yb^{3+}, growth, spectral and laser props. 80−45115
$Bi_4Ge_3O_{12}$:Nd^{3+} and $Bi_4Si_3O_{12}$:Nd^{3+} crysts., absorpt. and luminesc. spectra, 4.2-300K 80−34957
BiI_3, absorpt. spectra, role of impurities *(Russian)* 79−51994
BiI_3, lamellar single cryst., absorpt. depend. on surface defects *(Russian)* 77−28606
$Bi_{12}SiO_{20}$:Mn, Cr, reversible photochromic effects, absorpt. spectra before and after illum. 79−91471
BiTeI, melt and vapour grown, optical props. 80−84746

impurity and defect absorption spectra of inorganic solids continued
$^{12}C^{16}O$:CO isotopes, IR and Raman spectra, vibron band, vibron-phonon combination bands 78−68495
$CaCO_3$ calcite, neutron irrad. effects 77−39617
$CaCO_3$, γ-irrad. defects, absorpt. spectra obs. 77−63447
CaF_2, 0.36 μ absorptance/fluence dependence obs. 79−15506
CaF_2, additively coloured, Ca colloid form. and size evolution during annealing 77−20895
CaF_2, additively coloured, new type of F_3-centre, absorption bands obs. 78−35172
CaF_2, additively coloured, photothermal bleaching of Ca colloids 79−15500
CaF_2, bleaching characteristics of crystals coloured by low energy electrons 78−76497
CaF_2, F-centre growth by neutron irrad. 79−55788
CaF_2, localised vibrs. due to substitutional impurities 78−22803
CaF_2, natural fluorite colouring, effect of impurities on absorpt. spectra 79−56822
CaF_2, optical props. of cation colloidal particles 78−23503
CaF_2, rare earth doped, force const. changes near impurity site, calc. 77−47529
CaF_2, U-centre, electronic struct. and optical transition energies, SCF MS Xα calc. 79−4532
CaF_2, undoped, H-centre prod. by reactor neutron irrad., optical absorpt. meas. 77−59010
CaF_2:CaO, optical scatt., absorpt. at 205 nm 80−20669
CaF_2:Ce_3 Stark struct., phototransitions, g-factors 78−67995
CaF_2:Ce^{3+}, absorpt. peaks in the lowest 4f→5d band, effect of conc. 80−2798
CaF_2:Ce^{3+}, thermally modulated UV absorpt. spectra, 90K 77−28602
CaF_2:Co, X-irrad., F-centre form., optical absorpt. spectra and dichroism obs. 79−42998
CaF_2:Co, X-irradiated, optical absorption spectrum 78−35173
CaF_2:Co^{2+}, designation of optical transitions near 5.40 nm, temp. evolution of absorption spectra meas. 77−55806
CaF_2:Co^{2+}, elec. field effect on spectra induced by odd vibrs. 79−73973
CaF_2:Co^{2+}, MCD spectra 77−28603
CaF_2:Co^{2+}, parity-forbidden transitions, elec. field effect on electronic-vibr. spectrum 79−65905
CaF_2:Co^{2+}(Mn^{2+})(Ni^{2+}), far IR absorpt. spectra peaks 78−27265
CaF_2:Dy, TLD-200, thermolum. phosphor, photolum. and absorpt. spectra, thermolum. mechanisms 80−97321
CaF_2:Dy crystal with M centre, antiresonance line, mag. field effect 80−55138
CaF_2:Er, defect structure, quenching effect, dielec. relax. and optical absorption 80−65031
CaF_2:Er^{3+}, fluorite, defect equilibria cluster control 79−99231
CaF_2:Eu, oxidation and reduction of Eu, EPR and optical studies 80−25199
CaF_2:Eu^{3+}(Sm^{3+}), VUV absorpt. spectra, dopant clustering 80−108230
CaF_2:Fe^{2+}, electronic props., Mossbauer and far IR spectroscopy 79−99803
CaF_2:Gd, triply ionised, lowest energy 4f-5d transition 79−24345
CaF_2:M, M=Mn, Fe, Co, Ni, X-irrad., impurity effects on defect prod. 80−92525
CaF_2:M^{3+}, M=activator ion, redox processes during growth 77−85924
CaF_2:Mn, EPR and optical absorpt. spectra 80−93171
CaF_2:Mn, low temp. X-irrad., Mn centres, optical absorpt. and emission props. 80−60635
CaF_2:Na, single cryst., X-irrad., optical absorpt. and thermoluminesc. 80−34952
CaF_2:Na, tunable room temp. laser action of M-centres, luminesc. and absorpt. spectra 79−31907
CaF_2:Nd^{3+}, crystal field study, absorption spectra 80−20668
CaF_2:Nd^{3+}, Slater, Racah and Lande parameters, crystal bonding 80−16062
CaF_2:Ni, X-irrad., optical absorpt. spectra and dichroism meas. 80−108239
CaF_2:Ni, X-irradiated, optical and EPR meas. 80−108235
CaF_2:O, absorpt., ionic cond., and thermal depolarisation 79−14960
CaF_2:O, absorption, ionic cond. and thermal depolarisation 78−14502
CaF_2:O_2^-, OH^-, ion incorporation by reaction with surrounding atm. 80−55143
CaF_2:Pb_3O_4, UV absorption, impurity centres 78−68534
CaF_2:Pb^{2+}, band struct., Jahn-Teller effect, UV luminesc. and optical absorpt. spectra 80−66243
CaF_2:Pr^{3+}, multisite system, laser selective excitation and energy transfer 78−84634
CaF_2:Pr^{3+}, wavelength and temp.-modulated UV absorpt. 80−2799
CaF_2:RF_3, colour centre prod. by γ-irrad., absorpt. spectra obs. 78−72565
CaF_2:rare earth ion, hydrogenated, local lattice modes, spectroscopy 80−50375
CaF_2:Sm, charge transitions, positron annihilation exam. 78−92143
CaF_2:Sm^{2+}, coherent population oscills. and hole burning observed using polarization spectroscopy 80−71457
CaF_2:Sm^{2+}, optical absorption and magneto-optic. props. 77−59595
CaF_2:Sm^{2+}(Eu^{2+}), cubic crysts., vibronic spectra, induced dichroism method 77−81131
CaF_2:Tb, spectra of radn.-induced defect form. 80−2801
CaF_2:Tm temperature dependence of V_k-centre generation efficiency *(Russian)* 78−48203
CaF_2:Tm^{2+}, vibronic spectra and dynamics of impurity-contaiing lattice 79−1787
CaF_2:U single crystal, Czochralski-Kyropoulos grown, U ion localization 79−91580
CaF_2:U^{3+}, anomalous magnetooptic props., optical detection of ESR and cross-relax. resonances 80−93287
CaF_2:Y, absorpt. spectra, radiation defect formation energy, F to M centre conversion kinetics 79−65079
CaF_2:Yb^{3+} vacuum UV absorpt. spectrum, rel. to other rare-earth ions 79−43001
CaF_2-NaF crysts., F_A centres, 385 and 435 nm absorpt. bands of electron irrad. crysts. 78−2889
CaF_2.3Ca(PO_4)$_2$, apatite, fission damage detection, absorpt. spectra 78−84617
$CaLa_4(SiO_4)_3O$:Nd^{3+}, spectra, stimulated emission 77−85755
$CaMoO_4$, exam. of electrical conductivity, absorption spectrum 79−51301
CaO, absorpt. band identification of colour centres 77−40271

impurity and defect absorption spectra of inorganic solids continued
CaO, electron irradiated, symmetry assignment of new point defect 78−31261
CaO, electronic struct. calc. of F-centre, absorpt. and luminesc. bands 77−62859
CaO, electronic struct. of V^- and related centres 80−2355
CaO, luminesc. single cryst., sharp IR absorpt. lines 77−1704
CaO, neutron irrad., MCD, optical absorpt. lines 77−77255
CaO, spectra rel. to interstellar absorpt. features 77−57073
CaO:Li, thermally quenched, generation of Li^0 centres 80−50382
$CaO-Li_2O-Al_2O_3-SiO_2:Nd^{3+}$, CaO enriched, laser-type glasses, spectroscopic behaviour 78−60497
$Ca_{10}(PO_4)_6Cl_2$, nonstoichiometry effect on X-irrad. induced electron-excess centres 77−62525
$Ca_2PO_4Cl:MnO_4^{3-}$, polarised electronic spectrum 77−52137
$Ca_5(PO_4)_3F:Nd^{3+}$, luminesc. and absorpt. spectra, line shift and broadening 77−4678
$Ca_5(PO_4)_3F:Nd^{3+}$, selective site laser spectroscopy and ESR studies 79−19909
CaS, absorpt. band identification of colour centres 77−40271
CaS phosphor, deep capture centres obs. 78−10951
CaS:Ce, Na, photon sidebands in emission and excitation spectra, pseudolocalised vibrs. 79−28800
$CaSO_4$ phosphors:Ce(Eu)(Dy)(Tm), gamma-irradiated valency conversions in rare-earth ions 80−55198
$CaSO_4$:Dy(Tm), thermolum. thermolum. phosphor, photolum. and absorpt. spectra, thermolum. mechanisms 80−97321
$CaS(Se):Eu^{2+}$, emission and excitation spectra obs. 80−55162
$CaWO_4$:Er, spectroscopic parameters calcs. 80−50379
$CaWO_4:Nd^{3+}$, Slater, Racah and Lande parameters, crystal bonding 80−16062
$CaWO_4:Nd^{3+}$ $4f^3$ configuration, ground level energy state variation rel. to press. *(Russian)* 77−16358
$CaWO_4:Nd^{3+}$ absorpt. spectra, hypersensitivity of $^4I_{9/2}$ to $^4G_{5/2}$ $^2G_{7/2}$ transition 80−97309
$CaWO_4:Pr^{3+}$, anomalous hypersensitive $^3H_4 \rightarrow {}^3P_2$ transition 80−106296
$CaYAlO_4:Nd^{3+}(Er^{3+})$, absorpt. and luminesc. spectra 77−69901
$Ca_3Y_2Ge_3O_{12}:Eu^{3+}$, garnets, prep., struct., luminesc., absorpt. spectra, Eu^{3+} localisation 77−69884
$CaY_4(SiO_4)_3O:Nd^{3+}$, absorpt. and luminesc. spectra 77−85755
$CdBr_2$:Co, spectroscopic studies of interactions 80−29769
$CdBr_2:Co^{2+}$, exchange-coupled Co^{2+} pairs, optical absorpt. and Zeeman studies 80−66242
$CdBr_2:Co^{2+}$, polarised IR absorpt. spectra 77−40269
$CdBr_2:Cu^+$, polarised absorption spectra 77−59594
$CdBr_2:I_2$, layered extrinsic cryst., impurity absorpt. band, temp. anomaly *(Russian)* 77−8616
$Cd(Ca)F_2:Co^{2+}$, Jahn-Teller split $^4A_{2g} \rightarrow {}^4T_{1g}(P)$ absorption band, elec. field effect 78−15202
$CdCl_2$:Co, spectroscopic studies of interactions 80−29769
$CdCl_2:Co^{2+}$, optical absorpt. spectra, Zeeman study 78−6712
$CdCl_2:Co^{2+}$, polarised IR absorpt. spectra 77−40269
$CdCl_2:Cu^+$, polarised absorption spectra 77−59594
$CdCl_2:Fe^{2+}$, magneto optical study, ferromagnetically coupled Fe(II) pairs 78−6711
$Cd(ClO_3)_2$, irrad., bleaching and annealing expts., EPR and optical absorpt. 79−91476
$Cd(ClO_3)_2$ irradiated single crystal, ESR and annealing, trapped defect centre 80−55141
$CdCr_2Se_4$:Ag, magneto-optical effects in impurity spectral region 80−97313
CdF_2, colour centres, IR absorpt. and photocond. after UV irrad. 80−79784
CdF_2: $YF_3(YbF_3)$, photoconversion from insulating to semicond. state, IR absorption and elec. cond. 78−14759
$CdF_2:Co^{2+}$, MCD spectra 77−28603
$CdF_2:Co^{2+}$, parity-forbidden transitions, elec. field effect on electronic-vibr. spectrum 79−65905
$CdF_2:Co^{2+}(Mn^{2+})(Ni^{2+})$, far IR absorpt. spectra peaks 78−27265
CdF_2:Eu, role of solution and precipitation phenomena on ITC spectra 80−7265
CdF_2:Eu(Gd)(Nd), semicond., symmetry of optical centres, optical and elec. props. 77−59592
CdF_2:NaF(AgF), colour centres, IR absorpt. and photocond. after UV irrad. 80−79784
$CdF_2:YbF_3$, conversion processes into semiconductor 78−14730
CdF_2-YF_3, thermal ionisation energy of monovalent centres 80−80207
$CdGeAs_2$, optical and elec. props. 79−19590
$(CdGeAs_2)_{1-x}D_x$ amorphous films, property control in common target sputtering, elec. cond. 80−7494
CdI_2-Ni^{2+}, absorption and mag. circular dichroism, spectra, phonon density of states of CdI_2 deduced 79−19913
$CdIn_2S_4:CO^{2+}$, site symmetry, spectral meas. 79−78729
$CdIn_2S_4$:Co, optical absorption meas. 78−64384
$CdIn_2S_4$:Cr, absorpt. and photoluminesc. spectra, Cr conc. depend. 79−78712
$Cd_{1-x}Mn_xTe$, acceptor photoionisation and light-to-heavy hole absorpt. 79−65908
CdS, absorpt. spectra, 400-650 nm, electron irrad. defects and absorpt. edge shift 78−64382
CdS, characts. of interaction of light with dislocations 78−2137
CdS, dislocation structural optical absorpt., plastic deformation *(Russian)* 80−34959
CdS, influence of surface states on absorption edge 77−16344
CdS, interaction of excitons with charged impurities 78−43906
CdS, photoexcitation, effect of elec. field *(Russian)* 79−1751
CdS, photoplastic effect due to α, β dislocations, spectral depend. 77−90180
CdS, plastically deformed, optical and electronic transport anisotropies 77−8611
CdS, spatial dispersion and surface layer effects on the phase of reflected light *(Russian)* 78−35182
CdS sprayed film, prep., optical props., struct. and comp. 79−78875
CdS, transition metal centres, first-harmonic electromodulation spectra 78−35116
CdS, two-photon absorpt., influence of In and Cu impurities 77−16353
CdS:Cd,Cu crystal, formation and bleaching of optically-induced absorption bands 78−31221
CdS:Cl, extrinsic, exciton absorption 78−72569
CdS:Cu,Pb reflectivity of Ni-salt coated powder, pre-irrad. effect on defect form. 79−27973

impurity and defect absorption spectra of inorganic solids continued
CdS:Cu(In), two-photon and two-step absorption of light 80−7389
$CdS:Er^{3+}$, spectra of different emission centres *(Russian)* 77−16356
CdS:In, two-photon absorpt. spectra exam. of effects of screening of exciton continuum 79−8166
CdS:Li, anisotropy of the absorption by impurity centers in hexagonal crystals 78−88343
$CdS:Ni^{2+}$, Zeeman effect at Ni impurities 80−60633
$CdS-Co^{2+}$, IR spectrum, 4.2K, electron-phonon interaction effect on emission spectrum 78−27270
CdS-Li, hexagonal crystl., orientation degeneracy of anisotropic centres, dichroism of impurity photocond. 79−73981
CdS(Se), with dislocations, optical props. 79−83001
CdSb:Fe, self absorpt. edge, impurity effect *(Russian)* 80−97316
CdSe, recombination mechanism at dislocations, photoluminescence 80−103993
CdSe, reson. absorpt. of coherent IR radn. by acceptors, photocurrent and emission spectra 79−73974
CdSe:Cd, Cu, photo-induced changes in absorpt. spectra 78−80382
CdSe:Ti, optical and elec. investig. of shallow donor levels, reson. states 77−63437
CdTe and CdTe:Cl, semi-insulating, electroabsorpt. by impurities and defects, dichroism 77−40270
CdTe, average number of phonons emitted in optical transition 77−8614
CdTe, shallow donors, excited state transitions 78−6710
CdTe, shallow impurity spectral linewidths, 4-10K 77−63443
CdTe single crystal IR window for CO_2 laser 77−75566
CdTe:Be, impurity modes and IR absorption 78−76506
$CdTe:Cr^{2+}$, absorpt. and luminesc. of $Cr^{2+}(d^4)$, cryst. field theory interpretation 79−83000
CdTe:In, shift optical absorpt. edge with temp. and doping level 79−8165
CdTe:Li, excitation spectrum of Li acceptor and valence band parameters 79−28795
CdTe:Mn, photoionisation absorption spectrum 78−23502
$CdTe:Mn^{2+}$, exciton refl. spectra and mag. susceptibility 80−66253
CdTe:S, reson. interaction of local S vibr. with lattice phonons 77−11654
$CdTe:Ti^{2+}$, Jahn-Teller effect on $^3T_1(^3F)$ state, resonance on $^3T_1(^3P)$ state 78−27271
$CeF_3:Pr^{3+}$, 400-700 nm, 78K, 22 kbar press. effects 77−81133
$CeP_5O_{14}:Gd^{3+}$, EPR and emission spectra *(French)* 77−69686
CeSe:Fe, long-wavelength fundamental absorpt. edge formation, role of Fe 77−16351
Co^{2+} in ionic crystals, exchange-coupled, optical spectra *(Rumanian)* 79−87474
$CoO:Ni^{2+}$, far IR absorpt. by impurities and collective antiferromag. reson. mode 77−8576
CoO-containing glass, effects of γ-rays, electron beam and neutron flux on transmissivity *(Japanese)* 77−73156
Cr^{3+}, coupled in ionic crystals, optical spectra *(Rumanian)* 79−87474
Cr^{3+}, electronic states interactions with crystal odd vibrs., R-lines vibr. recurrences 78−84639
Cr^{3+} impurity spectra anal. with Trees' correction 78−68539
CrO_4^{2-} in halide salt aqueous solution, absorpt. spectra, 4.2 to 290K *(Russian)* 78−60499
$Cr_2O_7^{2-}$ centre in lattice, optical props., mol. orbital calcs. 79−15491
$CrVO_4$, adsorption of methanol, IR spectra *(Russian)* 79−51435
Cs halides, F-centres, first excited degenerate states, props. of electron-phonon interaction 78−63824
Cs-halide, optical response function from Jahn-Teller systems, F-band absorpt. band shape 79−43005
CsBr, F-centre absorpt., uniaxial stress effects 80−60634
CsBr, impurity absorpt. spectra after γ-irrad., aggregated colour centres 79−4829
CsBr, temp. depend. of Cs colloids absorption bands 80−40145
$CsBr:CrO_4^{2-}$, coupling and fine struct., IR electronic and vibr. spectra obs. 80−45118
CsBr:Cu, polarisation study of tetragonal Cu^{2+} aggregate centres 78−39590
$CsBr:Cu^-$, excitation and absorpt. spectra 80−108255
$CsBr:Cu^+$, off-centre, optical absorpt. meas. 79−33740
$CsBr:K^+(Na^+)(Rb^+)(Tl^+)$, impurity induced IR absorpt. spectrum, breathing-shell model 77−77256
$CsBr:MNO_4^{2-}$, optical and vibronic spectra 79−65909
CsBr:Pr, absorpt. and fluoresc. spectra, crystal field 78−2885
CsBr:Th, absorpt., excitation, fluorescence spectra 79−43032
$CsBr:Tl^+$, perturbed lattice dynamics, breathing shell model calculation 78−75744
CsBr(Cl)(I):K(Li)(Na)(Rb), optical absorpt. investig. of F_A-centres 77−44029
$CsCdCl_3:Co^{2+}$, Zeeman Raman scatt. and Zeeman IR absorpt. spectra 79−56782
CsCl, F- and F_H-centres, luminesc. meas. 78−10397
CsCl(Br)(I), doped F_{Z1}-centre exam. 78−14341
$CsCl(Br)(I):NO_2^-$, vibronic and reson. Raman spectra of BCC cryst. 79−87468
CsF, F-centre ground state distortion fields and optical absorption 80−55140
CsF, F-centre optical absorption bandshape calc. for transition to state with Jahn-Teller and spin orbit couplings 80−55135
CsI, and Na doped sample, elastically loaded, effect of annealing on optical absorption 77−44034
CsI, F- and F_H-centres, luminesc. meas. 78−10397
CsI, temp. depend. of Cs colloids absorption bands 80−40145
$CsI:CrO_4^{2-}$, coupling and fine struct., IR electronic and vibr. spectra obs. 80−45118
$CsI:MnO_4^{2-}$, multiple-order Raman scatt., and absorpt. spectra 77−40229
CsI:Na, localised excitons, absorption and emission 77−32425
CsI:Na, X-ray irradiated, optical and ESR studies in IR absorption band 80−80828
$CsMgCl_3:Co^{2+}$, Zeeman Raman scatt. and Zeeman IR absorpt. spectra 79−56782
$Cs_2O-B_2O_3:Tl^+(Pb^{2+})(Bi^{3+})$ glass, optical basicity, variation with probe ion and comp. 80−2800
$CsSiF_6:Mn^{4+}$, splitting of vibronic levels 78−60496
$Cs_2SiF_6:Mn^{4+}$, IR absorpt. band, electron-vibr. effect 80−108238
$Cs_2SnCl_6:ReCl_6^{2-}$, luminesc. and absorpt. spectra, relax. processes 77−85779
$CsSrCl_3$:Tl, absorpt. and luminesc. spectra 78−72586

impurity and defect absorption spectra of inorganic solids continued
$Cs_2TiF_6:Mn^{4+}$, spin-orbit and field splitting, Jahn-Teller effect, Zeeman meas. 80−80234
$Cs_2TiF_6:MnF_6^{2-}$, $^4A_g \rightleftarrows {}^2E_g$ transition of Mn^{4+}, absorpt., emission, linear and MCD, MCE 78−10929
Cs_2ZrBr_6, $PtBr_4^{2-}$-$PtBr_6^{2-}$ doped, mixed valence, absorpt. spectra, vibronic struct. 80−97308
$Cs_2ZrBr_6:Os^{4+}$, intraconfig. absorpt. and MCD spectra 80−80776
$Cs_2ZrCl_6:Os^{4+}$, intraconfig. absorpt. and MCD spectra 80−80776
$CuGaS_2$, coloration, pure and Fe doped, EPR and optical absorpt. obs. 78−88336
$CuGaTe_2$, elec. and optical props. 80−6829
$CuInSe_2$, influence of impurities and free carriers on optical props. 80−108225
Cu_2O, Cu inclusions and annealing, optical and IR absorpt. obs. 80−60630
Cu_2O, positive and negative photomemory, IR luminesc. spectra, illum. effect 79−69557
Cu_2O, yellow exciton series, silver impurity influence on spectrum 78−64388
$Cu_2O:Ag^+$, yellow series line width, exciton-impurity scatt. 78−64386
Cu_2O:Cd, dipolar and quadrupolar bound excitons, absorption spectrum *(Russian)* 78−92099
$Dy_3Al_5O_{12}:Ca^{2+}$, optical absorpt. spectrum, strong crystal field of tetragonal symm. 77−32410
Er^{3+} doped phosphors, IR excitation and absorpt. and emission spectra *(Russian)* 79−52021
ErAg, rare earth impurity, spectral probe of stoichiometry variations 77−85790
ErGG, rare earth impurity, spectral probe of stoichiometry variations 77−85790
EuO, Eu-rich, IR absorpt. spectra, 4.2 to 300K, transitions assoc. with O vacancies 77−52142
$Eu_{1-x}O$, optical absorpt. spectra at metal insulator transition 78−10928
(Fe, Ti) silicate glasses, optical absorption and Mossbauer spectra 80−55136
$FeBr_2:MnBr_2$, magnon modes and impurity spin reson. 79−15501
$FeCO_3:Mn^{2+}$, far IR host and impurity excitations, antiferromag. and paramag. temp. ranges 77−52140
$FeF_2:Co^{2+}$, impurity-induced magnon, influence of localisation 80−11182
α-Fe_2O_3 electrode, carrier density determ. by optical absorpt. and photoelectrolysis spectra 80−71462
Fe_3O_4, substituted magnetite, correl. between IR spectra, X-ray diffr., and struct. vacancy distrib. 80−84753
FeS_2, optical absorpt. 79−43002
GGG, GGG-ErGG, rare earth impurity, spectral probe of stoichiometry variations 77−85790
$Ga_{1-x}Al_xAs$ epitaxial layers, spectroscopic technique for imaging spatial distrib. of nonradiative defects 78−23498
$Ga_{1-x}Al_xP$, two-phonon optical absorpt. 78−88341
GaAs, amorphous layer formation, ion implantation 78−95063
GaAs, carrier conc. and compensation microprofiles 80−80820
GaAs, compensated, photoabsorption, expt. 78−19521
n-GaAs, crystal growth by Czochralski method kinetics, total emittance determ. 80−75193
GaAs, deep levels, optical and thermal spectroscopy, lattice relaxation *(French)* 80−66248
GaAs, donor van der Waals interactions, spectral lineshapes 80−11450
GaAs, electron-irrad., deep-level defect anal. using 2γ positron annihilation and IR absorption spectra 80−16120
GaAs, excitonic spectra broadening, influence of phonons and impurities 77−1711
n-GaAs, heavily doped, test of cond. band edge random fluctuations by MCD 77−63438
GaAs, IR absorption of isolated impurities 77−12407
GaAs, interaction of excitons with charged impurities 78−43906
GaAs, irradiated with fast neutrons, IR vibrational absorpt. 78−75776
GaAs, multilayer liquid phase epitaxy, transition to faceting 80−96750
GaAs, nonlinear light absorpt., photoluminesc. meas. 77−66528
GaAs p-n junctions, electron irrad. induced defect levels, hydrostatic press. effect 80−92858
GaAs Schottky barrier structure, defects from proton irradiation, thermal transients and optical capacity *(French)* 80−59534
GaAs, shallow donors, excited state transitions 78−6710
GaAs, shallow impurity spectral linewidths, 4-10K 77−63443
GaAs:Co, neutral state of Co impurities, optical absorption and mag. susceptibility 78−39578
GaAs:Co^{2+}, piezoabsorption meas. tunnel splitting and Jahn Teller effect in $^4T_1(P)$ state 79−15494
GaAs:Co(Ni), intra d-shell excitations of acceptors 80−84757
GaAs:Cr, deep levels, wavelength-modulated photocapacitance spectroscopy 80−76055
GaAs:Cr, impurity conc. and segregation coeff., optical absorpt. meas. 79−56819
GaAs:Cr, luminescence and absorption spectra, temp. depend. of fine structure 80−6779
GaAs:Cr, optical modulation study of proton bombardment 78−6720
GaAs:Cr, origin of sharp near IR transitions 80−10913
GaAs:Cr, photoionisation transition $Cr^{3+} \rightarrow Cr^{2+}$, EPR studies 80−60638
GaAs:Cr, photoluminescence, YAG laser or krypton laser 80−60668
GaAs:Cr, plane-parallel plate subjected to laser illumination, photocond. meas., photodetector for far IR 79−93221
GaAs:Cr, zero-phonon struct. in Cr^{2+} ($3d^4$) optical absorption 80−60640
GaAs:Cr semi-insulating substrate, photoluminescence obs. of surface degradation during LPE growth 78−6865
GaAs:Fe, profile of impurity optical absorption bands 78−56509
GaAs:Fe(Ni) O_2 effects on opt. props. 77−16350
GaAs:Ni, behaviour of Ni impurity in $3d^8$ state, optical absorption and photocond. meas. 78−47737
GaAs:O, annealing effects, optical absorpt. and I-V characts. 80−29037
GaAs:O, defect states, IR absorption spectra meas. 77−4666
GaAs:O, Fe, temp. depend. of ionisation energies of O and Fe levels, electroabsorption meas. 78−47736
GaAs:O, optical characterisation of deep O implants 77−55294
GaAs:Si, donor-acceptor pair defects absorpt. bands 80−16064
GaAs:Si, electron irradiated, LPE layers and Bridgman crysts., IR absorption and Hall meas. 77−16345
GaAs:Si, IR absorpt. bands, localised modes, Si-related defects 80−76054
GaAs:Si, ion-implanted, annealing with Nd:glass laser 79−73194

impurity and defect absorption spectra of inorganic solids continued
GaAs:Si, Li, IR absorpt., microstruct., charge compensation 80−107565
n-GaAs:Si LEC crystal, carrier conc., B acceptor centres, Hall meas. and IR spectra 78−6717
n-GaAs:Te, electron-irrad., absorpt. spectra *(Russian)* 78−15200
GaAs:Te, ion implanted optical transitions in modulated reflectivity spectrum 79−73972
p-GaAs:Zn, optical absorpt. spectra and photocond. after 2 MeV electron irrad. *(Russian)* 77−69859
GaAs-C, ion implanted; obs. of localised vibrational mode absorption, effects of annealing temp. 80−16068
$GaAs_{1-x}H_x$, amorphous, vib. props., Raman and IR meas. 80−50322
$GaAs_{1-x}P_x$, $0 \leq x \leq 1$, evidence for common nature of certain deep-level radiative centres 78−6767
$GaAs_{1-x}P_x$, electron irrad., radiation defects annealing 80−29059
$GaAs_{1-x}P_x$:N, film, optical absorpt. from photoluminesc. meas. 78−92134
$GaAs_{1-x}P_x$:N epitaxial layers, absorption and photolum. spectra meas. 77−24894
$GaAs_xP_{1-x}$ epitaxial film nonlinear light absorpt., photoluminesc. meas. 77−66528
n-$Ga_xIn_{1-x}P$, optical props. and energy spectrum of donors 78−72567
$Ga_xIn_{1-x}P$:Si, solid soln., splitting of ground state 79−51527
GaN:Zn, VPE grown, optical cross sections, photoluminesc. and optical absorpt. meas. 80−55160
$GaNbO_4$, diffuse refl. and luminesc. spectra 78−56516
Ga_2O_3-$R_2O_3:Nd^{3+}$ glass, prep., characts., X-ray diffr., absorpt. and thermal anal. obs. *(French)* 78−19704
GaP, donor-acceptor pair luminesc., excitation spectroscopy 80−25440
GaP, effects of hydrogen incorporation during deposition by sputtering 79−69981
GaP, electron irrad., radiation defects annealing 80−29059
GaP, IR absorpt. spectra depend. on compensating defects and thermal treatment *(Russian)* 80−71465
GaP, impurity-containing single crysts., refl. spectra 80−80823
GaP, optical absorption and struct. of acceptor centres 78−48205
GaP, shallow impurity states, free exciton binding energy 78−79960
GaP, spectral depend. of O photoneutralisation cross-section near threshold, and band gap 79−1788
GaP, VPE Ni contaminant detection, IR photoluminescence of Ni 78−15212
GaP:Co, optical spectra and Zeeman anal. of Co $3d^7$ state 80−66247
GaP:Cr, origin of sharp near IR transitions 80−10913
GaP:Cu, impurity absorpt. bands at 1.05, 0.75 eV 77−44032
GaP:Fe, diffusion, solubility, elec. activity and energy levels 77−55395
GaP:Fe, optical absorption spectrum and Faraday effect 80−108245
p-GaP:Fe, photoionisation spectrum of acceptor level 77−55810
GaP:Fe, profile of impurity optical absorption bands 78−56509
GaP:Fe^{2+}, absorpt. and luminesc. spectra 77−16388
GaP:Fe^{3+}, deep impurity states investig. 77−15794
GaP:N, bound exciton absorpt. line asymmetry, electroabsorption spectra 80−71459
GaP:N, epitaxial layers, N concentration determination by two independent methods 80−39142
GaP:N, N doping profiles in GaP grown by LPE, cathodoluminesc. data 79−23631
GaP:N(Te), ion implanted at 40 keV, refl. spectra, 210-2000 nm, annealing *(Russian)* 78−80386
GaP:Ni, absorpt. and luminesc. spectra 79−42996
GaP:Ni, Hall effect and absorpt. spectrum investig. of acceptor level 77−44033
GaP:Ni, optical and EPR study of two-electron-trap state 79−73806
GaP:Ni(Fe), multivalence impurities, EPR and optical absorpt. meas. 80−75844
GaP:O, wave functions and optical cross sections associated with deep centres 78−34801
GaP:O^-, two electron state, electron capture 78−39054
GaP:S, Se, Te, Si, shallow donors, excitation spectra 77−81128
GaP:S, shallow donor states, Stark effect and inversion splitting, electroabsorption spectral obs. 80−50385
GaP:S(Se)(Te)(Si)(C)(Zn), IR photocond. response spectra 79−56257
n-GaP:S(Te), IR absorpt. cross-section 79−38582
GaP:S(Te), photostimulation spectra, bound electron phonon interactions *(Russian)* 77−1712
GaP:Sb(Bi), gap vibrs. and impurity conc. determ. 79−69869
GaP:Zn, light attenuation by impurity precipitates 79−11441
GaS:Bi_2S_3, photocond. and optical obsorpt. 79−51634
n-GaSb:Te(Se), forbidden optical band gap, Moss-Burstein effect 78−88335
$GdAlO_3:Er^{3+}$, $^4S_{3/2}$ to $^4I_{9/2}$ transition laser action, optical and luminescence spectra 80−16082
$Gd_3Ga_5O_{12}:Nd^{3+}$, growth, stimulated emission, spectral props. 78−95593
$Gd_2(MoO_4)_3:Nd^{3+}$, optical spectrum, free ion wavefunctions, radiative transition probabilities 79−24339
Gd_2S_3, resonance excitation of Nd^{3+}, luminescence, absorption spectra *(Russian)* 80−50381
GdTe:P and CdTe:P,In(Ga)(Al), IR absorpt. investig. of localised vibr. modes of impurity centres 77−52136
$GdVO_4:Eu^{3+}$, absorption and fluoresc. spectra, SU(2) chain *(French)* 78−28912
$GdVO_4:Ho^{3+}$, optically excited doublet splitting in magnetically ordered state 78−19238
Ge, acceptor complex spectra, tunnelling H systems 80−89036
Ge, acceptor levels, ionis. energy and IR absorpt. 79−78033
p-Ge, depend. of saturation intensity on impurity conc. and residual absorption at 10.59 microns 80−45125
Ge, doped, electron or neutron irradiated, vibrational absorption 78−6718
Ge, excitation spectra of shallow acceptors, Zeeman effect, expt. 80−7381
Ge, exciton effects on intervalence band transitions 77−4297
Ge, group III acceptor impurities, oscillator strengths of dipole optical transitions 79−56823
Ge, impurity spectral linewidth meas., free electron effects 80−71463
Ge, internal Stark effect on impurity states, low-temp. magnet. absorption meas. 80−60636
Ge, lattice disorder influence on optical spectra in interband transition region 79−43006
Ge, optical absorpt. in samples with 60° dislocations 78−39577
Ge, piezospectroscopy of group V impurities 79−99915

impurity and defect absorption spectra of inorganic solids continued
Ge, plastically deformed, photocond. and absorpt. spectra, dislocation levels 77−28219
Ge shallow impurity bound states, IR spectroscopic obs. 77−39806
Ge, sum rule for intraband optical absorpt. of shallow acceptor impurities 79−28793
Ge surface ion implanted far IR composite bolometers 79−30549
Ge:As, far IR transmission spectra, singlet-triplet optical transitions in ground states of donors 78−2887
Ge:As, uniaxially stressed, electronic Raman scatt. from valley-orbit transitions 78−15166
Ge:As(Sb), D^- states in mag. fields, photocond. spectra, and far IR absorption spectra 79−95370
n-Ge:As(Sb), far IR absorpt. spectra 79−91469
Ge:B(Al)(Ga), shallow acceptor spectral line intensities 80−88517
Ge:H, amorphous, H content determ. by IR absorpt., gas evolution and nuclear reaction methods 80−44130
Ge:In, magneto-optical transitions between discrete levels of In acceptor, far-IR obs., 4.2K 78−2890
Ge:O, IR absorpt. at low temp. *(Chinese)* 80−108228
Ge:P, bound-exciton luminesc. and absorpt. 79−87469
Ge:Sb, bolometer element, absorpt. spectra, bias depend. 79−30553
Ge:Sb, excited donor states, double optical transitions, reson. absorpt. meas. 80−93371
n-Ge:Sb, exciton absorption 78−6688
Ge:Sb,Cu, exactly compensated, impurity absorpt. and photocond. spectra 78−56189
Ge:Sb(Ga), fast electron radiation defects, 0.52 eV absorpt. band, impurity photocond. and Hall effect meas. 78−27273
Ge:Si, impurity modes and IR absorption 78−76506
Ge:Zn^-, G and D lines, stress induced components 80−71447
Ge-S film, amorphous, photo-induced ESR and optical absorption edge shift 78−88374
Ge-S glass, melt-quenched photoinduced ESR, annealing behaviour and glass comp. depend. 80−71156
Ge-Si, imperfect homopolar cryst., lattice dynamics, IR spectra calc. 80−59601
GeO:Cr, dielectric thin film, transmission and EPR spectra 77−69676
GeO_2 based glasses, absorpt. and emission of Ho^{3+} 79−11439
GeO_2, radiation damaged, paramag. point defects, F-centres, ESR, absorpt. spectra 78−80213
GeO_2:Si, optical props. IR absorpt., UV reflection spectra 78−84619
GeO_2:V^{++}, crystal field splitting from ESR and optical absorpt. results 79−47063
GeO_2-P_2O_5-SiO_2 glass fibre, incorporation of OH in modified CVD process 80−50560
$Ge_{1-x}Si_x$, with Si implanted ions, optical and photoelec. props. 79−24014
H:T solid, collision induced IR lines caused by T_2 radioactivity 80−84756
H_xWO_y film, effect of struct. on optical and electrical props. 78−84671
HfS_2, intercalation-induced shift of absorpt. edge 79−82999
$HfSiO_4$:U^{4+}(U^{5+}), opt. spectra 78−88334
$Hg_{1-x}Cd_xTe$, theory of optical absorpt., contribution by quasilocal acceptor levels *(Russian)* 80−71451
$Hg_{1-k}Mn_kTe$, impurity magnetoabsorpt. 79−91473
N-InAs, Moss-Burstein effect, S, Sn, Te dopants 78−64389
InAs, neutron bombarded, optical absorption, struct. defect form. and nuclear alloying *(Russian)* 78−31206
InAs, radiation defect formation processes, effect on physical props. 78−2163
n-InAs, undoped, electron irrad., Hall coeff., elec. resistivity, optical absorption 77−89479
InAs:S(Mg), ion implanted, photocond., photo-EMF, and optical absorpt. spectra 80−70763
InAs:Zn, optical absorpt. and refl. spectra 79−91479
$In_xGa_{1-x}As$, epitaxial solid soln. film, spectral depend. of transparency, absorpt. spectra calcs. 80−45161
$In_{1-x}Ga_xAs_yP_{1-y}$ far IR reflection spectrum 80−60612
$In_{1-x}Ga_xP$:N_2, N-trap bound states, photoluminesc. and absorption data 77−1719
InP, excitons bound to neutral donors in VPE layers, luminesc. and absorpt. obs. 79−42460
InP, radiation defect formation processes, effect on physical props. 78−2163
n-InP, room temp. electron irrad., Hall coeff. meas. 77−89478
InP:Bi, isoelectronic impurity states, emission and absorpt. obs. 79−42491
InP:Fe, Fe acceptor charge states, photolum., absorpt. and ESR meas. 77−36123
InP:Fe, Hall and resistivity meas., optical absorpt. 80−10990
InP:Fe, influence of covalence on EPR spectra 78−26827
InP_xAs_{1-x}, radiation defect formation processes, effect on physical props. 78−2163
InSb, doping depend. of high-field donor spectra 77−90175
n-InSb, strongly compensated, ionized donor mol. optical absorpt. spectra characts., 1.5-2.5 mm 79−11422
InSb:Ge annealing effect on electrical parameters, absorption spectra and photocond. 77−11939
In_2Se_3, 77 and 300K spectra, freezing of absorpt. centres 77−24417
IrF_6, in mixed crysts., Jahn-Teller effect, $\Gamma_{8g}(t_{2g})^3$ state, 6800 Å 78−76032
K salts, spectral refl. changes and luminesc. during 2-10 keV proton bombardment, implications for Io 79−96950
K-β-Al_2O_3, far IR absorpt., Beevers-Ross sites, interstitials 80−66240
$KAl(SO_4)_2.12H_2O$:MnO_4^-, visible and UV absorpt. spectra interpretation 80−45116
KBr, cation defects creation mechanism 80−75224
KBr, colour centre form. under polarised UV irrad., dichroism in absorption spectra 80−107232
KBr, efficiency of V_k- and Ag^0-centres generation *(Russian)* 80−39080
KBr, electron irrad. at 4K, role of V_K centres in equilib. among centres 78−67712
KBr, electron irradiated, defect accumulation kinetics of low temps. 80−10577
KBr extrinsic absorpt. near 9.6 μ, using CO_2 laser calorimetry 77−16341
KBr, intra impurity local oscill. composition tone absorpt. band anharmonic temp. broadening *(Russian)* 80−60642
KBr, pure and Sr^{2+} doped, X-irrad., hole Br_3^- centre creation and destruction 77−15411
KBr, quenched, absorpt. spectra, role of Schottky defects 77−59599
KBr, Stark effect in F-centre emission 77−63434
KBr, stored energy after X-irrad. at low temp., 10-50K 77−76459
KBr, V- and X-centres accumulation *(Russian)* 80−54228
KBr, X-irrad. crysts., halogen aggregation, absorpt. spectra obs. *(Russian)* 80−66234
KBr:(CrO_4^{2-})(MoO_4^{2-})(MnO_4^-)(ReO_4^-), absorption spectra 78−10924
KBr:Ag, optical absorpt. spectra interpretation mol. orbital scheme 80−20671
KBr:Au^-, optical absorpt. bands and MCD, electron-lattice interaction 80−108236
KBr:BeF_4^{2-}, IR absorption spectra of impurity anions *(Russian)* 80−2807
KBr:CN^- tunnelling motion of dipolar impurities, absorption spectra 80−66239
KBr:Ca, X-ray re-irradiation effects on Z_1 centres 78−75664
KBr:$CaSO_4$, SO_4^{2-} vibr. spectra, press.-scanned Fermi reson. spectroscopy appl. 79−73937
KBr:H^-, U-centre absorpt. band shape, piezodichroism dispersion curve and electron-phonon interaction 77−24873
KBr:H^+(H_2^+), absorption bands, V_4- and M-centres 77−48204
KBr:In^+, B-band, optical absorpt. and mag. circular dichroism calcs. 80−29765
KBr:KI, microcrystalline powder, isothermal decay of colour centres 79−42995
KBr:Li^+(Na^+), electronic struct. of $(V_K e)_A$ 78−95269
KBr:Li(Na), low temp. radiation hardening mechanism, single halogen interstitials as hardening agent, Ha annealing 79−23634
KBr:MnO_4^-, optical and IR absorpt. spectra, internal vibr. of MnO_4^-, freq. and type of symm. 79−15466
KBr:MnO_4^-, vibronic spectra interpretation 79−37770
KBr:NO_2, Na effect of Na^+ impurity on self-trapped hole *(Japanese)* 78−67982
KBr:Na(Rb)(Cs), microcrystalline powders, isothermal decay of colour centres 80−2804
KBr:Rb, H-centre interaction with Rb^+ ion 78−75662
KBr:SO_4^{2-}, Ba^{2+}(Ca^{2+}), IR absorpt. band parameters, temp. depend. *(Russian)* 78−31226
KBr:SO_4^{2-}, IR absorpt. spectra, cation impurity influence *(Russian)* 78−10901
KBr:SeO_4^{2-}(WO_4^{2-}), IR absorpt. spectra, vibr. splitting *(Russian)* 79−51995
KBr:Sr, X-irradiated, first-stage F-centre production, absorption spectra 77−76395
KBr:TeO_3^{2-}, IR absorpt. of impurity complexes *(Russian)* 79−33746
KBr:Tl, A-band absorpt., sruct. high resolution spectroscopy 77−20896
KBr:Tl, impurity-induced first-order Raman scatt., critical-point and critical-line anal. 79−19884
KBr:Tl^+, thermally induced absorpt. transfer between impurity bands, electron-lattice interactions 77−77257
KBr-KI:Tl, spectral, polarisational and kinetic charact. 78−80385
KBr(Cl):Eu, Z_2-centre investig. by EPR and optical absorpt. 77−16177
KBr(Cl):OH^-, cc U_2 to H_2O^- defects conversion after UV photodecomp. 80−107230
KBr(F), orbital g-factor and spin-orbit splitting of F-centre excited state, magnetoabsorpt. and MCD 78−2886
KCL:Pb^{3+}, interpretation of optical absorption spectra 79−51993
KCN, F-centre emission spectrum 77−12420
KCN, F-centres, optical props. 78−2892
KCN, optical F centres and phase transitions 78−56504
KCN:H , U-centre, local mode meas. 77−1199
KCN-KCl mixed crystals, F-centre optical absorpt. half width 77−81134
$KCdCl_3$:Co^{2+}, Zeeman Raman scatt. and Zeeman IR absorpt. spectra 79−56782
KCl absorption and emission of F_A(Li) centres under hydrostatic pressure 78−92117
KCl, absorption spectra of F-aggregate centres, 2K 77−48207
KCl, absorption spectra exam. of H-bearing complexes 79−8167
KCl, additively coloured, colloid size distrib., replica microscopy, absorpt. spectra 77−47449
KCl, additively coloured photochromic crystals, spectral sensitivity *(Russian)* 80−91871
KCl and KCl:NO_2, X-irrad. crysts., Cl_3^- centres photodissoc., optical anisotropy and creation mechanisms *(Russian)* 80−66235
KCl, bulk and surface absorpt. in 9.2-10.8 μm region 79−95808
KCl, bulk and surface absorption comparison, 9.2 to 10.85 μm 80−33051
KCl, cryst., colour centres, ionic cond., X-ray effects, thermoluminesc. *(Russian)* 78−6056
KCl, cryst., two-layer colloidal K and Cu colour centre light absorption 77−12408
KCl crystals with NaF surface absorpt. regions, photoacoustic detect. 79−87466
KCl, doped, elec. conductivity and optical absorpt., quenching from 750°C 78−2289
KCl, doped with alkaline earth ions, Z_1-centres form. under X-ray irrad. 79−24338
KCl, electron irrad., F-centre absorpt., ellipsometric obs. 78−23501
KCl extrinsic absorpt. near 9.6 μ, using CO_2 laser calorimetry 77−16341
KCl, F_2 centres triplet state, radiative and nonradiative decay 79−11438
KCl, F_2-centre triplet-triplet transition at 685 nm, MCD obs. *(French)* 77−63433
KCl, F-center pairs, light excitation, mag. field and resonance effects on absorption bands 78−92094
KCl, F-centre form. and dissociation under pulsed electron irrad. 78−18643
KCl, F-centre phonon many-mode interaction, absorption band shape 78−2883
KCl, gamma-irradiated crystal, interrelation between V_2 and V_3 centres *(Russian)* 79−69862
KCl, γ-irrad., F-centre absorpt., flash-stimulated changes 80−92524
KCl, γ-radiation effect on 10.6 μ absorpt. coeff. assoc. with F-aggregate centres 77−4661
KCl, H_2O-related centres 78−67711
KCl, irrad., V_3-band in absorpt. spectra, model *(Russian)* 79−56821
KCl, irradiated, determ. of molar extinction coeff. and oscillator strength of V_2-centre *(Russian)* 78−80384
KCl, irradiated crystal, determ. of oscillator strength of V_3-centre *(Russian)* 78−92095

impurity and defect absorption spectra of inorganic solids continued
KCl, luminesc. excitation spectra of F-aggregate centres, 400-900 nm. *(Russian)* 78−10980
KCl, MCD, magneto-optical parameters of R-centre in H_3-mol. model 77−77253
KCl, photo-induced F-centres, hologram recording 80−28174
KCl, radiation damaged, proton and $^4He^+$ channelling, F-centre production, optical absorpt. meas. 78−79656
KCl, room temp. X-irrad., first stage F-centre form. 78−67709
KCl single crystals, F-band absorpt. and thermolum. under DC field and X-ray irrad. 79−65910
KCl surface, electron bombard., F-centre absorpt. investigated by use of lateral light waves 78−4707
KCl surface, vacuum UV radiation damage, spectroscopic study 78−71758
KCl, thermal and photothermal conversion of colour centres, after high-dose electronic interaction *(Russian)* 80−39156
KCl, undoped and Pb- or NO_3^--doped, colloid centre formation, absorpt. spectra, 300-1000 nm 79−78710
KCl, V- and X-centres accumulation *(Russian)* 80−54228
KCl:$(CrO_4^{2-})(MoO_4^{2-})(MnO_4^-)(ReO_4^-)$, vibronic absorption spectra 78−10924
KCl:Ag, optical absorpt. spectra interpretation mol. orbital scheme 80−20671
KCl:Au^-, absorption bands and MCD, electron-lattice interaction 77−55808
KCl:Au^-, absorption band shape in D-mode model 79−47485
KCl:Ba(Sr), Z-centre, luminesc. and absorpt. spectra obs. 80−49221
KCl:BeF_4^{2-}, IR absorption spectra of impurity anions *(Russian)* 80−2807
KCl:Ca, additively coloured, spectral and temp. depend. of initial yield of Z_3-centre form. 79−78716
KCl:Ca, optical studies of Z_4 centres 79−24336
KCl:Ca, thermolum. and optical absorpt. spectra of Z_1 centres 79−52029
KCl:Ca, Z_2-centres, optical absorpt. and ESR spectra 79−91480
KCl:Ca^{2+}, cryst., hydrolysed, IR absorpt. bands 77−32404
KCl:Ca^{2+}, Z_1-centre thermolum. 80−80879
KCl:$CaCl_2$, KOH, complex form., U-centre influence, optical absorpt. bands 77−80502
KCl:Ca(Ba)(Mg)(Sr), microcrystalline powders role of Z centres in stabilising coloration, optical absorption 80−54227
KCl:Ca(Yb), Z_2 and Z_2^+ centres, excited state, magnetooptical spectra 80−108233
KCl:Cu, EPR, optical absorpt. and luminesc. investig. of anisotropic Cu_F^0 centres 77−20893
KCl:Cu^-, absorpt. and emission spectra, $3d^{10}4s^2 \rightarrow 3d^9 4s^2 4p$ bands 79−24343
KCl:Cu^- excitation and absorpt. spectra 80−108255
KCl:Cu^+, exciton bands, optical absorpt. and MCD spectra 80−80821
KCl:Eu, impurity conc. determ. by optical absorpt. meas. 77−32409
KCl:Eu, luminescence and absorption of color centres in RbCl:Cu and KCl:Eu crystals 78−92118
KCl:Eu crystallophosphores, aggregation of $Eu^{2+}v_c^-$ centres *(Russian)* 78−43909
KCl:Eu, IR laser window lattice equilibrium obs. 79−14055
KCl:Eu^{2+}, F centres and 220-nm optical-absorption band, creation by X-rays 79−55778
KCl:Eu^{2+}, γ-irrad., photostimulated low temp. recomb. luminesc. 80−11435
KCl:Eu^{2+}, lattice defect equilib. optical absorpt. and cond. studies 80−29767
KCl:Eu^{2+}, optical absorpt. meas. for Eu^{2+} conc. determ. 79−51137
KCl:Ga(In), ESR of impurity centres, impurity optical absorpt. bands 80−29618
KCl:H, dichroic H- and U-centres by polarised bleaching of interstitial H, absorpt. spectra study 80−29766
KCl:I crystals, V-band development using X-rays 78−88337
KCl:I(Br), colouration under two-photon excitation, absorption spectra 78−84618
KCl:KOH, influence of anion impurities on mech. props. of alkali halide crystals 78−87736
KCl:Li, additively coloured, luminesc. material for IR region *(Russian)* 78−15209
KCl:Li, self-induced resonant optical rotation 79−65831
KCl:Li,H optical and EPR exam. of H centre, $(LiH)^+$ absorpt. spectra 79−99920
KCl:Li^+, defect induced tunnelling states, depend. on strain, pot. model calcs. 79−69865
KCl:Li^+, press. tuning of motional behaviour in shallow off-centre pots. 79−78718
KCl:Na, absorption from relaxed excited state by F_A and F_B centres 77−44031
KCl:Na, electron trapping from α_A and F_A-centres, low temp. depend. 80−11444
KCl:Na and pure, hologram recording through F→X conversion 80−48190
KCl:Na^+, OH^-, IR absorpt. spectra, Na^+ ions rel. to OH^- stretching vibr. 79−47442
KCl:Na^+, self trapped excitons, optical absorption and emission 77−43503
KCl:Na(Ag), UV irrad. anionic H and D atoms, ESR and optical absorpt. expts. 79−99187
KCl:OH, absorpt. in high-transparency region 80−89037
KCl:OH, low temp. spectrophotometry, impurity absorpt. band *(Russian)* 79−40635
KCl:Pb, colouring, room temp., influence of conc. and aggregation state of Pb 78−14339
KCl:Pb, impurity valence, heat treatment influence, absorpt. spectra obs. 79−38574
KCl:Pb, vibr. struct. of absorption band 79−33735
KCl:Pb exam. of simultaneous effect of heat treatment, Pb concentration on state, phase diagram construction 79−96008
KCl:Pb^{2+}, γ-irrad., rel. to props. 78−31262
KCl:Pb^{2+}, highly doped, state of dispersion of Pb^{2+} 77−1144
KCl:Pb^{2+}, pure and doped, electrolytically coloured, elec. cond. and optical absorpt. meas. 80−100668
KCl:Pb^{2+}, X-ray irrad., electron-trapped centres, Pb^+ and Pb^0, optical absorpt. spectra 80−71461
KCl:Pb^{2+}(0.005% Pb), A band fine structure, electron-phonon interaction 78−60491
impurity and defect absorption spectra of inorganic solids continued
KCl:$PbCl_2$, tablet, 272 nm absorpt. band 78−84612
KCl:$Pr^{3+}(Sm^{3+})$, absorption spectra at 4.2 K, anal. 80−7378
KCl:ReO_4 nonlinear absorption for CO_2 laser pulse compression and mode locking 80−74443
KCl:Ru, optical absorption bands, complex form. 77−1705
KCl:S, influence of anion impurities on mech. props. of alkali halide crystals 78−87736
KCl:SO_4^{2-}, $Ba^{2+}(Ca^{2+})$, IR absorpt. band parameters, temp. depend. *(Russian)* 78−31226
KCl:SeO_4^{2-} (WO_4^{2-}), IR absorpt. spectra, vibr. splitting *(Russian)* 79−51995
KCl:$SnCl_2$, Sn^+ centres, polarised luminesc. and EPR 79−65076
KCl:$SnCl_2$, X-ray irrad., polarised luminesc. and EPR study of Sn^{3+} centres 80−39868
KCl:Sr, triplet state of F_2-centres, ESR spectra 80−29616
KCl:$SrCl_2$, H_{Na} annealing, X-ray irrad., H centre capture by IV dipoles 78−10927
KCl:Sr(Ca), thermoluminescence and colour centre thermal stability in irradiated sample 78−43941
KCl:Tl, 475 nm emission, attributed to Tl^+ dimer 78−39611
KCl:Tl, impurity-induced first-order Raman scatt., critical-point and critical-line anal. 79−19884
KCl:Tl, mixed phosphor, dimer absorption bands, 200-300 nm 79−73976
KCl:Tl^+, absorpt. spectra, electrolytic coloration, migration in electric field, heat treatment 78−23504
KCl:Tl^+, cryst., electron transfer, optical and thermal excitation 79−4833
KCl:Tl^+, optical absorpt. spectra following X-irrad., F- and V-centres 79−99912
KCl:Tl^+ cryst., A band, mag. field effect 80−34897
KCl:Tl^{2+}, optical absorpt. spectra interpretation mol. orbital scheme 80−20671
KCl:Yb, Z_2-centres, optical absorpt. and ESR spectra 79−91481
KCl-KF:Pb^{2+}, point defects, ionic thermal currents and optical meas. 80−6403
KCl-KH, F- and U-centre redistrib. at end of proton tracks, microspectrophotometric anal. 80−10583
KCl-KI:Tl, spectral, polarisational and kinetic characts. 78−80385
KCl-Mg, thermolum. of Z-centre, optical absorpt. 80−55203
KCl-Mg, X-irrad. and F-bleached, optical and ESR spectra 77−48052
KCl-Tl^+,$Ca^{2+}(Sr^{2+})$, electrolytic colouring, colour centre form., optical absorpt. spectra 79−15497
KCl(:LiF), radiative Q-centres, opt. absorpt. and thermal conductivity 77−47450
KCl(Br), coloured, irrad. damage during positron bombardment 78−63791
KCl(Br), triplet state lifetime of F_2 centre, mag. field effect 78−35177
KCl(Br):OH^-, electron irrad., F_2^+ centre stabilisation 80−54231
$KCl_{0.5}Br_{0.5}$:Ca, X-ray irrad., Z_1-centres, thermoluminesc. and optical absorpt. meas. 80−16108
$KCl_{1-c}Br_c$, impurity centre local vibrs., comp. depend. of spectral parameters 80−79898
$KCl_{1-x}Br_x$:NCO , absorpt. band defect broadening *(Russian)* 78−72526
KCl_xBr_{1-x}, mixed crystals, thermolum. and optical absorption studies 80−104000
KCl(Br)(I), U_2 and U_1 centres, optical excitations 80−2803
KCl(Br)(I) with alkali and halogen impurities, colour centre deformation induced nonradiative decay 80−7387
KCl(Br)(I):Eu^{2+}, single cryst. optical absorpt. spectra 80−45117
KCl(Br)(I):PO_2^-, vibr. spectra and struct. of PO_2^- impurity ions 77−16354
KCl(Br)(I):Zn^+, optical absorpt. bands rel. to charge transfer 80−66245
$KCl_{1-x}I_x$:NCO^-, absorpt. band defect broadening *(Russian)* 78−72526
KClIn, absolute quantum output of low-inertial energy transmission *(Russian)* 77−32429
$KClO_4$:MnO_4^-, reson. Raman excitation profiles for totally symmetric mode, vibronic struct. 80−50309
K_2CoF_4:Mn^{2+}, impurity induced mag. excitations, magnon gap mode, far IR spectra obs. 80−44821
K_2CrO_4:SO_4^{2-}, IR absorpt. spectra, local symmetry of impurity ions *(Russian)* 78−2893
$K_2Cu_{1-x}Mn_xF_4$, Cu-Mn exchange interaction, optical determ. 78−72551
$KDy(WO_4)_2$, phase transition mechanism, absorpt. spectra, symmetry props. *(Russian)* 80−55130
KF, deformation coloration 77−76397
KF, F_2+-centre excited-state absorption spectrum, rel. to H_2^+ model 80−16066
KF, IR absorpt. spectra from relaxed excited states of F-centres 77−69868
KF:Pd^{2+}, pure and doped, two-step photoionisation, laser-active F_2^+ centre form. 79−963
$K(H_{1-x}D_x)_2PO_4$, single cryst., 77K, γ-radiation damage centres, and EPR obs. 78−68379
KH_2PO_4:Tl, 5.76 eV absorpt. band, temp. effects on doublet struct. 79−78713
KH_2PO_4:Tl, UV absorption bands obs. 78−27266
KI crystals, containing excess of halogen, V-centres *(Japanese)* 77−59596
KI, optical bleaching of V_2 and V_3 bands 79−33739
KI, oscillator strengths of defects, Smakula eqn. generalisation 80−108232
KI, quenched, absorpt. and emission spectra, α-centres 80−11442
KI, self-trapped excitons and F-centres, picosec. range form., absorpt. bands 78−19515
KI, Stark effect in F-centre emission 77−63434
KI, V-centres, optical and thermal bleaching of V_2 and V_3 bands 77−85751
KI:BH_4^-, far IR absorption in phonon gap 77−12406
KI:$CaSO_4$, SO_4^{2-} vibr. spectra, press.-scanned Fermi reson. spectroscopy appl. 79−73937
KI:Cu^-, absorpt. and emission spectra, $3d^{10}4s^2 \rightarrow 3d^9 4s^2 4p$ bands 79−24343
KI:Cu^+, exciton bands, optical absorpt. and MCD spectra 80−80821
KI:$Ga^+(In^+)(Sn^+)$, magnetic circular dichroism of A- and B-absorption band region 77−12412
KI:NO_2^-, first-order Raman scatt. meas. 77−52085
KI:OH^-, HF phonon studies under uniaxial stress 79−83002
KI:Pb_2 absorpt. spectra of Pb^{++} centres 80−76058
KI:Pb^{2+}, absorpt., excitation and luminesc. spectra 78−19519

impurity and defect absorption spectra of inorganic solids continued
KI:Pb^{2+}, UV absorpt. and mag. circular dichroism spectra 80−25418
KI:S^{2-}, impurity-vacancy dipole UV absorpt. and ionic thermocurrent, F-centre form. 77−36271
KI:S^{2-}, photochemical reaction, F-centre production, optical absorption and ionic thermocurrent meas. 78−64861
KI:S^{2-}, photoinduced polarisation and depolarisation 79−33738
KI:Tl, decay of fast component of impurity luminesc. excitation in A-absorption band *(Russian)* 80−84767
KI:Tl^{+}, phosphor, anomalous stress-induced dichroism 79−4828
KI:Tl^{+}, pre-resonant enhancement of Raman scatt. 80−7354
$KMgF_3$:Co^{2+}, γ-irrad. single cryst., visible and IR absorption, MCD, annealing data 78−10926
$KMgF_3$:Co^{2+}, MCD and linear dichroism, 3d→4s transitions 79−56768
$KMgF_3$:Co^{2+}(Fe^{2+})(Mn^{2+})(Ni^{2+}), high energy absorption spectra interpretation 78−6716
$KMgF_3$:Fe^{2+}, Jahn-Teller quenched spin-orbit, splitting of $^5T_{2g}$ state 77−63442
$KMgF_3$:Mn^{2+}, exchange and spin-orbit interactions, optical spectra study 79−95817
$KMgF_3$:Mn^{2+}, MCD and linear dichroism, 3d→4s transitions 79−56768
$KMgF_3$:Ni^{2+}, absorpt., MCD and emission spectra 79−51953
$KMgF_3$:Sm^{2+}, absorpt. spectra and Zeeman effect, 3000-12000 Å, 4.2-295K 79−24341
$KMgF_3$:Sm^{2+}, luminesc. spectra 4.2, 77 and 295K and Zeeman spectra, 4.2K 77−81146
$KMgF_3$:V^{2+}, first and second order Jahn-Teller coupling const. calc. 79−65906
$KMgF_3$:V^{2+}, MCD and linear dichroism, 3d→4s transitions 79−56768
K_2MnF_4:Co^{2+}, Raman spectra meas. 77−12389
K_2MnF_4:Ni^{2+}, and undoped, magnon spectra, Raman and far IR spectra meas. 77−20573
$K_{1-c}Na_cCl$ and $K_{1-c}Rb_cCl$, impurity centre local vibrs., comp. depend. of spectral parameters 80−79898
K_2NaGaF_6:Cr^{3+}, mag. circular dichroism and absorption spectra 77−77254
K_2O-Al_2O_3-B_2O_3:Fe_2O_3, glasses, liq.-liq. phase separation, Fe^{3+} ions rel. to mag., optical props. 77−15322
K_2O-AlF_3-B_2O_3 glass:VO^{2+}, opt. absorpt., Al atom bonding mode *(Japanese)* 78−11023
K_2O-B_2O_3 glass, γ- and UV- irrad., thermodecolorisation and thermolum. 80−20721
K_2O-BaO-GeO_2:Bi^{3+}, Nd^{3+}, absorpt. and excitation spectra, fluoresc. 77−90183
K_2O-BaO-SiO_2 glass, rare earth ion activated, spectral intensity, effect of number of 4f electrons 78−84602
K_2O-BaO-SiO_2:Nd^{3+} glasses, absorption and fluoresc. spectra, density 80−25417
$K_{1-x}Rb_cCl$:HF_2^-, dynamic inhomogeneous broadening of bands of local vibr. 78−92102
$K_xRb_{1-x}Cl$:HF_2^-,SO_4^{2-}, nonuniform broadening of IR vibr. absorpt. bands of impurities *(Russian)* 77−16357
$K_xRb_{1-x}Cl_aBr_{1-y}$, far IR absorption spectra 79−33695
K_2SO_4:XO_4^{2-}, X=Cr, Se, Mo, W, lattice-impurity interactions, IR spectra 78−19522
K_2SO_4-$ZnSO_4$ glass, transition metal ion doped, visible spectra 79−51990
K_2SnCl_6:$ReCl_6^{2-}$, (K_2PtCl_6:$ReCl_6^{2-}$), luminesc. and absorpt. spectra, relax. processes 77−85779
$KTaO_3$:OH^-(OD^-)(OT^-), IR spectra, spectrosc. consts. 80−100671
KX:SO_4^{2-}, X=Cl,Br, impurity ion IR spectra analysis *(Russian)* 77−85762
K(Zn,Mn,Co)F_3, crysts., Mn, Co distrib., as function of cryst. region *(German)* 78−14375
$KZnF_3$, Cu^{2+} and Mn^{2+} exchange interactions, luminesc. line temp. depend. 79−69480
$KZnF_3$:Mn^{2+}, exchange and spin-orbit interactions, optical spectra study 79−95817
$KZnF_3$:Ni^{2+}, absorpt., MCD and emission spectra 79−51953
$KZnF_3$:Ni^{2+}, Mn^{2+}, interference transition electric dipole mechanism 80−34896
$KZnF_3$:Ni^{2+}, temp. depend. of luminesc. 79−83016
KI:Tl^{+}, X-irrad., absorpt. spectra investig. of Tl_2^{+} centres 77−20887
Kr:S_2, absorption spectra of matrix-isolated S_2 molecules 77−52139
KrF, matrix isolated, mag. circ. dichroism, UV and vis. absorpt. and saturation 78−46379
$LaBr_3$:Np^{3+}, energy level anal., polarised absorpt. and fluoresc. spectra 80−76056
$LaCl_2$:U^{3+}($5f^3$), polarised absorption spectra and energy levels 80−16063
$LaCl_3$:Np^{3+}, energy level anal., polarised absorpt. and fluoresc. spectra 80−76056
$LaCl_3$:Np^{3+}, phonon-induced relax. in excited optical states, linewidth temp. depend. meas. 80−100688
$LaCl_3$:Pr_1 optical absorpt. and Zeeman spectra, zero mag. field splitting 79−91482
$LaCl_3$:Pr^{3+}, hyperfine struct. of 6011 Å line, laser-induced absorpt. line narrowing 78−15196
$LaCl_3$:Pr^{3+}, Nd^{3+}, single cryst., optical double reson. excitation, energy transfer and transform. 77−69891
$LaCl_3$:Pr^{3+}, satellite lines in optical absorpt. spectra, Zeeman effect 79−65911
$LaCl_3$:U^{3+}, cryst., spectrum anal., cryst. field parameters 80−76057
$LaCl_3(Br_3)$:Pr^{3+}, IR absorption, energy values for Stark manifolds 80−34955
LaF_3:Ce, cryst. field parameters, optical transitions and g-factor determ. 78−2456
LaF_3:Dy^{3+}, magnetospectroscopy with optically pumped far IR laser 79−33737
LaF_3:Eu^{3+}, absorpt and laser fluoresc. spectra 77−52159
LaF_3:Ho^{3+}, laser excited fluorescence absorption spectra, symmetry groups 78−60514
LaF_3:Nd^{3+}, cryst., $4f^3$ config., ground level energy state var. rel. to press. *(Russian)* 77−16358
LaF_3:Nd^{3+}, laser-excited fluoresc., self-adsorpt. 78−15210
LaF_3:Pr^{3+}, optical transition, spin decoupling and magic angle line narrowing 80−28286
LaF_3:Pr^{3+}, ultrahigh resolution photon echo spectroscopy 80−28285
LaF_3:Pr^{3+}, ultraslow optical dephasing 80−58648
LaF_3:Pr(Nd)(Sm)(Eu)(Gd)(Dy)(Ho)(Er)(Tm), cryst. field anal. of triply ionised ion spectra 80−2796

impurity and defect absorption spectra of inorganic solids continued
LaF_3:R^{3+}, R=rare earths, crystal field anal., intensity calcs. 80−100670
$La_2Mg_3(NO_3)_{12}.24H_2O$:$Ce^{3+}$, mag. circular dichroism of Ce^{3+} 77−69869
$LaNbO_4$:Eu^{3+}, single cryst., photoluminesc. obs., vibronic transition dichroism 77−69890
$La_{2-x}Nd_xTi_2O_7$, luminesc. and absorpt. props. 79−65928
La_2O_3-Y_2O_3-Al_2O_3-SiO_2, coloration by transition metal oxides, absorpt. bands *(Japanese)* 80−55148
$(La_{1-x-y}Pr_xA_y)Cl_3$ (A=Ce, Gd, Y), satellite lines in optical absorpt. spectra, Zeeman effect 79−65912
$La_2S.3GaS_3$:Ho^{3+}, fluoresc., visible and IR spectra assignments 77−52150
LiBr:Cu^{2+}(Ni^{2+})(Co^{2+})(Fe^{2+})(Mn^{2+}), optical absorpt., charge transfer spectra 80−2797
LiCl:Cu^{+}, 3d→4p transitions, near UV absorpt. spectrum assignment 78−27272
LiCl:Cu^{2+}(Ni^{2+})(Co^{2+})(Fe^{2+})(Mn^{2+}), optical absorpt., charge transfer spectra 80−2797
LiCl:V(Cr)(Mn)(Fe)(Ni)(Co)(Cu), electron transfer absorption bands 79−95810
LiF, 3 MeV electron induced F, F_2, F_2^{+}, R_1, R_2 and F_2 colour centre obs., IR spectra obs. *(Russian)* 77−48210
LiF, alkali ion implantation, migration, segregation, effect on optical props. 80−100269
LiF, coherent radiation generation in F_2-centres 78−50782
LiF, electron irrad., transport of valence band holes, optical absorpt. obs. 79−99188
LiF, F-centre, excited state, optical absorption 77−20267
LiF, high-energy particle bombard., F-centre creation, optical meas. and model 77−47497
LiF, influence of neutron irrad. temp. on F-aggregate centre form. 78−72561
LiF, irrad. at pile temp., higher F aggregate centres produced during thermal annealing 77−43212
LiF, M-centre vibronic absorpt. spectra, elec. field, method of moments 78−27186
LiF, radiation damaged, proton and $^4He^{+}$ channelling, F-centre production, optical absorpt. meas. 78−79656
LiF, restored thermoluminescence mechanism 78−19580
LiF, Stark effect, M-centre absorpt. bands 78−84614
LiF, TLD phosphor, Z_3 centre, thermolum. and optical absorption spectra 79−24374
LiF, TLD-100, trapping centres, optical absorpt. spectra defect and thermolum. mechanism models 80−50436
LiF:Fe^{3+}, optical absorpt., 200-750 nm 78−39576
LiF:Mg, dependence of optical absorpt. on temp. during X-ray irrad. 80−66237
LiF:Mg, TLD-100, thermolum. phosphor, photolum. and absorpt. spectra, thermolum. mechanisms 80−97321
LiF:Mg, X-irrad., colour centres, ESR and UV asborpt. meas. 80−108069
LiF:Mg, X-irrad. induced sensitisation mechanism, optical absorpt. spectra 80−60637
LiF:Mg, Z_2- and associated Z-centres, elec. cond., ionic thermocurrent, and optical absorpt. meas. 80−107229
LiF:Mg,Ti, (TLD-100), optical bleaching of defect centres 79−19911
LiF:Mg,Ti, thermolum. related Z-centres, optical absorpt. bands 78−23540
LiF:Mg,Ti crystals, Z_3-centres, correlation of thermoluminescence and optical absorption 80−45154
LiF:Mg cryst., Mg electron colour centers 80−100229
LiF:Mg^{2+}(CO^{2-}), X-ray induced UV absorpt., band shapes, F- and Z-centers 77−20889
LiF:Mg(Eu)(Co)(Si)(O), IR spectra and elec. cond. 79−7709
LiF:OH crystals, X-irradiated, H centres formation and annealing 80−54226
LiF:OH^-, electron irrad., F_2^{+} centre stabilisation 80−54231
LiF:OH^-, IR spectra 80−20676
LiF:U_3O_8, X- and γ-irrad., U^{3+} luminesc. molecular centres, optical and ESR expts. 77−48224
LiF:U^{5+}, absorption and laser-excited fluoresc. 79−99927
LiF+UO_2^{+}, optical spectra, 2000 to 6000 Å 77−81129
LiH, effect of surface hydrolysis to LiOH on IR absorption, X-ray luminesc. and EPR spectra 80−60660
LiH, formation and annihilation of Li colloids and H bubbles 80−107228
LiI crystal, irradiated at low temps., optical absorption spectra 80−45123
LiI, reactor irrad., absorpt. spectra 79−65902
LiI:Pb, absorpt. spectra of Pb^{++} centres 80−76058
LiI:Tl, absorpt. spectrum obs. 80−50378
α-$LiIO_3$:Cr^{3+}(Ni^{2+})(Mn^{3+}), absorption spectra, impurity environments 78−27275
$Li_{1-x}K_xI$, intrinsic optical absorpt. spectra 78−23500
$Li_{1-x}Na_xBr(I)$, intrinsic optical absorpt. spectra 78−23500
$LiNbO_3$ doped with transition metal oxides, absorption spectra temp. depend. 77−90176
$LiNbO_3$, OH^- groups effect on dielec. and optical props. of single crysts. 77−12327
$LiNbO_3$, OH^- ion conc., PMR calibration method, IR determ. *(German)* 77−55712
$LiNbO_3$, OH^- ion incorporation, mobility and optical absorpt. 77−35583
$LiNbO_3$, optical absorption of hole centres, polaron model 80−97314
$LiNbO_3$, pure, two-photon photorefractive recording 78−31220
$LiNbO_3$, two-photon and X-ray induced Nb^{4+} and O^- small polarons, ESR and optical absorpt. 78−76306
$LiNbO_3$:Co_3 optical props. 78−64383
$LiNbO_3$:Cu^{2+}, EPR and optical spectra 80−20453
$LiNbO_3$:Fe, characts. for holographic storage appls. 77−23630
$LiNbO_3$:Fe, optical damage, Fe ion conc., EPR and optical spectra evaluation 79−42933
$LiNbO_3$:Fe(Cu), photorefractive centres, optical absorption, EPR and Mossbauer spectra meas. 77−32403
$LiNbO_3$:M, (M=Cr,Mn,Fe,Co,Ni,Cu), absorpt. spectra, 0.3-2.0 μm *(Russian)* 77−20898
$LiNbO_3$:Ni optical absorpt. spectra 80−71450
Li_2O, neutron irrad. effects, optical absorpt. spectra 80−75271
Li_2O-Al_2O_3-P_2-O_5:V^{4+}, glass exam. of ESR spectrum of V^{4+}, optical spectra, and structure 78−88180

impurity and defect absorption spectra of inorganic solids continued
Li_2O-Al_2O_3-SiO_2 glass, crystn. aggregation and migration of ion-implanted Ag 77−55240
Li_2O-B_2O_3:Tl^+(Pb^{2+})(Bi^{3+}) glass, optical basicity, variation with probe ion and comp. 80−2800
Li_2O_1 fund. optical absorpt. edge, number of displaced atoms from $^6Li(n,\alpha)^3H$ reaction 78−51594
(Li_2O-Al_2O_3-SiO_2):Fe_2O_3, glass, pyroceramic form., colour centres, magnetochem. investig. 77−16537
$LiSO_4.H_2O$:Cr^{3+}, single cryst., EPR and optical absorpt. spectra 80−39855
$LiTaO_3$, picosecond study of colour centre translocation 80−40144
$LiYF_4$, electron-irrad. induced defects, optical and EPR study, impurity effects 80−66238
$LiYF_4$:Dy^{3+}, spectrum, Stark struct. 77−85756
$LiYF_4$:Ho^{3+}, optical absorpt. and luminesc. spectra 79−4844
$LiYF_4$:Pr^{3+}, polarized absorpt. and fluoresc. spectra, 10 to 300K, energy levels and line intensities 79−95836
$LiYF_4$:Pr^{3+}, spectroscopic determ. of ground config. energy levels 80−34969
$LiYFd_4$:Er^{3+}, optical spectra and multifreq. stimulated emission 79−56818
$LiYO_2$:Nd^{3+}, absorption and luminesc. spectra, energy level diagram 77−63441
$LuAlO_3$:Er^{3+}, $^4S_{3/2}$ to $^4I_{9/2}$ transition laser action, optical and luminescence spectra 80−16082
$Lu_3Al_5O_{12}$:Er^{3+}, absorpt., luminesc., stimulated emission 77−32402
$LuVO_4$:Eu^{3+}, absorption and fluoresc. spectra, SU(2) chain *(French)* 78−28912
$MgAl_2O_4$, spinel, γ-irrad. effect on optical absorpt. and thermolum. spectra 77−85759
$MgAl_2O_4$, thermochemical coloration and annealing 79−91468
$MgAl_2O_4$:Cr^{3+}, exchange parameters determ. from emission and luminesc. excitation spectra 77−52160
$Mg_xCd_{1-x}Te$:P, vibr. modes of defects, IR absorpt. expts. 77−62601
$MgCl_2$:Co, spectroscopic studies of interactions 80−29769
$MgCl_2$:Co^{2+}, Zeeman electronic Raman scatt. spectra 79−42962
MgF_2, 0.36 μ absorptance/fluence dependence obs. 79−15506
MgF_2 film, optical absorption meas., rel. to prep. conditions *(French)* 77−44078
MgF_2 films, electronic transitions near optical absorpt. edge, depend. on prep. conditions *(French)* 77−63429
MgF_2, optical absortion following pulsed electron irrad., 100-500K 79−8164
MgF_2:Co^{2+}, MCD and linear dichroism, 3d→4s transitions 79−56768
MgF_2:Co^{2+}(Mn^{2+}), Coulomb and exchange interaction consts. optical spectra line assignment, new technique 80−45124
MgF_2:Fe^{2+}, γ-irrad., F-centres, Fe^{2+} ion hole traps, absorpt. and EPR meas. 79−7598
MgF_2:Mn^{2+}, MCD and linear dichroism, 3d→4s transitions 79−56768
MgF_2:Ni^{2+}, temp. depend. of luminesc. 79−83016
MgF_2:V^{2+}, MCD and linear dichroism, 3d→4s transitions 79−56768
$Mg(NH_4)_2(SO_4)_2.6H_2O$:Cr_2O^{2-}, optical absorption study, $Cr_2O_7^-$ and CrO_4^{3-} centres 80−55128
MgO, electron irrad., V^--centres, stress-induced optical dichroism, absorpt. spectra 79−61406
MgO, Fe^{2+} and Fe^{3+} conc. and valency, optical density, EPR and MCD obs. 77−89462
MgO, Fe^{3+} and Cr^{3+} impurity ions valence conversion in single cryst. by UV irradiation *(German)* 78−84620
MgO film, vacuum deposited on NaCl-type alkali halides, struct. characterisation, IR impurity absorpt. 79−82490
MgO, ion irrad. induced vol. changes, optical absorpt. expts. 77−59053
MgO irradiated with Li^+ and K^+ ions, optical props. of metal aggregates 79−65907
MgO, neutron irrad., MCD, optical absorpt. lines 77−77255
MgO, spectra rel. to interstellar absorpt. features 77−57073
MgO, thermochemical coloration and annealing 79−91468
MgO, V^- centres, electronic struct., rel. to optical absorption 77−28140
MgO:Cr, Co, optical and ESR studies 80−50175
MgO:Cr, high resolution far IR spectroscopy of lower energy levels of Cr^{2+} 80−80822
MgO:Cr^{3+}, diffuse interstellar absorpt. bands origin 79−30101
MgO:Cr^{3+}, emission and excitation spectra 80−93387
MgO:Cr^{3+}, radiationless relax., photoacoustic spectra 78−27264
MgO:Cr^{33}(V^{2+}), $^4A_{2g}$→$^4T_{2g}$ spectra, new expt. results 80−11441
MgO:Fe crysts., oxidised and reduced, optical absorpt. spectrum at low temps. 77−63436
MgO:Fe^{2+}, $^5T_{2g}$→^5E_g adsorption, Zeeman effect meas. 77−12405
MgO:Fe^{2+}, Jahn-Teller effect in ^5E_g state, tunnelling splitting obs. 78−19517
MgO:Fe^{2+}, phonon-induced transition interf. in EPR and IR spectra, ion-lattice coupling 77−51945
MgO:Fe^{2+}, shock compressed absorpt. spectrum, appl. to Earth mantle 80−90039
MgO:Fe^{3+}, Mn^{2+}, X-irrad. induced anion Frenkel defects, stabilisation by Fe^{3+}, optical and ESR obs. 77−68969
MgO:Ga, γ-irradiated, EPR and optical studies 79−73809
MgO:K, implanted K aggregates, TEM and optical spectra obs. 78−83838
MgO:Li, $[Li]^0$ defect, high temp. and ionisation induced effects 78−34509
MgO:Li, $[Li]^0$ defect, stress induced optical dichroism 78−35179
MgO:Li, $[Li]^0$ defects, magneto-optical props. 77−12365
MgO:Li, mech. deformed crysts., imprinting of slip bands using Li impurities 80−59473
MgO:Li, oxidation and reduction up to 1700K, defect prod. 79−39013
MgO:Mn^{4+}, diffuse interstellar absorpt. bands origin 79−30101
MgO:Ni, optical absorpt. spectrum in mag. field, and 2p-3d charge transfer 77−52141
MgO:Ni^{2+}, temp. depend. of luminesc. 79−83016
MgO:OH^-, room temp. IR spectra, heat treatment and electron irrad. effects 79−51992
MgO:V^{2+}, first and second order Jahn-Teller coupling const. calc. 79−65906
MgO-Al_2O_3 spinel crysts., thermolum. spectra 79−65938
MgO-P_2O_5-Al_2O_3-$3P_2O_5$ glass, absorpt. shift, electron and hole traps, thermolum. meas. 79−65897
MgS:Eu^{2+}, emission and excitation spectra obs. 80−55162
MgS:Eu^{2+} phosphors, anal. of absorption spectra $4f^{N+1}$→$4f^N5d$-6s 80−7383

impurity and defect absorption spectra of inorganic solids continued
$MgSO_4.7H_2O$:($Cu[H_2O]_6$)$^{2+}$, EPR and optical spectra anal. 79−38377
Mg_2SiO_4:Tb, thermolum. phosphor, photolum. and absorpt. spectra, thermolum. mechanisms 80−97321
Mn^{2+} in ionic crystals, exchange-coupled, optical spectra *(Rumanian)* 79−87474
Mn^{2+}, in nearly tetrahedral clusters, ^4E levels, orbit-lattice interaction and Jahn-Teller effect, spectra obs. 80−24860
$Mn_3Al_2(SiO_4)_3$, Mossbauer spectra and absorpt. bands 80−55144
$MnCl_2$:Co^{2+}, polarised IR absorpt. spectrum 77−40269
MnF_2, radiation damage, optical absorpt. and luminesc. expts. 78−2161
MnF_2:Fe^{2+}, temp. depend. of magnon pair-mode energies, Raman scatt. meas. 77−20577
MnF_2:Zn, shift and broadening of optical transitions 79−38579
MoO_3, film, colour centre studies, optical absorpt. spectra 78−71724
MoO_3 film, optical absorpt. after ion irrad., appl. to ion beam profile monitoring 79−26181
MoO_3:Re, ESR and optical absorption obs. 77−36127
MoO_4^{2-}, in halide salt aqueous solution, absorpt. spectra, 4.2 to 290K *(Russian)* 78−60499
MoS_2, 2H phase, far IR magnetoabsorption and refr. index meas. 77−24847
N_2:CO, IR and Raman spectra, vibron band, vibron-phonon combination bands 78−68495
$NH_4Al(SO_4)_2.12H_2O$, CrO_4^{3-} centres, EPR and optical absorption spectra 79−91475
NH_4Br:Cu^{2+}, ESR and absorpt. spectra, 300-1500 nm 78−60492
NH_4Br:Tl, absorption, excitation and fluorescence spectra 79−33824
NH_4Cl, cryst., impurity overtone states, interference two-photon spectrum *(Russian)* 79−24344
NH_4Cl-TlCl, mixed phosphors, diffuse absorption spectrum 79−24342
NH_4ClO_4, formation of colour center by X-irradiation, optical absorption spectra 79−19247
NH_4ClO_4:Co^{2+}, optical absorpt. spectra 77−66523
$(NH_4)_2SO_4$:MnO_4^-, X-ray irrad. damage, optical absorpt. spectra study 80−66246
$(NH_4)_2Zn(SO_4)_2$:Ni^{2+}, optical absorpt. spectrum, room and liq. air temp. 79−15499
N_2O crystal, vibrational exciton bands, impurity modes 77−28560
Na, matrix isolated in Ne, absorpt. and emission spectra 80−99465
Na salts, spectral refl. changes and luminesc. during 2-10 keV proton bombardment, implications for Io 79−96950
Na_2-β-Al_2O_3, far IR absorpt., Beevers-Ross sites, interstitials 80−66241
NaA zeolite:S, optical spectra 78−88342
$Na_6Al_6(Si_{0.99}Ge_{0.01})_6O_{24}.2NaBr$, Ge-doped sodalite powders, UV absorpt. band 80−71452
$Na_4Al_3Si_3O_{12}Cl$:Br,Ge, sodalite, reflectance and luminescence obs. 79−4839
$Na_8(Al_6Si_6O_{24})Cl_2$, sodalite, electronic struct. of F-centre 80−2356
$Na_6Al_6Si_6O_{24}.NaX_{(2-n)}$, (X=Cl, Br, I), X-ray irrad., thermal-erase cathodochromism and dihalide mol. centres *(Russian)* 80−66236
NaBr powder coloured in electrodeless discharge, reflectance spectra, thermoluminescence props. 78−6796
NaBr, thermally processed cryst., optical absorption bands *(Russian)* 78−76513
NaBr:Ag^+, UV absorption bands, temp. depend. 80−20672
NaBr:Cu^+, absorpt. spectra, pressure effects up to 6 kbar, comparison with NaCl:Cu^+ 79−4826
NaBr:Cu^+, press. tuning of motional behaviour in shallow off-centre pots. 79−78718
NaBr:Pb^+, absorpt. and emission spectra of Pb centres 79−78717
NaBr:Tl^+, absorption spectra meas. 78−15197
NaBr:V, covalency effects, EPR and optical spectra 77−85557
NaCN, optical F centres and phase transitions 78−56504
NaCl , X-irrad., F-thermal bleaching 77−89433
NaCl, additively coloured, sensitised with O, photochromic props. 79−28792
NaCl, bulk and surface absorpt. in 9.2-10.8 μm region 79−95808
NaCl, bulk and surface absorption comparison, 9.2 to 10.85 μm 80−33051
NaCl crystals irrad. by high electron doses, annealing, colour centre prod. 80−2074
NaCl, defect formation during fast electron beam irrad. *(Russian)* 77−7716
NaCl, F-centers, laser irrad. optical bleaching kinetics 80−66244
NaCl, gamma irradiated, optical bleaching of colour centres, F-aggregate centre form. 79−95813
NaCl, gamma irradiation, optical and thermal bleaching of colour centres, trapped electron centre form. 79−95814
NaCl, γ-radiation effect on 10.6 μ absorpt. coeff. assoc. with F-aggregate centres 77−4661
NaCl, irradiated, determ. of molar extinction coeff. and oscillator strength of V_2-centre *(Russian)* 78−80384
NaCl, M-centre prod. processes, in-beam studies, 15-95°C 79−55737
NaCl, optically bleached and X-irrad., relation between F- and C-centres 77−72613
NaCl plates, γ-irrad., optical absorption spectra, hologram recording samples 78−17878
NaCl preirradiation effect on proton channelling, thermoluminescence study 80−19860
NaCl, radiation damaged, proton and $^4He^+$ channelling, F-centre production, optical absorpt. meas. 78−79656
NaCl, thermoluminesc. and optical absorpt., simultaneous DC field and X-irrad. 79−99956
NaCl, V- and X-centres accumulation *(Russian)* 80−54228
NaCl:$^{63}Cu^+$, resonant bandmode, stress spectroscopy with far IR laser 78−2847
NaCl:Ag, absorpt. spectra, influence of elec. field 80−2794
NaCl:Ca, Z_1 centre thermoluminescence study 80−16109
NaCl:Ca^{2+}, cryst., hydrolysed, IR absorpt. bands 77−32404
NaCl:Cu, UV absorpt., emission, excitation spectra, Cu^- centres 77−81127
NaCl:Cu^+, electrolytically coloured, electron trapping, optical absorpt. 80−100672
NaCl:Cu^+, X-irrad., anisotropic Cu centre anal. 79−78714
NaCl:Eu, secondary Eu phase dissolution, EPR and optical absorpt. study 80−96655
NaCl:Eu^{2+}, optical absorpt. meas. for Eu^{2+} conc. determ. 79−51137
NaCl:Eu^{2+}, single cryst. optical absorpt. spectra 80−45117
NaCl:Ga(In), ESR of impurity centres, impurity optical absorpt. bands 80−29618

impurity and defect absorption spectra of inorganic solids continued
NaCl:H^-, U-centre absorpt. band shape, piezodichroism dispersion curve and electron-phonon interaction 77−24873
NaCl:Mg^{2+}(Mn^{2+})(Ni^{2+})(Cd^{2+})(Pb^{2+}), Z_4-like centre, absorpt. spectra obs. 78−76498
NaCl:Mn^{2+}, radiation-induced colouring, room temp. kinetics 79−55736
NaCl:NaOH, $NaNO_3$, oxygen colour centres, spectral absorpt. rel. to annealing 200-600°C 77−69862
NaCl:NaOH($NaNO_3$), absorpt. spectra and dielectric losses 78−19524
NaCl:Ni single crystals, VUV spectrum, ionic conductivity, X-ray diffr. 78−92097
NaCl:O, hologram recording, colloidal type centre transformation *(Russian)* 80−55147
NaCl:O_2^-, excitation and absorpt. spectra at 2K, O_2^- excited state field 79−56843
NaCl:OH^-, UV and IR absorpt. spectra, colour centres transformation 79−28791
NaCl:Pb, colouring, room temp., influence of conc. and aggregation state of Pb 78−14339
NaCl:Pr^{3+}(Sm^{3+}), absorption spectra at 4.2 K, anal. 80−7378
NaCl:Ru, optical absorption bands, complex form. 77−1705
NaCl:V^{2+}, EPR and optical absorpt. spectrum temp. depend., crystal field theory 77−16163
NaCl:V^{2+}, elec. field effect on Z-like centres spectrum 80−2802
NaCl:Zn^+, interpretation of optical absorption spectra 79−51993
NaCl:Zn^+, X-irrad., EPR and optical absorpt. 78−43642
NaCl-Cu^-, absorpt. and emission spectra, $3d^{10}4s^2 \rightarrow 3d^9 4s^2 4p$ bands 79−24343
NaCl-NaF:Pb^{2+}(Eu^{2+})(Zn^{2+})(Mn^{2+})(Sn^{2+}), point defect ionic thermal current and optical meas. 80−6403
NaCl(Br), orbital g-factor and spin-orbit splitting of F-centre excited state, magnetoabsorpt. and MCD 78−2886
NaCl(Br), X-ray or UV irradiated, cation defects creation mechanism 80−75224
NaCl(Br)(I), U_2 and U_1 centres, optical excitations 80−2803
$NaClO_3$, X-irrad., thermal stability of radiation damage products 79−34324
NaF, excess electron colour centre obs. 77−16343
NaF, F_3^+ centre zero-phonon line, photochem. and population hole burning 79−42997
NaF, M-centre vibronic absorpt. spectra, elec. field, method of moments 78−27186
NaF, M-centres, dichroim absorpt., appl. to optical waveguide polariser 79−995
NaF, radiation damaged, proton and $^4He^+$ channelling, F-centre production, optical absorpt. meas. 78−79656
NaF, Stark effect, M-centre absorpt. bands 78−84614
NaF, X-irrad., colour centres and thermolum. 80−84790
NaF: Mn^{2+}, VUV absorpt. spectrum and EPR 80−55142
NaF:Mn^{2+}, two-step photoionisation, laser-active F_2^+ centre form. 79−963
NaF(Cl):OH^-, electron irrad., F_2^+ centre stabilisation 80−54231
NaI:Cu^+, luminesc. of iolated V_K-centres 78−84641
NaI:F, electron-lattice coupling of F-centres, optical props. 80−60641
NaI:Pb, absorpt. spectra of Pb^{++} centres 80−76058
$NaMgF_3$, defects induced by X- and vacuum UV irrad., optical and elec. study 80−107319
$NaMgF_3$, optical absorpt. of radiation produced defects 77−28604
$NaMgF_3$:Sm^{2+}, absorpt. spectra and Zeeman effect, 3000-12000 Å, 4.2-295K 79−24341
$NaMgF_3$:Sm^{2+}, luminesc. spectra 4.2, 77 and 295K and Zeeman spectra, 4.2K 77−81146
NaN_3, UV irradiated, polarised optical absorpt. of F_2^+-, F-centres 77−28605
$NaNO_2$, X-irradiated IR, UV and visible absorption 79−95811
$NaNO_2$:Ag^+, optical and MODR spectra, anion states spin-orbit perturbation 79−19908
($NaNO_3$-$Mg(NO_3)_2$):Nd^{3+}, glass, cryst., absorpt. luminesc. spectra, term struct. of Nd^{3+}, bonding 77−8624
Na_2O-3SiO_2 glass, high-temp. thermolum., colour centre absorpt. 80−16110
Na_2O-Al_2O_3-B_2O_3-SiO_2, CuCl crystal activated photochromic glasses, absorpt. spectra 79−27353
Na_2O-B_2O_3 glass, covered with PbO film, deep penetration of Pb^{2+} ions 78−79535
Na_2O-B_2O_3 glass, γ- or UV-irrad., laser and thermal bleaching of colour centre, absorpt. spectra 79−33744
Na_2O-B_2O_3 glass, PbO interdiffusion layer form. 79−51318
Na_2O-B_2O_3:Au glasses, Au solubility, oxidation state and opt. absorpt. 80−44321
Na_2O-B_2O_3:Cu^{2+}, glasses, ESR and optical absorpt. 80−34760
Na_2O-B_2O_3-CoO glass, Co^{2+} ion activated, magneto-opt. study 79−65844
Na_2O-B_2O_3-SiO_2 glass, type DB-1, exam. of distrib. of rare earth activators, by absorption study 79−4832
Na_2O-B_2O_3-SiO_2-Fe glass, near IR optical absorption of Fe (II) 78−84616
Na_2O-BaO-SiO_2:Nd^{3+} glasses, absorption and fluoresc. spectra, density 80−25417
Na_2O-CaO-P_2O_5:Co glass, bonding, symmetry meas. 79−46572
Na_2O-CaO-SiO_2:UO_2, energy spectrum of UO_2 ions, fluoresc. and absorption spectra 77−66531
Na_2O-GeO_2-CoO glass, Co^{2+} ion activated, magneto-opt. study 79−65844
Na_2O-K_2O-SiO_2 glasses, optical absorption of Ni (II) complex, complex co-ordination change, annealing effects 79−69870
Na_2O-P_2O_5, metaphosphate glass, active solute doped, absorpt. spectra of radiation products 78−64865
Na_2O-SiO_2 glass, magnetooptical props. 78−80318
Na_2O-SiO_2:Ce photochromic glass absorption centres 79−27352
Na_2O-SiO_2:Cu^{2+} glass ESR and optical absorption 79−77526
Na_2O-SiO_2:CuO glass, gamma-irradiated, EPR and optical spectra 80−103885
Na_2O-SiO_2:VO^{2+} glass, optical absorption spectra *(Japanese)* 78−42918
Na_2O-SiO_2-CoO glass, Co^{2+} ion activated, magneto-opt. study 79−65844
Na_2O-WO_3 glass containing transition metal ions optical absorption 78−27254
$Na_2O.3B_2O_3$, glass, effect of Fe_2O_3 conc. and temp. on UV absorption 77−16340

impurity and defect absorption spectra of inorganic solids continued
Na_2SO_4:XO_4^{2-}, X=Cr, Se, Mo, W, lattice-impurity interactions, IR spectra 78−19522
$Na_2S.9H_2O$-NaOH-H_3BO_3, glass, IR and Raman spectra of boro-ultramarine, exam. of S_3^- presence 78−68502
$Na_2Zn(SO_4)_2.4H_2$:Ni, divalent state obs. 78−76501
Nd:glass laser rod, piezoelectric detection of photoacoustic signals 78−54467
Nd^{3+}:glass, inhomogeneously broadened spectra, struct., selective laser excitation obs. *(Russian)* 78−35181
Nd^{3+}-Yb^{3+}:glass, excitation transfer, selective filling of levels in inhomogeneous contour 77−69898
$NdCl_3$, anhydrous, Nd^{3+} absorption spectra and quantum states *(Chinese)* 80−89032
Nd_2O_3-Al_2O_3-SiO_2 glass, exam. of spectroscopic and luminescent props. 78−88364
Nd_2O_3-SiO_2 glass, exam. of spectroscopic and luminescent props. 78−88364
Ne, solid, doped with Xe and benzene, energy transfer 77−32416
Ni-Co(Fe)(V)(Ti), dil., optical absorpt., electronic struct. 80−108227
Ni-Cu alloy, optical absorpt. meas. 78−19518
NiO doped glass, improved band-pass charact. 78−42394
α-O_2 crystals, absorpt. line polarisation biexciton existence *(Russian)* 80−108242
P_2O_5 glass, absorption spectrum of Nd^{3+} ion, chem. composition effects, group IV element effects *(Polish)* 78−10932
P_2O_5-GeO_2 glass, absorption spectrum of Nd^{3+} ion, chem. composition effects, group IV element effects *(Polish)* 78−10932
P_2O_5-K_2O-CdO-Na_2O glass:Nd^{3+}, highly doped, spectroscopic props. and CW laser action *(French)* 79−41385
PbBr(Cl)-Ag^+ IR absorpt. spectrum and vibr. of substitutional impurity 77−81135
$PbCl_2$:NaCl, trapped exciton states, absorption spectra 80−50383
β-PbF_2, γ-irrad., F-band region spectrum, impurity effects 77−44026
PbF_2-TlI graded coatings on KCl laser windows, photoacoustic spectroscopy 80−33052
PbI_2 film, photolyzed, refr. index change 78−11010
PbI_2:KI, trapped exciton states, absorption spectra 80−50383
PbI_2:KI alloys, fundamental abs. edge, potential as solar convertor 80−101128
$PbMoO_4$, colour study from absorption, fluorescence and thermoluminesc. exam. 78−31245
$PbMoO_4$, defect electron centres after X-irrad. 79−55738
$PbMoO_4$, optical absorption of hole centres, polaron model 80−97314
$PbMoO_4$:Nd^{4+}, optical absorpt. intensities, 300, 550 and 4.2K, expt. and Judd-Ofelt theory 77−20894
PbO-B_2O_3:Cu^{2+}, glasses, ESR and optical absorpt. 80−34760
PbO-B_2O_3(SiO_2) glasses, absorpt. spectra of Cu^{2+} ions and interpret. 78−27276
PbO-SiO_2 and Na_2O-PbO-SiO_2 system glasses, radiative paramag. and optical absorpt. centres 77−8402
PbO-SiO_2 glasses, absorpt. spectra of Nd^{3+} ions and interpret. 78−27277
PbSe:Tl, high temp. elec. and optical props., impurity states 79−60854
PbSe:Tl, impurity states, optical absorption and Hall effect meas. 78−18995
$Pb_{0.8}Sn_{0.2}$Te:In, absorption spectra meas., 475-725K 77−4664
$Pb_{1-x}Sn_x$Te film, Burstein-Moss effect, absorpt. and photocond. spectra 78−18961
$Pb_{1-x}Sn_x$Te film, pure and Bi doped, polycryst., struct., elec., optical props. 79−42542
Pb_xSn_{1-x}Te, oxide and Te monolayer films, Raman backscattering spectra 77−48211
PbTe, ion implanted, magneto-optical expts. *(German)* 79−28848
PbTe, undoped, nature of defects, X-ray diffr. and optical absorption meas. 77−43211
PbTe:In, absorption spectra meas., 475-725K 77−4664
PbTe:Tl, absorpt. coeff. spectral depend. 80−93370
PbTe:Tl, influence of Tl impurity states 80−20121
Pr^{3+} impurity, $4f^2$ config., semiempirical eqns. for deciphering spectrum 77−24874
$PrCl_3$, anhydrous, Nd^{3+} absorption spectra and quantum states *(Chinese)* 80−89032
RbBr, Stark effect in F-centre emission 77−63434
RbBr, suprapure, thermolum. glow and emission studies at room temp. 80−7423
RbBr:Ag^+, press. tuning of motional behaviour in shallow off-centre pots. 79−78718
RbBr(I), parallel and perpendicular Stark effect of F-centre 77−1703
RbCN, ferroelasticity and F- and M-centres absorpt. 79−87475
$RbCaF_3$, optical absorpt. of radiation produced defects 77−28604
RbCl:Ag, phosphor, luminesc., absorpt. and excitation spectra 77−12424
RbCl:Ag^+, press. tuning of motional behaviour in shallow off-centre pots. 79−78718
RbCl:Au^-, optical absorpt. bands and MCD, electron-lattice interaction 80−108236
RbCl:Ca^{2+}, thermolum. and optical absorption studies 80−104002
RbCl:Eu, luminescence and absorption of color centres in RbCl:Cu and KCl:Eu crystals 78−92118
RbCl:Eu^{2+}, optical absorpt. meas. for Eu^{2+} conc. determ. 79−51137
RbCl:Eu^{2+}, tetragonal sites, spin Hamiltonian parameters, EPR and UV absorpt. spectra obs. 80−50177
RbCl:H^-, defect pairs of F-centres and U-centres, Raman meas. 79−7599
RbCl:NO_2^-, first-order Raman scatt. meas. 77−52085
RbCl:Sn crystals, Sn-centres, X-ray and coloration effects 78−76500
RbCl:Tl, absorpt. spectra, 210-300 nm 79−87473
RbCl(Br), cation defects creation mechanism 80−75224
RbCl(Br):Eu^{2+}, single cryst. optical absorpt. spectra 80−45117
RbI, intra impurity local oscill. composition tone absorpt. band anharmonic temp. broadening *(Russian)* 80−60642
RbI, Stark effect in F-centre emission 77−63434
RbI:AgI, thermal reorientation kinetics of I_2^-, decay of optical anisotropy 77−52138
RbI:Pb, absorpt. spectra of Pb^{++} centres 80−76058
RbI:Pb^{2+}, optical and elec. props. 79−15493
RbI:ReO_4^-, IR absorpt., half width, temp. depend. *(Russian)* 79−78722
RbI:TeO_3^{2-}, IR absorpt. of impurity complexes *(Russian)* 79−33746
$RbMgF_3$:Mn, low-temp. radiation damage, optical absorption meas. 78−22761

impurity and defect absorption spectra of inorganic solids continued
$RbMnCl_3$, twinning struct., cryst. domains, orientation mag. transition *(Russian)* 80−107275
$RbMnF_3$, radiation damage, optical absorpt. and luminesc. expts. 78−2161
$RbMnF_3:Er^{3+}$, absorption, emission, excitation and lifetime meas. 80−71460
$RbNgF_3$, radiation defect F,M,R-centre absorpt., emission, excitation spectra 79−43000
$Rb_2SnCl_6:ReCl_6^{2-}$, luminesc. and absorpt. spectra, relax. processes 77−85779
ReO_4^-, in halide salt aqueous solution, absorpt. spectra, 4.2 to 290K *(Russian)* 78−60499
$(SN)_x$ polymer, Be_2 doped, influence of halogen on elec. and optical props. *(Japanese)* 79−51559
$Sc_2(WO_4)_3:Er^{3+}$, growth, solubility, absorption spectrum and thermal expansion meas. 77−36391
Si, acceptor levels, ionis. energy and IR absorpt. 79−78033
Si, ambient effect of O precipitation, self interstitial mechanisms, IR spectra, TEM study 80−66510
Si, amorphous, doping and absorption edge 80−29042
Si, amorphous film, RF plasma deposition from $SiCl_4$-H_2, characterisation 80−66435
Si, and Si:H, amorphous, sputter deposited, O_2 incorporation during and after fabrication 80−49541
Si, bound-exciton spectral lines, conc. broadening at high impurity concs. 80−80826
Si, compensated monocrystal, IR absorption spectra, Fourier transform obs. 80−60644
Si, Czochralski-grown crysts., thermally induced microdefects, annealing temp. and starting material effects 80−49141
Si, deformed, photo-EPR of dislocations 80−11267
Si, diffusion coeffs. for O impurity, determ. from optical absorpt. 79−69294
Si, dislocation-free, O_2 precip., IR and TEM obs. 80−29173
Si, divacancies due to proton irrad., IR absorpt., annealing effects 80−20673
Si, electron irrad., multivacancy-O complexes, EPR expt., correl. with IR absorpt. data 77−28443
Si, electron irrad., rod-shaped defects, electron microscopy and IR spectra obs. 80−39159
Si, electron irradiated, O-vacancy pair, EPR of optical absorption 77−16173
Si, far IR impurity spectra, effects of high uniaxial stress 78−56508
Si, heavily disordered, fast neutron irrad., IR absorption following heat treatment 78−2448
Si, impurity doping influence on free-exciton absorpt. 77−69861
Si, ion bombardment induced defect distrib., IR and electron diffr. study 80−65074
Si, ion implanted, spin density effect on laser annealing 80−11517
Si, ion irrad., temp. and dose depend. of defect profiles 80−29097
n-Si neutron and electron irrad., isochronous annealing influence on edge absorpt. 80−11449
Si, neutron irrad., point defects photopopulation and photoionis., IR spectra meas. 80−25423
Si, neutron irradiated, charact. of defect form. 78−14382
Si, neutron irradiated, direct band gap transition, IR absorpt. 79−73980
Si, neutron irradiated, intrinsic defect exam. by IR spectra 78−52534
Si, neutron transmutation doping, annealing, lattice damage 80−15163
Si, optical absorption by acoustic phonons related to shallow impurity levels 77−4665
p-Si, photoabsorpt. associated with divacancies 79−15502
Si, photoionisation of Group III acceptors, model 78−35174
Si, precipitation of O, 1000°C TEM, IR absorpt. and X-ray studies 80−34194
Si, precipitation of O, 650°C, IR absorpt. and X-ray diffr. 80−76258
Si, precipitation of O, annealing, IR spectra meas. 80−24606
Si, proton irradiated, IR absorption 79−33742
Si, radiation induced defects, IR absorpt. bands 80−25424
Si, resonant interaction of acceptor states with optical phonons 77−1394
Si, resonant interaction of optical phonons with acceptor continuum states 78−35178
Si shallow impurity bound states, IR spectroscopic obs. 77−39806
Si, sputtered, cluster formation, influence of HF plasma interaction 78−64441
Si, thermally induced microdefect form., C and O role 80−11439
Si wafer, heat treatment behaviour of microdefects and residual impurities, X-ray diffr. and IR absorpt. study 80−49214
Si wafer C impurity IR absorption spectrometry, thickness fringe elimination 80−55132
Si wafer O interstitial IR absorption spectrometry, multiple reflection correction 80−55131
Si: Li, absorpt. and luminesc. transitions involving exciton excited hole states 79−78038
Si:Al, absorpt. line broadening 78−95594
Si:Al, bound-exciton absorption 78−56507
Si:Al(In), acceptor levels, IR spectra 78−67972
Si:Au, IR absorption and elec. resist. meas., impurity centres 79−38580
Si:Au donor and acceptor centre obs. using IR absorpt. and dynamic nucl. polarisation with optical pumping 80−54639
Si:B, antiferromagnetic ordering of holes, recombination radiation polarisation *(Russian)* 80−45121
Si:B, ion implanted, laser annealed, Raman scatt., Fano interactions, lattice damage 79−78711
Si:B amorphous film, CVD prep., EPR, elec. and optical props. 79−4558
Si:B(Ga), IR spectra of acceptor levels 80−34953
Si:C, impurity determ. by IR absorpt. spectroscopy, room temp. and low temp. meas. comparison 80−108237
Si:F, amorphous alloys, RF sputtering prep. in SiF_4-Ar gas mixture, spectra 80−80772
Si:F,H, amorphous, elec. and optical props. 80−60031
Si:Ga, bound-exciton absorption 78−56507
Si:Ga, IR absorption of dopant centres, spectral depend. on doping, impurity conc. and temp. 80−76053
Si:Ga, LPE on Si, technique and characterisation 79−38751
Si:Gd, radiation defect form., effect of Gd impurities, elec. and optical meas. 78−71764
Si:H, amorphous, defect creation and H evolution 80−50392
Si:H, amorphous, glow discharge deposited, thermal dehydrogenation, IR spectra 80−44442
Si:H, amorphous, glow discharge deposited, laser annealing 80−49104
impurity and defect absorption spectra of inorganic solids continued
Si:H, amorphous, H content determ. by IR absorpt., gas evolution and nuclear reaction methods 80−44130
Si:H, amorphous, optical studies of excess carrier recomb., evidence for dispersive diffusion 80−76059
Si:H, amorphous, plasma-deposited, effect of DC elec. field superimposed during deposition 80−44643
Si:H, amorphous films, plasma-deposited, defect states, IR, ESR, and refractive index meas. 79−65944
Si:H, amorphous thin film, ion plating, IR absorpt. meas. 80−84857
a-Si:H, influence of H on optical props., H conc. and H bonds 80−76098
Si:H, new IR absorpt. bands 79−87472
a-Si:H, structural interpretation of vibr. spectra 79−69864
Si:H,F,O amorphous, plasma deposited, comp. and optical props. 80−50441
Si:H alloy, amorphous, dihydride model of vibrational spectra 80−80827
Si:H amorphous film, prop. by glow discharge deposition, and plasma parameter effects on props. 80−45240
Si:H amorphous film, sputtered in Ar-SiH_4 mixtures, props. 79−87023
Si:H amorphous film, sputtered IR vibr. spectra and photolum., effects of partial evolution of H 80−44413
Si:H amorphous films, role of Ar in deposition process, IR absorpt. and photocond. meas. 80−50321
Si:H amorphous glow discharge film, optical absorpt., near IR region 79−87518
Si:H amorphous sputtered films, optical gap, IR absorpt. meas. 80−50320
Si:H(B)(P), amorphous, UV absorpt. spectra 80−25420
Si:H(D), H-related defects, channelling and IR meas. 80−25422
Si:In, absorpt. spectra, impurity excited state lines 80−108243
Si:In, bound-exciton absorption 78−56507
Si:In, C, 0.111-eV acceptor level, X-level defect conc. from IR absorpt. and Hall meas. 79−51512
Si:In,P, photoinduced IR absorpt. and luminesc. 79−33828
Si:I, obs. of donor exciton in far IR transmission meas. 79−91477
Si:Mg, Zeeman effect of excitation spectrum of neutral donors 77−63439
Si:N(P), ion implanted, IR transmission and rel. spectra study 80−108244
Si:Na^+, inversion layer, far IR optical spectroscopy 80−20680
Si:Ni,Co,Mn, γ-irrad., interaction of deep-level impurity atoms with radiation defects 77−76457
Si:Ni,O, interaction of Ni with O, influence of heat treatment, IR absorption meas. 77−4667
Si:O, 9 μm absorpt. band attributed to dissolved O, from expts. on quartz particles 79−19914
Si:O, amorphous, sputtered, influence of O and deposition conditions 80−54693
Si:O, Czochralski crystal, oxygen striation and thermally induced microdefects 80−100275
Si:O, dislocation-free, Si-O complexes, heat treatment effects 77−62557
Si:O, IR absorpt. at low temp. *(Chinese)* 80−108228
Si:O, IR absorpt. spectra of Si:O complexes 78−19520
Si:O, impurity conc. profiles, scanning IR absorpt. using semicond. laser 80−50376
Si:O,C, electron irradiated, indirect vacancy-interstitial reco .b., IR absorpt. meas. 77−43209
Si:O,H amorphous, plasma-deposited, electronic and struct. props. 80−50391
Si:O film, near IR absorption, O impurity states 78−88333
Si:O film, near IR reflectivity at high temps. 78−56532
Si:O(C) wafers, impurity meas. by Fourier transform IR spectra 80−89030
Si:O(C) wafers, impurity meas. by Fourier transform IR spectra at low temp. 80−89031
Si:Os, P, photoelec. props., depend. on P conc. 79−91099
Si:P, absorpt. due to creation of bound excitons 78−23025
Si:P, heavily doped, glow-discharge-produced, elec. and optical props 80−2497
Si:P, IR absorpt. and D^--band 78−52533
Si:P, neutron transmutation doped, electron trap annealing, deep level transient spectra 78−14368
Si:P, satellite of bound excitons, transient decay 80−11466
Si:P, temp. depend. of anomalous struct. in wavelength-derivative absorption spectra 77−52143
Si:P film, polycryst., heavily doped, mobility and carrier conc., optical determ. 80−66314
n-Si:Pd, surface, photocond. and photo-emf spectra 79−73544
n-Si:Re diode photocapacitance spectra, Re centre dissociation 79−90997
Si:S(Se), IR absorption and photocond., donor levels 77−55809
Si-Au amorphous system, optical absorpt., IR photocond. 79−42582
Si-B amorphous film, plasma deposited, characterization 79−69828
Si-H, amorphous, plasma-deposited, H evolution and defect creation 80−44914
n-SiC (6H), doping effect on birefingence dispersion, effective electron mass 79−69807
SiC (6H), IR absorpt., UV illumination effects, defect levels 80−66251
α-SiC (6H), paramag. N impurity levels, IR absorpt. and ESR expts. 77−59598
SiC, electron trap depth, additional IR absorption induced by UV excitation *(Russian)* 79−78721
SiC ion implanted, laser induced ordering and defects 80−84754
SiC, struct. of spectrum of excitons bound to neutral B atoms 78−19523
SiC, synthesis by ion implantation of diamond, role of struct. imperfections 78−34529
SiC:B, electroabsorption, 0.35-0.45 eV, under UV illumination 79−4831
p-SiC:B (4H), absorption spectra of bound excitons 78−88338
α-SiC:H, prepared by reactive sputtering, layer props. *(Japanese)* 80−60695
SiC:Ti (6H), absorpt. spectra of n- and p-type cryst. 79−38581
n-SiC(6H), donor ground state splitting, IR spectra *(Russian)* 78−92104
SiH_1-like centres, in cryst. Si, vacancies and chem. trapping obs. 79−99916
a-$Si_{1-x}H_x$, oxygenated thin film, sputtered, elec. cond. and optical props. 79−15239
SiO_2, amorphous, optical and elec. props., comparison with chalcogenide semiconds. 78−6721
SiO_2 bricks, quartz estimation using IR spectra 78−48718

impurity and defect absorption spectra of inorganic solids continued
SiO_2, D-impregnated, vitreous, radiation induced isotope exchange 79−99240
SiO_2, E'-centre model, IR absorption spectra 79−37634
SiO_2 film, attenuated total reflectance study, impurity spectra 80−97311
SiO_2, fused, as-received and irrad., dielectric props. 79−65786
SiO_2, fused, γ-irrad., O-associated trapped-hole centres, optical absorpt. and ESR spectra obs. 79−65729
SiO_2, fused, high-temp. darkening and absorption spectra meas. 77−36258
SiO_2 glass, absorption spectrum of Nd^{3+} ion, chem. composition effects, group IV element effects *(Polish)* 78−10932
SiO_2 glass, optical props. of colour centres, intrinsic and modified defect states 79−60756
SiO_2, ion irrad., H capture, absorpt. bands *(Russian)* 78−76505
SiO_2, OH group interactions, IR and Raman spectra 78−80383
SiO_2, RF sputtered, stoichiometry and atomic defects obs. 79−60647
SiO_2, vitreous, Fe^{2+} absorpt. spectra in polarised light and struct. position 79−43007
SiO_2, vitreous, H impregnated, Raman spectroscopy 77−36230
SiO_2, vitreous, H impregnated, γ radiation effects, hydride, hydroxyl formation 79−87874
SiO_2, vitreous, hydroxyl free, reaction with H, diffusion, absorpt. spectra 80−85210
SiO_2, vitreous, intrinsic radiation defects, nonbridging O 80−19837
SiO_2, vitreous, substrate for PbO film, interdiffusion reactions, UV spectroscopy obs. 78−51750
SiO_2, vitreous, valence-attenuation pair defect, states, IR and Raman spectra 79−91442
SiO_2:Fe, vitreous and cryst., with or without Al_2O_3, Na_2O additions, exam. of Fe^{2+} coordination, IR spectroscopy 78−88344
SiO_2:Fe^{3+}, vitreous silica, absorpt. spectra and structural state 80−16071
SiO_2:GeO_2/SiO_2, SiO_2/SiO_2:B_2O_3, glass fibre waveguides, γ-radiation optical stability 80−23799
SiO_2:H(D), γ-irrad., hydroxyls and hydrides form., detect. by Raman scatt. 77−32817
SiO_2-Al_2O_3-Li_2O:TiO_2(ZrO_2),Fe_2O_3, pyroceramic glass, coloration, absorpt. spectra obs. 77−8615
SiO_2-GeO_2, synthetic, struct, IR spectra 79−42993
SiO_2-Na_2O-CaO:Fe(As)(Cr) glasses, optical absorpt. changes on heat treatment 78−31224
SiO_2-Si MOS system, ion irrad. effects on struct. and electrophysical props. 80−6995
SiO_2:B, P films doped by pyrolisis and ion implantation, IR absorpt. obs. of impurity conc. 77−72802
SiO_2 film, RF sputtered, stoichiometry and atomic defects obs. 79−90904
SiO_2:Ge, B, P, optical fibre, radiation induced optical absorpt. spectra, 0.4 to 1.7 μm region 80−58761
SnO_2, exciton luminescence spectra, absorpt. spectra 80−89064
$SrCl_2$:Cu^+, exciton bands, optical absorpt. and MCD spectra 80−80821
$SrCl_2$:Fe^{2+}(Co^{2+}) electronic absorption spectra in far and middle infrared 78−68537
$SrCl_2$:S, S_2^- and S_3^- mol. paramag. centres, investigation using EPR, Raman and optical spectroscopy 79−51855
SrF_2, 0.36 μ absorptance/fluence dependence obs. 79−15506
SrF_2, doped, far IR absorption spectra 78−76507
SrF_2, neutron irrad., role of F-centres in thermoluminesc. 79−19941
SrF_2, optical props. of cation colloidal particles 78−23503
SrF_2, U-centre, electronic struct. and optical transition energies, SCF MS Xα calc. 79−4532
SrF_2, undoped, H-centre prod. by reactor neutron irrad., optical absorpt. meas. 77−59010
SrF_2:Ce^{3+}, cryst. field energies 80−59941
SrF_2:CeF_3(GdF_3)(TbF_3), absorpt. spectra of γ-irrad. cryst., 77K, 200-700 nm 78−84615
SrF_2:Dy^{3+}, cluster form., IR absorption study *(French)* 80−108240
SrF_2:Na, tunable room temp. laser action of M-centres, luminesc. and absorpt. spectra 79−31907
SrF_2:Nd^{3+}, linear dichroism induced by electric field orientation kinetics of Nd^{3+} centres 79−69868
SrF_2:Pb^{2+}, band struct., Jahn-Teller effect, UV luminesc. and optical absorpt. spectra 80−66243
SrF_2:Pr, Nd, Tb, Dy, Ho, Er, Tm^{3+} far IR spectra 79−33736
SrF_2:Pr^{3+}, wavelength and temp.-modulated UV absorpt. 80−2799
SrF_2:R^{3+}, far IR vibr. spectra of F^- compensation ion 78−92059
SrF_2:R^{3+}, R=rare earth ion, hydrogenated, IR and EPR spectra meas. 77−69865
SrF_2:Sm^{2+}(Tm^{2+}), vibronic spectra and dynamics of impurity-contaiing lattice 79−1787
SrFCl, thermolum. and optical absorption spectra 80−66309
SrO, electronic struct. of V^- and related centres 80−2355
SrO:Co^{2+}, EPR, optical, MCD absorpt. spectra 78−43692
SrO:Ni, optical absorption spectra in visible and near IR region 80−45119
SrO:Ni^{2+}, linear Stark effect for zero-phonon optical absorpt. line 80−80830
$Sr_5(PO_4)_3Cl$:CrO_4^{3-}, polarised absorpt. spectra, visible and IR, ligand field transitions 79−95812
$SrSO_4$, celestite, colouring mechanisms 79−82998
$SrTiO_3$ and $SrTiO_3$:Nb, reduced samples, optical absorpt., effect of impurity-O vacancy complex *(Korean)* 79−8163
$SrTiO_3$, monodomain, O-D and O-H stretching vibrs., IR spectra 80−71449
$SrTiO_3$, pure and Nb doped, heat treated, Hall effect, electrical cond., optical absorpt., defect states 78−47812
$SrTiO_3$, tetragonal, effect of impurities on Raman spectrum 80−2770
$SrTiO_3$:Cr^{3+}, radiationless relax., photoacoustic spectra 78−27264
$SrTiO_3$:Eu(Sm), absorption spectra, Ti^{3+} ion and Z-centre formation 77−24871
$SrTiO_3$:Fe^{4+}, opt. absorpt. 77−16349
$SrTiO_3$:H(D), controlled doping, IR spectra 79−28007
$SrTiO_3$:Ni, photochromism, optical absorption spectra and EPR meas. 77−1708
$TbAlO_3$:Nd^{3+}, absorpt. and luminesc. spectra 79−91470
$Tb(OH)_3$:Er^{3+}, ferromag., anisotropic exchange effects in optical spectra 78−80141
Te, impurity spectroscopy 80−65499
Te, intervalence band absorption, press. and defects influence 80−55149
Te, negative photoconductivity, intraband absorpt. *(Russian)* 80−107854
impurity and defect absorption spectra of inorganic solids continued
Te, screw-dislocation-induced scatt. and acceptor states, galvanomag. and optical expts. 77−28142
TeO_2-Li_2O glass:Nd^{3+}, highly doped, spectroscopic props. and CW laser action *(French)* 79−41385
$ThBr_4$:U^{4+}, absorpt. spectrum, zero phonon line *(French)* 80−11443
$ThBr_4$:U^{4+}, single cryst., absorpt. and emission spectra 77−90174
$ThSiO_4$:U^{4+}(U^{3+}), opt. spectra 78−88334
Ti^{4+}, valence transition in fluorphlogopite, ESR and optical absorption data 77−16155
TiO_2, chemical implantation of 10-keV H^+ and D^+, resist. and optical absorpt. expts. 77−59031
TiO_2 electrode, carrier density determ. by optical absorpt. and photoelectrolysis spectra 80−71462
TiO_2, exciton luminescence spectra, absorpt. spectra 80−89064
TiO_2, K^+ implantation, extended defects and precipitates 80−49251
TiO_2, room temp. coloration by diffused Na and H from Na amalgam 78−84611
TiO_2, rutile, deuteron and alpha-particle implantation, chemical effects, optical and cond. meas. 78−67755
TiO_2:Cu, anodic, effect of Cu on optical props., rel. to possible appl. in solar energy conversion 80−16115
TiO_2:H(D)(T), IR spectra, 300, 77 and 8K 78−35175
TiO_2-SiO_2, semicond. glass, optical props. 78−60412
TlI coatings on KCl laser windows, photoacoustic spectroscopy 80−33052
V (d^3) in II-VI semiconductors, absorption and luminesc. spectra 78−15203
V_2O_5 and lower oxides, defect structures and related props. 80−59454
α-V_2O_5:Li(Na)(Cu), far IR absorption spectra meas. 77−73158
WO_3 electron density map of W^{5+} polarons, EPR and optical absorpt. obs. 80−44912
WO_3 film, optical absorpt. after ion irrad., appl. to ion beam profile monitoring 79−26181
WO_3 films on Si, sapphire, glass and metal substrates, colour intensity dependence obs. *(Russian)* 80−2430
WO_3, thin films, electrochem. coloration, optical and elec. props. 77−85345
WO_3:H^+, optical and elec. props., suggested band struct. model 77−4654
WO_3-electrolyte electrochromic cells, proton injection phenomena 80−71448
Xe, optical excitation of rotational transition of methane, 6K 78−60494
YA-O_3:Er^{3+}, pulsed laser action, $^4S_{3/2}$ to $^4I_{9/2}$ transition laser action, optical and luminescence spectra 80−16082
YAG, colour centres conceived as bound polarons 78−63990
YAG, optical absorption of hole centres, polaron model 80−97314
YAG, rare earth impurity, spectral probe of stoichiometry variations 77−85790
YAG, transient colour centres caused by UV radiation 77−84744
YAG:Ce^{3+}, excited-state absorpt. meas., tunable laser model system 79−42994
YAG:Ce^{3+}(Tb^{3+}), recomb. processes, spectral, kinetic and relative quantum intensity meas. 79−61443
YAG:Cr^{3+}, absorption and luminesc., spectra, Cr conc. depend. 77−12435
YAG:Cr^{3+}, cryst. field pot. expansion 77−36268
YAG:Cr^{3+}, radiation colour centres, absorpt. and thermolum. spectra 78−48206
YAG:Er^{3+}(Ho^{3+})(Tm^{3+}), oscillator strengths of impurities, 5000 to 30000 cm^{-1} 79−4830
YAG:Mn, impurity-induced O^- colour centres, absorpt. and fluoresc. spectra 77−1709
YAG:Nd,Ce,Cr, effect of γ-rays, fast electrons on optical props., annealing and colour centre destruction 77−8608
YAG:Nd^{3+}, Ce^{2+}, sensitisation, luminesc., absorpt. and emission spectra *(Russian)* 78−10982
YAG:Nd^{3+} and free Nd^{3+} ion, energy levels, absorption spectra 79−11076
YAG:V_2O_5, CaO, V^{4+} ion impurity spectral anal. 79−78719
$YAlO_3$, $YAlO_3$:Nd, colour centre form. rel. to growth conditions, absorpt. spectra 79−90652
$YAlO_3$:Pr^{3+}, ultrahigh resolution photon echo spectroscopy 80−28285
$YAlO_3$:Yb^{3+}, absorption and luminescence spectra, electron-phonon resonances, Stark splitting *(Russian)* 80−20674
$Y_3Al_5O_{12}$:Nd^{3+}, absorpt. spectra dependence on press. *(Russian)* 77−52183
YGG, YGG-ErGG, rare earth impurity, spectral probe of stoichiometry variations 77−85790
$Y_3Ga_5O_{12}$:Fe^{3+}, impurity absorpt. spectra to 5.5 eV 77−20892
$Y_3Ga_5O_{12}$:Nd^{3+}, $YGaO_3$:Nd^{3+}, spectroscopic characts. 77−12427
$Y_3Ga_5O_{12}$:Tb^{3+}, fluoresc. and absorption spectra 77−32422
$(Y_{0.8}Gd_{0.2})AlO_3$:Er^{3+}, spectroscopic props. 77−85791
$Y_{1-x-c}Gd_xNd_cScO_3$, crystal, absorption, luminescence, stimulated emission spectra 78−15220
YIG, Bi-substituted, LPE film, optical absorpt. changes due to impurity incorporation 77−1702
YIG, impurity absorpt. spectra to 5.5 eV 77−20892
YIG: Ca^{2+} epitaxial films, Fe^{4+} centres, MCD, optical absorpt., and thermoelectric power meas. 78−95595
YIG:B,Pb, IR spectrum, localised modes, rel. to impurities and O vacancies 80−50377
YIG:Ir, Ir on tetrahedral sites, contrib. to mag. anisotropy, optical absorpt. meas. 77−69867
YIG:Nb, tetrahedral Fe^{2+} detect. by induced anisotropy ang. variation 79−11311
YIG:Ru, optical absorpt. and MCD obs. of Ru^{4+} site occupancy 80−71456
YIG:Sn, mag. circular dichroism orientation depend., optical absorpt. 79−99914
Y_2O_3, formation and changes in point defects, EPR, optical transitions and thermolum. spectra 78−2118
Y_2O_3:Eu^{3+}, absorpt. spectra, fluoresc., electron beam excitation 78−92093
Y_2O_3:Nd^{3+}, absorpt. spectra, hypersensitivity of $^4I_{9/2}$ to $^4G_{5/2}$ $^2G_{7/2}$ transition 80−97309
Y_2O_3:ThO_2, IR absorpt., 2-4 μm 77−55805
YPO_4:Ce(Tb), luminesc. and optical spectra 79−65921
YVO_4:Bi^{3+}, absorpt. and emission props., excitons 77−38592
YVO_4:Eu, cluster electron struct., X-alpha calc., emission spectra 78−2898

impurity and defect absorption spectra of inorganic solids continued
$YVO_4:Eu^{3+}$, absorption and fluoresc. spectra, SU(2) chain *(French)* 78−28912
$YVO_4:Eu^{3+}$, absorpt. spectra, fluoresc., electron beam excitation 78−92093
$YVO_4:Nd^{3+}$, absorption and fluoresc. spectra of laser states 77−38900
$YVO_4:Nd^{3+}$, optical absorption intensities 79−24335
Yb^{3+} doped phosphors, IR excitation and absorpt. and emission spectra *(Russian)* 79−52021
Yb^{3+}:phosphate glass, relation between absorption and equilib. luminesc. spectra 77−85754
$Zn_{0.1}Cd_{0.9}S$, two-photon and two-step absorption of light 80−7389
$Zn_{0.1}Cd_{0.9}S$:Cu, doping effect on two-photon absorpt. spectra, deep levels 77−69870
$Zn_xCd_{1-x}Te$-P, vibr. modes of defects, IR absorpt. expts. 77−62601
$ZnCs_2(SO_4)_2.6H_2O:VO^{2+}$, optical absorpt. spectra obs. 80−40146
$ZnGeP_2$, electron irrad., elec. and optical props. 79−33743
$ZnGeP_2$, P vacancies, lattice parameters, optical props. depend. on thermal treatment *(Russian)* 78−71729
$ZnO:Co^{2+}$, polarised optical absorpt. spectrum, crystal field transitions 77−48206
ZnO:Cu, excited state, zero phonon lines in emission and Zeeman spectra 79−38026
ZnO:Cu, H(D), IR absorpt. line spectra, OH and OD vibr., optical excitation 79−15498
ZnO:Cu, H(D), OH and OD centres, IR-active absorpt. line spectra 79−15496
$ZnO:Cu^{2+}$, electronic struct., optical absorpt. and ESR 79−87312
$ZnO:Ni^{2+}$, Zeeman effect at Ni impurities 80−60633
$ZnO-B_2O_3:Cu^{2+}$, glasses, ESR and optical absorpt. 80−34760
ZnP_2:In(Ga)(Ge)(S)(Se), doped and undoped, optical absorpt. spectra in range 0.5 to 2.2 eV 80−66250
ZnS, additively coloured or neutron irradiated, near IR emission 77−90199
ZnS, high-resist., optical transmission thermal processing effects 77−63431
ZnS phosphor, deep capture centres obs. 78−10951
ZnS single cryst. distrib. coeffs. of transition metals, Pb and Sn 77−55298
ZnS:Al, IR studies of Al complexes 79−33741
ZnS:Al-Cu, localised vibrational modes 78−63827
ZnS:Be, far IR lattice absorpt., Green's function calc. 78−43865
ZnS:Be, impurity modes and IR absorption 78−76506
ZnS:Cl, single cryst., deep centre study by impurity electroabsorpt., photocond. meas. 77−12411
ZnS:Cr, anomalous temp. depend. of near IR absorption 79−28794
$ZnS:Cr^{2+}$, photoionisation, lattice relaxation energy 80−6778
ZnS:Cu 79−24350
$ZnS:Eu^{3+}$, origin of red fluoresc., occurrence of rare earth oxysulphide inclusions *(French)* 77−69875
ZnS:Fe, piezospectroscopic effect on electron-vibr. lines of Fe^{2+} 78−27269
ZnS:Ga(Cl), deep traps, impurity electroabsorpt. and photocond. meas. 78−6707
$ZnS:Mn^{2+}$, $^4T_2$ level, Zeeman splittings, Jahn-Teller effect 80−40141
$ZnS:Mn^{2+}$, heavily doped, anomalies in reflectivity 77−20891
$ZnS:Mn^{2+}$, Jahn-Teller effect in fluorescent level 78−52566
ZnS:Ni, IR luminesc. and absorpt. spectroscopy 80−108261
$ZnS:Ni^{2+}$, Zeeman effect at Ni impurities 80−60633
ZnS-CdS system, IR luminesc. and absorpt. centres, donor-acceptor pair model 77−44043
ZnS-O, single cryst., fast neutron irrad., optical props. 78−27331
ZnS(Se)(Te):Cr^{2+}, absorpt. and luminesc. of $Cr^{2+}(d^4)$, cryst. field theory interpretation 79−83000
ZnSe, CVD, laser window material, impurity absorpt. meas. 78−25909
ZnSe crystals, doped and undoped, optical absorption edge 80−60626
ZnSe, electron irrad., short-lived optical absorpt. 79−51989
ZnSe, impurity effects on two-photon absorpt. spectrum 77−59597
ZnSe, reson. absorpt. of coherent IR radn. by acceptors, photocurrent and emission spectra 79−73974
ZnSe, two-photon and two-step absorption of light 80−7389
n-ZnSe:Al, free carrier absorpt., 80-300K 77−63432
ZnSe:Co, effect of in-band position of states on photoelec. props. 78−23132
ZnSe:Co, optical props. in near IR 78−43924
$ZnSe:Co^{2+}$, depression of vibronic levels, transition of Jahn-Teller states from dynamic to static 78−43337
$ZnSe:Cr^{2+}$, photoionisation, lattice relaxation energy 80−6778
$ZnSe:Cr^{2+}$, stress-induced alignment of Jahn-Teller centres 79−78651
ZnSe:In, optical absorpt. spectrum, 0.4 to 0.7 μm 77−81136
ZnSe:Li(Na)(Ga) doped and pure cryst., donor-acceptor bands 80−11465
$ZnSe:Mn^{3+}$, Jahn-Teller effect in fluorescent level 78−52566
$(ZnSe)_{1-x}(GaP)_x$, two-photon absorpt. at ruby laser freq., clarification *(Russian)* 79−15505
ZnSe(Te), photolum. excitation spectra of tightly bound holes, valence band contrib. 80−60658
$ZnSiAs_2$, electron irrad., defects, elec. and optical props. 79−19282
ZnTe, doped with group I impurities, fluorescence spectra meas. 78−10949
ZnTe, nonlinear absorpt., temp. depend. *(Russian)* 77−20899
ZnTe, real structure effect on luminescence and absorption spectra, dislocations 80−16085
ZnTe, refined, undoped, Cu acceptor, optical absorption and photoluminesc. meas. 80−34970
ZnTe: group I element, absorption saturation *(Russian)* 78−35183
ZnTe:Ag, containing dislocation loops, optical absorption-edge fine struct. 78−43905
ZnTe:Ag, real structure effect on luminescence and absorption spectra, dislocations 80−16085
ZnTe:As(P)(Li), binding energy of shallow acceptors from photoluminesc. excitation spectra for donor-acceptor pairs 79−95809
ZnTe:As(P)(Li), electronic Raman scatt. and IR absorpt. spectra of shallow acceptors 79−73978
ZnTe:Au, impurity identification and characterisation, capacitance, luminescence and IR absorption 80−60639
ZnTe:Cr(Mn)(Fe), exciton refl. spectra 80−2806
ZnTe:Cu, red centre, electric and optical props. 80−20239
ZnTe:In(Al), pure and doped, Zn vacancy energy levels, elec. and optical props. 79−4827

impurity and defect absorption spectra of inorganic solids continued
ZnTe:P, pure and doped, electron and exciton excited states of neutral donor 80−34393
ZrF_4-ThF_4-$BaF_2:V^{3+}(Cr^{3+})$ glasses, absorpt. spectra *(French)* 79−99918
ZrO_2, cubic single crystal, colour centres 77−15410
ZrS_2, intercalation-induced shift of absorpt. edge 79−82999
$ZrSiO_4:U^{4+}(U^{5+})$, opt. spectra 78−88334

impurity and defect absorption spectra of solids
see also impurity and defect absorption spectra of inorganic solids
activated crystals, influence of temp. on energy transfer 79−28323
activated crystals, Jahn-Teller effect in optical bands of impurity centres 78−6706
adsorption spectroscopy of adsorbed atoms, plasmon satellites and relax. shifts 77−59204
alchohols, glassy, spectra shift of trapped electrons, after γ-irrad. 79−78709
alcohols, trapped electron spectral relax., random-walk model 78−60493
alkali halide:Ag film, EPR and optical exam. of Ag impurity centres 77−85562
alkali halides: $SCN^-(CNO^-)$, absorption bands temp. depend. *(Russian)* 77−77260
anharmonic molecules in condensed media, vibronic dephasing, intra- and intermolecular processes 80−2127
anisotropic condensed system, dipole-inductive interactions rel. to impurity spectra *(Russian)* 78−31225
anisotropic media, molecular distrib. determ., using polarised absorption and emission spectroscopy 78−27298
anthracene:2-aminoanthracene, polarised guest absorpt. spectra, transition dipole moment direction, cryst. packing 77−8610
anthracene:cyclohexadienyl type radicals, charge transfer reactions 78−52535
anthracene:tetracene, absorpt. spectra, energy transfer over highest vibronic levels 79−65904
anthracene:tetracene, electronic absorpt. spectrum, host-cryst. field effect 80−100669
anthracene:tetracene, upper excited vibronic states optically pumped energy transfer matrix fluoresc. 78−76512
anthracene, monocryst., additional absorpt. spectrum at low temp. 78−92096
antiferromagnet, IR absorption on impurity excitations near upper edge of spin-wave band 80−80829
antiferromagnetics, with displaced 3d-ions, mech. of electric dipole absorption of light *(Russian)* 77−32406
antiresonant electron-phonon system, in strong-coupling limit, moments and absorption line shape 77−24875
apatites, condensation of tetrahedra, IR absorpt. band exam. 77−85760
aromatic hydrocarbons, in organic glasses, nonphotochemical burning, impurity site relaxation 78−25548
atom pairs in solids, cooperative two-photon absorpt. lineshape 80−84706
band shapes, Poisson distrib. moments 80−25419
bandshapes, moments, absorption and emission spectra of impurities in solids 80−45122
benzene cryst., electron irrad., phenylcyclohexadienyl radical form., absorpt. and fluoresc. spectra study 80−89035
benzene-d_6:benzene-d_0, phonon side bands of specular optical transitions 78−26649
benzened_0:phenol, phonon side bands of specular optical transitions 78−26649
benzophenone: diphenylmethylene, mixed cryst., emission and absorpt. spectra, 2-30K, excitation-phonon coupling 79−99900
1, 12-benzperylene, in alkane matrices, zero-phonon lines, press. shifts *(Russian)* 78−76502
biphenyl:tetracene, electronic absorpt. spectrum, host-cryst. field effect 80−100669
biphenyl single crysts., γ-ray induced radicals, EPR and optical absorpt. studies 80−44921
bis(p-toluene sulphonate) diacetylene, partially polymerised, defect-induced absorpt. and fluoresc. 77−44030
CaF_2:Na, Stark effect on Na disturbed F_2-centres 77−69279
calcium tartrate tetrahydrate:Cr^{3+}, optical absorpt. spectrum, cryst. field parameters 80−16067
calcium tartrate tetrahydrate:Cu^{2+}, spin-orbit coupling, optical absorpt. spectra 80−45120
calcium tartrate tetrahydrate:Ni^{2+}, optical absorpt. spectrum 78−84610
calcium tartrate tetrahydrate:VO^{2+}, optical absorption spectrum 78−6713
carbazole:tetracene, electronic absorpt. spectrum, host-cryst. field effect 80−100669
o-chlorobenzoic acid: $Nd^{3+}(Pr^{3+})$ solid, vibrational spectra 80−84758
p-chlorobromobenzene, spectral meas. of static interaction changes in molecular crystals *(Ukrainian)* 78−6708
p-chlorobromobenzene in p-dichlorobenzene cryst., absorpt. spectra, mol. clusters static interaction 78−15198
colour centres, absorption wavelength, finite-pot. well models 78−12463
Condon approximation, shape of absorpt. and fluorescence bands, effect of electron-phonon coupling *(Russian)* 77−48212
coronene, in alkane matrices, zero-phonon lines, press. shifts *(Russian)* 78−76502
crystal, impurity, light absorpt. max. at Brillouin zone boundary 80−55139
crystal impurity centres, quadratic Stark effect, quantum mech. band shape calcs. 77−69863
crystal localised centres, inversion symmetry, Stark effect in wideband, electronic-vibr. spectra 77−69864
crystal with long range impurity states, vibr. spectrum *(Russian)* 80−6478
crystals, dipole-impurities, HF elec. cond., dielec. losses and light absorption 77−63363
cubic crystals, electrooptic absorption of anisotropic Jahn-Teller centres 78−27188
cyclodextrin, trapped electrons in cryst. matrices, ESR, optical absorption spectra 78−80768
deep impurities, charged, photoionisation allowing for Coulomb interaction 77−15793
diamond, radiation-induced optical absorption spectrum, 0.4-2.0 MeV electrons 77−84798
p-dibromobenzene, in p-dichlorobenzene cryst., absorpt. spectra, mol. clusters static interaction 78−15198

impurity and defect absorption spectra of solids continued
p-dibromobenzene, spectral meas. of static interaction changes in molecular crystals *(Ukrainian)* 78−6708
p-dichlorobenzene, spectral meas. of static interaction changes in molecular crystals *(Ukrainian)* 78−6708
3,6-dichloropyridazine, liq. and solid soln. spectra, fundamental freqs. and assignments 80−5541
dielectric medium, impurity dispersion self energy calcs. 78−52536
dielectric thin films, electron beam deposited, anomalous optical absorpt. 77−20947
diglycine barium chloride monohydrate:Cu^{2+}, optical absorpt. and EPR, lattice sites, hybridisation 77−43872
disordered crystal, biphonon spectra, light absorpt. coeff. and density of states, CPA calc. 80−84271
dispersive medium, many-photon scatt. of light by impurity centres 80−60622
dispersive medium, QED and multiphoton processes at impurity centre *(Russian)* 78−71141
doped cubic crystals, resonance absorption region, self-induced rot. of polarisation 80−2805
durene, mol. cryst., Stark effect origins, point dipole approx. soln. 77−77252
electroabsorption, and negative ion photodestruction in elec. field 77−20897
electron beam irradiated crystals, optical absorption and luminesc. meas. apparatus *(French)* 77−26378
electron localisation, evolution of optical spectra 77−90173
electron-phonon coupling from structured optical spectra, review 80−89038
electron-vibrational transitions in presence of several minima of adiabatic potentials 77−81150
energy percolation is multicomponent solids 77−31972
ethanol glass, trapped and solvated electrons produced in presence of applied electric field 80−7379
ethanol glasses containing anion radicals of fluorene and isologs, γ-irrad., optical absorpt. and EPR obs. after photobleaching 77−44491
ethylene, isotopically mixed, crystal, dilute guest probe orientational energy, IR, Raman spectra 78−68496
exciton absorption spectra, dislocations effect on band profile 80−16070
exciton-impurity interaction rel. to absorption band shape *(Russian)* 77−52146
Faraday rotation and dispersion associated with point-imperfections 78−19449
fluorene, photoconductive props., sample purity depend. 78−10508
hexagonal crystal, orientational degeneracy of anisotropic centres 79−73981
HMPA:alkali metal, density of states in band gap, EPR and optical correlations 79−61201
1-hydronaphthyl radical, in naphthalene single cryst., anisotropic oscill. strength 78−50591
hydroxyquinones, H-bonded, zero-phonon photochem., hole burning obs. 79−11802
impurity ion clusters in a two-dimensional lattice 78−23047
indoles, in glassy hydrocarbons, complexation vs. aggregation, absorption and fluoresc. obs. 79−98132
inhomogeneous solid, determ. of homogeneous impurity spectra 79−73982
inhomogeneously broadened spectra, dip contour saturation *(Russian)* 78−76503
interband optical absorption in solids, effect of impurity 79−38577
intercombination transition intensities in strong crystal fields, symmetry reduction method 78−84175
Jahn-Teller impurity centre, electroabsorption moments 77−48205
Jahn-Teller impurity centres, piezo-optics and magneto-optics 78−39579
Jahn-Teller problem, $T \times \varepsilon_g$, spin-orbit allowed tunnelling splitting, zero-phonon line splitting 78−19006
lanthanum ethyl sulphate nonahydrate:Pr^{3+}, 400-700 nm, 78K, 22 kbar press. effects 77−81133
line shapes, quantum-mechanical moments 78−72566
local vibration Fermi resonance, lattice with two-phonon spectrum 78−18723
localised centres in strong EM fields, multiquantum transitions 78−10936
magnetic circular dichroism 77−8556
magnetic crystal, with impurity centre, anomaly of width and lineshape of light absorpt. 78−76499
magnetic impurity ion in mag. ordered cryst., optical absorpt., exchange interaction effects 77−16355
many-valley semiconductor, two-photon transitions from deep neutral impurity centres, light absorpt. and drag effect 79−91478
methyl iodide, biexciton states, IR absorpt. exam. 77−89714
methylcyclohexane, trapped electron charge distribs., optical transitions 77−28139
3-methylpentane, trapped electron charge distribs., optical transitions 77−28139
2-methyltetrahydrofuran-methanol mixed glasses, annealed, γ-ray produced electrons transfer from IR to bisible traps 80−11440
mixed diatomic system, depend. of fine struct. on short-range order parameter 79−51991
molecular crystal, exciton scatt. by lattice defects, absorpt. line shape 79−38576
molecular crystal, high power light pulse coherent interaction with exciton-impurity centres 80−55146
molecular crystal, impurity reson. interaction effects 77−1396
molecular crystal, polar guest, stark shift, point-dipole approx. 77−1701
molecular crystal, sensitised luminesc. calc. for trapping models using momentum-space theory of exciton transport 80−11447
molecular crystals, effect of intermol. interaction of impurity on spectral props. 78−27268
molecular crystals, spectroscopy, bibliography for 1976 78−72585
multi-phonon processes due to absorption at localized centres in noncond. cryst. 78−27278
multiphonon effects on dispersion, Faraday rot., associated with point imperfections 78−43839
multiphonon nonradiative transition rates, quadratic impurity-phonon coupling 78−23506
naphthalene:1-hydrodynaphthyl, cryst., charge transfer optical transitions 77−44027
naphthalene:tetracene, electronic absorpt. spectrum, host-cryst. field effect 80−100669

impurity and defect absorption spectra of solids continued
naphthalene, β-naphthol impurity mol. distrib., spectral obs. *(Russian)* 79−82253
naphthalene, cryst., vibronic absorpt., impurity-vibronic spectrum, two-phonon spectra 79−4817
naphthalene, doped, zero-phonon lines and absorpt. spectra, temp. depend. of shift and broadening 79−69866
naphthalene, mol. cryst., Stark effect origins, point dipole approx. soln. 77−77252
naphthalene molecule in durene and xylene crystals, vibronic interactions 80−84755
naphthalene-β-naphthol, concentration effects in exciton absorption region 80−108241
naphthalene-β-naphthol mixed mol. cryst., multiplet struct. of electron absorption spectra 77−1706
naphthalene-d_4(d_8) crystal, with isotopic impurities, Rashba effect, luminescence spectra, impurity states 80−29768
naphthalene-d_8:β-methylnaphthalene-d_{10}, phonon side bands of specular optical transitions 78−26649
naphthalene-d_8:naphthalene, symmetry reduction obs. of deformed crysts. by absorbt. spectrum method 79−15504
β-naphtholate in methanol-methyltetrahydrofuran glasses, electron solvation, laser flash photoionis. compared with pulse radiolysis 79−74405
p-nitrobenzoic acid:rare earth laser materials, vibr. spectra, wavelength 125 to 500 mm 80−2769
non-equilibrium phonon distrib., in cryst., spectral line shape theory 80−60530
nonradiative decay, impurity ions and molecules in solids, book 80−2858
O-O absorption line for quasimolecular centres, effects of reson. laser radiation 78−6728
optical fibres, glass and plastic, neutron irradiated, optical absorpt. spectra 0.7 to 1.1 μm 80−58762
organic compounds, inhomogenously broadened absorption spectra, linear struct. detect. *(Russian)* 78−76504
organic molecular crystal, doped, two-particle electronic excitation, optical cooperative excitation 80−93368
palladium porphin, in n-alkane crystal, Zeeman and crystal field effects, absorpt. vibr. anal. 80−7372
palladiumporphin, in n-alkane, $S_1 \leftarrow S_0$ absorpt. spectrum, vibronic coupling and avoided crossing, field splitting 78−84613
pentacene in naphthalene crystal, relax. of vibronic states, photon-echo and ab absorpt. relax. expts. 79−95807
perylene, solid soln. in ethanol, fine struct. in absorpt. spectra, laser technique 77−90178
phthalimide derivatives, hidden vibr. band determ. method, fluorescence and excitation spectra meas. 80−40158
phthalocyanine-halogen complex, influence of halogen on elec. and optical props. *(Japanese)* 79−51586
point defects, Urbach's rule 79−91474
polarised light absorpt. spectra, forbidden transitions and discrete saturation 80−71464
polyacetylene, lightly doped, donor and acceptor states, IR absorpt. obs. 79−73979
polydextran, γ-irrad. frozen gel, electron trapping, EPR and optical obs. 78−20030
potassium oxalate monohydrate:VO^{2+}, cryst., IR absorpt. 80−55134
pressure effects of optical spectra of impurity centers in solids 80−108231
PVC film, metal doping effect on chain vibrs. 79−95868
quadratic electron-phonon interaction and impurity-ion band shape in impurity absorption and fluorescence spectra 78−6731
quadratic Stark effect in crysts. with wideband absorption spectra, semiclassical approx. 77−66526
quantum system interacting with nonequilibrium phonons, light absorption props. 78−88340
quinoxaline in durene (naphthalene) crystal, Stark effect, space charge, local field tensor and dipole moment 77−28601
quinzarin in alcohol glasses, electron-phonon coupling, photochemical hole burning 80−97265
radiative electronic transitions of impurities, effects of hydrostatic press. 80−11446
Raman scattering by impurity centre pairs, possibility of cooperative effects 78−60449
resonance Raman profile with consideration for quadratic vibronic coupling 80−55099
resonant localised impurity vibrs. at finite temps., spectral distrib. 77−7814
resonant scattering at impurity centres in solids *(German)* 80−7377
ruby, optical detect. of 10^{12} Hz acoustic phonons 77−36272
semiconducting solid solutions, optical transitions, review 78−2908
semiconductor, absorption in mag. field and resonant laser radiation 77−52145
semiconductor, absorption line profile in static elec. field, effect of impurities 78−92101
semiconductor, Coulomb screening influence 78−72568
semiconductor, deep impurity centres, elastic light scattering 80−97315
semiconductor, donor van der Waals interactions, spectral lineshapes 80−11450
semiconductor, donor-acceptor system, weak wave absorpt. in reson. laser radiation field 80−66252
semiconductor, doped, metal-insulator transition, anal. 80−88478
semiconductor, exciton absorpt. line shape calc. *(Russian)* 78−10934
semiconductor, extrinsic, resonance transitions between ground states of donor and acceptor impurities 80−45126
semiconductor, H^--H^+ type impurity complexes, spectra, and pseudointeractions of mol. energy levels *(Russian)* 78−92100
semiconductor, impurity study by visible and far-infrared laser spectroscopy 77−74524
semiconductor, intense light absorption by deep impurity electrons 77−69871
semiconductor, interimpurity absorption in strong EM wave field *(Russian)* 80−60631
semiconductor, ionisation energy of deep centres from absorpt. spectra, electron-phonon coupling 77−4663
semiconductor, nonlinear light absorption, influence of transition via deep impurity centres 77−63446
semiconductor, photocurrent spectra investig. of fund. absorption edge 77−4397
semiconductor, shallow donor states exam. by two photon spectroscopy 79−23925

impurity and defect absorption spectra of solids continued
semiconductor, strongly compensated, H-like impurity wavefunction overlap effect on optical absorpt. spectrum 77−8613
semiconductor, wave functions and optical cross sections associated with deep centres 78−34801
semiconductor, weakly polar, IR absorption by optical polaron in mag. field 77−66127
semiconductor or insulator, impurity optical spectra, p-phonon processes 80−16061
semiconductor thin quantised wire, with charged defects, interband light absorption *(Russian)* 77−59593
semiconductor with highly anisotropic bands, photoionisation cross section of deep impurity centres 78−56510
semiconductor with impurties, light absorpt. *(Russian)* 79−47484
semiconductor with superlattice, optical absorpt. by impurities 79−69867
semiconductors, deep impurity centres, photon drag effect in interband optical transitions 80−16069
semiconductors, impurity electro- and magnetoabsorpt. coeffs., deep levels 79−24340
semiconductors, impurity-induced free-carrier magnetoabsorption 79−42950
semiconductors, localised transition metal impurities, lattice relaxation in optical transition *(Polish)* 80−70345
semiconductors, luminescence and absorption spectra calcs. 79−99938
semiconductors, shallow impurity centre spectra, isotopic shift of zero-phonon lines 80−66249
semiconductors, weakly polar, free polaron IR absorpt. effect of DC field 77−81132
semiconductors materials testing deep-level transient spectroscopy appl., using HP-IB instruments and desk-top computer 80−37091
solid solutions, impurity centres, internal mol. vibrs., inhomogeneous band broadening 78−92103
strongly coupled Jahn-Teller system, cluster model for optical absorption spectrum 80−89034
strontium formate dihydrate:Cr^{3+}, optical absorption spectrum 80−50380
strontium formate dihydrate, EPR and optical absorption spectra of VO^{2+} ion 77−40112
TGS:Fe^{3+} and aq. soln., optical absorpt. spectra 79−82997
TGS, effect of Fe^{3+} admixture on phys. props. 80−76052
transition metal ions, in solid, nearly degenerate electronic levels, dynamical effects 78−68535
transition metal ions in crystals, thermal broadening and shift calcs. 77−48208
tris sarcosine calcium chloride:VO^{2+}, EPR and absorpt. spectra 78−60330
tunnel centres, resonant optical orientation, kinetic eqn. *(Russian)* 78−43911
xanthene dyes, hidden vibr. band determ. method, fluorescence and excitation spectra meas. 80−40158
zero-phonon impurity lines in absorption and fluorescence spectra, temp. broadening and shift 77−8643
zero-phonon transitions, spectral characts. 78−2884
zinc porphin, in n-alkane crystals. at 4.2K, Zeeman spectra for Jahn-Teller instability 78−27256
Al_2O_3, neutron irradiated, electron centres, optical spectra exam. 77−63440
CaF_2:Eu^{2+}, two-photon absorpt. spectra exam. of excited state of Eu^{2+} 77−77261
CdS, substitutional Ti^{2+} centres, linear electroabsorpt. 77−66525
$CdSiP_2$:Fe, EPR and optical absorpt. of Fe^{+}, Fe^{2+}, Fe^{3+} and Fe^{4+} on tetragonal sites 77−8397
Cl_2, Ar matrix, vibronic dephasing 80−6469
n-GaAs, epitaxial, ionised donor pair spectrum 77−63477
GaAs, nonlinear light absorption, effect of deep impurity levels 77−77259
GaAs:Co^{2+}(Ni^{3+}), mag. and optical props. 78−10763
GaAs:Cr, IR absorpt. determ., emissivity meas. 77−63421
GaP, radiation defect accumulation due to ion bombardment, optical absorpt. meas. 77−76438
GaSe, exciton absorpt. spectra, additional light wave 77−63445
$Gd_2Gi_2O_7$:Nd^{3+}, spectroscopic props. 77−69866
$Gd_2(MoO_4)_3$, cryst. field parameters for Gd^{3+} 77−66142
$Gd_2(MoO_4)_3$:Nd^{3+}(Dy^{3+}), cryst. field parameters 77−66142
n-Ge:O, Czochralski growth, O content rel. to props., IR, Li precipitation determs. 77−15445
InSe, exciton absorpt. spectra, additional light wave 77−63445
KBr and KBr:Sr X-irradiated, optical investig. of Br_3 centres 77−16348
KCl, photoconductivity during F→X transition *(Russian)* 77−43663
KCl:Pb, additive coloration 77−68967
$KMgF_3$:V^{2+}(Cr^{2+})(Fe^{2+}) 3d→4d absorpt. band exam. 77−63435
LiF:Mg, X-irradiated, Z_1-centre exam. 77−68968
$Li_{1-x}Rb_xI$, intrinsic optical absorpt. spectra 78−23500
MgF_2 crystal, $M(D_{2h})$ centre absorption and emission spectra obs. 79−19910
MgO, deformation induced damage, effect on optical props. 77−77258
Mn^{2+}, in nearly tetrahedral clusters, ^4E levels, orbit-lattice interaction and Jahn-Teller effect, spectra obs. 80−24860
NaCl, neutron irradiated, induced flow stress and optical absorpt. 77−62569
PbSe:Tl, elec. props. and IR reflection 78−6686
Si, doped and amorphous, $L_{2,3}$ threshold spectra 77−69934
SiC, radiation damage, review 77−80553
Si_3N_4, amorphous, $L_{2,3}$ threshold spectra 77−69934
SiO_2, amorphous, $L_{2,3}$ threshold spectra 77−69934
SrF_2:Eu^{2+}, two-photon absorpt. spectra exam. of excited state of Eu^{2+} 77−77261
V^{3+} in crystal field, intercombination transition intensities, symmetry reduction method 78−84175
$YAlO_3$:Nd^{3+}, thermal broadening and shift calcs. of Nd^{3+} energy levels 77−48208
$YAlO_3$:Tm^{3+}, cryst. field parameter determ. 77−15800
$Y_2Ti_2O_7$:Nd^{3+}, spectroscopic props. 77−69866

impurity clustering *see segregation*

impurity-defect interactions
see also impurity-dislocation interactions; impurity-vacancy interactions
alkaline earth fluorides, thermodynamics and kinetics of O incorporation 77−84778

impurity-defect interactions continued
diamond, natural, dislocation-N_2 impurity interaction, photoconductivity spectra, resistivity 79−91097
diamond, type IIa, electron irrad., EPR obs. of interstitial-impurity complexes 78−76310
diamond, type IIa, electron irradiated, annealed to high temps., EPR spectrum 77−90034
dislocation loop growth during intrinsic point defect-impurity atom mobile complex formation *(Russian)* 79−90653
externally stimulated interstitial release followed by vacancy-interstitial annihilation, kinetics 78−34535
homopolar crystals, imperfect, lattice dynamics 80−59601
hydrogen embrittlement due to H-inclusion interaction 78−30664
interstitial solutions, impurity subsystem free energy, impurity distrib., temp. depend. 80−44232
intrinsic point defect-impurity atom mobile complex form., influence on defect diffusive fluxes 80−2063
ionic crystal, defect pair, dielec. relax. meas. using EPR 78−23392
metal, electron irrad., selfinterstitial atomic defect interaction radii, recovery expts. and error sources 80−65049
metal, He migration and defect interactions, role in radiation damage processes 77−28041
metal, solute atom displacement in mixed dumbbell interstitials for FCC lattice 78−79631
metal, trapping of H, book contrib. 80−24491
metals, μ^+ diffusion, LAMPF results 80−71285
metals, heavy ion implantation, site populations in case of immobile defects 79−23624
metals, pure and alloyed, grain boundary relaxation model, *(Russian)* 80−39107
non-metallic crystals, electric field influence on defect creation mechanism 80−70251
semiconductors, Watkins-type radiation defects, low temp. form. mechanism 80−15153
solar cells, defects, rel. to elec. parameters, SEM electron beam induced current investig. 79−43772
steel, ferritic, radiation hardening and embrittlement 80−35199
thermal neutrons, inelastic scattering by one-dimens. defecton *(Russian)* 78−84169
transition metals, BCC, point defects chem. binding energy 79−82260
transition metals, electronic structure and ordering of sp defects 78−91639
d-transition metals, impurity integration with large-angle grain boundaries 80−39148
trapping and diffusion of particles near surface, attachment of mobile particles to non-saturable traps, theory 80−39417
void nucleation and growth, effect of point defect trapping on impurities 79−23637
Ag wires, LF internal friction peak due to O 78−3160
Ag-In, dil., interaction between recoil implanted impurities and lattice defects, TDPAC meas. 78−39467
AgBr:Pb^{2+}, cubic microcryst., ion influence on ionic cond. and space charge characts. 79−55928
Al alloys, dil., size effect of impurity atoms rel. to trapping radii for migrating self-interstitials 78−75690
Al alloys, dil., size effect, valency factor and point defect interactions 79−51143
Al, bicrystal, varying purity, breakaway of grain boundary from adsorbed impurity 77−31678
Al foil, electron-irrad., interstitial trapping on impurities 79−99242
Al, radiation damage with radioactive probes, TDPAC meas. 77−24336
Al:^{111}In, electron irrad., defect trapping at impurities 78−55892
Al-Ag(Ge)(Mg)(Zn) alloy, dil., electron-irradiated, impurity-interstitial interaction 77−15449
Al-Co, electron irradiated, self-interstitials trapped at Co impurities, Mossbauer line shape anal. 78−6615
Al-Cr, neutron irrad., Cr atom distribution NMR study 80−54957
Al-Cr(Ti), electron irradiated, interstitial trapping and detrapping at undersized impurity atoms 78−47424
Al-Cr(V)(Ti), dil., electron irradiated, interaction of self interstitials with undersized solute atoms 78−63789
Al-Fe, dil., defects and phases, Mossbauer studies 80−40004
Al-Mn(Cu)(Ag), solute atom displacement in mixed dumbbell interstitials for FCC lattice 78−79631
β-Al_2O_3, effect of halogen ion additions to structural state 78−76620
Al_2O_3:Ti^{2+}, corundum, point defect diffusion and interaction with impurity, Ti^{3+} to Ti^{4+} reaction 79−10985
Au-Er, dil., cold-worked, EPR expts. 80−39864
β-B, electron beam zone melting growth, crystn. and defect form. 80−15020
Bi, quenching and annealing of defects, elec. resist. meas. 78−87973
Bi:Sb(Te), quenching and annealing of defects, elec. resist. meas. 78−87973
CaF_2:Er^{3+} laser fluoresc. of Er^{3+} sites, defect equilibria 78−6748
CaF_2:rare earth metal, thermal cond., 80 to 300K, defect centre struct. 77−15638
Cd:^{116}Sn, quadrupole interaction, radiation damage effects 78−43752
Cd-Sb, dil., loss of nucl. alignment of ^{115}Sb by radiation induced defects 78−43344
CdTe:Cl, influence of lattice defects on electrical behaviour 78−2497
CdTe:Cl, interaction of impurities and lattice defects, elec. props. and photoluminescence. spectra 77−4685
CdTe:Ge, dopant behaviour 78−22742
Cu alloys, dil., size effect of impurity atoms rel. to trapping radii for migrating self-interstitials 78−75690
Cu alloys, dil., size effect, valency factor and point defect interactions 79−51143
Cu, elec. resist. under torsional deform., impurities and tensile strain 78−30898
Cu foi.foil, interstitial impurity interaction investigation by stage II isochronal recovery expts. 78−47423
Cu foil, electron-irrad., interstitial trapping on impurities 79−99242
Cu, ion-irradiated, impurity defect configuration, by DPAC-technique with ^{111}In 79−28021
Cu, radiation damage with radioactive probes, TDPAC meas. 77−24336
Cu, self ion irrad., determ. of the nature of defect clusters by Rutherford backscatt. of He ions 79−4342
Cu-Be, solute atom displacement in mixed dumbbell interstitials for FCC lattice 78−79631
Cu-Be (0.25 at.%), cryst., Cu self-interstitial atom, trapping, nucl. reactions and ion channelling obs. 78−14384

impurity-defect interactions continued
α-Fe, interaction of He with C impurities, computer simulation calc. 79−99235
Fe, nitrogen, impurity defect interaction influence on radiation hardening and embrittlement 80−35199
Fe:C, neutron irradiated at low temp., mag. disaccommodation 80−44881
Fe:He, BCC, process of interstitial trapping by impurities 79−46697
α-Fe:He, interaction of He with small self-interstitial platelets 79−60399
Fe:Xe(Te) interaction of impurities with point defects, Mossbauer spectroscopy exam. 78−47414
Fe-H system, effect of H on struct. during creep 77−16652
GaAs, impurity-point defect complexes 78−6097
GaAs:Co, effect of complex formation on impurity diffusion 77−11736
GaAs:Te, superdilation and defects, lattice parameter meas. and carrier mobility 80−10569
Ge, As impurity precipitation from solid soln., neutron irrad. effect 80−29177
n-Ge, electron irradiated, annealing at 6K, Watkins model explanation 78−47427
Ge, primary point defect-impurity interaction, mechanism 77−80501
Ge, quenched, defect annihilation process near 100°C 79−95047
p-Ge:Au, interaction of primary radiation defects with Au atoms, after irrad. and annealing 79−51145
p-Ge:Au,Sb,Hg(Zn), radiation-defect form., Au influence 80−92911
Ge:Cu, electron irrad. effects on carrier density, defect form. 80−19843
InSb, energy spectra of impurity atoms under 4.2K gamma irradiation 77−89471
KBr:Rb^+, elastic interaction of H-centre with impurity, dynamic effects 77−76396
KCl bicrystals, grain boundary migration kinetics, effect of solutes 78−43185
KCl, undoped and Pb- or NO_3^--doped, colloid centre formation, absorpt. spectra, 300-1000 nm 79−78710
KCl:Ba, γ-irradiation, defect struct., X-ray and chemical etching exam. 77−84793
KCl:F (Br^-)(I^-), U-centres, local defect modes, Green's functions calcs. 80−44280
K_2CoF_4:Mn^{2+}, impurity induced mag. excitations, magnon gap mode, far IR spectra obs. 80−44821
LiF, annealing effects on thermoluminescence, dipoles and dimers 77−12452
LiF:OH:Mg, γ-irrad. induced oxyhydryl complexes 80−92555
Li_2O, cation diffusion, NMR obs., MgO and LiF doping effects *(German)* 77−20112
Mg, defect solute atom interaction investigation using channelling techniques 78−47442
Mg-Ag, dil., ion irradiated, interaction between Ag and defects, channelling meas. 78−38766
MgF_2 film, vac.-deposited, origin of mech. stress 79−90925
MgO:Fe^{3+}, Mn^{2+}, X-irrad. induced anion Frenkel defects, stabilisation by Fe^{3+}, optical and ESR obs. 77−68969
MgO:Li, mech. deformed crysts., imprinting of slip bands using Li impurities 80−59473
Mo, diffusion of H(D), trapping at ion implantation induced defects 77−47622
Mo, irrad., defect configurations, PAC study 79−86817
Nb, diffusion of H(D), trapping at ion implantation induced defects 77−47622
Nb, neutron irrad. effects on mech. props. 78−91361
Nb-Zr(Nf)(Mo)(W)(Rh), dil., neutron irradiation at 4.6K, influence of impurities on defect prod. 79−55790
Ni, foil, electron bombard., impurity redistrib. during third stage of annealing, residual resist. meas. 80−6434
Ni, HVEM obs. of irrad. damage 77−35589
Ni, plastically deformed, recovery stages III and IV investig. by positron annihilation 77−31715
Ni-In, ion-implanted, impurity defect interaction and diffusion, Rutherford backscatter and TDPAC expts. 80−34039
Pd-Fe, dil., plastically deformed, positron annihilation study of recovery of crystal, imperfections *(German)* 77−85835
Pt, radiation damage with radioactive probes, TDPAC meas. 77−24336
p-Si, electron irrad., influence of acceptor impurity conc. and irrad. temp. on defect formation 79−19281
Si, grain boundary elec. props./impurity correl. using surface anal. of multigrained samples by SIMS and AES 80−79816
Si, interstitial swirl defect form. in dislocation free floating zone cryst. 77−7682
Si, models for irradiation effects on impurity diffusion 77−80654
p-Si, Na impurity diffusion, ion irrad., defect form. effects *(Russian)* 77−43386
Si, neutron and electron bombard., radiation defect recomb., photoelec. props. meas. 80−60039
Si, O impurity precipitation from solid soln., neutron irrad. effect 80−29177
Si single crystal surface, He^+ bombardment, damage production, defect diffusion 80−39181
Si, status of defect studies 77−84742
Si:Gd, radiation defect form., effect of Gd impurities, elec. and optical meas. 78−71764
Si:Ni,Co,Mn, γ-irrad., interaction of deep-level impurity atoms with radiation defects 77−76457
Si:O, C, impurity conc. profiles and process-induced defects 78−6094
Si:P, Cu(Au) radiation-doped, influence of growth defects on elec. props. 79−69144
Si(:Au), gamma-induced trapping levels 79−87059
SiO_2, ion irrad., H capture, absorpt. bands *(Russian)* 78−76505
SrF:rare earth $^{3+}$, reorientation of dipoles 77−8494
Ta-H, N interstitial trapping of H, hydride precip., resist. meas. 77−20293
Ti, influence of H_2 on the internal friction *(French)* 78−75723
V, electron-irradiated, positron annihilation study 80−70259
V, oxygen impurity defect interaction influence on radiation hardening and embrittlement 80−35199
V, radiation hardening and plastic instability *(Russian)* 78−39842
V, trapping of D by O interstitials, channelling study using ion induced nuclear reactions 79−4316
V-$D_{0.01}$, enrichment of D during the ion bombardment 80−54288
V-Zr-C, radiation hardening and plastic instability *(Russian)* 78−39842
W, electron irrad., or ion irrad., stage II, point defect struct., FIM 77−80542
impurity-defect interactions continued
W, trapping of He at Xe atoms, attachment of mobile particles to non-saturable traps 80−39418
Zn, grain boundary detachment from adsorbed impurity, conc. depend. 78−2144
ZnS film, vac.-deposited, origin of mech. stress 79−90925
Zr, defect solute atom interaction investigation using channelling techniques 78−47442

impurity-dislocation interactions
see also dislocation locking; dislocation pinning
austenitic steel, VN_x spherical misfitting particle precip. along dislocations, diffr. contrast 77−16595
axial channelling, effects of dislocations on energy loss of channelled ions 77−11610
charged impurity influence on dislocation motion in cryst. 80−103333
cubic crystal edge and screw dislocation−point defect elastic interactions 80−15151
dislocation loop-length distrib. and frequency-depend. damping for small impurity concs. 80−49232
dislocation percolation through absolute obstacles in impurity crystals *(Russian)* 80−70196
elastic stress field shape change kinetics depend. on inclusion-edge dislocation interaction 79−86815
FCC crystal, elastic interaction of 60° and screw dislocations with point defects 78−63786
gettering of impurities, by intentional double diffusion 80−75383
glissile dislocations, prod. by impurity atoms, Debye-Waller factor calcs. 78−2214
impurity crystal, microstructural plastic instability *(Russian)* 79−99190
inclusions, misfitting, precipitated close together on dislocation, electron diffr. contrast 77−27886
low temp. radiation hardening mechanism, single halogen interstitials as hardening agent, Ha annealing 79−23634
metal, dislocation-impurity interactions, electrical and elastic interactions *(Russian)* 78−22758
metal, trapping of H, book contrib. 80−24491
metals, BCC, dislocation processes, straining expts., electron microscope obs. 80−29025
metals, reversible H embrittlement 80−104292
microcreep, low temp., quantum effects *(Russian)* 78−71784
motion of dislocation in impure cryst., stochastic theory 77−11548
nonstationary temperature field, dislocation struct. dynamics *(Russian)* 77−27884
precipitation on dislocations, and competitive diffusion sinks 77−76455
semiconductor, containing screw dislocations, impurity centres 78−72111
semiconductor, defects, electron microscopy study 79−95021
solid solutions, conc. tetragonal substitutional, dislocation impurity segregation *(Russian)* 79−65114
steel, C, diffusion of H_2, effect of quenching and tempering 77−7908
steel, cold worked, alloying additions effect on 200°C internal friction peak *(Russian)* 77−8867
steel, cold-worked, state of cementite, nucl. gamma reson. meas., plastic deform. *(Russian)* 78−68706
steel, Cr, H-dislocation interaction 79−8307
steel, delayed fracture, hydrogen and impurities 78−84988
steel, stainless, 316, creep and rupture, 525 to 900°C, creep rate 79−11678
strain ageing effect on strength and toughness, susceptibility to strain hardening 79−57028
substitutional alloys, conditions for appearance of striations in stress/strain curves *(French)* 77−44319
supersaturation, of H, produced by dislocation motion 77−36640
Ag, polygonisation, impurity effects rel. to stacking fault energy 77−63685
AgBr:Cd^{2+}(Sr^{2+}), single cryst., stress-induced migration and aggregation of solute ions, internal friction 79−51200
Al dilute alloys, cold worked, internal friction peaks 80−97520
Al, electron irrad., interstitital loop nucleation at impurity site *(Japanese)* 77−43247
Al, resistivity decrement under torsional deform., impurity segregation at moving dislocations 77−4321
Al-Ag (7.27 wt.%), peculiarities exhibited during fatigue loading *(Chinese)* 80−71723
Al-Fe, dil., defects and phases, Mossbauer studies 80−40004
Al-Li, dil. alloy, cold-worked, annealing spectrum 78−39801
Al-Mg alloy, creep rate, effect of dislocation pinning by impurity atoms *(Russian)* 78−38719
Al-transition metal alloys, anomalous sp. ht. and nuclear spin-lattice relax. 79−46814
Al-Zn-Mg alloys, decomp. kinetics from Young's modulus obs., microprocesses *(German)* 78−64522
Au, work hardened, Hasiguti peaks, spectrum and recovery, impurity effects *(French)* 77−66670
Au-Cu(Ag)(Pt), cold worked, impurity conc. rel. to internal friction Bordoni peak, solid soln. hardening mech. 80−16363
Be, plastic strain mech., effect of impurities *(Russian)* 79−34101
$CaCO_3$, plastic deformation in compression parallel to (111) 78−38709
CaF_2, impurity effects on strengthening 77−63682
Cd, single crysts., plasticity study during deformation by twisting *(Russian)* 80−93597
Cu, polygonisation, impurity effects, rel. to stacking fault energy 77−63685
Cu single crystal, elec. resist. recovery due to impurity capture by dislocations 77−81304
Fe alloy, impurity-dislocation interaction and Snoek Koester relaxation *(Russian)* 78−59834
Fe, H_2 adsorption at dislocations and cracks 79−20146
α-Fe, He atom clustering at $^1/_2\langle 111\rangle\{110\}$ edge dislocation, calc. 78−2154
Fe, influence of H on slip process *(French)* 78−6965
Fe, pure, dislocation relaxation peaks under low temp. deform. *(French)* 80−100867
Fe, varying purity, internal friction, H-dislocation interactions 77−52377
α-Fe:He, impurity clustering in vacancies bound to edge dislocations 78−91358
α-Fe:He, interaction of He with small self-interstitial platelets 79−60399
Fe-C, ageing late stages, diffusional coalescence of precip. along dislocation lines *(Russian)* 77−25060
Fe-C (4 at.%), dislocation-C atom relax. 77−70074

impurity-dislocation interactions continued
Fe-Co-V alloys, effect of V on struct., electron diffr. and Mossbauer meas. *(Russian)* 77−77507
Fe-H, deformed, internal friction 79−57041
Fe-H, Snoek-Koster peak of internal friction, Schoeck model *(Polish)* 79−96076
Fe-H system, cold work internal friction peak, appl. of Schoeck's model 78−95771
Fe-Ni solid solution, deformation mechanism, softening phenomena, dislocation-solute atom interactions *(French)* 80−45344
Fe-Ni-C, martensitic, deformed, stress induced C distrib. *(Czechoslovakian)* 77−32641
GaAs autoepitaxial structure on heavily Te-doped GaAs substrate *(Russian)* 80−49556
GaAs, doped with Group IV elements, etching, electron spectra, cathodoluminesc. study of inhomogeneities 77−11556
GaAs, impurity effect on grown-in dislocation density *(Japanese)* 78−6063
GaAs:Sn(Te), epitaxial film, influence of impurities on stacking fault energy 80−103371
GaP LEC crystal, imperfections obs. by light scatt. 78−6074
$Gd_3Ga_5O_{12}$, precipitates assoc. with dislocation climb trails *(German)* 77−35567
Ge, heavily doped, microcreep breakdown 80−97549
n-Ge, plastic deformation, impurities and dislocations interaction, cond. *(Russian)* 79−47100
Ge, single cryst., ultrasound effects on dislocation struct. and impurity atoms diffusion 77−69119
H-dislocation, interactions rel. to H_2 embrittlement 79−42097
Hf-O(N), solid soln. hardening, impurity cluster and interstitial mechanisms 77−36523
InP, impurity effect on grown-in dislocation density *(Japanese)* 78−6063
KCl:Ca(Ba), effect of doping on dislocation distrib., in melt grown cryst. 80−6410
KCl:Ca(Ba)(Mg)(Sr), microcrystalline powders, role of Z-centres in stabilizing coloration 80−54227
LiF, crysts. containing rigid dislocation forest, mech. props. 79−99212
LiF, deformed in liquid He, penetration of He, dislocation effects 77−20131
LiF:Be(Mg), Maxwell-Wagner relax. induced by impurity clouds around dislocations, ionic thermocond. meas. 80−7281
LiF:Mg, origin of dislocations *(Russian)* 77−15425
Mg-Ag(Cd), anisotropic, dislocation interaction with tetragonal impurity, mobility 77−19953
MgEu, dil. alloy, cold worked, valence transform. of Eu due to defect association, mag. suscept. and Mossbauer meas. 77−51404
Mo deformed single crysts., struct. state and dislocation splitting *(Russian)* 80−29029
Mo, Mossbauer absorpt. spectrum in deformed cryst. 77−16234
Mo:He, at. config. of $^1/_2\langle 111\rangle$ screw dislocation 79−65081
Mo:He, interaction of He with edge dislocation, influence of interatomic pot. 79−33014
$NH_4ClO_4:Cu^{2+}$, dislocation etch pits exam., rel. to thermal decomp. 77−11555
NaCl, dynamic dislocation retardation, impurities effect 78−26577
NaCl, screw dislocation mobility under high hydrostatic press. 79−69109
$NaCl:Co^{2+}$, dynamic braking of dislocations *(Russian)* 78−6068
$NaCl:MnCl_2$, Suzuki phase precip. obs. by TEM, misfit dislocations 77−31776
NaCl:Tl, deformed phosphors, thermoluminesc., impurity conc. effects 77−63473
NaCl-Ca, single crysts., load-microhardness curves, heat treatment, impurity effects obs. 78−30694
Nb-O, cyclic creep, effect of O_2 conc. and temp. 78−48466
Nb-O(N), dislocation pinning, impurity interactions, strengthening *(Russian)* 80−92532
Ni, H diffusion, trapping and mobility near vacancies, dislocations and cracks 80−49426
Ni, H diffusion in imperfect lattice, annealing and cold rolling effect 80−49425
PbTe, and its alloys, rel. to microhardness as function of applied load 78−48493
Pd-Fe, dil., plastically deformed, positron annihilation study of recovery of crystal, imperfections *(German)* 77−85835
Pd-H, dil. α-phase, influence of deform. on low-temp. sp. ht. 77−31783
Pd-H(D), elastic energy dissipation peak 80−60905
Si, cryst., impurities rel. to lattice parameters, dislocation density, stresses *(German)* 77−51403
Si, crystal defects and impurities interaction obs. by electron microscopic methods 80−65003
Si, Czochralski grown, intrinsic gettering by oxide precipitate induced dislocations 77−27903
Si Czochralski wafer intrinsic gettering by oxide precipitate induced dislocations 78−6092
Si, diffusion of B and P, influence of dislocations 78−18840
Si, heavily doped, microcreep breakdown 80−97549
Si ion damage critical gettering microstructures 78−6098
Si, ion-implantation gettering effects, crit. microstructure 77−43229
Si, ion-implanted, disorders, nature and annealing behaviour, review 78−83836
Si, low dislocation density, plastically deformed, electron mobility anisotropy anomaly *(Russian)* 77−80777
Si, nucleation of stacking faults at oxide precipi tate-dislocation complexes, TEM 77−19967
Si, substrates, review of defects 77−39597
Si:Cu, interaction between vacancy emitting absorbing precipitates and dislocations, TEM obs. 78−71755
Si:Fe^0, solid soln. decomp., Fe deposition on dislocations 77−51943
Si:O wafer, dislocation pinning effect of O atoms 77−89437
Si:P, Au gettering by P diffusion and P-induced dislocations 78−91346
Si:Sb, heavily doped, TEM obs. of impurity effects in dislocation motion 77−43220
SiC:B(Be), dislocation induced deceleration of impurity diffusion 77−28043
Si(111):Pb ion implanted amorphous layers, recrystallisation, impurity out-diffusion model *(Chinese)* 80−88363
Ta-O, BCC, Snoek type reordering during strain ageing *(French)* 79−8312
Ta-O(N), dislocation pinning, impurity interactions, strengthening *(Russian)* 80−92532

impurity-dislocation interactions continued
α-Ti, initial stage of strain ageing *(Russian)* 77−81278
Ti, irradiated and cold worked, internal friction peaks 77−86074
Ti, plastic deform. dynamics, mech. characts. and phys. props., effect of O_2 *(French)* 80−45353
V-O, dislocation pinning, impurity interactions, strengthening *(Russian)* 80−92532
Y, plastic deformation props., deformation ageing, plastic flow, dislocation-impurity interactions *(Russian)* 80−66582
Zn-Ag(Cd), anisotropic, dislocation interaction with tetragonal impurity, mobility 77−19953
Zn-Al, dil., isotherm of internal adsorption at dislocations 79−37733

impurity distribution
see also doping profiles; segregation
AES depth profiling, appl. of tailored modulation techniques 77−15702
alkali halide, off-center displacement of univalent impurity ions 79−23632
alkali halide cryst., surface impurity distribution, Fick's 2nd law calc. 77−47673
alkali halides, divalent impurity dipole aggregation kinetics 78−79630
alkali metal:H(0), impurity investigation using residual resist. and optical absorpt. meas. 79−95816
n-alkanes, single cryst., γ-irrad., ESR, energy deposition rel. to alkyl radical form. 77−16844
alloy, BCC, ordered, implanted atom redistrib. at octahedral and tetrahedral interstitial sites *(Russian)* 78−34533
alloy, crystallising, impurity distrib. under suppressed natural convection temp. *(Russian)* 77−28795
alloy melt, impurity conc. field model, growth by Czochralski method *(Russian)* 80−75191
alloys, crystallisation, under conditions of temp.-conc. convective mixing of liq. nucleus, impurity distrib. *(Russian)* 80−40342
alloys, impurity diffusion and distrib. 79−33118
alloys, ion-implanted, integral Gaussian profile determ. method 80−107313
alloys, surface composition after fabrication by SIMS 80−65351
amethyst, Fe^{3+} diffusion, associated phenomena 77−36269
axial channelling, multistring model computer simulation, foreign atom location appl. 79−42128
backscattering anal. using 2 MeV $^4He^+$ ions *(Chinese)* 80−35590
barley seeds, N depth distrib., $^{14}N(d,p_0)$ reaction 79−5221
binary disordered continuous solid solns., thermal cond. calc. method, struct. model 77−43394
binary melt, thermoconcentration convection in solidification, influence on impurity distrib. *(Russian)* 79−73292
calcite, luminescence spectral anal. of polycyclic aromatic hydrocarbon impurities 80−71483
casting solidification, impurity distrib., effect of thermal-gravitational convection, numerical study *(Russian)* 78−19734
channelling of ions for atom location, continuum approx. calc. of scatt. yield 77−7778
coincidence measurements between scattered particles and X-rays to obtain high depth and mass resolution 80−54278
composite material, matrix impurity distrib. in melt crystallisation *(Russian)* 80−100277
compositional depth profiling by Auger electron spectroscopy 79−52053
conference on ion beam anal., Washington, USA (June-July 1977) 79−5194
corundum, defect cryst. struct. study 80−103316
crystal growth, cylindrical pores growth, numerical calcs. 80−92471
crystal growth, modified Czochralski method, variations of impurity distrib. 80−88193
crystal growth from melt, impurity distrib. ratios, kinetic depend. 78−43044
crystal growth from melt, kinetic factor effects 78−52656
crystals, obtained by directed crystallisation, nomogram for impurity distribution coefficients 79−51133
Czochralski growth, fluctuating growth rates effect on segregation, backmelting 80−59413
depth, effect of impurity fluoresc. by matrix X-rays 79−5224
depth profiles by sputtering in SIMS and AES 79−56891
depth profiling, dynamic range of 10^6 80−107302
depth profiling expts., $D(^3He,\alpha)H$, background reduction using electrostatic deflector 79−14841
depth profiling of H and He isotopes within near surface region of solids using ion beams 79−7622
depth profiling of light elements in materials with high-energy ion beams 77−59036
diamond: B, natural, sub PPM determ. of B, identification of acceptor centre 77−59035
diamond, Ar ion induced struct. changes, depth profiles, from XPS 78−34554
diamond, B doped, electron irradiated, threshold energy for atomic displacement, elec. cond. meas. 77−11594
diamond, natural, (110) and (210) defects, X-ray diffr. pattern weak extra reflections 79−82257
diamond, natural, high conc. of implanted Si ions, He backscatt. and IR absorption 77−89466
diamond, natural, $N_{S(111)}$ impurity segregation on diffuse X-ray scatt. 79−95046
diamond, natural, topography of impurity distrib. and neutron-induced colouring 77−39613
diamond, natural semicond., isothermal annealing of electron radiation damage 77−7764
diamond, paramagnetic N centres spatial distrib., EPR imaging method 79−65732
diamond, synthetic, γ-Mn cluster existence, neutron diffr. obs. 77−89464
diamond powder, explosion synthesized, impurity distrib. and thermal stability 80−15147
dibenzyl-tolane, single cryst. growth from melt, influence of supercooling and impurity conc. on growth rate of faces 79−14714
diffusion in cryst. solid with inhomogeneous layers, impurity distrib. calc. *(Russian)* 78−14500
diffusion layers, piezoresist. coefficient determ. allowing for two-dimens. impurity distribution *(Russian)* 78−6374
diffusion of interstitials in cryst. with random impurities, incoherent scatt. law 77−1266
durene-p-dibromobenzene system, phase diagram and X-ray diffr. expts. 78−79774
emerald, artificial single crystal, distrib. of Cr^{3+} impurity 80−59505

impurity distribution continued
epitaxial films, condensed from vapour or molecular ion beams, impurity distrib. 80−65032
epitaxial films, model for autodoping lateral variation 80−103595
Fick's equations solutions for impurity diffusion, dislocations, interstitials, vacancies 80−70469
film profiling using proton excited X-rays 79−4490
film sandwich structures Auger anal. 78−72030
film structure, low conc. ^{16}O depth profiling using $^{16}O(d,\alpha)$, α-particle energy anal. 79−5214
p-GaAs:Zn, diffusional doping, photoluminesc. in mag. field 77−16384
garnet, Stockbarger-grown, impurity capture and distrib. 77−28713
garnets, concentrational inhomogeneities, appl. of vacuum decoration method 79−14835
glass, diffusion coefficient equation 80−103521
glass, diffusion profiles analysis, grinding and etching techniques comparison 78−26732
glass, Li depth distrib., meas. using $^{7}Li(p,n)^{8}Be$ 77−35582
graphite, chemisorption of O_2, influence of Fe as impurity 80−96732
heavy atom impurity in light atom host 79−56903
heterojunction properties analysis and control, cathodolum. appls. *(French)* 79−69892
high resolution Rutherford backscatt. techniques, appl. to near surface anal. 79−5207
homogeneous doped semiconductor, influence of internal elec. field on diffusion of ionised impurity 79−55940
I-V impurity profiling under Schottky barrier 78−19148
II-VI compounds, acceptor state model 80−2059
III-V compounds, surface comp., low-energy ion scatt. spectrometry 80−100382
III-V semiconductor solid soln., LPE, doping with groups II and IV *(Russian)* 77−80705
III-V semiconductors, during epitaxial growth from liq. phase 80−88443
implanted crystals, ang. depend. of MeV H^+ backscatt. yield in glancing geometry 79−4874
impurity relaxation in nonresonance field, phonon amplification *(Russian)* 80−100310
inclusion emersion in vertical zone refining 78−52663
inhomogeneous material, implanted ion distrib. 78−18663
inhomogeneous semiconductor, impurity opt. absorpt. and photocond. spectral line profile variation 77−16352
inhomogeneous solid solutions with conc. expansion, thermodynamics, energy defect diffusion calcs. 80−24618
interstitial solutions, impurity subsystem free energy, impurity distrib., temp. depend. 80−44232
ion axial channelling analytical model, point defect scatt. 80−39192
ion beam induced atomic transport and conc. profiles 80−59723
ion channelling, flux peaking, lattice location 79−95062
ion implantation, metastable phases in metals, review 80−49254
ion implantation, range parameters, nucl. stopping power, ion backscatt. determ. 80−88232
ion induced optical emission for surface and depth profile analysis 79−4333
ionic crystals, aliovalent impurities, periodic distrib., self consistent approach 79−69149
ionized-cluster beam deposition and epitaxy 79−83137
isovalent impurity long range potential, role in electron scatt. 80−10966
lattice location, using channelling effect *(Japanese)* 80−24513
light atoms in crystal lattices, position determ. by α-particle channelling and backscatt. 79−65113
light element depth distrib. in materials, meas. with ^{6}Li beam 77−16888
light element profiles in heavy matrix materials, depth profiles and lattice locations using (n,p) and (n,α) 79−5205
long-range order 78−95061
low energy ion beam materials anal. with SIMS 79−49331
LWR fuel rods, power ramp induced I and Cs redistrib. 80−32343
martensite transformation mechanism, position of C atoms in cryst. lattice *(Russian)* 77−8820
mechanical stresses caused by growth centres 80−19735
melt crystallizing with conc.-depend. convection, impurity distrib. 80−10642
melt-grown crystals, striated impurity distrib. calc. 80−24488
metal, FCC, homovalent impurity migration energies, fluctuation theory model 79−95219
metal, H_2 diffusion profile, neutron radiography 77−24438
metal, H detect., SIMS method with quadrupole mass filter 77−32854
metal, impurity depth conc. profiles using nucl. reson. reactions and Rutherford backscatt. 79−52448
metal-semiconductor contacts with thin interfacial films 80−96969
metals, fraction of ions in unique sites, hyperfine interaction studies 77−15438
metals, gas-forming impurities in crystal inclusions, trends in modern anal. *(Russian)* 80−15123
metals, group VA, O and N determ. from internal friction meas. 79−39246
metals and alloys, segregation studies by imaging atom probe microscopy 80−66911
metals and alloys, trace element detection by atom probe microanalysis 80−66910
mica, Fe^{2+} distrib. on octahedral sites, PMR investig. 78−15041
mica, surface impurity levels by static SIMS, cleaning treatment effects 77−59190
molecular crystals of solid replacement solns., NQR investig. of impurity distrib. 77−12222
MOS struct. with nonuniformly doped semiconductors, depletion approx. anal. of differential C-V characts. 79−99625
MOS structure, flat-band capacitance, impurity concentration, approx. formulae 79−95497
MOS structure, use of mini-computer for rapid evaluation of C-V-plots *(Russian)* 79−28413
naphthalene:β-methylnaphthalene, impurity phosphoresc. centres *(Russian)* 77−81151
naphthalene, β-naphthol impurity mol. distrib., spectral obs. *(Russian)* 79−82253
nonconstant distribution coefficient, calc. from expt. data 78−75606
optical inhomogeneities obs. by spectral modulator, using scanning image convertor 78−59144
p-n junction, conc. profile of singly charged deep impurity, capacitance meas. 78−26945
p-n junction, diffused, conc. profile of deep-level impurity by capacitance method 77−55299

impurity distribution continued
p-n junction impurity profile meas., two-freq. method 79−23633
petrographic method of determ. of quantitative relation between phases in microcryst. structs. 78−35608
phase boundary, impurity conc. 80−34038
plagioclase:Mn^{2+} (Fe^{3+}), ligand field bands of impurity luminesc. centres and their site occupancy 78−88350
polyacetylene, pristine and acceptor doped isomers, EPR, DC cond., evidence against solitons 80−15782
polyisobutylene, impurity distrib. of tagged poly-cis-isoprene, individual and aggregate 79−68339
polymer, dye conc. distrib. determ., microdensitometry *(German)* 77−37962
polypropylene, impurities redistribution during crystn. 78−75577
porous powder struct., Gorskii effect *(Russian)* 79−65109
proton induced X-rays, impurity atom depth determ. 77−11582
quartz, H concentration profiles by nuclear reaction method 79−60396
quartz, high purity, impurity distrib., neutron activation anal. 80−24485
quartz, ion-implanted layers, total X-ray reflection investig. of clustering 78−6081
quartz, synthetic, Al centres conc. and anomalous pleochroism depend. on crystn. parameters 80−107311
quartz, synthetic, impurity anal. by X-ray method 79−52099
quartz, synthetic, lattice distortions, optical inhomogeneities by X-ray topography and optical birefringence meas. 78−55887
quartz glass, Ge and B dopants, OH impurities, preform material and fibre optic waveguide struct. 80−64173
quartz resonator, growth sector boundaries 77−39595
radiation induced segregation of impurities to voids, kinetic model 77−43245
radiational materials, spatial distrib. of H^+, He^+, D^+ ions in solids 80−6429
ruby, concentrational inhomogeneities, appl. of vacuum decoration method 79−14835
sapphire, concentrational inhomogeneities, appl. of vacuum decoration method 79−14835
Schottky diodes, space distrib. in near-contact region, meas. instrument 77−19976
scrape off layer of Tokamaks TFR 400 and 600 79−652
SEM cathodoluminescence analysis of impurities, localisation and sensitivity 78−95985
semiconductor, charged impurity diffusion 80−6563
semiconductor, distrib. of implemented ions near arbitrarily shaped mask edges 77−31689
semiconductor, dopant impurity redistrib., Chen and Chen series method 79−1457
semiconductor, doping reduction using zone recrystn. with temp. gradient 80−104062
semiconductor, impurity conduction, at very low temp. *(Japanese)* 80−20200
semiconductor, ion implanted, pulsed laser and electron beam annealing comparison 80−92547
semiconductor, lightly doped compensated, electric fields at impurity centres *(Russian)* 80−84198
semiconductor, MBE, doping impurity transport, free carriers effect 78−26793
semiconductor, multilayer spreading resistance anal., high-speed implementation and expt. evaluation 79−4324
semiconductor, nonuniformity monitoring by relative thermoEMF meas., limits of applicability 77−36702
semiconductor, VPE, mol. flow in vac., free carriers effect on doping impurity distrib. 78−47682
semiconductor concentration calc. in weakly doped sample, iterative method, GaAs appl. *(French)* 77−72634
semiconductor impurity distrib. and defect structure analysis by charge collection SEM 78−9924
semiconductor impurity profile determ., multilayer spreading resistance anal. using image method 77−68993
semiconductor materials, contamination equilibrium assessment 79−51134
semiconductor substrate surface, low loss electron and Auger images correl. 78−22944
semiconductor supersaturated solid solns., decomp., surface impurity content 78−51681
semiconductor with impurities, laser beam induced synergetic-phenomena 79−74021
semiconductor with inhomogeneous impurity distrib., irrad. effects 79−10875
semiconductors, charge neutrality produced by impurity diffusion 80−59724
semiconductors, multiply doped, donor-acceptor complexes and interactions, physicochem. nature 80−15472
semiconductors, SIMS characterisation of thin epitaxial layers and bulk material *(French)* 80−50904
Si:Au, step junction, mathematical model *(Rumanian)* 79−87148
solid, depth profiling of ^{3}He ion implantation 78−59830
solidifying melt thermal gravitational convection, impurity distrib. and transfer processes 80−19367
solubility of group III and V elements 77−84928
sputtering, cascade mixing in depth profiling 79−78811
sputtering use in depth profiling, review 80−40214
steel, austenitic stainless type AISI 304, surface comp. after different surface treatments 80−3253
steel, austenitic stainless type AISI 316, L sheet and LN plate surface comp. after different surface treatments 80−3253
steel, Cr-Mo, ferritic, grain boundary segregation, X-ray microanal. by STEM 80−66740
steel, Cr-Ni, microstructural distrib. of cathodic H_2, autoradiography *(French)* 79−99234
steel, Cr-plated, H_2 distrib., laser-mass spectrometer investig. 78−61113
steel, depth profiles of transition elements using (p,γ) react. 80−50910
steel, grain boundary P segregation, effect after quenching and tempering *(Russian)* 80−81145
steel, hydrogenated austenitic stainless ^{57}Mossbauer obs. 77−7758
steel, mild, implantation of Cu(Cr), annealing and rolling behaviour of conc. profiles 78−75684
steel, Ni-C, martensitic, microstructural distrib. of cathodic H_2, autoradiography *(French)* 79−99234
steel, nitride inclusions, identification by differential thermal anal. and evolved gas anal. 78−48721

impurity distribution continued
steel, quenched, local H distrib. and internal microstresses *(Russian)* 80−50654
steel, stainless, austenitic, microstructural distrib. of cathodic H_2, autoradiography *(French)* 79−99234
steel, stainless, D depth distrib. determ. using $D(^3He,p)^4He$ 79−4326
steel, stainless, spatial distribution of limiter material and impurities on the first wall of TFR 400 79−651
steel, transformer, texture formation tendency *(Russian)* 77−59803
steel surfaces, O and N profiles, Rutherford backscatt. and (d,p) reaction anal. 79−5216
steels, N-implanted, surface hardness and abrasive wear resist. 80−50746
strain distrib. meas. by X-ray Bragg reflexion rel. to dopant distrib. 77−19835
structural phase transition, interaction and diffusion of impurities 79−42083
surface contamination by H_2, shortening of ultracold neutron storage time 78−17461
surface deformation due to non-homogeneous distribution of solute atoms in crystals 79−33164
surface structure, appl. of imaging atom probe mass spectroscopy 79−23818
thin film, electron-induced X-ray spectrometry anal. *(French)* 79−43067
three-phase system, diffusion laws 80−107310
total current spectroscopy, review 80−45185
vapour deposition with simultaneous ion implantation, gaseous impurities 79−69146
vicinal faces grown from dil. soln., impurity incorporation, interface model 80−84127
wall and limiter materials for DITE Tokamak, H conc. meas. 78−94136
X-ray diffraction line broadening from small subgrains containing gradients of spacing 78−67612
X-ray emission, ion-excited, impurity atom position determ. *(Russian)* 78−47408
X-ray standing wave field excitation, meas. apparatus, appls. 77−15285
Ag films, electrodeposited and vac. deposited, AES depth profiling anal. 77−59232
Ag-In melt system, conc. depend. of component and impurity diffusion coeffs., radioactive isotope method *(Russian)* 80−107454
Ag-Pd, dil., elec. field gradients due to Pd near neighbour configs., TDPAC obs. 78−19391
Ag-Pt interface formed by electrodeposition, depth profile 77−16512
Ag-Pu (0.5 wt.%) deposited profiles, homogeneity, from hexagonal point source array 80−25559
AgBr:Cd^{2+}(Sr^{2+}), single cryst., stress-induced migration and aggregation of solute ions, internal friction 79−51200
AgBr:Pb, ion scattering spectroscopy obs. 77−19979
AgCl:$CdCl_2$, point defect model, free energy and radial distrib. functions 80−44201
AgCl:Na^+, Frenkel defect formation energy, impurity diffusion and migration 79−99179
AgCl-$AgNO_3$, eutectic mixture, estimation of impurity distrib. coeffs. 80−55290
AgI-AgCl, eutectic mixture, estimation of impurity distrib. coeffs. 80−55290
AgI-$AgNO_3$, eutectic mixture, estimation of impurity distrib. coeffs. 80−55290
Al ingot solidification by HV pulses, impurity distrib. and conc. region formation *(Russian)* 80−20919
Al, plastically deformed by pulsed mag. field, mobility of Fe atoms, radiotracer profiles 79−28584
Al:^{11}B, relax. mechanism for polarised implant 78−87693
Al:Ga, pulsed electron-beam annealing, lattice site location improvement 80−107303
Al:Sb(Zn), ion implanted electron beam annealing, ion backscatt. and TEM meas. 80−59500
Al-Bi(Cd)(Pb)-Ti, containing low-melting pt. inclusions, mech. props. 80−93632
Al-Cu, implanted metal system, Cu redistrib. after laser irrad. 79−69163
Al-Sb, laser induced surface alloy formation and Sb diffusion 80−54439
p- (AlGa)As:Zn, MBE grown, elec. props., shallow junction solar cell use 79−91175
$Al_xGa_{1-x}As$, epitaxial layer, distribution of Te and Ge impurities 78−43046
p-$Al_xGa_{1-x}As$:Ge layer on GaAs substrate, Hall and elec. cond. meas., Hall mobility 80−2402
$Al_xGa_{1-x}As$:Ge(Te)(Zn), photo- and cathodolum., comp. depend. *(Russian)* 77−48215
$Al_xGa_{1-x}As$-GaAs, epitaxial heterostructure, influence of defects on diffusive distrib. of group I impurities 78−43045
$Al_xGa_{1-x}P$, proportional ingredient content determ. by X-ray fluoroscopy 80−97747
$Al_xGa_{1-x}Sb$:Zn(Si)(Ge)(Sn)(Pb), doping of solid solns. during LPE *(Russian)* 77−85087
$AlMg_2Mn$, H impurity detection by $^1H(^{15}N,\alpha\gamma)$ reaction 80−55767
Al_2O_3 anodic films, H conc. profiles meas. 80−75261
Al_2O_3, dense, steam-enhanced Ca segregation, AES and SEM obs. 79−83352
Al_2O_3, sintered, containing $MgAl_2O_4$ precipitates, Mg distribution at grain boundaries 78−80498
Al_2O_3, sintered, electron microprobe anal. of impurity and additive distribs. 80−40359
α-Al_2O_3:Co,H, Co and proton ENDOR, IR and optical spectra charge compensator nature and defect struct. 80−44956
Al_2O_3-Al interface, AES depth profiling, appl. of tailored modulation techniques 77−15702
As_2S_3, glassy, diffusion, elec. transport and first group impurities effect on elec. and opt. props. 77−76623
As_2S_3, glassy, photoreactive diffusion of Ag 80−19991
Au, damage by ion implantation, spike threshold, TEM 79−90705
Au electrode, diffusion into polymer film, particle backscatt. anal. 79−77821
Au-Mo-Si multiple layer structure, bombarded with P ions, calc. of P ion profile in substrate *(Russian)* 79−55771
Au-Si contacts, O determ. by SIMS, nuclear reaction and Rutherford backscatt. anal. 79−4482
B concentration profiling in solids by neutron TOF using $^{11}B(p,n)^{11}C$ 79−51131

impurity distribution continued
B, preparation and purification, physical characterisation *(French)* 80−16189
$BaTiO_3$, ferroelec., elec. field in 90° domain walls 80−2713
$BaTiO_3$:Fe ceramic, dopant distrib., STEM obs. 79−82255
$BaWO_4$, single cryst. growth by Czochralski method and U incorporation, effective distrib. ratios, luminesc. characts. 79−42094
Be alloy, dil. metastable, produced by ion implantation, lattice location of impurities 79−51132
Be depth profiling in alloys, simultaneous α and d detection in $^9Be(p,d)$ and $^9Be(p,\alpha)$ reactions 79−5203
Be, ion-implanted, impurity lattice location, channelling meas., Monte Carlo calc. 80−107291
Be, lattice location results for implanted impurities, Rutherford backscatt./channelling technique 79−4329
Be:Li, lattice location of implanted ^6Li, ion beam channelling study 79−37730
Be-Cu dynode, depth profiling anal. of surface layer 80−2253
Bi and Bi-Sb (12 at.%), cryst. growth from melt, impurity distrib. control by electrotransfer method *(Russian)* 80−66418
$Bi_2Te_{3-x}Se_x$, thermoelec. mat., prep. effects on inhomogeneities 78−51576
C, trapping of 6 to 15 keV D, temp. depend. and depth profile 77−30664
CaF_2:Eu, CaF_2:Eu,Mn(Gd), single crystal predisintegration phenomena, SEM cathodolum. obs. 80−59502
CaF_2:Gd^{3+} evaporated film, struct. of impurity centres, substrate temp. effects 79−99943
CaF_2:Mn, CaF_2:Eu,Mn, single crystal predisintegration phenomena, SEM cathodolum. obs. 80−59502
CaF_2:U single crystal, Czochralski-Kyropoulos grown, U ion localization 79−91580
β-$Ca_{3-x}Mg_x(PO_4)_2$, struct. and impurity distrib., stabilising role of Mg 78−10020
$CaWO_4$, Czochralski grown, distrib. coeffs., cavity form., cellular struct. 77−11492
$CaWO_4$, single cryst. growth by Czochralski method and U incorporation, effective distrib. ratios, luminesc. characts. 79−42094
$Ca_3Y_2Ge_3O_{12}$:Eu^{3+}, garnets, prep., struct., luminesc., absorpt. spectra, Eu^{3+} localisation 77−69884
$Cd(NO_3)_2.4H_2O$:Mn^{2+} single cryst., low symm. effects in EPR 77−90020
CdS, charged impurity centres, drift during passage of photocurrent 80−70767
CdS, thin film, diffusion of Cu, 20 to 200°C *(French)* 80−15424
CdS:$CuCl_2$($CdCl_2$) sintered layer, distrib. of energy levels of local centres 80−15568
CdS:I_2 system, interface kinetics and vapour phase mass transport 80−19732
CdS:Li lattice, location of implanted Li atoms 80−6428
CdSe:In, epitaxial layer, effect of activator distribution on conductivity 78−43047
CdSe:Zn(Ga), epitaxial film, impurity distrib., current transfer features *(Russian)* 77−47908
CdTe, trace anal. by heavy ion induced X-ray emission and SIMS 80−55755
CdTe:Cl, grown by travelling heater method, carrier homogeneity investig. 77−39848
CdTe:Fe(Ni), luminesc. and refl. spectra, high temp. annealing effects 80−24472
Co-Ni (0.45 to 7.23 wt.%) theoretical analysis of cation distrib. in (Co, Ni)O scale 77−12747
Cr depth distrib. determ. using $^{52}Cr(p,\gamma)$ resonant react. 79−33011
Cr microcracked plate microanal. of F by $^{19}F(p,\alpha\gamma)^{16}O$ 79−79351
Cr steel, N depth distrib., $^{14}N(d,p_0)$ reaction, 3 MeV deuterons 79−5221
CsI:Na, crystal, kinetics of decay of surface solid soln. 79−23810
Cu, distribution between crude Cu, white metal and SiO_2 saturated slag 78−44055
Cu, doubly peaked He depth profile and blistering 78−10078
Cu, high purity, identification of imperfections by thermal resistivity meas. 80−59951
Cu, ion channelling, continuum approx. calc. of scatt. yield for atom location 77−7778
Cu single crystals Au ion implanted, pulsed electron beam irrad. 80−65019
Cu:^{85}Kr 80−15145
Cu-Be solid solutions, local oscill. conc. depend., impurity bands *(Russian)* 80−75318
Cu-CdS, Schottky barrier, Cu diffusion and photovolt. mechanism 80−6980
Cu-Ni alloy, sputtered altered layers, in-depth profile, model 78−19613
Cu_2O, switching channel electron probe microanalysis, switching cycle number (life) 77−32056
D depth profiling with $D(^3He,p)$, proton detection at backward angles 80−30309
D implantation in metals, lattice location of D using $D(^3He,p)$ for defect-impurity interaction study 79−5206
D, in solid absorber, large depth profile meas. by deuteron induced reactions 77−19978
ErD_2:He, tailored low Z impurity distribs. in solids, distrib. evaluation by proton backscatt. technique 79−5199
EuTe, high-temperature evaporation and reactivity 80−103469
Fe alloys, CC distribution ability of alloying elements *(Czech)* 80−29047
Fe alloys, ion-implanted, depth profile and diffusion coeff. 80−54277
Fe, cast, ferritic, Ce addition effect on impurity distrib. Mossbauer study *(Russian)* 78−18673
Fe, cast, Mg, despheroidising effect of Bi, Sn on graphite in alloy 78−56670
Fe, cast hypoeutectic, Ce distrib. in graphite grains 80−100279
Fe, defect trapping of ion implanted D, depth profile, diffusion eqn. calcs. 80−2047
Fe, diffusion and solid solubility of Sb, 773-873K, ion backscatt. anal., rel. to intergranular embrittlement 78−71880
Fe, grey cast, P effect on distrib. of alloying elements 77−12634
Fe, heavy impurity implanted, relation between hyperfine field and lattice-location meas., influence of radiation damage 80−6794
Fe, liq., of diffused alloying elements *(Russian)* 78−79791
Fe, plastically deformed by pulsed mag. field, mobility of Fe atoms, radiotracer profiles 79−28584

impurity distribution continued
Fe, segregation of impurities, physico-chemical aspects *(Czech)* 80−60866
Fe, surface, contamination in vac. depth selective conversion electron Mossbauer spectroscopy 80−2671
Fe, tetrahedral site occupation by C, study of possibility *(French)* 77−51508
Fe:^{169}Yb, lattice location of implanted Yb, annealing temp. depend., channelling meas. 77−48100
Fe:Bi, impurity site distrib., channelling and nucl. orientation obs. 77−15447
Fe:F, lattice location of implanted F rel. to mag. hyperfine fields 77−59041
Fe:Yb,^{18}O, interaction between implants 77−27921
Fe:Yb(Au), radiation-damage evolution, influence on lattice-location meas. 80−6426
Fe-C, dil., Hall-field electrotransport of C, effective valence numbers 79−28148
Fe-Cr, high-C, sulphide inclusion distrib. obs. 79−74168
Fe-Cr, surface covered with anodic oxide film, in-depth composition profiles 80−10763
Fe-Cr, surface segregation of impurities (C,N and S) *(French)* 77−56192
Fe-implanted alloys, residence sites of Fe, Mossbauer data 80−39299
Fe-Ni, grain boundary segregation, X-ray microanal. by STEM 80−66740
Fe-Ni, hydrogenated, Mossbauer effect meas. 78−92002
Fe-Ni electrodeposit, sectional analyses and impurities *(Japanese)* 80−21350
Fe-Sb system, α-phase, interdiffusion 79−73349
Fe-Ti (0.15 wt.%), H trapping obs. by high resolution autoradiography 79−73205
Fe-Ti (0.15 wt.%), Ti distrib., segregation, FIM anal. 80−84200
$FeGe_2$, single cryst. perfection depend. on growth rate and direction 80−55284
$Fe_{3-x}In_xO_4$, ferrospinels, cation distrib., Curie point and magnetisation meas. 79−42095
Ga, liq., electrodiffusion conc. of impurities 80−54414
GaAs, annealing with Si_3N_4, Cr profiles meas. 79−90693
GaAs, autoepitaxial layer, local impurity inhomogeneities *(Russian)* 79−23854
GaAs, electron trap at E_c-0.75 eV, direct evidence for nonassignment to O 79−90988
GaAs epitaxial layer, Be, O, Si, S, Zn and Sn impurity concentrations 80−49260
GaAs epitaxial layer, fast electron irrad., impurity distrib. profile obs. 77−76969
GaAs epitaxial layers, surface impurity gradients, Schottky barrier capacitance meas. 80−70782
GaAs, impurity distribs. by chemical methods 77−43237
GaAs, lattice location of S and Mn implanted impurities, ion channelling and ion induced X-ray meas. 79−4332
GaAs, qualitative anal. of oxygen in thin epitaxial layers by SIMS 79−5233
GaAs, semi-insulating, effects of heat treatment characterised by SIMS 78−6091
GaAs, semi-insulating, elec. characts., correl. with mass spectra anal. 78−39104
GaAs, semi-insulating, surface layer thermal conversion mechanism, Hall effect meas. 80−49772
GaAs, trace element conc. meas. by Zeeman atomic absorpt. spectroscopy 80−29046
GaAs VPE layers, back surface gettering, Cr out diffusion 80−10802
GaAs:B, incorporation of B during growth 80−93471
GaAs:B(Ge)(Mg), impurity conc. profile by glow-discharge optical spectroscopy 80−49258
GaAs:Be, implanted, determ. of Be concentration profiles by ^{9}Be(p,α) reactions and SIMS anal. 79−4335
GaAs:Co, effect of complex formation on impurity diffusion 77−11736
GaAs:Cr, bulk and epitaxial, ion implanted, Cr conc., depth distrib. and diffusion coeff. 80−49243
GaAs:Cr, Cr distrib. and heat-treatment migration studies by SIMS 80−107305
GaAs:Cr, impurity conc. and segregation coeff., optical absorpt. meas. 79−56819
GaAs:Cr, redistrib. of Cr during laser annealing 80−88192
GaAs:Cr, semi-insulating, Cr charge states conc., EPR determ. 80−20450
GaAs:Cr, semi-insulating, Cr redistrib. during thermal annealing as function of encapsulant and implant fluence 80−84199
GaAs:Cr, semi-insulating, damage gettering of Cr during annealing of Cr and S implants 80−107304
GaAs:Cr, Zn(Se) shallow impurity implantation, elec. props. after annealing 80−24465
GaAs:Cr substrates and LPE layers, Au film deposition and annealing, Cr redistrib. 80−15312
GaAs:Cu, supersaturated solid solns., decomp., surface impurity content 78−51681
GaAs:Mg(C)(Te)(Ge), ion implanted, laser annealing, ellipsometric and Hall meas. 79−73193
GaAs:Se, ion implanted, Cr redistrib. during annealing, SIMS anal. 80−10570
GaAs:Si, ion-implanted, annealing with Nd:glass laser 79−73194
GaAs:Si,Cr, under layer of SiO_2, effect of annealing, on electron concentration and mobility, and impurity distrib. 79−4323
GaAs:Si p-n junction LED, electroluminesc. efficiency 80−71491
GaAs:Sn(Te), epitaxial film, influence of impurities on stacking fault energy 80−103371
GaAs:Te, impurity cond., microcathode-luminesc. investig. 77−8666
$GaAs_{1-x}P_x$-SiO_2:N,Zn ion-implanted multiple layers, ion range distribs., secondary ion microprobe meas. 79−42129
GaAs;Cu, epitaxial and bulk conductivities compared *(Russian)* 78−10585
$Ga_xIn_{1-x}As_{1-y}P_y$:Ge(Sn)(Te), epitaxial film, elec. and optical props. 79−11251
GaP, effective partition coeffs. and elec. behaviour of group IV elements 77−7754
GaP, epitaxial layers, dislocation recomb., SEM cathodoluminescence studies 79−42558
GaP, epitaxial struct., cathodolum. in SEM 78−10991
GaP, impurity behaviour during crystallisation from melt 77−84772
impurity distribution continued
GaP, impurity distribution ratios, correl. with covalent and ionic radii 80−54276
GaP, LPE at 650°C from In solvent, low Si contamination 78−80480
GaP:Cr_2O_3, growth, dopant distribution, elec. resist. 78−34531
GaP:Fe, diffusion, solubility, elec. activity and energy levels 77−55395
GaP:O, impurity concentration determ. by donor-acceptor luminescence 78−6090
GaP:Sn(Sb), lattice location of implanted atoms, ion backscatt. and ion-induced X-ray obs. 77−84785
GaP:Zn, Sn doped epitaxial layers, Hall const., hole mobility and conc. 80−15143
GdF_3:H films, H, F profiles meas. by sputter-induced optical emission 78−47407
$(Gd_{1-x}Tb_x)_2O_2S$, phosphor, concentration quenching of Tb^{3+} luminesc., Tb^{3+} conc. determ. 80−29785
Ge, amorphous and crystn. films, contamination behaviour, XPS examin. 79−1815
Ge, amorphous film, ion-implanted, regrowth 79−15043
Ge amorphous film, O depth profiling by SIMS 80−39480
Ge, heavily-doped single cryst., macroinclusions, annealing in elec. field 77−47474
Ge, high-doped single crysts., impurity atom distrib. changes around growth dislocations in thermocyclic treatment *(Russian)* 80−107307
Ge, high-purity, with Al, B and P, residual impurities, photothermal cond. 80−24965
Ge, impurity cloud form., anal. using heat treatment effects on light scatt. in pure crystals 80−15146
Ge, melt growth conditions and doping level influence on impurity distrib. ratio 77−12516
Ge p^+-ν-n^+ structures, charge transport under impurity freezeout conditions 80−92965
Ge, pure, degree of compensation, capacitance meas., 4.2-150K 79−7624
Ge, ultra pure, method to determ. composition and struct. of non-elemental acceptor and donor centres 78−39658
Ge:^{6}Li, diffusion study using ^{6}Li(d,α) reaction 79−5202
Ge:Ba distrib. pattern, partition coeff., limiting solubility and energy levels 77−15444
Ge:H, amorphous, H content determ. by IR absorpt., gas evolution and nuclear reaction methods 80−44130
Ge:Li, supersaturated solid solns., decomp., surface impurity content 78−51681
n-Ge:O, Czochralski growth, O content rel. to props., IR, Li precipitation determs. 77−15445
Ge:O ion implanted, O localisation determ. 79−95040
Ge:Sb, Czochralski growth, orientation depend. of impurity distrib. coeff. 79−69976
H analysis in different materials problems, using ^{1}H(^{15}N, $\alpha\gamma$) and ^{1}H(^{19}F, $\alpha\gamma$) reactions 79−5196
H content of thin surface layers, nondestructive anal. by alpha-particle scatt. 77−56297
H depth distribution meas. by reson. nuclear reactions 77−81435
H depth profiling in materials, use of ^{1}H(^{15}N,$\alpha\gamma$) resonant reaction *(French)* 78−91357
H depth profiling in solids, using neutron TOF from H(t, n) 79−5198
H implantation in metals, profile distrib. determ. using ^{1}H(^{11}B,α) for defect-impurity interaction study 79−5206
H profiling, appl. of ^{1}H(^{15}N,$\alpha\gamma$)^{12}C, ^{15}N energy loss meas. 78−59845
H profiling using ^{15}N bombardment, method and appl. 79−5195
H_2 in plate subject to external stresses *(Russian)* 79−14836
H_2, mol. solid, atomic H impurities, dynamic local field approx. 79−69316
HF molecules in crystalline solvates, mol. diffusion and spatial symmetry of arrangement 79−42313
^{1}H profiling with 2.5 MeV van de Graaff accelerators 79−77626
^{2}H depth profiling with ^{2}H(^{3}He,p)^{4}He react. 80−49262
He concentration profiles meas., using ^{4}He(^{7}Li,γ)^{11}B reson. reaction at 1.68 MeV incident energy 79−5200
He depth profile meas. in thin metal foils 77−12858
^{3}He, in solid absorber, large depth profile meas. by deuteron induced reactions 77−19978
^{3}He profiling, depth resolution using ^{3}He(d,α)^{1}H reaction 78−58557
^{4}He, solid, quantum diffusion of ^{3}He, tunnelling jumping approx. *(Russian)* 78−87844
HgTe:Cu, effect of prep. conditions on impurity distrib., hole conc. 77−8743
In, electrodiffusive conc. of impurities for analysis 78−22752
In, liq., electrodiffusion conc. of impurities 80−54414
$In_xAl_{1-x}P$, proportional ingredient content determ. by X-ray fluoroscopy 80−97747
n-InAs, photoelectric props., inhomogeneous impurity distrib. 80−107867
InAs:Cd,Te interaction between impurities, effect on elec. props., Hall effect. 80−19832
InGaAsP, LPE growth, impurity depend. of distrib. coeff. 80−10843
InGaAsP:Sn(Te)(Zn), LPE growth, influence of growth-solution dopants on distrib. coeffs. 79−47640
$In_xGa_{1-x}P$, proportional ingredient content determ. by X-ray fluoroscopy 80−97747
InI directional crystallisation, behaviour of Ag, Cu, Sn, Ni impurities, partition coeffs. 77−16491
InP, Zn diffused single-crystal, substitutional dopant and hole conc. meas. 80−75260
InSb, charact. and phys. props., review *(Japanese)* 80−39576
InSb, during epitaxial growth from liq. phase 80−88443
InSb IR detector array, AES anal. of localised contaminants at interfaces 77−57391
InSb, undoped and Te-doped, anomalous impurity segregation, Hall and mass spectrum meas. *(Chinese)* 80−59501
InSb:Cr, Zn and InSb:Zn, impurity centre behaviour, impurity conc. and Hall coeff. meas. 80−65490
p-InSb:Cu(Ag), ionisation energy and distrib. of multiply charged impurities, compensation effects 78−18996
InSb:Sn, equilibrium distribution coefficient of Sn 79−10872
InSb:Te, cryst. growth from melt, pulling method, US effects on facet growth 80−76169
InSb-GaSb, directionally solidified, determination of non-constant distrib. coeffs. 78−76641
InSb-NiSb, eutectic alloy, Te-doped, electrophys. props. 77−35955
KCl:Ba (0.005 at.%), spatial diffuse X-ray scatt. intensity distrib. 77−7757

impurity distribution continued
KCl:Ba(Ca)(Sr), microstruct. and hardness, impurity distrib. effects 79−24529
KCl:Ca(Ba), effect of doping on dislocation distrib., in melt grown cryst. 80−6410
KCl:Eu^{2+}, optical absorpt. meas. for Eu^{2+} conc. determ. 79−51137
KCl:Pb, impurity distrib., light scatt. and microhardness study, heat treatment 80−96562
KCl:Pb crystal surfaces,,Au decoration, electron microscope study 80−15144
KCl:Pb crystals, development of mechanical stresses during growth 80−19735
KCl:Sr, single crystal, thermally stimulated topochemical reactions 79−28011
KCl-Ba, X-ray irrad. cryst., thermoluminescence spectra 80−20719
KCl-KBr, mechanism of aggregation of divalent impurities, dielectric loss meas. *(Japanese)* 79−60394
KH_2PO_4, elec. cond. and diffusion, Co dopant effects 77−72716
KI:Tl, crystallisation from melt by various methods, impurity distrib. 77−4733
K(Zn,Mn,Co)F_3, crysts., Mn, Co distrib., as function of cryst. region *(German)* 78−14375
$La_{1-x}Tb_xOBr$, phosphor, concentration quenching of Tb^{3+} luminesc., Tb^3 conc. determ. 80−29785
LiCl:Na (K,Rb,Cs,Ag), theoretical and experimental study of partition coeffs. of isovalent impurities 79−65111
LiF, alkali ion implantation, migration, segregation, effect on optical props. 80−100269
LiF, deformed in liquid He, penetration of He, dislocation effects 77−20131
Li_3N:H, ionic cond., impurity conc., IR transmission meas. 79−42305
Li_3N:H, ionic cond., nuclear reaction anal. 80−34454
$LiNbO_3$, OH^- ion incorporation, mobility and optical absorpt. 77−35583
Li_2O, C atom conc. profile determ. by proton backscattering 78−10079
Li_2O-Al_2O_3-SiO_2:Cd^+, glass, ESR study 80−103879
LiT, retention and distrib. of ^{3}He NMR studies 79−69153
^{6}Li, in solid absorber, large depth profile meas. by deuteron induced reactions 77−19978
MgO, single cryst. grown by arc fusion, C content 77−68991
MgO:Co ions, impurity distrib. from EPR 77−51401
$MgSeO_4.6H_2O$:Mn^{2+}, EPR obs., rel. to Mn crystallographic sites 78−79628
Mo, D and ^{3}He trapping and mutual replacement 80−59493
Mo, diffusion of H(D), trapping at ion implantation induced defects 77−47622
Mo films, sputtered from cylindrical-post magnetron with Ne, Ar, Kr and Xe, compressive stress and presence of inert-gas obs. 80−80140
Mo, fission fragment bombardment, channelling effects *(Russian)* 78−38762
Mo:H(He), depth profiles of implanted atoms, proton backscatter meas. 79−51136
Mo:He, accumulation and distrib., monolayer conc. by sputtering quantitative anal. 80−49253
Mo-Ca, ion implanted, range distrib. of Ca^+ ions, work function and AES obs. 78−27365
Mo-transition metal admixtures, equilib. distrib. coeff., functional dependence *(German)* 77−76566
$NH_4H_2PO_4$, elec. cond. and diffusion, Co dopant effects 77−72716
$NH_4H_2PO_4$:^{57}Fe, Mossbauer study, Fe^{3+} effect in habit 80−100627
$(NH_4)_{2(1-x)}Rb_{2x}SO_4$, stoichiometry defects, electron probe microanal. 80−39143
$(NH_4)_2SO_4$:Cu^{2+}, ferroelec., ESR, Cu^{2+} in trigonal bipyramidal coord. 78−23330
Na:O, evaluation of V wire equilibration method, for determining O content 78−79626
NaBr:Tl, impurity segregation with Kyropoulos growth 78−9977
NaCl, elec. cond. and distrib. of Ni^{2+} ions 79−33010
NaCl:Ca(K), impurity state from heat treatment on microhardness 77−80532
NaCl:Eu^{2+}, optical absorpt. meas. for Eu^{2+} conc. determ. 79−51137
NaCl:$MgCl_2$ (0.1 mol.%), thermoluminesc. glow curves, temp. distrib. and trapping centres 78−48241
NaCl:$PbCl_2$ crysts., melt grown, Pb distrib. determ., UV spectrochem. anal. 78−40101
Nb, diffusion of H(D), trapping at ion implantation induced defects 77−47622
Nb, He depth distrib. meas. 77−30665
Nb, He depth profile meas. by nuclear reaction methods 79−14839
Nb, O impurity distrib. determ. by neutron activation anal. *(Russian)* 80−70243
Nb, of He, replacement of implanted ^{3}He by subsequent ^{4}He bombardment, and vice versa, using ^{3}He(d, α) 79−4325
Nb single cryst., He ion implantation, depend. of blister deckeldicke and depth profiles on incidence angle 79−73226
Nb:Li, depth profiling using ^{7}Li(p,n) reaction 77−80534
Nb-H, interstitial position of H from entropy of soln. 77−65989
Ni, deuteron diffusion obs. by D(d,p)T reaction *(German)* 77−59150
Ni, foil, electron bombard., impurity redistrib. during third stage of annealing, residual resist. meas. 80−6434
Ni, growth direction orientation effect on impurity distrib. 78−47261
Ni, He depth profile meas. by nuclear reaction methods 79−14839
Ni, trapping and release of inert gases, thermal evolution mass spectrometry 78−95077
Ni:Bi, impurity site distrib., channelling and nucl. orientation obs. 77−15447
Ni:D, diffusion study using D(d,p) reaction 79−5202
Ni:F, lattice location of implanted F rel. to mag. hyperfine fields 77−59041
Ni:Mn, radiation-enhanced diffusion, effect of point defect fluxes 77−89588
Ni/Cr multilayers, AES depth profiling by sputtering with N_2^+ ions 79−95881
Ni-Fe-Mo(Cr), determ. of preferential locations of Mo or Cr on Fe and Ni sublattices, by X-ray intensity study 79−37662
Ni-S, S atom redistribution under high temp. electron irrad., residual elec. resist. reduction *(Russian)* 79−82256
Ni-Zn ferrite:Co^{2+}, synthesis of optimal quality recording head mat. 77−52272
Pb ceramic glaze, Cu^{2+} doped, Pb^{2+} release 80−49101
Pb-Au, interstitial and substitutional distrib. 80−84204

impurity distribution continued
PbF_2:Mn, mag. tagging of ion diffusion, ^{19}F NMR meas. 80−108106
$Pb_{1-x}Sn_xTe$, epitaxial layers, In doping, donor impurity singularities, distrib. coeff. 77−80526
$Pb_{1-x}Sn_xTe$:Cd, Cd diffusion obs. using Hall mobility and Cd solubility expts. 78−26584
$Pb_{1-x}Sn_xTe$:Cd, distrib. of Cd atoms in cryst. lattice after compensation metal vacancy sites 79−69292
$Pb_{1-x}Sn_xTe$:Cd, long-wavelength photosensitivity shift on annealing, Cd influence 78−26912
PbTe:Cd, Cd diffusion obs. using Hall mobility and Cd solubility expts. 78−26584
PbTe:Cd, distrib. of Cd atoms after compensation of metal vacancy sites 79−69292
PbTe:Ga, location, behaviour of Ga, electrophysical props. meas. 79−38016
$PbWO_4$, single cryst. growth by Czochralski method and U incorporation, effective distrib. ratios, luminesc. characts. 79−42094
$PbZr_{0.95}Ti_{0.05}O_3$:oxide doped, A and B site dopant distrib., antiferroelec.-ferroelectric transition 78−34532
Pd-Ag-H, alloys, 25-50% Ag, thermodynamic props., 555-700K 79−65216
Pd-H, interstitial position of H from entropy of soln. 77−65989
Pd-H, Mossbauer study of local environment of substitutional Co and Fe impurities 80−60475
$(Pd_{0.8}Au_{0.2})D_{0.04}$, lattice location of D, ion channelling obs. 78−67708
α-$PdD_{0.007}$, lattice location and thermal props. determ. of D by ^{3}He channelling 78−38747
Pt-Si:As, silicide form. during laser irrad., p-n junctions and ohmic contacts 80−84397
RbCl:Eu^{2+}, optical absorpt. meas. for Eu^{2+} conc. determ. 79−51137
Sb_2S_3 spherolite crysts., direct lattice resolution obs. of defect struct. 80−107255
ScH_x:Er, proton distrib. and site energies, ESR meas. 80−59509
Se:U, cryst. and amorphous, impurity conc. and distrib., solid state nuclear track detection 79−46694
Si, ^{75}As implantation, scanned CW electron beam annealing 79−99225
Si, amorphous, asymmetrical profile of ion implanted P 79−46693
Si, amorphous, H isotope backscattering, trapping, and depth profiles, model 79−99233
Si, amorphous, ion implantation method, B and P ions 80−100274
Si, amorphous film, EELS microanalysis 80−100722
Si amorphous film, ion-implanted, regrowth 79−15043
Si, and SiO_2 on Si, ranges of implanted B^+ and B^{2+} 77−31687
Si, annealing, using laser pulses, impurity incorporation at melt-cryst. interface 80−59504
Si, characterisation by photolum. method *(Japanese)* 79−38638
Si crystal growth, for electronic devices 80−66419
p-Si, Czochralski grown, microdistrib. of O, SEM and spreading resist. obs. 80−79830
Si Czochralski grown, O distrib. meas. 77−11580
Si, Czochralski grown crystal, radial impurity distrib. improvement 77−73225
Si, deep diffusion of B and P, expt. results 80−54437
Si, determination using anodic oxidation 80−40583
Si, diffusion coeff. of Se, by sheet Hall coeff. meas. 79−46843
Si, diffusion layers, B distrib. 77−7753
Si diffusion profiles, P and B diffusion determ. *(Rumanian)* 79−77615
Si diode, impurity profiles, scanning electron microprobe anal. 80−79832
Si, dislocation free, C and O impurity clouds, heat treatment influence on light scatt. 80−6427
Si, displacement of group III, IV, V, and VI impurities in Si by He^+ and H^+ analysing beam 79−4330
Si, doping impurity distrib., during cryst. growth by Czochralski method *(Russian)* 80−100276
Si, EFG ribbon, characterisation by ion beam tech. 80−79833
Si, effect of disorder on H content 80−75258
Si, epitaxial, minority carrier lifetime and impurity conc. meas. *(Japanese)* 80−25025
Si epitaxial layers, grown in vac. at low temps. P and Sb doping 80−88189
Si epitaxial layers, vacuum deposited, conditions for impurity migration from B, P, Sb doped sources *(Russian)* 80−107570
Si epitaxial structures, junction layer width and impurity conc. estimates *(Russian)* 80−49893
Si filamentary crystals, grown from vapour, electron probe microanal. 79−77538
Si film, solid phase epitaxy, Au and O distrib. 77−66095
n-Si, gamma ray irrad., impurity composition influence on recombination centre formation 80−6872
Si, H^+ and H_2^+ ion implantation profiles determ. by SIMS 79−4334
Si, high dose Pb^+ and Cs^+ distribs., determ. using low angle Rutherford He ion backscatt. 79−4327
Si, implanted ^{16}O, lattice location of ^{16}O by α-particle backscatt. method 78−10080
Si, implanted Bi distrib., planar oscills. effects, low angle He^+ backscatt. obs. 78−34534
Si, impurity conc. from MOS DC transfer characts. 78−2155
Si, impurity content characterisation, exciton luminesc. 80−60653
Si, impurity determination, by neutron activation analysis 78−11586
Si, impurity penetration depth, chemical-spectral determ. 80−19830
Si, ion implantation-induced damage after Ar and P implantation, defect density and distrib. *(German)* 77−24337
Si, ion implanted, laser-annealed, theoretical anal. of thermal and mass transport 78−91364
Si, ion-implanted, laser annealing at 1.06 μm, computer simulation 79−47556
Si, ion-implanted, thermally oxidised, Rutherford backscatt. analysis 78−19910
Si ion-implanted laser-annealed solar cells 80−93881
Si, ion-implanted layers, total X-ray reflection investig. of clustering 78−6081
Si large grain films on metallurgical Si substrates, metallic impurity distrib. and conc. 80−61357
Si layers, epitaxially grown on sapphire substrates, Al conc. as a function of depth using ^{27}Al(p,α_0) reson. reaction 79−4328
n-Si, magnetoresistance, growth layer influence, effect of randomly distributed inhomogeneities 80−20229
Si, melt grown crysts., impurity incorporation, calcs. 80−79718
Si, monocryst. plates, purification by thermal diffusion, impurity migration anal. 80−25553

impurity distribution continued
Si n/n^+ epitaxial layers, anomalies of Sb distrib. 80−65035
Si, neutron transmutation doping, ^{31}P conc. meas. 80−19833
Si, optical inhomogeneities obs. by spectral modulator 78−59144
Si oxidation, dopant redistrib., Cs^+ SIMS anal. appl. 79−39265
Si p^+-n junction diodes, flow fluence S implanted unequal defect densities, dynathermal obs. 80−20293
Si, p-n junction, dopant conc. diffusion length and lifetime variations, SEM obs. 79−82604
Si, precipitation of Au, supersaturated soln., Hall effect meas. 77−89465
Si, redistribution of impurities during single oxidation step, computer program calc. 80−2060
Si ribbon, EFG, C contaminant conc. determ. by nuclear techniques and SIMS 80−59506
Si, ribbon, impurity distrib. in EFG 78−91280
Si ribbons grown by capillary action shaping technique, surface quality and impurity distrib. 80−108343
Si single crystal ingot growth from metallurgical grade Si, inhomogeneities 80−59416
Si, sputtered, cluster formation, influence of HF plasma interaction 78−64441
Si, stacking fault form. model during oxidation and ageing, defect clustering 77−24322
Si, status of defect studies 77−84742
Si, surface, controlled stripping, automated system 78−31557
Si surface, ion bombardment enhanced mixing of Ag layers, Rutherford backscatt. meas. 80−65034
Si, surface-barrier detector, impurity distrib., influence on characts. 80−18766
Si, swirl defects, gettering effects, obs. by photoluminesc. meas. 78−84623
Si, thermally induced microdefect form., C and O role 80−11439
Si, thin sheet, Sb impurity profile eval. in p-n diffusion junction by anodisation and resist. meas. 79−46695
Si two-step impurity diffusion, effect of internal elec. field 77−76624
Si vacuum sublimated thin film structure impurity distrib. 78−95354
Si wafer, heat treatment behaviour of microdefects and residual impurities, X-ray diffr. and IR absorpt. study 80−49214
Si: (B, P, Ge), impurity-pair diffusion, influence of elastic stresses 78−87824
Si:^{85}Kr, ion-implanted, impurity distrib. 80−15145
Si:Ag, surface layer, ellipsometry 78−19121
Si:Ag (Zn,Fe), diffusion mechanism of fast impurities, distrib. in surface layers 77−11735
Si:Al(Ga), O_2 diffusion, conc. profile meas. 80−79990
Si:As, ion implanted layers in device structures, boundary effects in laser annealing 79−73188
Si:As, shallow junctions by high-dose implants 80−96694
Si:As, solid solubility and thermal behaviour of metastable 80−75359
Si:Au, impurity diffusion and distribution obs. by neutron activation analysis *(Japanese)* 77−84787
Si:Au, impurity induced internal friction, impurity centre symmetry 79−73252
Si:Au, P-induced point defects influence on Au gettering mechanism 80−65030
Si:Au(P)(B) whiskers, impurity inhomogeneity 80−39145
Si:B, diffusional impurity redistrib., elastic stress field effect *(Russian)* 77−72719
Si:B, distrib. profiles, high temp. treatment effects 79−69150
p-Si:B, high temp. treatment, effects on ion implanted impurity distrib. profile 78−79625
Si:B, implanted, free carrier conc. and impurity location, Raman scatt. obs. 77−55295
Si:B, implanted laser annealed, lattice strain, X-ray study 80−96554
Si:B, impurity conc. from photoluminesc. anal. 78−63785
Si:B, ion implanted, SOS device struct., nonlinear impurity redistrib. 79−1625
Si:B, ion implanted, structure defects formation and behaviour under annealing in various ambients 80−65033
Si:B, lattice location of implanted ions after laser annealing 78−30660
Si:B, sputtering influence on distrib. profile of ion-implanted impurities 79−42091
Si:B doping from BN sources, impurity transfer considerations 77−76441
Si:B ion implanted, strain profiles from X-ray rocking curves 80−107290
Si:B redistribution after oxidation, integro-differential eqn. 77−76453
Si:B sputtering by Ar^+, computer simulation of sputter broadening in impurity depth profiling 80−2908
Si:B^+, ion implanted, lateral spread of B^+ ions through SiO_2 mask 79−51130
Si:BF_2^+, ion implantation appl. in semicond. device production 80−103383
Si:B(Be)(Li) ion implanted, channelling and random equivalent depth distrib. 80−100293
Si:B(Ga), heavily doped, form of occurrence of acceptor impurities 77−11581
Si:B(P), impurity-peak form. during proton-enhanced diffusion 79−55772
Si:B(P), ion implanted crystalline and amorphous laser annealing 80−97509
Si:Bi, ion-implanted, solid phase epitaxial growth during annealing, supersaturated solid soln. form. 80−103384
Si:C(O)(Sb), striated impurity distrib. calc. in melt-grown crystals 80−24488
Si:Cr, ion implanted, Cr conc., depth distrib. and diffusion coeff. 80−49243
Si:Cu(Au), recoil implantation from thin surface films, backscatt. obs. 78−63783
Si:Fe, B thermally activated Fe interstitial, elec. and kinetics props. *(German)* 80−34035
Si:Fe, EPR and neutron activation anal. of thermal defects 78−91355
Si:Ga^+, impurity distrib. profiles using SIMS and Hall effect method 79−69152
Si:Ge B, strain compensation, X-ray Bragg reflexion 80−39137
Si:H, amorphous, exodiffusion of H, EPR expts. 80−49102
Si:H, amorphous, glow discharge deposited, thermal dehydrogenation, IR spectra 80−44442
Si:H, amorphous, H content determ. by IR absorpt., gas evolution and nuclear reaction methods 80−44130
Si:H, amorphous and crystalline, hydrogenation and dehydrogenation, luminesc. spectra 80−11477

impurity distribution continued
Si:H, ion implanted, anal. of methods used for H profiling in materials using ion beams 79−5197
Si:H, plasma-deposited amorphous film, proton mag. reson. 80−44931
Si:H amorphous film, plasma-deposited, growth morphology and defects 80−44128
Si:H amorphous film, plasma-deposited, elec. and comp. heterogeneity 80−44745
Si:H amorphous film, sputtered IR vibr. spectra and photolum., effects of partial evolution of H 80−44413
Si:H amorphous films, effects of glow-discharge prep. conditions on H content 79−46969
a-Si:H film, glow discharge deposited, H profiles, doping level 80−84202
Si:In, clustering and precipitation, time-dependent perturbed ang. correlation meas. 80−65234
Si:Ir, Ir diffusion and solubility 77−15448
Si:Li, strongly doped, piezoresist., gas-liq. type transition 77−43600
Si:O, 9 μm absorpt. band attributed to dissolved O, from expts. on quartz particles 79−19914
Si:O, annealing behaviour of O donor, conc. reductions via resistivity meas. 79−51129
Si:O, C, impurity conc. profiles and process-induced defects 78−6094
Si:O, comparision of depth profiling techniques 80−29048
Si:O, Czochralski crystal, oxygen striation and thermally induced microdefects 80−100275
Si:O, high temp. annealing effect on impurities 78−38745
Si:O, implanted O location, channelling effect meas. 78−26593
Si:O, impurity conc. profiles, scanning IR absorpt. using semicond. laser 80−50376
Si:O, impurity solubility and diffusion props. 78−6093
Si:O, specific resist. rel. to annealing, Si-O complex form., O_2 distrib. *(German)* 77−72863
Si:O, Xe, ion implanted, Xe retention, Rutherford backscatt., comparison with SiO_2+Xe 79−4320
Si:P, Au, neutron irradiated, distrib. of P and Au determ. 78−79627
Si:P, distrib. depth for dislocation loops and P precipitates 79−55756
Si:P, distrib. of implanted impurity after laser annealing, e.s.r. and neutron activation analysis 77−4122
Si:P, impurity conc. from photoluminesc. anal. 78−63785
Si:P, impurity redistrib. by Ar ion hot implantation 77−72633
Si:P, N implantation through Si_3N_4 film, depth distrib. of knock-on N, SIMS meas. 78−10066
Si:P(B), high temp. impurity diffusion via vacancies and self-interstitials 80−24667
Si:Pb, implanted and annealed, impurity redistrib. 78−75689
Si:Pt, implanted and laser annealed, segregation and increased dopant solubility 80−65016
Si:Sb, high dose implanted, orientation dependent annealing effects 78−18665
Si:Sb, ion implanted, Sb diffusion during oxidation, snow-plough effect 80−88366
Si:Sb, redistribution of thin impurity layers after laser annealing, theoretical model and expt. results 79−69147
Si:Te, laser melting, surface Te atom accumulation, profiles 80−100258
Si:Zn, implanted atom diffusion during laser annealing 79−37725
Si/surface porous oxide film, impurity distrib. during P diffusion 77−39944
Si-H, amorphous, H three-dimens. distrib., ion-induced AES and Rutherford backscattering 80−44132
Si-Si_3N_4-SiO_2-Si multilayer structs., impurity distrib., activation anal., autoradiography techniques 77−16881
Si-SiO_2 interface morphology, P pileup effect, Auger sputter profiling 78−72006
α-SiC, epitaxial layer, impurity macroincorporation, distrib. of Al, B, N and P 77−69192
Si_xGe_{1-x}, Ge distrib. in single crysts. grown by zone refining without crucible 78−22754
SiN_x, plasma deposited, H content meas. 78−63949
Si_3N_4 film, diffusion of Al, AES and depth profiling 78−51744
Si_3N_4, film, H_2 concentration profile, chem. bonding 79−33205
Si_3N_4, oxidised ceramic, O_2 depth profiling using ^4He backscatt. 77−89463
Si_3N_4:$(MgO+Al_2O_3)(Y_2O_3)$, hot-pressed and sintered, microstruct. and impurity distrib. 80−49261
Si_3N_4:H, film, impurity profile determ. by 1.2 MeV proton-proton scatt. 80−49256
Si_3N_4-SiO_2:N,Zn ion-implanted multiple layers, ion range distribs., secondary ion microprobe meas. 79−42129
SiO, film, effect of ion implanted O_2 on optical props. 80−45027
SiO_2 based optical fibre waveguides, water impurity 77−68270
SiO_2 based optical fibre rod preform, optical meas. of OH ion distrib. 78−87130
SiO_2 film, O, F, B isotopes in profiling by quantitative SIMS 77−9147
SiO_2 film on Si substrate, Na transport caused by ion and atom impact 80−6682
SiO_2, formed by Si oxidation in trichloroethylene-O_2, Cl incorporation and elec. props. 79−91827
SiO_2 in MOS struct., room temp. cond., mobile Na^+ location 78−39217
SiO_2, insulating films, neutron activation anal. and autoradiography 78−92574
SiO_2 prepared in O_2-HCl and H_2O-HCl ambients, Cl conc. profiles using SIMS 79−65110
SiO_2:^{85}Kr, ion-implanted, impurity distrib. 80−15145
SiO_2:Cl film, grown on Si surface in O_2-HCl mixture, Cl incorporation 79−70186
SiO_2:Ga film, impurity distrib. after annealing, neutron activation anal. 80−24484
SiO_2:Na, film, depth profiling by SIMS 78−79624
SiO_2:P films, P content determ. by IR absorpt. and activation anal. 79−51139
SiO_2:P_2O_5, GeO_2 fibre, anomalous conc. profile of P_2O_5 and GeO_2 77−79943
SiO_2:Xe, ion implanted, Xe retention, Rutherford backscatt., comparison with Si-O, Xe 79−4320
SiO_2-GeO_2, synthetic, struct, IR spectra 79−42993
SiO_2-Na_2O-CaO-MgO float glass, surface SnO_2 distrib., ellipsometry and XPS study 80−84346
SiO_2-P_2O_5 glass film, CVD, P conc. profile by etch rate technique 80−96450
SiO_xN_y films on Si, ^{16}O conc. profiles anal., using (d,p) and (d,α) reactions with mag. spectrom. 79−5215

impurity distribution continued
SiO_xN_y, low temp. films, comp., chem. bonding and contamination 78−47676
SiTe:Ge(Sn), substitution of Si, thermoelectric props. *(Russian)* 80−11023
Sn, liq., electrodiffusion conc. of impurities 80−54414
SnS(Te):O, impurity assoc. with Fe microtraces, Mossbauer effect meas. 77−20763
$SrWO_4$, single cryst. growth by Czochralski method and U incorporation, effective distrib. ratios, luminesc. characts. 79−42094
Ta film, determ. of thickness and O, N content 78−80824
Ta, thermally oxidised, ^{16}O conc. profiles anal., using (d,p) and (d,α) reactions with mag. spectrom. 79−5215
Ta-8W-2Hf wt.% (t-111) alloy, dissolution kinetics of small amounts oxygen, internal oxide disp. reactions, annealing 77−16612
Ta-H, interstitial position of H from entropy of soln. 77−65989
$TaD_{0.10}$, lattice location of D, ion channelling obs. 78−67708
Ti alloys, metallurgical characterisation using thermoelec. power meas. *(French)* 80−45462
Ti, thermally oxidised, ^{16}O conc. profiles anal., using (d,p) and (d,α) reactions with mag. spectrom. 79−5215
Ti:D, ion implanted, depth profiles, temp. depend. 80−100270
Ti:T, depth profiling by neutron TOF spectroscopy 77−73500
Ti-Al-V, VT6 alloy, butt welded joints, electron beam welding conditions effecting interstitial impurities distribution 80−39136
β-Ti-Mo-V-Fe-Al (8, 8, 2, 3, wt.%), exam. of stress induced H_2 migration 78−87823
TiAl, Ti_3Al, ordered alloys, Fe impurity atoms distrib. *(Russian)* 77−35584
TiC film, CVD, on WC, diffusion processes, ion beam anal. 80−49424
TiO_2:V, localisation and migration of V^+ ions, ESR and ESCA study *(French)* 79−33529
TlBr-TlI crystals, Pb halide impurity distribs. for various cryst. orientations 79−51135
U, γ- and β-hardened, recrystallisation, effect of impurity distrib. 78−70602
V, H_2 permeability, surface impurity layer effect 77−24440
V, neutron diffraction determ. of O, N, C interstitial sites 77−19944
$V\text{-}D_{0.01}$, enrichment of D during the ion bombardment 80−54288
W (110), D^+ depth distrib., effect of surface impurities, channelling model 79−1451
W:^{3}He, implanted ion positions, determ. using mol. deuteron beam 80−70240
W:K-Al-Si, state of bonding, distribution of impurities 78−92212
YAG, influence of facial growth effect on Yb ion incorporation 79−10822
$YFe_{5-x}Al_xO_{12}$, impurity redistrib. kinetics, temp. depend., vacancy effects 80−75263
$Y_3Fe_{5-z}Al_zO_{12}$, mixed garnet, cation distrib., temp. depend., magnetisation study 80−79831
$YFe_{5-x}Ga_xO_{12}$, impurity redistrib. kinetics, temp. depend., vacancy effects 80−75263
$Y_3Fe_{5-z}Ga_zO_{12}$, mixed garnet, cation distrib., temp. depend., magnetisation study 80−79831
YH_x:Er, proton distrib. and site energies, ESR meas. 80−59509
YIG, diamagnetically substituted, annealing effects on cation distrib. 79−1455
YIG:Ir, Ir on tetrahedral sites, contrib. to mag. anisotropy, optical absorpt. meas. 77−69867
YbTe, high-temperature evaporation and reactivity 80−103469
ZnO:Co ions, impurity distrib. from EPR 77−51401
ZnS ion beam etching, topographic changes, amorphisation, luminescence study 80−76078
ZnS, single cryst., grown from melt, distrib. coeffs. of transition metals, Pb and Sn 77−55298
ZnS:Ag film, photocapacitance IR quenching, hole photoionisation energy and spectral distrib. 79−87127
ZnS:Cu,Cl, exciton refl. spectra, hexagonal struct. 77−44021
ZnS.CdS, flux growth, processes accompanying roasting of CdS+NaCl 78−23590
ZnSe:Ag(In)(Cu), melt growth, dopant partition coeffs. 79−14837
Zr, deuteron implanted, temp. depend. depth profiles of deuterons 78−95076

impurity electron states
see also A-centres; Anderson model; charge compensation; deep levels; electron traps; heavily doped semiconductors; impurity scattering; OH^--centres; U-centres; Z-centres
acceptors, randomly distributed, direct energy transfer via exchange from excited donor 80−65483
activated crystal, electronic excitation energy migration efficiency, inverse transfer influence 78−19546
activated crystals, influence of temp. on energy transfer 79−28323
activated crystals, Jahn-Teller effect in optical bands of impurity centres 78−6706
activation energy number, spin degeneracy values *(Russian)* 79−69462
adatom, electronic states, correlation effects, self-consistent T-matrix calc. 80−44691
adatom density of states, impurity atom effects 80−92958
Al-Mn(Fe)(Co)(Ni)(Cu), alloy, dil., electronic states, XPS meas. 77−44117
alkali halide: $Ge^{2+}(Sn^{2+})(Pb^{2+})$, T-centres, absorpt. spectra, energy level diagram 77−73157
alkali halide: S_2^-, laser-excited spectra and reorientation of S_2^- 77−28563
alkali halide:Sn^{2+}, V_c^--centres, vacancy induced splitting of excited states, Sn^{2+} structure 78−51931
alkali halide:Sn, excited states producing polarised type A emission from Sn centres 78−10945
alkali halide=O_2^- soln., phonon wings in luminescence spectra *(Ukrainian)* 79−52001
alkali halide, far IR props. of lattice resonant modes, hydrostatic press. effects 77−28574
alkali halide, FCC, PO_4^{3-}-$Al^{3+}(Sb^{3+})$ anion-cation impurity mol. complex, IR absorpt. obs. *(Russian)* 77−16317
alkali halide crystal, activator centres, excited state transitions, bleaching dynamics 79−4527
alkali halides:Ga^+, optically detected EPR in relaxed excited states of Ga^+ 78−72437
alkali halides, F-centre, cluster-Bethe lattice treatment 78−63762
impurity electron states continued
alkali halides, luminescence of Tl^{-1}-like centres, Ga^+-centre polaris. effect 79−33806
alkali halides, polarization, photoinduced, rel. to exchange between vacancy and impurity 80−59914
alkali metal:halogen, charge transfer excitations 79−95815
alkali metal:inert gas, optical absorpt. by impurity, cluster Bethe lattice calc. 77−8612
alkali metal, HMPA frozen soln., Wannier-Mott impurity ground state, EPR 77−8054
alkali metal film, inert gas impurities, sharp pair spectra and excited states 77−24877
alkali metal halides, hyperfine struct. of V_K and $(XY)^-$ centres, valence band wave functions 77−11873
alkali metal with rare gas impurity, extra-orbital relax. model, hole-electron creation 79−4825
alkaline earth fluorides, rare earth doped, photoionis. thresholds 79−78132
alkane:toluene, radiolysis at 77K, luminesc., excited singlet toluene form., energy transfer mechanism 77−16846
n-alkanes, single cryst., γ-irrad., ESR, energy deposition rel. to alkyl radical form. 77−16844
alloys, dil., mag. field and impurity interaction effects on resist., Anderson model 79−51554
alloys, disordered, muffin-tin model, electronic struct. and density of states, theory 80−29301
amorphous semiconductors, conductivities, drift and diffusion 79−95413
Anderson model, asymmetric, perturbation theory 80−6766
Anderson model, direct interaction between impurities 80−54681
Anderson model, dynamical susceptibility of impurity electrons 77−12090
Anderson model, ground-state energy 79−99511
Anderson model, impurity pair interactions, local moment form., var. method 80−92854
Anderson model, non-orthogonal elec. resist. 80−59947
Anderson model, T-matrix approx., self-consistent soln. 78−43330
anisotropic crystal, exciton-impurity complexes *(Russian)* 77−80741
anisotropic crystal impurity states, perturbative theory 80−34390
anisotropic impurity centres, local relaxational phase transitions *(Russian)* 80−44220
anthracene:2-hydroxyanthracene cryst., site selective photochem. change, fluoresc. obs. 77−40273
anthracene:tetracene, delayed fluorescence excitation spectra 78−39594
anthracene, impurity effects on elec. cond. *(Russian)* 77−62930
antiresonant electron-phonon system, in strong-coupling limit, moments and absorption line shape 77−24875
Auger transition from excited Coulomb level of deep impurity centre to ground state 79−15116
band gap narrowing, physical mechanisms 80−15478
band modification caused by impurities and magnetophonon effect 79−42562
beat effect of sp. ht. due to impurities, in external mag. field 78−10401
benzene phenol crystal, asymmetry of phonon side bands, absorption, luminesc. and specular spectra 77−1730
beryl, channel constituents, electronic absorption spectra of Fe^{2+} 79−69863
binary alloy, determ. of distortion field 80−44536
bound excitons in local density approximation 79−47022
bound states in a random potential 77−47762
bulk trap energetic distribution props., space charge limited current meas. use 80−80293
capacitance transient spectroscopy, book contrib. 78−10548
carbazole, triplet state of X-traps, ODMR 79−24231
carrier conc., temp. depend., computer data anal., effect of band parameter errors *(Russian)* 78−52006
CdS, green edge luminescence spectrum, temp. depend. 80−108274
CDW, impurity effects on long-range order in incommensurate phase 77−51678
CDW dynamics, impurity pinning in single chain 78−47716
chalcogenide glass, localised gap states, Mott-street model 79−37968
chalcogenide glasses:Cu(Mn), elec. cond. increase on impurity addition 77−11920
chalcogenide glasses, conductivity, doping effect 79−38062
chalcogenide lone-pair semicond. charged impurities, effect on carrier concs., Street-Mott model 78−67984
chalcogenide semiconductor, density of valence-alternation centres, influence of additives 78−47733
charge densities, calc. method 79−42433
Condon approximation, shape of absorpt. and fluorescence bands, effect of electron-phonon coupling *(Russian)* 77−48212
conduction phenomena, review of exptl. work *(Japanese)* 80−49737
Covalency and hyperfine interaction on the impurity ion in crystals 78−23063
covalent semiconductors, optical absorption by acoustic phonons related to shallow impurity levels 77−4665
crystal, impurity, light absorpt. max. at Brillouin zone boundary 80−55139
crystal colour, lattice defects and impurities 78−72562
crystals, dipole-impurities, free-carrier absorpt. and dielec. losses calc. 77−63363
Cu-Ni, dil. alloy, optical reflectivity meas. virtual bound state model analysis 78−2873
Cu-Ni(Mn)(Fe)(V), dil., local mag. moments and Kondo effect, theoretical model 79−69651
cubic semiconductor, Zeeman split acceptor levels, calc. method 79−28322
cyclotron resonance width of impurity system in two dimens. 77−35892
d-band metals and alloys, s-d hybridisation 78−91644
DC Bi:Te, elastic consts., electronic contrib. 77−84826
degenerate d-electron alloys, dilute, local moment and ferromagnetic state formation 79−51748
degenerate semiconductors, impurity band struct. for dense donors and acceptors 80−29348
density of states for crystal with impurity levels near band edge, fluctuation states *(Russian)* 77−69274
detection by admittance-freq. dispersion 77−43536
deuteronaphthalene:β-deuteromethylnaphthalene crystal, asymmetry of phonon side bands, absorption, luminesc. and specular spectra 77−1730
diamond: B, natural, sub PPM determ. of B, identification of acceptor centre 77−59035
diamond:B, B conc. and impurity-to-band activation energy 79−56165

impurity electron states continued
diamond:Li, ion implantation, Hall effect and elec. cond. meas. 80−15526
diamond:N(B)(Si)(O), substitutional impurities 79−87056
diamond, effective supersystem cryst. simulation method, geometrical parameters, bulk moduli, impurity levels calcs. *(French)* 80−15430
diamond, ion-doped with Li electron transport 80−92917
diamond, N9 and ND1 energy levels, electron irrad. photocond. obs., thermolum. 78−6324
diamond, natural, N3 luminesc. decay time 78−76520
diamond, natural, N centres, thermolum., phosphoresc., low temp. 78−11000
diamond, semicond., energy band struct., elec. and optical props., review 77−35862
diamond, van Hove singularities, absorpt. and luminesc. electronic-vibr. spectra 80−70639
diatomic molecule in solid lattice, nonradiative relax. of intramolecular vibr. 77−52178
dibenzofuran, triplet state of X-traps, ODMR 79−24231
dibenzothiophene, triplet state of X-traps, ODMR 79−24231
dibenzyl: naphthacene, cryst., ground electron state, vibr. levels, relax. time determ. *(Russian)* 78−15195
4,4′-dichlorobenzophenone, cryst., X-traps, rel. populations, elec. field effect 77−12414
dilute alloy, electronic config. and vol. of formation 79−90991
dilute alloy, method of orthogonal operators 79−33254
dilute alloys, transitional and noble metal impurities in simple metals, electronic struct. 77−43528
dilute quasi-one-dimensional system, trapping model 80−54640
disordered condensed media, with impurities, energy transfer 80−80217
disordered semiconductors, recomb. radiation spectrum *(Russian)* 79−4855
disordered systems, fluctuation levels *(Russian)* 77−31981
disordered systems, simplified treatment of energy levels 77−76774
distorted one dimensional system with bond disorder, electron density of states, CPA calcs. 80−24778
domain boundaries, thermal impurity depinning in two dimensions 79−73565
donor excited state lifetime, delayed avalanche breakdown 77−85231
donor-acceptor electron transfer kinetics *(Russian)* 79−38029
donor-acceptor energy transfer, quantum statistical calcs. 77−1713
donor-acceptor energy transfer, reabsorpt. mechanism 79−78041
donor-acceptor pair lines, broadening due to potentials of ionised impurities 79−51522
donors with excited states, kinetics of electron transitions 80−39600
donors with excited states, non-equilibrium phenomena, theory of kinetics of electron transitions 78−79961
doped narrow gap semiconductor, two-channel vibronic mechanism of ferroelectric phase transitions *(Russian)* 79−56745
doped semiconductor, potential fluctuations, random impurity distribution 80−88512
doped semiconductors, impurity states, cluster model 80−20117
doped semiconductors, metal-insulator transition pretransition range anal., screening model 80−6724
electron correlation and bound excitons 77−85150
electron gas, spin-polarised, self-consistent screening of positive muon 78−47714
electron gas, uniform, electronic props. of H and He impurities 80−96807
electron penetration through barrier due to repulsive centre, anisotropy 79−65497
electron state density in Gaussian random potential, path-integral approach 79−69389
electron-phonon interactions, phonons and localisation at impurities 80−24812
electronic excitation energy transfer, electron-vibr. transitions *(Russian)* 77−48232
electronic excitation energy transfer in activated crysts., math. modelling 79−38028
electrons in disordered metals and at metallic surfaces, conf., Ghent, Belgium (Sept. 1978) 80−41946
elemental semiconductor, polarisability of donors 78−14693
energy percolation is multicomponent solids 77−31972
energy transfer, to randomly distrib. acceptors, conc. and time depend. 80−29345
energy transfer and two-centre optical transitions in OH^- and rare earth double-doped solid 80−7398
EPR, optical detection in excited state *(Japanese)* 77−81029
evanescent states and complex bound structure 80−34387
excitation migration effect on luminesc. spectrum with inhomogeneous broadening 80−60676
excitation transport, two-particle eqn. 79−69472
excited-state decay for strongly interacting donors 77−8651
exciton to neutral acceptor binding energy, calcs. using atomic-like variable wave function 78−79937
exciton-ionised donor complex, binding energy, effective electron-hole interaction pot. 78−67949
exciton-neutral donor complexes, dissociation energy 80−34364
extrinsic semiconductor, Fermi level eqns. 79−99472
extrinsic semiconductors, impurity interaction and metal-nonmetal transition 80−29325
Fano effect theory, electronic structure, d band metals and alloys 78−2402
Fermi level, effect of random var. in impurity conc., n-Si appl. 79−51470
ferrocene films, plasma-polymerised, carrier trapping, elec. cond. meas., 300 to 525K 80−100543
ferroelectric semiconductor, impurity carrier effects, vibronic theory 78−43803
ferromagnet with antiferromag. impurity with arbitrary spin, ground state calc. *(Russian)* 78−43585
ferromagnetic metal-rare earth, dil., hyperfine fields 78−87947
ferromagnetic semiconductor with defects, exchange Hamiltonian 79−82777
ferromagnetic semiconductors, bound mag. polaron 79−90976
ferromagnetic transition metal, Fano effect and hyperfine field of non-transition impurity 80−25128
finite chain, with random dil. impurities, localisation characts., amplitude anal. 80−96825
fluorene:pyrene-d_{10}, exciton-guest, triplet-triplet annihilation, impurity traps effects 80−25433

impurity electron states continued
fluorene, triplet state of X-traps, ODMR 79−24231
fracture, ionisation wave generation, microbreakdown mechanism 79−33032
Friedel sum rule in static mag. field, impurity-induced mixing between Landau levels 77−31976
p-GaAs:Zn, diffusional doping, photoluminesc. in mag. field 77−16384
gapless semiconductor, magnetic field resonance states *(Polish)* 80−88508
n-Ge US attenuation due to donors and acceptors 77−28223
glass, fluorescence linewidth, anomalous of impurity ions, theory 80−50404
Goldstone system with off-diagonal disorder, location of impurity band edges 79−60466
graphite, heteroatom doped, electronic struct., energy spectrum, HMO LCAO calcs. 77−43539
graphite vacancy and substitutional impurities, moderately-large-embedded-cluster approach 80−49663
Green function and electron density of states in field of randomly distributed impurities 77−8052
halide crystals, 3p→4d transitions of transition metal ions, assignment from expts. on $LiCl:Cu^+$ 78−27272
Hall effect in impurity bands and inversion layers 79−51609
heavily doped semicond., photoemission lineshapes of impurity levels, p-wave resonance 80−76154
heavily doped semiconductor, carrier Debye screening length, temp. depend. 80−88504
heavily doped semiconductor, impurity bands, review of expt. results 79−95367
heavily doped semiconductor, n-type, Mott transition, dielec. enhancement and conduction electron screening, unified treatment 78−72073
heavily doped semiconductor with overlapping electronic orbitals impurity bands, theory 78−56102
heavily doped semiconductors and devices, review 79−47039
highly doped semiconductors, far IR absorption 79−95787
HMPA:alkali metal, density of states in band gap, EPR and optical correlations 79−61201
hopping conduction, anal. in impurity bands in inversion layers 79−47171
hot electron distribution functions, expts., review 78−27231
hot luminescence and reson. Raman effect of impurity centres 77−81149
IGFET, interface and bulk-trap states, determ. using deep level transient spectroscopy 77−8199
II-VI compounds, acceptor state model 80−2059
II-VI compounds with transition metal impurity, SCF LCAO MO formalism in CNDO and INDO approx. 79−38017
II-VI semiconductor:Mn^{2+}, superhyperfine struct. tensor and g-shift 78−39056
II-VI semiconductor solid solutions, local levels 77−1395
II-VI semiconductors, impurity and defect centre energy states, luminesc. meas., review 80−55150
II-VI semiconductors, injection electrolum., review, book contrib. 77−73174
III-V semiconductor, acceptor levels, anisotropy of Zeeman splitting and polarization of luminesc. in mag. field 79−24365
III-V semiconductors, electronic Raman scatt. on donor levels, transition matrix element determ. 79−56792
III-V semiconductors, optical transitions, effect of perturbed k-selection and gap shrinkage 80−66257
III-V semiconductors, radiative recomb., optical evaluation review 80−60647
III-V semiconductors solid solutions, local levels 77−1395
impure crystal, nuclear quadrupole spin-phonon interaction mechanism 79−95674
impurities, conc. of C, O, Si 78−59832
impurity centre-external elec. field interaction, charge transfer processes influence 78−87944
impurity centres, electron-phonon coupling from structured optical spectra, review 80−89038
incommensurate-commensurate transition, impurity pinning effect on commensurate CDW state 79−65394
indirect coupling between localised impurities, virtual bound state model 78−64001
indirect gap semiconductor, valley-orbit interaction and effective-mass theory 78−23043
inert gas:H, quasifree electron energy, inference from ESR studies 79−69459
n-InSb, acceptor effect of plastic bending 80−6885
insulator, disordered, charged impurity states, Lloyd model 80−29360
insulator with uniform distrib. of traps, nonequilib. photocond. *(French)* 78−43433
insulators, improved effective mass for impurity levels 78−87941
interband optical absorption in solids, effect of impurity 79−38577
ion clusters in two-dimens. lattice 78−23047
ionic crystal:transition metal, excitation and trapping at impurity sites 79−33776
ionic crystals, nonradiative multiphonon transitions in impurity centres with extremely weak electron-phonon coupling 80−25436
ionised impurity scatt. 78−51984
isotopically mixed crystals, electronic energy transfer, crit. conc. 77−76771
IV-VI semiconductor, intergap interaction effects, T-matrix approx. *(Russian)* 77−31973
Jahn-Teller impurity centre, electroabsorption moments 77−48205
layered piezoelectric-semiconductor surface state acoustic memory 78−90615
layered semiconductor, exciton spectrum calc. rel. to shallow impurity centres *(Russian)* 77−1378
layered semiconductors 77−51666
level position depend. on interaction with bands, Wannier representation calcs. 80−54653
light diffraction by sound in impurity containing crystals 79−8119
lightly doped semiconductors, impurity band struct. 79−69461
linear chain, arbitrary number of impurities, analytic conditions 78−2443
linear chain crysts. containing impurities, Peierls instability and supercond. *(Chinese)* 79−51486
linear conductor, localized mag. moment formation and one and two impurity sites 80−50087
linear crystal, donor-acceptor complex, Frenkel excitons and ionic excited state mixing 79−99485

impurity electron states continued
liquid metal, integrated density of states, expression in Roth's effective-medium approx., generalisation of Friedel formula 79−99467
local impurity states, existence, levels, Green function, tight-binding calcs. 78−67981
localisation in impurity bands 80−20114
localised impurities, elec. dipole moment and local fields 79−90992
long range impurity states, electron spectrum *(Russian)* 79−56167
lower bounds, intermediate Hamiltonian approach, appl. to Kronig-Penney pot. 80−54643
luminescence band, deform. and shift, impurity centres, migration of excitations, math. modelling 78−48225
luminescence quantum efficiency, temp. depend. 78−35198
magnetic alloy, dil., thermopower, interconfig. fluctuations 79−65412
magnetic alloys, dil., spin correlation 78−84385
magnetic crystal, effect of impurity on local density of states 79−33263
magnetic cyrstal, semi-infinite, Green's function method *(Russian)* 79−51647
magnetic impurities and Kondo effect, theoretical model 79−33455
magnetic semiconductor, with impurities, semicond.-metal transition and instability phenomena 77−59257
magnetically ordered crystals with orbital degenerated impurities, single- and two-magnon absorpt. by localised excitations *(Russian)* 77−69858
many-valley semiconductor, dispersive screening and Bloch function interference, large binding 79−51525
many-valley semiconductor, effective mass theory of intervalley mixing 77−47763
many-valley semiconductor, electronic structure of D^- ion 79−95369
many-valley semiconductor, energy states calc. of negative donor ion, high stress and stress free cases 78−2444
many-valley semiconductor, impurity band for screened impurities 79−47053
many-valley semiconductor, two-photon transitions from deep neutral impurity centres, light absorpt. and drag effect 79−91478
many-valley semiconductor with shallow donors, Mott transition 77−47747
many-valley semiconductors, donor impurity levels and excitons, shallow-deep instabilities 80−75520
many-valley semiconductors, electron-impurity system *(Russian)* 79−69464
many-valley semiconductors with anisotropic masses, screened donor impurities 78−10399
metal, charge density perturbation around impurities 78−39058
metal, effect of impurities on electronic struct. 78−47692
metal, electron density behaviour near impurity charge 80−75518
metal, electron density surrounding impurity, Wannier function calc. 77−20262
metal, H and He impurities, electronic struct. 78−10402
metal, H-impurity, energy and electron density of states 80−34398
metal, H-like impurities electron. struct., μ^+ probes 79−56653
metal, Heine-Abarenkov model potential for ions 78−47731
metal, impurities and photoexcited ions, jellium model 80−39523
metal, impurity effects on cond. electrons, perturbation theory 79−60763
metal, impurity interactions and pseudo-molecule form. 78−47735
metal, k-wave electron state energy level shift due to impurity 77−39805
metal, localised atomic states, resist. and free energy calc. 77−8069
metal, localised non-mag. impurities, general theory 77−1392
metal, monovalent, impurity potential 79−78039
metal, nonlinear electron density distribution around point defects, applications 79−19549
metal, quasimagnetic impurity, exact solution of Wolff's model 78−56105
metal, quasiparticle bands, cond. electron mixing with impurity d(f) ions *(Russian)* 78−10409
metal, simple, electronic struct. of H impurity 78−67978
metal, single-particle density matrix, perturbation expansion 80−54635
metal, with stored H, electronic struct., many electron theory 80−49667
metal oxide surface, adsorption of electron acceptors, strength and distrib. of electron donor sites 78−84055
metal surface electronic density of states, random distribution of impurity atoms 78−6424
metal-H system, bond energy calcs. 78−51940
metal-nonmetal transition, universality aspects 78−56075
metals, charge perturbations around impurities 77−85582
metals, free-electron-like, electron struct. of single and interacting H impurities 79−95365
metals, Kondo effect, Anderson hamiltonian 80−60187
metals, light impurities, electronic struct. 80−34394
metals, local excitations, X-ray edge and recoil problems in optical excitation spectra 77−24879
metals, noncubic s-p, influence of impurities on solutes elec. field gradient 77−24770
MIM structure, isothermal current-time characts. and trap parameters determ. 77−89879
mixed diatomic system, depend. of fine struct. on short-range order parameter 79−51991
mixed valence compounds, electronic levels, impurity model 79−99513
mixed valence cpds., mag. susceptibility and sp. ht., periodic Anderson model, CPA alloy analogue method 80−15474
mixed valence impurity model, Fermi liq. theory, Ward identities 80−34401
mixed valence model, spinless, isolated f-level problem 80−107750
mixed valence problem, renormalisation group approach 77−89734
molecular crystal, disordered, transport of energy of electron excitations 77−40283
molecular crystal, energy spectrum *(Russian)* 79−78720
molecular crystal, exciton trapping and self-trapping 77−31947
molecular crystal, high power light pulse coherent interaction with exciton-impurity centres 80−55146
molecular crystal, impurity reson. interaction effects 77−1396
molecular crystal, mixed, electronic energy dispersive diffusion in impurity band 79−69458
molecular crystal, quasi-one-dimensional, exciton wave scatt. by impurity 79−78012
molecular crystal impure, exciton transport, local defect scatt. 77−8025
molecular crystals, disordered, incoherent, electronic energy transfer in impurity band 80−75525
molecular crystals, effect of intermol. interaction of impurity on band spectrum 78−27268
molecular crystals, ground electron state, vibr. levels, relax. time determ. *(Russian)* 78−15195
impurity electron states continued
molecular crystals, semi-infinite, with surface point defect, exciton states 80−20271
molecular crystals, shallow traps, spin triplet population temp. depend. 77−1371
molecular impurities in crystals, exclusion rules for librational-tunnelling states 78−84174
molecular solid, isotopically-mixed, electronic excitation localisation, off-diagonal disorder effects 79−99503
molecular solids, Raman, fluoresc. and nonlinear props. 79−33702
molecular solids, substitutionally disordered, Anderson localisation of mol. excitons 77−89733
MOS structure, irradiated, interface state effects 78−39218
MOS structure, quenched-in bulk defects and interface states, transient capacitance spectroscopy 79−24081
MOS transistor, Au-doped, Au surface-state energy levels 80−11092
multiphonon relax., localised electron radiationless decay, continuum and cluster modes 77−52158
multivalley semiconductor, donor binding energies, variational calc. 78−23041
naphthalene;β-methylnaphthalene, impurity phosphoresc. centres *(Russian)* 77−81151
naphthalene;β-naphthyl-n-biphenylylethylene, cryst., ground electron state, vibr. levels, relax. time determ. *(Russian)* 78−15195
naphthalene: pentacene, intermol. interaction dynamics and optical dephasing 80−64112
naphthalene, cryst., three-particle complex as impurity-exciton-phonon bound state *(Russian)* 77−62842
naphthalene, doped, fluoresc., impurity centre struct. depend. *(Russian)* 77−48231
naphthalene, doped, role of nonequilibrium phonons in stimulated radiation emission 80−103971
naphthalene, electron excitation energy transfer efficiency, temp. depend. *(Russian)* 77−52182
naphthalene, in naphthalene-d_8, Anderson-Mott transition model for excitation transport 80−96812
naphthalene, in naphthalene-d_8, energy trapping from localised states 80−100440
naphthalene, isotopically mixed crystals, electronic energy transfer, crit. conc. 77−76771
naphthalene, mol. cryst., impurity reson. interaction effects 77−1396
naphthalene cryst., anthracene doped, fluoresc., two-photon excited 78−68560
naphthalene-β-naphthol mixed mol. cryst., multiplet struct. of electron absorption spectra 77−1706
naphthalene-d_4(d_8) crystal, with isotopic impurities, Rashba effect, luminescence spectra, impurity states 80−29768
naphthalene-d_8:naphthalene, symmetry reduction obs. of deformed crysts. by absorbt. spectrum method 79−15504
narrow band gap semiconductor, 1D with impurities, density of states calc. *(Russian)* 77−39761
narrow band gap semiconductors, conference, Warsaw, Poland (Sept. 1977) 79−82582
narrow band gap semiconductors, conference, Warsaw, Poland (Sept. 1977) 80−49703
near-surface, adiabatic potential, symmetry props., group theory methods 80−70786
neutral donor, binding to exciton 77−31949
noble metal alloys, disordered, bulk electronic structure 80−44467
noble metal based, disordered alloys, dil., virtual bound states, reson. model pot. theory 79−23934
noble metal hosts, electronic props. of dil. impurities, exact Green function treatment 77−62856
non-orthogonal basis set, Green's function method *(Russian)* 79−15119
noncrystalline system, continuous and discontinuous metal insulator transitions 78−56076
nonmag., effect on nucl. spin-lattice relax. in two-band superconductor *(Russian)* 77−51845
nonradiative electron transitions in crystal, impurity molecule vibr. 80−103645
nonradiative transitions at impurity centre with participation of short-wavelength phonons 80−16099
nonresonant energy transfer interactions, randomly distrib. mols. in lattice, numerical anal. 77−8626
nonresonant transfer of energy between impurities in solids 78−23520
nonrigid impurity centres, symmetry groups *(Russian)* 80−65498
one-dimensional conducting chain array, long-range Coulomb effects, CDW dynamics 78−47717
one-dimensional conductor, charge density waves impurity pinning 80−6819
one-dimensional conductor, phonons effect on localisation and electro-cond. 78−6362
one-dimensional crystals, matching conditions, Bloch functions, logarithmic derivatives 80−15475
one-dimensional Kronig-Penney lattice, impurity levels, transfer matrix approach 79−42489
one-dimensional lattice, impurity perturbed electronic struct. using generalised Wannier functions 79−69468
one-dimensional metal, disordered, with half-filled band, rel. to elec. cond. *(Russian)* 77−80769
one-dimensional organic semiconductors, resonant states, mag. excitations and impurities 80−24839
one-dimensional strongly disordered conductor, localisation of electrons *(Russian)* 79−78046
one-dimensional system, phase fluctuations, disorder, nonlinearity 80−54331
one-dimensional systems with half-filled zone, singularity of electronic density of states due to impurities 78−6254
one-dimensional Tomonaga model, localisation and delocalisation 77−89735
one-dimensional Tomonaga model with impurities, localisation versus delocalisation 78−6311
optical absorption spectra evolution for localisation in trapping and solvation 77−90173
orbitally degenerate interacting impurity thermodynamics, stress field depend. due to point defects, dislocations 79−69477
organic solid, isotopically mixed, electronic energy transfer, Anderson localisation model 79−19557
organic solid, isotopically mixed, electronic energy transfer, Anderson transition 80−44545

impurity electron states continued
organic solid, isotopically-mixed, electronically excited states localisation model 79−47044
p^+-π-n^+ structure with low cond. region, double injection, IU characts. of single-level semicond. 79−56296
p-n junction, impurity centre mobility at room temp. *(Russian)* 78−34891
p-n junction impurity profile meas., two-freq. method 79−23633
p-n junction space charge region, thermally stimulated current, impurity centre parameters 77−85237
p-n junctions, minority carrier surface recombination velocity, lifetime, AM electron beam determ. 79−87145
p-n junctions, TSC, impurity centre parameter determ. 78−47857
p-n tunnel junctions, phototransitions accompanied by impurity scatt. 80−107901
p-type semiconductors, internal strain on bound hole-phonon interaction 78−91492
paraelectric defect relaxation process, quantum interference and multilevel aspects 79−95109
paramagnetic impurity centre interaction with external elec. field 77−89727
Peierls-Frohlich dielectric, metallic screening, with pinning to impurities at finite temps. *(Russian)* 79−56208
perovskite oxides, single cryst., photocond. and TSC meas. 78−43436
perturbed crystals in Kg representation, orthonormal localised states 78−6327
perturbed crystals in kq representation, impurity problem 77−39799
photoconductivity, monopolar injection *(Russian)* 79−24004
photoconductivity and autoionisation calc., impurity states 80−44648
photoconductivity due to optical transitions between excited states of impurity centers 79−73545
photoconductors with deep impurities, resist. inhomogeneity effects on photoelec. props. 77−8151
photoelasticity, nonlinear, in impure crystals, theory 80−108179
photoelectrons in crystals, scatt. by impurity centre, multipole wavefunctions 79−42490
photoluminescence activation conditions for binary inorganic crystals 78−10394
photon merging in disperse medium, on impurity centre scatt. *(Russian)* 80−55118
photovoltaic effect, impurity centre models *(Russian)* 78−60153
phthalocyanine-dodecane interface, photostimulated charge transfer flash expt., trapping model 77−66182
piezoelectric semiconductor, cascade capture of carriers by attractive impurity centres, cross section 78−56157
piezoelectric semiconductors, US ionisation of shallow impurities 77−43538
point defects, basis sets for study using Green's function methods 79−90994
point defects in crystals, book 77−47442
Poisson's equation for impurity ion in medium with spatially variable dielec. const., variational principle 78−60084
Poisson's equation for impurity ion in medium with strongly variable dielec. constant, variational principle 77−69271
polar semiconductor, exciton-neutral donor and biexciton complexes 79−90968
polar semiconductor, excitons bound to ionised donors, binding energy calc. 77−28128
polar semiconductor, impurity levels, influence of electron-phonon coupling 78−64007
polar semiconductors, chemical shift of Zeeman masses 78−10338
polyacetylene:AsF_5, mag. susceptibility, Fermi surface density of states, semicond.-metal transition 79−95566
polyacetylene, lightly doped, charged π-phase kinks 79−56163
polyacetylene, lightly doped, donor and acceptor states, IR absorpt. obs. 79−73979
polyacetylene, lightly doped, phenomenological theory of soliton formation 80−103644
polyacrylic acid:Fe^{3+}, electron state of Fe^{3+}, Mossbauer and magnetisation obs. 79−73872
polymer, Koster-Slater method, convergence and interleaving theorem 78−23051
proton in jellium, self-consistent screening 78−2441
pseudocontinuum approach to interaction theory for impurity defects in crystal lattice 79−69214
quartz:Cu, glassy and cryst., luminesc. centres 77−4679
quartz, electron capture by impurity ions, cross sections eval. using thermolum. data 79−95855
quartz, impurity microdefects. electron capture cross-sections *(Russian)* 78−76025
quasi-local level, line shape induced by impurity 80−100441
quasi-one-dimensional conductors, impurity effect on phase transitions 78−6297
quasifree excitons and electrons impurity trapping, finite coherence effects 80−59880
radiationless Auger-recombination of electrons on three centres *(Russian)* 79−78114
radiative and nonradiative recomb. at metal ions, core struct. effects, review 79−4834
radiative transitions, hydrostatic press. effects 79−38632
random impurity system, density of states tails, fluctuations and mobility edges 78−67983
rare earth metal impurity in metallic host, exchange interaction, electrical resistivity 80−84453
rare-earth impurities in s-p hosts, self-polarization hyperfine fields 79−33456
rare-earth ion spectra, effect of coordination polyhedron struct. 77−55807
recursion method for the extended impurity problem 80−96814
resonance energy transfer, donor excimers effect 79−95825
resonance fluorescence of impurity atom in solid, transient spectrum, intensity, and intensity correl. 80−84777
resonance Raman profile with consideration for quadratic vibronic coupling 80−55099
resonant localised impurity vibrs. at finite temps., spectral distrib. 77−7814
resonant scattering at impurity centres in solids *(German)* 80−7377
resonant secondary emissions by impurities in crysts. 80−93335
ruby, Raman effect to probe dynamical processes of Cr^{3+} photoexcited states 80−2740
sapphire, natural, origin of colour 79−70794

impurity electron states continued
scattering theory, in crystals, appl. to electronic states of impurities, review 77−85172
screening in strong mag. fields 79−47054
semiconducting solid solutions, optical transitions, review 78−2908
semiconductor:transition metal, Anderson model localised impurity states *(Russian)* 80−6788
semiconductor, μSR research 79−56672
semiconductor, absorption line profile in static elec. field, effect of impurities 78−92101
semiconductor, acceptor binding energies 77−69270
semiconductor, acceptor spectra, interpretation 78−43332
semiconductor, Auger transition probability, phonon-assisted 79−15120
semiconductor, bound excitons, review, book contrib. 80−44519
semiconductor, compensated, electron capture probability by Coulomb centre in case of optical phonon emission 80−20214
semiconductor, compensated, phase transition of impurity electrons interacting with lattice 77−24535
semiconductor, containing screw dislocations, impurity centres 78−72111
semiconductor, cryst. field coeff. of point defect 77−43537
semiconductor, deep impurity state characterisation 80−6776
semiconductor, defect electronic structure and lattice config., MO approaches 80−65495
semiconductor, density of states of impurity bands 77−31979
semiconductor, detection by junction capacitance and current techniques 78−10550
semiconductor, direct band gap, electronic Raman scatt. of polarised light on donor levels 80−93309
semiconductor, direct band gap type, polariton theory of reson. electronic Raman scatt. on neutral donor levels 80−108194
semiconductor, dislocation cond. process at low temp. 79−99551
semiconductor, donor levels, anomalous press. effects, Hall const. meas. 77−51693
semiconductor, donor van der Waals interactions, spectral lineshapes 80−11450
semiconductor, donor-acceptor pair in elec. field, anomalous Stark shift of ground state energy 79−19564
semiconductor, donor-acceptor pair luminesc. polarisation with optical orientation 77−24895
semiconductor, donor-acceptor system, weak wave absorpt. in reson. laser radiation field 80−66252
semiconductor, doped, Coulomb repulsion term in Hubbard model for impurities 79−42492
semiconductor, doped, impurity band density in atomic limit 80−107735
semiconductor, doped, metal-insulator transition, anal. 80−88478
semiconductor, doped, zinc blende type, electron-phonon interaction, reson. scatt. theory 78−64036
semiconductor, doped and strongly compensated, fluctuation pot. and density of states *(Russian)* 79−95366
semiconductor, doped with mag. impurity, ordering mechanism 80−2572
semiconductor, electron-donor recombination, Monte Carlo studies of transitions between excited donor states 79−38093
semiconductor, electron-hole liquid, 'neutrality' question of impurities 80−92822
semiconductor, exciton and impurity states, unified theory, for arbitrary mag. field 80−39511
semiconductor, exciton and impurity states theory 79−82526
semiconductor, extrinsic, resonance transitions between ground states of donor and acceptor impurities 80−45126
semiconductor, far IR spectroscopy, appl. of far IR lasers 80−31914
semiconductor, ferromag. shallow donor state anomalous carrier density mag. field depend. 80−49774
semiconductor, ferromagnetic, with mag. impurities, low-energy localised states *(Russian)* 79−19543
semiconductor, free carrier scatt. by nonhydrogenic charged impurity centre 79−11110
semiconductor, ground state energy of shallow impurity centres 77−4314
semiconductor, H^--H^+ type impurity complexes, spectra, and pseudointeractions of mol. energy levels *(Russian)* 78−92100
semiconductor, heavily doped, long range fluctuations in impurity pot. effects 80−93356
semiconductor, heavily doped, perturbation potential distrib. and density of states 79−47052
semiconductor, high field longitudinal magnetoresist and bound states 78−23113
semiconductor, impurity band, molecular model 78−76018
semiconductor, impurity band props. 79−23888
semiconductor, impurity band shift and width 78−6329
semiconductor, impurity characterisation from thermal carrier meas. 80−65595
semiconductor, impurity interaction and donor-acceptor recombination 80−16094
semiconductor, impurity ion pot., approx. equivalence of Csavinszky and Resta models 80−59901
semiconductor, impurity ion pot., nonlinear Poisson eqn. soln., variational principles 78−67976
semiconductor, impurity ion pot., nonlinear Poisson eqn. soln., var. principles 80−29350
semiconductor, impurity ion pot., nonlinear Poisson eqns. 77−20265
semiconductor, impurity ion pot., screening charge density expansion convergence 79−7799
semiconductor, impurity ion screening charge density expansion 80−107780
semiconductor, impurity ions screening 79−87062
semiconductor, impurity levels of transition metal ions in cryst. field 78−23059
semiconductor, impurity photocond., temp., elec. field and impurity centre conc. effects 78−56190
semiconductor, impurity photoconductivity for nonuniform impurity distrib. 79−82632
semiconductor, ionic., ionisation of doubly charged centres 79−11085
semiconductor, ionisation of impurity states by elec. field 78−47738
semiconductor, large-band-gap, self-compensation, role of impurities 80−92850
semiconductor, lightly doped, compensated, percolation level, Monte Carlo calc. 80−59923
semiconductor, localised states near displacive transition 80−70644
semiconductor, lone-pair effect of electronegativity difference on defect chemistry 78−72063
semiconductor, low temp. field ionisation of localised impurity levels 79−47600

impurity electron states continued
semiconductor, luminescence emitted from excited acceptor-donor complexes subject to external electric field 77−66544
semiconductor, magnetic freezeout in ultraquantum limit, appl. to GaAs 78−76017
semiconductor, magnetic phase transitions in impurity band *(Russian)* 80−50097
semiconductor, model energy spectrum, optimisation of parameters of neutrality equation *(Russian)* 78−6320
semiconductor, multiphonon recombination processes 79−38643
semiconductor, n-type, donor-polarizability enhancement as the insulator-metal transition is approached from the insulating side 80−80184
semiconductor, nonlinear impurity screening 78−67977
semiconductor, optical absorpt., Coulomb screening influence, shallow impurity centre photoionisation 78−72568
semiconductor, optical and IR characterisation 79−95846
semiconductor, photoconductivity and Dember effect, theory, allowance for long-range fields of charged impurities 79−24013
semiconductor, photodielectric effect associated with impurity excitation 79−82630
semiconductor, photoionisation of deep impurity levels 80−34386
semiconductor, photostimulated impurity absorpt. of US 77−62962
semiconductor, polaron aspects of generalised Haynes' rules 78−18978
semiconductor, quasilocal acceptor states, effects on band gap and electron mobility *(Russian)* 78−60082
semiconductor, quenching of luminesc. by charged defects 78−23531
semiconductor, radiative recomb. at donor-acceptor pairs, majority impurity config. average calcs. 80−40154
semiconductor, recomb.-enhanced defect reactions 77−51377
semiconductor, screened impurity in mag. field ground state energy of bound electron 78−72107
semiconductor, self-oscillatory medium, modelling 77−20811
semiconductor, shallow donor states exam. by two photon spectroscopy 79−23925
semiconductor, shallow impurity levels, effective mass approx. 80−6781
semiconductor, shielding by electron gas in magnetic field 80−107727
semiconductor, short range impurities in two band model 78−34803
semiconductor, spin relax., in quantising mag. field, effect of carriers 78−72388
semiconductor, strongly compensated, H-like impurity wavefunction overlap effect on optical absorpt. spectrum 77−8613
semiconductor, superlattice doping, electronic states, elec. props. 79−95480
semiconductor, techniques for detecting electrons and holes trapped at bulk and interface imperfections 77−11934
semiconductor, three impurity molecules, shallow hydrogenic donor interaction 77−31977
semiconductor, three-impurity clusters, ionisation energies and electron affinities 80−65496
semiconductor, transition metal impurities, localized electron states, Cluster-Bethe lattice method calcs. 79−56164
semiconductor, with defects or impurities, local density of electron states 80−92857
semiconductor, with neutral impurities, exciton spectrum, conc. depend. *(Russian)* 78−2894
semiconductor, with spatially varying dielec. const., impurity ion pot., variational calc. 79−7800
semiconductor, wurtzite structure, effect of local strain fields on shallow acceptor states 80−96821
semiconductor, zero-gap props. correlated to Γ_8 symmetry, review 80−6717
semiconductor, zinc-blende struct., shallow acceptor contribution to near-resonance spin-flip Raman scatt. 79−95754
semiconductor, zincblende struct., phonon attenuation in presence of internal strains and mag. field 78−76118
semiconductor, zincblende-type, exchange splitting of donor-acceptor pairs 77−20263
semiconductor capacitor, parameters of local states using thermally stimulated discharge, allowance for strong field effects 79−51528
semiconductor compounds, III-V and II-VI, H-like impurities interaction 79−82541
semiconductor crystal, spin-depend. luminesc. of donor-acceptor pairs 77−52173
semiconductor D^- centres, in mag. field, variational trial functions 79−38019
semiconductor defects, entropy of ionisation and temp. variation of ionisation levels 77−11871
semiconductor doped surfaces, inversion layers, quantum model 78−30961
semiconductor film, donor-acceptor pairs, polarisation of recomb. radiation in presence of quantum size effect 79−11462
semiconductor forward biased junctions, excess noise sources due to defects 79−38154
semiconductor gapless, with impurities, energy spectrum 78−67979
semiconductor impurities, photoionisation cross section calcs. 78−2450
semiconductor impurity bands, one-dimens. AMO-MT model validity 79−33256
semiconductor layer crystals, light absorption by shallow impurity centres 79−15503
semiconductor materials, shallow and deep level evaluation using Schottky contacts, conc. and distrib. 80−49669
semiconductor or semimetal, screened and localised impurity states in 'optical' and exciton insulators *(Russian)* 77−62870
semiconductor surface with incomplete impurity ionisation, quantum model 78−34877
semiconductor thin film, Coulomb interaction depend. on film thickness, exciton binding energies *(Russian)* 79−78027
semiconductor with impurities, light absorpt. *(Russian)* 79−47484
semiconductor with relativistic electron spectrum, bound and reson. states 77−51701
semiconductor with spatially variable dielec. const., impurity ion pot. 77−47769
semiconductor with superlattice, optical absorpt. by impurities 79−69867
semiconductor with superlattice, optical phonon excitation by light absorpt., impurity photoionisation 80−44275
semiconductor with surface doping, surface parameters determ. 77−15933
semiconductor with transition metal impurity states, EPR linewidth calc. 80−80599
semiconductor with uniform distrib. of traps, nonequilib. photocond. *(French)* 78−43433
impurity electron states continued
semiconductor-acceptor-donor complex model 77−51695
semiconductor-insulator boundaries, impurity electron states near interface 78−95320
semiconductor-metal transition, modified screened impurity pot. 79−99500
semiconductors, Auger and radiative recombination of acceptor bound excitons 79−47023
semiconductors, binding energy in exciton-impurity systems, Haynes rule 79−15112
semiconductors, cpd., large-lattice-relax. model for persistent impurity photocond. 77−85261
semiconductors, deep level impurity photoionisation cross-section 80−65485
semiconductors, depend., matrix elements in Matsubara-Toyozawa theory of impurity band 79−33261
semiconductors, doped, impurity bands, effect of nonorthogonality 77−59243
semiconductors, doped, light diffr. by sound 79−11404
semiconductors, doped, shallow impurity states, Hubbard bands and donor excitonic states, HF calc. 80−100443
semiconductors, doping of amorphous tetrahedrally bonded cpds. 80−2361
semiconductors, exciton-impurity state with low binding energy 80−103646
semiconductors, impurities and other point defects, electronic struct., review 79−7803
semiconductors, impurity electro- and magnetoabsorpt. coeffs., deep levels 79−24340
semiconductors, impurity electron scatt., resonance scatt., Hall and drift mobility 80−65487
semiconductors, impurity photoionisation, quantum-defect, billiard-ball model comparison 80−65486
semiconductors, impurity-induced free-carrier magnetoabsorption 79−42950
semiconductors, in neutral impurity field, cyclotron reson. fine struct. *(Russian)* 79−4727
semiconductors, interimpurity radiative recombination, intermediate exciton state *(Russian)* 80−49621
semiconductors, local centre parameter determ. from thermally stimulated excitation curve derivative singularities 80−11004
semiconductors, localised magnetic moment of transition metal impurities 80−60192
semiconductors, many-valley, localised impurity states with low binding energy 80−24835
semiconductors, multiple bound excitons, density functional calc. 80−10889
semiconductors, multiply charged impurity centers, energy spectrum 79−69469
semiconductors, multiply doped, donor-acceptor complexes and interactions, physicochem. nature 80−15472
semiconductors, nontrapping isoelectronic impurities, trapping in mag. fields 78−9097
semiconductors, photoelectric spectra of impurities 79−82623
semiconductors, two-dimensional, Mott exciton formation in high mag. fields *(Russian)* 80−65467
semiconductors, weakly doped compensated IR light absorption by small scale fluctuations *(Russian)* 80−66255
semiconductors with neutral impurity, transverse cond. in quantising mag. fields, finite radius scatterers *(Russian)* 80−29400
semiinfinite crystal with surface substitutional disorder, electronic struct. 77−72903
semimetal, mag. freeze-out of extrinsic carriers 77−59268
semimetal, phonon spectrum, influence of mag. field induced quasi-local levels 78−18946
semimetallic thin films, Coulomb interaction depend. on film thickness, exciton binding energies *(Russian)* 79−78027
sensitiser radiation quenching by activators in impure cryst., influence of collective phenomena 77−44052
shallow impurity centre conc. meas., junction capacitance technique, review *(Japanese)* 78−79958
shallow impurity centres near Curie point, influence of dielec. nonlinearity on temp. depend. of ionisation energy 80−10916
Si:B, isolated A^+ states under high compressive stress, long wavelength photocond. spectra 79−60765
n-Si, donor energy and polarisability in weak mag. field, rel. to hydrogenic atoms 79−3594
p-Si US attenuation due to donors and acceptors 77−28223
β-SiC, optical quenching of luminesc., acceptor ionisation energy 80−55178
silicate glasses:Cu^+, effect of UV irrad., absorption bands 78−31222
simple metals, screening of light impurities 77−85177
solid solution, nondiagonal disordered system, excitation spectrum 80−15429
spectrum of one electron Hamiltonians with impurities 79−1578
spin chain impurity zone fine struct. *(Russian)* 80−6787
Stark effect of localised electronic centres, impurities in semiconds. 77−66476
statistical mech. treatment of phase transitions impurity states 78−64004
statistical mechanics of impurity states 78−51930
stilbene:rhodamine-6Zh, luminesc. of adsorbed mols., excitonic energy transfer to surface 78−31255
substitutional impurities, Green's function calc. *(Russian)* 78−56101
substitutionally disordered material, impurity band triplet energy transfer 79−51513
superconducting localised state near dislocation, influence of impurities 80−10917
superconductors with transition metal impurities, density of electron states 77−63024
superlattice semiconductor impurity photoconductivity electron spectrum reconstruction 80−24966
supernonradiative phase transition, appl. to paramag. impurities in strong mag. field 79−14898
surface bound states, quantum and classical liquids 78−18859
symmetric Wolff model, weak-coupling−long-time−zero-temp limit 77−80907
TCNQ salt, Qn$(TCNQ)_2$, organic transfer salt, impurity effects on cond. 77−76799
1,2,4,5-tetrachlorobenzene, exciton migration and trapping, X-trap phosphoresc. 79−1780

impurity electron states continued
1,2,4,5-tetrachlorobenzene, impurity induced states, spin dephasing, spin coherence expts. 78−84498
1,2,4,5-tetrachlorobenzene, localised excitations thermal promotion to exciton band, impurity states effect 78−52539
tetramethylammonium manganese chloride, energy migration rel. to impurity trap behaviour 77−55811
thermal ionisation of an impurity in strong electric fields *(Russian)* 78−43410
thin crystal slab, impurity atom states, anal. 80−10910
three-dimensional crystal, Hartree-Fock theory of surface states 80−44468
three-dimensional organic chain conductors, one-dimensionalisation by impurities 78−91681
transition metal, BCC, rel. to solubility, heat of solution calcs. 78−6160
transition metal, charge perturbation due to impurities, theory 79−23924
transition metal, d-electron contrib. to impurity screening 77−62857
transition metal, impurities, as probes of critical points, in host band structure 78−91645
transition metal alloys, disordered, bulk electronic structure 80−44467
transition metal alloys, Wolff model of origin of localised mag. moments 79−61049
transition metal hosts, electronic props. of dil. impurities, exact Green function treatment 77−62856
transition metal ions in crystals, thermal broadening and shift calcs. 77−48208
transition metal-H systems, energy and electron density of states, improvements to theory 80−70636
transition metal-rare earth alloy, dilute limit model of mixed-valence effect 77−47768
transition metals, electronic structure and ordering of sp defects 78−91639
transition metals, Fe series, interstitial H, cluster model for bonding mechanism 79−60753
transition metals, ferromag., dil. H electronic struct. 80−70638
transition metals, ferromag., interstitial or substitutional sp impurity doped, electronic struct. 80−34384
transition metals, impurity scattering and residual resistivity 79−56192
triplet state population kinetics, of impurity molecules *(Russian)* 78−56519
TTF-TCNQ, 53 and 38K transitions, mag. and elec. props. meas., doping effect 77−66159
tunnel junction, resonance differential negative resistance in the Fredkin-Wannier inhomogeneous field model 80−80355
tunnelling of solitons and CDWs through impurities 78−51913
two-dimensional electron impurity system, quantum theory of cyclotron reson. lineshape 78−64083
two-dimensional electron-impurity system in strong mag. field, electron spectrum and cond. *(Russian)* 78−88016
two-dimensional impurity bands, carrier-density dependence of activation energies associated with hopping 80−88561
two-sublattice isotropic Heisenberg ferromagnet, impurity localised level theory 79−69471
ultrathin doping levels as model for 2-dimens. systems 78−60182
vacancy-impurity scattering, complex dispersion law 78−87957
vibronically coupled systems, cluster model 79−19540
XPS, solid-state and adsorbate shifts, equivalent cores calc. 79−28888
YAG crystals, EPR spectra of V^{2+} ions, ion energy levels 80−7157
zero gap semiconductor, magnetooptical and impurity effects 80−6721
zero gap semiconductors, electron scatt., thermoelec. power and Hall effect at low temp. 80−44628
zero-gap semiconductor, variational approach to resonances 79−82559
zero-gap semiconductors, reson. states, review 79−82558
zero-gap semiconductors of α-Sn group, impurity states model, appl. to HgSe(Te) 79−60758
zero-phonon impurity lines in absorption and fluorescence spectra, temp. broadening and shift 77−8643
zinc blende-type hosts, Co^{2+} impurities Huang-Rhys number rel. to props. of host lattice 79−83018
ZnS:V^{2+}, impurity states by Green's function method 80−92855
Ag, electronic and mag. structure calcs. of mag. impurities 80−80213
Ag halide, photographic image form., defect and impurity states, LCAO calc. 78−16876
Ag, virtual bound states due to 4d- and 5d-transition metal impurities 80−70667
Ag-Mn, dil., valence and core level spectra, XPS study 80−84838
Ag-Pd, thermoelectric force meas., test of virtual bound d-state model 77−32001
Ag-transition metal, dil., mag. impurities, electronic struct., KKR-Green's function calc. 80−65783
Ag_3AsS_3, proustite, elec. cond. rel. to impurities, melt stoichiometry deviations 77−11914
AgBr, pure and doped, identification of shallow electron centres 77−59267
AgBr, Stark effect on I-bound exciton 79−28719
AgBr:I, activator luminesc., energy model 79−28808
AgBr:Pd(II), photolysis-induced trapping behaviour, EPR study 80−54949
AgCl, pure and dopded, identification of shallow electron centres 77−59267
AgCl:Pt^{2+}(Pt^{4+}), single crystal EPR, substitution effects on photochemistry 79−15348
AgCl(Br), multivalent impurities 79−19556
$AgGaS_2$, elec. field influence on absorpt. spectrum, exciton parameters and energy of impurity levels *(Russian)* 77−69860
$AgGaSe_2$ single crysts., opt. quenching of photocond., temp. depend., slow centres activation energy *(Russian)* 77−69370
AgPd, dil. alloys, electronic states, virtual bound states model test *(French)* 77−62809
Ag_3SbS_3, pyrargyrite, elec. cond. rel. to impurities, melt stoichiometry deviations 77−11914
Al, 3d impurities, self-consistent spin density functional calcs. 80−70635
Al, adsorption of O_2, relation between energy-band and cluster model 78−52048
Al dilute alloys, 3d transition metal impurities, residual resist., influence of multiple scatt. effects 79−19570
Al matrix, capture radius of impurities 80−20110
Al:H, impurity energies and geometrics, self-consistent jellium calc. 79−99507
Al:H(He), interaction energy of two H(He) atoms, Hohenberg-Kohn-Sham density functional formalism 79−51519

impurity electron states continued
Al:He, pseudopotential calc. of screening of He atom 78−51917
Al-3d transition metal, dil., transport props., sp. ht. and supercond. ant. temp. calcs. 77−1393
Al-3d transition metal, dil. alloy, preasymptotic charge oscillations around 3d impurities 77−36055
Al-3d transition metal, dil., localisation of additional screening charge 79−47051
Al-3d transition metal alloy, dil., electronic charge density around impurities 78−34799
Al-Al_2O_3-Pd diodes, resonant tunnelling via localized inpurity states 79−28416
Al-Cu, dil., virtual bound states 77−43528
Al-Li, dilute substitutional alloy, impurity Knight shift and electric field gradient 80−44940
Al-M, dil. alloy, electronic states of 3d-transition metal (M) impurities 78−64005
Al-Mg, determ. of distortion field, induced by substitutional defect 80−44536
Al-Mn(Ni)(Cu), dil., core and valence band spectra, XPS study 80−84837
Al-transition metal, dil., residual resist. of 4d and 5d impurities 77−28155
Al-ZnS-Au structure, coulombic centres, thermal ageing, cond. and photovoltaic characts. *(French)* 77−43741
AlAs-GaAs LEDs, Ge or Zn-doped, mechanism of degradation 77−76911
$Al_2Be_3Si_6O_{18}$:Cu^{2+}, synthetic beryl, ESR, optical spectra and X-ray diffr. meas. 77−16166
AlGaAs p-n diodes, I-V characts., tunnelling 80−100510
AlGaAs-GaAs DH laser, impurity effects on relaxation oscillations 78−13710
$Al_xGa_{1-x}As$, Hall effect, press. temp. and composition depend. 80−49775
$Al_xGa_{1-x}As$, indirect-gap, laser oscill. involving N isoelectronic impurities 77−10919
$Al_xGa_{1-x}As$, pure and Ge doped, shallow acceptor photoluminescence 80−76064
$Al_xGa_{1-x}As$: Sn(Te), persistent photocond., due to donor-related centres, symmetry 80−15558
$Al_xGa_{1-x}As$:Cr, exptl. verification of Cr^{2+} models of photoluminescent transitions 78−27320
$Al_xGa_{1-x}As$:Cu, variable-gap semicond., impurity props., carrier recomb. 80−96907
$Al_xGa_{1-x}As$:Cu(Ag)(Au), LPE film, impurity levels, elec. and optical props. meas. 78−26862
$Al_xGa_{1-x}As$:N, luminescent material, appl. in optically pumped lasers and electrolum. diodes *(Japanese)* 77−44069
$Al_xGa_{1-x}As$:N, photolum. excitation spectra 77−63451
$Al_xGa_{1-x}As$:Si, charge state of impurity atoms, positron annihilation meas. 78−39062
$Al_xGa_{1-x}As$:Te, epitaxial film, elec. cond. and Hall coeff. rel. to donor levels 77−24630
$Al_xGa_{1-x}As$:Te, persistent photocond. trapping centre, donor complex model, photocapacitance meas. 79−65517
$Al_xGa_{1-x}P$, photoluminescence excitation spectra, bound excitons, Al conc. depend. 80−20687
$Al_xGa_{1-x}Sb$, soln.-grown, photolum. 80−71476
$Al_xGa_{1-x}Sb$:Zn(Si)(Ge)(Sn)(Pb), doping of solid solns. during LPE *(Russian)* 77−85087
AlH_3, photocond., photocurrent carrier-type 78−34855
AlN, absorpt. edge shape interpretation, Wannier excitons absorpt. in charge impurity elec. field 80−66233
AlN:Mn(Eu), luminescence at high excitation levels with and without doping 77−1721
AlN:O, UV spectra of deep impurity centres, radiative recombination 79−87490
α-Al_2O_3, energy levels of donor and acceptor dopants and electron and hole mobilities 80−59911
Al_2O_3, gamma irradiated single crystal, defect centres 79−65117
α-Al_2O_3, impurity energy levels, uniaxial stress effects 80−54642
Al_2O_3, transition metal ion doped, phonon spectroscopy using freq. crossing techniques 79−42193
α-Al_2O_3, unintentionally doped, defect struct. 79−60755
Al_2O_3:Mn^{3+}, electronic and vibronic Raman scatt. 78−2839
α-Al_2O_3:Ti, defect struct., electronic and ionic cond., optical absorption meas. 78−30603
Al_2O_3:V, V^{3+} pairs studied by phonon freq.-crossing spectroscopy 78−39068
Al_2O_3:V, valency changes of V ions, γ irradiation, thermal cond. optical absorption and EPR meas. 77−80541
α-Al_2O_3:V_2^{3+}(V^{4+})(Co^{3+})(Co^{2+}), optically and thermally stimulated reactions, absorpt. spectra 80−80825
α-Al_2O_3:V^{4+}, emission spectrum, Jahn-Teller effect in $^2T_{2g}$ and ^2E_g states 79−83007
Ar:H crystalline matrix, Xα scattered wave cluster model 79−73468
Ar:Xe, liq. 0-1.4 g cm^{-3}, vac. UV absorpt. spectra, Wannier impurity states 77−77232
As:Ni(Ge)(S)(Se)(Te) film, amorphous, chemical modification of props. 80−49250
As_2S_3, glassy, diffusion, elec. transport and first group impurities effect on elec. and opt. props. 77−76623
As_2S_3 vitreous, Ag, Cu, Sn and Ge impurities influence on electrophys. props. 77−76826
As_2S_3:Fe glass, photolum. and ESR, Fe impurities as non-radiative recomb. centres 80−29788
As_2Se_3, effect of impurities on paramagnetic gap states 80−24848
As_2Se_3:Fe, glassy, mag. susceptibility investig. of doping effect 77−77024
As_2Te_3, amorphous, defect and impurity states, hopping cond. obs. 80−54650
Au, virtual bound states due to 4d- and 5d-transition metal impurities 80−70667
Au-Fe, dil., thermopower, interconfig. fluctuations 79−65412
Au-Fe(Co)(Ni), dil., valence and core level spectra, XPS study 80−84838
Au-Ga, dil. alloys, dHuA meas. and phase shift analysis of electronic scatt. anisotropy 77−35932
Au-Pd dil. alloys, electronic states, virtual bound states model *(French)* 77−62809
Au-Ti, dil., virtual bound states, optical absorption meas. 78−2891

impurity electron states continued
Au-ZnSe:Ga(Al), Schottky diode, wavelength modulated photoresponse spectra 78−6714
α-Al_2O_3, thermoluminescent trap stability, 450 to 1400°C 79−24372
β-B, rhombohedral, influence of impurities on elec. cond. 77−4345
B_xCy, metal-insulator transition, elec. cond. and thermoelec. power, 80 to 700K 80−44673
BaF_2: rare earth, far IR electronic transitions 77−4657
BaF_2:U^{3+}, single crystal, superhyperfine interaction of tetragonal centres 79−42834
$Ba_2NaNb_5O_{15}$, ferroelectric, local states, thermoluminesc. study 80−60690
$Ba_3(PO_4)_2$ phosphor, ionisation of capture centres, thermolum. spectra 80−11487
BaS:Cu, thermoluminesc. and decay 78−80426
$BaTiO_3$, bulk photovoltaic effect in ferroelecs. 79−15181
$BaTiO_3$, ferroelec. inhomogeneous impurity distrib., distrib. of spontaneous induction 77−28530
$BaTiO_3$, phase stability as function of doped 3d elements 78−38835
$BaTiO_3$, photocond. of doped single cryst., photoexcitable levels 77−4391
$BaTiO_3$, polycryst., elec. resist. anomaly in phase transition region 78−43381
$BaTiO_3$:Mn^{2+}, electrooptical effect, charge transfer mechanism, defect. pair form. 79−38519
$BaVS_3$:Fe, Mossbauer and mag. studies, electronic state of Fe 80−108130
$Be_3Al(SiO_3)_6$:Cr^{3+}, Raman effect to probe dynamical processes of Cr^{3+} photoexcited states 80−2740
BeO, cryst., local centres, electronic struct. calcs. 80−100433
Bi, acoustic waves, giant quantum attenuation at high mag. fields, angular depend. *(Japanese)* 79−4585
BiI_3, doped, IR photolum. and EPR spectra 78−19558
$Bi_{72}SiO_{20}$:Sn(Mo), Raman scatt. spectra, impurity effect 80−80795
$Bi_2W_2O_9$:Mo(Eu), energy transfer and luminesc. props. 80−55177
$(CH_4)NMnCl_3$, nearly-one-dimensional cpd., energy migration rel. to impurity trap behaviour 77−55811
CaF_2, rare-earth-doped, cluster-associated relax., 5.5-400K 78−31153
CaF_2:Ce(Nd)(Dy)(Ho)(Yb), props. of ionic thermocurrents 77−7897
CaF_2:Dy(Tm), cryst. fields, overlap and covalency contribs. 77−1397
CaF_2:Eu^{2+}, Sm^{2+}, relaxed resonance acoustic phonons in vibronic anti-Stokes luminescence *(Russian)* 80−93404
CaF_2:R^{3+}, R=rare earth, dipole reorientation of charge compensation centres, ionic thermocurrents meas. 79−73880
CaF_2:Sm, charge transitions, positron annihilation exam. 78−92143
CaF_2:Sm, positron annihilation polarisation effects, electron momentum distribution 80−55225
CaF_2:U^{3+}, anomalous magnetooptic props., optical detection of ESR and cross-relax. resonances 80−93287
CaF_2:U^{3+}, charge compensation, struct. 79−15124
CaF_2:Y^{3+}, DC cond., high Y concs. influence 78−22887
CaF_2-SrF_2-BaF_2:Gd^{3+}, luminescence spectrum of Gd^{3+} ion and solid solution region obs. 78−84638
CaO, triplet state of F_A centres, ODMR obs. 79−28639
CaO:Cr^{2+} Jahn-Teller system, APR spectrum, zero strain site energy level diagram 79−99756
Ca_2PO_4Cl:MnO_4^{3-}, polarised electronic spectrum 77−52137
$Ca_5(PO_4)_3F$:Nd^{3+}, optical fluorescence intensity and cryst. field parameters 78−52570
CaS:Mn,Ce, phosphor, fluoresc. spectrum, fine struct., $^4T_{1g}(^4G)\rightarrow{}^6A_1(^6S)$ transition 80−45130
CaS:Pb^{2+} phosphors, luminesc., refl., emission, and excitation spectra 79−11456
CaS:Zr, Gd phosphors, thermoluminesc., trap distrib., activator effects 78−2929
CaSe: Sn^{2+}, dimer centre, emission and excitation spectra, temperature quenching *(French)* 79−99937
$CaWO_4$, type selfactivated luminophors, nature of optically active centres 77−69880
$CaWO_4$:Nd^{3+} $4f^3$ configuration, ground level energy state variation rel. to press. *(Russian)* 77−16358
$Cd_{1-x}Ag_xCr_2Se_4$, Ag acceptor states effect on exchange interaction 80−20397
$CdCl_2$:Mn^{2+}, null points in zero-field splitting of mag. impurity levels 79−87066
$CdCr_2S_{4-y}$, spinel, anomalies in paramag. susceptibility, Curie pt. *(Russian)* 77−80910
$CdCr_2Se_4$:Ag, impurity contrib. to low temp. ferromag. reson. linewidth 79−65743
$CdCr_2Se_4$:In , impurity band, photocond. spectral depend. 78−19088
CdF_2: rare earth, electronic props., compared to CaF_2 *(French)* 80−49662
CdF_2: $YF_3(YbF_3)$, photoconversion from insulating to semicond. state, IR absorption and elec. cond. 78−14759
CdF_2:Er^{3+}, selective monochromatic excitation of $^4S_{1/2}$-$^4I_{15/2}$ transition *(French)* 77−85765
CdF_2:Eu(Gd)(Nd), semicond., symmetry of optical centres, optical and elec. props. 77−59592
CdF_2:Ge^{3+}, Ce^{3+}, in semicond. state, elec. cond. and Hall meas. 78−10443
CdF_2:In, evidence for strong impurity-lattice coupling 80−6775
CdF_2:In, shallow versus deep donors 77−85176
CdF_2:Sm^{3+}, photoconverted, thermally stimulated relax. 80−84476
CdF_2-YF_3, thermal ionisation energy of monovalent centres 80−80207
$Cd_{1-x}Fe_xCr_2S_4$:Cu, effect of doping on elec. props. and Curie temp. 78−84214
$Cd_{1-x}Ga_xCr_2S_3$, spinel, anomalies in paramag. susceptibility, Curie pt. *(Russian)* 77−80910
$CdGeAs_2$, optical and elec. props. 79−19590
n-Cd_2GeO_4, electronic and cond. props. rel. to prep. conditions and defect struct. 80−107787
n-$Cd_{0.21}Hg_{0.79}Te$, excess generation-recombination noise 80−107880
n-$Cd_xHg_{1-x}Te$, recombination due to surface excitation, photoconductivity, impurity states *(Russian)* 80−60042
p-$Cd_xHg_{1-x}Te$ solid soln., thermoelec. effects 79−73538
$Cd_xHg_{1-x}Te$, solid solns., role of stoichiometry defects 77−47813
$Cd_xHg_{1-x}Te$, strong elec. field effect on galvanomagnetic effects 79−11159
$Cd_xHg_{1-x}Te$, variable-gap structures, galvanomagnetic effects 80−11014
$CdIn_2S_4$ single crystals, recombination process and localised levels 80−93383

impurity electron states continued
$Cd_{1-x}Mn_xTe$, acceptor photoionisation and light-to-heavy hole absorpt. 79−65908
CdS, Auger effects in donor acceptor pair spectra 80−20707
CdS, compensated, characts. of Auger excitation spectra of photoluminesc. and photocurrent 77−90194
CdS, donors, EPR and spin-lattice relax., Faraday rot. meas. 80−54939
CdS film, doping and recrystn. effect on photocurrent relax. time. 77−4409
CdS, hydrogenlike donor negative ion, ground and excited states, obs. 80−70645
CdS, IR stimulated edge emission 77−59613
CdS, influence of surface states on absorption edge 77−16344
CdS, interaction of excitons with charged impurities 78−43906
CdS laser, electron beam pumped, catastrophic and gradual degradation 77−61960
CdS, M_1-M_2 luminesc. band, assignment to exciton-impurity complexes 77−8649
CdS, magnetoabsorption, explained by D centres 79−38019
CdS, mol. model for exciton-impurity complexes 77−80740
CdS polycrystalline layers, electron trapping depend. on preparation conditions 79−78232
CdS, props. of shallow acceptors, photocurrent meas. 79−7805
CdS, spectroscopic study of local centre interaction, change with external illumination 80−80323
CdS, subMM radiation excitation by N_2 laser pulse 80−60678
CdS, substitutional Ti^{2+} centres, linear electroabsorpt. 77−66525
CdS, Wannier exciton-ionised donor complex, binding energy 80−44509
CdS:Ag, induced impurity photocond. spectrum obs. 77−1447
CdS:Ag, orange luminesc. at 77K and induced impurity photoconductivity 79−43035
CdS:Ag crystals, spectral shifts of induced impurity photocond. bands 80−39633
CdS:Cd(In), Cu- or defect-compensated, optical ageing rel. to storage cond. 78−84247
CdS:Cl, heavily doped, fluoresc. spectrum upper threshold calculated 78−52568
CdS:Cu, photosensitivity degradation mechanism 80−107851
CdS:Cu, spectral sensitisation by cyanine dyes 78−64064
CdS:$CuCl_2(CdCl_2)$ sintered layer, distrib. of energy levels of local centres 80−15568
CdS:In, impurity resist., Matsubara-Toyozawa theory extension 80−80264
CdS:In, spin flip Raman scatt., electron dynamics 78−80342
CdS:Li, nature of recombination centres responsible for 0.95 μm luminesc. band 77−69908
CdS:Li, O film, chemical bath deposited, photocond. and optical props., O trap level 80−2426
CdS:Li, subjected to elec. fields, drift of defects 80−6558
CdS:Li, thermochemical changes in microstructure of anisotropic centres, polarisation modulation method meas. 79−38027
CdS:$Li^+(N^+)(Ne^+)(P^+)$, ion-implanted, edge emissions 77−77274
CdS:Li(Cu), pure and doped, electrodiffusion of shallow donors, photocurrent, TSC, and exciton luminesc. meas. 80−79992
CdS:Na, Hagemark theory, green edge emission line intensity 80−75517
CdS:Ni, elec., photoelec. and luminesc. props. *(Russian)* 78−84259
CdS:Ni, impurity to band electronic transitions, photocond. and dark cond. obs. *(Russian)* 77−8150
CdS:Ni, nonradiative recomb., photocond. spectra 80−70764
CdS:Ni, recomb. parameters, photocond. spectra meas. *(Russian)* 80−49820
CdS-CdSe, unactivated film, calc. of induced impurity photocond. due to donor-acceptor pairs 77−43749
p-CdSb, elec. props. at low temp. 77−62866
p-CdSb, photoconductivity and absorpt. in submm region, electroluminesc. 77−32046
CdSb:Ge, anisotropy of elec., mag. props. 78−34829
CdSb:Te, photoconductivity characts. 77−43653
CdSe, mol. model for exciton-impurity complexes 77−80740
CdSe platelets, determ. of localised level energies by Fermi level statistics 77−31980
CdSe:Cu,Cl film, induced impurity photocond., 0.6 to 1.2 eV 79−24012
CdSe:Fe, exciton electroreflectance spectra, impurity effects 77−16335
CdSe:In, epitaxial layer, effect of activator distribution on conductivity 78−43047
CdSe:Ti, optical and elec. investig. of shallow donor levels, reson. states 77−63437
CdSe:Zn(Ga), epitaxial film, impurity distrib., current transfer features *(Russian)* 77−47908
CdTe, compensated single cryst., impurity centre parameters, elec. cond. and galvanomag. props. *(Russian)* 77−47811
CdTe, excitation spectra, resonant Raman scatt. versus hot electron effects 79−38645
CdTe, film, theoretical models of impurity levels 79−82557
n-CdTe, Hall effect and resist., close and distant donor-acceptor pairing effects 77−39881
CdTe, levels in energy gap at 100K determ. from photoelectric meas. 77−47862
CdTe, microwave cond. and dielec. permittivity using reson. cavity method 79−51620
CdTe, photoconductivity, extrinsic, contrib. by hopping through excited states of donors 78−6411
CdTe, shallow donors, excited state transitions 78−6710
CdTe, shallow impurity spectral linewidths, 4-10K 77−63443
CdTe, undoped, high-resist.- characterisation, impurity level investig. 77−39801
CdTe, undoped and halogen-compensated, defect conc. calc. 77−39602
CdTe:Cl, capacitance meas. and trapping, mol. centre model *(French)* 77−39872
CdTe:Cl, influence of lattice defects on electrical behaviour 78−2497
CdTe:Cl, interaction of impurities and lattice defects, elec. props. and photoluminescence. spectra 77−4685
CdTe:Cl, localisation of electrons, temp. depend. of cond. and Hall effect 78−14732
CdTe:Cl, semi-insulating, impurity photocond. spectra, local state distrib. in band gap 80−107865
CdTe:Cl, semiinsulating, Hall effect and elec. cond., impurity levels 77−55532
CdTe:Cr, impurity photoionisation transitions, EPR meas. 80−39857
CdTe:Fe, Mn, Cr, introduction of elec. active defects 80−103647

impurity electron states continued
CdTe:Li, excitation spectrum of Li acceptor and valence band parameters 79−28795
CdTe:Li(Cl), acceptor states study by donar acceptor pair excitation luminesc. 80−100683
CdTe:p, defect model, from Hall effect meas. 77−43620
CdTe:Ti^{2+}, Jahn-Teller effect on $^3T_1(^3F)$ state, resonance on $^3T_1(^3P)$ state 78−27271
CdTe(Se):Co, impurity luminescence no phonon line depend. on temp., Debye temp. 80−66273
$Cd_{3-x}Zn_xAs_2$, cryst., two-band and impurity conduction, 1.8 to 370K 78−19057
CeO_2:S, acceptor properties of S, free electron concentrations 80−34395
CeSe:Fe, long-wavelength fundamental absorpt. edge formation, role of Fe 77−16351
CoMn(Cr)(V)(Ti), dil., low temp. specific heat and magnetisation 80−65925
Cr-Au alloys, dil., elec. resist., 77-700K 78−64035
CsBr:Pr, absorpt. and fluoresc. spectra, crystal field 78−2885
CsCl, impurity and defect sites, elec. field gradient calc. 79−78034
CsCl:Cr^{3+}, ESR of Cr^{3+} centres, room temp. 78−91943
Cs_2GeF_6:Mn^{4+}, magnetically circularly polarised emission and MCD of vibronic lines 77−16377
$CsMnCl_3(Br_3)$, rare earth doped, energy transfer, emission spectra obs. 80−20684
$Cs_2UO_2Cl_4$, low-lying excited electronic levels, fluoresc. decay meas. 79−47491
Cu (100) film, chemisorbed N_2, electronic struct. 77−59315
Cu (111) surface, partially Cs covered, oxidation effect on UPS 79−78826
Cu, electronic and mag. structure calcs. of mag. impurities 80−80213
Cu-3d transition metal alloy, dil., electronic charge density around impurities 78−34799
Cu-Be solid solutions, local oscill. conc. depend., impurity bands *(Russian)* 80−75318
Cu-Cr, dil. alloy, Knight shift temp. depend., electronic struct. 78−84488
Cu-Cr(Mn)(Fe), dil., NMR satellite data, rel. to electronic struct. 78−68398
Cu-Cr(Mn)(Fe), dil., NMR data, ionic model and Kondo temp. 78−68399
Cu-Fe, dil., thermopower, interconfig. fluctuations 79−65412
Cu-Fe group, dil., NMR satellite data calc., struct. of mag. impurities 80−103894
Cu-Fe(Co)(Ni), dil., valence and core level spectra, XPS study 80−84838
Cu-Ni(Pd)(Pt), dil., screening charge density round $\Delta Z=-1$ impurities, vacancies, NQR study 80−103897
Cu-Ni(Zn)(Ga)(Ge), dil. impurity electron struct., self-consistent Korringa-Kohn-Rostoker Green's function calc. 79−78040
Cu-Pd dil. alloys, electronic states, virtual bound states model test *(French)* 77−62809
Cu-transition metal, dil., mag. impurities, electronic struct., KKR-Green's function calc. 80−65783
$CuAl_{1-x}Fe_xS_2$ system, delocalisation of d-electrons, mag., elec. and optical obs. 78−34804
CuCl, defect and impurity bands, lattice consts. 80−54638
CuCl, excitons bound to neutral donor impurities, magneto absorption spectra 79−56816
$CuCr_2S_{4-\gamma}$, spinel, anomalies in paramag. susceptibility, Curie pt. *(Russian)* 77−80910
$Cu_{0.83}Ga_{0.17}$, α-phase, photoelectron meas., impurity level 78−35247
$CuGaSe_2$ single crysts., Hall effect and resist., acceptor states 80−10975
$Cu_{0.87}Ge_{0.13}$, α-phase, photoelectron meas., impurity level 78−35247
$CuInS_2$, epitaxial thin film on GaAs, exam. of growth, electrical props. 80−24754
$CuInS_2$:Cd(Zn), elec. props. 77−62927
$CuInSe_2$, influence of impurities and free carriers on optical props. 80−108225
n-$CuInSe_2$, single cryst., elec. props. 78−43397
Cu_xNi_{1-x}, bulk electronic structure, comparison of CPA and ATA techniques 80−44467
Cu_xNi_{1-x}, disordered alloy, muffin-tin model, electronic struct. and density of states calc. 80−29302
Cu_2O, yellow exciton series, silver impurity influence on spectrum 78−64388
Cu_2O:Ag^+, exciton-neutral and exciton-charged impurity scatt. cross sections 80−70618
Cu_2S-CdS heterojunctions, electron trap characterisation by capacitance transient meas. 79−78163
Cu_xZn_{1-x}, disordered alloy, muffin-tin model, electronic struct. and density of states calc. 80−29302
donor polarisability, enhanced, below insulator-metal-transition, self-consistent calc. 80−7262
EuO, paramag. phase, decrease in microwave cond. due to impurity electron localisation 79−69544
EuO:Eu, doped ferromag. semicond., carrier density and mag. susceptibility rel. to M-S transition 77−72820
EuO:Yb(Sm), electron transition and valence state of impurities, X-ray spectroscopy and structural anal. 78−39064
$EuO_{1-x}N_x$, ferromag. semicond., elec. and mag. props. *(French)* 78−79993
EuS:Yb(Sm), electron transition and valence state of impurities, X-ray spectroscopy and structural anal. 78−39064
EuSe, polarisability of shallow donors, permittivity meas. 80−24833
EuSe:Gd, mag. props. explained by band struct. 78−43324
$Eu_{1-x}Sm_xS$, electronic transition in Sm impurity ions, rel. to exchange interactions, L absorpt. spectra 77−59644
EuTe, magnetic impurity states, mag. and transport props. 80−96913
$Eu_2(WO_4)_3$, mag. susceptibility, elec. cond. and dielec. const. meas. 77−11916
Fe, electronic structure of nontransition element impurity atoms 77−73023
α-Fe, interstitial or substitutional sp impurity doped, electronic struct. 80−34384
Fe_3 screening of non-transition element impurities, model 77−4312
Fe^{3+}, cubic spin-Hamiltonian parameters in inorganic compounds, superposition model anal. 80−20367
α-Fe:C, Hartree-Fock calc. 78−14692
Fe:Y, ion implanted, deep D traps due to Y-vacancy complex 80−103372

impurity electron states continued
Fe-Al alloy, soft X-ray emission 77−32471
Fe-In, superconducting Kondo alloys and alloys with strong electron-magnetic impurity interaction, EM absorpt. of light 80−39711
Fe-M, dil., M=transition metal, impurity electronic struct., multiple scatt. approach 80−92856
Fe-V-C melts, electron struct., mag. susceptibility meas. *(Russian)* 78−47729
$FeCO_3$:Mn^{2+}, far IR host and impurity excitations, antiferromag. and paramag. temp. ranges 77−52140
Fe_3O_4, hopping conduction and the Coulomb gap 80−44605
^{57}Fe implantation in metals, electric hyperfine interactions, conversion electron Mossbauer meas. 80−7241
(Ga,Al)As:Si(Ge), epitaxial layers, radiative recomb., compensation, cathodolum. study 80−66307
Ga chalcogenides, energy spectrum of local levels *(Russian)* 79−51517
n-GaAlAs:Sn LED DH donor-level analysis, DLTS obs. 79−47040
$Ga_{1-x}AlAs$:Zn, acceptor energy level and elec. props. 80−65482
$Ga_{1-x}Al_xAs$-GaAs:Si, momentum distrib. of valence electrons, positron annihilation meas. 79−51530
Ga(As,P):N, intermediate range model of N states 79−73467
Ga(As,P):N, isoelectronic impurity states, long-range, short-range model 80−75524
Ga(As,P):N, theory of bound states induced by disorder and isoelectronic pots. 77−35889
GaAs, acceptor bound exciton Auger and radiative transition rates, radiative recomb. 80−6733
GaAs and related cpds., conf., Edinburgh, Scotland (Sep 1976) 78−3039
n-GaAs, carrier Debye screening length, temp. depend. 80−88504
GaAs, complex luminesc. centres at 1.20 and 1.30 eV 77−16386
GaAs, conduction band effective mass, influence of high uniaxial stress 80−80162
GaAs, degenerate, impurity band struct. for dense donors and acceptors 80−29348
n-GaAs, density of states tail in heavily doped closely compensated semicond. 78−47689
GaAs donor characterisation by far IR photoconductive techniques 78−43501
GaAs, donor energy spectrum, mag. field effect, submm. photocond. meas. *(Russian)* 77−43666
GaAs, donor van der Waals interactions, spectral lineshapes 80−11450
n-GaAs, donor-acceptor pair recomb., isolated-pair model revisited 79−28825
GaAs, donor-acceptor type complex, mag. field splitting of photolum. line 79−15512
n-GaAs, electron and gamma ray irradiated, introduction and annealing of defects 78−67736
GaAs, electron trap at E_c-0.75 eV, direct evidence for nonassignment to O 79−90988
GaAs, electronic Raman scatt. of polarised light on donor levels 80−93309
GaAs epilayers, high-quality, sharp-line transitions due to donor-acceptor recomb. 78−6768
GaAs, epitaxial, residual donor identification by far IR photocond. 80−60047
GaAs, epitaxial, residual donor identification by far IR photoconductivity meas. 80−103717
GaAs, epitaxial film, positron annihilation, impurity centre study 79−15554
GaAs epitaxial film, surface trap exam. by surface doping and field effect 77−76896
GaAs epitaxial layer, laser mag. photoelec. spectra 79−82635
GaAs epitaxial layers, undoped, recomb. of non-equilib. carriers, steady-state photocond. 77−85357
GaAs epitaxial layers, surface impurity gradients, Schottky barrier capacitance meas. 80−70782
GaAs, field ionisation speed of shallow impurity levels, quantum-mechanical estimates 80−97412
n-GaAs, H-like impurities photocond., mag. field effect 79−82634
n-GaAs, heat treated, origin of 1.41 eV emission band, photolum. expt. 78−72579
GaAs, high-purity, residual donors, ionisation energies determ. 78−6333
GaAs homoepitaxial interface, thermal degradation 77−11988
n-GaAs, hot electron magnetophonon resonance, Fourier anal. 80−54718
p-GaAs, impurity band Hall mobility 80−70730
GaAs, impurity density of states, effect of doping and injections, models and calc. method 79−73466
GaAs, impurity states and core excitons, binding energies, perturb. theory 80−49659
GaAs, interaction of excitons with charged impurities 78−43906
n-GaAs, intrinsic emission intensity, role of local centres in determ. of conc. depend. 78−39599
n-GaAs, LPE, impurity compensation photolum. and free carrier conc. meas. 77−62558
GaAs, low temp. gamma irrad., donor-acceptor pair formation 79−69158
GaAs, magnetic freezeout in ultraquantum limit 78−76017
p-GaAs, magnetoluminesc. of cond. band to acceptor transition 77−1716
n-GaAs, metal-insulator transition in impurity band induced by loss of dimension 77−47732
n-GaAs, metal-insulator transition in impurity band induced by mag. field and loss of dimens. 78−52042
GaAs, model relating elec. props. to impurity concs. 77−51697
GaAs, neutron transmutation doping, shallow donors magneto-optical effects 80−20255
GaAs, O^+ implantation, energy levels, photoluminesc. 80−24838
GaAs, p-n junction, conductance oscillations in a two-dimensional impurity band 79−95477
GaAs, photoconductivity, impurity induced, low energy edge spectral shift 80−65630
GaAs, point defects, multiple scatt. Xα model 80−54636
GaAs pure and Se-doped, photoluminescence at dislocations, band gap electronic levels 79−99926
GaAs, self-compensation due to shallow and deep levels 80−24837
GaAs, semi-insulating, cond. mechanism, model explaining temp. depend. of elec. props. 79−51571
GaAs, semi-insulating, thermal conversion, Hall effect and luminesc. meas. 78−6405
n-GaAs, shallow donors, elec. cond. and Hall coeff. meas. 77−11942
GaAs, shallow donors, excited state transitions 78−6710

impurity electron states continued
GaAs, shallow donors, screening, energy spectrum of electrons and cond. mech. 79−7831
GaAs, shallow impurity spectral linewidths, 4-10K 77−63443
GaAs, striped DH lasers, anomalous behaviour at low temp. *(Chinese)* 80−87390
GaAs, surface, electron struct. and Fermi level pinning by O_2 and metals 80−11066
n-GaAs, temp. depend. density of states, short range impurity pot. calcs. 79−56109
GaAs, transmutation doped, shallow donors, magneto-optical study, photocond. meas. 78−87996
GaAs, two dimensional impurity bands, Hall mobility 79−95509
GaAs type FET with buffer, bias effects due to deep centres in struct. *(French)* 80−107917
GaAs, VPE, high purity, residual donors, photocond. expts. 77−85174
GaAs VPE, residual donor impurities 77−76679
GaAs, VPE growth by single flat temp. zone method, residual doping level 77−48352
GaAs: Cr (O_2), impurity levels charact. using dark capacitance and photocapacitance transient techniques 80−59920
GaAs:Be(C)(Ge)(Sn), MBE layers, photoluminesc. 80−29803
GaAs:C(Sn), diamagnetism quenching 80−6782
GaAs:Cd, lattice defects caused by quenching, elec. cond. 79−56160
GaAs:Cr, 0.84 eV no-phonon luminesc., fine struct. and origin 80−103980
GaAs:Cr, acceptor levels, photocapacitance meas. 79−95443
GaAs:Cr, Be, ion-implanted, semi-insulating, carrier mobility and conc. temp. depend. 77−76808
GaAs:Cr, carrier equilibrium effects, impurity states, elec. resistivity 80−65488
GaAs:Cr, carrier transport in p^+-ν junction based on relaxation semiconductors 79−65543
GaAs:Cr, deep levels, wavelength-modulated photocapacitance spectroscopy 80−76055
GaAs:Cr, EPR, annealing and IR excitation effect on Cr^+ signal, Cr content by colorimetry 77−69680
GaAs:Cr, exptl. verification of Cr^{2+} models of photoluminescent transitions 78−27320
GaAs:Cr, impurity electron states by Xα scattered wave cluster method, electron-electron interactions 80−6767
GaAs:Cr, local level near valence band, photocapacitance 79−11080
GaAs:Cr, luminescence and absorption spectra, temp. depend. of fine structure 80−6779
GaAs:Cr, origin of sharp near IR transitions 80−10913
GaAs:Cr, photoluminescence in strong electric fields 80−108270
p-GaAs:Cr, semi-insulating photoelectronic analysis 77−80804
GaAs:Cr, semi-insulating impurity photomagnetoelectric effect 78−34861
GaAs:Cr, semi-insulating, Cr charge states conc., EPR determ. 80−20450
GaAs:Cr, site symmetry of Cr ions, ground-state splitting, ballistic phonon expts. 78−95273
GaAs:Cr, VPE growth, carrier conc. profiles, impurity level model 79−74099
GaAs:Cr,O, semi-insulating, photocond. anal. of levels 80−20243
GaAs:Cr (Cr-Te), and undoped, transverse-acoustoelec.-voltage spectroscopy 79−99586
GaAs:Cr photoluminesc. meas. 78−6761
GaAs:Cr^{2+}, cluster calcs. of Cr^2 electronic states 79−87064
GaAs:Cr^{2+}, Jahn-Teller effect for ion impurities 80−107753
GaAs:Cr^{2+}($3d^4$), Jahn-Teller distortion, photoinduced charge conversion, EPR 78−10758
GaAs:Cr(W), deep trapping centre exam. by thermally stimulated capacitor discharge method and luminesc. 77−55495
p-GaAs:Cu, impurity photocond. and absorpt. coeff., Hall meas. 80−6770
GaAs:Cu, LPE, photoelec. meas. of electron density for different Cu introduction methods 78−43437
GaAs:Cu, multiple scatt. Xalpha cluster model, impurity electronic states, dangling bond effect elimination 79−99504
GaAs:Cu melt grown, 1.36 eV band luminescence studies, edge emission 79−87510
GaAs:Fe, impurity atom charge exchange, Mossbauer spectroscopy 79−47050
GaAs:Fe(Co)(Cu)(Ni), substitutional impurity elec. struct. 80−88513
GaAs:Ge, LPE, on semi-insulating GaAs, film-substrate interface characterisation 78−72017
GaAs:Ge, stress depend. of donor-acceptor recomb. energy 79−15113
GaAs:Ge,Se transmutation shallow donor transition obs. 80−59925
GaAs:Mg, photoluminesc. temp. depend., 4.2-293K 77−69878
GaAs:Mg ion implanted, photoluminesc. and annealing charact. 77−16361
GaAs:Mg(Be)(Cd)(Zn), implanted, low temp. photolum. spectra 78−39583
GaAs:Mn, LPE layer, near band edge photoluminescence, 2K, low excitation intensities 78−48218
GaAs:Mn, p-type semiconductors, internal strain on bound hole-phonon interaction 78−91492
GaAs:Mn epitaxial layers, fabrication and electrical props. 77−80859
GaAs:N, extended Huckel theory appl. 80−59916
n-GaAs:Ni, negative photocond. at low temps., impurity levels 80−6900
GaAs:O, defect states, IR absorption spectra meas. 77−4666
GaAs:O, electrolum., photolum., negative differential resist. rel. to recomb. processes 80−66304
GaAs:O, electronic struct., multiple-scatt. Xα mol. cluster model 80−15445
GaAs:O, evidence for metastable state of O centre, Schottky barrier photocapacitance meas. *(French)* 78−10556
GaAs:O, Fe, temp. depend. of ionisation energies of O and Fe levels, electroabsorption meas. 78−47736
GaAs:O, high-resist., extrinsic photocond. meas., impurity binding energy determ. 77−85255
GaAs:O, impurity photocond. in high elec. field, 90K 78−19095
GaAs:O, photocapacitance quenching effect 78−91727
GaAs:O, slow domains, origin 78−60132
GaAs:O epitaxial film, impurity states, photocapacitance spectra 80−65625
GaAs:Sb, resonance levels of isoelectronic impurities 80−107740
GaAs:Se, multiple scatt. Xalpha cluster model, impurity electronic states, dangling bond effect elimination 79−99504

impurity electron states continued
GaAs:Si, charge state of impurity atoms, positron annihilation meas. 78−39062
GaAs:Si, electrical activity of Si 79−15145
GaAs:Si, electron irradiated, LPE layers and Bridgman crysts., IR absorption and Hall meas. 77−16345
GaAs:Si, ion implanted, photoluminesc. 79−69887
GaAs:Si, momentum distrib. of valence electrons, positron annihilation meas. 79−51530
n-GaAs:Si, thermally treated, photolum., acceptor levels obs. 79−38587
GaAs:Si, thick LPE layer growth and characterization 77−12511
n-GaAs:Si LEC crystal, carrier conc., B acceptor centres, Hall meas. and IR spectra 78−6717
GaAs:Sn, 1.39 eV luminescence, injection level depend., freq. response and thermal quenching 78−19529
n-GaAs:Te, 0.93-0.99 eV luminesc. band charact. 78−19560
GaAs:Te, impurity cond., microcathode-luminesc. investig. 77−8666
GaAs:Te, ion implanted optical transitions in modulated reflectivity spectrum 79−73972
n-GaAs:Te, vibr. props. of 1.0, 1.2 and 1.3 eV luminesc. centres 77−55823
GaAs:W^{2+}, radiative transitions, photoluminesc. obs. 80−108271
GaAs:Zn, sign inversion of the linear photogalvanic effect *(Russian)* 80−80321
$GaAs_{1-x}P_x$, N^+ implantation photoluminesc. props. 77−68987
$GaAs_{1-x}P_x$:N, film, optical absorpt. from photoluminesc. meas. 78−92134
$GaAs_{1-x}P_x$:N, Koster-Slater model and N-states 78−47732
$GaAs_{1-x}P_x$:N, N isoelectronic trap, model calc. of N_Γ and N_x electronic states 78−10398
$GaAs_{1-x}P_x$:N, upper branch of N isoelectronic trap., photo- and electrolum. expts. 77−63462
$GaAs_{1-x}P_x$:N heterojunction, N_x and N_Γ bound states, high-press. effects on electroluminesc. meas. 77−11870
$GaAs_{1-x}P_x$(Te), bound exciton stress depend., piezoluminescence, photoluminescence 80−80206
n-$Ga_xIn_{1-x}P$, optical props. and energy spectrum of donors 78−72567
$Ga_xIn_{1-x}P$:N, Delta lattice parameter model, correl. with electronic props. 78−91560
$Ga_xIn_{1-x}P$:N layers, LPE growth, luminesc. and direct exptl. obs. of band struct. effects 77−52157
$Ga_xIn_{1-x}P$:Si, solid soln., splitting of ground state 79−51527
GaN:Al, VPE grown, luminesc. and elec. props. depend. on doping conc., bound excitons 80−20688
GaN:As(P), implanted single cryst. film, cathodolum. 78−60523
GaN:Zn, LED, blue, yellow and green emission, temp. depend. 77−8658
GaN:Zn, temp. and press. depends., electrolum. 78−19567
GaN:Zn, VPE growth, photoluminesc. rel. to doping conditions 80−55159
β-Ga_2O_3:Cr, temp. depend. of luminesc. charact. *(Russian)* 77−28621
GaP, complex form of donor energy levels, optical spectra anal. 78−23045
GaP, deep O^- state, model impurity calc. 80−6780
GaP, donor states theory, camel's back struct. influence 80−59921
GaP, donor-acceptor pair luminesc., excitation spectroscopy 80−25440
GaP, epitaxial layers, dislocation recomb., SEM cathodoluminescence studies 79−42558
GaP, excited 1s-level of S-bound excitons 79−82996
GaP, impurity interaction on excited acceptor states, luminesc. excitation spectra 79−15517
GaP, multiband and multivalley effective mass theory for impurities 79−65409
GaP, optical absorption and struct. of acceptor centres 78−48205
GaP, piezo-modulated spectroscopic investigation of N and N-N pairs, bound exciton 77−66474
n-GaP, quasidirect radiative recombination of free holes at neutral shallow donors 78−64410
GaP, reevaluation of bandgap and free exciton binding energy 78−60061
GaP, shallow impurity states, free exciton binding energy 78−79960
GaP, Stark effect at H-like impurity centres, forbidden electron transitions *(Russian)* 80−16009
n-GaP, uniaxially deformed, piezoresist. exam. of donor levels 77−4346
GaP:Bi,N, photoluminesc., electroluminesc., 4.2 to 300K, excitons and hole traps 80−108275
GaP:Cr, origin of sharp near IR transitions 80−10913
GaP:Cu, elec. and optical props., rel. to doping and heat treatment 80−16056
GaP:Cu, Raman scatt. from acceptor state 80−11408
GaP:Fe, diffusion, solubility, elec. activity and energy levels 77−55395
GaP:Fe, double Fe-thermal acceptor centre, energy states 80−96823
GaP:Fe, electron exchange via val. band between Fe acceptor centres, Mossbauer spectra 77−55741
GaP:Fe, impurity atom charge exchange, Mossbauer spectroscopy 79−47050
GaP:Fe, photo-EPR study Fe($3d^6$) centres and deep electron traps 80−44910
p-GaP:Fe, photoionisation spectrum of acceptor level 77−55810
GaP:Fe^{2+}(Co^{2+})(Ni^{2+}) d→d luminesc. spectra 80−7414
GaP:Fe(Cr), photo-ESR of annealed crysts. 80−15795
GaP:N, bound excitons, low temp. photoluminesc. thermal quenching 77−48228
GaP:N, Cd(Zn),(C), interimpurity recomb., acceptor binding energies 78−34796
GaP:N, electron binding by N pairs 79−90990
GaP:N, electron charge distrib. in vicinity of substitutional N 77−24531
GaP:N, electronic energy levels calc., optimisation 79−28315
GaP:N, excited states of excitons bound to NN_i pairs, fluoresc. obs. 77−44039
GaP:N, extended Huckel theory appl. 80−59916
GaP:N, radiative recomb. from electron-hole drops, impurity induced transition 78−19547
GaP:N VPE LED, deep level centres, DLTS studies 79−42493
GaP:Ni(Fe), multivalence impurities, EPR and optical absorpt. meas. 80−75844
GaP:O, multicharged state of O, TSC and photoinduced currents 79−7808
GaP:O, photoionisation of deep impurity levels 80−34386
GaP:S, effects of uniaxial stress on luminesc. 79−78739
GaP:S, Se, Te, Si, shallow donors, excitation spectra 77−81128
GaP:S, shallow donor states, Stark effect and inversion splitting, electroabsorption spectral obs. 80−50385

impurity electron states continued
GaP:S(Se)(Te), pot.-depend. g-values and quenched diamag., props. of donor states 77−62861
GaP:S(Se)(Te), pot.-depend. g-values and quenched diamag., pseudoacceptors D^0, X 77−62862
GaP:Si(s)(O)(Ta), donor centre struct. and conduction band nonparabolicity 78−14695
GaP:Sn, LPE growth from Sn soln., elec. resist. and Hall coeff. meas. 78−2593
n-GaP:Te, doping parameters calc., by means of Hall data analysis 78−51925
GaP:Zn, Raman spectra of Zn acceptor 77−77187
GaP:Zn,O, degradation of bulk luminesc. induced by laser excitation 77−1715
p-GaP:Zn,S, spin polarisation of donors and acceptors in mag. field, optical and microwave study 80−93393
GaP:Zn (Cr)(S) positron annihilation, deep acceptor level props. 79−11485
GaP_xAs_{1-x}:N, impurity energies and wavefunctions 79−42488
$(GaP)_x(ZnS)_{1-x}$ solid solutions, X-ray fluorescence spectra, photoluminescence *(Russian)* 79−74003
GaSb, carrier density depend. on impurity conc., multiple doping effects 77−8047
p-GaSb, cond. mechanisms, uniaxial compression effects 77−20312
GaSb, sputtered films, on GaAs, growth, Hall effect, impurity levels 80−20334
GaSb, surface, electron struct. and Fermi level pinning by O_2 and metals 80−11066
GaSb, undoped, impurity band parameters calc. 79−51516
GaSb:Fe, shallow acceptor level, electrical meas. 79−11087
GaSb:Li, dopant behaviour 77−51696
GaSb:S, cond. and Hall coeff. relax., impurity config. model 80−6786
n-GaSb:Se, resonant and bound impurity states, Hall effect and resistivity press. depend. 77−28143
p-GaSb:Te, effective radiative recombination centre nature, photoluminescence spectra 79−90998
n-GaSb:Te, heavily doped, electron-hole recomb., photoluminesc. spectra 78−84644
GaSb:Te, indirect gap photolum. 80−29797
n-GaSb:Te(Se), forbidden optical band gap, Moss-Burstein effect 78−88335
p-GaSe, resist. and Hall-mobility meas. at 77-850K 77−59295
GaSe:Sn, single crystal, space-charge-limited currents *(Russian)* 80−11001
Ga_2Te_3:Sn, impurity atom electron shell compression by matrix *(Russian)* 77−28146
$Gd_2O_2S:Tb_1$ recomb. processes and emission spectra *(Russian)* 78−6797
$GdVO_4:Ho^{3+}$, optically excited doublet splitting in magnetically ordered state 78−19238
$GdVO_4:R^{3+}$, R=Nd, No, Tm, Sm, Dy, Er, Eu, Tb, electronic struct. and spectra of VO_4, RO_8 clusters 78−10953
Ge, acceptor ground state, US attenuation meas. *(Japanese)* 78−19105
Ge, acceptor ground state, stress effects 80−34385
Ge, acceptor levels, ionis. energy and IR absorpt. 79−78033
Ge, acceptor spectra, interpretation 78−43332
Ge, acceptors, transitions from second excited state, photocond. meas. 79−11082
n-Ge accumulation layers, effect of low-energy Ar^+ ion bombardment on electron scatt. 77−66205
Ge, amorphous film, effects of alloying chalcogen atoms 80−49670
Ge, anomalous muonium states 80−34841
n-Ge, compensated, impurity photoconductivity 78−10512
n-Ge, D^- state struct. rel. to photocond. expts. 80−59924
Ge, deep and shallow levels of muonium, electronic struct. 78−39051
p-Ge, detector-grade single crysts., impurity background 79−11088
Ge detector; high-purity, effect of crystal growth direction on energy resolution 79−45541
Ge, donor energy spectrum, mag. field effect, submm. photocond. meas. *(Russian)* 77−43666
Ge, donor ion pot., small r behaviour of nonlinear Poisson eqns. 80−54652
Ge, donor-acceptor electron transfer at low temps., photocond. tail 78−84249
Ge, electron-hole drop drag, interaction with thermal pulses 80−103631
Ge, electron-hole droplet, attachment to donor 78−87916
n-Ge, electron-phonon interaction, internal strain and impurity elec. field effect 78−14418
Ge, electronic states of isolated negative donor ion, binding energy 79−65404
Ge, energy gap, impurity conc. depend., calc. 80−80170
p-Ge, energy spectrum of impurities and effect of mag. field *(Russian)* 77−47770
Ge, evidence for correlated hopping in impurity cond. at moderate impurity conc. 77−20317
Ge, excitation spectra of shallow acceptors, Zeeman effect, expt. 80−7381
Ge exciton and electron-hole drop decay, far IR magnetoabsorption obs. 77−40252
Ge, excitons bound to acceptors, Auger transition rates 78−34778
Ge, far IR magneto-absorption of donor-bound excitons, pseudo-acceptor model 77−63418
Ge, far IR magnetoabsorption, excitons, electron-hole drops and impurities 78−6664
Ge film, polycrystalline, structural and elec. props. 78−76173
Ge, gamma irrad. above threshold, defect formation impurity ionisation mechanism 80−6433
Ge, heavily doped, far IR props. of shallow impurity states 79−95786
Ge, high-purity, with Al, B and P, residual impurities, photothermal cond. 80−24965
Ge, hydrogen multivalent acceptor complexes 77−55491
Ge, impact ionisation of shallow donor states, 4 to 7K 78−30936
Ge, impurity determ. in very pure sample by photoelec. spectroscopy 77−39888
Ge, impurity levels of H and muons 79−56162
Ge, impurity photoconductivity 79−82631
Ge, impurity spectral linewidth meas., free electron effects 80−71463
Ge, light scattering, by pure single cryst., influence of photoexcitation 79−28780
Ge, localised states due to isocoric donor impurities 77−76768
Ge, low temp. recombination into shallow donors, transient case 79−38092

impurity electron states continued
Ge, nonradiative transitions at impurity centre with participation of short-wavelength phonons 80−16099
Ge p-i-n diodes, deep level transient spectroscopy 79−47105
Ge p-n junctions, impurity photoelec. effect 79−56300
Ge, photoconductivity, carrier lifetimes in excited states of impurities *(Russian)* 77−76864
Ge, photoconductivity spectra of shallow impurities 79−82625
Ge, photoelectric spectra of shallow impurities, mag. field effect 79−82624
Ge, photoelectric spectra of impurity groups 79−82627
Ge, photoelectric spectra of remanent impurities 79−87125
p-Ge, photoexcited charge carrier capture by shallow impurity centres *(Russian)* 80−15571
N-Ge, pressure influence on photoconductivity temp. dependence 78−76109
n-Ge, rel. to shock wave effects on elec. cond. *(Russian)* 78−87979
Ge shallow hydrogenic centres, ground states, isotope shifts, photoelectric spectrosc. 78−39055
Ge, shallow impurities, excited states, population and lifetime *(Russian)* 79−51532
Ge shallow impurity bound states, IR spectroscopic obs. 77−39806
Ge, spectral diffusion in acceptor-hole system at low temp., ultrasonic hole-burning expt. 80−92610
Ge, sum rule for intraband optical absorpt. of shallow acceptor impurities 79−28793
Ge, surface states, recombination centre formation *(Russian)* 80−29459
p-Ge, thermal conductivity meas. down to 50 mK, acceptor state exam. 77−80658
Ge, transmutation-doped, impurity cond., 1.5-4.2K 77−89758
n-Ge, US attenuation by impurities 77−69047
Ge, ultra pure, method to determ. composition and struct. of non-elemental acceptor and donor centres 78−39658
Ge:Ag(Ni), gamma ray effects on impurity states 80−96822
Ge:Al, acceptor levels, Zeeman splitting, far IR photoconductivity spectrum 78−43444
Ge:Al(B), uniaxially stressed, photoionisation of acceptors, impurity photocond. meas. 78−10509
Ge:Al(B)(P), impurity ground state levels from photo-thermal cond. in mag. field 77−51699
Ge:As, far IR transmission spectra, singlet-triplet optical transitions in ground states of donors 78−2887
Ge:As, NMR, conduction electrons in impurity band, metal-nonmetal transition 79−78544
Ge:As, recomb. of donor bound excitons, luminesc. intensity decay 80−25441
Ge:As, uniaxially stressed, electronic Raman scatt. from valley-orbit transitions 78−15166
Ge:As(P)(Sb), impurity photocond. spectra under uniaxial compression 80−44656
Ge:As(Sb), D^- states in mag. fields, photocond. spectra, and far IR absorption spectra 79−95370
Ge:As(Sb), D^- states investigated by long wavelength photoconductivity 78−6323
Ge:As(Se^+), energy spectra, multivalley effective mass calcs. 77−59266
Ge:Au, gamma-irradiated and electron irradiated, elec. props. meas. 77−62950
Ge:Au, Sb, Hall mobility, temp. dependence 80−96919
Ge:Au, Sb 79−69577
n-Ge:Au piezoresistance in presence of deep levels, stress anisotropy 80−10979
Ge:B(Al)(Ga), shallow acceptor spectral line intensities 80−88517
Ge:B(Al)(Ga)(In)(Tl), binding energy, excited state spectra, photolum., semi-empirical short range pot. 80−44534
Ge:Ba distrib. pattern, partition coeff., limiting solubility and energy levels 77−15444
n-Ge:Bi,O, plastically deformed, dislocation scatt. anisotropy, effect of state of O in Cottrell atm. 78−19028
Ge:Cd, compensated, complex oscillatory impurity photocond. spectrum 77−43656
Ge:Cu, degree of Cu contamination in heat treated Ge from impurity level density meas. 80−2359
Ge:Cu, press. effect on energy spectrum of carriers, elec. cond. and Hall coeff. expts. 79−23930
Ge:Cu, quenched, interaction between shallow-level defects and Cu atoms, Hall effect meas. 78−64002
n-Ge:D^-; energy spectrum of D^- impurity band 77−51702
Ge:Ga, magnetoacoustic resonance attenuation, Zeeman splitting of acceptor ground state 77−47869
p-Ge:Ga far IR absorption and photoconductivity obs. 77−39899
Ge:Ga(In), resonant phonon interaction with localised acceptor levels 80−6784
Ge:Ga(In), shallow acceptor ground state, thermal cond. meas. 77−43540
Ge:H, amorphous, H-states exam. 78−39059
Ge:H, interstitial impurity levels, pseudopot. calc. 80−44533
Ge:H, photoelec. spectra, acceptor and donor behaviour 80−29443
Ge:Hg, anomalous room-temp. impurity photocond. 78−39159
Ge:In(Hg), impurity characterisation from thermal carrier meas. 80−65595
Ge:Li, long wavelength photoconductivity spectrum 77−43641
Ge:Li, thermal cond., 0.4-20K, Li valley-orbit splitting 79−15111
Ge:Li-O, donor complex EPR and photoelectron piezoelectric spectra, dynamic tunnelling 79−1711
Ge:Mg, energy level behaviour, Hall coeff. and elec. cond. meas. 80−34396
Ge:Ni compensated, hot electron recomb. anisotropy 78−39125
Ge:O, elec. props., O donor levels determ. 77−8123
Ge:O, elec. props., O interaction with point defects 79−11081
n-Ge:O, impurity-saturated, dislocation-free, anomalously high magnetoresist., vacancy effects 77−43629
Ge:O, slow thermal relax. of cond. rel. to donor complexes 80−70704
n-Ge:P(As), nonlinear optical susceptibility, Raman scatt. cross-sections for impurities 77−46759
Ge:P(As)Ga, lightly doped semicond., electron-phonon scatt., role of compensation 79−60456
Ge:Sb, amorphous, electronic transport props. 80−44589
Ge:Sb, effect of degree of doping on surface state charact. 79−69577
n-Ge:Sb, electron irrad., impurity photoconductivity 77−15900
n-Ge:Sb, fast neutron irrad. effects on donor conc., and annealing 78−56107

impurity electron states continued
n-Ge:Sb, γ-irrad. effects on donor conc. and compensation by acceptors 78−56106
Ge:Sb, rel. to uniaxial stress effects on acoustic attenuation 78−59863
Ge:Sb,Au, photoelectronoc exam. of multilevel gold structure 77−69272
Ge:Sb,Cu, high resist. compensated, impurity of photocond., pulsed unipolar injection carriers 80−92935
Ge:Sb,In, lightly doped semicond., low temp., phonon cond., electron-phonon scatt. 79−60456
Ge:Sb (As), isolated D^{-} states and D^{-} complexes in mag. fields 80−15473
Ge-Sb, D^{-} complexes and band form., photocond. 78−84251
Ge-Si, electron irradiation and annealing 77−55305
Ge-Si alloy p-n junction, Sb-diffused, TSC 80−20289
Ge-Si solid solution film, elec. props. in range 4.2 to 500K 77−8214
Ge-Si:Sb, energy spectrum of Sb 80−34382
Ge-Si:Te, solid solns., donor states energy spectrum 80−88516
n-$Ge_{1-x}Al_xAs$:Te, long-lifetime photocond. effect obs., Hall effect meas. 77−89795
$GeO_2:Sc^{3+}(Y^{3+})(In^{3+})$, trapped-hole centres, ESR meas. 79−77597
p-GeS, crystalline, photoelectric props. 80−70769
$Ge_{0.8}Si_{0.2}$, elec. cond., density of states, impurity and temp. depend 80−65568
$Ge_{1-x}Si_x$, solid soln., local levels, matrix elements of valence band, perturbing pot. calc. 77−1395
He:Xe, liq., 0.04-0.1 g cm^{-3}, vac. UV absorpt. spectra, Wannier impurity states 77−77232
^3He-^4He, liquid solution, bound impurity pair effect on surface tension *(Russian)* 80−65332
hexamethylphosphoramide:Li glass, metallic condensation of Wannier-Mott impurity states 78−2420
$HfO_2:M^{n+}$, M=Ce, Pr, Tb, Eu impurity valence transitions 77−51694
$Hg_{0.77}Cd_{0.23}Te$, near reson. spin-flip Raman scatt. 79−82983
$Hg_{0.8}Cd_{0.2}Te$-ZnS MIS struct., nonparabolic bond semicond., surface state studies, capacitance measurements 79−78190
$Hg_{0.82}Cd_{0.18}Te$, electronic anomalous mass near reson. acceptor level, Shubnikov-de Haas meas. 80−80163
$Hg_{0.85}Cd_{0.15}Te$, acceptor states, galvanomagnetic effects study 79−82560
$Hg_{1-x}Cd_xTe$, acceptor bound exciton Auger and radiative transition rates, radiative recomb. 80−6733
$Hg_{1-x}Cd_xTe$, acceptor impurity band form. 80−20119
$Hg_{1-x}Cd_xTe$, acceptor levels due to local impurity potential 79−11084
$Hg_{1-x}Cd_xTe$, ionized intrinsic pt. defects, effect on carrier density 77−47835
$Hg_{1-x}Cd_xTe$, magnetooptical and impurity effects 80−6721
$Hg_{1-x}Cd_xTe$, photolum. and optical pumping 80−50424
$Hg_{1-x}Cd_xTe$, quasi-local acceptor levels and electron mobility 78−67974
$Hg_{1-x}Cd_xTe$, resonant acceptor level, single and multiple scatt. effect 77−47767
$Hg_{1-x}Cd_xTe$, semiconducting phase, acceptor states and galvanomagnetic effects 80−11017
$Hg_{1-x}Cd_xTe$, theory of optical absorpt., contribution by quasilocal acceptor levels *(Russian)* 80−71451
$Hg_{1-x}Cd_xTe$-type semimetals, kinetic props., local acceptor level effects 80−65557
$Hg_{a-x}Cd_xTe$, (x<0.16), semimetallic phase, acceptor states and galvanomagnetic effects 80−6882
HgI_2 crystals, native defect compensation, doping, mobility-lifetime and TSC meas. 77−55492
HgI_2:Ag, trapping effects, TSC, photocond. and photolum. meas. 77−32023
$Hg_{0.98}Mn_{0.02}Te$, resonance acceptor level 78−23048
$Hg_{1-x}Mn_xTe$, acceptor reson., states in high mag. field 80−49668
$Hg_{1-x}Mn_xTe$, magnetooptical and impurity effects 80−6721
α-HgS, cinnabar, donor-acceptor transitions, cathodolum. meas. *(French)* 77−48250
HgS, cinnabar powder, 1.65 eV pair recomb., thermal quenching and total light decay 78−27330
α-HgS, green cathodoluminesc., impurity effects 78−2924
α-HgS, natural, yellow emission 78−68567
HgSe, magnetooptical and impurity effects 80−6721
HgSe(Te), zero-gap semicond., impurity states model 79−60758
HgTe, acceptor reson., states in high mag. field 80−49668
HgTe, contrib. of resonant states to conductivity 79−51577
n-HgTe, far IR magnetoabsorption involving resonant acceptor states 79−69813
HgTe, Γ_8 symm. acceptor centre hole mag. props. *(Russian)* 80−88733
HgTe, long-wavelength magneto-absorptions 80−11397
HgTe, resonance states in scatt., variational methods 79−60754
HgTe, uniaxially compressed, anomalous magnetoresist. and band crossing 79−65501
HgTe, zero gap semiconductor, review 77−31944
HgTe, zero gap semiconductors, Coulombic resonance states 79−38020
HgTe, zero gap semiconductor, resonant acceptor states 80−6772
HgTe, zero-gap semiconductor, variational approach to resonances 79−82559
In-Mn, dilute alloy, local excited states, electron tunnelling observation 80−34565
n-InAs, edge luminescence band, shape depend. on degree of doping, band gap 80−7405
InAs, heavily doped, Burstein-Moss effect and near-band-edge luminesc. 79−47525
InAs, longitudinal magnetoresistance in extreme quantum limit *(Russian)* 80−11008
N-InAs, Moss-Burstein effect, S, Sn, Te dopants 78−64389
InAs:Cd, Te, donor-acceptor interaction, elec. cond. and Hall coeff. meas. 80−59988
InAs:Cd,Te interaction between impurities, effect on elec. props., Hall effect. 80−19832
n-InAs:Cr, Czochralski growth of high-resist. single crysts. 77−66587
InAs:Mn^{3+}, Jahn-Teller effect for ion impurities 80−107753
$In_{1-x}Ga_xP:N_2$, N-trap bound states, photoluminesc. and absorption data 77−1719
$In_{1-x}Ga_xP$:N(Te), composition depend. of bound state luminesc. transitions 78−39595
$In_{1-x}Ga_xP$:Te,Zn, photolum. and electrolum., direct transition region 77−8659
InP, acceptor excited states, luminesc. spectra 80−16091
InP, bulk grown, selective spectroscopy, acceptor level studies 80−29778
n-InP, compensated impurity conduction and negative magnetoresist. 79−28360
impurity electron states continued
InP, exciton localisation at impurity pairs 79−37999
InP, growth and props., Zn acceptor obs. 79−1822
n-InP, Hall effect, 10-300K ,thermal activation energy and influence of compensation 78−72171
n-InP, magneto-impurity resonances, obs. of central cell struct. 78−95303
n-InP Schottky barriers, photocapacitance effects of deep traps 78−43325
InP, surface, electron struct. and Fermi level pinning by O_2 and metals 80−11066
InP:Bi, isoelectronic impurity states, emission and absorpt. obs. 79−42491
n-InP:Cr, press. depend. of elec. resist. and Cr ionisation energy 80−80281
InP:Cr^{2+}, Jahn-Teller effect for ion impurities 80−107753
InP:Fe, deep levels 79−56166
InP:Fe, Fe acceptor charge states, photolum., absorpt. and ESR meas. 77−36123
InP:Fe, photocond., Fe^{2+} intracentre excitation model 80−29436
p-InP:Zn, vapour grown, prep. and props. 80−54268
n-InSb, absorption of millimetre radiation in mag. field 79−11083
InSb, donor excitation spectra in high mag. field 78−80027
InSb, donor impurities, magnetic freezeout in hyperquantum regime 80−10921
InSb, donor spectrum, effect of strong mag. field 79−7806
InSb, doping depend. of high-field donor spectra 77−90175
n-InSb, electron recombination between Landau-levels 79−38096
InSb, energy spectra of impurity atoms under 4.2K gamma irradiation 77−89471
n-InSb, galvanomag. props. at low temp., carrier localisation, metallic impurity cond. 77−28195
InSb, gamma irradiated, changes in energy spectrum of impurity spectrum 78−51937
n-InSb, H-like impurities photocond., mag. field effect 79−82634
n-InSb, Landau-level-electron lifetimes, saturation meas. of magnetoabsorption 78−48150
n-InSb, longitudinal magnetoresistance in extreme quantum limit *(Russian)* 80−11008
n-InSb, low temp., electric and mag. resonances, impurity level *(Russian)* 78−56159
InSb MOS structs., energy spectrum of traps in oxide layer 80−107922
InSb, magnetically frozen-out, evidence of surface cond. from etching expts. 79−47152
InSb, magneto-optical anomalies of impurity electrons, two-LO-phonon region 78−72415
p-InSb, uniaxially deformed, mag. field induced semicond.-metal transition 79−95457
InSb:Cr(Zn)(Mn)(Ge), recombination of nonequilibrium carriers 79−65496
p-InSb:Cu(Ag), ionisation energy of multiply charged impurities, compensation effects 78−18996
InSb:F, acceptor props. and diffusion coeff. of F 80−70643
InSb:Ge annealing effect on electrical parameters, absorption spectra and photocond. 77−11939
InSb:S(Se)(Te), reson. states and reson. scatt., elec. props. 80−49738
InSb:Zn, impurity centre behaviour, impurity conc. and Hall coeff. meas. 80−65490
InSb-NiSb, eutectic, intraband magneto-optical studies, far IR transmission spectra 79−61371
InSb-type semiconductors, shallow donor states in magneto-optical props. 80−6785
In_2Te_3-type semiconductor, mechanism of electrically inactive impurities 80−24834
Ir, chemisorption levels of CO and O on (100) and (110) faces 78−84704
K:F^{-}(Ne), ground states and core hole states, self-consistent soln. using density functional formalism 79−69467
KBr:Ag, optical absorpt. spectra interpretation mol. orbital scheme 80−20671
KBr:CN^{-} tunnelling motion of dipolar impurities, absorption spectra 80−66239
KBr:MnO_4^{-} (MnO_4^{2-}) Raman scatt. spectra, freq. and type of symm. of internal vibr. of impurity centres 79−15466
KBr:NO_2, Na effect of Na^{+} impurity on self-trapped hole *(Japanese)* 78−67982
KBr:PO_2^{-}, phosphorescence, triplet state sublevels, mixing 80−25446
KBr:TeO_3^{2-}, IR absorpt. of impurity complexes *(Russian)* 79−33746
KBr:Tl, A-emission, line shapes and relative efficiencies 79−83011
KBr(I):Co, coloured and uncoloured, Mossbauer effect, inhomogeneous hyperfine fields 77−32307
KCl, thermoluminesc., halogen and alkali impurity effects 80−97352
KCl:Ag, hole capture radius, scintillation luminesc. obs. *(Russian)* 78−39582
KCl:Ag, optical absorpt. spectra interpretation mol. orbital scheme 80−20671
KCl:AgCl, positron annihilation characts., positronium state form., X-irrad. effects 77−4700
KCl:Cu,Tl, plastic deform., charge exchange of hole centres *(Russian)* 77−11876
KCl:$In^{+}(Tl^{+})$, HF calc. for ground and excited states of impurity centre 77−72835
KCl:Li^{+}, press. tuning of motional behaviour in shallow off-centre pots. 79−78718
KCl:MnO_4^{2-}, Raman scatt. spectra, bands due to ν_1, vibr. of MnO_4^{2-} 79−15466
KCl:Na,Br, EPR of interstitial and diinterstitial $BrCl_2^{2-}$ centres 77−81007
KCl:Pb^{2+}, decay of luminescence emission 78−39593
KCl:Ru, optical absorption bands, complex form. 77−1705
KCl:$SnCl_2$, electronic struct. of Sn^{+} centres, model 77−43530
KCl:$SnCl_2$, photostimulated hole recombination luminesc. *(Russian)* 80−80833
KCl:Tl, 375 nm emission band 79−95834
KCl:Tl, energy level scheme, mol. orbital model 80−10912
KCl:Tl^{2+}, optical absorpt. spectra interpretation mol. orbital scheme 80−20671
KCl:V^{2+}, EPR spectrum temp. depend., crystal field theory 77−16163
KCl(Br)(I):Ga^{+}, polarisation of Ga^{+} centre A_T emission, temp. depend. 80−80842
KH_2PO_4:Tl, UV absorption bands obs. 78−27266

impurity electron states continued
KI:BH_4^-, far IR absorption in phonon gap 77−12406
KI:Pb, absorpt. spectra of Pb^{++} centres 80−76058
KI:Pb^{2+}, UV absorpt. and mag. circular dichroism spectra 80−25418
KI:Tl, $(Tl^+)_2$ centre luminesc. 78−84632
KI:Tl, decay of fast component of impurity luminesc. excitation in A-absorption band *(Russian)* 80−84767
$KLiSO_4$:Cr; optical activity characts. cryst.-chem. exam. 78−95569
KLu_3F_{10}:Eu^{3+}, crystal field and spin-orbit parameters 78−30892
$KMgF_3$:Co^{2+}(Fe^{2+})(Mn^{2+})(Ni^{2+}), high energy absorption spectra interpretation 78−6716
$KMgF_3$:Sm^{2+}, absorpt. spectra and Zeeman effect, 3000-12000 Å, 4.2-295K 79−24341
$KMgF_3$:Yb^{3+}, ^{19}F hyperfine interaction, anisotropic Fermi and isotropic dipolar interactions 79−78056
$KMnCl_3$, rare earth doped, energy transfer, emission spectra obs. 80−20684
$KNbO_3$, photoconductivity and TSC 78−2520
$KTaO_3$, depletion region and donor levels determ., appl. in surface barrier volume wave transducer 80−33403
KY_3F_{10}:Eu^{3+}, crystal field and spin-orbit parameters 78−30892
$KZnF_3$:Ni^{2+}, temp. depend. of luminesc. 79−83016
$LaCl_3$:Ho^{3+} parametric energy level anal. 78−18991
$LaCl_3$:Np^{3+}, phonon-induced relax. in excited optical states, linewidth temp. depend. meas. 80−100688
LaF_3:Nd^{3+}, cryst., $4f^3$ config., ground level energy state var. rel. to press. *(Russian)* 77−16358
La_2O_2S:Tb, recomb. processes and emission spectra *(Russian)* 78−6797
$La_{1-x}Pr_xP_5O_{14}$:Pr^{3+}, fluorescence spectrum 79−83014
$La_{1-x}Sr_xVO_3$, high-temp. transport meas. 77−11917
LiCl:Cu^+, 3d⟶4p transitions, near UV absorpt. spectrum assignment 78−27272
LiCl:Cu^+, luminescent centre, cluster MO calculation of energy levels 78−64411
LiCl:Cu^+, MO calc. of luminesc. Cu^+ centres 79−38609
LiF:Fe, dispersed ions, absorber Mossbauer spectra 78−15077
LiF:Mg,Ti, defect states, ESR and ionic cond. study 80−108058
LiI:Pb, absorpt. spectra of Pb^{++} centres 80−76058
$LiNbO_3$ doped with transition metal oxides, absorption spectra temp. depend. 77−90176
$LiNbO_3$:$^{57}Fe^{2+}$ Mossbauer spectra, EFG axis 77−20760
$LiNbO_3$:Cu^{2+}, EPR and optical spectra 80−20453
$LiNbO_3$:Cu(Fe), light induced charge transport, photovoltaic effects, impurity states 80−80317
$LiNbO_3$:Fe, bulk photovoltaic effect in ferroelecs. 79−15181
$LiNbO_3$:Fe, impurity valence state charge on X-ray irrad., Mossbauer meas. 80−7235
$LiNbO_3$:Fe, impurity charge states after UV irradiation 80−60462
$LiNbO_3$:Fe, state of impurity Fe cation, nucl. gamma reson. study 80−40014
$LiNbO_3$:Fe, X-ray and γ-ray irradiation effects on Fe charge state, Mossbauer study 80−40013
$LiNbO_3$:Fe^{3+}, electrooptical effect, charge transfer mechanism, defect. pair form. 79−38519
$LiNbO_3$:Fe(Cu), photorefractive centres, optical absorption, EPR and Mossbauer spectra meas. 77−32403
$LiNbO_3$:Ti, diffused waveguide, +4 valence state, XPS 77−11014
$LiTaO_3$:Cu(Fe), light induced charge transport, photovoltaic effects, impurity states 80−80317
$LiYF_4$:Tm^{3+}, cryst. field parameters, appls. 77−20277
$LiYO_2$:Nd^{3+}, absorption and luminesc. spectra, energy level diagram 77−63441
$LuRhO_3$, elec., mag. and photoelectrochemical props. 80−96925
$LuVO_4$:R^{3+}, R=Nd, No, Tm, Sm, Dy, Er, Eu, Tb, electronic struct. and spectra of VO_4, RO_8 clusters 78−10953
Mg:H, impurity energies and geometrics, self-consistent jellium calc. 79−99507
Mg:H(He), interaction energy of two H(He) atoms, Hohenberg-Kohn-Sham density functional formalism 79−51519
MgF_2:Ni^{2+}, temp. depend. of luminesc. 79−83016
MgO, electronic excitations and luminescence, review *(Russian)* 78−72575
MgO, Fe^{2+} and Fe^{3+} conc. and valency, optical density, EPR and MCD obs. 77−89462
MgO, transition metal ion doped, phonon spectroscopy using freq. crossing techniques 79−42193
MgO:Cr, high resolution far IR spectroscopy of lower energy levels of Cr^{2+} 80−80822
MgO:Fe crysts., oxidised and reduced, optical absorpt. spectrum at low temps. 77−63436
MgO:Li^+, quenched, elec. polarisation, thermal depolarisation and dielectric loss meas. 79−1738
MgO:Li(Al)(F), impurity-induced UV luminesc. 79−83037
MgO:Ni^{2+}, temp. depend. of luminesc. 79−83016
Mg_2SiO_4, forsterite, elec. props. 78−34833
Mn^{2+}, cubic spin-Hamiltonian parameters in inorganic compounds, superposition model anal. 80−20367
$Mn_{1+\delta}Sb$, Mn electronic state, neutron diffr. study 80−65806
Mo-Co Kondo alloy, Co impurity susceptibilities, Knight shift 80−88721
MoS_2, 2H phase, far IR magnetoabsorption and refr. index meas. 77−24847
$MoSe_2$:Nb(Re), layered, elec. props., semicond.-metal transition 77−11922
NH_4Br:Cu^{2+}, ESR and absorpt. spectra, 300-1500 nm 78−60492
NH_4Cl:Cr^{3+}, ESR of Cr^{3+} centres, room temp. 78−91943
Na:F^-, ground states and core hole states, self-consistent soln. using density functional formalism 79−69467
NaA zeolite:S, optical spectra 78−88342
$Na_{56}(AlO_2)_{56}(SiO_2)_{136}$:$Eu^{3+}$, Y-type zeolite, luminesc. props. 79−83017
NaBr:Cu^+, press. tuning of motional behaviour in shallow off-centre pots. 79−78718
NaBr:Tl^+, emission spectra, excitation in A-band 78−15218
NaCl, mechanoluminesc. peaks, microbreakdown mechanism, generation of ionisation waves 79−33032
NaCl, pure, indoped, luminesc. obs. 77−32412
NaCl:Ag, thermolum. light sum storage by ultrasoft X-rays 77−20939
NaCl:AgCl, positron annihilation characts., positronium state form., X-irrad. effects 77−4700
NaCl:Ga^+, polarisation of Ga^+ centre A_T emission, temp. depend. 80−80842
NaCl:Pb, γ-irrad., centres in thermoluminescent emission 77−85816
impurity electron states continued
NaCl:Pb^{2+}, decay of luminescence emission 78−39593
NaCl:Pb^{2+}, emission spectra obs., and luminesc. centre model 77−36286
NaCl:Ru, optical absorption bands, complex form. 77−1705
NaCl:V^{2+}, EPR and optical absorpt. spectrum temp. depend., crystal field theory 77−16163
NaF:Fe, dispersed ions, absorber Mossbauer spectra 78−15077
NaI:Pb_1 absorpt. spectra of Pb^{++} centres 80−76058
NaI:Tl^+, luminescence spectrum, excited states of monomer centre 77−66536
$NaMgF_3$:Sm^{2+}, absorpt. spectra and Zeeman effect, 3000-12000 Å, 4.2-295K 79−24341
$NaNO_2$, cryst., triplet excitons, localised states, zero-field ODMR, dopant effects 78−15062
($NaNO_3$-$Mg(NO_3)_2$):Nd^{3+}, glass, cryst., absorpt. luminesc. spectra, term struct. of Nd^{3+}, bonding 77−8624
$NaNbO_3$, elect. cond. mech., resist., Hall coeff. and thermoelec. power meas. 80−65603
$NaNbO_3$, photoconductivity and TSC 78−2520
Na_2O-Al_2O_3-B_2O_3-SiO_2:Ag, photochromic glass, EPR of Ag^0 and Ag_2^+ centres 77−24741
Na_xWO_3, Knight shift, spin-lattice and spin-spin relax., high press. NMR obs. 80−50211
Nb, electrotransport of H(D) at high H concs. 80−34246
Nb-H system, screening of H impurity and lattice distortion *(Russian)* 79−1577
$NdCl_3$, anhydrous, Nd^{3+} absorption spectra and quantum states *(Chinese)* 80−89032
$Nd_2(WO_4)_3$, elec. transport and mag. props. meas. 77−24668
$Nd_xY_{1-x}P_5O_{14}$, fluorescence quenching 77−69903
Ne, solid, pure and Xe, Kr, Ar doped, photoemission yields and reflectance spectra, exciton dynamics 77−28123
Ne:H, exciton states and $L_{\alpha_3}L_\beta$ emission 80−93372
Ne:Xe, liq., 0.1-0.65 g cm^{-3}, vac. UV absorpt. spectra, Wannier impurity states 77−77232
Ni, Ar ion implantation, $1S_{\Gamma/2}O$, $1S_{1/2}C$ and $2P_{3/2}Ni$ states, X-ray photoemission spectroscopy obs. 80−16149
Ni, cluster approach to single H atom in single crystal 78−47334
Ni, electronic structure of nontransition element impurity atoms 77−73023
Ni, FCC, H impurity self-consistent electronic screening charge density, cluster calc. 79−33255
Ni, ferromagnetic, electronic struct. and hyperfine field of nonmag. impurities, calc. 80−70658
Ni:B, impurity electronic struct. calc., ^{12}B NMR data anal., magnetisation decrease 79−47046
Ni:H, energy and electron density of states 78−51929
Ni-C interstitial alloys, electronic struct. 77−35886
Ni-Co(Fe)(V)(Ti), dil., optical absorpt., electronic struct. 80−108227
Ni-Cr(V)(Co)(Mn)(Mo)(Ru)(Fe), spin wave stiffness consts., RPA CPA band model 79−61088
Ni-Cu(Zn)(Ga)(Ge)(As)(Se)(Br)(Kr), dil., ferromagnetic, hyperfine field and relax. time obs. of impurity heavy nuclei 80−75533
Ni-H, ferromag., H impurities and μSR, self-consistent calc. 80−84447
Ni-H system, cluster calc. of electronic struct. of interstitital H 78−43326
Ni-Re, dil. alloys, two-band Mott conductivity *(Russian)* 78−60118
$Ni_{1-x}Rh_xS$, nonvolume effect of Rh substitution on paramag. metal-antiferromag. nonmetal transition 79−28277
P+Nb, dil. alloy, NMR obs. of ^{93}Nb 80−71203
$Pb_{1-x}Cd_xS$, metastable epitaxial films, elec. props. 78−26979
$Pb_{1-x}Cd_xTe$, IR absorpt. study of Cd impurity levels, energy gaps 80−45081
$Pb_{1-x}Ge_xTe$, ferroelectric phase transition effect on forbidden band width 80−24794
$Pb_{1-x}Ge_xTe$:Ga, Fermi level stabilization, transport props. meas., 77-400K 78−56065
PbI_2, TSC meas., localised levels in energy gap, depend. on purity and history 77−15856
PbO, single crysts., exciton and impurity luminesc. 80−60674
PbO-B_2O_3(SiO_2) glasses, absorpt. spectra of Cu^{2+} ions and interpret. 78−27276
PbO-SiO_2 glasses, absorpt. spectra of Nd^{3+} ions and interpret. 78−27277
$Pb_3(PO_4)_2$:Gd^{3+}(Eu^{2+}), EPR spectra of α- and β-phases 80−11261
PbS:Tl, Hall and Seebeck coeffs., Hall mobility, impurity states 80−15545
PbS:Tl, self-compensation of acceptors by vacancies, Hall coeff. meas. 80−92913
PbSe:Tl, high temp. elec. and optical props., impurity states 79−60854
PbSe:Tl, impurity states, optical absorption and Hall effect meas. 78−18995
PbSe:Tl, self-compensation of acceptors by vacancies, Hall coeff. meas. 80−92913
$Pb_{1-x}Sn_xSe(Te)$:I epitaxial layers, photoelectric props., doping donor impurity behaviour 77−80810
$Pb_{0.8}Sn_{0.2}Te$:Cd, defect struct., Hall effect and solubility meas. 77−11571
$Pb_{0.8}Sn_{0.2}Te$:Cd, influence of Cd doping on high field magnetoresist. and Hall effect 80−75590
$Pb_{0.8}Sn_{0.2}Te$:In, absorption spectra meas., 475-725K 77−4664
$Pb_{1-x}Sn_xTe$: Mn, Mn mag. and elec. active states, mag. impurity behaviour 80−44627
$Pb_{1-x}Sn_xTe$:Cd, impurity photocond. spectra 80−6902
$Pb_{1-x}Sn_xTe$:Cd(In), solid solutions, impurity states in photoluminescence spectra *(Russian)* 80−97333
$Pb_{1-x}Sn_xTe$:Ge, anomalous behaviour of impurity centres under press. *(Russian)* 80−65491
$Pb_{1-x}Sn_xTe$:In, energy spectrum under combined effect of mag. field and hydrostatic press. 79−65382
$Pb_{1-x}Sn_xTe$:In, energy spectra modifications due to comp. changes and press. appl. 80−10915
$Pb_{1-x}Sn_xTe$:In, impurity influence on photoluminescence at large excitation levels *(Russian)* 80−93384
$Pb_{1-x}Sn_xTe$:In, semiconductor-metal-semiconductor transitions under press. 80−34491
$Pb_{1-x}Sn_xTe$:In, tunnelling impurity self-localisation, anomalous props. nature *(Russian)* 80−59915
PbTe epitaxial layers, submillimetre spectroscopy 79−83048
p-PbTe, far IR obs. of shallow bound states in high mag. fields 78−23444

impurity electron states continued
PbTe, ion implantation induced damage and reson. levels 80−49255
PbTe, ion implanted, magneto-optical expts. *(German)* 79−28848
PbTe:Cd, defect struct., Hall effect and solubility meas. 77−11570
PbTe:Ga, location, behaviour of Ga, electrophysical props. meas. 79−38016
PbTe:In, absorption spectra meas., 475-725K 77−4664
PbTe:In, electron mobility, temp.-independent part, Hall effect and elec. cond. meas. 80−92914
PbTe:In, Shubnikov-de Haas oscillatory effects, quasilocal impurity level 80−92912
PbTe:In based solid solutions, impurity states, elec. props. 79−87054
PbTe:Tl, influence of Tl impurity states 80−20121
PbTe:Zn, defect struct., Hall effect and solubility meas. 77−11572
$PbTiO_3$, photocond. and TSC meas. 77−15911
$Pb(Zr,Ti)O_3:Nb_2O_5(Sc_2O_3)$, elec. cond. investigation with and without various dopants and stoichiometry 79−11120
Pd, dil. alloy, electronic struct. calc. using KKR method 80−15438
Pd:H, electron density of states of interstitial H 77−47766
Pd:H, energy and electron density of states 78−51929
Pd:H, energy of interstitial H 77−47765
Pd-Ag(V), H mobility and solubility, appearance pot. spectra obs. 80−55231
Pd-H dilute alloy, de Haas-van Alphen oscill. freq., absolute amplitude, Dingle temp. 80−49575
Pd-H dilute alloy, impurity elec. struct. 80−103643
Pd-H system, cluster calc. of electronic struct. of interstitial H 78−43326
Pd-H system containing d impurities, chem. binding energies of point defects 80−107214
Pd-H sytem, electronic struct. of H, mol. cluster and pseudojellium models 80−24832
PdNb, dilute, NMR obs. of ^{93}Nb 80−71203
Poisson's equations for impurity ion in medium with spatially variable dielec. const., variational principle 78−60085
Pr ion in free state and in crystal, change of spectra 79−33271
$PrCl_3$, anhydrous, Nd^{3+} absorption spectra and quantum states *(Chinese)* 80−89032
$PrCl_3$, rare earth ion overlap in crystal field theory, configuration interaction 80−44552
PtV, dil. alloys, NMR obs. of ^{51}V 80−71203
RbBr:Ag^+, press. tuning of motional behaviour in shallow off-centre pots. 79−78718
RbCl:Ag^+, press. tuning of motional behaviour in shallow off-centre pots. 79−78718
RbCl:Sn, γ-irrad. crysts., thermolum. and emission, 300 to 560K 79−15539
RbCl:V^{2+}, EPR spectrum temp. depend., crystal field theory 77−16163
RbI:Pb, absorpt. spectra of Pb^{++} centres 80−76058
RbI:TeO_3^{2-}, IR absorpt. of impurity complexes *(Russian)* 79−33746
$Rb_2InOH(SeO_4)_2.H_2O:Eu^{3+}$, synthesis and luminesc. 79−91488
$RbMg_xMn_{1-x}F_3$, impurity induced fluorescence, thermal depend. 77−85776
Rb_2MnCl_4, rare earth doped, energy transfer, emission spectra obs. 80−20684
Rh:H, energy and electron density of states 78−51929
S:Si, implanted, defect signature by thermally stimulated meas. 78−91643
$(SN)_x$ chain, isolated, effect of $(SCH_2)_2$ impurities, on electronic props., EHT calcs. 79−15067
$(SN)_x$, with H impurities, CPA calculations 80−44468
SbSI, electrical cond. and acceptor level shift temp. depend., para- and ferroelec. phases 77−28181
Sc, sp. ht. data rel. to electronic props. 78−83971
$ScVO_4:R^{3+}$, R=Nd, No, Tm, Sm, Dy, Er, Eu, Tb, electronic struct. and spectra of VO_4, RO_8 clusters 78−10953
Se, amorphous, O impurity addition rel. to elec. cond. 79−38067
Se, amorphous film, between metal electrodes, switching mechanism 78−39172
Se, trigonal single crystal, peak in temp. dependence of elec. cond. 80−44663
Se:As(Cl), trigonal, defect and impurity electron levels, surface photovoltage spectra 78−72108
Se:O(Cl)(K) amorphous, elec. cond. increase on impurity addition 77−11920
Se-Te, liq., localised impurity states, mag. susceptibility of Co and Mn solutes 77−51882
$Se_{60}Te_{30}Ge_{10}$, amorphous, neg. magnetoresist. 79−51603
Si (111) surface, clean, ESCA obs., Ni(Au) surface impurities 78−52640
Si, acceptor levels, ionis. energy and IR absorpt. 79−78033
Si, acceptor spectra, interpretation 78−43332
Si, amorphous, effective mass theory, impurity states in band gap 79−77992
Si, amorphous, elec. props., ion implantation effects 80−79828
Si, amorphous presence of acceptor states around Fermi level 78−2445
Si, Auger recombination, localized and free carrier comparison 79−38090
Si, bound exciton lifetimes for acceptors 77−80738
Si, bound exciton-dopant Auger lifetimes 78−18970
Si, bound-exciton spectral lines, conc. broadening at high impurity concs. 80−80826
p-Si, change of elastic const. due to presence of acceptor impurities 77−84831
Si, deep and shallow levels of muonium, electronic struct. 78−39051
Si, diffusion coeff. of Se, by sheet Hall coeff. meas. 79−46843
Si, donor bound excitons and bound multiexciton complexes 77−40282
Si, donor ground state wave functions 78−87937
Si, donor ion pot., small r behaviour of nonlinear Poisson eqns. 80−54652
Si, donors, dispersive screening and Bloch function interference, large binding 79−51525
Si, doped, basis functions for studying intervalley effects 79−69442
Si doping by thermal neutron irrad., annealing characts. of bulk electron traps obs. 80−49244
n-Si, effect of random var. in impurity conc. on Fermi level 79−51470
Si, effective supersystem cryst. simulation method, geometrical parameters, bulk moduli, impurity levels calcs. *(French)* 80−15430
n-Si, electron-phonon interaction, internal strain and impurity elec. field effect 78−14418

impurity electron states continued
Si, electronic states of isolated negative donor ion, binding energy 79−65404
Si, energy gap, impurity conc. depend., calc. 80−80170
Si, energy spectrum of Fe group impurities 79−23932
Si, exciton-impurity complexes, emission spectra, Zeeman splitting *(Russian)* 78−64413
Si, excitons bound to acceptors, Auger transition rates 78−34778
Si, far IR impurity spectra, effects of high uniaxial stress 78−56508
Si film, elec. props., effect of amorphous to polycryst. transition 79−28425
Si, He impurity props. investigation by EHT calcs. 79−99183
Si, heavily doped, bandgap narrowing 80−15479
Si, heavily doped, carrier recomb. through shallow donor and acceptor states 80−15535
n-Si, heavily doped, meas. of minority carrier transport parameters 80−15537
Si, high field electron transport, effect of ionised impurities 77−28186
Si, hole localisation, solid solubility, excitonic Auger lifetime of acceptors 80−20216
Si, impurity determ. in very pure sample by photoelec. spectroscopy 77−39888
Si, impurity levels of H and muons 79−56162
Si, impurity screening, local-field effects 79−60759
Si, impurity states, localised orbital approach 80−92851
Si, impurity states and core excitons, binding energies, perturb. theory 80−49659
n-Si, impurity-assoc. magnetophonon reson. 80−20221
n-Si inversion layer, electronic bound states, theory 78−60217
n-Si, ionisation of low donor levels and recomb. of hot electrons at low temp. 79−51596
Si, localised states due to isocoric donor impurities 77−76768
Si, multiband and multivalley effective mass theory for impurities 79−65409
Si, neutral undistorted vacancy 78−91638
n-Si, new small donors, energy spectra, photoionisation energy *(Russian)* 80−34391
n-Si, photocond. of negative donor ion states, for far IR detect. 77−59299
Si, photoconductivity, extrinsic, contrib. by hopping through excited states of donors 78−6411
Si, photoelectric spectra of remanent impurities 79−87125
Si, photoionisation of Group III acceptors, model 78−35174
n-Si, piezoresist. effect, influence of temp. and impurity conc. *(German)* 77−62924
Si pin diode, current filament temp. and Au acceptor level capture cross section temp. depend. 78−95351
Si, pn-product calc. as function of temp. and impurity conc. 77−35891
Si, point charge impurity screening 80−6783
Si, polarisation of recombination radiation from multiparticle exciton-impurity complexes, induced by uniaxial deform. *(Russian)* 79−78754
Si, polycryst. films, transport props. and grain boundary charact. by TEM 80−50980
Si, precipitation of Au, supersaturated soln., Hall effect meas. 77−89465
n-Si, quantum magnetoresist. results, using pulsed fields up to 35 T 79−73528
Si, resonant interaction of acceptor states with optical phonons 77−1394
Si, resonant interaction of optical phonons with acceptor continuum states 78−35178
Si, screening of donor ions by delocalised electrons 79−69466
Si, shallow donor states, substitutional donors 79−65403
Si, shallow donors, Zeeman interaction, relativistic corrections and very small g-shifts, contrib. to EPR 78−72393
Si shallow impurity bound states, IR spectroscopic obs. 77−39806
n-Si shallow impurity states for far IR heterodyne detection 77−38005
Si, spherical effective impurity electron mass 77−24532
Si, sputtered amorphous film, photocond. and electronic props., effects of annealing in plasma gas 80−44644
Si, surface potential, influence of metal impurities, surface photo-EMF obs. 78−19122
Si, surface with incomplete impurity ionisation, quantum model 78−34877
Si, thermal donor energy levels, Hall effect meas. 78−6335
Si, thermal donor generation in temp. range 600-800°C 79−11121
Si, two dimensional impurity bands, Hall mobility 79−95509
p-Si, US attenuation by impurities 77−69047
Si wafer doping, by thermal neutron irradiation, charge carriers behaviour obs. *(Japanese)* 79−42484
Si: Li, absorpt. and luminesc. transitions involving exciton excited hole states 79−78038
Si:0, electrical activity due to heat treatment, Hall effect meas. 80−15543
Si:Ag, photoexcitation of electrons from ionised AG acceptors 78−2519
Si:Al, bound exciton and multiple bound electron luminesc., fine struct. 77−48221
Si:Al, valley-orbit splitting of bound exciton states 79−28290
Si:Al(In), acceptor levels, IR spectra 78−67972
Si:As(Li)(P), luminesc., stress effects on donor exciton satellites 77−85786
Si:Au, carrier capture cross-section at low temp. *(Rumanian)* 79−15163
Si:Au, degeneracy factor of acceptor level 78−51927
Si:Au, electron capture cross section, energy level of Au acceptor centre 78−51926
Si:Au, IR absorption and elec. resist. meas., impurity centres 79−38580
Si:Au, impurity capture cross section and generation lifetime determ., MOS expts. 78−91772
Si:Au diodes, diffused, influence of gamma irradiation, Au levels monitored 77−66199
Si:Au donor and acceptor centre obs. using IR absorpt. and dynamic nucl. polarisation with optical pumping 80−54639
Si:Au p^+-n junction, small area, acceptor level conc., determ. from TSC curves 80−75631
Si:Au use in weakly absorbed nucl. radiation detectors 77−67947
p-Si:B, defect energy levels with 1 MeV electron irrad. and annealing, transient capacitance spectra 77−62860
Si:B, impurity excited state lifetimes 78−60083
Si:B, many-body exciton-impurity complexes, stress depend. of photolum. meas. 79−28833
Si:B, photolum. of heavily doped p- and n-type 80−20708
P-Si:B, US spectroscopy, energy splitting of acceptor ground state 79−33260

impurity electron states continued
n-Si:B,P, radiative recombination at thermal defects, luminescence centre electron struct. 79−91496
Si:B recombination emission polarisation of bonded multiple-exciton complexes in mag. field *(Russian)* 78−2905
Si:B(Al)(Ga)(In)(Tl), binding energy, excited state spectra, photolum., semi-empirical short range pot. 80−44534
Si:B(Ga), even-parity acceptor excited states, bound exciton two hole transitions 77−85793
Si:B(Ga), IR spectra of acceptor levels 80−34953
Si:B(P), photocond. spectra of H^--H^+-type complexes 79−95451
Si:B(P), recombination spectra of bound multiexciton complexes, Zeeman splitting *(Russian)* 79−38526
Si:B(P) polycrystalline thin film, plasma annealing, effect on elec. props. rel. to localised states 80−7005
Si:B(P)(Sb), multiparticle impurity complexes *(Russian)* 78−72601
Si:C, electron irrad., C interstitial, photo EPR 77−16175
Si:Co, study of impurity states 78−76020
p-Si:Cu, influence of Cu on diffusion of Au 77−62679
Si:Cu, parameters of Cu levels determ. by photocapacitance meas. 77−62869
Si:Cu, photocond. spectra and IR quenching 77−55568
Si:Fe, EPR and neutron activation anal. of thermal defects 78−91355
-Si:Fe, effect of γ-irradiation, photocapacitance meas., impurity centre conc. 78−18993
Si:Fe_0 photoconductivity and Hall effect 79−4579
Si:Fe^0 interstitial localisation, EPR spectrum 79−1582
Si:Fe(Au)(Pt)(Ag)(Ti), photoionisation cross-sections and energy levels 79−87060
Si:Ga, neutron irrad., Hall effect meas. of shallow donor levels 80−20124
Si:Ga(Al), edge luminesc. spectra of acceptors, multiexciton complexes 78−56517
Si:Ga(Zn), impurity ground states 79−28313
n-Si:Gd, depth of energy levels of As and P from impurity photocond. 79−90996
Si:Ge,Sn, role of interelectronic correl. in paramag. props. of impurity-vacancy complex 77−62858
Si:H, amorphous, band tail absorpt., photocurrent meas. for Schottky barrier solar cell 80−60032
Si:H, amorphous, electronic states of hydrogenated Si, theory 79−42494
Si:H, amorphous, luminesc., band tail states and thermalization 80−25455
Si:H, amorphous electronic struct. calc., rel. to UPS data 80−39527
Si:H, defects in monovacancy Si cluster, semi-empirical calc. 78−43329
Si:H, electron states 80−29355
Si:H, interstitial electronic struct., self-consistent pseudopotential calcs. 79−73469
Si:H,P, amorphous, heavily hydrogenated, high gap state densities 80−49803
Si:In, absorpt. spectra, impurity excited state lines 80−108243
Si:In, bound exciton photolum. obs. 78−95607
Si:In, C, 0.111-eV acceptor level, X-level defect conc. from IR absorpt. and Hall meas. 79−51512
Si:In, capture cross section of excitons on neutral In impurities, photoluminesc. decay 78−6760
Si:In, dopant energy levels, Hall meas. interpretation 80−107736
Si:In, neutron irrad. to compensate for residual B, photocond., IR focal plane array 78−67727
Si:In, new acceptor level determ. from Hall effect and photocond. meas. 77−66136
Si:In, photoluminesc., In acceptor excited level 79−47506
Si:In,P, photoinduced IR absorpt. and luminesc. 79−33828
Si:Ir, precipitation of solid soln., photocapacitance, electrical resistivity meas. 78−47833
Si:K, bound exciton luminescence in mag. field *(Russian)* 80−108278
Si:l, obs. of donor exciton in far IR transmission meas. 79−91477
Si:Li, bound exciton complexes associated with Li, photolum. meas. 79−28823
Si:Li, photolum. of bound exciton and bound multiexciton complex, Zeeman effect 80−108265
n-Si:Mg, energy levels and degeneracy ratios determ. by Hall effect meas. 79−90993
Si:Mg, Zeeman effect of excitation spectrum of neutral donors 77−63439
p-Si:Mn, temp.-elec. instability, photocond. meas. 77−1448
Si:Mn(Fe)(Ni) amorphous films, ESR and elec. cond. 80−50171
Si:Na ion implanted, Hall effect temp. depend., electron surface density and mobility 80−11018
Si:Na^+, variation of cond. in two-dimensional impurity band with Fermi level position 79−95510
Si:O, A centre, theoretical study 80−75521
Si:O, amorphous, sputtered, influence of O and deposition conditions 80−54693
n- Si:O, charge carrier scattering on neutral centres 80−49762
Si:O, cryst., donor form. during annealing, elec. resist. study 80−49653
Si:O, dislocation-free, Si-O complexes, heat treatment effects 77−62557
Si:O, IR absorpt. spectra of Si:O complexes 78−19520
Si:O, kinetics of donor formation, under heat treatment in 450-900°C range 80−75523
Si:O, specific resist. rel. to annealing, Si-O complex form., O_2 distrib. *(German)* 77−72863
Si:O film, near IR absorption, O impurity states 78−88333
Si:P, absorpt. due to creation of bound excitons 78−23025
Si:P, acceptor bound multiexciton complex recomb., shell model, luminesc. line splitting 78−6275
Si:P, amorphous, CVD, substitutional doping, electronic props. 79−23923
Si:P, CVD amorphous film, electronic density of states 79−46993
Si:P, Czochralski growth, dopant evaporation coeffs., resistivity distrib. 77−16487
p-Si:P, defect energy levels, ion implantation effects, Hall coeff., sheet resist. meas. 77−85173
Si:P, excitation spectrum of P donors introduced by neutron transmutation, high resolution study 79−47460
Si:P, exciton complexes bound to impurities, resolved fine structure 77−62843
Si:P, expt. evidence against shell model of bound multiexciton complexes 78−10368
Si:P, Gd, optical orientation of ^{29}Si nucleus, effect of donor level implantation depth *(Russian)* 77−8452

impurity electron states continued
Si:P, heavily doped, 100 GHz ESR of impurity band 79−95631
n-Si:P, heavily doped, carrier conc., Hall coeff. and elec. cond. meas. 77−8094
Si:P, heavily doped, IR bound-exciton luminesc. spectra 78−15211
Si:P, heavily doped, origin of photoluminesc. 79−56856
Si:P, heavily doped, sp. ht. near metal-nonmetal transition, generalized Matsubara-Toyozawa theory 79−73321
Si:P, heavily doped, sp. ht., calc. using AMO-MT scheme for impurity bands 79−95182
Si:P, heavily doped, thermal oxidation 78−56793
Si:P, hopping conduction and the Coulomb gap 80−44605
Si:P, impact excitation of P at low temps. 78−23098
Si:P, impurity band states calc. and photoluminesc. meas. 77−8046
Si:P, luminesc. lines, multiexciton complexes and unaixial stress 78−92114
Si:P, model for exciton bound to donor pair, photolum. data anal. 79−51498
Si:P, photolum. obs. of donor pairs 79−52014
Si:P, photoluminesc. associated with impurity clusters 79−38656
Si:P, submillimetre wave study of metal-insulator transition 79−95336
Si:P, variable range hopping conduction, in lowest temp. region 79−73511
n-Si:P,V, degeneracy ratios and impurity levels of V, resist. and Hall effect meas. 77−20260
Si:P bound multiexciton complexes, expt. evidence for shell model 78−39036
Si:P photochronic detector, IR detect. using delayed breakdown 79−58786
Si:P(As)(Sb) donors, polarisability binding energy in mag. field 79−1581
Si:P(B), multiple-particle exciton-impurity complex form. *(Russian)* 78−43925
n-Si:P(Sb)(As), characts. of piezoresist. 77−51750
Si:Pd, energy levels obs. 77−35890
Si:Pt, elec. props., deep-level transient spectroscopy and thermal emission meas. 79−82542
Si:Pt, hole capture cross-section at E_v+0.34 eV, capacitance meas. *(French)* 80−65493
Si:Pt, photoionisation cross-sections, photocurrent and photocapacitance meas. 78−10497
n-Si:Re, photon-capture cross sections of Re levels, spectral depend. 77−89726
Si:Re diode, photocapacitance and induced photocapacitance spectra 77−4404
n-Si:Re diode photocapacitance spectra, Re centre dissociation 79−90997
Si:Ru, photon- and carrier-capture cross sections of Ru levels 79−90995
Si:S, deep level characterisation, implantation predeposition technique 80−100444
Si:S, two-electron donor centre, photoionisation cross sections meas. 77−8044
Si:S(Se), IR absorption and photocond., donor levels 77−55809
Si:Sb, amorphous, electronic transport props. 80−44589
Si:Sb, polarisability of Sb donors in mag. field 79−95368
Si:Sb(As)(P), bound excitons and bound multiexciton complexes for shallow donors, luminesc. meas. 79−24363
Si:Sb(P)(As), shallow donor states with strong central cell perturbation theory 78−51933
Si:Sb(P)(As), shallow donor electrons, hyperfine interactions, reply to Onffroy's calcs. 78−51934
Si:Se, diffusion coeff., solubility and energy level determ. 79−35825
Si:Se, energy levels, resistivity and Hall coeff. 79−69528
Si:Se, impurity states, A- and B-centres, electron, hole thermionic emission rates 80−96813
Si:Se,B(Ga)(Al)(In), diffusion of Se, solubility and ionization levels, Hall effect and photocond. meas. 79−42486
Si:Ti, deep level impurity, Hall meas. 80−6768
Si:transition metal, electronic states of impurities 77−43531
Si:Zn, P^+-n-n^+ struct., deep doubly ionized centres, impedance calc. 79−11202
Si:Zn, photoionisation of deep impurity levels 80−34386
Si:Zn, trapping struct., analysis of TSC meas. 77−8045
n-Si-^{119}Sn resonant detector for Mossbauer spectroscopy 80−883
Si-Au amorphous system, optical absorpt., IR photocond. 79−42582
Si-H, amorphous film, in situ prepared, photoemission studies 80−35060
n-Si-Se, ion implantation studied by deep level transient spectroscopy 78−10392
Si-SiO_2, intentionally contaminated interface, transient capacitance meas. 79−33349
Si-SiO_2, interface, doping depend. of interface states and charges 80−92992
Si-SiO_2, interface, hopping conduction, anal. in impurity bands in inversion layers 79−47171
Si-SiO_2, n-type inversion layer, theory of impurity-shifted intersubband transitions 80−20324
n-Si-SiO_2, screening of charged impurity centre localised inside oxide and at interface of inversion layer 79−73563
Si-SiO_2 interface, Au surface state energy levels and Au diffusion 79−51652
Si-SiO_2 interface, Na^+ drifted, impurity bands in inversion layers 78−60211
Si-SiO_2 structures, B ions implanted, energy spectra of shallow traps at various implantation energies 80−80392
Si-SiO_3 interface, effect of Au recomb. centres on interfacial trapping states 79−38175
Si-type, semiconductor, interimpurity radiative recomb. with phonon cooperation 77−16385
Si(:Au), gamma-induced trapping levels 79−87059
n-SiC, 6H polytype, expitaxially grown, electronic props. meas. 77−39975
α-SiC (6H), paramag. N impurity levels, IR absorpt. and ESR expts. 77−59598
β-SiC, cubic, conduction band minima location and shape determ. 77−85141
n-SiC, cubic, piezoresistance meas. under hydrostatic compression 77−4344
p-SiC, inequivalent sites of IR luminescence centres *(Russian)* 77−1722
SiC:Al,N (6H), ODMR for effective-mass-like acceptor 80−93213
β-SiC:B, diffused structures, current-voltage characts. 78−47865
SiC:B, impurity distribution determ. by neutron activation anal. 77−76452

impurity electron states continued
p-SiC:B (4H), absorption spectra of bound excitons 78−88338
α-SiC:B(Be)(Ga), piezoresist. rel. to acceptor levels 78−60129
p-SiC:Be, Fermi level, Fermi distrib. and activity coeff. calc. 77−1365
SiC:Be, film donor impurity, diffusion influence on elec. and optical props. 78−87942
4H-SiC:Ga(Al), photoluminesc. spectra 77−66530
SiC:Ti (6H), absorpt. spectra of n- and p-type cryst. 79−38581
a-$Si_{1-x}H_x$, oxygenated thin film, sputtered, elec. cond. and optical props. 79−15239
SiO_2, mobility and trapping of ions, Si-SiO_2 interface states 80−92985
SiO_2:Ag, implanted atom, X-ray photoemission obs. 78−39050
SiO_2:Al, vitreous state, EPR of Al defects 78−91951
SiO_2:Au, implanted atom, X-ray photoemission obs. 78−39050
p-Si(111) surface inversion layer, Cs covered, negative magnetoresist. in 2D impurity band 78−64135
Sm-Fe, dil., valence impurity state, inference from mag. susceptibility 78−95270
SmS, electronic phase transition, mechanism, trivalent metal impurity effects 80−49604
SmS type cpd., fd mixing effect on impurity levels, local valence transition 80−24831
SnO_2, semiconductor, photoluminescence, depend. on lattice temp. and excitation intensity 80−45137
SnO_2:Mo^{5+}, hyperfine and superhyperfine interactions, EPR 77−8398
SnO_2-Cu_xS-ZnS:Mn,Cu-Al_2O_3-Al, light-emitting struct., cond. and electrolum., heat treatment 80−97345
$Sn_2P_2S_6$, illumination effect on soft mode and dielectric props., luminesc. study *(Russian)* 80−50420
p-SnS, IR photocond., double acceptor impurity 78−2514
$SrCl_2$:Fe^{2+}(Co^{2+}) electronic absorption spectra in far and middle infrared 78−68537
SrF_2:CeF_3(GdF_3)(TbF_3), absorpt. spectra of γ-irrad. cryst., 77K, 200-700 nm 78−84615
SrF_2:Gd, cryst. field parameters calc. and model of tetragonal Gd^{3+} centres 79−28328
SrF_2:Gd^{3+}, cryst. field parameters calc. 77−8048
SrF_2:Tb^{3+}, mag., thermal and hyperfine props. 80−29368
SrS:Hf phosphor, activation energy and freq. factor calcs. from glow curves 77−12451
$SrTiO_3$:Ni, photochromism, optical absorption spectra and EPR meas. 77−1708
Ta, electrotransport of H(D) at high H concs. 80−34246
$Ta_{0.97}Hf_{0.03}S_2$ (1T), charge density waves, ESCA, XPS investigs. 77−12490
$Ta_{1-x}Zr_xSe_2$ (1T), CDW stacking order, interlayer interactions and impurity effects 77−7699
$Tb(OH)_3$:Er^{3+}, ferromag., anisotropic exchange effects in optical spectra 78−80141
Te, impurity spectroscopy 80−65499
Te in MIS structure, impurity photocond. 78−72203
Te, liquid, localized impurity states, paramag. susceptibilities 78−64185
Te, photoconductivity in strong mag. fields, doping effects, impurity levels 80−75602
Te, pure and Sb doped, impurity state and impurity cond., press. effect 80−54723
Te, weakly doped, impurity spectroscopy, magnetoresist. meas. under nonohmic conditions 78−30942
Te:I, semicond., elec. efficiency *(German)* 78−84166
Te:Sb, impurity states and impurity conduction, hydrostatic pressure 80−39521
Te:Sb, surface carrier effects on Hall mobility at low temp. 77−80794
Th_3As_4-U_3As_4 solid soln., electronic props. 80−34469
ThO_2, pure and Tb^{3+} doped, impurities effect in absorboluminesc. and photoluminesc. 79−38597
Ti, polycryst., absorpt. of O at room temp., XPS and UPS 77−89645
Ti:C, molecular cluster approach to electronic struct. and bonding mech. for impurity C 77−20270
Ti-H system, cluster calc. of electronic struct. of interstitial H 78−43326
TiO_2:Cr(Ta), slightly doped, elec. cond. and defect struct., charge compensation and point defect model 80−75568
TiO_2:Cu, anodic, effect of Cu on optical props., rel. to possible appl. in solar energy conversion 80−16115
TiO_2:S, acceptor properties of S, free electron concentrations 80−34395
TiO_2:V(Cr)(Mn)(Fe), impurity levels, photocurrent and ESR meas. 80−29346
Ti_4O_7, hopping conduction and the Coulomb gap 80−44605
$TiSe_2$ impurity effects on elec. props. 80−80263
TlBr:I, isoelectronic donor, broad-band photoluminesc. meas. 77−8636
TlCl-TlBr mixed cryst., impurity-induced self-trapping of holes and minority-ion percolation 78−64398
TlCl(Br), Wannier exciton-ionised donor complexes, binding energy calc. 80−49609
$TlSbS_2$, photocond. characts. 77−4407
$U_xTh_{1-x}As$ (Sb), electronic struct., relativistic KKR-averaged T-matrix approx. method 80−107702
V, electrotransport of H(D) at high H concs. 80−34246
VO_2:Ga(Al)(Fe), phase transforms., influence of nonstoichiometry 77−85274
V_2O_5-P_2O_5 glass, in metal-semicond.-metal struct., TSC of dielec. relax. *(Russian)* 77−35998
V_5S_8:Fe, Mossbauer and mag. studies, electronic state of Fe 80−108130
YAG, undoped and Ce^{3+}-doped, cathodolum. intensity and decay time, 10-480K 79−99952
YAG:Cr^{3+}, Raman effect to probe dynamical processes of Cr^{3+} photoexcited states 80−2740
YAG:Eu^{3+}, reson. fluoresc. spectra, showing multiple Eu^{3+} sites 80−2812
YAG:Nd^{3+}, nonradiative multiphonon relaxation of isolated impurity level, transition probability calcs. 79−56853
YAG:Nd^{3+} and free Nd^{3+} ion, energy levels, absorption spectra 79−11076
YAG-Ce^{3+}(Eu^{3+})(Tb^{3+})(Gd^{3+}), cathodolum. intensity, temp. depend., comparative study 79−99953
$YAlO_3$:Nd^{3+}, thermal broadening and shift calcs. of Nd^{3+} energy levels 77−48208
$YAlO_3$:Yb^{3+}, absorption and luminescence spectra, electron-phonon resonances, Stark splitting *(Russian)* 80−20674
YIG, Bi-substituted, LPE film, optical absorpt. changes due to impurity incorporation 77−1702

impurity electron states continued
YIG:B,Pb, IR spectrum, localised modes, rel. to impurities and O vacancies 80−50377
Y_2O_2S:Tb, recomb. processes and emission spectra *(Russian)* 78−6797
YPO_4 phosphor, ionisation of capture centres, thermolum. spectra 80−11487
YVO_4 phosphor, ionisation of capture centres, thermolum. spectra 80−11487
YVO_4:Eu, cluster electron struct., X-alpha calc., emission spectra 78−2898
YVO_4:R^{3+}, R=Nd, No, Tm, Sm, Dy, Er, Eu, Tb, electronic struct. and spectra of VO_4, RO_8 clusters 78−10953
YVO_4:Tm^{3+}, cryst. field parameters, appls. 77−20277
Zn:^{115}In, 828 keV state, elec. quadrupole interaction meas. 77−8484
Zn:Al, residual resistivity, numerical calc., Fermi surface and multiple plane wave band struct. 77−51722
Zn-Al, dil., impurity quasi-particle lifetimes and pseudopotential form factor 78−47734
Zn-Mn, supercond., thermal cond. compared with Shiba's theory 77−8228
$ZnAl_2O_4$:Cr^{3+}, Raman effect to probe dynamical processes of Cr^{3+} photoexcited states 80−2740
$Zn_{0.35}Cd_{0.65}S$ binder layers, doped and undoped, xerographic characts. 79−56288
$Zn_xCd_{1-x}S$:Cl, Cu^+(Ag^+), high pressure luminesc. 78−19533
$Zn_xCd_{1-x}S$:Cu, photoluminescence 80−29783
$Zn_xHg_{1-x}Te$, impurity influence on thermomagnetic effects and elec. cond. 79−60856
ZnO, chemomechanical effects 79−82431
ZnO:Cu, excited state, zero phonon lines in emission and Zeeman spectra 79−38026
ZnO:Cu^{2+}, electronic struct., optical absorpt. and ESR 79−87312
ZnO:Li, luminesc. donor-acceptor pairs, exchange broadened optically detected EPR spectra 78−23373
ZnO:Li(Na), band-edge emission obs. 77−20933
α-ZnP_2, doped, single crystal, electrical properties 80−92892
ZnP_2, pure and doped, carrier mobility and conc., donor and acceptor energy levels, 190 to 380K 78−84217
ZnS crystals, luminescence kinetics, centre discrimination exam. 78−15215
ZnS, green-blue luminesc. characts., model of luminesc. centres 79−73999
ZnS, interimpurity high press. luminesc. 78−19532
ZnS, self-activated, trap distrib. and photoelectronic effect due to UV, IR and visible excitation 77−36282
ZnS, tight binding calc., F-centres, and isoelectronic defects 77−20266
ZnS:Ag, TSC and induced impurity photoconductivity, existence of two electron trapping centres 80−44655
ZnS:Al-Cu, localised vibrational modes 78−63827
ZnS:Cr^{2+}, excitation spectrum of IR emission 77−12421
ZnS:Cu, Al phosphors, mechanism of IR stimulated and quenching 77−69881
ZnS:Cu, Cl, I, anisotropy of blue Cu luminesc. centres 77−81137
ZnS:Cu, film effect of Cu valency on cond. 79−11246
ZnS:Cu, O(Fe,Co,Ni) photoconductors, killer impurities effect on electron escape probabilities and trap depths 77−4392
ZnS:Cu, polycryst. phosphor, excitation storage, recombination barrier participation 78−27316
ZnS:Cu,O, photocurrent spectral distrib., Fe, Co and Ni impurity effects 77−8135
ZnS:Cu crystal, powder, epitaxial film, luminescence anomalous thermal 80−76077
ZnS:Cu^{2+}, motional averaging in excited state 77−66137
ZnS:Fe, piezospectroscopic effect on electron-vibr. lines of Fe^{2+} 78−27269
ZnS:Fe^{2+}, low temp. Mossbauer spectra, in source and absorber expts. 77−28500
ZnS:Ga, self-activated emission, A-centre ODMR 79−95685
ZnS:In, polarisation of deep centre electroabsorpt., effect of random electric fields 77−48148
ZnS:In, recombination emission by optically detected magnetic resonance 80−66272
ZnS:Mn, self-activated and Mn^{2+} emission, high press. action 80−16093
ZnS:Mn^{2+}, $^4T_1$ state, magneto-optical meas. 77−20833
ZnS:Pb^{2+}(Mn^{2+}), high press. luminesc., localised excitations 78−19534
ZnS:Tm(Er)(Nd) phosphors, optical scintillation mechanism 79−56867
ZnS-CdS system, IR luminesc. and absorpt. centres, donor-acceptor pair model 77−44043
ZnS(Se):Ni, optical absorpt., impurity ionisation, optical phonon coupling 80−88505
ZnS_xSe_{1-x}, VPE, characterisation of defect centres by photoelectronic meas. 80−10914
ZnS(Se)(Te):Co, impurity luminescence no phonon line depend. on temp., Debye temp. 80−66273
ZnSe, exciton-impurity complex, electroabsorption meas. 79−15484
n-ZnSe, impurity band, Hall effect, elec. cond., mobility and magnetoresist. expts. 77−35888
ZnSe, ionisation energy of H-like impurities 80−20120
ZnSe, laser induced modulation of opt. absorpt. 78−88324
ZnSe, self-compensation, role of impurities 80−92850
ZnSe:Ag, low-temp. photolum. meas. 77−20912
ZnSe:Al(Ga)(In), single cryst., doping, blue luminesc. 78−39584
ZnSe:B(F), ion implantation, photocond. and cathodoluminesc. meas. 78−26586
ZnSe:Co, effect of in-band position of states on photoelec. props. 78−23132
ZnSe:Cr^{2+}, excitation spectrum of IR emission 77−12421
ZnSe:Cu, Cl, high press. luminesc. 78−19532
ZnSe:Cu, deep energy levels 80−6774
ZnSe:In, Li, binding energy of excitons bound to donor-acceptor pairs, electron-phonon coupling 77−4689
n-ZnSe:Li, semicond. selective pair luminesc., excited impurity state investigation 79−61439
ZnSe:Li(Na), shallow acceptor excited states, luminescence spectra, Rydberg energy 79−78750
ZnSe:Li(Na)(Ga) doped and pure cryst., donor-acceptor bands 80−11465
ZnSe:Ni, evidence for exciton binding at Ni impurity sites, photolum. excitation spectrum 80−45135
ZnSe(Te), photolum. excitation spectra of tightly bound holes, valence band contrib. 80−60658

impurity electron states continued
ZnSe(Te):Cr^{2+}, spin Hamiltonian parameters and wave function coeffs., LCAO theory 77−39804
p-$ZnSiAs_2$:Au(Tl)(S), photoluminesc., radiative recombination 77−24883
p-$ZnSiP_2$, single cryst., recomb. processes, photoelec. props. *(Russian)* 78−68053
$ZnSiP_2$:Ga, effect of doping conc. on elec. cond. and Hall effect 78−76077
p-ZnSnAs, LPE, electronic struct. obs. by laser excited photolum. 80−60654
ZnTe, band parameters from bound exciton, donor-acceptor pair excitation luminescence 78−92111
ZnTe, dominant acceptors, annealing and quenching 80−24463
ZnTe, doping and intrinsic stoichiometric defects, self-compensation 80−59918
ZnTe, effects of Zn anneals in 400-550°C range on acceptor conc. 80−10571
ZnTe, elec., SEM and TEM studies of impurity segregation during long annealing 80−30001
ZnTe, elec. field and impurity conc. effects on ionisation energy of impurities, appl. to acceptors 80−88514
ZnTe, electro- and cathodoluminesc., impurity segregation 79−43042
ZnTe, electronic and optical parameters of O related centre 77−24534
ZnTe, exciton localisation at impurity pairs 79−37999
ZnTe, excitonic complexes, stress splitting of luminesc. lines 77−4672
ZnTe, high quality p-type cryst., predominant acceptors 78−60504
ZnTe, I_4 bound exciton, magneto-optical meas. 77−20836
ZnTe, magneto-optical effect, I_2 bound exciton 77−12432
ZnTe:Al,Cl, photolum., complex acceptor, ionization energy 80−20693
ZnTe:As(P), spin flip acceptor scatt. 78−92072
ZnTe:Au, impurity identification and characterisation, capacitance, luminescence and IR absorption 80−60639
ZnTe:Cu, elec. and optical identification of persistent acceptor 79−60764
ZnTe:Cu, red centre, electric and optical props. 80−20239
ZnTe:Li, bleaching by green laser radiation 77−62015
ZnTe:Li, Li in Te precipitates, diffusion during thermal anneal 80−39358
ZnTe:Li, O, Hagemark theory, O modification isoelectronic trap 80−75517
ZnTe:Li, Zeeman splitting of ground and excited acceptor states, selective pair luminesc. 80−84780
ZnTe:P, pure and doped, electron and exciton excited states of neutral donor 80−34393
p-ZnTe:P, semicond. selective pair luminesc., excited impurity state investigation 79−61439
ZnTe:P, spin flip scatt., shallow acceptor states 77−8587
ZnTe:P(Li), luminesc. transitions, quantum efficiency 79−1783
ZnTe:Sb film, acceptor levels 78−76172
Zr-H alloy, soft X-ray emission spectra, electronic struct. 79−65959
ZrO_2, cubic single crystal, colour centres 77−15410
ZrO_2-Y_2O_3:M^{3+}, M=transition metal, X-ray luminesc. 77−44063

impurity scattering
used for carrier scattering by impurities
see also Kondo effect
alkali metal:halogen, charge transfer excitations 79−95815
alloy, dil., thermoelectric coeff., vertex and other electron-phonon corrections to impurity scatt. 79−95390
alloy, disordered, energy band struct. and elec. cond., effect of short-range order 80−10860
alloy systems, conc., Kondo type effects, phenomenological dilution model 77−72858
alloys, binary narrow-band, metal-dielectric transition, off-diagonal disorder *(Russian)* 79−4512
alloys, dil. mag., transport props. in mag. field, impurity-electron scatt. 80−65541
anisotropic, semiconductor, p-Ge type, theory *(Russian)* 78−39103
anisotropic metal, with impurities, long-range interactions of spins 79−47092
anisotropic superconductors, upper critical field theory 80−75692
anthracene, cryst., cyclotron reson. and carrier scatt. 77−76746
antiferromagnet, itinerant model, spin density wave transition, impurities effect 77−72986
Boltzmann equation method, derived from Kubo formula 78−95277
CDW drift velocity 78−56123
CDW transition temperature, scatt. effects 80−107720
charge carrier with anisotropic energy spectrum, cond. oscills. in quantised mag. field *(Russian)* 80−6886
clean superconductor, effect of impurity scatt. on thermally induced charge imbalance 80−60135
compensated semiconductors, low temp. mobility, unscreened charged impurities effects calcs. 80−75562
conduction phenomena, review of exptl. work *(Japanese)* 80−49737
conductor, EM wave penetration, effect of impurities and spatial dispersion 79−7813
conductor, high-frequency props., electron relax. time and impurity scatt. amplitude *(Russian)* 77−32033
crystals, dipole-impurities, HF elec. cond., dielec. losses and light absorption 77−63363
crystals, review of scattering theory 77−85172
cubic semiconductors, bulk hot-electron props., review 79−99553
cyclotron resonance 78−48045
cyclotron resonance width of impurity system in two dimens. 77−35892
DC electrical conductivity, microscopic fields and currents 78−56121
DC electron scattering, by spherical macroscopic pot. including screening 77−51739
DC resistivity as functional of generalised dynamical susceptibilities, solid state model 79−28330
de Haas-van Alphen effect, quasiparticle approach 80−10897
degenerate semiconductor, EM wave absorption 78−95308
degenerate semiconductors, ionised impurity scattering cross-section, variational calc. 80−20180
degenerate semiconductors, longitudinal thermo-EMF in quantising mag. field, scatt. mechanism *(Russian)* 80−24960
dilute alloy, electron scatt. by impurity cluster, lattice distortion and back-scatt. effects 77−20306
dilute magnetic alloy, cond. electron scatt. asymm. 77−62916
dilute magnetic alloy, kinetics, appl. to generating functional method *(Russian)* 77−43579
dirty superconductor, multiphoton absorption *(Russian)* 77−36022

impurity scattering continued
disordered alloy with strong impurity scatt., adiabatic approx. 77−66161
doped conducting media, low-freq. props., EM wave reflection 80−103715
electron gas, interacting, elec. cond. 78−95276
electron-electron scatt. and elec. resistivity of metals 79−95396
electron-hole droplet, motion damping, impurity and piezoelec. scatt. 78−67951
electron-hole pairing, suppression by impurities, thermodynamic and kinetic props. *(Russian)* 77−69318
electron-hole plasma current layering, electron cooling length, momentum scatt. 80−6890
electron-impurity system, elec. cond. anomalous behaviour, Coulomb interactions 79−95381
electron-ion metal system, dynamics eqns. in microscopic theory *(Russian)* 80−15198
exciton insulator, differential thermo EMF, temp. depend. *(Russian)* 78−72182
exciton insulators with spontaneous currents, impurity scatt. effect on phase transitions 80−80242
ferromagnetic metal, impurity resist., band model calcs. 77−39830
ferromagnetic metals, magneto-optical effects, electron scatt. 77−90133
ferromagnetic semiconductors, free carrier absorpt. of radiation 80−97227
graphite, anomalous galvanomagnetic properties, in strong mag. field 79−23986
Hall effect, AC, ferromag., in electron-impurity system, itinerant electron model 77−47796
heavily doped semiconductor, correction to static elec. cond. due to many-centre scatt. 80−2374
heavily doped semiconductors, static conductivity in terms of transport relax. time 79−56213
hopping promoted by electron-electron coupling 80−59987
impure metals at low temperatures, conductivity 80−103669
n-InSb, anomalous Hall effect, stress depend. 80−65598
insulator, Coulomb interaction effects on tunnelling 77−8051
intervalley impurity scatt. effects on non-metallic behaviour of two-dimens. systems 80−107803
ionised impurity scatt. limited mobility in semiconductors with spatially variable dielec. function 78−51986
isotropic scattering of current carriers in quantizing mag. field 78−51954
isovalent impurity long range potential, role in electron scatt. 80−10966
linear conductor, CDWs and impurity effects 80−59967
liquid binary alloys, dilute, conduction electron scatt. cross section and component effective charges *(Russian)* 77−8082
magnetic field effects 80−44559
Matthiessen's rule and its variation for cyclotron reson. width in two and three dimensions 78−6578
metal, compensated, with closed Fermi surface, rel. to Hall coeff. temp. depend. 77−8074
metal, cond. electron relax. time, review *(Japanese)* 78−30910
metal, deformed, transfer phenomena *(Russian)* 77−35906
metal, dirty, resist. temp. depend., causes of Matthiessen's rule deviations *(Russian)* 77−69291
metal, disorder surface, multiple scatt. of cond. electrons 80−10959
metal, electron-impurity scattering, lattice distortion effects, phase shifts, calc. 80−96860
metal, electron-phonon and electron-impurity collision frequencies, RF size effect method 77−20227
metal, general theory for elec. resist. temp. depend. 78−47757
metal, low temp. impurity cond. temp. depend., kinetic eqn. *(Russian)* 79−7817
metal, Matthiessen rule deviations, electron scatt. by dislocations, impurities and phonons 78−19026
metal, neutral and charged impurity scattering, Matthiessen's rule 79−47081
metal, nonlinear elec. resist. due to paramag. impurity scatt. 77−15826
metal cylindrical wire, elec. resist., scatt. processes, Monte Carlo calc. 80−75560
metal-H systems, temp. depend. of impurity resist. 80−65529
metal-insulator-metal junction, hopping model of zero-bias tunnelling anomalies, mag. field effect 79−60936
metal-insulator-superconductor junction, electron interactions with phonons and mag. impurities 77−16004
metallic crystal, RF size effect, electron scatt. by impurities diffuse layer boundary *(Russian)* 78−91717
metallic thin film, conductivity, Kubo formalism 79−7909
metallic thin films, low adsorption coverage, microscopic calc. of elec. cond. 79−15236
metals, magnetoresistance of localized impurities, multiple scatt. theory 78−43360
metals, polyvalent, Matthiessen's rule deviation crit. resist. 80−6811
molecular crystals, effects of impurity scatt. and transport topology on trapping, Frenkel excitons 78−95263
monovalent metal, resistivity, 1-4K, HF phonons role 77−15828
MOS two-dimens. systems under strong mag. field, many-body effect on level broadening and cyclotron resonance 79−78195
narrow gap semiconductor, resonant scatt., Green's function method and CPA 80−6827
narrow- and zero-gap semicond., mag. impurity scatt. effect on transport props. 77−15852
nondegenerate semiconductor with ionised impurity scatt., acoustic wave amplification 77−11965
one-dimensional conductors, impurity scattering effect on electron pairing 78−60112
one-dimensional metal, effect of impurities on electron pairing *(Russian)* 77−11903
one-dimensional Peierls-Frolich state, impurity pinning of charge density wave 78−6298
one-dimensional strongly disordered conductor, localisation of electrons *(Russian)* 79−78046
one-dimensional systems, impurity effects on ordered phases 80−24905
order parameter spatial variation near Kondo impurity 80−103813
p-n tunnel junctions, phototransitions accompanied by impurity scatt. 80−107901
parametrized model for obtaining electron scattering rates from radio-frequency size-effect data 79−69541
Peierls systems with dil. impurities, microscopic theory of pinning effect 77−15837

impurity scattering continued
point contacts, metallic, elec. cond., spectroscopy of phonons, impurities *(Russian)* 78−38797
quantised magnetic field effect *(Russian)* 78−47752
quasi one-dimensional metal, cond. at T=0 *(Russian)* 77−28169
quasi one-dimensional metal, static cond. at finite temp. *(Russian)* 78−10428
quasi-one-dimensional conductor, impurity effects, interchain interaction 78−72138
quasi-one-dimensional conductor, supercond. transition, impurity effect 77−15986
quasi-one-dimensional metal systems with random impurities, cond. at T=0 78−6360
rate, lattice distortion structure factor, anisotropy 77−76801
residual resistivity for electrons scatt. by spin-depend. potentials 77−39829
screening in strong mag. fields 79−47054
semiconducting surface inversion layer, cyclotron reson. of interacting electrons 78−34885
semiconductor, 1/f noise origin 80−11060
semiconductor, carrier collisions with impurity ions 80−34434
semiconductor, carrier scattering by impurity potentials with spatially variable dielec. functions 79−69507
semiconductor, compensated, cluster scattering, DC resist., energy-loss method 80−96862
semiconductor, conduction electron scattering by vibrating impurities 78−95297
semiconductor, degenerate electrons, relax. of spin and energy 80−10965
semiconductor, doped, zinc blende type, electron-phonon interaction, reson. scatt. theory 78−64036
semiconductor, electron scattering by layer struct., geometrical resonances, plasmon and free carrier freq. 79−56212
semiconductor, free carrier scatt. by nonhydrogenic charged impurity centre 79−11110
semiconductor, free-electron screening of short-range scatt. pot. 80−49704
semiconductor, heavily doped, scatt. mech., resist. and Hall effect maxima 80−75586
semiconductor, hole scatt. from impurity pots. in spherical-band approx. 77−76803
semiconductor, impurity acoustoconduction, nonlinear theory 77−15914
semiconductor, impurity ion pot., nonlinear Poisson eqns. 77−20265
semiconductor, impurity ion screening charge density expansion 80−107780
semiconductor, intrinsic, quantum theory of transverse galvanomag. phenomena, model of two standard bands *(Russian)* 77−62945
semiconductor, ionised impurity scatt. 78−51984
semiconductor, ionised impurity scattering, theory 80−20181
semiconductor, magnetoresistance quantum limit for impurity scatt. 79−91083
semiconductor, negative electron diffusivity in high fields 78−30935
semiconductor, Nernst-Ettingshausen effect, thermopower, strong elec. field 78−23122
semiconductor, photoexcitation phenomena, low density 78−27319
semiconductor, quantum transport theory under high elec. field 78−23099
semiconductor, Seebeck and Hall coeffs. Lorenz number, anisotropy, theory *(German)* 80−65608
semiconductor, spin relax. of deep impurity centres, exchange scatt. 77−43870
semiconductor, theory of charge transport partly dissociated excitons and impurity atoms 80−44581
semiconductor, unipolar, acoustophotoelectric effect theory 77−55577
semiconductor carrier scattering by ionized impurity potentials incorporating spatially variable dielectric functions 79−42535
semiconductor gapless, nonlinear effects in transverse quantising mag. fields 77−69353
semiconductor multilayer heterojunction struct., impurity and phonon scatt. 80−2456
semiconductors, charge carrier capture by attractive centres 79−82602
semiconductors, charged-impurity scatt., third-body interference, formulae 77−55520
semiconductors, elec. cond. in elec. and mag. fields, carrier scatt. mechanisms 79−65467
semiconductors, electron scattering by deep level impurities 80−10968
semiconductors, free electron scattering and dynamical cond. 78−2476
semiconductors, hot electron recombination at impurity centres 80−10995
semiconductors, intervalley acoustoimpurity resonance 80−107868
semiconductors, many-valley, localised impurity states with low binding energy 80−24835
semiconductors, mobility-fluctuation description of 1/f noise 80−84496
semiconductors, n-type, free carrier absorpt., ionized impurity scatt. 79−42999
semiconductors, quasi elastic hot electron impurity scatt. in quantising mag. field 80−24938
semiconductors, scatt. influence on Auger transition, depend. of impact ionisation on electron energy 80−44608
semiconductors, spatially variable dielectric functions, ionized impurity limited mobility 79−42534
semiconductors with neutral impurity, transverse cond. in quantising mag. fields, finite radius scatterers *(Russian)* 80−29400
semimetal, degenerate, quantum theory of transverse galvanomag. phenomena, model of two standard bands *(Russian)* 77−62945
semimetal, longit. cond. in extremely strong mag. field 77−89779
semimetals, giant quantum attenuation of sound, fluctuation effect of gas-liq. type transition 78−39168
strongly degenerate plasma, double injection, vol. controlled current regime 79−51658
superconducting film, ordering parameter and current density, depend. on paramag. impurity conc. and electron pair rel. *(Russian)* 78−6489
superconducting fluctuation effects on local electronic spin suscept., impure case 77−72943
superconducting tunnel junction, paramag. impurities effect on Josephson current *(Russian)* 80−70903
superconducting virtual bound state alloys with resonant impurity scatt. centres theory 79−99654
superconductor, Boltzmann kinetic equation, scatt. by paramag. impurities *(Russian)* 77−36015
superconductor, triplet pairing, strong Kohn anomaly *(Russian)* 78−19179

impurity scattering continued
superionic conductor, one-dimens., soliton Brownian motion and impurity effects 79−77814
superlattice semiconductor impurity photoconductivity electron spectrum reconstruction 80−24966
TCNQ salt, $Qn(TCNQ)_2$, organic transfer salt, impurity effects on cond. 77−76799
TCNQ salts, $Qn(TCNQ)_2$ impurity effects on electronic coherence length 79−73500
thin surface layer, interactions between nondegenerate electrons, effect on cyclotron resonance, mag. cond. *(Russian)* 80−15802
thin wires, Kubo formalism for heavy elec. cond., heavy impurity electron scattering 79−56191
transition metals, impurity scattering and residual resistivity 79−56192
transport equation and photocurrent of electrons, in EM field 78−26913
TTF-TCNQ, impurity effects on CDW fluctuations 80−44576
two-dimensional disordered systems, effects of interactions on non-metallic behaviour 80−92869
two-dimensional electron-impurity system, electron mobility, theory 78−43457
vacancy-impurity scattering, complex dispersion law 78−87957
Wannier Stark ladder existence studies in electron scatt. in elec. field 80−39569
zero-gap semiconductor, reson. scatt. of electrons 80−10938
Si:P, sheet resistance of Gaussian n-type ion-implanted layers 79−87103
Ag, metal and dil. alloys, electrical resistivity at low temp., ultra high resolution meas. 79−60795
Ag-Au(Cd), deviations from Matthiessen's rule 78−10420
Ag-Mn dilute, magnetoresist. and Hall effect, field-depend. electron scatt. 77−43581
Al alloys, dil., depend. of electron scatt. rate on lattice relax. 77−69311
Al alloys, dil., diffusion thermopower, inelastic electron-phonon interaction 80−96851
Al and dilute alloys with Ge and Zn, magnetoresist. depend. on temp., 4.2-70K 80−70682
Al, electrical resist. and magnetoresist., 2 to 40K, Matthiessen rule deviations *(Russian)* 77−31996
Al, impurity low-field galvanomag. coeffs., 4 OPW calcs. 77−69304
Al, magnetoresistance, path integral method calc. 80−65537
Al, quenched, irradiated, anisotropic electron scatt. on defects 79−95397
Al, superconducting, order parameter, spatial var. near Anderson impurity 79−60962
Al, superconducting and normal state, anisotropic impurity scatt. and EM surface resist. 78−30970
Al-3d transition metal, dil., pre-asymptotic charge oscills. 80−20099
Al-Ag, dil., deviation from Matthiessen's rule at high temps. 77−69294
Al-Ag (4 wt.%), scattering of conduction electrons, effect of size and internal struct. of GP zones *(Japanese)* 77−21149
Al-Cr, Al-Mn, Al-Cr-Mn, dil. alloys, Hall coeff. and elec. resist. 77−11898
Al-Cu, dil., anisotropic scattering of conduction electrons on dilute Cu impurities 79−47082
Al-Cu dil. alloys, elec. resist. temp. depend. 77−8068
Al-Cu(Ag)(Ge), dil., deviation from Matthiessen's rule at high temps. 78−64025
Al-Ga(Mg)(Zn), electrical resist. and magnetoresist., 2 to 40K, Matthiessen rule deviations *(Russian)* 77−31996
Al-Li, Fermi surface impurity scatt. 79−56114
Al-M, dil. alloy, electronic states of 3d-transition metal (M) impurities 78−64005
Al-Mn, dil., magnetoresist. meas. 77−28160
Al-Zn, GP zones, effect of Si, Ag, Mg on transport props. 77−16588
$Al_xGa_{1-x}As$, compensated, electron mobility temp. depend. 80−96868
As, thermal resist. due to carrier-impurity scatt. 79−19610
Au alloy, charge density perturbations, ^{197}Au isomer shift obs. 77−20771
Au alloys, electrical resistivity, deviations from Matthiessen rule and scattering anisotropy 78−76051
Au wire, thermal cond., 0.8-10K 77−89748
Au-Co, electron scatt. by mag. impurity pairs, de Haas-van Alphen obs. 77−66162
Au-Cr, dil. alloys., elec. resist., deviations fro Matthiessen's rule 80−75541
Au-Fe, anomalous Hall effect, asymm. scatt. of itinerant electrons 77−43569
Au-Ga, dil. alloys, dHuA meas. and phase shift analysis of electronic scatt. anisotropy 77−35932
Au-Gd(Y), dil., conduction electron-local moment exchange interaction meas. 80−60191
BP film, high temp. thermoelec. power, scattering processes 80−80305
Bi, attenuation coefficient of sound, effect of impurity on gas-liq. type phase transition 78−39167
Bi:Sn,Te, and undoped sample, low-temp. transport meas., electron scatt. 77−24551
Bi-Sn, thermopower from 50 mK to 25K 80−24880
$Bi_{2-x}Sb_xTe_{3-y}Se_y$ solid solution, density-of-states effective mass, carrier mobility temp. depend. 80−24931
Cd_3As_2, elec. resist. and HF dielec. const. calcs. *(French)* 77−59284
Cd_3As_2, ionised-impurity mobility and static dielec. const. at 4.2K 77−32017
p-$CdCr_2Se_4$:Ag, electrical props., 100-300K 80−54692
$CdCr_2Si_4$:Ga, negative magnetoresist. effects near Curie temp. 79−11152
n-Cd_2GeO_4, electronic and cond. props. rel. to prep. conditions and defect struct. 80−107787
$Cd_{0.2}Hg_{0.8}Se$, longitudinal Nernst-Ettingshausen effect, effect of disorder scatt. 78−84240
$Cd_{1-x}Mg_x$, energy spectrum pseudopotential calcs., mag. props., impurity scatt. *(Russian)* 80−65430
n-CdS single crystals, effect of high-temp. annealing on electrical transport props. 79−78098
CdSe:Au impurity light absorpt. for current control in negative resistance region 80−11052
CdSe:In, epitaxial layers, synthesis and elec. props. 77−47909
n-$CdSnP_2$, Hall coeff. and elec. cond. meas., 24-900K 80−54721
CdTe, compensated single cryst., impurity centre parameters, elec. cond. and galvanomag. props. *(Russian)* 77−47811
CdTe, purification, efficiency for extraction of Cu and Ag impurities, impurity scatt. meas. 77−8749
Ce, high temperature transport props., scatt. mechanisms, phase transitions 77−15825

impurity scattering continued
Cs-Ag, dil., electronic struct., density functional approach, appl. to elec. and mag. props. 80−44492
Cu and ilute Cu-Au alloy, magnetoresist. depend. on temp., 4.2-70K 80−70682
Cu, electrical cond., effects of impurities 78−43355
Cu, electrical resistivity, at low temp., temp. depend. 78−23071
Cu-Al(Ge)(Sn) alloy films, electron transport props. 77−76955
Cu-Al(Ge)(Sn) film, thermoelec. power, 80-350K 78−68096
Cu-Cr, dil. alloys, Frenkel defects, effects on anomalous resistivity and thermopower 77−8084
Cu-Mn, dilute, magnetoresist. and Hall effect, field-depend. electron scatt. 77−43581
Cu-Ni dil. paramagnetic alloys, sp. elec. resist., effect of Ni clusters *(German)* 78−95293
Cu+3d alloying impurities, solid soln., exam. of thermoelectricity *(Russian)* 79−28339
n-$CuInSe_2$, single cryst., elec. props. 78−43397
Cu_2O, hole mobility, scatt. mechanisms, elec. field effect 77−80786
Cu_2O, pure and Fe doped, carrier cyclotron resonance impurity scattering effects, polar mass extrinsic origin 79−56614
Cu_2S film, reactively sputtered, Hall effect meas., 90-300K 80−15541
Dy, ferromag., rel. to magnetoresist., fields up to 75 kOe, 1-70K 77−20297
Eu chalcogenides, anomalous Hall effect, impurity scatt. 78−39131
Eu, high temperature transport props., scatt. mechanisms, phase transitions 77−15825
EuO:Gd, electron mobility below Curie temp. 78−91696
Fe based ternary alloys, Coulomb and exchange scatt. amplitudes, spin dependent residual resistivities 78−64033
Fe, elec. resist. between 2 and 30K, deviations from Matthiessen's rule 80−10944
$(Fe_yNi_{1-y})_{1-x}(SiO)_x$, dielec. effect on magnetisation and Faraday rot. *(Russian)* 78−39298
$Ga_{1-x}AlAs$, LPE layers, electron mobility, scatt. processes 80−84519
GaAs, compensated, electron mobility temp. depend. 80−96868
GaAs compensated VPE thin film, electron Hall mobilities 80−107932
p-GaAs, electronic props. 78−68040
n-GaAs, heavily doped, impurity-band cond., DC cond., Hall mobility, and magnetoresist. meas. 80−49733
GaAs, impurity centres ionis. by Auger electrons, carrier relax. *(Russian)* 79−51594
GaAs, impurity scattering of current carriers in quantizing mag. field 78−51954
GaAs, LPE in graphite boat, total ionised impurity density 77−12550
n-GaAs, magneto-impurity effect, review 79−91081
GaAs, model relating elec. props. to impurity concs. 77−51697
GaAs, n-i-n three layer struct., transmitted phonon effect in strong mag. fields 77−20341
n-GaAs, photo-Hall effect meas. of ionised impurity scatt. 78−56182
n-GaAs, piezoelectric semiconductor, influence of acoustic phonon disturbances on conductivity 78−91697
p-GaAs, piezoresistance, relax. time for heavy and light holes determ. 79−19599
n-GaAs, transferred electron effects under hydrostatic press. 78−26871
GaAs, two-photon interband transitions, carrier drag 79−7858
$Ga_{1-x}In_xAs$ solid solns., electron scatt. by isoelectronic impurities in covalent crysts. 79−11129
$Ga_xIn_{1-x}Sb$, electron transport props. calc. by Monte Carlo method 77−76834
n-GaN elec. props., electron mobility calc. 78−30923
GaP complex band semicond. photogalvanic effect mechanism 80−11036
GaP:Fe^{3+}, deep impurity states investig. 77−15794
GaP:Te on GaAs, LPE growth fron Sn, exam. of impurity band conduction effects 79−11249
p-GaP:Zn, Hall effect determ. of hole mobility temp. depend., scatt. mechanisms 77−4364
n-GaSb, galvanomagnetic effects 78−72172
p-GaSb, heavy and light holes scattering 78−91692
n-GaSb:Te, elec. transport mechanism in cond. band from Hall mobility and transverse mangetoresist. meas. 79−73531
p-GaSb:Zn, hole transport props. from 77 to 300K 79−73530
Gd-Dy, dil. alloy, impurity component of elec. resist., meas. 1.5 to 390K 77−39831
Gd-rare earth metal, dil. resist. anisotropy due to impurities 77−62902
Ge, electron mobility is semiconductors based on dielectric function modification of Dingle pot. 79−60836
Ge, electron scatt. by charged impurities under cyclotron reson. conditions 77−63286
Ge, electron-hole drop interaction in stationary and alternating mag. field *(Russian)* 77−62845
n-Ge, Hall coeff. and cond. mech. in intermediate conc. at He temps. 79−95422
p-Ge, highly deformed, hole scattering 77−20309
Ge, hole diffusion 78−6372
Ge, hole drift velocity, effect of impurity scatt. 78−60127
Ge, hot hole distribution function, effect of impurity and hole hole scatt. 79−11139
n-Ge, impurity breakdown field, temp. depend. 79−24263
Ge, impurity-ion potential, electron-conductivity mobility, spatially variable dielectric function calcs. 79−78105
Ge, ionised impurity scatt. limited mobility in semiconductors with spatially variable dielec. function 78−51986
Ge, n- and p-type, magneto-impurity effect, review 79−91081
p-Ge, odd magnetoresist., ionised impurity scatt., theory 78−72178
Ge, partly dissociated excitons and impurity atoms system, collisional processes, charge transport theory 80−44581
Ge, photoconductivity, magnetoimpurity oscills. 79−82626
Ge, photomag. EMF, reson. struct., energy relax. mechanisms 78−2515
p-Ge, rel. to calc. of carrier mobility, 10-70K *(Russian)* 78−39103
n-Ge, single cryst. with dislocations, UHF cond. *(Russian)* 79−78128
n-Ge, thermal phonon scatt., piezo-thermal cond. 80−70482
Ge:Sb, heavily doped, mass anisotropy, and multiple scattering effects 80−107802
Ge:Sb,In, lightly doped semicond., low temp., phonon cond., electron-phonon scatt. 79−60456
$Hg_{1-x}Cd_xTe$, quasi-local acceptor levels and electron mobility 78−67974
$Hg_{1-x}Cd_xTe$-type semimetals, kinetic props., local acceptor level effects 80−65557
HgTe film, vac. deposited, elec. props., 78-420K 80−11119
impurity scattering continued
HgTe, gapless, nonlinear effects in transverse quantising mag. fields 77−69353
HgTe:Cu(In), dopant interactions 77−47834
In, electron scattering rates, RF size effect meas. under multiple-turn conditions 78−14654
n-InAs, transport props., influence of higher energy bands, calcs. 79−19598
InAs:Cd,Te interaction between impurities, effect on elec. props., Hall effect. 80−19832
InAs:Zn, optical absorpt. and refl. spectra 79−91479
In_2O_3 films, reactively evaporated, elec. props. 80−84521
n-InP, magneto-impurity effect, review 79−91081
n-InP, transferred electron effects under hydrostatic press. 78−26871
InSb, CESR at high mag. fields, scatt. mechanisms 80−93177
n-InSb, cond. electron spectra in quantised mag. field, impurity resonance scatt. *(Russian)* 80−93178
n-InSb, cyclotron reson. study of conduction electrons, strong mag. field 80−2639
n-InSb, elec. cond., press. dependence 80−6830
n-InSb, elec. props. changes during ht. treatment 77−85213
n-InSb electron heating and energy relaxation time in quantising mag. field 80−10996
n-InSb, heavily compensated, hopping cond. in mag. field 79−7842
n-InSb, ionized impurity scatt. limited mobility, expt. 80−80274
n-InSb, rel. to sign change of Hall effect, in quantum limit 77−15875
n-InSb, rel. to sign reversal of acoustomagnetoelec. effect 77−24592
p-InSb:Cu(Zn) film, heavily doped, ionized impurity scatt., Hall effect and DC cond. meas. 79−99643
InSb:NiSb, size reson. scatt. from hard cylindrical pot. obs. in magnetoresist. 79−95421
Insb, doped, electron scatt. by deform. pot. 77−72860
K, Matthiessen's rule, low temp. deviations 78−14724
K, thermal cond. electronic contrib., 1 to 330K 77−20291
K-Rb, dil., calc. of press. depend. of low-temp. transport props. 78−30905
K-Rb(Na), dil., anisotropy of electron-impurity scatt. in K, de Haas-van Alphen effect meas. 78−18943
K-Rb(Na), dil., anisotropic scatt. of conduction electrons by impurities 78−18944
$(La,Ce)Al_2$ and $(La,Gd)Al_2$, magnetic impurity effect on thermal cond., normal and supercond. states 77−63027
La-Gd (8 at.%), FCC, under hydrostatic pressure, resistivity meas., comparison with positive-J spin glasses 80−59958
Li, impurity and conduction electron scatt. at 4.2K *(Russian)* 77−35931
Li-Mg, Mathiessen's rule, elec. and thermal deviations, impurity scatt. 80−88536
Mg-rare earth metal dil. alloys, anisotropic magnetoresist. 77−62905
MnTe film, elec. props. 78−43498
$MoTe_2$, elec. cond. and thermoelec. power 79−91047
Nb, elec. resist. due to interstitial H (D) 80−96848
$NbSe_3$:Ta, elec. cond., anomalous, and microwave absorpt. 79−42527
Nd, high temperature transport props., scatt. mechanisms, phase transitions 77−15825
Ni alloys, anomalous Hall effect meas., two current model 77−62906
Ni based ternary alloys, Coulomb and exchange scatt. amplitudes, spin dependent residual resistivities 78−64033
Ni, ferromagnetic, Hall effect, anomalous, rel. to scatt. processes 80−44572
Ni, magnetoresistance anisotropy, planar Hall effect 79−23947
Ni-Cu, ferromagnetic, Hall effect, anomalous, rel. to scatt. processes 80−44572
Ni-Cu alloy, magnetoresistance anisotropy, planar Hall effect 79−23947
Ni-Fe, film, anomalous Hall and Nernst-Ettingshausen effect, contribution of phonon and impurity scatt. *(Russian)* 78−64145
Ni-Re, dil. alloys, two-band Mott conductivity *(Russian)* 78−60118
Ni-Sn(Sb), dilute ferromagnetic alloy, resistivity and magnetoresist. anisotropy 79−11106
Ni-transition metal alloys, deviation from Matthiessen's rule in elec. resist. 77−4319
Ni-V, magnetocryst. temp. and conc. depends., rel. to resistivity 77−40052
Pb alloys, dil., diffusion thermopower, inelastic electron-phonon interaction 80−96851
Pb dilute alloys, solute resist. meas., multiple point defect form. 78−10433
Pb-Au, dil., solute resist. meas., multiple point defect form. 78−10433
Pb-Sn-Te, solid solution, scattering mechanism of carriers 80−49710
p-$Pb_{1-x}Sn_xTe$, carrier mobility, acoustical phonon and impurity scatt., deform. impurity const., conc. depend. 80−39570
n-PbSe, polar semicond., mag. field influence on high-freq. relaxation time 79−95438
PbSe:Tl, scatt. of holes and phonons by impurities 78−19068
$Pb_{0.82}Sn_{0.18}Te$, Hall mobility, scatt. mechanisms, temp. and carrier conc. depend. 77−55548
p-$Pb_{1-x}Sn_xTe$, mobility meas., impurity and phonon scatt. mechanisms 78−23091
PbTe-InTe, solid solns., anomalies in electron mobility 77−80772
Pd, elec. resist. due to interstitial H (D) 80−96848
Pd-Co, normal Hall effect *(Russian)* 80−103676
Pd-Cr, dil., temp. dependent scatt. 80−59973
Pd-Cr alloys, dil., elec. resist., 7.4 to 300K, anomalous temp. depend. associated with cond. electron scatt. 79−73491
Pd-Fe, normal Hall effect *(Russian)* 80−103676
Pd-Ni, normal Hall effect *(Russian)* 80−103676
PdFe alloy, magnetoresistance meas. below 295K 79−78070
β′-PdIn, electrical resistance, mag. susceptibility and IR freq. dispersion *(Russian)* 80−107759
Pr, high temperature transport props., scatt. mechanisms, phase transitions 77−15825
Pt, impurities on grain boundaries 79−87076
Pt-Cr (0.3 and 0.5 at.%) anomalous resist. associated with conduction-electron scatt. from Cr impurities 79−99530
Pt-Cr alloys, dil., elec. resist., 7.4 to 300K, anomalous temp. depend. associated with cond. electron scatt. 79−73491
Pu-Np, elec. resist., reson. scatt. from Np and local spin fluctuations 77−28170
p-Sb_2Te_3, rel. to thermopower anisotropy 77−15884
Si, (100) inversion layer, electromigration in two dimensional electron gas, driving force 80−84441

impurity scattering continued
n-Si, carrier scatt. anisotropy, Hall mobility calcs. 77−24552
Si, electron mobility is semiconductors based on dielectric function modification of Dingle pot. 79−60836
p-Si, highly deformed, hole scattering 77−20309
n-Si, hot-electron diffusion, effect of ionised impurity scatt. 78−56151
Si, impurity-ion potential, electron-conductivity mobility, spatially variable dielectric function calcs. 79−78105
p-Si, interband transitions, contrib. to conductivity at submillimetre wavelengths 80−34473
Si, inversion layer, impurity scatt., self-consistent calc. 79−28415
p-Si, inversion layer, screening effect and quantum transport in strong mag. fields 78−19155
Si, ionised impurity scatt. limited mobility in semiconductors with spatially variable dielec. function 78−51986
Si:B, hole mobility calc. for dopant density and temp. var., resistivity meas., effective mass calcs. 80−54703
Si:B, hot-carrier scatt. and recomb. characts. 79−91069
Si:B(P), uniaxially stressed, impurity-assisted intervalley scatt., photoluminesc. obs. 80−34979
n- Si:O, charge carrier scattering on neutral centres 80−49762
n-Si:P, electron mobility and resist., dopant density and temp. depend. 77−76816
Si:P, heavily doped, influence of impurities and crystalline defects on electron mobility 79−78095
n-Si:P, low-compensated, Hall factor, electron-phonon interactions 79−4570
Si:P, polycryst., CVD, elec. activation of impurities, EPR obs. 80−34774
Si-Ge:As,P, heavily doped, electron scatt., Hall coeff., Seebeck coeff. and resist. meas., 4-300K 77−4379
n-SiC, 6H polytype, expitaxially grown, electronic props. meas. 77−39975
Si(100)-SiO_2 interface, mobility in Si inversion layers, screening and neutral impurity effects 79−28412
Sn, aggregate film, resist., temp. depend. 78−39230
$Sn_{1-x}Mn_xTe$, degenerate mag. semicond., thermoelec. power meas. 80−29392
SnTe-MnTe, degenerate semicond., anomalous Hall effect 80−29420
SrF_2, thermo-EMF meas., ion transfer characts. 77−7892
TTT_2I_3, neutron irrad. induced defects and chemical impurity effects on DC cond. 80−39565
Ta, elec. resist. due to interstitial H (D) 80−96848
p-Te, magneto-impurity effect, review 79−91081
Te, pure and Sb doped, impurity state and impurity cond., press. effect 80−54723
Te:Sb, 96 to 500K, cond. Hall const., hole mobility, conc., dislocation effects *(Russian)* 78−64039
V, elec. resist. due to interstitial H (D) 80−96848
W, low temp. transport props., phonon and impurity scatt. 78−10418
Zn:Al, residual resistivity, numerical calc., Fermi surface and multiple plane wave band struct. 77−51722
$Zn_xHg_{1-x}Se$, current carrier scattering mechanism 80−65546
ZnMn, dil., magnetoresist. meas., temp. depend. anisotropy 80−65532
n-ZnSe crystals, electron scatt. mechanisms, high mobility 80−34433
ZnSe:Al(As), high temp. electron mobility, lattice scatt. and ionized impurity scatt. 79−91042
n-$ZnSiP_2$:Ga, elec. cond. and Hall meas., 77 to 1000K, scatt. mechanisms 79−11153
$ZnY_{0.95}R_{0.05}$ resist. anisotropy due to impurities 77−62902
ZrS_3, quasi one-dimens. semicond., elec. transport props. 80−107790

impurity-vacancy interactions
β-AgI, valence state and impurity-vacancy dipole formation, Mossbauer effect meas. 78−68435
alkali halide:Me^{2+}, nearest-neighbour theory of dipole polarisation and depolarisation, cation vacancies 77−16243
alkali halide:VO^{2+}, impurity behaviour, elec. cond. and IR absorpt. obs. 77−8607
alkali halide, cation impurity-cation vacancy complex, equilib. conc. calc. 80−19834
alkali halide, divalent metal doped, dipolar relax. induced by AC field in various crystallographic directions 79−19833
alkali halide, impurity-vacancy dipole interaction with relaxed and nonrelaxed holes *(Russian)* 78−75661
alkali halides, doped, AC field induced impurity-vacancy dipole relax. 79−11385
alkali halides, implantation of ^{57}Fe, conversion electron Mossbauer spectroscopy technique 80−40012
alkali halides, impurity-vacancy complexes, association and orientation energies 78−51578
alkali halides, impurity-vacancy dipoles, activation energy 79−33013
alkali halides, trimer formation due to dimer-dipole aggregation 77−62561
alkali metal chloride: $F^-(Br^-)(I^-)$, anion impurities substitution, energies of soln., association and migration 78−83831
alloys, thermomigration, substitutional-vacancy and interstitial-vacancy mechanism 77−35744
chemical potential of impurity-vacancy pairs 77−11587
clustering of vacancies, effect of impurity atom 77−84789
defect diffusion coeffs., site blocking, correlated defect motion 80−84315
diffusion of impurity atoms *(Russian)* 80−19985
diffusion phenomena, vacancy-impurity complexes effect, appl. to nonequilib. segregation near grain boundaries *(Russian)* 80−44350
fusion reactor metals and alloys, microvoid form., gaseous impurity atom effects, positron annihilation study 80−49275
II-VI compounds, electron energy radiation damage threshold meas., EPR and luminesc. 77−84799
ionic crystal, solid soln. hardening by aliovalent cations 77−44265
ionic crystals, degree of association of point defects 78−2156
ionic impurity, drift mobility in electric field, computer simulation 79−82388
metal, interaction energies between point defects 78−47360
metal, vacancy-solute interaction 78−47409
metals, free-electron-like, electron struct. of single and interacting H impurities 79−95365
metals, point defect solute interactions 78−47410
metals and alloys, vacancies and lattice elec. cond. determ. method at high temp. 79−37695
Mossbauer impurity atoms trapped by vacancies, resonance energy shift 80−25265
neutron-irrad., void annealing, positron annihilation obs. 77−76469

impurity-vacancy interactions continued
noble metals, impurity diffusion, electrostatic interaction theory, impurity-vacancy pair 78−43181
point traps, effect on diffusion and diffusing element distrib. function in crysts. *(Russian)* 80−59692
substituent impurities in diamond-structure crystals, diffusion equation, complex formation, theory 80−24677
vacancy trapping by foreign atoms in FCC crystals 79−90696
Ag, recoil implanted ^{111}In impurities, interaction with radiation damage, TDPAC meas. 79−11362
AgBr, doped, neutralisation of trapped photoholes 78−76108
AgBr(:Pb^{2+}), ionic conductivity, Frenkel defects 77−51542
AgBr(Cl):$Ru^{3+,2+}$, dopant vacancy config., EPR 79−91288
AgCl:Cd^{2+}, heavily doped, free energy and point defect distrib., integral eqn. method 80−107219
AgCl:Pb^{2+}, ionic cond. and dielec. loss relax. vacancy-impurity complex. form. 77−1259
AgCl:Sr, effect of impurity doping on Sr^{2+} diffusion 78−84002
Al, impurity-vacancy binding energy, clustering effects calc. 78−47411
Al, interaction between ^{57}Co atoms and quenched-in vacancies, Mossbauer meas. 80−7234
Al, quenched, vacancy-Fe interactions 78−47412
Al, vacancy-solute interaction 78−47413
Al:^{111}In, electron irrad., defect trapping at impurities 78−55892
Al-Cr(Zr), dilute, vacancy-impurity interaction investig. by tempering method *(French)* 77−68995
Al-Fe, dil., annealing after cold working, impurity-vacancy interactions, Mossbauer meas. 80−7236
Al-Fe, dil., Mossbauer spectra of implanted ^{57}Fe, ageing behaviour 80−7233
Al-Fe, dil. solid soln., vacancy-trapped Mossbauer impurity Debye Waller factor 80−60468
Al-Mn (0.35 wt.%), quenched exam. of Mn-vacancy interaction 78−76676
Al-Sn, dil. alloy, vacancy-impurity interaction, exam. by electrical resistivity meas. at 77K *(German)* 78−83846
Al-transition metal, impurity binding energies 79−42096
Al-Zn-Mg alloys, decomp. kinetics from Young's modulus obs., microprocesses *(German)* 78−64522
Au(-Cu)(Sn) vacancy cluster form. in quenched pure Au and dil. alloys 77−62546
CaF_2, fluorite crysts., lattice O^{2-} effect on thermal, elec., and thermoelec. props. 77−76599
CaF_2, O^{2-}-F_v^- dipoles association from ionic conductivity 77−43242
CaF_2:Na, vacancy motion activation vol., complex dielec. const. meas. 80−39356
CdF_2:NaF, formation and reorientation of Na^+-anion vacancy complexes 78−84516
$Cd_xHg_{1-x}Te$, solid soln., pure and Ag(In) doped, defect struct. model, Hg self-diffusion coeff. 79−95213
CdTe, donor impurity compensation models, impurity-vacancy complexes 77−39601
CdTe:Cl, heavily doped, elec. and photoluminesc. investig. of defect interactions 77−39603
Ce, vacancy formation enthalpy in γ phase, positron annihilation meas. 79−99182
CeO_2:CaO(Y_2O_3), oxygen ion cond. and defect struct. 80−107553
CeO_2-rare earth oxides, complexes of the 'two impurity ions-vacancy' type 79−95004
CsBr:Ca^{2+}(Pb^{2+})(Ba^{2+}) (MnO_4^{2-}), reorientation of dipolar complexes, ionic thermo currents meas. 77−80642
Cu, He-vacancy clusters, computer simulation 77−39583
Cu, irradiation with 4 to 6 kV Ar^+ ions, Ar-vacancy cluster form. and stability 77−43259
Cu, vacancies-gas impurity interactions in vacuum condensates *(Russian)* 79−15036
Cu:H, interaction of H and vacancies, positron annihilation, Doppler broadening 78−80434
Cu-Ge, dil., point defect props., density functional approach 80−29013
Cu-Ge alloys, equilib. defects *(German)* 79−86789
Cu-Sc alloy, dil., impurity effects on annealing and resist., vacancy-Sc interaction 79−51142
$CuGaSe_2$ crystals, I_2 vapour transport grown, luminesc. spectra 78−88349
Fe, defect trapping of ion implanted D, depth profile, diffusion eqn. calcs. 80−2047
α-Fe, He interaction with vacancies, computer simulation 78−79604
Fe, heavy impurity implanted, relation between hyperfine field and lattice-location meas., influence of radiation damage 80−6794
α-Fe, interaction of foreign interstitial atoms with vacancies 78−6052
α-Fe:He, impurity clustering in vacancies bound to edge dislocations 78−91358
GaAs, interimpurity interaction effect on distrib. profiles of impurities diffusing simultaneously 77−76451
GaAs:Cd, lattice defects caused by quenching, elec. cond. 79−56160
GaAs:Si, hardening by solute-vacancy pairs 77−4794
GaAs:Si epitaxial films, elec. and photoelec. props., impurity distrib., impurity-defect interactions 80−7006
GaAs:Si(Ge) LPE layers, luminesc. props. rel. to substrate quality 78−52583
GaAs:Sn, solubility and point defect-dopant interactions 79−90688
GaAs:Te, heavily-doped, annealing-induced prismatic dislocation loops and elec. changes 78−51546
GaAs:Te, solubility and point defect-dopant interactions 79−90687
GaP, complex ^{119}Sn impurity-defect, Mossbauer study 80−75898
GaP, interimpurity interaction effect on distrib. profiles of impurities diffusing simultaneously 77−76451
n-Ge, electron irradiated, threshold energy for atomic displacement, carrier traps 80−29351
Ge, gamma irradiated, radiation defects, formation kinetics, successive capture of vacancies by impurities 79−10873
Ge, high-purity dislocation-free, divacancy-hydrogen complexes 78−2449
Ge, quenched, defect annihilation process near 100°C 79−95047
Ge, vacancy interactions with H atoms, positions and positive muons 77−80500
Ge:O, elec. props., O interaction with point defects 79−11081
InP:Co(Fe), diffusion solubility and elec. activity of Co and Fe 77−43240
KBr:Se^{2-} single cryst., dielec. relax. of impurity-vacancy dipoles, ITC meas. 79−91349

impurity-vacancy interactions continued
KBr:Sr, X-irradiated, first-stage F-centre production, ionic cond. meas. 77−76395
KBr(Cl):Mg^{2+}, dopant aggregation and precipitation 80−107306
KCl, Ba^{2+} diffusion, light scatt. meas., dipole mechanism *(Russian)* 78−22900
KCl, doped, elec. conductivity and optical absorpt., quenching from 750°C 78−2289
KCl, pure and Sr doped crystals, strengthening effects rel. to IV-dipoles and aggregates 78−55907
KCl, with divalent impurity, reorientation of impurity-vacancy complexes, thermally stimulated depolarisation 77−65977
KCl:Ca^{2+}, Z_3-centre thermolum. 80−80879
KCl:Ca(Pb)(Sr), structural state of impurities, hydrostatic press. effect, thermostimulated depolarisation exam. 77−39614
KCl:CrO_4^{2-}, reorientation of dipolar complexes, ionic thermo currents meas. 77−80642
KCl:Eu^{2+}, cation impurity-vacancy pairs, effect of X-rays 79−55778
KCl:Sr^{2+}, X-irrad., thermolum., impurity aggregation, trapping centre form. 78−88367
$KClO_4$:CrO_4^{2-}(SO_4^{2-}), AC electrical conductivity meas. between temp. range 25-325°C, automated technique 80−59699
$KHSO_4$:Co^{2+}, conduction and ^3H diffusion 77−15622
KI:Cl, dielec. relax. of impurity-vacancy complexes, ionic thermal current meas. 77−48124
KI:S^{2-}, impurity-vacancy dipole UV absorpt. and ionic thermocurrent, F-centre form. 77−36271
KI:S^{2-}, photochemical reaction, F-centre production 78−64861
LaF_3, ionic transport, NMR and cond. studies 80−107555
LiCl:Ni^{2+}, EPR meas. of Ni^{2+} vacancy dipoles 79−28594
LiF, annealing effects on thermoluminescence, dipoles and dimers 77−12452
LiF:Mg, role of impurity-vacancy pairs in thermolum. 79−8195
LiF:Mg, Z_2- and associated Z-centres, elec. cond., ionic thermocurrent, and optical absorpt. meas. 80−107229
Li_3N, photoluminesc. props. 80−50414
Li_3N:H, ionic cond., impurity conc., IR transmission meas. 79−42305
$LiO_{1/2}$-$2SiO_2$ glass, alkali motion ionic thermocurrent study, polarised impurity-vacancy dipole relaxation study 79−77806
Mo cryst., radiation induced vacancies and D_2^+ implantation 80−65076
Mo, He interaction with vacancies, computer simulation 78−79604
Mo:N single cryst., interaction of N with vacancies 79−82261
Mo-Nb, impurity diffusion and vacancy-impurity binding energy 80−15307
NH_4Cl:$[MoOCl_5]^{2-}$, single cryst., struct. investigations 77−66524
NaCl, evaluation of ionic thermocurrent technique in monitoring relaxation behaviour of impurity-vacancy dipoles 78−43778
NaCl, Mn^{2+}-□ reorientation, ESR elec. field effect meas. 79−8050
NaCl, pure and Sr doped crystals, strengthening effects rel. to IV-dipoles and aggregates 78−55907
NaCl:$(Mn^{2+}$-□$)_{Fanion}$, F^- assoc. complex, ionic thermocurrent and EPR 79−8086
NaCl:Ca, aggregation and precip. hardening in impurity vacancy, dipole decay 80−16322
NaCl:Ca^{2+}, dipole concs. determ. considering aggregation, expt. and theoretical comparison 80−59512
NaCl:Ca^{2+}, highly doped, aggregation of point defects, NMR and dielec. loss meas. 79−10847
NaCl:$CaCl_2$, quenched, aggregation process of Ca^{2+} ion-vacancy dipole, elec. cond. and dielec. loss meas. 77−80535
NaCl:Cd^{2+}, dielectric loss following plastic deform. 80−84690
NaCl:Eu^{2+}, reorient. of Eu^{2+}-vacancy complexes, ESR method using elec. field effect 79−99768
NaCl:Mg^{2+} (Ba^{2+}), dopant aggregation and precipitation 80−107306
NaCl:Mn, impurity-vacancy dipole aggregation, role of dimers and trimers, reanal. of dielec. and cond. data 79−1458
NaCl:Mn^{2+}, dimer detection, EPR and ITC expts. 78−59833
NaCl:Mn^{2+}, X-ray irradiated, thermolum. and EPR 77−81161
NaCl:Pb^{2+}, activation energy for clustering of Pb^{2+} vacancy pairs 77−72610
NaCl:S^{2-}, enthalpy of anion vacancy migration 80−15309
Nb-Ru(Pd), impurity diffusion and vacancy-impurity binding energy 80−15307
Ni, H diffusion, trapping and mobility near vacancies, dislocations and cracks 80−49426
Ni, lattice defect symmetry, time differential PAC meas. 78−15069
Ni, neutron irrad., void formation, C interstitial effects 77−76471
Ni-Fe (20at.%), vacancy-C interaction, Lomer's model insufficiency *(French)* 77−76456
Ni-Fe-C, 20 at.% Fe, vacancy-C interaction, induced mag. anisotropy *(French)* 79−55775
Ni-Sb, dil., vacancy-impurity binding enthalpy, positron annihilation 79−91525
NiO, undoped and Al doped, Ni self-diffusion, vacancy-impurity complex effects 80−107493
RbCl, with divalent impurity, reorientation of impurity-vacancy complexes, thermally stimulated depolarisation 77−65977
$RbCl_2$-$NiCl_2$, impurity ion and vacancy aggregation, thermally stimulated depolarisation investigation 78−18678
RbI:Pb^{2+}, optical and elec. props. 79−15493
Si, A-centre formation by vacancy-O_2 recomb., acceptor impurity conc. effect 77−43243
Si, carrier lifetime degradation at room temp. 78−95301
Si, electron beam scan annealed, deep levels 80−65481
Si, electron irradiated, EPR of C-O divacancy complex 77−69691
Si, electron irradiated, EPR of impurity-divacancy complex 79−19779
Si, extended Huckel theory calc. of hyperfine interactions of positive divacancy 77−89742
Si implanted layers, interaction of defects and impurities stimulated by induced ionisation, ESR 80−11270
Si, proton irrad., efficiency of form. and nature of defects, Hall meas. 80−6444
p-Si, radiation defects by annealing, kinetics anal. 79−33018
Si, Sn or Ge complex with vacancy, many-electron approach 78−67980
Si, stacking fault annihilation by impurity diffusion 77−19968
Si, vacancy interactions with H atoms, positions and positive muons 77−80500
Si:As, displacement effect beam energy depend., vacancy trapping 80−33996
Si:As, relation between total and electrically active As conc. produced by diffusion 79−55773

impurity-vacancy interactions continued
Si:B(P), impurity-peak form. during proton-enhanced diffusion 79−55772
Si:B(P), proton-irrad., impurity uphill diffusion, vacancy mechanism 80−92719
Si:Ge,Sn, role of interelectronic correl. in paramag. props. of impurity-vacancy complex 77−62858
Si:O, carrier recomb. processes, role of vacancy-O complexes 80−65592
p-Si:P, Cu, influence of Cu on diffusion of P meas. 77−1267
p-Si:P, defect energy levels, ion implantation effects, Hall coeff., sheet resist. meas. 77−85173
Si:P, diffusion eqn. numerical soln. 79−51311
Si:Sb, Mossbauer spectra of ^{119}Sn defect struct. 80−97174
Si:Te, Mossbauer spectra of ^{119}Sn defect struct. 80−97175
α-Sn, implanted with Sn, Sb or Te, impurity-defect structs., Mossbauer expts. 80−39129
$SrTiO_3$ and $SrTiO_3$:Nb, reduced samples, optical absorpt., effect of impurity-O vacancy complex *(Korean)* 79−8163
$SrTiO_3$:Fe, EPR, of Fe^{3+}-rhombic, Fe^{2+}-V_0 and Fe^{1+}-V_0 complexes 78−76302
ThO_2-CaO electrolyte, cond. rel. to dissociated vacancies and vacancy-impurity complexes 77−8156
(U,Ce)C, U self-diffusion 80−92711
(U,La)C, U self-diffusion 80−92711
(U,Y)C, U self-diffusion 80−92711
(U,Zr)C, U self-diffusion 80−92711
UC, quenched-in defects, formation, migration and resistivity 80−64990
UCN, quenched-in defects, formation, migration and resistivity 80−64990
V, electron-irradiated, positron annihilation study 80−70259
V, He interaction with vacancies, computer simulation 78−79604
W:Kr, He trapping at substitutional Kr, vacancy creation 77−43258
$^{133}Xe/^{133}Cs$, implanted in various hosts, isomer shift values, Mossbauer spectra 80−7240
$(ZrO_2)_{0.9}(Y_2O_3)_{0.1}$:Cr, Mn, stabilised single crystal, EPR of Mn^{2+} and Cr^{3+} obs. 80−66024
incandescent lamps *see filament lamps*
inclusions in crystalline material *see crystal inclusions*
inclusive reactions, elementary particle *see elementary particle inclusive interactions*
incremental computers *see digital differential analysers*
independent particle model *see nuclear optical model; nuclear shell model*
indeterminancy
alkali halide, lattice energy, binding, indeterminancy principle theory 78−59777
analytic observables in nuclear physics 80−105993
Brownian motion, generalised Einstein theory for nonequilibrium fluctuations 80−31672
causal theory, removal of Einstein's objections to quantum theory, unification 80−31572
coherence and randomness in quantum theory, uncertainty relations 80−22231
commutation and uncertainty relations, deterministic interpretation, Planck's const. as coupling condition 78−73875
correspondence principle, classical tests without corresponding quantum tests 80−62527
de Broglie waves of the second kind 79−6004
demonstration of uncertainty principle using single-slit diffraction pattern 78−69953
diffraction in time and the time-energy uncertainty relation 77−13518
Dirac field, nonlinear, kinks and the Heisenberg uncertainty principle 79−35943
Doppler effect, transverse, in six-dimensional space, hidden variables 80−82666
double slit experiment, quantum nonseparability and Bohr's complementarity principle 79−35582
education, classical and quantum uncertainties, particle in box, harmonic oscill. and atom 79−25789
education, Einstein and $\Delta t\Delta E$ 80−51986
Einstein, quantum mechanics, conceptual problems 80−46783
Einstein-Poddlsky-Rosen paradox, determinism, objectivity, completeness *(French)* 80−90721
electtrical conductivity and uncertainty principle 78−84182
entropic uncertainty relation from quantum mechs. state function 78−21009
entropy, relation between classical and quantum-mechanical entropy 80−73298
excited-mass states of the electron, chronon 78−21004
exclusion principle extended, particle classification anal. 78−49690
extremum uncertainty product and sum states 78−24687
Feynman path, trajectories in Hilbert space connecting any two states, dense measurements 80−82678
Feynman postulates, modifed set, superposition principle 80−82657
foundations of quantum mechanics and uncertainty principle, book 78−29000
generalised quantum meas., uncertainty relations, efficient meas. 77−37781
gravitational wave interferometer, quantum mechanical radiation press. fluctuations 80−90770
harmonic oscillator, quantum action angle variables 80−46842
harmonic oscillators, quantum nondemolition meas., gravit. wave detection 78−41198
Heisenberg's commutation rule, geometric interp., algebraic struct. of Pauli eqn. 78−93549
Heisenberg's microscope, uncertainty relation paradox 79−17254
Heisenberg microscope, crit. ang. aperture 80−41981
ideal experiments connected with uncertainty principle 77−5679
inequalities and uncertainty principles 78−36875
information propagation in a quantum-mechanical system between 2 physical parts 80−17832
interference and phase shift due to Earth's rotation 80−82679
locality, Bell's theorem and probabilistic character of quantum mechanics 80−90709
Lorentz deformation and jet phenomenon 80−105806
Lorentz-invariant minimum uncertainty product 79−6006
macroscopic oscillator motion parameter meas., quantum restrictions *(Russian)* 80−12943
minimal phase indeterminancy states, of photons *(Russian)* 79−18390
minimal time-energy uncertainty relation 79−67174
minimal uncertainty states for rotation and allied groups 78−4501

indeterminancy continued
minimum uncertainty states, conditions on Hamiltonian for stability 78−24683
minimum uncertainty states of angular momentum system 78−93559
momentum and positional uncertainty, for states of N identical fermions with spin 79−35583
momentum conservation and Heisenberg's interpretation of uncertainty formulas 77−45724
oscillator, Morse, anharmonic, position-momentum uncertainty products 80−68072
physical system, model of space-time from set theory concepts 80−82660
position-momentum, angle variable-momentum paradoxes in uncertainty principle boundary conditions 78−89280
position-momentum uncertainty products for exactly solvable potentials 80−12939
quantum mechanics, interpretation, spin and uncertainty, teaching approach 79−58481
quantum mechanics and determinism *(Hungarian)* 79−44766
quantum numbers, uncertainty, min. entropy and discrete spacetime 77−87659
realist interpretation, indeterminancy and measuring process 77−9898
Schrodinger equation, randomly fluctuating interaction term, uncertainty in nature 80−62499
self turbulence in free particle motion 78−86177
space-time events, nonlocalisability 80−94972
SU(1,1) non-compact group, existence of intelligent states 78−77753
subensemble of particles, uncertainty product 77−33886
time quantisation, relation between proton mass and ρ-meson lifetime 78−76
time-energy uncertainty principle failure 79−30279
time-energy uncertainty relation, quantum-mechanical derivation 78−73894
time-energy uncertainty relation 78−45492
topological shifts in the Aharonov-Bohm effect 80−82674
uncertainty measure for compact Lie group, minimised for max. weight vectors 78−20996
uncertainty relation, mathematical proof 79−84888
uncertainty relation 80−90722
uncertainty relation and Pauli's principles *(Hungarian)* 79−3339
uncertainty relation between angular momentum and angle variable 80−27073
uncertainty relation for symmetric operators, extension using sesquilinear form methods 78−81872
uncertainty relations, covariant harmonic oscillator forms 79−9137
vector-valued operators, uncertainty relns. 77−49637
weak signal detection, limitations by uncertainty principle 79−25898

indexing
see also information dissemination
chemical reaction information comparison 79−83541
electron diffraction patterns, computer assisted indexing 78−9918
ion milling (ion beam etching), bibliography for 1975-1978 period 80−4
mass spectra, classification, ion series-related index, fast library searching appls. 77−12837
structural search codes for on-line compound registration 78−90319
Zimdex audio indexing system, efficiency 79−92915

indicating devices *see indicators*

indicating instruments *see indicators*

indicators
see also alarm systems; standing wave meters
accuracy categories, absolute and relative errors *(Croatian)* 80−13063
acoustic temp. indicator, consisting of temp. sensitive resistor and operational amplifiers *(Spanish)* 80−13061
analogue versus digital, analogue meter advantages 80−13053
automatic plugging indicator for impurity conc. meas. in Na coolant 78−17283
balancing, use of conventional galvanometers *(Polish)* 77−10064
blood indicator dye microconcentration meas. instrument 79−39565
capacitance meas. instrument, operational amplifiers employing, for 10pF to 10μF range *(German)* 77−146
cardiostimulator, implanted, contactless rhythm indicator 79−39602
chemical, for testing poisonous and explosive gases *(German)* 77−4950
dial gauges reliability obs., manufactured in Rumania *(Rumanian)* 80−47049
diapositive graphical data stereoscopic image *(Russian)* 77−71308
differential temp. sensor with indicator system *(Spanish)* 79−54133
digital pressure indicator construction and application 78−21112
dust measurement engineering, survey *(German)* 79−35712
electrical instruments in photometric laboratory, selection, care, and use 80−86283
electrochemical voltage indicators, production, voltage response, resist. 77−1936
electromechanical, automatic torque measurement, torque meter appl. 77−87757
electronic balance, commercial products survey solid state technique appl. *(Polish)* 77−10065
extremal value indicator using glow-discharge thyratrons 77−17967
floating level indicator for meas. of fluid level in reservoir *(Russian)* 77−65018
hole diameter meas. with universal microscope and electronic contact indicator 77−79055
ice calorimeter reading unit with water indicator 80−31755
image quality indicators for crack detection in steel 77−25232
laser pulse energy digital indicator *(Russian)* 79−22995
lighting, effectiveness, ESI meter application 80−22417
liquid crystal indicator of variable light-reading angle 78−57932
micro-organism enzymic activity indicator 79−57819
microhole axis perpendicularity deviation meas. device 77−13739
microwave circular scanning indicator for 3.2 cm wave expts. *(Russian)* 77−26328
microwave diathermy equipment and power indicator 77−40901
nuclear reactor neutron flux level CRT state indicator 77−79444
pacemaker pulse generator replacement indicator 77−81692
parity indicators for DC voltages 77−142
photoresistor contactless temperature indicator *(Russian)* 77−10023
plugging indicator, liquid Na impurity deposition rate obs. 79−13557
position, capacitive, linear and angular *(German)* 80−57256
position indicator with freq. data transmission for distance meas. *(Russian)* 77−65019
profilometers 252 and 283, surface roughness parameters meas. 80−22329

indicators continued
quadrature, current and voltage, errors components determination 77−74442
recorders, one, two, three or four channel indicating types 77−18007
resistance meas., of quartz resonator, high-accuracy bridge instrument 77−10056
respiratory test performance indicator for subject motivation 79−57797
strain indicator, for semiconductor strain gauges 77−71313
surface flatness meas., moire angular readout device 79−93209
surface meas. instrument, modular *(German)* 80−57283
surface roughness meas., hand-held instrument with in-built data processor *(German)* 80−57255
thermogravimetric automatic temperature indicator 78−86257
thickness meter, eddy-current for thermal insulation meas. 80−73316
time interval meter, broadband, with digital display 80−31729
TTF-chloranil visual pressure or temperature indicator 80−87443
whistle, for He, N_2 or air presence indication, at low temperatures *(Czech)* 77−61069
Be crystal indicator, single, for high magnetic field measurements 79−63280

indium
see also nuclei with .....
$^2P_{3/2}$, at. quadrupole shielding factor 79−10222
acoustic emission characts. of twinning, nondestructive testing evaluation 77−4873
acousto-optical modulator coupling layer, freq. characts. 77−62069
additives to MnZn ferrites, effect on X-ray spectra *(Ukrainian)* 79−52046
adsorption of H_2 and O_2, surface reaction, thermal desorption and FEM obs. 79−52774
adsorption of O_2, CO, CO_2, and water, AES study 79−82451
adsorption on GaAs (110), UPS and EELS study, tight-binding calcs. 80−49496
adsorption on W, field emission, FIM 77−16470
in air, trace amounts, extraction and neutron activation determ. 80−12045
alkali halide: In^+, charge transfer absorpt. band 79−73977
alkali halide:In^+, cryst. field effect on spectral characts. 77−24880
alkali halide:In, high press. studies of luminesc. phenomena 79−43017
amorphization by ion implantation 78−52135
atom, 451.1 nm transition, HFS and ^{113}In-^{115}In isotope shift 78−82674
atom, absorption spectra, 320 to 1000 Å, inter-subshell correls. 4d spectrum 77−10617
atom, and isoelectronic ions, excited-state energy level k-ordering, l-patterns 77−88406
atom, electron affinity, meas. by dissoc. ionisation of InBr, InI *(French)* 80−63849
atom, electron impact excitation cross sections 79−54972
atom, excited state lifetime, delayed coincidence meas. 77−3315
atom, GTO basis sets, Hartree-Fock-Roothaan calcs. 79−97973
atom, HF oscillator strength calculations, relativistic, $np^2P_{1/2,3/2} \rightarrow (n+1)^2S_{1/2}$ and $np^2P_{1/2,3/2} \rightarrow nd^2D_{3/2,5/2}$ transitions 79−89609
atom, high-resolution laser spectroscopy of at. beam *(Dutch)* 79−50166
atom, integral K-shell Compton scattering, cross-section, for 1250 keV photons 78−90128
atom, $K\beta_3/K\beta_1$ and $K\beta_2/K\beta_1$ relative intensities 77−75088
atom, $K\beta/K\alpha$ rel. intensity obs. 80−32665
atom, K-fluorescence yield determ. from K-Auger electron emission rates 80−95569
atom, K-shell ionis. by electron impact, cross-sections, 300-600 keV 78−29853
atom, K-shell X-ray spectra $K\beta_2/K\beta_1$ determ. 77−23456
atom, Lα X-ray fluoresc. spectra, natural linewidth meas. 79−85934
atom, L X-ray yields from double-vacancy states 79−49977
atom, lowest S-state lifetime meas. 77−65436
atom, photoionisation cross section calc. for $4d^{10}$ subshell in RPA with exchange 77−23479
atom, quadrupole antishielding factors, Hartree-Fock perturbation theory 78−62723
atom, s^2p-$sp(^3P)np$ transitions, absorpt. spectra in 100-150 nm region 80−87067
atom, two-photon laser spectroscopy 79−6925
atom, XPS and XES, dynamical effects 80−52924
atom in metal-halide arc, laser Raman scatt. determ. of local density 77−11424
atomic electron impact excitation cross sections calc. *(Russian)* 78−55240
atomic fluorescence, intensity profile in acetylene-air flame 77−52680
atomic gas, Raman transitions, active reson. spectroscopy 77−27003
atomic oscillator strengths and radiative lifetimes 79−54811
atomic-transition lasers based on two-photon dissociation of metal-triiodide vapors 80−23679
atoms, laser saturation broadening in flames, fluoresc. excitation profile obs. 80−95568
atoms, VUV photoelectron spectra, pseudo-atomic beam technique 80−58225
atoms and ions, regularities within Stark widths of reson. lines 78−78662
Auger electron spectra, solid state effects 80−20739
chemisorption of O_2, XPS and static SIM spectral study 80−80055
coating on steel for watch part finishing, ion plating *(French)* 78−23879
concentration in a.c. arc, during interruption, time depend. *(Russian)* 78−22597
conducting flat plate, electrostatic pot. distrib. transverse magnetoresistance, electrode effects 78−60108
conduction-electron elec. field gradient, probe valence effects 78−47749
contact charge density, press. depend., trends for Ag-Te 78−39077
core level binding energies 80−71564
core level XPS energy loss study, angle and energy dependence 78−23582
crystal defects, study with muon probes 78−47314
desorption of Ba, conc. depend. of kinetic characts. of thermal desorption 78−2377
desorption of H from (110), thermal desorption mass spectrometry, order plots 80−44409
determ., by flame spectroscopy, absorpt. and emission, analogue data processing system 77−36804

indium continued
determination, by at. fluoresc. anal. with pulsed dye laser excitation *(Russian)* 78−35774
determination, in Italian chondritic meteorites, by destructive neutron activation anal. 78−12172
determination, in Sn or Cd by neutron activation analysis, substoichiometric method 78−76954
diamond:^{111}In, ion implanted, intrinsic limitations of doping 80−34019
diffusion, in Ni, temp. depend. *(Russian)* 78−75880
diffusion coefficient of Pb, RF size effect meas. *(Russian)* 78−91717
diffusion in GaSb, 520 to 712°C 80−79995
diffusion in Ge single cryst., effects of ultrasound 77−69119
diffusion in liquid Cu *(Japanese)* 78−10204
diffusion in Pb-Au (2.5 wt.%) film 78−22899
discontinuous film, DC resist. in normal and supercond. states 79−56357
discontinuous film, thermal hysteresis of phase transitions and mechanism of crystallisation 77−89679
dislocation dynamic props., investigation by impact loading *(Russian)* 78−85069
dislocation obs. by X-ray topography *(French)* 79−46661
divided superconducting thin film, superheating and supercooling field resistive meas. *(French)* 80−44751
double beam photoemission study of electronic struct. 79−83098
elastic constants, from room temp. to MP, US pulse echo meas. 77−24342
electric field gradient, magnitude and sign 77−80755
electric field gradient at nucleus calc. 78−39079
electric field gradients of recoil-implanted ^{19}F via ^{9}Be(^{12}C, np)^{19}F 77−8471
electrical resistivity measurement by eddy current decay method *(Korean)* 80−27275
electrode, annealing, effect on elec. resist. of metallic thin film 80−80416
electrodeposition, review 79−83144
electrodeposition from acid sulphate solns., electrode reactions 78−88436
electrodeposition on Si from glycerine soln., rapid method 77−32534
electrodiffusive conc. of impurities for analysis 78−22752
electron density at nucleus, press. depend., Hartree SCF calcs. 78−56411
electron MFP, conduction electrons injected from ferromag. 79−15135
electron scattering rates, RF size effect meas. under multiple-turn conditions 78−14654
Eliashberg gap equation, approx. BCS-like soln. 77−1513
enthalpy of fusion measured by adiabatic calorimetry 80−37037
epitaxial growth, cluster mobilities, in-situ electron microscopes obs. 80−15407
epitaxial layer, growth and desorption of W tips, high field microscopy obs. 79−69380
epitaxial layer on imperfect FEM/FIM W emitter 78−60037
face centred tetragonal, total cryst. energy with electronic screening effect, struct. stability 77−15345
Fermi surface dimensions, ab initio KKRZ calc. 77−89686
Fermi surface dimensions, RF size effect meas., KKRZ calc. 77−89687
fibres, supercond. transition at 6K *(Russian)* 77−80868
field evaporation patterns, multilayer 77−59675
film, $\sqrt{3}$ and $\sqrt{31}$ submonolayer superstructures on Si (111) isothermal desorption, RHEED meas. 79−86992
film, current-induced resistive state, fluctuations in flux nucleation process 79−38252
film, damping and vel. of longit. elastic waves at 9.4 GHz 80−10596
film, embedded with He particles, superconductor ion implantation study of inhomogeneities 78−52181
film, evaporated, resist., Hall effect and light transmittance, use as semitransparent electrode 77−39966
film, flux nucleation meas. in current induced resistive state 78−27002
film, freshly deposited, 77K, refl., annealing effect, thickness depend. 77−16413
film, friction and fear in ultrahigh vacuum, effects of speed, film thickness and substrate surface roughness 79−20202
film, growth by vacuum deposition, impurity presence, effect *(Hungarian)* 80−7495
film, MBE deposited, struct. by RHEED obs. 79−82491
film, oxidation, XPS excited by Zr Mζ radiation 80−40236
film, oxidized polycrystalline, spectra obtained from combined XPES and SIMS investigation of surface 80−52377
film, polycrystalline, optical transitions from d core states 77−85827
film, RF plasma oxidised, surface analysis using ESCA 80−50742
film, superconducting, He ion implantation effects on parallel crit. field, vortex state *(Russian)* 77−69459
film, transversal magnetoresist. meas. 77−72925
film, ultrathin on PbTe and Te, prep. and characterisation 77−7995
film, vac. deposited, influence of ion bombardment during condensation 79−82483
film, vacuum deposited, growth conditions effect on elec., optical, and structural props. 79−78215
film, vapour deposited on polymer, ageing, adhesion, elec. cond., electrochem. pot. *(Russian)* 79−33362
film, vol. plasmon dispersion and damping, electron energy loss spectra 79−7797
film cathodes, arc spot theory 77−39495
film growth on C, conductance meas. 79−82495
film on Au, ultrathin, quantum size effect *(French)* 77−20466
fine particles, prep. by gas evaporation technique, crystal habit 77−52239
foil, neutron activation cross sections meas. for generalised intermittent irradiation, fusion machines appl. 78−58283
gasification by atomic F, high temp. kinetics 78−53019
Gruneisen parameter, behaviour at high press. 78−83899
Hall field, reversal, 6-280K 78−72135
heat capacity and enthalpy of fusion, 300-1000K 79−14939
heat pipe meas. of corrosion and vapour press. 80−23878
helicon resonance acoustic satellites, flexural acoustic wave spectrum *(Russian)* 80−2415
immunology slide, darkening, Mie scatt., Maxwell Garnett theory 77−9315
intermediate state, dynamic, cooling effect *(Russian)* 78−26998
intermediate state, single cryst., helicon dispersion law and damping *(Russian)* 77−12066
intermediate state structure, hydrodynamic flow observation 78−43530
ion, HF calc. for ground and excited states, appl. to impurity centres 77−72835

indium continued
ion source using surface ionisation process 80−68999
island film, melting and crystn. kinetics, dark field electron microscopy 79−11026
isotope shift and HFS, isotope effects, UV spectra obs. 80−42973
J_1J_2 transition from LS, revised assignments for $d^9s^2p^2$, $d^9s^2p^3$ 79−45630
L shell prod. cross section of Zr, Mo, Ag, Cd and In for 75 to 150 keV p and e excitation 79−47552
lambda-tight In rings, simple demountable device for fixing 77−30160
laser, photodissoc. of InI, 451 nm 77−14698
lattice dynamics, pseudopot. computation *(Russian)* 80−92617
linear magnetoresistance increase by artificial voids 79−60799
liquid, contact angle with Nb and Zr substrates 79−77864
liquid, diffusion coeff. determ. of P, mathematical model, numerical method 79−23754
liquid, direct pair correl. function 78−38613
liquid, electrodiffusion conc. of impurities 80−54414
liquid, interatomic interaction potential, rel. to structure factor *(Russian)* 79−69006
liquid, isothermal compressibility, harmonic pot. model calc. 79−14870
liquid, nucl. quadrupole relaxation, Sternheimer antishielding and fluctuating elec. field gradients 77−55726
liquid, nuclear quadrupole relax. rate for ^{115}In, 170-650°C 77−36151
liquid, O_2 activity from electrochemical meas. 80−104123
liquid, PAC of ^{111}Cd 77−4584
liquid, pure, surface tension meas. *(German)* 77−35799
liquid, resist. and thermo-electric power using corrected parameters of Shaw model 79−19566
liquid, small-ang. X-ray scatt., at. microgrouping depend. *(Russian)* 78−14271
liquid, solubility and activity of O 77−43331
liquid, spreading kinetics on Cu surface 80−10742
liquid, struct. factor, Percus-Yevick equation perturb. treatment, square-well pot. approx. 78−75530
liquid, surface tension, low-temp. H_2 plasma influence, elec. double layer form. 79−33160
liquid, thermal conductivity meas. in Spacelab, measuring cell design and testing *(German)* 80−57303
liquid, thermal props. at high temp. 80−75536
liquid, thermoelectric power, pseudopotential calc. 80−59959
Madelung energy, stability of f.c.t. lattice 77−1097
magnetic breakdown exam., magnetoresist. meas. 78−6351
magnetic ground state props., simple one-electron theory 77−63063
magnetothermopower, phonon drag 79−69496
magnetothermopower giant oscills., mag. breakdown 77−8075
many-body effects, role of density of states 77−15777
melt, adhesive props. on Ti and graphite, 300 to 1200K *(Russian)* 77−15663
melting curve, effect by asymmetrical friction in piston-cylinder device 80−86292
metal cluster generator for gas-phase electron diffr., variation of microcryst. with size 78−63645
mixed state, two-dimensional effect study, destruction current *(Russian)* 80−93054
monolayers on W field ion image qualities and work function 78−35272
muon quadrupolar interaction expansion of crystal lattice *(Russian)* 79−15388
Nernst-Ettingshausen effect in solid and liq. states *(Russian)* 78−6353
neutron radiographic film imaging systems, MTFs and resolution capabilities 80−66758
nonequilibrium superconductivity in microwave field 79−42695
normal atom conc. determ. by resonance line broadening with Hg press. 80−43883
oxidation and vaporisation of volatile oxides, gravimetric exam. comparision with losses due to vacuum annealing *(Russian)* 79−57136
particles, grown in ultra-high vac. on KCl substrates, struct. and orientation 80−10814
photoelectric cross sections at 52.4, 60, 72.2 and 84.4 keV 80−69187
photoemission, transition from ordered solid to disordered liquid 80−45217
photoionisation cross section of d-core level synchrotron radiation study of spin-orbit branching ratio 79−74057
polarographic determination *(Japanese)* 77−77852
porous glass:In, effect of press. on transition temp. 80−97027
positron annihilation, 4.2-500K, Doppler broadening meas. 78−43957
positron annihilation, Fermi momentum and core electron contribution 77−81173
positron annihilation, vacancy form. vol. 78−15245
positron annihilation line Doppler broadening, self-trapping and vacancy form. 77−40298
positron annihilation lineshape meas., 74 to 430K 77−36308
positron annihilation rates, electron-electron and electron-positron correl. effects 78−76548
powders, uncoated and Cu-coated, fluctuation diamag. susceptibility above T_c 79−78309
pressure-mode soft-metal vacuum seal, for glass and ceramics 80−17952
quadrupole interaction of ^{69}Ge, TDPAD expts. 78−48089
quadrupole interactions, nuclear quadrupole alignment of ^{114}In^m 78−48090
reactive sputtering in Ar-N_2, N_2-O_2 discharges, mechanism, model 80−89109
reactive sputtering in DC triode config. 78−23618
recoil implanted ^{111}In impurities in Ag, interaction with radiation damage, TDPAC meas. 79−11362
recrystallisation of films prep. by vacuum evap. 79−4488
reflective coatings, refr. index, UV polariser mirror coating appl. *(Russian)* 77−34928
relativistic energy bands, density of states, and optical spectra, KKRZ calc. 79−51478
RF size effect signals, anomalous behaviour 79−4502
Si:In growth by Czochralski crystal pulling, characterisation for extrinsic IR detectors, focal-plane arrays 80−76168
size effect in metallic sandwiches 79−73604
slip and twinning relns. *(Russian)* 77−65982
solder for GaAlAs DH laser, deterioration and Au diffusion in In 80−33019
solder joints, thermal conductance at low temps. 77−30150
solubility in GeTe and SnTe, and thermo-EMF of ternary cpds. 78−43124
solubility in SnO_2 cryst. grown from Sn-In melt 77−11697

indium continued
sphalerites, in-determ. by nondestructive neutron activation anal. 79−87929
sputtering in Ar-N_2 discharge, mechanism, optical spectra study 80−89107
sputtering in N_2-O_2 discharge, mechanism, optical spectra study 80−89108
submonolayer growth on Si(111)7 surface, superstruct. 79−77930
supercond. crit. RF mag. field, rel. to superheating 78−2632
superconducting, expt. study of thermoelectricity 80−60138
superconducting, ideal superheating and supercooling limits 77−4465
superconducting, intermediate state, thermoelec. effects 79−65620
superconducting, thermoelec. transport effect 78−39257
superconducting bridge of large cross-section, Josephson effect, flux tube nucleation 77−36028
superconducting crit. temp., functional derivative with electronic density of states, Eliashberg eqns. 79−56368
superconducting critical temp., shell model for clad particles *(Chinese)* 79−69623
superconducting energy gap and phonon frequencies under press., tunnelling meas. 77−32112
superconducting film, crit. current hysteresis prod. by electron overheating 79−56449
superconducting film, Josephson arrays, proximity effect junctions 80−84553
superconducting film, metastable current states, mean free path variation *(Russian)* 80−2538
superconducting film, resistive transitions scaling behaviour 79−15248
superconducting film with dirty type II props., flux flow resistivity 77−51859
superconducting films, metastable states, supercooling fields 80−97031
superconducting films, sp. ht. discontinuity and transition temp. meas. 79−60969
superconducting films, thick, phonon damping of virtual levels 79−4626
superconducting intermediate state, doping effect on US attenuation 80−2522
superconducting microbridge, voltage locking and other interactions 80−39720
superconducting microbridges, non-equilibrium phenomena 79−56410
superconducting microbridges and arrays, I-V characts. temp. depend., Josephson radiation 79−28459
superconducting microbridges and tunnel junctions, half-harmonic generation at RF induced steps 79−56439
superconducting parameters, stress depend. 77−12045
superconducting thin film, crit. temp. enhancement *(Russian)* 80−93021
superconducting transition temp., electron-phonon mass enhancement, pseudopot. calcs. 78−2604
superconducting transition temp. from Eliashberg eqns. 79−51709
superconducting-normal interface, boundary resist. 80−50006
superconductive fixed points for temperatures above 0.5K 79−63221
superconductive penetration depth field depend. meas. 77−4464
superconductivity, Lifshits transition, electron-phonon interaction 80−29502
superconductivity, stimulation and enhancement by external micropower irradiation *(Russian)* 78−95394
superconductivity destruction singularities, intermediate state, hysteresis *(Russian)* 80−80460
superconductor, destruction in high amplitude LF varying field *(Russian)* 78−26999
superconductor, internal friction hysteresis *(Russian)* 77−36023
surface, (111), electron beam induced desorption and dissociation of chemisorbed CO 78−56043
surface, impurity precipitation and resolution at melting point 78−14553
surface, isotope effects in ion-scattering double spectroscopy curves for He^+ 77−59658
surface, X-ray prod. by 5 MeV/amu deuterons (oxygen ions), projectile Z depend. 80−42982
surface analysis, quantitative, comparison of XPS results with model 78−40091
surface coating on W field emitter, stability 77−12500
surface ionisation meas. after ion sputtering *(French)* 80−27374
surface layer of Ge, heterodiffusion due to H atom surface recombination stimulation *(Russian)* 80−59726
surface plasmon dispersion, high-energy electron loss spectroscopy obs. 77−20390
surface structure, (111) face, LEED 77−85040
surface superconducting layer in high amplitude LF EM field *(Russian)* 79−78261
thermal cond. in solid and liq. phases, Wiedemann-Franz law 80−39554
thin films, elec. props. effect of thickness and temp. 80−44742
transducer bonding material investigations, US delay lines *(Japanese)* 80−79097
transverse magnetothermoelec. props. 78−47768
twin boundary movement by creep 80−24460
twin layer broadening dynamics, in single crysts. 79−65098
two stage nuclear demagnetization experiments 79−65644
type I superconductor, thermoelec. power in intermediate state 78−34935
ultrasonic absorpt., intermediate state 77−72942
ultrathin metallic filaments, appearance of dielec. instability, coexistence with supercond. 80−103784
US absorption and dispersion, lineshape studies of quantum oscills., anomalous behaviour 78−63966
US attenuation in supercond. and normal state in transverse mag. field and zero field 80−54836
US velocity dispersion in external mag. field 80−20446
US wave polarisation plane and ellipticity rot. in mag. field *(Russian)* 79−15335
vacancy formation and activation volume, macroscopic model 80−54221
vacancy size effect, surface energy in small particles and bulk specimens 80−75223
vacuum seal fabrication by prepressing 80−101800
vapour pressure over $In+MgIn_2O_4+MgO$ mixture, 1095-1350K 78−91433
volume diffusion in Ni, activation energies, expt. and by Le Claire method *(Russian)* 79−99369
whisker, current carrying, breakdown of supercond. 80−60133
whisker, supercond. crit. temp., stress depend. 77−39988
wire, linear magnetoresist., effect of voids 78−51974

indium continued
X-ray cross sections, L-shell, proton induced, 1 to 3 MeV range 79−1799
XPS, outer core of level linewidths 77−44118
XPS and $M_{4,5}N_{4,5}N_{4,5}$ Auger spectra 79−61472
n-ZnSe:In, highly compensated, freq. depend. of cond. 79−99548
Ag/In/Ge ohmic contact to GaAs, solid phase epitaxy formation 79−60658
Ag-In multilayers, vapour quenched, supercond. transition temp. 80−20346
Ag-In thin film couple, room temp. interactions 80−2220
Al:^{111}In, electron irrad., defect trapping at impurities 78−55892
Al-In multicomponent binding layers, acoustic light modulator 80−87546
Al-Sb_2O_3-In films, negative resistance characts. 80−11103
Al|chlorophyll-a|Hg/In, sandwich cell, photovoltaic, rectifying and tunnelling effects 79−1628
As_2Se_3:In, amorphous, photoluminesc. fatigue, metallic additive effect 79−61434
a-As_2Se_3:In, doped film, photoluminescence intensity and lineshape study 80−50448
Au/In film structure, interdiffusion at room temp. 77−39703
Au/In proximity effect bridges, finite size array 79−78270
Au/In proximity effect bridges, square arrays, transition temps. 80−84557
Au-ZnO-In metal-semicond. diode, electrolum. spectra 79−99948
$BaNi_2M_xFe_{16-x}O_{27}$, effect of $M=Sc^{3+}$ or In^{3+} on props. 77−47978
Cd $CdCr_2Se_4$:In, elec. props., vac. heat treatment effect 80−15518
$CdCr_2S_4$:In, resist. and magnetoresist. meas., effect of donor impurities 79−19608
$CdCr_2S_4$:In, single cryst. prep. and elec. props. 79−38727
$CdCr_2Se_4$:In, elec. cond., annealing effect 79−87102
$CdCr_2Se_4$:In, elec. resist. and magnetoresist., 2 to 200K 80−96876
n-$CdCr_2Se_4$:In, electrical props., 93-168K 80−49713
$CdCr_2Se_4$:In, influence of Se-deficiency on props. 78−30921
$CdCr_2Se_4$:In, magnetic microregions caused by s-d exchange 77−77050
$CdCr_2Se_4$:In, photoconductivity, photomagnetoresistance near Curie point *(Russian)* 80−100485
$CdCr_2Se_4$:In, temp. driven metal-semiconductor transition, temp. and mag. field depend. *(Russian)* 78−88003
$CdCr_2Se_4$:In , impurity band, photocond. spectral depend. 78−19088
CdF_2:In, evidence for strong impurity-lattice coupling 80−6775
CdF_2:In, shallow versus deep donors 77−85176
$CdGa_2S_4$:In, photoluminesc. and photocond. meas. 78−60159
CdGeP$_2$:In, photolum. spectra and kinetic coeffs. 79−19927
CdGeP$_2$:In, polarisation of recombination radiation 78−19562
CdGeP$_2$:In based surface barrier diode, photosensitivity 79−33330
$Cd_xHg_{1-x}Te$:In, solid soln., defect struct. model, Hg self-diffusion coeff. 79−95213
CdS film, high cond., high transmittance, growth by evaporation method, and characterisation 77−77386
CdS vacuum evaporated film photoconductivity and In doping effects *(Japanese)* 79−87174
CdS:Cu, In, Ga, spray deposited film, struct., X-ray obs. 78−71713
CdS:In, cathodolum. on diffusion front 77−32447
n-CdS:In, containing excess Cd, effects of In on elec. props. 79−56217
CdS:In, Cu- or defect-compensated, optical ageing rel. to storage cond. 78−84247
CdS:In, diffusion of In, 729-1411K 78−22895
CdS:In, impurity resist., Matsubara-Toyozawa theory extension 80−80264
CdS:In, Photoluminesc., conc. quenching mechanism 80−97336
CdS:In, spin flip Raman scatt., electron dynamics 78−80342
CdS:In, two-photon absorpt., impurity effects 77−16353
CdS:In film, flash evaporated, prep. and elec. props. 80−20792
CdS:In films, vacuum deposited, growth, elec. and optical props. 79−51460
CdS:In whiskers, prep. by vapour deposition 78−75969
CdS-In, photosensitive granular superconductor 79−78246
CdS_xSe_{1-x} sputtered film contact, props. *(Russian)* 79−42642
CdS_xSe_{1-x}:In film, flash evaporated, prep. and elec. props. 80−20792
CdSb:In, p-n junction formation by laser radiation 80−96983
CdSe:Ag, In, cryst., photocurrent and electroreflection, 77 to 300K *(Russian)* 78−23136
CdSe:In, epitaxial layers, synthesis and elec. props. 77−47909
CdSe:In, photoluminesc. props. near fund. absorpt. edge, impurity conc. effects 79−52003
$CdSe_yTe_{1-y}$ sputtered film contact, props. *(Russian)* 79−42642
CdTe:In, electron-hole liq. form., luminesc. spectra 80−10884
CdTe:In, lightly- and heavily-doped, cathodoluminesc., temp., injection level and freq. depend. 78−52584
CdTe:In, photoconductivity exam. and IR quenching 79−11181
CdTe:In, photoelectronic investig. of trap depths, TSC and SCL cond. 77−39893
CdTe:In, shift optical absorpt. edge with temp. and doping level 79−8165
CdTe:In precipitation and out-diffusion of solute during cooling 80−100840
CdTe:P,In, IR absorpt. investig. of localised vibr. modes of impurity centres 77−52136
CdTe-In system, equilib. phase diagram and liq. phase epitaxial growth of CdTe from In soln. *(Japanese)* 80−71634
$Cd_{1-x}Zn_xS$:In, film, technical data, for low cost solar cell 79−48127
Cu:In, He, lattice defect struct., PAC meas. 80−70190
Cu-In solid/liquid interface, laws governing diffusive interaction *(Russian)* 78−95156
Cu-In thin film couples, room temperature interactions 80−96699
α-Fe_2O_3:In^{3+}, substitution effect on Morin transition, neutron diffr. study 80−44827
GaAs:$^{119}In^+$, Mossbauer study of resulting ^{119}Sn impurity-defect complex 80−59486
GaN-In contact, using GaN made by oxidation and subsequent nitridation of GaAs, I-V characts. 77−20436
n-GaP:In, LPE from In solvent, dislocation density reduction by doping 78−18919
GaP-In LPE layers, carrier diffusion lengths and escape probabilities optical absorpt. and photoemission meas. 79−87559
Ge:In, impurity characterisation from thermal carrier meas. 80−65595
Ge:In, kinetics of strain-confined large electron-hole drop and its clinging exciton system 80−75508
Ge:In, magneto-optical transitions between discrete levels of In acceptor, far-IR obs., 4.2K 78−2890

indium continued
Ge:In, resonant phonon interaction with localised acceptor levels 80−6784
Ge:In, shallow acceptor ground state, thermal cond. meas. 77−43540
Ge:In film, electronic props. 78−84330
Ge:Sb,In, lightly doped semicond., low temp., phonon cond., electron-phonon scatt. 79−60456
GeO_2:In^{3+}, trapped-hole centres, ESR meas. 79−77597
$Hg_{1-x}Cd_xTe$-In contact, diffusion of In 80−103520
HgSe:In, enrichment of doping substances at pseudo phase boundaries *(German)* 80−29036
HgTe:In, enrichment of doping substances at pseudo phase boundaries *(German)* 80−29036
^{127}I nucleus, resonance signals observed at liquid N_2 temp. using UHF NQR spectrometer 80−13114
In, elec. field gradient at ^{111}Cd, effects of high press., TDPAC meas. 80−25266
In I, $6^2S_{1/2}$ state lifetime meas. by Hanle effect method 78−90097
In I, radiative lifetimes, calcs. and beam-foil spectra 77−75223
In I, relativistic and cancellation effects in line strength ratios 78−82689
In I, Rydberg series, disctete levels and continua of finite bandwidth 78−74603
In V, spectrum, levels in $4d^8 6s$ and $4d^8 5d$ configs. 78−62748
In V fifth spectrum, $4d^8 5s$ and $4d^8 5p$ configurations, UV spectra (270 to 2400 Å) 78−33456
In^-, photodetachment cross-sections, crossed beam meas. *(German)* 77−42298
In^{2+}, emission spectrum, 340 to 6500 Å, ionisation pot. and dipole polarisability 78−78654
In:^{67}Ge, elec. quadrupole interaction temp. depend., PAC meas. 79−42877
In:Fe, impurity recoilless fraction calc. from mean square displacement 78−2216
In:Sn, phonon spectrum, electron-phonon interaction *(Russian)* 78−18722
In/(Zn-)phthalocyanine/Au, photovoltaic effects, illuminated thin-film cell props. 79−4605
In/(Zn-)phthalocyanine/Au, photovoltaic effects, dark elec. props. of rectifying cells 79−4604
In/Au-Ge ohmic contact to GaAs, solid phase epitaxy formation 79−60658
In-$Cd_{0.175}Hg_{0.825}Te$ contacts, photo-effect in the 77-300K range, barrier height estimation 80−107850
In-CdS ohmic contacts, by electrolytic deposition 77−8194
In-CdS-In Josephson junction, exhibiting nonuniform max. current distrib. self-resonant modes 78−56263
In-CdS-In structure, volt-ampere characts., carrier tunnelling emission *(Russian)* 80−49914
In-CdS-In(Te) contacts, ohmic nature, monitoring method 77−39935
In-CdTe contacts, photo-effect in the 77-300K range, barrier height estimation 80−107850
In-GaAs (110), Schottky barrier form., defect mechanism 80−49902
In-GaAs:Cu-In S-type diode, role of deep trapping levels in form. of current-volt. characts. 77−76948
In-GaAs:Cu-In structure, phototrigger effect 78−56238
In-GaAs(Ge)(Si) Schottky barrier interface, covalent bonding of metal atoms 77−20429
In-GaP, phase diag. cross section 77−48410
In-Ge:As, Schottky barrier tunnel junction, zero bias resistance, temp. depend. 78−72258
In-In_2O_3-Pb, Josephson tunnel junction fabrication for MM-wave detector 80−100427
In-In-P-GaP, liquidus surface obs. 78−22829
In-InCl, finely disperse system, supercond. props. 77−85376
In-Mn, relative activity ratios in natural UO_2 reactor fuel 78−58347
In-Pb-In thin film bridge, instability current enhancement in perpendicular mag. field 77−85396
In-PbTe contacts, fabrication and props. 80−60078
In-PbTe-In, semiconductor thin films, random noise measurements 80−15629
In-$SrTiO_{3-x}$ contacts, differential capacitance, elec. field depend. permittivity effect 80−54779
In-ZnO-Al metal-semicond. diode, electrolum. and photoluminesc. spectra 79−99948
In-ZnSe system residual conductivity, cathode quenching 79−7902
In-ZnSe:Al-In, MSM structure, mechanism of current flow *(Russian)* 79−78208
In-$ZnSiP_2$ Schottky diode, photovoltaic spectra 80−2423
In-ZnTe Schottky diodes, photocapacitance determ. of electron-hole recomb. *(French)* 79−47119
In+He^+, chem. effects on oscillatory cross sections in low energy scatt. 77−6889
In+Hg, spectral-line contours in high-press. arcs 79−3412
In+I^{16+}, double K-shell vacancies obs., K_α hypersatellite transitions, shift, shared double vacancies 79−72268
In+inert gas atom, diffuse series head lines, hyperfine components, broadening calcs. 80−32632
^{111}In, ^{113m}In, rapid method for labelling albumin microspheres 79−34669
^{111}In, human lymphocyte labelling 79−5354
^{111}In, human platelet labelling with ^{111}In 8-hydroxyquinoline 80−12259
^{111}In labeled transferrin, perturbed angular correls. study 79−39342
^{111}In labelled human platelets, dose obs. 80−94370
^{111}In, nucl. orientation coeffs., nucl. mag. moment 80−97168
^{111}In oxine, radiolabelled liposomes as metabolic and scanning tracers in mice 80−17073
^{111}In platelets, comparative deep-vein thrombosis imaging with ^{131}I fibrinogen 79−29607
^{111}In, tumour tracer accumulation, autoradiographic study, experimental infectious lesions 79−5348
^{115}In, $8P^2P_{3/2,1/2}$, HFS and lifetimes, fluoresc. decay and quantum beats, beam 80−32657
^{113m}In, liver scanning agents, comparison of ^{113m}In-phytate, ^{99m}Tc-phytate and ^{113m}In-colloid 79−96650
$^{115m,113m}In$, separation from ^{113}Sn and ^{115}Cd by chem. extraction 78−74783
^{113m}In-labelled transferrin, use in meas. of blood vols. in rat, rabbit 80−3878
^{113m}In-tripolyphosphate, new radiopharmaceutical for bone scanning 80−67247
^{114m}In, diffusion in Cu 80−65301
indium continued
^{114m}In, implanted in Fe and Co, nucl. orientation and NMR/ON meas. 79−47345
^{192}Ir orientated in Fe and Ni, nuclear mag. resonance 80−84661
KBr:In, type A long-wave luminesc., polarisation obs. 78−10944
KBr:In^+, B-band, optical absorpt. and mag. circular dichroism calcs. 80−29765
KBr:In^+, luminescence spectra, emission lifetimes, temperature dependence 79−78745
KBr:In^+, mag. circular dichroism meas. 79−42988
KBr:In^+, mag. circular dichroism spectra line shape, lattice mode calcs. 79−82957
KBr:In^+, optical absorption and MCD spectra, Gaussian quadrature calc. 80−7367
KCl:In, ESR of impurity centres, impurity optical absorpt. bands 80−29618
KCl:In, excitation in fund. absorpt. region, luminesc. and thermolum. 80−50433
KCl:In, injection electrolum., fields up to 10^4 V cm^{-1} 77−12445
KCl(Br)(I):In^+, Jahn-Teller split luminescence, high press. study 78−52565
KCl(Br)(I):In^+ phosphor, press. effects on triplet relaxed excited states, quadratic Jahn-Teller interaction 78−23510
KClIn, absolute quantum output of low-inertial energy transmission *(Russian)* 77−32429
KI:In, type A long-wave luminesc., polarisation obs. 78−10944
KI:In^+, luminesc. decay, excited state symm. and g-value 79−99922
KI:In^+, mag. circular dichroism meas. 79−42988
KI:In^+, magnetic circular dichroism of A- and B-absorption band region 77−12412
KI(Br):In, A-luminescence spectra and polarisation, Jahn-Teller minima 77−20914
LiF:In, optical absorption effects of ion implantation 80−70239
liquid, polyvalent, electrical resistivity by harmonic model potential 80−54668
MgF_2/In/MgF_2 struct., surface plasma wave optical excitation 79−91516
NaCl:In, ESR of impurity centres, impurity optical absorpt. bands 80−29618
Nb/In composite superconductor, transport props. 80−88658
Nb-Nb_2O_5-In Josephson junctions, props. of Nb_2O_5 thermally grown tunnel barriers 80−100568
Nb-Nb_xO_y-In Josephson junctions, preparation and props. *(Russian)* 79−91188
NbTi/In composite superconductor, transport props. 80−88658
NbTi/In granular composite, resistivity mag. field depend. 80−15654
NbTi-In granular supercond. composites, mag. field-induced dissipation 80−84545
Ni:In, He, lattice defect struct., PAC meas. 80−70190
Pb:In, type II superconducting film, penetration depth meas. 77−28285
Pb-CdS-In Josephson junction, light-sensitive, structural fluctuations *(Russian)* 78−56265
$Pb_{1-x}Sn_xGe$:In, press.-induced transition to gapless state, galvanomag. effects 78−19108
$Pb_{0.78}Sn_{0.22}Te$:In, transport phenomena, below 20K *(Russian)* 79−38074
$Pb_{0.78}Sn_{0.22}Te$:In epitaxial layers, dislocation density, Hall effect, conductivity, photoeffects 80−25024
$Pb_{0.8}Sn_{0.2}Te$:In, absorption spectra meas., 475-725K 77−4664
$Pb_{0.8}Sn_{0.2}Te$:In, implanted thin epitaxial films, laser annealing 79−65104
$Pb_{1-x}Sn_xTe$, In doping, donor impurity singularities, distrib. coeff. 77−80526
$Pb_{1-x}Sn_xTe$:In, carrier spectroscopic g-factors, magnetoresistance, temp. depend. 80−6705
$Pb_{1-x}Sn_xTe$:In, dielectric state, avalanche breakdown in strong elec. fields *(Russian)* 80−92901
$Pb_{1-x}Sn_xTe$:In, elec. props., dopant influence 79−51599
$Pb_{1-x}Sn_xTe$:In, energy spectrum under combined effect of mag. field and hydrostatic press. 79−65382
$Pb_{1-x}Sn_xTe$:In, energy spectra modifications due to comp. changes and press. appl. 80−10915
$Pb_{1-x}Sn_xTe$:In, Hall const. depend. on temp., autocompensation, band gap temp. depend. explanation 79−69527
$Pb_{1-x}Sn_xTe$:In, Hall effect and photoconductivity *(Russian)* 80−103720
$Pb_{1-x}Sn_xTe$:In, high temp. Fermi level position 79−90948
$Pb_{1-x}Sn_xTe$:In, impurity influence on photoluminescence at large excitation levels *(Russian)* 80−93384
$Pb_{1-x}Sn_xTe$:In, nonequilib. metallic state *(Russian)* 79−33300
$Pb_{1-x}Sn_xTe$:In, semiconductor-metal-semiconductor transitions under press. 80−34491
$Pb_{1-x}Sn_xTe$:In, solid solutions, impurity states in photoluminescence spectra *(Russian)* 80−97333
$Pb_{1-x}Sn_xTe$:In, tunnelling impurity self-localisation, anomalous props. nature *(Russian)* 80−59915
$Pb_{1-x}Sn_xTe$:In, with low carrier conc., transport phenomena 80−49783
$Pb_{1-x}Sn_xTe$:In epitaxial layers, growth, elec. props., and luminesc. 80−54542
$Pb_{1-x}Sn_xTe$:In film, anomalous elec. props. 78−10477
PbTe:In, absorption spectra meas., 475-725K 77−4664
PbTe:In, electron mobility, temp.-independent part, Hall effect and elec. cond. meas. 80−92914
PbTe:In, ion implanted, magneto-optical expts. *(German)* 79−28848
PbTe:In, mag. susceptibility, temp. depend., 4.2 to 200K 80−65773
PbTe:In based solid solutions, impurity states, elec. props. 79−87054
n-PbTe:In epitaxial films, elec. transport props. 80−75659
n-PbTe:In thermoelectric props., 300-750K 78−34851
PbTe:Na, In, high temp. Fermi level position 79−90948
p-PbTe-In, barrier props. 79−7898
$PbTe_{1-y}Se_y$:In, high temp. Fermi level position 79−90948
Pd-CdS-In, tunnel junction, light induced DC Josephson current 79−47204
Sb:^{111}Cd,In, elec. field gradient, TDPAC expts. 80−55002
Si (111)($\sqrt{31}\times\sqrt{31}$)R±9°-In struct., RHEED obs. 79−60612
Si:B,In, sharp line series in near-band-edge photolum. 80−16092
Si:In, absorpt. spectra, impurity excited state lines 80−108243
Si:In, acceptor levels, IR spectra 78−67972
Si:In, backward wave phonon spectroscopy 80−2357
Si:In, binding energy, excited state spectra, photolum., semi-empirical short range pot. 80−44534
Si:In, bound exciton photolum. obs. 78−95607
Si:In, bound-exciton absorption 78−56507

indium continued
Si:In, C, 0.111-eV acceptor level, X-level defect conc. from IR absorpt. and Hall meas. 79−51512
Si:In, capture cross section of excitons on neutral In impurities, photoluminesc. decay 78−6760
Si:In, clustering and precipitation, time-dependent perturbed ang. correlation meas. 80−65234
Si:In, dopant energy levels, Hall meas. interpretation 80−107736
Si:In, dopant solubility limit, laser irrad. effects 80−84295
Si:In, doping conc., meas. by Hall, C-V and junction breakdown methods 79−14824
Si:In, electron excited, recomb. radiation, high resolution investigation 78−15233
Si:In, electron irrad., Hall effect meas. 80−2401
Si:In, extrinsic detector material props. 77−89797
Si:In, gradient transport soln. growth, IR monitoring, 950-1300°C 79−100040
Si:In, implanted, laser annealing 79−52050
Si:In, incorporation of implanted impurities during amorphous layer regrowth 79−55761
Si:In, ion implantation and pulsed laser annealing, supersat. alloy form. 80−54267
Si:In, ion implanted, annealing behaviour, time differential PAC obs. 77−89455
p-Si:In, ion implanted, doping profiles from capacitance-voltage characts. 80−88203
Si:In, ion implanted film, elec. prop. impurity depend. 80−24467
Si:In, MIS structure, determ. of deep level parameters in surface layer of semiconductor 80−15612
Si:In, MOSFET device structure for characterising imperfection centres 79−73595
Si:In, mean square dynamic displacement of atoms, effect of electron-phonon interactions *(Russian)* 78−10145
Si:In, neutron irrad. to compensate for residual B, photocond., IR focal plane array 78−67727
Si:In, new acceptor level determ. from Hall effect and photocond. meas. 77−66136
Si:In, obs. of long lifetime lines in photolum. 79−47512
Si:In, photoelec. props. meas 77−89804
Si:In, photoluminesc., In acceptor excited level 79−47506
Si:In, surface characterised by negative electrochemical pot., electronic props. 80−44695
Si:In,P, photoinduced IR absorpt. and luminesc. 79−33828
Si:In amorphous films, EPR, elec. cond., and magnetoresist. 80−50160
Si:In extrinsic detectors, compensation of residual B by neutron transmutation 78−281
Si:In extrinsic detectors in IR imaging systems, focal plane temp. stability requirements 79−94324
Si:In extrinsic IR detectors with closely compensated residual impurities, model of responsivity temp. depend. 80−73453
Si:In extrinsic IR detector material with high responsivity compensated by neutron transmutation, float-zone growth 80−75597
Si:Se,In, diffusion of Se, solubility and ionization levels, Hall effect and photocond. meas. 79−42486
Si/In(-Cd), Si/Cd Schottky contacts, electrochemically deposited 80−88633
Si-In interface, electron energy loss spectra of Schottky barrier 77−48290
Si-In Schottky diode, X-ray effects on elec. props., irrad. induced diffusion 77−4439
Si-In Schottky diode, X-ray irradiated, radiation-accelerated diffusion of In in Si 78−26952
SnO_2:In, film, struct. and resist., impurity addition effect 77−20469
superconducting relaxation time determ. 77−55638
V-CdS-In Josephson structures, light-sensitive 79−99660
V-CdS-In preparation and behaviour obs. Josephson junctions 80−100559
(Zn, Cd, Hg)S:Cu,In, electroluminesc. temp. depend. 77−1732
(Zn,Cd,Hg)S:Cu,In, electroluminesc., brightness waves 77−59616
Zn:^{115}In, 828 keV state, elec. quadrupole interaction meas. 77−8484
$Zn_xCd_{1-x}S$:In, low resist. film for solar cell window 78−71200
$ZnCr_2Se_4$:In, magnetoresist. and elec. resist. above and below Neel temp. *(Russian)* 80−88576
ZnP_2:In optical absorpt. spectra in range 0.5 to 2.2 eV 80−66250
ZnS:In, polarisation of deep centre electroabsorpt., effect of random electric fields 77−48148
ZnS:In, recombination emission by optically detected magnetic resonance 80−66272
ZnS:In^{3+}, $Cu^{+}(Ag^{+})$, interimpurity luminesc. at high press. 78−19532
ZnSe:In, heavily compensated, galvanomag. props. and thermopower 79−51600
ZnSe:In, heavily compensated, negative magnetoresistance 79−91079
ZnSe:In, heavily doped, Hall effect and DC cond. expts., compensating acceptors 78−52013
ZnSe:In, heavily doped, impurity band cond., Hall coeff. and cond. expts. 78−72147
n-ZnSe:In, heavily doped, high field DC cond. 79−65490
ZnSe:In, highly compensated single crystals, thermally initiated current breakdown, current-voltage characts. 80−65579
ZnSe:In, Li, binding energy of excitons bound to donor-acceptor pairs, electron-phonon coupling 77−4689
ZnSe:In, melt growth, dopant partition coeffs. 79−14837
ZnSe:In, optical absorpt. spectrum, 0.4 to 0.7 μm 77−81136
ZnSe:In, single cryst., diffused, blue luminesc. 78−39584
ZnSe:In, single crysts., new vapour phase growth method, elec. cond. props. and photoluminesc. spectra 79−19982
ZnSe:In elec. transport props., effect of Zn-annealing, 300 to 77K 78−76075
ZnSe:In films, MBE growth, doping effect on photoluminesc. 80−10818
ZnTe:In, ion implanted and annealed, photoluminesc. meas. 78−15208
ZnTe:In, pure and doped, Zn vacancy energy levels, elec. and optical props. 79−4827
ZnTe:In, single cryst. film, MBE, quality obs. using photoluminesc. 77−77419

indium alloys
see also indium compounds
amalgam lamp, Hg vapour partial pressure meas. 78−67488
dilute, Nielsen-Taylor effect in thermopower meas. 77−66157
In-Cd-Sn, supercond. transition temp. and electronic props., Brillouin zone effect 79−56345

indium alloys continued
liquid, ^{117m}Sb nucl. spin relax., quadrupolar interaction 78−39437
liquid, $^{117}Sb^{m}$ nucl. quadrupole relax. rate, systematical trends 79−73849
liquid, concentration fluctuations, nucl. quadrupole spin relax. 78−91975
liquid amalgams mixing, excess entropy, vibr. contrib. *(Russian)* 79−51263
rare earth alloy, RIn_3, ^{111}Cd quadrupole coupling consts. and valence states, PAC meas. 77−48102
rare earth-Au-In, Fe_2P type phases 77−70033
superconducting transition temp. rel. to electronic struct. 77−80865
Wood's alloy, liq. enthalpy effects when solute is added 80−39314
Ag-^{112}In, dil., ^{112}In nucl. alignment, radiation damage, γ-ray spectra 78−19398
Ag-In, dil., elec. quadrupole interactions on ^{111}Cd probe nuclei, time differential PAC meas. 78−15066
Ag-In, dil., electron irrad., stage I_E recovery 77−39616
Ag-In, dil., interaction between recoil implanted impurities and lattice defects, TDPAC meas. 78−39467
Ag-In, dil., temp. depend. of elec. field gradient, impurity mass and conc. effects 78−48085
Ag-In, dil. alloys, single crystals, dynamic dislocation behaviour 77−4108
Ag-In, HCP ζ-phase, magnetic susceptibility 78−47946
Ag-In, liquid alloy, thermoelectric powder and magnetic susceptibility 77−8076
Ag-In, rapidly quenched from melt, stacking faults, TEM and X-ray diffr. meas. 77−59768
Ag-In, single cryst. elastic consts. 77−1164
Ag-In, temp. depend. of elec. field gradient, TDPAC meas. 77−32304
Ag-In, Zener relaxation, valency and dimensional effects *(Russian)* 78−19802
Ag-In alloy, α-phase, lattice sp. ht. calcs. 80−65246
Ag-In melt system, conc. depend. of component and impurity diffusion coeffs., radioactive isotope method *(Russian)* 80−107454
α-Ag-In solid solutions, lattice dynamics parameters *(Russian)* 80−96477
Ag-In-Ge alloyed contacts to GaAs 79−78174
Ag-In-Sn, internal oxidation, precipitation behaviour of oxide *(Japanese)* 80−66515
Ag-In-Sn, internal oxidation, solute element and O_2 behaviour *(Japanese)* 80−89479
Ag-Zn-Sn-In-Te, internally oxidised, oxide particle size control *(Japanese)* 80−89480
Al-Ga-In, liq. alloys, excess Gibbs functions 633 to 1173K 78−60655
Al-Ga-In system, thermodynamic anal. 79−60512
Al-Ga(In)(Sn), interpretation of metallic phase diagrams, entropy of mixing 79−42274
Al-In, dil., vacancy trapping and detrapping at ^{111}In, PAC spectra 78−39461
Al-In, enthalpy of mixing, 'const. vol. alloy' formulation 79−28111
Al-In, monotectic system, rapid cooling from melt, effect on struct. *(Russian)* 79−70053
Al-In, rapid quenching, struct. and decomp. 80−76244
Al-In (40, 70 wt.%), liq. phase immiscible system, solidification in microgravity 78−84770
Al-In alloy, dilute, electron irradiation, interstitial dislocation loop obs. 78−18681
Al-In alloys within miscibility gap, agglomeration in space environment 79−47672
Al-In emulsion, solidification mechanisms at zero gravity, review 78−88458
Al-insulator-$In_{1-x}Mg_x$ film tunnel junction, resistance zero-bias anomalies 80−107925
Au-Al-In solid soln., elastic strain energy depend. of supercond. T_c 79−38229
Au-Ga-In solid soln., elastic strain energy depend. of supercond. T_c 79−38229
Au-In, charge-transfer and valence-band behaviour using ^{197}Au Mossbauer and X-ray photoemission spectra 79−60695
Au-In, electrodeposited from acid cyanide electrolyte, exam. of wear and corrosion resistance 78−80482
Au-In, HCP ζ-phase, magnetic susceptibility 78−47946
Au-In, UPS exam. of valence bands 79−19511
Au-In liq. alloys, ΔG^E of mixing from ht. of melting and sp. ht. of cpds. 77−4920
Au-In-Pb, $AuIn_2$-In-Pb portion of phase diagram 77−32562
Au-Pb-In solder joints, layer growth, ageing 77−32764
AuIn-Pb pseudobinary system, DTA 78−23667
$AuIn_2$, core-level binding energy shifts and charge transfer 80−25268
$AuIn_2$, pulsed NMR expts, rel. to performance as nuclear refrigerant 79−61259
$AuIn_2$ superconductive device to provide reference temps. below 0.5K 79−63220
Au_2MnIn, Heusler alloy, ferromag., NMR meas. 78−76320
$Au_2(MnIn)_2$, Heusler alloy, magnetic order and coupling 79−38303
Bi-In, dilute, oxidation kinetics 80−25914
Bi-In, liq., Hall coeffs. 78−14711
$BiIn_2$, dHvA effect, Fermi surface determ., free-electron model 77−15744
Ca-In liquid alloy, thermodynamic exam. 78−75848
Cd-In diffusion into $Pb_{1-x}Sn_xTe$, changes in elec. props. 78−91348
Cd-In-Sb, liq. alloy, Cd thermodynamic activities, Gibbs free mixing enthalpy *(German)* 80−45279
Cd-In-Sb, liq. alloys, thermodynamic activity of Cd between 833 and 953K *(German)* 80−45278
(Ce, La)In_3, heat capacity and elec. resist. 80−71049
Ce-In, liquid, solubility and thermodynamic props. *(Russian)* 78−19717
Ce-In, phase equilibrium and cryst. struct. 80−66483
$CeAg_xIn_{1-x}$, cubic to tetragonal phase transform., conc. dependence by resist. meas. 78−2252
Ce(In, Sn)$_3$, heat capacity and elec. resist. 80−71049
Ce(In, Sn)$_3$, mag. susceptibility, temp. depend., intermediate valence 80−65779
$CeIn_3$, crystalline elec. field parameters, exchange and Coulomb contrib. 77−20278
$CeIn_3$, Kondo effect, mag. suscept. exam. 77−8270
$CeIn_3$, Kondo system, mag. susceptibility calc. in Anderson model 77−55661
$CeIn_3$, mag. struct., neutron diffr. study 80−80481
$CeIn_3$, magnetisation and sp. ht. 80−20418
$CeIn_3$, Neel temp., hydrostatic press. depend. 80−29549

indium alloys continued
$CeIn_{3-x}Sn_x$, conduction electrons role in valency fluctuations 78−47741
$CeIn_{3-x}Sn_x$ mixed valence system, low-temp. susceptibility, paramagnon study 80−97077
$CeIn_{3-x}Sn_x$, scaling behaviour near valence instability, mag. susceptibility and mag. transitions 80−25111
$CeIn_{3-y}Sn_y$, electrical resist. and thermal expansion meas., 1.5-300K 80−34400
$CoIn_3$, ordered phase, cryst. struct. determ. 78−2066
Cu-In, dil., point defect trapping after ion implantation, DPAC meas. 78−43728
β-Cu-In, directionally transformed eutectoid, morphology exam. by metallography *(German)* 78−92257
Cu-In, effect of alloying additions on electrical cond., and mech. strength 78−44233
Cu-In, electron work function, contact pot. difference meas. 78−80041
Cu-In, growth kinetics of discontinuous precipitation, third element effects 77−36511
Cu-In, lamellar eutectoids, calorimetric determ. of interfacial enthalpy 78−60668
Cu-In, liq., elec. cond., temp. and conc. depend., model interpret. and alloy struct. *(Russian)* 80−88528
Cu-In, liq., solubility and activity of O 77−43331
Cu-In, magnetic susceptibility, comp. and temp. depend., melting effects 78−52202
Cu-In, microconductors, cast, struct. and physical props. exam 78−44232
Cu-In, thermally cycled, effect on mech. props. and microstruct. 79−4987
Cu-In, undirectionally transformed, mechanical props. 78−48492
β-Cu-In, unidirectionally transformed eutectoid, lamellar microstructure, influence of grain boundaries on thermal stability 78−72795
Cu-In (20.15 at.%), eutectic systems, specific phase boundary enthalpy, calorimetric study *(German)* 79−29016
Cu-In alloy, thermodynamics, calorimetric exam. *(French)* 77−21105
Cu-In dilute, In^{114} impurity diffusion 79−65256
β-Cu-In eutectic, unidirectionally decomposed discontinuous coarsening reaction 78−27472
Cu-In eutectoid, coarsening at 829K 79−1885
Cu-In eutectoid, directional eutectoid decomposition growth, crystallography 80−29874
Cu-In liquid alloy, thermodynamic props., potentiometric exam. *(French)* 77−59126
Cu-In liquid alloys, heat of form meas. *(Korean)* 77−9116
Cu-Ti-Tin, wetting of Al_2O_3, alloying effects 80−107617
Cu_2MnIn, Heusler alloy, hyperfine field at ^{111}Cd, TDPAC meas. 78−43705
$Cu_{2.0}Mn_{0.94}In_{1.0}$, In-Heusler single crystal, elec. resist. 78−60107
$Cu_2MnIn_{1-x}Sn_x$ alloy, compositional SRO, hyperfine interactions 80−71065
$DyAg_{1-x}In_x$, elec. and Hall resist. 80−96844
$DyIn_3$, magnetisation 80−25106
Fe-In, dil., hyperfine field of In, clustering effect, nucl. orientation obs. 77−16188
Fe-In, superconducting Kondo alloys and alloys with strong electron-magnetic impurity interaction, EM absorpt. of light 80−39711
Ga-In, dil., elec. resist., temp. and impurity depend., deviation from Matthiessen's b-axis crystals 78−51970
Ga-In, liq., mag. susceptibility *(Russian)* 78−6513
Ga-In, liq., O diffusion coeff., thermodynamic activity and solubility 78−38860
Ga-In, liquid binary alloys, magnetic susceptibility *(Russian)* 77−24671
β′-Ga-In, metastable binary phase, X-ray diffr. determ. of cryst. struct. 80−1967
Ga-In (2 and 4 wt.%), binary, kinetic conditions for two phase zone form. *(Russian)* 77−66633
Ga-In eutectic system, diffusion coeff. depend. on composition *(Russian)* 80−59695
Ga-In liq. alloy, repetitive pulses electron emission 79−24416
Ga-In-Sn, thermal analysis, determination of liquidus and reactions 78−88446
GaIn, liq. alloys quad. relax. rates, 3-particle correls., ^{71}Ga and ^{115}Sn 77−12272
Gd-Ir, dil., hyperfine interaction of ^{193}Ir, Mossbauer effect meas. 78−52413
Gd-Ir, dil., mag. hyperfine field of ^{193}Ir, Mossbauer effect meas. 79−24242
$GdAg_{1-x}In_x$, elec. and Hall resist. 80−96844
$GdAg_{1-x}In_x$, magnetic transition temp., effect of hydrostatic press. 78−76244
$GdIn_3$, magnetisation 80−25106
Ge-In melts, short-range order, radial atomic distrib. functions 79−86673
Hg-In, dil. liq. amalgams, expanded, cond. at high temps. and press. 77−20287
Hg-In, liq., positron annihilation meas. 78−43955
Hg-In, liq., positron studies, trapping at solute-vacancy complexes 78−31271
Hg-In, liq. alloy, chem. diff. coeff. determ. 77−1249
Hg-In (3, 15, 30, 45 at.%) amalgam, viscosity meas. near melting point 80−70441
Hg-In (3 at.%), amalgam, thermodynamic and electron transport props. 79−23938
Hg-In-Bi, liquid alloy, elec. resist. *(Russian)* 79−51544
Hg-In-Zn, liquid alloys, thermodynamic props., 25 to 75°C *(German)* 77−73259
β-$Hg_{0.80}In_{0.20}$, cryst. struct. from powder patterns 79−51052
In-Ag, dil., TDPAC technique appl. to diffusion model 79−78589
In-Al(Ga) systems, thermodynamic anal. 79−60512
In-Bi, dil., supercond., ideal superheating and supercooling limits 77−4465
In-Bi, dil., supercond. penetration depth field depend. meas. 77−4464
In-Bi, liq., PAC of ^{111}Cd 77−4584
In-Bi, mixed state, pinning centre distrib. statistics, I-V characts. *(Russian)* 80−100571
In-Bi, single crystal, vacuum UV optical props. 77−1697
In-Bi, single spheres, supercond. props. 79−73617
In-Bi, small κ supercond., phase transitions higher than second order 80−88668
In-Bi, supercond. crit. RF mag. field, rel. to superheating 78−2632
indium alloys continued
In-Bi (2 at.%), supercond. film, thermal cond. in perpendicular mag. field 77−8229
In-Bi (2-33.3 at.%), phase diagram DTA, X-ray diffr. and supercond. T_c meas. 79−38795
In-Bi (22 at.%), directionally grown eutectic two phase superconductors, magnetisation behaviour 77−28293
In-Bi (2.5 at.%), supercond. foils, transport current effect on magnetisation 79−56379
In-Bi alloy system at high press. and temp. 78−92238
In-Cd, dil., elec. field gradient at Cd impurities, press. depend., TDPAC meas. 78−64302
In-Cd, elastic phase transition, US study 78−6919
In-Cd, high temp. deviation from Mattheissens rule 77−43560
In-Cd, shape memory *(Japanese)* 79−43243
In-Cd, soft mode, latent heats and entropies of fusion 79−46786
In-Cd alloy crystal, phenomenological study of FCC⇄FCT transform. *(Japanese)* 79−100140
In-Cd/p-InP contact evaluation 77−24619
In-Cr film, electronic thermal cond., 1.5 to 3K 77−47934
In-Cr films, supercond., sp. ht. discontinuity and transition temp. meas. 79−60969
In-Fe film, dil., supercond., Raman scatt. of light 79−73634
In-Ga, eutectic alloy, zero point determ. from uncharged surface pot. 77−90611
In-Ga, work function, electrochem. determ. rel. to Ga 77−44489
In-Ga alloy, electrode metal-solvent interaction rel. to elec. double layer struct., adsorpt. 78−61023
In-Ga liquid alloy, low-resistance ohmic contacts in ZnSe, LED fabrication appl. 80−70823
In-GaP, phase diag. cross section 77−48410
In-Ge film, random percolation, elec. resist. meas. 79−28418
In-Hg, liq., Knight shift of ^{115}In, temp. and conc. depend. 79−47343
In-Hg amalgam, EMF meas. of $In/InCl_3$/amalgam cell and thermodynamic quantities 79−33999
In-Hg amalgam, thermal and electric cond., temp.-conc. depend. 78−43349
In-Hg liquid alloy, activities meas. 77−86351
In-InCl, finely disperse system, supercond. props. 77−85376
In-Mg, ordered equiatomic, lattice specific heat meas., Debye temp., superconducting transition 80−54396
In-Mn, dil., film, ion implanted, supercond, and mag. props. 77−15987
In-Mn, dil., supercond. film, H_{c2} meas., mag. impurity effects, pair breaking theory 79−42708
In-Mn, dilute alloy, local excited states, electron tunnelling observation 80−34565
In-Mn, discontinuity in sp. ht. at supercond. transition 79−60971
In-Mn films, supercond., sp. ht. discontinuity and transition temp. meas. 79−60969
In-Ni(Bi), liq., spreading kinetics on Cu surface 80−10742
In-Pb, liquid alloy, thermodynamic activity determ. using Knudsen method *(German)* 79−34008
In-Pb, small κ supercond., phase transitions higher than second order 80−88668
In-Pb, thermal anal. solidus determ. 79−20030
In-Pb (7 at.%), supercond. cylinder, magnetisation change induced by current near upper crit. field 80−70890
In-Pb alloys, elastic consts. of three phases, acoustic mode softening 80−30006
In-Pb-Sn system, thermal anal. 80−35162
In-Sb, cryst. struct. after appl. of high press., supercond. transition temp. 80−70169
In-Sb, liq., mag. susceptibility, MP to 1000°C, anomalies due to electron-ion interaction 77−20546
In-Sb, metallic soln., association 78−15373
In-Sb, thermodynamic quantity meas. by quantitative thermal anal. of heating process 78−19730
In-Sb alloys, liq., spin relax. of ^{117}Sb and ^{115}Sn 77−16216
In-Sb liquid alloy, calorimetric investigation, rel. to association equilibrium *(German)* 77−16862
In-Sb liquid alloy, mixing enthalpy, temp. depend. *(German)* 80−84298
In-Sb(Sn), binary metallic melt, deviation from the Kopp law, specific heat *(Russian)* 80−39305
In-Sn, dil., intermediate state, doping effect on US attenuation 80−2522
In-Sn, phase diagram, and superconductivity of In_3Sn 79−38794
In-Sn, phonon spectra and superconductivity, single-particle electron-tunnelling expts. 77−40005
α-In-Sn, stress depend. of supercond. parameters 77−12045
In-Sn alloy, Lifshits transition, electron-phonon interaction 80−29502
In-Sn alloy crystals, phase changes and shape memory effect *(Japanese)* 80−108502
In-Sn film, supercond. transition temp. and crit. currents *(Russian)* 77−55632
In-Sn liquid alloy, 2-butanol vapour adsorption, effect on surface tension and surface comp. 79−14981
In-Sn-Sb, liquid state, structure of eutectic alloy 78−42890
In-Sn(Pb), liq., conc. and temp. depend. nucl. relax. rates meas. 78−19357
In-Sn(Pb)(Tl) whisker, supercond. crit. temp., stress depend. 77−39988
In-T alloys, relationship between struct. and thermodynamic props. *(German)* 78−91307
In-Te, elec. field gradient, at ^{111}Cd probes, temp. depend. 79−28643
In-Te, liq., atomic struct., X-ray diffr. meas. 79−41934
In-Te, liq., mag. susceptibility 77−51881
In-Te, liq., nucl. spin relax. of ^{117}Sb 77−52004
In-Te, molten thermodynamic props. determ. by EMF method 77−51504
In-Tl, BCC alloys, stability and elastic consts., US vel. 79−42133
In-Tl, crystallographic reversibility of martensitic transform. 78−6925
In-Tl, electrodeposition from aq. sulphate soln., X-ray struct. 78−84722
In-Tl, exam. of magnetic susceptibility in solid and liquid states, and X-ray data *(Russian)* 79−28503
In-Tl, first order displacive transformations, localized soft modes and US effects 79−73281
In-Tl, single crystal containing Li, X-ray study of FCC⇄FCT transform. *(Japanese)* 80−108435
In-Tl, small κ supercond., phase transitions higher than second order 80−88668
In-Tl, soft mode, latent heats and entropies of fusion 79−46786
In-Tl, supercond. transition in martensitic two phase region 77−72936
In-Tl alloy, FCC→FCT martensitic transformation, on cooling, enthalpy meas. and X-ray exam. 78−39773

indium alloys continued
In-Tl alloy, superconducting transition temp., phonon mode softening 79−1637
In-Tl liquid alloy, thermodynamic props. and struct. *(German)* 77−48400
In-Tl single crystal, phase transform. X-ray topographic study *(Japanese)* 78−31405
In-Zn, liq., Zn activity meas. by Knudsen torsion-effusion method 79−10950
In-Zn binary system, melts, elec. resist., 0-700°C 80−65517
In-Zn/p-InP ohmic contact evaluation 77−24619
In_4Ag_9, γ-brass with P cell, struct. determ. 77−24290
In_4Au_9, γ-brass with P cell, struct. determ. 77−24290
InBi, anisotropy of temp. depend. elec. resist., 4.2-293K 78−43354
InBi, Knight shift and quadrupole interaction of ^{115}In 77−55717
InBi, quadrupole interaction precession frequency of ^{111}Cd, TDPAC meas. 77−16224
InBi, single cryst. zone melting growth and etching 79−34189
In_2Bi, cryst. struct. and density *(German)* 80−24407
In_2Bi, de Haas-van Alphen effect 78−91594
In_2Bi, magnetisation curve, interpretation using boson formulation of supercond. 78−2619
In_2Bi, pre-melting absorption of sound 80−88277
In_2Bi, press.-induced supercond. phase transform. 79−24099
In_2Bi, quadrupole interaction precession frequency of ^{111}Cd, TDPAC meas. 77−16224
In_2Bi-In, thin lamellar eutectic strips, unidirectionally solidified, morphologic and crystallographic study *(French)* 77−55264
In_2Bi-In(Bi) laminar eutectic alloy, SNS struct., Josephson behaviour *(French)* 78−26996
In_3Ce, nucl. orientation meas. 78−39415
InGa-GaSe interface, microplasma electrolum. at 300K 79−11469
InMn, ion implanted, influence of O and lattice disorder on Kondo resist. 79−38061
$InMn_3$, crystallographic anal., new form of γ-brass struct. with a P cell 79−99116
InPb-covered manganin wire, level detector, depth gauge, demonstration of superconductivity 79−35751
InR_2 (R-Y, Nd, Sm, Gd, Tb, Dy, Ho, Er, Tm), mag. props., 4.2 to 270K 79−56512
$In_{1-x}Sb_x$, liquid, nucl. quadrupole relax. of Sb, time depend. PAD meas. 77−43899
In_3Sn, anisotropy of upper crit. field 80−20360
β-In_3Sn, band struct. and Fermi surface calc. using model pseudopot. 77−28103
β-In_3Sn, crystn., decomp. and superconductivity 79−91579
β-In_3Sn, decomposition, X-ray powder diffr. study 80−89196
In_3Sn, pulsed high field magnetoresist., 77K 79−73493
In_3Sn, tetragonal supercond., lower and upper crit. field, anisotropy and temp. depend. 80−97042
$In_{0.69}Tl_{0.31}$, supercond. transition temp., specific heat, pseudopotential form factor 80−97026
In−Gd film, dil., fluctuation induced cond. above supercond. transition temp. 79−47196
$IrMn_{1+x}Sb$ alloys, crystal struct., and mag. props. 78−34466
$LIAl_{1-x}In_x$, thermal expansion, comp. depend. 78−22869
La-In, heat of formation meas. using differential direct isoperibol calorimeter 77−21101
La-In alloys, cohesive and superconducting props. from electronic struct. calcs. 79−99113
$LaAg_xIn_{1-x}$, crystal struct., neutron diffr. obs. 80−49187
$LaAg_xIn_{1-x}$, phonon dispersion, elastic consts. and struct. instability, soft mode behaviour 80−103436
$LaAg_xIn_{1-x}$, structural instability 78−79562
$La_{3-x}Gd_xIn$, mag. impurity ordering and superconductivity, EPR exam. *(Russian)* 77−8400
La_3In, mag. susceptibility and normal state NMR meas. 78−31118
La_3In, supercond. T_c. alloying effects 79−38227
$LaNi_{4.6}In_{0.4}$, H_2 absorption props., desorpt. pressure calc., and decomp. pressures 79−24827
Li-Al electrode, In surface additives effect on performance 80−40698
Li-In, liquid alloy, elec. resist., Knight shift of ^{115}In and ^{7}Li nuclei 79−11352
Li-In, liquid alloys, calorimetry study *(German)* 80−25664
$Li_2Ag_{2-x}In_x$, optical props., struct., energy bands, interband transitions 78−72539
$Li_2Cd_{2-x}In_x$, optical props., struct., energy bands, interband transitions 78−72539
LiIn, elastic moduli and Debye temp., US meas. 79−91724
LiIn, electrical resist. and thermal expansion temp. depend., 30 to 400°C, vacancy form. 77−24547
LuIr:Gd influence of cryst. field on EPR 78−52346
$LuIr_2$-Nd^{3+}, dil., ESR, hyperfine crysts. of $^{143,145}Nd$, g-factor, crystalline field splitting 78−52349
Lu_5Ir_2, cryst. struct. 80−96473
Mg-In, catalytic effect of In on Mg/H_2 reaction, kinetics 78−76851
Mg-In, complex energy band, l-depend. pseudopot. 78−84124
Mg-In, short-range order, temp. and conc. depend. *(Russian)* 77−43173
Mg-In dil. alloys, effect of alloying on Fermi surface, de Haas-van Alphen effect meas. 77−76732
Mg-In dil. alloys, effect of alloying on Fermi surface, pseudopot. model 77−76733
Mg-In liquid solns., EMF and calorimetric meas. 80−55359
Mg-In-Ga(Tl), phase diagrams and electrochem. props. *(Russian)* 80−40330
Mg-Li-In, phase diagram, isothermal cross section *(Russian)* 80−20900
MgIn, atmospheric corrosion, SEM, electron diffraction and electron probe obs. 79−24681
MgIn, X-ray diffr. exam. of compressibility 78−51610
$Mg_{0.25}In_{0.75}$ sensitising layer, effect on laser machining and ageing charcts. of granular Bi film 77−62020
Mn-In, liq., elec. resist. meas. 77−51721
Mn_3In, antiferromag., mag. susceptibility, X-ray and neutron diffr. 79−11314
Na-In, dil., magnetic susceptibility, impurities effect, free electron gas model 79−91206
Na-In, dilute soln., thermodynamic props. 77−89553
NaIn, elastic moduli and Debye temp., US meas. 79−91724
Nb-Ir system glasses, form., crystn. and microhardness, resist. obs. 80−89178
Nb-NbO_x-PbIn tunnel junctions with ultra-thin Nb electrodes 79−56398

indium alloys continued
NbAlIr A′ phase, struct. 78−18587
Nb_3In, thin films with A-15 struct., prep. 78−80478
Nb_3Ir, A-15 struct. ^{93}Nb NQR spectra 80−20496
Nb_3Ir, X-ray $M_{IV,V}$ emission bands *(Russian)* 80−45170
Nb_3Ir, XPS of valence electrons meas. 77−21003
$Nb_3(SnIn)$ tapes, diffusion processed, high field props. 79−38266
$Nb_3(SnIn)$ wires, prep. by ductile fabrication process and props. 79−38265
$NdIn_3$, crystalline elec. field parameters, exchange and Coulomb contrib. 77−20278
$NdIn_3$, magnetisation 80−25106
Ni-In, dil., symmetry of lattice defect, DPAC meas. 78−43729
Ni-In, dil., uncorrelated radiation damage, TDPAC meas. 78−43343
Ni-In, elec. field gradient, at ^{111}Cd probes, temp. depend. 79−28643
Ni-In, electrical cond. and magnetic susceptibility of B 8_2-compounds *(German)* 79−42520
Ni-In, FCC, cellular precipitation kinetics 78−52823
Ni-In, FCC crystals, exam. of volume transform. kinetics of cellular precipitation 79−11625
Ni-In, implantation damaged, crit. behaviour, perturbed ang. distrib. meas. anal. 80−60476
Ni-In, ion-implanted, impurity defect interaction and diffusion, Rutherford backscatter and TDPAC expts. 80−34039
Ni-In, protective coating on Kovar, vacuum seal for borosilicate glass appl. *(Italian)* 80−40621
α-Ni-In, solid solution, lamellar microstructure, influence of grain boundaries on thermal stability 78−72795
Ni-In, thermodynamic props., phase diagram 77−55949
Ni_2MnIn, Heusler alloy, order-disorder phase transitions, X-ray diffr. meas. 77−66640
Ni_2MnIn, Heusler alloy, hyperfine field at ^{111}Cd, TDPAC meas. 78−43705
Pb-2n, work hardening in mixed state *(Russian)* 79−42707
Pb-I(-Au) base electrode film Josephson junctions, tunnel barrier oxide struct. 80−65750
Pb-In, CPA interpretation of positron annihilation *(Russian)* 80−11507
Pb-In, containing Ag particles, flux pinning in superconducting matrix 80−2534
Pb-In, series-connected Josephson tunnel junctions, fabrication procedure diagnostics 78−47909
Pb-In, strong coupling effects in temp. depend. of flux-flow resist. near H_{c2} 77−36036
Pb-In, superconductive, electron tunnelling under hydrostatic press. 77−51850
Pb-In, superconductive to normal transition due to external mag. fields, dynamic behaviour 80−39722
Pb-In, viscous drag on mobile dislocations, plastic deformation, critical temp. magnetic data 78−43514
Pb-In, vortex pinning on grain boundaries *(Russian)* 77−89910
Pb-In (1 to 20 at.%), upper critical field anisotropy 77−36033
Pb-In (21 at.%), dirty type II supercond., anisotropic thermal cond. 79−56385
Pb-In (40 wt.%), solid soln., single phase, superplastic behaviour 80−21048
Pb-In (40-60 at.%), type II superconducting Ettingshausen effect, transport entropy of vortices 78−56272
Pb-In (5%), supercond. mobile dislocation density, instantaneous flux change meas. 80−15670
Pb-In (50 wt.%), supercond., pinning effect 80−15669
Pb-In alloys, flux pinning at grain boundaries 80−34572
Pb-In alloys, supercond., AC losses of EM energy, critical current densities 79−33423
Pb-In alloys, supercond. energy gap determ. by pt. contact tunnelling 78−19185
Pb-In and Pb-In/Au, Josephson junction, oxide formation process, ellipsomesric meas. *(Japanese)* 80−11561
Pb-In cylinder, vortex-surface interaction, vortex field *(Russian)* 78−27003
Pb-In film, RF sputter anodisation, Josephson junction form., ellipsometry anal. 79−29258
Pb-In film, supercond. surface sheath, dynamic pinning model of elec. dissipation 77−28320
Pb-In film, superconducting tunnel junction, pulsed quasiparticle injection 80−84565
Pb-In films, atom redistrib., ion-ion emission obs. *(Russian)* 78−18926
Pb-In multilayered superconducting film, critical currents 79−61017
Pb-In/Pb couple, FCC, Kirkendall interdiffusion, conc. depend. 77−39702
Pb-In/Sn-In proximity sandwiches, crit. currents 79−60992
Pb-In-Ag, transport current distribution in longitudinal mag. field 80−25057
Pb-In-Au, film, supercond. penetration depth 78−72306
Pb-In-Au, series-connected Josephson tunnel junctions, fabrication procedure diagnostics 78−47909
Pb-In-Au alloy, Josephson junction electrode materials, strain relax. 79−38255
Pb-In-Au Josephson tunnel junctions, strain relax. effects 79−65617
Pb-In-Sn system, liquidus and solidus isotherms 78−44088
Pb-Tl-Bi-In, localised phonons studies by supercond. tunnelling 79−87210
Pb-Tl-In, localised phonons studies by supercond. tunnelling 79−87210
PbIn films strengthening, by preventing formation of misfit dislocations 80−84858
PbIn, flux flow, longitudinal geometry 78−14902
PbIn oxidised electrodes, symm. and asymmetric supercond. tunnel junctions, subharmonic gap struct. study 79−60981
PbIn superconducting films, penetration depth measured with Nb-NbO_x-PbIn Josephson junctions 79−42691
β′PbIn, thermodynamic analysis 77−36455
PbIn-oxide-Pb superconducting junction, two-particle tunnelling and microwave effects 78−43527
PbIn-oxide-Pb(PbTl) thin film tunnel junction, subharmonic group struct., multiparticle tunnelling theory 79−56438
$Pb_{0.8}In_{0.2}$, superconducting, flux-flow noise 79−95556
$Pb_{0.84}In_{0.16}$, barriers to flux entry and exit, magnetisation meas. 79−60963
$Pb_{1-c}In_c$, liquid alloys, local fluctuations and quadrupolar relaxation 80−66060
$Pb_{40}In_{60}$, mixed state supercond., Hall and Ettingshausen effects, vortex entropy transport 80−44780

indium alloys continued
$Pb_{80}In_{20}$, flux pinning and flux flow noise 79−56473
$Pb_{80}In_{20}$ foil, deformed, annealed, correlation between pinning strength and flux flow noise charges 77−43792
$Pb_{80}In_{20}$ foil, flux flow current-voltage charact., and their mag. field depend. 78−23217
$Pb_{83}In_{17}$, supercond. flux creep meas. 77−20508
Pb_xIn_{1-x}-Pb_yTl_{1-y} asymmetric supercond. tunnel junctions, subharmonic gap struct. 79−15260
PbInAu film, RF plasma oxidised, surface analysis using ESCA 80−50742
Pd-In, electronic structure from annihilation quanta ang. distribs. 77−66107
Pd-In alloys, thermodynamic props., 800 to 1000°C 79−20454
β′-PdIn, electrical resistance, mag. susceptibility and IR freq. dispersion *(Russian)* 80−107759
$PdIn_xH_y$ films, ion implantation prop., supercond. crit. temp. 79−87182
Pd_2MnIn, Cd impurities, hyperfine field meas. 78−15074
$Pd_2MnIn_{1-y}Sb_y$, Heusler alloy, mag. order obs. 80−29528
$Pd_2MnIn_{1-x}Sb_x(Sn_x)$, Heusler alloy, Mossbauer effect exam., mag. coupling 79−69755
$Pd_2MnIn_{1-x}Sb_x(Sn_x)$, Heusler alloy, Mossbauer effect exam., hyperfine interactions in ferromag. phase 79−69756
$Pd_2MnIn_{1-x}Sn$, and $Pd_2MnIn_{1-y}Sb$, Heusler alloys, mag. order, disorder effects 80−88723
$Pd_2MnIn_{1-x}Sn_x$-Cd, dil., Heusler alloy, hyperfine mag. field on Cd, TDPAC obs. 79−8075
$Pd_2MnIn_{1-x}Sn_{1-x}$, mag. order exam. 77−40036
$Pd_2Mn_{0.98}Sn_1In_{0.02}$, Heusler alloy, hyperfine fields at sp elements, spin echo NMR meas. 78−84496
Pr-In system, phase diagram determ. and intermediate phases characterisation 79−91621
$PrIn_3$, crystalline elec. field parameters, exchange and Coulomb contrib. 77−20278
$PrIn_3$, nucl. orientation of ^{144}Pm in singlet ground state, exchange interaction and cryst. field splitting obs. 80−71275
$PrIn_3$, two stage nuclear demagnetization experiments 79−65644
$PrIn_3$:Gd, EPR relax. of impurity in Van Vleck paramag., host ion fluctuation spectra 77−48049
$(Pr_xLa_{1-x})_2In$, mag. props. 80−108009
Pt-In, cryst. struct. determ. *(German)* 78−26494
Pt-In, dil., damage induced quadrupole interactions, DPAC exam. 78−39465
Pt-In, dil., radiation damage heating, TDPAC exam. 78−39466
Pt-In, Fermi energy influence on thermodynamic props. *(German)* 80−24619
Pt-In, solid soln., magnetic props. and lattice parameters *(German)* 79−87236
$Pt_{13}In_9$, exam. of crystal structure, and phase diagrams *(German)* 78−83779
Pt_3In, Ll_2 ordered alloy, positive temp. depend. on strength, phase destabilization 80−81203
$Pt_{50}In_{50}$, ordered BCC phases at high temp. 79−32948
Pu_5Tr_4, cryst. struct. determ. 77−55267
R_2In, R_3In, R=Gd, Tb, Dy, Ho, Nd, mag. props. 80−108009
Rh_2MnIn, mag. and cryst. props. 77−20568
Sb-In, electronic work function, contact pot. difference meas. 77−85299
Sc, In, itinerant electron ferromagnet, magnetovolume effects 80−60397
Sc-Ir, electronic struct., susceptibility, sp. ht. and Knight shift meas. 77−43485
Sc_3In, itinerant electron ferromagnet, spin fluctuations 77−73096
Sc_3In, itinerant electron ferromag., NMR and relax. 78−6586
Sc_3In, itinerant electron ferromag., low temp. sp. ht., mag. field depend. 79−42765
$Sc_3InC_{1-x}(B_{1-x})$, stabilising effect of C and B on alloying behaviour of Sc 77−36454
ScIr:Gd, influence of cryst. field on EPR 78−52346
Si/In(-Cd), Si/Cd Schottky contacts, electrochemically deposited 80−88633
Sn-In, dil., amplitude depend. US attenuation in normal and supercond. state 77−28299
Sn-In, dil., intermediate state, US attenuation 79−42694
Sn-In, dil., supercond., current-induced resistive state 79−51712
Sn-In, distribution function branch imbalance, relaxation 79−33401
Sn-In, nonlinear conductivity of thin films in mixed state *(Russian)* 80−80464
Sn-In, supercond. crit. RF mag. field, rel. to superheating 78−2632
Sn-In (50 wt.%), mech. state relations at low and high homologous temps. 77−63707
Sn-In (up to 6.0 at.%) whisker, supercond. crit. temp., stress depend. 77−39988
Sn-In dil. liq. alloy, electrodiffusion and electroconvection, effective diffusion coeff., apparent effective valence 78−87802
Sn-In multilayered superconducting film, critical currents 79−61017
Sn-In-Te system, SnTe based solid solns. formation 77−84929
$Sn_{0.99}In_{0.01}$, superconducting-normal interface, boundary resist. 80−50006
Ta-Ir film, amorphous, temp. stability 78−63948
Ta-Ir system glasses, form., crystn. and microhardness, resist. obs. 80−89178
$TbAg_{1-x}In_x$, elec. and Hall resist. 80−96844
$TbAg_{1-x}In_x$, mag. and transport props. 78−43572
Te-In alloys, direct reaction calorimetric study, 737 to 1340K *(French)* 80−49382
Te-In system, enthalpies of fusion, peritectic decomp. and allotropic transition, DTA *(French)* 80−76226
Tm_5Ir_2, cryst. struct. 80−96473
UIn_3, thermoelectric power, 5-300K 79−65444
UIr_3, uncompensated metal, topological props. of Fermi surface, magnetoresist. meas. 78−6350
UIr_2X_2 (X=Si,Ge), cryst. struct. 80−1964
V_3In, hypothetical, electronic struct., lattice parameters and possible supercond. transition temp. 79−23891
$V_{0.62}Ir_{0.38}$, supercond., Knight shift contrib. to reson. line shift meas. 77−4467
$V(Ir_{1-x}Pt_x)_3$, NMR study of ferromag. 79−65760
$YbInAu_2$, intermediate valence cpd., mag. susceptibility expts., 4.2-280K 78−39288
Zn-In alloy, solid-liq. equilib. roughening transition 80−96630
Zn-In-Cd, anal. calc. of phase diagram 79−91631
indium alloys continued
Zn-In-Cd soln., liquid, thermodynamic props. 79−83176
Zr_3In, Ll_2 ordered alloy, positive temp. depend. on strength, phase destabilization 80−81203

indium antimonide
1/f noise, Hooge's parameter 79−24040
(110) surface, LEED intensity dynamical anal. 80−88412
absorption edge, exciton struct. 80−93321
absorption processes near bandgap, laser-induced hot electron and photocond. meas. 79−42584
accumulation layer localised carriers interaction with LO phonons, Raman interference lineshapes 80−93338
acoustic waves, amplification and vel. change due to external temp. gradient 78−84260
acoustoelectric effect at 77K 78−72209
acoustoelectric gain coeff., nonlinear elec. field depend. 78−76115
acoustoelectric phonon attenuation of X-ray anomalous transmission 77−4160
adsorption of O_2 on clean (110), AES, LEED, RHEED and field effect meas. 80−49501
adsorption rel. to dopant admixture 78−95596
amorphisation due to ion bombardment, SRO struct. 80−79844
amorphous, localised gap states, hopping cond. and chem. bonding 78−23052
amorphous, localised gap states, variable range hopping 77−72866
amorphous, optical absorpt. edge shape, band edge fluctuations 77−20880
amorphous, pressure induced struct. transform., X-ray diffr. obs. 77−11690
amorphous film, effective medium theory and freq. depend of conductivity 79−24090
Anderson-Gruneisen parameter, bulk modulus temp. depend. 78−10154
anode oxide film coated, ellipsometric and interferential study, optical parameters *(Russian)* 80−50449
anomalous avalanche breakdown 80−80284
asymmetrical behaviour of 60° dislocation glide 79−7611
asymmetrical dislocation glide, expt. evidence for 79−82232
Auger recombination, calc. for diamond-like narrow-gap semicond., compared with expt. 78−63978
Auger-governed decay of laser-induced plasma, optical probing 80−76105
avalanche breakdown voltage for p-n junction, calc. 78−88020
avalanche formation, high intensity IR transmission limit 79−78684
band structure, of cryst. with zincblende and rocksalt type struct., semiempirical LCAO calc. 77−72816
Brillouin zone, spin depend. wave functions 79−56126
carrier concentration variations using electrolyte electroreflectance, topographical features 79−99562
carrier heating, optical temp. waves 77−89770
carrier heating by microwave field, inertia effects 80−65580
CESR at high mag. fields, scatt. mechanisms 80−93177
characterisation and physical properties *(Japanese)* 80−39576
charge injection IR imaging array 78−37995
chemisorption of Cl on (110) surface, photoemission spectra and tight-binding calcs. 80−6629
conduction and valence band effective mass parameters 79−60689
conduction band inversion asymm. splitting, Shubnikov-de Haas meas. 78−10348
conductivity anisotropy in strong electric field 78−19048
crystal growth by travelling heater method 80−11553
crystal growth by vertical and horizontal travelling heater method, growth parameters and cryst. quality 79−24421
crystal growth from melt, facets and twin formation obs. *(Chinese)* 80−59409
crystal structure stability, P-T diagrams 78−51886
current-voltage characteristics at room temperature and high hydrostatic pressure 80−88560
cyclotron harmonic transitions, warping and inversion asymm. effects 78−68383
cyclotron resonance, in zinc blende struct. semiconductor *(German)* 78−10337
cyclotron resonance lineshape 80−15801
cyclotron-phonon resonance, pinning struct., effect of nonequidistant Landau bands 77−11881
Czochralski growth, melting and regrowth, inclusion density and dislocation generation 77−21016
Czochralski growth, thermoelec. monitoring of interface temp. 78−31331
Debye temperature, atomic mean square displacement 78−87757
degenerate electrons, relax. of spin and energy 80−10965
degenerate four-wave mixing obs. at 5K 80−53355
degenerate n-type, acoustomagnetoelec. effect obs. 78−72207
degenerate surface photo-EMF 79−69580
depletion layer, plasma and vibr. plasma type guided polaritons *(Russian)* 80−96933
dielectric permittivity, electronic contrib. calc. 77−59265
difference frequency mixing via spin nonlinearities in far IR, book contrib. 77−46765
dislocations due to thermal stress, single and composite crysts. 78−2124
donor excitation spectra in high mag. field 78−80027
donor impurities, magnetic freezeout in hyperquantum regime 80−10921
donor levels, anomalous press. effects, Hall const. meas. 77−51693
donor spectra, high-field, doping depend. 77−90175
donor spectrum, effect of strong mag. field 79−7806
doped, electron scatt. by deform. pot. 77−72860
education, Shubnikov-de Haas oscills., InSb degenerate semiconductor, third-year undergraduate expt. 79−9051
effective g-value of electrons determ. by spin flip Raman scatt. and electric-dipole-excited ESR 78−52494
Einstein relation for inversion layers 80−103706
elastic constants, third-order, meas. at 300, 80K 77−31711
electon drift velocity in fields up to 800 V/cm in presence of impact ionization 78−39120
electric paramagnetic resonance and combined reson. of cond. electrons at 24 GHz 77−1596
electrical conductivity in intense mag. field, freeze out, hopping 77−20338
electrical effects of dislocation, galvomag. props. 78−23119
electrical properties, low-temp. annealing effect 77−8091
electrodes, anodic and cathodic processes 77−44487

indium antimonide continued
electroluminescence in anodic oxidation, InSb-oxide-electrolyte interface *(Russian)* 77−90201
electron heating dynamics in longitudinal electric and quantising magnetic fields 79−69520
electron irradiated, kinetics of changes in carrier density 79−56228
electron irradiation effects on elec. props. and recomb. 79−51584
electron mobility, low-field, Monte Carlo calc. 80−10973
electron mobility from soln. of Bolzmann eqn. for electron-LO phonon scatt. 79−19586
electron mobility low temp., theory and expt. 77−89759
electron momentum distribution, anisotropy, positron annihilation *(Russian)* 78−84676
electron spin levels resonant excitation, photolum. 80−25454
electron spin relaxation 80−25187
electron-electron spin-flip scatt. and spin relax. 80−44916
electron-hole plasma, LF instabilities in crossed fields 78−39146
electron-hole plasma instabilities, impact ionisation conditions, microwave emission 80−107840
electronic interband Raman scatt. 80−11407
electronic surface structure, Cs(Rb)(Na) adsorpt. processes, AES, LEED, EELS, study 78−68068
electroreflectance in MOS struct., band-population effects under heavy surface accumulation 77−48167
electsron irradiation effect, high purity samples, elec. props. 79−23650
epitaxial film, amorphous and polycrystalline, vol. plasmon energy and linewidth, electron scatt. obs. 80−50482
equation of state 79−82310
etching of {111} plane, rates and activation energies 77−12723
Ettingshausen and Nernst-Ettingshausen effect meas. *(Russian)* 77−28201
Ettingshausen effect, influence of surfaces, narrow-gap semicond. characterisation 77−24571
eutectic alloys, thermal cond. and diffusivity, 300-700K, phonon mechanism 80−103526
evaporation kinetics, rel. to film growth 78−3050
external photoelec. effect 78−27366
extrinsic and intrinsic, interaction of transverse magnetoresist. effects 80−65596
Faraday effect, interband, for 100 W average power 10.6 μm isolator 79−59706
Faraday effect, IR, standard measure of magnetooptical rotation of plane of polarisation 80−60551
Faraday rotation obs., intensity depend., saturation and reson. enhancement effects 80−108186
film, amorphous, AC conductivity, anomalous freq. depend. 77−4456
film, analysis by attenuation of substrate X-ray fluoresc. 78−27872
film, degenerate, concs. and ionisation energies of defect levels, Hall effect meas. 79−91087
film, E_0, E_1 absorption edge size quantisation, optical and electroreflectance spectra 80−34998
film, for monolithic elastic surface wave amplifier of continuous operation 77−80023
film, galvanomagnetic meas. of surface layer carrier conc. and mobility 77−55628
film, gamma-irradiated, struct., TEM and SEM obs. 79−15033
film, grown by MBE, RHEED study 80−100415
film, Hall mobility of carriers at room temp. 79−65568
film, heteroepitaxial, MBE growth and elec. props. 80−2301
film, light scatt. from interface, polaritons 79−8202
film, low energy electron irrad. effect on elec. props. 80−7009
film, MBE apparatus and AES 78−47875
film, melt-grown, point defect effect on elec. props., 77-300K 80−2502
film, nonintrinsic, magneto-conc. effect *(Russian)* 79−47113
film, p-type, elec. transport props. 78−72291
film, phase transition dynamics, investigating device 78−22967
film, polycryst., Hall and drift mobilities 79−95531
film, prep. by ionised cluster beam deposition *(Japanese)* 80−25576
film, prep. by rotary type flash method *(Japanese)* 77−40372
film, quantum size effects, transport props. 78−76171
film, synthesis by 2-source mol. beam technique and AES characterisation 78−72729
film, transverse 1/f noise and signal-to-noise ratio of related Hall elements, comment 79−99593
film, transverse 1/f noise and signal-to-noise ratio of related Hall element 79−99594
film cyclotron-frequency submillimetric oscillation generation model 77−80801
films, elemental incorporation probability modification by ion bombard. during growth 80−80118
films, transverse 1/f noise and S/N ratio of related Hall elements 79−42597
films, X-ray fluoresc. anal. method, long-term stability 80−61212
films on $LiNbO_3$, prep. and props. 80−35093
fine struct. in energy derivative reflectance spectra 79−78705
galvanomagnetic properties at low temp., carrier localisation, metallic impurity cond. 77−28195
galvanomagnetic properties of annealed single crystals 80−96909
gamma irradiated, changes in energy spectrum of impurity spectrum 78−51937
growth angle determ. from cryst. lateral face shape and solidified separation drops 80−103282
growth of low-defect single crysts. by InN doping, IR detector appl. 80−20780
Hall effect sensor for mag. fields up to 23 T 77−10066
Hall element for magnetic bubble field distrib. meas. 79−56585
Hall plates, temp. and pot. distribs. determ., temp. depend. cond. effect 79−60851
heats of transformation for high pressure, orthorhombic modification, exam. 78−56627
heavily doped, high press. effect on electron mobility and conc. 77−4390
helicon beam form. during microwave transmission in mag. field 80−80308
helicon damping in quantum limit 77−28205
heteroepitaxial film, orientation and struct. investigation 79−82480
high field polaron transport 78−30932
high field quantum magnetotransport theory 78−30941
high power helicons, harmonic generation 80−29426
high pressure effect on elec. props., 50-300K 77−47807
hopping conduction in mag. field in heavily compensated n-type 79−7842
indium antimonide continued
horizontal zone melting in vacuum 79−47624
hot electron energy relax. in quantizing mag. fields 78−31259
hot electron energy relax. time 77−80783
hot electrons, HF props. at 77K, calc. using Monte Carlo method 80−15553
hot electrons, Monte Carlo calc. of transport characts. and distrib. functions of hot electrons 80−6853
hot electrons relax. in quantising mag. field *(Russian)* 80−6876
hot photoexcited electrons, time evolution of electron temp. in high mag. field 80−54709
impact ionisation, influence of external mag. field on recomb. radiation and I-V characts. 79−56864
impact ionisation and magneto-transport, high crossed elec. and mag. fields 80−107797
impact ionisation at room temp., carrier generation rate 80−20207
impact ionisation by elec. fields in intrinsic material 77−39864
impact ionisation in crossed elec. and mag. fields 79−28355
impact-ionisation magnetoelec. effect 78−52016
impurity atom energy spectra under 4.2K gamma irrad. 77−89471
impurity segregation in undoped and Te-doped crysts., Hall and mass spectrum obs. *(Chinese)* 80−59501
impurity-level assisted two-photon interband absorption of laser radiation 78−23464
p-InSb:Cu, Ag, deep impurity centres, acceptor conc. effect on conduction type 80−44602
p-InSb:Ge, single cryst. field dependence of Hall effect, cond. and carrier mobility *(Bulgarian)* 78−34848
n-InSb Corbino disc, acoustic noise effect on I-V characts. *(Russian)* 80−100492
p-InSb-Au, surface barrier, structure, photosensitivity spectrum 79−51674
interband Faraday rotation, Roth theory calcs. 77−52046
interband magneto-optical transitions, arbitrary field orientation 79−42948
intraband photoconductivity in mag. fields 79−47123
intrinsic, elec. cond., carrier wave instability in elect. and mag. fields 79−82617
intrinsic, photoinjected electron hole pairs, Auger lifetime, photoconductive decay obs. 80−39629
intrinsic magnetoresistance 79−69534
inversion layer, electromagnetic mode 78−60080
inversion layer, spectroscopy of electron subband levels 78−10569
inversion layer, spectroscopy of electron subband levels 78−64364
ion implantation, anomalous radiation disordering 80−92553
ion implantation, dose rate and orientation dependence of radiation damage 77−89482
ion implantation at elevated temps. 79−10870
ion implanted, efficient void form., TEM obs. 80−44237
ion implanted, ellipsometric study 80−60537
ion implanted layers, amorphisation, recrystallisation 78−63782
ion irradiated, isothermal annealing effects 80−6424
ion-bombardment and defect annealing, n- and p-type cond. layer prod. 78−26606
IR detector, 714 to 1667 μm, liq. He temp., Fourier interferometric spectrometer 77−83765
IR detector, for pulse radiolysis, reversible component in response time 78−41353
IR detector array, AES anal. of localised contaminants at interfaces 77−57391
IR detectors, integrating premaplifier 80−90337
IR reflectivity, longitudinal optical phonon-plasmon coupling 77−59578
Landau level struct., magneto-electroreflectance 80−25349
laser, with two photon pumping by CO_2 laser radiation 79−86182
laser beam propagation, low-power nonlinear refraction effect 80−5801
laser beam self-focusing, effect of quantising mag. field 77−42578
lattice, static dielec. const. and carrier conc. meas. via gyrotropic sphere reson. 80−97143
lattice dynamics 79−14895
lattice thermal cond. from three phonon scatt. relax. rate 78−51755
lattice vibration, thermal expansion and pressure effect 80−39233
light scattering from bunched solid-state plasma, stationary energy transport velocity 79−95720
liquidus line, quantitative fits and high-temp. thermodynamic data 77−63637
localised defects, one-electron pseudopot. 77−24533
low intensity nonlinearities, induced by lasers 79−94300
n-, low temperature UHF detector, with low noise preamplifier 80−68230
LPE growth characteristics, substrate surface contamination dependence 80−39470
luminescence enhancement due to carrier heating in elec. field 77−44068
magnetic circular dichroism at E_1 edges 78−92051
magnetic freeze out *(Japanese)* 78−39130
magnetic susceptibility of light and heavy holes 79−42734
magnetically frozen-out, evidence of surface cond. from etching expts. 79−47152
magneto-optical anomalies of impurity electrons, two-LO-phonon region 78−72415
magneto-optical transitions, one- and two-photon 77−16284
magneto-optical transitions from deep levels, photocond. obs. 80−55069
magneto-photoconductivity, phonon assisted combined reson. magneto-optical absorpt. reson. 78−47831
magneto-surface transport props. 77−43693
magnetoacoustic wave excitation by acoustic wave propagation 80−88597
magnetoconcentration effect, nonlinear current carrier recomb. 79−33298
magnetophonon effect exam. using field modulation technique 78−26918
magnetophonon effect in non parabolic band 79−37962
magnetophonon effect temp. depend., 80 to 190K 77−59293
magnetophonon resonance, damping factor by mag. field modulation technique 80−6878
magnetoresistance effects in strong electric fields *(Russian)* 78−19056
magnetoresistance meas., transverse diffusion currents on source of error 79−7843
magnetoresistance transducer 79−67287
magnetoresistive elements, fundamental effects *(Japanese)* 80−11013
mangetophonon structure in magnetoresist., elec. field depend. 78−30943
micron size Hall probe for precision magnetic field mapping 79−75558
microwave magnetoplasma matching effect 78−14750

indium antimonide continued
MIS capacitance measurements, method of separating hysteresis effects, interface state density estimation 77−85324
MIS capacitors, gamma-ray radiation effects at cryogenic temps. 80−34517
MIS devices, large-amplitude hysteresis, model 79−19665
MIS diode, anodised, C-V characts, effect of high elec. field pulse 80−60092
MIS struct., C-V characts., interface state densities and storage times meas. 77−89861
MIS structure, background radiation effect on photoelec. processes 80−25015
MIS structure, effect of room background on noise props. 80−103755
MIS structures, charge accumulation in insulator layers 80−6993
MIS structures, props. of metal-borosilicate glass-InSb oxide-p-type InSb structures 77−80848
MIS structures, review 78−95372
MIS thin film capacitance, theory 79−87156
MISIM structure, photovaractor effect and CV characs. obs. 77−8205
molten, temp. depend. of vel. of sound and adiabatic compressibility 77−27944
morphological and structural changes due to ion bombardment 80−79843
morphological instability under constitutional supercooling during cryst. growth from melt and stabilising thermal gradient 79−4910
MOS capacitor, AC behaviour, semicond.-oxide interlayer effect 78−19151
MOS struct., capacitance of n-channel inversion layers, elec. field effects 80−80393
MOS structs., energy spectrum of traps in oxide layer 80−107922
MOS structure, anodic oxide on n-InSb base *(Russian)* 77−89874
MOS structure, props. 80−49947
n^+-p junctions, photocurrent spectrum near long wavelength edge of fundamental absorption band 80−100483
n type, plasma, nonequilibrium, magnetohydrodynamic instabilities, theory and expt. *(Japanese)* 78−10493
n-type, 2 mm wave radiation interaction with charge carriers *(Russian)* 78−87991
n-type, absorption of millimetre radiation in mag. field 79−11083
n-type, acceptor effect of plastic bending 80−6885
n-type, accumulation layer submillimetric cyclotron resonance obs. 77−39912
n-type, acousomagnetoelec. effect, 20-120K, sign reversal obs., and Hall mobility 77−24592
n-type, acoustoelectric amplification, temp. depend., 77 to 135K 79−51638
n-type, acoustoelectric instability, effect of nonparabolic band struct. 79−60875
n-type, acoustoelectronic interaction, effect of alternating electric field 79−11188
n-type, acoustohelicon waves, parametric excitation 79−38135
n-type, anomalous Hall effect at high mag. field 77−15876
n-type, anomalous three LO phonon assisted cyclotron resonance 80−108078
n-type, Brillouin instability in magnetostatic field 80−78909
n-type, characts. of Gunn effect 77−55538
n-type, coherent microwave emission in high mag. field 79−60863
n-type, compensated, impact ionisation temp. depend. 77−20331
n-type, compensated, LF current instabilities 79−7859
n-type, compensated cryst., influence of surface cond. on Hall coeff. and elec. resist. 79−69579
n-type, cond. electron cooling induced by CO laser and non-ohmic DC field 80−96941
n-type, conduction-band struct. from reflectivity meas. when subject to mechanical strain 79−42450
n-type, condution band effective mass anisotropy and nonsphericity 79−69414
n-type, convective instability in crossed mag. and elec. fields 77−62939
n-type, cyclotron reson. of conduction electrons, strong mag. field, hot electrons 80−2640
n-type, cyclotron reson. study of conduction electrons, strong mag. field 80−2639
n-type, damped surface magnetoplasmons, theory 79−7873
n-type, deformed, spectral oscills. of absorption in quantising mag. field 80−34486
n-type, dielec. in solid-plasma waveguide, effect on slow surface wave propag. 79−50862
n-type, directional temp. of hot electrons under elec. and mag. fields 78−84135
n-type, dispersion curves for surface polaritons 79−19646
n-type, doping and strain depend. of quantum props. 79−60690
n-type, effective mass and Lande factor, stress depend. calcs. *(German)* 79−95313
n-type, elec. cond., carrier wave instability in elect. and mag. fields 79−82617
n-type, elec. cond., press. dependence 80−6830
n-type, electron gas degeneration in strong mag. field 77−66173
n-type, electron heating and energy relaxation time in quantising mag. field 80−10996
n-type, electron mobility at 77K in avalanche regime 79−33295
n-type, electron recomb. between Landau levels 79−38096
n-type, electronic bolometer, appl. in system for millimetre and submillimetre wave detection 78−24860
n-type, EM radiation in amplified sounds, theory 77−80812
n-type, EM wave resonant absorpt. 78−2757
n-type, EPR, oscillations of transverse magnetoresistance in weak mag. field 79−91086
n-type, far IR cyclotron emission 79−61226
n-type, Faraday effect in strong EM fields 80−93286
n-type, ferroelec. semicond., transverse acousto-elec. effect *(Russian)* 78−30958
n-type, flicker-noise power spectrum, 0.1 Hz to 10 kHz 79−73555
n-type, freq. depend. cond. tensor in quantising mag. fields *(German)* 80−29419
n-type, freq. depend. of effective temp. of hot carriers 79−11135
n-type, frequency shift of combined resonance, influence of plasma oscills. of conduction electrons 79−7850
n-type, galvanomagnetic props. at low temp., mag. field induced metal-nonmetal transition 77−76845
n-type, Gunn domains, direct probe meas. 78−26877
n-type, Gunn effect, influence of impact ionisation 80−44609
indium antimonide continued
n-type, H-like impurities photocond., mag. field effect 79−82634
n-type, Hall coeff. and magnetocond. in mag. freeze-out regime 79−60849
n-type, Hall effect and magnetoresist. in extreme quantum limit, stress depend. 80−11021
n-type, Hall effect and magnetoresist. in mag. freeze-out region 79−15165
n-type, Hall mobility of free electrons, determ. using radioelectric effect 77−69327
n-type, heavily doped, electron activity coeffs. 77−39837
n-type, heavily doped, spontaneous radiative recomb., complete vel. and radiative capacity 79−11458
n-type, helicon wave propag., quantum mechanical features 79−42571
n-type, helicons, parametric decay 80−34472
n-type, HF EM and acoustic oscill. generation in LF electric field 78−64068
n-type, high field electron diffusion, Monte-Carlo calc. 78−10455
n-type, high power helicon, interaction with semiconductor-free space interface 79−38114
n-type, high-resist., prep. using radiation compensation 80−34016
n-type, high-resist., recomb. of carriers at 77K 77−51761
n-type, hole mobility temp. depend. after electron bombardment 79−33290
n-type, hopping photoconductivity *(Russian)* 77−89801
n-type, hot electron magnetophonon effect, 77K, mag. field modulation method 78−60140
n-type, hot electron noise temp., Monte Carlo calc. 80−107877
n-type, hydrostatically compressed, instabilities of current Gunn effect meas. 77−1432
n-type, impact ionised plasma, three stream instability 77−55557
n-type, inelastic scatt. of electrons by optical phonons 78−76073
n-type, influence of electron irradiation intensity on defect formation 79−73216
n-type, influence of mag. field on hot electron effects 78−2493
n-type, instabilities of electron-hole plasma under impact ionization and microwave emission 79−65508
n-type, intraband processes exam. by stimulated spin-flip Raman scatt. 77−19362
n-type, ionized impurity scatt. limited mobility, expt. 80−80274
n-type, Landau emission spectra, influence of bakcground radiation 78−43935
n-type, Landau-level-electron lifetimes, saturation meas. of magnetoabsorption 78−48150
n-type, laser induced magneto-photoconductivity, conduction band transitions 77−55566
n-type, longitudinal magnetoresistance in extreme quantum limit *(Russian)* 80−11008
n-type, longitudinally magnetized, laser beam modulational instability, phonon-helicon interaction 79−56254
n-type, magnetoacoustic effects using two-band model 78−60170
n-type, magnetophonon effect, temp. depend. below 90K 79−56247
n-type, magnetophonon oscillations by photomag. effect *(Russian)* 77−43665
n-type, magnetophonon reson. under hot electron conditions 77−24568
n-type, magnetophonon struct. obs. in transverse magnetoresist. 78−23120
n-type, magnetoresistance, odd, in HF elec. field 77−28198
n-type, magnetotransport experiments, surface treatment induced effects 80−34468
n-type, MCD due to free carriers 78−56462
n-type, microwave displacement effect in longit. elec. and transverse mag. fields 78−87992
n-type, microwave magnetoplasma and heliconlike reson., sample shape effects 77−85252
n-type, millimetre rare modulation in semicond. plasma, use of effects of high elec. field. 78−60149
n-type, MIS diode, time-dependent photovoltaic effect 80−75601
n-type, mobility in mag. field, extreme quantum limit, iterative technique 78−2498
n-type, narrow gap, appl. of effect of pot. fluctuations induced by cryst. inhomogeneities 80−49780
n-type, negative longit. magnetoresist., carrier conc. and mobility depend., 77K 80−60007
n-type, non-degenerate, linear longitudinal elec. cond., US wave effects in DC mag. field 80−88599
n-type, non-degenerate semicond., magnetoacoustic effect 80−20257
n-type, nonlinear optical susceptibility, cyclotron reson. meas. *(Russian)* 79−50341
n-type, nonlinear optical susceptibility spin reson. *(Russian)* 79−59749
n-type, optical phonon emission in intraband magneto-optical transitions, photocond. meas. 80−34481
n-type, optical SHG in rectang. waveguide 80−43401
n-type, optically pumped stimulated recomb. radn. in mag. fields 79−94284
n-type, parametric excitation of plasma oscills. 77−66179
n-type, phonon heating by hot electrons in quantising mag. field 77−4354
n-type, phonon-assisted cyclotron reson. strongly depend. on surface condition 80−70755
n-type, photo-induced magnetophonon reson., 4.2K, peak shifts 78−84250
n-type, photoconductive lifetime, surface pot. effects 80−11029
n-type, photoconductivity, recombination processes 80−11030
n-type, photoconductivity meas. in crossed fields 79−7852
n-type, photoconductivity mechanism, 4.2 to 77K 80−70766
n-type, photoconductivity of laser excited hot electrons 80−11045
n-type, photoconductivity relax. temp. depend., carrier recomb. processes 77−4363
n-type, photoconductivity with different surface treatment 78−2517
n-type, photoluminesc. in crossed EM fields *(Russian)* 77−24892
n-type, photomagnetic effect anomalies, 90 to 300K *(Russian)* 78−84257
n-type, photoresistors of Corbino disc shape in mag. field, enhancement of responsivity 78−56186
n-type, plasma filament form. under impact ionisation conditions 78−60147
n-type, powder, microwave propag., 90-300K, magnetoplasma and helicon wave excitations 78−72183
n-type, property changes during ht. treatment 77−85213

indium antimonide continued
n-type, proton irrad. defects energy level scheme, transport props. meas. 80−96576
n-type, quasi-helicon waves instability 80−70741
n-type, Raman spin-flip laser, hot-electron effect 80−23743
n-type, recomb. of hot electrons, photoelectromag. and dynamic photocond. meas. 79−38081
n-type, reversal of sign of acoustoconductivity effect 78−2527
n-type, Shubnikov-de Haas effect 80−11015
n-type, Shubnikov-de Haas effect expts. on optically heated electrons 79−73529
n-type, Shubnikov-de Haas transverse kinetic coeffs., quantum oscills. 80−49778
n-type, sign change of Hall effect, in quantum limit 77−15875
n-type, spherical samples, size resonances, magnetoplasma waves 79−11168
n-type, spin-magnetophonon resonance 80−96918
n-type, stimulated Brillouin scattering of helicon waves 79−99571
n-type, stimulated recomb. radiation 78−90456
n-type, strongly compensated, ionized donor mol. optical absorpt. spectra characts., 1.5-2.5 mm 79−11422
n-type, sub mm photocond. *(Russian)* 79−38134
n-type, subjected to mag. field normal to current, coherent HF oscills. 78−52026
n-type, submillimetric-wave free-carrier Faraday effect in strong longitudinal elec. field 80−66164
n-type, surface polaritons, excited by microwave magnetoplasma 79−19530
n-type, surface quality improvement by low temp. CVD of SiO_2, and characterisation 80−49932
n-type, surface recomb. velocity, temp. and α-bombardment dose effects 77−8173
n-type, three-phonon assisted cyclotron harmonic transitions in magneto-photoconductivity 80−44652
n-type, transparency, DC field induced enhancement 79−91407
n-type, transverse magnetophonon reson., oscillatory amplitude and damping 78−47813
n-type, transverse magnetoresist. in strong mag. fields 79−4571
n-type, transversely magnetised, parametric instability of acoustic waves 79−65521
n-type, tunable far IR Landau emission with subnanosecond rise time 79−32015
n-type, tunnel diode, with high reverse bias, V-I characts. 79−38158
n-type acoustoelec. current instabilities, threshold field dependence on sample length, 77K 78−76116
n-type anomalous Hall effect, stress depend. 80−65598
n-type Corbino disc power meter for 3 cm wavelengths 79−71428
n-type film, degenerate, electron conc. and resist. temp. depend., band struct. 77−76971
n-type MIS device interfaces, low-temp. CVD of SiO_2, characts. 80−16196
n-type noise, round trip acousto-electronic amplification, anodic piezoelectric transducers *(Russian)* 78−23139
n-type polar semiconductor, TO phonon-helicon coupling, Doppler shifted cyclotron reson. region 79−73539
n-type propagation of magnetoplasma waves, Faraday geometry, effect of strong electric field 79−65510
n-type quantum magnetophonon oscills. of piezoresist. 77−15880
narrow band gap semiconductor, optical nonlinearity due to free carriers 79−81491
negative electron diffusivity in high fields 78−30935
neutron bombarded, optical absorption, struct. defect form. and nuclear alloying *(Russian)* 78−31206
neutron irrad., defect cluster form., effect on elec. props. 80−65062
nonlinear absorption and pulse shaping for 10.6, 9.6 μm laser radiation 78−79077
nonlinear optical effects obs. using CW CO laser 79−3752
nonlinear optical properties, hot electron effects 78−71139
nonlinear refraction and absorpt. 80−9939
nonlinear transmission of picosecond 10.6 μm pulses 80−106559
one-photon absorption coeffs. calc. 77−20884
one-sided abrupt junctions, distinction between avalanche and tunnelling breakdown 78−56211
optical bistability, signal amplification, low power nonlinear effect applications 80−19066
optical constants and oxidation with various surface treatment *(Russian)* 80−88955
optical mixing by mobile carriers 78−25920
optical signal amplification and bistability 80−9937
optical spin resonant four-wave mixing, CW meas. and transient effects 80−48344
oscillatory electron drift rel. in non-ohmic regime at low temp. 79−33291
oxide films grown by anodization in electrolytes, electron spectroscopy exam. *(German)* 79−15837
oxidised surface, detection of excess crystalline Sb by Raman scatt. 78−19453
oxidised surface, photocond. meas. *(Russian)* 77−43664
p-n junction, minority carrier injection in mag. field, recomb. radiation obs. 80−11078
p-n junctions, diffused, avalanche multiplication and impact ionisation 80−15595
p-type, cyclotron reson. of nonequilib. photoelectrons, distrib. function and line profile 78−60336
p-type, deformed, giant negative magnetoresistance 78−87990
p-type, deformed, Landau levels, photocurrent spectra obs. 78−19097
p-type, effect of static mag. fields on transverse photocurrent spectrum 78−14766
p-type, elec. instability and oscills. of transparency in transverse mag. field 78−6407
p-type, heavily doped, LO phonon-carrier interaction, Raman interf. lineshapes 80−93319
p-type, high resist. compensated, generation of microwave radiation 80−34476
p-type, high-resist. compensated, elec. breakdown peculiarities 80−2398
p-type, impact ionization 78−26879
p-type, influence of plastic bending on galvanomag. props. 79−28349
p-type, ion bombardment using 30-80 keV ions, isochronous annealing, elec. props. obs. 79−19295
p-type, IR detector, photovoltaic operation, theoretical anal. 79−224
p-type, low-resistivity n-type layer form. by laser irrad. 77−69944
indium antimonide continued
p-type, magnetoconcentration effect, negative differential conductance 80−70729
p-type, magnetoconductivity and cyclotron reson. in inversion layers 80−49946
p-type, magnetophonon reson. of holes 79−95424
p-type, magnetophonon resonance due to non-equilib. electron injection 80−6881
p-type, mobility, diffusion and thermoelectric power of hot holes 80−39595
p-type, negative magnetoresist. under press. 80−20224
p-type, negative photocond. in strong mag. fields 79−82636
p-type, negative piezomagnetoresist. meas., antiferromag. order form. 78−19061
p-type, oscills. of microwave photocond. and cyclotron reson. of photoelectrons 79−28377
p-type, quantum oscills. of photocurrent due to relax. of photoelectron energies via acoustic phonons 79−73546
p-type, quantum resonances in valence band under uniaxial stress, far IR meas. 79−99481
p-type, radioelec. effect, 100-300K 79−56255
p-type, shift of fundamental absorpt. edge in crossed elec. and mag. fields 80−76034
p-type, spin-flip Raman scattering, review 80−108209
p-type, stimulated magneto-Raman scatt. obs. 77−83924
p-type, stress induced k-linear terms in band struct. 80−49595
p-type, two-phase polycryst. films, negative magnetoresist. 80−11011
p-type, uniaxially deformed, mag. field induced semicond.-metal transition 79−95457
p-type film, elec. transport props., effect of non-stoichiometric excess of In 79−95528
p-type inversion layer, magnetotransport 78−64138
p-type MIS struct., field effect studies 80−80386
p-type plate in crossed E and H fields, even magnetoconcentration effect *(Russian)* 77−85244
parametric excitation in Kane's semiconductor 78−52023
periodically doped crystal prod. by Peltier effect, helicon diagnostics *(German)* 77−48338
phonon assisted cyclotron harmonic transitions 78−48046
phonon assisted cyclotron resonance exact sol. of integral eqn. for Green's function 79−61227
phonon conductivity, 2 to 300K, scatt. mechanisms 79−4436
phonon conductivity, temp. depend., 2-300K 77−31812
phonon dispersion curves, appl. of deformable-ion model 78−59887
phonon dispersion relations, eight-parameter bond-bending forces model 80−70334
phonon viscosity tensor 78−34570
photoconductive and photoelectromag. effect spectral distrib., sample thickness depend. 77−4394
photoconductive laser detector, dynamic range increase 78−49899
photoconductivity, sub MM wavelengths, weakly compensated n-type semiconductor 80−15565
photoconductivity 1.8K, hot carrier and free carrier absorption effects 78−84254
photoconductivity for cryst. covered with thin oxide protective film 77−55578
photoconductivity under uniaxial deform. 79−82637
photoexcited exciton spin-flip scatt. 80−74434
photoluminescence and Raman scattering, interaction of exciton recombination with LO phonons 79−38647
photoluminescence exam. 79−28809
photoresistor in mag. field, increased responsivity 78−39162
pinch effect at room temp. 80−65615
planar p-n junction fabrication by Be ion implantation, CCD chip appls. 77−89833
plasma, drift wave instability 79−15175
plasma, sausage instability, theory and expt. *(Japanese)* 78−10492
plasma, transversely magnetised, instability of EM waves 80−2411
plasma waves parametric amplification 78−43428
polar semiconductor, longit. magneto-Seebeck coeff. in quantising mag. field 79−56250
polar semiconductor, resonant magneto-Raman scatt. 79−51958
polymorphism and cryst. struct. at high temp. and press. 78−95026
positron annihilation 78−72636
quasi-static transport characteristics, expt. and explanation 77−20335
radiation defect annealing following 50 MeV electron beam irrad. 80−15154
radiometer with InSb detector, radioastronomical appl. in 0.2-5 mm wavelength range 77−13241
Raman laser, pulsed, external cavity operation at 10.6 μm 77−71990
Raman laser, pulsed spin-flip, external cavity, low field operation at 10.6 μm 79−41394
Raman laser, pumping by IR multiline NH_3 laser 79−94216
Raman laser, spin-flip, oscill. characts. of external-cavity system 78−55383
Raman laser, spin-flip, Stokes output mag. field depend. 77−61959
Raman laser, spin-flip external cavity CO_2-pumped, with intracavity etalon 78−42345
Raman scattering study of unoxidised Sb in anodic oxide films 80−88985
rapid-scan polarising Michelson interferometer and InSb detector calibration 80−59305
reabsorbed radiative recomb. and photon recycling 80−76076
reaction with Ga 78−23682
recoil damage obs. by PAC with ^{111}Cd 77−89484
recombination processes in high resistivity p-InSb and crystals of n-InSb, photocond. and photomag. effect meas. *(Russian)* 80−88567
recombination processes using impact ionization capture cross sections 80−75577
recrystallised thin films on mica substrate, elec. props. 80−70867
refractive index and absorpt. coeff., cryst. orientation depend. 80−60536
refractive index dispersion 79−24280
relations pressure-volume under high pressure 80−39219
resistivity inhomogeneity meas. with single-sonde potential method 80−65549
resonance effects in mag. field, effect of additional laser illumination 78−72417
resonance Raman scatt. under uniaxial stress near E_1 gaps 79−42960
SBS of laser radiation in presence of mag. field, ion acoustic wave nonlinearity 80−45091
self-diffusion 79−65249

indium antimonide continued
semiconductor plasma, Raman scatt. of waves of fluctuations *(Russian)* 79−94299
semiconductors, plasma oscills. within submillimetre freq. range 80−84473
shallow acceptor contribution to near-resonance spin-flip Raman scatt. 79−95754
shallow donor states in magneto-optical props. 80−6785
Shubnikov-de Haas effect, CO_2 laser induced hot electron effects 78−30957
site selective doping by ion implantation of radioactive nuclei 80−34023
small-gap, electron scatt. and transport props. 78−95294
small-gap, electron scatt. and transport props. 78−95295
solid solns. with Bi, solubility limits, microhardness, microstruct. 78−35368
spin depend. wave functions and band parameters 77−72818
spin flip Raman scatt. from electrons in localised donor states 77−3630
spin flip Raman scattering, gain, linewidth, effective g-value 78−22167
spin flip relaxation time, Raman scatt. 77−3631
spin polarisation, anisotropic size effect, effect on CESR signal 80−70743
spin-flip Raman laser, cond. electron T_1 meas. 77−3593
spin-flip Raman laser, pumped by TE CO_2 laser, fund. characts. *(Japanese)* 77−42542
spin-flip Raman laser 77−50674
spin-flip Raman laser characts. *(Japanese)* 78−25883
spin-flip transitions in magneto-optics and magneto-transport in InSb type semicond. 80−50306
sputtered, NaCl type, compression 79−46751
stimulated spin-flip Raman scatt. and stimulated recomb. radn. 79−72623
stress-induced phase change of single cryst. 79−23719
submillimeter radiation diffraction by electron-density waves 80−7328
submillimetre detector, fast response 78−89541
subMM detector, fast response, for use in measuring electron cyclotron emission 80−27347
substrate, LPE of $InAs_{1-x}Sb_yP_{1-x-y}$, and $InAs_{1-x}Sb_x$ 78−3065
substrate, room temp. CVD of Si_3N_4 80−71597
superconducting in rapidly condensed film *(Russian)* 77−72937
superconducting phases at high press. 78−88063
superconductor-semicond. device research, future prospects 79−28467
surface, (110), cleaved, gap states, field effect meas. 80−84501
surface, (110), core level photoionisation spin-orbit branching ratio, initial and final state effects 79−83094
surface, (110), oxidation process, XPS study 79−15585
surface, (111), oxidation props., LEED and surface cond. meas. 78−15559
surface, Cu deposition, ohmic contact formation, SEM obs. 77−51817
surface, IR spectroscopy of subband levels 80−20277
surface, LEED and surface conductivity during gas adsorption 77−62760
surface, oxidation, water vapour and O_2 excitation effects, XPS obs. 79−100274
surface, plasmon dispersion, appl. to INSb 77−1464
surface, reson. excitation of electron subbands 80−49865
surface, RF etch sputtering under controlled atmosphere 77−44397
surface (110), energy distrib. of dangling-orbital surface states 80−80347
surface (110), initial oxidation, XPS and AES study 80−11542
surface (110), ion bombard. effect on surface struct. and electronic props. 80−6923
surface (110), struct. and electronic props., RHEED and field effect meas. 80−11068
surface (110), struct. determ. by LEED, UPS, and EPR 80−49475
surface (110), surface struct. by elastic LEED, comparison with GaAs(110) and ZnTe(110) 80−80040
surface accumulation layer, sub mm electron cyclotron reson. 78−6576
surface analysis, X-ray photoelectron spectra, surface oxidation-etchant correlation 78−56029
surface carrier accumulation in crossed elec. and mag. fields 80−20205
surface charges induced by chemical and ion etching, electron microscopy and XPS studies *(French)* 80−108614
surface contamination of Cu-coated InSb, ion microprobe meas analyser obs. 77−52729
surface electron and hole mobility and conc. in MISS struct. *(Russian)* 80−44701
surface helicons in semiconductor plasma, theory 80−60019
surface magnetoplasma wave struct. 80−6934
surface magnetoplasma waves, reson. spectrum and dispersion characts. 79−38148
surface plasmon-phonon modes in quantizing mag. field, nonlocal shift 77−72908
surface recombination velocity, repeated cyclic surface treatment effects 77−32065
thermal cond., elec. cond., and thermoelec. power, press. depend. 80−59744
thermoelectric power and relative resist. at press. up to 35 kbar 79−65505
thermoelectric power in longit. quantising field, phonon drag component 78−19064
thin film element having non-linear galvanomagnetic effect 80−34534
thin films, electrophysical props. obs. 80−103765
thin layers, melt grown, mag. field depend. of PEM effect 79−95445
threshold energy for displacement of atoms 78−47428
transistor mat. characterisation 78−87970
transport phenomena, review 79−19587
transversely magnetised plasma, surface-wave reson. 78−30948
tunnel diode, V-I characts., hydrostatic press. effects 79−38157
tunnel diodes, abnormal V-I characts. *(Russian)* 77−8184
two-phonon diffuse scatt. of X-rays 78−26374
two-photon absorption coefficient, 3-band model 79−78679
two-photon absorption spectra 80−20660
N-type, forward biased Schottky barriers on low doped surfaces, current transport 79−24074
undoped n-type, press. induced slow relax. of free electron conc., Hall coeff. meas. 77−47833
uniaxially stressed, elec. cond., Hall coeff. and photocond. at 15K 77−47828
US absorption in alternating elec. field *(Russian)* 78−30959
valence band struct. obtained by magnetophonon effect 77−76748
valence band structure, CPA, bond orbital calcs. 78−87909
variable range hopping cond., percolation theory *(Japanese)* 78−14733

indium antimonide continued
volume plasmon dispersion, anisotropy 78−56090
warm electron coeff. 78−10452
waveguide, nonlinear third harmonic generation of submillemetre waves 80−44632
Wigner crystal, long-wavelength excitations in strong mag. fields 79−82533
X-ray topographic evidence of asymmetrical pre-yield behaviour 80−75229
X-ray two-circle SSD diffractometer appl. in angle dispersive mode 79−14641
Zener tunnelling in mag. and elec. fields 79−91082
Al-Al_2O_3-InSb MIS structures, recomb. processes and carrier lifetimes 79−38177
$Al_xIn_{1-x}Sb$, DC sputtering and struct. 78−52674
Au-InSb Schottky-barrier, photovoltage, temp. effects 77−69415
CO_2 laser control using Ge and InSb 78−1203
Ga-In-As-Sb quaternary system, phase equilib. and heterojunctions 79−34016
Ga-In-As-Sb system LPE layers, pseudoquaternary phase diagram 78−10293
Ga-In-Sb, solidus isotherms and isoconcentration lines 78−56624
Ga-In-Sb system, precipitation of solid phase from liq. phase, thermodynamical formulation *(French)* 77−28003
$Ga_{1-y}In_yAs_xSb_{1-x}$, LPE on GaSb, miscibility gap in liq. phase and lattice mismatch 80−15404
$Ga_xIn_{1-x}As_ySb_{1-y}$, epitaxial film and DH, luminesc. props. 77−686
$Ga_xIn_{1-x}As_ySb_{1-y}$ laser, efficient room temp. stimulated emission, 1.8 to 2.4 μm spectral range 79−10307
$Ga_xIn_{1-x}As_ySb_{1-y}$ tunable electron-beam-pumped laser parameters 80−106524
GaInSb, Be ion implantation, device appl. 80−24478
$Ga_{1-x}In_xSb$, effective radiative recombination centre nature, photoluminescence spectra 79−90998
$Ga_{1-x}In_xSb$, epitaxial, vapour-phase growth using open-tube flow system 79−33943
$Ga_{1-x}In_xSb$, LPE on GaSb by stepwise grading, and characterisation 78−72745
$Ga_{1-x}In_xSb$, vapour phase epitaxial growth by open tube method 78−84109
$Ga_{1-x}In_xSb$:Zn(Te), photolum. and stimulated emission obs. 78−72595
$Ga_xIn_{1-x}Sb$, computer simulation of growth from In soln. 77−51332
$Ga_xIn_{1-x}Sb$, electron transport in RF field, Monte Carlo simulation 80−96932
$Ga_xIn_{1-x}Sb$, growth by LPE 78−27421
n-$Ga_xIn_{1-x}Sb$ Gunn diode, high field domain characts. 80−59992
$Ga_xIn_{1-x}Sb$ LO phonon obs. using Raman scatt. 78−35152
$Ga_xIn_{1-x}Sb$, LPE, growth by vertical dipping method and elec. props. 77−85949
$Ga_xIn_{1-x}Sb$ p-n junction photodiode fabrication, sensitivity as 1 to 2.5 μm detectors *(Japanese)* 80−52311
$Ga_xIn_{1-x}Sb$, transferred-electron effect, and device performance estimation 78−19049
GaSb-InSb solid solns., heavily doped, electronic props. 77−80727
(In, Ga)Sb, sputter deposited amorphous film, impulse stimulated explosive crystallisation 78−84098
In-Sb-Te, region of In-Sb-based solid solutions 77−36466
InAsSb, Be ion implantation, device appl. 80−24478
$InAs_{1-x}Sb$, disorder-enhanced Auger recomb. 79−43014
$InAs_{1-x}Sb_x$, epitaxial film, carrier recomb., elec. and optical props. 79−15164
$InAs_{1-x}Sb_x$, LPE on InAs substrate, $InAs_xSb_yP_{1-x-y}$ used as buffer layer 78−3065
$InAs_{1-x}Sb_x$ on GaSb, LPE growth 80−29293
$InAs_{1-x}Sb_x$, organometallic VPE growth on InAs 80−45233
$InAs_{1-x}Sb_x$-InAs, lattice parameter meas. in epitaxic layers 79−11040
$InAs_{1-x}Sb_x$-InAs backside-illum. narrow band photodetectors 77−61118
$InAs_{1-x}Sb_x$-InAs stepwise-graded struct., steady-state LPE, etching, investig. 77−21042
$InAs_xSb_yP_{1-x-y}$, efficient electron-beam-pumped laser at 3.1-3.7 μm 80−5738
$InAs_xSb_yP_{1-x-y}$, LPE on InAs substrate 78−3065
InGaAsSb based injection heterolaser, 1.9 μm stimulated emission 79−18420
InGaAsSb, LPE growth, and appl. in GaSb/AlGaAsSb/InGaAsSb/AlGaAsSb/GaSb DH 80−16205
InGaAsSb-AlGaAsSb DH laser, room temp. operation at 1.8 μm wavelength 80−43358
InGaSb, LPE growth characteristics, substrate surface contamination dependence 80−39470
$In_{0.58}Ga_{0.42}Sb$, interband magneto-optical transitions, arbitrary field orientation 79−42948
$In_{1-x}Ga_xSb$ alloy system, interband magnetooptical study using Schottky barrier 79−8124
$In_{1-x}Ga_xSb$, band parameter variations 80−20084
$In_{1-x}Ga_xSb$, drift velocity of electrons 77−20327
$In_{1-x}Ga_xSb$, energy gap, temp. depend. and photovoltaic effect 80−70746
$In_{1-x}Ga_xSb$ film, epitaxial growth by multitarget RF sputtering 77−44157
$In_{1-x}Ga_xSb$ films, elec. props., preparation 80−100473
$In_{1-x}Ga_xSb$-Au, photovoltaic effect and Schottky barriers 80−49897
$In_xGa_{1-x}Sb$, energy gap variation, CPA calcs. 78−43294
$In_xGa_{1-x}Sb$, vertical Bridgman Stockbarger growth, magnetic field effect 78−60565
InGaSbAs heterostructures and LED's luminesc. props. in 1-2 micron band 78−10988
In_2O_3-InSb system, with Al(Au) electrode interface state density and oxide charge meas. 77−8200
InSb, acoustic NMR, role of incoherent phonons *(Russian)* 78−80230
n-InSb based MIS struct., carrier generation under nonequilibrium conditions 80−88640
n-InSb, cond. electron spectra in quantised mag. field, impurity resonance scatt. *(Russian)* 80−93178
n-InSb, degenerate plasma, Coulomb collision photon absorpt. dynamic screening *(Russian)* 80−92924
n-InSb, drift induced plasma insolubilities, carrier temp. effects 77−35949
InSb film, threshold singularity on quantising mag. fields 78−87904
InSb, hydrostatically pressed, negative differential cond. at room temp. 79−19600

indium antimonide continued
InSb, impurity distribution, during epitaxial growth from liq. phase 80−88443
p-InSb, influence of plastic deform. on elec. props. 80−103711
InSb, intrinsic capacitance in transverse mag. field *(Russian)* 79−91070
InSb, irrad. real and clean surfaces, work function 78−95336
p-InSb, magnetoconcentration effect in extrinsic cond. range 80−65593
n-InSb, microwave helicon resonances, carrier density, mobility, dielectric const. 80−96930
n-InSb, piezoelectric nondegenerate semicond., magnetoacoustic effects of nonparabolic band struct. 80−96948
InSb, reverse biased diode, negative resist. 78−19129
InSb, US attenuation and Akhieser loss, temp. depend. 79−86842
n-InSb, ultrasound modulation in mag. field 79−69196
InSb:Cd, diffusion props. of Cd, modified C-V technique meas. 79−19401
InSb:Cd, thermal conductivity down to 0.38K 80−107582
InSb:Cd (Zn) (Ge), ion-irradiated, p-n conversion during heat treatment 80−96558
n-InSb:Cr, deep impurities, elec. cond. and Hall coeff. meas., 4.2 to 120K 80−107791
InSb:Cr, electron and hole lifetimes, recomb. at trapping and acceptor levels 77−51760
InSb:Cr, press. effects on transport props. 78−56146
InSb:Cr, Zn and InSb:Zn, impurity centre behaviour, impurity conc. and Hall coeff. meas. 80−65490
InSb:Cr,Zn, transport props. meas. 77−1424
InSb:Cr:Zn, magnetic freeze-out electrons at deep Cr level 79−15169
InSb:Cr(Zn)(Mn)(Ge), recombination of nonequilibrium carriers 79−65496
p-InSb:Cu(Ag), ionisation energy of multiply charged impurities, compensation effects 78−18996
p-InSb:Cu(Zn) film, heavily doped, ionized impurity scatt., Hall effect and DC cond. meas. 79−99643
InSb:F, acceptor props. and diffusion coeff. of F 80−70643
p-InSb:Ge, photocond. in quantising mag. field, uniaxial press. influence 77−15907
p-InSb:Ge, proton irrad. defects energy level scheme, transport props. meas. 80−96576
InSb:Ge, uniaxially compressed, anisotropy of elec. props. 78−19035
InSb:Ge annealing effect on electrical parameters, absorption spectra and photocond. 77−11939
InSb:Ge(Zn)(Mn)(Cd), heat treatment effects on elec. props. 78−43411
InSb:Mn, NMR, magnetoresist., Hall effect and mag. susceptibility meas. 78−26888
InSb:Mn, powder, quadrupole interactions in NMR spectra 79−51880
InSb:Mn^{2+} nondegenerate semicond., mag. impurity indirect interaction *(Russian)* 80−34591
InSb:NiSb, size reson. scatt. from hard cylindrical pot. obs. in magnetoresist. 79−95421
InSb:S, ion implanted, Hall effect meas. 77−20342
InSb:S(Se)(Te), reson. states and reson. scatt., elec. props. 80−49738
InSb:Se, exam. of defects in crystal 80−6423
InSb:Se p-n tunnel diodes, influence of doping on characts. 79−73575
n-InSb:Se(Te), drift tunnel diode, prod., current ratio meas. *(Russian)* 77−8185
n-InSb:Se(Te), heavily doped, anomalous press. depend. of thermoelec. power 77−47840
n-InSb:Se(Te), Moss-Burstein effect, optical energy gap depend. on doping conc. 77−8581
InSb:Sn, equilibrium distribution coefficient of Sn 79−10872
InSb:Te, anomalous anisotropy of magnetoresist. and g-factor 77−47831
InSb:Te, cryst. growth from melt, pulling method, US effects on facet growth 80−76169
InSb:Te, Czochralski cryst. growth, strain configuration study using X-ray anomalous transmission topography 79−23552
InSb:Te, heavily doped degenerate semicond., Kondo effect 79−61053
InSb:Te, periodically laminated plasma, 56.5 GHz transmission, helicon diagrams *(German)* 77−20348
n-InSb:Zn, Zn diffusion out of implanted layers 79−10984
InSb:Zn p-n junctions, ion implantation and diffusion spreading, elec. and photoelec. props. 79−73573
InSb/GaSb superlattice thin films, sputtered, ion-bombardment-enhanced diffusion during growth 78−87882
InSb/$LiNbO_3$ acoustoelectric convolver, gap-coupled, for IR imaging device 78−94492
InSb/$Pb_{0.79}Sn_{0.21}Te$ photodiodes, two-colour sandwich detector 77−82602
InSb-anodic oxide MIS struct., electrophys. props. *(Russian)* 77−39961
InSb-anodic oxide-Ni, energy band diagram, internal photoemission meas. 79−33356
InSb-Au Schottky barrier, photovoltaic spectra and magneto-optical transitions, Landau levels and excitons 77−47858
InSb-Bi system, molten, enthalpy change due to mixing *(German)* 79−86892
InSb-CdTe solid solns., electroreflectance spectra, Brillouin zone transitions 80−7330
InSb-CdTe(PbTe) superlattices, laser deposition of multilayer heteroepitaxial structs. 80−44450
InSb-Cu non-rectifying contacts by immersion plating 78−30984
InSb-GaAs, interface between two polar semiconds., optic-phonon-magnetoplasmons 78−23146
InSb-GaAs semiconductor plasmas, surface wave instabilities, temp. effects 79−78125
InSb-GaSb, compositionally modulated sputtered superlattice, growth and interlayer diffusion 79−56930
InSb-GaSb alloys, directionally solidified, composition variations, electron probe anal. 79−24513
InSb-GaSb solid solution ingots, orientation, twinning and orientation depend. reflectance 79−28001
InSb-GaSb superlattice, interlayer diffusion 77−85086
InSb-GaSb(AlSb), liq., mixing enthalpies *(German)* 79−77755
InSb-Ge eutectic alloy, effect of crystallisation rate on microhardness 79−96110
InSb-HgTe system solid solutions, elec. cond. and thermo-EMF 79−51570
InSb-$LiNbO_3$ layer structures, fabrication and use in SAW amplification 79−41540
InSb-$LiNbO_3$ SAW convolver, efficient struct. realisation, Hall mobility meas. 80−83705

indium antimonide continued
InSb-$LiNbO_3$ struct., electroacoustic interaction temp. depend. 79−69336
InSb-MnSb eutectic alloy, temp. depend. of conductivity and Hall effect, field depend. of Hall coeff. 77−24566
InSb-NiSb, 8 mm band noise generation *(Russian)* 78−39175
InSb-NiSb, eutectic, intraband magneto-optical studies, far IR transmission spectra 79−61371
InSb-NiSb, eutectic alloy, Te-doped, electrophys. props. 77−35955
InSb-NiSb, longit. thermomag. amplifier 77−47838
InSb-NiSb, photovolt. effects rel. to theory of semicond. with internal elec. short circuits 80−65620
InSb-NiSb eutectic, struct. and optical props., IR polariser appl. 80−45078
InSb-NiSb plate, nature of transverse photo-EMF 79−15186
InSb-NiSb plate, transverse EMF due to modulated illumination 77−55572
InSb-NiSb system, anisotropic, acoustomagnetoelec. effect, theory 79−24021
InSb-NiSb two-phase system, photomag. effect, orientational depend., 90-300K *(Russian)* 78−2524
InSb-NiSb two-phase system, electron scatt. mechanism *(Russian)* 78−6373
h-InSb-oxide system, interface recombination activity variation on annealing *(Russian)* 79−78199
InSb-PbSnTe sandwich two-colour IR detector 78−45692
InSb-Pb(Bi), thermodynamic prop. *(German)* 78−75847
InSb-Sb alloy, form of growth of Sb crysts., precip. temp. effects *(Russian)* 77−21144
InSb-Sb eutectic solidification, interface demarcation expts. 79−43228
InSb-SiO-Al MIS structure, prep. and characts. *(Italian)* 78−84715
InSb-Sn(Pb)(Bi), metallic soln., quasibinary alloy, association 78−15373
$InSb_{1-x}As_x$, cryst. struct. and far IR reflectivity 79−56752
$InSb_{1-x}As_xBi_y$, far IR reflectivity 79−56752
$InSb_{1-x}Bi_x$ disordered solid solns, ionisation energy of fluctuation levels 78−72116
$InSb_{1-x}Bi_x$, film, multitarget sputtering growth technique 78−84711
$InSb_{1-x}Bi_x$, metastable epitaxial film, phase diagram 80−76238
$InSb_{1-x}Bi_x$ metastable films, elemental incorporation probability modification by ion bombard. during growth 80−80118
$InSb_{1-x}Bi_x$, multitarget RF sputtering, metastable phase, conductivity transition 80−76178
$(In_2SnTe)_x$-$(2InSb)_{1-x}$ system, semicond., Mossbauer absorption line of ^{119}Sn 78−27146
$LiNbO_3$-InSb amplifier production, role of protective films 78−95220
n-type, highly doped semicond., transverse magnetoresistance in strong mag. field 79−56246
n-type, low temp. electric and mag. resonances meas., model *(Russian)* 78−56159
plastically bent single crysts., dislocation struct. obs. 78−59816
YIG-InSb system, surface magnetostatic wave interaction with drift electrons *(Russian)* 77−12185

indium compounds
see also indium alloys; indium antimonide
binary, with chalcogenides and pnictides, at. vol. and semicond. props. 77−20089
[CC] Ag−(100)InP, metal-semicond.cathode contact, metallurgical, physical, chemical processes 80−107911
chalcogenate and chalcogenite double salts, form. laws and acid-base props. 80−101070
chalcogenides, cryst. struct. types 77−15392
CU In_2O_3-V_2O_5, ceramic elec. resist., dielec. props., porosoty 77−8093
double oxides, elec. cond. 80−34438
$Ga_{1-x}In_xSb$, inverted diode, electron irradiation effect on props. *(Russian)* 78−14378
GaInAsP quaternary alloys, orientation effects in LPE growth 78−92203
GaP/$In_xGa_{1-x}P$/GaAs:(Cs-O) high sensitivity transmission photocathodes, photosensitivity, electron diffusion length 79−78832
halides, UV photoelectron spectra of valence d shells, gas-phase 78−62845
halides, Wasastjerna pot. function, force consts., internuclear separations and binding energies 80−14187
$In_{0.25}Te_{0.75}$, amorphous film, off-state recovery after nonosecond switching 80−44681
α-In_2Te_3. I phase, order-disorder transform. for DO_{22} struct., thermodynamic study 80−70155
InAs, gas-phase epitaxy, prep. thermodynamics, use of partial pressure diagrams 79−79279
inorganic and organometallic cpds., photoelectron spectra, valence bands, ligand field broadening 77−63525
n-InP, magneto-impurity resonances, obs. of central cell struct. 78−95303
InP-InGaAsP-InP, low threshold laser, threshold density temp. depend., LPE method *(Russian)* 78−22133
maximum electric field in high-field domain in Gunn devices 78−79996
MOS capacitors, single- and double-layer insulators 78−14835
n-type, propagation of high power helicons 78−19070
oxidised surface, bonding of cadmium arachidate monolayers, XPS 79−15011
3-phonon diffuse scattering of X-rays, intensity calcs. 80−84027
photoelectromatnetic effect sign inversion at intense photoexcitation 77−85263
plasma, EM wave instability, effect of density gradient 79−1607
pnictides, mixed, impurity induced Raman scatt. spectra 80−88983
ternary and quaternary oxides, prep., cryst. struct., and mag. props. 79−14771
VPE growth, high-purity, by $PCl_3/In/H_2$ technique, progress in control 78−6857
Ag-In_2S_3-Si layered struct., Hall effect, I-V characts., surface states *(Russian)* 80−97001
Ag-InP interface, AgP_2 formation during sintering 80−65309
$Ag_{1/2}In_{1/2}Cr_2S_4$, first order macro to microdomain transition 77−69562
$AgInS_2$, and $AgIn_5S_8$, spray pyrolysis, film struct., elec. and optical props. 80−71592
$AgIn_5S_8$, cryst. growth and props. 78−39677
$AgInS_2(Se_2)$-$SnS_2(Se_2)$, degree of solid solubility and phases characts. 78−35377
p-$AgInSe_2$, far IR props. 79−42976
$AgInSe_2(Te_2)$, phonons, far IR refl. obs. 78−60459

indium compounds continued
Ag_2S-In_2S_3-SnS_2 system quaternary and ternary sulphide spinels, solid solubility and struct. 78−35376
Ag_2WO_4-$In_2(WO_4)_3$, cpd. formation and polymorphism 77−86009
Al-In_2S_3-Si layered struct., Hall effect, I-V charcts., surface states *(Russian)* 80−97001
Al-InP Schottky barrier, increase 80−15603
$Al_xGa_{1-x-y}In_yAs$, LPE on InP, solid-liq. equilib. calcs. 78−84083
$Al_2In_{12}S_{21}$, thermal decomposition 78−20016
$(Al_xIn_{1-x})_2S_3$, x=0-0.33, cryst. struct., X-ray diffr. 79−55710
As-Te-In, glass-forming, density and microhardness 80−103257
As_2Se_3-InI_3, glass system, IR spectra 78−64365
Au-InS Schottky-barrier diode, tunnelling current due to thermionic-field emission 79−33340
BaO-In_2O_3 system, stability of synthesized compounds 77−36487
BiTe-In(Gn,Sn)Te system, physicochemical anal., eutectic type phase diagram with solid soln. region 77−16556
Bi_2Te_3-InTe, thermoelec. props. 77−85250
$Cd_{1-x}In_xCr_2S_4$, ferromagnetic spinel, Cr^{3+} exchange interaction mechanism, Cr^{2+} relaxation, EPR line width depend. 79−69715
$Cd_{1-x}In_xCr_2S_{4-x}P_x$, ferromagnetic spinel, Cr^{3+} exchange interaction mechanism, Cr^{2+} relaxation, EPR line width depend. 79−69715
n-$Cd_{1-x}In_xCr_2Se_4$, effect of doping on elec. cond. and magnetoresist. 78−72174
$Cd_{1-x}In_xCr_2Se_4$, electric, photoelectric and mag. props., metal-semicond. transition *(Russian)* 80−54738
$CdInGaS_4$, far IR refl. and transmission spectra, lattice vibrs. 79−91439
$CdInGaS_4$, layered structure crystals, refractive index meas. method 80−98966
$CdInGaS_4$:Au, single crystal, thermostimulated conductivity *(Russian)* 79−11142
$CdInGaS_4$:Er^{3+}, cryst. field parameters, thermal and mag. props. calc. 77−20540
$CdIn_2S_4$ cubic spinel, electronic band struct. and chem. bonds 78−34768
$CdIn_2S_4$, electronic states, sensitivity to cryst. struct., UPS study 80−45209
$CdIn_2S_4$ films, vac. deposited, struct. and photoelec. props. 79−87006
$CdIn_2S_4$, fund. reflectivity, 2 to 6 eV, band struct. implications 78−39574
$CdIn_2S_4$, photocond. and trap. distrib. 78−39164
$CdIn_2S_4$, photocond. and electron trap distrib. 79−28373
$CdIn_2S_4$, photoluminesc., thermal quenching and recomb. centres 79−24362
$CdIn_2S_4$, single cryst., oscill. behaviour of photocurrent and luminesc. 78−10501
$CdIn_2S_4$, valence band densities of states, XPS meas. 79−28892
$CdIn_2S_{4-x}Se_x$, struct. types anal., X-ray diffr. exam. 79−86756
$CdIn_2Se_4$, defect zincblende semicond., valence band, cryst. struct. effects 78−48278
$CdIn_2Se_4$, needle-like cryst. X-ray exam. 79−42031
$CdIn_3Se_4$, cryst. growth, photoresponse and optical props. 78−39165
CdS, granulated films, optical reson. 79−4863
n-CdS/n-InP/p-InP heteroface solar cell with ultrathin window layer, computer anal. 80−97788
CdS-InP solar cell heterojunctions, CVD fabrication, photovoltaic response 80−93878
$CdSnAs_2$-InP, n-p heterojunction, elec. props., electroluminesc., band struct. 80−75632
$CdSnP_2$-InP, n-n heterojunctions, growth, elec. charcts. 77−11992
CdTe-In_2Te_3, composition depend. of energy gap, optical absorpt. obs. 77−80728
Cu-In-Se system cubic ordered phase existence and charcts. 78−34495
$(CuCr_2S_4)_x$-$(Cu_{0.5}In_{0.5}Cr_2S_4)_{1-x}$ solid solution, piezoelectric effect, X-ray struct. anal. *(Russian)* 80−15978
$CuGa_xIn_{1-x}S_2$ solid soln., IR refl. spectra, comp. depend. 78−52498
$CuGa_{0.5}In_{0.5}Se_2/Zn_{0.29}Cd_{0.71}S$ heterojunction solar cell, preparation and props. 80−101110
$CuGa_xIn_{1-x}Se_2$, CVD, elec. and optical props., use as heterojunction solar cell absorber 79−52095
$Cu_{0.5}In_{0.5}Cr_2S_4$, piezoelectric effect, X-ray struct. anal. *(Russian)* 80−15978
$CuIn_{1-y}Ga_ySe_{2(1-x)}Te_{2x}$ pentenary alloy compounds for photovoltaic solar energy conversion 80−93971
$CuInS_2$, cathodolum. spectra, heat treatment and electron irrad. effects 78−10996
$CuInS_2$, film, spray pyrolysis prod. 79−95953
$CuInS_2$, fund. reflectivity, 2 to 6 eV, band struct. implications 78−39574
$CuInS_2$, homogeneity region and intrinsic dopant mechanism 78−34630
$CuInS_2$, minority carriers lifetime, photoelectromag. effect meas. 79−47125
$CuInS_2$, optical and elec. phenomena 78−39605
$CuInS_2$, p-n junction photovoltaic props. and detectors 79−99574
$CuInS_2$ single phase thin film prep. by flash evaporation 80−100796
$CuIn_{11}S_{17}$, defect spinel, cryst. growth, search for new superionic cond. cpds. 78−31307
$CuIn_5S_8$, single crystn. phase, CVD prep., X-ray cryst. struct. determ. 79−65990
$CuInS_2(Se_2)$-$GeS_2(Se_2)$, degree of solid solubility and phases charcts. 78−35377
$CuInS_2(Se_2)(Te_2)$, thin film, bulk polycryst. and single cryst. samples, AES 78−72648
$CuInSe_2$ epitaxial growth on GaAs 78−84104
$CuInSe_2$, film, spray pyrolysis prod. 79−95953
$CuInSe_2$, growth on CdS (0001) surface using MBE 79−56936
$CuInSe_2$, IR lattice vibr. spectra 79−28765
$CuInSe_2$, influence of impurities and free carriers on optical props. 80−108225
$CuInSe_2$, large single crystals growth by iodine transport and Bridgman methods 78−35300
$CuInSe_2$, melt-grown, EPR charcts. 78−35030
$CuInSe_2$, n- and p-type, elec. resist. and Hall effect, 80 to 500K 79−87096
$CuInSe_2$, Schottky diodes with tunnel device charcts. 78−39215
$CuInSe_2$ thin film fabrication by RF-sputtering for solar cell appls. 80−100786
$CuInSe_2$ thin films, prep. by spray pyrolysis, struct., elect. and optical props. for solar cell appls. 80−100781
$CuInSe_2$-CdS solar cell, polycrystalline thin film, high photocurrent, charcts. 80−61339
$CuInSe_2$-$CuInS_2$, melts, viscosity, elec. cond., density composition prop. graphs 79−14948

indium compounds continued
$CuInSe_2$-$CuInS_2$, solid soln., photo-EMF spectra 80−20248
$CuIn_2Se_{3.5}$, cubic ordered compound, optical gap 78−48175
$Cu_{0.5}In_{2.5}Se_4$, transition state and domain struct. by electron microscopy and diffr. studies 80−15095
$CuInSnS_4$, spinel, cryst. growth, search for new superionic cond. cpds. 78−31307
$CuInTe_2$, direct energy band gap determ., electroreflectance meas. 78−2418
$CuInTe_2$, electroreflectance data, direct gap obs., cryst. field splitting and hybridisation degree 78−39557
$CuInTe_2$, grown from near stoichiometric comp., elec. and optical props. 78−68504
$CuInTe_2$, optical transitions from valence band states 79−87416
$(CuInTe_2)_{1-x}$-$(2ZnTe)_x$, phase diagram and cryst. growth of $CuZn_2InTe$ from $ZnCl_2$ flux 80−16287
$Cu_xIn_xZr_{1-x}S_2$ system, struct. and cond. meas. *(French)* 80−88354
$Fe_{1-x}In_xBO_3$, synthesis, cryst. chem. and mag. props. 78−31058
$Fe_{3-x}In_xO_4$, ferrospinels, cation distrib., Curie point and magnetisation meas. 79−42095
(Ga,In)(As,P) DH lasers, 1.55 μm, low-threshold current densities 80−1221
(Ga,In)As, growth of epitaxial layers 77−12542
Ga-In-As-Sb quaternary system,-phase equilib. and heterojunctions 79−34016
Ga-In-Sb, ternary phase diagram, thermodynamic models of solidus and liquidus isotherms 79−24504
Ga-In-Sb system, phase diagram calcs. in Ga+In rich region 80−60842
$Ga_xIn_{1-x}P$, localised exciton-phonon complex as intermediate state in light scatt. 78−39543
GaAs/GaInP DH, MBE grown, optically pumped laser action at 77K 80−95890
GaAs-$Ga_{1-x}In_xAs$ heterojunction, thermally assisted tunnelling 78−19136
GaAs-$Ga_xIn_{1-x}P$ heterostructure, elastic stresses and substrate/epitaxial film mismatch, X-ray diffr. method 80−92794
GaAs-$Ga_xIn_{1-x}P$ multilayer epitaxial films, MBE technology and epitaxial layers props. 79−33945
GaAs-GaInAs structure, dislocation struct., TEM anal., appl. as IR LED 80−70206
GaAs-$In_{2-x}Sn_xO_{3-y}$ SIS heterostructure solar cells, spray-deposited 80−101106
GaAs-$In_yGa_{1-y}P$, CW room temp. DH lasers prep. by VPE 77−10942
GaAs-InAs, pseudobinary alloy, phase diagrams calc. 78−52786
GaAs-InP heterojunction laser output wavelength control 80−74384
GaAs-InSe, heterojunction, electronic processes *(Russian)* 79−56312
p^+-GaAs-n-(Ga,In)As heterostructure, thermally assisted tunnelling currents 77−20412
$GaAs_{0.7}P_{0.3}$-$In_{0.34}Ga_{0.66}P$, CW heterojunction laser, visible, laser operation 77−38886
$GaAs_{1-y}P_y$-$In_{1-x}Ga_xP_{1-z}As_z$, DH laser, low threshold visible spectrum 78−5471
$GaAs_{1-x}Sb_x$-$Ga_{1-x}In_xP_{1-y}As_y$ multilayer structure, continuously tunable electron beam pumped laser 78−50802
$Ga_yIn_{1-y}As_xP_{1-x}$-InP heterostructure, lattice matching and cryst. perfection 78−6437
GaInAs, efficient photodiode for near IR detection 78−16848
GaInAs, electron-pumped laser, far-field radiation pattern, optical confinement effects 79−86181
GaInAs, photocathode with negative electron affinity, photoemission, influence of strong elec. field 79−8227
GaInAs-InP, growth by low-pressure metalorganic CVD 80−71595
GaInAs-InP injection lasers with longer wavelengths for optical fibre communications, review *(Japanese)* 78−25892
$Ga_{0.47}In_{0.53}As$, electron and hole impact ionisation rates 80−49745
$Ga_{0.47}In_{0.53}As$, HF carrier mobility, temp. depend., theory 80−75593
$Ga_{0.47}In_{0.53}As$, homojunction avalanche photodiode, exam. of props. 78−37072
$Ga_{0.47}In_{0.53}As$ homojunction photodiode, avalanche photodetector for 1.0-1.6 μm region 79−6179
$Ga_{0.47}In_{0.53}As$, LPE growth and characterisation 80−10845
$Ga_{0.47}In_{0.53}As$, MBE, InP/$Ga_{0.47}In_{0.53}As$/InP DH laser fabrication and room temp. operation 78−74906
$Ga_{0.47}In_{0.53}As$ p-n junctions, band-to-band tunnelling current 80−107895
$Ga_{0.47}In_{0.53}As$, photodetector applications 80−95140
$Ga_{0.47}In_{0.53}As$/InP DH lasers double cladded with InP by LPE technique, 1.67 μm operation 79−50314
$Ga_{0.7}In_{0.3}As$ photodiodes, fibre optic appls. 79−40613
$Ga_{1-x}In_xAs$, and $Ga_{1-x}In_xAs_{1-y}P_y$, quantum magnetoresist. results, using pulsed fields up to 35 T 79−73528
$Ga_{1-x}In_xAs$ epitaxial layer growth by organometallic pyrolysis, homojunction LED prep. 80−76194
$Ga_{1-x}In_xAs$, IR reflectivity, cluster effect on optical phonons 80−97259
$Ga_{1-x}In_xAs$, optical detection of CESR 77−36155
$Ga_{1-x}In_xAs$, organometallic VPE growth using trimethylarsenic 80−60788
$Ga_{1-x}In_xAs$, photocathode, work function depend. of photoelectric emission 78−68071
$Ga_{1-x}In_xAs$ photocathode, negative electron affinity, photoelectron scatt. in Cs-O film 79−28899
$Ga_{1-x}In_xAs$ photodetectors for 1.3 micron PIN-FET receiver 80−13145
$Ga_{1-x}In_xAs$ solid solns., electron scatt. by isoelectronic impurities in covalent crysts. 79−11129
$Ga_{1-x}In_xAs$, VPE grown, refractive index, reflectance meas. 79−4780
$Ga_{1-x}In_xAs$, VPE layers, main electron trap, transient capacitance spectroscopy obs. 78−34800
$Ga_{1-x}In_xAs$:Mn grown by LPE, elect. props. 80−100541
$Ga_{1-x}In_xAs$-GaAs epitaxial interface with small misfits, TEM image contrast 80−2275
$Ga_{1-x}In_xAs$-GaAs low-misfit epitaxial interface, electron microscope contrast 79−73416
$Ga_xIn_{1-x}As$, alloy film surface processes controlling growth by MBE RHEED and AES exam. 78−84084
p-$Ga_xIn_{1-x}As$, Auger recomb., theory and luminesc. expts. 78−56518
$Ga_xIn_{1-x}As$, cryst. growth on (100) InP by LPE 78−56591
$Ga_xIn_{1-x}As$, far IR reflectivity spectrum, damped harmonic oscill. model 77−52070
$Ga_xIn_{1-x}As$, method for determ. of liquidus surfaces in Ga-In-As phase diagram 77−28787
$Ga_xIn_{1-x}As$, on ⟨111⟩B InP, LPE growth, characterisation of high purity lattice 80−104082

indium compounds continued
$Ga_xIn_{1-x}As$ on InP, lattice matched LPE film growth and characts. 78−72033
$Ga_xIn_{1-x}As$ p-n junction, growth and electrolum. spectra 77−20420
$Ga_xIn_{1-x}As$, prep. and props. 79−100047
$Ga_xIn_{1-x}As$, spontaneous and stimulated emission, electron beam excitation 77−58333
$Ga_xIn_{1-x}As$, substrate orientation effect on liq.-solid distrib. coeffs., 600-700°C 80−2278
$Ga_xIn_{1-x}As$, VPE growth, thermodynamic anal. 80−2933
$Ga_xIn_{1-x}As$:Ge LED, by LPE, radiation emitted at 1.02 μm 78−48235
$Ga_xIn_{1-x}As$-InP, lattice matched LPE film growth and characts. 78−15320
$Ga_xIn_{1-x}As$-InP, MBE film growth, composition control obs. 80−84399
$Ga_xIn_{1-x}As$-InP heterostructure, growth by MBE 79−8251
GaInAsP alloys, materials and devices for long wavelength optical communication 80−99854
GaInAsP DH laser diode CW modelocking 79−7126
GaInAsP DH laser emitting at 1.55 μm, threshold currents 80−83609
GaInAsP, diffusion-limited growth in LPE 80−10842
GaInAsP diode lasers, self-sustained pulsations in light output 80−64012
GaInAsP, electroabsorption 79−78652
GaInAsP LEDs, 1.3-1.6 μm, appl. in long haul high data rate fibre optic communication systems 80−102854
GaInAsP layers on InP substrate, conditions for lattice matching in LPE growth 78−6866
GaInAsP on InP substrate, epitaxially grown, fabrication of avalanche photodiode 78−37071
GaInAsP, rectifying and ohmic contacts 80−80376
GaInAsP, VPE growth and props. 80−16194
GaInAsP/InP, DH laser, low threshold current density, 1.3 μm emission 79−94249
GaInAsP/InP 1.5-1.6 micron integrated twin-guide lasers with distributed Bragg reflectors 80−74380
GaInAsP/InP buried heterostruct. laser, 1.6 μm, fabrication and room temp. CW operation 80−58568
GaInAsP/InP DH lasers, with (100) substrate, 1.2-1.5 μm, LPE growth conditions 79−15617
GaInAsP/InP DH lasers, direct modulation charact. meas. by sharp pulse method 80−1245
GaInAsP/InP DH lasers emitting at 1.3 μm, growth and characts. 80−64057
GaInAsP/InP DH stripe geometry lasers emitting at 1.3 μm, growth characterisation 80−69410
GaInAsP/InP DH lasers, 1.3 μm wavelength, LPE growth and characterisation 80−69411
(100)GaInAsP/InP DH lasers, 1.5-1.6 μm wavelength, two phase soln. LPE technique using anti-meltback layer 80−99750
GaInAsP/InP integrated twin-guide lasers with distributed Bragg reflector, spectral behaviour 80−74381
GaInAsP/InP lasers, 1.5 μm emitting, high temp. CW operation 80−95889
GaInAsP/InP lasers, LPE grown, effect of p-doping on carrier lifetime and threshold current density 80−99726
GaInAsP/InP narrow planar stripe lasers, lasing characts. 80−95897
GaInAsP/InP optical sources for 1.2 to 1.4 μm wavelength region, growth and props. 79−90023
GaInAsP/InP system, chemical etching, fabricating laser diodes and integrated optical circuits 80−38030
GaInAsP-InP, broad-area and stripe-geom. DH laser, for fibre optic communication 78−42356
GaInAsP-InP, lattice matched, emission spectrum half width rel. to peak wavelength 80−2820
GaInAsP-InP avalanche photodiode, fabrication and characts. 78−54454
GaInAsP-InP buried stripe DH laser, fabrication using meltback method and CW operation 79−3708
GaInAsP-InP buried heterostructure laser with mesa substrate, linear light/current characts. 79−36894
GaInAsP-InP buried heterostructure lasers, 1.6 μm wavelength 80−64055
GaInAsP-InP DH laser, 1.3 μm CW operation at room temp. 77−71986
GaInAsP-InP DH laser grown by newly designed vertical LPE furnace 78−9380
GaInAsP-InP DH laser, relaxation and delay in oscillations 78−13709
GaInAsP-InP DH layers, lattice deform. and misfit dislocations 79−19473
GaInAsP-InP DH lasers with low threshold, narrow-beam divergence 79−36892
GaInAsP-InP DH lasers, for fibre optic communications 79−31924
GaInAsP-InP DH laser, LPE and wet chem. etching techniques for integration 79−98388
GaInAsP-InP DH laser, room temp. CW laser 80−28235
GaInAsP-InP DH lasers made by melt-back method, operating characteristics 80−48287
GaInAsP-InP DH lasers, LPE growth and operational characts. 80−53313
GaInAsP-InP DH injection lasers prep. by LPE, 1.11-1.67 μm operation 80−53321
GaInAsP-InP double heterostructure laser, prep. by LPE growth and laser operation 77−3590
GaInAsP-InP facet lasers with chemically etched end mirrors 80−1228
GaInAsP-InP integrated twin-guide lasers with first-order distributed Bragg reflectors, 1.3 μm 80−58567
GaInAsP-InP lasers and detectors, for fibre optic communications at 1.0-1.6 μm 79−3803
GaInAsP-InP mesa substrate buried heterostruct. injection laser, fabrication and lasing props. 80−53319
GaInAsP-InP planar stripe lasers, sputtered SiO_2 film as Zn-diffusion mask 80−48249
GaInAsP-InP stripe-geometry monolithic laser with etched mirror and monitoring detector 80−64054
GaInAsP-InP stripe laser, etched mirrors fabricated by wet chem. etch 80−99744
GaInAsP-InP surface emitting injection laser, fabrication and lasing props. 80−28234
GaInAsP-InP Zn diffused stripe geometry DH diode laser fabrication 79−98386
$Ga_{0.08}In_{0.92}As_{0.18}P_{0.82}$, band struct., optical studies 79−47013
$Ga_{1-x}In_xAs_{1-x}P_x$, VPE growth and characterisation 78−22970
$Ga_{1-x}In_xAs_{1-y}P_y$-InP DH laser, carrier lifetime meas. 77−61955
indium compounds continued
$Ga_xIn_{1-x}As_yP_{1-y}$, conduction band and phonons, Shubnikov-de Haas effect, magnetophonon resonance, Raman scattering 80−24795
n-$Ga_xIn_{1-x}As_{1-y}P_y$, photoluminesc. of epitaxial films, isovalent substitution 80−16097
$Ga_xIn_{1-x}As_{1-y}P_y$, spontaneous and stimulated emission, electron beam excitation 77−58333
$Ga_xIn_{1-x}As_{1-y}P_y$:Ge(Sn)(Te), epitaxial film, elec. and optical props. 79−11251
$Ga_xIn_{1-x}As_{1-y}P_y$-InP, room temp. electron-beam-pumped laser with dielec. waveguide, output characts. 80−5761
$Ga_xIn_{1-x}As_xP_{1-x}$-InP buried-stripe DH diode laser, room temp. CW operation 77−50671
$Ga_xIn_{1-x}As_yP_{1-y}$, CVD by Ga-In-P-H-Cl system, 80−54159
$Ga_xIn_{1-x}As_yP_{1-x}$, epitaxial layers on InP, expt. determ. of effective masses 79−65370
$Ga_xIn_{1-x}As_yP_{1-x}$, thermal expansion coefficients, 25-400°C 79−46817
$Ga_xIn_{1-x}As_yP_{1-y}$, anodisation, effect of pH, current density and illumination 78−95823
$Ga_xIn_{1-x}As_yP_{1-y}$, electron effective mass, cyclotron reson. and magneto-phonon effect meas. 80−103618
$Ga_xIn_{1-x}As_yP_{1-y}$, IR refl. spectra 80−60602
$Ga_xIn_{1-x}As_yP_{1-y}$, LPE layers, growth and characterisation 78−38983
$Ga_xIn_{1-x}As_yP_{1-y}$ LPE layers matched to InP, comp. and lasing wavelengths 78−71103
n-$Ga_xIn_{1-x}As_yP_{1-y}$, transferred electron oscill., threshold field 77−85227
$Ga_xIn_{1-x}As_yP_{1-y}$/GaAs structure, LPE growth and lattice consts. matching conditions 80−59822
$Ga_xIn_{1-x}As_yP_{1-y}$-GaAs substrate, lattice matching 79−90901
$Ga_xIn_{1-x}As_yP_{1-y}$-InP, CW stripe-geometry lasers, fabrication and props. 77−10943
$Ga_xIn_{1-x}As_yP_{1-y}$-InP injection laser, partially loaded with distributed Bragg reflector 78−82986
$Ga_xIn_{1-x}As_yP_{1-y}$-InP, rib-waveguide injection lasers made by one-step LPE 79−59710
$Ga_xIn_{1-x}As_yP_{1-y}$-InP injection laser partially loaded with first-order distributed Bragg reflector 79−98387
$Ga_xIn_xAs_yP_{1-y}$-InP substrate, lattice matching 79−90901
$Ga_xIn_{1-x}As_yP_{1-y}$InP laser, DH, 1500 h continuous CW operation 77−42537
$Ga_{1-y}In_yAs_xSb_{1-x}$, LPE on GaSb, miscibility gap in liq. phase and lattice mismatch 80−15404
$Ga_xIn_{1-x}As_ySb_{1-y}$ tunable electron-beam-pumped laser parameters 80−106524
GaInP, composition dependence of phonon frequencies 78−75764
(GaIn)P, dislocation etching of (001) faces with H_3PO_4 etchant 80−15103
$Ga_{1-x}In_xP$, mixed cryst., IR absorption by zone edge lattice vibrs. 78−19487
$Ga_xIn_{1-x}P$ alloy films, surface processes controlling growth by MBE, RHEED and AES exam. 78−84084
$Ga_xIn_{1-x}P$, band struct. enhancement of indirect transitions, piezoreflectance meas. 77−20823
$Ga_xIn_{1-x}P$, diffuse X-ray scatt. investig. of cation distrib., segregation 77−24409
$Ga_xIn_{1-x}P$ electrode, in aqueous electrolytes, impedance meas. *(French)* 79−87153
$Ga_xIn_{1-x}P$, epitaxial film, diffusion of Cu(Au)(Zn), intrinsic impurity effects 78−87825
$Ga_xIn_{1-x}P$, film, energy band struct., photolum. meas. 79−7784
$Ga_xIn_{1-x}P$, flat band pot., impedance meas. and photoelectrochemistry *(French)* 80−49894
$Ga_xIn_{1-x}P$, LPE producing coherent interface, model 77−59229
$Ga_xIn_{1-x}P$ MBE layers, comp., Rutherford scatt. and X-ray diffr. meas. 80−75457
n-$Ga_xIn_{1-x}P$, optical props. and energy spectrum of donors 78−72567
n-$Ga_xIn_{1-x}P$ photoelectrochemical cells, bandgap energy, electronic transition mode, and diffusion length 80−72070
$Ga_xIn_{1-x}P$, real struct. exam. by electron microscopy and channelling 78−2143
$Ga_xIn_{1-x}P$, refractive index comp. depend., nonlinearity parameter *(German)* 77−32344
$Ga_xIn_{1-x}P$ solid soln. epitaxial layers, stabilisation of composition 78−18933
$Ga_xIn_{1-x}P$ solid solns., isothermal liq. epitaxy 80−60793
$Ga_xIn_{1-x}P$, undoped liquid epitaxial layers, effect of heat treatment on photoluminescence 78−60512
$Ga_xIn_{1-x}P$, VPE, recent advances, book contrib. 79−66011
$Ga_xIn_{1-x}P$, with indirect band struct., radiative recomb. of free excitons, cathodolum. meas. 77−90202
$Ga_xIn_{1-x}P$:Mn, ESR of Mn 79−11341
$Ga_xIn_{1-x}P$:N, Delta lattice parameter model, correl. with electronic props. 78−91560
$Ga_xIn_{1-x}P$:N layers, LPE growth, luminesc. and direct exptl. obs. of band struct. effects 77−52157
$Ga_xIn_{1-x}P$:Si, solid soln., splitting of ground state 79−51527
$Ga_xIn_{1-x}P$-GaAs heterostructures, photolum. props., assessment as laser struct. 80−20705
Ga_xIn_xP, LPE, with GaP saturation source wafer *(Polish)* 78−23633
$Ga_xIn_{1-x}P$, piezomodulation spectra of cond. band struct. 77−48191
GaInPAs, CW strip heterolaser, characts. 78−9382
GaInPAs heterostructures and LED's, luminescent props. in 1-2 micron band 78−10988
GaInPAs laser using multicomponent solid soln., room temp. operation 77−75516
GaInPAs, narrow-band tunable injection laser, 1.06 μm 79−76713
GaInPAs/InP heterostructure DFB laser under optical pumping, lasing characts. 80−87396
GaInPAs-InP, high-efficiency LED 79−65545
$Ga_{1-x}In_xP_{1-y}As_y$, carrier compensation and alloy scatt. 80−29490
$Ga_{1-x}In_xP_{1-y}As_y$, drift vel. elec. field characts., Monte Carlo simulation 77−39839
$Ga_{1-x}In_xP_{1-y}As_y$, electron transient drift vel., influence of effective mass and alloy scatt. 80−2384
$Ga_{1-x}In_xP_yAs_{1-y}$/InP DFB injection laser, one-step LPE 80−58575
$Ga_xIn_{1-x}P_yAs_{1-y}$, 111-A and 111-B faces, defect struct., etching and X-ray diffr. obs. 80−2026
$Ga_xIn_{1-x}P_yAs_{1-y}$, (0.5<y<0.9), LPE on InP, Ga, As distrib. coeffs., lattice matching 78−47673
$Ga_xIn_{1-x}P_yAs_{1-y}$-InP(GaAs), DH integrated optics development 80−33240

indium compounds continued
p-$Ga_xIn_{1-x}PyAs_{1-y}$/Au-Zn, specific contact resist. 80−84509
$Ga_xIn_{4-x}PyAs_{1-y}$, In rich bulk single crysts. growth from melt via gradient freeze method, and characterisation 78−68618
GaInSb, intervalley electron transfer, drift velocity and diffusion coefficient 80−39594
$Ga_{1-x}In_xSb$, press.-induced structural phase transition 78−30751
$Ga_{1-x}In_xSb$, temp. gradient zone melting 80−50550
$Ga_{1-x}In_xSb$-GaSb, lattice parameter meas. in epitaxic layers 79−11040
$Ga_xIn_{1-x}Sb$ diode, with Au metallisation, interdiffusion effect of heat treatment 78−14820
$Ga_xIn_{1-x}Sb$, electron transport props. calc. by Monte Carlo method 77−76834
$Ga_xIn_{1-x}Sb$, Ga-rich, prep. by Czochralski technique 80−60771
$Ga_{1-x}In_xSe$, energy spectrum and struct., X-ray diffr. and light absorption 79−11437
$Ga_{1-x}In_xSe$, exciton spectrum nature and anisotropy of electron bands near absorption edge *(Russian)* 79−51483
$Ga_{1-x}In_xSe$, layered, luminescence and photocond. obs., two-photon excitation 78−76521
$Ga_{1-x}In_xSe$, magnetic susceptibility anisotropy, chemical bonds, electron density distribution *(Russian)* 80−50073
$Ga_{1-x}In_xSe$, Raman scatt. spectra, optical phonon freq., cryst. vibr. freq. types 80−29744
$Ga_{1-x}In_xSe$ solid solution, IR spectra of static reflectivity 79−69849
$Ga_xIn_{1-x}Se$, fabrication, struct., elec. and optical props. 80−44180
GaP-InAs solid solns., energy band struct., edge absoprtion spectra 78−39018
GaP-InP, pseudobinary alloy, phase diagram calc. 78−52786
GaP-InP solid solution, quantitative analysis, use of internal calibration technique developed by AES 77−36834
$(GaP)_x(InAs)_{1-x}$ solid solution, IR reflection spectra 77−69830
GaSb-$Ga_{1-x}In_xSb$ p-n heterojunction, electrolum. spectra and elec. props. 77−12444
GaSb-InAs system, (110) surface and interface electronic struct. 80−100494
$GaSb_{1-x}As_x$-$In_{1-x}Ga_xAs$ heterojunction, prep. by MBE, transport props. 77−80827
GaSe-InSe, heterojunction, electronic processes *(Russian)* 79−56312
GaSe-InSe, heterostructure fabrication using laser radiation 79−73580
Ga_2Se_3-In_2Se_3, semiconducting props. of four stable phases 77−55528
Ga_2Se_3-In_2Se_3 solid solution system, X-ray diffr. exam. 77−63639
Gd_3InO_6, high press. synthesis, cryst. struct. 77−68955
Ge-In-Ga system, microscopic and X-ray phase anal. 77−12606
Ge-In-Te system, homogeneity region, struct., electrophysical props. 78−44091
Ge-In-Te system, region of solid soln. of In in GeTe 77−51499
Ge-InAs based MIS struct., avalanche carrier multiplication 80−88566
Ge-InP system, phase analysis 78−23674
Ge-S-In, chalcogenide glass, determ. of glass phases, phys. props. meas. 79−23526
Ge-S-In system glasses, photoinduced changes 80−24365
Ge-Se-In system glasses, vitreous phase struct. 77−76320
Ge-Te-As-In quaternary compounds, elec. resist. of thin sheets, Mott's theory *(Spanish)* 77−69320
Ge-Te-As-In quaternary compounds, elec. props., Hall effect *(Spanish)* 77−69344
Ge-Te-As-In quaternary compounds, thin sheets elec. props., thermoelec. power *(Spanish)* 77−69358
$(Ge_{1-x}In_x)_{1-x}Te$, rhombohedral and cubic phases, transport effects 78−2481
$(HfO_2)_y(In_2O_3)_{1-y}$, bulk resistivity 77−35936
$Hg/Na_2B_4O_7.10H_2O$ contacts, double-layer capacitance, temp. depend. 80−44707
Hg-InP Schottky-barrier diode, contact times, I-V charcts. 80−96971
$HgCr_2Se_4$-$CdIn_2S_4$ heterojunctions, prep. and photovoltaic prop. 78−34892
$Hg_3In_2Te_6$, complex ordered-vacancy cpd., struct. and lattice dynamics 78−34496
IN_2O_3:Sn, RF magnetron sputtered film, elec. and optical props. 80−104065
$_xI_{1-x}$ mixtures, high-temp. solids and melts, struct., thermodynamic props., Raman spectra obs. 80−66174
(In,GA)(As,P) binary, ternary and quaternary, hydride vapour phase epitaxy, cryst. growth and props. 80−66434
(In,Ga)P/Ga(As,P) DH laser, red-emitting, optical and elec. charcts. 78−66826
n-$(In_xSn)O_y$-p-InP solar cell, growth, efficiency 77−72910
n-In Ar:Te(Sn), heavily doped, cathodoluminescence, doping effect on luminesc. band position and spectral profile 80−45153
In complex, photoluminesc. spectra, $\pi \rightarrow \pi^*$ and charge transfer L→M transitions, Stokes shift 78−64407
In complexes, chlorocomplexes, digitised Raman band profiles 77−71802
In complexes, formation in aq. solutions, perturbed γ-ray directional correlation 77−12847
^{111}In complex, ^{111}In-DTPA, renal function meas. in dogs 77−66838
In-Ar mixture, metal-insulator transition, resistivity meas. 77−76883
In-As system, exam. of thermodynamic consistence of models, and QCE approx. for activity coeffs. *(German)* 80−24615
In-As system, p-T-x diagram 77−8801
In-As-P, liquidus surface in ternary phase diagram, simplex lattice method 77−7847
In-As-Se-I system, glass form. obs. 77−77466
In-EDTA tracer, for groundwater flow investig., neutron activation anal. 78−11921
In-Ga-As system, heterophase equilibrium, phase diagram calc. 79−43212
In-Ga-As-P, phase diagram rel. to lattice matched LPE 78−39708
In-Ga-P ternary system, low temp. phase diagram rel. to epitaxial growth 80−84916
In-In_2O_3-Pb, Josephson tunnel junction fabrication for MM-wave detector 80−100427
In-In_xO_y-Pb tunnel-junction barriers, evidence for chemical annealing effects 79−42701
In-In-P-GaP, liquidus surface obs. 78−22829
In-O film, AC behaviour, dielec. relax. 77−52019
In-P melt, diffusion coeff. of Ga 77−85927
In-P system, liquid-vapour equil., VP functional depend., 1023 to 1123K 79−42228
In-P-As-Sb, III-V quaternary alloy, $A_xB_yC_zD$ or $AB_xC_yD_z$, energy band gap and lattice constant 79−4296

indium compounds continued
In-S system, vac. deposited films, form., reacts. 78−43259
In-Sb-Bi system, solid solns., solubility limits, microhardness, microstruct. investig. 78−35368
In-Sb-Cd system, phase diagrams 79−87617
In-Sb-Te, region of In-Sb-based solid solutions 77−36466
In-Se, liq., mag. susceptibility meas., electron localisation and chem. bonding 80−60178
In-Te, liq., mag. susceptibility meas., electron localisation and chem. bonding 80−60178
In-Te, liq., reflectance, 0.65-3 eV, comp. depend. 78−72549
In-Te alloys, liq., transport props. interpret. using effective-medium theory 77−76806
In-Te liquid alloys, mag. susceptibility 77−59383
In-Te system, IR spectra *(Russian)* 78−84589
In-Te system, thermodynamic props. 77−12821
In-Te system cpds., degree of dissoc. from curvature of liquidus line 78−22828
In-Te-SnTe, phase equilib. 77−86006
(In+InP) melt, critical undercooling determ. and P content change after annealing *(Slovak)* 80−55430
p-$In_{0.77}Ga_{0.23}As$/Ag photocathode, field assisted photoemission to 2.1 microns 80−76130
$In_{1-x}Al_xAs$, band gap, IR absorpt. spectra meas. 80−66205
$In_xAl_{1-x}P$, proportional ingredient content determ. by X-ray fluoroscopy 80−97747
$In_{12}Al_2S_{21}$, preparation, struct. and elec. props. 77−59685
InAs (110) surface and InAs-GaSb (110) interface, electronic states, Green's function technique, tight binding approx. 80−49855
InAs, absorpt. rel. to dopant admixture 78−95596
InAs amorphous film, DC sputtered, optical absorpt. 78−19589
InAs and solid solutions, recombination mechanisms of excess carriers, luminesc. obs. 80−97337
InAs anodic oxide films prep. and props. 80−55553
InAs, anomalous avalanche breakdown 80−80284
p-InAs, Auger recomb., theory and luminesc. expts. 78−56518
InAs avalanche diode, noise meas. 77−4431
n-InAs, avalanche formation, high intensity IR transmission limit 79−78684
InAs, band gap and effective mass, depend on impurity conc. 79−69412
InAs, brittle, deform. during static indentation in single crystals 79−87714
n-InAs, cathodoluminescence, radiative recomb. of hot carriers 77−8667
p-InAs, charcts. of Pb supercond. contact 79−38254
InAs, chem. transport equilib. with I_2 in gaseous phase *(French)* 77−55876
InAs chem. transport equilib. with I_2 in gaseous phase *(French)* 77−55877
InAs, cyclotron resonance, in zinc blende struct. semiconductor *(German)* 78−10337
InAs, dislocation velocities, double etch technique exam. 78−30629
n-InAs, EPR, oscillations of transverse magnetoresistance in weak mag. field 79−91086
n-InAs, edge luminescence band, shape depend. on degree of doping, band gap 80−7405
InAs, elec. props. after heating for 300 to 900°C for 1 to 100 hours 78−47793
InAs, electrical conductivity and thermoelectric power charge due to melting 80−100490
InAs, electron beam excitation, luminesc. and stimulated emission 77−16339
n-InAs, electron irrad., carrier introduction rate, annealing 80−24948
n-InAs, electron irrad., rel. to thermal and electrophysical props. *(Russian)* 80−39154
InAs, electron irrad. at 50 MeV, elec. and optical props. 77−47486
n-InAs, electron mobility dependence on conc. Hall effect at 300K 78−47794
InAs, electron surface props., contact potential difference and photoemission expts. 77−47884
InAs, electroreflectance spectrum 78−19479
InAs, epilayer, MBE growth parameters, relationship with elec. props. 80−2296
InAs epilayers in MOS, carrier transport coeffs. determ. by multilayer model 78−2575
InAs, epitaxial, laser action mechanisms with electron beam excitation 80−28240
InAs epitaxial film on GaAs, far IR reflectivity obs. 77−40251
InAs epitaxial layers, on GaAs substrate, electron diffr. and SEM exam., electronic props. 79−1552
InAs, exam. of decomposition of donors 79−1605
InAs, far IR transmission spectrum 78−4713
InAs, film, CVD H_2O transport method, Hall element preparation 77−40377
InAs film, DC sputtering, struct. and elec. props. 77−66567
InAs films, MBE grown on GaAs, electron mobilities, lattice mismatch effect 80−80419
InAs, fine struct. in energy derivative reflectance spectra 79−78705
InAs, fine struct. of diamag. excitons, oscillatory magnetoabsorpt. obs. 78−18971
InAs, Hall effect sensor for mag. fields up to 23 T 77−10066
InAs, heat and entropy of melting, assessment by quantitative thermography 77−15550
n-InAs, heated electron gas, longitudinal optical phonon form., IR absorpt. modulation 80−45079
InAs, heavily doped, Burstein-Moss effect and near-band-edge luminesc. 79−47525
n-InAs, heavily doped, spontaneous radiative recomb., complete vel. and radiative capacity 79−11458
InAs, heteroepitaxial, charge transport obs. by gate-voltage-controlled meas. on MOS struct. 77−47912
InAs, heteroepitaxial, far IR refl. and transmission meas., surface and interface effects 80−16044
InAs, heteroepitaxial film, orientation and struct. investigation 79−82480
InAs heteroepitaxial layers, VPE grown, effect of $AsCl_3$ mole fraction on elec. props. 79−11255
InAs, heteroepitaxial layers, $AsCl_3$ mole, fraction and substrate orientation effects on elec. parameters 80−39690
InAs, high temp. thermodynamic data, quantitative fits to liquidus line 77−63637
n-InAs, hot electron temp. determ. by interference modulation of radiation 80−44610

indium compounds continued
InAs IR filter properties, operational characts. of antireflection coatings 79−14107
InAs, IR hot carrier diode mixer 78−29161
InAs, IR reflectivity, longitudinal optical phonon-plasmon coupling 77−59578
InAs, impact ionisation and Auger recomb. 77−20329
InAs, in MOS struct., electrorefl., band-population effects under heavy surface accumulation 77−48167
InAs, individual solubilities and cosolubilities of Zn, Cd, Te, microhardness 77−16552
InAs, interband Faraday rot., Roth theory calcs. 77−52046
InAs, intrinsic point defects, nature and influence on electrophys. props. 78−79609
InAs laser, electron-beam-pumped 77−50689
InAs, laser excitation, photocond., optical absorpt., electron-hole scatt. 77−43661
InAs, lattice dynamics 79−14895
InAs, liquid interaction parameters determ., 580-670°C 80−65197
InAs, longitudinal magnetoresistance in extreme quantum limit *(Russian)* 80−11008
InAs, MBE growth, SEM, RHEED, optical microscopy and elec. meas. 78−18925
InAs, MIS struct., C-V characts., interface state densities and storage times meas. 77−89861
InAs MIS struct., review 78−95372
n-InAs, magnetophonon resonance under hydrostatic press. 77−47832
InAs, melt, mutual diffusion of components 80−88345
InAs, migration of liq. inclusions, DC current and temp. effects 77−7910
InAs, narrow-gap semicond., externally induced band population effects on electroreflectance 77−66114
InAs, narrow-gap semiconductor, high intensity IR transmission limit 80−7361
n-InAs, negative magnetoresist. in extreme quantum limit 78−64051
n-InAs, negative photocond. and photomemory due to pot. barrier on surface 79−19620
InAs, neutron bombarded, optical absorption, struct. defect form. and nuclear alloying *(Russian)* 78−31206
n-InAs, nucl. maser effect 78−19345
InAs, obtained by liquid-seal method, deviation from stoichiometry 77−40345
InAs on GaAs, epitaxial-substrate system, far IR transmission and refl. 78−6802
InAs, on GaAs, heteroepitaxial layers, compositional profile, AES 77−20212
InAs, organometallic VPE growth on InAs and GaSb 80−16193
InAs, oriented single crysts., photoemissive props., photoelec. thresholds 77−59666
n-InAs, oscillations in photocond. and photomag. effects 77−4405
InAs, oxidised surface, detection of excess crystalline As by Raman scatt. 78−19453
InAs p-n junction, carrier multiplication and ionisation coefficients 77−8188
n-InAs phonon propagation, heat pulse obs. 79−46852
n-InAs, photoelectric props., inhomogeneous impurity distrib. 80−107867
InAs, photoluminescence exam. 79−28809
InAs, photovoltaic detector, photoelectric evaluation, for Gaussian incident pulse 79−63306
InAs, plasmon-phonon coupling, and IR refl. spectra of impure crysts. 79−56150
InAs, positron annihilation 78−72636
InAs, possibility of local epitaxy in depressions on unmasked substrates 79−42415
InAs, radiation defect formation processes, effect on physical props. 78−2163
InAs, Raman scatt. by LO phonons 77−20852
n-InAs, recomb. of nonequil. charge carriers at high photoexcitation levels 77−44053
InAs, resist. inhomogeneity meas. with single-sonde potential method 80−65549
p-InAs, saturation characts. over CO_2 laser spectrum 80−83646
InAs, second order Raman scatt., electron-two phonon deform. pots. determ. 78−60473
n-InAs, Shubnikov-de Haas oscills., conduction electron density, phonon scatt. 77−15768
n-InAs, Shubnikov-de Haas effect, effective mass, Dingle temp., and g-factor 79−51602
n-InAs, Shubnikov-de Haas transverse kinetic coeffs., quantum oscills. 80−49778
InAs, single crystal, exam. of microhardness using static indentation 79−52517
InAs, single crystal, stress-induced phase change 79−23720
InAs, site selective doping by ion implantation of radioactive nuclei 80−34023
InAs, soln. in liq. Sn, vapour phase partial press. meas., rel. to LPE 78−34610
InAs, supercond. of surface *(Japanese)* 78−14864
InAs, superconductor-semicond. device research, future prospects 79−28467
InAs surface, contact pot. difference meas. 77−20403
InAs surface accumulation layers, magneto-transconductance meas. 78−64137
InAs surface accumulation layers, magneto-transconductance study 80−49948
p-InAs, surface conductance of Ar-ion-bombard. samples 79−60910
InAs surface layers, oscillatory transport coeffs. 78−64136
InAs, surface potential and surface states rel. to n-, p-, compensated n-type behaviour 77−15932
InAs, surface space charge investig., reson. enhanced Raman scatt. 77−20849
InAs, temporary diffr. grating form. on surface 79−59801
InAs, thermal oxidation, growth rate and chem. comp., temp. depend. 80−108619
InAs, thin film prep. and elec. props. 79−1633
InAs, three-photon absorption, transition effects *(Russian)* 78−35147
InAs, transient dynamic response calculation by Monte Carlo techniques 80−107796
InAs, transport phenomena, review 79−19587
n-InAs, transport props., influence of higher energy bands, calcs. 79−19598

indium compounds continued
InAs, transverse acoustoelec. voltage spectroscopy 80−49828
n-InAs, tunnelling spectra in mag. field, dispersion law *(Russian)* 79−60923
InAs, two dimensional accumulation layer, Anderson localisation 80−107871
n-InAs, undoped, electron irrad., Hall coeff., elec. resistivity, optical absorption 77−89479
InAs, undoped n-type single crystals, dislocation velocity 77−11559
n-InAs, VPE layers, on GaAs substrate, electronic profile 79−95525
InAs, valence band structure, CPA, bond orbital calcs. 78−87909
InAs, X-ray thermal diffuse scattering measurements of phonon dispersion curves 79−77701
n-InAs:Cd, p-n junction, photosensitivity spectra depend. on mag. field 79−91137
InAs:Cd, Te, donor-acceptor interaction, elec. cond. and Hall coeff. meas. 80−59988
InAs:Cd,Te interaction between impurities, effect on elec. props., Hall effect. 80−19832
n-InAs:Cr, Czochralski growth of high-resist. single crysts. 77−66587
InAs:Cr, high-resist., energy positions of deep levels, elec. and optical props. 79−7807
InAs:Cu, contamination equilibrium assessment 79−51134
InAs:Mn, NMR, magnetoresist., Hall effect and mag. susceptibility meas. 78−26888
InAs:Mn powder, quadrupole interactions in NMR spectra 79−51880
InAs:Mn^{3+}, Jahn-Teller effect for ion impurities 80−107753
InAs:S(Mg), ion implanted, photocond., photo-EMF, and optical absorpt. spectra 80−70763
InAs:Sb (100) surface, Sb-induced surface states 78−10529
InAs:Sn, single crysts., defect formation 80−88606
InAs:Te(Se)(S), intrinsic pt. struct. defects 80−33998
InAs:Zn, optical absorpt. and refl. spectra 79−91479
InAs:Zn,S,(Se)(Te), exam of microhardness, Hall effect as function of dopant 79−95038
InAs:Zn,S(Se), solubility and donor-acceptor interaction 80−54263
InAs/GaSb (001) superlattices, electronic struct., two dimensional effects 80−11064
InAs/$LiNbO_3$ structure, SAW generated transverse acoustoelectric voltage, image scanning and signal processing appl. 80−49826
InAs-$Al_xGa_{1-x}Sb$ heterojunctions, elec. and photoelec. props. 79−11206
InAs-AlAs, phase diagram plotting by DTA and thermodynamic calc. 77−86016
p-InAs-Au contacts, influence of free surface on elec. behaviour 78−95362
InAs-CdTe, preparation, microhardness rel. to component interactions 77−24350
InAs-CdTe quasi-binary system, temp.-comp. diagram, physicochem. and thermodynamic analysis 80−104127
InAs-FeAs, eutectic, growth from melt, electrical props. 77−11911
InAs-GaSb (001) superlattice, electronic struct., tight binding calc. 78−95350
InAs-GaSb (001) superlattices, two-dimens. effects and effective masses 80−49883
InAs-GaSb (100) superlattice, electronic struct., self-consistent pseudopot. method 80−49884
InAs-GaSb heterojunction, photoelec. props. 77−28245
InAs-GaSb heterostruct. superlattice, props. in high mag. fields 79−73570
InAs-GaSb superlattices, two-dim. electronic structure 78−75995
InAs-GaSb superlattice energy struct. and semiconductor-semimetal transition 79−23893
InAs-GaSb superlattice, cyclotron resonance, energy level quantisation 79−73430
InAs-GaSb superlattice, electronic struct., self-consistent pseudopot. calc. 80−29470
InAs-GaSb superlattice, semiconductor-semimetal transition obs. 80−44710
InAs-GaSb superlattices, crystallography, Rutherford backscatt. and channelling obs. 80−49533
InAs-GaSb superlattices, semicond.-semimental transition obs. 80−49882
InAs-GaSb superlattices, mag. field induced semimetal-semicond. transition 80−65656
InAs-HgTe, phase diags. 77−52299
InAs-InP, phase equilib. and dissoc. 80−35170
InAs-oxide-$Pb_{50}Bi_{20}$ junction, hot electron temp. in InAs meas. by tunnelling 77−4352
$InAs_{1-x}P_x$, magnetophonon effect 79−65500
$(InAs)_{1-x}(CdSe)_x$ solid solution, elec. props. 79−15146
$(InAs)_x(CdTe)_{1-x}$, band gap and effective mass, IR spectra obs. 78−56491
InAs(P), avalanche breakdown voltage for p-n junction, calc. 78−88020
InAsP, intervalley electron transfer, drift velocity and diffusion coefficient 80−39594
$InAs_{1-x}P_x$, deep levels and semicond.-semimetal transition at high press. 80−11056
$InAs_{1-x}P_x$, electron effective mass cyclotron reson. and magnetophonon effect 80−24786
$InAs_{1-x}P_x$ epitaxial layers, sub-threshold velocity-field characts., intervalley separation 77−63010
$InAs_{1-x}P_x$, evidence for reduction in momentum matrix element P^2 due to alloy disorder 79−65853
$InAs_{1-x}P_x$, high field instabilities, press. and comp. depends. 78−26873
$InAs_{1-x}P_x$ quantum magnetoresist. results, using pulsed fields up to 35 T 79−73528
$InAs_xP_{1-x}$, continuously tunable electron beam pumped laser 78−50802
$InAs_xP_{1-x}$, method for determ. of liquidus surfaces in In-As-P phase diagram 77−28787
$InAs_yP_{1-y}$ alloy, composition effects in growth by MBE 80−59816
$InAs_xP_{1-x}(Sb_{1-x})$, energy gap variation, CPA calcs. 78−43294
InAsSb, Be ion implantation, device appl. 80−24478
InAsSb/GaSb broad-spectral-band IR detector, backside-illum. heterostructure approach 80−73450
$InAs_{0.85}Sb_{0.15}$, MIS struct., C-V characts., interface state densities and storage times meas. 77−89861
$InAs_{1-x}Sb$, disorder-enhanced Auger recomb. 79−43014
$InAs_{1-x}Sb_x$, epitaxial film, carrier recomb., elec. and optical props. 79−15164
$InAs_{1-x}Sb_x$, LPE on InAs substrate, $InAs_xSb_yP_{1-x-y}$ used as buffer layer 78−3065
$InAs_{1-x}Sb_x$ on GaSb, LPE growth 80−29293

indium compounds continued
$InAs_{1-x}Sb_x$, organometallic VPE growth on InAs 80−45233
$InAs_{1-x}Sb_x$ p-n junctions, avalanche multiplication 80−6965
$InAs_{1-x}Sb_x$-InAs backside-illum. narrow band photodetectors 77−61118
$InAs_{1-x}Sb_x$-InAs stepwise-graded struct., steady-state LPE, etching, investig. 77−21042
$InAs_xSb_yP_{1-x-y}$, efficient electron-beam-pumped laser at 3.1-3.7 μm 80−5738
$InAs_xSb_yP_{1-x-y}$, LPE on InAs substrate 78−3065
$In_{1.9}As_{0.1}Se_3$, growth by chem. vap. transport, characterisation as photoelectrode 78−43994
$InBO_3$, thermal expansion, up to 610°C, X-ray determ. 77−43352
$InBO_3:Fe^{3+}$, ESR spectra, lattice parameters 80−93170
In_2BRCl_6, B=Li,Ag,Na, systematic structs., X-ray Guinier-Simon method *(German)* 80−44186
InBi, Fermi surface and band struct., press. effects 77−39779
InBi, possibility of existence with sphalerite struct. 80−33950
InBi single crystal, deform. mode under dynamic indentation 80−88163
InBi single crysts., Knight shifts and quadrupole interaction 80−84662
InBr, electron impact dissoc. ionis., In electron affinity meas. *(French)* 80−63849
InBr, metastable exciton emission, electron excitation mechanism 77−66546
$^{115}In^{79}Br$, $^{115}In^{81}Br$, rot. J=1→2 hyperfine struct., quadrupole coupling consts. *(German)* 77−30866
$InBr_3$, specific and equivalent cond. of aq. solns., viscosity 77−35736
$InBr_3$, vibr. anal., pot. const. determ., mol., compliance and Coriolis coupling const. calc. 80−95579
$InBr_3$-In_2Te_3 quasibinary system, phase relations 80−100834
In_4CdI_6, fast ionic cond. and order-disorder transition 79−99363
In_4CdI_6, ionic conductivity, Raman spectra 77−69113
In_4CdI_6, solid electrolytes, ion transport mechanism and polarisability role, comparison with Cu^+ and Ag^+ cond. 80−107531
InCl, B→X system, rot. anal. 79−36619
InCl, discharge excited spectrum 4100-3900 Å, vibr. anal. 80−32732
InCl disproportionation under influence of high pressure 80−16660
InCl, ionisation energies, self-consistent-charge Hartree-Fock-Slater calcs. 77−6687
InCl powder, effect of thermal treatment on photographic props. *(Russian)* 80−291
InCl, red and yellow, X-ray structural anal. 79−4287
$InCl_2$, aq. soln., factor analysis and band contour resolution applications, book contrib. 78−21931
$InCl_3$, D_{3h} point group, mol. consts., struct. effects 79−54992
$InCl_3$, force and compliance consts., OVFF, UBFF and GVFF models 78−50663
$InCl_3$ in Kr lattice, Raman and IR spectra, vibr. assignments, force consts., isotope shift and config. 79−89671
$InCl_3$, intramolecular force fields, compliance consts. and vibr. amplitudes 80−58234
$InCl_3$, planar D_{3h} struct., IR matrix isolated spectra 77−75148
$InCl_3$, vibr. anal., pot. const. determ., mol., compliance and Coriolis coupling const. calc. 80−95579
$InCuAlO_4$, rhombohedral oxides, symmetry group *(French)* 80−84157
InF_3-MF_1 (M=alkalines, Tl, NH_4), crystallographic study *(French)* 79−46631
$InF_3.3H_2O$, cryst. struct. by X-ray diffr. 78−63729
$InFe_{1.75}Si_{0.25}O_4$, rhombohedral oxides, symmetry group *(French)* 80−84157
InGaAs detector, integrated optics appl. *(Czech)* 80−33227
(InGa)As film, growth kinetics for step-cooling LPE technique 77−40395
InGaAs, LED, 1.06 μm range, neutron and γ-irrad. effects 79−97433
InGaAs, LPE, diffusion-limited step-cooling technique, layer thickness and composition 80−84402
InGaAs, lattice-matched VPE on (100) InP, photodiode appl. 80−35102
InGaAs p-n junction, carrier multiplication and ionisation coefficients 77−8188
InGaAs, transferred electron photoemission to 1.65μm 78−68600
(InGaAs)/(InGa)P, DH laser, threshold current temp. depend. 79−81431
InGaAs/InP p-i-n small area photodiodes, fabrication, charact. and performance in 274 Mb/s receivers at 1.31 microns 80−53415
InGaAs-GaAs heterojunction with low misfit, misfit dislocation struct. 77−62783
InGaAs-GaSbAs periodic structures, with controlled emission 79−7880
InGaAs-$In_{1-x}Ga_xAs_yP_{1-y}$ DH laser, LPE fabrication, electroluminesc., lasing charact. 79−3709
InGaAs-InGaP vapour-grown ternary heterojunction laser struct., reliability 79−98385
InGaAs-InP heterojunction detector for 1.0-1.7 μm wavelength range 78−49895
InGaAs-InP punch-through type photodetector fabricated by VPE 80−68253
$In_{0.1}Ga_{0.9}As$, quantitative anal. with SIMS 80−101052
$In_{0.53}Ga_{0.47}As$, growth on (100)-oriented InP, from supercooled solution 79−70001
$In_{0.53}Ga_{0.47}As$, Hall mobility and Hall factor, temp. and donor conc. depend. 80−49773
$In_{0.53}Ga_{0.47}As$, incorporation of Ga during LPE growth on (111)B and (100)InP substrates 78−91557
$In_{0.53}Ga_{0.47}As$, interband magnetoabsorption study, quasi-Ge model application 80−50304
$In_{0.53}Ga_{0.47}As$, LPE growth on (100) InP, for field assisted photocathode appl. 78−15318
$In_{0.53}Ga_{0.47}As$, LPE layer on InP, electron mobility and energy gap 77−24627
$In_{0.53}Ga_{0.47}As$ p-i-n photodiodes, for long-wavelength fibre-optic systems 80−5826
$In_{0.53}Ga_{0.47}As$ p-i-n photodiode-FET photoreceiver for 1.0 to 1.7 μm wavelength optical fibre communications systems 80−58794
$In_{0.53}Ga_{0.47}As$, phase diagram at 650°C and LPE growth of lattice-matched layer 79−96009
$In_{0.53}Ga_{0.47}As$ photodiodes with dark current limited by generation-recombination and tunneling 80−107893
p-$In_{0.53}Ga_{0.47}As$:Zn on InP, elec. and optical props. 80−75662
$In_{0.53}Ga_{0.47}As$/InP avalanche photodetector 80−4764
$In_{0.53}Ga_{0.47}As$-InP, 1.7 μm heterojunction lasers and photodiodes fabrication 78−25880
$In_{0.53}Ga_{0.47}As$-InP avalanche photodiode with guard-ring struct., charact. 80−96939

indium compounds continued
$In_{0.53}Ga_{0.47}As$-InP avalanche photodiode structure for 1 to 1.6 μm region 80−98978
$In_{0.53}Ga_{0.47}As$-InP heterostructure, LPE growth 80−11582
$In_{1-x}Ga_xAs$-$GaSb_{1-y}As_y$ superlattice, optical absorption 79−19887
$In_{1-x}Ga_xAs$ alloy surface states obs., using electron energy loss spectra 79−15202
$In_{1-x}Ga_xAs$, disorder carrier scatt., Green's function calc. 77−11906
$In_{1-x}Ga_xAs$, LPE, electron mobility and max. drift vel., microwave device appls. 77−77431
$In_{1-x}Ga_xAs$, LPE growth on InP substrate, quasi grown layers, photoluminescence meas. 79−23862
$In_{1-x}Ga_xAs$, LPE layer on InP substrate, phys., elec. and optical props. 78−39235
$In_{1-x}Ga_xAs$, LPE on InP substrate, comp. latching phenomenon and lattice mismatching effects 79−28961
$In_{1-x}Ga_xAs$ layer on InP, misfit dislocation free, LPE growth 80−108364
$In_{1-x}Ga_xAs$, MBE-grown, substrate effect on lattice consts. 79−77942
$(In_{1-x}Ga_x)As$, scattering of electrons by potential clusters 77−15842
$In_{1-x}Ga_xAs$-$GaSb_{1-y}As_y$, semiconductor superlattices by MBE 79−95939
$In_{1-x}Ga_xAs$-$GaSb_{1-y}As_y$, superlattice electronic subband struct. 77−72815
$In_{1-x}Ga_xAs$-$GaSb_{1-y}As_y$, new heterostruct. charact. 78−72247
$In_{1-x}Ga_xAs$-$GaSb_{1-y}As_y$ superfine heterostruct., MBE 78−95348
$In_{1-x}Ga_xAs$-$GaSb_{1-y}As_y$ superlattice, with nonlinear energy-wave and energy-momentum relationships 79−7871
$In_{1-x}Ga_xAs$-$GaSb_{1-y}As_y$ heterostructure devices 79−42624
$In_xGa_{1-x}As$ (x=0.03 and 0.05), grown as GaAs substrate, with InGaAsP buffer layer, exam. of dislocation density 80−44447
$In_xGa_{1-x}As$ avalanche diode, noise meas. 77−4431
$In_xGa_{1-x}As$, electron drift vel. in high elec. fields 78−30928
$In_xGa_{1-x}As$ epitaxial layer, waveguiding at 1.06 μm, losses 78−18052
$In_xGa_{1-x}As$, epitaxial solid soln. film, spectral depend. of transparency, absorpt. spectra calcs. 80−45161
n-$In_xGa_{1-x}As$ film, epitaxial growth on GaAs, using CVD system 77−1812
$In_xGa_{1-x}As$, heteroepitaxial, MBE grown, props. 78−84328
$In_xGa_{1-x}As$, heterostructure composition profile by photoemission microanalysis 80−44717
$In_xGa_{1-x}As$, LPE growth on GaAs 79−61519
$In_xGa_{1-x}As$ layers, on GaAs substrate, MBE fabrication and laser operation 80−10820
$In_xGa_{1-x}As$, MBE layers on InP substrates, elec. props., photoluminesc., X-ray and Auger obs. 79−51450
$In_xGa_{1-x}As$ MBE layers on InP substrate, lattice deformation, misorientation 79−90896
$In_xGa_{1-x}As$ multilayer struct., photoluminesc. and X-ray spectroscopic microprobe analysis 77−4687
$In_xGa_{1-x}As$ on GaAs, heterojunctions, misfit dislocation banding, stress-induced birefr. 77−28542
$In_xGa_{1-x}As$, planar photodiodes made by VPE 79−49286
$In_xGa_{1-x}As$, thick LPE growth, electrolum. obs. 78−60589
$In_xGa_{1-x}As$, VPE on (100), (111)A, and (111)B InP substrates 80−15382
$In_xGa_{1-x}As$, Zn diffusion coeff. and surface conc. 80−39122
$In_xGa_{1-x}As$:Si, p-n junction form. in LPE layers, In content effect on inversion temp. 77−4266
$In_xGa_{1-x}As$:Si p-n structs., electrolum. spectra, 77 to 300K 80−93408
$In_xGa_{1-x}As$:Zn, lattice matching to InP, LPE growth conditions 80−70541
$In_xGa_{1-x}As$-Au Schottky contacts, interfacial oxide layers used to increase effective barrier height 79−7896
$In_xGa_{1-x}As$-$In_yGa_{1-y}P$ DH laser, CW room temp. operation at 1.06 μm 77−19250
$In_xGa_{1-x}As$-$InAs_xP_{1-x}$ VPE mixed crystal composition rel. to vapour pressure *(Japanese)* 77−55893
InGaAsP, 1.3 μm LED, for high-bit-rate fibre data link 78−46825
InGaAsP, anodic oxidation, refractive indices 80−97601
InGaAsP avalanche photodiodes, leakage current, shot noise, quantum efficiency, gain saturation 79−67381
InGaAsP avalanche photodiode, 1.3 μm, noise performance, −190°C 80−57370
InGaAsP avalanche photodiodes, breakdown mechanism, donor conc. effect 80−70710
InGaAsP, bandgap energy by electroreflectance and photoluminesc. spectra 80−107700
InGaAsP buried stripe laser, modulation charact. 79−98418
InGaAsP DH, luminesc., quantum efficiency determ. 80−108273
InGaAsP DH laser charact., temp. depend. 80−1223
InGaAsP DH lasers with etched reflectors, fabrication, current density 80−64050
InGaAsP, dual-wavelength demultiplexing photodiode 79−63304
InGaAsP, epitaxial layer, defect evaluation by cathodoluminescence 80−2866
InGaAsP, expitaxial growth by chloride CVD process, thermodynamic anal. 80−64936
InGaAsP heterojunction cathode, transferred electron photoemission 78−48272
InGaAsP, high radiance CW LEDs emitting at 1.30 μm 78−22196
InGaAsP IR heterojunction photodiode detector 79−21813
InGaAsP, injection heterojunction laser at 1.3-1.5 μm 79−89910
InGaAsP LED sources, for near-IR absorpt. meas. 80−77135
InGaAsP, LPE, diffusion-limited step-cooling technique, layer thickness and composition 80−84402
InGaAsP, LPE growth, orientation depend. of incorporation of Ga, As, and Zn 78−6869
InGaAsP, LPE growth on InP, influence of lattice mismatch on surface morphology 79−1553
InGaAsP, LPE growth techniques influence on composition 79−52130
InGaAsP, LPE growth, impurity depend. of distrib. coeff. 80−10843
InGaAsP, LPE grown, impurity effect on surface morphology 80−29291
InGaAsP LPE heterostructs., interface grading, Auger depth profile 80−103585
InGaAsP LPE layers on InP substrate, material selective chemical etching 79−70188
(InGa)(AsP) laser system, VPE growth using metal organic sources or halide transports 80−99748
InGaAsP, lattice matched, LPE growth on (100) InP, for 1.15-1.31 μm spectral region 78−64483

indium compounds continued
InGaAsP low-threshold 1.25-μm vapour grown CW lasers, emission charcts. 79−50308
p-InGaAsP, on InP surface, diffusion coeff. and surface recombination velocity 80−39598
InGaAsP photocathodes for astronomical detectors, UV response 77−57387
InGaAsP photodetector, improved two wavelength demultiplexing 80−58795
InGaAsP quaternary alloy IR heterojunction detectors, props. 79−2823
InGaAsP, quaternary alloy, physical props. *(Japanese)* 80−15449
InGaAsP single-mode CW ridge-waveguide laser emitting at 1.55 micron 80−58584
InGaAsP strip-buried-heterostructure high-output power laser 80−58540
InGaAsP strip-buried heterostructure laser, high output power, operation 80−58559
InGaAsP, with and without InP cladding layers, low photolum. regions 79−33754
InGaAsP:Be, avalanche photodetectors annealing temp. effect on photolum. spectra 79−69872
InGaAsP:Be ion-implanted avalanche photodiode, struct. and charcts. 79−17487
InGaAsP:Sn(Te)(Zn), LPE growth, influence of growth-solution dopants on distrib. coeffs. 79−47640
InGaAsP/InP, DH laser, 1.5 μm, with optical waveguide structure, fabrication 79−72587
(InGa)(AsP)/InP, DH laser, threshold current temp. depend. 79−81431
InGaAsP/InP, native oxide stripe laser 79−68405
InGaAsP/InP avalanche photodiode, ionisation coeff. 80−15590
InGaAsP/InP DFB injection lasers 80−5746
InGaAsP/InP DH, vapour phase growth by dual-growth-chamber method 80−50559
InGaAsP/InP DH lasers, Zn doping level 79−98373
InGaAsP/InP DH laser, self-aligned struct. 80−9893
InGaAsP/InP DH lasers, temp. depend. charcts. 80−58541
InGaAsP/InP DH stabilised 1.3 μm laser diode-isolator module for hybrid optical integrated cct. 80−58583
InGaAsP/InP heterojunction, X-ray characterisation of defects 78−95239
InGaAsP/InP heterostruct. lasers as optical source, CW operation at room temp. 80−1220
InGaAsP/InP injection lasers for long wavelength (1.1 to 1.6 μm) optical communication 80−58582
InGaAsP/InP lasers and detectors for LW optical fibre communication 80−9885
InGaAsP/InP phototransistors, fabrication by LPE, photodetectors 80−95139
p-InGaAsP-Au, Schottky barrier height comp. depend., photoelec. meas. 77−20433
InGaAsP-InP, anomalous luminesc., near heterojunction interface 79−65932
InGaAsP-InP, double heterostructure laser, temp. sensitive threshold current 79−59700
InGaAsP-InP, double heterostructure laser lifetime, point defect generation model calcs. 80−32992
InGaAsP-InP, Zn diffused DH structures, oxide defined transverse junction stripe lasers 79−98389
InGaAsP-InP 1.27 μm CW DH injection lasers, 1.1 Gb/s pseudorandom PCM 78−55390
InGaAsP-InP buried crescent injection laser emitting at 1.3 μm with low threshold current 80−87404
InGaAsP-InP buried heterostructure lasers emitting at 1.3 μm, accelerated ageing charcts. 80−95898
InGaAsP-InP CW lasers, 1.5-1.7 μm, VPE 80−78861
InGaAsP-InP DH laser emitting at 1.27 μm, fast pulse behaviour, high speed direct modulation 77−23676
InGaAsP-InP DH laser, room temp. operation, 1.27 μm emission 77−88743
InGaAsP-InP DH lasers, direct modulation 78−42363
InGaAsP-InP DH lasers, carrier lifetimes meas. 78−66828
InGaAsP-InP DH laser, threshold depend. on active layer thickness 79−7127
InGaAsP-InP DH lasers, threshold characteristic 79−81430
InGaAsP-InP DH laser, optical gain meas., low-intensity luminesc. and absorpt. spectra 79−98356
InGaAsP-InP DH lasers, low temp. behaviour of threshold current and carrier lifetime 79−98374
InGaAsP-InP DH lasers, degradation by In solder 79−98402
InGaAsP-InP DH laser with self-aligned struct., oscillation charcts. 80−38017
InGaAsP-InP DH laser, 1.55 μm, low temp. LPE growth for room-temp. CW operation 80−64045
InGaAsP-InP DH LED, high temp. aged, dark-spot defects, TEM obs. 80−66300
InGaAsP-InP DH lasers, interfacial recomb., influence on oscill. charcts. 80−87393
InGaAsP-InP DH lasers, spatial hole burning, spontaneous emission saturation, direct obs. 80−95892
InGaAsP-InP DH lasers, temp. dependence of threshold and elect. charcts. 80−99725
InGaAsP-InP DH lasers, perturbed InP growth, photoluminesc. study 80−106518
InGaAsP-InP DH laser, threshold current, temp. depend. 80−106521
InGaAsP-InP dual wavelength LED 80−15589
InGaAsP-InP embedded mesa strip lasers 80−14350
InGaAsP-InP heterojunction, LPE, lattice mismatch, Auger depth profile 79−87005
InGaAsP-InP high-gain heterojunction phototransistor 80−103745
InGaAsP-InP laser, LPE, 1.5 μm range, effects of double cladding struct. 80−48290
(InGa)(AsP)-InP laser system, 1 μm wavelength, lattice matching techniques 80−99748
InGaAsP-InP lattice-matched heterojunction, LPE growth and characterisation 77−21041
InGaAsP-InP lattice matched DH, growth by two-phase supercooled soln. technique 78−10296
InGaAsP-InP layers, grown by LPE techniques, lattice const., bandgap, thickness and surface morphology meas. 80−59818
InGaAsP-InP photodiodes, microplasma-limited avalanche multiplication at 1 to 1.3 μm 79−26128

indium compounds continued
InGaAsP-InP photodiodes antireflectively coated with InP native oxide 80−13137
InGaAsP-InP vapour-grown quaternary heterojunction laser struct., reliability 79−98385
InGaAsP-InP:Mg LEDS, for high-bit-rate optical communication systems 80−5823
$In_{0.79}Ga_{0.21}As_{0.54}P_{0.46}$, LPE layer, electroreflectance meas. 79−24290
$In_{0.8}Ga_{0.2}As_{0.5}P_{0.5}$, LPE growth 80−11557
$In_{0.83}Ga_{0.17}As_{0.37}P_{0.63}$, reactive ion etching of III-V compounds 80−58813
$In_{0.84}Ga_{0.16}As_{0.46}P_{0.54}$, refractive index, at laser oscillating wavelength of 1.2 μm 79−64224
$In_{0.85}Ga_{0.15}As_{0.39}P_{0.61}$, deep impurity levels 79−87058
$In_{0.9}Ga_{0.1}As_{0.22}P_{0.78}$, effective mass meas. by Shubnikov-de Haas oscills. 78−34754
$In_{1-x}Ga_xAs_{1-y}P_y$ layers on InP substrate, LPE growth, quaternary phase diagram, and band gaps 79−42403
$In_{1-x}Ga_xAs_xP_{1-y}$, p-n junction diodes, fabrication by Be ion implantation 79−47156
n-$In_{1-x}Ga_xAs_yP_{1-y}$, cyclotron reson., cond. band nonparabolicity 80−29311
$In_{1-x}Ga_xAs_yP_{1-y}$, DH laser material, spatially resolved photolum. characterisation and optically induced degradation 79−47486
$In_{1-x}Ga_xAs_yP_{1-y}$ DH laser, low threshold current density, near equilibrium LPE growth 80−19040
$In_{1-x}Ga_xAs_yP_{1-y}$ DH lasers for 1.3 and 1.5 μm optical fibre communications 80−91817
$In_{1-x}Ga_xAs_yP_{1-y}$, electron effective mass from Shubnikov-de Haas meas. 80−80298
$In_{1-x}Ga_xAs_yP_{1-y}$ epitaxial layer, far IR refl. spectra, lattice vibrs. 80−97282
$In_{1-x}Ga_xAs_yP_{1-y}$, evidence for alloy scatt. from press. induced changes of electron mobility 80−88548
$In_{1-x}Ga_xAs_yP_{1-y}$ far IR reflection spectrum 80−60612
$In_{1-x}Ga_xAs_yP_{1-y}$, Hall mobility, comp. depend. 80−75587
$In_{1-x}Ga_xAs_yP_{1-y}$, hole mobility over temp. range 77 to 300K 80−60111
$In_{1-x}Ga_xAs_yP_{1-y}$, LPE growth on InP (100), lattice matched composition 78−87881
$In_{1-x}Ga_xAs_yP_{1-y}$ LPE layers, background carrier conc. and electron mobility. 79−95523
$In_{1-x}Ga_xAs_yP_{1-y}$, lattice vibrs., Raman study 78−91391
$In_{1-x}Ga_xAs_yP_{1-y}$, lattice matched to InP, band gap vs. comp., and Vegard's law demonstration 79−7782
$In_{1-x}Ga_xAs_yP_{1-y}$, oscillatory magneto-transmission, band parameters 79−60707
$In_{1-x}Ga_xAs_yP_{1-y}$ quaternaries VPE 0.75 to 1.35 eV band gap range 79−69987
$In_{1-x}Ga_xAs_yP_{1-y}$, traps in device quality n- and p-type LPE material 80−10999
$In_{1-x}Ga_xAs_yP_{1-y}$, vapour grown, alloy comp., thermodynamic calc. 79−99094
$In_{1-x}Ga_xAs_yP_{1-y}$:Be, ion implantation, hole conc. and mobility, junction depth 79−46685
$In_{1-x}Ga_xAs_yP_{1-y}$/InP 1.5 μm room-temp. CW laser fabrication and operation 80−64070
$In_{1-x}Ga_xAs_yP_{1-y}$-InP DH laser, fabricated on (100)-InP substrate, 500-hr CW operation 77−83890
$In_{1-x}Ga_xAs_yP_{1-y}$-InP DH lasers, fabrication and performance 78−5500
$In_{1-x}Ga_xAs_yP_{1-y}$-InP DH laser on InP (100) substrate 78−29965
$In_{1-x}Ga_xAs_yP_{1-y}$-InP photodetectors, high-efficiency with selective wavelength response, 0.9-1.7 μm 79−21810
$In_{1-x}Ga_xAs_yP_{1-y}$-InP DH laser, 10000 h continuous CW operation, dark-line and dark-spot defects 79−98384
$In_xGa_{1-x}As_{1-y}P_y$ epitaxial layers, characterisation and relation to lattice matching 80−100540
$In_xGa_{1-x}As_xP_{1-x}$-InP photodetectors, construction and performance 78−65966
$In_xGa_{1-x}As_yP_{1-y}$ layers on InP, LPE and opt. props. characteris. 79−28849
$In_xGa_{1-x}As_yP_{1-y}$ photodetector diode on InP substrate dark currents, tunnelling, energy gaps, effective masses 80−70805
$In_xGa_{1-x}As_yP_{1-y}$, surface and dielec.-semicond. interface props. 80−93001
$In_xGa_{1-x}As_yP_{1-y}$, valence band struct., CPA calc. 79−73435
$In_xGa_{1-x}As_yP_{1-y}$-InP n-p heterojunction photodiode, charcts. 78−14800
InGaAsSb based injection heterolaser, 1.9 μm stimulated emission 79−18420
InGaAsSb, LPE growth, and appl. in GaSb/AlGaAsSb/InGaAsSb/AlGaAsSb/GaSb DH 80−16205
InGaAsSb-AlGaAsSb DH laser, room temp. operation at 1.8 μm wavelength 80−43358
$In_{1-x}Ga_xAs_{1-y}Sb_y$, LPE growth on (111)B-oriented InAs, growth conditions and lattice matching 77−24973
$In_xGa_{1-x}As_ySb_{1-y}$ laser, nonequilibrium carrier recombination, luminesc. study 80−50431
InGaP/InGaAs struct. for transferred electron photocathodes, VPE growth and characterisation 80−76193
InGaP-GaAs junction, effect of elastic strain on energy band gap and lattice parameters 79−24057
InGaP-InGaAs solar cell, high internal collection efficiency, low bandgap 80−26134
$In_{0.3}Ga_{0.7}P$, N free and implanted, photoluminescence study 80−97322
$In_{0.5}Ga_{0.5}P$-GaAs heterojunction, interfacial recomb. vel. determ. 77−51809
n-$In_{1-x}Ga_xP$, direct-gap semiconductor, cathodoluminesc., electron irrad. effects 80−108283
$In_{1-x}Ga_xP$, epitaxial film, cathodolum. obs., recomb. mechanisms 78−72613
$In_{1-x}Ga_xP$, epitaxial growth from melt, optimisation of growth conditions 79−52132
$In_{1-x}Ga_xP$, epitaxial growth on GaAs substrate, formation of intermediate layers 80−2304
$In_{1-x}Ga_xP$, epitaxial layers, compositional inhomogeneity 80−88444
$In_{1-x}Ga_xP$, homogeneous bulk, growth from soln. with predetermined cryst. comp. 78−11097
$In_{1-x}Ga_xP$ LEDs and electron-beam-pumped lasers, LPE and VPE growth 80−2281
$In_{1-x}Ga_xP$, LPE, conditions, reacts. in In-Ga-P system 79−11525
$In_{1-x}Ga_xP$, LPE, on $GaAs_{1-y}P_y$, photo- and cathodolum. 78−19559

indium compounds continued
$In_{1-x}Ga_xP$, non-isodisplacement of P atoms in long-wavelength optical phonons 79−47444
$In_{1-x}Ga_xP$, phonon density of states, cluster Bethe lattice treatment 80−6475
$In_{1-x}Ga_xP$, quantitative characterisation of chemical disorder from wavelength-modulated no-phonon absorpt. 79−15482
$In_{1-x}Ga_xP$, solid soln., evaporation of P during LPE 79−95948
$In_{1-x}Ga_xP$, solid soln. film, photoluminesc. meas. 78−27321
n-$In_{1-x}Ga_xP$ solid solns., electron scatt. mechanisms *(Russian)* 79−4568
$In_{1-x}Ga_xP$, temp. depend. of forbidden band width, photoluminesc. meas. 78−19556
$In_{1-x}Ga_xP$, two-phonon IR absorpt. 78−52493
$In_{1-x}Ga_xP:N_2$, N-trap bound states, photoluminesc. and absorption data 77−1719
$In_{1-x}Ga_xP$:N(Te), composition depend. of bound state luminesc. transitions 78−39595
$In_{1-x}Ga_xP$:Te,Zn, photolum. and electrolum., direct transition region 77−8659
$In_{1-y}Ga_yP$-GaAs heterojunction, VPE, energy band gap and lattice parameter, lattice mismatch effects 78−95345
$In_xGa_{1-x}P$ on GaP, heterojunctions, misfit dislocation banding, stress-induced birefr. 77−28542
$In_xGa_{1-x}P$, proportional ingredient content determ. by X-ray fluoroscopy 80−97747
$In_xGa_{1-x}P$, solid solns., gas phase epitaxy from Ga-In-HCl-PH_3-H_2 systems 78−34722
$In_xGa_{1-x}P$, TEM foil preparation, using polishing set 'Elypovist' *(German)* 79−9264
$In_xGa_{1-x}P$-GaAs heterojunction, interface recomb. velocity determ. 77−89838
$In_xGa_{1-x}P$-GaAs lattice mismatched heterojunction, recomb. props. 78−13707
InGaPAs LPE layers, compositional inhomogeneity, photoluminesc. obs. 80−75451
InGaPAs LPE multilayered DH lasers exhibiting quantum size effects 78−1227
InGaPAs, LPE-grown on (001)-InP, lattice mismatch study using X-ray double-cryst. diffr. 79−99440
InGaPAs-InP DH laser, threshold current temp. depend., potential barrier height influence 80−53296
$In_{1-x}Ga_xP_{1-y}As_y$ LPE films, hot electron and magnetotransport props. 78−26977
$In_{1-x}Ga_xP_{1-y}As_y$ lattice-matched epitaxial layers, LPE growth on GaAs(100), characterisation 80−75465
$In_{1-x}Ga_xP_{1-z}As_z$, DH, operated in external grating cavities, inhomogeneous and homogeneous line broadening 77−10921
$In_{1-x}Ga_xP_{1-z}As_z$, DH, diode and laser performance, limitations of direct-indirect transition 77−39927
$In_{1-x}Ga_xP_{1-z}As_z$ DH lasers, pulsed room temp. operation 77−10941
$In_{1-x}Ga_xP_{1-z}As_z$ DH laser, effective index of refr., wavelength depend. 77−61954
$In_{1-x}Ga_xP_{1-z}As_z$ DH lasers, multiple LPE, lattice matching 77−77421
$In_{1-x}Ga_xP_{1-z}As_z$ DH laser diode, defect and phonon assisted tunnelling 78−13708
$In_{1-x}Ga_xP_{1-z}As_z$ LEDs and electron-beam-pumped lasers, VPE and LPE growth 80−2281
$In_{1-x}Ga_xP_{1-z}As_z$ LPE DH laser with multiple thin layer active region 77−83887
$In_{1-x}Ga_xP_{1-z}As_z$, lattice matched to InP, electroreflectance obs. 80−93416
$In_{1-x}Ga_xP_{1-z}As_z$ near IR DH laser, constant temp. LPE, external grating cavity 77−75550
$In_{1-x}Ga_xP_{1-z}As_z$, room temp. visible heterojunction lasers 78−5501
$In_{1-x}Ga_xP_{1-z}As_z$ single thin active layer visible spectrum heterostruct. lasers 78−63120
$In_{1-x}Ga_xP_{1-z}As_z$ solid solution, radiative transitions 79−11476
$In_{1-x}Ga_xP_{1-z}As_z$, stimulated yellow-green emission under electron excitation, 80K 79−33846
$In_{1-x}Ga_xP_{1-z}As_z$ thin well in InP p-n junction, confined carrier luminesc. and laser modes 78−13703
$In_{1-x}Ga_xP_{1-z}As_z$, visible spectrum laser diode, continuous operation, 6280 Å, 77K 79−960
$In_{1-x}Ga_xP_{1-z}As_z$ well in InP, tunnel injection into confined particle states 78−19130
$In_{1-x}Ga_xP_{1-z}As_z$:Zn, x∼0.12, z∼0.26, LPE, DH lasers, tunnelling involving defects 77−65594
$In_{1-x}Ga_xP_{1-z}As_z$-$In_{1-x}Ga_xP_{1-z}As_z$ visible spectrum multiple-quantum-well heterostruct. lasers 80−106537
$In_{1-x}Ga_xP_{1-z}As_z$-InP, LPE heterojunctions, lattice matching and dislocations 78−23150
$In_{1-x}Ga_xP_{1-z}As_z$-InP, single and multiple layer heterostruct., LEDs and lasers 78−46626
$In_{1-x}Ga_xP_{1-z}As_z$-InP coupled multiple quantum-well heterostructure laser diodes, threshold current temp. depend. 80−78855
$In_uGa_{1-u}P_vAs_{1-v}$-InP, LPE, lattice matching, phase 80−54350
$In_xGa_{1-x}P$(As), energy gap variation, CPA calcs. 78−43294
$In_xGa_{1-x}P_yAs_{1-y}$, electron effective mass and Dingle temp., Shubnikov-de Haas oscills. 80−59859
$In_{1-x}Ga_xSb$, multitarget sputtering using decoupled plasmas 77−12529
$In_xGa_{1-x}Sb$, influence of annealing on microstruct., exam. 78−56669
$In_xGa_{1-x}Sb$, molecular beam epitaxy 79−47638
InGaSbAs heterostructures and LED's luminesc. props. in 1-2 micron band 78−10988
$In_xGa_{1-x}Se$ single crystals, exciton absorption spectra 80−20663
$In_2Ga_6Te_{10}$, X-ray cryst. struct. determ. *(French)* 79−23580
$In_{1-x}GaxAs$, MBE, RHEED meas. 78−18916
$(In(H_2O)_2\text{-}(SO_4)_2)^-(H_5O_2)^+$, cryst. struct. *(French)* 79−73146
$InH(SO_4)_2.4H_2O$, cryst. parameters and X-ray powder diffr. data *(French)* 79−14765
InI directional crystallisation, behaviour of Ag, Cu, Sn, Ni impurities, partition coeffs. 77−16491
InI, electron impact dissoc. ionis., In electron affinity meas. *(French)* 80−63849
InI, far IR spectra obs. 79−47435
InI, high temp. solid and melt., struct., thermodynamic props., Raman spectra obs. 80−66174
InI, impurity in AC metal halide discharge, atomic plasma characts., a priori method 80−44034
InI, orthorhombic, reflection spectra, exciton transition 79−24333
InI, photoluminesc., Raman scatt. 79−38593

indium compounds continued
InI, relativistically parameterized extended Huckel theory 79−49924
InI, vapour, excited by photodissociation, fluoresc. yields 78−55138
InI_2 far-IR spectra, valence states in InI_2 79−47435
InI_2, high temp. solid and melt., struct., thermodynamic props., Raman spectra obs. 80−66174
InI_3, D_{3h} point group, mol. consts., struct. effects 79−54992
InI_3, far IR spectra obs. 79−47435
InI_3, high temp. solid and melt., struct., thermodynamic props., Raman spectra obs. 80−66174
InI_3, molten, electrical cond., press. effect, 0-1 kbar 78−55963
InI_3, molten, isothermal compressibility obtained from adiabatic thermal press. coefficients 79−95065
InI_3, vibr. anal., pot. const. determ., mol., compliance and Coriolis coupling const. calc. 80−95579
InI_x, x=1,2,3, thermodynamic props. 77−40572
$In_{1-x}I_x$, molten mixture, NMR, reson. shifts, relax. rates, quadrupole relax. 80−2654
In(III) complexes with gluconate ions, reduction, polarographic behaviour 78−92568
InKr, low-lying electronic states, PE curves, transition moments, emission coeffs. 79−6894
$In_xMo_3S_4$, chevrel phase, charge transfer and valence electron conc. 78−6029
$In_xMo_6S_8$, Chevrel phase, lattice instabilities, X-ray diffr. meas. 78−34491
$In_xMo_6S_8$ Chevrel phase, synthesis, stability and characts. 80−71608
$InMo_6Se_8$, X-ray cryst. struct. determ. 80−103299
$In_2Mo_{15}Se_{19}$, superconducting chalcogenides containing Mo_6 and Mo_9 clusters 80−103804
$In_2Mo_{15}Se_{19}$, X-ray cryst. struct. determ. 80−103299
$In_{\sim 3}Mo_{15}Se_{19}$, containing isolated Mo_6 and Mo_9 clusters, single cryst. X-ray diffr. anal. 79−32952
$In_{\sim 3}Mo_{15}Se_{19}$, high field supercond., crit. temp. and crit. field 79−47211
$In_xMo_{15}Se_{19}$, new ternary Mo(II) compounds, containing Mo_6Se_8 and Mo_9Se_{12} units, X-ray diffr. study 79−65056
$InMo_3Se_3(Te_3)$, synthesis and struct. 80−92498
InN, epitaxial layer prep. using $InCl_3$-NH_3 system 78−3056
InN, epitaxial layer prep. and X-ray analysis 79−38747
InN film, refl. and transmission spectra, band struct. 78−72625
InN film, specular reflection spectra, lattice parameters 80−7428
InN film growth by reactive sputtering in Ar-N_2 discharge, mechanism 80−89107
InN, physical props. and appls. in integrated optics *(Czech)* 80−28355
InN preparation technology, powder, thin film and volume crystals *(Czech)* 78−3037
InN, RMS dynamic displacements of atoms and struct. amplitudes 79−99154
InN, thin film, characterisation using XPS electron energy loss spectra 79−87561
$In(NO_3)_3$, specific and equivalent cond. of aq. solns., viscosity 77−35736
InNbS(Se), struct., X-ray powder diffr. meas 80−44175
InO_3:Sn film, prep. by spray hydrolysis, struct., elec. and optical props. *(Japanese)* 79−42678
InO_3:Sn transparent conducting films, homeotropic orientation of liquid crystals *(Russian)* 80−108181
In_2O species, vapour press. over In+$MgIn_2O_4$+MgO mixture, 1095 to 1350K 78−91433
In_2O_3 additions to alkaline earth oxide cathodes 77−48298
In_2O_3, defect chemistry and struct. stability, impurity incorporation 77−35552
In_2O_3, effect on thermal oxidation of Si 77−12722
In_2O_3, elec. conducting film on glass substrate, measurement of optical constants and thickness 78−60525
In_2O_3, electro-conducting transparent film, props. rel. to production method *(Japanese)* 80−25557
In_2O_3, entropy of transform. from rare-earth ot corundum struct. 78−91433
In_2O_3 film, AC behaviour, dielec. relax. 77−52019
In_2O_3 film, conductive, transparent, optimal reactive sputtering conditions for prep. 79−95295
In_2O_3 film, evaporated, on ferroelec. ceramic, switching characts. 78−19107
n-In_2O_3 film, on Pb(Zr,Ti)O_3 ceramic, ferroelec. field effect 79−47177
n-In_2O_3 film, RF sputter grown, substrate bias effect on elec. and optical props. 78−64150
In_2O_3 film reactive sputtering gas composition and film growth rate *(Russian)* 80−50554
In_2O_3, films, activated reactive evaporation technique of prep. 80−80989
In_2O_3 films, electron beam evaporation, elec. and optical props. *(Japanese)* 80−60784
In_2O_3 films, reactively evaporated, elec. props. 80−84521
In_2O_3, grown from Sn-In melt, Sn solubility 77−11697
In_2O_3, in Al/tetracene/nesatron cell, electroabsorption and electrorefl., interfacial elec. fields 79−65548
In_2O_3, In_2O_3:SnO_2, transparent thin films for satellite temp. control 79−80187
In_2O_3, lattice defects, optimum prep. conditions w.r.t. stoichiometry 79−27974
In_2O_3 layer, in ohmic contact for $BaTiO_3$ 79−42638
In_2O_3 layers, chemically sprayed, prep. and intrinsic absorpt. in band edge 77−81169
In_2O_3, optically selective coating, for multiple-plate glass system design 78−74956
In_2O_3, polycrystalline, electron conc. and mobility, 25 to 700°C, O_2 partial press. depend. 77−76811
In_2O_3, reactive ion plating onto insulating substrates, and elec. and optical props. 79−87588
In_2O_3, Seebeck coeff., density of states effective mass 78−56171
In_2O_3 semiconductor electrode, sensitised photocurrent by energy and electron transfer in dye monolayers 79−38119
In_2O_3, smoke particles prep. by burning metal in Ar-O_2 gas, electron microscope obs. 77−52238
In_2O_3 smoke particles prepared by gas evap., morphology and coalescence growth 80−97738
In_2O_3, spray coated, reaction with Si, IR investig. 79−39197
In_2O_3, standard Gibbs energy of formation, meas. by electrochemical method *(Japanese)* 79−83499
In_2O_3, thermally evaporated film, struct. and elec. props. 80−104066
In_2O_3, thin film, characterisation using XPS electron energy loss spectra 79−87561

indium compounds continued
In_2O_3, thin film, sputter deposition form., optical and elec. props. 80−60123
In_2O_3 thin film on polyester substrate, struct. determ. by TEM 80−6674
In_2O_3, transparent conducting film, prep. by CVD, and characterisation 80−11571
In_2O_3 transparent conductive coating production 80−35092
In_2O_3, transparent electrode deposition on PLZT ceramic, elec. and opt. props. 78−74848
In_2O_3, transparent films, state of art *(Chinese)* 79−73610
In_2O_3, transparent heat mirror formation by ion plating on ambient temp. substrates and props. 80−25578
In_2O_3:Sn, coating on polyester film, elec. and optical props. 79−99959
In_2O_3:Sn, film, HF sputtered, cond., Hall mobility, oxidation, charge carrier density 78−72287
In_2O_3:Sn, film, optical modulation effects in electroreflectance spectra 78−6800
In_2O_3:Sn, films, activated reactive evaporation technique of prep. 80−80989
In_2O_3:Sn, glass like thin film, electron evaporated, conductive transport *(Chinese)* 80−49960
In_2O_3:Sn, HF sputtered films, temp. depend. studies of the elec. transport props. 78−76170
In_2O_3:Sn, sputtered films for selective transparent films, prep., elec. and opt. props. *(Japanese)* 77−68247
In_2O_3:Sn, sputtered film, optical and elec. props. 78−76177
In_2O_3:Sn, thin films, prep. by pyrolitic method, charact. by SEM, electron diffr. and SIMS, solar energy appl. 79−43143
In_2O_3:Sn, transparent conducting films, prep. by $InCl_3$ thermal decomp., transmittance, resistivity 79−33944
In_2O_3:Sn coated Si, temp. depend. of 10.6 μm refl., solar selective absorber appl. 77−58398
In_2O_3:Sn film, CVD and DC sputtered, electro-reflectance meas. 80−11496
In_2O_3:Sn film, electroreflectance effects 79−43055
In_2O_3:Sn film, RF sputtered, effect of O_2 press. during deposition on props. 78−19664
In_2O_3:Sn films, CVD prep. and elec. resist. meas. 79−52120
In_2O_3:Sn films, doping profiles and elec. props., appl. to optoelectronic devices 79−38203
In_2O_3:Sn films, elec. and optical props., solar energy conversion appl. 79−65945
In_2O_3:Sn films, prep. at low deposition temps. by ion-beam sputtering, elec. and optical props. 79−66004
In_2O_3:Sn films, pure and doped, prod. by ion plating, elec. and optical props. 80−2488
In_2O_3:Sn films, RF reactive sputtered, optical props. rel. to band struct. 79−91515
In_2O_3:Sn films; vac. deposited, elec. props. 80−100542
In_2O_3:Sn solar collector selective coating resistivity obs. 79−62034
In_2O_3:Sn transparent cond. films, hydrolysis deposition, elec. and optical props. 79−43144
In_2O_3:Sn/n-Si heterojunction solar cell, fabrication and charact. 78−15314
In_2O_3:Sn-Al_2O_3-Al tunnel junction, light emission via inelastic tunnelling effect 79−24076
In_2O_3:Sn-Si heterojunctions, current mechanisms and barrier height 80−11083
In_2O_3:Sn-Si solar cell, characterisation *(French)* 79−39306
n-In_2O_3/p-InP heterojunction solar cell, photovolt. effects 80−12014
In_2O_3-InN film growth by reactive sputtering in N_2-O_2 discharge, mechanism 80−89108
In_2O_3-InSb system, with Al(Au) electrode interface state density and oxide charge meas. 77−8200
In_2O_3-M_2SO_4.3MoO_3, M=Rb, Cs, phase diags., chem. reactions 77−86008
In_2O_3-Si highly photosensitive diodes, and their appl. 78−23152
In_2O_3-Si(Ge)(GaAs)(InP) heterostructure solar cells, photovoltaic and rectifying props., electron affinity determ. 79−1618
In_2O_3-SnO_2, magnetron RF sputtered electro-optical film for data storage and display 78−83047
In_2O_3-SnO_2, patterned thin films, strong electron emission obs. 77−8731
In_2O_3-SnO_2, thin films deposited on cold substrates, life stability 79−23867
In_2O_3-SnO_2, X-ray and optical meas. of solubilities 79−55894
In_2O_3-SnO_2 electro-optical film, for data storage and display 78−71176
In_2O_3-SnO_2 film, reactive DC diode sputtering, using large scale system 78−72723
In_2O_3-SnO_2 film, stress, and elec. and optical props. 78−51861
In_2O_3-SnO_2 film, XPS expts., energy band model accounting for phys. props. 77−90241
In_2O_3-SnO_2 film on Si, heterojunction, photovoltaic effect, sunlight induced 77−1470
In_2O_3-SnO_2 sputtered film, appls. in displays, vidicon tube windows, dielec. window surfaces 79−59778
In_2O_3-SnO_2 thin film, effects of heat treatment on resist. and optical absorpt. 78−43495
In_2O_3-SnO_2 thin film, Hall mobility, temp. depend., grain boundary effects 80−75658
In_2O_3-SnO_2/GaAs, solar cell, fabrication, charact. and interfacial chemistry 80−21401
In_2O_3-SnO_2/InP, solar cell, fabrication, charact. and interfacial chemistry 80−21401
In_2O_3-SnO_2/InP junction, ion probe analysis of chemical nature 79−73411
In_2O_3-SnO_2/Si solar cells, antireflection props. of oxide film 80−3513
In_2O_3-SnO_2/SiO_x/Si diode solar cells, loss mechanisms, charact., band struct. 80−26135
In_2O_3-SnO_2/polySi, solar cell response exam. using electron-beam-induced current and scanning light spot tech. 80−81477
In_2O_3-SnO_2-CdTe:P, p-n homojunction solar cell, elec., photovoltaic props., photoluminescence 80−81463
In_2O_3-SnO_2-InP solar cell junctions, efficiency, InP surface props. 80−85288
In_2O_3-SnO_2-Si heterojunctions, elec. and photovoltaic charact. 78−52070
In_2O_3-SnO_2-Si SIS heterojunction solar cells 80−85281
In_2O_3-SnO_2-Si SIS solar cells, reverse current-voltage charact. under illumination 80−89622
In_2O_3-SnO_2-SiO_x-pSi solar cells, comparison between MIS and SIS 80−81443

indium compounds continued
In_2O_3-TeO_2, phase diag. 77−81252
In_2O_3+Sb_2O_3(Sb_2O_5.H_2O) reacts., complex oxide form., struct. 77−16516
In_xO_y barriers in supercond. tunnelling junctions 77−36027
$In(OH)_3$, cubic, cryst. struct., X-ray and neutron diffr. obs. 79−77568
InO_xN_y, thin film, characterisation using XPS electron energy loss spectra 79−87561
InP (001), substrate for Ag film growth by at. beam epitaxy, elec. props. 77−59691
InP, (001) surface, MBE deposited Ag, struct. using TEM and RHEED 79−82492
InP (001)-Ag, contact, surface stoichiometry and struct., and electronic surface states 78−95361
n-InP (100), photovoltage transients by retarding pot. electron beam techniques 77−24586
InP (100) substrates, for MBE, ion-cleared, contamination, SIMS meas. 78−11353
InP, (100) surface, Auger depth profiling limitations 79−61473
InP (100) surfaces, chem. treatment effects on comp. and nature 79−47794
InP (110), low coverage adsorption, SIMS study 80−49500
InP (110), oxidation, initial stages, photoemission study 80−16529
InP (110) surfaces, cleaved and polished-sputtered-annealed, LEED and AES study 80−103550
n-InP, (110) surfaces, photolum. intensities in vac. and gas ambients 79−61412
InP (111), (110) and (001) substrates, Cd(S, Se) film growth, mismatch dislocations and lattice distortion 80−84406
InP (111) substrate, and homoepitaxial layers, characterisation by divergent X-ray beam diffr. 78−31352
InP, acceptor excited states, luminesc. spectra 80−16091
InP, ambient-enhanced photoluminesc. props., mol. adsorption and gas-flow effect 79−99925
InP, anal. of anodically oxidised (111) layers by MeV $^4He^+$ channelling effect meas. and AES 79−4492
InP, and InP_xAs_{1-x}, 111-A and 111-B faces, defect struct., etching and X-ray diffr. obs. 80−2026
InP anodically grown native oxide, antirefl. coating for InGaAsP-InP photodiode 80−13137
InP, anodisation, effect of pH, current density and illumination 78−95823
InP, automatic electrochemical carrier conc. profiling 79−99614
InP avalanche photodiodes, microplasmas, investigation 80−60018
InP, bulk grown, selective spectroscopy, acceptor level studies 80−29778
InP, CESR, optical detect. by spin orientation techniques, anal. 78−80251
InP carrier profiling using liq. barrier contact 78−76087
InP, chemisorption and oxidation states of (110) surfaces 79−24049
InP, cleaved surface, angle resolved photoelectron spectroscopy 80−55258
InP, cleaved surface, metal contact props. and influence of intermediate adsorbed layers 80−49905
InP cleaved surfaces, and interfaces with metal electrodes 78−10554
n-InP, compensated, elec. props., space-charge effects 80−65569
n-InP, compensated impurity conduction and negative magnetoresist. 79−28360
InP, compensation ratio, electron mobility and free-carrier absorpt. 80−80261
InP, concs. of C and O_2 in LEC grown cryst. determ. 77−39612
InP, critical implantation temp. and annealing 79−90691
InP, crystal growth by synthesis solute diffusion method 78−64454
InP, crystal growth by travelling heater method 80−11553
InP, current controlled LPE growth 77−77428
InP, current-controlled LPE growth, Peltier cooling at In-InP interface 77−8770
InP, cyclotron resonance, in zinc blende struct. semiconductor *(German)* 78−10337
InP cylindrical magnetron reactive sputtering, for solar cell appl. 78−39693
InP, Czochralski grown, etch pit obs., produced by new etchants HBr/HF or HBr/CH_3COOH 79−60370
InP, d-electron participation in chem. bonds 77−28682
InP, damage induced during handling for TEM obs. 80−2024
InP, deep level defects, review 80−24841
InP, deep level electron traps, emission and capture props. 80−29806
InP, deep level trap interaction with lowest and upper cond. minima 80−49654
InP, deep trap charact. by photocapacitance spectroscopy 78−6398
InP, deep trap study by free exciton refl. spectra 79−60761
InP, deep-level traps and cond.-band struct. 79−19542
n-InP, defects in homoepitaxial layers, on p-type substrate, accurate lattice parameters 78−47675
InP, depend. of phonon spectrum on hydrostatic press., Raman spectra 80−93315
InP detector, unbiased, using Schottky-barrier diode, operation in submm. wave region 80−105707
InP, diffusion and power spectral density of velocity fluctuations for electrons, Monte Carlo calc. 79−51572
InP, diffusion of Cd acceptors 79−82246
InP, dislocation etching of (001) faces with H_3PO_4 etchant 80−15103
InP, effects of baking time on purity and morphology 78−6862
InP, electrial props. at high temp. and in liquid state 77−11888
InP, electrical and optical props. at low temps. 80−39636
InP, electroabsorption spectra obs., reduced effective mass determ. 80−50301
InP electrode-electrolyte interface, Schottky barrier obs. 78−52079
InP electrodeposition, solvent systems, low melting point comps. in alkali metal metaphosphate/fluoride systems 79−28079
InP electrodes, photo-induced electrogenerated chemilum. and up-conversion 79−91510
InP electrodes in acetonitrile solns., photoelectrochem. behaviour 79−4600
InP, electron irrad. at 50 MeV, elec. and optical props. 77−47486
InP, electron transport props., mag. field and temp. depend. 80−92888
InP, electron-hole plasma, ground state energy 78−84244
InP, electronic structure of neutral phosphorus vacancy, empirical pseudopotential 79−78042
n-InP, epitaxial, Hall effect, electron mobility and density, temp. depend. 78−72288
InP, epitaxial, kinetics of VPE 80−60790

indium compounds continued
n-InP, epitaxial, subthreshold velocity-field charact., 77K 78−64038
InP epitaxial films, grown on heavily doped substrates, carrier mobility study, magnetoresist. meas. 80−60116
InP epitaxial growth, in vertical reactor, construction and expt. data *(Slovak)* 77−28081
InP, epitaxial growth, thermodynamic conditions 77−89661
n-InP, epitaxial layer, (100) surface chemistry, ESCA study 80−103552
InP, epitaxial layer, effective doping density, comparison of Hall and magnetoresistance meas. 77−11938
InP epitaxial layers, (100)-orientated, vapour phase deposited in closed-tube system, surface comp. variation 80−24752
InP, exchange interaction, analytical and nonanalytical parts, from polariton spectra in mag. fields 80−50367
InP, excitation by 2-4 KeV Ar^+ ions, electron energy spectra 80−11529
InP, exciton localisation at impurity pairs 79−37999
InP, excitons bound to neutral donors in VPE layers, luminesc. and absorpt. obs. 79−42460
InP, excitons detect., precision method 79−19906
InP, expt. studies on meltback morphology 78−31347
InP, far IR LPE photodetector performance 79−30546
InP, Faraday interband effect subjected to quantising mag. fields 80−97246
InP, Fermi level pinning on exposure to O_2 79−60637
p-InP field-assisted photocathodes, quantum efficiency 80−84831
p-InP film, CVD, growth charact. and CdS/InP solar cell efficiency 77−1813
InP film, CVD on preferentially etched Mo, initial growth behaviour 78−51855
InP film, electron-beam annealed, surface conduction 80−84500
InP film, liquid-phase epitaxial growth on (100) and {111} substrates *(Slovak)* 79−15037
InP film, on rough $Zn_xCd_{1-x}S$ substrate, film substrate lattice mismatch calcs. 78−43263
n-InP film, polycryst., deposited on Mo sheets, elec. props. obs., w.r.t. varying deposition conditions 79−4608
n-InP film, polycrystalline, elec. props. 77−76965
InP, film, prep. by low press. reactive deposition process 79−24449
p-InP film growth, by close space vapour transport 79−28944
InP films, organometallic VPE grown, props. 80−96753
InP, fine struct. in energy derivative reflectance spectra 79−78705
InP, free carriers, freq. depend. relax. time 80−2385
InP, free excitons in high mag. fields, band struct. 77−52129
InP, fused, SRO structure changes on heating 77−89367
InP grown by LPE, method for free In removal from surface 80−84860
n-InP grown by synthesis solute-diffusion method, electron traps 79−90987
InP, grown-in dislocation density, impurity effect 78−51543
InP, growth and props. 79−1822
InP growth from soln. and LEC, photolum. and elec. meas. 79−87575
InP Gunn diodes, population inversion condition 77−77251
InP, Gunn oscillator magnetoresist. meas. of mobility and noise, contact effects 77−62948
n-InP, γ-ray and electron irrad., annealing of radiation point defects, elec. cond. and Hall coeff. meas. 80−65051
n-InP, Hall effect, 10-300K ,thermal activation energy and influence of compensation 78−72171
n-InP, heat treatment effect on bulk grown and VPE grown material 77−11936
n-InP, heat treatment in controlled P vapour 80−88137
InP, heteroepitaxial deposition on GaAs substrate, using close-spaced method, X-ray analysis *(Czech)* 77−15710
InP, heteroepitaxy on CdS substrates using InI_3 as transport agent 79−56083
n-InP, high field props. under high press. 78−26872
n-InP, high resistivity layers produced by Fe^+ implantation 78−47404
InP, high-field transport 77−8107
InP, high-purity bulk, prep. from soln. 78−6839
n-InP, hole traps by deep level transient spectroscopy and transient capacitance methods 79−51514
InP, homoepitaxial film by MO-CVD process, for heterojunc. solar cell fabrication 79−8250
n-InP, hopping cond., nonohmic nature 79−23976
InP, hot carrier noise, Monte Carlo simulation 77−51792
InP hydrothermal oxidation kinetics, exam. 80−40566
InP, III-V semicond., electronic struct. of valence and conduct. bands 77−28110
InP, impact ionis. by electrons and holes 79−99554
InP, impact ionisation by electrons and holes 80−100467
InP, implantation of Si, Al, Hf, Ta into InP and GaAs, form. of protective oxide 78−79622
n-InP, impurity and minimum metallic cond. in mag. field 80−103731
InP, impurity effect on grown-in dislocation density *(Japanese)* 78−6063
InP injection laser, strong mag. field effect on emission 77−58329
InP, integrated optics appl., heterojunctions preparation and props. *(Slovak)* 80−33225
InP interface with anodic and thermal oxides, comparison of AES and ESCA 78−95980
InP interface with oxide, photoemission obs. of energy levels induced by adsorpt. 80−93000
InP, intervalley electron transfer, drift velocity and diffusion coefficient 80−39594
InP, inversion layers, C-V and surface transport meas. 80−49928
InP inversion-type MISFET with SiO_2 gate insulation interface props., elec. drift 80−93002
InP, ion implantation damage compensation 77−84770
InP, ion implantation used to create n-type, p-type and high resist. layers 78−6076
InP, ion implanted, anodic oxidation and elec. carrier conc. profiles 79−70185
InP, ion-implanted layers, close contact capless annealing, elec. props. 80−84192
InP, ion-implanted n- and p-type layers, charact. 78−6075
InP, ions coeffs. of electrons and holes 80−2394
InP, Kramers-Kronig electroreflection spectra 77−4655
InP, LEC growth of dislocation free crystals 80−89134
InP, LEC growth using pyrolytic BN crucibles 78−6841
InP, LPE, high purity, use of baking to reduce Si contamination 78−72744
InP, LPE grown, impurity effect on surface morphology 80−29291

indium compounds continued
InP, LPE grown, surface morphology 77−62771
InP, LPE growth 80−11557
InP, LPE growth on GaAs, etching and electron probe anal. 79−11526
InP Langmuir film MIS structures, surface state distrib. obs. 77−89859
InP, large size single crysts., synthesis, solute diffusion technique 79−33917
InP, laser-induced microscopic etching 80−76379
InP, lattice dynamics 79−14895
InP, lattice dynamics and phonon parameters bond bending force model 80−59595
InP, lattice matching to $In_xGa_{1-x}As$:Zn, LPE growth conditions 80−70541
InP layer growth method, model validity evaluation *(Slovak)* 80−54535
InP layers, grown by LPE from supercooled solns., thickness meas. 78−10307
InP layers, LPE growth from undercooled melts, numerical method 80−6665
InP, liq.-seal growth, protective props. of B_2O_3 flux 77−12519
InP, liquid encapsulated Czochralski cryst. growth, X-ray study 79−47619
InP, liquid interaction parameters determ., 580-670°C 80−65197
InP, low temp. diffusion of radioactive Ag 78−75884
InP, luminesc. emitted as a result of carrier heating 77−52185
InP, luminescence, hot electron effects 80−66277
InP, MBE, substrate temp. related degradation mechanisms 80−65385
InP, MBE and field emission deposition of Al and Au films, comparative study 79−87016
InP, MBE from In and P_2 beams, substrate temp. limits 80−15385
InP, MBE growth, expt. *(Japanese)* 77−4743
InP, MBE growth on InP substrate, orient.-depend. faceting 77−24966
InP, MBE growth surface, singular instabilities 77−24969
InP MIS capacitor, transient capacitance and C-V charact. 78−95374
InP MIS capacitor surface states 80−49931
InP MIS devices, diffusion, chemical reactions, contamination, AES and SIMS 80−72066
InP, MIS diode prep. by anodic oxidation 79−74270
InP MIS struct., review 78−95372
InP, MIS structures, dielec. and interfacial charact. appl. to microwave MISFETs 79−60933
n-InP, MOS solar cells, electrical and photovoltaic characteristics 80−85276
InP MOS structure, elec. charact. of InP surface meas. 77−20451
n-InP, magneto-impurity effect, review 79−91081
InP, manifestation of local vibrs. of dislocations in IR spectra 78−88339
InP, microstructs. assoc. with hardness indentations 78−80627
InP, model for ~1.10 eV emission band 80−66289
InP, molten stoichiometric, surface tension 78−39684
InP, multiphonon absorpt. bands *(Russian)* 77−85731
InP, n- and p-type, surface recomb. vel. meas., diffr. from transient optical grating 79−1604
InP, N- and p-type electrodes in acetonitrile solns., photoelectrochemical behaviour 79−99616
InP n^+-p-p^+ homojunction solar cells, high efficiency, LPE layer growth, photolithographic fabrication 80−93929
InP, n-type conductive regions produced by ion implantation 78−10067
InP, n-type doping by ion-implantation of S and Si, expt. 78−91351
InP, negative differential mobility and geometrical magnetoresist calc. 77−43624
InP, noise calc. using Monte-Carlo method 80−75575
p-InP, ohmic contact using Be-Au metallisation, low contact resist. 80−65677
InP ohmic contacts 79−28406
InP, ohmic contacts by thin film epitaxy, Gunn oscill. appl. 79−38159
InP, organometallic growth by cracking of $In(C_2H_5)_3$ and PH_3 80−11575
n-InP, oscill. intrinsic photocond. 79−60871
InP, oscillatory interband magnetoabsorption meas. 79−73909
InP p^+-n abrupt junctions, ionisation coeffs., photomultiplication meas. 80−65655
InP, p-i-ν diode, Franz-Keldysh effect 77−55790
InP p-n junction, grain boundary etching 80−96541
InP p-n junction diodes, fabrication by Be ion implantation 79−47156
n-InP, p-n junction form. by Be ion implantation 80−29474
InP photodiodes, dark current and breakdown charact. 80−70806
n-InP photoelectrode, stabilisation to photoanodic dissolution, in aqueous solutions of Te^{2-}/Te_2^{2-} 78−14814
n-InP photoelectrode, stabilisation to photoanodic dissolution in solns. containing Te^{2-} and Te_2^{2-} 78−19144
InP, photoemission and LEED meas., minority carrier diffusion length 77−69959
n-InP, photolum., evidence for low surface recomb. vel. rel. to n-GaAs 77−40272
InP, photolum. depend on surface treatment 79−78727
InP, photoluminesc. of epitaxial films, isovalent substitution 80−16097
InP, photoluminescence at dislocations, band gap electronic levels 79−99926
InP, photoluminescence intensity of cleaved surface, ambient gas influence 78−88345
InP, photoluminescence meas. using diamond-anvil press. cell 80−108256
InP, photovoltage transients, expt. and model 77−89802
InP, piezobirefringence above direct gap 79−51929
InP planar guarded avalanche diode prod. by ion implantation 79−95473
InP, planar reactive deposition on CdS, heterostruct. formation and elec. evaluation 78−72738
InP, planar Zn diffusion process for p-n junction formation 78−43040
InP, plastic deform. and scratch microhardness meas. 78−27583
InP, polar semiconductor, collisions between hot excitons and hot electrons 80−7415
p-InP, prep. of single and bi-crysts., epitaxial layer and polycryst. films 77−81211
InP, press. depend. of direct absorption edge 80−93365
InP, proton bombard. effects on resist. 77−80552
InP, proton range data and deep proton-isolated lasers 79−36923
InP, pure and S doped, VPE, exam. of molar fraction controlled impurity in In-PCl_3-H_2 78−56587
p-InP, RF sputtering on CdS and other substrates, and grain size obs. 77−90272
InP, radiation defect formation processes, effect on physical props. 78−2163
InP, reactive ion etching of III-V compounds 80−58813

indium compounds continued
InP, recoil damage obs. by PAC with ^{111}Cd 77−89484
InP, reflection spectra, optical functions, exciton peaks *(Russian)* 80−50372
InP, relaxation LSA mode obs. 77−8102
InP, reson. Raman scatt., deformation pots. 78−52495
n-InP, room temp. electron irrad., Hall coeff. meas. 77−89478
InP, Schottky barrier and semicond./insulator interface states formation 80−49906
InP Schottky barrier formation, Fermi-level pinning, defect mech. 78−95358
n-InP Schottky barriers, low leakage, near ideal 78−39212
n-InP Schottky barriers, photocapacitance effects of deep traps 78−43325
InP, Schottky diode, barrier height control by S diffusion 77−85309
InP, semicond., ^{31}P nuclear mag. shielding 79−33549
InP single crystals, uniaxial compression deform. characts. 80−84991
InP, site selective doping by ion implantation of radioactive nuclei 80−34023
InP solar cells, thin film growth tech. and characterisation 80−89631
InP, soln. in liq. Sn, vapour phase partial press. meas., rel. to LPE 78−34610
n-InP, submillimetre cond. and carrier heating, two-electron-temp. model 77−20349
InP substrate, LEC-grown, defect evaluation by cathodoluminescence 80−2866
InP substrate, LPE growth of GaInAsP on (100) and (111)B oriented crystal 78−92203
InP substrate, thermal damage suppression by adding Ar in H_2 atmosphere 79−100275
InP substrate, transient-mode LPE of GaAs 78−72746
InP substrates, chem. etching by H_2O_2-H_2SO_4-H_2O soln. 80−35360
InP substrates, control of thermal degradation in LPE growth with PH_2 partial pressure 79−33949
InP substrates HCl etching speed and polarity obs., with aid of laser beams *(Slovak)* 78−56575
InP substrates preparation, etching and polishing in Br-methyl alcohol solution *(Slovak)* 78−56576
InP, surface, electron struct. and Fermi level pinning by O_2 and metals 80−11066
InP surface, interaction with Cl, electron spectroscopic obs. 78−56036
InP, surface, pulsed electron beam processing, doping, annealing 80−75254
InP, surface (110) atomic struct. 79−69331
InP, surface and dielec.-semicond. interface props. 80−93001
InP, surface chemistry and electronic struct., adsorption of O_2, photoemission meas. 77−20985
InP, surface damage induced during SiO_2 deposition by RF sputtering 79−78879
InP surface decomposition prevention in LPE growth 80−96749
InP, surface passivation using composite Al_2O_3 and native oxide, MIS characts. 80−93004
InP, surface phonon polariton dispersion and damping, frustrated total internal refl. meas. 80−80792
InP surface preparation for Schottky barrier and ohmic contact formation 80−39671
InP, surface recomb. vel., psec. optical techniques 80−70784
InP, surface recombination velocity, diffr. from picosecond transient free carrier gratings 79−47109
InP, surface space charge layers and Schottky barrier form., Raman scatt. study 80−50319
InP, surface vacancies, bound state energy levels calc. 80−80340
InP, synthesis solute diffusion grown, elec. props., photoluminesc., etch pit profiles 79−4914
InP, temp. depend. of Fermi Level, calc. 80−39491
InP, terracing of LPE growth, doping effects 80−10846
InP, thermal degradation and its control in LPE growth 79−100343
InP, thermal oxidation, growth rate and comp. of oxide 80−55555
InP thin films for photovoltaic devices 80−93972
InP, transferred electron effect 77−39855
n-InP, transferred electron effects under hydrostatic press. 78−26871
n-InP, transferred electron instabilities, hydroststic press. effect 80−6869
InP, transferred electron device, relationship between microwave efficiency and metallurgical state of cathode contact 80−6981
InP, transferred electron effects under high press. 80−34453
InP, transient and steady-state electron transport props. 77−39812
InP, transport phenomena, review 79−19587
InP, twin-free, prep. using liquid encapsulated Czochralski growth 80−50546
InP VPE, growth kinetics and controlled doping 79−87569
InP VPE, In-H_2-PCl_3 chemistry 80−11549
InP, VPE, thermodynamics of transfer by water vapour 78−43260
InP, VPE growth for MESFET's 80−103602
InP, VPE layer props. control using boundary layer characts. 80−50561
InP, VPE using CVD 79−28927
InP VPE with new metalorganic compound 80−55278
InP, valence band fine struct. from light mod. with nonequilib. opt. phonons 78−39568
InP, valence band structure, CPA, bond orbital calcs. 78−87909
InP, vapour phase epitaxial growth in presence of O_2, elec. props. 79−46971
InP very high purity LPE layer growth 78−3061
n-InP wafer, defect studies by ASLEEP, SEM and scanning AES 79−19256
InP wafer diagnostics, using computer automated scanning low-energy electron probe 79−4214
InP, weak field Hall mobility and Hall mobility and Hall ratio 78−23116
InP, Zn diffused single-crystal, substitutional dopant and hole conc. meas. 80−75260
InP:Be, ion implantation, hole conc. and mobility, junction depth 79−46685
InP:Be, LPE, Be distrib. coeff., carrier conc. 79−90694
InP:Bi, isoelectronic impurity states, emission and absorpt. obs. 79−42491
InP:Bi, uniaxial stress effect on free and Bi-bound excitons 79−56854
InP:Cd, doping by UV laser photodeposition 80−84191
InP:Cd, p^+-p^--n^- junction form. by diffusion doping 80−84504
InP:Cd(Zn), avalanche photodiode characts., impurity diffusion effects 80−70709
p-InP:Cd(Zn), single cryst. growth by temp. gradient method 79−28907

indium compounds continued
InP:Co(Cr)(Fe), Hall and resistivity meas. 80−10990
InP:Co(Fe), diffusion solubility and elec. activity of Co and Fe 77−43240
n-InP:Cr, press. depend. of elec. resist. and Cr ionisation energy 80−80281
InP:Cr^{2+}, Jahn-Teller effect for ion impurities 80−107753
InP:Fe, deep acceptor levels, photocond. meas. 80−20116
InP:Fe, deep levels 79−56166
InP:Fe, Fe acceptor charge states, photolum., absorpt. and ESR meas. 77−36123
InP:Fe, influence of covalence on EPR spectra 78−26827
InP:Fe, photocond., Fe^{2+} intracentre excitation model 80−29436
InP:Fe, precipitate mixture 77−77485
InP:Fe, resonance photocond. 80−44651
InP:Fe shallow trap thermally stimulated cond. spectroscopy, photocond. spectrum under DC conditions 80−65585
InP:Fe^{3+} (Cr^{2+}), EPR, symm., spin Hamiltonian parameters 78−10759
InP:Ni^{3+}(Co^{2+})(Fe^{+}), EPR assessment of $3d^7$ transition metal impurity state 78−48031
InP:S, SSD growth of low dislocation density crystals 80−89135
InP:S^+(Se^+), ion-implanted VPE layers, laser annealing, elec. and struct. anal. 79−73199
InP:Se, implantation and laser annealing 80−24476
InP:Si, implantation at high temp., elec. mobilities 79−99541
InP:Si, pulse electron annealing, carrier activation and mobility 80−15124
InP:Si, vibr. modes of Si, IR absorpt. bands 78−55922
InP:Si(Mg), ion implantation and PH_3 ambient annealing under VPE conditions 79−42085
InP:Sn, LPE growth from Sn soln., elec. props., 80 to 300K 79−11250
InP:Sn film, mol. beam epitaxial growth 77−16505
InP:Te, mag. props. of conduction electrons 78−6510
InP:Te, powder, quadrupole interactions in NMR spectra 79−51880
InP:Te, quadrupole struct. of NMR line 80−20505
InP:Te(S), heavily doped, dislocation imaging using transmission cathodoluminesc. 80−29023
p-InP:Zn, electrical meas., doping levels hole conc. 78−14745
InP:Zn, isoconcentration diffusion of Zn at 800°C 78−6186
p-InP:Zn, vapour grown, prep. and props. 80−54268
InP:Zn heavily doped X-ray topography, cathodolum., and TEM obs. 79−99197
InP/(GaIn)(AsP) DH 1.27 micron lasers, nonradiative carrier loss and temperature sensitivity of threshold 80−43333
InP/anodic oxide interface, Auger analysis 77−90478
n-InP/Au-Ti Schottky diode, elec. characts. and barrier height 77−59329
n-InP/Au-Zn Schottky barrier diodes, fabrication and elec. props. 79−33348
InP/CdS epitaxial thin films on NaCl, HEED and TEM study 80−88446
InP/$Ga_{0.47}In_{0.53}As$/InP DH laser, lattice matched, MBE and room temp. operation 78−74906
InP/GaP system, two-layer structs., relaxation of internal stresses 80−34341
InP/$In_{1-x}Ga_xAs_yP_{1-y}$ heterostruct., optically induced degradation 79−86791
InP/In_2O_3-SnO_2, solar cell, fabrication, characts. and interfacial chemistry 80−21401
InP/$In_xGa_{1-x}As_yP_{1-y}$ interfaces, sputter-profiled, depth resolution degradation by cone form. 80−80094
p-InP/In-Zn(Cd) contact evaluation 77−24619
InP/InGaAs heterojunction phototransistor, high-sensitivity 80−100505
InP/InGaAs/InP field assisted photocathode, minority carrier electron transport across p-p heterojunction 78−95651
InP/InGaAsP avalanche photodiodes, with guard ring structure 80−100506
InP/InGaAsP/InP double heterostructure, grown on InP(111)B substrate, threading dislocation multiplication 80−54237
p-type InP/Langmuir film MIS diodes, characts. 80−80384
n-InP/SiO_2 capacitors, minority carrier generation 79−95496
InP/SiO_2 substrate/film system, interface formation during CVD, modelling 80−24764
InP-Ag, struct. of Ag contacts, TEM 77−62765
InP-Ag contact system, evaluation of Auger depth profiling technique 79−56893
InP-Ag Schottky barrier, hot electron attenuation length 80−49904
InP-Al interface struct., low temp. interaction, AES study 80−107661
InP-Al_2O_3 MIS struct., interface props. and MISFET fabrication 79−65557
InP-Al_2O_3-Al MIS struct., elec. props. 79−78184
n-InP-Al(Hg), Schottky barrier height and stability characterisation 80−54786
InP-Au, Schottky barriers, electroreflectance spectra 77−43698
InP-Au boundary, Schottky barrier height, interfacial layer effects 78−14824
InP-Au contacts, conditions of fabrication that control interfacial microstruct. 79−42643
InP-Au MIS Schottky barrier, interfacial parameters determ. 79−95505
InP-Au Schottky barriers, PES and depth profiling obs. 79−42641
InP-Au Schottky diodes, barrier height study 78−52088
InP-Au Schottky diodes, behaviour under heat treatment 79−78172
InP-CdS heterojunction, injection electrolum. 78−23153
InP-CdS heterojunction, prep. by CdS CVD and etching 78−52062
InP-CdS p-n heterodiodes, junction props. study by using injection electrolum. 79−82667
InP-CdS photovoltaic heterojunctions, growth and characts. 77−39931
p-InP-Cd(Zn), ohmic contact formation on InP by laser photochemical doping 80−80369
n-InP-chalcogenide glass heterojunction, fabrication, characterization, switching 80−49892
InP-Cu contact system, low temp. alloyed contact formation 80−100519
InP-electrolyte struct., field effect of photoluminesc. 79−99928
InP-$Ga_xIn_{1-x}As_{1-y}P_y$ heterojunctions, energy band diagram 77−16400
InP-$Ga_xIn_{1-x}As_zP_{1-y}$ systems, for optical devices in 1 to 1.6 μm region, LPE growth *(Japanese)* 79−28956
InP-$Ga_xIn_{1-x}As_yP_{1-y}$ DH, LEDs and lasers, fabrication and operation in 1.5 μm region 78−37893
InP-$Ga_xIn_{1-x}As$-InP, DH fabrication, crack form. due to lattice mismatch 77−15704

indium compounds continued
InP-$Ga_xIn_{1-x}P_yAs_{1-y}$ heterostruct. lasers, growth and characterisation 80−23691
InP-GaInAsP buried heterostructure lasers of 1.5 μm region, fabrication and characts. 80−74388
InP-GaInPAs DH lasers, misplaced p-n junctions due to Zn contamination 78−87051
InP-GaP, solid soln. crystallization from stoichiometric melt, solidus construction 77−85927
InP-$In_{1-x}Ga_xAs_yP_{1-y}$, DH lasers, dielectric-constant step 79−18418
InP-$In_{1-x}Ga_xAs_yP_{1-y}$-InP 1.55 μm DH room-temp. CW laser fabrication and operation 80−64071
InP-$In_{1-x}Ga_xAs_yP_{1-y}$-InP 1.53 μm single-mode CW ridge-waveguide laser 80−64072
InP-$In_{1-x}Ga_xP_{1-z}As_z$ quantum-well LPE heterostructure lasers, band filling and gain 79−22955
InP-$In_{1-x}Ga_xP_{1-z}As_z$ laser, phonon-assisted recombination 79−89906
InP-$In_{1-x}Ga_xP_{1-z}As_z$, valence band discontinuity, quantum well luminesc. 79−91483
InP-$In_{1-x}Ga_xP_{1-y}As_y$, LPE for optoelectronic devices *(German)* 79−95280
InP-$In_{1-x}Ga_xP_{1-z}As_z$ heterostructure laser, single and multiple quantum-well, liquid-phase epitaxial growth 80−38031
InP-In_2O_3 heterojunction solar cells, photovoltaic and rectifying props. 79−1618
InP-$In_xGa_{1-x}As$ alloy photocathodes, semiconductor photoemitters, field-assisted, 1-2 μm range 80−97396
InP-InGaAsP bias assisted photocathodes, photoemission in 1-2 μm range 78−48289
InP-InGaAsP p-n junction avalanche photodiodes, surface passivation techniques 80−100508
InP-InGaAsP-InP DH diode lasers, room temp. CW operation 80−1222
InP-InGaPAs heterojunction lasers and LEDs, 1.0 to 1.2 μm 80−74362
InP-metal contacts, intermediate adsorbed layer effect on electronic props. 80−39674
InP-metal contacts, metal beam epitaxy, struct. and elec. props. of films on ion bombarded InP 79−28922
InP-metal ohmic contacts, elec. and metallurgical props., heat treatment effects 80−34514
n-InP-metal Schottky barriers, effective lowering using thin VPE n^+ lasers 77−43717
InP-metal Schottky barriers, effects of heat treatment characterised by SIMS 78−6446
n-InP-metal surface barrier struct., props. 79−11223
InP-S(Te)(Zn), dislocation-free, TEM study of microdefects 79−82213
InP-$Si_3N_4(SiO_2)$, interface props., plasma deposited dielectrics, n-channel MOSFET action 80−93003
n-InP-SiO_2 capacitor, carrier generation and trapping 80−49929
InP-SiO_2 interface, CVD problems, ESCA profiles 80−93497
InP-SiO_2 MIS struct., with reduced interface state density near cond. band 78−26954
InP-SiO_2 MOS struct., capacitance-voltage and surface photovoltage meas. 79−60931
n-InP-SiO_2 system, interface and dielec. props. 80−49930
InP-SnO_2 heterojunctions, elec. and photovoltaic characts. 80−75628
InP(As), refractive index dispersion 79−24280
InP(As), surface (110), energy distrib. of dangling-orbital surface states 80−80347
InP(As), surface states, contact pot. difference, photoemission and low energy loss spectra expts. 77−85285
$InP_{1-x}As_x$, long wave and short wave phonons, Raman spectra obs. 80−50317
InP_xAs_{1-x}, absorption edge and band gap comp. depend., bowing effect 77−4653
InP_xAs_{1-x} alloys, thermoelectric characts. 77−11947
InP_xAs_{1-x}, radiation defect formation processes, effect on physical props. 78−2163
$In(PO_3)_2$, vitreous, microhardness 80−25864
$InPS_4$, $In_4(P_2S_6)_3$, $In_4(P_2Se_6)_3$, struct. chem. 78−51482
InP(Sb)(As) substrates for Al_2O_3 film, ion beam etching defect detection 80−89155
$In_{2/3}PSe_3$, cryst. growth and characterization 77−77357
InP(100) undoped homoepitaxial films grown by MBE, photoluminesc. props. 80−2809
InP(100)-Ag contacts, interface struct. 79−60922
$In_{1-x}Pb_xTe$, single crystals, mag. susceptibility 79−51738
InS, IR reflection spectra 80−11389
InS, layer semicond., Raman scatt. meas. 78−35134
InS, layer single cryst., Raman scatt. meas. 78−76478
InS, optical and nonlinear optical props. *(Russian)* 79−51943
InS, prep., and elec. and optical props. 77−77361
InS, Raman scatt. spectra and interpacket interaction 79−8146
In_2S_3, d-electron participation in chem. bonds 77−28682
In_2S_3 destabilisation of stabilised γ-phase, electron microscope obs. 78−71853
In_2S_3, film struct. and props. 77−80706
In_2S_3, valence band densities of states, XPS meas. 79−28892
In_2S_3-R_2S_3, intermediate combinations, cryst. types *(French)* 78−75648
In_2S_3-$ZnIn_2S_4$, nonlinear susceptibility, SHG 78−30019
In_6S_7, absorpt. band edge investigation 79−69840
In_6S_7, single crystal, switching effect and memory *(Russian)* 80−70774
In_6S_7, TSC at various cooling rates *(Russian)* 80−11000
InS(Se)(Te), fused, charge transfer nature 77−89757
InSb, (111) surface, anal. by low energy ion scattering spectroscopy, LEED and AES *(Japanese)* 80−20746
InSb, convection in melts, and cryst. growth under large inertial accelerations 80−66421
n-InSb, dynamical light scatt. from dielec. bulk waves, appl. of phenomenological theory 79−69829
InSb film, ion bombard. effects on elemental Sb incorporation probability during sputter deposition 79−83120
p-InSb, impact ionisation, electron-hole pair production 80−44611
InSb, narrow-gap semicond. externally induced band population effects on electroreflectance 77−66114
InSb, narrow-gap semiconductor, high intensity IR transmission limit 80−7361
InSb, noise calc. using Monte-Carlo method 80−75575
n-InSb substrates, MIS struct. form. by reactive deposition of Si_3N_4, C/V meas. 80−103752
InSb, surface (110) atomic struct. 79−69331
InSb, thin film prep. with remelting, elec. props. 77−52255

indium compounds continued
InSb thin films prepared by ion beam epitaxy system *(Japanese)* 78−22976
InSb thin layers, directed crystn. on sapphire, struct. 80−35112
InSb thin layers, interface stability during crystn. 79−65326
InSb-Au contact system, low temp. alloyed contact formation 80−100519
InSb-GaSb, directionally solidified, determination of non-constant distrib. coeffs. 78−76641
$InSb_{1-x}Bi_x$, film, multitarget sputtering growth technique 78−84711
$InSb_{1-x}Bi_x$ films, single-cryst. metastable semicond., growth and phase stability 80−80115
$InSb_{1-x}Bi_x$, metastable epitaxial film, phase diagram 80−76238
$InSb_{1-x}Bi_x$ metastable films, elemental incorporation probability modification by ion bombard. during growth 80−80118
$InSb_{1-x}Bi_x$, multitarget RF sputtering, metastable phase, conductivity transition 80−76178
$InSbO_4$, monoclinic high-pressure modification, structural type 80−33925
$In_{2-x}Sb_xO_{3+x}$, form., struct. 77−16516
$In_2Sb_4O_9$, form., struct. 77−16516
$InSbS_3(Se_3)$, prep., polymorphism, cryst. struct. 78−44002
$InSbSe_3$, cryst. prep. and props. 79−15601
$In_{1.8}Sb_{0.2}Se_3$, cryst. prep. and props. 79−15601
InSe, ^{110}Ag diffusion, temp. depend. and solution *(Russian)* 80−70467
γ-InSe, 3R struct. type refinement 80−64962
InSe (hexagonal), X-ray cryst. data redeterm. 80−19767
InSe, absorpt. edge fine struct. *(Russian)* 77−48176
InSe, ang. depend. of core level photoemission 79−43099
InSe, angle resolved photoemission, 15-29 eV, valence band struct. 77−48319
InSe, anomalous photocond. obs. 77−76869
InSe, band structure, pseudopotential calc. 80−24799
InSe, band structure, XPS, UPS and tight-binding calc. 77−47727
InSe, band structure calc., semi-empirical tight-binding method 77−47726
InSe based heterojunctions, props. 79−11210
InSe, characts. of photocond. in strong absorption region 77−66184
InSe, core-level photoemission anisotropy 78−11076
InSe, current induced by impurity-absorbed IR radiation 78−10511
InSe, direct gap exciton exam. by magneto-optics and photoconductivity 79−19527
InSe, directional dispersion of extraordinary phonons 79−65154
InSe, elastic props. temp. depend. 78−10119
InSe, electronic struct., tight-binding calcs. 80−15448
InSe, energy band structure, chem. bond polarity, photoemission, semiempirical tight binding method 80−44504
InSe, exciton absorpt. spectra, additional light wave 77−63445
InSe, exciton and polaron anisotropies, reson. Raman scatt. study 80−76033
InSe, excitonic absorpt. edge 78−88352
InSe film, photochem. production of holograms on surface *(Russian)* 79−7101
InSe film, structure, influence of laser beam 79−7761
InSe films, residual photocond., field quenching 80−60037
γ-InSe, fundamental absorpt. edge 80−2781
InSe, high field magnetoabsorpt. of hydrogenic excitons at second direct gap 80−6729
n-InSe, influence of elec. fields on anomalous photocond. 77−8147
InSe, LF oscills. of current 78−56187
InSe, large monocrysts., grown from nonstoichiometric melt., comp. and photovoltaic substrate 77−55882
InSe, layer compound, long-wavelength phonons and elastic consts. 80−65175
InSe, layer compounds, lattice instability, deformation dipole model 80−39249
InSe, layer cpd., reson. Raman scatt. at higher Mo exciton edge 79−28764
InSe, layer cryst., Raman and IR refl. spectra meas. 79−95777
InSe, layer semicond., electronic props. 79−28275
InSe, layer semicond., Raman scatt. meas. 78−35134
InSe, layer single cryst., Raman scatt. meas. 78−76478
InSe, layer single crystal, infrared and Raman spectra 78−92070
InSe, layer type, Raman spectrum exam. 78−23461
InSe, layered crystalline slabs, growth by Czochralski method 78−68619
n-InSe, layered semiconductor, current-voltage characts. investig., 130 to 400K 77−4342
InSe luminescent film, production and characterisation *(Russian)* 78−39581
InSe MOS structs. 79−69605
InSe, mag. susceptibility anisotropy, chem. bonding *(Russian)* 79−61045
n-InSe, negative photocond. and photocurrent quenching under impurity excitation conditions 77−4399
InSe, opt. props. new fundamental absorpt. edge 77−16330
InSe, optical and nonlinear optical props. *(Russian)* 79−51943
InSe, optical const. and interband transitions 77−20816
InSe, optical props. from 2-25 eV 80−29760
InSe, optical props. near fundamental absorption edge 77−12434
n-InSe, optical spectra, photocond. and resistivity 78−88321
InSe, photo-absorption of green exciton 80−80816
InSe, photoconductivity anisotropy at high optical excitation levels *(Russian)* 80−103721
InSe, photoelec. props., generation of elec. pulses 77−55574
InSe, photoelec. props. 79−73543
InSe, photoemission props. of III-VI layer compounds 79−65976
InSe, photosensitivity anisotropy in polarised light, pleochroism coeff., suitability as photoelec. analysers 79−60873
InSe, photovoltaic effect, appl. to solar energy conversion 79−29481
InSe, polar optical phonon ang. behaviour, IR refl. meas. 80−20633
InSe, polarisation selection rules for photoemission spectra, test of band struct. calcs. 77−52216
InSe, prep. and growth, book contrib. 78−19661
InSe, Raman scatt. spectra 79−69846
InSe, Raman scatt. spectra, optical phonon freq., cryst. vibr. freq. types 80−29744
InSe, Raman spectra, inter-, intra-layer interaction estimates 78−88313
InSe, reflectivity and low energy absorption 80−34944
InSe, reflectivity from 4 to 32 eV, Kramers-Kronig anal. 80−34943
InSe, SHG 79−81489
InSe, Schottky photovoltaic props. 79−7854

indium compounds continued
InSe, second order Raman spectrum and phase transition 79−38545
InSe, semiconductor layer cpds., band struct. calc. using tight-binding method 79−65376
InSe, semiconductor-metal contact, photovoltaic props. 77−59330
InSe solar cells, photovoltaic conversion efficiency 80−61356
InSe, spin orbit split off valence bands, exciton transitions, Hopfield's quasicubic model, visible absorpt. spectrum 80−50370
InSe thin film, sputter growth and chem. anal. by XPS/ESCA 80−80976
InSe, two and three dimensionality of electron states, normal photoemission obs. 77−32503
InSe, two-dimensional band struct., XPS meas. and tight-binding calc. 78−2419
InSe, valence and conduction bands, synchrotron radiation photoemission spectra 77−63536
InSe, vibr. energy spectrum *(Russian)* 79−51483
InSe, vibr. spectrum, IR refl. and absorpt. 500-100 cm^{-1} 77−81102
InSe, wavelength modulated optical absorption above fundamental edge 78−27255
InSe, X-ray crystallography, struct. determ. 77−4081
InSe, X-ray photoemission intensity, nearest-neighbour backscatter 79−65977
InSe-GaAs p-n junctions, 'optical' contacts, elec. props. 78−56222
InSe-SmSe system, microhardness and electrophys. props. 79−87093
InSe-SnO_2 n-n heterojunctions, photoelec. props. 80−96945
InSe-SnO_2 n-n heterostructures, photoelec. props., 80 to 300K 80−20297
InSe-SnSe system, phase diagram and lattice consts. of solid solns. 79−34014
n-In_2Se, influence of hydrostatic press. on elec. cond. and Hall coeff. 77−55552
In_2Se with p-n junctions produced by laser radiation, photoelec. characts. *(Russian)* 78−56226
In_2Se-InSe p-n junctions, 'optical' contacts, elec. props. 78−56222
γ-In_2Se_3 (hexagonal), X-ray cryst. data redeterm. 80−19767
In_2Se_3, chem. transport reactions with I, single cryst. growth 77−16480
In_2Se_3, cryst. struct. determ. by X-ray diffr. *(French)* 78−26501
α-In_2Se_3, far infrared optical study of ordered and disordered forms 78−84572
In_2Se_3, molar heat capacity and enthalpy of transition, 129 to 920K range 77−29030
β-In_2Se_3, rhombohedral, X-ray cryst. data redeterm. 80−19767
α-In_2Se_3, rhombohedral and hexagonal, X-ray cryst. data redeterm. 80−19767
In_2Se_3, thermodynamic and optical props. 77−24417
In_2Se_3, transitions of high temp. α form *(French)* 80−92473
In_2Se_3, vapour press. temp. depend., heat of evap. and form. 80−59642
α-In_2Se_3, X-ray diffr. line broadening 80−49047
In_2Se_3-Cu_2S system, electrophys. props., influence of 1-4% Cu_2S 80−20219
In_2Se_3-Sb_2Se_3 system, phase diagram 78−44090
In_4Se_3 layer crystal, three-dimensionalization of transport effects 79−73514
In_4Se_3, layered cryst., sp. ht. rel. to phonon spectrum *(Russian)* 79−90794
In_4Se_3, thermal cond., 2 to 30K, Umklapp processes and phonon boundary scatt. *(Russian)* 79−10991
p-In_6Se_7, electrophysical props. 110 to 400K *(Russian)* 77−35867
In_6Se_7, single cryst. prep. and electrophys. props. 79−43129
In_6Se_7 single crystals, absorpt. edge 79−87459
In_xSe_{1-x}, amorphous film, in metal-In_xSe_{1-x}-SnO_2 system, photovoltages 77−28215
In_xSe_{1-x}-SnO_2 amorphous film-SnO_2 system, photovoltic spectra, annealing effect *(Japanese)* 80−92926
In_xSe_{1-x}-SnO_2 heterostructure, anomalous temp. depend. obs. on photovoltage 78−56209
InSeI, X-ray cryst. struct. determ. *(German)* 80−100214
InSe(c), molar heat capacity and enthalpy of transition, 129 to 920K range 77−29030
$InSe_{1.2}$(c), molar heat capacity and enthalpy of transition, 129 to 920K range 77−29030
$In_2Si_2O_4$, high press. pyrochlore struct. 77−47426
$In_2Si_2O_7$, polymorphism at high press. and temp., thortveitite struct. stability *(French)* 80−10657
$In_xSi_yO_z$, thin film, sputter deposition form., optical and elec. props. 80−60123
$(In_{1-x}Sn_x)_2O_{3-y}$-Si solar cells, degradation 80−94047
$In_xSn_xMo_6S_8$, supercond. props. 80−97023
$(In_{1-x}Sn_x)_2O_2$-Si-N solar cell efficiency and elec. props. 80−35676
$(In_{1-x}Sn_x)_2O_{3-y}$, pyrolytic selective coating, Sn additions effect 78−43499
$In_{1.9}Sn_{0.1}O_3$ laser-damage-resistant transparent conductive coatings, appl. in Pockels cells 79−50333
In_2SnO_3 film, effect of ambient atmosphere during annealing, elec. props. 80−97510
$In_{2-x}Sn_xO_3$, sputter deposited, electrical and optical props. 79−47181
$In_{2-x}Sn_xO_{3-x}$ film, deposition with sputter gun 77−44162
$In_{2-x}Sn_xO_{3-y}$ film, deposited from organometallic composition, transparent cond. appl. 78−91793
$In_{2-x}Sn_xO_{3-y}$ film, magnetron DC reactive sputtering, X-ray diffr. meas. 77−44160
$In_{2-x}Sn_xO_{3-y}$ solar cells, majority carrier conduction effects 80−97796
$In_{2-x}Sn_xO_{3-y}$ thin films, optical transmission and elec. resist. 77−69926
n-$In_{2-x}Sn_xO_{3-y}$/p-Si, semicond.-insulator-semicond. solar cell, performance and spectral response, fabrication 79−83596
$In_{2-x}Sn_xO_{3-y}$-CdTe(InP) photovoltaic heterojunctions, surface and interface studies, efficiency 80−45691
$In_{2-x}Sn_xO_{3-y}$-$Ga_xIn_{1-x}P$(-InP_yAs_{1-y}) heterojunction solar cells, chemistry and prep. 80−94073
$In_{2-x}Sn_xO_{3-y}$-insulator-poly-Si solar cells, photovoltaic conversion parameters 80−101093
$In_{2-x}Sn_xO_{3-y}$-n-Si, electron deposited solar cell, photovoltaic props. 79−96446
$In_{2-x}Sn_xO_{3-y}$-poly Si SIS solar cells 80−97787
$In_{2-x}Sn_xO_{3-y}$-Si solar cells, SiO_2 detection of interface, Auger anal. 79−87991
$In_{2-x}Sn_xO_{3-y}$-SiO_x-Si SIS solar cells, loss mechanisms study for improvement of efficiency to above 12% 80−94080
$In_{2-x}Sn_xO_{3-y}$-ZnS:Mn thin film structure, surface morphology and electro-optical props. *(Russian)* 80−49554

indium compounds continued
$In_{2-x}Sn_xO_{3-y}$-ZnSe:Mn^{2+}-n-Ge thin film electrolum. cell with low-threshold voltage 80−84786
$In_{2-x}Sn_xO_{3-y}$[SnO_2]-CdSe-CdS:Cd,Cl sandwich photoconductor injection obs. *(Russian)* 80−54773
$(In_2SnTe)_x$-$(2InSb)_{1-x}$ system, semicond., Mossbauer absorption line of ^{119}Sn 78−27146
$InTa_{1-x}Nb_xO_4$ system, structural and luminescent props. 80−84769
$In_3Ta_2O_7$, new phase of mixed oxide 78−59787
InTaS(Se), struct., X-ray powder diffr. meas 80−44175
InTe, In_2Te_3, molten III-VI semiconductors, SRO 77−65945
InTe, Raman spectra, phonon modes 80−40109
InTe thin films, flash evaporation, electrical props. 80−65722
InTe-InSe p-n junctions, 'optical' contacts, elec. props. 78−56222
InTe-PbTe system, phase interactions and solid soln. form., physicochem. and elec. characteris. 80−104129
InTe-SnTe, melt temp. and composition dependence of elec. cond., and thermo EMF 79−95430
$In_{0.25}Te_{0.75}$ amorphous film, time evolution of nanosecond switching 80−6921
$In_{0.25}Te_{0.75}$ amorphous film, nanosecond switching, resist. fluctuations in low-resist. state 80−44676
$In_{1-x}Te_x$ amorphous films, elec. cond., optical absorpt. and transparency, band gap energy 79−56335
$In_{20}Te_{80}$, amorphous, splat cooled, thermoelectric props. 78−43426
In_2Te_3 defect semicond., photoconductivity kinetics 80−11035
In_2Te_3 film thermal deposition, transmission spectra and elec. cond. *(Russian)* 80−49555
In_2Te_3, liq., elec. cond. at high temps. and pressures 79−11119
In_2Te_3, liq., elec. resistivity meas. up to 30 kbar 79−38070
In_2Te_3, low temp. ordered phase and transition state, TEM obs. 79−28095
In_2Te_3, nuclear gamma resonance of ^{57}Fe, isomer shift scale construction *(Russian)* 78−35070
In_2Te_3, photoelectric props. 77−8144
In_2Te_3, photosensitivity on γ- and neutron-irrad., γ-ray dosimeter mat. applic. 77−85258
α-In_2Te_3 single crysts., elec. and photocond., temp. depend., linear thermal expansion coeff. 79−42541
In_2Te_3 type semiconductors, basis of ionising radiation detectors 78−86743
In_2Te_3-PbTe system, phase diagram, elec. props. 78−35361
In_2Te_3-type semicond. radiation-resistant fast-electron detectors 78−78559
In_2Te_3-type semiconductor, mechanism of electrically inactive impurities 80−24834
$(In_2Te_3)_x$-$(Hg_3Te_3)_{1-x}$, photoelec. and luminesc. props. 77−39889
In_2Te_5 (II), cryst. struct. determ. 78−26510
In_2Te_5, photocond. and absorption spectra, polarisation dependences 80−20642
In_3Te_2 amorphous film, pulse hologram recording 79−55091
In_3Te_4, ordered state, cryst. struct. determ. 78−26499
InTeBr, intermediate phase, cryst. struct. 80−100834
$(In_2Te_3)_x(Hg_3Te_3)_{1-x}$, characts. of photocond. in strong absorption region 77−66184
InTeI, X-ray cryst. struct. determ. *(German)* 80−100214
$(In_2Te_3)_{1-x}(In_2Se_3)_x$, thermal cond. exam. 79−28160
In_2TeO_6, crystal growth by high press. method, elec. and struct. props. 77−81206
$In_2Te_3O_9$, isolated in In_2O_3-TeO_2 system, cryst. struct. anal. *(French)* 79−32977
$(In_2Te_3)x$-$(Hg_3Te_3)_{1-x}$, $0.15 \leq x \leq 0.37$, E_g-comp. depend., spectral photo EMF meas. 77−47851
$InVO_4$, synthesis and thermal props. *(French)* 80−97443
$InVO_4$, X-ray cryst. struct. determ. *(French)* 80−39019
$InVO_4.2H_2O$, $In_4(V_2O_7)_3.14H_2O$, physicochem. props. 77−85702
$In_{0.30}WO_3$, struct. anal. *(French)* 78−59786
In_xWO_3 ($0.12<x<0.33$), structural evolution of bronze series *(French)* 79−73141
$InX(X_2)(X_3)$, $InAlX_4$, X=Cl,Br, Raman spectra, up to 1200K 80−48003
$In_2ZnBr_4(I_4)$, fast ionic cond. 79−99363
In_2ZnI_4, ionic conductivity, Raman spectra 77−69113
In_2ZnI_4, solid electrolytes, ion transport mechanism and polarisability role, comparison with Cu^+ and Ag^+ cond. 80−107531
^{114m}In-EDTA complex, method of determ., use as tracer in hydrology 77−73458
$K_2InCl_5.H_2O$, crystal structure and H-bonding 80−64978
KIn_2F_7, cryst. struct. *(French)* 78−18590
$KIn(SO_4)_2.4H_2O$, cryst. struct. 80−15082
$KIn(WO_4)_2$, ferroelastic domain struct. *(Russian)* 79−90719
La_3InS_6, cryst. struct., four-circle diffractometer data and Fourier synthesis determ. *(French)* 79−14739
$LiBO_2$-In_2O_3, phase composition, mag. props, elec. cond. 80−55365
Lu_3InO_6, high press. synthesis, cryst. struct. 77−68955
$MgIn_xFe_{2-x}O_4$, comp. effects on ferrite characts. 78−52305
$MgIn_2O_4$ free energy, entropy of form. 78−91433
$MgIn_2S_4$:Co(Cr), EPR powder spectra 80−25197
$NH_4In(SO_4)_2.4H_2O$, cryst. struct. 79−19231
$NH_4In(SO_4)_2.4H_2O$, H-bond system, X-ray diffr. obs. 80−6395
$Na_3In(SO_4)_3.3H_2O$, cryst. struct. by X-ray methods 80−6393
$Na_xIn_xSn_{1-x}S_2$ ($1>x>0$), intercalation-substitution system, NMR study *(French)* 79−69095
$Na_xIn_xSn_{1-x}S_2$, intercalation-substitution compounds, NMR study 80−44952
$Na_xIn_xSn_{1-x}S_2$, ionic conductors, ^{23}Na NMR and complex impedance meas. 79−91314
$Na_xIn_xZr_{1-x}S_2$, ionic conduction of phases *(French)* 77−47620
$Na_{1+x}Zr_{2-x}In_x(PO_4)_3$, three-dimens. solid soln., comp. depend. of ionic cond. *(French)* 80−34230
$Nd_4In_5S_{13}$, chalcogenide cryst. struct., diffr. and Patterson function anal. 80−39056
Pb/oxide/InAs structure, effective mass determ. by tunnelling spectroscopy *(Russian)* 80−44482
$PbIn_{0.5}Nb_{0.5}O_3$, ferroelectric, dielectric props. 80−103923
$Pb_{1-x}In_xTe$, $0.01 \leq x \leq 0.2$, elec. cond., Hall coeff. liquid He temp. 78−47815
$Pb_{1-x}In_xTe$, impurity-state conduction and temp. depend. of transport coeffs. 78−47795
PbO-In_2O_3 two-phase film, quantitative analysis, use of internal calibration technique developed by AES 77−36834

indium compounds continued
PbS-In_2S_3, phase investigation 80−66488
PbTe-InTe, solid solns., anomalies in electron mobility 77−80772
$RbIn(MoO_4)_2$:Fe^{3+} monocrystals, EPR spectrum in the phase transition neighbourhood 80−2624
$RbIn(SO_4)_2.4H_2O$, refinement of cryst. struct., interatomic distances, bonds 80−59448
a-Si/$In_{2-x}Sn_xO_{3-y}$, p-i-n heteroface solar cell, device physics and design 80−101113
Si/In_2O_3-SnO_2 thin film junctions, polarity dependent memory switching effects 80−70814
p-Si-$In_{2-x}Sn_xO_{3-y}$ solar cells, thermal degradation mechanisms 80−55841
Si-$In_{2-x}Sn_xO_{3-y}$ SIS heterostructure solar cells, spray-deposited 80−101106
Si-In_2O_3:Sn heterojunctions for solar cells 78−64107
SiO_2/InP interface formation, thermodynamic considerations 80−100529
SiO_2-InP, MIS struct., prod. by pyrolytic deposition resist., breakdown and interface states 77−15961
SiTe-InTe, solid solns., mag. suscept. meas., defects 78−43552
Sn-In-Te system, SnTe based solid solns. formation 77−84929
SnTe-In_2Te_3 system, thermoelec. props., phase diagram, transitions 78−43424
SnTe-InTe, SnTe-In_2Te_3, solid soln. region, lattice constant variation 77−35697
SnTe-InTe system, solid soln. films prep. under quasi-equilibrial conditions 79−33931
Ta-Ta_2O_5-InP thin refractory MIS struct. deposition 80−75647
Tb_3InO_6, high press. synthesis, cryst. struct. 77−68955
$Tb_3In_5S_{12}$, crystal struct. determ. *(French)* 77−43179
TiO_2:In_2O_3, impurity influence on polymorphic crystn. 79−78858
TiW-TiO_2-InP thin refractory MIS struct. deposition 80−75647
TlBr, He II photoelectron spectra 78−94285
TlCl, He II photoelectron spectra 78−94285
TlI, He II photoelectron spectra 78−94285
$TlInS_2$, electrical cond. of single crysts. with symm. and asymm. Ag-In contacts 80−6835
$TlInS_2$, layered structure crystals, refractive index meas. method 80−98966
$TlInS_2$, optical phonons, IR and Raman spectra *(Russian)* 79−10903
$TlInS_2$, Raman spectra, intralayer and interlayer modes 78−43876
$TlInS_2(Se_2)$, IR reflection spectra, lattice vibrs. *(Russian)* 77−85701
$TlInS_2(Se_2)$, optical and nonlinear optical props. *(Russian)* 79−51943
$TlInS_{2x}Se_{2(1-x)}$, layer solid soln., mixed one- and two-mode behaviour of optical phonons 79−47445
$TlInS_{2x}Se_{2(1-x)}$ layer solid soln., long wave lattice vibrs., IR reflection spectra 80−11388
$TlInS_xSe_{2-x}$ solid solution, optical and photoelectric props. 79−11179
$TlInSe_2$, electrical cond. of single crysts. with symm. and asymm. Ag-In contacts 80−6835
$TlInSe_2$, monocrystal, photoelec. props. *(Russian)* 80−70752
$TlInSe_2$, single cryst., elec. cond., photocond. and IR spectra absorpt. spectrum 79−47097
$TlInSe_2$, single crystals, optical phonons, Raman and infrared spectra studies 79−55842
$TlInSe_2$ single crystals, vibr. props. by light scatt. spectroscopy 79−56804
$TlInSe_2(Te_2)$, multilayer cryst., lattice vibr. symm., IR absorpt. and Raman scatt. selection rules 80−39231
Tl_2WO_4-$In_2(WO_4)_3$, cpd. formation and single cryst. growth 77−86010
Zn-In-S thin layers, ternary phases, optical props. near long-wavelength intrinsic absorpt. edge 80−80887
Zn-In-S ultraviolet detector *(Russian)* 80−18014
$ZnIn_2S_4$, and $ZnIn_2S_4$-In_2S_3 alloys, SCL currents, trap distrib. 78−52000
$ZnIn_2S_4$ crystals, switching effect, electric field distribution 80−107872
$ZnIn_2S_4$ film, photoluminesc. and photocond. 78−52677
$ZnIn_2S_4$, fund. optical consts., Kramers-Kronig analysis, reflectivity spectra 78−39573
$ZnIn_2S_4$, fund. reflectivity, 2 to 6 eV, band struct. implications 78−39574
$ZnIn_2S_4$, III(a) polytype, absorpt. spectrum tail changes due to microstresses 80−2788
$ZnIn_2S_4$ layered compound, phonon freqs., IR refl. and transmission spectra 77−77210
$ZnIn_2S_4$ layered semiconductor, fundamental optical constants, comparison with band structure calcs. and PES 79−56757
$ZnIn_2S_4$, S-type negative resist. and switching effects 80−65581
$ZnIn_2S_4$ single cryst., intense radiation effect on optical transmission, absorpt. saturation 80−53385
$ZnIn_2S_4$ switching investigation, negative resistance state instability, resistivity transitions 80−6920
$Zn_xIn_2S_{3+x}$, residual cond. 78−56185
$Zr_{1-x}In_{2x}O_{2-x}$, ionic conductivity, lattice const. 80−96688
$(ZrO_2)_x(In_2O_3)_{1-x}$ ceramic, bulk resistivity 77−35936

INDO calculations
absorption bands, vibronic intensification obs., floating-orbital method 80−63619
acetone, absorption bands, vibronic intensification obs., floating-orbital method 80−63619
acetylcholine neurotransmitter, PCILO-INDO calcs. 80−58153
N-acetylglycine, X-irrad., stable radical electronic and mol. struct., ENDOR and ESR 80−80637
acrylonitrile, dielectric constant effect on nuclear spin-spin coupling constants, INDO approx. 79−72240
alkali borate glass networks, π-electron distrib. SCF INDO LCAO-MO calc., O basicity 78−79924
alkoxy radical, trapped in nucleosides or nucleotides, EPR, INDO calcs. 77−90623
all-valence LCAO MO SCF INDO method, for mol. ground and excited state props. 78−37556
α-aminoisobutyric acid, cryst., γ-irrad., cation radicals, ESR obs.; SCF-MO-INDO calcs. 78−11537
aniline-chlorophenol complexes, ^{35}Cl NQR, inter- and intramol. interactions 80−63666
anthronyl radicals, ESR, temp. depend. phenyl twist angles 79−18210
aromatic hydrocarbons, mol. polarisability, INDO calc. 80−52886
azaaromatics, neutral and protonated, excited singlet and triplet states, charge densities, INDO calcs. 80−58152
azomethane, trans-cis isomerisation, INDO-SCF and CI calc. 78−25440

INDO calculations continued
benzene, monosubstituted, dipole moments, isomerisation and H bonding, INDO calcs. 77−54515
benzene and monosubstitutes, hyperpolarisabilities, perturbed INDO calc. 79−68189
benzene monosubstitutes, hyperpolarisabilities, perturbed INDO calc., substituent effects, σ-π contributions 79−68190
benzenes, monosubstituted, high resoln. ^1H coupled ^{13}C NMR, INDO calcs. 77−50457
1,4-benzosemiquinone, monoprotonated radical, spin distrib., INDO calcs. 77−14357
benzyl radicals, monomtheyl- and dimethyl-substituted, electronic spectra and electron affinity 80−63618
biphenyl, INDO geometry optimisation 78−74575
bond order, maximum principle, LCAO formalism 78−29728
bond polarity parameters, IR intensities, molecular orbital study 79−63914
cis- and trans-2-butene, proton-proton coupling consts., valence angle depend. 77−23508
butyl cation, H-elimination, energy partitioning, transition state geometry calc. using MINDO/3 80−104430
carbazole, spin-unrestricted study, donor and acceptor states 78−9077
chemisorption, iterative extended Huckel theory, INDO and CNDO methods 79−87875
chloroanisoles, ^{35}Cl NQR, inter- and intramol. interactions 80−63666
chlorophenols, ^{35}Cl NQR, inter- and intramol. interactions 80−63666
cyanoacetylene, IR absorpt. bands, integrated intensities, ab initio and LMO calcs. 79−72234
cytosine monohydrate single cryst., X-irrad., OH addition radical and decay product 77−86447
deoxycytidine 5′-phosphate, H_2O, X-irrad., 3αH radial. form., ENDOR, ESR 77−73453
N,N′-dialkyl dipyridinium cation radicals, struct., INDO calcs., EPR obs. 77−71821
dicarboxylic acids, D quadrupole coupling constants, ENDOR study 78−90195
5,5′-diethylbarbituric acid, EPR and INDO-MO study of radical formation after irrad. 80−93774
difluoromethane, dielectric constant effect on nuclear spin-spin coupling constants, INDO approx. 79−72240
dihydrophenazine derivatives, in 3-methylpentane (ethanol) (PMMA), radiationless processes, temp. depend. 80−43087
dimethylketene, thermal dimerisation mechanism, CNDO/2-INDO calcs. *(German)* 79−54771
dioxodiazacycloalkanes, electronic struct., mol. orbital theory 77−14359
DMSO-$PdCl_2$ complex semi-empirical INDO calc. of bonding 80−32611
ethylene, proton-proton coupling consts., valence angle depend. 77−23508
ethylenes, substituted, unstable twisted forms, excited states, DODS-NO CI calcs. 79−13643
fluorinated ethylenes, valence bond polar parameters, IR intensities, MO calc. 80−28013
force constants, semiempirical quantum mechanical method 78−62947
formamide, and related cpds., INDO-CI calc., transition moments 79−45637
free radicals, RHF CI INDO spin density calc. 80−919
glyoxal-photoreduction-product-radicals, kinetics and intramol. dynamics 77−32808
graphite, interstitial C atom, INDO calc. *(French)* 80−39068
heterocyclic conjugated compounds, electronic struct., spectra, ionisation pot., INDO-CI LACO-MO-SCF calcs. 79−54834
hippuric acid, X-irrad. single cryst., ^{14}N and ^1H ENDOR study; 80−71240
hydrocarbon, ^{13}C NMR shielding constants and tensors, finite perturbation calcs. 77−27092
hydrocarbons, ^{13}C chem. shifts, simplex optimised INDO calcs. 80−83284
hydrocarbons, proton NMR chem. shifts, mag. shielding effect of neighbouring C atoms 77−27094
hydrocarbons, small, electron momentum distribs. in π orbitals from (e,2e) expts. 80−14239
hydrocarbons proximity and conform. effects, ^{13}C chem. shifts at γ position, INDO computations 77−50451
II-VI compounds with transition metal impurity, SCF LCAO MO formalism in CNDO and INDO approx. 79−38017
invariance requirements in approx. SCF MO theory 79−6824
large unit cell semiempirical mol. orbital approach to props. of solids, general theory 79−87029
magnetic shielding, shielding anisotropies 78−21851
mass spectrometric fragmentation, MO-model and simulation 77−417
methanes, substituted, calculation of proton chemical shifts 79−45657
methanol, charged fragments, structure and stability 78−90085
methanol, field ionisation, geometry changes, INDO-SCF-MO calc. 77−38614
methyl groups, electric dipole moment, perpendicular component, orbital calcs. 77−68138
N-methyl-N-nitrosourea, electronic interactions with DNA, ESR obs. and INDO calcs. 80−94154
methylenes, substituted, INDO calcs. 77−30782
MINDO/3, unrestricted open-shell calcs., applics. to radicals 77−23429
molecular complex, bond lengths and heat of form., INDO calc. 79−54783
molecular complex, pot. energy curves, INDO calc. 79−54784
molecular orbital methods, speed and accuracy, comparison of methods 79−41106
NMR coupling constant, SCF INDO calc., zero overlap approx. *(French)* 79−50047
NMR parameters, chem. shielding, ^{13}C chem. shifts 80−23435
NMR screening constants of O and N in molecules, INDOS/S parameterisation scheme 79−76449
nonbonded interactions, pot. energy curves, CNDO/2, INDO and extended Huckel calcs. 77−27140
nuclear spin-spin coupling constants, directly bonded C-C and C-H, CDOE/INDO LMO calcs. 80−95546
nucleotide sugar-phosphate region, γ-irradiated, deoxycytidine 5′-phosphate alkoxy radical EPR 79−5249
open shell systems, energy partitioning theory at INDO level 79−68192
organic mols., relative Raman intensities, CNDO/2 INDO param. effect 80−95633
organic radicals, HFS coupling const. calcs., RHF+CI method in INDO approx. 79−770

INDO calculations continued
organic ring mol., INDO finite perturbation theory, contact proton spin-spin coupling 77−50361
PCILO method, modified, second-order energy using CNDO/2 and INDO Hamiltonian approxs. 79−36533
PCILO method at INDO level, σ-π exchange phenomena 78−62725
PCILO-INDO method, theory and appls. 80−58153
pentofuranosyl nucleosides, isomeric, ^{1}H NMR coupling consts., SCF FPT INDO approx. calc. 80−14156
phenol, PMR in absence of intermol. proton exchange, long-range coupling and conformations 77−34660
L-phenylalanine.HCl, X-ray induced radical form. 78−48755
9-phenylanthronyl radical, ESR, temp. depend. phenyl twist angle 79−18210
phenylpolyenes, donor-acceptor disubstituted, INDO calc. of hyperpolarisability 79−93924
poly(vinyl cinnamate), excited state, low-energy EELS and INDO/S calcs. 80−106407
propylene, proton-proton coupling consts., valence angle depend. 77−23508
pyrimidine bases, electron adducts, spin density distribs., INDO calcs. 77−71754
pyrimidine H-addition radicals in single crystals, long range proton hyperfine coupling, EPR and INDO 77−54568
pyrrole, free radicals produced by X-irrad. and decay of tritium atom, EPR study 78−48676
radical ions, conjugated, solvent effect in CNDO and INDO calcs. of electronic spectra by restricted methods 77−38624
Raman intensity of molecules, modified CNDO/2/INDO method 79−825
Raman line intensities, modified CNDO/2/INDO calc. 78−25621
rotational invariance, with d-orbitals included in basis set 78−41954
Rydberg INDO method, mol. Rydberg S←S and T←S transitions and oscill. strengths 78−17572
second-row elements, nucl. spin-spin coupling consts. to H, INDO calcs. 77−83621
second-row molecular orbital calcs., INDO calc. for Na to Cl 78−82643
semi-empirical INDO calc. of electronic struct. 80−32611
semi-empirical SCF-LCAO calc. including energy minimisation, GEOMO program 77−23428
SINDO/F theory of electronic struct., validity for transition metal cpds. 80−69075
spin-extended Hartree-Fock INDO calcs. 77−30781
spin-spin coupling consts., mol. vibr. contrib., calc. methods comparison 80−23402
stilbene aza-analogues, lowest excited states, INDO/S calcs. 80−95545
TCNQ, and anions, PRDDO method using Slater orbital basis 79−764
TCNQ, anions, screened INDO model, appl. to photoelectron, optical, Raman spectra 79−765
tetrafluorobenzene, microwave spectra, dipole moment, centrifugal distortion consts. 77−75133
TGS, X-irrad., glycine radicals, geom. struct. by ENDOR and INDO calc. 79−24230
transition metal compounds, SINDO theory 77−50359
transition metal compounds, SINDO/F theory of electronic struct. 80−69075
triallyl orthoformate, photoelectron spectra, ionisation pot. bands, conformation, SPINDO calc. 78−9194
trifluoroacetamide, single cryst., X-irrad., transient radical form., INDO and ESR calcs. 77−12814
1,2,4-trifluorobenzene, microwave spectrum, dipole moment and centrifugal distortion constants 78−37630
trifluoromethane, dielectric constant effect on nuclear spin-spin coupling constants, INDO approx. 79−72240
trimethyl orthoformate, photoelectron spectra, ionisation pot. bands, conformation SPINDO calc. 78−9194
L-tryptophan-HCl radical form. after X-irrad. 78−64940
two-centre integrals calculation in semi-empirical INDO method 80−32611
uracil, aq. soln., fast electron induced radical identification 79−24870
y_t-base, ground and excited states, dipole moment, CNDO/S and INDO/S calcs. 79−36534
As_2S_3 glass, localised paramag. states, As_4S_6, As_4S_4 units, mol. analogue models 78−60087
As_4S_4, electronic struct. and vertical electron affinities, INDO-type ASMO SCF calcs. 79−31402
$As_4S_4^-$, electronic struct. and vertical electron affinities, INDO-type ASMO SCF calcs. 79−31402
As_4Se_4, electronic struct. and vertical electron affinities, INDO-type ASMO SCF calcs. 79−31402
$As_4Se_4^-$, electronic struct. and vertical electron affinities, INDO-type ASMO SCF calcs. 79−31402
$Ba(NO_3)_2$, electric field gradient, quadrupole coupling consts. 77−89740
CH_2CCH radical, electronic struct., geometry, INDO calcs. 77−14358
CO, electron scatt., adiabatic polaris. pots. 79−10203
CO+e, static pot. calcs. by INDO/1s and INDOX/1s 77−27192
CO_2, elastic electron scattering and rot. excitation calcs. 79−22834
^{13}C-^{15}N spin-spin coupling consts. calcs., lone pair contribs. 77−480
Cl_2, semi-empirical INDO calc. of electronic struct. 80−32611
ClF_6, EPR spectra, mol. symmetry, INDO calcs. 77−46580
Co complex, $Co(NO_2)_6^{4-}$, bond. props. and Jahn-Teller distortion, INDO-LCAO-MO calcs. 80−75532
$CoCl_n$, electronic struct., INDO theory 80−42948
Cu complex, $Cu(NO_2)_6^{4-}$, bond. props. and Jahn-Teller distortion, INDO-LCAO-MO calcs. 80−75532
$CuCl_n$, electronic struct., INDO theory 80−42948
$CuCl_2(Cl_4^{2-})(Cl_6^{4-})$, electronic struct. studies by SCF, MSXα and INDO method 80−74119
$CuF_2(F_6^{4-})$, electronic struct. studies by SCF, MSXα and INDO method 80−74119
D quadrupole coupling const., semiempirical MO theory 79−10128
$FeCl_n$, electronic struct., INDO theory 80−42948
H^+ chemical shifts, INDO calcs. 80−32743
$H+CH_4 \rightarrow H_2+CH_3$, transition state, UHF method in INDO approx, 79−43578
HCl, semi-empirical INDO calc. of electronic struct. 80−32611
$HOO(H_2O)$, electronic struct., and config., semiempirical UHF INDOC calc. 79−59356
N-containing cpds., ^{13}C chem. shift calcs. using approx. SCF perturbation theory 77−18945

INDO calculations continued
N_2, 50 eV elastic electron scatt., centrifugal-dominant channel decoupling 80−32831
N_2, electron scatt., local exchange pot. comparison 80−78707
N_2, electron scattering, 13.6 eV, coupled channel treatment calcs. 79−64106
N_2, electron scattering, charge polarisation effects, SCF treatment 79−50132
N_2 fixation, semiempirical INDO study 80−16898
NCNCO, geometrical struct., INDO calcs. 79−22602
NF_2, ionis. pot., many-body diagrammatic RSPT calc. 79−31378
NH_3^+ radical, EPR in K_2SO_4:$(NH_4)SO_4$ 80−11272
NO_2, ionis. pot., many-body diagrammatic RSPT calc. 79−31378
N_2O^+, electronic ground state, INDO SCF MO calcs. 78−82644
^{15}N-^{13}C spin-spin coupling constants calc. using SCF and INDO method 80−32609
$NaBF_4$, electric field gradient, quadrupole coupling consts. 77−89740
NaNCO, val. band electronic struct., XPS meas., MOC and INDO calc. 80−95520
$NaNO_2$, electric field gradient, quadrupole coupling consts. 77−89740
$NaNO_3$, electric field gradient, quadrupole coupling consts. 77−89740
O_2, spin-forbidden transition intensities, selective heavy atom effects 80−58240
^{17}O, screening constants by CNDO/S and INDO calculations 77−46576
P-C, one-bond couplings, orbital and spin dipolar contribs., INDO approx. 79−31552
Pt complexes, INDO calcs. for predicting ground-state props., charge distributions and force const. determ. 80−83283
S_8^{2+}, electronic struct. and localised MOs, bonding nature and geom. struct. 80−18798
S_2N_2, polymerisation, mol. struct., INDO calcs. 77−70301
S_4N_4, electronic struct. and vertical electron affinities, INDO-type ASMO SCF calcs. 79−31402
$S_4N_4^-$, electronic struct. and vertical electron affinities, INDO-type ASMO SCF calcs. 79−31402
Se_8^{2+}, electronic struct. and localised MOs, bonding nature and geom. struct. 80−18798
Si-C, one-bond couplings, orbital and spin dipolar contribs., INDO approx. 79−31552
Si_2H_6O, geom. and electronic struct., ab initio MO calc. 79−97972
$TiCl_4$, photoelectron and UV spectra, SINDO theory 77−50360
VCl_4, photoelectron and UV spectra, SINDO theory 77−50360

INDOR
see also nuclear Overhauser effect
cytidine, pulse Fourier transform proton mag. resonance, equivalent to CW INDOR 77−32293
heteronuclear double resonance, line intensities in $A(X_2)$ and $A(X_3)$ systems 77−46583
heteronuclear selective decoupling, automatic, using Fourier transform NMR spectrometer, appl. 79−93185
ruby, consideration of dipole-dipole reservoir in nonstationary double reson 77−4580
2,3,4,- tri-O-acetyl-1,6,-anhydro-β-D-mannopyranose, pulse Fourier transform proton mag. resonance equivalent to CW INDOR 77−32293
uridine, pulse Fourier transform proton mag. resonance, equivalent to CW INDOR 77−32293
vinyl acetate, pulse Fourier transform proton mag. resonance, equivalent to CW INDOR 77−32293
Cu-Cs diluted deuterated Tutton salts, electron non-Zeeman system, nuclear relaxation study 80−44951
^2H quadrupole resonance, double transitions, appls. 79−3465
^{15}N-$^1H^+$ NMR, coupling consts., double reson., difference proton Fourier transform spectroscopy 79−3467
$NaAuCl_4.2H_2O$, ^{17}O and ^{23}Na pure quadrupole double reson., fine struct. 77−63323

induced anisotropy (magnetic)
amorphous ferromagnets, mag. fundamentals, props. and appl. *(German)* 79−28557
amorphous magnetic materials, review 79−82839
carnauba wax, magnetoelectret state, mag. anisotropy, quantum mech. effect 77−59379
carnauba wax magneto-electret, Struve function 78−76287
ferromagnet, dislocation effects on phys. props. at T≠0K *(Russian)* 77−8378
ferromagnetic amorphous system, directional order and induced anisotropy energy, theory 78−95431
ferromagnetic crystal with dislocations, mag. anisotropy *(Russian)* 77−8377
films, induced mag. anisotropy, temp. depend. *(Russian)* 79−42757
garnet, doped magnetic, ang. variation of induced anisotropy, symm. of centres 78−2676
garnet film bubble material, orthorhombic anisotropy and positive magnetostriction 77−85513
garnet LPE bubble film, growth-induced anisotropy, effect of La 77−85514
garnets, doped, site symm. exam., ang. variation of induced linear dichroism 78−95429
large aspect ratio expansion, toroidal magnetofluid equilibria, anisotropic pressure 78−26257
rare earth-Fe alloys, highly magnetostrictive, isotropy breaking magnetoelastic behaviour 78−72386
rhodopsin, visual pigment, mag. anisotropy estimation 80−51137
steel, C, residual stress induced by uniaxial deform., mag. meas. 77−73390
transition metal-metalloid amorphous alloys, mag. props. review 78−52300
$CdCr_2Se_4$, magnetisation, study of photoindduced charges 80−80567
$(Co,Fe)_{80}B_{20}$ glass, induced anisotropy and time changes of permeability 80−75815
Co, magnetic anisotropy induced by magnetic and stress annealing 78−35010
Co-Fe(Ni), magnetic anisotropy induced by magnetic and stress annealing 78−35010
Co-Gd(Nd)(Pr)(Sm), dilute, magnetic annealing effect, induced anisotropy 77−73054
Co-rare earth dilute alloys, mag. annealing, conc. depend. 78−35011
$(Co_{0.89}Fe_{0.11})_{72}Mo_3Si_{15}B_{10}$, metallic glass, strain- and field-induced mag. anisotropy 80−108004
$Co_{73}Mo_2Si_{15}B_{10}$, metallic glass, strain- and field-induced mag. anisotropy 80−108004

induced anisotropy continued
$Co_xNi_{1-x}Fe_2O_4$, conc. and temp. depend. 80—108001
CoNiZn ferrites, Fe excess, complex permeab. var. with annealing temp. 77—89979
$Er_3Fe_5O_{12}$, low temp. CVD epitaxial film growth and mag. props. 79—42406
$(Eu,Lu)_3Fe_5O_{12}$ epitaxial film, induced orthorhombic anisotropy 77—69640
$(Eu,Y)_3Fe_5O_{12}$, low temp. CVD epitaxial film growth and mag. props. 79—42406
$(Eu,Yb)_3Fe_5O_{12}$, low temp. CVD epitaxial film growth and mag. props. 79—42406
Fe, compression deformed single cryst., induced uniaxial anisotropy 78—52336
Fe, mag. anisotropy in crit. region, neutron polarisation-vector analysis 78—31065
Fe, residual stress induced by uniaxial deform., magnetic meas. 77—73390
Fe-Al (4 wt.%) alloy, mag. anisotropy induced by cold rolling *(Russian)* 80—84595
Fe-Al (4 wt.%) single crystals, rolling induced mag. anisotropy and its removal by annealing treatment *(Russian)* 79—61746
Fe-Al(25 at.%), mag. anisotropy induced by plastic deform., dislocations, long-range order 77—4544
Fe-Al(4 wt.%), ferromag. alloy, mag. anisotropy induced by cold rolling 80—30114
Fe-B, amorphous, induced anisotropy by heat treatment in mag. field and under applied mech. stress 80—75758
Fe-B-Si amorphous ribbon, strain induced anisotropy, and toroid diam. effect on mag. props. 80—34623
Fe-B(-Si), glassy, field-induced mag. anisotropy near eutectic comp. 80—93110
Fe-Co, film, magnetisation induced uniaxial anisotropy, dislocations effects 78—43618
Fe-Cr-Co-Al (27.5, 17.5, 0.5 wt.%) alloy, induced anisotropy 78—76239
Fe-Mn base alloy, mag. preferred directions 78—39370
Fe-Ni-B(-P) amorphous alloys, mag. annealing mechanism, induced anisotropy 78—95484
Fe-Ni-Co, rel. between induced uniaxial anisotropy and coercive force 78—91904
Fe-Ni-P-B amorphous alloy 77—89948
Fe-Si (3 wt.%), anisotropy induced by rolling in (001) and (111) planes *(Russian)* 77—80931
Fe-Si (3 wt.%), mag. anisotropy induced by rolling in (110) plane *(Russian)* 78—34978
Fe-Si (3 wt.%) alloy, mag. anisotropy induced by cold rolling *(Russian)* 80—84595
Fe-Si (3% wt.) polycrystalline, short-range order and induced anisotropy *(Russian)* 79—51772
Fe-Si(3 wt.%), ferromag. alloy, mag. anisotropy induced by cold rolling 80—30114
$(Fe_{0.07}Co_{0.93})_{75-x}Cr_xSi_{15}B_{10}$, amorphous, disaccommodation of mag. permeability and induced anisotropy 80—88741
$Fe_{3-x}Co_xO_4$, effect of Fe^{2+} content on coercivity instability 79—51820
$(Fe_{1-x}Co_x)_{77}Si_{10}B_{13}$ alloys, amorphous, induced mag. anisotropy by mag. annealing 79—4671
$Fe_5Co_{70}Si_{10}B_{15}$ amorphous magnetic alloy, decrease of permeability after demagnetisation, disaccommodation 80—39814
$(Fe_yNi_{1-y})_{80}B_{20}$, mag. anneal anisotropy in amorphous alloys 77—16069
(FeNi)PB amorphous wires, surface oxidation and annealing influence on induced anisotropy 80—100957
$(Fe_{1-x}Ni_x)_{80}P_{10}B_{10}$, amorphous, magnetostriction meas. by ferromag. reson., induced anisotropy 77—32232
$Fe_{40}Ni_{40}P_{14}B_6$, amorphous, stress-induced mag. easy axis 79—33516
Gd-Co, amorphous film, anisotropy due to resputtering effect 77—89989
Gd-Co, evap. amorphous film, mag. props. 77—24720
Gd-Co, evap. amorphous films, anisotropy, magnetisation and FMR meas. 77—66392
Gd-Co, evaporated amorphous film, perpendicular anisotropy by controlled O_2 contamination 77—89990
Gd-Co film, amorphous, selective resputtering-induced anisotropy 78—72376
Gd-Fe, amorphous film, stress induced anisotropy 77—89989
GdCo film, amorphous, sputtered, in-plane anisotropy induced by rare gas annealing 78—84458
HoCo film, amorphous, sputtered, in-plane anisotropy induced by rare gas annealing 78—84458
Li-Co ferrite, mag. anisotropy induced by thermomag. treatment, ionic order effect, magnetostriction meas. 80—103830
$Li_{0.5}Fe_{2.17}Al_{0.33}O_4$:Co, single cryst., domain struct., mag. annealing effect depend. on induced anisotropy 78—68290
$Li_{1-x}Fe_{5-x}O_8$:Co, single cryst., domain struct., mag. annealing effect depend. on induced anisotropy 78—68290
$Mn_{1+x}Cr_{2-x}O_4$, noncollinear ferrimagnets, uniaxial and unidirectional induced anisotropies 77—73022
MnFe ferrite, mechanically induced anisotropy, effect on mag. permeability 78—47970
MnZn ferrite, mechanically induced anisotropy, effect on mag. permeability 78—47970
Ni-Co, film, magnetisation induced uniaxial anisotropy, dislocations effects 78—43618
Ni-Fe, film, magnetisation induced uniaxial anisotropy, substrate temp. depend. 77—8367
Ni-Fe (19 wt.%) alloy, mag. anisotropy induced by cold rolling *(Russian)* 80—84595
Ni-Fe-Rh films, mag. and corrosion props. 80—34702
NiCo ferrite, induced mag. anisotropy, hysteresis loops, Barkhausen effect *(Russian)* 78—64203
Ni_3Fe, compression induced magnetic anisotropy, annealing effect 80—93112
Ni_3Fe, superlattice dislocations, compression induced mag. anisotropy 77—85442
Ni_3Fe, superlattice dislocations, compression induced mag. anisotropy 77—85443
$(Ni_{0.75}Mn_{0.25})_{82}Si_{10}B_8$, amorphous, exchange anisotropy, mag. susceptibility meas., 4.2K to room temp. 80—11186
$(Y,Sm,Ca)_3(Fe,Ge)_5O_{12}$ epitaxial films, mag. props., growth condition effects 80—97124
YCo_3, amorphous ferromagnet, exchange dominated surface modes 78—52359
induced anisotropy continued
YCo_3 film, amorphous, sputtered, in-plane anisotropy induced by rare gas annealing 78—84458
YIG, film, photoinduced mag. surface anisotropy spin wave reson. 77—4560
YIG, large growth-induced anisotropy to preferential occupation of Fe sites 80—75754
YIG:Co film, influence of stress induced anisotropy on domain struct. 80—100605
$(YRBi)_3(FeAl)_5O_{12}$ films, R=Gd, Yb, Faraday effect in transverse mag. field, orientation depend. 80—88971
$Y_{3-x}Sm_xFe_5O_{12}$, cubic and induced anisotropy, temp. depend., 100-300K, ferromag. reson. obs. *(Russian)* 78—39313
inductance
amorphous semiconductor, solid-state inductance, theory and expt. 78—56138
brass cylindrical shells, thickness determ. by inductive meas. 79—12760
co-axial single layer circular coils, accurate computation of force 80—32877
coils on infinite cylinder, mutual inductance 80—58443
complex mutual inductance concept for bioelectric impedance transformer bridge 80—63886
education, mechanical mutual inertia in spring coupled system, mutual inductance analogue 78—49590
elastic system incremental inductance, magnetoelastic instability of structures carrying electric current 79—73789
electric steel, induction above magnetisation curve knee from pole density texture 77—12151
II-IV-V_2 semiconductor, glassy, solid-state inductance, theory and expt. 78—56138
intrinsic, standardisation instruments *(Czech)* 78—32837
Josephson junction parametric inductance fluctuations, upconvertor 80—25052
nerve stimulation, contactless, electromagnetic induction technique 77—52779
plane eddy current problems, calc. method *(German)* 78—58881
rotationally symmetric mag. field expansions into zonal harmonic functions 79—31772
semiconductor, compensated, solid-state inductance, theory and expt. 78—56138
solenoid inductance, minimisation, mag. induction optimum profile 79—31769
solid electrolyte cells, inductive effects and AC meas. 78—6623
spheres and current carrying coils, integral representation of inductance 80—80469
SQUID, with V-VO_x-Pb Josephson tunnel junctions, quantum interference, critical currents 78—91821
teaching two-capacitor problem, using circuit self-inductance 79—62960
toroidal field coils, EM parameters calcs. of current paths in homogeneous media *(Japanese)* 80—106155
Cu cylindrical shells, thickness determ. by inductive meas. 79—12760
GaAs:Cr, semiinsulating solid-state inductance, theory and expt. 78—56138
Ge, epitaxial-diffusion p-n junction, inductive props. in secondary breakdown 80—15598
$(Li_{0.5}Fe_{2.5}O_4)_{0.8}(CuFe_2O_4)_{0.2}$, struct., magnetic props., rectangular hysteresis loop 77—20645
inductance measurement
10 mH or less, resonance circuit using self-excited oscillator and frequency meter 77—5867
62AD inductance meter, Boonton *(German)* 80—22344
AF impedance bridge, 4-terminal-pair, 40 Hz to 2 kHz 79—88978
antimonic caesium vacuum photocell, test instrument for contactless circuits *(Russian)* 79—58676
automatic, 1 μH to 100 H, with digital readout *(French)* 79—85152
bridge measurement methods and formulae for calculating inductance 79—44920
coaxial mutual-inductance standards, computation of parameters 80—4735
defibrillator, damped sine wave, intact, evaluation of operating parameters 78—57120
digital inductance meter, low-cost instrum. 78—32832
digital meter for inductance coil parameters meas. 78—12718
direct reading inductance meter 79—2787
inductance standard unit transmission techniques 77—53854
inductance standards, group storage errors, statistical analysis 77—53853
instrument for windings with steel magnetic yoke *(Bulgarian)* 79—88976
iron core inductor time invarying inductance meas. method 78—62207
method using laboratory oscilloscope and function generator 77—67463
mutual inductance bridge using operational amplifiers 78—54407
near infinite signal source impedance measuring system, errors reduction 77—30186
relays inductance measurement to TGL 24961 specification methods for Fe-cored coils *(German)* 80—4736
RLC bridge, with oscillator and having ten ranges 79—2785
small active resistance and inductance meas. AC bridge 78—86299
standards comparison, capacitance-inductance, transformer ratio bridge *(Polish)* 79—80645
stray, experimental methods with nanosec pulses 77—82548
student experiment, establishing $V=L(dI/dt)$ directly 77—37688
superconductor, accurate interferometric meas. technique 78—72306
universal bridge, digital meter used to measure L, R, and C 78—12715
induction, electromagnetic *see electromagnetic induction*
induction heating
see also electric furnaces; ovens
arc furnaces, stabilisation methods *(German)* 78—75402
automatic induction hardening equipment 78—92284
circular coil carrying AC in plane anisotropic cond. plates *(Rumanian)* 79—72456
cylindrical induction furnace, velocity and EM field distrib. calcs. *(Russian)* 77—47106
eddy currents in cylindrical core of induction coil considering winding helix *(German)* 80—95764
education, eddy currents, levitation, metal detectors and induction heating 78—61967
electrical resistance of metals, and semiconductors at high temp., using inductive heating 79—7816
EM induction, irregularity shaped plates, slow ramped field, eddy current heating, anal. 80—91722

induction heating continued
ferromagnetic material, induction heating for case hardening 78−15570
furnaces, cylindrical charge equivalent diameter *(Czech)* 79−50188
fusion crystallisation device for refractory block production 77−63606
fusion reactors, Large Coil Program, Westinghouse coil stability testing, pulsed induction heating 80−106194
heater, for static testing of riveted samples for short-term high-temp. strength determ. 79−87793
HF generators, calorimeter for power output investigation *(German)* 79−40571
induction heating coils, 50 kA prototype superconducting cable, critical current 80−106196
inductively heated high temp. furnace for photoelectron spectroscopy 77−82521
inductor-screen-ingot systems, EM fields calcs. *(Russian)* 77−46671
ion plating, induction-heated source, arcing elimination by top coil grounding 79−47639
ion plating industrialisation, appl. 77−8764
metal, packed powder, induction heating mechanism *(Japanese)* 79−59615
oven, for laser induced fluorescence spectroscopy of U 78−21230
permeability of saturated steel calc., with aid of formulae and charts *(French)* 77−28409
RF technique, for sample heating in surface science expts. 78−93691
salt baths, automatic temp. control 80−27300
semiconductor, inductively heated, computer simulation of temperature and EM fields 78−55961
slab heating at steel plant 80−71672
steel, heat treatment with induction heating, 78−92285
steel, rolls for cold-rolling mills, surface hardening, contact fatigue strength 79−24664
steel, sheet, thermomechanical bending, induction heating calc. 79−52280
steel, stainless, Cr-Ni, low temp. plastic deformation, in mag. field 79−83256
surface induction hardening universal feeders 79−83243
underground coal gasification, technical and economic advantages 80−3476
vacuum extraction device, with mass spectrum analyser, gas-forming admixture in metals determ. 80−22371
vacuum recrystallisation annealing apparatus for brass tubes 79−57021
Si, dislocation structure, effect of induction heating *(Russian)* 77−21180
ZrO_2 induction furnace for precision silica optical fibre drawing 78−1446

induction machines *see asynchronous machines*

induction motors
see also squirrel cage motors
3-phase, laminated cores, sound level theory, meas., and results *(Polish)* 80−92004
475 MVA pulsed motor generators for TFTR 78−58498
contactless double-supply motor, variable speed, props. *(Russian)* 77−17375
ferrofluid motion, in stator of asynchronous motor, rot. mag. field effects 77−950
frequency and speed meas. using piezoelectric pick-ups *(Russian)* 78−65911
linear, fluid flow induced in liquid metals, investigation 80−43800
linear asynchronous motor drive system, for rotating optical components inside vac. system 80−102874
linear motor slide drive system for optical machining 80−1366
noise abatement for induction motors in air/air heat-exchangers for ventilation *(Hungarian)* 80−102923
nuclear power plant appls., in safety-related function 77−3144
polyphase, at no-load, nonlinear magnetostatic field determ. 78−33647
three phase, heat flow model, locked rotor and running-up temp. rise calcs. *(German)* 79−90115
vibration generation techniques using induction motors 77−42790
vibrations caused by homopolar alternating fluxes, anal. 77−78981

inductor microphones *see microphones*

inductors
see also coils; power inductors; transformers
digital meter for inductance coil parameters meas. 78−12718
extensional trapped energy mode transducer bandwidth, influence of tuning inductor 79−55303
ferromagnetic, external field effect on MHD convertor, at finite mag. Reynolds nos. *(Russian)* 79−1351
fusion reactor, inductive and rotating machinery energy storage and transfer 79−85782
induction inspection unit with spaced windings, increasing sensitivity over magnetising and measuring length 78−56864
inductive motion transducers, design for information measurement systems 79−67284
iron core inductor time invarying inductance meas. method 78−62207
liquid metal mixing and refining in EM chute 79−77284
MHD liquid metal pump, conical MHD channel of single-phase inductor 79−77280
plasma-filled inductor, producing liq. metal MHD in trough *(Russian)* 79−1259
simulated inductors, large voltage swing, used for oscillator and floating coupling cct. 78−69227
steel, austenitic, intergranular defectiveness determ. using inductive instruments 78−53075
voltage divider, calibration by step-up method up to 1 MHz 77−18031
Fe-Si(6.5 wt.%) steel, core mat. development *(Korean)* 78−60852
SiO-Al multilayer capacitors and inductors, heat treatment effect on elec. props. 77−32082

industrial atmospheres *see air pollution*

industrial computer control
see also computerised materials handling; manufacturing computer control
conference on analysis instrumentation, Charleston, West Virginia, USA (May 1977) 79−16100
optical precision instrument manufacture, microcomputer appl. *(German)* 80−95116
petroleum industry, automation level affecting factors analysis 78−28327
stack gas monitoring system for warning and control in Chiba Prefecture 79−57561

industrial control
see also industrial computer control
cement kiln dust emission control by electrostatic precipitator, meas. 79−52989
cost-effective noise control 78−55515
machine vibration, suppression via force controlled vibr. isolation system 78−18100
neutron radiography using research reactors 79−11757
particulate matter dynamics in industrial manufacturing processes, appl. of radiotracer techniques 78−41398
robots and manipulators, symposium, Warsaw (Sept., 1976) 78−53574
temperature measurement techniques, sensor/instrument interface optimisation 77−5835
vibration control, active vibr.-mounting techniques 78−18102

industrial economics *see economics*

industrial plants
acoustic noise, random sampling techniques for in-plant use 79−27464
acoustic noise reduction system effectiveness study *(German)* 78−5612
acoustic pattern recognition, noise meas. *(German)* 77−80038
air pollution detection and control, health hazards in India 77−41145
aluminium plants electrolytic baths, power consumption limitation method *(Russian)* 80−3366
atmosphere submicroscopic asbestos fibre evaluation 79−74585
chimney design with air pollution considerations *(Dutch)* 78−81364
chromatograph dynamic error estimation 77−77853
chromatograph static error determ. and correction 77−81446
contactless speed meas., laser Doppler difference system *(German)* 77−17957
deafness risk, British Government code of practice 78−55513
electronics manufacturing plant waste treatment facility 77−73780
ELMO-G quiet running vacuum pumps and compressors for plant noise reduction 80−5872
fibre-optic data link integrated components 79−10392
furnaces, industrial, heat recovery from exhaust gases *(German)* 80−38224
hard X-ray channel-plate image intensifier 78−54517
hazards to nuclear power stations 80−78408
health service automated ECG analysis results 79−39563
hearing protection, types and limitations 78−55509
heat exchanger installations, heater min. furnace diameter determ. *(German)* 80−38234
impact/impulsive noise source study 78−1493
indirect heating systems, heat-carrying molten salt eutectic mixture *(German)* 80−38233
industrialisation of space, introductory outline *(French)* 78−77454
International Solar Energy Congress, New Delhi (1978) 79−57357
IR detector markets and device limitations 80−86432
IR instrumentation sources and optical components 80−87453
IR thermometry using fibre-optic lightguides 80−86302
large industrial hall reverberation time 78−38145
metal casting workplace lighting, vision problems, Swedish report *(Swedish)* 77−77896
methanol derivation from lignite, fuel appl. 80−61223
NDT computed transverse axial tomography system 80−89430
noise abatement by acoustically absorptive room boundaries 77−75741
noise control, choice of engineering or administrative controls or personal protection 78−33956
noise control, costs and legal requirements 78−33957
noise control services including acoustic enclosure with calculation of ventilation requirements 79−23138
noise hazard control programme 78−9490
noise level measurement techniques, legal implications 78−33955
noise level meter calibration procedures 77−62125
noise levels control in petrochemical process plant expansions 79−68480
noise onset effects on physiological and psychological functions 80−91959
nuclear safety exercises carried out in French industrial facilities *(French)* 78−55051
odorous pollution rel. to perceived sensory discomfort 77−37391
optical fibre applications to military and industrial systems 78−38021
outdoor process plant design, atm. noise attenuation calc. 79−70497
pollutant source emission meas. needs 77−41165
pollution, airborne metal conc. rels., nuclear anal. technique 80−72107
precision filter radiometer development and applications 79−21814
radioactive tracer techniques for meas. and testing *(German)* 77−70522
radioactive waste, vitrification, industrial scale plant, under construction in France 78−78478
rainwater chemical composition 30 km downwind from industrial complex 77−37395
refining factory, cost-effective noise control 79−23139
sheet-steel manufacturing plant, partial enclosures for noise control 79−29495
solar total energy systems in United States 79−96426
thickness meas., destructive and nondestructive methods compared *(French)* 78−15611
US equipment, review of BRH, FCC, CPSC, FDA and OSHA regulations 77−57311
X-ray film information processing methods *(German)* 78−15637
NO_2 and SO_2 pollution near industrial area, meas. and remote sensing equipment *(French)* 79−74928
SO_2 removal from waste gases, citrate process demonstration at 60 MW power plant 79−100553

industrial property
camera automatic focusing mechanism principles and designs 79−30595
electrophotography developments in Western Europe (1974-77) 79−71556
glass comp., patent information, automated retrieval system 79−24715
patent information system, appl. of microfilm camera DA 5 DOKUMATOR 79−75632
patent information time distrib. 79−97181
patents, significant aspects 79−17187

industrial research management *see research and development management*

industrial standards *see standards*

industries
this heading is restricted to those industries which are not covered by other specific headings
see also automobile industry; brick industry; cement industry; ceramic industry; chemical industry; construction industry; electricity supply industry; food processing industry; glass industry; manufacturing industries; metallurgical industries; mineral processing industry; paper indus-

industries continued
try; petroleum industry; plastics industry; printing industry; rubber industry; textile industry
acoustic noise meas., transducer function, basic theory *(German)* 77−80037
Bell Laboratories, origin of solid-state research 77−41449
conference, physics in industry, Dublin, Ireland (9-13 March 1976) 77−60887
European nuclear industry situation, review *(Dutch)* 77−3073
French private nuclear fuel cycle industries *(German)* 79−81055
gas, metrological service tasks 80−8981
history of industrial meteorology and weather modification 77−49542
industrial meteorologists, trade assoc. and National Council 77−53193
industrial meteorology, AMS 56th annual meeting (Philadelphia, 20 January 1976) 77−53098
industrial meteorology, future 77−53100
industrial meteorology, NOAA policy 77−53194
industrial meteorology and American Meteorological Society, history 77−49543
industrial meteorology policy of American Meteorological Society 77−53195
industrial weather service, starting difficulties 77−53099
machine noise measurement, conf., St. Louis, USA (Nov. 1974) 77−39151
meteorology, digital satellite imagery, industrial appls. 77−91282
noise control in industry, costs 80−16877
noise exposure control in heavy industrial plants 79−14153
nuclear, United States energy policy 78−5061
nuclear fuel cycle industry development, limiting factors *(French)* 78−66430
nuclear industry in Argentina, history and present status 77−65352
nuclear industry safety criteria 77−65302
nuclear power, safeguards in technology transfer to developing countries 77−65348
optics industry, business side, conf., San Diego, USA (Aug. 1978) 79−81354
pharmaceuticals, freeze drying 77−70010
phosphate and related industries, need for radiation controls 77−56483
plant site, local weather effects on air pollution, field studies 77−53165
power industry, need for continuing education 77−45633
radioisotope applications in agriculture, hydrology, medicine industry etc., booklet 78−35947
solar energy for process heat, energy requirement 80−76606
solar power industry, economic considerations and feasibility in Britain 80−26111
thermal energy storage in industry and power stations 80−67002
thermography appls. in industry 78−79112

inelastic electron tunnelling spectra *see tunnelling spectra*

inelastic electron tunnelling spectroscopy *see tunnelling spectroscopy*

inert anodes *see anodes*

inert gas compounds
see also argon compounds; helium compounds; krypton compounds; neon compounds; radon compounds; xenon compounds
alkali + inert gas molecule, far wing line broadening, quasistatic theory 79−22762
alkali metal-inert gas mol., gaseous transient, D-line emission obs. 77−38688
complexes, spectroscopic data, geometry, pot. energy curve, dissoc. energy, equilib. internuclear distance, determ. 80−53018
excited molecules formation, rate const. determ. 80−9859
excited rare gas complexes, optical excitation device 78−13629
fluoride exciplex laser pumping efficiency 78−74892
fluoride laser, using NF_3-inert gas mixture, long pulse UV emission *(French)* 78−58982
fluoride lasers, discharge and electron beam pumped, review 78−71083
fluorides, covalent and ionic states, ab initio CI calcs. 78−78634
fluorides, excimer emission bands *(Russian)* 77−71885
fluorides, formation in AC discharge 80−64817
halide electronic transition laser, quantum chem. 80−32971
halide excimer electronic struct., config. interaction, electrostatic model 78−927
halide excimer laser, electrode surface prep., metallisation techniques 80−19048
halide excimer laser, electron beam excited, efficiency 80−53278
halide excimer laser, gas recirculating system, purification by Ti gettering 78−46617
halide excimer laser, operating and beam characts. 79−59715
halide excimer lasers, book contrib. 79−81418
halide excimer lasers, high power and efficiency, review 78−33728
halide excimer lasers, power and efficiency, review 79−937
halide exciplex lasers, VUV and XUV pulse generation 79−3688
halide high power lasers, const. E/N pumping 77−88711
halide high-efficiency UV lasers 77−54706
halide high-power lasers, efficiency and energy scaling, review 79−36887
halide ions, form., mass spectrosc. obs. 79−29346
halide laser, discharge excited, gas composition and lifetime studies 80−53268
halide laser compatible materials, gas purification techniques 80−38037
halide lasers, at. and mol. collision processes 80−53263
halide lasers, development of miniature high-power high-press. UV and IR lasers 78−46642
halide lasers, discharge excited, optical loss mechanisms and tuning performance 80−32970
halide lasers, discharge excited, preionisation technique 80−23714
halide lasers, e-beam sustained, glow discharge stability 79−55117
halide lasers, emission spectra, efficiencies, pulse energy, appls. 78−58993
halide lasers, kinetic processes 78−63098
halide lasers, operation and use in photochem. 80−9860
halide lasers, pumped by transverse elec. discharge devices 79−41373
halide lasers, pumping technology 77−88767
halide lasers, stable-unstable resonator for beam control 80−23722
halide lasers, use in mol. photolytic dissoc. obs. of Se_2 80−11935
halide VUV lasers, pumped by travelling-wave discharges, 170 to 250 nm range 79−41372
halides, avalanche discharge lasers, characts. and parametric behaviour 80−37998
halides, B(1/2)-A(1/2) system, emission spectra 79−6934
halides, electronic transition dipole moments, excited state alignment 77−38698
halides, emission spectra, open-shell closed-shell interactions, electron gas model 77−30879
halides, excimer emission from electron beam produced plasma 80−43887
halides, exciplex mol. form., rel. to laser operation 80−81318
halides, III(1/2)-II(1/2) transition 79−94211
halides, laser mechanism, excitation methods and appls. 80−95871
halides, theory and application of excimer lasers 79−59684
halides, triatomic, as laser candidates 80−28220
halides, triatomic, optical emission 78−66558
halides, UV emission spectra, pressure and temp. depend. 80−28209
halides, UV excimer lasers, review 77−34877
halogen bearing molecule-inert gas three-component mixture, self-sustained electric photoionization discharge 80−54073
halogen excimer laser principles, performance and applications 78−55342
halogen excimer lasers, electron beam controlled discharge pumping 77−10893
halogen exciplex, spontaneous and superfluoresc. emission, pumping of I laser 77−34883
hydrides, laser active media, feasibility, energy storage 78−79014
inert gas-alkali metal excimer molecule, possibility of existence 79−76354
monohalides, hyperfine interactions, struct., valence bond calcs. 78−66473
oxide amplifiers, appl. and performance 78−63085
oxide excimer lasers, book contrib. 79−81417
oxide laser, electron beam pumped, rel. to fusion applic. 77−46403
oxides, low-lying electronic states, ab initio CI calcs. 77−57888
oxides, theory and application of excimer lasers 79−59684
stability of hypothetical $A^{(2)}B^{(8)}$ compounds 79−99110
BrF_2^--, $BrFCl^-$-, $BrCl_2^-$, inert gas cpds., localised MOs and bonding nature 78−9061
ClF_n-, ClF_n^+-, ClF_n^--, inert gas cpds., n=1-6, localised MOs and bonding nature 78−9061
CsHe(Ne)(Ar)(Kr)(Xe), excited state IR emission bands 80−14140

inert gases
see also argon; helium; krypton; neon; radon; xenon
absorbate-substrate system, surface phonons, superstructures 77−15676
abundance patterns in granite samples, Sudbury phenomenon *(Japanese)* 77−73735
abundances on Mars rel. to volatile outgassing on Earth and Mars 77−45342
adsorbates on simple metals, optical excitation, configurational switching, charge transfer 80−107643
adsorbed atoms, vibrational modes 77−69172
adsorbed layers, 2-dimens. condensation, crit. temps. 80−20032
adsorbed layers, order-disorder phase transforms., CDW and mass density waves 80−39281
adsorbed monolayer, Percus Yevick theory for gas to condensed phase transition 77−7968
adsorbed monolayer, thermal expansion and stability 79−69352
adsorbed on graphite, phase transition using Landau model 79−69243
adsorbed on graphite as microcluster, temp. depend., mol. dynamics study 80−80056
adsorbed on graphite surface, excitation spectrum 78−71943
adsorbed overlayers, LEED exam. 77−47306
adsorption, on alkali halides, pot. energy calcs. 78−67902
adsorption, on graphite, solidified layer struct. and density *(French)* 78−18893
adsorption, on graphitised C black, gas-solid virial coeffs. 78−75928
adsorption, on graphitised C black, Henry constant, rel. to intermol. interaction pot., review 78−22948
adsorption, on metal surfaces, excitation spectrum 79−23832
adsorption, on metallic surface, collective effects 79−19456
adsorption, on polycryst. transition metal surfaces, tangential momentum accommodation coeffs. meas. 79−95270
adsorption heat on alkali halide crystals, variation 77−85049
adsorption on Ag surface, physisorption energies 78−71944
adsorption on inert gas substrates, sp. ht. of adsorbates calc. 77−1302
adsorption on ionic crystals, initial heat of adsorption calc. 78−26773
adsorption on metal, interaction energy, quantum mech. density functional formalism calc. 78−67911
adsorption on metal surfaces, density functional approach 77−85061
afterglow, excimer form., VUV emission obs. at low press. 80−38755
afterglow plasma, anisotropic props. 79−1362
afterglow plasmas, cyclotron emission and electron thermalisation 77−84545
air monitoring systems for radioiodine and inert gases, evaluation 80−95480
alkali atom, in inert-gas solid, at level struct. calc. pseudopot. method 80−9532
alkali atom+inert gas, long-range interaction, S-state alkali atom 79−76480
alkali atom+inert gas, three-body interaction, secondary satellites of alkali line 77−83683
alkali atom+inert gas atom, $^2P_{1/2}$ state depolaris., mag. field effect 78−33590
alkali ion+inert gas, interaction pots., gaseous ion mobilities 77−54584
alkali metal:inert gas, optical absorpt. by impurity, cluster Bethe lattice calc. 77−8612
alkali metal+inert gas, adiabatic pots. 79−81254
alkali metal+inert gas, collisional shifts and broadening of Voigt contour 80−27983
alkali metal atom+inert gas, collisional broadening and shifts, semiempirical pots. calcs. 77−10727
alkali metal atom+inert gas atom, hyperfine transition spectral line shift, quantum corrections 78−82655
alkali metal-inert gas, inhomogeneous mixture, nonequilib. processes under conditions of T-layer form. 78−91079
alkali-inert gas system, mol. band profiles of induced dipole transitions 78−42135
alkali-rare gas atom systems, electronic collisionally induced transition dipole moments 79−98195
annealing atmosphere, inducing of in-plane anisotropy in rare earth-Co amorphous films 78−84458
arc, low-voltage, ionis. mechanism 79−27852
arc discharge, high current, anode near-electrode layer, spot formation and sheath breakdown 80−38835

inert gases continued
in atmospheres of Venus, Earth and Mars, abundances rel. to planetary interiors outgassing 79−48721
atom, charge capture to continuum, differential cross-section, cusp asymmetry 79−94082
atom, chem. radiative collisions *(Russian)* 78−23942
atom, correl. lines, Rydberg excitation and ionisation pots. 77−6705
atom, diamagnetic susceptibility relationship with electronic polarisability 77−14597
atom, dynamic polarisability, dispersion forces, at. levels light shifts, model pot. 77−31017
atom, electron impact double ionisation, binary encounter approx. calcs. 78−90294
atom, electron impact ionisation cross-sections for excited states 80−9742
atom, field ionis. and proton capture, critical energy deficits 78−82853
atom, first excited config., intermediate coupling coeff. 80−83450
atom, low energy electron elastic scatt. effective cross section, time of flight meas. 79−13823
atom, metastable, electron impact ionisation cross-section calcs. 77−46644
atom, metastable composition of inert gas beam from ion-neutral reaction 77−29008
atom, oscill. strength determ. from resonance radn. self-absorpt. 77−18847
atom, outer shell photoionisation, relativistic RPA calcs. 80−9571
atom, photoelectron ang. distribs., theoretical calcs. comparison 79−59412
atom, photoelectron spin polarisation, ab initio calcs. 80−18833
atom, photoionis. cross sections of excited levels, quantum defect method calcs. 80−37795
atom, photoionisation cross-section, multiconfig. Hartree-Fock calc. 78−17630
atom, positron elastic scatt., polarised orbital approx. 77−30996
atom, positron scatt., low energy, semiempirical polarisation pot. calcs. 80−9735
atom, primary ionisation by ~2 MeV relativistic electrons *(Russian)* 77−75309
atom, quasiadiabatic polarisation pot. for elastic electron-atom scatt. 77−6929
atom, radical cation+$NH_3(PH_3)$, thermal energy charge transfer reaction 77−16796
atom, screened potential model, for at. energy levels and oscill. strengths 79−36516
atom, spectral line width and shift in shock-tube plasma 77−23467
atom, two-photon excitations, interelectron correlation 80−957
atom+^{87}Rb, D_1-line hyperfine components perturbation, interferometer obs. 80−32635
atom+ $Ba^+(YB^+)$, ($^2P_{3/2}$) states relax. cross sections 78−13595
atom+alkali atom (ion), collision studies of quasi-one-electron systems 80−63750
atom+alkali halide, inelastic scatt., short-lived complex form. 79−13796
atom+alkali metal, nonresonant collisions, intramultiplet relax. 77−6902
atom+alkali metal atom, S-state, long range interaction 77−50490
atom+alkali metals, line profiles, width, shift and asymmetry, square well pot. approx. 80−52936
atom+alkaline earth ion, polarisation of emitted radiation, quasimol. interf. effect *(Russian)* 77−46633
atom+atom, excited state-ground state interactions 79−18259
atom+atom, total cross-section, glory struct. meas. apparatus 80−18901
atom+B, B emission line broadening in glow discharge lamp 77−3304
atom+Ca, Ca metastable ^3P-state, quenching reactions, fluoresc. meas. 80−102477
atom+Ca(Sr), $^1P_1$-$^3P_1$ excitation transfer 80−102559
atom+Cd, broadening of 5^1P_1 level 80−83479
atom+Cd, transitions between excited Cd states 78−17773
atom+diatomic molecule, collision in laser field, vibr. excitation 78−86937
atom+$Fe(CO)_5(Ni(CO)_4)$, dissoc. energy transfer, chemiluminesc. 80−55647
atom+Ga(In), (Tl) 80−32632
atom+$H_2(NO)$, cross section meas. with state selected beams 78−62910
atom+H^+, S-shell ionisation cross-sections calcs. *(French)* 78−42212
atom+H^-, charge transfer, ejected electron spectra 79−45828
atom+H^-, negative ion detachment cross section determ. 80−63796
atom+H(1^2S)(H(2^2S)), electron capture, electron loss and deexcitation cross sections meas. 78−22025
atom+H(2s), electron capture, H^- form., 4-25 keV 80−9729
atom+halogen mol., halide form., relax. and quenching 80−81314
atom+Hg, interaction potential *(French)* 78−25647
atom+high-Rydberg atom, thermal collision, l-changing cross section calc. 80−14190
atom+HX, (X=halide), rot. excitation 77−10742
atom+I_2, energy and ag. momentum transfer, polarised laser fluoresc. obs. 79−31590
atom+ion, electron capture cross section, 200-4000 eV 79−76512
atom+ion, radiative charge transfer coeffs. 79−7010
atom+ion (F^-) collisions, hyperfine interactions of recoiling fast ions 77−18469
atom+K(Rb), ground-state pots. from elastic cross sections 77−75258
atom+Li_2, collision induced transition rate consts., two-laser spectrosc. 80−9629
atom+Li, low energy, excitation, emission cross sections and polarisation fractions 80−37867
atom+Na, collisional redistrib., two-photon absorpt. with near-reson. intermediate state 80−23505
atom+$Ne^{2+}(Ar^{2+})(Kr^{2+})(Xe^{2+})$, low energy reactions, SIFT and drift tube obs. 80−97705
atom+O_3, rot. energy transfer, centrifugal sudden approx. 80−27933
atom+O^+, potential energy curves from elastic scatt. cross sections 80−23502
atom+O^{n+} (n=4 to 7) small impact parameter collisions, dynamic screening model 77−50525
atom+O(S)(Se), ^1S-^1D collision-induced transitions 78−33588
atom+O ion, small impact parameter scatt., charge distrib. 77−30989
atom+OH^-, collision-induced dissociation 78−29834
atom+positronium, fine struct., interval, collisional density shifts 77−34788
atom+Rb, spectral broadening and shift of Rb 79−22663
atom+Rydberg atom, ang. momentum mixing 79−10175

inert gases continued
atom+S^{n+}, electron promotion effects for small impact parameter 79−18278
atom+S^{n+}(n=5 to 9), small impact parameter collisions, charge exchanging processes 80−14227
atom+Tl($^2S_{1/2}$), long-range interaction, spectral line shifts and broadening 79−10174
atom+ZeCl, ground state destruction, quenching rate consts. meas. 80−63758
atom (^1S)+halogen atom (^2P), coupled channel study, rel. to elastic approx. 79−81255
atom and solid, excitons 78−39034
atom-atom collision induced polarisabilities, perturbation treatment 78−86778
atom-atom systems, spherically symm. van der Waals pot. theoretical model 77−34713
atom-solid surface beam-scatt. spectroscopy in eV range, nucl. channel, formal theory 79−78820
atomic electron elastic scatt., computer anal. of differential cross sections 77−58160
atomic electron scatt., effective collision cross sections 79−98222
atomic electron scatt., optical model, differential and inelastic cross-sections, spin polarisation 77−75299
atomic excited states in discharge, Hanle effect 79−76394
atomic inner-shell optical photon excitation, Auger, autoionisation, photoionisation processes, photoelectron spectra 77−18867
atomic ion recomb. with F^- 78−46574
atomic levels, fine struct., in field of intense reson. wave 78−9099
atomic multiphoton inoisation probability, Green's function model pot. 78−25498
atomic photoionisation, Dirac-Fock calcs., branching ratios and angular distrib. in p shells 80−63601
atomic polarisability, variation with density 77−68131
atomic positron scatt., total scatt. cross-sections at intermediate energies 77−3456
atomic scattering, metastable states 78−62906
atoms, electron impact excitation to high Rydberg states 79−89790
atoms, initial state wave functions for photoionisation cross-sections, multiconfigurational HF calcs. 80−47908
atoms, metastable states, laser excitation and fluoresc. 77−57921
atoms, multiple photoionisation, threshold to 280 eV, time of flight meas. 79−85939
atoms, polarisabilities, linear and nonlinear, screening consts. effects 79−31435
atoms, pot. energy curves analysis 80−53083
atoms, reson. widths, anomalous variation 79−31478
atoms+HgBr vibr. relax., rate coeffs., fluoresc. obs. 80−63697
basalts, oceanic, noble gas abundance patterns controlling factors 78−65220
binary inert gas systems, determ. of (m,6,8) pot. parameters 79−46414
binary mixture, unlike mol. force consts. from viscosity data, thermal cond. 78−33565
binary mixtures, thermal cond., 400-2500K 77−76020
binary mixtures, thermal diffusion factor meas. 80−79425
blood supersaturation by counterperfusion and diffusion of inert gases 77−90829
bound diatomic molecules, covalent bonding concept in undergrad. chem. courses 80−22177
bound-free excimer lasers, radiative and kinetic mechanisms 77−88697
buffer gas, H and alkali atoms hyperfine shift and interatomic pots. 80−5491
BWR power plant stack effluent inert gas nuclide monitor 79−3255
central potential models 77−54510
chondrite Kirin H, inert gas content interpretation *(German)* 80−46505
chondrite Yamato-74191, inert gas composition and neutron capture effects 80−46504
coating, on Al thin film, effect on supercond. 80−7026
collision-induced absorption, exact line shapes, rare gas mixture, appl. to He-Ar 78−66512
collision-induced translational absorpt., line shape 77−439
complex atom*+inert gas atom, model pot. curves, including CI 78−42154
compressed gases, intermol. interactions, translation absorption spectra, temp. depend. 78−46419
compressor for inert gas and mixtures 78−86286
corona discharge, ionisation instability 77−11430
crystal, acoustic velocity, theory 79−55831
crystal, bound self-localised hole states assoc. with lattice distortion 77−24530
crystal, correlation forces *(Russian)* 78−22686
crystal, dielec. const., Brillouin scatt., short-range at. interaction effect 78−43881
crystal, exciton-phonon interaction, scatt. and self-localisation phenomena *(Russian)* 77−62831
crystal, lattice vibrs. and radiative transitions of implanted ions *(Russian)* 80−69098
crystal, Monte Carlo calc. of conc. of lattice vacancies, method of overlapping distribs. 80−39077
crystal, quantum mech. calc. of elastic forces *(Russian)* 77−39555
crystal, quasi-atomic and quasi-molelcular exciton states *(Russian)* 80−103628
crystal, two-phonon bound states in high temp. limit 77−43291
crystal struct., induction energies, FCC and HCP 77−15343
crystallites of 5, 6, 7, 8 atoms, metastable states, Monte Carlo method 78−22687
crystals, dispersion binding energy 77−76351
crystals, intermediate-radius excitons *(Russian)* 79−11068
crystals, internal energy, Monte Carlo calcs. 77−72577
crystals, repulsive interaction energy, Born-Mayer parameters 78−26485
crystals, three-body forces and third-order elastic consts. 79−51185
crystals with imbedded impurities, struct. and diffusion props., review 80−10563
cyclobutane-t, chemically activated by nuclear recoil, vibr. energy transfer 77−66763
degenerate atom+inert gas atom, pairwise additivity, DIM calc. 79−89728
dense, positronium annihilation rate 78−55258
dense, rotational relax. of solute molecules reln. with local anisotropy fluc. 80−58183
dense gases and liqs., three-body nonadditive interactions, thermodynamics props., mol. dynamics simulation 79−7435

inert gases continued
desorbing atoms, from solid, apparatus for detection 78−32915
diatomic ions, mobility in parent gas meas. 78−63532
diatomic isovalent sequence, free-mol. electronic transition intensity consts., systematics 78−42137
diatomic mol. impurities, nonequilibrial dissoc. consts., vibr. relaxation 77−52632
diatomic systems, interactions, long-range dipoles, quadrupoles and hyperpolarisabilities 80−53161
dielectric liquids, high-field electron transport *(Japanese)* 78−2495
dimer+atom, IOSA calc. for total integral cross sections for excitation, exchange and dissoc. 80−1044
dimer formation, free-jet expansions, rate coeffs. 77−66745
dimer ions, electronic struct., chem. binding 79−31376
dimer ions, photofragment spectroscopy using fast ion beams 80−9755
dimers, Gordon-Kim intermol. force model 79−45781
dimers, Van-der-Waals type, electron impact ionis. 80−58400
discharge, crossed elec.-mag. fields, spatial mass division, mass spectra obs. *(Russian)* 78−5960
discharge, HF, continuous bremsstrahlung emission, radiation standard 80−1856
discharge, HF, continuous radiation source 80−1855
discharge, high-current, Z-pinch dynamic and radiative characts. 80−19631
discharge, ionisation waves in axial mag. field, crit. current 78−42848
discharge, isotope separation in travelling magnetic field 80−78719
discharge, low-press., electron energy distrib., elec. field and electron wall loss effects 80−24294
discharge, plasma electron ensemble, collision-dominated final periodic state and adjustment 78−71426
discharge, positive column contraction, medium press., vol. recombination 78−51379
discharge, reson. radiation imprisonment model 80−38756
discharge lamp, UV inert gas-type, monochromated, addition to XPS spectrometer 78−89601
discharge possibility, self-sustained, with bulk photoionisation impurities 80−75113
dissolved gases in seawater hydrophysical studies *(Russian)* 77−60425
Djermaia (H) chondritic breccia, spallogenic rare-gas data rel. to preirradiation history 80−36579
dye vapour-inert gas mixture, potential laser system 77−23672
(e,2e) reactions 200 to 2600 eV as probe of atomic and molecular struct. 77−88566
Earth inert gas composition, origin from solar nebula 80−61785
Earth mantle, noble gases, abundances and isotopic compositions 78−85521
earthquake prediction, changes in chemical composition, subterranean waters and gases *(Russian)* 79−84163
electric breakdown, by combined laser and microwave irrad. 77−35434
electric breakdown using single ps ruby laser pulses 77−19789
electroionisation discharge, negative cathode pot. drop 80−79615
electron beam excited, absorpt. characts. 78−82948
electron beam excited, transient absorpt. at XeF laser wavelengths 80−32644
electron drift velocities in mixtures, Monte Carlo simulations, rel. to neutron counters 80−48843
electron impact absolute ionisation cross section, 0.5 to 5.0 keV 80−53146
electron scattering, elastic, applic. of one-electron model from $1/r_{12}$ partition 77−14572
electronic excitation, mol. thermal strength depend. 77−46595
electrophotoionised discharge, inert gases-halide mols. laser mixtures, current voltage characts. 80−38821
electrophotoionization discharge, laser pumping 80−91781
elemental and isotopic ratios in Luna 24 drill core soil samples 80−26760
ethylene+inert gas, vibr. energy transfer, fluoresc. detect. 79−64026
excimer lasers, at. and mol. collision processes 80−53263
excimer lasers, book contrib. 79−81417
excimer lasers, stimulated emission kinetics in nonself-sustained elec. discharge 78−50753
excimer lasers, VUV and XUV pulse generation 79−3688
excimers, theory and application of excimer lasers 79−59684
excited complexes, instrument for quenching studies 79−17511
F ions recoiling in gases, hyperfine interactions 78−74735
field ion appearance potential spectroscopy, temp. effects 79−19978
field ion source with high angular current 80−68996
flash lamp, absolute spectral distrib. and radiant output 78−66510
fluoromethane+Br, isotope selective photobromination, using c.w. CO_2 laser irrad. in excess inert gas 78−76843
frequency conversion, fifth and seventh order, XUV coherent radiation generation 78−83033
fusion reactor, first wall, thermal response to X-rays, effect of inert gases 79−85776
gas, eqn. of state, second virial coeffs., intermol. pot. at low temp. 79−46416
gas, transport and equilib. props., using LJ (12-7) pot. 79−98849
gas laser, at. and mol. vibr. and electronic metastable states, book contrib. 77−50653
gas phase mixtures, dipole moments, IR absorpt. spectra obs. 80−28903
geothermal tracing with atmospheric and radiogenic noble gases 78−69502
glow discharge, origin of visible continuum radiation, bremsstrahlung theory 77−62421
glow discharge, polymer surface modification, ESCA obs. 78−3438
graphite/inert gas adsorption, modified Buckingham pot., virial coeff. anal. 79−65312
HCl-inert gas mixtures, van der Waals molecules, far IR spectra 80−95610
high press. discharge props. electrode influence, spectra obs. 80−38806
high pressure HF discharges and DC arcs, instability obs. 80−38807
high-pressure metal-vapour/inert-gas mixture discharge peculiarities 78−71620
hollow cathode arc, mol. beam sampling of metastable atoms as electron temp. probe 80−43967
hollow cathode tube, inert gas buffered U, time resolved optogalvanic effect 79−37564
HTGR, inert gas release core-survey calc. 79−67908
HTGR fuel particles, inert gas intrusion as charact. procedure for pyrocarbon coatings 79−54512
hydrogen halides rot. relax. with inert buffer gas, comment 80−69221
inert gases continued
hydrogen halides rot. relax. with inert buffer gas, reply 80−69222
impurities in alkali metal films, excitonic and mol. spectra, rel. to inert gas solids 77−24878
impurities in alkali metal films, metal-insulator transition, optical absorption and cond. 77−24598
impurities in alkali metal films, optical excitation spectra obs. 77−24876
impurities in alkali metal films, sharp pair spectra and excited states 77−24877
impurities in alkali metal films, X-ray edge and recoil problems in optical excitation spectra 77−24879
inelastic scattering from metal surfaces, generalised Langevin theory 77−85872
inert gas:Eu(Sm), absorpt. and emission spectra, phonon sidebands 79−43021
inert gas:H, quasifree electron energy, inference from ESR studies 79−69459
inert gas+diatom, dissoc. of HCl, HF and O_2, rot. energy depend. 79−100341
inert gas+H(2S), collisional quenching, mass spectral obs. 78−25685
inert gas+hydrogen halide, energy transfer as function of collision energy, luminesc. obs. 79−86043
inert gas+methane, vibr. energy transfer, fluoresc. 77−519
inert gas+methyl halide, vibr. relax. transition rates, anharmonicity effects 79−89747
inert gas+N_2O, $(CO_2)(O_2)$, (cyclopropane), reactant decomp., rot.-vibr. energy transfer, relax. analytic soln. 80−55650
inert gas+Xe, Xe three level system, collisional transfers, disalignment cross section 80−53098
inert gas metastable atom+$HgBr_2$, dissoc. excitation 80−63774
inert gas-Cs(Rb) molecules, excimer transitions, absorpt. spectra 77−475
inert gas-halogen mixture, ion form., ion-mole. reactions, mass spectra 77−61841
inert gas-halogen mixtures, UV laser output from elec. discharge after X-ray preionisation 79−64205
inert gases, atomic alignment in positive column *(Russian)* 80−87981
inert gases, photoionisation cross sections of excited atoms and dimers 78−66523
interactions, correl. and exchange energies, statistical methods calcs. 78−86931
interatomic potential, Gordon-Kim theory variants, appl. to inert gases and Hg_2 79−76478
interatomic potentials, absolute total cross-section data anal. 80−53093
interatomic potentials, book contrib. 77−46615
interatomic potentials, relativistic effects 79−3516
interatomic short and intermediate range forces, book contrib. 77−50494
intermolecular spectroscopy and dynamical properties of dense systems, conf., Varenna, Italy (1978) 80−82581
ion+alkaline earth atom, double ionisation, cross-section and defect energy *(Russian)* 77−83703
ion+atom, ionis., 200-4000 eV 77−27174
ion+atom electron transfer collisions, cross section meas. 79−5143
ion+H_2O (methane), thermal energy charge transfer 78−37739
ion+oxides, energy loss spectra 78−58798
ion beam, metastable fraction determ. by W surface impact, secondary electron obs. 79−28873
ion excitation of solids, vac. UV continua 80−25468
ion laser, high repetition rate operation 195 to 225 nm 78−82980
ion laser, high voltage-low press. discharges, stationary props. 80−92400
ion laser, wall confined, high CW power UV generation 77−19232
ion laser discharge, energy balance 78−74884
ion laser ion-acoustic wave excitation 78−74885
ion laser mixtures, hollow cathode, CW operation and excitation mechanism 80−69363
ion plating, inert gas handling 79−69994
ion scattering from crystal, quasi-single collisions, calculational approach 78−27360
ion source, inert gas duoplasmatron 80−32560
ion source, saddle-field type, gas depend. characts., at. spectroscopy appls. 78−78039
ion-atom collisions, momentum transfer rate consts., energy depend., polarisation pots. 77−75260
ion-surface bombardment, photon emission 78−11059
ionically pumped, thermal release 77−67450
ions, doubly charged, thermal energy charge transfer, quenching, association reactions 79−91946
ions, in parent gas, transverse diffusion coeff., reson. charge exchange effects 78−63533
ions, mobilities in He and Ne 79−90370
ions, $X^+(^2P_{1/2})$, conversion into dimer ions 78−70903
isoelectronic sequences, positive ion p-subshell photoionisation cross-sections calcs. 77−50374
isoelectronic series, polarisabilities and shielding factors 79−98008
isotopic anomalies in meteorites, origin, comment 80−26818
isotopic anomalies in Murchison meteorite evidence for stellar condensates 80−41772
isotopic anomalies in Nigorikawa geothermal area, Japan 79−88314
isotopically anomalous noble gases in carbonaceous chondrites 79−75163
josephinite and assoc. rocks, anomalous noble gases 79−79761
in Kakangari meteorite, unique chondrite, noble gases abundances and isotopic comps. 78−65570
laser development, visible absorpt. in electron beam pumped gases 78−63057
laser induced translational absorpt. *(Russian)* 78−31197
lasing, vacuum UV, from highly ionised inert gases 78−63060
lasing action in vacuum UV obs. from highly ionised inert gases 77−79798
liberation in multiposition metallic reactor 78−59978
lifetimes from collision induced absorption spectra, IR line broadening 78−33554
liquid, compressibility, long wavelength limit of liquid struct. factor 78−67633
liquid, density functional theory, localised excess electron states 79−55641
liquid, diffusion and NMR of H_2 79−61249
liquid, effect of nonelectronegative molecules on excess electron mobility 78−2534
liquid, electron absorpt. of light, one- and two-photon process probabilities *(Russian)* 77−43957
liquid, kinetic equation for electrons for strong ion-ion interaction 77−35908

inert gases continued
liquid, model for thermalisation of quasifree electrons rel. to electron mobility 77−40316
liquid, nucleation of freezing by positive ions 77−84893
liquid, photoelectric determ. of conduction state energies and electron ranges 77−89487
liquid, viscosity, density depend., theory 77−20105
liquid drop model, electronic structure extension of nucl. model 79−94769
liquid inert gas-propane systems, ground state energy of excess electrons 79−57346
liquid mixtures, collision induced absorpt. 77−4638
liquid phase mixtures, dipole autocorrelation function, IR absorpt. spectra obs. 80−28903
liquids, nucl. spin relax. of H_2 79−56623
low temp. plasma ionisation by fast electron beam, effective cross section calc. 79−14572
low voltage arc theory 80−38809
lunar soil samples from Luna 24, inert gas element and isotope composition 80−67593
lung, inert gas a-A differences, direct reflection of dV/dQ distrib. 79−20567
lung, intrapulmonary haematocrit maldistrib., effect on O_2, CO_2, inert gas exchange 80−8033
lung absorption, closed system study 80−30969
lung compartmental models, steady state inert gas exchange 80−26249
lung compartmental models, transient inert gas exchange 80−26251
lung elimination characteristics, computer model 79−20566
lung mathematical models, effect of common dead space on inert gas exchange 80−67126
lung model, ventilation-perfusion inequality, susceptibility of different gases 80−8089
lung models, inert gas elimination studies without mixed venous partial pressures 80−26250
Mars atmosphere, rare gases relative concs., effects of regolith adsorption 78−49358
mass spectrometer for noble gas anal., high-sensitivity pulse-counting spectrometer 80−95187
matrix, anisotropic hyperfine interactions with trapped H atoms 79−65728
matrix, metal cluster formation, models for aggregation processes 77−62630
matrix, OH radical, H-bonding and charge-transfer, fluoresc. 78−25602
matrix isolated impurities, freq. shift anal. 79−91472
metastable, at. collisions, intermediate energies 78−62904
metastable atom diffusion, state decay, VUV obs. from discharge afterglow 80−44061
metastable atom impact on Mo (110) surface, electron production 77−32486
metastable atom relaxation on Ta surface, energy distrib. of secondary electrons *(Russian)* 77−85861
meteorite, Unter-Massing iron, cosmic-ray exposure age and preatmospheric size *(German)* 80−46507
meteorite inert gas isotope and element anomalies, He and Xe 80−56779
in meteorite samples, noble gases and gas-rich fractions, stepwise heating study 78−49403
meteorite Springfield specimens, mass spectroscopic element and isotope anal. 77−60731
meteorites, Antarctic, stone, inert gas content, isotopic composition 80−46506
meteorites, noble gases abundance in separated minerals 77−33429
meteorites, noble gases in chondrites, exposure ages rel. to ^{26}Al ages 78−7949
meteorites, noble gases isotopic anomalies in separated minerals from Allende chondrite 77−33430
in meteorites, rare gases and fossil particle tracks in Kenna ureilite 77−41366
meteorites, thermal metamorphism, noble gases, C and S in Allende 79−92732
meteorites, trapped noble gases in bulk samples and C-rich veins of ureilites 78−40883
methane+inert gas, vibr. relax. time, spectrophone meas. 77−38669
methane-d_3 + inert gas, vibr. deactivation, laser-induced fluoresc. obs. 77−42377
methane-d+methane-d_4 (inert gas), vibr. relax. time meas. by photoacoustic effect 77−88541
mixture, binary, μ-capture, near 5 atm., X-ray yield 80−58419
mixture, collision induced light absorpt., density effects 77−42258
mixture, dipole autocorrelation function, Lennard-Jones and exponential dipole pots., classical calc. 80−64665
mixture, high-pressure arc characts. 77−19797
mixtures, high-press., collisional radiative recomb. 80−63595
mixtures, interatomic pots. and interaction dipole moments, IR spectra calcs. 77−75082
mixtures, internal forced convection, numerical calcs. 77−47005
mixtures, positron annihilation, conc. and elec. field depend. 79−43062
mixtures for particle detection high-pressure discharges in nonuniform elec. fields. 78−74545
molecular noble gas ions in hot cathode ion source 80−306
molecule, population inversion in high press. short discharge 77−71974
molecule+$CO(O_2)(N_2)$, state-to-state rates from press.-broadened linewidths, data reduction method 78−46430
molecules, Lennard-Jones 12:6 parameters calc. from viscosity data 77−46612
molecules, mean force constants and rectilinear law of mean force calcs. 78−33414
monolayer, adsorbed on graphite, commensurate-incommensurate transition 79−69244
monolayer, physically adsorbed, many-body interactions 78−84068
monolayers on graphite, nonregistered-registered phase transition 79−77894
multiphoton ionisation, by ultrashort laser pulses from tunable Nd:glass laser 77−58095
Murchison meteorite, inert gases as possible relics of s-process nucleosynthesis 79−21243
noble gas-rich separates from H-type chondritic meteorites 80−85907
nuclear pumped lasers, electron impact cross section meas. 80−63985
nuclear pumped lasers, prod. efficiency of excited states 80−63998
oceanic basalt glass, noble gas comp. of neutron activated samples 79−74866

inert gases continued
Ontario Hydro nuclear power plant stack effluent monitoring 79−3254
origin and abundances in terrestrial planets and meteorites 78−28559
partially ionised inert gases in travelling HF mag. field 78−75474
partly ionised, minimisation of effective electron-neutral particle collision cross section 79−64821
Penning ionisation processes investig. by electron spectroscopy 80−58364
photoabsorption, local field effects, density-functional formalism 80−78766
photoabsorption bound state and photoabsorption to continuum state (ionisation), comparison, HF calcs. 80−47910
photoionisation cross-sections, multiconfig. Hartree-Fock calcs. 77−50373
physisorbed, dipole moments of atoms 79−33175
planetary atmospheres, accretion from protoplanetary nebula, noble gas contents 80−109385
planetary nebulae, abundances of He, Ne, Ar, N, and Cl 80−109532
planetary-type rare gases in an upper mantle derived amphibole 78−96167
plasma, continuous spectrum of radiation 78−42729
plasma, electron-beam produced, laser action of ionized and neutral atomic lines 80−106929
plasma, emission continua, photoionis. cross sections, absorption coeffs. 300-10000 Å 78−42731
plasma, free-bound continuum determ. using photoionis. cross sections calc. 80−43878
plasmas, prod. by U fission fragments in nucl. reactor, props. 77−76147
point defect trapping and migration, calcs., in presence of rare gases and dislocations 79−77834
positive corona discharge, current oscills. 77−11431
positive discharge column, at. temp., interferometric meas. 77−35427
presolar gas components, isotopic anomalies in Murchison C2 chondrite 80−85904
primary ionisation relativistic growth 79−86554
primary specific ionisation, relativistic increase *(Russian)* 79−60102
proportional counters, inert gas mixtures, Penning ionisation effect on resolution 77−26936
pulsed microwave inert gas discharge, ion composition, mass spectra 79−14616
quantum EM processes, population var. and natural radiative decay *(Russian)* 77−32343
radioactive, concentration meas. by portable gas radiometer 80−32570
radioactive, emanation thermal analysis of solid state structures appl. 79−11834
radioactive gas analysis, calibration of Ge(Li) gamma-ray spectrometer 77−83442
radioactive inert gas release by nuclear reactors in West Europe 77−50305
radioactive inert gas treatment for safe environment 77−50306
radioactive isotope separation, using cell with two membranes of differing permeability 78−29590
radioactive rare gas separation performance of a two-unit series-type separation cell 79−41008
rare gas concs. in Fe meteorites rel. to cosmic-ray-produced nuclides 78−65473
rare gas diffusion as bubbles from lunar fires 79−48695
rare gas fractionation rel. to Earth-atmosphere evolution model 77−13077
rare-gas-rich separates from carbonaceous chondrites 79−62796
recombination afterglow, spectral line shapes 80−940
resonance ionisation spectroscopy for transuranic trace analysis 80−93833
rotating arc meas. in plasma centrifuge 78−75438
scintillation counters for energetic heavy ion detection 79−45550
slightly ionised plasma, hollow arc discharge in cylindrical hollow cathode, theory 80−38810
small clusters, structure, thermodynamic properties 80−88341
small clusters, three body interaction effects on thermodynamic props., comparison bulk props. 80−28128
solid, absorption of inert gases, sp. ht. of absorbates calc. 77−1302
solid, anharmonic crystals, unsymmetrised SCF approx. 78−63830
solid, band struct. and excitons, book contrib. 77−47731
solid, benzene-doped, luminescence excitation investig. 77−77276
solid, book 77−47296
solid, Brillouin scatt. intensity, elastooptical coefficients 78−10907
solid, collective excitations and EELS, calc. 80−92842
solid, Compton profiles, APW-Xα calc. 80−80894
solid, contact electrification of 'ideal' insulators 80−70797
solid, core excitons, nonstructural theory, appl. to core transitions 78−84148
solid, cryst. struct., book contrib. 77−51348
solid, cubic crystal, self-diffusion and melting 77−31803
solid, dead layer effects in UV reflectance of excitons 78−72553
solid, delocalisation probability of interstitials 79−7801
solid, doped, Rydberg states 79−69425
solid, elastic moduli vol. depend., Born-Durand melting hypothesis 79−60420
solid, electron impact excited, exciton recomb. spectrum, temp. variation 78−48239
solid, electronic excitations, nonstructural theory 78−79942
solid, exciton states, intermediate coupling interaction 78−67952
solid, exciton states, nonstructural theory using effective mass approx. 78−84147
solid, homology of lattice vibrations 79−77695
solid, isotherms 77−20041
solid, long range forces, book contrib. 77−51347
solid, long-range many-body interaction and monovacancy heat of form. 80−38996
solid, matrix isolation spectra of O_2, visible emission 77−14444
solid, melting curves, Lennard-Jones Devonshire theory 80−65201
solid, molecular dynamics exam. intensity and band shape of depolarised scattered light 77−51458
solid, non-linear and dispersive elastic continuum, wave eqns. of motion 80−15187
solid, phonon dispersion relation, anomalous terms at small wavenumber 78−2210
solid, photoelectron energy distrib. meas. 78−48271
solid, research history, book contrib. 77−49547
solid, self-consistent phonon theory, book contrib. 77−51460
solid, thermodynamic props. calc. 77−62653
solid, two-phonon Raman light scatt. 79−56783

inert gases continued
solid, unpaired elastic force model in lattice dynamical study 78−63820
solid, V_0-values, photoelectric determ. 80−92938
solid, vacancy entropy of formation due to anharmonic effects 77−62521
solid, vibr. relax. of NH, ND in amorphous host 77−7817
solid, VUV luminesc. from excitons 79−43020
solid layer, adsorption of H_2, sorption capacity meas. 79−90865
solids, benzene doped, energy transfer processes, excitons, photoemission, luminescence spectra 77−69886
solids, Debye Waller factors from unpaired elastic force model 80−19896
solids, luminesc., self-trapped exciton 79−38605
solubility in liquid metals 77−51506
solubility in liquid solvents, temp. depend. from scaled particle theory 80−24604
solubility in serpentine, meteoritic abundance 80−12712
solubility of inert gases in homogenates of canine lung tissue 80−46117
solutions in liquid alkali metals, calc. of enthalpy and elec. resist. 77−55225
speed of ultrasound at 298.15K *(French)* 79−82027
sputtering environment, contamination effects on uniaxial anisotropy of Gd-Co films 78−64232
St. Mesmin brecciated chondrite, noble gases abundances rel. to irradiation history 78−28593
steam-inert gas, uncondensable gas content effect on steam condensation heat transfer in vert. tube 78−75041
stochastic description of exchange in living organs 80−81520
substitutional solid solution formation on glow discharge interaction with metal 79−65202
supersonic jets as vacuum UV source 77−75639
thermal cond. meas., room temp., up to 35 MPa, transient hot-wire technique 80−48838
thermodynamic properties, perturbation calcs., density depend. 77−7504
Townsend avalanches, gas scintillation counter obs. 80−38805
transient absorption, electron-beam excited inert gases at XeF laser wavelenghts 80−83592
transport in the microcirculation, isobaric supersaturation risk 80−45939
trimers and tetramers, ground state energies, pairwise Morse pot., few-body methods 79−72378
vapour-inert gas mixtures, condensation, heat transfer coeff. calc. *(German)* 77−39724
Venus atmosphere, noble gases *(German)* 79−58289
viscosity, expt. and derived from statistical models *(French)* 77−35302
viscosity rel. to ionis., skin friction of wetted oscill. disc 78−34252
in volcanic rocks, isotopes mass fractionation as indicator of gas transport to or from magma 80−98292
weak shock wave struct. investig. 79−94679
xanthene dye N-92+inert gas buffer, electron beam excited, fluoresc., energy transfer 78−25877
Ar^++$CO(CO_2)(N_2)(N_2O)(NO)(O_2)$, charge transfer, thermal energy, product distrib. obs. 78−25656
atom+H^+, 4s-state electron capture cross-section meas. 78−82836
B^++inert gas atom, pot. interactions 78−55219
BF_3+$BF_3(D_2)$ (inert gas), US dispersion meas. 78−17758
Ba-inert gas, Ba reson. lines broadening, absorpt. cross sections anal. 80−32642
Be+Ar(Kr)(Xe), chemiluminesc. associative ionisation mechanisms 77−32781
CO+inert gas, collision-induced intersystem crossing, reversibility 77−50465
CO+inert gas, collision-induced intersystem crossing mechanism 78−74689
CO_2+inert gas, intramol. energy transfer, 153-393K, photoacoustic obs. 79−54943
CO_2+inert gas, vibr. and rot. energy transfer, quasiclassical trajectory study 78−33578
CS_2+inert gas, translational excitation, energy transfer, cross spectra 77−50559
Ca+inert gas, collision-induced dipole transitions, absorpt. study 80−37865
Ca+inert gas, collision-induced dipole transitions assoc. with high-lying states 80−37866
Cd($^3P_1$) radiation imprisonment lifetime, inert gas effect, phase-shift method 80−58213
Cl+inert gas, $3p^5(^2P_{1/2})$ state quenching 78−42192
Cl^-+inert gas atom, electron detachment and inelastic processes 78−42208
Cs inert gas, pot. energy curves, collision induced oscillator strengths 79−22659
Cs+inert gas, hyperfine struct., broadening and shift calcs. 77−58153
Cs+inert gas, three body interaction, fluoresc. spectra principal series lines and secondary satellites 80−83313
Cs+insert gas, $5d^2D_{5/2}$ level excitation by laser photon absorpt. 77−3438
Cs^++Ar(Kr)(Xe), elastic beam scatt., repulsive pots. 79−98184
CsF, rot. inelastic collisions, mol. beam meas. 80−1049
$Cs(5D_{5/2,m=1/2})$+inert gas, dipole-induced transitions, pot. curves, oscillator strength 80−32816
D+$H^+(D^+)(He^+)(Ne^+)(Ar^+)(Kr^+)$, reson. charge charge transfer from photoexcited donor state 79−22820
D_3^+ +inert gas, ion decay, 1-40 eV *(Russian)* 78−90286
$F^-+X_2^+ \rightarrow [X_2F]^*$, 300K, 50 atm., recombination rates 78−46576
F_2-inert gas mixtures, transport and attachment processes 78−59542
Ge:inert gas, ion implantation, UV photoemission exam. 78−80457
H-inert gas laser spark, emission spectra 79−82119
H+H(inert gas), negative ion form. 77−30988
H^++He(Ne,Ar), charge transfer into continuum 79−89765
H^++He(Ne)(Ar)(Kr), charge exchange, 80 to 1500 eV, total cross sections 77−61854
H^++inert gas, binary encounter calc., cross section calc. 79−72412
H^++inert gas, charge transfer into excited states, 10-150 keV, target at. struct. depend. 79−45830
H_2+inert gas, intermol. pot. anisotropy determ. from total collision cross sections, expt. 78−21988
H_2+inert gas, intermol. pot. anisotropy determ. from total collision cross sections, theory 78−21989
H_2+inert gas, vibr. relax. mechanism, master eqn. anal., density changes 79−76493
HCl-inert gas rot.-vibr. line pressure broadening and shift calc. 80−69124
inert gases continued
HCl+iert gas, weak collisions, HCl spectral line broadening of IR spectra 80−74161
HD-inert gas mixtures, $R_1(J)$ and $P_1(J)$ absorpt. spectra, positive intercollisional interference 79−54843
HD+inert gas, isotropic Raman Q branch, vibr. dephasing effects and motional narrowing 78−74738
$H_2(D_2)$-Ne-He(Ar) plasma, combustion driven shock tube, H_β central struct., ion mass effect 78−26327
HF+inert gas, press. broadening and shifting of vibr.-rot. absorpt. lines 77−27161
He-Ar(Kr)(Xe), intermol. forces, combining rules 78−66622
He+H (inert gas atom), long range interactions for (2^1S) and (2^3S) states 78−70895
He+Ne(Ar)(Kr)(Xe), absolute total elastic cross sections 77−30953
He^++$CO(CO_2)(N_2)(N_2O)(NO)(O_2)$, charge transfer, thermal energy, product distrib. obs. 78−25656
He_2^++inert gas, binary encounter calc., cross section calc. 79−72413
He^{2+}+inert gas atom, electron capture into different excited states in plasma 80−64679
$Hg(6^3P_{2,0})$+inert gas, diffusion in low-current discharge 78−63618
K+inert gas atom, resonance levels relax. 77−83684
K^++inert gas atom potential, determ. from total cross section meas. 77−68091
$K(4^2P)$+He(Ne)(Ar)(Kr)(Xe), collisional excitation, differential cross-sections 78−66643
Li+inert gas, Doppler and collisional broadening, correls. 77−14530
Li+inert gas, fluoresc. reson. line broadening 77−6734
Li+inert gas collisions, electron loss cross-section meas. *(French)* 78−86941
Li^++inert gas, elastic differential scatt., diffr. effects 77−511
$Li_2(B^1\Pi_u)$+inert gas, rot. inelastic collision, classical trajectory calc. 78−1054
LiF+inert gas atom, interaction anisotropy, Van der Waals forces 79−6985
Mg-inert gas, Mg reson. lines broadening, absorpt. cross sections anal. 80−32642
Mg+Xe(Ar)(Ne)(He)(Kr), collisional broadening of 285.2 nm line 77−79580
$MnCl_2$-inert gas laser, energy charact. *(Russian)* 77−665
N^++inert gas, electron capture (loss) by metastable (ground-state) ions, 2-30 keV 78−25695
N^{2+}+inert gas target, 60-200 keV single electron capture 80−43172
N_2O+inert gas ion, mol. ionis., emission obs. 79−31707
Na+inert gas, $4D_{3/2}$ and $4D_{5/2}$ levels relax. 78−50526
Na+inert gas, D line broadening 80−32663
Na+inert gas, fine struct. state changing cross-sections, crossed beam determ. 77−50496
Na+inert gas, Rydberg states, collisional ang. momentum mixing theory 77−10748
Na+inert gas atom, 4^2D fine struct. transition 79−850
Na+inert gas atom collisions, optical emission cross section, reson. lines 78−13584
Na+inert gases, 3S-4D and 3S-5S two-photon line broadening and shift 77−75105
Ne^++$CO(CO_2)(N_2)(N_2O)(NO)(O_2)$, charge transfer, thermal energy, product distrib. obs. 78−25656
O^{2+}+inert gas, electron transfer meas., 60-200 keV 80−83480
O_2+inert gas atom, absolute total elastic cross sections 78−9220
OCS, IR spectral moments and mean squared torques, rare gas effects 78−62944
O(^3P)+inert gas atom, absolute total cross sections, 0.6-2.0 km sec^{-1}, model pots. 77−19010
O(^5S)+inert gas, de-excitation cross sections 80−53118
Rb+inert gas, hyperfine struct., broadening and shift calcs. 77−58153
Rb^++Ar(Kr)(Xe), elastic beam scatt., repulsive pots. 79−98184
Rb(nP)+Rb(inert gas), collisional depopulation Rydberg P state 77−75281
S+inert gas (N_2)(H_2), rare gas sulphide S(^1S) emissions 78−82828
$S_2(B\ ^3\Sigma_u^-)$+inert gas (H_2)(N_2)(S_2), collision-induced energy transfer 79−3544
SF_6-inert gas mixture, high power cylindrical spark discharge, dynamic and visible charact. 80−64816
Se($^3P_1$)+inert gas, gas phase flash photolytic deexcitation obs., 1000K *(Russian)* 78−50626
Se(4^1D_2) atoms, electronically excited, direct obs., quenching by inert gases 78−25461
Si:As thermal diffusion retardation by inert gas ion implantation 79−77616
Te($^3P_1$)+inert gas, gas phase flash photolytic deexcitation obs., 1000K *(Russian)* 78−50626
Tl+inert gas, $6^2P_{1/2}$-$7^2S_{1/2}$ and $6^2P_{3/2}$-$7^2S_{1/2}$ line broadening 77−50475

inertial navigation
accelerometers, floated pendulum, performance meas. 80−31718
aircraft gyroscope accuracy increase 79−71421
aviation and astronautics, conference, Tel Aviv (1977) 78−81517
external gravity field calc., signal processing approach 78−24708
gravity detection, covariance analysis of periodic traversing 80−95087
gravity vector and geodetic position survey, inertial navigation system appl. 79−29914
gyro instruments, standards for metrological support 79−67262
gyroscope, optical fibre, based on Sagnac effect, background and development *(German)* 80−48431
gyroscope, two-degree-of-freedom with free rotor 77−41595
gyroscope-based systems performance improvement, permanent magnets flux stability enhancement, by thermomechanical treatment 80−50144
LaCoste and Romberg inertial navigation system for gravity meters 77−82022
optical rotation rate sensors, Air Force appls. 80−9932
relativistic effects for small deformable particle motion 77−67276
surveyor for automatic position, azimuth and gravity disturbance meas. 77−5353
vibrating sensitive element reliability improvement *(Russian)* 77−57302

inertial systems
centrifugal forces, simulation, on overhead projector, teaching appl. 77−41438
geodetic meas. systems, basic eqns. and error models *(German)* 80−56655
gyroplatform orientation in geographical meridan, effect of earth non-sphericity *(Russian)* 79−14240

inertial systems continued
photogrammetric inspection *(French)* 79−62603
surveying systems, geodetic appls. *(German)* 80−56656
Ne-Xe gas discharge, LF oscillations, modulation by gravitation and inertia forces 77−11429

infinite series *see series (mathematics)*

inflammability *see combustion*

information analysis
see also cataloguing; classification; indexing
astronomy, data growth anal. 79−21202
atomic absorption spectroscopy, development in USSR, 1965-1975, science metrics investig. 78−61104
data evaluation at Nuclear Safety Information Center, products and available services 78−17545
geophysics and astrophysics research worldwide growth, 1967-75 period 77−66884
multiphase medium plasma dynamics, Soviet literature growth and duplication parameters *(Russian)* 80−59191
scientific advance, objectivity vs. relevance techniques 79−58520
world's scientific journals, subject composition 80−36757
world science as input-output system 79−58521

information analysis centres *see information centres*

information centres
Biomedical Computing Technology Information Centre, for technology transfer 77−40824
Controlled Fusion Atomic Data Center 78−17432
data centres of NSRDS, role in technical information transfer 78−13402
National Neutron Cross-Section Center 78−13403
Nuclear Safety Information Center, products and available services 78−17545
Radiation Shielding Information Center, international technology resource 78−17543
Stellar Data Centre, Strasbourg, data surface distribs. on celestial sphere 77−2423
Strasbourg Stellar Data Centre 77−91447

information dissemination
CODATA, review of function and operation 79−49012
data centres of NSRDS, role in technical information transfer 78−13402
India, science and technology policy, secondary information sources 79−49009
international team research networks, CAITR, CAPS examples, cost-benefit analysis 79−35441
Nuclear Safety Information Center, products and available services 78−17545
scientific journals significance, Science Citations Index anal. 77−9831
selective information distribution system for international scientific co-operation *(Russian)* 79−179
stellar photometric data 80−105179
Strasbourg Stellar Data Centre, data distrib. 77−91447
teleprocessing innovation, role of US National Science Foundation 77−2504

information retrieval
see also information storage
associative holographic memory appls. *(German)* 77−3549
astronomical stellar data base, retrieval techniques and graphics display 77−78652
astronomy data growth, obs. of known objects, bibliographic inaccessibility problem 79−21202
chemical rotation evolution, changing role of symbol 77−87621
crystalline compounds, computer identification techniques using X-ray powder diffr. file 77−70389
crystallographic data, molecular geometry, computer retrieval and anal., general principles and methods 78−83643
crystallographic data, molecular geometry, computer retrieval and anal., variance and interpretation 78−83644
crystallographic data, molecular geometry, computer retrieval and anal., geometry of β-1′-aminofuranoside fragment 78−83645
IR spectra, binary coded, feature selection for automated interpretation 80−3428
IR spectrometry, computer program LISE (Literature Search and Edit) 78−85223
liquid-liquid equilibrium data, retrieval 79−46797
mass spectra, low-resolution, identification using combined forward-reverse library search system 80−30296
mass spectral data bases, information content of retrieval procedures calc. 80−30297
mass spectrum dictionary for library searching 79−89031
oceanographic data, retrieval-time data generation 77−5354
teleprocessing innovation, role of US National Science Foundation 77−2504
X-ray diffr. anal., computer searching of JCPDS powder diffr. file 77−70390
X-ray diffr. powder phase identification, manual computer search techniques 77−70387

information retrieval system evaluation
X-ray powder diffr. anal., computer search/match methods evaluation, manual search comparison 77−70391

information retrieval systems
see also information retrieval system evaluation
alloy, multicomponent phase diagram calc., NPL alloy data bank 78−92243
astronomical database, BADAS, design and realisation *(Italian)* 80−98580
automated, organisation of data banks and exchange operations *(Russian)* 77−1960
bibliographic star index, information retrieval system *(Japanese)* 79−101086
Cambridge crystallographic data centre: computer-based search, retrieval, analysis and display of information 80−1877
chemical information system, computer-based 77−33978
chemical reaction information comparison 79−83541
Chemical Registry System, tautomerism and alternating bonds, handling 80−63851
Chemical Registry System from Chemical Abstracts, augmented connectivity molecular formula appl. 79−83542
Chesapeake Bay pollution, data importance 80−3544
climate data archiving and quality control by computer 80−61907
climatic data service for USSR 77−70838

information retrieval systems continued
colour reversal film evaluation, microfilm retrieval systems appl. *(Japanese)* 79−97455
computerised bibiliographic data base for nuclear criticality data 80−13568
electrolytic solutions database, energy properties 80−3368
EPR saturation transfer data, tape library 79−51841
geophysics information system automation *(Slovak)* 77−56735
glass comp., patent information, automated retrieval system 79−24715
holographic, storage structures and technical feasibility *(Japanese)* 78−37829
holographic document retrieval and conversion to photographic microforms 79−76643
hydrometeorology, in USSR information retrieval publications, comparative study 80−36401
infrared spectra search 77−22535
Japanese reactor noise pattern library 79−3338
liquid chromatography, computer-based bibliography update 78−31736
mass spectra, classification, ion series-related index, fast library searching appls. 77−12837
mass spectra data identification, text search system based on Boolean logic 79−20480
mass spectrometry, on-line literature search system 78−15734
microcomputer use for hail topic, retrieval and storage system 80−17381
MOLARS system of British National Meteorological Library 80−82068
NMR data bank, ^{13}C, DARC PLURIDATA system 80−30298
nuclear safety inform. retrieval system, development 79−26551
number reactor operating data retrieval and evaluation system RECORDS 80−13690
oncological clinical research, data storage and retrieval system 79−48321
photomapping data collection, storage and retrieval system 79−71549
SIGMI user-oriented file-processing system for geological data 77−9506
SIINC laboratory instrumentation information system, proposed structure 80−98908
spectra search systems, computer-aided, efficiency eval. using information theory *(German)* 80−37003
spectroscopy, analytical systems comparison and development 79−49297
stellar bibliographic file for automatic information retrieval 77−78833
vapour-liquid equilibria correlation and prediction 80−2141
X-ray phase analysis, information retrieval system 78−79501
^{59}Co NMR line breadth and chemical shift data compilation *(Japanese)* 78−15045

information science
see also publishing
European physics publication output, by country 79−88776
Indian scientific and technical Journals critical evaluation 80−94906
Soviet physics publication output, 1910-79 79−88777
visual science research, the place of the library 80−30711
world physics publication output, by country 79−88778

information services
British Isles, 1978 guide to information sources in geology 78−88922
British National Meteorological Library, MOLARS automation 80−82068
Cambridge crystallographic data centre: computer-based search, retrieval, analysis and display of information 80−1877
Chemical Registry System, tautomerism and alternating bonds, handling 80−63851
Chemical Registry System from Chemical Abstracts, augmented connectivity molecular formula appl. 79−83542
CODATA, review of function and operation 79−49012
composite materials, Soviet service 78−8182
computer information, conference, London, England (Nov. 1979) 80−90599
geoscience information services, review, conf., April 1978, London 80−46183
hydrologic data networks, design 79−21022
India, science and technology policy, secondary information sources 79−49009
international team research, information networks, CAITR, CAPS examples, cost-benefit analysis 79−35441
isomer shift reference scales, Mossbauer Effect Data Centre 80−37147
materials science and engng. data sources, book contrib. 79−65986
mobile sonar technology (MOST), technical document information system 78−45003
Mossbauer Effect Data Centre 80−37148
NDT computer-based information system description and advantages 77−81366
Nuclear Code Centre, Japan, history, activities *(Japanese)* 79−13618
Nuclear Safety Information Center, products and available services 78−17545
ocean data and information services, changes and challenges 78−69463
ocean environmental data files, quick guide 80−12551
physics information sources, introductory guide 80−1
powder metallurgy, Soviet service 78−8181
Prestel system appls. 79−48979
Radiation Shielding Information Centre, available computer codes and data 77−65343
speech synthesis and recognition for information from data banks over telephone 80−1384
variable stars unpublished observations, IAU archives and 1978-79 data 79−88688

information storage
see also information retrieval
chemical rotation evolution, changing role of symbol 77−87621
climate data archiving and quality control by computer 80−61907
ferroelectric-semiconductor system, illuminated, voltage redistrib. 77−40194
geophysical data storage by metallic carrier electroerosion via liquid pulsed discharge *(Russian)* 78−61563
liquid-liquid equilibrium data, retrieval 79−46797
micrographic storage and image retrieval, perforated film, mag. striped film, pocket microfilm reader 78−16779
modelling of dynamic phase memory in self-excited wave media 79−79505
ocean environmental data files, quick guide 80−12551
PETROS data bank, igneous rock major element analyses 77−2249
in piezoelectric semiconducting single crystals 78−15101
SAW information storage and correlation in semiconductor diode arrays 78−9505

information storage continued
teleprocessing innovation, role of US National Science Foundation 77−2504
Vela seismological network, information storage and retrieval by datacomputer 78−81411
GdIG single crystal plates for magnetooptical information storage 79−7997

information storage systems *see information retrieval systems*

information systems, management *see management information systems*

information theory
see also channel capacity; codes; correlation theory; decision theory and analysis; estimation theory; filtering and prediction theory; modulation; signal detection; signal processing; speech intelligibility
acoustic emission sources, localisation 78−87220
analytic signal model, physical justification 79−909
atmospheric temperature, vertical profile, from satellite data, information retrieval 78−3959
atom+molecule, 3-dimens. vibrot. reaction probabilities from collinear results, information theoretic synthesis 79−74354
automated weather service rocket sounding system, information theory effectiveness rating 79−58057
biological information expression via message operators 77−29089
biological information processing *(Japanese)* 80−12049
biological system statistical, semantic and pragmatic information amounts calc. 80−30631
biological systems 77−29090
Boltzmann distribution in the distribution limit, maximisation of entropy of degree β *(Italian)* 79−93083
Boltzmann-Gibbs-Shannon generalised entropy, unique characterisation 77−5747
cardiac rhythm disturbances, Markov process model *(German)* 79−2019
cerebellum, neuronal organisation, informational capacity of Purkinje cell and climbing nuclear unit 77−25409
chance and origin of life 78−69269
chemical analysis applic. 78−3393
chemical reaction dynamics, Franck-Condon factors rel. to information theory for vib.-rot. distribs. and isotopic branching ratios 77−60041
chemical reactions, angular momentum disposal, information theory anal. 78−80730
chemical reactions, branching ratios calcs. for known conditional probabilities 78−13406
chemical system, nonlinear, open, information, critical fluctuations and phase-transition-like phenomena 79−24720
collision processes, information theoretic maximal entropy theory, rel. to scatt. theory 78−81888
communication problems, information, message and signal concepts *(German)* 78−46525
communication structures description *(German)* 77−12869
concert hall problem, coherence length and diffuse reflection formulation 80−91962
cosmology, maximum information universe 79−30157
curve information content, role of affinity and conservation of information *(French)* 78−24771
diffraction pattern diameter from theory of extremal functions *(French)* 80−46835
diversity indices computation, FORTRAN program 77−33076
ECG lead system information content *(German)* 78−69226
elementary particle interactions, statistical treatment of multipicity data using information theory 78−89682
entropy, generalised, basic props. 77−5746
entropy, information and statistical, and law of large numbers, opacity of statistics *(French)* 80−73288
entropy, stability criteria, fluctuations 80−8947
entropy, thermodynamic, relationship *(French)* 77−5788
entropy and information of comparison under generalized additivity and non-additivity 79−85105
entropy and macroscopic disequilibrium, isothermal vibr. relax 77−6896
entropy and macroscopic disequilibrium, Markovian relax. 77−14539
entropy and other thermodynamic props., analogy in information theory *(French)* 80−27247
entropy in operational statistics and quantum logic 80−17903
entropy in quantum information theory, comments on recent studies 77−17851
entropy which does not increase, quantum logic 77−17850
experiments, indirect, maximising information, optimal initial state 80−77744
Fraunhofer diffraction of apertures, analogy with SSB modulation 80−48138
Gaussian signals in Gaussian noise transmitted over digital channel, degradation of S/N ratio 80−64298
geodesy, physical interpretation of notion-system of information 77−64176
geological records, coding method based on data transmission theory *(Russian)* 80−17383
geophysical potential field data, interpretation methods 77−73861
gradation, information approach to recognition problem 79−17203
heat transfer in linear harmonic chain, nonequilib. steady states, information theoretic approach 80−19214
heterogeneous solid media, statistical continuum theory, information theory approach, static field theory 80−22198
holograms, relative information content of magnitude and phase components 80−43286
hydrocarbons, mol. thermodynamics, information-theoretic aspects 78−13409
hydrogen halides, rot. relax. rate consts., information theoretic synthesis 79−86044
image analysis, structural methods, in diagnostic image systems 77−86564
image restoration using maximum information norm 80−106476
impulse stochastic control on 3D crystallographic lattice 77−22499
information theory density matrix for a simple quantum system 79−58470
information uncertainty 79−40506
inversion problems, information theoretical approach 80−27210
IR spectra, feature selection, using numerical taxonomy and information theory 79−50012
irreversible energy conversion processes, information model *(Ukrainian)* 78−89419
isotope radiometry, nonlinear information processing in random signal detection *(Russian)* 80−22428

information theory continued
Jupiter clouds spectropolarimetry, lines equivalent widths information content 80−31215
knowledge distance, information extent and information distance, concepts evaluation 78−77687
liquids and amorphous solids, similarity and short range order parameters 78−83730
living systems, thermodynamic, informational and structural entropies *(Russian)* 79−20511
Lorentzian shape, deduction from maximum entropy principle 78−21056
lunar surface gravimetric surveying process optimization 79−8846
macroscopic system, vibrational relaxation, information-theoretic approach 77−58156
marginal distribs., appl. to energy disposal in exothermic reaction 78−15658
mathematical and thermodynamic aspects *(French)* 77−5789
maximal entropy distribution subject to constraints, algorithm 79−49183
Maxwell demon and correspondence between information and entropy 80−86241
measurement, theory, and information 79−71395
measurement device information-theoretic characts. estimation via radiation absorption *(German)* 78−65900
measurement dynamics rel. to system and information theory 78−8377
measurement information amount determ. approach 80−8949
measurement systems, construction using concept of entropy 79−93088
measurement techniques, error anal. using information, signal and system theory *(German)* 80−68164
medical imaging systems, information capacity considerations 80−98090
membrane potential and active transport, information theory approach 80−35855
memory, as process of information transmission, neuronal organisation 77−21503
molecular collisions, surprisal analysis of products' translational energy distrib. 77−38706
molecular physico-biological systems, informational interactions 77−25362
molecular scattering angular distrib. information content, angular entropy 77−54583
molecular vibr. states population distrib., information theory anal. 77−42380
nonlinear experimental design, information measures 80−62616
nonprobabilistic measures of information with biological applications *(French)* 77−9160
object perception criteria 78−44444
oil and gas exploration, information content of geochem. parameters *(Russian)* 79−39957
optical communication quantum effects 80−1147
optical structured image reproduction, quality, information rating 77−10851
particle multiplicity distribution application 77−38131
photographic images, information content 79−17548
planetary gravitational fields, inform. theory appl. 78−53835
plant information measures selection criteria nuclear reactor monitoring appl. 79−41006
point images resolution, decision theory 79−81375
probability distrib. of discrete scheme, maximisation of entropy of degree β *(Italian)* 79−93082
quantum, expressions for Shannon quantity of information, microwave, optical communications appl. 79−55075
quantum information theory and open systems 77−17848
quantum measurement 78−36863
quantum measurement as a communication with nature 79−17253
quantum-mechanical kinetic energy as measure of information in distribution 80−101725
radiation absorption measuring instrument characts. evaluation with reference to information theory *(German)* 78−86753
radioactive contamination in aquatic organisms, evaluation by statistical and information theory 78−53535
radiographic images, evaluation by entropy, appl. to development process 79−12914
radiography, medical diagnosis, information storage requirements 80−98086
random field reconstruction using theory of statistical decisions 79−72509
random signal, test for stationary behaviour using power spectrum 77−37817
reaction cross sections, information content of mol. beam state. vs. resolved product state distrib. expts. 77−28980
relative entropy, information-theoretic discussion 79−71360
role in physics 78−28933
seagull effect in π semi-inclusive distribs. by information theory, p_L-p_T correlations 78−86458
sensory information processing, parallel and sequential *(French)* 77−12873
Shannon's theory appl. to large information systems in biology 77−56325
signal quantisation, for photon and field channels 77−42493
solar energy collection anal. using information theory 80−97799
sound, structural information theory 77−14822
spectra search systems, computer-aided, efficiency eval. using information theory *(German)* 80−37003
speech recognition systems design *(German)* 79−46127
statistical inference and quantum mech. meas., information theory 78−20990
statistical mechanics, entropy, information theory *(French)* 79−63178
statistical mechanics, obs. prob. for stochastic variables *(Norwegian)* 79−80497
statistical mechanics, system in contact with a heat reservoir, for teachers 78−36770
stochastic neuron models, multi-input-output information transmission 80−30707
streamflow, model, identification of seasonal water supply forecasting models using Akaik's information criterion 80−67386
surface roughness computer-aided three-dimensional anal. *(Polish)* 77−67411
tachyon theory, information flow, causality 78−82261
thermodynamic process applied to biological systems 80−45855
transinformation functions, constrained, essential features 79−1997
transport processes, nonlinear, hydrodynamics 80−22310
turbulence, description and quantification *(German)* 80−106789

information theory continued
US imaging, clinical information, comparison of two types in detect. of focal intrahepatic lesions 77−64100
Venus clouds spectropolarimetry, lines equivalent widths information content 80−31215
von Neumann entropy and entropies of meas. 78−54229
X-ray structure determination, information theory aspects 77−51258
$D+Cl_2$, reaction probabilities, information theoretic anal. 77−16799
$F+H_2$, reaction probabilities, information theoretic anal. 77−16799
$F+H_2$ dynamics, Franck-Condon factors rel. to information theory for vib.-rot distribs. and isotopic branching ratios 77−60041
$F_2+X \rightarrow XF+F$ (X=Mu,H,D,T), isotope effects, quantum mech. and information theoretic calcs. 78−44360
$H+Cl_2$ dynamics, Franck-Condon factors rel. to information theory for vib.-rot. distribs. and isotopic branching ratios 77−60041
$H+F_2(Cl_2)$, reaction probability, information theoretic anal. 77−16799
$H+H_2$ dynamics, Franck-Condon factors rel. to information theory for vib.-rot. distribs. and isotopic branching ratios 77−60041
$H+NO_2 \rightarrow OH+NO$, energy disposal, information theory appl. 78−15658

information use
data centres of NSRDS, role in technical information transfer 78−13402

infrared astronomical observations
0957+561A, B, double quasar, IR obs. of quasar and intervening galaxy 80−73065
1980 S 2, new Saturnian satellite, discovery and possible orbital periods 80−46473
25 1702−363, IR candidate in error box, JHKL photometry 78−61934
2A 0311−227, AM Herculis type binary star, IR photometry and polarimetry 80−77517
2 A 0311−227, IR flickering obs. 79−40298
AFCRL Sky Survey objects, 2-14 μ spectrophotometry 77−22331
AFCRL Sky Survey sources, accurate photometric positions 77−45603
AFCRL sources, identification of southern objects 77−33682
AFCRL/AFGL sources obs., AFGL catalogue evaluation 78−28846
AFGL 333, far IR obs., evidence for star form. at ionization front 79−53932
AFGL 437, optical and IR obs., young star cluster embedded in nebulosity 78−4394
AFGL IR sky survey sources, ground-based obs. 79−71150
AFGL IR sources in revised catalogue, identifications from 3.5-12.5 μm obs. 79−25659
AFGL/CRL IR sources, spectroscopic obs. 78−32599
Air Force Geophysics Laboratory IR sky survey, extended source extraction 79−101088
Allen's obscured IR source in NGC 2264, spectrophotometric anal. 79−21370
Am stars, τ Ursae Majoris and 15 Vulpeculae, energy distrib. from spectral obs. 80−85949
AB Andromedae, W Ursae Majoris type star, 1.2 and 2.2 micron light curves 79−84822
Aquila region, near IR mapping at balloon altitudes 79−12514
Arakelian 120, optical and IR photometry of class 1 Seyfert 79−58423
asteroid 1976 AA, diameter and albedo, radiometric obs. 77−82145
asteroid 1976 AA, photometric obs. at 0.56 and 2.2 μ 77−82144
asteroids, IR (JHK), photometry 79−2531
asteroids, IR reflectance spectra obs. and search for water of hydration 80−77318
asteroids, photometry in 0.56-2.2 μ range for 30 objects 78−69725
asteroids, radiometric diameters and geometric albedos from 10 and 20 μ photometry 77−53456
asteroids, radiometry and surface props. of Apollo, Amor and Aten objects 79−75135
astronomical diffuse objects, strip photometry appl. to globular clusters multicolour obs. 78−89229
atmospheric turbulence effects on optical and IR image form. *(French)* 80−46257
RW Aurigae, IR spectroscopy with contact-type image tube 79−92768
B2 1225+317, IR and optical spectrophotometry, $H\alpha/L\alpha$ ratio 79−25749
B2 1225+31, high-luminosity quasar, H emission line intensity ratios 79−25748
B2 1308+326, BL Lacertae object, photometry and polarization during 1978 outburst 79−25718
B2 1308+326, optical and IR variability during 1978 outburst 80−51888
BD+30°3639, IR spectrum of planetary nebula 77−22297
BD+30° 3639, S III 18.7 μ fine-struct. forbidden line obs. in planetary nebula 77−37637
Be stars, polarimetry at 1.25 and 2.2 microns 79−44484
Be stars, spectroscopic obs. in near IR 77−56972
Be stars envelopes, observational study 77−13355
Be-stars, intrinsic polarisation 79−75213
Be-stars, photographic IR spectroscopy and near IR photometry 77−56991
Becklin's star, in Orion, 4 to 8 micron spectrum 77−29903
Becklin-Neugebauer object, Brackett-alpha emission obs. 78−36657
Becklin-Neugebauer object, CO band emission detect. 79−101184
Becklin-Neugebauer source in Orion, 3.3 to 5.5 microns spectrum 80−12796
Becklin-Neugebauer source in Orion, high resolution 1.5 to 5 micron spectroscopy 78−93368
1580 Betulia, broadband visual and 10.6 μ photometry 79−2511
binary stars, JHKLM photometry of close systems 80−46614
BL Lacertae-type objects, variable, IR and visible polarimetry and photometry 78−16528
α Bootis, comparison of predicted and observed spectral energy distrib. 80−46546
α Bootis, He I 10830 Å emission obs., high-temp. chromosphere 79−48792
44 i Bootis, W Ursae Majoris type star, 1.2 and 2.2 micron light curves 79−84822
α Bootis (Arcturus), CO fundamental bands, inhomogeneous chromosphere 78−36561
Brackett α line survey of compact IR sources 79−62882
bright IR star monitoring at 2.7 μm 78−16433
Butterfly Nebula M2-9 rel. to Be stars and protoplanetaries 79−48887
3C 120, IR variability, 2 μm obs. 79−30118
3C 227 and 382 radiogalaxies, spectral-flux distrib. in 0.36-3.5 μ range 78−36710

infrared astronomical observations continued
3C 273, quasar, IR polarisation obs. 78−4360
3C 273, quasar containing dust, IR spectra obs. 80−56970
3C 273, spectrophotometry of QSO at optical and IR wavelengths 79−17123
3C 279, variable quasi-stellar source, IR and visible polarimetry and photometry 78−16528
3C 345, large 2.2 μm polarisation obs. 79−80367
3C 371, polarisation at 2.2 μm, nonthermal emission 79−2566
C- and M-type stars near globular cluster NGC 419 in SMC, cluster membership 80−26921
Callisto, identification of water frost 78−4141
Callisto, IR emission spectra 80−82264
Canis Major R1, optical and IR props. of newly formed stars 78−93332
VY Canis Majoris, circumstellar shell heterodyne interferometry 78−8000
VY Canis Majoris, diameter upper limits 79−16974
VY Canis Majoris, expanding circumstellar cloud, SiO 8 μm band obs. 79−62840
VY Canis Majoris, IR obs. with new photometer 77−26017
27 Canis Majoris, spectroscopic obs. in 0.14-4.7 μ range 78−85957
α Canis Minoris (Procyon), CNO abundances from near IR spectrum 78−93222
Y Canum Venaticorum, C_3 and IR spectrophotometry of C star 78−65619
Y Canum Venaticorum, C star, IR spectrum between 1.2 and 30 microns 80−46544
Carina I and II H II regions, far IR obs. 79−25657
η Carinae, high angular resolution obs. (35-175 μ) 79−8925
η Carinae, high-resolution IR radiation maps of homunculus, spectral and spatial distrib. 80−12767
η Carinae, IR ang. diameter 78−93271
η Carinae, spectral obs. at 4 microns 78−4237
γ Cassiopeiae, Be star, coordinated IR and optical obs., (in late 1976) 79−25616
γ Cassiopeiae, Be star, IR excess 78−93257
SU and TU Cassiopeiae, short-period Cepheids, photometry and spectra rel. to radius anomalies 80−26864
o Cassiopeiae (HD 4180) Be star, IR photometric vars. rel. to optical spectrum vars. 79−58353
CD −31°622 as metal-deficient subdwarf 78−65618
V553 Centauri, C rich Cepheid, spectrum and photometry rel. to C and N abundances 80−4378
V553 Centauri, CH-type Cepheid, BVRI photometery rel. to chemical comp. and luminosity 79−62849
ω Centauri, JHK photometry of globular cluster, giant branch spread 78−16476
ω Centauri, near IR photometry, giant branch struct. 77−41397
ω Centauri, near IR photometry anomalous giant branch 78−16477
U Cephei, chem. comp. of secondary component of close binary system 79−35308
Cepheid variable stars, short-period, radial vels., BVRI photometry, radii 80−31309
Cepheids, in LMC, BVI obs., period-luminosity-colour relation 79−71055
Cepheids, in southern hemisphere, VBI photometry 77−53612
Cepheids, southern, BVI photometry 77−60772
Cepheus IV association, spectrophotometry of young stars 77−13328
Cepheus OB3 molecular cloud, obs. of new IR sources 79−67072
Ceres, carbonaceous chondrite mineralogies remote spectroscopic identification from IR obs. 79−96946
Ceres, evidence for water of hydration 78−32386
τ Ceti, Ca II 866.2 nm emission event 80−26860
UV Ceti, IR obs. of flares *(Russian)* 78−93278
o Ceti, vars. in spatial distrib. of 11 micron radiation 79−5828
o Ceti (Mira), diameter apparent var. at 10.2 μm 78−93267
o Ceti (Mira), spectropolarimetry 79−21302
o Ceti (Mira), strong TiO-related dia. vars. 78−16429
UV Ceti type stars, weak Ca II triplet absorpt. lines *(Russian)* 79−88691
Chamaeleon T association, JHKL photometry of stars, reddening 79−58384
Circinus X-1, Ariel 5 X-ray and IR brightness meas. 77−82325
Circinus X-1, IR magnitude drop (1978 March-April) 78−54080
Circinus X-1, JHKL photometry and IR brightness decline 77−74162
Circinus X-1, JHKLM photometry and light curve 78−54086
CIT fields, near IR vidicon images 77−33683
cluster of galaxies obs. at low galactic latit. 78−4373
CNO abundances from near IR spectrum 78−93222
S.Coalsack, obs. of IR sources 80−46652
Comet Bradfield (1978c), IR obs. 78−36529
Comet Bradfield (1978c) IR and total visual magnitudes (1978 March) 78−45283
Comet Bradfield (1979l), ephemeris and IR mags. (1980 Jan.-May) 80−41769
Comet Bradfield (1979l), spectroscopic and photographic obs. in near IR 80−105205
Comet Kohoutek (1973 XII), analysis of IR continuum 79−62792
Comet West (1975n), scatt. phase function of cometary dust, 0.5 to 18 μ 77−29731
Comet West (1976 VI), IR obs., results 78−81591
comets recent UV and IR obs. and prospects for Spacelab 77−33425
compact far IR source in W31 region assoc. with G10.6−0.4, early stage of stellar evolution 78−49504
compact galaxies, spectroscopic and photometric obs. 78−77603
compact H II regions, large beam IR obs. 78−16488
compact H II regions in areas of DR 21, W75N and K3-50, IR line obs., extinction determ. 80−12788
compact H II regions near class I OH maser sources, IR obs. 77−45525
compact IR sources assoc. with southern H II regions 77−45515
compact IR sources in molecular clouds, near IR slit scans 80−105300
compact nonthermal sources, polarisation at cm., mm., IR and visual wavelengths 79−5913
compact sources assoc. with H II regions and molecular clouds, polarimetry 78−41019
composite stellar systems, CO and JHK obs. of E and S0 galaxies 78−36684
cool giant stars, obs. and anal. of CO at 5 μm 78−36569
cool stars, effective temps; ang. dias. and reddening determ. from 1 to 5 μm flux curves 79−44458
cool stars, H_2O maser emission, catalogue of 82 objects 79−8909

infrared astronomical observations continued
cool stars, Ti isotopic abundance ratios 80−26840
cool stars, wavelength depend. of polarisation rel. to atmospheres struct. 77−2426
cool stars in near IR, spectrophotometry and Cassiopeia 79−88658
cool supergiant stars, near IR excesses 78−16406
R Coronae Austrinae dark cloud stars, interstellar absorpt. spectra rel. to dust grain growth 80−67834
R Coronae Austrinae interstellar molecular cloud, for IR study and dust temp. profiles 80−62237
β Coronae Borealis, H I Paschen lines and Ca II triplet study 80−26869
R Coronae Borealis, He I λ10830 line obs. at 1978 pre-maximum phase 79−16975
R Coronae Borealis stars, long-term IR behaviour 78−96490
cosmic background, new balloon-borne meas. in far IR *(Italian)* 79−48965
cosmic background radiation, IR limit on fine-scale anisotropy 78−28863
cosmic dust, IR observations at Jena University Observatory *(German)* 77−26047
cosmic glack body radiation meas. using low temp. optical techniques, 2-40 cm^{-1} 79−71161
CPD−56°8032, emission line object, red and IR spectrum 78−4249
CPD −62° 1837 (HDE 308122), long-period variable member of triple 80−105260
3CR, radio galaxies, spectrophotometry spectral energy distrib. 79−21413
Crab Nebula, far IR emission, upper limit 79−58406
Crab Nebula, mapping and total flux determ. at 1 mm wavelength 77−49460
Crab Nebula, millimetre and submillimetre meas. 79−75267
Crab Nebula, near IR photometry and spectral index 80−8675
CRL 2104, CRL 2179, late WC stars, 2 to 4 μm spectrophotometry and circumstellar dust 78−96491
CRL 2591, IR source rel. to radio and H_2O counterparts 77−22330
CRL 2688 (Egg Nebula), 8000-11000 Å spectrum 77−41400
CRL 2688 (Egg Nebula), bipolar nebula, optical and IR polarimetry 78−36658
CRL 3068, dust-enshrouded star 77−91664
CRL 3099, highly evolved C star, IR photometry and spectrum 78−49436
CRL 618 and 915 (HD 44179), IR spectra in 2-8 μ range 78−41080
CRL objects, IR polarization obs. 79−48901
V1500 Cygni, (Nova 1975), emission line profiles during early nebular stage 79−53826
V460 Cygni, cool C star, atmospheric $^{12}C/^{13}C$ ratio 78−93223
θ Cygni, F-type dwarf star, spectral type of faint distant companion 80−90481
V1057 Cygni, FU Orionis star, IR spectroscopy with contact-type image tube 80−17587
P Cygni, H Paschen α obs. 80−62156
V444 Cygni, IR eclipse obs. and Wolf-Rayet wind structure 78−45357
59=V832 Cygni, IR emission increase, spectrum scanner obs. 80−94809
NML Cygni, IR speckle interferometry 80−31216
V1016 Cygni, IR spectrum 78−93266
V1016 Cygni, near-IR spectrographic obs. 80−94810
V1500 Cygni, spectral development, visible and near IR obs. 78−4231
V1016 Cygni, symbiotic star, IR variability obs. from VJHKL photometry *(Russian)* 80−105263
CH Cygni, symbiotic variable, flickering obs. during outburst, binary model 79−8929
CH Cygni, visible and near IR spectra 77−82232
V645 Cygni (GL 2789), IR and EHF spectroscopy 80−72956
V1500 Cygni (Nova 1975), continuous energy distrib., IR obs., thermal bremsstrahlung 79−80315
V1500 Cygni (Nova 1975), multiband photometry 77−87445
V1500 Cygni (Nova 1975), near IR spectroscopy 78−36599
V1500 Cygni (Nova 1975), near IR spectrum 78−36606
V1500 Cygni (Nova 1975), photometric and spectroscopic obs. 78−36604
V1500 Cygni (Nova 1975), UBVRI photometry and polarimetry 78−36614
V1500 Cygni (Nova 1975), wide-band IR photometry 78−36615
V1668 Cygni (Nova 1978), JHKLM photometry 79−53828
V 1668 Cygni (Nova 1978), spectral development 80−51789
V1500 Cygni (Nova Cygni 1975), IR photometry and spectroscopy 77−53599
V1500 Cygni (Nova Cygni 1975), shell phase obs. 77−49392
V1500 Cygni (Nova Cygni 1975), spectrophotometric obs. 77−49402
V1500 Cygni (Nova Cygni 1975), UBVRI photometry 77−33509
Cygnus OB2 No.12, high resolution 2μ spectroscopy rel. to interstellar and stellar features 78−57613
Cygnus OB2 No.12 (VI Cygni No.12), C_2 detect. in interstellar spectrum 78−12332
Cygnus X region, far IR survey 80−82538
349 Dembowska, IR spectral obs., candidate for meteorite parent bodies 80−98595
diffuse interstellar bands in 6500-8900 Å region 79−21373
30 Doradus, IR survey, 2 μm sources in central region 78−32544
DR 21-W75, H II region, high-resolution, far IR obs. 77−33589
DR 21/W75 complex, detection of H_2 vibrationally excited 2 μm lines 80−94853
BY Draconis, spectroscopic binary flare star, BVRI obs. 77−53595
CM Draconis, spotted dM4e eclipsing binary flare star, absolute dimensions and masses 78−12289
dwarf novae and possibly related objects, IR photometry 78−8015
dwarf stars, late-type, broad-band IR colours, CO and H_2O absorpt. indices 78−4218
early-type stars, IR photometry, extinction ratio, 2200 Å interstellar absorpt. feature 78−53943
early-type stars in N. Milky Way, IR photometry, interstellar extinction determ. 77−78783
early-type stars in southern hemisphere, IR photometry 80−94786
early-type stars with gas-dust envelopes, IR spectral energy distrib. 80−67732
eclipsing binary stars, near IR photometry rel. to mass transfer rates 80−67784
emission line object, spectral obs., possible planetary nebula 77−49451
emission line star obs. rel. to star formation 79−58333
emission line stars, spectrographic obs., 8000 to 11000 Å *(French)* 79−48815
infrared astronomical observations continued
emission line stars in LMC, spectroscopy and IR photometry 77−13348
emission line stars in southern hemisphere, IR obs. 80−90496
emission-line galaxies with IR excesses, 8000-11000 Å spectra 77−67124
emission-line stars, far IR obs., cool dust cloud evidence 79−92771
Enceladus, IR photometry rel. to presence of water frost 78−12146
equatorial IR catalogue (EIC), 2.7 μ high-precision sky survey results 78−81560
433 Eros, thermal props. from radiometric and refl. light obs. 80−31231
ESA/NASA ASSESS II Mission, far IR spectroscopy *(Italian)* 79−48687
extended radiosource 1400+162, BL Lacertae object in group of galaxies 78−4339
extragalactic nonthermal sources, spectral flux var. in 0.36-3.5 μ range 79−35412
extragalactic objects, 1 mm continuum obs. 78−36720
extremely red stars at $l^{II}\approx113°$, $-10°\leq b^{II}\leq+90°$, photometry and spectra 78−57554
faint proper-motion stars, spectra and photometry to very low luminosity degenerates deficiency 80−17575
faint red stars, photoelec. photometry of complete sample, space density 79−71034
faint stellar images, colour-magnitude diagrams and clustering correl. functions rel. to star populations 80−82360
fast irregular variables, UBV and JHKL photometry *(Russian)* 78−28684
fine structure lines, [O III] 88.35 microns and [O I] 63.2 microns obs. 80−12794
fireball meteors, satellite-borne IR obs. 79−35196
FJM 3, 100 micron source, radio and near IR studies 77−26082
FJM 6, molecular cloud, far IR, near IR radio mol. line studies 80−26929
flare stars, photographic photometry of four new objects 78−89207
G12.2−0.1, radio and IR obs. of OH/H_2O source 78−57620
G333.6−0.2, compact H II region, S III 18.7 μ fine-struct. forbidden line obs. 77−37637
G333.6−0.2, G298.2−0.3, southern compact H II regions, IR emission lines obs. 78−96522
G333.6−0.2, Ne II 12.81 μm forbidden line obs. at high resolution 80−85983
G333.6−0.2, powerful H II region, 2 μm line emission detect. 78−54017
G333.6−0.2, southern H II region, IR line and continuum spatial study 77−49455
G45.1+0.1, 8-13 μm spectrophotometry of compact H II region 78−65672
G45.5+0.1, compact H II region, IR sources photometry 78−4396
G75.84+0.4, IR photometry and spectrophotometry 79−62889
G-type dwarfs, macroturbulence and age anticorrel. 78−93226
galactic center, variable IR extinction obs. 79−48909
Galactic central IR surface brightness obs. by balloon *(Japanese)* 78−61925
galactic central region, 2.4 μm mapping 77−29934
galactic central region, absolute surface photometry at 2.4 and 3.4 μm 77−57088
galactic central region and anomalous IR source, balloon-borne obs. at 2.4 μ 79−44588
galactic centre, 2.2 μm spectroscopy 78−36686
galactic centre, 4 to 8 micron spectrum 79−48922
galactic centre, forbidden O III 88 μm line emission obs. 78−49503
galactic centre, IR emission maps at 10, 34, and 56 microns 78−41037
galactic centre, IR obs., 1.25-12.5 μm interstellar extinction law 78−41039
galactic centre, IR obs. and nature of compact IR sources 78−24551
galactic centre, IR polarisation obs. 78−8109
galactic centre, IR polarization due to silicate dust grains 77−9794
galactic centre, linear polarisation in near IR 78−96534
galactic centre, Ne II 12.8 micron emission obs. 78−32572
Galactic Centre, polarisation obs. at 2.2 microns 77−64850
galactic centre, star density rel. to nature of IR source IRS 16 80−46671
galactic centre, struct. from 2.4 μm obs. 78−81689
Galactic centre obs. with balloon-borne IR telescope *(German)* 79−5906
galactic centre point source, 1.4-2.7 μ spectrum 77−5569
galactic centre region, 2.2 μ map 79−58424
galactic centre region, airborne far IR obs. 78−8110
galactic centre region, IR linear polarisation 77−91630
galactic core, H II obs. in near IR 79−53864
galactic diffuse IR radiation obs. at 2.4 μ 77−33656
galactic for IR emission, balloon obs. *(Japanese)* 80−36714
galactic H II regions, O III 51.8 μm forbidden emission line obs. 79−25685
Galactic IR obs. at 2.4 μ wavelength by balloon *(Japanese)* 78−61924
galactic IR radiation, balloon borne obs. *(Japanese)* 79−80351
galactic IR radiation, balloon obs. *(Japanese)* 79−80350
galactic plane, diffuse far IR emission, balloon obs. 79−35378
galactic plane, diffuse far IR emission detect. 77−33611
galactic plane, far IR diffuse emission, longit. profile 79−88742
galactic plane, far IR scans 77−60823
galactic plane, near IR photographic survey 79−62911
galactic plane far IR emission, obs. at galactic longit. ($l^{II}=27.5°$) 80−62231
galactic surface brightness obs. in anticentre direction 79−48935
galactic X-ray sources, IR photometric obs., identifications, reddening 79−71155
galaxies, active nuclei, IR obs., future prospects 78−57651
galaxies, active southern objects, JHKL obs. 79−40270
galaxies, bright, southern, photoelectric photometry 79−21436
galaxies, distance scale from IR magnitude/H I vel.-width relation 80−82480
galaxies, E and S0, UBVR and JHK photometric obs. 79−58412
galaxies, extinction in IR-emitting nuclei 79−44599
galaxies, H I vel. widths and IR magnitudes rel. to distance scale and expansion rate outside Local Supercluster 80−105325
galaxies, IR emission rel. to Byurakan classification *(Russian)* 77−22305
galaxies, IR luminosity/H I vel. width relation and distance scale 79−44596
galaxies, luminosity evolution from 2.2 μm of giant ellipticals 80−105358

infrared astronomical observations continued
galaxies, metallicity on integrated colours, calibration of early-type objects 78−89227
galaxies, V−K colours and IR Hubble diagram for giant ellipticals 80−105359
galaxies of E and S0 type, H_2O absorption and coolest stellar component at 2 μ 78−41034
galaxies with IR bright nuclei, photometry at 10 μ 78−41045
Galaxy central region, IR profile at 2.47 μm 77−29935
Galaxy surface brightness, balloon obs. *(Japanese)* 77−82308
Galilean satellites, near IR spectra rel. to surface composition 79−35180
Galilean satellites, water ice existence, IR spectral reflectance obs. 80−82263
U Geminorum, dwarf nova, M-type dwarf companion spectral type 79−62851
giant and supergiant stars, atm. $^{12}C/^{13}C$ ratio 77−13337
giant planets, atmospheric refraction indexes 80−98608
giant stars, late-type, O I 7773 Å triplet obs. 79−35250
giant stars in globular cluster M71, IR colours, CO band strengths and physical parameters 79−25650
giant stars in M3, M13, M92 and M67, IR photometry, bolometric magnitudes and effective temps. 78−57595
giants in globular cluster ω Centauri, CO absorption and effective temp. 80−51749
giants of G and K type, Fe abundances 79−16944
GL 2591, protostellar source, 3 μm ice absorpt. band, linear polarisation obs. 80−105303
GL 2636, star form. region in Cygnus-X, IR obs. 80−105302
GL 3068, IR spectrum of C star 79−12469
GL 490, GL 2591, obscured IR objects, K-band spectra anal. 79−92828
GL 490, IR obs. of low-luminosity pre-main sequence stars 79−53808
GL 915, 618, 2688, IR sources assoc. with double-lobed refl. nebulae, far IR obs. 78−54009
GL southern sources, 10 and 20 μm photometry 79−97097
glaaxies, far IR (30-300 μm) emission 80−51861
globular cluster assoc. with X-ray source MXB 730-335, IR obs. 77−9776
globular clusters, colours and interstellar reddening from integrated IR photometry 80−67575
globular clusters, metal-rich, TiO band strengths, reddening and metallicity determ. 79−40227
globular clusters, metal-rich, V, I_K photometry 77−45503
globular clusters, metallicity effects on integrated colours, calibration 78−89227
globular clusters near galactic centre, IR studies 80−82434
H-H 2, condensation H, spectrophotometric data 79−62826
H-H 7 and 11, spectrophotometry of very low-excitation objects 80−46549
HD 101065 (Przybylski's star), Ap-star model rel. to light vars. and temp. 79−101151
HD 152667 (V861 Scorpii), phys. props. and orbital parameters, supergiant star with black hole companion model 79−71067
HD 193793, shell condensation around W-R binary, IR obs. 79−12495
HD 193793, Wolf-Rayet binary, visible and near IR spectra 78−8023
HD 193793, Wolf-Rayet star, IR brightening rel. to circumstellar dust form. 80−31301
HD 193793, Wolf-Rayet star, IR obs., cooling of circumstellar dust shell 79−48823
HD 193793(=BD+43°3571), near IR magnitude increase 77−87413
HD 200775, possible protostar in reflection nebula NGC 7023, optical polarization and IR spectrum 80−85944
HD 44179, binary star, 3.3 micron unidentified feature, high resolution spectra 80−82466
HD 44179 (Red Rectangle), bipolar nebula, IR polarimetry 78−36658
HD 44179 (Red Rectangle), obs. and interpretation of IR spectrum 77−78859
HD 50138, Be star, model for shell from continuous spectrum obs. in IR 77−56976
HD 50896 and 151932, WN stars, IR spectra 78−8024
HD 51585, B[e] star, visible and near IR spectrum 77−45445
HD 87643, forbidden line Be star, IR obs. with new photometer 77−26017
HD 97048 (=HM 18), pre-main sequence star, unidentified IR features obs. 80−85943
HDE 245770, near IR photometry of OBe star, A 0535+26 optical counterpart 79−48826
HDE 245770, spectroscopic obs. of X-ray nova Ariel 0535+26 optical counterpart 77−45450
HDE 245770 (Ariel 0535+26), 1977 spectrum, objective prism study 78−61866
He2-442, UVRK photometry and spectroscopic obs. *(Russian)* 80−94817
624 Hektor, nature of Trojan asteroid 79−35176
Henize 2-38, symbiotic star, steam and CO absorpt. obs. 78−40970
Henize 715 (4U 1145−61), Be star, IR vars. rel. to circumstellar envelope disappearance 80−72979
Herbig Ae/Be stars, spectrophotometry 78−93258
Herbig-Haro 2, detection of H_2 vibrationally excited 2 μm lines 80−94853
Herbig-Haro object 1 exciting star, identification as T Tauri star 80−17633
Herbig-Haro objects exciting stars, 2 micron search 80−67720
α^1 Herculis, He I 10830 Å emission obs., high-temp. chromosphere 79−48792
AM Herculis, IR and visual monitoring, model constraints 79−17018
AM Herculis, IR spectroscopy, period, mass function 79−71066
AM Herculis, J and K light curves 77−74091
AM Herculis, polar, IR photometric obs. 80−98687
AK Herculis, R and I light curves, B and V light curves comparison, starspot 79−67064
AM Herculis (3U 1809+50), IR light curves 78−28727
AM Herculis (=3U 1809+50), near IR and violet mag. obs. 77−53643
HFE 2,3, molecular cloud, for IR radio mol. line studies 80−26929
HFE 2, 100 micron source, radio and near IR studies 77−26082
hot stars, IR photometry *(Italian)* 79−53829
HR 1099 (V711 Tauri), JHK photometry of noneclipsing RS Canum Venaticorum type star 80−72995
HR 1105, He I 10830 Å line obs. of cold giant *(Russian)* 80−17586
HR 5999 (V856 Scopii), multicolour photometry, circumstellar dust shell 79−48828
HR 6766, weak G-band star, light-element abundances 78−57548

infrared astronomical observations continued
HR 8752, spectrum var. of superluminous supergiant, near IR obs. 78−81630
Hyades, BVRI photometry of new possible cluster members 78−32533
Hyades cluster, possible members BVRI photometry 80−51821
Hyades stars, Hα and O I 7774 Å photometric obs. 77−22286
EX Hydrae, dwarf nova, IR and optical light curves 80−67747
VW Hydri, dwarf nova, IR light curves 80−67747
Hyperion, radius and albedo from 20 μ obs. 79−40136
Iapetus, near IR reflectivity of dark and light faces 80−26800
Iapetus, normal reflectance from lunar occultation obs. 78−85897
Iapetus, relative reflectance meas. at 1.6 and 2.2 μm 80−98607
IAU 13S6A, strong southern radiosource, optical identification 77−64865
IC 1396 interstellar molecular cloud, for IR study and dust temp. profiles 80−62237
IC 1848 A, bright-rimmed mol. cloud, IR source obs. rel. to star form. 79−5810
IC 2149, planetary nebula, absolute spectrophotometry in near IR 77−17669
IC 342, Scd galaxy, central regions IR emission and star form. 80−62256
IC 418, IR spectra, heated dust emission, atomic emission lines 80−46629
IC 418, near-IR spectroscopic obs. of planetary nebula 80−4421
IC 443, H_2 detection at 2.1 μm 80−17630
IC 4593, planetary nebula, absolute spectrophotometry in near IR 77−17669
IC 5146 dark cloud complex and cluster 78−89234
ice, interstellar, 45μ signature possible identification in Orion 79−17068
III-106, CH star in globular cluster M22, CO in IR spectra 80−62131
interstellar C_2, rot. fine-struct. lines obs. towards ζ Persei 80−67811
interstellar C_2 detect. towards ζ Ophiuchi 78−49505
interstellar C_2 molecules towards ζ Persei 80−12799
interstellar C in mol. clouds, 492 GHz line detection 80−90508
interstellar dark clouds motions, obs. with IR Fabry-Perot iterferometer 80−8672
interstellar extinction law correl. with wavelength of max. polarisation 78−61902
interstellar grains, interaction of light with small-particle system 77−74111
interstellar grains, organic compositon, IR obs. 80−77460
interstellar grains comprised of organic cpds., 3.4 microns absorpt. obs. 80−109514
interstellar IR and molecular line sources, 9400 Å photography 77−45602
interstellar linear polarisation, wavelength depend. at near IR wavelengths 80−51833
interstellar linear polarisation in 1-2.2 μ wavelength range 78−77588
interstellar matter, far IR emission between l=36° and l=55° galactic longitudes 78−54014
interstellar medium, far IR fine structure line obs. 80−62253
interstellar mol. clouds, relationship of submillimetre optical depth to ^{13}CO column density 77−45508
interstellar molecular clouds, Fourier interferometer for IR line emission obs. *(Italian)* 79−48679
interstellar molecules, vibr. excited, in grain mantles, IR emission lines 78−36670
interstellar reddening in near IR, new results from JHK photometry of reddened stars 80−94857
interstellar type I OH masers, positions, polarisation, nearby H_2O masers, radio and IR props. 79−25671
Io, 5 micron variability 80−46463
Io, absorpt. bands in near IR spectrum 79−5776
Io, gaseous SO_2 identified and upper limits for other gases 79−92704
Io, intense transient brightening obs. near 5 micrometres 79−101113
IO, IR reflectance spectrum, absorption features 79−92706
Io, reflectance spectrum, evidence for sublimates and adsorbates 79−92707
Io, surface composition, comparison of observed and lab. reflectance spectra 77−60716
ionized gas motion and distrib. in central parsec of Galaxy 79−25719
IR 12.4+0.5, compact far IR source discovery 79−40234
IR bright stars in region of galactic centre, catalogue and photometry 80−77299
IR source assoc. with Sh 2-149, spectral type and luminosity class 78−73772
IRC+10216, brightness distrib. at 11 μm 79−67115
IRC+10216, C star, near IR obs. of new mol. feature 79−92762
IRC+10216, C star, NH_3 obs. in circumstellar envelope 79−48793
IRC+10216, far IR obs. 77−29949
IRC+10216, spatial spectra from 2.2 to 20 microns, deviations from spherical symmetry 80−41911
IRC+10216, variable C star 80−90568
IRC+10420, IR emission lines from F-type supergiant star 78−4395
IRC+10°216, circumstellar acetylene in IR spectrum 77−5591
IRC +10216, C star, far IR size 80−82539
IRC +10216, high resolution IR spectrum 77−33681
IRC +10°216, circumstellar methane in IR spectrum 78−57694
IRC-10442 (GL5268S), near IR and radio obs. 80−4412
Jupiter, 5-8 μm spectrophotometry 77−29711
Jupiter, atm. acetylene abundance 78−16337
Jupiter, atmosphere, equatorial belt, spectrophotometry in 0.6-1.1 μm range 79−96960
Jupiter, atmospheric CO obs. at 5 μm, airborne spectroscopic obs. 78−36491
Jupiter, brightness temperature at sub-mm wavelengths 79−53743
Jupiter, C/H and D/H ratios from 8-9 μm IR spectrum 80−67638
Jupiter, cloud distrib. between Voyager 1 and 2 missions, 5 micron obs. 80−77345
Jupiter, CO IR spectrum and abundance 78−49374
Jupiter, D/H and C/H ratios from methane-d_1 spectrum 78−28572
Jupiter, evidence for telluric value of $^{12}C/^{13}C$ atmospheric ratio 78−20723
Jupiter, far IR spectra, airborne interferometry 77−25942
Jupiter, far IR spectral obs. 77−29681
Jupiter, far IR spectrum showing NH_3 rotational bands 78−85891
Jupiter, ground-based imaging rel. to Pioneer and Voyager cloud configurations interpretation 80−26787
Jupiter, high spectral resolution obs. around 80 μm 78−45267
Jupiter, high spectral resolution obs. between 30 and 50 μm 80−46462

infrared astronomical observations continued
Jupiter, high-resolution IR spectra in 10.2-13.4 μm range 79−96947
Jupiter, IR and visible spectrum, C/H ratio 79−48729
Jupiter, IR images at 5 microns wavelength during Voyager 1 encounter 80−26799
Jupiter, IR imaging in 8-14 μ spectral region 77−41350
Jupiter, IR multiple freq. sounding of anomalous clouds 79−2515
Jupiter, IR spatial scans 80−82268
Jupiter, IR spectral obs., 800-1000 cm^{-1} 78−16336
Jupiter, IR spectrum, 17-25 μ, comparison with thermal struct. models 77−45348
Jupiter, mean temp. struct. from far IR spectral obs. 80−17540
Jupiter, methane band photometry, absolute reflectivity, centre-to-limb vars. 79−53759
Jupiter, methane band photometry, SEB and STrZ reflectivity, atm. models 79−53760
Jupiter, methane line profiles near 1.1 μ as probe of cloud struct. and C/H ratio 80−62067
Jupiter, near IR polarisation studies 78−85899
Jupiter, near IR spectral albedo 80−31242
Jupiter, NH_3 1.56 band study 77−17422
Jupiter, NH_3 abundance from 2 μ spectrum 79−35182
Jupiter, NH_3 spectral line meas. using 10μm superheterodyne receiver 78−16335
Jupiter, PH_3 absorpt. in 5 μm window 80−31243
Jupiter, PH_3 obs. at 5 μ 77−33393
Jupiter, reflectivities during 1976 opposition 79−40124
Jupiter, spectrophotometry in 0.6 to 1.1 μ region, Jovian atmosphere optical parameters latit. vars. 80−46468
Jupiter, spectrophotometry in far IR 78−85890
Jupiter, spectrum between 10 and 13 μ, Jovian $^{15}N/^{14}N$ ratio estimate 79−8876
Jupiter, thermal radiation spectrum between 12 and 24 μ 77−17425
Jupiter, thermal structure from IR spectral meas., filtered iterative inversion method 78−7918
Jupiter, upper atmosphere aerosol content from Ganymede eclipse obs. 77−41349
Jupiter, vertical cloud struct. from 5 μm meas. 77−29710
Jupiter's ring detect. at 2.2 μm 79−66958
Jupiter and Galilean satellites, Voyager 2 IR obs. 80−77335
Jupiter and satellites, IR obs. from (Voyager 1) 80−26790
Jupiter atmosphere, GeH_4 abundance from IR spectrum anal. 78−61791
Jupiter atmosphere, IR obs. by Fourier transform spectroscopy 78−61747
Jupiter atmosphere, temporal characts., IR obs., north-south temp. asymm. 80−41760
Jupiter atmosphere, trace constituents upper limits from 5 μm spectrum anal. 78−61790
Jupiter ring, ground-based 2.2 μ obs., confirmation of Voyager 1 detection 79−40131
Jupiter tropical and temperate belts, 0.6 to 1.1 μm spectrophotometry, brightness distrib. and atmosphere optical parameters 79−92715
K3-50, H and He lines in obscured luminous H II region 80−51830
K3-50, ionized gas, IR and optical spectrophotometric meas. of compact H II region 79−53870
K-type giant stars, evidence for circumstellar shells from 0.4 to 20 μm photometry 80−90420
Kleinmann-Low Nebula in Orion, far IR polarization 79−12502
Kuwano's novalike object in Vulpecula, IR photometric obs. 80−62147
L1641 and Orion Nebula, submillimetre emission obs. 80−36685
L 43, CO mm wave and near IR obs. of filamentary cloud 79−62886
EV Lacertae, IR obs. of flares *(Russian)* 78−93278
Jupiter cloud zones, IR obs. 77−29712
Jupiter H_2 2-O quadrupole spectrum in atm. 77−45351
K3-50, compact H II region, 2 to 4 micron spectrophotometry 77−13422
K3-50, IR obs. of nearby H II regions and dust clouds 77−49457
Kapteyn's star, M-type subdwarf, IR spectrum and comp. 77−13330
Kleinmann-Low nebula, optically thin CO emission 78−4315
Kleinmann-Low nebula, spectrum from 29 to 125 microns 77−33680
BL Lacertae, polarisation at visible and IR wavelengths 77−9803
BL Lacertae, submillimetre photometry 78−4353
SW Lacertae, W Ursae Majoris type star, 1.2 and 2.2 micron light curves 79−84822
BL Lacertae objects, polarisation, visual and IR photometry and polarimetry 80−77480
late-type (K0 to M6) giant stars, IR photometry and effective temps. 80−46545
late-type dwarf stars, BVRI photometry, metal abundance index and galactic evolution 77−60754
late-type giant and supergiant stars, 1.25-3.25 μ airborne photometric obs. 78−40934
late-type stars, 4-8 μ spectral obs. 77−74054
late-type stars, anal. of balloon-borne near IR multicolour photometry 80−98654
late-type stars, ang. dias. by lunar occultation technique 77−74048
late-type stars, angular diameters from lunar occultations 79−44475
late-type stars, Ba oxide and halide identification in near IR 77−56926
late-type stars, balloon-borne near IR multicolour photometry 80−4356
late-type stars, balloon-borne near IR photometry 77−13345
late-type stars, Ca II 8542 Å line as chromospheric activity indicator 80−62108
late-type stars, in elliptical galaxies, IR obs. 77−91639
late-type stars, near IR multicolour photometry from BAT *(Japanese)* 80−31298
late-type stars, near IR photometry with balloon-borne telescope 78−73713
late-type stars, near IR photometry with balloon-borne telescope 80−4357
late-type stars, O-rich, 16 to 39 micron spectroscopy 80−22002
late-type stars, spectrophotometry, incident and emergent flux calc. 78−4200
late-type supergiants, C, N and O abundances for G AND K Ib stars 78−24509
R Leonis, circumstellar shell heterodyne interferometry 78−8000
R Leonis, IR atomic line spectrum of Mira variable 80−46557
R Leonis, IR spectroscopy of Mira variable, H_2O vibr. rot. bands 79−35258
87 Leonis, lunar occultation ang. diameter 79−25599
R Leonis, Mira variable, CO and OH IR vibr.-rot. overtone bands 78−36574

infrared astronomical observations continued
20 Leonis, possible eclipse obs. in triple system 78−12298
CW Leonis (IRC+10216), IR C star, intrinsic polarisation obs. and origin 80−67730
δ Librae, Algol-type eclipsing binary, IR detection of secondary 78−49475
AP Librae, polarisation at 2.2 μm, nonthermal emission 79−2566
Liller 1, optical candidate for X-ray burster MXB 1730−335, IR bursts detect. 79−44640
Liller I (MXB 1730−333), unusual burst in K-band (2.2 μm) 80−62319
Liller I/MXB 1730−333, IR burst detection from rapid X-ray burster 79−97105
LkHα101, 1-4 μ spectra, aircraft and ground-based obs. 77−5590
LkHα 101, IR spectra of emission line object, preplanetary disc obs. 78−16423
LMC, catalogue of 302 C stars 78−20654
LMC, far IR obs. of H II regions 78−81671
LMC supergiants, BVI photometry 77−33490
long-period variables, pulsation from near IR photometry 78−4248
long-period variables, SiO in 4 μ spectrum 77−13360
luminous blue variable stars in M31 and M33, IR detect. 78−49437
luminous C stars in LMC, photometry 78−28670
luminous cool stars, atm. $^{12}C/^{13}C$ ratio 77−13336
lunar, soils, mineral comp. determ. from spectral behaviour of albedo 79−21207
lunar mare grounds relative spectral reflectivity 80−12695
lunar regional basalt types from remote spectral refl. meas. 77−22118
lunar soil, near IR refl. coeff., Luna 24 obs. *(Russian)* 77−73983
β Lyrae, CNO abundances in atmosphere, IR spectra *(Russian)* 80−67794
α Lyrae, emission lines in IR spectrum, thin expanding extended atm. 78−53946
β Lyrae, optical and IR photometry, gaseous disc electron density distrib. 78−28722
α Lyrae (Vega), O I and Ca II emission in near IR spectrum 79−21289
RR Lyrae stars, in southern hemisphere, VBI photometry 77−53612
M101, spectra of H II regions, comp. gradient across spiral galaxy 78−65683
M17, far IR obs. rel. to H II region interaction with mol. cloud 80−22053
M17, high resolution radio and far IR maps compared 79−75263
M17 (Omega Nebula), O III 51.8 μm forbidden emission line obs. 79−25685
M17 SW, obscured IR point source spectroscopic anal. 79−48878
M22, globular cluster, membership and other problems 78−32537
M31, central region, near IR surface photometry 78−28791
M31, near IR polarization of nucleus 78−24556
M31, near IR vel. dispersion for nuclear bulge 78−49521
M31, near-IR energy distribs. 79−12512
M42, far IR polarisation obs. 77−53663
M43, emission nebula around NU Orionis, radio and IR obs. 78−54012
M6 field, supergiant IR photometry and interstellar matter towards galactic centre 78−16405
M81, near IR vel. dispersion for nuclear bulge 78−49521
M82, bright ridge detected in 2.2 μ emission 79−40269
M82, galaxy, 2 to 8 μm spectrophotometry 78−12363
M82, Ne II 12.8 micron emission obs. and galactic dynamics 79−17082
M82, nuclear source nature from IR obs. 80−82485
M82 nucleus, Brackett-line obs. 79−25704
M8, IR map 77−64817
M8, large-beam near IR and 24 GHz obs. 79−48882
M8, new IR-CO source obs. 77−64818
M8 (Lagoon Nebula), far IR obs. 80−4413
M-stars at $l^{II}=138°$, space density from objective prism spectral studies 77−9748
M-type dwarf stars, IR Fourier transform spectroscopy, abundance anal. 79−21279
M-type dwarfs and giants, near IR luminosity-sensitive features rel. to M31 and (M32) 78−49431
M-type dwarfs and S-type stars, FeH bands identification in spectra 78−7952
M-type giants and supergiants, circumstellar gas and dust shells, optical and IR obs. 79−21281
M-type stars, in Orion population, CaH and TiO band strengths 78−12227
M-type stars, spectral type and luminosity classification from near IR spectrograms 79−16952
M-type stars in direction of N galactic pole, photometry and spectroscopy 77−37594
M-type supergiants, in LMC, MK spectral types, luminosities 79−62820
M-type supergiants, photoelectric two-dimensional spectral classification 78−53936
Markarian 231, IR emission obs. 77−5570
Markarian 231, IR polarisation obs. 78−4360
Markarian galaxies, 3.2 mm and IR continuum obs. 77−22317
Mars, cloud obs. by Mars 2 in 0.36 to 1.38 μ range 77−53450
Mars, CO_2 IR heterodyne spectroscopy 77−41344
Mars, disc IR spectra compared with terrestrial analogues optical props. 78−85879
Mars, dust storm 1971-2, Mariner 9 IR spectra, composition and particle size distribs. 77−41345
Mars, extratropical cyclones, Viking Orbiter 1 obs. during summer season 79−44398
Mars, far IR brightness temp., appl. to planetary brightness temps. recalibration 77−9683
Mars, far IR spectral obs. 77−29681
Mars, IR photometric function and bolometric albedo 77−29698
Mars, isotopic ratios and minor constituents from Mariner 9 77−82142
Mars, near IR spectral reflectance, surface comp. determ. 79−21216
Mars, O_2 dayglow and O_3 abundance latit. var. 79−53750
Mars, occultation of ε Geminorum, obs. at Princeton 78−57482
Mars, photometric imaging in 0.35-1.10 μ range 1973 opposition 77−71044
Mars, spectral reflectance during 1973 opposition, 0.33-1.10 μ photoelectric photometry 77−60703
Mars, water vapour global seasonal var. and implications for permafrost 79−84714
Mars, water vapour obs. from Viking orbiters 78−20682
Mars atmosphere, water vapour mapping expt., Viking preliminary results 77−13263

infrared astronomical observations continued
Mars atmosphere thermal IR properties, 15 μm band meas. 79−84710
Mars atmosphere thermal IR properties, dust and ice clouds detect. from Viking IRTM spectral meas. 79−84712
Mars atmosphere thermal IR properties, global behaviour at 7, 9, 11 and 20 μm 79−84709
Mars atmosphere thermal IR properties, local dust clouds effects 79−84711
Mars surface and atmosphere, IR thermal mapping by Viking 77−13264
maser stars, late supergiants and long period variables 80−77410
maser stars, search for water vapour absorpt. lines 77−78804
Mauna Kea Observatory 33 μ photometry, calibration 77−67044
MD 101065, effective temp. and atm. electron press. 77−45468
Mercury, regolith containing Fe^{2+}, refl. spectra, 0.65-2.5 μm 80−56736
metal-deficient stars, CO obs. at 2.2 and 2.4 μm 79−58336
metal-poor stars, O abundances from O I IR triplet 80−36610
microwave background radiation polarisation, IR survey 78−73779
millimetre region cosmic background radiation, large scale anisotropy meas. 80−82553
Mira and semiregular variables, microwave and IR obs. of H_2O vapour maser emission 79−67037
Mira variables, airborne IR spectrophotometry, H_2O and CO absorpt. bands 78−32465
Mira variables, discovery of 123 new stars in Palomar 10 globular cluster region 78−40837
Mira variables, IR Photometry and OH maser pumping efficiency 80−82379
Mira variables and IR sources, angular dia. in near IR, 2-5 μm speckle interferometry 80−27010
molecular clouds, far IR emission 78−4313
molecular clouds, IR circular polarisation obs., interpretation 80−82469
Monoceros R2, far IR obs. of young assoc. 80−73010
Monoceros R2, IR obs. of CO line 79−25654
Monoceros R2, obs. in 40-400 μm range 78−69853
Monoceros R2 cloud, near IR and mol. obs. of rot. collapsing cloud 77−78840
1 Monocerotis, δ Scuti star, oscillation modes from photoelectric radial vels. and BVRI photometry 80−51787
N Monoceros region, two-micron IR objects survey 80−8555
V616 Monocerotis, A0620−00, transient X-ray source, spectrophotometry 77−33684
R Monocerotis, bipolar nebula, optical and IR polarimetry 78−36658
V616 Monocerotis, spectroscopic obs. of X-ray nova, Ariel 0620−00 optical counterpart 77−45450
Moon, 0.95 μm absorpt. strip intensity expression on colorimetric map *(Russian)* 79−44381
Moon, IR map of disk 79−25526
Moon, observational and theoretical temps. for total lunar eclipse 77−41328
Moon, regolith, IR spectra, Salyut 4 obs. in 3.5-7 μ range 78−69716
Moon, thermal emission at 350 μ 77−73980
MR 2251−178, X-ray quasar, IR obs. 79−44642
MS-stars, near-IR spectrophotometry *(Russian)* 78−20832
multiple systems in molecular clouds 79−101180
MWC 349, IR source optical identification with reddened high-luminosity star 80−56971
MWC 349, IR spectra of emission line object, preplanetary disc obs. 78−16423
MWC 349A, near-IR spectrographic obs. 80−94810
MXB 1728−34, X-ray burster, search for optical counterpart 77−33694
MXB 1730−335, 2.2 μm flashes from X-ray rapid burster 80−46706
MXB 1730−335, IR bursts detect. from Liller 1 optical candidate 79−44640
MXB 1730−335, Rapid Burster, IR bursts detect. confirmation 80−27020
MXB 1730−335, X-ray rapid burster, unsuccessful search for IR bursts 80−98740
MXB 1730−33, X-ray burster, globular cluster as possible optical counterpart 77−33694
Mz 3 (p-K 331−1°1), obs. of bipolar nebula, possible protoplanetary 78−45376
narrow-line emission galaxies, near IR broad-band photometric obs. 80−46659
Neptune, 5-20 micron obs. 78−32393
Neptune, albedo and brightness temp., 5 μm IR obs. 80−82300
Neptune, atmospheric changes and rotation period from IR photometric light curves 78−40869
Neptune, brightness temperature at sub-mm wavelengths 79−53743
Neptune, effective temp. from IR photometry 78−32394
Neptune, evidence for optically thin high-altitude cloud form. 77−53469
Neptune, IR refl. spectrum, evidence for weather 77−53468
Neptune, IR spectrum from 0.8 to 2.5 microns 80−21946
Neptune, methane and ethane emission detect. 78−16344
NGC 1023, SB0 galaxy, surface photometry, brightness distrib. 77−22316
NGC 1068, Seyfert galaxy, 2-2.5 μm spectrum, H_2 detect. 78−57636
NGC 1068, Seyfert galaxy, IR photometry and polarimetry 78−54035
NGC 1068, type 2 Seyfert, recombination spectrum and reddening 80−90519
NGC 1275, IR variability, 2 μm obs. 79−30118
NGC 1275, Seyfert galaxy, IR polarisation obs. 78−4360
NGC 1365 and 1386, IR and optical props. of emission-line galaxies 80−51867
NGC 1502, open cluster, IR photographs processing, discovery of faint source *(Russian)* 77−13250
NGC 2023, reflection nebula, far IR study 80−51831
NGC 2024, H II region, near IR obs. 79−58393
NGC 2024, obs. in 40-400 μm range 78−69853
NGC 2024 (Orion B) nebula, CO J=2 to 1 line obs. 80−8673
NGC 2071(IRS), IR obs. of low-luminosity pre-main sequence stars 79−53808
NGC 2264, far IR emission from compact sources 77−78841
NGC 2264, H II region, classification of optical, IR and radio obs. data 80−67818
NGC 2264, young open cluster, circumstellar shells, IR excess obs. 77−45410
NGC 253, Ne II 12.8 μm emission and galactic dynamics 79−92844
NGC 253, nuclear source nature from IR obs. 80−82485
NGC 253, Sc-type galaxy, two-micron spectrophotometry 80−4442
NGC 2903, spiral galaxy, nucleus identification and visual energy distrib. 80−62273

infrared astronomical observations continued
NGC 4151, Seyfert galaxy, IR polarisation obs. 78−4360
NGC 4151, Seyfert galaxy, optical polarimetry, circumnuclear dust envelope 78−61916
NGC 4631, spiral galaxy nucleus, IR photometry 78−45412
NGC 5128 (Centaurus A), dark lane, extended 10 μ emission 79−21429
NGC 520, tidal interaction in peculiar galaxy 79−48916
NGC 5506, IR obs. of X-ray Seyfert-like galaxy 78−65696
NGC 604 in M33, [S III] obs. and N/S abundance gradients 78−8083
NGC 6121 (M4), near IR photometry of metal-poor globular clusters 77−41398
NGC 6210, planetary nebula, absolute spectrophotometry in near IR 77−17669
NGC 6334 complex, 1 mm continuum map of cool IR sources 79−21390
NGC 6357A, O III 51.8 μm forbidden emission line obs. 79−25685
NGC 6572, 6891, 7662, near IR spectrophotometry of planetary nebulae 78−8105
NGC 6572, IR spectra, heated dust emission, atomic emission lines 80−46629
NGC 7009, spectral comparisons of ring and ansae 79−71101
NGC 7027, 16-38 μ spectral obs. and dust model of planetary nebula 78−93354
NGC 7027, interstellar extinction 164-2170 nm obs. of planetary nebula 79−67082
NGC 7027, IR spectrum of planetary nebula 77−22297
NGC 7027, planetary nebula, 0.9-2.7 μ spectrum 77−2461
NGC 7027, planetary nebula, 3.3 microns unidentified feature, high resolution spectra 80−82466
NGC 7027, planetary nebula, C abundance 77−87526
NGC 7027, planetary nebula, far IR obs. 77−22288
NGC 7027, planetary nebula, H_2 emission spatial distrib. obs. 80−98698
NGC 7027, planetary nebula 4 to 8 micron spectrum 78−12333
NGC 7027, planetary neubla, near IR obs. 78−73748
NGC 7027, S III 18.7 μ fine-struct. forbidden line obs. 77−37637
NGC 7027, S IV and Ne II IR emission line obs. of planetary nebula 79−21400
NGC 7027, search for vibrationally excited H_2 emission 78−93346
NGC 7129, refl. nebula, star form., CO mol. line and far IR obs. 79−17043
NGC 7213, IR photometry of lenticular Seyfert X-ray galaxy 78−89262
NGC 7538, H II region, IR study 79−84842
NGC 7538 (IRS 1+2), compact H II region, 2 to 4 micron spectrophotometry 77−13422
night sky background, 2.4 μm meas. 78−81715
Norma nova-like X-ray source, search for optical candidates 77−82322
GU Normae, Cepheid, BVI photometry and assoc. with (NGC 6067) 77−45464
northern sky photographic optical IR survey 79−21198
Nova, Aquilae 1975 (V1301 Aquilae), IR development 77−17570
Nova Cygni 1978, distance and interstellar reddening 79−21310
Nova Cygni 1978, photometric obs., light vars., IR obs. showing dust form. phase 78−96494
nova in LMC, IR obs. with HJKL filters 77−33518
Nova Sagittarii 1977, IR obs., high temp. dust shell form 77−60766
Nova Sagittarii 1978, identified with IRC *7a C−→C −20494=V3876 Sagittarii, IR obs. 78−49459
Nova Scuti 1975, spectrum, line identifications 78−45335
Nova Scuti 1975, UBVRI photometry 77−33520
Nova Serpentis 1978, IR magnitudes and BVR photometry 78−65629
Nova Serpentis 1978, IR photometry 80−4365
Nova Serpentis 1978, visible and IR photometry rel. to dust shell evolution 80−90430
Nova Vulpeculae 1976, IR energy distrib. 1976, Nov./Dec. 77−9757
Nova Vulpeculae 1976, IR spectrum *(Russian)* 78−16441
Nova Vulpeculae 1976, polarisation meas., reddening and distance 77−29855
Nova Vulpeculae 1976, spectra in range .38 to 1.12 microns *(French)* 77−53606
Nova Vulpeculae 1979, spectroscopic and photometric obs., (1958 and 1968) 79−58344
novalike object in Vulpecula, light curve, photometric and spectroscopic obs. 80−67758
O-stars, He II 10124 Å and H Paschen 7 line obs. 79−67003
O-type stars, C III 7901 to 9715 Å emission lines obs. 80−77401
O-type stars, He I 10830 Å to spectral line, rel. to mass loss 79−80304
OB-type stars, search for H Paschen α 80−62156
OBA supergiants and Of stars, IR photometry and mass loss rates 77−45414
UV Octantis, VBRI obs. of RRab star, radius determ. 79−8928
OH 0739−14, IR polarization obs. 79−48901
OH 0739−14, M-type giant in reflection nebula, IR obs. 80−46692
OH 205.1−14.1 in Lynds 1630 dark cloud, coincident IR source obs. 80−101630
OMC-2, detection of H_2 vibrationally excited 2 μm lines 80−94853
Omega Nebula (M17, W38, NGC 6618), S III, O III, N III, IR obs. 80−90495
Omega Nebula (M17), O I 63 μm forbidden emission line obs. 79−25684
XX Ophiuchi, emission-line star, near IR spectrum 77−49404
ζ Ophiuchi, search for C_2 in interstellar spectrum 77−45423
ρ Ophiuchi cloud, search for vibrationally excited H_2 emission 78−93346
ρ Ophiuchi dark cloud, high ang. resolution obs. of far IR source 79−40235
ρ Ophiuchi dark cloud, ice mantles and abnormal extinction 79−21376
ρ Ophiuchi dark cloud stars, interstellar absorpt. spectra rel. to dust grain growth 80−67834
ρ Ophiuchus dark cloud, IR polarimetry 79−40239
Ophiuchus dark cloud complex, IR study 78−93363
Ophiuchus dark cloud region, IR sources identifications 77−45522
Orion, Nebula 77−5557
Orion molecular cloud, 870 μm CO emission 78−12335
Orion Molecular Cloud, H_2 2.1 μm emission line vel. profiles 79−71094
Orion Molecular Cloud, H_2 quadrupole line reddening determ. 79−71095
Orion Molecular Cloud, H_2 S(2) 12.28 μm rotational line 80−41881
Orion Molecular Cloud, HCN J=4→3 354 GHz transition detection 80−101636
Orion molecular clouds, obs. in 40-400 μm range 78−69853
Orion Nebula, 2.1 μ H_2 emission , high spectral resolution obs. 78−20878

infrared astronomical observations continued
Orion Nebula, C I IR forbidden emission lines obs. 78−85987
Orion Nebula, Fabry-Perot high-resolution O I 8446 Å mapping 79−35344
Orion Nebula, fine-struct. lines obs. and elemental abundances 80−4410
Orion Nebula, forbidden Cl II and forbidden Fe II near IR high resolution mapping 80−62217
Orion Nebula, H_2 emission at 2.12 μm 80−17631
Orion Nebula, H_2 emission at 2 microns 78−93351
Orion Nebula, H_2 emission interstellar extinction meas. 79−25668
Orion Nebula, high resolution map at 33 μ 78−28757
Orion Nebula, IR obs. by Fourier transform spectroscopy 78−61747
Orion Nebula, IR polarisation, preferential extinction in Kleinmann-Low nebula 78−4311
Orion Nebula, lamellar grating obs. in 100-500 μm region 78−28743
Orion Nebula, near IR Fourier spectroscopy 77−57071
Orion Nebula, near IR Fourier spectroscopy of weak lines 79−35328
Orion Nebula, near IR photography with vacuum-cold camera 80−90341
Orion Nebula, O I 63 μm forbidden emission line obs. 79−25684
Orion Nebula, O III 51.8 μ forbidden emission line obs. 78−65510
Orion Nebula, O III 51.8 μm forbidden emission line obs. 79−25685
Orion Nebula, photographic obs. in Hα, Hβ and He I 10830 Å lines 78−81669
Orion Nebula, polarisation at 11.1 and 19.6 μm meas., aligned absorbing grains 80−36690
Orion Nebula, S III 9096 Å forbidden line, Fabry-Perot obs., abundance determ. 78−96515
Orion Nebula, S III emission at 534.37 cm^{-1} 77−73966
Orion Nebula, search for H_2 ground state S(2) line 79−8961
Orion Nebula, search for vibrationally excited H_2 emission 78−93346
Orion Nebula, submillimetre emission obs. 80−36685
Orion Nebulae, IR studies of ionization front 79−75261
Orion region, survey of extremely red stars with Schmidt telescope *(Japanese)* 78−20833
ζ Orionis, C III line obs. 77−87387
α Orionis, circumstellar shell heterodyne interferometry 78−8000
α Orionis, CO circumstellar absorpt. obs. in 4.6 micron spectrum 80−26858
42 Orionis, Copernicus UV spectra and IR photometry 77−49437
α Orionis, IR speckle images, two-dimens. obs. *(French)* 80−46553
FU Orionis, IR spectroscopy with contact-type image tube 80−17587
V380 Orionis, near IR spectrum line identifications, equiv. widths *(Russian)* 78−61861
α Orionis (Betelgeuse), circumstellar gas shell spatial extent 78−28673
α Orionis (Betelgeuse), K I 7699 å emission from circumstellar shell 77−22210
FU Orionis stars, composite spectra rel. to three models 78−65617
Pal 12, metal-rich globular cluster in outer galactic halo, optical and IR obs. 80−105290
Pallas, carbonaceous chondrite mineralogies remote spectroscopic identification from IR obs. 79−96946
S Persei, 1.2-10 micron data rel. to maser emission var. 78−49461
β Persei, 4.8 μ photometry 77−74092
X Persei, Be star, coordinated IR and optical obs., (in late 1976) 79−25616
β Persei (Algol), light curve at 10 μm near scondary min. 78−93315
β Persei (Algol) system, gravity darkening 79−44525
PG 0026+129, spectrophotometry of QSO at optical and IR wavelengths 79−17123
Phobos, composition, evidence for carbonaceous chondrite surface from spectral anal. 78−49365
Phobos, evidence for carbonaceous chondritic composition from multicolour obs. with Viking lander cameras 78−49366
Phobos, first encounter by Viking Orbiter-1, mass and density determ. 78−49364
PKS 0237−23, Lymanα/Hα intensity ratio from IR obs. of quasar 78−41078
PKS 0548-322, surface photometry of X-ray emitting BL Lacertae object 80−22069
PKS 2126−15, QSO (z=3.27), JHK photometric obs. 80−94888
planetary nebulae, 10 micron props. obs. 79−48879
planetary nebulae, 8 to 13 micron spectrophotometry 80−22057
planetary nebulae, absolute flux densities for emission lines in 6000-11000 Å range rel. to physical parameters 80−51857
planetary nebulae, advances in IR obs. 80−109525
planetary nebulae, dust temp. and mass, IR photometry obs. 80−94850
planetary nebulae, IR emission lines in 12 faint objects *(French)* 78−12337
planetary nebulae, moderately bright, spectroscopic study 79−84835
planetary nebulae, S abundance from IR and visible line meas. 80−82444
planetary nebulae, S abundance in 20 galactic objects, spectrophotometry 78−45375
planetary nebulae central stars, visible and near IR spectra 77−78785
planetary nebulae H_2 emission detect. from 5 objects 78−20879
planetary nebulae in southern hemisphere, IR and SHF obs. 80−90496
planetary satellites of outer solar system, IR photometry and identification of new class 78−12146
planets, brightness temps. at 1 mm wavelength 79−2496
planets, far IR and submillimetre obs. 77−71037
planets, far IR obs., temp. determ. 79−12431
Pleiades, Hα and O I photometry 79−35315
Pluto, 1.5 to 2.5 μm spectrum obs. 80−56765
Pluto, image tube spectra, 6800-9000 Å, search for possible atm., methane upper limit 79−16880
Pluto, methane frost, IR photometry obs. 77−22136
Pluto, surface and atmosphere from 1.4-1.9 μm spectrum 80−46480
Pluto, surface composition, IR photometry 79−53768
Praesepe, photometry in BVRI colours 80−26917
pre-main-sequence A and F stars in NGC 2264, nature of IR excesses 78−32461
RX Puppis, 2 μm spectroscopy, H_2O and CO absorpt., symbiotic binary model 79−67032
VV Puppis, polar, IR photometric obs. 80−98687
Q 0420−388, IR obs. of most luminous quasar 78−89272
Q 0420−388, QSO (z=3.13), JHK photometric obs. 80−94888
QSO 0957+561 AB, double quasar, IR spectrum confirms gravitational lens 80−77510
QSO absolute spectral energy distrib. in 0.3−10 μ range 79−62926
QSOs, JHKL obs. of four objects 79−40270
infrared astronomical observations continued
QSOs, new type, identified through IR meas. 80−8708
quasars, IR energy distribs. obs. 78−57645
quasars, IR spectra, H I line ratios 80−105391
quasars, optical identification problems 80−105392
quasi-stellar objects with low-redshift absorpt. systems, search for nearby faint objects 79−17121
R50 dusty star in SMC, IR photometry 77−45461
R associations, early-type stars in CMa R1 and Vel R2, JHKL photometry 77−45505
radiosources, coordinated photometric and spectroscopic observations of strong extragalactic 90 GHz sources 78−93440
red dwarf stars near north galactic pole, vel. dispersion 78−7989
Red Rectangle, refl. nebula assoc. with HD 44179, spectrum interpretation 77−49462
reddened star cluster in Ara, IR photometry 77−41395
Rhea, normal reflectance from lunar occultation obs. 78−85897
rich galaxy cluster 0004.8−3450, bri photometry 80−46685
Rosette Nebula, far IR emission from compact sources 77−78841
S106 IR, S235 B, obscured IR point sources, 2 μm spectroscopic anal. 80−12795
S140 interstellar molecular cloud, for IR study and dust temp. profiles 80−62237
S140 IR, far IR spectrum 78−93372
S140 molecular cloud, energetics, mol. line data, temp., density, abundances 78−36650
S140 molecular cloud, far IR emission detect. 77−33611
2S1728−337 vicinity, 5 IR sources detected by K-band photometry 78−54076
S255, molecular cloud, molecular line, radio continuum and IR data 78−8087
S88B, Hα knot, optical radio and IR obs. of vicinity 77−74115
2S 1702−363 field, IR object brightening and identification as Mira variable 78−81705
S-type stars, FeH and CeO identification 79−21280
S-type stars, Keenan and Wing bands, IR obs. 80−67722
S-type stars, Keenan band identification problem, IR obs. 80−72946
S-type stars in Southern Milky Way, objective prism survey and BVI photometry 78−61754
HM Sagittae, emission line variable, near IR spectrum *(Russian)* 78−81637
HM Sagittae, emission variable, optical spectrograms and IR magnitudes 77−67098
Hm Sagittae, eruptive variable, IR variability 79−25614
HM Sagittae, IR spectrum 78−93266
FG Sagittae, light vars. rel. to photometric radius and pulsation mass 78−36576
HM Sagittae, near emission-line object, optical and IR obs. 78−36575
HM Sagittae, near-IR spectrographic obs. of young planetary nebulae 80−94810
HM Sagittae, symbiotic star, IR variability obs. from VJHKL photometry *(Russian)* 80−105263
υ Sagittarii, absorpt. lines identification as Fe II high level transitions 78−93316
AQ Sagittarii, C star, ang. dia. from lunar occultation meas. 80−22008
RY Sagittarii, pulsating R Coronae Borealis star, IR variability 77−45462
Sagittarius A, 540 μ obs. of galactic centre 78−36699
Sagittarius A-west, IR obs. of Ne II forbidden line emission 78−36680
Sagittarius B2, 2.2 μ obs., origin in field stars 77−29908
Sagittarius B2, far IR spectrum obs. 78−8073
Sagittarius B2, H II region, high-resolution, far IR obs. 77−33589
SAO 158687, occultation of Uranus, 1977 March 10, rings discovery 78−69743
Saturn, 5-8 μm photometry 77−29711
Saturn, deuterated methane obs. in 5 μm spectrum 79−25543
Saturn, equatorial limb scans at 20 microns 79−2517
Saturn, evidence for telluric value of $^{12}C/^{13}C$ atmospheric ratio 78−20723
Saturn, far IR photometry, atm. thermal models 79−75151
Saturn, far IR spectral obs. of planetary disc and rings 78−16341
Saturn, H_2 2-O quadrupole spectrum in atm. 77−45351
Saturn, IR scans (1977 to 1978) 80−90363
Saturn, IR spectrum, 17-25 μ, comparison with thermal struct. models 77−45348
Saturn, near IR polarisation studies 78−85899
Saturn, near IR spectral albedo 80−31242
Saturn, PH_3 abundance, IR obs. 80−82278
Saturn, rings, 22.7 μ brightness versus solar declination 78−20724
Saturn, South Pole temp. enhancement, spatially resolved IR obs. 79−25541
Saturn, spectrophotometry in far IR 78−85890
Saturn, thermal profile from IR meas. inversion 78−4144
Saturn's rings, 2-4 μ spectrum 77−82159
Saturn and rings, brightness temps. at 39 μ 77−41351
Saturn atmosphere, Pioneer 11, IR radiometry data 80−82290
Saturn NH_3 1.56 μ band study 77−17422
Saturn rings, IR brightness and eclipse cooling obs. 80−56763
Saturn rings, unilluminated side, 20 μm brightness temp. 80−109392
Saturn spatially resolved IR obs., 10 and 20 μm disc scans at (B′=−11°.8) 79−84741
Sc galaxies, nuclear regions stellar content 77−9793
α Scorpii, circumstellar shell heterodyne interferometry 78−8000
V861 Scorpii, IR obs. of black hole candidate 79−44538
V861 Scorpii, near IR meas. rel. to orbital phase 78−93324
V861 Scorpii (OAO 1653−40), near IR obs. of single line spectroscopic binary 80−8652
RZ Scuti, JKL IR obs., light curves for eclipsing binary 80−101615
RY Scuti, silicate grains IR emission from early-type supergiant binary system 80−41827
seasonal phenomena from $3\nu_3$ methane band obs. 80−26803
seeing, wavelength depend., atm. inhomogeneity effects 78−92979
Serpens X-1, no IR bursts assoc. with Type I X-ray burst 80−98742
CV Serpentis, IR photometry and CRL 2120 identification 77−78825
Seyfert 1 galaxies, O I 8446 Å emission excitation mechanism, visible and IR obs. 80−85991
Seyfert galaxies, Fe XI 7892 Å forbidden line emission 78−49520
Seyfert galaxies, IR emission obs. 79−17083
Seyfert galaxies, IR energy distribs. obs. 78−57645
Seyfert galaxies, near IR broad-band photometric obs. 80−46659
Seyfert galaxies, submillimetre photometry 78−4353

infrared astronomical observations continued
Seyfert galaxy nuclei, spectroscopic obs. 77−9792
Sh2-149, near IR photography with vacuum-cold camera 80−90341
Sharpless 106, excitation and nature of bipolar nebula from IR obs. 79−48888
Sharpless 106 IR sources, 8-13 micron spectrophotometry 80−105305
Sharpless 140, compact source, strong far IR emission obs. 78−36649
Sharpless 140 IR source, detect. of assoc. near-IR complex 79−25686
Sharpless 235A, optical, radio and IR obs. of H II region 80−4415
sky fluctuating emission in airborne astronomy, meas. and interpretation 78−81552
sky noise at telescope focus, photometry of atmospheric IR emission, statistical props. *(French)* 78−53731
sky survey, large beam, at millimetre and submillimetre wavelengths made from balloon altitudes 79−97045
slow novae and symbiotic stars, late-type components spectral classifications 80−94813
SMC, photoelec. UBV and RI sequences 77−82307
SN in NGC 4321, JHKL mags., 1980 Jan. obs. 80−41847
SO -alaxies, radio and IR photometry 78−16531
solar active regions, submillimetre obs. 78−12177
solar atomic lines identification, 3.3-8 μ spectral region 77−45383
solar brightness temperature, 85-250 μm, with balloonborne lamellar grating interferometer 77−13308
solar brightness temperature near its minimum, meas. by balloon-borne lamellar-grating interferometer 78−85921
solar chromosphere, wave propagation, near IR and Ca II line obs. 77−78746
solar CO spectrum, centre to limb behaviour of first overtone vibr.-rot. transitions 79−8889
solar coronal Fe XIII emission line polarisation, near IR polarimeter obs. 78−61740
solar coronal holes, solar wind streams and geomag. activity during 1976-77 period 79−25570
solar far IR brightness temp. minima rel. to sunspot activity 80−62035
solar Fe I line spectrum, photosphere Fe abundance determ. *(Russian)* 80−12720
solar five-minute oscillation, IR continuum obs. 77−78745
solar flare of 1975, August 10, magnetic field reconstruction 77−13302
solar flux in Venus atmosphere, meas. by Pioneer Venus multiprobe mission radiometer expt. 79−48718
solar limb darkening in 1-4 μ range *(French)* 77−74023
solar limb darkening in 7404-24018 Å wavelength region 77−71099
solar photosphere, wavelength depend. of granulation, 0.38-2.4 μm region 78−12188
solar polarisation upper limit in mm. and far IR regions 77−49354
solar quiescent prominance spectra, meas. of Ca^+ 8542 and 8498 Å 80−90373
solar quiescent prominences, Hβ, He D_3 and Ca II 8542 Å line emission meas. 78−32427
solar quiescent prominences, He I 10830 Å line emission obs. 77−29787
solar quiescent prominences, spectra meas. 78−40886
solar quiet chromosphere, velocity waves propag. 77−22198
solar radial velocity, meas. using HF absorpt. cell 80−12681
solar spectra atlas, 775 to 950 cm^{-1} and 1050 to 1300 cm^{-1} 79−48745
solar spectrum, absorpt. lines asymmetry *(Russian)* 80−72901
solar spectrum registration using double-pass spectrophotometer with digital registration, precision *(Russian)* 79−96917
solar total eclipse, 1973 June 30, Si vidicon spectrometer obs. 77−9657
solar undisturbed chromosphere, He I 10830 Å line obs. 77−71102
southern galactic plane, near IR surface brightness 79−71128
southern hemisphere IR sources, search for H_2 2.1 μ emission 80−22059
southern stars, IR obs. with near photometer 77−26017
SS 433, enormous periodic Doppler shifts obs. 80−17593
SS 433, IR and visible obs., IR excess and emission processes 80−4387
SS 433, IR energy distrib. obs. 80−31312
SS 433, IR excess and variability from JHKL obs. 79−58346
SS 433, IR light curves from BVIJHK photometry, period and ephemeris 80−8642
SS 433, IR spectral obs., reddening and emission 80−4388
SS 433, IR variability obs. 80−98676
SS 433, near IR (600 to 1100 nm) spectra, 1979 June and September 79−97009
SS 433, near IR spectrum obs. 79−84803
SS 433, visible and IR photometric and polarisation obs. 79−80321
SS 433, visible and JHKL photometry and light vars. periodicity 79−53821
standard stars, polarisation obs. by Hatfield near IR polarimeter 79−2482
standard stars defining near two-colour photometric system for near IR, obs. 79−62759
standard stars for VRI photometry with S25 response photocathodes, obs. 77−2422
star dust, interstellar and circumstellar 77−41404
star formation, observational studies conclusions 79−25592
star formation, review 78−7988
star formation regions, IR spectroscopy of assoc. lineless objects 79−44586
star formation regions 78−32564
star formation regions near SNR W44, IR obs. 79−58399
stars, 1.25-11.1 μm photometry of late type objects 80−41823
stars, 20 μ, broadband photometry 77−9807
stars, Equatorial Infrared Catalogue development from satellite data 79−101091
stars, late-type, IR spectral observations *(Japanese)* 79−80307
stars, near IR photometric obs. 78−69795
stars IR colours, meas. rel. to diffuse interstellar bands strengths 78−93198
stars spectral obs. *(Japanese)* 77−82218
stars with IR emission line peculiarities 77−29862
stellar airborne spectrophotometry, 1.2-5.5 μm, spectra and absolute calibration 80−62117
stellar angular diameter meas. IR interferometry 77−53576
stellar BVRI photometry, secondary standards 79−70962
stellar BVRI photometry, with photometer using Si diodes as light detectors 78−20651
stellar flares *(Russian, English)* 79−75216
stellar IR fluxes, obs. for stellar ang. dias. and effective temps. determ. 79−92682
stellar IR spectral obs. in 1-2.5 μ range from balloon-borne telescope *(Japanese)* 78−61850

infrared astronomical observations continued
stellar occultations by Uranus' rings, existence of rings confirmation and radii calc. 78−53872
stellar secondary spectrophotometric standards, obs. in 5840-10800 Å range 79−29995
stellar speckle interferometry, modulation transfer function and evidence for log-normal statistic 79−101079
stellar spectra, atlas 78−20657
Stephenson's planetary nebula, optical, near IR and radio obs., position 79−67086
Stephenson-Sanduleak 433, 1.2-2.5 μm spectroscopy, photometry and polarimetry 80−41838
subdwarfs, old disc population, CaH and TiO band strengths 78−40930
Sun, absolute brightness temp. meas. in far IR with balloon-borne interferometer 80−62095
Sun, asymmetry of selected Fraunhofer lines 78−4175
Sun, CO molecular layer optical depth and rotational temp. 79−96988
Sun, comparison of He II 304 Å and He I 10830 Å spectroheliograms 78−20799
Sun, evidence for long-period global oscills. 79−2539
Sun, He I 10830 Å spectroheliograms from Kitt Peak 60 cm vacuum telescope *(Norwegian)* 77−60613
Sun, He I 10830 Å triplet in umbral spectrum *(Russian)* 80−36604
Sun, meas. of Fraunhofer lines asymmetry *(Russian)* 78−40892
Sun, polar coronal holes, evolution from He I 1083 nm synoptic maps 80−56801
Sun, quiet-time near-IR variability 80−12729
Sun, short millimetre wave radiation obs. by wide-band radiometer 79−62750
Sun, temperature measurement, chromosphere photosphere boundary *(German)* 80−51721
Sun, temperature minimum in far IR, var. with solar cycle 80−94769
Sun, Ti I lines meas. and solar Ti abundance 77−29743
sunspot umbrae, IR Ca II lines 80−85918
sunspots, FeH bands identification in spectra 78−7952
sunspots, umbral intensity rel. to phase in solar cycle 78−69773
supergiant, B-type, assoc. IR source GL 2636, IR and visible obs. 80−105302
supergiant stars, late-type, in Magellanic Clouds, IR photometry 79−35254
symbiotic stars, IR variability and nature 77−49399
symbiotic stars and slow novae, late-type components spectral classifications 80−94813
45 Tauri, Hyades cluster star, CNO abundances from near IR spectrum 78−93222
SU Tauri, visible and IR photometry and polarimetry *(Russian)* 78−61860
T Tauri star, extremely young, and assoc. nebula, fading 78−93236
T Tauri stars, H_2 emission obs. 78−93230
T Tauri stars, photometric and spectral props. 79−21282
T Tauri stars and Herbig Ae-Be stars, broad-band IR photometry 78−4217
T Tauri stars and related objects, IR meas. 78−8002
Taurus dark cloud complex, IR study 79−8963
RR Telescopii, symbiotic star, steam and CO absorpt. obs. 78−40970
Titan, 16-30 μm spectroscopy 80−56760
Titan, IR spectrum from 0.8 to 2.5 microns 80−21946
Titan, normal reflectance from lunar occultation obs. 78−85897
Titan, search for H_2 (3,0) S1 line in spectrum 78−4143
Titan, suspected near IR variability 80−46469
Triton, image tube spectra, 6800-9000 Å, search for possible atm., methane upper limit 79−16880
Triton, narrow band spectrophotometry 79−16879
Triton, satellite with atmosphere, IR spectrum obs. 80−21945
Tycho's supernova remnant, filaments spectrum 78−73747
4U 1608−52, optical identification and transient source outburst 78−41088
UBVRGI photometric measurements of 1297 stars, catalogue on mag. tape 78−40839
unidentified 3.3 μ emission feature obs. 77−33601
upconversion for astronomy 80−46412
Uranus, 5-20 micron obs. 78−32393
Uranus, albedo and brightness temp., 5 μm IR obs. 80−82300
Uranus, albedo and spectral features from IR obs. 80−82299
Uranus, brightness temperature at sub-mm wavelengths 79−53743
Uranus, disc profiles, narrow waveband, 6000-8500 Å region 79−66960
Uranus, IR spectrum from 0.8 to 2.5 microns 80−21946
Uranus, new satellite occultation of SAO 158687, Kavalur obs. 77−53473
Uranus, SAO 158687 occultation obs. rel. to upper atmosphere temp. struct. 79−62791
Uranus, satellite rings, KAO obs. of SAO 158687 occultation 77−53471
Uranus, satellite rings, Perth Observatory obs. of SAO 158687 occultation 77−53472
Uranus, thermal structure from IR meas. 78−36509
Uranus, unsuccessful search for ethane emission 78−16344
Uranus and rings, obs. of stellar occultation, (1980 August 15 to 16) 80−98610
Uranus occultation of SAO158687, obs. possibilities in methane bands 77−29719
Uranus occultation of SAO 158687, obs. rel. to upper atmosphere mean temp. and temp. vars. 80−46477
Uranus ring system, obs. of occulation of (SAO 158687) 77−67068
Uranus rings, BD−15° 3969 occultation obs. 78−89118
Uranus rings, optical search 77−67067
Uranus satellites, narrow band spectrophotometry of Ariel, Umbriel, Titania and Oberon 79−16879
AN Ursae Majoris, polar, IR photometric obs. 80−98687
variable far IR source detect. in NGC 6334 group of nebulae 80−8671
variable stars, USAF satellite obs. 77−49406
VB10, spectrophotometry rel. to low luminosity M-type dwarfs optical spectral classification 79−58339
AI Velorum, BVRI photometry and photoelectric radial vels. rel. to nature of variable star 80−94815
Venus, atmospheric, scattering coeff. from Venera 9 and 10 photometry 80−8572
Venus, atmospheric aerosol distrib. changes, 1972-75 period 77−64681
Venus, atmospheric net radiation meas. by Pioneer small probe 80−46435
Venus, atmospheric temp. and press. from high resolution IR spectra 77−60701

infrared astronomical observations continued
Venus, brightness temperature at sub-mm wavelengths 79−53743
Venus, cloud and temp. struct., from 12-20 μm spectrum 79−66946
Venus, cloud properties from airborne obs. of near-IR reflectivity spectrum 78−53850
Venus, clouds, IR radiation, Venera 9 and 10 radiometer meas. 77−78699
Venus, CO_2 8689 Å band high-dispersion spectroscopy near superior conjunction 79−75129
Venus, CO_2 band spectroscopic obs. at 7820 Å 77−37540
Venus, CO_2 equivalent widths, phase variation obs. 77−37539
Venus, CO_2 IR absorpt. bands, 3900-10000 cm^{-1}, assignment 78−7896
Venus, CO_2 line profiles, phase variation 77−82139
Venus, emission spectrum, 17-38 μm, aqueous H_2SO_4 droplets in CO_2 atm. 78−40855
Venus, equatorial and polar limb-darkening 79−88613
Venus, equatorial IR brightness diurnal vars., obs. during 1975 apparition 79−16858
Venus, far IR photometry, atm. thermal models 79−75151
Venus, far IR spectral obs. 77−29681
Venus, global thermal emission and radiometric albedo *(Russian)* 78−4132
Venus, high spectral resolution ground-based obs. in 450 to 1250 cm^{-1} region 77−91456
Venus, IR image obtained at time of Pioneer Venus probe encounter 79−48714
Venus, IR spectrometer obs. on Venera 9 and 10 spacecraft 77−78698
Venus, $O_2(^1\Delta)$ airglow and nightglow emission 80−17515
Venus, polar clearing in clouds, Pioneer Orbiter 1 obs. at 11.5 μm 79−70978
Venus, sunlight absorption in atmosphere, Pioneer radiometer meas. 80−46434
Venus, surface dust detected by Venera 9 and 10 radiant flux obs. 80−72803
Venus, temp., cloud structure and dynamics from IR remote sensing 80−46429
Venus, thermal anomalies persistence and size 78−85876
Venus, thermal asymmetry from Venera 9 and 10 obs. 77−53447
Venus, thermal radiance maps, anomalous features 79−101102
Venus, thermal radiometry by Venera 9 and 10 of cloud tops 80−46424
Venus, upper atm. temp. and dynamics from Pioneer Orbiter IR radiometer meas. 80−26766
Venus, UV and IR simultaneous images, correl. of features 79−53744
Venus, winds, spectroscopic obs., techniques and data reduction 79−75130
Venus atmosphere, cloud particles, Venera 9 and 10 nephelometric meas. 77−78695
Venus atmosphere, first results from Pioneer Venus large probe IR radiometer expt. 79−48719
Venus atmosphere, lighting conditions in 0.5-1.1 μ range, Venera 9 and 10 meas. 77−78696
Venus atmosphere, scattered solar radiation, day sky spectrum, Venera meas. 80−56573
Venus cloud layer, entry probes and orbiters obs. rel. to optical model 78−4130
Venus cloud layer, Venera 9 and 10 narrow-band photometric probing 77−78697
Venus day sky spectrum, Venera 11 and 12 spectrophotometric obs. *(Russian)* 79−66949
Venus middle atmosphere, IR remote sounding from Pioneer orbiter 79−48712
Venus retrograde winds, possible periodic vars. 79−25530
Vesta, IR spectral obs., candidate for meteorite parent bodies 80−98595
Vesta, spectral refl. meas., pyroxene absorpt. band 77−82146
W Virginis stars, in southern hemisphere, VBI photometry 77−53612
NQ Vulpeculae (Nova 1976), IR photometry, dust form. in exploded shell 79−48832
NQ Vulpeculae (Nova 1976), isothermal dust condensation phase, broad-band photometry 78−36586
W31 region, high resolution far IR survey 78−12389
W33 A, 4.5-8 μm spectrum 79−101181
W33 A, OH source, IR spectrophotometric and polarimetric obs. 79−21451
W3, 8 to 13 micron spectrophotometry of compact sources 77−57070
W3, IR maps from 4.9 μm to 20 μm 78−49495
W3 IRS 1, fine structure line radiation, dust UV opacity 80−90505
W3 region, near IR obs. of far IR sources G133.8+1.4 (W3N) and G133.982+1.14 (BS4) 80−22058
W40 and W48, near IR and CO mm wavelength obs. 78−65667
W49, H II region, high-resolution, far IR obs. 77−33589
W50 (SS 433), supernova remnant, optical filamentary nebulosity discovery 80−56916
W51, O III 51.8 μm forbidden emission line obs. 79−25685
W51, W49, airborne for IR spectroscopic obs. rel. to dust cloud model 80−36684
W51 (IRS 2), compact H II region, 2 to 4 micron spectrophotometry 77−13422
W51 (IRS 2), H and He lines in obscured luminous H II region 80−51830
W51-IRS 2 and W49 NW, compact H II regions, IR spectra obs. 80−90497
Walker No.67 in NGC 2264, interstellar linear polarisation meas. rel. to circular polarisation existence 78−12223
WC stars, near IR spectrometry 80−94816
weak-G-band stars, CO 2.3 μ band strength 78−12228
white dwarfs, cool, IR photometry, atm. comp. 79−16950
Wing-Ford 9910 Å molecular band as mass function constraint in old galaxy populations 77−17673
Wolf Rayet stars, late type, 8-13 micron spectral obs. 80−101599
Wolf-Rayet stars, 2 to 4 μm spectrophotometry of late WC stars 78−96491
Wolf-Rayet stars, IR light vars. 77−9750
Wolf-Rayet stars, near IR spectra emission line characts. 79−53825
X-ray quasar 0241+622, IR obs. 79−44642
X-ray source fields from Einstein Observatory, RI photometry with CCD camera 80−62315
young stars, accreting, ang. dimensions 79−44482
young variable stars, absorpt. and emission features, IR spectrophotometry obs. 80−72954
zodiacal dust cloud, thermal emission at 11 and 20 microns 80−90367
zodiacal light IR radiance model and meas. 78−81588

infrared astronomical observations continued
III Zw 2, IR variability, 2 μm obs. 79−30118
Ba II stars, JHK photometry 77−74053
C and M-type giant stars distrib. in galactic nucleus and Magellanic Clouds 78−32460
C stars, $^{12}C/^{13}C$ ratio determ. 78−73710
C stars, 3 μm absorpt. band obs. 78−28682
C stars, 3.9 micron absorpt. band identification 78−93231
C stars, IR CN spectra rel. to $^{12}C/^{13}C$ ratios 79−35257
C stars, in LMC, VRI photometry, optical spectroscopy and evolutionary implications 79−71019
C stars, JHKL photometry 80−46555
C stars, photometry at 1-2.5 μm, circumstellar dust shells 79−88652
C stars, polyatomic molecular line search in photographic IR 77−78786
C stars, variable, IJHKL photometry obs. 80−98657
C stars in Cygnus, new discoveries and BV photometry 80−46551
CO in giant stars in globular clusters 78−93339
H II compact regions, far IR obs., (40-150 μ) 79−62883
H II regions, 1-1000 μm wavelength obs. 79−67084
H II regions, compact, IR obs. in 3.4 to 33 microns range 77−22287
H II regions, forbidden O III 88 μm line emission obs. 78−49503
H II regions, galactic, forbidden S III 18-71 micron emission obs. 79−97046
H II regions, He II abundance and IR excess 78−86000
H II regions, IR line emission, airborne obs. 78−93353
H II regions, obs. at 10 μ using ESO 3.6 m telescope 79−35337
H II regions, southern, 1 mm continuum obs. 79−8968
H II regions, spectrophotometry from 4 to 8 μ of compact regions 79−35321
H II regions and galactic centre, far IR spectrometry 77−53668
H II regions in M33 galaxy 78−61923
H II regions near galactic centre, far IR obs. 78−41012
Hα emission stars in young cluster NGC 2264, UBVRI obs., pre-main sequence stars 79−35267
He variable stars, IR excesses obs. 80−67733
OH 0739-14, IR source assoc. with double-lobed refl. nebulae, far IR obs. 78−54009
OH 26.5+0.6, spectrophotometry from 2 to 40 microns 78−24568
OH maser source OH 0739−14, IR polarization obs. 79−48901
OH masers, obs. of new assoc. IR objects 78−12407
OH/IR stars, IR search and identifications 78−24510

infrared astronomy
see also infrared sources (astronomical)
3.8-m telescope on Mauna Kea, UK instrument 78−96397
3-m telescope on Mauna Kea, NASA/Univ. of Hawaii instrument 78−96398
32.5 cm IR airborne telescope 78−28523
accreting stars, model IR spectra for dusty circumstellar shells 78−85934
airborne, fluctuating sky emission meas. and interpretation 78−81552
airborne far IR Fabry-Perot astronomical spectrometer 80−109371
airborne far IR Fabry-Perot spectrometer for astronomical fine structure lines 80−62026
airborne IR observations, methods and instruments 78−69688
artificial satellite telescope and detector arrays 78−45226
astronomical instrumentation conference, Tucson, Arizona (29 January to 1 February 1979) 79−75108
atlas of stellar spectra 79−88649
atmosphere extinction, 0.65 to 2.50 μm above Mauna Kea, obs. 80−12546
atmospheric transmission rel. to precipitable H_2O at Gornergrat Obs., Switzerland 79−34941
Australian Astronomical Society, conf. Melbourne, Australia (May-June '77) 78−69655
automated spectrum scanner, 3000-11000 Å region 79−53724
balloon-borne IR telescope for absolute surface photometry of night sky 78−36453
balloon-borne telescope IR and sub-MM astronomy, review 80−8547
bandpass interference filters for 1-3 mm window 80−109368
bolometer, composite, for submm. wavelengths 78−65964
British large IR telescope on Mauna Kea, construction 78−69686
Cassegrain scanning system for IR images 80−82204
chopper for deep space IR interferometer/spectrometer 78−81545
conference, IR and MM waves and appls., Miami Beach, USA (Dec. 1979) 80−57009
conference, Zurich, Switzerland (Mar. 1979) 80−4783
conference proc. (Lecce, Italy, 1977 September 22-24) *(Italian)* 79−48685
conference proc. (Lecce, Italy, 1977 September 22-24) *(Italian)* 79−101077
cooled instrumentation for space platform use 78−16298
cosmic background, new balloon-borne meas. in far IR *(Italian)* 79−48965
Cosmic Background Explorer, satellite instrumentation 80−61988
Cosmic Background Explorer Satellite, IR and mm wave techniques 78−49344
cosmic background radiation, ang. momentum 79−80374
3K cosmic background radiation, star form., nuclei of active galaxies 80−67958
cosmic dust grains, observed IR props. 80−26943
cosmic ray Cherenkov photons, effect on IR interferometric search for non-solar planets 80−98523
cryogenically cooled sensors, calibration in space, AFGL expts. 79−5753
cryogenics appls., 1 mK to 10K temp. range, survey 78−93712
data processing 79−101087
detection techniques, for low background satellite expts. 78−49343
detector, low-temp. modulated calibration method, space appls. 77−79152
detector performance, operating characts. of thermal and photon detectors 78−45231
detectors, conf., Los Angeles, CA, USA (1978) 79−2822
detectors, trends in low-temp. thermal and photon detectors *(Russian)* 80−72778
diffuse galactic emission in far IR 79−67092
ESA programmes *(Italian)* 79−48646
ESA/NASA ASSESS II Mission, far IR spectroscopy *(Italian)* 79−48687
extended source extraction from AFGL IR sky survey data 79−101088
extinction in 3.98-4.07 μm wavelength region, atmospheric effects 79−96808

infrared astronomy continued
extragalactic IR background radiation, meas. technique 80−17496
Fabry-Perot etalons as high-resolution IR interferometers 77−45888
Fabry-Perot interferometer for astrophysics 80−8672
far IR astronomy, calibration source for balloon-borne telescopes 80−62027
far IR astronomy, detectors and sources, review 80−56726
far IR bolometric and photoconductive detectors 77−41305
far IR interference filters 77−22592
far IR polarimeter for balloon astronomy 79−35094
Far IR Sky Survey Expt., 8-120 microns, objective 79−5751
flux collector on Tenerife 78−69684
flux method for stellar temps. and diameter determ. 80−62030
focal plane IR detector arrays for planetary missions 80−85862
Fourier interferometer for IR line emission obs. of molecular clouds *(Italian)* 79−48679
Fourier spectrometer, lamellar grating type for balloon-borne telescope 78−16294
Fourier transform spectrometer applic. 78−16309
Fourier transform spectroscopy, airborne IR obs. 78−61747
Fourier transform spectroscopy appl. to remote identification of solids in solar system 77−87273
galactic dust and IR astronomy, review *(French)* 78−12352
galactic nuclei radiation 77−53433
galaxies, active nuclei, IR obs., future prospects 78−57651
galaxies, UVK colour plane rel. to morphology 78−49539
giant stars, IR radiation emission in final stages 80−72931
grating spectrometer, liquid He cooled, for far IR astronomical obs. 79−66925
Hadamard techniques in optics and their relationship to other multiplexing schemes 79−80242
Hadamard transform IR imaging device 77−13240
heat trap field optics, compact lens-mirror system 78−55422
heterodyne detect. of stars, atm. turbulence effects, corrections *(French)* 80−46409
heterodyne detection, optical IR tuning, wavefront distortions effect *(French)* 79−62755
heterodyne spectroscopy 78−85859
high resolution image prod., use of totally computer controlled telescope 80−72785
high resolution spectrometer, used for satellite astronomical measurements, cryogenically cooled 80−90914
image coding in near IR, multiplex technique 77−53428
image contrast of diffraction-limited telescopes for circular incoherent sources of uniform radiance 80−82194
image processing technique appls. to scanned radiometer data of stellar sources 77−49312
image restoration appls., conf., Bordeaux, France (Mar. 1979) 80−41935
image scanning systems, tilting plane mirrors 77−83944
Infrared Astronomical Satellite, features and performance 80−61989
instrumental developments review 78−61737
instrumentation at U.C. Berkeley, current status 78−16293
instrumentation of Calar Alto telescopes 78−16295
instrumentation on NASA airborne observatories 78−45224
integrated IR photometry and wide field techniques for globular clusters 80−67574
integrated IR photometry using wide field photometer for globular clusters 80−62029
interference filter for submillimetre astronomy 80−48393
interferometer, 11 μm heterodyne system *(French)* 80−46397
interferometer, IR spatial, design and operation 78−45232
interferometer, Michelson far IR 78−93118
interferometry, high spatial resolution methods, speckle and aperture synthesis *(French)* 80−46405
interstellar 10 micrometer absorpt. band, comparison with phyllosilicates laboratory spectra 79−80344
interstellar diatomic oxide grains, IR absorption features 78−49509
interstellar silicate absorption bands rel. to IR laboratory spectra of protosilicate particles 80−56907
interstellar submillimetric lines, possible detect. via laser heterodyne techniques 79−44377
IR and sub-MM spectroscopy, conf., Bonn, Germany (Mar. 1977) 78−12778
IR technology, conf. II (San Diego, California, 1976, August 26-7) 77−45891
IR-array spectrometer 7-25 μ astronomy 77−22081
Jupiter, atmospheric structure and 5 μ limb-darkening 79−25539
large aperture IR optical system, design 77−2339
Large Infrared Telescope on Spacelab 78−12070
light collector for near IR, for stellar spectroscopy 77−73960
limb-darkening coeffs. for late-type giant model atmospheres 79−71029
long wavelength IR heterodyne detection 77−45892
long wavelength IR telescope, ang. response meas., off-axis rejection performance 78−61739
long-wave focal plane array, for astronomical satellite telescope, test facilities 79−5755
long-wave IR sensors, ground calibration 79−5749
low-background astronomical integrated IR detector array development 80−85860
low-temperature narrow-bandpass interference filter construction 79−32049
low-temperature star automatic recognition by two-channel IR systems 79−75118
measurements at liquid He temperatures *(German)* 79−5760
Michelson interferometer for airborne IR obs. of interstellar media 77−73966
Michelson interferometer for airborne IR obs. of interstellar media 77−73967
Michelson interferometer for balloon-borne IR spectroscopy 80−51654
Michelson interferometer on Voyager 80−77290
Mira phenomena, AlO IR bands 78−69801
mirror design, economical construction of large lightweight glass mirrors *(French)* 77−17370
MOSFET preamplifier, liquid He-coooled, for use with astronomical bolometer 77−61123
Multiple Mirror Telescope, brief description and early discoveries 80−12669
multiple mirror telescope, design, review 78−69687
multiplex image coding, astronomical IR speckle interferometry appl. *(French)* 80−67580
NASA 91 cm aircraft-borne telescope for IR astronomy 77−22075
infrared astronomy continued
non-thermal emission mechanisms 79−48667
nonsolar planets, search methods, IR interferometry from Earth orbit 79−53737
observation development progress *(German)* 77−67138
observation technique, space research appl. 78−61738
observational sites in high-mountain regions, astronomical-climatic conditions evaluation 79−62566
observatory sites, water vapour data 79−21181
orbiting astronomical telescopes, IR detector cryogenic cooling requirements 78−96400
Palermo four-colour far IR program *(Italian)* 79−48688
photoconductive detectors, low-noise preamplifiers 77−61124
photodiode array, self-scanned, for high dispersion astronomical spectrophotometry 78−45230
photographic photometry, processing techniques for revealing faint objects *(Russian)* 77−13250
photography, near IR, with vacuum-cold camera 80−90341
photometer, far IR, for Kuiper Airborne Observatory 79−66926
photometer, sub-mm, for ESO 3.6 m telescope 78−16296
photometer, sub-mm, opt. components 78−16297
photometer, wide field for extended stellar sources 77−82582
photometer for solar intensity obs. in 1.5-2.4. μm range 79−101069
Pioneer Venus orbiter, IR radiometer 80−36469
Pioneer Venus Orbiter cloud photopolarimeter 78−57429
Pioneer Venus Sounder Probe IR radiometer 80−67509
Pioneer-Venus large probe infrared radiometer optical system 78−81543
planetary nebulae, advances in IR obs. 80−109525
planetary radiometers for space probes 77−49299
polarimeter, near IR, for solar corona emission line obs. 78−61740
polarimeter, near IR, of Hatfield Polytechnic Observatory, design 79−2482
review 79−35153
review of IR and submillimetre astronomy *(Russian)* 80−72773
Salyut 6 Ge:B receiver for 60-130 μm studies 80−67566
satellite telescopes, control of contamination due to cryogenic cooling 80−31209
scanning Fabry-Perot interferometer for balloon-borne astrophysical obs. 79−35092
scanning Fabry-Perot interferometer for far IR balloon astronomy 79−35093
Schmidt achromatic corrector plates for near IR, spherical aberration elimination 78−28515
Shuttle IR Telescope Facility, detector performance conditions 79−5752
Shuttle IR telescope facility 77−49297
Shuttle Telescope Facility, focal plane design 79−5750
Shuttle/Spacelab, platform for cooled IR astronomical telescope 77−73921
silicates, emission and extinction in 4-14 μ range 79−44581
simulation of the infrared astronomical satellite (IRAS) telescope system 79−29976
Skibotn, N.Norway, min. precip. H_2O in atmosphere, rel. to IR astron. obs. 79−92572
sky noise at telescope focus, photometry of atmospheric IR emission, statistical props. *(French)* 78−53731
sky noise correl. for IR telescope focal plane *(French)* 78−53725
sky simulation 79−29975
sky survey telescope for wide field photography 80−105167
solar IR spectra, computer simulated appl. to atm. fluorocarbon detect. 77−53217
South Pole as obs. site, atm. water vap. meas. 77−81954
space telescope, IR Astronomical Satellite, focal plane design 79−5750
space-borne interferometers, astrometry and planetary detection 80−109357
Spacelab telescope facility 77−45283
spatial interferometer, space-borne, exposure time 79−35131
speckle interferometry, principle, performance and appl. to NML Cygni 80−31216
spectra of galactic sources and evidence for polysaccharides 77−78857
spectral features, unidentified, review 80−26936
spectrometer, high resolution Fabry-Perot 79−53722
spectrometer, Si diode vidicon, IR capability for solar research 77−9657
spectrometer for near IR stellar spectra obs., automatic system *(Russian)* 80−51664
spectroscopy, future objectives *(Italian)* 79−48686
spherical lamellar grating interferometer for airborne far IR astronomy 77−25942
star formation rate in inner Galaxy, IR obs. 80−67704
star interplay with interstellar medium 77−53433
stellar angular diam. determ. from IR photometry, appl. to Arcturus 77−64760
stellar angular diameters and effective temperatures determination, IR flux method appl. 79−92682
stellar near IR photometry, effects of atmospheric extinction 80−51539
stellar photometry, response functions in red and near IR 80−56715
stellar speckle interferometry, modulation transfer function and evidence for log-normal statistic 79−101079
stellar speckle interferometry in near IR 79−53734
stellar spectra, near IR low dispersion ground based obs. *(Italian)* 79−48689
stratospheric balloons, appls. *(Italian)* 79−48683
submillimetre sky emission and absorpt., freq. spectrum of fluctuations 77−41308
submillimetre waves and applications, conference, Guildford, England (1978) 79−31916
submillimetric multicolour photometry and calibration 79−35143
Sunyaev-Zel'dovich effect in cosmic microwave background, obs. via IR detectors 79−25765
survey data processing techniques 78−81553
system for radiating source meas., calibration and spectral props. 77−49300
telescope, 102 cm balloon-borne, for far IR obs. of celestial sources 78−45227
telescope, 41 inch, with composite bolometers, for far IR balloon astronomy 78−45228
telescope, rocket-borne cryogenically cooled IR system technology 78−45225
telescope for Infrared Astronomical Satellite 77−49298
telescope on Space Shuttle, contaminant environment effect 77−91398
TIRGO project *(Italian)* 79−48678

infrared astronomy continued
TV detector, intensified-Si intensity target, near IR astronomy appls. 78−81544
TV imaging, astron. appl. 79−92678
UK 3.8 m IR telescope, description 78−16300
UK 3.8 m IR telescope in Hawaii, features 79−75103
upconversion for astronomy 80−46412
upconversion to visible, detect. method for astronomy 78−45240
upconvertor for astronomical imaging 78−7883
utilisation of IR technology, conf., San Diego (1977) 78−77984
Venus, clouds, IR absorption and scattering, particle size dispersion effect 80−109384
Venus, subcloud lower atmosphere, IR radiation absorption calc. method 77−53446
Viking IR thermal mapper, design 78−57440
Voyager IR spectroscopy and radiometry experiments 78−24428
water vapour comparison for IR observatory sites 78−11973
Wyoming Infrared Telescope (Jelm Mountain), IR universe exploration 78−85848
Ge:Be photoconductive detectors for obs. from space platform, 30-55 micron 79−5754
Ge:Ga, uniaxially stressed, far IR photocond. meas., appl. in IR detection 78−10496
Ge:Ga photoconductive detectors for obs. from space platform, 50-120 micron 79−5754
InSb IR detectors, integrating premaplifier 80−90337
Si extrinsic photoconductive IR detectors, VLF behaviour 78−81542
Si:As photoconductive detector for IR astronomy, responsivity and system noise 80−51665

infrared communication *see optical communication*

infrared detectors
see also bolometers; photodetectors
3-channel far IR detector based on coded Si;B, Ge:B, n-GaAs photoresistors 80−101839
aberration sensor for high-energy laser system, interference problems 79−98422
Air Force Geophysics Laboratory IR sky survey, extended source extraction 79−101088
air pollution meas. by incoherent optical heterodyne detection 79−48203
airborne IR scanners, temp. calibration 80−41572
airborne IR system performance 78−82039
angular displacment transducer 80−86257
antenna design and simulation 79−30552
antenna-coupled, noise-equiv. power, theory 77−57390
aspheric mirror optical systems for the infra-red 79−36983
astronomical appl., current developments review 78−61737
astronomical application, operating characts. of thermal and photon detectors 78−45231
astronomical far IR bolometric and photoconductive detectors 77−41305
astronomical satellite telescope and detector arrays 78−45226
astronomical submillimetre detector-telescope systems, for spectroscopy 77−49305
atomic vapour quantum counter, Stark tuning 80−53242
atomic vapour quantum counter for upconversion of narrowband IR radiation in 1.5-20 μm region, expt. results 80−73455
avalanche photodiode detectors, 1.0 to 1.4 μm region, for high data rate fibre optic systems 79−54188
balanced common module coolers 80−95142
Balloon Altitude Mosaic Measurements Program 78−81455
biotelemetry appl. 77−90926
BLIP systems, effect of f-number and other parameters on FLIR performance 78−77981
bolometer, laser narrow pulse recording appl. *(German)* 78−4692
book, optical and IR radiation detection 79−2821
C-CD appl. for IR detection and imaging *(German)* 78−63190
calibration for space appls., modulation method 77−79152
calibration of long wavelength IR sensor, uncertainty terms 77−170
calibration standards requirements survey 80−57248
calorimetric energy meters, KDM and BKDM, for pulsed laser radiation 79−17494
calorimetric energy meters, KDS and BKD, for high-power laser pulses 79−17496
charge transfer device imaging arrays 78−77990
charge transfer devices with Si detectors 77−83991
chopping pyrometer for remote meas. below 200°C *(German)* 80−86313
coherent detection of partially coherent sources 80−47109
combustion technology, IR applications 80−86431
compact four-mirror optical system design and testing 79−23049
composite superconducting transition edge bolometer 77−71371
conference, IR and MM waves and appls., Miami Beach, USA (Dec. 1979) 80−57009
conference, optical phenomena in IR materials, Annapolis, MD, USA (Dec. 1976) 78−25933
conference, Zurich, Switzerland (Mar. 1979) 80−4783
contactless temperature meas., IR techniques and detectors *(German)* 80−86314
conversion, two-stage, of IR radiation to visible, high sensitivity detector appl. 79−59761
cooling element for radiation detector, shape effect on heat removal efficiency 78−12691
cooling systems for space appls., He II flow through porous plugs 78−49842
Cosmic Background Explorer Satellite, IR and mm wave techniques 78−49344
cryogenic, expt. using closed-cycle mech./adsorption refrigeration 78−93708
cryogenic package, non-evacuated 79−97395
cryogenic sensors, CAD and evaluation 79−85184
cryogenically cooled sensors, calibration in space, AFGL expts. 79−5753
data processing in infrared astronomy 79−101087
development, operating principles, performance, appls. 78−12757
development and applications 77−5934
development and characteristics 78−77986
developments, review 78−12753
DH photodiodes, diffusion limited transient response 80−70809
dicalcium lead propionate, improper ferroelectric, dielectric props., IR radiation pyroelectric detection 80−80711
differential reactor, single-pass, and IR cell, combined device 79−80683

infrared detectors continued
digital radiometer/photometer (Tektronix) optical transmission characts. meas. *(French)* 79−89000
digital thermometer improvement *(Japanese)* 78−41306
dimensions of IR detector, rapid meas. by Fresnel diffr. *(French)* 78−89435
diode, point contact, metal-metal and metal-semiconductor, subMM wave mixing 80−4769
discontinuous metal film millimetric-wave and IR detectors *(Japanese)* 77−49771
doped semiconductor system at cryogenic temps. 78−45710
electric apparatus and power lines, temp. rise meas. by infrared radiometer *(Russian)* 78−89537
electronic gas detection, Pellistor, VQ and TGS sensors *(Spanish)* 80−93832
emitter/receiver device which detects objects by beam interruption or reflection *(Spanish)* 79−67389
energy analysis for system with narrow band interference filters 78−16846
epitaxial graded gap semiconductor layer appl. 78−74060
Ettingshausen-Nernst detector, sensitivity-time const. relationship *(German)* 77−37980
Ettingshausen-Nernst detectors with one- and two-phase detector layers *(German)* 80−27344
evaporated thermoelec. detectors, theoretical/practical performance limits 79−2830
far IR and near MM wave power energy meter calibration 80−57373
far IR Josephson junction voltage-tunable differential heterodyne spectroscopy 79−30578
far IR laser output detection by MOM point-contact diodes *(Japanese)* 79−21811
Far IR Sky Survey Expt., 8-120 microns, objective 79−5751
far IR technology and applications, conf., Reston, USA, (Apr. 1977) 78−45711
far IR thin crystal pyroelectric detector development 77−37994
fast-response thermoelectric radiation detector, construction and sensitivity 77−22597
figures of merit for characterizing detector performance 79−2825
film thermal device appl. 78−70189
focal plane IR detector arrays for planetary missions 80−85862
focal planes in intrinsic semiconductors 78−37994
forest fire alarm system 80−86429
FP and FPU electron-trap photocells, for laser flux intensity meas. 78−286
frequency conversion, two-stage process in $AgGaS_2$, α-HIO_3, for thermal radiation recording 79−46002
frequency mixing and detect. by interaction of radiation with metallic and semicond. films 77−75614
FT-IR detector with gas chromatograph (collects, stores spectral data, monitor functional groups) 78−92560
fusion reactor, Doublet III, neutral beam interlock system using IR detector 80−106228
N-GaP and p-GaP, photon drag-optical rectification detectors, performance in 2 to 33 μm range 79−35834
gas analyser, non-dispersive, for industrial processes and environment protection *(Hungarian)* 80−55735
general theory for wideband radiometers *(Russian)* 77−21926
glow discharge detection, gas breakdown theory 78−58035
Golay detector, housing for Grubb Parson modular cube interferometer 79−26113
group specific detectors for gas chromatography 78−92557
heterodyne detection, optical IR tuning, wavefront distortions effect *(French)* 79−62755
heterodyne detection, using interferometer and backscatt. radiation system, nonlinearities *(French)* 77−37991
heterodyne detection of random gaussian signals, pulse duration optimisation 79−12848
heterojunctions, metal layer between two dissimilar semiconductors 77−74501
HgCdTe/CdTe, limited diffusion volume photodiode, characterisation 80−75627
hot carrier diode mixer 78−29161
HV equipment temperature meas. by IR instrument 77−10039
hybrid IR focal plane modules, construction and operation 77−87825
hybrid IR/CCD focal planes, performance, appls. 79−3798
III-V semiconductor heterostructure avalanche photodiodes, high speed response, high quantum efficiency 79−80682
imaging, CCD, modelling and appl. of HgCdTe MIS struct. 78−80058
with immersed lenses, performance characts. *(Russian)* 79−27358
impurity photoresistor in interferometer, threshold charact. 80−31856
industrial IR detector markets and device limitations 80−86432
industrial IR thermometry using fibre-optic lightguides 80−86302
industrial precision filter radiometer development and applications 79−21814
p-InSb-Au, surface barrier, structure, photosensitivity spectrum 79−51674
integrated focal plane arrays for thermal imaging 77−19448
integrated MOM device, detect. expts. at 10.6, 3.39, 1.15 and 0.6328 μm 77−89878
intensified-Si intensity target vidicon application to IR astronomy 78−81544
interferometer for NDT 79−8419
intrinsic semiconductor IR detector array data acquisition system 78−77991
IR and sub-MM spectroscopy, conf., Bonn, Germany (Mar. 1977) 78−12778
IR defectoscopy, optimum algorithm in case of noncontent temp. meas. 78−60947
IR emissivity meas. method and equipment 79−35812
IR imaging, imaging systems design, operation and performance, applications 80−47111
IR streak camera, high speed, appls. 77−79093
IV-VI narrow gap semiconductors, fabrication, IR laser and detector appls. 77−77415
IV-Vi semiconductor film, quantum efficiency 79−75596
IV-VI semiconductor lateral-collection photodiodes, for 3-5 μm region 78−32871
Josephson effect heterodyne receivers 78−12754
Josephson junction, millimetre-wave, far-infrared and infrared detectors *(Japanese)* 78−32872

infrared detectors continued
Josephson junction detector of microwave and far IR radiation, response 77−61119
Josephson junctions, applications in plasma physics 80−103194
Josephson junctions mounted in a waveguide, wide-band detect. characts. 80−4767
Josephson point contact for use at sub mm. wavelengths 77−22600
Josephson self-oscillator mixer 77−34026
lag correction network ccts. 78−288
lag effect on thermal imaging system basic parameters 78−89544
Landsat multispectral scanner, calibration of thermal band 79−97438
Large Infrared Telescope on Spacelab 78−12070
laser irreversible damage in IR detector materials 78−25914
laser low-level pulse meas. system at 1.064, transfer standards 80−86253
laser pulse detector, fast nondamageable, using gaseous plasma 80−95138
laser pulse recording, semicond. ionisation-type photographic system 78−49903
laser radiation energy photoelectric meter, digital output 78−58040
laser techniques in mol. spectroscopy, book contrib. 78−8455
leaf temp. meas. method in connection with plant physiology *(Japanese)* 78−31993
least-mean-square spatial filter for IR sensors 80−38092
Limb Infrared Monitor of Stratosphere, radiometer spatial frequency response 79−101048
linearity, device for checking 80−101841
long wavelength IR heterodyne detection 77−45892
long-wave, cold spectral filters appl. problems 79−3799
long-wave, for astronomical obs., ground calibration 79−5749
long-wave focal plane array, for astronomical satellite telescope, test facilities 79−5755
low background satellite experiments 78−49343
low scatter mirror degradation by particle contamination 77−65618
low-background astronomical integrated IR detector array development 80−85860
low-temperature thermal and photon detectors, astronomical appls. *(Russian)* 80−72778
material exposure threshold meas. at 10.6 μm 78−90471
matrix pyroelectric detector for laser oscills. investigation 77−74502
measurement of temperature distribution in weld of thermoplastic foil *(Polish)* 80−22362
measuring cup for the blind, electronic, 50 μl indications 77−78054
metal film, laser induced transverse voltages, detector appl. 0.33 to 10.6 μm 77−39824
metal whisker diode, with thermally enhanced field emission, elec. fields, calc. by antenna theory 77−47889
metal-Ge Schottky barrier quantum detectors, optoelectronic props. 80−13146
metal-oxide-metal diode for IR detection, fabrication by positive photoresist process 77−67496
metal-oxide-metal wide band IR detector, long life 77−5916
metal-semiconductor transition, i.r. detection model 77−1442
micrometer detectors using pulsed Pb salt tunable diode laser 80−13148
microwave-biased extrinsic photoconductors, equivalent circuit model 78−49898
millimetric and IR discontinuous-metal-film detector 78−289
MIM discontinuous metal film, fast detector for MM-wave through optical freq. range 77−18092
MIM point contact diodes, freq. response, effect of d-electrons 77−47898
MIM tunnelling diode, detector performance, IR and microwave freqs. 79−12844
MIS structure, charge current and band to band tunnelling *(French)* 77−1487
modern IR technology, theory, practice and applications *(German)* 80−37088
monolithic Si detector array, design, processing and performance 77−74498
MOSFET Si:In(Ga) IR sensor, characts. 3 to 5 and 8 to 14 μm 77−74503
multichannel IR receiver performance 79−76596
multichannel system, MIK-48, for laser pulse energy meas. 79−17497
multichannel system, MIS-20, for laser pulse energy recording 79−17495
multidetector spectrometer for atm. temp. sounding 79−25365
multielement IR detector array technology 77−45893
multiple pulse detection in atmospheric turbulence 78−92974
nanosecond recorder of radiation at 10.6 μ wavelength 77−37990
narrow band gap semiconductor IR devices, advances 80−48464
near IR (1 to 2 μm) optical communications, colloquium, London, England (May 1980) 80−86040
near IR absorption analysis, differential compensation method 78−80819
near IR mapping spectrometer design and testing for Galileo Jupiter Orbiter 80−90336
Nernst-Ettingshauser effect based radiation detectors 79−58795
noise caused by turbulent flows, IR detector obs. 79−31799
non-coaxial aspherical IR optical system, automatic design *(Chinese)* 80−5810
nondispersive analyser Infralyt 4 dynamic characts. *(German)* 78−88676
nondispersive IR photometer selectivity improvement *(German)* 80−90880
nonlinear responsivity characterisation 80−77853
nonlinear tunnelling devices, photon detection, theory 79−6177
nuclear materials safeguards applications of far infrared radiometric techniques for the detection of contraband 80−73925
on-chip signal processing to overcome IR detector nonuniformities 77−79154
one-beam spectrophotometer with two radiation detectors 79−71536
optical communication systems *(Japanese)* 79−27406
optical fibre absolute power meas. thermistor sensor 78−65971
optical meas. of semicond. temps. *(French)* 79−35743
optical system design *(Japanese)* 78−55428
optical system design for low light and thermal imaging 79−37041
optical systems design, future computer program requirements 79−86260
optically pumped ruby far IR quantum counter 77−38001
optoacoustic detection using Stark modulation 79−94325
optoacoustic detector, background signal 80−31913
optoacoustic IR detector, micromodularisation 79−49291
optoacoustic laser radiation detector, spatial resolution 79−17493
infrared detectors continued
optocator system, precision measurements non involving contact *(German)* 80−82823
orbiting astronomical telescopes, IR detector cryogenic cooling requirements 78−96400
orbiting IR detector cooling by multimission solid cryogen cooler 80−86423
orbiting IR sensor systems interfering space radiation background 77−22011
ore Au content determ. 78−35076
p-i-n laser detector, Si, wavelength and temp. depend. characts. 80−13134
p-i-n photodetector under transient conditions, simulation and expts. 79−58793
p-i-n photodiode, for rocket-borne photometry of near IR airglow 77−13128
p-n junction photovoltaic diode, appl. as IR detector 78−86330
parametric up conversion process, coherence effect of generating radiations 79−76756
performance criterion of radiation detectors for thermal viewing systems 80−73459
performance evaluation of IR sensors and assoc. signal processing 77−49313
performance of nearly BLIP detectors 77−61121
photoconductive detectors, low-noise preamplifier 77−61124
photoconductive IR detectors, microwave-biased, noise performance 80−9037
photodetector, microwave biased, module construction 80−9038
photodiode array, self-scanned, for high dispersion astronomical spectrophotometry 78−45230
photodiode array, thermal behaviour *(French)* 80−37083
photodiode optimisation for higher temp. operation by excess volume reduction 79−2824
photographic films, Kalvar and Polaroid, damage threshold variation with spot size at 10.6 μm 79−36945
photometry, NDIR, partially layered detector, function and properties 80−105696
photon drag detector design and choice of semiconductor 80−57374
photon drag detectors, spectral responsivity meas. 78−12756
photoresistor, PbSe base, thermal stability over range 0°C to 60°C 80−73458
photoresistor detectors for optical investigation at high pressures 78−21217
photovoltaic, absolute detectivity determ. 77−13535
photovoltaic detector, antenna coupled 77−87824
Pioneer Venus Sounder Probe IR radiometer 80−67509
point contact and Schottky diodes, submm. mixing for heterodyne detect. 77−5910
point contact IR detector tunnelling and rectification characteristics, geometrical and multiple image interactions 80−57376
point contacts between identical metals, HF rectification at low temp. 80−105706
point-contact diode tunnelling and rectification rel. to electrode geometry 80−57378
point-contact diodes, use as far IR detectors 79−6180
polarized dielectric appl. *(French)* 79−51902
polyvinylidene fluoride film, pyroelec. camera tube for IR imaging, thermal diffusivity of Bi-Bi_2O_3 black layer 80−57369
portable ^{3}He detector cryostat for far IR 78−41352
practical IR optics, conference, Los Angeles, USA (Jan. 1978) 79−23085
preamplifier capabilities of CO_2 laser, for low level 10.6 μm direct detectors 77−53976
principles, and potential appls., book contrib. 78−37069
principles, appls. of main types, book contrib. 78−37068
probe, for internal interfacial wave motion meas. 79−18981
pulsed LED source detects objects on a conveyor belt 78−45700
PVDF pyroelectric detector *(Japanese)* 80−105714
PVF_2, plastic film sensors 79−99826
PVF_2 film pyroelectric radiation detector sensitivity *(Japanese)* 79−93222
pyroelectric, direct meas. of IR laser radiation multiphoton mol. absorpt. 80−102545
pyroelectric, radiometer appl. *(Czech)* 79−40611
pyroelectric, sub-100 ps, 10.6 μm damage threshold meas. 80−77859
pyroelectric, technology review 79−2827
pyroelectric, user's guide 79−35823
pyroelectric 80−82820
pyroelectric detector, performance evaluation method 80−82819
pyroelectric detector, temp. noise 78−89542
pyroelectric detector, temperature noise and dielec. loss 77−17975
pyroelectric detector, temporal exam. of IR pulses 78−37056
pyroelectric detector, use in horizon sensors 80−37086
pyroelectric detector array for IR and far-IR studies, improvement of sensitivity using digital averaging technique 79−49290
pyroelectric detector for subnanosecond CO_2 laser pulse meas. 80−78884
pyroelectric detector of transmitted power, coordinate-sensitive, for laser beam displacement determ. 79−75599
pyroelectric detectors, effect of substrate on current responsivity 80−73454
pyroelectric detectors and materials 78−49901
pyroelectric detectors for submillimetre waves 79−30545
pyroelectric ionisation upconvertor for IR detection 80−77860
pyroelectric polymers detector *(Japanese)* 80−105713
pyroelectric self-scanning IR detector arrays 79−58785
pyroelectric thin film detector, temp. fluctuation noise 80−77861
pyroelectric vidicon, CO_2 laser beam meas. 78−49907
pyroelectric vidicons for instrum. with IR lasers 78−59150
pyromagnetic, for Nd laser pulse detect. 77−82606
pyrometer, portable, noncontact temp. meas. *(German)* 80−42229
pyrometer performance parameters and applications *(German)* 80−86315
pyrometer using non-cooled $Hg_{1-x}Cd_xTe$ detector, 0-700°C range *(Polish)* 78−41313
pyrometry, high speed, review of problems and technology 77−26299
pyrometry, radiation laws and practical instruments *(German)* 77−5844
radiant flux gauge, IR optical materials for thermoradiation chambers *(Russian)* 80−48366
radiant heat flux detector, method of interpreting readings 78−211
radiant-flux detectors, comparison 79−35831

infrared detectors continued
radiation standards for source spectral emission and detector spectral sensitivity 77−39007
radiation thermometer with fibre-glass bundle, up to 1000°C *(German)* 79−35745
radiometer, distant-focused system, thin film thermal-profile meas. 77−169
radiometer optical head thermostabilisation structure 78−86316
radiometer with pyroelectric radiation receptor 80−101842
radiometric meas. of object true temp., 240-570K range 77−57326
rapid-scan polarising Michelson interferometer and InSb detector calibration 80−59305
ray-tracing techniques for infrared scanners 79−36984
receiver design principles 78−45714
red/IR oximeter operating cct. 78−28101
refracting objectives for 8 to 13 μm 80−86421
refractory metal thin film laser detector 78−41350
remote sensing appls., atm. effects *(German)* 77−9567
response and sensitivity of thermistor, thermopile and pyroelec. detectors 79−35832
review of detectors in 10 μm region *(Japanese)* 78−24862
RF and photodetection techniques at 10 μm, comparison 78−89539
ring laser, solid state, beat regime with nonlinear absorber, appl. to ang. vel. sensor *(Russian)* 78−1273
rocketborne IR spectrometer 78−81460
ruby, optical pumped, tunable quantum counter for far IR radiation 77−53977
Rydberg atoms, selective field ionisation, 300K blackbody radiation detect. 79−58787
Rydberg atoms transitions to detect far IR radn. 80−4763
satellite digital data, radiometric correction and equalisation 79−74587
satellite image plane scanner for earth observations 79−97436
satellite thermal imager for Defense Meteorological Satellite Program 79−97435
scanning background-limited IR sensor with adaptive threshold signal processing logic, performance 80−37082
scanning IR microscope, photodetector field of view correction using additional mirror 80−52304
scanning radiometer data interpretation 79−30541
scanning sensor optimisation, SNR, sensor sizing parameters 79−58792
Schottky barrier, nomographs for parameter evaluation, 77K 80−31870
Schottky barrier photovoltaic IR detector 80−9040
Schottky diode, point-contact, for detection of 10 μm radiation 77−37979
Schottky-barrier diode, heavily doped, without substrate, noise equivalent power 77−24618
Schottky-barrier diode IR capacitive mixing and detect. at high, intermediate or modulation freqs. 80−77864
self-oscillating Josephson mixer as submillimetric and far IR detector 77−38004
self-scanned photodiode array as multichannel spectrometric detector 80−73466
semiconductor, narrow band gap, characts. *(German)* 77−20356
semiconductor alloy, for appl. in IR detector arrays, comp. control 80−31872
semiconductor IR photodetectors, comparison of extrinsic and intrinsic devices, temp. limitations 80−73456
semiconductor superlattice microwave/infrared detectors 80−13138
seminar, optical radiation meas., San Diego, CA, USA (Aug. 1979) 80−86036
sensor figures of merit 80−86419
Shuttle IR Telescope Facility, detector performance conditions 79−5752
Si:In growth by Czochralski crystal pulling, characterisation for extrinsic IR detectors, focal-plane arrays 80−76168
signal processors, continuous-time, for IR surveillance 80−78781
signature classification system 80−86430
slow-acting IR radiaion receivers, meas. value correction *(German)* 80−105708
small-spot scanning IR spectrophotometer head 78−29133
solid state pyroelectric IR detector array 80−9036
solid thermal cond. and interface resistance meas. by radiation thermometry 80−86289
spacecraft, cooling down to 85K using solid cryogen cryostat. 79−54122
spectrometer, cryogenic, detector-preamplifier, optimization 80−95164
spectroradiometer systematic error calc. 79−75629
spot scan system for photodetector props. evaluation, 0.5-2 micron 79−2826
staring, military space and reconnaissance appln. 80−86406
steam fraction determ. in flowing air/stream mixtures by meas. of IR rad. attenuation 80−75010
step-stare IR sensor design for aerospace vehicle detection 80−86418
stratospheric composition, IR meas. radiometer, H_2O vapour profile 79−8718
submillimetre and IR review *(Russian)* 80−72773
submillimetre planar sandwich receiving antenna 79−40609
submillimetre wave heterodyne radiometry, for upper atm. comp. meas. 78−49183
submillimetre wavelengths, techniques and devices for the detect. and sensing of radiation 78−93759
submillimetre waves and applications, conference, Guildford, England (1978) 79−31916
submillimetric low-noise Schottky-barrier coherent detector materials 77−37995
subminiature Schottky-barrier diode video detection and heterodyne mixing 77−37996
superconducting, space appl. 80−85836
superconducting double multivibrator used as near- and medium-infrared radiation detector *(German)* 80−90892
superconducting microbridges, basic props. and appls. 77−26400
superconducting normal electron tunnel elements, interaction with 0.6-40 μm EM radn., radn. detection appl. *(German)* 79−24103
superconducting point contacts, sub mm band mixer 77−49774
superconductive FIR detectors, Josephson-junction direct devices and transition edge bolometers, review 80−77865
superconductivity, space applications 80−41694
surface temperature contactless meas. instrument 78−57946
survey of different detector characts. 77−10106
system limitations 78−77988
systems and equipment, design and appls. *(German)* 80−52316
techniques and appls., conf., Los Angeles, CA, USA (1978) 79−2822
technology, detector selection, trends beyond 40 μm 77−53974
technology, radiator and detector designs *(German)* 80−22430
technology and technical anal., book 78−37066
technology fundamentals 77−61120
technology utilisation, symposium, San Diego, CA, USA (Aug. 79) 80−86037
temperature meas., minimum resolvable temp. difference charts 77−82509
temperature meas. devices developments *(German)* 80−8986
temperature units, USSR special standards 77−30148
test facilities 77−65647
TGS, capacitive bolometer effect in paraelectric phase 77−57389
TGS, proper and improper ferroelec., direct meas. of figure of merit 79−95711
TGS, pyroelec., permanent polarisation due to X-rays, optimum non-ferroelec. behaviour 77−41684
TGS, pyroelectric figures of merit 77−59519
TGS pyroelectric detector, compared with W-C point contact, appl. to temporal coherence meas. of HCN laser 80−31871
TGS thin film pyroelectric detectors, far IR absorption 77−38010
TGS vidicon tube, used with optical multichannel analyser as IR detector 78−86329
thermal IR scanner meas. technique for cooling water temp. 80−40947
thermal radiation detector sorbent test 79−29403
thermistor bolometers, reliability anal. 78−24795
thermoelectrically cooled, features and appls. 79−2828
thermographic diagnosis, high resolution dynamic method, detector system 80−41167
thermometer, non-contact *(Polish)* 80−90845
thermometer and pyrometer calibration methods and standards 79−88958
thermometers, calibration and standards 79−85141
thermometry, temp. monitoring and thermal inspection 78−45622
thermophotographic paper for recording long-wavelength IR laser radiation 79−40636
thermopile pyranometer, accelerated response tests 77−10110
thermopiles appl. thin-film commercial detectors specs. and appl. 80−47104
thin-film techniques appl. *(German)* 78−62226
thin-film thermometry, efficiency in meas. radiant flux density of pulsed lasers 77−38967
three-dimensional thin pyroelectric IR detector simulation 80−57375
three-level quantum counters for far IR radiation 77−53977
tightness control by IR gas method 79−66236
time-magnifier, IR-range, construction 80−13139
tracking receiver with holographic information processing 78−78970
Trombay IR pneumatic detector, operational characteristics 79−12843
turbine blade surface temperature meas. IR pyrometer 77−17983
TV system for building heat loss meas. 77−45837
two-scatter-plate low-speckle-noise integrator for atmospheric laser beam transmission meas. 80−90252
United States Air Force infrared reconnaissance set 78−81458
upconversion to visible, detect. method for astronomy 78−45240
utilisation of IR technology, conf., San Diego (1977) 78−77984
very-fast-response uncooled photodetector based on intraband μ-photoconductivity 79−30562
visual micropyrometer 28 kV power source features *(Russian)* 78−12701
whisker diodes sub-MM receivers, antenna characts. 78−12755
wide-gap diode detectors of IR radiation, positive feedback 78−24863
wideband 1064 nm laser communications detector evaluation 77−18097
$AgGaS_2$, IR signal detection by mixing with dye laser radiation 77−88846
Al-Ge photovoltaic cell, charact. 79−40612
AlGaSb, growth and characts. for 1.0-1.8 μm heterojunction devices 78−6870
AuSi, response characts. obs. 80−52308
$Ba(NO_2)_2.H_2O$, pyroelectric IR radn. detector 79−80685
$Ba_{0.25}Sr_{0.75}Nb_2O_6$, fast-response pyroelec. cryst. detector 78−49904
CO concentration meas. in coal pulverising plant, IR gas analysers 80−89572
(Cd,Hg)Te, photoconductive detector, uncooled, for 8-14 μm region 80−31868
Cd_xHg_{1-x} Te, photodetectors, recomb. processes, photoconductive decay obs. 79−38129
Cd_xHg_{1-x} Te type, props. and manufacture *(German)* 77−2693
CdHgTe detectors, high-performance, for thermal imaging 79−40616
CdHgTe detectors for CO_2 laser appls. 79−40615
(CdHg)Te photoconductive detector, thermal figure of merit limit 78−89540
(CdHg)Te photoconductive IR detectors, ultimate detectivity 79−58788
CdHgTe photoelectromagnetic detector for 10.6 μm radiation, non-cooled, performance 80−82818
$Cd_{0.2}Hg_{0.8}Te$ IR photoresistors/detectors, lateral geometry requirements *(German)* 79−93213
$Cd_{0.2}Hg_{0.8}Te$, ion implantation doping for realisation of IR detectors, responsivity meas., ion range straggling 80−73452
$Cd_{0.2}Hg_{0.8}Te$ recrystallisation for supercooled IR detector production *(German)* 80−86403
$Cd_xHg_{1-x}Te$, epitaxial layer p-n junction, current-voltage characteristics of photovoltaic detectors, 1 to 15 μm 80−86407
$Cd_xHg_{1-x}Te$ graded-gap epitaxial layers, photocond. meas. 0.5 to 6 μm, detector appl. 79−60869
$Cd_xHg_{1-x}Te$, IR detector appls., prep., elec. props. *(German)* 78−86332
$Cd_xHg_{1-x}Te$, narrow gap semiconductor, charge transfer device for IR detection in 3-5, 8-15 μm bands *(French)* 79−30563
$Cd_xHg_{1-x}Te$ photoconductive detectors, 77 to 300K, normalised thermal figure of merit 80−31878
$Cd_xHg_{1-x}Te$ photodiode, high efficiency, energy level diagram 77−15891
$Cd_xHg_{1-x}Te$ photodiode, IR responsivity and detectivity 78−19139
CdSb:Al, p-n junction formation by laser emission, photoelectric effects *(Russian)* 80−70815
CdTe-Ge heterojunction, photoelec. props., sensitivity in near IR region *(Russian)* 77−69405
$CuInSe_2$ polycrystalline thin film anomalous photovoltaic effect *(German)* 78−68102
D_2O leak detection, on-line infrared analyzers, CANDU report 78−82038
$Fe_3B_7O_{13}I$, improper ferroelectric, dielectric props., IR radiation pyroelectric detection 80−80711

infrared detectors continued
$Ga_{0.72}Al_{0.28}Sb$ avalanche photodiodes, ionization coeff. 79−17488
GaAs, electroabsorpt. avalanche photodiode, waveguide detector for 1.06 μm 78−16842
GaAs, electroabsorpt. avalanche photodiode waveguide detectors 78−65965
GaAs, electroabsorpt. avalanche photodiode waveguide detector, freq. demultiplexing 79−17486
GaAs extrinsic photoconductor detectors, DC and microwave bias comparison 77−37998
GaAs injection photodiode IR radiometer 79−75597
GaAs, p-i-n avalanche photodiode, temp. depend. characts. 79−35835
GaAs, photocapacitive MIS IR detector, spectral response, noise characts. 80−75644
p-GaAs photon drag optical rectification detectors, performance in 2 to 33 μm range 79−35834
p-GaAs photon-drag photodetector, responsivity comparison with p-Ge detector 79−11185
GaAs Schottky barrier diode, detection down to 70.5 μm 77−10103
GaAs single-cell radiometer for artificial satellite measurement system 80−13147
GaAs:Cr, IR spectral detectivity 78−70184
GaAs:Cr, plane-parallel plate subjected to laser illumination, photocond. meas., photodetector for far IR 79−93221
GaInAs, efficient photodiode for near IR detection 78−16848
$Ga_{0.47}In_{0.53}As$, homojunction avalanche photodiode, exam. of props. 78−37072
$Ga_{0.47}In_{0.53}As$ homojunction photodiode, avalanche photodetector for 1.0-1.6 μm region 79−6179
$Ga_{0.47}In_{0.53}As$, photodetector applications 80−95140
$Ga_{0.7}In_{0.3}As$ photodiodes, fibre optic appls. 79−40613
GaInAsP on InP substrate, epitaxially grown, fabrication of avalanche photodiode 78−37071
GaInAsP-InP avalanche photodiode, fabrication and characts. 78−54454
GaInAsP-InP avalanche photodiode IR detectors, 1.1 to 1.3 μm, fibre optics appls. 80−14360
GaInAsP-InP lasers and detectors, for fibre optic communications at 1.0-1.6 μm 79−3803
GaInSb, Be ion implantation, device appl. 80−24478
$Ga_xIn_{1-x}Sb$ p-n junction photodiode fabrication, sensitivity as 1 to 2.5 μm detectors *(Japanese)* 80−52311
n-GaP low absorption monitors for HF laser 79−31964
n-GaP, optical rectification due to free carriers, detector appl. 77−10967
GaSb mesa photodetectors with very high quantum efficiency between 1.3 and 1.6 μm 80−47102
Ge and Ge-diamond bolometers operated at 4.2, 2.0, 1.2, 0.3, 0.1K, design and construction 80−77868
Ge, based on carrier photon drag 77−74507
Ge cryogenic bolometer, for 20 to 500 μm spectral region 78−70187
Ge far IR photoconductive detector speed, limitation 79−30550
Ge IR photon drag detector, photosensitivity spectrum 79−12853
Ge, intrinsic photodiode as IR detector, fabrication and performance 77−57388
Ge MIS photocapacitative IR detector 80−47106
Ge, p-i-n avalanche photodiode, temp. depend. characts. 79−35835
p-Ge photon drage detector, performance in 2 to 33 μm range 79−35834
Ge photon-drag detector submillimetric-wave performance 79−30547
Ge surface ion implanted far IR composite bolometers 79−30549
Ge:Au, based on Ga impurity photoconductivity, characts. *(German)* 78−82036
Ge:Be for far IR astronomical obs. from space platform, 30-55 micron 79−5754
Ge:Cu, based on Ga impurity photoconductivity, characts. *(German)* 78−82036
Ge:Ga, for far IR astronomical obs. from space platform, 50-120 micron 79−5754
Ge:Ga, uniaxially stressed, far IR photocond. meas., appl. in IR detection 78−10496
Ge:Ga photoconductor detector performance in low optical background 77−37999
Ge:Ga photoconductors in low IR backgrounds 79−63305
Ge:Hg photoconductive detector, laser damage thresholds calc. 78−90443
Ge-metal Schottky barrier photodetectors, near IR interband transitions and optical parameters 80−73449
n-Ge-metal Schottky barrier contacts, IR optoelectronic props., quantum detector appls. 80−75640
Ge-$Pb_{1-x}Sn_xTe$, amorphous/crystalline heterojunction, rectification props., IR detector appl. *(Japanese)* 78−60197
He-cooled LWIR spectrometer for exo-atmospheric airglow measurement, calibration 79−97450
(Hg,Cd)Te detector array, 72-element, 8-12 micron, performance, FLIR system appl. 79−2829
(Hg,Cd)Te photodiode for 2 μm IR detection 77−82603
(Hg,Cd)Te photodiode IR detectors, planar technology 80−9043
(Hg,Cd)Te photodiodes, wide-bandwidth 10.6 μm IR heterodyne detect. 80−9042
(Hg,Cd)Te photovoltaic detector, 5 μm, direct coupling with CCD multiplexer 77−83987
HgCdTe, for 8-14 μm range, review *(Italian)* 78−54451
HgCdTe IR photovoltaic detectors, imperfections and surface conditions using electron induced current technique 79−67385
HgCdTe, in skin temp. meas., influence of cosmetics and ointments on spectral emissivity 77−9285
HgCdTe, nonlinear responsivity characterisation 80−77853
HgCdTe photodiode IR detector, selection 79−58791
HgCdTe reverse-biased photodiodes for wideband appls., excess noise 80−107876
HgCdTe Schottky barrier diode and n-p diffused junction IR detectors, comparison 80−9039
HgCdTe short-wavelength IR photovoltaic detectors, radiation testing 80−37084
HgCdTe solid solution photodiode for CO_2 laser active medium study 80−95868
HgCdTe-CdTe IR detector arrays, 3 to 11 μm, fabrication techniques 80−9041
$Hg_{1-x}Cd_xTe$ and $Pb_{1-x}Sn_xTe$ quantum detector selection for 8 to 14 μm 79−80681
$Hg_{1-x}Cd_xTe$, for appl. in IR detector arrays, comp. control 80−31872
$Hg_{1-x}Cd_xTe$, high-pressure reflex growth technique, IR detector appl. 77−40347
infrared detectors continued
$Hg_{1-x}Cd_xTe$ IR detector technology 78−77989
$Hg_{1-x}Cd_xTe$ IR focal plane status and performance 78−77987
$Hg_{1-x}Cd_xTe$ IR photodetectors for night vision appl. 80−22429
$Hg_{1-x}Cd_xTe$ implanted detector 8 to 14 μm, performance, p-n junction characts. 77−15941
$Hg_{1-x}Cd_xTe$, material capabilities for 1 to 1.3 μm room temp. photodiodes 78−24859
$Hg_{1-x}Cd_xTe$, nonlinear optical effects 80−14389
$Hg_{1-x}Cd_xTe$ photoconductive IR detector, optimum bias attainment with batteries 79−58789
$Hg_{1-x}Cd_xTe$ photodiodes, long cutoff wavelength, effect of trap tunnelling on IR detector performance 80−73451
$Hg_{1-x}Cd_xTe$ Schottky barrier photodiodes, 3 to 5 μm and 8 to 12 μm 80−13144
InAsSb, Be ion implantation, device appl. 80−24478
InAsSb/GaSb broad-spectral-band IR detector, backside-illum. heterostructure approach 80−73450
$InAs_{1-y}Sb_x$, epitaxial heterojunction photodiodes, IR detector appls. 77−79155
$In_{0.53}Ga_{0.47}As$-InP avalanche photodiode structure for 1 to 1.6 μm region 80−98978
$In_xGa_{1-x}As$, planar photodiodes made by VPE 79−49286
InGaAsP avalanche photodiode, 1.3 μm, noise performance, −190°C 80−57370
InGaAsP, dual-wavelength demultiplexing photodiode 79−63304
InGaAsP IR heterojunction photodiode detector 79−21813
InGaAsP quaternary alloy IR heterojunction detectors, props. 79−2823
InGaAsP:Be ion-implanted avalanche photodiode, struct. and characts. 79−17487
InGaAsP-InP high-gain heterojunction phototransistor 80−103745
InGaAsP-InP photodiodes, microplasma-limited avalanche multiplication at 1 to 1.3 μm 79−26128
InGaAsP-InP photodiodes antireflectively coated with InP native oxide 80−13137
$In_{1-x}Ga_xAs_yP_{1-y}$-InP photodetectors, high-efficiency with selective wavelength response, 0.9-1.7 μm 79−21810
InP, far IR LPE photodetector performance 79−30546
InS, liq. He temp., Fourier interferometric spectrometer, 714 to 1667 μm 77−83765
InSb charge injection device IR imaging arrays 77−79962
n-InSb electronic bolometer, appl. in system for millimetre and submillimetre wave detection 78−24860
InSb fast response submm. detector 78−89541
InSb, IR detector, for pulse radiolysis, reversible component in response time 78−41353
InSb IR detector array, AES anal. of localised contaminants at interfaces 77−57391
InSb IR detectors, integrating premaplifier 80−90337
InSb, in skin temp. meas., influence of cosmetics and ointments on spectral emissivity 77−9285
InSb, low defect crystal growth by InN doping, IR detector appl. 80−20780
InSb n^+-p and p^+-n photodectors fabrication by S and Be ion implantation 78−49906
p-InSb, photovoltaic operation, theoretical anal. 79−224
InSb/$Pb_{0.79}Sn_{0.21}Te$ photodiodes, two-colour sandwich detector 77−82602
InSb-PbSnTe sandwich two-colour IR detector 78−45692
$LaBr_3$:Pr, continuous wave and pulsed laser pumped Pr IR quantum counters 79−93219
$LaCl_3$:Pr, continuous wave and pulsed laser pumped Pr IR quantum counters 79−93219
$LiIO_3$ crystals with optical freq. conversion, IR detect. characts. 77−87832
$LiIO_3$, IR radiation parametric upconversion with pulsed ruby and CW Ar lasers 77−72026
$LiNbO_3$ crystals with optical freq. conversion, IR detect. characts. 77−87832
$LiNbO_3$ intracavity upconvertor for IR detect., limits to low noise equivalent power operation 80−74430
$LiTaO_3$ monolithic pyroelectric array, IR detectors 80−77857
$LiTaO_3$ pyroelectric detectors, temp. noise effects on performance 77−79156
$LiTaO_3$/CCD hybrid focal plane, IR imaging and detection, crosstalk 80−77856
Na vapour, quantum counter, IR detection 78−30016
Nb Josephson point-contact far IR detector props. 79−30543
Nb point contacts, Josephson effects in far IR, high freq. behaviour 79−1643
Nb superconducting point contact, high freq. props. in far IR 80−54840
Nb thin film microbridge, video detection of far IR radiation *(Japanese)* 80−97038
Ni-NiO-Ni, integrated MOM junctions, characts. at DC and optical freqs. 78−41349
PLZT, light scattering, IR laser radiation recording 78−4695
PLZT pyroelectric detectors, fast response to MW CO_2 laser pulses 79−54187
PLZT pyroelectric detectors, piezoelectric oscillations, in response to CO_2 laser pulses 79−61305
(Pb,Sn)Te, (Pb,Sn)Se IR detector diodes, junction resist. comparison, minority carrier lifetimes 78−24858
Pb-SnTe semiconductor, spectral response calcs. 77−87826
$PbHPO_4$ cryst. for pyroelectric detector 77−82600
$Pb_{1-x}Hg_xS$ film, IR detector material, struct. and IR props. 78−26775
$Pb_{1-x}Hg_xS$, soln. growth, variable gap film for i.r. detector 77−1796
$Pb_{0.97}Hg_{0.03}Te$ photovoltaic detector produced by Sb^+ ion implantation 80−82821
PbS, chem. deposited thin film, effect of morphological struct. on photosensitivity 80−70760
PbS, chemically deposited film, photosensitivity, effect of morphological struct. 79−82647
PbS film detector performance, review 77−53975
PbS IR staring mosaic detector array module development 80−86413
PbS mosaic array pulse-bias modulation 80−86414
PbS-Si heterojunction, related optical and IR detector props. 80−77866
PbS-Si heterojunction detector, direct injection readout 80−4765
PbS-Si p-n heterojunction characts. and operation 78−52075
PbS_xSe_{1-x}, Schottky-barrier IR detector, comp. tuning 78−12752
PbSe, pollution detection and control appl. 78−24378

infrared detectors continued
$Pb_{0.93}Sn_{0.07}Se$ crysts., sublimation growth, controlled carrier concs. for IR lasers and detectors 77−52237
$Pb_ySn_{1-y}Se$, multispectral photovoltaic IR detectors 80−105710
PbSnTe detector and preamplifier modules for heterodyne detection of CO_2 laser radiation 78−32875
PbSnTe detector arrays for thermal imaging 79−37047
PbSnTe, for 8-14 μm range, review *(Italian)* 78−54451
PbSnTe IR detectors, spectral response depend. on surface carrier concentration *(Japanese)* 79−44929
PbSnTe long-wavelength IR photovoltaic detectors, radiation testing 80−37084
PbSnTe/PbTe inverted heterostructure mosaics, long wavelength, energy gap-Fermi level temp. depend. 79−85182
$Pb_{0.8}Sn_{0.2}Te$, film photodiodes, quantum efficiency 79−75596
$Pb_{1-x}Sn_xTe$ and $Hg_{1-x}Cd_xTe$ quantum detector selection for 8 to 14 μm 79−80681
$Pb_{1-x}Sn_xTe$, cryst. growth rel. to IR detector fabrication 77−85911
$Pb_{1-x}Sn_xTe$ film, sputtered, for IR detector appl. elec. and optical props. 80−35084
$Pb_{1-x}Sn_xTe$ IR detector, ESCA meas., surface leakage currents 77−20402
$Pb_{1-x}Sn_xTe$, impurity defused IR detector, spectral response depend. on impurity conc. *(Japanese)* 78−58036
$Pb_{1-x}Sn_xTe$ LPE film IR detector performance 80−86422
$Pb_{1-x}Sn_xTe$, VPE crystals, X-ray diffr. data interpretation 77−15712
$Pb_{1-x}Sn_xTe$-PbTe, amorphous/crystalline heterojunction, rectification props., IR detector appl. *(Japanese)* 78−60197
$Pb_xSn_{1-x}Te$, for appl. in IR detector arrays, comp. control 80−31872
$Pb_xSn_{1-x}Te$, RF sputtered film IR detector, photocond. response speed improvement by annealing 79−58790
PbSnTe(Se) Schottky barrier diode and n-p diffused junction IR detectors, comparison 80−9039
PbTe detector arrays, planar oxide-insulated 79−40614
PbTe, film photodiodes, quantum efficiency 79−75596
p-PbTe MIS capacitors 5 μm IR detector appl. 78−52101
PbTe photovoltaic detector, detectivity limits 80−105709
PbTe, semiconductor polycrystalline thin films, low-frequency 1/f noise meas. 80−15629
$Pb(Zr, Ti)O_3$ ceramics for IR detectors, pyroelectric characts. 79−56736
$PbZrO_3$ pyroelectric detector, low temp. behaviour, expt. 80−31869
Pr based, IR quantum counter imaging system, resolution, sensitivity 79−81541
PtSi Schottky-barrier monolithic IRCCD focal plane 80−86427
p-Si, compensated with radiation centres, current responsivity and detectivity 79−17492
Si, dopant survey for IR detector appl., 2 to 2.7 and 3 to 5 μm 77−15433
Si extrinsic IR detectors, As doped, low-level γ-ray irrad. effects 80−37085
Si extrinsic IR monolithic focal plane array detectors, I-V characts. of p^+-p-p^+ and n^+-p-p^+ structs. 80−77863
Si extrinsic photoconductive IR detector, counterdoping scheme 78−49896
Si extrinsic photoconductive IR detectors, VLF behaviour 78−81542
Si, free carrier absorption 78−37060
p-Si, heavily doped contact layers on IR detectors, IR transmissivity 80−108190
Si IR 'two-colour' detector, packaging approaches, review 77−10108
Si inversion layer, far IR photoresponse 77−38002
Si low-temperature far and middle IR bolometers 79−71529
Si, MIS photocapacitive IR detector 78−62223
Si, neutron transmutation doping for IR detector material 80−15136
Si, p-i-n avalanche photodiode, temp. depend. characts. 79−35835
Si, photocapacitive MIS IR detector, spectral response, noise characts. 80−75644
n-Si, photocond. of negative donor ion states, for far IR detect. 77−59299
Si, photodiode, 1.06 μm range, neutron and γ-irrad. effects 79−97433
p-Si, photon drag detection 78−43440
p-Si, photon drag detector, performance in 2 to 33 μm range 79−35834
Si position-sensitive detector for CW and pulsed laser beams 80−78883
n-Si shallow impurity states for far IR heterodyne detection 77−38005
Si vidicon, performance at low signal levels, astronomical spectroscopy appl. 77−22085
Si vidicon optical detector, laser data acquisition/analysis system 78−58041
Si:As, neutron damage mechs. in IR detectors 78−30668
Si:As detector, high-low junction contact at low temp. 77−39925
Si:As photoconductive detector for IR astronomy, responsivity and system noise 80−51665
Si:Au, impurity photocond., for IR electrophotographic system 77−24589
Si:Au planar extrinsic IR detector, use of multiple internal refl. for increased sensitivity 80−77862
Si:Ga (Al)(In) extrinsic detector material props. 77−89797
Si:In, MOSFET device structure for characterising imperfection centres 79−73595
Si:In, neutron irrad. to compensate for residual B, photocond., IR focal plane array 78−67727
Si:In extrinsic detectors, compensation of residual B by neutron transmutation 78−281
Si:In extrinsic detectors in IR imaging systems, focal plane temp. stability requirements 79−94324
Si:In extrinsic IR detectors with closely compensated residual impurities, model of responsivity temp. depend. 80−73453
Si:In extrinsic IR detector material with high responsivity compensated by neutron transmutation, float-zone growth 80−75597
Si:P photochronic detector, IR detect. using delayed breakdown 79−58786
Si:S, background-limited photodetector near 77K 77−122
Si:S IR detectors, performance and elec. transport props. 78−45702
Si:Se, detector for 3-5 μm appl. development 79−35825
p-Si-Au, Schottky barrier IR detector 77−37985
n-Si-Cr, Schottky barrier IR detector 77−37985
SnO_2 far IR photoconductivity response obs. 77−38000
SnO_2:Sb, prep. and material characts. for far IR detector 78−4697
$SrF_2:Sm^{2+}$, cryst., i.r. radiation, high-speed detect. appls. 77−4677
$Tb_2(MoO_4)_3$, improper ferroelectric, dielectric props., IR radiation pyroelectric detection 80−80711
infrared detectors continued
$Tb_2(MoO_4)_3$, proper and improper ferroelec., direct meas. of figure of merit 79−95711
Te detector for CO_2 pulsed laser radiation, using photon drag and optical rectification 78−21216
p-Te photon-drag detectors for CO_2 lasers 77−5911
TeO_2 noncollinear IR tunable acousto-optical filter 79−23086
p-Tl_xSe_y, IR bolometer detector performance 78−24856
VO_2, film, visualisation of microwave and IR radiation 80−5839
W-C point contact, compared with TGS pyroelec. detector, appl. to temporal coherence meas. of HCN laser 80−31871
W-Ge whisker diode, 337 μm IR detector *(French)* 78−8445
W-Ni point contact diode, IR antenna characts. 77−49772
W-Ni point contact diode detectors at 10.6 μm, mech. and props. 78−24861
W-Ni point contact diode fast acting detector for modulated CO_2 laser beams 79−3730
Zn_3P_2, photocond. and Dember effect meas., 0.5 to 1.2 μm, possible detector appl. 78−91721

infrared imaging
8.5 m IR imaging system performance in degraded atmospheres 77−19445
aerial photography for agriculture, potato blight detection 80−13174
aerothermodynamic test techniques at AEDC von Karman gas dynamics facility 80−14863
air-sea search and rescue appl. of line scanner imagery 79−21519
airborne IR system performance 78−82039
airborne system, resolution, object contrast depend. 77−2285
aircraft IR segmented composite window design 80−106621
applications, conf., London, England, June (1977) 78−58042
aspherical lens and surface evaluation 77−39019
aspherical surface diamond turning machine development 80−1372
astigmation and spherical mirrors 78−33804
astronomical applications of IR TV imaging 79−92678
astrophysical applications of image restoration, conf., Bordeaux, France (Mar. 1979) 80−41935
atmospheric remote sensing, theoretical problems 79−80052
atmospheric turbulence effects on optical and IR image form. *(French)* 80−46257
ATP-12M infrared imaging system (USSR), body temperature meas. 80−67280
automatic target screener for tactical thermal imaging system 79−32083
autoscreener with secondary screener for target screening 79−32082
background suppression algorithm 78−77985
basic parameters of thermal imaging system, effect of radiation detector lag 78−89544
benzothiazoline products, bicondensed, for thermographic recording 79−24767
black body radiation IR imaging system 78−21220
blackbody radiant flux calc. simplification 80−106710
blood perfusion measurement by thermography 80−56167
breast cancer 30 GHz and 68 GHz telethermography *(French)* 80−3765
breast cancer screening by thermography, progress and prospects 77−48915
breast disease, importance and limitations of thermography in diagnosis and treatment *(French)* 78−7419
breast examination by radiography, thermography and US, reviews *(French)* 78−7472
breast examination methods including radiography, thermography and cytology, review 78−3656
breast pathology, liq. cryst. thermography *(French)* 78−7420
breast thermograms, automated diagnosis of abnormality using minicomputer 77−21593
breast thermography, use of liq. cryst. sheets 80−41166
breast thermography vein-finding algorithm 78−40393
building heat loss diagnostics, IR image evaluation requirements 80−86424
C-CD, modelling and appl. of HgCdTe MIS struct. 78−80058
C-CD appls., book contrib. 78−38026
C-CD multiplexer, direct coupling with 5 μm (Hg,Cd)Te photovoltaic detector 77−83987
C-CDC image sensors, operation *(German)* 78−63190
calibration curve of digital thermal field analyzers and method of obtaining it 80−27293
cancer detection by microwave thermography 78−24172
cancer diagnosis, breast, computer analysis *(Japanese)* 77−5099
cancer thermographic diagnosis enhancement by US irradiation 79−79614
cancerous mouse hyperthermia meas., microwave, IR and thermocouple methods *(French)* 80−3768
cathodoluminescence topography recording, crystal lattice defects appl. 78−22201
centimeter- and millimeter-wave thermography−a survey on tumor detection 79−100690
change detection using IR imagery 79−32080
charge injection and CCD focal plane arrays 77−39088
charge transfer device imaging arrays 78−77990
charge transfer devices with Si detectors 77−83991
cholesteric liquid crystal, pseudoencapsulated film, selective light scatt. 77−16289
cholesteric liquid crystal IR visualizer, wide dynamic range 77−79955
cholesteric liquid crystal panel, energetic sensitivity, as IR registrator *(Russian)* 79−89995
cholesteric liquid crystal photographic plate, for images in IR, extreme characts. *(Russian)* 79−89994
clinical microwave focusing thermography 80−3771
clinical thermography, eval. of distortion 80−3750
cloud determination, SMS IR data appl. during GATE 80−31113
coherent fast IR wavefront aberration sensor interference problems 80−74499
colour-IR photographic filters 77−71396
compact four-mirror optical system design and testing 79−23049
composite materials, thermographic technique, for examining damage extent 79−43540
composite thermal/visual display superposition technique 78−77992
computer tomographic thermography, numerical simulation 79−83889
computerised breast thermographic interpreter, comparison with human interpretation 77−81547
computerised pattern recognition for breast cancer screening 77−21652

infrared imaging continued
continuous zoom forward-looking IR optical system design and implementation 79−23046
coronary artery blood flow thermographic visualisation during by-pass surgery 79−53265
crack detect. using IR scanning 79−83400
CRT thermal image recording, scale and luminance distortion elimination 79−50398
data processing of thermal images, optimal projection to human eye 78−38038
detection techniques, for low background satellite expts. 78−49343
detector peak wavelength selection, optimum performance 77−2692
development trends, optical-mechanical, electronic and solid-state technologies *(Czech)* 79−97383
devices and appls., conf., Los Angeles, CA, USA (1978) 79−2822
devices and appls., conf., Washington DC, USA, 1978 79−32085
diagnostic methods, non-invasive, seminary, Brno, Czechoslovakia (Sept. 1976) *(Czech)* 77−17001
digital processing technique appl., thermal imager pictures delining 80−106466
digital thermal field analysers 78−82034
digital thermal inertia image construction and interpetation 78−4001
digital thermal IR scanner data temporal correlatibility 77−78525
digitisation and analysis of thermographic images 77−16960
direct view type night vision aids 79−72711
doped Si detector photoresponse measurement problems 78−37000
dual-channel ratio thermograph counteracting skin emissivity errors 77−40892
Earth resource thermal imaging by airborne system, possible LED use 78−93010
Earth scene dynamics, satellite-borne mosaic sensor performance 80−90321
Earth surface, i.r. remote sensing *(German)* 77−9567
ecosystem succession detection by aerial IR photography 78−81459
electron beam high resolution thermal wave microscopy 80−95158
electrosurgical dispersive electrodes, thermal performance evaluation method 79−74735
emissivity meas. of good heat conducting materials *(French)* 80−103507
energised polluted insulators, temp. distrib. meas. 79−97385
evaporographic image, formation and recording, anal. 79−32066
evaporographic recording for far IR plasma diagnostics 78−5929
fabrication of IR optical components, diamond turning appl. 78−5590
far IR optics testing and specification for night vision thermal imaging 80−48440
far IR technology and applications, conf., Reston, USA, (Apr. 1977) 78−45711
far IR two-dimensional plasma interferometry with evaporographic and pyroelec. recording 77−39468
fast response system with 50 element detector 78−18064
fibre composite structure, thermal field techniques for NDT 80−66737
fibreglass laminates, thermal NDT using liq. crysts. 80−93709
flood-plain delineation by multispectral data analysis 77−73885
flow meas., IR camera for separated flow regions diagnosis in wind tunnels 80−10335
fluorescent screens for thermophotography 77−171
focal plane IR detector arrays for planetary missions 80−85862
focal planes in intrinsic semiconductors 78−37994
fog in Cheddar Gorge, England, oblique false-colour photograph 78−57290
forward looking IR system, radiometric accuracy 77−82604
forward-looking IR sensor image segmentation by maximum likelihood parameter estimation 80−99662
forward-looking IR system improvement by aspheric elements 79−23048
forward-looking IR type optical system design programs 79−23047
frost prone areas, Niagara fruit belt, defined by thermal imagery 79−25314
geothermal research by IR scanning, image processing 77−64458
glass, IR transmitting, as optical material in passive systems, preparation and characterisation 79−23034
glasses for 8 to 12 μm thermal imaging systems, Ge-As-Se glass props. 78−25935
gradient index fibre image intensifier system 80−14484
Gulf Stream meanders, GOES IR meas., time series anal. 79−34842
Gulf Stream rings distrib. and number, 1975 spring period 79−39725
Hadamard transform astronomical IR imaging device 77−13240
haemangiomata betatherapy, diagnostic value of thermography *(French)* 79−5356
hand pathology, role of thermography 80−8120
heat-camera system for panorama spectroscopy of extended laser medium 80−1257
high resolution image prod., use of totally computer controlled telescope 80−72785
holographic reflector, computer-generated, for IR image construction 78−25814
holographic scanner imaging systems, active and passive, 8 to 13 μm, characts. 80−91755
hybrid IR/CCD focal planes, performance, appls. 79−3798
IC thermal analysis by IR microimager 78−45619
image conversion tube, low-cost apparatus for teachers 79−71207
image processing technique appls. to scanned radiometer data of stellar sources 77−49312
image registration and differencing by coherent optical pattern recognition 80−99648
image segmentation based on second-order grey level statistics 80−99663
imaging systems design, operation and performance, applications 80−47111
industrial appl. *(German)* 80−13072
industrial IR detector markets and device limitations 80−86432
inflammatory joint disease assessment by quantitative thermography 78−31881
infrathermograms properties and evaluation in nonblack radiators *(Hungarian)* 78−65922
inland wetland photointerpretation evaluation, cell analytical method 79−29898
insulating material monitoring by electroluminescent screens, defect imaging 78−53083
integrated focal plane arrays for thermal imaging 77−19448
intrinsic semiconductor IR detector array data acquisition system 78−77991
invisible information imaging techniques 77−5819
infrared imaging continued
IR non-destructive testing of bonded materials, theory and practice 80−93708
IR photographic methods 79−93243
land and sea surface temp. fields, seasonal vars., NOAA 5 satellite IR obs. 78−85676
land use classification by thermal IR scanning imagery 77−26422
large-screen visualiser using ZnS-CdS phosphor coating 78−18070
laser components, fast thermal monitoring system 79−80614
laser nozzle, chemical, temperature profiles meas. 80−14376
laser pulse recording, semicond. ionisation-type photographic system 78−49903
laser radiation visualiser 77−38974
laser tracking system testing by 1 m unobscured IR collimator 80−78991
lasers, imaging methods for measurements of 3-dim. energy characts. 79−76842
lens system, large diameter, for pyroelec. vidicon 80−19086
Limb Infrared Monitor of Stratosphere (LIMS) radiometer, design and performance, expt. goals 78−61601
line scanner, Reconofax XIII A, improved recording system using LED 79−25335
liquid crystals, cholesteric, radiation visualisation instrum. 80−13071
low light and thermal imaging, conf. Nottingham, England, 1979, Apr. 79−36856
low light and thermal imaging systems, atmospheric effects 79−39860
low-background astronomical integrated IR detector array development 80−85860
luminescent screens sensitivity threshold determ. 80−31873
malignant melanomas, value of IR thermography 80−36062
mammary thermography classification by statistical filtering of spatial freqs. *(French)* 79−20610
marine thermal imaging system material and design considerations 80−42259
material and lens evaluation interferometer 77−39121
medical applications of thermography 77−44737
medical images, formation, perception and measurement, conference, Leeds, England (Mar. 1976) 77−86561
medical imaging techniques, developments, review 80−26324
medical thermograph, use of pyroelectric vidicon camera 79−25060
medical thermographic system model parameter calc. 79−79477
medical thermography, quantitation 78−31946
membraneous image translators, theory of basic characts. *(Russian)* 80−90838
meteorological satellite, A/D conversion for digital processing *(Japanese)* 78−7711
Meteosat in-orbit calibration, appl. to lunar thermal props. obs. 80−17511
microwave dosimetry, thermographic comparison of temp. probes 79−96521
microwave thermography, appl. in cancer diagnosis *(Spanish)* 80−67195
microwave thermography, for cancer diagnosis 80−26320
microwave-enhanced thermographic turnover detection, sweep-freq. illum. investigation 78−73194
military, staring IR sensors, space and reconnaissance appln. 80−86406
mirror, C-fibre reinforced resin laminate, design and production *(French)* 77−54770
and missile-borne tracker optics, selection guidelines 79−23050
mm-wave thermography, application to breast cancer 79−100693
modern IR technology, theory, practice and applications *(German)* 80−37088
mosaic IR image differencing for track assembly 80−86420
MOSFET Si:In(Ga) IR sensor, characts. 3 to 5 and 8 to 14 μm 77−74503
mountain aerial photography, colour film types compared 77−29500
MTF equipment testing in IR using standard reference lens 78−50898
multidetector spectrometer for atm. temp. sounding 79−25365
multispectral aerial imagery capabilities for military geographic information acquisition 77−82054
near-millimetric wavelength military systems 80−86428
neurosecretory cell IR photomicrography 80−30959
night viewing by thermal imaging systems 77−19447
night vision devices, new components including InSb-, HgCdTe-, PbSnTe-photodetectors, heat cameras appl. *(German)* 79−49287
night vision system testing image scanner 77−39102
night vision system with refractive optics, glare characts., surface defect influence 79−32024
noise equivalent temperature difference calc., radiation slide rule 77−124
noise reduction algorithms, Monte Carlo evaluation 80−95824
nonlinear image upconvertor systems 78−59091
nonlinear optical upconversion, for IR imaging 78−79070
nonstationary thermal fields of flat or cylindrical items, with one axis optomech. scanning 79−7218
nuclear fuel rods, thermographic imaging 77−42085
on-chip signal processing to overcome IR detector nonuniformities 77−79154
optical characterisation for IR diamond-turned aspherical elements 80−1373
optical components testing for thermal imaging systems 78−33911
optical heterodyne line-scan imagery, speckle noise model 79−50337
optical system design for low light and thermal imaging 79−37041
optical systems design, future computer program requirements 79−86260
parametric system, two-stage, up-conversion for IR image visualisation 77−83994
passive image dissector for time-resolved IR spectroscopy 77−41705
passive thermal screen for IR scene simulation 77−62060
performance criterion of radiation detectors for thermal viewing systems 80−73459
performance estimate, thermal imaging system, photon or thermal detectors 77−83973
phosphor convertor camera for near IR laser beam profile recording 79−81468
photoelasticity meas. using IR polariscope 79−94567
photographic information recording, new techniques, review *(German)* 77−26411
photography, principles and appls., book 78−82068
photography on wax films at 10 μm 80−4784
photon detector for geophysical and astrophysical research 80−86405
pick-up tube, pyroelectric, sensitivity and geometrical resolution improvement *(German)* 80−105715

infrared imaging continued
plasma sources, cooling pattern of acceleration grids meas. by IR scanning 80−86303
polyvinylidene fluoride, optimised target for IR vidicon camera tube, human body image recording 79−32050
power plant stack emission vel. and SO_2 conc., IR TV appl. 77−49197
practical IR optics, conference, Los Angeles, USA (Jan. 1978) 79−23085
pryroelectric vidicon, thermography appl. 77−54798
pupil, closed-circuit TV infrared electropupillometer design *(Japanese)* 77−66870
pyroelectric IR visualisation gauges 79−68432
pyroelectric recording for far IR plasma diagnostics 78−5929
pyroelectric target performance improvements 77−39103
pyroelectric vidicon, appls. 77−65635
pyroelectric vidicon, CO_2 laser beam meas. 78−49907
pyroelectric vidicon for thermal imaging *(Japanese)* 77−27359
pyroelectric vidicon thermal imager principles and performance 77−39093
pyroelectric vidicons, figures of merit, material parameters 80−77855
pyroelectric vidicons for thermal imaging 77−19449
quasi-staring IR sensor clutter rejection processor design 80−86417
radiometrically calibrated imagery for thermography 77−40893
real-time macro- and microthermography 79−9217
refracting objectives for 8 to 13 μm 80−86421
remote sensing, ground truth meas. 77−91318
remote sensing, operational meteorological satellite system GEOS 79−5727
remote sensing, recent developments 77−23752
remote sensing, sensors and detectors in NASA's future mission 79−5656
remote sensing measurements, conceptual considerations and surface temp. estimation, review 79−34984
remote sensing of atmosphere, land and sea props. 78−93015
remote sensing of ocean surface currents, recent progress 77−87114
remote sensing system specification using computer image simulation 80−48439
residential building heat loss estimation by aerial IR imaging 79−74586
reticulated sensing layers, thermal props., analytical solns. and design parameters 78−49897
retinal camera with infrared TV obs. *(German)* 79−2145
rheumatology, quantitative IR tele-thermography *(German)* 78−92684
riverine and coastal effluents, remote sensing of thermal alterations and circulation patterns 79−57524
rocket engine plume radiation, measurements in space simulation chamber 79−97437
satellite solid-state imaging for meteorology and astronomy 77−39074
scanning by SAW modulation 79−80687
scanning system modular design, assembly and alignment 80−78989
Schottky IR C-CD staring sensors, operation and performance 80−10029
sea ice and surface temp. meas., enhanced IR satellite imagery 77−37422
semiconductor thermocamera, thermojunction method appl. *(Russian)* 78−45693
sensibility equation modification *(Chinese)* 80−102806
shallow aquifers detection using thermal infrared imagery 79−84326
Shroud of Turin, IR reflectance spectrosc. and thermographic investigations 80−87578
Shroud of Turin, scientific investigation 80−87576
Shuttle Orbiter re-entry, remote IR imagery and tracking 80−82171
single-line scanning camera, portable, battery-operated 78−58029
skin, influence of cosmetics and ointments on spectral emissivity 77−9285
Skylab conical multispectral scanner IR data statistics 80−90223
Skylab spectral channel evaluation for classification and thematic mapping 77−78500
smoke/dust cloud temporal analysis algorithm 80−98484
soft tissue temp. increases due to US Doppler blood flowmeters, thermographic meas. 79−62294
solar energy collector array flow imbalance detection by thermography 79−83634
solid state pyroelectric IR image convertor 80−9036
Soviet Meteor satellite imagery, reception and processing in USA 79−39872
specification preparation guide 77−62059
Spectral Infrared Experiment equipment and objectives 78−81456
spinning cryogenic IR sensor, integrated thermal/structural/optical evaluations 78−82040
staring mosaic sensor background suppression and tracking 80−86415
staring mosaic sensor performance, effect of spacecraft-induced line-of-sight jitter 80−86416
static performance model 77−65636
statistical thermogram classifiers using coherent and incoherent light 79−96644
steel, mild, exam. of fatigue damage, using thermography 78−92356
steel against Al_2O_3, elastohydrodynamic contact, lubricated by naphthenic hydrocarbon, IR meas. of surface temp 79−15807
step-stare spaceborne optical system image motion compensation 80−90322
stratified media for IR image visualisation 79−32071
stress pattern analysis by thermal emission 80−33552
structural stress distrib. determ. by remote IR thermometry 80−87749
submillimetric imaging, speckle effects and specular reflections 77−39071
submillimetric imaging system for inclement weather 77−39070
submillimetric reflectivity of common materials 77−39005
submillimetric wavelength bad-weather vehicle recognition system 77−19450
superficial temperature testing, thermographic method *(Polish)* 79−67299
superficial vasculature visualisation using Vidicon camera with Si target 77−21592
superficial vein imaging by infrared television 77−81546
systems and components, educational film 77−45658
target discrimination methodology in remote sensing 80−58470
technology fundamentals 77−61120
technology utilisation, symposium, San Diego, CA, USA (Aug. 79) 80−86037
telephoto lens design, Ge, 8-14 μm region 77−39011
infrared imaging continued
telescope, large aperture, for near IR imaging onto detector array 77−2339
temperature meas., thermograms anal. *(Hungarian)* 78−65923
temperature meas. by IR camera, plastic processing industry appls. *(German)* 79−58685
thermal band imaging, glare in optical systems 79−32025
thermal imaging scanners, mirror rotation axis optimisation 80−86426
thermal imaging screens for visual display of infrared laser beams 78−66903
thermal imaging system design for graphic arts, laser scanning unit 80−14487
thermal imaging system resolution and S/N ratio, optical aberration effect 79−81552
thermal imaging systems, pyroelectric technology, review 77−14794
thermal imaging with pyroelectric vidicon camera 80−86288
thermal inertia mapping by IR imagery, mathematical model 80−109280
thermal IR scanner analogue data digital processing 77−82045
thermal spectrozonal aerial photography, capabilities and future prospects 80−18036
thermal TV camera, noise, synchronisation, spatial resolution and lifetime characts. 79−35833
thermal viewing system, image integral scanning effectiveness 79−50402
thermal viewing system LF noise suppression 78−82035
thermally induced index gratings Bragg refl., IR optical image conversion, thermal index changes 79−59753
Thermatrace, operating principles, appls. improvements 79−30565
thermo-optical convertor with liq. modulating medium 80−91927
thermogenesis, harmonic analysis and inverse filter 80−27304
thermogram enhancement by tissue-condition correction 79−39460
thermogrammetric temp. meas. method *(Hungarian)* 78−65924
thermographic camera, calibration, transmittance and emittance meas. 78−45628
thermographic diagnosis, high resolution dynamic method, detector system 80−41167
thermographic imaging, breast screening 77−86585
thermographic instrument, types 78−86266
thermographic meas., three-dimensional signal detection, expt. 78−3662
thermographic observability of tumours with microwave heating 78−73193
thermography, biomedical appl. aspects 78−61279
thermography, clinical, effect of obliquity 77−9286
thermography, colour, environmental physiology appl. 78−58043
thermography, NDI method for damage detection 80−35445
thermography, pyroelectric vidicon camera use 79−93143
thermography, reflectance errors 80−62661
thermography, skin temp. meas. appl. 78−61280
thermography appls. in industry 78−79112
thermography in clinical diagnosis and monitoring 78−57113
thermography of breast, feature extraction for mass screening 77−60237
thermography of high-power neutral beam target 80−33820
thermoplastic layers, isothermal smoothing of surface deformation *(Russian)* 80−76394
thermoviewer principle and industrial appl. 78−45614
thermovision flaw detector 'Stator-1', meas. channel 80−76449
thermovision system, AGA 680, calibration procedure to extend versatility 78−4680
tissue stess state intensity measures, hospital patient pressure sore prevention appl. 77−48923
triglycine sulphate, deuterated, reticulated target for pyroelectric vidicon, IR imaging 80−77858
tumour detection, computer processing of microwave enhanced thermographic images 80−8125
tumour detection by microwave enhanced thermography and computer-aided image analysis 79−70604
tumour microwave heating for thermographic detection enhancement 79−2124
TV camera, Pyricon thermal imaging tube 78−9437
TV system for building heat loss meas. 77−45837
uncontrolled thermographic mosaic compilation and videotape processing 77−29502
United States Air Force infrared reconnaissance set 78−81458
upconversion for astronomy 80−46412
US intensity pattern characterisation, thermographic-photographic technique 80−106689
US vibration visualization in piezoelectric ceramics using IR telethermography 78−33966
utilisation of IR technology, conf., San Diego (1977) 78−77984
video camera 10 μm, human body surface visualisation 79−94326
Viking IR thermal mapper, design 78−57440
visible and infrared imaging radiometers for ocean observations 78−69536
Visible and Infrared Radiometer evaluation from SeaSat-A surface temp. obs. 80−46325
vision systems, active and passive, 0.35-14 μm, atm. effects *(German)* 77−9500
wheelchair sent evaluation by time-lapse and quantitative thermography of skin after sitting 80−51205
Ag halide film for nanosecond photography, 10.6 μm CO_2 laser pulse spatial distrib. recording 79−89016
CdHgTe detectors, high-performance, for thermal imaging 79−40616
CdS:Ag, Ni thermographic phosphor luminesc. screen, for IR laser pulse recording 79−64342
Cu_2S, $Cu_{1.8}S$, $\alpha \rightarrow \beta$ transition, thermographic investigation of heats, entropies and activation energies 80−88314
gaAs photocathodes for low light level imaging 79−37043
Ge IR optical characteristics and performance requirements 80−48363
Ge, polycrystalline thermal-imaging lens, optical requirements 80−69495
Ge transparent IR window design for uniform pressure loading 79−23088
(Hg,Cd)Te n^+-p photodiodes, 8 to 12 μm IR imaging appls. 80−9044
$Hg_{1-x}Cd_xTe$ IR photodetectors for night vision appl. 80−22429
$Hg_{1-x}Cd_xTe$ photodiodes, implanted n^+-p, improved performance using insulated field plates 80−52309
InAs, heat and entropy of melting, assessment by quantitative thermography 77−15550
InSb charge injection device IR imaging arrays 77−79962
InSb charge injection imaging array 78−37995
$InSb/LiNbO_3$ acoustoelectric convolver, gap-coupled, for IR imaging device 78−94492

infrared imaging continued
InSb/$LiNbO_3$ gap-coupled convolver operation at 77K 79−50242
$LiTaO_3$/CCD hybrid focal plane, IR imaging and detection, crosstalk 80−77856
Pr based, IR quantum counter imaging system, resolution, sensitivity 79−81541
Pu safeguards, eval. of thermography 79−93719
Si, process stress analysis by IR photoelastic meas. 78−11488
Si:In extrinsic detectors in IR imaging systems, focal plane temp. stability requirements 79−94324
Si:S, background-limited photodetector near 77K 77−122
SiC heat-exchanger tubing, IR techniques for evaluation 80−76435
Si_2N_2O, emissivity determ. by IR thermography 77−59130
SiO_2-Al_2O_3-CaO-MgO-NaO-K_2O-B_2O_3-ZrO_2, glaze, exam. of zircon crystallisation 79−19155
TiN, synthesised in SHF discharge plasma, exam. of props. *(Russian)* 80−7524
VO_2, film, visualisation of microwave and IR radiation 80−5839
ZnS CVD IR window, optical and physical characteristics 80−106620
ZnS CVD window, IR lattice absorption, phonon assigments and image spoiling 80−33104
ZnS:Ag, Ni thermographic phosphor luminesc. screen, for IR laser pulse recording 79−64342
Zn_2SiO_4:Mn, energy storage effect and retrieval 80−100684

infrared-infrared double resonance *see optical double resonance*

infrared radiometers *see radiometers*

infrared sources
35 Mb/s optical fibre cable transmission using IR LED optocouplers 80−33156
astronomical telescope calibration, visible nd IR source, VISIR 80−36506
atmospheric emission obs. by Fourier transform IR spectrometer *(Japanese)* 80−12541
'blackbody' IR sources 78−83059
blackbody for energy calibration of infrared equipment 80−86377
blackbody radiant flux calc. simplification 80−106710
brightness determination of thermal source, use of optical parametric converter 80−98979
capillary discharge mode selection for IR brightness standard *(Russian)* 79−55198
carbon furnace for IR source, practical consideration 78−81976
Cherenkov light source, intense, 60 nm to IR range 79−59784
ChT-2R electric oven (USSR), calibration of radiometers using blackbody models 80−62722
classification system for isolated IR signatures 80−86430
coherent tunable efficient source 80−5789
communication sources, 1 μm range, LED and laser diodes 80−48448
communications transmitter, multipurpose IR emitters 78−30053
conference, IR and MM waves and appls., Miami Beach, USA (Dec. 1979) 80−57009
conference, Zurich, Switzerland (Mar. 1979) 80−4783
continuum source, improved design 77−39008
diffuse wall cavity, radiation pattern, nonuniform temp. and emissivity 77−80053
effective emissivity meas. by natural cooling *(Japanese)* 78−29117
electron beams, modulated, IR emission in magnetic field *(Italian)* 77−3525
far IR calibration source for balloon-borne telescopes 80−62027
far IR laser line frequency meas. by klystron harmonic comparison 77−7113
far IR laser spectroscopic sources and applications 77−57415
fibre-optic communication system performance at 1.55 μm with single-longitudinal-mode laser 80−87556
fibreglass laminates, thermal NDT using liq. crysts. 80−93709
fluoromethane, $^{12}CH_3F$, far IR Raman laser line obs., CO_2 laser pumping 80−69381
fluoromethane high-power laser, tuning behaviour 80−63994
Fourier spectrometer, choice of radiation source 80−27362
gas laser for remote meas. of atmospheric gases 77−49199
glass fibre, stimulated Raman emission, 1-1.3 μm source 77−42568
grating tuned (1.9-2.4 μm) picosec. travelling wave IR generated 80−5793
IKS-12 IR spectrophotometer, illumination system improvement 79−2838
industrial IR instrumentation sources and optical components 80−87453
integrated coherent IR generator, difference freq. generation in nonlinear optical waveguide 80−33084
laser, mass spectroscopic analysis of gaseous impurity microconcentrations in nonconducting materials 80−73518
laser absorption spectroscopy with ATR prism 79−98480
laser power transmission waveguides 77−19430
lasers, and laser techniques in mol. spectroscopy, book contrib. 78−8455
LED, industrial appl. of fibre optics 78−59123
LED system, pulsed output at 0.95-1.1 μm 77−72041
methanol far IR laser, twin optically pumped, for plasma diagnostics 80−59306
methanol twin optically pumped far IR laser for plasma diagnostics 80−103189
methyl fluoride, Dicke superradiance obs. in far IR emission 77−38841
multimegawatt tunable IR source up to 7.7 μm, using dye laser and H_2 78−1301
near IR (1 to 2 μm) optical communications, colloquium, London, England (May 1980) 80−86040
non-image forming classification system, exp., simulation results, military appl. 79−49296
photoionisation, multiple, infrared laser 80−69194
Pockels cell system, with 2.25 cm^2 aperture, for IR pulsed radiation production 80−5806
quartz lamps, emitter for permeable walls cooling characts. investig. 80−64535
radiation standards for source spectral emission and detector spectral sensitivity 77−39007
Raman laser, powerful, tunable IR and far IR 80−5787
scalable tunable IR laser operating characteristics and limitations 77−54713
semiconductor DH laser diode IR torch 77−39101
semiconductor light source for fibre optical communication 80−58653
stimulated EM shock radiation from relativistic electron beam 77−38997
stimulated Raman scattering, appls. *(German)* 79−27320

infrared sources continued
stimulated Raman scattering, coherent source tunable down to 16 μm 77−65605
storage ring design considerations for parasitic use of synchrotron radiation in the infrared 80−91340
storage ring synchrotron radiation far IR source 79−30577
submillimetre laser sources for magnetic resonance spectroscopy, standard frequencies 77−13788
subMM radiation, monochromatic, simple tunable source using harmonic generation 80−5788
synchrotron radiation, IR, from Orsay storage ring, photometric anal. 77−34922
technology, radiator and detector designs *(German)* 80−22430
thermometer and pyrometer calibration methods and standards 79−88958
tunable CO_2 laser source, 2.75 GHz 77−14786
tunable coherent IR and FIR sources utilising modulational instability 80−95967
tunable IR solid-state laser characteristics and principles 80−87406
tunable laser for semiconductor multiphoton spectroscopy *(French)* 80−82836
UV and IR radiation effects on eyes, safety measures *(Japanese)* 78−35881
UV and IR rays, effect on skin, safety measures *(Japanese)* 78−35882
W33 A, OH source, IR spectrophotometric and polarimetric obs. 79 21451
W3, IR maps from 4.9 μm to 20 μm 78−49495
Ar high-pressure arc plasma, IR continuum emission obs. 78−71604
CdS, subMM radiation excitation by N_2 laser pulse 80−60678
Co:MgF_2, tunable transition-metal-doped solid state lasers 80−58549
Cs vapour, IR picosecond pulse generation by stimulated Raman scatt. 80−53371
n-GaAs tunable far IR Landau emission with subnanosecond rise time 79−32015
GaAs:Si LEDs grown from restricted soln.-alloy bulk, props. *(Russian)* 79−43043
Ge, four wave mixing, intense tunable IR source for photochemistry 77−88852
Ge, four wave mixing, tunable IR generation 79−98444
H_2 four-wave interactions for tunable IR generation 77−54759
HCl, tunable far IR generation by stimulated Raman scatt. 79−31983
HF resonantly enhanced stimulated Raman scatt. for tunable IR generation 77−54759
He-Ne laser reference IR frequency meas. installation 77−79068
He-Ne lasers, standard wavelength sources 78−74957
$Hg_{0.77}Cd_{0.23}Te$ nonlinear optical IR generation 80−58642
n-InSb tunable far IR Landau emission with subnanosecond rise time 79−32015
$LiGaO_2$:Fe IR emitting phosphor preparation and props. 78−6789
$LiIO_3$, 5.3 μm down-conversion, IR source appls. *(German)* 78−90452
$LiIO_3$, pulse-period parametric oscillator, tunable 0.63 to 3.4 μm, for nonlinear spectroscopy 78−59083
$LiNbO_3$ computer-controlled IR parametric oscillator source 77−19365
$LiNbO_3$ computer-controlled Nd:YAG-pumped parametric oscillator 77−54758
$LiNbO_3$ grating-tuned picosecond IR source with CdSe down-conversion 80−74435
$LiNbO_3$, IR parametric oscillator source for remote air pollution monitoring 77−21936
$LiNbO_3$, Nd:YAG laser pumped parametric oscillator 77−46767
$LiNbO_3$, polariton excitation for tunable coherent far IR generation 79−31982
$LiNbO_3$, transient parametric generation of far IR radiation 79−94293
N_2 laser near-threshold IR enhancement by He additive *(Japanese)* 80−14324
N_2 laser UV-IR pulse time lag theory *(Japanese)* 80−14325
Ni:MgF_2, tunable transition-metal-doped solid state lasers 80−58549
OCS laser, for 16 μm range, review *(Rumanian)* 80−87408
Pb salt DH lasers for IR gas spectroscopy 77−19325
Pb salt tunable diode laser-integrating sphere system, output intensity characts. 80−78881
$PbS_{0.1}Se_{0.9}$ 4.6 μm LED, room temp., band gap and electrolum. 80−66302
Si inversion layer electronic transitions for voltage-tunable far IR emission 77−39962
Si MOSFET, far IR emission on high index surfaces 78−48232
SiC cavity radiator, spectral emissivity and radiance 77−83939

infrared sources (astronomical)
3 μm absorption feature, identification with water ice questioned 78−49499
5 GHz survey 78−69906
10 and 20 μm absorpt. bands, comparison with Nogoya meteorite IR spectrum 79−48741
0957+561A, B, double quasar, IR obs. of quasar and intervening galaxy 80−73065
2A 0311−227, AM Herculis type binary star, IR photometry and polarimetry 80−77517
accreting stars, model IR spectra for dusty circumstellar shells 78−85934
AFCRL 618, thermal radio emission from young planetary nebula 78−12343
AFCRL Sky Survey objects, 2-14 μ spectrophotometry 77−22331
AFCRL Sky Survey sources, accurate photometric positions 77−45603
AFCRL sources, identification of southern objects 77−33682
AFCRL sources, optical, IR and radio studies 78−4393
AFCRL Survey, subcatalogue of brightest sources 77−87283
AFCRL/AFGL sources obs., AFGL catalogue evaluation 78−28846
AFGL 2789 (V645 Cygni), Ae star, perplexing spectrum 80−73066
AFGL 333, far IR obs., evidence for star form. at ionization front 79−53932
AFGL 437, optical and IR obs., young star cluster embedded in nebulosity 78−4394
AFGL IR sky survey sources, ground-based obs. 79−71150
AFGL IR sources, mol. line obs. 80−51856
AFGL IR sources in revised catalogue, identifications from 3.5-12.5 μm obs. 79−25659
AFGL/CRL optically identified sources, spectroscopic obs. 78−32599
Allen's obscured IR source in NGC 2264, spectrophotometric anal. 79−21370
R Aquarii, 43 and 86 GHz obs. of SiO maser 79−71036

infrared sources continued
R Aquarii, symbiotic star, radio mol. maser line obs. 80−72960
R Aquarii, UBVRI polarimetric obs., orbital motion effect *(Russian)* 80−36646
Be stars, correl. between presence of Paschen emission lines and IR excess 77−22234
Becklin's star, in Orion, 4 to 8 micron spectrum 77−29903
Becklin-Neugebauer object, Brackett-alpha emission obs. 78−36657
Becklin-Neugebauer object, CO band emission detect. 79−101184
Becklin-Neugebauer source in Orion, 3.3 to 5.5 microns spectrum 80−12796
Becklin-Neugebauer source in Orion, high resolution 1.5 to 5 micron spectroscopy 78−93368
bipolar nebula, new, in Centaurus, discovery, photometry and spectral type 79−84837
bipolar nebulae, study of general phenomenon 78−41026
BL Lacertae-type objects, variable, IR and visible polarimetry and photometry 78−16528
3C 273, quasar, IR polarisation obs. 78−4360
3C 273, quasar containing dust, IR spectra obs. 80−56970
Calar Alto IR objects, search for continuum radio emission 77−41418
VY Canis Majoris, diameter upper limits 79−16974
VY Canis Majoris, IR obs. with new photometer 77−26017
VY Canis Majoris, OH/IR star, 1612 MHz OH maser multibaseline VLBI obs. 80−12766
Y Canum Venaticorum, C star, IR spectrum between 1.2 and 30 microns 80−46544
carbonaceous material in IR sources, origin and nature 78−24543
Carina I and II H II regions, far IR obs. 79−25657
η Carinae, high-resolution IR radiation maps of homunculus, spectral and spatial distrib. 80−12767
η Carinae, IR Fe II lines and interpretation of IR excesses 78−32478
η Carinae, spectral obs. at 4 microns 78−4237
η Carinae and Carina Nebula, polarimetric study 79−67043
R Cassiopeiae, late-type giant, possible H_2O thermal emission identification 78−81628
μ Cephei, late-type supergiant, possible H_2O thermal emission identification 78−81628
Cepheus OB3 molecular cloud, obs. of new IR sources 79−67072
o Ceti, vars. in spatial distrib. of 11 micron radiation 79−5828
Circinus X-1, changes in optical, IR and radio emission 80−67910
circumstellar clouds, scattered stellar radiation circular polarisation theory 78−96428
circumstellar dust shells, radiative transfer and radiation emission 77−13318
CIT 6 (IRC+30219), IR C star, CO obs. of mass outflow 80−12761
CIT fields, near IR vidicon images 77−33683
S.Coalsack, obs. of IR sources 80−46652
cocoon stars, calculated IR spectra 77−64824
cocoon stars, numerical soln. of radiation transfer eqn. in spherical geometry 80−90329
cocoon stars, relation to maser sources and compact dust bounded H II regions 77−26032
cometary coma, IR continuum rel. to dust grains props. 78−7923
compact far IR source in W31 region assoc. with G10.6−0.4, early stage of stellar evolution 78−49504
compact H II regions, fine struct. IR line emission 78−16482
compact H II regions, large beam IR obs. 78−16488
compact H II regions in areas of DR 21, W75N and K3-50, IR line obs., extinction determ. 80−12788
compact IR sources, dust shell models 77−29948
compact IR sources in molecular clouds, near IR slit scans 80−105300
compact sources assoc. with H II regions and molecular clouds, polarimetry 78−41019
compact sources assoc. with southern H II regions 77−45515
cool stars, effective temps; ang. dias. and reddening determ. from 1 to 5 μm flux curves 79−44458
cool stars, H_2O maser emission, catalogue of 82 objects 79−8909
cool stars, polarisation wavelength depend. 77−2426
R Coronae Austrinae interstellar molecular cloud, for IR study and dust temp. profiles 80−62237
R Coronae Borealis, origin of 1100 day periodicity in IR excess 77−45462
R Coronae Borealis stars, long-term IR behaviour 78−96490
cosmic dust grains, observed IR props. 80−26943
cosmic dust grains surrounding variable source of heating radiation, IR flux development 80−105324
Crab Nebula, millimetre and submillimetre meas. 79−75267
CRL 2104, CRL 2179, late WC stars, 2 to 4 μm spectrophotometry and circumstellar dust 78−96491
CRL 2591, IR source rel. to radio and H_2O counterparts 77−22330
CRL 2688, bipolar nebula, search for OH emission 78−41016
CRL 2688, Cygnus Egg Nebula, optical spectropolarimetry 77−33602
CRL 2688 (Egg Nebula), 8000-11000 Å spectrum 77−41400
CRL 3068, dust-enshrouded star 77−91664
CRL 3099, highly evolved C star, IR photometry and spectrum 78−49436
CRL 437, microwave spectral line profiles, rotation effects 78−45426
CRL 618 and 915 (HD 44179), IR spectra in 2-8 μ range 78−41080
CRL objects, IR polarization obs. 79−48901
NML Cygni, IR speckle interferometry 80−31216
V1016 Cygni, IR spectrum 78−93266
NML=V1489 Cygni, OH/IR star, 1612 MHz OH maser multibaseline VLBI obs. 80−12766
V1016 Cygni, symbiotic star, IR variability obs. from VJHKL photometry *(Russian)* 80−105263
V645 Cygni (CRL 2789), bipolar nebula, O-type exciting star 78−4392
V1500 Cygni (Nova 1975), fine-struct. lines rel. to 10 micron excess 78−93269
Cygnus OB2 No.12, high resolution 2μ spectroscopy rel. to interstellar and stellar features 78−57613
Cygnus X region, far IR survey 80−82538
Cygnus X-3, cocooned X-ray binary pulsar model 78−36723
dark clouds and cocoons, rel. to star form. *(French)* 79−67087
dark globules, IR radiation theory 78−53999
diffuse radiation, upper bound on metagalactic flux 77−29964
30 Doradus, IR survey, 2 μm sources in central region 78−32544
dust grain emission near variable primary sources 79−44358
dust temperatures in IR sources showing 10 μm silicate absorpt. feature 79−101217
dust/molecular clouds in Galaxy, props. 80−26925

infrared sources continued
Dyson spheres, stellar energy requirements and IR emission 78−69710
early-type stars, disc struct. in extended atms. 78−93206
early-type stars in southern hemisphere, search for IR excesses from JHKL photometry 80−94786
early-type stars with gas-dust envelopes, IR spectral energy distrib. 80−67732
embedded sources, optical spectrophotometry 78−96520
emission line stars in southern hemisphere, IR obs. 80−90496
emission-line galaxies with IR excesses, 8000-11000 Å spectra 77−67124
Equatorial Infrared Catalogue development from satellite data 79−101091
Equatorial Infrared Catalogue No.2 astronomical source distrib. 80−90346
equatorial IR catalogue (EIC), 2.7 μ high-precision sky survey results 78−81560
expanding molecular envelopes around evolved stars, CO emission line obs. 77−22219
extended source extraction from AFGL IR sky survey data 79−101088
extragalactic H II regions, observed, IR flux 77−87501
extragalactic IR sources, synchrotron radiation model 80−31387
extragalactic objects, 1 mm continuum obs. 78−36720
far IR astronomy, detectors and sources, review 80−56726
far IR background contrib. at high galactic latitudes 77−53712
far IR fine structure lines, obs. of [O III] 88.35 microns and [O I] 63.2 microns 80−12794
field stars at North Galactic Pole, props. 78−81622
FJM 3, 100 micron source, radio and IR studies 77−26082
FJM 6, molecular cloud, far IR, near IR radio mol. line studies 80−26929
G12.2−0.1, radio and IR obs. of OH/H_2O source 78−57620
G333.6−0.2, G298.2−0.3, southern compact H II regions, IR emission lines obs. 78−96522
G45.1+0.1, 8-13 μm spectrophotometry of compact H II region 78−65672
in G45.5+0.1, compact H II region, IR sources photometry 78−4396
galactic 2 μm radiation, mean intensity in solar neighbourhood 80−36744
galactic center, variable IR extinction obs. 79−48909
galactic central region, 2.4 μm mapping 77−29934
galactic central region and anomalous IR source, balloon-borne obs. at 2.4 μ 79−44588
galactic centre, 2.2 μm spectroscopy 78−36686
galactic centre, 4 to 8 micron spectrum 79−48922
galactic centre, forbidden O III 88 μm line emission obs. 78−49503
galactic centre, IR obs. and nature of compact IR sources 78−24551
galactic centre, linear polarisation in near IR 78−96534
galactic centre, Ne II 12.8 micron emission obs. 78−32572
galactic centre, near IR mapping at balloon altitudes 79−12514
Galactic Centre, polarisation obs. at 2.2 microns 77−64850
galactic centre, radiating dust cloud 77−78863
galactic centre point source, 1.4-2.7 μ spectrum 77−5569
galactic centre region, sources and obscuration 80−77487
galactic diffuse IR emission, rel. to extended low-density H II region and star form. 79−17047
galactic distrib. of IR sources 77−64842
galactic dust clouds, far IR emission rel. to translational anisotropy of cosmic microwave background 77−33706
galactic IR radiation, balloon borne obs. *(Japanese)* 79−80351
galactic IR radiation, balloon obs. *(Japanese)* 79−80350
galactic IR sources, 3 μ spectral feature identification 80−62227
galactic plane, near IR photographic survey 79−62911
galactic plane far IR emission, obs. at galactic longit. (l^{II}=27.5°) 80−62231
galactic sources, IR fluxes calcs. for polysaccharide grain model 78−54008
galaxies, distance scale from IR magnitude/H I vel.-width relation 80−82480
galaxies, IR emission rel. to Byurakan classification *(Russian)* 77−22305
galaxies, IR magnitude/H I vel. width relation rel. to distance scale and Universe expansion rate outside Local Supercluster 80−105325
galaxies, nearby, interstellar CO survey 80−62276
galaxies, star formation rates and IR radiation 78−49526
Galaxy central region, IR profile at 2.47 μm 77−29935
giant H II regions, radio and IR maps interpretation 78−85994
giant stars, survey for circumstellar OH emission 79−48787
GL 2591, angular dia. in near IR, 2-5 μm speckle interferometry 80−27010
GL 2591, protostellar source, 3 μm ice absorpt. band, linear polarisation obs. 80−105303
GL 2636, star form. region in Cygnus-X, IR obs. 80−105302
GL 2789 (V645 Cygni), IR and EHF spectroscopy 80−72956
GL 333, vels. as affected by W4 ionisation front and assoc. shock 80−94843
GL 490, GL 2591, obscured IR objects, K-band spectra anal. 79−92828
GL 490, IR obs. of low-luminosity pre-main sequence stars 79−53808
GL 915, 618, 2688, IR sources assoc. with double-lobed refl. nebulae, far IR obs. 78−54009
GL southern sources, 10 and 20 μm photometry 79−97097
globular cluster assoc. with X-ray source MXB 730-335, IR obs. 77−9776
globular clusters near galactic centre, IR studies 80−82434
h 4636, binary star in young cluster NGC 5367, IR photometry rel. to circumstellar shell 77−82294
HD 190073, a0ep star, Ca II lines struct., nightly vars. and line profiles interpretation 77−17578
HD 193793, Wolf-Rayet star, IR brightening rel. to circumstellar dust form. 80−31301
HD 44179 (Red Rectangle), obs. and interpretation of IR spectrum 77−78859
HD 50896, Wolf-Rayet star, wind struct. determ. from IR continuum 77−78793
HD 87643, forbidden line Be star, IR obs. with new photometer 77−26017
HD 97048 (=HM 18), pre-main sequence star, unidentified IR features obs. 80−85943
He2-442, UVRK photometry and spectroscopic obs. *(Russian)* 80−94817
Herbig-Haro object 1 exciting star, identification as T Tauri star 80−17633

infrared sources continued
Herbig-Haro objects vicinity, exciting stars search and IR sources discovery 80−67720
AM Herculis, 1.2 and 2.2 μm light curves interpretation, model parameters 79−8949
AM Herculis, accretion onto highly magnetised white dwarf 79−92764
HFE 2,3, molecular cloud, for IR radio mol. line studies 80−26929
HFE 2, 100 micron source, radio and IR studies 77−26082
HFE 64-70, 100 μm objects in Cygnus X, identifications with H II regions 77−17663
hot stars, effect of winds and coronae on IR and radio continua 77−29817
IAU 13S6A, strong southern radiosource, identification with IR non-stellar object 77−64865
IC 1396 interstellar molecular cloud, for IR study and dust temp. profiles 80−62237
IC 1795 (W3), N II forbidden line unusual profiles over giant H II region 80−46645
IC 1805, radio identification of IR object assoc. with passage of shoc front 78−93369
IC 1848 A, bright-rimmed mol. cloud, IR source obs. rel. to star for 79−5810
IC 2149, planetary nebula, absolute spectrophotometry in near IR 77−17669
IC 342, Scd galaxy, central regions IR emission and star form. 80−62256
IC 4593, planetary nebula, absolute spectrophotometry in near IR 77−17669
image processing technique appls. to scanned radiometer data of sar sources 77−49312
interstellar 10 μm silicate absorpt. band equivalent widths and du temps. 78−57614
interstellar 10 micrometer absorpt. band, comparison with phyllocates laboratory spectra 79−80344
interstellar clouds spectral line widths, influence of extended conuum source 79−12398
interstellar dark clouds, obs. with IR Fabry-Perot interferometer 80−8672
interstellar dark clouds far IR emission, implications of 2 μm r:ation intensity in solar neighbourhood 80−36744
interstellar dense clouds, dust condensation, cooling, IR emissi(79−62897
interstellar dust grains, temp. fluctuations effects on far IR en sion spectrum 80−26938
interstellar grain mantle molecules, middle IR fluoresc. and aorpt. spectra 79−88716
interstellar H_2 line emission from OH maser regions 80−1?0
interstellar IR and molecular line sources, 9400 Å photograp 77−45602
interstellar IR sources, polysaccharides and related hydrocarons identification 78−28763
interstellar medium, far IR fine structure line obs. 80−62?3
interstellar mol. clouds, relationship of submillimetre opticalepth to ^{13}CO column density 77−45508
in interstellar molecular clouds containing Herbig-Haro objcts, IR sources rel. to mol. props. 80−36689
interstellar molecules, vibr. excited, in grain mantles, IR eission lines 78−36670
interstellar radiating dust clouds, review 77−78863
interstellar submillimetric lines, possible detect. via laser terodyne techniques 79−44377
interstellar type I OH masers, positions, polarisation, neay H_2O masers, radio and IR props. 79−25671
IR 12.4+0.5, compact far IR source discovery 79−40?4
IR stars, review of observational data *(Russian)* 77−?377
IRC+10216, angular dia. in near IR, 2-5 μm speckle interferometry 80−27010
IRC+10216, brightness distrib. at 11 μm 79−67115
IRC+10216, butadiynyl N=12→11 doublet study 80−51829
IRC+10216, C_4H (butadiynyl) radical detect. 78−9374
IRC+10216, C star, HC_5N and HC_7N detect. 79−?126
IRC+10216, C star, near IR obs. of new mol. feature 79−92762
IRC+10216, C star, NH_3 obs. in circumstellar envelope 79−48793
IRC+10216, C star, possibility of detecting cyanoacetylene-d_1 (DC_3N) 78−69901
IRC+10216, circumstellar dust shell model rel. to IF energy distrib. 80−56972
IRC+10216, far IR obs. 77−29949
IRC+10216, isotope abundance anomalies in C star 79−5814
IRC+10216, late type C star, circumstellar envelope 78−4189
IRC+10216, luminous C star, ^{14}C search 77−53652
IRC+10216, molecular abundances in cool C star 80−4354
IRC+10216, poss. C_3N detect., Hartree-Fock calcs. 77−26041
IRC+10216, spatial spectra from 2.2 to 20 microns, deviations from spherical symmetry 80−41911
IRC+10216, variable C star, IR spectra obs. 80−90568
IRC+10216 (CW Leonis), IR C star, intrinsic polarisation 80−67730
IRC+10216 and related objects, CO obs. at 230 GHz 79−62931
IRC+10374, IRC+10523, IR stars, H_2O maser emission detect. 80−62298
IRC+10420, high-resolution OH maser obs. at 1612 MHz 79−44471
IRC+10420, IR emission lines from F-type supergiant star 78−4395
IRC+10420, stellar OH maser VLBI obs. rel. to mag. field 79−25742
IRC+10420, supergiant star, new OH maser feature spatial struct. 79−48946
IRC+10°216, circumstellar acetylene in IR spectrum 77−5591
IRC+30219, variable C star, optical emission-line phase obs. 80−90569
IRC +10216, C star, far IR size 80−82539
IRC +10216, detection of vibrationally excited CO at 114 GHz from C star 78−40941
IRC +10216, high resolution IR spectrum 77−33681
IRC +10216, tentative C_3N detect. 77−29913
IRC +10°216, circumstellar methane in IR spectrum 78−57694
IRC −20494, identified with Nova Sagittarii 1978=V3876 Sagittarii 78−49459
IRC and CRL sources, CO emission from late-type giants, molecular envelopes and planetary nebula origin 78−40940
IRC catalogue, reddest stars at 2 μ 79−62841
IRC comparison with UV Celescope Catalogue, common objects identification 77−9676

infrared sources continued
IRC stars, angular diameters from lunar occultations of nine objects 79−44475
IRC-10442 (GL5268S), near IR and radio obs. 80−4412
IRS 16, in galactic centre, nature, rel. to star density 80−46671
IRS 5, in W3, assoc. with H_2O sources 78−4332
K3-50, compact H II region, 2 to 4 micron spectrophotometry 77−13422
K3-50, H and He lines in obscured luminous H II region 80−51830
K-type giant stars, IR excesses rel. to presence of circumstellar shells 80−90420
Kleinmann-Low IR nebula, possible ethylene oxide detect. 77−53662
Kleinmann-Low i.r. nebula in Orion, high-vel. gas obs., CO 115 GHz line 77−5554
Kleinmann-Low nebula, ^{12}CO line profile rel. to radially moving cloud model 78−20865
Kleinmann-Low nebula, nature of broad molecular line emission 77−5556
Kleinmann-Low nebula, NH_3 nonmetastable levels obs. 79−25665
Kleinmann-Low nebula, optically thin CO emission 78−4315
Kleinmann-Low nebula, spectrum from 29 to 125 microns 77−33680
Kleinmann-Low Nebula in Orion, far IR polarization 79−12502
Kleinmann-Low nebula in Orion, ice 45μm signature possible identification 79−17068
L1641 and Orion Nebula, submillimetre emission obs. 80−36685
late-type stars, anal. of balloon-borne near IR multicolour photometry 80−98654
late-type stars, ang. dias. by lunar occultation technique 77−74048
late-type stars, balloon-borne near IR multicolour photometry 80−4356
late-type stars, near IR photometry with balloon-borne telescope 78−73713
late-type stars, near IR photometry with balloon-borne telescope 80−4357
late-type stars, O-rich, 16 to 39 micron spectroscopy 80−22002
late-type stars with OH, H_2O or SiO maser emission, catalogue 79−70965
LkHα101, 1-4 μ spectra, aircraft and ground-based obs. 77−5590
long-period variable and IR stars, discovery of new 1665/1667 MHz OH/IR sources 77−64763
M17, far IR obs. rel. to H II region interaction with mol. cloud 80−22053
M17, Platt particles and spatial temp. fluctuations 78−61907
M17 SW, obscured IR point source spectroscopic anal. 79−48878
M1-92, bipolar nebula, OH emission obs. 78−41016
M3-99, bipolar nebula, search for OH emission 78−41016
M42, far IR polarisation obs. 77−53663
M82, galaxy, 2 to 8 μm spectrophotometry 78−12363
M82, implications of IR sources for explosion model 79−75279
M82, model with galaxy drifting through dust 77−33632
M82, Ne II 12.8 micron emission obs. and galactic dynamics 79−17082
M82 nucleus, Brackett-line obs. 79−25704
in M8, IR map 77−64817
M8, large-beam near IR and 24 GHz obs. 79−48882
M8, new IR-CO source obs. 77−64818
M8 (Lagoon Nebula), far IR obs. 80−4413
M 1-92, Minkowski's Footprint, optical spectropolarimetry 77−33602
M-type supergiants, highly reddened IRC objects, IR photometry and near IR spectra 79−84796
M-type supergiants in reddened Ara cluster, IR photometry rel. to thermospheres 77−41395
Markarian 231, IR polarisation obs. 78−4360
maser emission from IR sources, role of dust in pumping 78−36716
maser stars, search for water vapour absorpt. lines 77−78804
Michigan 239, peculiar extragalactic or extreme halo emission-line star, obs. 80−4380
middle IR polarisation by dust, model 79−67078
millimetre temps. of planets, galactic and extragalactic sources 78−28556
molecular clouds, CH radio emission obs. 77−87512
molecular clouds, far IR emission 78−4313
Monoceros R2 cloud, near IR and mol. obs. of rot. collapsing cloud 77−78840
N Monoceros region, two-micron IR objects survey 80−8555
multiple systems in molecular clouds 79−101180
MWC 349, IR source optical identification with reddened high-luminosity star 80−56971
MXB 1730−335, 2.2 μm flashes from X-ray rapid burster 80−46706
MXB 1730−335, Rapid Burster, IR bursts detect. confirmation 80−27020
MXB 1730−335, X-ray rapid burster, unsuccessful search for IR bursts 80−98740
NGC 1068, Seyfert galaxy, IR photometry and polarimetry 78−54035
NGC 1068, Seyfert galaxy, radiative transfer in dust rel. to spectral flux distrib. 77−29914
NGC 1275, Seyfert galaxy, IR polarisation obs. 78−4360
NGC 1502, open cluster, IR photographs processing, discovery of faint source *(Russian)* 77−13250
NGC 2023, reflection nebula, far IR study 80−51831
NGC 2024, H II region, near IR obs. 79−58393
NGC 2024 (Orion B) nebula, CO J=2 to 1 line obs. 80−8673
NGC 2071(IRS), IR obs. of low-luminosity pre-main sequence stars 79−53808
NGC 2264, far IR emission from compact sources 77−78841
NGC 2264, open cluster, CO obs. of mol. cloud 79−21363
NGC 2264, young open cluster, circumstellar shells, IR excess obs. 77−45410
NGC 2264 IR source, formaldehyde kinematics and distrib. 80−4418
NGC 253, Sc-type galaxy, two-micron spectrophotometry 80−4442
NGC 2903, spiral galaxy, nucleus identification and visual energy distrib. 80−62273
NGC 4151, Seyfert galaxy, IR polarisation obs. 78−4360
NGC 6210, planetary nebula, absolute spectrophotometry in near IR 77−17669
NGC 6334, far IR sources positions rel. to H_2O masers 80−73025
NGC 6334 complex, 1 mm continuum map of cool IR sources 79−21390
NGC 7027, planetary nebula, far IR obs. 77−22288
NGC 7027, planetary nebula, H_2 emission spatial distrib. obs. 80−98698
NGC 7027, planetary neubla, near IR obs. 78−73748
NGC 7538, H II region, IR study 79−84842
NGC 7538, IRS 1, formaldehyde maser, SHF band obs. 80−67822

infrared sources continued
NGC 7538 (IRS 1+2), compact H II region, 2 to 4 micron spectrophotometry 77−13422
Nova Serpentis 1978, IR magnitudes and BVR photometry 78−65629
Nova Serpentis 1978, IR photometry 80−4365
O-type stars, C III 7901 to 9715 Å emission lines obs. 80−77401
OB stars, newly formed, IR sources assoc. with nearby H_2O masers 78−12390
OH 0739−14, IR polarization obs. 79−48901
OH main lines, IR pumping 80−46632
OH/IR sources, microwave spectra, galactic distrib., radial velocity 78−16432
OMC-1, IR emission rel. to methanol masers excitation 80−67891
ρ Ophiuchi dark cloud, high ang. resolution obs. of far IR source 79−40235
ρ Ophiuchi dark cloud, near IR point source rel. to C II and S II regions 78−49500
Ophiuchus dark cloud region, IR sources identifications 77−45522
Orion molecular clouds, obs. in 40-400 μm range 78−69853
Orion Nebula, H_2 emission interstellar extinction meas. 79−25668
Orion Nebula, near IR photography with vacuum-cold camera 80−90341
Orion Nebula, search for H_2 ground state S(2) line 79−8961
Orion Nebula, submillimetre emission obs. 80−36685
Orion OB 1 association stars, photometric anal. rel. to IR excesses 77−82288
Orion-KL nebula, VLBI obs. at 43 GHz of SiO maser 79−92836
Parsamyan 21, bipolar nebula, search for OH emission 78−41016
photometric histories of six objects 79−5916
photometric monitoring from Earth orbit 78−16433
planetary nebula IC 418, search for absorpt. in CO fourth positive system 80−46647
planetary nebulae, 10 micron props. obs. 79−48879
planetary nebulae, 8 to 13 micron spectrophotometry 80−22057
planetary nebulae, advances in IR obs. 80−109525
planetary nebulae, IR photometry of (Abell 30 and 78) 77−91602
planetary nebulae, IR radiation energy balance 77−13424
planetary nebulae, molecular abundances and IR spectra 78−53998
planetary nebulae, OH emission search 79−48787
planetary nebulae, southern, IR obs. 80−90496
pre-main sequence stars, observational study conclusions 79−25592
pre-main-sequence A and F stars in NGC 2264, nature of IR excesses 78−32461
primaeval giant elliptical galaxies, observable props. 78−89260
protostellar clouds, dynamical evolution and IR radiation 77−17543
protostellar envelope evolution, radiative transfer and spectrum 80−77384
protostellar envelopes of masses 3 M⊙ and 10 M⊙, coupled radiative transfer/hydrodynamics eqns. and IR appearance 80−36616
protostellar sources, IR polarisation rel. to nearby interstellar polarisation 80−4347
quasar-like objects, black hole model for IR and optical emission 78−20905
quasars, continuous and emission-line spectra and relationship with Seyfert galaxies 79−2571
quasars, IR energy distribs. obs. 78−57645
quasars, optical identification problems 80−105392
R50 dusty star in SMC, IR photometry 77−45461
radiation transfer and 10 micron silicate feature, effect of multiple grain components 78−36659
radiative transfer in nongray extended dust shell models, Eddington approx. generalization 78−73627
radiative transfer in spherical dust shells, generalised two-stream Eddington approx. 79−35120
Red Rectangle, refl. nebula assoc. with HD 44179, spectrum interpretation 77−49462
Red Rectangle (HD 44179), precessing jets model 80−4422
review of IR and submillimetre astronomy *(Russian)* 80−72773
Roberts 22, bipolar nebula with OH emission, visual, radio and IR obs. 80−94859
Rosette Nebula, far IR emission from compact sources 77−78841
RSO 1 catalogue cross correl. with IRC, AFGL and EIC catalogues 80−77511
S106 IR, S235 B, obscured IR point sources, 2 μm spectroscopic anal. 80−12795
S140 interstellar molecular cloud, for IR study and dust temp. profiles 80−62237
S140 IR, far IR spectrum 78−93372
S140 molecular cloud, far IR emission detect. 77−33611
2S1728−337 vicinity, 5 IR sources detected by K-band photometry 78−54076
S255, H II region, compact IR sources correl. with CO emission small-scale struct. 80−46637
S255, molecular cloud, molecular line, radio continuum and IR data 78−8087
2S 1702−363 field, IR object identified as Mira variable 78−81705
S-type stars, list of brightest stars in IR 77−41382
HM Sagittae, emission line variable, near IR spectrum *(Russian)* 78−81637
Hm Sagittae, eruptive variable, IR variability 79−25614
HM Sagittae, IR spectrum 78−93266
HM Sagittae, symbiotic star, IR variability obs. from VJHKL photometry *(Russian)* 80−105263
HM Sagittae, variable emission object, spectrophotometry 80−17599
RY Sagittarii, pulsating R Coronae Borealis star, IR variability 77−45462
Sagittarius A, IR polarisation obs. 78−8109
Sagittarius B2, far IR spectrum obs. 78−8073
Sagittarius B2, NH_3 nonmetastable levels obs. 79−25665
V818 Scorpii (Scorpius X-1), UV, visible, IR and X-ray obs. 80−82541
Seyfert galaxies, continuous and emission-line spectra and relationship with quasars 79−2571
Seyfert galaxies, IR emission obs. 79−17083
Seyfert galaxies, IR energy distribs. obs. 78−57645
Seyfert galaxies, thermal IR emission vars. 80−67865
Seyfert galaxies, type 1, dust as source of IR luminosity 78−12357
Sh2-149, near IR photography with vacuum-cold camera 80−90341
Sh 2-149 assoc. IR source, spectral type and luminosity class 78−73772
Sh 2-158 (NGC 7538), bright high excitation galactic nebula, stellar IR sources obs. 79−40241
Sharpless 106 IR sources, 8-13 micron spectrophotometry 80−105305

ared sources continued
harpless 140, compact source, strong far IR emission obs. 78−36649
harpless 140 IR source, detect. of assoc. near-IR complex 79−25686
harpless 254, 255 and 257, triple emission nebula in Orion, obs. 7−13430
harpless 88A-B and 106, compact H II regions, optical obs. 79−8969
w novae and symbiotic stars, late-type components spectral classifications 80−94813
thern hemisphere IR sources, search for H_2 2.1 μ emission 80−22059
ctral features, unidentified, review 80−26936
433, IR energy distrib. obs. 80−31312
433, IR photometry, and search for short period variability −58346
433, IR variability obs. 80−98676
s dust, interstellar and circumstellar 77−41404
formation regions, IR sources membership rel. to population cates and mol. clouds evolution 80−17645
st 20 μ, broadband photometry 77−9807
sta IR bright, in region of galactic centre, catalogue and photometry 8 77299
sta late-type, IR spectral observations *(Japanese)* 79−80307
sta search for 18 cm OH emission 78−8026
sta very long baseline interferometric obs. of assoc. OH masers 7 3699
star ith IR excesses, optical emission intrinsic linear polarisation origin 78 6481
stell point sources, modulation transfer function for speckle interfeomy 79−101079
subm meter wavelength sources, large beam sky survey from balloon altit s 79−97045
supern a remnants in molecular clouds, struct. and emission 80−82450
symbi c star candidates in LMC, optical spectroscopy and IR photome 80−62139
symbi stars, survey at 1612 MHz 80−12774
symbi stars and slow novae, late-type components spectral classifications −94813
SU Tau R Coronae Borealis star, IR excess discovery from optical and IR photometry 80−101601
RV Tau and yellow semiregular variables, IR excess correl. with metallicity −26865
Taurus d k cloud complex, IR study 79−8963
thermal ission spectrum from small interstellar grains with temp. fluctuation 8−69864
Trapezi d IR sources 79−44557
Trapezium-like objects, visual and IR photometric obs. 79−92805
Type II OH/IR maser sources near galactic centre, systematic search at 1612 MH 79−35415
unidentifie 3.3 μ emission feature obs. 77−33601
unidentifie emission features, possible mechanism 80−82452
variable fai R source detect. in NGC 6334 group of nebulae 80−8671
variable sta H_2O maser source in circumstellar envelope 78−73724
variable sta USAF satellite obs. 77−49406
NQ Vulpecu e (Nova 1976), CO emission and η Carinae stage 79−25609
W33 A, 4.5-μm spectrum 79−101181
W3, 8 to 13 icron spectrophotometry of compact sources 77−57070
W3(OH), pr uction by moving compact object 78−54064
W3 IRS 1, fi structure line radiation, dust UV opacity 80−90505
W3 region, ne IR obs. of far IR sources G133.8+1.4 (W3N) and G133.982+14 (BS4) 80−22058
W3/W4/W5 rection, IR sources correl. with heavy optical obscuration 80−62301
W40 and W48 near IR and CO mm wavelength obs. 78−65667
W49 NW, compact H II regions, far IR spectrum 80−90497
W51, W49, air rne for IR spectroscopic obs. rel. to dust cloud model 80−36684
W51 (IRS 2), compact H II region, 2 to 4 micron spectrophotometry 77−13422
W51 (IRS 2), H and He lines in obscured luminous H II region 80−51830
W51-IRS 2, compact H II regions, IR spectrum obs. 80−90497
white dwarfs, highly magnetised, accretion theory 79−92764
Wolf-Rayet stars, 2 to 4 μm spectrophotometry of late WC stars 78−96491
Wolf-Rayet stars, truct. of winds from obs. of IR continua 77−78793
yellow semiregular and RV Tauri variables, IR excess correl. with metallicity 80−26865
young stars, accreting, ang. dimensions 79−44482
young stellar objects, origin of polarisation 79−8911
II Zw 40, dwarf galaxies, radio obs. rel. to IR excess 79−8992
C stars, search for HCN and CH maser emissions 80−51856
H II blisters, dusty, appearance at radio and IR wavelengths 80−85979
H II Brackett α line survey of compact IR sources 79−62882
H II regions, anisotropic, with axial symmetry, models rel. to IR brightness distribs. 78−85993
H II regions, compact, IR obs. in 3.4 to 33 microns range 77−22287
H II regions, forbidden O III 88 μm line emission obs. 78−49503
H II regions, galactic, comparative study of high-radiofrequency and far IR obs. 78−49497
H II regions, galactic, forbidden S III 18-71 micron emission obs. 79−97046
H II regions, IR emission from dust 79−71091
H II regions, IR obs., 1-1000 μm wavelength 79−67084
H II regions, models of IR emission from dusty and diffuse regions 78−41010
H II regions, newly formed, in interstellar dark clouds, physical props. from radio continuum interferometry 80−105301
H II regions, southern, 1 mm continuum obs. 79−8968
H II regions and galactic centre, far IR spectrometry 77−53668
H II regions is IC 1795/1805, IR luminosity compared with exciting star total luminosity 78−96519
H_2 IR line emission, shock model appl. to Orion Nebula 78−8086
H_2O masers, accurate interferometric positions at 1.35 cm 78−45374
He variable stars, IR excesses obs. 80−67733
OH 0739-14, IR source assoc. with double-lobed refl. nebulae, far IR obs. 78−54009
OH 26.5+0.6, IR spectrum, polysaccharide grain model 78−12342
OH 26.5+0.6, spectrophotometry from 2 to 40 microns 78−24568
OH emission sources, low latitude search at 1612 MHz 77−49452
OH maser source OH 0739−14, IR polarization obs. 79−48901
OH masers, obs. of new assoc. IR objects 78−12407

infrared sources continued
OH sources in CRL objects and late-type stars, 18 cm obs. 79−35427
OH type I maser sources, model 80−90556
OH type II stars, unidentified, search for H_2O emission 79−75286
OH/IR stars, IR search and identifications 78−24510
OH/IR stars, new SiO transition detect. 78−53954
OH/IR stars, OH main lines masers inversion 78−28664
OH/IR stars maser emission, role of plasma effects in generating high-rel. and symmetric spectral features 80−31378
OH/IR Type II sources, radial diameters from 1612 MHz OH line obs. 78−36713
OH/IR unidentified Type II sources, 1612 MHz obs. at low galactic latits. 77−17704
OH/IR unidentified Type II stars, galactic distrib. and kinematics from 1612 MHz survey 78−49450
SiO masers in IR stars 79−71036

infrared spectra of diatomic inorganic molecules
alkaline earth dimens., heteronuclear, matrix-isolated, laser photoluminesc., van der Waals ground state 79−41192
bond polarity parameters, IR intensities, molecular orbital study 79−63914
collision-induced, overlap dipole moment determ. 77−18924
diatomic molecule, vibr.-rot. states, high accuracy wave functions and energies 80−74159
diatomic molecule in strongly interacting solvent, IR band shape, field theoretic methods appl. 79−27038
diatomic molecules, matrix isolated, vibr. spectrosc., IR line shape calcs. 79−72307
diatomic molecules, shortening of energy relax. time of excited mol. vibr. in dense medium by form. of H-bonds 80−91553
diatomic molecules vibr. consts. determ., IR spectroscopic, quantum chem. teaching project 79−84914
diatomic polar molecules, in simple liquids, interactions, far IR absorpt. spectra 78−25527
diatomic polar molecules, in simple liquids, interactions, statistical theory and spectra 78−29779
dilute solutions, IR and Raman spectra temp. depend. anal. model *(French)* 77−88456
far IR atmospheric emission and absorption spectrum calc. program 79−35020
free radicals and molecular ions, matrix isolation spectra 79−50008
gases, high resolution vibr. spectra by Fourier transform far IR spectroscopy 80−86461
homonuclear diatomics, in zeolite matrices, induced IR spectra 78−46333
hydracids, monatomic matrix-trapped, assoc. forms, struct. and spectral response, intermol. pot. calcs. 79−93996
intensity prediction, at. polar tensor method, F containing mols. 78−62854
intensity relation, IR to Raman intensity, matrix notation 78−62853
line shape, rotational lines, influence of collision duration, diatom-atom gas mixture 80−43110
linear molecular gases, IR radiation in Q branch 79−54850
$^{14}N^{16}O$, 1-0 band at 1900 cm^{-1}, meas., interpret. 78−58651
radiating molecules, in upper atm., rot. relax., IR emission and vibr.-rot. transitions calcs. 77−65462
sooting flame, absorpt. spectrosc. using tunable diode laser 80−55660
stratospheric far IR emission, balloon-borne obs. 79−34896
upper atmosphere, IR radiation from mol. vibr.-rot. transitions 79−5695
AlO stellar IR bands rel. to Mira phenomena 78−69801
Ar_2, near IR absorpt. spectra 78−66547
ArF_2 laser spectra, absorpt. lines 80−9604
$Ar_2(^3\Sigma_u^+)+N_2$, quenching, fast absorption spectrophotometry 79−54940
AuCa radicals, rotational analysis for near IR bands *(French)* 77−61741
AuLi, vibr. freq. determ., IR spectra, matrix depend. 77−75146
AuSi radicals, rotational analysis for near IR bands *(French)* 77−61741
Bi_2, in Ar matrix, electronic states, vis. and near IR absorption spectra 78−5213
BiN, form., IR matrix spectra, comparison with group V nitrenes 80−18853
BrO free radical in Ar matrix at 10K 79−89669
C_2, IR flame emission spectra, Ballik-Ramsay system 79−63999
C_2, interstellar, rot. fine-struct. lines obs. towards ζ Persei 80−67811
C_2, Phillips system, 2.3-0.9 μm, rot. consts. 78−21925
C_2, Phillips system, rot. depend. of Franck-Condon factors 77−27058
CN, Fourier spectrometry of $A^2\Pi \rightarrow X^2\Sigma$ transition 77−57995
CO, $a^3\pi$ state, IR radiative decay of vib. levels 77−30870
CO, absolute intensity meas., 4-0 vibr.-rot band 77−6854
CO, absorpt. spectra around 2100 cm^{-1}, Fourier transform spectroscopy appl. 78−58068
CO, adsorbed, lateral interactions on vibr. spectrum 79−46954
CO, adsorbed on Pd/Al_2O_3, IR study 80−108193
CO, adsorbed on Ru (001), temp. depend. ordering processes 80−80773
CO, adsorption on evaporated Ir films, IR refl.-absorpt. spectroscopy 80−34925
CO, adsorption on Pt (111), adsorption site investigation by IR reflection spectra 78−14565
CO, adsorption sites of Ni (111), LEED, AES, thermal desorption, work function, and IR system meas. 79−77903
CO, and isotopic forms, fundamental bands, absolute wavenumbers, mol. consts. 79−59458
CO, and isotopic forms, laser freqs., Dunham coeffs. 79−64207
CO, appl. of technique for IR spectroscopy of mol. beams. 77−46655
CO, Autler-Townes power splitting of rovibr. lines, direct obs. using intense IR laser 79−54854
CO, CO-air, mol. rot. temp. determ., absorpt. spectra calcs. 77−30851
CO, chemisorbed, CNDO calcs. of mol. struct. *(German)* 79−96368
CO, chemisorbed on Pt {111}, IR spectra, evidence for strong absorbate coupling interactions 78−14604
CO, chemisorbed on Rh, IR spectra, species identification 79−39198
CO chemisorbed on $Rh/\gamma\text{-}Al_2O_3$ disperse δ-phase, IR spectra, site distrib., mol. mobility 78−72496
CO, chemisorbed on supported Rh, activated surface processes, IR spectra 80−16724
CO, chemisorbed on W, IR vibration spectroscopy 78−14603
CO, computation of multiphoton IR rovibration spectrum 79−89660
CO, ground-state, absorpt. oscillator strengths for vibr. rot. transitions 78−62846

infrared spectra of diatomic inorganic molecules continued
CO, high resolution lifetime meas., perturbation and collisional transfer correl. 78−78699
CO, hole burning in single quantum power spectrum due to Autler-Townes splitting 80−9671
CO, IR band absorpt. derivation from vibr.-rot. band spectroscopic variables 77−14434
CO, IR band nonrigid rot. absorption 78−91060
CO, in Ar matrix, vibr. line shape, vibr.-phonon interaction 79−3493
CO in giant stars in globular clusters, IR obs. 78−93339
CO in IR spectra of III-106, CH star in M22 globular cluster 80−62131
CO in solar faculae, spectra rel. to mols. rot. temp. 77−78740
CO, in solar spectrum, centre to limb behaviour of first overtone vibr.-rot. transitions 79−8889
CO j=2→1 IR line obs. of Monoceros R2 assoc. 79−25654
CO, laser lines, spectral coincidences with NO absorpt. lines 77−54559
CO, line parameters appl. to IR spectrometer performance testing 77−91275
CO, matrix-isolated, librational relax., IR line broadening 80−978
CO molecular layer optical depth and rotational temp. on Sun 79−96988
CO on Ni (111), adsorption sites using IR reflection-absorption spectroscopy 79−69355
CO, on Pt surface, IR spectrum obs. in presence of free CO 78−74654
CO, oxidation on Ir films, IR absorpt. spectroscopy 80−71398
CO, P(6) line absorpt. coeff. and halfwidth, temp. depend. 80−78618
CO, rot. distrib. in supersonic beam, IR bolometry using tunable diode laser 80−63869
CO, rot. spectra, 714-1667 μm, Fourier interferometric spectrometer 77−83765
CO, rovibr. multiphoton spectra comput., hole burning effect 80−9672
CO, solid and matrix isolated, IR and Raman spectra 78−48156
CO, vibr.-rot. absorpt. line., shock tube spectroscopy 77−71890
CO, vibr.-rot. interaction, high excitation transitions in solar IR spectrum 77−68040
$^{12}C^{16}O$, $^{13}C\ ^{16}O$, Heizberg system, rot. anal. 79−59423
CO-^{3}He nuclear pumped laser, optimisation with 2 MeV protons 80−64000
CO-alkane, liq. soln., vibration-rot. IR spectra, rot. diffusion 77−83584
CO-cycloalkane solns., CO IR vibr.-rot. spectra, solvent mol. struct. 77−83585
CO-myoglobin, mol. tunnelling, isotope effect, time resolved IR Fourier transform obs. 80−72126
CO+Ar(CO), rot. band, line shape, collisional broadening, impact approx. 78−42134
$CO+Hg(6^3P_1)(6^3P_0)$, electronic-vibr. energy transfer collision, IR obs. 79−45716
$CO+N_2(CO_2)$, line broadening, short range force effects, semiclassical calcs. 79−98085
CS, isotopic variants, IR absorpt. spectra, ν=2←1 hot band 79−45721
CS, isotopic variants, IR absorpt. spectra, vibr.-rot. transitions 79−45720
CS, rotation analysis of $d^3\Delta_i\text{-}a^3\Pi_r$ transition, IR spectra 80−78591
$^{12}C^{32}S$, ($^{12}C^{34}S$), IR spectra, 2-0 vibr.-rot. bands, spectroscopic consts. 77−75153
$^{13}C^{16}O$, IR emission, vibr.-rot. lines 77−3355
Ca_2, matrix isolated, vis. and near IR spectra 78−5214
Ca_2, vibr.-rot. states, high accuracy wave functions and energies 80−74159
^{44}Ca substituted oxides, matrix isolated, IR spectra 78−9151
CdO, formed by matrix reactions, IR, Raman and visible spectra 80−87110
ClO, bandstrength determ. of fundamental vibr.-rot. spectrum 78−70872
ClO, fundamental vibr.-rot. spectrum, rel. to remote sensing 77−42317
ClO radical, IR vibr.-rot. spectra, background data for atm. meas. 78−58679
ClO, vibr.-rot. bands, intensity parameters 78−17722
CoO, matrix isolated IR spectra, ground state vibr. freqs. 80−28015
CoO, vibr. IR absorption spectrum, mol. consts. 79−89666
CrH (CrD), molecular vibration, IR spectra electron spin resonance, 4K 79−98084
Cs_2, concealed weak absorpt. band, detect. by saturation spectroscopy 77−10675
Cs_2, dimer and higher polymer IR absorpt. bands, triplet state 80−63629
CsBr, far IR spectra, matrix isolated, monomers, dimers, trimers 78−66545
CsCl, far IR spectra, matrix isolated, monomers, dimers, trimers 78−66545
CsF, far IR spectra, matrix isolated, monomers, dimers, trimers 78−66545
CsHe(Ne)(Ar)(Kr)(Xe), excited state IR emission bands 80−14140
CsI, far IR spectra, matrix isolated, monomers, dimers, trimers 78−66545
CuI dissoc. energy A-X system vibr. bands 77−50434
D_2^+,(DT^+), IR transition freqs. calcs. 77−88452
D_2, elec. quadrupole vibr.-rot. spectrum, 2.8 to 3.9 μm 79−805
D_2, in zeolitic matrix, IR active fundamentals obs. 77−71800
D_2, matrix isolated, IR spectra, mol. rot. and vibr. const. determ. 80−78617
D_2 matrix shift, CoM freq., in solid Ar, Kr and Xe 79−6969
DBr, IR absorpt. in 5-0 band, high-resolution spectra 77−14431
$D^{79}Br$, $D^{81}Br$, IR absorpt. spectra of 1-0, 2-0, 3-0, 4-0 bands 77−3360
DCl, IR matrix isolation spectra, N_2 matrix effects 79−36634
DCl, vib.-rot. spectra in hexadecane solvents of different mol. shapes 77−34623
$D^{35}Cl$, $D^{37}Cl$, IR absorpt. 3←0 band, dipole moment series expsn. 77−61747
DCl-cycloalkane solns., CO IR vibr.-rot. spectra, solvent mol. struct. 77−83585
DF, IR laser spectra 79−45936
DF* prod. from D+PTFE, Fourier transform IR spectroscopy 80−87105
DI, IR absorption bands 4←0 and 5←0 79−98091
DT, vibr. rot. Raman anal. 80−87126
FO free radical, detection by CO_2 laser mag. reson. 80−45594
FeH, 9900 Å band profile rel. to identification in M dwarfs and S stars 77−45418
FeH, FeD, matrix isolated IR spectra, mol. vibr. 79−93992
FeH, wavelengths and line intensities for 4920 Å, 5320 Å and 8690 Å bands 77−10680

infrared spectra of diatomic inorganic molecules continued
FeO, matrix isolated IR spectra, ground state vibr. freqs. 80−28015
FeO, vibr. IR spectra, $X(^3\Delta)$ and the ground state 79−63998
H bonding molecules, self assoc., intermolecular interactions, matrix isolation vibr. spectra obs. Raman and IR spectra 80−52995
H_2 2.121 μ emission line vel. and width meas. towards Orion Nebula 79−17061
H_2 emission at 2 microns from Orion Nebula 78−93351
H_2, far IR absorpt., collision-induced at 77.4, 195 and 292K 78−13495
H_2, ground state S(2) line, search in Orion Nebula 79−8961
H_2, $H\bar{H}^1\Sigma_g^+$ state $H^1\Sigma_g^+$-$B^1\Sigma_u^+$ transition, $1<R<20$ a.u. 79−98094
H_2, interstellar, rot. transitions rel. to hot gases cooling 79−12505
H_2, lifetimes from collision induced absorption spectra, IR line broadening 78−33554
H_2, matrix isolated, IR spectra, mol. rot. and vibr. const. determ. 80−78617
H_2, predissociation of $^1\Pi_u^+$ state vibr. and rot. levels, dissoc. yields meas. 80−32784
H_2 S(2) 12.28 μm rotational line in Orion Molecular Cloud 80−41881
H_2+Ar, induced IR spectrum, overlap dipole moment determ. 77−18924
H_2+D(O)(Cl)(Br), relax. and chem. reaction, time resolved IR fluoresc. and mass spectrometry obs. 80−69177
H_2+H_2, quadrupolar $S_1(J)+S_0(J)$ double transitions, IR fundamental band, 77K 80−52986
H_2+He, far IR absorpt., collision-induced at 77.4, 195 and 292K 78−13495
H_x+H_2, hexadecapolar U-branch transitions in IR fundamental band 80−91631
HBr, and DBr, in monatomic matrices, near IR spectra and aggregate structs. 79−89667
HBr, far IR Ar matrix isolated spectra, 4.2K, press. and conc. effects 78−62801
HBr, fundamental IR band, solvent effect *(Russian)* 78−13501
HBr, IR matrix isolation spectra, N_2 matrix effects 79−36634
HBr, isotopic struct. and spectral characts. of vibr. band, using liq. N_2 Raman laser source 78−50859
HBr, vibr.-rot. absorpt. spectra at very high foreign gas densities 78−78687
HBr-Ar, IR fundamental region, line intensity, line breadth, tunable laser meas. 78−46328
HBr(Cl), absorpt. coeffs. meas. in Nd laser emission band 80−78620
HCl, 1-0 absorption bands, absolute wavenumber meas. 77−3361
HCl, absorption coeffs. for DF laser radiation, pollution detection appl. 77−27059
HCl, and DCl, in monatomic matrices, near IR spectra and aggregate structs. 79−89667
HCl, anhydrous conc. solns. in methanol, Raman and IR spectra 78−82724
HCl, coherent spectroscopy of anharmonic vibrations 79−18187
HCl, dissolved in carbon tetrachloride, far i.r. absorpt. intensity 77−463
HCl, far IR Ar matrix isolated spectra, 4.2K, press. and conc. effects 78−62801
HCl, IR matrix isolation spectra, N_2 matrix effects 79−36634
HCl, in dil. solution IR absorpt. fundamental shape temp. depend., solvent-solute interaction 79−26977
HCl, in inert solvents, far IR absorpt., free rotational models 77−450
HCl, spectral data analysis using graphics display terminal 78−54473
HCl, spectral line parameters in IR 79−22766
HCl, vibr.-rot. absorpt. spectra at very high foreign gas densities 78−78687
$H^{35}Cl$, collision broadened vibr.-rot. linewidths and shifts in fund. band, low temp. obs. *(French)* 77−68076
$H^{35}Cl$, $H^{37}Cl$, IR Fourier absorption spectra, press. induced shifts 78−74706
HCl-dimethylether complex, gaseous, H-bond IR spectra, temp. depend. theory 78−62804
HCl-Kr, rot. for IR spectra, anisotropic density fluctuations 79−54848
HCl+D(O)(Cl)(Br), relax. and chem. reaction, time resolved IR fluoresc. and mass spectrometry obs. 80−69177
HCl+iert gas, weak collisions, HCl spectral line broadening of IR spectra 80−74161
HCl+$N_2(O_2)(D_2)(H_2)$, HCl ν_0-ν_1 band perturbations, linewidth and shifts calcs., IR spectra obs. *(French)* 80−58251
HCl(-acetone)(-acetonitrile), soln., IR absorption, H-bonding, solvent effect 78−29778
HD, IR absorpt. spectra, collision induced fundamental band 77−79613
HD^+, ground state vibr.-rot. spectrum, high resolution laser-ion beam reson. expt. 78−82733
HD^+, IR hyperfine struct. of rot.-vibr. transitions calc. 77−42323
HD^+, spontaneous IR rot.-vibr. emission probability 78−50535
HD+Kr(Xe), collision-induced fundamental band in room temp. IR absorpt. spectra 77−34627
HF, 1-0, 2-0 absorption bands, absolute wavenumber meas. 77−3361
HF, cluster and chain dipole moments, ab initio calc. 77−26967
HF, far IR line shift, meas. using Michelson spectro-interferometer *(French)* 77−61875
HF, IR absorption in Born-Oppenheimer approx., vibronic gauge function for vibr. intensity 78−966
HF, IR Fourier absorption spectra, press. induced shifts 78−74706
HF, IR laser spectra 79−45936
HF in absorption, anomalous dispersion meas. 80−95881
HF, near IR absorpt. spectra, collisional broadening, line shapes and half-widths 79−89673
HF, pressure broadened linewidths in 2.5 μm band, influence of polymer form. 80−32777
HF, rot. population transfer using IR-laser double-resonance expt. 79−55128
HF rotational line shift, far IR Fourier transform spectrometry improvement 79−30582
HF+$O_2(a^1\Delta_g)$, E-V energy transfer 77−30960
$H_2^+(HD^+)(HT^+)$, IR transition freqs. calcs. 77−88452
HI, 1→0 IR absorpt. band 78−86863
HI, line strength meas., 0→4 and 0→5 absorpt. bands, dipole moment *(French)* 78−62847
HI nuclear quadrupole HFS in IR spectrum, obs. using tunable diode laser 80−58412
$H_2{}^{17}O$ and $H_2{}^{18}O$, centrifugal distortion anal. of ground vibr. states 78−70834
He H^+, formation and destruction in gaseous nebulae, assoc. IR emission line spectrum 79−44589
infrared spectra of diatomic inorganic molecules continued
He-Ar mixture, translational IR spectrum at 165K, binary and ternary absorptances 77−68042
He+Ar mixture, collision induced absorpt. calcs. 77−6777
$^4HeH^+$, IR rot.-vibr. spectrum obs. 80−23420
HfN, vibr. IR spectrum, mol. consts. 79−68230
HgH, predissoc. by rot., continuous rot.-vibr. spectrum, Weyl's theory 77−18996
HgH, predissoc. by rot., continuous rot.-vibr. spectrum, resons. and eigenvalues, Weyl's theory 77−18997
I_2, A-X system 79−63995
I_2, N_2 and Ar matrix isolated, magnetic circular dichroism spectrum 80−5567
I_2, $X^1\Sigma_g^+$ ground state, Le Roy's theory, continuous wave oscillation 79−94006
I_2-benzene, N_2 and Ar matrix isolated, magnetic circular dichroism spectrum 80−5567
ICl, ^{35}Cl and ^{37}Cl, $B^3\Pi_{0+}$ state IR spectra, mol. consts. 80−28016
ICl, $A^3\pi(1)$-$X^1\Sigma^+$ absorption spectrum, rotational analysis 80−47990
ICl, $A^3\pi(1)$-$X^1\Sigma^+$ emission spectrum, near-IR, rotational analysis 80−47991
K_2 saturated vapour, absorption coeff. 77−34625
K_2, vapour, IR absorpt. bands obs. 79−31527
KCl far IR complex permittivity meas. by dispersive Fourier transform spectroscopy, 7 to 300K 80−15940
KF, KCl and KI, monomers and dimers, Ar matrix-isolated, IR spectra, vibr. assignments and calcs. 79−45718
Kr_2, near IR absorpt. spectra 78−66547
KrF, laser spectra, absorpt. lines 80−9604
LiF, aggregation, microcryst. form., IR spectra obs. 78−46331
Mg_2 matrix isolated, vis. and near IR spectra 78−5214
MgO, from Mg+O_3 matrix reaction, IR spectra, isotope shifts and blue matrix shift 78−80736
^{24}MgH, transition probabilities, oscill. strengths, rot.-vibr. bands fine struct., stellar atm. appl. 77−18918
N_2, $B'^3\Sigma_u^- \rightarrow B^3\Pi_g$ (0,0) emission band 78−58690
N_2, collision induced far IR absorption at high press. 78−5161
N_2, collision-induced far IR absorpt., quadrupole moment 77−27163
N_2 continuum absorpt. contrib. to atm. transmission, 4.0 to 5.3 μm 79−92589
N_2 continuum rel. to atm. absorpt. spectra near 2400 cm^{-1} 78−11968
N_2, dispersive Fourier transform spectrometry using modular interferometer 78−89567
N_2, energy levels, low lying triplet states, infrared emission analysis 78−58691
N_2, gaseous, collision-induced absorpt., temp. depend., rel. to atm. far IR transmission 79−62584
N_2, gaseous, density behaviour of rototranslational spectrum, IR spectral obs. 80−28002
N_2 HP collision-induced translational-rotational far IR absorption obs. 77−38628
N_2, high-resolution electronic emission spectrum, 15300 Å 78−66549
N_2, in auroral upper atmosphere, vibr. excitation rel. to IR emissions 77−33247
N_2, in zeolite matrix, IR active fundamentals obs. 77−71800
N_2, liquid, Q-band position, width in cryogenic mixtures *(Russian)* 78−46401
N_2, multipole moments, far IR spectrum determ., pot. function effects 77−50435
N_2 solid matrix, ^{57}Fe Mossbauer spectra, Fe_xN mol. form., IR spectra confirmation 77−59496
N_2, spectroscopic data review 77−38680
$^{14,15}N_2$, Fourier spectrometry and IR emission spectra 80−83368
N_2+Ar(Xe), $A^3\Sigma_u^+$ state energy pooling in flowing afterglow, Herman IR system 80−83503
NH, IR emission studied using Fourier spectroscopy 80−95628
NO, absorpt. lines, spectral coincidences with CO laser lines 77−54559
NO, absorpt. lines spectral coincidences with CO laser lines 79−86162
NO, adsorbed on SiO films, infrared spectra exam. 79−45725
NO, and isotopic forms, $X^2\Pi$ state, IR obs., mol. consts. 78−42045
NO, and isotopic forms, $\nu=0$ electronic states, spin-rot. doubling 80−5540
NO, $b^4\Sigma^- \rightarrow a^4\Pi$ band system, rot. consts. 79−72312
NO, chemiexcited, form. in $N(^2D)+O_2$, 90-180K, IR obs. 78−90163
NO, chemisorption on goethite, IR spectra 80−7855
NO, far IR spectral lines and absorptance calcs. 77−46564
NO, Fourier transform spectra, intensity and self-broadening coeff. meas. 80−102503
NO, fundamental band spectrum, determ. of rotational, spin-orbit coupling and Λ type doubling consts. *(French)* 77−6768
NO, fundamental intensity and linewidth of IR absorpt. spectra, press. broadening 78−25530
NO, high resolution absorpt. spectrum in region of first ionization limit 77−461
NO, IR band absorpt. derivation from vibr.-rot. band spectroscopic variables 77−14434
NO, IR band nonrigid rot. absorption 78−91060
NO, IR spectra in O_2 matrix, vibr. freqs. 78−23936
NO, intracavity Zeeman modulation detect., passive Q-switching, CO IR laser obs. 80−9597
NO isotopes, spectrophone meas. at selected CO, CO_2 laser wavelengths 78−57310
NO, press.-broadened linewidths of $R(9.5)_{3/2}$ transition 78−70824
NO, Q-branch spectra, external-resonator controlled Raman laser pumped by CW CO laser 80−9624
NO $R_{1/2}(25/2)$ transition, extinction coeff. at 8-7 P(11) CO laser line 79−45711
NO, reson. absorpt. meas. with CO laser, spectroscopic data for pollution monitoring 77−37350
NO, rot. spectra, 714-1667 μm, Fourier interferometric spectrometer 77−83765
NO, rot.-vibr. fundamental obs., mol. consts. 77−57971
NO, Salyut 4 IR spectral obs. in upper atmosphere mid-latitudes 78−16223
NO, selectively excited rovibrational states, multiphoton ionisation spectra 80−69202
NO, sub-Doppler resolution IR spectra 78−86860
NO, Zeeman modulation IR spectroscopy using spin-flip Raman laser 79−18181
NO, Zeeman modulation spectroscopy, line shape analysis 80−74197
NO^+, interstellar transitions in mm and IR wavelengths 80−56906

infrared spectra of diatomic inorganic molecules continued
^{15}NO, vibr.-rot. transitions, Λ-doubling, optoacoustic spectroscopy meas. 78−42062
NO+$ClONO_2$, react., gas phase, kinetics, mechanism, IR photometric investig. *(German)* 78−76834
NO+Hg(6^3P_1)(6^3P_0), electronic-vibr. energy transfer collision, IR obs. 79−45716
NO^+(v=1,2)+N_2, vibr. transfer, vibr. absorption coeff. 79−6994
$^{14}N^{16}O$, overtone region IR emission spectra, vibr.-rot. Dunham coeffs. 79−41164
$^{14}N^{16}O$, v=2←0 overtone band IR spectra, Λ doubling, hyperfine struct. 79−41165
Na_2 vapour, IR absorpt. bands 80−102507
Na_x, matrix-isolated, formed in supersonic nozzle beam, 400-800 nm absorption and mass spectra obs. 79−76439
NaBr, far IR spectra, matrix isolated, monomers, dimers, trimers 78−66545
NaCl, far IR spectra, matrix isolated, monomers, dimers, trimers 78−66545
NaF, far IR spectra, matrix isolated, monomers, dimers, trimers 78−66545
NaI, far IR spectra, matrix isolated, monomers, dimers, trimers 78−66545
NaNe, laser spectroscopy, interat. pot. curves 78−86871
Ne_2, near IR absorpt. spectra 78−66547
NiO, matrix isolated IR spectra, ground state vibr. freqs. 80−28015
O_2 1.27 μ A-band intensity in lower atmosphere *(Japanese)* 78−61486
O_2 1.27 μm airglow emission, zenith angle dependence 77−45216
O_2 1.27μ emission, auroral enhancement 78−81485
O_2 7594 Å telluric A-band on objective prism spectra of stars, radial vel. meas. appl. *(Japanese)* 78−89083
O_2, (0,1)$b^1\Sigma_g^+ - X^3\Sigma_g^-$ band, integral absorption coeff. 78−20512
O_2, adsorbed on SiO films, infrared spectra exam. 79−45725
O_2, dispersive Fourier transform spectrometry using modular interferometer 78−89567
O_2, in auroral upper atmosphere, vibr. excitation rel. to IR emissions 77−33247
O_2, in zeolite matrix, IR active fundamentals obs. 77−71800
O_2 metastable states obs. in electron-beam controlled discharges *(French)* 77−30880
O_2, multipole moments, far IR spectrum determ., pot. function effects 77−50435
O_2 singlet energy transfer in quenching, vibr. excited mols. 77−71828
O_2, spectral line shape, Fourier representation of Voigt profile 78−90223
O_2^+, IR spectra, rot. anal. of b Σ_g^- a $^4\pi_u$ first negative band 78−5219
OH far IR rotational lines in stratosphere, column densities 80−36367
OH, ground state Λ doublet maser emission, overlapping far IR transitions 77−45533
OH, isotope effects, Zeeman effect, far IR laser mag-reson. spectra obs. 80−63674
OH, laser absorption spectrum, scanning technique, appl. to atmospheric monitoring 78−17664
OH, Pt catalytic oxidation of H_2 and D_2, matrix isolation and laser fluoresc. obs. of prods. 80−66865
OH radical, in Earth's atmosphere, pure rot. lines 79−92593
OH, vibr. ground-state, MFS, rot. spectra and electronic band anal. 78−5206
$^{12}O^{16}O$, $^{12}C^{18}O$, IR emission, vibr.-rot. lines 77−3355
$^{18}O_2$, Herzberg transition I in absorpt. spectrum 79−72313
P_2, ($A^1\Pi_g \rightarrow A'^1\Sigma_u^-$), IR emission spectra, Fourier spectroscopy, mol. parameter determ. 78−42056
P_2, $b^3\Pi_g$-$w^3\Delta_u$ and $A^1\Pi_g$-$W^1\Delta_u$ systems, IR emission spectrum 78−94244
P_2, intersystem transition obs. in absorpt. spectrum 80−48008
P_2 radical, $b^3\Pi_g$-$a^3\Sigma_u^+$ transition, perturbed by $l^3\Sigma_g^+$ state *(French)* 80−18855
PD^+, IR emission spectra, rot. anal. and mol. parameters 80−69134
PH^+, IR emission spectra, rot. anal. and mol. parameters 80−69134
PN, matrix IR spectra, aggregation to P_3N_3 77−83599
PO, in Ar matrix, IR and UV absorpt. spectra 80−47985
PbF, rot. anal. of B-X_2, B-X_1 and A-X_1 systems 77−58001
PuN, in Ar matrix, IR spectra, stretching freq. and isotope shifts 78−78690
PuO, in Ar and Kr matrices, IR absorption spectra, normal coord. anal., assignments, force consts. 78−78681
PuO, matrix isolation studies with Fourier transform IR 78−45740
RbF, RbCl and RbI, monomers and dimers, Ar matrix-isolated, IR spectra, vibr. assignments and calcs. 79−45718
S_2, $^1\Delta_g$ and $^1\Sigma_g^+$ states, near IR emissions 80−18852
SCl(Br), unstable radicals, matrix-isolated, IR spectra force const. *(German)* 80−43053
SD, $X^2\Pi_{3/2}$-state, far IR LMR spectra 79−6954
SF_6+N_2, simultaneous vibr. transition, absorpt. band intensity 77−50474
SO, and isotopic forms, $X^3\Sigma^-$ state, CO_2 laser mag. reson. spectroscopy 80−9602
SbF, ($f0^+$, $e0^-$)-$X_2$1 transition, rot. anal. 78−74657
ScD, emission bands in 5580 and 8603 Å regions 78−990
ScH, emission bands in 5580 and 8603 Å regions 78−990
ScS, $B^2\Sigma$-$X^2\Sigma$ system, rot. struct. and hyperfine effects near IR spectrum 80−5544
ScS, IR spectrum, vibr. consts. 77−10669
Se_2, $b^1\Sigma^+ \rightarrow X^3\Sigma^-$ near IR emission obs. 80−91556
SeH($X^2\Pi$), IR LMR spectrum, spin-orbit coupling const. direct determ. 79−76429
SeH($X^2\pi_{3/2}$), far IR LMR spectrum 78−66564
SeO, $b^1\Sigma^+ \rightarrow X^3\Sigma^-$ near IR emission obs. 80−91556
SeO, IR bands of 10296 and 10491 Å, rot. struct. 78−5224
SeS, $b^1\Sigma^+ \rightarrow X^3\Sigma^-$ near IR emission obs. 80−91556
SiBr, $B^2\Sigma^+ \rightarrow X^2\Pi$ transition, rot. anal. *(French)* 79−50013
SiC and IR excess of C stars 78−16413
SiO, isotopic lines in sunspots, $^{28}Si/^{29}Si/^{30}Si$ isotopic abundance ratio determ. 79−30044
SiO vibration rotation bands in sunspots, equiv. widths at 8 μ 78−40903
SiS, matrix IR spectra, aggregation to Si_2S_2 77−83599
Sr_2, matrix isolated, vis. and near IR spectra 78−5214
Te_2, $B0_u^+ - b^1\Sigma_g^+$ system, transition assignment, IR and visible spectra obs. 80−58298
$Th^{14}N$, $Th^{15}N$, matrix isolated IR spectra 79−59457
TiN, vibr. IR spectrum, mol. consts. 79−68230
TiO Φ system, near IR emission spectrum 80−69131

infrared spectra of diatomic inorganic molecules continued
TiO, $X(^3\Delta)$ state, vibrational IR spectrum using microwave powered molecular source, rotational analysis 80−9596
UN, identification in AR matrix, IR spectra, vibr. freqs. 77−9066
UN, matrix isolation studies with Fourier transform IR 78−45740
UO, matrix isolation studies with Fourier transform IR 78−45740
Xe_2, near IR absorpt. spectra 78−66547
XeF_4 matrix-isolated, search for IR fundamental 77−58017
YF, $^3\Phi$−$^3\Delta$ system, rot. anal. 78−9149
YH, YD, 3800-9000 Å negative glow spectra, triplet and singlet systems 77−79608
YI, IR $^1\Pi \rightarrow {}^1\Sigma$ system, Fourier spectrometry, rovibrational anal. 80−83360
ZnO, formed by matrix reactions, IR, Raman and visible spectra 80−87110
ZrN, vibr. IR spectrum, mol. consts. 79−68230
ZrO, predicted IR spectrum and possible presence in S-type stars 80−62124
ZrO spectrum, new $^3\Pi$-$^3\Delta$ system identification 80−23414
ZrO, $X(^1\Sigma)$ state, vibrational IR spectrum using microwave powered molecular source, rotational analysis 80−9596
ZrO^+ spectrum, $^2\Pi$-$^2\Sigma$ system identification 80−23413
$^{90,92,94}ZrO^+$, rot. anal. in near IR 80−74162

infrared spectra of inorganic solids
absorption spectrum, effect of electron-phonon interaction on vibronic peaks and phonon lines 78−43086
actinide (V) dioxocation containing compounds, coordinating props. 77−27869
actinolite, optical spectra obs. 77−40284
adsorbed layers, reflection-absorption IR spectroscopy, review, book contrib. 80−84747
adsorbed molecules, IR frequency shifts, coverage dependence 79−19464
adsorbed species, catalytic reaction, high temp. IR obs. 78−88655
adsorbed species, IR ellipsometric spectroscopy 80−39434
β-Al_2O_3-Na_2O, IR high temp. amplitude-phase spectroscopy 79−35860
alkali borate glass, IR absorption spectra and structure 79−8148
alkali germanate crystals and glasses, struct. and stability, IR spectra meas. 80−64911
alkali halates, NQR freq. temp. depend., phonon spectra interpretation 77−12226
alkali halide:H^-(D^-), local modes and colour centre absorpt. bands, analogy 80−60632
alkali halide:VO^{2+}, impurity behaviour, elec. cond. and IR absorpt. obs. 77−8607
alkali halide, adsorption of CO_2, field induced vibr. splitting, IR spectra 78−46334
alkali halide, electron trapping by alkali ion impurities 78−47809
alkali halide, far IR props. of lattice resonant modes, hydrostatic press. effects 77−28574
alkali halide, FCC, PO_4^{3-}-Al^{3+}(Sb^{3+}) anion-cation impurity mol. complex, IR absorpt. obs. *(Russian)* 77−16317
alkali halide, lattice dynamics calc., extended three body force shell model 78−47491
alkali halide, lattice props. from interorbital-distance-related-repulsion approach 78−22809
alkali halide, lattice vibrs., effect of NO_2^- impurity molecule, theory 77−35654
alkali halide, ReO_4^- doped, saturable absorber at 10.6 μm 80−53384
alkali halide, SH^- and SD^- impurities, shift of IR absorption band centre 77−16346
alkali halide crystal, containing mol. centres, IR absorpt. spectra, 77-630K 79−99863
alkali halide high-pressure submillimetric-wave spectra 79−33694
alkali halide thin films, photoacoustic determ. of optical absorptance of highly transparent solids 79−40632
alkali halides: SCN^-(CNO^-), absorption bands temp. depend. *(Russian)* 77−77260
alkali halides, absorpt. in molecules, clusters and microcrystals 78−80363
alkali halides, compressibility, force const. and IR absorpt. freq. 77−27955
alkali halides, cryst., force consts., IR absorpt. freq., logarithmic pot. function calcs. 78−2832
alkali halides, far IR reststrahlen spectra, γ-induced changes 77−40244
alkali halides, IR absorption spectrum, lattice vibrs., freq. and temp. depend. 79−65864
alkali halides, IR spectra, freq. and temp. depend. of charact. lattice vibrs. 79−65861
alkali halides, multiphonon absorption, quasiselection rules 77−24844
alkali halides, shift and broadening of local vibr. bands, temp. depend. 78−87755
alkali halides, temp. and press. depend. of transverse-optic modes and anharmonic self-energies 77−11649
alkali hydrides, thermodynamic props. calc. using ionic pots. 78−10155
alkali metal hexachlorotellurates, $A_2(TeCl_6)$, (A=Cs, Rb, K), IR and Raman spectra, lattice and internal modes, phase transition 78−6659
alkali metal metaniobates, electron spectra of polycrystals, 0.06 to 25 μm 77−20868
alkali metal metatantalates, electron spectra of polycrystals, 0.06 to 25 μm 77−20868
alkali metal polyphosphates, vitreous IR spectra 80−16043
alkali metal tetracyanoplatinate (FHF), one-dimens. conductors, IR spectra 77−77184
alkali metal tetrafluoroborates, intramol. force fields and mean vibr. amplitudes 80−2743
alkali phosphate glasses, colour and absorption spectra of Fe 77−85752
alkali silicate glasses, struct. and thermal props. 80−84075
alkali-alkaline earth silicate glasses, IR refl. spectra *(Japanese)* 78−52505
alkali-alkaline-earth silicate glasses, IR reflection spectra *(Japanese)* 78−19491
alkaline earth fluorides, hydrogenated mixed cryst., local mode absorpt. 77−81130
aluminate glasses, new families, light transmission, 0.4 to 6 μm 77−24843
aluminoborate glass, Fe and Cr ion interaction, mag. and spectral props. 80−103883
aluminophosphate glass:Mn:Mg(Sr), optical props. H_2O effects 77−28600

infrared spectra of inorganic solids continued
aluminophosphate glass, multicomponent, 3.2 micron broad absorption band computer anal., residual H_2O vibr. 78−52478
alunite-jarosite, spcae group refinement by means of vibr. spectroscopy 79−94981
amethyst, 3400 cm^{-1} IR spectra fine struct., H impurities 78−43910
amethyst, Fe^{3+} diffusion, associated phenomena 77−36269
amorphous, annealing effect on absorpt. edge *(Korean)* 79−15142
amorphous materials for IR and microwave absoprtion, temp. and freq. depends. 78−39539
amorphous pyramidally bonded solid, phonon density of states, spectra interpretation 77−8001
amorphous semiconductor, local order as determined by electronic and vibrational spectroscopy 79−37627
amorphous semiconductors optical absorpt. edge shape, band edge fluctuations 77−20880
amorphous solid, very far IR props. 78−80344
anfiferromagnet, superexchange, charge transfer light absorpt. 78−34975
antiferromagnet, IR absorption on impurity excitations near upper edge of spin-wave band 80−80829
antimonates, $M_4^{II}M^{III}Sb^{V}O_8$ spinels, struct. determ., IR and Mossbauer spectra 79−91431
apatites, condensation of tetrahedra, IR absorpt. band exam. 77−85760
aqueous glass, γ-radiolysis, photolysis of trapped electrons, quasi-free electron IR absorpt., luminesc. 77−21401
arsenates, $M^{II}M^{IV}(AsO_4)_2$, (M^{II}=Ba,Sr; M^{IV}=Ge,Ti,Sn,Zr,Hf), vibr. spectra, cryst. struct., bonding 77−36225
B_2O_3-Li_2O-LiCl, ionic conductor, IR refl. Raman study 80−66173
barium titanyl oxalate exam. of chemical production and thermal dissocation *(German)* 79−4935
benzil, phase transition, far IR spectroscopy meas. 80−71407
$Bi_{1-x}Sb_x$ narrow band gap semiconductors, galvanomagnetic, optical and photoelectric props. 80−15544
biotite, Mossbauer and optical spectra, Fe^{2+}-Fe^{3+} interactions 80−60470
bis(p-toluene sulphonate)diacetylene, monomer and polymer, solid state phase transformation, far IR transmission spectra obs. 80−55077
boracite, single cryst. prep. and phys. props. 80−100763
borate glass: Ni, absorption spectra, mag. props., coordination behaviour *(German)* 80−40147
borate glasses:Cu^{2+}, near IR electronic spectra, effect of alkali contents 78−27267
borosilicate glass, assignment of IR reflection spectra *(Japanese)* 78−10902
borosilicate glass, Fe and Cr ion interaction, mag. and spectral props. 80−103883
borosilicate glass, influence of Ti on absorption spectra of transition metals in glass 77−12403
borosilicate glass, IR refl. spectra resulting from phase separation *(Japanese)* 78−39542
borosilicate glass film, vapour-deposited, structural model, IR spectra meas. 77−1084
borosilicate glass sputtered film, phys. and chem. props., B diffusion into Si, SiO_2 80−29040
borosilicate glasses, porous, IR spectroscopic obs. of coordination state of B atoms 77−24268
butoxybenzylidene-aminobenzonitrile, crystalline and liq. cryst. states, low freq. spectra 78−34437
CaO:OH^-, room temp. IR spectra, heat treatment and electron irrad. effects 79−51992
CdSe two-photon absorption, laser calorimetric obs. 80−33076
cement, hot-pressed paste, strength, X-ray diffr., DTA, Ir spectra, microstruct. exam. 77−8864
ceramic crystalline materials, IR transmission, review 78−55417
ceramics, piezoelectric, photoacoustic effect 80−84252
chabazite type zeolite, cation substituted, IR spectra 30 to 470 cm^{-1} 78−10933
chalcedonies, structural disorder by IR spectroscopy 79−87450
chalcogenide glass films, reversible photostructural change obs. in IR absorption spectra 78−10897
chalcogenide semiconductors, optical and elec. props., comparison with SiO_2 78−6721
chalcopyrite type ternary crystals, IR dispersion *(Russian)* 78−76451
chemisorbed atoms and mols., vibrational motion dynamics, infrared absorpt. line shape 78−51814
o-chlorobenzoic acid: Nd^{3+}(Pr^{3+}) solid, vibrational spectra 80−84758
trans-1,4-chloroiodocyclohexane, liquid, crystalline and amorphous state, conformation and vibr. spectra, IR obs. 80−60568
chrysotile asbestos, photoacoustic spectrum using CW HF laser 80−7980
citrine, 3400 cm^{-1} IR spectra fine struct., H impurities 78−43910
complex band shapes, resolution by IR polarisation meas. 79−12873
complex contours interpretation of IR refl. bands, dispersional analysis 78−72508
complex disordered systems, IR absorption spectra, chem. bond. *(Russian)* 77−90155
condensed gas films, thermal radiation absorpt. 78−32824
continua, phonon theory 80−29729
corundum, complex reflection spectra, dispersional anal. 77−36239
corundum, optical, polished, surface layer obs. by IR reflection spectra *(Russian)* 78−19458
cross section, comparison with 77−85729
crystal, molecular lattice vibr. IR intensities, mol. polarisability calc. 80−11372
crystals, vibr. spectra, approx. calc. method *(Russian)* 78−35148
crystals of C_{4h}, D_{2d} and D_4 symmetry at second-order structural transform., spectroscopic props. 78−22845
Cu, adsorption of CO, on (110), LEED, surface pot., IR spectra 77−66092
p-$CuInTe_2$, single cryst., IR study of lattice and free carrier effects 80−45074
desert varnish, importance of clay minerals 77−86893
diamond:B, B conc. and impurity-to-band activation energy 79−56165
diamond:B, epitaxial layer, charge transfer and acceptor state 78−19169
diamond:B, photoconductivity and electroabsorpt. spectra 77−4647
diamond, GR1 band, anal. of satellite lines by quadratic Jahn-Teller computing 80−97295
diamond, N aggregates, partial dissoc. by high press.-high temp. treatment, IR spectra obs. 78−43904
diamond, natural, high conc. of implanted Si ions, He backscatt. and IR absorption 77−89466
diamond, natural, polycryst., distinctive features of struct. 79−92530

infrared spectra of inorganic solids continued
diamond, natural, rate of donor defect introduction by 2 MeV electrons, 0.348 eV absorption band 77−89477
diamond, natural, topography of impurity distrib. and neutron-induced colouring 77−39613
diamond, natural type IB, thermal conductivity anomaly, defects obs. 77−85003
diamond, optical absorption and luminesc. spectra, review 80−2848
diamond, optically active centre effect on strength props. 80−40462
diamond, semicond., electron irrad., charge carrier mobility 77−11921
diamond, semicond., energy band struct., elec. and optical props., review 77−35862
diamond, synthetic, transition metal impurity effect on IR absorpt. 79−82980
diamond, synthetic and natural, neutron irrad., optical and elec. props. *(Russian)* 78−59841
diamond, synthetic semiconductor, IR spectroscopy and cathodoluminesc. *(Ukrainian)* 79−78758
diamond, thermal cond. at low temp., correl. with IR absorpt. features 80−49435
diamond, type Ia, max. lattice freq., IR absorpt. spectra 80−16026
diamond, vacancy enhanced N aggregation, electron irradiation effects IR spectra 80−70245
diamond electron irradiated, photochromism 80−71454
dickite, unusual crystal habit, structural disorder 80−59445
dielectric absorpt. spectrum, charact. lattice vibrs. 80−2766
diffuse reflectance Fourier transform IR spectroscopy using diamond anvil cell 80−101855
trans-1,4-dihalocyclohexanes, far IR spectra of high press., using diamond anvil cell 79−12874
dimethylammonium cadmium tetrachloride, far IR refractive index, extinction coeff. and dichroism obs. 80−66144
disordered solids, rel. between simple analytic models 78−76473
electron reflection from metal surfaces, surface roughness, IR absorpt. 80−71526
enstatite ($MgSiO_3$) effects of irradiation with MeV protons 77−45534
exciton polariton attenuation, spatial dispersion effect 80−20097
far IR absorbent solid dispersive reflection meas., using Fourier spectrometer and cryostat 79−30580
far IR transmission spectral bandshape 77−32363
far IR transparent solid dispersive transmission meas., using Fourier spectrometer 79−30581
ferrites, EM wave effects on mag. and optical props., lecture 78−27031
ferroelectric semiconductors, props., book 80−82590
ferroelectrics, temp. depend. of soft mode freq. and its damping 79−38484
ferromagnetic alloy, disordered, intraband magnetooptic absorpt., theory 77−12366
ferromagnetic semiconductor, free carrier absorption below Curie temp. 79−47440
fibreglass insulating materials, radiative heat transfer rel. to optical props. 80−100367
fluorapatites, $M_4R_6(SiO_4)_6F_2$, (M=alkaline earth; R=Nd, Y, or Yb), synthesis and characterisation 77−24992
fluoride coating materials, refractive index, spectroreflectometry meas. 250 to 2000 nm 79−32006
fluorite structures, superionic props., IR spectra 80−107483
fluoroapatite, IR spectra, H motion in nonstoichiometric cryst. 78−35125
fluorophosphate system glasses alkali free and crystn. products, struct. and IR spectra 79−94913
frosts, Na and K doped, reflectance spectra and implications for Io surface 78−84561
fused silica, GeO_2-, P_2O_5-, B_2O_3-doped fibres, charact. *(Japanese)* 78−37981
garnets, IR refl., ATR, Voigt and Faraday expts. 80−66180
garnets from Sharns, IR absorption spectra *(Chinese)* 79−20831
Gd, optical conductivity meas., 0.5-3.1 eV *(Russian)* 80−45100
germanate glasses:Cu^{2+}, near IR electronic spectra, effect of alkali contents 78−27267
glass:Eu^{3+}, vibronic spectra, impurity complex model 78−19516
glass:Nd, surface struct., laser beam effects, IR spectra appl. 79−95250
glass, BK 7, ethoxysilane adsorption obs. *(German)* 78−30834
glass, far IR anomalous excitation obs. 77−40245
glass, IR total internal refl. spectrum, surface polaritons *(Russian)* 77−20861
glass, molecular water, IR spectra 77−43992
glass, porous Vycor, surface phonons, Raman and IR reflectivity spectra meas. 78−38931
glass, refractive index freq. depend., dispersion enq. calc. 80−40083
glass, surfaces joined by optical contact, spectral absorpt. of water layer 78−46852
glass fibre waveguide, γ-irrad., reversible optical bleaching of induced absorpt. 80−14462
glass high-temperature transmission/wavelength characteristics *(French)* 79−7188
glass interface with anodic electrolyte solution, simultaneous transfer of different cations in elec. fields 78−30800
glass structure, vibr. spectroscopy studies 80−84732
glass with hydrophilic protective coatings 78−85019
glasses, elec., mag., and optical props., conference, Troy, NY, USA (Aug. 1979) 80−105417
graphite, IR active optical vibrations, IR reflecting meas. 77−69837
graphite, IR optical properties, refl. data and complex dielec. function 78−10889
graphite, magnetoreflection under press., Landau level transitions 80−50303
graphite, optical probe of lattice dynamics 78−35131
graphite, pyrolytic, IR reflectance, dielec. props. 77−55781
graphite, reflectivity in near IR and hydrostatic press. 79−91423
graphite, reflectivity in near IR under hydrostatic press., lineshape anal. 79−91424
graphite and graphitic intercalation compounds, lattice dynamics 78−34574
graphite intercalate with SbF_5 and AsF_5, optical reflectance 78−35163
graphite intercalated with Br_2, Fermi level, far IR magnetorefl. expts. 77−40228
graphite intercalation compounds, band struct. model, dynamical dielec. function, reflectivity 80−34348
graphite intercalation compounds, interband Landau level transitions, magnetorefl. 77−52095

infrared spectra of inorganic solids continued
graphite intercalation compounds, low energy optical transitions, refl. spectra, and X-ray diffr. 80−25371
graphite intercalation cpds., K-point effective masses and Fermi level shifts, magnetorefl. study 80−50305
graphite intercalation cpds., Raman scatt. and IR refl., review 80−45066
graphite nitrate, $(C_{3.24})^+(NO_3)^-3HNO_3$, DTA, NMR and refl. meas., dynamical and electronic props. 77−59478
graphite-$AlCl_3$, well-staged, Raman and IR spectra 80−50339
graphite-alkali metal intercalation cpds., IR, active lattice mode obs. 80−45072
graphite-$FeCl_3$ intercalation complex, IR and Raman spectra study of optical modes 79−56797
graphite-$SbF_5(Cl_5)$ intercalation compounds, compacts, elec. resistivity, C fluorination 80−34493
graphite-SbF_5 intercalation compounds, elec. cond. and opt. reflectance 77−62970
group V, transition metal dichalcogenides, layered, thermoreflectance spectra 77−52120
gypsum, struct., vibr. spectroscopic obs. *(Russian)* 78−15175
highly absorbing solid, dispersive refl. meas. using modular interferometer 78−89568
highly doped semiconductors, far IR absorption 79−95787
hot electron distribution functions, expts., review 78−27231
hydrides, near-IR spectra, in Teflon powder matrix 78−3401
hydroxylapatites, IR spectra, H motion in nonstoichiometric cryst. 78−35125
hydroxylapatites, stretching and librational bands of OH groups, and hindered rotation 78−2841
ice, 3 μm absorpt. band rel. to identification in IR sources 78−49499
ice, amorphous, 2500-4000 cm^{-1} Raman and IR spectra, vibr. anal. 77−59562
ice, cryst. Ic and Ih phases, diffr. patterns and far IR spectra, isotope effects 78−6662
ice, cubic, D_2O isolated, H^+ exchange and Bjerrum defect migration, direct spectroscopic obs. 80−88356
ice, D_2O, H_2O, intramolecular potential from overtone spectrum anal., H-bonding dependence 79−93972
ice, disordered phase TO-LO splitting 79−91420
ice, H_2O:D_2O, I_c phase cryst., IR spectra, H exchange activation energy 79−99866
ice, hexagonal, i.r. polarisability rel. to mol. vibrs, anharmonicity 77−4639
ice, Ih, polycryst., vibr. spectrum anal., OH stretching region 79−11412
ice, II and IX, deuterated forms, 10K, OD stretching bands interpretation 78−2836
ice, IR ν_s absorption band profile of isotopically diluted OH group in crysts. 79−69821
ice, IR absorpt., O-H stretching vibrs., orientation polaris. 78−31177
ice, IV, 4000-400 cm^{-1} IR spectra, H-bonding and assignments, orientational disorder 80−16022
ice, O-H and O-D bond stretching vibrs., Raman spectra at atmospheric press. 80−66166
ice and amorphous solid water, D_2O-H_2O, intramolecular stretching spectrum, role of Fermi resonance 79−93973
ice I, assignment of O-H stretching bands in disordered state 78−19454
ice I, OH stretching region anal. of vibr. spectra 77−59563
ice I, polycryst., 2500-4000 cm^{-1} Raman and IR spectra, vibr. anal. 77−59562
ice platelets radiation attenuation effectiveness factor determ., IR absorpt. 80−66141
impurities, conc. of C, O, Si 78−59832
incommensurate structure, IR and Raman activity of soft modes, appl. to K_2SeO_4 79−28738
Inconel 600, PWR primary corrosion products 80−13578
inert gases, solid, absorption spectra of self-trapped excitons 78−43879
inorganic glasses, IR transmitting materials, appl. in 1 to 6 μm range, mech. props., review 79−4250
insulating thin film, thickness meas. by IR refl. spectroscopy *(German)* 79−58671
intermolecular interactions in condensed medium, long-wavelength IR spectroscopy 80−34927
intermolecular spectroscopy and dynamical properties of dense systems, conf., Varenna, Italy (1978) 80−82581
ion bombarded surfaces, spectral refl. 77−55308
ionic conductors, polaritonic spectra 79−23908
ionic crystal powdered stratified layers, lattice frequency 77−40222
ionic crystal spheroids, calc. using point matching method 77−32377
ionic crystallite, on substrate, IR active modes 77−1667
ionic rectangular crystallites, IR absorpt. calcs. 78−95583
IR active modes in large clusters of spheres, appl. to NiO powder 79−42964
IV-VI semiconductors, transverse effective charge from one dimens. band struct. calc. 80−15038
IV-VI semiconductors, transverse effective charge from three dimens. band struct. calc. 80−15039
Jahn-Teller multimode effect for E-term with strong vibronic coupling, IR and Raman spectra band shapes 80−20139
kaolinite, optical spectroscopy study of structural changes at 700-1000°C 79−65193
kaolinite-mullite reaction sequence, interpretation from IR absorption spectra, comment 78−48720
laser window material extrinsic absorption 79−14049
layered compound, anisotropy of lattice vibrs., polarisable ion model 77−35642
layered compounds, book contrib. 77−44023
leucosapphire, spectral absorption coeff., 0.25-1.25 micron, up to 1800K, and 3.5-5.2, up to 1200K 78−27204
ligand-metal overlap, rel. to ligand field and charge transfer interaction intensity 79−87067
lunar soils, IR spectra compared with astrophysical IR features 80−26728
magnetic materials, far IR absorpt. meas. by Fourier transform, apparatus 77−177
Maxwell Garnett theory, validity range 78−68507
metal, change in refl. on adsorption of molecular monolayer 79−65877
metal, highly reflecting, determ. of IR optical constants by surface plasmon excitation 78−76418
metal, IR absorption, contribution of conduction electron scattering 79−42971
metal, laser irrad., time-resolved specular reflectivity 79−69819
infrared spectra of inorganic solids continued
metal oxide metaphosphate glasses, vibr. study of metal cation reduction at surface 78−56797
metal particles, small, dielectric function and IR absorption 80−60607
metal particles, small, far IR absorption 79−61383
metal particles, ultrafine, eddy current nonlocal calc. 79−60744
metal surface oxidation, refl. spectra obs. 78−39958
metal surfaces, investigation by IR spectroscopy *(Japanese)* 78−19470
metal-insulator composite films, optical props., rel. to solar collector appls. 78−72622
metal-insulator composite solar selective absorbers optical props. 79−52037
metallic mirror coatings, protected and unprotected specular reflectance 79−76792
metallic particles, low-freq. EM absorption, particle size depend. 78−88311
metallic particles, small, far IR absorption cross-section calcs. 78−10879
metallic particles, ultrafine, far IR absorpt. calc. 78−60454
metallic particles, ultrafine, retardation effect on optical props. 78−6677
metallic powders, far IR absorption, self-consistent theory 78−56442
metallised coating on polyethylene terephthalate film, fracture under laser irrad. *(Russian)* 80−76333
metals, coated, IR surface wave interferometry 80−63913
meteorites, IR spectra compared with astrophysical IR features 80−26728
methanation catalysts, nonreduced, IR spectra 78−88288
$MgSiO_3$, Mg_2SiO_4, vapour condensed, mid IR optical props. 80−31337
mica tetrahedra, cation-apical O vibrs., IR spectra 79−47420
microstruct. depend. of optical props., SEM, XPS, and sputter depth-profiling 79−43049
minerals, IR spectra appl. to identification 79−62589
minerals, IR spectra exam. 78−84567
minerals, near IR spectra of hydrothermally altered rocks 80−81871
mixed alkali glasses, IR reflection spectra *(Japanese)* 78−19491
mixed alkali glasses, Raman and far IR spectra, vib. at cation site, struct. 78−60435
mixed crystals, diatomic linear chain model 77−39649
mixed valence compounds, anomalous IR absorption 80−66210
molecular crystal, lattice vibr., Raman and IR obs., review 78−43079
molecular crystal, two-phonon resonances, bound states absorpt. coeff. 78−47486
molecular crystal IR spectral line shape and polarisation temp. depend. 80−88991
molecular crystal lattice vibrs., IR intensities, dynamic multipoles model 80−11372
molecular glass, density of states for IR active internal modes of tetrahedral mols. 78−75788
molecular reorientation barrier, from LF lattice vibr. spectra 77−69824
molybdates, hydrated, water mol. bending vibrs. at low freqs. *(French)* 79−78670
molybdates, nonstoichiometric, IR spectra rel. to vacancy struct. *(French)* 78−43867
montmorillonite, Co^{2+} form, optical spectroscopy study of structural changes at 700-1000°C 79−65193
near IR diffuse reflectance analysis anomalies 80−86383
negative photoresist, KMR-747, transmission and refr. index 2 to 10 μm, interferometric meas. *(French)* 79−76780
neutron bombarded, optical absorption, struct. defect form. and nuclear alloying *(Russian)* 78−31206
NH_4 halides, halides, simple, complex, polycryst., hydrogen bonding, NH_3D^+ probe ion IR spectra 79−82966
nickeliferous limonites, pressure leaching for Ni extraction, using H_2SO_4 78−39717
niobates, columbite struct., IR and Raman spectra *(French)* 78−19485
noble metal complexes, hexafluoro, review of struct. obs., pseudorot., press. effects 78−6045
nosean identification, in sodalite and conversion of nosean sodalite 80−84907
olivine, heavy ion irradiated, and amorphous, IR extinction rel. to interstellar dust 79−53873
olivine, optical absorpt. spectra and radiative heat transport at high temp. 79−79818
olivine (Mg_2SiO_4), effects of irradiation with MeV protons 77−45534
opals, crystal struct. and IR spectra 80−40117
optical coating refl. spectroscopy 79−61448
optical fibres, glass and plastic, neutron irradiated, optical absorpt. spectra 0.7 to 1.1 μm 80−58762
optical glass, TI-20, IR transmitting semicond., dn/dT, wavelength depend. 77−77163
optical glass attenuation and optical density spectral curves 79−50361
oxide coating materials, refractive index, spectroreflectometry meas. 250 to 2000 nm 79−32006
oxide crystal, IR spectra at high temps. 77−48155
oxide crysts., Fourier transform Ir spectroscopy of vibr. states at high temp. 80−97256
oxofluorotitanates, preparation and characterisation 79−99872
oyster shell, IR and atomic mineral anal. 78−61116
PAA, liq. cryst., solid-state polymorphism, IR spectra meas. 77−4200
palygorskite, uncoupled H_2O, isotopic dilution IR obs. 77−8568
perovskites, ordered cubic, cationic effect on intramolecular forces, stretching force const. 80−88979
phase form. and relations, phys. props. 79−43218
phosphate glass: Ni, absorption spectra, mag. props., coordination behaviour *(German)* 80−40147
phosphate glasses, cation-site interactions 80−2744
phosphates, $M^{II}M^{IV}(PO_4)_2$, (M^{II}=Ba,Sr; M^{IV}=Ge,Ti,Sn,Zr,Hf), vibr. spectra, cryst. struct., bonding 77−36225
phosphosilicate films, deposited, P conc. meas. 79−69014
phosphosilicate glass film, vapour-deposited, structural model, IR spectra meas. 77−1084
photoacoustic spectroscopy using open membrane spectrophone 79−225
photoelasticity meas. 79−30443
photothermal absorber stacks on Ag, stabilisation 77−32459
phyllosilicates, laboratory spectra comparison with interstellar 10 micron absorpt. band 79−80344
plagioclases, singularities of IR spectra, struct. and composition depend. 77−78166
PLZT ceramics as electro-optic shutter material for IR appls. 79−72679
pnictide amorphous semiconductors, absence of photodarkening 80−103970
polar mode crystals, IR dispersion 77−73141

infrared spectra of inorganic solids continued
polar phonons, directional dispersion meas. by i.r. reflection 77−1665
polar semiconductor crystalline thin films, surface vibr. states, IR absorpt. spectra obs. *(Russian)* 80−60606
polaritons, appl. of IR reflectivity and Raman scatt. expt. 77−40237
polydiacetylene-toluenesulphonate, photocond. meas., 0.62-3.1 eV 80−70757
polyethylene, epitaxial crystallisation, IR investig., macromol. struct. changes 77−35493
polymer concretes, hydrothermally stable, hydraulic cement-type fillers 80−85144
polyoxyethylene, epitaxial crystallisation, IR investig., macromol. struct. changes 77−35493
polysilicic acid, IR spectra, struct., crystallisation effects *(Russian)* 78−72528
polyurethanes, epitaxial crystallisation, IR investig., macromol. struct. changes 77−35493
porous glass, adsorbed water molecule interaction with surface hydroxyls, IR spectra 78−43244
Pyrex, ion bombardment, form. of cpds., IR spectrosc. exam. *(German)* 80−88173
quartz:Co^{2+}, far IR absorption spectra, effect of phonons *(French)* 78−31186
quartz, amorphous and crystalline, surface polaritons and splitting of optical frequencies 78−72090
α-quartz, Au film coated, surface polariton dispersion, IR spectra obs. 78−48249
quartz, cryst., far IR complex refr. index spectra determ., new method, for transparent solids 77−28566
quartz, cryst. and melt, irrad., optical absorpt. spectra, computer calcs. *(Russian)* 78−92091
quartz, crystal growth in fluoride environment, growth features and props. 80−6373
quartz, electron irradiated, optical and anelastic absorptions and resonator freq. 78−64385
quartz, electron irradiation effects on optical, dielec., elastic props. 80−59521
quartz, Fourier transform Ir spectroscopy of vibr. states at high temp. 80−97256
quartz, fused, IR total internal refl. spectrum, surface polaritons *(Russian)* 77−20861
quartz, high-grade low-temp. impurity band IR absorption spectra 79−56825
quartz, hydrolytic weakening of natural and synthetic crystals, mech. and IR study 78−61410
α-quartz, IR absorption 79−42959
quartz, IR radiation extinction coeff. rel. to mechanical Q 80−100653
quartz, IR reflection spectra of rough surfaces *(Russian)* 77−48175
quartz, irradiated, fused, crystalline, absorpt. spectra, colour centres 80−7384
quartz, natural and synthetic, 3400 cm^{-1} IR spectra fine struct., H impurities 78−43910
quartz, OH^- impurity IR absorpt., electron irrad. effects 79−99913
quartz, pleochroic amethyst, optical absorpt. of d^4 ion Fe^{4+} 78−15201
quartz, pure, fused, optical consts. in far IR, 20 to 120 cm^{-1} 78−79080
γ-quartz, reaction, with NaCl-kCl melt, exam. of struct., IR absorption spectra 80−55706
quartz, shock-loaded, IR spectroscopic studies, solid-state glass prod. 79−19157
quartz, synthetic, characterisation by IR adsorption 79−56824
quartz, synthetic, deuterisation, EPR and IR absorpt. characterisation 80−92721
quartz, synthetic, electron beam irrad.-induced interstitial ion mobility, ESR centres and IR spectra meas. 80−39153
quartz, synthetic, lattice distortions, optical inhomogeneities by X-ray topography and optical birefringence meas. 78−55887
quartz cylindrical fibres in regular struct., multiple frustrated total internal refl. calc. 78−83094
quartz fibre, ESR and IR obs. of microinhomogeneities 77−8401
quartz glass, spectral absorpt. coeff., 0.25 to 1.25 μ and 1300 to 1700K 80−20622
quartz glass, spectral absorption coeff. in 2.0 to 4.8 micron region, up to 800°C 77−43985
quartz glasses, spectral adsorptance in 0.25-1.25 μ wavelength, 293-1273K temp. ranges 77−36212
quartz particles, embedded in NaCl, IR spectra, rel. to state of O impurity in Si 79−19914
quartz radiation defects, effect of annealing on absorpt. spectrum *(Russian)* 77−47495
rare earth compounds, R_2MoO_5, cryst. struct., IR spectra, elec. and mag. props. 80−33954
rare earth double orthophosphates with alkali metals, spectroscopic obs., struct. and chem. nature 80−100674
rare earth fluorides, as antirefl. coatings, evaluation 77−61963
rare earth gallium borates, high temperature crystallisation, composition, struct., props. 80−40253
rare earth garnets, prep. and props. book contrib. 80−44193
rare earth metal film, optical cond., rel. to cryst. struct. and electronic config. 77−36303
rare earth metal films, room temp. cond. free electron contrib., rel. to mag. transitions 77−1745
rare earth molybdo-perrhenates, synthesis and props., cryst. struct., IR spectra *(French)* 79−32976
rare earth orthophosphates, RPO_4 (R=Tb, Dy, Ho, Er, Tu, Yb, Lu), IR and Raman spectra 80−34904
rare earth orthotitanates and orthovanadates, interrelationship between cryst. struct., IR spectra and physiochem. props. 77−24835
rare earth oxide film, transmission of refl. spectra, opt. consts. and parameters 79−95864
rare earth oxide films, optical absorpt., refractive index, band gap and zone struct. *(Russian)* 78−76544
rare earth oxides, binary, struct. and props., book contrib. 80−45292
rare earth oxymolybdates and oxytungstates, R_2MO_6, spectroscopic props. and crystallochem. laws 77−36215
rare earth oxyphosphates, IR and Raman spectra, vibr. assignments, cryst. struct. characts. 80−97258
rare earth selenides of yttrium subgroup, powder prep. conditions and energy of optical transitions 77−63581
rare earth substituted lead apatites, $Pb_{10-2x}R_xM_x(PO_4)_6Z_2$, M=Na or K and Z=F or Cl, cryst. struct. and IR spectra 80−107167

infrared spectra of inorganic solids continued
rare earth sulphides-1.8 Ga_2S_3 glasses, vibr. spectra, electronic transitions, short range order 77−69820
rare earth systems, mag. field depend. of polaritons 79−33246
rare earth thiohafnates, thermal stability and oxidation products in air 79−83346
rare earth thiosulphate, $R_2(S_2O_3)_3.4H_2O$, possible evidence for nonexistence of cpd. of given formula *(French)* 77−24279
rare earth titanates, pseudoperovskite struct., nonlinear spectral and luminesc. characts. 80−29771
rare earth vanadites, X-ray fluoresc., IR and UV spectra 77−77206
rare earth-gallium sulphide glass, R_2S_3-1.8Ga_2S_3, vibr. and electronic spectra, short-range order 78−27228
rare-earth oxides, absorption spectra and energy levels of trivalent ions 77−63420
refl. depend. on angle of incidence, 8 to 12 μm 78−37960
resonant far IR absorption by impurities 78−6715
rhombic distortion of cryst. lattice at low temp. 78−2253
Rochelle salt, ferroelectric, Raman and IR study 80−71406
rocks, IR spectra exam. 78−84567
rocks, metamorphic, visible and near IR spectra rel. to comp. 77−17087
rocks, sedimentary, visible and near IR spectra rel. to comp. 77−17086
rocks from Cr-rich areas, visible and near IR spectra, remote sensing appls. 80−4000
rocks of volcanic origin, refl. characts., 400-800 nm 80−90073
ruby, E, 2A levels, laser excitation, Zeeman spectra 78−43908
ruby, spectral absorption coeff., 0.25-1.25 micron, up to 1800K, and 3.5-5.2, up to 1200K 78−27204
ruby colouring due to specific growth, annealing and irrad., exam. of visible, infrared and UV spectra 79−11440
sapphire substrate surface evaluation for SOS 77−76653
scheelite crysts., Davydov splitting of vibr. levels, short range interaction 80−71418
semiconductor, carrier intrinsic conc. and effective mass determ. by IR refl. 79−51580
semiconductor, direct gap, one-photon Keldysh absorption 77−8599
semiconductor, inhomogeneously doped, computed IR refl. spectra 78−27205
semiconductor, intervalley cyclotron-phonon reson., IR absorption in mag. field 78−60448
semiconductor, IR plasma reflectivity spectra analysis 78−52480
semiconductor, nonequilibrium optical phonons generated by electrons in laser radiation field 78−71802
semiconductor, nonlinear light absorption in presence of laser wave field 78−13747
semiconductor, optical and IR characterisation 79−95846
semiconductor, p-type, infrared absorption and plasma reflection 80−97284
semiconductor, surface space charge layer spectroscopy 77−20386
semiconductor, vibr. IR excitons, spectra *(Russian)* 78−15173
semiconductor, weakly polar, IR absorption by optical polaron in mag. field 77−66127
semiconductor film, quantised, one-phonon light absorption 78−60527
semiconductor materials, optical characterization 80−50352
semiconductor-insulator system, contact interaction mechanism, optical props. 78−88375
semiconductors, amorphous, optical absorption, theory 80−80818
semiconductors, doped, IR absorpt. in Drude tail, effect of finite electron densities 79−47449
semiconductors, elemental amorphous, vibr. props., review 77−84873
semiconductors, laser window materials, residual lattice absorpt., freq. and temp. depend. 78−25910
semiconductors, light absorption, amplification and luminescence, saturation effects *(Russian)* 78−13771
semiconductors, n-type, free carrier absorpt., ionized impurity scatt. 79−42999
semiconductors, optical props. due to phonons, book contrib. 80−80805
semiconductors, weakly doped compensated IR light absorption by small scale fluctuations *(Russian)* 80−66255
semiconductors, weakly polar, free polaron IR absorpt. effect of DC field 77−81132
serpentine minerals, IR specta, comparison with Orgueil, type C-1 chondrite 80−17556
Si:P(As)(Sb)(Bi), high resolution study of group V impurities absorption 80−7388
Si, ion implanted by high energy C ions structural and optical props. 80−107292
Si inversion layers, prep. domain studies of intersubband optical transitions 80−20637
silica gel, infrared absorpt. spectra *(Russian)* 77−55794
silica gel, IR spectra of dry transparent plates, surface struct. study 79−87884
silica gel, struct., dielec. polarisation, IR spectral investigs. *(French)* 77−81427
silica gels, surface treatment, adsorption properties *(Japanese)* 78−95855
silicate glass, assignment of IR reflection spectra *(Japanese)* 78−10902
silicate glass, hydration in steam atmosphere 80−85211
silicate glass, IR refl. spectra resulting from phase separation *(Japanese)* 78−39542
silicate glass, IR reflection spectra relation to corrosion state of surface *(Japanese)* 78−88554
silicate glass corroded by moisture, IR refl. spectra change *(Japanese)* 78−53013
silicate glass. IR reflection spectra change due to moisture corona *(Japanese)* 78−19914
silicate glasses:Cu^{2+}, near IR electronic spectra, effect of alkali contents 78−27267
silicate glasses, relation between IR reflection spectra and corrosion state *(Japanese)* 78−23850
silicate glasses, struct. and phase transform. 78−64538
silicate minerals, thermodynamics and lattice vibr. props. 79−100830
silicate smokes, vapour condensed, IR absorpt. peaks compared to interstellar extinction curve 80−82180
silicates, amorphous, IR extinction meas., rel. to interstellar dust 77−12352
silicates, IR spectra compared with astrophysical IR features 80−26728
small metallic particle, theory of far-IR absorpt. 79−19881
small-particle metal-insulator composites, anomalous far IR absorption 80−71427

infrared spectra of inorganic solids continued
SmS film, metallic, interpretation of optical absorption spectrum 78−27344
sodalites, aluminogermanate- and aluminate-, IR spectra rel. to T-O bond length and T-O-T ang. 79−91445
solid surface, microgravimetric-IR study 80−76577
space group refinement by vibr. spectroscopy methods, possibility 78−79507
sputter-deposited materials, electrical and optical props. 79−47181
stainless steel, 304, cryogenic constructing material, far IR spectral refl. 77−24855
steel, BN extraction, and identification, IR anal. 80−85254
steel, stainless, 304, partially ordered, i.r. absorptance, 0-600°C 77−4632
steel, stainless, hard, and mild, optical constant dispersion and emissivity, up to 900K 78−52464
steel, stainless, PWR primary corrosion products 80−13578
substrate, surface quality determ. by optical reflectance methods 78−43862
substrate heating in vac., heating method rel. to spectral characts. 77−7223
superconducting film, with spatially varying order parameter, far IR absorption 77−28284
superionic conductors, light scatt. and IR absorpt. book contrib. 80−25382
surface, use of vacuum ultramicrobalance 79−71465
surface films on metals, using spectrophotometer multiple reflection attachment 79−71543
surface polariton interaction with periodic surface struct. 77−47879
TCNQ salt, MTPA $(TCNQ)_2$, IR refl., dielec. function and cond. 80−34924
tellurite glasses, binary, struct. and props. *(Japanese)* 79−32917
ternary alloys, vibr. freq. distrib. spectra, small cluster statistical theory 79−24317
tetracyanoplatinate conductors, IR and Raman spectra, cyanide stretching vibrs. 79−11415
tetracyanoplatinates, energy band calcs. 77−39780
tetrahedral glass AX_2, band limits and vibrational spectra 79−73935
tetramethylammonium hexabromotellurate, far IR and Raman spectra and phase transitions 80−11376
TGS, ferroelec., phonon contributions to anomalous sp. ht. near phase transition temp. 77−52023
TGS(Se), optical phonons near T_c, IR refl. and Raman spectra 77−48136
TGS(Se), optical phonons near T_c, nonlinear pseudospin-phonon interaction 77−48137
thiourea, ferroelectric, Raman and IR study 80−71406
$(TMTSF)_2X$, $(X=PF_6^-, AsF_6^-, SbF_6^-, BF_4^-, NO_3^-)$ highly conducting salts, props. 80−59969
transition metal, optical consts. 12 to 24 μm, anomalous skin effect region 77−20842
transition metal carbides and nitrides, surface energy for brittle fracture from phonon freqs. 79−86837
transition metal chalcogenophosphates, intercalation with n butyl-lithium, possible appl. in Li batteries 80−71446
transition metal complex anion, vibr. spectra in solid and soln., struct. and fundamental mode assignment 78−62803
transition metal dichalcogenides, optical phonon modes and localised effective charges, reflection spectra 78−76453
transition metal hydrides, IR spectra, vibr. levels, struct., H_2 chemisorpt. appl. 77−48686
transition metal monoantimonides, 3d-states, optical evidence for analogy with transition metals 77−62816
transition metal surface, spin orientation effect of shallow electrons by magnetization 79−65881
transition metals, BCC, thin films, optical props. 79−78781
tremolite, optical spectra obs. 77−40284
TTT_2-$(I_3)_{1+x}$, physical props., elec., mag. and optical meas. 80−24908
uniaxial crystal, dispersion of bulk phonon polaritons meas. by IR refl. 78−59902
vermiculite, interlayer space struct. anal., by replacing exchange cations with NH_4^+ 77−7700
vibrational spectra crystals with split configuration interstitial *(Russian)* 78−76450
VPE, growth processes, in-situ obs. *(Japanese)* 80−35104
water, continuity of state between liquid and amorphous solid, IR obs. 79−8130
water, low-density amorphous solid, IR spectrum, OH stretching region 79−11411
water, low-density amorphous solid, OH stretching spectrum 79−11413
water cryofilm, on specular and diffusing surfaces, bidirectional reflectance 78−88274
zeolites, and Ga analogues, IR spectroscopy to investigate structure 79−95744
zeolites, type Y, containg catalysts, cryst. struct., IR spectra 79−42958
zero-gap semiconductors, anisotropy of IR absorpt. coeff., k.p. calc. 80−97285
zero-gap semiconductors, reson. two phonon absorpt. 79−55847
Zircaloy, PWR primary corrosion products 80−13578
γ-Al_2O_3, physisorption and reaction of $Mo(CO)_6$, IR spectra obs. 80−80064
Ag, absorpt. coeff. temp. depend., IR, 3 to 30 μm 78−74953
Ag, chemisorbed ethylene, IR refl. obs. 77−31903
Ag electrodeposition, on (100) face of single crystal Ag in presence of sulphadiazine 80−89161
Ag film, electroreflectance effects 79−43055
Ag film, evaporated, chemisorption effects on reflectance and elec. resist. 80−11495
Ag halide photochromic glasses, optical properties, effect of Cu ions 80−93364
Ag halides, temp. and press. depend. of transverse-optic modes and anharmonic self-energies 77−11649
Ag, intraband optical conductivity, electron-electron scatt. 78−35166
Ag sphere, ultrafine, with dielectric cores, optical absorpt. 78−60455
Ag, surface polariton absorption and emission spectra, edge effects 78−10375
Ag ultrafine particles evaporated on glass, optical transmittance meas. 79−78772
Ag-Cu, metastable alloy film, optical props. 77−12460
Ag-Cu, optical spectra, 0.5-6 eV, d-band struct. 77−48168
Ag-Hf(Ta)(Pt) film, optical absorption spectra meas. 77−85823
Ag-SiO_2 film, elect. and struct. props., ion beam sputtering 78−80071

infrared spectra of inorganic solids continued
Ag-Zr(Nb)(Mo) film, dielec. const., optical props., DC resist. and thermoelec. power 77−85824
Ag_3AsS_3, proustite, cryst., vibr. spectra 78−48172
Ag_3AsS_3, proustite, reflectivity and optical constants at 80K and 300K from 18 to 700 μm *(French)* 77−36235
AgBr, far IR spectra, cond., cation local motion 79−1754
AgBr, lattice dynamics, 295K, three-body-force shell model 77−15517
AgBr, one-phonon sidebands, rel. to anal. of 4.4K neutron scatt. data 77−39643
AgBr, pure and doped, identification of shallow electron centres 77−59267
AgBr:Li^+, time-depend. infrared absorpt. due to Li-localised mode 79−8133
AgBr:Li^+(Na^+), impurity induced IR absorpt. 80−7386
AgCl, pure and dopded, identification of shallow electron centres 77−59267
$Ag_{0.85}Cu_{0.15}Br$, far IR spectra, cond., cation local motion 79−1754
$AgGaCr_4S_8$, IR spectra obs. of ordering *(German)* 78−6669
$AgGaS_2$-$AgGaSe_2$ system, phase diagram, lattice consts., and IR spectra 80−60841
$AgGaSe_2$, growth by Bridgman method, optical characts. 77−69980
$AgGaSe_2$, optical phonons, IR reflectance meas. *(French)* 77−81095
$AgGaSe_2$, polarised IR refl. spectra, optical phonon modes 77−16304
$AgGaSe_2(Te_2)$, phonons, far IR refl. obs. 78−60459
$AgGaTe_2$, optical phonons, IR reflectance meas. *(French)* 77−81095
Ag_8GeS_6, fundamental absorpt. edge changes due to polymorphic transitions 77−20240
$Ag_8GeS_6(Se_6)(Te_6)$, Ag_8SiSe_6, $Ag_8SnS_6(Se_6)$, absorpt. edge investigs. at phase transitions 78−35149
Ag_8GeSe_6, fundamental absorpt. edge changes due to polymorphic transitions 77−20240
Ag_8GeTe_6, optical props. and polymorphism 80−45082
$Ag_2H_3IO_6$, paraelec. and antiferroelec. phases, IR vibrational study 77−85697
AgI, density of states, IR cond., and Raman scatt., lattice dynamics calc. 78−30709
AgI, superionic conductor, dynamical aspects 78−79695
AgI type solid electrolytes, expt. props. 78−63877
AgI-Ag_2O-MoO_3, superionic conducting glass, IR spectra and struct. 79−10804
AgI-Ag_2O-MoO_3 glass glass superionic cond., struct. and transport props. 80−88602
$AgInCr_4S_8(Se_8)$, 1:1 ordering on tetrahedral sites obs. *(German)* 78−6669
$AgInSe_2$, far IR refl. spectra, polarised light 78−43870
$AgInSe_2$, far IR refl. spectra, ionic bonds 79−55695
p-$AgInSe_2$, reflectivity 40 to 400 cm^{-1} range 79−42976
$AgInSe_2(Te_2)$, phonons, far IR refl. obs. 78−60459
$AgInTe_2$, far IR refl. spectra, polarised light 78−43870
$AgInTe_2$, far IR refl. spectra, ionic bonds 79−55695
Ag_8MSe_6, (M=Si, Ge, Sn), forbidden energy gap changes under high press., polymorphic transitions 77−51649
$AgNO_3$, cryst. and molten salt, Raman and IR spectra, vibr. anal. 77−16311
$AgNO_3$, differences between diffr. and vibr. spectroscopic results 79−69818
Ag_2S, metal-nonmetal transition, crystallographic, optical, mag. and transport props. 78−6418
Ag_3SI, superionic conductor, dynamical aspects 78−79695
Ag_3SbS_3, IR refl. spectra, permittivity, lattice vibrs. 79−65862
Ag_2Se, metal-nonmetal transition, crystallographic, optical, mag. and transport props. 78−6418
Ag_8SnS_6, fundamental absorpt. edge changes due to polymorphic transitions 77−20240
Ag_8SnSe_6, fundamental absorpt. edge changes due to polymorphic transitions 77−20240
Ag_2WO_4, preparation and characterisation 79−99873
$Ag_2W_2O_7$, preparation and characterisation 79−99873
$Ag_2W_4O_{13}$, preparation and characterisation 79−99873
Al alloy, 5083, cryogenic constructing material, far IR spectral refl. 77−24855
Al, anodized, as cryogenic material, IR reflectance 79−61387
Al, condensed film, phase and struct. nonuniformity *(Russian)* 80−54536
Al, diamond-turned, surface reflectivity meas. 1 to 12 μm 80−1298
Al film, optical cond., energy derivative spectrum 77−66551
Al, IR laser reflectance, anomalous absorpt., plasma ignition 80−7439
Al, low vacuum condensates, struct., IR refl. obs. *(Russian)* 78−30850
Al saponite, differential thermal anal., IR absorpt. spectra, chlorite-like mineral 78−88816
Al, surface oxide layer, Fourier transform IR emission studies 79−67399
Al, transient reflectivity at 10.6 μm 79−11408
Al, ultrafine particles, far IR absorpt. 77−52084
Al ultrafine particles, optical props., 0.3-2.5 μm 80−76020
Al-Mg alloys, 3004 and 5182, oxide films, IR refl. spectra characterisation 77−77644
$Al_{0.4}Ga_{0.6}As$:Te, saturable optical absorpt. of deep Te-complex centre 79−99917
$Al_{1-x}Ga_xP$, IR phonons, lattice reflection spectra 78−51626
$Al_xGa_{1-x}P$, solid solutions, refr. index dispersion characts. *(Russian)* 77−81080
AlGaSb, growth and characts. for 1.0-1.8 μm heterojunction devices 78−6870
$Al_xGa_{1-x}Sb$ mixed crystal, two-phonon absorption meas., 15-48 μm 77−1682
AlN, ultradispersed powder, IR spectra 80−50312
$Al(NO_3)_3.9H_2O$, cryst., deuteration rel. to NO_3 ion vibr. spectrum *(Russian)* 77−40240
$AlNbO_4$, diffuse refl. and luminesc. spectra 78−56516
β-AlO_3-(Na,Li)$_2O$, NMR, Raman and IR spectra, and X-ray diffr., heat treatment induced changes 80−107508
Al_2O_3, adsorption of linoleic acid, under carbon tetrachloride immersion, IR obs. 79−24822
Al_2O_3 anodic films, formed on Al, optical reflectance method anal. 80−37073
Al_2O_3 anomalous absorpt., in far IR region 78−56464
Al_2O_3, corundum, Fourier transform Ir spectroscopy of vibr. states at high temp. 80−97256
Al_2O_3, film, form. in discharge, IR absorpt. spectra *(Russian)* 77−12461

infrared spectra of inorganic solids continued
Al_2O_3 film, on Al, IR refl. obs. 78−35591
Al_2O_3 film, RF sputtered by planar magnetron, phys. props. 77−43448
Al_2O_3 film on Al substrate, IR photoacoustic spectra 80−13163
Al_2O_3 films, amorphous, self-supporting, vac.-tight, from electrochem. oxidation of Al in $(NH_4)_2CO_3$ solns. 80−16177
Al_2O_3 films, DC reactive sputtering prep., IR spectra characterization 79−11513
Al_2O_3 films obtained by pyrolysis of Al acetylacetonate, struct. and props. 77−85098
Al_2O_3, films on Al, photoacoustic refl.-absorption spectroscopy 78−31264
γ-Al_2O_3, heat treated, SO_2 adsorpt., IR spectra 79−56070
γ-Al_2O_3, hydrate covering, surface struct., IR spectra meas. 77−89622
Al_2O_3, hyperfine film on metal, IR refl.-absorpt. spectra *(Russian)* 78−11014
α-Al_2O_3, IR absorpt. spectra of OH , OD , and OT^- 80−55145
α-Al_2O_3, IR intensities, valence-band dynamic and electrooptic models 80−34906
Al_2O_3, IR spectra, comparison to inelastic electron tunnelling spectra *(French)* 78−68489
Al_2O_3, noncrystalline films, opt. and elec. props. 77−51627
α-Al_2O_3, single crystal transmission and reflectance IR phonon spectra, polariton dispersion 80−66170
β-Al_2O_3, stoichiometric, Raman and IR spectra, Frenkel defects, order-disorder transition and cation cond. 80−55086
β-Al_2O_3 structures, superionic props., IR spectra 80−107483
Al_2O_3 surface, acidity, rel. to topochem., IR determ., adsorption method 80−35611
Al_2O_3, surface microstructural changes due to reduction by C *(Russian)* 80−100378
Al_2O_3:Co, spectra, heat treatment and irrad. effects 77−4659
α-Al_2O_3:Co,H, Co and proton ENDOR, IR and optical spectra charge compensator nature and defect struct. 80−44956
Al_2O_3:Cr^{2+}, multiple-ion phonon absorpt. 79−82971
Al_2O_3-B_2O_3-SiO_2 sheet glass, solar energy appl., optical and mech. props. 80−87447
β-Al_2O_3-H_3O^+ protonic cond., struct. investig. 79−19213
β-Al_2O_3-$H^+(H_2O)_n$, IR and Raman spectra, OH stretching freqs., struct. and cond. 78−27210
β''-Al_2O_3-$H^+(H_2O)_n$, IR study 80−16037
B-Al_2O_3-M_2O, M=Na, Ag, Rb, K, far IR absorption and ionic cond. 78−72512
β-Al_2O_3-NH_4^+, protonic cond., struct. investig. 79−19213
β-Al_2O_3-Na_2O, cation vibrations, disorder and hydration, IR and Raman spectra *(French)* 80−7343
β-Al_2O_3-Na_2O-K_2O, cation interstitial pair modes in vibr. spectra 79−37788
β-Al_2O_3-Na_2O-Rb_2O, cation interstitial pair modes in vibr. spectra 79−37788
Al_2O_3-SiO_2, struct., localised radiation centres, spectroscopic investig. *(Russian)* 77−69844
Al_2O_3-SiO_2 system, andalusite and kyanite powders, shock induced transformations 80−45301
β-Al_2O_3-X_2O, (X=Na,K,Rb,Ag,Tl), infrared and Raman spectra 79−1761
γ-AlOOH and γ-AlOOD, struct. and D_{2h}^{17} space group anal. 80−89000
γ-AlOOH, boehmite, lattice vibrs., evidence for C_{2v}^{12} space group 79−28756
$Al(OOH)_3$, formed by reaction of methyl esters and $Na_2Al_2O_2$, exam. of props. 78−48346
AlPO cristobalite form, polymorphic transform. investig., X-ray diffr. and IR spectra 77−4199
$Al(PO_3)_3$-NaF system, glasses, IR spectra and struct. 79−65882
$Al(PO_3)_3$-NaF-LiF glasses, mixed-alkali effect 80−19715
$\alpha AlPO_4$ as SAW substrate material, piezoelec. props. 80−80710
α-$AlPO_4$, IR and Raman spectra, optical phonons 80−2767
Al_2SiO_5, andalusite, phonon spectra and rigid-ion model calcs. 80−11391
AmO_2, IR spectra, values of transverse vibr. frequencies 77−28585
Ar, optical absorpt. and luminesc. spectra, obs. of relaxed exciton states 77−52082
As, amorphous, bonding coordination defects, Raman scatt. and IR absorption meas. 78−60498
As, amorphous, optical, vibr., transport and defect-related props., review 79−51935
As, amorphous, refr. index meas. near absorpt. edge 78−2819
As, amorphous, vibr. excitations at defect sites, IR and Raman spectra calc. 80−49329
As, amorphous, vibrational excitations of defect sites 80−49332
As, amorphous and cryst., phonon density of states calc., comp. to IR absorpt. and neutron scatt. data 78−55924
As amorphous solid dielectric loss meas. by submillimetric waveguide laser 79−33603
As, interband, magnetorefl. for circularly polarised radiation 78−2840
As, magnetoreflection of circularly polarised IR radiation, band struct. 77−52094
a-As, opt. and elec. props. 77−39894
As-Ge-Se based glasses, refr. index, 1-11 μm 78−39520
As-Ge-Se system glasses, alkali-free, optical absorpt. 79−65883
As-S, glass, IR vibr. spectra, optical charact. calc. 80−40119
As-S-Br glasses 79−95780
As-S-I system glasses, IR transmission spectra, structure-chem. comp. 79−42974
As-Se amorphous films, photo-induced changes in IR vibr. spectra 79−91514
As-Se based glasses, refr. index, 1-11 μm 78−39520
As-Se-Ge(-S), photostructural change in Urbach tail 80−76021
AsD_3, IR spectra, vibr. relax., rot. reorientation in solid phase 78−19463
AsF_5-graphite intercalation compound, metallic. optical reflectance meas. 78−6683
AsGe amorphous film, far IR absorpt. spectra, refractive index 80−80785
AsH_3, IR spectra, vibr. relax., rot. reorientation in solid phase 78−19463
AsH_3, plastic cryst., dipolar autocorrelation function, phonon contrib., IR absorption 78−42928
$AsO_{3/2}$-$BO_{3/2}$, glass, props. and struct. *(Japanese)* 77−27836
As_2O_3, vitreous, local struct. and vibrational spectra 80−55091
As_2O_3, vitreous, Raman and IR spectra 79−73933
As_2O_3-SO_3, polarised Raman and IR spectra, force field calc. *(French)* 78−6674

infrared spectra of inorganic solids continued
$(As_2O_3)_n$, claudetite I, vibr. spectra, force field calc. *(French)* 78−60447
As_2O_5-$Rb_2O(Rb_2CO_3)$ system, phase diagram, polymorphic transform. 79−83181
As_2S_3 amorphous films, photo-induced changes in IR spectrum 79−52033
As_2S_3, cryst. and glassy, two-photon spectrum at room temp. 79−24334
As_2S_3, crystalline, two phonon vibrational spectra 78−35142
As_2S_3 evaporated film, optical props., depend. on light exposure and heat cycling 78−68572
As_2S_3 film, amorphous, deposited at different temps., IR spectra 80−40102
As_2S_3 film, amorphous, opt. const. changes under illumination 77−77316
As_2S_3 film, effect of light exposure and heat cycling 78−94417
As_2S_3 glasses, quasi-eutectic structure, X-ray and IR investig. 77−15320
As_2S_3, glassy, diffusion, elec. transport and first group impurities effect on elec. and opt. props. 77−76623
As_2S_3, non-cryst., Faraday rotation, 0.7-2 μm 77−16307
As_2S_3, photoacoustic spectroscopy, app. of expt. system for powdered samples 77−87846
As_2S_3, two-phonon vibrational spectra, crystalline and amorphous forms, Raman and IR spectra 78−39537
As_2S_3-HgS, phase diag., IR spectra 77−36479
As_2S_3-Tl_2S and As_2Se_3-Tl_2Se system glasses, comp. depend. of IR absorpt. props. 77−16292
As_2S_5, amorphous, struct., vibr. and electronic spectra 80−64908
As_2S_5-AsSI glasses, IR and Raman spectra, struct. rel. to comp. *(Russian)* 77−81107
As_2S_x glass, Raman and IR spectra, struct. model 78−80330
$(As_2S_3)_{1-x}(As_2Se_3)_x$ and $(As_2Se_3)_{1-x}(As_2Te_3)_x$ pseudobinary glasses, comp. depend. of opt. props. 77−90157
$As_2S_3Ge_x$ glasses, vibr. props. and struct., IR refl. and Raman scatt. 79−78682
$(As_2S_3)_{1-x}(GeS_2)_x$ and $As_2S_3Ge_x$ glasses, struct. and vibr. spectra 79−91440
$(AsSI)_x(GeS_2)_{1-x}$ glasses, Raman and long-wave IR spectra obs. of struct. 79−51964
$As_{1-x}S_x(Se_x)$, bulk-quenched glasses, opt. freq. dielec. const., chem. ordering effects 78−23472
$As_2S_3(Se_3)$, vitreous, photostimulated light absorpt. 77−77221
AsS(Se)I films, electrophys. and opt. props. 77−51741
$As_2S_{3-x}Te_x$, opt. and mag. props., comp. influence 77−77225
$As_{0.2}Sb_{0.8}SI$ cryst., ferroelec., soft mode Raman and IR spectroscopy 80−76016
As_2Se_3, amorphous, photocond. and photoinduced optical absorpt. 79−82645
As_2Se_3, amorphous chalcogenides, optically broadened lattice vibration spectra 79−77712
As_2Se_3, cryst. and amorphous, optically induced absorption in band gap, picosec. dynamics 79−87439
As_2Se_3, glassy, IR spectra and intrinsic band assignments 77−77223
As_2Se_3, photodarkening and photostructural effects, Raman, IR and NQR studies 80−16036
As_2Se_3-$GeSe_2$ glass, bulk and impurity IR absorpt. 80−71455
As_2Se_3-InI_3, glass system, IR spectra 78−64365
$As_4Se_5Ge_1$, amorphous chalcogenides, optically broadened lattice vibration spectra 79−77712
$As_xTe_{90-x}Ge_{10}$, $As_{35}Te_{55}Ge_{10-x}Si_x$ glasses, elec. and optical props., comp. depend. 77−24555
$As_xTe_xS_xSe_{100-3x}$ glasses, IR absorpt. spectra 77−12378
$As_xTe_xSe_{100-2x}$, x=2.5 and 5.0, chalcogenide glasses, IR absorpt. spectra 77−24842
Au, absorpt. coeff. temp. depend., IR, 3 to 30 μm 78−74953
Au, discontinuous film, optical absorption 77−69927
Au discontinuous films, optical transmittance, effect of island morphology 78−84673
Au film, electroreflectance effects 79−43055
Au film, modifications of optical and elec. props. as function of struct. during deposition 79−78777
Au, intraband optical conductivity, electron-electron scatt. 78−35166
Au, metallised coating on polyethylene terephthalate film, fracture under laser irrad. *(Russian)* 80−76333
Au, single cryst. electrodes, electroreflectance obs. in aqueous solns. 80−25342
Au solar black, optical props., microstruct. influence 79−42937
Au ultrafine particles, optical props. 78−19481
Au-Ag, optical spectra, 0.5-6 eV, d-band struct. 77−48168
Au-Cr, cosputtered films, optical props. 0.2 to 6.1 eV 77−32454
Au-Cu, optical spectra, 0.5-6 eV, d-band struct. 77−48168
$AuCu_3$, ordered, band struct. and optical props. at 30K 79−60696
$Au_{1-x}Si$ amorphous metallic films, optical props. as function of composition 79−95865
$Au_{1-x}Si_x$, amorphous film, spectra 0.01-6.2 eV, $0.13 \leq x \leq 0.5$ 78−68574
B, α-, β-rhombohedral and amorphous, struct. changes on Zn incorporation 78−79596
B, β-rhombohedral, optical absorption band in 8 μm region, anomaly of temp. dependence 80−29735
B, IR-active phonons, reflectivity and absorption spectra 79−82294
β-B, rhombohedral, localised states charact., review, book contrib. 78−47728
β-B, rhombohedral, optical absorpt. band, temp. depend., anomalies *(Russian)* 79−28772
B:C,H amorphous film, IR absorpt. spectra 77−77312
B:H amorphous CVD films, IR, visible, and near UV optical props. 80−50442
BC_x, IR-active phonons, reflectivity and absorption spectra 79−82294
$B_{12}C_x$, phonon energies and electronic props., x depend., refl. spectra and thermoelec. power meas. 80−16052
BN, self focusing high current relativistic electron beam for structural and chemical transformations *(Russian)* 80−15190
B_2O_3 glass, struct. and phonon spectra 80−50324
B_2O_3-NaF-$NaBF_4$, crystalline compounds and glasses 78−11210
B_2O_3-SiO_2 glass film, CVD, differential IR studies 80−55213
BaB_2O_4-RF_2, R=Mg, Ca, Sr, Ba, glass form., struct. and props. 80−84077
$BaBr_2$:Sm^{2+}, radiationless coupling, $4f^5 5d$ band effects, spectra 77−8627
BaBrF, reacted flux growth, dislocation density, dielec. const. and loss, IR spectra 77−36214
$BaBr_2.2H_2O$, pure and deuterated, low temp. IR and Raman spectra *(German)* 79−19874

infrared spectra of inorganic solids continued
$BaCa_2Mg[SiO_4]_2$, synthesis and struct. characterization 78−22698
$BaCl_2$:Sm^{2+}, radiationless coupling, $4f^5$5d band effects, spectra 77−8627
$Ba(ClO_3)_2.H_2O(HDO)(D_2O)$, hydrate group vibr., IR spectra, isotope effects 77−8557
$BaCl_2.2H_2O(D_2O)$, lattice vibr., IR and Raman spectra 79−15443
BaF_2, F^- interstitial and substitutional trivalent cations, phonon reson. and IR absorpt. 80−84752
BaF_2, optical ceramic, hot pressing in vacuum, rel. to spectral transmission 78−52730
BaF_2, rare earth and transition ion doped, far IR absorption and Zeeman effect 77−40246
BaF_2, strain induced splitting and oscillator strength anisotropy of IR transverse optic phonon 80−92625
BaF_2: rare earth, far IR electronic transitions 77−4657
BaF_2:Co^{2+}(Mn^{2+})(Ni^{2+}), far IR absorpt. spectra peaks 78−27265
BaF_2:Dy^{3+}, far IR absorption 80−40143
BaF_2:Mn^{2+}, far IR absorption spectra 78−76507
BaF_2:R^{3+}, far IR Stark and Zeeman splitting 77−48190
BaF_2:Sm^{2+}(Tm^{2+}), vibronic spectra and dynamics of impurity-contaiing lattice 79−1787
BaFBr, X- and γ-irrad., thermolum. and optical absorpt. spectra 79−95857
$Ba_2Fe[Ge_2O_7]$, hydrothermal growth, struct. and opt. props. 77−65971
$Ba_2Ga_2GeO_7$, gehlenite struct., synthesis and physicochem. props. 79−43181
$BaGeO_3$-(0.25MgF_2.0.75YF_3)-Ga_2O_3 glass, synthesis and props. 80−25648
$BaNB_2O_6$, IR and Raman spectra, vibr. anal. *(French)* 79−91446
$Ba(NO_3)_2$, dynamical props., IR reflection spectra meas., 10-300K 77−1676
$Ba(NO_3)_2$, IR reflection spectra, dynamical props. 77−16303
$Ba(NO_3)_2$, vibrations of isotopic impurities, IR reflection and Raman spectra meas. 77−51465
$BaNb_xY^{III}Ti_{x}^{III}Ti_{1-x}^{IV}O_3$, A and C-domain crysts., elec. cond. and absorption spectra 77−47805
Ba_2NiF_6, quadratic layer antiferromag., optical spectra obs. 77−16326
BaO-GeO_2-Na_2O-H_2O system, hydrothermal crystn., phase formation laws 79−46636
BaO-WO_3-P_2O_5 glass, struct. and IR spectra 80−64914
$Ba(PO_3)_2$-AlF_3-BaF_2 (SrF_2), elec. cond., density, and IR spectra 79−95215
$Ba(PO_3)_2$-AlF_3-CaF_2, glass, elec. cond. and IR spectra 80−89005
$Ba(PO_3)_2$-AlF_3-MgF_2, glass, elec. cond. and IR spectra 80−89005
$Ba(PO_3)_2$-BaF_2, IR absorption spectra exam. of hydrolytic stability 80−39291
$Ba(PO_3)_2$-CaF_2, IR absorption spectra exam. of hydrolytic stability 80−39291
$Ba(PO_3)_2$-MgF_2, IR absorption spectra exam. of hydrolytic stability 80−39291
$Ba(PO_3)_2$-SrF_2, IR absorption spectra exam. of hydrolytic stability 80−39291
α-$Ba_2P_2O_7$, Raman, IR spectra, factor group anal. and band assignment 78−35126
$BaPO_3F$-Al_2O_3-B_2O_3 system, liq. phase separation, IR spectra, microstruct. 80−29940
$Ba_{10}(PO_4)_6(OH)_2$, cryst., IR spectra, band assignments 78−60442
$BaPb_{1-x}Bi_xO_3$, semiconductor-metal transition and supercond., IR absorpt. and struct. meas. 77−28278
$BaSO_4$, polarised IR refl., absorpt. and laser Raman spectra 77−43997
$BaTa_2O_6$, structural study X-ray diffr., IR absorpt. and Raman spectra *(French)* 80−107173
(BaTi) citrates, thermal decomp., thermal anal., IR and X-ray diffr. obs. 79−24735
$BaTiO_3$, A_1-modes reflectivity meas. 79−65875
$BaTiO_3$, ferroelec. cryst., IR and Raman spectra, mode coupling 80−66194
$BaTiO_3$, OH^- impurity IR spectra meas. 80−20679
$BaTiO_3$, paraelec. phase, stabilisation of soft mode 80−75985
$BaTiO_3$, permittivity, temp. depend., submm. spectroscopy 77−176
$BaTiO_3$, soft mode spectroscopy IR refl. meas. 80−88982
$Ba_2TiSi_2O_8$, fresnoite, Czochralski growth and phys. props. 78−3026
$Ba_2TiSi_2O_8$, luminescence of TiO_5 group, decay time, IR and Raman spectrosc. 80−2819
$Ba_{0.15}VO_2$, electrical cond., thermo-EMF, and lattice consts. 80−54685
$Ba_3(VO4)_2$, determination of enthalpies of formation, from heats of solution 80−2182
(Be, Al)B_{12}, wide-gap semicond., elec. cond., refl. and absorpt. spectra 80−20188
$Be_3Al_2(SiO_3)_6$, beryls, optical absorpt. spectra in the near IR (900-2500 nm) 80−89004
$BeCl_2.4H_2O$, IR and Raman spectra *(French)* 80−20618
BeF_2 glass, IR and UV transmission spectra 80−89019
BeF_2, vitreous, band limits and vibrational spectra 79−73935
BeF_2, vitreous, IR and reduced Raman spectra, weak Raman bands 78−68498
BeF_2, vitreous, Raman and IR spectra 78−39549
BeF_3, water free vitreous, preparation and props. 79−66033
BeO, small crystal, surface phonon modes, IR transmission spectra 80−11398
BeO_2-Al_2O_3-SiO_2-MF_2 (MF) glasses, M = Mg, Ca, Sr, Ba, Li, Na, fluoride ion role during crystn. 79−65176
$BeSO_4.4H_2O$ and deuterated analogue, 110K, 1200 to 250 cm^{-1} 77−8582
$BeSO_4.4H_2O$, IR and Raman spectra *(French)* 80−20618
Bi hole pocket, far-IR magnetospectroscopy, electron-electron interaction effects 77−77211
Bi, magnetoreflection of circularly polarised IR radiation, band struct. 77−52094
Bi, magnetoreflection spectra, reson. Landau level transitions 77−52096
Bi-SiO_2 cermet films, elec. and optical props. 79−78775
BiF_3 thin films, optical props. 79−32005
$Bi_{12}GeO_{20}$, $Bi_{12}SiO_{20}$, IR reflection spectra studies of lattice vibrations 79−99879
$BiH(PO_3)_4$, condensed, thermal behaviour 80−19912
Bi_2O_3 and sillenite struct. derivatives, $MO_x.6Bi_2O_3$, IR and Raman spectra, vibr. anal. 78−76464
Bi_2O_3, transmission spectra of thin films 78−76440
BiOCl, cryst. growth, Raman and IR spectra *(German)* 77−21012
BiOI, synthesis, thermal decomposition in dry O_2 *(French)* 78−53205
25 $Bi_2O_3.P_2O_5$, hydrothermal growth, vib. spectrum 77−63555

infrared spectra of inorganic solids continued
BiP_5O_{14}, condensed, thermal behaviour 80−19912
$Bi_{1-x}Sb_x$, far IR magnetoabsorption, band struct. study 80−50351
$Bi_{1-x}Sb_x$, far IR transmittance meas. *(Russian)* 77−44006
$Bi_{1-x}Sb_x$, reson. Landau level transitions, magnetorefl. 77−52096
$Bi_{1-x}Sb_x$:Te(Sn), band struct., plasma refl. spectra and galvanomag. tensor 77−16315
$(Bi_{0.25}Sb_{0.75})_2Te_3$, opt. props. of bulk and films 78−27206
n-Bi_2Se_3, cryst. nonparabolic cond. band., IR refl. and Hall voltage meas. 77−31940
n-Bi_2Se_3, IR, reflectance, Seebeck coeff. and Hall voltage meas. 79−60692
Bi_2Se_3, Raman spectra, Raman and IR-active modes 79−56776
Bi_2Se_3:Hg point defects in crystal lattice, Hall coefficient and IR spectra determ. 80−55129
$Bi_2(SeO_4)_3$, single cryst. growth in silica gels, X-ray diffr., IR and emission spectroscopy study 79−74075
$Bi_xSi_yO_z$ films on Si, form. kinetics and props. 80−35358
Bi_2Te_3, Bi_2Se_3, $Bi_2(Te_{1-x}Se_x)_3$, Raman and far infrared investigation of phonons 78−23453
Bi_2Te_3, Raman spectra, Raman and IR-active modes 79−56776
BiTeI, melt and vapour grown, optical props. 80−84746
$Bi_8Te_7S_5$, anisotropic dielec. const., oblique incidence reflectivity data 77−73124
$Bi_4Ti_3O_{12}$, IR refl. spectrum, 60-2000 cm^{-1} 77−69843
β′-$Cu_xV_2O_5$, mag. and spectroscopic study, semiconductor to metal transition 80−2628
C, amorphous film, spin resonance, IR spectra, microhardness 80−71157
C, amorphous grains, extinction coeffs., 0.21-340 μm, lab. meas. rel. to interstellar grains 80−73020
C, arc evap. film, optical props., 0.6-3.8 eV 77−81166
C black, IR-, UV- and NMK spectra, props. after extraction with organic solvents *(Polish)* 79−70010
C film, amorphous, growth under ion impact in butane plasma, and IR transparency 78−52688
C film, oxidation, IR spectroscopic study 79−96162
C, film with random struct. growth from ion impact damage in butane plasma 79−83139
C, pyrolysis mechanism, electron microscopy, DTA, IR, ESR obs. 78−56593
CO, adsorbed on Pt (111), oxidation process, reflection-absorpt. IR study 78−76468
CO adsorpt. on MgO, IR spectra 80−2751
CO, chemisorbed on metals, electronic struct., vibr. spectra, and chem. 79−42390
CO chemisorbed on Pt, IR refl.-absorpt. spectra, absorbate island struct. 80−84385
CO, chemisorption on AgNa mordenite 80−2752
α-CO, IR and Raman spectra, vibron band, vibron-phonon combination bands 78−68495
CO, solid and matrix isolated, IR and Raman spectra 78−48156
$^{12}C^{16}O$:CO isotopes, IR and Raman spectra, vibron band, vibron-phonon combination bands 78−68495
CO-N_2O-NH_3-methanol, solid mixture, vibr. modes, IR spectra 80−90504
CO_2, adsorption on η-Al_2O_3, IR and microgravimetric meas. 78−14578
CO_2 ice spheres, IR scatt. and absorpt. props. 80−97269
CO_2, isotopically mixed crysts., IR spectra ν_2 vibr. exciton band 77−73136
CO_2, solid, IR spectra and refr. index, Martian implications 80−72821
CO_2-type cryst., transl.-vibr. absorpt., hexadecapole moment effects 77−90134
CS_2, crystalline, far IR spectra 77−24834
$Ca_2Al_2GeO_7$, gehlenite struct., synthesis and physicochem. props. 79−43181
$CaBa(PO_3)_4$, struct. from IR spectra 77−47421
$CaCO_3$, aragonite-calcite transformation, effect of impurities, DTA and IR studies 78−51662
$CaCO_3$, IR reflectivity, oblique phonons 78−60440
$CaCO_3$, Iceland spar natural crystals, optical characts. 77−10988
$CaCO_3$+SiO_2, in presence of NaF, thermal decomposition of Ca_2SiO_4 formation 78−68889
$CaCl_2(Br_2)$, adsorption of NH_3 and ND_3, complex formation, IR and for IR spectra obs. 80−80063
$CaEuAl_3O_7$, mechanism of solid-phase reactions of formation and physicochem. props. 77−52622
CaF_2, additively coloured, photothermal bleaching of Ca colloids 79−15500
CaF_2, adsorbed water film internal reflection spectroscopy 79−15549
CaF_2, fluorite, transmission spectrum 1200-800 cm^{-1} band, spectrophotometer scale calibration 79−12837
CaF_2, localised vibrs. due to substitutional impurities 78−22803
CaF_2, rare earth doped, force const. changes near impurity site, calc. 77−47529
CaF_2, rare-earth and transition ion doped, far IR absorption and Zeeman effect 77−40246
CaF_2, strain induced splitting and oscillator strength anisotropy of IR transverse optic phonon 80−92625
CaF_2, surface, adsorption of water, IR internal reflection spectra 79−77920
CaF_2 trapezoid, ThF_4 and ZnSe coated, IR characterisation by internal-refl. spectra 78−71161
CaF_2:Co^{2+}(Mn^{2+})(Ni^{2+}), far IR absorpt. spectra peaks 78−27265
CaF_2:D^{2+} submm. magnetospectroscopy, tunable far IR laser potential 78−52481
CaF_2:Er, hydrogenated and deuterated, optical and EPR specra 79−61209
CaF_2:Fe^{2+}, electronic props., Mossbauer and far IR spectroscopy 79−99803
CaF_2:Nd^{3+}, crystal field study, absorption spectra 80−20668
CaF_2:O_2^-, OH^-, ion incorporation by reaction with surrounding atm. 80−55143
CaF_2:R^{3+}, far IR Stark and Zeeman splitting 77−48190
CaF_2:Sm^{2+}, coherent population oscills. and hole burning observed using polarization spectroscopy 80−71457
CaF_2:Sm^{2+}(Eu^{2+}), cubic crysts., vibronic spectra, induced dichroism method 77−81131
CaF_2:Tm^{2+}, vibronic spectra and dynamics of impurity-contaiing lattice 79−1787
CaF_2-Ge(Si), cosputtered composite semiconductors, selective solar energy absorbers 79−56876

infrared spectra of inorganic solids continued
$CaF_{2-x}H_x$, IR spectra 80−34920
$CaFe_2^{2+}Fe^{3+}(OH)O(Si_2O_7)$, ilvaite, IR spectrum and Mossbauer effect obs. *(French)* 78−80321
$Ca_3Fe_2Ge_3O_{12}$ garnet, light absorpt. spectral study 80−93322
$3CaGeO_3.H_2O$, synthesis, IR spectra 77−43986
$CaHPO_4.2H_2O$ powder and crystals, vibrational spectra, factor group anal. 80−45076
$CaIr_xRe_{1-x}O_3$, perovskite struct., X-ray and IR obs. 79−90621
$CaIr_xTi_{1-x}O_3$, semiconductor, struct., mag. and elec. props. 79−91046
$Ca_8La_2(PO_4)_6O_2$, IR and Raman spectra 79−78671
$Ca_8La_2(PO_4)_5(VO_4)O_2$, IR and Raman spectra 79−78671
$Ca_4La_6Si_4P_2O_{26}$, and derivatives, synthesis, physicochemical props. 77−21066
$Ca_8La_2(VO_4)_6O_2$, IR and Raman spectra 79−78671
$CaMg(Si, Ge)_2O_6$, solid solns., IR spectra 77−48156
$CaMgSi_2O_6$, single cryst., IR reflection spectra, vibr. spectrum calc. 77−73142
$CaNb_2O_6$, columbite, polarised Raman and IR spectra, normal coord. anal. 77−76500
CaO, luminesc. single cryst., sharp IR absorpt. lines 77−1704
CaO, spectra rel. to interstellar absorpt. features 77−57073
CaO-(CaF_2)-Al_2O_3, IR absorption spectra and X-ray emission spectra obs. *(Japanese)* 77−52075
CaO-Al_2O_3-B_2O_3-SiO_2-FeO, glass, IR spectra at room and melt temp. 80−88986
CaO-Ga_2O_3, vitrification, spectroscopic and petrographic anal. 77−15556
CaO-Ga_2O_3-Bi_2O_3, vitrification regions 77−15557
CaO-SiO_2 system glasses, IR absorpt. struct. obs. of phases and struct. 80−34918
$Ca(OH)_2$ and $Ca(OD)_2$, molecular and lattice dynamics by IR^2 and Raman spectra 77−73134
β- and γ-$Ca_2P_2O_7$, IR and Raman vibr. spectra 80−25355
α-$Ca_2P_2O_7$, Raman, IR spectra, factor group anal. and band assignment 78−35126
$Ca_5(PO_4)_3$, fluorapatite, far IR reflectivity to polarised light 79−56778
$Ca_5(PO_4)_3F:Nd^{3+}$, luminesc. and absorpt. spectra, line shift and broadening 77−4678
$Ca_{10}(PO_4)_6(OH)_2$ halogenated derivatives, IR absorpt. spectra *(Spanish)* 78−52489
$Ca_{10}(PO_4)_6(OH)_2$, hydroxyapatite, prep. by hydrotherm. recrystn., composition and props. study 79−33913
$Ca_{10}(PO_4)_6(OH_2)$, polarised Raman and LF IR spectra, lattice vibr. 77−77192
$Ca_5(PO_4)_3OH$, prep. from sulphate, X-ray diffr. and IR spectrosc. 80−29893
$CaSO_4$, anhydrite, resonance splitting of complex anion internal vibrs. 80−55081
$CaSO_4$, anhydrite and gypsum, phonon spectroscopy, lattice dynamical calc. 80−19889
$CaSO_3.1/2H_2O$-$CaSO_4$ solid solution, prepared by coprecipitation from solns., exam. 79−20034
$CaSO_4.2H_2O$-$CaHPO_4.2H_2O$ system, solid solns., IR study *(French)* 80−66165
$CaSiO_3$, structural transform. during hydration, IR spectra and X-ray diffr. meas. 77−76548
β-Ca_2SiO_4, stabilisation, IR and Raman spectra 79−42265
Ca_2SiO_4, structural transform. during hydration, IR spectra and X-ray diffr. meas. 77−76548
Ca_3SiO_5, P containing, hydrated, microstruct. and IR struct. 79−29074
Ca_3SiO_5, structural transform. during hydration, IR spectra and X-ray diffr. meas. 77−76548
$Ca_{10-x}Sr_x(PO_4)_6(OH)_2$, continuous cation migration, IR spectra study 80−93297
$Ca(UO_2PO_4)_2.6H_2O$, calc. and meas. of vibr. spectrum 77−76499
CaVG, polycryst. IR transmission spectra rel. to Faraday rotator and modulator appl. 78−10900
$Ca_{0.15}VO_2$, electrical cond., thermo-EMF, and lattice consts. 80−54685
$CaWO_4:Nd^{3+}$ $4f^3$ configuration, ground level energy state variation rel. to press. *(Russian)* 77−16358
$CaY_2Mg_2Ge_3O_{12}:Nd^{3+}$, optical absorpt. and fluoresc. intensities 80−29793
$CaZrO_3$-$CaHfO_3$, solid soln. formation obs. 77−86003
CdA_2X_4 (A=Ga,In; X=S,Se), Fourier IR and Raman spectra, cryst. struct. and symm. *(German)* 79−24313
Cd_3As_2 film, optical absorption edge 80−50450
Cd_3As_2 film, transmission spectra, crystalline and amorphous films 78−11013
$CdBa(PO_3)_4$, $CdSr(PO_3)_4$, struct. from IR spectra 77−47421
$CdBr_2$ crystal, transverse and longitudinal lattice mode freq., IR reflection spectra meas. 78−27227
$CdBr_2$, lattice vibr., IR absorpt. meas. 79−4380
$CdBr_2:Co^{2+}$, polarised IR absorpt. spectra 77−40269
$CdCl_2$ crystal, transverse and longitudinal lattice mode freq., IR reflection spectra meas. 78−27227
$CdCl_2:Co^{2+}$, polarised IR absorpt. spectra 77−40269
$CdCr_2S_4$, ferromag. semicond., IR refl. spectra, phonon props. and dielec. function 80−66191
$CdCr_2S_4$, polycrystalline films, mag. semicond., spinel-type, magneto-optical effects *(Japanese)* 79−47415
$CdCr_2Se_4$, crit. behaviour of optical absorption edge 78−35143
$CdCr_2Se_4$, energy structure, magnetooptic effects 80−71394
$CdCr_2Se_4$, mag. semicond., spinel-type, magneto-optical effects *(Japanese)* 79−47415
$CdCr_2Se_4$, mag. semicond. effect of illum. on domain struct. 79−99726
$CdCr_2Se_4$, optical absorption due to transitions between bands and local levels 79−38537
$CdCr_2Se_4$, photoinduced infra-red optical absorption 78−23455
$CdCr_2Se_4$, reflectance magneto-circular dichroism 77−81120
$CdCr_2Se_4$:Ag, magneto-optical effects in impurity spectral region 80−97313
$CdCr_2Se_{4-x}S_x$, influence of anion substitution on red shift of optical absorption band edge 77−32399
$CdCr_2Sr_4$, press. depend. optical aborption edge shift and compressibility 79−28714
CdF_2, colour centres, IR absorpt. and photocond. after UV irrad. 80−79784
CdF_2, rare earth and transition ion doped, far IR absorption and Zeeman effect 77−40246
CdF_2: $YF_3(YbF_3)$, photoconversion from insulating to semicond. state, IR absorption and elec. cond. 78−14759
infrared spectra of inorganic solids continued
$CdF_2:Co^{2+}(Mn^{2+})(Ni^{2+})$, far IR absorpt. spectra peaks 78−27265
CdF_2:NaF(AgF), colour centres, IR absorpt. and photocond. after UV irrad. 80−79784
$CdF_2:R^{3+}$, far IR Stark and Zeeman splitting 77−48190
CdF_2:YbF_3, conversion processes into semiconductor 78−14730
CdF_2-YF_3, thermal ionisation energy of monovalent centres 80−80207
$Cd_{1-x}Fe_xCr_2S_4$, mag. semicond., spinel-type, magneto-optical effects *(Japanese)* 79−47415
$Cd_{1-x}Fe_xCr_2S_4$ series of magnetic semiconductors, magneto-optical effects, expt. *(Japanese)* 77−40212
$CdGa_2S_4$, IR light transmission, IR refl. spectra and cryst. struct. 79−56777
$CdGa_2S_4$, IR refl. spectra 80−60604
$CdGa_2S_4$, vibr. spectra, 33-400 cm^{-1}, symm. transform. *(Russian)* 78−23465
$CdGaS_4(Se_4)$, absorption and refl. spectra anisotropy, band struct. 77−69840
$CdGa_2Se_4$, IR refl. spectra and cryst. struct. 79−56777
$CdGa_2Se_4$, IR refl. spectra, optical phonon dispersion 80−29746
$CdGa_2Te_4$, IR refl. spectra and cryst. struct. 79−56777
$CdGeAs_2$, elec. and optical props., acceptor levels and energy gap determ. 77−85218
$CdGeAs_2$, optical and elec. props. 79−19590
$CdGeAs_2$, polarised IR reflectivity, optical modes, optical phonons 77−69836
n-$Cd_{0.2}Hg_{0.8}Te$, fundamental absorption edge, influence of temp. 80−20640
$Cd_{1-x}Hg_xTe$, lattice dynamics of low conc. of Hg atoms, perturbation model impurity description 79−55853
n-$Cd_xHg_{1-x}Te$, conduction band struct., IR refl. spectra obs. 80−39502
$Cd_xHg_{1-x}Te$, gap width temp. depend., absorpt. band edge meas. 78−72521
CdI_2 crystal, transverse and longitudinal lattice mode freq., IR reflection spectra meas. 78−27227
CdI_2, optical phonon anisotropies and intralayer bonding forces from IR refl. 77−59573
$(CdI_2)_x(PbI_2)_{1-x}$, reflection and luminesc. spectra obs. 77−8648
$CdInGaS_4$, far IR refl. and transmission spectra, lattice vibrs. 79−91439
$CdIn_2S_4$, partial inverse spinel struct., detection by Fourier transform spectroscopy 80−108197
$CdIn_2S_4$, Raman and IR spectra 78−48181
$CdIn_2S_4$:Co, optical absorption meas. 78−64384
$CdIn_2S_4$:Cr, absorpt. and photoluminesc. spectra, Cr conc. depend. 79−78712
$CdIn_2Se_4$, cryst. growth, photoresponse and optical props. 78−39165
$Cd_xM_{10-x}(PO_4)_6X_2$(M=Ca, Sr, Ba, Pb; X=F, Cl) apatites, IR spectral study *(French)* 80−93316
$Cd_{1-x}Mn_xTe$, acceptor photoionisation and light-to-heavy hole absorpt. 79−65908
CdO, elec. cond. and IR refl. spectra after sintering and compaction 79−56945
CdO-Bi_2O_3-Al_2O_3, glass formation and IR transmission *(Japanese)* 80−54146
CdO-SnO_2 film, DC reactively sputtered, transparent electrode props., optimum sputtering conditions 80−11116
CdP_2, cryst., tetragonal, 2-phonon IR absorpt. 80−66176
CdP_2, polarised spectra of IR absorption and emission of single crysts., oscillatory states *(Russian)* 77−28583
Cd_3P_2, free carrier and interband absorption 78−23446
$CdPS_3$, layered, organometallic intercalates, X-ray diffr., optical absorpt. and mag. props. 80−45103
$Cd_3(PS_4)_2$, synthesis by roasting, and exam. of props. 79−4926
$Cd_{10}(RO_4)_6X_2$(R=As, P, V; X=Cl, Br) apatites, IR spectral study *(French)* 80−93316
CdR_2S_4, (R=Sc, Yb, Tm), IR and Raman spectra, force consts. 78−68503
CdS 80−11398
CdS, chemically precipitated film, optical spectra, annealing effects *(Russian)* 79−11424
CdS films, electrolessly deposited, annealing effect on optical spectra 80−2884
CdS films, precip. from soln., phase comp. change during annealing in air at 200-600°C 80−15393
n-CdS, new type photoconduction due to magneto-phonon reson. 77−55565
CdS, photoexcitation, effect of elec. field *(Russian)* 79−1751
CdS, photophoretic spectroscopy, broadband 80−86469
n-CdS, piezoelectric polaron and polaron pinning 77−35872
CdS sprayed film, prep., optical props., struct. and comp. 79−78875
CdS sprayed films, elect. and optical props. 78−39241
CdS, transition metal centres, first-harmonic electromodulation spectra 78−35116
CdS:Cd,Cu crystal, formation and bleaching of optically-induced absorption bands 78−31221
CdS:Cu,Pb reflectivity of Ni-salt coated powder, pre-irrad. effect on defect form. 79−27973
$CdS:Ti^{2+}$, linear electroabsorption due to Ti^{2+} centres 77−66525
$CdS-Co^{2+}$, IR spectrum, 4.2K, electron-phonon interaction effect on emission spectrum 78−27270
CdS(Se), optical spectroscopy, absorpt. coeff., lattice vibr. modes, band gap, acoustic approach 77−69822
$CdS_{1-x}Se_x$ film, resonance between Se atom dipole vibr. and interference modes, IR spectra obs. *(Russian)* 80−2888
$CdS_{1-x}Se_x$, zone edge phonon, IR absorpt. and Raman scatt. meas. 77−76508
$CdS_{1-x}Se_x$, zone edge phonons 78−76475
p-CdSb, photoconductivity and absorpt. in submm region, electroluminesc. 77−32046
CdSe, fundamental vibrs., Raman scatt. and IR refl. obs. 78−60451
CdSe, photocond. film, plasma reson., IR refl. obs. 80−11037
CdSe, undoped and Cr doped, far IR transmission and reflectance spectra 80−71429
$CdSiP_2$:Fe, EPR and optical absorpt. of Fe^+, Fe^{2+}, Fe^{3+} and Fe^{4+} on tetragonal sites 77−8397
n-$CdSnAs_2$, optical absorption rel. to energy spectra *(Russian)* 78−75994
$CdSn_xO_y$, DC reactively sputtered film, elec. and optical props. 79−87022
$CdSn_xO_y$ films, transparent conducting, deposited by RF sputtering from CdO-SnO_2 target 80−76179

infrared spectra of inorganic solids continued
Cd_2SnO_4 film, optical transmission and reflection, evaluation for solar heat collectors 77−52191
CdTe, energy bands and optical props. calc., tight-binding model with spin-orbit interaction 80−65448
CdTe, far IR absorpt., two-phonon density of states 78−15155
CdTe, IR transmitting semicond., dn/dT, wavelength depend. 77−77163
CdTe, lattice mode, dispersive refl. meas. using modular interferometer 78−89568
CdTe, near-edge absorpt., effect of light illumination and elec. field 79−38547
CdTe optical applications, review 77−42580
CdTe, shallow donors, excited state transitions 78−6710
CdTe single crystal IR window for CO_2 laser 77−75566
CdTe sputtered films, deposition conditions effects on struct. and props. 77−43452
CdTe thin films, oriented, VPE growth, infrared transmission, photovoltaic cells 80−59825
CdTe, transmission spectrum under uniaxial compression 80−29714
CdTe two-photon absorption, laser calorimetric obs. 80−33076
CdTe:Be, impurity modes and IR absorption 78−76506
CdTe:Cr^{2+}, absorpt. and luminesc. of $Cr^{2+}(d^4)$, cryst. field theory interpretation 79−83000
CdTe:Li, excitation spectrum of Li acceptor and valence band parameters 79−28795
CdTe:S, reson. interaction of local S vibr. with lattice phonons 77−11654
CdTe:Ti^{2+}, Jahn-Teller effect on $^3T_1(^3F)$ state, resonance on $^3T_1(^3P)$ state 78−27271
CdTe:Tl, growth by travelling heater method, elec. and optical characterisation 77−40356
CdTe-CdS-CdSe system solid soln. single crysts., forbidden band width determ., comp. depend. 80−55083
CdTe-In_2Te_3, composition depend. of energy gap, optical absorpt. obs. 77−80728
CdTe-PbTe(InSb) superlattices, laser deposition of multilayer heteroepitaxial structs. 80−44450
$CdTe_{1-x}S_x$, long-wavelength optical phonons, composition depend., IR and Raman spectra 78−67788
$Cd_{1-x}Zn_xS$ 10 μm film optical and electrical characterisation *(French)* 78−64153
$Cd_xZn_{1-x}S$, vibr. spectra, microscopic theory 79−73949
Ce_2ASe_5, A=Ge, Sn, diffuse refl. spectra and band gaps 79−51963
CeB_6, mag. and electronic props. 80−71048
$CeCl_3$, mag. field depend. of polaritons 79−33246
CeH_x, phonon features in IR and Raman spectra 80−93310
CeN, optical props. and valence mixture 78−56450
$CeNH_4P_4O_{12}$ and $Ce(NH_4)_2(PO_3)_5$, synthesis by solid-phase reaction, characts. 80−60778
CeO_2:Y_2O_3, bias sputtering, film growth and characts. 77−40366
CeP_5O_{15}, IR absorpt. and luminesc. spectra 80−55079
$CePd_3$ fluctuating-valence compound, anomalous far IR absorption 80−66210
$CeVO_4$, monazite struct., IR and NMR spectra 79−78534
$^{249}CfBr_x$, spectral and X-ray diffr. data, 25 to 700°C 77−28584
CmO_2, IR spectra, values of transverse vibr. frequencies 77−28585
(Co,M)$SiF_6.6H_2O$, (M=Mg,Mn,Zn), phase transition at low temp., IR spectra 79−24302
Co complex, C0(l-spartein)Cl_2, IR circular dichroism spectra, vibr.-electronic interaction 80−55074
Co complexes, $[Co(H_2O)_x(NH_3)_{6-x}][Co(CN)_c]$, x=1,2, hydrogen bonding 77−42437
Co, HCP, low energy interband absorption, electronic struct. exam. 79−73930
$Co_4(CO)_{12}$, heptane soln. Co-Co force consts., prereson. Raman spectra, rel. to solid IR spectra *(French)* 78−31193
$CoCO_3$ far IR spectrum, HF antiferromag. resonance and two-magnon absorption 77−40136
$CoCO_3$, long wave IR spectrum, high freq. antiferromag. reson. *(Russian)* 78−31115
$CoCO_3$-LiCl-H_2O system, complexing during cryst. growth, of spherocobaltite, electron diffr., neutron diffr. and spectroscopic obs. 77−44144
$CoCl_2$, polarised IR absorpt. spectra 77−40269
$CoCl_3$, interlayer force constants 78−14406
$CoCl_2.2H_2O$, wagging and rocking band intensities of water 78−27200
$CoFe_{2-x}Ga_xO_4$, IR reflection spectra, permittivity spectra and effective ionic charges 79−69841
$Co_{1-x}Fe_xSi$, elec. and optical props. 80−49740
$Co_{1-x}Fe_xSi$, solid solution, optical props. 78−72556
$Co_xMg_{1-x}Al_2O_4$, struct., catalytic activity, Co^{2+} ion distrib. 78−30595
$Co(NH_3)_6FeF_6$, anomalous Raman intensities, due to interionic coupling by H bonding 78−27230
$Co_{1-x}Ni_xSi$, IR refl. spectra in plasma refl. region 78−27233
$Co_{1-x}Ni_xSi$, solid solution optical props. 78−72556
CoO:Ni^{2+}, far IR absorpt. by impurities and collective antiferromag. reson. mode 77−8576
CoP metallic glasses, elec. and optical props., annealing effects 79−38565
$CoSO_4.H_2O$, hydrate librational modes in IR spectra 78−48161
CoSi, IR refl. spectra in plasma refl. region 78−27233
CoSi solid solution, optical props. 78−72556
CoSi, thermoelectric and optical props. 78−91714
$CoSiF_6.6D_2O$, phase transition, mag. anisotropy and IR absorption spectra 77−89537
$CoSiF_6.6H_2O(.6D_2O)$, near IR spectrum, 80K, assignments 78−48164
Co_2SiO_4, IR absorpt. spectra 80−60591
Cr black films, electrodeposited, visible and IR reflectance 77−81168
Cr complexes, $[Cr(H_2O)_x(NH_3)_{6-x}][Co(CN)_6]$, x=1,2, hydrogen bonding 77−42437
Cr, emissitivty and reflectivity, oxide film thickness effect 79−82364
Cr, lattice dynamics, improved Fielek model 80−59598
Cr, optical absorpt. spectrum 0.25-21 μm *(Russian)* 77−81118
Cr, ultrafine particles, coatings for selective absorpt. of solar energy, efficiency 78−18060
Cr-Co (4 wt.%) alloy, antiferromag. transitions effect on opt. props. 77−12371
Cr-Cr_2O_3, black chrome films, surface microstruct. rel. to optical props. in solar absorbers 79−52036
Cr-Cr_2O_3, black chrome solar selective absorber, microstruct. 79−56875
Cr-Cr_2O_3 black chrome, commercial, solar absorber coating characterisation 80−80111
infrared spectra of inorganic solids continued
Cr-Ni-Ti alloy and steel, emissitivty and reflectivity, oxide film thickness effect 79−82364
$Cr(CO)_6$, solid and matrix isolated, Raman spectra 79−28755
Cr_2O_3, IR active phonons 78−34578
Cr_2O_3, optical generation of longit. phonon modes 77−43288
Cr_2O_3-CrO_3-ZrO_2.CrO_3H_2O, exam. of thermal transitions 79−100116
Cr_2O_3-Mo_2O_3, catalyst, effect of Al_2O_3 additives on catalytic activity, in oxidation of methanol to formaldehyde *(Russian)* 79−66346
Cr_2O_3-MoO_3, physicochem. investig. of phase struct. 77−8807
CrSb, optical props., 0.05 to 5 eV 77−48194
$CrVO_4$, adsorption of methanol, IR spectra *(Russian)* 79−51435
Cs salts, Raman and IR spectra of the dicyanoiodate (I) ion 80−60572
Cs_2AF_6, A=Si, Ge, Sn, IR absorpt. spectra, integrated intensity 79−73944
$CsAl_xFe_{(1-x)}(SO_4)_2$, solid soln., Raman and IR spectrum study *(French)* 79−47453
CsB_3H_8, IR, Raman and inelastic neutron scatt. spectra 79−42966
$Cs_5Bi(MoO_4)_4$, synthesis, X-ray and thermal investigations 77−36390
CsBr, impurity absorpt. spectra after γ-irrad., aggregated colour centres 79−4829
CsBr, temp. depend. of Cs colloids absorption bands 80−40145
CsBr:CrO_4^{2-}, coupling and fine struct., IR electronic and vibr. spectra obs. 80−45118
CsBr:$K^+(Na^+)(Rb^+)(Tl^+)$, impurity induced IR absorpt. spectrum, breathing-shell model 77−77256
CsBr:MNO_4^{2-}, optical and vibronic spectra 79−65909
CsBr:Tl^+, perturbed lattice dynamics, breathing shell model calculation 78−75744
$CsCaCl_3$, optical characts. over wide spectral range 80−34875
$CsCdCl_3$:Co^{2+}, Zeeman Raman scatt. and Zeeman IR absorpt. spectra 79−56782
$CsCd(NO_2)_3$, pure and metal ion doped, cryst. struct., reflectance spectra and thermal decomp. 79−51081
Cs_3CoBr_5, optical anisotropies of mechanism of vibronic transitions in spectra 77−12372
$CsCoCl_3$, 10 Ising antiferromag., mag. excitations, electronic Raman and IR absorption spectra 78−2668
Cs_3CoCl_5, optical anisotropies of mechanism of vibronic transitions in spectra 77−12372
$Cs_3CoCl_5(Br_5)$, polarised single cryst. reflectance spectra 78−39535
$CsCr_xFe_{(1-x)}(SO_4)_2$, solid soln., Raman and IR spectrum study *(French)* 79−47453
$CsCuCl_3$, cryst., gyrotropy, anomalous dispersion curves 80−2719
$CsCuCl_3$, Jahn-Teller effect induced phase transitions 79−47439
$CsCuCl_3$ submillimetre spectra phasons, low freq. modes, phase fluctuations *(Russian)* 80−50333
$CsDy(MoO_4)_2$, effect of 38K phase transition on phonon spectrum, IR reflection spectra *(Russian)* 79−10902
$CsFeCl_3$, linear chain ferromag., optical absorpt. and dichroism in mag. field 77−77237
$CsGa_3Br_{10}$, cryst., vibr. spectrosc. *(French)* 78−6667
Cs_2GeF_6, IR absorpt. spectra, integrated intensity, 100-300K 79−73945
$CsHSeO_3$, and deuterated analog, vibr. spectra 79−24311
$CsHg(CN)_3$, CN and HgC stretching vibrations and HgCN bending vibration assignments 80−69140
CsI, far-IR optical props., shell-model calcs. 77−28557
CsI, temp. depend. of Cs colloids absorption bands 80−40145
CsI:CrO_4^{2-}, coupling and fine struct., IR electronic and vibr. spectra obs. 80−45118
CsI:MnO_4^{2-}, multiple-order Raman scatt., and absorpt. spectra 77−40229
CsI:Na, X-ray irradiated, optical and ESR studies in IR absorption band 80−80828
$Cs_2LiCo(CN)_6$, mol. vibr. in cryst., normal mode anal., Raman and IR obs. 77−76494
$Cs^+M^{III}(SO_4)_2$, M=Al^{3+}, Cr^{3+}, Fe^{3+}, Raman and IR spectrum study *(French)* 79−47453
$CsMgCl_3$:Co^{2+}, Zeeman Raman scatt. and Zeeman IR absorpt. spectra 79−56782
CsN_3, polycryst., IR active lattice vibr., optical consts. 77−77185
CsNCS, vibr. spectra, multiphonon modes 77−40230
$CsNO_3$, phase transition, IR spectra 80−7350
$Cs_2NaErCl_6$, mag. susceptibility and IR and Raman spectra meas., crystal field splitting determ. 80−100652
$CsNiF_3$, 1D ferromag., optical absorption and spin dynamics 80−71417
$Cs_2Ni_3(P_2O_7)_2.nH_2O$, thermal dehydration 80−35513
Cs_2O-MgO-SiO_2 system, glasses, crystn. prods., composition, props. 79−41961
$CsPO_3$-$Sr(PO_3)_2$ system, physicochem. investigation 77−35666
$Cs_{1.75}(Pt(CN)_4).1.5H_2O$, 1-D cond., IR spectra 77−85703
Cs_2ReF_6(-Cs_2GeF_6) cryst., $ReF^{-2}{}_6$ ion electronic absorpt. spectra, Raman, visible, IR and UV, liq. H and room temps. 77−77193
Cs_2SO_4, IR absorpt. spectra, polymorphism, site group approx. and SO_4 stretching mode 78−52510
$CsSbF_6$, high press. phase relations, vibr. spectra, and cryst. chemistry 80−108200
$CsSbF_4(OH)_2$, solid, IR and Raman spectra 80−40114
$CsSbF_5OH$, solid, IR and Raman spectra 80−40114
Cs_2SiF_6, lattice dynamics from neutron scatt., Raman and IR absorpt. meas. 79−60449
Cs_2SiF_6:Mn^{4+}, IR absorpt. band, electron-vibr. effect 80−108238
$Cs_2(TeBr_6)$, far IR and Raman spectra and phase transitions 80−11376
Cs_2TiF_6:MnF_6^{2-}, $^4A_g \rightleftarrows {}^2E_g$ transition of Mn^{4+}, absorpt., emission, linear and MCD, MCE 78−10929
$Cs_4(UO_2)_2F_8$-$2H_2O$, IR absorpt. and Raman spectra, normal coordinate anal. *(French)* 78−52509
$CsUO_2(NO_3)_3$, ^{15}N isotope shifts in electronic spectrum, internal mode identification 80−55098
$Cs_2Zn(N_3)_4$, IR and Raman spectra 77−43999
Cs_2ZrBr_6:Os^{4+}, intraconfig. absorpt. and MCD spectra 80−80776
Cs_2ZrCl_6:Os^{4+}, intraconfig. absorpt. and MCD spectra 80−80776
Cu (111), chemisorption of CO, IR spectra, LEED, and surface pot. meas. 80−39438
Cu, cryogenic constructing material, far IR spectral refl. 77−24855
Cu film, complex impedance, IR transmission and refl. meas. 79−78216
Cu, fine interaction of surface electrons, IR spectra 80−16041
Cu, intraband optical conductivity, electron-electron scatt. 78−35166
Cu light pipe, submm. wave transmission, and refl. of surfaces 50-10 cm^{-1} 78−18050

infrared spectra of inorganic solids continued
Cu, metallised coating on polyethylene terephthalate film, fracture under laser irrad. *(Russian)* 80−76333
Cu surface, fine interaction of conduction electrons 80−34500
Cu, surface polariton absorption and emission spectra, edge effects 78−10375
Cu-Ni alloy, dil., far IR absorptivity meas. using multireflection cell 77−18075
Cu-Sb-I system, glass form., struct. and IR spectra 80−64915
Cu-Xe film, metal-nonmetal transition, optical and resist. meas. 77−89818
$CuAl_{1-x}Fe_xS_2$ system, delocalisation of d-electrons, mag., elec. and optical obs. 78−34804
β-CuBr, far IR spectra, cond., cation local motion 79−1754
CuBr, two-phonon optical absorpt. spectra 78−52485
CuCl, absorpt. coeff., 0.4-25 μm, band struct. determ. 77−73155
CuCl, anomalous TO-doublet origin for light scatt. study 78−43872
CuCl, electronic struct. by LCAO and LMTO methods, IR absorpt. 80−59868
CuCl, two-phonon optical absorption 77−63406
CuCl, two-phonon optical absorpt. spectra 78−52485
CuCl(Br), multiphonon far IR absorpt., 2-80K 78−60462
$CuCr_2O_4$ and $CuCrO_4$, IR spectrometry and EPR study *(French)* 79−47452
CuFe film, metastable polycrystalline optical props. 79−83044
$CuGaCr_4S_8(Se_8)$, 1:1 ordering on tetrahedral sites obs. *(German)* 78−6669
$CuGa_xIn_{1-x}S_2$ solid soln., IR refl. spectra, comp. depend. 78−52498
$CuGa_xIn_{1-x}Se_2$, CVD, elec. and optical props., use as heterojunction solar cell absorber 79−52095
$CuGaS_2$, IR lattice reflectivity spectra obs. 78−19477
$CuGaS_2$, lattice vibr. modes, Fourier transform spectroscopy 79−33701
$CuGaS_2$-CuGaSe, solid solutions, IR lattice reflectivity spectra obs. 78−19477
$CuGaSe_2$, IR lattice reflectivity spectra obs. 78−19477
$CuGaTe_2$ and $CuInTe_2$, electroreflectance data, direct gap obs., cryst. field splitting and hybridisation degree 78−39557
$CuGaTe_2$ film, flash evaporated, growth and optical props. 79−95296
$CuGaTe_2$, IR lattice vibr. spectra 79−28765
$CuInCr_4S_8(Se_8)$, 1:1 ordering on tetrahedral sites obs. *(German)* 78−6669
n-$CuInSe_2$, effective electron mass, IR free-carrier Faraday rot. meas. 77−55783
$CuInSe_2$, far IR refl. spectra, ionic bonds 79−55695
$CuInSe_2$ film, MBE growth, AES and optical absorpt. obs. 79−78903
$CuInSe_2$, IR lattice vibr. spectra 79−28765
$CuIn_2Se_{3.5}$, cubic ordered compound, optical gap 78−48175
$CuInTe_2$, direct energy band gap determ., electroreflectance meas. 78−2418
$CuInTe_2$, far IR refl. spectra, ionic bonds 79−55695
$CuInTe_2$, grown from near stoichiometric comp., elec. and optical props. 78−68504
$CuInTe_2$, infrared optical properties 79−82974
$Cu_xMg_{1-x}Al_2O_4$, spinel solid solns., solid-state and surface props. 77−66415
CuO-MgO system, Cu ions valence states, electronic refl. spectra 78−35168
Cu_2O, Cu inclusions and annealing, optical and IR absorpt. obs. 80−60630
Cu_2O, refl.-absorpt. IR spectroscopy 78−84555
Cu_2O-CuO-MoO_3, subsolidus phase diagram, mag. props. 80−50615
Cu_2S:Cd(Zn), effects of doping on elec. and optical props. 78−38743
Cu_xS, layers produced by reactive RF sputtering, struct., elec. and optical props. 79−90908
$CuSO_4$, single cryst., IR optical consts., comparison with soln. 77−66470
$CuSO_4.5H_2O$ and $CuSO_4.5D_2O$, Raman and IR spectra, mode assignments 77−66493
$CuSO_4.5H_2O$, IR spectra, internal modes and pot. environment, isotope effects 77−8563
$CuSeO_4.5H_2O$, Raman and IR spectra, mode assignments 77−66493
Cu_2ZnGeX_4, (X=S,Se), optical and electrical props. 77−35941
Cu_2ZnSiX_4, (X=S,Se), optical and electrical props. 77−35941
p-D_2, far IR absorpt. in ordered state 79−91430
D_2, solid, compressed, anomalons double peaked one-phonon for IR absorption 79−56788
D_2, solid, far IR absorption by phonons and librons in ordered state 78−80331
p-D_2, solid, orientationally ordered state, anomalous far IR absorption spectrum 78−10876
D_2, solid, phonon absorption line shape as function of density 80−50329
D_2, solid, press. depend. of phonon lineshape in ordered state, far IR spectra 79−56023
DI, crystalline, Raman and IR spectra, mol. vibr., libration and translation 80−2757
D_2O, isolated in glassy H_2O, IR spectrum 78−27207
D_2S, solid, low-temp. phase, IR, far IR and Raman spectra 78−27218
D_3SiNCS, IR and Raman spectra, vibr. anal., LF bending mode 78−70842
DT, liquid and solid, collision induced infrared spectra 79−45717
$DyFeO_3$, spin reorientation, Faraday rot. meas. 77−8547
Dy_2S_3, vibr. spectra, factor-group anal. 80−80793
$Dy_2(SeO_4)_3.8H_2O$, thermal decomp. and IR spectra 80−3319
(Er,Tb,Gd_3)Fe_5O_{12} plate, pseudouniaxial, domain struct., magneto-optical obs. 80−11221
Er, paramagnetic and antiferromagnetic states, optical absorption *(Russian)* 78−56497
Er^{3+} doped phosphors, IR excitation and absorpt. and emission spectra *(Russian)* 79−52021
$ErFeO_3$, far IR spectra 78−88303
$ErPO_4$, cryst., IR spectra, complex anions internal vibrs. resonance splitting 80−34907
$Er_2(SeO_4)_3.8H_2O$, thermal decomp. and IR spectra 80−3319
(ErSm)FeO_3, spin reorientation, Faraday rot. meas. 77−8547
$^{253}EsBr_x$, spectral and X-ray diffr. data, 25 to 700°C 77−28584
Eu complex, $(Et_4N)_3$ [$Eu(NCS)_6$], Eu^{3+} ion site symm. 78−84656
Eu-As-S, glass forming region, Raman and IR obs. *(French)* 79−99080
EuO, Eu-rich, IR absorpt. spectra, 4.2 to 300K, transitions assoc. with O vacancies 77−52142
EuO, ferromagnetic piezotransmission behaviour in magnetic field 80−97272
EuO, mag. semicond., dielec. and optical props. 78−10824

infrared spectra of inorganic solids continued
EuO, stoichiometric, crit. behaviour of piezotransmission at Curie temp. 77−85688
EuO, transmission and resistivity, stress modulation effect near Curie temperature 80−96874
EuO:Gd, pure and doped, elec., mag., and optical props. rel. to electronic conc. 80−96880
$EuO_{1-\delta}$ films, Faraday effect dispersion rel. to electronic struct., visible and IR spectra 80−45162
$EuO_{1-\delta}$ single crystals, Faraday effect, near IR, effect of carriers 80−71395
$Eu_{1-x}O$, optical absorpt. spectra at metal insulator transition 78−10928
$Eu_5(PO_4)_3OH$, prep. from sulphate, X-ray diffr. and IR spectrosc. 80−29893
EuS, conduction band density of states, redistrib. near ferromag. saturation 78−67939
EuS film, struct., elec. and opt. prop. changes during annealing in air 77−7983
EuS, pure and Gd doped, electronic struct., mag. exchange and elec. transport props. 78−87974
EuSe, dynamical conductivity in high mag. fields 79−78118
$Eu_3VTa_2O_9$, prep., characterisation and mag. props. 78−26535
Fe, BCC, low energy interband absorption, electronic struct. exam. 79−73930
Fe hexacyanoferrates, $M_4Fe(CN)_6.nH_2O$, Mossbauer and IR spectra 80−2739
Fe, optical and electronic props., temp. depend., 20, 1400 and 1600°C 79−87412
Fe, optical constant dispersion and emissivity, up to 900K 78−52464
Fe-Al, optical props. rel. to order-disorder transformations 80−29736
Fe-Al (45%), ordered and disordered states, optical and elec. props. 77−85826
Fe-Co alloy, optical characts., 0.073-4.92 eV, quantum absorption 79−56814
Fe-Co alloys, optical and spectrosc. props. *(Russian)* 78−72529
Fe-Co films, optical props. order-disorder transformation influence, absorpt. band existence *(Russian)* 79−65942
Fe-Ni alloy, optical and electronic characts., 20-1750°C, comp. depend. *(Russian)* 78−84601
Fe-Si-Mn (3, 0.004 to 0.1 wt.%), Mn effect on oxidation in H_2O-H_2 atmos. 78−31560
$(Fe_{6-y}Al_y)O_9$, IR spectra, lacunar γ-phase to corundum α-phase transform. 80−108199
$FeBO_3$, antiferromag., vibr. spectra, 6000-30 cm^{-1} 78−19473
$FeBO_3$, mag. linear dichroism and absorpt. spectra, Jahn-Teller effect 80−54662
Fe_3BO_6, polarised absorpt. spectra in range of $^6A_1 \rightarrow {}^4T_1$, $^4T_2$ transitions 77−52092
$FeBr_2$:$MnBr_2$, magnon modes and impurity spin reson. 79−15501
$FeCO_3$:Mn^{2+}, far IR host and impurity excitations, antiferromag. and paramag. temp. ranges 77−52140
$Fe_2(CO)_9$, solid, Raman and IR spectra, vibr. exam. 78−27214
$Fe(CO)_2(NO)_2$, vib. assignment using ^{15}N isotopic substitution, solid, liq. and soln. spectra 77−48152
$FeCl_2$, far IR absorpt. meas. by Fourier transform apparatus 77−177
$FeCl_2$, interlayer force constants 78−14406
$FeCl_2$, light scatt., metamagnetic transition effects 77−4513
$(Fe_2Cr_{4-y}Al_y)O_9$, IR spectra, lacunar γ-phase to corundum α-phase transform. 80−108199
$FeCr_2O_4$, $FeAl_2O_4$, solid solns. and oxidation products (lunar spinels), IR spectra 77−81099
$(Fe_{6-y}Cr_y)O_9$, IR spectra, lacunar γ-phase to corundum α-phase transform. 80−108199
FeF_2, dielectric properties, IR spectra, lattice dynamics *(French)* 80−76026
FeF_2, IR reflectivity spectrum 79−51952
FeF_2, interacting phonon-magnon states, theory of Raman scattering and IR obs. 80−71426
FeF_2, magnon-acoustic phonon hybridisation in far IR absorpt. spectra 78−60271
FeF_2:Co^{2+}, impurity-induced magnon, influence of localisation 80−11182
FeF_2:Mn, mag. polariton, impurity mode enhancement and superradiance effects 79−28622
FeI_2, far IR magnetoabsorption, excitation of two spin deviations 78−80339
FeI_2, spin waves and two magnon bound states, mag. field IR absorption meas. 80−65840
FeO, Fe_3O_4, Fe_2O_3, absorption spectra, 0.1-6 eV, one electron energy level diagram 78−52487
$Fe_{1-x}O$, IR reflectivity obs. 77−43996
β-Fe_2O_3 film, CVD and characterisation 77−44172
Fe_2O_3, haematite, anal. of refl. spectrum by Kramers-Kronig relations 80−16058
α-Fe_2O_3, IR lattice vibr. and dielectric dispersion 78−6679
α-Fe_2O_3 microcrystals, surface phonon modes, IR study 80−55089
α-Fe_2O_3, surface struct., adsorptive interactions rel. to rusting process, IR spectra 79−34363
xFe_2O_3-(1−x)PbO-$3B_2O_3$ glass, Mossbauer study of Fe cations 79−91325
γ-Fe_2O_3-organic interfaces, mag. struct., Mossbauer effect, IR absorpt., and magnetisation meas. 80−44869
Fe_3O_4 and $Fe_{3-x}Ti_xO_4$, IR transmission spectra changes at Verwey temp. 77−85714
Fe_3O_4, IR refl., ATR, Voigt and Faraday expts. 80−66180
Fe_3O_4, magnetite, optical props. in IR 80−97271
Fe_3O_4, optical props. in spectral range 0.03 to 12 eV 79−51977
Fe_3O_4, substituted magnetite, correl. between IR spectra, X-ray diffr., and struct. vacancy distrib. 80−84753
Fe_3O_6, O_2 annealed, optical absorpt., spin struct., polaronic absorpt., cryst. field transitions 78−68493
α- FeOOH, goethite, surface OH groups, D_2O isotopic exchange, IR investig. 80−2254
α-FeOOH, surface struct., adsorptive interactions rel. to rusting process, IR spectra 79−34363
$FePO_4$ coating on Armco Fe, Fourier transform IR absorpt.-reflection spectra 80−71500
FeS_2, band gap temp. depend., optical absorpt. studies up to 425K 79−95758
FeS_2, optical absorpt. 79−43002

infrared spectra of inorganic solids continued
$Fe(SO_3F)_2$, Mossbauer and electronic spectra, cryst. field splittings, mag. hyperfine interactions 77−48096
$FeSi_2$ films, structural and Anderson transitions, cond. and IR reflectance meas. 79−15200
$FeSiF_6.6H_2O(.6D_2O)$, near IR spectrum, 80K, assignments 78−48164
$FeSiO_4$, spinel, IR absorpt. spectra 80−60591
Fe_2SiO_4, fayalite, Czochralski growth under controlled O_2 fugacity conditions 80−84843
$FeSnO(OH)_5$, mag. props. and cryst. struct. 78−43574
Fe_xZrSe_2, intercalation compound, IR spectra 78−88300
$Fe_3[Co(CN)_6]_2.12H_2O$ struct. dehydration fluorescence and IR studies 80−28976
Ga, optical properties in 0.3 to 5 eV range 78−31196
Ga selenites, binary, effect of nature of alkali metals on composition and props. of hydrothermal reaction products 77−24941
Ga, thermoreflectance, in near IR, down to 0.3 eV 77−85722
Ga-Xe film, metal-nonmetal transition, optical and resist. meas. 77−89818
$Ga_{1-x}Al_xAs$, IR refl. spectra and Raman spectra 80−20623
$Ga_{1-x}Al_xAs$, surface phonon polaritons, frustrated total internal refl. expts. 78−47656
$Ga_{1-x}Al_xAs$:Te, plasmon-LO-phonon coupling, IR refl. obs. 80−50335
$Ga_{1-x}Al_xP$, long-wavelength optic phonons, IR reflectance meas. 77−7804
$Ga_{1-x}Al_xP$, two-phonon optical absorpt. 78−88341
$Ga_{1-x}Al_xSb$, surface oxidation, Raman spectra, residual Sb layers 80−71419
GaAs, absorption edge broadening by piezoelec. phonon fields 77−16302
GaAs, amorphous layer formation, ion implantation 78−95063
n-GaAs, and Te doped, homogeneity, IR introscopy investig. 79−15446
GaAs anodic oxide, refl. and transmission, 0.01-6 eV 78−95613
GaAs anodic oxide, refr. index meas., Sellmeier eqn. 77−12454
GaAs anodic oxide film, ellipsometric and IR spectroscopic studies 80−11493
n-GaAs, bulk and epitaxial film, IR reflectance meas. 77−32364
GaAs, compensated, photoabsorption, expt. 78−19521
GaAs, conduction band effective mass, influence of high uniaxial stress 80−80162
n-GaAs, conduction band nonparabolicity and coupled plasmon-phonon modes, IR refl. spectra 80−55110
n-GaAs, crystal growth by Czochralski method, kinetics, total emittance determ. 80−75193
n-GaAs, electron mobility, free-carrier absorpt., and compensation ratio 79−56218
GaAs, electron-irrad., deep-level defect anal. using 2γ positron annihilation and IR absorption spectra 80−16120
n-GaAs, epitaxial, ionised donor pair spectrum 77−63477
GaAs epitaxial film on GaAs substrate, IR characterisation 78−23544
n-GaAs epitaxial wafers, IR reflectance and elec. characts. 79−56293
GaAs, exciton-polariton reflectance spectra, exciton impact ionization and illum. intensity effects 79−42943
GaAs, far IR transmission spectrum 78−4713
GaAs film, electroreflectance effects 79−43055
GaAs, high-energy ion layer implanted, layer thickness and refr. indices meas. 77−24837
GaAs, highly transparent semicond. crysts., multiphonon IR absorpt. 78−10885
GaAs, highly transparent semicond., multiphonon IR absorpt. 78−60461
GaAs, IR absorption of isolated impurities 77−12407
p-GaAs, IR plasma reflectivity spectra calc. 78−52511
GaAs, IR scanning absorption, microcharacterisation for device appls. 80−10922
GaAs, IR spectra, multiphonon absorpt., phonon density of states interpretation 77−69833
n-GaAs, implanted, IR refl. meas. of free carrier parameters 77−36244
GaAs, irradiated with fast neutrons, IR vibrational absorpt. 78−75776
GaAs, isolated impurities, local mode sideband IR absorption and second harmonic intensity calc. 77−85707
n-GaAs, Landau level lifetimes for electrons 79−87112
GaAs, magnetoplasma reflectivity effects, difference method *(German)* 77−12363
GaAs, manifestation of local vibrs. of dislocations in IR spectra 78−88339
n-GaAs, mechanical polishing damage effect on IR refl. and ATR spectra 77−20848
GaAs, nonlinear light absorption, effect of deep impurity levels 77−77259
GaAs, opt. consts. in 0.6 to 4.2 eV range 79−51928
GaAs, optical conductivity, constants, refractivity from IR absorption spectra 78−43873
GaAs, optical inhomogeneity, physical basis 79−15430
GaAs, optically pumped, absorption spectrum, band filling, hot electron effects 78−31199
GaAs oxide growth kinetics and physical props. 79−77937
GaAs p-n junctions, electron irrad. induced defect levels, hydrostatic press. effect 80−92858
GaAs, peculiarities of plasma region reflection, effect of surface treatment methods *(Russian)* 79−69827
GaAs, photoexcited, band edge absorpt. dynamics 79−19879
GaAs, plasma-grown oxides, physical props., Auger and IR spectral anal. 79−91821
GaAs, plasmon-phonon coupling, and IR refl. spectra of impure crysts. 79−56150
GaAs, reactor irrad., opt. props. 77−90137
GaAs, Schottky barrier electrorefl. under uniaxial stress, band struct. 77−48193
GaAs, shallow acceptor states exam. by far IR Fourier transform spectroscopy 78−31185
GaAs, shallow donors, excited state transitions 78−6710
GaAs surface impurities, struct. and comp. of compounds using IR spectroscopy 78−63918
GaAs, transmission spectrum under uniaxial compression 80−29714
GaAs, two-photon 1.06 μm absorption coeff., absolute meas. 78−19527
GaAs, two-photon absorpt. spectrum, band gap luminesc. 78−10888
GaAs:Be, ion-implanted, IR refl. and transmission meas. 80−34908
GaAs:Co, neutral state of Co impurities, optical absorption and mag. susceptibility 78−39578
GaAs:Co^{2+}(Ni^{3+}), mag. and optical props. 78−10763
GaAs:Co(Ni), intra d-shell excitations of acceptors 80−84757

infrared spectra of inorganic solids continued
GaAs:Cr, deep levels, wavelength-modulated photocapacitance spectroscopy 80−76055
GaAs:Cr, IR absorpt. determ., emissivity meas. 77−63421
GaAs:Cr, impurity conc. and segregation coeff., optical absorpt. meas. 79−56819
GaAs:Cr, origin of sharp near IR transitions 80−10913
GaAs:Cr, zero-phonon struct. in Cr^{2+} ($3d^4$) optical absorption 80−60640
GaAs:Fe, profile of impurity optical absorption bands 78−56509
GaAs:Ni, behaviour of Ni impurity in $3d^8$ state, optical absorption and photocond. meas. 78−47737
GaAs:O, defect states, IR absorption spectra meas. 77−4666
GaAs:O, Fe, temp. depend. of ionisation energies of O and Fe levels, electroabsorption meas. 78−47736
GaAs:P^+, ion-implanted, refr. index, IR reflection and transmission meas. 77−1671
n-GaAs:Si, B, IR absorpt. spectra, reson. and localised modes 80−66172
GaAs:Si, electron irradiated, LPE layers and Bridgman crysts., IR absorption and Hall meas. 77−16345
GaAs:Si, IR absorpt. bands, localised modes, Si-related defects 80−76054
GaAs:Si, ion-implanted, annealing with Nd:glass laser 79−73194
GaAs:Si, Li, IR absorpt., microstruct., charge compensation 80−107565
GaAs:Si, neutron irrad., strain detection by local mode IR absorpt. meas. 77−69828
GaAs:Si, thick LPE layer growth and characterization 77−12511
n-GaAs:Si LEC crystal, carrier conc., B acceptor centres, Hall meas. and IR spectra 78−6717
n-GaAs:Sn epitaxial layer, free carrier relax. time, transverse magnetoplasma refl. 77−90212
p-GaAs:Zn, optical absorpt. spectra and photocond. after 2 MeV electron irrad. *(Russian)* 77−69859
GaAs-AlAs alternating monolayers, zone folding effects on phonons 78−72510
GaAs-polyethylene, for i.r. characts. rel. to powder band-pass filter design 78−90468
GaAs-polyethylene mixture, optical transmission spectra, IR filter prep. using computer appl. 80−2763
$GaAs_{1-x}H_x$, amorphous, vib. props., Raman and IR meas. 80−50322
$GaAs_xP_{1-x}$, surface phonon polaritons, total internal refl. *(Russian)* 79−38688
ε-GaAse, optical consts. for ⊥ and ∥ light polarisation, reflectivity, interf. meas. 77−52077
$Ga_{1-x}In_xAs$, IR reflectivity, cluster effect on optical phonons 80−97259
$Ga_{1-x}In_xAs$, VPE grown, refractive index, reflectance meas. 79−4780
$Ga_xIn_{1-x}As$, far IR reflectivity spectrum, damped harmonic oscill. model 77−52070
$Ga_{0.08}In_{0.92}As_{0.18}P_{0.82}$, band struct., optical studies 79−47013
$Ga_xIn_{1-x}As_{1-y}P_y$:Ge(Sn)(Te), epitaxial film, elec. and optical props. 79−11251
$Ga_xIn_{1-x}As_yP_{1-y}$, IR refl. spectra 80−60602
$Ga_{1-x}In_xP$, mixed cryst., IR absorption by zone edge lattice vibrs. 78−19487
$Ga_{1-x}In_xP$, zone edge phonons 78−76475
n-$Ga_xIn_{1-x}P$, optical props. and energy spectrum of donors 78−72567
$Ga_{1-x}In_xSe$ solid solution, IR spectra of static reflectivity 79−69849
GaN, magnetoplasma reflectivity effects, difference method *(German)* 77−12363
$GaNbO_4$, diffuse refl. and luminesc. spectra 78−56516
Ga_2O_3-Na_2O, β- and β″-phases, IR spectra 78−39552
GaP, complex form of donor energy levels, optical spectra anal. 78−23045
GaP, high-energy ion-implanted, layer thickness and refr. indices meas. 77−24837
GaP, IR absorpt. spectra depend. on compensating defects and thermal treatment *(Russian)* 80−71465
GaP, manifestation of local vibrs. of dislocations in IR spectra 78−88339
n-GaP, many-valley semiconductor, relative displacement of D_1 and D_2', bands under shear deform. influence 79−15080
GaP, optical absorption and struct. of acceptor centres 78−48205
GaP, optical inhomogeneity, physical basis 79−15430
n-GaP, optical rectification and photon drag 77−36224
GaP, polariton dispersion, IR reflection spectroscopy 80−11415
GaP, refr. index, 100 to 420K, permittivity calcs. *(Russian)* 77−90156
GaP, upper polariton branch obs. by ATR 78−68510
GaP:Co, optical spectra and Zeeman anal. of Co $3d^7$ state 80−66247
GaP:Cr, origin of sharp near IR transitions 80−10913
GaP:Cu, elec. and optical props., rel. to doping and heat treatment 80−16056
GaP:Fe_3^{3+}, profile of impurity optical absorption bands 78−56509
GaP:Fe^{3+}, deep impurity states investig. 77−15794
GaP:N(Te), ion implanted at 40 keV, refl. spectra, 210-2000 nm, annealing *(Russian)* 78−80386
GaP:Ni, absorpt. and luminesc. spectra 79−42996
GaP:Ni, optical and EPR study of two-electron-trap state 79−73806
GaP:Ni(Fe), multivalence impurities, EPR and optical absorpt. meas. 80−75844
GaP:O^-, two electron state, electron capture 78−39054
GaP:S, Se, Te, Si, shallow donors, excitation spectra 77−81128
GaP:S(Se)(Te)(Si)(C)(Zn), IR photocond. response spectra 79−56257
n-GaP:S(Te), IR absorpt. cross-section 79−38582
GaP:S(Te), photostimulation spectra, bound electron phonon interactions *(Russian)* 77−1712
GaP:Sb(Bi), gap vibrs. and impurity conc. determ. 79−69869
GaP/Te(S), IR lattice band profile, electron spin reversion in mag. field, Nf-R curve 79−28771
$(GaP)_x(InAs)_{1-x}$ solid solution, IR reflection spectra 77−69830
$GaPO_4.2H_2O$, orthorhombic, thermal dehydration 79−79234
GaS, Davydov splitting of degenerate lattice modes 79−61382
GaS, indirect excitons *(Russian)* 77−89709
GaS, infrared optical props., polarisation depend., vibr. modes 80−100658
GaS layer semiconductor, IR derivative absorpt. spectra 78−6666
GaS:Bi_2S_3, photocond. and optical obsorpt. 79−51634
Ga_2S_3, IR refl. spectra, linear chain model for lattice vibrs. 78−27235
αGa_2S_3, single crystal, lattice phonon exam., Raman and IR spectra of polycrystalline samples *(French)* 78−27229
Ga_2S_3-La_2S_3-Nd_2S_3:Nd^{3+} chalcogenide glass, Nd^{3+} emission and absorption spectra, nonradiative relax. 77−40268

infrared spectra of inorganic solids continued
GaS(Se), layered, optical phonons, IR and Raman scatt. meas. 78−59903
GaS(Se), optical and nonlinear optical props. *(Russian)* 79−51943
GaS(Se), polar optical phonon ang. behaviour, IR refl. meas. 80−20633
$GaS_{1-x}Se_x$, mixed crystals, IR reflectivity spectra 80−66204
GaS_xSe_{1-x}, IR reflectivity and transmission spectra, stacking transform. 77−32371
GaS_xSe_{1-x} layered system, neutron diffr., IR and Raman scatt. 79−87443
GaS_xSe_{1-x} solid solutions, two-mode behaviour of optical phonons, IR reflect spectra 79−78680
GaS_xSe_{1-x}, two photon absorpt. 77−69841
GaSb, bulk and epitaxial, IR reflect. meas., carrier conc. and mobility determ. 80−80769
GaSb, cond. band L-states, i.r. absorption, uniaxial stress 77−1674
GaSb films, amorphous and cryst., vac. evaporated, Elec. cond. thermoelec. power and optical absorpt. 80−2504
GaSb, manifestation of local vibrs. of dislocations in IR spectra 78−88339
GaSb, oscillatory magnetoabsorption and excitons 77−55777
GaSe, exciton absorpt. spectra, additional light wave 77−63445
GaSe films, optical props. at lattice vibr. freqs., IR and Raman spectra 80−60696
ε-GaSe films, optical props. in IR region, metal substrate effect 80−71502
GaSe layer semiconductor, IR derivative absorpt. spectra 78−6666
GaSe, long wavelength IR refl. spectra 80−11401
GaSe, luminescence and absorpt. spectrum in region of high-energy resonance 77−44044
GaSe, refr. index 0.45 to 330 μm, interf. and refl. meas. methods 77−63387
GaSe, single cryst., dispersion of refr. indices and exciton absorption 79−73947
GaSe, thin layers, far IR refractive index 80−80799
Ga_2Se_3, IR refl. spectra, linear chain model for lattice vibrs. 78−27235
Ga_2Se_3-Ga_2S_3 solid solutions, IR refl. spectra, linear chain model for lattice vibrs. 78−27235
GaTe, layer cryst., polarised IR refl. spectra 80−97279
GaTe, long wavelength phonons, Raman and far IR spectra obs. 79−69210
GaTe monocrystal, far IR polarised complex reflectivity obs. 80−60609
GaTe, vibr. spectrum 77−89513
Gd, ferromag., magneto-optical reson., optical consts. determ. 78−6657
Gd, optical constants, reflectance meas. *(French)* 78−2869
Gd, optical properties, 0.5-3.1 eV *(Russian)* 79−11432
Gd, thermoreflectance meas. 79−69816
Gd-La, magneto-optic reson. *(Russian)* 79−47426
Gd-La alloy, optical freq. cond. in 0.5-3.1 eV range, paramag.-ferromag. transition 80−29761
Gd_2ASe_5, A=Ge, Sn, diffuse refl. spectra and band gaps 79−51963
$GdCrO_3$, Faraday rot. and linear birefr. meas., 0.8 to 2 μm 77−77180
$Gd_3Ga_5O_{12}$, IR refl., ATR, Voigt and Faraday expts. 80−66180
$Gd_3Ga_5O_{12}$:Nd^{3+}, optical absorpt. and fluoresc. intensities 80−29793
$Gd_2Gi_2O_7$:Nd^{3+}, spectroscopic props. 77−69866
GdIG, IR refl., ATR, Voigt and Faraday expts. 80−66180
GdP, electronic struct., mag. exchange and elec. transport props. 78−87974
$(GdPrBi)_3(FeGaIn)_5O_{12}$, pure and In^{3+} doped, near IR absorpt. and Faraday rot. 78−95580
GdS, electronic struct., mag. exchange and elec. transport props. 78−87974
GdTe:P and CdTe:P,In(Ga)(Al), IR absorpt. investig. of localised vibr. modes of impurity centres 77−52136
Ge (111), spectroscopy of electron subbands 80−71422
Ge, absorption edge, hydrostatic press. effects 77−43994
Ge, amorphous, electronic struct., far infrared absorption 80−45051
Ge, amorphous, far IR absorption 78−88306
Ge, amorphous, IR absorpt , first-order effective charges due to at. displacements 77−48164
Ge, amorphous, O_2^+ ion implanted, influence on electrical and optical props. 77−89891
Ge amorphous film, disorder induced phonon absorpt. meas. using double beam Fourier spectrometer 80−105725
Ge, amorphous film, optical consts. in near IR range *(Korean)* 79−8137
Ge amorphous solid dielectric loss meas. by submillimetric waveguide laser 79−33603
Ge, compensated by thermal defects, recomb. and optical props. 80−64989
Ge, diamagnetic excitons, fundamental absorption edge, Faraday config. 79−8144
Ge, direct transition absorpt. coeff. modulation by electron-hole drops 77−90153
n-Ge, doped, dopant distrib. from carrier drift distrib. in high elec. field 79−51140
Ge, doped, electron or neutron irradiated, vibrational absorption 78−6718
Ge, electron hole drop far IR absorpt., damping, size effects, Mie theory 79−78685
Ge, electron-hole drop and exciton atmosphere 80−6748
Ge, electron-hole drop velocities as probe of phonons 78−68517
Ge, electron-hole droplets, conc. in mag. field, magnetoplasma absorpt. spectra meas. *(Russian)* 77−24854
Ge, electron-hole drops, far IR absorption 78−56467
Ge, electron-hole drops, far IR magneto-optical effects 78−84565
Ge, electron-hole drops, IR absorpt. spectra 79−87423
Ge, electron-hole drops, IR magnetoplasma absorptions 80−6728
Ge, electron-hole drops, spatial distrib., time and spatially resolved absorption at 3.4 μm 78−92075
Ge, electron-hole drops size effect on far IR absorption and scatt. *(Russian)* 78−10903
Ge, electroreflectance, field reversal asymm. at direct gap 77−69802
Ge, electroreflectance spectra, meas. on Al-SiO_2-Ge struct. 77−1677
Ge exciton and electron-hole drop decay, far IR magnetoabsorption obs. 77−40252
Ge, exciton effects on intervalence band transitions 77−4297
Ge, exciton energy gap and LA and LO momentum-conserving phonon energies 79−90965
Ge, far IR magneto-absorption of donor-bound excitons, pseudo-acceptor model 77−63418

infrared spectra of inorganic solids continued
Ge, far IR magnetoabsorption, excitons, electron-hole drops and impurities 78−6664
Ge, far-IR absorpt. spectra interpret. 77−40233
Ge film, amorphous, O implantation effects on absorpt. edge and elec. cond. 77−39970
Ge film, electroreflectance effects 79−43055
Ge films, adsorption of H_2O, IR spectra 80−6628
Ge, free carrier, intervalence band indirect absorpt., at high optically created carrier densities 79−42961
Ge, free-carrier plasma edge, fast transient spectroscopy 77−8558
Ge, heavily doped, far IR props. of shallow impurity states 79−95786
Ge, high density electron-hole plasma, infrared absorpt. at low temp. 78−92078
p-Ge, hot hole relax., IR saturated absorption, LO phonon emission 77−28569
Ge, hot light hole distrib. function and light absorpt. 79−60844
Ge, hydrogenated amorphous and cryst., IR spectra 79−61359
Ge, IR absorption and scatt. by electron-hole drops 78−51903
Ge, IR absorption by laser-excited nonequilibrium holes *(Russian)* 79−95752
Ge, IR absorption coeff. by holes, temp. depend., effective mass *(Russian)* 80−50350
p-Ge, IR light free hole absorpt., nonvertical optical transitions *(Russian)* 80−80802
Ge, impurity modes due to point defects, comparison with IR and Raman meas. 79−4386
Ge, impurity spectral linewidth meas., free electron effects 80−71463
Ge, inhomogeneous stressed, electron-hole drop light scatt. and absorption 80−108212
Ge, interband Faraday ellipticity 78−92052
Ge, internal Stark effect on impurity states, low-temp. magnet. absorption meas. 80−60636
Ge, lattice disorder influence on optical spectra in interband transition region 79−43006
Ge, local IR transmission 80−7357
Ge, matrix isolated cluster, optical absorpt. 80−16045
Ge, multioscillatory electrorefl. spectra *(Russian)* 77−8590
Ge, neutron irrad., absorpt. edge 80−93320
p-Ge, nonlinear IR absorpt., theory 79−65868
Ge, nonpolar semiconductor, IR free carrier absorpt., two short wavelength phonon scattering 79−78665
Ge, optical absorpt. in samples with 60° dislocations 78−39577
Ge, optical absorption from indirect transitions at high mag. fields 79−47441
Ge optical props. in 2.5-15 micron region 80−80775
Ge, optical pulse transmission, pulsewidth depend., phonons and plasmons role 78−31198
Ge optical windows, contaminated by NH_3, CO_2, CO, HCl, methane, cryocooled, IR transmission 79−32007
p-Ge, photon drag spectrum 77−32044
Ge, picosecond optical absorption, at high optically created carrier densities 79−47462
Ge, piezospectroscopic determ. of electron-phonon to hole-phonon interaction 79−95783
Ge, reactor irrad., opt. props. 77−90137
Ge, reflectivity, picosec. laser pulses and electron-hole plasma 79−47463
Ge, Schottky barrier electrorefl. under uniaxial stress, band struct. 77−48193
Ge, solid-state plasma, ultrafast transient response, theory and expt. 77−80748
Ge strain-confined large electron-hole drop characteristics 80−65469
p-Ge, tunable laser induced grating dip for sub-picosecond relax. meas. 77−75623
Ge, two photon absorption of light with optical transitions between heavy- and light-hole states 79−11421
Ge, two-phonon difference absorption spectra 78−76452
Ge:Al, Zeeman effect in excitation spectra, photoelectric spectroscopy 79−82633
Ge:As, far IR transmission spectra, singlet-triplet optical transitions in ground states of donors 78−2887
Ge:As(Bi), donor bound exciton luminesc. and absorpt. 80−29777
Ge:As(Sb), D⁻ states in mag. fields, photocond. spectra, and far IR absorption spectra 79−95370
n-Ge:As(Sb), far IR absorpt. spectra 79−91469
p-Ge:Ga, saturation behaviour at CO_2 laser wavelengths 78−1307
p-Ge:Ga far IR absorption and photoconductivity obs. 77−39899
n-Ge:Ga(P), uniaxial compression, 0.6-2.9 mm radn. absorpt. 79−82629
Ge:H, amorphous, H content determ. by IR absorpt., gas evolution and nuclear reaction methods 80−44130
Ge:In, magneto-optical transitions between discrete levels of In acceptor, far-IR obs., 4.2K 78−2890
Ge:Li,O, EPR and piezospectroscopy 80−25338
n-Ge:O, Czochralski growth, O content rel. to props., IR, Li precipitation determs. 77−15445
Ge:P, bound-exciton luminesc. and absorpt. 79−87469
Ge:Sb, bolometer element, absorpt. spectra, bias depend. 79−30553
n-Ge:Sb, exciton absorption 78−6688
Ge:Sb(Ga), fast electron radiation defects, 0.52 eV absorpt. band, impurity photocond. and Hall effect meas. 78−27273
Ge:Si, impurity modes and IR absorption 78−76506
Ge-Al film, elec. resist. and IR transmission, comp. and substrate temp. depend. 78−52112
Ge-Bi-S system, semicond., elec. cond., glass transition temp. and optical absorption meas. 77−16329
Ge-Bi-S system glasses, opt. props. and glass transition temp. 77−77224
Ge-Ga alloys, amorphous, far IR absorption 78−88306
Ge-Ga amorphous alloy, co-evaporated elec. and optical props. 80−70860
Ge-metal Schottky barrier photodetectors, near IR interband transitions and optical parameters 80−73449
Ge-S-Sb glasses, microgravity effect on recrystn., optical and elec. props. 80−49127
Ge-Se based glasses, refr. index, 1-11 μm 78−39520
Ge-Se glass, vibr. props., Raman and IR spectra obs. *(Japanese)* 77−43989
Ge-Se glass system, effect of changes in local surrounding of atoms on optical props. *(Russian)* 78−80414
Ge-Si, dil. alloy, IR absorpt. and first-order Raman scatt. due to single and paired impurity atoms 79−82976

infrared spectra of inorganic solids continued
Ge-Si, imperfect homopolar cryst., lattice dynamics, IR spectra calc. 80−59601
Ge-Si, solid soln., local IR transmission 80−7357
Ge-Si alloys, defect modes and optical spectra 80−11413
Ge-Te alloy films, amorphous, semicond. props., refr. index, struct. study 78−26978
$Ge_xAs_xS_xSe_{100-3x}$ and $Ge_xTe_xS_xSe_{100-3x}$ glasses, IR absorpt. spectra 77−12378
$Ge_xAs_xSe_{100-2x}$, x=2.5 and 5.0, chalcogenide glasses, IR absorpt. spectra 77−24842
$Ge_xAs_xTe_xSe_{100.3x}$, glassy 78−23448
$GeFe_2O_4$, single crysts., elec. and mag. props, optical absorpt. spectra 80−54719
GeH_4, phase transforms and vibrs. 77−36226
GeH_4, crystalline, determ. of mol. symm. from IR spectrum 78−9969
GeH_4:$SiHD_3$, symmetries of GeH_4 cryst. phases, IR spectra meas. 79−19886
GeH_3NCS, liq. and solid, IR and Raman spectra 79−89663
GeO_2, amorphous, obtained by hydrolysis of $GeCl_4$, exam. of props. 79−95956
GeO_2, glassy high freq. vibr. bands, central force model 80−49330
GeO_2, ultrathin layers on Ge substrate, ATR spectra, thickness depend., struct. obs. 80−55214
GeO_2, vitreous, band limits and vibrational spectra 79−73935
GeO_2, vitreous, LO vibrational modes, Raman and IR spectra 77−7819
GeO_2-P_2O_5-SiO_2 glass fibre, incorporation of OH in modified CVD process 80−50560
GeO_2-$PO_{5/2}$ glass, struct. and props. *(Japanese)* 77−27837
GeO_2-PbO glasses, IR transmittance and thermal expansion, effect of oxides and fluorides 77−63405
GeS, far IR reflectivity spectra, lattice vibr. and dielec. const. 77−52068
GeS, IR reflectivity meas. 77−8570
GeS, thin layer cryst., far IR transmission spectra 79−56870
GeS_2, energy gap and optical props. in IR region 79−51948
GeS_2, glassy, high freq. vibr. bands, central force model 80−49330
GeS_2, single cryst., IR polarised reflectivity spectra, 79−56775
GeS_2, single crystal, far IR transmission 80−80800
GeS(Se), dielec. function, optical and electron energy loss spectroscopy 78−15189
GeS_xSe_{1-x}, form. of solid soln. and phys. props. *(Russian)* 77−1232
GeS_xSe_{1-x}, IR spectra, differential calorimetry, phase diagram *(Russian)* 78−52513
$Ge_{1-x}S_x(Se_x)$, bulk-quenched glasses, opt. freq. dielec. const., chem. ordering effects 78−23472
GeSe, amorphous film, optical properties 78−39620
GeSe, optical absorption edge meas. 77−63430
GeSe, single crystal, optical absorption 80−25383
$GeSe_2$, far IR reflectivity meas. 77−28565
$GeSe_2$, far IR reflectivity spectrum, dielec. const. and lattice vibrs. 77−52069
$GeSe_2$, IR and Raman spectra 78−95585
$GeSe_2$ multimode layer cryst., far IR transmission and reflection spectrosc., comparative merits 80−76019
$GeSe_2$, single cryst., IR polarised reflectivity spectra, 79−56775
$GeSe_2$, single crysts., 3 polymorphic forms, DTA, photolum., IR and Raman sepctroscopy 80−33923
$Ge_{1-x}Se_x$ film, EPR, elec. and optical props. meas. 78−48038
Ge_ySe_{1-y}, glass, bulk and film, IR transmission and reflectivity meas., struct. mode assignments 78−79537
$Ge_xSn_{1-x}S(Se)$, lattice parameters, optical energy gap and IR refl. 78−23021
GeTe film 79−43055
GeTe, heterophase state, plasma refl. spectra, twinning domain distrib. study 79−69845
GeTe, heterophase state with nonuniform distribution of free carriers *(Russian)* 78−2849
GeTe, heterophase state with nonuniform free carrier distrib. 79−56798
p-GeTe, reflectance, and thermorefl. spectra 80−80814
$Ge_xTe_xSe_{100-2x}$, x=2.5 and 5.0, chalcogenide glasses, IR absorpt. spectra 77−24842
Ge(111)2×1, oxide layer, surface states detect optical reflectivity obs. 80−50368
Ge(111)2×1, surface electron states detected by external reflectivity 78−80036
H:T solid, collision induced IR lines caused by T_2 radioactivity 80−84756
H-bonded crystal, IR absorpt. spectra band shape, X-H stretching vibr. temp. depend., isotope effect 78−76445
H_2, chemisorption on AgNa mordenite 80−2752
p-H_2, cryst., hexadecapolar induced absorption intensities 78−88290
O-H_2, far IR absorpt. in ordered state 79−91430
H_2, IR fundamental band, U-branch transitions 78−64361
H_2, phonon absorption line shape as function of density 80−50329
H_2, solid, far IR absorption by phonons and librons in ordered state 78−80331
p- H_2, solid, induced near IR absorption spectrum, freq. shift, intensity, up to 10 kbar 78−6658
$HAl_{11}O_{17}$, H β-alumina, IR absorpt. study 80−100655
HBO_2, cubic, monoclinic and orthorhombic forms, H bonding, IR and Raman spectra 80−76029
HCl, cryst., internal vibr. electrostatic interactions and IR bandshape 79−91417
HCl-DCl mixed crystal, IR spectra, freqs., bandwidths and ν_{01} simultaneous transition 77−28564
HD-T_2, liq. and solid, vibr.-rot. IR spectra 80−50313
$HEu(PO_3)_4$, vibr. spectra 80−34905
HF, cluster and chain dipole moments, ab initio calc. 77−26967
HI, crystalline, Raman and IR spectra, mol. vibr., libration and translation 80−2757
α-HIO_3, dispersion anal. of IR reflection spectrum *(Russian)* 78−56493
α-HIO_3, near IR absorpt., influence of deuteration 78−27237
H_2O ice, amorphous, IR spectrum rel. to 3.1 μm absorpt. in interstellar mol. clouds 80−26956
H_2S frost, near IR reflectance spectra, tetragonal to cubic phase transition 77−81094
H_2S, solid, low-temp. phase, IR, far IR and Raman spectra 78−27218
HSO_3F crystal, indication of molecules existing as infinite chains *(French)* 80−989
H_2SeO_3, and deuterated analog, vibr. spectra 79−24311
H_2SeO_3, cryst., vibr. spectra in O-H stretching region 79−51949

infrared spectra of inorganic solids continued
H_2SeO_3, IR overtone spectra and temp. depend. 79−47456
H_3SiNCS, IR and Raman spectra, vibr. anal., LF bending mode 78−70842
HT-T_2, liq. and solid, vibr.-rot. IR spectra 80−50313
$HUO_2AsO_4.4H_2O$ and $HUO_2PO_4.4H_2O$ layered cpds., struct. investigs. below antiferroelec. transition temps., H bond ordered structs. 80−107416
H_xWO_3, amorphous, Anderson transition, disorder depend. and optical detection 78−47840
H_xWO_y film, effect of struct. on optical and electrical props. 78−84671
Hf-C-N-O-H, solid solns. of H, exam. of props. 80−29172
HfF_4-BaF_2-LaF_3 glass system, IR transmitting, synthesis and props. 80−71623
HfF_4-BaF_2-ThF_4-(ZrF_4) glass system, IR transmitting, synthesis and props. 80−71623
HfO_2-La_2O_3 system, phase form. and relations, phys. props. 79−43218
HfO_2-MgO system, intermediate phases existence, X-ray diffr. and IR obs. 79−38805
HfS_3, quasi one-dimens., optical phonon anisotropy, IR spectra study 80−40112
$HfS_3(Se_3)$, phonon study of chemical bonding 80−20645
Hg films, superconducting, far-IR and electrodynamic props. meas. 80−103957
Hg-As-S-I system, glasses, optical and acousto-optical props. 78−83053
HgA_2X_4 (A=Ga,In; X=S,Se), Fourier IR and Raman spectra, cryst. struct. and symm. *(German)* 79−24313
$Hg_{2.86}AsF_6$, anisotropic linear-chain conductor, optical reflectance meas. 77−77247
$Hg_2(BrO_3)_2$, Raman and IR spectra, vibr. anal. 77−66492
$Hg_{1-x}Cd_xSe$, IR absorpt. spectra, band struct., refr. index 80−50337
$Hg_{1-x}Cd_xSe$, zinc blende structure, optical and electronic properties 80−6723
$Hg_{0.74}Cd_{0.25}Te$ thin film deposition on Si substrates by RF triode-sputtering, large-area photodetector arrays 80−80965
$Hg_{0.75}Cd_{0.25}Te$, single crystal, reflection spectra 80−40140
$Hg_{1-x}Cd_xTe$, avalanche formation, high intensity IR transmission limit 79−78684
$Hg_{1-x}Cd_xTe$, carrier conc., Hall effect, photocond., IR spectra meas. 80−49771
$Hg_{1-x}Cd_xTe$, far IR cyclotron resonance in inversion layer 77−69396
$Hg_{1-x}Cd_xTe$, high intensity IR transmission limit 78−79074
$Hg_{1-x}Cd_xTe$, IR optical absorpt. and refr. index, 80 to 300K 79−91418
$Hg_{1-x}Cd_xTe$, narrow-gap semiconductor, high intensity IR transmission limit 80−7361
$Hg_{1-x}Cd_xTe$, semimetallic state, magneto-optical investig. of Landau levels and band parameters 77−63410
Hg_2Cl_2, cryst., birefringence and dichroism, 200-500 nm and far IR 78−27257
Hg_2Cl_2 single crysts., IR refl. spectra and ferroelasticity 79−99889
n-$HgCr_2Se_4$, ferromagnetic semiconductor, plasmon refl., 86 to 320K 80−50346
HgI_2, IR lattice vibr. and dielec. dispersion 80−76018
Hg_2I_2, large single crystal far IR spectra 78−92057
$HgIn_2Se_4$, IR refl. spectra and cryst. struct. 79−56777
$Hg_3In_2Te_6$, complex ordered-vacancy cpd., struct. and lattice dynamics 78−34496
$Hg_{1-k}Mn_kTe$, impurity magnetoabsorpt. 79−91473
$Hg_{1-x}Mn_xTe$, exchange interaction effect on $\Gamma_8 \rightarrow \Gamma_8$ magnetoabsorption 79−61351
$Hg_{1-x}Mn_xTe$, far IR interband absorption obs. 79−33696
$Hg_{1-x}Mn_xTe$, far IR studies of lattice and free carrier effects 78−39544
$Hg_{1-x}Mn_xTe$ mixed crystals, zero gap, effect of exchange on interband magneto-absorption 78−23443
$Hg_2(NO_3)_2.2H_2O$, Raman and IR spectra, vibr. anal. 77−66492
Hg_2SO_4, Raman and IR spectra, vibr. anal. 77−66492
$Hg_{2.91}SbF_6$, anisotropic visible and IR refl. rel. to metallic cond. 77−8602
HgSe, dielec. function at 2, 95, and 300K, reflectivity spectra meas. 79−15458
HgSe, interband absorpt. and Γ-point band structure parameters 79−47010
HgSe, interband $\Gamma_6 \rightarrow \Gamma_8$ magnetoabsorption, temp. study 80−76032
HgSe, optical determ. of Γ-point band struct. parameters 79−82523
HgSe, two-phonon resonant effect, far-infrared reflectivity 80−108203
HgSe(Te), dynamic dielectric function, IR absorpt. meas. 78−68508
HgTe, energy bands and optical props. calcs., tight-bonding model with spin-orbit interaction 80−65448
p-HgTe, far IR reflectivity spectra, experimental and theoretical study of the dynamic dielectric function 78−92069
p-HgTe, inverted band struct., negative energy gap from IR absorpt. meas. 77−62820
HgTe, long-wavelength magneto-absorptions 80−11397
HgTe, magnetooptical study of Γ_8 bands anisotropy 79−82984
HgTe, optical absorption 77−28572
HgTe, zero-gap semicond., absorpt. spectrum in mag. field 80−11370
$Hg_xZn_{1-x}Cr_2Se_4$, absorption spectra near the absorption edge 78−80340
$HoPO_4$, cryst., IR spectra, complex anions internal vibrs. resonance splitting 80−34907
$Ho_2(SeO_4)_3.SH_2O$, thermal decomp. and IR spectra 80−3319
$IN(OH)_3$, cubic, IR spectra comparison with $In(OD)_3$ 79−77568
In, film, vac. deposited, influence of ion bombardment during condensation 79−82483
In-Te system, IR spectra *(Russian)* 78−84589
$In_{1-x}Al_xAs$, band gap, IR absorpt. spectra meas. 80−66205
InAs amorphous film, DC sputtered, optical absorpt. 78−19589
n-InAs, avalanche formation, high intensity IR transmission limit 79−78684
InAs, electroreflectance spectrum 78−19479
InAs epitaxial film on GaAs, far IR reflectivity obs. 77−40251
InAs, far IR transmission spectrum 78−4713
InAs, fine struct. of diamag. excitons, oscillatory magnetoabsorpt. obs. 78−18971
n-InAs, heated electron gas, longitudinal optical phonon form., IR absorpt. modulation 80−45079
InAs, heteroepitaxial, far IR refl. and transmission meas., surface and interface effects 80−16044
InAs, narrow-gap semiconductor, high intensity IR transmission limit 80−7361
InAs, neutron bombarded, optical absorption, struct. defect form. and nuclear alloying *(Russian)* 78−31206

infrared spectra of inorganic solids continued
InAs on GaAs, epitaxial-substrate system, far IR transmission and refl. 78−6802
InAs, plasmon-phonon coupling, and IR refl. spectra of impure crysts. 79−56150
InAs:Cr, high-resist., energy positions of deep levels, elec. and optical props. 79−7807
InAs:S(Mg), ion implanted, photocond., photo-EMF, and optical absorpt. spectra 80−70763
$(InAs)_x(CdTe)_{1-x}$, band gap and effective mass, IR spectra obs. 78−56491
InAs(P), electron irrad. at 50 MeV, elec. and optical props. 77−47486
$InAs_{1-x}P_x$, evidence for reduction in momentum matrix element P^2 due to alloy disorder 79−65853
InAs(Sb), IR reflectivity, longitudinal optical phonon-plasmon coupling 77−59578
InAs(Sb), in MOS struct., electrorefl., band-population effects under heavy surface accumulation 77−48167
$In_{1-x}Ga_xAs$-$GaSb_{1-y}As_y$ superlattice, optical absorption 79−19887
$In_xGa_{1-x}As$, epitaxial solid soln. film, spectral depend. of transparency, absorpt. spectra calcs. 80−45161
$In_{0.79}Ga_{0.21}As_{0.54}P_{0.46}$, LPE layer, electroreflectance meas. 79−24290
$In_{1-x}Ga_xAs_yP_{1-y}$ epitaxial layer, far IR refl. spectra, lattice vibrs. 80−97282
$In_{1-x}Ga_xAs_yP_{1-y}$ far IR reflection spectrum 80−60612
$In_{1-x}Ga_xP$, non-isodisplacement of P atoms in long-wavelength optical phonons 79−47444
$In_{1-x}Ga_xP$, phonon density of states, cluster Bethe lattice treatment 80−6475
$In_{1-x}Ga_xP$, two-phonon IR absorpt. 78−52493
$In_{1-x}Ga_xP_{1-z}As_z$, lattice matched to InP, electroreflectance obs. 80−93416
InI, InI_2 and InI_3, far-IR spectra, valence states in InI_2 79−47435
InN film, refl. and transmission spectra, band struct. 78−72625
InO_3:Sn film, prep. by spray hydrolysis, struct., elec. and optical props. *(Japanese)* 79−42678
n-In_2O_3 film, RF sputter grown, substrate bias effect on elec. and optical props. 78−64150
In_2O_3:Sn film, CVD and DC sputtered, electro-reflectance meas. 80−11496
In_2O_3:Sn film, electroreflectance effects 79−43055
In_2O_3:Sn films, RF reactive sputtered, optical props. rel. to band struct. 79−91515
In_2O_3-SnO_2, X-ray and optical meas. of solubilities 79−55894
InP, manifestation of local vibrs. of dislocations in IR spectra 78−88339
InP, multiphonon absorpt. bands *(Russian)* 77−85731
InP, p-i-ν diode, Franz-Keldysh effect 77−55790
n-InP, room temp. electron irrad., Hall coeff. meas. 77−89478
InP, surface phonon polariton dispersion and damping, frustrated total internal refl. meas. 80−80792
InP:Fe, deep levels 79−56166
InP:Fe, influence of covalence on EPR spectra 78−26827
InP:Si, vibr. modes of Si, IR absorpt. bands 78−55922
InS, IR reflection spectra 80−11389
In_6S_7, absorpt. band edge investigation 79−69840
InS(Se), optical and nonlinear optical props. *(Russian)* 79−51943
InSb, absorpt. edge, exciton struct. 80−93321
InSb, absorpt. saturation by nonequilib. electron-hole plasma, luminesc. 78−9418
InSb, avalanche formation, high intensity IR transmission limit 79−78684
InSb, doping depend. of high-field donor spectra 77−90175
InSb inversion layer, spectroscopy of electron subband levels 78−64364
InSb, narrow-gap semiconductor, high intensity IR transmission limit 80−7361
p-InSb, shift of fundamental absorpt. edge in crossed elec. and mag. fields 80−76034
n-InSb, strongly compensated, ionized donor mol. optical absorpt. spectra characts., 1.5-2.5 mm 79−11422
InSb surface, IR spectroscopy of subband levels 80−20277
n-InSb:Se(Te), Moss-Burstein effect, optical energy gap depend. on doping conc. 77−8581
InSb-NiSb, eutectic, intraband magneto-optical studies, far IR transmission spectra 79−61371
InSb-NiSb eutectic, struct. and optical props., IR polariser appl. 80−45078
InSb-PbTe(CdTe) superlattices, laser deposition of multilayer heteroepitaxial structs. 80−44450
$InSb_{1-x}As_x$, cryst. struct. and far IR reflectivity 79−56752
$InSb_{1-x}As_xBi_y$, far IR reflectivity 79−56752
InSe, absorpt. edge fine struct. *(Russian)* 77−48176
InSe, exciton absorpt. spectra, additional light wave 77−63445
InSe, layer cryst., Raman and IR refl. spectra meas. 79−95777
InSe, layer single crystal, infrared and Raman spectra 78−92070
InSe, optical props. near fundamental absorption edge 77−12434
InSe, polar optical phonon ang. behaviour, IR refl. meas. 80−20633
InSe, vibr. spectrum, IR refl. and absorpt. 500-100 cm^{-1} 77−81102
α-In_2Se_3, far infrared optical study of ordered and disordered forms 78−84572
In_2Te_3 film thermal deposition, transmission spectra and elec. cond. *(Russian)* 80−49555
In_2Te_5, photocond. and absorption spectra, polarisation dependences 80−20642
$InVO_4.2H_2O$, $In_4(V_2O_7)_3.14H_2O$, physicochem. props. 77−85702
Ir complexes with adenosine, xanthosine, prep., elec. cond., IR spectra, characterisation 78−92065
IrP_2, prep. and characterisation 78−39679
K double fluorides, IR refl. spectra, vibr. modes, optical vibr. freq., Kramers Kronig anal. 80−66190
K, Mayer-El Naby optical absorption anomaly 77−4643
K salts, anion exchange, in tablet pressure for IR spectroscopy *(Russian)* 78−95927
K, surface electron states and optical props. in IR spectral range *(French)* 80−54757
K-β-Al_2O_3, far IR absorpt., Beevers-Ross sites, interstitials 80−66240
K_2AF_6, A=Si, Ge, Sn, IR absorpt. spectra, integrated intensity 79−73944
$KAlSi_3O_8$, feldspar microwedge, melting by CO_2 laser, deform. of IR absorpt. spectra 77−19984
K_3AsO_4-$KAsO_3$, glass and cryst., Raman and IR spectra 79−99862

infrared spectra of inorganic solids continued
$KB_5O_8.4H_2O$, polariton Fermi reson., spontaneous parametric light scatt. 78−87923
$K_5Bi_{1-x}Nd_x(MoO_4)_4$ solid soln., growth, spectroscopic and laser props. 78−2901
KBr, amplitude and phase spectra, 80 to 280 cm^{-1}, Fourier spectroscopy technique 77−45903
KBr extrinsic absorpt. near 9.6 μ, using CO_2 laser calorimetry 77−16341
KBr, IR laser window appl., crystal growth, polishing and optical absorpt. 77−7102
KBr pellet spectroscopy, H_2SO_4 effect 79−88034
KBr, Stark effect in F-centre emission 77−63434
KBr, transient infrared absorption of bound polarons 78−92071
KBr:BeF_4^{2-}, IR absorption spectra of impurity anions *(Russian)* 80−2807
KBr:$CaSO_4$, SO_4^{2-} vibr. spectra, press.-scanned Fermi reson. spectroscopy appl. 79−73937
KBr:HS^- (HF_2^-), anharmonic interaction of impurity intramol. vibrs. with cryst. phonons 77−77217
KBr:MnO_4^-, optical and IR absorpt. spectra, internal vibr. of MnO_4^-, freq. and type of symm. 79−15466
KBr:SO_4^{2-}, IR absorpt. spectra, cation impurity influence *(Russian)* 78−10901
KBr:TeO_3^{2-}, IR absorpt. of impurity complexes *(Russian)* 79−33746
$KBrO_3$, polarised IR reflection spectra, surface damage effects 79−19872
$KBrO_2F_2$, struct. data, vibr. spectra 77−39563
KCN, dynamics of CN^- ions near phase transitions at 83K 80−80717
KCN, F-centre emission spectrum 77−12420
KCN, librational and phonon sidebands of IR CN^- stretching mode 79−15457
KCN, multidomain birefr. solid, light scatt. and IR transmission spike 80−60587
KCN, optical F centres and phase transitions 78−56504
KCN, Raman diffusion spectra, IR absorpt. in phases II and III *(French)* 80−84741
KCN:H^-, U-centre, local mode meas. 77−1199
KCN_xCl_{1-x}, finite field local field catastrophe phenomena in spectra 80−92830
KCN_xKCl_{1-x}, phase transition and OCN^- vibr. spectrum 78−43093
KCNS, single cryst., IR and Raman multiphonon bands, factor group anal. 77−4644
K_2CO_3, molten, IR emission spectra *(Japanese)* 78−19469
K_2CO_3-D_2O, glassy matrix, absorpt. spectra after X-irrad., solvated electrons 79−65903
$KCdCl_3$:Co^{2+}, Zeeman Raman scatt. and Zeeman IR absorpt. spectra 79−56782
KCl, absorpt. coeff. meas., using pulsed CO_2 laser, calorimetric method 78−18028
KCl, bulk and surface absorpt., 2 to 10 μm, calorimetric meas. 78−71160
KCl, bulk and surface absorpt. in 9.2-10.8 μm region 79−95808
KCl crystals with NaF surface absorpt. regions, photoacoustic detect. 79−87466
KCl, electron trapping by alkali ion impurities 78−47809
KCl extrinsic absorpt. near 9.6 μ, using CO_2 laser calorimetry 77−16341
KCl, IR absorpt. calcs. in rectangular crystallites 78−95583
KCl microcrystal boundary influence on IR spectrum 77−40243
KCl, surface and bulk absorpt. at 10 μm, temp. depend. 77−28576
KCl, TSM study of lattice statics and dynamics 79−82292
KCl, undoped and Pb- or NO_3^--doped, colloid centre formation, absorpt. spectra, 300-1000 nm 79−78710
KCl:Au^-, absorption band shape in D-mode model 79−47485
KCl:BeF_4^{2-}, IR absorption spectra of impurity anions *(Russian)* 80−2807
KCl:Ca, optical studies of Z_4 centres 79−24336
KCl:Ca^{2+}, cryst., hydrolysed, IR absorpt. bands 77−32404
KCl:Eu IR laser window lattice equilibrium obs. 79−14055
KCl:$KNO_2(KNO_3)$, anion exchange during tablet pressing, IR spectroscopy appl. 80−2764
KCl:Li, additively coloured, luminesc. material for IR region *(Russian)* 78−15209
KCl:Li^+, defect induced tunnelling states, depend. on strain, pot. model calcs. 79−69865
KCl:Na, absorption from relaxed excited state by F_A and F_B centres 77−44031
KCl:Na^+, OH^-, IR absorpt. spectra, Na^+ ions rel. to OH^- stretching vibr. 79−47442
KCl:OH, absorpt. in high-transparency region 80−89037
KCl:RbCl, $SrCl_2$, IR window material, cryst. growth and props. 78−31333
KCl:SO_4^{2-}, Ba^{2+}(Ca^{2+}), IR absorpt. band parameters, temp. depend. *(Russian)* 78−31226
KCl:Tl^+, optical absorpt. spectra following X-irrad., F- and V-centres 79−99912
KCl-Al(Pd) composite, far IR absorption 78−56466
KCl(Br):OH^-, electron irrad., F_2^+ centre stabilisation 80−54231
$KCl_{1-x}Br_x$:NCO^-, absorpt. band defect broadening *(Russian)* 78−72526
KCl(Br)(I), far IR complex refr. indices, dispersive Fourier transform 78−80322
KCl(Br)(I):PO_2^-, vibr. spectra and struct. of PO_2 impurity ions 77−16354
$KCl_{1-x}I_x$:NCO^-, absorpt. band defect broadening *(Russian)* 78−72526
K_2CoF_4:Mn^{2+}, impurity induced mag. excitations, magnon gap mode, far IR spectra obs. 80−44821
K_2CrO_4, IR reflection spectra, Davydov splitting and mol. interaction 79−8147
K_2CrO_4:SO_4^{2-}, IR absorpt. spectra, local symmetry of impurity ions *(Russian)* 78−2893
K_2CrO_4+$La_2(NoO_4)_3$, ($Nd_2(NoO_4)_3$), X-ray phase analysis, IR absorption spectra, and thermogravimetric anal. 79−1944
$K_xCs_{(1-x)}Al(SO_4)_2$, solid soln., Raman and IR spectrum study *(French)* 79−47453
K_2CuF_4, two-dimens. ferromag., magneto-optical props., absorpt., MCD and MLD 79−87419
$K_2Cu(H_2O)_6(SO_4)_2$, IR and Raman vibr. spectra 79−28743
$KD_{2x}H_{2(1-x)}PO_4$ crystals, $0<x<0.98$, light scatt. by polaritons 80−96802

infrared spectra of inorganic solids continued
KD_2PO_4, high temp. phase transition, dielec. const., elec. cond. and IR refl. meas. 78−43118
KD_2PO_4, IR and Raman polarised spectra, rel. to crystal struct. 78−56489
$KDy(MoO_4)_2$, polarised IR and Raman struct., $^{92}Mo/^{100}Mo$ isotope effect 80−108198
$KDy(WO_4)_2$, low temp. phase transitions *(Russian)* 78−87787
$KEu(PO_3)_4$, synthesis of K_2CO_3, Eu_2O_3 and phosphoric acid, exam. of structure 79−1837
α-$KEu(PO_3)_4$, vibr. spectra 80−34905
$K_3Eu(PO_4)_2$, synthesis and IR spectra 80−16019
KF, IR absorpt. spectra from relaxed excited states of F-centres 77−69868
$KF(HF)_n$, (n=2,3,4), cryst., anion struct., H bonding, IR spectra 77−54560
$K_3Fe(CN)_6$-KCl, press. induced reduction, IR spectra after pressurization 80−66776
$KFeCl_3$, linear chain ferromag., optical absorpt. and dichroism in mag. field 77−77237
K_2FeF_4, two dimensional planar antiferromag., mag. excitations, Raman and far IR spectra obs. 78−72343
K_2GeF_6, IR absorpt. spectra, integrated intensity, 100-300K, phase transition 79−73945
KH_2AsO_4, high temp. phase transition, dielec. const., elec. cond. and IR refl. meas. 78−43118
$K(H_{1-x}D_x)_2PO_4$, for IR response exam. by asymmetric Fourier spectroscopy 77−28570
KHF_2, IR refl. spectra 78−80324
KH_2PO_4, and isomorphs, IC spectra and phase transitions, under pressure 78−31180
KH_2PO_4 crystals, polarisation of unbound many particle states, IR spectra *(Russian)* 78−84556
KH_2PO_4, far IR c-axis transmission spectrum obs. 77−8571
KH_2PO_4, far IR dispersive reflection spectra 77−36213
KH_2PO_4 far IR dispersive reflection obs. with asymmetric polarising interferometer 77−40249
KH_2PO_4, ferroelectric phase transition exam. by spontaneous parametric light scatt. 78−19427
KH_2PO_4, IR overtone spectra and temp. depend. 79−47456
KH_2PO_4, near IR absorpt., influence of deuteration 78−27237
KH_2PO_4, soft mode behaviour, dispersive Fourier transform spectroscopy 77−7823
KH_2PO_4, spontaneous electrooptic effect in far IR 79−95734
$KHSeO_3$, and deuterated analog, vibr. spectra 79−24311
$K_2HgCl_4.H_2O$, cryst., IR spectra, water mol. struct., H-bonding 77−81089
KI, far IR, quartic damping, and quasiselection rule for gap compounds 78−31195
KI, Stark effect in F-centre emission 77−63434
$KI:BH_4^-$, far IR absorption in phonon gap 77−12406
$KI:CaSO_4$, SO_4^{2-} vibr. spectra, press.-scanned Fermi reson. spectroscopy appl. 79−73937
$K_2InCl_5.H_2O$, crystal structure and H-bonding 80−64978
$(K_{0.5}La_{0.5})_xBa_{1-x}TiO_3$, cryst. struct., dielec. and IR spectral meas. 79−46614
$KLa(PO_3)_4$ (α and β forms), vibr. spectra 80−34905
$K^+M^{III}(SO_4)_2$, M=Al^{3+}, Cr^{3+}, Fe^{3+}, Raman and IR spectrum study *(French)* 79−47453
$KMgCl(ClO_4)_2.nH_2O$, IR spectra and struct. features 79−15452
$KMgCl_3.nH_2O$, IR spectra and struct. features 79−15452
$KMgF_3$ residual IR absorption, freq. and temp. dependence obs. 79−15468
$KMgF_3:Co^{2+}$, γ-irrad. single cryst., visible and IR absorption, MCD, annealing data 78−10926
$KMgF_3:Fe^{2+}$, Jahn-Teller quenched spin-orbit, splitting of $^5T_{2g}$ state 77−63442
$KMgF_3:Ni^{2+}$, absorpt., MCD and emission spectra 79−51953
$K_3Mg_4LiSi_{12}O_{30}$, cryst. struct., X-ray diffr. and IR spectra *(French)* 80−107158
$K_2Mg_3M_2Si_{12}O_{30}$ (M=Cu, Fe, Zn, Mg), cryst. struct., X-ray diffr. and IR spectra *(French)* 80−107158
$K_2Mg_4Mo_4O_{16}.(OH)_2(H_2O)_2$, dehydration processes rel. to stoichiometry *(French)* 79−24734
$K_2Mg(S_2O_3)_2.6H_2O$, isolation, struct., decomposition *(French)* 78−52506
$KMnF_3$, IR-active phonons in tetragonal phases 80−2748
K_2MnF_4, IR active modes, interlayer and intralayer forces 77−59575
K_2MnF_4, perovskite type layer struct., far IR reflectivity and Raman spectra 77−15511
$K_2MnF_4:Ni^{2+}$, and undoped, magnon spectra, Raman and far IR spectra meas. 77−20573
KN_3, IR refl. spectra, fundamental lattice modes, azide ion dipole derivatives 78−48166
KN_3, mono- and polycrysts., IR active lattice vibr., optical consts. 77−77185
KNCO, polycryst., IR and Raman spectra, lattice and internal modes 77−32369
KNCSe, IR and Raman spectra, internal and external modes 77−16312
KNO_3 characteristic features of electronic structure 79−47436
KNO_3, far IR study of dielec. function by asymmetric Fourier spectroscopy 79−51947
KNO_3 in alkali halides tablets, phase transition and ion exchange, IR spectra 80−79937
KNO_3, Raman and IR spectra and lattice vibrs. 80−60565
KNO_3, vibrations of isotopic impurities, IR reflection and Raman spectra meas. 77−51465
KNO_3-urea solid eutectic mixtures, Raman, IR spectra, line shifts, width 77−55793
$K_3N(SO_3)_3.2H_2O$ and ^{15}N derivative, Raman and IR spectra, $N(SO_3)_3^{3-}$ normal coord. anal. 79−91433
$K_3N(SO_3)_3.2H_2O$, cryst. binding of H_2O, IR spectra 78−75620
$K_2NaGaF_6:Cr^{3+}$, magneto-optical study of $^2T_{1g}$, $^4T_{2g}$, ^2E_g-$^4A_{2g}$ transitions 80−71384
$KNbO_3$, ferroelec. cryst., IR and Raman spectra, mode coupling 80−66194
β-$KNd(PO_3)_4$, vibr. spectra 80−34905
$K_3Nd(PO_4)_2$, synthesis and IR spectra 80−16019
K_2NiF_4, quadratic layer antiferromag., optical spectra obs. 77−16326
$K_2Ni_3(P_2O_7)_2.nH_2O$, thermal dehydration 80−35513

infrared spectra of inorganic solids continued
K_2O-Al_2O_3-P_2O_5-Nb_2O_5 glasses, struct. singularities, IR spectra *(Russian)* 78−2861
K_2O-B_2O_3 glass, laser decolorisation of colour centres 79−43008
K_2O-PbO-SiO_2, glass, mech. and optical props. *(Russian)* 77−20860
K_2O-SiO_2 glass, IR reflection spectra change due to moisture corrosion *(Japanese)* 78−19914
K_2O-SiO_2 glasses, IR reflection spectra, computer resolution *(Japanese)* 77−69832
K_2O-TiO_2-SiO_2 glass, Si-O bonding, Si Kβ X-ray fluorescence and IR spectra 80−10500
$K_2O.4TiO_2$, new fibrous phase 80−20917
$K_2Pt(CN)_4Br_{0.3}.3H_2O$, IR absorption peak theory 77−43991
$K_{1.75}(Pt(CN)_4).1.5H_2O$, 1-D cond., IR spectra 77−85703
$K_{1.62}Pt(C_2O_4)_2.2H_2O$, plasma resonance absorpt. from small particles 77−24841
K_2PtCl_4, far IR reflection spectra, assignments, effective ionic charges, force consts. 77−66488
$K_2PtCl_6:Os^{4+}$, sharp line luminesc. band at 10K, vibr. assignment 78−95600
$K_xRb_{1-x}Cl:HF_2^-,SO_4^{2-}$, nonuniform broadening of IR vibr. absorpt. bands of impurities *(Russian)* 77−16357
$K_xRb_{1-x}Cl_6Br_{1-y}$, far IR absorption spectra 79−33695
$K_xRb_{1-x}Cl_yBr_{1-y}$, IR reflection spectra 78−76474
K_2ReCl_6-K_2ReBr_2 solid soln., mixed ligand complexes 77−72585
$KReO_4$, vibr. spectrum, Raman and IR spectra obs. 80−55104
$K_2(RuCl_5NO)$, polarised Raman and IR spectra, vibr. anal. 77−69819
K_2SO_4, IR absorpt. spectra, polymorphism, site group approx. and SO_4 stretching mode 78−52510
$K_2SO_4:XO_4^{2-}$, X=Cr, Se, Mo, W, lattice-impurity interactions, IR spectra 78−19522
KSO_3F, disordered cryst., IR and Raman spectra, internal modes assignment, space group *(French)* 79−95742
K_2SeO_4, incommensurate structure, IR and Raman activity of soft mode 79−28738
K_2SeO_4, incommensurate and ferroelec., far IR and mm dielectric response 79−73955
$KTaO_3$, complex refr. index meas. in far IR, by dispersive Fourier transform spectroscopy 78−92042
$KTaO_3$, dielec. response temp. depend. meas., dispersive Fourier transform spectroscopy 79−15449
$KTaO_3$ pseudodisplacive ferroelec., temp.-dependent dielectric response obs. 77−40247
$KTaO_3:OH^-(OD^-)(OT^-)$, IR spectra, spectrosc. consts. 80−100671
KTb_3F_{10}, Faraday rotation, optical absorpt. spectra and refr. index 78−72542
$K_2(TeBr_6)$, far IR and Raman spectra and phase transitions 80−11376
$K_5(UO_2)F_9$, optical spectra, vibr. freqs. calcs. *(Russian)* 78−31205
$K_2(UO_2)_3F_8.4H_2O$ and $K_3(UO_2)_2F_7.2H_2O$, IR and Raman vibr. spectra *(French)* 79−51937
$KX:SO_4^{2-}$, X=Cl,Br, impurity ion IR spectra analysis *(Russian)* 77−85762
K_2XY_6 (X=Sn, Te, Y=Cl, Br), low temp. vibr. spectra, lattice dynamics and phase transitions 79−73917
$KZnF_3:Ni^{2+}$, absorpt., MCD and emission spectra 79−51953
$K_2Zn(H_2O)_6(SO_4)_2$, IR and Raman vibr. spectra 79−28743
$K_2Zn(H_2O)_6(SeO_4)_2$, IR and Raman vibr. spectra 79−28743
La compounds, plasma light reflection by free charge carriers 80−11403
La_2ASe_5, A=Ge, Sn, diffuse refl. spectra and band gaps 79−51963
LaB_6 film, prep. by electron beam evaporation, and optical and elec. props. 80−20793
$La_2Be_2O_5:Nd^{3+}$, optical absorpt. and fluoresc. intensities 80−29793
$LaBr_3:Np^{3+}$, energy level anal., polarised absorpt. and fluoresc. spectra 80−76056
$La(BrO_3)_3.9H_2O$, IR and Raman spectra, vibr. asignments 78−84569
$LaCl_2:U^{3+}(5f^3)$, polarised absorption spectra and energy levels 80−16063
$LaCl_3:Np^{3+}$, energy level anal., polarised absorpt. and fluoresc. spectra 80−76056
$LaCl_3(Br_3):Pr^{3+}$, IR absorption, energy values for Stark manifolds 80−34955
$LaF_3:Dy^{3+}$, magnetospectroscopy with optically pumped far IR laser 79−33737
$LaF_3:Nd^{3+}$, $4f^3$ configuration, ground level energy state variation rel. to press. *(Russian)* 77−16358
LaF_3-$La(OH)_3$, high pressure phases, X-ray diffr. and IR spectroscopic anal. 79−47679
$LaNbO_4:Eu^{3+}$, single cryst., photoluminesc. obs., vibronic transition dichroism 77−69890
γ-La_2S_3, indirect electron transitions, diffuse refl. and vibr. spectra 78−84576
La_2S_3 single crystals, optical props. 79−87458
La_2S_3, vibr. spectra, factor-group anal. 80−80793
La_xS_y, stoichiometry and opt. props. during hot pressing 78−23653
$LaVO_4$, monazite struct., IR and NMR spectra 79−78534
Li aggregated deposits, optical props., 1-6 eV 77−66549
Li aluminosilicate, formation of glass-ceramic in $LiCl_3$ vapour 77−16536
Li deposits, optical consts., 0.5-10.7 eV, Kramers-Kronig anal. 77−40201
Li MIM struct., electron-phonon interaction function investigation by microcontact spectroscopy 79−95108
β-LiAl, optical dispersion, room temp. reflectance spectra 80−66195
$LiAl_xFe_{5-x}O_8$, IR spectra, ionic ordering in absence of fine struct. 77−8583
$LiAlSi_2O_6$, IR refl. spectra dispersion anal. 79−99877
$LiBaPO_4$, vibrational spectra and cryst. struct. 78−39536
Li_2CO_3, molten, IR emission spectra *(Japanese)* 78−19469
$^7Li_2CO_3$, and $^6Li_2CO_3$, polycryst., low freq. IR and Raman bands assignments 79−42970
LiCl-D_2O, aq. 10 M glass, optical absorpt. spectra after X-irrad., electron scavenging efficiency 79−83476
LiCl-D_2O glass, trapped and quasifree electrons optical transitions, bound-continuum character 78−6660
$LiCr_xFe_{5-x}O_8$, IR spectra, ionic ordering in absence of fine struct. 77−8583
$LiErF_4$, spectroscopic anal. Er^{3+} polarised absorpt. spectra, cryst. field parameters 79−95756
$LiEu(PO_3)_4$, vibr. spectra 80−34905
LiF, 3 MeV electron induced, F, F_2, F_2^+, R_1, R_2 and F_2 colour centre obs., IR spectra obs. *(Russian)* 77−48210
LiF, ATR IR spectrum from rough surfaces 77−20850
LiF, aggregation, microcryst. form., IR spectra obs. 78−46331

infrared spectra of inorganic solids continued
LiF, alkali ion implantation, migration, segregation, effect on optical props. 80−100269
LiF film, ATR spectrum, reson. between longit. phonons and substrate surface polaritons *(Russian)* 77−32384
LiF, manifestation of local vibrs. of dislocations in IR spectra 78−88339
LiF, microcryst. and polymers, IR absorpt. 77−63412
LiF microcrysts., matrix isolated in Ar, aggregated and isolated samples 77−55782
LiF, Stark effect, M-centre absorpt. bands 78−84614
LiF thin film boundary influence on IR spectrum 77−40243
LiF:Mg(Eu)(Co)(Si)(O), elec. cond., influence of impurity ion 79−7709
LiF:OH crystals, X-irradiated, H centres formation and annealing 80−54226
LiF:OH^-, electron irrad., F_2^+ centre stabilisation 80−54231
LiF:OH^-, IR spectra 80−20676
LiF:U_3O_8, X- and γ-irrad., U^{5+} luminesc. molecular centres, optical and ESR expts. 77−48224
LiF-$Al(PO_3)_3$ glass, phase decomp., X-ray diffr. and IR spectra study 80−30003
LiF-$NaPO_3$-MeF_x (Me=Mg, Ca, Al) glasses, IR spectroscopy study 80−16042
$Li_{0.5}Fe_{2.5}O_4$-$CuFe_2O_4$-$ZnFe_2O_4$, order-disorder transition, quadratic transformation *(French)* 78−76447
$Li_{0.5}Ga_{0.85}Cr_{1.625}O_2$ spinel, tetrahedral coordination of Cr^{3+} ion, electronic spectra, X-ray and neutron diffr. *(French)* 79−65031
$LiGaCr_4S_8$, 1:1 ordering on tetrahedral sites obs. *(German)* 78−6669
$Li_{0.5}Ga_{2.5}O_4$-$CuCr_2O_4$ system, phase diagrams, IR spectra, Cu^{2+} electronic spectra *(French)* 78−51461
$Li_2Gd_4(MoO_4)_7$, Czochralski growth, struct. and optical props. 78−27397
LiH, effect of surface hydrolysis to LiOH on IR absorption, X-ray luminesc. and EPR spectra 80−60660
$Li_{1-x}H_xIO_3$, dielec. behaviour, Raman and IR spectra 77−32357
LiH_2PO_3, Raman and IR spectra of transverse and longitudinal modes *(French)* 80−60573
$LiHSeO_3$, and deuterated analog, vibr. spectra 79−24311
$LiH_3(SeO_3)_2$, IR and Raman spectra, internal modes, intra- and inter-H-bond tunnelling 78−43853
$LiHoF_4$, spectroscopic anal., Ho^{3+} polarised absorpt. spectra, cryst. field parameters 79−95756
α-$LiIO_3$, attenuated total reflection spectra of anisotropic surface polaritons 78−87919
α-$LiIO_3$, Fermi resonance in surface polariton spectra *(Russian)* 80−71423
α-$LiIO_3$, hexagonal cryst., vibrs. and force consts. 79−69220
α-$LiIO_3$, single cryst., opt. and physicochem. props. 77−8566
$LiIO_3$, surface polariton spread length by modified DCIR method *(Russian)* 79−73566
$LiInCr_4S_8$, 1:1 ordering on tetrahedral sites obs. *(German)* 78−6669
$LiKSO_4$, polarised Raman and IR reflection spectra, internal and external mode assignments 77−16293
$(Li_{0.5}La_{0.5})_xBa_{1-x}TiO_3$, cryst. struct., dielec. and IR spectral meas. 79−46614
LiN_3, evidence for N_3^- from static and dynamic props. 78−60465
LiN_3, polycryst., IR active lattice vibr., optical consts. 77−77185
Li_3N, IR and Raman spectra and lattice dynamics 78−48177
Li_3N phonon spectra and lattice dynamics 77−59580
Li_3N, superionic conductor, cryst. growth and struct., phys. props., book contrib. 79−42308
Li_3N, superionic conductor, far IR absorption, temp. and isotope effects 79−51969
Li_3N:H, ionic cond., impurity conc., IR transmission meas. 79−42305
Li_3N:H, ionic cond., nuclear reaction anal. 80−34454
$^{6,7}LiNO_3$, cryst. vibr., Raman and IR spectra 79−15445
$LiNO_3$-$NaNO_3$(KNO_3) solid eutectic mixtures, Raman, IR spectra, line shifts, widths 77−55793
$LiNbO_3$ and $LiTaO_3$, IR reflectivity spectra and phonon self-energy effect 77−63413
$LiNbO_3$, asymm. phononlines, IR refl. analysis 78−27197
$LiNbO_3$, comparative frustrated total refl. and Raman scatt., fundamental mode freq. and phonon dispersion 77−28579
$LiNbO_3$, ferroelec., displacive type phase transition, far IR reflection spectra 80−71339
$LiNbO_3$, ferroelec. phase, soft vibr. modes, far IR refl. meas. 79−87407
$LiNbO_3$, Fourier transform Ir spectroscopy of vibr. states at high temp. 80−97256
$LiNbO_3$, IR reflectivity temp. depend. 78−27202
$LiNbO_3$, OH^- ion conc., PMR calibration method, IR determ. *(German)* 77−55712
$LiNbO_3$, optical phonon modes and anharmonic couplings 78−60466
$LiNbO_3$, spontaneous parametric scatt. line profile, IR absorpt. coeffs. 80−25377
$LiNbO_3$, transition metal doped, photovoltaic effects, spectroscopic investigation 77−20365
$LiNbO_3$:Fe, characts. for holographic storage appls. 77−23630
$LiNbO_3$:M, (M=Cr,Mn,Fe,Co,Ni,Cu), absorpt. spectra, 0.3-2.0 μm *(Russian)* 77−20898
LiO_2-Al_2O_3-SiO_2, anal. of composition by IR reflection spectra 80−40783
Li_2O, neutron irrad. effects, optical absorpt. spectra 80−75271
Li_2O-Al_2O_3-SiO_2, kinetics of glass-ceramic formation, by modified broken total internal reflection method 77−36444
Li_2O-Al_2O_3-SiO_2 glass, aq. corrosion 79−61753
Li_2O-GeO_2 glass, synthesis, Ge coordination state 77−24271
Li_2O-LiX-B_2O_3 glass, X=halogen, high anionic cond. of new solid electrolytes 80−107546
Li_2O-SiO_2 glass, protonated, field-driven guest proton redistrib. 80−107474
Li_2O-TeO_2 glasses, struct., IR reflection spectra 78−68516
(Li_2O-Al_2O_3-SiO_2):Fe_2O_3, glass, pyroceramic form., colour centres, magnetochem. investig. 77−16537
$Li_2O.3MoO_3.5.7H_2O$, fibrillar cryst., IR and NMR investig. of water bonding 77−12370
$LiPbPO_4$, vibrational spectra and cryst. struct. 78−39536
$LiRF_4$, R=rare earth, laser matrices prep. and characterisation 77−24945
Li_2SO_4, IR absorpt. spectra, polymorphism, site group approx. and SO_4 stretching mode 78−52510
$Li_2SO_4.H_2O$, $^6Li/^7Li$ and H/D substituted, IR and Raman spectra, vibr. and librational modes 77−85716

infrared spectra of inorganic solids continued
$Li_2SO_4.H_2O$, far IR spectra, H_2O flipping motion, lattice modes 80−84258
$Li_2SO_4.H_2O$, X-ray diffr., IR and Raman spectra, internal optic modes, mol. dipole model 77−76493
Li_2SiO_3, IR and Raman spectra, normal coord. anal. of unit cell vibrs. 77−81090
$Li_2Si_2O_5$, laminated cryst., IR spectra, dispersion anal. 77−1675
$LiSrPO_4$, vibrational spectra and cryst. struct. 78−39536
$LiTaO_3$, asymm. phonon lines, IR refl. analysis in paraelec., ferroelec. phases 78−27197
$LiTaO_3$, far IR complex refl. coeff. and refr. index, dispersive Fourier transform meas. 79−2841
$LiTaO_3$, ferroelec., displacive type phase transition, far IR reflection spectra 80−71339
$LiTaO_3$, ferroelec., IR high temp. amplitude-phase spectroscopy 79−35860
$LiTaO_3$, Fourier transform Ir spectroscopy of vibr. states at high temp. 80−97256
$LiTaO_3$ high-temp. ferroelec. transition, soft mode IR reflectivity spectroscopy 79−33692
$LiTaO_3$, optical phonon modes and anharmonic couplings 78−60466
$LiTaO_3$, paraelectric phase, soft vibr. modes, far IR refl. meas. 79−87407
$LiTbF_4$, $LiTb_{0.5}Y_{0.5}F_4$, and $LiTb_{0.25}Gd_{0.75}F_4$, Faraday rotation, optical absorpt. spectra and refr. index 78−72542
$LiTbF_4$, Tb^{3+} absorption spectra, 4000 to 25000 cm^{-1} 78−72550
$LiTmF_4$, spectroscopic anal., Tm^{3+} absorpt. spectra, cryst. field parameters 79−95757
Li_2WO_4, high press. modifications, IR spectra *(German)* 78−23459
Li_4WO_5, IR, Raman, luminesc. spectra meas., cryst. struct. investig. 77−52074
$LiYF_4$:Pr^{3+}, polarized absorpt. and fluoresc. spectra, 10 to 300K, energy levels and live intensities 79−95836
$LiZnVO_4$, high press. spinel modification, vibr. spectra 78−35124
$Li[Mn_2]O_4$ spinels, crystallographic, electronic and mag. props. *(German)* 79−60324
LuH_2, electronic struct., optical studies, 0.2-5 eV, 4.2-340K 79−78005
$Lu_2(SeO_4)_3.8H_2O$, thermal decomp. and IR spectra 80−3319
$Lu_{2-x}Si_2O_7$:Eu_x, synthesis and spectroscopic study 80−84846
$Lu_2Si_2O_7$, IR and Raman spectra, internal and external modes 79−61365
Mg film, optical cond., energy derivative spectrum 77−66551
$MgAl_2O_4$, IR spectrum exam. 78−76454
$MgAl_2O_4$, lattice dynamics, rel. to space group of spinel 78−59898
$MgAl_2O_4$ spinel, optic frequencies, evidence for membership of F43m space group 78−48168
$MgAl_2O_4$, spinel materials press forged, mech. props., IR appl. 78−39722
Mg_xCd_{1-x} Te:P, vibr. modes of defects, IR absorpt. expts. 77−62601
$MgCl_2.nH_2O$, IR spectra and struct. features 79−15452
MgF_2, transparent, multiphonon IR absorption spectra 80−7348
$MgHPO_4.3H_2O$ and $MgDPO_4.3D_2O$, IR absorpt. and Raman spectra, vibr. assignments 80−97257
MgO, adsorpt. of H_2O vapour, at high temps., IR spectra 77−47687
MgO, clumping on substrate, effects on infrared extinction spectra, bulk absorption freq. 78−43875
MgO, Fe^{2+} and Fe^{3+} conc. and valency, optical density, EPR and MCD obs. 77−89462
MgO film, IR spectroscopy and RHEED analysis 77−89664
MgO film, vacuum deposited on NaCl-type alkali halides, struct. characterisation, IR impurity absorpt. 79−82490
MgO, IR absorpt. spectra, 2300K, elec. furnace appl. *(French)* 80−27311
MgO irradiated with Li^+ and K^+ ions, optical props. of metal aggregates 79−65907
MgO microcrystals, IR absorption 78−92074
MgO microcrystals, IR absorpt. 79−42963
MgO small cubes, surface vibr. modes, IR transmission obs. 78−22947
MgO, spectra rel. to interstellar absorpt. features 77−57073
MgO:Cr, high resolution far IR spectroscopy of lower energy levels of Cr^{2+} 80−80822
MgO:Fe crysts., oxidised and reduced, optical absorpt. spectra at low temps. 77−63436
MgO:Fe^{2+}, $^5T_{2g}\rightarrow{}^5E_g$ adsorption, Zeeman effect meas. 77−12405
MgO:Fe^{2+}, far IR absorpt. meas. by Fourier transform, apparatus 77−177
MgO:Fe^{2+}, Jahn-Teller effect in ^5E_g state, tunnelling splitting obs. 78−19517
MgO:Fe^{2+}, phonon-induced transition interf. in EPR and IR spectra, ion-lattice coupling 77−51945
MgO:Li, $[Li]^0$ defects, magneto-optical props. 77−12365
MgO:Mo catalyst, adsorpt. of propylene, oxidation reactions, surface structs., IR absorpt. spectra obs. 80−66868
MgO:OH^-, room temp. IR spectra, heat treatment and electron irrad. effects 79−51992
MgO-BaO-Al_2O_3-SiO_2, glass, IR absorpt. spectra and solid struct. exam. 78−88314
MgO-ZnO-Fe_2O_3-Cr_2O_3 system spinels, IR absorpt. spectra, short-range order 79−42957
$Mg(OH)_2$, sintering, IR spectra, X-ray anal. 80−66452
$Mg_2P_2O_7$, α- and β-phase, vibr. spectra, Raman and IR spectra 78−19467
$Mg_2P_2O_7$-$Mg_2As_2O_7$ solid solns., formation of mixed anions $PAsO_7$, IR absorption spectra exam. 79−1508
$Mg(PO_4)_2.xH_2O$, x=8, 22, dehydration and water bonding 77−44456
MgR_2S_4, (R=Sc, Yb, Tm), IR and Raman spectra, force consts. 78−68503
Mg_2SiO_4, fosterite, lattice dynamics, IR and Raman spectra meas. 79−65153
$Mg_3(VO_4)_2$, determination of enthalpies of formation, from heats of solution 80−2182
$(MgV_2O_4)_c(FeFe_2O_4)_{1-c}$, struct. parameters, IR spectra, cluster-component analysis 77−47425
MnAs, optical props., 0.3-14 eV 77−52122
$MnAs_{0.85}P_{0.15}$, optical props., 0.3-14 eV 77−52122
$MnAu_2$, helical antiferromagnetic compound, optical props. and electronic struct., visible and IR obs. *(French)* 80−45101
$MnAu_2$, helical antiferromag., optical absorpt., density of states 80−66224

infrared spectra of inorganic solids continued
$MnAu_2$, optical consts., 0.5-3.5 eV, intra-and interband absorpt. *(French)* 78−10916
$Mn(CN)_3.(H_2O)_{0.57}$, mag. interactions, theory 80−97085
$Mn_xCd_{1-x}Te$, far IR refl. spectra, phonon spectra 78−52497
$Mn_xCd_{1-x}Te$, lattice vibrs., Raman and IR spectra meas. 80−93311
$Mn_xCd_{1-x}Te$, phonons, Raman scatt. and IR absorpt. meas. *(French)* 80−97275
$MnCl_2$:Co^{2+}, polarised IR absorpt. spectra 77−40269
$MnCl_2.2H_2O$, wagging and rocking band intensities of water 78−27200
$Mn_3(Co(CN)_6)_2.xH_2O$, mol. vibr. in cryst., normal mode anal., Raman and IR obs. 77−76494
MnF_2, ATR spectra and surface EM wave dispersion anisotropic case 77−77215
MnF_6^{2-}, $A_2{}^1M^{IV}F_6$ hosts, luminesc., IR and Raman spectra, 5K, assignments 77−20904
$MnHPO_4.3H_2O$ and $MnDPO_4.3D_2O$, IR absorpt. and Raman spectra, vibr. assignments 80−97257
$Mn_xHg_{1-x}Te$, long wavelength optical phonons, IR refl. obs., 50-300 cm^{-1}, 90 and 295K 77−36243
MnMg ferrite, products of reaction with ferrogel with $MnCl_2$ solution 77−12582
$Mn_2NaSi_3O_8(OH)$, serandite, synthesis, struct., physicochem. props. 79−43187
MnO, Jahn-Teller effect on optical absorption spectra 78−52484
$Mn_xRe_{1-x}(CO)_5X$(X=Cl, Br), $0<x<5$, vibr. spectra in the 2000 cm^{-1} region of mixed and isotopic crystals 78−84585
$MnSO_4.H_2O$, hydrate librational modes in IR spectra 78−48161
MnSb, optical props., 0.05 to 5 eV 77−48194
$MnSe_2$, IR lattice vibrs., dielectric dispersion 79−28735
$MnSi_x$, X=1.72 to 1.75, IR absorpt., transmission, refl., spectra 80−60600
Mn_nSi_{2n-m}, thermoelectric and optical props. 78−91714
$MnSiF_6.6H_2O(.6D_2O)$, near IR spectrum, 80K, assignments 78−48164
$MnTa_2O_6$, columbite struct., X-ray diffr., IR and Raman spectra *(French)* 78−63727
MnTe, optical props. and electronic struct. 78−6682
$Mn_3(VO_4)_2$, X-ray powder diffr. and IR spectra 78−10016
MnZn ferrite, optical refl. and electroreflection spectra obs. 78−27262
$Mn_{1-x}Zn_xF_2$, antiferromagnetic reson. freq. from far IR transmittance spectra 77−69695
Mo, CVD films of high IR reflectance 79−52119
Mo complex, $MoOCl_3.2Ph_2SO$, prep. and characterisation 78−30592
Mo complexes, bis-carboxylate Mo(V), struct. and catalytic reactivity 77−77804
Mo complexes, oxo-bridged dimers, ^{16}O and ^{18}O-substituted synthesis, IR spectra 77−77188
Mo complexes derived from electron-rich olefins, cryst. chem. 77−76372
Mo complexes with poly(iminoethylene)-dithiocarbamate polymer, synthesis and spectra 77−77189
Mo complexes with thousands and L-cystein, formation and Ir-spectra 77−81096
Mo cpds, chemistry and uses, conf., Oxford, Eng., Sep (1976) 77−77749
Mo film, CVD, with high IR refl. and large solar absorpt., prep. and props. 80−26163
Mo halides, $[Mo_6X_8]$ cluster group identification in IR spectra of solids, normal vibrs. 78−64359
Mo, lattice dynamics, improved Fielek model 80−59598
Mo, thermoreflectance spectra, 0.3 to 6 eV rel. to band struct. calcs. 77−66521
$MoCl_5$-MoF_5 system, magnetochem. and IR study of phase struct. 77−85710
MoO_3, Raman scatt. and struct. props. 77−55780
MoS_2, 2H phase, far IR magnetoabsorption and refr. index meas. 77−24847
$2HMoS_2$, far IR optical and magneto-optical absorpt. 77−52078
$MoSCl_3$, prep. and characterisation 77−59705
$MoSe_2(Te_2)$, IR and Raman spectra, lattice vibrs. interlayer bonding 80−40110
$(Mo_xV_{1-x})_2O_5$, mag. and spectroscopic investigation 80−25206
α-N, low freq. absorpt. spectra, libration modes *(Russian)* 80−55078
N_2 matrix N-N stretching vibr., IR activation, guest mol. depend. 80−60570
N_2, solid, β-phase, for IR absorption spectra 80−11385
N_2, solid, far IR 4.2K absorption apparatus 79−30583
α-N_2, solid, $w^1\Delta_u$-$X^1\Sigma_g^+$ intensity and band shape 79−47427
α-N_2, temp. depend. of IR spectra, Gruneisen parameters determ. 80−84730
N_2:CO, IR and Raman spectra, vibron band, vibron-phonon combination bands 78−68495
ND_4DS, polycryst., vibr. spectrum, lattice dynamics 77−90138
ND_4DSeO_4, crystals, struct., IR spectra, dielec. props. 80−75919
ND_4I, librational motion of ND_4^+ ion, far IR spectra obs. *(Japanese)* 79−8142
NH_3, and liq., vibr. spectra 77−32360
NH_3 frost, near IR refl. spectra, appl. to Saturn upper clouds 79−8135
NH_3, IR and Raman intensity of lattice vibrs., theory 80−11381
NH_3 solid film, absorpt. coeffs. determ. 50 to 7000 cm^{-1} 80−97356
$(NH_4)_2AF_6$, A=Si, Ge, Sn, IR absorpt. spectra, integrated intensity 79−73944
NH_4AlCl_4, crystal struct., X-ray, Raman, IR and NMR 78−63720
NH_3BF_3 and d_3, polycryst., for IR spectra, lattice vibrs., cryst. and mol. struct. interpret. 80−2771
$(NH_4)_2BeF_4$, far-infrared and submillimetre dielectric response 80−80782
$(NH_4)_2BeF_4$, powder, IR spectra, assignments, mol. libration, in paraelec. and ferroelec. phases 78−88299
NH_4Br:Cl^-, impurity mode, far IR transmission obs. 77−16308
NH_4Br:Cu^{2+}, ESR and absorpt. spectra, 300-1500 nm 78−60492
NH_4Br-NH_4I mixed crysts., far IR spectra, phase transition and NH_4^+ libration 77−85719
NH_4Cl, orientational disorder, Raman and far IR spectra 78−23447
NH_4Cl, vibrations of isotopic impurities, IR reflection and Raman spectra meas. 77−51465
NH_4Cl:$[MoOCl_5]^{2-}$, single cryst., struct. investigations 77−66524
NH_4ClO_4:Co^{2+}, optical absorpt. spectra 77−66523
$(NH_4)_2Cr_2O_7$ crystal hypomorphism and hypermorphism 80−59427
$(NH_4)_2CuCl_4.2H_2O$, HDO and NH_3D^+ species, IR spectrum, low-temp., phase transitions 77−77182
NH_3D^+, IR spectrum in NH_4ClO_4 and weakly H-bonded cpds., mol. motion 77−36232

infrared spectra of inorganic solids continued
$(NH_4)GeF_6$, IR absorpt. spectra, integrated intensity temp. depend. 79−73946
$(NH_4)_2GeF_6$, cryst., highly bent H bonds, IR spectrosc. investig. 80−93292
$(NH_4)_2H_3IO_6$, paraelec. and antiferroelec. phases, IR vibrational study 77−85697
$NH_4H_2PO_4$, high temp. phase transition, IR spectra, differential 80−25319
$NH_4H_2PO_4$, IR overtone spectra and temp. depend. 79−47456
NH_4HS, polycryst., vibr. spectrum, lattice dynamics 77−90138
NH_4I, orientational disorder, Raman and far IR spectra 78−23447
$(NH_4)_2M(SO_4)_2.6H_2O$, Tutton's salts, correl. of vibr. freq. and N...O distance for NH_3D^+ 78−92066
$(NH_4)_2M(SO_4)_2.6H_2O$, M=Ni, Co, Mg, IR spectra 80−97280
$(NH_4)_2Mg(S_2O_3)_2.6H_2O$, isolation, struct., decomposition *(French)* 78−52506
NH_4NO_3, phase transition, IR spectra 80−7350
NH_4NO_3, shear-stress-induced phase transitions at high press. 77−32368
$(NH_4)_2Ni_3(P_2O_7)_2.nH_2O$, thermal dehydration 80−35513
$(NH_4)_{0.8}Ni_{1.1}PO_4.xH_2O$, ion exchange props., Cs^+ ion sorpt., struct., IR spectra 77−9121
$(NH_4)_2(RuCl_5NO)$, polarised Raman and IR spectra, vibr. anal. 77−69819
$(NH_4)_2SO_4$, IR photoacoustic spectra 80−13163
$(NH_4)_2SO_4$ powder and aqueous soln., photoacoustic spectra in middle IR 77−81101
$(NH_4)SiF_6$, IR absorpt. spectra, integrated intensity temp. depend. 79−73946
$(NH_4)_2SiF_6$, cryst., highly bent H bonds, IR spectrosc. investig. 80−93292
$(NH_4)_2SnF_6$, cryst., highly bent H bonds, IR spectrosc. investig. 80−93292
$(NH_4)_2(TeBr_6)$, far IR and Raman spectra and phase transitions 80−11376
$(NH_4)_2(TeCl_6)$, IR and Raman spectra, lattice and internal modes, phase transition 78−6659
$(NH_4)_2TiF_6$, cryst., highly bent H bonds, IR spectrosc. investig. 80−93292
$^{14}(NO)_2$, solid, for IR spectra at 20K 77−73139
NO_2^- ion in nitrite salt cryst., $^{1,3}B_1$−$^1A_1$ transition spectra, reasons for diffuseness 80−97276
N_2O crystal, vibrational exciton bands, impurity modes 77−28560
N_2O_2, IR spectra of solid, Raman spectra of solid and liq., vibr. anal. 77−81093
Na, IR and optical props., surface-plasmon-mediated absorpt. mechanism 80−93308
Na MIM struct., electron-phonon interaction function investigation by microcontact spectroscopy 79−95108
Na polysilicates, IR spectra, struct., crystallisation effects *(Russian)* 78−72528
Na-NaO-Na struct., inelastic tunnel effect, spectra, potential barrier parameters 79−95511
Na_2-β-Al_2O_3, far IR absorpt., Beevers-Ross sites, interstitials 80−66241
Na_2O-SiO_2-MgO glass, melt viscosity and IR meas. to study MgO behaviour *(Japanese)* 78−14495
Na_2AF_6, A=Si, Ge, Sn, IR absorpt. spectra, integrated intensity 79−73944
$NaAl(CO_3)(OH)_2$, cryst. struct., IR spectral investig. 77−8567
Na_3AlF_6, film on Si, fused quartz substrates, H_2O absorpt., IR anal. 80−75446
$NaAlSi_2O_6$ melts quenched at high press., IR radiation data rel. to struct. 79−32907
NaBr:V, covalency effects, EPR and optical spectra 77−85557
$NaBrO_3$, IR and Raman spectra, vibrs., dipolar coupling effect 78−43852
NaCN, crystal props., log potential model calc. 78−63829
NaCN, librational and phonon sidebands of IR CN^- stretching mode 79−15457
NaCN, multidomain birefr. solid, light scatt. and IR transmission spike 80−60587
NaCN, optical F centres and phase transitions 78−56504
NaCN, Raman diffusion spectra, IR absorpt. in phases II and III *(French)* 80−84741
Na_2CO_3, molten, IR emission spectra *(Japanese)* 78−19469
$Na_4Ca(SO_4)_3$, cryst. data and IR spectra 78−42986
$Na_8Ca_3SiO_{1.5}[Si_2O_7][PO_4]_3$, synthesis conditions, cryst. struct. and IR spectra characts. 80−108335
NaCl, bulk and surface absorpt., 2 to 10 μm, calorimetric meas. 78−71160
NaCl, bulk and surface absorpt. in 9.2-10.8 μm region 79−95808
NaCl, electron trapping by alkali ion impurities 78−47809
NaCl, far IR dispersive-reflection meas. at room temp., comparison with calc. 78−35139
NaCl, search for IR absorption by triplet self-trapped excitons 78−56473
NaCl, single cryst., for IR dispersive refl. meas., low temp., rel. to anharmonicity calcs. 80−11371
NaCl, surface and bulk absorpt. at 10 μm, temp. depend. 77−28576
NaCl, transient infrared absorption of bound polarons 78−91642
NaCl transverse optic mode anharmonic self-energy meas. by dispersive Fourier transform spectroscopy 77−39642
NaCl, transverse optical mode anharmonic self energy, far IR spectrum 78−6131
NaCl:$^{63}Cu^+$, resonant bandmode, stress spectroscopy with far IR laser 78−2847
NaCl:Ca^{2+}, cryst., hydrolysed, IR absorpt. bands 77−32404
NaCl:OH^-, UV and IR absorpt. spectra, colour centres transformation 79−28791
NaCl-kCl melt, reaction with LiO_2-$2SiO_2$ X-ray, IR exam. 80−55706
NaCl(Br) (F) (I), lattice dynamics and statics, three-body-force shell model 80−49323
$NaClO_3$, IR and Raman spectra, vibrs., dipolar coupling effect 78−43852
$NaClO_3$-$NaBrO_3$ mixed crystals, internal optic modes, Raman and IR spectra meas. 79−95746
$NaClO_4$, anhydrous, Raman, IR and FIR spectra, 90 to 600K *(German)* 79−78687
$NaClO_4$, Brewster type surface mode dispersion, IR refl. meas. 80−11415

infrared spectra of inorganic solids continued
$NaClO_4$-D_2O, glassy matrix, absorpt. spectra after X-irrad., solvated electrons 79−65903
$NaCrS_2$, antiferromag. semicond., Raman and far-IR spectra 79−47454
$Na_3Eu(PO_4)_2$, synthesis and IR spectra 80−16019
NaF, Stark effect, M-centre absorpt. bands 78−84614
NaF-SrF_2-CrF_3, glass transition, crystn. and melting temps., optical transmission *(French)* 80−64910
NaF(Cl), far IR complex refr. indices, dispersive Fourier transform 78−80322
NaF(Cl):OH^-, electron irrad., F_2^+ centre stabilisation 80−54231
Na_2GeF_6, IR absorpt. spectra, integrated intensity, 100-300K 79−73945
$NaHF_2$, IR refl. spectra 78−80324
$NaHSeO_3$, and deuterated analog, vibr. spectra 79−24311
$NaH_3(SeO_3)_2$, IR and Raman spectra, internal modes, intra- and inter-H-bond tunnelling 78−43853
$NaH_3(SeO_3)_2$, $NaD_3(SeO_3)_2$, IR and Raman spectral interpretation of ferroelectric phases 79−24312
NaI, long wave phonon modes, IR absorpt. 78−79686
$NaIO_4$, normal coord. anal., internal and external modes 79−23684
$NaKMg_3M_2^{II}Si_{12}O_{30}$ (M=Cu, Mg), cryst. struct., X-ray diffr. and IR spectra *(French)* 80−107158
$(Na_{0.5}La_{0.5})_xBa_{1-x}TiO_3$, dielec. and IR spectra exam., ferroelec. transition 78−23418
$Na_3M_2^{III}Li_3F_{12}$, M=Sc, Ti, V, Cr, Mn, Fe, Ce, Ni, IR spectra 79−38544
$Na_3M_2^{III}Li_3F_{12}$ garnets, M=Al,Cr,Fe, synthesis from aq. soln., props. 77−44184
$Na_3Mg_4LiSi_{12}O_{30}$, cryst. struct., X-ray diffr. and IR spectra *(French)* 80−107158
$Na_2Mg_3M_2^{II}Si_{12}O_{30}$ (M=Cu, Fe, Zn, Mg), cryst. struct., X-ray diffr. and IR spectra *(French)* 80−107158
$Na_2MoO_4(S_4)(Se_4)$ crystals, charge transfer spectra of MoX_4^{2-} complexes 80−54658
NaN_3, polycryst., IR active lattice vibr., optical consts. 77−77185
$NaNO_2$, ferroelec., lattice dynamics, two-phonon Raman scatt. and IR absorpt. 79−33684
$NaNO_2$, ferroelec., X-ray diffr. topographic study of polarisation reversal 79−38441
$NaNO_2$, ferroelectric, second-order vibr. spectra and dispersion of phonon branches 79−69847
$NaNO_2$, mechanism of ordering type ferroelec. transition, vibr. spectroscopy 78−76402
$NaNO_2$, Raman and IR spectra, destructive Fermi reson. 77−16309
$NaNO_2$, vibr. spectrum, interference effects 78−87752
$NaNO_2$, X-irradiated IR, UV and visible absorption 79−95811
$NaNO_3$ characteristic features of electronic structure. 79−47436
$NaNO_3$, isotopically mixed, vibr. spectra, IR and Raman spectra 79−28770
$NaNO_3$, lattice vibrs., order-disorder transform., IR spectra study 80−65176
$NaNO_3$ shear-stress-induced phase transitions at high press. 77−32368
$NaNO_3$, vibrations of isotopic impurities, IR reflection and Raman spectra meas. 77−51465
$Na^{14}NO_3$, $Na^{15}NO_3$, polarised IR reflection spectra, surface damage effects 79−19872
$Na^{15}NO_3$, $Na^{14}NO_3$, multiphonon transitions in microcryst. reflectivity 78−72499
Na^ANO_3, (A=14,15), anomalous IR reflectivity min. in transverse-longitudinal band gap 79−56796
$NaNO_3$-urea solid eutectic mixtures, Raman, IR spectra, line shifts, width 77−55793
$(NaNO_3$-$Mg(NO_3)_2)$:Nd^{3+}, glass, cryst., absorpt. luminesc. spectra, term struct. of Nd^{3+}, bonding 77−8624
$Na_2Nd(PO_4)_2$, synthesis and IR spectra 80−16019
$Na_2Ni_3(P_2O_7)_2.nH_2O$, thermal dehydration 80−35513
Na_2O-(CaO)-SiO_2, corroded, quantitative anal. by IR frequency shifts 78−19909
Na_2O-Al_2O_3-$SiO_2.xH_2O$, fibrous crystal growth in silica gel, X-ray, electron probe and IR spectra obs. 80−25541
Na_2O-B_2O_3-SiO_2-Fe glass, near IR optical absorption of Fe (II) 78−84616
Na_2O-CaO-P_2O_5:Co glass, bonding, symmetry meas. 79−46572
Na_2O-CaO-SiO_2 glass, optical props. characteris. in 0.006 to 22 eV region 77−16328
Na_2O-$GeO_2(TiO_2)(SnO_2)(ZrO_2)(ThO_2)$-$SiO_2$ glass, density, refractive index, thermal expansion, hardness IR spectra, DTA *(Japanese)* 78−15535
Na_2O-Li_2O-β-$Al_2O_3.H_2O$, water mol. vibrs., IR and Raman spectra 80−89006
Na_2O-SiO_2 glass, IR reflection spectra change due to moisture corrosion *(Japanese)* 78−19914
Na_2O-SiO_2 glass, ion bombardment, form. of cpds., IR spectrosc. exam. *(German)* 80−88173
Na_2O-SiO_2 glasses, Na_2O effect on Si-O bonds *(Japanese)* 78−42918
Na_2O-SiO_2-NaF, elec. cond. of melt, and IR absorpt. spectra of glassy phase *(Japanese)* 77−62657
Na_2O-TiO_2-SiO_2 glass, IR refl., Raman and EPR spectra, struct. *(Russian)* 78−2860
Na_2O-TiO_2-SiO_2 glass, Si-O bonding, SiKβ X-ray fluorescence and IR spectra 80−10500
Na_2O-WO_3 glass containing transition metal ions optical absorption 78−27254
NaOH-D_2O, glassy matrix, absorpt. spectra after X-irrad., solvated electrons 79−65903
$Na_2O.xSiO_2.yH_2O$, x71, y71, cryst., IR spectra 79−51951
$NaPO_3$-$NaAsO_3$ system solid solutions, four-mode type IR spectra 79−51942
NaRhY zeolite, Rh complexes with CO and methyl iodide ligands; spectrosc. obs. 80−85159
Na_2S, dielectric const., transverse and longitudinal optical mode, static dielectric const., effective charge 79−73892
Na_2SO_4, IR absorpt. spectra, polymorphism, site group approx. and SO_4 stretching mode 78−52510
Na_2SO_4:XO_4^{2-}, X=Cr, Se, Mo, W, lattice-impurity interactions, IR spectra 78−19522
$Na_2S.9H_2O$-NaOH-H_3BO_3, glass, IR and Raman spectra of boro-ultramarine, exam. of S_3^- presence 78−68502
$NaSbClF_3.H_2O$, cryst. and mol. struct. *(French)* 77−43200
Na_3SbS_4, vibrational spectra, internal SbS_4 vibr. assignments 80−66199
$Na_3SbS_4.9H_2O(D_2O)$, vibrational spectra, internal SbS_4 and $H_2O(D_2O)$ vibr. assignments 80−66199

infrared spectra of inorganic solids continued
α-$Na_2Si_2O_5$, laminated cryst., IR spectra, dispersion anal. 77−1675
$Na_3UO_2F_5$, IR and Raman spectra, struct. *(French)* 79−11409
$Na_2W_2O_7$, Raman and IR spectra 80−25356
Na_xWO_3, optical props., analysis of free- and bound-electron contribs. 77−77248
$Na_4[M^{II}(NH_3)_4][M^I(S_2O_3)_2]_2.L$, ($M^{II}$=Cu, Ni), ($M^I$=Cu, Ag), (L=$H_2O$, NH_3), IR spectra, vibr. anal. *(French)* 78−52477
$Na_4[UO_2(CO_3)_3]$, vibr. and low temp. optical spectra, rel. to U recovery from oceans 79−73939
Nb alloys, optical props., 0.1-25 eV, band models 78−10892
Nb, BCC lattice, optical prop. in range λ=0.265−18 μ, polarimetric meas. 79−15075
Nb complex, $NbCl_5$ complex with O- and S-containing ligands, prep., and characterisation 79−14729
Nb complex, $NbOCl_3.2L$ (L=Ph_2SO, Ph_3PO and $(Me_2N)_3PO$), prep. and characterisation 78−30592
Nb complex, prep. by halide reaction with tetramethylurea and tetramethylthiourea, and characterisation 79−15972
Nb, electronic struct., thermoreflectance studies 80−76047
Nb film, far IR reflection and transmission spectra, room temp. 77−55792
Nb-C-N-O-H, solid solns. of H, exam. of props. 80−29172
Nb_3Ge film, far IR reflection and transmission spectra, room temp. 77−55792
$NbH_{0.453}$, influence of H on bulk band struct., optical absorptivity spectra obs. 77−89692
NbO_2, IR dispersion 79−65854
$NbOAsO_4$ and $NbOAsO_4$ $4H_2O$, crystal growth, composition, struct. and crystallographic charact. 80−54198
$Nb(OR)_2Cl_3.L$, halo-alkoxide complex, prep. and props. 78−18605
$NbSCl_3$, prep. and characterisation 77−59705
$NbSe_2$(2H)-hydrazine, intercalation cmpd., kinetic studies by transmittance meas. at 1600 nm 78−71981
Nd^{3+}:glass, inhomogeneously broadened spectra, struct., selective laser excitation obs. *(Russian)* 78−35181
Nd_2ASe_5, A=Ge, Sn, diffuse refl. spectra and band gaps 79−51963
$NdAl_3(BO_3)_4$, LPE for thin film miniature lasers 79−74101
$Nd_4Al_2O_3$ film, struct. charact., IR spectra 77−48157
$Nd(BO_2)_3$, single cryst., IR absorpt. spectra 80−34903
$Nd(BrO_3)_3.9H_2O$, IR and Raman spectra, vibr. asignments 78−84569
NdF_3, Zeeman splitting in mag. fields up to 100 kG 78−52483
$Nd_{1/3}NbO_3$, $NdNbO_4$, structural characteristics and residual polarisation 77−15361
NdP_5O_{14}, fluoresc. lifetime meas., IR and photoacoustic spectroscopy 80−60652
NdP_5O_{14}, spectral line intensity anal. 78−43888
Nd_2S_3, vibr. spectra, factor-group anal. 80−80793
$NdVO_4$, monazite struct., IR and NMR spectra 79−78534
$Nd_2Zr_2O_7$-$Nd_2Hf_2O_7$, struct., elec. cond. and melting point 80−54197
Ni (110), chemisorption of N_2, mol. and dissociative mechanisms 80−39431
Ni (111), adsorption sites of CO using IR reflection-absorption spectroscopy 79−69355
Ni catalyst, Al_2O_3 supported, adsorpt. of CO in H_2-He, effect of H_2S on IR spectrum 78−71945
Ni complex, 1,2-benzoquinonedioximates, refl. spectra, 0.5-2.5 eV, Young's modulus and internal friction 78−39562
Ni complex, Ni(l-spartein)Cl_2, IR circular dichroism spectra, vibr.-electronic interaction 80−55074
Ni, emissitivty and reflectivity, oxide film thickness effect 79−82364
Ni, metallised coating on polyethylene terephthalate film, fracture under laser irrad. *(Russian)* 80−76333
Ni, optical absorption in near IR 79−38539
Ni Tulton salts, cryst. field spectra in visible and near IR regions, solid dilution effect 80−100666
Ni/$Al_2O_3(SiO_2)$ methanation catalysts, nonreduced, IR spectra 78−88288
Ni/SiO_2, adsorption of CO, scavenging effect of H_2, in situ Fourier transform IR spectra obs. 80−39410
Ni/SiO_2, chemisorption of NO, desorpt. and IR expts. *(German)* 78−30835
Ni-Cr, interband absorpt. and refractive index, photoconductivity dispersion function 77−36263
Ni-Fe alloys, cond. electron charact. *(Russian)* 77−48173
Ni-NiO_x-NiS_y, black Ni, struct.-depend. thermal and optical props., rel. to solar thermal conversion 79−79404
Ni-pigmented anodic Al_2O_3, for selective absorpt. of solar energy, optical and struct. props. 80−55892
β'-NiAl, electronic struct. and optical props. 80−97228
NiAs, optical props., 0.05-5 eV 77−48194
$Ni(ClO_4)_2.6H_2O$, EPR and IR spectra, 98-298K, phase transition at 224K 78−84477
$Ni_{1-x}Co_xS_2$, elec. cond., thermoelec. power and optical meas. 80−59986
NiI_2, far IR study of lattice dynamics 78−80359
Ni_3Mn thin films, transmission spectra, structural order depend. 80−66318
$Ni(NH_3)_6X_2$, (X=Cl, Br, I, ClO_4, BF_4) and d, far IR, Raman spectra, 80-300K 78−31190
NiO, absorption spectrum temp. depend. 77−48162
NiO electrodes, effect of $Co(OH)_2$ on self-discharge, IR spectra obs. 80−21295
NiO powder, IR active modes in large clusters of spheres 79−42964
NiO, temp. depend. of thermal expansion and IR lattice vibrational mode 77−84950
NiO-Cr_2O_3-$MgAl_2O_4$, methanation catalyst, struct. changes, IR obs. 79−73912
NiO-Cr_2O_3-$MgSiO_3$ methanation catalyst, S-resistant, IR and Raman spectra 80−93290
NiP_4O_{11}, formation in phosphoric acid melts 78−27394
$NiSO_4.H_2O$, hydrate librational modes in IR spectra 78−48161
NiSb, optical props., 0.05 to 5 eV 77−48194
$NiSiF_6.6H_2O(.6D_2O)$, near IR spectrum, 80K, assignments 78−48164
$(NiV_2O_4)_c(MgFe_2O_4)_{1-c}$, struct. parameters, IR spectra, cluster-component analysis 77−47425
NiZn ferrites, Mossbauer effect and IR spectra 78−64300
Ni_xZrS_2, fundamental optical absorption edge 79−99904
NpO_2, IR spectra, values of transverse vibr. frequencies 77−28585
O_2 isotopically mixed crystals, IR absorption spectra (7000-15000 cm^{-1}) at 1.5K *(Russian)* 77−32362

infrared spectra of inorganic solids continued
OCS, lattice dynamics and phonon sidebands of vibr. excitons calc. 77−20028
P, amorphous, red, far IR absorpt. spectra 80−34923
P, amorphous, vibrational excitations of defect sites 80−49332
P, amorphous red, Raman scattering 80−11416
P, bulk red amorphous, Raman scatt. and IR absorption 79−24323
P-As-Se glasses, mag. susceptibility, dielec. const., opt. props. 78−64184
P-Se glass system, IR spectra 78−64365
$PF_2H(D)$, Raman and IR spectra 80−14147
γ-$PH_{3-x}D_x$, Raman and IR spectra, phase transition, internal and external modes 77−77191
$PMo_{12}O_{40}$, vibr. anal., symmetry coords. and force field anal., IR and Raman spectra 77−15522
P_2O_5, glassy, high freq. vibr. bands, central force model 80−49330
P_2O_5-SiO_2 glass film, thickness and IR spectrum changes on heat treatment in H_2 80−70549
$POCl_3$-$SnCl_4(ZrCl_4)(TiCl_4)$, splitting of Sm^{3+} near IR absorpt. bands 80−2750
Pb, aq. corrosion film, IR and Raman spectroscopy 80−55567
Pb chalcogenides, interband transitions, absorpt. coeff., multiband calc. 80−29738
Pb complex formation with oxyacids, IR and PMR study *(Russian)* 77−28582
Pb, patination, IR spectroscopic study 77−56140
Pb, superconducting, phonon density of states determ. 77−20493
Pb-As-S semiconductor glasses, far IR transmission and Raman scattering 77−63419
Pb-Ge-S semiconducting glasses, far IR transmission and struct. 79−65855
$Pb_5(AsO_4)_3Cl$, mimetite, vibr. spectra, normal coord. anal. 78−88305
$PbBr(Cl)-Ag^+$ IR absorpt. spectrum and vibr. of substitutional impurity 77−81135
$PbCO_3.PbX_2$ (X=Cl,Br), vibr. props. 79−24319
$Pb_{1-x}Cd_xTe$, IR absorpt. study of Cd impurity levels, energy gaps 80−45081
$PbCl_2$, single cryst., far IR refl. spectra, effective ionic charges 79−87430
PbF_2-AlF_3 glass, optical props., crystn. and thermal expansion 80−48367
PbF_2-AlF_3 glass, prep. and props. 80−49120
$Pb_2Fe_2O_5$, IR absorpt., Mossbauer spectra, Neel temp., cryst. cell *(French)* 79−42759
$Pb_5Ge_3O_{11}$, ferroelec. phase transition, for IR transmission meas. 79−38478
$PbGeS_3$, vitreous and cryst., IR and Raman spectra *(Russian)* 78−72527
$Pb_5Ge_{3-x}Si_xO_{11}$, ferroelec. phase transition, for IR transmission meas. 79−38478
$Pb_{1-x}Ge_xTe$ epitaxial layers, phase transition obs. by far IR reflectivity spectroscopy 79−33691
$Pb_{1-x}Ge_xTe$, ferroelec. phase transition, IR refl. and resist. meas. 80−11353
$Pb_{1-x}Ge_xTe$ magnetoplasma reflectivity and transmission spectra 80−71428
$PbHAsO_4$, ferroelec., far IR and submillimetre dielec. dispersion 79−38528
$PbHAsO_4$, ferroelec., far IR and microwave dielec. props. 80−55108
$PbHPO_4$, ferroelec., far IR and submillimetre dielec. dispersion 79−38528
$PbHPO_4$, microwave permitt. and far IR refl. spectra in paraelec. and ferroelec. phases 80−40033
$Pb_{1-x}Hg_xS$ electroless-deposited films, optical and elec. props. 80−7011
$Pb_{1-x}Hg_xS$ film, IR detector material, struct. and IR props. 78−26775
PbI_2, 2H polytype, anisotropy of lattice vibrs., optical modes analysis 77−7807
PbI_2, optical phonon anisotropies and intralayer bonding forces from IR refl. 77−59573
PbI_2, single cryst., far IR refl. spectra, effective ionic charges 79−87430
PbI_2, single cryst., luminesc., photocond. and absorpt. after thermal treatment 79−56855
PbI_2:KI alloys, fundamental abs. edge, potential as solar convertor 80−101128
$Pb_2M_2^{III}Ge_2O_9$, (M^{III}=Fe,Mn,Sc,In), synthesis, X-ray diffr. and vibr. anal. 79−61360
$Pb_2M^{II}M^{IV}Si_2O_9$, (M^{II}=Mg,Ni,Co,Cu for M^{IV}=Sn; M^{II}=Co, Ni for M^{IV}=Ti), synthesis, X-ray diffr. and vibr. anal. 79−61360
$PbMg_{1/3}Nb_{2/3}O_3$, vibr. spectrum and dispersion of optical consts., coexisting ferro- and paraelec. phases 77−63422
$Pb(NO_3)_2$, dynamical props., IR reflection spectra meas., 10-300K 77−1676
$Pb(NO_3)_2$, IR reflection spectra, dynamical props. 77−16303
$PbNb_2O_6$, IR absorpt. spectra and diffuse Raman scatt., normal coord. anal. *(French)* 80−66198
PbO-Bi_2O_3-Al_2O_3, glass formation and IR transmission *(Japanese)* 80−54146
PbO-GeO_2, glass, structure of anionic network, IR spectra 80−103256
PbO-GeO_2 glass, synthesis, Ge coordination state 77−24271
PbO-MoO_3-MO and PbO-WO_3-MO systems, M=Ca, Ba, Mg, Sr, perovskite type cpds. detection 80−108404
PbO-SiO_2, corroded in acid, IR reflectance spectra 77−20846
PbO-SiO_2, glass IR and Raman spectra, heat treatment conditions effect 79−66088
PbO-SiO_2 and PbO-SO_3-SiO_2 system glasses, struct. and IR absorpt. spectra 79−41967
PbO-SiO_2 glass, IR and Raman spectra interpreted in terms of struct. 78−27213
PbO-SiO_2 glass, modifier release in acid soln. 79−43450
Pb_3O_4, IR and Raman study of structural phase transitions *(French)* 78−84582
$(PbO)_x(SiO_2)_y$ glass, vibrational spectroscpic exam. 79−11417
$PbO.B_2O_3$ glass, additional IR absorpt. *(Russian)* 77−85730
$15PbO.3B_2O_3.2WO_3$, struct. and electrophys. characts. 77−84716
$12PbO.6SiO_2.PbSO_4$, crystn. from 2PbO-SiO_2-xSO_3 melts, struct. and vibr. spectra 80−59400
$Pb_3(PO_4)_2$, crit. behaviour of polar modes near ferroelastic phase transition 79−95750
$Pb_3(PO_4)_2$, IR dispersion at room temp. 79−15460
$Pb_5(PO_4)_3Cl$, pyromorphite, vibr. spectra, normal coord. anal. 78−88305
$Pb_{10}(PO_4)_6(OH)_2$, cryst., IR spectra, band assignments 78−60442
$Pb_5(PO_4)_3OH$, prep. from sulphate, X-ray diffr. and IR spectrosc. 80−29893

infrared spectra of inorganic solids continued
$Pb_3(P_xV_{1-x}O_4)_2$, ferroelastic phase transitions, lattice dynamics, dielec. and optical props. meas. 77−55334
PbS film, form. by chem. spraying, elec. and optical props. 78−2588
PbS film, polycryst., chem. deposition from soln. and characterisation 78−72743
PbS film, vac. deposited, optical and phys. props. 80−2315
PbS, low carrier conc., prep. and props. 77−39846
n-PbS, natural galenite, reflectivity, 10-40 μm 79−42975
p-PbS, struct. of valence band, transport processes study 80−20081
PbS-Sb_2S_3 semicond., optical and photoelec. behaviour 80−96938
PbSe epitaxial film on NaCl, far IR reflectivity obs. 77−40251
PbSe on NaCl, epitaxial-substrate system, far IR transmission and refl. 78−6802
n-PbSe, polar semicond., mag. field influence on high-freq. relaxation time 79−95438
p-PbSe, valence band structure, IR refl. and absorpt. meas. 77−55791
PbSe, valence band struct., Hall and transverse Nernst-Ettingshausen effects, optical absorption 79−11064
PbSe:Tl, elec. props. and IR reflection 78−6686
PbSe:Tl, high temp. elec. and optical props., impurity states 79−60854
$PbSe_{0.5}S_{0.5}$, valence band struct., absorpt. spectra, elec. props. 80−44505
p-$(PbSe)_{1-x}(SnTe)_x$, absorpt. edge temp. depend. *(Russian)* 78−34765
$(PbSe)_{1-x}(SnTe)_x$ solid solution, band struct. and some optical props. *(Russian)* 77−76752
$PbSe_{1-x}Te_x$, for-IR reststrahlen spectra, mode behaviour 80−7345
$PbSe_{1-x}Te_x$, symmetry change in cond. levels, photovoltaic effect and reflectivity obs. 78−34766
Pb_2SiO_4-$PbSiO_3$, Raman and IR spectra of crystalline phases 80−3013
$Pb_xSi_yO_z$ films on Si, form. kinetics and props. 80−35358
$Pb_xSn_{1-x}O_2$ film, optical props. 78−39616
n-$Pb_{0.94}Sn_{0.06}Se$ solid solns., Burstein-Moss effect and energy band struct. 80−40118
n-$Pb_{1-x}Sn_xSe$, absorption spectra investigation 80−2768
$Pb_{1-x}Sn_xSe$, plasma reflection spectra, carrier effective masses and relax. times determ. 78−2858
$Pb_{1-x}Sn_xSe$, thin film, opt. props. *(Japanese)* 77−1750
$Pb_{1-y}Sn_ySe$, characts. of IR absorption 77−1681
PbSnTe and PbSnTe, epitaxial-substrate system, far IR transmission and refl. 78−6802
PbSnTe/PbTe inverted heterostructure mosaics, long wavelength, energy gap-Fermi level temp. depend. 79−85182
$Pb_{0.79}Sn_{0.21}Te$ epitaxial film on $Pb_{0.79}Sn_{0.21}Te$, far IR reflectivity obs. 77−40251
p-$Pb_{0.79}Sn_{0.21}Te$, free-carrier optical absorption 77−52101
$Pb_{0.8}Sn_{0.2}Te$, single cryst. and epitaxial film, far IR refl. spectra, carrier density, Hall const., and plasma freq. 80−20629
$Pb_{0.8}Sn_{0.2}Te$:In, absorption spectra meas., 475-725K 77−4664
$Pb_{1-x}Sn_xTe$, absorption edge shift, energy gap determ. 78−88308
$Pb_{1-x}Sn_xTe$ anodic oxide film form. conditions, IR absorpt. spectra 80−11494
$Pb_{1-x}Sn_xTe$, characts. of IR absorption 77−1681
$Pb_{1-x}Sn_xTe$, electroreflectance, Faraday rot., elec. band struct. parameters 77−66113
$Pb_{1-x}Sn_xTe$, energy band parameters from IR Faraday rotation 78−48154
$Pb_{1-x}Sn_xTe$ epitaxial films, adsorption-induced accumulation layer form. on surface 80−60117
$Pb_{1-x}Sn_xTe$, far IR magneto-optical meas. 79−61343
$Pb_{1-x}Sn_xTe$ film, Burstein-Moss effect, absorpt. and photocond. spectra 78−18961
$Pb_{1-x}Sn_xTe$, heteroepitaxial film, fundamental absorpt. edge and Shubnikov-de Haas effect 79−24381
$Pb_{1-x}Sn_xTe$, hole effective mass near zero bandgap, IR refl. study 80−108205
$Pb_{1-x}Sn_xTe$, interband absorpt. edge for single cryst. epitaxial films 78−43948
$Pb_2Ta_{2-x}M_2xO_{7-x}$, (M=Ti, Sn Zr), oxygen deficient, form., IR spectra, dielec. const. *(Japanese)* 77−48171
$PbTa_2O_6$, IR absorpt. spectra and diffuse Raman scatt., normal coord. anal. *(French)* 80−66198
p-PbTe, absorpt. coeffs. meas. 77−24850
PbTe epitaxial film, many valley semicond., band population effects, intraband magneto-optical props. 79−78007
PbTe epitaxial film, stimulated emission, absorption spectra and recombination 78−80409
PbTe, far IR magnetorefl., band struct. 80−76010
n-PbTe, far IR magnetotransmission and refl., dielec. function 77−52091
p-PbTe, far IR obs. of shallow bound states in high mag. fields 78−23444
PbTe, far IR spin flip reson. 79−82979
PbTe film, characts. of photocond. spectra and reflectivity 77−55624
p-PbTe film, for IR magneto-optics, 8-30K 78−23543
n-PbTe, free carrier absorpt. and electron mobility 78−43392
p-PbTe, IR reflection and Faraday rotation angle meas. 77−1680
PbTe, index matching far i.r. method for static dielectric const. meas. 77−1678
PbTe, ion implanted, magneto-optical expts. *(German)* 79−28848
p-PbTe, magneto-optics of free and bound carriers 79−82985
PbTe surface space charge layers, far IR magnetoreflectance meas. 78−64349
PbTe, TO phonon mode softening, sub mm spectra 78−6665
PbTe, TO phonon softening, free carriers and defects effects 78−79720
PbTe, TO-phonon mode softening, far IR Fourier transform spectroscopy 77−40248
PbTe:As, hole conc. control, in LPE layers, plasma reflectivity and thermoelec. probe meas. 79−99640
PbTe:In, absorption spectra meas., 475-725K 77−4664
PbTe:Ti, effect of impurities on transport props. 79−11158
PbTe:Tl, absorpt. coeff. spectral depend. 80−93370
PbTe:Tl, thermoelectric power, elec. cond., Hall coeff. and optical absorpt. coeff. 80−39584
PbTe-CdTe(InSb) superlattices, laser deposition of multilayer heteroepitaxial structs. 80−44450
$Pb_5(VO_4)_3Cl$, vanadinite, vibr. spectra, normal coord. anal. 78−88305
$PbWO_2$, IR and Raman multiphonon spectra, struct. 77−90143
$PbWO_4$, reflectivity, dispersion parameters and optical const. temp. depend. 77−28575
Pd (100), adsorption of Xe and CO, lateral interactions, effect on work function, UPS, and IR spectra 79−77904

infrared spectra of inorganic solids continued
Pd, adsorption, of CO(NO) on SiO_2-supported surface, IR spectrosc. obs. 80−92780
Pd complex, 1,2-benzoquinonedioximates, refl. spectra, 0.5-2.5 eV, Young's modulus and internal friction 78−39562
Pd complex, linear ionic mixed valence cpd., IR and resonance Raman spectra rel. to lattice modes 80−25393
Pd, optical properties, 0.1 to 6 eV 78−92092
Pd surface, chemisorption of CO, IR spectroscopic evidence for localised site adsorption 78−47669
Pd-Fe alloy, IR absorpt. characts., 0.9 to 19 μm, mag. order effect 78−84577
Pd-Pt, adsorption of CO(NO) on SiO_2-supported surface, IR spectrosc. obs. 80−92780
β′-PdIn, electrical resistance, mag. susceptibility and IR freq. dispersion *(Russian)* 80−107759
PdIn, refractive index, reflectivity and band struct., APW calcs. 80−40139
PdO, optical props., 0.5-5.4 eV 79−56813
Pr compounds, plasma light reflection by free charge carriers 80−11403
Pr_2ASe_5, A=Ge, Sn, diffuse refl. spectra and band gaps 79−51963
PrB_6 film, prep. by electron beam evaporation, and optical and elec. props. 80−20793
$Pr(BO_2)_3$, single cryst., IR absorpt. spectra 80−34903
$PrCl_3$, one-dimensional X-Y system, far IR absorpt. spectra, cooperative spin excitations 78−95584
$Pr(OH)_3$, low temp. heat capacity, thermophys. props. optical spectra, anal. of Schottky contributions, review 80−24611
$PrVO_4$, energy levels, opt. and NMR measurements 78−80226
$PrVO_4$, monazite struct., IR and NMR spectra 79−78534
$Pr_xY_{3-x}Fe_{5-y}O_{12}$ film, IR absorpt. and Faraday rot. spectra 77−52093
Pt {111}, chemisorpt. of CO, refl.-absorpt. IR spectroscopy 77−1306
Pt {111}, chemisorpt. of N_2, refl.-absorpt. IR spectroscopy 77−47676
Pt, adsorbed CO, IR reflection absorpt. spectra, 1875 cm^{-1} band 79−65852
Pt, chemisorbed ethylene, IR refl. obs. 77−31903
Pt complex, 1,2-benzoquinonedioximates, refl. spectra, 0.5-2.5 eV, Young's modulus and internal friction 78−39562
Pt complex, bis(1,2-benzoquinonedioximato)platinum(II), intrinsic elec. cond. and refl. spectra 78−6377
Pt complex, linear ionic mixed valence cpd., IR and resonance Raman spectra rel. to lattice modes 80−25393
Pt/MgO catalyst, H_2 adsorption, 300-873K *(French)* 78−38967
PtO film, electrochemically formed, anisotropy of optical constants, reflection spectroscopy and Kramers-Kronig analysis 77−32456
$Pt_{0.97}S_2$, optical props. at absorption edge 78−35140
Pu(IV) oxide polymer, potential pollutant from fuel reprocessing, IR spectrum 78−76456
α-quartz, reflection and surface polariton spectra, ion implantation effect *(Russian)* 79−47451
Rb_2AF_6, A=Si, Ge, Sn, IR absorpt. spectra, integrated intensity 79−73944
RbBr, Stark effect in F-centre emission 77−63434
RbCN, crystal props., log potential model calc. 78−63829
RbCNS, single cryst. factor group anal. of IR and Raman multiphonon bands 77−4644
Rb_2CO_3, molten, IR emission spectra *(Japanese)* 78−19469
$RbCl_xBr_{1-x}$, IR refl. spectra, temp. depend. 77−28573
RbCl(Br)(I), far IR complex refr. indices, dispersive Fourier transform 78−80322
$RbClO_3/RbBrO_3$ mixed crystals, internal optic modes obs., Raman and IR reflectance spectra 80−76024
$RbDy(MoO_4)_2$, Dy^{3+} doublets, temp. anomaly in splitting separation due to structural phase transformation *(Russian)* 80−39274
$RbDy(MoO_4)_2$, low temp. phase transitions *(Russian)* 78−87787
$RbEu(PO_3)_4$, vibr. spectra 80−34905
$Rb_3Eu(PO_4)_2$, synthesis and IR spectra 80−16019
$RbFeCl_3$, linear chain ferromag., optical absorpt. and dichroism in mag. field 77−77237
$RbFeCl_3$, one-dimens. ferromagnet, lowest excitation, far IR study 80−66186
$RbFeCl_3$, singlet ground state 1-D ferromag., far IR Zeeman spectra 77−52098
$RbFeCl_3$, singlet ground state one-dimens. ferromag., 2-magnon excitation, far IR spectra obs. 77−69831
Rb_2FeF_4, two dimensional planar antiferromag., mag. excitations, Raman and far IR spectra obs. 78−72343
$RbGa_3Br_{10}$, cryst., vibr. spectrosc. *(French)* 78−6667
Rb_2GeF_6, IR absorpt. spectra, integrated intensity, 100-300K 79−73945
RbH_2PO_4, high temp. phase transition, dielec. const., elec. cond. and IR refl. meas. 78−43118
RbH_2PO_4, IR overtone spectra and temp. depend. 79−47456
RbHSeO4, ferroelec., far IR spectra 80−71404
RbI, Stark effect in F-centre emission 77−63434
$RbI:HF_2^-$, anharmonic interaction of impurity intramol. vibrs. with cryst. phonons 77−77217
$RbI:ReO_4^-$, IR absorpt., half width, temp. depend. *(Russian)* 79−78722
$RbI:TeO_3^{2-}$, IR absorpt. of impurity complexes *(Russian)* 79−33746
$Rb^+M^{III}(SO_4)_2$, M=Al^{3+}, Cr^{3+}, Fe^{3+}, Raman and IR spectrum study *(French)* 79−47453
Rb_2MnCl_4, IR active modes, interlayer and intralayer forces 77−59575
Rb_2MnCl_4, perovskite type layer struct., far IR reflectivity and Raman spectra 77−15511
RbN_3, polycryst., IR-active lattice vibr., optical consts. 77−77185
RbNCO, polycryst., IR and Raman spectra, lattice and internal modes 77−32369
$RbNO_3$, phase transition, IR.spectra 80−7350
$RbNaMg_3M_2Si_{12}O_{30}$ (M=Cu, Fe, Mg), cryst. struct., X-ray diffr. and IR spectra *(French)* 80−107158
$Rb_3Nd(PO_4)_2$, synthesis and IR spectra 80−16019
Rb_2NiF_4, quadratic layer antiferromag., optical spectra obs. 77−16326
$Rb_2Ni_3(P_2O_7)_2.nH_2O$, thermal dehydration 80−35513
RbO_2-Na_2O-P_2O_5 glasses, Raman and far IR spectra, vib. at cation site, struct. 78−60435
Rb_2O-Li_2O-P_2O_5 glasses, Raman and far IR spectra, vib. at cation site, struct. 78−60435
$RbPO_3$-$Mn(PO_3)_2$ system, $Rb_2Mn(PO_3)_4$ and $RbMnP_3O_9$ form. 79−78943
$Rb_{1.75}(Pt(CN)_4).1.5H_2O$, 1-D cond., IR spectra 77−85703
$Rb_2(TeBr_6)$, far IR and Raman spectra and phase transitions 80−11376

infrared spectra of inorganic solids continued
$Rb_4(UO_2)_2F_8$-$2H_2O$, IR absorpt. and Raman spectra, normal coordinate anal. *(French)* 78−52509
Rb_2ZnBr_4, modulated struct., far IR transmission, temp. depend. 80−71408
Rb_2ZnBr_4, soft modes at phase transforms., far IR spectrum study 80−107398
$Re(^{12}CO)_{5-y}(^{13}CO)_yX$(X=Cl, Br), 0<y<5, vibr. spectra in the 2000 cm^{-1} region of mixed and isotopic crystals 78−84585
ReF_6, cryst., Raman and absorpt. spectra, Jahn-Teller effect 78−6675
ReO_3 type lattice, group-theoretical symmetry anal. of vibr. *(Russian)* 80−10610
Rh, adsorption of CO_2+H_2 mixtures, reflection-absorption IR and thermal desorpt. obs. 78−6226
Rh complexes with adenosine, xanthosine, prep., elec. cond., IR spectra, characterisation 78−92065
Rh/Al_2O_3 catalyst, surface interaction between NO and CO, IR study 79−70369
Ru (001), adsorption of CO, IR spectra, LEED, and thermal desorption meas. 80−70533
Ru complexes, carbonyl hydrides, pre-reson. Raman spectra, Ru-Ru and Ru-C modes 78−43854
Ru complexes with adenosine, xanthosine, prep., elec. cond., IR spectra, characterisation 78−92065
Ru, optical props. 79−24282
α-$RuCl_3$, reflectivity and absorpt. spectra, thermo-reflectance 79−47438
RuP_2, prep. and characterisation 78−39679
$Ru_xTi_{1-x}O_2$ films, elec. props. and IR spectra 79−38207
Ru(001) surface, adsorption of CO, IR spectra and LEED 79−37914
S, orthorhombic, far IR absorpt. spectrum 77−8560
SF_6, cryst., IR and Raman spectra at 9 and 97K, cryst. struct. 79−87427
SF_6, IR rot. spectra, orbital level splitting in octahedral symmetry, high J levels 77−69815
SF_6, IR rot. spectra orbital level splitting in octahedral symmetry, high J levels 77−69816
S_2F_{10} 77−6775
SF_5Br, Ar matrix and solid phase Raman and IR spectra, vibr. assignments 77−6775
SF_5Cl AR matrix and solid phase Raman and IR spectra, vibr. assignments 77−6775
SF_4O, vibr. spectra, struct. and thermodynamic props. 77−63416
$(SN)_x$, electronic struct. and opt. props. 78−6256
$(SN)_x$ film and crystal, acoustic and optical phonons, Raman, i.r. and transmission spectra 77−4642
$(SN)_x$, IR spectra 79−56781
$(SN)_x$, IR transmission spectrum assignment 78−15160
$(SN)_x$, phonon evolution during polymerisation of SN units 78−79711
$(SN)_x$, reflectivity spectra meas. by synchrotron radn. 79−91513
$(SN)_x$, single cryst., elec. anisotropy, polarised refl. spectra 77−36264
$(SN)_x$, X-ray and optical props. 78−39632
$(SN)_x$:Br, IR spectra 79−56781
S_4N_4, solid and soln., IR and Raman spectra, vibr. assignment 78−74659
$(SNBr_{0.4})_x$, metallic, transport and optical props. 77−85724
$S_3N_3Cl_3$, solid and soln., IR and Raman spectra, vibr. assignment 78−74659
$S_4N_4H_4$, and -d_4, solid and soln., IR and Raman spectra, vibr. assignment 78−74659
S_7NH, solid and solns. vibr. spectra, force consts. isotope effects 77−66490
$S_{8-x}(NH)_x$, (x=1,2,3,4), and deuterates, IR and Raman spectra, isotope shifts, mol. vibr. assignment 79−10110
$(SN)_n^*$ radicals polymerisation to $(SN)_x$ in thin films, optical spectra 80−16656
SO_2, frost, IR spectra and implications for Io 80−77331
SO_2, IR and Raman spectra, mol. and lattice vibrs. 78−19464
$S(SiD_3)_2$, Raman spectra of gaseous, liquid, solid phases, IR spectra of gaseous and solid phases 78−25547
$S(SiH_3)_2$, Raman spectra of gaseous, liquid, solid phases, IR spectra of gaseous and solid phases 78−25547
Sb, amorphous, vibrational excitations of defect sites 80−49332
Sb electrodeposit, amorphous explosive crystn., semicond-semimetal transition and IR absorpt. 78−51849
Sb film, electroreflectance effects 79−43055
Sb, magnetoreflection of circularly polarised IR radiation, band struct. 77−52094
Sb, thin films, IR absorpt. and intraband transitions 80−16114
Sb-Se-I system, exam. of glass formation, IR transmission spectra 78−88452
$SbBr_x^{-y}(I_x^{-y})$, low freq. Raman and IR spectra, force consts. 80−55097
SbF_3, IR spectra of solid and gas, rel. to struct. *(French)* 78−78692
$SbF_3.(NH_2)_2CS$ and $SbF_3.[(NH_2)_2CS]_2$, X-ray cryst. struct., IR spectrum *(French)* 78−87643
$SbO_{3/2}$-$BO_{3/2}$, glass, struct. and props. *(Japanese)* 77−27836
Sb_2S_3 film, amorphous and crystalline, optical props. 79−95867
Sb_2S_3, vitreous, prep. elec., opt. and struct. props. 77−76889
Sb_2S_3-SbI_3, amorphous phase formation in vacuum condensates, TEM study 79−86712
SbSBr glass, IR reflectivity spectra 80−71403
SbSI-SbSBr system, ferroelec., anharmonic effects in far IR reflectivity spectra 80−76014
$Sb_2S_3(Se_3)$, IR spectra rel. to bonding, amorphous film and cryst. 77−16410
Sb_2Se_3, energy gap, light absorpt., elec. cond., photocond. meas. 78−47826
Sb_2Se_3, Raman spectra, Raman and IR-active modes 79−56776
$Sb_xSi_yO_z$ films on Si, form. kinetics and props. 80−35358
Sb_2Te_3, $(Bi_{1-y}Sb_y)_2Te_3$, Raman and far infrared investigation of phonons 78−23453
Sc, HCP, optical examination of electronic struct. 77−89694
ScF_3, metastable high press. phases, X-ray diffr. and IR absorpt. expts. 77−11499
ScH_2, electronic struct., optical studies, 0.2-5 eV, 4.2-340K 79−78005
ScH_2, optical interband struct. and low energy plasmons 78−31200
ScO(OH), ScOF, and $Sc(OH)_3$, metastable high press. phases, X-ray diffr. and IR absorpt. expts. 77−11499
$Sc_2Si_2O_7$, IR and Raman spectra, internal and external modes 79−61365
Se, amorphous, far IR investigation of structure, ring and polymeric chain components *(Japanese)* 77−76311

infrared spectra of inorganic solids continued
Se amorphous films, structural relax., viscosity, creep, heat capacitors, and IR spectra meas. 79−42424
Se amorphous solid dielectric loss meas. by submillimetric waveguide laser 79−33603
Se film, amorphous, struct. and crystn., far IR transmission spectrum and DSC obs. 77−85106
Se, glass, sp. ht. excess rel. to far IR absorption 77−84874
Se, rhombohedral, IR absorpt. spectrum 80−103949
Se, trigonal, model of lattice dynamics using long and short range interactions 78−59893
Se-As_2Se_3 system glasses, vibr. spectra and partial vols. of components 79−42973
Se-Ge glass, lattice vibr. spectra, photostruct. change, far IR absorpt. 78−72494
Se-Ge glasses, extreme far IR absorpt. meas. 80−50318
Se-Si system glasses, vibr. IR spectra 80−20643
Se-Te crystallised glasses, struct. transforms. and IR spectra 80−19712
Se-Te-As-Ge glasses, absorpt. spectra, diffuse reflectivity loss correction 79−82995
$Se_{0.84}Ge_{0.16}$ glass, sp. ht. excess rel. to far IR absorption 77−84874
$Se_{1-x}Ge_x$, amorphous, IR absorption spectra *(French)* 77−73146
$SeMoOCl_7$, prep., cryst. struct., characterisation *(French)* 78−63722
Si (100), surface space charge layer, inter-subband optical transitions 77−15931
Si, (100) surface space-charge layer, intersubband cyclotron combined resonances 79−69571
Si (111)7×7, dangling-bond surface states and O_2 adsorption, reflectometric study 79−99600
Si accumualtion layers, temp. depend. of inter-subband transitions, many-body effects 79−60899
Si, ambient effect of O precipitation, self interstitial mechanisms, IR spectra, TEM study 80−66510
Si, amorphous, electronic struct., far infrared absorption 80−45051
Si, amorphous, hydrogenated, soft H plasma effect, IR absorpt. *(French)* 80−45054
Si, amorphous, IR absorpt., first-order effective charges due to at. displacements 77−48164
Si, amorphous, pure and hydrogenated, far IR absorption coeff. meas. 80−108213
Si, amorphous film, IR and Raman spectra of Si-H bonds 78−19482
Si, amorphous film, RF plasma deposition from $SiCl_4$-H_2, characterisation 80−66435
Si, amorphous film, RF-sputtered, influence of O_2 and deposition conditions, elec. cond., IR absorpt. and ESR 80−2949
Si, amorphous film prepared by CVD, optical props. and struct., solar absorber appl. 79−52035
Si, amorphous films, RF sputtering prep. at high Ar press., props. obs. 80−80418
Si, and Si:H, amorphous, sputter deposited, O_2 incorporation during and after fabrication 80−49541
Si, CVD, amorphous and polycryst., solar thermal absorber, temp. variation of absorpt. edge 80−12028
Si, carrier concentration distribution by scanning IR absorption 79−61356
Si, compensated by thermal defects, recomb. and optical props. 80−64989
Si, compensated monocrystal, IR absorption spectra, Fourier transform obs. 80−60644
Si complex reflectivity determ., absolute method 79−30584
Si Czochralski wave, oxid. induced stacking fault, oxygen content influence 78−10062
Si, Czochralski-grown crysts., thermally induced microdefects, annealing temp. and starting material effects 80−49141
Si, dislocation-free, O_2 precip., IR and TEM obs. 80−29173
Si dislocation-free crystal O precipitation obs. 78−6095
Si, divacancies due to proton irrad., IR absorpt., annealing effects 80−20673
Si, electron irrad., limiting position of Fermi level, elec. cond. and optical absorpt. meas. 79−65484
Si, electron irrad., multivacancy-O complexes, EPR expt., correl. with IR absorpt. data 77−28443
Si, electron irrad., rod-shaped defects, electron microscopy and IR spectra obs. 80−39159
Si, electron irradiated, EPR of C-O divacancy complex 77−69691
Si, electron irradiated, O-vacancy pair, EPR of optical absorption 77−16173
Si, electron-hole drops, far IR absorpt. spectrum 78−47706
Si epitaxial film, correlation between electrooptical and electrical props., IR absorpt. spectra *(Russian)* 78−60453
Si, epitaxial wafer, saucer pit microdefects reduction by intrinsic gettering 80−75450
Si, exciton and deformation pot. fine struct. 78−88301
Si, excitons, far IR absorption 78−31201
Si, far IR complex refr. index spectra determ., new method, for transparent solids 77−28566
Si, far IR impurity spectra, effects of high uniaxial stress 78−56508
Si film, polariton resonance obs. from reflectivity meas. 77−69251
Si, heavily disordered, fast neutron irrad., IR absorption following heat treatment 78−2448
p-Si, heavily doped contact layers on IR detectors, IR transmissivity 80−108190
Si, high-dose implantation damage, reflectivity, Rutherford backscatt. and TEM obs. 77−7743
Si, high-resistivity, local IR refraction and transmission 79−15429
Si, highly transparent semicond. crysts., multiphonon IR absorpt. 78−10885
Si, highly transparent semicond., multiphonon IR absorpt. 78−60461
Si, IR absorption spectra, Si-H bonds, crystal defects *(Chinese)* 80−55073
Si inversion layer, IR spectrum, 10^5G effect on linewidth 78−946
Si inversion layer, inter-subband optical absorpt. in mag. field 77−32375
Si inversion layers, discrepancies between absorption and photocond. meas. 78−6451
Si inversion layers, far IR transmission spectra, two-dimensional plasmons 77−76931
Si inversion layers, far IR reson. magnetotransmission, temp. and band gap light depend. 78−64363
Si inversion layers, low density, far IR resonant magnetoabsorption 77−55789

infrared spectra of inorganic solids continued
Si, ion bombardment induced defect distrib., IR and electron diffr. study 80−65074
Si, ion implanted amorphous layers, free carrier plasma effects 77−73133
n-Si, irradiated with large neutron doses, defect annealing 80−19849
Si MOSFET inversion layers, IR photocond. and absorption 78−64123
n-Si, many-valley semicond., relative displacement of D_1 and D_2' bands under shear deform. influence 79−15080
Si, mass-anisotropy exciton splitting determ. 78−6685
Si, matrix isolated cluster, otpical absorpt. extended Huckel calcs., electron energy levels 80−16045
n-Si neutron and electron irrad., isochronous annealing influence on edge absorpt. 80−11449
Si, neutron irrad., point defects photopopulation and photoionis., IR spectra meas. 80−25423
Si, neutron irradiated, characts. of defect form. 78−14382
Si, neutron irradiated, direct band gap transition, IR absorpt. 79−73980
Si, neutron irradiated, intrinsic defect exam. by IR spectra 78−52534
Si, neutron transmutation doping, annealing, lattice damage 80−15163
Si, nonequilibrium carrier density relax., lifetime determ. using light absorption 78−15170
Si, nonpolar semiconductor, IR free carrier absorpt., two short wavelength phonon scattering 79−78665
Si, O content determ. by spectral analysis, phonon absorpt. effects *(Russian)* 77−48177
Si, optical spectroscopy, absorpt. coeff., lattice vibrs. modes, band gap, acoustic approach 77−69822
Si, oxide layer form. by O^+ ion implantation, Rutherford backscatt. and IR transmission obs. 79−51141
p-Si, photoabsorpt. associated with divacancies 79−15502
Si, piezo−spectroscopic study of ratio of electron−TO phonon to hole−TO phonon interaction 79−24289
Si, piezospectroscopic determ. of electron-phonon to hole-phonon interaction 79−95783
Si plasma deposited amorphous hydrogenated film, optical props., annealing effect 79−56874
n-Si plate, effect of nonequilibrium carriers on IR transmission 79−38548
Si polycrystalline CVD film optical props. 77−77315
Si, porous layer, oxidation, and oxide film props. 80−55556
Si, precipitation of O, 1000°C TEM, IR absorpt. and X-ray studies 80−34194
Si, precipitation of O, 650°C, IR absorpt. and X-ray diffr. 80−76258
Si, precipitation of O, annealing, IR spectra meas. 80−24606
Si, proton irradiated, IR absorption 79−33742
Si, radiation induced defects, IR absorpt. bands 80−25424
Si, resonant interaction of acceptor states with optical phonons 77−1394
Si, resonant interaction of optical phonons with acceptor continuum states 78−35178
Si, splitting of 1s excitons, derivative spectra of optical absorption 77−69249
Si, sputtered, cluster formation, influence of HF plasma interaction 78−64441
Si surface, metal doped, recomb. of nonequilib. carriers at high excitation rates 79−7835
Si, surface inversion layers, intersubband optical absorpt., Auger-type transition 80−29741
Si, surface space charge layer, anisotropic and tilted valley systems, absorption 77−85726
Si, thermally induced microdefect form., C and O role 80−11439
Si, thinly oxidised wafer reflectance at normal incidence, calc. 79−78641
Si, vibrational properties of the ⟨001⟩ split interstitial 78−91405
Si wafer, heat treatment behaviour of microdefects and residual impurities, X-ray diffr. and IR absorpt. study 80−49214
Si wafer C impurity IR absorption spectrometry, thickness fringe elimination 80−55132
Si wafer O interstitial IR absorption spectrometry, multiple reflection correction 80−55131
Si:Al, absorpt. line broadening 78−95594
Si:Al(In), acceptor levels, IR spectra 78−67972
Si:As, annealed, dopant profile parameter contactless probing by IR spectroscopy 79−77629
Si:Au, IR absorption and elec. resist. meas., impurity centres 79−38580
Si:Au donor and acceptor centre obs. using IR absorpt. and dynamic nucl. polarisation with optical pumping 80−54639
Si:B, ion implanted, laser annealed, IR and Raman spectra 79−73914
Si:B(Ga), IR spectra of acceptor levels 80−34953
Si:C, impurity determ. by IR absorpt. spectroscopy, room temp. and low temp. meas. comparison 80−108237
Si:F, amorphous, heat resistant, prep., elec. cond., IR absorpt., annealing 80−65719
Si:F, amorphous, pure and doped, vibr. excitations at defect sites, IR and Raman spectra calc. 80−49329
Si:F, amorphous alloys, RF sputtering prep. in SiF_4-Ar gas mixture, spectra 80−80772
Si:F, H amorphous films, optical props., photoconductivity, photostructural changes 80−11034
Si:Ga, IR absorption of dopant centres, spectral depend. on doping, impurity conc. and temp. 80−76053
Si:Ga, LPE on Si, technique and characterisation 79−38751
Si:H, amorphous, defect creation and H evolution 80−50392
Si:H, amorphous, glow discharge deposited, thermal dehydrogenation, IR spectra 80−44442
Si:H, amorphous, glow discharge deposited, laser annealing 80−49104
Si:H, amorphous, H content determ. by IR absorpt., gas evolution and nuclear reaction methods 80−44130
Si:H, amorphous, plasma-deposited, effect of DC elec. field superimposed during deposition 80−44643
Si:H, amorphous film, prep. by plasma decomp. of SiH_4 under mag. field, and characterisation 80−45239
Si:H, amorphous films, plasma-deposited, defect states, IR, ESR, and refractive index meas. 79−65944
Si:H, amorphous thin film, ion plating, IR absorpt. meas. 80−84857
Si:H, amorphouse film, optical and elec. props. 79−82694
a-Si:H, influence of H on optical props., H conc. and H bonds 80−76098
Si:H, new IR absorpt. bands 79−87472
a-Si:H, structural interpretation of vibr. spectra 79−69864
Si:H,F,O amorphous, plasma deposited, comp. and optical props. 80−50441

infrared spectra of inorganic solids continued
Si:H,Li, amorphous, DC electrical conductivity, absorption edge and IR meas., role of H 80−54694
Si:H amorphous film, sputtered in Ar-SiH_4 mixtures, props. 79−87023
Si:H amorphous film, sputtered IR vibr. spectra and photolum., effects of partial evolution of H 80−44413
Si:H amorphous films, IR spectrum and struct. 80−97277
Si:H amorphous films, photovoltaic and photocond. spectra, photoluminesc. 80−44645
Si:H amorphous films, role of Ar in deposition process, IR absorpt. and photocond. meas. 80−50321
Si:H amorphous glow discharge film, optical absorpt., near IR region 79−87518
Si:H amorphous sputtered films, optical gap, IR absorpt. meas. 80−50320
Si:H(D), H-related defects, channelling and IR meas. 80−25422
Si:In, absorpt. spectra, impurity excited state lines 80−108243
Si:In, C, 0.111-eV acceptor level, X-level defect conc. from IR absorpt. and Hall meas. 79−51512
Si:In, gradient transport soln. growth, IR monitoring, 950-1300°C 79−100040
Si:In,P, photoinduced IR absorpt. and luminesc. 79−33828
Si:I, obs. of donor exciton in far IR transmission meas. 79−91477
Si:N, ion implantation, refractive index, IR spectra, ion range and straggling meas. 80−34020
Si:N(P), ion implanted, IR transmission and rel. spectra study 80−108244
Si:Na^+, inversion layer, far IR optical spectroscopy 80−20680
Si:Ni,Co,Mn, γ-irrad., interaction of deep-level impurity atoms with radiation defects 77−76457
Si:O, 9 μm absorpt. band attributed to dissolved O, from expts. on quartz particles 79−19914
Si:O, amorphous, sputtered, influence of O and deposition conditions 80−54693
Si:O, Czochralski crystal, oxygen striation and thermally induced microdefects 80−100275
Si:O, dislocation-free, Si-O complexes, heat treatment effects 77−62557
Si:O, electrial and infrared spectroscopic investigations 80−34389
Si:O, IR absorpt. spectra of Si:O complexes 78−19520
Si:O, impurity conc. profiles, scanning IR absorpt. using semicond. laser 80−50376
Si:O,C, electron irradiated, indirect vacancy-interstitial recomb., IR absorpt. meas. 77−43209
Si:O,H amorphous, plasma-deposited, electronic and struct. props. 80−50391
Si:O film, near IR absorption, O impurity states. 78−88333
Si:O film, near IR reflectivity at high temps. 78−56532
Si:O(C) wafers, impurity meas. by Fourier transform IR spectra 80−89030
Si:O(C) wafers, impurity meas. by Fourier transform IR spectra at low temp. 80−89031
Si:P, absorpt. due to creation of bound excitons 78−23025
Si:P, amorphised by Ne^+ implantation, high fluence P implants, plasma region obs. 79−86807
Si:P, characterisation by IR reflectivity 78−56501
Si:P, excitation spectrum of P donors introduced by neutron transmutation, high resolution study 79−47460
Si:P, high fluence ion implantation, layer thickness and refr. indices, IR refl. meas. 79−82248
Si:P, IR absorpt. and D^--band 78−52533
Si:P, submillimetre wave study of metal-insulator transition 79−95336
Si:Tl, IR excitation spectra 78−88289
Si:Tl, optical absorption and photolum. of bound exciton 78−88359
Si-Au amorphous system, optical absorpt., IR photocond. 79−42582
Si-B amorphous film, plasma deposited, characterization 79−69828
Si-C:H, amorphous film, vibr. spectrum 79−61450
Si-containing films, formed by reaction of Si with organic compounds of N, struct. investigation 79−87009
Si-H, amorphous, on Nb or W, spectrally selective absorber, IR spectra 80−26164
Si-H, amorphous, plasma-deposited, H evolution and defect creation 80−44914
Si-H (up to 15 at.%), amorphous, ion implanted, laser annealing obs. 79−69133
Si-H amorphous film, reactively sputtered, prep. and props. 79−78889
Si-H(-D), film, IR and Raman spectra, H bonding effects 78−72515
Si+metal oxides, spray coated, IR investig. 79−39197
SiAs-Au surface barrier diodes, optical props. of SiAs 79−8145
$Si_{1-x}Au_x$ amorphous films, IR absorpt. spectra 80−16034
Si_xB_y formed when Bi_2O_3 is diffused in Si, anal. study 79−19269
SiC (1 OH), phonon spectrum, dispersion curves energy discontinuity and vibr. modes, IR spectra obs. 80−44274
SiC (6H), IR absorpt., UV illumination effects, defect levels 80−66251
α-SiC (6H), paramag. N impurity levels, IR absorpt. and ESR expts. 77−59598
SiC, electron trap depth, additional IR absorption induced by UV excitation *(Russian)* 79−78721
SiC fibre reinforced Ni-Cr alumina coated fibres, hot pressed, annealed, IR study 78−60623
SiC fibres obtained from polycarbosilane fibre 80−50582
SiC film, amorphous, reactively sputtered, effects of S/C ratio and H content on elec. and optical props. 79−90906
α-SiC, lattice absorpt. bands in IR spectra, surface treatment effects 77−52071
β-SiC layer synthesized by C ion implantation in Si, IR absorpt. 78−56492
β-SiC, pyrolytic, optical and elec. props. 79−78093
SiC smokes, vapour condensed, IR absorpt. peaks compared to interstellar extinction curve 80−82180
SiC, sputtered, comp. and struct. props., effect of target materials 80−54549
SiC, sputtered amorphous film, struct., elec. and optical props. 79−78236
β-SiC, submicron powder, prep. by siliconization of C black, props. *(Japanese)* 79−66192
SiC, synthesis by ion implantation of diamond and silicon, struct. charcts. 77−76434
SiC, synthesis by ion implantation of diamond, role of struct. imperfections 78−34529
SiC:B, electroabsorption, 0.35-0.45 eV, under UV illumination 79−4831

infrared spectra of inorganic solids continued
α-SiC:H, prepared by reactive sputtering, layer props. *(Japanese)* 80−60695
SiC-Si struct. formation on ^{12}C ion implantation in Si, optical and photoelectric props. 79−91136
$Si_xC_{1-x}H_z$ amorphous films, IR absorpt. bands 80−100705
$Si_xC_yH_z$ films, reactive plasma deposited, comp., IR anal., and optical props. 79−95945
n-SiC(6H), donor ground state splitting, IR spectra *(Russian)* 78−92104
SiF_4, mol. cryst., coupled phonon modes and IR band shapes 78−26641
SiGe, matrix isolated cluster, optical absorpt. 80−16045
Si_xGe_{1-x}:H, amorphous, photoinduced optical absorption 79−82973
SiH_1-like centres, in cryst. Si, vacancies and chem. trapping obs. 79−99916
SiH_4, low temp. oxidation, film growth rates, IR absorption spectra 80−15399
$Si_{1-x}H_x$ amorphous sputtered films, IR vibr. spectra 79−43051
SiH_3D, in polycryst. SiH_4, mol. motions and symmetries, IR obs. 78−48163
$SiH_3PH_2BD_3$, vibr. analysis, spectra and structure of P-B compounds 78−84586
$SiH_3PH_2BH_3$, vibr. analysis, spectra and structure of P-B compounds 78−84586
β-Si_3N_4, β′-$Si_2Al_4N_4O_4$, combined X-ray and IR analyses 78−79579
Si_3N_4, CVD, chem. bound H, NH_3/SiH_4 ratio and annealing depend. 77−76680
Si_3N_4, CVD, effect of deposition parameters 77−55272
Si_3N_4, CVD, struct., optical and mech. props. 77−1816
α-Si_3N_4, exam. of chemical vapour deposition, and IR transmission and reflectance 79−19993
Si_3N_4, film, absorption, refr. index, freq. dispersion 78−48248
Si_3N_4, film, H_2 concentration profile, chem. bonding 79−33205
Si_3N_4 film formation by $^{14}N_2^+$ ion implantation into Si 79−99455
Si_3N_4 film in MNOS memory struct., distrib. and role of N-H and Si-H bonds 79−33358
Si_3N_4 films, amorphous, CVD, IR spectra 77−21031
Si_3N_4, films, ion-beam synthesis, IR spectra, struct., crystallisation on annealing 77−16705
Si_3N_4 layers, prep. by N_2 ion implantation into Si, TEM and IR absorpt. obs. 79−46974
Si_3N_4 thin film, CVD, multiple internal refl. IR spectroscopy 80−11499
Si_3N_4:C film struct., oxidation, defects 79−51455
Si_xN_y, film, chemical nonuniformity of films produced by ammonolysis of monosilane 77−1334
SiO evaporated film, dielec. function 8 to 33 μm, spectrophotometric and refl. meas. 80−80883
SiO film, vacuum evaporation on NaCl single cryst., IR absorption spectra 80−35098
SiO film on Al, radiative cooling surface 80−50439
SiO films, adsorption of $NO(N_2O)(NO_2)(O_2)$, infrared spectra exam. 79−45725
SiO_2, adsorption of diketones, under carbon tetrachloride immersion, IR obs. 79−24821
SiO_2, adsorption of pentan-3-one, under carbon tetrachloride immersion, IR obs. 79−24821
SiO_2, amorphous, and layers on Si substrate, IR optical props. 79−56780
SiO_2, amorphous, intrinsic surface phonons, Raman scatt. and IR refl. 80−24728
SiO_2, amorphous, optical and elec. props., comparison with chalcogenide semiconds. 78−6721
SiO_2, amorphous, phonons, neutron, IR and Raman spectra calcs. 78−10150
SiO_2, amorphous and crystalline, surface polaritons and splitting of optical frequencies 78−72090
SiO_2 and SiO_2-B_2O_3 glasses, struct. and phonon spectra 80−50324
SiO_2 based glasses, highly absorbing anomalous IR absorption at low temps. 78−43871
SiO_2 based optical fibre waveguides, water impurity 77−68270
SiO_2 bricks, quartz estimation using IR spectra 78−48718
SiO_2 coatings on SiO_2 substrate, cathodoluminescence spectra, electron irrad. 80−76085
SiO_2 deposited on Ge, optical constants, reflection spectra by Kramers Kronig method 80−76099
SiO_2, doped and nondoped fused silica, IR charcts. of optical fibres 79−18537
SiO_2, E′-centre model, IR absorption spectra 79−37634
SiO_2 fabric, structural stability rel. to brittleness, X-ray diffr. and IR spectrosc. studies 80−96634
SiO_2 fibres, LF optical phonons, Raman spectra 80−80789
SiO_2 film, IR spectra and elec. props., influence of prep. conditions 79−87176
SiO_2 film, ion bombarded, attenuated total refl. method obs. of H capture 79−95863
SiO_2 film, on GaP substrate, N ion implantation, optical refl. and EPR meas. 80−84197
SiO_2 film, on Si, SiOH and SiH groups, IR absorpt. results 78−26779
SiO_2 film, spin-on oxide, phys. and cond. meas. 77−43762
SiO_2 film on Cu substrate, surface EM wave absorpt., optical consts. *(Russian)* 80−108216
SiO_2 films, CVD at reduced press., optical props. 80−2957
SiO_2 films, dehydroxylation, sintering, IR investig. *(Russian)* 78−75967
SiO_2 films, microporous, sintering effects, IR ATR, transmission investigs. 79−66031
SiO_2 films, prep. from tetraalkoxysilanes, by activation pyrolysis 79−87583
SiO_2, fused, for sealed ampoule cryst. growth, thermal transmission function 80−84731
SiO_2, fused, surface crystn. by Li^+ ion implantation and annealing 80−89383
SiO_2 gel. struct., IR spectra obs. 78−88297
SiO_2 glass, formation by hydrolysis of $Si(OC_2H_5)_4$ with NH_4OH and HCl soln., and characterisation 80−71622
SiO_2 glass, IR spectral emissivity and absorpt. coeff. at 600 to 1700K 80−16018
SiO_2 glass, ion bombardment, form. of cpds., IR spectrosc. exam. *(German)* 80−88173
SiO_2 glass, low loss optical fibre, radiation-induced IR absorpt. 80−87521
SiO_2 glasses, opt. consts. in IR and vacuum UV 78−27238

infrared spectra of inorganic solids continued
SiO_2, heat of adsorption of various mols. by IR spectroscopy 77−55447
SiO_2, ion irrad., H capture, absorpt. bands *(Russian)* 78−76505
SiO_2 layers, crystallisation, structural props. rel. to annealing 78−34724
SiO_2 layers, room temp. transforms induced by diethyl ether vapour 79−99456
SiO_2, OH group interactions, IR and Raman spectra 78−80383
SiO_2, P-doped amorphous, porous and hydrophilic, water adsorpt. and IR spectra obs. 80−80061
SiO_2 powder, surface modes, IR spectra 78−92063
SiO_2 thermal film, freon ion beam etching, IR study *(Russian)* 80−76095
SiO_2 thin film CVD, multiple internal refl. IR spectroscopy 80−11499
SiO_2 thin films, comparison of RI and IR spectra 80−11497
SiO_2, ultrathin layers on Ge substrate, ATR spectra, thickness depend., struct. obs. 80−55214
SiO_2, vitreous, band limits and vibrational spectra 79−73935
SiO_2, vitreous, LO vibrational modes, Raman and IR spectra 77−7819
SiO_2, vitreous, multiphonon IR absorpt. 80−25381
SiO_2, vitreous, valence-attenuation pair defect, states, IR and Raman spectra 79−91442
SiO_2:B_2O_3 doped, IR spectra 79−78664
SiO_2:Fe, vitreous and cryst., with or without Al_2O_3, Na_2O additions, exam. of Fe^{2+} coordination, IR spectroscopy 78−88344
SiO_2:P films, P content determ. by IR absorpt. and activation anal. 79−51139
SiO_2:TiO_2, prep., amorphous struct., effect of roasting, bonds 78−44061
SiO_2-Al_2O_3-CaO-MgO-NaO-K_2O-B_2O_3-ZrO_2, glaze, exam. of zircon crystallisation 79−19155
SiO_2-B_2O_3 glass system, gel hot pressing synthesis and characterisation *(French)* 80−66468
SiO_2-BPO_4, glasses and devitrificates prep., IR spectra *(Polish)* 80−71624
SiO_2-C mixture, nitridation to form. Si_3N_4 additives effects, exam. 78−44068
SiO_2-GeO_2, synthetic, struct, IR spectra 79−42993
SiO_2-Na_2CO_3, sodium Erevanit-25, sintering, struct. 79−43284
SiO_2-Na_2O-CaO:Fe(As)(Cr) glasses, optical absorpt. changes on heat treatment 78−31224
SiO_2-NaAlSiO$_4$ glasses and devitrificates, prep. and vibr. spectroscopy study *(Polish)* 80−93530
SiO_2-$PO_{5/2}$ glass, props. and struct. *(Japanese)* 77−27837
SiO_2-Si MOS system, ion irrad. effects on struct. and electrophysical props. 80−6995
SiO_2-TiO_2 films, obtained from $Si(OC_2H_5)_4$ and $TiCl_4$, exam. of props. 79−95934
SiO_2-TiO_2 glass phonons, IR and Raman spectra meas. 79−91447
SiO_2-TiO_2(Al_2O_3)(ZrO_2), noncrystalline film form., IR study *(Japanese)* 77−59634
SiO_3:B, P films doped by pyrolisis and ion implantation, IR absorpt. obs. of impurity conc. 77−72802
SiO_3-Na_2O-CaO-MgO-Al_2O_3 charge, silicate formation during heating 80−55342
SiO_x, anodic, on SiC *(Russian)* 78−11376
SiO_x film, reactively evaporated, substrate temp. depend. of optical props. 77−70006
SiO_x thin films, deposition and characterisation study 80−80133
SiO_2(-GeO_2)(P_2O_5)(B_2O_3), 3 to 25 μ, rel. to attenuation in optical fibres 77−75665
SiO_xN_y thin film, CVD, multiple internal refl. IR spectroscopy 80−11499
$Si_xO_yN_2$ film, opt. props. rel. to reactive sputter prep. conditions 77−81165
SiO_2.H_2O, (x<1), cryst., IR spectra 79−51951
Si_2Te_3, cryst., IR reflection, Raman spectra 77−12393
$Si0_2$:Ge, B, P, optical fibre, radiation induced optical absorpt. spectra, 0.4 to 1.7 μm region 80−58761
Si(111)2×1, oxide layer, surface states detec., optical reflectivity obs. 80−50368
Si(111)2×1, surface electron states detected by external reflectivity 78−80036
Sm monochalcogenides, electronic struct., optical props. 0.03 to 12 eV 77−28594
Sm monochalcogenides, valence related optical and other studies, review 78−31215
Sm_3ASe_5, A=Ge, Sn, diffuse refl. spectra and band gaps 79−51963
SmB_6 film, prep. by electron beam evaporation, and optical and elec. props. 80−20793
$Sm(BO_2)_3$, single cryst., IR absorpt. spectra 80−34903
SmS, metallic, optical refl. investig. of valence fluctuations 77−63428
SmS, optical props. and electronic struct., Kramers-Kronig model anal. 79−69859
SmS, relative intensity of optical bands calc. 77−8603
SmS, semicond. thin film, absorpt. and refl. spectra, fine struct., cond. band extremum 79−69897
Sm_2S_3 films, refl. and transmission spectra at 300K 80−80889
Sm_2S_3-Sm_3S_4, valence related optical and other studies, review 78−31215
$Sm_{1-x}Yb_xS$, $Sm_{1-x}Tm_2S$ and $SmS_{1-x}As_x$, optical investig. of substitution effects on metal-semicond. transition 77−63427
Sn borate glasses, IR and ^{119}Sn Mossbauer spectra 78−60438
Sn, film, vac. deposited, influence of ion bombardment during condensation 79−82483
Sn-Au(Cu), amorphous film, optical props. 79−69895
Sn-KCl granular superconductors, far IR absorpt. 80−84548
$(Sn)_x$, superconducting polymer, elec. cond., heat capacity and optical props. 80−7028
$Sn(HPO_4)_2$.H_2O and its alkali metal salts, struct. and vibr. spectra 80−39030
$Sn(HPO_4)_2$.H_2O, struct., vibr. spectra 79−15447
SnO-SiO_2 glass, struct., X-ray density, IR obs. 79−46574
SnO_2 film, growth by DC sputtering from compressed target, cond. and optical props. 77−59690
SnO_2, review 77−1673
$Sn_2P_2S_6$, ferroelec., IR and Raman spectra, photocond., edge absorpt. spectra, spontaneous polarisation, forbidden gap 78−68514
SnS, coupling of plasma waves with optical phonons 78−31204
SnS, far IR optical props. 77−12375
SnS_2, crystal growth and optical props. in visible and IR regions 77−52114
SnS_2, refl. using Kramers-Kronig anal., optical functions 79−95798

infrared spectra of inorganic solids continued
SnS_2, single cryst., far IR reflectivity 79−56774
Sn_2S_3, mixed valence semicond., long wavelength phonons, full space group theoretical anal. 79−65873
Sn_2S_3 mixed valence semiconductor, far IR refl. spectra 80−108191
SnS(Se), dielec. function, optical and electron energy loss spectroscopy 78−15189
SnS(Se), IR reflectivity and Raman spectra, phonon frequencies and dielec. const. 77−48166
SnS(Se), layer crystals, optical phonons, Is and Raman spectra 77−73148
SnS_2(Se_2), optical phonon anisotropies and intralayer bonding forces from IR refl. 77−59573
SnS_xSe_{2-x}, thermal changes in optical props. 78−19504
SnSe, far IR reflectivity spectra, lattice vibr. and dielec. const. 77−52068
SnSe, IR-active optical phonons, vibr. spectra 79−69848
SnSe, lattice refl. spectra in long-wavelength IR range 78−27236
$SnSe_2$, refl. using Kramers-Kronig anal., optical functions 79−95798
SnTe film, electroreflectance effects 79−43055
SnTe film, evaporated, electro-reflectance meas. 80−11496
SnX_6^{2+}, (X=Cl,Br,I), spectroscopic consts., environmental cation effects 79−56779
$Sr_5(PO_4)_3OH$, prep. from sulphate, X-ray diffr. and IR spectrosc. 80−29893
$Sr_{F2}:R^{3+}$, R=rare-earth ion, hydrogenated, IR spectra meas. 77−69865
$Sr_2Al_2GeO_7$, gehlenite struct., synthesis and physicochem. props. 79−43181
$Sr_{1-x}Cd_xF_2$, lattice dynamics 78−75763
$SrCl_2$:Fe^{2+}(Co^{2+}) electronic absorption spectra in far and middle infrared 78−68537
SrClF, SrBrF, reacted flux growth, dislocation density, dielec. consts. and losses IR spectra 77−36214
$SrCl_2$.2(H,D)$_2O$, IR and Raman spectra, force fields 80−2753
$SrCl_2$.$2H_2O$, IR and Raman spectra, force fields 80−2753
SrF_2, doped, far IR absorption spectra 78−76507
SrF_2, strain induced splitting and oscillator strength anisotropy of IR transverse optic phonon 80−92625
SrF_2:Ce^{3+}, cryst. field energies 80−59941
SrF_2:Dy^{3+}, cluster form., IR absorption study *(French)* 80−108240
SrF_2:Pr, Nd, Tb, Dy, Ho, Er, Tm^{3+} far IR spectra 79−33736
SrF_2:R^{3+}, far IR vibr. spectra of F^- compensation ion 78−92059
SrF_2:Sm^{2+}(Tm^{2+}), vibronic spectra and dynamics of impurity-contaiing lattice 79−1787
$SrFeO_{3-x}$, NO absorpt., IR spectroscopic study 79−78675
$Sr_3M_6Si_4O_{26}$, M=Nb,Ta, IR spectra and cryst. struct. *(French)* 79−11418
$Sr(NO_3)_2$, dynamical props., IR reflection spectra meas., 10-300K 77−1676
$Sr(NO_3)_2$, IR reflection spectra, dynamical props. and phase transition 77−16303
$Sr(NO_3)_2$, Raman and infrared spectra, structure of nitrate ion from space groups 78−43002
$SrNd_2S_4$, specular IR reflectance 78−2844
SrO:Ni, optical absorption spectra in visible and near IR region 80−45119
SrO-Ga_2O_3, vitrification, spectroscopic and petrographic anal. 77−15556
α-$Sr_2P_2O_7$, Raman, IR spectra, factor group anal. and band assignment 78−35126
$Sr_5(PO_4)_3Cl$:CrO_4^{3-}, polarised absorpt. spectra, visible and IR, ligand field transitions 79−95812
$Sr_{10}(PO_4)_6(OH)_2$, cryst., IR spectra, band assignments 78−60442
$SrSb_2O_5$, $SrSb_4O_9$, $SrSb_6O_{10}$, mixed valence cpds., prep., IR and X-ray investigation *(French)* 78−88292
$SrTa_2O_6$, structural study X-ray diffr., IR absorpt. and Raman spectra *(French)* 80−107173
$SrTiO_3$, complex refr. index meas. in far IR, by dispersive Fourier transform spectroscopy 78−92042
$SrTiO_3$, monodomain, O-D and O-H stretching vibrs., IR spectra 80−71449
$SrTiO_3$, optical props. above 0.14 eV 79−38546
$SrTiO_3$, permittivity, temp. depend., submm. spectroscopy 77−176
$SrTiO_3$, plasmon-phonon reson., IR reflection spectra 78−56093
$SrTiO_3$ pseudodisplacive ferroelec., temp.-dependent dielectric response obs. 77−40247
$SrTiO_3$, surface EM wave propag., IR refl. expts. 78−39553
$SrTiO_3$:H(D), controlled doping, IR spectra 79−28007
$Sr_{0.15}VO_2$, electrical cond., thermo-EMF, and lattice consts. 80−54685
$Sr_3(VO_4)_2$, determination of enthalpies of formation, from heats of solution 80−2182
$Sr_3VTa_2O_9$, prep., characterisation and mag. props. 78−26535
T_2, liquid and solid, collision induced infrared spectra 79−45717
Ta, and α-TaH_x, electronic struct., thermoreflectance studies 80−76047
Ta complex, prep. by halide reaction with tetramethylurea and tetramethylthiourea, and characterisation 79−15972
Ta complex, $TaCl_5$ complex with O- and S-containing ligands, prep., and characterisation 79−14729
Ta, electronic props. and reflectivity, iterative empirical pseudopot. calc. 77−76745
Ta-W optical props., temp. depend., 4.2-1100K 78−2874
$TaH_{0.257}$, influence of H on bulk band struct., optical absorptivity spectra obs. 77−89692
Ta(OR)$_2Cl_3$.L, halo-alkoxide complex, prep. and props. 78−18605
TaS_2 (1T), commensurate and incommensurate CDW state, far IR reflection spectra 79−95755
$TaSCl_3$, prep. and characterisation 77−59705
$TaSe_2$, 2H phase, CDW band struct. and IR and visible thermoreflectance meas. 77−28556
$TaSe_2$ (1T), commensurate and incommensurate CDW state, far IR reflection spectra 79−95755
$TaSe_2$ (2H), optical absorpt., band struct., plasmons, and CDW 80−45104
$Tb(NO_3)_3$-$Fe(NO_3)_3$-$(NH_4)_2CO_3$-H_2O system, cpd. form., comp. and props. 80−100832
Tb_2O_3-H_3PO_4-H_2O system, cpd. form., comp. and props. 80−100832
TbP_5O_{14}, IR absorpt. and luminesc. spectra 80−55079
$Tb_2(SeO_4)_3$.$8H_2O$, thermal decomp. and IR spectra 80−3319
Te, acoustoelectric domain induced transparency near 11 micron 77−85727
Te, energy gap meas. under press., photocond. and transmission spectra 77−85267

infrared spectra of inorganic solids continued
Te, intervalence band absorption, press. and defects influence 80−55149
Te intrinsic, intermediate IR optical absorpt., 5-20 μm 78−84562
Te, natural optical activity and features of struct. of electronic energy spectrum 79−8110
Te, opt. props. under high press., band struct. transform. 80−55112
Te, oriented films, semiconducting props., Hall coeff., band structure 80−70854
Te, photo-excited carriers, far IR magneto-spectroscopy 80−50343
Te, trigonal, model of lattice dynamics using long and short range interactions 78−59893
Te-Si glassy alloys, IR transmission and sp. ht. changes in glass interval, vibr. modes, struct. models 78−23474
TeO_2, paratellurite, atomic motions corresponding to zone centre phonons 78−76461
TeO_2, paratellurite, lattice dynamics, IR refl. and Raman scatt. expts. 77−15518
TeO_2, paratellurite, phase transition at high-press., Raman and far IR spectra 78−80328
TeO_2-Fe_2O_3 system, glass structure 79−90562
TeO_2-V_2O_5-$Li_2O(Na_2O)(K_2O)(Cs_2O)(Ag_2O)$, glass, IR spectra of crystalline phases 79−38536
TeX_6^{2-}, (X=Cl,Br,I), spectroscopic consts., environmental cation effects 79−56779
Th complexes, O-donor complexes of cyclopentadienyl Th (IV) halides, prep. and characterisation 79−15974
Th complexes, Th(IV) poly(pyrazol-1-yl)borate complexes, prep. and characterisation 79−15978
Th, interband structure and role of 5f electronic states, optical reflectivity meas. 77−76744
$ThBr_4$:U^{4+}, single cryst., absorpt. and emission spectra 77−90174
$Th(NO_3)_4$-K_2HPO_3-H_2O, mixed phosphites formation and characterisation 77−52304
ThO_4, prep., IR spectra and thermal exam. 77−89402
Ti complex, $Ti_2Cl_8(CH_3NO_2)_2$, single cryst., struct., IR and Raman spectra, X-ray diffr. 78−43000
Ti, cryogenic constructing material, far IR spectral refl. 77−24855
Ti, electropolished, optical props. from 1.8 to 3 eV 80−85088
Ti garnets, synthetic, IR spectra, Ti struct. role 80−7346
Ti, oxidation kinetics, refl. interf. meas. of film thickness 77−90498
Ti-Al-Sn (5, 2.5%) alloy, cryogenic constructing material, far IR spectral refl. 77−24855
Ti-Al-V(6,4 wt.%), partially ordered, i.r. absorptance, 0-600°C 77−4632
Ti-C-N-O-H, solid solns. of H, exam. of props. 80−29172
Ti-Nb, IR absorption peculiarities 79−65876
Ti-Ni, electron phase transition XPS, optical spectra and mag. susceptibility meas. 80−19943
Ti-Ni, martensite transform. B2-B19′, optical props. and electron struct. *(Russian)* 80−34878
Ti-V, IR absorption peculiarities 79−65876
$TiCl_3$, vib. spectra 77−40231
$(TiCl_4.POCl_3)_2$, solid, IR and Raman spectra, vibr. assignments 78−43868
TiN, optical props. at 300K 78−19466
TiO_2 amorphous film, alkali resistance, refractive index, IR spectra *(Japanese)* 78−23546
TiO_2, chemical implantation of 10-keV H^+ and D^+, resist. and optical absorpt. expts. 77−59031
TiO_2, IR spectra, up to 1635K 77−48155
TiO_2, non-stoichiometric rutile, LO phonon-plasmon coupling, IR refl. spectrum 77−32376
TiO_2, rutile, adsorption of acetic acid-d_4, IR obs. 78−30827
TiO_2, rutile, deuteron and alpha-particle implantation, chemical effects, optical and cond. meas. 78−67755
TiO_2:H(D)(T), IR spectra, 300, 77 and 8K 78−35175
TiO_2-ZrO_2-SiO_2 amorphous film, alkali resistance, refractive index, IR spectra *(Japanese)* 78−23546
TiO_{2-x}, plasmon and polar optical phonons 77−39794
TiO_3, water adsorpt. IR spectra 78−14577
TiO_x, reactive sputtering, film prep. conditions rel. to stoichiometry 77−40370
Ti_2O_3, IR refl. spectra, IR active phonons, Ti 3d electronic effects 78−35145
Ti_2O_3, metal-semicond. transition, refl. spectra study 80−10880
Ti_4O_7, optical absorpt. and metal-insulator transitions 78−15165
$(Ti_2O_3)_{1-x}(V_2O_3)_x$, lattice polarisability, electronic contribs. IR refl. obs. 78−59904
TiS_2, evidence for semicond. props., Hall coeff., refl., cond., thermoelec. power 80−20220
TiS_2, transport props. and semicond. nature 80−44598
$TiS_2(Se_2)$, modelling contrasting semimetallic characters 78−43393
$TiSe_2$, IR reflectivity, phonons and free carriers 79−61379
$TiSe_2$, semimetal, IR props. 79−24318
$TiSe_2$, superlattice formation, Raman and far IR spectra 78−35135
$Ti_{1+x}Se_2$, superlattice form., phase transform., IR reflectivity meas. 77−15383
$Ti_{1+x}Se_2$, superlattice form. and phase transition, IR reflectivity meas. 79−24322
$TiSe_2(S_2)$ (1T), electronic and vibronic struct. 80−44500
Tl $GaS_2(Se_2)$, optical and nonlinear optical props. *(Russian)* 79−51943
Tl halide single crystals, spectral transmission meas. 77−59581
Tl halides, temp. and press. depend. of transverse-optic modes and anharmonic self-energies 77−11649
$TlAsS_2$, Tl_3AsS_3, and Tl_3AsS_4, Raman and IR spectra *(Russian)* 77−66512
Tl_3AsS_4, optical phonons, Raman and refl. spectra 80−11400
$Tl_xAs_{2-x}S_{3-x}$ glasses, opt. and mag. props., comp. influence 77−77225
TlBS, synthesis, struct., optical, spectral props. 79−15631
TlBr, complex refr. index meas. in far IR, by dispersive Fourier transform spectroscopy 78−92042
TlBr pseudodisplacive ferroelec., temp.-dependent dielectric response obs. 77−40247
$TlBr_{0.42}I_{0.58}$, KRS-5 crystal, 10.6 μm absorption obs. by laser calorimetry 79−50360
$TlBrO_3$, polycryst., Raman and IR spectral assignments, room temp. 78−15156
TlCl, phonon difference band absorpt., far IR laser spectroscopy 80−93325
$TlCl_{0.7}Br_{0.3}$, KRS-6 crystal, 10.6 μm absorption obs. by laser calorimetry 79−50360

infrared spectra of inorganic solids continued
$TlClO_3$, polycryst., Raman and IR spectral assignments, room temp. 78−15156
$TlGaS_2$, IR refl. spectrum., LO phonons *(Russian)* 77−40221
$TlGaS_2$, IR refl. spectrum, Kramer-Kronig analysis, transverse optical phonons 78−19489
$TlGaS_2$, layer ternary semicond., polarised Raman, IR reflect. spectra 78−68513
$TlGaS_2(Se_2)$, IR reflection spectra, lattice vibrs. *(Russian)* 77−85701
$TlGaS_2(Se_2)$, optical phonons, IR and Raman scatt. meas. 78−59903
$TlGaS_{2x}Se_{2(1-x)}$ layer solid soln., long wave lattice vibrs., IR reflection spectra 80−11388
$TlGaSe_2$, layer ternary semicond., polarised Raman, IR reflect. spectra 78−68513
$TlGaSe_2$, Raman and IR spectra, zone centre optical phonons 78−76462
$TlGaTe_2$, IR refl. and Raman scatt. spectra, lattice vibrs. 80−40108
$TlGaTe_2$, multilayer cryst., lattice vibr. symm., IR absorpt. and Raman scatt. selection rules 80−39231
$TlGaTe_2$, $TlInTe_2$, and $TlInSe_2$, IR refl. spectra 80−60605
TlH_2PO_4, calorimetric and dielectric exam. of phase transition, nearly crit. case. 77−40171
$Tl_6I_6M_{2/n}^{n+}(I_4)^{2-}$, (M=Pb, Ag, Au, $(Bi_{0.5}Tl_{0.5})$), struct., rel. to phonon spectra 80−71425
$TlIO_3$, polycryst., Raman and IR spectral assignments, room temp. 78−15156
β-$TlInS_2$, layer ternary semicond., polarised Raman, IR reflect. spectra 78−68513
$TlInS_2$, optical phonons, IR and Raman scatt. meas. 78−59903
$TlInS_2$, optical phonons, IR and Raman spectra *(Russian)* 79−10903
$TlInS_2(Se_2)$, IR reflection spectra, lattice vibrs. *(Russian)* 77−85701
$TlInS_2(Se_2)$, optical and nonlinear optical props. *(Russian)* 79−51943
$TlInS_{2x}Se_{2(1-x)}$ layer solid soln., long wave lattice vibrs., IR reflection spectra 80−11388
$TlInSe_2$, single cryst., elec. cond., photocond. and IR spectra absorpt. spectrum 79−47097
$TlInSe_2$, single crystals, optical phonons, Raman and infrared spectra studies 79−55842
$TlInSe_2(Te_2)$, multilayer cryst., lattice vibr. symm., IR absorpt. and Raman scatt. selection rules 80−39231
$TlInTe_2(Se_2)$, IR refl. and Raman scatt. spectra, lattice vibrs. 80−40108
Tl_2MoO_4, prep., characterisation 78−63731
$Tl_3Na(SO_3)_2$, α-phase, IR and Raman spectra, order of cryst. struct. *(French)* 77−85718
$TlPO_3$, vitreous and polycrystalline, NMR and IR exam. of cation motion 77−66041
TlS_2, amorphous, spectral depend. of absorpt. and refr. indices 77−77222
$TlSbS_2$, single cryst., spectral transmission distrib., polaris. effect, refractivity, dispersion 77−59551
TlSe, optical phonons, IR and Raman scatt. meas. 78−59903
TlSe, vibr. props., Raman and far IR spectra meas. 78−71800
TlSe, vibrational spectrum, IR spectra meas. 78−35146
$Tl_{1-x}Se_x$, amorhpous, IR spectra, structure 77−77194
Tl_xSe_{1-x}, amorphous and cryst., IR transmission spectra and struct. interpret. 78−23471
$Tl_2(TeCl_6)$, IR and Raman spectra, lattice and internal modes, phase transition 78−6659
Tm monochalcogenides, valence related optical and other studies, review 78−31215
Tm, polycryst., optical props., temp. depend., photocond., relaxation parameters 78−84603
TmS(Se)(Te), far IR refl. and DC resist., 1-300K, interconfig. fluctuation effects 78−35136
TmSe, metallic, optical refl. investig. of valence fluctuations 77−63428
$Tm_2(SeO_4)_3.8H_2O$, thermal decomp. and IR spectra 80−3319
α-U, polycryst., optical absorption meas. 0.15 to 2.0 eV 80−108223
U-O system, infrared spectroscopy 77−8573
$U(BH_4)_4$, and d-16, IR specra, gas, matrix, isolated and film 79−36639
$U(BH_4)_4$, in $Hf(BH_4)_4$, excited state assignments and E-symmetry ground state, near IR MCD obs. 80−66153
UCl_5, IR absorpt., ground config. splitting, spin-orbit coupling 77−55778
UCl_5, single crystal, thermal broadening of IR energy levels 78−35121
UO_2, 5f-magnetic semiconductor, spectroscopic data, review 80−97299
UO_2, electronic transitions, crystal field effects and phonons, phase transition 80−97303
UO_2 fluorides, $M_2^I[M^{II}(H_2O)_6][(UO_2)_2F_8]$, M^I=K, Rb, or Cs and M^{II}=Mn, Co, Ni, Cu, Zn or Cd, struct. and IR spectra 77−35525
UO_2, optical props. and electronic struct. 78−68527
UO_2, temp. depend. of 5f to $6de_g$ absorption edge and intra-5f transitions 79−24314
$UO_2(NH_2O)_2(H_2O)_2.H_2O$, cryst., Raman and IR spectra 77−63409
$UO_2S_2O_3.H_2O$, possible evidence for nonexistence of cpd. of given formula *(French)* 77−24279
UOX_2 (X=Cl, Br, I) crystal struct., IR spectra, and mag. meas. *(French)* 79−60331
$UO_3.HCONH_2.0.5H_2O$, prep., cryst. struct. and charact 80−29010
US(Se)(Te), electronic struct. and exchange band splitting, optical refl. meas. 80−66226
V, electronic struct., thermoreflectance studies 80−76047
V, film, vac. deposited, influence of ion bombardment during condensation 79−82483
V, lattice dynamics, vibr. spectrum and sp. ht., CGW model 78−22793
V, optical absorpt. spectrum, 0.25-14 μm *(Russian)* 77−81118
V phosphate glasses, vibr. spectra 77−52064
$V_{1-x}Cr_xO_2$, VPE and characterisation 78−3053
VO_2, amorphous thin films, phase transition, resistivity and opt. transmission discontinuities 77−47871
VO_2, change in optical props. at semicond.-metal transitions 77−28597
VO_2 film, optical props. meas. near semicond.-metal transition 77−1742
VO_2 film, semicond.-metal transition, light absorption by metallic drops *(Russian)* 77−59579
VO_2, V_2O_3, film, absorption spectra, semicond.-semimetal transition 78−19512
VO_2, VPE and characterisation 78−3053
V_2O_5 and lower oxides, defect structures and related props. 80−59454
V_2O_5 and lower oxides, electronic, optical, structural and surface props., review 80−88120
V_2O_5 bronze catalysts, α- and β-phase, rel. to decomp. mechanism determ. for isopropanol 78−11553
V_2O_5 film, optical absorption in 1.0 to 5.5 eV range 78−19586

infrared spectra of inorganic solids continued
V_2O_5, interaction with adsorbed propene, IR emission spectra obs. 79−90881
V_2O_5, optical characts., far IR transmission spectra 78−72525
α-V_2O_5:Li(Na)(Cu), far IR absorption spectra meas. 77−73158
V_2O_5-MoO_3 system, X-ray diffr., IR absorption spectra, NMR and thermal analysis 77−24379
V_3O_5, semiconductor metal transition, IR spectra obs. *(German)* 78−23456
V_6O_{13}, optical props. in metallic and semicond. phase 80−40135
V_6O_{13}, semicond., vibration spectra 80−88997
V_xO_y, film, preparation by calcining vanadium naphthenate, formation process exam. *(Japanese)* 78−30849
α-$VOPO_r$, VPO_4, $V_4(P_2O_7)_3$ and $(VO)_2P_2O_7$, IR absorpt. spectra, bond freqs. 80−108192
$VO[UO_2(SO_4)_2].6H_2O$, synthesis and crystallographic data 78−26532
VPO_5, cryst., vibr. spectra 77−52064
V_3Si, complex refr. index and reflectivity of thin film, microscopic characts. and superconductivity 78−31267
V_3Si film, far IR reflection and transmission spectra, room temp. 77−55792
V_3Si superconductor film, Fourier and laser spectroscopy comparison in far IR-sub. mm. range 79−93237
V_3Si thin film far IR laser thermal spectroscopy 80−60144
V_3Si thin films, Holstein processes and electron-phonon spectral function, far IR meas., 19K 79−87445
V_3Si, thin films in supercond. and normal states, far IR laser spectroscopy 79−61453
W (100), chemisorbed H, ν, vibrational mode IR study 80−60582
W, chemisorbed H, surface cond. and intrinsic surface states, surface refl. spectra 80−15378
W, chemisorbed H_2, vibr. spectra characts., adsorption sites 80−70535
W surface, (110), chemisorpt. effects on dielec. function, refl. spectra 80−75616
W, thermoreflectance spectra, 0.3 to 6 eV, rel. to band struct. calcs. 77−66521
W-complex, $WOCl_4.Ph_3PO$, prep. and characterisation 78−30592
W-Re, optical props., temp. depend., 4.2-300K 78−2874
$W_xMo_{1-x}O_3$, mixed cryst., structural phase transition, Raman and IR spectra 78−79766
WO_3 electrodes, vac. evaporation and anodic oxidation prep., electrochromic process kinetics 79−100390
WO_3 electron density map of W^{5+} polarons, EPR and optical absorpt. obs. 80−44912
WO_3, thin films, electrochem. coloration, optical and elec. props. 77−85345
WO_3:H^+, optical and elec. props., suggested band struct. model 77−4654
WO_3-electrolyte electrochromic cells, proton injection phenomena 80−71448
$WSCl_3$, prep. and characterisation 77−59705
WSe_2, refl. spectra and photovoltaic effect, 1.5-3.2 eV, 4.1-300K 79−47470
$WSeF_4$, cryst. struct., and preparation 78−63730
Xe-MF_6, M=W, Mo, U, Re, Ir, charge transfer interactions, VUV and IR obs. 78−50664
Y-Si-Al-O-N glass, prep. and props. 80−25647
YAG:Er^{3+}(Ho^{3+})(Tm^{3+}), oscillator strengths of impurities, 5000 to 30000 cm^{-1} 79−4830
YAG:Nd^{3+}, Ce^{2+}, sensitisation, luminesc., absorpt. and emission spectra *(Russian)* 78−10982
YAG:Nd^{3+} and free Nd^{3+} ion, energy levels, absorption spectra 79−11076
YB_{68}, melt grown, props. meas. 77−11518
$Y_2(CO_3)_3.nH_2O$, tengerite, single cryst. hydrothermal growth 80−97417
$Y_{3-2x}Ca_{2x}Fe_{5-x}V_xO_{12}$, single cryst., Faraday effect and opt. props. 77−1660
$YFeO_3$:Co^{2+}, Ti^{4+}, spin reorientation, Faraday rot. meas. 77−8547
$Y_{3-x}Gd_xFe_{5-y}Al_yO_{12}$, solid solns., IR absorpt. spectra, physical props. 80−55082
$Y_{3-x}Gd_xFe_5O_{12}$, solid solns., IR absorpt. spectra, physical props. 80−55082
YH_2, electronic struct., optical studies, 0.2-5 eV, 4.2-340K 79−78005
YIG, Bi-substituted, LPE film, optical absorpt. changes due to impurity incorporation 77−1702
YIG:B,Pb, IR spectrum, localised modes, rel. to impurities and O vacancies 80−50377
YIG:Ir, Ir on tetrahedral sites, contrib. to mag. anisotropy, optical absorpt. meas. 77−69867
YIG:Sn, IR absorpt. and MCD 78−19447
YIG:Sn, mag. circular dichroism orientation depend., optical absorpt. 79−99914
YIG:Zr, near IR absorpt. and magnetic circular dichroism 80−60580
$(YLaBi)_3(FeGa)_5O_{12}$, pure and In^{3+} doped, near IR absorpt. and Faraday rot. 78−95580
Y_2O_3 sintered pieces, optical transmittance 80−40561
Y_2O_3:ThO_2, IR absorpt., 2-4 μm 77−55805
$Y(OH)_3$-α-FeOOH, physicochem. props. rel. to growth of $Y_3Fe_5O_{12}$ 77−40418
$Y(OH)CO_3$, ancylite like phase, hydrothermal cryst. growth *(French)* 80−108340
YPO_4, cryst., IR spectra, complex anions internal vibrs. resonance splitting 80−34907
$Y_2(SeO_4)_3.8H_2O$, thermal decomp. and IR spectra 80−3319
$Y_2Ti_2O_7$:Nd^{3+}, spectroscopic props. 77−69866
Yb^{3+} doped phosphors, IR excitation and absorpt. and emission spectra *(Russian)* 79−52021
Yb^{3+}:phosphate glass, relation between absorption and equilib. luminesc. spectra 77−85754
YbP_5O_{14} and $Yb_{0.9}Tb_{0.1}P_5O_4$, IR absorpt. and luminesc. spectra 80−55079
$Yb_2(SeO_4)_3.8H_2O$, thermal decomp. and IR spectra 80−3319
$Yb_2Si_2O_7$, IR and Raman spectra, internal and external modes 79−61365
Zn complex, Zn(l-spartein)Cl_2, IR circular dichroism spectra, vibr.-electronic interaction 80−55074
ZnA_2X_4 (A=Ga,In; X=S,Se), Fourier IR and Raman spectra, cryst. struct. and symm. *(German)* 79−24313
Zn_3As_2, optical band-gap, absorption meas. 80−25372
Zn_3As_2, p-type semiconductor, absorption edge spectra, energy gap 79−56793

infrared spectra of inorganic solids continued
$ZnAs_2(P_2)$, monoclinic, lattice vibr. symm., IR and Raman active frequencies *(Russian)* 77−69055
ZnB_2O_4-RF, R=Mg, Ca, Sr, Ba, glass form., struct. and props. 80−84077
$Zn_xCd_{1-x}S(Te)$, solid soln., broadening of exciton states, depend. on conc. 79−73449
$Zn_xCd_{1-x}Te$-P, vibr. modes of defects, IR absorpt. expts. 77−62601
(ZnFe)S, marmatite, optical properties 78−39555
$ZnGeP_2$, electron irrad., elec. and optical props. 79−33743
$ZnIn_2S_4$, IR refl. spectra and cryst. struct. 79−56777
$ZnIn_2S_4$, lattice dynamics, IR and Raman spectra 77−81106
$ZnIn_2S_4$ layered compound, phonon freqs., IR refl. and transmission spectra 77−77210
$ZnIn_2S_4$, Raman and IR spectra 78−48181
$Zn_{1-x}Mg_xTe$, long wavelength optical phonons, IR ref. and Raman obs. *(French)* 78−60433
n-ZnO film, highly degenerate, IR absorption by free polarons 77−4697
ZnO, IR spectra, surface phonon modes 79−78668
ZnO, microcryst., surface microscopic modes, IR detection 79−38527
ZnO, optical surface phonon modes, far IR transmission 77−31863
ZnO particles, average dielectric const. generalised theory, appl. to IR spectra 79−28667
ZnO, polariton dispersion, IR reflection spectroscopy 80−11415
ZnO, single cryst. and film, emission band characts. *(Russian)* 77−52133
ZnO, small crystal, optical surface phonon modes 78−71940
ZnO, small crystal, surface phonon modes, IR transmission spectra 80−11398
ZnO:Cu, H(D), IR absorpt. line spectra, OH and OD vibr., optical excitation 79−15498
ZnO:Cu, H(D), OH and OD centres, IR-active absorpt. line spectra 79−15496
ZnP_2, cryst., tetragonal, 2-phonon IR absorpt. 80−66176
ZnP_2, polarised spectra of IR absorption and emission of single crysts., oscillatory states *(Russian)* 77−28583
ZnP_2, second-order vibr. spectra and dispersion of phonon branches 80−25376
ZnP_2:In(Ga)(Ge)(S)(Se), doped and undoped, optical absorpt. spectra in range 0.5 to 2.2 eV 80−66250
Zn_3P_2, multiphonon absorption in IR spectra 78−39554
Zn_3P_2, optical props., transition energies from transmission and refl. meas. 80−60532
$Zn_3(PO_4)_2.4H_2O$, thermal transitions, thermographic investig. 77−9063
ZnS CVD window, IR lattice absorption, phonon assigments and image spoiling 80−33104
ZnS, cubic, IR-active phonons obs. 80−55084
ZnS, film on Si, fused quartz substrates, H_2O absorpt., IR anal. 80−75446
ZnS, two-photon absorption in crossed elec. and mag. fields 77−85693
ZnS:Al, IR studies of Al complexes 79−33741
ZnS:Al-Cu, localised vibrational modes 78−63827
ZnS:Be, far IR lattice absorpt., Green's function calc. 78−43865
ZnS:Be, impurity modes and IR absorption 78−76506
ZnS:Cr, anomalous temp. depend. of near IR absorption 79−28794
ZnS:Cr^{2+}, photoionisation, lattice relaxation energy 80−6778
ZnS:Cu 79−24350
ZnS:Fe, piezospectroscopic effect on electron-vibr. lines of Fe^{2+} 78−27269
ZnS-MgF_2 alloy films, struct. and optical props. 79−90910
$ZnSO_4.H_2O$, hydrate librational modes in IR spectra 78−48161
ZnS(Se), highly transparent semicond. crysts., multiphonon IR absorpt. 78−10885
ZnS(Se), highly transparent semicond., multiphonon IR absorpt. 78−60461
ZnS(Se), IR transmitting semicond., dn/dT, wavelength depend. 77−77163
ZnS(Se)(Te):Cr^{2+}, absorpt. and luminesc. of $Cr^{2+}(d^4)$, cryst. field theory interpretation 79−83000
$ZnSc_2S_4$, IR and Raman spectra, force consts. 78−68503
ZnSe, CVD, laser window material, impurity absorpt. meas. 78−25909
ZnSe cryst., IR absorpt., annealing effect 80−80774
ZnSe, exciton refl. spectra, temp. depend. 80−59886
ZnSe film, surface polaritons, thermostimulated emission *(Russian)* 78−10904
ZnSe films, long wavelength IR polariton emission band thermal shift and broadening 80−92833
ZnSe, IR absorpt., temp. depend. 78−48155
ZnSe, IR laser window coating absorption rel. to deposition conditions 79−14061
ZnSe laser windows, AR coated, photoacoustic chopping freq. studies using CO_2 laser 80−83629
ZnSe, reactor irrad., opt. props. 77−90137
ZnSe, refr. index meas. and nonlinear moment parameters 77−85681
ZnSe:Co, optical props. in near IR 78−43924
ZnSe:Cr^{2+}, photoionisation, lattice relaxation energy 80−6778
ZnSe:Cu, discovery of bound exciton, electroabsorption 80−45038
ZnSe:Mg, local vibrations of impurities, IR absorpt. spectra exam. 77−7815
$ZnSiF_6.6H_2O(.6D_2O)$, near IR spectrum, 80K, assignments 78−48164
$Zn_4Si_2O_7(OH)_2H_2O$, hemimorphite, polarised IR refl., vibr. modes *(French)* 77−85698
n-$ZnSiP_2$, IR absorption 77−12377
ZnTe:As(P)(Li), electronic Raman scatt. and IR absorpt. spectra of shallow acceptors 79−73978
ZnTe:Au, impurity identification and characterisation, capacitance, luminescence and IR absorption 80−60639
ZnTe:Cu, elec. and optical identification of persistent acceptor 79−60764
$Zn_3(VO_4)_2$, determination of enthalpies of formation, from heats of solution 80−2182
$(ZnV_2O_4)_c(MgFe_2O_4)_{1-c}$, struct. parameters, IR spectra, cluster-component analysis 77−47425
Zr-C-N-O-H, solid solns. of H, exam. of props. 80−29172
ZrF_4-THF_4-BaF_2 glass, IR-transparent, synthesis using reactive atm. processing technique 80−100826
ZrN, optical props. at 300K 78−19466
ZrO_2 amorphous film, alkali resistance, refractive index, IR spectra *(Japanese)* 78−23546
ZrO_2, optimum sintering characts., density, X-ray diffr., IR spectrum, UV spectrum obs. 78−76617

infrared spectra of inorganic solids continued
ZrO_2, stabilized, thermal barrier coating system, spectral emission and absorpt., 300 to 1590K 79−24672
ZrO_2:Y_2O_3, bias sputtering, film growth and characts. 77−40366
ZrO_2:Y_2O_3, cryst., IR refl., refr., absorpt. 77−12382
ZrO_2-MgO system, intermediate phases existence, X-ray diffr. and IR obs. 79−38805
ZrO_2-Y_2O_3-Nd_2O_3, spectral determ. of crystal stabilisation 78−27203
$ZrOS_2O_3.8H_2O$, possible evidence for non existence of cpd. of given formula *(French)* 77−24279
$ZrS_3(Se_3)$, quasi one-dimens., optical phonon anisotropy, IR spectra study 80−40112
$ZrS_3(Se_3)(Te_3)$, phonon study of chemical bonding 80−20645
$ZrSe_3$, long wavelength optical phonons, Raman scatt. and IR refl. 80−34921
$ZrSiO_4$, mechanochemical effect by mechanical grinding *(Japanese)* 78−84754
$ZrSiO_4$, zircon, resonance splitting of internal vibr. freq. of complex anion 80−55080

infrared spectra of organic molecules and substances
see also molecular rotation; molecular vibration
1,1-dimethyl-1-silacyclopentane, IR and Raman spectra 80−60577
1,4-dithiane-1-oxide, cryst., IR and Raman spectra 79−69839
2-chloronaphthalene, vibr. and calorimetric investigation of polymorphism 78−87641
2-fluoronaphthalene, vibr. and calorimetric investigation of polymorphism 78−87641
2-furanmethanethiol, mol. struct., electron diffr. and IR spectroscopic examination 79−10106
1,3-butadiene-1-one, spectroscopic consts., IR and microwave spectra, prep. 80−18859
3,3,3-trifluoropropene, struct. and vibr. spectra, IR, Raman polarisation study 80−18845
ABS polymers, deposited in internal magnet magnetron sputtering system, adhesion of Cu films 79−83121
absorption spectra, nonuniformly broadened, hidden fine struct. 79−93999
acenaphthene, vibr. spectra, mol. crystal dynamics, librational modes 78−64356
acetaldehyde, Coriolis resonance bands in IR spectrum 80−47995
acetaldehyde, soln., C-O stretching band intensity calcs., intermol. interaction effects 77−68081
acetaldehyde, torsional fundamental and combination bands, K-struct. anal. 78−78696
acetaldehyde, UV photolysis, transient species IR spectra 80−86464
acetaldehyde photolysis products, time resolved Fourier transform spectrum 78−58071
acetamide, IR spectra, amino group inversion transitions and pot. functions 80−43041
acetate crystal hydrates, bonding determ. from IR spectra 77−42321
acetic acid, and derivatives, vibr. spectra in soln. 80−63633
acetic acid, chemisorption on goethite, IR spectra 80−7855
acetic acid, cryst., and isotopic species, H-bond, ν_s-ν_σ coupling and ν_s anharmonicity, IR spectra at 10K 79−15450
acetic acid, protonated complexes, IR and Raman spectra *(French)* 78−78691
acetic acid, self association, factor analysis and band contour resolution applications, book contrib. 78−21931
acetic acid dimer, vibr. spectra at low temp., Witkowski-Marechal theory 78−46314
acetic acid-d_0, -d_1, -d_4, cryst., IR spectra, H bonding 77−40217
acetic acid-d_0, -d_1, -d_4, H bonding in solid, IR spectra, vibr. and librational modes 78−43843
acetic acid-d_0(-d_1,-d_3,-d_4), cryst., H bonds, stretching, temp., isotope effects 79−51938
acetic acid-d_0(-d_1), Fermi reson., IR spectra band profiles 80−60569
acetic acid-d_4, adsorbed on TiO_2 (rutile) IR obs. 78−30827
acetone, adsorbed on ZnO, decomp., IR and kinetic obs. 80−59780
acetone, solvent effects on oscillator integrated strength, IR absorpt. bands 78−84575
acetone in mixed protic-aprotic solns., C=O stretching, IR spectra 80−45056
acetones, fluorinated, absorpt., fluoresc. spectra, quantum yields, decay times meas., mechanism 77−3410
acetonitrile, adsorbed on ZnO, IR spectrum species identification *(French)* 79−82967
acetonitrile, adsorption on MgO, IR and TPD study 80−70528
acetonitrile, electrolyte solns., IR and Raman spectra interpretation, CN-stretching region 79−73941
acetonitrile, in dilute CCl_4 soln., far IR spectra and mol. dynamics models 79−99876
acetonitrile, in liq. phase, Ramon band profiles, calc. using IR intensities 80−2741
acetonitrile, IR spectra, vibr. and reorientational and energy transfer width separation, rot. const. determ. 80−87131
acetonitrile, liq. and solns., IR absorpt. band intensity, temp. depend., CC and CN bonds 77−75157
acetonitrile, soln., IR perpendicular bands, profiles, rot. models 78−58695
acetonitrile-HCl complex in liq. Xe, IR spectral study 80−95626
acetophenone, liquid, far IR absorpt., mol. vibrs., internal rot., dipoles *(French)* 77−24827
acetophenones, spectrosc. characts. using PPP SCF CI calcs. 80−102448
acetophenones, substituted, IR absorpt. spectra, vibr. anal. 77−10672
acetyl cyanide, IR and Raman spectra, vibr. spectrum and vibr. anal. 77−10676
acetyl halide-titanium tetrahalide adducts, coordination, IR and Raman spectra 78−42050
acetylene, absorpt. coeffs. meas. in Nd laser emission band 80−78620
acetylene, absorpt. spectrum, 9240-9520 cm^{-1}, rot. anal. and consts. 79−54855
acetylene, absorption spectrum, LiF F_2^+-centre laser intracavity spectroscopy appl. 80−32999
acetylene, and -d_1, 1.1 μm band, rot. struct. 77−27069
acetylene, and -d_2, integrated IR intensities, effective charges 77−18921
acetylene, and -d_2, integrated IR intensity, meas. and interpretation 78−66551
acetylene, chemisorbed on Ni and Pd films, IR refl. study 79−69343
acetylene, chemisorbed on W, IR vibration spectroscopy 78−14603

infrared spectra of organic molecules and substances continued
acetylene, He-Ne laser line, high temp. absorpt., anal. by high resolution IR spectra 80−91554
acetylene, IR spectra, rot. and vibr. struct. 78−21922
acetylene, line search in C star spectra 77−78786
acetylene, Q-branches, diode laser IR spectra, rot. consts. and struct. 79−45723
cis-acetylene, triplet state, near IR electronic absorption spectrum, and form. 79−63997
acetylene, vibr.-rot. IR spectra, mol. force field determ. ^{14}C effects 77−61748
acetylene(-d_1,d_2), integrated IR intensities 80−23457
acetylene(-d_2) solns., IR absorpt. band profile *(French)* 77−83597
acetylene smoke, optoacoustic meas. of absorpt. at 0.5145, 10.6 μm 80−43060
acetylene-d_0, (−d_2), IR intensities, relative error anal. 78−58686
acetylene-d_1, vibr. bands, IR spectrum in region of bending fundamental ν_4 80−23418
acetylene-d_2, IR spectra of ν_5 bending fundamental, and $^{12}C^{13}CD_2$ isotope 79−50020
acetylene-d, IR absorpt. spectra around 700 cm^{-1} 79−50021
acetylenic compound, 1,5-hexadiyne, hydrogen bonding effects on Raman line ν(≡C-H) *(French)* 77−75167
2-acetylfuran, IR spectra, cis/trans equilib. 77−469
acetylpyridines, vibr., IR and Raman spectra 78−74653
acid oxalate ion in aq. soln., vibr. studies, IR and Raman spectra 80−95589
acridine, Ar matrix-isolated, lowest triplet state IR and visible absorption spectra 79−68228
acrylamide-acrylic acid (acrylic acid salts) copolymers, composition determ., IR spectra *(Russian)* 80−7358
adipic acid, monoclinic crystals, IR absorption and dichroism 78−88293
adipic acid crystals, H bonds, harmonic couplings, IR vibr. modes, isotope effect origin 80−34902
adipic acid crystals, IR spectra, O-H(O-D) stretching bands 79−91422
adsorbates on SnO_2 hydrous gel, transmission IR spectroscopy 77−55465
adsorbed layers, reflection-absorption IR spectroscopy, review, book contrib. 80−84747
adsorbed species, catalytic reaction, high temp. IR obs. 78−88655
alanine-d_3, vibr. circ. dichroism, mechanism 78−33505
alcohols, OH-stretching vibr. band in overtone region, IR-Fourier spectral investig. *(German)* 80−976
alcohols, opt. consts. in IR, stretch band obs. 79−91421
alcohols, vapour and liq. IR spectra, bandwidth, directional mol. rot., H-bonding 79−78661
alicyclic ring compounds, vibrational spectra and structure, book 78−78700
alicyclic ring cpds., vibr. spectra, conformational props., book contrib. 78−78702
aliphatic ethers-HF, H bonded complex, gas phase, first overtone reconstruction 80−43040
aliphatic ketones, freq.-topology-milieu relation, IR study, struct. and solvent effect *(French)* 80−95623
alkali-anthracene ion-pairs and triple-ions in solution, far IR spectra 79−78663
alkanes, IR spectral intensity for electro-optical parameter 79−54835
alkanes, liq., mol. struct., selective deuteration and IR vibr. spectra 80−96432
alkanes, overtone spectra, local mode anal., discrete excitation of nonequivalent CH oscills. 78−78688
alkenes, IR absorpt. curves calc. using standard fragments computer library 80−982
alkenes, IR multiphoton dissoc., IR detection of H atoms 80−83356
n-alkoxy-α-methyl-p′-cyanophenyl cinnamate, orientational order, tricrit. behaviour 79−27907
p-alkoxybenzylidene-p,n-butylanilines, IR absorpt. spectra, elec. field effects, orientational order parameter determ. by IR dichroism 80−80778
p-alkoxybenzylidene-p-aminocyanoanilines, IR absorpt. spectra, elec. field effect, orientational order parameter determ. by IR dichroism 80−80777
n-alkyl carboxylic acids, vibr. spectra, C-H stretching mode assignments 79−47429
alkyl metal carbonyls, phosphine monosubstituted, LF vibrs., IR and Raman spectra 80−95585
alkyl sulphides, C-S stretching vibrs. 78−25533
alkylammonium tetrachloromanganate (II) IR and Raman spectroscopic exam. 78−31189
alkylcyanobiphenyls, far IR absorpt. in nematic and isotropic phases, order parameter determ. *(French)* 80−50330
allene, rot. diffusion in CS_2 soln., IR spectral profiles 79−87426
allene(-d_4), IR absorption intensities 80−1026
allene-d_4, high resolution IR spectra 80−83365
allene-d_4, Raman and IR spectra, rot.-vibr. bands, ground state constants 78−25545
allylamine, laser-microwave double and triple reson. 80−83397
amide group in soln., interactions, IR, Raman spectral investigs., peptide, protein struct., review 78−90330
amidofluorosulphuric acid, and Hg salt, IR spectra *(French)* 80−18858
amines, aliphatic and aromatic, H-bonding, strong, stochastic model and IR spectra temp. effects 78−62805
amino acid block copolymers, morphology and mech. props. 78−91264
2-amino-4-chlorophenol in solutions, IR absorpt. spectra 80−69135
2-amino-5-chloropyridine, IR absorption, vibr. assignments 80−979
2-amino-p-cresol in solutions, IR absorpt. spectra 80−69135
4(6)-amino-uracil, IR absorpt. spectra, vibr. anal. 78−61143
aminoarsines containing As-NH group, IR spectrometry, configuration isomers and hybridization state of N *(French)* 77−23495
γ-aminobutyric acid, cryst., film, matrix IR spectra, low temp., neutral and zwitterion forms. 77−18920
aminopyrazine, far IR spectra, barrier to planarity, pot. function and energy levels 80−69137
4- aminopyridine hemiperchlorate, struct. determ. by neutron diffr. and IR spectra 80−92515
2-aminopyrimidine(-d_1), amino inversion vibr., planarity, far IR obs. 79−31515
ammonium benzoate, IR spectrum, cryst. struct. 78−19455
ammonium bioxalate monohydrate, refractive indices in IR region 78−52512
ammonium hydrogen bisbenzoate, IR spectrum, cryst. struct. 78−19455
ammonium hydrogen glutarate, H bonding, vibr. spectra 78−43860

infrared spectra of organic molecules and substances continued
ammonium oxalate monohydrate, IR refl. and Raman spectra, internal and external modes *(French)* 77−36231
ammonium uranyl formate, struct. determ. from X-ray diffr. and IR spectrum *(French)* 78−75653
analgesic group commercial tablet samples 78−74652
anharmonic molecules in condensed media, vibronic dephasing, intra- and intermolecular processes 80−2127
anilides of 1-piperidine carboxylic acids, $CDCl_3$,$CHCl_3$ solns., intramol. easily polarisable H-bonds, IR spectra 78−25523
aniline, amino group inversion and torsion, far IR spectra 77−10670
aniline, far IR absorpt. spectra, 20 to 60 cm^{-1}, temp. depend. 79−59450
aniline, IR absorpt. and MCD spectra, Rydberg transitions 77−27068
aniline, liq., far IR absorpt. spectra, electric field effects 80−95625
aniline black, superconductivity at room temp. 78−80089
aniline-ND_2(-NHD), far-IR vap. phase spectra, assignments pot. function calcs. 77−75144
anthracene, IR spectra, strong anharmonicity effects *(Russian)* 77−66511
anthracene, mol. cryst., polariton fusion, two-photon excitation spectra 77−90139
anthracene, soln. and melt, second vibronic transition, spectroscopic charcts., effective field dispersion calcs. 80−55102
9,10anthraquinone, lower triplet states, interactions and position, matrix isolation spectra 80−63634
p-(9-anthryl)-N,N-dimethylaniline derivatives, excited emitting states in polar solvents, fluoresc. 78−5263
antimony ethyl derivative, Et_3Sb, IR and Raman spectra, rot. isomerism 79−41167
aromatic hydrocarbons, IR spectra and high-pressure phase transitions 80−10659
arsenic ethyl derivative, Et_3As, IR and Raman spectra, rot. isomerism 79−41167
aryl ammonium hydrogen difluorides, IR vibr. spectra and NMR reson. obs. 80−34788
2-aryl-3-benzylidenamino-4-thiazolidones, IR and NMR spectra, solvent effects and isomer conform. *(Italian)* 79−3596
L-ascorbic acid, cryst. isolated OH iscillators, IR absorption, temp. and H-bond effects 80−7351
asphaltenes, from coal liquefaction, IR characterisation 77−52683
1-azacarbazole, IR spectra, Fermi reson., H-bonding *(German)* 77−12392
7-azaindole, IR spectra, Fermi reson., H-bonding *(German)* 77−12392
azo polyamide, solutions, spectra and viscosity 79−68340
azulene vapour, IR and CO_2-laser absorpt. spectra 80−87120
bacteria, E. coli B, microwave radiation effects on colony formation and mol. struct. 78−24097
band intensities, hybrid orbital rehybridisation model, mol. charge distrib. 78−74630
band intensities and polar tensors, effective charge and dipole moment derivs. sign 77−34695
benzaldehydes, para-halogenated, IR and Ramam spectra, vibr. assignments, thermodynamic functions 80−14139
benzamide, single cryst., far i.r. absorpt. spectrum *(French)* 77−4637
benzene, 1036 cm^{-1} band, optical consts. correction 77−61145
benzene, 607-μm line absorption curve 78−95581
benzene, adsorbed on γ-alumina, high-temp. IR spectra *(German)* 79−28757
benzene, Ar and Kr matrix isolated, IR spectra, vibr. freqs. and intensities 78−50548
benzene, cryst., IR and Raman intensity of lattice vibrs., theory 80−11381
benzene, cryst., IR spectrum assignments rel. to benzene Br_2 complex 77−36217
benzene, in benzene-d_6 soln., IR and Raman spectra, line breadths, rot. diffusion consts. 79−56772
benzene, in Br_2-carbon tetrachloride soln., complex form., IR spectra 78−70828
benzene, IR spectra, fine struct. of rot.-vibr. bands 80−102504
benzene, IR spectra, vibr. exciton cluster states, percolation and pairwise interactions 78−43844
benzene, liq., spectral broadening of mol. transitions, librational broadening 79−51939
benzene, liq., vibr. excitons, reson. energy transfer and local struct., IR spectra 77−75145
benzene, optical consts. determ. from IR absorpt. spectra *(Spanish)* 77−69787
benzene, p-disubstituted, MCD and absorpt. spectra, PPP calcs. 78−66574
benzene, plasma polymerisation in glow discharge, thin film IR and free radical EPR obs. 80−2964
benzene, Raman and IR intensity anal. 78−70829
benzene, Raman and IR spectra at high press. 78−35127
benzene, T_1-S_0 intersystem crossing vibronic interactions IR absorpt. spectrum obs. 80−28042
benzene, vibronic coupling and IR intensities, CNDO/S semiempirical calc. 79−36596
benzene adsorbed on metal surface, obs. of vibrational modes 80−6649
benzene cryst., electron irrad., phenylcyclohexadienyl radical form., absorpt. and fluoresc. spectra study 80−89035
benzene derivatives, solid, phase transition under press., IR spectra 79−38531
benzene derivatives, symmetrically substituted, IR spectra, high press. solid-state phase transform. 77−43984
benzene-^{13}C, liq., vibr. spectra, band assignments 78−13500
benzene-Br_2 complex, cryst., IR spectrum assignments, site symmetry, rel. to benzene 77−36217
benzene-d_0 (-d_6), polar tensors and at. effective charge, calculated from IR intensity 78−74703
benzene-hexa-n-hexanoate, phase transitions and mesophase form., sp. ht. and IR spectra, 13 to 393K 80−79955
benzenes, adsorbed, IR multiple refl. spectra recording via cuvette attached to spectrophotometer 78−298
benzenes, IR spectral intensity for electro-optical parameter 79−54835
n-benzoates, MP and rot. mobility of struct. groups *(Russian)* 77−69074
1,3-benzodioxole, far IR spectrum anal., pot. function 79−76427
benzoic acid, and p-deuterobenzoic acid, sensitivity of inelastic electron tunnelling spectroscopy 77−88605
benzoic acid, dimer, cryst., IR and Raman spectra, vibr. assignments 78−31191
infrared spectra of organic molecules and substances continued
benzoic acid, IR absorpt. spectra, fundamental assignments 80−5542
benzonitrile, IR absorpt. and Raman bands, half-band width conc.-depend. 80−74171
benzophenone in cyclohexane dilute soln., far IR absorption obs. 77−40250
benzotrifluoride, and mono-substituted derivatives, vibr. spectra, internal rot. 77−83598
(β-benzyl D- and L-aspartate) obtained by polymerisation of N-carboxylic anhydride IR spectra 77−55784
benzyl radical, IR absorpt. spectra, matrix isolated at 77K 79−22706
benzyne, struct. and IR spectrum, MNDO calc. 79−31403
bianthryls, vibronic anal. of circular dichroism and absorption spectra 77−38683
bicyclo(3.2.0)hept-6-ene, LF vib. spectra, conformations 78−58685
biphenyl in Ar matrix, mol. struct., IR spectra 77−30875
biphenyl in Ne or Ar matrix, biphenyl ring torsion by vibronically resolved spectra 79−81228
bis(cyclopentadienyl)Ti(IV)chloride, reactions with oximes, IR spectra 78−92471
bis(methylthio)alkanes, model compounds of polythioethers, vibr. spectra 80−58430
bis(p-toluene sulfonate) diacetylene polymer cryst., second order phase transition 79−73922
bis(trifluoromethyl)peroxide, gas and solid, Raman, IR spectra, internal rot. barrier of CF_3 78−29789
bis (methylammonium) tetrachlorometallates (II), IR spectra and phase transitions of 10-25 kbar at 25°C 80−10658
bis [4-(n-butyl)-styryl dithiolato] Pt nematic complex with strong IR absorption 80−88305
bisphenol A-phthallic anhydride epoxy resin, diglycidyl ether, Rayleigh scatt., Brillouin and IR spectra 80−66211
block copolymers, IR spectroscopy for struct.-props. relations 78−91268
bromanil and radical anion, Raman and IR freq. shifts 78−33516
1-bromo-1-chloroethylene, vibr. assignment, IR and Raman spectra 77−18925
1-bromo-2,2-dimethylpropane, Raman and IR spectra, vibr. anal. 78−90173
1-bromo-2,3 dimethylbenzene, IR vibr. spectrum, internal modes, overtones, combination freqs. 78−9146
1-bromo-2,4 dimethylbenzene, IR vibr. spectrum, internal modes, overtones, combination freqs. 78−9146
1-bromo-2,4-dimethylbenzene, liq., IR and Raman spectra 78−42049
1-bromo-2,5 dimethylbenzene, IR vibr. spectrum, internal modes, overtones, combination freqs. 78−9146
1-bromo-2,6 dimethylbenzene, IR vibr. spectrum, internal modes, overtones, combination freqs. 78−9146
1-bromo-2,6-dimethyl benzene, IR and Raman spectra, vibr. anal. 77−57997
2-bromo-4-nitrotoluene, IR absorpt. spectra, vibr. assignments 78−42048
2-bromo-5-nitrotoluene, IR absorpt. spectra, vibr. assignments 78−42048
5-bromo-uracil, IR absorpt. spectra, vibr. anal. 78−61143
bromoacetic acid, cryst., films, polarised IR spectra, struct. 78−72502
bromobenzene-d_0, -d_1, -d_4, vibr. spectra and force fields 77−65463
bromocyanoacetylene, cryst., IR, far-IR and Raman spectra, vibr., struct. 77−63407
bromodifluoromethyl radical, IR matrix isolation spectrum, stretching fundamentals 78−27788
bromoform, polycryst., cryst. struct., IR spectrum 77−44000
bromoform and Cl substitutes, VUV photoionis. during condensation with Ar, IR spectra of (CHX_2^+)X and X^--HCX_2 ions 79−13773
4-bromoisoquinoline, UV and IR spectra, f-values and ground state vibr. freqs. 78−58714
bromomethane, IR spectra, $2\nu_2$, $2\nu_5$ and $\nu_2+\nu_5$ 78−42059
bromomethane-d_3, IR spectra of ν_3 band, $^{79/81}Br$ substitution 79−64000
β-bromonaphthalene, IR absorption spectra, forbidden character 77−58002
α-bromotoluene, liq., IR absorpt. spectrum 78−979
bromotrifluoromethane-^{79}Br (^{81}Br), vibrational spectra and force constants of symmetric tops, rotational analysis 79−98090
bromotrifluoromethane-^{12}C, -^{13}C, matrix IR spectra and harmonic force fields *(German)* 79−76431
1,3-butadiene, matrix isolation, trapping from thermal mol. beam, IR spectra 78−46330
butadiene elastomers, influence of intermol. interaction on durability *(Russian)* 78−76746
butadiene-nitrile elastomers, high temp., and press. chem. transformations *(Russian)* 79−52659
butadienes, optical activation energy and dipole moment, electron repelling and attracting groups 78−46341
n-butane, LF vibr. spectrum, methyl torsional pot. function, internal rot. 79−89670
butane, liq., enthalpy difference between rot. isomers, IR spectrosc. obs. 80−106404
1-butanol, IR and Raman spectra, vibr., conformers 78−25532
1-butene, adsorbed on δ-Al_2O_3, isomerisation, IR study 80−76554
trans-2-butene, Raman and IR spectra, torsional mode pot. function 79−89676
1-butene adsorption on delta alumina, microgravimetric-IR study 80−75432
butene-1, solubility in liq. N_2 80−39286
t-butyl alcohol, and deuterates, gaseous and matrix IR spectra, liq. Raman spectra, vibr. assignment 79−10113
t-butyl alcohol, struct. determ. from vibr. spectra, H-bonding and heat of mixing *(Russian)* 78−3368
n-butyl bromide conformers, IR and Raman spectra, vibr. anal. *(German)* 77−88451
t-butyl cyanide-HF, hydrogen bonded heterodimer, spectroscopic consts. from IR and microwave spectra 80−43039
t-butyl formate, deuteration effects, IR and Raman spectra 79−50016
tri-n-butyl phosphate, quantitative IR absorpt. meas. 80−87106
n-butyl radical, matrix isolation IR spectrum 78−33510
p-n-butyl-p′-heptanoyloxyazoxybenzene oriented on NaCl MgF_2 coated NaCl, surface phenomena and IR spectra 80−79678
N-tert-butylacrylamide-styrene copolymers, struct., composition, IR, DTA investigs. *(Polish)* 79−31751
butylsilane-d_0,(−d_n), vibr. spectra, normal vibrs. and rot. isomerism 79−31523
3-butyn-1-ol, vibr. spectra, assignments, rot. isomerism 80−58257
calcium behenate monolayers, mol. orientation determ. by IR absorpt. 79−11423

infrared spectra of organic molecules and substances continued
calcium dipicolinate trihydrate, IR and Raman spectra, isotopic frequency shift, mol. vibr. obs., point groups determ. 80−89001
calcium oxalate, anhydrous, IR and Raman spectra, vibrational studies 80−69139
calcium oxalate monohydrate, IR and Raman spectra, vibrational studes 80−69139
camphor, optical isomers, separated, IR Lamb dip obs. 78−90197
Camphor Fourier transform IR vibrational circular dichroism 79−99845
carbon tetrachloride, solid, Raman and far IR spectra 79−33680
carbon tetrafluoride, intensities of binary overtones and combinations in IR spectrum 78−55172
carbon tetrafluoride, lasing action, spectroscopy of features near 9 μm lines 79−22944
carbon tetrafluoride, liquid, comparison on interaction induced light scatt. and IR absorption 80−60561
carbon tetrafluoride, weak absorpt. spectra of $\nu_2+\nu_4$ vibr. using CO_2 laser 80−5762
carbon tetrafluoride $^{12}CF_4$ laser, Doppler-limited absorption spectroscopy 80−74347
carbon tetrafluoride laser, CF_4 molecule $\nu_3+\nu_4$ band optical pumping 80−74349
carbon tetrahalides, matrix photodissoc. and photoionisation by inert gas reson. radiation 77−83587
carbonaceous insulating films, RF diode sputtering growth, IR absorpt. and Rutherford backscatt. meas. 79−99458
carbonyl frequency correlation of aromatic derivatives with nonaromatic analogues 79−22709
n-carboxylic acid, IR-spectra and dimeric molecules normal vibr. *(Russian)* 77−77218
carboxylic acid systems, H(D) complexes and dimers, ν_{CO} IR band intensities 80−63715
carboxylic acid-ethanol systems, proton exchange process kinetics, effect of H bond strength in intermediate state *(Russian)* 79−96306
n-carboxylic acids, IR spectra, normal vibrs. forms and freqs. *(Russian)* 79−91450
cellulose diacetate as solid state heavy ion track detector 78−17523
cellulose hydrated film, orientational heterogeneity, IR spectra and dichroism obs. *(Russian)* 78−38990
cellulose macromolecule, conform. states and IR dichroism calcs. 80−55986
cellulose triacetate, vibr. spectra, theory 79−54836
cellulose trinitrate, in soln., gel-like aggregate form. rel. to configuration 77−31036
cetyliodide, cryst. phase transitions, mol. dynamics, spectroscopic and dielectric meas *(Russian)* 79−51965
CF_3X^+ cations, (X=Cl, Br, I, H), IR spectra in Ar matrix 78−74710
chloranil and radical anion, Raman and IR freq. shifts 78−33516
p- chloraniline cryst., lattice vibr., IR and Raman spectra, lattice energy 78−56481
3-chloro-1-butene, rot. isomerism, vibr. spectra assignments 78−58702
1-chloro-2,2-dimethylpropane, IR and Raman spectra, vibr. assignment 80−74169
3-chloro-2-methylpentane, IR spectra of film, rot. isomerism 79−59595
1-chloro-2-methylpropane, IR and Raman spectra, vibr. assignment 80−74169
2-chloro-2-nitropropane, far IR-microwave estimation of binary collision approx. 80−55095
4-chloro-3-nitrotoluene, IR absorpt. spectra, vibr. assignments 78−42048
2-chloro-4-methylpentane, IR spectra of film, rot. isomerism 79−59595
2-chloro-6-methyl benzonitrile, vibr. spectra 79−89665
chloroaluminium phthalocyanine, sublimed layer, IR absorption, vibr. assignments 78−55174
p-chloroaniline, IR spectra of cryst. at low temp. 79−38533
p-chlorobenzaldehyde and deuterated derivs., vibrational spectra 79−3441
chlorobenzene in cyclohexane dilute soln., far IR absorption obs. 77−40250
p-chlorobenzylidene-p-n-pentylaniline, metastable phases formed by rapid cooling of mesophase, IR and Raman spectra and DSC obs. 80−34919
o-chlorobromobenzene, phase transition evidence from far IR absorption and Raman spectra 79−33693
p-chlorobromobenzene, single cryst., polarised Raman and IR spectra, assignments 78−60431
trans-1,4-chlorobromocyclohexane, liquid, crystalline and amorphous state, conformation and vibr. spectra, IR obs. 80−60568
2-chlorobuta-1,3-diene, far IR and Raman spectra, internal rot. 79−89668
4-chlorobutyrylchloride, Raman and vibr. IR spectra of solid and liq., rot. isomerism 78−62810
chlorocyanoacetylene, cryst., IR, far-IR and Raman spectra, vibr., struct. 77−63407
chlorodifluoromethane, IR multiphoton dissoc., mag. field effect 80−93772
chlorodifluoromethane, photoacoustic spectra meas. at CO_2 laser wavelengths 80−18849
2-chloroethanol, IR and Raman spectra, normal coord. anal., isomerism 78−74661
chloroethylene, CO_2 laser absorption, Stark modulation 78−17671
chloroform-d_0(-d_1), Raman and IR intensity anal. 80−18857
chloroform-d, and di-n-butyl ether, complex formation, factor analysis and band contour resolution applications, book contrib. 78−21931
chloroform-d-acetonitrile-d_3, IR spectra liq. and solid at −180°C. *(French)* 78−15154
trans-1,4-chloroiodocyclohexane, liquid, crystalline and amorphous state, conformation and vibr. spectra, IR obs. 80−60568
chloromethane, and −d_3, cryst., IR and Raman spectra of lattice vibrs. 79−95741
chloromethane, and isotopes, $\nu_2+\nu_3$ band, Coriolis reson. with $\nu_3+\nu_5$ band *(French)* 78−5229
chloromethane, IR spectrum, evidence for $2\nu_3$ overtone 79−68226
chloromethane, rot. dynamics, far IR spectra 77−19864
chloromethyl formate, conformation potential energy surfaces, ab initio calcs. 80−69065
m-chloronitrobenzene, cryst., low freq. vibrs., polarised Raman and IR spectra study *(French)* 80−16029
chloronitrobenzene, IR spectral intensity, N-O group in aromatic ring 79−41199
β-chlorophenetole, UV and IR electronic and vibr. spectra, model assignments 77−10673

infrared spectra of organic molecules and substances continued
chlorophyll, -a and -b in cyclohexane soln., far IR and reson. Raman spectra 77−48753
chlorophyll-a, mol. interaction in monolayers and multilayers, IR obs. 77−71799
chlorophyll-a, nonlinear absorpt. spectra 78−25522
chloroplasts, in suspension, near IR radiation dispersion *(Russian)* 78−24045
chlorotrifluoremethane, IR rovibr. spectrum *(German)* 80−47998
chlorotrifluoromethane, 11.8 μm band, statistical model anal., integrated intensity 77−460
chlorotrifluoromethane, IR absorption spectrum, binary overtone and combination bands 78−46342
chlorotrifluoromethane, matrix IR spectra and harmonic force fields *(German)* 79−76431
cholesteric helix surface, elec. field-induced high-order ref. 78−35115
cholesterol, adsorbed monolayer on aerosil 78−15753
cholesterol, in carbon tetrachloride, self-assoc., IR absorbance 79−47920
chymotrypsin, charge relay system, H-bond models, IR spectra 78−64935
coal, chem. struct., NMR and IR obs. 77−40590
coal, cleaved surface, photoacoustic IR spectra 80−87104
cobalt, phthalocyanine, sublimed film, absorption spectra and association 78−48174
complex band shapes, resolution by IR polarisation meas. 79−12873
complex biological systems, Fourier transform. IR obs. 78−68945
conformation, IR spectra 78−1116
conformers, dynamic interaction between ground states, effect on IR spectra 78−58767
continua, phonon theory 80−29729
copper phthalocyanine, sublimed film, absorption spectra and association 78−48174
copper porphin, IR spectra and vibr. anal., and deutero-derivatives 79−22705
copper-porphin-d_4, reson. Raman and IR spectra 77−75164
coronene-TCNQ, solid complexes, spectra, stoichiometry 78−23435
m-cresol, vibr. spectrum determ. using Al-insulator-Pb tunnel junction 77−6782
cryst., IR spectra in polarised light, cryst. struct. 78−27223
crystals of C_{4h}, D_{2d} and D_4 symmetry at second-order structural transform., spectroscopic props. 78−22845
cyanoacetylene, ν_3 vibr.-rot. band, diode laser spectrum 80−91563
cyanoacetylene, and-d_1, cryst., IR, far-IR and Raman spectra, vibr., struct. 77−63407
cyanoacetylene, IR absorpt. bands, integrated intensities, ab initio and LMO calcs. 79−72234
cyanoacetylene, vibrational excitation in Orion molecular cloud 80−22067
α-cyanoacrylate adhesive in first monolayer on bulk Al surface, IR spectra, H-bond form., stretching vibr. 80−87119
cyanomethane-d_0,-d_3, soln., for IR spectra, band shape and moment anal. 80−58252
1,1-cyclobutane dicarboxylic acids and K salts, IR and Raman vibr. spectra *(French)* 80−2758
cyclobutane-d_0(d_8), cryst. modifications, low. freq. Raman and IR spectra 80−7342
cyclobutanone, absorpt. of pulsed IR radiation and decomp., joulemeter and opto-acoustic obs. 80−58328
cyclobutanone, clathrate hydrate, struct. II, for IR spectra, 4-100K 79−13707
cyclobutylmethylether, IR and Raman spectra, config. 79−31525
1,3-cycloheptadiene, Raman and IR spectra, normal coord. analysis, conform. 77−77203
cycloheptanone, vibr. spectra, pot. functions and conformers 77−83569
cyclohexane, in benzene soln., mol. motion, correl. functions 80−96431
cyclohexane, IR absorption in Ar matrices and perdeutero-cyclohexane, vibrational anal. *(French)* 77−6769
cyclohexanol, low temp. solid phases, far IR absorpt. spectra, 93 to 303K 79−56785
cyclohexanol, struct. information from OH-stretching freqs., axial/equatorial hydroxyl ratio 79−72438
cyclohexene vapour, IR spectra anal. 80−63628
1,5-cyclooctadiene, liq. and solid phases, IR and Raman spectra 79−19877
cyclooctanone, vibr., rot. spectra and conformations, pot. function 78−78707
cyclopentadienyl Ho(III), cyclooctadienyl sandwich compound, mag. circular dichroism and absorption spectra, anal. 80−23449
cyclopentadienylhafniumdichloride, gaseous, far IR and Raman spectra 80−95624
cyclopentadienyltitanium dichloride, gaseous, far IR and Raman spectra 80−95624
cyclopentadienyltitaniumtrichloride, gaseous, far IR and Raman spectra 80−95624
cyclopentadienylzirconiumdichloride, gaseous, far IR and Raman spectra 80−95624
cyclopentylamine, vibr. spectra and struct. 80−102516
cyclopropane, clathrate hydrate, struct. II, for IR spectra, 4-100K 79−13707
cyclopropane, IR band intensities using press. broadening technique 79−41172
cyclopropane, IR spectra studied by tunable laser, $\nu_{10}+\nu_{11}$ band anal. 80−95615
cyclopropane, lattice vibrs., IR and Raman spectra, 4 to 78K 78−27209
cyclopropane-d_0, d_6, absolute IR intensities, dipole moment derivatives and polar tensors 78−90165
cyclopropane-d_6, high resolution IR spectra, vibr. rot. band anal. 80−95621
cyclopropyl bromide, IR absorption, Raman scatt., assignments, thermodynamic functions 80−984
DL-cysteine, phase transition obs. at 10°C *(French)* 80−49355
cytochrome a, a_3, noninvasive monitoring of cerebral and myocardial O_2 sufficiency and circulatory parameters 78−44583
DBTTF$(BF_4)_{0.8}$, new conducting compound, synthesis, elec. and mag. props. 79−28341
DBTTF halogen complexes, IR, UV spectra, EPR study 80−108215
decanoic acid, mol. config. change in cryst., IR spectra, normal coord. anal. 78−33506
decomposition products of CO in corona discharge, qualitative anal. 78−60992

infrared spectra of organic molecules and substances continued
decyloxybenzoic acid, vibr. bands., IR dichroism, phase change effects *(Russian)* 78−15174
deoxyhaemoglobin high spin ferrous ion, low lying electronic states, far IR mag. reson. 80−48110
deoxymyoglobin high spin ferrous ion, low lying electronic states, far IR mag. reson. 80−48110
dextran, aqueous, solns., IR spectra 80−2761
1,2-di(N-piperidyl)ethane-bis-N-oxide tetrahydrate, synthesis, cryst. and mol. struct. obs. 79−32985
p,p′-di-n-alkoxyazoxybenzene series, C_1-C_7, submillimetre wave absorpt. investig. 80−34910
diacetylene, obs. of ν_4 band near 3 microns 80−47977
dialkylammonium copper chlorides, mag. and struct. transitions, IR absorption 77−52097
dialkylammonium manganese chloride, order-disorder transition mechanism 78−79772
2,4-diamino-6-hydroxy-pyrimidine, IR absorption spectrum, vibr. anal., tautomerism 80−58253
diammonium layer compound, $(CH_2)_2(ND_3)_2MnCl_4$, mag. and optical props. 79−51760
diammonium layer compound, $(CH_2)_n(NH_3)_2CuCl_4$, mag. and optical props. 79−51760
diatomic molecules, shortening of energy relax. time of excited mol. vibr. in dense medium by form. of H-bonds 80−91553
diazonium salts in aqueous solns. and polymer matrices, IR absorpt. spectra 80−76030
meso-2,3-dibromo-1,4-dichlorobutane, rot. isomerism, IR and Raman spectra 80−981
1,3-dibromobutane, IR and Raman spectra, normal coord. anal., C-halogen stretch bands and conformers 79−31522
dibromofluorobenzene, IR absorpt. spectra, vibr. assignments 78−17665
dibromomethane, IR spectra, local mode description for overtone spectra 78−42047
1,12-dicarbaclosododecaborane, plastic solid, phase transitions, 10-320K, Raman and IR obs. 79−28744
dicarbonyl compounds in soln., internal motion, dielectric relax., ^{13}C NMR relax., far IR spectra 77−28517
dicarboxylic acids, IR spectra Davydov splitting, methylene chain pendular vibrs. *(Russian)* 80−89008
2,5-dichloro-1,4-benzoquinone, mol. cryst., transition moment directions 78−64351
3,5-dichloroaniline, 250 to 4000 cm^{-1}, C_{2v} point group symmetry anal. 79−13717
2,3-dichloroaniline, 250 to 4000 cm^{-1}, C_s point group symmetry anal. 79−13717
2,6-dichlorobenzamide, IR spectrum, vibr. assignment 80−95608
o-dichlorobenzene, phase transition evidence from far IR absorption and Raman spectra 79−33693
4,4′-dichlorobenzophenone, cryst., $T_1 \leftarrow S_0$ singlet-triplet absorption profiles, temp. depend., phonon-exciton anal. 78−60436
dichlorobromobenzenes, IR absorpt. spectra, vibr. assignments 78−17665
1,3-dichlorobutane, IR and Raman spectra, normal coord. anal., C-halogen stretch bands and conformers 79−31522
2,2-dichlorobutane, liquid and solid., vibr. spectra, IR and Raman obs. 80−60567
1,1-dibromo-2,2-dichlorocyclopropane, IR and Raman spectra 79−41170
dichlorodifluoromethane, diode laser spectra near 10.8 μm, air-broadening effects 78−61555
dichlorodifluoromethane, IR spectrum and mol. force field 79−72309
dichlorodifluoromethane, study of ν_6 fundamental 79−31526
1,2-dichloroethane, conformer equilibrium by effusive beam-matrix IR spectroscopy 80−48100
2,2-dichloroethanol, vibr. spectra, normal coordinate anal. 79−22694
dichlorofluorobenzene, IR absorpt. spectra., vibr. assignments 78−17665
dichlorofluoromethane, IR absorpt. spectra, 1155-1163 cm^{-1} 80−37807
dichlorofluoromethane, photoacoustic spectra meas. at CO_2 laser wavelengths 80−18849
dichloromethane, (-d_2), liq. and vap., IR spectra, intensity anal. 79−64003
dichloromethane, high press. and temp. IR absorpt. spectra, stretching fundamentals *(German)* 80−47999
dichloromethane, IR spectra, local mode description for overtone spectra 78−42047
dichloromethane, liq. and dil. CCl_4 soln., far IR spectra and Rayleigh scatt. for planar itinerant oscillator 78−47229
dichloromethane, liq. state dynamics, models 79−73087
dichloromethane-d_0,-d_2, soln., far IR spectra, band shapes and moment anal. 80−58252
1,3-dichloropropyne and -d_1, vibr. spectra, normal coord. anal. and centrifugal distortion constants 78−70832
3,6-dichloropyridazine, liq. and solid soln. spectra, fundamental freqs. and assignments 80−5541
1,1-dichroethane and d, IR and Raman spectra, βCH stretching interaction force consts. 77−79616
dicyanobenzene, deuterated isomers, vibr. spectra 79−31521
dicyanoethylenes, substituted, vibr. spectra, intramol. effects 79−31528
diene rubbers, highly filled, supermolecular struct. *(Russian)* 78−76627
diethylammonium cadmium tetrachloride, first order phase transition, optical phonon line broadening, spin-phonon coupling model 80−7335
diethylammonium manganese tetrachloride, IR active modes, interlayer and intralayer forces 77−59575
N,N-diethylaniline, IR absorpt. and MCD spectra, Rydberg transitions 77−27068
diethylcarbonate, liq., alkoxy group internal torsion, extended microwave/far IR anal. 78−19457
diethylsilane-d_0(−d_n), vibr. spectra, normal vibrs. and rot. isomerism 79−31524
diethynylbenzenes, vibrational spectra, deuterated isomers 78−58705
difluoroacetic acid, soln., polarisable H bonds, IR spectrosc. obs. 80−58408
1,2-difluorobenzene-d_0, -d_4, IR spectra, vibr. anal., force field 77−27063
difluorodichloromethane, high-resolution polarisation spectroscopy in 10 μm region 79−6196
difluorodichloromethane, spectral data evaluation for atm. sensing 79−62582
1,2-difluoroethane, gauche-trans conformers, IR and Raman spectra, vibr. 78−17667
1,2-difluoroethane, in Ar matrix film, interference enhanced IR ATR spectra 79−9248
infrared spectra of organic molecules and substances continued
1,2-difluoroethane, internal rotation temp. frozen in supersonic jet, matrix IR spectroscopy 80−9594
1,2-difluoroethane, matrix isolation, trapping from thermal mol. beam, IR spectra 78−46330
1,1-difluoroethane, rot. relax., anharmonic shifts and excited state absorpt. 80−43154
1,2-difluoroethane in Ar matrix, IR hole burning and lineshape, vibr. transition 79−76425
2,2-difluoroethanol, vibr. spectra, normal coordinate anal. 79−22694
difluoroethylene, absorption coeff. at 10.6 μm 77−23654
1,1-difluoroethylene, diode-laser heterodyne spectrosc. meas. 80−43051
1,1-difluoroethylene, optically pumped, far IR laser line assignment 79−31865
1,1-difluoroethylene, rot. dynamics, far IR spectra 77−19864
1,1-difluoroethylene near-MM-wave emission assignments 80−58260
1,1-difluoroethylene submillimetric wave emission assignments 80−102708
difluoromethane, IR spectra, local mode description for overtone spectra 78−42047
difluoromethane cation, in solid Ar, IR spectra, vibr. modes 79−68231
difluoromethyl cation, in solid Ar, IR spectra, vibr. modes 79−68231
1,5-difluoronaphthalene, IR and Raman study of crystal dynamics 78−80346
dihalobenzenes, IR and Raman spectra, phase transitions *(French)* 78−84557
2,2-dihalohexafluoropropane, IR and Raman spectra, gas, liq. and solid, normal coord. anal. 79−72314
2-5-dihydrofuran, liq. phase far IR spectra, ring puckering *(French)* 78−92068
2,3-dihydropyran vapour, IR spectra anal. 80−63628
1,5-dihydroxyanthraquinone-d_0,-d_2, mol. vibr., IR spectra 77−467
p-diiodobenzene, far IR single cryst. transmission spectrum, temp. and polaris. depends., assignments 78−72498
diiodomethane, IR spectra, local mode description for overtone spectra 78−42047
1,2-diiodotetrafluoroethane, Raman and far IR spectra, conformation 78−78715
diketones, adsorbed on SiO_2, under carbon tetrachloride immersion, IR obs. 79−24821
dimerized organic linear chain conductor, electron mol. vibr. coupling consts. 78−14686
dimethoxybenzaldehyde, IR absorpt. spectra, 400-4000 cm^{-1} 79−41163
dimethoxymethane, vibr. spectra and rot. isomerism 80−106325
N,N-dimethyl acrylamide (−d_3,d_6,d_9), force field, IR and Raman spectra obs. 80−47979
dimethyl aniline, IR spectra, 250-4000 cm^{-1}, vibr. anal. 78−62797
dimethyl di(trifluoromethyl) germanium, and perdeuterated analogues, vibr. spectra, normal coord. anals. *(German)* 80−5547
dimethyl ether -d_0, -d_3, -d_6, internal rot., far IR and Raman spectra 77−79612
dimethyl oxalate, oriented cryst. film, polarised IR spectrum 80−29730
dimethyl phosphine-d_4, isolated CH stretching frequencies, bond strength, bond lengths 78−90167
dimethyl sulphide-d_4, isolated CH stretching frequencies, bond strengths, bond lengths 78−90167
dimethyl sulphoxide, 1:1 and 1:2 complexes with H_2O and D_2O, H-bonding, IR and Raman vibr. spectra 77−34633
dimethyl sulphoxide-d_6, intensities in inelastic electron tunnelling, IR, and Raman spectroscopy *(French)* 79−822
dimethylamino radical+O_2(NO)(NO_2), reaction rate constants, FTIR obs. 80−16652
dimethylammonium copper chloride, magneto-optical props., 0.03-13.5 eV 77−52132
dimethylammonium manganese tetrachloride, IR active modes, interlayer and intralayer forces 77−59575
dimethylboric anhydride, IR and Raman spectra, vibr. and struct. 78−25531
2,3-dimethylbuta-1,3-diene, IR, Raman spectra, torsional pot. function, thermodynamic function 80−43046
dimethylcarbonate, liq., alkoxy group internal torsion, extended microwave/far IR anal. 78−19457
trans-dimethyldiazene-1, 1, 1-d_3, IR and Raman spectra, vibr. assignments and pot. functions 78−33507
1,2-dimethyldiborane, IR and Raman spectra of cis and trans isomers 78−86868
dimethyldihalostannanes, cryst., IR spectra bandwidth, CH_3 group internal rot. 78−52490
dimethylether, ab initio SCF calcs., force field, IR and Raman intensities 77−79601
dimethylether-HCl(I)(Br) mixture in N_2 matrix, IR induced proton transfer isotope effects, bond strengths 79−29335
3,3-dimethyloxetan, far IR spectra, ring puckering vibration 78−42058
dimethylphosphines, -d_0 (-d_n) force field interpretation of coupling between methyl rocking, PH bending and PC stretching 80−69141
N,N-dimethylselenourea, deuterated forms and methyl derivatives, fundamental IR vibr. assignments 80−961
dimethylsolphoxide, effects on water struct., Raman and IR spectral study 80−14143
dimethylsulphate, cryst., liq., and oriented film, vibr. spectra, internal rot. 79−91444
dimethylsulphide, liq., solvated electrons, optical absorpt. spectrum obs. 80−97250
dimethylsulphide, Raman spectra, torsional pot. consts. and kinetic coeffs. 78−5233
dimethylsulphite(-d_6), cryst., liq., and oriented film, vibr. spectra, force fields 79−91443
dimethylsulphoxide, aqueous solns., IR spectra *(Italian)* 79−63994
N,N-dimethylthiourea, deuterated forms and methyl derivatives, fundamental IR vibr. assignments 80−961
m-dinitrobenzene, oriented film, intermol. vibr. coupling, polarised IR spectra 80−97264
2,2-dinitropropane-d_0(-d_6), phase polymorphism, vibrational assignments, IR and Raman study 80−16031
2,4-dinitrotoluene, laser optoacoustic absorpt. spectra of explosive vapours 78−76941
dioxane, 1:1 and 1:2 complexes with H_2O and D_2O, H-bonding, IR and Raman vibr. spectra 77−34633
dioxane-$HgCl_2$ complexes, IR and Raman vibr. spectra, inter- and intramol. forces 77−66489

infrared spectra of organic molecules and substances continued
1,3-dioxolane, clathrate hydrate, struct. II, for IR spectra, 4-100K 79−13707
diphenyl anion salts, sublimed layer, electronic and IR absorpt. spectra 80−66189
dipicolinic acid, IR and Raman spectra, isotopic frequency shift, mol. vibr. obs., point groups determ. 80−89001
dipolar fluid dielectric relaxation, far IR absorption spectrum models 80−15954
dipolar liquid, far IR absorpt. rel. to Mori continued fraction for autocorrel. function 78−2875
dipotassium malonate, aq. soln., IR and Raman vibr. spectra *(French)* 79−26989
1,4-disilabutane, rot. isomerism, Raman and IR spectra 80−74168
1,3-disilacyclobutane, ring-puckering combination band spectra in SiH_2 stretching region 78−70836
disordered solids, rel. between simple analytic models 78−76473
1,2-disubstituted imidazole compounds, IR and Raman spectra, vibr. anal. *(French)* 79−45713
dithiocarbamate complexes of Cr, Mn, Sn and Pb IR, electronic and mass spectra, mag. susceptibility, cond. meas. 80−97270
DNA, Na salt, freeze-dried layers, unpolarised IR spectrum, temp. dependent spectral shift 77−48755
DNA hydrate, struct. conversions of sugar phosphate chain and nitrogenous bases 80−81530
DNA-lipid interaction, IR spectroscopic obs., DNA compactisation on disperse particles 80−104550
E. coli B irrad. with 0.8 MeV electrons in oxygenated and anoxic states, mol. alterations 78−24031
EBBA, IR absorpt. spectra, elec. field effects, orientational order parameter determ. by IR dichroism, bend elastic consts. 80−80778
EBBA, liq. cryst., IR and far IR spectra, vibr. assignments 77−16298
EBBA, metastable phases formed by rapid cooling of mesophase, IR and Raman spectra and DSC obs. 80−34919
EBBA, orientational order in glassy and nematic phases, IR dichroism meas. 80−64891
EBBA-MBBA mixture, differential IR spectroscopy determ. of orientation of molecules 77−7670
eosin, photoacoustic spectra in soln. 80−9606
epifluorohydrin, IR and Raman spectra and conformations 80−60576
episulphide network polymers, mech. relaxation 79−96061
epoxy, curing composition, viscoelasticity in critical region 77−62228
epoxy, Stycast 1266, very low temp. thermal conductivity and optical props. 78−55992
epoxy films, in polished metal mirrors, refl.-absorpt. IR spectrosc. and ellipsometry obs. 79−78765
erythrocyte ghost IR spectra in region of amide I and II bands on microwave irrad. 77−86531
esters, long-chain, X- and Y-type multilayers, form. conditions and struct. characterisation 80−80127
ethane, ground state parameters and IR absorpt. spectra 80−47986
ethane, high resolution IR spectrum using $Pb_{0.93}Sn_{0.07}Te$ laser 78−33511
ethane, in air, IR spectra, optical-acoustic investig. *(Russian)* 78−74663
ethane, intensity of $^RQ_0$ branch in ν_9 fundamental 77−6856
ethane, IR obs. spectra meas. using $Pb_{1-x}Sn_xTe$ diode laser *(Japanese)* 79−49306
ethane, liq., IR torsion band, 98-173K mechanism, Coriolis coupling 77−38662
ethane, nonlinear IR absorpt. spectra 78−13492
ethane, spectral parameters, Lamb dip method investig. 78−89560
ethane($-d_6$,d_3,d_1), electro-optical parameters from IR intensities, least-squares calc. 80−9584
ethane-1,1,1-d_3, gas-phase IR spectra, rot. fine struct. obs. 80−83359
ethane-d_0,-d_6, normal coord. and IR intensity anal. 79−36604
ethane-d_n, IR spectra, r_0, r_z and r_e structs. 79−59453
ethaneselenol, IR, Raman and microwave spectra, barriers to internal rot. 77−38666
ethanol, dissoc. adsorption on porous glass, IR obs. 79−23830
ethanol, solns., local struct. equilib., light scatt. and IR spectra obs. 78−84564
ethanol mols. reorientation in ethanol-water mixtures, Raman and Rayleigh spectra 78−76449
ethene, general valence force field, ab initio calcs., IR and Raman intensities 77−71746
ethers, and solid alkane solns., far IR spectra *(French)* 79−4793
N-p-ethoxybenzylidene-p′-cyanoaniline, nematic, mol. reorientation in DC elec. field, IR ATR spectra study 80−45064
ethyl acetate, photoacoustic spectra meas. at CO_2 laser wavelengths 80−18849
ethyl alcohol, solution, struct. determ. from vibr. spectra, H-bonding and heat of mixing *(Russian)* 78−3368
ethyl methyl sulphide, low freq. vibr. spectra, methyl torsional pot. functions and internal rot. 80−5543
ethyl radical, C-C bond barrier rot., IR spectra 80−76536
ethyl-furan-2-carboxylate, skeletal vibr. of IR spectra, conformational props., solvent polarity effect 80−87118
ethyl-p-azoxybenzoate, far IR and Raman spectra, smectic polymorphism 80−76022
ethylammonium cadmium tetrachloride, order-disorder transition, far IR reflectivity obs. 79−65870
ethylcyclopropane, solid, liquid, vapour phase, IR and Raman vibr. spectra 80−84740
ethyldifluoroborane, microwave, Raman, IR spectra, conform., dipole moments, vibr. assignment 78−90155
ethylene, 10 μm absorption line profile, high resolution meas. 77−42359
ethylene, absorpt. cross sections at CO_2 laser wavelengths, temp. and press. depend. 80−78613
ethylene, chemisorbed on Ni and Pd films, IR refl. study 79−69343
ethylene, compressed gas, far IR dipolar absorpt., meas. and theory 77−14425
ethylene, dipole moment derivatives, IR vibr. intensities, STO-3G, 4-31G, calcs. 77−6750
ethylene, He-Ne laser line, high temp. absorpt., anal. by high resolution IR spectra 80−91554
ethylene, high pressure polymerisation investig. using near IR spectroscopy *(German)* 77−21384
ethylene, high resolution heterodyne absorption spectra 78−267
ethylene, in air, IR spectra, optical-acoustic investig. *(Russian)* 78−74663
ethylene, IR absorpt. spectra of ν_1, ν_{10} and ν_4 interacting band 80−83369

infrared spectra of organic molecules and substances continued
ethylene, IR and near IR spectra, high press. cell meas. *(German)* 78−12769
ethylene, IR and Raman intensities calc., efficient ab initio computation method 79−45698
ethylene, IR double reson. obs., external-resonator controlled Raman laser pumped by CW CO laser 80−9624
ethylene, IR spectra, solid and matrix isolated, dimer config. 79−36638
ethylene, isotopically mixed, crystal, dilute guest probe orientational energy, IR, Raman spectra 78−68496
ethylene, laser spectroscopy with CO_2 and N_2O lasers 79−59455
ethylene, liq., far IR absorption spectrum, quadrupole induced dipole interaction 78−86857
ethylene, narrow resonances of multiple-photon IR absorpt. 80−99529
ethylene, near IR absorption at high press. and temps. 77−14435
ethylene, pure, IR absorption obs. of C-H stretching fundamentals up to 2 kbar and 200°C 79−22701
ethylene, quadrupole moment tensor determ. by collision-induced absorpt. spectrum 80−91555
ethylene, solubility in liq. N_2 80−39286
ethylene($-d_4$) clusters, IR photodissoc. 80−89506
ethylene and propylene adsorbed on Ag, enhanced Raman spectra obs. 80−95607
ethylene carbonate, Fermi reson., isotopic substitution meas. 78−86870
ethylene glycol, IR spectra, ab initio calcs., vibr. anal., conformations of isotopic modifications 78−5210
ethylene glycol dinitrate, laser optoacoustic absorpt. spectra of explosive vapours 78−76941
ethylene oxide, cryst. symmetry, X-ray diffr., far IR and Raman spectra 78−35123
ethylene-d_0,-d_4, IR band intensity and Coriolis interactions 79−54851
ethylene-d_1, ν_9 B-type band analysis, ground state rot. parameters 77−42316
ethylene-d_1, IR absorpt., ν_{12} and $\nu_2+\nu_9$ bands, rot. consts., Fermi and Coriolis coupling consts. 77−27070
ethylene-methacrylic acid copolymer, dielectric relax. and IR obs. 79−69772
ethylene-vinyl alcohol copolymers, H bonding study by near-IR spectra *(Japanese)* 80−78734
ethylenediammonium metal chlorides, $(NH_3CH_2CH_2NH_3)MCl_4$, M=Ni,Pd,Cu,Cd,Mn, struct. and mag. props., vibr. spectra 79−10842
ethylenes, optical activation energy and dipole moment, electron repelling and attracting groups 78−46341
ethylgermane, microwave, IR and Raman spectra, struct., internal rot., dipole moments 77−79605
ethylmethylamine, low freq., vibr. spectra, methyl torsional pot. functions, mol. struct. 80−43045
ethylmethylether($-d_3$), low freq. vibr. spectra, methyl torsional pot. functions, internal rot. 79−26978
ethylmethylsilane-d_0($-d_n$), vibr. spectra, normal vibrs. and rot. isomerism 79−31524
ethyloxirane, solid, liquid, vapour phase, IR and Raman vibr. spectra 80−84740
exciton spectra, Fermi resonance and two particle excitation 79−69436
explosive vapours, laser optoacoustic absorpt. spectra 78−76941
far IR transmission spectral bandshape 77−32363
ferricenium complex, Franck-Condon light scatt. transitions 77−57999
fibre reinforced composite, stress meas. by IR spectroscopy 79−52559
fluoranil-macrocyclic polyether mol. complexes, configs., IR and NMR obs. 78−33529
fluorinated ethylenes, valence bond polar parameters, IR intensities, MO calc. 80−28013
1-fluoro 2:4-dinitrobenzene, laser Raman and infrared spectra 79−22711
2-fluoro ethanol, Ar matrix, induced conformational isomerisation by IR irrad. 80−101010
3-fluoro-4-chloroaniline, Raman and IR spectra, vibr. anal. 79−81198
2-fluoro-5-bromotoluene, IR and Raman spectra 78−70830
2-fluoro-5-chloro-toluene, IR vibr. spectra 79−68232
3-fluoro-6-chloro-toluene, IR vibr. spectra 79−68232
fluoroacetylene, absorpt. spectra, ν_4 C-H bending fundamental near 17 μm 77−75151
fluoroacetylene-d_1, bending vibr.-rot. band ν_4, IR spectrum 77−75149
4-fluoroaniline, amino group inversion and torsion, far IR spectra 77−10670
4-fluoroaniline, far IR spectrum, efficiency of heatable long path gas cell 79−58807
m-fluoroaniline, vap. (liq)., Raman and IR spectra, vibr. assignments 78−58699
fluorobenzene, IR vibr. spectra 79−13713
fluorobromomethanes, matrix photoionisation and radiolysis, IR spectra of free radicals 79−24765
fluorocarbon ether bibenzoxazole polymers of low glass transition temp., preparation and characts. 79−51006
2-fluoroethanol-d_0,-d_1, IR spectra in Ar, N_2 and Ar-N_2 matrices, normal coordinate anal. 78−25538
fluoroform, ν_3, ν_6 and hot bands, high resolution IR spectrum 79−81204
fluoroform, absolute IR intensities of fundamental vibrs. 77−79655
fluoroform($-d_1$)-trimethylamine-Ar(Kr), cryospectroscopic IR study of association 77−468
fluoromethane, ν_3 band Lamb dips, effects of RF elec. field modulation on Stark spectra 80−52989
fluoromethane, in liq. O_2(Ar), vibr. energy relax. obs. 78−5208
fluoromethane, IR absorpt., CW saturation, theory 77−83933
fluoromethane, optically pumped laser, IR-FIR transferred Lamb dip spectra 80−1193
fluoromethane, vel.-tuned multiphoton processes in laser cavity 77−27134
fluoromethane, very high resolution IR spectrum anal. 77−34630
fluoromethane+fluoromethane, collision induced mode selective energy transfer, fluoresc. obs. 80−69177
fluoromethane+HCl, IR spectra, intermol. interactions 80−9605
fluoromethane-^{13}C, IR spectra, pulse Fourier transform technique 77−26405
fluoromethane-d_2, matrix isolated, vibr. energy transfer at low temps. 80−37860
fluoromethane-d_3, laser Stark spectra, ν_6 band, vibr.-rot. consts., dipole moment 78−5277
fluoromethanes, dipole moment derivatives and infrared intensities, transferable polar tensors 78−17668
fluoromethyl formate, conformation potential energy surfaces, ab initio calcs. 80−69065

infrared spectra of organic molecules and substances continued
fluoromethyl methyl mercury-d_0, -d_3, vibr. spectra, normal coord. anal. 79−50017
fluoromethylene cation, in solid Ar, IR spectra, vibr. modes 79−68231
2-fluoropyridine, IR and Raman spectra, vibr. assignments 78−25534
fluorotrichloromethane, spectral data evaluation for atm. sensing 79−62582
formaldehyde, 17(2,15)→17(2,14) line press. broadening relationship 79−98093
formaldehyde, 3.5 μ region spectrum, ground state consts. 79−13712
formaldehyde, absorpt. coeff. meas. using optothermal detector 79−40634
formaldehyde, chemisorbed on Rh, catalytic decomposition, transmission IR spectra 79−39199
formaldehyde, CO laser Stark and IR absorpt. spectra, dipole moment and rot. consts. 77−75150
formaldehyde, Doppler-limited spectra of C-H stretching fundamentals 78−70831
formaldehyde, IR Doppler-limited spectrum, wavenumbers, line strengths and assignments 79−72310
formaldehyde, IR intensities by electron impact spectroscopy 77−6851
formaldehyde, IR spectra, Coriolis-coupled ν_4, ν_6 and ν_3 fundamental bands 78−5227
formaldehyde, IR spectrum, rot. anal., P-and Q-branch assignments 77−18923
formaldehyde, isolated Voigt line, off-peak spectral absorpt. coeff. 80−106355
formaldehyde, low-temp. matrix photolysis, hydroxymethylene intermediacy, IR obs. 78−76877
formaldehyde, photolysis in Ar matrix, role of cage dimer 79−91973
formaldehyde, solid soln. in Xe, precipitation, IR spectra obs. 80−45059
formaldehyde+Ar(N_2O), mol. isolated Voigt line, off-peak spectral absorpt. coeff. 80−106355
formaldehyde dimers, matrix isolated, struct., IR spectra 80−99504
formaldehyde-d_0(-d_1)(-d_2), matrix isolated, IR spectra, monomer absorpt. 80−99503
formaldehyde-d_1, ν_3 fundamental band, IR absorpt. and laser Stark spectra 77−34629
formaldehyde-d_1, absorpt. spectra, 9-11 μm, ν_5 and ν_6 fundamental bands 78−70827
formaldehyde-d_2, laser Stark spectra, Coriolis coupled ν_4 and ν_6 fundamentals 77−27065
formaldehyde-H_2O complex, IR spectrum in solid Ar, N_2 matrix 80−43042
formamide, far IR spectrum, efficiency of heatable long path gas cell 79−58807
formamide, intermol. H bonding, vibr. spectrosc. obs. 79−50018
formamide, IR spectra, amino group inversion transitions and pot. functions 80−43041
formamide, near-IR spectra, anharmonic pot. 77−14430
formamide, partly deuterated, in electrolytic soln., IR spectra, anion-solvent H-bonding 78−84558
formamide(-d_2), vibr. spectra NH_2 stretching modes assignment 79−89675
formate, Fermi reson. of optical phonons with two particle state zone, interference effects *(Russian)* 77−90149
formate esters-d_1, Fermi reson. parameters 80−48103
formic acid, cryst., H bonded, IR spectrum computer simulation 80−97253
formic acid, soln., polarisable H bonds, IR spectrosc. obs. 80−58408
formic acid, vibr. states, rot. and Coriolis parameters 1R Fourier transform spectra 80−32709
formic acid anhydrides, valence force consts., IR spectra, isotope effects 79−93997
formic acid crystals, low temp. IR spectra 77−48153
formic acid dimer, vibr. spectra, CNDO/2 interpretation *(French)* 80−58155
formic acid monomer, vib. spectra and normal coordinate analysis 77−58003
formic acid-d_0, -d_2, OH(OD) stretching, vibr. band struct. 77−6751
formic acid-d_0(-d_1)(-d_1)(-d_2), vibr. spectra, CNDO/2 interpretation *(French)* 80−58155
formyl fluoride (-d_1), IR absorption intensity anal. 78−70813
formyl radical, atmospheric oxidation, IR Fourier transform spectroscopic obs. 79−66785
formyl radical, laser mag. reson. spectrum at 5.3 micron 80−47981
Fourier transform IR spectroscopy, use in polymer research as vibr. spectroscopy tool 80−55744
Fourier transform of spectroscopy for pharmaceutical anal. quality control 79−97449
Fourier transform spectroscopy appl., far IR 78−58069
free radicals and molecular ions, matrix isolation spectra 79−50008
Freon 123-d and natural 123, selective absorpt. cross section at 10.2 and 10.6 μm 80−5546
Freon IR mass absorption coefficients, 3 to 15 μm 79−76422
Freon-12, absorpt. coeffs. for CO_2 laser radiation, press. and temp. depend. 78−55170
Freons, IR absorpt. band intensities meas. in atm. window region 77−30871
furan, adsorbed on NaCl, evidence of new condensed phase, IR spectra *(French)* 80−16028
furan, photoacoustic spectra meas. at CO_2 laser wavelengths 80−18849
furane, cryst., low freq. vibr. spectrum, temp. depend., 12 to 253K 80−84743
gases, IR fluoresc. by CO_2 laser 80−78619
gelatin, fine struct., IR spectroscopic study of effects of impurities and other actions *(Russian)* 78−58083
gelatin film, deuterated, IR absorpt. spectra, heat treatment and ageing *(Russian)* 78−39621
gelatin films with Fe,Cu,Ag and S containing compounds, IR spectra *(Russian)* 78−49928
germanyl acetylenes, fine structure due to internal rotation in IR-active perpendicular bands 79−98096
glass fibre reinforced plastics, coupling agent/matrix interface investigation by Fourier transform IR spectroscopy 80−20884
glucose powder and aqueous soln., photoacoustic spectra in middle IR 77−81101
L(+)-glutamic acid hydrochloride, deuterium isotope effect, cryst. struct., IR spectra and SHG 77−46755
glycylglycines, isotope substituted, IR and Raman vibr. spectra 78−42051

infrared spectra of organic molecules and substances continued
gramicidin A in biomembrane channel, IR spectroscopic obs. 80−16901
graphite-epoxy resin, hydrothermal ageing 77−52367
guanine, ^{15}N and D substituted, in acid and base solutions, vibr. anal. 79−26994
halfwidths transferability in related mols. series 79−54921
1-halo-1-n-propylcyclohexanes, conform. equilib., and pot. barriers, IR spectra *(Russian)* 78−21928
haloacenaphthenes in n-heptane, quasi-line phosphoresc. spectra, vibronic spin-orbit interaction 80−43096
haloalkyl peroxy radical+NO_2, haloalkyl peroxynitrate form., FT IR obs. 79−34283
haloanilines, far IR spectra, vibr. assignments 78−82726
2-haloethanols, torsional interaction, IR spectra, ab initio calcs., 2-dimens. model 80−74160
halogenated propanes, IR and Raman spectra, LF vibrs. 79−10105
halogenobenzenes, dipolar liquid, far IR absorpt. rel. to Mori continued fraction for autocorrel. function 78−2875
halomethanes, -d_0 and -d_3, IR intensity anal. 77−58082
halomethanes, absorpt. coeffs. meas. in Nd laser emission band 80−78620
heparin, aqueous, solns., IR spectra 80−2761
α-heptacyclene, in solid matrix, photodissoc. quantum yields, fluoresc. temp. depend., phosphoresc. IR spectra 77−25292
n-heptyl cyanobiphenyl, near IR dichroic spectrum, using unpolarised radiation 78−27201
hexa(trifluoromethyl) germanium, gas and liq., IR and Raman spectra, normal coord. anal. *(German)* 79−72315
hexabromobenzene, cryst., IR and Raman spectra, vibr. normal coordinate anal. 77−79602
hexafluorobenzene, polar tensors and at. effective charge, calculated from IR intensity 78−74703
hexafluorobenzene-benzene, liq., mol. interactions, IR and Raman lineshape obs. 80−28907
hexafluoroethane, far IR multipole induced absorpt. 78−37639
hexafluorohalopropanes, gas and solid, IR and Raman spectra, normal coord. anal. *(German)* 79−72317
hexafluoropropane(-d_2), IR and Raman spectra, gas and liq., normal coord. anal. 79−68235
hexafluoropropene, struct. and vibr. spectra, IR, Raman polarisation study 80−18845
hexaidobenzene, cryst., IR and Raman spectra, vibr. normal coordinate anal. 77−79602
hexamethylbenzene, IR polarised spectra 79−28758
P-hexamethylcyclotriborophosphanes, substituted, struct., vibr. spectra 77−65460
hexamethyldisiloxane, polymer film, struct. determ., IR spectra, elemental anal. *(German)* 77−59224
n-hexatriacontane, cryst., orthorhombic modification, vibr. spectra 80−50314
4-n-hexyloxybenzylidene-4′-n-hexylaniline, liquid crystal, exam. of orientation order of dissolved molecules 80−44112
histone H4 N-terminal oligopeptide struct., circular dichroism and IR spectroscopy 78−24025
hydrocarbons, high-temp. absorptivity of 3.39 μm laser line 78−86856
hydrocarbons, IR intensities, C-H bond moments and bending modes 77−10703
hydrocarbons, IR intensities, polar tensors, atomic population densities 77−23497
hydrocarbons, nonlinear absorpt. spectroscopy 79−63315
hydrocarbons, saturated, thermal cond., rad. effect interferometry method 77−11745
hydrogen chloride/dimethyl ether complex, temp. depend. of IR spectra of H bond in gaseous state 77−34624
hydrogen-bonded ion-pair complex, anomalous isotropic freq. ratio of stretching $\nu_{N(+)H}$ vibrs. 77−3366
hydroperoxy-hydroxy-methane, metastable mol., IR spectra of formaldehyde photooxidation products 79−93994
imidazole, vibr. spectra, mol. crystal dynamics, librational modes 78−64356
in cyclohexane-ethanol mixtures, UV spectra, solvent effect 79−22770
indigoid dyes, Raman, IR and Shpolskii spectra 79−65866
intensity prediction, at. polar tensor method, F containing mols. 78−62854
intensity relation, IR to Raman intensity, matrix notation 78−62853
intermolecular interactions in condensed medium, long-wavelength IR spectroscopy 80−34927
intermolecular spectroscopy and dynamical properties of dense systems, conf., Varenna, Italy (1978) 80−82581
intramolecular H bond energy determination, by competing equilibria, IR spectra obs. *(Russian)* 78−29783
1-iodo-2-methylpropane, IR spectra, vibrational anal., stretching bands 78−90168
1-iodo-3-methylbutane, IR spectra, vibrational anal., stretching bands 78−90168
iodocyanoacetylene, cryst., IR, far-IR and Raman spectra, vibr., struct. 77−63407
iodomethane, liq. (liq. mixtures), vibr. relax. and reorientation, symmetric C-H bending mode 1st overtone 78−62884
iodomethane, P-line and ν_6 band spectra using CO_2 laser absorpt. 80−69142
iodomethane, thin single cryst., IR spectra anal., Fermi-Davydov intensity distrib. 77−59577
iodomethane-d_3, ν_2 band, laser Stark and laser-microwave double resonance spectra 77−27067
α-iodonaphthalene, IR absorption spectra, forbidden character 77−58002
2- and 3-iodopyridine, IR and Raman spectra, vibr. assignments 78−25534
iodotrifluoromethane, high vibr. state excitation in high-power laser field, spectral characts. 80−91562
ionised ethylene-acrylic acid copolymer, heterogeneous ionomer, dynamic mech. props. *(Japanese)* 77−59843
iron (III) salicylates, Mossbauer and IR spectra, mag. susceptibility 80−50242
isobutene-d_0, -d_6, torsional pot. functions, spectra anal. 78−25528
isobutyl alcohol, adsorpt. on Al_2O_3, gravimetry, IR investigs. 79−1546
isocyanic acid, molecular structure and centrifugal distortion constants 80−47974
isomer identification by vib. spectra analysis, for similar structs. *(Russian)* 77−83577

infrared spectra of organic molecules and substances continued
isopropyl alcohol, adsorbed on ZnO, decomp., IR and kinetic obs. 80−59780
isopropyl radical, Ar matrix isolated, IR spectra and UV photolysis 80−66827
isopropylcyclopropane, solid, liquid, vapour phase, IR and Raman vibr. spectra 80−84740
isoquinoline semiperchlorate, H-bonding, strong, stochastic model and IR spectra temp. effects 78−62805
K-vitamins, IR absorpt. spectra, vibr. anal., quinonoid struct. 78−61139
ketene, IR spectra, rot.-vibr. anal. of Coriolis coupled bands 78−86859
ketocyanines alcohol solns., spectral-luminesc. props. 80−2835
ketones, in soln., IR spectral line halfwidths determ., rot. Brownian motion investig. 77−36248
ketones, solns., IR absorpt. band parameters rel. to temp. 80−2762
lecithin, adsorbed monolayer on aerosil 78−15753
ligand-metal overlap, rel. to ligand field and charge transfer interaction intensity 79−87067
linoleic acid, adsorbed on Al_2O_3, under carbon tetrachloride immersion, IR obs. 79−24822
linuron, herbicide, interaction with soil, Fourier transform IR spectra 77−9142
liquid, barrier to internal rot., IR spectral linewidths meas. 78−72507
liquid, far IR absorpt., rot. dynamics studies *(French)* 78−39534
liquid, molecular reorientation, autocorrelation functions 77−80400
liquid, orientational correlation functions for dipolar and induced dipolar absorpt. in far IR 77−11451
liquid, thermal lens effect meas. by photomixing method, laser system 77−42577
liquid chromatography effluents on line anal., micro liq. chromatograph-interfaced Fourier transform IR spectrophotometer 80−73483
liquid complex refractive, index 5 to 500 cm^{-1}, Fourier transform interferometric determ. 77−13798
liquid crystals, solid state polymorphism, differential scanning calorimetry and IR and Raman spectra obs. 80−55094
liquid differential absorpt. in far IR, novel cell type for meas. 78−24872
liquids, H-bonded, IR and Raman spectra, elec. anharmonicity on H-stretching bands 78−48167
Liquids, nonpolar, far infrared absorption 80−50331
liquids and solids, gas chromatography-IR spectroscopy using Sadtler CIRA 101 analyser 80−93809
lithium formate, and deuterated, polaritons, spontaneous parametric light scatt. 77−90150
lithium oligopentadienyl and complexes, IR spectra *(Russian)* 80−71424
lithium salt electrolyte submillimetric absorption obs. 80−60611
lossy liquid, for IR refr. spectrum meas. 77−2700
low-temperature materials, IR spectra rel. to heat shield prod. for changing mag. fields 77−74408
maleic acid, acid slats, melts, H_2 bonding, IR, NMR investigs. 79−65859
maleic anhydride, and its photochem. transform. products *(Russian)* 77−66761
malonic acid, aq. soln., IR and Raman vibr. spectra *(French)* 79−26989
malonic acid, phase transition at 360K, IR study 80−44311
malononitrile, cryst., phase transitions, Raman and IR obs. 80−88980
malononitrile, solid phases I-IV, vib. spectra 77−20840
manganese formate dihydrate, IR absorption spectra 79−19893
manganese stearate Langmuir-Blodgett layers on Ag, IR surface EM wave prism spectroscopy 78−52587
manganese stearate monolayer, two-dimensional mag., prep. and characterisation 78−31097
MBBA, IR absorpt. spectra, elec. field effects, orientational order parameter determ. by IR dichroism, bend elastic consts. 80−80778
MBBA, liq. cryst., IR and far IR spectra, vibr. assignments 77−16298
MBBA, metastable phases formed by rapid cooling of mesophase, IR and Raman spectra and DSC obs. 80−34919
MBBA, orientational order in glassy and nematic phases, IR dichroism meas. 80−64891
MBBA, solid phase polymorphism, IR and Raman spectra study *(French)* 79−87438
MBBA, solid phase polymorphism and phase transforms., IR spectra obs. 79−8128
β-melanocyte stimulating hormone and β-lipotropic hormone fraction, spectral study 77−36863
metal phthalocyanines, IR spectra, vibr. transitions during intermol. interactions 79−54857
methane, $2\nu_3$ band, R_1 line, spectrum reconstruction using test response 80−77884
methane, $2\nu_4$ band, IR spectral assignments *(French)* 77−42319
methane, $2\nu_4$ band anal. *(French)* 79−41168
methane, 4350-10600 Å bands, intensity profile, vibr. assignments, rel. to major planets spectra 78−42084
methane, ^{12}C and ^{14}C, line parameters for ν_2 and ν_4 bands, isotope shifts, appln. to planetary atmospheres 80−95622
methane, ^{13}C and ^{12}C, line strength ratios of $2\nu_3$ singlet 80−78616
methane, ^{13}C enriched, IR spectrum, ν_3-band forbidden lines, ground state consts. 77−18922
methane, $\nu_1+\nu_4$ vibration-rotation spectrum, spectroscopic constants *(French)* 79−13709
methane, ν_1 line contour anomalous behaviour on pressure changes *(Russian)* 80−43052
methane, $\nu_3=1$ state, dipole moment and IR-radiofrequency double reson. spectra 80−14161
methane, ν_3 band, IR spectrosc. meas. and anal. 79−98098
methane, ν_3 P(6) transition, Doppler-free intracavity polarisation spectroscopy 80−5537
methane, ν_4 fundamental, Q and R branch absolute line intensities 80−5539
methane, ν_4 fundamental band strength, line-intensity meas. 79−22700
methane, absolute line strengths meas. using dual-beam diode laser spectrometer 80−101853
methane, absorpt. meas. in 3.3 μm band, temp. depend. 78−90159
methane, absorpt. of 3.39 μm He-Ne laser line, 300-2400K 78−90166
methane, absorption and press. coeffs., 4500-10500 Å, band model calcs., astronomy appls. 77−83593
methane, absorption spectra, 3.5-4.1 μm, appl. of pulsed source spectrophone 77−23494
methane, absorption spectrum, LiF F_2^+-centre laser intracavity spectroscopy appl. 80−32999
infrared spectra of organic molecules and substances continued
methane, and d_4, Raman scatt. activity and IR intensity, finite field method 79−59462
methane, and methane-d_4, rotational transition in condensed Xe, 6K, optical excitation 78−60494
methane, anharmonic molecular vibrations, coherent spectroscopy 79−18187
methane, collision-induced light scatt., spectral features 78−13493
methane, fluid, collision-induced light scatt. 78−68509
methane, hyperfine struct. of $F_2^{(2)}$ line, appl. of laser spectrometer 77−58201
methane, in air, IR spectra, optical-acoustic investig. *(Russian)* 78−74663
methane, in liq. SF_6, ν_3 band IR profile, temp. depend. 78−58696
methane, in SF_6, CCl_4 soln. and Ar, IR band profile *(French)* 79−54913
methane, intensity pertubations due to ν_3/ν_4 coriolis interaction 79−98087
methane, IR anal. of ν_2 and ν_4 bands *(French)* 80−87113
methane, IR bands identification in Triton atmosphere 80−21945
methane, IR intensities, C and H atomic polar tensors 78−50592
methane, IR line intensities 78−58687
methane, IR spectra, 2862-3000 cm^{-1}, line positions and strengths 78−5217
methane, IR spectra of ^{13}C mol: isotope, ν_4 band line strengths 79−94036
methane, IR spectral atlas for 1120-1800 cm^{-1} region 80−23415
methane, isotopic variants, IR intensity anal. 77−58081
methane, J-multiplet intensity meas., ν_4 fundamental at 300K 77−68080
methane, Jovian line profiles near 1.1 μ as probe of cloud struct. and C/H ratio 80−62067
methane, liq., optical consts. meas. in IR, possible planetary cloud cover component 78−64341
methane, liquid, comparison on interaction induced light scatt. and IR absorption 80−60561
methane, liquid, vibrational overtone spectrum, planetary appls. 79−2497
methane, mag. hyperfine struct., laser spectroscopy 77−88757
methane, multipole moments, far IR spectrum determ., pot. function effects 77−50435
methane, nonlinear laser spectroscopy, inside Doppler line *(Russian)* 78−21231
methane, obs. in IR spectra of Uranus, Neptune and Titan (0.8 to 2.5 microns) 80−21946
methane, phase II, IR and Raman spectra of ν_3 and ν_4 modes 78−2834
methane, saturated absorpt. meas. at 3.39 μm using multipath cell 80−74442
methane, saturated absorpt. reson. shape, geometry and field intensity effects *(Russian)* 80−32778
methane, saturated absorpt. resonances, shift and broadening due to curvature of laser wave fronts 77−18981
methane, simultaneous analysis of ν_2 and ν_4 bands 77−10662
methane, solid, far IR spectra, and lattice vibr., 4.2K, 0.4-4.5 kbar 79−19868
methane, solid, orientational order of molecules in phase III 79−51042
methane, solid, phase II and in Kr, Ar matrices, IR spectra quantum rot. 77−28562
methane, V-V energy transfer 80−83469
methane, vibr. induced rot. spectrum in $(u_4=1)$ state 79−18184
methane, vibr. relax. time, spectrophone meas. 77−38669
methane, vibration-rotation energies, $2\nu_2$ and $\nu_2+\nu_4$ bands 80−47963
methane+inert gas, vibr. relax. time, spectrophone meas. 77−38669
methane(-^{13}C), absorpt. spectra. optoacoustic laser meas. 78−37635
methane(-d_1,d_2,d_3), electro-optical parameters from IR intensities, least-squares calc. 80−9584
methane in condensed inert gas matrices, optical excitation of rotational transition, far IR absorption spectra 80−37808
methane-d_1, 9613 Å band rot. anal. 78−86861
methane-d_1, ν_3 band anal., 7.6 micron 80−47980
methane-d_1, ν_6 band at 8.6 μm, vibr.-rot. band 78−21923
methane-d_1, and -d_3, reorientation in simple fluids, IR band profiles 77−36237
methane-d_1 absorpt. spectrum in 6000-12000 Å region 77−42318
methane-d_2, IR spectrum, ν_2 and ν_8 bands, rot. struct. and consts. 77−27066
methane-d_4, ν_2 and ν_4 IR bands meas. and anal. 80−18851
methane-d_4, B_0 determ., from ν_3 Raman band and IR spectrum 77−88455
methane-d_4, IR laser sideband obs., ro-vibr. struct., isotope shifts, line widths 79−72306
methane-d_4, laser sideband spectroscopy *(German)* 79−26975
methane-d_4 4.5 μm absorpt., $2\nu_6$ overtone band anal. 80−91557
methanes, $^{12}CH_4$ and $^{13}CH_4$, IR spectra obs., anal of $\nu_2+\nu_3$ band 80−95614
methanol, absorption spectrum, LiF F_2^+-centre laser intracavity spectroscopy appl. 80−32999
methanol, adsorbed on CsCl(Br)(I), IR spectrometric obs. *(French)* 78−46343
methanol, and dimer, CNDO/2 calcs. of O-H stretching vib. freqs. and intensities 77−18927
methanol, C-O-H bending mode in α- and β-forms at 85K 77−8588
methanol, excited by CO_2 laser, sub-Doppler optoacoustic spectrum 80−5545
methanol, H-bonded struct., IR spectra, assignments 78−62800
methanol, IR absorption using opto-acoustic rapid scan Fourier spectroscopy 79−30585
methanol, IR spectra in soln., OH group fundamental and first overtone bands *(French)* 77−27071
methanol, optically pumped laser, IR-FIR transferred Lamb dip spectra 80−1193
methanol, pure liq. and soln., Raman and IR intensity, polymerisation degree *(French)* 79−28740
methanol (d_3), OH stretch fund., torsion-rot. levels, IR spectra obs. 80−32711
methanol far IR laser line Stark splitting obs. 80−58313
methanol far IR Stark spectroscopy and 9-P(34) CO_2 laser line 80−69145
methanol solns., IR spectroscopic detection of free lone-pair groups or terminal methanol mols., PMR 79−19869
methanol-^{13}C, torsion-rotation transitions, C-O stretch fundamental, FIR spectra obs. 79−93998

infrared spectra of organic molecules and substances continued
methanol-acetonitrile, solns., H bonding, IR and Raman band profiles 77−42320
methanol-CO-H_2O-NH_3 solid mixture vibr. modes, IR spectra 80−90504
methanol-d_1, H-bonded in soln., ν_s(OD) band 79−18183
methanol-d_1(-d_4), far-IR internal rotation spectrum 80−47989
methanol-d_3(d_1) in freon 11, self-associated, OH frequency temp. depend. 80−37809
methanol-proton acceptor binary systems, hydrogen bonded, anharmonicity of OH stretching vibr. 77−6772
p-methoxy benzonitrile, IR absorpt. spectra, vibr. assignments 80−95609
methoxydifluorophosphine-d_0 and -d_3, IR and Raman spectra, mol. vibr. and struct. obs. 80−87103
methoxytrifluorosilane and -d_3, IR and Raman spectra, vibr. anal., barrier to internal rot. 79−18185
methoxytrimethylsilane-d_0,(−d_3) 78−86853
methyl 2-bromopropionate, IR and Raman liq. phase spectra, rot. isomerism 78−58680
methyl 2-chloropropionate, IR and Raman liq. phase spectra, rot. isomerism 78−58680
methyl acetylene, IR absorpt. intensities 79−10103
methyl alcohol, and -d_3, far IR spectra of internal rot. 78−5222
methyl alcohol, photoacoustic spectra meas. at CO_2 laser wavelengths 80−18849
methyl alcohol gaseous, diode laser spectra of C-O stretch band 79−59449
methyl alcohol IR absorption, diode laser obs. 79−31518
methyl anilines, IR spectra, 250-4000 cm^{-1}, vibr. anal. 78−62797
methyl bromide, ν_6 band, CO_2 and N_2O laser Stark spectroscopy 78−78698
methyl bromide, and isotopic modifications, rotational spectrum in vibr. ground state 79−54853
methyl bromide, far IR laser lines, rot. anal. of ν_6 perpendicular band 77−3359
methyl bromide, pure rot. spectrum, fundamental and ν_3=1 levels *(French)* 77−18919
methyl bromide, rot. absorption spectrum of ν_3 and $2\nu_3$ excited vibr. states, mol. consts. determ. 78−82732
methyl chloride, ν_1 band absorpt. strengths 77−75226
methyl chloride, absorption strength of perturbed ν_4 band 78−70833
methyl chloride, far IR laser lines, vibr. isotopic shift value 78−42055
methyl chloride, rot. anal. of IR absorpt. spectra, mol. vibr., rot. const. determ. 80−99505
methyl chloride-d_3, 9.4 μm region laser Stark spectrum, ν_2 and ν_5 bands 77−27112
methyl chloroform, vap., multiphoton dissoc. by CO_2 laser beam 80−61123
methyl chloroformate, struct., microwave, Raman, far IR and NMR spectra 77−34614
methyl cyanide, IR rot.-vibr. spectrum, ν_2 and ν_3 and ν_4 bands anal. 77−75159
methyl cyanide, isotopically substituted species, IR spectra, vibr. freq. displacements, harmonic pot. function 78−42057
methyl cyanide, submm. rot. spectra in ground vibr. state *(Russian)* 77−34636
1-methyl cyclohexanol, struct. information from OH-stretching freqs., axial/equatorial hydroxyl ratio 79−72438
methyl fluoride, IR spectra deconvolution in real time 77−38034
methyl fluoride, solid, IR and Raman spectra, cryst. struct., and deutero deriv. 77−36218
methyl fluoride, tunable diode laser spectroscopy, 9-10 μm 77−54558
methyl furan-2-carboxylate, skeletal vibr. of IR spectra, conformational props., solvent polarity effect 80−87118
methyl furan-2-thiolcarboxylate, skeletal vibr. of IR spectra, conformational props., solvent polarity effect 80−87118
methyl halides, mol. force fields, IR intensities, and vibr. props. 80−47879
methyl indoles, UV and IR absorpt. spectra, f-values and ground state vibr. freqs. 78−58716
methyl iodide, biexciton states, IR absorpt. exam. 77−89714
methyl isocyanide-d_2, IR spectrum, rovibr., ground state struct. 78−25537
3-methyl l-butanethiol, Raman and vibr. IR spectra of solid and liq., rot. isomerism 78−62810
methyl mercapto acetate, Raman and vibr. IR spectra of solid and liq., rot. isomerism 78−62810
methyl methacrylate methacrylic acid copolymer, hydrogen bonding effect on mol. relax., IR obs. of dissoc. process 77−58959
methyl nitrite, internal rotation temp. frozen in supersonic jet, matrix IR spectroscopy 80−9594
methyl nitrite, IR multiphoton dissoc., time resolved IR emission from prods. 78−29822
methyl phosphine-d_2, isolated CH stretching frequencies, bond strength, bond lengths 78−90167
methyl propionate−H_2O(Ba^{2+}) mixtures, in DMSO, acetonitrile solns. IR, assoc., solvent, catalytic effects *(French)* 79−87827
methyl sulphoxide, photoacoustic spectra meas. at CO_2 laser wavelengths 80−18849
methyl symmetric stretching vibr. bandwidths, vibr. and reorientational effects, IR and Raman spectra 78−78686
methyl thionine chloride, intramol. vibr. spectra 80−977
methyl torsion modes, vibrational optical activity, inertial contrib. 80−5524
methyl tri(trifluoromethyl) germanium, and perdeuterated analogues, vibr. spectra, normal coord. anals. *(German)* 80−5547
methyl vinyl ether, and -d_3, IR and Raman spectra, vibr., torsion and internal rot. 78−94250
1-methyl-2-thiomethyl imidazole, IR and Raman spectra, vibr. anal. *(French)* 79−45713
5-methyl-uracil, IR absorpt. spectra, vibr. anal. 78−61143
N-methylacetamide, solid, Fermi resons. 80−97266
N-methylacetamide, vibr. spectra and normal coord. calcs. 79−36632
N-methylacetamide-N-d_3, vibr. spectra and normal coord. calcs. 79−36632
methylacetylene, ν_5 band, microwave and IR laser Stark spectrosc. 80−91558
methylamine liquid, 293K, solvated electron decay kinetics obs. 80−71928
methylanilines, far IR spectra, pot. energy barriers 80−43043
N-methylanilines, substituent effects on geometry, IR spectra obs. 79−10107

infrared spectra of organic molecules and substances continued
methylbenzene sulphinate, vapour and soln. UV spectra, solid IR spectrum, assignments 77−50444
methylborodichloride-d_0(-d_3), vibr. spectra and force constants *(German)* 79−26982
methyldisilylamine, and -d_3, vibr. assignment and barriers to internal rot., IR and Raman spectra 78−13496
methylene radicals, rotational transitions, laser mag. resonance spectra 80−5538
methylenimine, ν_4 fundamental band, laser Stark spectroscopic obs. 79−64039
methylfluoride, rot. IR spectra, line width study 79−76426
N-methylformamide, cis-isomer rot. struct., IR absorpt. spectrosc. obs. 80−14138
3-methylisoquinoline, semiperchlorate, H-bonding, strong, stochastic model and IR spectra temp. effects 78−62805
3-methylpentane, C-H stretching diagonal local mode anharmonicity, intermol. perturbation 78−25524
methylphosphinosilane, IR and Raman spectra, vibr. assignment and asymmetric potential function 79−85962
methylpropylsilane, vibr. spectra, normal vibrs. and rot. isomerism 79−31524
2-methyltetrahydrofuran-methanol mixed glasses, annealed, γ-ray produced electrons transfer from IR to bisible traps 80−11440
1-methylthymine cryst., theory of IR spectra of H-bond 77−40223
Michelson type Fourier interferometer and gaseous molecular spectra 80−68275
microbial cell vibratory spectra, interpretation 77−70425
molecular crystal, lattice vibr., Raman and IR obs., review 78−43079
molecular crystal IR spectral line shape and polarisation temp. depend. 80−88991
molecular crystal lattice vibrs., IR intensities, dynamic multipoles model 80−11372
molecular crystals, intermolecular interactions, spectroscopic studies, review 80−103958
molecular crystals, IR absorpt. spectra, intermol. reson. interaction, temp. depend. 78−72506
molecular crystals, IR intensity of lattice modes 77−47516
molecular crystals, mol. orientation defects, effect on polarised IR and Raman spectra 80−88989
molecular crystals, theory of IR spectra of H-bond 77−40223
molecular fragmentary composition, determ. by IR, EPR and US mag. reson. spectra *(Russian)* 78−13624
molecular glass, density of states for IR active internal modes of tetrahedral mols. 78−75788
molecular liquids, depolarised Rayleigh-wing scatt. and far IR absorpt. spectra 78−39532
molecular liquids, IR absorpt. lineshape, orientation density fluctuation effects 78−48171
molecular liquids, IR spectra, calc. involving vibr. and reorientational relax. 78−48170
molecular monolayers, IR absorpt. enhancement by thin metal overlayers, ATR technique 80−88995
molecular reorientation of symmetric top molecules, in liquid state, book contrib. 78−22623
molecular rotation, model for IR and Raman studies in liqs. and gases 80−11390
molecular vibr. freq. tables, up to 13 atom mols., and Raman and IR values 77−79614
monochloroacetic acid, isolated molecules, internal rotation, CNDO/2 calcs., IR spectra 80−69254
monofluoromethane, ν_6 band, Q-branches, diode laser IR spectra, mol. consts. 79−45722
monofluoromethane, force consts. and IR intensities, ab initio SCF finite difference method 78−86783
2(4)-monooxopyrimidines, gaseous, matrix, soln., tautomeric equilib., IR and UV absorpt. spectra 80−58256
Mori formalism for far IR and microwave absorption 77−24833
mucochloric acid-d_0, -d_1, vibr. spectra, struct. 78−46326
muscle, skeletal, IR spectra of mitochondria and endoplasmic reticulum 77−70434
MXY_2 type molecules, IR intensity anal., dipole moment 78−62806
N-hetrocyclic biomolecules, IR absorpt. spectra, vibr. assignment 77−10671
[n-]alkanes, cryst., vibr. correl. splitting and chain packing 80−7338
Nafion cation exchange membranes, IR spectrum assignment 79−89818
naphthalene, and deutero derivatives, fluoresc., absorpt. spectra under Shpolskii conditions 80−2825
naphthalene, doped crysts., fine struct. strengths in vibronic spectra 77−44004
naphthalene, far IR spectrum, efficiency of heatable long path gas cell 79−58807
naphthalene, in nonpolar solvents, IR absorpt. bands 79−6939
naphthalene, mol. cryst., polariton fusion, two-photon excitation spectra 77−90139
naphthalene, soln. and melt, second vibronic transition, spectroscopic characts., effective field dispersion calcs. 80−55102
naphthalene and −d_8, vibronic spectra 79−51956
naphthalene crystal, multiphonon i.r. absorption 77−1686
naphthalene radical anion, ethereal soln., far IR spectra 78−62796
naphthalene-h_8 and -d_8, gas phase far IR 78−37638
naphthalene-h_8 and d_8, isotopic mixed crystals, exciton spectra in IR region 80−71400
α-naphthol, ν(O-H) k=0 phonon band, width and splitting 77−52066
β-naphthol, IR dichroic ratio, oriented gas and effective charge models calcs. 78−60437
naphthols, IR spectra, assignments 78−58681
napthalene-$d_{0\text{-}8}$, fluoresc. and absorpt. Shpolskii spectra *(Russian)* 78−90208
nematic liq. crystal, dielectric anisotropy, IR spectra, effect of AC elec. field 78−64355
nematic liquid crystal, 7CB, far IR spectra 79−33688
nematic liquid crystal, vibrational IR and Raman spectra 79−73913
nematic liquid crystals, IR absoprtion, strong positive dielec. anisotropy, elastic consts. 78−75545
nickel-porphin, reson. Raman spectra 77−75164
nitriles, in soln., IR spectral line halfwidths determ., rot. Brownian motion investig. 77−36248
nitriles, solns., IR absorpt. band parameters rel. to temp. 80−2762
n-nitroaniline, IR and Raman spectra, internal modes 79−61366

infrared spectra of organic molecules and substances continued
nitroaniline, IR spectral intensity, N-O group in aromatic ring 79−41199
nitrobenzene, intensities in inelastic electron tunnelling, IR, and Raman spectroscopy *(French)* 79−822
nitrobenzene, IR absorpt. and Raman bands, half-band width conc.-depend. 80−74171
nitrobenzene, substituted, IR spectra, vibr. modes 77−68039
nitrobenzene-d_0(p-d)(d_5), vibr. spectra 79−26966
nitrobenzene-d_5, vibr. spectra 79−22695
p-nitrobenzoic acid:rare earth laser materials, vibr. spectra, wavelength 125 to 500 mm 80−2769
nitrobenzoic acid, IR spectral intensity, N-O group in aromatic ring 79−41199
nitrocyclopropane, vibr. spectra struct. and bonding 80−102520
nitroglycerine, laser optoacoustic absorpt. spectra of explosive vapours 78−76941
nitromethane, far IR reflection meas. and plasmon model relevance 79−33687
nitromethane, torsional barriers, electronic spectrum 79−59424
n-nitrophenol, H-bonded complexes, IR absorpt. band struct., freqs. and intensities *(Russian)* 77−18928
nitrophenol, IR spectral intensity, N-O group in aromatic ring 79−41199
o-nitrophenol, solvent effects on oscillator integrated strength, IR absorpt. bands 78−84575
p-nitrosodimethylaniline, solid and CCl_4, H_2O solns., Raman and IR absorpt. spectra 77−79615
p-nitrotoluene, in nematic mixture of octyl cyanobiphenyl, octyloxy cyanobiphenyl, dichroic exam. 78−27201
nitrotoluene, IR spectral intensity, N-O group in aromatic ring 79−41199
p-nitrotoluene, low-freq. vibr. spectrum, Raman and IR spectra 78−56484
p-nitrotoluene, vibr. spectra, normal mode calcs. 77−65482
p-nitrotoluene crystal film, exciton spectrum, IR absorpt. and Raman scatt. 80−80771
nonafluorobutane(-d_1), and halo-substituted forms, gas and liq., IR and Raman spectra, normal coord. anal. *(German)* 79−72318
nonafluoroisobutane, IR spectra, spectral bandshape and intensity of C-H chromophore 80−83355
nucleic acid films, oriented, IR linear dichroism 80−8013
nucleoside cyclic monophosphates, phosphodiester stretching vibrs., IR and Raman spectra 77−65461
nylon, H-bridge interactions, far IR spectra study 80−11374
nylon-11, folded-chain crystal, pressure-induced crystallisation from melt, annealing 77−84671
Nylon-12 film, casting conditions effect on polymorphism 80−84903
nylon-6, pressure-crystallised, morphology and structure 77−84669
nylons 6, 66, 610, change in cryst. struct. with temp. 77−15324
octadecylacrylamide films, oriented ultrathin, radiation-induced solid state polymerisation 80−80128
p-n-octadecyloxybenzoic acid, thermal props. 77−47345
octafluoronaphthalene, phase transitions at elevated press., Raman and mid-IR spectroscopy obs. 80−45062
octamethylcyclotetrasilazane, gas, liq., cryst., CCl_4 soln. IR and Raman spectra, assignments, struct. *(French)* 78−29790
oil, lubricating, ageing parameter determ. by IR spectroscopy *(German)* 80−27360
one-dimensional conductor, IR and Raman activity 78−60441
optical fibres, glass and plastic, neutron irradiated, optical absorpt. spectra 0.7 to 1.1 μm 80−58762
optoacoustic spectra of some far IR laser active molecules 79−59448
organic compounds, low freq. anharmonic vibr., pot. function determ., Raman and IR spectra obs. 80−52997
organic conductors, Fano anti-resonance and IR props. 79−15465
organic N bases, solutions in organic solvents, IR spectra and struct. 79−38534
organo-arsenic compounds, $(CF_3)_2AsSCH_3$ and $(CF_3)_2AsSeCH_3$, gas phase IR and liq. Raman spectra, normal coord. anal. *(German)* 80−32725
organometallic amines, IR spectra *(German)* 80−87133
organometallic compounds, vibr. spectra, book 77−38671
organonitrogen derivatives of Si, Ge and Sn, prep. and props. 78−60456
organophosphorus compounds, $(CF_3)_2PSCH_3$ and $(CF_3)_2PSeCH_3$, gas phase IR and liq. Raman spectra, normal coord. anal. *(German)* 80−32725
organosilane coupling agent interphase of glass-fibre reinforeced plastics, molecular organisation 80−44195
orthocarboranes, IR spectra, CH intra-, intermol. perturbations, hydrogen bonds *(French)* 77−68044
7-oxabicyclo-[4,1,0]-hept-3-ene, far IR spectrum, Q-branch transitions calcs. 77−6770
1,3,4-oxadiazole derivatives, in soln., IR absorpt. and fluoresc. spectra, vibr. anal. 78−66597
oxalic acid, monomeric, IR matrix-isolation spectra, vibr. anal. 78−66550
oxalic acid diamide, mol., PMR and IR spectra, easy polarisable H-bonds 79−31516
oxalic acid in aq. soln., vibr. studies, IR and Raman spectra 80−95589
oxanilide, IR and Raman spectra, cryst. struct. and vibr. 79−42954
oxetane, clathrate hydrate, struct. II, for IR spectra, 4-100K 79−13707
2-oxybicyclo(3.2.0)hept-6-ene, LF vib. spectra, conformations 78−58685
PA-6, polymer fibre, orientation changes during stretching, IR spectra 78−75568
PAA, solid state polymorphism 78−42945
palladium bis-β-diketonates, IR and Raman spectra 78−46327
palladium porphin, IR spectra and vibr. anal., and deutero-derivatives 79−22705
PAN, spectroscopic analysis of electrically polarised films 78−68443
PAN fibre, pre-oxidised, IR absorpt. 77−28561
PAN fibres, SO_2 treatment 79−52403
2,2 paracyclophane, dimer vibration influence on emission spectrum 80−69133
n-paraffins, IR spectra, −180°C, two-phonon absorpt. bands 78−72495
pattern recognition anal. of IR and Raman spectra for cpd. classification 77−75158
pentacene, first excited singlet state, butterfly motion studied by fluoresc. spectra 80−78615
pentacene in naphthalene, intersystem crossing rates following single-mode laser excitation 80−43085

infrared spectra of organic molecules and substances continued
pentachloro aniline, far IR spectra, mol. crystal orientational dynamics 78−60428
pentachloronitro benzene, far IR spectra, mol. crystal orientational dynamics 78−60428
pentachloronitrobenzene, single cryst., far IR absorption 79−73940
pentachloronitrobenzene crystal, anomalous microwave permittivity, IR absorption and Raman spectra *(Japanese)* 78−15169
pentafluorophenol, liq. IR absorpt. spectrum, fundamental freqs. and combinations 79−36633
pentan-3-one, adsorbed on SiO_2, under carbon tetrachloride immersion, IR obs. 79−24821
pentane, liq., enthalpy difference between rot. isomers, IR spectrosc. obs. 80−106404
pentanol activity in bulk phases, distribution and surface activity *(French)* 80−24712
perchloro-[4]-radialene, IR and Raman spectra 77−77198
perdeuteropolyethylene, IR and Raman intensities by electro-optical parameters, single chain 78−1115
perfluoro-1,3-butadiene, vibr. spectra, struct. and barrier to planarity 78−9147
perfluorocyclobutane, matrix isolation Raman and IR spectra, pot. function 77−3352
perfluorocyclobutanone, IR and Raman spectra, vibr. anal. 77−38661
perfluorotertiarybutanol, IR spectra in soln., OH group fundamental and first overtone bands *(French)* 77−27071
perhalonitrosomethanes, gas phase IR spectra, assignments, isomerism 80−28017
peroxyacetic acid, and isotopic forms, matrix IR spectra, force spectrum, force const., thermodynamic props. calc. 77−14427
perylene, α- and β-crysts. and soln., polarised reflection and absorption spectra 77−8598
(perylene)$_3$TCNQ, prep. and spectra, electron-mol. vib. coupling 77−16290
PET, biaxial orientation, refr. index meas. by Raman and IR spectrosc. 80−60583
PET, IR, spectra of prefractured state 77−69032
PET, uniaxially drawn, comparison of polarised fluorescence, polarised Raman and IR dichroism measurements 79−99084
PET film, relation between deform. and rotational isomerism 77−52438
PET film interatomic bond determ. by IR transmission and reflection spectroscopy 77−65958
PET films, dyed, local mech. stresses, IR spectrosc. determ. 80−65418
PET films, one-way drawn, constant strain effects, IR meas. 80−60584
petroleum, weathered, source identification using IR spectra and correl. coeffs. 78−15153
phase transitions at high pressure, IR spectra of 11 compounds 79−95743
phenacyl halides, IR spectra, $\delta(CH_2)$ vibrs. correlation with structs. *(French)* 80−23417
phenanthrene, IR and Raman spectra, lattice and internal mode coupling 77−20843
phenanthrene, vibr. spectra, mol. crystal dynamics, librational modes 78−64356
phenetole, in cyclohexane-ethanol mixtures, UV spectra, solvent effect 79−22770
phenol, cryst., mol. vibrs., factor group splittings 80−16021
phenol, H-bonded complexes, IR absorpt. band struct., freqs. and intensities *(Russian)* 77−18928
phenol, in cyclohexane ethanol mixtures, UV absorption, solvent effects 79−22767
phenol, self association, factor analysis and band contour resolution applications, book contrib. 78−21931
phenols, halogenated, internal rot. barriers, torsional vibr. freqs. 77−68041
phenyl propargyl ether, dimerised, H getter 77−18001
phenylsilanetriol-d_0,(-d_3), cryst. and liq. vibr., IR and Raman spectra 78−86855
phosgene, spectrophone meas. at selected CO, CO_2 laser wavelengths 78−57310
phosphine, IR spectrum, ν_1 and ν_3 band analysis 80−83366
phosphine 3R hydrochloride, interaction with aliphatic acids and alcohols, IR and electron spectra *(Russian)* 78−21930
photoacoustic rapid-scan Fourier spectroscopy and methyl alcohol interferograms 79−30585
photoacoustic spectroscopy using open membrane spectrophone 79−225
photoionisation, multiple, infrared laser 80−69194
phthalic acid, IR absorpt. spectra, fundamental assignments 80−5542
phthalic acid diamide, mol., PMR and IR spectra, easy polarisable H-bonds 79−31516
phthalic anhydride, vibr. excitons reson. interaction in IR and Raman spectra *(Russian)* 79−61386
phthalocyanine, in n-alcanes and polyethylene, absorpt. and fluoresc. spectra, 4.2 and 77K 78−976
phthalocyanine, sublimed film, absorption spectra and association 78−48174
1-piperidine carboxylic acids, intramol. H bonds, struct., IR spectra 77−14426
plasma proteins adsorbed on polymer surface, Fourier transform IR spectrometry 80−16899
plastics, filled and reinforced, optical const. determ. 78−19472
PMMA, molecular interaction in frictional-contact zone, absorpt. spectra 79−78688
PMMA film, Plexiglas, penetration depth of 10.6 μm laser radiation, transmission, refl. and absorpt. meas. 79−74010
polar molecules in nonpolar solvent, far IR spectra and dielec. relax. 80−71312
polaritons, appl. of IR reflectivity and Raman scatt. expt. 77−40237
poly(2-vinyl pyridine), electronic struct., molecular-ion states and dielectric props. 79−37969
poly(β-benzyl L-aspartate), conformational transitions 77−88613
poly(ϵ-caprolactone)-PVC system, Fourier transform infrared spectroscopic exam. 80−25361
poly(m-methylene terephthalate) polymers, IR and Raman spectra 77−52088
poly(octadecyl ethylene), temp. depend. of 720 cm^{-1} IR band 80−97281
poly(octadecyl ethylene oxide), temp. depend. of 720 cm^{-1} IR band 80−97281
poly(p-phenylene), AsF_5 doped, highly cond. charge transfer complexes, elec. and optical props. 80−70778
poly(S)-2-methylbutyl vinyl ether, conformation, IR spectra 78−1116

infrared spectra of organic molecules and substances continued
poly(tetramethylene terephthalate), IR obs. of reversible stress induced crystal-crystal phase transition 80−20627
poly(tetramethylene tetraphthalate), IR studies of α crystal phase 77−62486
poly(vinylidene fluoride) film, phase-III, IR study 80−20624
poly(vinylidene fluoride) orientation, solid state deformation by coextrusion 80−40394
poly N,N-diallyldimethylammonium chloride, soln. props., struct. 79−94861
poly-1,3-pentadiene, microstruct., IR, NMR, X-ray determs. 79−37637
poly-4-vinylpyridene, protonated and deuterated vibr. spectra *(Russian)* 77−19120
poly-4-vinylpyridine N-oxide, aqueous, solns., IR spectra 80−2761
poly-α-deuteroacrylonitrile, thermal degradation under reduced press., Fourier transform IR studies 79−87437
poly-β-benzyl-L-aspartate films, circular dichroism, IR spectra, α, β, ω conforms. 77−48197
poly-β-benzyl-L-aspartate films, conformational stability, effect of organic solvents, IR spectra 78−70988
poly-γ-benzyl-L-glutamate, monolayers, struct. studies, IR, ATR, and TEM obs. 80−44396
poly-γ-benzyl-L-glutamate solution orientation of liq. cryst. domains, IR spectroscopy *(Russian)* 77−62477
poly-bis-phenyl glutarate diacetylene, cryst., solid-state synthesis, struct. 79−15638
poly-m-phenylene isophthalamide-ε-caprolactam, complex polymer cryst. 78−9967
poly-n-butylisocyanate, conformation, IR spectra *(Russian)* 77−19123
polyacetylene: Br(Cl)(I)(AsF_5) electrical conductivity, metal-to-insulator transition 78−10525
polyacetylene, doping with AsF_5, mechanism, effect on elec. cond. and spectra 80−24473
polyacetylene, lightly doped, donor and acceptor states, IR absorpt. obs. 79−73979
polyacetylene, pure and heavily doped, optical and IR studies, electronic struct. calcs. 80−7347
polyacetylene, vibr. excitations of charged solitons 80−108201
polyacetylene films, doping effect on elec. cond., chem. and optical props. 80−65572
polyacids, unsaturated carboxylic, in organic solvents, hydrogan bonding, structurisation *(Russian)* 78−71666
polyacrylonitrile, film, IR attenuated spectra determ. of chem. origin of TSC 77−55746
polyacrylonitrile, thermal degradation, Fourier transform IR obs. 78−92474
polyamide-polyurethane, enamel lacquer, far IR transmission, encapsulation of optical devices 79−55194
polyamidoimide film, thermomech. props. rel. to mol. struct. *(Russian)* 79−57029
polyarylbutadiene, microstructure, NMR and IR obs. *(Japanese)* 79−24488
polyatomic fluid, local dynamics, spectroscopic studies, summer school lecture series 80−6343
polyatomic liquids, vibr. relax. and energy transfer, ultrafast dynamics obs. 77−50506
polyatomic molecules, dil. solns., IR spectral band shapes of fundamentals 78−66544
polyatomic molecules, structure recognition, from IR, UV, NMR and mass spectra, computer method 78−25737
polyatomic molecules in C star 3 μ band 79−5807
polybut-1-ene, cryst. forms I and II, far IR spectra 79−33708
polybutadiene, adsorption behaviour, surface tension exam. *(Japanese)* 78−31690
polycaproamide, molecular interaction in frictional-contact zone, absorpt. spectra 79−78688
polycaproamide, oriented, molecular rearrangements during deformation, IR spectra exam. 80−7644
polycarbonate, colour appearance during oxidation *(Russian)* 79−24643
polycarbonate, glassy, IR dichroism at small strains 78−56475
polychloroprenes, microstruct., IR digital subtraction method, struct. irregularities effect on copolymer IR bands 79−38543
polychloroprenes, microstruct., IR digital subtraction method, struct. irregularities 79−42965
polydeoxyribonucleotides, poly(dA).poly(dT) and poly(dAT).poly(dAT), HF vibr. modes, Raman and IR spectra 80−32698
polydiacetylene polymer crystals, one dimensional conjugated, optical props. 77−43993
polyether-amidourethane, segmented, polymer domain struct., IR spectra and optical microscope *(Russian)* 78−51453
polyethyl ethylene and deuterated derivatives, modification I, vibrational spectra and normal coordinate anal. 79−87434
polyethylene, amorphous, glass temp. 77−66017
polyethylene, brominated, single cryst., IR analysis 80−25362
polyethylene, crystalline struct. transitions 77−51496
polyethylene, deformed cryst., IR spectrum, C-H stretching, effect of polymorphism 79−15453
polyethylene, FIR absorpt. freqs. using proved semiempirical pot. function 77−52090
polyethylene, high density, cold-drawn, IR spectroscopy and X-ray diffr. 77−4764
polyethylene, high density, fracture fatigue kinetics, IR absorption spectra 78−11323
polyethylene, IR and Raman intensities by electro-optical parameters, single chain 78−1115
polyethylene, IR spectra, −180°C, two-phonon absorpt. bands 78−72495
polyethylene, linear, far IR absorpt. spectrum, temp. depend., 14K to melting pt. 79−1758
polyethylene, linear, single cryst., surface melting, X-ray diffr. 77−31755
polyethylene, melt crystallized, amorphous phase, IR spectrum 78−76463
polyethylene, modified with phosphonate ester pendant side group, thermal and mech. props. 78−11195
polyethylene, molecular interaction in frictional-contact zone, absorpt. spectra 79−78688
polyethylene, NMR, IR spectra and elemental anal. 80−29681
polyethylene, partially crystalline, far IR absorption and thermal props. 79−33690
polyethylene, perdeuterated, skeletal vibr. spectrum 78−23445
infrared spectra of organic molecules and substances continued
polyethylene, photodegradation study by Fourier transform IR spectroscopy *(Japanese)* 79−24772
polyethylene, polarised Raman studies of crystalline and amorphous orientation 78−67660
polyethylene, single crysts. chain end location, IR spectra 78−71687
polyethylene, solid, IR spectra, interference distortion of 73 cm^{-1} absorpt. line 80−11375
polyethylene, structural changes induced by high elec. field *(Japanese)* 79−23532
polyethylene, supermolecular structure study, IR spectroscopy *(Spanish)* 79−77532
polyethylene, uniaxially oriented, relation between deform. and rotational isomerism 77−52438
polyethylene, vinyl group reactions during γ-irrad., crystallinity effect, absorbance obs. 80−81346
polyethylene (orthorhombic), intermol. pot. functions, force consts., vibr. assignments, thermodynamic props. 77−39639
polyethylene electret, internal pot. topography, Raman and IR spectra 80−7362
polyethylene electrets, charge trapping mechanism, TSC, DTA and optical meas. 80−11322
polyethylene far IR absorption rel. to crystallinity 77−40242
polyethylene film, gauche-trans transition, activation energy meas. by IR spectra 79−57220
polyethylene glycol, aqueous, solns., IR spectra 80−2761
polyethylene oxide, low mol. wt., effect of end-group on crystallinity and fusion 77−84897
polyethylene oxide homo and copolymers, monomer link lengths determ., IR spectral method *(Russian)* 77−32383
polyethylene reinforced with graft polymers, molecular failure mechanism, IR spectra 77−16682
polyethylene single cryst., FT IR spectra, CH_2 rocking mode 78−2843
polyethylene single cryst., FT IR spectra, CH_2 wagging mode 78−2842
polyethylene single crystal in suspension, Fourier transform IR study 78−10877
polyethylene terephthalate, fatigue failure under cyclic loading, overstress in chem. bonds 79−57106
polyethylene terephthalate, film, optical consts., frustrated total internal refl. obs. 77−55763
polyethylene terephthalate, film, two-stage orientation in monoaxial extension *(Russian)* 77−62488
polyethylene terephthalate, isotropic and oriented, refr. index meas. 40 to 300 cm^{-1} 78−52482
polyethylene terephthalate, molecular interaction in frictional-contact zone, absorpt. spectra 79−78688
polyethylene terephthalate, simultaneous mech. loading, UV rad. effects on overstrained chem. bonds 79−52706
polyethylene terephthalate fabric, surface struct., props. rel. to plasma surface treatment 78−95831
polyethylene terephthalate far IR absorption rel. to crystallinity 77−40242
polyethylene terephthalate film, gauche-trans transition, activation energy meas. by IR spectra 79−57220
polyfluorocarbon, synthesis and opt. spectra 78−23657
polyglycine, IR spectra calc. for helix and β configs. 80−45853
polyhexamethylene adipamide, calorimetric, X-ray and IR study 80−10512
polyisocyanides, solns., struct. and acidification 80−19915
polymer, deformation of interatomic bonds, IR spectral meas. 79−38918
polymer, oriented, under load, crystallite stability, X-ray diffr. and IR spectra meas. 77−70126
polymer film, conformational transitions, activation energy determ. *(Russian)* 78−48186
polymer film, supermolecular structure and mech. stress distrib. among chem. bonds 78−75562
polymer orientation measurement, in solid, by spectroscopic techniques, mech. anisotropy 78−75558
polymer solution, short-range solvent orientational order, IR dichroism and photoelasticity obs. *(Russian)* 78−26415
polymer spray coatings, struct. investig. by multiple-external-refl. method 78−6235
polymer thin films formed in RF discharge using monomer organic semicond., elec. props. obs. 80−80432
polymers, aliphatic and aromatic, mean mol. orientation factors, from IR spectra and acoustic method 80−70142
polymers and crysts., vibr. anharmonicity, intensities of overtones and component freqs. 77−69052
polymethacrylic acid-polyethylene oxide polymer complex, H bond form., thermal behaviour *(Japanese)* 79−15454
polymethine dye layer, vibr. spectrum anal., inelastic electron tunnelling spectroscopy 79−13716
polymethinium dye, cryst. metallic refl., damping theory 77−16294
polymethylene chain, vibr. spectra, CH stretching region, struct. and assignments 78−70991
polyoxymethylenes, dielec. relax. and IR spectra, 90 to 300K *(Russian)* 79−28678
polypeptides, helical sense characterisation by IR spectra 78−17831
polypeptides, poly-L-lysine based, comb-like, struct., physicochem. props. *(Russian)* 79−55644
polyperdeuteroethylene, IR and Raman spectra, 77K and room temp., vibr. anal. 78−72517
polyphenyl ether fluid operating in elastohydrodynamic contacts, IR emission spectra 79−91807
polyphenylene oxide, with and without impact resisting polystyrene, photo-oxidative ageing, Cu and Fe trace effects *(German)* 79−100191
polyphenylene oxide-polystyrene blends, spectroscope exam. of chain conform. and bonding 78−42925
polyphenylene oxides, high temp. ageing effect on struct. and props. *(Japanese)* 77−70078
polypropyl ethylene and deuterated derivatives, modification I, vibrational spectra and normal coord. anal. 79−87435
polypropylene, effect of corona treatment on dielectric props. for capacitor appl. 79−33607
polypropylene, Fourier transform IR study of ordered and amorphous phases 78−27225
polypropylene, molecular interaction in frictional-contact zone, absorpt. spectra 79−78688
polypropylene monofilaments, tensile props., orientation degree depend., IR dichroism obs. 78−3163

infrared spectra of organic molecules and substances continued
polypropylene reinforced with graft polymers, molecular failure mechanism, IR spectra 77−16682
polypropylenes, iso- and syndio-tactic, Raman tacticity bands, vibr. spectrum 80−66193
polyquinazolones with N-phthalimide groups in side chain, prep., props. *(Japanese)* 79−15642
polysaccharides, 2.5-15 μm spectra rel. to interstellar mols. identification 78−28763
polysiloxene, irrad., linear, IR and solubility obs. 80−93775
polystyrene, and copolymers, optical fibre waveguides, spectral characts. 80−14461
polystyrene, atactic, stereoregularity study using Fourier transform IR spectroscopy 79−59612
polystyrene, atactic, uniaxially oriented, Fourier transform IR spectroscopic exam. 80−25360
polystyrene, film, optical props. from near IR to X-ray, sum rules 77−48195
polystyrene, glass-like, intermol. interactions temp. depend., IR spectra *(Russian)* 79−51967
polystyrene, glassy, intermol. interaction during inelastic deform., optical spectral obs. 77−59878
polystyrene, isotactic, normal vibrational anal. 78−43869
polystyrene, isotactic gel film, Fourier transform IR spectrum 80−104465
polystyrene, methacrylic acid/(PSMA) ionomers, far IR studies of ion clustering 79−87436
polystyrene, stress cracking, pressure-induced, mechanism 80−35361
polystyrene, substituted, Raman, IR and neutron spectra of LF vibs. 78−2848
polystyrene amorphous film, cyclically fatigued, molecular behaviour 80−35310
polystyrene and styrene copolymers, amorphous, intermolecular interaction and disintegration 79−86723
polystyrene film, Fourier-transformed IR photoacoustic spectra 80−34993
polystyrene lattice cleaning, dialysis, steam stripping and ion exchange effectiveness 80−3414
polystyrene-polydivinylbenzene, interpenetrating network, IR, NMR and chromatographic anal. of intermediate regions 77−55711
polythylene, and perdeuteropolyethylene, crysts., IR and Raman intensities, factor group splittings 79−65851
polyurethane, interpenetrating network, IR, NMR and chromatographic anal. of intermediate regions 77−55711
polyurethane, variation of packing charact. near solid surface, IR obs. *(Russian)* 79−65349
polyurethanes under tension loads, spectral exam. *(Ukrainian)* 78−92058
polyvinyl acoustal, enamel lacquer, far IR transmission, encapsulation of optical devices 79−55194
polyvinyl formate, far IR molecular vibrational spectroscopy by inelastic electron tunnelling 78−50546
polyvinylalcohol, aqueous, solns., IR spectra 80−2761
polyvinylidene chloride, vibr. spectra, amorphous and cryst. state conforms. 79−27930
polyvinylidene electrets, IR and Raman spectra 80−7359
polyvinylidene fluoride, corona-charged, surface effects 80−66102
polyvinylidene fluoride, poling by corona charging, pyroelec. effect 78−19423
polyvinylidene fluoride film, cryst. dipole orientation in elec. field 78−80286
polyvinylidene fluoride films, stretched and rolled, electrostriction and piezoelectric effects *(Japanese)* 80−55041
polyvinylidene fluoride-PTFE, thermoelectret, IR spectra, struct. modifications and dielec. props. 77−55785
polyvinylpyrrolidone, aqueous, solns., IR spectra 80−2761
porphin free base, vibr. and normal mode anal. 80−69122
porphin-d_n, (n=2-14) electronic-vibr. interaction, quasi-line absorption (fluoresc.), mirror symmetry 78−55197
potassium chloranil, IR spectra, mag. and optical props., phase transition and solvation 77−43983
potassium formate, IR absorpt. spectra, sampling effects, Davydov splitting and struct. 78−52508
potassium hydrogen glutarate, H bonding, vibr. spectra 78−43860
potassium hydrogen malonate, aq. soln., IR and Raman vibr. spectra *(French)* 79−26989
potassium hydrogen malonate single cryst., IR and Raman spectra 78−60444
potassium oxalate, anhydrous, phase II, vibr. spectra and cryst. struct. 80−34901
potassium oxalate monohydrate:VO^{2+}, cryst., IR absorpt. 80−55134
potassium tetrachlorophthalimide, polycrystalline, IR and Raman band assignments 79−50015
principal component analysis, using computer *(Japanese)* 80−69143
propanal, methyl torsional pot. functions, LF Raman and IR vibr. spectra 80−95612
propane-Ar, reson. absorpt. of 10.6 μm light, shock wave in Ar mixture 79−64002
1-propanol, low temp. pulse radiolysis, solvated electrons, absorpt. spectral changes 77−12813
propenoyl chloride, far IR and Raman spectra, internal rot. 79−89668
propenoyl chloride, IR bands, torsional struct. 80−28018
propenoyl fluoride, far IR and Raman spectra, internal rot. 79−89668
propiolyl chloride(-d), 357-333 nm absorpt. system 80−69161
propionitriles (-O, NH, S), conformational investig., NMR, IR and semiempirical MO methods 80−95650
N-p-propoxybenzylidene-p-pentylaniline, orientational order in glassy and nematic phases, IR dichroism meas. 80−64891
n-propyl alcohol-α-picoline, donor-acceptor complex form., solvent effects, IR spectra 77−38660
isopropyl chloride, torsional pot. function, far IR and Raman obs. 80−28022
n-propyl radical, matrix isolation IR spectrum 78−33510
n-propylbenzene, broad band far IR absorpt., temp. depend. 78−2835
propylene, He-Ne laser line, high temp. absorpt., anal. by high resolution IR spectra 80−91554
propylene, solubility in liq. N_2 80−39286
propylene and ethylene adsorbed on Ag, enhanced Raman spectra obs. 80−95607
propylene ozonide formation mechanism, Fourier IR spectra 77−33132

infrared spectra of organic molecules and substances continued
propylene-alkyl acrylates alternating copolymers characterisation 79−51950
propylene-butadiene, alternating copolymer, struct., fractional composition obs. *(Russian)* 79−65011
1,3-propylenediammonium manganese tetrachloride, vibr. study of phase transitions, IR and Raman spectra 80−40103
propylsilane-d_0(−d_n), vibr. spectra, normal vibrs. and rot. isomerism 79−31523
propynal, IR-microwave double reson. and two-photon expts. 80−83396
propynal, rovibronic populations, collisionless IR multiphoton spectra, energy deposition, photoacoustic determ. 80−83354
propynal-d, in ground vibrational state, IR microwave double resonance spectra, rot. and centrifugal distortion const. determ. 80−83358
propyne-d_0(-d_3), absolute and integrated IR intensities of fundamental modes 80−87179
PTE, polymer fibre, orientation changes during stretching, IR spectra 78−75568
PTFE, γ-ray effects on 19 and 30°C phase transitions, Fourier transform IR spectroscopy 80−103387
PTFE, molecular interaction in frictional-contact zone, absorpt. spectra 79−78688
PTFE, surface layer optical consts. in 1000-1300 cm^{-1} region 79−51957
PTFE, vib. assignment, far IR spectrum 77−48170
PTFE, vibrational assignment problem, far infrared spectrum 77−52087
PTFE films, plasma-polymerized, cond. mechanism, AC cond. and capacitance meas. 79−24093
purple membrane, anomalous amide I IR absorpt. 80−12058
purple membrane, polarized IR spectroscopic struct. study 79−43809
purple membrane of halophil cells, homogeneity based on IR spectra 78−69003
PVA, photooxidation, kinetic eval. for carbonyl form. *(Japanese)* 79−39007
PVC:Fe(Cu) film, struct. and optical props., soln. growth technique 78−51837
PVC, highly syndiotactic, X-ray diffr. and IR studies of annealed material, crystallinity 78−2022
PVC, mechanochemical degradation in primary struct., mech. vibration effects, IR spectra *(German)* 78−19769
PVC, reduced, NMR, IR spectra and elemental anal. 80−29681
PVC, with stabiliser, dielec. and mech. characts. under γ-irrad., plasticisers effects *(Korean)* 77−81054
PVC+Br_2(I_2), reaction in surface-modified film subject to thermal-radiative and photochem. action *(Russian)* 77−21385
PVC branching, origin, extent 79−7048
PVC chain branching, CH_2Cl group production mechanism, IR data evaluation 79−7047
PVC film, metal doping effect on chain vibrs. 79−95868
PVC plastisol films, thermally hardened, struct. and props. *(German)* 79−70097
PVC-THF-H_2O, precipitation fractionation, influence of stereoregularity 79−7046
pyrazine, phase transitions, sp. ht., X-ray diffr., LF vibr. spectra 78−43122
pyrazine, triplet-triplet absorpt. related to state splitting 80−47917
pyrene, appl. of new force field for condensed aromatics, inplane vibrs. 79−81201
pyrene, far i.r. spectra, phase transition effects 77−1685
pyridine, chemisorption on goethite, IR spectra 80−7855
pyridine, deuterium substituted, Raman and IR vibr. spectra 80−84739
pyridine, IR spectra, adsorpt. on $Zr(HPO_4)_2$, acidity 78−92377
pyridine, i.r. spectra and electronic struct. 77−3363
pyridine-2,3,5,6-d_4, vibr. spectra, IR and Raman, assignment 80−102519
pyridine-3,4,5-d_3, vibr. spectra, IR and Raman, H exchange rates meas. 80−102518
pyridine-3,5-d_2, vibr. spectra, IR and Raman, H exchange rates meas. 80−102518
pyridine-Ag_5I_6, superionic conductor, dynamical aspects 78−79695
pyridine-d_5, vibr. spectra, IR and Raman, assignment 80−102519
pyridine-I_2(Br_2) charge transfer complexes, vibr. spectra, vibronic contrib., intensity enhancement 80−53048
pyridinium pentasilver hexaiodide, solid, far IR refl. spectra, low freq. optical modes 78−2291
2-pyridone, dimer, vibr. Hamiltonian for IR spectra of H bonding 78−37620
di-α-pyridyl hydroperchlorates, intramol. H bonds, steric conditions and polarisability obs. 80−53160
pyrimidine bases, water vapour effect on struct. and amorphous-cryst. transition 77−70408
β-quinol, low frequency mode investig. by IR absorpt. and neutron scatt. *(French)* 77−36220
β-quinol clathrate, CH_3OH mol. reorientation investig. by IR and dielec. meas. 77−12369
rare earth formate, IR spectra and phase transitions, under pressure 78−31179
resin vulcanisation, effect of Sn halides, IR spectra *(Bulgarian)* 79−33994
resin vulcanisation, effect of Zn halides, IR spectra *(Bulgarian)* 79−33993
retrieval system for IR spectra 77−22535
rhodamine 6G, aqueous soln., absorpt. spectra, ground and triplet state photoprotonation pH depend. 80−42961
rhodamine 6G, photoacoustic spectra in soln. 80−9606
rhodamine dyes in soln., bleaching, electronic and vibr. absorpt. spectra, fluoresc. 80−42960
ring compounds, three-membered, vibr. spectra and struct., book control 78−78701
Rochelle salt, cryst., oriented intrinsic absorpt. edge shape 77−66505
rubidium hydrogen glutarate, H bonding, vibr. spectra 78−43860
rubidium tetramethylborate, vibr. spectra and force constants *(German)* 79−26981
saccharose, far IR absorpt. spectra, pyroelec. coeff. temp. depend. *(French)* 78−72503
saccharose, far IR absorption, low temp. pyroelectricity 78−80348
salicylic acid, IR absorpt. spectra, fundamental assignments 80−5542
samarium oxalate, IR and Raman spectra exam. *(French)* 78−48159
scandium oxalate, IR and Raman spectra exam. *(French)* 78−48159
selenoacetamide (-d_n), IR spectra, vibr. assignments, normal coord. anal. 79−22708
semicarbazide hydrochloride, phase transition, IR spectra and thermal study 79−37833

infrared spectra of organic molecules and substances continued
semicarbazide hydrochloride, vibr. spectra, normal coord. anal. 80−58255
semicarbazide-d_0, -d_6, vibr. spectra, normal coord. anal. 80−58255
semiconductor, vibr. IR excitons, spectra *(Russian)* 78−15173
semitetrafluoroborates, H-bonding, strong, stochastic model and IR spectra temp. effects 78−62805
L-serines-d_0 and -d_4, IR and Raman spectra, rot. isomers *(French)* 79−45714
silane coupling agent deposited on E-glass fibre, hydrolysis and drying effect on siloxane bonds 80−85072
silk fibroin films, conformational changes induced by water immersion 80−10498
silyl acetylenes, fine structure due to internal rotation in IR-active perpendicular bands 79−98096
smectic liquid crystal, vibrational IR and Raman spectra 79−73913
sodium formate(-d_1), far IR and IR absorpt. spectra, lattice mode assignment 77−85717
solution, mol. vibr. spectral linewidth, conc. fluctuations effect 78−70880
sorbitol, relax. processes, optical probe obs. 79−47430
squaric acid and deuterated derivative, vibrational study, IR and Raman spectra 78−92076
squaric acid thin films, Raman and IR spectra, Davydov splitting rel. to interlayer interaction 79−99878
steel, rusted, exam. of tannin treatment action mode 78−88564
stilbene, thin single cryst., IR spectra anal. Fermi-Davydov intensity distrib. 77−59577
strong H bonded systems, vibr., Raman, IR spectra, biology appls. 78−82735
strontium uranyl tetraformate hydrate, struct. determ., orthorhombic unit cell, UR spectrum *(French)* 78−22705
styrene, and isotopic forms, IR and Raman spectra, normal vibr. assignments 77−18930
styrene, plasma polymerisation in glow discharge, thin film IR and free radical EPR obs. 80−2964
styrene anions, electron affinities, transition energy, comparison for gaseous liquid and solid 80−29731
styrene-β-d_2, IR and Raman spectra, vibr. assignments 79−13711
styrene-divinylbenzene grafted copolymer, structure investigation by IR spectroscopy *(Russian)* 77−62487
styrene-methacrylic acid copolymer, glass-like, intermol. interactions temp. depend., IR spectra *(Russian)* 79−51967
styrene-methacrylic acid copolymer, glassy, intermol. interaction during inelastic deform., optical spectra obs. 77−59878
succinic acid and its alkaline salts in aqueous soln., Raman and IR spectra *(French)* 80−32723
succinic acid diamide, mol., PMR and IR spectra, easy polarisable H-bonds 79−31516
symmetric top mols., gas phase IR rot. velocity correl. functions, appls. to CH_3F, CHF_3 *(French)* 78−62778
TBBA, smectic and cryst. phases, far IR absorpt., struct. and dynamical props. 77−84636
TCND, IR and Raman spectra, vibr. anal. 79−36630
TCNE-benzene, charge-transfer complex, change of C≡N and C=C band intensities 77−88448
TCNE-paraxylene, charge-transfer complex, change of C≡N and C=C band intensities 77−88448
$TCNQ_2$-TEA, quasi 1-D cryst., interaction between electronic and vibr. states 77−52102
TCNQ, cryst., metallic refl., damping theory 77−16294
TCNQ, optical IR antireson. absorption, characts. rel. to cryst. parameters 77−77183
TCNQ, salt, $(NMe_3H)(I)(TCNQ)$, semicond. 'metal-like' complex, optical props. 79−95761
$(TCNQ)_2TEA$, refl. spectra 77−90154
TCNQ alkali salts, charge transfer enhanced IR absorpt. spectra 77−28558
TCNQ alkaline salts, in dimethylsulphoxide, and aq. solns., Raman and IR spectra 78−46344
TCNQ alkaline salts, phase transitions, vibronic intensity enhanced IR spectra 78−23441
TCNQ complexes with pyridine, polarised IR refl. spectra, evidence for electron-vibr. coupling 79−47448
TCNQ ion radical salt, $DECA(TCNQ)_2$, IR absorpt. spectra obs. of first-order transition 80−71397
TCNQ salt, decamethylferrocenium, monomeric and dimeric, optical and EELS study 80−100660
TCNQ salt, HMTTF-TCNQ, electron-electron interactions, mag. susceptibility and optical reflectivity 77−81104
TCNQ salt, K-TCNQ, energy gap, electron-phonon interaction, IR spectrum 78−15167
TCNQ salt, K-TCNQ, single crystal, charge transfer band interpretation, refl. spectrum obs. 80−25353
TCNQ salt, $MeDABCO(TCNQ)_2$, elec. cond. and IR and visible spectra meas. 79−42526
TCNQ salt, $MeDABCO(TCNQ)_2$, optical, elec., and mag. props. 80−65539
TCNQ salt, n-methyl-n-ethylmorpholinium, unpaired electron states, IR refl. study 80−75491
TCNQ salts, anomalous infra-red activity and the determination of electron-molecular vibration coupling constants 80−25389
TCNQ salts, complex, optical absorption meas. 79−4824
TCNQ salts, elec. and optical props. 79−73498
TCNQ salts, electron localized and band motion, IR spectra 77−66487
TCNQ salts, IR, X-ray electron spectra, tetrathiotetracene $(TCNQ)_2$ cond. investig. 77−44005
TCNQ salts, K(TCNQ), $Ba(TCNQ)_2$ and $Ca(TCNQ)_2$, electronic absorpt. spectra, vibronic struct., charge transfer bands 79−24331
TCNQ salts with alkali metals, intensities of IR absorpt., electronic transfer magnitude 78−6691
TCNQ-HMTSeF, polarised single cryst. reflectance obs. and one-dimens. behaviour interpret. 78−6690
TCNQ-perylene, electronic absorpt. spectra, vibronic struct., charge transfer bands 79−24331
TCNQ-TSef, Drude optical edge, press. depend. 79−19882
$TEA(TCNQ)_2$, linear chain semicond., phase phonons, intramol. electron-phonon coupling 77−32373
TEA $(TCNQ)_2$, mixed electronic-vibr. states in far IR spectra, dielec. const. *(Russian)* 77−36249
terephthalate liquid crystals, vibr. spectra, vol. struct. 78−18547

infrared spectra of organic molecules and substances continued
terpenes, IR absorption bands of α- and β-pinenes above forests 80−12539
p-terphenyl, far IR absorption spectra, 300-1.3K, phase transition obs. *(French)* 77−90140
p-terphenyl, substituted, dye laser and spectral characts., output power, conversion efficiency 80−23681
tetra(trifluoromethyl) germanium, gas and liq., IR and Raman spectra, normal coord. anal. *(German)* 79−72315
tetra-alkylammonium halide interionic potential models and far IR spectra 79−33689
tetra-alkylammonium halides, far IR spectra, interionic pot. energy 78−27217
tetra-n-butylammonium halides in benzene, chloroform, CCl_4, far IR spectra, ion-ion, ion-mol. interactions 80−60562
tetraalkylammonium halides in methanol, struct., IR spectra 77−23500
1,2,4,5-tetrabromobenzene, lattice vibrs., Raman and far IR spectra 78−76444
1,2,4,5-tetrabromobenzene, structural phase transition, Raman and IR spectra meas. *(French)* 77−66503
meso-1,2,3,4-tetrabromobutane, IR and Raman spectral studies 80−32722
1,1,2,2-tetrabromocyclopropane, IR and Raman spectra 79−41170
tetrabromomethane, liq. and plastic cryst., rot. Brownian motion, far IR absorpt. 77−36234
tetrabutylammonium halides, solutions in organic solvents, IR spectra and struct. 79−38534
tetrachloro-p-benzoquineone, IR and Raman spectra of phase transition *(French)* 78−60445
1,2,4,5-tetrachlorobenzene, structural phase transition, Raman and IR spectra *(French)* 77−66503
meso-1,2,3,4-tetrachlorobutane, IR and Raman spectral studies 80−32722
2,2,3,3-tetrachlorobutane, vibr. spectra, liq. and solid-state, conform. struct. 79−73936
tetrachloroethylene, cryst., IR spectra in polarised light, cryst. struct. 78−27223
tetrachlorophthalic anhydride, polycrystalline, IR and Raman band assignments 79−50015
N-d-tetrachlorophthalimide, polycrystalline, IR and Raman band assignments 79−50015
1,1,1,3-tetrachloropropane, Raman and IR obs. of rot. isomerism, entropy difference between vapour and liq. phase isomer *(Russian)* 79−31529
1, 2, 4, 5-tetracyanobenzene and -d_2, IR and Raman spectra, vibr. anal. 79−36629
tetracyclo[4,2,2,$O^{2,5}$,$O^{3,7}$] decane-10-carboxylic acid, lactone substituted, molecular, crystal struct. 79−90640
1,1,2,2-tetrafluoroethane, anti- and gauche-rotamers, struct., spectra, electron diffr. 77−50439
tetrafluoromethane, $\nu_2+\nu_4$ band, high resolution diode laser spectra 80−69138
tetrafluoromethane, ν_4 fundamental of three isotopic species 78−70835
tetrafluoromethane, collision-induced light scatt., spectral features 78−13493
tetrafluoromethane, collision-induced rot. spectrum 79−98101
tetrafluoromethane, IR spectrum, Fermi reson. sequences, cubic pot. energy, anharmonicity consts. 77−10674
tetrafluoromethane, multipole moments, far IR spectrum determ., pot. function effects 77−50435
tetrafluoromethane, pot. consts., IR spectra 78−82808
tetrafluoromethane, spherical top mol. vibr.-rot. spectrum with tunable diode laser 78−82734
tetrafluoromethane+He gas mixture, collision induced for IR translational spectra 80−83353
tetrafluoromethane molecule, laser spectrosc. and optical pumping from CO_2 laser 80−74202
tetrahydrofuran, clathrate hydrate, struct. II, for IR spectra, 4-100K 79−13707
1,4,5,8-tetrahydroxyanthraquinone-d_0,-d_4, mol. vibr., IR spectra 77−467
tetramethyl germanium(-d_{12}), vibr. spectra, normal coord. calcs. 79−22717
tetramethyl lead(-d_{12}), vibr. spectra, normal coord. calcs. 79−22717
tetramethyl silicon(-d_{12}), vibr. spectra, normal coord. calcs. 79−22717
tetramethyl tin(-d_{12}), vibr. spectra, normal coord. calcs. 79−22717
tetramethylammonium cation(-d_{12}) aqueous solution, Raman and IR spectra 78−82741
tetramethylammonium compound, $(TMA)_2C_2S_6.1/2CS_2$, IR spectra in 200 to 4000 cm^{-1} range *(French)* 79−33711
tetramethylammonium hexachloroplatinate, order-disorder phase transition, IR and Raman spectra 78−92060
tetramethylammonium hexachlorotellurate, IR and Raman spectra, lattice and internal modes, phase transition 78−6659
tetramethylethyl-cyclopentadienyl thorium trichloride, prep., NMR and IR spectra 79−76428
tetramethylethyl-cyclopentadienyl uranium trichloride, prep., NMR and IR spectra 79−76428
tetramethylsilane, IR and visible spectral intensity data and the universal intensity concept 80−28066
tetramethylsiloxane dicarbonxylic acid Langmuir films on Cu surface, surface EM wave absorpt. study 80−97359
tetramethyltetraphenyltrisiloxane film, DC-704, on Ge, Al and KRS-5, IR refl. spectra anal. 77−59630
tetramethylurea-d_0,-d_{12}, IR spectra, normal coord. anal. 78−978
tetraphenylarsonium, Raman and IR spectra of the dicyanoiodate (I) ion 80−60572
tetraphenylphosphonium, Raman and IR spectra of the dicyanoiodate (I) ion 80−60572
tetraselenatetracene bromide complex, optical props. 78−6680
tetrathiotetracene salts, IR, X-ray electron spectra, tetrathiotetracene $(TCNQ)_2$ cond. investig. 77−44005
tetrohydrofuran-$HgBr_2$ complexes, IR and Raman vibr. spectra, inter- and intramol. forces 77−66489
tetrolyl fluoride, IR and Raman spectra 79−41171
1,3,5,7-tetroxocane, vibr. spectra and intermol. forces 77−36216
TGFB, IR spectra and optical consts. *(French)* 79−95748
TGS, cryst., characteristic absorption edge shape 77−85712
TGS, cryst., vibr. bands, ferroelec. and paraelec. phase H bonds *(Russian)* 78−15172
TGS epitaxial thin film, IR absorption spectra *(French)* 78−35129
TGS-d, TGSe-d, single cryst. films, epitaxial growth method, IR transmission spectra *(French)* 78−72742

infrared spectra of organic molecules and substances continued
TGSe, IR trichroism, epitaxial prop. process 77−63475
thermoplastic enamel lacquer, far IR transmission, encapsulation of optical devices 79−55194
thermoplastics, wideband optical transmission meas. 79−76771
2-thiapyridone, dimer, vibr. Hamiltonian for IR spectra of H bonding 78−37620
thiazolidine, IR spectroscopy of mol. association *(French)* 79−50178
thiazolidine, mol., vibr. anal., IR and Raman spectra *(French)* 79−26964
Δ-2 thiazoline and alkyl derivatives, IR and Raman vibr. spectra, conformation *(French)* 79−10104
thick liquid films, absorbance ratio, IR spectra determ. 78−48710
thieno(3,2-b)thiophene, electronic and vibr. spectra, vapour phase and cryst. 77−34654
thiirene and deuteroderivatives, Fourier transform IR spectra using Ar matrix isolation, vibr. band assignments 80−14142
thiirene-d_0(-d_1)(-d_2), IR spectra, normal coordinate anal. 80−87107
2-thio alkyl (allyl, benzyl) pyrimidines, IR and Raman spectra anal., mol. vibr. and symmetry *(French)* 80−87123
thioacetamide, IR spectra, amino group inversion transitions and pot. functions 80−43041
thioamides, characteristic pattern in IR and Raman spectra 78−29818
thiocarbonyl bromide, IR spectra, gas, liq. and matrix isolated, mol. force consts. *(German)* 79−36640
thioformaldehyde, $\tilde{a}^3A_2 \leftarrow \tilde{X}^1A_1$ IR absorpt. spectra 80−83362
thiones, N-H-S weak and medium strong H bonds, IR spectra 80−69132
thiophosgene, IR spectra, gas, liq. and matrix isolated, mol. force consts. *(German)* 79−36640
thiosemicarbazide, mol. cryst., transition moment directions 78−64351
thiourea, dielec. const. and IR spectra in ferroelec. and antiferroelec. phases 79−33589
thiourea, ferroelec., soft mode and Debye relax., IR reflection spectra 77−90111
thiourea, IR reflectivity study of ferroelec. and antiferroelec. phases, dielec. function model 79−33686
thiourea, order-disorder transitions, soft modes 78−80361
thiourea, phonon modes near order-disorder transforms., hard-core modes due to pseudospin-phonon coupling 80−44285
thiourea, phonon modes near phase transitions, IR and Raman spectra 80−45084
thiourea, soft mode and Debye relaxations 78−80347
thiourea crystal, ferroelec., i.r. reflection spectra meas., shift of soft mode obs. *(French)* 77−4635
tissue IR absorption, photoacoustic spectroscopy obs. 79−79604
TMMC linear chain antiferromag., optical absorption, magnon sideband intensities calc. 77−59569
TMNB, and deuterated derivative, low temp. far IR spectra 79−24309
TMNC, phase transition, low temp. far IR spectra 79−24309
TMTTF fluoroborate, transmission spectra with electron-phonon coupling phenomenological model 79−19891
toluene, asymmetric bending vibrs. 79−13696
toluene, in benzene soln., mol. motion, correl. functions 80−96431
toluene sulphonate diacetylene polymer, electronic and vibr. excitations, press. and temp. depend. 78−31188
toluene-sulphonate-diacetylene, thermal polymerisation, near IR absorpt. and low lying states obs. 80−71399
p-toluidine, vibr. spectra, normal mode calcs. 77−65482
transition metal oxalates, crystal growth in silicate gel, characterisation 77−4724
tri(trifluoromethyl) germanium halides, gas, liq. and solid, IR and Raman spectra, normal coord. anal. 79−72316
tri-i-propygermylamine, and isotopomers, IR and Raman spectra, normal coord. anal. *(German)* 80−32716
tri-t-butylstannylamine, and isotopomers, IR and Raman spectra, normal coord. anal., Mossbauer spectrum *(German)* 80−32716
trialkyl silanes, IR absorption vibration spectra, true parameters of isolated bands calc. *(Russian)* 77−83586
s-triazine(-d_3), gas phase IR band contours obs., computer simulation 77−6774
tribenzo [12] annulene, monovalent anion, MCD and absorpt. spectra 78−70859
2,4,6-tribromophenol, Raman and IR spectra, hydrogen bonds 80−84735
tribromotrifluoroethane, IR and Raman spectra, normal coord. anal. *(German)* 80−32726
trichloracetonitrile, IR dispersion, complex refractive index and permittivity, time correl. function 80−45057
trichloroacetic acid, self association, factor analysis and band contour resolution applications, book contrib. 78−21931
trichloroanilines in solutions, IR absorpt. spectra 80−69136
1,2,3-trichlorobenzene, low freq. vibs. 77−32365
2,2,2-trichloroethanol(-d_2), vibr. spectra and normal coord. anal. 79−72319
trichlorofluoromethane, 8-12 μm band model calcs. 80−43112
trichlorofluoromethane, 8-12 μm bands intensities, temp. depend. 80−43048
trichloromethane, matrix isolation IR spectra, $^{35/37}Cl$ and $^{12/13}C$ isotope shifts 78−977
trichloromethane-d_0,-d_1, soln., far IR spectra, band shape and moment anal. 80−58252
2,4,6-trichlorophenol, Raman and IR spectra, hydrogen bonds 80−84735
1,3,5-trichlorotrifluorobenzene, IR and Raman vibr. spectra 77−3356
trichlorotrifluoroethane, IR and Raman spectra, normal coord. anal. *(German)* 80−32726
triethylsilylamine, and isotopomers, IR and Raman spectra, normal coord. anal. *(German)* 80−32716
1,1,1-trifluoro-3-chloropropane, Raman and IR obs. of rot. isomerism, entropy difference between vapour and liq. phase isomer *(Russian)* 79−31529
trifluoroacetic acid, soln., polarisable H bonds, IR spectrosc. obs. 80−58408
1,3,5-trifluorobenzene, IR rot.-vibr. band contours 79−76430
trifluorobromomethane, $CF_3{}^{79}Br$, precision IR spectra from IR-microwave double reson. 77−14428
trifluorochloromethane, Raman and IR spectra, $^{35/37}Cl$ isotope splitting and mol. constants *(German)* 77−83595
trifluoroethane(-d_3), IR and Raman spectra, normal coord. anal. *(German)* 80−32726
2,2,2-trifluoroethanol(-d_2), vibr. spectra and normal coord. anal. 79−72319
infrared spectra of organic molecules and substances continued
trifluoroiodomethane, laser microwave double reson. spectroscopy with CO_2 laser lines 80−87156
trifluoromethane, IR spectra, spectral bandshape and intensity of C-H chromophore 80−83355
trifluoromethyl hypochlorite, vibr. spectra and normal coord. anal. 80−102517
trifluoromethyl hypofluorite, vibr. spectra and normal coord. anal. 80−102517
trifluoromethyl trimethyl germanium (tin)(lead), and perdeuterated analogues, vibr. spectra, normal coord. anals. *(German)* 80−5547
trifluoromethylperoxy radical, in Ar:O_2 matrix, IR spectra 80−50845
trifluorotriiodoethane, IR and Raman spectra, normal coord. anal. *(German)* 80−32726
triglycerides, diacid and triacid, IR spectra, diathesis (vibr. moieties) anal. 77−44525
1,1,1-trimethoxyethane, mol. struct., electron diffr., vibr. spectra 78−37765
trimethyl phosphine-d_6, isolated CH stretching frequencies, bond strengths, bond lengths 78−90167
trimethylaminegallane, microwave, IR and Raman spectra, struct., vibr. assignment 80−95600
2,4,5-trimethylbenzaldehyde, in durene, cryst., photochem. and photophys. processes 77−60092
trimethylborane, vibr. spectra and force constants *(German)* 79−26981
trimethylcarbinol complexes in soln., weakly H-bonded, IR bandshapes 80−106354
trimethylchlorosilane, chemisorption on goethite, IR spectra 80−7855
trimethylene sulphoxide, ring puckering vibr., IR spectra obs. 80−32710
trimethylgermylisocyanate, IR and Raman spectra, struct. 78−37637
trimethylgermylisothiocyanate, IR and Raman spectra, struct. 78−37637
trimethylsilyl azide, vibr. spectra, normal mode assignment 78−86867
trimethylsilyl isocyanate, vibr. spectra, normal mode assignment 78−86867
trimethylsilyl isothiocyanate 78−86867
trimethylvinylsilane, IR spectra, struct., vibr. assignment, barriers to internal rot. calc. 80−87102
trimethyoxybenzenes, liq. and solid, IR and Raman spectra, vibr. assignments 78−58701
1,3,5-trioxane, vibr. spectra and intermol. forces 77−36216
triphenylamine in 3-methylpentane and ethanol glasses, γ-radiolysis, IR spectra, trapped electron 77−16842
triphenylcarbinol complexes in soln., weakly H-bonded, IR bandshapes 80−106354
triphenylmethane dyes, IR and Raman vibr., spectra, vibr. anal., vibronic theory of Raman scatt. 77−68048
triphenylphosphine compounds, $(C_6H_5)_3PM_xM'_{1-x}(CO)_5$, M,M′=Cr, Mo, W, mixed cryst., CO vibr. spectra, modal anal. 78−35128
tropolone vibr. spectra and proton tunneling 80−28014
TTF^+, cryst., vibr. assignments, IR spectra 79−99869
$(TTF^+)_2$ dimer, cryst., vibr. assignments, IR spectra 79−99869
TTF, cryst., vibr. assignments, IR spectra 79−99869
$(TTF)_{12}(SCN)_7$ and $(TTF)_{12}(SeCN)_7$, charge-transfer salts, elec., mag. and optical props. 77−43575
TTF and derived cpds., intramolecular vibrs. and vibronic effects, IR and Raman spectra 80−25387
TTF-d_0, -d_4, IR and Raman spectra, vibr. assignments 78−23436
TTF-I_n, single cryst. optical props., polarised specular reflectance meas. 77−12400
TTF-TCNQ, optical evidence for Coulomb interactions, review 78−6704
TTF-TCNQ, ^{15}N, ^2H isotope labelled, IR, Raman spectra, mol. vibrs., electron-phonon interactions 77−69835
TTF-TCNQ, conductivity model 79−51557
TTF-TCNQ, Drude optical edge, press. depend. 79−19882
TTF-TCNQ, electron-molecular distortion coupling near Peierls transition, IR spectra obs. 80−25390
TTF-TCNQ, IR absorption peak theory 77−43991
TTF-TCNQ, IR reflectance in conducting phase 80−25388
TTF-TCNQ, irradiated, IR reflectance, optical and low-freq. transport comparison 79−51961
TTF-TCNQ, pinned CDW in very far IR 80−25391
TTF-TCNQ film, mag. field effects on IR spectra *(French)* 77−48260
TTF-TCNQ film on KBr, IR spectra in mag. field 77−16310
$TTF_2I_xBr_{3-x}$, charge transfer complex, optical and elec. props. 79−4554
$(TTF)_2I_3$, optical, spin-reson., magnetoresist. study, nature of ground state 78−68023
TTT salts, charge transfer salts, optical props. 79−73970
TTT salts, IR spectra, mixed-valence salts 80−40121
TTT-I_n, charge transfer salt, electronic spectra in soln. and solid state 78−2878
unstable conformations, matrix isolation, trapping from thermal mol. beam, IR spectra 78−46330
uracil cryst., theory of IR spectra of H-bond 77−40223
uracil derivatives, effects of UV radiation, IR spectra obs. 78−27801
urea-$NaNO_3(KNO_3)$ solid eutectic mixtures, Raman, IR spectra, line shifts, widths 77−55793
urethane elastomer, temp. strain relaxation investigation by opticomechanical method and IR spectroscopy 77−4805
vanadyl phthalocyanine, sublimed layer, IR absorption, vibr. assignments 78−55174
vibrational spectra, theory vibr. spectra, theory *(Russian)* 78−13502
vinyl acetate, monomer and polymer, Raman and IR spectra, liq. and solid 78−58700
vinyl alcohol-vinyl acetate copolymers, mol. architecture and physiochem. props. 80−44103
vinyl chloride, IR laser induced photoreactions, product identification 79−57257
vinyl chloride+O_3 reaction, IR matrix and microwave spectroscopy 77−90587
vinyl sulphides, divalent S linking with multiple bonds, spectrosc. obs. *(Russian)* 78−21929
vinyloxirane, Raman and IR vibr. spectra and conformations 80−83379
vinylsilanetriol-d_0,(-d_3), soln., vibr., IR and Raman spectra 78−86854
volatile substances, cryostat for low-temp. investig. of IR spectra 79−54136
water, H-bonded struct., IR spectra, assignments 78−62800
xanthoporphinogen, IR electronic excitation spectra, CNDO/S calcs. *(German)* 77−79617
XH_2 molecules 1:2 complexes, H-bonding fluctuation hypothesis, IR and Raman vibr. spectra 77−34632

infrared spectra of organic molecules and substances continued
XH-Y complexes, IR absorpt. spectra, intramol. coupling influence, pot. energy surfaces derivation 80−91624
yeast cell IR spectrum, effect of membrane components 77−70433
yeast cell wall component contrib. to IR spectra 79−39371
zinc tetraphenylporphin anion, IR spectra and vibr. anal. 79−54852
Ag complexes of 2-amino-5-methyl-1,3,4-thiadiazole and 2,5-dimethyl-1,3,4-thiadiazole, conductometric and IR meas. 80−87121
BCl_2NCO, soln., force fields and normal modes, vibr. spectra, IR and Raman obs. *(French)* 80−58266
$BX_2{}^{15}NCS$ (X=Cl, Br, I), soln., force fields and normal modes, vibr. spectra, IR and Raman obs. *(French)* 80−58266
BeF_2, aq. glass, 76K, solvated electron spectrum evolution, following ns radiolysis 78−88295
1-bromo-1-chloro-1-fluoroethane(-2-d_1), IR and Raman spectra, vibr. assignments, normal coord. anal. 78−42053
t-butyl chloride, dipolar liquid, far IR absorpt. rel. to Mori continued fraction for autocorrel. function 78−2875
C-H, isolated IR stretching freqs., LeFevre bond parameter anal. 77−57965
$(CD)_x$, polymer, heavily doped, IR spectra, vibronic intensity enhancement 80−28124
CF_2, absolute IR intensity of fundamental vibrs. 78−58743
CF_2, in Ar matrix, conc. determ. by intensity calcs. 78−68941
CF_3, absolute IR intensity of fundamental vibrs. 78−58743
CF_3, in Ar matrix, conc. determ. by intensity calcs. 78−68941
CF_3^+ cations, IR spectra in Ar matrix 78−74710
CF_2Br^+, CF_2Cl^+, IR spectra, matrix isolation study, C-F stretching fundamentals 78−37632
CF_2Cl^+, and parent cations, IR spectra in matrix radiolysis and photoionis. of Freons 78−80767
$CF_2Cl_2^+$, CF_3Cl^+, IR spectra, in matrix radiolysis and photoionis. of Freons 78−80767
CF_2X^+ cations, (X=Cl, Br, I, H_2), IR spectra in Ar matrix 78−74710
CF_3X^+ cations, (X=Cl, Br, I, H), IR spectra in Ar matrix 78−74710
CH_2, line search in C star spectra 77−78786
CH_3, CH_2 and CH deformation vibration group frequencies and MO electron densities, interaction force const. 80−87101
CH_3-d_n, matrix isolation IR spectra, rot. and vibr. struct. 77−83589
$(CH)_x$, polymer, heavily doped, IR spectra, vibronic intensity enhancement 80−28124
CH_2F, far IR laser mag. reson. spectrum 78−9174
CNC radical vibr. and electronic spectra, in VUV photolysis of matrix-isolated cyanomethane 78−85180
CSFCl, vibr. spectrum, anharmonicity corrections *(German)* 79−41173
α-chloronaphthalene, IR absorption spectra, forbidden character 77−58002
Cl+formaldehyde, photolysis, Fourier transform IR studies, metastable species detection 80−81293
Cl+vinyl bromide-d_3 reaction, IR chemiluminesc. 80−102506
ClH-dimethyl ether, H bonded complex, IR and Raman spectra, mech. and elec. anharmonicity 79−89672
ClH-dimethyl ether, vibr.-rot. IR spectra, quantum and classical mechanics 80−91561
Co complex, $CoCl_2$(indazole)$_2$, linear chain ferromagnetism 79−56519
Co complex, $CoCl_2$(pyrazole)$_2$, linear chain ferromagnetism 79−56519
$Co[Ag(SeCN)_2]_2$, and complexes, softness values and struct., IR spectra 79−59459
Cu complex, bis(1,5-cyclooctadiene)copper(I) perchlorate, IR and Raman spectra 79−19877
Cu complex, di-μ-chlorobis[(1,5-cyclooctadiene)copper(I)], IR and Raman spectra 79−19877
Cu complex, glycylglycine, isotope substituted, IR and Raman vibr. spectra 78−42051
Cu complexes of 2-amino-5-methyl-1,3,4-thiadiazole and 2,5-dimethyl-1,3,4-thiadiazole, conductometric and IR meas. 80−87121
4-cyano-4′n-heptyl biphenyl, nematic phase, torsional absorptions 77−48161
Eu complex Eu dibenzoylmethane chelate with piperidine, vibronic and IR spectra 79−82981
F+ethylene (benzene) derivatives, deuterated, IR chemiluminesc. 80−102506
F+methane, reaction in Ar matrix, IR spectra obs. 79−96293
FCO, form. in Ar matrix, vibr. and electronic spectra, valence force potential determ., mol. photodissoc. obs. 80−85170
Fe complex, 2,2′-bipyridine, visible spectra of cryst. 79−47424
α-fluoronaphthalene, IR singlet-singlet absorption and emission spectra, forbidden character 77−58002
H bond dynamics in soln. 78−84573
H-bonded complexes, OH stretching vibr. band, temp. effect 78−90158
H-bonded crystal, IR absorpt. spectra band shape, X-H stretching vibr. temp. depend., isotope effect 78−76445
H-bonded systems, frequency shift rel. to IR bandwidth 80−99502
HCCN, free radical, matrix isolation spectra and ab initio calcs. 78−46329
HCCN, matrix isolation IR and UV spectra, vibr. anal., struct. 77−65457
HCl-dimethylether complex, gaseous, H-bond IR spectra, temp. depend. theory 78−62804
HCl-X, matrix isolation vibr. spectroscopy, complex form. studies 78−62952
HF-cyclic ethers H-bonded complexes, calorimetry, IR spectra and MO calcs. 79−52738
HF-fluoromethylene anion, in solid Ar, IR spectra, vibr. modes 79−68231
IBr-benzene in n-decane soln., IR line broadening by chemical exchange 80−87111
K salt of β-ketoaldehyde, configurations of anions in solutions studied by IR spectroscopy, H-bond form. 80−87117
$K^+CF_3SeO_2^-$, IR and Raman spectra, normal coordinate anal. for $CF_3SeO_2^-$ anion 80−87122
Li salt of β-ketoaldehyde, configurations of anions in solutions studied by IR spectroscopy, H-bond form. 80−87117
methane $2\nu_4$-ν_4 and $\nu_2+\nu_4$-ν_2 hot bands, difference bands 80−63632
Mn III chloro complexes, IR and Raman vibr. spectra 77−68038
$NH_4{}^+CF_3SeO_2^-$, IR and Raman spectra, normal coordinate anal. for $CF_3SeO_2^-$ anion 80−87122
NH_2D, dipole moments effects of RF elec. field modulation on IR stark spectroscopy 80−52989
NO_2+ROO→ROONO_2, (R=C_nH_{2n+1}), Fourier transform IR spectroscopic meas. 78−53194
infrared spectra of organic molecules and substances continued
Na salt of β-ketoaldehydes, configurations of anions in solutions studied by IR spectroscopy, H-bond form. 80−87117
Na zeolite, molten salt inclusion in intracrystalline canals, spectrosc. charact. *(Rumanian)* 79−74463
Na-chlorofluoromethane, matrix radiolysis, photoionis., IR spectra of CF_2Cl^+ and parent cations 78−80767
NaK, laser induced $D\,^1\Pi$-$a\,^3\Sigma$ fluorescence, mol. vibr. 80−87160
Ni catalyst, chemisorption of ethylene-(d), Raman and vibr. spectra 80−108747
Ni complex, bis-[4-(n-butyl)-styryl-dithiolato] Ni nematic complex, IR absorption 80−49342
Ni complexes, Ni(glycinate)$_2$(pyrazine) and Ni(glycinate)$_2$(pyridine)$_2$, and isotopic forms, IR band assignments 79−22710
trans-$Ni(S_2N_2CH_3)_2$, IR and Raman spectra, normal coord. anal. 80−28019
O_2, $b'\Sigma_g^+$-$X^3\Sigma_g^-$ electronic transition, absorpt. coeffs. and transition moments 80−43061
OH, radical, far IR laser mag. reson. spectra, fine struct. transition 79−76454
Os complex, 2,2′-bipyridine, visible spectra of cryst. 79−47424
PbO, laser excitation IR spectra, photoluminescence obs., rot. anal., rot. const. determ. 80−95619
Pd complex, tetrabenzo tetra-azacyclohexadecine, I_2 oxidation product, synthesis and characterization 79−47900
$Pd(S_3N)_2$, IR and Raman spectra, normal coord. anal. 80−28019
$Rb^+CF_3SeO_2^-$, IR and Raman spectra, normal coordinate anal. for $CF_3SeO_2^-$ anion 80−87122
Rh complex, di-μ-chlorobis[(1,5-cyclooctadiene)rhodium (I)], IR and Raman spectra 79−19877
Ru complex, 2,2′-bipyridine, visible spectra of cryst. 79−47424
SCF_2, IR, Raman and matrix isolation spectra, isotopic shifts, anharmonicity consts. *(German)* 77−83600
$SeCF_2$, IR, Raman and matrix isolation spectra, isotopic shifts, anharmonicity consts. *(German)* 77−83600
SiO_2-liquid heptane interface, adsorption of organic liqs., IR spectra obs. 79−57295
$Si_2O(Cl_3)_2$, IR and Raman spectra, vibr. anal. 78−66552
TCNQ ion-radical salts, struct. disorder 79−99885
TCNQ salts, $Cs_2(TCNQ)_3$, quasi-one-dimens., IR spectra, electron-vibr. interaction 78−88309
TGSe, Raman and far IR spectra, lattice vibrs. in para- and ferroelec. phases 77−77190
Ti complex, dichloro bis-cyclopentadienyl titanium+dialkoxy bis chelated titanium compounds reaction, IR spectra 79−79239
U complex, binding, by brown coal, from seawater, IR spectroscopic obs. 78−82855
UO_2 complexes, cubic crysts., low temp. optical spectra *(Russian)* 78−92083

infrared spectra of polyatomic inorganic molecules
alkali halides, IR absorpt. in molecules, clusters and microcrystals 78−80363
alkali metal uranyl nitrates, IR spectra, force constants, bond orders 77−30873
alkali tetrafluoroaluminates, matrix isolated IR spectra 80−985
anharmonic molecules, stochastic multiphoton absorpt. processes, classical model 79−45778
band intensities and polar tensors, effective charge and dipole moment derivs. sign 77−34695
bond polarity parameters, IR intensities, molecular orbital study 79−63914
bromomethane-$d_{0,1,2,3}$, IR spectra intensities, dipole moment, bond charge, force consts. 77−83588
$^{13}C^{16}O_2$, ν_3 band, absorpt. spectrum 78−58693
collisionless dissociation by multiphoton IR absorption 77−54580
conformers, dynamic interaction between ground states, effect on IR spectra 78−58767
DSO, radical, electronic spectrum and struct. 77−75147
far IR atmospheric emission and absorption spectrum calc. program 79−35020
free radicals and molecular ions, matrix isolation spectra 79−50008
gases, high resolution vibr. spectra by Fourier transform far IR spectroscopy 80−86461
group IV tetrahalides, isotope shifts, Coriolis coupling and force consts., isotope substitution and matrix isolation 77−42322
H_2O 1.38μm band absorption meas. of precipitable water 80−4108
HCl-inert gas mixtures, van der Waals molecules, far IR spectra 80−95610
heterodyne spectroscopy, stratospheric sounding 79−100971
high temp. gas phase species, mol. beam mass spectrometry 80−52235
high temp. molecules, matrix isolation studies, review 80−57399
inhomogeneous molecular gas radiation calc. using spectral comp. modelling 80−32697
inorganic and coordinated cpds., IR and Raman spectra, book 79−807
intensity prediction, at. polar tensor method, F containing mols. 78−62854
intensity relation, IR to Raman intensity, matrix notation 78−62853
iodomethane-d_3, Stark tuned level crossings and saturated absorpt., RF elec. field modulation effects 80−52989
IR bands transmission functions 80−106324
IR intensities, fundamental, overtone and combination band calcs. 78−29780
isomer identification by vib. spectra analysis, for similar structs. *(Russian)* 77−83577
lanthanides in molten $LiNO_3$-KNO_3, transition probabilities in absorpt. and fluoresc. spectra 79−50085
linear molecular gases, IR radiation in Q branch 79−54850
ljquid polyatomic molecule vibrational mode obs. with picosecond laser pulses 77−58007
$M^IM^{IV}IO_6$, vibr. spectra (M^I=Na,K,Rb,Cs,NH_4; M^{IV}=Ge,Sn,Pb) 77−42325
metal surface, adsorbed molecule, IR spectra exam. by surface EM wave spectroscopy 78−71967
methyl group meas. in plastic industry, computer-infrared method 77−27073
molecular fragmentary composition, determ. by IR, EPR and US mag. reson. spectra *(Russian)* 78−13624
molecular vibr. freq. tables, up to 13 atom mols., and Raman and IR values 77−79614
molecular vibration, IR spectra 79−98084

infrared spectra of polyatomic inorganic molecules continued
$(MX)_n$, $(MX_2)_n$ ionic clusters, struct. and vibr. freqs. calcs. 78−94348
MXY_2 type molecules, IR intensity anal., dipole moment 78−62806
orthoborates, dolomite type, vibr. spectra, vibr. coupling effects *(French)* 77−65464
polyatomic molecules, dil. solns., IR spectral band shapes of fundamentals 78−66544
polyatomic symmetric molecules, collisionless dissoc. and vibr. spectum of degenerate modes 80−18893
quasi-linear molecules, low frequency anharmonic vibrations, pot. function determ., Raman and IR spectra obs. 80−52997
rare earth complex, $R(DMMP)_6(ClO_4)_3$ and $R(TBPO)_4(ClO_4)_3$, synthesis and characterisation 77−23498
rare earth oxalates, struct., IR absorpt. and Raman spectra *(French)* 80−32714
SF_6 IR mass absorption coefficients, 3 to 15 μm 79−76422
silane, coupling agent on E-glass fibre, structure, Fourier transform infrared spectroscopy 78−60643
silane, coupling agent on porous silica, Fourier transform infrared spectroscopy 78−60642
silica gel, microporous amorphous toroidal, spectroscopic and thermal analysis, adsorption properties 79−57305
solvated halide ions, in methanolic alkali halide solns., IR obs. 79−22703
stratospheric far IR emission, balloon-borne obs. 79−34896
strong H bonded systems, vibr., Raman, IR spectra, biology appls. 78−82735
structure recognition, from IR, UV, NMR and mass spectra, computer method 78−25737
transition metal complex anion, vibr. spectra in solid and soln., struct. and fundamental mode assignment 78−62803
transition metal complexes, excited states geometrical parameters, Franck-Condon anal. 77−27047
transition metal complexes, isothiocyanates with pyridine, far IR spectra, vibr. bands 78−25535
transition metal complexes, of 4-methylpyridine, IR and Raman spectra, vibr. anal. 78−25536
transition metal porphyrins, quasiline absorpt. spectra, metal and substituent effects 77−34628
trifluoroformamide, photodissoc., obs. of NO (v=1) 78−74712
upper atmosphere, IR radiation from mol. vibr.-rot. transitions 79−5695
uranyl complexes, IR spectra, complexation effects on force consts. and bond lengths 78−980
uranyl complexes, IR spectra and bond distances 80−74167
van der Waals complexes, IR continuum spectrum at low temps. 80−980
vibrational spectra, theory vibr. spectra, theory *(Russian)* 78−13502
water, and isotropic forms, IR band intensities estimation 78−86916
water, thin layer between quartz plates 79−56773
water cluster evidence from phase transition changes in IR mol. absorpt. coeff. 79−10100
water cluster interpretation of IR water vapour continuum, comments 79−12262
water cluster interpretation of spectra in 8-14 μm region 79−98081
water vapour, atmospheric, IR continuum absorpt. calc. *(Russian)* 78−96293
water vapour continuum absorption (3.5 to 4 μ) temp. dependence obs. 80−61903
water vapour-N_2, absorption at CO_2 laser frequencies 79−50011
water-carbon tetrachloride soln., fundamental H_2O IR spectrum, liq. struct. 80−23419
X_3Y_3 molecules, isotopically substituted, IR freq. and intensity patterns 78−21926
XH-Y complexes, IR absorpt. spectra, intramol. coupling influence, pot. energy surfaces derivation 80−91624
$AlBr_2$, IR spectra in Ar matrix, struct. 79−31520
$AlBrCl_2$, matrix isolated, vibr. spectrum, struct., vibr. freqs. 78−46339
$AlBr_2Cl$, matrix isolated, vibr. spectrum, struct., vibr. freqs. 78−46339
$AlCl_3$, matrix isolated, vibr. spectrum, struct., vibr. freqs. 78−46339
$AlCl_3$, soln., IR spectra 78−74649
$AlCl_4^-$, IR spectra in $AlCl_3$-MCl (M=Li, Na, K) melts 79−806
Al_2Cl_6, matrix isolated, vibr. spectra, isotopic fine struct. and valence force field calcs. 80−58258
AlClBr, IR spectra in Ar matrix, struct. 79−31520
$AlCl_2Br$, IR spectra in Ar matrix, struct. 79−31520
$Al(OH)_xCl_{3-x}$, soln., IR spectra 78−74649
Ar-HCl, van der Waals mol., far IR spectra 77−79611
Ar-HCl, Van der Waals mol., far IR spectrum, anisotropic intermol. force effects 78−62869
ArHBr, bond energy, IR spectra determ. 77−58000
Ar.HBr(DBr), van der Waals complexes, rot. spectra and struct. 80−48055
Ar.HCl bond energy from IR spectra 77−27061
As_4O_6, IR and Raman spectra vibr. spectra, valence force field calc., pot. function *(French)* 78−50549
As_4O_6, matrix isolated, IR isotope freq. and intensity patterns 78−46338
BCl_3, high-resolution IR Ar matrix-isolation spectra, 10K 80−32708
BCl_3, high-resolution polarisation spectroscopy in 10 μm region 79−6196
BCl_3, in solid Ar, Kr, high resolution IR absorpt. spectra, isotopic splitting 80−87109
BCl_3, intense IR radiation absorption singularities 79−76432
BCl_3, ν_3 vibr. level, fine struct., nonlinear reson. 77−6783
BCl_3-$COCl_2$, impurity removal by laser irrad., IR spectra meas. 78−15686
BCl_2F, in solid Ar, Kr, high resolution IR absorpt. spectra, isotopic splitting 80−87109
BCl_2SH, BCl_2SD, Raman and IR spectra, barrier to internal rot. 78−5223
BF_3, IR intensity anal. 77−58081
BF_3, pure rot. spectra of ground vibronic state, calc. 79−63975
$^{10,11}B_5H_9$ gas (liq.) phase, vibr. dephasing and Raman spectra 80−48101
BO_2, reson. fluoresc. assignment of vibr. and vibronic transitions 78−17663
$Ba(ClO_4)_2$, solutions in amides and esters, structure *(French)* 80−7343
$Ba(ClO_3)_2.H_2O(HDO)(D_2O)$, hydrate group vibr., IR spectra, isotope effects 77−8557
BaN_2O_3, vibr. spectra, assignments 77−38670
Br+NOBr, primary and secondary photochemistry, vibrationally excited NO, IR fluoresc. obs. 80−48030
BrF_5, IR intensities, fundamental, overtone and combination band calcs. 78−29780
$BrHCN^-$, $BrDCN^-$, IR spectra, rel. to mol. geom. 79−22702

infrared spectra of polyatomic inorganic molecules continued
BrOBr and BrBrO mols. in Ar matrix at 10K 79−89669
$BrONO_2$, stratospheric photolysis, UV and IR spectra 78−53227
CCN radical in solid Ar, emission and excitation spectra 78−70868
CF_2+H, IR matrix isolation spectra 80−97706
CO, catalytic oxidation on ferrites, IR spectrosc. investig. 80−89524
CO, ground level abundance, simultaneous determ. of CO_2, N_2O and H_2O 78−11969
^{14}CO, pure rot. far IR spectra, rot. consts. 80−47996
CO_2, 10 μm absorption line profile, high resolution meas. 77−42359
CO_2, 10^00-$00^00_{1,11}$ absorpt. band profile temp. depend., integral and spectral binary absorpt. coeffs. 80−43049
CO_2, 10.6, 9.4 μm laser bands high-press. absorpt-spectra 78−66543
CO_2, 10.6 μm absorption, 300-650K 78−5207
CO_2 15 μ band radiant energy inflow in disturbed LTE *(Russian)* 78−40657
CO_2, 15 μm band rel. to non-LTE radiative transfer in Earth atmosphere *(Russian)* 78−36341
CO_2, 201_{II}←000 band, press. broadened coeffs. and absolute intensities, temp. depend., IR obs. 80−53054
CO_2, 30^01_{II}←00^00 band, meas. at different temps. of absolute intensities, line half-widths and broadening by Ar and N_2 78−86865
CO_2, 30^01_I←00^00 and 30^01_{IV}←00^00 bands, absolute intensity meas. at different temps. 78−86864
CO_2, 4.3 micron band, band model parameters 80−43026
CO_2 4.3 μ band radiance meas. of internal combustion engine gas temp. *(Japanese)* 78−29119
CO_2, 4.3 μm airglow, excitation mechanism involving OH and N_2 79−16731
CO_2, 4.3 μm band, spectral absorpt. coeff. 78−5211
CO_2, 9.6 μm region emission spectrum, rot. consts. 77−3353
CO_2, absorpt. in regions of weak absorpt., lab. meas. rel. to atm. windows 79−64005
CO_2, absorpt. spectrum recorded by intracavity Nd:glass laser spectrometer 77−74530
CO_2 absorption at 2.7 μ in atmosphere at large optical thicknesses, mechanisms *(Russian)* 78−40659
CO_2, absorption bands integrated intensities, liquid and gas 77−493
CO_2, absorption spectra calibration, 14-15 μm, using diode laser source 77−18917
CO_2, absorption spectrum line parameters *(Rumanian)* 77−42326
CO_2, and isotopic forms, bending fund. region, IR spectra, rot. consts. 80−47988
CO_2 and isotopic species, high-resolution Fourier spectra near 4.3 micron 80−47982
CO_2, atm. absorpt. and emission over mean long optical paths 77−49163
CO_2 atmospheric line freqs. in 4.3 μ region 78−88910
CO_2, band model parameters prediction, 4.3 micron, 200-3000K 80−43047
CO_2, chemisorption on goethite, IR spectra 80−7855
CO_2, combination and difference bands, IR intensities 77−466
CO_2 continuum absorpt. contrib. to atm. transmission, 4.0 to 5.3 μm 79−92589
CO_2, continuum rel. to atm. absorpt. spectra near 2400 cm^{-1} 78−11968
CO_2 dimers in rare gas matrices, struct. determ. from IR spectra 79−10101
CO_2, dispersive Fourier transform spectrometry using modular interferometer 78−89567
CO_2, electro-optical parameters determ. from IR absorpt. 79−98128
CO_2, electron excitation-relax., time resolved Fourier spectra 78−58070
CO_2, electrooptic constants, IR absorption spectrum in $2\nu_3$ vibration band 79−3442
CO_2 enriched in $^{17,18}O$, diode laser spectroscopy of Q branches 80−78621
CO_2, excited by CO_2 laser, sub-Doppler optoacoustic spectrum 80−5545
CO_2, fundamental vibr. bands in liq. phase 79−54856
CO_2 gasdynamic laser, IR spectroscopic determ. of vibr. level populations 80−32952
CO_2 gasdynamic laser, vibr. temp. meas. method 80−9854
CO_2, ground level abundance, simultaneous determ. of CO, N_2O and H_2O 78−11969
CO_2, high temp. absorpt. meas. in 10.4 μm laser band 79−36870
CO_2, IR absorpt. spectrum, press. and conc. depend. 77−3362
CO_2, IR absorption spectrum using Nd:glass intracavity spectrometer *(Russian)* 78−33512
CO_2, IR band intensity 80−83425
CO_2, IR band nonrigid rot. absorption 78−91060
CO_2, IR bands transmission functions 80−106324
CO_2, IR energy levels and line intensities 78−85691
CO_2, IR spectra, 401←000 and 411←010 absolute intensities 78−21976
CO_2, IR spectra, lineshape and Q-branch head absorpt. profile 79−59452
CO_2 IR Zeeman spectra utilizing copropag. wave reson., diamag. shift obs. 80−53055
CO_2, in alkali halide cryst., field induced vibr. splitting, IR spectra 78−46334
CO_2, in N_2, 20-140 bar, dipolar correlation function meas., IR band shape anal. 77−61743
CO_2, in various solvents, IR absorpt. spectrum, Fermi-reson. doublet and intermolecular interactions 80−18856
CO_2 induced absorpt., 3-4μm, temp. depend. 80−983
CO_2 laser heterodyne meas. of 01^11-11^10 hot band transition frequencies 77−7063
CO_2, laser sideband spectroscopy *(German)* 79−26975
CO_2 laser small-signal gain coefficient calc. 80−78831
CO_2 lasers, high-power, book contrib. 77−50651
CO_2, lifetimes from collision induced absorption spectra, IR line broadening 78−33554
CO_2, line parameters, spectral transmittance function *(Russian)* 77−57998
CO_2, liq. and gas, state of aggregation effect on 1-4 μm absorpt. bands intensities 79−27042
CO_2, liq. phase vibr. spectra, anharmonicity effects 79−50022
CO_2, matrix isolated Raman and IR spectra, fundamental freqs., isotope effects 77−88457
CO_2, near IR absorpt. band props. 77−30872
CO_2, ν_2 fundamental, absolute IR intensities, Fourier transform spectrosc. obs. 79−93993
CO_2, optical reson. widths, nonlinear press. depend. 77−42358
CO_2, P-branch transitions, accurate wavelength meas. 77−38667
CO_2, P(26)-P(32) laser transitions, high temp. absorpt. meas. 80−14137

infrared spectra of polyatomic inorganic molecules continued
CO_2, press. broadening coeffs. at 4.2 μm, rot. quantum number 78−74704
CO_2, R-branch head of ν_3 band, up to 985K laser spectrometer 80−47983
CO_2 R-branch line intensities and press.-broadened line widths at 15 μm 80−102508
CO_2, rot. Raman and IR lines, self-broadened linewidths 77−42357
CO_2, rot.-vibr. bands, absorpt. coeff. calc. method, Fermi reson. effect on spectral lines 80−32696
CO_2, spectral line breadth in 15 μm band, N_2 broadened, 200-300K 79−22765
CO_2, supercooled, IR absorpt. spectrum 77−23574
CO_2, time-resolved IR single-shot absorpt. spectra 79−58808
CO_2, transition calibration, rotational constants, absorption spectrum, 4.82-μm region 78−58868
CO_2, transition moment and probabilities 79−3498
CO_2, transition moment of IR band near 7740 cm^{-1} 78−90224
CO_2, transition moment of IR band near 7740 cm^{-1} 78−90225
CO_2, transmission functions for 15 μm band, calc. and expt. *(Russian)* 77−64428
CO_2, turbulent flow field, mol. vibr.-rot. bands, spectral absorpt. coeff., temp. depend. 80−52987
CO_2, Venus IR absorpt. bands, 3900-10000 cm^{-1}, assignment 78−7896
CO_2 vibr. luminesc., excited by DC discharge, rot. and vibr. mol. consts. 78−58867
CO_2, vibr.-rot. spectrum, absolute line intensity, vibr. transition moment 77−83655
CO_2 wave numbers, intercomparison at 800 to 600 cm^{-1} with diode laser spectrometer 79−98082
$^{12}CO_2$, absorpt. spectrum at 4.3 microns 78−58692
$^{12}C^{16}O_2$, ν_3 band, IR single line strength 80−83370
$^{13}C^{16}O_2$, emission spectrum near 4.5 μm, nu_3 region spectroscopic consts. 77−38664
$^{13}C^{16}O_2$, IR line strength 80−83371
$^{13}C^{16}O_2$, ν_3 fundamental at 4.4 μm 78−86862
$^{13}C^{16}O_2$, Q-branch spectrum of $(01^{1}0\text{-}00^{0}0)$ transition 78−42061
$^{14}C^{16}O_2$, band centre at 4.5 μm, tunable diode laser spectroscopy 78−33503
CO_2+Ar(N_2), 301_{III}-000 band, intensities, press.- and self-broadening coeffs. meas. 78−78695
CO_2+CO_2(N_2), IR spectral absorpt. induced by press. in atmos. *(Russian)* 80−56600
CO_2+N_2, near IR absorpt., collisional broadening 77−30872
C_3O_2, far IR absorpt. spectra, 20 to 100 cm^{-1}, temp. depend. 79−59450
C_3O_2, far IR and Raman spectra, vibr. mode and quasilinear config. 78−62940
C_3O_2, Fourier transform spectroscopy, interaction between vibr. levels 77−75152
C_3O_2, IR spectra, P-branch of ν_6 fundamental 79−98092
C_3O_2, $\nu_2+\nu_7$ bands, Q-branch spectra, 12 μm region, l-doubling const. 77−65459
C_3O_2, $\nu_4+2\nu_7^0$ and $\nu_4+3\nu_7^1-\nu_7^1$ bands, high resolution IR spectrum 79−72311
C_3O_2, vibr. IR spectra anal. 80−47984
C_3OS, vibrational assignment, calc. of normal modes and valence force consts., IR spectra 79−50014
CS_2, condensation vibr. shift, intermol. interaction, vap. press. isotope effect 77−61742
CS_2, fundamental vibr. bands in liq. phase 79−54856
CS_2, IR spectra, $\nu_1+2\nu_2^0+\nu_3$ band *(French)* 79−41162
CS_2, isotopic variants, $2\nu_1+\nu_3$ band IR spectra, rot. and rovibr. consts. 79−41166
CS_2, liq. phase vibr. spectra, anharmonicity effects 79−50022
CS_2, matrix isolated Raman and IR spectra, fundamental freqs., isotope effects 77−88457
CS_2, ν_2 bending fundamental, high resolution IR spectrum 80−91559
CS_2, ν_3 band, dipole moment correl. function, isotope splitting and band contour 78−74650
CS_2, vibr.-rot. bands at .46 μm, isotope effects 78−94245
$^{12}CS_2$, $^{13}CS_2$, vibration-rotation bands 2700-2900 cm^{-1} *(French)* 78−25521
$^{12}C^{32}S_2$, ν_1-ν_2 difference band assignments 79−45719
$^{12}C^{34}S_2$, $^{13}C^{34}S_2$, high resolution IR spectra *(French)* 80−58249
CS_2+He(Ar)(N_2), perturbed rot. diffusion of CS_2, IR spectra 78−75245
$^{14}CO_2$, tunable diode laser spectroscopy, absorption coeffs., appls. 77−83583
Ca^+NO^-, $Ca^+NO_2^-$ in solid Ar, IR spectra at 15K 77−57996
CaN_2O_3, vibr. spectra, assignments 77−38670
CdFCl, CdFBr, existence and vibr. characterisation, IR and Raman matrix isolation obs. 78−78706
CdF_2(FCl)(FBr), matrix isolated IR and Raman spectra, assignments, force consts., isotope effects and thermodynamic props. 80−63631
$CdFe(CO)_4$, IR and Raman spectra, vibr. anal. 78−66553
$Cd(^{15}NH_3)_4^{2+}$, IR spectrum, force consts. *(German)* 77−6781
CdN_2O_3, vibr. spectra, assignments 77−38670
CdO_3, formed by matrix reactions, IR, Raman and visible spectra 80−87110
CdX_2, CdXY, (X,Y=Cl,Br,I), matrix isolated vibr. spectra, isotopic effects, force consts. 77−3358
CdX_2, CdXY, (X,Y=Cl,Br,I), matrix isolated, far IR spectra, thermodynamic props. 78−86869
Cl+NOCl, primary and secondary photochemistry, vibrationally excited NO, IR fluoresc. obs. 80−48030
$ClHCN^-$, $ClDCN^-$, IR spectra, rel. to mol. geom. 79−22702
ClNO+Cl_2O→ClONO+Cl, reaction kinetics, IR spectra 78−35641
$ClNO_2$, form. in matrix reaction, IR absorpt. obs. 78−15667
$ClNO_3$, far IR rot. and torsional spectra 77−79609
ClO_2, laser mag. reson. spectra tuned by Zeeman level crossing avoidance, perp. spectra 79−68229
ClO_2, laser mag. reson. spectra tuned by Zeeman level crossing avoidance, high-field spectra 79−76424
ClO_3^-, in $MClO_3$ and $MClO_4$ matrix, vibr. spectra, anion site asymmetry 77−27062
ClONO, form., reaction kinetics, IR spectra 78−35641
ClONO, form. in matrix reaction, IR absorpt. obs. 78−15667
ClONO, prod. via Cl+NO_2 react., FT IR obs. 79−8427
$ClONO_2$, high resolution IR absorptivity 77−33184
$ClONO_2$+NO(ClNO) react., gas phase, kinetics, mechanism, IR photometric investig. *(German)* 78−76834

infrared spectra of polyatomic inorganic molecules continued
Co complex, S_4N_4 with $CoCl_2$, mass and IR spectra, config. 78−13494
$CoSO_4.H_2O$, IR spectra, H_2O external modes temp. depend. 78−58683
$Co[Ag(SeCN)_2]_2$, and complexes, softness values and struct., IR spectra 79−59459
$Cr(CO)_6$, bonding, IR intensity anal. 78−25526
$Cr(CO)_6$, ν(CO) region, IR and Raman spectra in organic solvents 79−41169
$Cr(CO)_6$, solid and matrix isolated, Raman spectra 79−28755
CrO_2Cl_2, inert gas matrices, IR spectra, emission spectra, photoselection 77−14443
CrO_2Cl_2, matrix isolation IR spectrum and force constants 79−3445
CrO_2Cl_2, multiphoton induced inverse electronic relax. 80−66836
CsBrICN, Raman and IR vibr. spectra, struct. 80−102513
CsClICN, Raman and IR vibr. spectra, struct. 80−102513
CsI_2CN, Raman and IR vibr. spectra, struct. 80−102513
Cs_2ReF_6, absorpt. spectra, splitting of $\Gamma_8(^4A_{2g})$ ground state 78−74658
$CsReO_4$, IR matrix-isolation spectra 80−87108
Cs_2SO_4 molecules isolated in inert gas matrices, low freq. IR spectra 78−50547
$Cs_2UO_2Br_4$, force consts., IR spectra 78−5216
Cu_nCO, interaction of Cu small particles with CO, matrix isolation spectra obs. 77−20195
D_3^+, IR spectrum, vibr.-rot. assignment 80−95627
D_3^+, rot.-vibr. spectrum, ab initio calcs. 80−95595
DBr, (1,0) fundamental IR band meas., isotope shifts 78−42052
DCN, integrated IR intensities of fundamental modes 79−98083
DCN, $\nu_1+\nu_3$ combination bands, transition moments, integrated intensities 77−79610
DCN, self-assoc. in matrices, IR vibr. spectra of multimers 78−86858
$D(CN)_2^-$, IR spectra, rel. to mol. geom. 79−22702
DNO, fundamental vibr. bands, laser Stark spectra 77−38692
DNSO, IR spectra obs., mole. vibr., anharmonicity constant determ. 80−83357
DO_2, IR spectra, config. of $^2A'$ and $^2A''$ states 79−36636
D_2O, $(D_2O)_2$, isotopic forms, Ar matrix isolated IR spectra, assignments, config. 77−6779
D_2O, far IR absorpt. coeffs. by H_2O laser meas. 80−9599
D_2O, heterodyne meas. of IR absorpt. freqs. 78−55175
D_2O, IR and Raman spectra, bonding, vibr., band shapes 79−6938
D_2O, IR spectra, $\nu_2+\nu_3$ band shape 78−62855
D_2O, matrix isolation spectra, vibr.-rot. lines, nucl. spin interconversion 78−46336
D_2O, mol., Raman scatt. activity and IR intensity, finite field method 79−59462
D_2O, vap., 9.7 μm radiation absorption rel. to laser design 77−31098
D_2O, vibrational and rotations meas. by laser spectrosc. 80−43050
$D_2{}^{16}O$, IR spectra, ν_2 band, rot. struct. 78−982
D_2O-H_2O, IR absorption spectra, statistical charact., continuous model of liq. struct. confirmation 78−6671
D_2O-H_2O-HDO, gaseous mixture, absorpt. meas. by Michelson inclined mirror interferometer, high spectral resolution 80−9023
$(D_2O)_2$, and isotopic species, Ar isolation IR spectra, band assignments, struct. 77−3364
$(D_2O)_2$, and isotopic species, Ar matrix IR spectra, Xe, HCl, $(CH_3)_2O$ doping, struct. 77−3365
$(D_2O)_2$, isotopic forms, Ar matrix isolated IR spectra, assignments, config. 77−6780
D_2SO_4, pure, IR and Raman spectra in liq. state, assignments and cryst. spectra comparison *(French)* 79−33699
D_3SiNCO, low freq. bending mode, pot. function 78−82728
D_3SiNCS, IR and Raman spectra, vibr. anal., LF bending mode 78−70842
$Dy(NO_3)_3$ in nonaqueous solvents, anharmonic vibrs. in electronic energy degradation 77−23541
$ErCl_3(AlCl_3)_x$, vap. complexes, absorpt. spectra, 6000-44000 cm^{-1}, relax. props. 78−62799
FCN, IR laser Stark spectra, C-F stretching mode, dipole moments, rot. consts. 78−1022
FCN+N_2, rot. spectra and geom. struct. of FCN 78−82725
FNO, Stark spectroscopy of ν_1 band, rot. consts., dipole moment 79−13710
F_2O, absorpt. band freq. and intensities, electro-optical parameters, pot. energy, IR spectra 80−37812
F_3SiAsH_2, liq. Raman, gas phase IR spectra, normal coord. anal., assignments *(German)* 77−6778
$F_3SiOSiF_3$, vibr. anal., normal coordinates, siloxane bridge vibr. band struct. 79−50003
Fe complex, Fe (III) acetylacetonate, solvent effects on oscillator integrated strength, IR absorpt. bands 78−84575
$Fe(CO)_4$, IR spectra and laser photochem., matrix isolated at 20K 78−74651
$FeCl_4^-$, effective charge, from IR and Raman scatt. intensity obs. 78−62809
FeO_2, matrix isolated IR spectra, cyclic complex struct. 77−88449
FeOOH, H-bonding, strong, stochastic model and IR spectra temp. effects 78−62805
GeF_4, $\nu_3(F_2)$ IR band contour, isotopically pure cpds., mol. consts. 77−61746
GeH_2, centrifugal-distortion dipole moment, CO_2 laser spectroscopy 77−75331
GeH_4, IR laser sideband obs., ro-vibr. struct., isotope shifts, line widths 79−72306
GeH_4, laser sideband spectroscopy *(German)* 79−26975
GeH_4, ν_3 and 2 ν_3 bands, high resolution IR spectra, rel. to Jovian atm. 78−37636
GeH_4, ν_3 band obs., molecular const. determ. *(French)* 77−462
GeH_4, ν_3 fundamental, Jovian atm. absorpt. profile, computer simulation 78−81584
GeH_4, ν_3 fundamental, theoretical absolute J-manifold intensities 78−74707
$^{74}GeH_4$ mol. vibr., IR and CARS spectra *(Russian)* 80−102509
GeH_3.NCS, mol., IR, Raman and microwave spectra, ^{70,72,74}Ge and ^{1,2}H isotopes 79−89663
Ge_3O_3, isotopically substituted, IR freq. and intensity patterns 78−21926
Ge_3O_3, matrix isolated, IR isotope freq. and intensity patterns 78−46338
H bonded species, line broadening, kinematic and electronic coupling mechanisms 77−68043
H-bonded systems, frequency shift rel. to IR bandwidth 80−99502
H_2-H_2, overlap parameters from IR spectrum in binary collision-induced H_2 band 77−54561

infrared spectra of polyatomic inorganic molecules continued
H_2-inert gas, bound complex form., anisotropic intermol. pot., IR spectra anal. 78−37634
H_2+SF_6 (tetrafluoromethane), collision-induced simultaneous transitions, IR spectra 77−50438
H_3^+, ab initio calcs. of vibr. spectrum 77−6753
H_3^+, IR spectrum, ν_2 band obs. 80−99506
H_3^+ rot.-vibr. spectrum, ab initio calcs. 80−95595
$HAlCl_2$, IR matrix spectrum, vibrs. and force consts. *(German)* 79−11786
H_3AsO_4, polarisable acid-acid and acid-water hydrogen bonds 79−76423
HBO_2, band strengths, shock tube IR spectrosc. meas. 80−106358
HBr, far IR Ar matrix isolated spectra, 4.2K, press. and conc. effects 78−62801
HBr-nN_2 aggregates, near IR spectra in monatomic matrix 78−21921
$(HBr)_2$, IR matrix isolation spectra, N_2 matrix effects 79−36634
$(HBr)_2$, intermol. distances, dipole moments, MINDO/3 and IR intensities and shifts calcs. 78−46335
HCCl, IR spectra, ν_4 and ν_5 vibr. bands, rot. struct., rot. and vibr. consts. 77−38665
HCN, absorption, spectrum calibration, 14-15 μm, using diode laser source 77−18917
HCN, and stable isotopic species, mol. struct., ground vibr. rot. transitions and consts. 77−10666
HCN, IR and Raman vibr. intensity changes due to Li^+ interaction 79−45712
HCN in smoke, tunable diode laser meas. 80−89559
HCN, integrated IR intensities of fundamental modes 79−98083
HCN, J=4→3 354 GHz transition in Orion Molecular Cloud 80−101636
HCN laser processes, mm. and submm. microwave spectroscopy 78−13685
HCN, line search in C star spectra 77−78786
HCN, $\nu_1+\nu_3$ combination bands, transition moments, integrated intensities 77−79610
HCN ν_2-lines, IR tunable diode laser spectroscopy, techniques and calibration 79−71542
HCN, self-assoc., matrix isolation vibr. spectroscopy, complex form. studies 78−62952
HCN, self-assoc. in matrices, IR vibr. spectra of multimers 78−86858
HCN wave numbers, intercomparison at 800 to 600 cm^{-1} with diode laser spectrometer 79−98082
$(HCN)_2$, IR spectra in Ar matrix, vibr. bands, H-bonds 78−29782
$H(CN)_2^-$, IR spectra, rel. to mol. geom. 79−22702
HCNO, far IR spectrum, weak vibr. transitions 77−3357
HCNO, IR spectrum, ν_1 and $3\nu_1$ bands 77−3354
HCO, IR spectra of ν_2 fundamental, laser elec. reson. 78−5226
HCP, ν_1 and $\nu_1+\nu_2-\nu_2$ IR absorpt. bands 78−42060
HCP, ν_3 band, high-resolution IR absorption spectrum 80−47994
HCl, far IR Ar matrix isolated spectra, 4.2K, press. and conc. effects 78−62801
HCl-DCl(HBr)(DBr)(HI), absorpt. spectra near 3.5 μm, equilib. config. of complexes *(French)* 78−42046
HCl-nN_2 aggregates, near IR spectra in monatomic matrix 78−21921
HCl-X, matrix isolation vibr. spectroscopy, complex form. studies 78−62952
$(HCl)_2$, absorpt. spectra near 3.5 μm, equilib. config. of complexes *(French)* 78−42046
$(HCl)_2$, IR matrix isolation spectra, N_2 matrix effects 79−36634
$(HCl)_2$, intermol. distances, dipole moments, MINDO/3 and IR intensities and shifts calcs. 78−46335
HClF, neutral free radicals, in Ar matrix, IR spectrosc. evidence 78−66546
$HClO_4$-H_2O, aq. soln., IR and Raman spectra, conc. depend. *(Russian)* 80−53002
HDSe, high resolution IR spectra, anal. of $2\nu_1$ band, rot. ground state const. determ. 80−95616
HF_2, neutral free radicals, in Ar matrix, IR spectrosc. evidence 78−66546
HF_2^-, IR spectra and mol. struct. 79−63996
HF_2^-, matrix isolated, IR spectra and struct. 78−74655
H_2F_3, struct. H bonding, IR spectra obs. 77−54560
$H_3F_4^-$, struct., H bonding, IR spectra obs. 77−54560
$H_4F_5^-$, struct., H bonding, IR spectra obs. 77−54560
HNC, and stable isotopic species, mol. struct., ground vibr. rot. transitions and consts. 77−10666
HNCO, rot. spectrum, ground and vibr. state reson., centrifugal distortion coupling 80−83364
HNCS, ground state spectroscopic const., microwave, millimeter and IR spectra 80−28010
HNO, fundamental vibr. bands, laser Stark spectra 77−38692
HNO_2, trans and cis, ν_2 fundamental vibrational bands, intracavity CO laser Stark spectroscopy 80−47992
HNO_3, aq. soln., H bonds, IR spectra 78−94243
HNO_3, high resolution spectral meas. of 11.3 μm band, using tunable diode lasers 78−33504
HNO_3, high resolution spectral meas. of 5.9 μm band using tunable diode laser 80−32707
HNO_3 IR spectra, 865.5-871.0 and 884.5-887.0 cm^{-1} regions, equiv. width meas., atm. spectrum appl. *(French)* 80−87114
HNO_3, IR spectra rel. to abundance in stratosphere 80−12464
HNO_3, ν_5 band rot. struct., anal., band centre and rot. consts. 79−10109
HNO_3 vapour line parameters meas. by CO laser transmittance 79−26976
HNO_3, vibr.-rot. spectrum, 855-915 cm^{-1} *(French)* 78−50543
HO_2 and HOCl, struct., vibr. freqs., IR intensities, ab initio calcs. 79−98007
HO_2, IR spectra, 1.43-1.51 μm emission bands 79−36635
HO_2 radical, near IR emission bands, vibr. and vibronic transitions 78−37633
HO_2+HO_2, gas phase reaction mechanism, FT IR spectrosc. obs. 80−85163
$H_2O_2(H_2O)_2$, isotopic forms, Ar matrix isolated IR spectra, assignments config. 77−6779
H_2O 79−63992
H_2O 79−72308
H_2O, $4\nu_2$ band, hot vap., Fourier transform spectrum, rot. consts. 80−32712
H_2O, absorpt. in regions of weak absorpt., lab. meas. rel. to atm. windows 79−64005
infrared spectra of polyatomic inorganic molecules continued
H_2O absorption and coolest stellar component of E and S0 galaxies at 2 μ 78−41034
H_2O, absorption spectrum, LiF F_2^+-centre laser intracavity spectroscopy appl. 80−32999
H_2O, adsorbed in monolayer hydrate of halloysite, NMR obs. of mol. motion 78−95226
H_2O at interfaces, mol. struct. and dynamics 77−31873
H_2O, band spectra after HF combined mag. treatment *(Russian)* 79−15682
H_2O, computation of absorpt. near 4250 cm^{-1} 78−82729
H_2O, continuum IR absorpt. near 1200 cm^{-1}, temp. depend. 78−85687
H_2O dimer, continuum absorpt. spectra in 8-13 μm range *(Chinese)* 80−109237
H_2O dimer, props., influence on tropic meteorology 79−2349
H_2O, dimer config., vib.-rot. band intensities, rel. to 8-13 μm atmospheric extinction 80−9610
H_2O, dimers, IR spectra in N_2 matrix, assignments and force consts., isotope effects 77−61744
H_2O dimers, IR spectra in N_2 matrix, temp. and IR irrad. effects 77−61745
H_2O, dispersive Fourier transform spectrometry using modular interferometer 78−89567
H_2O droplet, IR emissivity 80−36394
H_2O, effect of mag. field on rotational IR spectra 79−54849
H_2O electro-optical harmonicity of OH bond 77−34634
H_2O, electro-optical parameters determ. *(Russian)* 77−14466
H_2O, far IR absorpt. coeffs. by H_2O laser meas. 80−9599
H_2O, ground level abundance, simultaneous determ. of CO, CO_2 and H_2O 78−11969
H_2O, higher ro-vibr. levels, high resolution flame spectra 77−58033
H_2O, IR absorpt. spectra, band profile temp. depend. 77−30869
H_2O, IR continuum absorpt. due to librational mode of dimer 78−66542
H_2O, IR line and band strengths, 5000-5750 cm^{-1} 78−5292
H_2O, IR line intenisties and widths, ν_2 rot.-vibr. band 78−9200
H_2O, IR spectra, linewidths 79−59454
H_2O, IR spectrum, rot. anal., isotope effects 78−78694
H_2O, IR spectrum rot. nonequilib. *(Russian)* 79−50023
H_2O, in D_2O ice I_c, decoupled vibr. spectra 80−52984
H_2O isotopes, spectrophone meas. at selected CO, CO_2 laser wavelengths 78−57310
H_2O, laser Stark and IR-RF double reson. at 6 μm 79−45760
H_2O, linewidths and press. shifts, in N_2 and air, Anderson theory and quantum many-body theory 78−74708
H_2O, low density flow temp. and density meas. by submillimetre spectroscopy 80−43816
H_2O, matrix isolation spectra, vibr.-rot. lines, nucl. spin interconversion 78−46336
H_2O, mol., Raman scatt. activity and IR intensity, finite field method 79−59462
H_2O, $\nu_1+\nu_3$ combination band, evolution with temp. 78−66548
H_2O, polymolecular adsorbed layers, on quartz surface 80−9595
H_2O, Pt catalytic oxidation of H_2 and D_2, matrix isolation and laser fluoresc. obs. of prods. 80−66865
H_2O, pure rot. band, exponential wide band parameters 79−31498
H_2O, Raman and IR spectrum in overtone OH stretching region 80−58263
H_2O, solutions in organic solvents, IR spectra and struct. 79−38534
H_2O, spectral line wave number, intensity and width near 5.3 μm *(French)* 77−50432
H_2O spectrum, 4200 to 5000 cm^{-1} 77−58005
H_2O, superheated steam, AFCRL atm. absorpt. line parameters in 2900-3000 cm^{-1} atm. window 80−36396
H_2O, theoretical IR transition matrix elements 79−85953
H_2O, time-resolved IR single-shot absorpt. spectra 79−58808
H_2O, ultrahigh resolution IR absorpt. spectra using tunable PbTe laser diode 79−75628
H_2O vapour, absorption at 1 to 8 μm, rel. to atm. spectra 78−81402
H_2O vapour, IR absorpt. spectrum, contrib. by molecular clusters 80−9598
H_2O vapour, line shape functions in absorpt. coeff. calc. 80−9600
H_2O vapour absorpt. coeff. at HF laser wavelengths 79−80010
H_2O vapour and liquid far IR spectroscopy 80−60610
H_2O, vapour bands, 2.7 and 1.9 μm, adiabatic pressure depend. 78−33509
H_2O vapour continuum absorpt., 4.5-5.0 μm 80−36395
H_2O, warm fog and steam clouds, emission spectra variations, evidence for clusters in vapour phase 79−39849
H_2O, weak spectral absorpt. of vap., visible and near IR 80−82062
H_2O^+, electronic spectrum, predicted IR and microwave lines, comet tail bands 77−473
$H_2{}^{16}O$, 6.3 μm region hot bands, intensities 77−75156
$H_2{}^{16}O$, $H_2{}^{18}O$, determ. of line intensities from Fourier absorpt. spectra *(French)* 79−18186
$H_2{}^{16}O$, laser spectroscopy using an optothermal receiver 80−37810
$H_2{}^{16}O$, vibr.-rot. intensities of $3\nu_2$, $\nu_1+\nu_2$, and $\nu_2+\nu_3$ bands 78−5291
$H_2{}^{17}O$, $H_2{}^{18}O$, Stark spectra with CO laser, Lamb dip spectra of ν_2 band 78−62840
$H_2{}^{18}O$, $H_2{}^{17}O$, IR spectra, 5030-5640 cm^{-1}, line centre positions 78−5220
$H_2{}^{18}O$, $H_2{}^{17}O$, IR spectra, 6974-7387 cm^{-1}, line centre positions 78−5221
$H_2{}^{18}O$, $H_2{}^{17}O$, rot. spectra, 650-50 cm^{-1} 77−65458
$H_2{}^{18}O$, line positions and intensities, $\nu_1+\nu_2$ and $\nu_2+\nu_3$ bands 78−74656
H_2O:D_2O, ice Ic, vibr, decoupling, IR spectrum 79−13706
H_2O-CO_2, IR radiation transfer 79−80028
H_2O-HCl(HBr)(DBr) complexes, IR matrix isolation spectra, struct. 78−29781
$(H_2O)_2$, and isotopic species, Ar isolation IR spectra, band assignments, struct. 77−3364
$(H_2O)_2$, and isotopic species, Ar matrix IR spectra, Xe, HCl, $(CH_3)_2O$ doping, struct. 77−3365
$(H_2O)_2$, isotopic forms, Ar matrix isolated IR spectra, assignments config. 77−6780
$H_3O_2^-$, in HCl and KOH aq. solns., vibr. freq. assignments 79−73916
$H_5O_2^+$, aq. soln., IR continua with polarisable H-bonds 79−26979
$H_5O_2^+$, in HCl and KOH aq. solns., vibr. freq. assignments 79−73916
HOCl, high resolution spectrum of ν_1 band 79−98095
HOCl, photolysis product of Cl_2-O_3-H_2 dil. mixtures, absolute integrated IR band intensities 80−26033

infrared spectra of polyatomic inorganic molecules continued
$2HOCl=H_2O+Cl_2O$, equilib. const., Fourier transform IR determ. 80−7765
HOD, IR band intensities in ice and water 79−3443
HOD, IR spectra in D_2O, combination vibr. 80−9609
$H_3O^+(H_2O)_n$, IR spectra, OH stretching vibrs. 78−25529
HOI, $O_3(O)+HI$ matrix reaction, IR spectra, isotope shifts and band assignments 78−80737
HO_2NO, unimol. dissoc., rate consts., temp. depend., atmospheric implications 78−7175
$HOONO_2$, FT IR spectral obs. of $HOO+NO_2 \rightarrow HOONO_2$ 77−28993
$H_2O.H_2S$, IR spectra of complex in solid nitrogen, 20K 79−10102
HPO, in Ar matrix, IR and UV absorpt. spectra 80−47985
H_3PO_2, H_3PO_3, H_3PO_4, polarisable acid-acid and acid-water hydrogen bonds 79−76423
H_2S, absorbed on zeolites with varied Si/Al ratios 78−60029
H_2S, absorpt. coeffs. meas. in Nd laser emission band 80−78620
H_2S, rot. spectra, 714-1667 μm, Fourier interferometric spectrometer 77−83765
HSO, radical, electronic spectrum and struct. 77−75147
H_2SO_4, dissociation and absorpt. consts., ultrahigh resolution obs. of 8.2, 11.3 μm bands 78−70825
H_2SO_4, pure, IR and Raman spectra in liq. state, assignments and cryst. spectra comparison *(French)* 79−33699
H_2SO_4, vap. IR absorption coeff., 1190-1260 cm^{-1} 77−68036
H_2SO_4, vapour, foreign gas broadening diode laser spectroscopy in IR 78−36261
HSO_3F, liquid, indication of molecules existing as mixture of cyclic dimers and infinite chains *(French)* 80−989
$HSiCl_3(DSiCl_3)$, Raman and IR spectra, mol. motion 78−64353
H_3SiNCO, low freq. bending mode, pot. function 78−82728
H_3SiNCS, IR and Raman spectra, vibr. anal., LF bending mode 78−70842
$H_3SiOSiH_3$, pot. function governing low freq. bending mode 77−58016
H_20, vibr. transition moment and band intensity 79−27036
HeH_2 collision induced dipole IR spectra, ab initio SCF LCAO calc. 79−89737
Hg complex, methylethynylmercury(II)($-d_1$,$-d_3$,$-d_4$), vibr. spectra and normal coord. calcs. 80−58259
$Hg(CN)_3^-$ ion, CN and HgC stretching vibrations and HgCN bending vibration assignments 80−69140
HgFCl, HgFBr, HgFI, existence and vibr. characterisation, IR and Raman matrix isolation obs. 78−78706
$HgF_2(FCl)(FBr)$, matrix isolated IR and Raman spectra, assignments, force consts., isotope effects and thermodynamic props. 80−63631
$HgFe(CO)_4$, IR and Raman spectra, vibr. anal. 78−66553
$HgX_2(HgXY)$, (X,Y=Cl, Br, I), IR and Raman matrix isolation spectra, bending force consts. 77−465
IF_5, IR intensities, fundamental, overtone and combination band calcs. 78−29780
$InCl_3$ in Kr lattice, Raman and IR spectra, vibr. assignments, force consts., isotope shift and config. 79−89671
$InCl_3$, planar D_{3h} struct., IR matrix isolated spectra 77−75148
$K_2(Cd(CN)_4)$, vibr. spectra, isotope substitutions, force consts. determ. *(German)* 77−61750
KF, KCl and KI, monomers and dimers, Ar matrix-isolated, IR spectra, vibr. assignments and calcs. 79−45718
$KReO_4$, matrix isolated, IR spectra 80−28012
K_2SO_4, IR and Raman spectra of vap. over heated matrices 78−25525
K_2SO_4 molecules isolated in inert gas matrices, low freq. IR spectra 78−50547
$K_2UO_2Br_4$, force consts., IR spectra 78−5216
$K_2(Zn(CN)_4)$, vibr. spectra, isotope substitutions, force consts. determ. *(German)* 77−61750
LiCNS, ether solns., dimer struct. and force consts., IR and Raman spectra 79−72442
$LiClO_4$, solutions in amides and esters, structure *(French)* 80−7343
$(LiF)_n$, 'polymers', aggregation, microcryst. form., IR spectra obs. 78−46331
Li_3F_3, isotopically substituted, IR freq. and intensity patterns 78−21926
$LiReO_4$, IR matrix-isolation spectra 80−87108
Mg complex, bis-pyridal-Mg-tetrabenz-porphyrin, disagreement with diffuse interstellar bands 80−56905
MgO, wavelengths and relative intensities of IR bands 79−2407
$MgO_2(O_3)$, from $Mg+O_3$ matrix reaction, IR spectra, isotope shifts and blue matrix shift 78−80736
$Mn(CO)_5Br$, ν(CO) region, IR and Raman spectra in organic solvents 79−41169
MnO_4^- ion, ^{18}O enriched, matrix isolated IR spectra, force consts. 80−52985
$MnSO_4.H_2O$, IR spectra, H_2O external modes temp. depend. 78−58683
Mo complexes, oxo-bridged dimers, ^{16}O and ^{18}O-substituted synthesis, IR spectra 77−77188
$Mo(CO)_6$, bonding, IR intensity anal. 78−25526
$MoCl_6^n$, n=1,2,3, vibr., IR meas. 79−68234
MoF_6, in Ar matrix, photolysis, MoF_5 form., IR spectrum 80−87115
$N_2+CO_2(O_2)(N_2)$, IR spectral absorpt. induced by press. in atmos. *(Russian)* 80−56600
N_3, spectroscopic data review 77−38680
N_3^-, high press. IR vibr. spectroscopy *(German)* 80−74170
NCO, $A^2\Sigma$ state, Fermi resonance and vibr. relax. in solid Ar 78−5212
$^{14}ND_3$, $^{15}ND_3$, ν_2 fundamentals and isotope shift 79−59456
$ND_2(NH_2)$, ν_2 band, laser mag. reson., 9-10 micron 80−9601
NF_2, IR spectra, ν_1 and ν_2 bands, vibr. excitation and spin-rot. interaction, doublet splitting 80−28011
NF_3, gas and liquid Ar soln., IR spectra, binary overtone and combination band intensities 77−79658
NF_3, IR intensity anal. 77−58081
NF_3, IR spectrum in liquid Ar, vibr. anal. 78−21927
NF_3, shock induced decomposition in Ar, IR emission, reply 77−63907
NF_3 shock-induced decomposition in Ar, IR emission, comment 77−63906
NH_2, ν_2 band, laser mag. reson. 80−83523
NH_2, radical, laser mag. reson. spectra in 9 μm region, ν_2 band 79−45724
NH_3, 10 μm absorption line profile, high resolution meas. 77−42359
NH_3, 10.6 μm region absorption lines, diode laser meas. 78−58689
NH_3, 2sQ(1,1) meas. in $2\nu_2-\nu_2$ band, using heterodyne spectrometer 79−75626
NH_3, 800-1200 cm^{-1} region 79−98086
NH_3, 9.5 μm region diode laser spectra 78−58688

infrared spectra of polyatomic inorganic molecules continued
NH_3, absorpt. coeffs. meas. in Nd laser emission band 80−78620
NH_3, absorpt. cross sections at CO_2 laser wavelengths, temp. and press. depend. 80−78613
NH_3, adsorbed on $CaCl_2$ and $CaBr_2$, IR and far IR spectra 77−24478
NH_3, and $-d_n$ IR matrix isolation spectra, rotation and inversion 78−5218
NH_3, collisional broadening, vel. depend., IR optical saturable absorpt. technique, book contrib. 78−9201
NH_3, Coriolis and l-type interactions, ν_2, $2\nu_2$ and ν_4 states, IR spectra 80−47993
NH_3, decay of saturation reson., IR ν_2 as Q(8,7) transition 78−25609
NH_3, decomposition, on supported FE catalyst, kinetics, IR obs. 79−11792
NH_3, fuse of $Pb_{1-x}Sn_xTe$ injection laser in high-resolution spectroscopy 79−76714
NH_3, gaseous, IR obs. spectra meas. using $Pb_{1-x}Sn_xTe$ diode laser *(Japanese)* 79−49306
NH_3, high-resolution absorpt. spectra obs. using pressure-tuned diode laser 80−82835
NH_3 high-resolution spectroscopy using pulsed $Pb_{0.955}Sn_{0.045}Se$ laser 79−64252
NH_3, IR absorption band integrated intensities, ab initio and LMO studies 80−23458
NH_3, IR intensity anal. 77−58081
NH_3 IR intensity formulations 77−58004
NH_3, IR spectra, fine struct. of rot.-vibr. bands 80−102504
NH_3 in benzene(CCl_4)(pentane) Fermi resonance, solvent and phase depend. 80−47960
NH_3, in inert solvents, far IR absorpt., free rotational models 77−450
NH_3, laser saturation time-delayed IR spectroscopy 78−86976
NH_3, laser-induced excitation at 1076 cm^{-1} in megawatt region 80−10354
NH_3, line intensities in 2 μ band, Doppler broadened lines 77−75155
NH_3, lone pair contributions to the IR intensities, ab initio calcs. 80−63630
NH_3, ν_2 band as R(1, 1) line self-broadening coeff. 79−98158
NH_3, ν_2 IR band, vibr,-rot. lines, self-broadening and intensities 77−34635
NH_3, $\nu_3+\nu_4$ band anal. 77−75154
NH_3, photoacoustic spectroscopy at 9 μm, 10 μm $^{12}C^{16}O_2$ laser wavelengths 79−21014
NH_3, pure rot. spectrum 20 to 120 cm^{-1}, Fourier transform spectrometry meas. method 77−45902
NH_3, saturated absorpt. at 888 cm^{-1} using tunable diode laser 78−94239
NH_3, spectral line meas. using 10μm superheterodyne receiver on Earth and Jupiter 78−16335
NH_3, spectral lines near 11 μm, precise meas. using IR heterodyne technique 78−5230
NH_3, weak IR absorpt. meas. using double-beam Fourier spectrometer 80−105725
$^{14}NH_3$, $^{15}NH_3$, CW and pulsed $Pb_{1-x}Sn_xSe$ diode laser spectroscopy 79−26980
$^{14}NH_3$, $^{15}NH_3$ and $^{14}NH_2D$, IR laser Stark spectroscopy 80−47978
$^{14}NH_3$, Doppler free spectroscopy, 16 micron generation applications 79−94049
$^{14}NH_3$, IR saturated absorpt. spectra, vibr. depend. of hyperfine quadrupole const. 77−27072
$^{14}NH_3$, Jupiter atmos. comp., IR spectral obs., 800-1000 cm^{-1} 78−16336
NH_3-CO_2 complex, matrix isolation IR spectrum, struct., ab initio SCF calcs. 78−5209
$N_2H_2(N_2D_2)$, ground and first excited state small vibr. coupling, ab initio CI calc. 78−62791
$NH_4(NH_3)_n^+$, n=0 to 4, gas phase IR spectra 80−43044
NH_4NO_3, IR spectra and vibr. bands 80−69144
$NH_4UO_2(NO_3)_3$, IR spectra, force consts., bond orders 77−30873
NO dimer, asymmetric, characterisation, Raman, IR spectroscopy 79−41176
NO, IR emission Fourier transform spectroscopy, mol. rot.-vibr., RKR potential curve calc. 80−95618
NO_2, 7390 Å band, vibronic transition within ground state manifold 78−21919
NO_2, 8170-8280Å absorption spectrum, rot. struct., assignments 79−6937
NO_2, 8920 Å band temp. depend., location of 000-000 band of A^2B_2-X^2A_1 transition 78−70826
NO_2, (101) band, line strengths, spin-splittings and forbidden transitions 80−47987
NO_2, absolute integrated intensity for 3.44 μm band 77−3418
NO_2, adsorbed on SiO films, infrared spectra exam. 79−45725
NO_2 excited, fluoresc. spectrum, IR multiphoton vibr. pumping, photon absorpt. probability distrib. study 80−18854
$(NO)_2$, IR spectra in O_2 matrix, vibr. freqs. 78−23936
NO_2, rot. Q-branch effective line strength at 37.7 cm^{-1} 77−6859
NO_2^-, high press. IR vibr. spectroscopy *(German)* 80−74170
NO_2^-, solvated, in H_2O, ethanol, cyanomethane, and DMF lowest n-π* transition 79−85960
$^{14}N^{16}O_2$, IR spectra, $2\nu_2+\nu_3$ and $\nu_1+\nu_2+\nu_3$ bands, vibr. and vibr.-rot. consts. 78−983
$^{14}N^{16}O_2$, ν_1 band, high resolution IR spectra 78−55173
$^{14}N^{16}O_2$, $\nu_1+\nu_3$ band, IR absorpt. spectra 78−78693
NO_3^-, in $MClO_3$ and $MClO_4$ matrix, vibr. spectra, anion site asymmetry 77−27062
N_2O, 12°1 band lines, precise meas. with compact vacuum IR spectrometer 80−95157
N_2O, 40°00-00°0 band, IR high press. absorpt. spectra profiles 80−52988
N_2O, adsorbed on SiO films, infrared spectra exam. 79−45725
N_2O, combination and difference bands, IR intensities 77−466
N_2O, diffraction-limited IR spectroscopy, normalised slit width appls. 77−71388
N_2O, fundamental vibr. bands in liq. phase 79−54856
N_2O, ground level abundance, simultaneous determ. of CO_2, CO and H_2O 78−11969
N_2O, IR absorpt. spectra, N_2-broadened lines of ν_3 band 78−5228
N_2O, IR band nonrigid rot. absorption 78−91060
N_2O, IR bands, parametric deconvolution method 78−78697
N_2O, IR emissivity and band-model parameters, 200-500K 77−83591
N_2O, IR intensities by electron impact spectroscopy 77−6851

infrared spectra of polyatomic inorganic molecules continued
N_2O, IR spectrum in liquid Ar, vibr. anal. 78−21927
N_2O, in soln., IR and Raman band shapes, mol. dynamics, ν_3 band 77−36238
N_2O, in soln., Raman and IR ν_1 and ν_2 band shapes, mol. motion dynamics 78−64352
N_2O, liq. phase vibr. spectra, anharmonicity effects 79−50022
N_2O, multiple reflection cell, laser spectroscopic meas. 78−86359
N_2O, ν_2 band as freq. standard in 17 μm spectral region 79−63991
N_2O, ν_3 and $2\nu_3$ IR bandshape and dipole correl. functions 80−91560
N_2O quadrupole hyperfine struct., vibr. depend. obs. using twin-laser spectrometer 80−43097
N_2O, rot. spectra, 714-1667 μm, Fourier interferometric spectrometer 77−83765
N_2O+N_2, vibroluminesc., V-V transfer consts., quadrupolar transition moment, IR spectra 79−10112
$N_2O+N_2^*$, vibr. population studied by IR emission spectra *(French)* 77−14544
$(N_2O)_2$, IR continuum spectrum at low temps. 80−980
N_2O_4, IR spectra in O_2 matrix, vibr. freqs. 78−23936
N_2O_4, vibr. assignment 79−6940
N_2O_5 gaseous, integrated band intensity data, stratospheric detection implications 80−58250
N_2O_5, IR spectra in O_2 matrix, vibr. freqs. 78−23936
N_2O_5, spectrum rel. to stratospheric abundance 77−5299
NO_2Br, formation and IR spectrum 79−98097
NO_2I, formation and IR spectrum 79−98097
NSF_3 band contours of E fundamentals, IR spectra 79−98089
NSF_3, IR spectra, matrix isolated, force const. calc. 78−62802
$^{14}NH_2D$, i.r. absorption coeff., press. broadening 77−464
$^{15}NH_3$, spectral parameters, Lamb dip method investig. 78−89560
Na_x, matrix-isolated, formed in supersonic nozzle beam, 400-800 nm absorption and mass spectra obs. 79−76439
$(NaCl)_n$ (n=1-7) equilib. configs., total energy calcs., far IR spectra 78−29872
$NaClO_4$ aqueous soln., IR absorpt. spectra, band profile temp. depend. 77−30869
$Na_2N_2O_3$, vibr. spectra, assignments 77−38670
$NaPF_6.H_2O$, IR and Raman spectra 77−61749
$NaPO_2$, mol. identification by matrix isolation IR spectrosc. 80−104485
$NaPO_3$, mol. identification by matrix isolation IR spectrosc. 80−104485
$NaReO_4$, matrix isolated, IR spectra 80−28012
Na_2SO_4, IR and Raman spectra of vap. over heated matrices 78−25525
$Nb_nW_{6-n}O^{(n+2)-}$, config., IR and Raman spectra 77−42324
Nd complex, with ortho-phenanthroline and $\alpha\alpha'$-dipyridyl tris-trifluoroacetate, absorption spectra 79−98113
NdX_3,(X=Cl,Br,I) far IR spectra, planar D_{3h} symm. 77−88450
Ni complex, S_4N_4 with $NiCl_2$, mass and IR spectra, config. 78−13494
$Ni(CO)_4$, bonding, IR intensity anal. 78−25526
$NiSO_4.H_2O$, IR spectra, H_2O external modes temp. depend. 78−58683
$O+H_2S$, matrix reactions, IR spectra of products, chemiluminesc. 77−60057
O_2, (0,0)$b^1\Sigma_g^+$-$X^3\Sigma_g^-$ band, press.-induced line shift 79−98160
$O_2+O_2(N_2)$, IR spectral absorpt. induced by press. in atmos. *(Russian)* 80−56600
O_3, (010) and (020) states, 14 μm diode laser spectra, assignments 79−98079
O_3, atmospheric, IR heterodyne spectroscopy 77−45160
O_3, combination bands ($\nu_1+\nu_2$) and ($\nu_2+\nu_3$), anal. 78−9150
O_3, high resolution spectroscopy of ν_3 band, rel. to atm. O_3 monitoring 79−63993
O_3, IR absorption spectrum using CO_2 TEA laser injection locked, tunable single longitudinal mode operation 80−33018
O_3, IR and microwave spectra, ν_3 vibr.-rot. band 77−38663
O_3, IR spectroscopy 79−98088
O_3, infrared spectra of vibr.-rot. bands 79−64001
O_3, line and band strengths in IR spectra, variational calcs. 80−87112
O_3, line position and intensities of $2\nu_3$, $\nu_1+\nu_3$ bands 80−87181
O_3, microwave and IR spectra, ν_2 state, ($\nu_3+\nu_2$)−ν_2 band, 10 micron lines 78−82718
O_3 soln., IR spectra, nonlinear absorpt. 79−98100
O_3, stratospheric, spectroscopy with CO_2 waveguide laser 77−13117
O_3 stratospheric 10 μ absorption line obs. with IR heterodyne spectrometer 78−61494
OAlCl and OAlF, IR matrix spectra, vibr. freqs. *(German)* 79−11785
OBF, band strengths, shock tube IR spectrosc. meas. 80−106358
OBrO free radical in Ar matrix at 10K 79−89669
$OCBr_2$, IR spectra in Ar matrix, force consts. *(German)* 79−36641
OCS, 5.3 μm vibr.-rot. bands, rot. consts., spin-flip Raman laser obs. 77−34631
OCS, fundamental vibr. bands in liq. phase 79−54856
OCS, IR spectra, diode laser calibration 80−83363
OCS, IR spectra using spin-flip Raman laser, combination band near 1890 cm^{-1} 78−37640
OCS, IR spectral moments and mean squared torques, rare gas effects 78−62944
OCS, IR spectroscopy 79−98088
OCS in Ar soln., IR spectra, solvent shifts, vibr. band assignment and anharmonic force consts. 80−9607
OCS in n-alkane, rot. relax., solvent hydrodynamic props., Raman and IR spectra 80−45055
OCS, laser Stark spectra, 9.5 micron, band origins, dipole moments 77−18969
OCS, mol. consts. of ν_2 levels 77−14429
OCS, ν_3 band absolute wavenumbers *(French)* 79−98099
OCS, spectroscopic reference freqs. in 9.5 μm band, heterodyne freq. meas. 80−18850
$^{16}O^{12}C^{34}S$ and $^{16}O^{13}C^{34}S$, IR spectra, v_3 band anal. 80−95620
OCSe, isotopic species, microwave and IR spectra 77−38658
OClNO, form. in matrix reaction, IR absorpt. obs., photoisomerisation 78−15667
$O_2F(Cl)(Br)$ radicals, matrix IR spectra, bonding 78−90160
OGaF, matrix IR spectrum, vibrs. and force consts. 79−11787
$ON^{81}Br$, anharmonic force field from IR and microwave data 78−82809
ONCN, far IR spectra, pure rot. and vibr.-rot. bands 78−82731
$ON^{35}Cl$, anharmonic force field from IR and microwave data 78−82809
ONI, IR matrix isolated spectra, force consts. 79−10111
O_3O_2, $3\nu_7^{11}+\nu_2\leftarrow 2\nu_7^0$ $4\nu_7^0+\nu_2\leftarrow 3\nu_7^{11}$ Q-branches, diode laser analysis 78−74660
$OSiF_2$ prod. from SiO+F_2 matrix reactions, IR spectra and force consts. calcs. *(German)* 80−97718
infrared spectra of polyatomic inorganic molecules continued
OsO_4, and isotopic forms, stretching fundamental, 961 cm^{-1}, high resolution spectroscopy 78−90162
OsO_4, IR vibr.-rot. spectrum, theoretical interpretation 77−6776
OsO_4, spectroscopy using tunable high-press. CO_2 waveguide laser 80−43054
OsO_4, tunable diode laser spectrosc. obs. 78−82061
OsO_3F_2, OsO_4 matrix-isolated IR and Raman spectra 77−75166
P_2, perturbations in $b^3\Pi_g$ state, existence of $^2\Sigma_g^+$ state, visible and IR systems *(French)* 77−68035
PF_2D, gas, normal coordinate analysis of vibrational spectra 79−68233
PF_2H, gas, normal coordinate analysis of vibrational spectra 79−68233
$PF_2H(D)$, vibr. spectra and normal coordinate anal., Raman and IR spectra 80−14147
$(PF_2)_2O$, IR and Raman spectra, vibr. assignment 78−50544
PH_3, dipole moment in ground and excited states, submm. spectrum obs. 80−28056
PH_3, IR intensity anal. 77−58081
PH_3, IR intensity formulations 77−58004
PH_3, IR spectrum rel. to absorpt. in Jupiter 5 μm window 80−31243
PH_3, Jupiter atmos. comp., IR spectral obs., 800-1000 cm^{-1} 78−16336
P_3N_3, matrix isolated, IR isotope freq. and intensity patterns 78−46338
P_4O_6, IR and Raman spectra vibr. spectra, valence force field calc., pot. function *(French)* 78−50549
POF_3, IR rot.-vibr. spectrum, mol. consts., laser Stark spectroscopy obs. 78−33508
POF_3, level anticrossing effects, vibr., laser Stark spectra obs. 80−32771
PbN_2O_3, vibr. spectra, assignments 77−38670
Pd complex, $Pd^{II}Pt^{II}(CNCH_3)_6(PF_6)_2$, vibr. spectra, M-M bonds. *(French)* 80−47997
Pd complex, S_4N_4 with $PdCl_2$, mass and IR spectra, config. 78−13494
Pr complex, with ortho-phenanthroline and $\alpha\alpha'$-dipyridyl tris-trifluoroacetate, absorption spectra 79−98113
Pt complex, $Pt^{II}(CNCH_3)_4(PF_6)_2$, $Pt_2^{I}(CNCH_3)_6(PF_6)_2$, and $Pt^{I}Pd^{I}(CNCH_3)_6(PF_6)_2$, vibr. spectra, M-M bonds. *(French)* 80−47997
Pt complexes, cyano and cyanohalide hydrates, IR absorpt. spectra 77−6771
$PtCl_4^-$, effective charge, from IR and Raman scatt. intensity obs. 78−62809
PuF_6, near IR spectrum, isotope shifts, vibronically induced transitions 77−6773
PuN_2, in Ar matrix, IR spectra, stretching freq. and isotope shifts 78−78690
PuO_2, in Ar and Kr matrices, IR absorption spectra, normal coord. anal., assignments, force consts. 78−78681
PuO_2, matrix isolation studies with Fourier transform IR 78−45740
RbF, RbCl and RbI, monomers and dimers, Ar matrix-isolated, IR spectra, vibr. assignments and calcs. 79−45718
$RbReO_4$, IR matrix-isolation spectra 80−87108
Rb_2SO_4 molecules isolated in inert gas matrices, low freq. IR spectra 78−50547
$Re_2Cl_8^{2-}$, in acetonitrile and dichloromethane solns., 300K, emission spectra and lifetimes 79−59447
$(Re_2OCl_{10})^{3-}$, reson. Raman, IR and electronic spectral studies 79−10118
Rh supported surface, CO chemisorption, activated surface processes, IR spectra 80−16724
RuO_4, $\nu_3(F_2)$ IR band contour, isotopically pure cpds., mol. consts. 77−61746
S_7, Raman and IR spectra, vibr. anal., force consts., thermodynamic functions 78−50545
SBr_2, SI_2, matrix isolated, IR spectra 80−58254
$^{32}SF_2$, $^{34}SF_2$, matrix IR spectra, vibr. and force fields, bond angle *(German)* 78−74662
SF_5, IR spectrum, form. by VUV photolyses in Ar matrices 78−981
SF_6 10.5 μm spectrum, high-J assignments, identification of levels pumped by CO_2 P(12) and P(22) 78−70837
SF_6, $3\nu_3$ band anal., IR spectra 78−90161
SF_6, absorption of intense IR radiation, statistical model 77−34626
SF_6 and S_2F_{10}, absorpt. of intense laser radiation, vibr. excitation 80−9667
SF_6, CO_2 laser excited, optoacoustic meas. of energy absorpt. 77−83667
SF_6, CW CO_2 laser spectroscopy 80−83367
SF_6, collisions, laser spectroscopy investig. 80−9697
SF_6, Doppler-limited spectroscopy of $3\nu_3$ band, rot. const. and anharmonic parameters calcs., mol. photodissoc. 80−83361
SF_6, dynamics of 10.4 μm absorption, vibr. bath model 78−17666
SF_6, electron impact, vibr. excitation, dissociative attachment 77−3481
SF_6, emission spectrum of ν_3 band, 1780K, dissoc. effects 78−62795
SF_6, excitation by strong IR laser field, spectral characts. 80−32713
SF_6, excited to dissoc. threshold, IR absorption 79−81245
SF_6, gas, thermodynamical and spectral props., effect of angle-dependent part of dispersion forces 80−43138
SF_6, gaseous, IR obs. spectra meas. using $Pb_{1-x}Sn_xTe$ diode laser *(Japanese)* 79−49306
SF_6, high-resolution IR Ar matrix-isolation spectra, 10K 80−32708
SF_6, highly excited, time-resolved IR absorpt. obs. 80−9666
SF_6, IR absorpt. spectra of vibr. excited mols. *(Russian)* 79−36643
SF_6, IR absorption peak shift at high intensity *(Russian)* 77−42327
SF_6, IR laser isotopic enrichment in low temp. matrices 78−90318
SF_6, IR laser radiation multiphoton absorpt. direct meas. by pyroelec. detector 80−102545
SF_6, IR radiation induced mol. excitation and heating effects, time resolved 77−75142
SF_6, IR spectra, fine struct. of rot.-vibr. bands 80−102504
SF_6, IR spectra, ν_4 vibr. band strength 78−94240
SF_6, in cryogenic liqs., vibr. kinetics, IR spectrosc. obs. 79−18182
SF_6, intramode anharmonicity const., vibr. linear absorpt. spectrum 80−18893
SF_6, laser spectroscopy using an optothermal receiver 80−37810
SF_6, matrix isolated, CO_2 laser irrad., IR absorpt. spectra obs. *(Russian)* 77−6877
SF_6, matrix isolated, IR spectrosc., temp. reversible site structural changes 80−95613
SF_6, matrix photolysis, vac. UV, using windowless discharge, IR spectra 77−71798
SF_6 molecule, resonant energy absorpt. struct. in IR laser field *(Russian)* 80−5592
SF_6 molecule absorption of IR laser radiation *(Russian)* 80−986
SF_6, mulitphoton absorpt., pulsed CO_2 laser radiation absorpt., press., freq., fluence depend. 80−28080

infrared spectra of polyatomic inorganic molecules continued
SF_6, multiphoton-excited, $\nu_2+\nu_6$ absorption and emission 80−63626
SF_6, multiple photon absorpt., laser pulse intensity and collisions influence 80−95699
SF_6, multiple reflection cell, laser spectroscopic meas. 78−86359
SF_6, multiple-photon excited, double reson. spectroscopy 80−53030
SF_6, multiple-photon two-freq. IR laser pumping, optoacoustic spectroscopy 79−36717
SF_6, nonlinear absorpt. spectrum using Doppler-free polarisation spectroscopy 79−3440
SF_6, ν_3 band, IR spectra, in supersonic mol. beam 78−66541
SF_6, ν_3 manifold, $3\nu_3$ transition, 3-quantum transition probabilities, IR spectrum 78−86866
SF_6, partial saturation of ν_3 ladder in IR absorpt., rate process model 80−58645
SF_6, pumped by OC_6 laser, transition strengths 77−14416
SF_6, relax. mechanism, narrow reson. obs. by amplitude-modulated wave method 79−10155
SF_6, soln. in liquid Kr, resonant IR radiation, nonlinear absorpt., vibr. relaxation estimate 79−36642
SF_6, spectral parameters, Lamb dip method investig. 78−89560
SF_6, spectroscopy using tunable high-press. CO_2 waveguide laser 80−43054
SF_6, spherical top mol. vibr.-rot. spectrum with tunable diode laser 78−82734
SF_6, supercooled, IR absorpt. spectrum 77−23574
SF_6, time-resolved IR absorpt. meas. using injection-locked single mode TEA CO_2 laser 80−9665
SF_6, transmission meas. of multiple photon absorpt. 77−83668
SF_6, tunable diode laser spectrosc. obs. 78−82061
SF_6, vibr. anharmonicity consts., ν_4 region laser absorption obs. 78−94242
SF_6, vibr. spectra, rot. consts., IR spectra, Raman spectra obs. 80−32719
SF_6, vibr. strength, IR intensities calcs. 77−34608
SF_6^-, matrix isolated, IR spectra, evidence for form. 77−68037
$^{32}SF_6$, point group symmetry breakdown, vibr.-rot. state, saturation spectroscopy 80−87116
SF_6-Ar, condensing flow, gasdynamic and IR meas. 80−6501
SF_6+N_2, simultaneous vibr. transition, absorpt. band intensity 77−50474
S_2F_{10} 77−6775
S_2F_{10}, IR laser irrad., absorpt., reaction parameters 78−94241
SF_6Ar, multiple photon excitation, saturation and linear absorpt., pulsed optoacoustic detect. 78−42148
SF_5Br, Ar matrix and solid phase Raman and IR spectra, vibr. assignments 77−6775
SF_5Br, vibr. spectrum and normal coord. anal. 77−18926
SF_5Cl AR matrix and solid phase Raman and IR spectra, vibr. assignments 77−6775
SF_5NF_2, multiphoton excitation, absorption and dissoc., isotope selection 79−100408
SF_4O, vibr. spectra, struct. and thermodynamic props. 77−63416
S_4N_4, solid and soln., IR and Raman spectra, vibr. assignment 78−74659
$S_3N_3Cl_3$, solid and soln., IR and Raman spectra, vibr. assignment 78−74659
$S_4N_4H_4$ ($S_4N_4D_4$), vibr. spectra, force consts. *(German)* 78−13499
$S_4N_4H_4$, and -d_4, solid and soln., IR and Raman spectra, vibr. assignment 78−74659
SO_2, 4 μm $\nu_1+\nu_3$ band, Doppler-limited and atmospheric spectra 77−27064
SO_2, absorpt. coeffs. for ν_2 and ν_3 bands 77−38668
SO_2, atmospheric transmittance over IR spectral bands, model 80−51535
SO_2 frost or adsorbate on surface of Io, IR reflection spectrum 79−92708
SO_2 IR absorption spectra *(Russian)* 79−25328
SO_2, IR bands, emissivity, line shape and band model parameters 78−94246
SO_2, IR bands, line-shape parameters, 300-1200K 79−36704
SO_2, IR multiphoton excitation and inverse electronic relax., mol. vibr. and fluoresc. 80−106349
SO_2, IR obs. spectra meas. using $Pb_{1-x}Sn_xTe$ diode laser *(Japanese)* 79−49306
SO_2, IR spectra, Coriolis intensity perturbations 80−95617
SO_2, IR spectra, $\nu_1+\nu_2$ combination band, rot.-vibr. anal. 78−5225
SO_2, IR spectroscopy 79−98088
SO_2, matrix isolated, ν_3 vibr. spectrum, diode laser spectroscopy, temp. depend. 77−50433
SO_2, ν_1-bands, absolute integrated intensity 77−6858
SO_2, rot. spectra, 714-1667 μm, Fourier interferometric spectrometer 77−83765
$^{34}SO_2$, $\nu_1+\nu_3$ band, high resolution IR spectrum *(French)* 77−71801
SPF_3 band contours of E fundamentals, IR spectra 79−98089
SPF_3, IR spectra, matrix isolated, force const. calc. 78−62802
SPF_3, isotopic forms, microwave spectra, centrifugal distortion consts., vibr. and rot. states, IR matrix spectra 77−10665
SPF_3 vibr. spectrum, assignment using matrix isolation and isotope substitution *(German)* 78−13498
$SSBr_2$, IR matrix isolation spectra in Ar matrix at 9K 79−93995
$SSCl_2$, IR spectra, prod. in S_2Cl_2 photolysis 78−61033
SSF_2, FSSF, and ^{34}S isotropic forms, matrix IR and Raman spectra *(German)* 79−89674
$S(SiD_3)_2$, gaseous and solid phases, molecular vibr. exam. 78−25547
$S(SiH_3)_2$, gaseous and solid phases, molecular vibr. exam. 78−25547
$SbCl_3$, dynamic coeff., molecular interaction effects of media *(Russian)* 77−83601
$SbCl_5$, nitrile addition compounds, mol. vibr., IR and Raman spectra *(French)* 77−23499
SbF_3, IR spectra of solid and gas, rel. to struct. *(French)* 78−78692
Sb_4O_6, IR and Raman spectra vibr. spectra, valence force field calc., pot. function *(French)* 78−50549
SeF_6, IR vibr. band contours, isotope substitution, force consts. 78−17670
SeF_6, in Kr matrix, temp. reversible IR spectral changes, site struct. dynamics 80−102505
Sf_6, absorpt. of pulsed CO_2-laser radiation at 140K 79−22707
Sf_6, IR-IR double reson. following IR laser excitation, ν_3 mode 79−54872
Sf_6, integrated IR band intensities and transition moments 80−95611

infrared spectra of polyatomic inorganic molecules continued
Si_6Br_{12}, and Si_6Cl_{12}, vibrational spectra and force constants, rel. to Si_5Cl_{10} and Si_5Br_{10} *(German)* 79−22716
Si_5Cl_{10}, and Si_5Br_{10}, vibrational spectra and force constants, rel. to Si_6Cl_{12} and Si_6Br_{12} *(German)* 79−22716
$(SiCl_3)_2O$, IR matrix isolation spectrum, Raman spectrum 78−82730
SiF_4 molecule, saturated absorpt. of CO_2 laser radiation 80−37811
SiF_4, $\nu_3(F_2)$ IR band contour, isotopically pure cpds., mol. consts. 77−61746
SiF_6, saturation absorpt. spectra, evidence of tumbling multiplets 79−36637
SiH_4, IR spectra, ν_2 and ν_4 band anal. 78−9153
SiH_4, ν_3 and ν_1 IR bands, anal. 79−22704
SiH_4, ν_3 band assignment in IR and Raman spectra, ν_1-ν_3 coupling 77−75124
SiH_4, ν_4 fundamental, laser sideband direct freq. reading IR spectra, electro-optical, press. broadening 78−21920
$^{28}SiH_4$, analysis of ν_4 band interacting with ν_2 band *(French)* 78−9152
Si_6H_{12}, and Si_6D_{12}, Raman and IR spectra, vibr. force consts., config. *(German)* 79−22715
SiH_3D, in polycryst. SiH_4, mol. motions and symmetries, IR obs. 78−48163
$^{28}SiH_3D$, IR spectrum ν_1 and ν_4 bands, rot. const. 77−83590
$(SiH_3)_2O$, vibr. spectra, coupling of large amplitude vibrs. 78−37619
Si_3O_3, isotopically substituted, IR freq. and intensity patterns 78−21926
Si_3O_3, matrix isolated, IR isotope freq. and intensity patterns 78−46338
Sm complex, mono-, di-, tri-glycolate, IR absorpt. spectra, vibr. freq. and co-ordination number 78−58684
Sm complex, with ortho-phenanthroline and $\alpha\alpha'$-dipyridyl tris-trifluoroacetate, absorption spectra 79−98113
$SnBr_4$, matrix-isolation and $^{79/81}Br$ and $^{116/124}Sn$ isotope shifts in IR spectra 77−46561
SnI_4 in cyclohexane, using model for absorpt. band shapes 77−71794
$TeO_{11}Cl_2$ thermal decomposition, matrix isolation IR and mass spectra 80−81306
$Th(N_2)$ complex, IR matrix isolation spectrum 79−59457
$TiCl_4$, IR absorpt. bands, absolute integrated intensities, obs. and calc. 78−78689
$TiCl_2(SO_3X)_2$.DMSO complex, X=F, Cl, IR spectra 78−42054
$TiCl_2(SO_3X)_2$.acetylacetone complex, X=F, Cl, IR spectra 78−42054
$TiCl_2(SO_3X)_2$.pyridine complex, X=F, Cl, IR spectra 78−42054
$TiCl_2(SO_3X)_2$.quinoline complex, X=F, Cl, IR spectra 78−42054
Tl_2Cl_2, mol. consts., IR and Raman freqs. assignments 78−17648
Tl_2F_2, mol. consts., IR and Raman freqs. assignments 78−17648
$Tl_2F_2(Cl_2)$, assignment of vibr. Raman and IR spectra bands 80−58268
$TlNO_3$, ion pair, in Ar matrix, solvation effects, IR spectra 77−46563
$TlReO_4$, IR matrix-isolation spectra 80−87108
U complexes, tetranuclear halogenocomplexes, preparation, vibr. spectra *(French)* 77−83596
$U(BH_{4-x})_y^+$, identified in vap. above $U(BH_4)_4$, IR spectra 79−36639
$U(BH_4)_4$, and d-16, IR specra, gas, matrix, isolated and film 79−36639
$U(BH_4)_4$, IR and UV spectra of gas phase 78−62798
UF_4, matrix isolated, IR spectra, interactions with frozen gas 78−9148
$UF_4+F_2 \rightarrow UF_5$, UF_6, IR matrix isolation spectra 77−12787
UF_5, monomer struct. and pot. consts., IR and Raman spectra in inert gas matrices 78−5215
UF_5, transient mol., IR absorption spectrum, 580-630 cm^{-1}, assignments, mol. struct. 79−68227
UF_5, transient species formed in UF_6 laser flash photolysis, 17 micron IR spectrum 79−45715
UF_6, CW CO_2 laser spectroscopy 80−83367
UF_6, matrix isolation spectra and photolysis 79−50043
UF_6, ν_3 manifold 3-quantum transition probabilities, spectral assignment 78−58648
UF_6, room temp., IR absorpt. obs., isotope shift of fund. band and combination bands, freq. depend. 80−23421
UF_6, supercooled, IR absorpt. spectrum 77−23574
UF_6, vibr. strength, IR intensities calcs. 77−34608
UN_2, matrix isolation studies with Fourier transform IR 78−45740
UO_2, molecular geometry determ. from IR spectra vibr. assignments 77−50437
UO_n (n=2,3), matrix isolation studies with Fourier transform IR 78−45740
$UO_2(NO_3)_2$ complexes, IR spectra, normal coordinate anal., vibr. assignments, force consts. and ligation effects 80−9608
$W(CO)_6$, bonding, IR intensity anal. 78−25526
WCl_6, force fields, IR spectra, isotope shifts 77−14432
WCl_6^{n-1}, n=1,2, vibr., IR meas. 79−68234
WF_6, CW CO_2 laser spectroscopy 80−83367
WF_6, supercooled, IR absorpt. spectrum 77−23574
WO_3, IR spectra, normal coord. anal. 78−58682
$ZnCl_2$, aq. solns., complex IR refr. indices, IR spectra, mechanisms, spectrometer system 78−43831
ZnFCl, existence and vibr. characterisation, IR and Raman matrix isolation obs. 78−78706
$ZnF_2(FCl)(FBr)$, matrix isolated IR and Raman spectra, assignments, force consts., isotope effects and thermodynamic props. 80−63631
ZnO_3, formed by matrix reactions, IR, Raman and visible spectra 80−87110
ZnX_2, ZnXY, X and Y=halogen, matrix isolation IR and Raman spectra 78−55171
ZnXY, (X,Y=Cl,Br or I), matrix isolation, vibr. spectra, isotope effects, force consts. and geometry 78−46337

infrared telescopes *see telescopes*

infrared transmitters *see infrared sources*

infrasonic waves *see acoustic waves*

initial value problems
α^2-dynamos, finite amplitude, with large scale in compressible circulation, theory 78−81534
adiabatic stability of rotating gaseous masses 77−91516
aerodynamics, non-stationary pipe flow solution, numerical methods comparison *(German)* 80−33621
aerodynamics, one-dimensional unsteady flow, numerical solution *(German)* 80−6095
Alfven waves collisionless damping in inhomogeneous plasma, initial value problem soln. 79−64864
anelastic deformation, generalised representation by num. sol. of initial boundary value problems *(German)* 79−12610
antenna radiation field, soln. as initial value problem *(Chinese)* 78−9294

initial value problems continued
articial satellite motion, orbitally stable multistep methods 78−85834
asymmetric elastodynamics with homogeneous initial conditions, Boggio's type theorem 78−26037
atmosphere, dynamic initialisation for barotropic flow 77−21855
atmosphere baroclinic instability, normal modes of primitive and quasi-geostrophic eqns. 77−5286
atmospheric circulation, forced by heating, transient mass flow adjustment 79−53455
atmospheric radiative transfer, doubling initialization, interaction of ang. and initial-layer error 77−70996
atmospheric radiative transfer, doubling initialization and ang. discretization errors 77−70997
beam, homogeneous, initial boundary value problem of transverse vibr. 79−40367
beam, homogeneous, initial boundary value problem of transverse vibr. 79−41601
Benard convection, initial and boundary condition effects, book contrib. 80−1591
Boltzmann eqn., spatially non-homogeneous, uniqueness and local existence anal. 78−29065
Boltzmann eqn. approach to equilibrium for spatially homogeneous solutions 79−26007
Boltzmann equation, global soln. 79−44883
Boltzmann equation, nonlinear, with soft potential, spatially periodic problems 80−77731
Boltzmann equation in an exterior domain 80−90797
boundary layer flows, behaviour of small velocity perturb. 79−94588
Burgers equations, in two dimens., finite element anal. 80−1532
canonical decomposition of the general relativistic initial value problem 79−71304
catalyst pellet, transient diffusion-react. eqns., approximation using Galerkin technique 79−96357
Cauchy problem, global soln. in discrete kinetic theory *(French)* 79−12710
Cauchy problem for Liouville eqn., global solns. in case of singular initial data 80−4509
Cauchy problem for Milne's integral eqn., radiative transfer 77−2513
Cauchy problem in kinetic theory of gases, global soln., two dimens. model *(French)* 77−68727
classical elastodynamics as linear symm. hyperbolic system, differentiability of solns. 78−57783
coherent excitations interacting in dispersive medium, envelope-soliton propagation 79−2639
Comptonization of X-rays by low-temperature electrons, rel. to X-ray sources spectra 79−35108
damped linear integrodifferential eqns., dielectric appl., concavity arguments and growth estimates 79−28703
discrete kinetic theory, maths. and numerical aspects, Couette flow appls. 80−19413
dynamical astronomy simulation, new Runge-Kutta algorithms for differential eqns. soln. 79−12387
Earth atmosphere vertical temp. profile estimation, system identification method 77−91342
Einstein field eqns., linearised 77−57208
Einstein field equations, characteristic initial value problem in general relativity 80−73238
Einstein-Cartan theory of gravitation, generalized 78−73895
elastic-plastic initial value problem, iterative numerical integration 77−62170
elastodynamics, linear, discrete time approx. of initial boundary value problems, error estimates 80−73175
elastodynamics, linear theory, stability anal. 77−13610
elastoplastic bodies, quasistatic deform., models, initial boundary value problems *(German)* 78−42549
evolution systems and convection-diffusion, stiffness and stability, Gershgorin theory 80−77626
finite element, unconstrained variational approach 77−67256
finite element method of soln., unconstrained variational formulation 77−87637
fins, nonlinear problems, 1-D conduction, initial value problem 80−83726
flames, premixed, laminar, time-depend. soln. determ. 78−67282
flow depend. expansion process, initial value problem, two step difference method *(German)* 78−57877
fluid dynamics, plane Couette flow, resonance mechanism, small 3-D disturbances 80−79269
fluid dynamics, Rayleigh-Benard convection, randomly forced 80−79314
fluid mechanics, num. methods and associated problems, book contrib. 77−89087
fluids, Newtonian, eqns. of motion, initial value problem 80−62477
forced oscillations in rotating stratified liquid, initial value problem 78−63478
galactic dynamo models, initial-value formulation 79−40262
galaxy clustering depend. on cosmological density parameter 79−48971
gas, two dimensional, initial value problem for model Boltzmann eqn. 79−44885
general relativistic fluids, rot. and non-rot., initial-value problems and singularities 78−112
general relativity, 'thin sandwich conjecture' 78−4539
general relativity, conformal changes of metrics 77−79009
general three body problem, stability of solns. 77−53408
generalised Feller eqn., initial condition solns. 79−12579
geodesy, soln. of downward continuation problem by initial value method *(German)* 77−86750
glow discharge theory 77−39496
gravity waves, created against vertical cliff, uniform asymptotic soln. 78−67210
Green and Ampt infiltration eqn. parameters depend. on initial water content 79−79899
harmonic oscillator EM field interaction 80−47223
heat conductivity, partial differential equations solution, inverse problems *(German)* 80−1404
heat exchanger, dynamic analysis, digital algorithm for initial value problem 77−42727
Hilbert asymptotic expansion method for evolution equations in Banach spaces 79−17368
hydrodynamic stability problems with time-depend. boundary conditions, numerical simulation methods 80−19411
hydroelastic shell opening in fluid flow numerical soln. *(Ukrainian)* 79−50592
initial value problems continued
hyperbolic differential eqn., charact. initial value problems, interval-analytic soln., iterative procedure *(German)* 78−8234
hyperbolic initial boundary value problems with damping, Galerkin-Obrechkoff numerical methods 77−45686
inertial waves and an initial-value problem for a thin spherical rotating fluid shell 78−55656
inflows, density currents, and fronts 79−10542
integrable evolution equations, general struct. 79−30201
KdV equation, perturbative expansion and initial value problem 80−62487
Klein-Gordon-Schrodinger coupled equations 79−35955
Korteweg-de Vries eqn. solns., existence and regularity 79−71265
Korteweg-de Vries-Burgers equation, time evolution, stability, of shock soln. 77−37743
lake, variable depth circular model, time dependent response to wind stress 78−24320
Langmuir soliton formation with ion-acoustic densiton emission 78−75328
line thermal numerical model, initial conditions influence 78−92932
linear dynamic viscoelast., stability conditions for solns. 79−30240
linear elasticity, finite error approx., error estimates for continuous time approx. 80−52024
linear hyperbolic initial boundary value problems, hydraulic system appl. *(German)* 79−9115
linear supersonic flow round a yawed elliptic cone *(German)* 77−65762
Lorentz-Dirac equation, nonlocal generalisation 77−13622
magnetic islands coalescence, in plasma MHD 80−19564
magneto-elastic plates under mixed boundary conditions 79−7328
massive Thirring model, sine-Gordon eqn., soliton struct., Coleman correspondence 78−8509
Maxwell's initial boundary value problem, horizontal line (Rothe) method, convergence and error estimates 80−94957
Maxwell's vacuum field eqns. 77−57208
Maxwell-Hopkinson dielectric theory electric displacement fields, growth estimates 79−24278
mechanical response and the initial value problem 79−2620
MHD Couette flow stability in presence of mag. field 79−23373
micropolar fluids, initial boundary value problems 79−14373
mixture of two elastic solids, variational theorem in linear theory for quasi-static case 78−9561
Navier-Stokes eqns., steady flow prod. by rot. disc, series soln., integral method 78−71308
Navier-Stokes eqns. in domains with non-compact boundaries *(Russian)* 78−30255
Navier-Stokes initial value problem for boundary-free incompressible flow, bounds on solns. 77−11163
neural system model, excitation propagation 78−96044
neutron diffusion, time-dependent continuous-energy equation, weak solns. 77−65244
neutron nonlinear transport, initial value problem, integro-differential eqns. 77−61474
nonlinear initial-value problem arising from kinetic theory of vehicular traffic 79−163
nonlinear reaction-diffusion models for interacting populations 78−65886
nonlinear Schrodinger eqn., global solns. in 1,2,3-dimens. 79−5993
null gravidynamics, initial value problem and Dirac-bracket relations 78−77781
numerical weather prediction, initialization with data assimilation method 78−57282
ocean continental shelf waves, generation by alongshore vars. in bottom topography 80−51424
oil shale, transient temp. distrib. due to combustion flame in retort 79−37110
one-dimensonal heat equation with nonlinear time-dependent boundary conditions, global attraction 78−16754
operational-differential equations of arbitrary order, regularisation of improperly posed initial-value problem *(Russian)* 77−67206
ordinary differential eqns., suppression of inherent instabilities in initial value methods 79−9090
parabolic, numerical soln. using Volterra integral eqns. 77−68437
peeling mechanics of elastic strip from rigid substrate, large bending 77−80122
perturbed spherically symmetric collapsing star, initial value problem in quasi-Newtonian background 79−5842
perturbed wave eqn., Pettis integration initial-value problem 79−71285
pipe, curved, in creep, flexibility 78−34039
planetary accretion dynamics, computer simulation, sensitivity to initial conditions 77−82131
plasma, drift waves and trapped particle modes, non-Hermitian radial eqns. 77−89244
plasma oscillations, Vlasov theory, linear approx., electron distrib. initial value problem 77−84423
protogalaxies, rot. and star form. rate 79−35374
quartz resonators, anisotropic circular plate initial stress effect calc. 79−55300
quasi-linear, variational formulation, appl. to wave problems and transonic flow 77−13579
randomly perturbed one dimens. wave eqn., multiple-scales space-time anal. 78−8247
Rayleigh problem, exact transform soln. 77−53844
Rayleigh-Taylor instability of viscous fluids 79−1159
reactor coolant accidents, appl. of self-initialized RELAP4 momentum eqn. 78−13287
reactor heat conduction and fluid flow, local Green's function method for initial value problems 79−89359
resistive MHD instabilities, diffuse pinch configs., numerical study 77−58853
Roberts, min. degree algorithm appl. 78−89311
rotating dust sphere, slow rotation limit, maximal slicing condition 80−73246
Rothe's line method, three dimensional heat equation *(German)* 78−30147
Schrodinger time dependent eqn., initial value problem, fund. soln. 79−25902
second order hyperbolic differential equations *(German)* 78−20952
singular perturbations for initial value problems, hyperbolic nonlinear partial differential eqns. 78−58111
small-amplitude internal waves due to an oscillatory pressure 79−72906
spin 3/2 field theories, constraints, positivity and obscure representations 79−2909

initial value problems continued
spray, numerical computation, appl. to engines 79−37378
stellar dynamics, global particular solution to initial value problem 79−35314
stratified fluid flows, transient solns. 77−35196
string, nonlinear semi-infinite, initial value problem 79−49044
summed progressing wave formalism for initial value problem calcs. 80−92039
superfluid, Poisson's formulas for wave propagation 78−38891
surface waves under gravity, uniformly analytic initial domains 79−72901
symmetric top on horizontal surface, computer program for initial value problem 79−44714
symmetrical free vibrations of a thin elastic plate with initial condition as a generalized function 79−59939
Taylor instability, in inverted atmosphere 77−9476
thermal elastoplastic stress analysis based on initial strain method *(Japanese)* 80−77620
thermoelasticity, nonlinear, initial value prob. for dynamic eqns. 77−7304
thermoelasticity, stress-flux initial boundary value problem 80−61
thermoelasticity with microstruct., existence and uniqueness theorems 80−60
third-order difference schemes, stability and boundary conditions, smoothing of discontinuities use 77−53762
thrown string problem 78−89331
Toda lattice, Kac-Moerbeke's eqn., scatt. problem 78−12647
transient field initial-boundary value problems, hybrid simulation 77−41469
transient vibration problems, solution bounds 77−67226
two layer shear flow, radiation field and baroclinic eddy development in β-plane 79−81897
two-dimensional steady-state and transient eddy current problem soln. 79−41289
unconstrained variational statements 78−93518
unconstrained variational statements for initial and boundary value problems, comment and reply 79−75327
vibrations of string with time-varying length 79−25870
viscoelastic displacement vector growth estimates 79−27552
viscoelastic liquid channel flow, boundary-initial value problem 79−4045
viscous incompressible inhomogeneous fluid flow, uniqueness and existence of soln. of initial value problem 77−51019
Volterra eqn., growth estimates for solns., appl. to viscoelastic initial-boundary value problems 77−74195
water wave initial value problem *(German)* 79−77155
wave equation in several space dimensions, Rothe method 80−82651
wave equation solutions decaying at prescribed rate with respect to time 77−58230
wave front set of soln. of simple initial boundary value problem with glancing rays 77−41458
wave interaction, resonant, three-wave, separable initial-value problem of initially nonoverlapping envelopes 80−68058
wave motion in one dimens. nonlinear, periodic, exponential lattice 78−12646
wave quadratic path solns. for initial-value problem 77−67298
waves, theory of generation, amplification and damping in nonlinear media *(Russian)* 79−75361
weather, severe convective event numerical simulation and prediction, Navier-Stokes eqns. initialisation 80−31111
weather forecasting scheme, determ. of initial wind field 79−39833
white dwarf stars, rapidly rotating, oscills., numerical calc. 80−46554
^{3}He, superfluid B phase, soliton-like spin waves 80−44385

injection lasers *see semiconductor junction lasers*

injury by radiation *see biological effects of radiation*

inorganic insulators *see insulating materials*

inorganic molecule configurations
see also isomerism
AB_4, non-transition element complexes, shapes and other props. 78−82648
AB_5, non-transition element complexes, shapes and other props. 78−86790
AB_6, non-transition element complexes, shapes and other props. 78−82647
actinide (VI) ions, AnO_2^{2+}, in CO_3^{2-} media, Raman scatt. 79−13718
alkali halide molecular clusters, equilib. geom., form. energy and vib. spectrum 78−55269
alkali halide surfaces, adsorbate binding energies and struct. at surface defects 77−59206
alkali halides, geometries, force consts., charge distribs., FSGO model pot. calcs. 77−88379
alkali metal trimers, spin population, config. determ. 80−42937
alkali trimers, LEPS pot. energy surfaces, equilib. geometries, vibr. force consts. 79−22624
alkali trimers, London pot. energy surfaces 79−6893
alkaline earth chlorides and iodides, photoelectron spectra, geometry 78−29816
boranes, polyhedral, bonding topology, graph-theoretical interpretation 78−33408
carboranes, bonding topology, graph-theoretical interpretation 78−33408
chalcogen and pseudochalcogen mols., stereochem. using nonrigid mol. model 78−62788
chloramine, HOCl, isoelectronic mols., vap. phase UV photoelectron spectra, struct. 78−66600
conference, Crystal XII, Canberra, Australia (Jan.-Feb. 1980) 80−62388
diatomic molecules, equilibrium parameters and Morse anharmonic consts., electron diffr. determ. 78−58818
diatomic molecules, polarisability correl. with mol. dimens. 80−23288
diatomics, harmonic oscillators, R-centroid props. 77−50421
diatomics, spin coupled theory of mol. wavefunctions, struct. and props. 77−50337
DSO, radical, electronic spectrum and struct. 77−75147
Faraday effect measurement in pulsed mag. field 80−80758
first-row hydrides (CH_n, NH_n, OH_n, FH_n), equilib. geometries calcs. 78−33435
group IV hydrides, pseudopot. FSGO calc. 79−22591
halide vapour molecules, MX_2 and MX_3 mols., vibr. freq. and geom. struct. 80−1081
high temperature electron diffraction, review 80−52237
homonuclear diatomics, equilib. geometries, Gaussian-based model pot. calcs. 78−94183

inorganic molecule configurations continued
hydracids, monatomic matrix-trapped, assoc. forms, struct. and spectral response, intermol. pot. calcs. 79−93996
hydrides, first row, bending pot. calc. using MINDO approx., force const., equilib. geometry 80−95544
inert gas complexes spectroscopic data, geometry, pot. energy curve, dissoc. energy, equilib. internuclear distance, determ. 80−53018
interconversion pot. energy surfaces, geometries, electronic structs. 78−35660
ionic solutions, in liq. HCl, coord. sphere radius, vibr. spectrosc. investig. 80−50843
metal clusters, bonding topology, graph-theoretical interpretation 78−33408
methylsilylene, closed shell states, isomerisation, config. calcs. 78−35652
monolayer on graphite, sp. ht. and u.p., size and steric effects 77−85073
MX_4 mole cules, distortion from T_d symm. appl. to PO_4, SO_4, $AlCl_4$ 78−63706
MX_4 molecules, distortion from T_d symm. kernel, co-kernel and averaged configs. 78−63705
$(MX)_n$, $(MX_2)_n$ ionic clusters, struct. and vibr. freqs. calcs. 78−94348
sym-N_2O_3, mol. vibr. in N_2 matrix, normal coord. anal. 79−59432
polyatomic mol. gas phase spectra, struct., review and tabulation 80−14136
pyrophosphatase, inorganic, of yeast, cryst. growth, derivatives formation, heavy atoms positions 80−108842
quasi-linear molecules, low frequency anharmonic vibrations, pot. function determ., Raman and IR spectra obs. 80−52997
rare earth complex, $R(DMMP)_6(ClO_4)_3$ and $R(TBPO)_4(ClO_4)_3$, synthesis and characterisation 77−23498
rare earth complexes, formation and props., book contrib. 80−43204
rare earth ions, aquo complex form., in aq. chloride soln., coord., X-ray diffr. obs. 79−64975
rare earth metal orbital radii, quantum-mech. calcs. rel. to inner series contraction 77−83514
rare earth oxalates, struct., IR absorpt. and Raman spectra *(French)* 80−32714
second-row hydrides, equilib. geometry, FSGO model pot. calcs. 77−50347
second-row molecular orbital calcs., INDO calc. for Na to Cl 78−82643
1,2,5-selenadiazole, partially oriented in mesophase, r, struct. PMR obs. 78−58719
tetramethyl-p-benzoquinone, mol. struct., gas phase electron diffr. obs. 80−58386
thiocarbonates, mol. struct., S-substitution effect *(French)* 80−23335
thionitrates, mol. struct., S-substitution effect *(French)* 80−23335
third-row hydrides, core d-electrons, FSGO struct. optimisation method 77−50382
transition metal clusters, bonding capabilities, MO calcs. 79−22589
transition metal complex anion, vibr. spectra in solid and soln., struct. and fundamental mode assignment 78−62803
transition metal complexes, excited states geometrical parameters, Franck-Condon anal. 77−27047
transition metal complexes, mol. dissymmetry, book 80−27057
transition metal dihydrides, gas phase geometrical struct. calcs. 80−42951
transition metal trifluorides, mol. and electronic structs., ab initio restricted Hartree-Fock calcs. 79−63900
triatomic isoelectronic molecules, electronic struct., one-electron props. 80−42935
valence ionisation pots., SCF-MS-Xα calcs., mol. space partitioning 79−36529
valence shell electron pair repulsion model, ab initio calc. of geometry variations 80−5472
water, config. and vibr. heat capacities, H-bonds 79−99331
ZXF_5, heavy central atom, vibr. mean amplitudes and mol. geometry, charact. vibr. method 80−5522
Ag_3, Raman spectra, matrix isolated in Kr, linear config. 78−46347
$Ag(CO)_2^+$, laser Raman spectra, CO stretching region 79−59469
$(AgCl)_3$, photoelectron spectrum and valence shell struct. 78−62843
Al_2 (Al_2^-)(Al_2^+) configurations, ab initio study, LCAO, STO, MO-SCF and CI calcs., binding energy *(French)* 80−91447
$AlBr_2$, IR spectra in Ar matrix, struct. 79−31520
$AlCl_3$, matrix isolated, vibr. spectrum, struct., vibr. freqs. 78−46339
Al_2Cl_6, ab initio LCAO SCF minimal basis set calc., struct. 79−49943
AlClBr, IR spectra in Ar matrix, struct. 79−31520
$AlCl_2Br$, IR spectra in Ar matrix, struct. 79−31520
Al_2F_6, ab initio LCAO SCF minimal basis set calc., struct. 79−49943
AlH_3, AlH_3^-, ground electronic states and geometries, ab initio calcs. 77−57863
$Al^{3+}(H_2O)n$ (n=1,2,4,6), FSGO-pair-pot. calcs. *(German)* 80−74278
Al_2O_2, thermochem. evidence rel. to mol. structure 77−38738
AlOH→HAlO system, intramol. rearrangement, ab initio calc. of pot. surfaces and min. energy paths, geom. parameters 80−32623
Ar-O_3 Van der Waals complex, struct. and props., RF and microwave obs. 80−32704
$ArCO_2$, struct. determ. by mol. beam elec. reson. spectrosc. 79−64019
Ar_2F, electronic states, ab initio POL CI calcs. 78−66474
ArHBr, ArHCl, and isotopic forms, rot. spectra, mol. struct., mol. consts. 80−58246
ArHF, van der Waals complex, ab initio RHF calc., struct. 79−76339
$Ar_nH(H^+)$, excited and ground state struct. energies and binding energy, vibr. modes, LCAO-SCF-MO calc. 79−3608
ArHO, van der Waals complex, ab initio RHF calc., struct. 79−76339
$Ar_{N-1}K^+$ clusters, equilib. configs. and binding energies 80−48115
$ArSO_3$, weakly bound complex, struct., MBER obs. 80−95701
$AsBr_3$, gas-phase electron diffr., mol. struct., force consts., vib. unharmonicities 77−546
$AsBr_3$, microwave spectra, rot. consts., mol. struct. 77−3485
AsF_3, inversion barrier, STO SCF calc. 80−63567
AsH_3, forbidden millimetre-wave transitions 78−55165
B-containing mols., MNDO calcs. for ground-state 77−88391
B-O(S)(Se)(Te)(Po) compounds, prep. and struct., book contrib. 78−47306
$BClF_2$, microwave spectrum, struct., quadrupole coupling consts. 77−57986
BF_3^-, geometric struct. of ground state, ab initio calc. 78−5130
BF_3^-, radical, struct., EPR spectrum 77−8406
B_2F_4, molecular structure, barrier to internal rotation, temperature effects 78−13625
BFHOH, transient mol. form., microwave spectroscopic obs. 78−74643

inorganic molecule configurations continued
$BF(OH)_2$, identification, rot. and centrifugal consts., mol. struct., microwave spectra obs. 80−32705
BH_3, electronic wave function determ., genealogical technique using Clebsch-Gordan coeff. 80−95529
BH_4^-, pot. energy surfaces and mol. deform. induced by external cation 80−106285
$(B_{12}H_{12})^{2-}$, icosahedral cage, symmetry coords. and vibration freq. 80−47966
$B_2H_5^+$, FSGO ab initio calc. of geometry, CNDO/2 calc. 78−41943
B_2H_6, mol., static electron densities 78−79552
B_2H_6, molecular charge distrib., quantum topology, bonding theory and molecular structure 80−5463
B_2H_n, struct., ab initio SCF calcs. *(French)* 79−22598
B_3H_n, struct., ab initio SCF calcs. *(French)* 79−22598
$^{10,11}B_5H_9$ gas (liq.) phase, vibr. dephasing and Raman spectra 80−48101
BH_3CO, struct., quadrupole coupling consts., dipole moment, microwave spectra 77−54557
BH_2NH_2, microwave spectra, rot. consts., dipole moment, mol. struct. 79−85957
$BH(OH)_2$, transient mol. form., microwave spectroscopic obs. 78−74643
BO, spectroscopic properties, PNO-CI and CEPA calcs. 78−41961
B_2O_2, thermochem. evidence rel. to mol. structure 77−38738
B_2O_3, bipyramidal struct., stability, ab initio SCF-MO calcs. 80−99446
BOH—HBO system, heterovalent isomerism, ab initio calc. of pot. surfaces and min. energy paths, geom. parameters 80−32622
$BaH[AsCr_2O_{10}]$, X-ray cryst. struct. determ. 79−42019
$Ba_4Sb_4S_{11}$, cryst. struct., selenoantimonate (III) anions *(German)* 80−103305
$BaVO(EDTA).6H_2O$, cryst. and mol. struct., X-ray diffr. obs. *(Russian)* 78−30601
Be compounds, electronic structure, configs., energy, bonding, of small mols. and complexes 78−13420
Be^{2+}, ion compexes with HF, H_2O, and NH_3 solvent molecules, structural and electronic props. calc. 77−57873
$BeBH_5$, H bridged system, floating spherical Gaussian model 80−78518
BeF_2^-, ground state, conform., electron affinity, extended basis SCF calcs. 79−72253
BeH_3, FSGO model of mol. struct., energy terms 79−63904
$Be^{2+}(H_2O)_n$, (n=1,2,3,4,6), FSGO-pair-pot. calcs. *(German)* 80−74277
BeOH, struct. and electronic props., ab initio calcs. 80−74113
$BiCl_3.GaCl_3$ complex, NQR of ^{209}Bi, $^{69,71}Ga$ and $^{35,37}Cl$ 78−25569
BrF_3 complexes with BF_3, PF_5 and AsF_5, F NMR, struct. and stability 78−37658
BrF_5, gas phase electron diffraction and microwave rot. consts. data anal., mol. struct. 79−76363
$BrHCN^-$, $BrDCN^-$, IR spectra, rel. to mol. geom. 79−22702
$Br(H_2O)_n^-$, geometric and electronic struct., CNDO/2 calc. 79−41113
C-containing mols., MNDO calcs. for ground state 78−911
C_2N_2, satellite struct. of electron spectra, CI and vibronic coupling, dynamical calc., equilib. geometry 80−53044
CO, photoelectron ang. distributions, wavelength and vibr. state depend., reson. effects, asymmetry parameters 80−91602
CO, vibr. struct., core and valence ESCA spectra, Frank-Condon and HF anal. 80−32602
CO_2, ab initio SCF calcs., force consts., vibrs., pot. energy surface 78−5209
CO_2, anomalous energy minima surfaces 78−86791
CO_2, asymmetry parameter, angle resolved photoelectron spectra, multiple scatt. method 80−63708
CO_2, dimer, geom. struct., by mol. beam deflection 79−27102
CO_2, dimer struct. CNDO/2 and ab initio calcs. 77−71753
CO_2 dimers in rare gas matrices, struct. determ. from IR spectra 79−10101
CO_2, elastic and inelastic electron scatt. differential cross section, obs. and calc., struct., binding energy 80−28110
CO_2H^+, geom. struct., ab initio mol. orbital study 78−62939
CO_2, ionised states, core and valence, ab initio HF calcs. 77−79597
CO_2, polarisabilities, quadrupole and dipole moments, nucl. geom. effects 79−63899
$(CO_2)_2^-$, struct., stability, electron affinity of neutral dimer, Hartree Fock calc. 79−63912
CO_3, and isotopic forms, struct., normal coord. anal. 78−965
C_2O_3, liq., mol. conform. and orientation correlation 79−32877
C_3O_2, far IR and Raman spectra, vibr. mode and quasilinear config. 78−62940
C_3O_2, semirigid bender, rot.-vibr. energy level separations obs., struct. and pot. functions determ. 80−83446
CO_2H^+, SCF CI equilib. struct. calc., CO_2 proton affinity 77−10599
COS, asymmetry parameter, angle resolved photoelectron spectra, multiple scatt. method 80−63708
CS_2, asymmetry parameter, angle resolved photoelectron spectra, multiple scatt. method 80−63708
Ca-water interactions, in crystalline hydrates, geometry 80−39024
CaI_2, mol. struct. parameters and geom. config., gaseous electron diffr. obs. 80−37883
^{44}Ca substituted oxides, matrix isolated, IR spectra 78−9151
Cd complex, $(Cd[SC(CH_3)_2CH_2NH_2]_2CdCl_2)_2.2H_2O$ cryst. and mol. struct. 78−74787
$CdFe(CO)_4$, IR and Raman spectra, vibr. anal. 78−66553
$CeCl_3.7H_2O$, X-ray cryst. struct. determ. 79−46606
$Ce_6Mo_{10}O_{39}$, 22 77−76373
$(Cl_2)_2$, config., ab initio calc. 79−41098
ClCO radical, struct. and props. calcs. 80−74112
ClF_4 radical, geom., ab initio MO calcs. 79−89610
ClF_5, microwave spectrum, rot. transitions, dipole moment, struct., nuclear quadrupole coupling consts. 77−14423
$(Cl_2F)^+$, structure, theoretical investigation 80−904
$ClFH^+$, structure, theoretical investigation 80−904
$ClHCN^-$, $ClDCN^-$, IR spectra, rel. to mol. geom. 79−22702
$ClHCl^-$, deuteron quadrupole coupling const., nuclear mag. shielding, geometry depend. 78−58586
ClNSO, ground state geometry, ab initio calcs. 80−106259
ClO_2, analytical pot. functions, several surface minima 78−5158
ClO_n^+, ClO_n and ClO_n^- (n=1 to 3), ab initio calcs., localised MO and nature of Cl-O bond 80−69070
cis-ClONO, microwave spectrum, rot. consts., inertial defects and config. 79−59439
ClOO radical, struct. and props. calcs. 80−74112
$(Cl_3PNPCl_3)(PCl_6)$, X-ray cryst. struct. determ. 80−88095

inorganic molecule configurations continued
$Cl_nSi(CH_3)_{4-n}$, ^{35}Cl NQR, geminal and vicinal interactions on substituents electronic effect 80−63663
$Cl_nSi(OCH_3)_{4-n}$, ^{35}Cl NQR, geminal and vicinal interactions on substituents electronic effect 80−63663
$Cl_3SiOSiCl_3$, normal vibs. and force field, calcs. using electron diffr. struct. determ. *(Russian)* 78−46317
Co complex, $(NH_3C_6H_5)[Co(SO_3)DH_2(NH_2C_6H_5)](NH_3C_6H_5)ClO_4.H_2O$, cryst. and mol. struct. 80−33980
Co complex, bisdimethylglyoxime (thiosemicarbazide)-cobalt (III) nitrate, mol. and cryst. struct. of dihydrate 78−83803
Co complex, O_2CoCl_4 and $O_2CoCl_4NH_3^{2-}$, struct. and bonding model, CNDO-UHF calcs. 80−95541
Co complex, S_4N_4 with $CoCl_2$, mass and IR spectra, config. 78−13494
Co complexes, Co II tetraphenylporphyrins, constraint, ESR and optical detect. 80−83394
Co complexes with H_2S, formation and mol. struct. 77−75323
Co-complex, dichlorobis(pyridinium-2-thiolate)Co(II), cryst. and mol. struct. 80−28963
$CoCl_2$-LiCl-glycerin-water system, Co^{2+} ion coordination transition, spectral investig. 79−42953
$Co[Ag(SeCN)_2]_2$, and complexes, softness values and struct., IR spectra 79−59459
$CrAl_3Cl_{12}$, gas, mol. struct., ligand field spectrum *(German)* 78−37762
$Cr(NO)_4$, XPS and UV photoelectron spectra, compared to NO data 80−58317
$(CrO_3)_4$, identification of polymer species by vapour phase electron diffraction 80−53135
$CsBO_2$, mean geometrical config., vapour phase electron diffr. 77−50554
$CsBO_2$, mol. struct. determ. by gas phase electron diffr. 79−10227
CsBrICN, Raman and IR vibr. spectra, struct. 80−102513
CsClICN, Raman and IR vibr. spectra, struct. 80−102513
CsI_2CN, Raman and IR vibr. spectra, struct. 80−102513
Cu complex, Cu (II)-substituted ethylenediamines and monocarboxylates, cryst. and mol. struct., X-ray diffr. obs. 79−82182
Cu complex, $Cu(NH_3)_2(NCX)_2$, X=O, S, electronic struct., stereochem. 80−58156
Cu complex (acetylacetonate), in vitreous liq. cryst. matrix, ang. depend. of EPR spectrum 78−9175
Cu complexes, Cu(I)-P tetrahedral, ^{63}Cu FT-NMR 80−53021
Cu complexes, of polyamines, ESR in soln., coordination around Cu(II) ions 78−5254
Cu II complex, bis(pyrrolidonecarbodithioato) copper II, ESR, solvent effects 78−1008
Cu II complexes, 5-coord., ESR, optical absorpt., solvent effects 78−5253
Cu^{2+} complex, in water-ethanol soln., struct., EPR 78−50565
$CuAl_2Cl_8$, Raman resonance spectra of vapour 78−94251
$(CuBr)_3$, photoelectron spectrum and valence shell struct. 78−62843
$Cu(CO)_4^+$, laser Raman spectra, CO stretching region 79−59469
$(CuCl)_3$ photoelectron spectrum and valence shell struct. 78−62843
$(CuI)_3$, photoelectron spectrum and valence shell struct. 78−62843
$D(CN)_2^-$, IR spectra, rel. to mol. geom. 79−22702
DNC, vibronic coupling and linear to bent transitions 79−45694
DO_2, IR spectra, config. of $^2A'$ and $^2A''$ states 79−36636
D_2O, $(D_2O)_2$, isotopic forms, Ar matrix isolated IR spectra, assignments, config. 77−6779
D_2O bond length, angle, high momentum transfer liq. phase neutron scatt. 77−27195
$(D_2O)_2$, and isotopic species, Ar isolation IR spectra, band assignments, struct. 77−3364
$(D_2O)_2$, and isotopic species, Ar matrix IR spectra, Xe, HCl, $(CH_3)_2O$ doping, struct. 77−3365
$(D_2O)_2$, isotopic forms, Ar matrix isolated IR spectra, assignments, config. 77−6780
DSiCl, $^1A''$ states, geometry, bending pot. and vibr. freqs. 79−59593
Er complex, $ErL_6(ClO_4)_3$, L=tetramethyl, urea, struct. 77−62512
Eu compounds tetrahedral, ligand struct., rel. to luminesc. spectra satellite intensity *(Russian)* 78−72603
F compounds, ground states, mol. parameters, MINDO calcs. 78−41955
$FBrO_3$, gas-phase electron diffr., mol. struct., force field, vib. amplitudes 77−547
$FCN+N_2$, rot. spectra and geom. struct. of FCN 78−82725
FCO, radical, struct. and props. calcs. 80−74112
F_2CS, pot. surfaces, X^1A_1, a^3A_2 and $a^3A_2(b_1)$ states, ab initio SCF calcs. 78−86795
$FClO^+$, radical cation, struct. and electronic props., ab initio RHF SCF MO calc. 80−52883
FH_3^+, stability, ab initio calcs. 77−30775
$FHCl^-$, deuteron quadrupole coupling const., nuclear mag. shielding, geometry depend. 78−58586
FHF radical, struct. and stability, ab initio SCF and CI calcs. 77−71887
FHF^-, deuteron quadrupole coupling const., nuclear mag. shielding, geometry depend. 78−58586
$F^-(H_2O)n(n=1,2)$, FSGO-pair-pot. calcs. *(German)* 80−74278
FNNF, mol. struct., cis effect 80−91434
F_2O, geometry, electron spectrum, vert. ionis. pot. ab initio calc. 80−58187
F_2O_2, geometry, SCF CI calcs. 78−55126
FOO radical, struct. and props. calcs. 80−74112
F_2S_2, electronic struct. and stability of isomers, gaussian SCF MO calc. 79−93921
FSO (FOS), struct. and props., SCF calcs. 80−106260
FSO_2OF, wide-line NMR anal. of mol. struct., chem. shielding tensor 77−83622
FSS, struct. and props., SCF calcs. 80−106260
$FeBr_2$, electron diffr. determ. of mol. struct., evidence for Fe_2Br_4 species 78−37767
$Fe(CO)_5$, microwave dielec. relax., fluxional mechanism 78−94235
$FeCl_2$, electron diffr. determ. of mol. struct. 78−37767
$FeCl_3$, Fe_2Cl_6, matrix isolation Raman spectra, assignments 77−65480
$FeCl_3$, matrix isolation Raman spectra, mol. config., thermodynamic props. 78−46346
Fe_2Cl_6, matrix isolation Raman spectra, mol. config., thermodynamic props. 78−46346
$FeMo_3S_4$, triclinic, containing Fe pairs, X-ray cryst. struct. anal. 80−54193
FeN_2 complexes, electronic configuration calc. using SCCC-LCAO-MO method *(Chinese)* 80−1082
FeO_2, matrix isolated IR spectra, cyclic complex struct. 77−88449

inorganic molecule configurations continued
$GaBr_3$, D_{3h} point group, mol. consts., struct. effects 79−54992
$GaCl_3$, D_{3h} point group, mol. consts., struct. effects 79−54992
$GaCl_3(I_3)$, gaseous, Raman spectra, struct., Fermi reson. and thermodynamic functions 77−18929
$GeCl_2$, combined electron diffr. and mass spectra mol. struct. determ. 79−89783
GeH_2, struct. determ., restricted HF calcs. 80−87030
Ge_2H_6, valence electronic struct., model pot. in floating spherical GO formalism 78−74563
$(GeH_3)_3P$, vibr. force fields and amplitudes zero point, structs. 77−54551
$GeH_3.NCS$, mol., IR, Raman and microwave spectra, $^{70,72,74}Ge$ and $^{1,2}H$ isotopes 79−89663
H halides, polarisability, correl. with mol. dimens. 80−23288
H-bonded systems, cyclic and bifurcated, ab initio MO calcs. 79−41100
H-bonded systems, MINDO/3 geom. optimis. calcs., heats of form. of monomer and dimer 79−31399
H-containing mols., MNDO calcs. for ground state 78−911
$H^+ + CO$ ($^1\Sigma$), ground state pot. energy surface, ab initio SCF calc., protonated equilib. geometry 80−83301
H_2, repulsive intermol. pot. 80−32794
H_2-H_2 dimers, hyperfine struct. in zero mag. field 80−95700
H_3, Rydberg states energies and equilib. geometry calcs. 80−9493
H_3^+ expt. determ. struct. 78−74752
H_3^+, struct. props., in mag. fields, var. calcs. 78−21843
H_4 and H_4^+, H_4^- ions rectangular configurations, stability, SCF MO LCAO calcs. 77−42235
H_4 excimer, electronic and geom. struct., ab initio CI calc. 79−76348
H_4, excited potential energy hypersurfaces, 'triply right' (C_{2v}) tetrahedral geometries 77−83501
H_4, FGSO open-shell calcs., pot. energy surface, electronic energies of configurations 79−10025
H_4, pot. energy surfaces, valence bond calcs. 80−74129
H_4, square config., $^1B_{1g}$, $^1B_{2g}$ states, quantum chem. calcs., random walk method 79−36518
H_4^+, ground and excited state pot. energy surfaces and geom. struct., SCF and CI calcs. 78−78769
H_n^- (n=5 to 13), ion-induced dipole clusters, binding energies and geometries 79−41261
H_n^+ (n=3,5,7,9,11), stability, struct., ab initio MO calcs. 78−74810
HBF_2 and DBF_2 harmonic force field and ground-state average struct. determ. 80−83342
HBr, and DBr, in monatomic matrices, near IR spectra and aggregate structs. 79−89667
HBr, photoelectron angular distrib. 80−58318
HCC^+, equilib. struct., rot. const. 79−98003
HCN, and stable isotopic species, mol. struct., ground vibr. rot. transitions and consts. 77−10666
HCN, dipole moment derivative, sign anomaly, CGTO ab initio calc. 78−74795
HCN, Fermi and Coulomb correl. holes, SCF and CI wave functions 80−69085
HCN, HNC, electronic reorganisation, with core ionisation 78−94196
HCN, HNC, molecular electronic struct., unlinked cluster effects 78−94185
HCN, intravalence triplet-triplet electronic transition, geometrical struct. and rel. energies determ. 80−99586
HCN, nuclear quadrupole coupling and mol. deformations 78−90191
HCN, semi-empirical excited state Morokuma's EHP calc., geometry and order of states 78−46256
$H(CN)_2^-$, IR spectra, rel. to mol. geom. 79−22702
HCNO, isomers, geometry, spectra, rot. and force consts., ab initio calcs. 77−34574
HCN...HF, hydrogen bonded heterodimer, spectroscopic consts. from microwave spectrum 80−43037
HCO_2^+, geom. struct., ab initio mol. orbital study 78−62939
H_2CO^+, geom. struct. optimisation, open-shell restricted HF and MC SCF calcs. 79−98004
HCl, and DCl, in monatomic matrices, near IR spectra and aggregate structs. 79−89667
HCl, nuclear quadrupole coupling and mol. deformations 78−90191
HCl-DCl(HBr)(DBr)(HI), absorpt. spectra near 3.5 μm, equilib. config. of complexes *(French)* 78−42046
$(HCl)_2$, absorpt. spectra near 3.5 μm, equilib. config. of complexes *(French)* 78−42046
$HCo(CO)_4$, mol. struct., gas phase electron diffr. expt. 78−13623
HF dimer, stabilisation energies, harmonic force constants, intermolecular vibrations, SCF and CEPA PNO calcs. 79−98177
HF, geometries, props. and protonation, ab initio mol. orbital study 79−22588
HF H-bonded dimers, PCILO calc., energies, geometries 78−37557
HF^+, ab initio valence band calcs. 79−6869
HF-ClF complex, and isotopic forms., mol. beam elec. reson. spectra, config., bonding, spectroscopic consts. 77−30860
HF-HCl, H bonding , struct., mol. beam-elec. reson. spectra 78−29777
HF+H′→H+H′F, transition state geometry, SCF CI calcs. 78−20009
HF_2^-, IR spectra and mol. struct. 79−63996
$(HF)_n$, n=1-∞, ab initio hydrogen bond and electronic parameters, phonons 77−14342
HFF radical, struct. and stability, ab initio SCF and CI calcs. 77−71887
$H_2Fe(CO)_4$, mol. struct., gas phase electron diffr. expt. 78−13623
$HFeN_2$ complexes, electronic configuration calc. using SCCC-LCAO-MO method *(Chinese)* 80−1082
H_2^+He, total energy, interat. dist., geometric configurations, LCAO MO SCF calcs., stability, binding energy 77−42236
HI, photoelectron angular distrib. 80−58318
$HMn(CO)_5$, mol. struct., gas phase electron diffr. expt. 78−13623
HN_3, ground $^1A'$ state, SCF and CI calcs., conform., geom., vibr. freqs. and dissoc. 80−18806
HNB,(HNBH), spectroscopic properties, PNO-CI and CEPA calcs. 78−41961
HNC (DNC), anharmonic force field, equilib. struct., rot. consts. and bond lengths 78−90147
HNC, and stable isotopic species, mol. struct., ground vibr. rot. transitions and consts. 77−10666
HNC, millimetre spectrum, rot. consts., force consts., U90.7 interstellar line, struct. parameters 77−57989
HNC, vibronic coupling and linear to bent transitions 79−45694
HNCSe, struct., microwave spectrum 79−18178
HNF_2, force consts., geometry, ab initio Hartree-Fock calcs. 77−57864
H_2NF, force consts., geometry, ab initio Hartree-Fock calcs. 77−57864
HNNN, substitution struct., rot. consts. calcs. 80−91534
HNO, HON, electronic reorganisation, with core ionisation 78−94196
HNO^+, ab initio pot. surface, and isomerisation barrier of lowest states 79−22622
HNO^+, ab initio SCF and CI comparison of struct. and spectra, rel. to NOH^+ 77−26972
HNO^+, vertical spectra, heat of form., ab initio MRD-CI calcs. 79−49934
HNO_2, and protonated forms, electrostatic pot. predictions, basis set depend. 78−74786
$(HNO_3)_2$, gas phase, H-bonded complex struct. from elec. dipole moment obs. 78−74791
HNSi, struct. and microwave freqs. calcs., rel. to interstellar emission lines 78−36648
HO_2, analytical pot. functions, several surface minima 78−5158
HO_2 and HOCl, struct., vibr. freqs., IR intensities, ab initio calcs. 79−98007
HO_2, struct. and props., SCF calcs. 80−106260
HO_2^+, ab initio calc. of three lowest states 78−62711
$H_2O.(H_2O)_2$, isotopic forms, Ar matrix isolated IR spectra, assignments config. 77−6779
H_2O, $(D_2O)(HDO)$, photoelectron spectrum, Franck-Condon, factor calc., geometry and vibrs. *(French)* 77−83652
H_2O, $(H_2O)_2$, mag. shielding rel. to hydrogen bonding 77−14348
H_2O, ab initio calcs., VSEPR model and Pauli exclusion principle 79−31380
H_2O, ab initio SCF CI calcs., ground state energy, config. and force consts. 77−18782
H_2O, chemisorbed on Ru(001), conformation, electron stimulated desorption ion ang. distribs. 77−89637
H_2O dimer, partially deuterated, microwave spectra and struct. 80−74212
H_2O dimer, props., influence on tropic meteorology 79−2349
H_2O, dipolar correlation factor and dipole moment, in ice III 79−77548
H_2O, ESCA and soft X-ray emission, vibr. excitation 80−23433
(H_2O), electron affinity, ab initio SCF calcs. 79−76343
H_2O, electron affinity, mol. geom. effects calcs. 78−82618
H_2O, electronic ground state, SCF HF and CI calcs, pot. energy hypersurface, spectroscopic consts. 78−50473
H_2O, empirical potential model EPEN/2 for conform., intermol., solvation studies 79−50102
H_2O, equilib. struct., ab initio SCF calcs., general valence force field 77−3265
H_2O, geom. and electronic struct., ab initio SCF calc. 79−76331
H_2O, geometry, SCF and CI calcs., basis set effects 78−62715
H_2O, H bonding, electronic struct., geometries, moments, dimerisation energies, charge distrib., pseudopotential calcs. 80−27942
H_2O H-bonded dimers, PCILO calc., energies, geometries 78−37557
H_2O, liq. surface, spreading vel., rel. to mol. struct. *(German)* 78−95209
H_2O, Politzer's k and V/T variations, mol. geom. effects 79−54766
H_2O, shape, electrostatic force study with floating wavefunction 78−37545
H_2O, VB minimal Slater basis set calcs., comparison with H_2S, MO calcs. 79−36536
H_2O^-, electron affinity, mol. geom. effects calcs. 78−82618
H_2O^+, ab initio potential energy surface study by CI techniques, equilibrium conform. determ., mol. dissoc. pathways 80−78550
H_2O^+, spin and rot. fine struct., orbital angular momentum 80−83247
H_2O^+, states geometries, electronic vibr. coupling consts. HF calcs., comparison with Xalpha calcs. 80−27946
H_2O^+, X^2B_1 and B^2B_2 states, pot. surfaces, SCF and CI calcs. 77−3338
H_2O-HCl(HBr)(DBr) complexes, IR matrix isolation spectra, struct. 78−29781
(H_2O)-HF complexes, (x=1 or 2), geometry, CNDO/2 calc. 79−36531
H_2O-HF heterodimer, H bonding, microwave rot. spectrum, mol. geometry and moment 80−99501
$(H_2O)_2$, and isotopic species, Ar isolation IR spectra, band assignments, struct. 77−3364
$(H_2O)_2$, and isotopic species, Ar matrix IR spectra, Xe, HCl, $(CH_3)_2O$ doping, struct. 77−3365
H_2O_2, geometry, internal rot. barriers, electron correl. calcs. 78−70751
H_2O_2, hindered rot. pot., strongly orthogonal geminal calcs. 77−71751
H_2O_2, hindered rot. pot. recreation, electron pair wavefunction transferability 77−71752
$(H_2O)_2$, isotopic forms, Ar matrix isolated IR spectra, assignments config. 77−6780
H_2O_2, struct. and barrier to internal rot., HF and Rayleigh-Schrodinger perturbation calcs. 79−13636
$(H_2O)_2$, struct. from mol. beam elec. reson. spectra 77−54555
$(H_2O)_2$, struct. studied by CNDO/2 method 80−69081
H_2O_2, structural parameters of vibr. ground state 80−28116
$(H_2O)_3$, geometric config. energies, SCF LCAO MO calcs. 80−63551
H_2O_3, struct., barrier to int. rot., HF and RS-MP perturb. calcs. 79−13637
H_3O^+ inversion barrier, high-order replacements inclusion in CI calcs. 80−63504
$H_6O_4^{2-}$, cluster anion tetrahedral struct. and stability, polarisation model 80−53181
HOB,(HBO), spectroscopic properties, PNO-CI and CEPA calcs. 78−41961
HOCl, photodissoc., ab intio SCF CI calcs. 78−50604
$H_3O^+(H_2O)_n$, H^+ motion energetics, ab initio calcs. 78−25413
$H_2O.H_2O$ and $H_2O.Ne$, excited, first order interaction energy, ab initio calc. 80−32598
$HO_2.H_2O(NH_3)$ complex form., ab initio calcs., min. energy configs. 77−14340
$H_3O.^+2H_2O$, in 2,5-dichlorobenzenesulphonic acid trihydrate, neutron diffr. obs. 78−58855
HPO, mol. struct. and props., ab initio, calc., Gaussian lobe orbital 78−62713
HS_2, ground and first excited states, geometry, ab initio SCF calcs. 78−50657
HS_2 radical, ab initio calcs. of geometry and spectra 77−34552
H_2S, VB minimal Slater basis set calcs., comparison with H_2O, MO calcs. 79−36536
H_2S-H_2O complexes, equilib. config., H-bond energies and electron densities, CNDO/2 method 80−14084

inorganic molecule configurations continued
H_2S_2, electronic struct. and stability of isomers, gaussian SCF MO calc. 79−93921
HSO (HOS), struct. and props., SCF calcs. 80−106260
HSO, ground and first excited states, geometry, ab initio SCF calcs. 78−50657
HSO, radical, electronic spectrum and struct. 77−75147
H_2SO_4, anhydrous, cryst. struct. refinement 80−19770
HSO_3F, gas, indication of molecules existing as cyclic dimers *(French)* 80−989
HSO_3F, liquid, indication of molecules existing as mixture of cyclic dimers and infinite chains *(French)* 80−989
HSS, struct. and props., SCF calcs. 80−106260
HSiBr, $^1A''$ states, geometry, bending pot. and vibr. freqs. 79−59593
HSiCl, $^1A''$ states, geometry, bending pot. and vibr. freqs. 79−59593
HSiN, struct. and microwave freqs. calcs., rel. to interstellar emission lines 78−36648
H_3SiNCS, far IR and Raman spectra, vibr. mode and quasilinear config. 78−62940
$HSiO^+$, $HOSi^+$, quantum mechanical study 78−37541
$H.HF_2$, H-bonded complex, ab initio calcs. *(French)* 80−52866
He_2H^+, quantum-mechanical calculations 78−33424
HeI_2, rot. fluoresc. spectra, nonlinear equilib. struct. 78−37672
$HfBr_4(HfI_4)$, struct., force field and Coriolis const. calcs. 78−86843
HfF_4, mol. struct. and vibr. freqs., gaseous electron diffr. obs. 80−32836
Hg complex, methylethynylmercury(II)-(d_1-,d_3-,d_4), vibr. spectra and normal coord. calcs. 80−58259
Hg complex, trihalogenomercurate II ions in amide solvents, config. equilib. 79−26997
$Hg(CN)_2$, phonon freq. anomalous press. depend., mol. struct. distortion 80−88981
$HgFe(CO)_4$, IR and Raman spectra, vibr. anal. 78−66553
HgI_2, mol., gas-phase electron diffr. for geom. struct. 79−97368
HgI_2, mol. struct. and vibr. pot. function, gas-phase electron diffr. obs. 79−31689
I-containing molecules, geom. struct. and dipole moments, CNDO/2 calc. 79−94103
I_2, electron diffr. data for geom. struct., non-parametric estimation method 79−86066
I_2, equilibrium parameters and Morse anharmonic consts., electron diffr. determ. 78−58818
I_2, mol., gas-phase electron diffr. for geom. struct. 79−97368
I_3^-, geom. and electronic struct., effective pot. calc. 78−74788
I_5^-, geom. and electronic struct., effective pot. calc. 78−74788
ICN, microwave spectrum, vibr.-rot. const., equilib. struct. 78−58677
IF_5, gas phase electron diffr. and B_0 rot. const., struct. determ. 79−89782
$I(H_2O)_n^-$, geometric and electronic struct., CNDO/2 calc. 79−41113
$I_2Ne_aHe_b$ van der Waals complexes photodissoc. 80−50864
$InCl_3$, D_{3h} point group, mol. consts., struct. effects 79−54992
$InCl_3$ in Kr lattice, Raman and IR spectra, vibr. assignments, force consts., isotope shift and config. 79−89671
$InCl_3$, planar D_{3h} struct., IR matrix isolated spectra 77−75148
$(In(H_2O)_2\text{-}(SO_4)_2)^-(H_5O_2)^+$, cryst. struct. *(French)* 79−73146
InI_3, D_{3h} point group, mol. consts., struct. effects 79−54992
IrF_6, in mixed crysts., Jahn-Teller effect, $\Gamma_{8g}(t_{2g})^3$ state, 6800 Å 78−76032
$K_2Mo_2O_7.H_2O$, cryst. and mol. struct. 77−76373
$K_8Mo_4V_8O_{36}.12H_2O$, single cryst. X-ray cryst. and mol. struct. 79−99131
$K_2NH(SO_3)_2$, X-ray cryst. struct. refinement 79−69062
$K_3N(SO_3)_2.H_2O$, X-ray cryst. struct. determ. 79−69062
$KPbI_3.2H_2O$, X-ray cryst. struct. determ. 80−64958
K_2SO_4, IR and Raman spectra of vap. over heated matrices 78−25525
$K_2[UF_2O_2(SO_4)].H_2O$, X-ray cryst. struct. determ. 80−54194
$K_4[V(CN)_6(NO)].1/2KOH.1/2H_2O$, cryst. and molecular struct. 77−80469
KrF, electronic states, ab initio POL CI calcs. 78−66474
Kr_2F, semi-empirical VB calcs. of hyperfine interactions and struct. 79−85902
KrHBr, KrCHl, and isotopic forms, rot. spectra, mol. struct., mol. consts. 80−58246
KrHCl, van der Waals complexes, struct., RF and microwave spectra, isotope effects 80−37806
KrHCl, weak complex, rot. spectra 80−52980
LaF^+, electronic spectra, rot. anal. and orbital configurations 80−83240
LaS, chemiluminesc. vibr. analysis of $C^2\Pi \rightarrow X^2\Sigma^+$, D_0^0 determ. 77−48645
Li compounds, electronic structure, configs., energy, bonding, of small mols. and complexes 78−13420
Li^+ ion complexes with HF, H_2O, and NH_3 solvent molecules, structural and electronic props. calc. 77−57873
Li_{2n}, (n=1, 2, 3), stable cluster configs., ionisation pots., binding energies, vibr. freqs., al initio SCF and CEPA calcs. 80−14265
Li_3, geom. struct. and binding energy, diatomic-in-molecules 78−74785
Li_3, potential energy surface and config., RHF CI calc. 77−34562
Li_3, spin populations, restricted Hartree-Fock calcs. 77−57906
Li_4, geom. struct. and binding energy, diatomic-in-molecules 78−74785
$LiAlF_4$, struct. pot. energy surface, Li^+ migration, ab initio LCAO SCF calcs. 80−23305
$LiAlH_4$, $LiBH_4$, ab initio calc. of geom. struct., charge distrib., bonding and pot. energy surfaces 80−18796
Li_5B_4, molecular and electronic struct. 80−20107
$LiBF_4$, nonrigid mol. struct. and stability, ab initio calcs. 80−83259
$LiBH_4$, H bridged system, floating spherical Gaussian model 80−78518
$LiBH_4$, non-rigid complex molecule, ab initio calcs. of pot. energy surface and geometric struct. 77−6678
$LiBH_4$, pot. surface and geometry, ab initio calcs. 78−86771
$LiBH_4$, struct., pot. surface, ab initio calcs. 79−41092
$LiBeF_3$, pot. energy surface, struct., stability and internuclear distances, ab initio calc. 80−58147
$LiBeH_3$, ab initio calc. of pot. surfaces and geometry 79−10024
$LiBeH_3$, H bridged system, floating spherical Gaussian model 80−78518
$LiBeH_3$, pot. surface, struct., ab initio calcs. 77−88385
$LiCH_5$, H bridged system, floating spherical Gaussian model 80−78518
LiCNS, ether solns., dimer struct. and force consts., IR and Raman spectra 79−72442
Li_2Cl^+, mass spectra, struct., stability, expt. and theory 77−554
LiF oligomers, struct., stability SCF and CEPA-PNO calcs. 78−78640
Li_2F^+, mass spectra, struct., stability, expt. and theory 77−554

inorganic molecule configurations continued
Li_2F_2, struct., force fields and normal mode freqs., ab initio calcs. 80−83260
Li_2F_2, struct., internuclear-distances and mean amplitude of vibr. determ. by electron diffr. 80−69252
LiH oligomers, struct., stability SCF and CEPA-PNO calcs. 78−78640
$LiH\text{-}NH_3$, struct. and props., SCF ab initio calcs. 80−106250
$(LiH)_3$ complex, SCF interaction energy nonadditivity 80−91437
$Li(H_2O)^+$, config. ab initio GAUSSIAN 70 calcs. 79−49939
LiH_2O^+, geom., electronic struct. FSGO model calcs. 78−82614
$Li^+(H_2O)_n$, (n=1,2,3,4,6), FSGO-pair-pot. calcs. *(German)* 80−74277
LiN_2, geom., electronic struct. FSGO model calcs. 78−82614
LiNC, metal atom motion, WKB calcs. 78−82623
LiNC, struct. vibr. states and pot. energy calcs. 78−86776
$LiNH_3^+$, geom., electronic struct. FSGO model calcs. 78−82614
$LiNO_3$, mol. struct. ab initio calcs. 79−26884
Li_2O^-, electronic struct. and config., ab initio SCF study 79−85898
LiOH, geom. and electronic struct., ab initio SCF calc. 79−76331
$LiOH^-$, electronic struct. and config., ab initio SCF study 79−85898
$LuCl_3$, pyramidal struct. and force field coeffs., electron diffr. obs. 78−9250
Mg^{2+} ion complexes with HF, H_2O, and NH_3 solvent molecules, structural and electronic props. calc. 77−57873
$MgCl_2$, mol. struct. parameters, average values, geom. config., gaseous electron diffr. obs. 80−37904
Mg_2Cl_4, equilib. config., pot. energy curves, ion model calc. 77−65540
MgF_2^-, ground state, nonempirical LCAO SCF calcs. 78−66469
MgF_2^-, ground state, conform., electron affinity, extended basis SCF calcs. 79−72253
$Mg(H_2O)_n^{2+}$, geometric and electronic struct., CNDO calc. 79−36532
$Mg^{2+}(H_2O)n$ (n=1,2,4,6), FSGO-pair-pot. calcs. *(German)* 80−74278
MgOH, struct. and electronic props., ab initio calcs. 80−74113
$(Mn_2(CO)_8\{GeMn(CO)_5I\}_2)$, X-ray cryst. struct. determ. 80−54190
Mo complex, μ-oxo bridged oxomolybdenum(V) dimers, conform. anal. by ang. overlap method, triplet ground states 78−5119
Mo complexes, electron-rich bis(phosphine) dicarbonyl, chemistry and props. 77−77754
Mo complexes, hydrazine, hydrazido, amido, alkoxy 77−75324
Mo complexes, μ-oxo, di-μ-oxo, di-μ-oxo-μ-carboxylato bridged oxodimolybdates (v), structures 77−76370
Mo complexes, organic derivs. of heteropolymolybdates 77−79701
Mo complexes organonitrogen derivs., chem. reactions, struct. 77−77752
Mo cpds, chemistry and uses, conf., Oxford, Eng., Sep (1976) 77−77749
Mo nitrido complex, with multiple Mo-N bonds, prep., struct. and reactivity 77−83758
$Mo(CO)_5Kr$, dispersion energy, stabilisation energy, Mo-Kr separation 79−98241
MoF_5, mol. and electronic struct., vitreous, liq., and tetrameric states, ^{19}F NMR obs., mol. mobility 80−34787
Mo_7O_{24}, C_{2v} symmetry model, force field anal. 79−81200
MoS_2, struct., XES and XPS obs. 80−43105
N-containing mols., MNDO calcs. for ground state 78−911
N_2 asymmetry parameter, angle resolved photoelectron spectra, multiple scatt. method 80−63708
N_2, elastic and inelastic electron scatt. differential cross section, obs. and calc., struct., binding energy 80−28109
N_2, polarisabilities, quadrupole and dipole moments, nucl. geom. effects 79−63899
N_2, vibr. struct., core and valence ESCA spectra, Franck-Condon and HF anal. 80−32602
N_3, polarisability correl. with mol. dimens. 80−23288
NCNCO, geometrical struct., INDO calcs. 79−22602
ND_3, cryst. struct. between 2-180K, neutron powder profile refinement 79−73134
ND_3, in $TaS_2(TiS_2)$, intercalation system, wideline NMR, temp. effects 77−16184
ND_4NO_3, cubic, mol. orientation determ. by multipole anal. 79−73136
NF_3, NF_3^-, and NF_3^+, optimised struct. and bonding, ab initio SCF MO calc. 80−23334
NH_2, geometry, SCF and CI calcs., basis set effects 78−62715
NH_2, spin and rot. fine struct., orbital angular momentum 80−83247
NH_2^-, mol. geom., diffuse functions in SCF calcs. 79−10226
NH_3, ab initio SCF calcs., force consts., vibrs., pot. energy surface 78−5209
NH_3, ESCA and soft X-ray emission, vibr. excitation 80−23433
NH_3, Franck-Condon factors calcs. 78−17723
NH_3, geometry changes during inversion, ab initio calcs. 78−5154
NH_3 H-bonded dimers, PCILO calc., energies, geometries 78−37557
NH_3, HF geometry calcs. and SCF calcs. 80−47877
NH_3, lowest triplet state geometry, SCF and CEPA-PNO calc. 80−914
NH_3, NH_3^+ ion, electrostatic force theory appl. to mol. geometry ab initio verification 79−98002
NH_3, vibr. excitation in soft X-ray emission and core ESCA spectra 80−69163
$NH_3\text{-}CO_2$ complex, matrix isolation IR spectrum, struct., ab initio SCF calcs. 78−5209
$(NH_3)_3$, open-chain and cyclic structs. 80−45480
$(NH_3)_n$, (n=1-6), mol. beam elec. deflection obs. 79−72371
NH_4^+, nuclear quadrupole coupling and mol. deformations 78−90191
N_2H_2, model rearrangement system, electron correlation and basis set effects 80−3317
N_2H_2, $N_2H_2^+$, ab initio calcs., electronic struct., geometries relative energies 77−46487
N_3H_3 radical, lowest two electronic states 80−925
$NH_3(D_3)$, liq., longitudinal proton and deuteron relaxation rates, press. and temp. depend. 80−44941
NH_xF_{3-x}, geometry changes during inversion, ab initio calcs. 78−5154
$NH_2(F_2)(Cl_2)$, SCF-MO-HF calc., struct. and one-electron props., population anal. indices 79−76338
NH_4I, $(NH_4)_{0.16}K_{0.84}I$ and $(NH_4)_{0.84}K_{0.84}Br$, reorientation motion of NH_4^+ 78−79542
$(NH_4)_4Mo_8O_{26}.4H_2O$, Lindqvist octamolybdate, cryst. and mol. struct. 77−76373
NH_4NO_3 crystals, NH_4^+ ion symmetry in phases II-V, Raman spectra obs. 80−66200
$NH_4PbI_3.2H_2O$, X-ray cryst. struct. determ. 80−64958
$NH_2.HF$, H-bonded complex, ab initio calcs. *(French)* 80−52866
NO_2, laser-induced fluoresc. spectrum near 6125 Å 77−58069
NO_2^- hydrate clusters, ground-state HF pot., Monte Carlo simulation, energy surfaces and rot. barriers 80−106412
$^{15,14}NO_2$, predissoc. rot. struct. in 2490 Å band 80−87192

inorganic molecule configurations continued
$(NO_2)_2$, struct. and force fields of isomers, ab initio calcs. 77−18783
NO_3, mag. hyperfine interactions, MO LCAO UHF calcs. 77−14369
NO_3^{2-}, coupling consts., geometry, LCAO UHF and ENDOR data calcs. 77−14369
NO_x biradicals, conform., spin probe appls. 78−86895
N_2O, satellite struct. and momentum distrib., binary (e,2e) spectroscopy 80−69125
NOCN, struct., dipole moment, quadrupole coupling, microwave spectra 78−94238
NOF and ONF, ab initio calcs. of geometry and electronic struct. 79−76342
NOH^+, ab initio pot. surface, and isomerisation barrier of lowest states 79−22622
NOH^+, ab initio SCF and CI comparison of struct. and spectra with HNO^+ 77−26972
NOH^+, vertical spectra, heat of form., ab initio MRD-CI calcs. 79−49934
$N_2O_4 \rightleftharpoons 2NO_2$, chem. equilib., struct., statistical mech. calcs. 77−9111
$N_3P_3Br_6$, ^{81}Br NQR, conformation investig. 80−63665
NSF, geometry and stability, LCAO-MO SCF calcs. 79−31391
Na^+ ion complexes with HF, H_2O, and NH_3 solvent molecules, structural and electronic props. calc. 77−57873
Na-ice condensate, EPR lineshape second moment, electron solvation struct. 78−3440
Na_3, electronic struct., pot. energy surface, ab initio CI study 78−70996
Na_n ($n \leq 8$), equilibrium geometries and ionization energies calcs. 80−1099
$NaAlH_4$, $NaBH_4$, ab initio calc. of geom. struct., charge distrib., bonding and pot. energy surfaces 80−18796
$NaBH_4$, struct., pot. surface, ab initio calcs. 79−41092
$Na_2CO_3.1.5D_2O_2$, neutron profile refinement and deuterium positions 79−90602
NaCl dimer, electron diffr. study of mol. struct. 80−28951
$(NaCl)_n$ (n=1-7) equilib. configs., total energy calcs., far IR spectra 78−29872
Na_2Cl^+, mass spectra, struct., stability, expt. and theory 77−554
NaF oligomers, struct., stability SCF and CEPA-PNO calcs. 78−78640
Na_2F^+, mass spectra, struct., stability, expt. and theory 77−554
NaH oligomers, struct., stability SCF and CEPA-PNO calcs. 78−78640
$Na_5HMo_6P_2O_{23}(H_2O)_{11}$, mol. and cryst. struct., X-ray diffr. anal. 79−32951
$Na^+(H_2O)n$ (n=1,2,4,6), FSGO-pair-pot. calcs. *(German)* 80−74278
Na_2SO_4, IR and Raman spectra of vap. over heated matrices 78−25525
$NaSbClF_3.H_2O$, cryst. and mol. struct. *(French)* 77−43200
$Na_6W_7O_{24}.14H_2O$, crystal and molecular struct. X-ray determ. 79−82188
NbO_2, vapour phase molecular struct., high temp. electron diffr. 79−68330
$Nb_{10}O_{28}^{6-}$, mol. config. from cryst. structs. 77−71886
$Nb_nW_{6-n}O^{(n+2)-}$, config., IR and Raman spectra 77−42324
NdX_3,(X=Cl,Br,I) far IR spectra, planar D_{3h} symm. 77−88450
Ni complex, cis-dichloro-bis(1,2,cyclohexadionedioxime) cryst. and mol. struct. 80−44198
Ni complex, Ni (II)-substituted ethylenediamines and monocarboxylates, cryst. and mol. struct., X-ray diffr. obs. 79−82182
Ni complex, S_4N_4 with $NiCl_2$, mass and IR spectra, config. 78−13494
Ni_3, in solid Ar, reson. Raman spectra 80−63638
$Ni(CO)_4$, mol. struct. by gaseous electron diffr., quadratic force field refinement 79−64115
O-containing mols., MNDO calcs. for ground state 78−911
O_2, excited state geometries and energies, ab initio pot. energy surfaces 78−5151
O_2, symmetry adapted wave function generation using group theoretical projection operators 80−102428
$(O_2)_2$, struct., energy transfer, high resolution electronic spectra 78−25550
O_3, conformation, ab initio HFS method calc. 79−36526
O_3, metastable cyclic ozone predictions 77−46511
O_5^{2-}, hypothetical, mol. self-consistent study, possible prep. method *(French)* 80−91717
$OCS_+ r_m$ struct. determ. from rot. consts. 78−42236
OCl_2^+, radical cation, struct. and electronic props., ab initio RHF SCF MO calc. 80−52883
OH-HF, H-bonded complex, ab initio calcs. *(French)* 80−52866
OH_4^+, stability, ab initio calcs. 77−30775
O_3H^+, isomeric structs. ab initio MO calcs. 80−83270
ONF, geom. and electronic struct., ab initio calcs. 79−76342
$OPBr_3$, mol. struct., electron diffr. and spectroscopic vibr. amplitude 80−58387
OsO_3F_2, OsO_4 matrix-isolated IR and Raman spectra 77−75166
PH_3, equilibrium structure and harmonic force field, ab initio calc. 80−9502
PH_5, equilibrium structure and harmonic force field, ab initio calc. 80−9502
PH_5, rearrangements, CI calcs. in large at. orbital basis 79−94106
PH_xF_{3-x}, geometry changes during inversion, ab initio calcs. 78−5154
$PH_2(F_2)(Cl_2)$, SCF-MO-HF calc., struct. and one-electron props., population anal. indices 79−76338
$PbCl_2$, mol. struct. determ. from gas phase electron diffr. 78−25742
Pd complex, bis(N-allylsalicylaldiminato)-palladium(II) cryst. and mol. struct. 79−32972
Pd complex, S_4N_4 with $PdCl_2$, mass and IR spectra, config. 78−13494
$PdAl_2Cl_8$, Raman resonance spectra of vapour 78−94251
Pd(II)-Gly-Tyr complexes, aq. soln., PMR obs., conform. 77−50450
PrO, D_0^0-state struct., dissoc. energy, mass spectrometric obs., 79−10228
Pt complex, bis(1,2-benzoquinonedioximato)Pt(II), cryst. and mol. struct. 79−60327
Pt complex, tris[bis(1,2-diaminoethane)Pt(II)dichlorobis(1,2-diaminoethane)]Pt(IV)tetrakis[tetrachlorocuprate(I)], cryst. and mol. struct. 80−28964
$PtCl_2(NH_3)_2$, cis- and trans-isomers, electronic struct., SCF-Xα study 80−18795
$Pt(SeC(NH_2)_2)_4Cl_2$, crystal and mol. struct. 78−59794
$RbBO_2$, mean geometrical config., vapour phase electron diffr. 77−46651
$RbPbI_3.2H_2O$, X-ray cryst. struct. determ. 80−64958
Re complex, $AsPh_4ReOCl_4$, cryst. and mol. struct. determ. 77−47390
S atom, van der Waals radius, mean statistical value 77−83515
S_2 $^{35}Cl_2$, microwave spectra and double reson., assignments, distortion consts. and struct. 79−89664

inorganic molecule configurations continued
S_3, conformation, ab initio HFS method calc. 79−36526
S_4^x, x=2−, 0, 2+, struct. differences explained, SCF Xα scatt. wave MO calcs. 78−74784
S_8, in α-S, under hydrostatic press., deformable mol. lattice statics 80−49175
S_8^{2+}, electronic struct. and localised MOs, bonding nature and geom. struct. 80−18798
$(SCN)_2$, prep., UV photoelectron spectrum and structure 80−28059
SF_2, ab initio LCAO MO SCF calcs., elec. struct., mol. props. 77−14344
SF_2, microwave spectrum inertia defects, ν_1, ν_3, ν_2, equilibrium structure, vibration rotation constants, anharmonic potential functions 79−93988
SF_5, anisotropic ESR spectrum in γ-irrad. SF_6 77−21400
SF_6 and S_2F_{10}, absorpt. of intense laser radiation, vibr. excitation 80−9667
SF_6, clusters, collision induced polarisability, mol. frame distortion 80−32798
$^{32}SF_6$, point group symmetry breakdown, vibr.-rot. state, saturation spectroscopy 80−87116
SF_4O, vibr. spectra, struct. and thermodynamic props. 77−63416
SH_3^+ geometry and inversion barrier, basis set depend. 80−921
SH_3^+, struct., ab initio HF calcs. 79−31371
SN_2 struct., vibr. spectra, ab initio calcs. 78−66475
SN^+, struct., vibr. spectra, ab initio calcs. 78−66475
S_2N_2, polymerisation, mol. struct., INDO calcs. 77−70301
S_2N_2, struct., vibr. spectra, ab initio calcs. 78−66475
S_4N_4, Raman scatt. and opt. absorpt., press. and temp. depend. 77−36227
SNF, geometry and stability, LCAO-MO SCF calcs. 79−31391
$S_4N_4.AsF_5$, molecular adduct cyclotetra(azathiene), X-ray cryst. struct. determ. 80−54180
SO_2, $^1B_2$ state, force field and asymm. struct. 79−22685
SO_2, analytical pot. functions, several surface minima 78−5158
SO_4, and isotopic forms, struct., normal coord. anal. 78−965
S_2O, 3400 Å bands, rot. anal., upper state struct. 78−13506
SOH, ground and first excited states, geometry, ab initio SCF calcs. 78−50657
SOH radical, ab initio SCF and CI calcs., electronic states and transitions 77−46488
$SPBr_3$, mol. struct., electron diffr. and spectroscopic vibr. amplitude 80−58387
SbF_3, IR spectra of solid and gas, rel. to struct. *(French)* 78−78692
ScF_3, pyramidal struct. and force field coeffs., electron diffr. obs. 78−9250
Se_8^{2+}, electronic struct. and localised MOs, bonding nature and geom. struct. 80−18798
SiF_3Cl, radical anion struct. and ESR spectrum 78−25571
SiH_2, $1B_1$-state, geometry calcs., avoided crossings 80−53085
SiH_4^+, struct, stability, ab initio calcs. 79−13632
Si_2H_4, ab initio GO calc., geom. optimisation 78−94187
Si_2H_6, valence electronic struct., model pot. in floating spherical GO formalism 78−74563
Si_6H_{12}, and Si_6D_{12}, Raman and IR spectra, vibr. force consts., config. *(German)* 79−22715
SiH_3D, in polycryst. SiH_4, mol. motions and symmetries, IR obs. 78−48163
SiH_2DF, $SiHD_2F$, microwave spectra, harmonic force field, mol. struct. 77−18913
SiH_3NCO, geometric struct., ab initio MO calc. 79−13834
$(SiH_3)_2O$, and d_6, Raman spectra, vibr. mode and config. 78−62940
Si_2H_6O, geom. and electronic struct., ab initio MO calc. 79−97972
SiH_3X^-, X=Cl, Br, I, and isotopic forms, EPR spectra, mol. struct. 79−94023
$(SiH_3)_3Y$, (Y=As, P, Sb), vibr. force fields and amplitudes, zero point struct. 77−54551
SiO_2, mol., ab initio SCF calcs., ground state stability, struct., vibr. freqs. 78−86781
SnH_2, struct. determ., restricted HF calcs. 80−87030
SrI_2 mol. struct. parameters and geom. config., gaseous electron diffr. obs. 80−37883
$Sr[Fe(CN)_5NO].2H_2O$, cryst. and mol. struct. 78−91311
$Sr[Fe(CN)_5NO].4H_2O$, cryst. and mol. struct. 77−58982
$TaBr_5$, gaseous, electron diffr. obs. of vibr. assignment, mol. struct. and barrier to pseudorot. 79−81293
$(TaI_5)_2$, X-ray cryst. struct. determ. *(German)* 80−19754
TeF_6, gas phase electron diffr. patterns, mol. struct., three-at. scatt. 78−66662
Ti (III) halides, bonding, struct., ligand field splitting, electron gas calcs. 78−17557
$TiBr_4$, (TiI_4), struct., force field and Coriolis const. calcs. 78−86843
TiF_4, equilib. config., force field, Coriolis consts., vibr. freqs. and amplitudes 80−32835
$TlBO_2$, mean geom. config., gas-phase electron diffr. 77−83759
Tl_2Cl_2, mol. consts., IR and Raman freqs. assignments 78−17648
Tl_2F_2, mol. consts., IR and Raman freqs. assignments 78−17648
$TlNO_3$, molten and aqueous soln., Raman spectra 79−78673
UF_5, electronic struct. and geometry, ab initio calcs. using relativistic ECP 80−32606
UF_5, monomer struct. and pot. consts., IR and Raman spectra in inert gas matrices 78−5215
UF_5, transient mol., IR absorption spectrum, 580-630 cm^{-1}, assignments, mol. struct. 79−68227
UO_2, molecular geometry determ. from IR spectra vibr. assignments 77−50437
VBr_4, mol. struct., vibronic interactions, dynamic Jahn Teller effect, gas phase electron diffr. 79−31711
$V(CN)_5NO^{3-}$, struct., FSGO calcs. 78−70736
$V(CN)_6NO^{4-}$, struct., FSGO calcs. 78−70736
$V(CO)_6$, cryst. and mol. struct., Jahn-Teller distortion, mol. vib. and librational correction 79−32949
β-$VOSO_4.5H_2O$, X-ray cryst. struct. determ. and refinement *(French)* 80−107121
$W(CO)_6$ dissolved in oriented compensated nematic mixture, distortion of cubic mol., linear dichroism obs. 79−95797
$(WO_3)_3$, identification of polymer species by vapour phase electron diffraction 80−53135
WOF_4, gas phase electron diffr., mol. struct. 77−34775
X_2H^+, X=Li, Na, K, equilib. geom. and dissoc. energy, pseudopot. calc. 78−94329

inorganic molecule configurations continued
X_2Y^+, X,Y=Li, Na, K, equilib. geom. and dissoc. energy, pseudopot. calc. 78−94329
XeF_2, pseudopotential SCF-MO studies, equilib. struct., stretch-stretch interaction force const. 80−95525
XeF_2, stereochem. of structs. and valence bonds 79−69066
XeF_4, pseudopotential SCF-MO studies, equilib. struct., stretch-stretch interaction force const. 80−95525
XeF_4, stereochem. of structs. and valence bonds 79−69066
XeF_5^+, pseudopot. SCF MO studies, steric aspects of struct. and force fields, Jahn-Teller effect 80−99444
XeF_6, monomeric charact., electron ionisation mass spectra 77−75322
XeF_6, pseudopot. SCF MO studies, steric aspects of struct. and force fields, Jahn-Teller effect 80−99444
XeO_3, stereochem. of structs. and valence bonds 79−69066
ZnXY, (X,Y=Cl,Br or I), matrix isolation, vibr. spectra, isotope effects, force consts. and geometry 78−46337
$ZrBr_4(ZrI_4)$, struct., force field and Coriolis const. calcs. 78−86843
ZrF_4, mol. struct. and vibr. freqs., gaseous electron diffr. obs. 80−32836
inorganic molecule electronic structure *see molecular electronic states*
input-output media (computers) *see computer peripheral equipment*
insolubility *see solubility*
inspection
see also quality control; reliability; testing
acoustic emission, transducer for inspecting weld quality 79−94444
acoustic methods, review 79−43504
acoustic ranger for tube and pipe inspection 78−85092
acoustic spectral inspection unit piezoreceiver, operation conditions 79−64465
active thermal NDT, review 79−70282
air tightness inspection by gas anal. method 78−41323
airtightness, total lack of, automatic system for measurement 79−52593
airtightness inspection by hydrostatic method, correcting to standard conditions 79−91898
airtightness inspection using halogen leak detector, automation 79−52595
airtightness of joints, foam indicator for inspection 79−52594
amorphous materials, high resolution imaging 79−99039
amplitude and time analyzer for flaw detect. 79−70288
AMUR-6 instrument to detect defects and indicate their location 80−104402
austenitic weld joints and surface claddings, eddy current testing *(German)* 77−1895
automated US units for inspecting thin walled tubing 78−88606
automatic inspection of materials using lasers 80−66734
automatic magnetic inspection system for oil country tubular goods 77−81361
automatic surface flaw inspection of nuclear fuel pellets 79−30939
automatic US inspection of heated objects by SGK-2Ts system 78−95894
automation of measuring equipment state-inspection results, USSR Krasnodar territory 80−52152
babbitting tester, semiautomatic, for US inspection 79−66245
bar insulation in stator winding of large turbogenerator, inspection using microwave defectoscope 80−35474
biomedical electronic equipment maintenance, inspection, hospitals appl. 79−96684
boiler tube corrosion monitoring by gamma ray meas. instrument 77−9011
boiler tubes in service inspection, creep testing techniques assessment *(Japanese)* 77−81356
butt welds inspection, using multielement US probe 77−90569
BWR, boilers and pressure vessels, in-service inspection, General Electric's code 77−3152
BWR, in-service inspection and external base-line tests, instrumentation 80−784
BWR, revised Inservice Inspection program, implementation at Millstone Unit 1 80−23020
BWR, surface inspection methods, in-service inspection of reactor pressure vessel 80−27759
BWR power plant, routine checks and radiation protection 78−74462
CANDU fuel, post-irradiation test facilities at Chalk River 80−30206
cast stoneware, quality control, use of US methods 78−11490
chromatographic method of calibrating leaks 80−77800
circuit for electrochemical recording of defect records in US inspection 79−66246
coarse-structure materials, inspection of part quality using LF US methods, review 80−81264
coating thickness, mounted eddy-current transducer error correction 80−77775
cold rolling rolls, magnetic inspection at heat treatment quality 78−88613
cold strip surface, flaw inspection with optoelectronic equipment 78−60967
complex shape product inspection, local eddy current transducer 80−108671
complex surface shape inspection, coherent optical method evaluation 79−81578
component inspection by speckle pattern interferometry 77−37975
component profile inspection equipment 80−105608
composite piezotransducer for LF acoustic inspection using electrical models 80−104393
condenser, tubular, rotating eddy-current probe method *(German)* 77−1897
contact fluid for US inspection 79−52586
contact layer thickness optimization for resonance method inspection 79−34236
contact lenses, back surface aspheric 80−66711
contact media for US thickness meas. and defect inspection over wide temp. range 80−104395
contactless laser interferometer sweep gauge for diamond-turned surfaces 80−73441
continuous self-inspection of acoustic emission instruments 79−96275
CRT, speckle patterns appl. to surface inspection 77−26385
cyclically loaded structures, effects of periodic proof and nondestructive testing 79−15946
cylindrical articles of small diameter, monitoring by automatic X-ray apparatus 79−70280
cylindrical part edge quality determ., acoustic method and equipment 80−35491
inspection continued
cylindrical products, diameter meas., interfering factors elimination 80−77755
dark-field surface inspection using total internal reflection 80−74519
defect classification, automatic, by US spectral method 79−66240
defect coordinate determ. by calibration of AE method 80−35473
defect depth determ. by radiographic inspection 79−66241
defibrillators, review of instruments and maintenance 78−69251
delaminations in thin sheets, elongated, interaction with Lamb waves, book contrib. 79−98574
density of materials on supply line, neutron radiometric inspection 80−21205
deposited metal, US echo inspection procedure 80−89425
device for checking airtightness by parameter changes in object and medium 80−104404
dielectric material, electro-optical inspection of internal defects 78−56869
dielectric tube, electrospark inspection unit for defect obs. 78−92431
diesel nozzle sprayer castings, heat treatment quality inspection 80−35471
drill pipe with welded end couplings, US inspection 79−5124
EBR-II steam generator tube bore side inspection probe and drive 79−9850
eddy current inspection, possibilities of phase generator circuits 78−88614
eddy current inspection of fastener holes, computer automation, exam. 78−53040
eddy current probe, high saturation with internal reference, design and specifications 80−40658
eddy current testing of wire and bar 80−71819
eddy current transducer part geometry effect on inspection 78−53078
eddy current transducer with electrical commutation of excitation field, NDT 80−105633
eddy-current feed-through transducer, approx. calc. of mag. field, nonferromag. media 80−78746
eddy-current phase thickness gauge, automatic error corrections 79−9204
eddy-current probes, rotary, for defects scanning and detection 77−90557
electric and magnetic props. change with depth, electromagnetic transducer 79−52603
electrical contact tip for magnetic inspection 79−66248
electromagnetic, parameter calc. using nomographs 79−79215
electromagnetic inspection of railway rails, high speed, objective rating 79−47858
electromagnetic inspection review 80−35468
electromagnetic inspection units, type MD-3 and 77PMD-3M, improvements 79−100318
electromagnetic NDT, digital method of edge effect suppression 78−56866
electron beam welds, defect detection by acoustic emission *(German)* 77−56193
electronic component hermetic package water content anal. by mass spectroscopy 78−21263
electronics microstructure analysis by SEM 79−80723
elongated part of noncircular cross section, straight through eddy current transducer inspection 79−47860
equipment, circuit for selecting signals in specified phase range 78−56863
failed steam accumulator anal., role of metallography and NDT 78−95877
fast breeder reactor boiler tubes, eddy current probe insertion for in service inspection, method development *(Japanese)* 80−822
fatigue, fracture, statistical treatment, maintenance procedures 79−43538
fatigue detection and rating by acoustic emission, review 80−104380
FBR and HWR, in-service inspection, Japanese practices 77−366
feed through eddy current transducer, numerical anal. or operating mode during ferromagnetic rod inspection 80−108670
ferrites, void, conc. and dimensions determ. by acoustic charact. 80−35472
ferromagnetic material, electromagnetic props. inspection by electromagnetic transducer with frequency output singal 78−53131
ferromagnetic material, inspection by method of two harmonics 78−88608
ferromagnetic object, investigation of the through-transducer signal spectrum 80−35487
ferromagnetic object inspection, method of higher harmonics, difference schemes 80−89444
ferromagnetic probe coercimeter for inspecting the quality of parts with variable geometric dimensions 80−35488
ferromagnetic probe inspection unit for automatic inspection of welded tubing 78−56860
ferromagnetic probe unit, MD-10F, automatic 78−56861
ferrous metal rolled repetitive sections, ultrasonic quality inspection 79−87770
ferrous metallurgy, nondestructive inspection and quality control review 80−21201
fission reactor pressure vessel walls, ultrasonic inspection reliability 79−24713
flaw detection in welded joints, X-ray television systems appl. and characteristics 77−81380
flaw detection probability estimation from inspection data 79−24712
flaw detector, UD-22UM, materials with large US attenuation appl. 79−52585
flexible scanning industrial X-ray fluoroscopic inspection 80−100971
flexible scanning industrial X-ray/fluoroscopic inspection 80−89459
fluorometallic intensifying screens suitability in X- and gamma-radiography *(German)* 77−180
fracture toughness testing, acoustic emission, inspection technique 78−68860
friction material, US inspection 78−60931
fuel elements, quality inspection by eddy currents, unit 79−100315
gas cooled fast breeder reactor core element fabrication technology 77−18682
gas turbine sand casting, US inspection 78−88594
glass fibre reinforced plastic, thermal inspection, one sided for separation of parts 79−79206
glassware dimensional and sidewall inspection using digital camera and computer 78−16890

inspection continued
glued members, low frequency acoustic flaw detector inspection 78−60954
graphite, US inspection apparatus for complex profiles 79−5109
graphite reinforced epoxy, NDT 79−96254
heat treatment, electromagnetic quality inspection with specified intensity of internal field 80−108677
high density polyethylene tube flash welding, IR spectrometer appl. 78−21109
high-speed digital image processing 78−12680
high-temperature contactless testing by EM acoustics 78−85095
honeycomb panels, holographic interferometry appl. 77−34843
hot-rolled rods, surface defect detection without scale removal by NDT 78−95890
hydraulic component fatigue crack acoustic emission inspection 77−40513
IAEA safeguards, instruments and techniques for nondestructive assay 78−33302
image dissector tube with minicomputer control suitable for IC mask inspection 79−55065
impact excitation of vibrations in the acoustic spectral inspection method 79−70273
impedance inspection unit for inspecting joints in multilayer parts 78−44335
impedance method charact. and inspection transducer 79−96270
impedance type ferromagnetic probe sensors for magnetic inspection 78−48599
induction inspection unit with spaced windings, increasing sensitivity over magnetising and measuring length 78−56864
inservice inspection of nuclear power plants in Japan, appl., problems *(Japanese)* 77−50255
instrument for crack detection by AE 79−52582
interferometer for precision linear displacement meas. 80−27285
international collaboration among calibration services 80−101773
irradiated fuel sipping, inspection and repair 79−9844
joint, welded, through defects, study using vacuum bubble method of airtightness inspection 79−52599
kerosene appl. for airtightness inspection 79−52579
laminate, bonding inspection, by acoustic amplitude method 78−48591
large monocrystal X-ray reflection/scanning and transmission topographic methods 80−96415
large-scale angle inspection unit 78−77864
linear accelerator for nondestructive inspection appl. 79−41046
LMFBR, inservice NDT methods 77−38357
LMFBR vessel, US testing of austenitic steel welds 77−1903
LWR, heavy water moderated, prototype, pressure tube monitoring with US devices 77−88268
LWR power plants, inservice inspection 79−30944
LWR pressure vessels testing, using ultrasonic probe 78−17339
machine tool geometry using laser interferometry 77−9997
magnetic induction defectoscope with adjustment 78−53105
magnetic particle inspection, combined magnetization of parts by rectified single half-period fields 79−52575
magnetic particle inspection, nature of magnetic inks and powders 80−100974
magnetic particle inspection fundamentals 78−44285
magnetized samples, defects, magnetostrictive conversion of US waves into EM fields 80−66008
magnetizing device for inspection of products of ferromagnetic materials according to parameters of Barkhausen discontinuity 80−89457
magnetizing flaw detection system for underground pipeline inspection 78−53103
magnetodynamic method of part inspection 79−96272
manometric tightness control, increased reliability 79−79214
manufactured part rejection validity, influence of random meas. errors 77−17947
measurement facility inspection, confidence and productivity improvement 78−77840
measuring instrument inspection, optimal error correction signal 78−77829
medical equipment technical servicing, determ. of quality 80−3834
metall, thin section fusion weld, US inspection 79−15916
metallic and non-metallic surface defects, optical method 77−28973
metallic objects with complex shape, eddy-current inspection 80−89446
metrological provisions for thermal methods of inspection 79−100314
metrology use in material inspection 78−95899
microinterferometer transducer, air-bearing, for use with universal inspection machines 78−57899
microtrons, appl. in nondestructive inspection of industrial products 80−81267
MIRA series of impulse X-ray apparatus 79−34252
moving material fault test rig *(German)* 80−11855
multichannel US inspection unit, indicator of working order of electronic-acoustic circuits 78−92425
multicomponent assemblies, moire inspection 80−35434
multilayer cylindrical parts, thermal inspection unit for NDT 79−52606
multilayer parts, thermal quality inspection two dimensional problem soln. 79−70283
multilayer product, theory of laid-on shielded transducers for inspection 78−88610
multivariant inspection methods, theory 78−88609
NDT, book 78−44340
NDT, equipment for production line inspection 79−29320
NDT, penetrant inspection, modern techniques *(French)* 77−9028
NDT, X-ray apparatus, Toshiba, Japan 79−57193
NDT inspection reliability in quality control 79−66229
nondestructive inspection methods, review 79−43535
nondestructive quality test, holographic interferometry appl. *(French)* 78−42305
nondestructive technique optimisation, as operations research problem 77−90548
nuclear facilities in USA, IAEA inspections effect, (1960s to 1978) 79−85680
nuclear fuel, inspection by neutron radiography, review 78−60890
nuclear fuel element assembly, X-ray technique appl. 78−72940
nuclear fuel pellet inspection system for remote operation and maintenance 79−89480
nuclear fuel pellets, automated inspection 80−13766
nuclear fuel pin bundle tomographic visualisation, maximum entropy method 79−63883
nuclear fuel rods, thermographic imaging 77−42085
inspection continued
nuclear fuel shell inspection, mag. method for detecting ferromag. particles 80−66746
nuclear materials supervision in West Germany, by Euratom and IAEO *(German)* 80−18415
nuclear plant, safety requirements for remote and continuous inspection 80−5295
nuclear plant safety system redundancy, cable routine inspection 78−735
nuclear power plant, in-service inspection methods and limitations 77−3169
nuclear power plant piping welds by in-process acoustic-emission monitoring 77−14823
nuclear power plants, in-service inspection requirements, impact of changes 79−54589
nuclear power plants, utility requirements for in-service inspection 79−54588
nuclear power station, inservice examinations, effective quality assurance 79−97861
nuclear power station, inspection practices and decisions for safety and availability 77−46304
nuclear pressure vessels, ultrasonic testing techniques review 77−74899
nuclear reactor, in-service inspection, using acoustic emission technique 77−34409
nuclear reactor components, weld seam inspection, steam supply system, quality assurance *(German, English)* 77−83052
nuclear reactor containments, in-service leakage tests 79−67895
nuclear reactor pressure vessels, remote controlled US pre-service and in-service inspections 78−89955
nuclear reactor vessel, recording instrument for US inspection results 79−5104
nuclear research facilities, inventory verification 79−85600
nuclear steam generators, inservice inspection, book contrib. 79−100322
oil seal lubrication static contact shape and kinetic behaviour 80−97598
optical fibre end face cut prep. and inspection techniques, review 80−74483
optical fibre endoscope type OD-20Eh, internal surface inspection 79−79216
optical gauging by remote image tracking used in production 79−86264
optical heterodyne interferometer, appl. to surface inspection 77−90529
optical microscope, large field, for use in semiconductor manufacture 80−82812
optical microscope as production tool 77−41679
part inspection with surface temp. up to 500°C, transducer 79−98584
penetrants, high temp., precautions in use 80−30192
periodic inspection of meas. facilities, probabilistic confidence characteristic selection 78−77839
phase defect inspection for determ. of moment of origin of fatigue cracks 79−52578
phase meters checking, by comparison with angular measure 77−10057
photographic materials, automatic inspection by IR laser beam 79−30593
piezoceramic transducers 80−104392
piezoelectric transducer with oblique bottom immersion chamber inspection of plane parallel objects 78−53111
piezoelectric transducers for contactless US product inspection 79−34238
pipe, thick walled, increasing efficiency of automated ultrasonic inspection of segregate defects 79−11755
pipe, transverse oscillation effect on measurement accuracy in radiometric inspection 79−34245
pipeline welding flaw detection 78−19984
pipes, soldered, device for automatic scrapping 79−29308
plastic encapsulated and hermetic modules corrosion model 80−100937
plastic pipe inspection by rotational ultrasonics 79−20323
pneumatic tyre, X-ray testing in automated production line *(French)* 77−5969
polymer, thermal inspection by one side method 79−52604
portable comprehensive irradiated-fuel inspection stand 79−9836
precision image isocon X-ray TV camera 80−101263
pressure vessel crack detection by magnetic crack detection and dye-penetrant inspection 80−100994
pressure vessels, acoustic emission inspection during water pressure testing 77−1901
pressure vessels, AE during fatigue crack expansion 80−108675
pressure vessels weld quality assessment, NDT methods and equipment 78−56871
profile multiaxis meas. with vector drive 80−105609
PWR assemblies, pool-site fuel inspection and exam. techniques 80−18567
PWR primary circuit, in-service inspection *(French)* 79−22385
PWR primary coolant system, in-service inspection programs 79−22384
PWR reactor, pressure vessel US testing *(Czech)* 78−29658
pyroelectric vidicon appls. 77−65635
quality assurance *(German)* 79−52548
radiation inspection improved effectiveness of differential circuits used to suppress low-frequency noise 79−52608
radio wave inspection with one sided access to object, conditions of coating and compensation 80−108679
radiographic inspection algorithm speedup by array processor 80−108659
radiographic inspection method, productivity 80−71861
radiographic inspection of welded joints, effectiveness investigation 78−56872
radioscopic inspection data of pore defects, statistical anal. 78−48606
raw material acceptance testing for dielectric applications 80−97646
reactor pressure vessel, automatic compound scanning US inspection system 77−1892
reactor vessel inspection techniques *(Dutch)* 80−27758
receiver-transmitter for ultrasonic inspection units 80−89458
recording system, for automatic US flaw detection system 78−76815
rectangular probe under impulse conditions, directivity of emission curves 79−96276
reinforced plastic, fatigue mech., charact. and defect detection 79−24687
reinforced plastics, low frequency acoustic flaw detector inspection 78−60954
resistance introduced by a defect in modulation inspection method 79−91892
road construction, nondestructive testing principles, instruments and methods *(German)* 79−11742
rolled sheet thickness effect in magnetic inspection of mech. props. 79−91894

inspection continued
rotatable microscope stage, used for hybrid microcircuits inspection 80−90889
rotor forgings, crack detection, US holography method 77−66730
rubber gasket inspection, US system, gas pipe appl. 80−30178
scanner development, for surface inspection of cold rolled sheets *(German)* 79−43533
scanning acoustic microscopy for study of interfaces in solid-state devices 80−99907
scanning optical microscope for semicond. materials and devices 80−95136
semiconductor manufacturing, interferometric method for surface deform. meas. 78−32793
semiconductors, SEM electron beam irradiation damage and contamination, failure analysis 78−29217
service life of equipment in creep, AE appl. to technical diagnostics 79−96271
sheet material, Lamb wave inspection, pulsed and impact excitation of transducer 79−34244
SNR 300, pumps, heat exchangers and manipulator systems 79−97784
solar reflector paraboloid surface inspection using LG-75 gas laser system 77−75643
soldered joint, thermal inspection system design 79−91897
soldering inspection using optical projection microscopes *(German)* 80−77849
specimen with varying thickness for US inspection 78−53137
spectacle lens inspection apparatus *(French)* 79−7235
stamped disc surface inspection by automated eddy current unit 78−92430
steam pipe, crack detection, electrical potential probe method *(German)* 77−1898
steel, 11YuA, cold worked, heat treated, electromagnetomech. props. NDT 79−4980
steel, 20A, melt, tube blanks, mech. props., statistical determ. 79−29316
steel, 38KhS, heat treatment quality inspection by magnetic method 79−52574
steel, austenitic, tubing, heavy walled, US inspection 79−39107
steel, austenitic stainless, pipe welds, US inspection pattern recognition reflector classification feasibility study 80−16615
steel, ball bearing rods, inspection installation 80−81268
steel, billet, high speed automatic surface inspection, MIDAS 79−83420
steel, C, wear of Cr, Zn protective coatings, exam. using nuclear radiation excited X-ray fluorescence 80−21206
steel, casting, C-scan method of US inspection, developments 79−29294
steel, castings for use at high temp., correlation between US and radiographic inspection *(German)* 78−88599
steel, circular hot rolled stock, magnetic inspection of external surface, zond automated installation 79−79210
steel, coarse grained Kh18N9T, US amplitude inspection, efficiency estimation 78−48592
steel, cold rolled strip, surface defects, online automatic system, design study 79−34231
steel, cold-formed, NDT of mech. props., coercimeter results 79−34240
steel, electrical sheet, wattmeter unit for measuring specific losses, system errors 79−91893
steel, heat treated, electromagnetic device for quality inspection 78−53104
steel, heat treated small parts, electromagnetic hardness inspection 79−34241
steel, hot, US inspection 78−88586
steel, hot rolled strip and plate shape meas. device 80−35498
steel, low alloy, welded joints, cracking during heat treatment, simple detection method 80−7724
steel, low alloy and C, hardened and tempered parts, nondestructive magnetic inspection 78−95889
steel, low alloy and C, hardened and tempered parts, nondestructive magnetic inspection 79−1929
steel, massive object inspection, coercimeter with attached electromagnetic appl. 79−70277
steel, neutron quasialbedo thickness meas. of single layer product, optimization 80−105611
steel, nitrided layer depth, electroinduction meas. method 80−104379
steel, round bar inspection, EM-acoustic techniques 78−60973
steel, square parts, surface inspection, defect depth meas., eddy current method 79−29307
steel, stainless, pipe, small-diameter ribbed-bore, Lamb-wave ultrasonic inspection for defect detection 79−15944
steel, stainless, US methods for intergranular corrosion inspection 78−95898
steel, stainless austenitic welds, US inspection 80−71821
steel, strip, US inspection by differential method using binary comparative probes 79−70285
steel, strip inspection for cracks, magnetic instrument 79−52584
steel, structural ties, NDT by eddy current transducer, optimum parameters and capabilities 80−108669
steel, tape, US inspection for segregate type defects 79−15943
steel, US attenuation, defect effects in US inspection *(Italian)* 78−48609
steel case depth after quench hardening, inspection using coercimeters 80−104377
steel industry online US internal flaw detection system 77−66717
steel products, hot thick, US inspection system 80−40661
steel stainless, intergranular corrosion, effect on acoustic props. for US inspection 79−11745
strobe impulse former in inspection zone of part with variable thickness 79−39100
surface finish automatic inspection by laser scanning *(German)* 78−170
surface roughness of small-diameter channels, non-destructive inspection by replicas 77−30136
Symphonie communications satellite components, NDT *(German)* 77−1899
thermal inspection of plates with internal defects, one and two sided, heat transfer intensity effect 78−88616
thermal methods and apparatus for NDT of weld joints 78−88615
thermal methods of NDT, review of theoretical and experimental problems 78−44325
thermocouples and meas. line, using computer-controlled capacitor discharging method *(German)* 80−13079
thermovision flaw detector 'Stator-1', meas. channel 80−76449
thickness meas., US resonance method 78−48590
thickness meas. US inspection, variability of meas. 79−24704
thin walled bearing races eddy current inspection of hardening and tempering quality 78−95892
tightness inspection, sensitivity determ. using holographic interferometry 79−36862
tightness of mating parts 79−66234
tolerance gauging, Mercer electronic unit 79−12780
transducers, alternating-voltage, analogue, Soviet methods development 80−98872
tube inspection, magnetic leakage flux method 78−95891
tube testing, relationship between ultrasonic field and testing zone *(German)* 77−1893
tubes, new acoustic device characteristics 77−68343
tubing, ferromagnetic probe coercive force meter, different heads 78−60943
two layer medium with metallic base, dielectric charact. determ. using reflected electromagnetic wave 79−35688
two-dimensional periodic structures, spatial filtering 77−38819
ultrasonic, welded joints in sugar extraction diffusion apparatus 80−93703
ultrasonic inspection, sensitivity adjustment by use of new measuring scales 79−52567
ultrasonic testing of austenitic collars in a computer controlled immersion test-plant *(German)* 79−96256
US, coarse grain anisotropic structure materials 77−16767
US, homogeneity improvement of inspection trace of line focused US probe *(German)* 79−94428
US, inspection of metallic atomic power station equip., portable unit 80−104394
US, nomogram for determ. of damping coeff. of transverse waves 78−56867
US, of seamless drill casting and linepipe, review 78−95879
US, online inspection, steel plate manufacture appl. 78−80702
US, with given reliability, optimal conditions 78−95895
US adhesive bond eval., computer controlled 79−96253
US automatic inspection of tubing 78−56865
US echo method of inspection for complicated shapes 78−44317
US inspection, automatic, thin walled large diameter pipes, flaw size classification 78−60949
US inspection of large diameter pipe and stock 78−48593
US inspection of rails for flakes, mechanised US unit 78−44330
US inspection result reproducibility on welded joints of tubes in boiler surfaces 78−60948
US inspection slanted probes, prism material choice 78−92428
US nondestructive inspection system, microprocessor utilization 80−71845
US rail-inspection transducers lateral position automatic control 79−57200
US shadow flaw detectors, metrological peculiarities when inspecting thick rolled steel sheet 80−81263
US thickness gauge, Kvarts-6, design of automatic control block 78−73005
US wave damping in solid material, instruments for determ., review 78−92429
weld joint, furnace welded pipe inspection unit for above 1000°C 78−53134
weld joint, US inspection probe 78−92426
weld joint, use of flux sensitive magnetic heat for magnetographic inspection 78−44328
weld testing, automated US installations *(German)* 77−1894
welded joint, radiographic inspection, standardization of sensitivity and flaw size 80−89455
welded joint inspection by X-ray TV intrascope, photographic recording of images 80−86485
welded joint inspection using special US scanning system 79−34235
welded joints, radiographic inspection, real flaws detectability evaluation 80−81266
welded joints, US inspection of defects, recording nominal length and height 79−52577
welded joints of tube headers, US inspection feasibility study 79−11746
welded lengthwise seam, US inspection of cylindrical testpieces 79−39087
welded pipe joint, efficency of various methods of NDT 79−39103
welded T-joint, US inspection possibility by normal entry probe on far side of main member 79−52570
welding seams, automatic US inspection system 79−29310
welds, US examination, handbook 78−48608
wrap-soldered tubing, inspection using UDT-6Sm us apparatus 78−3276
X-ray inspection of welded seams in heavy engineering using Philips MG 420 and MG 300 systems 79−93269
x-rays and vidicon TV combine for instant inspection of precision components 79−74321
Ag solder strip continuity, US inspection 79−52605
Ag_3Mg, ordered alloy, projected pot. image of defect obs. 79−99176
Al, A999, US inspection of purity and dislocation struct. 79−70286
Al alloy, US inspection of overheating in parts 79−52607
Al alloy, US testing of cold worked surface, quality evaluation 78−48602
Al parts, radiographic testing *(German)* 77−1900
Fe, cast, parts inspection of unmachined surfaces using fluorescent penetrant method 79−11754
Li-I cell solid state, cardiac pacemaker power source, testing 79−66584
Pb, parts, albedo thickness meas., neutron technique 79−29309
Si devices, oxidation induced stacking fault detection by refl. X-ray topography 77−84767
Ti alloy, tubing, heavy walled, US inspection 79−39107

instability *see stability*

installation
see also commissioning; computer installation
EM flowmeter theory and application 80−96328
fibre-optic Bell System Chicago installation 78−42434
intersecting storage ring supercond. solenoid installation and performance 79−31270
mine concentrator X-ray on stream anal. system 78−35778
nuclear fuel reprocessing plant, optimal installation program 77−46370
nuclear power station installation policies analysis using TOTEM-3 code 77−65323
optical fibre cable, development and experience 78−9460
optical fibres, transmission, applications and cable techniques *(Japanese)* 80−87493

installation continued
solar battery installation and performance in mid-European latitudes *(German)* 80−21399
solar energy for domestic dwellings, installation practice *(Italian)* 79−100499
solar systems installation for domestic heating *(German)* 80−94103

installation, computer *see computer installation*

instrumentation
see also aerospace instrumentation; computerised instrumentation; digital instrumentation; digital readout; display instrumentation; nuclear instrumentation; physical instrumentation control; signal generators; signal sources
200 kW Gedser windmill in Denmark, performance and structural response meas. 80−61431
accuracy and repeatability 78−21090
analogue simulation of measuring equipment and testing means 79−80564
analogue versus digital measuring instruments *(Italian)* 80−37015
calibration optimal interval determ., generalised method *(Rumanian)* 78−49787
cells failure analysis, Ag-Zn, test methods evaluation 79−48105
chemical research, appl. of physical instrumentation and computers, review 79−70295
cloud electric fields measuring instruments, review 77−41226
coal gasification, in situ, diagnostic and remote monitoring instrumentation development 79−48055
dissolved O_2 in water, automatic analyser *(Japanese)* 80−35812
dynamic force meas. device comparison *(German)* 77−79089
dynamics, averaging time as equivalent dynamic parameter *(Polish)* 78−29081
electrodeposits thicknesses meas., multilayer, based on destructive coulombmetric method *(Czech)* 80−8980
electromechanical force meas. devices, long-term stability tests *(German)* 77−79088
electronic measurements, book 80−31805
electronics influence on laboratory technology and instrumentation over last 25 years 77−67422
EM meas., conf., Ottawa, Canada, 1978 79−21731
EM precision meas., conf., Ottawa, Canada 1978 78−89462
environmental and pollution control 78−24363
experiment design *(Japanese)* 78−62190
experiments design, statistical methods *(Japanese)* 78−41299
experiments design *(Japanese)* 78−70087
fibre optics appl. survey 80−83665
field instruments, winterisation without accessory heat 80−82758
fluid dynamics research facilities, California Institute of Technology, 1976 77−51147
general purpose measuring instruments, microprocessor techniques appl. *(Spanish)* 80−62655
health care and instrumentation, Indian scene 77−40813
instrument block optimal precision synthesis *(Russian)* 78−70092
instrumentation and control technology, decentralisation, past developments and future trends 80−4701
interface buses, for instrumentation link-ups 77−22565
linear parameter estimation, for chem. anal. 79−24843
magneto-optical effects appl. *(Japanese)* 79−14099
mathematical models of instruments, fundamental principles 78−93641
measurement accuracy, evaluation 79−17380
measurement techniques 78−8391
measuring systems, systematic design 80−95094
metrological reliability, standardization 79−80568
microwave, Intern. Microwave Power Symposium, Minneapolis, Minn., USA May 1977 77−70492
microwave survey instrument evaluation and calibration 77−37946
MIS structure capacitance-voltage charact. gauge 77−37923
modular units assembly, mathematical aspects of design *(Russian)* 80−37021
photolysis and radiolysis, kinetic data acquisition, and anal., by computer based system 79−39180
precise elec. meas., conf., Brighton, UK (Sep. 1977) 77−82551
probabilistic representation of quantities 78−49788
R&D instrumentation, selection of power supply 78−246
radiation chemistry, in Inst. Nuclear Res., Warsaw 78−76888
reliability, activities at National Institute for Metrology (INMB), Bucharest *(Rumanian)* 79−40522
reliability assessment using mathematical models 80−22348
research and production process investigations, development *(Polish)* 77−10003
RF instrumentation based on superconducting quantum interference 78−57995
scientific, in India, review 77−79087
statistical time interval analyser with visual display 77−37850
synchrotron radiation instrumentation, conf. Gaithersburg, MD, USA, June 1979 80−90607
systematic design of instrumentation systems 78−24781
temperature control, use of thermosensor indications 77−41599
tolerance gauge, Mercer electronic unit 79−12780
undergraduate course, in advanced physical instruments 79−21486
in undergraduate engineering curriculum 78−8206
USSR State Bureau of Standards, metrological resource programmes 80−90809

instruments
see also individual types of instruments, e.g. astronomical instruments, bridge instruments, optical instruments
aerosol electrical analyzer, performance under nonideal conditions 79−66372
analytical instrument use and planned acquisitions 78−88684
aspirator saturator, performance, dew point data of air *(Japanese)* 79−40580
battery-powered portable instruments, LSI ccts. for versatility and economy 77−33999
CAD considerations *(Hungarian)* 79−93134
conductometer, type DG-1, for solution conductivity meas., features *(Polish)* 78−41330
double insulation reduces measuring problems, safety aspects 78−32802
electric shock, safety precautions may result in health hazards 77−34001
electrical measuring instruments, new CEI standards *(Italian)* 80−31789
electrical measuring instruments, portable, securing and calibrating, description *(German)* 77−2665

instruments continued
electrode process research, instruments and appls. review 78−21174
electronic industry, Spain measuring equipment choice, criteria *(Spanish)* 78−36963
electronic instrument design, modern circuit technologies impact 77−5861
electronic measurements, book 80−31805
Epstein permeameter, 25 cm, parallel stray mangetic flux compensation *(Polish)* 79−2798
feedback in instruments and its applications 79−21687
ferroelectric film switching transition meas. instrument, operating principle 79−17443
flame ionisation detector measures fluctuating concentrations hydrocarbon gases 77−57312
flatness deviation meas. instrum. with aerostatic basis 79−6083
flue gas measuring, NO_x, calibration and checking 79−53015
History of Sciences Collections, Royal Swedish Academy of Sciences, catalogue 78−81789
indicating measuring instruments, error estimation *(Croatian)* 78−57886
inductometer calibrator, U-738, description 78−74034
innovation and business opportunity in instrument development 80−98909
inspection, optimal erorr correction signal 78−77829
instrument science, introductory article 77−53847
linear mechanism anal., error statistics *(Hungarian)* 78−49823
low-speed motion irregularity meas. equipment, portable 78−54346
magnetic characteristics determination, construction *(Rumanian)* 77−79131
measurement facility inspection, confidence and productivity improvement 78−77840
measuring instruments as tools of knowledge and control, book 80−41968
metrological support in linear accel. meas. 78−45601
operation in adverse environments, conference, London (1976) 78−189
operation speed increase, additive-iterative correction method *(Russian)* 78−89423
performance unified representation *(Japanese)* 78−70090
periodic inspection of meas. facilities, probabilistic confidence characteristic selection 78−77839
plastometer, cone type, for strength props. determ. of plastoviscous disperse systems 80−76426
pneumatic feedback-monitoring, pressure variation effects 80−77743
psychrometer, direct indication, of temp. difference and temp. type *(Japanese)* 79−40581
quality not maintained by frequent calibration, statistical evidence 79−93090
rack and pinion type, indication error reduction *(Polish)* 78−49818
RF signal level measurement, calibration reference 77−115
sieves, Fourier transform method for verification of wire screens 77−53874
sorption and diffusion, low-molecular liqs. meas. in polymer films 79−100305
testing of measuring instruments, determ. of valid interval between tests values 80−57284
thermocouple thermal inertia meas. *(Russian)* 80−62665
thermographic instrument, types 78−86266
undergraduate course, in advanced physical instruments 79−21486
vibration measurement, logarithmic, error estimation *(Russian)* 77−2648
O_2 meter, type 648, mains-free, features *(German)* 78−94858
Zn sulphate electrolyte cathodic-current meas. 78−35707

insulated gate field effect transistors
carrier density and mobility meas. using a long gate MOSFET structure 79−47178
n-channel MOSFET, Si inversion layer, negative differential resistance 78−30996
charge pumping effect, applic. to surface states density determ. 77−69421
dopant profile determ. from enhancement mode DC meas. 78−30987
dosimetric properties *(Czech)* 77−86636
effective mass and collision time of (100) Si surface electrons, oscillatory magnetoconductance meas. 78−34909
electrolyte double layer potential change meas., transistor method 77−85298
electrometer, current noise meas. 78−54398
electron and hole drift vels. in high elec. field, Monte Carlo calc. 78−60224
field effect potentiometric sensor for biomedical appl. 78−44644
galvanomagnetic props., theory and expt. *(German)* 77−76926
high energy electron irrad. effects on MOST, 15-35 MeV 78−34907
high temperature MOSFET characteristics for geothermal instrumentation, up to 300°C 78−73553
hole mobility determ. in high resist. diffusion layers in Si 77−66204
hot electron emission from Si into SiO_2 78−30997
hot electron emission into gate insulator, threshold instabilities 77−32084
integrated micro multi-ion sensor using IGFET 78−40439
interface and bulk-trap states, determ. using deep level transient spectroscopy 77−8199
inversion layer, two-dimens. semicond., Gunn instability 78−84305
inversion layers, (100) and (911), IR photocond. and absorption 78−64123
inversion layers, near threshold at low temps., cond. anomalies and electronic states 77−59333
inverted MOSFET surface, evidence for Lande factor g=2, finite valley splitting 80−6989
inverted MOSFET surfaces, quantum oscills., valley splitting, lineshape in state density effects 79−56318
ion implanted, spatial position of deep levels near Si-SiO_2 interface 77−12008
ion implanted MOSFET, surface charact. of Si-SiO_2 struct. 77−80850
ion selective electrochemical electrode with MOSFET 79−34411
ion sensitive, appl. of semiconductor interface system *(French)* 80−6935
ion sensitive FET, ion selectivity and temp. depend. 79−34409
ion sensitive FET's development review, biological applications *(French)* 77−70578
ion sensitive FET micro pH sensor, for biomedical appl. 78−44643
ion-selective, microcircuit prod. technique 77−16872

insulated gate field effect transistors continued
IR sensing, Si:In(Ga) MOSFET, characts. 3 to 5 and 8 to 14 μm 77−74503
Josephson FET, hybrid, feasibility 80−80451
MAOS memory element, stored charge volatility 78−52100
MIS, mobility in inversion channel calc. *(German)* 80−6996
MNOS, degradation, rel. to negative bias stress of MOS devices at high elec. field 77−62996
MNOS, dharge distribs. in Si_3N_4 film exam. 79−38184
MNOS devices, switching characts. at low fields 79−56311
MNOS p-channel transistor, memory characts., H_2 anneal effects 80−80388
MNOS structures, charge pumping investigations 77−43729
MNOS transistors, p-channel, transport processes of electrons 80−34523
MNSFET, thermally grown Si_3N_4 films for high performance devices 78−48322
MOS, defect spatial distrib. in Si, transient capacitance meas. 77−11973
MOS, defects, SEM 79−23507
MOS, dosimeter appl., response functions obs. *(Czech)* 79−49874
MOS, n-channel, Hall meas. on trap states at 77K 80−44732
MOS, n-type inverted surface channel, reproducibility of electronic props. 79−99628
MOS, Si, voltage tunable far IR emission from inversion layers 77−12440
MOS, surface states, density and capture cross section determ. *(German)* 78−23173
MOS, unwanted effects of ions in SiO_2 layers on Si, review 80−92985
MOS dopant profile, DC method 80−70244
MOS electron inversion layers, temp. depend. of subthreshold currents 79−73596
MOS field-effect devices, mag. quantisation effect on surface capacitance 80−70834
MOS inversion layers, negative magnetoresist. 80−49922
MOS phototransistor with Si-SiO_2 systems, spectral characts. *(Russian)* 79−42657
MOS struct. with nonuniformly doped semiconductors, depletion approx. anal. of differential C-V characts. 79−99625
MOSFET, conductance oscills., source-drain limited cond. 80−20316
MOSFET, fabricated on MBE Si layer. 79−78179
MOSFET, far IR emission on high index surfaces 78−48232
MOSFET, flicker noise theory 80−11100
MOSFET, ionic scatt. effect on Shubnikov-de Haas amplitudes in Si inversion layers 79−42653
MOSFET, method to determine effective channel length 79−69601
MOSFET, n-channel, Si ⟨100⟩, Shubnikov-de Haas oscills. on mag. fields up to 35 T 79−91154
MOSFET, n-channel voltage-tunable far IR emission 80−25018
MOSFET, n-Si inversion layers, electronic g-factor, spin-split Landau levels 80−80346
MOSFET, n-Si inversion layers, resist. temp. depend. at liq. He temps. 80−80391
MOSFET, near-ideal Si-SiO_2 interfaces using CVD, props. 80−80382
MOSFET, negative magnetoresistance, 2-D random system 80−70728
MOSFET, p-channel, anal. of surface states on semiconduc.-dielectric interface 79−42648
MOSFET, periodic stepped struct. on vicinal planes of Si (100) 80−24725
MOSFET, recomb. lifetime determ. 80−62683
MOSFET, Si-SiO_2 inversion layer carrier mobility, theory 80−60094
MOSFET, surface quantum states, two-dimensionality of many-body effects 80−103740
MOSFET, surface states at GaAs-oxide interface, modified DLTS meas. 80−11094
MOSFET, two-dimens. electron gas, determ. of fine struct. const. based on quantised Hall resist. 80−96997
MOSFET impedance transforming stage in C film bolometer detection system with <0.1 μs response time 79−63226
MOSFET inversion layer, localised highly correl. phase cond. 79−33354
MOSFET research in high mag. fields 80−13110
MOSFET structure for characterising impurity centres in Si:In 79−73595
MOSFET structures, photocond. rel. to intersubband transitions 78−64127
MOSFETs, short channel, fabrication by ion implantation and laser annealing 80−20312
MOSFETs, Shubnikov-de Haas oscills. from electron irrad. induced two-dimens. leakage channel 79−19671
MOST, comparison of Shubnikov-de Haas effect and cyclotron reson. under uniaxial stress 80−20320
MOST, high freq. props., channel behaviour *(French)* 79−78196
MOST, sensitivity to γ-radiation 79−67966
MOST, short channel, carrier saturation velocity, temperature effect *(French)* 80−70837
MOST, short channel, output conductance, effect of ionising radiation 80−70836
MOST, short channel, output impedance, thermal feedback effects *(French)* 80−15609
MOST, threshold voltage shift, influence of ion implantation parameters 79−69598
MOST channels, quasi-Fermi level gradient distrib., Hall voltage 80−29481
MOST structure modelling, using hybrid computer, Poisson partial differential equation solution *(Slovak)* 80−75643
MOST structures with process-induced defects, elec. props. 80−54788
MOST-transistor struct., breakdown-initiated negative resist. device 80−20314
NMOS VLSI circuits manufacture process and problems *(Norwegian)* 80−60090
p-channel MOST, quantum galvanomagnetic effects in p-type accumulation channels 78−64134
photocurrent spectral response, bias depend. 77−69422
phototransistor, current-illumination and spectral characts., 0.22 to 2.5 μm *(Russian)* 77−35996
piezoresistivity effects, use as press. transducer 80−4695
quasi-saturation mechanism associated with low doping level in drain region *(French)* 80−107920
radiation dose measurement using radiation induced changes *(Japanese)* 78−78504
radiation-induced positive charge, thermal annealing 80−75648
reference ion sensitive FET for compensation, biomedical appl. 78−44642
insulated gate field effect transistors continued
resistive gate, velocity-field curves for surface-free carrier in Si 80−60095
semiconductor transport simulation using coupled and decoupled soln. techniques 80−65695
SOS, cryst. perfection rel. to MOS transistor mobility 78−75956
submicron MOST fabrication, influence of lateral diffusion of B in polycryst. Si 78−26588
subthreshold range under illumination 79−69599
surface depletion and inversion, arbitrary doping profile, theory 80−107912
surface states, spin orbit interaction and many-body effect 78−64132
two-dimensional electron gas, influence of one-dimensional superlattice magnetoconductance and DC cond. meas. 77−43683
two-dimensional impurity bands, carrier-density dependence of activation energies associated with hopping 80−88561
V-groove multichannel power MOST, non-pinched off regime, elec. props. *(French)* 78−23174
VMOS transistors used to give linear thermal response characts. 79−9216
$AlGe_3N_3$-GaAs structures and MISFETs based on them 79−60932
Au doped MOS transistors, Au surface-state energy levels 80−11092
BN insulated gate, fabrication and characts. 77−20459
$BaTiO_3/SiO_2$ charge storage memory films for IGFETs 80−11566
GaAs for MOSFETs, native oxides, annealing effects and inversion layer mobilities 78−6452
GaAs, MIS structures, dielec. and interfacial characts. appl. to microwave MISFETs 79−60933
GaAs MOSFET, fabrication using thermal oxidation technique 80−11808
GaAs, ohmic contact formation with thin film 77−8756
GaAs-Al_2O_3 MIS struct., interface props. and MISFET fabrication 79−65557
GaAs-native oxide interface, electronic props. 79−73590
Ge IGFET cryogenic temp. operation 79−69604
Ge, MIS transistor, MIS struct., electrophysical characts. 79−82680
InP inversion-type MISFET with SiO_2 gate insulation interface props., elec. drift 80−93002
InP, MIS structures, dielec. and interfacial characts. appl. to microwave MISFETs 79−60933
InP-Al_2O_3 MIS struct., interface props. and MISFET fabrication 79−65557
InP-$Si_3N_4(SiO_2)$, interface props., plasma deposited dielectrics, n-channel MOSFET action 80−93003
InSb MOSFET fabrication with ion implanted source and drain regions, CCD chip appls. 77−89833
n-Si, (111) inversion layers, valley splitting, Shubnikov de Haas oscills. 80−65698
Pd gate, fabrication and elec. characts. for H_2 detection applic. *(French)* 78−2569
Pd gate MOS, to monitor H_2, H_2S and NH_3 78−44645
n-Si channel ⟨100⟩ inversion layer MOSFET, valley splitting, conductivity 80−70840
Si deep level determ. using deep depletion MOSFET test structure 78−10571
Si, inversion layers, nonmetallic cond. at low temp. 80−70833
Si, inversion layers, submillimeter cyclotron reson. at low electron density 79−60925
Si, lattice scattering mechanism in quantised inversion layers 79−78187
p-Si MOSFET, intersubband reson. photoresponse, mechanism 79−82677
Si MOSFET, n-type inverted, surface, mag. field depend. of valley splitting 79−19650
Si, n-type inverted MOSFET (100) surfaces, quantitative determ. of valley splitting 79−51678
Si:H, amorphous, density of states determ. using field effect 80−49937
Si-SiO_2 (111) interfaces, sixfold valley degeneracy in electron inversion layers 80−49936
Si-SiO_2 interface, elec. props. and influence on service performance and stability 78−23171
Si-SiO_2 interface, inversion layer transport, radiation hardness effects, review 79−19673
Si-SiO_2 interface in IGFETs, anal. of CVD SiO_2 on (100) and (111) surfaces, near-ideal structs. 80−100528
Si-SiO_2 structures, scanning analyser of electrophysical parameters *(Polish)* 79−91145
SiO_2, in IGFET struct., thermal reemission of trapped electrons 79−42650
SiO_2 irradiated film, electron and hole trapping 80−11098
SiO_2 layer used for MOSFETs, electron trapping behaviour 80−92981
SiO_2 thin films, radiation-induced trapping centres, rel. to MOS transistor technology 80−107804
TiO_2/SiO_2 charge storage memory films fo IGFETs 80−11566

insulated wires
absorbed dose for electron irradiation for polymeric part of electrical wire 79−46708
corona impulse energy spectrum under high AC voltages 78−71621
insulating and sheath materials for wire and cable, crosslinking by irradiation 80−66845
polyolefin, cross-linked, insulation system for wire and cable for locomotives 80−66851
polyolefin, cross-linked, irradiation appl. to provide improved insulation props. to wires and cables 80−66850
PVC, cross-linked, irradiation appl. to provide improved insulation props. to wires and cables 80−66850
PVC materials, cross-linkable, for wires and cable insulation 80−66849

insulating coatings
see also varnish; waxes
anode, surface and excess vol. charge meas. in presence of flare discharge 77−11426
barium aluminosilicate glass coating on NbZr, d and He ion irrad., blistering 77−35605
formvar coating on composite superconductors, cryostatic influence 79−61633
glazed ceramic insulators, surface quality monitoring 79−61813
multilayer coating, radiation breakdown and microscopic inhomogeneities 80−7294
oxide films, passivating, transient growth kinetics 80−93672
pipes, flow of gas-solid suspensions, electrification 77−77811

insulating coatings continued
polymer electrophoretic coating, effect of silicone additive on electrophys. props. *(Russian)* 79−15615
rare earth aluminate, scandate and zironate film coatings, electrophys. props. w.r.t. prep. technology 80−60781
semitransparent filled polymer coating, thermal radn. characts. 77−35731
space shuttle, combined load testing at 1100°C 79−34261
space-shuttle thermal-protection coating, testing techniques at 870°C 78−35604
steel, transforms CC types M6 and M3N, elastoplastic bending, insulating coating influence on magnetic losses *(Russian)* 79−100284
thermoregulative coatings, radiation effects on reflectivity, space vehicle appl. *(Russian)* 78−76542
Al_2O_3, sputtered insulating film contouring over substrate topography 77−8752
Fe-Si, grain oriented, phosphate coating anal. by IR spectroscopy 80−89570
Fe-Si, grain-oriented, surface coating effect on transverse magnetostriction 77−66402
Fe-Si (3 wt.%) cores with insulative coatings, morphological and struct. SEM characteris. 78−23881
$MgAl_2O_4$-Al_2O_3 powder prep., for plasma arc spraying, coating props. 77−66612
MgO-based, effect on domain struct. in grain oriented Fe-Si sheet, high voltage SEM obs. 77−1565
Si_3N_4, sputtered insulating film contouring over substrate topography 77−8752
SiO_2, sputtered insulator film contouring over substrate topography 77−8752

insulating materials
see also asbestos; ceramics; composite insulating materials; dielectric materials; glass; insulating thin films; mica; organic insulating materials; thermal insulating materials
air, predischarge-stabilised breakdown voltage *(German)* 78−63608
capacitors, power, dielectric liquids flammability and degradation 80−88944
ceramics, granular, electrophysical props. depend. on porosity, temp., solid-phase props. 77−69764
cordierite electroceramic, thermal expansion coeff. meas., 80-300K 79−60526
corona discharge, ageing process, expt. 77−43095
current runaway, impact ionisation and recomb. effects 77−4601
direct scanning electron microscope viewing without charging, modification to Cambridge SEM 80−47150
electric field numerical soln. *(Slovak)* 78−66710
electrical properties, three-terminal cell for investigating the elec. props. of insulating materials over wide freq. and temp. ranges 80−37053
ESCA, X-ray type, C 1s contaminant buildup on conductors and insulators 78−95981
ferric solution ferromagnetic liquid insulation in redox flow battery, quantum parameters separation 80−61338
fibreglass insulating materials, radiative heat transfer rel. to optical props. 80−100367
gaseous, electric potential meas. by corona probe 80−82790
glass, temp. depend. of elec. resist. determ., expt. *(Croatian)* 77−74426
growth of insulating crystals, mechs., practical techniques, review 77−69975
high energy radiation effects 80−19835
inorganic polymers, viscoelastic materials, physical props. *(Japanese)* 77−72569
intense electric fields, tree-shaped phenomena in solid insulating materials *(Rumanian)* 80−63885
ion-induced kinetic electron ejection, pot. emission, semiconductors and insulators, review 77−44109
KER 110 hard porcelain corrosion in conditions of practical use *(German)* 79−100270
mullite-corundum electroceramic, thermal expansion coeff. meas., 80-300K 79−60526
porcelain, charge carrier prod. by degradation in SF_6 80−7707
pretinax, temp. depend. of elec. resist. determ., expt. *(Croatian)* 77−74426
semi-insulating material, elec. stressed, storage of charge caused by cond. gradient 80−25306
SF_6 compressed, breakdown threshold, surface roughness and pressure effects 78−75449
shirasu volcanic-ash ceramics, sintered and bloated, props. and appls. *(Japanese)* 77−73252
steatite electroceramic, thermal expansion coeff. meas., 80-300K 79−60526
surface analysis using ion microprobe analyser 77−16887
surface arc discharge effects and arc resist. 79−37563
synthetic, dielec. strength correl. with other parameters, expt. 77−43933
textile insulating tapes, tensile strength, low temp. testing, −196 to +20°C 79−61692
Al_2O_3 based electroceramic, thermal expansion coeff. meas., 80-300K 79−60526
Al_2O_3, insulator, electrical puncture strength at high temps. *(German)* 79−70175
Al_2O_3 porcelain for high voltage insulators, increased mech. strength 78−11269
BN, high temp. compatibility with insulating oxides 77−24995
CO_2, electric breakdown, Paschen curves *(French, English)* 77−76221
H_2, electric breakdown, Paschen curves *(French, English)* 77−76221
H_2+SF_6 mixture, equilib. composition and transport props., 300 to 15000K 77−24051
He, electric breakdown, Paschen curves *(French, English)* 77−76221
SF_6 arcs in axial flow at const. press., steady-state characts. 78−1940
SF_6 avalanche breakdown as stochastic process 78−67574
SF_6 breakdown distributions, low-value fractile determ. 78−67578
SF_6 breakdown field strength, electrode surface roughness tolerance 78−67577
SF_6 breakdown mechanisms, review 78−59699
SF_6 coaxial gap breakdown probability determ., influence of meas. procedure 78−67579
SF_6, compressed, ion mobility and recombination 79−60098
SF_6, compressed, low probability first breakdown voltage determ. 80−38787
SF_6 dielectric strength, conductor surface irregularities influence 80−14946

insulating materials continued
SF_6, elec. discharges, expt. *(German)* 79−10726
SF_6 electric strength, electrode surface roughness effects *(German)* 78−63609
SF_6 electric strength as statistical charact. *(Russian)* 79−41787
SF_6, electrical conductivity calc., 2000 to 50000K 79−14512
SF_6, equilib. composition and transport props., 300 to 15000K 77−24051
SF_6, equilibrium composition calc., in 20000 to 50000K range, in dependence on pressure 79−14511
SF_6, gas chromatography in design of switching installations and devices *(German)* 78−88668
SF_6 high-temp. electrical breakdown parameters 78−67567
SF_6, impulse breakdown, polarity effect, thin dielectric coating influence 80−38773
SF_6 impulse breakdown characteristics for nonuniform field gaps for switchgear design 80−84024
SF_6 insulation breakdown characts. under operating conditions in HV apparatus 80−96414
SF_6, partial discharge overvoltage dependence 77−76243
SF_6 positive-point corona phenomena, breakdown voltage/press. characts. 80−38859
SF_6, predischarge-stabilised breakdown voltage *(German)* 78−63608
SF_6 rod-to-plate corona discharge characteristic obs. 78−67584
SF_6 with gaseous contaminants, arc decomposition kinetics investigation by combined gas chromatograph-mass spectrometry methods 80−92250
SF_6/N_2 mixtures, positive-point corona phenomena breakdown voltage/press. characts. 80−38859
SF_6/N_2 pressurized mixtures, electric breakdown investigation 80−14877
SF_6-gas mixtures electric breakdown 79−37438
SF_6-N_2 mixture, discharge inception voltages, calc. 79−68966
SF_6-N_2 mixture in rod-plane gaps, static field breakdown 79−68965
SiO_2 based materials, degradation due to SF_6 gas dissociation products formed by arc discharges 80−44005
SiO_2 fabric, prep. from E-glass, structural stability rel. to brittleness, X-ray diffr. and IR spectrosc. studies 80−96634

insulating materials, acoustic *see noise abatement*

insulating materials, thermal *see thermal insulating materials*

insulating oils
breakdown in long gaps, impurity effects 79−91359
cable oil, EHD pumping 78−87414
co-field motion, effect of dissolved gases, organic additives and field configuration 79−37407
composition, physical and chemical props. and determ. of free radicals *(Rumanian)* 80−97745
dimethyl silicone oil, laser-induced breakdown mechanism *(Japanese)* 77−43935
electric breakdown at solid-liquid interface with EHD motion, expt. 77−76226
electric breakdown mechanism, high speed photography expts. 79−91367
electric strength for switching surges and long flash-over distances, expt. *(Czech)* 78−56427
film transient heat exchange in transverse electric field *(Russian)* 79−94607
high field conduction and breakdown in dielectric liquids, anal. 77−8506
laser-induced breakdown, threshold fields 79−91363
liquid dielectrics, thermal performance estimation 80−88582
mineral oil, apparent zero-gap breakdown voltage, surface oxide film effects 77−28519
mineral oil, breakdown voltage, live electrode polarity depend. for non-uniform field 78−75450
mineral oil, electrical breakdown under uniform fields 77−80387
mineral oil in large gaps, electric strength study 79−38452
oil immersed transformers, dissolved gas causes and phenomena, anal. *(German)* 80−76570
polybutene oil, direct voltage elec. strength 79−91360
power transformer operating state determination by chromatography anal. of gases *(Czech)* 79−87894
power transformers, fault diagnosis, dissolved gas analysis of insulating oils 80−26097
Senftleben effect, under uniform DC elec. stress 77−31395
silicon fluids, positive discharge propag., rel. to transformer oil 80−88926
silicon oil, behaviour under HV stress 79−91368
silicone fluid, discharge propag. 79−91362
silicone oil, props. determ. by harmonical shear vibr. *(German)* 78−67164
transform oil, polarity effect on breakdown voltage in inhomogeneous field 77−52018
transformer, diagnosis by chromatographic analysis, computerised evaluation of results *(Czech)* 80−97744
transformer, oil ion mobility and fluid motion, effect of additives and dissolved gases 78−47543
transformer oil, nondestructive acoustic elec. field probe meas. 80−47076
transformer oil, optical obs. of pre-breakdown and breakdown 77−80386
transformer oil, positive discharge propag., rel. to silicone fluids 80−88926
transformer oil electrohydrodynamic flow, jet dynamic pressure obs. *(Russian)* 80−59117
transformer oils, under 60 Hz stress elec. stress induced motion 79−90346
white mineral oil, electronic processes in elec. breakdown, streamer growth 77−89333

insulating thin films
see also dielectric thin films; electronic conduction in insulating thin films
alumina, anodic, dielec. breakdown 77−1637
anodic oxide film, ionic cond. determ., open-circuit transient method, rel. to other techniques 80−24650
Auger depth profiling by angle lapping 78−53287
Auger line shape changes effect on depth profiles, correction 77−40605
barium stearate, in MIM struct., thickness depend. of internal voltage 77−72920
barium stearate in MIM struct., diode characts. obs. 77−4449
breakdown strength, statistical analysis 78−2603
cadmium stearate based Langmuir films, deposition on p-CdTe, characts. and MIS struct. 80−92998
carbonaceous film, deposition on RF target in butane plasma 77−16507
carbonaceous film, hard, phys. props. 77−39752
carbonaceous films, RF diode sputtering growth, IR absorpt. and Rutherford backscatt. meas. 79−99458

insulating thin films continued
charge migration kinetics, MIM struct. nonstationary VI charact. anal. 77−76943
chemical shift meas. by ESCA *(Japanese)* 79−4891
chlorophyll a film, charge injection and storage 78−53317
corona charged insulating film high-field conduction and breakdown 80−15975
CVD, low press. techniques, IC fabrication process anal. 79−100058
deposition techniques, on semiconductor devices, review 78−23611
depth profiling, line shape changes correction 77−40605
disordered, electronic energy spectrum calcs. extended Halpern Green's function technique 80−20066
effective electron mass determ. 77−1506
electric charging by X-radiation *(Japanese)* 79−61488
electrical breakdown by impact ionisation, models 79−91373
electrical breakdown mechanisms 78−76385
ellipsometric monitoring on semiconducting substrate 79−49272
fatty acid monolayers, electron tunnelling 77−69428
fluorocarbon foil, Ftoroplast, homogeneity study *(Polish)* 80−35278
gelatin, in MIS struct., C-V charact., irrad. effects *(Russian)* 77−51823
glassy passivation films on Si substrates, appl. of silicates to flaw detection 77−39745
guided optical waves for refr. index and thickness determ. 78−74049
hexamethyldisiloxane plasma polymerised thin film, charge trapping charact. 80−96895
homogeneity during growth, determ. using vacuum automatic ellipsometer 80−101825
hot electron energy distribs., Monte Carlo study 77−51832
impact ionisation, models for current runaway 78−6630
inorganic, plasma deposition review 80−50564
instability phenomena in films on Si, review 77−12037
IR surface wave selective absorpt. of film on metal substrate *(Russian)* 77−1754
multilayer structure of semiconductor, dielectric and mag. film, constant EMF 79−69583
multiple insulating layers on GaAs, Auger exam. 79−83345
organic films, electronics and communications engineering appls. *(German)* 78−44011
organic photoconductor, electric field-induced fluoresc. quenching 80−34967
oxide, on electrode, effect on apparent zero-gap breakdown voltage in mineral oil 77−28519
oxide film, thermal and anodic, space charge effects on steady-state transport 80−11124
oxide film on metal electrode, nonadiabatic theory of electron transfer 77−28237
oxide films, As doped, thermal stress effects on roughening 79−23813
[p-]quinquaphenyl film between metal electrodes, memory switching 80−2484
paracyanogenlike films, deposition by C reactive RF sputtering in N_2 79−78886
pentacene films, luminesc., struct. 80−11461
PET, charge effects at Al electrodes obs. 80−75625
phosphosilicate glass, growth on contaminated Si wafer, Au redistrib. during growth 77−4121
phosphosilicate glass, on Si or Al, corrosion in high temp. water and moisture 77−48564
polarisation dispersion charact. meas. under high DC elec. fields *(Japanese)* 77−63013
poly(p-xylylene), electron MFP as function of kinetic energy, XPS 78−52114
polyacetonitrile in MIM capacitor, electroforming, negative resist., electron emission 80−80406
6-polyamide, cond. and relax. under very high press. 77−35748
polyethylene:$Br_2(I_2)$, films, electron-beam induced carrier mobility and elec. breakdown 80−80429
polyethylene, elongated, elec. impulse breakdown strength temp. depend., 20 to 80°C 77−73113
polyethylene, elongated low density film, TSC 79−47106
polyethylene terephthalate, between metal electrodes, electrochem. effects as source of EMF 78−72278
polyethylene terephthalate, lateral motion of charge 78−43458
polyferrocene film, plasma polymerised, dielec. props., 40 kHz to 50 MHz, 30-400°C 78−52439
polyimide, dielectric breakdown in high-temperature region 78−84522
polyimide film, thermally stimulated depolarization anal. 79−69766
polyimide thin film vacuum deposition 78−39695
polymer, viscoelastic props., capacitance change meas. *(Japanese)* 78−23752
polystyrene:$Br_2(I_2)$, films, electron-beam induced carrier mobility and elec. breakdown 80−80429
polytetrahydrofuran in MIM capacitor electroforming, negative resist., electron emission 80−80406
powders, SAW interactions, for various directions of propagation 80−49486
preparation and properties, for semicond. devices, conf., Boston, MA, USA (Nov. 77) 78−23610
properties, rel. to deposition conditions, appl. in semicond. devices 78−23612
PTFE film, reactive sputtering in Ar-CF_4 mixture, MSCA 78−92191
PTFE films, sputtering conditions effect on comp. and optical props. 79−52115
quartz microcrack growth, electron microscope obs. 77−69037
rare earth aluminate, scandate and zironate film coatings, electrophys. props. w.r.t. prep. technology 80−60781
rare earth oxide films, non-stoichiometric phases 79−7755
rare earth oxides, in MOS struct., elec. props. and band struct. 80−7013
SCL currents, effects of finite contact energy barriers and traps 79−38209
self-drifting of ionic charges, detection by surface potential decay method 78−72295
silane layers, reactive ion etching and Auger electron spectra 79−24394
silicone, film deposition, glow discharge polymerisation, elec. and thermal charact. 78−6467
soft magnetic mat. prep. by precip. of insulating film on Fe powder in polishing bath 78−23637
Teflon, negatively corona charged, new model of isothermal charge transport 80−34536
tetracene, polycrystalline, charge carrier drift mobility 78−34835

insulating thin films continued
thermal conductivity normal to layer, meas. method, error anal. 78−90682
thickness meas. by IR refl. spectroscopy *(German)* 79−58671
thickness measurements determ. using ellipsometer with nonmonochromatic source *(Russian)* 78−51862
trap analysis, influence of spatial trap distrib. on SCLC charact. 79−56343
TSEE from insulating layers, Monte Carlo method simulation *(German)* 80−2932
vinyl chloride-vinyl acetate copolymer film between metal electrodes, depolarisation current studies 80−2691
VLSI multilayer metallisation interlayer dielectrics, CVD films 80−45235
Young's modulus measurement by micromechanics 80−33548
AgBr, surface space charge region 77−1508
AgBr, thin epitaxial layer, surface ionic cond., lattice disorder, space charge region 77−11730
Al-Al_2O_3-Al junctions, Dy doped at Al_2O_3-Al interface, electron transport mechanisms and barrier height 78−91778
Al-SiO_2-Si structure, photocurrents, 1.4 to 3.1 eV 79−65514
AlF_3, RF sputtered, dielec. props. meas. 77−36173
AlN, chemical and plasmachem. vapour deposition, optical and other props. 77−28727
AlN film, Si doping by DC glow discharge 78−19674
AlN-Si_3N_4 CVD film preparation and props. 77−77408
AlO_x, obtained by oxidation of Al magnetron sputtering target in Ar/O_2 mixtures 80−55291
Al_2O_3, amorphous anodic film, struct. anal. 79−51452
Al_2O_3, amorphous film, non-thermal switching in Al-Al_2O_3-Al struct. *(Russian)* 78−80069
Al_2O_3 amorphous films, struct., electron diffr. investigation 80−20046
Al_2O_3 amorphous layers in MIS structures, prep. and physical props. *(Slovak)* 78−64122
Al_2O_3, anodic, luminesc. during growth on high purity Al 77−48589
Al_2O_3 anodic film, gas emission, mass spectrometer study *(Polish)* 77−9157
Al_2O_3, anodic film, trapped O_2 and effect on dielec. stability 80−100634
Al_2O_3 anodic films, H conc. profiles meas. 80−75261
Al_2O_3 anodic films, trapping levels study using TSC 80−103768
Al_2O_3, CVD film on III-V semicond. substrate, ion beam etching, defect detection 80−89155
Al_2O_3, CVD on Si, chem., phys. and elec. props. 77−12543
Al_2O_3, composite film, barrier layer, ellipsometric meas. 78−67918
Al_2O_3 composite film props., form. by water reaction and anodic oxidation 78−15606
Al_2O_3, DC reactively sputtered, in MIS structs., effects of annealing on C-V charact. 77−51822
Al_2O_3, elec. breakdown during anodic growth 80−55034
Al_2O_3 electrical breakdown by impact ionisation, models compared with expt. 79−91373
Al_2O_3, electron beam deposition, heating of multiple layer structs. *(Russian)* 78−92192
Al_2O_3, electron trapping due to neutron irradiation 80−2505
γ-Al_2O_3, enhanced activated reactive evaporation process, ion effect 79−66013
Al_2O_3 film, Al embedded, non-ohmic conduction behaviour 78−64157
Al_2O_3 film, MBE-growth on GaAs, MOS GaAs capacitor appl. 79−77943
Al_2O_3 film growth on MBE GaAs 78−39706
Al_2O_3 films, DC reactive sputtering prep., IR spectra characterization 79−11513
Al_2O_3, films, form., cross-sections, struct. obs. 78−67917
Al_2O_3 films obtained by pyrolysis of Al acetylacetonate, struct. and props. 77−85098
Al_2O_3, films on Al, photoacoustic refl.-absorption spectroscopy 78−31264
Al_2O_3, growth by anodisation of sintered Al, and elec props. 79−95964
Al_2O_3 layer prep. by reduction by carbon in vacuum 77−8757
Al_2O_3, MOS gate insulator, photoconductive processes 77−8216
Al_2O_3, metal layer interdiffusion, Rutherford backscatt. 77−85000
Al_2O_3, noncrystalline films, opt. and elec. props. 77−51627
Al_2O_3 on Al, anodic oxide film, effect of interface roughness on cracking 78−76755
Al_2O_3, on Al, IR refl. obs. 78−35591
Al_2O_3, on Au layer, stopping power and energy straggling meas., Li ion backscatt. anal. 79−3328
Al_2O_3, on GaAs, prep. and surface states 77−85336
Al_2O_3, on Si, dissolution and corrosion in high temp. water and moisture 77−48564
Al_2O_3 plasma anodised films, dielec. props. and high-field cond. *(Japanese)* 78−23185
Al_2O_3, polycryst., on Si, anodisation, MAOS struct. form. and elec. props. 77−48563
Al_2O_3, RF sputtered by planar magnetron, phys. props. 77−43448
Al_2O_3, RF sputtered film, transient current meas. 78−52113
Al_2O_3, self-drifting of ionic charges, detection by surface potential decay method 78−72295
Al_2O_3, thermoluminesc., in H_2O vap. atm., temp. depend., time decay *(Russian)* 77−44074
Al_2O_3, thick vacuum condensates, electron microscopy struct. investig. *(Russian)* 78−95242
Al_2O_3 thin anodised film conduction and internal field obs. 80−15639
Al_2O_3 thin film used in inelastic electron tunnelling spectroscopy, X-ray photoelectron spectrum 80−108319
Al_2O_3-Si MIS struct., fabrication from UV irradiation converted organometallic cpds. *(Russian)* 80−45245
BN on Si substrate, elec. charact. of BN-Si interface, expt. 77−20459
BN, prep. and I-V charact. of Al-BN-Au device *(Japanese)* 77−73230
BaO, film, emission props. in relation to struct. 80−100501
BaO, film, initial struct., field electron emission microscopy and LEED determ. 79−11033
BaO thin films, on (110) face of W, struct. study by LEED 79−60659
$BaTiO_3$ on Si substrate, prep. and elec. props., expt. 77−20460
BeO, film, TSEE, low energy electron impact excitation 77−12505
BeO reactively evaporated film, elec. and optical props. 77−32512
$Bi_{12}GeO_{20}$ vacuum-deposited film elec. and photoelec. props. *(Russian)* 78−60237
$Bi_{12}GeO_{20}$ wide-zone dielectric injection contact characteristics *(Russian)* 78−60236
Bi_2O_3, anodic film, dielec. props. 77−20794

insulating thin films continued
Bi_2O_3 anodic films, struct. and electronic props., photoeffects 80−44749
Bi_2O_3, thin film capacitor elec. props. under reduced press. 80−80397
$Bi_4Ti_3O_{12}$, coaxial magnetron sputtering technique 79−83123
C, amorphous, growth under ion impact in butane plasma, and IR transparency 78−52688
C, film with random struct. growth from ion impact damage in butane plasma 79−83139
C, films, hard and transparent, prep. by condensation of ionised organic species 79−83132
CaF_2 thin films, initial ionic thermocurrent meas. 80−97018
CaF_2, thin insulating film, lattice parameter meas. by electron microscope 77−65940
CeO_2:Y_2O_3, bias sputtering, film growth and charact. 77−40366
CoO film on thermally aged Co hardened Au, mech. film breakdown and ESCA, expt. 77−4436
CsCl, kinetic electron emission when penetrated by H^+ ions with 0.3 to 30 keV energy 79−91554
Cu-Cu_xO film, numerical anal. of normal reflect. data 79−99457
Cu_2O films arc cathode emission study 78−23583
Cu_xO, film, thermoelec. power, activation energy variation with electrode spacing in DC sputtering 78−76099
Eu_xO_y film, dielec. props. rel. to annealing 79−99636
Fe_2O_3 thin films, reactively sputtered, mechanical stresses rel. to deposition conditions 80−80146
Fe_xO_y, prep. by reactive sputtering, struct. and props. *(Japanese)* 78−92190
$Ga_{0.64}Al_{0.36}As$, plasma grown oxide, phys. and elec. props. 78−48550
GaAs anodic oxide, electrical props. 79−38170
GaAs anodic oxide, leakage currents 79−38169
GaAs anodic oxide, refl. and transmission, 0.01-6 eV 78−95613
GaAs anodic oxide, self drifting of ionic charges, detection by surface potential decay method 78−72295
GaAs, anodic oxide film, annealing effect on carrier density profile 78−88040
GaAs anodic oxide film, ellipsometric and IR spectroscopic studies 80−11493
GaAs anodic oxide film growth obs. by in situ differential refl. 80−50732
GaAs film plasma oxidation process 77−77614
GaAs oxide, anodic, evidence for growth-induced damage from photolum. expts. 78−75953
GaAs oxide, anodic, optical props., 1.5-6.0 eV 77−90209
GaAs oxide, formation by plasma oxidation, and props. 78−95825
GaAs oxide, growth by thermal oxidation, optical obs. and model 77−56120
GaAs oxide, passivated layers, quantitative in-depth profile, AES-SIMS thermal, anodic and plasma oxidations 78−84087
GaAs oxide, plasma grown, anal. by combined ion beam techniques 79−7760
GaAs oxide, thermal and anodic, in-depth profiles, XPS expts. 78−84086
GaAs oxide, thermally grown, elec. props. 78−2601
GaAs oxide film, ellipsometry study 79−69894
GaAs oxide film growth in As_2O_3 vapour, As incorporation 79−77928
GaAs oxide films grown by anodization in electrolytes, electron spectroscopy exam. *(German)* 79−15837
GaAs thermal oxide film, fabrication and characterisation 80−11808
GaN, reactive sputtering, GaAs MIS struct. fabrication and props. 78−39686
Ga_2O_3 film, growth by reactive vapour deposition, optical and elec. props. 77−48347
Ga_2O_3, prep. by anodic oxidation of Ga film on GaAs or Si 77−81338
Ga_2O_3 reactively evaporated, props. *(Japanese)* 79−99648
GaP, anodically grown insulating layers, prep. and props. *(German)* 78−64158
GaP oxide, anodic, optical props., 1.5-6.0 eV 77−90209
GaP oxide films grown by anodization in electrolytes, electron spectroscopy exam. *(German)* 79−15837
$GaPO_4$ film growth on GaP, XPS exam. 78−31552
GaSb oxide, anodic, optical props., 1.5-6.0 eV 77−90209
GaSb oxide films grown by anodization in electrolytes, electron spectroscopy exam. *(German)* 79−15837
Ge_3N_4 films, synthesis and principal props. 77−24960
GeO, supermultilayer dielectric film, elec. strength *(Russian)* 77−85648
GeO_2, film, optical and electrophysical props. *(Russian)* 77−85821
GeO_2, growth from liq. phase for MIS struct. *(Russian)* 80−40273
GeO_2, ultrathin layers on Ge substrate, ATR spectra, thickness depend., struct. obs. 80−55214
HfN, deposition by HfC reactive RF sputtering in N_2 79−78886
HfO_2, CVD growth, struct., elec. and optical prop. characterisation 77−55891
Hg-Xe solid films, optical absorpt., localised states 79−61452
InAs anodic oxide films prep. and props. 80−55553
In_2O_3-P_2O_5, thermal oxide on InP, growth rate and comp. 80−55555
InP anodic oxide, anal. by MeV $^4He^+$ channelling effect meas. and AES 79−4492
InP oxide, MIS diode prep. by anodic oxidation 79−74270
InSb oxide films grown by anodization in electrolytes, electron spectroscopy exam. *(German)* 79−15837
KBr, field enhanced secondary emission, energy spectrum obs. 77−1771
KBr, porous insulator films, field enhanced secondary emission, energy spectrum 77−20969
KCl, field enhanced secondary emission, energy spectrum obs. 77−1771
KCl, porous insulator films, field enhanced emission, energy spectrum 77−20969
LaB_6 film, structure, stoichiometry, elec. properties 78−60043
LiF, thin insulating film, lattice parameter meas. by electron microscope 77−65940
MgO, dissoc. under heat and electron bombardment 80−7834
MgO film, delayed secondary electron emission 78−19617
MgO film, ion induced secondary electron emission 77−44104
MgO, film, low energy electron absorpt., struct. and absorpt. centres 79−7763
MgO thin film, DC conduction 78−88051
MoO_3, film, colour centre studies, optical absorpt. spectra 78−71724
NaCl, thin single-crystal film, hot electron emission 79−15244
NaF, thin insulating film, lattice parameter meas. by electron microscope 77−65940
Nb-Ta-N sputtered films and their anodic oxides, elec. props. of resist. and dielec. films 80−11126

insulating thin films continued
Nb_2O_3 in MIM structure, space charge density *(Russian)* 78−10579
Nb_2O_5, amorphous, in MIM struct., Schottky barrier effects on dielec. props. 77−8203
$NdAlO_3$ films, preparation, electrophys. props. in MIM structs. 77−24956
$Nd_4Al_2O_3$ film, struct. charact., IR spectra 77−48157
NiF_2 film preparation and characterisation 80−59815
Ni_xO, film, thermoelec. power, activation energy variation with electrode spacing in DC sputtering 78−76099
PLZT, coaxial magnetron sputtering techniques 79−83123
P_2O_5-SiO_2 glass film, thickness and IR spectrum changes on heat treatment in H_2 80−70549
PbI_2, thin films, photolysis kinetics 77−36769
$Pb_2Nb_2O_7$, electric cond. and dielect. props. of cathodic-sputtered films *(French)* 79−33371
PbO layers on Pb films, optical props. 79−83042
$Pb_{1.8}Zn_{0.15}Na_{0.05}Nb_2O_{6.95}F_{0.05}$, electric cond. and dielect. props. of cathodic-sputtered films *(French)* 79−33371
RbCl films, breakdown on appl. of electric voltage pulses 80−66109
SF_6, film, IR laser induced processes at low temp. and under ultrahigh vac. 79−69914
S_4N_4, Raman scatt. and opt. absorpt., press. and temp. depend. 77−36227
Si oxide film, porous Si layer oxidation, dielec. props. 80−55556
Si-containing inorganic films, for microelectronics appls., plasma deposition and characterisation 79−78904
Si-N, passivation layer, density comp., and ref. index, Lorentz-Lorenz correl. 78−39697
Si-Si_3N_4-SiO_2-Si multilayer structs., impurity distrib., activation anal., autoradiography techniques 77−16881
Si-SiO_2, SiO_2 layer charging in UV irrad. of MISS struct., photoinjection currents *(Russian)* 80−39680
Si-SiO_2 interface, light induced reson. centres, photocond. reson., EPR obs. 80−50184
Si-SiO_2 interfaces, carrier transport processes, electron states, conference, Durham, England (July 1979) 80−90612
SiC coatings for first-wall candidate materials by RF sputtering 80−25563
SiC, dielectric coating effect on surface polaritons, optical consts. *(Russian)* 80−88489
SiN film, on Si substrate, thermal stresses and cracking resist. 78−63958
SiN_x, film by magnetron sputtering, composition, hardness and optical props. 78−3047
SiN_x film reactive plasma deposition enhancement 77−77405
SiN_x film reactive plasma deposition and characterisation 77−77406
Si_3N_4, amorphous, AES and EELS characterisation 79−90905
Si_3N_4, amorphous, CVD, IR spectra 77−21031
Si_3N_4, amorphous, CVD, core and valence electron excitations, low energy electron loss spectroscopy and AES 80−2365
Si_3N_4 amorphous films, CVD mech. and thermal props. *(Japanese)* 77−90280
Si_3N_4 amorphous films, struct., short-range order, and crystn. kinetics 79−28240
Si_3N_4, CVD, chem. bond nature, Compton scatt. expts. 80−49539
Si_3N_4, CVD, chem. bound H, NH_3/SiH_4 ratio and annealing depend. 77−76680
Si_3N_4, CVD, ion implanted, compressive stress buildup 77−89456
Si_3N_4, CVD, multiple internal refl. IR spectroscopy 80−11499
Si_3N_4, CVD amorphous film, X-ray diffr. 79−87013
Si_3N_4, CVD anal. using hydrodynamics 77−40384
Si_3N_4 CVD film etching in acidic fluoride media 78−7071
Si_3N_4, CVD films, chemically trapped H reflection spectrometry 78−10081
Si_3N_4 CVD films, microstruct. and MNS struct. charact. 79−65339
Si_3N_4 CVD films on Si, dark currents 79−78240
Si_3N_4, CVD from $SiCl_4$ and NH_3, mass spectroscopic anal. of intermediates 79−43149
Si_3N_4, CVD in hot-wall diffusion system 79−19996
Si_3N_4, conditions for thermal current runaway and breakdown 77−43760
Si_3N_4 degradation due to high-temp. processing 78−6454
Si_3N_4, deposited Ga and As concentration measurement by CAMECA probe *(French)* 77−86411
Si_3N_4, deposition by plasma stream transport method, use of charge exchange plasma source 79−15613
Si_3N_4, deposition by pyrolysis of SiH_4-NH_3 mixture, struct. and props. of deposit *(French)* 77−40382
Si_3N_4, deposition by SiC reactive RF sputtering in N_2 79−78886
Si_3N_4 dielectric film on Ge, dislocation interactions 80−39472
Si_3N_4, dielectric films made by NH_3-silane reaction, TEM study 80−84413
Si_3N_4, diffusion of Al, AES and depth profiling 78−51744
Si_3N_4 film, absorpt. meas. 79−78769
Si_3N_4 film, CVD, etching in acidic fluoride media 78−39927
Si_3N_4 film, grown by direct thermal reaction with N_2 78−52665
Si_3N_4, film, H_2 concentration profile, chem. bonding 79−33205
Si_3N_4 film, MNOS device, high temperature annealing, effect on Si_3N_4 stress, interface charge density and memory props. 79−87158
Si_3N_4 film, on Si substrate, thermal stresses and cracking resist. 78−63958
Si_3N_4 film, on W-coated Si, photocond., 1.31-3.10 eV, mechanism 79−19679
Si_3N_4 film, thermal oxidation rate and masking effect against Si oxidation 78−64749
Si_3N_4 film deposited from SiH_2Cl_2 and NH_3, characterisation 79−11521
Si_3N_4, film edge induced stress in Si substrate 78−30839
Si_3N_4 film formation by $^{14}N_2^+$ ion implantation into Si 79−99455
Si_3N_4, film growth by reaction of NH_3 with Si (111) surface 79−100441
Si_3N_4 film in MNOS memory struct., distrib. and role of N-H and Si-H bonds 79−33358
Si_3N_4 film on Si substrate, dislocation generation at film edge, suppression effect of SiO_2 80−2025
Si_3N_4, films, ion-beam synthesis, IR spectra, struct., crystallisation on annealing 77−16705
Si_3N_4 films, plasma deposited over substrate steps, fast etching phenomenon 79−34168
Si_3N_4 films, prep., props. and appls., bibliography 80−94939
Si_3N_4 films, prep. by thermal nitridation of Si in NH_3, comp. and oxidation resist. 80−3215

insulating thin films continued
Si_3N_4 films, reactive plasma sputtering prep. 79−43147
Si_3N_4 films, struct. 80−54545
Si_3N_4 films on Si, photocurrents 79−24092
Si_3N_4, formation by N ion implantation into Si 79−90692
Si_3N_4, growth by plasma-activated CVD, optical prop. depend. on growth conditions 77−55892
Si_3N_4, growth technique 79−43141
Si_3N_4, HF plasma deposition *(German)* 80−7507
Si_3N_4, high-speed electron irradiation effect on charge storage 77−69430
Si_3N_4, highly insulating film, current cond., CV curves, and IR absorpt. 79−38208
Si_3N_4, kinetic model for RF plasma-activated CVD 78−27416
Si_3N_4 layers, on GaAs, encapsulation, low-energy ion beam sputtering 79−78882
Si_3N_4 layers, prep. by N_2 ion implantation into Si, TEM and IR absorpt. obs. 79−46974
Si_3N_4 layers, RF plasma deposition and props. 79−43155
Si_3N_4 layers deposition, high-temperature, in resistance furnace, temperature gradient and nitrogen flow influence obs. *(Bulgarian)* 80−80981
Si_3N_4 layers produced by ion implantation, oxidation inhibition and etching 80−103374
Si_3N_4, low press CVD film, steady-state electron and hole space charge distrib. 80−29493
Si_3N_4, MNOS struct., mechanical stress and elec. props. as function of nitride deposition temp. 79−42651
Si_3N_4, non-stoichiometric films, struct. 79−42412
Si_3N_4, on Si, conc. profiles of ions and recoiled N after implantation through Si_3N_4 films 79−55764
Si_3N_4, on Si, dissolution and corrosion in high temp. water and moisture 77−48564
Si_3N_4, on Si, implantation effects on substrate hardening and film stress reduction 78−71748
Si_3N_4, on Si, influence of induced stresses on B diffusion in Si 80−29224
Si_3N_4, on Si, struct. stability 80−54564
Si_3N_4, on Si. crysts. from amorphous state 79−28225
Si_3N_4, penetration of As and P ions, 50 to 500 eV 77−76444
Si_3N_4, plasma etching, MOS processing appl. 80−40577
Si_3N_4, plasma-activated, passivation *(Japanese)* 80−85073
Si_3N_4, preparation, characterisation and appl. 80−40268
Si_3N_4, preparation by reaction of active N with SiI_4 vapour 77−24963
Si_3N_4, reactively sputtered, MNS struct. hysteresis elimination 79−99633
Si_3N_4, room temp. CVD on InSb 80−71597
Si_3N_4 sample substrates, high resoln. electron beam fabrication using STEM 80−104104
Si_3N_4, self-drifting of ionic charges, detection by surface potential decay method 78−72295
Si_3N_4, separation, effect of reactor geometry *(German)* 78−60583
Si_3N_4, Si rich, CVD film prep. and props. 78−76607
Si_3N_4, synthesis mechanism 77−12538
Si_3N_4, thermally grown films for high performance MNS devices 78−48322
Si_3N_4, thermally stimulated depolarisation current meas. 80−88643
Si_3N_4, thin intergranular phase, imaging by high-resolution electron microscopy 79−90895
Si_3N_4 ultra-thin film composites of FET wafers and devices, thickness determ. by microprobe technique 77−36397
Si_3N_4, with varying refr. index, AES and XPS 78−72029
Si_3N_4:C film struct., oxidation, defects 79−51455
Si_3N_4:Ge films, intrinsic stress rel. to deposition conditions 80−39467
Si_3N_4:H, film, impurity profile determ. by 1.2 MeV proton-proton scatt. 80−49256
Si_3N_4:Si, amorphous, optical and electrical props. 77−76987
Si_3N_4-SiO_2, double dielec. layer on Si substrate, ellipsometric parameter meas. methodology 77−63474
Si_3N_4-SiO_2, interface, electron and hole cond. at moderate elec. fields 78−95376
Si_4N_4, ion-implanted, enhanced etching in buffered HF solns. 78−72903
Si_xN_y, amorphous, prepared by glow discharge method, elec. and optical props. 77−21035
Si_xN_y, film, chemical nonuniformity of films produced by ammonolysis of monosilane 77−1334
SiNH films, thickness and refractive index meas., comparison of techniques 80−8957
$Si_xN_yH_z$, film, prep. from plasma-induced CVD from Si-NH_3 79−83132
$Si_xN_yO_z$ film, band diagram, optical props. and elec. cond. meas. 78−84333
SiO, alumina surface deposited film, SiH bond form., inelastic electron tunnelling spectra 79−69375
SiO amorphous film, optical transmittance and reflectance, bulk optical props. determ. 80−88954
SiO, binding energies, XPS meas. 77−7989
SiO, effect of heat treatment on chemical and electronic struct., electron spectroscopy 77−48320
SiO, effect of ion implanted O_2 on optical props. 80−45027
SiO, elec. breakdown voltage vs. thickness 78−2602
SiO, electrode effects in TSC and capacitance meas. 79−78203
SiO film, Au coated, thickness meas. using stereo technique, TEM 77−30220
SiO, for low tilt angle nematic alignment compatible with frit sealing 77−68910
SiO, obliquely evaporated, topography rel. to liquid crystal orientation 77−69190
SiO supermultilayer dielectric film, elec. strength *(Russian)* 77−85648
SiO thin films at 60 mK, high-freq. phonon propagation 79−19347
SiO-Al multilayer capacitors and inductors, heat treatment effect on elec. props. 77−32082
SiO_2, 10-22 Å, on Si wafer, production 77−76690
SiO_2, action of plasma in capacitive electrode HF discharge *(Russian)* 78−95818
SiO_2, Al implanted, in MOS struct., electron traps characts. obs. 79−15226
SiO_2, amorphous, shock crystn. obs. 80−10828
SiO_2, amorphous, thermal, core and valence electron excitations, low energy electron loss spectroscopy and AES 80−2365
SiO_2, and $SiO_{0.7}$, amorphous sputtered thin film, US anomalies, 0.5-300K 80−34145
SiO_2, CVD, multiple internal refl. IR spectroscopy 80−11499
SiO_2, CVD anal. using hydrodynamics 77−40384

insulating thin films continued
SiO_2 CVD layer, high current injection from Si rich SiO_2 film 80−80430
SiO_2 charge effects at Al electrodes obs. 80−75625
SiO_2, clean film prep., use of poly-Si oxidation tubes 78−39924
SiO_2 controlled electrode area ratio sputtering system operation and film props. 77−77382
SiO_2 deposited on Ge, optical constants, reflection spectra by Kramers Kronig method 80−76099
SiO_2, deposition by plasma stream transport method, use of charge exchange plasma source 79−15613
SiO_2, depth profiling, AES 77−40605
SiO_2 dielectric film on Ge, dislocation interactions 80−39472
SiO_2, drift mobilties of Na^+ and K^+ ions 78−10213
SiO_2, elec. breakdown voltage vs. thickness 78−2602
SiO_2, electric strength in MOS structures obs., under unidirectional, alternating and combined voltages *(Slovak)* 78−88034
SiO_2, electrical breakdown by impact ionisation, models compared with expt. 79−91373
SiO_2, electron-beam-induced cond., appl. to obs. of voltage contrast in SEM 79−21856
SiO_2, ellipsometry of anodised layers on clean and ion bombarded Si surfaces *(Russian)* 79−24382
SiO_2, evaporated film, Debye-type dielec. dispersion props. 78−56421
SiO_2 film, form. by reactive sputtering, effect of defects in Si wafer 77−89676
SiO_2, film, formation from tetraalkoxysilanes in O_2 current, props. 77−44170
SiO_2 film, from oxidation, in dry O_2 and H_2O ambients, initial oxidation regime obs. 79−29240
SiO_2 film, grown on Si surface in O_2-HCl mixture, Cl incorporation 79−70186
SiO_2 film, localised states, low-temp. photocurrent spectroscopy 78−19090
SiO_2 film, on GaP substrate, N ion implantation, optical refl. and EPR meas. 80−84197
SiO_2 film, on Si, radiation damage structures, EPR obs. 78−95097
SiO_2 film, on Si, structure determ. by electron diffr. anal. 79−15050
SiO_2 film, on Si substrate, thermal stresses and cracking resist. 78−63958
SiO_2 film, prep. using high press. O_2, residual stress, chemical etch rate, refr. index and density meas. 80−71768
SiO_2 film, thermally stimulated depolaris. current, model *(Russian)* 79−56342
SiO_2, film, transmission, photocond. and band gap meas. 79−73540
SiO_2 film covered Si:P, implanted, laser annealing behaviour 79−86808
SiO_2 film deposition by SiH_4 oxidation, kinetics and physicochemical model 79−42419
SiO_2 film deposition on high-resistance Ge substrate by pyrolysis of tetraethoxysilane 77−1818
SiO_2 film growth technology *(Japanese)* 77−40381
SiO_2, film on Si, electron beam damage, obs. using scanning AES 80−2070
SiO_2 film on Si, irradiation behaviour anal. 78−26957
SiO_2 film on Si, negative bias instability 78−91773
SiO_2 film on Si substrate, Na transport caused by ion and atom impact 80−6682
SiO_2 film preparation and props., Si planar technology 78−10589
SiO_2, film thickness and field depend. of saturation defect density 78−56250
SiO_2 films, amorphous to cryst. transform. induced by diethyl ether vapour 79−55667
SiO_2 films, CVD at reduced press., optical props. 80−2957
SiO_2 films, DC plasma Si anodisation, dielectric const., O_2 pressure influence 80−70564
SiO_2 films, dehydroxylation, sintering, IR investig. *(Russian)* 78−75967
SiO_2 films, growth on Si, role of defect structure 80−65403
SiO_2 films, on Si, role of H_2 79−69376
SiO_2 films, Si-rich, amorphous Si region obs. 80−84400
SiO_2 films, spin-on diffusion sources, debris-induced effects 80−39465
SiO_2 films, stabilised by ion bombardment and heat treatment, crystn. and phase separation 79−77931
SiO_2 films, thickness and dielectric const., elec. cond. mech. *(Japanese)* 79−8084
SiO_2 films, thickness and refractive index meas., comparison of techniques 80−8957
SiO_2 films on Si, ellipsometric spectra, thickness determ. *(Chinese)* 80−86379
SiO_2 films on Si, mobile Na ion instability 79−82503
SiO_2, form. by thermal oxidation in Cl-H-O ambient, gas phase comp. considerations 77−48562
SiO_2, formed by trichloroethane oxidation of Si wafer, props. 79−70193
SiO_2 grown anodically over Si, optical and electrophys. props. 77−72934
SiO_2, growth and thermal evaporation kinetics of oxide film on Si surface 78−3246
SiO_2, growth by oxid. of silane 78−3038
SiO_2, growth kinetics on Si by low-temp. oxidation of monosilane 77−8763
SiO_2, growth on contaminated Si wafer, Au redistrib. during growth 77−4121
SiO_2 HF plasma sputtered dielectric layer thickness and refractive index obs. 79−56931
SiO_2, high-field electron trapping, I-V characts. of MOS capacitor 78−6449
SiO_2, IR spectra and elec. props., influence of prep. conditions 79−87176
SiO_2, in IGFET struct., thermal reemission of trapped electrons 79−42650
SiO_2, in MIM struct., dye sensitisation of photocond., steady state and pulse photoelectric props. 78−6408
SiO_2, in MOS struct., charge transport, TSD obs. 77−89870
SiO_2, in MOS struct., thermally stimulated ionic cond. 78−10565
SiO_2 in MOS structures, elec. props. with DC voltage *(Slovak)* 80−88634
SiO_2, insulating films, neutron activation anal. and autoradiography 78−92574
SiO_2, ion bombarded, attenuated total refl. method obs. of H capture 79−95863
SiO_2 irradiated film, electron and hole trapping 80−11098
SiO_2 layer, ultra thin, Si substrate, surface cond. mechanism 79−38149

insulating thin films continued
SiO_2 layer anodically grown on high resistivity n-Si wafer, improved homogeneity 79−24642
SiO_2 layer formation on polycryst. Si, morphological aspects 80−76388
SiO_2 layer of MOS structs., centroid location of implanted ions by photo I-V technique 79−24079
SiO_2 layer used for MOSFETs, electron trapping behaviour 80−92981
SiO_2 layers, anodic oxidation growth on p-Si, transmission electron diffr. obs. 79−28241
SiO_2 layers, dielectric strength, dislocation effect 78−31154
SiO_2, layers, on Si substrate, IR optical props. 79−56780
SiO_2 layers, passivating, deposition by plasma decomp. in planar reactor 78−88430
SiO_2 layers, room temp. transforms induced by diethyl ether vapour 79−99456
SiO_2 layers, thermally grown, undoped and ion implanted, elec. props. 78−23187
SiO_2 layers on Si, ionis. thresholds of electron traps 80−92983
SiO_2, localised cond. regions, obs. by liq. cryst. technique 77−1507
SiO_2 magnetron sputtered film, oblique deposition effect on growth rate, etching rate, and struct. *(Japanese)* 80−54555
SiO_2, mobility and trapping of ions, Si-SiO_2 interface states 80−92985
SiO_2, neutralisation of mobile ions, in Al-SiO_2-Si MIS diode *(Japanese)* 79−73591
SiO_2, noncryst., in MOS struct., Na ion impurities motion 78−10223
SiO_2, numerical anal. of kinetics of space charge formation, rel. to irradiation *(Russian)* 79−78243
SiO_2, O_2 partial press. depend. of fixed surface state charge due to thermal oxidation of N-Si (100) 79−70179
SiO_2, obtained by oxidising SiH_4 in HF gas discharge plasma 77−11804
SiO_2, on n-GaAs, Ga content after annealing at 730-940°C neutron activation anal. 78−43255
SiO_2, on semiinsulating GaAs:Cr,Si, annealing 79−4323
SiO_2, on Si, dissolution and corrosion in high temp. water and moisture 77−48564
SiO_2, on Si, H_2 and D_2 ion bombardment effects 80−34086
SiO_2, on Si, influence of induced stresses on B diffusion in Si 80−29224
SiO_2, on Si, internal stresses 77−24499
SiO_2 on Si, range distrib. of implanted As, He^+ backscatt. obs. 77−39611
SiO_2, on Si, SiOH and SiH groups, IR absorpt. results 78−26779
SiO_2, on Si, struct. stability 80−54564
SiO_2, on Si, thermal growth kinetics, oxidation profile meas. 78−88551
SiO_2, on Si wafer, surface roughness by gas adsorption techniques 80−15398
SiO_2, on Si. crysts. from amorphous state 79−28225
SiO_2, oxidation kinetics of Si in low O_2 partial press. *(Japanese)* 78−27665
SiO_2, penetration of As and P ions, 50 to 500 eV 77−76444
SiO_2, plasma deposition in prod. planar reactor 80−2966
SiO_2, plasma etching, MOS processing appl. 80−40577
SiO_2, plasma etching, role of chemisorpt. of CF_4, CF_3H, CF_3Cl, CF_2Cl_2 and CCl_4 79−11714
SiO_2, preferential etching on Si substrate, plasma reactive sputter etching 77−20448
SiO_2, produced by thermal oxidation of Si, control of oxide defects 77−20477
SiO_2, prop. of insulating film for tunnelling study on zero bias anomaly in Pb-SiO_2-$Pb_{0.8}Sn_{0.2}Te$ 79−15608
SiO_2, pyrolytic, on Ge substrate, ellipsometry, TEM, electron diffr. studies of struct. 78−10297
SiO_2, RF sputtered, stoichiometry and atomic defects obs. 79−60647
SiO_2, RF sputtered, stoichiometry and atomic defects obs. 79−90904
SiO_2 RF sputtered film, Na^+ motion, small-voltage elec. response 79−90822
SiO_2, RF sputtered films, anomalous etching phenomenon 80−3226
SiO_2, RF sputtered films, AC conductivity and conduction mechanisms 80−20338
SiO_2 RF sputtering, homogeneity improvement using mag. quadrupole field, expt. *(Croatian)* 78−48316
SiO_2, reactive ion etching damage, electron trapping characts. in MOS struct. 79−90704
SiO_2, self drifting of ionic charges, detection by surface potential decay method 78−72295
SiO_2, Si rich, CVD film prep. and props. 78−76607
SiO_2, spin-on oxide, phys. and cond. meas. 77−43762
SiO_2, sputter deposition onto GaAs, and MIS struct. characts. 77−89864
SiO_2 sputtered films in thin film transistors, trapping centres 80−7014
SiO_2 sputtered layers for semicond. devices, effect of impurities on elec. props. *(German)* 77−16495
SiO_2, stoichiometric condensate form. during electron beam evaporation of quartz, electrophysical props. 77−16496
SiO_2, struct., rel. to elec. props. of Si-SiO_2 interface *(Russian)* 77−15967
SiO_2, surface charge, effect of doping with P+B, differing vacuum deposition conditions *(French)* 77−85286
SiO_2, technology rel. to semicond. prod., bibliography 77−12038
SiO_2, thermal, elec. stressed film, dielec. breakdown 78−64322
SiO_2 thermal films, hole and electron trapping density reduction 80−2400
SiO_2 thermal growth, stress meas. 79−91812
SiO_2, thermal growth kinetics, in O_2/N_2 mixture, 950- 1100°C 77−86202
SiO_2, thermal oxide layer on Si, chemical shift meas. by ESCA *(Japanese)* 79−61761
SiO_2, thermally grown, pore size influence of punch-through voltage 78−6632
SiO_2, thermally grown, thickness, XPS obs. 80−11540
SiO_2, thermally grown film, optical absorption and photocond. 78−64421
SiO_2, thermally grown films, thicknesses 30-600 Å, defect density meas. 80−84412
SiO_2 thermally grown insulating film on Si, electron injection 78−23176
SiO_2, thermally grown or sputtered, electrostriction and piezoelectricity 77−12010
SiO_2, thermoluminesc., in H_2O vap. atm., temp. depend., time decay *(Russian)* 77−44074
SiO_2, thin film, prep. from low-temp. oxidation of tetraisopropoxysilane, dielec. props. 77−8759
SiO_2 thin films, mobile Na ion passivation in HCl oxides 79−70187
SiO_2 thin films, radiation-induced trapping centres, rel. to MOS transistor technology 80−107804

insulating thin films continued
SiO_2, thin films on rough polycryst. Si surfaces, oxide thickness and refractive index meas. 80−93422
SiO_2 thin thermally grown oxide layers etching in HCl, ellipsometric control of Si surface form. *(Russian)* 80−104315
SiO_2, transient charge relax., continuous time random walk, simple approx. solns. 77−43584
SiO_2, tunnelable film form. using vap. O_2 source at liq. N_2 temp. 78−76774
SiO_2 ultra-thin film composites of FET wafers and devices, thickness determ. by microprobe technique 77−36397
SiO_2 ultrathin layers, refr. index meas. 80−103936
SiO_2, ultrathin layers on Ge substrate, ATR spectra, thickness depend., struct. obs. 80−55214
SiO_2 undoped film, cathodoluminescence *(Russian)* 80−40164
SiO_2, uniform film prep. by pyrolysis of tetraethoxysilane 77−40379
SiO_2 vitreous film on Si, defect struct. comparison with crystalline SiO_2 and Si-O bond nature 80−54557
SiO_2, vitreous films on Si, channel and network defects 80−54142
SiO_2, vitreous layers, thermal growth on Si 80−93675
SiO_2:Al film, ion-implanted, electron trapping behaviour 78−67729
SiO_2:As^+ implanted layers in MOS struct., electron trapping and detrapping characts. 80−92982
SiO_2:B, ion implanted, props. 79−65106
SiO_2:B implanted, thin films, props. *(Polish)* 80−39692
SiO_2:B(P) film, high temp. deposition and evaluation 79−69989
SiO_2:Cs(B), implanted, electronic cond. mechanism in MOS struct. 77−15983
SiO_2:F-ion implanted, mobile-ion drift compensation 79−19664
SiO_2:Ga film, impurity distrib. after annealing, neutron activation anal. 80−24484
SiO_2:Na_3 film, depth profiling by SIMS 78−79624
SiO_2:Nd^{3+} films, cathodoluminesc. 80−20717
SiO_2:P films, P content determ. by IR absorpt. and activation anal. 79−51139
SiO_2:W, electron trapping characts., obs. by avalanche injection techniques 77−89862
SiO_2/InP film/substrate system, interface formation during CVD, modelling 80−24764
SiO_2-PSG-Si_3N_4 composite layer, on Si, crack occurrence, PSG film thickness and comp. effects 77−72806
SiO_2-Si, low-energy neutral particle bombardment of SiO_2 film, degradation 80−54790
SiO_2-Si interface, props. variation in SiO_x region 80−49548
SiO_2-Si MOS system, ion irrad. effects on struct. and electrophysical props. 80−6995
SiO_2-TiO_2 films, obtained from $Si(OC_2H_5)_4$ and $TiCl_4$, exam. of props. 79−95934
SiO_2:B, P films doped by pyrolisis and ion implantation, IR absorpt. obs. of impurity conc. 77−72802
SiO_2-$LiTaO_3$, temp. compensated SAW device fabrication 79−76923
SiO_x, amorphous, AES and EELS characterisation 79−90905
SiO_x, amorphous, acoustic study using Rayleigh waves 80−75312
SiO_x, amorphous, dispersion of refr. index and chem. comp. 80−7429
SiO_x, amorphous and recrystallised layer, optical props. 80−25474
SiO_x amorphous films, high energy electron diffr. study 80−38911
SiO_x, Cole-Cole diagrams of ionic hopping systems 77−66217
SiO_x film, vacuum evaporated, phase comp., electron spectroscopy obs. 78−60042
SiO_x, grown in HCl/O_2 ambients, phase separation and Na passivation 80−3219
SiO_x, growth on passive n-Si, kinetics, thickness, ellipsometric investig. 77−1885
SiO_x, in MIM struct., electroformed, struct. and elec. props., 4-300K 79−78206
SiO_x layers, grown in HCl/O_2 ambients, struct. and comp. 79−42404
SiO_x, metal layer interdiffusion Rutherford backscatt. 77−85000
SiO_x, on Si exposed to O_2, phase comp., electron spectroscopy obs. 78−60042
SiO_x, oxidation, film defect equilibria and growth reactions 78−11377
SiO_x, reactively evaporated, substrate temp. depend. of optical props. 77−70006
SiO_x semi-insulating polycryst. films, AES and PES studies 80−107939
SiO_x thin films, deposition and characterisation study 80−80133
SiON/GaAs film/substrate system, interface formation during CVD, modelling 80−24764
SiO_xN_y, CVD, multiple internal refl. IR spectroscopy 80−11499
SiO_xN_y, deposition kinetics in SiH_4-CO_2-NH_3-H_2 system 77−48346
SiO_xN_y, low temp. films, comp., chem. bonding and contamination 78−47676
SiO_xN_y, on Si, ^{16}O conc. profiles anal., using (d,p) and (d,α) reactions with mag. spectrom. 79−5215
SiO_xN_y, on Si, struct. stability 80−54564
$Si_lO_mN_p$, CVD from SiH_4-CO_2-NH_3-H_2 system, physicochem. props. 78−38978
$Si_xO_yN_z$, on Si. crysts. from amorphous state 79−28225
$Si_xO_yN_z$, amorphous, shock crystn. obs. 80−10828
$Si_xO_yN_z$, non-stoichiometric films, struct. 79−42412
$Si_xO_yN_z$, pyrolytic, on GaAs, evidence for growth-induced damage from photolum. expts. 78−75953
$SiO_{2-x}Nx$ thin CVD film processing and characteristaion 77−77413
$(SiO_2)_x(Si_3N_4)_{1-x}$ on GaAs, deposition method and props. 78−91796
SnO_2 films, cohesive energy, free electron density effect 79−60655
SnO_2 layers, study using Mossbauer effect 78−31124
on Ta, anodic film, electrochem. reactions by tunnel current 77−81340
TaN film, press. depend. of elec. props. appl. to press. meas. 79−78241
Ta_3N_5, polycryst. film, cryst. struct., electron diffr. *(French)* 77−76677
Ta_2O_5, anodic, on sputtered Ta_2N, dielec. props., 20-10^5 Hz, 150-500K 79−87386
Ta_2O_5 anodic oxide film, model for ionic cond. 80−2197
Ta_2O_5, defective anodic film on Ta, elec. characts. 77−12039
Ta_2O_5, elec. breakdown during anodic growth 80−55033
Ta_2O_5, electrical breakdown by impact ionisation, models compared with expt. 79−91373
Ta_2O_5, film, dielec. props. meas., two layer Maxwell-Wagner model 78−76373
Ta_2O_5, for MIS device, CVD and characterisation 77−4742
Ta_2O_5, reactive DC sputtering deposited films with magnetron-plasmatron, mechanical elec., optical props. 80−25566
Ta_2O_5, sputter deposition onto GaAs, and MIS struct. characts. 77−89864

insulating thin films continued
Ta_2O_5, temp. and time characts. of breakdown *(Russian)* 77−55751
Ta_2O_5 thermoluminesc., in H_2O vap. atm., temp. depend., time decay *(Russian)* 77−44074
Ti-anodic oxide-Au(Al), electronic cond. *(French)* 79−95512
TiC, CVD rate, depend. on gas composition 77−40386
TiN, deposition by TiC reactive RF sputtering in N_2 79−78886
TiN film, struct. and elec. props. 78−26788
TiO_2, anodic film, AES study 79−5072
TiO_2 anodic film, optical indices as function of crystallisation 77−66552
TiO_2, anodic film, polarisation behaviour, stoichiometry 79−5073
TiO_2, laser CVD 79−78897
TiO_x, reactive sputtering, film prep. conditions rel. to stoichiometry 77−40370
Ti_xO_x film, interference enhanced Raman scatt. 80−40105
V_2O_5, amorphous, electronic cond., effect of random glass struct. 79−23972
WO_3, amorphous, struct. and crystn., TEM obs. 80−103606
WO_3, amorphous, sublimed under different conditions, elec. transport props. 80−7015
WO_3 amorphous film, elec. cond. and dielec. const. 78−60238
WO_3, single cryst. and amorphous film, ESR of defects 78−10770
Y_2O_3, film, anodic glow in Y-Y_2O_3-electrolyte system 77−12447
Y_2O_3 film in Y-Y_2O_3-metal junction, electroforming and conduction 78−26969
Y_2O_3 film in Y-Y_2O_3-Au junction, defect struct. and local conduction 78−26970
Y_2O_3, in MIM struct., electroforming props. 80−65705
Y_2O_3, struct. and elec. resist., electron diffr. meas. 78−87888
Y_2O5d3 films, preparation, electrophys. props. in metal-oxide-metal structs. 77−24956
Yb_2O_3, amorphous, electron beam deposited, dielec. props. 79−91339
ZrO_2 film, CVD from organometallic cpds. and characterisation 78−23626
ZrO_2:Y_2O_3, bias sputtering, film growth and characts. 77−40366

insulation
see also cable insulation; electric breakdown; insulating coatings; insulating materials; insulators; machine insulation; transformer insulation
air gap corona pulse delay obs. and HV insulation design 79−19117
conference, Electrochem. Society fall meeting, Las Vegas, USA (Oct. 1976) 77−16831
conference, electrochem. society fall meeting, Las Vegas, USA (Oct. 1976) 77−77787
dielectric conduction and breakdown, conf., Gainesville, FL, USA (Oct.-Nov. 1979) 80−82564
double insulation for electronic instruments advantages 78−32802
electric arc deformation by narrow insulating slot *(Russian)* 80−28861
electrical diagnostic stimulator with insulated sources of power *(German)* 79−16324
electromagnets for nuclear fusion and high energy research, insulation systems, features 78−89506
gases as electrical insulators, nature and practice 78−83632
laminated insulating element, vac. drying in inert heat-transfer vap. 78−56875
microelectrode, chronically stable, reproducible, using parylene 77−40942
moistening diffusion kinetics, forecasting *(Hungarian)* 80−96692
PMMA, ageing characts., sub-atm. pressure partial discharge obs. 80−1867
self-magnetic insulation in vacuum for coaxial geometry 78−78520
solar energy utilization, all year domestic heating, in Europe *(Czech)* 79−83564
solid, discharges, elec. strength and degradation 78−83631
superconducting magnet HV insulation problems 79−30512
turbulent thermal insulation in magnetoplasma device, ion wave effects 80−106914
X-ray tubes, rotary anode, HV insulation, discharges due to back scattered electrons elimination *(German)* 80−105758
H_2O, as dielectric insulator, in plasma devices, electron accelerators and impulse current generators *(Russian)* 78−75430
N_2-SF_6 mixture, electrode surface roughness effect 77−39490

insulation, thermal *see thermal insulation*

insulation testing
air gaps, critical impulse voltage stress determ. 77−4018
air-gaps, breakdown tests with ramped impulse voltage 77−15266
cap-and pin-type insulators, resistance to high current arcing for 110 and 400 kV power transmission lines *(Polish)* 80−70049
composite insulating materials, fatigue behaviour, influence of superposition of elec., mech. and environmental stresses 80−97590
composite insulation breakdown under AC and impulse voltages 78−23398
crack inspection in foam insulation, using dye solution or X-ray opaque solution 80−76440
electric insulating oils, composition, physical and chemical props. and determ. of free radicals *(Rumanian)* 80−97745
electrical resistivities of some common insulators, temp. depend. meas. *(Croatian)* 77−74426
epoxy polymers, unfilled and filled effect of specimen size on elec. strength expt. 77−8505
epoxy resin insulation, adapted models selection problems for electric ageing *(German)* 80−89365
flameproof coating for PVC insulated cables, composition, tests *(Russian)* 78−68828
flammability testing, problems, language and scientific basis 79−5092
fusion reactors, TFTR mag. field coil electrical insulation system and test results 80−95429
high energy radiation effects 80−19835
insulating material monitoring by electroluminescent screens, defect imaging 78−53083
insulators, HV for transmission lines, power arcs occurring in networks and laboratories, comparisons 80−87983
JET Tokamak toroidal field coil manufacture 79−31206
lapped paper and plastic insulated cables, butt gap distribution and spliced joints study using X-ray method 77−77726
liquid dielectric gassing rate and discharge energy loss meas. 80−15965
loss-angle and capacitance test trolley *(Russian)* 77−10041
machine windings, wound wires, enamel insulated, elongation plus flexibility 80−20999
nuclear power station cables, deterioration test *(Japanese)* 80−27743

insulation testing continued
organic insulating material, arc tracking, comparative tracking index 77−90528
plastic, arc resistance test *(Japanese)* 78−27697
plastic, of HV and MV cables, dielectric breakdown obs., distribution law parameters estimation *(French)* 77−24794
polyethylene, ageing prediction by isothermal differential scanning calorimetry 78−11485
polyethylene life test needle electrode selection 80−15969
polyethylene surface field strength under DC stress 80−15967
polymeric, insulating materials, partial discharges, simulation and meas. *(German)* 77−77146
power transformers, electromagnetic testing of partial discharges for failure and breakdown prevention *(Russian)* 80−97743
solid dielectric specific resistance meas. instrument 77−79109
Space Shuttle external insulation, acoustic emission inspection 78−16276
three-terminal cell, for investigating the elec. props. of insulating materials over wide freq. and temp. ranges 80−37053
trifluorotrichloroethane, liq., as insulating material and coolant, dielectric strength, HVDC convertor appl. *(German)* 77−76218
N_2, compressed, insulation breakdown at cryogenic temp., obs. 78−51368
SF_6 breakdown characts. in non-uniform field gaps, at 0.8-2 MV range 77−15269
SF_6 under impulse voltage stress, effects of pressure and vol. on firing delay *(German)* 80−87959

insulator-metal boundaries *see metal-insulator boundaries*

insulator-semiconductor boundaries *see semiconductor-insulator boundaries*

insulators
i.e. insulating devices. For materials see insulating materials
see also bushings; insulation
ceramic insulator rings, for Tokamak fusion test reactors 78−55022
contact electrification, expts. with solid rare gases 80−70797
contaminated insulators, flashover under DC conditions 79−68967
electric breakdown, of gas, liq., and solid insulators *(Japanese)* 79−19837
energised polluted insulators, temp. distrib. meas. using IR thermography 79−97385
fission fragment sputtering 80−40207
glazed ceramic insulators, surface quality monitoring 79−61813
HV, influence of air pollution on dielectric rigidity *(Slovenian)* 80−64801
HV for transmission lines, power arcs occurring in networks and laboratories, comparisons 80−87983
magnetically insulated vacuum diode, μs pulse insulation, ion beam generation 77−26431
parameters meas., freq. and mode variation in cavity 80−13102
refractive index meas. using continuously recording spectrograph, instrum. 79−17467
thermal conductivity meas. of cast insulation materials 80−86293
thermionic technology development, for space nuclear propulsion, NASA's program 1978 status, objectives and plans 79−48159
transient and alternating currents, influence of deep traps 79−73525
transient radiation induced ionisation effects 77−80788
Al_2O_3 porcelain for high voltage insulators, increased mech. strength 78−11269
Al_2O_3 rod, damaged, mech. strength, surface defects effect, appl. as insulators *(German)* 80−76330

integer programming
BWR, optimal fuel pin enrichment distribs. 77−83008
energy planning, national, optimisation model 79−57350
heat exchange network synthesis, mixed integer optimisation 78−30152
national energy policy anal. and planning models 80−101071
nuclear fuel reprocessing plant, optimal installation program 77−46370
nuclear power stations, optimal size and location in energy parks 80−95489
PWR refuelling fuel shuffle scheduling 79−9866
teaching simplification 79−17163

integral equations
see also integro-differential equations
Γ-integral, invariance props. *(Russian)* 77−71187
a mixed boundary value problem in elasticity 79−23274
Abel's integral eqn., least squares finite element method appl. 79−25830
Abel eqn. for rigid indentor sliding over power law viscoelastic half space 79−27602
Abel integral eqn., numerical soln., optical diagnostics of axisymmetrical objects 79−7488
Abel integral eqn., numerical soln., plasma spectroscopy appl. *(French)* 78−30415
Abel integral eqn. inversion in astrophysical problems 80−26732
Abel integral eqn. solution by orthogonal polynomials 78−67436
acoustic radiation problem, Schenck numerical method *(French)* 80−69589
acoustic wave diffr. by parallel strips 79−1015
adhesively bonded metallic panels, 2-ply, finite element and integral eqns. anal. of fatigue crack growth 78−92347
adsorption, from multicomponent mixtures, on heterogeneous solid surfaces *(German)* 80−44430
adsorption integral equation, new method of solution 77−28076
aerodynamics, discrete vortices method and multidimensional singular integral eqns. theory 80−19421
airfoil, oscillating, exact soln. by integral eqn. 77−84270
alloys, binary, surface segregation kinetics 80−80044
Ambartsumian's function derivatives w.r.t. single scatt albedo *(Russian)* 77−49698
anisotropic slab, thermoelastic crack problem 80−23960
annulus, infinite, with two pairs of cracks at inner boundary, plain strain problem 77−14963
applications of integral equations in particle-size statistics 78−62050
approximate method for solving the integral equation of transport theory 77−87707
approximate solution, dynamic errors in linear conversion calc. 77−5796
approximation method for solution of nonlinear integral equation with error estimation for problems in heat or mass transfer *(Russian)* 78−57879
arbitrarily shaped body, integral approach to acoustics prediction 77−84040
asymptotic behaviour of group integrals, infinite rank limit 78−62051
asymptotic long time behaviour 77−74197

integral equations continued
asymptotic series coefficient, generalised calculus using steepest descent method *(Rumanian)* 78−89304
atoms, molecules, pair energies, numerical soln. 78−90065
Ball-Zachariasen model of diffractive scattering, numerical soln. near singularity of Frechet derivative 80−9158
Banach algebra, Hilbert boundary problems, associated abstract singular integral eqn. *(Russian)* 77−22370
bar, homogeneous isotropic, shearing stress in Saint-Venant torsion, integral eqn. method 79−80445
bar with two natural freqs., minimum mass design 79−46246
beam, impulsively loaded, clamped end bending moment, Bessel function eval. 79−92937
bending, axisymmetric elastic bodies with arbitrary boundary conditions, semianal. boundary integral 80−102969
Benjamin-Ono eqn., props. 79−63050
Benjamin-Ono equation, meromorphic solns. 79−62998
Bernouilli and Lagrange-Cauchy integrals, p/γ term 78−65779
bifurcation of crystalline solutions and freezing 78−67814
bifurcation of solutions with crystalline symmetry 77−7650
Blasius type boundary layer subject to blowing or suction, transition behaviour 79−18869
book, mathematical methods for physics 77−45670
Born-Green-Yvon eqn., electrical double layer theory 80−35539
bosons, analytical treatment of hypernetted-chain and Percus-Yevick eqns. 79−30359
boundary element methods, using weighted residual techniques potential problems and engineering appl. 78−36803
boundary integral eqn. method, appl. to creep of metals 79−46231
boundary integral eqn. method in stress anal., resolution of tension discontinuity problem *(French)* 77−71215
boundary integral eqn./finite element anal. of cracked solids 77−72178
boundary layer and freestream with separated flow, simultaneous soln. 78−38271
boundary value problems, numerical soln. through integral eqns., review 78−81808
boundary-integral equation method, stress anal. fracture mechs., computer calcs. 77−80111
boundary-layer development, on moving wall, use of integral theory 77−23933
boundary-value problems, appl. of method of singularities 77−67254
boundary-values with shift, approx. 77−77795
bounded elastic body containing a crack, mode 1 deform., integral eqn. soln. 79−3976
branched cracks in 2-D, numerical soln. 79−46269
Brownian motion, generalized multiple Wiener integrals 79−30370
butadiene-styrene gum elastomers, compounds, viscoelastic props., stress relaxation meas. 77−7321
calculation of scattered sound fields near three dimensional objects 80−74558
capacitor, coaxial and planar magnetoplasma, impedance characts. 78−42837
Cauchy type, anal. of elastic layer on substrate, frictional slip caused by normal load 80−33541
Cauchy type singular integral eqns. with complex singularities, numerical soln., stress intensity factors 78−55611
celestial mechanics, formal integrals for autonomous Hamiltonian system near equilib. point 78−89047
celestial mechanics, quasi-integrals from Von Zeipel transformations 80−46372
Chandrasekhar's X-function, reln. to eigenvalues of integral operators with difference kernels 77−71280
Chandrasekhar H-equation, Banach space anal. 77−13224
Chandrasekhar nonlinear H-eqn., iteration 79−58652
Choquard nonlinear eqn. minimising soln. existence and uniqueness 78−67315
circular bar in elastic half-space, longitudinal harmonic excitation 79−10518
circular crack under general asymmetric loads, related integral eqns. 80−64483
circular disc, stress intensity factors and crack energy 78−79260
clarinet, integral equation anal. of self sustained oscillations 78−94490
classical liquids, in equilib., mol. theory, integral eqns. 77−39522
classical molecular fluids at equilibrium, integral equation derivation 80−64861
classical particles in box, continuous system, phase transform. 77−82444
Coanda effect, potential model 79−77198
collocation variational method for solving Fredholm integral eqns., convergence condition 78−57764
complex Gauchy type singular integral eqn., curvilinear crack anal. 79−37246
complex resonator with internal diaphragm, diffr. losses and field distribs., integral eqns. 80−95921
composite particle scatt., integral eqns. taking Pauli principle into account 78−86496
computer treatment of images, from high-speed image convertor camera 78−42295
concave grating mirror stable resonator, self-consistent integral eqn. *(Chinese)* 79−50324
conducting body of revolution covered with thin layer of dielectric, axisymmetrical excitation 79−81327
conducting rectangular cylinder, losses due to finite length coils, exact analysis 77−10806
conical cavity, local effective emissivity, analytic approx. soln. 80−23874
conical flow, Pohlhausen method appl. to 3-D boundary layers 77−65746
conjugated heat transfer in plate in flow, integral eqn. 78−87345
connectivity theory for formally symmetric operators 78−49651
constrained systems, quantum treatment using path integrals based on distrib. theory 78−65815
continuum mech. linear mixed problems, two effective soln. methods *(Russian)* 77−82388
continuum mechanics, suction force, interpretation of Rice integral 78−49658
convective heat transfer, with conjugate boundary conditions *(Russian)* 77−23956
convective heat transfer in porous layers, Karman-Pohlhausen method 79−7408
convolution type integral equation for seismic obs. digital processing, steady solns. *(Russian)* 79−53317
Coulomb scattering, Green's functions, integral eqns. soln. 77−37789
integral equations continued
Coulomb T-matrix, modified integral eqn. using Green's functions 79−35976
coupled anharmonic oscillator energy levels, large quantum number behaviour, path integral method 80−91
coupled singular eqns., solns. for shell containing crack 77−50997
crack, in semiinfinite thermoelastic solid with heated boundary 78−55610
crack branching, asymmetric, plane stressed and loaded plate 78−59344
crack edge stress field three dimensional anal. using integral equation system 77−46968
crack-edge stress field anal. method 77−68530
cracks, curvilinear, star-shaped array in infinite isotropic elastic medium 78−55609
cracks problem in elasticity, singular eqn. soln. 79−68639
crystal orbital calculations, deformation density method, transferable integrals 80−38992
crystal orbital calculations, deformation density method, transferable integrals, neutral atom pots. 80−38993
curved space-time quantum stochastic processes, covariant Kolmogorov-Klein-Fock eqn. 80−18083
cylindrical shell mixed boundary value problem, heat cond. and crack torsion 77−35
cylindrical shells, stress conc. anal. by integral eqn. method 77−75806
cylindrical viscoelastic waves, diffraction by circular obstacle, calc. *(Russian)* 77−54895
cylindrical wave, diffr. from slit, above interface, paired integral eqn. calcs. 77−50613
definite integrals of generalized functions 79−50200
deformation localised function, integral eqn. 77−50932
deformed boundary determ. by method of caustics 77−89077
dense, quadrupolar, hard sphere fluid, integral eqn. approx. 78−63652
dense dipolar hard sphere fluid, integral eqn. theory 77−76278
dense simple fluid near wall, density profile calc., integral eqn.−Monte Carlo comparison 80−54083
dielectric coated gratings, general integral theory 78−66909
diffraction, scalar, null field approach, general method 78−13656
diffraction at shadow boundaries and transition regions, spectral domain formulation 77−75381
diffraction gratings, Fredholm integral eqn. formalism 78−63192
diffraction integral transform, sampling theorem 77−45678
diffraction on transparent structures, soln. using integral equations method *(Russian)* 77−68154
diffuse reflection problem for combination of Rayleigh and isotropic scatt., integral eqn. 79−84661
diffusion of particles, time-depend. problem, spectral anal. 78−45582
dipolar liquids, hypernetted-chain eqn., perturbation theory soln. 80−49072
dipole fluid theory in hypernetted chain approx. *(Russian)* 80−14988
Dirac system, nongrassmann quantisation, path integral approach in phase space 79−97496
Dirichlet-Neumann mixed boundary value problem for harmonic functions, integral eqn. method 77−67223
distributed parameter reactor core, optimal control by function space method, numerical experiences 77−54317
distribution functions and Green functions *(Russian)* 78−65890
drag on a sphere moving axially in a long rotating container 79−50734
drift-diffusion problem with special boundary conditions, numerical soln. by integral eqns. 77−76591
drop motion in immiscible liquid, integral eqn. for Stokes flow 78−71389
drops in liquid, diffusional interaction 79−81947
dual, anal. of coplanar Griffith cracks in infinite elastic medium, dynamic stress conc. 79−46270
dual, appl. to elastic thin semi-circular plate containing edge crack 78−13972
dual eqns., appl. to half-space steady state vibr. elastic contact problem 78−18219
dual unitarisation scheme, planar amplitudes, Regge cut cancellation 77−87954
duct, nonuniform, finite element method for acoustic transmission 78−83140
duct acoustics, integral equation methods for nonuniform duct with variable impedance 77−58498
Duhamail integral, rel. to river runoff travel time *(Russian)* 77−53089
Duhamel's integral numerical evaluation, earthquakes response spectra calc. appl. 79−21035
dynamical systems, global first integrals, connections with critical phenomena 78−32667
Earth-ionosphere waveguide excitation by low-freq. sources in inhomogeneous ionosphere 79−66873
eccentric spheres, interior and exterior boundary-value wave problems 77−75384
ECG forward problem, relationships among Green's theorem, Helmholtz theorem and integral eqn. methods 78−57090
eclipsing variable stars Fourier anal., $B_{n,m}{}^{q}$ integrals explicit expression 79−35298
eddy current calculations 77−83783
eddy current problem soln., integral eqn. method developments 79−41292
edge crack pair in circular disc 78−46914
edge dislocation interactions in infinite array, elastic energy 78−55871
elastic, isotropic, incompressible solid, plane deform., integral eqn. formulation 78−51081
elastic bimaterial problems and cracks, integral equations 79−44741
elastic cylinder contact problems, approx. soln. of Shtaerman's eqn. 80−38355
elastic dissimilar semiinfinite strips, different widths, plane symmetric contact problem 78−55615
elastic eqns. of uniform systems, general integral solns., appl. *(Russian)* 79−14272
elastic linear, material of hexagonal symm., half-space, indentation by circular punch 78−34020
elastic plug in elastic region contact problem, influence coefficient technique appl. 77−53747
elastic stress intensity factor calcs. using elastostatics M-integral conservation law, plane cracks 78−46913
elastic system, composite, interface flaw, appl. of dynamic Green function method 77−84153
elastic unitarity integral, angle-dependent lower bound on soln. and new uniqueness condition 79−40414

integral equations continued
elastic unitary eqn., soln. uniqueness 79−5981
elastic-viscoplastic materials, stress concentrations determ. by integral eqn. methods *(French)* 77−72194
elasticity, anisotropic, stress concentration around holes, formulation of problems 79−64509
elasticity, nonlocal, fundamental 1-D solns. 79−67163
elasticity, nonlocal theory, stationary boundary problems, reciprocity principle and Green's tensors 80−68046
elasticity, plane, inclusion problem, numerical soln. of Cauchy-type integral eqn. 78−54194
elasticity, plane theory, singular integral eqn. for mixed problem soln. *(Ukrainian)* 78−89339
elasticity, pot.-type singular integral approx. algorithm 80−27132
elasticity, variational formulation of integral eqns. *(French)* 77−72181
elasticity axisymmetric problems, numerical soln. using integral eqn. method 77−22421
elasticity problem, dual integral equation solns. *(Ukrainian)* 79−88809
elasticity problems, axisymmetric bodies with arbitrary boundary conditions, boundary integral approach 79−75344
elasticity singular integral eqns., regularisation of differential props. 77−17820
elasticity theory, boundary-value problem, index of integral operator *(German)* 80−5945
elasticity theory, plane problems, integral eqn. soln. 77−75810
elastodynamics, numerical boundary integral eqn. method 79−63036
elastostatics, appl. of modified integral eqn. method 79−14254
electric arc, steady-state, energy eqn. soln., boundary value problem 80−79601
electrodynamic suspension system, current coil interaction with semiinfinite superconducting sheet *(Russian)* 80−83539
electron beam interaction with target, integral eqns. *(Ukrainian)* 80−32549
electron gas, classical and quantal treatment involving integral eqns. 78−41228
electron in multicentre Coulombic field of nuclei, integral Schrodinger eqn. soln. 79−30285
electron integrals over cartesian Gaussian functions 78−37538
electron propagator, Dyson-Schwinger eqn. solns. 78−24984
electron transport in one-dimensional finite systems 79−54077
electrostatic two-dimensional problem anal. 77−31043
ELF propag. in nonstratified Earth-ionosphere waveguide, integral eqn. method 80−61959
elliptical disc in viscous liquid, slow broad-side motion anal. 77−58635
EM eccentric spherical cavity, resonant frequencies 79−72457
EM field calc. using integral equation method 79−64157
EM field calculation using integral eqn. method *(Russian)* 78−82887
EM field laws, finite element method equations derivation 80−18961
EM field penetration into conductive spherical cavity 78−86990
EM field penetration into thick, finitely conducting shell, anal. 78−62990
EM field time domain reflection from inhomogeneous and dispersive slabs 78−62985
EM induction, H-polarisation problem soln. by wavenumbers integral eqn. method 77−44913
EM radiation scatt. by dielectric spheroids and ellipsoids, Fredholm integral eqn. 77−19142
EM radiation scattering by dielectric spheroids and ellipsoids, numerical soln. 78−85622
EM scatt. integral eqn. resonant solution elimination 79−45895
EM scattering by multiple rectangular cylinders, numerical anal. 78−62992
EM scattering by spherical shell with arbitrarily located circular aperture, anal. 78−62989
EM scattering from corrugated conducting surfaces with inhomogeneous surface impedance, anal. 78−62987
EM scattering from dielectric cylinders, surface integral representations 78−42263
EM wave, of sinusoidal ring current, diffr. by cond. cone 79−27140
EM wave diffraction, from nonintersecting plates 79−10248
EM wave diffraction by elliptic cylinder of finite conductivity *(Russian)* 78−17844
EM wave diffraction in radial array of nonintersecting 1/2-planes 80−28147
EM wave direct scattering from one-dimensional inhomogeneous media, anal. 79−10244
EM wave impinging homogeneous layer transmission and refl. coeffs. *(German)* 78−82907
EM wave propag., nonlinear media, integral eqns. 77−58375
EM wave scatt. from dielectric infinite cylinder embedded into another 79−59620
EM wave scattering by dielectric circular cylinders, elimination of resonant solns. of integral eqns. 80−63896
EM waves diffraction from nonhomogeneous anisotropic bodies 80−18972
EM waves in cavity, integral eqn. *(French)* 78−42259
energy resource usage, conservation effects 78−69941
epicardial and body surface potential distributions related by geometric transfer coeffs. 77−21671
epithermal 1/V self-shielding of reactor poisons using Nordheim integral method 78−17306
equilibrium liq.-solid coexistence line, phase instability and direct correl. function integral eqn. 80−65196
excitation of conductive body, covered with thin dielectric layer *(Russian)* 79−18322
explicit integrals in celestial mechanics, new exact method for Hill's eqn. *(Chinese)* 80−105152
exponential integrals, general method for accurate numerical evaluation 78−36
exterior problems of acoustics, integral eqns. soln. 79−27455
extremum sufficient condition in classical action integral, eigenvalue problem, education 80−105462
Faddeev equations, generalised, for many-cluster problems 77−88058
Faddeev integral eqns. for three charged particles *(Russian)* 80−8830
Fadeev integral eqns. for 3 particles in boundary condition model, wave function determ. 78−54248
farfield scatt. from prolate spheroid, meas. and anal. 78−94459
FEBIE−a combined finite element-boundary integral equation method 79−2633
Fermi-Dirac integrals of arbitrary order, expansions and approx. 79−85065
integral equations continued
Feynman's path integrals, continuum calculus 77−5691
Feynman path integral, pointwise convergence 80−8778
field theory problems, alternating continuity principle in piecewise solutions 79−84959
fission reactor neutron transport theory, reduced three-dimensional transport equation with anisotropic scattering 80−18368
flat galaxies dynamics, integral eqn. for normal modes in matrix form 77−33637
flow, separated, internal, computation using coupled boundary layer-inviscid core, elliptic representation 80−1549
flow, separated incompressible boundary layer prediction, including viscous-inviscid interaction 80−1548
flow, separating boundary layer, subsonic, integral prediction method 80−1623
flow, swirled, in pipe, friction law and form parameters 79−37329
flow, viscous, time-dependent, integral representation approach to simulation 80−38375
flow, viscous incompressible, integral eqn., soln. by function-theoretic method 78−69990
flow in pipe, swirled, integral calc. method 79−37402
fluid, of hard-spheres, with dipoles and quadrupoles, integral eqns. approx. 80−24334
fluid with surfactant surface layer, slow rot. of axisymmetric solid 80−10284
fluid-structure coupling problem soln. using boundary-integral eqn. method 77−54920
flute oscillation suppression by automatic EM control *(Russian)* 78−30464
flux calculation in complex heterogeneous reactor cells by imbedding element method *(Russian)* 78−58321
force-free fields, Neumann's type boundary-value problem soln. 78−12585
four particle problem in resonating group approx. 77−2960
Fredholm, anal. of elastic cylinder with internal circular crack *(Russian)* 79−59944
Fredholm, anal. of granular layer on elastic foundation, axisymmetric contact problem 79−27600
Fredholm, anal. of heat transfer in composite solids with heat generation 79−76949
Fredholm, anal. of stress distrib. in vicinity of external crack 80−23954
Fredholm, approx. soln., degenerate-kernel methods convergence 78−12543
Fredholm, contact problem of elasticity for space with spherical hollow *(Ukrainian)* 79−50669
Fredholm, first kind, appl. in electromag. field theory 78−94357
Fredholm, forced torsional vibrations of a semi-infinite piezoelectric medium of (622) class 79−51910
Fredholm, mathematical analysis of decomposition *(Italian)* 77−45677
Fredholm, plane stress state anal. in macroscopic model of composite material *(Russian)* 77−80069
Fredholm, second kind, appl. to elastic deformation anal. of large thick plate 79−90132
Fredholm, second kind, with Cauchy type singular kernels, approx. solns. using Chebyshev series 79−2611
Fredholm, soln. for cylinder containing radially stretchable disc, axisymmetric problem 77−58551
Fredholm, soln. for elastic cylinder embedded in elastic half space 79−27524
Fredholm, soln. for penny-shaped crack in a sphere embedded in an infinite medium 79−27585
Fredholm, type two, inviscid gas, nonequilibrium flow past thin profile 77−84344
Fredholm 1st kind for acoustic calc. *(Russian)* 80−58834
Fredholm elastic, axisymmetric shrink fit problems of cylinder of infinite length 77−75803
Fredholm eqn. of the second kind for current distrib. in antenna theory *(Chinese)* 78−66708
Fredholm eqns., criticality anal. of slab reactor 79−26475
Fredholm eqns. from strip with one-sided constraint under moving load 77−7305
Fredholm eqns. soln. *(Russian)* 78−86120
Fredholm eqns. with kernels $K(z-z_0)$, resolution by operational calculus 79−88794
Fredholm equation, for plane EM wave diffr. by grating at interface 79−27139
Fredholm equations solns., error bounds, appls. to pot. scatt. and bound state problems 77−71234
Fredholm integral eqn., soln. by collocation variational method 77−71229
Fredholm integral equation, free-knot spline inversion using nonlinear least squares method 79−2486
Fredholm integral equations in computational methods for solving static field and eddy current problems 79−68344
Fredholm integral first kind eqns., soln. via Ricatti differential eqns. depending on parameter *(Russian)* 78−54153
Fredholm linear eqns. of first kind, failure to satisfy Picard's condition 79−2601
Fredholm non-singular eqns., numerical soln. 78−16630
Fredholm-Poincare integral eqn., induced potential problem in 3-D 78−58880
free convection laminar flow, viscous dissipation and pressure stress effects importance 78−63428
free-molecule flow, through circular tube with sudden enlargement or contraction 78−14047
freely gravitating charge, radiation, in field of weak plane gravitational wave *(Russian)* 78−89381
Fresnel-Kirchhoff integral equation, analytical solns. for marginally stable resonators 79−94262
frictionless elastic contact problems, approximate soln. 78−16646
Galaxy stellar orbits, applicability of approximate third integral of motion 80−67798
galaxy two-point correlation function, integral constraint on evolution 77−5578
Galerkin solution using cubic splines 77−26189
Galerkin-finite element formulation in viscous flow 79−14367
Gaussian integrals, evaluation by backwards recursion or Taylor expansion 80−31488
generalised finite element method for magnetostatics 79−41270
generalised integrals involving elliptic functions, appl. to stellar structure 77−71107

integral equations continued
geodesy, soln. of downward continuation problem by initial value method *(German)* 77−86750
geophysical fields, props. of linear integral transforms *(Russian)* 79−35007
geophysical inverse log.-potential problems, integral and functional eqn. analysis 77−40968
glow curve integral, computation technique 79−8199
Griffith crack in nonhomogeneous medium under shear, asymmetric problem 79−18813
Griffith crack-antiplane shear wave interaction at interface of two bonded elastic half-spaces, geophys., seismological appl. 80−92087
groundwater two-dimensional unconfined saturated flow, boundary integral solns. 78−77291
guided light propagation mode computing, in fibres with non-circular cross sections 79−76874
hard particle fluids, short range solvation forces 80−38885
hard sphere fluid, radial distrib. function, in semiclassical limit, integral eqn. theory 80−54089
heat conduction, inverse problem, integral eqns. calcs. 80−74695
heat conduction, inverse problems, two-dimensional linear integral eqns. 79−37120
heat conduction in axisymmetric body-duct configuration 79−32185
heat conduction inverse problems, soln. 77−42689
heat transfer between bodies in gas-filled contact, numerical solution 79−37130
heat transfer dynamics in channel, anal., impulse function method 79−37317
heat transfer in domains with sources having variable power, soln. 79−72891
heavy ion-solid surface collision cascade theory and expt. *(Japanese)* 80−11527
Helmholtz equation for region with corners, boundary distribution soln. method 79−58532
Helmholtz equation for two dimens. polygonal regions, numerical soln. method 79−63005
Helmholtz homogeneous equation, numerical soln. methods *(German)* 78−90337
high temperature gas diagnostics by spectral remote sensing 78−74002
Hilbert space, quantum mechanics and integration, functional integrals 79−97246
homogeneous kernels, Mellin transformation of generalised functions 77−49572
hydrodynamics, half-immersed cylinder, virtual mass, integral equation method 80−87783
hydrogenic one particle Green's function power moments, 1s-type orbital reduction 78−9051
image restoration by Gauss LU decomposition 79−76600
impact response of layered composite containing a crack, integral transform technique 77−50991
inclined derivative type boundary value problem, geometric criteria for Fredholm case *(Russian)* 77−49566
incompressible laminar boundary layer, three-dimensional, hyperbolicity of integral equations of momentum 77−27505
inductor-screen-ingot systems, EM fields calcs. *(Russian)* 77−46671
inhomogeneous many-body system integral equations for quantum liquids and solids 80−22732
initial boundary value problem for three dimensional heat equation, Rothe's line method *(German)* 78−30147
integrable evolution equations, general struct. 79−30201
integral eqn. with approximation of direct correl. function in pot. rigid core region 77−84611
integral inequality 77−82373
integral transport eqn., asymptotic props. near curved material interface 79−63175
interface penny-shaped crack, Fredholm integral eqn. soln. 78−90784
interface transonic separation due to plane stress pulse 79−68624
intermediate anomaly for Keplerian motion, elliptic integral of first kind 78−45209
inverse scattering problem, class of singular integral eqns. 77−17878
inversionlike integral eqn. in multidimensional case 78−62054
inversionlike integral equations generalisation, appl. to nonlinear partial differential equations soln. 78−86117
ion-atom collisions, charge transfer, new integral eqn. calc. method 79−45832
ionic liquids, hypernetted chain eqn., Newton Raphson soln. 80−49071
irreversible processes, nonlinear, memory function calc. 77−26265
Ising ferromagnet, transition temp. in integral representation 77−77059
isochronous cyclotron sector magnet field calc. 79−41053
isoparametric, finite element variational solution 77−87635
iteration algorithm *(Russian)* 77−53765
Ito-Doob, martingale model for estimation in nonlinear stochastic physiological systems 77−77865
K-transforms, theorems 77−17776
Kepler motion, generalised, Lie groups of motor integrals 78−85831
kernel approx. in axially symmetric temp. problem 79−35643
Kinnersely-Chitre transforms for spinning mass solns. to Einstein eqns., integral eqn. method 79−97267
Kinnersley-Chitre transformations, integral eqn. method 80−17844
Kirchhoff shells, static and dynamic anal. based on mixed finite element formulation 79−32328
Kirkwood-Salzburg integral eqn. solns. for boson and fermion systems *(Ukrainian)* 79−93036
Kondo effect, in finite mag. field, Suhl's dispersion eqns. 77−24673
laminar boundary layer flow, convection anal. 78−34137
Landeu model, critical multiple correlations 79−75440
Laplace's equation, numerical soln. by integral eqn. method without Green's function 79−12564
Laplace eqn., axisymmetrical Koshi problem *(Russian)* 80−101713
large algebraic eqn. systems, direct and iterative solns. 79−41274
laser theory integral eqn., concept of 'approx. eigenvalue' 77−67217
Lennard-Jones low temp. gas, eqn. of state, integral eqn. and perturbation method 78−26228
lifting surface integral eqn. solution *(Russian)* 78−73836
lifting-line theory, alternative treatment as perturbation problem 79−27663
light diffusion in optically finite shell, linear integral eqn. *(Russian)* 77−13236
light scatt. from three-dimensional obstacles with complex refractive index 77−75415
light scatt. in anisotropic two layer medium, auxiliary functions *(Russian)* 77−54671
Lighthill nonlinear integral equation, soln. 79−6061
linear random integral eqns., approx. solns. by method of moments 77−64934
linear rarefied gas dynamics, integral transport equation functional anal. 79−50756
Lippmann Schwinger eqns. for three charged particles 80−4580
Lippmann-Schwinger equation, numerical soln. 78−81802
liquid, simple, equilib. theories, review 80−38887
liquid metals, radial distrib. function and thermodynamic characts., interparticle interaction pot. *(Russian)* 80−49086
liquid structure, integral eqns., numerical solns. new method 80−28896
liquid-vapour interfacial density profiles by integral eqn. approach 77−35682
liquids, simple, thermodynamically self-consistent theories, radial distrib. function, functional derivative 80−92435
longitudinal wave diffraction, geometrical theory for three-dimensional elastodynamics, integral transforms 77−46829
magnet immersed in ferrofluid, force on, surface integral calc. 78−94350
magnetic field calc., two-dimens., boundary integral eqn. method 78−94355
magnetic field problems, numerical techniques 80−32878
magnetic induction determ., current distributions in presence of ferromagnetic bodies 80−18958
magnetoelastic waves, shear, horizontal, integral representation 77−90009
magnetostatic problems, 3-dimens., soln. using scalar potentials 79−22879
magnetostatic problems with thin plates or shells 78−50675
magnetostatics 79−72453
master equation, path integral soln. 79−12715
materials with memory, nonlinear integral representations 77−42732
mathematical modelling of highly parametrised integral or differential equations 79−35492
Maxwell equations, time-harmonic, exterior boundary-value problem of EM reflection 80−28148
megnetic deflection yokes, mag., integral eqn. method for anal. 79−50183
mesometeorological stationary problem of flow around obstacle 78−81271
meson bound state eqn. and solutions 78−78101
metal, spatially dispersive, EM waves and plasmons, propagation 80−15549
metal creep, nonlinear integral eqn., existence and approx. solns. 78−13931
Milne equation with Pincherle-Goursat kernel, Cauchy problem 77−2513
Mindlin plate elements, free vibration anal. 79−46244
minimally coupled N-particle scatt. integral eqns. 77−88090
mixed boundary value problem in three dimens. 77−71184
mixed boundary value problems for Helmholtz eqn., integral eqn. method 78−57751
mixed continuous mechanics problems, orthogonal functions *(Russian)* 78−49659
mixtures of reacting gases, extension of Chapman Enskog method *(Russian)* 78−57878
mm EM wave scattering from precipitation particles, calcs. 79−22882
model nuclear matter, hypernetted chain integral eqns. 79−490
molecular Hartree-Fock integral eqns., soln. 79−76325
molecular integral explicit expressions, generalised Chong method 78−892
molecular quantum mechanics, $F_m(y)$ function, improved computation 79−63892
molecular theory of fluids, integral eqn. equivalence 79−86670
momentum space, electron molecule. scatt. 80−48087
motion integral disappearance in multi-resonance conditions 78−77471
multi-part mixed boundary value problems, numerical solns. 77−68430
multidimensional singular integral eqns., numerical methods, anal. of elastic solids 77−17818
multiple integrals, evaluation, correl. functions of Legendre ensembles 77−22396
multiple integrals in waveguide scatt. problems 79−3796
multiple integrals of transfer theory 78−4568
multiregion problems in plane geometry for neutron transport 78−17274
multispectral radiance method for temp. distribution meas. *(Japanese)* 78−77912
Muskhelishvili Omnes integral equation, soln. procedure 77−13577
N particle systems, one-dimens., completely integrable, construction technique 78−57768
N-body integral eqns. and orthogonality scatt. 77−17861
N-particle quantum scattering theory, spurious solns. of integral eqns. 78−65812
N-particle scattering, combinatorics 78−24693
natural convection film boiling, from spheres to saturated liquids, integral calcs. 78−34129
neural network models, excitation and inhibition structures 79−2044
neutron hot perfect fluid relativistic stars, asymptotic eigenfrequency distrib. for even parity perturbations 78−49668
neutron transport, collision probability integrals in annular geometry, properties 79−22361
neutron transport, eqn. soln. in x-y geom. by numerical method 77−3066
neutron transport integral eqn., iterative and direct approaches to critical dominant eigenfunction 77−38313
neutron transport theory, F_N method 79−30877
neutron transport two-group integral eqn., asymptotic solns. 77−14203
non-linear uniaxial integral constitutive equation incorporating rate effects, creep and relaxation 80−28436
non-Maxwellian distribution integral representation and approach to equilib. 80−10343
non-Newtonian pulsatile laminar flow in tube 78−79346
non-self-adjoint linear operators, bivariational bounds 77−49569
nonequilibrium statistical mechanics, path integral formalism based on Onsager's principle 77−67373
nonhomogeneous elastic layer bonded to nonhomogeneous half-space, torsion by circular die, Fredholm eqn. 78−87263
nonlinear, periodicity threshold theorem 79−5973
nonlinear, soln. for sluice gate problems with gravity 77−39349
nonlinear creep problems in symm. press. vessels, uniqueness of integral eqns. positive solns. 77−65694

integral equations continued
nonlinear elasticity strain energy, integral bound for displacement boundary value problem 79−37171
nonlinear optics, extinction theorem 77−14770
nonlinear transient heat transfer, through multilayer wall *(Russian)* 77−23857
nonmonotone stochastic integrals and stochastic differential calculus *(French)* 80−90779
nonsingular integral eqn. for three body scatt. problem 78−62106
nuclear coupled two-body channel scatt., nonsingular eqn. 77−30526
nuclear medicine, fourier reconstruction with a distortion function 80−8174
nuclear physics nonlinear integral eqn. solution *(Chinese)* 78−74324
nuclear scattering N-particle transition operators in channel coupling scheme 78−569
numerical anal. in applied engineering science (conf. May 1977) 77−67249
numerical calc. of eigenvalues, of scalar Helmholtz equation 77−78964
numerical inversion of Laplace transform and Fredholm integral eqns., eigenvalues and eigenfunctions 78−81800
numerical methods, book 78−41143
numerical props. of integral eqns. in which boundary values and solns. defined on different curves 77−68428
numerical soln., improvement of Sastry's method by Richardson's extrapolation 78−28924
numerical soln. by boundary integral eqn. method 78−92850
numerical soln. by multi-part mixed boundary value problems 78−62056
numerical solution, computer-aided, dynamic temperature meas. data recovery 77−5839
numerical solution of a class of integral equations arising in two-dimensional aerodynamics 78−62086
numerical solutions of integral equations with kernels containing poles, interpolative technique 78−41141
numerical solutions of problems in quantum mechanics and quantum field theory 77−2526
numerical treatment of boundary integral eqns., three-dimens. elastostatic anal., fracture mechs. appls. 77−46909
one dimensional wave function for the effective Hamiltonian of non-local potential 80−46847
one group, integral transport eqn. for homogeneous sphere, neutron scatt., classical diffusion, anal. 78−62589
optical wavefunctions, inversion of integral equation for system distorted by aberrations 79−98304
optical waveguide, diffused, energy distribution determ. by rigorous solution 78−63200
organ flue pipes, self-sustained oscillations, integral eqn. soln. 78−51015
Ornstein-Zernike eqn., rel. to pair pots. calc. 77−1054
orthotropic laminate composite, broken layer 78−38254
partial-wave Schrodinger differential and integral eqns., comparison of numerical solns. 78−16671
path integral representation for U- and S-matrix, scalar meson model renormalised S-matrix elements 78−78103
path integral representation of QFT for S-matrix, meson field-nucleon field interaction 79−2947
path integrals in Riemannian spaces, smooth path spectral anal. 80−52059
penny-shaped crack, sudden twisting in a finite elastic cylinder, stress calcs. 78−67110
Percus Yevick eqn. for square mound pot., perturbation soln. 78−22619
Percus-Yevick eqn., existence and local uniqueness of solutions 80−36936
Percus-Yevick eqn., orthonormal series expansion soln. 80−49065
periodic curvilinear cracks in isotropic medium, integral eqn. soln. 78−51118
periodic Green's function, solution electric potential problems, appl. 77−82370
periodic interface scattering, rigorous method derived from integral formulation 79−13896
phase space functional integrals of quantum mechs., Hamiltonian quantization 78−41194
piecewise-uniform plane, curvilinear cracks, integral eqns. of heat conductivity and thermoelasticity *(Russian)* 78−38250
plane crack, in infinite solid, stress intensity factor under normal pressure 79−72855
plane crack displacement field, integral eqn. formulation *(French)* 79−55338
plane elasticity, cracks, Cauchy type integrals and integral eqns. with logarithmic singularities 79−30252
plane elasticity, periodic contact and crack problems, closed form solns. 77−42783
plane elastostatic boundary value problems, formulation as integral eqns. by singularity method 79−35556
plane elastostatic boundary value problems, integral operators, eigenvalue num. calc. 80−36848
plane elastostatic boundary value problems, Rizzo's integral and Kupradze's functional eqns. 80−57093
plane elastostatics, boundary value problems, spectra of integral operators 78−57782
plane elastostatics, integral equations for mixed boundary value problem 80−79143
plane elastostatics, numerical props. of integral eqns. describing boundary value problems 78−34013
plane electron-optical system, electrostatic field anal. with integral eqns. of first kind 77−19157
plane isotropic elasticity, crack stress intensity factors using singular integral eqns. 79−72858
plane permanent magnet system field distrib. model *(Russian)* 80−28133
plane-fronted gravitational waves, integrals of wave equations in space time *(Russian)* 78−89380
plasma, nonequilibrium, nonlinear EM fluctuation field correlation functions *(Russian)* 78−9756
plasma cylinder short-wave probe, inverse diagnostics problem formation 78−67423
plasma diagnostics of radial profiles axisymmetric plasma Abel eqn. soln. accuracy 77−84506
plasma magnetic field determ. using Abel eqn. inversion 80−28825
plastic torsion and integral inequality anal. 80−10155
plate, circ., thin, elastic, containing Griffith crack, in infinite elastic medium, stress distrib. 79−32374

integral equations continued
plate, elastic, under uniform twisting, periodic collinear cracks *(Japanese)* 78−67097
Pocklington integral eqn. basis function continuity requirements 77−74208
polymer chains, zero component field *(French)* 80−69280
polymerisation, multicomponent, differential and integral rate eqn. 78−23944
polyoxymethylenes, dielectric property relaxation, unidentical relaxator system activation model *(Russian)* 80−80694
porous medium, drying, evaporation characteristics determ. *(Russian)* 79−37134
Possio equation, approx. unsteady thin airfoil theory for subsonic flow 77−23978
potential approach appl. 77−68429
potential flow problems, partition technique integral eqn. method 78−49652
potential problem, numerical soln. by integral eqns. without Green's functions 77−26162
potential problems, numerical solution, integral equations without Green's function 78−20950
potential problems, two-dimens., numerical soln. by boundary integral eqn. method 79−58533
potential problems with source function not located on boundary 78−24643
potential theory, higher-order approximations 79−22877
power measurement in three phase AC circuits *(German)* 77−74458
principal value collision integrals, reduction scheme 77−57234
product integration, choice of point, convergence 80−68396
projections, reconstructions and orthogonal functions 77−41463
proper functions of two-dimens. field, air pollution appl. 79−21002
quadrupole trigonometrical integral eqn. soln., appl. to crack problems 79−72852
quantal hyper-netted chain eqn., Kohn-Sham theory derivation 78−47225
quantum gravity and path integrals, supersymmetric theory, virtual Planck-mass black holes 79−2706
quantum mechanical perturbation problems, resolution using integral eqn. 80−58112
quantum mechanics, Feynman path integrals with Gaussian measure, Laplace transform method 80−62522
quantum oscillator, phase automatic freq. control parameters, optimal values *(Russian)* 80−77814
radiation fields from polygonal sources, Fock method 78−83060
radiation from vertical electric vibrator, located on axis of ideally conducting disc 80−106418
radiation theory, equivalence of some integrals 77−49285
radiation transport, integral equation methods 77−53843
radiation transport, multidimensional, in plane-parallel atmosphere, appl. to 4.3 μm auroral arc 78−88917
radiation transport in absorbing medium, analytic solns. 77−14886
radiative flux local characteristics calculation using Monte Carlo method modification *(Russian)* 79−35648
radiative source function, isotropically scatt. medium, refr. index effect 77−83805
radiative transfer, general integral transform of exponential integrals 79−88577
radiative transfer, integral eqn. spectrum calc. for semi-infinite medium 80−67540
radiative transfer, invariance principles and integral eqns. for radiation fields in plane atmosphere 80−67559
radiative transfer, inverse problems method in transport and filter theory 79−29920
radiative transfer, linear eqns. for spectral line broadening by electron scatt. *(Russian)* 77−17347
radiative transfer, unified treatment of reflected and transmitted intensities, integral eqn. 78−85838
radiative transfer albedo problem in inhomogeneous isotropically scatt. atmospheres 80−36398
radiative transfer eqn. exact soln. for semiinfinite plane-parallel isotropic scatt. atm. 79−12396
radiative transfer equation, quadratic integrals for monochromatic isotropic scatt. 77−33332
radiative transfer exponential integrals, Λ-transform determ. 79−35114
radiative transfer in expanding homogeneous sphere *(Russian)* 78−73945
radiative transfer in fibrous media 78−94571
radiative transfer in finite plane parallel media, linear Fredholm eqns., imbedding in infinite medium 78−81532
radiative transfer in finite plane parallel media, linear Fredholm eqns., imbedding in semiinfinite medium 78−81533
radiative transfer X- and Y-equations, new representation using Wiener-Hopf technique 79−53710
radioactive pollution, atmospheric, concentration time integral *(German)* 80−26378
rapidly varying integrands, asymptotic expansions, Sommerfeld integrals for microstrips appl. 80−14272
rarefied flow, low-speed flow over sphere, convergence of integral methods 78−22375
rarefied gas mixture Poiseuille flow 79−14438
recirculation maths. and cardiac output meas. 77−56404
recurrence relations for integrals of associated Legendre functions 79−29690
reduced Bessel functions, three dimens. convolution integrals evaluation 78−32654
reflection from moving boundary between two dielectrics in waveguide 77−584
renewal equations system, extension of Feller's renewal theorem 77−33841
resolution method for second problem of elastic limits for plane *(French)* 78−57779
resonant thermonuclear reaction rate integrals, closed-form evaluation and approximation considerations 80−8535
retina, Limulus, oscillatory responses 80−101166
retina of Limulus, spatially synchronised oscillatory response theory 78−73158
Rice's polynomial, integral eqn. soln. 77−22371
ring laser, open cavity matrix eqns. in diffraction theory 80−69429
rotating disk, in liquid surface with adsorbed film, torque 78−32685
round buoyant jets in stratified flows, integral eqns. 79−27680
Roy eqns., multiple solns., N/D method on finite interval 78−16949

integral equations continued
Saint-Venant torsion problem, classical, integral and functional eqns. 78−57780
Salpeter equations, integral transform and relativistic radial eqns. 80−4835
scalar Helmholtz equation, integral formulations 78−36796
scattering amplitudes with positivity constraints, analytic extrapolation, integral eqns. 79−35589
scattering by several fixed scatterers, wave mech. 77−78996
scattering from randomly rough surfaces *(French)* 80−53193
scattering integral equations for distorted transition operators, N- particle scatt., DWBA 79−6532
scattering of neutral atoms by exponential corrugated pot. 80−25512
scattering theory integral eqns., close coupling method *(Russian)* 77−74268
scattering theory of ≥4 particles, on the unique soln. 78−21005
Schrodinger eqn. for atomic evolution operator, transitions to continuum, Fredholm method 79−72223
Schrodinger integral equation, soln. using El-Gendi approx. method 78−77749
screw dislocations, moving in elastic nonlinear medium, displacement field *(Russian)* 80−44206
seismic data migration in two and three dimens., integral formulation 78−77342
seismic wave-equation datuming technique, Kirchhoff integral formulation 80−51553
seismology, waves integral spectral parameters method for geological section prediction *(Russian)* 79−8705
semiclassical path integrals in terms of catastrophes 80−8860
semiconductor, minority carrier conc. determ., integral eqn. approach to abrupt depletion approx. 77−32022
semiconductor magnetoconductivity, practical approx. to integrals 77−15870
shallow water with moving boundaries digital simulation, finite element method appl. 78−92847
shock tube flows, unsteady non-equilibrium, discretisation of boundary layer terms 80−14742
simultaneous, anal. of 3-D wave propagation in cracked elastic solid 79−46251
simultaneous Wiener Hopf eqns., Fredholm integral type soln., wave diffraction appl. 80−57100
singular, anal. of anisotropic discs *(German)* 78−87272
singular, numerical soln. 78−32661
singular, two-group problems with anisotropic scatt., closed-form solns. 78−4569
singular eqns. of airfoil class, generalised Theodorsen soln. 78−1682
singular integral eqns. of first kind, finite element method 77−64935
singular integral equations, for acoustic surface-wave diffr. and guidance anal. 78−13828
singular integral operators with integral eigenvalues and polynomial eigenfunctions 79−62997
singular integrals, 2-dimens., used in 3-dimens. elasticity 79−35561
singularities in Feynman integrals of quantum field theories 79−40661
solenoid, windings, nonlinear eqn. for equal loading 79−55028
solid body radiation problem, soln. 80−77734
solitary Rossby waves, atmospheric, associated integral invariant 80−56539
solution by optical spatial filtering 79−3643
space-time integral eqn. scattering by finned cylinders 77−75390
spatial-correlation theory, evaluation of integral 77−88981
spherically stratified medium and bounded obstacle, integral equation 79−32120
spin correlation function for free induction decay, appl. to CaF_2 77−8421
spin lattice models, continuous-integral method 78−93615
spin-orbit potentials, quantum scattering theory inverse problem, fixed energy Jost functions *(Russian)* 80−68082
stability criteria, appl. to gas chromatography 78−62049
stellar accretion magnetospheres, general solns. 77−45400
stellar dynamics, construction of formal third integral of motion in reson. cases 77−53647
stellar dynamics, formal third integral approximations for reson. orbits 80−56889
stellar orbits in rotating galactic bar, isolating integrals of motion 80−4404
stellar orbits near galaxy particle resonance, reson. integral of motion 80−26914
stochastic integral equations, nonlinear, mixed type, existence, uniqueness and stability of solutions 80−68131
stochastic Volterra eqn., existence and uniqueness of soln. 78−89405
stochastically macro-inhomogeneous medium, integral equation of mean radiation intensity *(Russian)* 78−5639
Stokes equation, appl. to gravity pot. calc. 79−62428
Stokes problem of motion of Cassinian cylinder in viscous fluid 78−71312
streaming, uniform, past fixed semicirc. infinite strip 79−23299
stress analysis, connection between finite element and integral equation methods *(French)* 77−87649
stress analysis, three dimensional, by boundary integral eqn. method 79−58546
stress intensity factors FOR X-formed arrays of cracks 78−67121
stress singularity at the corner of a wedge-shaped crack or inclusion 79−46268
summation formula for integral computation over sphere 79−29689
supersonic boundary layer flow about cones, method of integral relations 79−10589
supersonic lifting surface, finite element anal. and collocation method 78−1687
surface integral calc. in numerical investigation of 3D fields *(Russian)* 79−64143
surface lattice dynamics and density response 78−71930
surface plasmon, eigenmodes, Fredholm integral eqns. *(French)* 78−56195
surface scatt., electric field integral eqn. formulation 77−38784
surface wave, scattering, by submerged sphere 78−34145
temperature integral, approximative eqns., accuracy analysis 80−36834
thermal conductivity infinite and finite integral transforms solution 77−75773
thermal diffusion, integral eqn. method 77−17928
thermally induced stress, intensity factors calc. using contour integral method 79−37243
integral equations continued
thermoelastic periodic problems for infinite solid with disc shaped cracks, integral eqn. solns. *(Ukrainian)* 78−55559
thermoelastic punch problem for elastic layer overlying elastic half-space 77−42742
thermoelasticity, advanced boundary integral eqn. method 77−72175
thermoelasticity problem, plane, for solids with curvilinear hole and cracks *(Ukrainian)* 77−31257
thermoelastoplastic 3-D problem formulation by integral eqns. 79−7292
thermoelastoplasticity three-dimensional integral eqns. *(French)* 78−90718
thermonuclear reaction rate, parameter-depend. integral evaluation 79−29985
thin finite dielectric cylinder, scattering and absorption of EM waves 80−74281
thin plates, treatment of boundary conditions on distinct boundary curves by integral eqns. *(German)* 79−49042
three- and two-dimensional eddy current problems, Fredholm integral eqns. 79−41298
three-body problem, doubly averaged elliptical restricted, first integrals 80−17479
three-body problem, generalised twice restricted, generalised energy integral *(Russian)* 80−51643
three-body problem, restricted plane case, formal integrals 79−96900
three-dimensional radiation and scatt., surface-type integral eqn. approach 77−38782
three-dimensional single-phase Stefan problem 77−7300
torsion of connected bars *(German)* 78−34024
torsion of elastic layer, by annular die, Fredholm integral equation anal. 79−3969
torsion problem for elastic cylinder with holes, integral eqn. method soln. 80−36849
transient heat conduction, Laplace transform and boundary integral eqn. 77−72129
transient piezoelectric wave scatt. from crack 79−52615
transition metal surface, electronic perturbations 78−95334
transonic, integral eqn. formulation for lifting profiles and wings 78−38363
transonic flow, past thin two-dimensional airfoil 77−58721
transonic flow, three-dimensional, integral eqn. derivation 80−10259
transonic subcritical flow, numerical soln. by integral eqn. method 77−65756
transonic unsteady flows calc. using integral eqn. method, aerodynamics 79−32554
transport theory, nonlinear integral equations 79−30393
transport theory, optimum biasing of integral equations in Monte Carlo calculations 79−54078
transport theory, two-group integral transport equation, variational method 80−68156
transport theory integral eqn. soln. in Green's function formalism, scatt. amplitudes 80−4566
turbine blades, subsonic gas flow integral eqn. method *(Russian)* 79−27662
turbulence-degraded image a posteriori restoration using multiframe imagery 77−60469
turbulent boundary layer, compressible, extended mixing length appls. 78−94655
turbulent boundary layer development with fluctuating mainstream, integral method for calculation 79−94597
turbulent boundary layer with separated flow, integral method 80−1547
turbulent boundary layer-transonic shock wave interaction, integral computation method 79−1213
turbulent flow over body, Fredholm integral eqn., spline fit approx. 79−37302
unified Radon inversion formula 79−2598
uniform approximations to integral and integrodifferential equations 78−57742
unilateral contact problem integral eqn. approach 80−8798
vapour-liquid multicomponent equilib., Gibbs-Duhem eqn. 79−23714
viscoelasticity, dynamical problems, approx. soln. of integral eqns. 80−10164
viscoelasticity, Il'yushin kernels, analytical representation 78−67055
viscoelasticity equations, numerical soln. via Volterra integral eqns. 77−89042
viscoplasticity anal., boundary integral eqn. method *(French)* 78−90728
viscous flow, numerical boundary conditions 77−23929
viscous flow theory, exact soln. of integral eqn. 77−65764
visual activity lateral impedance theory, Markov processes appl. 79−2046
visual impedance, nonlinear integral equation 79−100599
Volterra, approx. soln. in polymer mech. 79−50614
Volterra, for heat conduction problems with variable heat transfer coeff. 77−14876
Volterra eqns., classes solvable using Laplace transform techniques 78−8224
Volterra eqns., numerical soln. of parabolic system 77−68437
Volterra equations, frequency domain methods 77−9854
Volterra integral equations, uniformly valid solns. 78−8225
Volterra nonlinear eqn. for gas absorption in liquid 77−72754
Volterra nonlinear eqns., soln. using two-point rational approximants 79−40351
Volterra nonlinear integral eqn., Mellin transform for asymptotic soln. 77−5636
Volterra nonlinear integral eqns. solns., existence, continuous depend. *(Chinese)* 77−67213
Volterra stochastic integral eqns. of second order, anal. of dynamic system of variable inertia 77−57166
Volterra stochastic nonlinear integral eqns., interconnected systems stability 79−71368
Volterra type in viscoelasticity theory, existence and uniqueness of solns. 77−62173
volume integrals of real part of nucleon optical pot. for A=10-238 78−78339
vortex motion, integrals of hydrodynamic equations, Helmholtz 1858 paper 79−9072
water wave diffr. and radn., numerical methods, book contrib. 78−59412
wave-induced oscillations in harbours of variable depth 79−4023
Weichert-Herglotz integral for low-vel. seismic zone inversion 80−21829
whistler propagation times eqn., inversion via spectral expansion 80−8495

integral equations continued
Wiener-Hopf eqns. in non-LTE radiative transfer, rapidly convergent iterative method 78−12089
WKB method for systems of integral equations 80−98787
X-ray small angle scattering, slit-height correction, exact soln., general method 78−42852
Yang-Mills 2-D theory in leading 1/N expansion 79−26242
yawed slender wings, Abel integral eqns. for wake strength 79−32552
Yukawa fluid, fluid-solid interface 80−38883
zodiacal light brightness integral inversion, three-dimensional eqn. 79−75155
d-α elastic scatt. three body eqns., Pade technique 78−46074
AgCl:Cd^{2+}, heavily doped, free energy and point defect distrib., integral eqn. method 80−107219
AgCl:$CdCl_2$, point defect model, free energy and radial distrib. functions 80−44201
BH_3-ethylene complex, semiorthogonalised orbitals, integral approx. scheme 80−83262
H+H interaction, second order dispersion energy, Borel integral investigation 80−74218
Pb particles, evaporation in arc plasma, integral eqn. method calcs. 78−1942

integral transforms *see transforms*

integrated circuit manufacture
Used for commercial manufacture only
see also masks; photolithography
dioptric lens applications 78−46754
microminiature cooler, thermoelectric, 3-stage, for stabilisation of microelectronics elements 80−31763
optical microscope, large field, for use in semiconductor manufacture 80−82812
plasma etching, chemically selective anisotropic 78−64755
production equipment, high vacuum cryopumps optimisation using thermal design criteria 80−22377
temperature monitoring, low-temperature radiometer with conical light pipe 80−47105
vacuum coater, automatic, using minicomputer or microprocessor 78−48317
VPE, reduced pressure, advances 80−40242
Ti-W magnetron sputtered films metallisation 80−45231

integrated circuit technology
See also under specific integrated circuit headings
see also semiconductor technology
acoustic microscope appl., using piezoelectric transducers 80−1387
biomedical electronics in MBE *(Japanese)* 79−44014
bipolar, collector diffusion isolation technology, assessment of radiation tolerance 79−45430
bipolar, epitaxial, pattern shift comparison in vertical, horizontal, and cylindrical reactor geometries 78−27408
cochlear implantable prosthesis realisation, hybrid technology 80−46099
CVD dielectric thin films, multiple internal refl. IR spectroscopy 80−11499
CVD of dielectric films, low press. techniques 79−100058
dielectric-isolated substrates, deform., and control by multilayer poly Si support struct. 80−107681
diffusion barrier layer evaporation, improved Cr-Zr source 80−76163
dry etched inorganic resist. for lithographic appl. 79−24633
dry etched line edge profiles, computer simulation 80−71780
electroless deposition of Au, substrate structure influence 77−8771
electron beam microfabrication, variable aperture projection and scanning system design 78−74836
electron-beam annealing of ion-implantation damage 79−77622
gas chromatographic air analyser fabricated on Si wafer 80−73343
gettering of impurities by intentional double diffusion 80−75383
hybrid IC monolithic crystal filter 77−39171
impurity predeposition diffusion profiles, errors in iterative numerical calcs. 78−26591
inorganic lithography using metallo-organic photoresists 80−79024
ion implantation, controlled doping profiles, angular sensitivity 78−30659
ion microprobe analysis, elemental imaging errors, polarity role 78−20103
IV-VI material production and physical props. for microelectronics *(Russian)* 78−11108
laser annealing to round edges of Si structures 80−25742
laser processing of thin films, review 77−23684
linewidth control, and pattern overlay errors, automatic meas., using EL-1 lithographic system 79−21868
lithography, optical and electron-beam, MTF evaluation 80−4801
LSI, lithographic manufacturing techniques *(German)* 79−71547
metal film wet-chemical etching, galvanic effects 80−25915
metallurgical coatings conf., San Francisco (1977) 78−2394
microanalytical method for IC with Si substrate *(French)* 78−35760
microelectronic component thermal stresses, photoelastic anal. 77−62217
microfabrication by ion-beam etching 79−78807
micrometallurgy and mats. development, review *(Russian)* 77−55874
microstructure fabrication, using STEM and X-ray lithography and reactive ion etching, appl. 79−15844
monolithic optical IC, based on Si, fabrication 77−19461
MOS, As diffusion through SiO_2, diffusivity and masking oxide thickness 80−39350
MOS, dielectric breakdown in electrically stressed films of thermal SiO_2 78−64322
p-MOS, master slice, appl. of B diffusion into Si from CVD Bn covered with Si_3N_4 80−107564
MOS, properties of sputtered WSi_2 as gate electrode and interconnecting material 80−70831
MOS compatibility of RF sputtered polySi films 78−6455
MOS LSI passivation using reactive plasma deposited Si-N films 78−56584
MOS processing, appl. of plasma etching techniques 80−40577
NDT wire bonds on Si chips, IR microscopy 78−95867
optical grating circuit fabrication by electron beam direct writing 80−64214
optical projection printer for IC fabrication, wavelength and coherence effects 80−64136
photomask and wafer linewidth meas. using optical spatial coherence 80−77850
photoprojection method of image formation of submicron patterns 78−71180

integrated circuit technology continued
plasma chemistry, appl. to IC fabrication 79−79252
plasma CVD equipment for formation of insulating films 80−25572
plasma etching control using optical reflection methods 79−57127
plasma etching process, Si removal from thin oxides and thin metal films 80−76384
plasma reactor for materials research good processing 77−40362
PMOS, deep diffusion of B at solid solubility limits 78−10070
positive photoresist., computer simulation of exposure and development 79−54208
positive photoresist, formulation, photochem. props., teaching appls. 78−89284
positive photoresists, optical system MTF meas. 78−9337
pressure transducer, miniature implantable, biomedical appl. IC fabrication techniques 80−76849
reactive sputter etching, plasma gas temp. determ. 78−63586
RF plasma etching, mechanistic considerations for selective etching 78−64754
sapphire ribbon microvoid distribution control in edge-defined film-fed SOS growth 77−77370
single crystals under large loads, theoretical elastic behaviour, review and appl. 80−71681
SOS, gettering effect by O implantation, Hall and Rutherford backscattering meas. 79−65103
SOS etching method 78−7070
SOS for LSI/VLSI technology *(German)* 79−95918
spark machining of thin films, with and without stencils *(Russian)* 78−27651
sputtered insulator film contouring over substrate topography 77−8752
superconducting IC fabrication technology 79−28493
surface mapping, interferometric method with variable sensitivity, IC manufacturing appl. 78−45592
template fabrication, SEM and electron lithography optics 79−75662
thermal analysis by IR microimager 78−45619
thin and thick film technology, conference, Augsburg, Germany (1977) *(German)* 78−39685
thin film capacitors using rare earth metal oxide dielectrics, characts. and design considerations *(Russian)* 77−1638
thin film circuit preferential sputtering process *(German)* 78−39691
thin film field ionisation source fabrication 80−52359
thin film resistors on Si, photoexcitation effects during laser trimming 80−64093
thin films in restricted geometry 78−72044
transition metal silicides, refractory for ICs, review 80−100820
vector scan electron beam lithographic system, deflection distortion 78−74835
VLSI, low temp. differential oxidation for double poly Si devices 80−16521
VLSI metallisation, Al and Al alloy metallisation sputter deposition 80−66429
VLSI multilayer metallisation interlayer dielectrics, CVD films 80−45235
VLSI processing by low-pressure CVD, review 79−87581
X-ray lithography fabrication of microcircuits 77−34059
X-ray lithography using synchrotron radiation, resist sensitivity 80−62820
Ag electroplated lead frames, surface struct. rel. to bonding behaviour, IC prod. *(German)* 79−11010
Al film, magnetron sputtered deposition, characts. 79−91587
Al-Cu film, magnetron sputtered deposition, characts. 79−91587
Al-Si alloy metallisation by rate controlled dual electron beam gun evaporator 79−11516
Al-Si contacts, effect of vacuum ambience 77−43718
Al-Si film, magnetron sputtered deposition, characts. 79−91587
Al-SiO_2-Si, void form. in Al interconnection lines at Si-SiO_2 boundaries 80−2476
Au electroplating, selective, on Pd-Ti conductor patterns, Si IC manufacturing appls. 79−95951
GaAs planar p-n junctions, Be ion implantation, fabrication and characts. 78−88022
P in PSG protective film, X-ray fluoresc. technique for rapid determ. 77−40612
Pt, sputtered film, Al and Mg contamination, AES, SIMS 77−11822
Si accelerometer, batch fabricated 80−73328
Si dry pressure-oxidation for low-temp. IC processing 78−7068
Si epitaxy and oxidation, first-order process models 78−72049
Si, polycryst., anisotropic plasma etching 80−85069
Si, reactive ion beam etching expts., selectivity, anisotropy 80−104308
Si substrate package for integrated GaAs laser arrays, fabrication 79−18555
Si, surface roughness evaluation by UV refl., appl. to IC fabrication 80−39393
Si, thinly oxidised wafer reflectance at normal incidence, calc. 79−78641
Si:B doping from BN sources, impurity transfer considerations 77−76441
Si-based technology for hemispherical laser fusion target fabrication 79−89495
Si-metal contacts, low temp. reactions 78−2567
Si-PVF_2 integrated acoustic transducer arrays 80−74683
SiN_x film reactive plasma deposition enhancement 77−77405
SiN_x, plasma deposited dielectric film, elec. props. 78−68103
Si_3N_4 film, laser coupling, new technique for refr. index and thickness meas. 77−88965
Si_3N_4 films, plasma deposited over substrate steps, fast etching phenomenon 79−34168
Si_3N_4, low temp. deposition using microwave-excited active N_2 78−84718
SiO_2 film, laser coupling, new technique for refr. index and thickness meas. 77−88965
SiO_2, low-pressure deposition from tetraethylorthosilicate, modelling 79−87582
SiO_2, reactive ion beam etching expts., selectivity, anisotropy 80−104308
SiO_2:B(P) film, high temp. deposition and evaluation 79−69989
SiO_x thin films on Si, anal. by backscattering techniques 79−96385
Ta-Al_2O_3 microelectrode array, design and fabrication 80−76868
Ti line fabrication, shadow deposition method using optical lithography for 0.15-0.3 μm widths 79−43148
Ti/Cu/(Au) thin films thermocompression bonds degradation by thermal ageing 80−66546
Ti-Cu, evaporated adhesion after electroplating 79−82475

integrated circuit testing
acoustic microscopes, nondestructive testing appls. 80−48537
cardiac pacemaker semiconductor component reliability trends 80−30943
defective struct. tests using scanning acoustic microscope 80−38190
fault detection by scanning acoustic microscopy 77−80040
function testing with stroboscopic microcomputer-controlled SEM 80−68294
laser microellipsometer appl. *(Czech)* 77−61109
leak test, automatic, nondestructive, design, evaluation and implementation for IC assemblies 78−53180
local voltage measurement by SEM 79−54156
LSI circuits, wafer defect classification using modified scanning electron microscope 79−21876
metal-oxide system characterisation by high-resolution electron spectroscopy 77−40624
microanalytical method for IC with Si substrate *(French)* 78−35760
microprocessor, SBP9900, radiation test 77−75002
monolithic integrated circuits, digitised layouts and impurity profiles, particle induced X-ray fluoresc. obs. 79−52804
multiplexer IC, MHz, microcomputer controlled stroboscopic scanning electron microscope for meas. signal waveforms 79−21871
NDT wire bonds on Si chips, IR microscopy 78−95867
nondestructive, ellipsometry appl. 79−85161
nondestructive evaluation by improved reflective scanning acoustic microscope 79−50551
nondestructive testing by acoustic microscopy 79−37094
pacemaker electrostatic discharge sensitivity grouping 80−30941
photoacoustic microscopy appl. 80−14525
plastic-encapsulated IC, metallisation corrosion test 78−11486
radiation hardness design, of microcircuits, SEM as diagnostic tool 79−21869
reliability, scanning electron microscope appl. 78−24902
scanning acoustic microscope examination of Si IC 78−13877
scanning electron microscope appl., ISI Model (7) 79−89044
SEM voltage contrast mode at semiconductor surfaces, anal. of conditions *(Czech)* 79−35897
voltage coding, LSI circuits, appl. of electron beam meas. techniques for verification of computer simulations 79−21875
Al_2O_3 moisture sensor for sealed hybrid packages 77−87754

integrated circuits
see also digital integrated circuits; hybrid integrated circuits; large scale integration; linear integrated circuits; masks; microwave integrated circuits; monolithic integrated circuits; substrates; thick film circuits; thin film circuits
amplifier, muscle potential monitor applic. 77−40899
biomedical IC differential amplifiers 77−48891
in broadband frequency multiplier for type KM-2 quantum magnetometer using optical pumping 77−37951
cardiac pacemaker, reliability technology conf., Gaithersburg, USA, (Jul. '76) 78−57129
conference, nuclear and space radiation effects, San Diego, Calif., USA (July 1976) 77−20376
conference Calcutta, India (Jul. 79) 80−96755
design improvements, digital measuring instruments appl. *(Rumania)* 77−74451
diagnostic ultrasonic instrumentation, effect of integrated electronics technology 80−17029
electronics technology development, teaching 80−31470
flaw detection in welded and soldered seams, Fourier holograms appl. 79−52580
health care expansion aided by integrated electronics 78−11751
linear convertor, for acoustic emission signals 78−9512
magnetic field meas., based on Hall generator *(German)* 80−52276
microcircuits 133 series, scaling decade circuit 77−18754
microelectronics and microprocessor impact on metals prod. and NDT 79−74320
microelectronics revolution, appl. in telecommunications, medicine, education 80−31446
pacemaker IC advantages and disadvantages 77−81725
Robinson oscillator, for NMR detection 77−74475
skin conductance meas. IC operational amplifier cct. 77−25566
strain measurement, in 10 μm spots using X-ray microdiffractometer 78−86262
telemetry system, implantable, multichannel, for animal physiological data recording 77−86661
telemetry systems, totally implantable, integrated circuit approach 80−67291
temperature controller, use of ICs, at cryogenic temps. 80−90856
thermoelectric coolers for micromodules 79−6120
time-amplitude convertor for 20 to 100 ns 77−50334
NbO_x-Pb Josephson junction, fabrication, integrated circuit technology 77−24645

integrated control systems
fission power reactor, zone regulation, intra- and extrareactor sensors 77−61525
nuclear power station, B&W system performance improvement 78−8946
pulsed ion cyclotron resonance spectrometer, integrated control system 79−71560
PWR operation and controls concept 77−88259

integrated data processing *see data processing*

integrated logic circuits
CMOS, for diffusion pump monitoring 77−5855
CMOS logic, basics 77−78925
digital frequency meter, for LF meas., using TTL ICs 78−86296
digital logic using integrated circuit modules, for teachers 78−81755
emitter-coupled integrated circuits, application to nanosecond nuclear electronics 78−5101
junction isolated, ionising radiation performance, black box modelling 77−83467
processor, fast mass depend. trigger for muon pair detection 79−97954
programmable combinatorial logic trigger system for high energy particle physics expts. 77−38589
seven segment display, for oscilloscopes 77−37933
shaper amplifier for proportional chambers, logical microcircuits and high time resolution 78−5103
signal interface element survey, low cost quantisers, fast ADC's, high energy physics appl. 79−45584
strain gauge transducer, digital output obtained from counter and logic ccts. 79−67281
TTL ICs, use of dry cells as power source, teaching 77−17745

integrated logic circuits continued
CdTe single-crystal film, switching and memory effects 78−76174
$LiNbO_3$/CdS integrated optical half adder circuit 79−76877

integrated memory circuits
ambulatory activity monitor with solid-state digital memory 77−52894
CMOS static memory, eight channel 64-bit scalar applic. 78−17531
layered piezoelectric-semiconductor surface state acoustic memory 78−90615
MNOS structures, discharge behaviour 79−38174
MOS RAM, influence of point like and extended defects 79−82679
MOS RAM, Siemens HYB 4116 16 384-bit, failure anal. using modified scanning electron microscope 79−21876
nonvolatile, book 77−78906
optical waveguide-hologram memory design approach 80−32940
Random-Access Memory-Interval Timer and buffered storage system 79−84066
SAW/CCD buffer memory device, operation 79−46137
VMOS dynamic memory, 65536-bit, investigation of alpha-particle induced soft errors 80−88223
CdTe single-crystal film, switching and memory effects 78−76174

integrated optics
see also fibre optics; optical films; optical modulation; optical waveguides; semiconductor junction lasers
4-bit digitally driven integrated optical amplitude modulator for data processing 80−53476
A/C convertor using channel waveguide modulators, design and analysis 79−55249
A/D convertor based on bulk acousto-optic interaction 80−69552
absorption spectroscopy in scattering samples using integrated optics 77−29232
acousto-optic Bragg deflector, wideband guided-wave, using tilted finger chirp transducer 80−74510
acousto-optic bulk interactions in thin film waveguides, for GHz modulators 78−42471
acousto-optic planar guided-wave Bragg modulators, integrated optic communication appls. 80−38131
acousto-optic tunable TE-TM mode convertor on diffused waveguide 80−53477
acousto-optical spectral analyser waveguide geodesic lens correction 79−50241
acousto-optics, guided-wave, with appls. to wideband communications and signal processing, progress review 80−58801
acoustooptic Bragg deflector, wide-band guided wave, using tilted-finger chirp transducer 80−14440
acoustooptical film deflector, efficiency for Gaussian beam 78−13791
active dielectric waveguide, symmetric first-order Bragg interactions 78−46765
active medium guided by reactive surface with reactance modulation, wave characts. 77−75710
active optical devices, seminar, San Diego, CA, USA (August 1979) 80−101664
active periodic media, stability of higher-order Bragg interactions 77−42629
active Y-junction switching devices in Ti diffused $LiNbO_3$ optical waveguides 79−23091
additional film in thin film slab waveguide, effect on waveguide propag. 79−81543
AlGaAs laser array with Si detector array for stabilization 80−58817
alkaline glass, ionic diffusion and exchange, integrated optics study *(French)* 77−88940
amplifier based on resonant tunnelling between passive and active optical waveguides 79−59838
anisotropic graded-index waveguide, optical mode propag. consts. calc. 80−69540
anisotropic medium, optical wave reflectance, general formula *(Japanese)* 78−87012
anisotropic optical waveguides based on Langmuir organic films 80−64177
anisotropic optical waveguides of $LiNbO_3$ type, guided and semileaky modes 79−18530
anisotropic waveguide for integrated optics, monomolecular layered film 78−66954
application to branching, switching, modulation in light systems including multimode fibres 78−87169
arachidate monolayers, optical props. integrated optics meas. 78−35214
aspherical geodesic lenses for integrated optical circuits, signal spectral analysis appl. 79−27437
astable multivibrator using Mach-Zehnder interferometric optical switches 80−87560
asymmetric three-layer optical waveguide, radiation losses due to discontinuities 80−53446
balanced-bridge switch modified config. with two straight waveguides 79−98506
beam splitter using variable thickness film 77−65626
bending losses of dielectric rectangular waveguides for integrated optics 78−63205
bent Guide structure semiconductor lasers, optimal ICs, appl. 79−41462
bibliography 78−66959
BIOD used as switch, amplifier, limiter and memory logic element 79−32090
birefringent prism couplers, for thin film optical waveguides 78−55468
bistable nonlinear Fabry-Perot resonator switching speed and energy calc. 80−64095
bistable optical device, transient response and applications 80−33214
bistable optical device development from integrated two-arm interferometer, appls. *(French)* 80−69555
bistable optical device using Mach-Zehnder interferometric optical waveguide 79−59843
bistable optical devices: an overview 80−58625
bistable optical devices 78−46763
bistable optical devices for integrated optics and fibre optics appls. 79−55175
bistable optical multivibrator using electro-optically controlled directional coupler switches 80−19111
bistable switch, based on waveguide coupler, exam. 78−38086
blazed dielectric gratings, Bragg-reflection approach 79−1013
blazed dielectric gratings, surface wave scattering 80−48136
blazed dielectric gratings for integrated-optics applications, microwave models 80−87564
blazed dielectric gratings with high beam coupling efficiencies 80−64211

integrated optics continued
blazed replica grating coupler for optical waveguides, design and fabrication 77−88972
blazed waveguide corrugations, loss coeffs. 77−34948
Bloch waves in periodic planar optical waveguides 80−58777
Bragg deflection of guided optical wave by surface acoustic waves in $LiNbO_3$ Ti-diffused waveguides 79−14118
Bragg deflector, using photorefract. effect in $As_{40}Se_{15}S_{35}Ge_{10}$ film loaded on $LiNbO_3$ waveguide 80−58673
Bragg diffraction grating, guided light refl., deflector appl. *(French)* 77−65621
Bragg effect waveguide coupler analysis 78−33827
Bragg interactions in active medium, first and second order 78−50747
Bragg mirror, corner-reflector type, laser beam divergence reduction 80−91822
Bragg mirror reflectance, dielectric waveguide inhomogeneity effect 80−28356
Bragg reflection in planar dielectric waveguides with periodic thickness modulation 77−79970
Bragg reflector statistical analysis 78−66882
Bragg spectrum analyser design 80−33237
Bragg switch, thin film 78−38088
Bragg switch for optical channel waveguides 78−75002
Bragg-effect polarizer/analyzers and lens-less waveguide beam expanders 80−58807
branching filter using three-dimens. input waveguide, nonradiative condition 80−38130
branching waveguide directional coupler, for GaAs-GaAlAs injection laser 78−38047
branching waveguide stripe injection laser, beam scanning and wavelength modulation 79−7138
Brillouin scattering in thin film waveguide 78−35153
broad band grating filters for thin film waveguides 77−83962
broadband chirp transducers for integrated optics spectrum analyzers 80−74514
bulk acousto-optic interactions in thin film waveguides, gigahertz modulators 79−32091
buried 2D waveguide with asymm. graded refr. index profile, modal solns. 79−41431
bypass dielectric waveguide mode order convertor 79−81570
C-CD parallel signal injection using integrated optical channel waveguide array expt. 78−37996
cell type optical circuitry fabrication using photopolymer 77−42633
chalcogenide glass films, kinoform optical elements and integrated optics elements prod. 77−75634
chalcogenide glass films, opt. inform. recording uses 77−75633
channel waveguide array, coupled to integrated CCD, fabrication and operation 78−38077
channel waveguide array CCD transversal filter 80−58797
channel waveguide array coupled to integrated C-CD, appl. 80−102860
channel waveguide array in fan-out pattern for high resolution optical imaging 80−38129
channel waveguide arrays coupled to integrated CCD 80−33244
channel waveguide coupling with fibres on Si substrate 78−46761
channel waveguide double-pole double-throw switch/coupler, using total internal refl. 78−71233
channel waveguide electro-optic switch, low crosstalk operation 80−38126
channel waveguide interferometric modulator for EM field detection 80−74498
channel waveguides, single-mode, prism coupling efficiency meas. 80−99878
channel waveguides and directional couplers with graded-index profile, analysis 79−81542
chirp-grating lens for guided-wave optics 79−7232
'Chirped' grating coupler: a holographic approach 79−76854
chirped grating lenses anal. 80−87563
chirped gratings, fabrication and optical props. 77−34963
chirped gratings, improved holography 80−102667
chirped gratings in broad band filters, theory 78−25994
circular strip waveguide, fabrication by Ag ion migration 80−96042
codirectionally coupled waveguides with weighted coupling, filter characts. 79−23068
coherent correlator for real-time signal processing 80−79007
coherent mode coupling at waveguide bends 78−38060
colloquium, London, England (May 1980) 80−79008
communication, conference, Amsterdam, Netherlands (Sep. 1979) 80−46733
communication, hybrid fibre optics and integrated optical circuit advances 77−75716
communication appls., future trends 79−3808
communication conference, Munich (1977) *(German)* 78−33854
communication devices, optical circuits *(Japanese)* 79−27408
for communications, present status 77−46822
component developments 80−1356
components for optical communication systems, review 80−87539
composite light-controlled waveguide struct., polystyrene film with methyl red dye as active medium 80−14464
composite waveguide laser with end-fire excitation, output characts. 80−23738
compound optical crosspoint with low crosstalk, using $LiTaO_3$ 78−33915
conference, Incline Village, NV, USA, January 1980 80−58772
conference, optical fibres and integrated optics, London, England (May 1977) 78−38063
conference, Reston, VA, USA, (Mar 1976) 77−46811
conference on integrated and guided wave optics, Salt Lake City, UT, USA (Jan. 1977) 78−38072
contradirectional frequency-selective couplers for guided-wave optics 80−102803
convex dielectric thin film fibre optical modes, conformal mapping 77−83996
convolution of ps optical signals 80−58629
corrugated dielectric waveguide, radiation loss calcs. 79−41461
corrugated dielectric waveguide, radiation loss calcs. for TM polarisation 80−43445
corrugated dielectric waveguide, second order stop band numerical study 80−23807
corrugated planar waveguides in the mid-IR region 79−98494
corrugated waveguide, guided mode diffr., coupled-wave eqns. 80−48434
corrugated waveguide, resonant wave conversion 80−74505

integrated optics continued
corrugated waveguide boundary, TM-polarized light diffraction, zero diffraction effect 79−64339
corrugated waveguide filters, mode conversion and filtering of obliquely incident waves 79−81571
corrugated waveguide filters, sidelobe suppression 77−84008
corrugated waveguide leaky modes, anomalies of dielec. coated gratings *(French)* 77−79969
corrugated waveguides, effective index approach to distrib. feedback, TE polarisation 80−102859
corrugated waveguides and lasers, improved coupled mode analysis 78−46842
corrugated waveguides and lasers, improved coupled mode analysis for TM mode 78−83117
corrugated-waveguide optical demultiplexer mode couplings 80−64194
coupled optical waveguides, coupling coeff. meas. by detuning 78−30066
coupled optical waveguides involving anisotropic or gyrotropic materials, theory and appl. 77−54789
coupled thin-film dielectric waveguides with tapered edges, EM surface waves 79−3792
coupled wave analysis, DFB and DBR lasers 77−27305
coupled waveguide modulator with p-n junction, multilayer planar waveguide config. 78−71235
coupled-waveguide optical modulators with Schottky contacts, embedded- and rib-waveguide configurations 79−23093
coupled-waveguide TE/TM mode sputter 80−99855
coupler, directional, operation and manufacture *(German)* 77−75673
couplers, double diffraction grating coupler with high efficiency 79 3812
coupling between single-mode fibres and integrated optical components, novel method and appls. 80−43442
coupling between substrates, tapered block coupling and mode conversion 79−50442
coupling coefficient modification by periodic modulation of propag. consts. 77−72092
coupling methods in single mode fibre integrated optics systems, review 78−59162
coupling to waveguides with linearly tapered horns, theory 78−33917
covered groove, optical surface wave scatt. and refl. 77−75707
crossed gratings appls. *(French)* 79−50441
crossed-beam diffraction gratings theory 79−23071
crossed-beam volume gratings, three dimens., diffr. characts. 80−78975
curved dielectric waveguides, coupling characteristics, coupled-mode equations 80−48455
curved-line grating form., use as reflectors and laser resonators 77−88971
deep dielectric gratings, light diffr., transform. props. 80−99835
deflector using chalcogenide amorphous film on graded index $LiNbO_3$ waveguide 80−48463
demultiplexer, using coupling between nonidentical waveguides 79−10380
demultiplexer with matrix of Si waveguide photodetectors 79−32095
detection of light in dielec. waveguide by photodiode through direct evanescent field coupling 78−30094
detectors development, with and without optical coupler *(Czech)* 80−33227
development trends, integrated optics vs. integrable optics 77−65643
developments in optical ccts. 80−48459
developments in USSR 77−88969
devices and applications 79−14117
devices fabricated by MBE 79−95943
DH injection laser coupling to optical fibre waveguide 78−33851
DH lasers, symmetric waveguide, near and far-field analytical approx. for fundamental mode 79−50296
dielectric branching waveguide mode order convertor 78−1379
dielectric film refractive index meas., synchronous angle integrated optical method 80−15976
dielectric gratings, arbitrary profiles, scatt. and guiding of EM waves 80−96005
dielectric optical waveguide characts. determ., far-field radiation patterns, semiconductor laser structure appl. 80−48407
dielectric rib waveguide, propag. and radiation characts. 77−79933
dielectric slab waveguide, scatt. characts. of beam mode 79−55230
dielectric waveguide, active, asymmetric first order Bragg interactions 79−3807
diffraction, at corrugated surface, Brewster affect analogues 79−13901
diffraction grating, curved, coupled-mode theory 80−83668
diffraction grating and optical waveguide coupler, fabrication by laser beam interference 78−1440
diffraction grating form. on optical waveguide surface, ion-beam etching through photoresist mask 80−14492
diffraction grating generation for integrated optics, interference method 80−48460
diffraction gratings, photoresist and GaAs, exposure and etching time optimalisation 80−23816
diffractive logic elements for optical computers 80−78993
diffused channel waveguides, direct index meas. 80−87562
diffused corrugated waveguide, diffr. emission and excitation of E and H-waves 78−25984
diffused microwaveguide, refr. index profile determ. 77−23764
diffused rectangular anisotropic waveguide, modal characts. rel. to integrated optics devices 79−27443
diffused strip-loaded waveguide, modal analysis by variational method 78−46776
diffused waveguide, acoustooptic interaction efficiency of TE modes, freq. depend. 80−53455
diffused waveguide, attenuation characteristics of TE modes and surface scatt. 80−5822
diffused waveguide, characts. determ. by profile approx. with parabola and exponential function 79−64341
diffused waveguide, corrugated section, H and E wave refl. and emission 77−34954
diffused waveguide, effective thickness meas. 79−32070
diffused waveguide, generalised parameters describing acoustooptic interaction 80−91924
diffused waveguide, refractive index profile determ. by inverse scatt. theory 80−5838
diffused waveguide tunnel excitation and emission 78−59146
diode laser wavelength monitoring using fibre interferometer 80−74413
diode lasers coupled to external resonators, tutorial review 79−94231
diode pumped miniature solid lasers 78−9392

integrated optics continued
diode twin-guide laser, narrow radiation angle for optical fibre coupling 78−46628
directional coupler, coupling length adjustment by loading a metal film 79−23055
directional coupler, made from plane gyroscopic, anisotropic light guides 79−18547
directional coupler as 2×2 switch, coupling length adjustment 79−94370
directional coupler as waveguide tap with infinitesimal insertion loss 80−99883
directional coupler modulator, 1 Gbit/s 80−38125
directional coupler switch, electrooptic, used as amplitude modulator, exam. 78−42467
directional coupler switch, polarisation independ., using weighted coupling 80−28352
directional coupler switches, modulators and filters using $\Delta\beta$ reversal techniques, review 80−38132
directional coupler theory, accuracy in fibre or integrated optics appls. 79−3810
directional couplers with graded index profile, variational analysis 80−96037
directional optical coupler, phase tuning 77−75680
directional waveguide couplers, parameter meas. using radiation patterns 79−3771
distributed Bragg deflector, multifunctional integrated optical device 78−83115
distributed Bragg reflector filter, polystyrene-collodion (polyvinyl alcohol) multilayers, fabrication 79−76838
distributed Bragg reflector for saturable resonator, bistability using Kerr effect 77−46737
distributed Bragg reflector injection lasers for integrated optics 78−42472
distributed Bragg reflector laser design, waveguide struct. 77−27306
distributed feedback radiating structure, refl., emission and transmission calcs. 79−10414
distributed feedback structures, hybrid modes 79−27441
distributed feedback waveguide structure, refl., emission and transmission calcs. 78−13819
distributed-feedback waveguide structure, dispersion characts. 78−66949
dye DFB laser with integrated Si and polyurethane channel waveguide 80−74373
dye doped polyurethane film, photoinduced guided light stopping 77−23739
edge MOM diode, integrated optical nonlinear device 77−88963
educational course, graduate, at Georgia Inst. of Technology 80−62414
elastic rubber waveguide, multimode thinfilm optical component fabrication 80−102857
elastomeric modulators 77−75715
electro-optic A/D conversion using channel waveguide modulators 78−66898
electro-optic devices, guided wave, for logic and computation 78−66946
electro-optic guided-wave A/D convertor, high speed 80−33234
electro-optic modulators, review 79−37058
electro-optic multimode waveguide modulator or switch 80−23783
electro-optic multimode waveguide switch 79−10383
electro-optic waveguide deflector performance characteristics 80−33213
electro-optical A/D convertor, using branching waveguide modulator channels 78−42474
electro-optical active components for guided light 78−42470
electro-optical Bragg deflection modulators in corrugated waveguides 79−59844
electro-optical channel waveguide switch for computer communication bus 80−9987
electro-optical devices for multimode optical switching 79−76882
electro-optical integrated two arm interferometer, optical bistability expts. 79−76883
electro-optical linear interferometric modulator for electromagnetic field detection 80−58782
electro-optical modulator, 12 GHz continuous tuning of CO_2 laser lines 77−83907
electro-optical multivibrator operation, in optical bistable device 80−58674
electro-optical nonlinear Fabry-Perot resonator, for optical signal processing 78−42460
electro-optical waveguide 3×3 switch, tuning and control theory 79−41458
electro-optics, conference, Utrecht, Netherlands (Oct. 1978) 80−31420
electron-beam and photolithographic fabrication of guided-wave optical components 78−13818
electrooptic analogue-digital conversion, using channel waveguide modulators 78−38051
electrooptic phased array light beam deflector, application to analogue-digital conversion 78−38052
electrooptic polarisation switch for multimode fibres 77−27335
electrooptic polarization modulated injection laser 80−58591
electrooptic radiation modulators utilizing semiconductor ridged waveguides 80−91925
electrooptic waveguide array deflectors, performance criteria and limitations 80−5821
electrooptical channel waveguide matrix switch using total internal reflection 80−58810
electrooptical distributed Bragg relfection modulators 77−27388
electrooptical oscillator, integrated cutoff modulation 80−48424
EM surface-wave modes in integrated optical systems, ray theory 79−64360
EM wave propagation in periodic structs., theory 79−45892
end fire coupling between fibres and diffused channel waveguides 77−79922
end-fire coupling between optical fibres and diffused channel waveguides 79−86252
endface coupling of planar and strip waveguides *(German)* 79−3795
endfire coupler efficiency calc. and expt. 80−102863
fabrication on ferroelectrics and semiconductors, research at Bell Laboratories 79−37055
Fabry Perot resonator containing electrooptical element, light processing appls. 78−38001
Fabry-Perot nonlinear electro-optic device, using refl. light feedback 78−55457
Fabry-Perot resonator, bistable, use as optical switch, limiter or memory element 77−39024

integrated optics continued
fact directional coupler switch/modulators, novel ps optical pulse sampling method 80−58784
far IR IC, antennas and waveguides for integration, review 80−69553
ferrite-garnet film, waveguide light propag. charact., integrated optics appl. *(Russian)* 78−1346
ferroelectric devices for optical systems 78−90473
ferroelectric materials, use in guided wave devices, review 78−38048
fibre and film waveguides, local normal modes, superlocal modes, ideal modes 80−14466
fibre butt-joining to Ti-diffused $LiNbO_3$ waveguide 79−76812
fibre communication systems 80−43487
fibre communications development and need for standardisation *(Italian)* 79−23066
fibre coupling, high efficiency single mode fibre/channel waveguide flip-chip coupling 80−58799
fibre coupling, simple permanent connection method for single-mode fibres 77−72097
fibre gyroscope, possible integrated optics soln. 80−10041
fibre optic multimode planar coupler device, formation using ion-exchange process 79−50429
fibre optic rotating sensor, Sagnac interferometer preliminary results 80−10040
fibre optic rotation sensor, all-waveguide configuration, key element tests 80−58796
fibre optical communication system with thin-film modulator 79−10407
fibre optical coupling to film 78−87167
fibre-optic communication and integrated-optics sources *(Italian)* 79−94371
fibre-optic integral data source/receiver package 78−63179
fibres, single-polarisation, slab model, strain birefr. 79−50381
film applications, review 78−71234
film mode excitation by Hertzian dipole 77−75709
film waveguide spectrum analyser with prism coupling 77−62071
filter, multilayer frustrated-total-internal-refl., spatially limited 80−96014
filter with surface corrugated diffr. grating, characts. for oblique incidence 78−50949
first order waveguide grating filters, random fluctuations 79−94369
fluoromethane DFB gas laser, construction and operation 80−23715
fluoromethane TEM_{00} far IR laser with integrated pump laser 80−58578
focusing diffraction grating, for integrated optics, holographic production *(Russian)* 77−84009
four-channel integrated-optics coupler and frequency-channel multiplexer 80−91936
four-layer isotropic waveguides, TE and TM modes 77−58433
four-layer waveguide diffractive injection efficiency optimisation *(Russian)* 80−64206
Fourier transform cct. 77−39111
Fourier transform signal processing in integrated optical format 78−50950
frequency multiplexing light source, integrated DFB diode lasers 77−702
Fresnel lens for thin-film waveguide 78−94452
Fresnel lens in thin film waveguides 78−38075
Fresnel lenses in BaO optical waveguides 80−96034
fulgimide planar photochromic structures for optical waveguide components 80−64196
functional components, fabrication of microstructs. in micrometre/submicrometre range, microlithographic techniques *(German)* 80−106637
functional elements based on vol. holographic gratings in As_2S_3 film waveguides 77−79972
future appls. 79−37053
GaAs epitaxial layer photoelastic channel optical waveguides 80−48457
GaAs homojunction rib waveguide directional coupler switch 80−69554
GaAs photo-FET high speed photoconductive integrated optical receiver 80−58816
garnet optical waveguide, with high Faraday rotation, mode degeneracy 78−94454
garnet thin film waveguide, magneto-optical effects 77−54802
Gaussian beam propagation in thin film waveguides 78−79102
Gaussian beams, divergence reduction using phase masks *(Russian)* 79−27308
Gaussian beams, waveguided, coupled by misaligned or curved grating effect 80−33228
Gaussian light beam propagation in thin films 78−33817
geodesic aspherical perfect lens, general sol. for integrated optics 80−10049
geodesic diffraction limited lens for integrated optic cct. 80−1357
geodesic lens, aberration corrected, for integrated optics circuits 78−38074
geodesic lens, axially symmetric, geometrical theory 80−33238
geodesic lens, diffraction-limited, in polyurethane waveguide struct. 78−94453
geodesic lens design for integrated optics signal processing 80−33247
geodesic lens formation in diffusion fabricated optical waveguides 80−91937
geodesic lenses, aberration-corrected rounded edge, profile calcs. 80−10048
geodesic lenses, anal. by beam propag. method 80−58686
geodesic lenses, axially symmetric, design parameters 78−83114
geodesic lenses, change of focal length as function of depth change due to fabrication errors 80−38128
geodesic lenses, edge-rounding effects 77−7216
geodesic lenses, spherical aberration correction and fabrication tolerances 79−27435
geodesic optical lens prod. by anisotropic etching 80−10047
geodesic optical waveguide lens analysis: comment 79−76879
geodesic optics: new components 80−58800
glass 7059, film acousto-optical props. for integrated optical Bragg cell 79−55251
glass diffused and thin-film waveguides, light interf. 79−14115
glass optical waveguide fabrication by effusion 80−5850
glass waveguide, in-plane scatt. and loss mechanisms 80−33216
glass waveguides, control of refractive index profile 79−27442
graded index planar lightguide, electrooptical diffraction 80−78995
graded index slab waveguides, exact solns. for TM modes 79−27397
grating circuit fabrication by electron beam direct writing 80−64214
grating circuit for guided-beam multiple division fabricated by electron-beam direct writing 80−91934
grating coupler fabrication in waveguide photoresist. *(Czech)* 80−28354

integrated optics continued
grating direct writing using SEM 78−83121
grating formation, asymm. line profile, on glass waveguide surface, ion etching method 79−10418
grating lenses, fabrication by electron beam pattern generation, chem. etching and printing 78−75004
grating profile evolution under ion beam erosion 79−94374
grating reflector for thin film Fabry-Perot laser 78−55471
grating single beam coupler with large grating periodicity 77−39114
guided wave acoustooptics, fundamental principles and wideband appls. 79−37038
guided wave electro-optic structures, elec. field and refractive index distribs. 77−72068
guided wave optical devices, using electrooptical switches and modulators, to perform logic and computation 78−38089
guided wave optical systems and devices, conf. Washington DC, USA, 1978, Mar. 79−37031
guided wave optics, appls. review 79−37054
guided-beam splitter, refl. meas., fabrication method 80−74473
guided-wave acousto-optic interaction on Si substrate 79−37050
guided-wave optical signal processing, diode laser sources and photodetectors 80−48465
guided-wave optical systems and devices, seminar, Washington, USA (April 1979) 80−31418
guided-wave optics, design of devices, laser beams in thin transparent films 79−64337
guided-wave signal transformers, synthesis guided-wave signal transformers, synthesis 80−1358
gyrator, thin-film waveguide, theoretical analysis 78−25993
gyrotropic waveguide switching elements at optical wavelengths 79−37049
Hadamard transformation, using optical waveguides, cct. synthesis 78−22221
harmonic generation in thin-film integrated optics, field analysis 79−98509
heterojunction lasers for fibre optic appls., technological advances 79−36933
heterojunctions appl., based on GaAlAs, technology advancements and heterostructure types *(Slovak)* 80−33226
heterostructure applications 77−39112
high density multichannel optical waveguides with integrated couplers 77−794
high quantum efficiency waveguide coupled photodetectors on Si substrate 80−58805
holographic gratings as beam-couplers and splitters 78−25821
holographic interference lithography for integrated optics 79−14116
holography with guided optical waves, diffr. efficiencies, theory 80−83563
horn for mode coupling in waveguides 78−1434
horn structures, linear and shaped, coupling efficiencies 77−34964
horn-shaped coupling structures and linear waveguides fabrication 77−23782
hybrid-type integrated photodetector using partially metal-clad dielectric-slab waveguide struct. 77−11050
III-V nitride semiconductors, physical properties and appls. *(Czech)* 80−28355
III-V semiconductor technology for integrated optical communication components, overview 80−79012
III-V semiconductor technology in integrated optics, overview 80−79010
indiffused waveguides with thin metal buffer, TE_0-TM_0 mode splitting device 80−106638
industrial fibre-optic data link integrated components 79−10392
information transmission appl., system components construction and operation *(German)* 79−18553
information transmission by laser, review *(German)* 77−54810
infrared microwaveguides with a mode-guiding layer of chalcogenide glass 80−28329
inhomogeneous dielectric-slab waveguide, synthesis 79−94337
inhomogeneous planar dielec. waveguides for integrated optics structs., synthesis *(Russian)* 80−38135
inhomogeneous slab, propag., rigorous soln. 78−18055
inhomogeneous waveguide lens anal. 78−5561
injection heterojunction laser with short resonator, construction and output radiation characteristics 79−98408
injection laser, high-power coupled-multiple-stripe phase-locked, beam characts. 79−50307
injection laser diode, single freq., for integrated optics and fibre optic appls. 80−1237
injection laser diode coupling to planar waveguide 80−33245
injection laser integration with Gunn oscillator on semi-insulating GaAs 78−71232
inorganic lithography using metallo-organic photoresists 80−79024
insulator-metal multilayered structs. *(Japanese)* 79−38191
integrated retardation technique, rotationally symmetrical bodies, thermal stress 80−38362
integrated twin guide lasers, axial mode selectivities 77−75519
interferometric reflector with elec. control for laser reflector 77−58490
introduction to integrated optics techniques, appls. in fibre communication and broadband RF signal processing 80−79009
ion exchanged waveguide, thin film overlay effect on mode props. 80−33191
ion implantation applications 77−23781
ion implanted integrated optic devices, fabrication parameters *(German)* 78−83119
ion polishing of optical coatings, for multilayer interf. systems and integrated optics 80−33261
ion-exchanged optical waveguide repeatability improved by melt dilution 80−53493
IR electrooptic waveguide for CO_2 laser modulation 77−27349
IR planar waveguide with chalcogenide glass-BaF_2 emitting grating, mech. fabrication 79−50443
IR waveguides, development for fibre and integrated optics 79−98491
isolator using Faraday and Cotton-Mouton effects 77−79966
isolator using Faraday and Cotton-Mouton effects 77−88964
Langmuir film applications 77−75711
Langmuir-Blodgett films, lightguiding 80−79006
laser, epitaxial waveguide type, with surface diffr. grating *(Russian)* 78−29973
laser coupling, new technique for refr. index and thickness meas. 77−88965
laser diode end-fire coupling into $LiNbO_3$:Ti waveguides 79−94368
integrated optics continued
laser diode structure improvements using DFB, integrated optical elements suggested as alternatives *(German)* 79−89920
laser diode-isolator module, 1.3 μm stabilised, for hybrid optical integrated cct. 80−58583
laser diode-to-diffused waveguide coupling efficiency, waveguide mode asymm. effects 80−9990
laser gyro applications 80−1345
laser-fibre coupling with optical transition structures 78−42449
laser-waveguide transition coupling struct. fabrication 78−38029
lasers, semiconductor injection, integrated optical components 79−36932
leaky dielectric waveguide, planar hollow structure, eigenmode analysis 80−78973
leaky-mode propagation in Ti-diffused $LiNbO_3$ and $LiTaO_3$ waveguides 78−87149
LED coupling to optical fibre, efficiency 80−48416
LED coupling to optical fibres, truncated spherical lens efficiency 79−76813
lenses, thin-film waveguide, progress 78−66950
light trapping in fluid media, teaching, approach 79−71179
light wave transmission technology, survey 79−55213
light waves in thin-film optical waveguides *(Polish)* 78−33849
$LiNbO_3$ single-mode planar waveguides for integrated optics, fabrication *(Korean)* 80−43448
liquid crystal waveguides 77−34960
lithographic focused laser system, integrated optical device fabrication appl. 78−55477
long-term role in optical and electronic systems 80−33232
lossy corrugated structures, plane wave scatt., quantitative results 80−96005
lossy planar waveguide, radiating normal modes 79−55220
LPE, selective, for integrated optical circuits 78−6868
Luneberg geodesic lenses 79−76880
Luneburg guided-wave optical thin-film lens, fabrication technique and props. 80−33223
Luneburg lens index profile for planar waveguide 78−5562
Mach-Zehnder interferometer, switch, integrated optical format 78−38084
Mach-Zehnder interferometric switch for integrated optical multivibrators 80−53479
Mach-Zehnder interferometric waveguide modulator, polarization-independent operation 79−18552
Mach-Zehnder type modulator, RF modulation characts. meas. method 80−74480
Mach-Zehnder waveguide modulators in Ti-diffused $LiNbO_3$ 80−33203
magneto-optical TE-TM mode convertor, coupling and phase matching coeffs. 77−54816
materials and fabrication techniques for integrated and guided wave optics 80−23809
MBE, device appls. 80−25570
MBE of injection lasers, integrated optics device fabrication 79−90042
metal clad waveguide as cutoff polariser for integrated optics 77−27386
micro-optics *(Japanese)* 79−37051
microfabrication for guided-wave optical devices 80−58812
microfabrication techniques, review 78−38091
microgratings for guided-beam deflection, electron-beam direct-writing fabrication 80−102856
micromechanical light modulator array fabricated on Si 78−1433
microoptic signal processing research, review 78−38073
microoptical switch, Mach Zehnder interferometer, for use with optical fibre transmission lines, exam. 78−38085
mirrorless electrooptic device with feedback, optical multistable operations 79−32051
mixer in waveguide based on phase diffr. gratings, for multichannel optical communication lines 79−18554
mode conversion at corner bends in waveguides 77−42594
mode filters using coupling between two nonidentical waveguides 78−46757
mode interaction phenomena, exact anal., and its appl. to acousto-optics 78−42465
mode selection in plane waveguide using organic Langmuir films 79−98495
modes of propagating light waves in thin film waveguides for integrated optics *(Japanese)* 79−98510
modulator, coupled waveguide with pn-junction, strip loaded channel waveguide, design 78−46843
modulator analysis, using MIC formulas 77−39108
modulator switch, balanced bridge, using Ti-diffused $LiNbO_3$ strip waveguides 78−63201
modulator using electro-optic phase shifter pair with optical waveguide couplers 78−66952
modulators and deflectors development, review 77−79973
monolithic integration for new devices 77−75714
monolithic integration of laser and amplifier/detector by twin-guide struct. 78−42466
monolithic integration of laser and laser amplifier or detector, using AlGaAs twin guide structure 78−38082
monolithic laser-waveguide coupling by evanescent fields 77−39110
monolithic SAW amplifier and periodic grating oscillator 79−50447
monolithically integrated lasers and amplifiers using cleaved substrate technique 80−58590
monolithically integrated optical repeater, fabrication and characts. 80−28353
monomode fibre, step discontinuity radiation characts., anal. 77−62047
multichannel data preprocessor, preliminary testing 79−3813
multichannel data processor using holography 79−36853
multifunction integrated optic device with mag. alterable phase grating 77−11048
multilayer anisotropic structures, impedance matching effects 79−7233
multilayer gyrotropic structures, light propag. anal. *(Polish)* 79−3809
multilayer gyrotropic structures for nonreciprocal light propagation 78−90529
multilayered dielectric structures with planar grating, scattering beam characteristics 77−42630
multilayered structures containing anisotropy, EM wave anomalies 79−41460
multilayered structures containing optically active medium, absorption and amplification of light *(Japanese)* 80−19052
multimode, modified thick film technology 79−32093
multimode 3×2 fibre optical matrix switch 80−58764
multimode fibre bussing, active fail-safe terminal 78−55438

integrated optics continued
multimode fibre optic switching devices, computational approach to predict optical behaviour 79−59845
multimode optical systems-power coupling between waveguides 78−42473
multimode strip-waveguides made by thick film technology, loss meas. 79−59846
multimode waveguides, Fourier domain propagation calc. 80−64219
multiple beam spectral analyser with thin film waveguide feed, prism radiation tap 77−34944
multiple fibre end fire coupling with single-mode channel waveguides 79−7230
multiply reflected Gaussian beams in circular cross section 79−18343
multiport coupling between single mode fibres and indiffused channel waveguides 78−38061
multiwavelength monolithic integrated fibre-optic terminal development 80−33243
narrow band gap semiconductor IR devices, advances 80−48464
narrowband optical wave filter with stacked directional coupler 79−7226
network methods for integrated optics devices 78−38070
m-nitroaniline single crystal fibre waveguide core, melt growth and charcts. 77−34965
nonlinear distributed feedback structures, bistability theory 80−5780
nonlinear Fabry Perot devices, integrated optic format 78−38087
nonparallel dielectric waveguides, degenerate mode coupling 79−37006
nonreciprocal integrated optical devices, design considerations 77−793
nonreciprocal optical IC mode convertor analysis 77−84010
nonreciprocal optical systems in ferrite-film light guides 80−99880
oblique Bragg grating, mode conversion 79−27444
offset straight integrated optical waveguides, length optimisation of S-shaped transition 78−46838
offset waveguides, length optimisation of S-shaped transition 78−38059
optical communication appl. 78−87159
optical communications, integrated optical circuits design *(Italian)* 78−55467
optical component and LOC-DBR laser integration 78−38081
optical data processor, satellite data processing appls. 80−48458
for optical fibres, progress and components, review *(French)* 80−69524
optical processing systems, seminar, Huntsville, USA (May 1979) 80−46732
optical switches for integrated optics and fibre optics appls. 79−37057
optimisation of props. of $\Delta\alpha$ waveguide 79−32076
optoacoustic deflector planar, expt. 78−74995
optoacoustic device, planar, SAW loss meas. using light beam diffraction 78−74996
optoelectronic Si devices, optical signal processing and communications, fibre-channel waveguide coupled 79−59847
optoelectronic Si devices for optical signal processing and communications 79−37056
organic materials for volume phase holographic recording media and integrated optical devices 79−3755
oxidizing furnace design, for integrated optics processing 78−9461
parabolic-index slabs and fibres with bent axes, radiation losses 78−46758
parabolic-index waveguides with distorted optical axis, beam propag. 79−46035
parallel end-butt coupling for optical ICs 77−58488
passive components for integrated-optics signal processing 80−48466
passive optical rotation sensors using guided waves, developments 80−58781
passive planar optical element construction from thin film optical waveguides 79−27440
periodic corrugated waveguides, grating coupled radiation and distrib. feedback 78−59161
periodic media diffr., equiv. of multiwave coupled-wave and modal theories 79−41331
periodic media with gain or loss, higher-order Bragg coupling 77−54814
periodic stratified medium, EM propag., general theory 77−65565
periodic structure with varying permittivity, EM wave refl. 79−86109
periodic surface corrugation generation by holography 78−55469
periodic thin film waveguides, theory and appls. 77−39109
phase distribution controlled correction, thin-film optical waveguide with diffr. grating 79−76850
phase grating testing and meas., visual demonstration of non-uniformities 77−34966
phase profiles, waveguides and gratings by optical methods 78−38071
phase profiles generation, recent advances, book contrib. 79−76644
photochromic film waveguide, acousto-optical props., integrated optics appl. 80−33207
photoconductive detector with integrated waveguide struct. 80−48456
photodetector array, waveguide and modulator, based on Si technology 77−11049
photolithography and electron beam lithography techniques 78−46844
photorefractive effect, appl. to optical memories, holographic interferometry, and integrated optics 79−3756
photoresist, Shipley AZ-1350B, linearity and enhanced sensitivity 77−72090
photoresist grating structures with variable period, fabrication 77−19460
photoresist microlens production for semiconductor lasers 78−9398
photoresist testing and phase filter synthesis 77−39116
physical principles and Czechoslovak development *(Czech)* 80−19090
picosecond signal processing with nonlinear integrated optics 80−99882
planar, comparison of normal mode and total field analysis techniques 80−38134
planar dielectric branching waveguide, coupled mode analysis 79−997
planar dielectric waveguide, interacting discontinuities, anal. 79−27445
planar diffused waveguide, WKB approx. for refr. index profile determ. 78−30086
planar diffused waveguides, refr. index distrib. function 79−55227
planar electrodes, distributed capacitance, optic and SAW device appls. 77−27387
planar multilayered structure, resonant polarization conversion and beam shift 78−1438
planar multimode couplers for fibre optics 79−18531
planar multimode coupling structure fabrication by ion exchange 80−64233
planar optical elements, dispersion props. 79−3811
planar optical waveguide interconnection method 80−58671
planar optics, goals, methods, potential appl., principles and trends 80−33231
planar technology, future of electro-optic devices *(Czech)* 77−46820

integrated optics continued
planar waveguide, fabricated by diffusion and ion exchange, refr. index distrib. 79−27429
planar waveguide, fabricated by ion exchange in glass, refractive index profile 80−14460
planar waveguide, isotropic, polarisation conversion by Bragg deflection coupled mode theory 80−48461
planar waveguide, isotropic, polarisation conversion by Bragg deflection, expt. results 80−48462
planar waveguide blazed dielectric diffraction gratings, anal. and design 80−58779
planar waveguide structure, props. *(Czech)* 80−96018
planar waveguide with interacting step discontinuities, field and network anal. 79−55214
planar waveguides and fibres, book 78−42426
planar waveguides prepared by solid-state diffusion, refr. index distrib. function 79−10404
plane four-layer waveguide with diffr. grating, surface light waves 79−55250
plane waveguide formed by K^+ diffusion 79−90043
plastic film, interconnections in thin-film guided-wave optics 77−58487
plastic optics for optoelectronics, moulding techniques for single, multi-element systems 78−63210
PMMA, direct writing of gratings by electron beam 79−46091
polarisation insensitive integrated optical switch, electrode design 77−79967
polarisation-independent optical switch using weighted directional coupler 80−58798
polariser, reduced cladding-medium, fabricated in ion-exchanged guides 80−14489
polygonally bounded waveguides, hybrid finite element analysis 77−27358
polymer films, plasma polymerisation, light propag. expt. *(Japanese)* 78−6846
polymer films for waveguides and dye laser, prep. and characts. *(Japanese)* 78−5551
polymeric film optical properties meas. 78−27342
polymeric medium, guided light diffr. by holographic grating 77−7215
polymers, Raman, spectroscopy of thin films, integrated optical techniques 80−22432
polyurethane optical solid cct., preferential doping of rhodamine 6G 77−62075
prism, symmetrical, as input coupler for integrated optics 79−10412
prism coupler, EM theory, tutorial approach *(French)* 77−37694
prism coupler fabrication technique 80−83685
prism coupler for optical waveguides 78−94431
prism coupling efficiency optimisation for surface IR wave excitation 77−75708
prism coupling into clad uniform optical waveguides 80−96003
prism coupling into optical waveguide second harmonic generation 80−102763
prism or grating couplers, determ. of ray directions coupled out of waveguides 79−59841
prism-waveguide coupling efficiency for waveguides with arbitrary refr. index profile, WKB approx. 79−7231
prism-waveguide dual coupler theory and exptl. performance 80−33236
programmable planar waveguide components formed by optically writing Bragg diffraction gratings into photochromic structs. 80−79011
progress in 1977, review 78−33916
propagation of optical mode in guided interlayer struct. with variable thickness *(French)* 79−23089
quantum electronics, conf., New York, USA (Jun. 1980) 80−90614
quartz, anisotropic waveguide, for IR propag., coupling 77−34938
quartz, fused, waveguide struct. form. by H_2^+ ion irrad. 78−18072
quasimonolithic and hybrid integrated optical circuits on Si substrates 80−64218
radiating distributed feedback structures, calc. and optimisation of parameters 79−27438
radiation loss caused by discontinuities in dielectric slab waveguide, anal. 79−7227
reactive ion etching of III-V compounds 80−58813
receiver characts., influence on optical fibre system performance 77−83984
reduced depth polariser for integrated optics 77−84006
refractive index distribution for prescribed two-dimens. ray path. 79−59633
refractive index profile calc. from measured coupling angles 80−78954
relief grating, diffr. anomalies near crit. angle for total internal refl. 80−10035
remote sensing multichannel data sets, integrated optical comparator 80−64213
residue arithmetic computation, integrated-optical methods 79−76886
resonant tunnelling in film optical waveguides 79−27430
review, integrated optics and guided wave devices 78−42468
review and unsolved problems 78−1435
review of device principles 78−1429
review of integrated optics and optical waveguide devices 78−66948
review of integrated optics and thin-film technology 77−54815
review of optical IC developments *(Japanese)* 77−62077
RF spectral analyser 77−27389
RF spectral analyser acousto-optical readout scheme 79−50446
RF spectrum analyzer, feasibility 78−5431
rhodamine 6G solution, stimulated emission under internal refl. conditions 77−58327
rib wave guides, field expansion analysis, measurements at mm-wavelengths, approx. solutions comparison 77−54778
rib waveguide switches with MOS electrooptic control, monolithic integrated optics in GaAs-$Al_xGa_{1-x}As$ 78−87168
rib waveguide with trapezoidal cross section, numerical analysis 80−96009
ridge waveguide, trapezoidal cross-section, propag. characts. 78−55436
ring resonator, high-Q, asymmetric three-layered dielectrics, design 78−83118
S-shaped dielectric waveguide, guided leaky waves 80−28341
sandwich ribbon fibres for hybrid integration in high-index materials 80−79013
sandwich-ribbon optical fibre, near-field intensity patterns of mixed modes 77−62073
saturable optical resonator with distributed Bragg refl. 77−3684
saturable resonator with distrib. Bragg reflectors, bistability, bleaching and loss effects 77−27309

integrated optics continued
SAW acousto-optic modulators 79−90032
SAW Broadband modified chirp transducers for integrated optics spectrum analyser 80−58802
SAW integrated optics spectrum analyser, development progress 80−58803
SAW oppositely propagating in optical waveguide, light diffr., signal processing appl. 79−41453
SAW signal convolution using acoustooptic interaction in film waveguide 77−27428
second- and higher-order waveguide grating filters, refl., transmission and loss coeffs. meas. 80−19110
second- and higher-order waveguide grating filters, spectral response calcs. 80−19109
self-filtering multilayer S-waveguides with absorption and radiation losses 80−38102
self-filtering S-type strip waveguides 80−33219
self-imaging multiplexer and branching couplers 80−106629
self-scanned photodiode array, evaluation for integrated optics spectrum analyser 80−58806
SEM written diffraction gratings for integrated optics, characts. 79−68450
SEM written gratings in chalcogenide films, for optical integrated circuits 79−32087
semiconductor, IR switching, ultrafast optically controlled 80−58626
semiconductor etalon, optical bistability and ns modulation 80−64096
semiconductor heterostructures, elec. and optical phenomena, discrete devices, review 78−72250
semiconductor layer structure, laser-induced photolum. and collective effects *(Russian)* 79−95830
semiconductor nonlinear interferometer, logical element *(Russian)* 79−49279
semiconductor source matching to thin-film planar and stripe waveguides 80−64174
semiconductor waveguide switches, and modulators, review of development progress 78−38045
semiconductor-waveguide lasers in bent-guide structs., characts. *(Japanese)* 78−87062
semiconductor-waveguide-laser amplifier, with anisotropic gain by drift carriers 77−79818
sensitivity analysis of waveguides dimensional tolerances 79−76833
SHG, phase-matched, in four-layered optical waveguide struct. 78−74950
SHG by guided radiation mode coupling in thin film optical waveguide 80−106567
short-range fibre optics 78−46786
signal and image processing, US Air Force research programme 80−78791
signal processing, fibre and integrated optics techniques 77−27379
signal processing activities of United States Army 80−48172
signal processing fibre and integrated optical devices 79−76887
signal processing research programme of United States Air Force 80−48171
signal processing with fibre and integrated optical devices 80−33233
signal processor, performance limits 79−36854
signal processor, using geodesic thin film lenses 78−42475
single mode coupling of fibre to indiffused waveguide 77−34959
single mode fibre coupling structure fabrication 78−33899
single mode fibre network, coupling and integrated optical switches 78−59159
single mode fibre optic system coupling techniques 78−33901
single mode grating coupling between thin-film and fibre optical waveguides 79−1012
single mode inhomogeneous fibre problems, scalar wave approach 79−64312
single-mode optical waveguides with inhomogeneous index variations 79−76804
sinusoidal interface light diffraction 79−13900
slab-type directional coupler with activated rhodamine 6G top layer, amplified oscill. 80−99718
soda lime glass, Ag^+ ion exchanged, planar optical waveguide, manufacturing tolerances 78−71212
spatial digital filter based on Bragg effect 80−96036
spatially periodic media, modal theory 77−7218
spatially periodic media, second-order coupled-mode eqns. 78−13655
spectral analyser, 1978 advancements 79−46086
spectral analyser design and fabrication 79−50445
spectrum analyser, design of Bragg cells 80−74515
spectrum analyser design and fabrication 79−72720
spectrum analyzer dynamic range, waveguide scatt. effect 78−59163
spheroidal geodesic lenses for integrated optical processing, design 77−27385
sputtered films, optical props. and appls. 78−72623
sputtered optical waveguides, out-of-plane scattering meas. 80−38127
stepped switched optical directional couplers with unequal section lengths 80−33235
stigmatically focusing grating coupler 79−59842
strip line, optical, theory and numerical anal. 77−79956
strip waveguide analysis, reflection-transmission of obliquely incident wave on strip side 79−50378
strip waveguide directional coupler, leaky-wave 78−38058
strip waveguides, leakage and reson. effects, anal. 78−66953
strip-guides, polarisation filtering 80−102861
stripe geometry injection lasers, rigorous boundary value soln., for lateral modes 78−71100
stripe waveguide, Ag^+/Na ion exchanged, propag. characts. 80−83664
stripe waveguide in glass, fabrication by low-temperature diffusion process 80−102867
stripline waveguides, dispersion characts. and radiation fields 80−64155
sub-ps gate 80−58809
submerged diffused waveguide prep., refr. index distrib. determ. 78−18068
submicron structures, National Research and Resource Facility at Cornell 78−38101
submillimetre-wave optical design approach 79−32048
subpicosecond gate, velocity-matched directional coupler 80−74512
superconductor junction/optical waveguide combination 78−66955
surface acoustic wave scattering of guided optical beams 79−98508
surface acousto-optic interaction on nonpiezoelectric substrates 79−46090
integrated optics continued
surface EM wave coupling efficiency, prism gap height depend. 78−33914
surface wave, momentum exchange with moving atom 79−64359
surface waveguide electrooptical deflector, high-resolution, prism model 80−48454
surface waves in integrated-optics elements with distributed coupling, review 79−64361
surface-diffused and buried waveguides, scatt. losses caused by surface imperfections 79−64332
switch, 3×3, using single-mode waveguides in electrooptical material 78−55470
switch, bistable, using $LiNbO_3$ phase modulator 78−79145
switch, optically controlled two channel, based on directional coupler 78−83116
switch, polarization-independent, for use with single-mode optical fibres 79−37059
switch, total internal refl., theoretical evaluation 79−18551
switch array, mirror-type, integrated on $LiNbO_3$ substrate 79−27436
switch constructed of graded-index rod lenses, for multimode fibre systems 79−27439
switch for fibre data transmission system 77−27384
switch/modulator, optically activated, using photoconductor and two channel waveguides 78−1437
switching device using leaky surface wave, controlled by electro-optic effect 79−23090
switching system with input modulator 80−99884
symmetric slab waveguide in birefr. media, coplanar optical axis slab, modes 79−32053
taper couplers utilizing SiO_2, photolithographic fabrication processing sequence 79−41464
tapered beam to film couplers, coupler eqns. 78−55472
tapered coupler, coupled-mode eqns., parabolic cylinder functions 77−46821
tapered coupling problems, use of Bloch vector model 78−22219
tapered gap prism couplers for high index materials 77−72091
tapered highly reflective surface-wave grating, refl. spectrum, distortion 78−13867
tapered horn shaped channel waveguide coupling 77−42619
tapered light guide condenser design approach 80−33218
tapered optical waveguide structs., mode coupling in terms of local modes 80−38126
tapered velocity coupler application, freq. discrimination 78−38057
tapered waveguides, permitting efficient fiber to waveguide coupling 79−50376
TE-TM mode splitter for optical waveguides, glass comp., r.f. sputtered fabrication 78−46841
techniques for fibre-optic communications *(German)* 78−38069
telecommunication appls., manufacturing technology *(French)* 78−50946
theory, technology and appl. *(Czech)* 80−33229
thick film optical waveguide integration with fibre-optic connectors 80−33246
thick planar films, transmission method for index meas., modal effects 80−102862
thin dielectric film optical waveguides, ideal fabrication technology, comparison of four techniques 80−79025
thin film and integrated optics review, theory, expt. techniques, waveguides 78−22220
thin film detector for integrated optical systems, description and exam. 78−38080
thin film electrooptic deflector using induced grating with variable blaze angle 80−99862
thin film glass lightguide boundary refraction expts. 80−106639
thin film lasers and waveguides with arbitrary refr. index distribs., optical processes 77−79971
thin film optical circuit fabrication using CO_2 laser 80−99881
thin film optical waveguide, attenuation due to roughness-induced mode coupling 79−10408
thin film optical waveguide, with emitting diffr. grating, inhomogeneity in thickness 80−48425
thin film preparation and properties, symposium, Loughborough (1976) 77−77376
thin film refractive index meas., modified Abeles method *(Italian)* 78−1427
thin film rib waveguide, numerical anal. by mode-matching method 80−48421
thin film technology appls. to integrated optical circuits 78−38068
thin film waveguide, anisotropic, field excited by sources 79−7198
thin film waveguide, mode conversion by two-stage coupling process 79−32034
thin film waveguide, phase distrib. along emitting aperture 79−55226
thin film waveguide component interconnection and signal processing 78−55847
thin film waveguides, optical damage thresholds 79−46033
thin-film chirped gratings, mode coupling 80−23808
thin-film laser logic element, operation *(Russian)* 79−10413
thin-film laser with a two-dimensional diffraction grating 80−9906
thin-film laser with spatially separated multiple-frequency outputs 80−43368
thin-film lenslike light guide focusing properties 77−54786
thin-film micro-optics, hybrid communication systems 77−11051
thin-film multimode waveguides, higher order mode amplification 80−96012
thin-film optical disc 80−106641
thin-film periodic structures, optoelectronic devices appls. *(Polish)* 78−50947
thin-film strip waveguide on dielectric substrate, optical dispersion 80−53478
thin-film two parallel waveguides, numerical anal. 80−106626
thin-film waveguide, on Si substrated, optical power losses calc. and obs. 80−106640
thin-film waveguide, refr. index meas. using diffr. method 79−30532
thin-film waveguide, TE and TM modes phase-matching, dielectric constant relations *(Japanese)* 80−58677
thin-film waveguide, with plane diffr. grating, radiation fields and spectrosc. characts. 79−3790
thin-film waveguide with liq. cryst. boundary modulation of refr. index, mode switching 80−23800
thin-film waveguides, propag. modes 78−71218
thin-film waveguides fabrication, review *(Polish)* 79−3775

integrated optics continued
thin-film waveguides of dense crown glass, HF sputtering prep. 79−10415
three-dimensional diffraction grating, Al diffusion into glass 78−42480
three-layer heteroepitaxial struct., strip waveguide optimum width *(Russian)* 77−7200
three-waveguide system, interference effects on couplings 80−78969
total reflection region, refracted beam field distrib. 79−27169
total-internal-reflection hologram grating, diffr. efficiency 79−64347
transition fibre fabrication for coupling fibres to integrated optical films 77−39061
transmission technique for planar film index-profile measurements 80−33230
travelling wave optical modulator using a directional coupler $LiNbO_3$ waveguide 80−96035
triangular gratings, surface wave guiding, quantitative results 80−96005
tunable coupler filter, composed of coupled nonidentical $LiNbO_3$ strip waveguides, description 78−38083
tunable narrow-band thin-film waveguide grating filters, performance 80−38124
tunable optical waveguide directional coupler filter 78−79144
tunable switched directional couplers of two thin film waveguides using SAW 78−75003
twin guide laser, coupled wave theory 77−27307
twin-guide laser, AlGaAs, mode selectivity 77−88723
twin-guide lasers theory, oscillation conditions and efficiency calc. 77−62076
two-dimensional waveguide analysis with misaligned or curved gratings 79−23092
uniaxial graded-index waveguides, mode propag. and conversion 79−55204
volume diffraction gratings with inclined layers in thin-film optical waveguides, coupling efficiency 79−90028
W-shaped fibre waveguide with rectangular core and two-layer shell, eigenmodes 80−28340
waveguide, refractive index smoothly graded, near and far fields 79−72705
waveguide, thick, highly multimode, fast fabrication method 78−18043
waveguide 4×4 switching network 77−3683
waveguide analysis methods and improvements 77−79974
waveguide and CCD image array 77−34962
waveguide grating, diffraction efficiency, Brewster's law 80−91935
waveguide hologram using optical thin films high-efficiency relief-type hologram 78−66958
waveguide holograms, recording and reconstruction, integration 77−14674
waveguide interferometer using modular holographic elements 77−61116
waveguide intersection, higher refr. index, without light leak 77−58489
waveguide lens technologies for RF spectrum analyser 77−34961
waveguide lenses, Bragg and Luneburg type 80−10050
waveguide lenses, review *(Japanese)* 80−10019
waveguide Luneburg lenses, diffr. limited, mask synthesis for sputtering production 78−38076
waveguide modal characts. determ. for integrated optics 78−1439
waveguide modified mode propag. due to perturbing overlayer 77−65624
waveguide optical collimator, Luneberg lenses with plane connecting waveguides 79−68446
waveguide props., mode anal., prism coupling method 78−66947
waveguide refractive index meas., method and results 77−83965
waveguide tapers, multimode coupling and transmission characts. 79−27378
waveguide-hologram memory design approach 80−32940
waveguides, new wave phenomena, review 77−54817
waveguiding in semiconductor injection lasers and integrated optics 77−14807
wavelength division multiplexing, review of recent developments 78−38079
wideband repeater, for fibre optic communications 77−14813
wideband signal processors, review 79−89864
wideband thin film modulators and switches, for optical communication 78−63206
X-ray lithography for fabrication of submicrometer period gratings with precisely defined profiles for integrated optics applications 80−58814
AlAs-GaAs heterostructure, fabrication by selective liq.-phase epitaxy 79−15618
AlGaAs DH laser epilayer struct. optimization for integrated optical circuits 80−99879
AlGaAs heterostructures with periodic optical inhomogeneities 77−75713
AlGaAs integrated twin guide laser with distributed Bragg reflectors 77−88744
AlGaAs laser array on Si heat sink, optical power detection 80−74383
AlGaAs resonant laser amplifier, gain and saturation power 80−53315
AlGaAs rib waveguides, characts. 80−33177
AlGaAs-GaAs DH lasers, coupling efficiency between gain-induced guides 79−23094
$Al_{0.42}Ga_{0.58}As$-GaAs-$Al_{0.42}Ga_{0.58}As$, etalon, optical bistability and modulation 80−58628
$Al_xGa_{1-x}As$, fabrication of mesa-type waveguides by laser irrad. 80−5849
$Al_xGa_{1-x}As$, solid soln., controlled electrochemical and selective etching, integrated optics appl. 77−14814
$Al_xGa_{1-x}As$, waveguide heterostruct. epitaxial growth with gradual composition change 79−42416
$Al_yGa_{1-x}As$-GaAs, DH integrated optics development 80−33240
$Al_yGa_{1-y}As$-$Al_xGa_{1-x}As$ laser struct., for integrated optics, MBE 78−13817
$Al_yGa_{1-y}As$-$Al_xGa_{1-x}As$, electrooptic rib waveguide modulators and switches 78−38046
$Al_yGa_{1-y}As_{1-x}Sb_x/GaAs_{1-x'}Sb_{x'}$, buried heterojunction electroabsorption modulator, report of operation 78−38044
Al_2O_3 optical waveguide, fabrication by reactive Al sputtering in O_2-Ar atm. 80−33262
As-S film, guided light reversible control by electron beam irrad. 78−1331
As-Se glass thin-film waveguide, for 10.6 μm range 77−50770
As-Se-S-Ge chalcogenide glass films, appls. to passive optical waveguide components 79−37048
As_2S_3 amorphous film waveguide and grating coupler 80−53448
As_2S_3, film waveguide, acoustooptic deflection and modulation of light by stationary phase grating struct. 80−5841
As_2S_3 focusing diffraction grating with const. spacing 79−23096
integrated optics continued
As_2S_3 polyethersulphone sandwich ribbon fibre for coupling high refractive index integrated optics 79−32089
As_2S_3 thin films for integrated optics, photodetector elements, relief-type diffraction gratings 79−32094
As_2S_5, thin film optical waveguide, for acoustooptic modulators 78−83051
B_2O_3-SiO_2 optical fibres, exposed cladding technique, birefr. and polarization props. 79−14094
BaO crown and flint glasses, Ag and Cu diffusion for optical waveguide fabrication 78−59166
$Bi_{12}SiO_{20}$ crystal, for programmable optical guided-wave device 79−23069
$Bi_{12}SiO_{20}$ crystal, programmable optical integrated circuit, exam. 78−38078
$Bi_{12}SiO_{20}$, optically controlled multimode planar switch 78−42476
$Bi_{12}TiO_{20}$, RF sputtered epitaxial film on $Bi_{12}GeO_{20}$, for optical waveguiding 78−9462
CdS semiconducting thin-film optical waveguide polariser 80−33180
CdS_xSe_{1-x}, photosemiconductor, optically controlled deflector based on thin-film waveguide 80−33206
CdTe, H^+ ion implanted, optical waveguiding and electrooptic modulation 77−75679
GaAS, (110) oriented, preferential chemical etching of blazed gratings 79−37067
GaAlAs DH laser-diode-to-diffused-waveguide coupling calcs., Gaussian beam model 79−94372
GaAlAs embedded DH stripe laser with GaAsP strip-waveguide modulator 78−66957
(GaAl)As heterojunction laser with distributed Bragg refl., mode switching 80−43336
GaAlAs injection laser, monolithic integration with Schottky-gate FET 80−48275
GaAlAs light intensity modulators using p-n junctions 80−99871
GaAlAs-GaAs epitaxial heterostructures for integrated optics functional elements 78−50948
$Ga_{0.64}Al_{0.36}As$, plasma grown oxide, phys. and elec. props. 78−48550
$Ga_{0.7}Al_{0.3}As$-GaAs chemically etched mirror lasers, optical coupling effect 77−72000
$Ga_{1-x}Al_xAs$ integrated optical waveguide LPE 77−75703
$(Ga_{1-x}Al_x)As$ LOC DBR laser integration with p-n junction detector 78−38066
$Ga_{1-x}Al_xAs$ low threshold stripe geometry DH laser, Be implanted, on semi-insulating substrate 80−69409
$Ga_{1-x}Al_xAs$ Schottky directional coupler switch, construction and operation 78−25960
$Ga_{1-x}Al_xAs$-GaAs injection laser, branching waveguide coupler fabrication by LPE 78−63202
$Ga_xAl_{1-x}As$ embedded stripe DH laser monolithically integrated with strip waveguide 78−59025
$Ga_xAl_{1-x}As$ injection heterojunction distributed output laser, exptl. study 80−43369
$Ga_xAl_{1-x}As$ layer, optical guiding in Bragg configuration 78−1431
GaAs, and its alloys, as integrated optics materials, book contrib. 79−64362
GaAs and related compounds appl., properties and preparation 77−65644
GaAs CW injection laser diode specification for integrated optical circuits 80−33034
GaAs devices, recent advances 77−75712
GaAs directional couplers and electrooptic switches, wavelength depend. 78−79143
GaAs, directional-coupler switch with stepped $\Delta\beta$ reversal 77−79968
GaAs directional-coupler switch with stepped $\Delta\beta$ reversal 77−88962
GaAs double-cavity laser with branching output waveguides 78−63128
GaAs electro-optic rib waveguide directional-coupler switch with stepped $\Delta\beta$ Schottky electrodes 79−98507
GaAs, electroabsorpt. avalanche photodiode, waveguide detector for 1.06 μm 78−16842
GaAs, electroabsorpt. avalanche photodiode waveguide detectors 78−65965
GaAs, electroabsorpt. avalanche photodiode waveguide detector, freq. demultiplexing 79−17486
GaAs, epitaxial layer, controlled electrochemical and selective etching, integrated optics appl. 77−14814
GaAs epitaxial layer, strain induced optical waveguiding 79−27388
GaAs, exam. as cladding material, for optical waveguides as cutoff polariser 78−55474
GaAs film optical components, prep. by MBE using Si shadow masking technique 80−28358
GaAs, Franz-Keldysh effect modulator parameters for integrated optics systems 80−106624
GaAs integrated optical circuits by wet chemical etching 79−32092
GaAs, interference grating blazed by ion-beam erosion 80−1302
GaAs, ion etching, effects on optical props. and lattice disorder 78−83122
GaAs laser array, integrated, Si substrate package fabrication 79−18555
GaAs laser array source package, with collimating lens and fibre light-guides 77−84007
GaAs laser array to channel groove waveguide coupling prism 78−38067
GaAs laser arrays, Si substrate packaged, thermal performance and limitations 78−46613
GaAs laser with integrated interferometric reflectors 77−65642
GaAs layer grown by MBE, direction coupler switch 79−76878
GaAs, MBE prep., device props. 77−77417
GaAs oxide confined optical waveguides formed by lateral epitaxial growth 80−58815
GaAs, p^+-n^--n^+ electro-optical directional-coupler switch 77−7217
GaAs p-n-i-n^+ semi-insulating struct. as integrated optical coupler 80−64212
GaAs patterned epilayer structures, MBE writing, for integrated optics 78−56590
GaAs rib-waveguide directional-coupler switch with Schottky barriers 78−63204
GaAs, semi-insulating substrates, monolithic integration of optical and electronic devices, review 80−58543
GaAs signal processing optical electronic devices 80−33242
GaAs, technology and device develop. 77−46823
GaAs waisted-rib optical waveguides 80−74487
GaAs:Zn waveguide, light coupling at fundamental absorption edge 79−23082

integrated optics continued
GaAs/AlGaAs integrated twin guide injection lasers prepared by LPE, coupling coeff. and coupling length meas. 79−81458
GaAs/GaAlAs crowding effect lasers using whispering gallery mode on semi-insulating GaAs substrates 80−58589
GaAs/GaAlAs diode lasers, with distributed feedback 77−46721
GaAs-(Ga,Al)As light modulators and distributed Bragg reflector laser, monolithic integration 78−50944
GaAs-(GaAl)As DH injection laser with pillbox resonator, characts. and fabrication 80−58581
GaAs-$Al_xGa_{1-x}As$, integrated twin-guide laser with distrib. Bragg reflectors 77−19310
GaAs-$Al_xGa_{1-x}As$, high resolution and high aspect ratio structs., dry processing 77−27383
GaAs-$Al_xGa_{1-x}As$, single mode optical rib waveguides, MOS control of switches 78−1432
GaAs-$Al_xGa_{1-x}As$, single-mode rib waveguide switches electro-optical modulation 78−46839
GaAs-$Al_xGa_{1-x}As$ electro-optic frequency- and polarisation-modulated injection laser 80−91810
GaAs-$Al_xGa_{1-x}As$ films for optical devices, masked MBE 78−38100
GaAs-$Al_xGa_{1-x}As$ integrated injection lasers and detectors with etched reflectors 77−62074
GaAs-$Al_xGa_{1-x}As$ integrated lasers and detectors fabricated by wet chemical etching 77−88961
GaAs-$Al_xGa_{1-x}As$ multilayer struct., MBE, selective area growth using Si shadow masks 77−85946
GaAs-$Al_xGa_{1-x}As$ MOS rib waveguide polarizers 80−64207
GaAs-$Al_xGa_{1-x}As$ MOS rib waveguide polariser, modulator and isolator 80−64217
GaAs-$Al_xGa_{1-x}As$ single mode rib waveguide COBRA switches, MOS control 77−88970
GaAs-AlGaAs distributed Bragg reflector integrated twin-guide laser, temp. characts. 78−87064
GaAs-AlGaAs laser array packaged with fibre lightguide array on Si substrate 78−46611
GaAs-AlGaAs multilayer stack, optical surface wave propag. 78−38090
GaAs-$Ga_{0.8}Al_{0.2}As$ layered struct., LPE, optical surface waves 78−48244
GaAs-$Ga_{1-x}Al_xAs$ DH laser, curved stripe, operation and appl. 78−42341
GaAs-$Ga_{1-x}Al_xAs$ stripe geometry lasers 79−94245
GaAs-GaAlAs, injection laser and MESFET monolithic integration on GaAs substrate 79−64242
GaAs-GaAlAs, transverse Bragg-reflector injection lasers 78−74926
GaAs-GaAlAs bipolar transistor and heterostruct. laser, monolithic integration 80−102858
GaAs-GaAlAs DH injection laser, integrated optics techniques 80−33033
GaAs-GaAlAs DH laser, beam scanning with twin-stripe injection lasers 79−10334
GaAs-GaAlAs large optical cavity injection layer with low loss DBRs 78−1430
GaAs-GaAlAs laser, high-spectral radiance source 79−36931
GaAs-GaAlAs monolithically integrated DFB lasers as freq. multiplexing source 77−34958
GaAs-GaAlAs multiple-stripe phase-locked laser array, behaviour 79−45955
GaAs-GaAlAs room temp. DBR lasers, highly collimated broadside emission 78−1428
GaAsP epitaxial waveguide, electro-optic phase modulation of laser radiation 79−10417
$Ga_{0.47}In_{0.53}As$, homojunction avalanche photodiode, exam. of props. 78−37072
GaInAsP on InP substrate, epitaxially grown, fabrication of avalanche photodiode 78−37071
GaInAsP/InP integrated twin-guide lasers with first order distrib. Bragg reflector, room temp. operation at 1.3 μ 80−64077
GaInAsP/InP system, chemical etching, fabricating laser diodes and integrated optical circuits 80−38030
GaInAsP-InP DH laser, LPE and wet chem. etching techniques for integration 79−98388
GaInAsP-InP integrated twin-guide lasers with first-order distributed Bragg reflectors, 1.3 μm 80−58567
$Ga_xIn_{1-x}P_yAs_{1-y}$-InP(GaAs), DH integrated optics development 80−33240
GaN epitaxial films, planar waveguides for integrated optics appls. 79−10416
GaP-AlGaP, stripe-geometry electrooptical modulator 80−23798
GaP-GaAsP planar heterostructure strip ridged waveguide under mech. load, polarisation modulation 80−96038
$In_xGa_{1-x}As$ epitaxial layer, waveguiding at 1.06 μm, losses 78−18052
InP, heterojunctions preparation and props. *(Slovak)* 80−33225
$K_3Li_2Nb_5O_{15}$ films for optical waveguides epitaxial growth and characterisation 80−79016
$K_3Li_2Nb_5O_{15}$ optical waveguides fabricated on sapphire by RF sputtering 79−98488
Li(Nb,Ta)O_3, LPE growth of thin film waveguides on $LiTaO_3$ substrates 79−41467
$LiNbO_3$, anisotropic diffused optical waveguides, polarisation and spectral characts. 79−32073
$LiNbO_3$, anisotropic planar waveguide, TE to TM mode conversion *(Russian)* 77−11039
$LiNbO_3$ balanced bridge modulator/switch with ion-etched slot 79−89993
$LiNbO_3$ branching waveguide, optical TE-TM mode splitter 80−96033
$LiNbO_3$, bulk, Ti-diffused spectrum analysers, H implantation effects, pot. uses 80−43486
$LiNbO_3$, channel waveguide to single-mode fibre high-efficiency flip-chip coupling 80−99833
$LiNbO_3$ corrugated optical waveguide, electrooptic scanning of coupled light 78−38050
$LiNbO_3$, diffused waveguide for acoustooptical signal processing 79−90029
$LiNbO_3$ diffused waveguide, induced diffr. grating, integrated optics applications 79−98511
$LiNbO_3$, electro-optical modulator/switch, switched directional coupler principle 77−7191
$LiNbO_3$, Fi diffused, single-mode waveguide, comparison of bending losses in integrated optical circuits 80−83684
$LiNbO_3$ geodesic lens fabrication by single-point diamond turning 80−33239

integrated optics continued
$LiNbO_3$ graded-index planar waveguide, $As_{40}Se_{50-x}S_xGe_{10}$ film strip-loaded 78−74965
$LiNbO_3$, high freq. plane acousto-optical light modulators *(Russian)* 78−79106
$LiNbO_3$ layers, Li out-diffused, SHG phase matching temp. variation 80−69455
$LiNbO_3$ lenses, diamond-turned aspheric geodesic waveguide lenses 80−58804
$LiNbO_3$, optical filter, for integrated optical waveguide structures 77−58443
$LiNbO_3$ optical waveguides, electrooptic modulation and switching, recent progress 78−50945
$LiNbO_3$ optical waveguide, diffused with mag. garnet film top layer, non-reciprocal props. 79−41444
$LiNbO_3$ optical waveguide, beam-to-waveguide coupler 79−90003
$LiNbO_3$, planar lightguide, optical mode interaction with standing elastic surface waves 80−99836
$LiNbO_3$ planar waveguide, light beam switching and modulation using built-in dielectric channel 77−88967
$LiNbO_3$ planar waveguide, light beam switching and modulation using built-in dielec. channel 78−46840
$LiNbO_3$ planar waveguide mode conversion and intensity modulation 79−10410
$LiNbO_3$, ridge struct. fabrication by CF_4 plasma etching 80−28357
$LiNbO_3$ substrate based ICs_s performance obs. *(Japanese)* 79−86265
$LiNbO_3$ TE-TM mode convertor, using collinear acoustooptic interaction 77−19407
$LiNbO_3$, Ti diffused, mirror type optical branch and switch 78−33834
$LiNbO_3$, Ti diffused, optical waveguide isolator using electrooptic branching waveguide 79−18532
$LiNbO_3$, Ti diffused, optical directional couplers, characts. 80−33145
$LiNbO_3$, Ti diffused optical waveguides, efficient prism-coupling 79−46089
$LiNbO_3$ Ti diffused single-mode waveguide coupling to single-mode fibre 79−81547
$LiNbO_3$, Ti diffused waveguide, refr. index and thickness precise determ. 79−41446
$LiNbO_3$, Ti diffused waveguide, leaky mode loss coeffs., calc. 80−19094
$LiNbO_3$, Ti diffusion and characts. of graded-index lightguide 79−27433
$LiNbO_3$ Ti-diffused waveguide for cutoff modulator 80−9991
$LiNbO_3$ very high throughput damage resistant waveguide modulator 80−58788
$LiNbO_3$ waveguide, corrugated, electro-optic scanning of light diffr. from grating output coupler 78−63172
$LiNbO_3$ waveguide, diffusion fabricated, angular variation calcs. using mode propag. consts. 80−69540
$LiNbO_3$ waveguide, form. of geodesic lenses 77−88966
$LiNbO_3$ waveguide, holographic writing technique based on multiphoton photorefractive processes 77−38824
$LiNbO_3$ waveguide, horn struct. and thin film optical switch 77−88968
$LiNbO_3$ waveguide, planar electro-optic prism array beam splitter 80−64209
$LiNbO_3$ waveguide, thin-film optical filtering using acoustooptic interaction 79−81572
$LiNbO_3$ waveguide absorption losses, laser calorimetric meas. 79−64311
$LiNbO_3$, waveguide and modulator form. by ion implantation 80−48469
$LiNbO_3$, waveguide formation using organometallic solns. as diffusion sources 80−23810
$LiNbO_3$ waveguide modulators and switches, Ti-diffused, fabrication on directional coupler principle 80−83678
$LiNbO_3$ waveguides, optical scattering phenomena 80−58786
$LiNbO_3$:Ti, broad-band travelling wave waveguide modulator 77−39036
$LiNbO_3$:Ti, diffused strip waveguide, refractive index changes, two-dimensional distrib. 79−86254
$LiNbO_3$:Ti, dopant conc., refr. index profile rel. to integrated optics 78−5583
$LiNbO_3$:Ti, electrooptical modulator and switch *(French)* 78−30074
$LiNbO_3$:Ti, in-diffused waveguide, integrated bistable optical device development 78−75001
$LiNbO_3$:Ti, in-diffused waveguides, optical damage thresholds 79−46033
$LiNbO_3$:Ti, planar and channel optical waveguides, anisotropic diffusion expts. 80−64200
$LiNbO_3$:Ti, planar optical waveguides, processing and props. 80−78965
$LiNbO_3$:Ti, two mode waveguide coupler electrooptical switch 77−83961
$LiNbO_3$:Ti, Y-cut thin film waveguide, acousto-optical deflector, electro-optical modulator *(Russian)* 77−39115
$LiNbO_3$:Ti 3-dB optical waveguide mode convertor using chirped gratings, power transfer 80−79014
$LiNbO_3$:Ti branched waveguide amplitude modulator 77−39037
$LiNbO_3$:Ti channel waveguide high-speed cutoff modulator 80−64195
$LiNbO_3$:Ti diffused optical waveguide, guided light scatt. sources 80−78966
$LiNbO_3$:Ti diffused strip waveguide, optical insertion losses 78−74985
$LiNbO_3$:Ti digitally driven integrated optics amplitude modulator 80−58808
$LiNbO_3$:Ti electro-optic TE-TM mode convertor structure 80−64215
$LiNbO_3$:Ti in-diffused optical waveguide fabrication 79−76892
$LiNbO_3$:Ti narrow ridge optical waveguides and electro-optical, ion-bombardment-enhanced etching 80−38133
$LiNbO_3$:Ti optical waveguides, pyroelectric loss meas. 79−46046
$LiNbO_3$:Ti optical waveguides, elec. field tuning of SHG, phase-matching condition 79−41412
$LiNbO_3$:Ti optical waveguide channel branches 80−58811
$LiNbO_3$:Ti optical waveguide, SiO_2 thin film grating, surface wave mode conversion, static strain-optic effect 80−87561
$LiNbO_3$:Ti planar and channel optical waveguides, Ti diffusion coeff. meas. 80−19096
$LiNbO_3$:Ti planar waveguide, edge coupling to GaAlAs DH laser diode 80−87559
$LiNbO_3$:Ti single mode electrooptic waveguide modulator, high-speed operation 80−91915
$LiNbO_3$:Ti single-mode waveguide, fabrication by sequential combination of Ti diffusion and masked ion-implantation 80−58785
$LiNbO_3$:Ti single-mode waveguides, losses due directional changes 80−58789
$LiNbO_3$:Ti thin film acousto-optic deflector 77−75698
$LiNbO_3$:Ti waveguide, diffused, Mg diffusion effects on characts. 78−66905
$LiNbO_3$:Ti waveguide, integrated bistable Fabry-Perot resonator fabrication 79−41459

integrated optics continued
$LiNbO_3$:Ti waveguide, in-plane scatt. obs. and countermeasures 80−33215
$LiNbO_3$:Ti waveguide, operation of geodesic lens, anisotropic and curvature losses 80−48453
$LiNbO_3$:Ti waveguide, ps signal processing with planar, nonlinear integrated optics 80−64208
$LiNbO_3$:Ti waveguide geodesic lens 77−84005
$LiNbO_3$:Ti waveguide directional coupler type modulator 78−66951
$LiNbO_3$:Ti waveguide for lightwave communications and data processing systems 79−37052
$LiNbO_3$:Ti waveguide thin film electrooptic Bragg modulator, bistable optical element 80−10034
$LiNbO_3$:Ti waveguide and cryst., absorpt. loss and photorefractive index changes 80−48368
$LiNbO_3$:Ti waveguide directional coupler switches, optically-induced crosstalk 80−48417
$LiNbO_3$:Ti waveguide electro-optic TE⇄TM mode converter-wavelength filter 80−64210
$LiNbO_3$:Ti waveguides, nondegenerate four-wave mixing 79−46088
$LiNbO_3$:Ti Z-cut crystals, Ti diffusion process parameters 80−102849
$LiNbO_3$/CdS integrated optical half adder circuit 79−76877
$LiNdP_4O_{12}$, glass clad, slab waveguide laser 78−46625
$LiTaO_3$, multimode electro-optical 2×2 crossbar switch 78−55473
$LiTaO_3$ optical waveguide, Ag-Li ion exchange 80−91888
$LiTaO_3$, Ti diffused, electrooptic diffraction modulation 79−10381
$LiTaO_3$:Cu, waveguide with periodic electrodes, mode conversion 78−33840
$LiTaO_3$:Ti, diffused waveguide prep., parameters determ. 80−14465
$LiTaO_3$:Ti waveguide modulator structs., high optical power capabilities 77−39023
MgF_2 film applicability assessment, vacuum deposited, destruction props. obs. *(Slovak)* 80−33224
MgO:Cu, dopant conc., refr. index profile rel. to integrated optics 78−5583
Nb_2O_5 waveguide, in-plane scatt. and loss mechanisms 80−33216
Nd^{3+} miniature laser principles, materials and integrated optical design 80−33004
Nd:glass films for integrated optics, RF sputtering and optical characts. 79−46087
$Nd_{0.14}Y_{0.86}P_5O_{14}$ epitaxial layer an $Gd_{0.33}Y_{0.67}P_5O_{14}$, growth lasing 77−46722
PLZT ceramic, modulator for optical communication 80−78964
P_2O_5-SiO_2 glass, flow for integrated optical cct. fabrication 80−79005
PbO-SiO_2 interdiffusion layer optical waveguide, prep. and props. 80−43489
PbTe, high mobility polycrystalline layer, mol. beam deposition 79−83138
Se amorphous Au clad waveguides piezoelastic modulator for 10.6 μm radiation 78−66956
Si guided-wave acousto-optical devices 80−102864
Si monolithic optical IC fabrication 77−19461
Si monolithic optical integrated circuits for laser system applications 78−1436
Si photodiode array for integrated optical spectrum analyser 80−33241
Si-SiO_2-$Si_xO_yN_z$ waveguide model *(Russian)* 79−10374
Si_3N_4 film acousto-optical props. for integrated optical Bragg cell 79−55251
Si_3N_4 on Si, optical waveguide, fabrication, propag. consts. 78−33826
Si_3N_4, RF-sputtered thin-film optical waveguide, effect of deposition parameters on optical loss 79−76881
Si_3N_4 waveguide layer, as electro-optic phase modulator 79−23081
SiO_2 thin film grating for $LiNbO_3$:Ti waveguide mode convertor and reflector 80−64216
SiO_2-Ta_2O_5 film, refr.-index-adjustable, for integrated optical ccts., prep. and props. 78−63203
Ta_2O_5 film acousto-optical props. for integrated optical Bragg cell 79−55251
Ta_2O_5 film with protective coating, optical waveguide prod. 79−72682
Ta_2O_5, RF-sputtered thin-film optical waveguide, effect of deposition parameters on optical loss 79−76881
Ta_2O_5 sputtered film, refr. index meas. *(Italian)* 79−32088
Ta_2O_5 waveguides, colinear interaction between acoustic and optical waves in planar waveguide, radiation into substrate 80−53452
TiO_2 film applicability assessment, vacuum deposited, destruction props. obs. *(Slovak)* 80−33224
YIG substituted film waveguides, TE→TM mode conversions 78−66904
YIG thin film gyromag. waveguide, on GGG substrate, optical propag. props. Faraday effect 80−74513
ZnO, CVD films on sapphire substrates, use as optical waveguide 78−90500
ZnO film, optical waveguide fabrication, CVD on sputtered ZnO film on sapphire 79−86269
ZnO film acousto-optical props. for integrated optical Bragg cell 79−55251
ZnO, high rate epitaxy on sapphire by planar magnetron RF sputtering 79−28916
ZnO integrated optical transducer arrays 79−50444
ZnO low-loss optical waveguides on amorphous substrates 80−58793
ZnO, RF sputtered epitaxial film, appl. to integrated optics 77−14821
ZnO thin films, surface acoustic-optic interaction, diffr. 77−3685
ZnS film applicability assessment, vacuum deposited, destruction props. obs. *(Slovak)* 80−33224
ZnS leaky waveguide electro-optic modulator limitations 78−22218
ZnTe ion implanted planar waveguides, refr. index profiles 77−62039

integrating circuits
400 Mb/s optical fibre communications, integrating and transimpedance front end performance comparison *(German)* 78−33879
analogue, for dosimeter to meas. ion-beam current integrated flux 78−49865
automatic reset integrator, respiratory activity obs. in expt. animals 79−29683
averaging meter for nonelectric periodic quantities, dual slope principle *(German)* 78−73983
boxcar integrator instruments, automatic baseline correction, appl. to plasma chromatography 77−52717
boxcar integrator/US recording unit using sample-and-hold circ., for student lab. 80−27083
capacitance meter, linear 79−6146
digital calculating integrator for Calvet-type twin calorimeter 80−77786

integrating circuits continued
digital display adaptor for Victoreen 440 survey meter 79−70644
digital electronic integrator, for radioastronomical obs. processing *(Russian)* 78−57465
digital integrator, automatically triggered, for flame AAS with discrete nebulization 80−35610
digital integrator, for flameless at. absorpt. spectrometry 77−38014
digital integrator for Auger SEM 80−37131
digital integrator for chemiluminescent analysis 78−21196
digital leaky integrator 79−22560
electric heating regulator using a FET amplifier and Schmitt trigger convertor *(French)* 79−58681
electrometer transducer, with time-pulse output 77−74443
fluorimeters, weak fluoresc. detect., analogue method 77−40581
integrator for use in bombardment experiments 79−18092
marine seismic survey, modified integrating A/D convertor *(Russian)* 78−49142
microprocessor integrators for chromatography, development, operation, capabilities 77−56287
microprocessor-controlled digital integrator for quantitative NMR measurements 80−11971
multi-channel, for plasma magnetic-probe meas. 78−75413
phase detector produces unambiguous output 78−4627
phasic signal integrator with automatic drift correction 78−35985
preamplifier, for InSb IR detectors 80−90337
preamplifier in Fourier spectrometer, InSb photodiode improved noise compensation 80−73474
precision full-wave rectifier/integrator for physiological signals 79−83988
pulsed integrator for EMG analysis 80−61719
pulsed NMR, digital integrator 77−26372
respiratory flow integrator with improved stability 79−16331
respiratory flow-volume integrator 77−48914
signal shape reconstruction from derivative using synchronous filter 77−37870
two channel boxcar integrator with A/D conversion for pulsed NMR spectrometer 79−80657
variable-potential coulometer analyser integration error analysis 80−93831

integration
Adams-Moulton-Cowell multistep integrator for satellite orbit, time regularisation 78−45208
ADIF, a FORTRAN IV program for solving the shallow-water equations 79−84493
Airy function products, indefinite integrals 77−37731
analytical angular integration technique for generating multigroup transfer matrices in transport calcs. 80−68722
anisotropic solid fluid flow with free or artesian surface analysis, finite element method soln. 78−92872
annulus with rotating inner cylinder, momentum integral soln. of developing flow 77−35149
artificial satellite motion, numerical integration of near-parabolic orbits 77−25925
asteroids orbital perturbations, analytical integration using regular proximities concept 80−72843
astronomy, numerical integration of stellar orbits 79−21361
atoms, variation-iteration procedure, by numerical integration scheme 78−17551
Cauchy integrals, appl. to geomagnetic bidimensional inhomogeneous direct problem *(Russian)* 79−35013
Cauchy type singular integral eqns. with complex singularities, numerical soln., stress intensity factors 78−55611
celestial mechanics, 2101 Adonis problem soln. by recurrent power series integration 80−72842
celestial mechanics, major planets motion using numerical integration method 79−92657
cell nuclei, human lung, determ. of mean caliper diameter using serial section reconstruction models 79−29679
chemical reaction kinetics, temp. integral approximating eqns. accuracy 78−92445
circular cylindrical shells, integral calc. involving characteristic beam functions 78−63359
circulation models, numerical integration method for improving soln. stability 78−69118
classical trajectory calcs., empirical testing of nonrandom integration method 78−50607
coherent optical hybrid space- and time-integrating spectrum analysis 80−48177
collision theory integral, analytic determ. 78−28987
cometary equations of motion, recurrent power series integration 80−72882
commutator theorems, integration of Lie algebras representations and commutation relations 77−53732
complex variables method for soln. of large nonlinear differential eqns. systems 78−62062
continuity eqn., boundary conditions for integration 78−3342
cool flame explosion, during piston compression, time predicted by Livengood-Wu integral method 78−15675
cosmology, BBGKY eqns. integration for development of nonlinear clustering in expanding universe 78−8175
curved rectangular conductor magnetic field calc. 77−61895
curvilinear domains, quadratures *(Russian)* 79−63006
dam unsteady compressible fluid flow digital simulation, finite element method appl. 78−90820
demagnetising field, calc. by FFT 79−38355
detector integration acouto-optic signal processing 79−72519
dynamical grid method for time-dependent simulations of axisymmetric instabilities in tokamaks 79−10702
Earth gravity field, associated Legendre functions integration for spherical harmonics expansion *(German)* 78−61311
elastic-perfectly plastic von Mises material, accuracies of numerical soln. constitutive eqns. 78−59315
elastic-viscoplastic constitutive equations, incremental, represent. of high strain rate behaviour 80−85138
electron microscopy, image processing by linear integration technique, periodic structures obs. *(Japanese)* 80−52363
electron repulsion integrals, computation involving Gaussian basis functions 78−58572
EM cascade eqns., numerical integration, results for air, Cu, Pb and Fe 78−20602

integration continued
Euclidean 0^4 theory, simple Feynman graph evaluation 78−41404
Euler equation for compressible flow, integration scheme 79−81913
exact Slater integrals determ. for H wave functions, computer method 78−90074
fermion systems, integral evaluation 79−40449
finite element isoparametric quadrilaterals, integration formulas 78−89317
finite element method, reduced integration, appl. to elastostatics 78−75066
finite geometry effects in scatt. expts., numerical integration method 78−82596
first-order linear differential eqns., optimum integration operators 77−78962
fission reactor digital simulator software development, kinetic equations integration, numerical solution method 80−68901
fission reactor point kinetics equation, integration with improved steady-state behaviour 79−22378
flow meas. traverse methods, techniques comparison *(French)* 77−75871
fluorescence decay, nontrandom errors, moment index displacement calcs. 77−6835
Fokker-Planck eqn., integration method 78−91067
Fourier transformation, singularity expansions and product integration 78−89316
free electron lasers, equations of motion, approx. technique for integration 79−64193
Gaussian plume model parameters determ. from diffusion-convection eqn. integration 78−81399
generalised WKB method simplification 79−7767
generalized calculus and its applications, review 79−35527
generalized WKB method, sufficient conditions for rapid convergence of iterations 80−53195
long geodesics computation on ellipsoid through Gaussian quadrature 79−100806
grid points condensation in process of solving and using high order schemes in numerical integration of viscous gas flows *(Russian)* 78−59363
groundwater flow analysis, finite element method soln. 78−92875
Hankel transforms, related, of orders 0 and 1, numerical integration by adaptive digital filtering, FORTRAN IV algorithms 79−92599
heat conduction, steady-state, soln. using heat balance integral method 77−14880
highly oscillatory functions, numerical integration 77−13593
Hilbert space, quantum mechanics and integration, functional integrals 79−97246
Hough harmonic expansions for numerical integration of global barotropic primitive eqns. 77−78442
hydrological system tracer digital simulation, finite element method soln. 78−92881
hypersonic viscous shock layer equations, num. soln. scheme 79−90280
hypersonic viscous shock-layer equation, method for successive approximations for integration *(Russian)* 78−59421
hypoelastic compressible rate-sensitive material flow, integrable generalized wave eqns. 78−38213
improper integrals, programmable pocket calculator calcs. 80−101696
incompletely integrated shape functions, numerical stability, finite element stiffness matrices 78−1567
inelastic deformation, stiff constitutive models, numerical integration 80−96208
infinite range oscillatory integrals evaluation 77−5652
integral estimation w.r.t. density of states 78−41224
internal stresses, calc. with integration methods, X-ray stress meas. 79−32415
invariant integration over SU(N) 79−243
IR radiation spectral absorptance and transmittance, accurate modelling technique 78−91062
isentropic perfect fluids, integration of relativistic equations of motion 78−7872
isoparametric linear bending element and one-point integration 79−3919
Kirchhoff surface integral calc. of acoustic field due to disc radiator, simplification 79−86275
Laplace equations in thin regions, mixed boundary-value problem 77−35016
large amplitude water wave digital simulation, finite element method soln. 78−92851
laser light pulse parameter meas., integral method 77−72018
laser resonator standing wave simultaneous forward and backward integration 79−94258
lifting wing calcs., spanwise integrations, computational economy improvement 78−71344
linear inhomogeneous differential eqn. systems with variable coeff., integration using Runge-Kutta-Nystrom algorithm *(German)* 78−8235
linear lattices, integration of vector valued functions 79−63157
linear system mean square response to nonstationary random excitation 80−57085
linearized evolution eqns. 78−32657
magnetic film, micromagnetic dynamics in domain walls, numerical model 78−72382
many-body problems with pair interaction, involute set of integrals 77−22448
matrix exponential method, dynamic response via digital simulation 77−72149
Maxwells eqn. integration, implicit scheme, space and time discretisation 80−90688
mechanical equations with slowly varying coefficients, approx. integration *(Italian)* 77−5627
mechanics equations with slowly varying coeffs. *(Italian)* 77−78968
metal, cyclic and damage constitutive laws, calculation methods *(French)* 79−43408
meteorology, limited area forecasting model, forward-backward integration scheme 77−87084
meteorology, primitive eqns., semi-implicit and filtered integration schemes 77−86976
meteorology, viscous forecast eqns., boundary conditions for limited-area integration 77−86979
Mie scattering between any two angles 77−65576
molecular dynamics simulation, of liquids with ionic interaction 80−54097
Monte Carlo code, RISO, for resonance integral calc. in reactor cell lattice 77−3088

integration continued
Monte Carlo event generation with limited tranverse momentum 79−3001
Monte Carlo iterative scheme for adaptive multidimensional integration 78−57762
MOS photosensor charge integration and storage 77−39079
multidimensional integrals, numerical calc. 78−89323
multidimensional nonlinear partial differential eqns., integration by inverse scatt. problem method 77−60905
multilayer solids, soln. of heat conduction and thermoelasticity problems *(Russian)* 78−38177
N twisting gravitational field soln. to Einstein eqn., integrability conditions 78−86203
Navier-Stokes equations, photoabsorpt. convection in horizontal tube 80−33594
Navier-Stokes equations solution for incompressible three-dimens. internal flows 77−58795
near resonant oscillating systems, integration in slow-fluctuation approx. 80−62483
nonconservative systems, integration of motion eqns. *(Ukrainian)* 78−81827
nonlinear differential eqns. of compressible plane subsonic flow *(German)* 77−11218
nonlinear wave propagation, spectral and pseudospectral methods, turbulent sound wave appl. 77−5672
Norsett methods for implicit time integration of partial differential eqns. 77−82376
nuclear field theory of Fermi systems in an external field, path integrals 78−93954
nuclear reactor dynamic structural anal., comparative evaluation 77−3091
nuclear reactor thermal-hydraulic conservation eqns., analytic integration 77−83012
numerical, computer aided linear physical systems analysis, with periodic inputs 79−51
numerical, EM plane waves scattering calc., by metal cone, near its symmetry axis 80−106426
numerical, error estimation by means of Fourier series *(Japanese)* 79−2612
numerical, in shell problems finite elements *(French)* 77−74206
numerical, of diffusion eqn. using time level schemes 79−2609
numerical, of harmonic motion differential eqns., programmable calculator, teaching appl. 78−86083
numerical, SNIFF self-adaptive algorithm 77−67261
numerical for viscous dissipation effect on nonlinear convection at high Rayleigh number 77−54994
numerical integration, one-step methods, quadrature formulae *(Russian)* 77−37747
numerical integration formulas, asymptotic behaviour of coeffs. *(French)* 77−37742
numerical integration of eqn. system for nonadiabatic compressible gas flow in tube *(Russian)* 78−83427
numerical integration over solid angle and vol. of Brillouin zone, any crystal symm. 77−27843
numerical surface integration, expressions for element base area unified with integration formulas 79−53967
numerical weather prediction, split explicit integration scheme 79−12210
objective and regular differentiation and integration, constitutive law and transport *(French)* 80−57090
optimum filter design for discrete integration 80−200
orbit calculation, past and future, for 1977 UB, Object Chiron 79−35171
ordinary and partial differential equations, appl. of semi-implicit Runge-Kutta methods 78−12542
ordinary differential eqns., error estimation 77−9874
ordinary differential eqns., suppression of inherent instabilities in initial value methods 79−9090
ordinary differential eqns., with numerous discontinuities, numerical anal. 79−21535
path integral, canonical to covariant change 78−73877
path integrals in quantum theory, basic concepts, review 80−52066
path integration in phase space 78−128
photoelectron spectra of cryst. solids, numerical integration within linear analytic approx. 78−60545
pitch angle diffusion eqn. of trapped particles in presence of loss. cone, finite difference integration 79−70931
Planck blackbody radiation function integration for meteorology 77−45059
plasma, rapidly changing, numerical integration of ionisation rate eqns. 78−55734
plasma drifting, cold or hot, radiation potential of immersed point antenna, DRFT computation 80−14906
plate bending, reduced and selective integration techniques in finite element analysis 78−42552
plate bending elements, quadrilateral, finite element anal. with reduced integration 78−75071
plates, piecewise-constant coeff. of heat transfer, thermoelasticity, method of integral charact. *(Russian)* 78−38188
Poincare-Chetaev's equations, integration *(Russian)* 79−35547
Poisson's equation integration for complex system with arbitrary geometry 77−47705
polaron theory, Bessel function integral, asymptotic evaluation 78−56082
polyatomic molecules, quadrupolar and dipolar, numerical evaluation of second virial coeff. 78−91050
product integration with applications to differential eqns., book 80−41967
propagator method for set of classical trajectory equations 77−57233
pseudospectral dispersion model, inter grid sources representation 79−12259
pseudospectral method for atmospheric pollutant dispersion eqn. numerical integration 77−56727
quadrature formulae of high algebraic precision for sphere *(Russian)* 77−5643
quadrupole mass spectrometry, numerical calcs., book contrib. 77−22611
radiation field of extended rectangular source, numerical integration 78−66424
radiative transfer in real spectrum, calc. using integration over freq. method 80−33430
reactor shielding materials, Pb, and steel, γ leakage spectra, numerical integration of Boltzmann eqn. 78−58350

integration continued
resolvent integration techniques for generalized transport equations 79−76051
rigid body with discrete symmetry, conditionally-linear integration of eqns. of motion *(Russian)* 78−86135
rivers, St. Venant eqns. integration rel. to morphometric and hydraulic channel characts. determ. 78−3838
Runge-Kutta-Nystrom condition equations, resolution through eighth order 77−22398
satellite motion, numerical integration of differential eqns. of motion 77−33327
Schrodinger eqn., time depend., explicit integration method, comment 79−72224
Schrodinger eqn. for quantum system subject to random pulses, Blume's integration 79−97232
Schrodinger eqn. with double-minimum potential, numerical integration 78−58573
Schrodinger equation, numerical integration, using WKB approx., eigenvalue estimates 78−12486
sea ice, relationship between mean stresses and internal forces local values in drifting cover 80−31056
sea pollution simulation, higher accuracy predictor-corrector method 79−66431
second order linear partial differential eqns. of math. phys., integration by separation of variables *(Italian)* 78−81798
shells of resolution, transient dynamic and inelastic anal., survey of programs 77−3767
singular integral, construction related with local props. *(Russian)* 77−22382
Slater type orbitals, analyt. calc. of two-centre Coulomb and hybrid integrals 77−83479
Slater type orbitals, analyt. calc. of two-centre Coulomb and hybrid integrals with correlation factor 77−83481
solid shaft, elliptic cross section, elastic torsion, polynomial soln. to approx. of any order *(Italian)* 78−13897
solid transient dynamic problems, finite element formulations using explicit time integration 78−18162
Sommerfeld integral in radiowave propag., numerical approximations for fast convergence 78−66727
sorption kinetics in porous granules, integration of nonlinear eqns. 77−7967
stability of explicit-implicit mesh partitions in time integration 79−1101
star clusters, evolution, Fokker-Planck eqn. numerical integration 80−36675
stationary satellite eqns. of motion numerical methods *(Japanese)* 78−85837
steady-state laminar flow in turbulence amplifier, numerical method *(Bulgarian)* 80−106779
stiffened plates, structural and by finite element and integration methods 77−3753
STO basis set, removal of singularities in numerical integration 79−6847
stochastic and ordinary differential eqns., connections *(French)* 77−37734
Stokes Theorem, surface of mixed physical properties, mathematical method *(Italian)* 77−50589
structure-fluid mesh partitions of explicit-implicit integration appl. to reactor safety 77−46238
supersonic boundary layer, prediction by hybrid marching integration procedure 77−65761
surface scattering integrals, asymptotic approx. 77−42468
Takagi-Taupin equations, boundary conditions in numerical integration, appl. to Bragg and Laue cases 80−1886
three dimens. turbulent boundary layer, fourth order Mehrstellen integration 77−3816
three-centre integrals calc. for chem. shifts determ. *(French)* 79−31550
time integrating acousto-optic signal processors 80−48176
time transformations and Cowell's method 78−77466
time-varying signal coherent detection using multiple obs. 80−43553
transient response of orthotropic plates to uniformly distributed transverse load, computer calcs. 77−68503
transonic small-disturbance theory, leading-edge singularity, num. integration methods eval. 80−6080
triangular finite elements and numerical integration 78−33
triangular finite elements containing corrective rational functions 77−13591
triple systems, non-rotating, exact mean time of decay *(Russian)* 78−32523
two body problem, time transformations and local truncation errors 77−22053
two body problem, time transformations effect on local truncation errors 77−22052
two-dimensional radiative transfer in planar geometry, Hermitian integration formula 78−40810
unsteady flow in open channels, num. analysis method, teaching aid paper 77−29972
unsteady squeezing of viscous fluid from tube 79−90296
viscoelasticity equations, stability of numerical soln. 78−16647
Vlasov eqn. integration in configuration space 77−7512
wave eqn. numerical integration by digital integrators 77−53760
wave equation in n-space dimensions, approx. integration formulae 78−16659
work hardening-recovery type constitutive eqns., numerical integration, improved method 78−6949
Fe, cast, US flaw detection by boxcar integration 80−89437

integro-differential equations
see also Boltzmann equation; Fokker-Planck equation; Liouville equation; master equation; Vlasov equation
absorbing-emitting media, integro-differential energy eqn. soln., validity range of differential approx. 78−5644
aerofoil in unsteady viscous flow, numerical soln. procedures 78−75165
aerosol coagulation, simplified model 77−56254
anisotropic scattering media, neutron transport formulae 79−17959
asymptotic long time behaviour 77−74197
base excited cantilever beam, whirling motion, comments 80−48488
Benjamin-Ono eqn., conservation laws 80−31524
Benjamin-Ono equation, periodic wave and soliton solns. 79−35570
Benjamin-Ono equations, two-parameter Miura transform. 80−14720
boomeron equation, asymptotic behaviour (in t) of solutions 79−9082
Born-Green-Yvon eqn., two-dimensional, with anisotropic interac. 78−79882
integro-differential equations continued
Born-Green-Yvon equations, for strongly interacting Fermi systems 79−49161
boundary elements in potential and elasticity theory 79−35560
Brownian motion, generalised scalar case, computer simulation 80−77704
Brownian motion, theory 77−26242
charged particle in box, nonlinear integrodifferential eqns. with delay, soln. existence 79−27124
coagulation, with breakdowns, exact solution of integrodifferential equation 78−53272
conducting screen, excitation of object through aperture 79−13871
continuity equations, for transverse multipole amplitudes, EM and gravitational fields 79−58609
cylindrical shell, viscoelastic, forced axisymmetric oscillations 77−50933
damped linear integrodifferential eqns., dielectric appl., concavity arguments and growth estimates 79−28703
degenerative, reduction method convergence and generalisation *(German)* 80−33
dielectric, damped integrodifferential eqns., asymptotic bounds to system of solns. 80−62493
differential operator and integro-differential eqn. for thermospheric tides *(Chinese)* 80−56660
diffusion kinetics, crystallisation of salts from supersaturated solns. 79−23553
diffusion model, statistical distribution of particles over given volume 77−82467
discrete particle diffusion in turbulent fluid, finite difference method anal. of integro-differential eqn. 79−77089
dissipative gasdynamic system, nonlinear interaction model *(French)* 79−14427
Earth equilibrium figure, integro-differential eqns. 79−44077
eigenvalue problems, numerical soln., nuclear theory *(Russian)* 77−57641
elastic body vibrations, justification of two scale method for class of integro-differential eqns *(French)* 78−28947
elastically clamped variable-stiffness annular plate, thermostability 77−89052
elasticity, nonlocal, fundamental 1-D solns. 79−67163
electric fields in non-conducting material dielectrics, stability and growth estimates 79−71262
electrochemical machining, approx. method for solving problems 78−44241
electromagnetic scatt., time depend., boundary value formulation, integro-differential eqns. 78−66726
electron-atom collision theory, soln. of coupled integro-differential eqns. by computer program 78−86948
EM field penetration through small apertures, first order correction 79−64156
EM wave propagation, 1-dimens., calc. of refl. and transmission coeffs. 77−23599
EM wave two-dimensional transient scattering, new space-time integral eqn. 78−78861
evolution equations for heat cond. with memory 80−38220
exact derivation of a generalized master equation for the motion of excitons 78−87911
flame front, laminar, hydrodynamic instability, nonlinear integro-differential eqn. 78−51253
flame front, laminar, hydrodynamic instability, numerical solns. 78−51254
flow boundary layer, stochastic model of fluctuations 78−90818
fluid monolayer at solid surface, density distrib. calcs. 80−49492
fog clearing by laser beam, thermal self-defocusing effect 77−64432
Fredholm second kind in stationary system impulse response function, Cauchy problem reduction 77−37729
frequency domain stability for a class of equations arising in reactor dynamics 79−54475
gas kinetics, integro-differential eqn. approx. by Fokker-Planck type 78−91049
generalised kinetic theory with memory 79−35625
grain boundary groove profile, effects of surface free energy anisotropy 79−7734
groundwater flow in unconfined aquifers, theory 79−5522
heat cond. for materials with memory, linear theory 79−14206
heat flow eqn., asymptotic stability theorems 77−67216
hereditary elasticity, integro-differential problems 79−67162
higher order Benjamin-Ono equation, N-soliton and N-periodic wave solns. 80−12915
Hodgkin-Huxley reduced model, speed of spread of excitation 77−21509
homogeneous kernels, Mellin transformation of generalised functions 77−49572
immiscible fluids in one dimensional porous medium, regularity and asymptotic behaviour 79−72936
infinite depth fluid, steady free surface gravity-capillary waves, integro-differential formulation 80−6072
interacting systems, general theory of natural states, use for calc. of intermol. forces 78−82807
interacting systems, natural states in the asymptotic 1/R expansion, use for calc. of intermol. forces 78−86930
ions, electron impact excitation close-coupling formalism, perturbative treatment 80−48091
laser modelocking, soln. of 2nd order integro-differential eqns. 78−66796
leaky aquifiers, integrodifferential eqns., numerical method of unlimited appl. 78−11935
Lindhard's equation, radiation damage by energetic heavy particles *(Japanese)* 80−29094
linear spectral problem of arbitrary order, general form of integrable eqns. and their Backlund transform. 80−52002
linear viscoelastic material vibrations, integro-differential eqn., two-scales method soln. 79−72839
linear waves, asymptotic behaviour and wave patterns construction *(Czech)* 80−69
materials with memory, linear theory of heat cond., final value problem, existence, uniqueness theorems 78−59266
Maxwell-Hopkinson dielectric theory electric displacement fields, growth estimates 79−24278
metal surface, integro-differential eqn. for electron density and formula for surface tension of jellium 80−44689
modified Lame eqn. with integral term, exact soln. 78−63052
modulated electron beam in inhomogeneous isotropic plasma, nonlinear wave generation 78−1852

integro-differential equations continued
nerve fields, topographic organisation 80−89742
neutron diffusion, time-dependent continuous-energy equation, weak solns. 77−65244
neutron transport, nonlinear, initial value problem 77−61474
neutron transport theory, Monte Carlo method applicability *(Spanish)* 79−6721
nonLie method for mathematical physics eqns. group props. investigation 80−36832
nonlinear, appl. of min. of non-convex functional *(French)* 79−53963
nonlinear mixed systems with polyvibrating operators, possible soln. determ. *(French)* 77−37726
nonlinear noisy sine wave oscillator, optimal control 80−27218
nonlinear quantum mechanics, Gauss transform. appl., Schrodinger eqn., nonlinear integro-differential eqn. 79−6013
nonlinear system with unknown boundary, solvability 79−84940
nonlinear transfer processes, optimisation *(Russian)* 80−8934
nonlinear Volterra integro-differential equation, heat flow appl. 79−18668
nuclear deformation meas., coupled integro-differential eqns. treatment 79−451
olfactory bulb model, spatial and temporal charact. freqs. of interactive neural masses 77−25476
one-dimensional nonstationary problems of gas dynamics, estimates of shock wave motion 79−18912
open systems, eqns. of motion in nonequilib. statistical mechanics 80−82710
operator, limiting irradiance distribution of light in random media appl. 80−5695
operator eqn. model of reactor with delayed neutrons 77−50213
oscillators, nonlinear stochastic, triangular wave, optimally controlled, Weiner process and Poisson process, numerical studies 80−52128
partial, early time anal. space depend. reactor transients 77−3077
partial distrib. functions of statistical mechanics, BBGKY hierarchy 77−61006
particle scattering, low-energy, two-pot. formulation with r^{-4} interaction 80−31552
particle transport theory, integro-differential eqn. soln. 80−36955
plane steady temp. field, effect of biperiodic system of plane inclusions 80−19224
plasma, Vlasov, mathematical model 79−55503
plasma high temp. transport process, numerical soln. 80−19559
plasma sheath, integro-differential eqns., nonlinear, nonlocal, soln. formalism 80−43936
Pocklington type, finite cylindrical scatterer near imperfectly conducting ground 78−71003
polymer rheology nonlinear singularly perturbed Volterra integrodifferential eqn. 79−23290
polyvibrant Mangeron equations, study of different classes *(French)* 77−33839
Prandtl's eqn., deduction 77−29997
pulse propag., uniaxial, in viscoelastic medium, formulation using Boltzmann superposition integral 79−12619
radiating electron, stability of motion 78−65789
radiative transfer, time-dependent, exact soln. of integro-differential eqn. via Laplace transform 80−94703
radiative transfer in diatomic gas, vibr. nonequil., probabilistic modelling 80−33434
radiative transfer in finite atmosphere, exact soln. of basic eqn. via Laplace transform 80−94702
Rayleigh waves, finite heterogeneous media, effective elastic props. *(German)* 78−22291
resonance phenomena in systems described by eqns. with divergent arguments *(Russian)* 78−73832
retarded argument, higher approx. solns. *(Russian)* 78−12545
retarded Josephson equation, adiabatic and pendulum approx. 78−68119
retarded Josephson equation 79−19697
scattering, low-energy, by long-range pot. 78−74723
Schrodinger equation, free, invariance algebra 78−81
singular, using spline methods 77−13595
Stefan problems, two-dimensional, approx. of integro-differential eqn. 77−80050
stratified fluid of finite depth, exact multi-soliton soln. for nonlinear waves 80−22199
stratified fluid with finite depth, internal wave eqn. governing long gravity waves 79−97217
thin film eddy current calc., finite element method solution 78−90343
three-dimens. solitons 78−62053
three-dimensional neutron transport, discrete ordinate solution 80−63222
turbulent diffusion, nonlinear integrodifferential eqn., numerical soln. 78−38306
turbulent flow problems 79−32468
unbounded linear transformation arising in kinetic theory of gases, spectral representation 79−55441
unsteady filtration with unknown boundary, nonlinear integro-differential eqn. 80−43769
viscoelastic displacement vector growth estimates 79−27552
viscoelastic media, deform. theory with account of thermodiffusion *(Ukrainian)* 78−67052
viscoelastic structures, strength and stability, a method of solving integral eqns. used 80−10167
viscoelasticity, existence and asymptotic stability of solns. 79−12608
viscoelasticity, integrodifferential eqn. system, Cauchy problem soln. 77−50931
viscoelasticity, nonlinear, one-dimens. model 77−67290
viscoelasticity, solns. for eqns. with small parameter *(Russian)* 78−62078
viscoelasticity dynamics, solving methods in integro-differential eqns. 80−14586
viscoelasticity linear, isotropic integro-differential models *(French)* 79−80443
Volterra eqn., growth estimates for solns., appl. to viscoelastic initial-boundary value problems 77−74195
Volterra equation, nonlinear, compactness of bounded trajectories of dynamical systems 80−82636
Volterra type in viscoelasticity theory, existence and uniqueness of solns. 77−62173
vortex sheet, unsteady, self-similar, rolled-up, large scale struct. 79−32531
vortex sheets, calculation of three-dimensional unsteady flows *(French)* 78−14025
integro-differential equations continued
wave equations, asymptotic solns. using methods of averaging and two-timing 78−59
wave reflected from randomly inhomogeneous layer description, by series satisfying causality condition 80−106420
wavefunctions for electron+atom or electron+ion system, coupled integro-differential equations 80−18924
waves, gravity, on deep water, finite-amplitude steady irrotational inviscid waves 80−64575
H_2^+, electron scatt. eqns. convergence, H_2 continuum states, appl. to photoionis. 78−66663
N, high intensity arcs, anode contraction region modeling 80−103210
intelligence, artificial *see artificial intelligence*
intelligibility, speech *see speech intelligibility*
intensification *see amplification*
intensity measurement
see also acoustic intensity measurement
absolute luminous intensity meas., apparatus *(Danish)* 78−62217
electron gun, LaB_6 cathode, current beam intensity and brightness meas. *(French)* 77−590
Gaussian laser beam focus, intensity distrib. determ. 79−14002
illumination engineering measurements using photometry and spectroradiometry 80−22416
intensity correl. spectroscopy, spherical particle continuous distrib. meas. 78−21228
laser beam diameter fluctuations meas. 78−87086
laser radiation intensity fluctuation in fine-droplet water aerosol at 630 nm 80−4109
laser radiation TV analyser for intensity distrib. anal. 79−3702
LEED intensity measurement by photographic method with digital image processing appl. to Si (111) surface 79−60234
lighting, effectiveness, ESI meter application 80−22417
liquid light scatt. coeff. absolute determ. apparatus 78−86319
monochromatic speckle patterns, statistical props. 80−53215
noise signal, nonstationary, modulation radiometer, noise 77−61048
nonstationary Poisson train intensity meas. error analysis 79−67246
photoelectric radiation flux density meas. technique 78−89521
photoionisation collision radiation spectrometer, for absolute intensity distrib. meas. of light sources 79−93233
photometric meas., digital meter, cct. and operation *(Polish)* 78−65943
pulsed X-ray thermionic tube intensity and dose angular distrib. obs. 79−67450
trichlorofluoromethane, 8-12 μm bands intensities, temp. depend. 80−43048
AlO, $B^2\Sigma$-$X^2\Sigma$, Einstein A coeffs., band strength and band oscillator strength 80−43113
He-Ne laser radiation, spatial and temporal correlation of intensity fluctuations 79−81473
He-Ne single mode lasers, meas. of intensity of sources of inherent fluctuations 80−32958
interacting control systems *see multivariable control systems*
interactive programming
see also interactive systems
biostereochemical modelling, interactive computer graphics, appl. to DNA-protein interaction 78−88693
chemical synthesis computer design, interactive strategy 79−91945
IFECS interactive software, thermal stress modelling appl. 79−80440
image processing software, structure and design philosophy 78−58940
lake survey programme for water resource surveillance 78−81257
minicomputer optical design and analysis program 79−14075
musculoskeletal complex shape cross-sectional props., interactive graphics software package 79−79595
myocardial electrical activity modelling, dialogue mode *(Russian)* 79−2021
PAL, highly tutorial interactive, pattern recognition program for seismic anal. 77−81833
particle track data in plastics, rapid anal. using interactive programming and graphic displays 78−66456
radiography, interactive meas. in computerised tomographic imagery 77−77984
signal analysis and simulation program 79−79678
water resource problem with multiple objectives, interactive optimisation, Yodo River basin, Japan appl. 79−57516
interactive systems
see also interactive programming; interactive terminals; online operation
air pollution data analysis using combined interactive graphic presentation and clustering technique 79−83656
astronomical plate analysis, interactive imaging technique appls. 79−58266
bacterial cell wall structure study 79−5427
B.I.P. An interactive graphic system for indexing energy bands of model polymers 79−59608
CAD of windows as passive solar collectors, for buildings heating and cooling 79−62146
conversational statistical analysis program, COSTAT, DEMOS-E library *(Japanese)* 79−2614
digital image processing, interactive system for computer reduction and display of two-dimensional data 79−58257
echocardiographic and systolic time interval processor 79−83869
electric field computation using SCOFF program *(German)* 80−78740
epithelial tissue pattern recognition 79−25145
graphic computing system linked with signal enhancement seismograph, description and application 80−4131
Graphic Interactive System for Processing of Electrocardiographic Maps 79−39552
image data analysis, Meteosat project MISS IDA 80−36404
image processing system 79−13916
incremental compiler for data acquisition 79−89550
interactive graphics system developed for NDT 80−66729
microprocessor based interactive radiographic image display 79−25092
microprocessor-controlled hologram interferometry analysis using intelligent TV system 79−76648
minicomputer, real-time, portable, for dynamic ocean data acquisition and display 80−12552
molecular analysis system, MOLY, design of biologically active compounds 80−63852
morphometric cytology pictorial pattern recognition appl. 79−25179
multiuser facility, experimental data processing 79−88922
POL, data analysing interactive system 79−31347

interactive systems continued
resistivity soundings over horizontally stratified earth, man/computer interpretation 78−45014
Rietveld neutron profile refinement, interactive computer system, POWDER 80−1900
satellite video display systems for atmospheric analysis 79−58229
sea ice, airborne laser profiles, interactive correction and anal. system 79−25338
seismic surface waves analysis 77−81818
solar buildings, climatological design assessment interactive CAD techniques 80−61289
Spectronic 2000 spectrophotometer, interactive microprocessor-controlled instrument 80−105716
surveying and cartography, interactive graphical systems appl. *(German)* 79−21023
X-ray imaging and measuring method using interactive display terminal for X-ray microbeam scan system *(Japanese)* 77−81563

interactive terminals
see also interactive systems; remote consoles
agriculture acreage estimates using LANDSAT data, appl. 77−78504
astronomical appls. of graphic routines for interactive Tektronix video unit and Printronix printer *(Italian)* 80−8553
computer data input/output control panel, for thermophysical experimentation 79−17401
computer-aided optical design, optimisation and interactive graphics improvements 80−78933
coronary intensive care unit, computerised monitoring system 77−21656
data terminal with voice indication for general practitioner use, ECG analysis via telephone network appl. 77−81613
device coupler for interactive systems 78−24767
ECG data interactive display system 78−53550
engineering design curricula, computer appls. 80−27065
image analyser FAS II, scanning electron microscope appl. 78−89597
intelligent communication device, design parameters 77−52928
linguistically oriented computer system for recognition natural continuous speech 80−23845
microprocessor speech synthesiser terminal 79−81660
oceanography, intelligent terminals and calculators as alternative to minicomputer systems 80−12553
photogrammetric model deformation, interactive demonstration program 77−74183
thermogravimetric data acquisition and reduction program 78−64901
X-ray microbeam scan system with interactive display terminal *(Japanese)* 77−81563

interatomic potentials *see potential energy functions*

intercalation compounds
alkali graphite intercalation compound, evidence for alkalilike cond. bands 80−45201
alkali graphite intercalation compounds, evidence for alkali-like conduction band, UPS study 80−45208
alkali graphite intercalation cpds., selection rules and restricted valence band self-convolution for KVV Auger transition 80−29832
alkali intercalated graphite, C XVV Auger lineshape anal. 80−104019
alkali ionic conductors with sheet structures, ion mobility and influences 80−107522
alkali metal, prep. methods and cryst. struct. 79−99156
alkali metal intercalation compounds, ionicity, struct., size, intercalation amount, ion mobility anal. 80−39041
alkali metal ternary chalcogenides, $M_{0.33}TaS_2$ and $M_{0.5}NbS_2$, supercond. props., alkali cation and topotactic solvation influences 79−87180
alkali metal ternary sulphides, A_xMoS_2 and $A_xMo_3S_4$, cryst. struct. 78−42989
alkali metals in graphite, organic molecule effects, aromatic hydrocarbons *(French)* 78−27433
$C_{24}K$, order-disorder transition, X-ray study 80−33922
$C_8^+MF_6^-$, (M=Os,Ir,As), struct. and elec. props. 80−70183
CDW suppression in layered compounds 78−14856
dichalcogenide hosts, intercalation and substitution-intercalation cpds., factors affecting ion mobility 80−59707
dichalcogenide layer compounds, interface plasmon-phonon interactions, transverse cond. 80−49641
DNA double helical fragment intercalator complex, molecular struct. 79−16140
DNA-adduct systems, binding geometry, determ. by induced circ. dichroism 80−55988
drug-nucleic acid interactions, conformational flexibility at intercalation site 78−96005
electrical properties, anisotropy, rel. to chem. bond struct. 80−24888
electrode materials, thermodynamic and transport props. 80−66963
electron energy loss spectra for characterisation 79−95054
ethidium bromide E-DNA, intercalated birefringent fibres, microspectrophotometric investig. *(German)* 80−57392
graphite, a-axis conductivity model 78−10435
graphite, conf., La Napoule, France (May 1977) 78−27428
graphite, Cs-intercalated, melting and staging, X-ray scatt. obs. 79−19180
graphite, diffusion coeffs. of Br_2, HNO_3, and $PdCl_2$ 79−42310
graphite, dispersion relations of intercalate modes 80−34379
graphite, electrochemical insertion of $BF_3(C_2H_5)_2O$ *(French)* 78−27438
graphite, electrostatic interactions and staging, nonlinear Thomas-Fermi eqns. 80−107732
graphite, Fermi surface and transport props., LCAO model 80−80159
graphite, intercalation compound, C_8Rb, elastic and inelastic neutron scatt. 78−30597
graphite, intercalation compound with AsF_5, high elec. cond. 78−26838
graphite, intercalation compound with $AuCl_3$, reduction by H_2 *(French)* 78−27820
graphite, intercalation compounds as cathodes 78−27780
graphite, intercalation compounds with alkali metals and halogens, intralayer crystal struct. and order-disorder transform., electron diffr. 78−26540
graphite, intercalation compounds with AsF_5, elec. cond. meas. with high anisotropy 78−26837
graphite, intercalation mechanism and physical chemistry 78−27430
graphite, intercalation of chlorides in chlorosulphonic acid *(French)* 78−27436
graphite, intercalation of metal chlorides and bromides 78−27435
graphite, K-point effective masses and Fermi level shifts, magnetorefl. study 80−50305
graphite, Raman scatt. and IR refl., review 80−45066

intercalation compounds continued
graphite, struct. and phys. props., symposium, San Jose, USA (March 1979) 80−62379
graphite, trifluoromethanesulphonate intercalate, prep. by anodic oxidation 78−27439
graphite, two-dimensionality, structural phase transitions 80−19938
graphite, with K, Rb, or Cs, phase transitions, resistive anomalies, electronic props. 79−95405
graphite acceptor compounds, band struct. model and electrostatic effects 80−92814
graphite acceptor cpds., C_nBr and C_nNO_3H, electronic struct., quantum-magnetothermal oscills. 80−44478
graphite acceptor intercalation cpds., modulated electronic struct. 79−95310
graphite $AlCl_3$ intercalation compound, electrochem. characterisation method 80−55666
graphite compound, metallic electronic props. and correl. with chemistry 80−44567
graphite compounds, C_nK, de Haas-van Alphen effect, cyclotron reson., and transport props. 80−44479
graphite compounds, C_nK, electronic struct. and elec. props. 80−44471
graphite $FeCl_3$ intercalate, interpenetration of 'stages' direct imaging 80−84037
graphite intercalaction compounds with acceptor molecules, CESR 78−48042
graphite intercalate with SbF_5 and AsF_5, optical reflectance 78−35163
graphite intercalated with AsF_5, HNO_3 and $SbCl_5$, Raman scatt. in low stage cpds. 80−20638
graphite intercalated with AsF_5, quantum oscillatory phenomena 80−107823
graphite intercalated with Cs(K) donor atoms, Raman scatt. 78−10890
graphite intercalated with nitrate, galvanomagnetic props. 78−76092
graphite intercalated with $PdCl_2$, $RuCl_3$ and $OsCl_3$, synthesis and cryst. struct. 79−8253
graphite intercalates, coherency strains and staging 80−44167
graphite intercalates, struct. and order-disorder transforms. 78−71710
graphite intercalation acceptor lamellar cpds., charge distrib. and transport props. 79−95411
graphite intercalation compound, $C_{8.8}K$, mag. susceptibility fluctuations near supercond. transition temp. 79−78259
graphite intercalation compound, elastic coherency strain 79−60306
graphite intercalation compound, interaction between one or two s orbitals *(French)* 80−65440
graphite intercalation compound, LiC_6, ^7Li NMR *(French)* 78−35050
graphite intercalation compound, RbC_8, first stage intercalation cpd., X-ray crystallographic obs. *(French)* 79−32966
graphite intercalation compound with halogens, ionisation 78−26489
graphite intercalation compound with SbF_5, texture 78−31355
graphite intercalation compounds, alkali and halogen, electronic props., conductivity and optical reflect. *(German)* 80−49837
graphite intercalation compounds, as catalysts for polymerisation *(French)* 78−27822
graphite intercalation compounds, band struct. model, dynamical dielec. function, reflectivity 80−34348
graphite intercalation compounds, C_8M, (M=K, Rb, Cs), Breit-Wigner line shape anal., Raman spectra 80−50336
graphite intercalation compounds, charact. by electron inelastic scatt. anal. 79−95055
graphite intercalation compounds, characterisation by electron energy loss spectra 79−95054
graphite intercalation compounds, electronic props. review 78−30860
graphite intercalation compounds, KC_8 and CsC_8 polarised reflectance 78−31213
graphite intercalation compounds, low energy optical transitions, refl. spectra, and X-ray diffr. 80−25371
graphite intercalation compounds, magnetic resonance determ. of oxidation state 78−35051
graphite intercalation compounds, nomenclature 80−1948
graphite intercalation compounds, props. and appls. 78−71711
graphite intercalation compounds, X-ray charact. 80−19780
graphite intercalation compounds, X-ray struct. factor meas. applications 80−54207
graphite intercalation compounds *(French)* 78−27431
graphite intercalation compounds struct., elec. props. 78−27446
graphite intercalation compounds with alkali metals and halogens, physical props. 78−31050
graphite intercalation compounds with Br, K, ^{13}C NMR spectra 80−66048
graphite intercalation compounds with Br, magnetoreflectivity in high fields under press., energy band parameters 79−61346
graphite intercalation compounds with $FeCl_3$, prep. *(French)* 78−27445
graphite intercalation compounds with $FeCl_3$, struct. expt. data for domain theory 78−30596
graphite intercalation compounds with K, Rb, Cs, resistivity anomalies and phase transform. 78−26839
graphite intercalation compounds with K and Cs, low temp. specific heat meas. and XPS 78−26693
graphite intercalation compounds with K and tetrahydrofuran *(French)* 78−26692
graphite intercalation compounds with Rb Raman scattering 78−35130
graphite intercalation compounds with $SbCl_5$, K and bisulphates, development as reagents in organic synthesis 78−27444
graphite intercalation cpd., C_6Li, charge distrib. 78−34743
graphite intercalation cpd., C_6Li energy band struct. 78−30861
graphite intercalation cpds., acceptor type, elec. cond. theory 80−44686
graphite intercalation cpds., electronic props. 78−34744
graphite intercalation cpds., high elec. cond., engineering appl. 80−70780
graphite intercalation cpds., mag. susceptibility, tight-binding model 80−44796
graphite intercalation cpds. with alkali metal, interlayer screening and mag. susceptibility 80−44794
graphite intercalation cpds. with AsF_5 and SbF_5, synthesis and elec. props. 80−70781
graphite intercalation cpds. with H_2SO_4 and sulphuric oleums, elec. resist. evolution 80−45518
graphite intercalation with Eu and Yb, struct. 80−44184
graphite intercalation with Hg and alkali metal 80−44183
graphite interclation with Li, Raman scatt. study 80−88999
graphite lamellar cpds., ^{13}C NMR studies 80−44936

intercalation compounds continued
graphite lamellar cpds. with Li, K, Rb, HNO_3 and SO_3, EPR studies 80−44902
graphite lamellar derivatives, KC_{24}(tetrahydrofuran)$_m$, (m=1 and 2) ^1H NMR study 80−44932
graphite layered material prep. and growth, book contrib. 78−19647
graphite nitrate, charge transfer, ionic salt model 79−11780
graphite nitrate, chem. of intercalation 79−43564
graphite nitrate, structural ordering in intercalation compounds 78−26539
graphite nitrate, X-ray obs. *(French)* 78−27440
graphite nitrates, elec. props. perpendicular to layers, resistance, magnetoresistance, charge transport mechanisms 80−80268
graphite struct. effect on intercalation rate 78−31356
graphite with K, staging classical model variations, EXAFS results 80−45166
graphite with K and Cs, low temp. sp. ht. 78−71868
graphite-$AlCl_3$, well-staged, Raman and IR spectra 80−50339
graphite-alkali metal, electronic props. 80−45202
graphite-alkali metal intercalation cpds., IR, active lattice mode obs. 80−45072
graphite-alkali metal intercalation cpds., large anisotropy and stage depend. 80−44795
graphite-alkali metal lamellar cpd., reversible intercalation of tetrahydrofuran 80−16211
graphite-alkali metal-benzene ternary intercalation compounds thermal and X-ray anal. *(French)* 78−27434
graphite-AsF_5, resist. and magnetoresist. 79−99590
graphite-AsF_5 intercalated species, fractional ionisation and identification 80−97397
graphite-AsF_5 intercalation compounds, de Haas-van Alphen effect, charge transfer rate 80−54595
graphite-Br_2, in-plane intercalate lattice modes, Raman scatt. 79−42163
graphite-Br_2, intercalation process 78−63965
graphite-Br_2 intercalation cpds., EXAFS study 80−71515
graphite-Br_2 stage 2 cpds., Raman spectra 80−80787
graphite-Br, effect of oxidation and residual Br on intercalation 79−43565
graphite-Br system, intercalation threshold, ellipsometric investigation 78−26760
graphite-$FeCl_2$($FeCl_3$) intercalation cpds., lattice dynamics, Mossbauer spectra 80−15925
graphite-$FeCl_{3-x}$ intercalation compounds, Mossbauer spectra 80−20538
graphite-$FeCl_3$, electronic excitation spectrum, high resolution EELS meas. 80−45182
graphite-$FeCl_3$, form., effect of added O, Cl, and water vapour *(German)* 79−52634
graphite-$FeCl_3$, form. kinetics and microstruct. *(German)* 79−43560
graphite-$FeCl_3$, IR and Raman spectra study of optical modes 79−56797
graphite-$FeCl_3$ layered compound, lattice modes, Raman spectra 79−95785
graphite-halogen intercalation compound, calorimetric study of order disorder transform. 79−52206
graphite-HNO_3, differential scanning calorimetry investigation 79−42234
graphite-HNO_3 intercalate, HNO_3 mol. orientation, model 80−24432
graphite-HNO_3 intercalation compound, in-plane elec. resistivity 80−34435
graphite-HSO_3F insertion compounds *(French)* 79−52635
graphite-HSO_3F intercalation compound, Raman spectral study *(French)* 80−60581
graphite-ICl, anomalous sp. ht. due to order-disorder transform. 79−42235
graphite-ICl residue compounds, struct., X-ray diffr. 78−47287
graphite-K, dielec. function, EELS study 80−45183
graphite-K, effect of H addition on superconducting transition temp. 80−70872
graphite-K, electronic props., resistivity, Hall effect and magnetoresistance 80−75585
graphite-K inclusion compounds, paramagnetism after treatment by π or n donors *(French)* 78−10749
graphite-K intercalation compounds, electronic props., de Haas-van Alphen effects and Fermi surfaces 80−75498
graphite-K intercalation compounds, Fermi surface, transport and supercond. props. 79−65367
graphite-Li, nucl. relax. times 80−44947
graphite-metal chloride intercalation compound, reduction 78−27821
graphite-metal fluoride intercalation cpds., prep. and props. 80−40686
graphite-Na-N-H intercalation compounds *(French)* 79−52633
graphite-Rb, Raman scatt. from in-plane lattice modes 78−15168
graphite-Rb, superlattice struct., electron diffr. study 80−75214
graphite-SbF_5, carrier density from ^{19}F NMR line shapes 80−25224
graphite-SbF_5(Cl_5) intercalation compounds, compacts, elec. resistivity, C fluorination 80−34493
graphite-SbF_5/Cu intercalated composite wires, elec. cond. 80−44687
graphite-$TlBr_3$, prep. *(German)* 79−43563
graphite-$TlCl_3$ *(German)* 79−43562
graphite-UF_6, NMR exam. 78−39416
graphite/AsF_5 intercalate, first stage, rel. to synthesis of first stage graphite salt $C_8^+AsF_6^-$ 79−24738
graphitic, lattice vibrations 78−34574
inorganic-organic layered complexes, effects of intercalation on elec. and mag. props. *(Japanese)* 79−8255
intercalated with DNO_3, mol. dynamics, NMR line shape and spin-lattice relax. 79−28631
ionic conductivity, of two dimensional alkali metal intercalation compounds 79−28138
lamellar graphite acceptor type, charge distrib. and Fermi surface 78−87935
lamellar intercalation compounds, NMR studies 80−39882
laminar chalcogenides and alkaline intercalates *(French)* 78−27442
layer and tunnel compounds, fast ion transport and electrochem. storage 80−61324
layer structures, intercalation with N_2H_4, charge density waves or artefacts 80−100221
layered compounds and intercalates, TDPAC studies 80−39890
layered materials and intercalates, International Conference, Nijmegen, Netherlands (Aug. 1979) 80−36771
layered structures, intercalation, crack propag. theory 80−97559
layered transition metal dichalcogenide, diffuse intensity contours in electron diffr. patterns, struct. interpretation 80−38878
metal guests in chalcogenide hosts, struct., review 79−46627

intercalation compounds continued
metal halide intercalated graphite, acceptor sites 80−49218
N-methylformamide intercalate, cryst. struct. determ. using film-scanned data 79−55729
neutron scattering from adsorbed mols., surfaces and intercalates, review, book contrib. 80−84394
NMR investigation in solid soln. electrodes, review 80−60432
order-disorder phase transforms., CDW and mass density waves 80−39281
photo-intercalation: possible application in solar energy devices 80−108803
piperidine solution of PbI_2, crystn. of intercalation cryst. 80−16170
polyacetylene:I charge transfer complex, struct. 79−74052
polyacetylene, doping with AsF_5, mechanism, effect on elec. cond. and spectra 80−24473
pyridine intercalation cmpd. of layered transition metal dichalcogenide, ionic bonding model 79−65052
pyrographite, elec. resist., during electrochem. insertion of H_2SO_4 *(French)* 80−2437
resistivity meas. 78−26836
review of intercalation props. *(Japanese)* 80−49838
solid state chemistry of batteries, electrodes, and electrolytes, conference, Miami Beach, Florida, USA (Sept. 1978) 79−100393
staged, phase diagrams 80−60849
structure, physical and chemical props. 79−19209
synthesis, reaction mechanism, struct. and bonding 80−39047
synthesis, review *(French)* 78−27429
TaS_2, amine intercalation, water effects, X-ray diffr. meas. 80−44178
transition metal dichalcogenides, octahedral intercalate ordering study by electron diffr. 80−15076
transition metal intercalates of Ni and Ta dichalcogenides, Hall coefficient and resistivity 80−39610
transition metal intercalates of Ni and Ta dichalcogenides, magnetic susceptibility, function of temp. 80−39756
transition metal layered dichalcogenides and their intercalation compounds, physical props., review 78−27443
transition model chalcogenophosphates, intercalation with n butyl-lithium, possible appl. in Li batteries 80−71446
trapped species in host lattice, teaching 78−16594
Ag_xTiS_2, intercalation cpd., Raman scatt. and electron diffr. meas. 79−24321
$Al(OH_3)$, intercalation with Li ions, X-ray diffr. patterns and comp. determ. 80−76502
AsF_5 intercalation with graphite and benzenoid systems, EPR, NMR and X-ray diffr. obs. 80−19775
AsF_5-graphite, lamellar, highly two dimensional synthetic metal, room temp. elec. cond. 78−6349
AsF_5-graphite, metallic optical reflectance meas. 78−6683
AsF_5-graphite intercalation compound nature 80−103308
AsF_5-intercalated graphite, mag. spin susceptibility, density of states at Fermi energy 79−7966
BiNbS(Se), struct., X-ray powder diffr. meas 80−44175
BiTaS(Se), struct., X-ray powder diffr. meas 80−44175
Br-graphite, intercalation cpd., magnetothermal oscill. and charge-density waves 80−11199
Br_2-graphite systems, adsorbed and intercalated, EXAFS 78−72638
C cathode, intercalation props. in Al reduction cell 79−43559
C fibre layered compounds with alkali metals, prep. 80−20809
C, partially graphitised, K intercalation-desorpt. cycle rel. to stacking faults 78−47396
$C_{8n}AsF_5$, electrical cond. theory 80−44686
$C_{12.6}AuCl_3$, intercalation compound, struct. *(French)* 78−42982
CBr_x, graphite intercalated, de Haas-van Alphen effect and cyclotron reson. 80−44479
$C_{16}Br_2$, Br_2 intercalation in graphitised C fibres and its removal 79−43561
$C_8Br_xCl_{1-x}$ intercalate, crystallographic, elec., mag. props. 80−107184
$C_{12}Cl$ and $C_{16}Cl$, form. and struct. *(French)* 80−40674
$C_{24}Cs$ and $C_{36}Cs$, graphite intercalated, ordering of intercalant layers, X-ray diffuse scatt. 80−44182
$C_{24}Cs$, positional and orientational correlations 80−33970
C_8Cs, intercalation cpd., theory of order-disorder phase transitions 80−19908
$C_6Eu(Yb)(Ba)$ intercalation compounds, three dimensional continuous melting 80−59631
$C_{6.6}FeCl_3$ intercalation compound, charge transfer, acceptor sites, XPS study 80−49218
$C_{6.6}FeCl_3$, stage 1, dielec. response and intraband plasmon dispersion 80−59902
C_8FeCl_3, behaviour with H_2 and CO, effect of activation 79−43623
C_8ICl, ICl intercalation in graphitised C fibres and its removal 79−43561
$C_{12n}K$, graphite intercalated, two-dimens. structurally disordered phases, X-ray diffr. profiles 80−44181
C_8K graphite intercalation compound, band structure calc., charge transfer effect 80−6692
C_8K, intercalation cpd. with graphite, supercond. props. 80−44755
C_8K, superconductivity 78−91827
$C_8K(Rb)$, graphite intercalated, phonon dispersion relations and Raman spectra 80−44272
C_6Li, intercalate ordering in first stage graphite-Li 80−6380
C_8Li, theory of order-disorder phase transitions 80−19908
$C_{11.3}NiCl_{2.13}$ intercalation compounds, cryst. struct. *(French)* 80−33947
$C_{12}^{2+}PtF_6^-$, struct. and elec. props. 80−70183
$C_{24}Rb$, intercalated graphite, resistivity and specific heat anomalies 80−107440
$C_{24}Rb$, graphite intercalated, de Haas-van Alphen effect, cyclotron reson., and transport props. 80−44479
$C_{24}Rb$, intercalated graphite, order struct. determ. by neutron scatt. 80−107143
C_8Rb, intercalation cpd., theory of order-disorder phase transitions 80−19908
$C_{12n}(SbCl_5)$, magnetothermal oscill. and electronic struct. 78−84129
$CdPS_3$, layered, organometallic intercalates, X-ray diffr., optical absorpt. and mag. props. 80−45103
Co, electron microscopy 80−84164
Co_xZrS_2, ($0<x\leq0.50$), intercalation compounds, ordered phases obs. 80−33962
$CrPS_4$-Li intercalation cpd., phys. props. 79−19788
$CrS_2(Se_2)$-alkali metals, phys. props. 80−44179
Cs graphite, structural ordering in intercalation compounds 78−26539

intercalation compounds continued
CsC_8 intercalation compound, cryst. atomic struct. study *(French)* 79−42021
Cu-intercalated electrodes, cyclable solid-state cell 79−100511
Cu_xMS_2, ($0<x\leq0.50$) (M=Zr, Hf), intercalation compounds, ordered phases obs. 80−33962
D_xTaS_2, struct., form. by cathodic reduction, neutron diffr. obs. 79−73150
EuC_6, intercalation cpd. with graphite, synthesis and struct. 80−44184
Fe complex, $FeOCl[(ethyltetramethylcyclopentadienyl)_2Fe]_{0.16}$ synthesis and struct. 80−44176
Fe complexes, $FeOCl[Co(cyclopentadienyl)_2]_{0.16}$ and $FeOCl[Fe(cyclopentadienyl)_2]_{0.16}$, Mossbauer and mag. susceptibility meas. 80−44176
Fe, electron microscopy 80−84164
Fe-graphite, intercalate, prod. by slow electrochemical reduction *(French)* 78−27437
$FeCl_2$-graphite, formation by reduction of Fe(III) compounds with $Fe(CO)_5$ 78−63721
$FeCl_3$ intercalated with graphite, vibrational excitations, polarised Raman spectra 79−19888
$FeCl_3$-graphite, intercalation compound, Fermi level lowering and core exciton spectrum, EELS study 79−74036
$FeCl_3$-graphite intercalation compound, dielec. function, band struct. EELS study 80−49643
$FeCl_3$-intercalated graphite, plasmon spectra 79−38011
$Fe_{0.33}NbS_2$, lattice dynamics and hyperfine interactions, Mossbauer spectra study 80−108135
FeOCl, cathodic reduction in organic electrolytes, intercalation complex production 79−1833
FeOCl intercalation cpds. with Li and amines, cryst. struct. 78−51512
FeOCl/ferrocene (cobaltocene) intercalation cpds., X-ray diffr. obs. 79−65066
FeOCl-pyridine intercalate, mechanism, nucleation and diffusion 80−49420
Fe_xTiS_2, lattice dynamics and hyperfine interactions, Mossbauer spectra study 80−108135
Fe_xZrS_2, ($0<x\leq0.50$), intercalation compounds, ordered phases obs. 80−33962
Fe_xZrSe_2, intercalation compound, IR spectra 78−88300
graphite, intercalation compounds with $FeCl_3$ intercalation kinetics 78−31354
H_xNbS_2, struct., form. by cathodic reduction, neutron diffr. obs. 79−73150
H_xTaS_2, nonstoichiometric, incoherent neutron spectra, X-ray diffr. 78−42998
HfS_2, intercalation-induced shift of absorpt. edge 79−82999
InNbS(Se), struct., X-ray powder diffr. meas 80−44175
InTaS(Se), struct., X-ray powder diffr. meas 80−44175
K-intercalated graphite (stage-1), electron energy loss expts. and band struct. theory 79−100001
KC_{24}, intercalated graphite cpd., anisotropic mag. susceptibility and phase transitions 79−19370
KC_{24}, intercalated graphite, struct. phase transitions, X-ray diffr. 79−65189
KC_{24}, press. induced staging transition 80−79938
KC_{24}, reduction of aromatic compounds 80−3306
KC_8, H_2 chemisorption *(French)* 79−43624
KC_8, intercalated graphite, electronic and cryst. struct. 80−44472
$KC_8H_{2/3}$, H_2 chemisorption *(French)* 78−27432
$KC_8H_{2/3}$, struct., X-ray anal. *(French)* 78−26538
$KHgC_4$, and $KHgC_8$, intercalation cpds., synthesis and struct. 80−44183
K_xZrS_2, intercalation cpd., X-ray K absorption edges 78−39627
Li incorporated transition metal oxides, topochem. reactions, chem. prep. and characterisation 80−61115
Li intercalated atoms, host lattice strain effects 80−88082
$Li/TiS_2(TiSe_2)(Ti_{1.1}S_2)$, electrochem. obs. of Li intercalation 80−61216
Li-graphite, prep. from Na-Li melts *(French)* 80−2970
Li-graphite intercalation compounds, synthesis, elec. and optical props. 79−74108
Li-pyrographite intercalation cpds., synthesis and elec. resist. 79−91601
Li-transition metal dioxide intercalation compounds, mag. props., decomposition effects 80−25075
LiC_6, and LiC_{12}, electronic struct. calcs. 80−70613
LiC_6, intercalated, charge-transfer and non-rigid-band effects 80−44496
LiC_6, intercalated graphite, band struct. determ. by angle-resolved photoemission 80−45203
LiC_6, intercalation compound with graphite, sp. ht. meas., 4-300K 80−44332
LiC_6, intercalation compound, electronic struct., XPS meas. 80−59850
LiC_6, prep. from Na-Li melts *(French)* 80−2970
LiC_6, Raman spectrum, rigid band model anal. 79−4800
LiC_6, synthesis method and reflectivity spectrum 79−15600
$LiCrS_2$, NMR 77−90048
$Li_xCr_yV_{1-y}S_2$, Mossbauer and mag. studies 79−73869
$Li_xFePS_3(Se_3)$, Li_xMnPSe_3 and $Li_xNiPS_3(Se_3)$, NMR and neutron diffr. obs., mag. props. 80−60433
$Li_xFe_yV_{1-y}S_2$, Mossbauer and mag. studies 79−73869
$Li_xM_yV_{1-y}S_2$ (M=Fe, Cr) physical props., effect of metal substitution of Li intercalation 79−100395
Li_xNiPS_3, antiferromag., mag. props. and ionic mobility, NMR meas. 79−24223
Li_xNiPS_3, ionic conductivity, activation energies, NMR study 79−28138
Li_xTaS_2 and Li_xTiS_2, chem. diffusivity of Li at 30°C 80−59737
$LiTiS_2$, band struct., tight-binding calc. 79−95323
$Li_{1-y}Ti_{1+y}S_2$, intercalation chemistry and electrochemical energy storage 79−100541
Li_xTiS_2, ($0\leq x\leq3$), intercalation in TiS_2, possible electrochem. cathode 80−19772
Li_xTiS_2, alkali ion ordering, X-ray study 80−107165
Li_xTiS_2, electrochemically intercalated, ion ordering, X-ray diffr. meas. 80−44177
Li_xTiS_2, Li ordering, electrochem. obs. 78−59795
Li_xTiS_2, Li ordering in intercalation battery, theory 79−77580
Li_xTiS_2, struct. determ. by neutron diffraction 80−54196
$Li_xV_{1-y}Fe_yS_2$, intercalated battery cathode material, Mossbauer studies 80−44984
$Li_xV_2O_5$ ($0.1<x<1.0$), phase relationship in ambient temperature system 80−20912
$Li_{0.8}VOCl$, magnetic, optical and electrical props. 79−95402
$LiVS_2$, NMR 77−90048
$Li_2VS_2(Se_2)$ based topochemical cells, low voltage behaviour 79−92069
Li_xVSe_2, intercalation cpds., electron chem., ionicity 80−89501
Li_xWO_2/Li_yTiS_2 cyclable organic electrolyte cell, using 2 intercalation electrodes 80−76625
$LixTiS_2$, mechanism of Li intercalation, optical and X-ray studies 79−100394
$Mn_{0.25}NbS_2$, mag. anomaly rel. to struct. disordering 78−43557
MoF_6-graphite 78−27441
MoS_2 intercalation compounds, reaction with alkali and alkali earth metals, band struct., superconductivity 78−26541
Na-graphite intercalates, preparation, struct. 80−103307
$NaCrS_2$, NMR 77−90048
$Na_xIn_xSn_{1-y}S_2$ ($1>x>0$), intercalation-substitution system, NMR study *(French)* 79−69095
$Na_xIn_xSn_{1-x}S_2$, intercalation-substitution compounds, NMR study 80−44952
$Na_xIn_xSn_{1-x}S_2$, ionic conductivity, activation energies, NMR study 79−28138
$Na_xIn_xSn_{1-x}S_2$, ionic conductors, ^{23}Na NMR and complex impedance meas. 79−91314
$Na_xIn_xZr_{1-x}S_2$, ionic conductivity, activation energies, NMR study 79−28138
Na_xMS_2 (M=Ta,Ti), Na chem. pot. and free energy of intercalation, electrochemical meas. 79−100396
Na_xTiS_2, alkali ion ordering, X-ray study 80−107165
Na_xTiS_2, electrochemically intercalated, ion ordering, X-ray diffr. meas. 80−44177
$NaVS_2$, NMR 77−90048
$Na_xVS_2(Se_2)$, physical props. 80−44179
$Na_xY_xZr_{1-x}S_2$, ionic conductivity, activation energies, NMR study 79−28138
$Na_xY_xZr_{1-x}S_2$, ionic cond. and NMR mobility obs., comp. depend. *(French)* 80−70459
NbS_2 intercalate with tetraalkylammonium hydroxide, prep. and struct. 80−79752
NbS_2, intercalation cpd. with pyridine, nucl. spin-lattice relax. meas. 80−54962
NbS_2 intercalation cpdr., octahedral, microstruct. obs. 77−84729
NbS_2-(pyridine)$_{1/2}$ intercalation complex, superlattice struct., NMR meas. 80−70180
$NbS_2(Se_2)$ complexes with 3d transition metals, mag. and metallic transport props. 80−44814
$NbS_2.Sn$, $NbS_2.Sn_{1/3}$ intercalation cpds., lattice dynamics, hyperfine interactions 79−61273
$NbSe_2$ (2H), intercalated with TCNQ, elec. resistivity temp. behaviour anomaly *(Russian)* 80−10953
$NbSe_2$ intercalated with Rb, EXAFS 80−2897
$NbSe_2$, intercalated with Rb, EXAFS meas. 80−40185
$NbSe_2$ pure and intercalated with ethylenediamine, positron annihilation study 80−84801
$NbSe_2Cu_x$, ordering study using electron diffr. and microscopy 80−39043
$NbSe_2$(2H)-hydrazine, intercalation cmpd., kinetic studies by transmittance meas. at 1600 nm 78−71981
$nbSe_2$ (2H) single crystal, elec. resistivity, effect of hydrogen intercalation *(Russian)* 78−84338
Ni, electron microscopy 80−84164
$NiPS_3$-Li, chemical and electrochemical intercalation *(French)* 78−38679
Ni_xZrS_2, ($0<x\leq0.50$), intercalation compounds, ordered phases obs. 80−33962
Ni_xZrS_2, fundamental optical absorption edge 79−99904
PbI_2 intercalated with organic donor mols., cryst. struct. and phys. props. 78−26543
PbI_2 intercalated with organic mols., energy band splitting *(Russian)* 78−76027
PbI_2 intercalated with organic mols., superlattice and quantum dimens. effect *(Russian)* 79−46628
PbI_2 intercalated with aniline, NQR meas. *(Russian)* 79−91311
PbI_2-piperidine intercalations rel. to NQR, spin-lattice relax. temp. depend. *(Russian)* 78−27108
PbI_2-piperidine(aniline)(pyridine), heat capacity of low temp., intercalation effect *(Russian)* 80−92682
PbNbS(Se), struct., X-ray powder diffr. meas 80−44175
PbTaS(Se), struct., X-ray powder diffr. meas 80−44175
Pt, electron microscopy 80−84164
RbC_8, intercalated graphite, band struct. determ. by angle-resolved photoemission 80−45203
$RbHgC_4$, and $RbHgC_8$, intercalation cpds., synthesis and struct. 80−44183
Rb_xZrS_2, intercalation cpd., X-ray K absorption edges 78−39627
SnNbS(Se), struct., X-ray powder diffr. meas 80−44175
$SnSe_2$, intercalated with cyclopropylamine, photoelectron spectra study of electronic struct. 78−84698
SnTaS(Se), struct., X-ray powder diffr. meas 80−44175
TaS_2 (2H), intercalation with deuteropyridine, neutron diffr. meas. 79−90612
TaS_2 (2H) intercalated with pyridine, ionic bonding model 79−65052
TaS_2 (aniline)$_{3/4}$, low-field magnetisation meas. on small cryst. in supercond. phase 79−87188
TaS_2, alkali metal and alkali metal hydroxide intercalates, lattice parameters, supercond. transition temps. 80−25029
TaS_2 and $TaS_{1.6}Se_{0.4}$, intercalated with organic cpds., supercond., upper crit. fields and reduced dimensionality 80−70910
TaS_2 complexes with 3d transition metals, mag. and metallic transport props. 80−44814
TaS_2 intercalate with tetraalkylammonium hydroxide, prep. and struct. 80−79752
TaS_2 intercalated with NH_3, charge transfer, PAC meas. 78−76366
TaS_2 intercalated with methylamine, supercond. layer cpd., crit. field enhancement and reduced dimensionality 80−60152
TaS_2 intercalates with alkali metals, prep., X-ray anal. and supercond. transition temp. 78−31007
TaS_2 intercalation complexes, superconductivity 78−91803
TaS_2, intercalation cpd. with pyridine, nucl. spin-lattice relax. meas. 80−54962
TaS_2 intercalation cpds., octahedral, microstruct. obs. 77−84729
TaS_2 polytypes, in situ intercalation in TEM, using N_2H_4 gas 79−8254
TaS_2, TDPAC meas., CDW, structural and charge transfer effects 78−39468
TaS_2:NH_3, mol. motion, neutron quasielastic scatt. obs. 79−90827

intercalation compounds continued
TaS_2/pyridine intercalated, struct. and bonding 78−91323
TaS_2-2H electrodes, topotactic reduction nechanism, neutron diffr. obs. and intercalation cpd. form. 80−108748
TaS_2-copper tetra-4-dimethylaminophthalocyanine, dye intercalated layered cpd., struct. and superconductivity 78−84342
TaS_2-NH_3 intercalation complex, press. induced diffusion effects, NMR study 79−19797
$TaS_2(NH_3)$ and $TaS_2(NH_3)_{1/3}(H_2O)_{2/3}$, incoherent inelastic neutron spectra 80−84163
$TaS_2(NH_3)_x$, NMR spectral densities and two-dimens. diffusion 80−50215
$TaS_2(Se_2)$, intercalated with ethylenediamine, Raman spectra 78−48182
TaS_2(2H), Li intercalation, electrochemical studies 80−39048
$TaS_2.NH_3$, tracer exchange by liquid ND_3, neutron diffr. meas. 79−29350
TaS_2(pyridine)$_{1/2}$ intercalation complex, supercond. transition temp., upper crit. field, and interlayer coupling strength 79−56406
TaS_2(pyridine)$_{1/2}$, pyridine orientation, X-ray diffr. meas. 79−55679
TaS_2(pyridine)$_{1/2}$, superconducting intercalation complex, proton spin lattice relaxation time 78−80096
TaS_2(pyridine)$_{1/2}$, upper and lower critical fields, supercond. props. from Ginzburg-Landau theory 79−56456
$Ta_yTi_{1-y}S_2$, Li intercalation, electrochemical studies 80−39048
Ti complex, TiOCl[Co(cyclopentdienyl)$_2$]$_{0.16}$, sxnthesis and struct. 80−44176
$TiCl_4$-graphite intercalation compound 80−40675
$(TiNbO_5)^-$ oxide layers, intercalation of alkylammonium ions 80−64985
$TiS_2(NH_3)_{1.0}$, NMR spectral densities and two-dimens. diffusion 80−50215
$TiS_2(Se_2)$-alkali metals, phys. props 80−44179
V complex, VOCL [Co(cyclopentadienyl)$_2$]$_{0.16}$, synthesis and struct. 80−44176
$VS_2(Se_2)$-alkali metals, phys. props. 80−44179
WF_6-graphite 78−27441
WO_3M_x (M=H, Li, Na, K, Ag), bronzes, atom motion 78−75874
YbC_6, intercalation cpd. with graphite, synthesis and struct. 80−44184
ZrB_2, self-consistent band struct., XPS, reflectance, NQR, Hall effect and density of states meas. 80−107689
ZrS_2, intercalation-induced shift of absorpt. edge 79−82999
$ZrS_2Cs_{0.37}$, lamellar cpd., gas absorpt. 80−44418
ZrS_2Cs_x, adsorpt. of H_2, mol. sieving effect *(French)* 79−65305

interdiffusion *see diffusion*

interface electron states
adsorption for noncoplanar geometry 78−79887
amorphous semiconductor-insulator boundary, density of states determ. from field effect data 80−107688
anisotropic transition layer, surface polariton spectra in presence of resonance 80−88484
anthracene, cryst., with electrolytic contacts, photocurrent anomalous behaviour, current-volt. characts. 77−39933
anthracene, cryst.-electrolyte system, pot. well, hole residence time 77−8190
band models, appl. of Green's function matching procedure 77−59320
bimetallic interface energies 78−2545
bimetallic junction, van der Waals interaction 79−24048
biometallic interfaces, dynamic response of electrons and dispersion force fields 78−47845
C-CD, surface channel, interface trapping noise calc. 80−11058
charge layer at interface between dielec. media, response to external charge density 77−69260
chemisorption of hydrocarbons on metals, correlation between energy levels and occupied molecular orbitals 79−19449
cluster Bethe-lattice method appl. 80−49852
compound semiconductor interfaces, conf., Los Angeles, USA (Jan. 1978) 78−91756
conference on solid-vacuum interface, Amsterdam, Netherlands (June 78) 79−42342
contact levels for two ideal subsystems *(Russian)* 77−62973
covalent semiconductors, electronic interface states in intrinsic stacking-faults 80−75522
Cu_2S-CdS solar cell, interface recombination and junction field studies, exptl. technique 80−45683
defects, scatt. theory 80−84498
deformed heterojunctions, one-dimens. model 78−64100
degenerate junctions with position-dependent band struct., density-voltage relations 79−87150
desorption, time dependent escape rate from potential well 78−79888
diamond Schottky barrier, electronic struct., pseudopot. calc. 78−95364
diamond Schottky barrier, electronic struct., pseudopotential method, jellium model 79−38162
dielectric continuum theory of van der Waals interaction 77−11976
dielectric function, inverse RPA calcs. at metal-vacuum interface 78−14789
dielectric-semiconductor interface, anal. of fast surface states 79−42648
dipolar plasmon in liq. multilayer struct., freq. and dispersion relations 77−59323
disorder at surfaces and interfaces, effect on electronic props. 78−26932
double layer barrier, deform. of electron spectra *(Russian)* 78−84292
double layers, image forces influencing capacitance and interaction 79−29367
dual-dielectric charge storage cells, electron-electron effects in writing and erasing 78−34900
effective mass approximation, interface effect 78−64082
empirical tight-binding method, critique 80−49854
energy determ. during capture of electrons and holes using DLTS 79−87107
epitaxial heterostructure superlattice, construction of bound states in continuum 77−32076
epitaxial thin films with neg. electron affinity, photoelectron energy distrib. 80−100755
Green's function and generalised phase shift for surface and interface problems, Green's function and generalised phase shift 79−60895
Green's function for surface physics, partial differential eigenvalue eqn. 80−6929
Green's function formulation of n-interface problem 80−54760
heterojunction, energy barriers and interface states 79−56295
heterojunction, interface state parameters from differential admittance 77−15944
heterojunction energy band lineups, orientation depend. 78−95344

interface electron states continued
heterojunction interface, effective band edges, due to quantum and grading effects 80−20305
heterojunction superlattices, Green's function of electron in periodic field 80−49857
heterojunction thin film solar cells, survey or semiconductor combinations 80−50974
heterojunctions, between narrow-gap semiconds. interface states 77−55603
heterojunctions, deformed and undeformed, interface boundary effect on interface states 78−47855
heterojunctions between monatomic semicond., interface spacing effect on interface states 79−95478
IGFET, interface and bulk-trap states, determ. using deep level transient spectroscopy 77−8199
III-V oxide interface state and Schottky barrier form., unified mechanism 80−44724
III-V semiconductor based layered multielectronic systems, electronic process investig. survey *(Russian)* 80−107891
III-V semiconductor n-channel inversion layers, subband struct. and gate-controlled Gunn effect 77−76929
III-V semiconductor surfaces and interfaces, Green's function technique, tight binding approx. 80−49855
III-V semiconductor-oxide interface states, photoemission obs. of energy levels induced by adsorpt. 80−93000
image charge pot. at interface of two semi-infinite media, Thomas-Fermi soln. 79−87155
image potential near dielectric-dielectric interface 78−84274
interface energies, appl. to stacking faults 79−19547
inversion layer, EM modes 78−80030
inversion layer in quantising mag. field, Einstein relation 78−19156
inversion layers, implications of coupled electron-phonon system in two dimensions 78−6425
Ising model, phase transition in 2-dimens. Coulomb gas, interfacial roughening transition 77−20394
junction field effect structures, 2-D subbanding 78−64125
laminarly-nonuniform media, surface polaritons, spectrum, rel. to transition layer at each interface *(Russian)* 77−35982
LED, DH, output power and response time, thickness depend. 79−95479
localisation in two-dimens. systems 78−60213
many-valley semiconductor, inversion layers, electronic ground state 77−43731
metal, electrodynamics at boundary, including plasma waves 77−59317
metal surface or metal-metal interface, plasmon dispersion 78−52053
metal-amorphous Si barrier, electronic props. 80−11089
metal-dielectric contact, exciton quenching and excited state props. 77−4416
metal-gelatin-n-GaAs struct., C-V characts. and gelatin-semiconductor interaction rel. to photographic process *(Russian)* 80−49944
metal-InP contacts, intermediate adsorbed layer effect on electronic props. 80−39674
metal-insulator interface, Hubbard model, possibility of insulator-metal transition 78−52084
metal-insulator interface region, band gap closure in insulator 80−11086
metal-metal contact, electron tunnelling stimulated by surface plasmons *(Russian)* 78−30974
metal-metal interface, simple, electronic props. 78−72234
metal-metal junction, effect of non-local exchange correlation pot. on charge density profile and electrostatic pot. 77−28239
metal-NaCl system, sliding and rolling electrification 78−14796
metal-non-metal interface, existence of localised electronic states 77−32081
metal-semiconductor contact, axial pressure effects on surface-state density redistrib. *(Russian)* 77−89847
metal-semiconductor disordered interface, supercond. transition temp. enhancement by bipolaron interface centres 80−84528
metal-semiconductor interface, electronic structure 78−72261
metal-semiconductor interface, Schottky barrier formation, microscopic model 78−52087
metal-semiconductor junction photoelec. phenomena, effect of dielectric gap and surface states *(Russian)* 78−84299
metal-semiconductor junctions, capacitance, temp.-depend., by space-charge methods 78−91758
metal-semiconductor junctions, Schottky barrier heights for low ionicity semiconds. 79−42640
metal-semiconductor structure, quasitwo dimens. excitons and plasmons at different carrier conc. 78−60063
metal-tunnel oxide-Si junctions, processing condition depend. 80−80380
metal-ZnO-SiO_2-Si structures, charge injection 80−49919
metals, free-electron like, interface energy and charge oscills. 77−62984
MIM tunnel junctions, roughened, photon emission, calc. 80−44738
MIS capacitance measurements, method of separating hysteresis effects, interface state density estimation 77−85324
MIS capacitor, freq. and temp. tests for lateral nonuniformities, C-V characts. 78−10563
MIS capacitor, thermally stimulated discharge in differential regime 79−15214
MIS capacitors, theory of nonequilibrium props. including charge exchange of interface states 79−42659
MIS dielectrics, charge centres, removal by RF annealing 78−88035
MIS interface states and deep level impurities, DLTS, charge storage and charge release modes 80−49923
MIS Schottky barrier and conducting diodes with interface traps, capacitance and conductance 78−10564
MIS Schottky barriers, photocurrent suppression and interface state recomb. 78−39222
MIS solar cells, computer simulation studies rel. to interface state meas. 80−72048
MIS solar cells, interface-state Fermi level change from dark to illuminated conditions 79−66407
MIS struct. on III-V narrow bandgap compounds, C-V characts., interface state densities and storage times meas. 77−89861
MIS structure, accumulation regime, C-V data anal., insulator capacitance determ., interface states effects 77−12016
MIS structure, Al_2O_3 insulating layer, electron gun evaporated, HF C-V characts. and surface state density 78−84310
MIS structure, interface states, deep level transient spectroscopy 79−78183
MIS structure, interface states, thermally stimulated surface pot. 78−68091

interface electron states continued
MIS structure, photovoltaic efficiency, influence of interface states 78−39227
MIS structure, photovoltaic efficiency, interface states effect 77−80844
MIS structure, quasitwo dimens. excitons and plasmons at different carrier conc. 78−60063
MIS structure, surface state density, determ. from surface saturation photo-EMF meas. 80−75652
MIS structure surface characterisation by C(V) curves 78−72276
MIS structures, surface potential distributions *(Russian)* 78−80065
MIS structures, surface recombination and photoeffect, statistics *(Russian)* 78−39221
MIS tunnel diodes, photoionisation of states 80−11099
MIS tunnel solar cell, interface states, kinetic and electrostatic props. 79−52933
MIS tunnel structure, injection and extraction effects, self-consistent model 80−92996
MIS/SIS solar cells, automated surface states anal. 80−93966
MNOS device, high temperature annealing, effect on Si_3N_4 stress, interface charge density and memory props. 79−87158
MNOS structure, Au-diffused, with chem. oxidised ⟨100⟩ substrate Si-SiO_2 interface traps 77−62995
MNOS structures, charge pumping investigations 77−43729
MNOS system, interface states 78−84309
modelling, Xα-scatt. wave cluster approach 80−49851
MOS, many-body effects in n-Si inversion layers, excitation to higher subbands 77−62997
MOS capacitor, interface state parameter determ. by DLTS 80−65642
MOS capacitor, polycryst. Si gate, surface state annealing 77−39946
MOS capacitor, TSC meas., suppression of meas. interferences from interface states and mobile ions 80−29479
MOS capacitors, irrad., interface state buildup depend. on hole generation and transport 77−20446
MOS capacitors, n-type, optically active interface states study 80−60096
MOS charge layer n-channel (001) surface induced valley splitting 79−28414
MOS devices, interfacial and bulk trap props., expt. characterization techniques 80−49950
MOS diode, bulk traps and interface states determ., deep-level transient spectroscopy appl. *(Japanese)* 79−42645
MOS diode, impurity profile effect on density of interface states 79−33359
MOS electron inversion layers, temp. depend. of subthreshold currents 79−73596
MOS interface states, capture cross-sections 78−64129
MOS interface states density, photoemission obs. using photocurrent and photocapacitance meas. 80−92990
MOS inversion layer, 2-dimens. disordered electron systems in strong mag. fields 77−76930
MOS inversion layer, hot electron effects in Landau levels 80−6998
MOS inversion layers, freq. response of charge transfer 80−88638
MoS processing-related interface state meas., transient capacitance method 78−10574
MOS radiation sensitivity, influence of Si surface defects 77−20445
MOS solar cell, IV characteristics obtained under dark and illuminated conditions 79−48126
MOS solar cell, role of interface states 79−15228
MOS solar cell operation, role of interface states 79−61979
MOS struct., surface state density determ., error caused by numerical differentiation of Q-V data 78−43483
MOS structure, B ion implanted, form. and annealing of radiation damage 79−56321
MOS structure, C-V characts., temp. and Si dislocation density effects *(Russian)* 78−6447
MOS structure, distrib. of interface states conc., method for determ. 80−44733
MOS structure, dynamic props. of interface states 78−95373
MOS structure, flatband shift induced by electron beam radiation, Si dopant effects 77−32085
MOS structure, hole emission from interface states, transient capacitance meas. 78−14830
MOS structure, interface states, evidence for multiphonon emission 78−39220
MOS structure, interface states induced by amorphous SiO_2 77−28254
MOS structure, irradiated, interface state effects 78−39218
MOS structure, leakage effects 79−91155
MOS structure, model for ion-electron (configurational) interface states 80−29478
MOS structure, quench-in defects and interface states exam. by transient capacitance techniques 78−39225
MOS structure, quenched-in bulk defects and interface states, transient capacitance spectroscopy 79−24081
MOS structure, semiconductor conductance and capacitance, extended AC conductance−bias method 80−96995
MOS structure, space charge layer physics 80−92980
MOS structure, tail states of London subbands under strong mag. field 77−15962
MOS structures, interface state density evaluated from charge-voltage data 79−11234
MOS structures, quasistatic and nonequilibrium phenomena with constant gate-current bias 80−80385
MOS structures, thickness dependence of radiation charging, hole trapping model 77−20442
MOS structures, total dose effects on density of states 77−20443
MOS system containing interface traps, equilibrium and nonequilibrium response to linear voltage ramp 79−38173
MOS tunnel device, interface props. 78−34911
MOSFET, near-ideal Si-SiO_2 interfaces using CVD, props. 80−80382
MOSFET inversion layer, localised highly correl. phase cond. 79−33354
MOSFET structure, artificial superlattice near carriers 78−64130
MOST, charge pumping effect, applic. to surface states density determ. 77−69421
MOST struct., gamma irrad., interface states and carrier mobility 79−73593
MOST structures with process-induced defects, elec. props. 80−54788
non-local density based self-consistent surface calculations, Thomas-Fermi soln. 77−28227
one-dimensional crystals, matching conditions, Bloch functions, logarithmic derivatives 80−15475
one-dimensional theory, Green's function soln. *(Russian)* 77−59311

interface electron states continued
p^+-n diode under forward bias, effects of radiation-induced deep levels on admittance 78−23157
p-n heterojunction differential admittance theory in the presence of surface electron states 80−96981
p-n junctions, capacitance, temp.-depend., by space-charge methods 78−91758
polar semiconductor, optical phonon-magnetoplasmon interface oscills. 78−43467
polar semiconductor-polar semicond. interface, optic-phonon-magnetoplasmons 78−23146
polar semiconductors, phonon-plasmon-polariton mode propag. at interface 79−60731
polariton modes at interface between two conducting or dielec. media, review 78−87922
polyvinylcarbazole-Hg interface, contact electrification, internal photoemission study 78−60191
pseudopotential surface and interface calculations 80−49853
quantised inversion layer, hot carrier transport 78−30993
quantum chemical calc. methods 80−49849
quasi-two-dimensional electrons, electrodynamics 77−89829
quasiparticle interaction near interface of two media 79−65532
rectifying barrier formation with metal-semiconductor junction *(Russian)* 78−84296
SAW convolver in monolithic MIS struct., basic characts. 77−23791
Schottky barrier, theory and complex band struct. 79−15220
Schottky barrier formation and shape determ. factors *(Russian)* 78−84295
Schottky barrier solar cell, rel. to efficiency 80−76637
Schottky barrier theory at jellium-semicond. interface, role of ionicity, pseudopot. method 77−47888
Schottky barriers, Bardeen and Schottky limits of interface index 80−49868
Schottky barriers, T_0 anomaly, comparison of Levine and Bardeen models 77−39938
Schottky-barrier diodes, resonant tunnelling spectroscopy, deep centre detection 80−96968
Schottky-barrier metal-semiconductor junction carrier migration and equivalent cct. analysis *(Russian)* 78−84294
Schottky-barrier metal-thin oxide-semicond. structures, physical processes and microelectronics applications *(Russian)* 78−84307
semiconductor, electronic struct. calc., scattering theoretic approach 80−6940
semiconductor, electronic struct. of point defects, surfaces and interfaces, Green's function scatt. theoretic method 79−33258
semiconductor, ionic, -oxide interface, plasmon-phonon interactions 80−44730
semiconductor, meas. of surface and interface states *(Japanese)* 80−20269
semiconductor, polycryst., electronic processes at grain boundaries under optical illum. 77−55561
semiconductor, potential barrier height, temp. depend. *(Russian)* 78−68070
semiconductor, techniques for detecting electrons and holes trapped at bulk and interface imperfections 77−11934
semiconductor, transfer of electrons and ions *(French)* 80−6935
semiconductor electrode, electrolum. due to hole injection from electrolyte 77−20926
semiconductor heterojunction, band-edge discontinuities and interface pot. step, two-band narrow-gap approach 80−39665
semiconductor heterojunction, interface states, two-band-narrow gap approximation 79−24059
semiconductor heterojunction, thin, energy band diagram 77−43712
semiconductor heterojunctions, calcs. 79−1613
semiconductor heterojunctions, electrostatic effects of interface states on carrier transport 79−78160
semiconductor heterostructure, multipass, effective lifetime of nonequilibrium carriers 78−6435
semiconductor heterostructure, potentials supporting continuum-embedded positive-energy eigenstates 77−47894
semiconductor interface, scattering-theoretic approach and its appl. to Ge-GaAs 78−95340
semiconductor interface and overlayer electronic struct., review 80−49841
semiconductor interfaces, conf., San Diego, Calif., USA (Feb. 1976) 77−20377
semiconductor metal interface, Schottky barrier, chemical reaction and charge redistrib. 78−95365
semiconductor surface eval. using SAW convolver 80−97677
semiconductor with polytype layers, interface exciton states 78−26819
semiconductor-insulator boundaries, impurity electron states near interface 78−95320
semiconductor-insulator interface, effective-mass approx. 79−99629
semiconductor-insulator interface, microcomputer-aided interface-state analysis 80−80383
semiconductor-insulator interface, surface wave spectrum, theory 79−19674
semiconductor-insulator interfaces, electronic props. 79−42662
semiconductor-insulator structure, charge transport in insulators 77−20452
semiconductor-insulator structure, light refl. and absorpt. control, boundary state population rearrangement 77−69795
semiconductor-metal, surface exciton modes for plane and spherical interfaces 78−64113
semiconductor-metal boundary, magnetoplasma polaritons at the interface 79−38163
semiconductor-metal boundary, Schottky barrier form., chem. mechanisms 80−49869
semiconductor-metal interface, barrier height anal. including virtual surface states 77−69416
semiconductor-metal interface, calcs. 79−1613
semiconductor-metal interface, electronic struct. self-consistent pseudopot. method 77−20428
semiconductor-metal interfaces, intrinsic surface states and Fermi-level pinning 78−95319
semiconductor-metal Schottky barrier interfaces in pairing model, covalent-ionic trend 78−95367
semiconductors, magnetoplasmon-type surface polaritons at interface 77−85292
semiconductors, surface and interface electronic struct., book contrib. 79−42619

interface electron states continued
semiconductors and insulators in contact with metals, charging of bulk states 80−54781
simiconducter heterojunctions, energy band profile and interface states calcs. 79−78162
solar cell, interface state and energy barriers effect on efficiency 78−43464
solar cells n-type Schottky barrier, theoretical anal. of band edges, Fermi levels 80−50975
solid surface, theory, book 80−36787
solid-liquid interface, optical methods of study *(French)* 80−7318
superconducting proximity effect, effect of non-mag. localised states at interface 78−64170
superconductor-oxide interface, surface states, enhanced tunnel conductivity 80−80456
surface Green's function formalism for N-interfaces 78−39179
tetrahedral semiconductor/oxide interface, continuous random network and tight-binding models 77−89866
thin-oxide MIS thyristor devices, interface state charge 79−38172
tight binding method, first principles 80−49564
tight-binding Green's functions for surfaces, thin films, and solid interfaces using random-walk theory 80−54753
transition metal interfaces, localised electron states 77−59313
tunnel junction, plasma radiation in Ag layer, expt. interpretation 77−31966
two-dimensional system, electronic props., conf. Berchtesgaden, Germany (Sept., 1977) 78−60177
two-dimensional system, random attractive electron-electron interactions 78−60183
two-metal systems, plasmon dispersion 79−82656
Ag, adsorbed on Si (111), electronic and cryst. struct., Schottky barrier form. obs. 78−84091
Ag film, initial stages of growth on Si (111) 7×7, LEED, AES and UPS expts. 78−38988
Ag grating, with LiF coating, surface plasmons, rel. to reson. anomalies in reflected light intensity 77−3665
Ag surface, optical props. of organic dye monolayers by surface plasmon spectroscopy 79−11480
Ag-Si (111) interface, chemisorption, AES 78−14589
Al/III-V interfaces, photoemission 80−25526
Al-Al_2O_3, local struct. and interface states using surface soft X-ray absorpt. and photoemission spectroscopy 79−69595
Al-Al_2O_3-InP MIS struct., elec. props. 79−78184
Al-Al_2O_3-SnTe structure, tunnelling characts., model anal. 80−29480
Al-Al_2O_3-(a-Ge)-Al, electron tunnelling into a-Ge, press. effect 80−49938
Al-Al_2O_3-p-GaAs MOS diode, capacitance-voltage characts. 80−107914
Al-anodised Ta_2O_3/native oxide-n-GaAs MOS structure evaluation 80−84514
Al-GaAs Schottky barrier diode, Richardson const. 77−20424
Al-SiO_2 interface, internal photoemission and photon-assisted tunnelling 80−6982
Al-SiO_2-Si, MOS diodes, defects due to electron beam lithography obs. *(Japanese)* 80−54787
Al-SiO_2-Si capacitor, N_2 gas reaction, elec. and structural characts. 77−39950
Al-SiO_2-Si Schottky barrier solar cells, recomb. effects 79−39310
Al-SiO_2-Si structures, effect of β-radiation on fast surface states and space charge 77−55610
Al-SiO_2Si, mobile ion kinetic behaviour 79−56315
Al-$TiSi_2$-n-Si struct., elec. props., charge transfer mechanism across $TiSi_2$-Si interface *(Russian)* 80−34515
AlAs-GaAs (001) interface and superlattice, electronic props., band struct. 79−95485
AlAs-GaAs (100) interface, tight binding calc. of electronic struct. 78−95342
AlAs-GaAs (110) interface, self-consistent calc. of interface states and electronic struct. 78−52066
AlAs-GaAs abrupt (110) interface, electronic struct. 78−95339
AlAs-GaAs double heterostructure, effective lifetime of nonequilibrium carriers 78−6435
$Al_{0.35}Ga_{0.65}As$-GaAs N-p heterojunction diodes, current suppression by cond. band discontinuity 80−80362
$Al_xGa_{1-x}As$-GaAs, heterojunction, interface width, AES obs. 80−20290
Al_2O_3-Si boundaries, insulator charges evaluation *(German)* 79−82682
Al_2O_3-SiO_2-Si boundaries, insulator charges evaluation *(German)* 79−82682
As_2S_3-Si, isotype amorphous-crystalline heterojunctions, electrophys. props. 79−24063
As_2Se_3 disordered films in flash evap. systems, nonsteady-state behaviour of interface states 77−76952
Au-GaAs Schottky barrier diode, Richardson const. 77−20424
Au-n-GaAs Schottky diodes, interface state density model 77−39937
Au-Si interface, electron energy loss and AES meas. 80−89096
Au-Si interface, valence band and core levels, Si diffusion, alloy form., photoelectron spectra obs. 80−45205
Au-Ti/SiO_2/p-Si MOS struct., interface state distrib., DC tunnelling spectra determ. 80−75611
Au-ZnSe:Ga(Al), Schottky diode, wavelength modulated photoresponse spectra 78−6714
Bi film, oxidation kinetics and interfacial bonding using final states 77−56127
$Bi_xSb_{2-x}Te_3$, 2-dimens. cryst. interface props. of Bi overlayer UPS obs. 78−34881
CdS-Au contacts, electronic states, vacuum UV photoelectron spectra 80−70827
CdS-Cu_2S heterojunction, influence of surface recomb. on photoelec. props. 77−43711
CdS-Cu_2S heterojunction, energy-band struct., capacitance-voltage characts., illumination effects 80−96982
CdS-$CuInSe_2$ solar cells, grain boundary and interface recomb. effects 79−39311
CdS-Ge heterojunction, grown by chemical transport, props. 77−4422
CdS-metal interface, chemical reactions and local charge redistrib. 79−19661
CdS-SiO_2-Si structures, elec. props., role of interface states 79−56286
CdS(Se)-Al function formation, coupled interface plasmons, low energy electron energy loss spectra 77−24621
CdSe-As_2S_3($AsSbS_3$) heterostructure, energy bands and interface props., photoelectron spectroscopy 78−2551

interface electron states continued
CdSe-Au contacts, electronic states, vacuum UV photoelectron spectra 80−70827
CdSe-metal interface, chemical reactions and local charge redistrib. 79−19661
$CdSnAs_2$-InP, n-p heterojunction, elec. props., electroluminesc., band struct. 80−75632
CdTe-Au contacts, electronic states, vacuum UV photoelectron spectra 80−70827
CdTe-CdS heterojunctions, growth by closed-tube chem. transport, elec. props. 80−60070
CdTe-CdS heterojunction, photocapacitance and photocond. 80−96978
CdTe-HgTe ideal superlattice, electronic props. calc. 80−49885
p-CdTe-Langmuir film interface, prep., characters. and MIS struct. 80−92998
$Cd_zZn_{1-z}S/Cu_2S$, heterojunction interface double layer, space charge distrib. 79−7855
Cr/polymer interface, electronic struct., XPS study 80−45204
Cr-Si, cleaved junction, interface states, capacitance meas. 79−91118
Cr-SiO_x-Si MIS solar cells, photovoltaic performance and interface states, nucl. radiation effects 80−94004
Cu (111), adsorbed Cs, XPS exam. of Cu surface state and Cs valence electrons 79−19647
Cu (111)/Na interface, UPS study of surface electronic struct. 80−80350
Cu/polymer interface, electronic struct., XPS study 80−45204
P-Cu_{2-x}-n-CdS, heterojunction, energy band diagram 79−24070
Cu_2S-CdS heterojunction solar cells, carrier transport, nonmonotonic band profiles 80−61361
Cu_2S-CdS solar cells, interface recombination phenomena and tunnel effect 80−66978
$Cu_{2-x}S$-CdS heterojunction, current flow characts. and energy band struct. 77−43709
Fe film bounded by dielec. layers, surface polariton in ATR angular spectra 79−15545
(Ga, Al, As) heterostructures and compounds, electronic props., empirical pseudopot. calc. 80−80366
Ga-GaAs heterojunctions, electronic struct., tight-binding and pseudopot. models 79−42633
GaAS(P)(Sb)-anodic oxide MOS struct. oxide and interface props. 79−60929
$Ga_{1-x}Al_xAs$ electrodes, interface capacitance meas., flatband pot., conduction and valence band boundaries *(French)* 79−33339
GaAs (001)-Ag contact, surface stoichiometry and struct., and electronic surface states 78−95361
GaAs (110), chemisorption site geometry and interface electronic struct. of Al and Ga, photoelectron spectra 80−49843
GaAs (110), with Al or Ga overlayers, interfacial electron states, UPS and LEED obs. 80−80377
GaAs (110)-Al(Ga) interface, interface states, photoemission study 78−95359
GaAs (110)-Au Schottky barriers on ordered and disordered GaAs surfaces, props. 78−95360
GaAs anodic MIS system, dynamic props. of interface state bands 80−49933
GaAs anodic MOS structs., interface-state band model 80−11093
GaAs, deep level photoionisation, absorpt. by derivative surface photovoltage spectroscopy 79−99575
n-GaAs, epilayer, on semi-insulating substrate, elec. field distrib. *(French)* 80−20333
GaAs, epitaxial film on GaAs substrate, two-interface surface polariton modes 78−60180
GaAs, film and solar cell on graphite, struct. and elec. props. 80−2286
GaAs, GaO_xN_y-passivated, surface state density 80−11809
GaAs homoepitaxial interface, thermal degradation 77−11988
GaAs, intrinsic, on degenerate n-Ge, surface polaritons, hydrodynamical model 80−6752
GaAs, low temp. plasma oxidation and MIS struct. characts. 78−31546
GaAs MIS diodes, interface states determ., by deep-level transient spectroscopy *(Japanese)* 80−49917
GaAs MOS diodes, interface states, deep-level transient spectroscopy 80−44727
GaAs MOS system, elec. meas. interpretation 78−43484
GaAs MOS system, surface and interface exam. by derivative surface spectroscopy 79−82674
GaAs, oxidation in multipole plasma, MOS elec. props. 80−44737
GaAs, plasma anodisation in DC discharge, AES and MIS diode expts. 78−95826
n-GaAs Schottky barrier diode, electron processes at interface *(Russian)* 78−84301
GaAs Schottky-barrier diode, elec. props. 77−59331
GaAs, surface passivation using Si_3N_4, interface characts. 80−93005
GaAs type FET with buffer, bias effects due to deep centres in struct. *(French)* 80−107917
GaAs/anodic oxide interface, characterisation of proposed model 80−103754
p-GaAs/electrolyte soln., electrode photoemission, energy diagram, Volta pot. 77−62990
GaAs/oxide interface, interface states obs. by electrochem. method 79−99626
p-GaAs/thermal oxide interface fabrication and characterisation 80−11808
GaAs-Al interface, metal overlayer effect on semicond. (110) surface states 77−4441
GaAs-$Al_{0.4}Ga_{0.6}As$, p-n heterojunction, quantum confinement and compositional grading effects on band struct. 79−87151
GaAs-Al_2O_3, in MIS struct. surface states 77−85336
GaAs-Al_2O_3 MIS struct., interface props. and MISFET fabrication 79−65557
GaAs-$Al_xGa_{1-x}As$ differentially doped heterojunction interface, two-dimens. electron gas obs. 80−49886
GaAs-$Al_xGa_{1-x}As$ heterojunctions, MBE grown, photocollection efficiency and interface charges 79−11199
GaAs-$Al_xGa_{1-x}As$ heterojunctions, LPE grown, 2D electron gas obs. 79−99606
GaAs-$Al_xGa_{1-x}As$ heterojunction interface, two-dimensional hole gas obs., Shubnikov-de Haas meas. 80−80357
GaAs-$Al_xGa_{1-x}As$ LPE heterojunction, interface states 78−19128
GaAs-AlAs, heterostructure, effects of cation order on energy bands 80−11081

interface electron states continued
GaAs-AlAs and related monolayer heterostructures, pseudopot. calc. 78−60198
GaAs-AlGaAs heterojunction superlattices, inelastic light scatt. by two-dimens. electron gas 80−93360
GaAs-AlGaAs:Si heterojunction interface, two-dimens. electron gas, Hall effect and cyclotron reson. meas. 79−65530
GaAs-anodic oxide MOS struct., interface state band 79−60930
GaAs-Au Schottky barriers, PES and depth profiling obs. 79−42641
n-GaAs-Au(Al) Schottky diodes, interface state density model 77−80840
GaAs-electrolyte interface, energetic barrier height hypothesis 79−19657
GaAs-Ga, (110) interface electron states, photoemission study, chemical shift, surface charge redistrib. 78−72259
GaAs-$Ga_{1-x}Al_xAs$, ultrathin layer heterostruct., pseudopot. calcs. 78−95343
GaAs-$Ga_{1-x}Al_xAs$ heterostructures, quantum size effect in superlattices, electronic props. 80−29471
GaAs-GaAlAs, superlattice, subband related anisotropy in negative magnetoresistivity 80−11082
GaAs-GaAlAs (100) abrupt interface, carrier transmission and refl. coeffs. 79−69588
GaAs-GaSe n-p heterojunction, elec. props., interface states 80−65670
GaAs-Ge, electronic struct., self-consistent calc. 77−24611
GaAs-Ge abrupt interface, electronic struct., self-consistent wave mechanical calcs. 77−89837
GaAs-metal interface, metal-induced chem. reactions and surface states 80−20311
GaAs-metal interface form., chem. and electronic struct. 80−25009
GaAs-metal Schottky barrier, surface states and barrier height, I-V (C-V) characts. meas. 77−85310
GaAs-NaOH interface, inversion layer form. and surface states 80−2465
GaAs-oxide interfaces, local atomic and electronic struct., high resolution XPS 80−49927
GaAs-Pt interface states energy distrib. and relaxation time 79−33345
n-GaAs-SiO_2 interface, MOS capacitors, surface states from conductance and capacitance meas. 80−100533
GaAs-ZnSe (110) interface, electronic struct., self-consistent calc. 79−95486
$GaAs_{1-x}P_x$ electrodes, interface capacitance meas., flatband pot., conduction and valence band boundaries *(French)* 79−33339
GaAs(Sb), Schottky barrier and semicond./insulator interface states formation 80−49906
$GaAs_{1-x}Sb_x$ epitaxial n-n heterostructures, gap energies and interface pots., modulation electroabsorpt. meas. 79−11201
GaAs(110), surface and interface states, effects of atomic and electronic rearrangements 77−85284
GaN, reactive sputtering, GaAs MIS struct. fabrication and props. 78−39686
GaP anodic MOS structs., interface-state band model 80−11093
GaP, deep level profiles at substrate-epitaxial interfaces, photoionisation meas. 79−38025
n-GaP, inversion layers, broken-symmetry ground states 77−47873
GaSb, photoemission investig. of surface states, effects of O_2 and alkali metals 77−48312
GaSb-Au Schottky barriers, PES and depth profiling obs. 79−42641
GaSb-InAs system, (110) surface and interface electronic struct. 80−100494
GaSb;Au overlayer, adatom interactions, photoemission obs. 79−33898
GaSe MSM struct., inelastic tunnelling investigation of lattice dynamics, electron-phonon interaction 80−20330
n-Ge inversion layers, broken-symmetry ground states 77−47873
Ge, Schottky barrier, electronic struct., pseudopot. calc. 78−95364
Ge Schottky barrier, electronic struct., pseudopotential method, jellium model 79−38162
Ge/electrolyte soln., photoemission, energy diagram, Volta pot. 77−62990
Ge/GaAs (110) heterojunction, valence band discontinuity in XPS spectra, precise determ. 80−84834
Ge-GaAs, (100) interface, electronic struct. calc. 80−49861
Ge-GaAs, heterojunction, electronic structure 79−73572
Ge-GaAs (100) interface, electronic struct., scattering-theoretic approach 78−95340
Ge-GaAs (110) interface, self-consistent calc. of interface states and electronic struct. 78−52066
Ge-GaAs (110) junction, interface states and electronic struct. 77−69408
Ge-GaAs abrupt (110) interface, electronic struct. 78−95339
Ge-GaAs abrupt interface, orientation depend. of interface dipole energies, XPS expts. 78−39196
Ge-GaAs heterojunction, electrostatic dipole shifts contrib. to valence band discontinuities 79−51657
Ge-GaAs heterojunctions, electronic struct. 78−19138
Ge-GaAs interface, electronic struct. of Ge overlayers on (100) GaAs 80−49880
Ge-GaAs interface, surface and interface states of (111) surfaces 79−15206
Ge-GaAs interface, XPS obs. of electronic struct. 78−95341
Ge-GaAs superlattice and interface, electronic struct. 78−52065
Ge-metal contacts, surface electron state spectrum surface treatment effects *(Russian)* 80−34497
Ge-metal oxide, elec. props., molecular deposition method 80−34525
Ge-metal Schottky barrier junction, surface electron states spectrum *(Russian)* 78−84297
Ge-Na interfaces, interdiffusion, electron states, EELS study 80−50484
Ge-ZnSe, (100) interface, electronic struct. calc., scattering theoretic approach 80−6940
Ge-ZnSe, (100) interface, electronic struct. calc. 80−49861
Ge-ZnSe abrupt (110) interface, electronic struct. 78−95339
Ge-ZnSe p-n heterojunctions, effect of interfacial condition on optoelectronic props. 79−24061
He, liq., surface with trapped electron, parallel mag. field effect on interband transition 78−87835
$Hg_{1-x}Cd_xTe$ interface with native oxide, elec. props. 80−20318
$Hg_{1-x}Cd_xTe$-oxide interfaces, MIS capacitance characts. 80−49926
In-GaAs(Ge)(Si) Schottky barrier interface, covalent bonding of metal atoms 77−20429
p-InAs-Au contacts, influence of free surface on elec. behaviour 78−95362
InAs-GaSb (001) superlattice, electronic struct., tight binding calc. 78−95350
interface electron states continued
InAs-GaSb superlattice energy struct. and semiconductor-semimetal transition 79−23893
InAs(Sb), in MOS struct., electrorefl., band-population effects under heavy surface accumulation 77−48167
In_2O_3-InSb system, with Al(Au) electrode interface state density and oxide charge meas. 77−8200
In_2O_3-SnO_2/GaAs, solar cell, fabrication, characts. and interfacial chemistry 80−21401
In_2O_3-SnO_2/InP, solar cell, fabrication, characts. and interfacial chemistry 80−21401
InP (001)-Ag, contact, surface stoichiometry and struct., and electronic surface states 78−95361
InP, and $In_xGa_{1-x}As_yP_{1-y}$ binary and quaternary cpds., surface and dielec.-semicond. interface props. 80−93001
InP inversion-type MISFET with SiO_2 gate insulation interface props., elec. drift 80−93002
InP MIS capacitor surface states 80−49931
InP, Schottky barrier and semicond./insulator interface states formation 80−49906
InP-Al_2O_3 MIS struct., interface props. and MISFET fabrication 79−65557
InP-Au Schottky barriers, PES and depth profiling obs. 79−42641
InP-CdS p-n heterodiodes, junction props. study by using injection electrolum. 79−82667
InP-$Ga_xIn_{1-x}As_{1-y}P_y$ heterojunctions, energy band diagram 77−16400
InP-$In_{1-x}Ga_xP_{1-z}As_z$ quantum-well LPE heterostructure lasers, band filling and gain 79−22955
InP-Si_3N_4 (SiO_2), interface props., plasma deposited dielectrics, n-channel MOSFET action 80−93003
InP-SiO_2 MIS struct., with reduced interface state density near cond. band 78−26954
n-InP-SiO_2 system, interface and dielec. props. 80−49930
n-InSb based MIS struct., carrier generation under nonequilibrium conditions 80−88640
InSb, covered with thin oxide protective film, intrinsic photocond. 77−55578
n-InSb, forward biased Schottky barriers on low doped surfaces, current transport 79−24074
n-InSb, in MIS struct., accumulation layer submillimetric cyclotron resonance obs. 77−39912
InSb MOS capacitor, AC behaviour, semicond.-oxide interlayer effect 78−19151
InSb MOS structure, props. 80−49947
n-InSb, surface quality improvement by low temp. CVD of SiO_2, and characterisation 80−49932
InSb-anodic oxide-Ni, energy band diagram, internal photoemission meas. 79−33356
h-InSb-oxide system, interface recombination activity variation on annealing *(Russian)* 79−78199
InSe MOS structs. 79−69605
$In_{2-x}Sn_xO_{3-y}$-Si solar cells, SiO_2 detection of interface, Auger anal. 79−87991
MNOS structure, temp. depend. of flat band voltage 77−20456
MOS capacitor, photoionisation cross section and interface state density 80−92974
Mo-n-Si Schottky barrier, sputtered, freq. cond. charact. 77−20426
Na, metallic, Auger cross relaxation energy, SCF cluster model calc. 79−46945
Ni, adsorption of CO, binding and energy level shifts, NiCO and Ni_2CO electronic struct. 78−34882
Ni/polymer interface, electronic struct., XPS study 80−45204
Ni-Se interface, reactive diffusion, electronic struct., UPS study 78−51748
$Pb_{1-x}Hg_xS$-Si heterojunctions, elect. props. 80−100513
PbS-Si heterojunction, space charge capacitance, PbSn film thickness depend. 80−88630
PbTe substrate for MIS capacitor, C-V and G-V characts. 78−26962
Pd-SiO_2, work function changes due to adsorbed H_2, surface and interface dipoles 80−96972
Pt, electron wave interference in adsorbed CO film 79−33332
Pt-electrolyte interface, electron states, photoemission studies 78−85171
Pt-$SrTiO_3$ (100) interface, struct. and electronic props., AES, LEED, EELS, and UPS study 80−24986
Pt-$SrTiO_3$ (100) interface, Auger and photoemission studies, relax. and chem. shift effects 80−54749
Si (001)-SiO_2, n-inversion layer, valley splitting without effect mass approx. 80−15586
p-Si (100) inversion layers, intersubband spectroscopy by photocond. and absorpt. 78−10566
Si (100) surface accumulation layer, subband struct. and inter-subband absorption in strong mag. field 78−39177
Si (110), (111) surfaces, inter-subband spectroscopy in hole space charge layers 77−32064
Si (111), chemisorbed Cl layer, SCF LCAO band struct. calcs. 78−88010
Si (111), with chemisorbed Al, self-consistent pseudopotential calc. 78−34880
Si (111)-Au interface, chemically driven intermixing, UPS study 80−50533
Si (111)-SiO_2, sixth-valley state stability a priori calc. 80−49859
Si, amorphous, in contact with electrolyte, Schottky barriers at interface 79−78169
Si, amorphous film, interface charge, influence on transfer meas. 79−15237
Si, annealed, ion-implanted, in MOSFET, defect spatial distrib. 77−11973
Si, cast polycryst. p-n junction solar cell, hydrogenation effects 80−93916
Si, electron inversion layer on vicinal plane, minigaps 80−20282
Si, high-index surface, valley-valley splitting in inversion layers 78−39219
Si, inversion layer, dynamic conductivity of electrons, temp. depend. 78−19115
n-Si inversion layer, electronic bound states, theory 78−60217
Si, inversion layer, Hall effect meas. 78−56199
Si, inversion layer, impurity scatt., self-consistent calc. 79−28415
Si inversion layer, in strong mag. fields, electron localisation 78−60219
Si inversion layer, inter-subband optical absorpt. in mag. field 77−32375
Si, inversion layer, on vicinal plane, band structure 80−24994
n-Si inversion layer, resist. minima in surface quantum oscills. 78−60215

interface electron states continued
p-Si, inversion layer, screening effect and quantum transport in strong mag. fields 78−19155
Si, inversion layer, temp. depend. of subband energies, exchange and correlation effects 80−20281
Si inversion layer electronic transitions for voltage-tunable far IR emission 77−39962
Si inversion layers, Anderson transition, random field origin, substrate bias effect 77−28255
Si, inversion layers, far IR emission from hot electrons 78−30995
n-Si inversion layers, in strong mag. field, quantum galvanomag. expts. 78−60214
Si, inversion layers, intervalley transitions and subband splitting 77−20455
Si, inversion layers, magnetic localisation of electrons 78−43481
Si inversion layers, near threshold at low temps., cond. anomalies and electronic states 77−59333
Si inversion layers, review 77−80842
Si inversion layers, stress effects on electronic props. 78−43476
Si inversion layers, stress and intersubband correlation 78−60227
Si, inversion layers, two-subband screening and transport 78−64126
Si MOS (111) inversion layers, angular dependent negative magnetoresist. 78−80062
Si MOS diodes, P^+ implanted, DLTS of bulk traps and interface states 79−33350
Si MOS inversion layer, subband struct., many body effects 78−64131
Si MOSFET inversion layers, IR photocond. and absorption 78−64123
Si MOSFET structures, photocond. rel. to intersubband transitions 78−64127
Si, n-type inversion layer, theory of impurity-shifted intersubband transitions 80−20324
Si p-n heterojunction, DC sputtering growth, photocond. and photovoltaic effects 79−33337
Si solar cells, interface states effects on performance 78−76153
Si surface, high index, theory of inversion layers 80−44697
Si surface interacting with adsorbed gases, paramag. props., EPR study 80−34772
Si, two-dimensional electrons in superlattice, HF cond. 78−64055
Si wafer, trichloroethane oxidation, effect on SiO_2 and Si props. 79−70193
a-Si:H Schottky barrier diodes, capacitance studies 80−49908
Si/Al interfaces, chemical bonding states, low energy AES 80−6985
Si/SiO_2, CCD, incomplete charge transfer, fringing fields and interface states effects 77−15964
Si/SiO_2 interface, slow-trapping instability, kinetics, 78−76151
n-Si-Ag(Au) evaporated contact photoelectric props. *(Russian)* 78−43473
Si-Al_2O_3, inversion layer subbands, magnetocond. oscills. 78−64124
Si-Al(Ga)(In) interface, electron energy loss spectra of Schottky barrier states 77−48290
Si-Au, interface study using EELS 80−97391
n-Si-Au Schottky barrier, role of surface states in appearance of photo EMF 79−11222
Si-Au(Ag) contacts, Schottky barrier heights and interface states 77−85317
Si-BN interface, elec. characts., expt. 77−20459
Si-CdSe n-n heterojunction, photovoltage sign reversal, energy band profile *(Korean)* 80−29469
Si-electrolyte interface, energetic barrier height hypothesis 79−19657
Si-GaSe n-p heterojunction, elec. characts., interface states 80−70812
Si-Ge heterojunction form., microscopic aspects, EELS meas. 80−80368
Si-Ge junction, Si monocryst. and Ge film, elec. props. 79−51660
Si-metal Schottky barriers, surface states and barrier heights 77−80838
p-Si-metal Schottky contact surface state spectra and current transport mechanism *(Russian)* 78−43472
Si-metal systems, interfacial reaction and Schottky barrier 80−39672
n-Si-Ni surface barrier junction, rectifying, struct. and elec. characts., effect of low temp. annealing 78−14821
Si-Ni surface barrier struct., surface electronic states, annealing effects *(Russian)* 78−6441
Si-Ni(Pt)(Al) Schottky diode, type II localised interface states, Si surface prep. effects 78−39210
Si-PbS heterojunction, effect of Si substrate orientation on struct. and interface props. 80−80097
Si-polymer interface states in MOS structure, capacitance and cond. meas. 77−20438
Si-sapphire interface charge trapping, effects of sapphire type and epi growth conditions 77−20447
Si-sapphire interface states exam. by transient current anal. 77−43736
Si-Si interface, elec. cond. rel. to interface state population 80−65672
Si-Si_3N_4 interface in MNS capacitors, surface state density investigation 80−60100
Si-Si_3N_4(SiO_2) boundary, electrophysical properties, effect of ionic processes in dielectric layers *(Russian)* 78−10562
Si-SiC p-n and n-n heterojunctions, prep. by ion implantation, tunnelling cond. 77−43710
Si-SiO_2, Al-implanted, low-temp. annealing effect on charge and surface state density 77−85337
Si-SiO_2, distinction between donor and acceptor character of surface states 78−39216
Si-SiO_2, ESR centres, interface states and oxide fixed charge 80−2474
Si-SiO_2, effects of processing on radiation damage 78−39223
Si-SiO_2, electron-beam annealing of ion-implantation damage 79−77622
Si-SiO_2, generation of interface states due to emission of leaky electrons 77−62972
Si-SiO_2, intentionally contaminated interface, transient capacitance meas. 79−33349
Si-SiO_2, interface, doping depend. of interface states and charges 80−92992
Si-SiO_2, interface, morphology and electronic struct. 79−78194
Si-SiO_2, interface, reconstructing states 80−49925
Si-SiO_2, interface defect states obs. by constant capacitance DLTS 80−49924
Si-SiO_2, interface groups of states, C-V meas. 78−2541
Si-SiO_2, interface states from capacitance-voltage term spectra anal. 77−4446
Si-SiO_2, inversion layer, electronic ground state, stress, temp., mag. field and gate voltage depend. 78−60226
Si-SiO_2, ion bombardment by H_2^+, D_2^+, changes in annealing behaviour 79−78185
Si-SiO_2, ion implantation effects on charges 77−32086

interface electron states continued
Si-SiO_2, MOS interface states density, meas. techniques and model development 80−92988
Si-SiO_2, props. of surface states reviewed 77−20449
Si-SiO_2, Si lattice constraints on structure of interface states 77−20379
Si-SiO_2, surface state annealing 77−39946
Si-SiO_2, surface states, oxide charge centres, annealing effects 78−2570
Si-SiO_2, thermally oxidised, origin of fixed charge, Si diffusion in transition region 77−20381
Si-SiO_2 boundary, origin of interface states and oxide charges generated by ionising radiation 77−20380
Si-SiO_2 boundary, surface charge transport in valence band of Si 80−70789
Si-SiO_2 interface, amorphous, electronic states, Cayley trees appl. 79−65373
Si-SiO_2 interface, Au doping, trap distribution 80−20319
Si-SiO_2 interface, Au surface state energy levels and Au diffusion 79−51652
Si-SiO_2 interface, density of states, theory 80−80395
Si-SiO_2 interface, effect of thin transition layer on electron mobility and energy levels 77−20458
Si-SiO_2 interface, effect of hot electron injection on interface charge density 80−49921
Si-SiO_2 interface, elec. props. and influence on service performance and stability 78−23171
Si-SiO_2 interface, electronic struct., field depend. internal photoemission probe 77−20450
Si-SiO_2 interface, electronic props. of n-Si inversion layers, stress and temp. depend 78−19113
Si-SiO_2 interface, electronic states, review 78−30992
Si-SiO_2 interface, electronic struct., EELS study 79−99596
Si-SiO_2 interface, electrically active paramag. centres detect., photocond. reson. obs. 80−50185
Si-SiO_2 interface, electronic struct. calc. 80−100531
Si-SiO_2 interface, evolution of surface states density during bias temp. treatment 78−14832
Si-SiO_2 interface, form. and struct., AES obs. 79−56314
Si-SiO_2 interface, improved characterisation, refined quasistatic and cond. methods 80−96990
Si-SiO_2 interface, in MOS struct., fast surface states density, electron irrad. effects 78−88042
Si-SiO_2 interface, in MOSFET struct., electronic props. 79−42662
Si-SiO_2 interface, intermediate chem. state of Si during sputter profiling, Auger spectra 79−11230
Si-SiO_2 interface, interface-state parameters near band edge, MOS conductance meas. 79−11226
Si-SiO_2 interface, ion implantation induced interface states, effect of oxidation and N_2 annealing 77−39949
Si-SiO_2 interface, Na^+ drifted, impurity bands in inversion layers 78−60211
Si-SiO_2 interface, O_2 plasma effects on elec. props. 80−100523
Si-SiO_2 interface, props. 78−23170
Si-SiO_2 interface, props. variation in SiO_x region 80−49548
Si-SiO_2 interface, quasistatic capacitance-voltage determ. of interface state density, sources of error 77−12011
Si-SiO_2 interface, surface states and elec. defects obs. using ESR 78−23169
Si-SiO_2 interface, surface states characterization, expt. techniques review 80−49949
Si-SiO_2 interface, thermally grown, surface pot. inhomogeneities after stress ageing 80−92993
Si-SiO_2 interface, trapping props. from electrochemical current-voltage behaviour 79−69597
Si-SiO_2 interface, unwanted effects of ions in SiO_2 layers, review 80−92985
Si-SiO_2 interface charge inhomogeneities effect on surface state density meas. by MOS AC cond. technique 78−14833
Si-SiO_2 interface in MIS struct., B^+ ion implanted, elec. props. due to laser irrad. 78−72272
Si-SiO_2 interface in MOS device, indirect tunnelling involving intermediate states 80−92994
Si-SiO_2 interface in MOS solar cells, operational characts. and struct. 80−93901
Si-SiO_2 interface state density in MNOS structures 78−47873
Si-SiO_2 interface state spectrosocpy using MOS tunnelling strucures 80−6991
Si-SiO_2 interface state distribution, Br incorporation effects 80−11091
Si-SiO_2 interface state density, dependence on thermal oxidation process variables 80−15607
Si-SiO_2 interface state density in ion-controlled diodes, acid-base exposure effects 80−96984
Si-SiO_2 interface states, effect on memory characts. of thin-oxide MNOS devices 79−82681
Si-SiO_2 interface states, deposition of H containing layers and annealing 80−92991
Si-SiO_2 interface traps energy distribution meas., in MOS devices, under non-steady-state *(Korean)* 78−64119
Si-SiO_2 interfaces, carrier transport processes, electron states, conference, Durham, England (July 1979) 80−90612
Si-SiO_2 interfaces, local atomic and electronic struct., high resolution XPS 80−49927
Si-SiO_2 inversion layers, applied stresses, cyclotron masses and CDWs 77−55596
Si-SiO_2 inversion layers, bound states at interface 79−42655
Si-SiO_2 MOS capacitors, relationship between trapped holes and interface states 80−70830
Si-SiO_2 MOS interface states density, transient capacitance meas. eval. 80−92989
Si-SiO_2 new type of interfacial charge 78−23168
Si-SiO_2 surface states, influence of $\Phi ms(T)$ 79−99597
Si-SiO_2-Si_3N_4, surface states, density and spectrum 77−69423
Si-SiO_2-Si_3N_4 MNOS structure, chem. comp. and electronic states, Auger and energy loss spectra obs. 80−92999
n-Si-SiO_2-ZnO-Al, SAW convolver in monolithic MIS struct. 77−23791
Si-SiO_3, effect of Au recomb. centres on interfacial trapping states 79−38175
Si-SiO_x interface, localisation in inversion layer due to states in gap of oxide 77−12012
SiO_2 film on thermally oxidised Si substrate, interface props., sputter deposition parameters effects *(German)* 80−40257
SiO_2 in MOS struct., exciton transport rel. to surface states 78−34901

interface electron states continued
SiO_2-InP, MIS struct. prod. by pyrolytic deposition 77−15961
SiO_2-Si, low-energy neutral particle bombardment of SiO_2 film, degradation 80−54790
SiO_2-Si boundaries, insulator charges evaluation *(German)* 79−82682
SiO_2-Si in MIS, interface states, thermally stimulated charge decay 77−12009
SiO_2-Si interface of hardened MOS capacitors, radiation effects 78−26958
SiO_2-Si interfaces, surface state form. during bias-temp. stress aging 79−78193
SiO_2-Si MOS capacitor, two-stage process for building up of radiation induced interface states 80−20313
SiO_x, chem. shift of Si 2p core level, relax. contrib. 79−47141
SiO_x-GaAs, vacuum evaporated system, acoustoelec. signal, interface props. 80−75646
Si(100), inversion layer, interaction induced transition at low density 80−15581
Si(100) inversion layers, magnetoelec. and piezoresist. evidence for mobility domains 77−4447
n-Si(100) inversion layers on sapphire, surface quantum oscills. 78−19158
p-Si(111) surface inversion layer, Cs covered, negative magnetoresist. in 2D impurity band 78−64135
Su-SiO_2 interface states, exptl. study of charge model 79−65554
n-TiO_2 electrode in photoelectrochem. cell, anomalous photoresponse 77−11998
TiO_2-Ni (100) interface, electronic props., struct., comp., chemical bonding 80−84499
W-EuS interface, electron spin polarisation in field emission 78−35265
ZnO based varistor, analysis of highly nonlinear current-voltage characts. 77−11983
ZnO/Si SAW structs., anal. of charge injection 80−80049
ZnO-Bi_2O_3, heterojunction, current-voltage characts. 79−56291
ZnO-grainboundary-ZnO junction in ceramic varistor, capacitance-voltage characts. 80−65689
ZnS-metal interface, metal-induced chem. reactions and surface states 80−20311
ZnS-metal interface in MIM struct., photoexcitation level assignment *(French)* 80−15622
ZnSe:Mn-n-GaAs, single cryst. substrate low threshold DC electrolum. 77−63465
ZnSe-Ge (100) interface, electronic struct., self-consistent pseudopot. calc. 78−91747
ZnTe-electrolyte interface, electrochem. behaviour of single crysts. 79−91138
Zn0 based varistor, analysis of highly nonlinear current-voltage characteristics 77−39917

interface phenomena
see also adsorption; crystal surface and interface vibrations; interface structure; Kapitza resistance; semiconductor-electrolyte boundaries; surface phenomena
3 GHz surface and lateral EM wave meas. 80−103742
adhesion, interfacial energy-contact angle relation 79−91904
adhesion, surface and interfacial aspects, review 80−108690
adhesion, surface chemistry studies, anal. appls. 80−88440
adhesion between solid surfaces 80−88438
adsorbed molecules at metal-solution interface, enhanced light scatt. 79−82989
adsorbed monolayers, permeation and evaporation resistance, attractive forces effects 78−67892
air entrainment at solid/liquid/gas interface 77−1276
air-dielectric interface, EM wave reflection and transmission in terms of polarisation, education 80−105458
air-water interface, adequacy of theories of capillary wave damping 77−72750
air-water interface, effects on gravity waves 79−57947
air-water interface, fine struct. of thermal boundary layer in water *(Russian)* 78−22332
air-water interface, turbulent heat and mass transfer 79−68551
air/water interface, monolayer transfer to rot. square pillar 77−59184
alloys, binary dilute, solidification, planar interface stability *(Czech)* 80−89212
amino acid residues, form. of mixed micelles and relative compatibility at interface 80−71951
anisotropic insulators, interaction of point charge and interface 79−69584
anthracene single cryst., Frenkel exciton spectra at dielectric and conducting layer interfaces 80−44510
anthracene-Au interface, energy transfer 77−85775
binary alloy indirectional solidification, convective and interfacial instabilities 80−60851
binary alloys, magnetic interface struct. 80−29564
blood-fluorocarbon, biocompatibility of continuously generated and collapsed interface related liq. oxygenator 77−48944
bonded ductile half planes, plastic yielding through interface from cracks under antiplane deformation 77−14960
brass, morphological stability of α/β phase interface, interface moving direction effect 77−15700
brass/water interface leaky Rayleigh wave reflectivity loss meas. 78−59187
capillary condensation, Kelvin eqn., direct exptl. verification 79−33159
capillary wave propagation, experimental test of theories 80−69847
carbon tetrachloride-perfluoroethylcyclohexane, crit. mixture, brilliant total refl. from liq.-liq. interface 79−90786
cation-exchange membranes, electrochem. props. rel. to interfacial polarization during electrodialysis 79−16038
cellulose acetate polymer-solution interface props. from liq. chromatographic data 79−16039
charge deposition profiles, thin layers near irrad. material interfaces 77−27906
charged, surface pressure, electrostatic contrib. of divalent ions 79−24752
charged hard spheres near charged hard wall, nonlinear Debye-Huckel theory rel. to HNC approx. 79−64970
charged hard-sphere fluid, electrified interface pot., extended mean spherical approx. calcs. 80−84502
charged particle beam, influence of thin inhomogeneities 78−69219
charged particle beam, influence of thin inhomogeneities 78−69220
coexisting phases, interfacial profile near tricrit. points 80−19906

interface phenomena continued
coexisting thermodynamic phase interface, Ginzburg-Landau-Wilson model, drumhead model derivation in low temp. limit 80−42180
colloid interfaces, elec. double layer struct. 78−40088
colloid system, forces of mol. attraction between solids, effect of EM lag 80−71949
composites, single fibre-brittle zone model, fracture behaviour 80−97570
computational techniques in interface problems, conference, San Francisco, CA, USA (Dec. 1978) 79−41655
condensing vapour region, interface kinetics 79−69321
conference, San Juan, Puerto Rico (June 1976) 77−25318
conference on surface science, Cambridge, England (March 1979) 80−36773
contact behaviour of surfaces, of small nominal area 80−64493
contact conductance, heat transfer between solid surfaces 78−46888
contact deformation of elastic solids, role of mol. forces 79−23824
contact deformations of elastic solids, role of mol. forces 79−23823
contact fusion in complex metallic systems 78−26664
contact interaction between spherical surfaces under press. in various media *(Russian)* 77−7958
contact interface temp., internal thermal radiation effect 78−18151
copper phthalocyanine film, photoelectrochem. behaviour on SnO_2 electrodes 80−15626
covalent or ionic-covalent crysts., dislocation-free contact 80−80096
crack between dissimilar media, biaxial load effects 80−99968
critical fluid interface, in gravit. field, renormalisation calc. in three-dimens. 78−83911
crystal growth of two component systems, multilayer solid-on-solid interface model 80−28935
crystal with island film, dislocations and stresses 79−87015
crystal-met interface of Lennard-Jones substance, Monte Carlo simulation 79−60622
cylinder, stable conditions for phase change problem with internal heat generation 80−10130
cylindrical particle at fluid interface, equilib. position, force and free-energy anal. 77−55428
cylindrical rod, periodic structure, torsional vibrations, interfacial elastic parameters 80−96215
deformational instability of plane interface with transfer of matter 77−46994
dendrite, interface kinetics effect on growth rate 79−90927
dendritic growth, interfacial instabilities 79−82506
dense liquids, structure at solid wall interface, NVT Monte Carlo method 79−65310
designed monolayers assemblies 79−37915
desorption, damped oscillatory evaporation of single crysts., empirical discussion 79−65327
desorption, nonstationary evaporation of single crysts., phenomenological model 79−65328
diamond solid-fluid interface roughening transition, Monte Carlo simulation 79−99088
dielectric fluid-fluid interface, stability in elec. and gravit. *(Russian)* 77−27617
dielectric fluid-fluid interface, stability in elec. field *(Russian)* 77−27616
dielectric fluid-vacuum, wave packet propag. across abrupt boundary 77−17828
dielectric liquids, interfacial profile, elec. field effects theory 80−2244
dielectric-ferrite interface, physics of microwave reflection, Renard analysis of lateral shift 79−76557
diffusion bonding, in Ar atmosphere, aspects *(Japanese)* 78−11491
dilute binary alloy monocrystal, thermodynamics of growth, model *(French)* 78−87635
dimpled draining film, axisymm., model 77−59180
disperse system, fluid interface, dynamic properties 77−25313
dispersed medium freezing, origin of water aspiration 77−60130
DNA entrapment mechanism at air-water interface 77−60181
dose distributions across air-tissue, polythene-tissue and graphite tissue interfaces for 14 MeV neutrons 77−52889
dosimetry, transport of energy by electrons 77−86647
double layer diaphragm, electro-osmosis of different arrangements of layers, rel. to poles of current source 79−70373
drop coalescence at liquid-liquid interface drop surface velocities 77−43406
drop deformation and orientation in shear and extensional flow fields, dynamic interfacial props. 80−107611
drop dynamics in shear fields, role of dynamic interfacial effects 80−107612
duality transformations, interfacial energies and correlation functions, 2D Ising model 78−24741
dynamic surface tension excess at compressed interface, bulk-to-surface diffusion interchange 79−56042
EHD, liq. dielectrics interface equilib. and instability, curved wall effects *(Russian)* 78−5807
elastic interactions between defects and interfaces 80−39147
elastic SH wave reflection in presence of slip and friction 79−98519
elastic waves, reflection and refraction in presence of separation at solids interface 77−75848
electric conductor, elastic strain state, contact phenomena effects *(Russian)* 78−9564
electric double layer capacitance meas., potentiostatic method 78−85169
electrochemical fused soft systems, solid films and interfaces, review 77−77783
electrochemical noise generated by anodic dissolution or diffusion 77−25277
electrode surface, anisotropy of optical props. 80−60534
electrode systems of second kind, quantum mech. relations 79−100398
electrode-electrolyte interface, solid film props., review of expt. techniques 77−77780
electrode-solution interface, use of specular reflection methods 77−63926
electrode-solution interfaces, role of water 78−40058
electrodes, smooth, solid, double-layer capacitance freq. dispersion 79−20379
electrokinetic and surface potentials, for interfaces with two types of ionising groups 78−76136
electrolyte-gas interface motion in electric field 77−35248
electrolyte-solid interface, electrochemistry of surface 78−80798
electrolytic ion distribution near phase boundary *(German)* 78−56901
electrostriction-induced surface acoustoelectric waves at interface 77−16255

interface phenomena continued
EM waves, total refl. at interface between relatively moving media 79−55032
entrapped liquid lenses at elastomer-glass interface, formation and geometry 77−85021
entropy, due to elec. and mag. interfacial polarisation *(French)* 79−7050
entropy inequality for material interfaces 77−15678
enzymatic charge transfer across oil-water interface, effect of dielec. const. 77−70419
enzyme dynamics, statistical phys. 80−21439
equilibrium segregation of dil. solutes to grain boundaries, free surfaces, interphase interfaces 78−31411
evaporating interface, Marangoni instability 77−908
ferrite-austenite (α-γ) interface, Fe self-diffusion compared with grain boundaries diffusion 80−65306
ferromagnet-semiconductor contact, spin-depend. recomb. and scatt. on electron injection 80−65654
fibre reinforced polyester composite, interface strength *(Japanese)* 78−15646
fibre-resin composite, interfacial interactions and bonding, fibre surface props. 80−80046
film-transition layer-substrate, theorem of electrical images *(Rumanian)* 79−74064
fluid interface, perturbations surface tension and gravity effects *(Russian)* 78−10256
fluid interface problems, simple line interface calculation method 77−58777
fluid interfaces, isothermal and deformable, mass transfer and surface tension 80−33564
fluid interfaces, Marangoni instability, dissipative structures and nonlinear kinetics 80−33565
fluid interfaces dynamics and instability, conf., Lyngby, Denmark (May 1978) 80−31423
fluid surface correlations, density profiles 78−6196
fluid-fluid interface mass transfer, thermodynamic non-idealities 77−80683
fluid-solid surface interaction, two-particle correlation function 78−79880
fluid/fluid interfaces, capillary phenomena, review 80−70506
force transmission through incompressible viscous fluid-isotropic elastic solid interface 78−43252
forces and interactions, roughness and ductility depend. 77−24476
free energy for phase interface, solar-prod. expression, Ising model and cluster approx. 78−34591
frictionless contact problem for elastic layer under axisymm. loading 78−83341
gas-liquid annular two-phase flow, wave and interfacial friction characts. 78−67249
gas-liquid interface, irreversible thermodynamics, eqn. of state 78−51800
gas-liquid interface, mass transfer, ultramicroprobe method obs. 78−63901
gas-liquid interface of rising bubbles, adsorption rate determ. *(Japanese)* 80−6595
Gibbs adsorption equation, phenomenological interface theory 79−23834
glass fibres-resin interface studies 80−93531
glass interface with anodic electrolyte solution, simultaneous transfer of different cations in elec. fields 78−30800
glass-electrolyte solution interface chemistry 79−79256
graphite, interfacial tension determ. between C saturated liquid Fe by buoyancy meas. *(German)* 80−34273
graphites, ARV, VPP, MPG-6, contact thermal resistance, surface finish and compression depends. 78−79829
Hamaker constants, struct. effects, dispersion forces calcs. 78−43215
hard spheres permeation through hard disc monolayers, interfacial mass transfer 80−107460
hard-sphere fluid, density profile near container wall, mean spherical approx. 77−15149
hard-sphere fluid, interacting with wall, virial coeffs., in surface tension 79−23808
hard-sphere fluid, three particle interaction with wall 78−47223
hard-sphere fluid/soft wall interface, nonuniform fluid in external field 78−34413
heat transfer between bodies in gas-filled contact, integral equation numerical solution 79−37130
heating surfaces, furring, mass transfer, convective heat transfer, mathematical model *(German)* 77−23854
n-hexadecane-acetone, noncritical interface near crit. end point, surface tension meas. 79−69322
hydrocarbon drops levitated in water, acoustically forced shape oscill. 79−47987
hydrocarbon layer, influence on laser-induced surface damage 78−60533
hydrodynamic interfacial instability, mechanical, chem. and elec. constraints, review 80−34278
ice, melting, in porous solid, NMR and differential scanning calorimetry obs. 77−62621
ice surface layer, viscosity, from thermal contraction meas., 0 to −50°C 80−49469
ice-substrate interface, liq.-like layer in between, model, appl. to wire regelation and particle migration 79−46893
ice-water interface, local temp. meas. and convective flow 79−73293
immiscible fluids, interface hydrodynamic reponse and free surface modes 78−34681
immiscible incompressible fluids, interfacial convective instability, diffusional exchanges, adsorption-desorption processes 80−70504
immiscible liquid replacement, in capillary tube, moving contact line 77−55414
impedance of graphite electrode/graphite-βZnS mixture electrode in acidic aq. soln. *(Japanese)* 77−52648
inorganic solid, interfacial endothermic reaction, abnormal thermal decomp. rate 78−76852
interface of two phases or liquids, selective processes induced by resonance laser radiation 78−64867
interfaces, co-segregation of metallic and non-metallic impurities 80−60868
interfacial stability with heat and mass transfer, appl. to Rayleigh-Taylor and Kelvin-Helmholtz cases 78−67253
interfacial tension var. with supersaturation, one-layer adsorpt. model 80−103563
ionic crystals, coupling of interfacial charge transfer and bulk transport 80−79986

interface phenomena continued
ionic distribution function, discreteness-of-charge effects 79−100399
ionic distribution function, discreteness-of-charge effects in inhomogeneous dielectrics 79−100400
Kapron fibre reinforced phenolic resin, fracture kinetics, interface props. 80−66640
lamellar liquid cryst. phases, form. at liquid-liquid interface, rheological props. 79−99063
Lennard-Jones 12-6 fluid, liq.-vap. interface, density and surface tension 79−90772
Lennard-Jones fluid in contact with Lennard-Jones wall, interfacial density profile 78−67901
Lennard-Jones system, molecular dynamics simulation of interfacial and co-existence props. at triple point 78−83916
linear elastic fracture mechanics, stress singularities interfaces 78−34079
lipid films, at fluid interfaces, phys. chem., review, book contrib. 77−39725
liquefied natural gas spilled on water, spreading and evap. investig. 78−26748
liquid alkali-metal solid metal interfaces, chemistry and physics 77−51576
liquid boundary layers, struct. and thermodynamic peculiarities 80−88408
liquid dielectric-liquid conductor, separation surface equilib. and stability 78−91510
liquid film draining deformation between rigid sphere and gas-liquid interface 77−66078
liquid interface, mol. light scatt., heat fluctuations *(Russian)* 78−23477
liquid interfacial instability, mass transfer under high press. 79−94601
liquid metal-vibrating solid surface, equipment for investigating interaction at US freqs. 77−51589
liquid phases interface, hydrochemical stability 78−22933
liquid zone stability, static or rot. 77−59182
liquid-air interface, dipole layer, electrolyte effect 78−51796
liquid-gas, deform. in inhomogeneous elec. field *(Bulgarian)* 80−54474
liquid-gas interface, Stefan flow of binary mixture, with evap. or condensation 79−37381
liquid-liquid interface, adsorbed monolayer mol. orientation, electrolyte effects, reson. Raman obs. 78−60430
liquid-liquid interface, nucleate boiling 78−2342
liquid-liquid moving boundary, reflected freq. conversion *(Russian)* 77−7152
liquid-liquid system interfacial instability and longitudinal waves 80−33566
liquid-rigid wall, and liq.-cryst. interfaces, Monte Carlo simulations 79−27896
liquid-solid, measurements of voltage-induced reflectance changes 79−58804
liquid-solid interface, waves generated at interface with viscoelastic solid 79−68729
liquid-solid interface transmission IR spectroscopy 80−98985
liquid-solid interfaces, scanning laser probe for acoustic wave phenomena observation 80−100386
liquid-vapour interface, kinetic eqn. at mean field level 79−37905
liquid-vapour interface, location of surface of tension 79−37909
liquid-vapour interface struct. from uniformity of chemical pot. 79−60241
liquid-vapour interfacial density profiles by integral eqn. approach 77−35682
liquid-vapour system in gravit. field, interface correlations 77−1275
liquids, immiscible, convection at interface induced by coupling between chem. reacts., hydrodynamics *(French)* 79−41682
liquids, laminal flowing, concurrent, in horizontal cylindrical channel, mass transfer across interface of liquids 80−79397
liquids, low-press. evaporation, interface thermodynamic model 80−2252
liquids, potential and flux conserving static equilibria in elec. or mag. fields, determ. 80−88399
liquids rapidly evaporating at reduced press., stability rel. to lateral press. variations 79−95146
lossy liquid-lossless isotropic solid interface, reflection coeff. acoustic wave reflection coeff. 79−72733
lyotropic liquid crystal, ^{6}Li, ^{7}Li, and ^{23}Na NMR, metal ion-polar head group interaction 79−4243
lyotropic liquid crystals, orientation in mag. field, glass interface effects 79−1390
magnetic alloys, binary, spinodal decomp., computer simulation study of interface behaviour 80−84913
mass transfer through spherical particle interface, unsteady state 78−47017
mass transfer through spherical particle interface, unsteady state 78−47018
membrane-solution interface, phase jump of osmotic press., theory 79−11826
meniscus, three-dimens. numerical simulation by finite elements 77−59183
metal AC anodic dissolution rate, effect of H^+ evolution *(Russian)* 80−16693
metal drops in electrolytes, electrocapillary motion, elec. field strength effects 78−3346
metal surface struct. and initial stages of reactivity, review 78−68837
metal-cellulose-metal sandwich system, spontaneous elec. current induced by heating 80−40700
metal-electrolyte boundary, elec. refl. and photoemission relationship 80−45211
metal-electrolyte boundary, electrodynamics in visible and near UV range, microscopic effects 80−45521
metal-electrolyte boundary, photoemission effect on elec. refl. 80−45212
metal-electrolyte double layer, dual capacitor model 77−60071
metal-electrolyte interface, optical methods of study *(French)* 80−7318
metal-electrolyte interface, vibratory process meas. apparatus 77−39732
metal-electrolyte interfaces, optical reflectance specta, interpretation 80−93263
metal-epoxy resin adhesion, fracture mech. study 77−4888
metal-liquid interface, laser generated MHz elastic waves 79−73387
metal-metal interface, effect on adhesion and friction 77−24488
metal-metal interface, EM wave propag., plasmon polaritons, computer simulation 78−84276
metal-polymer friction pairs, triboelec. effects 80−11784
metal-semiconductor system, interfacial reaction, dynamical obs. at room temp. using AES 80−10798

interface phenomena continued
metal-solid electrolyte interface, DC and current-voltage charact. 77−28251
metallic glass, thermal stability, validity of energy and entropy interfacial tension models 78−91255
metals, contact melting, state of cryst.-liq. boundaries, influence of impurities and hydrostatic pressure *(Russian)* 79−37812
metals in molten salts, mass and electron transfer meas. via recording coulometer 78−3344
mica surfaces, interaction forces at small separations in polar and non-polar liquids 80−39458
MIS solar cells, interface problems, AES, SIMS and XPS study 80−89627
molecular forces, theory 78−40087
molecular models of condensed systems and interfaces *(German)* 80−20062
molten metals *(French)* 79−43632
monolayers, surface pressure at air-water interface, meas. technique 80−89526
monolayers on liquid-liquid interfaces, interfacial tension *(French)* 79−73376
multicomponent systems, nonequilib. thermodynamics 77−33966
multilayer assembly, freq. depend. cond., electron transitions between localised states 77−43699
nematic liquid crystals, surface and interfacial free energy, Van der Waals dispersion force contrib. 79−99399
neutron bottles, surface physics and chem. rel. to storage time anomaly 79−85575
non-equilibrium thermodynamics of two bulk interfaces including Em effects 80−13021
nonideal fluid mixtures, generalised film model for mass transfer across interfaces 77−67387
ocean, acoustic imaging of New England shelf-slope water mass interfaces 78−3784
octane-water, proton transfer coupled with ATP hydrolysis by chloroplast ATPase 77−36876
octane-water interface, electron transfer in presence of chlorophyll 77−81474
octane-water interface, generation of pot. jump by Na^+,K^+-ATPase 77−81484
octane-water interface, water photo-oxidation in presence of adsorbed porphyrins 78−64933
oil-water interface, chem. and hydrodynamic instabilities *(French)* 80−7789
oil-water interface, electroadsorption and electrocapillarity 80−44393
oil-water interface, fatty alcohol adsorbed layer phase transition, high-press. effect 79−99395
oil-water interface, long-range attraction of red cells 77−77874
optical surface wave at a nonlinear interface 80−91867
orthodontic direct bonding systems, stress anal. 77−56513
outgassing from surface, Monte Carlo method in one-dimens. 78−47001
paraffin, solid-liq. interface motion during melting, convection effects, photographic obs. 79−18890
passivated semiconductor surface, net surface charge determ. using floating field ring devices 78−88037
penny-shaped crack, Fredholm integral eqn. soln. 78−90784
n-pentane-water interface, nucleate boiling 78−2342
phase interfaces, balance eqns. and struct. models 78−59453
phthalocyanine-alkane interface, charge transfer, rel. to photoelectrophoretic image form. 80−65616
phthalocyanine-dodecane interface, photostimulated charge transfer flash expt., trapping model 77−66182
planar double layers, Derjaguin force formula 80−107890
plane interface between two viscoelastic superposed cond. fluids, instability in mag. field 80−1694
plasma-vacuum, wave packet propag. across abrupt boundary 77−17828
poly(dihydroxypropyl methocrylate), surface charact., by contact angle methods 80−61140
poly(hydroxyethyl methacrylate), surface charact., by contact angle methods 80−61140
poly(methoxyethyl methacrylate), surface charact., by contact angle methods 80−61140
polymer soln., colloid stability near repulsive wall 80−21326
polymers attached to inert interface, conformations 79−94120
polypropylene fibre reinforced polyoxyethylene, fracture kinetics, interface props. 80−66640
polystyrene interfacial colloidal crysts., microscopic obs. 80−97737
propyl stearate monolayers, elasticity and viscosity determ. by laser light scatt. 77−72749
protein adsorption and immunological reactions at liq./solid interface, ellipsometry obs. 77−52948
protein film, at liq. interfaces, dilatational props. 80−94255
protein-solvent interface area rel. to protein packing and struct. 77−86441
pyrene dodecanoic acid, lateral diffusion at air-water interface, monomer excimer dynamics 80−92693
radiation dose enhancement due to backscatt. secondary electrons at interface 77−2058
radiation propagation analysis, layer decomp. method *(French)* 80−95772
Rayleigh-Taylor instability, method of generalised coords. 78−65771
reflection from moving boundary between two dielectrics in waveguide 77−584
reflectivity of superconducting-normal metal interface and applications 78−91822
renormalisation group approach to interfacial order parameter profile near critical point 78−6200
rough interfaces, light reflection, scattering in homogeneous media *(French)* 79−50211
roughening transition dynamics, renormalisation group method 78−45574
roving cloth fibre reinforced plastic, strength of fibre/matrix, matrix/matrix and FRP/FRP interfaces *(Japanese)* 78−27608
rubber, Schallamach waves, rel. to friction of elastomers 79−29225
SAW, harmonic generation at unbonded interfaces and fatigue cracks 78−90562
Schottky barrier, thermal emission from damage near interface, effect on TSC and transient current expts. 77−11982
screw like dislocations behaviour with lattice frictional forces 80−64999
semiconductor film-substrate boundary, epitaxial interface form. and transition regions 80−10821

interface phenomena continued
semiconductor physics, conf., Edinburgh, Scotland (Sept. 1978) 79−95303
semiconductor-electrolyte boundary, hot carrier injection, tunnelling from semiconductor states in depletion region 80−75637
semiconductors, conference, Pacific Grove, USA (Jan.-Feb. 1979) 80−46725
semiconductors, interface and surface physics, review 80−49872
shock wave generation, liq.-liq. interface with temp. discontinuity 78−51197
shock wave refraction, at slow-fast gas interface 79−32573
singular densities and currents at dividing surface 80−17907
sintering, appl. of stereological charact. of interface interaction 77−63589
slag-metal interface determination using electrochem. conc. element 78−7114
sliding mechanism without slipping, interface of two solids 78−51136
slip zones along interface, caused by plane horizontally polarised SH stress pulse 80−53648
sludge/water, vel.-displacement phase difference *(Japanese)* 80−45580
soft metal, effect of loading time on contact area *(Japanese)* 78−6230
solid films and surfaces, conference, Tokyo, Japan (Jul. 78) 80−10739
solid-fluid interface, wetting and adhesion, thermodynamic aspects 80−89525
solid-liquid flashover, permittivity matching effect 78−1945
solid-liquid interface, optical methods of study *(French)* 80−7318
solid-liquid interface free energy anisotropy clustering influence 80−80054
solid-nematic interfaces, reflection and refraction of obliquely incident shear wave 79−86691
solid-on-solid model, roughening transition, Temkin approx. 77−39739
solid-solid interaction, crystallographic interfacial fit *(French)* 79−73410
solid-solid interface chemistry, characterisation, theory 80−75448
solid/liquid interface interactions, IR spectroscopy obs., review 80−40733
solidification interface in reduced gravity, bubble interactions 78−84787
solitons in condensed matter physics, theory 80−50122
solvent structure, at polarisable interfaces, mol. models, review 80−59359
sound scattering by spherical body 79−94387
spherical inclusion embedded in bonded dissimilar half-spaces, eigenstresses 77−23886
spherical particle at fluid interface, equilib. position, force and free-energy anal. 77−55429
spherical particles, force exerted by freezing interface 80−107083
spinning drop interfacial viscometer, liquid-gas interface, surface viscosity meas. 80−44395
spreading of liq. Ni over α-SiC single crystals 79−86962
stability of interfaces which separate compressible bulk phases 80−107610
stability problem, diffusion, reaction and convection 80−33567
stable surface chemical reactions, interfacial hydrodynamic instability 80−66874
statics, differential eqn., micromech. derivation 79−46882
statistical mechanics of short chain mols. 77−43426
steel, austenitic stainless, MC precipitate comp., APFIM study 80−104161
steel, ferrite-austenite welded joints, corrosion cracking resist. *(Russian)* 79−52437
steel 45-antifrictional alloys friction pairs, electrochem.-mech. investigation *(Russian)* 80−76367
stereological counting measurements, use in testing growth rate theories 80−16311
Stoneley US waves on boundaries, surface bonding effects 79−56059
stresses in viscoelastic adhesive layers due to moisture sorption 79−90145
succinonitrile solid/liquid interface energy determ. by Abel-Cahn method 78−67909
superconducting ultra-thin films, transition temp., interface and fluctuation phenomena 80−84527
supersaturated soln., shape stability of growing cylindrical particle due to diffusion and interface kinetics 80−79720
surface science in metallurgy, review 79−42388
surface thermodynamics, fundamental eqns. 80−107630
surface viscosities at high pressure gas-liquid interfaces 78−75907
suspensions, concentrated, of shell-spheres, dielectric theory, interfacial polarisation, anal. of biological cell suspensions 80−45563
system with an interface, dynamical eqns. mol. derivation 78−38914
tetrabutylammonium iodide/I solid/liquid electrolyte interface, impedance study 80−26031
thermal resistance of contact between wavy surfaces in vacuum 77−7293
thermodynamics, nonequilib., of discontinuity surface, appl. to n-component viscoelastic mixture 78−93638
thermodynamics and dynamics of pure interfaces, rel. to Spacelab 79−28910
thermoelectric cooling equipment, welded joints, heat emission effects on temp. distrib. *(Russian)* 80−69635
thermoelectric phenomena, irreversible homogeneous materials, single (double) bimetallic junctions *(French)* 78−95291
thin films, segregation effects at surfaces and interfaces 80−39475
tibial plateau fixation, biomech. factors 77−56534
total reflection and surface wave obs. 80−108292
turbulent heat transfer across membrane between two liquids *(Russian)* 78−38180
two-dimensional interface, sine-Gordon chain model 80−29272
two-layer baths, dynamic rectification effect calcs. 78−95934
two-layer dielectric interface polarisation charge expt. 80−15946
two-phase anisotropic medium, interfacial dislocation, stresses, displacements and energy calc. 80−79786
two-phase flows, transient, theoretical interfacial constitutive models 79−86497
two-phase system with interface, derivation of dynamical eqns. 79−49155
vapour-liquid interface, mol. orientation, theoretical and computer simulation 79−73377
vapour-liquid interface, surface thickness determ. assuming linear density profile 79−69324
viscoelastic interface, constitutive equation 78−84028
viscoplastic medium, formation of contact with solid surface under pressure 79−69320

interface phenomena continued
viscous liquid spreading on water surface 80−49466
volatile liquid droplets, impaction on hot liquid surfaces 77−39330
water, at biological interfaces, struct. and functional aspects 78−40121
water, simulated, cooperative effects rel. to interfacial props. 80−28906
water, supercooled emulsified droplets, relative permitt. and cond., Maxwell-Wagner interfacial polarisation 78−52423
water-air interface, wind vel. profiles and drift current along wind-generated wave profile *(Russian)* 78−61429
water-ice interface struct., fluctuations during solidification 78−59935
water-nitrobenzene interface, mechanoelectrical energy conversion using interfacial tension changes 79−14982
water-sediment interface US reflection with bidirectional displacement 78−60017
Yukawa fluid, fluid-solid interface 80−38883
Yukawa fluid, hard planar wall interactions with exponential tail, mean spherical approx. 80−38884
Ag electrode, intense Raman spectra in presence of Cl^- and pyridine 80−55076
Ag/α-Ag_2S, interface, electrochemical transfer across phase boundaries 78−73046
AgI, interfacial electrochem., review 78−80748
Al contacts sintering in vacuum and O_2, room temp. 80−7512
Al-Pt film sandwich, interdiffusion and intermetallic form. 77−24448
$Al_{0.5}Ga_{0.5}As$-GaAs minimum heterojunction width determ. by sputter Auger techniques, interface broadening 79−69586
Al_2O_3, fine grained, interface-controlled diffusional creep 80−60915
Au-Ag bilayers, conc. profile by AES, interdiffusion coefficient determ. *(French)* 78−84077
Au-GaAs interface, atomic modulation of interdiffusion, effect of reactive Al monolayers 80−49432
CO_2 film, adsorbed on KBr, density fluctuations 79−42391
$Ca_{10}(PO_4)_6(OH)_2$, hydroxyapatite, aq. solution system, interfacial props. and equilibria 79−77751
CdS:I_2 system, interface kinetics and vapour phase mass transport 80−19732
Cl_2, vapour-liquid interface, mol. orientation, theoretical and computer simulation 79−73377
Co, plated film, magnetisation and mag. interface anisotropy 77−85510
Cr-(Pd_2Si)-Si, $CrSi_2$ form. kinetics 77−24492
Cr_2O_3-Al_2O_3, solid soln., effect of Cr on point of zero charge 78−61021
Cu, molten surface layer thickness, emissivity and AES meas. 80−39261
Cu, sintered, appl. of stereological charact. of interface interaction 77−63589
Cu-Al(In), lamellar eutectoids, calorimetric determ. of interfacial enthalpy 78−60668
Cu-Constantan junction, elec. response to shock compression 79−95470
CuCl, interface superconductivity? 80−39696
Fe, ferrite/austenite interface, prep. and charact. *(French)* 79−95272
Fe liquid, C saturated, decarburization by CO_2, effect of S 79−11726
Fe, passive, interfacial impedance *(Japanese)* 77−48581
Fe-C, lamellar eutectoid, calorimetric determ. of interfacial enthalpy 78−60668
Fe_2O_3-Al_2O_3, solid solns., effect on Fe on point of zero charge 78−61021
GaAs MIS solar cells, effects of thin oxide layers on characts. 80−89624
GaAs-Au(Ag) Schottky barrier solar cells, interface problems, AES, SIMS and XPS study 80−89627
$Gd_3Ga_5O_{12}$, Czochralski grown, effect of melt flow phenomena on perfection 78−88419
Ge films, adhesion to substrates, effect of Ar^+ ion irrad. 79−11047
^{4}He, superfluid against solid ^{4}He, surface tension and contact angle 79−42339
^{3}He-^{4}He mixture film, 2-D interface excitation spectrum 80−96718
^{3}He/solid interface, refl. of transverse zero sound *(Russian)* 80−70492
^{3}He-^{4}He, charged interface, ripplon softening 80−34269
^{3}He-^{4}He mixtures, ion trapping at crit. interface 79−65285
^{4}He, liq., phonon energy spectrum due to thin-film heater 77−76633
^{4}He, liquid-solid boundary, capillary sound motion, Kapitza resistance *(Russian)* 80−92737
^{4}He, superfluid, interface with sapphire, 0.25K, ballistic phonon pulse transmission 79−19415
^{4}He, superfluid, interface conditions between liq. and vapour 80−10723
Hg/aqueous solution interface, elec. double layer in presence of adsorbed ions 79−83469
Hg-aqueous electrolyte interface, double layer charge relax., thermal jump meas. 78−53216
Hg-electrolyte interface, polarizable, dynamics of double layer 79−24756
In, electron MFP, conduction electrons injected from ferromag. 79−15135
LiF, deformed in liquid He, penetration of He, dislocation effects 77−20131
Na conductive glass-Na amalgam interface, electrochem. obs. 78−76870
NaCl-KCl, interdiffusion and demixing, electron microprobe anal. *(French)* 80−54444
Ni films, electronic struct. calc., effects of chemisorption; contact pot. and surface magnetisation 80−103734
Ni, plated film, magnetisation and mag. interface anisotropy 77−85510
Ni-Al (42 at.%), Al_2O_3 growth, form. of voids at metal-oxide interface 78−53030
Ni-Al system, spreading kinetics of Al 80−24717
Ni-Fe, electronic struct. calc., effects of chemisorption; contact pot. and surface magnetisation 80−103734
Ni-Sn intermetallic phase growth kinetics at liq. Sn-solid Ni interface 80−71638
$PbSnF_4$, anionic conductor, thin films and ceramics 80−107556
Pt/Y_2O_3-ZrO_2/Pt cell, Faradaic reaction kinetics, impedance dispersion anal., electrode/electrolyte interface process 79−11798
Si-electrolyte interface, incident radiation image form. *(Russian)* 77−7199
Si-SiO_2, interface, stress meas. technique 80−84395
Si-SiO_2 interface, in MOS structure, effect of irrad. with low energy electrons *(French)* 77−55617
Si-SiO_2 interface, optical props. 79−99908
Si-SiO_2-KCl_{aq}, interface, capacitance meas. 78−80051
Si-undoped poly Si interface, in oxidation process, defects generation 80−40571
SiO_2, on Si, viscous flow meas., 960 to 1075°C 77−39729
SiO_2-liquid heptane interface, adsorption of organic liqs., IR spectra obs. 79−57295

interface phenomena continued
Sn melt in contact with Fe, Fe distrib. on thermal cycling *(Russian)* 80−16562
Ti metal-metal interface, adhesion energy, surface treatment and ion implantation effects 80−107660
Ti-Mn (0.4 and 12 wt.%), bonding between α-β interfaces, subsequent deform. 78−14517
U extraction by transfer between liq. phases, laser radiation effect 80−66795
UO_2-(Ni), surface, grain boundary and interfacial energies 78−71905
V_2O_5-$AlNbO_4(GaNbO_4)(TiNb_2O_7)$ systems, interfacial reactions, efficient boundary conditions and solid state reactivity 80−76542
V_2O_5-TiO_2 interface, role of struct. props. in interfacial reactions 78−31688
Zn alloy, flux adhesion, and spreading coefficient 80−15379
ZrC-Ni, refractory-liquid metal, interfacial reactions, C effect, electron microprobe analysis 77−12829

interface structure
$\alpha\gamma$ interface, struct., thickness, intermediate phase effects 78−71831
acetone-chloroform solution, Monte Carlo calcs. for interface struct. with directed intermol. forces *(Russian)* 78−1975
adhesion, surface anal. techniques appl. 80−65381
adhesive failure, rel. to interfacial structure 80−50820
adsorption of liq. mixture on solid, equilib. thermodynamics 78−84045
AES depth profiling, appl. of tailored modulation techniques 77−15702
alloy solidification, interface stability, interfacial wave 77−86019
alloy-casting interface struct. investig. after mould flame spraying *(Japanese)* 77−48586
analysis by combined Auger, X-ray and SEM studies 80−81413
atomic structure, interface roughness, calc. *(Russian)* 80−103587
bicrystals, symmetry and interfacial struct. 80−2274
bimetallic strip, interface struct., scanning Auger microprobe study 80−34322
binary alloys, magnetic interface struct. 80−29564
binary metallic system, conc. profiles across solid-liq. interfaces 80−55382
bonded interface defect testing by differential interferometric Stoneley wave meas. 80−76444
α-βbrass, interface struct. of two-phase bicrysts. made by solid state diffusion couple method, X-ray Laue and TEM study 79−28214
brass, two phase α/β bicrystal, transgranular slip and fracture across an interface 80−81150
brass, two-phase α/β bicrystal, diffusion induced twins in α-phase 79−46967
brass, two-phase α/β bicrystal, morphology and crystallographic relationships between phases 79−46966
brass α-β two-phase bicrystals, interface sliding studies 80−54248
coherent interphase boundary energy anisotropy between cubic-type crystals 80−54252
coincidence site lattices, and pattern shift lattices *(French)* 79−69035
compound semiconductor interfaces, conf., Los Angeles, USA (Jan. 1978) 78−91756
compound semiconductor-metal reactions, book contrib. 79−1622
conductor-insulator-semicond. (CIS) solar cells, noncrystalline (poly and amorphous), interface importance 80−81466
crystal-melt interface, computer built random model 77−20165
depth profiling techniques for thin film interdiffusion and interfacial reactions, book contrib. 79−1564
dielectric multilayer coated optical surface, diffr. and diffuse scatt. 79−50220
dislocation model for loss of coherence across interface 78−6057
dislocations, Burgers vector determ. using electron microscopy 78−34720
double-layer structure, electrohydrodynamical determination 78−95960
dynamic displacement, and air entrainment prediction 78−2337
edge dislocation, induced interface tractions 78−14345
elastic interaction of point defects and volume defects near interfaces 79−65115
electrode-electrolyte interface, orient. models for solvent 78−61017
electrolyte-solid interface, electrochemistry of surface 78−80798
fatty alcohol solid monolayers in H_2O, interface struct., model 80−54505
FCC crystal-melt interfaces, mol. dynamics simulation 80−79913
film, interdiffusion and reactions, book 79−1561
film, interdiffusion and reactions, book contrib. 79−1562
film reactions, $^{16}O^{2+}$ effect elimination in backscatt. 78−23575
film sandwich structures Auger anal. 78−72030
film-substrate bond strength, meas. by laser spallation 80−50821
finite two-phase bodies, response to internal and external stresses, geometrical considerations 80−24741
finite-two phase bodies, response to internal and external stresses, numerical considerations 80−24742
fluid, inhomogeneous, pair and density correl. functions 79−27887
fluid interfaces, mol. theory 77−7949
fluid interfacial stress and struct., gradient theories 79−19428
gas-solid interfaces, topographic and thermodynamic aspects 78−68927
glass surface, ellipsometric study of zone of optical contact 80−4754
glass/polymer, exam. using ion scattering spectroscopy and scattered ion mass spectrometry 78−60641
glaze/glass-ceramic, interface reactions, electron microprobe anal. 80−84398
grain boundaries, interfacial structure effects on high temp. mechanical behaviour 80−59480
graphite fibre reinforced Al, temp. and press. effect on interface chemistry, mech. prop. meas. 78−64595
hard sphere fluid, surface tension at wall 79−73081
heteroepitaxial structures, misfit, strain and dislocations, book contrib. 79−82499
heterojunctions, deformed and undeformed, interface boundary effect on interface states 78−47855
ice-metal, mech. behaviour and crack prod. of single cryst. 78−43230
III-V semiconductor compound structures, TEM analysis 77−89836
III-V semiconductors, surface and interface anal., secondary ion mass spectrometry technique 80−59763
interface study by Auger spectroscopy 80−76587
interfacial roughening transition, renormalisation group theory 79−2734
ion-etch profiles, interface position determ., nomographic method 77−89658
LEED anal., book contrib. 79−42358
Lennard-Jones (100) crystal-liquid interface, structure 78−91284
liquid-vapour interface, fluctuation theory 78−95204

interface structure continued
liquid-vapour interface, pair correl. function at triple pt., Monte Carlo method 80−10753
liquid-vapour interface, struct. at 110K, Monte Carlo method, for Ar-like fluid 80−54477
liquid-vapour interface struct., Ar like fluid in equilib., thermodynamic states 78−10259
liquid-vapour interface struct. and thermodynamics, density fluctuations, grand ensemble formulation 78−22932
liquid-vapour interface structure near hard wall 80−14983
liquid/solid, mol. dynamics simulation of struct. 78−26764
metal and oxide surfaces, and interfaces, slow exchange processes study using SIMS 80−55653
metal film, on pyrex, surface roughness meas. by ellipsometry and TEM 77−20205
metal semiconductor contact, elec. characts., interfacial reaction effects, book contrib. 79−1623
metal-dielectric interface, static point charge in dielec., pot. distrib. *(Russian)* 80−60088
metal-InP contacts, intermediate adsorbed layer effect on electronic props. 80−39674
metal-metal interface, effect on adhesion and friction 77−24488
metal-semiconductor interfacial reaction, AES study *(Japanese)* 80−96701
metal-semiconductor system, interfacial reaction, dynamical obs. at room temp. using AES 80−10798
MNOS structure, Auger depth profiling and ion sputtering of interfaces 77−20200
MNOS structures, electron-beam-irrad., interface defects, high temp. H_2 anneal 80−96745
molecular fluid, computer simulation of liquid-vapour surface 80−54478
MOS 78−2381
multilayer superlattice stacks, very thin nonideal, wavelength variation of transmissivity, refl. 80−100701
multilayer thin film, optical scatt., effect of interfacial roughness 79−31804
nonuniform fluid state, Van der Waals theory, thermodynamics, struct. and phase stability 79−77475
optical fibre preform diagnostics, nondestructive noncontacting method 79−27376
ordered structure conditions, pairwise interaction model *(Japanese)* 79−51018
organo tin polymers, glow discharge formed, interface composition and adhesion 79−82467
oxide layer-metal interface, ion-beam effects, ESCA obs. 78−52612
oxide-electrolyte interface, transition layer model 78−68895
p-n junction with one-sided step model internal field topography, TEM image interpretation 79−82129
periodic misfit-dislocation networks, electron diffr. 78−59815
point defect interaction with volume defects near interface 79−14843
polarisable interface, solvent struct., mol. models 80−59359
random distributed steps at interfaces and surfaces, quantitative LEED evaluation 78−63912
review of surface science 79−19427
rough surfaces computer simulation of contact 79−19470
rubber-brass interface, adhesion failure, XPS study 80−40671
rubber-metal interface, adhesion mechanism, XPS study 80−65382
sapphire ribbon crystal, interface growth feature rel. to voids 78−34456
sapphire-Si interface structure, SIMS obs. 77−76675
segregation, influence of cooling rate 78−72010
semiconductor film growth, multilayer systems, spectroscopic ellipsometry, review 80−103603
semiconductor with polytype layers, interface exciton states 78−26819
semiconductor-metal interfaces, Schottky barriers, chemical trends 78−95363
silane, coupling agent on E-glass fibre, structure, Fourier transform infrared spectroscopy 78−60643
silane, coupling agent on porous silica, Fourier transform infrared spectroscopy 78−60642
SIMS, interfacial impurities, quantitative anal. 80−84396
solid-solid interface, chemistry and physics, book contrib. 79−1551
solid-solid interface, circ. prismatic dislocation loop 79−82468
solid-solid interface chemistry, characterisation, theory 80−75448
spinodal decomposition, near interface, continuum mechanics *(German)* 80−45272
sputtered coatings, columnar boundaries, diffusion and interfacial structure 79−28253
steel, austenite/ferrite interface, struct. and diffr. effects, TEM exam. 80−16308
steel, austenitic stainless, Ni-alloyed, Cr_2N precipitation, interface struct. and morphology 80−11644
steel, continuously cast slab, liquid-solid interface obs. by Pb additions to mould 77−21128
steel, dual phase HSLA, compositional anal., TEM 80−85253
steel, galvanised, interface struct., scanning Auger microprobe study 80−34322
steel, galvanised, with paint coating, adhesion failure, XPS study 80−40671
steel, interface model of $(3, 15, 10)_F$ martensite 78−31408
steel, spheroidization of pearlite, global microstruct. evolution 80−108482
steel, stainless, interface with sputtered Nb film 79−74089
steel, stainless, with Ni base filler metals, brazed joint strength *(Japanese)* 80−16636
steel fibre reinforced Mg, fibre-matrix interfacial reactions 80−20043
steel plates, explosively clad, fatigue crack propagation behaviour *(Japanese)* 80−104262
surface dislocation model, Z-phase interface boundary problem 80−39085
synchrotron radiation and sputter Auger techniques 78−61130
tetrahedral semiconductor/oxide interface, continuous random network and tight-binding models 77−89866
thin films and interfaces, analytical techniques, review 80−80120
X-ray diffractometric study of polycrystalline junction structures 77−20406
zinc phthalocyanine film, between Au or Ag layers, microstruct. characterisation by TEM method 78−95241
Zircaloy-4/stainless steel, diffusion bonding in presence of Fe intermediate layer 79−10987
α-Zr(Al)/Zr_3Al interfaces, struct., TEM study 79−74156

interface structure continued
Ag (112) chalcopyrite films, lattice mismatch with (0001)CdS substrates 79−87012
Ag, epitaxially grown, on (001) Fe substrate, interface struct. 77−55470
Ag film growth on Pd substrate, interface cpd. form., AES study *(French)* 80−80131
Ag-(100)InP contacts, interface struct. 79−60922
Ag-Al (26 at.%), massive transform, $\beta \rightarrow \zeta$, crystallography and morphology 80−97475
Ag-Au, pseudoalloy behaviour at interfaces, grain boundary diffusion 80−6567
Ag-InP interface, AgP_2 formation during sintering 80−65309
Ag-liquid Ga interface, γ-phase interlayer growth, two-dimens. electron diffr. 79−19487
Ag-Pd, composition modulated foils, layer struct. and mech. props. 79−95300
Ag-Pt, formed by Ag electrodeposition on Pt film 77−16512
AgMg two phase bicrystal growth, orientation, interface struct. 80−60773
Al film, epitaxial growth on MgO, effect of weak interfacial interactions 77−1325
Al/Al_xO_y vacuum deposited laminates, struct. and mech. props. 79−28219
Al/Cu thin film couples, TEM study of intermetallic nucleation at interface 80−65305
Al-Al_2O_3, local struct. and interface states using surface soft X-ray absorpt. and photoemission spectroscopy 79−69595
Al-Cu (0.1 wt.%) alloy, unidirectional solidification, stability of planar solid liquid interface 77−86020
Al-Ge (100) interfaces, MBE prep. and geometrical struct., total refl. X-ray diffr. study 80−49531
Al-Ge(001) interface, struct., total-reflected X-ray diffr. 80−88441
Al-Mg/Al_2O_3 composites, interface phase, Auger and electron diffr. study 80−25646
Al-Si Schottky barrier solar cell, metallurgical reactions 77−72914
Al-SiO_2, surface reactions and interdiffusion, photoemission study 80−49532
Al-SiO_2 film-substrate interface, obs. of Al_2O_3 and free Si 78−91571
Al-SiO_2 interface, chem. struct., deposition conditions depend. 78−72007
Al-SiO_2 interface, stress and microstruct. via TEM 78−26797
Al-SiO_2-Si, void form. in Al interconnection lines at Si-SiO_2 boundaries 80−2476
Al-SiO_2-Si structure, Auger depth profiling and ion sputtering of interfaces 77−20200
Al-$TiSi_2$-n-Si struct., elec. props., charge transfer mechanism across $TiSi_2$-Si interface *(Russian)* 80−34515
Al-Zn alloy on mild steel 79−52466
Al-Zn alloys, interfacial stability of planar solid-liq. interface during solidification 80−104145
Al-Zn alloys, interfacial holes distrib. at beginning of interfacial instability in solidification 80−104146
Al-Zn-Mg alloy, welded, solute profiles at weld bead/parent metal interface 78−19942
Al-Zn-Mg/Al-Mg filler welds, weld fusion boundary structure 80−39459
(Al+Si)-Si thin films, struct. transitions and phase comp. 80−49537
$Al_xGa_{1-x}As$ epitaxial layers on GaAs, struct. study by scanning Auger electron microscopy 80−80110
$Al_xGa_{1-x}As$, LPE, effect of doping on interface morphology 77−81231
$Al_xGa_{1-x}As$-Au interface, Auger depth profiling 77−89657
$Al_xGa_{1-x}As$-GaAs abrupt LPE heterojunction, Auger profiling 77−85101
$Al_xGa_{1-x}As$-GaAs interface, Auger depth profiling 77−89657
$Al_xGa_{1-x}As$-GaAs n-n heterojunction, interface width determ. 80−49887
β-Al_2O_3/metal, field assisted bonding 80−45474
Al_2O_3-Al interface, AES depth profiling, appl. of tailored modulation techniques 77−15702
Al_2O_3-glass seals, diffusion of Al, electron microprobe study 80−107577
Ar, liquid-vapour interfacial width near central pt. 78−22931
Au, epitaxially grown bicrystal on (001) Fe substrate, interfacial dislocation behaviour 77−51622
Au film, interface reaction with n-type $Ga_{0.7}Al_{0.3}As$ and GaAs 80−39482
Au film, on Si and CaF_2 substrates, interphase coincidence boundaries 79−1560
Au film, on Si or CaF_2, oriented crystn., formation of coincidence orientations on interphase boundary 79−90922
Au/AuPd, bicrysts., in situ relax. of interphase interfaces 80−39455
Au/Fe epitaxial double layer system, interfacial dislocations 78−30847
Au-Ag, bicryst. thin film couples, interphase interfaces, TEM 80−70540
Au-Ni, composition modulated foils, layer struct. and mech. props. 79−95300
Au-Pb-In solder joints, layer growth, ageing 77−32764
Au-Pd, bicryst. thin film couples, interphase interfaces, TEM 80−70540
Au-Pt epitaxial film system, mismatch dislocations obs., electron microscopy 77−4268
Au-semiconductor system, room temp. interfacial reaction, AES obs. 78−18913
Au-Si contact, O determ. by SIMS, nuclear reaction and Rutherford backscatt. anal. 79−4482
Au-Si system, transition layer struct. form. and heat treatment influence, amorphisation obs. 80−54529
Au-Si thin film double layer, silicide form., electron diffr. study 80−80005
Au-TiC, multilayer struct., microhardness and elec. resist. 80−2950
Au-W, FIM obs. 80−65384
B fibre reinforced Mg, fibre-matrix interfacial reactions 80−20043
BN, contact reactions with Ti and WC-Co at high pressures 80−61029
Ba film, on SiO_2, interfacial chemistry, AES obs. 80−44434
CdGeAs, vertical Bridgman growth with control of interface shape and orientation 80−66420
Cd(S, Se) film grown on InP substrate, mismatch dislocations and lattice distortion, dangling bond density 80−84406
CdS-Al(Au) interfaces, bonding and interdiffusion, XPS obs. 80−80000
CdS-Cu_2S solar cells, microstructural study of heterojunction materials 80−93978
Cl_2, liquid-vapour surface, computer simulation 80−54478
Co-Mo, multilayer films, depth resolution determ. in Auger depth profiling meas. 79−78800
Co-Si film system, diffusion marker expts. 78−79824
Co-Si film system, interaction kinetics 78−79823
Co-Si interface, glassy layer, ellipsometric charact. 80−103589

interface structure continued
Cr film on Ni, prep. by evap. and ion plating, AES determ. of comp. profiles 77−89675
Cr/Au layered films, microstruct. and interdiffusion during ageing, 423 to 573K 79−46965
Cr-SiO_2-Si structure, solid-phase interaction between Cr and SiO_2, X-ray spectral obs. 78−10560
Cu (112) chalcopyrite films, lattice mismatch with (0001)CdS substrates 79−87012
Cu and Cu alloy, unidirectionally solidified, morphology of solid liquid interface and solute redistribution *(Japanese)* 77−21133
Cu on Fe (001) substrate, orientation relationship 80−65415
Cu substrate, ion induced intermixing of Au or Ag surface film 80−15420
Cu/Ni double layer evaporated film, misfit dislocation effect on strength *(Japanese)* 79−42425
Cu-mild steel explosively welded interface, SEM examination *(German, English)* 80−96746
Cu-Ni(Pd), composition modulated foils, layer struct. and mech. props. 79−95300
Cu_2S-Zn_xCd_{1-x}, heterojunction, composition meas. near interface using aqueous ion-exchange 80−29465
Fe, epitaxial growth on Au, two types of dislocation dependent on deposit thickness *(French)* 77−85109
Fe film, vacuum deposited on Au (111), interaction layer formation mechanism 80−54559
Fe-Ag-Cu melts, phase interface props., Cu influence *(Russian)* 79−51261
Fe-Al interface, O_2 content, reson. α-scatt. from ^{16}O 78−64778
Fe-Au (111) interface, nature of interaction layer 79−99433
Fe-fluoro compounds, triboelectric charging, effects of fluorinated compounds 78−60188
Fe-Ge system, cryst. growth forms and interface struct. 79−61515
Fe-Si (3 wt.%) layers, with ceramic coating, interface struct., electron microscopy and Mossbauer obs. *(Russian)* 79−28216
Fe_3O_4, orientation on α-Fe_2O_3 after low-temp. reduction, X-ray texture analysis *(French)* 77−39738
(Ga,Al)As, LPE growth of multilayered struct., explanation for meniscus lines on surfaces 77−76681
$Ga_{1-x}Al_xAs_{1-y}P_y$-GaAs quaternary heterojunction, misfit dislocation charact. by synchrotron radiation white beam topography 78−63771
GaAs (001)-Ag contact, surface stoichiometry and struct., and electronic surface states 78−95361
GaAs, anodised, interfacial reactions, Raman scatt. obs. 80−49544
GaAs based MOS capacitors, scanning photovoltage investigation 80−80396
GaAs MIS struct., elec. props., effect of interface As domains 78−88032
GaAs, plasma-grown oxides, in situ anal. using spectroscopic ellipsometer 79−79138
GaAs, polycryst., wet and dry oxides, comparative study by AES, SIMS and XPS 80−80116
GaAs-Al, X-ray total-external-refl.-Bragg diffr. study 80−34321
GaAs-$Al_xGa_{1-x}As$ epitaxial layer heterointerface, toroidal defect obs. 79−77933
GaAs-Al(Ga)(Ge), surface reactions and interdiffusion, photoemission study 80−49532
GaAs-anodic oxide interfaces, struct. and chem. props., Raman scatt. obs. 79−47168
GaAs-$Ga_{2.2}Al_{0.8}As$:Be, LPE, diffusion of Be into GaAs substrate 80−103517
GaAs-GaAs oxide interface layer characterisation by spectroscopic ellipsometry 80−50738
GaAs-Ge, heterostructure, zincblende-on-diamond type systems, MBE growth, (110) orientation as preferred orientation 80−80099
GaAs-metal Schottky barrier contacts, interface chemistry 79−74049
n-GaAs-metal Schottky barrier, ultrathin native oxide, thickness determ. from C-V and photoresponse meas. 80−70821
GaAs-oxide, interface layer determ. by spectroscopic ellipsometry 79−95275
GaAs-oxide interface, physical struct. 79−60644
GaAs-oxide interfaces, local atomic and electronic struct., high resolution XPS 80−49927
GaAs-ZnS p-n heterojunction, struct., multibeam electron microscopy obs. 79−11031
GaInAsP-InP DH layers, lattice deform. and misfit dislocations 79−19473
GaP, single-crystal, anodically oxidised layers, AES measurements 78−91556
GaP, VPE layer structures for LED's, SEM, and TEM obs. of dislocation density reduction expt. 80−100425
GaP-Si, heterostructure, zincblende-on-diamond type systems, MBE growth, (110) orientation as preferred orientation 80−80099
GaSb-Au contacts, interface struct., technology rel. to elec. props. *(German)* 77−72915
Ge (110) surface, sublimation of deposited GeS film, LEED meas., structural transitions 77−59195
Ge, interface structural model between amorphous and crystalline phase 78−63941
Ge-GaAs, heteroepitaxial systems, misfit dislocations obs. using HV electron microscopy 80−100242
Ge-GaAs heterojunction, electrostatic dipole shifts contrib. to valence band discontinuities 79−51657
Ge-GaAs heterojunction, elec. and recomb. props., interface defect effects 80−80365
Ge-GaAs heterojunction, interface geometry, model 80−49879
Ge-GeO_2, MIS struct., electrophysical charact. 79−82680
Ge-Si, UHV-produced epitaxial structs., electrophys. props. 78−3060
Ge-SiO_2, MIS struct., electrophysical charact. 79−82680
Ge-SiO_2-Si_3N_4, MIS struct., electrophysical charact. 79−82680
Ge-ZnSe heterojunction, change in interfacial microstruct. on high temp. annealing 77−28242
Ge-ZnSe p-n heterojunctions, effect of interfacial condition on optoelectronic props. 79−24061
^{4}He, solid-superfluid interface, struct., surface tension 80−88380
^{4}He, solid-superfluid interface, roughening transition 80−103536
Hf film on Si substrate, ion-beam induced silicide form. 79−46718
Hg, liq.-vap. interface, density profile near triple point, X-ray refl. 78−75821
InAs, heteroepitaxial, far IR refl. and transmission meas., surface and interface effects 80−16044
interface structure continued
InAs, on GaAs, heteroepitaxial layers, compositional profile, AES 77−20212
InAs-GaSb superlattices, crystallography, Rutherford backscatt. and channelling obs. 80−49533
InGaAsP LPE heterostructs., interface grading, Auger depth profile 80−103585
$In_{1-y}Ga_yP$-GaAs heterojunction, VPE, energy band gap and lattice parameter, lattice mismatch effects 78−95345
In_2O_3-SnO_2/GaAs, solar cell, fabrication, charact. and interfacial chemistry 80−21401
In_2O_3-SnO_2/InP, solar cell, fabrication, charact. and interfacial chemistry 80−21401
In_2O_3-SnO_2/InP junction, ion probe analysis of chemical nature 79−73411
InP (001)-Ag, contact, surface stoichiometry and struct., and electronic surface states 78−95361
$InP/In_xGa_{1-x}As_yP_{1-y}$ interfaces, sputter-profiled, depth resolution degradation by cone form. 80−80094
InP-Al interface struct., low temp. interaction, AES study 80−107661
InP-Au contacts, conditions of fabrication that control interfacial microstruct. 79−42643
InP-$Ga_xIn_{1-x}As$-InP, DH fabrication, crack form. due to lattice mismatch 77−15704
InSb IR detector array, AES anal. of localised contaminants at interfaces 77−57391
KCl, molten, vapour-liq. interface, mol. dynamics model 80−54362
Li_3N thin film, vacuum evaporation on WO_3, retarded deposition 80−108351
MgO-CdO, interface, coincidence-site-lattice relations 80−103588
Mo-Mn-Fe-Si/Al_2O_3 ceramic seal, interfacial phases 78−72011
Mo-Si diffusion couples, $MoSi_2$ or Mo_3Si/Mo_5Si_3 form. 79−77836
Mo-Si film-substrate interface, reaction on heat treatment, silicide formation 80−79999
Mo-SiO_2-Si, Mo-Si pelicular structures, struct. transitions during vacuum thermal treatment *(Russian)* 78−95238
N_2, liquid-vapour surface, computer simulation 80−54478
NaCl-KCl system, interdiffusion, miscibility, Kirkendall effect 80−107568
Nb-Fe, formed on laser irradiation of Nb-Fe interface, Mossbauer spectra *(Russian)* 79−60560
Nb_3Ge, sputtered on Cu, film-substrate interface obs. by electron microscopy 80−65398
Ni film on Si, formation of Ni_xSi_y, effect of substrate nature 77−15703
Ni film on Si substrate, ion-beam induced silicide form. 79−46718
Ni on Fe (001) substrate, orientation relationship 80−65415
Ni, sputtered, on Si, annealing effects on transmission electron diffr. patterns, silicide form. 78−91562
Ni/Fe interfaces sputter profiling, by AES 79−15572
Ni-Al-Ta dendritic monocrysts., directionally solidified, coarsening kinetics 80−108425
Ni-Cr-TaC eutectic-like composite, obs. of interfacial diffusion by high resolution TEM 79−4432
Ni-Cr(Fe)(Cu) alloy, matrix effect in SIMS anal. using O_2^+ primary beam 80−76576
Ni-Ge-Au evaporated contacts on GaAs, TEM obs. 80−75449
Ni-Mo, multilayer films, depth resolution determ. in Auger depth profiling meas. 79−78800
Ni-Si(111), interface, reactivity and struct., ion channelling meas. 80−92788
Ni-Ti, near equiatomic alloy, TEM exam. of austenite-martensite interface 78−51401
Ni-V system, interdiffusion, kinetics of phase growth *(Russian)* 80−29230
NiO-Al_2O_3 reaction at film-substrate interface, Rutherford backscatt. obs. 80−59733
Pb chalcogenide films, epitaxial, orientation on fluorite struct. substrate 77−35824
PbS-Si heterojunction, struct. and comp. 80−54530
PbS-Si heterojunction, chem. struct., AES anal. 80−76115
$Pb_{1-x}Sn_xTe$ LPE grown heterostructures, dislocation etch pitch, interfaces 80−2023
PbTe-In contacts, fabrication and props. 80−60078
PbTe-PbSnTe heterjunction, misfit dislocations, etch pit and electron probe study 79−77926
$Pb_{1-y}Te$-$Pb_{1-x}Sn_xTe$ (x,y≲0.3), double heterostruct., LPE growth, heterointerface morphology 80−70550
Pd film, VPE growth on Au(111) 79−95297
Pd/Si interface, chem. and struct. props. during silicide form., AES and TEM obs. 80−49430
Pd-MgO, reaction and bonding, below MP of starting materials, obs. in TEM 77−21419
Pd-Si structure, epitaxial silicide growth, LEED and AES study 80−103590
Pd-SiO_2, reaction and bonding, below MP of starting materials, obs. in TEM 77−21419
Pt film on Si substrate, ion-beam induced silicide form. 79−46718
Pt-electrolyte interface laser speckle movements related to electrode pot., H_2 adsorb. 78−40052
Pt-$SrTiO_3$ (100) interface, struct. and electronic props., AES, LEED, EELS, and UPS study 80−24986
PtSi-Si, impurity effects 80−80037
Se film on brass, ESCA interface study 78−43269
Se-Ni-Mylar multilayered struct., interfacial bonding effect on adhesion, ESCA obs. 79−95274
Si based MOS capacitors, scanning photovoltage investigation 80−80396
Si, epitaxial film on sapphire, optical absorption and interface comp. profiles 77−12459
Si, interface structural model between amorphous and crystalline phase 78−63941
Si on sapphire, deposition kinetics and interface characteris. 79−28234
Si, polycrystalline, thermal oxide anomalous stress 80−93661
Si substrate, ion induced intermixing of Pd or Pt film 80−15420
Si, thin single crystal, MeV ion scatt. and channelling obs. of interfaces 80−50492
p-Si-Al, ohmic contacts, Si dissoln. and recrystn. effects, computer calc. 80−103749
Si-C interface on polycryst. Si ribbon, effect on solar cell efficiency *(French)* 80−54531
Si-Ge heteroepitaxial system, imperfections and morphology, electron microscope and electron diffr. obs. 79−42420

interface structure continued
Si-metal interface, silicide formation, interface marker technique obs. 80−59734
Si-Ni(Pd)(Pt) film struct., silicide form. He^+ back scatt. and X-ray diffr. obs. 79−51442
Si-PbS heterojunction, effect of Si substrate orientation on struct. and interface props. 80−80097
n-Si-Pd_2Si contact, interface struct. and Schottky barrier height, correl. obs. using TEM 80−100504
Si-$Pd_{80}Si_{20}$, amorphous, Pd_2Si layer form., shallow contact 80−103586
Si-Pt(Ni)(Pd), laser-induced reactions of metal films with Si, surface struct. obs. 79−19471
Si-refractory metal structs., interface modification by ion implantation 80−70475
Si-SiO_2, bonding at (111) interface, stoichiometry and kinetics, synchrotron radiation photoemission spectroscopy 80−24744
Si-SiO_2, fitting stress and its effect on vacancy generation and distrib. 77−28087
Si-SiO_2, morphology and electronic struct. 79−78194
Si-SiO_2, separation boundary charact., surface oxidation after Ar^+ bombardment *(Russian)* 79−15028
Si-SiO_2, Si lattice constraints on structure of interface states 77−20379
Si-SiO_2, transient region, SIMS and metal microscopy 77−85115
Si-SiO_2 abrupt interface form. by very high dose O^+ ion implantation 80−75253
Si-SiO_2 bonding layer, EPR exam. 78−15022
Si-SiO_2 interface, Auger sputter profiling and photoelectron spectroscopy obs. 78−10287
Si-SiO_2 interface, Auger sputter profiling 78−43254
Si-SiO_2 interface, backscattering-channelling study 80−34320
Si-SiO_2 interface, defects, intimate valence attenuation pairs 80−54132
Si-SiO_2 interface, form. and struct., AES obs. 79−56314
Si-SiO_2 interface, high-resolution electron microscopy study 78−56046
Si-SiO_2 interface, in MOS structure, effect of irrad. with low energy electrons *(French)* 77−55617
Si-SiO_2 interface, local at. struct., XPS obs. 80−20042
Si-SiO_2 interface, MeV backscatt. channelling meas. of Si monolayers 79−11020
Si-SiO_2 interface, props. variation in SiO_x region 80−49548
Si-SiO_2 interface, thermal SiO_2 sputter induced roughness, Auger sputter profiling study 80−75424
Si-SiO_2 interface, thermally grown oxide, spectroscopic ellipsometric anal. 80−107659
Si-SiO_2 interface layer characterisation by spectroscopic ellipsometry 80−50738
Si-SiO_2 interface morphology, P pileup effect, Auger sputter profiling 78−72006
Si-SiO_2 interface struct. by cross-sectional TEM, amorphous oxide layer 77−24487
Si-SiO_2 interface study by XPS 80−50507
Si-SiO_2 interfaces, local atomic and electronic struct., high resolution XPS 80−49927
Si-SiO_2 interfacial regions obs., by XPS, ultrathin oxide films 79−15039
Si-SiO_2 interfacial region on TCE/O_2 and CCl_4/O_2 oxidised Si, struct. and comp. 80−50741
Si-SiO_2 layer formation by O_2^+ ion implantation, interface struct. and C-V charact. 77−1142
Si-SiO_2 structure, alkali metal ion migration and accumulation, interface struct. 80−107574
Si-SiO_2 transition region width, SIMS depth profiling 80−39454
Si-SiO_2-Si structures, P, As depth profiles, ion microanal. *(Japanese)* 78−85251
Si-$SiO_2(Si_3N_4)$, interface layer determ. by spectroscopic ellipsometry 79−95275
Si-transition metal interface, silicide formation, book contrib. 79−1530
Si-transition metal silicide interface, chemical state, AES expts. 78−91767
Si-V interface effects in growth of VSi_2 thin films 78−2395
SiC, high period polytype at interface of two interacting spirals 80−20041
SiC, polytypic transform., interface struct. exam. by TEM 80−15033
SiC-SiO_2 interface, Auger anal. 78−95375
Si_yGe_{1-x}-GaAs, heterojunction, elec. and recomb. props., interface defect effects 80−80365
SiO_2/GaAs, interface reaction during high-temp. heat-treatments 80−88439
SiO_2/InP film/substrate system, interface formation during CVD, modelling 80−24764
SiO_2/InP interface formation, thermodynamic considerations 80−100529
SiO_2/Si interface, obs. of chem. struct. 78−27654
SiO_2-Al and SiO_2-Si in MOS, electrochemical obs. 78−2381
SiO_2-Si (n-type) interface, electrochem. etching 77−11799
SiO_2-Si interface, interaction of point defects, electron microscope exam. 77−7979
SiO_2-TiO_2 antireflection coatings, 1064 nm 150 ps laser pulse damage rel. to barrier layering and smoothness 79−14018
SiO_x ultrathin oxide on Si, struct. obs. by high-resolution electron microscopy 80−103592
SiON/GaAs film/substrate system, interface formation during CVD, modelling 80−24764
Sn/CU electroplated bimetallic films, interfacial reaction 80−96765
SnO_2 chemically sprayed antireflecting films on Si solar cells 79−72639
Ta-Nb-Ta sheet, interface topology, exam. method 77−72797
Te/Ag double films, interdiffusion and struct. modifications *(French)* 77−62682
Te-Ag thin film system, stress-relief appearance conditions 80−65416
Te-Au thin film interface, evolution, switching effects *(French)* 80−6660
Te-Bi thin film system, stress-relief appearance conditions 80−65416
^{122}Te-Au interface, target fabrication for cyclotron isotope prod. 77−83406
Ti film, ultra-thin, AES and XPS anal. 78−91573
α-β Ti Widmanstatten alloy interfaces, elastic interact. stresses, effect on plastic flow onset 80−104218
Ti-Al-V (6,4 wt.%), α/β interface phase, formation charact. 79−52272
Ti-Al-V (6,4 wt.%), α/β interface phase influence on tensile props. 80−30034
TiC, CVD coating on Co-bonded multicarbide substrate, SEM, RHEED, AES interface study 79−77927
TiC, RF sputtered film on steel, transition region 78−39956
interface structure continued
TiO_2-Ni (100) interface, electronic props., struct., comp., chemical bonding 80−84499
U_3Si-ZI_4 interface, 700 to 800°C, exam. using metallographic and local X-ray spectral anal. 79−90831
(V,Ti)C+(Ni,Mo) cermets, carbide-binder interface ledges 80−29283
β-VH, precipitation crystallography, TEM obs. 77−77480
W fibre reinforced Cu, interface porosity formation, on thermal cycling 80−30092
W-Cu fibre reinforced composites, interface shear strength, critical aspect ratio 77−4826
YIG, Al- and Ga-substituted, floating zone method growth, interface shape and horizontal variations of Al and Ga contents by electron pulse anal. 79−33929
ZnO-Si(SiO_2) interface, XPS and Auger LMM anal. 79−90893
ZnSe, VPE on GaAS, role of interaction between gas and solids *(French)* 77−62769
ZnSe/water, laser-induced damage in ZnSe 80−102746
ZnSe-Ge(GaAs)(mica) epitaxial heterostructs., growth struct. 78−43257
ZnTe:Ag, dislocation loops creation in region of interface 79−82210

interface tension *see surface tension*

interface vibrations *see crystal surface and interface vibrations*

interfaces, computer *see computer interfaces*

interfaces, mechanical *see mechanical contact*

interfacial energy *see surface energy*

interfacial tension *see surface tension*

interfacial waves *see surface waves (fluid)*

interference
see also interference (signal); interference (wave)
acoustic, eigenmode analysis of the interference patterns in reverberant sound fields 80−96112
general relativity, quantum mechanical one-particle state, interfering neutron beam expt. 80−95025
grey-scale US images, local diagnoses and artefacts identification *(German)* 77−86571
short-term recall, phonological interference effect 79−96537
statistical interference as maximal entropy state 77−61040

interference (signal)
see also crosstalk; electromagnetic interference
antennas, nonlinear interference, theory of EM scatt. by vibrator with nonlinear contact 80−1110
astronomical image-tube systems, effects of phosphor decay on time-modulated meas. 79−88602
atmospherics, sweepers modulation struct. in HF and VHF bands 79−5707
biopotential recording interference and motion artifact sources and suppression 77−81634
birth monitoring by cardiotocography, interference effect by infusion pumps *(German)* 78−85416
digitisation noise in Fourier transform IR spectroscopy and gain ranging 79−97448
dynamic bioradiotelemetry noise reduction methods 77−86672
ECG, grounded, resistance to coherent mains interference, exptl. evaluation 78−85419
EEG artifact detection technique for automated anal. 78−31941
electrodes, ECG, EEG, interfering signals arising by cable motion 80−41296
fibre optic systems, digital, error probability with inter-symbol interference and additive noise 79−89855
film-grain noise, low-contrast image detection 78−94370
foetal heart rate recording, interference due to infusion pump *(German)* 78−85414
lunar noise effect obs., on satellite links *(Japanese)* 80−82239
magnetic recorder, output characteristics rel. to carrier velocity fluctuations 77−26279
Mossbauer effect, coherence and interference 78−27123
nuclear multichannel radiometer automatic channel separating system *(Russian)* 80−58094
optical fibres, modal noise in multimode systems 79−46083
optical waveguide, signal distortion, intensity distrib., single and coupled waveguides 80−33202
pacemaker interference simulation by models 78−81069
patient monitoring, computer-aided, interference problems *(German)* 78−3628
plasma density IF phase meas. using three-mirror interferometer 78−75414
PWR temp. sensor response time charact., estimation by noise anal. method 79−59216
RF SQUIDs, extension to noise theory rel. to gravit. radiation detectors 77−87685
seismology, noise-resistance of optically generated correlograms *(Russian)* 78−40699
VHF and UHF radio reception, RF energy deposition in biological tissue 77−73541
VLF, sunrise modal interference over west-east paths 77−53296

interference (wave)
see also acoustic wave interference; electromagnetic wave interference
band counter, active laser interferometer, digital readout, automatic systems appl. 77−67492
beats, interference phenomenon demonstration 79−75307
education, diffraction grating and interference effects, electronic cct. analogue 79−9052
education, electron interference using standard electron microscope and electron biprism as interferometer 78−62005
electron interference effects, Lande approach experimental contradictions 79−49081
field emission electron beams, two beam interference 78−63002
field interface of moving particles in statistically inhomogeneous medium 79−6063
gravity wave interference with ocean EM current meter recordings 77−78456
low intensity interference effects, hidden variable theories 78−70009
neutron interference fringes due to gravitational potential, role of gravity in quantum mechanics 80−62495
phase evaluation by electron diffr. by electron interfs. *(German)* 78−74112
plane wave interference in inverse scatt. theory 78−57
quantum interference, gravitational and rotational effects 77−45734
seismic interfering wave separation problem soln. *(Russian)* 77−91042

interference continued
seismic signal separation from records by interference system spectral synthesis *(Russian)* 77−91043
seismic wave Weber function computation in the interference reflected-head wave amplitude 77−78117
seismic waves, interference method for lower mantle radial vel. anomalies identification 79−25209
seismic waves interference effects in thin layers 78−92780
seismology, statistical algorithm for interfering seismic wave correl. *(German)* 77−25787
surface waves, method for separation of interfering waves and dispersion comp. 77−73649
tsunami simulation, Hawaii, open boundary reflection interference 80−17232
Young's double beam interference experiment with spinor and vector waves 78−89363

interference spectrometers
100 GHz to 1 THz atmospheric emission and absorption meas. 79−34980
airborne far IR Fabry-Perot astronomical spectrometer 80−109371
anomalous dispersion by band shift method, interference max. position 79−75578
astronomical CCD spectrometer for 500 to 900 nm range 80−82207
atmospheric pollutant interferential detector 80−108830
atmospheric submillimetric-wave interferometric spectrometry 79−34979
atomic emission DC plasma multielement spectrometer, spectral interferences 79−100459
background spectral radiance and contrast in the 1.5 to 13 micrometer region 79−8694
beam splitter and reflection reducing coatings on ZnSe for 3-14 μm 79−76811
Brillouin spectrometer with high contrast and resolution, fully stabilized 80−57386
computer-controlled Gabry-Perot interferometer for Brillouin spectroscopy 79−40622
confocal interferometer light-scattering sample cell 79−6182
curved crystal spectrometer, geometrical aberrations analytical and numerical study 78−78002
demonstration of Fourier transform spectroscopy for students 78−57722
diaphragm scanning system for Michelson interferometer 78−12764
dispersive refl. Fourier interferometer, sample holders for use at 4.2K and 300K 79−30587
elastic parallelogram mechanism 78−16859
etalon-spectrograph system, improved resolution over wide spectral range 80−101843
Fabry Perot spectrom., transformation of interference orders 80−263
Fabry-Perot, instrumental function influence on spectral profiles 77−67503
Fabry-Perot, multilayer broadband dielectric mirror coatings 77−18101
Fabry-Perot, press. scanning, 15000-30000 cm^{-1} 77−82617
Fabry-Perot, separation between maxima of interference fringes, difference record calcs. 80−62731
Fabry-Perot, signal noise limitations in data retrieval, winds, temp. and emission rate 78−93763
Fabry-Perot, stable multipass, design and anal. 78−274
Fabry-Perot etalon, piezoelectrically controlled, linear scanning cct. 78−4704
Fabry-Perot etalons in series with filter, spacing ratios 77−79160
Fabry-Perot grid and conventional spectrometers, luminous flux amplification 79−26139
Fabry-Perot high resolution spectrometer for IR astronomy 79−53722
Fabry-Perot interferometer as refractometer 80−264
Fabry-Perot interferometer data inversion algorithm 79−75604
Fabry-Perot interferometers with 20 cm^{-1} free spectral range *(Japanese)* 77−87847
Fabry-Perot laser spectrometer, for nonlinear superhigh-resolution spectroscopy 78−49912
Fabry-Perot scanning interferometer with piezoelec. spacers, appl. to solar UV spectrum 80−12678
Fabry-Perot spectrometer, optimisation for min. uncertainties in Doppler widths (shifts) determ. 80−27350
Fabry-Perot spectrometer, pulsed plasma emitted line profile meas. for vel. determ. 79−41869
Fabry-Perot spectrometer, reference channel for path difference determ. of interfering beams 80−77882
Fabry-Perot spectrometer for airglow studies, with large aperture and high resolution 80−67424
Fabry-Perot spectrometer for solar vel. field meas. 80−90333
Fabry-Perot spectrometer instrumental function, HFS pressure effect determ. from absorption coeff. profiles 80−106299
Fabry-Perot spectrometer instrumental function determ., Voigt function assignation *(Spanish)* 80−52322
Fabry-Perot spectrometer luminous flux amplification 79−75600
Fabry-Perot spectrometer luminous flux amplification comparison 79−75601
Fabry-Perot spectrometer parameter evaluation, deconvolution methods 80−105705
far IR absorbent solid dispersive reflection meas., using Fourier spectrometer and cryostat 79−30580
far IR apparatus, absorpt. meas. of molecular solids at high press., 4.2K 79−30583
far IR complex reflectivity meas., automated asymmetric interferometer 79−30534
far IR Fourier transform spectrometry improvements 79−30582
far IR interferometric spectrometer, sampling comb generation and precision 80−47122
far IR modular Fourier interferometer construction, very high resolution 80−57401
far IR spectrometer with interference selective AM 78−86362
far IR transparent solid dispersive transmission meas., using Fourier spectrometer 79−30581
fast-scanning Fourier spectrometer automatic adjustment method 79−80705
Febry-Perot interferometer, with automated data acquisition and stabilisation system 78−70180
field-widened interferometer spectrometers 80−95146
field-widened Michelson spectrometer with no moving parts 79−93223
Fourier, UFS-01 high-resolution, for IR molecular investigations 79−35862
Fourier and Hadamard transform spectrometers comparison 77−5922

interference spectrometers continued
Fourier spectrometer, 0.010 cm^{-1} working resolution, 20 to 1200 cm^{-1} 79−75603
Fourier spectrometer, 714 to 1667 μm, InSb detector at liq. He temp., rot. spectra of mols. 77−83765
Fourier spectrometer, amplitude-phase characts. of electrical channels 78−82058
Fourier spectrometer, balloon-borne, using focal plane detector array 80−95147
Fourier spectrometer, effect of random errors in sampling interval on spread function 80−18020
Fourier spectrometer, electrodynamic drive system 78−82059
Fourier spectrometers, sinusoidal interference modulation and path difference control *(Russian)* 78−29176
Fourier spectrophotometer, for far IR thermal emission meas. 77−45900
Fourier transform, Doppler-limited high-accuracy, 10^6 samples 78−58068
Fourier transform, history, current status and commercial future 78−58072
Fourier transform, problems in optical measurements 79−85187
Fourier transform hologram spectrograph, parameters 78−37858
Fourier transform interferometric IR spectrometer, performance evaluation 78−29181
Fourier transform spectrometer, high resolution ruggedized 80−95152
Fourier transform spectrometer, rapid scanning, very high resolution, data processing aspects 80−95150
Fourier transform spectrometer, simplified, for on-line anal. appl. 78−58074
Fourier transform spectrometer performance, instrumentation for assessment 80−95165
gas cell, heatable long path for IR, of light pipe type, design and efficiency 79−58807
gas refractive index meas., 150 GHz to 6 THz 77−5892
grating spectrometers and spectrographs, design method 80−62742
high resolution, appl. to study of laser modal configuration *(Spanish)* 80−86458
high resolution, with Fabry-Perot cell, for visible and near UV *(French)* 77−57410
high resolution Fourier transform spectrometer, 0.005 cm^{-1}, for 0.6 to 100 μm spectral range 78−70204
high-resolution optical heterodyne spectrometer 78−82048
holographic grating, calc., for very wide field camera *(French)* 78−81547
instrument function of spectral devices with multiple diffraction 80−37093
instrumental response deconvolution for asymmetric spectral lines 79−58802
interferometer calibration for atomic and molecular transition wavelength meas. 79−80696
interferometer-grating spectrograph for high resolution spectroscopy in middle UV 78−77490
IR, interferogram data acquisition interface *(German)* 77−87854
IR analyser, single-component, based on attenuated total reflection technique 78−58074
IR and mm wave techniques, for Cosmic Background Explorer Satellite 78−49344
IR Fourier spectrometers, grid polarisers 80−105724
IR interferometric spectrometer, slow scan, resolution and performance 80−42274
IR Michelson interferometer on Voyager 80−77290
IR multidetector spectrometer for atm. temp. sounding 79−25365
IR spectrometers, dispersion and FT interferometric types, comparison 77−82624
IR spectrophotometers, grating and FT types, rel. advantages of interferometers and monochromators 78−16861
IR tunable diode laser spectrometer, techniques and calibration with HCN ν_2-lines 79−71542
lamellar grating Fourier spectrometer for sub-mm and mm spectroscopy *(Japanese)* 77−67504
lamellar grating interferometer, for optical props. meas. of solids in far IR 79−58774
lamellar-grating Fourier transform spectrometer, high resolution, for submm. region 78−70203
large angle laser interferometer for 'curved' crystal spectrometer, precision 78−77973
laser spectrometer, high-speed, high resolution, for shortwave absorpt. spectral meas. in gases 79−54201
laser wavelength comparison with standard using interferometric digital wavemeter 77−162
linear motion gas bearing for Fourier spectrometers 80−31893
liquid complex permittivity meas., 100 GHz to 18 THz 77−8490
Lummer-Gehrcke interferometer for spectroscopy of dielec. films 77−5898
Martin-Puplett interferometer, use as Fourier spectrometer and for OTF meas. 78−70179
MATEC (matched tandem etalon camera), appl. to auroral obs. 80−101442
Michelson Fourier spectrometer modified for far IR spectroscopy 78−45741
Michelson interferometer, all-refl., for far IR Fourier spectroscopy 78−70205
Michelson interferometer for balloon-borne IR spectroscopy 80−51654
Michelson interferometer for Fourier transform. IR spectroscopy 78−49914
Michelson interferometer misalignment nonlinear phase errors 79−30535
Michelson interforometer, form. of bands of equal thickness as function of mirror and beam splitter positions 80−52298
Michelson type Fourier interferometer and gaseous molecular spectra 80−68275
Michelson-Fourier transform spectrometer for night airglow visible spectra 80−36424
microcomputer based scanning instrument controller, for Fabry-Perot interferometer 78−93764
moderate-resolution spectrometer with interf. selective amplitude modulation, construction of prototype 79−30588
modular Michelson interferometer for Fourier transform spectrochemical meas. 78−29177
modulation-interference spectrum analyser 77−79161
moire fringe analysis for interferometric grilles with Airy profiles *(Spanish)* 80−27354
monochromator, near IR meas. of parameters 79−75625

interference spectrometers continued
moving grating, analysis of spectral imaging capabilities 79−58799
multipass Fabry-Perot Brillouin scatt. spectrometer, optical alignment 79−35854
multiplexing, S/N ratio in high background 78−49339
multislit spectrometer for the night airglow observation 78−73542
near IR wide band spectroscopy, 27 MHz resolution 77−87853
optical background suppression by selective modulation interferometric spectrometer 79−97443
OTF measurement and image correction in spectroscopic system 78−37083
photoacoustic cell for mirror scan Michelson interferometer 80−68277
piezoelectric scanning of Fabry-Perot spectrometers, nonlinearities 79−6183
plane grating spectrometers, adjustment method 77−82611
plane-mirror two-beam interferometer analysis 79−2812
pupil-mounted opaque band effect on SISAM spread function 79−12871
rapid-scanning, appl. to low-level thermoluminesc. emission, use in archaeological dating 78−12773
real Fourier spectrometer, spread function determ. 80−31892
reflection dispersive Fourier interferometer window eliminating backlash error 80−57402
resolution of Fourier spectrometer, determ. using solid-state Fabry-Perot etalon 78−89569
rocket-borne cryogenically cooled field-widened interferometer for the 2 to 8 μm spectral region 80−95163
scanning Fabry-Perot interferometer for balloon-borne astrophysical obs. 79−35092
scanning interferometer designs for Fourier spectroscopy 79−75612
scanning interferometric multiplex photometer, airglow appls. 78−62216
selective modulation interference spectrometer, far IR 80−57397
selective modulation interference spectrometer, operation and props. 77−74519
selective modulation interferometric spectrometer, appl. to background suppression in optical target detection 79−97445
selective modulation interferometric spectrometer, simultaneous multiple monochromatic image obs. 79−75611
selective modulation interferometric spectrometer, theory, design 78−58054
SEMIDS, (selectively modulated interferometric dispersive spectrometer) anal. capabilities 77−44521
SISAM employing contracircular design, adjustment by prism system 80−31894
SISAM for amplitude spectrometry 80−27353
Sisam single-double pass spectrometer far near infrared 77−30208
SISAMs, sinusoidal interference modulation and path difference control *(Russian)* 78−29176
SISAMs, wavelength tuning by diffr. grating, interferometer type effects 79−26143
slit interference spectrograph, with diffr. grating and Fabry-Perot etalon 78−24866
solar interference spectrograph 80−109362
stratosphere trace molecule Fourier transform spectrometer optical design 80−82099
Tokamak far IR Fourier transform spectroscopic Michelson interferometer 80−59294
twin hollow cathode interferometer-spectrometer, strongly cooled, imaging system *(German)* 77−61143
Twyman-Green Fourier transform spectrometer alignment, for high temp. reflectivity meas. 79−17498
variable-thickness cell for liquid MM-wave Fourier transform and laser spectroscopy 80−57403
wavelength-modulating spectrometer implemented with photovoltaic photodiodes, comments 80−98981
wide-field spectrometers with selective interf., limiting value of gain 79−54203
X-ray interferometric moire pattern, analyser B diffusion effect *(Russian)* 79−44994

interference spectroscopy
see also Fourier transform spectroscopy
aliasing distortion in power spectra, digital processing of interferograms 77−45904
amplitude and phase spectra synchronous detection, using double-beam interferometer *(Russian)* 79−44937
anomalous dispersion near absorpt. line, meas. using interference fringes shift 77−34033
atmospheric temp. sounding with partially scanned interferograms 77−41176
atomic absorption spectra, anomalous dispersion meas. by interference fringe shift 77−71891
axial patterns diffracted from optical pupils, Fourier analysis of Fabry-Perot spectrograms 79−27188
background rejection method, for remote sensing using Fabry-Perot interferometers 77−71384
Brillouin spectra, multipass Fabry-Perot spectroscopy, linewidth correction 77−59583
coal and mineral content characterisation by Fourier transform IR spectroscopy 80−104474
coherent anti-Stokes Raman spectra of crystals lacking symmetry centre, cancellation by nonresonant background 79−14039
dispersive Fourier transform spectroscopy, mode of operation of polarising interferometer 78−78003
dispersive reflection spectroscopy using commercial Michelson interferometer 77−45903
Doppler free two photon resonances, optical Ramsey fringes 78−29167
Fabry-Perot etalon fringes, tunable diode laser source 77−18917
Fabry-Perot interferometer, far IR spectroscopy 80−9054
Fabry-Perot interferometer, instrumental convolutions, linewidth anal. determ. 80−31904
Fabry-Perot interferometer in far IR spectroscopy 80−27361
Fabry-Perot spectrograph, self-scanned photodiode array for image detect. *(French)* 80−73465
Fabry-Perot tandem and multipass interferometers, review 77−34038
faint Raman scatt. recording by interference contrast system 79−67393
far IR complex refr. index spectra determ., new method, for transparent solids 77−28566
far IR interferometry, (1950-76) 78−4456
far IR spectrum determined from Fabry-Perot interferogram 79−2840
Fourier decomposition technique appl. 77−49784

interference spectroscopy continued
Fourier interference spectrometric detection of atmospheric pollutants 80−35813
Fourier interferometer for IR line emission obs. of molecular clouds *(Italian)* 79−48679
Fourier spectrograph with wedge fringes, method using spectrum recorded in parts *(German)* 77−41698
Fourier spectrometric absorption meas. method 79−49300
Fourier spectrometry, optimal apodisation 80−99641
Fourier transform, comparison of refl. and refr. optics in condensing element of two-beam interferometer 78−77968
Fourier transform IR spectroscopy, multiple order spectra 77−74527
Fourier transform spectroscopy of imperfect blackbody sources 77−38032
Fresnel reflection coeff. of 3-phase system determ. by modulated reflectance spectroscopy and interferometry 77−82621
Galatry profile convolved with Fabry-Perot instrument function 77−78642
high resolution spectroscopy *(Chinese)* 77−67502
high resolvance interference spectrometry, visible spectrum 79−26145
hook meas. in wall-stabilised arc 78−13628
hook vernier method 80−31880
hypersonic flow, excitation temp. meas., hook method 77−58200
interferometric data from GC Fourier transform IR spectroscopy, functional group anal. 80−89548
IR ATR-matrix spectroscopy, interference-enhanced, appl. to 1,2-difluoroethane in Ar matrix film 79−9248
IR high temp. amplitude-phase spectroscopy, heater cell 79−35860
IR matrix interference enhanced attenuated total reflection spectroscopy, new technique 79−21823
IR spectroscopy-gas chromatography data, chromatogram reconstruction method 78−35737
laser pulse autocorrelation by optical processing of Fabry-Perot spectrograms 80−58465
laser wavelength, comparison of 2 beams, two-wave interference, book contrib. 78−9408
line deconvolution by Fourier analysis 79−12861
liquid complex refractive index, 5 to 500 cm^{-1}, Fourier transform interferometric determ. 77−13798
matched filtering, real time spectral recognition 78−37822
multi-pulse spectroscopy with Ramsey fringes, resolution and signal strength 78−82869
narrow linewidth meas. using Fabry-Perot interferometer of limited resolution 77−26408
noise reduction by averaging over optical path 77−18080
nonlinear processing of interferogram 78−89553
nuclear double resonance interference spectroscopy, appl. to ^{23}Na satellites in $NaNO_3$ 79−4745
optical Ramsey fringes in two-photon spectroscopy, time delayed pulsed Doppler free technique 78−82708
optical screw, path difference meas. and control device, anal. of periodic errors 78−77972
phase fluctuation optical heterodyne spectroscopy for molecular trace detect. 80−68266
photoacoustic rapid-scan Fourier spectroscopy and methyl alcohol interferograms 79−30585
power transmission spectrometry, use of approx. expressions 80−98982
Ramsey fringes in saturation spectroscopy 78−82868
Ramsey fringes in spectroscopy without Doppler broadening *(French)* 77−50560
range resolved Brillouin scattering using pulsed laser 80−38055
Rayleigh lines in presence of elastic scatt., Fabry-Perot expt. 78−4703
reflected light phase shift meas., complex refl. index determ., IR region *(French)* 77−87812
refractive index determ. from spectrally resolved interference pattern 77−49763
sampling error investigation, expt. 79−75613
saturable reflection spectroscopy, interference phase shift 77−2696
saturated absorption optical Ramsey fringes 79−54204
saturation spectroscopy, improved S/N ratio 78−70193
saturation spectroscopy using Jamin interferometer 78−74079
short pulse spectroscopy 79−54191
SISAM, diffracted light from grating affecting modulation 79−6187
solar rotation induced Doppler spectral shift meas. by scanning Fabry-Perot interferometer 80−77298
spectral line profile recording, high resolution, using Fabry-Perot interferometer and monochromator 80−42268
subnanosecond pulses, stretching and spectroscopy using Fabry-Perot interferometer 77−42555
Tokamak electron cyclotron emission spectrometry by plasma-scanned Michelson interferometer 79−32814
TV recording of interference images, spectral line contours 79−2833
water optical constant submillimetric wave meas. 79−33656

interference suppression
see also echo suppression
60 Hz harmonic eliminator, for biomedical signals 78−77124
acoustic noise in speech, nonstationary, reduction using LMS adaptive noise cancellation 79−64414
acoustic noise in speech, suppression using spectral subraction algorithm 79−64413
acoustic noise in speech based on spectral noise subtraction method 79−64415
acoustic signals, matrix formulation of coherence rel. to unwanted signals removal 77−46831
adaptive filter based on SAW monolithic storage correlator, appl. to CW interf. suppression 78−87208
amplifier, phase-sensitive, appl. to interference suppression and light detection *(Czech)* 78−86331
array processor for noise and interference suppression 77−23815
array processors for noise and interference suppression and signal-to-noise resolution enhancement, error corrections 78−30132
artifact-free electrodes for recording biopotentials in strong EM fields 78−40452
astronomical plates deconvolution by maximum entropy, appl. to M87 jet 80−62032
asynchronous cardiostimulators, increasing interference immunity 80−3868
atmosphere numerical model, modified forward- backward scheme for two-grid-interval noise 80−26575
automobile ignition RFI suppression at distributor rotor gap 79−55586

interference suppression continued
avian heart rate meas. using autocorrel. techniques 78−31989
bioelectric potential smoothing using controlled filter 78−40357
bioelectrode motion artefact model and artefact reduction by amplifier input stage design 80−56261
biopotential recording interference and motion artifact 77−81634
biotelemetry interference minimisation techniques *(Russian)* 79−29685
bolometer, using cooled low-noise, preamplifier 78−4698
computed, low-dose X-ray imaging system 80−98092
computerised tomography, non-linear smoothing filters and noise struct. 80−17118
computerised tomography, X-ray filtration, noise and artifacts 80−17119
decrepitometric recorder, noise interference suppression via electronic filter *(French)* 79−48571
demand pacemaker interference sensing functions 78−57123
demodulation system, microprocessor based 78−44627
dental drill with noise, vibr. radiointerference reduction 78−85450
detector array spatial noise reduction, controlled lateral shifts 80−53436
deterministic signals spectral anal., noise reduction using nonrecursive technique 79−58112
diagnostic probe for intense electron beams, noise reduction 78−12787
discharge-flow systems, noise reduction in EPR studies 79−39256
double-beam interferometry with optical background suppression 79−75576
dynamic bioradiotelemetry noise reduction methods 77−86672
dynamic spatial filtration of coded optical image signals from noise 80−95826
ECG, computerised, time-selective filtering 80−89895
ECG, grounded, standardisation of resist. to external cophasal power line interference for isolated patients 78−57085
ECG ambulatory monitoring, adaptive algorithm for noise rejection 79−66571
ECG fine structure analysis by noise reduction *(German)* 78−73268
EEG computerised artifact rejection, contamination by drowsiness 77−90932
electron micrograph optical and digital spatial freq. filtering 78−70231
electron microscopy, microdensitometer−computer correlation analysis of ultrastructural periodicity 80−85553
electronic circuit, pulse duration methods threshold sensitivity anal. *(Russian)* 78−45593
EM wave absorber with good reflection characts. at both normal and oblique incidence, synthesis 80−32891
evoked potential estimation, method for evaluation of Wiener filtering method 78−24190
evoked potential optimal filtering in sequential range *(German)* 78−85401
exercise ECG analysis, noise-impervious pattern recognition approach 78−7515
extracellular action potential recording, interference suppression 78−61294
fibre optics, modal noise suppression by dithering laser's operating point 79−94357
finger tremor amplitude and freq. artefact reduced routine meas., portable equipment *(German)* 78−85407
foetal ECG adaptive real-time noninvasive extraction using near-orthogonal functions 78−28110
foetal heart rate variability anal. using spectral anal. 78−28111
geomagnetic field changes determ., noise reduction techniques 80−26636
geomagnetic noise reduction, appl. in field gradient meas. in Colorado 77−29249
geophysical EM sounding using multicoil II airborne system, geologic noise reduction 80−51554
GEOS, booms/mechanisms for equipment protection against interference 78−4073
gravitational force on electrons meas., elec. and mag. field effects reduction 77−30080
high-voltage vacuum feedthrough, noise pick-up screening 78−24814
holographic reader-copier development and speckle suppression 79−81395
improved effectiveness of differential circuits used to suppress low-frequency noise 79−52608
IR background suppression algorithm 78−77985
IR staring mosaic sensor background suppression and tracking 80−86415
LF noise suppression in thermal viewing system 78−82035
light feedback suppression, from optical fibre into diode laser 79−1004
linear dichroism measurement, fictitious signal elimination via polarisation scrambling 78−4683
lung compliance loop recovery eliminating cardiac interference by digital filter 79−20570
magnetometers, induction-coil, optimisation theory at audio and higher freqs. 79−85156
magnetotelluric measurements, noise bias elimination using remote mag. reference 79−88245
marine seismograms, source signatures debubbling 79−16692
maximum entropy method, accuracy improvement via autocorrel. method 80−56712
microscopy, signal-to-noise enhancement by superposition of bright-field images obtained under different illumination tilts 80−6329
Mollenstedt electron vel. analyser high-order energy loss lines removal 78−93786
MOS capacitor, TSC meas., suppression of meas. interferences from interface states and mobile ions 80−29479
multiplex holographic representations of space-variant optical processors 80−48192
myopotentials, prevention of unipolar demand pacemaker inhibition 77−81709
natural speech interference separation technique 79−94417
NMR, use of noise-reduction filter for resolution enhancement 80−73403
noise compensation in Fourier spectrometer, using improved InSb photodiode preamplifier circuit 80−73474
noise suppression circuit for automatic flaw indicator 79−5111
optical background suppression by selective modulation interferometric spectrometer 79−97443
optical background suppression technique in double-beam interferometry 79−97428
optical communication using two-photon laser, optimum control of quantum noise 78−71049
optical fibre communication systems, digital 77−65631
optics, spatial frequency plane filtering by dynamic coherent illumination 80−95825
orthotics parameter assessment based on telemetric heart rate monitoring, paediatric patient appl. 78−31974
oscillator, band I, 10 GHz, with noise compressed by acoustic delay line *(French)* 78−16818
plasma emission spectroscopy, background reduction method using flame atomic absorpt. 79−16069
positron focused tomogram object reconstruction 78−40314
radar reflection from clouds and clutter target, broad-band noise technique 80−51454
radio astronomy, interference-excising correlator 79−75110
radiocardiography, equilibrium left ventricular ejection fraction determ., background noise estimation 80−94365
radioisotope imaging, digital low-pass filtering, random noise removal 77−5065
Raman spectra, time-resolved, fluoresc. suppression 77−53984
random nucleated halftone screen 78−62192
Reticon spectrophotometer at Asiago Observatory, data anal. procedure *(Italian)* 80−98565
RF mass spectrometer, background current elimination, using energy filter, expt. results *(Japanese)* 80−82844
RFI enclosure for Coulter Counter, design and construction 79−96721
satellite imagery, filtering to remove cloud cover 77−56744
satellite IR pictures, random noise reduction and oceanic features enhancement and extraction 79−5682
SEASAT-A satellite intersystem interference minimisation 78−49294
seismic digital signal detect. system *(Russian)* 77−29515
seismic linear multichannel systems for regular waves separation, random noise attenuation *(Russian)* 79−39922
seismic optimum stacking filters in suppressing uncorrelated noise 77−64216
seismic prospecting, minimisation of distortion caused by geophone-ground coupling 79−44256
seismic records, surface multiples suppression 80−56402
seismic signal interference separation using least squares method *(Russian)* 78−15969
seismology, comparative evaluation of methods for multiple waves suppression *(Russian)* 78−40515
sonar, interference rejection by amplitude shading of transducer arrays 77−62094
sonar, vertical sidelobe suppression in cylindrical arrays 77−46848
space geodesy, twin probes method for atmospheric drag elimination 79−25443
speech communication systems, narrowband, frequency domain noise cancelling preprocessor 79−68511
stimulus artifact suppression, sample and hold amplifier system 78−77163
submillimetre astronomy, sky emission and absorpt. noise reduction 77−41308
superconductive gradiometers, for measuring magnetic effects of geophysical origin 80−101463
synchroniser clock circuit, improves signal-to-noise quality of evoked response measurements 78−24155
tectonomagnetism, improved signal discrimination and volcanomag. effect at Kilauea, Hawaii 79−92629
TEM, high resolution, low-noise B supports 80−8236
TEM images of dislocation core, optical filtering for noise removal 80−107254
transducer, technique *(Polish)* 77−54837
transducer flow noise, rejection using coherence function method 77−84067
transient stimulated scattering, phase locking 80−53378
underwater acoustic communications, swept carrier method for multipath interference suppression 79−3835
underwater sound, cancellation of turbulent boundary-layer press. fluctuations 77−88978
US attenuation reconstructive tomography 80−30822
vertical ionosonde receivers *(Polish)* 78−88950
visual evoked cortical potential meas., signal optimisation using Kalman filter *(Japanese)* 80−72348
voice digitizer, linear predictive coding, with background noise suppression 79−64417
H I emission at high galactic latits., 21 cm line profiles correction for antenna stray radiation 80−51844
$LiNbO_3$ 400 MHz saw filters 79−23158

interferometers
see also acoustic wave interferometers; electromagnetic wave interferometers; interferometry
double Josephson junction interferometer, dynamics 78−68118
electron double crystal interferometer 78−83687
electron interferometer, modified Marton type 78−37111
fast interferometric chopper for neutrons and X-rays 78−82088
Josephson symmetric two-junction interferometers, self-induced reson., theory 80−107962
laser, for sensing of respiratory sounds 77−90872
Mollenstedt-Duker electron biprism, use of Wollaston wire 78−54512
neutron interferometer, rotating, phase shift due to Doppler effect 80−18006
neutron interferometer, two cryst. component 79−46512
neutron interferometer, with two cryst. components, construction 78−83654
neutron interferometer expt., role of gravity in quantum theory 80−86176
neutron Michelson interferometer for ultracold neutrons 80−33858
neutron perfect crystal interferometer, coherent scatt. length meas. 79−46517
neutron prototype interferometer at Grenoble high flux reactor 79−19127
solid state pulse interferometer to measure ultrasonic velocities in crystals 79−23154
two-junction Josephson interferometer, reson. phenomena, anal. 78−47910

interferometry
see also acoustic wave interferometry; electromagnetic wave interferometry; holographic interferometry; interferometers
calibration two-coordinate measuring devices *(German)* 78−89433
DNMR technique, AX spin system relax. times 78−6603
electron, appl. to Au-Ag contact PD meas. 77−32069

interferometry continued
electron beams interference, Bohm-Aharonov experiment without an electron microscope 79−894
electron interferometry for thin film studies 80−6328
epitaxial layers, on monocryst. supports, degree of disorientation, determ. by interferometry *(Russian)* 80−24748
neutron, determ. of scatt. lengths, and magnetic spin rotations 77−24248
neutron, exact spin rotation by precession 80−32584
neutron, spin rotation and phase shift, polarisation props. 77−18763
neutron and X-ray, principles, techniques and appls., book contrib. 78−42862
neutron interference, gravity and inertial effects, principle of equivalence at quantum level 80−77669
neutron interference fringes due to gravitational potential, role of gravity in quantum mechanics 80−62495
neutron interferometer and fundamental expts. 79−45000
neutron interferometer expt. as search for nonlinear variants of Schrodinger eqn. 79−92984
neutron interferometry, determ. of neutron phase wave, obs. of spinor periodicity 79−59113
phase detection using LSI-11 microcomputer and high-speed digital techniques 78−71545
Schrodinger equation, nonlinear variant search using neutron interferometry 80−52064
X-ray interferometry, appl. of synchrotron radiation 80−90954

intergalactic matter
see also clusters of galaxies; galaxies
Abell 1367 cluster, intergalactic matter rel. to peculiar radio sources obs. 79−2574
Abell 2118 cluster, extent of hot intergalactic gas 78−86021
Abell 2256, rich cluster, steep-spectrum radiosource obs. 79−9016
Abell 2256, X-ray cluster of galaxies, radio props. rel. to intracluster environment 80−36726
Abell 401, X-ray galaxy cluster, hot intracluster gas rel. to radio emission distrib. 80−98731
Abell clusters, intracluster medium parameters from complex radio sources obs. at 2.7 GHz 79−92881
abundances, gas loss from S0 galaxies 78−28784
accretion by the galaxy in solar neighbourhood 80−67863
accretion of gas having specific heat ratio 4/3 by a moving gravitating body 79−70951
accretion wake model of galactic and quasar jets in clusters 79−71135
anticorrelation rel. to dark intergalactic matter in galactic haloes 79−2567
Arp 205 (NGC 3448 and UGC 6016), aperture synthesis obs. of H I 79−53916
AWM 4, poor galaxy cluster, extended X-ray emission detect. surrounding cD galaxy (NGC 6051) 80−51884
background radiation in far-UV as probe of dense hot intergalactic medium 79−92897
black holes, primordial, number density limits from galactic radio spectrum 80−62179
3C 105, struct., polarisation and mag. field direction 79−35413
3C 132, 3C 192, radio galaxies, study of bridges rel. to intracluster medium props. 77−91658
3 C 31, isothermal gas cloud rel. to radio jet brightness and shape 79−25741
4C 32.69, quasar, radio jet confinement by circum-quasar hot gas press. 80−105375
3C 351, quasar, interaction with intergalactic gas 80−105376
capture by galaxies, theory of disc accretion in soft potential well 80−8532
charged intergalactic medium, cosmological implications 79−25766
clouds and QSO absorption lines 80−62311
clouds rel. to origin of universe *(French)* 80−67874
cluster X-ray sources evolution, subcluster collisions 79−53915
clusters of galaxies, gas content meas. by obs. of microwave background at 10.6 GHz 78−96551
clusters of galaxies, hot gas distrib. 79−17089
clusters of galaxies, hot gas X-ray emission rel. to radio sources props. 78−12398
clusters of galaxies, intergalactic background rel. to dynamical evolution 78−12384
clusters of galaxies, intracluster gas and galaxies dynamical interaction 77−13473
clusters of galaxies, intracluster gas dynamical collapse and hot plasma form. 77−22322
clusters of galaxies, numerical models for X-ray line emissions 78−8149
clusters of galaxies, radiative regulation of gas flow, X-ray source model 78−4371
clusters of galaxies, unborn, microwave and X-ray emission 78−8131
clusters of galaxies, viscosity rel. to intracluster gas heating 79−9011
clusters of galaxies, X-ray emitting gas evolution 79−40266
clusters of galaxies, X-ray temps. rel. to bremsstrahlung and emitting gas mass 77−91668
clusters of galaxies missing mass problem, evolutionary approach 77−37658
clusters of galaxies rel. to infalling intergalactic matter and X-ray luminosity 78−93487
collapsing pre-galactic H gas cloud, local stability, linear perturbation anal. 80−82513
Coma, Perseus and Virgo clusters, X-ray emitting intracluster gas models 77−45577
Coma cluster, diffuse background light photographic meas. 77−91655
Coma cluster, intergalactic mag. field from radio flux spatial distrib. 77−33686
Coma cluster, intracluster mag. field from halo radio source meas. 78−86027
Coma cluster, mass segregation and missing mass 77−45581
Coma cluster, photoelec. surface photometry, intergalactic gas luminosity upper limit 77−64858
Coma cluster, photometry of intergalactic optical surface brightness 77−87550
Coma cluster of galaxies, origin and transport of electrons in halo radio source 77−26073
Coma cluster X-ray source, X-ray brightness distrib. prediction 79−92896
Coma galaxy cluster, low energy X-ray absorpt. obs. 78−86025
Coma galaxy cluster, relativistic electrons streaming at speeds above Alfven vel. 79−40068

intergalactic matter continued
cosmic rays of highest energy, diffusion from Virgo cluster 80−4208
dark cloud near ι Microscopii, galaxy counts re-examined 80−36710
dense hot gas, heated by exploding galaxies 78−4345
diffuse H I clouds as probes of hot intergalactic medium 77−5568
dust, effect on meas. of cosmological deceleration parameter q_0 77−5564
dust, extinction effects on quasar distrib. in visible 80−17651
dust, possible existence 77−53678
dust cloud collision with M82, dynamical evidence for Ne II 12.8 micron emission 79−17082
dust in galaxy clusters, evidence from Zel'dovich effect 78−54041
dust in M81 group, appl. to explosionless model of (M82) 77−33632
dust model for irregular galaxy M82, constraints on nature of intergalactic dust 77−87543
dust obs. near NGC 300 77−45553
dwarf nearby galaxies, search for intergalactic H I clouds 79−71126
dynamical evolution of hot intracluster gas from galaxies, Fe abundance in X-ray clusters 79−12530
electrically polarized Universe model 78−36738
enriched gas in clusters and dynamics of galaxies and clusters rel. to galaxy formation 78−77596
evolution in clusters of galaxies, model 80−85992
existence, relevance to galaxies origin and early evolution 80−17669
extragalactic matter, infall rate in solar neighbourhood from cosmic ray nucleosynthesis 79−17084
extragalactic radio sources, problems and advantages *(German)* 77−67134
Faraday rotation of polarization plane for extragalactic radiosources 77−26066
galactic evolution, effects of intergalactic matter, review 80−109543
galactic infall rel. to cosmic ray accel. 77−78583
galactic ring structs. form. by collisions with gas clouds *(Russian)* 78−93425
galaxies with radio tails, rel. to intracluster medium *(French)* 78−41054
galaxy bridges and jets, hydromagnetic break-up into aligned objects 77−49475
galaxy cluster relaxation effect on intergalactic gas and X-ray emission 80−46684
galaxy cluster X-ray sources, intracluster medium gas supply rate rel. to luminosity function evolution 80−62314
galaxy clusters, missing mass, N-body expts. 80−41904
galaxy clusters at cosmological distances, X-ray emission detect. 80−26993
galaxy superclusters, X-ray emission, Uhuru meas., intergalactic gas 78−41064
gas accretion onto collapsed objects, source of cosmic X-ray background 80−90581
gas cloud enveloping bound Abell 401-399 system, evidence from diffuse X-ray emission 79−25736
gas clouds, Local Group and Local Cloud of galaxies 77−91642
gas clouds, rotation measures, intergalactic magnetic field and cosmology 78−28800
gas envelopes round disk galaxies, infall and ejection 80−82483
gas in galaxy clusters, Compton scatt. of microwave background radiation 78−24575
gas in rich clusters of galaxies, origin and distrib. rel. to cluster X-ray sources evolution 78−28770
gas secondary ionization causing microwave background fluctuations *(Russian)* 78−36736
gas stream in M81-82 system, 2.7 GHz continuum survey 78−36691
gaseous halos rel. to cluster and galaxy evolution 80−17675
general problems 79−97068
graphite, pyrolitic, whiskers, absorpt. effects rel. to cosmic microwave background 80−94866
graphite whiskers, RF adsorpt. props. rel. to microwave background radiation 80−31357
H I associated with galaxies NGC 4631/NGC 4656, aperture synthesis obs. 78−54043
H I clouds, search in NGC 1023 and Canes Venatici II 79−35389
H I search in nearby groups of galaxies 79−30121
He II 304 Å line redshifted to 1450 Å in far UV background 80−41893
head-tail radio galaxies in poor clusters, radio and optical obs. 78−96530
head-tail radio galaxies velocities with respect to intracluster medium 78−49516
Hercules supercluster, evidence for intracluster medium 80−22092
high positive velocity H I clouds, spatial and vel. struct. 77−13442
high velocity clouds, evidence against intergalactic interpretation 77−41399
high-velocity H I cloud near M33, obs. rel. to M33 H I tail 80−12815
high-velocity H I clouds, map 80−26923
hot clumpy intergalactic medium emission contrib. to X-ray background 80−62335
hot gas formation by ejection from galaxy in early explosive era 78−45408
hot gas in clusters of galaxies, review 78−12374
hot gas in clusters of galaxies, temp. and entropy 80−17660
hot gas in distant richness class 4 clusters of galaxies, detection 78−12369
hot gas rel. to X-ray source clustering in nearby superclusters 78−41065
hot intergalactic medium, rel. to diffuse X-ray background spectrum from 3 to 50 keV 80−41916
hot intracluster gas, as source of clusters X-ray emission 78−12387
hot intracluster gas, Sunyaev-Zel'dovich effect in millimetric region 79−25765
Hydra I cluster, ram-pressure sweeping, optical evidence 78−93429
II Zw 70/II Zw 71, compact galaxies, H I maps, tidal interactions 78−96531
intercluster dust tests and CGCG selection effects 79−9012
intercluster medium, theory for expanding cosmologies 80−4426
intracluster gas, heating by relativistic electrons rel. to cluster X-ray and radio emission 78−57655
intracluster gas, origin and evolution, interaction with interstellar gas in cluster galaxies 78−45407
intracluster gas, rel. to cluster X-ray luminosity and galactic content 78−32585
intracluster gas, thermal bremsstrahlung model and X-ray luminosity function prediction 79−101208
intracluster gas flow patterns and X-ray emission 78−65705
intracluster gas in Abell 2029, X-ray emission rel. to SAS 3 obs. 80−82519

intergalactic matter continued
intracluster gas in Zwicky clusters, implications of cluster radio sources interferometer obs. 80−22099
intracluster hot gas, extent from cluster halos density and vel. distribs. 80−22122
intracluster hot gas, props. from OSO 8 X-ray spectra 79−25734
intracluster hot gas, search for extended X-ray halos in Perseus, Virgo and Coma clusters 80−56953
intracluster hot gas, X-ray source evolution 79−17133
intracluster hot gas, X-ray spectra and relationship to other cluster props. 80−22093
intracluster hot gas in compact groups, X-ray emission 80−90574
intracluster hot gas stability problem, role of massive photons *(Russian)* 79−44614
intracluster intergalactic medium, in review on clusters of galaxies 77−64862
intracluster matter, radio sources Faraday rot. obs. 79−75285
intracluster medium, influence on hot gas in elliptical galaxies rel. to head-tail radio sources form. 80−36703
intracluster medium, mass and metal abundance from elliptical galaxies chemical evolution 80−67843
intracluster medium, origin rel. to galactic coronae and quasar absorpt. lines 80−31355
ionised gas in clusters of galaxies, microwave search 80−82477
ionization during bright phase of galactic evolution 77−26065
ionized gas in rich clusters of galaxies, angular broadening of distant compact radio sources 79−35380
lenticular galaxies, H I 21 cm line obs. 79−67090
local mean mass density and galaxy clustering 78−45436
M82, intergalactic cloud encounter model 79−75279
M87/Virgo cluster X-ray source spectrum, 1.1 keV Fe line emission discovery 79−25758
Magellanic Stream, dynamics, origin theories and model fitting 77−33648
Magellanic Stream, high sensitivity obs., small-scale struct. 79−35385
Magellanic Stream, kinematics rel. to Hypergalaxy mass 77−5573
Magellanic Stream, models and tidal origin 77−91647
Magellanic Stream, observations and origin theories 77−33647
Magellanic Stream, origin and dynamics 79−44594
Magellanic Stream, possibly assoc. C star, visible obs. 80−77411
Magellanic Stream, simulation to estimate total mass of Milky Way 77−91622
Magellanic Stream, turbuelnt wake of Magellanic Clouds in galactic halo 78−69884
Magellanic Stream, vel. structure from H I obs. 79−97078
Magellanic Stream and adjacent HVCs, Jodreel Bank 21-cm obs. 77−91650
Magellanic Stream and galactic wakes 79−48904
Magellanic Stream and gas concs. in Local Group 77−91646
Magellanic Stream from LMC close approaches to Galaxy 77−91648
Magellanic Stream H I regions, fine struct., 21 cm obs. 80−90523
magnetic field, interpretation of rot. measures of extragalactic radio-sources 77−60836
magnetic field, rel. to galactic spiral structs. origin 79−25714
magnetic field interaction with hot intergalactic gas, magnetosphere existence 80−67876
magneto-ionic medium, upper limit to contrib. to radio sources rot. measures 77−5584
magnetoionic medium, rotation meas. 78−20906
matter-antimatter hydrodynamics, annihilation rate calc. 78−73780
Microscopium, proposed intergalactic dust cloud, photometry of RR Lyrae stars 80−56851
microwave background distortion by hot intergalactic medium 79−97107
microwave background obs. in direction of clusters of galaxies, cool ionized gas mass limit 78−41098
missing dark mass rel. to primordial star generation 78−61946
MKW 3s, poor galaxy cluster, extended X-ray emission detect. surrounding cD galaxy (NGC 5920) 80−51884
neutral clouds, collisions with galactic discs rel. to interstellar super-rings form. 80−98717
NGC2805, 2814, 2820 and IC2458, H I 21 cm obs. of close galaxy group 79−53917
NGC 1275, ionization and excitation mechanisms in surrounding filaments 79−71107
NGC 2146, peculiar spiral galaxy, extensive H I obs. 77−17676
NGC 315, NGC 6251, very large radio galaxies intergalactic mag. fields from 11.1 cm obs. 78−86014
NGC 4631 group of galaxies, intergalactic neutral H rel. to tidal interactions model 78−54059
NGC 4945, late-type spiral galaxy, evidence for infalling gas 80−109547
NGC 6251, isothermal gas cloud rel. to radio jet brightness and shape 79−25741
non-uniform gas at high z, spectral appearance 79−92898
nonspherical galaxy clusters, hydrostatic struct. of hot plasma and X-ray morphology, rel. to Perseus cluster rot. 79−35406
opacity rel. to pregalactic fluctuations visibility, upper limit on q_0 80−8717
Perseus cluster of galaxies, soft X-ray struct. rel. to hot gas distrib. 79−9009
Perseus galaxy cluster, low energy X-ray absorpt. obs. 78−86025
Perseus X-ray cluster, form. of optical filaments in cooling gas round NGC 1275 galaxy 80−67862
pressure gradient, determ. from double radio sources asymmetry and components flux ratio 80−67892
prestellar gas clouds, spectral lines prediction *(Russian)* 78−77628
primaeval hot gas clouds fragmentation and diffuse X-ray background radiation 78−28861
primary cosmic rays origin, intergalactic suprathermal grains, accel. mechanisms 79−25412
protogalactic gas cooling mechanisms *(Russian)* 79−17107
protogalaxy interactions in newly formed clusters rel. to luminosities, colours and intergalactic gas 78−41060
QSO absorbing cloud, model for redshift doublets 77−22325
QSOs directions, intervening primordial gas rel. to absorpt. line regions physics 78−57680
quasar absorpt. line problem, visible obs. 80−67899
quasar absorption line clouds, radiative accel. 78−57683
quasars absorption line problem, optically selected high-redshift objects spectrophotometry 79−25746
quasars absorption lines, survey in QSOs of small and intermediate emission redshift 80−31218

intergalactic matter continued
quasars absorption lines origin, evidence for cosmological hypothesis 78−57684
quasars extinction, rel. to Dirac cosmology and microwave background 78−8176
radiative accretion flow onto giant galaxies in clusters 78−93433
radio sources, double, intergalactic medium rel. to gas dynamics 79−67107
radio sources extended, dynamical evolution and intergalactic gas props. 79−88757
radio sources variable at low freqs., intergalactic scatt. rel. to microarcsecond struct. 78−16550
radiogalaxy interaction with intergalactic medium *(Italian)* 77−87562
radiosource structure and intergalactic medium 79−62921
reddening determ. method 78−54039
relativistic and non-relativistic dust grains, rel. to high energy particles in EAS 80−61975
relativistic and nonrelativistic gas flows, general symm. soln., low press. limit 77−9655
relativistic dust grains, as source of cosmic gamma-ray bursts 79−88764
relativistic electrons in intracluster space, hard X-ray spectra and gas heating 79−25735
Sculptor high-velocity cloud, 21 cm obs. 77−64843
shock waves, rel. to giant ellipsoidal shells around normal elliptical galaxies 80−86000
shock waves generated by galaxies and quasars at large redshifts 79−21442
Shostak high-velocity cloud, possible intergalactic gas cloud, H I obs. 78−32575
spherical clouds in hot gas, radiation effects on evaporation 77−78842
star formation before galaxies, missing mass soln. 78−57654
structure, evidence for hot clouds 77−67129
supercluster candidate 4U0134−11, no X-rays from hot gas 78−8164
superclusters, X-ray emission, matter infall 79−67106
supernova radio pulses, intergalactic scatt. and dispersion rel. to instrumental sensitivity improvements 78−40975
suprathermal grains, prod. by scatt. on intergalactic mag. fields 79−48911
temperature and density, determ. from interaction with extended H I regions around spiral galaxies 78−12354
temperature and ionisation structure, effect of UV stars 77−13455
thermal evaporation of gas within galaxies by hot intergalactic medium 77−41413
transition radiation from relativistic intergalactic dust grains 79−75272
twin jet model for radio trails 79−75290
Universe global structure and nonhomogeneous large scale mag. field *(Russian)* 77−82335
Virgo, Perseus and Coma clusters, Fe abundance from X-ray Fe line obs. 77−49485
Virgo, Perseus and Coma clusters, X-ray obs., spectral evidence for hot evolved gas 77−17695
Virgo cluster, evidence for confining environment for Virgo A (M87) from 610 MHz map 80−62302
Virgo cluster, intracluster gas interaction with hot interstellar gas in elliptical galaxy (M86) 80−90535
Virgo cluster, intracluster gas/galaxies interaction rel. to spiral galaxies H I deficiencies 80−62277
Virgo Cluster, M87 massive halo rel. to extended X-ray source model 78−28775
Virgo cluster, X-ray obs. of galaxies, rel. to dynamical evolution 80−26995
Virgo galaxy cluster, low energy X-ray absorpt. obs. 78−86025
X-ray background source possibility after heating by quasars 80−94898
X-ray clusters of galaxies, gas stripping from spirals 78−32586
X-ray clusters of galaxies, large-scale struct. 80−82524
X-ray clusters of galaxies, radio limits on ionised gas 78−89243
X-ray emission from rich clusters, clusters extended halos and superclusters, search 80−26988
X-ray emitting clusters of galaxies, spatial distrib. of heavy elements 77−91654
Zwicky clusters of galaxies, intergalactic medium rel. to radio sources props. 78−4378
C model abundance, X-ray absorpt. effects 80−62270
Fe mass and distrib. in intracluster space of rich clusters of galaxies 79−5895
Fe-enriched gas in clusters of galaxies, origin and evolution 78−93390
H I, improved limits for intergalactic intracluster gas in Coma cluster of galaxies 79−75276
H I, obs. in inner M101 group of galaxies 80−67885
H I bridge between M81 and NGC 3077, structure and kinematics 79−67093
H I cloud in NGC 1023 galaxy group, discovery and redshift 80−67886
H I clouds, search in radiogalaxies directions 78−12316
H I clouds search in Sculptor group of galaxies 79−30122
H I content of intracluster medium 79−5896
H I high velocity clouds, high sensitivity survey 78−65686
H I high-velocity clouds, intergalactic interpretation and adiabatic theory of galaxy form. 80−46677
H I in clusters of galaxies, search for broadband emission 80−46667
H I in field of elliptical galaxy NGC 1052, evidence from 21 cm emission mapping and line profiles 80−98719
H I in spectra of large-red shift quasars, consequences of neutrino rest mass *(Russian)* 80−105414
H I search in galaxy clusters 78−49544
H, recomb. kinetics in presence of low mass primordial black holes *(Russian)* 79−17152
H_2O, gravitational wave absorpt. by mols. 80−82189
O VIII emission line detect. from M87 in Virgo cluster 80−26977

intermediate bosons
γ-W^0 mixing as an alternative to unified weak-electromagnetic gauge theories 79−2966
annihilations prod. spin-1/2 and spin-0 pairs, weak effects 77−18219
axion, astrophys. implications of new light Higgs boson 79−22007
axion effect on two-dimens. CP problem 80−42358
axion emission in ^{12}C excited state decay 80−32235
axions and Higgs particles, astrophysical mass bounds 79−5745
bilocal gauge field theory 80−31986
charged Higgs boson in SU(2)×U(1) gauge field theory, production and decay 79−13015
charged Higgs boson properties; Weinberg Salam model 79−40719

intermediate bosons continued
charged vector mesons, Compton scatt. cross section meas. 79−22102
charmed meson lifetime, 6 dominance and W^+ exchange dominance 80−37254
chiral SU(3)×SU(3), ρ-meson as dormant Goldstone boson 80−368
classical Yang-Mills solns., W meson condensation, superdense matter composition symmetry 79−93292
colliding e^+e^- beams accelerator expts., 100 GeV, particle prod., weak currents, etc. *(Russian)* 78−58194
corrections, to spin $^3/_2$ heavy lepton decay 80−73761
current algebra theorems for U(1) Goldstone boson 79−89081
decay, neutrino number and isotropy of Universe in grand unified theories 80−85852
decay, QED and QCD radiative corrections, hadronic jets 80−73759
dim 5 and 6 operator mixing induced by Higgs scalars 80−86654
Drell Yan production of intermediate vector bosons, μ prod. in pp, $\bar{p}p$, $\pi^{\pm}p$ reactions 78−29364
dynamical pseudo Goldstone bosons, production and decay characts., colour interactions 80−22557
electron nucleus weak currents, atomic X-ray spectra, parity violation *(Russian)* 79−22642
electroweak gauge models with heavy W bosons, $SU_2\times U_1\times U_1'$ scheme *(Russian)* 80−86652
electroweak gauge models with sequential W and Z bosons 80−101971
electroweak theory in SU(2|1) 79−63402
exceptional groups, patterns of symmetry breaking 80−42356
fermion asymmetry of the Universe and the W condensate, Weinberg Salam model *(Russian)* 80−73087
fermion mass generation, regularisation 80−9090
fermion-fermion scatt., very high energy weak interaction effects 79−9327
gauge boson masses in flavour $SU_3\times U_1$ model, quark and lepton weak and EM interactions 79−97554
gauge bosons, unified field theory of weak interactions of leptons and quarks 80−22556
gauge hierarchies beyond the tree approximation 79−67470
gauge models of weak and EM interactions, quantisation and renormalisation of gauge theories, book contrib. 79−30669
gauge symmetry, dynamical symmetry breakdown, appl. to intermediate vector boson mass relations 79−54269
gauge theory, suppression of flavour changing effects from neutral spinless meson exchange 79−40716
Glashow-Weinberg-Salam model, one-loop corrections to vector boson masses 80−57548
goldstino couplings and neutral currents, mass relation for lepton and quark superpartners 79−75717
hadron resonance decay, intermediate vector boson and high energy weak interaction detect. 79−22012
hadronic matter, Pomeron and critical temp., Yang-Mills gauge boson pairs 80−22566
hadronic neutral current in neutrino interactions and single Z-boson hypothesis 79−54295
heavy Higgs boson decay in Weinberg-Salam model 80−95241
heavy leptons, weak gauge boson and neutrino trimuon prod. 78−4851
heavy Weinberg-Salam type neutral Higgs boson, possible LEP prod. 79−75718
Higgs boson, bremsstrahlung prod. with heavy fermion pair in e^-e^+ collisions 78−86449
Higgs boson, spontaneously broken gauge theory phenomenon, possible weak interaction model 78−74200
Higgs boson couplings, charged, K_L-K_S mass-differences 80−62917
Higgs boson critical mass, baryon asymmetry from boson pair decay 80−90590
Higgs boson decay, gluon final states, differential spherocity and thrust distrib. 80−86655
Higgs boson decay, QED and QCD radiative corrections 80−95275
Higgs boson interactions with nucleons 79−2973
Higgs boson mass, 10 GeV? 79−63406
Higgs boson mass, perturbation constraint 79−67493
Higgs boson mass, relationship between coupling constants 80−353
Higgs Boson nature, test in $e^+e^-\rightarrow HHZ$ 79−63405
Higgs boson photoproduction 80−78068
Higgs boson production by high-energy lepton-nucleon interactions 80−27449
Higgs boson production in $e^+e^-\rightarrow H\mu^+\mu^-$ 80−32111
Higgs bosons, effects on experimental observables, and fermion mass scale 80−32061
Higgs bosons, masses, gauge hierarchies, SU_5 model 80−47236
Higgs bosons, photoproduction 80−22558
Higgs bosons, Weinberg model, input mass scale 80−22554
Higgs bosons in gauge models with right-handed charge currents 77−49892
Higgs bosons in SU(2)×SU(2)×U(1) left-right gauge field, coupling strength 79−13017
Higgs charged bosons and decays of heavy flavoured mesons 79−22014
Higgs coupling constraints from axionatics, Weinberg-Salam model Higgs extension 79−40706
Higgs induced neutral currents, symmetries leading to flavour conservation, Cabibbo angle 79−63407
Higgs new light boson, search 78−70319
Higgs particle search at PETRA using Wilczek mechanism 80−105838
Higgs pots. and SO(3) isotropy subgroups 78−37132
High energy behaviour of weak interactions and renormalisable theories, book contrib. 78−78164
high energy neutrino interactions, quark parton model anal. 79−30730
irreducible gauge theory of a consolidated Salam-Weinberg model 79−40707
left-right symm. gauge model, neutral gauge boson 78−29289
lepton-quark model, supermultiplet of weak bosons and Higgs scalar 78−62345
leptonic production calcs., anomalous electric quadrupole moment *(Russian)* 77−34148
light Higgs boson, Weinberg-Salam model 78−45835
light neutral gauge boson in SU(2) gauge model consequences for e^+e^- and pp($\bar{p}$) reactions 78−58154
mass bounds on spontaneously broken gauge theory 77−46007
massive Schwinger model, asymptotic completeness and confinement 78−66028
muonic atoms, long range parity violating interaction from γ-Z^0 conversion 80−48108
neutral current effects in Berthe-Heitler pair prod. 78−33022

intermediate bosons continued
neutral current interactions in $SU(2)_L\times SU(2)_R\times U(1)$ gauge models, natural parity conservation, gauge bosons 79−321
neutral intermediate boson decay calcs. using neutral hadronic weak current 77−38118
neutral light vector boson, possible exist., quark model construction 77−49898
neutrino interactions, appl. to weak interaction and nucleon struct. investigations, review 79−80823
neutrino interactions at high energy, book contrib. 79−30729
nonleptonic hyperon decay, octet dominance in nonrelativistic quark model 79−388
P violation, neutral currents, $SU(2)_L\times SU(2)_R\times U(1)\times U(1)$ 79−6308
parity nonconservation, coupling constants, intermediate boson mass ratio 79−9516
parity violation in He and Cs atomic electrons and e-e interaction effects 79−54788
perturbative QCD and exptl. signatures of weak bosons 78−93916
photoprocesses in few-nucleon systems, exchange meson currents role *(Russian)* 79−22269
photoprod. of charged intermediate vector bosons 78−45855
pp and $\bar{p}p$, associated prod. cross section for Higgs and Z particles 79−410
production and detection in pp and $p\bar{p}$ collisions 77−54072
production in pp($\bar{p}$) collisions, single lepton inclusive cross sections from decay 77−41868
production possibility in future multi-TeV colliding hadron rings 77−49897
pseudo-Goldstone bosons in Pati-Salam model 77−87933
purely leptonic processes, hypothesis test, purely diagonal single Z boson neutral currents 79−40713
QCD, decays of heavy leptons and intermediate weak bosons 78−8524
QCD corrections at Z_0 for hadron initiated lepton pair prod., renormalisation appl. 80−86678
QCD corrections for Higgs-boson production 80−68419
quark-lepton correspondence, multigeneration $SU(2)_L\times U(2)$-based model 80−22584
quarks, flavour number determination using Higgs scalar particle 80−13288
relativistic cosmology 80−90590
rishon model, topological bootstrap approach 80−78046
rishon model for quarks and leptons, topological bootstrap approach 80−78047
Schwinger model, equivalent boson theory, anomaly-free Ward-Takahashi identities 80−82873
search in p+nucleus 70 GeV muon yields 77−18367
short distance analysis of weak interactions, asymptotically free theory 77−54068
single-Z-boson hypothesis, neutral-current processes 77−74639
SO_{10} hierarchical breaking and neutrino masses 80−22550
spin, relation to isospin, strangeness and charm 80−37183
spontaneously broken gauge theories with heavy Higgs bosons 80−13209
standard electroweak gauge model with light W and Z bosons 80−95236
strongly interacting Higgs bosons, gauged nonlinear σ-model, $SU(2)_L\times U(1)$ extension 80−86656
$SU_2\times U_1\times U_1'$ electroweak model, Weinberg-Salam intermediate bosons 80−105831
$SU_4\times U_1$ and the origin of the Cabibbo angle, charged gauge boson mixing 80−73639
$SU_L(4)\times U(1)$ four-quark model, lepton quartets and W bosons 77−87934
$SU(2)_L\times(T_3)_R\times U_V(1)$ gauge group, grand unification, symmetry breaking and Z bosons 80−73641
$SU(2)\times U(1)\times SU_F(2)$ gauge model, CP violation and off-diagonal neutral currents 79−13008
SU(2)×U(1) gauge model, chiral SU(2)×SU(2) symmetry and electron mass 80−57542
SU(2)×U(1) gauge model, muon anomalous mag. moment, charged Higgs boson contrib. 80−78011
SU(2)×U(1) gauge model, symmetry breaking pattern with two Higgs doublets 79−12978
SU(2)×U(1) gauge models, CP violation origin, Yukawa interaction 79−40712
SU(2)×U(1) model, fermion and Higgs multiplet structure, universality 80−62909
SU(3)×U(1) gauge models, generalised mixing and CP violation in hadron decays 78−41473
SU(3)×U(1) gauge theory, charged intermediate boson mixing 77−87910
$[SU(4)]^4$ unifying symmetry for light neutral Z^0 boson, PETRA and PEP expts., $e^+e^-\rightarrow\mu^+\mu^-$ 78−37154
SU(5), unification of weak, EM and strong interactions, review 80−105814
SU(5) and O(10) grand unified theories, fermion and Higgs boson mass bounds 80−9134
SU(5) grand unification, heavy coloured Higgs scalars, b-quark mass 80−57543
subquark model of leptons and quarks, unification, currents and exotic states 80−86683
superheavy Higgs particles, proportional renormalisation corrections to W and Z mass, Weinberg-Salam model 79−276
supersymmetric Weinberg-Salam model 79−67490
superweak CP violation mediated by neutral Higgs bosons 80−363
superweak gauge theory of CP-invariance violation 79−75710
U(1) problem in generalised θ-vacua, Goldstone boson and QCD 80−52399
unification of EM, weak and strong interactions, massless fermions coupling to vector mesons 80−73637
unified gauge theories of weak currents of hadrons 79−80786
unified weak and EM theory without scalar fields, determ. of quark and lepton mass 79−75709
universal CP noninvariant superweak interaction and baryon asymmetry of the universe 78−66072
vector boson masses, weak and EM radiative corrections 80−52513
vector boson model from SL(2,C) gauge theory of gravitation and Yang-Mills theory 79−322
W-boson production by prompt high energy atmospheric neutrinos, $\bar{\nu}_e e^-\rightarrow W$ 79−3014
W-boson propagator effects in the neutrino-nucleon scattering 79−13098
weak gauge boson doubling in standard SU(2)⊗U(1) model, W, Z bosons 80−62916

intermediate bosons continued
weak interaction physics, present status and future prospects, review 79−67492
weak interaction studies with the DUMAND detector, 2 to 50 TeV 79−63463
weak interaction theory review, Higgs bosons 78−78131
weak interactions of ultra heavy fermions 78−93838
weak interactions with large dimensionless coupling constant, neutral currents as second order processes 77−61244
weak quark and lepton chiral symmetries, dynamical breaking gauge interaction 80−47215
Weinberg model, upper limit on mass differences determ. 77−61245
Weinberg-Salam model, extended, Higgs-induced neutral processes, natural-flavour conservation, K-symmetries 80−57539
Weinberg-Salam model, fermion and Higgs boson mass constraints 79−49437
Weinberg-Salam model, Higgs mechanism *(French)* 80−77999
Weinberg-Salam model, Yang-Mills theory, Higgs particle 80−4905
Weinberg-Salam model reformulation, for lepton scheme with 4-component ν-effects of Higgs scalar bosons *(Russian)* 79−80784
Weinberg-Salam model with two massless Higgs doublets, particle masses, perturbation constraint 80−57541
Weinberg-Salam model Yang-Mills theory of electro-weak interactions 80−73638
Z-boson and two-boson models, neutral current phenomena, μ-e universality 80−18109
Zweig forbidden processes, intermediate vector particle model, neutral vector mesons *(Chinese)* 80−62918
$B^0 \rightarrow D^+X(F^+X)$, W-exchange dominance, decay rates 80−86706
D^0 hadronic decay modes, W boson exchange model clean test 80−57592
D^0-$\bar{D}^0$ mixing, flavour-changing Higgs bosons 80−62915
D^+ decay, Cabibbo suppression, strong 20-plet dominance and W exchange 80−42453
(e,e+axion), bremsstrahlung mechanism for axion prod. *(Russian)* 79−54431
$e^+e^- \rightarrow Z^0\gamma \rightarrow \mu^+\mu^-\gamma$, Weinberg model anal. of Z^0 decay ang. distrib. 80−47275
e^+e^-, $SU_L(2)\times U(1)$ and $SU_L(2)\times SU_R(2)\times U(1)$ predictions at high Q^2, neutral currents, Z-bosons 80−63029
e^+e^-, W boson prod. calcs. in Weinberg-Salam model 77−30301
e^+e^-, weak corrections to three-jet angular distributions 80−22629
e^+e^- annihilation, charge asymmetry anal. 78−12898
e^+e^- annihilation, charged Higgs boson prod. signatures, Weinberg-Salam parametrisation 80−57620
e^+e^- annihilation, superheavy flavour prod., weak current effects, Z^0 effects 80−57614
e^+e^- annihilation, W^+W^- and Z^0Z^0 pair production 79−40820
e^+e^- collisions, weak neutral current effects, unified theories of dimension *(Hungarian)* 79−9326
$e^+e^- \rightarrow e^+e^-$, Coulomb interf. near Z^0 pole, Bhabha luminosity monitor 79−85289
$e^+e^- \rightarrow$heavy leptons, coupling of heavy leptons to W^0 anal. 78−33051
$e^+e^- \rightarrow$Higgs boson+γ in standard $SU(2)\times U(1)$ model, resonance enhancement 79−54331
e^+e^- high energy annihilation, possible signature of charged Higgs particles, $SU(2)\times U(1)$ model 79−35995
$e^+e^- \rightarrow H\nu\bar{\nu}$, 40-70 GeV, neutrino counting from Higgs boson production 79−97612
e^+e^- inclusive hadron prod., neutral weak currents 78−50041
$e^+e^- \rightarrow l^+l^-$, polarisation studies at Z^0 pole, expt. feasibility 79−97615
$e^+e^- \rightarrow \mu^+\mu^-$, early weak gauge boson restrictions from PETRA QED cut-off 80−52487
$e^+e^- \rightarrow \mu^+\mu^-$, radiative corrections around Z^0, Weinberg-Salam model 80−99103
$e^+e^- \rightarrow \mu^+\mu^-X$, possible Higgs boson detection in missing mass plot 80−4977
$e^+e^- \rightarrow \mu^+\mu^-X$, search for Higgs boson 80−27496
e^+e^- production cross-section in six-fermion interaction model *(Russian)* 77−34147
$e^+e^- \rightarrow \tau^+\tau^-$ near Z^0 pole, heavy lepton polarisation and radiative effects 79−22085
$e^+e^- \rightarrow \tau^+\tau^-H^0$, Higgs scalar boson production, Weinberg model calcs. *(Russian)* 80−68442
$e^+e^- \rightarrow V^+V^- \rightarrow e^+\nu_e\text{-}\mu^-\bar{\nu}_\mu$, beam polarisation, anomalous events 77−74669
$e^+e^- \rightarrow W^+W^-$, charact. of μe events anal. in Weinberg model 77−71478
$e^+e^- \rightarrow W^+W^-$, polarisation amplitudes 80−42484
$e^+e^- \rightarrow W^+W^-$, radiative, corrections in Weinberg model 80−52512
$e^+e^- \rightarrow W^+W^-\gamma(e^+e^-W^+W^-)$, Yang-Mills coupling 80−68443
$e^+e^- \rightarrow W^\pm$+hadrons, single $W^\pm$ prod. 77−46061
$e^+e^- \rightarrow W$+hadrons, from Z^0 pole to threshold 80−105917
$e^+e^- \rightarrow ZZ$, polarisation amplitudes 80−42484
$eN \rightarrow eX$, $SU(2)_L\times U(1)$ gauge theory distinguished from $SU(2)_L\times SU(2)_R\times U(1)$, neutral currents, z-bosons 80−62908
eN interactions, parity nonconservation, $SU(2)_L\times SU(2)_R\times U(1)$ gauge model anal., Z boson decay widths 80−47302
$ep \rightarrow W^+(Z^0)+X$, inclusive cross sections, quark-parton model calcs. 79−71755
$e^-p \rightarrow W\nu$, from Z^0 pole to threshold 80−105917
$\gamma p \rightarrow W^+(Z^0)+X$, inclusive cross sections, quark-parton model calcs. 79−71755
$\gamma p \rightarrow W^+n$, current algebra and sum rules high energy W^+ prod. 80−102039
Higgs meson prod., possible signals in high energy collisions, gauge groups 78−89649
$\lambda n\gamma(Z)$ vertex in vector-like model of weak and EM processes, appl. to K decay 77−6071
μ anomalous mag. moment in $SU(3)\times U(1)$ gauge model 79−3026
$\mu p \rightarrow \mu n W^+$, current algebra and sum rules high energy W^+ prod. 80−102039
ν mass, second-order effect in Higgs coupling 79−75716
$\nu(\bar{\nu})e$, differential cross-section calc. in gauge theories, W-boson exchange 77−82728
ν production, prompt sources, and axion decays and interactions, pN beam-dump experiment 80−63028
$\bar{\nu}e$ scatt., single Z boson hypothesis tests, non-diagonal neutral current inclusion 79−40714
$\nu e \rightarrow W^\pm Z^0(\gamma)X$, high energy behaviour and hard photon prod., cosmic rays 80−5028
intermediate bosons continued
$\bar{\nu}_e e^- \rightarrow W^- \rightarrow$hadrons, 30 to 100 GeV W-boson underwater detection from cosmic ν *(Russian)* 77−38159
νN, above W prod. threshold energy, QCD effects, cross sections and neutral currents *(Russian)* 79−67537
νN, charm and strangeness production, role of gluons 79−13104
$\nu N \rightarrow e^- N\phi^+$, phi meson as light scalar boson in unified weak and EM interactions 79−17706
$\nu n \rightarrow \mu^- p$, Higgs boson exchange effects on second-class currents 80−91075
$\nu N \rightarrow \nu X$, $SU(2)_L\times U(1)$ gauge theory distinguished from $SU(2)_L\times SU(2)_R\times U(1)$, neutral currents, z-bosons 80−62908
$\nu N \rightarrow \nu\psi X$, neutral current ψ prod., Z^0-gluon fusion model 80−78015
νN production cross-section in six-fermion interaction model *(Russian)* 77−34147
νN scatt., QCD effects above W prod. threshold, structure functions 79−71738
$\bar{\nu}p \rightarrow \mu^+n$, Higgs boson exchange effects on second-class currents 80−91075
$p(\bar{p})p \rightarrow W^\pm Z^0(\gamma)X$, high energy behaviour and hard photon prod. 80−5028
$p(\bar{p}p) \rightarrow W^\pm X$, QCD perturbative predictions 79−40812
pN, W boson and lepton pair prod. off nuclei, cross section enhancement 80−5014
$p\bar{p}$, equal sign lepton pairs, cleaner W-signal 79−13012
$p\bar{p}$, hadronic jets, possible intermediate bosons 80−18149
pp, polarised p, W prod. estimates for hadron jet decay detection, parity violating asymmetries 79−40821
$p\bar{p}$, pp, pol. and unpol. beams, hadronic jets, vector bosons, QCD and weak interference 80−57648
$p\bar{p}$, pp, $SU_L(2)\times U(1)$ and $SU_L(2)\times SU_R(2)\times U(1)$ predictions at high Q^2, neutral currents, Z-bosons 80−63029
$pp,p\bar{p}$, Z^0 high p_T bremsstrahlung, Higgs versus quark or gluon jets 80−32063
pp and $p\bar{p}$, Higgs-boson production at large transverse momentum in quantum chromodynamics 79−40745
$\bar{p}p \rightarrow \gamma, Z^0+X$, charge asymmetry, QCD-parton model study 79−93349
pp interactions, polarised beam, P violating asymmetries and estimates of W prod. 79−63538
pp or $p\bar{p}$ colliding beams, inclusive W^+W^- and Z^0Z^0 pair production 79−40820
$pp(\bar{p}) \rightarrow W^\pm(Z^0)X$, QCD perturbation theory struct. function predictions 80−42505
pp scatt., exchange degeneracy violating A_1-Z Regge amplitude and dibaryon resonances 80−4971
$p\bar{p} \rightarrow W^\pm X$, front back asymmetry in QCD and Weinberg-Salam model 79−97579
$pp \rightarrow W^\pm\gamma X$, mag. moment parameter meas. 79−97640
$p\bar{p} \rightarrow Z^0 \rightarrow l\bar{l}$+anything, cross section for Z^0 production, Weinberg model *(Russian)* 77−10296
$p\bar{p} \rightarrow Z$+anything, front-back asymmetry differential cross section, $W^\pm$ prod. 79−6352
$pp,\bar{p}p$, polarised and unpolarised, jet cross sections vector boson signals, QCD-weak interference 80−5026
production in $pp(p\bar{p})$, asymptotic freedom and scaling violations 77−26554
$Q\bar{Q}$ bound states mixing with Z^0 intermediate boson 79−75719
$\sigma \rightarrow 2\gamma$, Higgs meson decay amplitude, low energy theorems *(Russian)* 80−13309
t-quark mass in $SU(2)\times U(1)$ 79−40710
$\Upsilon(9.5)$, nature of heavy particle anal. *(Chinese)* 78−86443
W, mass in SU(5) grand unified theory 80−68411
W, production in hadronic collisions, appl. of quark parton model 79−30715
W boson, determ. of mass limit from neutrino scatt. data 79−3012
W boson magnetic and quadrupole moments, Weinberg model 77−30383
W searches with hadron beams, parton model anal. 80−91046
W-boson interaction, possibility of b-quark weak interactions 79−26285
W-boson mass and neutral electron-type heavy lepton 78−66100
W-boson prod. cross sections and hadronic jets in pp and $p\bar{p}$ collisions 78−8707
W-boson prod. in ep and pp collisions 77−61247
W-bosons, charged, mass spectrum, E_6 model of unified interactions, asymptotically free 80−73642
W-bosons, pp and $p\bar{p}$ collision, Weinberg-Salam model 80−9186
w-meson mass determ., 2-level vac. polarisation concept 79−40766
W-production via Z-decay in Weinberg-Salam model 80−101979
W^-, prod. in $\bar{\nu}_e e^- \rightarrow W^- \rightarrow X$ induced by direct neutrinos from cosmic ray protons *(Russian)* 80−12627
W^0 effects in e^+e^- interactions on a^- resonances 80−42386
W^+ production in π, p scattering in nuclear Coulomb field, cross section calcs. *(Russian)* 77−46086
W^{+or-} bosons, lowest order g-2 Weinberg-Salam model, Feynman diagrams 80−47291
$W^\pm$, Z^0 prod. anal. in asymptotically-free parton model 78−12865
Z, mass in SU(5) grand unified theory 80−68411
$Z \rightarrow H\gamma$, decay rate determ. in $SU(2)\times U(1)$ gauge theory 79−40717
$Z \rightarrow l^+l^-$, deviations from lepton universality in renormalisable gauge models 80−91122
Z-mass prediction as test of standard model 80−47239
Z^0, prod. in e^+e^- collisions, important landmark 79−97567
Z^0 flux loops, more heavy particles in the Weinberg-Salam model 78−82136
$Z^0 \rightarrow H^0l^+l^-$, leptonic decay into light Higgs boson, grand unification test 80−42381
Z^0 leptonic decay, weak-EM interference effects, LEP studies 79−97614
Z^0-bosons, pp and $p\bar{p}$ collision, Weinberg-Salam model 80−9186
$^4He(\gamma,\pi^0)$, P-odd effects, Regge and boson pole interference *(Russian)* 79−6564

intermediate-frequency amplifiers
30 MHz amplifier for EPR spectrometer 80−98955
for amateur radiotelescope 79−21189

intermediate state
domain structure near penetration field 77−16009
dynamic, cooling effect *(Russian)* 78−26998
dynamic resistance, linear response theory 79−87214
electric field penetration and collective oscillations, review 80−88678
electric resistance, Andreyev reflection at S-N boundary *(Russian)* 77−43789
layer structure in supercond. plate, theory 77−20505

intermediate state continued
magnetic flux quanta, obs. using decoration and electron vortex microscopy 77−47945
magnetoacoustic size effect *(Russian)* 80−7047
Meissner effect explicable in terms of classical electrodynamics 80−11134
nonequilibrium, phase transition to normal state under light irrad. *(Russian)* 77−80883
obliquely incident sound absorption *(Russian)* 78−39263
plate, finite thickness, Landau's laminar model 78−26987
reflectivity of S-N interface, application for Rowell-Tomasch oscills. amps. and thermal cond. 78−91822
structure, effect on supercond. destruction by current *(Russian)* 79−33412
superconducting wire, intermediate state dynamics 80−88697
superconducting-spot and normal-spot models 79−11275
superconductor, kinetic props. of corrugated and thread struct., sound attenuation *(Russian)* 80−54843
superconductor geometric resonance *(Russian)* 79−95551
superconductors, type I, mixed state, Josephson condition, phase jumps *(Russian)* 80−107967
thermal conductivity, Fermi surface shape and topology effects *(Russian)* 78−72314
thermal conductivity giant fluctuations *(Russian)* 78−34922
thin slabs, simplified model of intermediate state 79−61001
thread-like structure, sound attenuation *(Russian)* 77−32118
type II superconductor, bounded, intermediate state struct. form. near crit. field, role of surface 80−80465
Ga, ultrasonic absorpt., intermediate state 77−72942
Ge, Al-type superconducting thin film, critical mag. field 78−31023
In, dynamic, cooling effect *(Russian)* 78−26998
In, ideal superheating and supercooling limits 77−4465
In, intermediate state, doping effect on US attenuation 80−2522
In, intermediate state structure, hydrodynamic flow observation 78−43530
In, single cryst., helicon dispersion law and damping *(Russian)* 77−12066
In, superconductivity destruction singularities, intermediate state, hysteresis *(Russian)* 80−80460
In, thermoelectric effects 79−65620
In, ultrasonic absorpt., intermediate state 77−72942
In-Bi, single spheres, supercond. props. 79−73617
In-Bi dil., ideal superheating and supercooling limits 77−4465
In-Sn, dil., intermediate state, doping effect on US attenuation 80−2522
Pb film, hypersonic attenuation investig. of crit. field, intermediate state 77−8246
Pb film, shadow electron microscopy 79−11276
Pb, hardening in intermediate state 78−47917
Pb intermediate state, Meissner effect investigation by muon technique *(Russian)* 80−107954
Pb, nonbranching laminar intermediate state structs. 80−54846
Pb, supercond., internal mag. field meas. by μ^+ method *(Russian)* 79−33391
Pb superconducting film, interaction between crystal lattice and vortices 77−28307
Pb, thermal cond. measurements below 1K *(German)* 80−49984
Pb, thermal resist. of normal-supercond. interphase boundary 79−56384
Pb-Tl, low κ type II supercond., vortex motion anisotropy, intermediate-mixed state 78−47918
Si, Al-type superconducting film, critical mag. field 78−31023
Sn, Al-type superconducting thin film, critical mag. field 78−31023
Sn intermediate state, US attenuation 79−42694
Sn, intermediate state structure, single and poly cryst. cylindrical samples *(Russian)* 78−43528
Sn, thermoelectric effects 79−65620
Sn, thin layers, EM field penetration, depend. on temp. in mixed and intermediate states 79−65598
Sn-In, dil., intermediate state, US attenuation 79−42694
Ta, mag. props. and N-S surface energy 78−2633
Ta, muon spin rotation in intermediate state 79−56446

intermediate valence compounds *see mixed valence compounds*

intermetallic compounds *see alloys*

intermodulation
amplitude hologram intermodulation noise, effect of hologram thickness 79−50249
ionospheric cross-modulation of radio signals between two nearby stations 78−93048
laser diode characterisation, for multichannel applic. 78−87165
nonlinear holography, multiple-reference-beam, intermodulation background noise suppression appl. 80−99674
optical communication, TDM pulse analogue modulation, diode laser nonlinearity 78−55455
optical video discs, pit spacing frequency pit length frequency intermodulation 79−50338
thin ferromagnetic resonators, intermodulation distortion, spin waves 78−48048
volume phase holograms, non-sinusoidal high order modes 80−102665
$^{127}I_2$, weak rot. R(98), 58−1 line, HFS struct., saturated intermodulation fluoresc. 79−94024

intermodulation measurement
No entries

intermolecular forces
see also Van der Waals forces
ab initio calculation, including CI, correction for basis superposition error 79−85904
ab initio calculations applicability and accuracy 80−18898
acetone-toluene-tetrachloromethane, mol. interaction and thermodynamic props. 80−71935
acetonitrile, liq. and solns., IR absorpt. band intensity, temp. depend., CC and CN bonds 77−75157
acetonitrile-toluene-benzene, mol. interaction and thermodynamic props. 80−71935
acetylene, orientation depend. intermol. force, solid struct. 77−50487
adamantane, elastic props., press. depend. rel. to intermol. forces 80−54297
air, viscosity rel. to ionis., skin friction of wetted oscill. disc 78−34252
albumin, bovine serum, macroion soln. viscosity and diffusion, quasielastic light scatt., electrostatic interaction 79−70508
alkali halide solutions in DMSO, modelling of interactions 79−77469

intermolecular forces continued
alkali metal scattering at high-energies, intermol. potential determ. 77−46609
n-alkane+Ar mixtures, intermol. pot. using Kihara model with spherical cores 77−54591
angular dependence between linear molecules 78−37704
anisotropic atom-molecule interaction pot., influence on transport cross sections, appl. to He-alkali dimer 80−9677
anthracene, soln. and melt, second vibronic transition, spectroscopic charcts., effective field dispersion calcs. 80−55102
anthracene dimer anion, charge reson. transition anal. 80−42931
atom+diatom, anisotropic interaction pot., total cross-section calcs. 78−29835
atom+diatom potential, asymmetric, isotope substitution effect, Legendre expansion coord. transformation 78−70894
atom+diatom scattering eqns., generalised phase shift, semiclassical series soln. 80−43142
atomic beam, highly expanded free jet, quantum and intermol. pot. effects 77−61823
atoms, identical, dispersion intermolecular pot. anomaly prod. by intense radiation field 80−58336
benzene, $\pi\pi^*$ and Rydberg bands, cryogenic solvent effects 78−55182
benzene, in Br_2-carbon tetrachloride soln., complex form., IR spectra 78−70828
benzene, vapour, transport coeffs., theoretical study 77−3904
binary gas mixture, intermol. force parameters 79−22784
bromobenzenes, intermol. forces in cryst. 77−76349
carbonyl groups, intermol. interactions in H_2CO-H_2CO system, quantum chem., classical calcs. 78−86932
carboxylic acids, crystals, empirical interatomic potential functions 79−7567
chlorobenzene, in CCl_4 soln., quadratic changes in elec. permittivity, intermol. interactions 77−73107
chlorophyll-a, mol. interaction in monolayers and multilayers, IR obs. 77−71799
cholesteric mixture, molecular statistical theory with regard for steric repulsion forces *(Russian)* 78−34438
cholesterol benzoates, intermolecular interaction, influence on optical props. *(Russian)* 79−77516
cholesterol cinnamates, intermolecular interaction, influence on optical props. *(Russian)* 79−77516
cholinesterase-acetylcholine soln., anion-cation site interactions, solvent effects on aggregate stability 80−61070
closed-shell system, isotropic intermolecular forces evaluation using semi-empirical approach 79−36726
closed-shell systems, interactions, correl. energy, RPA calcs. 78−25646
collinear triatomic system, binding, crit. pot. strengths 77−6883
colloid system, forces of mol. attraction between solids, effect of EM lag 80−71949
conformational props. rel. to spatial electron density determs., computer simulations 78−70763
conjugated molecule, charge distrib. calcs., short range forces 77−3258
Coulomb force for molecular dynamic calculations 80−91627
coupled attractive square well pots., exactly soluble model, multichannel calc. 77−42368
crossed fibres, mol. attraction forces meas., depend. on air gap width 77−27216
cyclobutadiene, π face bonding with CO, HCN, benzene 79−98180
dense gas, of dipolar mols., electron localisation, density fluctuation, mol. orient. 78−38446
diatomic gas, vibr. cross section, orientation depend. of interaction pot. *(French)* 77−515
diatomic molecule in strongly interacting solvent, IR band shape, field theoretic methods appl. 79−27038
p-dichlorobenzene, bicentric expansion of potential function of mol. interaction 79−94056
p-dichlorobenzene($-d_4$), mixed cryst. phases, mol. reorientations and intermol. interactions, Raman obs. 79−28751
dichloromethane in nematic liq. crystal, $A_2(^{12}CH_2Cl_2)$ nuclear relax., dipole-dipole interaction 77−54567
dielectric medium, continuous, free energy due to Coulomb and hard-core pots., activity coeffs. 80−45537
dielectric molecular fluid, optical props., internal forces effects, theory 77−28534
dilute aqueous solutions, Monte Carlo studies of struct., review 80−54101
dilute gas simulation, pattern recognition algorithm for mol. formation 77−75249
dipolar solvent, ionic mean force, pot. anal. 77−56234
dipole properties and dispersion energies additivity, using atoms and small mol. models 80−53091
dipole-dipole coupling, inertial effect 80−40049
dispersion energy consts., dipole oscill. strength sums, refractivity, for Li, N, O, H_2, N_2, O_2, NH_3, H_2O, NO, N_2O 77−50492
distance force consts., pseudocritical volumes 78−58765
DNA base pairs., Coulomb interaction energy calcs, electron correlation role 79−96509
DNA conformation, influence of intermol. interactions 80−16900
DNA interactions with cations, UV difference spectrosc. and Marcus theory 80−94153
doublet with singlet ground state electronic system, long range interaction energy, CNDO approx. 80−53089
Drude oscillator model, atomic and molecular props. for different oscillator freq. 80−37846
effective potential examination for critical volume, rel. to mol. struct. 79−41122
electron exchange perturbation theory, direct spatial localisation 77−79668
electron gas approximation, scaled 79−98181
electron gas model, self-exchange corrected 77−46608
electron gas-Drude model, generalised 79−98182
ethane gas, local mode overtone bands 80−83444
ethylene, dimer interaction, lattice energy, multipole expsn., at.-at. pots. 78−9218
ethylene, pure, IR absorption obs. of C-H stretching fundamentals up to 2 kbar and 200°C 79−22701
ethylene+Cl_2(Br_2) complex, intermolecular interaction and struct. SCF-MO-LCAO CNDO/2 calc. 78−58763
ethylene dimer, exchange forces, Hellmann-Feynman theorem calc. 77−54589
ethylene dimer, intermol. pot., dissoc. energy, CNDO/2 calcs. 79−31641

intermolecular forces continued
ethylene-vinyl alcohol (<36.3 mol.%) copolymer, elastic moduli of crystalline region *(Japanese)* 79−15715
ethylene-vinyl alcohol (>40 mol.%) copolymer, elastic moduli of crystalline region *(Japanese)* 79−15716
exchange forces, Hellmann-Feynman theorem calc. 77−54589
exchange interactions, generalised Jansen's perturbation theory 79−6981
exchange perturbation theory, primitive function 78−37701
π-exciplexes, aromatic hydrocarbons-amine, intermolecular interactions 80−43134
factor VIII, native and modified, surface adsorption and mol. interactions, ellipsometric obs. 80−104555
fibrinogen, native and modified, surface adsorption and mol. interactions, ellipsometric obs. 80−104555
fluid, anisotropic, of hard rods, correlation function, to 1st order in density 79−86675
fluid, atomic, classical, with repulsive pair pot., perturbation method 79−68997
fluid, dense of polarisable dipolar hard spheres, Monte Carlo study 79−86665
fluid, intermolecular potentials, coulombic and multipolar, 2-dimens. mol. dynamics simulation 78−75520
fluids with polar, quadrupolar, octupolar mols., thermodynamics, vapour-liq. equilibria 78−95127
fluoranil-macrocyclic polyether mol. complexes, configs., IR and NMR obs. 78−33529
formaldehyde-water, heuristic intermol. pot. function, ab initio MO calcs. 78−33566
gas, Boltzmann collision operator with cut-off for intermolecular potentials 78−42697
gas, diatomic, spherical source expansion 80−58356
gas, intermol. pot. energy from viscosity meas., demonstration 77−13556
gas, of interacting particles, quantum momentum distribution, asymptotic form 79−98850
gas phase, EPR linewidths and intermol. pots., quantum calcs. 77−34665
gas phase nucl. mag. relax., DWBA cross sections from S-matrix formalism 77−27151
gas-liquid phase change, intermolecular pot. vibr. freq. shift depend. 77−23488
gas-liquid surface of mol. fluids, mol. dynamics computer simulations 80−39387
gas-solution phase change, intermolecular interaction pot. vibr. freq. shift depend. 77−23487
glycine, neutral and zwitterion interaction with water, Monte Carlo simulation 79−53026
Gordon-Kim model, appl. to inert gas dimers 79−45781
halogen molecular crystal, bond charge model, for lattice dynamics 78−79692
hard sphere fluid near hard wall, diffusion coefficient, mol. dynamics simulation 80−64858
hard spheres permeation through hard disc monolayers, interfacial mass transfer 80−107460
hexamethylbenzene in tetrachloromethane soln., local mode overtone bands 80−83444
HF subsystems, long range induction and dispersion interactions 80−53092
hot-atom collisional energy density function, stochastic calc. 79−29342
hydracids, monatomic matrix-trapped, assoc. forms, struct. and spectral response, intermol. pot. calcs. 79−93996
hydrogen-bonded liquids, HF, H_2O, NH_3, computer simulation, intermolecular potentials 80−38890
identical molecules, dispersion intermolecular pot. anomaly prod. by intense radiation field 80−58336
induced dipole-induced dipole potential, capture rate const., for ion-molecule collisions 79−13783
induction energy, coupled Hartree-Fock calcs. 80−43139
induction force, retardation correction from second-order perturbation theory and canonical transforms. 78−37703
inert gases, viscosity rel. to ionis., skin friction of wetted oscill. disc 78−34252
inorganic molecular crystals, metal complexes electronic spectra and intermolecular interactions 80−55137
interacting systems, general theory of natural states, use for calc. of intermol. forces 78−82807
interacting systems, natural states in the asymptotic 1/R expansion, use for calc. of intermol. forces 78−86930
interaction energy calc. by quantum chem. and atom-atom schemes 79−59529
intermolecular interaction energies, calcs. in terms of local contrib. 77−30755
internal scalar pressure determ. in atom or molecule, density functional theory 80−47857
invert emulsion, aggregation equilibrium 79−66356
iodomethane, liq. (liq. mixtures), vibr. relax. and reorientation, symmetric C-H bending mode 1st overtone 78−62884
ion-dipole capture in noncentral field, variational and trajectory investigation 80−63739
ion-ion, ion-dipole, and dipole-dipole interactions, teaching 78−10
ion-molecule forces, generalised electron gas Drude model, appl. to $Li^+ + H_2(N_2)$ 79−98183
ion-molecule repulsive potential reconstruction from ion mobility in gas data 80−23486
IR and Raman vibrational intensity changes due to long-range interactions 80−53084
isotropic, approx. method, crit. test using H-H ($^3\Sigma_u^+$) as model 78−78771
Jeziorski-Piela perturbation theory 77−65523
kinetic molecular theory teaching, expt.-oriented approach 80−12868
lipid bilayer membrane interaction forces in zone of contact 78−53345
lipid membrane order, mol. theory 79−66452
liquid, associated, radial correlations, comparison of Monte Carlo and Ewald mol. dynamics calc. methods 80−14984
liquid, interatomic and intermolecular forces, summer school lecture series 80−6342
liquid, molecular, struct., reference systems with spherical interactions 80−24337
liquid, Rayleigh scattered light, spectral and intensity distrib., mol. statistical theory, Racah algebra approach 79−99890
liquid, simple equilib. theories, review 80−38887
liquid, universal intermolecular interactions, semiempirical pot. derivation using continual model assumptions *(Russian)* 79−90514

intermolecular forces continued
liquid, vibr. relax., line widths, intermol. forces dephasing 77−47315
liquid crystal ordering and theory of mol. dispersion forces and pair pots. 80−64886
liquid metal, effective interionic potentials 78−91221
liquid mixtures, intermol. forces effect on phase diagram and excess props., perturbation theory 80−39287
liquids, long-range dipolar interactions in computer simulations of polar liquids, Monte Carlo calc. 78−87603
liquids, nonpolar, b.p. calc. as function of mol. polarisability, ionisation energy, and size 79−95148
liquids with noncentral interactions, struct. contrib., perturbation method and partition function separation 80−24341
long range, van Hove, correlation function asymptotic behaviour *(German)* 77−38707
long-range interaction coeffs. computed from Frost-model wave functions 77−23533
macromolecular interactions, effects of intervening medium and polar mode energy feeding 79−13857
macromolecules, interacting, spherical, light scatt., conc. fluctuations, transport eqn. 79−1775
MBBA, calc. of order parameter from X-ray diffraction data 79−69009
MBBA, nematic-isotropic transition, intermolecular forces, IR N_2O mol. probe obs. 80−29155
MBBA/EBBA, nematic, mol. interaction energy 80−33881
metal phthalocyanines, IR spectra, vibr. transitions during intermol. interactions 79−54857
methane, ^{13}C and proton medium shifts in gas phase and in soln. 77−88467
methane, intermol. pair pot. energy function 77−10721
methane+methane(He)(Ne)(Ar), dispersion forces 78−13565
methane + H_2O, pairwise interaction pot. function, ab initio SCF MO calc. 79−22786
methanol dimer, intermol. function from ab initio calcs. 80−32629
N-methyl-N-nitrosourea, electronic interactions with DNA, ESR obs. and INDO calcs. 80−94154
mica surfaces, interaction forces at small separations in polar and nonpolar liquids 80−39458
microphysics to macrochemistry, discrete simulations, review 80−54102
modern state of theory, rel. to large mols. 80−14186
molecular aggregates, nonvalidity of SCF vibronic spectra calcs. 77−10655
molecular cryst., dipolar exciton band struct., optical model 77−15770
molecular crystal subclasses from intermol. interaction energy calcs. 77−4064
molecular crystals, NQR freq., intermol. force effect 80−66065
molecular fluid, optical props., intermol. forces effects, theory, appls. 77−28535
molecular liquid, mol. dynamics simulation, multiple time step methods and improved potential function 80−54098
molecular solids, intermol. forces and eqn. of state, pseudoharmonic approx. calcs. 78−30731
multipole expansion invariance properties w.r.t. coord. system choice 79−85918
multipole results validity, 1st order forces, charge overlap effects, rel. to H_2, N_2, CO_2, and HF 79−89730
naphthalene, soln. and melt, second vibronic transition, spectroscopic charcts., effective field dispersion calcs. 80−55102
nematic liquid crystal, intermol. forces, in anisotropic mean field, hard spherocylinder model 77−35468
neopentane, diamond force const., rel. to crystal elastic consts., Raman freq., bulk compressibility and freq. assignments 80−65183
neopentane liq., local mode overtone bands 80−83444
nitroxide groups in crystals, H bonds and short intermolecular contacts 80−63855
NMR intermolecular relaxation operator, dipole coupling 77−68057
n-octane fluid, gauche-trans. relax. 79−69002
organic ternary liquid systems, intermolecular interaction, US vel. meas. 80−79879
organometallics, intermolecular interaction, Mossbauer spectra 80−15899
orientationally ordered liquids, Helmoholtz free energy, generalised van der Waals theory 80−44119
oscillatory forces between two solid surfaces arising from struct. in intervening liquid, meas. 80−70521
pair potential of attractive dispersion interaction in dense media 77−66787
paradichlorobenzene, NQR freq., intermol. force effect 80−66065
paraffin oil, aq. emulsion, polyelectrolyte stabilised, mech. props. 79−39223
paraffins, solid and liquid, diamagnetic susceptibility 78−14923
PCILO method for fixed wavefunctions 78−17571
perturbation theory, Pade approximants and convergence 79−31635
perturbation theory for fluid of rod-like mols. interacting via Kihara potential 77−11291
phenanthrene, phase transition, Raman spectral obs. 77−59112
phospholipid inter-and intra-molecular interactions, PCILOCC and pot. function calc. 80−3570
photon exchange interaction between neighbouring atoms and cooperative radiation 77−27141
planar structures, hexagonal and cubic models, surface forces 80−20022
point charge model approach to intermol. interaction coeffs. 80−18897
polar fluid, complex, modified free-energy averaged pot. 80−48833
poly-α-methylstyrene, in cyclohexane, crit. opalescence *(Russian)* 77−62463
poly-γ-benzyl-L-glutamate, soln., liquid crystal transitions anal. 80−65207
polyacrylamide, aq. solns., conform. changes, intermol. interactions, optical mixing spectroscopy 79−10770
polyatomic fluid mixtures, thermodynamics, phase equilib. calcs. 79−1485
polyatomic molecule, atomic force correlation functions for determ. vibr. relax. rates, role of mol. symmetry 80−83337
polyatomic molecule, crit. consts. evaluation from intermol. force consts. 80−37844
polyatomic molecule+atom, many body approach 79−31645
polyatomic molecules, vibr. spectrum, intermolecular interaction effects *(Russian)* 78−37621
polyatomic mols. in liqs., vibr. energy relax. 80−63611
polycyclic aromatic quinone, epitaxy on alkali halides, adsorbed water effect 79−28239
polyethylene, intermolecular force field and normal vibrs. 79−73265

intermolecular forces continued
polyethylene, uniaxial, deuterated, interchain forces effects on acoustic phonon branches, neutron scatt. study 79−51228
polyethylene (orthorhombic), intermol. pot. functions, force consts., vibr. assignments, thermodynamic props. 77−39639
polymer, liq., Brillouin scatt. and segmental motion, appl. to polypropylene glycol 78−91217
polymer film, in adhesive joint contact layer, intermol. interaction with substrate and filler *(German)* 79−8421
polymer formation, trimer, tetramer and pentamers 78−5313
polymer solution, dilute, aq., appl. of Hildebrand's fluidity model, apparent viscosity temp. depend. *(German)* 79−37366
porphyrin in n-octane Shpolskii matrix, defect props., Monte Carlo obs. 80−63533
potential determ. from elastic scatt. phaseshifts, generalised WKB method 77−58116
potential energy functions, determ. from gas transport coeff. data inversion 77−35293
potential function, of mol. interaction, bicentric expansion 79−94056
primitive wave function in theory of intermolecular interactions 80−95703
pure gases, mol. pot. parameters calc. using second virial coeff. data *(Spanish)* 77−47133
pyrazine, dimer interaction, lattice energy, multipole expsn., at.-at. pots. 78−9218
quartz fibres crossed in air, mol. attraction meas. as function of dist. 78−13566
radial distribution function, perturbation theory, three-body pot. 77−35456
Raman scatt. obs., review 80−23427
Raman spectra of liq. phase weak H-bonds, short range order and anharmonicity effects 78−64357
real fluids, short range repulsions and long range attractions, simple pair pot. model 80−64850
rotational energy transfer, sensitivity anal. 80−63762
S-matrix factorisation, in mol. collision problems 79−72380
scattering, low-energy, by long-range pot. 78−74723
scattering of beams to give intermol. pots., light scatt. anal. *(Dutch)* 79−50104
semiempirical calc. for simple systems 77−27138
short-range, non-additivity, pseudopot. anal. appl. to Ar_2, Ar_3 and Ar_4 79−50179
simple fluid, mol. dynamics simulation, including three-body interactions 80−54100
simple liquid intermolecular interaction, extremal values 78−87602
solutions, electronic and vibr. absorpt. spectra, repulsive intermol. forces 77−79671
square well fluid, viscosity, transport processes 79−98847
state change collisions, attractive intermolecular forces, temp. depend. 80−23515
steam, effective spherically symmetric pots., applicability to viscosity calc. 78−1779
Stockmayer molecules, two dimens. fluid, static props., dielec. const. mol. dynamics calcs. 80−54094
strongly coupled systems, one dimens. barriers, transfer rate 80−63735
supermolecule calcs. with additive procedure, intermolecular interactions and binding energy 80−52880
TCNE, K salt, in nematic liq. crystal solvent, ion pairing, EPR spectra 78−73020
tertiary phosphine oxide+aliphatic alcohol, $p\pi$-$d\pi$ conjugation, electronegativity and H-bond energy 78−82863
tetrabromomethane, in disordered phases, IR active mode Raman line shape, dipole-dipole interaction 80−9603
tetrafluoromethane, in disordered phases, IR active mode Raman line shape, dipole-dipole interaction 80−9603
tetrafluoromethane, intermolecular pot., lattice energy and heat of sublimation 80−38995
tetramethylbutane in hexachlorobutadiene soln., local mode overtone bands 80−83444
thermal diffusion data for intermol. pot. energy function determ. 77−54590
thermodynamic parameters determ. from chem. shifts of functional groups 79−64068
thermotropic systems of rodlike molecules with orientation-depend. interactions 80−33883
torsional ground state splitting of tetrahedral mol. in cryst. field, intermol. forces probe 80−15019
transition metal, paramagnetic-NO· radical interactions, EPR spectra rel. to dipolar interactions 79−95647
triangular-potential fluid, Zwanzig's perturbation theory, appl. to thermodynamic props. 79−41920
trichloromethane in nematic liq. crystal, $AX(^{13}CHCl_3)$ nuclear relax., dipole-dipole interaction 77−54567
tris-butadienyl metal D_3 complex pairwise chiral discriminations, stereochem. basis, extended transition monopole model 78−74725
two identical molecules, level shifts due to overlap of MO's 77−46494
van der Waals dimers, struct. rel. to dielectric second virial coeffs. 77−46611
water, IR spectra, thin layer between quartz plates 79−56773
water, liq., Monte Carlo studies of struct., review 80−54101
water, long range forces in mol. dynamics calcs. 78−79517
water, Monte Carlo simulation 80−54113
water+glycine(serine) zwitterions, interaction pots., ab initio SCF LCAO calcs. 78−48747
xanthine, planar autoassoc. energy 80−53086
$I^{129}Xe$, chem. shift in NO gas, chem. shielding 77−6706
air, viscosity rel. to ionis., skin friction of wetted oscill. disc 78−34252
$Al^{3+}(H_2O)n$ (n=1,2,4,6), FSGO-pair-pot. calcs. *(German)* 80−74278
Ar, intermolecular pot. energy function determ. from thermal diffusion data 77−54590
Ar, solid state props., statistical thermodynamic calc. using gas phase intermol. pair pot. *(German)* 77−20083
Ar-HBr, intermol. pot. energy surfaces calcs. 80−91625
Ar-N_2 interaction, electron gas pot. calc., Gordon-Kim model, ang. orientation depend. 78−70893
Ar-Ne(H_2), liquid solution, dielectric props., intermolecular interactions *(Russian)* 80−88904
Ar+CO_2(N_2), short-range intermol. pots., combined interatomic pots. calcs. 80−87198
Ar+HCl, line broadening, short range force effects, semiclassical calcs. 79−98085
intermolecular forces continued
Ar+N_2(CO), intermolecular pots. from Thomas-Fermi-Dirac functional 77−19009
Ar_2, interatomic potential single parameter 80−48059
Ar_2 van der Waals dimer, intermol. pot., SCF CI ab initio calcs. 80−106274
$AsBr_3$($AsCl_3$), Raman scatt. spectrum, intermol. interaction and dimeric assoc. *(Russian)* 77−54562
BO_2, laser saturation spatial spectroscopy of diffusion coeff., interaction pot. 77−75341
BaO+Ar(CO_2), in Ar flame, rot. and translational relax. by sub-Doppler optical-optical double reson. 80−95583
BeF_2, molten, symm. stretching freq. calc. using mol. dynamics method 77−71790
$Be^{2+}(H_2O)_n$, (n=1,2,3,4,6), FSGO-pair-pot. calcs. *(German)* 80−74277
CO, line broadening, short range force effects, semiclassical calcs. 79−98085
CO+N_2(CO_2), line broadening, short range force effects, semiclassical calcs. 79−98085
CO_2, in various solvents, IR absorpt. spectrum, Fermi-reson. doublet and intermolecular interactions 80−18856
CO_2, induced absorpt. spectral moment, mol. calcs. 80−63737
CO_2, line broadening, short range force effects, semiclassical calcs. 79−98085
CO_2, viscosity rel. to ionis., skin friction of wetted oscill. disc 78−34252
CO_2-type cryst., transl.-vibr. absorpt., hexadecapole moment effects 77−90134
CO_2+Ar, short-range intermol. pots., combined interatomic pots. calcs. 80−87198
CO_2+Ne, intermol. pot. in repulsive short-range region, ab initio 80−69204
CS_2, condensation vibr. shift, intermol. interaction, vap. press. isotope effect 77−61742
CS_2, liquid, Raman spectra, effects of intermolecular forces 79−41177
CS_2, $\pi\pi^*$ and Rydberg bands, cryogenic solvent effects 78−55182
CS_2, X-ray scatt., reference-site-interaction model, intermol. pot. function 77−11459
$^{12}C^{16}O+^{13}C^{16}O$, vibr. distrib., electron impact excitation, isotopic composition, interaction depend. 79−29332
Cl_2, mol. liquid, mean squared torque and mean squared force, interaction energy spherical harmonic expansion 80−54093
D_2, intermolecular pair potential, from solid-state data 79−14727
DCN, self-assoc. in matrices, IR vibr. spectra of multimers 78−86858
$F^-(H_2O)n$(n=1,2), FSGO-pair-pot. calcs. *(German)* 80−74278
H bonded ν_{X-H} band, dynamic theories survey 80−52983
H bonding molecules, self assoc., intermolecular interactions, matrix isolation vibr. spectra obs. Raman and IR spectra 80−52995
H, triple-dipole energy calcs. using pseudo spectral theory 78−46418
H+Br_2(Cl_2), nonreactive scatt., long range anisotropic pot. determ. 78−66626
H+H_2, anisotropic interaction pot., total cross-section calcs. 78−29835
H+H_2, integral cross section meas. at thermal energy 77−10724
$H+H^+$, interaction energy, perturbation expansion, symmetry forcing 79−22785
H^++2HF, interaction pot., monopole approx., supermol. SCF and perturbation schemes 77−27139
H_2, expressions for calc. Coulomb repulsion between electrons using adiabatic basis 80−91427
H_2 H_2, intermol. energy, CI ab initio calc. 79−85904
H_2, interaction energy, non-additive effects 79−50099
H_2, intermolecular pair potential, from solid-state data 79−14727
H_2 molecule dimer, ab initio SCF intermolecular interaction energy calcs. 80−78537
H_2, nucl. mag. shielding and susceptibility, elec. field depend., SCF-Hartree Fock method 80−18791
H_2, orientation depend. intermol. force, using charge density and dispersion force data 77−50487
H_2, repulsive intermol. pot. 80−32794
H_2, short range intermolecular forces, scattering of molecular beam 79−36727
H_2, triple-dipole energy calcs. using pseudo spectral theory 78−46418
H_2-Ar(Kr)(Xe) mixtures, intermol. forces 78−62867
H_2-H_2, mixed-pole terms in anisotropy of long-range interaction coeffs. 77−30950
H_2-He, mixed-pole terms in anisotropy of long-range interaction coeffs. 77−30950
H_2+H_2(He), anisotropic intermol. repulsion, pot. energy models 77−46610
H_2+He, vibr. relax. cross section 80−99494
HCN, self-assoc. in matrices, IR vibr. spectra of multimers 78−86858
HCl, intermol. partial struct. factors, isotopic substitution and neutron diffr. obs. 80−53157
HCl-dimethylether complex, gaseous, H-bond IR spectra, temp. depend. theory 78−62804
HCl+$N_2(O_2)(D_2)(H_2)$, HCl ν_0-ν_1 band perturbations, linewidth and shifts calcs., IR spectra obs. *(French)* 80−58251
$(HCl)_2$, vibr. freqs. in inert gas matrix, force const., MINDO/3 calcs. 78−41952
HD+Ne, j=0 to 1 scatt. differential cross section, interaction pot. anisotropy 77−42382
HF dimer, stabilisation energies, harmonic free constants, intermolecular vibration, SCF and CEPA PNO calcs. 79−98177
HF, nucl. mag. shielding and susceptibility, elec. field depend., SCF-Hartree Fock method 80−18791
HF+HF, interaction energy, MCF and perturbation calculations 77−27139
$(HF)_2$, energy decomp. anal. of H-bonding, ab initio SCF MO calcs. 77−57868
$(HF)_2$, intermol. force model, rel. to liq. struct. 78−78773
H_3N-HF, energy decomp. anal. of H-bonding, ab initio SCF MO calcs. 77−57868
H_2O, liquid, diamagnetism, temp. dependence, NMR chemical shift calcs., molecular interactions data 80−75707
H_2O, triple-dipole energy calcs. using pseudo-spectral theory 78−46418
$H_2O+H_O(F^-)(CH_4)$, interaction energy calc. using minimal basis sets 80−9678
H_2O+H_2O, interaction energy, MCF and perturbation calculations 77−27139
H_2O+H_2O, pair pot. near H bonded equilib. config., amorphous and crystalline solid and liq. 80−64946

intermolecular forces continued
$H_2O+H_2O(Na^+)(K^+)(NH_4^+)$, supermolecule calcs. with additive procedure, intermolecular interactions and binding energy 80−52880
$(H_2O)_2$, energy decomp. anal. of H-bonding, ab initio MO calcs. 77−57868
$(H_2O)_2$, exchange forces, Hellmann-Feynman theorem calc. 77−54589
$(H_2O)_3$, geometric config. energies, SCF LCAO MO calcs. 80−63551
$H_3O^+ + 2HF$, interaction pot., monopole approx., supermol. SCF and perturbation schemes 77−27139
H(1s)-H(1s)($^3\Sigma_u^+$) isotropic intermol. force, model for approx. method, crit. test 78−78771
He, accurate empirical intermol. pot. 79−68291
He, triple-dipole energy calcs. using pseudo-spectral theory 78−46418
He-Ar(Kr)(Xe), 208 and 707K, intermol. forces, virial, diffusion, and viscosity coeffs. 77−75256
$He+H_2$, anisotropic interaction pot., total cross-section calcs. 78−29835
$He+H_2$, exchange forces, Hellmann-Feynman theorem calc. 77−54589
He+He, weak intermol. interactions, intramol. correl. effects, perturbation anal. 79−86038
He+He(Li), intermol. forces, ab initio VB calc. using nonorthogonal basis set 80−23490
$He+N_2$, intermolecular pots. from Thomas-Fermi-Dirac functional 77−19009
$He+N_2(O_2)(CO)(NO)$, anisotropic intermol. pots., crossed beam expts. 79−31639
He_2, exchange forces, Hellmann-Feynman theorem calc. 77−54589
He_2, intermol. forces, Gaussian basis function calcs. 78−21993
^{3}He-^{4}He in liquid ^{4}He, non-additive interaction in solvent effect 79−41120
$^4He+H_2$, inelastic collision, R-matrix study 80−87204
$HgCl_2$, NQR freq., intermol. force effect 80−66065
I_2, laser saturation spatial spectroscopy of diffusion coeff., interaction pot. 77−75341
Kr, intermolecular pot. energy function determ. from thermal diffusion data 77−54590
Kr, molecular dynamics simulations, three effective interactions 79−69224
Kr-HCl, intermol. pot. energy surfaces calcs. 80−91625
Kr-He(Ne)(Ar)(Xe), gas, diffusion coeffs. meas., 350-1200K 80−14869
Kr+carbon tetrachloride, differential elastic scatt. cross-section 79−45784
LaB_6, synthesis and props. *(Japanese)* 80−40255
Li, triple-dipole energy calcs. using speudo-spectral theory 78−46418
Li^+, hydrated, polarisation model, review 80−54115
LiF oligomers, struct., stability SCF and CEPA-PNO calcs. 78−78640
LiF+Ar, polarised rot. state-selected cross sections, anisotropic intermol. pots. 79−72398
LiH oligomers, struct., stability SCF and CEPA-PNO calcs. 78−78640
$Li^+(H_2O)_n$, (n=1,2,3,4,6), FSGO-pair-pot. calcs. *(German)* 80−74277
$Mg^{2+}(H_2O)n$ (n=1,2,4,6), FSGO-pair-pot. calcs. *(German)* 80−74278
N, triple-dipole energy calcs. using pseudo-spectral theory 78−46418
N_2, line broadening, short range force effects, semiclassical calcs. 79−98085
N_2, liq. and gas, induced absorpt. spectral moment, mol. calcs. 80−63737
N_2, mol. liquid, mean squared torque and mean squared force, interaction energy spherical harmonic expansion 80−54093
N_2, orientation depend. intermol. force, using charge density and dispersion force data 77−50487
N_2, Raman spectra, intermol. torques and orientational correlation times 80−48006
N_2 structural second virial coeff., intermol. pot. and mag. scatt. 80−78678
N_2, tripledipole energy calcs. using speudo-spectral theory 78−46418
N_2, viscosity rel. to ionis., skin friction of wetted oscill. disc 78−34252
N_2-N_2 anisotropic interaction pot. model, comparison with solid state data 77−34712
N_2+Ar, short-range intermol. pots., combined interatomic pots. calcs. 80−87198
NH_3, assoc. mols., struct. and dynamics, atom-atom pots., gas, solid and liq., props. 80−23487
NH_3, ND_3, crystals, rotation mol. motion *(Russian)* 78−87762
NH_3, triple-dipole energy calcs. using pseudo-spectral theory 78−46418
$(NH_3)_2$, dimer, intermol. pot. calc. 78−58764
NO, triple-dipole energy calcs. using pseudo-spectral theory 78−46418
N_2O, triple-dipole energy calcs. using pseudo-spectral theory 78−46418
$N(^2S)+N^+(^3P)=N^+(^3P)+N(^4S)$, gerade-ungerade splitting of N_2^+ pots., cross sections 77−30987
$^{14}N^{14}N+^{14}N^{15}N$, vibr. distrib., electron impact excitation, isotopic composition, interaction depend. 79−29332
Na, liq., effective interionic potentials 78−91221
Na^++ether(thioether)(amide) interaction, pair pots., ab initio SCF LCAO MO calc. 79−36721
$(NaCl)_n$ (n=1-7) equilib. configs., total energy calcs., far IR spectra 78−29872
NaF oligomers, struct., stability SCF and CEPA-PNO calcs. 78−78640
NaH oligomers, struct., stability SCF and CEPA-PNO calcs. 78−78640
$Na^+(H_2O)n$ (n=1,2,4,6), FSGO-pair-pot. calcs. *(German)* 80−74278
NaN_3, struct. phase transform., microscopic model 79−65022
$Na^*(3p)+Na_2$, collisional and radiative processes, fluoresc. decay obs. 78−66638
$NeCO_2$, energy transfer, anharmonic coupling terms, semiclassical calcs. 80−37861
O, triple-dipole energy calcs. using pseudo-spectral theory 78−46418
$O+N_2$, intermolecular pots. from Thomas-Fermi-Dirac functional 77−19009
O_2, liq., photoluminesc., dimer effects 78−31233
O_2, liq. and gas, induced absorpt. spectral moment, mol. calcs. 80−63737
O_2, structural second virial coeff., intermol. pot. and mag. scatt. 80−78678
O_2, triple-dipole energy calcs. using pseudo-spectral theory 78−46418
O_2, viscosity rel. to ionis., skin friction of wetted oscill. disc 78−34252
OCS, IR spectral moments and mean squared torques, rare gas effects 78−62944
PBr_3, Raman scatt. spectrum, intermol. interaction and dimeric assoc. *(Russian)* 77−54562
Pb, liq., effective interionic potentials 78−91221
Pt fibres crossed in air, mol. attraction meas. as function of dist. 78−13566
Rb, liq., effective interionic potentials 78−91221

intermolecular forces continued
SF_6+N_2, simultaneous vibr. transition, absorpt. band intensity 77−50474
SO_2-$^{18}O_2$ mixtures, IR laser pumped, intermol. vibr. energy transfer dynamics obs. 80−87207
SbI_3, intermolecular bonding study using ^{129}I Mossbauer effect 78−72438
^{129}Xe, chem. shift in CH_4, CF_6 and SiF_4, chem. shielding 77−6707

intermolecular mechanics
see also association; intermolecular forces; kinetic theory of gases; liquid structure; liquid theory; Morse potential; potential energy functions
absorption profiles, relax. mechanisms effects 78−58664
acetaldehyde, soln., C-O stretching band intensity calcs., intermol. interaction effects 77−68081
acetone, ^{17}O chemical shift and NMR linewidth meas., self-association equilib. const. determ., mol. reorientations obs. 80−87148
adamantane-adamantane interactions, expansion of intermol. energy in set of symmetry-adapted functions 80−106371
aggregation in membranes, fluctuation-induced interactions in liquid crystals 77−90732
n-alkanes, anisotropic London dispersion forces, surface effects 80−74214
alkanes, solvent effects, quantum mech., macroscopic electrostatic contribs. 77−30801
alkylammonium iodides, solns., MCD spectra of iodide ions 78−94268
aminoborylpolyynes, intermolecular interaction through triple bonds, internal rot. 80−106370
4-aminomethylphthalimide-decalin-n-propanol, electronic spectra of 3-component solns., temp. depend. 79−4822
aminopolyynes, intermolecular interaction through triple bonds, internal rot. 80−106370
aniline-chlorophenol complexes, ^{35}Cl NQR, inter- and intramol. interactions 80−63666
anisotropic intermolecular potentials, mol. beam investig., review 79−72376
anthracene, vibronic absorpt. spectra in soln. and cryst., universal mol. interactions effects 77−68031
antimalarials, interaction with coenzyme-Q_{10}, theory 78−27885
athermal model chains, pair distrib. function, Metropolitan Monte Carlo calcs. 78−17827
atom+symmetric harmonic oscillator, vibr. energy transfer, 1-D and 3-D rate consts. calcs. 78−50611
azabenzenes, multipole moments, polarisabilities and long-range interaction coeffs. calcs. 79−89599
benzene+acetone, energy transfer cross-sections, generalised oscill. strength calcs. 79−10173
benzene binary liquid mixtures, US study of mol. interaction 77−15494
benzene-d_6, intermol. dynamics, neutron scatt. obs. 79−863
bimolecular potentials, forces and torques, S- and V-function expansions 78−74730
binary gas mixtures, force consts., intermol. pots. calcs. 78−66624
binary liquid mixtures, excess Gruneisen parameter and intermolecular interactions 77−20082
binary liquid mixtures, mol., intermol. props. from excess enthalpies 77−44503
biomolecular aqueous solution, attractive and repulsive dispersion forces 78−44447
biosystems, informational interaction, cooperative mechanism 78−15756
bromoethane, liq., relative mol. orientation appl. of nucl. mag. relax. data 79−41933
bromoform, Raman spectra, intermol. interactions 79−76436
butene-cis-Li^+ complex, intermolecular interaction energy, PCILO calc. 77−34572
carbon tetrachloride, isotropy, mol. interactions, effects, Raman scatt. obs. 78−58697
carbon tetrachloride-chloroform (methyl cyanide) solutions, anisotropic light scatt., interactions between solvent and solute mols. 78−27239
carbon tetrachloride-pyridine(anisole)(acrylontrile)(acetyl-acetone) mixtures, excess volume of mixing, mol. interactions 79−57281
cationic dyes, adsorbed ionisation energy, local environment effects 79−34337
chains, one-dimensional, shock wave effects, mol. dynamics study 79−4371
chiral molecules, averaged discriminatory interactions, chem. effects 78−13562
chloroanisoles, ^{35}Cl NQR, inter- and intramol. interactions 80−63666
chloroform-d_1, isotropy, mol. interactions, effects, Raman scatt. obs. 78−58697
chlorophenols, ^{35}Cl NQR, inter- and intramol. interactions 80−63666
collision broadening, short-range interaction effects 77−42355
complex-energy states in molecular dynamics 79−72374
compressed gases, intermol. interactions, translation absorption spectra, temp. depend. 78−46419
computer modelling of matter, conf., Anaheim, USA (March 1978) 80−51954
conformers, dynamic interaction between ground states, effect on IR spectra 78−58967
correlated Π-electron systems, mol.-interactions, linear response theory 80−53090
Coulomb centres with different charges, asymptotic expansions 80−69211
coulombic potentials, two virial theorems 77−3429
cyclohexanol plastic cryst. phase, glass transition temp., press. depend. 80−49135
cytochrome c-phospholipid interaction, studied by pulse radiolysis 78−48746
dense systems, intermolecular spectroscopy and dynamical props., conf., Varenna, Italy (1978) 80−82581
derivative autocorrelation functions, atom-atom pot. calcs. 77−58117
diatomic liqs., computer simulation of mol. dynamics 77−50493
diatomic polar molecules, in simple liquids, interactions, far IR absorpt. spectra 78−25527
diatomic polar molecules, in simple liquids, interactions, statistical theory and spectra 78−29779
differential cross sections, rainbow and diffr. oscills. damping, anisotropic pots. 78−50608
difluoromonochloromethane, parameters of Lennard-Jones 12-6, Stockmayer 12-6-3, 6-Exp, Kihary intermol. pots. 77−34711
dilute solutions, Monte Carlo algorithm for preferential sampling near solutes 77−51287

intermolecular mechanics continued
1,3-diphenylisobenzofuran, oxidation, dissoc. oxciplex relax., solute reencounter probabilities 79−34285
dipolar media, 0-10^{12} Hz freq. polarisation, dipole-dipole interaction effects 79−59525
dipolar molecules, IR absorpt. bands., temp. effects *(Russian)* 78−90228
DNA, B-configuration double helix, interaction with H_2O, isoenergy contour maps 79−20504
double well damped motion, proton tunnelling, transfer rate temp. depend. *(German)* 80−87058
dynamics, synchrotron radiation obs. appls. 80−66830
ethane, inclusion of nonbonded interactions in vibr. freq. calcs. 80−95590
exchange potentials, Bonham series representation Born-Oppenheimer calcs. 79−10169
excimer, fluorescence, relative yield following triplet-triplet annihilation, re-encounter effects 78−33538
excitation to coherent state, resonant energy transfer calcs. 79−98178
fermions, constrained variation in Jastrow method at high density, neutron system, liquid ^{3}He appls. 77−5753
fluid, one dimens., Kirkwood modified Tait eqn. of state 78−8372
fluid mol. theory, Kihara pot. *(Spanish)* 77−68902
fluids interacting with Kihara potential, thermodynamic props. using cell theory with holes *(Spanish)* 77−72400
fluids with Lennard-Jones and soft sphere pots., thermodynamic props. using method of mol. dynamics *(Spanish)* 77−72533
fluorescence in presence of strong driving field, stochastic Liouville eqn. 79−59503
fluorinated hydrocarbons, mol. recognition and self-organisation, information storage appls. 78−82806
Fokker-Planck eqns., stochastic modeling 80−43128
formamide, hydration by H_2O mol., point charge model 77−34569
free-length determination in liquids at cryogenic temp. 79−82131
gas, forbidden volume, van der Waal's gas equation 77−60864
gaseous relax. phenomena, few-level approx. validity 80−53097
gaussian overlap model potentials 77−75251
ground state alkali molecules, mag. shielding and spin-rot. interaction 80−87186
guest/host mixed crystal systems, thermally activated intermolecular effect of deuteration on guest phosphoresc. 79−43010
haemoglobin, in salt soln., diffusion rel. to intermol. interactions, light scatt. investig. 77−44585
Henry constant, rel. to intermol. interaction pot., review 78−22948
heterocyclic N-containing compounds, crysts., intermol. pots. calcs. 80−49169
heteronuclear dumb-bell fluid, local struct., reference interaction intersite model 77−11458
hexafluorobenzene-benzene, liq., mol. interactions, IR and Raman lineshape obs. 80−28907
hexamethylbenzene, mol. dynamics, allotropy, solid-state phase transitions effects, Raman spectra *(French)* 77−42372
homonuclear diatomic mols., force-torque correls. 80−87196
hydrocarbons, thermodynamic props., multiparameter conformal solution theory 78−18796
hydrodynamic friction on moving molecule 79−27732
hydrophobic interactions 78−37777
inert gas interactions, correl. and exchange energies, statistical methods calcs. 78−86931
inert gas mols., Lennard-Jones 12:6 parameters calc. from viscosity data 77−46612
interaction pot., extended law of corresponding states 79−81251
intermolecular correlation, approximation scheme 79−26905
ion molecule collisions, energy transfer, modified statistical theory 79−50107
Kirkwood superposition approximation, $\chi'(r)$ nondiagrammatic cluster props. 77−47129
Lennard-Jones gas, Ising model, critical parameters from cluster integrals 77−11297
Lennard-Jones molecules, dilute gas, density fluctuations, dynamic struct. factor 79−99044
linear molecules, dispersion forces calcs. 80−9675
linear molecules, forced rot. diffusion, nonlinear aspects 79−90503
linear rigid rotors, scattering calcs., ab initio intermol. pots. fitting 77−83680
lipid films, at fluid interfaces, phys. chem., review, book contrib. 77−39725
liquid, intermolecular nucl. relax. by translational and rot. diffusion, effect of pair correl. functions *(French)* 79−19794
liquid, NMR in Earth field range 80−50206
liquid crystal, chain ordering model 80−24357
liquid structure and dynamics from light scatt. spectra 80−55105
liquids, solute-solvent interactions, moment anal. of IR absorpt. bands 78−58766
long-range anisotropic interactions between molecules of arbitrary symmetry, derivation by irreducible tensor method 80−69207
luminescence of solutions under powerful excitation, intermol. relax. effect 79−85985
Manoxol OT-cyclohexane-water reversed micellar system, singlet-singlet energy transfer 80−9531
matrix isolation vibrational spectra, appls. 78−46416
MBBA/non-mesogenic cpd., binary nematic mixtures, dielec. relax. and intermolecular interaction 79−91350
methane, intermolecular interaction energies calcs. using minimal basis sets 80−78681
methane, Lennard-Jones 12:6 parameters calc. from viscosity data 77−46612
methane, solid, plastic phase, mol. dynamics simulation 80−79715
methane-methane interactions, expansion of intermol. energy in set of symmetry-adapted functions 80−106371
3-methylpentane, C-H stretching diagonal local mode anharmonicity, intermol. perturbation 78−25524
microdrop, two-dimensional, on solid body surface, stability dynamics 78−51790
moderately dense gases, molecular interactions, neutron scatt. 79−50144
molecular beam scattering experiments and techniques *(German)* 78−86971
molecular crystals, intermolecular interactions, spectroscopic studies, review 80−103958
molecular crystals, PCILO calculations 77−34571
molecular dynamics, allotropy, solid-state phase transitions effects, Raman spectra *(French)* 77−42372
molecular fluid, pair correlation function, perturbation theory 78−55799
molecular fluids, diatomic, struct. and dynamics 80−38889
molecular liquids, glass transition temp., press. depend. 80−49135
molecular structure theory, quantum topology 80−106247
momentum distrib., binary cluster term evaluation, 3D Lennard Jones gas, 1D hard rod gas 77−37808
n-body potential energy functions, for teachers 79−40318
nonane dimer, intermolecular interaction energy, PCILO calc. 77−34572
nonlinear oscillators, 1-D, intramolecular vibr. energy transfer, quantal, classical and statistical behaviour 80−91641
nonpolar molecules, intermol. interactions in intense radiation field 80−78679
nucleic bases, interactions and self-organisation, ionisation and solvent salt comp. effects 80−55985
nucleotides, interactions and self-organisation, ionisation and solvent salt comp. effects 80−55985
optically active and inactive molecules, electric and mag. dispersion forces interaction 80−99533
organic molecular crystals, intermolecular interactions, spectroscopic studies, review 80−103958
organic molecules, complexes with rare earth ions, energy transfer in strong donor solvents 79−54930
orientational correlation functions, dipole-dipole coupling 79−36798
pentyl ion+methane, energy transfer, modified statistical theory 79−50107
phase and population relax., semigroup formalism 80−78519
phase diagrams, step pot. particles, 2- and 3-dimens., mol. dynamics 79−28072
phosphine 3R hydrochloride, interaction with aliphatic acids and alcohols, IR and electron spectra *(Russian)* 78−21930
phthalimide derivatives, solns., ultrafast mol. relax. 79−85984
picosecond phenomena, conf., Hilton Head, USA (May 1978) 79−44940
plastic crystal, dipolar autocorrelation function, phonon contrib., IR absorption 78−42928
plastic crystal, glass transition temp., press. depend. 80−49135
PMMA, secondary loss peaks, effect of structural features 79−11649
polar fluids, intermol. and thermodynamic potentials, angle-depend. pot. 78−22618
polar fluids, intermol. and thermodynamic potentials, preaveraged pot. 78−22617
polar gas, second virial coefficients for four-parameter model 78−14121
poly N,N-diallyldimethylammonium chloride, soln. props., struct. 79−94861
polyatomic asymmetric top molecules, solns., IR spectra 78−58694
polyatomic molecular mixtures, Waldmann-Snider collision integrals, transport phenomena study 80−18900
polyatomic molecules, force and interaction consts. of ang. coords. 79−27054
polyatomic organic molecules, electronic excitation transport in inhomogeneity broadened 79−54884
polyethylene oxide in benzene solns., ^{1}H relaxation times, intermol. interactions 77−32281
polymer crystals, melting, intramol. and intermol. interactions effects 78−18745
polymer solution, intermolecular interaction phenomena *(Russian)* 77−21414
polymer solution, Rayleigh scattering, intermolecular correlations effect 80−75146
polymer solutions, order, conf., Midland, USA, (Aug 1973) 79−10769
polynucleotides, interactions and self-organisation, ionisation and solvent salt comp. effects 80−55985
polyphenyl ether, glass transition temp., press. depend. 80−49135
polyynes, intermolecular interaction through triple bonds, internal rot. 80−106370
potential energy wave calculations, and interactions, review 80−43140
purple membrane of Halobacterium halobium, energy transfer 78−44467
pyrene, micellar system, fluoresc., solubilisate distrib. statistics, kinetic model 79−34366
pyridine-H-bond donors, D spin-lattice relax. meas., mol. interactions anal. *(French)* 80−87151
quantum chemical intermolecular integrals, calc. using truncated Gaussian expansions of atomic orbitals 77−88520
quantum intramolecular dynamics: criteria for stochastic and nonstochastic flow 80−53082
real gases, thermodynamic props. and intermol. pots. *(German)* 78−17743
rigid polyatomic molecules, classical statistical mechanics 78−16718
Schwinger and Kohn variational phase shift calculations, comparison 80−78672
simple liquid, new integral eqn. for struct. calcs., interparticle pot. reconstruction 78−5999
solution, electronic bands statistical broadening depend. on intermol. interaction 77−71837
spin polarisation, analysis using intermolecular interactions theory, chemical polarisation, exchange repulsion 80−76510
stable molecules, matrix isolation spectroscopy obs., appls. 78−46320
statistical method, appl. to interactions theory, supermolecular density calcs. 79−6983
Stockmayer-type polarisable mols., N-particle dynamics 77−68089
surface tension, of liquid in equilib. with vapour, lattice model 77−43409
T_1 and T_2, by microwave meas., zero- and non-zero field 79−45738
TCNE, electron donor-acceptor complexes, EPR *(German)* 78−55187
TCNQ, electron donor-acceptor complexes, EPR *(German)* 78−55187
ten-atom model, interaction forces 79−59528
tetracene molecules in Ar clusters, excited state intramol. dynamics, laser-induced fluoresc. spectra obs. 80−78674
thiazolidine, IR spectroscopy of mol. association *(French)* 79−50178
three-body Coulomb interaction, adiabatic representation, exchange interactions 79−31640
triatomic molecules, C_{2v} symm., vector statistical distrib., mol. dynamics computer simulation 80−63734
bis-triazolopyridazines, conformation calcs. by mol. mechanics and CNDO/2 method 80−69079
bis-triazolyls, conformation calcs. by mol. mechanics and CNDO/2 method 80−69079
two-body interaction coefficients, C_8 and C_{10}, point-charge model calcs. 79−36719
velocity redistribution by optical processes 78−38448

intermolecular mechanics continued
wetting, mechanism, mol. dynamics 78−51789
Ar, fluid, vel. autocorrel. functions calcs. 77−58944
Ar, liq. nuclei, thermodynamic props. mol. dynamics calc. *(Russian)* 77−47325
Ar, Paschen (1s) reson. state, decay mechanism and kinetics 79−27021
Ar-Kr, internal pot. function calcs. 79−68292
Ar-methane (iodomethane), mol. interactions, differential scatt. cross-sections meas. 79−89732
$Ar+Br_2$, effective vibr. pot. of Br_2 in Ar gas, Monte Carlo simulation 79−59526
$Ar+N_2(O_2, CO)$, molecular fluid mixtures, equilibrium props. 80−64867
ArHCl, mol. interactions, differential scatt. cross-sections meas. 79−89732
ArKr, intermol. pots., differential cross-sections inversion calcs. 78−66619
ArKr, mol. interactions, differential scatt. cross-sections meas. 79−89732
AsH_3, plastic cryst., dipolar autocorrelation function, phonon contrib., IR absorption 78−42928
$BaCl_2.2H_2O(D_2O)$, lattice vibr., IR and Raman spectra 79−15443
CO, Lennard-Jones 12:6 parameters calc. from viscosity data 77−46612
CO, second virial coeffs. 80−83440
CO_2, Lennard-Jones 12:6 parameters calc. from viscosity data 77−46612
CO_2 refractive index meas., intermolecular interaction effects 80−33728
$CO(v=1)+He$, vibr. relax., collinear and 3D rate consts., temp. depend. 77−38717
$CO(v=1)+He$, vibr. relax., collinear and 3D rate consts., temp. depend. 77−38718
CS_2 liquid, Rayleigh and Raman bands, intensities of interaction induced components 80−63645
Cl_2, liq., mol. motion, Raman spectrum 78−5236
Cr^{3+} hydration model, external water interactions 78−78772
Cu_2Se-Cu_2Te, intermolecular interaction, thermodynamic anal. of dissociation pressure 80−53088
DCl, plastic cryst. phase, struct. and dynamics 80−92469
D_2Ne, mol. interactions, differential scatt. cross-sections meas. 79−89732
p-dichlorobenzene, mol. dynamics, allotropy, solid-state phase transitions effects, Raman spectra *(French)* 77−42372
$F+H_2$, collision in intense laser field, formalism for mag. dipole interaction 79−98190
o-H_2, in solid p-H_2, interactions 77−68088
H_2, ortho-para mixtures, 10 to 23K, rot. Raman spectra, quantum calcs. 77−6700
H_2-H_2 dimers, hyperfine struct. in zero mag. field 80−95700
H_2+H_2, dispersion forces calcs. 80−9675
H_β, Stark broadening, wings calc. 79−31464
$(HBr)_2$, intermol. distances, dipole moments, MINDO/3 and IR intensities and shifts calcs. 78−46335
HCL, fluid states, mol. dynamics simulation 80−79671
HCl, liquid, struct. and mol. dynamics studied using intermolecular force models 80−83445
$(HCl)_2$, intermol. distances, dipole moments, MINDO/3 and IR intensities and shifts calcs. 78−46335
HF+HF, interaction energy, multipole anal., charge overlap, orientation and bulk props. 77−34715
H_2Ne, mol. interactions, differential scatt. cross-sections meas. 79−89732
H_2O, intermolecular interaction energies calcs. using minimal basis sets 80−78681
H_2O, liq., intermol. coupling, isotope and salt effects, Raman spectra 78−90169
H_2O, mol. interactions, nonadditive pot. model, quantum mech. data fitting 78−1047
H_2O-lysozyme, interaction, intermol. pot. calcs. 77−75250
H_4O_2, intermolecular interaction energy, PCILO calc. 77−34572
He-Ne(Ar)$(N_2)(CO_2)$, thermal diffusion factors, (m,6,8) pot. calcs. 79−50835
$He+CO_2$, anisotropic intermol. pot. for differential scatt. cross-section 79−13788
I_2, photolytic cage effect in gas phase 80−81345
IF_5, second virial coeff. meas., Lennard-Jones pot. determ. *(German)* 77−19658
$K+N_2(CO)$, anisotropy of the repulsive intermolecular potential from rotationally inelastic scattering 79−41226
Kr, molecular dynamics simulations, three effective interactions 79−69224
Kr, potential, predictive ability for dilute gas, bulk and microscopic data 79−81250
Kr-Ar, mol. interactions, thermodynamic props.. mol. dynamics calcs. 77−61044
Li projectiles, electronic stopping cross section meas., intermolecular interactions 80−75279
$Li^+ + H_2O$, ab initio GTO calc. of vibr. intensity changes of spectroscopic parameters 78−58583
LiF+Ar(Kr), anisotropic system intermol. pot. determ. 77−58121
$(LiF)_n$, 'polymers', aggregation, microcryst. form., IR spectra obs. 78−46331
LiH+LiH, interaction energy, multipole anal., charge overlap, orientation and bulk props. 77−34715
MgH, Morse and Lippincott pots., r-centroids, dissociation energy 78−13446
$Mg^{2+}.nH_2O+PO_4H_2^-$, binding mechanisms, SCF ab initio calcs. 79−22586
MnII-ATP system, exchange mechanism, FT NMR and EPR obs. 79−22733
MoF_6, second virial coeff. meas., Lennard-Jones pot. determ. *(German)* 77−19658
N_2, ab initio MO-LCAO-SCF and Gordon-Kim intermolecular pot. for seven different orientations 80−95522
N_2, Lennard-Jones 12:6 parameters calc. from viscosity data 77−46612
N_2, liq., computer-simulated ang. correlations and rot. motion 77−11461
N_2, pair pot. 2nd virial coeff., nonproduct integration algorithm calc. 77−47128
N_2, second virial coeffs. 80−83440
N_2+N_2, dispersion forces calcs. 80−9675
N_2+N_2, interaction energy, multipole anal., change overlap, orientation and bulk props. 77−34715
N_2+O_2, molecular fluid mixtures, equilibrium props. 80−64867
$^{14}N_2+CO$, vibr.-vibr. energy transfer, long and short range pot. effect 80−99556
$^{15}N_2+CO$, vibr.-vibr. energy transfer, long and short range pot. effect 80−99556
$(N_2)_2$, Van der Waals molecule, struct. and internal rot. barriers determ., interaction pot. from ab initio calcs. 80−91626
NH_4Cl, aq. soln., struct. props., mol. dynamics simulation 79−82142
$^{14}N^{15}N+CO$, vibr.-vibr. energy transfer, long and short range pot. effect 80−99556
NO, adsorbed on MgO, dimer form., heat of dissoc., EPR obs. 78−82755
NO, Lennard-Jones 12:6 parameters calc. from viscosity data 77−46612
NO_2^- hydrate clusters, ground-state HF pot., Monte Carlo simulation, energy surfaces and rot. barriers 80−106412
$Na^+.nH_2O+PO_4H_2^-$, binding mechanisms, SCF ab initio calcs. 79−22586
Ne-Ar(He), thermal diffusion factors, (m,6,8) pot. calcs. 79−50835
Ne-Xe, equilibrium of coexisting phases 80−87197
O_2, Lennard-Jones 12:6 parameters calc. from viscosity data 77−46612
O_2, mol. dynamics, solid-state phase transitions effects, Raman spectra *(French)* 77−42372
PF_5, second virial coeff. meas., Lennard-Jones pot. determ. *(German)* 77−19658
S, mol. dynamics, solid-state phase transitions effects, Raman spectra *(French)* 77−42372
SF_6, refractive index meas., intermolecular interaction effects 80−33728
SO_2-H_2O microwave absorption, 94 GHz by mol. interaction 79−31507
Si_xO_y structures, $Si(OA)_4$ clusters, A=H,Li,K, HMO calcs., energy stability, charge distrib. *(German)* 79−89822
WF_6, second virial coeff. meas., Lennard-Jones pot. determ. *(German)* 77−19658
Xe-Ar, mol. interactions, thermodynamic props., mol. dynamics calcs. 77−61044
Xe-inert gas mixtures, far UV spectra, press. (temp.) depends., interaction consts. 77−61698
$ZnCl_2$, aq. solns., complex IR refr. indices, IR spectra, mechanisms, spectrometer system 78−43831

intermolecular vibrations *see molecular rotational-vibrational energy transfer*

intermolecular vibrations (molecular crystals) *see lattice dynamics of molecular crystals*

internal combustion engines
acoustic emission, exhaust manifold design and cylinder firing order effect on short term spectrum 77−14845
automobile air-intake flowmeter using corona discharge principle 80−33716
carburation enhancement by electrostatic atomisation of petrol 78−27829
concentration fluctuations, meas. 80−71973
diesel, combustion chamber flow meas., transit time of spark charged plasma cloud determ. *(German)* 80−14861
diesel, environmental pollution effects *(Croatian)* 80−55961
diesel, exhaust noise, single monopole very low freq. noise source in air duct 80−64282
diesel, open chamber, knock-induced cavity resonances 79−81624
diesel, piston slap, assessment of contribution to overall noise and vibration 80−79055
diesel, transient fuel jet droplet photography using light pipes 80−23784
diesel engine composite pistons, heat transfer calc. method *(French)* 78−63424
diesel engine noise, Lucas CAV research 79−50507
diesel engine noise analysis, diagnosis and control 80−58857
diesel engine noise radiation mechanisms 79−32135
diesel engine noise research at Perkins Engines 79−32136
diesel engine pistons, simulation of slap at TDC 77−72222
diesel engine radiating surface identification by partial coherence technique 78−42490
diesel engines, corrosion-resistant plasma-sprayed coatings 79−24675
diesel engines, high-speed, influence of piston slap and crankshaft torsional vibration on engine struct. noise 80−53555
diesel-driven chiller system simulation, with multi-tank thermal storage system, for large commercial buildings appl. 79−48187
efficiency of small engines, effect of mixture strength fluctuations 80−30526
efficient studies using laser anemometer 80−53307
exhaust air pollution in Netherlands *(Dutch)* 80−101138
exhaust system, acoustic characts. in presence of mean flow 77−837
exhaust systems, appl. of transmission matrices for noise control 80−53554
fuel, alcohols as auxiliary fuels 80−61230
generator noise control 79−43800
heat exchange, b.c.s of 1st kind determ. from b.c.s of 2nd kind, numerical method *(Russian)* 79−68554
heat pump drives, economic advantages *(German)* 79−74535
highly loaded, exhaust gases temp. and velocity meas. using two thermometer method *(German)* 80−31754
ignition by plasma jet 78−38555
laser Doppler anemometry in internal combustion engine cylinder 79−77296
marine two stroke compression ignition engines, heat exchange modelling 80−30529
microwave heating of flame plasma for enhanced combustion 79−20369
muffler design, scaling rules using Buckingham's pi principle 79−14152
piston impact noise, prediction models 80−53553
pulsating temp. and vel. measurements using US flowmeter 80−1704
pumps appl., economic comparison with solar pumps 79−74507
Rankine cycle, waste heat recovery from ceramic tunnel kilns, using tetra-chloroethylene as working fluid 79−52955
rotary expander engine, 250 hp, development program 80−30527
spray, numerical computation, appl. to engines 79−37378
Stirling engine powered heat pump, heat activated, system level performance 79−48164
temperature and species noninvasive meas. by CARS 80−30293
thermo-nuclear fusion based, using electron beams, progress and technical problems *(French)* 78−746
torsional vibr. dampers using silicone oil, props. of oil at various freqs. *(German)* 78−67164
velocity meter, appl. of photodiodes, for internal combustion engine 77−57303
vibration, transmission path and dynamic behavior, background and static tests 80−43520

internal combustion engines continued
vibrations, transmission path and dynamic behavior, motoring tests 80−48487
viscous boundary layer, hybrid random choice method, internal combustion engine appl. 80−38461
CO_2 4.3 μ band radiance meas. of internal combustion engine gas temp. *(Japanese)* 78−29119
H_2 powered, electronic fuel injection techniques 80−72094
H_2-fuelled cf. battery electric vehicles 80−45819
H_2-powered, electronic fuel injection techniques 80−45622
NO, combustion gas sampling system and valves for sampling during engine expansion process 78−24380
Pb concs. in petroleum rel. to airborne particulate Br levels 77−91254

internal conversion
see also conversion electron spectra
γ-ray internal pair conversion, form. of monoenergetic e^+ 79−6502
anthracene, carbonyl derivatives, triplet state population, picosec. laser obs. 78−13544
atomic electron screening and correlations, effects on internal conversion coeffs. 80−18237
atomic inner shell ionisation phenomena, conf., Freiburg, West Germany (March.-Apr. '76) 77−27040
atomic shells, internal conversion coefficients, numerical solution of Dirac equation 80−47434
atomic shells $30 \leq Z \leq 104$, Hartree-Fock-Slater model calcs. 79−36199
coefficient calculation discrepancies, reasons 79−9512
coefficients, higher approx. and near-threshold behaviour 79−6501
conference on nuclear spectroscopy and structure, Alma Ata, USSR, (Mar. 78) 79−75809
conference on nuclear struct. spectroscopy and atomic nucleus struct., Tashkent (Mar. 77) 79−6470
double K-shell vacancy creation per internal conversion 79−45212
E0 conversion, reduced probability, quadrupole moment effects 80−18235
E0-conversion, reduced probability, quadrupole moment effect 80−78138
E2 α_k conversion coeffs. for $2^+ \rightarrow 0^+$ transition, review 78−17143
even-even nuclei, internal conversion coeffs. of $2^+ - 0^+$ E2 transitions 80−9268
gamma-ray internal conversion coeffs. for all at. shells, $30 \leq Z \leq 104$ 79−45206
hadron-hadron, e^+e^- pair prod. calc., high energy internal conversion of bremsstrahlung photons 79−420
haloazulenes, S_2-state deactivation, intersystem crossing and heavy atom effects 78−13545
Hartree-Fock-Slater and Hartree-Fock models 80−18238
heavy nuclei, quadrupole moment effect on internal conversion coeff. *(Russian)* 77−82867
in-beam electron spectroscopy meas. of internal conversion coeff. 78−13374
inner shell electron rearrangements in radioactive decay 77−18881
inner-shell vacancy filling detector, scintillation counter 77−18749
isomer shifts, total conversion coefficients, nuclear electron and gamma transitions importance 79−85411
K X-ray nuclear satellites from (p,xn) reacts. on heavy elements 80−27599
K- and L_1-subshells internal conversion coeffs., relativistic effects 78−66245
K-shell internal conversion coeffs. for pure E2 transitions compilation anal. 79−75910
light elements, γ-ray internal conversion coeffs. 77−82866
M1 transitions, conversion nuclear parameters of odd spherical nuclei, penetration matrix elements 80−22763
mesoatoms, prompt fission internal γ-ray conversion, fragment radiative transitions *(Russian)* 80−86944
mono-energy pair conversion of nuclear multipoles, form factors, Hartree-Fock-Slater wave functions *(Russian)* 79−93555
multipolarity mixing parameter determ. program 80−52626
pair conversion particles, angular distribs. 79−6498
pair formation high resolution in-beam studies with magnetic+Si(Li) spectrom. 79−18073
penetration effects and nuclear structure 79−75907
penetration effects in total internal conversion probability 78−13026
polarisation of conversion electrons, parity violating nuclear forces 78−50125
radioactive decay lifetimes, influence of chemical environment, review 79−75911
radioactive nuclide decay data for reactor calcs., activation products and related isotopes 78−82426
radionuclide decay, computer simulation, levels, transitions, internal conversion 80−63136
renormalisation of g_s factors in conversion transitions, spin-force consts. 77−61347
screening effects L_1, K-shell internal conversion coefficients, nonrelativistic dipole approx. calcs. 77−71588
superheavy collision systems, positron prod., internal conversion 80−5168
weak neutral currents, internal conversion probe from M1 decay, nuclear matrix elements 79−67712
$Z = 30$ to 104, E5, M5 transition coeffs. 79−26396
$Z \leq 30$, internal conversion coeffs. 77−46136
μ-mesic conversion of γ-rays 77−82865
(n,e^-) high precision spectroscopy, internal conversion coeffs. for nuclear struct. 80−37353
^{A}Ag, A=105, 107, 109, 111, isomeric transition internal conversion, γ-transition energies and e intensities 79−6503
^{108}Ag transition multipolarity and conversion electrons from ^{107}Ag(n,e^-) 80−52627
^{109}Ag, internal conversion of high-multipolarity transition 77−2945
^{242}Am, mag. dipole moment-atomic electron satellite states, influence on E0 conversion 80−18236
^{242}Am, reduced E0 conversion due to mag. moment effects 80−83034
^{72}As, populated in ^{72}Ge(p,nγ), level scheme determ. 77−14032
^{208}At energy levels and transitions, IC electrons from ^{208}Rn decay 80−18242
^{191}Au, monopole conversion, magnetic dipole transitions, latent penetration effect 79−9464
^{195}Au decay, K-shell capture fractions, internal conversion electrons, coincidence techniques 80−57743
^{137m}Ba, internal conversion decay, double K-hole creation 77−18887
^{204}Bi excited states, γ rays, conversion electrons and $\gamma\gamma$ coincidences from ^{204}Po, EC 80−18241

internal conversion continued
^{76}Br, new isomeric state with half-life 1.49 sec 79−17858
^{12}C, internal pair emission branch of 7.65 MeV, stellar triple-α reaction 77−54183
^{109}Cd, 11 μs isomeric level, spin and parity determ. by ^{108}Pd$(\alpha,3n)$ *(French)* 78−8738
^{109}Cd decay, double K-shell vacancy creation per internal conversion 79−45212
^{109}Cd, double K-shell vacancy creation probability 77−54182
^{114}Cd(n,e^+e^-), thermal 77−26624
^{A}Ce, A=124-127, half lives, low energy γ-data, β decay probabilities 79−499
^{141}Ce decay, internal conversion coefficient, efficiency extrapolation technique 79−30806
^{144}Ce, low energy conversion lines resolution using fast discriminator cct. 80−5450
^{139m}Ce, internal conversion of N=81 isotones 78−13027
^{250}Cf two-quasiparticle states populated by ^{250}Es^{m} EC decay 77−46140
^{252}Cf spontaneous fission, prompt element yields determ. from X-ray multiplicities 77−30643
^{245}Cm, from ^{249}Cf α-decay, γ-spectra and internal conversion spectra 79−6477
^{127}Cs, 66-keV decay, $T_{1/2}$, K conversion coeff. 77−54184
^{133}Cs, 161 keV transition M1-E2 mixing ratio and nucl. struct. parameter 78−74332
^{137}Cs decay determ. by β-ray spectrometry 79−26397
Dy atom K-shell ionisation and X-rays from ^{158}Gd(α,xn) 79−93960
Dy K-shell internal conversion yields, gamma transition multipolarities from (α,xn), $(^{12}C,xn)$ 80−78215
^{151}Dy decay, ^{151}Tb lower excited state lifetimes, ^{151m}Tb isomer 79−75919
^{153}Dy β-decay to ^{153}Tb, decay scheme, weak deform. in ^{153}Tb 77−41884
^{155}Dy, γ-ray angular correlations 79−6494
^{160}Dy, quasi-continuum transitions multipolarities from ICC via ^{160}Gd$(\alpha,4n)^{160}$Dy 77−82945
^{17}Eu, transitions in ^{147}Gd decay 79−6475
^{153}Eu, EM transitions, multipole, internal conversion coeffs. *(Russian)* 80−63121
^{154}Eu, level scheme, populated by thermal neutron capture, conversion electron spectra 77−61374
^{156}Eu$\rightarrow$^{156}Gd, elec. monopole transitions from excited 0^+ states in ^{156}Gd 77−18478
^{56}Fe low lying levels, J^π, γ-γ coincidences, internal conversion from ^{56}Co β^+-decay 80−86815
^{57}Fe, 14 keV state excitation by synchrotron radiation 78−25147
^{57}Fe conversion electron Mossbauer spectroscopy at low temps., proportional counter 77−10542
^{224}Fr$\rightarrow$^{224}Ra, γrays, internal conversion, eγ coincidence spectra meas. 80−78216
^{146}Gd, 3^- 1579 keV first excited state 78−41670
^{146}Gd decay, γ- and internal conversion electron spectra 79−75916
^{67}Ge, from ^{64}Zn(α,n), coupling consts., M1, M2, E3 transitions 78−89823
^{67}Ge, mass excess and low lying states, comparison with ^{63,65}Ni, ^{65,67}Zn and ^{69}Ge, from ^{65}Zn$(\alpha,n\gamma)$ 78−66213
HBr^{n+}, highly charged, repulsion energies, nucl. internal conversion, ab initio calcs. 79−76341
^{158}He^{g,m} decay, obs. of ^{158}Dy collective excitations 78−82270
^{180}Hf, penetration effect in M2-component of K-forbidden transition 79−6500
^{199}Hg, internal conversion coeffs., HF calcs. and expts. 77−57628
^{197m}Hg, anomalous K/L conversion coefficients 77−26623
^{157}Ho$\rightarrow$^{157}Dy decay, internal conversion electron spectra and eγ coincidences *(Russian)* 80−68604
^{129}I, γ-ray and X-ray radiation, internal conversion coeff. 79−6499
^{129}I, internal conversion electron and Mossbauer spectra, calibration of isomer shift 80−39921
^{108}In high spin struct., in-beam spectroscopy, conversion electrons from ^{98}Mo$(^{14}N,4n\gamma)$ 80−73782
^{109}In high spin states, transitions, isomeric state, negative parity bands from ^{107}Ag$(\alpha, 2n\gamma)$ 80−451
^{113}In, internal conversion of high-multipolarity transition 77−2945
^{114m}In, K-shell internal conversion, $K\alpha_1$ hypersatellite line energies, intensities 77−18885
^{185}Ir levels populated in ^{185}Pt^{m+g} decay 80−9269
^{81}Kr levels, J^π, ICC via ^{81}Rb 77−79309
^{A}La, A=123-5, half lives, low energy γ-data, β decay probabilities 79−499
^{139}La, 166 keV hindered M1 transition, internal conversion, algorithm for data anal. 77−46137
^{139}La, nuclear structure effect on internal conversion of l-forbidden transitions 79−63632
^{139}La, total IC coefficient for 166 keV transition 79−13613
^{141}La, γ-γ coincidence and elec. conversion meas. 79−13252
^{A}Lu, A=169 to 172, internal conversion electron reference lines, energy value refinement 79−75908
^{169}Lu, internal conversion electron spectrum $E_\gamma < 100$ keV, ^{169}Yb ground state population probability 79−6497
^{172}Lu, decay scheme, γ-ray, conversion electron spectra 79−75913
^{172}Lu, internal conversion electron spectra 79−75906
^{172}Lu, radioactive decay, γ-ray spectra, internal conversion electron spectra 79−75912
^{99}Mo, short lived isomers from photonuclear reactions, internal conversion coeffs. 78−37308
Nb, A=90, 92, short lived isomers from photonuclear reactions, internal conversion coeffs. 78−37308
^{A}Nb, A=92, 94, γ-ray multipolarities, internal conversion coeffs., energy levels 79−63625
^{90}Nb, decay rate perturbation by implantation in metals 77−22944
^{93}Nb^{m}, γ-ray transitions of isomeric level, K-conversion coeff., exchange effects 77−6304
^{93}Nb$(\alpha,2n\gamma)^{95}$Tc, 17 to 27 MeV, band struct. of high momentum states in TC 78−33109
^{150}Nd$(^{20}Ne, xn\gamma)$, multipolarities of yrast and statistical cascades, total γ conversion coeff. 78−70484
^{141m}Nd, internal conversion of N=81 isotones 78−13027
^{191}Os, K-shell internal conversion, $K\alpha_1$ hypersatellite line energies, intensities 77−18885
^{141}PM struct. determ. from ^{141}Sm^{g} decay 77−46142
^{231}Pa α-decay, γ-rays and internal conversion spectrum, ^{227}Ac levels and bands 79−45217

internal conversion continued
^{203}Pb in-beam electron conversion from high spin states from ^{204}Hg(α,5n) 79−93554
^{206}Pb, level scheme including conversion electrons ≲40 eV 78−21518
^{109}Pd decay, double K-shell vacancy creation per internal conversion 79−45212
^{139}Pm decay, states in N=79 ^{139}Nd 77−41929
^{147}Pm decay, K-orbital shake off electrons and X-ray spectra 77−46141
^{147}Pm, internal bremsstrahlung photon intensity and energy yield 78−86509
^{147}Pm, level struct. via ^{148}Nd(p,2nγ) 12.1-20.2 MeV 78−510
^{147}Pm levels, transitions, $\gamma\gamma$-coincidences and IC electrons from ^{147}Nd decay 80−18243
^{204}Po, γ-rays, conversion electron spectra, $\gamma\gamma$ coincidences 80−83061
^{141}Pr, double K-hole creation in 145 keV internal conversion 77−18823
^{141}Pr, internal conversion decay, double K-hole creation 77−18887
^{141}Pr, nuclear structure effect on internal conversion of l-forbidden transitions 79−63632
^{192}Pt, lifetimes of first four excited states 77−294
^{194}Pt, populated in ^{194}Ir decay, level scheme determ. 77−2900
^{193m}Pt decay, K-shell conversion coeff. of 135.5 keV, M4 transition 77−2944
^{225}Ra rotational band level diagram from α-decay and conversion electrons 80−18156
^{90}Rb level scheme, transitions, J$^{\pi}$ assignments and internal conversion coeffs. from ^{90}Kr β-decay 79−67663
^{184}Re decay, energies, relative intensities, of conversion electrons and γ rays 77−61381
^{187}Re, 36.23 keV transition, penetration coeff. and mixing ratio determ. 77−50080
^{210}Rn decay, ^{210}At excited states, spins, parities and rate of population 79−75917
^{224}Rn→^{224}Fr±^{224}Ra, γ−rays, internal conversion, eγ coincidence spectra meas. 80−78216
^{224}Rn→^{224}Fr→^{224}Ra decay, γ-rays IC electrons and eγ coincidences 80−18239
^{101}Ru, short lived isomers from photonuclear reactions, internal conversion coeffs. 78−37308
^{106}Ru β-decay, e^{+} spectra, ^{106}Pd levels and E0 transitions 79−75894
^{113}Sb mean nuclear lifetime from X-ray spectrum in ^{112}Sn(p,p′) 80−9267
^{79}Se, 96 keV transition, conversion coeff., γ-spectrum 80−63131
^{148}Sm levels from ^{148}Eu decay, struct. interpretation from boson expansion model *(Russian)* 78−78261
Sn, internal conversion coeffs. for inner shells of atomic ions and relativistic ionic potentials 80−68600
^{121}Sn^{m}→^{121}Sn^{g}→^{121}Sb, branching fraction, K-shell IC coeff. 78−82319
^{132}Sn level struct., lifetimes, γ-γ coincidences, internal conversion from ^{235}U fission 80−52584
^{91}Sr, decay scheme, gamma-ray spectra 77−71587
^{180}Ta^{m}, β^{-} and EC branching ratios, K-internal conversion coeff., γ-intensities, T 1/2 80−68601
^{181}Ta, anomalous M1-conversion, 482-keV transition, penetration parameter meas. 77−61382
^{182}Ta decay, K-conversion coeff. of γ-rays above 800 keV 77−14069
^{148}Tb, high spin states, transitions J$^{\pi}$ assignments from (Li,xn) and (^{10}B,xn) 79−49582
^{149}Tb, high spin states obs. 80−18158
^{150}Tb, obs. of ^{150}Gd negative parity yrast states 77−88033
^{153}Tb low excited states, γ-ray angular distrib. in ^{153}Dy decay 79−6471
Tc, A=98, 100, 101, short lived isomers from photonuclear reactions, internal conversion coeffs. 78−37308
^{A}Tc, A=94 to 98, γ-ray multipolarities, internal conversion coeffs., energy levels 79−63625
^{93}Tc 17/2^{-} isomer, internal conversion coeffs., parity mixing search from ^{92}Mo(α,2np) 43 MeV 78−78255
^{96}Tc, high spin states, γ-energy, intensity, coincidence, ang. distrib. and electron conversion from ^{93}Nb(α,n) 80−52554
^{100}Tc internal conversion, isomeric level half life from ^{100}Mo(p,n), 3.7 MeV 78−78313
^{99m}Tc, supercond. effect on decay rate, lattice consts., transition temp. 78−41671
^{99m}Tc, X$_{\alpha}$-SW-calc. of chemically induced decay constant variation of Tc in TcO$_4^-$ and hexahalides 79−54769
^{m}Te, A=125,127,129, internal conversion of M4 transitions at 109.27, 88.26, 105.50 keV 77−65214
^{120}Te quasi-rot. band based on proton 4p-2h state, level scheme, transitions from ^{118}Sn(α,2nγ) 80−78119
^{124}Te^{M}, internal conversion in valence shell for M1 and M4 transitions, effect of chemical environment 78−33149
^{125}Te, 109 keV transition, K-conversion coeff. determ. 78−552
^{228}Th decay, γ-ray and internal conversion intensities 78−41669
^{231}Th, L2/L3 vacancy ratio for internal conversion by γ-X-ray coincidence technique *(Spanish)* 79−97682
^{233}Th, vibrational states determ. following (n,e^{-}) 77−30514
^{190}Tl→^{190}Hg→^{190}Au, decay spectra and periods 77−6317
^{203}Tl, nuclear structure effect on internal conversion of l-forbidden transitions 79−63632
^{169}Tm, anisotropic ang. correlation between γ-rays and K X-rays following internal conversion 77−6305
^{169}Tm, double K-shell vacancy creation by internal conversion in ^{169}Yb, EC decay 77−57627
^{230}U decay chain, γ-ray single and coincidence meas., internal conversion spectra obs. 77−6319
^{232}U high spin states and ground state rot. band from ^{232}Th(α,4nγ) 80−47349
^{235}U fission fragments, internal conversion cascading 78−94036
^{235}U internal conversion from 1/2^{+} isomeric state, U^{4+} electron configuration 80−58146
^{235}U(n,e^{-}), ^{236}U low lying levels from 4^{-} isomer decay 80−47396
^{235}U(n$_{th}$,f) ionic charge distrib., effect of internal conversion 78−78428
^{236}U, populated in (n, γf), X-ray prefission yield depend. on fission width 77−10453
^{238}U, nuclear excitation rate in high-temp. environment 78−66244
^{238}U+^{238}U (^{136}Xe), nuclear Coulomb excitation, inner shell ionisation and internal conversion, quasimol. formation 78−94026
^{45}V level scheme, γ-rays, level lifetimes, internal conversion from ^{40}Ca(Li,xn) 80−63085
^{182}W 100 keV E2-transition, L-subshell internal conversion coeff. from ^{182}Ta decay 79−75909
Xe, A=118,120,122, level struct., J, π, following Cs β-decay 77−57601

internal conversion continued
^{136}Xe+Th(Au)(Al), 624 MeV, internal pair conversion positron spectra 77−67769
^{140}Xe, μ-mesic conversion of γ-rays 77−82865
Yb isotopes, A=160-165, decay spectra meas. 77−22959
^{169}Yb, K-shell internal conversion, Kα_1 hypersatellite line energies, intensities 77−18885
^{100}Zr, lifetime meas. of 331.3 keV 0$_2^{+}$ state 78−21523

internal conversion in atoms *see Auger effect*

internal conversion in molecules *see nonradiative transitions*

internal fields, crystal *see crystal field interactions*

internal friction
see also Bordoni effect; damping; Snoek effect; Zener relaxation
alkali halide crystals, dislocation internal friction, orientation depend. 78−48439
alkali silicate glasses, influence of red/ox ratio of multivalent ions 78−31447
alkali silicate glasses, secondary relax. transitions 80−88261
alloy, cold worked, internal friction peak rel. to back reaction annealing kinetics 78−3161
alloys, decomposing, internal friction peaks in grain boundary model *(Russian)* 78−35418
alloys, omega forming 78−19796
amplitude dependence data, statistical processing 80−3114
anelastic relaxations and magnetic aftereffects in solids, conf., Katowice, Poland (Jan. 1978) *(Polish)* 79−96072
austenitic steel, ageing after deform. in pre-martensitic state, internal friction meas. *(Russian)* 77−77477
automated resonance bar damping meas. system 77−2649
automatic resonant-bar apparatus for plotting of internal friction against strain amplitude 79−14358
Bordoni relaxation, theoretical aspects, numerical calcs. from thermally activated double kink formation 78−63805
Bordoni relaxation models, internal friction and microdeformation rel. to dislocations *(French)* 79−37758
α-brass, acoustic harmonic generation by long-range dislocation motion 79−42150
α-brass, reson. vibrs. of metal spheres, elastic consts. and internal friction 78−15443
brittle materials, apparatus for Q-factors meas. 77−27499
ceramic, electrical transducers for automatic recording of mechanisms occurring during drying 77−52561
circular plate, elastic moduli meas., appl. of contactless vibr. excitation and detection method *(Polish)* 79−94571
Collette torsion pendulum, limits of applicability to internal friction meas. 79−14359
complex theory of hysteretic friction 79−18746
composite bar technique for Young's modulus and internal friction meas., multiple reson. 78−35612
concrete, running fatigue test, determ. of loading-deform. charact. and internal damping *(German)* 77−25229
construction element, optimal design in case of impulsive loading 79−86382
Cotac 74, directionally solidified composite, creep behaviour prediction *(French)* 78−68754
creep, high-temp., friction stress meas. validity 79−74219
crystal with impurities, dislocation internal friction *(Russian)* 77−73297
Cu, single cryst., peaking effect existence in kHz internal friction meas. 80−24531
curves, numerical anal., program in ALGOL-1900 *(Polish)* 79−95079
cyclic inelastic behaviour of metals, friction stress method 77−4855
Debye relax. eqns. for stand. solid with high relax. strength 77−20011
direct meas. of friction in solids with continuous variation of freq. 80−99979
dislocation behaviour, in fatigue, friction and back stress from hysteresis loops 80−3176
dislocation damping during electron irrad. 77−35632
dislocation damping during electron irradiation, new model for peaking effect 78−87683
dislocation motion, effect of anisotropic elastic medium, appl. to martensitic transform. 77−28811
dislocation motion, extended model of effects of point defect dragging 78−10083
dislocation motion, Kê peak anal. by internal friction meas. during deform. 78−18705
dislocation pinning, linear stress effect on diffusion, internal friction *(Russian)* 77−80505
dislocation-defect elastic force in dragging model 80−39104
double-cantilever beam, forced vibration technique for meas. of material damping 78−19964
E-glass epoxy beams, dynamic mech. behaviour, meas. and analysis 77−28844
elastic waves at frictional boundary, transmission (reflection), approx. anal. method 78−63371
elasto-plastic metal-dislocation system, stress-activated dislocation motion, thermodynamic theory *(Chinese)* 78−83868
elastomers, relax. transitions from relax. spectrometry and internal friction *(German)* 80−34136
electric circuitry modifications for meas. on thin wire U-shape specimens 80−59579
enstatite, elastic modulus and internal friction in single crystal 78−85550
epoxysilicon organic tar DFM-135 cement composition, internal friction meas. by composite oscill. method *(Russian)* 80−54312
epoxytitansilicon organic tar TK-75 cement composition internal friction meas. by composite oscill. method *(Russian)* 80−54312
fatigue failure testing, automatic unit 77−56209
ferrite, internal friction, rel. to dislocation movement *(Polish)* 79−95026
ferroelectric ceramic, mech. and elec. losses, correl., theory and expt. 80−66133
forsterite, elastic modulus and internal friction in synthetic polycrystal 78−85550
Fourier transform method for elastic consts. and internal friction meas. in small specimens 79−14357
Gentalloy, in Fe-W system, damping capacity *(Japanese)* 79−20094
glass, in region of transition to viscous-flow state 79−66101
glass, internal friction 79−52286
glass, network forming, oxide, internal friction *(Japanese)* 77−70096

internal friction continued
glass, relaxation phenomena and Raman spectroscopy, review of developments 78−22665
glass fibre reinforced epoxy resin, dynamic Young's modulus and internal friction 80−25754
glass-plastic, Young's modulus, expt. study 77−52389
glasses, oxide type, H bond interpretation 80−92605
grain boundary internal friction in magnetics, elastic moduli anomalies *(Russian)* 77−35633
grain boundary peaks, activation energy determ. *(Russian)* 77−43276
grain boundary relaxation, peak parameters, calcs. 80−2117
Granato-Lucke model, fitting of expt. data 77−43213
granular materials, intergrain slip in flowable zone, stress distrib., internal friction 79−99261
hydrocarbon crystal, calc. of internal friction resulting from molecular defects 78−31448
ice:HF, I_c, Bjerrum defects *(French)* 78−6122
ice I_h, grain boundaries *(French)* 79−55754
III-V compounds, point defects, internal friction meas. 78−71787
III-V semiconductor, dislocations, velocities and internal friction 79−82231
inelastic solids, anelastic relaxation anal., extended to creep at high temp., appl. to internal friction *(French)* 78−63806
inorganic materials, programmed controlled test equipment 77−90541
inorganic oxide glasses, review *(Polish)* 79−95078
ionic single crystals, elec.-mech. coupling of dislocations 78−75676
Kester peak, plastic deform. effects *(Russian)* 80−29118
magnetostrictive core dimens., influence on internal friction and shear modulus 'defect' 78−95506
martensitic steel, disloc. struct. obs. by amplitude independ. internal friction *(Bulgarian)* 77−19966
martensitic transformation, thermoelastic, factors affecting internal friction peak 77−28812
material anelastic behaviour, anal. using 3-lumped vibr. model *(Japanese)* 78−47473
measurement, via automatic internal friction and modulus apparatus using phase-locked loop 78−13981
measurement apparatus, for elevated temps. *(Polish)* 79−96279
measurement apparatus for freqs. up to 200 Hz, automated control 78−22308
measurement by resonant specimen with a dumb-bell shape 80−48660
measurement from dynamic hysteresis loop area and specimen cross section in deform. 78−23897
measurement in solid metal via inverted torsion pendulum *(French)* 79−18847
measurement servo system 77−39265
measurement system using one-crystal composite oscillator 77−42789
measurement using automated Marx's composite oscillator method 80−37151
measurement within solid metals *(Spanish)* 80−6002
measuring instrument for use at high temps. 78−13977
melting region, temp. depend. of internal friction 79−23675
metal, damageability determ. by meas. of elastic, inelastic, internal friction charact. 79−66133
metal, internal friction determ. using sound emission during vibration 77−77715
metal, torsional pendulum oscillation damping meas. system *(Polish)* 77−71314
metal and alloy polycrystals, internal friction amplitude depend. *(Russian)* 79−90726
metal film, vac. deposited, internal friction *(Japanese)* 78−47685
metal-H systems, anelastic and plastic props., review 80−49298
metal-metalloid amorphous systems, thermal instability, crystn. charact. 77−4044
metals, BCC, under elastic stress, Snoek peak height determ. 80−65153
metals, group VA, O and N determ. from internal friction meas. 79−39246
metals, porous, plastic flows, microscopic frictional effects, J_2-flow potential and yield function 80−64384
metals, pure and alloyed, grain boundary relaxation model, *(Russian)* 80−39107
metals and alloys, polycrystalline, LF viscosity meas. 78−80576
metals executing US torsional vibrations 80−58856
metals subjected to high intensity US flexural vibrations 80−6460
minerals, ultrasonic damping due to internal friction, freq. depend. *(German)* 80−90078
nondestructive eval., internal friction technique, computer-assisted digital processing system 79−43537
nonlinear effects, due to mechanisms with high activation volume *(French)* 79−77677
oriented transversely isotropic solid, yielding and failure 78−13915
peak shapes, harmonic analysis for relax. processes investig. 79−52284
pearlitic steel, P internal friction peak *(Russian)* 78−38774
peridotite, elastic modulus and internal friction 78−85550
piezoelectric transducer automatic setup, for continuous meas. of internal friction and elastic moduli of solids 80−108652
plastic, static strength determ. from elasticity and internal friction 77−70094
plastic strain rate, and internal friction, phenomenological rel. 80−75301
plate, deform. vibrs., acoustic thermal relax. method for thermophys. props. determ. of group V metals at high temp. 79−85143
polyester resin, POLIMAL 190, influence of MgO, BeO and TiO_2 on dynamical mechanical props. *(Polish)* 79−96074
polymer, crystallising, defects and mech. relax. *(Russian)* 78−22789
polymer chain, viscoelastic, local relax. props. anisotropy, internal friction influence *(Russian)* 78−37780
polymer melt, viscoelastic, 2-dimens. nonisothermal processing between calender rolls, mathematical model 79−68670
polymer solns., entangled, relax. dynamics, viscoelastic response functions 77−31578
polymer solution, rheological eqns. of state, macromol. elasticity and internal viscosity effects 77−80127
polymeric materials, inelasticity degrees estimation, hysteresis friction model appl. rel. to US testing 80−3136
polystyrene, atactic, isothermal internal friction meas. of glass transition 79−74191
polystyrene, intermol. interaction, conform. *(Russian)* 79−23539
polyvinylidene fluoride, γ-irradiated, low temp. internal friction 78−83874
powder cohesive strength and internal friction determination for small quantities of material 77−40495
internal friction continued
powdered minerals, adsorbed films influence on cohesion and angle of internal friction 77−25084
PZT, polycrystn., thermal expansions, elasticity and internal friction 80−35238
quartz, strain amplitude depend. of internal friction, role of dislocations 77−27939
quartz single cryst., mech. Q depend. on soln. growth rate 78−9978
rare earths, elastic and mechanical properties, review 79−70132
refractory metals, internal friction meas. from 20 to 2000°C in superhigh vac. 77−86249
reinforced UP resin laminate under dynamic stress, anisotropic, mech. behaviour determ. *(German)* 79−83268
relaxation processes activation energy determ. method, sample and holder design 78−39966
RIM-3 relaxator, for internal friction meas. *(Polish)* 79−94572
rocks, fracture regularities with internal friction and dilatancy 78−85537
rocks, friction rel. to seismic attenuation 79−34755
rocks, internal friction and resonant freqs. 78−65268
rubber under cyclic compression, heat generation and thermal conduction 79−52283
sapphire, low temp. peak of internal friction 80−2033
semiconductor, simple recording system using electronic circuit 79−37260
shafts, noncircular cross section, effect of external forces and internal friction on rotary motion *(French)* 78−63274
silicate glass, mechanical stress field influence on structural mobility 80−103421
sliding condensed-matter system model for dynamical friction 80−44258
soil, plastic flows, microscopic frictional effects, J_2-flow potential and yield function 80−64384
statistical mechanics, response theory for systems nonlinearly displaced from equilibrium, graphical approach 80−22285
steel, 110G13L, P content, effect on elastic moduli and internal friction 78−23753
steel, 7.1% Cr, α→γ transformation, studied by internal friction meas. *(French)* 77−25043
steel, austenitic, age-hardening kinetics, study by resistivity, Young's modulus and internal friction *(Czech)* 80−29970
steel, austenitic, alloyed with N, decomposition of solid solution 78−23712
steel, austenitic, alloyed with N, model of relaxation processes *(Russian)* 79−11650
steel, austenitic, Cr-Mn-N, plastic deformation influence on internal friction, relaxation processes *(Russian)* 80−100870
steel, austenitic, N alloyed, relaxation model *(Bulgarian)* 78−19806
steel, austenitic stainless, due to H_2 *(Japanese)* 77−48469
steel, austenitic stainless, internal friction due to H_2 gas molecules 80−71682
steel, austenitic stainless, Mn-N interaction, internal friction obs. 78−84883
steel, C and Co, carbide transitions during post-strain ageing and tempering *(Russian)* 78−95741
steel, cold strained, defects interaction with carbide strengthening phases, carbide decomp. degree *(Russian)* 80−84955
steel, cold worked, alloying additions effect on 200°C internal friction peak *(Russian)* 77−8867
steel, Cr, H-dislocation interaction 79−8307
steel, Cr maraging, internal friction, 120 to 700K *(Polish)* 79−96075
steel, deformed, Kh18N10T, ageing under gradually increasing load 77−90383
steel, graphitised, elastic modulus and internal friction, temp. depend. 80−35242
steel, high-strength reinforcing, 20GS2, local microstresses on creep strength in hydrogenating media *(Russian)* 77−52462
steel, low alloy, crack propag. anal. in delayed fracture under repeated load, internal friction model 79−79064
steel, low C, apparatus for elevated temp. meas. *(Polish)* 79−96279
steel, low C, increased damping capacity, mathematical planning method *(Russian)* 80−45332
steel, maraging, ageing study by internal friction meas. 77−12660
steel, martensitic, Cr-Ni deform., effect of phase composition and struct. *(Russian)* 77−25102
steel, mild, work hardening and strain ageing during fatigue *(Japanese)* 77−8931
steel, Mn-Cr-Ni-N, N effect on relaxation behaviour, internal friction temp. depend. *(Russian)* 78−52872
steel, Ni-Mn (16, 2 wt.%), 40N16G2, single crystal, stabilisation and destabilisation mechanisms *(Russian)* 78−23732
steel, Ni-Mn-C, austenitic, proof stress change meas. by internal friction with martensitic transform. 78−56638
steel, recrystn., structural inheritance charact., X-ray and friction obs. 79−57017
steel, stainless, reinforced glass matrix, vibr. damping anal. rel. to internal friction 80−40413
steel, thin sheets, C and N contents determ. by internal friction *(German)* 78−27715
steel, type Kh12M, rel. between structural inhomogeneity and wear resist. *(Russian)* 80−66672
steel, type KVK, deform. strengthening of bayanite phase *(Russian)* 80−100851
steel, VN precipitation after heat treatment 79−29067
steel sheet, mechanical anal. of meas. apparatus 77−32752
steels, ferritic and martensitic, C and N migration at low temps., monograph 80−22149
stress relaxation test, appl. to discerning frictional and internal stresses 77−63712
stress wave dislocation damping, strain-amplitude depend., KGL String model 77−4101
styrene-methacrylic acid copolymer, intermol. interaction, conform., composition depend. *(Russian)* 79−23539
superconductor, dislocation-point defect interaction, rel. to internal friction *(Russian)* 77−36018
superconductors near critical temperature at acoustic frequencies, internal friction 80−100305
superplastic alloys, internal friction 77−16635
Ta, single crystals, microyielding, high amplitude damping 77−52396
TCNQ salt, $(N(CH_3)_3H)(I)(TCNQ)$, elastic props., semicond. transitions 79−95072
technological strength and nondestructive methods of testing during heat treatment 78−85090

internal friction continued
test device for thin-walled tubular specimens 80−71836
test method, for plastic deform. *(Hungarian)* 80−97662
TGS:($CuSO_4$), internal friction 80−44257
thermal instability of amplitude depend. internal friction 77−84838
thin film, internal friction meas. during plastic deformation, 4.2 to 300K 79−71442
thin films under plastic deform., internal friction meas. apparatus for 4.2-300K 79−5093
threadlike crystals, precision method of internal friction investig. 78−36997
torsion pendulum, with anelastic solids of discrete relaxation spectra, resonant system 80−69687
torsion pendulum oscillations recording equipment for internal friction meas. 78−36998
torsional pendulum for internal friction meas. as function of freq. 78−13980
transient dislocational internal friction, freq. depend., under periodic stress *(Russian)* 79−65092
ultrasonic absorption in high dislocation density crystals dislocation internal friction *(Russian)* 80−34146
ultrasound resonance absorption by moving dislocation 80−54318
V, polycrystalline, 20 keV protons penetration depth, ultrasonic meas. technique 78−30677
viscoelasticity rods with nonlinear elasticity relation and nonlinear internal friction, parametrically excited oscills. 80−99947
viscoplastic flow, coupling of dissipative mechanisms 78−38206
vitreous solids, internal friction and relaxation *(French)* 77−72651
Ag, Bordoni effect during recrystallisation 77−90388
Ag, electron irrad., elastic moduli and internal function *(French)* 78−87703
Ag, pressure effect on shear modules and internal friction, EM reson. technique 77−31709
Ag, vac. deposited film, vibr. real technique 78−43276
Ag, wires, polycryst., internal friction and rigidity modulus, O removal from grain boundaries 78−3160
Ag-Mg, low temp. internal friction, 150 to 300K *(Polish)* 79−96077
AgBr:Cd^{2+}(Sr^{2+}), single cryst., stress-induced migration and aggregation of solute ions 79−51200
AgBr:Sr, stress induced anomalies in internal friction, logarithmic decrement 79−66095
Al and Al-Mg (5.7 at.%), test, appl. to discerning frictional and internal stresses 77−63712
Al, cold-worked, plastically deformed, internal friction spectrum, Hasiguti peaks associated with dislocations 80−7618
Al, deformation, internal friction, dynamic modulus and creep meas. 79−91727
Al dilute alloys, cold worked, internal friction peaks 80−97520
Al, dislocation velocity, from amplitude-dependent internal friction 79−11653
Al, electron-irradiated, anelastic relax. due to clustered self-interstitial atoms 77−39628
Al, fluxural oscillations in longitudinal mag. field, sound attenuation, magnetoelasticity *(Russian)* 80−54844
Al foil, internal friction changes during low temp. plastic deform. *(Russian)* 80−100304
Al, high-temp. internal friction peaks, deformation and annealing effects 77−32615
Al, internal friction, dislocation glide and jog climbing *(French)* 78−11261
Al, internal friction, strain amplitude dependent, hydrostatic press. effect 77−77520
Al, internal friction at medium temps. *(French)* 78−39826
Al, internal friction due to dislocation-loop interaction *(French)* 79−79017
Al, pressure effect on shear modulus and internal friction, EM reson. technique 77−31709
Al, pure, Bordoni effect during recrystallisation 77−90388
Al, pure, cold worked, internal friction peaks 80−97520
Al, reson. vibrs. of metal spheres, elastic consts. and internal friction 78−15443
Al, strain amplitude dependent damping at 8.3×10^{-3} Hz 77−1172
Al, strength changes on US treatment in programmed loading *(Russian)* 77−32583
Al, stress induced ordering of self-interstitial clusters 78−47358
Al wire, grain boundary internal friction after recrystn. annealing *(Russian)* 80−66561
Al-Ag, precipitation study by internal friction *(French)* 80−35190
Al-Ag (up to 40 at.%), exam. of anelastic phenomena and structural state 78−76693
Al-Cu, high temp. internal friction peaks 77−48470
Al-Cu (4 wt.%) alloy, coherency loss of θ'-phase due to deform. 77−15424
Al-Cu(Mg), low freq. internal friction during plastic deform. *(Chinese)* 80−103420
Al-Fe, electron irradiated, interstitial-solute complexes, internal friction spectra 78−92289
Al-Fe dil. alloy, bamboo struct., grain boundary internal friction peak 79−43306
Al-Ga alloy, internal friction and shear modulus, temperature and concentration dependence 77−86077
Al-Ge, internal friction and shear modulus after neutron irrad. at 80K 79−1468
Al-Li alloy, dil., quenched and irrad., recovery, resist. and internal friction obs. 78−52848
Al-Li alloys, precipitating, annealing spectrum 78−31429
Al-Mg, elastic and anelastic props. in relation to Guinier-Preston zones, US investigation *(French)* 79−38833
Al-Mg, plastic deform., separation of internal friction components *(Russian)* 79−52282
Al-Si, internal friction and Si precipitate nucleation 78−60690
Al-Si alloy, rod, tensile loaded, internal friction and Young's modulus measuring equipment, inelastic phenomena exam. *(Hungarian)* 79−52546
Al-steel profiled composite, pulling from melt, mech. props. 78−3075
β-Al_2O_3, internal friction and Na transport 80−59578
β-Al_2O_3-($Na,Li)_2O$, ionic motion obs. using NMR and internal friction 80−108099
β-Al_2O_3-Na_2O, Young's modulus and internal friction obs. 77−35624
Au, rod, tensile loaded, internal friction and Young's modulus measuring equipment, inelastic phenomena exam. *(Hungarian)* 79−52546

internal friction continued
Au, work hardened, Hasiguti peaks, spectrum and recovery, impurity effects *(French)* 77−66670
Au-Ag alloy, vacuum-deposited monocryst., 200-3000 Hz, 20-850°C *(Russian)* 77−21197
Au-Cu(Ag)(Pt), cold worked, impurity conc. rel. to internal friction Bordoni peak, solid soln. hardening mech. 80−16363
B fibre reinforced Al, dynamic Young's modulus and internal friction 80−25754
B fibre reinforced Al, residual stress, internal friction anal. 80−45339
B fibre reinforced epoxy, dynamic Young's modulus and internal friction 80−25754
B fibres, amplitude depend. of internal friction 80−20990
Be, internal friction, temperature spectrum and dislocation damping, anelastic relaxation *(Russian)* 80−2118
Bi, dislocation internal friction, HF, rel. to temp., freq., amplitude *(Russian)* 78−26574
Bi, evaporated film, internal friction 77−7998
Bi, Young's modulus and internal friction, 20°C to melting point *(Russian)* 80−89278
Bi:Sn(Pb)(Sb)(Te) polycrystal elastic constants for US velocity obs. 79−69180
C fibre coated with Si or ZrC, mech. props. 77−70197
C fibre reinforced Al composite, C-Al contact interaction kinetics 79−20007
C fibre reinforced epoxy, dynamic Young's modulus and internal friction 80−25754
Cd, dislocation internal friction, orientation depend., for single crysts. 78−52882
Cd, internal friction, cryst. orientation depend. *(Russian)* 77−7730
Cd, Young's modulus and internal friction, 20°C to melting point *(Russian)* 80−89278
Cd-Zn, cryst., internal friction, dislocation interactions 79−87673
Ce and Ce-Nd, reversible mech. memory effect, α to γ transition *(Russian)* 78−15396
Co, internal friction anomalies in spin reorientation temp. range *(Russian)* 80−49299
Co, internal friction meas. during polymorphic transform. *(Russian)* 79−29049
Co-Fe, internal friction anomalies in spin reorientation temp. range *(Russian)* 80−49299
Co-Pt, amplitude depend. of internal friction *(Polish)* 79−95627
$Co_{35}Dy_{65}$, metallic glass, internal friction peaks 80−25753
$Co_{35}Y_{65}$, metallic glass, internal friction peaks 80−25753
Cr, electrolytic, −200 to 800°C, hydrogenation effect *(Russian)* 77−39626
Cr, internal friction and segregation effects *(Russian)* 77−66669
CsH_2AsO_4, and deuterated derivative, attenuation of LF elastic oscills. 77−7791
Cu -Sn (0.05 at.%), grain boundary relax., misalignment angle effect *(Russian)* 78−3159
Cu, acoustic losses due to strong ultrasonic and static stress fields 80−79886
Cu, amplitude depend. modulus effect 78−64573
Cu, cold worked, determ., of dislocation pinning and unpinning stages, using internal friction meas. 78−92278
Cu, dil. alloy, dislocation inertial effects in plastic deform., internal friction meas. 77−36609
Cu, dislocation damping strain amplitude depend. on 1 MeV electron irrad. and quenching 79−95023
Cu, dislocation pinning rate, neutron and electron irrad., meas. by internal friction method 80−96570
Cu, elastic modulus and internal friction during plastic deform., dislocation props. determ. 80−35244
Cu, electron irrad., migration and thermal conversion of defects, 100 to 330K 80−59519
Cu, electron irradiated, dislocation defect dragging, 4.2 to 350K 78−43027
Cu, electron irradiation damage, dislocation pinning investig. of crowdion model 77−69000
Cu, fatigued, structural changes, damping and modulus 77−28906
Cu film, Gorsky effect, internal friction maxima, atom diffusional mobility *(Russian)* 80−70446
Cu, internal friction, impurity effect *(Russian)* 79−87677
Cu, low temp., internal friction and microplastic strain 77−84839
Cu, microplastic deform. and amplitude depend. of internal friction *(Russian)* 80−45349
Cu, neutron and electron irrad., interstitial formation, dislocation pinning, internal friction meas. 80−100284
Cu, neutron irradiated, effect on internal friction 78−15445
Cu, pressure effect on shear modulus and internal friction, EM reson. technique 77−31709
Cu, rod, tensile loaded, internal friction and Young's modulus measuring equipment, inelastic phenomena exam. *(Hungarian)* 79−52546
Cu, stress induced ordering of self-interstitial clusters 78−47358
Cu, whiskers, hardening during uniaxial extension, preliminary torsion deform. *(Russian)* 78−15420
Cu, wire, polycryst., internal friction, ultrasonic vibrations effect *(Russian)* 78−76685
Cu-Ag (0.1 wt.%), cold-worked, internal friction peaks in kHz range 80−89276
Cu-Al-Ni, sintered, internal friction after heat treatment *(Japanese)* 80−11686
Cu-Al-Ni (13.8, 7.9 wt.%), cooling rates effect on internal friction *(Japanese)* 80−39217
Cu-Al-Ni (14, 8 wt.%), γ'-martensitic, sintered high damping 80−50577
Cu-Au, (0.02-5 at.%), cold worked, internal friction peaks 79−11652
Cu-Ni alloy, dil., dislocation damping, 95-297K, at high strain amplitudes 78−39824
Cu-Ni(Au), elastic modulus and internal friction during plastic deform., dislocation props. determ. 80−35244
Cu-Ni(Zn), elastic modulus and internal friction during plastic deform., dislocation props. determ. 80−35244
Cu-Ti, ageing effect on internal friction and elastic props. *(Russian)* 77−28842
Cu-Ti (3.5 wt.%), internal friction in dissociating alloy following deform. by US *(Russian)* 78−35419
Cu-Zn-Al, internal friction, temp. and amplitude depend. 78−11262
Cu-Zn-Al, Zener relaxation *(Russian)* 77−21198
Cu-Zn-Al (19.5, 6.35 wt.%), martensitic, static stresses influences on damping behaviour 80−10594

internal friction continued
$Cu_{50}Zr_{50}$, metallic glass, internal friction peaks 80−25753
Dy, magnetic transitions and internal friction temp. depend. *(Russian)* 78−39317
Er-Tb, elasticity modulus, ΔE-effect, internal friction, magnetic transformations *(Russian)* 79−91723
Eu_2O_3-Ta_2O_5, microcracking, elastic props., internal friction 78−92326
α-Fe, (1$\bar{1}$2) [$\bar{1}\bar{1}$1] anti-twinning slip system, low temp. strengthening, dislocation struct. 77−21164
α-Fe, alloying with Ti, V, G, Mo, W and Mn, effect on dislocation mobility *(Russian)* 77−31671
Fe and Fe alloys, internal friction and US attenuation at large strain amplitudes 77−1182
Fe, Armco, cumulative fatigue damage at US freqs., thermal activation 77−70181
Fe, Armco, dislocation struct. after hot and cold rolling *(Russian)* 77−8847
Fe, Armco, recrystn., structural inheritance characts., X-ray and internal friction obs. 79−57017
Fe, C and Cr diffusion, US effects *(Russian)* 77−59144
Fe, damping during and after deformation 79−43344
α-Fe, dislocation density determ. after quenching, internal friction meas. 78−18658
Fe, domain wall-dislocation interaction, magnetoelastic damping 78−14980
Fe, effect of H_2 on phys. and mech. props. 80−101657
α-Fe, high purity, neutron and electron-irrad., interstitial migration at 200K 79−55920
α-Fe, internal friction for low temp. deform. 80−40420
Fe, internal friction in plastic deformation process *(Chinese)* 80−88259
Fe, internal friction near Curie point 79−24567
α-Fe, internal friction peaks from dislocation relax. in plastically deformed and/or neutron irrad. sample 78−48438
α-Fe, magnetic aftereffect correlations with internal friction after low temp. neutron irradiation 78−10733
α-Fe, magnetic aftereffect spectrum after low temp. neutron irradiation 78−10732
α-Fe, plastically deformed and/or irrad., high purity, internal friction peaks due to dislocation relax. 77−86075
α-Fe, polycrystalline, shear modulus, H_2 effects 77−36561
Fe, pure, deformed, internal friction, dislocation relax. and dislocation-defect interactions 79−29125
Fe, pure, strain ageing and fatigue *(Japanese)* 79−20161
Fe, relaxation process effect on initial stages of flow *(Russian)* 79−74189
Fe, reson. vibrs. of metal spheres, elastic consts. and internal friction 78−15443
Fe, varying purity, internal friction, H-dislocation interactions 77−52377
Fe-Co, damping capacity of Gentalloy, internal friction meas., mech. and mag. depend. *(Japanese)* 78−52875
Fe-Co (5 to 25 wt.%), exam. of damping capacity of Gentalloy 78−72800
Fe-Cr, damping capacity *(Japanese)* 79−70104
Fe-Cr alloys, cold worked, internal friction due to H *(Japanese)* 80−70305
Fe-Cr alloys, damping capacity 79−100206
Fe-Cr-Al (12, 3 wt.%), strain amplitude-depend. damping and modulus *(Japanese)* 80−92606
Fe-H, deformed 79−57041
Fe-H system, cold work internal friction peak, appl. of Schoeck's model 78−95771
Fe-Mo, damping capacity 77−86082
Fe-Mo, damping capacity *(Japanese)* 78−11259
Fe-Ni, internal friction study, tempering effects *(French)* 77−81286
Fe-Ni alloy, N27T2 and N28, internal friction peaks after reverse martensitic transform. *(Russian)* 78−92287
Fe-Ni alloys, ordering on annealing and electron irrad., mech. props. change *(Russian)* 80−29981
Fe-Ni base metallic glass, annealing embrittlement 78−64635
Fe-Ni-C, internal friction anomaly with reheat transform. 79−100204
Fe-Ni-C, martensitic, internal friction 77−16633
Fe-Ni-Mo, martensitic transformation, annealing, influence on struct. of austenite *(Russian)* 80−81057
α-Fe-P, grain boundary adsorption of P, internal friction *(Russian)* 77−32609
Fe-P-C, amorphous, at 0.5 Hz, room temp. to 550°C 77−25085
Fe-Si, anisotropy in longit. and circular fields *(Russian)* 78−2194
Fe-Si, internal friction, domain boundary area *(Russian)* 79−24562
Fe-Si, microplastic deform. and amplitude depend. of internal friction *(Russian)* 80−45349
Fe-Si (3 at%), deformation and electron bombardment, influence on dislocation struct., 20-500°C *(Russian)* 80−92536
Fe-Si (3 wt.%), internal friction, instantaneous, depend. on phase of torsional oscills. *(Russian)* 80−71142
Fe-Si (3 wt.%) alloy, H containing, H influence on internal friction *(Russian)* 79−38877
Fe-Si-C (2.86, 0.07 wt.%), internal friction peak at about 300°C *(Russian)* 77−81284
Fe-W (5%), internal friction, mag. and nonmag. components *(Russian)* 78−48018
Fe-W system, damping capacity of Gentalloy, internal friction, mech. and mag. props. 79−77679
$Fe_{80}B_{20}$, $Fe_{78}Mo_2B_{20}$ glasses, internal friction and shear modulus 79−52287
$Fe_{36}Cr_{12}Ti_7Mo_3$, high temp. precipitation kinetics, internal friction study 79−43254
$Fe_{0.49}Ni_{0.415}Mo_{0.095}$, Vibralloy, high-temp. vibrating reed meas. 79−55811
$Fe_{40}Ni_{40}P_{14}B_6$, $Fe_{29}Ni_{49}P_{14}B_6Si_2$ glasses, internal friction and shear modulus 79−52287
$Fe_{40}Ni_{40}P_{14}B_6$ metallic glass, dynamic mechanical props. 79−10894
FeO-P_2O_5 glasses, electrical and mechanical losses 78−80283
Fe_3Pt, stoichiometric composition, internal friction, microdeform. and memory effect, rel. to martensitic transform. *(French)* 77−52323
$Fe_2(Tb_{0.3}Dy_{0.22}Ho_{0.58})$, highly magnetostrictive alloy, vibrating-reed meas. of ΔE effect and internal friction 79−42819
GaP, containing matrix metal inclusions, internal friction study 79−42145
GaP, internal friction calc. 80−2116
Gd-Cu(Fe) splat-cooled, internal friction exam. 77−20012
internal friction continued
Gd-Tb, elasticity modulus, ΔE-effect, internal friction, magnetic transformations *(Russian)* 79−91723
Ge:Cu, anelastic relax., internal friction temp. depend. meas. 79−65143
Ge:Cu, solubility and behaviour of Cu, internal friction investigations 80−92678
HFO_2, polycrystalline, monoclinic, elastic props. at room temp. 78−27548
He, solid, energy absorpt. and size effect, point defect diffusion *(Russian)* 77−4243
^4He, solid, pure and with ^3He admixtures, effect of plastic deform. and impurities on internal friction *(Russian)* 79−77860
HfO_2, monoclinic, microcracking, elasticity, internal friction, thermal expansion meas. 79−29195
In, supercond. and normal states, internal friction hysteresis *(Russian)* 77−36023
KCl, γ-irrad., photoplastic effect and internal friction aftereffect 80−24529
$K(D_xH_{1-x})_3(SeO_3)_2$, ferroelastic, anelastic and elastic infra-low freq. props. 80−70304
KH_2PO_4 and deuterated derivative, attenuation of LF elastic oscills. 77−7791
KH_2PO_4, ferroelec. crystals, torsion pendulum technique 78−72474
$KH_3(SeO_3)_2$, ferroelastic, low-frequency elastic props., −190 to 50°C 79−37759
La-Al amorphous alloys, internal friction, relaxation process 80−92607
LiF, viscous drag of dislocations, internal friction, 4.2-300K 77−11566
$LiNbO_3$, damping of LF elastic vibrs., internal friction meas. 79−28043
$LiNbO_3$, LF sound attenuation, internal friction 78−63804
Mg, dislocation internal friction, orientation depend., for single crysts. 78−52882
Mg, internal friction, cryst. orientation depend. *(Russian)* 77−7730
Mg, internal friction spectrum after plastic deform. *(French)* 79−15737
Mg, pure, Bordoni relax. behaviour after plastic deformation 80−20997
Mg-Al(Sn)(Ni)(Cu), damping capacity 77−48474
MgF_2:LiF crystal, defect struct., anelastic and dielec. relax. meas. 77−27938
MgO, a/2 ⟨110⟩ edge dislocations, lattice friction stress, atomistic calc. 78−18648
MgO, plastically deformed, recovery of internal friction at room temp. *(French)* 78−80577
MgO, single crystal, elastic consts. and internal frictions meas. by rectangular parallelepiped reson. 77−78165
MgO:(Li), polycrystn., internal friction *(German)* 80−59577
MgO:Li, internal friction, mech. and dielec. relax. *(German)* 80−34135
γ-Mn-Fe, Mn rich, damping capacity 79−83252
MnF_2:LiF, anelastic relax. of Li^+-Li^+ split interstitial defect 79−77678
$Mn_{0.82}Fe_{2.18}O_4$, anelasticity, 280 to 730K, 125 kHz vibr. study 78−87740
MnZn ferrites, internal friction and ΔE effect depend. on demagnetisation method 80−80584
Mo, internal friction and segregation effects *(Russian)* 77−66669
Mo, internal friction peaks, induced by work hardening, low temp. relax. spectra *(French)* 77−1844
Mo monocrystal, dislocation motion, study by internal friction *(Russian)* 77−1133
Mo, strain induced damping, micro- and macro-, and dislocation structures in single crystals 78−19797
Mo, strength and internal friction 77−63711
Mo-Re, solid soln., dislocation internal friction *(Russian)* 78−23748
NH_4Cl, acoustic absorption by soft modes of defects 80−59584
NaCl, changes in internal friction and discharge following plastic deform. 79−99191
NaCl, dislocation microplasticity, internal friction expts. 78−47388
NaCl, γ-irrad., F-stimulated inversion of sign of dislocation charge 80−59475
NaCl, γ-irrad., photoplastic effect and internal friction aftereffect 80−24529
NaCl, interrupted neutron irrad. expts. involving dislocations 79−99208
NaCl, plastic deformation influence on shape recovery effects 80−6684
NaCl, point defect interaction with dislocations, internal friction meas. 79−90662
NaCl, viscous drag of dislocations, internal friction, 4.2-300K 77−11566
NaCl whiskers, plastically deformed, internal friction amplitude depend. 77−15727
NaF, dislocation microplasticity, internal friction expts. 78−47388
Na_2O-$3SiO_2$:Fe^{2+}, Fe^{3+} glasses, Mossbauer and ESR spectra and internal friction 80−100865
Na_2O-B_2O-SiO_2 glasses, high temp. mech. relax. 79−96071
Na_2O-FeO-P_2O_5 metaphosphate glass, 0.5 to 15 Hz, 120 to 670K *(Polish)* 79−96078
Na_2O-K_2O-Al_2O_3-SiO_2, structure of modified surface layer, internal friction method 80−103258
Na_2O-Si_2O glass, high-temp. peak of internal friction 80−39218
Na_2O-SiO_2, effect of annealing on absorbed H_2O action on temp. spectra of internal friction 78−88487
$Na_2O.SiO_2$ fibre, reactivity to atmospheric moisture below annealing range, internal friction measurement 78−92288
Nb, cold-worked, Snoek-Koster relaxation transient period, comparison with Schoeck's theory 79−34086
Nb, deformed, α-peak, internal friction meas. between 90 and 300K 79−100205
Nb, deformed, α′-peak in internal friction spectra 80−16368
Nb, deformed polycryst., γ-peak obs. and interpret. in internal friction, 300-500K 80−81098
Nb, diffusion coefficient calc. of O and N from internal friction meas. 77−89586
Nb, dislocation damping, amplitude depend. 80−59469
Nb, H_2 loaded, cold worked, plastic deformation, exam. of α internal friction peak 78−92307
Nb, high purity, dislocation relaxation by internal friction meas. over wide freq. range 79−38876
Nb, internal friction peaks, induced by work hardening, low temp. relax. spectra *(French)* 77−1844
Nb, neutron irradiated, radiation anneal hardening *(Japanese)* 80−89243
Nb, plastically deformed, hydrostatic pressure effect on dislocation relaxation, US exam. 78−76696
Nb, relaxation from room temp. to 114°C, computer optimization of elastic aftereffect curves 77−90390

internal friction continued
Nb, relaxation intensity due to interstitial O, temp. effect *(French)* 77−86080
Nb, reson. vibrs. of metal spheres, elastic consts. and internal friction 78−15443
Nb, solute trapping of H, symmetry of O-H pair 80−108488
Nb wire, neutron irrad., internal friction meas. 79−70077
Nb:H, lattice distortion and migration energy of H impurities 78−30796
Nb-H, behaviour of H in Nb, relation to mech. props. 78−80572
Nb-H, incoherent spinodals, meas. by Gorsky effect 78−19712
Nb-H, spinodals and diffusion coefficients of H, sample shape depend. 78−19713
Nb-H alloys, evidence of internal friction peak 78−52881
Nb-H system, temp.-stimulated acoustic emission, hydride precip. 80−3044
Nb-O, Snoek mechanism and long distance diffusion under strain ageing *(French)* 77−81279
Nb-Zn-N alloys, Zr-N complex formation, internal friction temp. depend. *(Russian)* 80−54311
Nb-Zr, deformed, α-peak, internal friction meas. between 90 and 300K 79−100205
Nb-Zr (1 wt.%), internal oxidation state of O_2, dispersion hardening by diffusion alloying, X-ray diffr. and internal friction *(Russian)* 79−70102
Nb-Zr-N, deformed and annealed, internal friction, rel. to structural state *(Russian)* 78−6957
Nb_xC powders, plastic deform. characts. on vibratory milling 78−11183
Nb_3Ge, metallic glass, internal friction peak obs. 78−79666
$Nb_3Ge(Si)$, amorphous films, thermally-activated internal friction peaks, structural obs. 80−80147
NbH, internal friction 78−6962
NbN_x, solid soln, strain ageing, internal friction, elec. cond. kinetics *(Russian)* 78−76667
NbN_xO_y, solid soln, strain ageing, internal friction, elec. cond. kinetics *(Russian)* 78−76667
NbO_x, solid soln, strain ageing, internal friction, elec. cond. kinetics *(Russian)* 78−76667
Ni, cold-worked, rel. between dislocation and ferromag. damping 80−107369
Ni complex, 1,2-benzoquinonedioximates, refl. spectra, 0.5-2.5 eV, Young's modulus and internal friction 78−39562
Ni, electroplated layers, internal friction and ΔG effect, rel. to bath comp. and annealing 78−19296
Ni ferrites, internal friction and modulus defect at US freqs. 79−19762
Ni, grain boundaries, mobility, effect of impurities *(Polish)* 79−96073
Ni, grain boundary internal friction, B solid solubility as function of grain size 80−60903
Ni, H-charged cold-worked, internal friction peak 80−107368
Ni, internal friction, instantaneous, depend. on phase of torsional oscills. *(Russian)* 80−71142
Ni, internal friction near Curie temperature 78−44163
Ni, magnetic internal friction peak bifurcation in rot. mag. field *(Russian)* 78−39380
Ni, magnetoelastic effects, ΔE-effect and macroeddy current damping, internal friction meas. 78−64253
Ni, porous, internal friction and effective elasticity modulus, temp. depend. *(Russian)* 79−29118
Ni, pure and doped, mech., mag. relax. meas. dumb-bell self-interstitital reorientation *(German)* 78−52879
Ni, strain amplitude-depend. damping and modulus *(Japanese)* 80−92606
Ni wire, internal friction, influence of orientation of mag. field *(Russian)* 79−24559
Ni-B, grain boundary internal friction, B solid solubility as function of grain size 80−60903
Ni-Cr complex alloy with good creep resistance, friction stress/flow stress relation 79−8337
Ni-Ti/Cu composite, plastic deform. influence on internal friction *(Russian)* 80−100871
Ni-Zn ferrite, high temp. behaviour of grain boundaries under bending stress *(Japanese)* 77−1875
Ni_3Fe, nondislocation origin friction stress in alloys, deformation hardening 80−21050
NiTi, martensitic transform. rel. to low frequency internal friction peaks 79−96024
Ni_3V, ordered, domain size effect on mech. props. 79−79027
NiZn ferrites, internal friction and ΔE effect depend. on demagnetisation method 80−80584
Nichrome, plasma spray coatings, relaxation phenomena 80−19876
PLZT, mech. and elec. losses, correl., theory and expt. 80−66133
Pb, activation energy and primary characts. of Bordoni relax. peak 77−69040
Pb, dil. alloy, dislocation inertial effects in plastic deform., internal friction meas. 77−36609
Pb, dislocation electron drag coeff. temp. depend., internal friction method, superconducting state 80−29031
Pb, dislocation inertial effects, internal-friction meas. on normal and superconducting states 79−38883
Pb, dislocation internal friction changes under the action of US vibr. 79−69630
Pb, fluxural oscillations in longitudinal mag. field, sound attenuation, magnetoelasticity *(Russian)* 80−54844
Pb, high purity, polycrystalline, Bordoni relaxation peak high vacuum annealing effect 78−39828
Pb impregnated porous Ni, porous, internal friction and effective elasticity modulus, temp. depend. *(Russian)* 79−29118
Pb, plastic deform. rate rel. to supercond. transition, temp. depend. *(Russian)* 78−31015
Pb, US oscillations and dislocation unpinning in supercond. and normal states *(Russian)* 79−11648
Pb, Young's modulus and internal friction, 20°C to melting point *(Russian)* 80−89278
Pb-Bi, elastic moduli, internal friction from US velocity meas. 79−15717
Pb-Sn, dil., dislocation inertial effects, internal-friction meas. on normal and superconducting states 79−38883
$Pb_{0.95}Sr_{0.05}(Zr_{0.53}.Ti_{0.47})O_3$, low temp. internal friction in ferroelectric ceramic 77−21200
$xPbTiO_3+(1-x)PbCd_{1/3}Nb_{2/3}O_3$, phase transition spread, polarisation relaxation, dielectric susceptibility *(Russian)* 80−75922
$Pb(Z,Ti,Mg,W)O_3$, low-Q ceramics, props. and transducer appl. 80−75944
internal friction continued
Pd complex, 1,2-benzoquinonedioximates, refl. spectra, 0.5-2.5 eV, Young's modulus and internal friction 78−39562
Pd-H alloy, 50K transition, internal friction, LF torsion pendulum meas. 77−15490
Pd-Si, amorphous, at 0.5 Hz, room temp. to 550°C 77−25085
Pt complex, 1,2-benzoquinonedioximates, refl. spectra, 0.5-2.5 eV, Young's modulus and internal friction 78−39562
RbH_2AsO_4, ferroelec., attenuation of LF elastic oscills. 77−7791
RbH_2AsO_4, ferroelec. crystals, torsion pendulum technique 78−72474
RbH_2AsO_4, phase transition, dielec. pyroelec. and internal friction meas. 77−16261
RbH_2PO_4, ferroelec., attenuation of LF elastic oscills. 77−7791
RbH_2PO_4, ferroelec. crystals, torsion pendulum technique 78−72474
Sb, dislocation drag constant temp. depend. 77−11565
Sb, dislocation internal friction depend. on high ampliutde US vibrations *(Russian)* 79−90727
Sb, dislocation internal friction changes due to high-amplitude US oscills. *(Russian)* 80−10556
Se, amorphous, struct. relax. effects, obs. by mech. props. *(French)* 79−51201
Se, amorphous, US attenuation at low temp., internal friction peak 80−65152
Se, vitreous, micromech. props., anelastic behaviour, internal friction *(French)* 77−72652
Si, neutron irrad., internal friction obs. of defects 78−51597
Si, plastic properties, internal friction, dislocation motion *(Russian)* 80−54305
n-Si plate, illumination effects, 50-250°C *(Russian)* 77−20010
Si plate, internal friction temp. depend. 77−15491
Si, polished plate, internal friction *(Russian)* 78−15441
Si, vacancy cluster props., effect of natural anisotropy *(Russian)* 77−62522
Si:Au, impurity induced internal friction, impurity centre symmetry 79−73252
Si-Au substrate-film system, relax. effects, internal friction meas., temp. range 20 to 900°C 78−18886
SiO_2 glass fibres, exam. of phase separation effect on internal friction 78−88455
SiO_2 vitreous fibres, relax. props. near glass transition interval 80−34137
SiO_2-Al_2O_3-MgO-TiO_2 glasses, internal friction during crystn. 79−52285
Sn crystal, white, time-dependent internal friction 80−7610
Sn, Young's modulus and internal friction, 20°C to melting point *(Russian)* 80−89278
TGSe:D,L-α-alanine crysts. with large unipolarity, dielec., piezoelec., elastic props. and internal friction 79−33615
Ta, acoustic emission induced by hydride formation 80−76257
Ta, at supercond. T_c, struct. effects *(Russian)* 77−36026
Ta, bamboo struct., wire, high-temp. rheology 77−1851
Ta, internal friction measurements, of O_2 and N_2 diffusion 78−75888
Ta, internal friction peaks, induced by work hardening, low temp. relax. spectra *(French)* 77−1844
Ta, proton implanted, anelasticity, internal friction meas. 79−24560
Ta, reson. vibrs. of metal spheres, elastic consts. and internal friction 78−15443
Ta:H, lattice distortion and migration energy of H impurities 78−30796
Ta-H, incoherent spinodals, meas. by Gorsky effect 78−19712
Ta-H, spinodals and diffusion coefficients of H, sample shape depend. 78−19713
Ta-O, BCC, Snoek type reordering during strain ageing *(French)* 79−8312
Ti, acoustic harmonic generation by long-range dislocation motion 79−42150
Ti, cold worked, annealed, internal friction meas. of H degassing *(French)* 79−43304
Ti, exam. of whether interstitial O can cause internal friction 78−48537
Ti, influence of H_2 on the internal friction *(French)* 78−75723
Ti, irradiated and cold worked, internal friction pdaks 77−86074
Ti-Al-Mo-Sn-Si (2.25, 4, 11, 0.25 wt.%), type IMI 680, internal friction study of martensitic transformations 80−7573
Ti-Al-Mo-Sn-Si (2.25, 4, 11, 0.25 wt.%), type IMI 680, stability of martensitic phases 80−7574
Ti-Al-Mo-Sn-Si (4, 4, 4, 1/2 wt.%), type IMI 551, internal friction study of martensitic transformations 80−7573
Ti-Al-Mo-Sn-Si (4, 4, 4, 1/2 wt.%), type IMI 551, stability of martensitic phases 80−7574
Ti-Al-V (6, 4 wt.%), type IMI 318, internal friction study of martensitic transformations 80−7573
Ti-Al-V (6, 4 wt.%), type IMI 318, stability of martensitic phases 80−7574
Ti-Ni, internal friction and US props. *(Russian)* 80−84247
Ti_3Al, phase transitions and physical props. 77−25068
TiNi, imperfect elasticity, elastic after-effect on basis of martensitic transformation theory *(Russian)* 79−100198
$TiSe_2$ Young's modulus and internal friction obs., 1.3 to 300K 79−46750
$TlSe.As_2Se_3$, $Tl_2Se.As_2Se_3$, γ-irrad. effects on mech. props. 77−80567
V and V-Fe (5.0 at.%), stress relaxation test, appl. to discerning frictional and internal stresses 77−63712
V, dehydrogenation by annealing with Zr foils, internal friction meas. 80−96736
V, diffusion of O and N, least squares computer technique 78−38881
V, fluxural oscillations in longitudinal mag. field, sound attenuation, magnetoelasticity *(Russian)* 80−54844
V, internal friction, low temp., H_2 effects 80−40419
V, internal friction α-peak origin 78−95773
V, interstitial impurity and substitutional solute interaction, internal friction meas. 78−10082
V, reson. vibrs. of metal spheres, elastic const. and internal friction 78−15443
V wire, deformed in torsion, internal friction, H effect 80−76300
V:H, lattice distortion and migration energy of H impurities 78−30796
V-D alloys, low frequency internal friction study 78−48444
V-H, incoherent spinodals, meas. by Gorsky effect 78−19712
V-Ti-O single crystal alloy, mech. props. 77−25112
V=O, lattice distortion and migration energy of O impurities 78−30796
W, plasma spray coatings, relaxation phenomena 80−19876
W, reson. vibrs. of metal spheres, elastic consts. and internal friction 78−15443
W, strain induced damping, micro- and macro-, and dislocation structures in single crystals 78−19797

internal friction continued
Zn, background damping in vicinity of grain boundary peak 77−28843
Zn, deformed, internal friction meas. 77−86067
Zn, dislocation internal friction, orientation depend., for single crysts. 78−52882
Zn, internal friction anomalies in temp. initiated brittle-plastic transition *(Russian)* 80−96648
Zn-Ag, dil., polycryst., amplitude-depend. internal friction *(Polish)* 79−96079
α-Zr, internal friction and O_2 pair diffusion 77−16634
Zr, terminal solid solubility of H, optical metallography, internal friction meas. 78−83962
Zr-O(2.85 at.%), Pr effect on internal friction of single crystal 77−4155
ZrV_2, supercond., Young's modulus and internal friction meas. 79−11654

internal friction of liquids *see viscosity of liquids*

internal mechanics, molecular *see molecular vibration*

internal mechanics of atoms *see atomic structure*

internal modes *see molecular vibration in solids*

internal stresses
β-eucrypite, glass-ceramics, internal stresses 79−15770
β-spodumene, glass-ceramics, internal stresses 79−15770
activation area, stress depend., critical assessment of method of internal stresses meas. 79−59955
activation volume stress depend. 80−54304
additive pulses from internally stressed magnetostrictive wire bundle 79−99742
adhesion joints, calc. of internal stresses under temp. variation *(Russian)* 77−70273
alkali halides, thermally stimulated depolarisation of NCO^- centres 80−80678
alloy V93, fatigue strength, effect of residual stresses and cold working 77−56101
alloying, electrospark, of Ti to transition metals and their compounds, and steel and Cu to Ag *(Russian)* 77−56145
alumina film, RF sputtered, stability 78−22993
amorphous ferromagnetic alloys, micromagnetic eqns. for case of dipolar and magnetocryst. fluctuations 80−11171
amorphous solid, structural defects, computer simulation study 80−88040
anelasticity influence, on internal stress meas. in creep 80−70306
anisotropic elastic medium, elastic energy of plate inclusion 78−38687
antiferromagnet, residual stress induced domains, specific heat meas. anal. 78−60286
Armco iron specimen, elastic const. meas., X-ray diffr. technique 78−5714
axisymmetric bodies, integrated photoelasticity, nondestructive anal. 79−18842
axisymmetric cylinder, experimental numerical hybrid method for stress anal. 80−48657
bakor beams, residual thermal stresses, expt. determ., theoretical anal. 77−66667
bars and tubes, anal. of axially symmetrical residual stresses 79−18734
bearings, plain, fracture 80−81170
biaxial residual stress distrib., meas. method for determ. throughout workpiece height *(German)* 78−35596
bicrystal, elastic incompatibility stresses *(Japanese)* 80−107361
bimetal, high-speed steel + machine steel, chem. comp. influence on magnitude of residual stresses in cooling *(Russian)* 79−74183
bimetallic tube, residual stress after thermal cycling 77−90465
blind hole drilling technique for residual stress measurement: application in NDT 80−40660
blind hole method with off centre hole, for residual stress meas. 79−20300
bonded bodies, internal stress/strain relations *(German)* 79−90143
bonded joints, device for automatically recording internal stresses 80−25963
Bordoni relaxation, theoretical aspects, numerical calcs. from thermally activated double kink formation 78−63805
bounded domain undergoing sequential crystallisation, stress and strain investigation 80−100183
brass, adsorpt. of Hg, effect on mech. strength, creep, fatigue, embrittlement, work hardening, roller burnishing effects *(Russian)* 79−29267
brass, delamination effects during grinding 79−52470
brittle crystal grown from melt residual stress rel. to dislocation density 78−2042
brittle solid, residual stress about pointed indentation impression 77−12686
calc. with integration methods, X-ray stress meas. 79−32415
carbon fibre reinforced composites, filament-wound, thermal residual stresses 80−49290
carnauba wax electrets, residual strain and crystal size of orienting crystallites and their effect on charge behaviour 80−11319
cemented carbides, physical and chem. nature 80−76265
ceramics, structural stress meas. using X-ray diffr. meas. *(German)* 78−52744
chinaware, semivitreous, eval. of crazing resistance by stress meas., after autoclaving *(Japanese)* 79−20235
circular blank, stress-strain state during forging *(Russian)* 79−52231
close-packed crystals, elastic moduli of polytypic modifications 79−51187
coated fibre and cable unit structure optimisation 80−53466
coated optical fibre cable unit, internal stress due to compressive loads, optimum design 80−58717
coating, diffusion solution, relaxation of residual stresses *(Russian)* 77−70195
component hydropressing, residual stress distribs. *(Russian)* 80−93567
composite beams, exam. of contact problem, using boundary value problem soln. 78−42532
composite beams, shearing stresses distrib. under three point flexure, fracture due to surface peeling 78−44183
composite laminates, transient moisture sorption induced stress field 78−34021
composite materials, density depend. of strength *(German)* 78−94592
composite materials, internal stress depend. on density gradients *(German)* 79−1105
composite three-layer cylindrical shells, initial stressed and deformed state 80−102974
compressed crystals, dislocations and point defects *(Russian)* 78−75666
continuum theory, nonlocal, using kinetic theory, stress, energy density *(Japanese)* 78−32677

internal stresses continued
corundum, defect cryst. struct. study 80−103316
Cr film, vacuum deposited, macrostruct. due to intrinsic stress, cracks following scratches in substrates 78−6238
crack propagation, fracture of practical materials, anal., recent developments, review 79−43428
crack tips, blunting during conc. plastic flow *(Russian)* 78−7013
cracked plate with periodic system of internal parallel cracks with asymmetrical loading *(Russian)* 77−50988
Crazing under applied compression 78−19875
creep, high temp., steady state, anelasticity and measured internal stress 78−35456
creep rupture strength at nonstationary loading, stress conc. influence 78−31514
crystal, residual stresses with gradient, determ. by X-ray diffr. 77−28944
crystal defects, elastic interaction under high hydrostatic press. 80−96512
crystal growth, creation of stress and dislocations *(Russian)* 80−103277
cubic crystals, response to (111) loading, internal energy, elastic moduli 80−84230
cubic single crystal, integrated photoelasticity 79−33671
cylinder, infinite circular elastic inhomogeneous, stressed state calc. body containing foreign components 77−89035
cylinder, solid, residual tangential stress determ. from segment sections, appl. 78−60902
cylinder with oblate spheroidal cavity or internal penny shaped crack under tension, stresses 80−69736
cylinders, rational utilisation of Gein and Bauer's method 77−54893
cylindrical shell, three layer, with strap reinforcement under internal pressure, stress-strain state calc. 78−30184
cylindrical testpieces, axial residual stresses determ. problem 78−7115
cylindrical vessel, residual stress in multilayer wall calc. 77−19540
cylindrical welded rod with interlayer of lower elastic modulus, stresses in tension 79−24557
data sheets, changes due to fatigue *(Japanese)* 77−4841
definition, classification and symbolisation *(German)* 79−91907
deformation rate, kinetic anal. of internal stress field effect 80−25787
deforming material, theoretical study of macroscopic meas. of mean internal stress 80−25788
deforming stress relaxation, non-uniform internal stress field effect 77−21204
diamond, synthetic, N impurity effect on strength characts. and thermal stability 80−11726
diamond anvil cell for high pressure measurement, with uniform internal stresses at 200 kbar 79−67334
diamond composite with Cu-Ti matrix, microstresses, X-ray diffr. exam. 78−56679
diamond type crystals, internal strain parameter 78−43090
diffusion coated plate, stress analysis with allowance for phase transform. *(Russian)* 78−11357
diffusion motions of macroscopic inclusions in nonuniform compressive stress fields *(Russian)* 80−88351
discs, circularly symmetric, rupture, ductile-brittle creep 80−69735
discs, impact stresses, photoelastic investigation 79−37182
dislocation dynamics theory, stress field produced by motion and creation 77−62530
dislocation interaction with point obstacle in non-uniform stress field, localised force approx. 80−15150
dislocation loop, plane, self-stress field singularity in anisotropic elastic medium 77−19952
dispersed particles, in plastic matrix, contrib. of load transfer to internal stress, approx. method 80−21047
dispersion hardened alloy, calc. of back stress decrease, due to Orowan dislocation loop climb 78−83812
double-wall piping welded joint residual stress study *(Russian)* 78−27541
Duralumin, adsorpt. of Hg, effect on mech. strength, creep, fatigue, embrittlement *(Russian)* 79−29267
Duralumin, D16AT alloy, residual stresses in samples with hole in static and cyclic tension 80−3149
Duralumin, lifetime after preliminary plastic deform., kinetic theory of strength 79−43395
dynamic thermoelasticity of body with crack, two- and three-dimensional *(Russian)* 77−68400
Earth crust, in situ stress in N. America, compilation 79−29728
edge stresses in multilayer laminates, calc. by substructuring 78−34022
elastic bodies, cylindrical, damping rate of stresses 77−53786
elastic deformation incompatibility, deform. mechanics model of residual stress *(Russian)* 80−54300
elastic/viscoplastic plate, combined longitudinal/torsional stress wave propag. *(Japanese)* 78−38227
elasto-plastic contact problem 78−46917
elastoplastic system, dynamic deformation, internal state variables and internal forces 80−53660
elastoviscoplastic system, work hardening due to residual stresses constitutive eqns. for rates *(French)* 77−70068
electrodeposition stress measurement, of sphere by X-ray in depositing method 77−36409
electroplated coatings, theory and meas. review, effects in Ni and Zn *(German)* 78−56049
enamel slips, control of rheological props. 79−29136
entropy of internal stress fields caused by lattice defects 80−39067
fastener hole, cold worked, residual strain 79−29088
fatigue crack closure, computer model, based on surface roughness and residual strain 77−73347
fatigue crack growth in vacuum 78−56729
fatigue crack propagation, in shaft or axle type components, problems specification 78−51120
FCC alloy, hardening by spinodal modulated structure 80−60874
ferrite film, determ. by ferromag. reson. method *(Russian)* 77−16126
ferroelectric phase formation energy in inhomogeneous inclusion under press. 77−12338
ferromagnet, mech. behaviour in microplastic strain region *(Russian)* 78−39838
ferromagnet, stress indication by transverse and longitudinal internal induction 77−16138
ferromagnetic alloy, 35KFN10, X-ray diffr. investig. after thermomech. treatment *(Russian)* 77−48457
fibre reinforced composite, hygrothermal microstresses, in material exhibiting inelastic behaviour 77−84141

internal stresses continued
fibre reinforced composite, imperfections, piezo- and elasto-optical effects under longitudinal shear *(Russian)* 78−56457
fibre reinforced composite, mech. behaviour, axial residual stress effect 77−36573
fibre reinforced composite, stress meas. by IR spectroscopy 79−52559
fibre reinforced composites, transverse plane, elastic, failure behaviour *(Japanese)* 78−48510
fibre reinforced materials, prod. of uniform plane stress states 78−85064
fibre reinforced plastic, regular struct., shrinkage stress calc. 77−70125
fibrous composite, residual stress form. during hardening 78−1575
fibrous material failure kinetics, internal stresses, computer simulation *(Russian)* 80−40479
film, domain size and internal strain, studied by electron diffraction line broadening 78−30840
film, rel. to peeling off from substrate 77−24501
film, spontaneous macrostress meas., improved methods 77−35100
film, stress measurement method using real-time holographic interferometry 78−84099
film on single cryst. substrate, X-ray meas. method 78−51860
film/substrate, two-layer structs., relaxation of internal stresses 80−34341
finite two-phase bodies, response to internal and external stresses, geometrical considerations 80−24741
finite-two phase bodies, response to internal and external stresses, numerical considerations 80−24742
friction machine, residual stresses meas., appl. to wear resist., surface wear 78−60906
frozen food, hydrostatic press. effect on phys. props. 78−26706
gelatin film, 20-240°C *(Russian)* 79−87645
GFRP, shrinkage stress calc. 78−19869
glass, chemically strengthened, ion exchange temp. and time influence on stress profiles and strengths 78−31417
glass, tempered, surface residual stresses from indentation fracture mechanics 77−90439
glass, thermal stresses, temporary and residual, monitoring by semiautomatic heating polariscope-polarimeter 78−16833
glass ceramic, second-order microstresses 78−27468
glass ceramic rods, strengthened, residual stress determ. 78−23830
glass fibre, residual stress meas. by strain gauge, metrological charact. 77−120
glass fibre preforms, elastic stresses 79−64343
glass fibre reinforced bakelite, laminate, internal stresses occurring during production 79−66034
glass fibre reinforced composite, thick-walled shell, crack prevention during heat treatment 77−52376
glass fibre reinforced plastic, dynamic stress conc. around defects, discrete model 80−30024
glass fibre reinforced plastic stiffened shells 79−100108
glass rods, compressively clad, residual stresses, comparison of optical and fractographic meas. 80−108539
glass-C fibre composite, mech. props. and residual stresses in wound components 77−52436
glass-ceramic, randomly oriented, physical props. 78−48501
glass-ceramic composite, internal stress effects on mech. props. 77−21250
glass-ceramics 78−30542
glasses, crystallised, internal stress depend. of hardness 80−16439
glasses, partially leached rods, contact-damage resist. 80−50707
graphite, artificial, residual macrostresses 77−16642
graphite, CVD anisotropic thick hollow cylinder, residual stress due to uniform cooldown 79−42423
graphite, reactor grade, irrad. creep, 850 to 1100°C 78−44167
graphite fibre reinforced epoxy resin, hygrothermal microstresses, in material exhibiting inelastic behaviour 77−84141
graphite intercalation compound, elastic coherency strain 79−60306
graphite intercalation compounds, coherency strains and staging 80−44167
graphite/polyimide laminates, effect of ply stacking sequence and orientation on residual stresses 77−52378
grid method for residual deforms. meas. 77−52572
ground and lapped metal surfaces, residual stresses determ. 79−34211
growth centres rel. to mech. stresses 80−19735
haematite-magnetite two-phase system, internal stresses porous bodies *(Russian)* 80−16319
hard-alloy/U8 C alloy steel weld, local internal stress region boundaries 77−59846
hardened components, residual stress, elastic characts. after surface plastic stress 78−60901
heteroepitaxial film deformation, causes and countermeasures *(Russian)* 80−49561
heterogeneous composite materials, influence of prestress and limited deformations 78−38205
high-speed stress detection and imaging, 100-element acoustic phased array 79−47876
hockey stick heat exchanger, elbow centroid 80−9329
Homalite-epoxy duplex specimens, crack arrest study via dynamic photoelasticity 78−31515
hyperelastic systems, discrete and continuum mech. 77−864
ice, polycrystalline cores, creep laws for various stress states *(French)* 77−53077
impression method for plastic deforms. determ. at apex of stress concentrator, bare choice considerations 77−52571
incremental deformations of initially stressed media with couple stresses 78−62077
indentation of hard metals, residual stresses, exptl. verification 77−21249
infinite cylindrical shell containing filler, reinforced by ring, influence of arbitrary load 78−42533
infinite transversely isotropic solid containing penny shaped crack, stress intensity factor *(French)* 80−43663
inner elastic constants, symm., depend. on symm. of interlattice tensors 79−28028
inner elastic constants, tensor notation and relation to lattice dynamics 79−28027
Invar, mag. susceptibility in technical saturation region and internal stress 77−85429
ionic crystal, dislocation mechanism of electrification during cleavage 77−24353
ionic crystal, exposed to high-current electron beam pulses, min. size of excited region for crack initiation *(Russian)* 78−84961

internal stresses continued
jacketed optical fibre residual stress diagnosis, pulse delay technique 80−53469
Jahn-Teller system, thermodynamic properties, internal stress effects 80−59679
lacquer coating, brittle, plasticizer *(Japanese)* 77−52479
laminate, residual stress form. during hardening 78−1575
laminate, shock wave propag., stress history recording 78−38242
laminated paper, decorative, deform. and internal stresses 79−61671
laminates, residual thermoelastic stresses 80−106721
laser optical component props. depend. on material flow props. *(Russian)* 80−38047
linear elastic and post yield fracture mechs., thermal and residual stresses 77−89066
liquids, Berthelot tube method, theory for tension before breaking 77−24341
Lochseiten limestone, differential stress in Glarus overthrust 78−88822
macrostress in deposits, spontaneous, calc. 77−36710
macrostress in deposits, spontaneous, dilatometric meas. 77−36709
magnetostrictive pulse-producing wire plating 80−2618
martensitic transformation, internal stress relax. effect on microstruct. and kinetic features 77−44250
meas., nondestructive, acoustoelasticity appl. 79−34259
measurement, Alignment Error of the hole-drilling method 79−81823
measurement, bending deflection and stress source methods *(French)* 79−34265
measurement, high-temp. 80−64498
measurement, X-ray diffr. equipment, comparison 80−82858
measurement using elastic punching method 79−34264
measurement using optical microscope stage polarisation adapter 80−31863
measurement with hole-drilling strain gauge method 79−39108
metal, BCC, intracrystalline fracture *(Russian)* 79−5031
metal, internal stress meas. by decremental unloading technique 78−64576
metal, internal stresses during rolling friction and their evaluation 77−28912
metal, oxide film growing by cation diffusion, stress generation 78−60865
metal, stress concentration sensitivity, scale factor effect on fatigue strength 79−39064
metal, textured cubic, residual stress evaluation 80−89435
metal and alloys, hot twisting differential method of shear stress determ. 77−56026
metal faced cylinders and discs, residual stresses determ. by combined method of Zaks 77−52568
metal matrix composites, thermal expansion effects, fibre length depend. 78−51708
metal sputtered film, compressive stress transition 78−10310
metal-dielectric-semiconductor structure, ponderomotive force effect on dielec. breakdown 79−15230
metal-H system, lattice strains, expt. methods, book contrib. 79−82202
metallic film, sputtered, internal stresses, effect of substrate orientation and rotation 79−77968
metallic films, deposited by cylindrical magnetron sputtering, internal stresses 80−24773
metals, BCC, solid soln. hardening, crystal resolved shear stress depend. on dislocations 80−40373
metals, determ. using internal boring technique 80−3263
metals, dislocation-core movement and frictional stress 80−92529
metals, inelastic cyclic strain under nonuniform stress state conditions, residual stresses effect 80−81132
metals, plastic deform., stored energy determ., temp. recording method 79−87775
metals, residual stress and deformation, due to quenching, elastic-plastic anal. *(Japanese)* 78−83268
metals, residual stress on drawing calcs. by stress state changes variational principle *(Russian)* 80−65125
metals, single phase FCC, cyclic deform. long range stress changes 80−54308
metals porous, mean principal stress in rolling without lateral expansion 80−25803
mica, syntectonic nucleation of new grains 79−65102
mirror/flaw-size relations, residual contact stresses effect 80−107363
misfitting inclusion deformation field 77−36505
molecular internal stresses, stress tensor, one electron system 78−62686
moulding mixtures, consolidated residual stress meas. 79−87791
multilayer cylindrical parts, residual stresses determ. 80−96206
multilayer heteroepitaxial structure, stress calc. 77−72798
Nabarro-Herring creep, internal stress 78−43067
NDT, failure prevention, test methods and equipment *(German, English)* 79−52560
non- homogeneous hollow cylinders stress determ. *(French)* 79−32423
non-linear viscoelastic behaviour, numerical anal. 78−59318
nuclear fuel can designs for Safety Test Facility, structural analysis 77−46310
nuclear fuel compacts for HTR, irrad.-induced creep 78−44168
nuclear reactor fuel rod bundles, square array, shear stress distribution, axial flow 80−47679
Nylon 6, injection moulded, residual stresses 80−38950
oblate spheroidal inclusion, internal stress, misfit, inhomogeneity and plastic deform. 78−60701
optical fibre, refractive index profile distortion, stress-induced 80−91889
optical fibre, single mode, bending induced birefringence 80−87537
optical fibre cables, measurement of longitudinal internal stress 79−64350
optical fibre cables, modular, composite strain analysis 79−64351
optical multifilm manufacturing, large scale, function stress testing 79−81576
optimal composite sheets, fixed upper bound on number of layers 78−30177
orbitally degenerate interacting impurity thermodynamics, stress field depend. due to point defects, dislocations 79−69477
oxide single crystals, Czochralski grown, thermoelastic stresses 78−55822
Ozhennite, yield point, effect of ageing stress 77−21223
Permalloy, high-permeability, influence of grain struct. and non-mag. particles on mag. props. *(German)* 77−16112
Permalloy film, perpendicular anisotropy, structural and thermal stresses *(Russian)* 79−4708

internal stresses continued
PET film, interatomic bond determ. by IT transmission and reflection spectrocopy 77−65958
PET films, dyed, local mech. stresses, IR spectrosc. determ. 80−65418
photoelastic measurement for crysts., appl. to Si 80−48656
pinned dislocation arrangements, TEM obs. 77−43217
plate, orthotropic multilayered, vibr. modes, acoustic transmission 78−83142
plate of variable thickness, defined applied theories construction, asymptotic method *(Russian)* 80−53634
plating, residual stress meas. by improved ring-core method *(German)* 79−34272
PMMA, atactic, elastic strain detection by X-ray scatt. 80−25751
PMMA, shock loaded, lateral compressive stresses meas. using Yb piezoresist. gauges 80−103007
point source modelling for extended source stresses 77−72609
polarisable dielectric crystals, mean internal stress pot. *(Italian)* 79−65797
polyamide-polyurethane copolymer dispersions, structurisation and relax. props., coating from props. 80−76559
polycarbonate, ductile, large strain cyclic deform. 80−85000
polycrystal, HCP, microstress and starting boundary of plasticity *(Russian)* 78−30695
polycrystalline metals, stored energy and strain hardening 79−82276
polyester-polyurethane interpenetrating polymeric network glues, props. 80−16640
polyethylene, anisotropic surface stress 78−14562
polyethylene, high density, ductile, large strain cyclic deform. 80−85000
polyethylene, injection moulded high density, tensile stresses, chemical cross linking effects 79−57035
polyethylene, stresses at spherulite boundaries causing black lines 77−72568
polyethylene film minimum running thickness, critical rupture stress 80−100993
polyethylene terephthalate, fatigue failure under cyclic loading, overstress in chem. bonds 79−57106
polyethyleneterephthalate film, influence of crystallisation on adhesive and cohesive props. 79−56100
polymer, amorphous, injection moulded, residual thermal stress calc. by FEM 79−55322
polymer, crystalline, stress transmission 80−35240
polymer agglomerates, forces in dispersive mixing 77−29052
polymer filled, internal stresses influence on glass transition temperature 80−10645
polymer film, in adhesive joint contact layer, intermol. interaction with substrate and filler *(German)* 79−8421
polymer film, supermolecular structure and mech. stress distrib. among chem. bonds 78−75562
polymer films and sheets 78−80590
polymer matrix laminate 77−25007
polymer solutions, intrinsic stress, birefringence tensor, bead/spring model, freq. depend. 78−42574
polymeric materials, stress meas., X-ray diffr. technique, review 78−5713
polymers, deformation under combined action of shear stress and hydrostatic pressure, testing equipment 77−56184
polymers, semicryst., and filled, elastic modulus, strength, rel. to crystallite shape 80−45335
polymers, wear in thermally stressed state 80−3202
polymethyl methacrylate, direct obs. of zero field surface 80−16133
polypropylene, ductile, large strain cyclic deform. 80−85000
polystyrene conc. sols. in toluene, rheological behaviour *(German)* 78−55618
porcelain, relation of crazing to stress in porcelain glaze, method of stress determ. *(Japanese)* 78−31537
porcelain wave, crazing resistance, glaze fitness *(Japanese)* 79−74278
porous body of simple shape, internal stress distrib., expt. and calc. *(Russian)* 79−68569
portable X-ray analyser for residual stresses, design, operation and testing 78−53058
powder, one sided die compaction, internal stresses 78−23641
Prandtl-Reuss plastic materials, with general work hardening, constitutive equations *(Japanese)* 78−92276
precipitate strain energy and elastic strains *(Korean)* 79−65201
pressmold materials, stand for high-temp. mech.-props. test 77−56183
punch, axisymmetric, contact with semi-infinite transversely isotropic elastic body *(French)* 80−23969
pyrographite, initial stress state, neutron irrad. effect 80−97555
quartz, α and β phases coexistence state, elastic light scatt., birefringence 79−47412
quartz, impact structs., peak shock press., X-ray diffr. investig., lunar rock bombard. appls. 78−7002
quartz, plate and fibre, internal stress and birefringence microanal. using optical phase microscope interference-polarisation 79−39109
α-quartz, Raman FTIR spectra, surface layer and vol. spectra comparison 78−52491
quartz, stress buildup due to UV irrad. *(Japanese)* 79−19278
rail steel NDT, residual stresses meas. using magnetoelastic effect 77−81379
rectangular twist disclination loops, elastic energy and stresses 79−27987
refractories, sintered, X-ray diffraction method for assessing local stress levels 79−96265
reinforced composite pull-out forces, effect of matrix stresses 77−21334
residual pseudo-macrostress, X-ray meas. errors due to plastic deform. 77−68544
residual stress determ. by NDT 79−96267
residual stress determ. for slightly curved rods 78−30185
residual stress effects in failure from flaws 79−66228
residual stress formation in explosive welding 79−83285
residual stress measurement using holographic interferometry and etching 77−52577
residual stresses, effect of triacetylpyridine and polyethylene glycol additives to NH_4Cl electrolytes 80−21190
residual stresses, methods of detecting, review *(German)* 78−44291
residual stresses determination in rod specimens with stresses varying along rod length 78−38260
residual stresses in shells of revolution, cut-out element method glass-plastic composite, thermoelastic residual stresses in shells of revolution, cut-out element method 80−38271
residual stresses in thin specimens, layer-by-layer X-ray diffr. analysis, additional strains and corrections 78−39964
internal stresses continued
residual stresses rel. to grinding and cutting directions, X-ray diffr. obs. *(Japanese)* 78−23847
review 80−44245
ring, axially cracked, numerical anal. of residual stress effect on crack closure 79−77012
rings, multilayer, circumferential residual stresses *(Russian)* 80−74729
rock, trends in relationships between meas. in situ stresses and depth 79−29729
rock bodies, cooling, residual stress development 78−88819
rocks, primary stress meas. at Eisenhower Memorial Tunnel, Colorado 79−29727
rocks, residual stress meas., microcracking effects 77−91118
rocks, stress state determ. in transversely isotropic rock mass 77−56752
rod, variable residual stress meas. by holographic interferometry 79−29312
Sachs method determ. 77−54894
sapphire, RF sputtering of Hf, high stress in graded interfacial layers, AES meas. 77−43446
sapphire, white, brittle fracture, microstruct. depend. 80−16469
scragged torsion bar, residual shear stress meas. 79−59954
sea ice dynamics in Arctic (May 1975), simulation 78−36192
seals, glass-metal and glass-ceramic, annealing effect on internal stresses 80−40389
self stresses, expt. and numerical study *(German)* 79−90142
semicircular inclusion in semi infinite plane experiment and analysis *(Japanese)* 77−65672
semiconductor, elastic stresses effect on diffusion processes 78−10226
sharp contact cracking, residual stress effects 79−100245
sheet, cold rolled, texture form., model *(French)* 78−68705
shell, cylindrical, inelastic with initial shape imperfections and residual stresses, buckling and carrying capacity *(Ukrainian)* 77−50937
shells of revolution, thin, numerical anal. thermal stress relief 77−89041
shot peening residual stress effects on plastic microstrain in isotopic media *(French)* 79−77675
single crystals, internal stresses determ. with multicryst. X-ray spectrometer 80−64832
sintered granules, onset of stresses of first kind, mechanism *(Russian)* 78−80485
soft-interlayer welded joint bending and torsion endurance, residual stress effects 79−83287
solid, finite stressed, surface dislocation model 79−73247
solid electrolyte, transition temperature to high cond. state as function of press. 80−44365
solid solution, diffusion, influence of conc.-induced stresses *(Russian)* 78−55969
solid solutions, conc. tetragonal substitutional, dislocation impurity segregation *(Russian)* 79−65114
solid solutions, dislocation-core movement and frictional stress 80−92529
solidification front propagation, residual stress levels, polymerisation 80−59635
Somigliana dislocations and pure inclusions, internal stresses 78−30615
SOS MOS devices, elec. characts., cryst. defects and residual stress effects 78−34906
spheroidal inclusion stress conc. *(Japanese)* 80−16320
spinning disc of radially inhomogeneous piezoelectric material, transient voltages and stresses 80−55039
static flow stress, decrease, by superimposition of ultrasonics 79−7652
steady-state heat conduction of solids with inclusions and cracks, analogy with longitudinal shear *(Russian)* 77−68371
steel, 1045, elastic const. meas., X-ray diffr. technique 78−5714
steel, 22K and 09G2S, residual stress change in conc. zone in cyclic loading 78−3224
steel, 45, EHI961, EHI437B, fatigue strength, effect of residual stresses and cold working 77−56101
steel, alloy, Ni-Cr-Mo, alloys SNCM8, SAE 4161, heat treated, residual stress at fatigue fracture surface *(Japanese)* 78−64622
steel, and alloy, fatigue strength improvement, by subcritical quenching 78−44153
steel, annealed low C, X-ray stress anal. using position-sensitive proportional counter 80−1498
steel, austenitic, measured internal stress and anelasticity in creep *(Czech)* 79−38909
steel, austenitic and martensitic, structural sensitivity of Bauschinger effect *(Russian)* 79−52303
steel, austenitic stainless, Cr-Ni (18,8 wt.%), X-ray meas. of residual stress in ground surface layer *(Japanese)* 77−48491
steel, austenitic stainless, Cr-Ni (25, 25 wt.%) grain size, temp. and stress influence on creep 80−30021
steel, austenitic stainless, intercrystalline corrosion, stressed state effect 80−55582
steel, austenitic stainless, type SUS 304, welded joint, polarisation behaviour, boiling $MgCl_2$ soln. *(Japanese)* 80−93695
steel, austenitic stainless, X-ray stress anal. by new position sensitive proportional counter with uniform angular resolution *(Japanese)* 80−30190
steel, brass clad plate/roll bonded Ni clad, fatigue crack growth behaviour 80−40484
steel, C, fatigue, residual stress and crack growth expts., notch and surface treatment effects 79−8356
steel, C, fatigue subsurface crack initiation, result of residual stresses 80−25833
steel, C, hardened, cold-drawn or shot-peened, residual stresses rel. to temp. *(French)* 77−77494
steel, C, magnetomechanical acoustic emission for residual stress NDT 80−71149
steel, C, predeformed, anisotropy temp. effect on yield point 78−39878
steel, C, residual stress induced by uniaxial deform., mag. meas. 77−73390
steel, C, wear, struct. changes in centres of galling 79−38985
steel, C, wear charact. of worn surface layer under lubrication *(Japanese)* 78−35526
steel, C, X-ray diffraction correlation between cyclic loading and residual stress *(German)* 78−48583
steel, C and alloy, nitriding, effect on struct. and internal stresses 80−30162
steel, C-Cr (1.0, 1.5 wt.%), 52100 bearing steel, control of surface residual stress by heat treatment 80−97501
steel, C-Mn, corrosion cracking, role of microstresses and crystal lattice stresses *(Russian)* 77−25190
steel, carbon, fastener holes, cold-worked, residual stress meas. 78−7163

internal stresses continued
steel, carburised, with non martensitic microstruct. at surface, fatigue *(Japanese)* 77−48535
steel, carburized and quenched, residual stresses *(Japanese)* 80−89262
steel, carburized fatigue, non-martensitic struct. effect, rel. to mean stress and residual stress *(Japanese)* 78−7024
steel, case carburised, residual stress effect in mech. performance 79−24659
steel, cold formed tubes, residual stresses 79−61605
steel, Cr, hypereutectic, structural, critical rates of impact, kinetics of failure 80−35325
steel, Cr plated, factors influencing durability 80−108643
steel, Cr-Mo:P (2.25, 1 wt.%), stress relief cracking, effect of P segregation 80−89324
steel, Cr-Mo, high tension, delayed fracture, fundamental study *(Japanese)* 77−48531
steel, Cr-Mo-V, cyclic oxidation and crack growth during high strain fatigue 78−31586
steel, Cr-Mo-V, high temp. main steam pipe, residual stresses in butt welds 80−21059
steel, Cr-Ni-Mo-Cu, ε phase particle precipitation from martensite, local internal stress relaxation *(Russian)* 79−78969
steel, Cu-Zn, brass clad, fatigue crack growth behaviour 80−40484
steel, cylinder, quenched without transform., residual stresses *(German)* 80−25725
steel, deformed strain-aged St.3 and 09G2S, stress conc. susceptibility, H_2 effect 78−95774
steel, endurance, effect of surface diffusion alloying 77−81344
steel, ferritic, magnetomechanical acoustic emission for residual stress NDT 80−71149
steel, ferritic, underclad cracking mechanism, effects of residual strain and heat affected zone ductility 77−25158
steel, free plate elastoplastic stress condition during phase transformation 78−95781
steel, heat treated, residual stress calc. with finite element program *(German)* 79−66075
steel, heat treated high strength, X-ray diffr. anal. of residual stress 80−3200
steel, high C, plate, rolling residual stress meas. by X-ray diffr. *(Japanese)* 79−66081
steel, high strength, fine grained, quenched and tempered, residual welding stresses, stress relieving temp. *(German)* 78−72793
steel, high-strength reinforcing, 20GS2, local microstresses on creep strength in hydrogenating media *(Russian)* 77−52462
steel, high-strength structural, stress-strain curves, shape effects *(German)* 80−45343
steel, HSLA control-rolled, surface residual stress meas., X-ray diffractometer 78−5716
steel, HY140 and HY180, fatigue crack init. at notch tip, early stage propag. *(Japanese)* 78−7021
steel, induction hardened sheet, inhomogeneity and distrib. of residual stresses effect on fatigue *(Japanese)* 78−31518
steel, Kh17N2, endurance limit, effect of residual stresses caused by Cr plating and cyaniding 77−86184
steel, low alloy, cladded with monolayer austenitic stainless steel, heavy section, residual stresses *(German)* 78−35420
steel, low alloy, high strength, fatigue crack growth, in presence of welding residual stresses *(Russian)* 80−71739
steel, low alloy, high strength, residual stresses during low cycle fatigue 79−29201
steel, low C, dynamics of cyclic plastic deform. and fatigue life at low temps. 77−16670
steel, low C, effective stress determ. during the loading cycle 79−38879
steel, low C, yield point, effect of ageing stress 79−96091
steel, low-alloy sheet, welded hydraulic turbine volute chamber, strength and toughness 78−68820
steel, low-C, sheet, thin, residual stresses determ. after bending 78−60708
steel, martensite, brittle fracture resistance, struct. after quenching effects, tempering effects 79−57104
steel, martensitic, ageing, effect of H_2 on stresses in process of $\gamma \rightarrow \alpha$ transformation *(Russian)* 80−76252
steel, martensitic transform., stress calcs. using statistical model *(Russian)* 80−93557
steel, medium, C, US attenuation, mag. field effect 80−89428
steel, medium C, ground, residual stresses, X-ray evaluation 80−79863
steel, medium C quenched, tempered, relation between wear and work surface layers *(Japanese)* 77−52499
steel, middle and low C, clad plate, inhomogeneity and residual stresses, heat treatment effects *(Japanese)* 78−6955
steel, mild, residual stress meas., acoustoelastic, in a patch-welded disc 79−27604
steel, mild, rolled, critical angle US reflectometry of stressed bar, book contrib. 79−100324
steel, mild, tensile and cyclic loading effect in Barkhausen noise 80−40560
steel, Mo and Cr-Mo, X-ray elasticity constants at high specimen temp. *(German)* 80−35239
steel, Ni, 11.6%, quenched cylinder residual stresses, boring/turning and X-ray diffr. obs. *(German)* 80−93586
steel, Ni-Cr-Mo-V, fatigue crack growth rate, specimen thickness and stress relief effect 77−40445
steel, nitrided EN41B, effect of residual stresses on fatigue failure 78−64698
steel, notched bar, plastic zone determ. near rupture *(French)* 78−88515
steel, plain C, type 304 and type 316 stainless, fatigue damage indicators, non-desructive 80−25932
steel, plastic deform. resist. during continuous hot rolling *(Russian)* 80−55462
steel, quenched, local H distrib. and internal microstresses *(Russian)* 80−50654
steel, quenched, martensite, rel. to tensile and compressive deform. resist. *(Russian)* 78−19819
steel, relaxation of residual stress with fatigue loading 77−56051
steel, residual quenching stress determ. in cylinder, consideration of transform. *(German)* 80−35213
steel, residual stress determ. by X-ray integration *(German)* 79−52551
steel, residual stress influence on mech. props. *(German)* 78−27587
steel, residual stresses, X-ray appratus for meas. 77−60016
internal stresses continued
steel, residual stresses meas., using position sensitive X-ray detector 77−56211
steel, Si-Mn-P-S-Ni-Cr, residual stress meas. by X-ray diffr. 80−71688
steel, spheroidized, Bauschinger effect and work hardening 78−64596
steel, stainless, fast neutron irradiated, solution annealed tubing, residual stress behaviour 80−65054
steel, stainless, fibre reinforced Al alloy, tensile props., cryogenic cooling effect 79−61623
steel, steam pipes, 12Cr1MoV, selection of allowable stresses based on minimum possible strength data 80−104237
steel, strain-hardened subsurface layer, residual stress change in fatigue 80−81185
steel, structural, brittle fracture, intermediate fracture stress, fracture initiation mode transition 78−60802
steel, structural martensitic, corrosion resist. under stress effect of strain ageing with hydroextrusion *(Russian)* 79−38853
steel, tempered StE70, water quenched, residual stress field in centrally welded plates *(German)* 78−72794
steel, transforms CC types M6 and M3N, elastoplastic bending, insulating coating influence on magnetic losses *(Russian)* 79−100284
steel, tufftrided, residual stress and fatigue crack propag. *(Japanese)* 77−48536
steel, type Ck22 and St52-3, under cyclic stress, damping behaviour and fatigue strength correlation *(German)* 80−39211
steel, US strengthening treatment effect on fatigue resistance 80−81193
steel, wear resist., mech. props. and struct. effects 80−35338
steel, welding residual stresses, sources, X-ray meas. *(German)* 77−86265
steel bearing, surface-ground, residual stress fatigue property comparison 80−60975
steel bearing rings, optimisation of thermomechanical working parameters *(Russian)* 80−93579
steel butt weld structure and mech. props., explosive treatment effects 79−24541
steel casting, meas. and significance of residual stresses 80−21253
steel components, residual stress distrib. on surface cold working *(Russian)* 77−59975
steel cylinder, electrodeposition internal stress meas. using X-rays 78−27693
steel fibre reinforced Al alloy, stressed state nondestructive testing method *(Russian)* 80−40631
steel mild, plastically deformed, X-ray meas. of stress and TEM 77−48496
steel N22, crack movement rate during cyclic deform., internal microstress effects 78−3225
steel plates, explosively clad, fatigue crack propagation behaviour *(Japanese)* 80−104262
steel shaft, residual tangential stress determ. after elastoplastic twisting 78−60902
steel ShKh15, fatigue strength and residual stress distrib., machining method effects 78−31528
steel surfaces, machined, X-ray diffr. residual stress meas. methods, comparison 77−56212
steel wire, magnetically hard Kh13N13M2-type, electroplastic drawing *(Russian)* 80−20967
steels, alloy, stress relax. data anal. using total strain-time parametric method *(Japanese)* 80−104198
stellarator device, stress analysis of supporting tube of helical winding 77−19776
Stepanov method shaped cryst. growth, physical problems, thermoelastic stresses 80−103279
stochastic model for dip test in steady-state creep 80−58915
stored energy, and increment in heat capacity due to plastic deform. 80−54302
stress relaxation in crystals, review 79−73248
stress relaxation test, appl. to discerning frictional and internal stresses 77−63712
stress tensor in nematic liquid crystals, micropolar continuum mechanics 78−67647
stress tensor in nematic liquid crystals, micropolar continuum theory 78−67648
strip with circular hole, visco-elastoplastic stress conc. 77−68455
styrene-butadiene-styrene block copolymer, stress relax. following steady-state flow, residual shear stress development 80−83772
substrates, deposits spontaneous mactrostress calc. 80−15412
supercooled, struct. refinement mech. *(Russian)* 80−20975
surface dislocations, universal concept, rel. to disclinations and grain boundaries 80−100231
surfaces, machined, X-ray diffr. residual stress meas. methods, comparison 77−56212
swelling and shrinkage stresses, automatic installation for meas. 80−55605
tempered glass discs, meas. of nonuniform distribution of residual stresses 78−95865
textures materials, residual stress evaluation by X-rays *(German)* 80−40670
theory, rel. to X-ray topography data 78−64254
thermoplastics, internal stresses revealed by artefacts produced in SEM 78−35634
thin film intrinsic stress determ., cantilivered plate method anal. 80−54570
thin films, intrinsic stress determ. by cantilevered plate method, substrate bending 80−54571
transition metal hydrides and deuterides, conc.-temp. depend. of mag. susceptibility 80−29523
transparent dielectrics, with inclusions, laser-induced stresses 79−28012
trident seal, thermal expansion differential test 79−61815
tube with hexagonal bore, crack formation during rolling *(Russian)* 78−80622
turbine components *(German)* 79−32414
type II superconductor, dielastic, interaction of flux line lattice with internal stresses of cryst. imperfections 78−14906
type II superconductor, dielastic interaction of flux line lattice with internal stresses of cryst. imperfections 78−56270
vacancy formation vol. in solids, stress-assisted diffusion theories 79−95201
vacuum deposited films, mech. props. 78−75968
volume change in internal stress fields 79−90138
water drops, ice envelope splitting during freezing *(Russian)* 77−27982

internal stresses continued
wedge disclinations near surface of semi-infinite cryst. *(Russian)* 80−49224
welded component fatigue life and crack propag. analysis with internal stresses 77−77576
welded dissimilar cylindrical shells under service loading, stress/strain calc. and expt. 79−83284
welded joints in dissimilar Al alloys, fishbone testpiece axis of symmetry, residual stress investigations 80−7725
welded pressure vessels, residual stresses, determination 78−40014
welds, residual stresses, evaluation by Barkhausen noise meas. 80−76436
wire, device for uniform electrolytic removal of surface layers for residual stress determ. 78−60918
X-ray evaluation, treatments for nonlinear distribs., review 80−25966
X-ray line-shape anal., simplifications using Fourier series, appl. to Mo film on Si 79−82123
X-ray measurement 79−97484
X-ray residual stress meas., use of position sensitive proportional counter *(Japanese)* 80−11853
X-ray stress meas., computer-aided system *(Japanese)* 80−104366
zinc blende type crystals, internal displacements 80−34127
zincblende crystals, internal strain and piezoelectric coefficient 78−39505
zincblende-type crystals, sublattice displacement from elect. or mech. deform. 80−81123
Ag, evaporated film, density, adhesion, intrinsic stress, substrate temp. effects 77−15709
Ag film, in situ struct. determ. by internal stress meas. 80−54569
Ag film, intrinsic stress meas. 80−71696
Ag film, on MgF_2 and SiO substrates, internal stresses correl. with struct. 79−87026
Ag film, vac. deposited, internal stress and its depend. on gas adsorption 80−6683
Ag film, vacuum-deposited, removed from substrate, internal strain *(Japanese)* 78−22872
Ag film deposition thermal effects, influence on internal stress meas. 80−96767
Ag powder, ultrafine, sintering, coalescence growth stage 80−89174
Ag ultra-thin film, deposited on MgF_2 and SiO substrates, struct. and internal stress 78−91572
Ag-Sn, splat-quenched, X-ray diffr. study 80−81094
AgCl, surface layer stress distrib. after mech. treatment, polarisation-optical obs. 78−18887
Al alloy, residual stress relax. rel. to temp., load cycling, aircraft struct. appl. 78−7053
Al alloy, residual stress gradient meas., modified hold-drilling technique 79−29300
Al alloy 2024, relief of residual quenching stresses *(Korean)* 79−70091
Al alloy 2024-T351, fatigue crack propag., residual stress distrib. 79−70146
Al alloy AMg6, residual stress change in conc. zone in cyclic loading 78−3224
Al alloys, quenching rate rel. to mech. props., residual stresses, optimum quench coolings *(French)* 78−64562
Al and Al-Mg (5.7 at.%), test, appl. to discerning frictional and internal stresses 77−63712
Al bicrystal, plastically deformed, slip heterogeneities 80−79858
Al film, deform. under He ion bombardment 80−65073
Al film, H incorporation effect on stress and electromigration 80−80139
Al film, internal stress, effect of residual gas press. 77−66100
Al film, intrinsic stress meas. 80−71696
Al, He implanted surface deform., integrated lateral stress 77−31697
Al, lattice resistance stress, Bordoni relax., microdeform. and US attenuation results 80−25747
Al, orthogonal cut surface, effect of cutting condition on residual stress *(Japanese)* 78−85035
Al, plastic deformation thermal activation parameters from creep kinetics and stress relaxation 80−71717
Al, polycrystalline, acoustic emission energy release, grain size and flow stress depend. 80−11722
Al thin films, vacuum deposited, influence of film thickness on internal stresses magnitude *(Russian)* 79−37938
Al thin films 1/f noise, depend. on internal mech. stresses 80−65711
Al-Cu-Mg alloy, influence of plastic deformation on fatigue limits, for prestrained components 78−68799
Al-Cu-Mg-Si-Mn alloy AK8, fatigue strength, effect of residual stresses and cold working 77−56101
Al-Mg, oxidation induced stresses, dislocation network form., HVEM obs 80−14978
Al-Mg (2.2 at.%), creep at 573K 79−20145
Al-Mg (5.5 at.%), internal stress during creep at high temp. 79−91749
Al-Mg (5.5 at.%), theory of internal stress for class I high temp. creep 78−19807
Al-Mg alloy, superplastic behaviour, effects of bidirectional twisting 77−70129
Al-Si alloy, eutectic, quasiisotropic 80−79165
Al-Zn, type 7075-T6, coldworked hole specimens, residual stresses, fracture mech. anal. 80−97587
Al-Zn-Mg, welded section stress in rolled plate edges, mechanical surface treatment and environment effects 80−21193
Al-Zn-Mg-Cu alloys, heat treatment optimisation 80−60888
$Al_xGa_{1-x}As$:Cu, variable-gap semicond., impurity props., carrier recomb. 80−96907
$Al_xGa_{1-x}As$/GaAs heterojunction laser, appl. of stress distrib. calc. for multilayer heteroepitaxial struct. 77−72798
$Al_{2x}Ga_{2(1-x)}O_3:Cr^{3+}$, luminesc., lifetime, 77 and 4K, struct., energy transfer 79−28798
AlN film, CVD, characterisation of film props. 78−43496
AlN-Si_3N_4 mixture film, CVD, characterisation of film props. 78−43496
Al_2O_3 film, RF sputtered by planar magnetron, phys. props. 77−43448
Al_2O_3, residual stress reduction by ultrasonics 79−24575
Al_2O_3, sintered, residual stress meas., piezospectroscopic technique 78−52704
Al_2O_3-Cr_2O_3, crystalline soln., microstrain rel. to lattice energy and strain energy 77−24411
β-Al_2O_3-Na_2O, thermal expansion 79−55910
Al_2O_3-SiO_2 clad with B_2O_3-SiO_2 effect of drawing tension on residual stresses 78−64554
Al_2O_3-SiO_2 glasses, thermally toughened, residual compressive stresses evaluation 78−31523
internal stresses continued
Au, electrodeposited and sputtered, hard, reactive softening, X-ray diffr. studies 80−100414
Au, electroplated, polyphosphate, citrate-phosphate and sulphite baths comparison 79−7756
Au film, ion plated, defect growth structs., SEM obs. 80−24768
Au film, on MgF_2 and SiO substrates, internal stresses correl. with struct. 79−87026
Au film, vac. deposited, internal stress and its depend. on gas adsorption 80−6683
Au film deposition, thermal effects, influence on internal stress meas. 80−96767
Au film electrodeposition, substrate effects on film props. 80−81329
Au powder, ultrafine, sintering, coalescence growth stage 80−89174
Au-Ni, supermodulus effect, one-dimens. modulated structs. 79−95068
Au-Ni, surface segregation, strain effects 80−80042
B fibre reinforced Al, residual stress, internal friction anal. 80−45339
B fibre reinforced Al, stressed state nondestructive testing method *(Russian)* 80−40631
B fibre reinforced Al, X-ray investigation of internal stresses *(Russian)* 77−73290
BN film, undoped and P-doped, effect of CVD parameters on props. 80−25571
BN films, elastic stiffness and thermal expansion 80−49559
$Ba_xSr_{1-x}Nb_2O_6$ crystals, optical defects and edge dislocation distributions 80−19806
$BaTiO_3$, effect of phase transformation on fracture behaviour 78−48507
$BaTiO_3$, ferroelectric ceramic, internal stress and strength, failure mechanism 80−66128
$BaTiO_3$, ferroic materials, fracture processes 80−79869
Be, RF sputtered film, props. rel. to deposition conditions 77−39965
$Bi_{2-x}Sb_xTe_3$, solid soln. film on mica substrate, effect of stresses on elec. cond. 78−51859
C steel, fatigue, residual stresses, surface cracks *(Japanese)* 77−25121
CaF_2, fine-grained, forging and bulk optical props. 80−33103
CaO, relax. in $^3T_{1u}$ state of F centres 80−24443
Cd films, struct. and props., X-ray diffr. spectra anal. 80−80119
Cd, thin film, vac.-deposited, X-ray diffr. struct. obs., props. 79−37937
$CdCr_2Se_4$, optical reflectivity, dielectric const. by expt. data Kramers-Kronig anal., spinel struct. 79−99903
CdS film preferred orientation, internal stress, and interface characteristics 78−26795
Co-Mo alloy electrodeposits, codeposited impurities rel. to H_2 permeation, props. 79−19493
Co-Ni alloys, electrodeposited, struct., internal stress, and mag. props. 78−95471
Co-P, amorphous foil, complex permeability and eddy currents, annealing induced short-range order 77−8360
$Co_{80}B_{20}$, amorphous metal ribbon, stresses, magnetoelastic anisotropy and zero-field mag. domain struct. 80−44896
$Co_3B_7O_{13}I$, intermediate phase between paraelectric and ferroelectric phase *(Russian)* 78−68465
$CoFe_2O_4$, epitaxial layer prod. by chem. transport 77−81224
Cr coatings, electrodeposition, conditions rel. to H_2 conc., internal stresses 77−1933
Cr condensates, lattice const., internal stresses *(Russian)* 80−107141
Cr electrodeposit on steel, stress meas., X-ray methods 79−29298
Cr film, evaporated, concurrent ion bombard. effects 80−80142
Cr film, evaporated, on die-cast Zn, microstruct. and intrinsic stresses, substrate temp. effects 78−10304
Cr film, residual stress meas. by X-ray diffr. using $\sin^2\psi$ method 79−15059
Cr, sputtered wafer, 0.1-0.3 μm, deposition parameters effect 77−39753
Cr-Mo, structural carbonitrided at low temps., rotating bending fatigue strength *(Japanese)* 77−48534
Cs_2O profiled silicate glass, residual stresses 80−2107
Cu electrodeposits, bright, low conc. of ions effect on internal stress 80−25909
Cu film, in situ struct. determ. by internal stress meas. 80−54569
Cu film, internal stress determ. by stress relaxation method *(Russian)* 77−62787
Cu film deposition, thermal effects, influence on internal stress meas. 80−96767
Cu, friction stress in high temp. creep 80−11723
Cu, internal stress meas. by decremental unloading technique 78−64576
Cu, internal stresses in plastically deformed crystals *(Russian)* 78−79615
Cu, ion plated, defect growth structs., SEM obs. 80−24768
Cu, plastic deformation thermal activation parameters from creep kinetics and stress relaxation 80−71717
Cu single crystals, in high temp. creep, meas. of internal stress 78−80608
Cu, stress removal during annealing after hydrostatic extrusion 79−83215
Cu-Al-Ni(Mn), duplex shape memory effect after nonuniform plastic deform. *(Russian)* 80−25759
Cu-Au (50 at.%), ordered, influence of elastic stresses on mech. props. *(Russian)* 78−92298
Cu-Ge(Sn)(Sb) alloys, stress removal during annealing after hydrostatic extrusion 79−83215
Cu-Ni, foils, supermodulus effect, one-dimens. modulated structs. 79−95068
Cu-Ni (10 at.%), creep, substruct. and internal stresses *(Russian)* 80−97527
Cu-Ni-Fe, age hardenable, dislocation interactions with internal coherency stresses 77−36528
Cu-Ni-Fe, age hardened, yield strength correlation with internal coherency strains 77−44254
Cu_xO, sputter deposited on Cu, induced stresses 80−24774
Dy, anomalous thermal expansion, interferometric meas. 78−52333
$DyPO_4$, metamagnet, phase diagram, influence of internal strains 79−28544
Fe, Armco, ground, residual stresses, X-ray evaluation 80−79863
Fe electrodeposited foils, microstruct., internal stress and mech. props. 80−20807
Fe, electroplated with soft Fe coating, fatigue fracture, struct. charact. 80−55524
Fe, high-purity, magnetic 90° domain wall-dislocation tangle interaction, magnetomechanical damping expts. 79−78496
Fe, internal stress meas. by decremental unloading technique 78−64576

internal stresses continued
Fe, low temperature deform., strain-rate cycling and stress relaxation tests *(Japanese)* 78−52876
Fe, magnetomechanical acoustic emission for residual stress NDT 80−71149
α-Fe, nitrided, aging at room temp. 80−71679
Fe, plastically deformed, high field suscept. anisotropy and domain struct. 78−15002
Fe, residual stress induced by uniaxial deform., magnetic meas. 77−73390
Fe, stress relaxation in high purity single crystal with controlled amounts of C *(French)* 79−70105
Fe/Cu composite, prop. of fatigue crack crossing interface under residual thermal stress effect 80−45371
Fe-Al (0.069 and 0.158 wt.%), internally oxidised, low temp. deform. *(Japanese)* 78−52876
Fe-Co, amorphous alloy, stress effect on mag. domain struct. 79−33502
Fe-Co-Cr (27, 0.5 wt.%) brittleness in ordered state *(Russian)* 79−61698
Fe-Cu composite plates, vol. fraction and residual stress, effect on fatigue strength *(Japanese)* 79−8349
α-Fe-Fe_3C alloys, ground surface layer exam. of props. 78−84840
Fe-Mo(4.1 wt.%), steady state creep at high temps. 80−89316
Fe-N, precipitated $Fe_{16}N_2$ nitride distrib. during isothermal ageing 77−21143
Fe-N (0.03 at.%), single cryst., stress distrib. around spherical inclusion, TEM study 79−34038
Fe-Ni (28 wt.%), martensitic reversion, effect of internal stresses *(French)* 77−21142
Fe-Ni film, vacuum-deposited, thickness and comp. effects *(Russian)* 77−80713
Fe-Ni-Cr, Elinvar, struct. and mag. props., singularities during tempering *(Russian)* 80−50627
Fe-Ni-Cr austenitic alloy, homogeneous and dispersion strengthened, internal stresses and high temp. creep 78−19841
Fe-Ni-Cr-Ti-Al Elinvar alloys, dispersion-hardened, structural transform. *(Russian)* 79−1872
Fe-Pd (50 at.%) alloy, structural changes during ordering *(Russian)* 77−77471
Fe-Si, grain-oriented, surface coating effect on transverse magnetostriction 77−66402
Fe-Si, maze domains upon appl. of horizontal mag. field or mech. tension 80−11218
Fe-Si (3 wt.%), deform., effect of superimposed US oscillatory stress *(Japanese)* 78−31461
Fe-Si (3 wt.%) layers, with ceramic coating, interface struct., electron microscopy and Mossbauer obs. *(Russian)* 79−28216
Fe-Si (3 wt.%) locally deformed, EM loss depend. on cryst. struct. and orientation *(Russian)* 80−7694
Fe-Si (3 wt.%) sheet, obs. through surface coating of domain struct., SEM 77−85482
Fe-Si (3.5 wt.%), Barkhausen noise strain depend., domain wall dislocation stress field interactions 77−12155
Fe-Ti (0.056 at.%), mobile dislocations during stress relaxation 78−68722
Fe-Ti (0.056 at.%), stress relaxation curves, anal. interpretation 77−59847
$(Fe-Ni)_{1-x}(SiO)_x$, cermet film, internal strsses *(Russian)* 78−75951
$Fe_{1-x}B_x$, amorphous films, mag. props. and thermal stability 79−78446
$Fe_{81.5}B_{14.5}Si_4$, amorphous metal ribbon, stresses, magnetoelastic anisotropy and zero-field mag. domain struct. 80−44896
$(Fe_{1-x}Co_x)_{78}Si_{10}B_{12}$, amorphous alloys, magnetic anisotropy meas., effect of internal stress relief 80−2570
(FeNi)PB amorphous wires, surface oxidation and annealing influence on induced anisotropy 80−100957
Fe_2O_3, pelletised, internal stresses, X-ray investigation *(Russian)* 78−19684
Fe_2O_3 thin films, reactively sputtered, mechanical stresses rel. to deposition conditions 80−80146
Fe_2O_3-Fe_3O_4-Fe_2SiO_4 system, haematite-magnetite-fayalite nodules, stressed state parameters *(Russian)* 80−40336
Fe_3O_4, effect of residual stresses on sp. ht. and elec. cond. 77−59308
Fe_3Pb, reversible shape memory effect, rel. to microstruct. memory and residual stresses 77−90419
n-GaAS epitaxial film, radiative recomb. under influence of mech. stresses 80−66291
$Ga_{0.65}Al_{0.35}As$ epitaxial layer on GaAs, two-dimensional lattice mismatch parallel to interfacial boundary 79−51439
$Ga_{1-x}Al_xAs$, epitaxial layers, on GaAs substrates, X-ray double-cryst. diffractometry, state of strain 79−19480
$Ga_{1-y}Al_yAs$ laser diode, hetero-isolation stripe geometry for IR and visible radiation *(Japanese)* 80−83607
GaAs:Si, neutron irrad., strain detection by local mode IR absorpt. meas. 77−69828
GaAs-GaAlAs DH lasers, strain-enhanced luminesc. degradation, photoluminesc. obs. 80−69392
GaAs-GaP heterostructure, radiative recomb. under influence of mech. stresses 80−66291
$Ga_{1-x}In_xAs$-GaAs epitaxial interface with small misfits, TEM image contrast 80−2275
Gd-Co amorphous films, mag. anisotropy, static and ferromag. reson. expts. 79−33477
Gd-Co amorphous sputtered films, magnetoelastic contrib. to perpendicular anisotropy, internal stress meas. 78−95490
Gd-Co(Fe) amorphous films, microstruct. and mag. anisotropy 79−82838
Gd-Fe amorphous films, stress contrib. to perpendicular anisotropy 80−75819
Gd-Fe amorphous sputtered films, magnetoelastic contrib. to perpendicular anisotropy, internal stress meas. 78−95490
Gd-Y alloy, anomalous thermal expansion, interferometric meas. 78−52333
$Gd_3Ga_5O_{12}$, high energy heavy ion irrad., lattice strain 80−49278
n-Ge, electron-phonon interaction, internal strain and impurity elec. field effect 78−14418
P-Ge, heteroepitaxial film, galvanomagnetic effects, influence of mechanical stresses 79−91171
n-Ge, internal stress effect on electron-phonon interaction, thermal cond. anal. 79−42468
Ho_xCo_{1-x} amorphous films, microstruct. and mag. anisotropy 79−82838
In_2O_3-SnO_2 film, stress, and elec. and optical props. 78−51861

internal stresses continued
$KAlSi_3O_8$, orthoclase, impact structs., peak shock press., X-ray diffr. investig., lunar rock bombard. appls. 78−7002
KCl, strain hardening during relax. of deforming stresses 77−7786
KCl surface texture and optical props. after forging between polished dies 80−33102
KCl:Pb crystals, development of mechanical stresses during growth 80−19735
KCl-KBr solid soln., highly conc., computer simulation of dislocation motion *(Japanese)* 77−68972
KH_2PO_4, cryst. growth, splitting due to colloidal inclusions 77−7681
$LaNi_5$-Gd, dil., ESR spectra, fine struct. and random stresses 80−25203
LiF crystal, gamma irradiated, shear stress depend. on oriented dipoles conc. 79−28013
LiF, dislocation mechanism of electrification during cleavage 77−24353
LiF film, intrinsic stress meas. 80−71696
LiMnSc ferrites, role of intergranular microstresses in control of coercive force 77−20640
$LiNbO_3$:Fe, lattice-strains induced by light, X-ray topography 77−76458
Li_2O-Al_2O_3-SiO_2, glass, study of elastic props. 80−104205
Li_2O-Al_2O_3-SiO_2 glass, crystallised, grain size and internal strain 80−103259
Mg films, struct. and props., X-ray diffr. spectra anal. 80−80119
Mg single crystal, anelastic internal stress field in easy glide region 78−48442
MgCd wire, elongation during disorder-order transform. *(Russian)* 80−104148
MgF_2 film, vac.-deposited, origin of mech. stress 79−90925
MgF_2 film, vacuum deposited, tensile stress, meas. and calc. 79−87027
MgMn ferrite film, determ. by ferromag. reson. method *(Russian)* 77−16126
MgO, granular, first-order stresses due to thermal shock 77−40409
MgO, lattice misorientation and displaced vol. for microhardness indentation 78−64617
MgO polycrystals, hot-pressed, changes in residual strain on annealing 79−34073
MgO single cryst., internal stresses and dislocation mobility, stress relaxation method 80−6413
MgO, stresses on hot pressing 77−36425
MgO-NiO, crystalline soln., microstrain rel. to lattice energy and strain energy 77−24411
Mn-Cr-Ti layers on low C steel, composite, residual stresses rel. to arc-spraying parameters *(German)* 80−104077
Mo alloys, intercryst. fracture in ductile-brittle transition region, local internal stresses effect 80−81200
Mo deformed single crysts., struct. state and dislocation splitting *(Russian)* 80−29029
Mo fibre reinforced Cu, rule of mixtures of deform. parameters in stage III 80−97532
Mo film, deposited by cylindrical magnetron sputtering, internal stresses, optical reflectance and elec. resist. 77−43449
Mo film, on Si, X-ray line-shape anal., simplifications using Fourier series 79−82123
Mo film, on SiO_2/Si substrate, effect of heat treatment after deposition on internal stress 78−22973
Mo film, sputtered on Si, annealing effect on uniform and nonuniform strains 79−82504
Mo, film, vacuum deposited, elec. cond., internal stresses, surface corrosion, MOS gate appl. *(Japanese)* 78−80073
Mo films, sputtered from cylindrical-post magnetron with Ne, Ar, Kr and Xe, compressive stress and presence of inert-gas obs. 80−80140
Mo, He implanted surface deform., integrated lateral stress 77−31697
NH_4Cl, order parameter, electro-optic measurement 78−88280
NH_4Cl, order-disorder transition, slip bands 78−22848
NH_4Cl, order-disorder phase transform., effect of plastic deform. and electrooptic effect 79−33672
NH_4HSO_4:VO^{2+}, ferroelastic, inernal strains, ferroelec. transitions, EPR 79−47400
Na silicate glass temp. depend. of rate of nucleation of acicular crystals 77−19875
NaCl, exposed to high-current electron beam pulses, min. size of excited region for crack initiation *(Russian)* 78−84961
NaCl, internal stresses and dislocation mobility 78−48440
NaCl, rock salt, quenched, residual stresses, optical study 80−55061
Na_2O-B_2O_3-SiO_2 glass, fracture toughness, effect of microheterogeneous struct. 80−104256
Na_2O-CaO-SiO_2 glass, sharp contact cracking, residual stress effects 79−100245
Nb alloys, solid solution hardening, crystal resolved shear stress depend. on dislocations 80−40373
Nb and Nb alloys, cold plastic deform., oriented microdistortions *(Russian)* 78−39840
Nb, electron drag on mobile dislocations, flow stress meas. 79−91197
Nb film, low temp. thermal stresses *(Russian)* 79−11036
Nb film, magnetron-sputtered, intrinsic stresses and supercond. props. 80−24772
Nb, He implanted surface deform., integrated lateral stress 77−31697
Nb heteroepitaxial layers on sapphire, residual mechanical stress and strain influence on superconductivity 80−15644
Nb, supercond., influence of plastic deform. 77−85378
Nb-H, lattice strains, book contrib. 79−82202
$NbH_{0.3}$, α-α′ phase transition, sp. ht. anomaly 78−39764
NbSn multifilamentary superconducting composites, micromechanics 79−38878
Nb_3Sn fatigue effects in unidirectional composites, computer simulated model 80−35289
Nb_3Sn, supercond. composite, residual stress state, crit. currents 80−80468
Ni alloys, welding crack resist. during welding, heating, stress reduction by hardening 79−24618
Ni base superalloy, internal stresses due to dislocation walls around second phase particles 79−99210
Ni, creep, struct. and activation charcts., effective stress, electron microscopy and resistometric obs. *(Russian)* 80−40427
Ni, creep, substruct. and internal stresses *(Russian)* 80−97527
Ni, cyclically deformed, polarisation stress field, dislocation shuttling, computer calcs. 79−96095
Ni, dislocation structure evolution after hydroextrusion *(Russian)* 80−96530
Ni, electrodeposited film, thermal anal., occlusion of gases rel. to mag. props. 80−59823

internal stresses continued
Ni electrodeposition, structure-internal stress relationship 80−70561
Ni electrodeposition from alkaline citrate electrolytes, coating impurity quantities and props. *(Russian)* 79−8252
Ni, electroless, on stainless steel, proximity meas. method 79−64611
Ni epitaxial electrodeposition, surface-stress phenomena at start 80−35542
Ni film, deposited by cylindrical magnetron sputtering, internal stresses, optical reflectance and elec. resist. 77−43449
Ni film, evaporated at oblique incidence, residual stress, mag. anisotropy meas. 78−22992
Ni films, electrodeposition, current modulation, pulse freq. rel. to struct., props. *(German)* 79−11528
Ni, grain boundary cavities growth under applied stress and internal pressure 80−29032
Ni, H diffusion in imperfect lattice, annealing and cold rolling effect 80−49425
Ni, Hopkinson effect, mag. field depend. *(Russian)* 79−4657
Ni, magnetoelastic effect on longitudinal compression, weak field spin rotation model 79−82851
Ni, residual stress determ. by X-ray integration *(German)* 79−52551
Ni, sputter deposited on Cu, induced stresses 80−24774
Ni sputtered coating microstructure on mechanically activated cathode *(Russian)* 79−91586
Ni superalloy, dispersion strengthened, creep stress component rationalisation *(Korean)* 79−66115
Ni, supercooled, struct. refinement mech. *(Russian)* 80−20975
Ni-Co (5(66) wt.%), internal stresses during creep 80−3142
Ni-Fe (36 to 50 wt.%), initial permeability, domain struct. model 80−88811
Ni-Mo alloy electrodeposits, codeposited impurities rel. to H_2 permeation, props. 79−19493
Ni-P, electrodeposited film, thermal anal., occlusion of gases rel. to mag. props. 80−59823
Ni-S, electrodeposited film, thermal anal., occlusion of gases rel. to mag. props. 80−59823
$(Ni_{1-x}Cu_x)Ti$, martensitic, shape memory effect kinetics and thermodynamics 80−3021
$NiFe_{2-x}Al_xO_4$, stress-induced anisotropy in LPE grown single cryst. films, stripe domains and mag. bubbles struct. 79−28238
NiO, lattice parameters, microstrains, non-stoichiometry, comparison between mosaic microcrysts. and quasi-perfect single microcrysts. 80−24414
NiPt, quenched, ordering kinetics and domain struct. form. during isothermal tempering *(Russian)* 80−66502
NiTi, martensitic, shape memory effect kinetics and thermodynamics 80−3021
Pb, film, deposited on Si substrate, residual strains 78−18915
Pb film, reactive ion beam sputtering 78−19666
Pb film, thermal strain, depend. on cryst. orientation 78−10311
Pb film, thermal strain, strain relax. mech. 79−42427
Pb films, vapour deposited FCC, normal and oblique incidences, microstructure, X-ray diffr. study 80−20048
$PbMoO_4$, hollock growht origin in gel growth 80−49139
$Pb(Ti,Zr)O_3$ solid solutions, phase coexistence discrepancies 80−96662
$Pb(Zr,Ti)O_3$ ceramics, DC field sintering preparation, piezoelectric props., ageing behaviour 80−81211
$Pb(Zr,Ti)O_3$, ferroic materials, fracture processes 80−79869
Pd-H, lattice strains, book contrib. 79−82202
Pd_2Si and PdSi films, on Si, stress obs. 80−80145
PtSi films, on Si, stress obs. 80−80145
α-Pu, during deform. of fine and coarse grained specimens 77−28880
S, elasto-optic coefficient of orthorhombic crystal, dielectric theory of strained mol. cryst. 79−65836
Sb evaporated film crystallisation rel. to substrate temp., −50° to 170°C 78−47680
Se amorphous film, spherulite formation and role of stresses due to volume changes in crystallisation 77−1083
Si, appl. of photoelastic stress. meas. technique 80−48656
Si, critical resolved shear stress, 800 to 1050°C indentation dislocation rosettes 79−24577
Si, cryst., impurities rel. to lattice parameters, dislocation density, stresses *(German)* 77−51403
Si, cryst. growth, temp. field, stresses rel. to dislocation density *(German)* 77−51335
Si crysts., deformed, strain distrib. characterisation, annealing response 77−70140
Si, deformed surface, defect struct. rel. to elec. props. 78−72231
Si, dislocation generation, influence of film stress and thermal oxidation 79−23609
n-Si, electron-phonon interaction, internal strain and impurity elec. field effect 78−14418
Si, epitaxial layer on sapphire, shear strain, TEM 78−51835
Si, film, CVD, low press., struct. and stability, X-ray diffr. and TEM obs. 78−91559
Si, film on Si substrate, stress meas., X-ray topography technique 78−5710
Si, high-dose Ar implantation, X-ray topographic obs. of strains and damage 80−59496
Si, implantation induced strains, X-ray interferometry and topography 78−43039
Si, implanted annealed layers, amorphised structure formation mechanism and crystallographic nature 80−29091
n-Si, internal stress effect on electron-phonon interaction 79−42468
Si, ion bombard. induced residual stress in amorphous implanted surface layers 77−35610
Si, ion implantation damage, annealing, role of stresses 78−75679
Si, local mechanical defects, annealing and effect on autoepitaxial growth *(Russian)* 80−7701
Si particle reinforced Al, internal stresses, X-ray diffr. meas. *(Russian)* 78−23765
Si, polycrystalline, thermal oxide anomalous stress 80−93661
Si, residual stress and defects induced by scribing 80−60990
Si, small defects in Czochralski grown and zone-floated monocrystals, TEM identification 79−95001
n-Si, strained cryst., role of phonon reson. scatt. in phonon cond., appl. to Si:Li 79−19407
Si substrate, stress field, induced by Si_3N_4 film edge, indentation-injected dislocation half-loops obs. 78−30839
Si wafer, stresses generated by thermomigration of liquid inclusions 79−37875
internal stresses continued
Si wafer, thermally oxidised, stress and strain meas. *(Russian)* 78−11375
Si: (B, P, Ge), impurity-pair diffusion, influence of elastic stresses 78−87824
Si:B, implanted laser annealed, lattice strain, X-ray study 80−96554
Si:B, with insulating coating, mechanical stress influence on B diffusion, strained surface layers 80−29224
Si:Li, thermal cond., low temp. phonon scatt., internal strain effects 80−96706
Si:P, Ge, simultaneous diffusion processes, elastic stress influence 77−89591
Si:P, shallow strain distrib. near cryst. surface, asymmetric X-ray Bragg reflexion 77−76252
Si:P epitaxial layer, strain distrib. at interface with substrate, obs. by X-ray double cryst. method 79−99461
Si:Pb, ion-implanted and annealed, dose depend. of residual lattice disorder 77−43228
Si:Sb, ion implanted, annealing behaviour of stress 78−63778
$Si-SiO_2$ structure, mechanical stress at Si(111) surface 78−63921
$Si-SiO_2$-Al structure, mechanical stress at Si(111) surface 78−63921
SiC, CVD anisotropic thick hollow cylinder, residual stress due to uniform cooldown 79−42423
SiC:N, impurity effect on stress gradients and dislocation development 77−4116
SiN film, on Si substrate, thermal stresses and cracking resist. 78−63958
Si_3N_4 film, CVD, ion implanted, compressive stress buildup 77−89456
Si_3N_4 film, in MNOS struct., mechanical stress and elec. props. as function of nitride deposition temp. 79−42651
Si_3N_4 film, on Si substrate, thermal stresses and cracking resist. 78−63958
Si_3N_4, film on Si substrate, stress meas., X-ray topography technique 78−5710
Si_3N_4:Ge films, intrinsic stress rel. to deposition conditions 80−39467
Si_3N_4/ZrO_2, hot-pressed, compressive surface stresses developed by oxidation induced phase change 80−60992
SiO_2 film, on Si 77−24499
SiO_2 film, on Si substrate, thermal stresses and cracking resist. 78−63958
SiO_2 film, prep. using high press. O_2, residual stress, chemical etch rate, refr. index and density meas. 80−71768
SiO_2, film on Si substrate, stress meas., X-ray topography technique 78−5710
SiO_2 glass, stressed state investigation by NDT using UHF waves 78−11460
SiO_2 thermal growth, stress meas. 79−91812
SiO_2, vitreous, electron irrad., vol., refr. index and stress changes 77−47482
SiO_2-Al_2O_3-B_2O_3-MgO-CaO-Na_2O, strengthened by ion exchange, exam. of internal stresses using polarising microscope 78−88549
SiO_2-Na_2O-CaO-MgO, glass, fibre and plate, internal stress and birefringence microanal. using optical phase microscope interference-polarisation 79−39109
$Si_lO_mN_p$, CVD from SiH_4-CO_2-NH_3-H_2 system, physicochem. props. 78−38978
Sn-In (50 wt.%), mech. state relations at low and high homologous temps. 77−63707
Steel, C, fibre reinforced Cu matrix, deformation parameters controlling dislocation motion, flow stress, activation volume 79−57055
Ta film, deposited by cylindrical magnetron sputtering, internal stresses, optical reflectance and elec. resist. 77−43449
Ti alloy RMI 38644, shock loaded, residual strength 78−27574
α+βTi alloy VT3-1, drop forgings, grain orientation and props., combined mech. working, hardening and high-temp. heat treatment influence *(Russian)* 80−20973
Ti film, deposited by cylindrical magnetron sputtering, internal stresses, optical reflectance and elec. resist. 77−43449
Ti, film, reactive ion beam sputtering 78−19666
Ti, internal stress meas. by decremental unloading technique 78−64576
Ti, martensitic transformation, strain energy minimisation 77−21140
Ti-Al, hardening of Ti by addition of Al *(French)* 78−23715
Ti-Al, structural and phase changes due to annealing *(Russian)* 80−55440
Ti-Al-V (6, 4 wt.%) cylinders, residual stresses introduced by quenching elastoplastic anal. *(French)* 80−45355
Ti-Al-V-Cr-Zr-Mo-Fe (3.4, 8.3, 5.8, 3.9, 4.2, 0.06 wt.%), shock loaded, residual strength 77−36589
Ti-Al-V-(Sn), surface finishing effect on internal stresses, X-ray study *(German)* 79−34210
Ti-Al-V(Sn) alloys, plastic deformation and fracture characts. at low temps. *(Russian)* 80−7624
Ti-Al(−V)(Mo), impact strength anisotropy, influence of texture *(Russian)* 80−20952
Ti-H, lattice strains, book contrib. 79−82202
TiNi, strain recovery, memory effect, in martensite phase *(Russian)* 77−4806
Ti_nO_{2n-1}, reduced rutile, elastic strain energy due to crystallographic shear plane arrays 78−55880
TlBr-TlI, KRS-5, periodic strain anisotropy, optical and X-ray diffr. study 80−54167
UO_2, mag. ordering lattice internal rearrangement transition, theory 80−20402
V and V-Fe (5.0 at.%), stress relaxation test, appl. to discerning frictional and internal stresses 77−63712
V, supercond., influence of plastic deform. 77−85378
V, zone-refined, deform. behaviour, stress relax. and slip plane patterns 79−29163
V_3Ge, bronze-processed, stress-induced enhancement of supercond. T_c 78−64159
VO_2, reactively sputtered film, influence of manufacturing parameters on film struct. and props. *(French)* 77−81218
W fibre reinforced Cu composite, work hardening 77−52341
W fibre reinforced Cu composites, correl. between thermal cycling-induced microstructural changes at interphase boundaries and tensile behaviour *(Japanese)* 80−71674
WC-Co, VK type hard alloy, influence of residual stresses on static strength 77−1862
WC-Co (10 to 30 wt.%) transverse rupture strength, residual stresses due to surface grinding effects 77−63789
WC-Co alloys, microstresses in two phases, mag. investig. 77−59879

internal stresses continued
WC-Co and WC-Co-TaC-TiC-NbC cemented carbides, microstructure, high temp. deformation, uniaxial plastic compression 80−40451
WC-Co hard alloy composite, calc. of weakest link in struct. 80−11730
WC-Co sintered hard alloy, yield stress, internal thermal stress effect 79−100230
WC-TiC-Co alloys, microstresses in two- and three-phases, mag. investig. 77−63758
Y_xFe_{1-x} amorphous films, microstruct. and mag. anisotropy 79−82838
YIG and Ga-substituted YIG, high energy heavy ion irrad., lattice strain 80−49278
Zn, electrodeposited coatings, residual stress diagrams 80−16588
Zn hexagonal films, residual stress meas. from X-ray peak shift anal. 77−72807
Zn, plastic deform., effect of hydrostatic press. stress relax. meas. *(Russian)* 79−96102
Zn single crystals, fatigue failure at low temp., under low-freq. cyclic loads *(Russian)* 79−61697
Zn, strengthening by electroplastic strain, surfactant effect *(Russian)* 80−20953
Zn, wear resistant coating, effect of surface-active substances in electrodeposition on props. *(Russian)* 78−11359
$ZnIn_2S_4$, III(a) polytype, absorpt. spectrum tail changes due to microstresses 80−2788
ZnS, elastic moduli of polytypic modifications 79−51187
ZnS, film, intrinsic stress meas. 80−71696
ZnS film, vac.-deposited, origin of mech. stress 79−90925
ZnS type structure solids, contrib. of many body forces to elastic consts. 78−2188
Zr film, reactive ion beam sputtering 78−19666
Zr, structural changes during plastic deform. *(Russian)* 77−8880
Zr-Rh alloys, amorphous, thermal relax. effects on electronic and supercond. props. 79−65575
ZrO_2, anodic films, growth stresses 77−16716
ZrO_2, anodic films, growth and morphology 77−16717
ZrO_2, stabilised, coating for turbine components, degradation due to internal stresses 79−24671

internuclear double resonance *see INDOR*

interplanetary magnetic fields
see also interplanetary matter
1972, August, field direction correl. with cosmic rays north-south anisotropies 78−89018
A_p-index, 1964-1976, rel. to geomag. field and interplanetary field states 80−104866
Alfven waves, influence of shock waves rel. to solar particle propag. 77−49250
annual variations, phase reversals rel. to Sun polar mag. fields reversals 78−40780
auroral arcs, quiet time pattern rel. to IMF in X-Y plane 79−25382
auroral electrojet, empirical relations to interplanetary parameters 80−105118
auroral electrojet intensity influenced by interplanetary mag. field 80−51602
auroral midday gap relationship and auroral substorms, photographic study 80−12592
auroral oval and polar cap mag. field perturbs., rel. to charged particles and interplanetary mag. field 78−45160
auroral oval dynamics, influence of interplanetary mag. field B_z component 79−62641
B_y and B_z components, origin *(Russian)* 80−98611
B_y-component sign rel. to longit. position of magnetosphere polar cap plasma flow entry region 80−67472
B_z component, direction rel. to Earth bow shock three-dimensional shape 80−85832
B_z component, dusk-dawn asymmetry in magnetosphere response 77−2310
B_Z component fluctuations effect on equatorial electrojet 79−53697
B_z component influence on geomag. field vars. and auroral dynamics 79−62689
B_z component rel. to evening sector auroral oval dynamics, DMSP photographs 79−96853
B_z component vars. and Dst vars., time displacement 79−101032
B_z-component, magnetosphere response dusk-dawn asymmetry 78−89006
B_z-component, pulses rel. to geomag. field disturbances 78−73583
B_z-component, search for correl. with counterelectrojet 78−88983
charged particle acceleration to relativistic energies in interplanetary shock waves 79−80123
charged particle diffusion in presence of Alfven waves, perpendicular particle flux 77−84406
charged particles acceleration, role of mag. mirrors in shock waves 79−80122
charged particles acceleration on shock front, temporal characts. 79−80121
charged particles transport in fluctuating mag. fields, Fokker-Planck eqn. soln. 79−27752
comet tails, hydromagnetic models rel. to mag. field strength 80−56773
cometary plasma, mag. structs. rel. to accel. 80−46486
cometary plasma tail disconnection events, rel. to sector boundary crossings and high-speed stream encounters 80−46482
cometary tails, small-scale turbulence theory 79−44411
cometary type 1 tails, origin of mag. fields 77−13288
comets, magnetic tail, laboratory simulation 79−62793
control of geomagnetic storm development 78−85771
coronal magnetic struct. from solar wind energetic particles and interplanetary field obs. 77−71076
coronal-interplanetary field, topological structure 78−49273
coronal-interplanetary mag. fields modelling, sheet current approach 78−20807
corotating mag. sector struct. assoc. with Jupiter's decametric radio emission 80−26710
corotating regions, nucleon accel. and modulation of Jupiter electrons 78−61690
correlation with interplanetary cosmic ray protons 80−77243
cosmic radiation intensity on Earth and in Galaxy, diffusion restriction by mag. fields 77−13191
cosmic ray current density and diffusion coeff. 77−49247
cosmic ray daily variation, 50-200 GeV particle motion in magnetic field 80−17455
cosmic ray diffusion coefficients, calcs. from diurnal intensity var. 79−29952

interplanetary magnetic fields continued
cosmic ray diffusion theory, vel. correl. function 77−73913
cosmic ray intensity diurnal variation rel. to interplanetary mag. field, two approaches 79−29953
cosmic ray intensity fluctuations, two-particle distrib. function eqn. 78−28457
cosmic ray intensity fluctuations 77−78585
cosmic ray intensity solar diurnal variation, interplanetary mag. field north-south component correl. 78−93057
cosmic ray interplanetary scintillations at 250 GV, statistical props. 80−8496
cosmic ray modulation and solar activity 79−80135
cosmic ray motion in field, kinetic eqn. 77−53346
cosmic ray neutrons short period vars., rel. to interplanetary mag. field direction *(Russian)* 79−96865
cosmic ray particles propag. in interplanetary region, transport eqn. 79−44315
cosmic ray propag., diffusion approx. of kinetic eqn. 77−13193
cosmic ray propagation, 10^{11} eV particles, sidereal variation 80−17452
cosmic ray propagation, applicability limits of quasilinear approximation to kinetic eqn. 77−91383
cosmic ray scatt. in stochastic mag. field, solar wind fluctuations, above 1 GeV 78−61689
cosmic ray scattering on magnetic inhomogeneity, spectrum, transport range 77−53345
cosmic ray streaming perpendicular to mean mag. field, gyrophase distrib. function 78−53778
cosmic ray transport, particle drift effects, galactic cosmic ray modulation numerical models 80−31180
cosmic ray transport, particle drift effects and analytical soln. to modulation problem 78−28456
cosmic ray transport, particle drift effects on solar modulation 77−45263
cosmic rays, quiet-time anisotropies rel. to mag. field data 78−77442
cosmic rays, scatt in simulated interplanetary mag. field fluctuations 80−51626
cosmic rays coherent propag. in random mag. field, perturb. calc. 77−17303
cosmic rays propagation, non-field-aligned diffusion effects on neutral monitor diurnal anisotropy 78−32304
cosmic rays short-period variations, interplanetary shock wave struct. determ. 79−80125
cosmic rays spatial diffusion coeffs., computation using nonlinear particle trajectories 77−45262
cosmic-ray fluctuations, charged-particle scatt. in interplanetary mag. field 77−53352
current sheet in compressible plasma, self-similar resistive decay 80−1755
current sheets struct. at 1 AU 77−87324
current sheets struct. in mag. holes at 1 AU 79−35087
dayside south polar cusp, field-aligned currents rel. to interplanetary mag. field 79−35059
dipole structure, rel. to galactic cosmic rays solar mag. cycle depend. semiannual var. 79−16777
direction, influence on magnetosphere hydromag. energy spectra 80−67476
direction, rel. to mag. substorm phase and daytime ionospheric absorpt. surges 78−73575
directional medium-scale variations, effect on galactic cosmic rays diffusion and solar cycle var. 77−29605
discontinuities, causing cosmic rays isotropy 78−4045
discontinuities in 1-8.5 AU range, temporal var. and radial gradient 79−101116
disturbances and cosmic ray Forbush decreases 77−60551
disturbances generated by solar wind vel. perturbations, MHD soln. 77−29615
disturbances rel. to mag. and cosmic ray storms 77−33313
early field intensity determ. from remanent magnetisation of Kirin meteorite *(Chinese)* 78−89136
Earth atmosphere elec. current systems and interplanetary field 80−105126
Earth bow shock, DC mag. field obs. 80−90306
Earth bow shock, initial ISEE mag. field obs. 80−90307
Earth bow shock, theory of magnetic shocks in collisionless plasma 80−85854
Earth bow shock interaction, backstreaming ions and interplanetary mag. field 80−101500
Earth bow shock region, mag. field topology rel. to upstream particle events 80−77247
Earth bow shock tangential mag. field line rel. to upstream energetic electrons 80−90308
Earth bow shock vicinity, low-freq. waves obs. 80−90311
Earth magnetosphere interaction, dayside merging rel. to substorm currents and dayside aurora 79−96852
Earth magnetosphere interaction, mag. curl in front of magnetosphere boundary 80−85804
Earth satellite observations by Isee-1 and -3, reliability of method 80−85895
Earth to Jupiter field line, struct. rel. to Jovian low-energy electrons increases 77−2367
effect of interplanetary mag. field on geomag. activity *(Hungarian)* 79−25544
effect on high latitude tropospheric pressure 80−56515
electron diffusion along field nonuniformities 77−53349
electron plasma obs. in vicinity of mag. holes 80−26808
electrostatic noise at solar wind plasma freq. beyond Earth's bow shock, mag. field-shock connection 79−70939
enhanced field regions, rel. to interplanetary accel. of nucleons in corotating interaction regions 77−9635
equatorial ionosphere vars. rel. to interplanetary mag. field vars. 79−84572
excursions and effect on magnetosphere, negative impulse at equatorial stations during SSC 79−16768
field line reconnection with geomag. field, untenability of models 77−22007
field line reconnexion by localised enhancement of resistivity 79−92644
fluctuations, correl. with cosmic ray transient diurnal var. 79−25416
fluctuations, power spectra rel. to geomag. field fluctuations at synchronous orbit 78−96358
fluctuations and noise, effects on neutron monitor diurnal anisotropy 77−45264
fluctuations spectrum, rel. to auroral pulsations harmonic anal. 79−8736

interplanetary magnetic fields continued
Forbush decreases and interplanetary mag. field structure 77−53365
frequency spectra of fluctuations rel. to mean field direction 78−85905
galactic cosmic rays, particle drift effects on solar modulation 77−37488
galactic cosmic rays density and current inside interplanetary mag. sector 79−80120
geomagnetic activity, cyclical nature due to interplanetary field 80−81813
geomagnetic activity depend. on solar wind and interplanetary mag. field, statistical anal. 79−48402
geomagnetic activity indexes rel. to interplanetary magnetic field *(Russian)* 78−16249
geomagnetic daily variations influenced by interplanetary field 80−85591
geomagnetic field disturbance, low latit. interplanetary mag. field effect 79−35090
geomagnetic field quiet time var. rel. to interplanetary mag. field, autocorrel. effects 78−61697
geomagnetic indices impulse response to interplanetary mag. field 80−51622
geomagnetic long-period pulsations rel. to interplanetary mag. field parameters 77−29583
geomagnetic polar cap activity during undisturbed periods, rel. to interplanetary mag. field 77−33295
geomagnetic pulsations, Borok B-index as probe of interplanetary mag. field 77−29589
geomagnetic pulsations, connections with interplantary mag. field 78−85773
geomagnetic pulsations affected by interplanetary medium 80−77228
geomagnetic variations correl. with interplanetary mag. fields 80−41642
geomagnetic variations in N. polar cap region, rel. to interplanetary field 80−41644
Gold bottle model rel. to bidirectional anisotropies in solar cosmic ray events 78−40778
Hale sector boundary, effect on geomag. activity 79−75055
Halley-Venus mission, Planet-A project for mag. meas. in interplanetary space *(Japanese)* 80−94672
heliocentric distance dependence 78−73675
Helios 1 and 2 observations, of interplanetary mag. field between 0.3 and 1 AU 80−21887
heliosphere, mag. field effects on charged interstellar dust particles motion in interplanetary space 80−4300
heliosphere magnetic field configuration, three-dimensional model 80−94670
HEOS-2 magnetometer data rel. to interplanetary diffusion coeff. for energetic particles 78−96364
Imp-J of N-S component, auroral zone electric and geomagnetic responses 78−77431
imperfect corotation, as possible source of cosmic ray semidiurnal var. 80−8497
inhomogeneity during periods of Forbush effects from galactic cosmic ray currents obs. 79−80124
inhomogeneity spectrum correl. with cosmic ray intensity spectrum 77−53348
inner solar system, mag. fields, plasmas and coronal holes 79−58212
intensity, vars. during geomag. storms with gradual commencements *(Russian)* 80−105127
intensity enhancements at 1 AU, solar cycle 20 obs. 80−41765
intensity rel. to geomag. perturbs. *(Russian)* 79−40055
intensity var. with solar cycle 80−26809
interaction with solar wind, equatorial ionosphere elec. fields and geomag. storms 77−78578
ionospheric equatorial elec. fields during mag. disturbances, interplanetary mag. field effect 80−26676
Jovian electron intensity modulation by corotating interaction regions 77−13283
large scale disturbances, effects on solar particle propag. during November 18, 1968 event 77−29607
large scale properties, effects of solar wind vel. vars. 77−17318
large-scale structure, between 1 and 0.3 AU during Helios 1 primary mission 79−29962
large-scale three-dimensional structure 78−28480
lunar plasma wake three-dimens. struct. 77−29613
magnetic holes, theory 79−29961
magnetopause, compressible reconnection model 77−37485
magnetosheath, dayside, field compression rel. to plasma press. anisotropy 77−37483
magnetosheath, high latit., mag. field lines rel. to ≲2 MeV electrons transport 80−90296
magnetosheath, mag. field direction rel. to obs. of energetic electrons of magnetospheric origin 80−90310
magnetosphere, dayside, particle meas. and mag. perturb. rel. to interplanetary mag. field 79−75044
magnetosphere, high-energy protons produced by substorms, interplanetary conditions 80−51615
magnetosphere boundary, mag. field from laboratory simulation data 78−57396
magnetosphere current systems, N.polar cap mag. variations associated with interplanetary field 80−41645
magnetosphere double substorm, rel. to interplanetary field southward component 77−53330
magnetosphere interaction, comprehensive model current system rel. to interplanetary mag. field 79−92636
magnetosphere interaction, correl. with auroral convection over ($60° \leq \Lambda \leq 75°$) 80−67454
magnetosphere interaction, dayside cleft field perturbations rel. to interplanetary mag. field 79−40023
magnetosphere interaction, effect on energetic electrons distrib. in geomag. field 77−22006
magnetosphere interaction, field rot. rel. to dayside magnetopause merging and cusp geometry 79−66884
magnetosphere interaction, force lines reconnection in two-sheet configuration 78−45140
magnetosphere merging with interplanetary field, half-wave rectifier response 80−72710
magnetosphere penetration, rel. to solar wind flow and magnetopause position 78−49236
magnetosphere response to interplanetary mag. field changes, substorms 78−4038
magnetosphere substorms, prediction of occurrence by solar wind and IMF obs. 80−41648
magnetosphere-solar wind dynamo affected by IMF vector 80−85824
interplanetary magnetic fields continued
magnetospheric polar cap electron accel. regions rel. to interplanetary mag. field direction 80−26698
magnetospheric tail interaction, strong Alfven pulse-excited instability *(Russian)* 80−1768
magnetotail plasma at lunar distance response to changes in interplanetary mag. field, solar wind and substorms 79−70932
Mars 2-7 meas. of field and solar wind vel. 78−16252
Mars interaction, field configuration rel. Martian mag. field 78−49359
Mars interaction, mag. field lines configuration from 'Mars 5' 78−49360
meteorological index, effect of interplanetary magnetic field 77−86994
MHD solitons in solar wind, nonlinear dispersion eqn. qualitative anal. 80−4217
microscale magnetic fluctuations during quiet conditions, probability distrib. functions 78−4053
N-S component variations correl. with geomag. activity at low latits. 78−44772
north to south component, correlated field and equatorial electrojet changes during mag. storm. 78−85766
north-south component, effect on mag. substorm occurrence probability 78−32298
north-south component, rel. to equatorward boundary of instantaneous nightside auroral oval 78−32289
north-south component, vars. rel. to equatorial ionosphere EM state rel. to interplanetary mag. field vars. 78−77413
north-south component in 1972 rel. to geomagnetic bays and geomagnetic activity 80−105124
north-south component rel. to auroral dynamics, DMSP photographs results 77−13146
north-south component rel. to polar cap current system 79−101023
north-south field component, solar cycle dependent configurations in solar wind interaction regions 80−98529
northward field, polar cap electric field structure 79−44305
northward magnetic field, assoc. convection in magnetosphere polar cap 80−94658
northward turning assoc. with anomalous equatorial ionospheric elec. fields 79−70914
orientation, correl. with geomag. Pc 3, 4 activity 77−25870
orientation, possible relationship with magnetic storms 79−12349
orientation, rel. to zodiacal light circular polarisation 78−96428
orientation and solar wind velocity, joint distrib. rel. to geomag. Pc 3-4 pulsations 79−53672
orientation changes rel. to magnetospheric substorms 78−28478
orientation hourly distribs. rel. to geomag. Pc 3 and Pc 4 pulsation activity 79−75046
outer solar system, fields and plasmas 79−58213
Pc 3 magnetic pulsations, synchronous orbit obs. and assoc. interplanetary mag. field conditions 78−28438
plasma field characteristics of directional discontinuities 77−29722
plasma flow, mag. field line reconnection rel. to geomag. Pc 1 pulsations 78−45142
plasma flows from strong flares, props. and nature of mag. regions 77−91397
plasma inhomogeneities, anisotropy rel. to magnetosonic turbulence *(Russian)* 80−36468
plasma mechanisms, mag. field modifications theories, review 77−73946
plasmas with arbitrary orientation of mag. field, two-stream instability 80−41715
polar cap electron precip. dawn-dusk gradient rel. to interplanetary mag. field 78−28408
polarity, heliographic latitude depend. Pioneer 10 and Heos 1, 2 data 77−49260
polarity, rel. to afternoon counter-electrojet events occurrence in Indian region 80−56672
polarity, solar wind speed and geomagnetic index 77−78593
polarity and 180°W low-pressure trough size 80−8511
polarity changes, rel. to D-region radiowave absorpt. 77−33272
polarity effects on equatorial geomagnetic field and ionosphere 78−36416
polarity on March 6, 1970, rel. to plasma sheet thinning and substorm occurrence 77−25874
power spectra, meas. with mean field radial or transverse to Sun 77−29617
primaeval field intensity determ. from Jilin chrondrite *(Chinese)* 78−85917
primitive solar nebula field 79−16847
radial component, correl. with 5-50 mHz geomag. pulsations 77−29590
radial dependences between 1-5 AU, Pioneer 10 obs. 79−2456
radial direction rel. to geomag. ULF pulsations obs. at large longit. separations 77−87201
radial orientation, correl. with magnetosphere ULF activity in Pc 3-4 range 78−28434
radial variation, 0.3-1 AU, Helios 1 obs. 78−20729
radio mapping expt. in International Sun-Earth Explorer C spacecraft 78−85796
radio obs. of out of the ecliptic structures 77−78592
recurrent interplanetary streams, mag. field sources 79−2457
recurrent magnetic field patterns, rel. to coronal holes and solar mag. fields 79−58312
recurrent magnetic storms, interplanetary magnetic field and plasma data 78−20585
restructurings, correl. with evolution of photospheric mag. field patterns 78−20798
reversals rel. to equatorial spread-F 79−16747
rotation, correl. with geomag. field vars. and weather, spectral anal. 77−5308
sector boundaries, geomag. Kp index var. 77−64202
sector boundaries, rel. to Swan Cloud in Comet Kohoutek (1973 XII) and cometary plasma tails general morphology 80−98612
sector boundaries and assoc. low-energy proton events 77−45265
sector boundaries and comets, plasma tail disconnection due to mag. field line reconnection 78−93155
sector boundaries at 1 AU, (1971-1973) 80−94668
sector boundaries config. rel. to certain days of solar rot. 80−41764
sector boundaries rel. to Sun-weather relation, troposphere energetics anal. 78−81285
sector boundary distortion in interplanetary medium 77−70967
sector boundary followed by MeV, proton streams, effect on troposphere 79−53491
sector boundary passage effect on equatorial geomagnetic field, daily variations 80−67335

interplanetary magnetic fields continued
sector boundary surface morphology, 1976 obs. of inner solar system 80−41766
sector boundary transits and assoc. tropospheric circulation 79−74936
sector changes, geomag. polar cap field responses 77−5134
sector field polarity, modulation of geomagnetic lunar component var. 78−15963
sector polarity, rel. to annual var. in occurrence of quiet and disturbed intervals 77−86767
sector polarity from cosmic ray north-south asymmetry 79−30009
sector polarity influence on equatorial geomag. bays 80−8489
sector polarity rel. to occurrence of low latit. geomag. bays 77−40982
sector struct. relation of solar cosmic ray proton fluxes in polar regions 77−49251
sector structure, correl. with lower ionosphere ionisation 80−4167
sector structure, effect on mid-latit. nighttime ionosphere 79−58151
sector structure, form. by large scale spiral waves in solar wind 80−85831
sector structure, influence on lower ionosphere and lower atmopshere in winter 80−8510
sector structure, rel. to atmospheric electrification modulation and Sun-weather relationship 78−57261
sector structure, rel. to ionosphere global scale electrodynamic coupling of high and low latit. regions 80−77194
sector structure, rel. to O I 557.7 nm nightglow intensity in central polar cap 77−33238
sector structure, rel. to occurrence of high-speed solar wind streams (1962-1974) 77−9734
sector structure, rel. to solar mean mag. field polarity pattern obs. 78−20800
sector structure, rel. to zodiacal cloud charged dust particles motion in interplanetary space 80−4299
sector structure (1926-1970), deduced from geomagnetic data 80−90368
sector structure and 50-1000 GV cosmic ray anisotropy 79−48639
sector structure and anisotropy of 50-1000 GV cosmic rays 80−62072
sector structure correl. with atmospheric circulation changes 80−17340
sector structure correl. with meteor radar rates and geomag. activity 78−65553
sector structure effect on cosmic ray diurnal var. 79−84622
sector structure effect on LF absorpt. in midlatit. ionosphere 77−29546
sector structure effects on auroral oval and plasmapause 79−80186
sector structure inferred from geomag. ap indices daily vars. 78−93066
sector structure rel. to galactic cosmic ray vars. 78−16253
sector structure rel. to geomag. activity aa index *(Russian)* 79−21261
sector structure rel. to ionosphere elec. pot., obs. over solar cycle 77−33271
sector structure rel. to mesospheric temp. vars. 79−34905
sector structure rel. to Pi 1 in mid-latitudes *(Russian)* 78−12066
sector structure rel. to solar mean mag. field, 1968-74 period 77−71082
sector structure up to 16° heliographic latitude, Pioneer 11 meas. 78−45281
sectoral struct. due to large scale spiral waves in solar wind 80−12633
sharp northward and southward transitions, dayside aurora response 77−87148
shock wave, 1978 January 3 to 4, Prognoz-6 energetic particle and solar wind meas. 80−90315
shock waves, assoc. plasma wave turbulence obs. 79−53700
shock waves, collisionless, mag. structs. thickness 80−90314
shock waves, effects on $^4He/H$ ratio vars. in energetic storm particle events 77−9636
shock waves, identification by computer on board HELIOS-1 and (HELIOS-2) 79−92679
shock waves, ISEE magnetic field profiles 79−58196
shock waves, parameters correl. with energetic storm particle events 79−35079
shock waves during August 1972 solar-terrestrial events, mag. field obs. and vels. 77−25903
shock waves interaction with Earth's magnetosphere, influence of mag. field direction 78−16243
shocks during August 1972, mag. field meas. at 2.2 AU 77−45276
sign reversal and equatorial ionospheric anomaly 79−2430
solar corona, mag. field from Crab nebula polarised radioemission occultation obs. *(Russian)* 78−77527
solar cosmic rays intensity vars. assoc. with interplanetary disturbances 78−40779
solar cosmic rays propag., diffusion in mag. fields, convection in solar wind, dimens. method soln. *(Chinese)* 78−81511
solar current sheet, radial deformation rel. to geomagnetic storms 79−84623
solar cycle var. of N-S component 78−49274
solar cycle variation of interplanetary mag. field config. 80−12632
solar flare particles propag. in interplanetary medium, model 79−80128
solar flare streams mag. field struct. 78−7969
solar high latitude field rel. to geomagnetic activity 79−44308
solar large-scale magnetic fields spatial distrib. rel. to interplanetary mag. field 79−84772
solar magnetic field three-dimens. struct. in interplanetary space 80−31191
solar magnetic sector crossings, lack of effects on troposphere 78−57244
solar nebula, evidence for strong mag. fields from ureilites mag. props. 80−8602
solar nebula, mag. field reversals regions rel. to meteoritic chondrules origin 80−4310
solar particle event, 1973, April 29-30, anal. of interplanetary mag. field behaviour 78−20593
solar plasma regime, rel. to cosmic ray storm symmetrical equator-pole anisotropy obs. 78−89020
solar proton flux affected by photosphere and interplanetary field 80−41672
solar relativistic protons, guiding by interplanetary mag. field rel. to anisotropy 77−22022
solar sector crossings, mid-latitude ionosphere response 79−35030
solar sector structure, long term evolution 77−53389
solar sources of mag. field and solar wind 77−45275
solar wind, Alfven instabilities in streaming plasmas with anisotropic press. 77−49259
solar wind, alignment of plasma anisotropies and mag. field direction 78−32311
solar wind, current sheets resistive instabilities 80−4218
solar wind, density and mag. field orientation rel. to magnetopause three-dimensional shape 79−101029

interplanetary magnetic fields continued
solar wind, dynamic mag. struct. of large amplitude Alfvenic vars. 80−72734
solar wind, EM field in Earth magnetosphere 78−28419
solar wind, field from time-depend. solar mag. field 77−9646
solar wind, instability of finite amplitude circularly polarised Alfven waves 78−28502
solar wind, interplanetary plasma turbulence 79−53693
solar wind, mag. field direction rel. to obs. of energetic electrons of magnetospheric origin 80−90310
solar wind, mag. field effect on MHD shock waves propag. speed 78−77449
solar wind, mag. field fluctuations rel. to plasmadynamical processes *(German)* 80−109323
solar wind, mag. field parameters rel. to magnetospheric ring current plasma injection 78−96363
solar wind, mag. field rel. to Alfven wave accel. 80−85923
solar wind, mag. field rel. to plasma irregularities anisotropic struct. 80−67489
solar wind, mag. field struct. rel. to effect on Earth weather *(Swedish)* 79−79910
solar wind, mag. fields and flows between 1 and 0.3 AU during Helios 1 primary mission 79−29963
solar wind, mag. fields in noncompressive density enhancements 78−28479
solar wind, magnetic data anal. rel. to MHD turbulence 80−61977
solar wind, magnetosonic instability driven by alpha particle beam 79−35089
solar wind, multispacecraft obs. of microscale fluctuations 77−87224
solar wind, obs. of fully developed anisotropic MHD turbulence 80−94669
solar wind, origin in coronal holes, mag. evidence 77−2394
solar wind, spherically symmetric, galactic cosmic rays propag. 79−53681
solar wind, thin layered field aligned currents distrib. 79−12375
solar wind azimuthal field radial var., effect of stream-assoc. fluctuations 77−45278
solar wind azimuthal vel. structure, min. variance direction of mag. field fluctuations 77−5408
solar wind corotating interaction regions, energetic particles shock accel. 80−82159
solar wind discontinuities, substorms triggering 77−29596
solar wind during Maunder Minimum, mag. field characts. 79−75069
solar wind fast mag. fluctuations, Helios 1 obs. at 1 AU 77−87225
solar wind field, rel. to hydromagnetic struct. of 1972, August 4 flare 78−28475
solar wind high velocity streams, mag. fields rel. to source struct. in high corona 77−53530
solar wind high-speed streams, fields rel. to geomag. activity 77−37487
solar wind irregularities impulsive penetration into magnetosphere by interplanetary mag. field direction 79−29939
solar wind large amplitude Alfven waves propag. direction rel. to average interplanetary mag. field 80−26709
solar wind mag. field, cosmic ray energy loss 77−53347
solar wind mag. holes, satellite obs. near 1 AU 77−64586
solar wind magnetic dips 79−75072
solar wind magnetic field rel. to geoefficiency of solar flares 77−29618
solar wind magnetic fluctuations, directional anisotropy and Landau damping of Alfven waves 80−21885
solar wind pulsations rel. to Pc 3-4 pulsations 78−65476
solar wind southward field component at beginning of 20th century 79−2464
solar wind streams magnetic classification 80−41692
southward component, correl. with dayside magnetosphere mag. flux transfer 78−96355
southward component, correl. with plasma sheet thinning during magnetospheric substorms 80−72705
southward component, rel. to ring current development and midlatit. convection elec. fields 78−57395
southward component, relation to mag. substorms, model 77−29587
southward component rel. to magnetospheric substorms, statistical anal. 78−49237
southward field, rel. to field-aligned currents in magnetosphere dayside cusp 77−29591
southward turning after mag. calm period, substorm and auroral activity development 78−28435
spatial variation, importance for EM radiation direct generation from beam-plasma system 80−54007
spiral field inhibition of thermal conduction in two-fluid solar wind models 78−96372
spiral struct., Pioneer 10 obs. 77−5495
stable solar wind and geomagnetic activity 79−53696
structures between 0.3 to 1 a.u., two-spacecraft obs. comparison 79−25429
Sun high-latitude magnetic field, possible connection with Earth rot. nonuniformity 80−46119
theories, effects on geomagnetic activity *(Hungarian)* 77−74010
three-dimens. structure 79−5778
transverse component rel. to polar cap geomag. variations 78−20733
turbulence, character rel. to mean free path of low-rigidity cosmic rays 80−98524
variation effects on solar flare cosmic ray particle intensity 80−77372
variations rel. to geomag. S_q var. at mag. conjugate points 78−69287
Venus magnetic tail interaction, unipolar induction effects 80−62060
vertical component, rel. to geomag. bays and geomag. activity on (1968) 79−53654
vertical component origin and recurrency 80−90369
Voyager magnetic field experiment 78−24431
weather-Sun relation, vorticity area index to interplanetary mag. sector struct. 80−46222
Y-component effect on low-latit. geomag. field, diurnal and seasonal vars. 80−56354
Z-components, variations causing magnetic storm main phase 80−4200
zodiacal light, circ. polarisation 77−53474
zone structure and energetic particle intensities 79−80267

interplanetary matter
see also comets; cosmic dust; interplanetary magnetic fields
ε parameter, rel. to magnetosphere ring current growth 79−75057
acceleration effect on solar cosmic rays, soln. to Fokker Planck eqn. 80−77242

interplanetary matter continued
Alfven waves, Fokker-Planck theory for cosmic ray diffusion 77−29606
antenna in plasma, detect. of natural noises 80−24181
boulders, mass distrib. and sources 78−89119
carbonaceous chrondritic matrix material planet forming unit, occurrence, formation review 78−53892
charged dust grains, Lorentz scatt. 79−70996
charged particle acceleration to relativistic energies in interplanetary shock waves 79−80123
charged particles, meas. instruments review *(Russian)* 77−17368
charged particles acceleration, role of mag. mirrors in shock waves 79−80122
charged particles acceleration on shock front, temporal characts. 79−80121
charged particles transport in fluctuating mag. fields, Fokker-Planck eqn. soln. 79−27752
circumsolar dust cloud, inner F-corona, model and composition 80−82162
circumsolar dust grains, dynamical effects 78−20730
circumsolar plasma, Venera 10 radio signal spectral meas. 80−109326
cold-cloud aggregates, chemical energy and meteorite chondrule origin 80−105210
collisional growth to planetesimals, relative vel. 80−82247
cometary erosion by interplanetary plasma, lab. simulation 77−87323
cometary plasma tail disconnection events, rel. to sector boundary crossings and high-speed stream encounters 80−46482
cometary tails, small-scale turbulence theory 79−44411
comets, origins, research and interplanetary relationships 78−57507
comets and asteroids population in circumterrestrial space 78−73599
comets plasma tails, disconnection rel. to mag. field line reconnection at interplanetary sector boundaries 78−93155
comets plasma tails disruption, triggering by flute instability 78−93156
complex solar particle event, 1973, April 29-30, anal. 78−20593
convection and field-aligned diffusion rel. to cosmic ray diurnal var. 80−56685
coronal-interplanetary space, subsonic flows in closed field lines regions 78−28624
corotating energetic particle events, origin 80−82161
corotating energetic particle streams radial var. in inner and outer solar system 79−16883
corotating interaction regions, rel. to interplanetary accel. of nucleons 77−9635
corotating nucleon fluxes separation from solar-flare fluxes by radial gradients and nuclear comp. 79−25413
cosmic dust, book 78−57498
cosmic plasma properties from magnetospheric research, use in astrophys. 78−93051
cosmic ray anisotropic diffusion in interplanetary space, radial and transverse gradients 77−49248
cosmic ray anomalous ^{4}He component, solar latit. and radial depend. 79−35080
cosmic ray diffusion average properties in solar wind streams 79−75067
cosmic ray diffusion eqn. soln., isotropic diffusion for random energy depend. 77−9632
cosmic ray diffusion with allowance for second spherical harmonic 79−80118
cosmic ray energetic particles intensity meas., 1973 Sept., by interplanetary probes 77−29604
cosmic ray intensity gradient, 1973 April-August, Pioneer 10 and 11 meas. 77−13192
cosmic ray intensity variations of interplanetary origin, Sayan spectrograph data 79−84606
cosmic ray modulation and solar activity 79−80135
cosmic ray nuclei, low energy, ionisation states and origin 78−69634
cosmic ray nuclei, low energy, props., Skylab expt. 78−69632
cosmic ray nuclei recurrent fluxes, 1-8 MeV/nucleon energies, Prognoz-4 meas. 79−21112
cosmic ray particles propag. in interplanetary region, transport eqn. 79−44315
cosmic ray propagation, applicability limits of quasilinear approximation to kinetic eqn. 77−91383
cosmic ray propagation, Mars spacecraft meas. 78−53779
cosmic ray propagation, Venera 9 and Venera 10 meas. rel. to interplanetary irregularities 77−91388
cosmic ray protons, 1-4.5 MeV, spectral anal. and correl. study 80−77243
cosmic ray protons diffusive Sunward flow at 1 AU 77−33302
cosmic ray steady-state transport eqn., Green's theorem and Green's functions 77−87214
cosmic ray steady-state transport eqn., monoenergetic source solns. 77−82088
cosmic ray streaming perpendicular to mean mag. field, gyrophase distrib. function 78−53778
cosmic ray sunward flowing proton and alpha particle fluxes, characts. 78−89016
cosmic ray transport, particle drift effects, galactic cosmic ray modulation numerical models 80−31180
cosmic ray vars., rel. to Dhajala chondrite cosmogenic radioisotopes 79−35207
cosmic rays, anisotropic diffusion in interplanetary space rel. to annual vars. 77−60550
cosmic rays, diffusion in solar wind deformed by interstellar medium 79−53680
cosmic rays, drift as essential energy loss process 80−8498
cosmic rays, flow lines and energy changes 80−82158
cosmic rays, galactic propag. in spherically symmetric solar wind 79−53681
cosmic rays, low energy, interplanetary heavy ions population discovery by Skylab 80−56689
cosmic rays, low-rigidity, weak turbulence diffusion theory rel. to mean free paths 80−98524
cosmic rays, quiet time interplanetary anisotropies obs. from Pioneer 10 and 11 78−77442
cosmic rays, scatt. in simulated interplanetary mag. field fluctuations 80−51626
cosmic rays, scatt. mean free path, energy depend. 77−9633
cosmic rays accel., one-dimens. model with moving MHD shock wave 79−80119
cosmic rays accel. on front of shock wave, regular mechanism 78−36410
cosmic rays acceleration to relativistic energies 79−21111
cosmic rays anisotropic inhomogeneous diffusion around Sun 79−21113
interplanetary matter continued
cosmic rays coherent propag. in random mag. field, perturb. calc. 77−17303
cosmic rays interplanetary anisotropic diffusion, solar daily vars. vector computation 80−4209
cosmic rays propagation, evidence for two modulation zones from neutron intensity vars. 79−84604
cosmic rays propagation, mag. field imperfect corotation as source of semidiurnal var. 80−8497
cosmic rays propagation, rel. to large amplitude wave-trains of neutron intensity 80−94660
cosmic rays short-period variations, interplanetary shock wave struct. determ. 79−80125
cosmic spherules from deep-sea sediments, surface features and origin 77−41361
density discontinuities rel. to radiosource scintillations 77−17314
distant geomagnetic tail, Pioneer 7 and 8 obs. 77−64548
disturbances caused by 1972 August solar flares, Pioneer 9 obs. 77−2317
disturbances generated by simulated solar wind vel. perturbations, MHD soln. 77−29615
dust, causing dark patches in zodiacal light 78−93153
dust, effect of spin and solar radiation on motion *(Japanese)* 78−20732
dust, large fluffy particles as explanation of optical props. 78−57499
dust, light scatt. intensity, theory 80−109324
dust, symmetry plane in inner solar system 80−56767
dust, two independent populations suggested 79−21227
dust, zodiacal light indications 78−57500
dust and electrons spatial distrib. round Sun, contrib. to corona 80−46514
dust between 1 and 5 Au, conflicting Pioneer 10 and 11 data 79−44410
dust cloud, large grains contrib. from Periodic Comet Encke 78−85908
dust cloud, origin and composition, review 79−75154
dust complex, azimuthal asymmetry mechanism from restricted three-body problem 80−85843
dust components in inner Solar System 80−85914
dust concentration toward Venus orbital plane, zodiacal light obs. 79−21228
dust free zone around Sun, search with Helios 1 solar probe 78−45277
dust grain trace element anal., stratosphere collected particle 80−82319
dust grains, H-implanted, role in upper atmosphere H chemistry 78−56445
dust grains in outer planetary magnetospheres, physical and dynamical processes 80−41745
dust in stratosphere, visible absorpt. spectra 80−101554
dust origin and evolution 80−101555
dust particles, effects of solar radiation on orbits 77−5493
dust particles, Mg isotopic composition 80−72879
dust particles, rot. bursting caused by solar radiation press. 77−9644
dust particles optical properties, Helios meas. 78−24484
dust particles orbit distribution, Pioneer 8 and 9 obs. 78−89031
dust spatial distrib. near 1 AU, Helios 1 and 2 obs. 78−36511
Earth bow shock, conference, Strasbourg, France (1978 August 31 to September 1) 80−82573
Earth bow shock, first evidence and early studies, historical introduction 80−85816
Earth bow shock, initial ISEE mag. field obs. 80−90307
Earth bow shock, kinetic models of shocks in collisionless plasmas 80−90330
Earth bow shock, obs. of backstreaming protons in upstream solar wind 80−90309
Earth bow shock, orientation and shape in three dimensions 79−101030
Earth bow shock, review of upstream energetic-particle meas. 80−90308
Earth bow shock, theory of magnetic shocks in collisionless plasma 80−85854
Earth bow shock, three-dimensional shape 80−85832
Earth bow shock interaction, model for ion thermalisation 77−25876
Earth bow shock ions in upstream solar wind, two distinct populations obs. 79−21124
Earth bow shock plasma, possible generation mechanisms of low-freq. waves (≲50 Hz) 80−90312
Earth bow shock vicinity, low-freq. waves obs. 80−90311
electric currents, generation by solar activity rel. to solar wind energy source 80−94768
electron bursts, low energy, Jovian origin 77−2367
electron density fluctuations rel. to interplanetary RF scintillation, weak scatt. approximation anal. 77−9706
electron density profile from Mariner 6 and 7 time delay meas. 77−33435
electron plasma obs. in vicinity of mag. holes 80−26808
electron plasma oscills. assoc. with type III solar radio bursts, heliocentric radial var. 79−2454
electrons, energetic, of magnetospheric origin in magnetosheath and solar wind, obs. 80−90310
electrons, meas. instrumentation on International Sun-Earth Explorer spacecraft 78−85786
electrons, penetration into magnetosphere, satellite obs. 78−73587
electrons from Jupiter, interplanetary modulation and transport 78−45175
electrons with energy 0.3 to 3 MeV, Prognoz 4 obs. 79−62693
electrostatic noise at solar wind plasma freq. beyond Earth's bow shock, mag. field-shock connection 79−70939
EM wave propagation, thin screen scintillation theory for spherical wave 78−13645
energetic particle flux meas. by International Sun-Earth Explorer A and B spacecraft 78−85799
energetic particle intensities and mag. field zone struct. 79−80267
energetic particles, ISEE obs. 79−40036
energetic particles, obs. 80−31186
energetic particles acceleration by transit time damping 77−2311
energetic particles acceleration mechanisms 77−2312
energetic particles from flares, interplanetary shock waves 78−49276
energetic particles pitch distrib. distortion by Earth's bow shock 79−35088
energetic props. at Earth's orbit following solar flare 77−49261
energetic proton bursts, simultaneous multispacecraft obs. 79−2440
energetic protons assoc. with forward-reverse shock pair at 1 AU 78−4052
energetic protons assoc. with interplanetary active regions at 1-5 AU 78−45176
energetic protons near Earth's bow shock, pitch angle distribs. 80−26683

interplanetary matter continued
fast ion stream front arrivals at Earth, prediction from solar wind meas. at 0.3-1 AU 79−58216
flux from flare of August 4, 1972, hydromagnetic struct. 78−28475
focused interstellar gases, planetary cones 77−5494
galactic cosmic modulation, isotropic and anisotropic diffusion, asymm. conditions 78−40777
galactic cosmic ray gradient meas. 78−49243
galactic cosmic ray interplanetary density distrib. 77−17305
galactic cosmic rays, energy spectra between 1-9 AU 78−4046
galactic cosmic rays, latit. depend. modulation 77−2314
galactic cosmic rays, particle drift effects on solar modulation 77−37488
galactic cosmic rays access at polar heliographic latits. 77−25893
galactic cosmic rays anisotropic diffusion, 11-year var. 77−25891
galactic cosmic rays intensity modulation taking into account royal zones in solar activity distrib. 79−80138
galactic cosmic rays modulation depth in interplanetary space, pitch-angle depend. 79−80139
gas, radial temp. and flow vel. 79−96875
gas, stochastic and dynamic temp. charges 78−49271
grain accretion in protoplanetary nebula, liquid drop effects 78−85862
grain motions in the solar nebula 79−84686
gravitational instability of composite plasma, effect of gyroviscosity and ion viscosity 77−87255
hectometric and kilometric radio emission in August 1972, satellite obs. 77−25994
HELIOS 1 and 2 and STIP Intervals I and II participation 78−49295
Helios 1 and 2 mission, general aspects 78−20615
heliosphere, model of mag. field configuration 80−94670
heliosphere, props. of dust in plasma environment 80−26930
heliosphere, scale size from cosmic ray modulation in 1974-1975 near solar minimum 77−33304
hydromagnetic surface waves, theory 79−25462
ice grains in interplanetary and interstellar media, low energy cosmic ray erosion 78−45177
ice particles in solar system, lifetime 77−29721
inflowing interstellar gas, heating by solar electrons 79−16881
inner solar system, mag. fields, plasmas and coronal holes 79−58212
interplanetary Lyman α emissions, Mariner 10 obs., rel. to solar wind latit. struct. 79−35085
interstellar charged dust grains, motion in interplanetary space 80−4300
interstellar gas parameters change in stellar-wind-dominated environment, rel. to solar system 78−61904
interstellar particles, optical detection during out-of-ecliptic mission 78−85906
interstellar wind, Mariner 10 meas. of Lyman α and He I 584 Å interplanetary emissions 78−65474
interstellar wind, Mariner 10 UV obs. and solar radiation models 79−48736
interstellar wind effect on interplanetary environment 79−5721
interstellar wind properties from Lyman α and He I 584 Å interplanetary emissions 78−65475
ion fluxes from Jupiter, Voyager 1 and 2 obs. 80−94667
irregular particle scattering, meas. results versus Mie theory 78−58918
Jovian electron intensity modulation by corotating interaction regions 77−13283
Jovian electrons, propag. close to Sun ($\lesssim$0.5 AU) 79−101034
Jovian electrons obs. at 1 AU 78−4150
Jovian relativistic electron distrib., 1 to 11 Au, continuously emitting point source 78−4149
Jupiter as source of electrons observed at Earth orbit 80−90357
near-Jupiter interplanetary plasma, low-energy charged particle environment 80−26797
near-Jupiter interplanetary plasma, Voyager 1 plasma waves obs. 80−26795
Lα polar enhancement through solar wind asymmetries 78−20605
laboratory and space plasmas, conference, Nagoya, Japan (1977 December 8 to 9) 80−4470
local interstellar medium, He component anal., UV obs. 79−30100
low energy charged particle measurements, Compton-Getting effect complications 78−49269
low-energy particles, interplanetary background meas. on Venera 9 and (Venera 10) 78−4049
lunar plasma wake three-dimens. struct. 77−29613
Lyman α emission in antisolar direction on Earth's night side 77−87138
Lyman α sky background, Copernicus high-resolution obs. 77−29963
Lyman alpha scattering meas. by Venera 9 in interplanetary space, interstellar medium parameters determ. 79−80180
m wavelength scintillation, bispectral anal. 78−12153
magnetic fluctuations, Helios 1 search-coil magnetometer expt. 78−20607
magnetic holes, theory 79−29961
magnetic measurement in interplanetary space during Halley-Venus mission, Planet-A project *(Japanese)* 80−94672
magnetosheath, plasma depletion obs. at dayside magnetopause 79−66876
magnetosheath, Prognoz 4 obs. of $\lesssim$2 MeV electrons and cold plasma 80−90296
magnetospheric storm, interplanetary shock wave with increased solar wind energy deposition 80−77237
Mariner 10 UV spectrometry results 77−45337
Mariner-Jupiter-Saturn low energy charged particle expt. 77−70971
mass ejection from solar corona 78−49417
meteor streams detection in interplanetary space 77−87338
meteoric material density distribution in vicinity of planet 78−20762
meteoritic material, meas. from spacecraft near Earth and in interplanetary space 77−53486
meteoroids from Periodic Comet d'Arrest, contrib. to interplanetary dust cloud 78−53876
MHD discontinuities with Hall effect 77−25899
MHD waves, nonlinear steepening and Landau damping 78−28477
MHD waves due to solar surface oscillations, geophysical effects 79−8777
micrometeoroid data from Helios 1 78−24485
micrometeoroid orbits, Helios obs. 78−20731
micrometeoroids, rel. to meteoric night-glow 77−91488
micrometeoroids within 10 R_E, HEOS-2 dust expt. 79−48740
microparticle studies by space-borne instrumentation 78−57460
nuclear and ionic charge distrib. particle expts. on International Sun-Earth Explorer spacecraft 78−85790
out-of-ecliptic space research, by Sun polar-orbiting probe 77−87228
interplanetary matter continued
outer solar system, fields and plasmas 79−58213
particle acceleration into interplanetary medium during 1972, August 4 solar flare *(Russian)* 77−33303
particle dynamics 78−57501
particle reflection by MHD shock waves, energy spectrum and pitch angle distrib. 79−35126
particle scattering brightness integral, phase function isotropy *(French)* 78−45279
particles, sampling techniques 78−57459
particles accelerated by Alfven waves, distrib. function self-similar solns. 79−32757
pattern motion, spaced sensor obs. 79−25427
piston problem, one-dimensional, in non-ideal gas, time-dependent soln. 80−82185
planetesimal formation, effect on asteroid form. *(Chinese)* 80−8579
planetesimals scattered from Jupiter zone, bombardment of asteroid belt 78−53859
plasma, collisionless, stability of contact discontinuity, solar wind and magnetosphere boundary appls. 80−62002
plasma, moving randomly-inhomogeneous medium, freq. fluctuations statistical characts. *(Russian)* 77−7545
plasma, multifreq. interrogation with coherent response dispersion interferometer 77−22038
plasma blobs, rel. to mag. storms and ionosphere total electron content changes 80−31164
plasma disturbances caused by charged Helios spacecraft in solar wind 78−24416
plasma dynamics from temporal scintillation spectral data 77−25980
plasma field characteristics of directional discontinuities 77−29722
plasma flow, hydromagnetic struct. rel. to geomag. Pc 1 pulsations 78−45142
plasma flow, rel. to cosmic ray Forbush decreases struct. 77−91385
plasma flow around planets, collisionless hydrodynamics rel. to Larmor freq. 78−69637
plasma flow from strong flare, 1972, August 4 to 5, struct. rel. to mag. storm 79−53653
plasma flow in curved mag. field 78−67329
plasma flows from strong flares, props. and nature of mag. regions 77−91397
plasma front parameter determ. by noncoherent response 77−45274
plasma inhomogeneities, anisotropy *(Russian)* 80−36468
plasma inhomogeneities, turbulence 78−28578
plasma meas. by satellite to Earth signals, radio interferometers oscillator stability 77−60571
plasma measurements near Venus using wide-angle instruments on (Venera 9 and 10) 77−91396
plasma physics, book 79−84625
plasma physics basic problems 78−69672
plasma shock waves and solitons effects on satellite signal phases 77−45273
plasma wave expt. on International Sun-Earth Explorer C spacecraft 78−85794
plasma wave propagation, magnetoacoustic wave transverse to mag. field 80−12629
plasma-neutral gas interaction in cosmic physics 78−69669
plasmas with arbitrary orientation of mag. field, two-stream instability 80−41715
primitive grain clumps and organic compounds in carbonaceous chondrites 77−2374
proton flux rel. to geomagnetic Dst var. 77−67018
proton flux rises, 1973 Aug.-Sept., correl. with solar wind vars. 79−21123
protons, low energy, expt. on International Sun-Earth Explorer C spacecraft 78−85791
protons, low-energy, interaction with shock waves, 1975 January, Helios 1 obs. 78−20609
protons and alpha-particles intensity increases at shock wave front 79−53695
protons and electrons, medium-energy, Helios 1 and 2 particle spectrometer meas. 78−20608
protoplanetary nebula formation of inhomogeneous Earth 80−90348
radiation forces on small particles in solar system 80−17461
radio scintillations, freq. correlation *(Russian)* 77−17427
radiowave phase scintillation rel. to search for VLF gravit. radiation 79−70995
recurrent proton streams, 1.3 to 2.3 MeV protons radial diffusion coeff. 79−16774
response to solar events, dynamic modelling 78−49418
rotational shock waves as bow and return shock waves in interplanetary plasma flows 77−17315
scintillation, appl. for solar wind probing 78−45178
scintillation, appl. to solar wind recurrence determ. at high heliographic latits. 80−62106
scintillation, joint Gaussian statistics appl. 77−2316
scintillation, obs. using fully automatic system 79−101064
scintillation meas. in conditions of strong radio interference 80−46413
scintillation obs. and solar wind vel. meas. 78−49278
scintillation obs. of solar wind plasma 78−49279
scintillation observations, solar wind vel. determ. *(Russian)* 79−80185
scintillation of faint radio sources, statistical study at 81.5 MHz 80−51893
scintillation pattern, nature of temporal restructuring 78−45280
scintillation pattern, rearrangements 79−96879
scintillation phenomena, theory, and appl. 79−8880
scintillation spectra, radio spectrograph obs. rel. to electron density vars. physical form 80−72741
scintillations, obs. rel. to solar wind plasma irregularities anisotropic struct. 80−67489
scintillations, radiosource size influence 79−25545
scintillations of PSR 0531+21 at 74 MHz, obs. and anal. 78−36625
scintillations spectra, influence of source sizes, obs. 80−46361
SCOSTEP project, Study of Travelling Interplanetary Phenomena (STIP) 77−17316
sheet-current approach to coronal-interplanetary space modelling 78−20807
shock acceleration of electrons and ions 78−49285
shock wave, 1978 January 3 to 4, Prognoz-6 energetic particle and solar wind meas. 80−90315
shock wave at 9.7 AU generated by solar flare, Pioneer 10 obs. 78−57422

interplanetary matter continued
shock wave from 1972 August 4 solar flare, energy characts., plasma and mag. field struct. 78−49268
shock wave parameters connection with energetic storm particle events 79−70935
shock wave propag., numerical soln. of two dimensional problem *(Russian)* 77−41277
shock waves, assoc. plasma wave turbulence obs. 79−53700
shock waves, assoc. with solar type III radio burst enhancements 77−2409
shock waves, collisionless, mag. structs. thickness 80−90314
shock waves, collisionless shocks simulation and laboratory expts. 80−87893
shock waves, during August 1972, rel. to high-energy cosmic ray obs. 77−25894
shock waves, during August 1972, vels. from solar wind plasma obs. 77−25902
shock waves, effects on ^{4}He/H ratio vars. in energetic storm particle events 77−9636
shock waves, flare generated, during second STIP interval (1976, March 15-May 15), obs. 78−81514
shock waves, flare-generated, scintillation obs., 1977 Sept. 79−48638
shock waves, generated emission in 100-700 kHz range, Prognoz obs. 78−69636
shock waves, identification by computer on board HELIOS-1 and (HELIOS-2) 79−92679
shock waves, inclination rel. to transient north-south anisotropy of cosmic rays 77−9634
shock waves, influence on solar particle events 77−49250
shock waves, interaction with Earth's magnetosphere, computer simulation 78−16243
shock waves, parameters correl. with energetic storm particle events 79−35079
shock waves, three-dimens. geometry 77−22033
shock waves and tangential discontinuities study by noncoherent response method 77−49230
shock waves at large heliocentric distances, Pioneer 10 studies 79−84621
shock waves during August 1972, directions rel. to cosmic rays N-S anisotropies 78−89018
shock waves generation by solar flares *(Italian)* 78−96377
shock waves in August 1972, meas. by radio source scintillation obs. 77−25901
shock waves in August 1972, summary of solar/interplanetary events 77−25991
shock waves in turbulent medium, energetic particles interaction 80−4210
shock waves interaction with bow shock-magnetopause system 80−26712
shock waves interaction with cometary atmospheres 77−22032
shock waves interaction with Earth's bow shock, magnetopause and plasmapause, noncoherent response method 77−64587
shocks during August 1972, obs. at 2.2 AU 77−45276
silicates, optical props. in far UV 78−53875
simulation studies of space 79−58217
Skylab contaminant particulate environment, coronagraphic technique 77−78633
slow MHD shock waves in solar wind 78−12068
solar accelerated particles escape into interplanetary space, influence of solar mag. fields 79−62807
solar cosmic ray event, 1973 April 29, mean free paths near Earth 78−89017
solar cosmic rays, anisotropy rel. to interplanetary medium characts. 77−60553
solar cosmic rays, injection processes and interplanetary propag. influence on intensity and anisotropy 78−12195
solar cosmic rays, origin, nature and effects, interplanetary propag., review *(Russian)* 79−66893
solar cosmic rays and shock waves interaction, 1973 April 29-30 events 79−21122
solar cosmic rays interplanetary propag. *(Chinese)* 79−101035
solar cosmic rays propag., correl. of characts. meas. by Mars-7 and (Prognoz-3) 77−82089
solar cosmic rays propag., diffusion in mag. fields, convection in solar wind, dimens. method soln. *(Chinese)* 78−81511
solar electrons-interplanetary plasma wave interaction, numerical anal. 78−7853
solar energetic particle event of 1974 July 4, Fe/O charge comp. spatial and temporal vars. 77−22199
solar equator vicinity, daily cosmic ray flows during solar cycle 78−69622
solar fast electrons assoc. with type III radio bursts, interplanetary scatt. 77−2411
solar fast electrons flux and type III radio burst intensity at 1 AU 77−2407
solar flare associated shock waves, from radiosource scintillation obs. 77−2318
solar flare cosmic rays, complete model of propag. 77−2313
solar flare electrons, peculiarity of ejection into interplanetary space *(Russian)* 78−77445
solar flare energetic particles, convection and adiabatic decel. effects on time to max. flux 77−2420
solar flare energetic particles, interplanetary propag. model 78−65468
solar flare energetic particles time dispersion, vel. and species depend. 77−2419
solar flare generated shock waves during 1972 August 79−16916
solar flare particles propag. in interplanetary medium, model 79−80128
solar nonrelativistic electron stream, interplanetary propag. and type III radio bursts 78−28623
solar nonrelativistic electrons coherent propag. 77−91506
solar particle propagation from 1 to 5 AU 78−20594
solar particle propagation in interplanetary environment, study of November 18, 1968 event 77−29607
solar particles from E45° flare, 1973, July 29, coronal and interplanetary propag. 77−82090
solar plasma EM wave propag., observations using Mars-2 and Mars-7 probes 78−49345
solar plasma inhomogeneous structure, Venera-9, 10 dispersion-interferometer meas. 79−8789
solar plasma inhomogeneous structure, Venera-9 and 10 radio sounding meas. 79−8788
solar plasma regime, rel. to cosmic ray storm symmetrical equator-pole anisotropy obs. 78−89020
interplanetary matter continued
solar proton and electron events, scatt. mean free path 78−57421
solar proton characteristics near Earth from radio burst obs., longit. attenuation function 78−45309
solar proton event, 1970, April 16, features in interplanetary space and magnetosheath 77−87215
solar protons, 1970, April 16, pitch angle distribs. transform. from solar wind into magnetosheath 77−87216
solar spectral lines propagation, profiles modification 79−66973
solar type III radio bursts, 1972 May-Aug., obs. in interplanetary space 79−62805
solar type III radio bursts, electron density along burst trajectory 78−20808
solar type III radio bursts, electron exciters obs. near 1 AU 80−46513
solar type III radio bursts, nonlinear stability theory 80−26826
solar wind, Alfven waves local instabilities in high speed streams 78−77546
solar wind, corotating streams, three-dimens. model, theory 79−35086
solar wind, current sheets resistive instabilities 80−4218
solar wind, evidence for solar cycle vars. 78−49266
solar wind, evidence of latit. gradient in vel. 77−25900
solar wind, expansion in high-speed streams 78−45298
solar wind, He^+ flux after interplanetary shock, Imp 7 obs. 80−101520
solar wind, interplanetary plasma turbulence 79−53693
solar wind, ion cyclotron instability 78−77547
solar wind, LF oscills. generated by accel. magnetosheath protons 77−33310
solar wind, long-term vars. of selected props., Imp 6, 7 and 8 results 78−77452
solar wind, low freq. continuum from ISEE 3, thermal electrostratic noise, LF obs. 80−101519
solar wind, mag. fields and flows between 1 and 0.3 AU during Helios 1 primary mission 79−29963
solar wind, magnetosonic instability driven by alpha particle beam 79−35089
solar wind, MHD solitons theory 80−4217
solar wind, models with Alfven waves 79−16789
solar wind, multispacecraft obs. of microscale fluctuations 77−87224
solar wind, nonlinear Langmuir waves during Type III radio bursts 78−93173
solar wind, plasma instability theory 79−96877
solar wind, plasma props. during August 1972, near-Earth obs. 77−25904
solar wind, plasmadynamical processes review *(German)* 80−109323
solar wind, proton temp. heliocentric gradient from Pioneer 10 obs. 79−40052
solar wind, radio meas. of second moment field 78−16369
solar wind, search for general vel. gradient at low solar latits. 77−33312
solar wind, spatial distrib. of tangential discontinuities 77−9648
solar wind, time-depend. two-fluid model with thermal cond. 79−92643
solar wind, unstressed deceleration model 79−53692
solar wind, vel. estimation from multi-station interplanetary scintillation 78−73601
solar wind, velocity out of ecliptic from interplanetary scintillation obs. 77−5409
solar wind, very low electron and proton temps., statistical anal., origin 78−65477
solar wind 74 MHz interplanetary scintillation and IMP 7 obs. during 1973 78−89033
solar wind alpha particle component, results of Prognoz satellite meas. 77−53385
solar wind corotating events, energetic particles comp. 79−25414
solar wind corotating stream, compression region interaction with Comet Kohoutek (1973 XII) ion tail 78−49267
solar wind corotating stream interaction regions obs. by Pioneer 10 and 11, dynamic MHD modelling 79−2461
solar wind corotating structures, MHD model 80−90304
solar wind D-sheets, interplanetary plasma characts. vars. 77−29616
solar wind density fluctuations near Sun from Pioneer 6 spectral broadening meas. 77−13199
solar wind density struct. var., interplanetary scintillation response 79−2455
solar wind discontinuities, substorms triggering 77−29596
solar wind disturbances during 1972 August solar flares, MHD modelling 78−45174
solar wind flow rel. to coronal open mag. structs. 79−2459
solar wind flux depletion at high ecliptic latits., Mariner 10 UV obs. 78−96371
solar wind heat flux regulation by ordinary mode instability at 1 AU 77−71097
solar wind high speed streams, rel. to coronal holes and solar mag. fields 79−58312
solar wind high-speed streams, proton-driven EM instabilities 79−53701
solar wind interaction regions, N-S mag. field component solar cycle dependent configurations 80−98529
solar wind ion acoustic waves, high-resolution spectrograms 79−96878
solar wind large-scale density fluctuations, meas. using dual freq. phase scintillations 77−13198
solar wind plasma and mag. field parameters at 0.3 AU from meas. at 1 AU 77−53387
solar wind plasma electrons, subthermal, thermal and extrathermal populations 80−41688
solar wind proton parameters changes assoc. with 1972 August flares, Pioneer 9 and 10 obs. 77−33314
solar wind protons cooling, evidence from Mariner 2 data 78−40789
solar wind protons preshock perturbs., two-spacecraft study 78−12067
solar wind pulsations rel. to Pc 3-4 pulsations 78−65476
solar wind spatial struct., latit. gradients in obs. averaged over solar longit. 79−2458
solar wind sputtering rate 80−85835
solar wind streams, Helios 1 plasma expt. results 78−20606
solar wind turbulence rel. to interplanetary scintillation, synoptic anal. 79−2460
solar wind turbulent plasma, radio wave propag. meas. using three satellites 80−101518
solar wind velocities, latit. and longit. struct. from interplanetary scintillation obs. 79−40049
solar wind velocity determ. from interplanetary scintillation effects on 3C 279, SHF obs. *(Russian)* 80−77248
solar-induced phenomena, rel. to differences between new and old comets 78−36513

interplanetary matter continued
space weathering effects, microprobe studies 77−60725
stationary solar cosmic-ray particles modulation 77−25896
structure in three dimens. 78−49280
sub-micron interplanetary dust, rel. to zodiacal light 77−13284
submicron dust, cometary origin 79−30008
submicron grain orbits, gravit. attraction, radiation press. and electrodynamics 79−8879
Sun and heliosphere, conference, London, England (1979 April 3 to 4) 80−82574
travelling interplanetary phenomena, space expts. related to Solar Maximum Year project 80−90404
travelling phenomena, symposium (Tel Aviv, 1977 June 7-10) 78−49275
turbulent interplanetary plasma, radio imagery 79−92645
turbulent plasma, Volterra integral eqns. for charged particle transport 78−8225
two-fluid shock waves propag., model 80−26711
two-frequency dispersion interferometers for space plasma nonuniformity 79−70964
type II emission mechanism 78−28476
velocity distrib. from scintillation obs. 80−105143
Venus environment, plasma wave investigation by Pioneer Venus Orbiter 80−67497
Voyager cosmic ray detector system, energetic particle studies in outer heliosphere 78−24434
Voyager low energy charged particle experiment 78−20618
Voyager mission objectives 78−24426
Voyager plasma experiment 78−20617
Voyager plasma wave system 78−24432
Voyager radio science experiment 78−24430
zodiacal cloud, symmetry plane from photopolarimetry and brightness annual vars. 78−45276
zodiacal dust cloud, charged dust particles motion in interplanetary space 80−4299
zodiacal dust cloud, thermal emission at 11 and 20 microns 80−90367
zodiacal light, new model for scatt. by irregular absorbing particles 80−67543
zodiacal light, photometric axis 78−20727
zodiacal light, spatial distrib, of interplanetary dust *(German)* 79−80268
zodiacal light, three-dimensional eqn. for brightness integral inversion 79−75155
zodiacal light dust, orbits from Doppler shift meas. 78−85904
zodiacal light Fraunhofer lines Doppler shift, dust dynamics 78−45278
H atoms, energetic, from Earth radiation belts 77−9645
H atoms, interstellar, Lyman α emission obs. 77−67120
H atoms from heliosphere, ionis. in near Sun region 80−105145
H I, hot, interstellar, between Sun and Earth, solar Lyman α absorpt. 80−31185
H I, interstellar, interaction with solar wind 80−101506
H I, Lα emission profiles reanal. rel. to local interstellar gas temp. and vel. 80−105141
H I, parameters from OSO-8 high resolution meas. of solar H Lyman-alpha profile 79−2452
H I Lyman α and β obs. by Voyager UV spectrometer 78−81673
H I Lyman α profile 80−8586
H, Lyman α radiation meas. with absorpt. cell spectrophotometer 78−28519
H of interstellar origin, temp. meas., Prognoz-5 obs. 78−7922
H, review of theory and obs. 78−49272
H_2, plasma, thermally anisotropic, cyclotron instabilities 78−1814
He, dynamical effects in 584 Å reson. scatt. 80−8509
He I, II in interplanetary space, EUV photometer obs. of 58.4, 30.4 nm lines 77−45309
He I, interstellar, obs. with gas absorpt. cell, implications for local interstellar medium struct. 80−62234
He, interaction of solar wind with Sun's gravity focused He 80−105144
He, rocket borne resonant absorption spectrometer and photometer for 58.4 nm line obs. 80−4155
He^+, obs. in driver gas of interplanetary shock wave 80−72735

interplanetary medium *see interplanetary matter*

interpolation
see also function approximation
Abel integral eqn., numerical soln., plasma spectroscopy appl. *(French)* 78−30415
acoustic waves in solar atmosphere, efficiency of one-dimens. hydrodynamic codes 78−57520
air pollution spatial distrib., objective interpolation formulae 78−65412
analogue interpolation system for incremental transducers used in position measurement *(German)* 80−17929
anisotropic strip with elliptic aperture, successive approx. method for determ. of elastic equilib. *(Russian)* 78−13907
astronomical optical surface control, Hartmann method, use of splines 79−35149
Bernstein's polynomials, differentiation and integration 78−40
bicubic spline, quantitative accuracy and efficiency test 80−17405
biomedical surface mapping 80−81750
bordering functions based interpolation method 78−81816
chemical kinetics, sensitivity analysis, numerical Green's function procedure 79−100334
computer aided tomography, Fourier transform reconstruct. by exact interpolation 80−21538
computerised tomography, fan-beam to parallel-beam conversion by rubber sheet transformation 80−109009
computerised tomography image reconstruction, interpolation effect 78−77110
cubic spline interpolation of unequally spaced data points 79−30210
cyclical data collection, linear method for second degree interpolation 78−45473
data sets with jump discontinuities, interpolation method 79−30211
digital image coding techniques, performance analysis 77−58277
distributed parameter system identification using doubly cubic spline, underground aquifer appl. 78−69391
ECG computerised acquisition, compression, and retrieval 78−36019
elastic-plastic finite element analysis, interpolation vs. iterative soln. for Tresca yield condition 78−59312
electrochemical data interpolation, fast Fourier transform method 79−16061
error estimates 80−29
error operator, digital time series error detect. and correction 78−3963

interpolation continued
finite elements construction for natural boundary conditions satisfaction 79−2610
fission reactor blanket neutronic performance, influence of design variations, variational interpolation techniques 77−34437
fission reactor theory, resonance reaction rates, group averaged, correl. technique 79−59129
flow field, multiply connected, curvilinear coords. and macro-elements 80−19318
formant frequency and bandwidth conversion to reflection coefficients 80−91975
function of two variables, thin plate bending energy approx. *(French)* 77−45700
gamma-ray detection, scintillator response, pulse height spectra unscrambling, computer program 78−55092
gas chromatography, programmed temp., retention index calcs. by linear interpolation 78−27844
generalized quadrature technique for transport eqn. soln. 79−22363
geodesy, interpolation method using multiquadratic eqns. *(German)* 78−15951
geodetic data, azimuth-dependent statistics 77−90982
geophysical unit vectors, time series interpolation 79−92625
glow discharge sheath RF impedance, scatt. and ionisation effects 79−86630
Hermite, and convective difference schemes 78−63268
high-precision data, improved interpolation method 77−45838
hologram spatial filter, computer-generated, for large object formats, interpolation 78−22099
Lagrange's interpolation formula program for Texas Instruments SR-56 78−77699
magnetic field anal. in cylindrical symmetry 78−25769
metal, strength, long-term charact. interpolation calc. using generalized curves and computer 77−86121
molecular potential energy data, spline interpolation method 78−46412
molecule, diatomic, electronic pot. rot.-vibr. eigenfunction, analytic expression 80−52964
moment-method solutions, convergence improvement using interpolants 79−18335
multidimensional interpolation by polynomial roots 80−18778
multirate digital filtering approach, appl. to common-depth-point stacking 79−29876
Navier-Stokes eqns., incompressible, finite-element soln. procedures using equal order variable interpolation 80−10226
neutron physics continuous energy Monte Carlo code VIM, cross section preparation 77−23166
NMR spectral segments, Fourier transform interpolation 77−26374
numerical solutions of integral equations with kernels containing poles, interpolative technique 78−41141
one-dimensional discrete ordinates, theoretical properties 79−76053
parabolic problem exact control finite element collocation method 77−26156
plasma drifting, cold or hot, radiation potential of immersed point antenna, DRFT computation 80−14906
plate bending and plane elasticity, finite element analysis 77−35033
polynomial spline interpolation for fluid dynamics 77−58636
profile digitised diffractographic data processing 77−58276
radiation integral transfer problems, splines under tension calcs. 77−53419
radiative energy loss of electrons in thick layers of material, interpolation formulae 78−21829
rainfall frequency relationships study for Karnataka region, India 80−31094
rectangular plate static stability soln. with fully conforming element 77−62184
refractive index data, collection of program library 80−55056
relative entropy and Wigner-Yanase-Dyson-Lieb concavity 77−49580
ruled steel grating system for length meas. 80−13039
seismic reflected waves, interpolation algorithm for vel. determ. *(Russian)* 79−88494
seismograms, interpolation of digitized curves 77−40999
singular isoparametric elements properties 77−13592
smooth interpolation and approximation of data by anal. curve method 77−26159
sparse data interpolation methods, appl. to atmosphere wind and conc. fields 80−51575
spline interpolation of γ-ray spectrometer response function 78−82561
surveying, interpolation via groups of triangulation data points of different statistical charact. *(German)* 77−9321
tetrahedra boundary data interpolation, appl. to finite elements 77−5645
thermal conductivity and viscosity of pure liquids and gases, extrapolatable formulae *(Dutch)* 78−12661
three-dimensional interpolation method, appl. to phonon spectrum determ. for Pb 78−59890
tracking of high speed bodies, appl. of sub-tabulation 77−60915
transaxial scanning X-ray tomography, oblique viewing plane reconstruction 78−77114
transition operator, interpolation model for Markov and non-Markov processes 80−8910
trend analysis and interpolation theory, geophysical appl. 77−45684
two-beam interference fringe interpolation method 80−105703
two-dimensional isoparametric Hermitian element for field problem soln. 77−60914
two-dimensional wave propagation, method of characteristics 78−73863
US pulse echo digital processing 77−32948
Van der Waal's interaction of 2 parallel cylinders, simple interpolation formula 79−92122
variational interpolation of linear functionals of inhomogeneous eqns. 78−49638
vibr. freq. calc., hybrid element method 77−26173
viscous fluid unsteady periodic flow, Galerkin finite element method 77−75872
X-ray spectra, energy dispersive, peak separation from background 78−7310
Co (VII), semiempirical investigation of spectra 78−33434
Cs, photoabsorption oscillator strengths, $17<n<\infty$ transitions, interpolation formula 80−9559
Ni (VIII), semiempirical investigation of spectra 78−33434

interpreters (program) *see program interpreters*
interpretive programs *see program interpreters*
interstellar dust *see cosmic dust*
interstellar magnetic fields
see also interstellar matter
alignment of interstellar grain 78−41017
amplification in collisionless shock waves 77−49459
anisotropic MHD turbulence, generation by cosmic rays 77−45532
B 0844+31, extended radio galaxy, mag. field distrib. from multifreq. obs. 80−56963
3C 219, double radio galaxy, mag. field configurations from obs. at 1.48 and 4.89 GHz 80−77500
3C 310, extended radio galaxy, projected mag. field distrib. from multifreq. obs. 80−51890
3C 31, radio galaxy, mag. field struct. in radio jets 80−82526
3C 33, radio galaxy, mag. field in compact head from optical emission lines 80−51892
3C 58, supernova remnant, radioemission from mag. field interaction with relativistic electrons 80−73023
3C 84, 3C 273, quasars, field strengths from circular polarisation vars. obs. 77−33673
Cassiopeia A, mag. field decrease rel. to radio spectrum secular flattening 80−101637
charged dust grains in mag. field, coagulation 78−28766
clouds, ambipolar diffusion, rel. to star form. 79−40237
clouds angular momentum problem and mag. braking, time independent soln. 79−62884
clouds containing magnetic fields, stability 79−5876
cold gas clouds with mag. field, gravit. contraction, star form. 78−8102
cosmic radiation intensity on Earth and in Galaxy, diffusion restriction by mag. fields 77−13191
cosmic ray diffusion in large-scale turbulent magnetic field 79−58203
cosmic ray diffusion theory, vel. correl. function 77−73913
cosmic ray electron spectrum determ. from galactic radio background 78−93056
cosmic ray electrons, confinememt and radio emission 77−73910
cosmic ray electrons, detect. by synchrotron radiation in geomag. and interstellar mag. fields 78−57412
cosmic ray propagation, anisotropy of 1-100 TeV particles 80−17451
cosmic rays acceleration by moving magnetic mirrors, efficiency 79−44310
cosmic rays spatial diffusion coeffs., computation using nonlinear particle trajectories 77−45262
Crab Nebula, small-scale polarisation rel. to mag. field 79−25656
Crab nebula, static mag. field rel. to magnetoparametric instabilities 79−8829
dark cloud complexes, magnetic field struct. 77−17648
dark cloud evolution, role of magnetic fields 77−67117
dark clouds, H I 21 cm Zeeman effect obs. 79−8977
dark clouds, mag. compression rel. to star form. 78−73744
dense cloud complexes, mag. fields determ. via Zeeman splitting obs. 79−5757
dense clouds, heating by magnetic ion slip, constraint on cloud field strengths 77−45513
dense clouds, mag. fields and energetic secondary electrons rel. to radio emission 77−33593
dense molecular clouds, mag. diffusion and ionization fractions, role of charged grains 80−12785
dense molecular clouds, mag. field upper limit from SO obs. 79−21375
direction correlation with planetary nebula major axes, hydromagnetic model 80−82473
discontinuities, causing cosmic rays isotropy 78−4045
electrodynamic and gravitational effects of Proca stresses in astrophys. 78−93098
equilibrium configurations stability, hydromagnetic energy principle 80−82448
Faraday rotation of extragalactic radiosources 79−58430
fluctuations, correl. length and fluctuating angle from starlight polarisation theory 80−82442
force free fields near Reissner-Nordstrom black hole 78−77572
galactic corona, closed mag. field lines 79−25709
galactic disc $\alpha\omega$ dynamo theory for mag. field generation 80−46663
galactic dynamo, numerical models 79−40262
galactic dynamo model, appl. to mean mag. field calc. 78−81685
galactic field, review of obs. 80−73042
galactic field, struct. rel. to interpretation of galactic continuum radiation 77−13465
galactic halo, mag. field rel. to diffusion models for low-freq. radio emission 78−12433
galactic halo, mag. field strength from radio obs. 78−96544
galactic halo, regular magnetic field component *(Russian)* 80−67872
galactic large-scale magnetic features 79−58418
galactic magnetic field, interstellar polarisation rel. to protostellar sources IR polarisation 80−4347
galactic magnetic field, rel. to gas hydrostatic equilib., cosmic ray confinement and radio emission 77−29919
galactic magnetic field configurations, rel. to synchrotron radiation 78−20884
galactic magnetic field from radioastronomy obs. 78−24548
galactic magnetic field from radiopolarisation obs. 78−24547
galactic magnetic field scale and strength from pulsar data 78−28752
galactic matter distrib., relation with cosmic ray dynamics and γ-ray production 78−4349
galactic rot. effect, corona prod. 80−82492
galaxies, mag. fields from light polarisation obs. 78−69872
galaxies, nearby, mag. fields meas. from radio continuum polarisation obs. *(German)* 80−109544
Galaxy, synchrotron radiation in inhomogeneous mag. field 77−67127
Galaxy magnetic field, turbulent struct. from extragalactic sources Faraday rot. 78−20885
Galaxy magnetic field and cosmic rays distrib., deduction from synchrotron radio and gamma-ray obs. 80−4207
galaxy origins, galactic angular momenta and magnetic fields 78−93405
gas hydrostatic equilib. in solar neighbourhood 79−30098
heliosphere boundary, mag. field direction rel. to cosmic rays ang. distrib. 79−80116
hydrodynamic turbulence in weak large scale mag. field, effective mag. viscosity 77−33340
IC 5146, young star cluster, starlight polarisation and cluster mag. fields 77−5550
interstellar magnetic fields continued
interstellar clouds, mag. fields rel. to gravit. collapse 77−13420
ionisation fronts, models with mag. fields and cooling 77−33594
irregular fluctuations, effect on starlight interstellar polarisation 80−26926
isothermal gaseous disc, mag. field effects on gravit. instability 80−4424
LMC, mag. field rel. to spiral struct. 77−29924
local inter-arim region field from absorption bands in O, B and A stars, polarized intensities 79−8915
M104, galactic-scale magnetic field from optical polarisation obs. 77−22313
M17, dusty H II region, optical polarisation meas. rel. to mag. field struct. 78−45379
M31, M51, M81, spiral galaxies, discs mag. field struct. from radio polarisation obs. 77−5575
M31, polarised radio emission detect. rel. to mag. field alignment 78−86017
M31, polarised radio emission distrib. rel. to large-scale mag. field 80−41899
M51, spiral galaxy, mag. fields config. from Faraday rot. data 79−48934
M87 jet, expanding mag. field struct. rel. to synchrotron emission *(Russian)* 80−8694
M87 radio/X-ray halo, mag. field strength from Faraday rot. 80−67844
magnetic braking of self-gravitating, oblate interstellar clouds 79−35325
microturbulence, effect on interstellar matter instability criterion 80−82454
molecular cloud, mag. field from near main line OH maser Zeeman pattern 80−56908
molecular clouds, cosmic ray penetration 79−8979
molecular clouds, magnetic field 79−67075
molecular clouds, nonthermal galactic radio background rel. to field magnitude limit 78−49527
NGC 1275, Seyfert galaxy, nucleus, radio brightness distrib. rel. to mag. field struct. *(Russian)* 80−62288
NGC 315, radio galaxy, mag. field struct. in radio jets 80−82526
NGC 654, young star cluster, starlight polarisation and cluster mag. fields 77−5550
NGC 7822 (W1), supernova remnant with mag. field local enhancement 78−54028
NGC 891, edge-on disc galaxy, mag. field from radio continuum obs. 78−28786
OB associations, mag. fields influence on subgroups sequential form. 80−4408
origin and superdense cosmogony *(Russian)* 79−8985
Orion Nebula, SO 36 GHz emission line detect., rel. to mag. fields 80−46642
Orion Nebula, Zeeman splitting in OH masers 78−16493
Parker instability in 2-dimens., using MHD energy principle *(French)* 77−64831
Parker instability with curved field lines 79−5889
α Persei star cluster, polarisation wavelength depend. rel. to mag. field strength 79−48865
plasma mechanisms, mag. field modifications theories, review 77−73946
protostellar cloud rotation, mag. braking of aligned rotator during star form., exact time-depend. soln. 80−90493
pulsar rotation measures 80−85966
radio galaxies with tail-bridge struct., spectral index, radio polarisation, mag. field 79−58416
radio sources, extragalactic, expanding mag. fields rel. to variable radio emission temporal characts. *(Russian)* 80−62307
radio sources, form. of universal and diffusion regions of relativistic electrons non-linear spectra 80−109555
regular field structure and stellar polarisation 78−69869
review 77−26048
rotating magnetic cloud, mag. braking during star form. 79−58319
rotating magnetic cloud, mag. braking during star form. 79−58320
S232, H II region, mag. field strength meas. 80−51840
self-gravitating gas masses containing axisymmetric mag. fields, equilib. structs. 80−94708
starlight linear polarisation meas., catalogue and vector maps 77−13255
stellar protoclusters, mag. fields rel. to system mass loss and dynamic evolution 80−51815
superluminal radio sources, mag. dipole model 80−56959
supernova remnants, intestellar mag. fields rel. to radio evolution and population characts. 79−75254
supernova remnants, mag. field distribs., Faraday rot. and depolarisation 77−13428
turbulent galactic mag. field and cosmic ray diffusion 79−48627
Vela supernova remnant, extended X-ray source obs. rel. to mag. field strength 78−41095
Vela supernova remnant, field struct. rel. to change in pulsar rot. measure 77−29867
W3, dusty H II region, optical polarisation meas. rel. to mag. field struct. 78−45379
weak MHD turbulence, inertial range 77−45528
Zeeman effect in OH maser emission from W3 (OH) 78−93377
$e^+e^- \rightarrow \nu\bar{\nu}$, in strong mag. fields, rate of energy loss 78−29326
H II regions, search for Zeeman effect in RF recomb. lines 77−60809
OH maser, OH removal by magnetic heating 79−98328

interstellar matter
see also cosmic dust; H I regions; H II regions; interstellar magnetic fields; nebulae
3.3 microns unidentified feature in NGC 7027 and HD 44179 spectra, high resolution obs. 80−82466
10 and 20 μm absorpt. bands, comparison with Nogoya meteorite IR spectrum 79−48741
10-micrometer absorpt. band, comparison with phyllosilicates laboratory spectra 79−80344
2175 Å absorpt. feature, effects of stellar Fe II and Fe III emission 77−13364
2200 Å interstellar absorption feature, identification 78−12346
absorption band at 10 μ, curves of growth for terrestrial and meteoritic olivine particles 77−78846
absorption effects in visible and UV *(Italian)* 77−87517
absorption effects on Balmer discontinuity strengths 78−89238
absorption effects on stellar absolute spectrophotometric gradients *(Russian)* 79−92752
absorption features, optical, in spectra of Wolf-Rayet stars HD 192163 and 191765, obs. 80−17640

interstellar matter continued
absorption lines in ζ Puppis spectrum 78−65665
absorption lines in UV spectrum of γ Velorum 79−35324
absorption lines of Na I, K I, Ca II, in stellar spectra rel. to galactic gas distrib. 80−26963
accretion by stars, stability of Bondi accretion 79−44359
accretion onto binary systems, numerical simulation 79−21358
accretion onto magnetised rot. neutron stars, possible instabilities 77−13377
accretion onto star, gas pressure effect, stagnation point 78−53932
accretion onto stellar surface, fractionated process 80−51734
acetonitrile emission obs. in Sagittarius B2 77−64835
acoustic nonlinear adiabatic waves in self-gravitating gas, astrophys. appl. 78−28512
in active galaxies nuclei, plasmons, particle accel. and flux vars. 77−13479
AFGL IR sources, mol. line obs. 80−51856
amorphous silicates, laboratory IR extinction meas. 77−12352
antiparticles in primary cosmic radiation and collisions in interstellar medium 80−77241
Ara, IR photometry of highly reddened cluster 77−41395
atomic b_n factors at low temperatures, appl. to interstellar C II regions 80−36696
atoms, fine struct. levels population ratios 79−35351
atoms, reson. transitions, radiative lifetimes, lab. meas. 78−62767
B335, mol. cloud, continuum emission mapping at 89.6 GHz 80−94842
B, A and F stars in selected areas, intrinsic uvby β indices, distances and colour excesses 78−89171
B 35, bright rimmed molecular cloud, CH obs. 80−62238
bacterial grains, prod. of 3 μ spectral feature in galactic IR sources 80−62227
Barnard globules evolution 80−82462
barred spiral galaxies gas dynamics, gaseous density waves and galactic shocks 80−12819
Becklin's star, in Orion, 4 to 8 micron spectrum 77−29903
Becklin-Neugebauer object, Brackett emission obs. rel. to visual interstellar extinction 78−36657
Becklin-Neugebauer source in Orion, high resolution 1.5 to 5 micron spectroscopy 78−93368
birefringence meas. from polarisation obs. of Cygnus OB2 association 77−33577
black holes, primordial, number density limits from galactic radio spectrum 80−62179
Bochum 15 stellar aggregate direction, photoelectric photometry and colour excesses 77−87490
Bok globules, search for neutral H 77−29904
Bok globules 77−78860
bubbles, structure and evolution 78−12318
butadiynyl in IRC+10216, N=12→11 doublet study 80−51829
Byurakan 2 stellar cluster, UBV photometry and interstellar reddening 77−2345
3C 120, Seyfert galaxy, interstellar reddening from IUE and visual spectrophotometry 79−92856
3C 286, quasar, optical absorpt. lines detect., redshift 80−4454
α Canis Majoris (Sirius), search for surrounding nebulosity 78−93242
carbonaceous compounds in interstellar dust 77−87519
carbonaceous material in Galaxy, origin and nature 78−24543
carbyne and interstellar grains 78−69859
carbyne as possible constituent 80−90514
Carina Nebula, extinction determ. from open cluster UBV photometry obs. 80−90513
Carina spiral feature, distrib. of stars and interstellar dust along inner side 80−51871
Carina-Crux-Centaurus region of Milky Way, interstellar extinction investigation 79−40242
VY Carinae, cepheid variable, intersteller reddening and absolute magnitude 77−64764
η Carinae, dust condensation 79−17066
η Carinae, interstellar colour excess rel. to distance 77−64744
α Carinae (Canopus) spectrum, effects of interstellar Compton scatt. 78−53938
celestial chaos related to Earth's climatic and biological catastrophes 79−53509
S.Celestial Pole region, nebulosity obs. 79−92839
ω Centauri, cluster reddening from RR Lyrae stars UBV photometry 78−73719
ω Centauri region, faint filamentary nebulosity obs. near globular cluster 80−56914
VV Cephei system in Puppis, interstellar reddening and distance 80−51810
Cepheid variables, intrinsic colours and colour excesses from Walraven VBLUW photometry 78−28696
Cepheus A mol. cloud, OH maser lines obs., star form. region 80−36691
Cepheus IV star formation region, continuum and recomb. lines, SHF obs. 80−90501
Cepheus OB2 association direction, interstellar line spectra anal. 80−22052
charged dust grains accretion, role of induced charges 79−8966
charged dust grains in mag. field, coagulation 78−28766
charged grains, thermal coagulation in dense interstellar clouds 79−53872
charged interstellar grains, motion in interplanetary space 80−4300
chemical and isotope fractionation by grain size separates 80−67831
Circinus, interstellar extinction of large new galaxy 77−41409
circular polarization, wavelength dependence, HD 183143 an exception 79−92819
circumstellar dust shells, models rel. to compact IR sources spectra 77−29948
Cloud 2, mol. cloud, detect. of HC_5N (cyanodiacetylene) and HC_7N (cyanohexatriyne), SHF obs. 80−101627
cloud accretion by white dwarfs, spectral evolution 79−35252
cloud material, contribution to planetary atmospheres 79−25698
cloud model, intragalactic factor in external objects apparent distrib. 78−96552
cloud stability, cosmic ray screening effect 79−67077
cloud surfaces, O VI absorption 79−97049
cloud-cloud collisions, time dependent numerical simulations 80−94844
clouds, ambipolar diffusion, rel. to star form. 79−40237
clouds, collisional excitation by charged particles, model exact soln. 77−74114
clouds, cooling rates 79−62887
clouds, diffuse UV radiation penetration 80−56901
clouds, gas phase chem. reactions amongst C, N and O compounds 80−105319
clouds, interaction with Vela supernova remnant 77−2463
clouds, mass spectrum, mol. clouds lifetime 79−53863
clouds, rotation rate, connection with binary star periods 77−33584
clouds and H_2 78−16491
clouds angular momentum problem and mag. braking, time independent soln. 79−62884
clouds cooled by C atoms and ions, struct. *(Russian)* 80−12801
clouds formation induction by OB-type stars, effects of eqns. of state 80−109506
clouds mass distribution, non-linear relationships between N(Ca II), N(K I) and N(H) 79−92832
CO isotope mapping of L 134 N 79−30108
Coalsack dark cloud, finding list of Hα emission objects 77−22115
cocoon stars, calculated IR spectra 77−64824
cold clouds and interstellar grains *(Italian)* 77−87516
cold diffuse cloud towards 3C 225.0, UHF and EHF obs. 80−105311
cold gas clouds with mag. field, gravit. contraction, star form. 78−8102
cold grains as seeds of life 77−91606
cold-cloud aggregates, chemical energy and meteorite chondrule origin 80−105210
collapse dynamics and models 78−32566
collapse of nonrotating magnetic gas clouds, numerical calcs. 80−105299
collapsing dust cloud, grain motions rel. to star form. 78−69788
collapsing isothermal spheres, predictability limit, rel. to star form. 79−75088
collapsing molecular clouds, line radiation transfer 78−73626
collapsing molecular clouds, self-reversed CO profiles 77−33581
collisional excitation by charged particles in interstellar clouds 77−57075
collisionally induced transition rates, estimation from lab. data, rel. to interstellar mols. 79−45787
collisionless shock waves, mag. field amplification 77−49459
colloidal plasmas in space: some aspects of condensation and growth of solids 79−41795
μ Colombae line of sight, Copernicus UV obs. 77−33591
comet interstellar origin hypothesis 77−37569
comets, long-period, evidence for interstellar origin from distrib. of nodes and perihelia 80−67661
comets possible origin in interstellar gas cloud 79−8882
complex molecules in clouds, synthesis 79−92826
composition and properties, review 79−53900
compressible fluid flow past degenerate star-red giant interacting binary stars 80−67779
Compton effect, electron gas-radiation field interactions, instability development 80−77274
conference, IAU, Grenoble, France, 1976, Aug. 78−16504
contracting clouds, molecular evolution 78−85986
contracting CO clouds, fragmentation 80−67838
contracting interstellar clouds, influence of turbulence on solid particles growth 80−62251
cool stars, effective temps; ang. dias. and reddening determ. from 1 to 5 μm flux curves 79−44458
Corona Austrina dark cloud, interstellar reddening law meas. 79−17050
R Coronae Austrinae interstellar molecular cloud, for IR study and dust temp. profiles 80−62237
coronal gas temp. and interstellar nature in five stars, Copernicus obs. 77−33598
cosmic dust, book 78−57498
cosmic dust, grain growth by radiation pressure induced coagulation 80−94851
cosmic dust, grains sudden nucleation and growth in supernova and nova ejecta 80−26941
cosmic dust condensation onset, role of association reactions 80−26931
cosmic dust condensation processes investigation, expt. techniques 80−26940
cosmic dust in spiral galaxies, optical anal. method, visible obs. 80−101638
cosmic gas clouds, fragmentation and initial stellar mass function 77−56907
cosmic masers, role of dust in pumping 78−36716
cosmic masers and star formation *(German)* 79−58410
cosmic ray confinement, effect of interstellar MHD turbulence 77−49246
cosmic ray deuterons and antiprotons production mechanisms 79−29955
cosmic ray electron spectrum determ. from galactic radio background 78−93056
cosmic ray electron spectrum in local interstellar medium, determ. from bremsstrahlung gamma radiation 79−25417
cosmic ray interactions with interstellar gas, X-rays prod. 77−68110
cosmic ray ionization and D abundance in clouds 79−17063
cosmic ray scattering irregularities spectrum, evidence from nuclei charge comp. and energy spectra 78−93059
cosmic rays interaction, deposition of momentum and energy by MHD waves 77−37493
Crab Nebula, interstellar O edge in X-ray spectrum 79−67079
Crab Nebula, interstellar shock waves hydrodynamics rel. to diffuse soft X-rays 78−85997
Crab Nebula, search for associated and nearby extinction 77−67118
Crab Nebula direction, characts., soft X-ray and radio obs. reconciliation 78−12328
CTB 80, peculiar supernova remnant, central radio source reddening and distance 80−56896
cyanoacetylene, 36.4 GHz rotational transition detect. 77−87515
cyanoacetylene, and ^{13}C substituted species, in Sagittarius B2 and Orion A, relative isotope fractionation 79−21374
cyanoacetylene, cyanodiacetylene in interstellar clouds, obs. 80−46634
cyanoacetylene, lab. study of ion-molecule reactions, rel. to interstellar synthesis 79−1940
cyanoacetylene, microwave spectrum, mol. consts. 78−74647
cyanoacetylene, Orion Molecular Cloud 1 obs. 78−4322
cyanoacetylene, rate coeffs. for reactions with ions of interstellar significance 79−57221
cyanoacetylene, vibrational excitation in Orion molecular cloud 80−22067
cyanoacetylene, vibrationally excited state detect. in Orion molecular cloud 77−13436
cyanoacetylene ^{13}C distribution at thermodynamic equilib. 79−59590

interstellar matter continued
cyanoacetylene in Sagittarius B2, evidence for chemical fractionation, ^{13}C isotopes 77−87532
cyanodiacetylene, 2663 MHz transition obs. in Sagittarius B2 77−33669
cyanodiacetylene, cyanotriacetylene, detect. in C star (IRC+10216) 79−17126
cyanodiacetylene, detect. of J=9 to 8 transition 77−91603
cyanodiacetylene, form. in RF discharge 79−5156
cyanodiacetylene, lab. study of ion-molecule reactions, rel. to interstellar synthesis 79−1940
cyanodiacetylene (HC_5N), J=2-1 transition detect. 79−25692
cyanodiacetylene (HC_5N), obs. in (Heiles's cloud 2) 80−22054
cyanodiacetylene emission at 24 GHz assoc. with Heiles 2 cloud collision 78−65675
cyanodiacetylene in Sagittarius B2, 5 and 7 GHz obs. 79−92817
cyanodiacetylene weak maser action in Sagittarius B2 77−5555
cyanohexatriyne, detect. at 14.7 GHz in Heiles Cloud 2 and Sagittarius B2 78−73745
cyanohexatriyne detection in Heile's Cloud 2 at SHF 78−41018
cyanopolyynes and related molecules, interstellar synthesis 80−12793
cyanotriacetylene, discovery, implications for theories of interstellar molecule formation 78−41029
P Cygni, extreme B-type supergiant, UV spectroscopy and interstellar extinction 80−22004
Cygnus, colour excesses of two obscured galaxies 77−29922
Cygnus A direction, galactic foreground reddening 77−9802
Cygnus direction, stars and dust space distrib. *(Russian)* 78−20893
Cygnus Loop, forbidden Fe XIV emission radial distrib. 78−32545
Cygnus Loop, radio struct. at 25 MHz 78−54027
Cygnus Loop, X-ray image rel. to interstellar medium inohomogeneities 79−25663
Cygnus OB2 No.12, high resolution 2μ spectroscopy rel. to interstellar and stellar features 78−57613
Cygnus OB 2 association, H content, radio continuum emission search 77−64809
Cygnus superbubble 80−105323
Cygnus X region, gamma-ray flux prediction and nature of (CG 78+1) 79−92895
Cygnus-Vulpecula direction, stars and dust cloud space distrib. *(Russian)* 78−20892
cylindrical clouds, two-dimensional collapse calcs. 79−40247
D and density of matter in open, expanding Universe 79−12548
dark cloud complexes, magnetic field struct. 77−17648
dark clouds, anisotropic scatt. and formaldehyde lifetimes 78−8080
dark clouds, formaldehyde as a probe, EHF and SHF obs. 80−105317
dark clouds, radio continuum interferometric search for newly formed H II regions 80−98699
dark clouds, radio continuum interferometry rel. to newly formed H II regions physical props. 80−105301
dark clouds, search for radio continuum radiation 77−33585
dark clouds and cocoons, rel. to star form. *(French)* 79−67087
dark clouds chemical and thermal equilib., grain surface reactions rel. to mol. form. 79−44593
dark clouds in Gum Nebula, evidence for stark form. 77−29821
dark clouds with assoc. young stellar objects, radio obs. of mol. lines 79−58390
dark globular filaments, catalogue 80−26756
dark globules, IR radiation theory 78−53999
dark interstellar clouds motions, obs. with IR Fabry-Perot interferometer 80−8672
dark nebulae, visual extinctions determ. via star counts 78−57612
dark nebulae and globules, star form. regions 78−12347
HR Delphini (Nova 1967), interstellar reddening from simultaneous X-ray, UV and optical obs. 80−109440
dense cloud complexes, mag. fields determ. via Zeeman splitting obs. 79−5757
dense cloud encounter with solar system, terrestrial consequences 78−57292
dense clouds, CO self-absorpt. towards embedded stars 77−53670
dense clouds, differential rotation producing MHD waves causing heating 78−8096
dense clouds, distrib. of energetic secondary cosmic ray electrons 77−33593
dense clouds, dust condensation, cooling, IR emission 79−62897
dense clouds, grain size control 77−33607
dense clouds, heating by magnetic ion slip, constraint on cloud field strengths 77−45513
dense clouds, kinematics and dynamics 78−32563
dense clouds, methane abundance calcs. 77−33608
dense clouds, molecular composition 77−29892
dense clouds, unified theory of form. of objects from meteors to stars 77−9739
dense clouds and diffuse production of gamma-rays 78−54011
dense clouds and X-ray burst origin 77−78896
dense clouds encounters with stars 77−87497
dense clouds mol. cooling and thermal balance 78−65666
dense gas clouds, interaction with stars *(German)* 80−109500
dense interstellar clouds, radiative association reactions 80−82441
dense molecular clouds, distrib., phys. conditions, origin *(Polish)* 79−101187
dense molecular clouds, mag. diffusion and ionization fractions, role of charged grains 80−12785
dense molecular clouds, mag. field upper limit from SO obs. 79−21375
density fluctuations caused by cosmic ray streaming, effect on pulsar scintillations 80−51845
density fluctuations effect on pulsar scintillations 80−46649
density wave interaction in differential rotating spiral system 78−69871
deuterated molecules, obs. and implications for interstellar chemistry 79−5891
diatomic molecules, form. and dissoc. in interstellar medium 80−23471
diatomic oxide grains, IR absorption features 78−49509
diffuse 4430 Å feature in LMC supergiant spectra 80−73033
diffuse λ4430 band, obs. in Carina Nebula, NGC 3603 and VI Cygni 78−32555
diffuse absorpt. bands origin, Ti depletion, accretion onto oxide grains 79−53879
diffuse absorption bands, origin, transition metal ions in oxide grains 79−30101
diffuse absorption bands, origin in zero phonon lines in MgO and CaO 77−57073
interstellar matter continued
diffuse bands, 2175 Å band correl. with other features in stellar spectra 77−60813
diffuse bands, possible origins 78−16483
diffuse clouds, C 166α recombination line 78−8099
diffuse clouds, detailed models, atomic and mol. abundances 77−87498
diffuse clouds, HCl abundance and chem. models 80−91570
diffuse clouds, thermal balance, struct. and characts. 79−88713
diffuse clouds temperatures, determ. from HD and OH column densities 78−93385
diffuse EUV radiation field obs. 79−30099
diffuse interstellar band at 5780 Å, photoelectric meas. 78−93350
diffuse interstellar bands, catalogue of meas. 77−64666
diffuse interstellar bands, strengths rel. to stars IR colour excesses 78−93198
diffuse interstellar bands at far UV wavelengths, obs. 78−32554
diffuse interstellar bands due to dust, possible appearance in nebulae spectra 79−53874
diffuse interstellar bands in 6500-8900 Å region 79−21373
diffuse interstellar cloud towards gamma Arae, model from stellar spectra anal. 80−105312
diffuse interstellar features at 6379 and 6614 A, high resolution profiles 78−4314
diffuse interstellar line at 6284 Å, obs. and relation to interstellar reddening 80−51843
diffuse interstellar lines, identification 77−87518
diffuse interstellar lines 79−21401
dimethyl ether, review of microwave spectrum, tabulated data 80−51965
disc galaxies nuclei, superdense gaseous cores form. 80−90526
distorted interstellar bubbles discovery around two stars 79−71088
distribution from obs. of OB stars near Carina arm, UBVβ photometry 80−85941
distribution in spiral galaxies, density wave theory 78−16540
distribution rel. to radioactive cosmic ray isotopes, two-zone propag. model 79−66891
30 Doradus central object (HD 38268), interstellar and nebular lines obs. 80−51839
30 Doradus complex, in LMC, UV reddening law 78−96516
30 Doradus nebula, in LMC, interstellar Ca II and Na I obs. 80−46643
30 Doradus region, far UV extinction anomaly 78−45386
30 Doradus region, in LMC, interstellar extinction and stellar population 78−96517
30 Doradus region, interstellar extinction and stellar population 77−13413
30 Doradus region, UV absorpt. by interstellar gas in stellar spectra 80−85978
DR15, H II region, 408 to 2695 MHz obs. and visual extinction 80−94881
DR 21, anomalous NH_3 absorpt. obs. 77−53669
DR 21 OH, relationships of N_2H^+, HCO^+, HCN and CN 77−33587
Draco direction, reddening of dwarf spheroidal galaxy 79−97077
drag effects on minimum time trajectory, of thrust limited relativistic rocket 78−49286
dust, Apollo 17 far UV search for starlight scatt. 78−65726
dust, chemical composition 78−57624
dust, cloudlike distrib. rel. to integrated starlight synthetic spectrum between 3000 and 10000 Å 80−62200
dust, composition, origins *(French)* 79−30116
dust, condensation in interstellar clouds, theoretical aspects 80−26939
dust, disequilib. condensation environments as frontier in thermodynamics 80−26942
dust, extinction curve, rel. to plasma reson. in Fe granular deposits 79−21387
dust, models for diffuse galactic light interpretation 78−8118
dust, new model for scatt. by irregular absorbing particles 80−67543
dust, new model of mixed oxide grains 80−26934
dust, scattering of starlight, origin and composition 79−88729
dust, turbulence effect on coagulation 79−35356
dust, UV opacity effects on stellar spectra 80−90505
dust and gas near 20 Tauri (Maia) in Pleiades 78−28734
dust cloud, internally heated, numerical soln. of radiative transfer eqn. in spherical geometry 80−90329
dust cloud complex in Taurus, radio obs. of fragmentation and localised multiple vel. components 78−4308
dust cloud in Corona Austrina, mm wavelength obs., nonhomologous collapse, rel. to star form. 79−30102
dust cloud with embedded stars, heating and model 80−26952
dust clouds, among brightest IR sources of AFCRL Survey 77−87283
dust clouds, low mass, in solar vicinity, photometric survey results 80−36512
dust clouds, OH excitation 78−4318
dust clouds above galactic plane, light scatt. detect. possibility 79−30124
dust clouds heating due to molecules desorption from grains 77−9786
dust clouds rel. to diffuse galactic light and Milky Way brightness fluctuations 78−61921
dust distribution from UBVβ photometry of OB stars in Puppis 80−85937
dust dynamics in collapsing protostellar cloud, planet formation 79−58401
dust for IR emmission, large-beam sky survey at millimetre and submillimetre wavelengths 79−97045
dust formation in space medium thermodynamics and kinetics, workshop, Houston, Texas (1978 September 6 to 8) 80−22131
dust globules, microwave spectral lines obs. 78−57609
dust grain growth in interstellar clouds, theory and obs. 80−67834
dust grain props. in H II regions *(Italian)* 79−48897
dust grain size, polarimetric obs. of four deviating stars 80−12792
dust grain vels. in turbulent gas in protostellar cloud 79−58402
dust grains, characts. near stars with peculiar interstellar polarisations 77−53659
dust grains, IR props. 80−26943
dust grains, temp. fluctuations 80−26938
dust grains distrib. in intercloud medium, from K-type giant stars colour excesses 79−40251
dust grains in hot gas 79−92820
dust grains in SNRs, effect on X-ray spectra 80−94849
dust grains surrounding variable source of heating radiation, IR flux development 80−105324
dust in cosmic plasma environment, props. 80−26930
dust in galaxies, effect on optical surface brightness 80−90518

interstellar matter continued
dust in refl. nebula NGC 7023, optical and UV extinction of (HD 200775) 80−109515
dust in thick slabs, light reflection 79−62881
dust lane origin, explosion model for active radiogalaxies 79−62910
dust penetration of solar system, Lorentz force versus gravit. focusing 77−13315
dust shell around α Orionis, scattered polarized light 79−12473
dust temperature statistical distrib. resulting from star random distrib. 80−98700
dust/molecular clouds in Galaxy, props. 80−26925
dusty plasma clouds, physics rel. to star form. 78−73744
dynamics of agglomerating ensembles of clouds 80−67813
dynamo model, appl. to galactic mean mag. field 78−81685
E/S0 radio galaxies, ionized gas obs. 79−17105
early-type galaxies, in Virgo cluster, H I survey 79−30123
early-type stars near Sun, space vels., ages and interstellar reddening 78−61858
effects on correlation functions for galaxy counts *(Russian)* 79−25740
electrodynamic and gravitational effects of Proca stresses in astrophys. 78−93098
electron abundances determ. in interstellar clouds, new method 80−41866
electron density, determ. from low-latit. pulsars dispersion meas. and distances 80−101606
electron density determ. from decorrel. bandwidth of pulsar scintillation 77−78850
electron density determ. from H I absorption in spectra of pulsars 79−92792
electron density irregularities from pulsar scintillations freq. time struct. 80−101608
electron temperature gradients with distance from galactic centre 79−88744
electron transfer in ion-dust grain collisions 78−77591
element abundances in galaxies 78−16542
elemental depletions in interstellar medium, model 78−36654
elements enrichment, contrib. of thermally pulsing high luminosity stars 78−40917
in elliptical galaxies, clouds props. rel. to star form. 77−33636
elliptical galaxies, hot gas interstellar medium rel. to head-tail radio sources form. 80−36703
elliptical galaxies, search for H I emission 78−65681
EM wave polarisation in thick weakly anisotropic layer with random irregularities 77−10822
EM wave propagation, thin screen scintillation theory for spherical wave 78−13645
embedded IR sources, optical spectrophotometry 78−96520
equilibrium configurations stability, hydromagnetic energy principle 80−82448
ethyl cyanide, mm wave emission line detect. in OMC-1 and Sagittarius B2 78−12317
ethylene oxide, possible detect. in Kleinmann-Low IR nebula 77−53662
ethynyl radical, mm wave emission obs. of interstellar clouds 80−90503
ethynyl radical abundance and distrib. 78−65664
EUV spectrum of hot, optically-thin interstellar plasma 78−81665
EUV/soft X-ray background, Apollo-Soyuz sky survey results 79−71160
evaporation of spherical clouds in hot gas, classical and saturated mass loss rates 77−33583
excitation temps. and column densities in direction of supergiant HD 154368, spectra 79−8981
expanding shell assoc. with loop structures in Orion and Eridanus 79−53866
external galaxies, diffuse [O I] emission and Hα lines, warm interstellar gas 78−4312
external galaxy spiral arms, CO emission detect. 77−33641
extinction, average model, from planetary nebulae obs. 80−62221
extinction, influence on galactic globular cluster system apparent flattening 79−48908
extinction, planetary nebulae spectra correction 77−53677
extinction, UBVRI equatorial star network 79−84827
extinction and distrib. of stars in Galaxy *(Russian)* 78−73701
extinction and reddening of IC 2149 planetary nebula 77−41402
extinction and stellar space density in Ophiuchus region 77−64839
extinction at UV wavelengths, role of biochemical chromophores 80−26945
extinction curve, comparison with visible and UV extinction of silicate, C and SiC smokes 80−82180
extinction determ. from IR photometry of early-type stars in N. Milky Way 77−78783
extinction determ. from planetary nebulae optical and radio obs. 77−22295
extinction determination in planetary nebulae direction 77−17660
extinction feature at 220 nm and diffuse 443 nm band, ANS obs. 80−62244
extinction in Monoceros region 77−9777
extinction law, results from IR photometry of southern early-type stars 80−94786
extinction law correl. with wavelength of max. polarisation 78−61902
extinction law for O-type stars towards Carina Nebula 80−105240
extinction law in dust clouds and young southern cluster NGC 6250, evidence for high R-values 78−16490
extinction law in visible region, refl. nebulae obs. with polarimeter 80−26964
extinction laws from 13-colour photometry 78−81676
extinction near N.Galactic Pole, determ. from polarisation meas. 79−62814
extinction ratio depend. on galactic longitude 77−64833
extinction towards NGC 7582, narrow emission line X-ray emitting nucleus, UV spectra 80−101640
extinction towards South Galactic Pole from A and F star reddening 77−60812
extragalactic CO emission obs. at 2.6 mm 77−45543
faint optical emission lines, limits on temp. and ionization state of emitting gas 77−37634
far IR emission between l=36° and l=55° galactic longitudes 78−54014
far IR fine structure line obs. 80−62253
far UV radiation field, prediction 77−64739
FJM 3, 100 micron source, radio and IR obs. of assoc. mol. cloud 77−26082
interstellar matter continued
FJM 6, molecular cloud, far IR, near IR radio mol. line studies 80−26929
flare stars, large-scale winds driven by mass loss, effects on interstellar matter 78−32464
flow past Sun, model of solar wind unstressed deceleration 79−53692
fluoromethane, search in mol. clouds for $J_K = 1_0$-0_0 transition 77−60808
formaldehyde, 5 GHz absorpt. spectra obs. in directions towards galactic centre regions 79−84855
formaldehyde, ^{18}O isotope, 4389 MHz obs. 79−44591
formaldehyde, absorpt. in four small dust clouds 77−5558
formaldehyde, abundance in ρ Ophiuchi dark cloud 79−71100
formaldehyde, collisional excitation 78−89237
formaldehyde, detect. at 1.3 mm in mol. clouds 79−25683
formaldehyde, detect. in M31 79−48929
formaldehyde, excitation temp. in dust cloud L134 77−5552
formaldehyde, interstellar absorption line in galactic radio source, SHF obs. 80−77472
formaldehyde, kinematics and distrib. near Cone nebula and NGC 2264 IR source 80−4418
formaldehyde, microwave doublet cooling by collisional pumping, calcs. 77−3436
formaldehyde, normal and deuterated solid films, UV dissociation at 77K 77−29021
formaldehyde, obs. along galactic plane 79−48893
formaldehyde, polymer formation in interstellar space 77−78858
formaldehyde, prod. in diffuse interstellar clouds 79−40246
formaldehyde, survey in Orion dust cloud L1641 79−71099
o-formaldehyde+He, rot. excitation at interstellar temps., coupled states cross sections 77−54593
formaldehyde absorption and visual extinction in several dark clouds near NGC 2264 79−88715
formaldehyde absorption in direction of Cassiopeia A obs. 78−45381
formaldehyde and CH abundance 79−48883
formaldehyde and H110α recomb. lines, obs. towards bright rims in diffuse nebulae 77−87510
formaldehyde excitation, effects of microwave background radiation observed spectrum 80−36681
formaldehyde in galactic centre region 80−94852
formaldehyde in giant molecular clouds, H_2 densities and $^{12}C/^{13}C$ ratio 80−51837
formaldehyde in NGC 5128 (Centaurus A), 14 GHz absorpt. obs. 80−17657
o-formaldehyde in rho Ophiuchi dark cloud, excitation temp. and optical depths 80−51846
formaldehyde polymer formation mechanism 78−54032
formaldehyde-d_1, detect. in interstellar clouds 80−8670
formaldehyde-d_1, unsuccessful search in dark clouds 79−12500
formamide, ^{13}C isotope detect. in galactic centre 79−25680
formic acid (-d), microwave spectra and rot. consts., astrophysical appl. 80−91550
formyl ion ($HC^{18}O^+$), detect. in Sagittarius B2 79−35346
formyl radical ion, mm wave emission obs. of interstellar clouds 80−90503
fragmentation of cosmic gas clouds, opacity limited star formation 77−49365
free radical recombination onto grain surfaces, isotope effects by hyperfine interaction 77−33609
G292.0+1.8, supernova remnant, optical identification, spectrum and interstellar reddening 79−84839
G48.6+0.0, galactic H II region, direction, H I, OH and H_2CO absorpt. line meas. 78−85996
galactic γ-rays from low energy cosmic ray interactions with interstellar medium 80−8678
galactic absorption revealed by Rubin et al. Sc-type galaxies sample, anal. 78−49533
galactic abundances of stable isotopes of common elements 79−44615
galactic anticentre, space distrib. of stars and dust *(Russian)* 78−73754
galactic bulge wind, interaction with gas disc, hydrodynamic model 80−77476
galactic central region, 2.4 μm mapping and interstellar extinction obs. 77−29934
galactic centre, gas, dust, high energy particles and star form. 80−36713
galactic centre, ionised gas dynamics from Ne II 12.8 micron emission obs. 78−32572
galactic centre, IR obs., 1.25-12.5 μm interstellar extinction law 78−41039
galactic centre, radiation model, dust grains heating by O-stars and K-giants 78−36697
galactic centre, struct. from 2.4 μm obs. 78−81689
galactic centre, variable IR extinction obs., role of formaldehyde mol. clouds 79−48909
galactic centre direction, 4 to 8 micron spectrum rel. to interstellar extinction 79−48922
galactic centre direction, near IR polarisation due to aligned interstellar grains 78−96534
galactic centre point source, 1.4-2.7 μ spectrum 77−5569
galactic centre region, eruptive phenomena 78−57647
galactic centre region, IR linear polarisation 77−91630
galactic centre region, shock wave model of expanding ring 78−4365
galactic centre region, shock wave model of kinematic features of H I and molecules 77−91629
galactic centre region, sources and obscuration 80−77487
galactic corona, origin and props. 79−25709
galactic corona, plasma parameters and heating mechanism 80−82492
galactic coronae, ionisation struct. and absorpt. line spectra 77−13448
galactic density wave, molecular clouds and star formation 78−8088
galactic density waves, maintenance and phase shifts between stellar and gaseous arms 79−44618
galactic density waves influence on star form. rate 79−88743
galactic disc, primordial gas inflow problem rel. to chemical evolution 80−62279
galactic disc emission at 4 cm wavelength, large-scale and small-scale cloud structs. 78−28795
galactic disc gas, corrugation waves in differentially rotating layer 77−5571
galactic distrib. of interstellar absorpt. from Celescope catalogue, UBV and Hβ obs. 77−60810
galactic dust and IR astronomy, review *(French)* 78−12352
galactic equator, H I recomb. line emission, 408 MHz obs. 77−13451
galactic gas-to-dust ratio determ. from globular cluster obs. 79−88747

interstellar matter continued
galactic gaseous warps persistance, test particle calc. for NGC 5907 79−71112
galactic globular clusters colour excess ratio, rel. to interstellar absorpt. law 78−28797
galactic H_2O vapour sources, maser phase duration galactic distrib. 79−35343
galactic Hα background emission, high spatial and spectral resolution pictures 80−56897
galactic H I absorption spectra in direction of extragalactic radiosources 78−24541
galactic halo, evidence for hot gaseous component from IUE UV obs. of (3C 273) 80−94886
galactic interstellar extinction law, vars. 78−85990
galactic light extinction, A_B coeff. amplitude 80−17664
galactic matter distrib., relation with cosmic ray dynamics and γ-ray production 78−4349
galactic photometric disc model, direct starlight intensities and interstellar dust clumping effects 80−22077
galactic plane, dark cloud near 140° longit. 77−9797
galactic plane, interstellar dust distrib. within 3 kpc 80−109512
galactic spiral structure, density wave theory and very hot interstellar gas 80−31356
galactic winds, supernovae-driven, rel. to Hubble sequence 79−8989
in galaxies, criteria of local gravit. instability of double gaseous discs *(Chinese)* 79−17099
galaxies, gas spiral density wave caused by orbiting retrograde companion 78−96533
in galaxies, kinetic theory of differentially rotating interstellar medium *(Russian)* 77−91617
galaxies, nearby, interstellar reddening law and dust content *(German)* 80−67850
galaxies active nuclei, contrib. of irradiated stars mass loss to broad line emission regions 80−56949
in galaxies in dense groups, effects of collisions 77−45573
galaxies material arms, tidal disturbances by spiral density waves *(German)* 79−17086
Galaxy, dark clouds and emission nebulae review 79−25723
Galaxy, gas, dust and molecules review 78−54006
Galaxy, interstellar medium rel. to one-dimensional spiral shocks struct. 77−64849
Galaxy central region, vacuum cleaner effect of stellar bar 77−45565
Galaxy central region gas distribution, barlike model based on improved H I data 80−67845
galaxy clusters, intracluster gas origin and evolution, interaction with interstellar gas 78−45407
Galaxy coronal gas, statistical anal. of O VI absorpts. 78−36653
Galaxy high latitude nebulosity, as source of enigmatic dark lines crossing (M81) 80−56947
galaxy rotating gravitating disc, nonlinear stability theory 80−17488
gamma-ray line emission from nucleus de-excitation following energetic particle reactions 80−18219
gas, hydrostatic equilib. rel. to cosmic ray confinement and Galaxy radio emission 77−29919
gas, in disc galaxies, effects of dissipation on response to oval distortions 78−12355
gas, in external galaxies, density rel. to star form. rate 77−45555
gas, isentropic instabilities 77−17644
gas, self-gravitating flow in barred spiral galaxies 80−90521
gas, semitorrid, obs. in direction of γ^2 Velorum and Gum Nebula 79−48890
gas accretion by pregalactic black holes in Galaxy 78−8039
gas chemical composition differences within and among galaxies 78−4369
gas cloud gravitational collapse and molecule form. 77−78848
gas clouds, effect on supernovae remnant kinematics and evolutionary sequence 80−67823
gas clouds, equilib. states during cooling in gravitational fields 80−94862
gas clouds, high-velocity, abundance vars. 77−26039
gas clouds, masses 79−17046
gas clouds, non-uniform collapse stability 80−101631
gas clouds, radiation diffusion *(Russian)* 77−41297
gas clouds, rotating isothermal, gravit. collapse, fluid-in-cell method 77−5523
gas clouds, spherically symm., gravitational collapse, effect of H_2 form. 80−101628
gas clouds, stability of self-gravitating magnetized system 79−21170
gas clouds, thermal instability in nonstationary medium, rel. to star form. 79−21178
gas clouds, whistler mode radiation during gravit. collapse 78−28509
gas clouds gravit. collapse, caustic and critical times for one-dimens. model 78−93367
gas clouds in Seyfert galaxies and quasars, containment by particle flux 79−8820
gas clouds spherical gravitational collapse, unsteady hydrodynamics 78−45212
gas density, implications of light isotopes abundances in galactic cosmic rays 80−17456
gas density, results from galactic cosmic rays ^{10}Be abundance 78−12060
gas density in M83 and Milky Way 80−51870
gas distribution in Galaxy, implications of galactic gamma-ray obs. 77−26083
gas evolution in galaxies, review 80−77486
gas flow stability in disk-halo galaxies 80−56933
gas flowing into interplanetary space, heating by solar electrons 79−16881
gas globule, ionisation and expansion, weak R-type ionisation front effects 77−78864
gas heating and ionization by X-ray photoelectrons 80−46383
gas heating by galactic UV radiation, rel. to two phase model 80−67839
gas heating during star formation, maintenance of spiral structure in galaxies *(Chinese)* 77−60830
gas hydrostatic equilib. in solar neighbourhood 79−30098
gas in active galactic nuclei, cosmic ray driving 77−29915
gas in diffuse interstellar regions, Copernicus UV obs. *(Italian)* 78−32552
gas in disc-halo galaxies, boundary layer circulation 78−57627
gas in M81 spiral galaxy, dynamics 80−105336
gas interaction with solar wind *(Russian)* 80−36467
gas mixing rel. to abundances in unevolved stars *(Russian)* 79−40192
gas motion in rotating disc-shaped galaxies 79−21424

interstellar matter continued
gas of galactic discs, kinetic energy, rel. to origin of spiral arm instability 77−13456
gas parameters change in stellar-wind-dominated environment, rel. to solar system 78−61904
gas phase chemistry in interstellar clouds, nonequilib. processes and temp. and activation energies effects 80−105298
gas phase element depletion anomalies and ionization potentials 80−31342
gas pressure and density *(Danish)* 78−4335
gas properties from spectral line surveys 79−5879
gas replenishment rates in galaxies, stripping of spirals to form S0 galaxies 79−40253
gas response to rotating stellar bar 79−48930
gas self-gravity effects on galactic shock waves 78−73761
gas-dust clouds assoc. with open star clusters, effect on cluster dynamics 80−101622
gas/dust ratio in disc galaxies 79−53903
gaseous component of flat galaxies, with double-peaked rot. curves, spiral struct. generation 80−46679
gaseous nebulae, riddle of spectra, history 80−8676
Gassiopeia-Taurus association, 2200 Å extinction feature anomalous strength 80−77469
giant grains formation 77−9787
giant molecular cloud near M17, H I abundance, 21 cm obs., chem. evolution 79−21383
giant molecular clouds, collisional growth 79−48877
giant molecular clouds, gravit. field probing 80−62242
giant molecular clouds in Galaxy, ^{13}CO emission distrib. in galactic plane 79−101183
giant nebular shells in LMC, dynamics 80−46674
GL 2591, protostellar source, 3 μm ice absorpt. band, linear polarisation obs. 80−105303
GL 2636, star form. region in Cygnus-X, IR obs. 80−105302
globular clusters, gas glow and contents 80−8666
globular clusters, interstellar reddening from six-colour photometry 77−13407
in globular clusters, ionisation by UV radiation, evidence from OAO photometry 80−73009
globular clusters, nova-driven winds 78−57596
globular clusters, southern, gas content upper limits 80−22047
globular clusters, UBVR photometric obs., dust patches 78−81662
globular clusters in Galaxy, Fornax and M31, integrated colours, reddening and metallicity 78−16469
globular clusters near galactic centre, interstellar extinction from IR studies 80−82434
globules, large, struct. and dynamics 80−62246
glycine, 22-83 GHz search in mol. clouds 79−30115
Gould's belt, anomalous extinction, grain growth 79−44603
Gould Belt, high-energy gamma-ray emission, SAS-2 obs. 77−33688
grain clouds gravit. contraction, star form. 77−53575
grain destruction by chemical reactions, collisions and photodesorption 78−54021
grain destruction by sputtering 78−54020
grain destruction mechanisms 79−92825
grain formation by nucleation, astrophysical environment 78−16501
grain formation in cool stellar envelopes 80−56814
grain mantle growth in UV-shielded dense clouds 78−54022
grain mantle molecules, middle IR fluoresc. and absorpt. spectra 79−88716
grain size distrib. 79−21388
grain size versus colour excess ratios 79−17040
grain sputtering and disruption in intermediate vel. clouds 79−21378
grain streaming in solar system 80−26810
grain synthesis and Be and B abundances in meteorites 79−16894
Grain unified model, alignment efficiency, grain model size and cosmic abundance 80−105306
grains, accretion by chemically peculiar A-type stars 79−67017
grains, charge distrib., induced charge effects 79−25679
grains, chemical role in interstellar medium 80−82470
grains, composition constraints from 10 μm data 80−82471
grains, destruction by sputtering 78−45382
grains, disorientation in suprathermal rotation 79−92824
grains, ice mantle and silicate core, emission props. *(Italian)* 79−48898
grains, interaction of light with small-particle system 77−74111
grains, luminesc. emission 79−8967
grains, magnetic alignment 78−41017
grains, narrow gamma-ray line emission 77−13437
grains, organic composition, IR obs. 80−77460
grains, possible identification with bacteria, algae and virus particles 80−31341
grains, size distrib. from 0.11-1.0 μm obs. 78−8084
grains, spin-related magnetism 79−5883
grains, suprathermal rotation 79−92823
grains, surface chem. activity, adsorbed mol. ions rel. to diffuse spectral bands 77−26040
grains, temperature fluctuations and size distrib. 79−71087
grains, UV scatt. props. and size distrib. 80−26932
grains and molecules, UV obs. from Spacelab 80−41871
grains destruction by cosmic rays, hydrodynamic mechanism 78−24546
grains formation, time-depend. nucleation theory 80−26946
grains in interplanetary space, optical detection during out-of-ecliptic mission 78−85906
grains in IR sources, possible origin for unidentified IR features 80−82452
grains shape, spheroidal model, rel. to polarization and extinction 79−40236
graphite grain surface reactions in interstellar and protostellar environments 78−4316
graphite grains, chemical sputtering 79−62880
graphite grains, porous, rel. to 2200 Å extinction hump 80−62228
graphite grains temperature, effect of IR optical consts. 78−12324
gravitational instability in presence of suspended particles and rot. 79−64633
gravitational instability of composite plasma, effect of gyroviscosity and ion viscosity 77−87255
Gum Nebula, Herbig-Haro objects spectrophotometry 78−36565
HD 101205 region, spectrographic and photometric obs. of stars and interstellar medium 77−49383
HD 153919 (3U 1700-37), X-ray binary interstellar absorpt. and distance 77−29877

interstellar matter continued
HD 200775/NGC 7023 complex, star intrinsic and interstellar reddening 80−51832
HD 28497, distant unreddened star, Copernicus UV obs. 77−33591
HD 44179 (Red Rectangle), obs. and interpretation of IR spectrum 77−78859
HD 50896, Wolf-Rayet star, UV spectral energy distrib. and interstellar extinction 77−22211
HD 97950 direction, interstellar features in spectrum 80−101586
He abundance, rel. to stellar models and cosmological models 78−16518
heating due to weak shock waves dissipation 78−81674
heating processes, rel. to delayed star form. in galaxies 80−105349
heavy haloes in spiral galaxies rel. to primordial star generation 78−61946
heavy nuclei synthesis rel. to interstellar radioactivity 77−2501
Heiles 2 dark cloud, NH_3 hyperfine struct. 77−78852
Heiles 2 dust cloud, NH_3, and cyanobutadiyne emission relative distrib. 80−17641
Heiles Cloud 2, obs. of H I self absorpt. 77−29901
Henize 788 (Wray 977), counterpart of 3U 1223-62, interstellar reddening 77−29846
Herbig-Haro object, far UV spectrum obs. rel. to nature of object 80−67714
HFE 2,3, molecular cloud, for IR radio mol. line studies 80−26929
HFE 2, 100 micron source, radio and IR obs. of assoc. mol. cloud 77−26082
high vel. ions, survey 78−8074
high velocity cloud near ζ Orionis, density, temp. and comp. 77−22291
high velocity clouds, absorption line obs. by Copernicus, review 77−37640
high velocity clouds at low galactic latits., H I absorpt. 78−49506
highly excited atoms, collision processes, review 77−58146
hot component information from np^q ions 80−83305
hot gas, nature, origin and evolution 78−16506
hot gas, sound wave propag., effect on Galaxy spiral struct. 80−109511
hot interstellar gas, evidence for retention in elliptical galaxies 80−90535
hot interstellar medium 79−25699
hot interstellar medium filling factor, implications of metal depletions 80−17634
hot optically thin plasma, soft X-ray spectrum, interstellar medium appl. 78−34275
hot plasma, evidence from diffuse soft X-rays distrib. and energy spectrum 78−28853
hot regions, rel. to extended 0.1-2.0 keV soft X-ray emitting regions 78−16581
hot tenuous gas, cosmic ray particle streaming at speeds above Alfven vel. 79−40068
hot tunnels, simulation of interacting supernova remnants 77−17645
hot white dwarfs, EUV flux interstellar absorpt., local clumpiness factor determ. 80−36627
hydrocarbon formation on graphite grains 80−82458
hydrocarbons, long chain, interstellar formation mechanism expt. 80−46653
hydrodynamic model for winds from discs of spiral galaxies 78−45397
hydrodynamic turbulence in weak large scale mag. field, effective mag. viscosity 77−33340
hydromagnetic surface waves, theory 79−25462
hydroocarbon chain synthesis in interstellar clouds, ion-molecule scheme 80−12786
IC 1318 b and c, H_2CO absorpt. 78−16484
IC 1396 interstellar molecular cloud, for IR study and dust temp. profiles 80−62237
IC 1848 A, bright-rimmed mol. cloud, IR source obs. rel. to star form. 79−5810
IC 2149, planetary model, near IR spectrophotometry and interstellar absorpt. 77−17669
IC 2581, young open cluster, ratio of total to selective extinction determ. 79−5870
IC 2944, stellar aggregate surrounding HD 101205, vels. from interstellar lines 77−17636
IC 342, Scd galaxy dust thermal IR emission obs. rel. to star form. in central regions 80−62256
IC 361, open cluster, preliminary photometry and colour excess 78−89228
IC 4593, planetary nebula, near IR spectrophotometry and interstellar absorpt. 77−17669
ice, 45μm signature possible identification in Orion 79−17068
ice, identification as carrier of 3 μm absorpt. in IR sources questioned 78−49499
ice grains in interplanetary and interstellar media, low energy cosmic ray erosion 78−45177
inhomogeneous cosmic masers, numerical calcs. of saturation behaviour 78−20898
instabilities, absolute and convective, distinction 80−98539
instability criterion for mag. field parallel to galactic plane 80−82454
interaction with planetary nebulae, disruption timescale calcs. 79−101179
interaction with stellar winds, cosmic ray origin and accel. 80−77512
intercloud cosmic ray ionisation rate 78−85989
intercloud medium, ionisation by single O star 77−9782
intercloud medium and spiral galaxy struct. 77−17664
intermediate-velocity gas in local interstellar medium, obs. 78−36655
International Solar Polar Mission, predictions for zodiacal light and local interstellar dust obs. 79−92717
interplanetary Lyman α emissions, Mariner 10 obs., rel. to solar wind latit. struct. 79−35085
in interplanetary space, Mariner 10 UV obs. 79−48736
interstellar *(Russian)* 80−36698
interstellar linear polarisation, wavelength depend. at near IR wavelengths 80−51833
interstellar UV and optical absorpt. lines, comparison with H I 21 cm obs. 78−24532
ion chemistry in interstellar plasmas 80−62254
ion-molecule reactions, isotopic exchange, interstellar implications 80−61087
ion-molecule reactions, review 78−33563
ion-molecule reactions rel. to cyanide chemistry in dense clouds 77−82297
ionisation-coupled acoustic instability, theory 79−97044
ionised interstellar medium, recomb. emission line obs. in galactic plane 77−13433

interstellar matter continued
ionization front propag. in inhomogeneous medium 80−46379
ionized gas motion and distrib. in central parsec of Galaxy 79−25719
ions, interstellar, in solar wind, flux motion rel. to plasma instability 79−96877
IR and molecular line sources, 9400 Å photography 77−45602
IR astronomy investigation of star interplay with interstellar medium 77−53433
IR emission, airborne obs. using Michelson interferometer 77−73966
IR emission from dust in stellar aggregates *(Italian)* 79−48869
IR molecular line emission from grain surfaces in dense clouds 78−61905
IR observations of star form., review 78−7988
IR source in 2S 1702−363 field, identification and interstellar visual absorpt. 78−81705
IR sources, 10 μm silicate absorpt. band equivalent widths and dust temps. 78−57614
IR sources, galactic, IR fluxes calcs. for polysaccharide grain model 78−54008
IR sources identification in Ophiuchus dark cloud region, spectral types and extinction 77−45522
IR spectra, unidentified features review 80−26936
IR spectral features, laboratory simulation 80−26728
IRC-10442 (GL5268S), radio obs. rel. to low-temp. extended CO cloud 80−4412
isocyanoacetylene theoretical study and rot. const. 78−33633
isocyanoethynyl radical, theoretical study and rot. const. 78−33633
isothiocyanic acid, detect. in Sagittarius B2, mm wave spectrum 80−41878
isotope fractionation, expts. under simulated space conditions 78−73623
isotopic composition, evidence from cosmic ray isotopes 78−53781
K-type giant stars, reddening determ. from David Dunlap Observatory (DDO) photometry 78−4222
ketene, microwave detect. in Sagittarius B2 77−37638
ketene+H, reaction rate consts., lab. meas., rel. to interstellar cloud processes 79−74359
kinetic energy equipartition breakdown in colliding systems with fragmentation 79−88586
Kirchoff's laws of spectral analysis, computer laboratory exercises 78−73790
L134, cool dust cloud, HNC quadrupole coupling constant determ. 78−1101
L134 N dark cloud, NH_3 hyperfine struct. 77−78852
L1544, L1521B, interstellar clouds in Taurus, HC_5N detect. 80−26957
L1641 and Orion Nebula, submillimetre emission obs. 80−36685
L 183 (L 134 N) dust cloud, NH_3 and cyanoacetylene mapping at 23 GHz 80−105307
large molecules, deuterated species 77−53665
large molecules formation, nucleation centres for grain growth 77−78844
lenticular galaxies, H I 21 cm line obs. 79−67090
ρ Leonis, non-anomalous diffuse interstellar absorpt. features 78−16418
line accretion by stars, effects of gas press. 78−32525
line spectra in interstellar clouds, weak lines below 3400 Å in ζ Persei 77−45509
linear molecules CO, CS, OCS and cyanoacetylene, collisional excitation 78−81664
linear polarisation in 1-2.2 μ wavelength range 78−77588
linear polarization of 313 nearby low galactic latitude 80−46641
LMC, far UV spectra rel. to interstellar reddening 77−13461
LMC, interstellar 4428 Å feature 79−35335
LMC, interstellar extinction meas., UV sky-survey telescope obs. 79−35384
LMC, IUE obs. and 2200 Å feature detection 79−16959
LMC interstellar extinction, visible and UV obs. 80−51877
LMC OB associations, for UV spectra and interstellar reddening 77−33634
Lo 807, open cluster, two-colour photographic photometry and interstellar reddening 78−96512
Local Group galaxies, interstellar gas 77−91644
local H and D densities, Copernicus obs. 78−16487
local H and D Lyman α towards cool stars 79−5886
local interstellar gas in southern sky, single 21 cm component study 79−84834
local interstellar medium, ionisation state 80−90502
local interstellar medium and cosmic ray anisotropy 79−44313
local mass density from AF stars near N.Galactic Pole 79−40267
long chain C molecules rel. to diffuse interstellar lines 79−53897
low density clouds, chem. and thermal equilib. model predictions 77−22290
low-density hot gas, influence on supernova outbursts frequency estimate 80−62168
Lyman α emission, line profile, temp. and polarisation meas. from geocoronal absorpt. 77−67120
Lyman α intensity, lower values 78−36675
Lyman α sky background, Copernicus high-resolution obs. 77−29963
Lyman alpha scattering meas. by Venera 9 in interplanetary space, interstellar medium parameters determ. 79−80180
Lynds 134, dust cloud, isotope ratios and CO chemical fractionation 77−87531
Lynds 134 dust cloud turbulence, formaldehyde obs. at 6 cm. 80−94845
β Lyrae, H emission profiles rel. to pattern of gaseous flow in system 78−57576
RR Lyrae stars, interstellar reddening from VBLUW photometry 79−48806
RR Lyrae variables in globular cluster NGC 6121 (M4), UBV photometry and interstellar reddening 80−22018
M17, discovery of extended mol. cloud assoc. with star forming complex 77−37635
M17 SW, obscured IR point source spectroscopic anal. 79−48878
M31, CO and H I distrib. comparison 78−36694
M31, globular clusters colour indices, rel. to interstellar absorpt. law 78−28796
M31, interstellar polarization, wavelength depend. 79−92835
in M31 (Andromeda galaxy), interstellar gas assoc. with Cepheids and star complexes *(Russian)* 80−90455
in M31 and companions, prod. rate from planetary nebulae numbers 80−109520
M33, ionisation of interarm medium 77−67131
M4, globular cluster, direction, reddening from UBV photometry of RR Lyrae stars 77−78802
M51, ionized gas velocities 79−75268

interstellar matter continued
M52 (NGC 7654), open cluster, four-colour and Hβ photometry rel. to interstellar extinction 78−8067
M81, kinematics of gas in nuclear disc 77−9795
in M81, M51, spiral galaxies, phase shifts between gaseous arm and stellar arm *(Chinese)* 79−17098
M82, galaxy, interstellar HCN and CS search 77−53661
M82, interstellar scatt. and absorpt. rel. to nucleus compact radio source VLBI obs. 80−22078
M82, irregular galaxy, OH absorption and emission obs. 77−5565
M82 nucleus, λ6 cm formaldehyde absorpt. detect. 79−17088
in M87, interstellar gas vel. dispersion rel. to presence of large central mass 80−94873
M87, model for optical knots in jet 79−30127
M87 nucleus, hot gas emission model for compact X-ray source 78−28847
Maffei 2 galaxy, CO emission obs. rel. to interstellar medium struct. 78−16530
Magellanic Cloud supernova remnants, optical emission from shocks 79−92831
Magellanic Clouds, gaseous corona, evidence from stellar spectra 80−82490
in Magellanic Clouds, giant and supergiant interstellar shells obs. 80−94858
Magellanic Clouds, ratio of total-to-selective absorpt. from Cepheid obs. 77−29927
in Magellanic Clouds, reddening of Cepheids 77−2435
magnetic braking of self-gravitating, oblate interstellar clouds 79−35325
magnetic charges, detect. using pulsar radio emission dispersion 79−75704
magnetic clouds, gravit. collapse 77−13420
magnetic clouds fragmentation by ambipolar diffusion, star formation 77−91608
magnetised gaseous discs, gravitational instability 80−4424
magnetite grains, stellar light circular polarisation, two-cloud model 77−78838
Markarian 335, Seyfert galaxy, gas props. from spectroscopic investigation *(Russian)* 79−101204
Markarian 3, 231, Seyfert galaxies, evidence for asymmetric dust envelopes from optical polarisation 80−90533
Markarian 79, Seyfert galaxy, interstellar reddening from IUE and visual spectrophotometry 79−92856
Mars bow shock, positions, rel. to Mars mag. field, Mars 5 evidence 78−49362
maser emission, role of plasma effects in generating high-rel. and symmetric spectral features 80−31378
maser emission by nebular regions and stellar atmospheres 78−89242
masers, Λ-doublet population inversion in OH, OD, CH, CD and NH^+ collisions 80−22065
masers, collision-collisional pumping model collisions *(Russian)* 80−90560
masers, review of physics 79−21455
masers, time vars. and radiative stability 79−35340
massive molecular clouds dispersal by young O-type stars 79−25693
massive protostellar clouds, dynamical evolution 77−17543
mechanical heating of interstellar medium, source and rate 80−36682
metal abundances, three-level models of chemical evolution 79−48873
metastable isomers 79−48872
methane, detect. in Orion A molecular cloud 79−17060
methane, possible microwave interstellar maser lines 78−41020
methane in Orion A, first detection at 76 GHz 78−16503
methanol, 84.5 GHz and 96.7 GHz lines obs. in Sagittarius B2 and Orion A 80−62245
methanol, and deuterates, dissoc. ionisation mechanisms, photoionisation mass spectra, ionic struct., interstellar formation 79−3503
methanol masers, search for microwave emission 78−32543
methanol-d_1, (CH_2DOH), microwave torsional-rot. spectrum, rel. to interstellar search 80−99498
methanol-d_1, laboratory freqs. of J=2-1, a-type transitions 80−63624
methyl alcohol, obs. 79−25666
methyl formate, microwave spectra, rot. consts., moments and struct., radio astronomy appl., review 80−17637
methyl mercaptan, detect. in Sagittarius B2, mm wave spectrum 80−41877
methylamine-d_1, probable detect. 77−33610
methylamine-d_1, unconfirmed from 10 GHz obs. 79−92822
methylidyne, obs. in Sagittarius B2 direction 78−65671
MHD shocks, grain disruption 78−4317
microwave spectroscopy, appls. to obs. of interstellar mols. 79−41160
microwave spectroscopy, modern aspects, book 80−51973
microwave spectrum lines, review 77−71138
N. Milky Way fields, interstellar extinction from early-type stars photometry 77−2424
mirror instability growth effects on pulsar scintillations 80−46648
molecular Λ-doublets transitions 80−14132
molecular abundance variations in interstellar clouds 79−17055
molecular and thermal equilib. in low density clouds, chem. reaction network 77−60816
molecular chemical tunnelling, facts and hypotheses 79−59520
molecular cloud complex assoc. with bright rim near VY Canis Majoris, CO obs. 78−24536
molecular cloud complex near M17, detailed obs. 77−33603
molecular cloud complexes, origin, lifetimes and mass 80−82453
molecular cloud in NGC 2264, NH_3 and OH line emission mapping, SHF and UHF 80−94847
molecular cloud near RCW 36, H_2CO and OH obs. 78−69862
molecular cloud struct. from 2 cm formaldehyde and 2.6 mm CO lines 79−80341
molecular clouds, 3.1 μm absorpt. attributed to amorphous H_2O ice 80−26956
molecular clouds, bimolecular reactions of positive ions, laboratory studies 77−63896
molecular clouds, bright-rimmed, heat sources 78−36664
molecular clouds, C recomb. line broadening by ions 77−49450
molecular clouds, chem. evolution 78−28749
molecular clouds, chemical evolution and formaldehyde abundance 77−13421
molecular clouds, CO(J=2-1) emission obs. 79−92827
molecular clouds, cosmic ray penetration 79−8979
molecular clouds, cosmic ray penetration rel. to nonthermal galactic radio background 78−49527
interstellar matter continued
molecular clouds, cosmic rays exclusion 77−13190
molecular clouds, critical mass rel. to supernova phase 77−78770
molecular clouds, detect. of new transitions of H, OCS and CH_2O, search for F 77−60808
molecular clouds, embedded supernova remnant struct. and emission 80−82450
molecular clouds, far IR emission 78−4313
molecular clouds, Fourier interferometer for IR line emission obs. *(Italian)* 79−48679
molecular clouds, H I and CO obs. comparison 78−24538
molecular clouds, high density, assoc. with type IIc OH radio emission sources in (W33) *(Russian)* 80−62247
molecular clouds, IR circular polarisation obs., interpretation 80−82469
molecular clouds, isotopic abundances 78−16513
molecular clouds, line formation, radiative transfer effects 79−5884
molecular clouds, location with respect to galactic plane 77−74127
molecular clouds, mag. fields influence on OB associations subgroups sequential form 80−4408
molecular clouds, magnetic field 79−67075
molecular clouds, microturbulence, systematic motions and spectral line form. 77−33586
molecular clouds, near IR slit scans of compact IR sources 80−105300
molecular clouds, props. from molecular lines 77−57079
molecular clouds, radiation transport and kinematics 78−93347
molecular clouds, relationship of submillimetre optical depth to ^{13}CO column density 77−45508
molecular clouds, shock front propag. rel. to subgroups form. in OB associations 77−60800
molecular clouds, shock waves rel. to massive stars birth 79−2542
molecular clouds, southern, $^{12}C/^{13}C$ abundance ratio derived from H_2CO obs. 79−84838
molecular clouds, summary of obs. 78−16512
molecular clouds 78−32562
molecular clouds and star formation, Cepheus OB3 cloud obs. 78−28750
molecular clouds as galaxy spiral struct. tracer, 2.6 mm CO survey 80−105346
molecular clouds assoc. with Herbig Be/Ae stars, star form. process 78−32542
molecular clouds associated with refl. nebulae, CO emission, EHF obs. 80−82447
molecular clouds containing H II regions, H II region evolution, O star wind effects 80−94846
molecular clouds containing Herbig-Haro objects, mol. obs. and physical props. 80−36689
molecular clouds evolution, IR polarisation rel. to nearby interstellar polarisation 80−4347
molecular clouds of Cepheus OB3 and Perseus OB2 associations, star form. from mol. obs. 80−12798
molecular clouds rel. to cosmic rays and spiral struct. in Galaxy 77−87544
molecular complexes in Orion, radio obs. 78−4310
molecular composition of planetary nebulae, atomic and mol. data 80−109528
molecular evolution, ion chemistry in dense clouds 80−31346
molecular isotopic abundance ratio $H_2{}^{13}CO/H_2C^{18}O$ determ. from 6.8 cm obs. 79−35347
molecular lifetime in dark dust cloud model 78−85999
molecular low-velocity cloud obs. near Sagittarius A 79−53898
molecular shell, expanding, surrounding Pelican Nebula (IC 5070=W80) H II region, CO obs. 80−105296
molecular spectra, predicted radioastronomical freqs. accuracy, determ. from OH spectrum 79−48666
molecular spectral lines, intensities appl. to interstellar medium kinetic temp. and density determ. 79−97056
molecular synthesis, lab. meas. 78−12314
molecular synthesis in interstellar clouds, radiative association reaction $H+OH \rightarrow H_2O+h\nu$ 80−90509
molecular transitions, rest freqs. 80−62218
molecule abundances in clouds, steady-state calc., chem. reactions 79−21381
molecule formation, grain surface reactions contrib. 77−9784
molecule formation and IR emission in shocks, physical processes 80−62219
molecule formation by surface reactions on interstellar grains 78−28753
molecule formation chemistry 80−12803
molecule formation in clouds from singly or multiply ionized atoms 79−17039
molecule formation in contracting clouds 77−22294
molecule formation in grain mantles, laboratory analogue expts. results and implications 80−26944
molecule formation processes and reactions 78−16515
molecule synthesis by ion implantation, photon emission studies of N^+ and $N_2{}^+$ bombardment of Si 77−70297
molecules, collision-induced dissociation 80−17632
molecules, collisional excitation theory 77−67119
molecules, determ. of galactic isotope distrib. 80−109550
molecules, discovery, chemistry and identifications 77−82300
molecules, distrib. in vicinity of young B-type stars *(Russian)* 80−105321
molecules, effect on cosmic background radiation spectrum *(Russian)* 80−8719
molecules, form., column densities, rel. to space communication and origin of life 79−84836
molecules, form. in diffuse interstellar clouds 77−26033
molecules, form. rel. to interstellar grains max. temps. 77−49449
molecules, galactochemistry and origin of life 78−12338
molecules, identified and unidentified, R&D progress *(German)* 77−67122
molecules, list of identifications before 1979 Sept. 80−51852
molecules, matrix isolation spectra, review 78−46340
molecules, microwave astronomy, modern aspects, book contrib. 80−56921
molecules, pioneering investigations 1935-42 period 78−69855
molecules, prod. on interstellar oxide grains 79−25690
molecules, radio obs., review 77−33616
molecules, radio obs. of Taurus Molecular Cloud 1 condensation 78−69858
molecules, reactions, review 77−9790
molecules, rel. to volatiles in cometary nuclei 78−12154
molecules, review 77−78856

interstellar matter continued
molecules, rot. excitation by electrons, appl. to HCN and DCN 77−22292
molecules, rotational-level populations 79−97054
molecules, unobservable by radioastronomy, indirect obs. possibility 78−4307
molecules, vibr. excited, in grain mantles, IR emission lines 78−36670
molecules and chemical reactions, summary 78−93384
molecules collisional excitation by H_2, theory for linear mols. CO, OCS, SiO, HCN and HC_3N in $^1\Sigma$ state 80−109508
molecules in grain mantles, IR absorpt. line interpretation 80−90504
molecules in planetary nebulae, abundances and IR spectra 78−53998
molecules of low electron abundance in dense clouds 79−21384
molecules synthesis, laboratory studies of ion-atom reactions 80−67812
Monoceros R1 molecular clouds ring struct., CO obs. 80−12784
Monoceros R2 cloud, near IR and mol. obs. of rot. collapsing cloud 77−78840
N Monoceros region, IR interstellar extinction curve from two-micron objects survey 80−8555
V616 Monocerotis (Ariel 0620-00), colour excess rel. to distance 77−64744
MWC 349, IR source identification and interstellar reddening 80−56971
N51D, giant filamentary shell in LMC, nature and dynamics 80−105343
N70, giant filamentary shell in LMC, dynamics 80−90511
nearby interstellar cloud, impending encounter with solar system 78−93352
nearby interstellar gas, optical and kinetic props. 77−29910
nebulosity associated with O-stars, rel. to galactic struct. and stellar spectral type 80−105236
neutral gas, critical vel. effect in solar wind interaction region 80−94666
neutral H, weak R-type ionisation front approaching a contact discontinuity 78−49510
in NGC 1068, Seyfert galaxy, mol. clouds as source of far IR emission 77−29914
NGC 1068, Seyfert galaxy, nucleus, H_2 existence and form. 80−12816
NGC 1275, Seyfert galaxy, nucleus, ralation between gas and radio source structs. *(Russian)* 79−48936
NGC 1904, globular cluster, BV photometry and reddening 77−13415
NGC 1999, reflection nebula, optical polarisation map and struct. 80−94856
NGC 2264, mol. cloud, continuum emission mapping at 89.6 GHz 80−94842
NGC 2264, open cluster, CO obs. of mol. cloud 79−21363
NGC 2264, open cluster, reddening, blanketing and metallicity from spectroscopic obs. 80−26916
NGC 2264, young open cluster, differential reddening due to intracluster dust clouds 78−53996
NGC 2264 and other Bok globules, formaldehyde absorpt. obs. at 6 cm 77−45511
in NGC 2403, Cepheids reddening rel. to galaxy distance 77−2471
NGC 2439 association, photometric study and interstellar reddening 78−16470
NGC 2527, galactic cluster, UBV photometry and foreground colour excess 78−16479
NGC 253, galaxy, interstellar HCN and CS search 77−53661
NGC 3105, young open cluster, UBV photometry and colour excess 77−64811
NGC 3201, globular cluster, BV photometry and interstellar reddening 77−2458
NGC 3227, 3516, Seyfert galaxies, evidence for asymmetric dust envelopes from optical polarisation 80−90533
NGC 3293, open cluster in Carina, interstellar reddening from UBVRI photometry 80−90490
NGC 3324, young open cluster in Carina, UBV β photometry and interstellar reddening 77−22282
NGC 362, globular cluster, BV photometry and reddening 77−13416
NGC 4151, Seyfert galaxy, optical polarimetry, circumnuclear dust envelope 78−61916
NGC 4321 (M100), interstellar Na I and Ca II absorption 80−51847
NGC 4594, search for O I 6300 Å forbidden line from warm neutral interstellar medium 79−71129
in NGC 4945, late-type spiral galaxy, excited gas kinematics, obs. 80−109547
in NGC 5236 (M83), Sc galaxy, CO obs. 78−65689
NGC 5367, young open cluster, photometry rel. to visual extinction 77−82294
NGC 6087, galactic cluster, colour excess and distance modulus from four-colour and Hβ photometry 80−62208
NGC 6144, globular cluster and neighbouring region, photometric obs. rel. to interstellar reddening 80−51816
NGC 6210, planetary nebula, near IR spectrophotometry and interstellar absorpt. 77−17669
NGC 6334, relationships of N_2H^+, HCO^+, HCN and CN 77−33587
NGC 6366, metal-rich globular cluster, BV photometry and interstellar reddening 77−5462
NGC 6528, metal-rich globular cluster, interstellar reddening and distance 80−4406
NGC 6530, open stellar cluster, broadband photometry rel. to cloud temp. and absorpt. 77−45504
NGC 6546, open cluster, interstellar reddening rel. to assoc. with Cepheid AV Sagittarii 79−58387
NGC 654, open star cluster, variable interstellar reddening meas. from UBV photometric study 80−109502
NGC 6717, globular cluster, colour excess meas. 80−46624
NGC 6823, UBV photometry and spectra, extinction study of young open cluster 80−4407
NGC 7027, planetary nebula, interstellar, local and internal dust extinction from UV spectrum 80−82459
NGC 7380, young cluster, interstellar polarization obs. 77−17649
in NGC 7469, Seyfert galaxy, spectrum rel. to interstellar clouds densities 77−57089
NGC 752, interstellar reddening from DDO astrophysical study 79−48864
NGC 7538 and Sherpless 159, H II region/mol. cloud complex, H I aperture synthesis obs. 80−90510
NGC 7538 region, IR study 79−84842
NGC 7654 (M52), open cluster, four-colour and Hβ photometry rel. to interstellar extinction 78−8067
NGC 7789, open cluster, photometry rel. to distance modulus and reddening 77−53648
interstellar matter continued
NGC 7793, late-type galaxy, ionized gas phys. conditions and mass-luminosity distrib. 80−26967
NGC 7822, NGC 281, bright rimmed mol. clouds, CH obs. 80−62238
NGV 6266, globular cluster, photometry, interstellar extinction and distance 78−61894
Norma dark cloud, struct. from stellar photometry 78−16494
GU Normae, Cepheid variable, reddening rel. to assoc. with cluster (NGC 6067) 77−45464
North Polar Spur, radio continuum obs. at 1420 MHz 80−22100
Nova Cygni 1975, interstellar extinction rel. to distance and absolute magnitude 77−2437
Nova Cygni 1978, distance, colour excess and absolute magnitude 78−89212
Nova Cygni 1978, interstellar polarisation obs. 78−89213
nova remnants shapes, effects of white dwarf rotation 80−105244
NP 0532, Crab Nebula pulsar, variability of dispersion and scatt. 77−49409
O VI, spectroscopic tracer for hot interstellar gas, Copernicus obs. 78−16505
O-B stars, spectrophotometry and colorimetry rel. to interstellar extinction *(Russian)* 77−17569
OH 205.1−14.1, unusual OH maser, new flare report and 1667 MHz line obs. 80−98734
OH absorption in direction of Cassiopeia A, obs. 78−45381
OH masers, obs. near Orion population stars 80−67716
OH near galactic plane, 18 cm lines survey 79−75265
OMC-1, methane-d_1 abundance upper limits from rot. spectrum obs. 80−56705
Oort model for colliding coalescing clouds, Monte Carlo simulation 78−12331
in open clusters, determ. of R from variable extinction anal. 77−37627
open star clusters, gas loss rel. to dynamical evolution early stages 79−8958
χ Ophiuchi, foreground interstellar material optical obs. 79−25673
ζ Ophiuchi, identification of interstellar lines in UV spectrum 78−93212
ζ Ophiuchi cloud, density from CO absorpt. obs. by Coperniucus 78−36656
ζ Ophiuchi cloud, model, atomic and mol. abundances 77−87498
ρ Ophiuchi cloud, search for vibrationally excited H_2 emission 78−93346
ρ Ophiuchi dark cloud, ^{13}CO self absorpt., EHF obs. 80−90500
ρ Ophiuchi dark cloud, atomic and mol. obs. 78−41013
ρ Ophiuchi dark cloud, C II and S II regions obs. 78−49500
ρ Ophiuchi dark cloud, extinction curves and R values from stellar photometry 77−13443
ρ Ophiuchi dark cloud, ice mantles and abnormal extinction 79−21376
ρ Ophiuchi dark cloud complex, anisotropic light scatt. and formaldehyde lifetimes 78−8080
ρ Ophiuchi direction, large interstellar grains origin 80−41870
ζ Ophiuchi direction, RF mol. emission spectra obs. 80−26958
ρ Ophiuchi mol. cloud, continuum emission mapping at 89.6 GHz 80−94842
optical interstellar lines towards stars of low reddening 78−57603
optical obscuration in W3/W4/W5 direction, distrib. 80−62301
organic chemistry, interstellar and prebiotic molecules 77−37641
organic compounds, uncooled millimeter wave receiver for radioastronomical observations *(Swedish)* 78−24461
organic compounds and graphite dust grains formation, influence of Fe condensation 80−26927
organic compounds comprising interstellar grains, 3.4 microns absorpt. obs. 80−109514
organic grains in interstellar medium, existence questioned 79−21397
organic molecules, astrochemistry and rel. to origin of life 78−73660
organic molecules, mm emission lines obs. in Orion A 77−2477
organic molecules in interstellar dust, possible spectral signature at 2200Å 77−57074
organonitrogen molecules, synthesis in interstellar clouds, ion-molecule scheme 80−12786
oriented non-spherical particles, polarisation characts. 79−81362
Orion, far-UV rocket survey 77−64762
Orion, shock chemistry 79−21391
Orion A, 22 GHz water line giant outburst 80−8703
Orion A, C recomb. lines and H I clouds obs. 78−57605
Orion A, relationships of N_2H^+, HCO^+, HCN and CN 77−33587
Orion A, SiO and H_2O maser obs. 78−8085
Orion A SiO maser intensity vars. 78−93256
Orion methanol masers, interferometric and multitransitional study 80−67891
Orion Molecular Cloud, HCN, HNC and HCO^+ J=3-2 lines detect. 79−25669
Orion Molecular Cloud, mag. field limit from Zeeman obs. in H II region 77−60809
Orion Molecular Cloud, new dynamical model 78−93373
Orion Molecular Cloud, rotational explanation of high-vel. mol. emission 80−36688
Orion Molecular Cloud 2, relationships of N_2H^+, HCO^+, HCN and CN 77−33587
Orion Molecular Cloud (OMC-1), SiO 86.2 GHz masers polarisation props. 80−4449
Orion Nebula, intracluster dust, circumstellar shells and wavelength depend. of polarisation 77−78839
Orion Nebula molecular cloud, anomalous var. of $N_2H^+/HCO^+/SO_2$ rel. to ion-molecule reactions 77−26034
Orion OB1 assoc., expanding gas shell, UV obs. 79−71086
Orion OB1 association direction, Copernicus obs. of interstellar matter towards ε Orionis and $^3\pi^3$ Orionis 80−22050
Orion OB 1 association, stellar colour excesses from photometric study 77−82288
oscillations, in stellar component gravitational field *(Russian)* 80−41883
partially ionised medium near NGC 2024 and W 3, recomb. line obs. 77−57077
particle acceleration in collisionless shocks, regulated injection and high efficiency 79−44311
particle size distribution from linear polarisation calcs. 80−12787
Perseus II complex, ζ Persei direction, Copernicus obs. 78−4301
perturbed grains, optical and thermal props. 77−45523
photoelectric heating of interstellar gas 77−29909
photoelectric heating of interstellar gas 78−77587
photoionization by galactic X-ray sources causing UV absorpt. lines 77−13439
physical processes, book 78−65679

interstellar matter continued
Pismis 6 and 8, open clusters, non-uniform interstellar reddening 79−88712
piston problem, one-dimensional, in non-ideal gas, time-dependent soln. 80−82185
PKS 0735+178, BL Lacertae object, spectrum, multiple components in z=0.424 absorpt. system 79−25707
planetary cones of focused interstellar gases 77−5494
planetary nebulae, interstellar extinction from absolute flux densities for emission lines in 6000-11000 Å range 80−51857
planetary nebulae, interstellar reddening rel. to synthetic distance scale 78−89240
planetary nebulae extinction rel. to turbulent interstellar medium in Galaxy 80−62220
planetary nebulae in M31, form. rate rel. to interstellar matter distrib. 78−28737
planetary nebulae role in heating stirring and ionisation of interstellar medium, review 80−109540
planetesimals, capture by solar system rel. to terrestrial catastrophism 80−31043
plasma, as source of ultrasoft X-ray background, obs. in S galactic hemisphere 77−45615
plasma, ion+mol., interstellar species form. radiative assoc., reaction types 80−31348
plasma, rotating, effect of suspended particles on gravit. instability 80−109347
plasma clouds, interpretation of anticorrelation between galactic radio and soft X-ray sources 80−82514
plasma irregularities, space-freq. correl function rel. to radiosource scintillation 77−13444
plasma irregularities space distrib. spectrum 77−53674
plasma-neutral gas interaction in cosmic physics 78−69669
plasmas, mirror instability, mag. field first adiabatic invariant breaking 80−67546
Pleiades, wavelength depend. of interstellar polarisation 77−45500
Pleiades cluster, reddening-face colours, photometric zero age main sequence definition 80−26920
Pleiades reflection nebulosity, model for filamentary struct. 78−8082
polarisation by clouds in elliptical galaxies 78−93399
polarisation in α Persei star cluster, wavelength depend. 79−48865
polarisation in irregularly fluctuating medium, statistical anal. 80−26926
polarisation of Nova Vulpeculae 1976, reddening and distance determ. 77−29855
polarisation of scattered radiation, in medium with internal energy sources 80−67541
polarisation of stars within 25 pc of Sun, obs. 78−12202
polarisation of Walker No.67 in NGC 2264, possibility of circular polarisation 78−12223
polyatomic ion-electron dissociative recomb. reactions, neutral products, statistical theory 78−57604
polymer formation, interstellar molecules and prebiological evolution 79−92842
polyoxymethylene co-polymers on grains 77−87500
polysaccharides, evidence in IR astronomical spectra 77−78857
polysaccharides and related hydrocarbons, identification from IR spectra 78−28763
porous grains, free-space equilib. temps. calc., rel. to optical props. 80−62223
pre-stellar interstellar dust 79−84844
prebiological evolution, occurrence in interstellar mols. 80−94726
prebiotic polymers, possibilities in IR spectra of galactic sources 78−4336
presolar grains in meteorites, prod. by supernovae 78−24520
presolar interstellar grains in Allende meteorite, evidence from ^{40}Ar-^{39}Ar ages 80−98621
prestellar gas, element separation by gravitational diffusion 79−21386
propyne, microwave spectra and mol. consts., rot. anal. 79−76411
proto-planetary nebulae, props. and comparison with planetary nebulae 80−109538
protosilicate particles, IR laboratory spectra rel. to interstellar silicate absorption bands 80−56907
protosolar nebula, dust grain motion time evolution 80−82234
protostellar cloud, rotating, collapse and stability, turbulent viscosity effect 80−109510
protostellar cloud, rotating isothermal axisymm. collapse 79−62737
protostellar cloud ang. momentum problem, mag. breaking 80−82342
protostellar cloud fragmentation processes, evidence from solar neighbourhood mass distrib. 80−98649
protostellar cloud rotation, mag. braking of aligned rotator during star form., exact time-depend. soln. 80−90493
protostellar clouds, rotating, ring form. during dynamic collapse 80−56820
protostellar clouds and star form., review 80−101589
protostellar clouds evolution, three dimens. dynamics 79−16929
protostellar clouds fragmentation, three-dimensional hydrodynamical calcs. 80−62236
protostellar envelopes of masses 3 M⊙ and 10 M⊙, struct. and hydrodynamic evolution 80−36616
protostellar formation in rotating interstellar clouds, nonaxisymmetric collapse 80−85927
protostellar rotating cloud, two-stage fragmentation 80−22061
protostellar rotating gas clouds, fragmentation 80−51827
PSR 1858+03 direction, galactic ridge obs. rel. to pulsar distance 77−64785
PSR 1919+21, radio pulse broadening rel. to interstellar scatt. 77−87466
pulsar dispersion and Hα emission meas., limits on interstellar electron density and ionized gas filling factor 78−8078
pulsar low freq. radiation in interstellar medium 77−26044
pulsar pulse scattering, resulting pulse shape *(Russian)* 77−78855
pulsar scintillations, freq. cross-correl. and finite bandwidth effects 80−4392
pulsar signal scattering by turbulent interstellar plasma 79−5854
pulsars scintillation patterns, rel. to vels. 77−78811
ζ Puppis, UV spectral energy distrib. and interstellar extinction 77−22211
quasar-like objects, interstellar clouds rel. to IR and optical emission 78−20905
radiating dust clouds, review 77−78863
radiation-driven instabilities 79−53880
interstellar matter continued
radiative shocks, thermal instability rel. to maser condensations form. 80−67821
radiative shocks and UV precursors, theoretical models 79−25660
radio emission, obs. at l=31.2° and (31.9°) 77−17724
radio galaxies, interstellar medium model from double sources asymmetry and component flux ratio 80−67892
radio galaxies, narrow line, interstellar extinction rel. to optical spectra 77−33664
radio recombination line obs., review *(Russian)* 77−57080
radioastronomical obs. of galactic struct. *(Spanish)* 79−40275
radiowave gravitational focusing in interstellar medium, model *(Russian)* 78−81905
radiowave propagation, cosmic background spectrum vars. along declination (+50° 30′) 77−17723
rare earth elements, atomic partition functions, Chebyshev approximations 80−67544
Red Rectangle, refl. nebula assoc. with HD 44179, spectrum interpretation 77−49462
reddening, distance of Nova Cygni 1978 determ. 79−21310
reddening, parameters for UBV and RGU multicolour stellar photometric systems 78−28528
reddening, vector space methods of photometric anal. 78−49338
reddening and intercloud density in solar vicinity 79−88720
reddening and quasars intrinsic spectra 79−67113
reddening freq. distrib., selection effects in SMC *(German)* 77−74113
reddening in δ Cephei direction 77−22243
reddening in clouds near Sun from SA colour excesses 79−30111
reddening in direction of low latit. globular clusters 77−22299
reddening in high-latit. field around ω Bootis 79−101185
reddening in Hyades, Coma and M67 clusters 80−62222
reddening in Markarian 3, class 2 Seyfert galaxy, visible spectral obs. 80−85999
reddening in near IR, new results from JHK photometry of reddened stars 80−94857
reddening in NGC 1068, UV, visible and IR spectra obs. 80−90519
reddening in S. Milky Way from stellar distrib. and colour excess obs. 80−85997
reddening law derived using kinematically determined distances 77−45521
reddening law from normal and Be star energy distribs. 77−74109
reddening law in Carina OB 1 association 79−8957
reddening material, distrib. in solar neighbourhood from stellar colour excesses 78−49502
reddening of 1610−771, QSO with steep optical spectrum, effects on spectral index 80−94887
reddening of β Doradus, nearby star UBV photometry 80−101598
reddening of Be and shell stars, colour excess and absorption law 80−90438
reddening of high galactic latitude southern B-type stars 80−82357
reddening of Nova Cygni 1975 (V1500 Cygni) 78−4230
reddening of open cluster Berkeley 11 UBV obs. 80−94840
reddening of RR Lyrae stars in Microscopium rel. to distance of proposed intergalactic dust cloud 80−56851
reddening relations in UBV, uvby and Geneva systems 77−22303
refractory grain destruction in low-velocity shocks 79−17041
refractory grains formation and destruction 78−16517
relativistic and nonrelativistic gas flows, general symm. soln., low press. limit 77−9655
relict circumstellar matter in young clusters 80−41865
Roberts 22, bipolar nebula with OH emission, visual, radio and IR obs. 80−94859
Rosette Nebula, far IR emission from compact sources 77−78841
rotating cloud collapse, isothermal rings fragmentation, star form. 78−93205
rotating clouds, multiple star system formation 78−93366
rotating clouds, protostellar formation, numerical methods and tests 80−56902
rotating clouds, structure and evolution under external pressure 78−61898
rotating gas cloud collapse, equatorial ring formation, Lagrangian method 78−12628
rotating interstellar clouds, axially symmetric collapse and protostellar form. 80−77380
rotating magnetic cloud, mag. braking during star form. 79−58319
rotating magnetic cloud, mag. braking during star form. 79−58320
S106, H II region, radio obs. of assoc. mol. cloud, CO, HCO^+ HCN, OH and formaldehyde lines 78−61906
S140 interstellar molecular cloud, for IR study and dust temp. profiles 80−62237
S140 IR, far IR spectrum 78−93372
S140 molecular cloud, energetics, mol. line data, temp., density, abundances 78−36650
S140 molecular cloud, far IR emission detect. 77−33611
S255, H II region, CO emission small-scale struct. from lunar occultation obs. 80−46637
S255, molecular cloud, molecular line, radio continuum and IR data 78−8087
SA 133 field near galactic centre, interstellar reddening from three-colour photometry *(German)* 80−36618
HM Sagittae, interstellar polarisation meas. rel. to colour excess and distance *(Russian)* 80−36649
AV Sagittarii, Cepheid, interstellar reddening rel. to assoc. with open cluster (NGC 6546) 79−58387
Sagittarius A, aperture synthesis obs. of H I absorpt. 77−26037
Sagittarius A, radio emission scattering from compact object 78−54049
Sagittarius B2, mol. cloud, detect. of HC_5N (cyanodiacetylene) and HC_7N (cyanohexatriyne), SHF obs. 80−101627
Sagittarius B2 molecular cloud, chemical fractionation of ^{13}C isotopes of cyanoacetylene 77−29900
scattering from a cylindrical dust cloud in an isotropic radiation field 79−30107
scattering props. of interstellar grains, in reflection nebulae 79−53867
scintillation method for quasar and galaxy superfine radiostructure *(Russian)* 80−77297
scintillation of low-freq. variable radio sources, evidence for relativistic expansion 79−9018
scintillation of pulsar radio emission, decorrelation bandwidth rel. to dispersion measure 80−85964
scintillation of pulsar radio emission, scale height determ. 80−85965

interstellar matter continued
scintillation of pulsar signals, analytic soln. of second-order moment eqn. 80−26726
scintillation of radio sources, compact source discovery in supernova remnant (G78.1+1.8) 79−101213
ζ^1 Scorpii, extreme B-type supergiant, UV spectroscopy and interstellar extinction 80−22004
V818 Scorpii (Scorpius X-1), colour excess from UV, visible, IR and X-ray obs. 80−82541
Scorpius X−1, interstellar extinction and UV flux distrib. 79−25754
Scutum Cloud direction, interstellar reddening distrib. from stellar RGU photometry 79−35242
sedimentation of grains in interstellar clouds 78−93349
self-gravitating gas masses containing axisymmetric mag. fields, equilib. structs. 80−94708
self-gravitating gas-particle suspension, magneto-gravitational instability, with conduction 79−29989
Seyfert and radio-galaxy nuclei, optical spectra of ionis. gas region, model 78−93420
Seyfert galaxies; suprathermal protons interaction with neutral gas rel. to broad H lines emission *(Russian)* 78−57642
Seyfert galaxies, exploratory obs. of gas near nuclei 79−48906
Sharpless 159 and NGC 7538, H II region/mol. cloud complex, H I aperture synthesis obs. 80−90510
Sharpless 254, 255 and 257, triple emission nebula in Orion, extinction meas. 77−13430
shock heated gas in supernova remnants, X-ray emission, ionisation effect 80−82475
shock wave models 79−58389
shock waves, CH^+ prod. in diffuse clouds 80−56898
shock waves, cosmic ray particles accel. 78−49241
shock waves, mol. diagnostics 80−56899
shock waves, post-collisional propag. and amplification *(Russian)* 79−44360
shock waves, vel. determ. from high vel. H I absorpt. features 79−48891
shock waves structure, first stages 79−88714
shock-compressed layers, role in star form. 78−40919
shocked dense molecular clouds, nonequilib. chemistry 79−21377
shocks, analytical results for post-shock gas temp., density, vel. and comp. 80−56911
shockwaves and their radiations: problems and prospects 79−48899
silicate absorption feature at 9.7 microns in Sharpless 106 IR sources spectra 80−105305
silicate grain condensation, laboratory expt. 78−54015
silicates, emission and extinction in 4-14 μ range 79−44581
silicates, optical props. in far UV 78−53875
SMC, lack of absorption of 1 keV diffuse X-rays 79−35381
SMC, ratio between total and selective interstellar absorpt. *(German)* 80−67851
SN 1181 (3C 58), remnant interstellar extinction and supernova absolute magnitude and type classification 80−56862
solar accretion, props. of surface contaminated dirty solar models 79−44436
solar neighbourhood, galaxy counts/H I column densities relation rel. to local interstellar cloud 80−26953
solar neighbourhood, interstellar gas temp. and vel. determ. from interplanetary H I Lα emission profiles 80−105141
solar neighbourhood, interstellar reddening, distrib. 80−62239
solar neighbourhood, UV interstellar lines in α Virginis line of sight 79−35323
solar neighbourhood electron density determ. from pulsar distance estimates by trigonometric parallax 79−88694
solar resonance radiation, multiple scatt. in nearby interstellar medium 80−41874
solar system collisions with interstellar clouds, obs. explanation *(French)* 77−74036
solar system formation, supernova trigger for collapse of interstellar cloud 77−37512
solar wind cavity deformation by interstellar medium, effect on cosmic ray diffusion 79−53680
solar wind interaction region struct., rel. to H atoms penetrating solar wind 80−41686
solar wind interaction with interstellar matter in heliosphere *(Polish)* 78−61696
south polar cap, radio sources optical identifications rel. to interstellar obscuration 79−75284
Southern Coalsack, CO emission obs. 77−29902
southern dark clouds, survey for Herbig-Haro objects and Hα emission stars 78−28536
southern dark dust clouds, catalogue 77−56844
southern dark dust clouds, catalogue and formaldehyde obs. 77−13434
Southern Milky Way, extinction curves and R values from stellar photometry 77−13443
southern sky, obs. in 2-20 MHz range 77−45563
spectral lines, form. and widths rel. to vel. fields 79−12398
spectrum near X-ray source Vela X-1 (=HD 77581), effect of X-rays 80−94892
spherical clouds in hot gas, radiation effects on evaporation 77−78842
spherical galaxies, gravit. stability of rotating embedded gas discs *(Russian)* 78−61915
spherically symmetric accretion with self-gravitation, criteria for enhanced accretion 79−71098
spherically symmetric radially moving clouds, spectral line shapes 78−20865
in spheroidal galaxies, equilib. forms of interstellar medium *(Russian)* 77−91616
spiral galaxies, gas fraction rel. to morphological type in stochastic star form. model 80−12818
in spiral galaxies, hydrodynamic flows in regions of Lindblad resons. 78−96527
in spiral galaxies, internal absorpt. rel. to intrinsic flattening 80−36701
spiral galaxies, light absorpt. by interstellar dust 79−35393
spiral galaxies, normal, post-explosion gas depletion in central regions 80−62272
spiral galaxy gas disc, non-linear corrugation waves theory 80−67859
spiral structure and dust lane gravitational collapse 79−92849
near SS 433, faint, highly-contorted nebular filament discovery 80−94855
stability of magnetic interstellar clouds 79−48885
star dust, interstellar and circumstellar 77−41404
interstellar matter continued
star formation, IAU Symposium 75 (Geneva, 1976 September 6-10) 78−32561
star formation, influence of initial vel. fields in interstellar medium 80−21985
star formation, rel. to density waves accretion-induced overstability in self-gravitating galactic disc 78−73752
star formation and interstellar gas density in Galaxy 78−86008
star formation and interstellar matter *(German)* 79−84787
star formation regions, rel. to galactic spiral struct. in vicinity of Sun *(Russian)* 80−62290
star formation regions structure, population categories and mol. clouds evolution 80−17645
star formation through accretion shock, model for H II blisters 80−21994
starlight polarization, intrinsic and interstellar components separation 79−30079
stellar debris clouds, in quasars and related objects 78−32597
stellar kinematics and interstellar turbulence 79−35313
stellar mass loss material, fate in galactic nuclei 80−67858
stellar photometry, reddening effects in Walraven VBLUW system 77−17377
stellar protocluster, effect of residual gas loss on system dynamic evolution 80−51815
stellar winds, turbulent mixing with interstellar gas 80−67701
structure, pictorial analysis of radio signals 78−54026
submillimetric lines, possible detect. via laser heterodyne techniques 79−44377
super-rings, form. by neutral clouds collisions with galactic disc 80−98717
supergiant stars intrinsic colours rel. to interstellar reddening material distrib. 79−8908
supernova blast waves and the interstellar medium *(Italian)* 79−53845
supernova ejecta, chemical condensation sequences 79−58365
supernova radio pulses, interstellar scatt. and dispersion rel. to instrumental sensitivity improvements 78−40975
supernova remnant W44, expansion into surrounding interstellar medium, dense cloud encounter 77−22298
supernova remnants, evolution of line intensity ratios in Galaxy and LMC 77−17656
supernova remnants, formation probability from neutron stars form. rate 78−49471
supernova remnants, H abundance rel. to H deficiency in Type I supernovae 78−53969
supernova remnants, optical emission from shock waves 77−64816
suprathermal grain production by radiation pressure 79−58391
T Tauri stars, props. of assoc. ionized regions 80−36624
Taurus Cloud, flare stars, comparison with ρ Ophiuchi flare stars, visible obs. *(Chinese)* 80−85957
Taurus dark cloud, gas temps. and motion 77−78851
Taurus dark cloud complex, IR study 79−8963
Taurus Molecular Cloud 2 (TMC-2), HC_5N and NH_3 obs. 80−26957
thermal emission spectrum from small interstellar grains with temp. fluctuation 78−69864
thermal sputtering in high-velocity shocks, heavy element depletion model 77−17662
thioformaldehyde (H_2CS), 3 GHz absorpt. transition obs. 80−67837
thioformyl ion, theoretical study 78−37553
tholins, complex organic solids prod. from cosmically abundant mols., rel. to interstellar grains and gas 79−25695
three component model regulated by supernova explosions in inhomogeneous substrate 78−16486
Trumpler 15 in η Carina, open cluster, age and reddening from UBVRI obs. 80−90487
Trumpler 27, young open cluster with supergiants, visual extinction 77−78836
turbulence, rel. to pulsars, modified Rickett diagram 77−17609
turbulence in interstellar gas, effects on grain collisions 80−77470
turbulent interstellar clouds collapse, three-dimensional numerical models 80−56910
turbulent plasma, maser effect in H I 21 cm line *(Russian)* 79−88727
two-phase model, intercloud wind theory 78−85991
two-phase model, rel. to obs. towards unreddened stars 77−74110
ultracold molecular gas toward galactic centre 80−51826
α Ursae Minoris (Polaris), interstellar reddening from field stars uvbyβ photometry 79−58356
α Ursae Minoris (Polaris) region, excited H decametric radio lines obs. *(Russian)* 80−12822
α Ursae Minoris B (Polaris B), spectral type and interstellar reddening 78−8005
UV absorpt. at 2175 Å, correl. with interstellar features 77−45401
UV absorption lines assoc. with Vela SNR 77−33604
UV absorption lines in HR 1099 direction, Copernicus obs. 78−93358
UV and optical spectral obs. towards λ Andromedae, absorpt. lines 79−30087
UV extinction, satellite obs. 79−67083
UV extinction obs. in galactic plane from TD1 satellite 78−93382
UV obs. by Voyager in 500-1700 Å range 79−53878
UV observations of interstellar lines towards 15(=S) Monocerotis 80−90494
UV radiation field, obs. from S2/68 sky-survey telescope 80−77523
UV radiation field from ionization equilib. of C, S, Fe and Ca 77−87508
UV radiation field in interstellar clouds, attenuation theory *(Russian)* 80−73026
UV spectrum, comparison with spectra of organic compounds 78−61913
velocities, evidence for discrete states 77−22307
velocity distrib. of interstellar gas, UV absorption line obs. 78−89235
vinyl cyanide, microwave spectra data tables 79−59445
volatile dust effects in H II regions *(Italian)* 79−21394
Vulpecula OB2, interstellar reddening rel. to membership of 67 day Cepheid S Vulpeculae 80−41831
NQ Vulpeculae (Nova 1976), interstellar absorpt. and polarisation rel. to distance 78−89205
W33, OH radio emission sources obs. *(Russian)* 80−62247
W3(OH), OH maser struct. from VLBI synthesis obs. 80−105368
W3 molecular cloud complex, model from mol. obs. 80−94843
W3-W4-W5 complex, CO emission mapping 79−17059
W40 and W48, near IR and CO mm wavelength obs. 78−65667
W44, supernova remnant, associated molecular cloud obs. 78−8079
W49 A, H_2O masers and H II regions obs. at 23 GHz 79−71136

interstellar matter continued
W49 H_2O vapour maser source, correlated variability 79−35352
W49B, supernova remnant, interstellar radio absorpt. 77−13431
W50, interstellar reddening rel. to distance and assoc. with (SS 433) 79−92783
W50, supernova remnant, optical spectrum rel. to interstellar reddening 80−51851
W50 SNR, interstellar medium interaction with SS 433 relativistic jets visible obs. 80−101629
W51, W49, airborne for IR spectroscopic obs. rel. to dust cloud model 80−36684
W51 H_2O source obs. with Crimea-Haystack interferometer *(Russian)* 78−69865
W58, galactic star-forming region, CO obs. 80−67810
Wat 6, open cluster, non-uniform interstellar reddening 79−88712
water ice mantles on grains, max. interstellar polarisation wavelength 79−5882
wave-wave interactions in rotating gravitating gas cloud, theory 80−105154
weak MHD turbulence, inertial range 77−45528
weak optical lines in stellar spectra 77−74124
white dwarfs rejuvenation due to interstellar accretion 77−17550
wind, effect on interplanetary environment 79−5721
X-ray burst propag. through interstellar dust, small-angle scatt. effects 78−57433
X-ray photoabsorpt. cross-sections for dense clouds and intercloud regions 78−12327
XUV emission, review of obs. *(German)* 80−109372
young stars, circumstellar mols. 80−22013
^{26}Al, galactic source of γ-ray line emission from beta-decay 77−33692
Ar, interstellar depletion rel. to grain temps. in diffuse clouds 80−51848
B, interstellar, detect. in front of κ Orionis 80−51841
B, V, Cr, Co, abundances and depletion models 80−46630
^7Be, cosmic ray accel. probe 78−81512
C, amorphous grains, extinction coeffs., 0.21-340 μm, lab. meas. 80−73020
C atom fine struct. excitation by H impact 77−42384
C chain molecules in interstellar clouds, form. schemes 80−26935
C depletion, from Cygnus Loop UV spectrum obs. 79−21398
C depletion, rel. to 2175 Å feature strength and origin 80−17638
C, ground state fine struct., laser mag. reson. obs., appl. to astronomy 80−87062
C I, abundances, UV grain albedos and pressures in interstellar medium 79−92818
C I, interstellar lines obs. in ζ Puppis and ζ Ophiuchi 79−35332
C II region, narrow radio recomb. lines prod. around X-ray source 79−8972
C IV column density towards early-type stars 80−73018
C in molecular clouds, 492 GHz line detection 80−90508
C isotope fractionation in interstellar molecules 77−87533
C isotope ratio 79−57656
C rich dust cloud in front of Wolf-Rayet star HD 193793, photometric evidence 80−26861
$C^+ + H_2$, C^+ fine-struct. excitation, interstellar cloud cooling 78−25675
C_2 absorption bands in stellar spectra, 876 nm obs. 80−12805
C_2, detect. in interstellar spectrum of Cygnus OB2 No.12 (VI Cygni No.12) 78−12332
C_2 detect. towards ζ Ophiuchi 78−49505
C_2 molecules towards ζ Persei 80−12799
C_2, rot. fine-struct. lines obs. towards ζ Persei 80−67811
C_2, search in IR spectrum of ζ Ophiuchi 77−45423
CH, CH^+, chem. processes rel. to abundances, book contrib. 77−33625
CH, detect. in NGC 4945, NGC 5128 and LMC 80−46673
CH, excitation temps. and abundance rel. to H_2CO 79−48883
CH, ground state inversion, collisional excitation 78−28503
CH in diffuse intersellar medium, optical and radio obs. 78−93356
CH, obs. of 3.3 GHz ground state transitions 78−77592
CH, radio emission obs. towards W49 region 77−87511
CH, radio emission obs. towards various galactic objects 77−87512
CH, radio obs. 78−28751
CH_2, rot. levels struct. excitation mechanisms 78−21908
CH^+ 3957 A line towards ζ Ophiuchi rel. to $^{12}C/^{13}C$ ratio 77−87529
CH^+ abundance, implications of predissociated levels obs. 80−37838
CH^+, CD^+, $A^1\Pi$-$X^1\Sigma^+$ band system, spectroscopic consts. and radiative lifetimes 78−5237
CH^+, electron impact excitation, rot. transitions 79−41244
CH^+, expt. oscillator strength 77−34693
CH^+ formation, problems 79−75266
CH^+ formation in hot gas behind interstellar shock fronts 78−61910
CH^+ ion dissociative recombination 77−53671
CH^+, photodissociation to C^+ and H, wavelength depend. and photofragment kinetic energies, visible obs. 80−58275
CH^+ upper limit towards τ Scorpii 78−4309
CH^+ $X\ ^1\Sigma^+$, dissoc. recomb. rate coeff., rel. to interstellar mol. form. 78−56884
CH_2^+, radiative association, rate const. 77−45512
CH_3^+ ion, radiative assoc. reactions in interstellar clouds 78−41021
CH_3^+ +small molecules, binary and ternary reactions at thermal energies, rate coeffs., product distribs. 78−44358
CH_n^+ +COS(H_2S)(formamide)(methanol)(methylamine), (n=Q-4), reactions at 300K 78−44357
C_4H (butadiynyl) radical, detect. towards (IRC+10216) 78−93374
CN towards interstellar clouds, EHF emission obs. 79−17037
CN^+ ions, radio search 78−24534
C_3N, Hartree-Fock calcs. rel. to poss. detect. in IRC+10216 77−26041
C_3N, tentative detect. in IRC +10216 77−29913
CNO depletion, interpretation of Copernicus data 77−87534
CNO isotope abundances in interstellar clouds 77−87527
CNO isotope importance in astrophysics 77−87263
CNO isotopes as probes of chem. evolution of Galaxy and spiral galaxies 77−91636
CNO isotopes in astrophysics, conf. Grenoble, France, 1976, Aug. 77−87262
CNO isotopes in interstellar clouds, interpretation of obs. 78−4356
CO and H comparative distrib. in Galaxy 78−16537
CO, band emission detect. in Becklin-Neugebauer object 79−101184
CO clouds, blister model for assoc. H II regions 79−25681
CO, column density towards 9 Cephei (B2 Ib) 80−94795
CO, detailed struct. in NGC 6334 mol. cloud complex 78−4324
CO, detect. in direction of supernova remnant (S147) 80−67836
CO, distrib. around (l=30°, b=0°) 80−41868

interstellar matter continued
CO distrib. in central region of Galaxy 79−21416
CO, distrib. in Galaxy rel. to spiral pattern speed 78−54036
CO distribution in galactic equatorial plane, 115 GHz obs. 78−36689
CO emission and visual extinction in dark cloud L134 77−13425
CO emission from late-type galaxies 78−89250
CO emission in external galaxies, upper limits 78−36693
CO emission obs. from molecular clouds 77−33612
CO emission obs. from supernova remnants 78−8071
CO, emission obs. in galactic H I self-absorpt. features 79−35350
CO formation in contracting clouds, thermal instabilities 78−81675
CO, in M31, partial radial distrib. meas. 78−8117
CO in molecular cloud complexes, structure of W75-DR 21 region 78−89232
CO, in molecular clouds, obs. rel. to Galaxy rot. curve to R=16 kiloparsecs 79−97081
CO in nearby galaxies, survey 80−62276
CO in the inner Galaxy 78−8072
CO, isotope fractionation in Lynds 134 dust cloud 80−26924
CO, isotopic abundance in interstellar clouds 77−29912
CO, isotopic fractionation in dark clouds 80−46638
CO, J=2 to 1 line obs. in NGC 2024 (Orion B) nebula 80−8673
CO kinematics within 1° of galactic centre 77−33597
CO line radiation transfer in collapsing dark cloud, Monte Carlo method appl. 79−44357
CO, obs. along ionisation front of NGC 1499 (California Nebula) 78−24537
CO obs. at 115 GHz in southern H II regions 77−87506
CO, obs. in Perseus OB2 dark cloud and W44 mol. cloud 77−64836
CO, obs. in young cluster (IC 5146) 79−48881
CO obs. of molecular cloud assoc. with NGC 7023 at 2.7 mm wavelength 78−41008
CO obs. of southern H II regions, RCW 38, RCW 122 and G316.8−0.1, star form. regions 79−35353
CO, out-of-plane survey at 115 GHz 78−12334
CO, population inversion mechanism for rot. levels 79−21406
CO, radio emission rel. to cold mol. clouds in inner Milky Way 80−4425
CO, reson. transitions, radiative lifetimes, lab. meas. 78−62767
CO, time-dependent form. and chem. fractionation 78−57602
CO^+ ions, radio search at 118 GHz 78−24534
CO/H_2 ratio in dark clouds, meas. 78−96513
CO_2 in dark clouds, abundance 79−35322
$(CO)_2$, RF lab. meas. and interstellar search 80−43035
CS J=1-0 transition at 49 GHz in southern molecular clouds 78−65674
CS, numerical solns. to radiative transfer and statistical equilib. eqns. 78−12319
CS, population inversion mechanism for rot. levels 79−21406
CS, turbulent cores in giant molecular clouds 80−51822
$CSiH_3$ matrix Hartree-Fock calcs. 79−5874
$^{12}C/^{13}C$ ratio, rel. to ^{13}C enriched matter ejection from red giants 77−9788
$^{12}C/^{13}C$ ratios from radioastronomical obs. 77−87530
$^{12}C^{16}O$ emission, unsuccessful search at 2.6 mm wavelength of globular clusters 78−41000
$^{12}CH^+/^{13}CH^+$ abundance ratio, meas. 80−67809
^{12}CO emission intensity rel. to H I absorption column density, EHF meas. 79−35319
^{13}CH, predicted Λ-doubling spectrum 77−30857
Ca II, interstellar lines obs. towards 47 stars 79−25676
Ca II, unique interstellar K-line profile in 30 Doradus direction 80−51850
Ca II K-line in α Cygni, core asymmetry 80−85981
Cl abundance towards 10 stars, Copernicus obs. 78−36646
Cl, depletion on oxide grains 80−17635
Co emission in Markarian and Seyfert galaxies, unsuccessful search 80−26975
D absorption line at 327 MHz, search towards galactic centre 78−77599
D abundance in Galaxy rel. to cosmology 78−69883
D enrichment in HCN and HNC 78−16500
D, galactic distrib., radial gradient, from $DCN/H^{13}CN$ and $DCO^+/HC^{18}O^+$ ratios 79−40232
D I absorption in direction of HR 1099 (V711 Tauri) 80−8658
D/H ratio in lines of sight to ζ Puppis and γ Cassiopeiae 77−37633
D/H ratio towards δ, ε and ι Orionis 79−53865
DCN in the Galaxy mm line obs. 77−33580
DCO^+ and electron density in dark clouds 78−12336
DCO^+, radio detect. in NGC 2264 L134 and DR 21(OH) 77−2460
DCO^+/HCO^+ abundance ratio in cool interstellar clouds 78−65673
DNC, detect. at 152.6 GHz in NGC 1333, 2264, Orion A and L134 dark cloud 78−4334
DNC detection, difficulties of chemical equilibrium hypothesis for D enrichment 77−82298
DNC in HNC interstellar clouds, temp. effects and D fractionation 79−44578
FCN, search in mol. clouds for J=2-1 transition 77−60808
Fe, gaseous depletion from Fe II resonance line UV obs. 79−44584
Fe, Mn and Mg, interstellar depletion derived from S 59 obs. of 67 stars 79−2563
FeH and FeH_2 formation in interstellar clouds 80−98704
GeH_4, possible microwave interstellar maser lines 78−41020
H and D, obs. towards α Canis Minoris 79−21275
H and D, solar Lyman alpha radiation pressure effects 79−92686
H and trace gases, review of galactic morphology 77−26070
H, as extraterrestrial source of atmospheric water vapour 78−69416
H, at periphery of galaxies, effects of ionising background radiation 78−65729
H atom survival in interplanetary system, near Sun trajectories and ionization 80−105145
H I, hot, interstellar, between Sun and Earth, solar Lyman α absorpt. 80−31185
H I, rel. to interplanetary neutral H 78−49272
H I 21 cm absorption towards extragalactic radiosources, catalogues of 819 sources 78−57638
H I absorption in direction of HR 1099 (V711 Tauri) 80−8658
H I absorption in galactic centre direction 80−77465
H I absorption lines high-resolution mapping in direction of NGC 2024, M17, W49 and Orion A 78−81667
H I column densities and galactic reddening determ. 79−5875
H I deficient region in Hercules, O VII emission line obs. in diffuse soft X-rays 79−25759

interstellar matter continued
H I gas, pervasiveness of intercloud medium 80−51825
H I large-scale distrib. in early type galaxies 80−8685
H I Lyman α and β obs. by Voyager UV spectrometer 78−81673
H I Lyman α profile and interstellar wind dynamics 80−8610
H I Lyman α profile in interplanetary space 80−8586
H I Lyman-α 1216 Å flux rel. to physics of interstellar medium 77−2459
H I radio recombination lines obs. in direction of pulsars 77−74155
H I supershell form. at OB assoc. interaction with interstellar medium 80−82468
H I survey from Lyman α absorption meas. towards 100 stars 78−93357
H I temperature distribution at high galactic latits. 77−22293
H II regions, gas dynamics axisymmetric calcs. rel. to interstellar medium kinetic energy input 80−12791
H I+molecular/H II shells from 1 to 2000 pc dia., wind-driven or supernova remnants 79−25678
H in solar system, temp. meas., Prognoz-5 obs. 78−7922
H-C, thermal desorption, one-phonon at. scatt., 3-dimens., continuum model 78−87860
H+CO, total different collision cross section meas., interstellar gas clouds appl. 79−45786
H_2 abundances and enhanced metal depletions 77−91605
H_2 clouds, instabilities 80−17629
H_2 clouds, ionisation by supernovae 78−69856
H_2 collisional excitation 78−77586
H_2, column densities, Copernicus UV obs. 78−8070
H_2 cooling, dissociation and IR emission in shocked clouds 78−41009
H_2 densities from CO obs. 79−25687
H_2, departure from translational equilib. 78−8081
H_2 dissociation fronts 79−5881
H_2, efficiency of ionisation, dissociation and heating by cosmic rays 78−28454
H_2 emission at 2 microns from Orion Nebula 78−93351
H_2 emission from Orion Nebula, interstellar extinction meas. 79−25668
H_2, emission line obs. from vicinity of T Tauri 78−93230
H_2, form., catalytic prod. on transition metal grains 78−57616
H_2, form. by catalysis process 78−54005
H_2, form. on amorphous ice grains and importance for planetary atmospheres 80−26933
H_2, form. on interstellar grain surfaces 79−21367
H_2 formation, reaction rates and chemical kinetics 79−17070
H_2 formation and excitation 78−16514
H_2 IR line emission, shock model appl. to Orion Nebula 78−8086
H_2, in intercloud medium 77−71136
H_2 line emission from OH maser regions 80−12800
H_2, ortho/para abundance ratio 79−40252
H_2 ortho-para ratio in dense clouds, protoplanets and planetary atmospheres 78−89233
H_2, recombination on interstellar grains, translational and rot. energy 79−17045
H_2, reson. fluoresc. with Lyman α 79−8821
H_2, rot. transitions rel. to interstellar hot gases cooling 79−12505
H_2, search for 2.1 μ emission in southern hemisphere IR sources 80−22059
H_2 vibrational excitation in intense UV fluxes 78−36647
H_2, vibrationally excited, search for 8150 Å emission line 78−93346
H_2, vibrationally excited in Orion 78−8076
H_2^+, role in star form. from hot matter with primordial chemical comp. *(Russian)* 78−40924
H_n^- (n=5 to 13), ion-induced dipole clusters, binding energies and geometries 79−41261
H_n^+ clusters with odd and even mass number 79−92840
HCN, absorpt. lines obs. towards Cassiopeia A 80−101624
HCN and HNC, mm wave emission obs. of interstellar clouds 80−90503
HCN confirmed in galaxies M82 and NGC 253, 89 GHz obs. 79−44582
HCN dimer, interstellar abundance, upper limit 78−54004
HCN emission detect. in Sagittarius A mol. cloud 78−73750
HCN, HNC formation, role of H_2CN^+ isomers 78−81672
HCN, isotopic abundance vars. meas. 77−53657
HCN, J=1-0 transition obs. in southern mol. clouds 79−8983
HCN, J=4→3, 354 GHz transition in Orion Molecular Cloud 80−101636
HCN^+ ions, radio search 78−24534
$H^{13}CN$ in the Galaxy mm line obs. 77−33580
HC_5N, HC_7N, obs. in dark dust clouds 78−54023
HC_9N, detect. in interstellar space 78−93370
HCO^+ detected toward M82 galaxy, 89 GHz obs. 79−44582
HCO^+ isotopes, anomalous line intensities towards dark clouds 79−17054
HCS^+ formation 79−17038
HD colling function in primary gas condensation and star birth *(Russian)* 77−33623
HD, IR emissivity *(Russian)* 78−36676
HD molecules, rate coeff. for $H^+ + D \rightarrow H + D^+$ near threshold 78−89239
HD, rotationally excited, towards ζ Ophiuchi, column density 79−25674
H_2D^+, interstellar and circumstellar search, upper limit determ. 79−2562
HNC, millimetre spectrum, rot. consts., force consts., U90.7 interstellar line, struct. parameters 77−57989
HNC, quadrupole coupling constant determ. 78−1101
HNC^+ ions, radio search 78−24534
$HN^{13}C$ and HNC, hyperfine structure in dark interstellar clouds 79−101182
$H^{15}NC$, J=1→0 emission obs. in DR21(OH) 77−82299
HNO, chem. reactions, form. and destruction rates 78−28764
HNO, radio detect. in Sagittarius B2 and NGC 2024 78−8098
HNO^+, HON^+, candidate mols. formed by NO ion-molecule reactions 78−28739
HNSi, structures and microwave freqs. calcs. 78−36648
H_2O, 183 GHz line emission obs. 80−41869
H_2O 22 GHz maser emission from W3(OH), 49N and 51, spatial distrib. 78−93355
H_2O cosmic masers, influence of dust on collisional pumping 78−54030
H_2O, gravitational wave absorpt. by mols. 80−82189
H_2O, high abundance in Orion, dynamical explanation 79−48876
H_2O maers, obs. with resolution of 0.0008 arcsec 77−74154
H_2O maser, collisional pumping in circumstellar shock wave 77−53675
interstellar matter continued
H_2O maser emission, new sources detect. emission, new sources detect. 80−62298
H_2O maser emission, VLBI obs. in W49 N 77−26038
H_2O maser emission from external galaxies, detects. 78−45417
H_2O maser emission in W49N, W51 and Sagittarius B2, high vel. features 77−9779
H_2O maser emission increase in W3(OH) 77−53672
H_2O maser line evidence for circumstellar ring systems 78−89195
H_2O maser source in Orion A, obs. of outburst *(Russian)* 80−105320
H_2O maser source near NGC 2071, discovery 78−73768
H_2O maser sources, near IR pumping 77−78862
H_2O maser sources in different stages of evolution, new VLBI maps 80−26954
H_2O maser sources in W3, accurate positions 78−4332
H_2O masers, 22 GHz galactic plane survey, 14 new sources 80−77464
H_2O masers, 22 GHz obs. with resurfaced Parkes radiotelescope 77−33347
H_2O masers, Herbig-Haro objects and interstellar bullets 79−35329
H_2O masers, high vel. structures, origin *(Russian)* 79−25697
H_2O masers, in dense interstellar mol. clouds, high sensitivity survey 78−85988
H_2O masers, in mol. clouds assoc. with small Hα emission regions 79−17042
H_2O masers assoc. with mol. clouds, VLBI aperture synthesis obs. 79−21368
H_2O masers associated with compact H II regions in Sagittarius B2 77−13486
H_2O masers in H II regions, time variability 77−82296
H_2O masers in H II regions, time vars. obs. 79−88725
H_2O masers in NGC 6334, positions and spectra rel. to star form. 80−73025
H_2O masers located near Herbig-Haro objects, discoveries 79−21369
H_2O masers survey in southern hemisphere 77−91599
H_2O, oscill. strengths of UV lines, rel. to abundance in interstellar clouds 78−90104
H_2O sources, linear polarisation of 22 GHz line emission 78−77612
H_2O sources, spectra and autocorrel. anal. 78−65713
H_2O sources in Galaxy, sites of newly formed OB stars 78−12390
H_2O vapour sources struct. and kinematics in OB star form. regions 78−61901
H_2O^+, unsuccessful search and interstellar abundance 78−69860
$H_2{}^{18}O$, detect. in Orion mol. cloud and DR 21(OH), H_2O abundance estimate 78−57621
H_2O+He, collisional excitation of interstellar molecules, rate consts. 80−67816
HSiN, structures and microwave freqs. calcs. 78−36648
$HSiO^+$, $HOSi^+$, quantum mechanical study 78−37541
H300 α recombination line obs. towards galactic centre 78−20873
He, abundance variations rel. to interstellar dust UV absorpt. cross section *(Italian)* 78−32551
He component of local interstellar medium, UV obs. 79−30100
He I, obs. with gas absorpt. cell, implications for local interstellar medium struct. 80−62234
He I local density from EUV obs. 78−4331
He, increasing galactic content rel. to chemical enrichment of disc dwarfs 79−88733
He, interaction of solar wind with Sun's gravity focused He 80−105144
He, local interstellar density correction 79−92834
HeH^+, electron impact excitation, rot. transitions 79−41244
^{3}He abundance implications for red giant evolving to planetary nebula 80−105237
^{3}He from dM stars 79−48810
$^3He^+$, probable detect. and significance 79−25689
high-velocity clouds, dynamic coronal gas flows 80−56928
K, Ar, in interstellar grains, isotopic anomalies 78−28761
K I, 4044 Å line obs. 78−24533
K I, quadratic depend. of column density on N_H 78−20872
LiH in diffuse clouds 78−93361
^{7}Li and ^{7}Be gamma ray lines from $\alpha\alpha$ reactions 77−87248
^{7}Li I and Li abundances towards ζ Persei and ε Aurigae 78−49494
Mg complex, bis-pyridal-Mg-tetrabenz-porphyrin, disagreement with diffuse interstellar bands 80−56905
Mg I 2852A line obs. towards moderately reddened stars 78−20874
Mg I interstellar line structure, balloon UV obs. of ζ Orionis spectrum 79−35251
Mg II column density towards nearby stars 78−41023
Mg II density along line of sight to nearby stars 78−45391
Mg, interstellar lines obs. in stellar spectra rel. to existence of circumstellar clouds 80−94782
Mg ionization zones around stars 77−45517
MgH, X→A and X→B′ band systems, oscill. strengths and photodissoc. cross-sections 79−94045
MgO and CaO grains, rel. to origin of diffuse interstellar absorpt. bands 77−9785
N bearing molecules, gas phase reactions 78−28754
N I interstellar absorption in γ Cassiopeiae direction, UV obs. 80−51823
N IV+H charge exchange cross section rel. to intercloud gas 77−45514
N, overabundance in nucleus of NGC 6946 spiral galaxy *(French)* 78−89257
N V, hot interstellar gas diagnostic, IUE obs. 80−101634
N/O abundance ratio in galaxies 80−8686
$N^+ + H$, charge transfer reaction in nebulae rel. to ionization struct. 80−46384
N_2 in diffuse clouds, Copernicus search, upper limits 79−25661
NCO as possible interstellar species 79−17065
N_2D^+, dissociative recomb., interstellar mols. appl. 79−31704
N_2D^+, lab. rest frequencies 78−1102
N_2D^+, radio detect. 78−16492
NH^+, radioastronomical freq. prediction at 13625 MHz 78−24544
NH_2, lab. obs. of 16 GHz rotational transition 77−3389
NH_3, absorpt. in Sagittarius B2 direction 79−35341
NH_3 emission and absorption at 23 GHz toward radiosource W3(OH) 78−36714
NH_3 emission line in Orion, 23 GHz obs. 79−30109
NH_3 emission obs. from galactic regions 78−28780
NH_3 in galaxies 79−48886
NH_3, non-metastable absorption at 23.1 GHz, first obs. towards W3 (OH) 78−65677
NH_3, nonmetastable levels obs. 79−25665

interstellar matter continued
NH_3, obs. in DR 21, NGC 1333 and NGC 6334 N 79−17044
NH_3, obs. in mol. cloud near (S106) 79−84840
NH_3, obs. in Orion Molecular Cloud 80−36687
NH_3, obs. in southern H II regions 78−69863
NH_3 survey of dark clouds 78−49507
N_2H^+, dissociative recomb., interstellar mols. appl. 79−31704
N_2H^+, HCO^+, HCN and CN, relative distribs. 77−33587
NH_2D, detect. in Klefnmann-Low Nebula 78−20881
NH_2D, microwave detect. in Sagittarius B2 78−20880
NO, microwave detection in Sagittarius B2 direction 78−93378
NO^+ transitions in mm and IR wavelengths 80−56906
NS molecule, radio emission theory 78−54031
^{14}N, search for radioemission regions 80−41886
$^{15}NH_3$, detection at 23 GHz 79−44590
Na I, interstellar lines obs. towards 47 stars 79−25676
Na I, possible detect. of 17 cm hyperfine emission in W 51 region 78−8139
Na I, quadratic depend. of column density on N_H 78−20872
Na I interstellar D-lines in WRA 977 spectrum 79−101148
Na I lines hyperfine struct. in α Cygni 78−24542
NaH in diffuse clouds 78−93361
NaH, search in diffuse clouds 78−4325
O atom fine struct. excitation by H impact 77−42384
O edge detectability and possible interp. 77−60811
O I, oscillator strengths interstellar O abundance 78−16498
O VI, rel. to three-band obs. of soft X-ray background 77−45604
O VI gas, circumstellar or interstellar origin 78−57528
O VI survey, UV spectra of OB stars 78−36679
O^- ions, ionisation and interstellar medium heating by photoelectrons 78−36666
OCS+methanol (H_2)(He), collisional rot. energy transfer, microwave-microwave double reson. obs. 77−19016
OH, 1720 MHz transition survey, comparisons with 1612, 1665 and 1667 MHz obs. 77−45586
OH 18 cm line obs. of young stellar clusters 79−25655
OH 1.6 GHz maser emission from W3(OH), 49N and 51, spatial distrib. 78−93355
OH 205.1-14.1, unusual OH maser source, 1667 MHz emission monitoring 77−64819
OH 26.5+0.6, IR spectrum, polysaccharide grain model 78−12342
OH absorbing clouds towards galactic centre, struct. determ. using regularisation method 80−17505
OH and H_2O maser lines intensity vars. due to induced Compton scatt. 78−4319
OH and H_2O masers, radial vel. struct. 77−33617
OH and H_2O masers, scintillation, solar wind vel. meas. *(Russian)* 78−69704
OH and H_2O masers assoc. with compact H II regions, model 78−81666
OH and H_2O searches in diffuse clouds, Copernicus UV obs. 79−40233
OH clouds in direction of extragalactic radiosources, survey 77−64822
OH emission sources, 13 GHz OH features obs. 77−33619
OH emission sources, low latitude search at 1612 MHz 77−49452
OH, exact hyperfine struct. and Einstein A-coefficients, astrophys. appl. 77−83762
OH, excitation in molecular clouds 78−65669
OH excitation towards dust clouds 78−4318
OH, inverted populations of Λ doublets 80−32694
OH, J=9/2 Λ-doublet line detect. in W3(OH) 78−65670
OH large-scale sky survey at 1612 MHz 78−32358
OH, Λ-doublet transitions induced by ion collisions 78−9222
OH main line maser in interstellar cloud, pumping mechanism 80−67824
OH maser, OH removal by magnetic heating 79−98328
OH maser, temporal var. 78−53817
OH maser clouds, saturation effects 77−91657
OH maser emission from W3 (OH), Zeeman effect 78−93377
OH maser sources, accurate position meas. 80−46646
OH maser sources, radiative transport effects on inversion 80−17681
OH maser sources, search at 1612 MHz, large-scale survey 79−58395
OH masers, 18 cm lines pumping by H+OH collisions 79−48892
OH masers, class I, IR obs. of nearby compact H II regions 77−45525
OH masers, ground state Λ doublet emission as result of overlapping far IR transitions 77−45533
OH masers assoc. with IR stars, very long baseline interferometric obs. 77−53699
OH masers in direction of H_2O masers, new discoveries 78−12393
OH molecules, detection of monopoles by nonlinear effects in interstellar masers 77−91609
OH, new main line maser obs. with probable Zeeman pattern 80−56908
OH, nonthermal main lines in interstellar dust clouds and OH abundance 80−36683
OH, radical, microwave spectra, search possibilities 79−26972
OH radicals, microwave spectra data tables 78−50542
OH, radio lines absorpt. obs. in galactic radio sources 78−54068
OH, radio obs. towards ζ Ophiuchi and evidence for interstellar shock 79−97052
OH, rot. excitation by H_2 at interstellar temps. rel. to maser emission 80−62232
OH rotational excitation by collisions with H or H_2 78−4306
OH, search for 18 cm absorpt. lines in high latit. H I clouds 80−67841
OH, search for emission in bipolar nebulae 78−41016
OH weak masers detect. in H_2O masers direction 77−33618
OH^{2+} in interstellar clouds 80−67828
$OH(^2\Pi)+H$, rel. to interstellar OH maser action 79−101186
$^{17}O/^{18}O$ abundances in interstellar clouds 77−87528
P abundance towards 10 stars, Copernicus obs. 78−36646
S chemistry 80−101632
S, depletion on oxide grains 80−17635
S II in ζ Ophiuchi interstellar spectrum, abundance upper limit 80−82445
SO, 36 GHz emission line detect. in Orion nebula, rel. to mag. fields 80−46642
SO, millimetre wave emission obs. 78−24535
SO_2 in Orion Molecular Cloud-1 (OMC-1), rot. temp. 79−25670
$^{32}S_2$, in interstellar molecular clouds, upper limits on abundance 78−28738
Si, chemistry in interstellar clouds 77−45507
Si III, high vel., shock model 78−8075
Si IV column density towards early-type stars 80−73018
interstellar matter continued
$Si^{2+}+H$, charge transfer reactions 77−9789
SiCH, matrix Hartree-Fock calcs. 79−5874
SiH, optically derived lambda splitting 77−17657
SiH, SiH^+, line positions and oscill. strengths of rot.-vibr. bands, interstellar medium appl. 78−58644
SiH, SiH^+, rot. transition freqs. calc., rel. to search in interstellar space 78−93100
SiH_4, possible microwave interstellar maser lines 78−41020
SiO, 8 μm band obs. in circumstellar cloud around VY Canis Majoris 79−62840
SiO circumstellar maser 78−16511
SiO maser line evidence for circumstellar ring systems 78−89195
SiO, nonmaser emission lines from expanding envelopes around evolved stars 78−28650
SiO particles and 9.6 μ interstellar extinction feature 78−45378
SiO, population inversion mechanism for rot. levels 79−21406
SiO, rot. and vibr. consts., millimetre-wave spectrum 77−34619
^{30}SiO detect. in Orion Nebula and Sagittarius B2 78−8097
Ti II 3384 Å line obs. towards ζ Persei, interstellar Ti vel. distrib. 79−53877
Ti, obs. of interstellar Ti II 3384 Å line 78−57611
TiO^+, TiO, prod. by associative ionisation 77−29893

interstitials
see also Cottrell atmospheres; crowdions; Snoek effect
β-Al_2O_3-Na_2O, mechanism of diffusion 80−2202
alkali fluorides, ESR study of interstitial atomic H centres 79−56609
alkali halide, crystal, irradiation-induced defects 80−107316
alkali halide crystals, defect fermion properties, ionic cond. calcs. 80−59457
alkali halides, influence of purity of crystals on stability of F-centres and interstitials 78−91336
alkali halides, interstitial motion during radiation damage and sputtering processes 80−54230
alkali metal:H(0), impurity investigation using residual resist. and optical absorpt. meas. 79−95816
alkali metal halides, irradiated, annealing 78−92494
alkaline earth fluoride, doped with trivalent rare earths, migration entropy for bound fluorine motion 80−71303
alkaline earth fluoride based solid solns., ion transport 80−107545
alkaline earth fluoride crysts., ion transport, defect energies calc. 77−55382
alloy, BCC, ordered, implanted atom redistrib. at octahedral and tetrahedral interstitial sites *(Russian)* 78−34533
alloy, Cu_3Au-type struct., redistribution of interstitial atoms after temp. change *(Russian)* 77−62523
alloy, dil., interstitial solute in multicomponent substitutional solvent, quasi-chemical approach to thermodynamics 77−28784
alloy, FCC, CuAu type, interstitial atom redistribution in octahedral and tetrahedral interstices *(Russian)* 77−55280
alloy, FCC, impurity atom position determ. from ion-excited characteristic X-ray emission *(Russian)* 78−47408
alloy, free energy calc. for any conc. of implanted atoms, diffusion current in chem. pot. gradient *(Russian)* 78−34657
alloy, HCP, low temp. interstitial struct., statistical-thermodynamic theory *(Russian)* 79−51100
alloy, thermodynamic and structural changes in deform. twinning 78−2139
alloys, conc., radiation induced, segregation of preferential defect migration, theory 79−77633
alloys, distrib. and kinetics of redistrib. of interstitial atoms in interstices *(Russian)* 77−43207
alloys, effects of temp. an order-depend. elec. resist. 77−31992
alloys, FCC, anisotropic ordering of interstitial impurities *(Russian)* 77−76389
alloys, interstitial atomic arrangement and mobility at high degrees of interstice filling *(Russian)* 80−107223
alloys, interstitial solid solns., HCP ordering type transitions within thermodynamics theory framework 80−49162
alloys, irradiated, segregation, inverse Kirkendall effect, effect of constitution on void swelling 78−91472
alloys, liquid dilute binary, interstitial index, definition and variation with temp. *(French)* 80−2011
alloys, storage of H_2, review 79−10956
atomistic computer experiments of point and extended defects 78−30610
BCC crystal lattice containing interstitial atom in split config., reson. and localised vibrs. *(Russian)* 80−84268
BCC lattice, low temp. interstitial hardening 79−20060
binary alloys, BCC lattice, ordered structs. of interstitial solutes 79−82196
borides, B_{12}, cryst. chem. classification, book contrib. 78−47302
α-brass, electron irradiated, defect production and interdiffusion 78−67739
α-brass, electron irradiated, vacancy migration props., effect on enhanced atomic mobility 79−46829
chemical potentials of structural elements of compounds and face or dislocation specificity, thermodynamic parameters 80−96514
cluster nucleation, effect of trapping at onset of irradiation 79−78974
cluster nucleation at onset of irrad. 78−79635
continuum model for diffusion in region with multiple diffusivity 79−77801
creep, irrad. induced in transient irrad. environments 80−92598
creep, swelling and growth, radiation induced, bias factors estimated from self-consistent model 80−88249
creep and growth, irradiation induced, solute effects on defect precip. rate 80−88252
creep and growth, radiation induced, fundamental mechanisms 80−92596
crowdion elastic interaction with extended at. defects in isotropic media 77−76454
crystal with interstitials, lattice dynamics 80−2128
cyclic creep, enhnaced, high temp. theory for polycrystalline materials 78−7018
defect clusters, nucleation and growth due to energetic particle radiation, chemical rate reaction theory, computer program 80−49263
defect diffusion coeffs., site blocking, correlated defect motion 80−84315
diamond, Fresnel diffraction platelets, defect struct. anal. by 3 Å phase-contrast microscopy 78−87701
diamond, irradiated, optical study of TR12 and 3H defects 77−85772

interstitials continued
diamond, natural, topography of impurity distrib. and neutron-induced colouring 77−39613
diamond, natural semicond., isothermal annealing of electron radiation damage 77−7764
diamond, platelets, giant, on cube planes, electron microscopy 77−84765
diamond, radiation-induced optical absorption spectrum, 0.4-2.0 MeV electrons 77−84798
diamond, structure and motion of self-interstitials 79−37700
diamond, type IIa, electron irrad., EPR obs. of interstitial-impurity complexes 78−76310
diamond, type IIa, electron irradiated, annealed to high temps., EPR spectrum 77−90034
diamond, type-II_a, electron irradiated, thermal cond. reduction at low-temps. 77−47631
diffusion, chemical, highly defective solids, steady-state computer simulation method for lattice gas 80−49401
diffusion, correl. factor estimation 78−43167
diffusion, influence of impurities 78−38879
diffusion, retardation by point defects *(Russian)* 77−59143
diffusion in crystal with random impurities, incoherent scatt. law 77−1266
diffusion in crystals, nonadiabatic quantum theory 78−79818
diffusion of light interstitial impurity, quasi-optical model *(Russian)* 77−24433
diffusion tensor for atomic migration in crystals 79−7705
dilute alloy, ternary, substitutional solute element effect on diffusivity of interstitial solute element 78−59969
dilute alloy in dissociative equilibrium, solute and solvent diffusion 77−76593
dislocation bias and point defect relaxation volumes 79−99248
dislocation loop diffusion growth in saturated soln. of point defects 77−68974
dislocation motion, lattice resist., effect of impurity interstitials 80−84170
disordered binary alloys of ferromag. crystals, mag. dipole fields at interstitial sites 80−97176
displacement spike annealing, Mont Carlo method computer expteriments 78−30672
distribution of dissimilar atoms among interstices of various types, appl. to isotopic ordering *(Russian)* 78−67706
edge dislocation interaction with interstitial atoms, influence on Peierls stress 78−34537
electron irrad. effect on electrolum., defects form. and quenching obs. 80−55194
electron micrographs, possible source of error in determ. of small lattice defect type 77−65941
electron solid, two-dimens., defects and implications for melting 80−39076
electronic structure and useful phys. props. of interstitial compounds 77−89683
EPR of thermally induced defect 77−81005
EXAFS in photoelectron yield spectra 80−16123
exotic atoms, conf., Erice, Sicily, (1979) 80−67939
externally stimulated interstitial release followed by vacancy-interstitial annihilation, kinetics 78−34535
FCC crystal, field-ion images, computer simulation of contrast of dislocation loops 77−11561
FCC crystal, interstitial and solute concentration gradients, flux expression derivation *(French)* 80−54219
FCC lattice, computer simulation of low energy displacement cascade 78−47367
FCC lattice, elastic interaction between point defects, nonlocal theory 78−38689
FCC metals, ⟨100⟩-split interstitials, internal modes reson. hybridization 79−42194
FCC metals, dynamics of multiple interstitials and interstitial impurity complexes 78−75775
FCC soln., thermodynamics based on kinetic considerations 77−62651
ferromagnetic BCC and HCP crystals, anisotropy of dipole fields, at interstitial sites 79−33584
Fick's equations solutions for impurity diffusion, dislocations, interstitials, vacancies 80−70469
field ion microscopy, developments, lattice imperfections 79−67445
fission oxide fuels, intergranular densification model due to the diffusion of pt. defects and pore destruction 79−73345
fission reactor materials, point defect nucleation and growth, rate theory model for simultaneous clustering 80−13604
fluorite structured crystals, high temp. disorder and elastic consts. 78−30689
Fokker-Planck eqn. describing evolution of interstitial loop microstruct. during irradiation 80−107215
Frenkel defects, form. and collapse, defect migration, electron irrad. effects, computer simulation 80−92523
fusion reactor metals, irradiated, defect cluster nucleation, He injection effect 80−34091
fusion reactors, inertial confinement, interstitial loop formation, point defect clustering 80−63378
glass, ionic conductivity, weak electrolyte theory 80−84322
Gorsky effect for low interstitial conc., theory 79−10896
graphite, fast neutron irrad. damage, chem. rate theory applic. effect of annealing and thermal equilib. defect concs. 77−67804
graphite, fast neutron irrad. damage theory and modifications 77−67805
graphite, interstitial C atom, INDO calc. *(French)* 80−39068
graphite, irrad., lattice expansion, vacancies and interstitials contrib., bond order role 80−65042
graphite, neutron irrad., annealing of radiation damage 79−1465
graphite, neutron-irradiated, EPR, rel. to electronic struct. *(Japanese)* 78−19326
graphite, point defects and self diffusion 78−63758
graphite, surface morphology changes after irrad. with energetic He ions 78−21767
graphite intercalation compound, LiC_6, ^7Li NMR *(French)* 78−35050
growth of point defect aggregates during irradiation, model 77−89468
halides, vacancy-interstitial pair prod. by electron-hole recomb. 79−4530
hardened irradiated metal, flow stress temp. depend., effect of interstitial atom clustering and embrittlement *(Russian)* 78−34538
hardening during creep, effect of interstitial and vacancy dislocation loops *(Russian)* 77−81271
HCP lattice, Huang diffuse scatt. from interstitials 80−88142
ideal solution, const. press. and vol. effect on nonideality 79−7698
interstitials continued
ideal solution const. press. and vol. effect on nonideality 79−7697
inert gas solid, delocalisation probability of interstitials 79−7801
intercalation compounds, physical and chemical props. 79−19209
intermetallic compounds, correl. between interstitial hole sizes and hydride thermodyn. props. 78−18798
intermetallic hydrides, interstitial site occupation by H atoms, quantitative model 80−96517
interstitial site determ., μSR technique 80−71287
ion implantation, net recoil density 80−88175
ionic compounds, hopon mechanism for ion transport 79−14957
irradiation creep due to dislocation and glide 77−69009
irradiation creep mechanisms, theoretical assessment 79−55817
irradiation enhanced diffusional mass transport 79−14844
irradiation induced creep, point defect absorption at dislocations 78−19842
irradiation produced point defects, rel. to stress induced mass transport, anal. soln. 79−60401
irradiation-induced, recombination rate with vacancies 80−96516
laser stimulation of light interstitial diffusion in semiconds. and insulators, theory 77−15630
Laves phase AB_2 intermetallic compounds, H_2 sorption, capacity and preferred location 79−43791
light interstitial diffusion, quantum theory *(Russian)* 77−15632
LMFBR materials, interstitial loop nucleation and growth during irradiation, Fokker-Planck equation, numerical soln. 80−57857
LMFBR materials, interstitial loop nucleation and growth during irradiation, Fokker-Planck equation, numerical soln. 80−68796
long-lived point defect formation from unstable vacancy-interstitial pairs 77−59008
loop finite, modelling of growth under irrad. 79−23607
low temperature depend. of elec. resist., mag. suscept., heat capacity, Hall const. *(Russian)* 78−30900
mass flux, irradiation enhanced, dislocation interactions 80−88206
metal, atomic defect config. from X-ray and neutron scattering studies 78−47322
metal, atomic defect configuration from high resolution TEM 78−47324
metal, atomic defect props., conf., Argonne, IL, USA, (Oct. 1976) 78−47318
metal, BCC, diffusion of heavy interstitial atoms 79−90829
metal, BCC, quantum diffusion model of light interstitial atoms 80−2212
metal, BCC, strain depend. elastic dipole tensor for interstitial impurities, nonlinear Snoek effect 79−8311
metal, BCC, tensor of deform. of cryst. lattices by impurity atoms *(Russian)* 77−7711
metal, BCC small-polaronic diffusion in light interstitials 79−42315
metal, diffusion of H(D), slow neutron scatt. obs., review 80−34248
metal, diffusion of interstitial atoms through crystal lattice interstices *(Russian)* 77−24425
metal, diffusion of interstitial solute 77−62672
metal, dynamic study of defect mobility using HVEM 78−47327
metal, electron irrad., selfinterstitial atomic defect interaction radii, recovery expts. and error sources 80−65049
metal, electron scatt., effect of surface on lattice defects, surface Landau level reson. 79−65534
metal, FCC, investigation of stage-I_E interstitial nature by TEM 78−47329
metal, FCC, structure and dynamics of multiple interstitials 78−47330
metal, FCC, vibr. behaviour of self interstitials 77−4175
metal, FCC and BCC, dipole-interactions and trapping effects of positive muons 78−47342
metal, H(D) diffusion, role of tunnelling, reson./nonreson. approaches 80−59718
metal, H and He impurities, electronic struct. 78−10402
metal, HCP, long-range interstitial migration rel. to c/a ratio 79−28125
metal, HCP, regular soln. model for interstitial soln. 77−15591
metal, HCP structure, interstitial ordering *(Russian)* 78−79610
metal, interstitial diffusion, cooperative nature 78−47556
metal, interstitial soln., conversion of thermodynamic functions from const. press. to const. vol. 77−7877
metal, ion beam damage, distinguishing between models of radiation damage using TEM *(German)* 78−30680
metal, ion implanted H(D), interstitial positions and vibr. amplitudes, fast ion channelling study, review 80−79848
metal, irrad., containing pre-existing dislocations, interstitial loop form. kinetics 80−65040
metal, irrad., containing self-interstitials and vacancies, electronic transport props. 78−60105
metal, irrad., self-interstitial type defects, combined single-double alignment channelling backscatt. 78−34561
metal, point defects, μSR studies 79−56703
metal, point defects, lattice theory 78−47321
metal, quadrupole effect on dipolar field width 78−2457
metal, quantum theory of light interstitial diffusion 79−56690
metal, radiation damage and hyperfine fields 78−38752
metal, refractory, BCC, free migration of self-interstitials 78−47574
metal, self-interstitial atoms, review 78−47332
metal, solute atom displacement in mixed dumbbell interstitials for FCC lattice 78−79631
metal, unstable vacancy-interstitial atom pair, scatt. of electrons 79−15129
metal, vacancies and interstitials, electronic struct. 78−47320
metal cluster, H site, SCF-Xα-MS calc. 78−47730
metal halides, fluorite structure, retarded ionic motion 80−88361
metal hydride form. for H storage, interstitial hole size and electron conc. effects 80−45789
metal tritide, ^3He detrapping and release after ^3H decay, strain model 77−60101
metal-H system, basic props., book 79−82349
metal-H system, lattice strains, expt. methods, book contrib. 79−82202
metals, BCC, diffusion of H_2 and its isotopes, phonon-assisted quantum-mechanical tunnelling of interstitials 80−59730
metals, cubic, relationship between defect resist. and bulk resist. at melting temp. 78−6344
metals, diffusion of H, theory, book contrib. 79−82389
metals, dissolution of interstitial H_2 and D_2, diffusion coeffs., reverse isotope effect *(Russian)* 80−88368
metals, dynamical props. of point defects, book contrib. 80−103317
metals, FCC, H_2 diffusion, isotope depend. 80−59727
metals, FCC, pair potentials calc., appl. to point defect props. 80−19798

interstitials continued
metals, FCC, small vacancy clusters, structures and energies, computer simulation 80−39073
metals, FCC and BCC, grain boundary struct., and segregated impurity sites, computer simulation 79−73173
metals, group VA, O and N determ. from internal friction meas. 79−39246
metals, HCP, vacancy and interstitial config. 79−65071
metals, interstitial atom struct. and vibr. air table simulation 79−71186
metals, interstitial loop growth, pulsed irrad. effects 80−88210
metals, irradiated, solute segregation and annealing kinetics at sinks 79−23640
metals, irradiation creep strain, produced by vacancy loops, calc. of magnitude 78−72815
metals, irradiation induced swelling, bias factor 80−2062
metals, light interstitials, self-trapped, quantum diffusion 79−19405
metals, light interstitials diffusion, multiphonon transition modes classification 80−70448
metals, point defect diffusion controlled reaction theory, book contrib. 80−103318
metals, point defect dynamic props. and diffusion controlled reactions, book 80−101674
metals, point defect relaxation volumes, dipole tensors and Kanzaki forces 80−54222
metals, point defect simultaneous clustering during irrad. 79−95000
metals, radiation damage production in stage II, temp. and impurity effects 77−68997
metals, two and one interstitial model explanation of elec. cond. variations 80−88143
metals and alloys, FCC, interstitial diffusion, theory *(Russian)* 80−65296
metals and alloys, radiation damage prediction and measurement 78−75693
metals irradiated, heavily, exam. of percolative mass transfer 78−79639
metastable alloy formation by ion implantation 80−15130
migration kinetics and thermodynamics 80−107461
mobility and interactions 78−47328
Nimonic alloy PE-16, irradiated, numerical simulation of void nucleation, dislocation densities, pt. defect conc. 79−73208
Nimonic PE16, He injected, bubble-void transitions in Ni ion bombard. 80−34095
NMR spin relaxation, motion-induced, in low. temp. HF limit 80−60443
noble metals, lattice distortion around interstitials 77−1122
non-metallic crystals, electric field influence on defect creation mechanism 80−70251
non-perfect solvent crystals, thermodynamics and diffusion of interstitial solute atoms 79−90825
nonmetallic crystals, collapse of tracks formed by fission fragments 80−24510
nonstoichiometric compounds, physicochem. props. depend. on short-range order struct. 80−100227
nuclear fuels, creep, irradiation induced, transient state, kinetic eqn. treatment 80−88251
ordering alloy, CuAu type struct., interstitials distrib. *(Russian)* 77−47542
ordering alloys, BCC lattice, diffusion of insterstitial atoms *(Russian)* 79−19400
oxide, defect struct., nonstoichiometry and elec. cond., pentavalent oxide dopant effect 80−24442
oxide films, diffusing pt. defects recomb. 79−19475
oxide fuels, in-pile densification by vacancy boil-off and vacancy knockout, model 79−8259
oxides, nonstoichiometry influence on plasticity *(German)* 79−24592
phonon perturbation by complex defects, expt. studies review 79−42190
point defect distrib. in bounded media under irradiation 77−7712
point defect trapping and migration, calcs., in presence of rare gases and dislocations 79−77834
point-defect clustering during irradiation 80−92521
pore nucleation in radiation damaged solid solns. 79−99237
quartz, synthetic, electron beam irrad., defect form., annealing and migration effects, ESR obs. 80−50180
quartz, synthetic, electron beam irrad.-induced interstitial ion mobility, ESR centres and IR spectra meas. 80−39153
radiation creep, contrib. of stress induced preferential attraction of interstitials to dislocations 80−2064
radiation damage cascades, stochastic theory of particle transport 80−54291
radiation damage tetragonal R2 centre, optical and EPR spectra 78−2888
radiation defect production, exact solns. of models for continuous and pulsed irrad., implications for stability and fluctuations 80−65041
radiation effects, distrib. functions of point defects and moving gas filled holes 77−55302
radiation enhanced diffusion, approx. solns. of chem. rate eqns. and appl. to expts. 79−73344
radiation induced solute segregation, kinetic model, GEAR package of subroutines 78−30673
rare earth metals, electrotransport of solutes 77−51548
recombination of vacancies and interstitial atoms in primary cluster of radiation defects *(Russian)* 79−1429
refractory metal solid solutions, thermodynamic study *(Ukrainian)* 79−37845
selfinterstitials and He interstitials, interaction with vacancies and vacancy clusters, Monte Carlo simulation 78−71754
semiconductor, elastic stresses effect on diffusion processes 78−10226
semiconductor, ion implantation, radiation defect form. in presence of force fields 79−51126
semiconductor, large-band-gap, self-compensation, role of impurities 80−92850
semiconductor displacement energy threshold 77−89430
semiconductors, annihilation processes of radiation-produced vacancies and interstitials 77−89432
semiconductors, asymmetry in displacement energy for Frenkel-pair prod. 78−2116
semiconductors, cryst. defects induced by radiation, review 79−55776
semiconductors, defect processes, electronic stimulation 80−24665
semiconductors, radiation damage studies on implanted Te, Sb and Sn by Mossbauer spectroscopy 78−2176
semiconductors, Watkins-type radiation defects, low temp. form. mechanism 80−15153
semiconductors, Z 80−19799
interstitials continued
p-Si, interstitial Fe and thermal defects, Hall effect and resist. meas. 79−82200
silicates, nonstoichiometry influence on plasticity *(German)* 79−24592
simple cubic lattice, drift mobility correlation of interacting ions 79−37868
simple metals, screening of light impurities 77−85177
solid electrolyte dielectric permeability, phase transition to superionic state *(Russian)* 80−49403
solid electrolyte with structural disorder, current flow mechanism 80−19982
solid electrolytes, two-state model, cationic disorder theory 79−73337
solid solution, binary, radiation-induced instability, contrib. of dissipative processes 80−65039
solid solution, deform. interaction of interstitial atoms, pseudopot. calc. *(Russian)* 78−18636
solid solution, diffusion, influence of conc.-induced stresses *(Russian)* 78−55969
solid solution, growth rate of layer of new phase containing impurity atom traps 77−76620
solid solution, with repulsive interactions, statistical treatment 77−72611
solid solutions, interstitial phase struct., reconstructive transition struct. symm. relationships 79−69246
solid solutions, self-diffusion activation energy rel. to partial molar energy 80−15291
solute-induced jump correlations during diffusive processes 79−51297
solutions, impurity subsystem free energy, impurity distrib., temp. depend. 80−44232
spatial pore lattice, parameter of vacancy pores, temp. depend. 79−27976
spin migration amongst tetrahedral or octahedral interstitials in FCC cryst. symmetric and asymmetric jump model 79−15127
steel, austenitic, dislocation struct. formed by interstitial diffusion of C 77−4223
steel, austenitic stainless, H_2 induced strain in single crystal *(Japanese)* 77−48530
steel, austenitic stainless, HVEM irrad., point defect trapping influence on void swelling 79−23652
steel, C, strain ageing and fatigue limit 80−40378
steel, C martensite, electron irrad., reversible C at. redistrib. 77−65991
steel, cold-worked, state of cementite, nucl. gamma reson. meas., plastic deform. *(Russian)* 78−68706
steel, ferritic, with interstitial N, continuous precipitation and clustering 80−7585
steel, lattice hardening due to dissolved H_2 77−8952
steel, rare earth addition effects and behaviour, review *(Chinese)* 79−43257
steel, Si, electron irrad. in HVEM, void swelling, Si role 80−54285
steel, stainless, irradiation creep and swelling, microstructural modelling 77−52407
steel, stainless, solution treated, irradiated to low doses with 22 MeV C^{2+} and 46.5 MeV Ni^{6+} ions, interstitial loops 79−14855
steel, stainless, type 316, neutron irrad., Ni ion bombard. effects of injected interstitials on void volume 80−34092
steel, stainless, type 316, point defect simultaneous clustering during irrad. 79−95000
steel, stainless, void swelling, Si point defect trapping, interstitial loop growth rate temp. depend. obs. 80−49270
steel, stainless 316, Fokker-Planck eqn. describing evolution of interstitial loop microstruct. during irradiation 80−107215
steel, stainless type 316, effect of damage rate on void growth, point defect conc., microstruct. development 79−73209
steel, thin sheets, C and N contents determ. by internal friction *(German)* 78−27715
stressed crystal, point defect interaction with dislocation 77−80537
strontium acetate hemihydrate:Cu^{2+}, EPR of cryst. 78−19312
strontium tartrate tetrahydrate Co^{2+} electronic absorpt. spectrum 78−92098
structural materials, radiation effects, review 80−49267
superionic crystal, domain formation, thermodynamic theory 77−84963
superionic crystals, structural transition theory 79−23731
superionic fluorites, disordered anions exam. 79−42299
superionic fluorites, structure and transport 80−84318
superionics, with fluorite structure, Brillouin scattering and lattice defect energetics 78−80369
swelling during self-ion bombardment, effect of implanted interstitials 78−10099
ternary BCC alloys, ordering process, effect of short-range order *(Russian)* 80−84908
tetrahedral semiconductor, interstitial type dislocation loop form. by vacancy precipitation 78−67715
TGS:nitroanilines, permittivity, elec. cond. and Curie temp. 80−25273
thermal neutrons, inelastic scattering by one-dimens. defecton *(Russian)* 78−84169
thermodynamic relationship between chemical diffusion coeff., true diffusion coeff. in interstitial phases 80−49397
transition metal, BCC, neutron spectroscopy of fast H diffusion 80−59731
transition metal, penetration of interstitial elements during surface treatment 77−12737
transition metal dichalcogenides, octahedral intercalate ordering study by electron diffr. 80−15076
transition metal hydrides, interstitial solid soln., H coordination 77−24289
transition metal-H dilute solns., pair potential anal., unrelaxed lattice model 79−65070
transition metal-H systems, energy and electron density of states, improvements to theory 80−70636
transition metal-hydrogen systems, eqn. for multiplateau isotherm, lattice expansion role 80−39252
transition metals, BCC, interaction energy between self-interstitial and screw dislocation, calc. 80−70248
transition metals, Fe series, interstitial H, cluster model for bonding mechanism 79−60753
transition metals, ferromag., electronic struct. of interstitials 77−62867
transition metals, ferromag., interstitial or substitutional sp impurity doped, electronic struct. 80−34384
transition metals, H interstitials, wave-packet motion in Eckart and quadratic pots. 80−52067
transition metals electrical transfer of O, N, exam., using heat transfer of interstitial atoms *(Russian)* 79−55931

interstitials continued
triglycine calcium bromide:Cu^{2+}, ESR studies 80−97136
vibrational spectra crystals with split configuration interstitial *(Russian)* 78−76450
void, and interstitial loop evolution in pulsed fusion reactors 80−84217
void coalescence kinetics in cryst. with dislocations and volumetric generation of point defects 77−68996
void swelling rate, vacancy dislocation loop effect 80−2084
void swelling simulation, effect of self ion injection 78−22772
voids, coated, capture efficiency 80−96515
zinc blende-type semiconductors, interstitial PDs, electronegativity diff. and effective ionic charges 77−76766
Zircaloy, in-pile temp. depend of yield strength and growth, under neutron irrad. 79−73219
Zircaloy-2, interstitial/vacancy nature of neutron induced dislocation loops, TEM study 79−42110
Zircaloy-2, irradiation growth, reaction rate theory calcs. 80−88212
Zircaloy-2, irradiation growth, shape and volume changes 80−92562
Zircaloy-2 irradiation growth at 353 and 553K, texture and temp. cycling effect 79−46709
Zircaloy-4, quenched, strain ageing behaviour, ageing time and temp. effects 78−56657
Zircaloy-4, quenched and annealed, strain ageing 77−25071
Ag, Ag-Cd(In) dil. alloys, electron irrad., stage I_E recovery 77−39616
Ag, electron irrad., elastic moduli and internal function *(French)* 78−87703
Ag film, defect density, thickness depend., elec. resist. obs. 80−70568
Ag halide, photographic image form., defect and impurity states, LCAO calc. 78−16876
Ag halide grains, photographic sensitivity and response to charged particles, interstitial generation 77−10124
Ag, production and annealing of radiation defects 78−47362
Ag, TEM exam. of ion damage in FCC metals 78−87727
Ag-Co, dil., binding and caging of impurities and trapped interstitials 78−39462
Ag-Zn, electron irrad. self-interstitials, migration and elimination charcts. 79−37872
Ag-Zn (30 at.%), electron irrad., mobilities of self-interstitials and vacancies 77−84795
Ag-Zn(Cd), production and annealing of radiation defects 78−47362
AgAu, recovery and formation of mixed dumbbells after thermal neutron irradiation 79−69161
AgBr, Ag speck formation, ionic and electronic effects in photographic process 77−4917
AgBr, Ag^+ migration vol. for vacancy and interstitial motion, influence of anharmonicity 79−14965
AgBr and AgBr:$PbBr_2$, emulsion grains, dielec. loss, ionic cond. and surface space charge 77−28038
AgBr, film and microcrystal, interstitials and surface conductance 79−23776
AgBr, Frenkel defects, interstitials, neutron scatt. study 79−42059
AgBr thin film interstitials, Frenkel and space-charge contributions 79−18494
AgBr(I) microcrystal dispersed in gelatin, effect of I^- on interstitial Ag ions 78−26726
AgCl, Frenkel defects, interstitials, neutron scatt. study 79−42059
AgCl(Br), point defect form. energies, atomistic calc. and surface pot. meas. 80−107221
α-AgI, structural and dynamical behaviour 80−107544
AgI:Cd, polycrystalline, thermoelectric power meas. 80−59698
β-Ag_2S, electrogalvanic and elec. props., and range of existence *(French)* 78−43175
Al, Al-Ag(Mg) dil. alloys, electron irrad., stage I_E recovery, interstitial trapping 77−15405
Al alloys, dil., size effect of impurity atoms rel. to trapping radii for migrating self-interstitials 78−75690
Al, atomic defects, computed electron microscope images 78−26392
Al, electron irrad., interstitital loop nucleation at impurity site *(Japanese)* 77−43247
Al, electron irradiated, di-interstitial formation within small defect clusters 78−26566
Al, electron-irrad., NQR, EFG around vacancies and interstitials 78−88220
Al, electron-irradiated, anelastic relax. due to single self-interstitial atoms 77−39627
Al, electron-irradiated, anelastic relax. due to clustered self-interstitial atoms 77−39628
Al, f.c.c., lattice distortion around interstitials 77−1122
Al, film, superconducting transition temp. and lattice dynamics 80−93028
Al foil, electron-irrad., interstitial trapping on impurities 79−99242
Al, foil, influence of O_2-pressure on oxidation rate, TEM study 80−104355
Al, interstitial clustering following electron irradiation at low temp. 79−19243
Al, interstitial loop form., effects of repeated electron irrad. 80−75220
Al, interstitial trapping configuration study by ion channelling 78−47455
Al matrix, capture radius of impurities 80−20110
Al, neutron irradiation, mobile interstitials production 80−34080
Al, proton irradiation, Al atomic displacement position study 80−103401
Al, pure, electron irradiation damage 77−19988
Al, quenched, irradiated, and quenched plus irradiated, grain boundary hardening 80−3162
Al, reactor irradiated, neutron inelastic scattering meas. of phonon dispersion curves 78−75758
Al, rigidity modulus, neutron irrad. and quenched, point defects 78−27546
Al, self-interstitial interaction with solutes, resistivity meas. 78−47331
Al, stress induced ordering of self-interstitial clusters 78−47358
Al thin foil, thin foil, electron irrad., observation of triangular loops at twin boundaries 80−34005
Al:^{111}In, electron irrad., defect trapping at impurities 78−55892
Al:H, impurity energies and geometrics, self-consistent jellium calc. 79−99507
Al-^{57}Co, implanted, Mossbauer effect obs. of annealing 80−39126
Al-Ag, dil., radiation damage by channelled and random He^+ ion beams 79−46719
Al-Ag (0.10 at.%), channelling meas. of trapping efficiencies of solute atoms for self-interstitials 79−86829
Al-Ag(Ge)(Mg)(Zn) alloy, dil., electron-irradiated, impurity-interstitial interaction 77−15449
interstitials continued
Al-C interstitial solid solns., atomic static displacements and deform. interaction *(Russian)* 80−64953
Al-Co, defect structs. introduced by electron irrad., Mossbauer study 80−7239
Al-Co, dil., binding and caging of impurities and trapped interstitials 78−39462
Al-Co, dil., electron and neutron irradiation, interstitital atom clustering at ^{57}Co impurity, Mossbauer meas. 78−30607
Al-Co, electron irradiated, self-interstitials trapped at Co impurities, Mossbauer line shape anal. 78−6615
Al-Co, electron irradiated, quadrupolar relaxation effect in Mossbauer effect 78−39459
Al-Co alloy, dil., fast neutron radiation damage, interstitial trapping, Mossbauer spectra and elec. resist. meas. 77−27914
Al-Cr, neutron irrad., Cr atom distribution NMR study 80−54957
Al-Cr(Mn), anisotropic electron scattering, Hall coefficient, path integral calc. 79−91027
Al-Cr(Ti), electron irradiated, interstitial trapping and detrapping at undersized impurity atoms 78−47424
Al-Cr(V)(Ti), dil., electron irradiated, interaction of self interstitials with undersized solute atoms 78−63789
Al-Cu (up to 0.5 at.%), neutron damage rate, interpretation of results 78−63794
Al-Fe, electron irradiated, interstitial-solute complexes, internal friction spectra 78−92289
Al-Ge (0.1 wt.%), channelling meas. of Al interstitial atom trapping by Ge atoms 80−59537
Al-Ge (0.2 at.%), exam. of interstitial trapping by X-ray diffuse scatt. 78−47363
Al-In alloy, dilute, electron irradiation, interstitial dislocation loop obs. 78−18681
Al-Mg 0.1 at.%, neutron-irradiated, dislocation loop characterisation by TEM 79−23614
Al-Mg (5 wt.%), static strain ageing at low temp. 79−29116
Al-Mn(Cu)(Ag), solute atom displacement in mixed dumbbell interstitials for FCC lattice 78−79631
Al-Si alloy, dilute, electron irradiation, interstitial dislocation loop obs. 78−18681
AlH_x, electronic struct. and electron-phonon interaction, hydrogenation effect, rel. to supercond. 80−107694
β-Al_2O_3, conduction and dielec. loss mechanisms, paired interstitialcy model 80−107468
Al_2O_3, defect microstructure due to ion bombardment, TEM study 80−34100
Al_2O_3, sapphire, edge dislocation loop obs. by high resolution lattice imaging 80−103346
β-Al_2O_3-Na_2O, cond. plane struct. and energetics 80−92715
β-Al_2O_3-Na_2O ^{23}Na asymmetry parameter, temp. variations 80−6540
β-Al_2O_3-Na_2O-K_2O, cation interstitial pair modes in vibr. spectra 79−37788
β-Al_2O_3-Na_2O-Rb_2O, cation interstitial pair modes in vibr. spectra 79−37788
AlO_xN_y spinel, crystal struct. model 78−91333
Ar:H, solid, struct., pair pot. calcs. 78−2215
Ar:Li^+, interstitial interaction energy calc. 78−38692
Au, atomic defects, computed electron microscope images 78−26392
Au, calc. images and diffraction patterns 80−100152
Au, electron irradiated, interstitials and their clusters, diffuse X-ray scatt. study 80−33997
Au foil, radiation damage, in situ study by HV electron microscopy 78−6101
Au, heavy ion irrad., cascade energy density effect on defect cluster type 80−107340
Au, irrad., self-interstitial type defects, combined single-double alignment channelling backscatt. 78−34561
Au, proton irrad. at 0.3K, resistivity annealing 77−76475
Au, sputtering, by point defects, time-of-flight spectra 79−47573
Au, TEM exam. of ion damage in FCC metals 78−87727
Au, work hardened, Hasiguti peaks, spectrum and recovery, impurity effects *(French)* 77−66670
Au-Cu, dil., electron irradiated, interstitials and their clusters, diffuse X-ray scatt. study 80−33997
B, in transition metals, electronic structure 79−1583
B-C-Cr, paramagnetic centre struct. and defect form. 80−66034
BaF_2, F^- interstitial and substitutional trivalent cations, phonon reson. and IR absorpt. 80−84752
BaF_2, NMR relax., ionic cond. and self-diffusion 78−23362
BaF_2:Dy^{3+}, far IR absorption 80−40143
BaF_2:Y^{3+}, diffusion of bound and free $F_{(i)}^-$ interstitials, NMR meas. 79−78542
$(BaF_2)_{1-x}(YF_3)_x$, crystal growth and struct. 77−12520
$(BaF_2)_{1-x}(YbF_3)_x$ and $(BaF_2)_{1-x}(NdF_3)_x$, crystal growth and struct. 77−12520
$Ba(N_3)_2$, thermal decomp., role of defects 78−73033
$BaTiO_3$:C, solubility of C at low O_2 potentials, 800°C 80−100334
$Ba_{1-x-y}U_xCe_yF_{2+2x+y}$, solid soln., ionic cond. 79−99356
Be, ion-implanted, impurity lattice location, channelling meas., Monte Carlo calc. 80−107291
Be:Li, ion-implanted, interstitial props. 79−37876
BeF_2, radiation induced defects, nuclear Hanle effect 78−43734
Bi-Cu, liquid, interstitial index, definition and variation with temp. *(French)* 80−2011
Bi-Zn, liquid, interstitial index, definition and variation with temp. *(French)* 80−2011
Bi_2WO_6, ionic cond. and relaxation polarisation, capacitance, losses 80−24657
$Bi_2W_2O_9$:Mo(Eu), energy transfer and luminesc. props. 80−55177
β-AgI, ionic cond. and dielec. meas., Frenkel defect formation energy 78−87814
C, in transition metals, electronic structure 79−1583
CaF:Eu(Gd)(Dy)(Tb), dimer reorientation activation volume 80−107285
CaF_2, (n,γ) induced point defects, struct. and annealing 78−59842
CaF_2, anion-void superlattices *(Danish)* 79−14796
CaF_2, F^- interstitial and neighbours, mean-square displacements 80−29011
CaF_2, impurity modes due to interstitials, Green function formalism 80−24554
CaF_2, superionic, computer simulation 78−43173
CaF_2:alkali metal cation, thermal depolarisation study 80−108147
CaF_2:Dy^{3+}, Mossbauer obs. 78−64303

interstitials continued
$CaF_2:O^{2-}$, $CaF_2:Na^+$, O^{2-} and $CaF_2:Y^{3+},O^{2-}$, thermal depolarisation obs. of defect clusters 80−71299
CaF_2:rare earth, defect model for nonlocally compensated trivalent impurities 77−72629
CaF_2:rare earth metal, thermal cond., 80 to 300K, defect centre struct. 77−15638
$CaF_2:Y^{3+}$, diffusion of bound and free $F_{(i)}^-$ interstitials, NMR meas. 79−78542
$CaF_2:Y^{3+}$, ionic cond. and thermal depolarisation obs. of defect clustering 80−71298
$CaF_2.3Ca(PO_4)_2$, apatite, fission damage detection, absorpt. spectra 78−84617
$Ca_{1-x-y}U_xCe_yF_{2+2x+y}$, solid soln., ionic cond. 79−99356
Cd, electron radiation damage in HVEM, nature of defect clusters 78−59838
Cd, faceting of interstitial loops 78−47381
CdF_2:Eu, role of solution and precipitation phenomena on ITC spectra 80−7265
CdF_2:Na(Nd), ionic cond. investigation by complex admittance method 80−100352
$CdF_2:Sm^{3+}$, photoconverted, thermally stimulated relax. 80−84476
$Cd_xHg_{1-x}Te$, diffusion and struct. of defects 77−84775
$Cd_xHg_{1-x}Te$, long term stability at 300K, rel. to device appl. 80−59978
CdS, 200 keV electron induced defects, low temp. annealing 77−80796
CdS, defect struct. and config. produced by irrad., elastic scatt. expts. 80−84178
CdS polycrystalline layers, electron trapping depend. on preparation conditions 79−78232
CdS:Cu, diffusion doping, photolum. 79−91493
CdS:Li, subjected to elec. fields, drift of defects 80−6558
CdS:Li, thermochemical changes in microstructure of anisotropic centres, polarisation modulation method meas. 79−38027
CdSe, defect struct. in Se vapour 78−64043
CdTe, diffusion of Cu at 250 to 500°C, interstitial process 77−11737
CdTe, diffusion of Sn and intrinsic defects role 79−33116
CdTe, Li diffusion, 300°C 77−43383
CdTe, Yb^{3+} implantation, nonstoichiometry effect 77−15440
CdTe:Cl, LPE from $CdCl_2$ soln., elec. props., defects 80−39689
γ-Ce, FCC, localised vibration of interstitial H impurities 80−75322
Co, dipole field anisotropy, at interstitial sites, lattice-deformation effects 79−33584
Co, electron irradiated, mag. after-effect spectrum, 20-350K 77−1570
Co, interstitial site determ., μSR technique 80−71287
Co, local magnetic fields probed by μ^+ 78−48103
Co, muon resonance meas. of local mag. dipole field at interstitials 79−95699
Co-C, ferromag., prep. by splat-quenching, obs. of electronic struct. of interstitial C 77−62868
Co_5R-H(D) system, R=rare earth, mag. orientation aftereffect 80−50148
Cr, neutron irradiated at 24.5K, elec. resist. exam. of radiation damage *(French)* 78−30671
$(Cr_{1-x}Fe_x)_{1+\delta}Sb$, interstitial occupancy, Cr:Fe distrib., X-ray and neutron diffr. study 79−42012
Cs halides:H, luminesc. of interstitial atomic H 80−103986
Cu alloys, dil., size effect of impurity atoms rel. to trapping radii for migrating self-interstitials 78−75690
Cu, Ar^+ ion irradiated, defects study by electron microscopy *(German)* 80−2087
Cu, Ar^+ ion irradiated, small defect clusters, electron microscopy contrast *(German)* 79−99253
Cu, defect-phonon perturbations after neutron irrad., neutron scatt. study 80−44278
Cu, diffusion of interstitial O_2, sink/barrier phenomena 79−60553
Cu, diffusion of muons and protons 79−56689
Cu, dislocation pinning rate, neutron and electron irrad., meas. by internal friction method 80−96570
Cu, electron irrad., migration and thermal conversion of defects, 100 to 330K 80−59519
Cu, electron irrad., rel. to stage III recovery kinetics 78−63792
Cu, electron irrad., secondary defect formation, effect of refl. condition *(Japanese)* 77−43248
Cu, electron irrad. at 100K, dislocation vel. meas. etch pit technique 80−49271
Cu, electron irradiated, dia- and paraelastic effects 77−76482
Cu, electron irradiated, evidence for vacancy migration in stage III 78−38693
Cu, electron irradiated, temp. depend. of threshold energy for atom displacement 80−34055
Cu, electron radiated, formation of Frenkel pairs 79−23598
Cu, electron-irradiated crystals, electron diffr. channelling effect on atom displacement 80−39158
Cu, FCC, single and multiple interstitials 77−68964
Cu foi.foil, interstitial impurity interaction investigation by stage II isochronal recovery expts. 78−47423
Cu foil, electron-irrad., interstitial trapping on impurities 79−99242
Cu, H_2 diffusion, isotope depend. 80−59727
Cu, He-vacancy clusters, computer simulation 77−39583
Cu, interstitial trapping configuration study by ion channelling 78−47455
Cu, ion bombard. by 5 keV Ar^+, sub-surface damage 80−103399
Cu irradiated, exam. of dislocation bias for interstitials to edge dislocations 78−79612
Cu, muon localisation and lattice dilation, μSR 79−56694
Cu, muon spin rot., EFG, site of localisation 78−2785
Cu, μ^+ diffusion data anal., theory of incoherent direct and indirect multiphonon transitions 80−70448
Cu, neutron and electron irrad., interstitial formation, dislocation pinning, internal friction meas. 80−100284
Cu, neutron irradiation, mobile interstitials production 80−34080
Cu neutron production of free interstitials 80−34071
Cu, point and planar defects, computer simulation 80−59455
Cu, self interstitial struct. determ., and vacancy clustering, X-ray exam. 78−47351
Cu, self-interstitial interaction with solutes, resistivity meas. 78−47331
Cu, stress induced ordering of self-interstitial clusters 78−47358
Cu, TEM exam. of ion damage in FCC metals 78−87727
Cu:μ^+, lattice distortions, microscopic calc. 78−87665
α-Cu-Al (15 at.%) alloys, low temp. neutron irrad. induced point defects behaviour 77−43251

interstitials continued
Cu-Be, solute atom displacement in mixed dumbbell interstitials for FCC lattice 78−79631
Cu-Be (0.0182 at.%), radiation induced Be segregation 78−23710
Cu-Be (0.25 at.%), channelling meas. of trapping efficiencies of solute atoms for self-interstitials 79−86829
Cu-Be (0.25 at.%), cryst., Cu self-interstitial atom, trapping, nucl. reactions and ion channelling obs. 78−14384
Cu-Co, dil., binding and caging of impurities and trapped interstitials 78−39462
Cu-M-O ternary liquid alloys, thermochem. calcs. 80−85209
$CuAl_2$, single cryst., embrittlement and subboundary hardening via interstitial segregation *(Russian)* 77−12679
CuAu type structures, interstitial atom redistrib. in octahedral and tetrahedral interstices *(Russian)* 77−55280
CuCl, pure and Cu_2S doped, rel. to ionic cond., 60-370°C 77−47617
CuI and CuI:CdI_2, ionic cond., vacancy and interstitial mobilities, phase transitions 77−20116
CuI, pure and CdI_2 doped, ionic cond. obs. 77−15626
$Cu_{0.5}In_{2.5}Se_4$, transition state and domain struct. by electron microscopy and diffr. studies 80−15095
$Cu_{2-x}S$, and related disordered crystals, diffr. pattern, cluster theory 80−75123
$Cu_{2-x}S$, digenite related phases, electron microscope study 79−10840
p-Cu_3VS_4, mixed conduction due to cationic interstitials 80−70772
Dy, interstitial site determ., μSR technique 80−71287
Er, ^{198}Au diffusion, anisotropy, interstitial solute diffusion mechanism 80−29223
Fe, Armco, discontinuous laser beam effect on mass transfer *(Russian)* 79−33109
α-Fe, BCC, stress-induced interaction and ordering 79−42057
Fe base ternary soln., containing interstitials and substitutional solutes, thermodynamic and kinetic props. 78−2297
α-Fe, C, electromigration, current density and temp. effects 77−59145
Fe, defect trapping of ion implanted D, depth profile, diffusion eqn. calcs. 80−2047
α-Fe, H ordering 79−7597
α-Fe, high purity, neutron and electron-irrad., interstitial migration at 200K 79−55920
Fe implanted alloys, residence sites of Fe, Mossbauer data 80−39299
α-Fe, interaction of foreign interstitial atoms with vacancies 78−6052
α-Fe, interaction of He with C impurities, computer simulation calc. 79−99235
α-Fe, internal friction for low temp. deform. 80−40420
α-Fe, interstitial or substitutional sp impurity doped, electronic struct. 80−34384
Fe, lattice hardening due to dissolved H_2 77−8952
α-Fe, mag. aftereffect after neutron irrad. at 77K 78−2705
α-Fe, mag. aftereffect spectrum after low temp. electron irrad. 78−2704
α-Fe, magnetic aftereffect disaccommodation between 30 and 300K after low-temp. neutron-irrad. 80−29585
Fe, magnetic aftereffect of interstitial O 78−91903
Fe, μ^+SR, theory of spin depolarisation rate 78−80271
Fe, pure, deformed, internal friction, dislocation relax. and dislocation-defect interactions 79−29125
Fe, pure and doped, electron irrad., mag. aftereffect 80−88838
α-Fe, stress induced interaction of point defect pairs, in BCC solutions 78−79608
Fe, structural stabilisation, influence of C interstitials, HF calc. 79−11611
Fe, trapping of H, average trapping depth and trapping sites density 80−84297
Fe, varying purity, internal friction, H-dislocation interactions 77−52377
Fe, vibrational spectrum with interstitial C atoms 78−67796
Fe, zone melted, H_2 diffusion, reversible lattice dilation 77−11732
α-Fe:B(C)(N)(O), valency effect of interstitials 80−65502
α-Fe:C, electronic struct., Hartree-Fock calc. 78−14692
Fe:C(N), small concs. determ., mag. and mech. relax. methods 80−7879
Fe:He, BCC, process of interstitial trapping by impurities 79−46697
α-Fe:He, interaction of He with small self-interstitial platelets 79−60399
Fe-Al, Al effect on softening in solid soln. *(French)* 79−52226
Fe-Al, hyperfine field meas. using muon-spin-rotation method 80−10933
Fe-Al (38.5-47 at.%), type B_2 ordered alloys, elec. resist. recovery stages after neutron irrad. *(French)* 77−69010
Fe-Al (40 at.%), ordered, plastically deformed, neutron irrad. damage and recovery, resist. meas. 77−19993
Fe-Al-C, gamma irrad., crystal lattice parameter reversible changes *(Russian)* 80−10576
Fe-Al(Ti), O containing, mag. aftereffect and disaccommodation meas., time depend., activation energy, and ageing props. 80−88836
Fe-C, ferromag., prep. by splat-quenching, obs. of electronic struct. of interstitial C 77−62868
Fe-C interstitial solid solutions, self-diffusion activation energy rel. to partial molar energy 80−15291
Fe-C-Cu (0.21, 0.2 wt.%), neutron irradiated, torsional props. effect of Cu additions and annealing temp. 78−56699
α-Fe-C(N), containing substitutional atoms, mag. permeability disaccommodation *(Polish)* 79−95612
Fe-Cr(Ni), use of electrochemistry in understanding $\alpha \rightleftarrows \gamma$ transform., interstitials role *(French)* 77−63662
Fe-Mn (8.25 wt.%), irreversible temper embrittlement, Mossbauer spectra, impact strength depend. on interstitials *(German)* 79−74235
Fe-Mo (3 wt.%), substitutional solid soln. with cubic faced symmetry, Portevin-Le Chatelier effect *(French)* 78−23785
Fe-Mo(V), nitrided by const. activity ageing, X-ray studies 77−32720
Fe-N(C), solid soln., metastable and stable, interstitial atom config. 77−36512
Fe-Ni, dil., point defect relax. after low temp. neutron irrad. 78−52316
Fe-Ni-C, martensitic, deformed, stress induced C distrib. *(Czechoslovakian)* 77−32641
Fe-Ni-V, nitrided austenitic alloys, modulated substitutional interstitial solute atom clustering 79−74160
Fe-Pd, magnetic after-effect of H isotopes 80−75817
α-FeC(P) solid soln., deform. interaction of atoms, pseudopot. calc. *(Russian)* 78−18636
FeCo, ordered and disordered alloy, annealing of point defects created by neutron irrad. at 20K *(French)* 79−1467
$Fe_{50}Co_{50}$, neutron irradiation, close pair recombination *(French)* 80−39162
$FeCo_2V$, ordered and disordered alloys, annealing of point defects created by neutron irrad. at 20K *(French)* 79−1467

interstitials continued
$Fe_{49}Co_{49}V_2$, neutron irradiation, close pair recombination *(French)* 80−39162
$Fe_{0.49}Mn_{0.01}Ti_{0.5}H_x$, localised vibrs., sp. ht. obs., room temp. 80−65248
$Fe_{1-x}O$, wustite, vacancy and interstitial ion order, equilib. conditions, neutron diffr. obs. *(French)* 78−14336
$Fe_{1-z}O$, wustite, struct. at high temp., neutron diffr. obs. *(French)* 79−86754
$Fe_{1-z}O$, wustite, struct. at high temp., neutron diffr. *(French)* 80−1982
$Fe_{0.545}Sb$, temperature effect on lattice consts., Mossbauer spectra and density 80−88124
$Fe_{1+\delta}Sb$, nonstoichiometry influence on mag. props. *(Russian)* 80−65813
$Fe_{1+x}Sb$, Mossbauer meas. of lattice and interstitial Fe atom mag. ordering 79−99807
Fe_2SiO_4, nonstoichiometry influence on plasticity *(German)* 79−24592
$FeTe_2Fe_2Te_3$, defect struct. compounds, room temp. ^{57}Fe Mossbauer spectra 79−47371
α-$FeTiD_{0.057}$, solid soln., interstitial D, neutron diffr. study 80−39071
GaAs, electron and neutron irrad., defect clusters 80−2077
GaAs:B, electron or neutron irradiated, low symmetry interstitial B centre 78−79605
GaAs:S(Te)(Zn), dislocation-free, TEM study of microdefects 79−82213
GaAs:Sn, implantation, annealing, impurity-defect struct., Mossbauer study 80−54269
GaAs:Sn, nature and conc. of point defects over conc. range 10^{17} to 6.10^{18} cm^{-3} 79−14802
GaAs:Te, superdilation and defects, lattice parameter meas. and carrier mobility 80−10569
GaN:Zn(Fe)(Ni)(Cr), influence of self-interstitials on lattice parameters 79−73153
GaP, electronic props. of paramag. antisite P(Ga) defect 78−43327
Gd, dipole field anisotropy, at interstitial sites, lattice-deformation effects 79−33584
Gd, interstitial site determ., μSR technique 80−71287
Gd, local magnetic fields probed by μ^+ 78−48103
$Gd_3Ga_5O_{12}$, decorated dislocations, large interstitial climb loops round precip. particles 77−19960
Ge (111) surface, clean and CO-covered, UPS and ion-neutralisation spectroscopy 80−10785
Ge, deep donor character of muons and protons 80−10911
Ge, defect form. under radiation-accelerated diffusion conditions 80−19854
Ge, defects, radiation effects 80−29016
Ge, electron beam irrad., {113} faults, nature and origin 80−70258
Ge, electron irrad., defect growth, struct. rel. to temp. 77−11591
n-Ge, electron irradiated, threshold energy for atomic displacement, carrier traps 80−29351
Ge, form. of divacancies anchored to self-interstitials under electron bombard. 77−80501
n-Ge, group V doped, point defect form. due to γ-ray irrad., carrier density, mobility meas. 78−71759
Ge, impurity levels of H and muons 79−56162
Ge, ion beam irrad., defects prod. by individual displacement cascades, TEM study 80−70265
Ge, ion bombarded, radiation defect formation, atom-atom collision cascades modelling 80−10582
Ge, irradiation at about 6K, low temp. annealing of defect 78−2162
Ge, migration energy of intrinsic point defects in different charge states 77−89582
Ge, neutron irrad., substitution of impurity atoms by self-interstitials, Ge(n,γ) reaction 80−39166
Ge, polarisation of implanted ^{12}B 78−43653
Ge, self-diffusion mechanism 79−90824
Ge, self-interstitials, vacancies and their clusters 77−80500
Ge:Cu, anelastic relax., internal friction temp. depend. meas. 79−65143
Ge:Cu, solubility and behaviour of Cu, internal friction investigations 80−92678
Ge:Fe, amorphous film or ion-implanted, comparison of ^{57}Fe Mossbauer data 77−40159
Ge:H, interstitial impurity levels, pseudopot. calc. 80−44533
H in metal, rel. to μ^+ trapping in Cu(V)(Nb)(Ta) expt. 80−50247
H_2, random walk diffusion models, generalisation to correlations over two jumps 78−79794
HF with interstitial O, quantitative TEM obs. of small agglomerates 80−107227
Hf-O(N), solid soln. hardening, impurity cluster and interstitial mechanisms 77−36523
HfV_2D_4, disordered solid solution, order-disorder transition 80−88321
Hg-S binary system, phase relations, bulk resist. meas. 79−66040
HgSe, point defect model rel. to elec. props. and phase diagram 77−4339
HgTe, single crystal, diffusion of transition metals 79−77818
In_2O_3, defect chemistry and struct. stability, impurity incorporation 77−35552
In_2O_3, lattice defects, optimum prep. conditions w.r.t. stoichiometry 79−27974
InSb, thin film, carrier scatt. by vacancies and interstitials 79−65568
K-β-Al_2O_3, far IR absorpt., Beevers-Ross sites, interstitials 80−66240
KBr, defect accumulation under electron irrad. at 4K 80−107233
KBr, dislocation interaction with radiation-induced single halogen interstitials 78−34536
KBr, electron irrad., F-centre formation kinetics, interstitial stabilisation mechanism 79−69103
KBr, electron irradiated, defect accumulation kinetics of low temps. 80−10577
KBr, irrad., colour centres and thermolum. 77−85815
KBr, pulse radiolysis of metastable interstitial centre of high temp. 80−20658
KBr, thermolum. and reactions of freed interstitial and trapped hole centres 78−23538
KBr, X-irradiated, at 80K, interstitial K ions associated with interstitial Br ions *(Russian)* 78−75655
KBr:I^-, OH^-, luminesc. of interstitial atomic H 80−89062
KBr:Li(Na), low temp. radiation hardening mechanism, single halogen interstitials as hardening agent, Ha annealing 79−23634
KCl, Born-Mayer parameters of He and Ar, interstitial interaction with neighbouring ions 80−100228
KCl, gamma irrad. relationship between thermolum. and deform. luminesc. 79−19942

interstitials continued
KCl, γ-irradiated, photo- and thermoluminesc., F-centre interstitial recomb. 77−44036
KCl, X-irrad. induced deform. effects, glow curves *(Russian)* 79−52022
KCl, X-irradiated, formation of cation defects 78−91359
KCl:Br^-(I^-), interstitial atomic H centres, formation kinetics and struct. MO calc. and EPR studies 80−75854
KCl:H, dichroic H- and U-centres by polarised bleaching of interstitial H 80−29766
KCl:H, dynamical superhyperfine interaction 80−2663
KCl:$I^-$$_2^1$H, fluorescence of interstitial H-centres 79−73987
KCl:Li^+, restricted interstitial motion of $H_A(Li^+)$ centre, ESR and uniaxial stress expts. 77−48053
KCl(Br)(I), U_2 and U_1 centres, optical excitations 80−2803
KN_3, migration of K^+ and N^0 interstitials, activation energies 79−77813
K_2OsCl_6, Cl NQR spectra by Fourier transform methods 80−75879
K_2OsCl_6, impurity H^+ ion motion, ^{35}Cl NQR obs., 77 and 298K 80−60451
K_2OsCl_6, single cryst. with H^+ interstitials, protonic cond. from dielec. meas. 80−107515
$LaNi_5$/H system, thermodynamics of H trapping 80−107444
$LaNi_5D_6$, cryst. struct., neutron diffr. obs. 79−19221
LiF, γ-irrad. pure and Mg-doped, phonon scatt. and interstitial clusters 80−70254
LiF, V_1 centre (F_3^{2-}) identification, ESR spectrum anal. 80−7164
LiH, cluster cryst., extended HMO calc. of defects 79−51521
LiH, defect form. at low temp., EPR, thermolum. and TSC study 80−107222
Li_3N, interstitial sites and anharmonic thermal vibrs. in cryst. struct., ionic cond. mechanism 80−107190
$LuMn_2$, Lu_6Mn_{23}, H_2 absorption effect on mag. props. 77−89931
Mg, HCP, vacancy and interstitial config. 79−65071
Mg, HCP, vacancy clusters and interstitials, computer simulation study 80−64992
Mg, HCP lattice, Huang diffuse scatt. from interstitials 80−88142
Mg:H, impurity energies and geometrics, self-consistent jellium calc. 79−99507
Mg-Ag, dil., ion irradiated, interaction between Ag and defects, channelling meas. 78−38766
Mg-Ag (0.18 at.%), channelling meas. of trapping efficiencies of solute atoms for self-interstitials 79−86829
$MgAl_2O_4$, faulted defect aggregates prod. by neutron-irrad. 80−107331
MgF_2:Li^+, defect struct., theory 77−47472
MgF_2:LiF crystal, defect struct., anelastic and dielec. relax. meas. 77−27938
MgO, electron irradiation damage, cryst. defects 80−107320
MgO, radiation induced O interstitials, EPR meas. 78−55866
MgO:H(D), electron irrad. induced diffusion of interstitial impurity 77−15452
MgO:Li, oxidation and reduction up to 1700K, defect prod. 79−39013
Mg_2SiO_4, directional depend. of transport for Mg interstitials and vacancies 79−69285
Mn film, heat treated, lattice distortion energy, resist. meas. 79−19492
Mn-MgF_2 cermet, heat treated, lattice distortion, resist. meas. 79−19492
MnD_x, synthesized at high pressures, neutron diff. anal. of struct. 80−28977
MnF_2:LiF, anelastic relax. of Li^+-Li^+ split interstitial defect 79−77678
α-MnS, defect energetics and range of homogeneity 78−47317
MnSb, interstitial cations, mag. and crystallographic study 79−55698
$Mn_{1+\delta}Sb$, ferromag., mag. disturbance around Mn interstitials 80−54868
Mo alloys, dil., HVEM bombarded, neutron damage simulation, defect cluster and dislocation obs. 80−107330
Mo, competition between interstitial atoms during segregation at grain boundaries, AES obs. *(Russian)* 77−25008
Mo, desorption of He, during stage III annealing, vacancy model 77−1123
Mo, elastic aftereffect after fast neutron irrad. at 5K 77−89431
Mo, electron radiation damage and props. of point defects 77−11590
Mo, H_2 diffusion enhanced by self-interstitial atoms, surface reaction const. determ. 80−75386
Mo, He ion irradiated, TEM 77−19994
Mo, interatomic pot. from phonon spectra 77−76355
Mo, ion bombardment by Ni^{2+}, TEM study of damage depth distrib. 78−10101
Mo, neutron dose depend. of elec. resist., vacancy-interstitial recomb. *(Russian)* 77−80546
Mo, neutron irradiated single crystals, vacancy reactions in III recovery 79−73220
Mo, pure and He doped, at. config. of $^1/_2\langle 111\rangle$ screw dislocation 79−65081
Mo sheet, 45° brittleness due to partial recrystallisation, 45° crack formation and propagation *(Russian)* 79−100238
Mo sheet, conc. of interstitial elements on lamination surface 77−86038
Mo:N, ion implanted proton-irradiated, annealing behaviour 78−91362
Mo:N film, high T_c amorphous phase stabilisation by interstitial nitrogen 78−23622
Mo-C dilute alloy defect cluster nucleation and growth under 1250 keV electron microscope *(Japanese)* 78−87663
Mo-Mn alloy, plasticity, fracture, strength depend. on C content *(Russian)* 80−35257
Mo-N solid solution, exam. of enthalpy of solution, variation with temp. 79−10947
Mo_2C, free energy of form. and thermodynamic props. of C in solid Mo 80−15266
N, in transition metals, electronic structure 79−1583
NH_4Br:Cu^{2+}, ESR and absorpt. spectra, 300-1500 nm 78−60492
$(NH_4)_2SO_4$:Cu^{2+}, ESR parameters, effect of pH of mother soln., trapping sites 80−15791
Na, adsorbed on Al, adatom valence-level position variation 80−88611
Na, thermodynamics of light interstitials, rel. to delocalised particles 79−46653
Na_2-β-Al_2O_3, far IR absorpt., Beevers-Ross sites, interstitials 80−66241
NaA zeolite:S, optical spectra 78−88342
NaCl, Born-Mayer parameters of He and Ar, interstitial interaction with neighbouring ions 80−100228
NaCl, X-irrad., F-thermal bleaching 77−89433
NaCl:H (Cl) interstitials repulsive parameters from electronic charge density overlap, diffusion 77−59006
NaCl(Br)(I), U_2 and U_1 centres, optical excitations 80−2803
$Na_2HAsO_4.7H_2O$:Cu^{2+}, ESR, Cu lattice location 78−52342

interstitials continued
$NaMgF_3$, defects induced by X- and vacuum UV irrad., optical and elec. study 80−107319
$NaMgF_3$, optical absorpt. of radiation produced defects 77−28604
NaN_3, X-irrad., EPR of N_2^- 77−66421
$NaNO_3$, dielec. loss anal., Debye type loss peaks 80−50260
Na_2O-K_2O-SiO_2, Na diffusion 78−26724
Na_2O-SiO_2 glass, conduction and dielec. loss mechanisms, paired interstitialcy model 80−107468
$NaPO_3$ glass, Na diffusion 78−63875
Nb, and alloys, interstitial impurity effects on strength 78−3194
Nb, BCC, stress-induced interaction and ordering 79−42057
Nb, channelling study of $^4He^+$ irradiation damage, effect of irradiation temp. 79−82271
Nb, channelling study of irradiation damage by $^4He^+$, effect of dissolved O_2 79−82270
Nb, defect annealing in 7 MeV-irrad. samples, positron annihilation obs. 80−24497
Nb, deformed, temp. effects on ageing, interstitial conc. depend. *(French)* 77−21182
Nb, diffusion of H, influence of H-H pairing, jump model 78−75878
Nb, diffusion of interstitial O_2, sink/barrier phenomena 79−60553
Nb, elec. resist. changes with plastic deform. 77−89749
Nb, elec. resist. due to interstitial H (D) 80−96848
Nb, electrotransport of H(D) at high H concs. 80−34246
Nb, ion bombard. by 5 keV Ar^+, sub-surface damage 80−103399
Nb, lattice distortion due to di-interstitial clusters 78−71726
Nb, low temp. diffusion of H and D from quenching and annealing study 80−6555
Nb, mobile interstitials after electron irrad., resistivity recovery meas. 79−55783
Nb, muon diffusion, μ^+SR meas. 78−39487
Nb, muon localisation and lattice dilation, μSR 79−56694
Nb, muon$^+$ depolarisation rate, anomalous temp. depend. 78−48104
Nb, neutron induced defect structs., TEM exam. 77−84802
Nb, neutron irradiated, TEM obs. of interstitial clusters 79−19288
Nb, relaxation intensity due to interstitial O, temp. effect *(French)* 77−86080
Nb, residual resistivity, effect of interstitial atoms of O, N and C *(German)* 77−11895
Nb, resistivity studies of interstitial He mobility 79−14800
Nb, resistivity variations caused by H and D interstitials, isotope effects 77−89750
Nb, solute trapping of H, symmetry of O-H pair 80−108488
Nb, stress induced interaction of point defect pairs, in BCC solutions 78−79608
Nb:Fe, diffusion mechanism, self diffusion enhancement 77−84992
Nb:H, lattice distortion and migration energy of H impurities 78−30796
Nb:N, H, atomic tunnelling of interstitial pair, specific heat meas. 78−47600
Nb:N,H(D), thermal cond., 0.07 to 1.5K, influence of N interstitials 79−65601
Nb:O, $^4He^+$ irrad.-induced lattice site change 79−99252
Nb-D, density fluctuations, small angle neutron scatt. study 79−60359
Nb-D, Huang diffuse scattering of neutrons 80−10544
Nb-D-H, equilib. H/D separation factors 80−59668
Nb-H, acoustic phonon anomaly at small wavevectors 78−59882
Nb-H, BCC, tetrahedral interstitial site H band modes, neutron scatt. obs. 79−55852
Nb-H, interstitial position of H from entropy of soln. 77−65989
Nb-H, modulated ordering, elastic free energy theory 79−94945
Nb-H interstitial alloy, props. and synthesis 79−69265
Nb-H system, Huang diffuse scatt. of X-rays from displacement field 77−15446
Nb-H systems, supercond., H conc. depend. *(Russian)* 77−47932
Nb-N, diffusion of H, incoherent neutron scatt., interstitial effects 79−60558
Nb-N, dil., low temp. interstitial hardening 79−20060
Nb-O interstitial diffusion coeff., effective charge *(German)* 77−35759
Nb-Si liquid quenched alloy, metastable A-15 and amorphous phases, interstitials 80−54394
Nb-Ta(V)(Ti)(Mo), resistivity due to H incorporation 80−70666
Nb-TiN(HfN)(ZrN), BCC solid soln., nitride solubility, alloying effects *(Russian)* 79−51262
Nb-Y, and Nb, mech. props., neutron irrad. and Y scavenging effects 77−90394
$NbH_{0.026}$, nucl. acoustic reson. of interstitial H 79−51867
$NbH_{0.11}$, incoherent struct. factor of H, neutron scatt. exam., quasielastic energy spectrum 79−99186
NbH_x, structural transform. rel. to order-disorder transform. 80−60858
NbH(D), ordered, TEM obs. of anisotropic lattice distortions 79−7579
$NbH_x(D_x)$, cryst. struct., phase diagrams, order-disorder transition 78−55836
$NbH_{0.004}N_{0.007}$, H-diffusion, interstitial trapping, quasielastic neutron scatt. study 79−42298
NbO_x, interstitial O, diffuse neutron scatt. 78−83809
$Nb_{12}O_{29}$-Nb_2O_5, oxide defect structures of stable and metastable phases, 800 to 1100°C 79−46651
Nb_3Sn, A-15 struct. Nb based superconductors, irrad. type influence on radiation defects 80−15093
$Nb_{53}Ta_{47}$, pure and hydrogenated crysts., effect of pressure on elastic consts. 80−7614
$Nb_{1-x}V_xH_x$, interaction between interstitial H and V, NMR meas. 77−59471
Nb-H, possibility of H ordering, DTA meas. 79−52174
Ni 200, C interstitial effect of yield point develop. during static strain ageing, model 78−88498
Ni binary alloys, constituent segregation during irradiation 79−55791
Ni, cluster approach to single H atom in single crystal 78−47334
Ni, computer simulation of point defects and planar defects 78−43013
Ni, electron irrad. in HVEM, interstitial loop growth 80−107326
Ni, ferromag., Knight shift of hyperfine field at positive muon 77−43925
Ni, ferromagnetic zero point motion effect on hyperfine field at interstitial positive muon site 80−2681
Ni, Frank loops, growth kinetics and 'preference factor' during electron irradiation 78−22723
Ni, HVEM obs. of irrad. damage 77−35589
Ni, interstitial diffusion of C in single crystals, stress distrib. changes 77−47626
Ni, interstitial site determ., μSR technique 80−71287
interstitials continued
Ni, irradiated, numerical simulation of void nucleation, dislocation densities, pt. defect conc. 79−73208
Ni, lattice distortion around interstitials 77−1122
Ni, neutron irrad., void formation, C interstitial effects 77−76471
Ni, plastically deformed, recovery stages III and IV investig. by positron annihilation 77−31715
Ni, pure and doped, mech., mag. relax. meas. dumb-bell self-interstitital reorientation *(German)* 78−52879
Ni, self interstitial migration and crowdion conversion, dislocation pinning expts. 77−84762
Ni, solubility of C *(Czech)* 79−77757
Ni superalloy powders, removal of interstitial contaminants 78−84735
Ni, TEM exam. of ion damage in FCC metals 78−87727
Ni:B, impurity electronic struct. calc., ^{12}B NMR data anal., magnetisation decrease 79−47046
Ni:C, H(D), isotope effects of C-H and C-D complexes 77−20129
Ni:H, energy and electron density of states 78−51929
Ni:He, defect props., quantum-chemical and lattice-defect hybrid approach 79−4528
Ni:He, implanted, profile meas. technique 77−80524
Ni:Mn, radiation-enhanced diffusion, effect of point defect fluxes 77−89588
Ni-C, ferromag., prep. by splat-quenching, obs. of electronic struct. of interstitial C 77−62868
Ni-C interstitial alloys, electronic struct. 77−35886
Ni-Cu, hydrogenated, Curie point, cluster magnetism 78−14960
Ni-Fe (20at.%), vacancy-C interaction, Lomer's model insufficiency *(French)* 77−76456
Ni-Fe-C, 20 at.% Fe, vacancy-C interaction, induced mag. anisotropy *(French)* 79−55775
Ni-Ge , defect-solute interactions and radiation-induced segregation 80−25705
Ni-H system, cluster calc. of electronic struct. of interstitital H 78−43326
Ni-Mn, hydrogenation kinetics, magnetisation, interstitial H influence 80−35528
Ni-Mn-H, hydride phase form. and decomposition in hygh-press. gaseous H_2, magnetisation meas. 79−56953
Ni-Si, defect-solute interactions and radiation-induced segregation 80−25705
Ni-Si solid solution alloys, irrad., γ phase precipitation, interstitial dislocation loops 77−1839
NiAl, nonstoichiometric, interstital defect cluster obs. 80−107226
NiD_x synthesized at high pressures, neutron diffraction anal. of struct. 80−28977
Ni_3Fe, disaccommodation meas. after low temp. electron and neutron irrad. 80−88832
Ni_3Mn, fission neutron disordering at 5K, exam. 78−47434
$Ni_{1-x}O$, electronic cond. at high temp., vacancies and interstitials effect *(French)* 78−79990
β-Ni_3S_2, formed during sulphidation of Ni, defect struct. and chemical diffusion 78−2115
$Ni_{1.1}Sb$, temperature effect on lattice consts., Mossbauer spectra and density 80−88124
Ni_3Sn_2, single cryst. embrittlement and subboundary hardening via interstitial segregation *(Russian)* 77−12679
O, in transition metals, electronic structure 79−1583
Pb and Pb alloys, interstitial substitutional model for anomalous diffusion 80−84330
Pb, charged particle irrad., damage and recovery processes 77−69002
Pb, electron irradiation at 4.7K and below 3K, annealing expts. 77−11595
Pb-Ag, solid soln. hardening due to metal interstials 77−52337
Pb-Au, interstitial and substitutional distrib. 80−84204
Pb-Au (0-0.0918 at.%), lattice parameter changes due to Au dissolution 79−77558
Pb-Cu, charged particle irrad., damage and recovery processes 77−69002
$Pb_{1-x}Al_xF_{2+x}$, ionic cond. of quenched and annealed specimens, interstitial cond. mechanism 80−2199
$Pb_{1-x}Bi_xF_{2+x}$, solid soln., struct. and ionic cond. correl., neutron diffr. study *(French)* 80−84324
PbF_2 based solid solns., ion transport 80−107545
PbF_2, cubic and orthorhombic, press. and temp. depends. of ionic cond. 79−95207
PbS_xSe_{1-x}, chalcogen interdiffusion, electron microprobe obs. 79−28145
Pd, elec. resist. due to interstitial H (D) 80−96848
Pd, H(D) interstitial interactions rel. to diffusion and ordering transition 80−34249
Pd:H, energy and electron density of states 78−51929
Pd-Ag-H, alloys, 25-50% Ag, thermodynamic props., 555-700K 79−65216
Pd-Ag-H(D), elastic energy dissipation peak 80−60905
Pd-Cu-H(D) dilute alloy soln., thermodynamic props. at high-temp. 79−99334
Pd-D-H, equilib. H/D separation factors 80−59668
Pd-Fe-H alloy, Mossbauer line shift with H conc. *(Russian)* 77−40165
Pd-H, interstitial position of H from entropy of soln. 77−65989
Pd-H system, cluster calc. of electronic struct. of interstitial H 78−43326
Pd-H system containing d impurities, chem. binding energies of point defects 80−107214
$Pd-H_2$, dilute soln., high temp. thermodynamics, partial molar props. 77−15597
Pd-H(D), elastic energy dissipation peak 80−60905
Pd-Pt-H(D), elastic energy dissipation peak 80−60905
$Pd_{1-x}Ag_xH_n$, positron annihilation examination of electronic structure *(German)* 77−69931
$(Pd_{0.8}Au_{0.2})D_{0.04}$, lattice location of D, ion channelling obs. 78−67708
α-$PdD_{0.007}$, lattice location and thermal props. determ. of D by ^3He channelling 78−38747
α-PdH_x, electronic states and Fermi surface props. 80−29310
PdH_x, PdD_x, ordering, resistivity, annealing and neutron diffr. obs. 79−34030
PdH_x:Co(Fe), diffusion and interstitial site occupancy, Mossbauer spectra 80−20555
$Pd_{13}Pb_{9.r}$, cryst. struct., X-ray study 80−103293
Pt, crowdion conversion to dumbbell, two-interstitial model, thermal neutron irrad. 80−33992

interstitials continued
Pt, deuteron irrad., energy release and resist. recovery, self-interstitial-atom interaction energies 79−95002
Pt, electron irradiated, interstitials activation vol. 79−51154
Pt, Frenkel defect migration and reactions, by subthreshold recoil events, exam. 78−47364
Pt, interstitial thermal conversion study by elec. cond. meas. 80−15096
Pt, ion irrad. damage, temp. depend., electron microscopy obs. of defect kinetics 80−107339
Pt, radiation damage, recovery of elec. resist., interstitial migration and clustering 77−11604
Pt, radiation damage, self-interstitials migration modes and thermal conversion 79−65126
Pt, radiation damage recovery curves, evidence for two self-interstitial configs. 77−7773
Pt, recovery spectrum after thermal neutron irrad., resist. obs., Au addition effect and defect conc. depend. 80−65057
Pt, TEM exam. of ion damage in FCC metals 78−87727
Pt, thermal and fission neutron produced defect configurations 78−47432
Pt-Au, ion-irradiated, self-interstitial migration in stage II recovery, FIM obs. 77−59140
Pt(Au), ion irradiated alloys, stage II recovery 78−47440
Pu, diffusion of Co in FCC and BCC phases, diffusion coeff. and mechanism 77−28046
RbBr:I^-, OH^-, luminesc. of interstitial atomic H 80−89062
$RbCaF_3$, optical absorpt. of radiation produced defects 77−28604
RbCl:Br^-(I^-), interstitial atomic H centres, formation kinetics and struct. MO calc. and EPR studies 80−75854
RbCl:Co^{2+}, dielectric loss, impurity sites 79−91348
RbCl:H, dynamical superhyperfine interaction 80−2663
RbCl:I, H, fluorescence of interstitial H-centres 79−73987
$RbMgF_3$, irradiated, thermal conductivity 78−22909
$RbMgF_3$:Mn, low-temp. radiation damage, optical absorption meas. 78−22761
$RbMnF_3$:Fr, pure and doped, unirradiated and electron irrad., energy transfer 80−108254
Rh:H, energy and electron density of states 78−51929
Sb, muon precession freq., anomalous shift 78−39488
Sc_2O_3, elec. cond. rel. to defect struct. 77−80814
Se, single crystals, fast neutron irradiated, annealing expts., dark conductance, reflectivity spectra 77−85266
n-Si, 300 keV proton irrad., temp. depend. of defect prod. 78−6113
Si, ambient effect of O precipitation, self interstitial mechanisms, IR spectra, TEM study 80−66510
Si, amorphous layer prod. by ion implantation, diffusion broadening, ESR study 80−92552
Si, atomic displacements damped by chemical bonds, computer calc. 78−47370
Si, Czochralski grown, dislocation free, swirl defect form., doping effect 80−92519
Si, Czochralski grown crystal, O precip., nucleation behaviour and dislocation loop form. *(Japanese)* 80−59664
Si Czochralski wafer, interstitial oxygen, rel. to oxide induced stacking faults 78−10062
Si, deep donor character of muons and protons 80−10911
Si, defect form. under radiation-accelerated diffusion conditions 80−19854
Si, defects, divacancy and split 100 interstitial, electronic structure calc. 80−65494
Si, diffusion mechanism of P, migration channels along vacancies and interstices 80−79996
Si, diffusion of self-interstitials and As, B and P, radn.-enhanced 80−29216
Si, dislocation free, C and O impurity clouds, heat treatment influence on light scatt. 80−6427
Si, dislocation free, O_2 precipitation, stacking fault form. 78−38731
Si, electron beam irrad., {113} faults, nature and origin 80−70258
Si, electron irrad., rod-shaped defects, electron microscopy and IR spectra obs. 80−39159
Si, electron irrad. induced defects, bulk photo-EMF meas. 80−39160
Si, electron irradiated, photolum. due to interstitial complex 77−44048
Si, electron-hole droplets nucleation at swirl defects 79−15095
Si, electron-irradiated, {113} loops obs. 79−82225
Si, fast electron irradiated, models of luminescence centres, role of interstitials 77−81153
Si, foreign interstitial atoms rel. to thermal intrinsic defects 80−29018
Si, H-related interstitial defects, vibr. electronic struct., extended Huckel theory 77−62604
Si, He impurity props. investigation by EHT calcs. 79−99183
Si, high dose self-irrad., spatial correl. between primary and secondary defect profiles 80−59536
Si, impurity interstitials, EHT calcs. 80−24845
Si, impurity levels of H and muons 79−56162
Si, interstitial swirl defect form. in dislocation free floating zone cryst. 77−7682
Si, interstitials and lattice vacancies 78−10038
Si, interstitials in radiation defect formation 77−15461
Si, ion beam irrad., defects prod. by individual displacement cascades, TEM study 80−70265
Si, ion bombarded, radiation defect formation, atom-atom collision cascades modelling 80−10582
Si, ion implanted, interstitial generation and loop form. during annealing in oxidising medium 80−107225
Si, ion irradiation prod. of stable vacancy-interstitial pairs 77−27925
Si, ion-implanted, secondary defects development, three-stage model 78−87725
Si, irradiated, nature of 0.97 eV A band luminesc. 77−44049
Si, migration energy of intrinsic point defects in different charge states 77−89582
Si, nearly perfect crysts., point defect aggregates, high resolution diffuse X-ray scattering study 80−49211
n-Si neutron and electron irrad., isochronous annealing influence on edge absorpt. 80−11449
Si, neutron irrad., EPR, ⟨100⟩ split di-interstitial, positive charge state 77−20698
Si, neutron irrad., internal friction obs. of defects 78−51597
Si, neutron transmutation doping, at. displacement effects 80−19852
Si, oxidation induced stacking fault growth, role of point defects 78−10061

interstitials continued
Si, oxidation stacking faults, shrinkage and growth, bulk O_2 effects 80−96546
Si, oxidation-induced stacking faults, influence of annealing ambient on shrinkage kinetics 80−29035
Si, P diffused sample, stacking faults and dislocations formation from interstitials 78−95059
Si, point defects, negative-U props. 80−49660
Si, precipitation of O, 1000°C TEM, IR absorpt. and X-ray studies 80−34194
Si, proton irrad., efficiency of form. and nature of defects, Hall meas. 80−6444
p-Si, radiation defects by annealing, kinetics anal. 79−33018
Si, rel. to oxidation effects on diffusion of P 79−51309
Si resistivity and carrier mobility effects of dissolved interstitital O_2 77−76824
Si, self-diffusion coeffs. between 1320K and 1660K, extended-interstitial mechanism 77−84985
Si, self-diffusion mechanism 79−90824
p-Si, self-interstitials, influence of white light on annealing process *(German)* 79−19245
Si, self-interstitials, vacancies and their clusters 77−80500
Si, small defects in Czochralski grown and zone-floated monocrystals, TEM identification 79−95001
Si, stacking fault growth, oxidation-induced, HCl and interstitial effects 80−49241
Si, status of defect studies 77−84742
Si swirl defect characterisation in floating-zone cryst., comment 77−4098
Si, swirl defect formation in floating-zone cryst., reply to comments 77−4099
Si, swirl defects, formation by agglomeration of self interstitials 77−80507
Si, thermal oxidation, mechanism of appearance of surface roughness and surface defects 77−7956
Si, thermal oxidation kinetics, steady-state transport anal. 80−71773
Si, thermal oxidation kinetics, theoretical perspective 80−76387
Si, vacancies and interstitials 80−29015
Si, vibrational properties of the ⟨001⟩ split interstitial 78−91405
Si wafer, Czochralski grown, interstitial O gettering 77−86196
Si wafer, heat treatment behaviour of microdefects and residual impurities, X-ray diffr. and IR absorpt. study 80−49214
p-Si wafer, self-interstitials form. during chemicomech. polishing *(German)* 79−34175
n-Si wafer, trap centres of self-interstitials 80−75516
Si wafer O interstitial IR absorption spectrometry, multiple reflection correction 80−55131
Si:Al, electron irrad. induced defects, transient capacitance study 80−59516
Si:Al, recomb. enhanced migration of interstitial Al 79−82201
Si:As, displacement effect beam energy depend., vacancy trapping 80−33996
p-Si:B, defect energy levels with 1 MeV electron irrad. and annealing, transient capacitance spectra 77−62860
Si:B, ion implanted, struct. of rod defects, TEM obs. 78−71744
Si:B, irrad. with fast neutrons true profiles of impurity photocond. bands from piezodichroisms 79−91103
p-Si:B, piezo-spectroscopic study of defects *(Russian)* 77−28607
Si:B, self-interstitials location by Rutherford backscatt. of channelled ions 80−2101
Si:B (0.2 wt.%) ion implanted, B atom displacement due to low temp. irrad. 80−88234
p-Si:B(Al), radiation defect form. and annealing study using Hall effect, cond. and carrier diffusion length 80−84214
Si:B(N)(O), interstitial Si atom formation by light ion bombardment 78−47406
Si:B(Sb)(P), microdefect formation depend on doping, Cu decoration, X-ray transmission topography, preferential etching 79−69120
Si:C, electron irrad., C interstitial, photo EPR 77−16175
Si:Co, Mossbauer spectra unstable line due to interstitial Co 79−11631
Si:Cr, photoconductivity exam. 77−20361
Si:D, ion implanted, struct. of impurity centre 79−7623
Si:Fe, B thermally activated Fe interstitial, elec. and kinetics props. *(German)* 80−34035
Si:Fe, EPR and neutron activation anal. of thermal defects 78−91355
Si:Fe, interstitial form., Au dopant effect 80−29611
Si:Fe, solubility study by EPR and neutron activation anal. 80−75361
Si:Fe^0 interstitial localisation, EPR spectrum 79−1582
Si:Gd, radiation defect form., effect of Gd impurities, elec. and optical meas. 78−71764
Si:H, interstitial electronic struct., self-consistent pseudopotential calcs. 79−73469
Si:In, electron irrad., Hall effect meas. 80−2401
Si:Li, amorphous, interstitial doping by in-diffusion and implantation and elec. characterisation 78−26585
Si:O, dislocation-free, Si-O complexes, heat treatment effects 77−62557
Si:O, effect of interstitial O on elec. props. 77−76846
Si:O, electrial and infrared spectroscopic investigations 80−34389
Si:O, implanted O location, channelling effect meas. 78−26593
Si:O, impurity conc. profiles, scanning IR absorpt. using semicond. laser 80−50376
Si:O,C, electron irradiated, indirect vacancy-interstitial recomb., IR absorpt. meas. 77−43209
Si:P, interstitial supersaturation near P-diffused emitter zones 79−65541
Si:P, ion implantation defect annealing investig. by CESR 77−8404
Si:P, metallic, heat treatment effects, EPR and photoluminesc. 77−77262
Si:P bipolar transistors, interstitial supersaturation and misfit dislocation climb, TEM study 80−70203
Si:P(B), high temp. impurity diffusion via vacancies and self-interstitials 80−24667
Si:Sb, Mossbauer spectra of ^{119}Sn defect struct. 80−97174
Si:Sm, implanted impurity location, Mossbauer and channelling expts. 80−39128
Si:Sn, Mossbauer study of defects due to ^{119}In implantation 80−80641
Si:Te, Mossbauer spectra of ^{119}Sn defect struct. 80−97175
Si-H, amorphous, struct. anomalies, theoretical interpretation 79−90556
Si-O system, modern view 78−10045
Si-SiO_2 interface, oxidation stacking faults, growth rel. to self-diffusion 80−49239

interstitials continued
SiO_2, g-tensor of interstitial O and broken Si-O bond, MO model calc. 79−78520
SiO_2, vitreous, fast neutron irrad. effect on struct., interstitials role 78−26599
SiO_2, vitreous and cristobalite, interstitial struct. anal. from gas solubility data, review 79−23525
SiO_2-Si interface, interaction of point defects, electron microscope exam. 77−7979
Sm, electron radiation damage, elec. resistivity change rates 80−59954
$SmCo_5$, magnetic aftereffect of H and D 79−56573
SmS type semiconductors, electronic struct., influence of point defects 80−70650
β-Sn, configuration of ^{57}Fe, Mossbauer effect measurements 78−47333
β-Sn, dissociative diffusion of ^{57}Fe, Mossbauer expts., 90-462K 79−7714
α-Sn, ion implanted, defect struct., Mossbauer spectra 80−80214
SnO_2 CVD coating on glass, elec. resist. rel. to cryst. microstruct. 80−84520
SnO_2:Mo^{5+}, hyperfine and superhyperfine interactions, EPR 77−8398
$SnSe_xTe_{1-y}$, semicond. chalcogen interdiffusion coeffs., antifrenkel defects, interstitials *(German)* 77−43375
$SrCl_2$, anion diffusion mechanism 80−2201
$SrCl_2$, ionic cond., self-diffusion, rel. to defect motion, mol. dynamics study 80−65282
$SrCl_2$, point defect parameters, ionic cond. study 80−107490
$SrCl_2$, pure and doped, disorder and defect props. 80−107217
SrF:rare earth $^{3+}$, reorientation of dipoles 77−8494
SrF_2:Er, activation vol. for interstitial motion, dielec. const. meas. 80−49412
SrF_2:La, type-I dipole reorientation, activation vol. determ. from dielec. const. 80−88916
SrF_2:Y^{3+}, diffusion of bound and free $F_{(i)}^-$ interstitials, NMR meas. 79−78542
SrO:Co, noncentral and interstitial ion complexes, ESR obs. 80−71169
SrO:Ni, optical absorption spectra in visible and near IR region 80−45119
$Sr_{1-x-y}U_xCe_yF_{2+2x+y}$, solid soln., ionic cond. 79−99356
Ta, BCC, stress-induced interaction and ordering 79−42057
Ta BCC lattice, strain ordering in interstitial solutions 80−107420
Ta, diffusion of interstitial O_2, sink/barrier phenomena 79−60553
Ta, elec. resist. due to interstitial H (D) 80−96848
Ta, electrotransport of H(D) at high H concs. 80−34246
Ta, internal friction meas. of O, N diffusion 78−75888
Ta, interstitial ordering, O effect, $Ta_{64}C$ artifact 79−99185
Ta, low temp. diffusion of H and D from quenching and annealing study 80−6555
Ta, muon diffusion, μ^+SR meas. 78−39487
Ta, resistivity due to H incorporation 80−70666
Ta, resistivity variations caused by H and D interstitials, isotope effects 77−89750
Ta, stress induced interaction of point defect pairs, in BCC solutions 78−79608
Ta, with mobile H impurities, anomalous nuclear acoustic reson. line shape 77−20730
Ta:H, lattice distortion and migration energy of H impurities 78−30796
Ta-H, BCC, tetrahedral interstitial site H band modes, neutron scatt. obs. 79−55852
Ta-H, interstitial position of H from entropy of soln. 77−65989
Ta-H, N interstitial trapping of H, hydride precip., resist. meas. 77−20293
Ta-H alloy, high conc., Huang diffuse X-ray scatt. from lattice strains 78−38746
Ta-O solid soln., interstitial ordering and precipitation at 100 to 270°C, exam. 78−52813
$TaD_{0.10}$, lattice location of D, ion channelling obs. 78−67708
Ta_2D_{1+x}, atomic displacement of Ta determined by deuteron magnetic resonance 79−37701
Ta_2H, single cryst., X-ray diffr. study on H ordering 79−14736
$TaH_x(D_x)$, cryst. struct., phase diagrams, order-disorder transition 78−55836
TaS_2 (1T) electron irradiated, lattice contraction 80−59520
Te:Ta, quadrupole interaction at ^{181}Ta, TDPAC meas. 80−20521
Th, diffusion and electrotransport of Fe, Co and Ni, 965-1625°C 79−90828
$ThMn_2$, Th_6Mn_{23}, H_2 absorption effect on mag. props. 77−89931
Ti alloy, BT22 quenched from 850-1200°C, X-ray study of structure *(Ukrainian)* 80−24402
Ti, commercial-purity, Portevin-Le Chatelier effect, mechanism 77−8886
Ti, effects of strain rate, temp. interstitial contact on electroplastic effect 79−83279
Ti, neutron irradiated, characterization of dislocation loops 80−88155
Ti:O, channelled ions, flux peaking study using protons, H_2^+ and H_3^+ ions 79−1450
Ti-Al-Sn (5, 2.5 wt.%), fracture mechanism at cryogenic temps. 78−64642
β-Ti-Al-V, annealed, differing interstitial O content, fatigue crack propag. resist. 79−11696
Ti-Al-V, VT6 alloy, butt welded joints, electron beam welding conditions effecting interstitial impurities distribution 80−39136
$Ti-C_x(N_x)(O_x)$, solid soln. film prep. by reactive sputtering, solubility and effect on props. 79−28231
Ti-Fe, diffusion of stored H, Mossbauer study 80−34838
Ti-Fe-H(D) system, struct. phase diagram, thermodynamics and diffusion *(German)* 79−56963
Ti-H system, cluster calc. of electronic struct. of interstitial H 78−43326
Ti-O, dil. HCP solid soln., O interstitial distrib. effect on lattice parameters 78−30588
Ti-Ta (4.37 wt%), oxidation kinetics, 1258-1473K, and at pressure of 0.013, 0.133 and 1.0 bar 80−89411
Ti-V-H system, BCC, hydrogen effects on anisotropic elastic props. 79−24565
Ti-V-Mo alloy system, phase equilibria and interstitial effects, TEM and X-ray diffr. study 79−43204
TiC, low-temp. reactor irrad., calorimetric investig. 77−80547
TiC_x, effect of structural vacancies on neutron radiation damage 77−35591
TiC_xO_y, structural mechanism of O inclusion into lattice 78−22707
TiFeD, cryst. struct., Mossbauer and neutron diffr. obs. 80−34839
γ-TiH_x, interstitial H diffusion mechanism, NMR spin-lattice relax. study 80−103515

interstitials continued
TiN_x, cryst. and internal structs., electron diffr. and microscopy 77−27861
TiNi-H system, thermodynamic rels. and struct. transformations 80−49385
$TiO_{0.42}$, diffuse X-ray and neutron scatt. due to out-of-step configurations of O atoms 77−62518
TiO_2, nonstoichiometry study, thermal emission of electrons 80−108317
TiO_2, slightly reduced rutile, diffusion of Ti 78−79799
TiO_2:Cr(Ta), slightly doped, elec. cond. and defect struct., charge compensation and point defect model 80−75568
TiO_2:Mo^{5+}, interstitial EPR, g-tensor and hyperfine tensor 80−84647
TiO_2:Nb and TiO_2, reduced, thermoelec. power meas. at high temp., point defect model 77−32030
TiO_2:$Nb_2O_5(Ta_2O_5)$, conduct. rel. to defect structure, obs. 77−76392
TiO_{2-x}, nonstoichiometric and Nb_2O_5 doped rutile, defect struct. and thermodynamic props. 79−86790
TiO_{2-x}, nonstoichiometric and Nb_2O_5 doped, defect struct. and thermodynamic props. 79−90650
TiO_{2-x}, reduced, cond. between elec. props. in equil. at 1100°C and after quenching, defects role *(French)* 80−44582
TiO_{2-x}, slightly reduced rutile, Ti interstitials, proton channelling obs. 77−35551
TiO_{2-x}, slightly reduced semiconducting, channelling expts. with 6 MeV protons, defect structs. 78−2117
TiO_x, interstitial alloy, electronic state, XPS, mag. susceptibility and elec. resist. 77−12486
Tm-H solid solution, struct., 20-500°C 79−90643
U, irradiation growth during fission fragment and proton bombard. 80−92568
UC, fission dose depend. of lattice parameter changes 77−24333
UO_2, irradiation induced vol. change 78−67740
UO_2, O diffusion mechanism 78−33249
UO_2, thermodynamics, defect props. 77−67810
$UO_{2\pm x}$, model of response of fission gas bubbles to dynamic behaviour of point defects 79−37735
$UO_{2.12}$ hyper-stoichiometric, defect struct., anal. of neutron diffr. data 78−26562
V, anomalous slip, suppression by O interstitials 77−28875
V, BCC, stress-induced interaction and ordering 79−42057
V, elec. resist. due to interstitial H (D) 80−96848
V, electron-irradiated, positron annihilation study 80−70259
V, electrotransport of H(D) at high H concs. 80−34246
V, interstitial impurity and substitutional solute interaction, internal friction meas. 78−10082
V, lattice distortion due to di-interstitial clusters 78−71726
V, muon diffusion, μ^+SR meas. 78−39487
V, muon localisation and lattice dilation, μSR 79−56694
V, neutron diffraction determ. of O, N, C interstitial sites 77−i9944
V, polycrystalline, strength, ductility, 4.2 to 400K, O_2 effect 77−36529
V, pure and hydrogenated crysts., effect of pressure on elastic consts. 80−7614
V, purification and plastic props. 80−25810
V, resistivity variations caused by H and D interstitials, isotope effects 77−89750
V, stress induced interaction of point defect pairs, in BCC solutions 78−79608
V, trapping of D by O interstitials, channelling study using ion induced nuclear reactions 79−4316
V:H, lattice distortion and migration energy of H impurities 78−30796
V:O, lattice location study, of 0, 1 MeV deuteron channelling 79−10846
V-H, BCC, tetrahedral interstitial site H band modes, neutron scatt. obs. 79−55852
V-H single crysts., elastic consts., temp. depend., H effects 80−66563
V-O alloys, quenched, local ordering of O, electron microscopy and diffr. 80−59453
V-O solid soln., BCC, modelling of interstitial solute behaviour 79−77748
α-$VD_{0.7}$, interstitial vibr., coherent neutron scatt. study 79−42196
α-$VD_{0.7}$, vibrations of interstitial D, coherent neutron scatt. 80−96612
V_2D, BCC α-phase, metal atom-induced diffuse X-ray scatt. from short range order 79−60358
V_2D, short-range interstitial order above crit. temp., diffuse X-ray scatt. obs. 79−95159
$VO_{1.30}$, ordered phase, X-ray anal. of defect struct. 79−99177
VO_x, defect ordering, electron diffr. obs. 79−23595
VO_x, defect struct., local ionic arrangements in disordered phase 80−10532
$V_{0.97}O_{0.03}$, lattice dynamics exam., neutron scatt. 79−23689
α-V_2O_5:Li(Na)(Cu), far IR absorption spectra meas. 77−73158
V=O, lattice distortion and migration energy of O impurities 78−30796
$VaH_x(D_x)$, cryst. struct., phase diagrams, order-disorder transition 78−55836
W, competition between interstitial atoms during segregation at grain boundaries, AES obs. *(Russian)* 77−25008
W, electron irrad., or ion irrad., stage II, point defect struct., FIM 77−80542
W, Frenkel pair creation and stage I recovery of electron irrad. cryst. near threshold 79−1463
W, ion implantation, $^4He^+$ range profile and ^4He diffusivity meas. 79−33022
W, neutron irrad., at thermal energies, annealing exam. of recovery 78−47355
W, self-interstitial diffusion, fully dynamic computer simulation 77−39687
W, single crystals, electron irradiated, recovery of resistivity, 4.5-380K *(German)* 78−87714
W, split crowdion interstitial, (111), computer simulation of TEM imaging 78−71723
W, substruct. stability of single crysts. on high temp annealing *(Russian)* 77−66666
W, thermal neutron irradiated, radiation damage and stage III defect annealing 78−51586
Y, electron radiation damage, elec. resistivity change rates 80−59954
YAG:rare earth metal, US absorpt. meas., relax. model 80−24539
YH_2, location of H, PMR rigid-lattice second moment meas. 80−71198
YMn_2, Y_6Mn_{23}, H_2 absorption effect on mag. props. 77−89931
Y_2O_3, nonstoichiometry study, thermal emission of electrons 80−108317
Yb, electron radiation damage, elec. resistivity change rates 80−59954
Zn, 6.1 MeV α-particle irrad., stage III and IV recovery kinetics, defect diffusion 77−76474

interstitials continued
Zn, α-irradiation damage and stage I recovery 78−38759
Zn, defect recovery after low temp. electron irrad. 78−10090
Zn, electron irradiated, diffuse X-ray scatt. exam. of self interstitials 79−73213
Zn, electron irradiated, diffuse X-ray scatt. exam. of interstitial clustering during thermal annealing 79−73214
Zn, electron radiation damage in HVEM, nature of defect clusters 78−59838
Zn, faceting of interstitial loops 78−47381
Zn, HCP lattice, Huang diffuse scatt. from interstitials 80−88142
Zn single cryst., dislocation velocity and plastic deform. 80−64998
ZnO, dislocation loop nucleation on prismatic faults in high voltage electron microscope 77−72620
ZnO, electron irrad., vacancies and interstitials, EPR meas. 79−14803
ZnO, irradiation in high voltage electron microscope dislocation loops study 80−88157
ZnO, vaporization from spinel solid solns. 77−76541
Zn_3P_2, elec. cond., Hall effect, P interstitial effects 80−84465
ZnS:Al, IR studies of Al complexes 79−33741
ZnSe, heat-treated in controlled partial press. of Zn or Se, TSC 80−59910
ZnSe, pure and Cu doped, elec. props. after heat treatment in Zn or Se vapour 79−99505
ZnSe, self-compensation, role of impurities 80−92850
Zr alloys, creep and growth, irradiation induced, rate theory approach 80−89294
Zr alloys, creep and growth, irradiation induced, microstruct. depend. 80−93602
Zr and alloys, neutron irrad. at 573 to 923K, damage struct. 80−107334
Zr, electron irradiated, interaction of self interstitials with O_2 atoms 79−65118
α-Zr, H location in HCP phase 78−18637
Zr, irradiation growth, reaction rate theory calcs. 80−88212
Zr, neutron irradiated, dislocation loop nature 77−47489
α-Zr, point defect props., effect on irradiation behaviour of Zr alloys 78−30609
Zr, void swelling during electron irrad., HVEM study 80−92559
α-Zr:H, energy of interstitial H calc. 79−23596
Zr-Au (0.3 and 0.2 wt.%), irradiated, backscattering meas. of Zr self-interstitial atom trapping by Au 77−69014
Zr-base alloy as reactor core material, microstruct., deform. and fracture 78−4988
Zr-H alloy, soft X-ray emission spectra, electronic struct. 79−65959
Zr-Nb alloy, direct imaging of point defects using TEM 77−35453
Zr-O(2.85 at.%), Pr effect on internal friction of single crystal 77−4155
Zr-Rh, absorbed interstitial H_2 energy 79−82198
ZrC, low-temp. reactor irrad., calorimetric investig. 77−80547
ZrC, sintering shrinkage, effect of struct. vacancies in interstitial phases 78−60630
$ZrH_{1.8}$, radiation-induced defects in hydrogen sublattice 79−37739
$ZrH_{1.9}$, neutron irrad. induced defects, nature and thermal stability 77−50246
ZrH_x, laser irrad. effect on interstitial phases, metallographic obs. 79−37734
$ZrMn_2D_3$, deuterated hexagonal Laves-phase, D atoms interstices and diffusion paths, positional disorder 79−73334

intersymbol interference
digital fibre optical communication system, average error probability calc. 80−53228
digital fibre-optic transmission system average error probability 77−27380
error probability anal. of digital fibre optic communication systems 78−46775
optical channel conditioning against intersymbol interference and timing errors *(Italian)* 77−23622
optical communication channel, error probability calc. charact. function method, intersymbol interference 80−53227
optical fibre communication systems, computer design aids 80−28350
optical fibre digital transmission error probability, quantum noise effects *(Italian)* 77−23623
optical fibre system, intersymbol interference and transmission medium instability 77−65638

intersystem crossing *see nonradiative transitions*

intramolecular potentials *see potential energy functions*

intramolecular vibrations *see molecular vibration; molecular vibration in solids*

intrinsic magnetisation *see spontaneous magnetisation*

Invar
amorphous alloy, mag. and elastic props. *(Japanese)* 79−20100
antiferromagnetic Cr-Fe-Mn Invar alloy, Elinvar charact., US wave propag. charact. 77−11640
Arrott plots rel. to itinerant electron charact. 77−73009
atomic structure, phase diagram 79−94964
band structure contribs. to shear consts., deform. pot. formalism and Stoner model 79−91280
bulk modulus anomaly, rel. to itinerant electron model of ferromag. 77−48025
conference, Nagoya, Japan (Sept. 78) 79−56481
crystal field model of Invar effects in weak and strong ferromagnets 79−56484
Curie temperature and elec. resist., effect of press. 77−85449
deformed, magnetism and temp. depend. of effective field on ^{57}Fe *(Russian)* 79−24234
dislocation motion anomaly 80−10554
elastic and magnetoelastic effects 79−56589
electrical resistivity temp. depend., 300-1300K *(Ukrainian)* 77−69290
electrical transport props. and Invar features *(Russian)* 78−14710
electronic structure, influence of temp. X-ray photoelectron study 77−28681
exchange interactions between ferromag. and antiferromag. components 80−29545
Fe-Ni-C spin pinning effect in RF collapse studies, Mossbauer spectroscopy 80−44971
ferromagnetic, influence of magnetoelastic effects on lattice vibrs., neutron scatt. meas. 78−2722
ferromagnetic, lattice dynamics 79−55838
ferromagnetism and antiferromagnetism coexistance at low temp. 77−66320
film, mag. props. and elec. resist. 77−32221

Invar continued
films, exchange interaction depend. on lattice parameter, spin-wave reson. and magnetisation meas. *(Russian)* 79−42751
Hall effect, and transverse magnetoresist., single cryst. specimens, 4.2-120K *(Russian)* 77−59277
heat capacity from AC calorimetry at high press. 77−41616
hysteresis loop displacement 78−52312
itinerant electron character 77−66240
itinerant electron ferromagnetism, press. effects on mag. props. 77−66241
linear expansion coefficient, mag. component *(Russian)* 77−76580
local moment model for the Invar effect 79−56505
magnetic and thermal anomalies 80−34603
magnetic inhomogeneity, ^{57}Fe and ^{61}Ni NMR 79−19803
magnetic phase transitions, linear expansion coeff. and mag. susceptibility meas. 77−69553
magnetic structure, absorbed H_2 effect 80−20534
magnetic structure, depend. on absorbed H, Stoner's band model calcs., Mossbauer spectra 80−65787
magnetic structure, small angle neutron scatt. study 79−47249
magnetic susceptibility in technical saturation region and internal stress 77−85429
magnetically insensitive, ternary alloys based on Cr-Fe and 4d transition metals 77−28026
magnetisation and magnetoresistance under high mag. fields 77−80764
magnetisation curves in high mag. fields above Curie point 77−66386
magnetisation reversal, fast, forced by external RF mag. field, Mossbauer obs. 78−52311
magnetocrystalline anisotropy 77−63173
magnetocrystalline anisotropy rel. to magnetisation 77−16070
magnetoelastic contribs. to US vel., elastic consts., and susceptibility 80−75829
magnetomechanical effects of Invar-type alloys, review 78−52330
magnetoresistance, magnetovolume contrib. to temp. variation 77−31999
Mossbauer effect at high press. 80−15858
Mossbauer spectra, heat treatment effect 80−15855
N36 melt, cast metal struct. depend. on heat treatment, subgrain struct. *(Russian)* 80−40343
Nernst-Ettingshausen effect and galvanomagnetic effect anisotropy *(Russian)* 79−91030
neutron small angle scatt. magnetocrystalline anisotropy 77−85420
phase stability, spinodal decomposition 80−88327
plastic deformation, effect on magnetisation, hyperfine field, elec. resist. and X-ray linewidth 77−48556
plastically deformed, struct. inhomogeneities, positron annihilation meas. 79−33859
rare earth alloys, RCo_2 and R_2Fe_{17}, Invar props. 79−56593
review of ferromag. materials which exhibit Invar charact. 79−56489
RF collapse and thermal effects, Mossbauer study 80−100624
RF collapse studies, skin depth effect, Mossbauer spectroscopy 80−39953
specific heat, temp. depend. *(Russian)* 78−56341
sputtered atoms, photon emissions, obs. of apparent local thermodynamic equilib. in excitation 78−72672
stainless, thermal expansion, elastic props. and Mossbauer effect 79−56502
superfine mag. struct. *(Russian)* 80−80572
Superinvar alloy casting for optical instruments 79−81580
thermal expansion, linear coeff., temp. and comp. depend. *(Russian)* 77−80634
thermal expansion, ultraprecise meas. 77−1247
thermal expansion coeff. at low temp. 79−86911
thermal expansion coefficient, analysis *(Japanese)* 79−65225
thermal expansion coefficient, origin of anisotropy 77−84951
thermal expansion coefficient, relationship to magnetisation 80−15269
thermal expansion meas. at const. temp. 77−45824
thermally excited electron transitions in FCC Fe-alloys 79−56559
thermodynamic props., anomalous 80−39313
transition metal alloys, AFe_2 and ACo_2, Invar effect, magnetovolume meas. 79−56592
transition metal alloys, local environment effect on magnetic states 79−56491
transition metal alloys, volume anomalies 79−56490
volume magnetostriction 79−56590
X-ray K-absorpt. spectra, depend. on composition and temp. changes *(Russian)* 80−55226
XPS of valence electrons, temp. effects, 122-580K *(Russian)* 77−8727
Fe alloys, FCC, Invar effect, model 80−25105
Fe base amorphous alloys, Invar and Elinvar charact. 80−29592
Fe-B, binary alloys, giant ΔE effect and Elinvar charact. 78−76291
Fe-B amorphous Invar alloy, elastic props., Elinvar charact. and ΔE effect 79−56595
Fe-Cr, Invar alloy, explanation of phys. anomalies *(Russian)* 78−88112
Fe-Cr-B, amorphous, Elinvar and Invar charact. *(Japanese)* 80−11832
Fe-Cr-B amorphous alloys, corrosion resistance, Invar and Elinvar charact. *(Japanese)* 79−96213
Fe-Cr-b amorphous Invar alloy, elastic props., Elinvar charact. and ΔE effect 79−56595
Fe-Ni, (35 wt.%), transport props. and Invar features *(Russian)* 78−51973
Fe-Ni, Curie point, annealing effects and time depend. 80−80508
Fe-Ni, Invar alloy, explanation of phys. anomalies *(Russian)* 78−88112
Fe-Ni, Invar problem, vibronic state model 79−56492
Fe-Ni, low temp. struct. 79−55856
Fe-Ni, magnetic inhomogeneous struct. model 79−56503
Fe-Ni, spin transition theory of anomalous props. 79−56558
Fe-Ni, virtual miscibility gap and interdiffusion coefficient 79−55891
Fe-Ni (308-44.1 at.%) Invar alloys, anomalous mag. anisotropy and thermal expansion 80−75755
Fe-Ni (36 wt.%), alloy 36N, effect of melting conditions on thermal expansion coeff. 80−65256
Fe-Ni alloys, anomalous thermal expansion, Gruneisen eqn. 78−83980
Fe-Ni alloys, thermal expansion rel. to X-ray emission spectra *(Russian)* 77−32470
Fe-Ni FCC alloys, invar effect by local moment model 77−90006
Fe-Ni film, electrodeposited, struct. and mag. props. 80−107668
Fe-Ni Invar, magnetovolume coupling enhancement factor, temp. depend. 80−88851
Fe-Ni Invar, Mossbauer exam. 79−56639
Fe-Ni Invar alloy, bulk modulus anomaly, mag. effect 79−91728
Fe-Ni Invar alloy, effect of hydrogenation, Mossbauer spectra 79−56641

Invar continued
Fe-Ni Invar alloy, electron irrad. effects 79−56638
Fe-Ni Invar alloy, mag. phase mixing effect on thermodynamic props. 80−54891
γ-Fe-Ni Invar alloy, phase mixture produced by long annealing 79−5065
Fe-Ni Invar alloys, forced and spontaneous magnetostriction 78−48019
Fe-Ni Invar alloys, splat quenched, mag. props. 80−75799
Fe-Ni Invar alloys, thermodynamic props. 79−56560
Fe-Ni Invar alloys of crit. conc., mag. props., flow theory methods *(Russian)* 80−65894
Fe-Ni Invar anomalies, explanation in terms of itinerant electron magnetism 80−75705
Fe-Ni magnetisation and high field susceptibility 79−56518
Fe-Ni-C, coated, Mossbauer spectra, effect of applied RF mag. field 80−80645
Fe-Ni-Cr, Invar alloy, ^{57}Fe effective field distrib., Mossbauer obs. *(Russian)* 78−19381
Fe-Ni(-Al)(Mn), mag. heterogeneities *(Russian)* 77−66251
Fe-Ni(Pt), magnetic excitation exam. by neutron diffr. 79−56521
Fe-Ni(Pt) Invars, elastic and mag. props., magnetoelastic interaction effects *(Russian)* 80−84631
Fe-Ni(35.4 at.%) Invar alloys, T^2 term contribution to magnetisation 80−71096
Fe-Ni(41.3 at.%) Invar alloy, asymmetric Mossbauer spectra 77−63346
Fe-Pd Invar, low temp. FCT phase obs. 80−93538
Fe-Pd Invar alloy, Young's modulus, magnetostriction, Curie temp. 80−65988
Fe-Pd Invar alloys, elec. and mag. props. and thermal expansion 80−75732
Fe-Pt, Invar alloy, paramag. susceptibility 80−70940
Fe-Pt, Invar alloy, strong ferromagnetism, magnetostriction and thermal expansion 79−8037
Fe-Pt, magnetoelastic contribs. to US vel., elastic consts., and susceptibility 80−75829
Fe-Pt, thermodynamic properties, effects of forced magnetostriction 79−11331
Fe-Pt Invar, magnetovolume effects 79−56597
Fe-Pt Invar alloy, bulk modulus anomaly, mag. effect 79−91728
Fe-Pt Invar alloy, homogeneous strong ferromagnet, thermal expansion and mag. props 79−91278
Fe-Pt Invar alloy, magnetocryst. anisotropy energy, itinerant electron model 80−54884
Fe-Pt Invar alloys, magnetocrystalline anisotropy const. determ. 80−65861
$Fe_{0.66}Ni_{0.34}$, magnetic form factor 79−56504
Fe_3Pt, ordered ferromagnetic alloy, magnetic excitation obs. 80−70978
$Fe_{0.65}Ni_{0.35}$, UPS, density of states determ. 78−52623
$Fe_{0.7}Ni_{0.3}$, bulk moduli, pressure effect on lattice spacing 79−55805
$Fe_{65}Ni_{35}$ ferromagnetic alloy, zero sound anomaly, inelastic neutron scatt. 79−46764
$Fe_{65}Ni_{35}$, ferromagnetic Invar alloy, lattice vibrations 78−91403
$Fe_{65}Ni_{35}$, H-infused, internal mag. field determ., Mossbauer effect 78−23382
$Fe_{65}Ni_{35}$, quasi-localised spin system, neutron scatt. 78−68194
$Fe_{65}{}^{60}Ni_{35}$, electron irradiated, small angle neutron scatt. 78−52218
$Fe_{70}Ni_{30}$, short range order, diffuse elastic neutron scatt. study 78−52219
$Fe_{70}{}^{60}Ni_{30}$, small angle neutron scatt., magnetisation inhomogeneity 78−52218
$Fe_{0.65}(Ni_{1-x}Co_x)_{0.35}$, Mossbauer spectra, ^{57}Fe hyperfine field distrib. 80−20533
$Fe_{0.65}(Ni_{1-x}Mn_x)_{0.35}$, Mossbauer spectra, ^{57}Fe hyperfine field distrib. 80−20533
$Fe_{65}(Ni_{1-x}Mn_x)_{35}$, H solid solutions magnetisation behaviour in pulsed mag. fields 79−65674
$Fe_{66}Ni_{31}Mn_3$, H-infused, internal mag. field determ., Mossbauer effect 78−23382
Fe_3Pt Invar alloy, anomalous Curie const., susceptibility meas. 80−75731
Fe_3Pt Invar alloy, mag. props., martensitic transform. 79−78365
Fe_3Pt, Invar alloy, theory of elastic-anomalies 78−95505
Fe_3Pt Invar alloy, thermal expansion and spontaneous magnetisation, Invar anomalies, low spin model 80−71001
Fe_3Pt Invar alloys, elec. resist. anomalous crit. behaviour 79−78067
Fe_3Pt, quasi-localised spin system, neutron scatt. 78−68194
Fe_3Pt:Sn Invar alloy, Mossbauer shift temp. depend. 80−100626
$Fe_{72}Pt_{28}$, ferromagnetic Invar alloy, lattice vibrations 78−91403
$(Mn_{1-x}Cr_x(Fe_x))B$, Invar charact. 77−15602
Ni-Fe, FCC, Invar behaviour, spin waves stiffness consts., neutron scatt. study 79−51769
Ni-Fe, thermoelectric power temp. and mag. field depend. 78−26849
Ni-Fe Invar, thermal expansion and spontaneous magnetisation, Invar anomalies, low spin model 80−71001
Ni-Fe-H, Curie points, mag. props. of H solutions FCC metal sublattice parameter behaviour 79−69671

invariance
see also conservation laws
adiabatic invariance of particle in selfgravitating spherical dust shell 80−105459
charged particle interaction with linearly polarised MHD plane wave, first adiabatic invariant approximations 77−78580
conformal space-time group, invariant tensors for maximal subgroups 79−85239
critical exponents for renormalisation groups generated by flow vector 77−67402
differential approximation method analysis of difference scheme props. 77−57172
Dirac monopoles, invariance props. 77−61208
education, classical mechanics gauge invariance, derivation of Maxwell's eqns. 80−73131
gauge invariance, Lorentz covariance and EM props. of elementary systems 80−32037
Hamiltonian continuum mechanics, differential geom. foundation 78−77708
heavy lepton model for rare μ and K decay modes 78−45898
Lagrangian systems with one degree of freedom, invariance and conservation laws 78−62067
Lie derivative of a differential form, invariance conditions and phys. laws 78−65748
limit cycle theory *(French)* 78−36813

invariance continued
molecular geometry optimisations, invariance criteria, symmetry conservation rules 80−58406
non-Noether invariant origin, relation to Euler eqn. transformation props. 80−31493
nonlinear first order evolution problem, MHD appl. 79−97197
nonlinear wave equations, symm. of solitons and general solns. 79−85210
orthogonality, radial orbitals, energy invariance 78−84
phase transitions, superradiant, gauge invariance theory 78−66795
physical systems, principle of stability of invariance 77−26164
Poisson brackets, canonical invariance, for teaching 79−25810
QCD, renormalisation group, confining and asymptotically free soln. 80−62881
quantum field theory, conformal-invariant, composite field operators 78−81886
radiative capture and Galilean invariance 77−38730
renormalisation group, invariance props. of crit. exponents 77−22512
rotating plane-fronted waves and their Poincare-invariant differential geometry 80−332
single quark transition model, parity violating charmed hadron decays, current-current interaction 78−12907
space-time transformations leaving Einstein eqns. invariant *(French)* 78−62123
two-electron atoms, channel invariants and SU(3) classification 78−41906

inverse Nyquist diagrams *see Nyquist diagrams*

inversion layers
cyclotron resonance lineshape, temp. depend. 78−64086
cyclotron resonance linewidth, mag. field depend. 78−56380
dielectric-semiconductor interface, anal. of fast surface states 79−42648
disordered system, props. of mobility edge 77−4330
effective-medium theory in two-dimens., appl. to macroscopic inhomogeneity model 79−95504
electrical conduction, effect of electron-electron scatt. 80−2477
electron-electron and electron phonon contribs. to carrier effective mass 78−64087
electron-impurity system, two-dimens., quantum theory of cyclotron reson. lineshape 78−48045
electron-phonon system, coupled, in two dimens., implication for inversion layers 78−6425
Hall effect, models 79−51682
Hall effect in disordered systems, conf., Cambridge, England (May, 1978) 79−51604
Hall effect in impurity bands and inversion layers 79−51609
hopping conduction, anal. in impurity bands in inversion layers 79−47171
hopping conduction, semiclassical theory 79−91052
III-V compounds, electron transport in quantised inversion and accumulation layers 79−60935
interface barrier effects 77−89867
interface effect on effective mass approx. 78−64082
lateral PNP transistors, hot electron reliability effects 77−41569
many-valley semiconductors, electronic ground state 77−43731
many-valley semiconductors, optical props. of CDW ground states 77−43732
metal-insulator transition, mag. field induced 79−65383
metal-insulator-Si(n)-Si(p^+) device, switching voltage criteria 80−15610
MIS inversion layer solar cells, two-dimensional model 80−89641
MIS solar cells, effects of pinholes, oxide traps, and surface states 78−80055
MIS tunnel diode, minority-carrier, pot. barrier height 80−96998
MISIM struct. inversion layer, symmetrical, carrier conc. calc. 80−75651
MNOS structure photoelectric writing operation 78−95382
MOS, hot electron effects in Landau levels 80−6998
MOS capacitors, establishment of inversion layer in Si substrate under high oxide field conditions 77−66202
MOS capacitors, stacking fault effect on capacitance relax. times 78−76157
MOS devices, inversion layer, pot. and carrier distrib., quantum mechanical determ. 80−29483
MOS electron inversion layers, temp. depend. of subthreshold currents 79−73596
MOS interface states density, photoemission obs. using photocurrent and photocapacitance meas. 80−92990
MOS inversion layer, hot electron effects in Landau levels 80−20315
MOS inversion layers, electron-phonon interaction and cyclotron reson. 80−25014
MOS inversion layers, freq. response of charge transfer 80−88638
MOS structure, 2D electron gas, for IR Faraday rotation 80−80389
MOS structure with nonuniformly doped semiconductors, heavy inversion, definition for onset 80−96994
MOS structures, inversion layer near electrode edge, pot. and charge density distribution 80−88642
MOS structures, ion-implanted, C-V and G-V characts. depend. on geometrical struct. of implanted region 77−55615
MOS structures, quasi-2-dimens. system, review 79−33352
MOS structures, surface piezoacoustic waves, interaction with two-dimens. plasmons 79−28683
MOS structures of small-gap semicond., capacitance, effect of quantising mag. field 80−84513
MOS structures with superthin gate dielectric, hole mobility in inversion layers 80−29482
MOSFET, ionic scatt. effect on Shubnikov-de Haas amplitudes in Si inversion layers 79−42653
MOSFET, localised state wave functions 77−4417
MOSFET, method to determine effective channel length 79−69601
MOSFET inversion layer, localised highly correl. phase cond. 79−33354
MOST channels, quasi-Fermi level gradient distrib., Hall voltage 80−29481
n-type, collective modes in charge density wave state 79−78200
narrow gap semiconductor, modification of Einstein relation for inversion layers in strong elec. field 80−96959
one-dimensional inversion (enrichment) layers in MOS structure semicond. surface, production method 79−42663
quasi-two dimensional space charge layers, transport phenomena 79−95508
quasi-two-dimensional electrons, electrodynamics 77−89829
semiconducting surface inversion layers, exchange and correl. 80−75618

inversion layers continued
semiconductor, narrow gap, boundary conditions, energy spectrum, and optical transitions 79−42614
semiconductor, quasi-two-dimens., electron scatt. by polar optical phonons 78−72237
semiconductor, quasi-two-dimens., hot carrier crit. conc. 77−35977
semiconductor, surface depletion and inversion, arbitrary doping profile, theory 80−107912
semiconductor spectroscopy in high mag. fields, review 79−60889
semiconductor surface, electromag. modes of inversion layer 78−80030
semiconductor surface space charge layers, subband struct., perturbation theory 80−84497
semiconductor surfaces, doped, quantum model of inversion layers 78−30961
semiconductor surfaces, electron-electron interaction and electronic props. of space-charge layers 78−60210
semiconductors, carrier mobility-meas. technique on inverted surfaces near cond. threshold, appl. to Si 79−69602
semiconductors, two-dimens., transient response of hot electrons, calc. 80−49747
Si, mobility temp. depend., Coulomb and surface roughness scatt. 80−80390
Si inversion layers, prep. domain studies of intersubband optical transitions 80−20637
solar cells, numerical modelling 80−81444
threshold conduction 78−43450
two-dimensional semiconductor, Gunn instability 78−84305
two-dimensional white noise problem and inversion layer localisation 78−84271
Wigner transition, mag. field induced 77−89869
Al-SiO_2-Si, MOS struct., lateral photovoltaic effect 79−4601
(CdHg)Te, ion implanted graded gap photodiodes 78−39192
n-$Cd_xHg_{1-x}Te$, action of laser pulses, elec. characts. 79−11212
CdSe, MIS thin film capacitance, theory 79−87156
p-CdTe-Langmuir film interface, prep., characters. and MIS struct. 80−92998
GaAs for MOSFET's native oxides, annealing effects, and inversion layer mobilities 78−6452
GaAs MOS structure, props. of surface carriers 77−20454
GaAs, obs. of localisation in two-dimens. systems 78−60213
GaAs, two dimensional impurity bands, Hall mobility 79−95509
n-GaAs-anodic oxide MIS devices, inversion and accumulation layer form. at elevated temps. 79−60934
GaAs-NaOH interface, inversion layer form. and surface states 80−2465
GaAs-SiO_2 MIS structures, fabrication and elec. props. 79−47166
Ge (111) surface, n-channel inversion layer, subband energies 80−11063
Ge, electronic inversion channel anomalous Hall factors *(Russian)* 79−95467
$Hg_{1-x}Cd_xTe$, Einstein relation for inversion layers 80−103706
$Hg_{1-x}Cd_xTe$, far IR cyclotron reson. in inversion layer 77−69396
$Hg_{1-x}Cd_xTe$, n-surface inversion layers study 80−25017
$Hg_{1-x}Cd_xTe$-oxide interfaces, MIS capacitance characts. 80−49926
InAs, superconductivity of surface *(Japanese)* 78−14864
InP, and $In_xGa_{1-x}As_yP_{1-y}$ binary and quaternary cpds., surface and dielec.-semicond. interface props. 80−93001
InP, C-V and surface transport meas. 80−49928
InP inversion-type MISFET with SiO_2 gate insulation interface props., elec. drift 80−93002
InP-Si_3N_4 (SiO_2), interface props., plasma deposited dielectrics, n-channel MOSFET action 80−93003
InSb, Einstein relation for inversion layers 80−103706
InSb, electromagnetic mode 78−60080
InSb inversion layer, spectroscopy of electron subband levels 78−64364
InSb, ion irrad., isothermal annealing effects 80−6424
InSb, MIS thin film capacitance, theory 79−87156
InSb MOS struct., capacitance of n-channel inversion layers, elec. field effects 80−80393
p-InSb, magnetoconductivity and cyclotron reson. in inversion layers 80−49946
p-InSb, magnetotransport in inversion layer 78−64138
InSb, spectroscopy of electron subband levels 78−10569
n-inversion layers, (001), $K_{\parallel}$-depend. of subband energies 80−103738
n-Si, (111) inversion layers, valley splitting, Shubnikov de Haas oscills. 80−65698
p-PbTe, MIS struct. inversion layer sub-bands, IR magnetoreflectance obs. 80−44731
p-PbTe, quantum oscills. in inversion layer 77−85245
PbTe substrate for MIS capacitor, C-V and G-V characts. 78−26962
PbTe, surface space charge layers, magnetorefl. study 78−52475
PbTe surface-space-charge layers, magnetorefl. study 78−64349
Si, 1/f noise and percolation in impurity bands 79−24029
Si (001) surface, energy gaps in inversion layer band struct., spectroscopic determ. 79−82658
Si (001)-SiO_2, n-inversion layer, valley splitting without effect mass approx. 80−15586
p-Si (100), intersubband spectroscopy by photocond. and absorpt. 78−10566
Si (100), surface space charge layer, inter-subband optical transitions 77−15931
Si (100) inversion layer, hot electron drift velocity, Monte Carlo calcs. inc. 3 subbands 78−91752
Si, (100) inversion layer, electromigration in two dimensional electron gas, driving force 80−84441
n-Si (100) inversion layer mobility depend. on intersubband scatt. at low temps. 79−95506
Si (100) surface electrons, effective mass and collision time 78−34909
Si (100) surface electrons, effective mass and collision time 78−64081
Si, (100) surface space-charge layer, intersubband cyclotron combined resonances 79−69571
Si (100)-SiO_2 system, exchange and correl. contribs. to subband energies 79−42654
p-Si, (100)-oriented, n-channel inversion layers, MOS field-effect devices, mag. quantisation effect on surface capacitance 80−70834
Si (110) and (111) surfaces, inter-subband spectroscopy in hole space charge layers 77−32064
Si (111) inversion layers, CDWs, effect of four valley interaction terms 79−33324
Si, (111) surface, electron inversion layers, obs. of sixfold valley degeneracy 79−38176
Si (111)-SiO_2 interfaces, sixth-valley state stability a priori calc. 80−49859
inversion layers continued
n-Si channel ⟨100⟩ inversion layer MOSFET, valley splitting, conductivity 80−70840
Si, elec. break-through, exactly solvable model 78−56234
Si, electron inversion layer on vicinal plane, minigaps 80−20282
Si, far IR cyclotron emission 79−61226
Si, far IR reson. magnetotransmission, temp. and band gap light depend. 78−64363
Si, Hall effect, consistency with presence of macroscopic inhomogeneities 79−51681
Si, high index surface, natural orientational superlattice in 2D electron gas 79−99598
Si high-index surface, valley-valley splitting 78−39219
Si, inter-subband optical absorpt. in mag. field 77−32375
Si, intervalley transitions and subband splitting 77−20455
Si inversion layer, cyclotron resonance in extreme quantum limit, collective ground state 80−50191
Si inversion layer, Γ and X electric breakthrough interference effect 79−47137
Si, inversion layer, impurity scatt., self-consistent calc. 79−28415
Si, inversion layer, magnetoplasmon reson. lineshape theory 79−1615
Si inversion layer, transient response of hot electrons, calc. 80−49747
Si, inversion layer electrons, temp. depend. cyclotron reson. lineshape 78−10568
Si inversion layer in MOS struct., carrier-phonon interaction, nonohmic transport 80−49943
n-Si inversion layers, broken symmetry states 79−15229
n-Si inversion layers, electronic g-factor, spin-split Landau levels 80−80346
Si, inversion layers, first order intervalley scatt. 80−29484
Si inversion layers, harmonic generation due to hot electrons 80−65694
Si, inversion layers, nonmetallic cond. at low temp. 80−70833
n-Si inversion layers, stress and temp. depend. of subband struct., plasmon-pole approx. 79−95461
Si, inversion layers, submillimeter cyclotron reson. at low electron density 79−60925
p-Si inversion-channel photoelectric cell characteristic *(Russian)* 80−49941
n-Si ion implanted surface pot. barriers, $LiN60_3$ SAW obs. 77−28234
Si, lattice scattering mechanism in quantised inversion layers 79−78187
Si MIS-inversion layer solar cells 80−76632
n-Si MOS inversion layers, Hall cond. meas. 80−39676
Si, MOS inversion layers, negative magnetoresist. 80−49922
n-Si MOSFET, resist. temp. depend. at liq. He temps. 80−80391
Si MOSFET, surface quantum states, two-dimensionality of many-body effects 80−103740
Si MOSFET structs., photocond. meas. rel. to intersubband transitions 78−64127
Si, MOSFETs, Shubnikov-de Haas oscills. from electron irrad. induced two-dimens. leakage channel 79−19671
Si, magnetoconductivity in ground Landay level, defect diffusion in Wigner cryst. 77−39914
Si, n-channel (100) inversion layers, valley splittings due to elec. break through 79−4592
Si, n-channel inversion layers, multivalley effective mass theory 79−47136
p-Si, n-channel inversion layers, mag. susceptibility of electrons in presence of quantising mag. field. 80−75650
Si, n-type, thermally oxidised, natural inversion layer, UV photodiode construction 79−30559
Si, n-type inversion layer, theory of impurity-shifted intersubband transitions 80−20324
Si, n-type inverted MOSFET (100) surfaces, quantitative determ. of valley splitting 79−51678
Si, on sapphire, MOS inversion layer, magnetoconductance oscillations 80−20325
Si, on vicinal plane, band structure 80−24994
Si, phase diagram in strong mag. fields 80−88492
Si, polaron model for localisation 80−20280
Si, quantum magnetoresist. results, using pulsed fields up to 35 T 79−73528
Si, quasi-two dimensional space charge layers, transport phenomena 79−95508
Si, resolution of Shubnikov-de Haas paradoxes 80−39648
Si, screening effect and quantum transport in strong mag. fields 78−19155
Si superlattice and two-dimens. electron gas 78−64080
Si surface, high index, theory of inversion layers 80−44697
Si surface, interaction with oxygen gas discharge plasma 78−83840
Si surface, MOS struct. band structure, minigaps, magnetoresistance, cond., space charge layers 80−92980
Si, surface inversion layers, intersubband optical absorpt., Auger-type transition 80−29741
Si, surface space charge layer, electron subbands, mag. field effect 77−20393
Si, temp. depend. of subband energies, exchange and correlation effects 80−20281
Si, thermally oxidised surfaces, electron mobility in inversion and accumulation layers, MOS devices 80−103753
Si, two dimensional impurity bands, Hall mobility 79−95509
Si, two-dimensional inversion layer on surface, minigap and conductivities 80−20267
Si, under stress, density functional calc. of subband struct. 80−20321
Si, valley splitting, effects of misorientation 79−73564
Si, velocity-field curves for surface free carriers, meas. on IGFET 80−60095
Si, voltage tunable far IR emission 80−25018
Si:Na^+, far IR optical spectroscopy 80−20680
Si:Na^+, variation of cond. in two-dimensional impurity band with Fermi level position 79−95510
Si-Al_2O_3, inversion layer subbands and magnetocond. oscills. 78−64124
Si-sapphire, interface radiation induced charge trapping, rapid anneal phenomena 79−19666
Si-SiO_2, broken symmetry states obs. in inversion layers 78−95125
Si-SiO_2, interface, hopping conduction, anal. in impurity bands in inversion layers 79−47171
Si-SiO_2, interface free carrier mobility in inversion layer, influence of polar phonon scatt. 79−73597
n-Si-SiO_2, screening of charged impurity centre localised inside oxide and at interface of inversion layer 79−73563

inversion layers continued
Si-SiO_2 (111) interfaces, sixfold valley degeneracy in electron inversion layers 80−49936
Si-SiO_2 boundary, surface charge transport in valence band of Si 80−70789
Si-SiO_2 in MOSFETs, inversion layer carrier mobility, theory 80−60094
Si-SiO_2 interface, (001) vicinal planes, minigaps in inversion layers, far IR absorpt. meas. 80−107919
Si-SiO_2 interface, inversion layer transport, radiation hardness effects, review 79−19673
Si-SiO_2 interface, Na^+ drifted, impurity bands in inversion layers 78−60211
Si-SiO_2 interface, radiation hardness, carrier localisation in inversion layer 77−85332
Si-SiO_2 interface, remote polar phonon scatt. in Si inversion layers 80−80095
Si-SiO_2 interface, valley degeneracy splitting in n inversion layer, effective-mass approx. 79−99629
Si-SiO_2 inversion layer, n-channel, anomalous magnetoresist., model 80−96996
Si-SiO_2 MIS systems, dynamic props. of switching, appl. to charge transfer devices 80−92997
Si-SiO_2 system, bound states at interface 79−42655
Si-SiO_x interface, evidence for superlattice 77−89868
Si-SiO_x interface, localisation in inversion layer due to states in gap of oxide 77−12012
Si-Sn heterojunction, RHEED, Mossbauer spectroscopy and I-V characts. 80−70828
SiO_2-Si solar cells, ionising radiation effects 77−43244
Si(100), inversion layer, interaction induced transition at low density 80−15581
Si(100) inversion layers, effects of uniaxial stress on cyclotron reson. 80−20322
Si(100)-SiO_2 interface, mobility in Si inversion layers, screening and neutral impurity effects 79−28412
Ta_2O_5 inversion layers for Si solar cells 80−94075
Te inversion layers in mag. fields 80−44690
Te, surface quantum levels, calc. from Shubnikov de Haas meas. and triangular surface pot. well 79−15207
ZnO-grainboundary-ZnO junction in ceramic varistor, capacitance-voltage characts. 80−65689

invertors
frequency response anal. and steady-state oscillations calc. *(Russian)* 77−53761
magnetic field measurement, using invertor circuit with toroidal core 77−82577
piezoelectric drive, implantable, for left ventricular assist device, improvement 78−15927
solar cell arrays, DC to AC power conversion and utility interfacing, technqiues, requirements and components used 80−45703
solar cells DC output conversion *(Spanish)* 80−35683
solar energy DC-AC inverter design, effect of meterological conditions, computer simulation 80−61373
Synchrotron Radiation Source booster magnet power supply 79−31272
variable speed wind power generator, control strategy for 3-phase output *(French)* 80−76591

iodine
see also nuclei with .....
^{131}I fixation in solid/liquid systems 79−13530
$^{29}I/^{127}I$ early solar system chronometer 80−62043
absolute quantum yields of ($^2P_{1/2}$), ($^2P_{3/2}$), photolysis of C_3F_7I, CF_3CFICF_3 and $CF_3OCF_2CF_2I$ 79−34339
absorption cell for He-Ne laser 77−79867
absorption on ion exchange resins in aqueous solns. 80−47610
absorption site on Ag(111) EXAFS 78−84679
adsorbed layers, on unroughened Pt electrode, Raman spectra 78−31689
adsorbed on Ag(111), Cu(111), and Cu(110), surface EXAFS study 80−40186
adsorbed on Ag(111), photoelectron diffr. aximuthal patterns, struct. sensitivity 80−107644
adsorbed on Ag (111), geometry and bond length, surface EXAFS 78−71952
adsorbed on CC LaB_6, polycrystalline, negative surface ionisation of I atoms, negative ion desorption heat 79−78848
adsorption, on silica, reson. Raman spectrum 78−42066
adsorption on activated C, pore struct. 77−31870
adsorption on Ag(111), surface EXAFs exam. 79−82446
adsorption on Ag(111) surface, cluster calc. with Xα scattered wave method 77−31894
adsorption on Cu (111) and (110), surface EXAFS exam. 79−82446
adsorption on Fe (100), AES, LEED, thermal desorption, and work function study 80−15374
adsorption on W(100) at room temp., LEED and AES study 80−84389
adsorption on W (100) and (110) surfaces, chemical effects in N_7 VV Auger spectra 77−32474
adsorption on ZnO, γ-irrad. induced centres 80−54513
air monitoring systems for radioiodine and inert gases, evaluation 80−95480
alkali metal chloride: $F^-(Br^-)(I^-)$, anion impurities substitution, energies of soln., association and migration 78−83831
alkyl iodide-$I_{(atom)}$ complex, multiple charge-transfer bands in liquid-phase 77−32776
14-aminopyridine-I_2, charge-transfer complexes, hyperpolarisability 77−34568
Atlantic Ocean, equatorial, I distrib. in upper layers 77−60422
Atlantic Ocean, particulate I distrib. 77−5237
atom, $5^2P_{1/2}$ state, collisional quenching, isotope effects 77−34583
atom, $^2P_{1/2}$ state, relax. between hyperfine levels 80−18880
atom, chemical generation of population inversion between spin-orbit states 78−17767
atom, collision-induced $5^2P_{1/2}$-$5^2P_{3/2}$ radiative transition 79−31461
atom, diffusion coeff. in laminar flames 78−51272
atom, electronically excited, collisional release and photocomp. kinetics of I_2 78−66819
atom, ESR spectra, broadening by He, O_2 and HI 79−68205
atom, excited ($5^2P_{1/2}$), quenching by mols. with C-I bonds 79−64076
atom, GTO basis sets, Hartree-Fock-Roothaan calcs. 79−97973
atom, He (I) photoelectron spectrum by I_2 photodissoc. 80−83325
atom, $M_{4,5}N_{4,5}N_{4,5}$ Auger spectra, kinetic energy shift rel. to molecule 80−5516

iodine continued
atom, metastable, produced in UV photodissoc. of alkyliodides, time-resolved obs. of I($^2P_{1/2}$) reactions 80−11940
atom, orbital calc., model potential method 79−36513
atom, partial photoionis. cross sections, rel. intensities, irreducible tensor anal. 79−98048
atom, photodissoc. ring laser, lasing regimes, emission and polarization characts. 80−48236
atom, photoelectron spectra, strong many electron effects from core levels 77−18862
atom, photoionisation cross sections and ang. distribs., outer p subshell 80−9572
atom, recomb., in presence of inert gas atoms and mols. 80−45496
atom, state determ. following photodissoc. of KI, time of flight meas. 79−18105
atom, stripping in gaseous targets, equilib. charge state distrib., statistical anal. 80−5610
atom, X-ray emission line chem. shift, interpretation 77−50395
atom, XPS and XES, dynamical effects 80−52924
atomic recomb., shock heating in unsteady Ar expansion, vibr. relax. effect 77−16794
atomic saturable absorpt. cell for I 1.315 μm laser wavelength 77−10985
atomic vapour, self-induced transparency and reson. self focusing 80−64114
atoms, Mossbauer isotopes, isomer shift 80−78573
benzene:I_2, charge transfer spectra line shape 79−78700
benzene-I_2, binary soln., charge transfer spectrum 78−90183
biomedical absorption-edge transmission technique using ^{139}Ce for stable I conc. meas. 80−56194
carbon tetrachloride-I_2-water system, mass transfer in pulsed perforated plate column 78−71385
α-cellulose iodination for dietary fibre analogue tracing 79−48339
chemical laser, electronic transition 78−55347
chemical laser, photodissoc. of C_3F_7I, CF_3I, CF_3CFICF_3, quantum yields 78−3355
chemical transport equilib., with group III arsenides *(French)* 77−55877
chemical transport equilib. with group III arsenides *(French)* 77−55876
chemisorbed on Au surface, AES and LEED study 80−100405
chemisorbed on zeolites, Raman spectra 80−93301
chemisorption, on Ag clusters, UPS obs. 80−84830
coherent optical transients observed by polarisation switching 79−81492
complex formation with pyrazine, n-σ-type, effect on intensity of intercombination transitions *(Russian)* 77−26980
computerised X-ray tomography, selective I imaging using K-edge energies 78−24131
desorption from W, field ion microscope exam. 78−35270
determination, in water, by neutron activation and X-ray fluoresc. analyses 78−3428
determination by high press. liq. chromatography, I-specific detector *(German)* 79−87920
determination in biological materials by neutron activation anal. 79−57828
determination in environmental water samples by neutron activation, isotope exchange 77−44550
diatom dissociation and recombination mechanisms, bound complex and triple collision mechanisms 80−23478
diffusion in copper phthalocyanine polycrysts., amorphous cpd. prep. *(Russian)* 80−66016
diffusion in mixed solvents, activation enthalpy of diffusion 78−14492
dissolved I in Yarra River estuary water 79−34855
dopant, in (SN)x, temp. depend. of elec. cond. 79−65563
doping effect on cellulose acetate electrical properties 80−49757
elastic scattering amplitudes, for high energy electron scattering, by ionised atoms, numerical calcs. 80−49057
electrode, in $RbAg_4I_5$ electrolyte, thermodynamcis and electrochem. behaviour 79−70348
excimer oscillatory emission, analytic quantum mech. model 79−59675
excitation spectroscopy, relation between I_2 bound exciton line and CdS excitonic molecule line 80−40153
extraction from liquid Na using molten chlinak in Na cooled fast reactor 80−27702
filter, absorpt. lines removal from 514 nm excited Raman spectra 78−70200
fission I increased release from defective fuel rods during PWR shutdown 79−49710
fission product, sorption and diffusion in concrete and containment uptake 79−67898
fission reactor fuel solns., I removal as insoluble PdI_2 77−42164
fission waste product, distribs. and concs. in reactor core 78−58322
flashlamp excited photodissociation laser 79−72558
frequency stabilisation of He-Ne laser 77−83915
frequency stabilisation of He-Ne lasers 78−87070
frequency stabilisation of He-Ne lasers 78−87071
frequency stabilisation of He-Ne lasers by ref. to absorption transitions 77−83913
frequency stabilised He-Ne laser, instrumental freq. offsets 78−87084
frequency stabilised He-Ne laser status 78−87072
frequency stabilised He-Ne laser with hot wall I_2 cell 78−87073
frequency stabilised He-Ne lasers, beat freq., international comparison *(French)* 78−87090
frequency stabilised He-Ne lasers, conf., Germany (Feb. 1977) 78−87069
frequency stabilised He-Ne lasers, length metrology *(French)* 78−87074
frequency stabilised He-Ne lasers, technological principles *(French)* 78−87075
gain measurements in chem. produced I system 78−63115
gas, dynamic friction coeff. meas. by saturation spectroscopy, radiative lifetimes 78−18368
gas fission product release, effect on LWR fuel performance calcs. 79−31054
gaseous effluents from LWR and reprocessing plants, treatment and control 77−61589
geochemical behaviour in sediments from Namibian shelf 78−32062
heat of sublimation, laser photometric meas. 79−5942
heavy ions with energy 0.4-0.9 MeV/A, stripping by C foils, straggling, foil behaviour 78−33351
high-power lasers, review 80−32950
hot wall cell, freq. stabilisation of He-Ne laser 77−65598
hot wall cell for He-Ne laser freq. stabilisation 77−83914
hydrolysis, reaction rate const. 80−11883

iodine continued
I_2, air pollutant, spectroscopic analysis using scanning tunable dye laser 78−81362
impurity in Li aluminosilicate glasses, ESR spectra 80−66027
Iodox process for iodine removal from air with hyperazeotropic nitric acid 79−31107
ion+Au collisions, mol. M-X-rays, self-consistent relativistic HF-Slater many electron correl. diagrams 77−14567
ion+target collisions, K-X-ray yields, 1sσ excitation 77−19051
ion+target collisions, K-X-ray yields, K-vacancy sharing 77−23548
ion+target collisions, K-X-ray yields 2pσ excitation 77−23549
ion+target collisions, X-ray yields, K-L level matching 77−19052
ion collisions, 15-80 MeV, K-vacancy production, multiple and single collisions in mol. orbital excitation 77−83717
ion tracklength in mica 78−38767
ion-atom collision, K-vacancy prod., mol.-orbital method 77−68095
ions, beam-foil spectra from 20 to 238 MeV energy, 5 to 60 nm, lifetime meas. problems 80−9722
ions, specific adsorption to Hg-KI solution interface, electrical double layer, interface excess activity coeff. 80−49523
laser, 100 ps pulse generation and amplification 77−19301
laser, 1.315 μm, Ni complex BDN II as saturable absorber 79−27297
laser, 1.315 μm, oscill. freq. selection hyperfine transition 77−10952
laser, 1.315 μm, transverse discharge excitation in i-C_3F_7I 77−19243
laser, 1.315 μm, transverse discharge excitation in i-C_3F_7I, kinetic model 77−19244
laser, 1.315 μm transition line struct. 78−59000
laser, 1 TW high power system, Asterix III 77−88765
laser, $^2P_{1/2}(F=3)\rightarrow{}^2P_{3/2}(F'=4)$ transition, stimulated emission cross section determ. 79−13961
laser, active medium refr. index change meas., delay method 77−58336
laser, angular spectrum form. of stimulated radiation, theory 77−14702
laser, Asterix III, light-plasma interaction expt. and light pulse props. 80−53349
laser, Asterix III, nuclear fusion D, T, appl. *(German)* 78−13744
laser, Asterix III and German laser fusion programme 78−63136
laser, at 1.315 μ, passive mode locking *(French)* 77−68203
laser, chem. changes in active media, IR spectrochem. analysis 77−14704
laser, chemically pumped by $O_2(^1\Delta)$ 79−98348
laser, continuously variable water filter for linearity testing of photoresistors 78−55397
laser, current design aspects, pumping system, optical arrangement and gas flow 79−31945
laser, flashlamp pumped photodissociation, local optical inhomogeneities 80−53284
laser, high power, developmental possibilities 79−975
laser, high power, operation, props. *(French)* 78−33731
laser, high power system, Asterix III, development 77−710
laser, high-power, for fusion reactor appl. 77−7062
laser, high-power, pulse amplification 80−48234
laser, high-power photodissociation, pulse propag. in amplifier 78−46592
laser, hollow cathode ion, freq. meas. by harmonic mixing 77−83919
laser, ICF_2CN photodissociation 78−50769
laser, large-scale, implications of n-C_3F_7I Raman spectrum and cross sections 79−23022
laser, methyl iodide photodissoc., kinetic model, cross-section calcs. 80−58530
laser, optical pumping using high current plasmdynamic discharges 77−38923
laser, optically pumped, four-level model *(Korean)* 80−28224
laser, optically pumped I_2, 1 μs pulse emission at 342 nm 77−79811
laser, photodissoc, dye laser pumped 78−63064
laser, photodissoc., ns 200 J output 77−27301
laser, photodissoc. of C_3F_7I with C_6F_{14}, energy of generation *(Russian)* 77−38877
laser, photodissociated by nucl. induced excimer fluoresc. 80−78846
laser, photodissociation, active medium gain in mag. field 77−79816
laser, photodissociation, characts. of dye comps. for passive switches 80−91826
laser, photodissociation, continuously pumped continuous flow 78−59027
laser, photodissociation, diffr. limited output beam 79−27286
laser, photodissociation, gain-switched, multi-atmospheric press. operation 79−76681
laser, photodissociation, high power system, nanosecond or shorter pulse prod. 77−38879
laser, photodissociation, press. induced freq. shifts 78−37875
laser, photodissociation, pumped by high-current discharge with return current conductor 80−28225
laser, photodissociation, Q-switched, optically thick active medium, chemical kinetics and gasdynamics 79−64218
laser, photodissociation, reaction rate consts. of CF_3, n-C_3F_7 and i-C_3F_7 79−52671
laser, photodissociation, stimulated emission pulse temporal characts. with active-medium gain control 80−28226
laser, photolytic, atomic, rel. to fusion applic. 77−46403
laser, photolytically pumped, chem. kinetics 80−48235
laser, pulsed photodissociation, based on methyl iodide 78−50767
laser, pumping by inert gas halogen fluoresc. emission, C_3F_7I photolysis 77−34883
laser, Q-switched, emission at two frequencies 79−18413
laser, quenching rate const. of I metastable atoms by I_2 78−13691
laser, radial oscills. of medium, effect on laser output 78−5507
laser, SAIL-1, performance characts. for laser fusion 77−88766
laser, short pulse amplification, multilevel paraxial Maxwell-Bloch eqn. 79−36889
laser, short-pulse, preamplifier stages characts. 79−94227
laser, smooth pulse oscillator for single mode operation 78−59057
laser, terawatt, ASTERIX III system 79−3713
laser, three-level, pumped by CW dye laser 80−63993
laser, using I to group V element bonding mols., $(CF_3)_2AsI$ laser characts. 77−14703
laser, with programmed mag. field 78−33750
laser amplifier pumped by open high-current discharge radiation, physical parameters 79−89904
laser intracavity absorption of I_2 vapour 79−22992
laser of high efficiency, low-press. Hg lamp pumped 79−31929
laser oscillator or amplifier, photodissociation, Faraday rot. in active medium 79−10296
laser pulse shaping 77−23691
iodine continued
laser pumpband UV spectral efficiencies of surface spark discharges 77−75496
laser radiation, 2nd, 3rd and 4th harmonic generation 80−91844
laser radiation wavefront instability and optical inhomogeneity evolution dynamics 80−9876
laser radiation wavelength stabilisation, He-Ne laser *(Czech)* 78−87061
laser with repeated use of regenerated mixture 80−28251
lattice dynamics, bond charge model 77−84858
lattice dynamics, internal and external modes 78−18719
lead phthalocyanine:O_2(I), Schottky barrier effect on AC current response 80−75623
liquid, static structure factor, neutron diffraction 80−103236
LWR, LOCA, fission product source terms 80−13654
LWR containment vessel, I removal by spray after LOCA, MIRA-PB code 80−47593
LWR fuel rods, power ramp induced I and Cs redistrib. 80−32343
LWR fuel-cladding gap, Cs-U-Zr-H-I-O system, chemical thermodynamics 78−82440
metallic, mol. and monatomic phase, elec. resist. at high press. and low temp. 80−65638
metallic A1-type modification, normal conductivity and superconductivity 80−20348
metallic solid, high press. struct., phase transition, X-ray diffr. study 78−87647
molecular, predissociation, electric-field induced 80−37839
molecular, reson.-enhanced three-photon absorption, CW intracavity absorption 79−10160
molecular absorption spectra, line identification band atlas, 19000 to 18000 cm^{-1} 78−42079
molecular beams ang. momentum polarisation 77−46635
molecular cell, impurity gas detection, He-Ne laser stability appl. *(French)* 77−73496
molecular crystal, bond charge model, for lattice dynamics 78−79692
molecular crystal, effective mol. polarisability calcs. 77−12298
molecular effusive collisionless beam, optical Rabi coherent transient damping, time resolved obs. 77−75231
molecular ion cluster emission in SIMS, parity rule applics. *(French)* 80−63882
molecular laser, optically pumped, review 80−58519
molecular static polarisability, ab initio SCF wave functions 80−74106
molecular transition freqs. in resonant optical field, Stark shift 77−14487
molecular vapour, saturable absorpt., self-focusing and nonlinear susceptibility 80−83647
molecule, 2- and 3-photon absorpt. obs. 80−18864
molecule, 2-step reson. scattering, subnatural linewidths in vapour 79−76419
molecule, 5350 Å band rot. anal., Fourier transform spectroscopy 77−27081
molecule, A-X system 79−63995
molecule, anomalous visible band effects near B state dissoc. limit 77−6816
molecule, $B^3\pi o_u^+$ state deactivation efficiency, temp. depend. 78−70869
molecule, B←X(0-0) band, visible spectrum obs. 78−5238
molecule, B state, effective hyperfine Hamiltonian 78−58598
molecule, B-X band system, intensity factors 78−25551
molecule, B-X fluoresc. band system, intensity and relative band strengths meas. 80−102540
molecule, B-X lines, Franck-Condon factors, Ar^+, Kr^+ and He-Ne laser excitation 80−58320
molecule, B-X system, mol. consts. and Dunham expansion parameters 80−87095
molecule, B-X transitions, rot.-vibr. hyperfine coupling consts., extension to other levels 80−63625
molecule, B-X transitions near 5145 Å, reassignment 77−3374
molecule, band system, MC SCF pseudopot. calcs. 78−78632
molecule, blue-green fluoresc., ArF laser excitation 80−14166
molecule, coherent multiphoton transitions, nonlinear resonant photoionis. 77−61814
molecule, coherent optical transients and optical dephasing in mol. collisions 80−9966
molecule, collision-induced predissoc., Landau-Zener model, method of analytic continuation 77−83687
molecule, collisional release and photocomp. kinetics, I* prod. 78−66819
molecule, conc. profiles, shock tube unsteady expansion wave technique, applic. 78−61011
molecule, dissoc. attachment by 0-8 eV electrons 78−74776
molecule, dissoc. electron attachment, negative ion prod. rates 80−18938
molecule, Doppler-free optoacoustic spectra 80−995
molecule, doubly resonant third harmonic generation, spectrosc. 79−93984
molecule, electron attachment coeff., 35-110°C, vibr. states interpretation 79−98219
molecule, electron diffraction parameters, spectrosc. calc. 78−70932
molecule, energy levels near B-state dissoc. limit, two-photon spectra 78−9210
molecule, equilibrium parameters and Morse anharmonic consts., electron diffr. determ. 78−58818
molecule, excited by circ. polaris. light, mol. collisions, emission depolaris. 78−33577
molecule, fluoresc. in 340 nm band, buffer gas press. depend. 79−13762
molecule, fluoresc. obs. in CW intracavity dye laser spectroscopy 80−13155
molecule, fluorescence, CW dye laser emission wavelength locking by intracavity gain 80−99721
molecule, fluorescence and quenching of 3400 Å 77−3398
molecule, folded Doppler broadened system, interaction with two reson. laser fields 80−53007
molecule, high-dispersion polarisation-labelled spectrum 80−990
molecule, high-resolution saturated absorpt. spectroscopy with short light pulse coherent trains 80−64110
molecule, hyperfine component classification, suitability for laser wavelength stabilisation 78−86965
molecule, hyperfine predissoc., Doppler-free spectrosc. obs. 78−89558
molecule, hyperfine predissociation, saturated absorpt. expt. 77−58103
molecule, hyperfine struct. in B-X transition, laser spectroscopy of pure I_2 jet 79−81234
molecule, hyperfine structure, 612 nm and 640 nm, saturated absorpt. expt. 78−66871
molecule, hyperfine structure obs. in saturated fluoresc. 78−50569

iodine continued
molecule, hyperfine transition saturation intensities, saturated absorpt. technique 80−43208
molecule, in Ar, emission spectrum interpretation 80−95634
molecule, in CCl_4 soln., $B^3\pi_0{}^+{}_u$ state ps excitation, ultrafast decay and spectrum 78−9184
molecule, in seeded supersonic beams, vibr. and rot. relax., laser-induced fluoresc. obs. 80−23522
molecule, laser dissociation, in gas and soln. *(German)* 78−90240
molecule, laser fluoresc., relax. of oriented ground and excited mols. 78−46390
molecule, laser fluoresc., spectral assignments at 5145 Å 78−46389
molecule, laser fluoresc. state selected and detected mol. beam mag. reson., hyperfine transitions 80−63731
molecule, lifetime of R(127) line of 11-5 band of $B^3\Pi_{ou}{}^+$-$X^1\Sigma_{og}{}^+$ transition 77−6861
molecule, line near 520 THz, HFS, direct freq. meas. 80−53266
molecule, low conc. detect. by laser fluoresc. excitation 78−27871
molecule, $M_{4,5}N_{4,5}N_{4,5}$ Auger spectra, kinetic energy shift rel. to atom 80−5516
molecule, $M_{4,5}N_{4,5}X$ Auger electron spectra, many-body effects 79−59415
molecule, matrix isolated in N_2 and Ar, magnetic circular dichroism spectrum 80−5567
molecule, model potential SCF calcs. 80−95528
molecule, molecular dissociation limit, two-photon technique 77−3425
molecule, multiphoton ionis. spectroscopy, sequential 79−50163
molecule, multiphoton reson. ionis. bands, 360-600 nm 78−90233
molecule, nonlinear photodissoc., at. reson. UV fluoresc. and photoionis. obs. 78−37692
molecule, optical dephasing, emitting mols. coherent oscills., optical T_1 and T_2 meas. 77−79644
molecule, Phillips, Kleinman pot. derivation, pseudpot. for ground state, orbitals bond length, vibr. freq. 77−65418
molecule, photodissoc., atomic He (I) photoelectron spectrum 80−83325
molecule, photodissoc., theory of resonant Raman scattering *(Russian)* 78−55180
molecule, photodissoc. cage effect, computer simulation 79−24771
molecule, photolytic cage effect in gas phase 80−81345
molecule, picosecond relax., fluoresc. spectroscopy, solvent effects 78−58737
molecule, polarisability anisotropy, laser assisted mol. beam spectroscopy 80−78646
molecule, props. as test mol. in modern spectroscopy, review 78−90317
molecule, pseudopotential calcs., dissoc. energy, bond length, force const. 77−26964
molecule, relativistic effects, photoelectron spectra, Hartree-Fock-Slater method, perturbation theory approach 80−27962
molecule, relativistically parameterized extended Huckel theory 79−49924
molecule, reson. CARS spectrum, electronic resonance enhancement 79−14033
molecule, reson. Raman lines, Stokes-antiStokes intensity ratio meas. 77−6786
molecule, reson. Raman scatt., time delay 77−34641
molecule, reson. Raman scatt. *(German)* 79−26983
molecule, reson.-enhanced CARS, band contours, assignments 78−86980
molecule, resonance Raman scatt. and collision-induced redistrib. scatt. 77−14439
molecule, resonance-enhanced multiphoton ionis. and fragmentation of mol. beam 79−100411
molecule, RF optically heterodyned saturation spectroscopy, reson. degenerate four-wave mixing 80−74211
molecule, rotationally inelastic collisions selection rules, reson. fluoresc. obs. 77−58133
molecule, rovibronic and gerade states, two-photon excitation 77−14508
molecule, saturated absorpt. lines press. and power broadening 79−76765
molecule, saturated absorpt. obs. using interferometric spectroscopy 78−74079
molecule, stepwise two-photon excitation, E-state vibr. bands, B-state vibr. rot. levels 79−26962
molecule, time-resolved reson. Raman and reson. fluoresc., hyperfine splitting effects 77−30874
molecule, two-photon sequential absorpt. spectroscopy 77−54581
molecule, UV laser, quartz flashlamp pumped, pulse-periodic operation 80−53279
molecule, UV laser transition, vibr. anal. 77−75170
molecule, vac. UV absorpt. cross section 80−91574
molecule, vibr.-translational relax., collisional predissoc., opto-acoustic effect obs. 80−43157
molecule, vibrational relaxation and dissoc. behind a shock front, absorpt. spectroscopy *(Russian)* 77−88536
molecule, visible absorpt. spectra, Fourier transform spectroscopy appl. 78−58060
molecule, visible spectrum, Fourier transform spectroscopy, B-X system 79−94007
molecule, $X^1\Sigma_g{}^+$ ground state, Le Roy's theory, continuous wave oscillation 79−94006
molecule+Ar(Ne)(tetrafluoromethane), D-state lifetime and UV laser action 77−14471
molecule photoluminesc. of matrix samples, laser spectroscopy, evidence for $(I_2)_2$ species 78−58735
molten, electrical cond., press. effect, 0-1 kbar 78−55963
naphthalene-I_2 soln., elec. cond., thermoelec. power, conc. depend., 120°C 77−39845
nonaqueous solution for selective etching for GaAs 77−40453
nonlinear spectroscopy, coherent background noise elimination from saturation spectrosc. signals using freq. offset pump 80−62733
optical frequency standard, highly stable, utilising an atomic beam 79−35685
optical rotary echoes, Bloch eqns. perturbative solns. 80−43407
oxidation of phthalocyanines to produce highly conducting mixed valence solids 77−47800
partition equilibrium between air and NaOH aq, effect of CO_2 conc. 78−78474
passive switch for 1.315 μm radiation 77−23685
photochemical laser, book contrib. 77−10912
photochemical laser, max. storable energy *(Japanese)* 77−38876
photodissociation laser, excited beam accumulation, kinetic eqns. 77−3576
photodissociation laser, free oscill. conditions, kinetic model 77−3577
photodissociation laser, pulse duration, mag. field control 77−75585
photodissociation laser, quartz:Ti tube for C deposit elimination 77−10945
photodissociation laser, short-pulse high-press., line broadening and saturation parameters 77−3575
poly-2-vinylpyridine-iodine, semicond. film, elec. cond., depend. on I conc. and temp. 79−73606
polyacetylene:I_2, synthesis, elec. cond., thermoelec. power 80−60016
polyacetylene:I, dc microwave cond., permittivity 80−107843
polyacetylene:I, electric props. in semicond. and metallic regions 80−29432
polyacetylene:I, electronic excitations, momentum depend., EELS study 80−76121
polyacetylene:I, electronic structure, XPS and UPS meas. 80−66385
polyacetylene:I, NMR investigation of struct. 80−39011
polyacetylene:I, NMR struct. investigation 80−108082
polyacetylene:I, reson. Raman spectroscopy 80−66208
polyacetylene:I, semiconductor-metal transition, thermoelec. power meas. 79−56271
polyacetylene:I charge transfer complex, struct. 79−74052
polyacetylene:I film, Raman scatt. 79−47457
polyacetylene-I_2, highly conducting, Raman, XPS and X-ray diffr. obs. 78−80454
polyethylene:I_2, films, electron-beam induced carrier mobility and elec. breakdown 80−80429
polynaphthoquinone-SO_2-I_2 system for H_2O decomposition for H_2 production 80−16825
polystyrene:I_2, films, electron-beam induced carrier mobility and elec. breakdown 80−80429
polystyrene:I films, thermally stimulated discharge, I conc. and polarisation temp. depend. 80−107937
polyvinyl acetate, thick film, pure and I_2 doped, electrical cond. 77−85234
polyvinyl fluoride:I_2, thermally stimulated currents 78−64315
polyvinylidene fluoride drift mobility meas., I_2 charge transfer from surface charge decay technique 80−49744
polyvinylquinazoline-I_2 complexes, absorpt. spectra and elect. cond. 80−92891
PVC+$Br_2(I_2)$, reaction in surface-modified film subject to thermal-radiative and photochem. action *(Russian)* 77−21385
pyrene-I_2 soln., elec. cond., thermoelec. power, 155°C, conc. depend. 77−39845
pyridine-$I_2(Br_2)$ charge transfer complexes, vibr. spectra, vibronic contrib., intensity enhancement 80−53048
pyridine-I_2(ICl), charge-transfer complexes, hyperpolarisability 77−34568
radical recombination in dense liquids, stochastic trajectory simulation 80−45487
radioactive, airborne, diffusion coeffs. 79−2142
radioactive I adsorption on charcoal filter, safety evaluation *(Japanese)* 78−33267
radioactive I behaviour during PWR steam generator tube rupture accident 79−59230
radioactive I spiking in LWR, release mechanism and its verification in plant operation 79−59229
radioactive I spiking in PWR fuel rods, cause and effects 79−59227
radioactive I spiking in PWR fuel rods, general model of origin and behaviour 79−59228
radioactive isotopes, nuclear fuel cycle radiation safety problem *(Russian)* 80−18560
radioactive waste, solidification in concrete, leach rates 78−703
radiographic meas. of I in tissue, appl. of filtered bremsstrahlung spectra 79−74747
radiography, I isolated images using spatial frequency encoding 79−39485
radioiodination, microelectrolytic, of polypeptide hormone, using Pt microcell 79−48340
radioiodine accumulation in thyroids of pasture animals, rel. to ^{129}I meas. *(German)* 77−52891
radioiodine environmental transport from air to milk rel. to deposition vel. 77−66866
radioiodine release from U_3O_8 in O_2 and inert gas atm., chem. identities 77−57712
radioisotope adsorption by minerals 80−83203
radioisotopes, A=123 to 135, derived air concs. annual limits 78−31909
radioisotopes, environmental and biological effects from nuclear fuel cycle *(Russian)* 80−52768
radioisotopes, high efficiency mixed species air sampling, readout and dose assessment system 78−57074
radioisotopes, meas. of crit. environmental exposure for reactor accidents 78−57081
reactor poison, stress corrosion cracking of Zircaloy LWR fuel rod cladding 80−71810
reversible photoredox system, thionine type and I_2 type, chem. equilibria *(German)* 77−90630
saturate absorber, transmission tests using AO coupled Ar-ion laser 78−30031
saturated absorption, He-Ne laser stabilisation, freq. shifts 77−50697
saturated absorption, He-Ne laser stabilisation 77−46740
saturated absorption for Ar^+ laser freq. stabilisation 79−22965
saturated absorption for He-Ne laser stabilisation 79−22964
saturated absorption signal for stabilized He-Ne laser 77−75481
solid, acoustic wave velocity calc. from phonon curves *(French)* 77−1180
solid, FCC metallic, self-consistent APW Xα electron-band calc., up to 22000K 77−39762
solid, metallic, insulating-metal transition at high-press., exptl. and theoretical shock-compression curves 77−39781
solid, press.-induced struct. phase transition, X-ray obs. 79−65192
solutions, vibr. and rot. relax., reson. Raman lineshape meas. 79−31616
solutions, visible absorpt. spectra, temp. effects 77−61760
sorption, by dextran struct. modifications, porosity depend. *(Russian)* 79−23535
stress corrosion cracking of LWR Zircaloy cladding 79−89380
stress corrosion cracking of Zircaloy, temp. and stress depend., threshold press. determ. 80−16595
stress corrosion cracking tests, nuclear fuel rod pellet clad interaction failures 78−58351
stress corrosion of reactor fuel element cladding tubes 77−3100

iodine continued
supersonic chemical laser flowfield, laser induced I_2 fluorescence meas. 80−38008
surface chemi-ionisation by Rb_2 beam 78−7231
switch, active modulation of transmission based on Zeeman effect 79−22994
tetrabutylammonium iodide/I solid/liquid electrolyte interface, impedance study 80−26031
thyroid, accumulation curve of radioiodine and its role in diagnostics *(Hungarian)* 80−94341
thyroid, microscopic dose distribs. due to I isotopes 79−39522
thyroid gland, X-ray fluoresc. tomography 80−61664
tissue content, meas. by coherently and Compton scatt. photons 79−88220
tissue stable I conc. determ. by X-ray photographic method 77−70540
tumour localisation expts. using heat-denatured radioiodinated calf thymus DNA 79−96651
UV laser possible pumping by synchrotron radiation, NaCl:I(Br) luminesc. 78−66835
vapour, absorpt. lines meas. using FM spectrosc. 80−42262
vapour, CARS, electronic reson. enhancement 78−29793
vapour, chemical composition at high temps. 77−36781
vapour, passive Q-switch for ruby laser 77−79872
vapour cell as narrow band opt. filter 78−74993
Zircaloy cladding stress corrosion cracking due to I *(Japanese)* 80−78361
Zircaloy-2, I_2 stress corrosion cracking, Cs_2O and Cs influence, in- and out-of-pile 80−3252
Zircaloy-2, iodine environment, plane strain tension test 80−22944
Zircaloy-4 cladding rubes, burst strain and stress corrosion cracking, I influence 80−3248
Zircaloy-4 tubes, I stress corrosion cracking *(Korean)* 79−34195
Zircaloy-4 tubing, unirradiated, under internal pressurisation, threshold conditions for I-induced stress corrosion cracking 79−66206
$Ag+I^+$, impact parameter depend. of K X-rays 78−94308
AgBr:I, activator luminesc., energy model 79−28808
AgBr:I, isoelectronic trap 79−43016
AgBr:I, refilling of recombination centres during thermal stimulation 78−10464
AgBr:I emulsion, photocond. and luminesc. at −186°C, rel. to incident light intensity 78−64063
$AgBr:I^-$, emission spectra at 4.2K 79−4841
AgCl-AgBr:I, lattice defect parameters, Frenkel defect form. energy, ionic cond. 80−44359
$AgI-I_2$ system, isotope exchange study, 115 to 195°C 77−77756
Ar^+ and Ar^+-Kr^+ ion lasers, I_2 stabilized, beat frequency 80−95916
Ar^+ laser 582 THz stabilisation by I_2 cell, improvements 80−102741
$Ar-I_2$, low electron beam excitation rates 79−86163
As_2Se_3:X (X=Cu, Ag, Tl, I, Ge), effect of doping, NMR meas. 80−11282
atom, recombination, shock tube unsteady expansion wave technique, applic. 78−61011
Au+I, noncharacteristic X-ray emission, self-consistent relativistic many-electron correl. diagram 77−19023
BWR, primary containment vessel, spray I_2 removal characteristics 80−73972
$Ba+Br_2(I_2)\rightarrow BaBr(BaI)+Br(I)$, time-of-flight chemiluminesc., mol. bond energies determ. 78−40051
$Br^*+I_2(Br_2)(Cl_2)(IBr)(ICl)(BrCl)$, deactivation rates of $Br^*(^2P_{1/2})$, collision complex form model 78−42179
CdS:I single cryst., I detection by argentometric titration DEP 77−16875
$CdS:I_2$ system, interface kinetics and vapour phase mass transport 80−19732
CuBr(Cl):I, lattice-dynamical study of impurity modes 80−29129
$F+I_2\rightarrow IF+I$, energy partitioning, vibr. populations and rot. temp., population inversion 80−50832
Fe:I, ^{131}I NMR, vacancy associated impurity sites 78−91964
Fe-I system, photochemical conversion efficiency 80−71923
$2Fe^{2+}+I_3^-$, solar photochemical decomposition for H_2 prod. 80−16822
n-GaSe:I, SCL currents, expt. test of theory for insulator with two sets of traps distribution in energy 77−89768
Ge-I, gas phase equilib. comp. 77−36776
$Ge_{42}S_{58}$:I, glass, impurity effect on e.p.r., dangling bonds 77−4553
GeTe:I, ferroelectric transition exam. 78−88264
H production, thermochem. H_2O decomposition using S-I cycle, process eng. and bench-scale studies 80−35770
$H_2+I\rightarrow HI+H$, collinear reaction, reson. effects, quantum mech. calcs. 77−52625
HBr^*+I, reaction rate, vibr. excitation effect, isotope enrichment 77−90581
$HF+I^*(5^2P_{1/2})$, electronic-vibr. energy transfer fluoresc. decay meas. 77−71846
He-Cd positive column laser power, effect of I_2 additive *(Japanese)* 79−7121
$He-I_2$ laser, sequential separate multicolour output operation *(Japanese)* 80−28205
He-Ne laser, I_2-stabilised, with long path interferometer, optical feedback effect 77−9544
He-Ne laser, I_2-stabilised, stability and reproducibility of wavelength 78−1270
He-Ne laser stabilisation, I_2 absorption cell power densities 80−99767
He-Ne laser stabilisation by I_2 612 nm saturated absorption 80−99765
He-Ne laser stabilisation by I_2 611.8 nm saturated absorption 80−99766
$He+I_2^*$, sudden rot. approx., rot. and vibr. cross sections 77−30966
$He+I_2^*$, sudden rot. total rot, inelastic cross section 77−30967
$^3He-^{20,22}Ne/^{127}I_2$, 0.63 micron laser generated contrasting power resons. *(Russian)* 77−23651
Hg-I ANL-4 cycle for thermochem. H prod. 80−35785
Hg-Tl-I discharges, 50 H_z, Tl atoms axial segregation 80−38781
Hg-Tl-I discharges, 50 Hz, axial segregation effect on elec. field strength 80−59320
$Hg+I_2$ reaction, adiabatic pot. energy surface 78−15666
$Hg+I_2\rightarrow HgI+I$, endoergic reaction, prod. ang. distrib. 78−15665
$I(5^2P_{1/2})+HBr$, reactive and inelastic channels rate, temp. depend., AAS obs. 78−35657
I I, isoelectronic sequence, multiconfiguration HF calc. of sp^6-s^2p^4d interaction 78−9072
I I,II, radiative lifetime meas., rel. to I and $He-I^+$ laser transitions 79−54810
iodine continued
I II, reson. lines, oscill. strengths determ. by absorption method 80−58214
I laser, high-power, beam quality, gain saturation effect, for fusion ignition 78−63149
I laser medium, CF_3I, UV absorption modification, by vibr. excitation for fusion ignition 78−58717
I nanosecond single pulse laser, open electric discharge pumping 80−5763
I photodissociation laser, tuning using Zeeman effect 79−50316
I photodissociation laser using CF_3I, n-C_3F_7I, optical inhomogeneity losses 79−55129
I, recomb. laser, possible use of alkali metals to obtain population inversion 79−94221
I, recombination in inert gas buffer, computer simulation, rate const., press. depend. 77−25261
I, spectral transition probabilities, 500-1050 nm 78−82676
I VI, beam-foil spectrum, 400 to 1300 Å 79−86059
I VI and I VII, beam-foil obs. of lifetimes, spectral assignments, 400 to 1300 Å 80−9556
I VII, beam-foil lifetime meas., cascading problem 80−14249
I VII, beam-foil spectrum, 400 to 1300 Å 79−86059
I^-, 3d photoabsorpt. spectra, continuum and discrete states 79−81176
I^-, $3d^94f$ config., collapse of 4f electron, X-ray spectral obs. *(Russian)* 80−58204
I^-, anal. in groundwater by X-ray fluorescence spectrometry 80−45829
I^- and I_2^- formed in CeI_3 by electron irradiation 77−27190
I^-, aq., in supercooled water, and glass forming solns., charge transfer to solvent spectra 77−50447
I^- beam, duoplasmatron ion source for SIMS, $Ar-I_2$ medium 77−18123
I^-, fluoresc. quenching of organic excited singlet states, rate meas., mechanism 77−38685
I^-, free-ion polarisability, empirical values 77−20792
I^-, in althylamminium iodides, in solns. of low parity, MCD spectra 78−94268
I^-, in He, ion reduced zero field mobility and free diffusion coeff. 77−47139
I^-, ion mobility in Ar, flow drift tube meas. 77−72405
I^- ions, labelled, adsorbed on Ag, surface diffusion 80−39413
I^- ions of 15 MeV, stripping and charge state fluctuations in O_2 77−79522
I^-, photo-oxidation at n-TiO_2 electrode 80−81331
I^-, plasma, broadening of free-bound radiation thresholds 80−53940
I^-, promotion of phosphoresc. in aromatic rigid solns. 80−50387
I^-, Thomas-Fermi-Amaldi eqn., approx. variational soln. 80−52870
I^{-2} ions in gas phase 79−36449
I^+, lasing in CdI_2-He hollow cathode discharge 77−10951
I^{53+}, 40 GeV beam, propag. through fusion target chamber, stability 78−26303
I-CdI_2 mixture, molten, nuclear spin relax. 80−88887
I-Xe dating of silicate and troilite in Fe meteorites, group IAB 80−17554
I^+-He laser discharge, positive column, particle densities 80−103215
I+Au, relativistic effects in variable-screening model 77−14516
I+Au, slow collision, M MO radiation anisotropy 79−72269
I+Au collisions, average ionisation probability of Au meas. 77−68005
I+Fe, Fe K-α X-ray emission, high-resolution meas. 80−37871
$I+H_2$, activation energy and trajectory calcs., temp. and isotope effects 78−76835
$I+H_2$, atom transfer reactions, reaction rate computing, trajectory calcs. 79−74371
$I+H_2$, collinear trajectories, pattern recognition 80−45481
$I+H_2$, thermal rate constants, quasiclassical trajectory calcs., detailed balance 79−87822
$I+H_2(HD)(D_2)$, intramultiplet transitions 77−54597
I+HCl, quenching of $I(5^2P_{1/2})$, temp. depend., time resolved at. absorpt. spectrophotometry 80−32655
$2I+He\rightarrow I_2+He$, energy transfer mechanisms studied using trajectory calcs. and Monte Carlo method 80−66785
$I+I+O_2\rightarrow I_2+O_2$, photolysis, rate const. obs., mechanism 77−63883
$I+I\pm I_2$, termolecular chemiluminesc. reaction, rate const. for interaction with n-C_3F_7I 79−96291
I+methane $^-d_0(^-d_3),(^-d_4)$, excited atoms, quenching, isotope effects, time resolved reson. fluoresc. 80−32656
$I+O_2$, near-resonant electronic energy transfer, surface-hopping model 79−86030
I+target atom, 15-80 MeV, K-vacancy cross sections, target depend. 77−19026
I+Z (total $Z\geq100$) adiabatic collision, inner shell X-ray prod., vacancy prod. 79−31675
I^-+CO, endoergic ion-molecule reaction 77−25262
$I^-+COS(CS_2)(H_2S)$, endoergic reaction, time of flight mass spectral obs. 77−12786
I^-+He, term parameters, electron spectra and scatt. cross sections 77−27148
I^-+methane(fluoromethane), excitation functions, reactive scatt., eV region *(German)* 78−35677
I^-+Ne, electron detachment collision, 1-3 keV, differential cross-section 79−72403
I^-+O_2, 0.2-100 eV, reaction differential cross sections energy depend. meas. 77−63902
$I^-+SF_6\rightarrow SF_5+F+I$, electron affinity of SF_5 radical 80−45495
I^-+SO_2, endoergic reaction, time-of-flight mass spectral obs. 77−12785
I^-+sulphorhodamine G, physical and chem. kinetics competition, fluoresc. quenching obs. 79−43567
I^{16+}+In, double K-shell vacancies obs., K_α hypersatellite transitions, shift, shared double vacancies 79−72268
$I^{25+}+Te^{24+}$, $I^{43+}+Au^{69+}$, $I^{25+}+Au^{51+}$, correlation diagrams, inner-shell vacancy prod., characteristic X-rays 77−83503
$I^{5+}+Xe(Ar)(N_2)$, 20 MeV, electron loss cross sections, pot. model data anal. 79−27082
I_2, $(B^3\pi_{0+u})$, dissoc. reaction, computer simulation 78−48639
I_2, absolute absorption spectrum measured by Fourier transform spectroscopy 79−75622
I_2, absorpt. spectrum, visible region, wavenumber meas. by Fourier transform spectroscopy *(French)* 77−57407
I_2 absorption cell for He-Ne laser, narrow nonlinear resonances at 0.63 μm *(Russian)* 79−59672
I_2, angular momentum transfer, elastic, inelastic collisions, orientation and polarised fluoresc. 78−90271

iodine continued
I_2, B state, fluorescence yield, individual hyperfine components 77−68067
I_2, B-X system superfluoresc. emission obs., 1.1 to 1.3 μm 79−81412
I_2 complex formation, thermodynamic values 80−45540
I_2 containing radioactive ^{124}I, ^{126}I, nucl. reson. fluoresc. in ^{124}Te, ^{126}Te obs. 77−2953
I_2, continuum reson. Raman scatt. 77−71809
I_2, dissociative attachment, thermal energy electrons 78−82850
I_2, dissociative mol. pot. functions from continuum reson. Raman spectra 77−38673
I_2, efficient laser action on 342 nm band, ArF laser pumping 80−99703
I_2, electron diffr. data for geom. struct., non-parametric estimation method 79−86066
I_2, electronically excited states, vis. and UV laser techniques, book contrib. 78−9277
I_2 frequency stabilised He-Ne laser 78−90429
I_2, gas phase flash photolysis, in ethane and propane, cage effect temp. depend. 78−80770
I_2, HFS and mag. parameters of B state, ab initio calc. 79−45865
I_2, HFS using Doppler-free stimulated-emission technique 78−93765
I_2, hyperfine struct., saturated absorpt. at 612 nm, stabilisation of He-Ne laser 79−59730
I_2, in CCl_4 (cyclohexane) soln., ps dye laser excitation, fluoresc. and resonance Raman emission 80−28021
I_2 laser, CW, optically pumped, performance 78−17912
I_2 laser, CW optically pumped, laser oscill. 0.57 to 1.35 μm 79−943
I_2 laser, quasi-tunable IR emission, appl. to absorption meas. 77−42551
I_2, laser saturation spatial spectroscopy of diffusion coeff., interaction pot. 77−75341
I_2, mol., gas-phase electron diffr. for geom. struct. 79−97368
I_2, mol. dephasing, radiationless decay meas. by laser-acoustic diffr. spectroscopy 78−37667
I_2 molecule, fluorescence decay study, dye laser app' *(Japanese)* 77−58341
I_2 molecule B-X electron transition during Cu vapour laser optical pumping *(Russian)* 80−78845
I_2 molecule pumped by Cu vapour laser, pulsed stimulated emission due to electronic transitions 80−14330
I_2, multiphoton ionis. and dissoc. vibronic/mass spectra method 79−3507
I_2, optically pumped, lasing obs. on 342 nm band 78−79008
I_2, optically pumped CW dimer lasers 80−14322
I_2, optically pumped continuous laser, 583-1338 nm 78−17962
I_2, photolytic cage effect in high-press. gases, laser wavelength depend. 80−11925
I_2, propan-1,3-dioic acid, H_2O_2, KIO_3, $MnSO_4$, $HClO_4$, periodic chem. reactions, bi- and tristability, rel. to biological mech. *(French)* 78−80726
I_2, quenching of laser-excited O_2 80−99515
I_2, saturated absorpt., freq. stabilisation of He-Ne laser *(French)* 79−31935
I_2 seeded in supersonic free jet, collision-induced rotational relax. 80−102556
I_2, stabilised He-Ne lasers, hyperfine struct. spacings, international intercomparison meas. 78−87088
I_2 stabilised He-Ne laser, practical approach to design and construction 80−19051
I_2, transition moment of BO_u^+-$X^1\Sigma_g^+$ system in I_2 laser 79−54917
I_2, UV laser transitions, electronic designation 79−944
I_2 vapour concentration monitoring, secondary laser cavity for weak absorptions 78−92551
I_2^-, pot. curve calc. 77−10596
I_2^+, fragmentation ang. distrib., energy disposal, branching, photoelectron-photoion coincidence spectra 79−68263
I_2^+, impact dissoc. cross-section, excitation energy, mass spectral obs. 77−3489
$^{127}I_2$, saturation resons., recoil shift meas. 79−93985
$^{129}I_2$, energy levels near B-state dissoc. limit, two-photon spectrosc. obs. 80−106367
$^{129}I_2$, frozen soln. in o- or p-xylene, Mossbauer effect obs. 80−78637
I_2:Li(Na) (K) (Cs) (Be) (mn) (Fe) (Cr), doping effect on elec. cond., semicond. props. 80−49732
I_2-aromatic complexes, photodissociation, I-aromatic complex in soln. formation ps laser studies 80−40711
I_2-benzene, N_2 and Ar matrix isolated, magnetic circular dichroism spectrum 80−5567
I_2-benzene, π-σ charge-transfer complex, frozen soln., Mossbauer spectra obs. 80−91655
I_2-He-Xe, gaseous mixture with one low conc. component, thermal diffusion calcs. 77−19661
I_2-methylated benzene, π-σ charge transfer complex, frozen soln., Mossbauer spectra obs. 80−91655
I_2-pyridine, n-σ charge-transfer complex, frozen soln., Mossbauer spectra obs. 80−91655
I_2-SO_2 water splitting cycle, thermochem. H prod. 80−30600
I_2-triethylamine, n-σ charge-transfer complex, frozen soln., Mossbauer spectra obs. 80−91655
I_2-Xe, UV transient absorption following flash photolysis 79−61879
I_2+acetylene, laser-induced 1,2-diiodoethylene form., isomerisation 80−85157
I_2+Ar, mol. rot. axes, collisional alignment calcs. 77−42376
I_2+Ar*, ion-pair form. differential cross-section, 25-133 eV, metastable Ar 78−78787
I_2+CO, E-V energy transfer reactions, electronically excited I_2 78−64814
I_2+CO_2, collisional energy transfer, quenching effects 80−14193
I_2+Cs(Na)(K), ionising collision, trajectory surface hopping calc. 77−50509
I_2+Cu(^{2}D), beam-gas chemiluminesc. reactions 80−85151
I_2+H_2, vib. relax. in supersonic jet 77−58134
I_2+He, collisional relax. of vibr. excited mol., reson. enhanced 79−64081
I_2+He, energy transfer, centrifugal sudden approx., classical infinite order sudden approx. 80−27933
I_2+He, vibr. relax. cross section, in I_2He_n photodissoc. expt. 79−100410
I_2+I_2, collisional energy transfer, selection rules for elastic collisions 77−50467
I_2+I_2, collisional energy transfer, ground and excited states, polarisation spectra 80−32805
I_2+I_2, optical coherent transients detected by frequency-switched tunable laser 77−54762
iodine continued
I_2+I_2, potential well depth estimation method 79−86034
I_2+$K_2(Cs_2)$, ionisation reactions, absolute cross sections 80−99565
I_2+Na(K)(Cs), at. negative ion prod. cross sections 77−531
I_2+Na(K)(Cs), ion-pair form. cross section, 15-120 eV, mol. props. depend. 77−28996
I_2+Na(K)(Cs), ion-pair form., differential cross sections, I_2 internal energy effects 77−61840
I_2+Na(K)(Cs), ion-pair form., energy transfer and differential scatt. 77−75272
I_2+O_2→IO, flash photolysis reaction mechanism 77−32813
I_2+SiAs(GeAs), high temp. Raman spectra, cryst. growth mechanism *(French)* 79−26999
I_2^++N_2→I^++I+N_2, 0.65-3.2 keV, dissoc. cross-section, internal excitation effects 78−64813
I_3^-, geom. and electronic struct., effective pot. calc. 78−74788
I_3, VB pseudopot. calcs. on electronic states 77−26984
I_4^+, electronic struct., binding energy, charge distrib. from free electron model *(German)* 78−29741
I_5^-, geom. and electronic struct., effective pot. calc. 78−74788
$I_2^-(I^-)$, formed by electron impact from SnI_4 ionis. efficiency curves 77−61865
$I_2(I_2^+)(I_2^-)$, HF and SCF calcs., pot. curves, electron affinity and quadrupole moment determ. 80−95527
$I(^2P_{1/2,3/2})$, from ICN A-state photolysis, branching ratio wavelength depend. 80−81335
$I^2P_{1/2}$→$^2P_{3/2}$, collision induced emission (Ar)(Xe), dipole transition moment by perturbation theory 77−83528
$I(^2P_{1/2})$ energy transfer and reactive collisions, laser pumping possibility 79−949
$I(^2P_{1/2})$+n-iodopropane (iodoethane), quenching rate coeff., in UV photolysis of n-iodopropane (iodoethane) 79−11799
$I(^2P_{1/2})$+NF($a^1\Delta$) system, electronic angular momentum transfer, chem. kinetic model 78−63104
$I_2X^1\Sigma_g^+$, collisional relax. of highly excited vibr. levels, using I_2 optically pumped laser 80−43155
^{A}I, A=123, 125, labelling of cyclosporin A, prep. and biodistrib. 80−85496
^{A}I, A=131-2, comparative effects in rat thyroid glands 80−104670
^{53}I, $L\gamma_{2,3}$ X-ray emission spectra, line breadth 78−62760
^{121}I labelling of radiographic contrast media 80−26350
^{121}I, production on Heidelberg compact cyclotron, dosimetry studies 80−21539
^{123}I labelled Hippuran dosimetry, physiological parameters 79−53251
^{123}I, labelling of o-iodohippuric acid for diagnostic nuclear imaging 79−39503
^{123}I labelling of radiographic contrast media 80−26350
^{123}I, prep. from gaseous TeF_6, nuclear medicine appl. *(French)* 80−98137
^{123}I, prod. and use in nucl. medicine diagnosis *(German)* 78−28061
^{123}I prod. from ^{127}(p,5n)^{123}Xe→^{123}I, at 58 MeV 80−94369
^{123}I, prod. using 6 MeV Van de Graaff accelerator 79−53243
^{123}I, production in LASL radiochemistry hot cells 80−72326
^{123}I, radiopharmaceuticals newly developed, conf., London, England (Feb. 1979) 79−92329
^{123}I-Na, thyroid scintigraphy, clinical comparative study with $^{99m}TcO_4^-$ *(Japanese)* 80−81728
^{125}I accidental inhalation, bioassay and thyroid monitoring results 78−24151
^{125}I airborne vapour detection 80−51027
^{125}I, counting device with automatic efficiency correction 80−42897
^{125}I, determ. of exposure rate constant using a scintillation detector 80−89863
^{125}I, encapsulated, and other photon sources, microdosimetric props. 80−36146
^{125}I fibrinogen, detection of deep venous thrombosis 79−16282
^{125}I in the thyroid, 2-probe meas. method 80−81718
^{125}I interstitial seed implants, new afterloading technique 79−34652
^{125}I, intramol. effects of decay in o-iodotyrosine 80−108973
^{125}I, intranuclear atoms not bound to DNA, radiotoxicity 80−104655
^{125}I labelled compounds, rat prostrate imaging expts. 80−51215
^{125}I labelled DNA, pot. tumour imaging agent 80−30892
^{125}I labelled DNA, prep. method and in vivo studies of tumour localisation 80−51249
^{125}I labelled estradiol, a γ-emitting estradiol analogue that binds to the estrogen receptor 80−61697
^{125}I labelled estrogen derivatives 80−81734
^{125}I labelled human serum albumin, geometrical dilution *(French)* 80−104742
^{125}I labelled prostaglandins *(Hungarian)* 80−94368
^{125}I, labelling facilities for biomedical appls. 80−41235
^{125}I labelling hazards, reommended code of practice 80−51270
^{125}I, medical imaging with a scintillation camera 79−49359
^{125}I microelectrolytic labelling of polypeptide hormones 80−12255
^{125}I, oxytocin radioimmunoassay, human plasma 79−5353
^{125}I photons, absorbed fractions in the thyroid 80−109032
^{125}I, procedures for safe working in labs. 79−35698
^{125}I, radiotherapy interstitial implants, dose inhomogeneity 79−100746
^{125}I, rel. to ^{99m}Tc in thyroid imaging 80−36077
^{125}I, release in autoclave sterilization of radioimmunoassay kit *(Japanese)* 80−81727
^{125}I seed implants in prostatic cancer, preoperative extended field radiation 80−72303
^{125}I, shielding of *(Japanese)* 80−63404
^{125}I, spleen damage after partial thyroid blockage, rat expt. 79−96631
^{125}I thyroid dose calc., air and water conc. limits 79−88195
^{125}I, tumour tracer accumulation, autoradiographic study, experimental infectious lesions 79−5348
^{125}I, variation of γ-counting efficiency with sample composition 80−83238
^{125}I worker thyroid meas. 80−36151
^{125}I-7-iodo-6-demethyl-6-deoxytetracycline HCl use for bone mineralisation obs. 80−12214
^{125}I+methane, γ irrad. effects on organic iodide form. and decomp. *(Japanese)* 77−81418
^{127}I, ^{129}I isotope separation possibility using photodissociation I laser 79−7030
^{127}I atoms in Xe matrices, ESR spectrum 80−1005
^{127}I, isomer shift calibration, using lifetime variations in electron capture decay of ^{123}I 80−39925
^{127}I, Mossbauer isomer shift 80−39922

iodine continued
^{127}I saturated absorpt. for He-Ne laser stabilisation, wavelength standard development *(German)* 78−79034
$^{127}I_2$, $^{129}I_2$, $B^3\Pi 0_u^+$-$X^1\Sigma_g^+$ systems, fluoresc., mol. consts., Franck-Condon factors 77−34680
$^{127}I_2$, absolute frequencies of ten hyperfine components, freq. meas. in visible 79−93104
$^{127}I_2$, B-X band system, nucl. HFS, coupling consts. 77−6794
$^{127}I_2$, B-X band system, nucl. HFS, octupole coupling const. effects 77−6795
$^{127}I_2$, B-X electronic transition, systematic hyperfine struct. meas. 78−9267
$^{127}I_2$, Doppler-free optoacoustic spectroscopy 80−57396
$^{127}I_2$, hyperfine struct. in electronic spectrum, saturated absorption spectroscopy 78−37645
$^{127}I_2$, laser stabilisation, gas cell 78−17971
$^{127}I_2$, saturated absorption, in laser cavity 77−58393
$^{127}I_2$, single saturated-absorption feature obs. using optically pumped Hg laser 77−83932
$^{127}I_2$, two photon excitation, rot.-vibr. structure of E-state 79−41213
$^{127}I_2$, visible spectra, HFS at 586.82 nm 78−9395
$^{127}I_2$, weak rot. R(98), 58−1 line, HFS struct., saturated intermodulation fluoresc. 79−94024
$^{127}I_2$, weakly saturable absorber for He-Ne laser, high contrast power reson. 78−29976
$^{127}I_2$ absorption lines at 582 THz, Ar^+ laser freq. stabilisation 78−90430
$^{127}I_2$ hyperfine structure components, stabilization of doubly resonant intracavity SHG of 1153 nm radiation 80−33077
$^{127}I_2$ rovibronic absorpt. lines, hyperfine struct. 80−78596
$^{127}I_2$ saturated absorption for Ar laser freq. stabilisation at 582.49 THz 77−79850
$^{127}I_2$ saturated absorption stabilised He-Ne laser, wavelength meas. *(Russian)* 79−22996
$^{127}I_2$ saturated absorption for He-Ne laser stabilisation, wavelength international comparisons 80−95872
$^{127}I_2$ stabilised He-Ne laser, freq. shifts, limitations 78−90440
$^{127}I_2$ stabilised He-Ne laser 80−106544
$^{127}I_2$ stabilised ion laser, beat freq. intercomparisons at 514.5 nm 80−74338
$^{127}I_2$ wavelengths at 633 nm and H_α, precision interferometer calibration for wavelength meas. 79−80696
$^{127}I^{5+}$ + atom (molecule), multiple electron loss cross sections meas. 79−45818
$^{127}I(p,5n)^{123}Xe \rightarrow ^{123}I^-$ production, separation and radiopharmaceutical labelling 79−79649
^{129}I, dose to world population from nucl. power industry 80−47619
^{129}I, hyperfine struct. and isotope shift of 1.3 μm transition 80−102486
^{129}I impurities implanted in semiconductors, isomer shift 80−20522
^{129}I in bovine thyroid glands, activation anal. obs. 80−94380
^{129}I, in iodyrite and marshite, determ. by radiogenic ^{129}Xe meas. 77−63983
^{129}I in man, cow and deer 78−80975
^{129}I, in reactor waste, sorption by minerals 79−49721
^{129}I in transition metals, calibration of Mossbauer isomer shift 80−20520
^{129}I, internal conversion electron and Mossbauer spectra, calibration of isomer shift 80−39921
^{129}I, isomer shift calibration, using lifetime variations in electron capture decay of ^{123}I 80−39925
^{129}I, limits to radiological dose, dog retention data 77−60253
^{129}I, long-lived, immobilization by fixation of $Bn(IO_3)_2$ in Portland cement 79−59208
^{129}I, mag. hyperfine field in Fe, press. depend., nucl. gamma reson. 80−71256
^{129}I, Mossbauer isomer shift 80−39922
^{129}I, nuclear reactor radioactive gaseous effluents, abatement techniques 79−3221
^{129}I photons, absorbed fractions in the thyroid 80−109032
^{129}I radioactive waste, fixation with Portland cement, radiation stability tests 80−83200
^{129}I radioactive waste storage, IO_3^- adsorption by hematite 80−22992
^{129}I, tandem accelerator mass spectrometry 80−86494
$^{129}I_2$, $^{129}I^{127}I$, $^{127}I_2$ high resolution saturated absorption spectra at 633 nm using He-Ne laser 80−95637
$^{129}I_2$, complete hyperfine spectrum obs. at 612 nm 80−95638
$^{129}I_2$, hyperfine struct., saturated fluoresc. obs. 79−31591
$^{129}I_2$, selective excitation and separation in $I_2+C_2H_2$ laser induced chem. reaction 80−68962
$^{129}I_2$ absorption cell, freq. stabilisation of He-Ne 0.63 μm laser 80−53333
$^{129}I_2$ rovibronic absorpt. lines, hyperfine struct. 80−78596
^{131}I, adrenal medulla imaging with an antiadrenergic agent 79−83910
^{131}I after surgery, thyroid carcinoma treatment 78−85373
^{131}I, age-related radiosensitivity obs. of guinea pig thyroid glands 80−104671
^{131}I air concentrations, comparison of calculated and meas. values 77−34477
^{131}I, air concs. during thyroid therapies 79−25122
^{131}I, airborne conc. at Swierk nuclear research centre 1975-1977 80−7978
^{131}I, airborne conc. in nuclear medicine lab. 79−34674
^{131}I, airborne release from operating BWRs 80−23033
^{131}I airborne release from PWR, determ. of sources 80−17138
^{131}I, airborne short-lived radionuclides of unknown origin in Sweden (1976) 78−32219
^{131}I and antithyroid drugs, simultaneous treatment of toxic diffuse goiter 80−56193
^{131}I, behaviour during rinsing in in-pile loop after fission product release expt. 80−73879
^{131}I, blood plasma, vol. meas. in man using labeled serum albumin 79−29602
^{131}I concentrations in air, milk and antelope thyroids in southeastern Idaho 80−89871
^{131}I determination in vegetation, ashing procedure 78−15930
^{131}I, diagnostic rel. to thyroablative distrib. in thyroid cancer evaluation 79−83903
^{131}I dosimetry of the rat thyroid, accurate method 80−46063
^{131}I, dynamic sorption from gas phase of dissociating N_2O_4 *(Russian)* 78−58356

iodine continued
^{131}I, estimation of γ dose to gastric wall after administration of isotope *(Japanese)* 80−98141
^{131}I fibrinogen, comparative deep-vein thrombosis imaging with ^{111}In platelets 79−29607
^{131}I filters, design against weathering 80−32524
^{131}I, hepatobiliary disorder scintiscanning, evaluation of labelled iogly-camic acid 80−36072
^{131}I, hepatobiliary study of liver-transplant patients 80−3793
^{131}I, high thyroid dose associated with adrenal scanning 79−29629
^{131}I in human thyroid gland, rapid monitoring using Ge(Li) detector 79−2134
^{131}I in milk, rapid method of detect. 80−46106
^{131}I, kidney function studies following radiation therapy of spleen 79−20615
^{131}I labelled chorionic gonadotropin, use in ovarian imaging, rat expts. 80−41186
^{131}I labelled Hippuran, evaluation of renal grafts 80−46017
^{131}I labelled Hippuran dosimetry, physiological parameters 79−53251
^{131}I labelled o-iodohippurate, in vitro stability 80−16668
^{131}I, long-term retention in Indian workers, dose commitment 78−35960
^{131}I, low level detection in milk rel. to population dose 78−31911
^{131}I, malignant thyroid disease treatment 80−36108
^{131}I manipulated in syringes, radiation exposure obs. 80−67252
^{131}I meas., radioactive release from Institution of Nuclear Research *(Czech)* 77−6568
^{131}I measurement in human thyroid gland, use of NaI(Tl) scintillation survey meter 78−80970
^{131}I, milk transfer coeff., review of meas. values 79−2141
^{131}I population thyroid dose in USA after Chinese atm. nucl. weapons tests 78−77116
^{131}I, probability distrib. for release in PWR steam generator tube rupture 80−13668
^{131}I produced radiation, low-dose, somatic mutations induction in Tradescantia 80−72266
^{131}I radionuclide pollution, protection of thyroid gland 79−66560
^{131}I renograms, single injection technique for subtraction of blood background 79−29581
^{131}I, separation from water by ion exchange *(Japanese)* 77−60099
^{131}I spiking phenomenon in accidents involving coolant leakage, expt. *(Japanese)* 77−54320
^{131}I therapy, role in childhood hyperthyroidism treatment 80−41182
^{131}I, thyroid, scintigraphic volume and dose estimation 79−16302
^{131}I thyroid activity meas., improvement in precision 79−29635
^{131}I, thyroid dose eval. following accidental release from reactor spent fuel 80−26366
^{131}I, thyroid uptake determ. *(Hungarian)* 80−94339
^{131}I treated patients, monitoring of I excretions and used materials 80−89873
^{131}I, treatment of benign thyroid disease, review 80−36107
^{131}I treatment of hyperthyroidism, carcinogenesis, comparison with surgery 78−85374
^{131}I, use in hyperthyroidism treatment of children and adolescents 80−46013
^{131}I, use in the treatment of metastatic thyroid cancer 80−36084
^{131}I waste in urine, filter system 77−60319
^{131}I, whole-body metastatic survey as aid in determ. functional thyroid metastases 79−96657
$^{131}I_2$ transport via pasture-cow-milk pathway, stat. anal., thyroid dose uncertainty 79−83950
^{131}I-4-iodoantipyrine preparation from ^{131}I-iodide 80−12256
^{131}I-iodomethyl-norcholesterol, adrenal imaging in primary aldosteronism 79−79634
^{131}I-iodomethylnorcholesterol, human adrenals absorbed dose 79−79660
^{131}I-ortho-iodohippurate absorbed kidney dose calc., literature review 80−76841
^{131}I + propane, U_3O_8 released radioiodine relative reactivity in O and He atmospheres 79−52644
^{135}I in liq. Na in fission reactor, ^{135}Xe isotopes production, degassing 77−34410
$I^* + H_2O(D_2O)(HDO)$, $5^2P_{1/2}$ electronic to vibr. energy transfer, quenching and time resolved IR fluoresc. 79−3537
$I^* + I_2(Br_2)(Cl_2)(IBr)(ICl)(BrCl)$, collisional deactivation and reaction rate consts., obs. 78−80738
I_2^* + He, low energy collisions, energy redistrib. 80−63765
I_2^* + He(Ne), energy depend. of collision induced intramolecular energy transfer 80−83470
$I^*(^2P_{1/2}) + Br_2 \rightarrow IBr + Br^*(^2P_{1/2})$, rate const., chemiluminesc. obs. 77−40520
$I^*(5^2P_{1/2})$ + HF(HCl)(HBr)(HI), collisional quenching rate consts. meas. 77−3299
I2 fluoresc., Ar^+ laser excited, high resolution and sub-Doppler Fourier transform spectroscopy 80−43089
$I(5^2P_{1/2})$, prod. by ICN photodissoc. 79−94047
$I(5^2P_{1/2})$, time-resolved reson. fluoresc., quenching rate coeffs. 78−25466
$I(5^2P_{1/2})$ + benzene-d_0(-d_6), fluoresc. quenching, spin-orbit interaction, isotope effect obs. 78−62763
$I(5^2P_{1/2}) + Br_2$, deactivation kinetics, time-resolved spectrosc. obs. 78−95916
$I(5^2P_{1/2}) + Br_2$, deactivation kinetics, $Br(4^2P_{1/2})$ prod., time-resolved spectrosc. obs. 78−95917
$I(5^2P_{1/2}) + H_2(HD)(D_2)$, electronic to vibrational energy transfer 79−68259
$I(5^2P_{1/2})$ + HBr(DBr)(methane)(propane), collisional deactivation, rate consts. meas. 77−86300
$I(5^2P_{1/2})$ + HCl(HBr)(NO), electronic-vibrational energy transfer, fluoresc. obs. 78−66579
$I(5^2P_{1/2})$ + iodomethane-d_0(−d_3), temperature dependence for quenching 79−45755
$I(5p^5(^2P_{1/2}))$, time-resolved kinetics, mean radiative lifetime, radiation trapping, HFS 78−5171
$I(5p^5P_{1/2}) + I_2$, metastable relax., rate const. 77−19022
K + I chemi-ionisation, integral cross section calc. for two state model 79−18282
K + I chemiionis. differential cross-section calc. for two-state model 79−18283
$K + I_2$, stripping reactions at hyperthermal energies 77−16815
$K + I_2(IBr)(Br_2)(ICl)(Cl_2)$, ion-pair form., bond stretching effect on cross sections 78−1064
$KBr{:}Br_2^-$, triplet luminesc. kinetics, 0.4-4.2K 79−87482

iodine continued
KBr:I, energy transfer due to excitons and holes under host sensitization 79−15526
KBr:I, luminesc., exciton and hole migration to I^- sites 79−38626
KBr:I^-, OH^-, luminesc. of interstitial atomic H 80−89062
KCl:I, colouration under two-photon excitation, absorption spectra 78−84618
KCl:I, luminesc. at low temp. 80−2818
KCl:I crystals, V-band development using X-rays 78−88337
KCl:I^-, H, fluorescence of interstitial H-centres 79−73987
KCl:I^-, interstitial atomic H centres, formation kinetics and struct., MO calcs. and EPR studies 80−75854
KCl:I^-, low-temp. heat capacity enhancement due to impurities 80−107442
KCl:I^-, modes of vibr. due to U-centre and additive anion impurities 80−44280
KI:I_2^-, triplet luminesc. kinetics, 0.4-4.2K 79−87482
Li-I_2, primary battery, self-discharge rates using microcalorimeter 79−61963
Li-I_2 pacemaker cell end-of-life characteristic approximation 80−30937
Li-I_2 power cell accelerated discharge test for battery longevity model 80−30938
Mg-I cycle for thermochem. decomposition of H_2O for H prod. 80−35786
MoO_2-I_2, heterogeneous equilib., vapour transport and cryst. growth 78−27405
$MoSe_2$-I^-, photoelectrode, time resolved photocurrent, nanosecond excitation 80−45708
molecule, vertical valence excited states, CI nonempirical pseudopotential calc. 77−71757
N_2+I_2, ($A^3\Sigma_u^+$) state quenching 78−13580
NO+I, vibr. relax. rate const. determ. 77−19013
$NO^+ + X^- \rightarrow NO + X$ (X=Cl, Br, I), rate const. determ. in flames 78−48633
NaBr:I, exciton ionisation and decay, photoluminesc. in elec. field 77−44046
NaCl:I, UV laser generation by optical pumping 78−82973
NaCl:I^-, energy of migration of I^- 77−43380
Na_2O-P_2O_5:I_2, metaphosphate glass, absorpt. spectra of radiation products 78−64865
NbB_2, vapour transport in temp. gradient in presence of iodine 79−19997
Ne-Ar-I_2, low electron beam excitation rates 79−86163
$O+I_2(CS_2)$(OCS), crossed-beam investigation of translational energy 79−5145
O_2-I_2 100 W transverse-flow chem. laser 79−41374
$O_2(^1\Delta_g)+I(^2P_{3/2})$, possible electronic transition chem. laser 78−63116
PVC:I, photoconductivity study, charge transfer complexes 80−44646
$Pb_{1-x}Sn_xSe$(Te):I epitaxial layers, photoelectric props., doping donor impurity behaviour 77−80810
Pd_2MnSb:^{129}I, mag. hyperfine field of ^{129}I, Mossbauer spectra 78−43706
PrP-I, heterogeneous equilib. 77−36777
RbBr:I^-, OH^-, luminesc. of interstitial atomic H 80−89062
RbCl:I, H, fluorescence of interstitial H-centres 79−73987
RbCl:I^-, interstitial atomic H centres, formation kinetics and struct., MO calc. and EPR studies 80−75854
S-I cycle for thermochem. prep. of H_2 by H_2O dissoc. 80−16823
$SO_2/H_2O/X_2$ reactions (X_2=Br_2, I_2), appl. to thermochem. H prod. 80−35773
Sb-I-Ca process for thermochem. H_2 prod. by H_2O dissoc. 80−16824
Se:I, liq., DC cond., temp. depend. *(French)* 77−69322
Se:I, liq., thermopower, temp. depend. *(French)* 77−69360
Se:I, vitreous, crystn, kinetics determ. *(German)* 80−79936
Se:I liquid, DC cond. and thermoelec. power *(French)* 79−56223
Si:In, neutron irrad. to compensate for residual B, photocond., IR focal plane array 78−80733
SiC:I, α- and β-phases, isomer shift in Mossbauer spectra of implanted ^{129}I 78−15067
Sn:I, α- and β-phases, isomer shift in Mossbauer spectra of implanted ^{129}I 78−15067
TaB_2, vapour transport in temp. gradient in presence of iodine 79−19997
Te:I, semicond., elec. efficiency *(German)* 78−84166
TiP-I_2, exam. of equilibrium gas-transport reaction 79−95911
TlBr:I, isoelectronic donor, broad-band photoluminesc. meas. 77−8636
Vo_2+I_2 transport react., thermochem., appl. to MoO_2:V cryst. growth 79−43116
Xe-I_2 mixtures, electron beam excitation, XeI* emission spectrum 77−6843
^{122}Xe-^{122}I short-lived positron emitter generator 79−100740
(ZnO-ZnS)Cu:I, double band electroluminophors, form., props. 78−19568
ZnS:Cu, Cl, I, anisotropy of blue Cu luminesc. centres 77−81137
ZnSe:Cu, I, ceramic, electroluminesc., electric field induced switching effect under illum. 77−1460
ZnSe:Cu, I ceramic, injection electroluminesc. of p-n microjunctions 80−40163
ZnSe:I, Schottky diode, direct impact excitation of luminescent centres 79−7900
ZnSe:I crystals, I vapour transport prep. 79−100035
ZnSe:I/aqueous electrolyte junction, electrochem. behaviour in dark and under illum. 80−25003

iodine compounds
caesium iodide screen for X-ray image intensifier 78−21311
chalcogenide glass film, M-Sb-S-I, (M=Ge, Sn, Pb, Cd, Cu), prep. and characterisation 77−12533
copper phthalocyanine-iodine, amorphous cpd. prep. by I_2 diffusion in polycrysts., triplet EPR signals obs. *(Russian)* 80−66016
5,10-dihydro-5,10-diethylphenozinium-iodide, average struct. 79−90636
hydration complexes, gas phase, electrostatic calcs. 80−100055
I_2He, I_2He_3, and I_2He_3, photodissoc. products energy distrib. 79−100410
inorganic, chemical bonds using Kα_1 line chem. shifts, Mossbauer isomer shifts 77−27089
iodide, charge transfer to solvent spectra, spectral shift data, Madelung const. determ. 80−85204
tetrachloroiodates, ^{35}Cl NQR freqs., correl. with crystallographic data 79−33559
XPS, binding energies and bond orders 77−18976
$Ag_{26}I_{18}W_4O_{16}$, cryst. struct. and ionic conductivity 77−80647

iodine compounds continued
As-S-I system glasses, IR transmission spectra, structure-chem. comp. 79−42974
As-Sb-S-I system glasses, vitrification and volt-ampere characts. 77−31756
As_2Se_3, effect of Cu and I, investigated by Mn^{2+} EPR spectra 77−73075
Bi-Sb-S-I system glasses, vitrification and volt-ampere characts. 77−31756
ClF_5-IF_5, determ. of phase diagram, using DTA 79−4955
Cu-Sb-S-I amorphous film formation and stimulated crystallisation, electrophysial props. *(Russian)* 78−30838
Ge-I_2, equilibrium study 700 to 1300K, vapour transport rate of Ge *(French)* 78−64476
$Ge_{10}As_{40}Te_{40}I_{10}$, chalcogenide glass film, switching delay time 78−26926
$H+ICl \rightarrow HCl+I$, IR chemiluminesc., product energy distrib. 78−23926
$H+ICl \rightarrow HCl+I$, product energy distrib., rate const., IR chemilum. obs. 77−81391
I complexes, charge transfer states, Mossbauer spectra 80−15907
I complexes, ICl.L (L=organic radical), charge transfer and quadrupole-interaction consts. calc. 77−10590
I^- in aq. soln., anthracene sulphonate sensitised photooxidation via singlet $^1O_2$ 77−32812
I^--$S_2O_8^{2-}$ aqueous redox mixtures, γ-radiolysis 79−16017
$I+H_2$, gas phase H-atom transfer reactions, struct.-reactivity correl., pot. energy surfaces 80−104433
I_2 solid charge-transfer complexes, determ. of thermodynamic form. values 80−45540
I_2-quinoline (pyridine) complexes, stability const. determ. by spectrophotometric methods 80−87056
I_2Ar^*, product state distrib. and binding energy 80−63857
IBr, $B^3\Pi(0^+)$ excited state, laser-induced fluoresc. 80−58309
IBr, $B^3\Pi(0^+)$ states, Franck-Condon factors, RKR turning pts. 77−34681
IBr, elec. dipole moment, rot. transition Stark shift obs. 77−75207
IBr, laser fluoresc. study of $B'O^+$-$X^1\Sigma^+$ system 78−70867
IBr, magnetic rot. spectrum, rot. and vibr. anal. 78−70861
IBr, photodissoc., $Br^*(4^2P_{1/2})$ yield, wavelength depend., collisional release 78−64857
IBr, photodissoc., curve crossing of $Br(^2P_{3/2})$ and $Br(^2P_{1/2})$ 78−62859
IBr, predissoc. and photodissoc., intermed. coupling strength 77−16850
IBr, relativistically parameterized extended Huckel theory 79−49924
IBr^+, fragmentation ang. distrib., energy disposal, branching, photoelectron-photoion coincidence spectra 79−68263
IBr:CO_2 photolysis, electron-vibr. pumping, 2.7 μm Br and 4.3, 10.6 μm CO_2 laser transitions 80−28196
IBr-benzene in n-decane soln., IR line broadening by chemical exchange 80−87111
IBr-CO_2 IR laser with $Br^* \rightarrow CO_2$ electronic-vibr. energy transfer as pump mechanism 80−53260
IBr-graphite intercalation compound, Raman scatt. 77−12390
IBr-graphite intercalation compound, interband Landau level transitions, magnetoref. 77−52095
IBr+Br*, deactivation rates of $Br^*(^2P_{1/2})$, collision complex form model 78−42179
IBr+Na(K)(Cs), at. negative ion prod. cross sections 77−531
IBr($B^3\pi_0^+$), lifetimes determ. from time resolved fluoresc. 78−46385
ICN, A-state photolysis, $I(^5P_{1/2,3/2})$ branching ratio wavelength depend. 80−81335
ICN, A-system photodissociation mechanism 77−38701
ICN, BrCN, and isotopic forms, force field calc., freqs., rot. consts. 79−22693
ICN, Franck-Condon transition amplitudes for mol. dissoc., semiclassical evaluations 78−62860
ICN, general quartic force field, Machina-Overend parameters 78−50532
ICN, laser photolysis, CN radical form. and energy partitioning 77−16853
ICN, microwave spectrum, mag. hyperfine struct., I nucl. shielding tensor 78−17661
ICN, microwave spectrum, vibr.-rot. const., equilib. struct. 78−58677
ICN, photodissoc., CN internal state distrib. 77−36773
ICN, photodissoc., efficient $I(5^2P_{1/2})$ prod. 79−94047
ICN, photodissoc., polarised fluoresc. from fragments 79−98130
ICN, photodissoc., product rot. distribs. 79−66310
ICN, photodissoc. and predissoc., cyanide radical fluoresc. excitation spectrum and laser emission 78−76892
ICN, photodissoc. dynamics, moment anal. 78−13557
ICN, photodissociation, absorpt. lineshape 77−79662
ICN, photodissociation, coupled eqns. calcs., final states interactions 78−25637
ICN, photofragmentation, vibr. and rot. distrib., quantum anal. 77−14504
ICN, rotational distribs. in photodissociation 77−9097
ICN, vacuum UV photodissociation spectroscopy quantum yield, fluoresc. polarisation vacuum UV photodissociation spectroscopy, quantum yield, fluoresc. polarisation 80−32736
ICN^+, fluoresc. quantum yields and lifetimes, meas. method, ion form. 77−6815
ICl, ^{35}Cl and ^{37}Cl, $B^3\Pi_{0+}$ state IR spectra, mol. consts. 80−28016
ICl $A^3\Pi(1)$, excited, laser induced fluorescence, quantum-resolved dynamics of excited states 80−69178
ICl, $A^3\pi(1)$-$X^1\Sigma^+$ absorption spectrum, rotational analysis 80−47990
ICl, $A^3\pi(1)$-$X^1\Sigma^+$ emission spectrum, near-IR, rotational analysis 80−47991
ICl, $B^3\Pi(0^+)$ states, Franck-Condon factors, RKR turning pts. 77−34681
ICl, $B^3\Pi(0^+)$-$X^1\Sigma^+$ fluoresc., predissoc. 77−34682
ICl, energy levels, near first dissoc. limit, 2-photon sequential absorption obs. 78−90246
ICl, fluoresc. decay lifetimes and quenching cross-sections for excited $B^3\Pi(0^+)$ states 78−1030
ICl intercalation in graphitised C fibres and its removal 79−43561
ICl, laser excited fluoresc. 79−50077
ICl, lifetimes of $A^3\Pi_1$ state vibr. levels, 6070-7300 Å 78−66605
ICl, microwave-optical double reson. obs. in $B^3\Pi_{0(+)}$ state 79−85979
ICl, mol. beam focusing in rot. states 79−18317
ICl selective photoaddition to acetylene, isotope enrichment, influence of press., buffer and wavelength 80−11927
ICl, two photon UV absorpt. spectrosc. 79−89687
ICl, XPS, binding energies and bond orders 77−18976

iodine compounds continued
ICl^+, fragmentation ang. distrib., energy disposal, branching, photoelectron-photoion coincidence spectra 79−68263
$I^{35}Cl$, predissociations in $B^3\Pi_{0+}$ state 80−1033
$I^{37}Cl$, predissociations in $B^3\Pi_{0+}$ state 80−1033
ICl-graphite intercalation compound, Raman scatt. 77−12390
ICl-graphite intercalation compound, interband Landau level transitions, magnetorefl. 77−52095
ICl-graphite intercalation compounds, anomalous sp. ht. due to order-disorder transform. 79−42235
ICl-graphite residue compounds, struct., X-ray diffr. 78−47287
ICl-pyridine, charge transfer complex, hyperpolarisability 77−34568
ICl+acetylene, isotopically selective photoaddition, ^{37}Cl enrichment 77−60084
ICl+Br*, deactivation rates of $Br^*(^2P_{1/2})$, collision complex form model 78−42179
ICl+CO, E-V energy transfer reactions, electronically excited ICl 78−64814
ICl+F reactions, product state analysis using laser-induced fluoresc. 80−11915
ICl+H, three dimens. collision, exponentiating trajectories and statistical behaviour 80−5595
ICl+Na(K)(Cs), at. negative ion prod. cross sections 77−531
$(ICl)_2$, mol. beam. elec. deflection obs. 80−53080
$(ICl)_3$, mol. beam. elec. deflection obs. 80−53080
ICl_4^-, force consts., bond polarizability 78−5201
$ICl(A^3\Pi_1)$, zero-press. lifetimes, fluoresc. quenching 79−68266
ICl(Br), rot. spectra in millimeter wave region, rot. transitions obs., equilib. const. determ. 80−78607
IF, $B^3\Pi(0^+)$, radiative and predissoc. lifetimes, laser-induced fluoresc. 79−31589
IF, $B^3\Pi(0^+)$ states, Franck-Condon factors, RKR turning pts. 77−34681
IF, $B^3\Pi(0^+)$-$X^1\Sigma^+$ fluoresc., predissoc. 77−34682
IF chemical laser, pumping using F reactions with CH_3I, CF_3I and ICl 80−11915
IF, elec. dipole moment, Stark effect 79−18233
IF emission spectrum and form. kinetics in electron-beam-produced plasma 80−102533
IF, fluoresc. decay lifetimes and quenching cross-sections for excited $B^3\Pi(0^+)$ states 78−1030
IF, He(I) photoelectron spectra, interpretation 79−13766
IF, in solid Ar, emission and excitation visible spectra at 12K 80−87137
IF internal vibr.-rot. product distrib., formed in F+CH_3I(CF_3I), fluoresc. obs. 80−48078
IF, laser excited fluoresc. 79−50077
IF+H→HF+I, reaction product energy distrib. 80−30219
IF_4, statistical thermodynamic functions calcs., force consts., vibr. amplitudes, between 250-1000K *(French)* 79−31504
IF_5, gas phase electron diffr. and B_0 rot. const., struct. determ. 79−89782
IF_5, IR intensities, fundamental, overtone and combination band calcs. 78−29780
IF_5, microwave spectra obs., rot. assignments, mol. parameters *(French)* 78−55163
IF_5, second virial coeff. meas., Lennard-Jones pot. determ. *(German)* 77−19658
IF_5, vapour press., phase transform. enthalpy *(German)* 78−51654
IF_6, NMR and NQR of ^{127}I and ^{19}F, solid-solid transitions and mol. motions 79−99784
$^{127}IF_6$, radical, prep. and EPR comparison with other hexafluoride radicals 78−68381
IF_7, generalised quadratic valence pot. calcs., Wilson's F-G matrix 79−93966
IF_7, molecular vibr. calc. 79−18169
IF_7, vapour press., phase transform. enthalpy *(German)* 78−51654
$I(H_2O)_n^-$, geometric and electronic struct., CNDO/2 calcs. 77−79542
$I(H_2O)_n^-$, geometric and electronic struct., CNDO/2 calc. 79−41113
I_2He, Van der Waals mol., photodissoc. lifetime, I_2 vibr. depend. 79−6977
I_2He^*, product state distrib. and binding energy 80−63857
I_2He^* Van der Waals complex, vibr. relax. processes and decomposition 80−63765
INCO, VPS obs., comparison with ab initio and semi-empirical calcs. 80−53043
$I_{0.33}NbSe_4$, cryst. growth and struct. *(French)* 77−15375
$I_2Ne_aHe_b$ van der Waals complexes photodissoc. 80−50864
I_2Ne^*, product state distrib. and binding energy 80−63857
IO, free radical, Ar matrix absorpt. and emission spectra, mol. vibronic states obs., spectroscopic const. determ. 80−83387
IO, role in reaction $2I+O_2 \rightarrow I_2+O_2$ 77−63883
IO^-, electron affinity formed in I^-+O_2 reaction 77−63902
IO_3^-, adsorption desorption by TiO_2 suspension, kinetics, relax. technique 80−93804
IO_3^-, determ. in rainwater by neutron activation anal. 78−76953
IO_3^- in $NaClO_3$, Raman spectra, fundamental vibr. modes 78−78711
IO_4^- ion in solns., UV spectra 80−2786
IO_4^--NO_2^- aqueous redox mixtures, γ-radiolysis 79−20392
I_2O_5, ^{127}I NQR spectra 80−39889
I_2O_5, NQR freqs. of ^{127}I 78−72433
I_2O_5, XPS, binding energies and bond orders 77−18976
I_2^*He, vibrational predissociation, van der Waals molecules, vibration-translation scaling theory 80−43135
In-As-Se-I system, glass form. obs. 77−77466
K+I_2(IBr)(Br_2)(ICl)(Cl_2), ion-pair form., bond stretching effect on cross sections 78−1064
KI, effect of addition on corrosion of Cu in seawater 78−80670
Li+ICl, product mag. deflection slotted disc velocity analysis 77−16806
$Mg(IO_3)_2.4H_2O$, crystal struct., unit cell, X-ray study 80−59447
Ni-I single crystals, mag. and dielectric props. 80−93095
Sb-Se-I system, exam. of glass formation, IR transmission spectra 78−88452
Se-Bi-I, amorphous, high sensitivity visible-near IR photoconductor development and characterisation 78−39153

ion-atom collisions *see atom-ion collisions*

ion beam effects
see also ion-surface impact; ionoluminescence; plasma-beam interactions
accelerator irradiation, heavy ion irradiation damage 80−100291
alkali halides, ion irradiated, using 1 MeV He^+, Pooley excitation mechanism 80−2093

ion beam effects continued
alkali halides, local vibr. modes excitation by ions, moving dislocation steps *(Russian)* 77−31696
alloy, binary, surface dehomogenisation during evaporation and ion sputtering 77−73207
alloys, preferential sputtering, surface binding and mass difference effects 79−83077
alloys and compounds, recoil implantation and ion-beam-induced comp. changes 80−34021
amorphisation, energy spike generation and quenching processes 78−47448
amorphisation due to ion bombardment, SRO struct. 80−79844
amorphous semiconductor film, ion bombardment effect on electronic props. 79−65125
amorphous target, ion range, Lindhard-Scharff-Schiott theory refinement 77−15473
aromatic polyamide fibre, sputter etching 80−21147
atomic collision processes rel. to vacuum system, review 80−54290
atomic transport and conc. profiles 80−59723
backscattering under planar channelling conditions, ion-atom pot. and stopping power 80−24519
barium aluminosilicate glass coating on NbZr, d and He ion irrad., blistering 77−35605
biological acute and late reactions, mice, comparison of heavy particles for therapy 78−85338
$(biphenol)^+/(biphenol)^-$ ion-radical pair, ODMR, hyperfine struct. *(Russian)* 80−15829
blister formation after He ion irrad., mechanism involving displaced atom transport 80−39178
bombardment, electron microscopical anal. of surface effects and volume defects, review *(Rumanian)* 80−29093
bombardment, simultaneous with He, H_2, heavy ions to simulate microstruct. damage from fission or fusion neutrons 79−46723
bounded media, dislocation loop growth and void swelling by charge particle damage 78−6110
brain, irradiation with C ions, recovery from pot. lethal damage, rat expts. 80−72234
carbides, brittle materials, swelling, blistering, p, d, and He ion irrads. porosity effects 77−35603
cascade mixing, diffusion approx. 80−6443
cell survival, OER and RBE, comparison of heavy particles for therapy 78−85337
cell survival vs. depth, comparison of heavy particles for radiotherapy 78−85336
cellulose nitrate, proton, H_2^+ mol. ion, and heavy ion irrad., track prod., etching obs. 78−86757
ceramics, ion beam irradiation techniques for simulation of 14 MeV neutron irradiation 80−10584
channelling, general description 79−95061
channelling, material characterisation, conf., Aleria, Corsica (Sept. 1976) 79−96403
channelling of ions for atom location, continuum approx. calc. of scatt. yield 77−7778
charge exchange in solids, studies with Van de Graaff tandem *(French)* 79−4339
charged particle beams in liqs., elastic wave excitation, microscopic bubble acoustic emission 80−43516
chemistry of bombarded compounds and energetic ions in gas phase 77−25290
Chinese hamster V79 cells, mutation and inactivation by heavy ion beams 80−35982
cleaning, plasma accelerator with closed drift of electrons for ion beam formation *(Russian)* 79−38993
collision cascades, computer simulation, Monte Carlo code 78−67756
condensed film on NaCl, ion bombarded, film growth, thermally stimulated exoelectron emission 80−50537
conference, physics of ionised gases, Dubrovnik, Yugoslavia, (Aug.-Sep. 1976) 77−42961
corrosion, conf., Manchester, England, (Apr. 1975) 77−8962
corrosion 77−8963
crystal, axial blocking shift of scatt. nuclear products 79−82268
crystal, electron-positron pair production coherent effect 80−88222
crystal surface morphology development during sputter erosion 80−88414
CTR first wall, high power ion-irrad. test 80−78443
CTR first-wall irradiation environment, appl. of dual-ion accelerator 78−13325
cylindrical ion implosion fusion using radially convergent beams 80−23137
damage correlation with neutron effects, predicted temp. shift on swelling with radiation dose rate change 79−7630
dechannelling by dislocation loop, energy depend. 79−42127
diamond, accelerator irradiation, heavy ion irradiation damage 80−100291
diamond, defects and impurities 80−29017
diamond, structural changes induced by Ar ion bombardment, depth profiles, using XPS 78−34554
dimethyl sulphoxide radioprotection of mammalian cells, exposed to X-rays, heavy charged-particle beams 79−79609
disorder accumulation, saturation and sputter limitation 78−67753
disorder distribution extraction, semiempirical method of applying dechannelling correction 78−22781
displacement spike annealing, Mont Carlo method computer expteriments 78−30672
dual beam irrad. expts., used for void swelling simulation, theoretical exam. 78−79646
electron gas coding influence in ion-bombarded layers 80−108272
electron-collision cross-section data for atom or molecule, rel. to radiation physics 80−63829
energy spike development and quenching depend. on thermal diffusion 80−88367
Escherichia coli K-12 rec and uvr mutants, LET-depend. radiosensitivity 78−15874
etching, by oblique incidence, pattern fabrication *(Japanese)* 79−74271
fast charged particle traversing ferromag., dynamic mag. field, RPA 79−73230
fast charged particles, prod. and impact effects 79−45492
fast molecular ions, transmission through thin foils 80−65065
fast moving ions traversing solid, wake-bound states, dispersive and surface effects 79−73231

ion beam effects continued
ferromagnet, magnetic field asymmetry correction on fast moving ions 79−14862
field-ion microscope specimens, field corrosion caused by polymer gaskets 80−57425
fusion devices, controlled, surface effects, conf., San Francisco, USA (Feb. 1976) 77−30659
fusion materials, heavy ion irradiation, swelling theory 80−34090
fusion reactor materials, in-situ analysis of ion irradiation and implantation effects 79−45408
fusion reactor materials, ion bombarded, swelling induced stresses, crystalline orientation effects 80−34093
fusion reactors, primary wall swelling, ion bombardment 78−17418
garnet epitaxial films, easy magnetisation axis orientation, ion bombard. effects 80−60383
gas ions, ion collector for expt. investigation of absorpt. and reliberation 79−99254
Ge:P, radiation-accelerated diffusion 80−6559
glass, blister formation by 150 keV He^+ irrad., effects of gas diffusivity 77−35604
glass, electromigration in ion bombardment 78−26601
glass, swelling, blistering, 140 keV p, d and He ion irrads., porosity effects 77−35603
graphite, cloth erosion by 20 keV H_2^+ and He^+ ions 79−46725
graphite, conditioning of surface by atomic H 80−93665
graphite, CTR material, the ion injection effect 78−34557
graphite, D^+ bombardment, surface damage, sputtering, SEM study 80−32459
graphite, energetic deuteron irradiated surface struct. quantitative meas. 78−95210
graphite, energetic ion sputtering, appl. of AES-SIMS (IMA)-FDS combined systems to physical and chemical processes 78−95636
graphite, H^+, D^+, He^+ ion bombardment, Raman scatt. and SEM anal. 77−35609
graphite, ion bombarded, light gases, structural study using TEM 80−92570
graphite, irradiated with MeV He ions, exptl. study of effects 79−4341
graphite, permeable, 0.6, 3.5 MeV He^+ irrad., surface erosion, porosity effects 77−35602
graphite, pyrolytic, Ar^+, N^+ and He^+ ion bombardment numerical discussion of flaking 78−52947
graphite, pyrolytic, ion bombard., flaking, stress fields around penny-shaped cracks 78−52946
graphite, pyrolytic, ion bombarded, surface deformation *(Japanese)* 78−18879
graphite, pyrolytic crystals, surface topography, bombarded with Ar^+, N^+, He^+ ions 78−6820
graphite, radiation damage by $^4He^+$, depth depend. and current density effects 80−2091
graphite, sputtering yield, use as first wall material 78−95629
graphite, surface alteration by interaction with Ar^+ and Xe^+ beams 78−91347
graphite, surface erosion by 100 keV $^4He^+$ and 200 keV H_2^+ 78−23569
graphite, surface erosion by ion bombardment crystal anisotropy effect 78−23845
graphite, surface morphology changes after irrad. with energetic He ions 78−21767
graphite, wall and limiter material for Tokamaks, induced desorption diffusion and gas production by 100 eV electrons and ions 79−675
graphite, X-ray photoelectron diffraction, influence of radiation damage 79−19970
graphite monofluoride, surface alteration by interaction with Ar^+ and Xe^+ beams 78−91347
graphite sputtering by low energy H and D 78−95630
Hasteloy B, equilibrium surface bombarded with high dose He^+ ions 78−95091
heavy ion beam inertial confinement fusion, US programme 80−23136
heavy ion beam targets, damage, lifetime, uniformity, book contrib. 79−31291
heavy ion induced collective electron emission 80−80926
heavy ion irradiated target, number of point defects in displacement cascade, computational code *(French)* 79−19300
heavy ion radiation transport computer codes for thick targets 80−39180
heavy ion simulation of neutron radiation damage 80−29071
heavy ion stopping, prediction using ion effective charges 80−88229
heavy ions, high energy, dosimetry for radiobiology expts. 77−66849
heavy ions, low vel., channelling stopping power oscills. 80−103404
heavy ions in solids, electronic stopping cross-section, Z_2-oscills., target struct. effects 80−70285
heavy-dose implantation, defect centre study, amorphous phase profile 77−80531
heavy-ion simulation of neutron radiation damage, HT ultra-high facility for potential reactor materials 77−57786
heavy ion lateral range calc., adaption of energy/depth distrib. program E-DEP-1 77−62571
human diploid fibroblasts, mutation and inactivation by heavy ion beams 80−35983
hydroxide surface, XPS exam. of chemical changes induced by Ar^+ ion bombardment 79−14993
III-V semiconductors, radiation-induced defects, review 77−80544
implantation, surface treatment process in production engineering 80−34028
implanted ion detection by X-ray emission anal. in TEM 78−51575
impurity depth profiling of H and He isotopes within near surface region of solids using ion beams 79−7622
Inconel, sputtering and blistering from H^+ and He^+ bombardment 78−79649
Inconel 600, equilibrium surface bombarded with high dose He^+ ions 78−95091
Inconel 675, wall and limiter material for Tokamaks, induced desorption diffusion and gas production by 100 eV electrons and ions 79−675
Inconel-718, blistering and exfoliation by 2 MeV He^+ beam 79−46722
intense ion beam propag. in z-discharge plasma channels, straight and tapered 80−83948
interstellar H II/OH maser regions, heating by ion streams 80−56912
ion acoustic solitons in beam plasma system with nonisothermal electrons generated by ion-beam 80−103151
ion impact induced shock processes in solids 80−89104
ion implanted layers, strain and damage distribs., X-ray diffr. model calcs. 79−69116
ion irrad., tertiary effects in pyramid form. 80−2090
ion milling (ion beam etching), bibliography for 1975-1978 period 80−4
ion plating, inert gas handling 79−69994
ion technology advances, conf., Murray Hill, USA (May 1976) 77−12476
irradiated materials, cascade damage and self-ion injection effects on swelling 78−34549
irradiation creep facility, materials testing for fast and fusion reactors 79−57192
isocitrate dehydrogenase from Azotobacter vinelandii, essential amino-acid residues identification 80−76538
Kapton, optical, elec. props., struct., ion textured surface 78−72904
Kevlar 49, fibre, mech. props., environmental effects incl. sunlight, ionising rad. 77−36560
kidney cells, inactivation by high-energy monoenergetic heavy-ion beams 80−72256
lamellar eutectic, specimen thinning for TEM *(German, English)* 78−95885
laser annealing, optical constants, ellipsometry observation 80−34024
laser-fusion reactor, surface heating of 1st wall by pulsed photon and ion irrad. 78−89979
lateral ion scattering in amorphous and polycryst. solids *(German)* 80−24508
magnetically insulated coaxial line, ion beam effects 80−87297
mammalian cell mutation and activation by radiations of differing LET 77−56431
mammalian cells, cultured, interpretation of mutation and inactivation obs. 80−72229
mammalian cells, drastic G_2 arrest after heavy-ion beam irrad. 80−45979
mammalian cells, heavy ion effects, irrad. facilities and methods 80−35981
mammalian cells, influence of radiation quality on effectiveness of small doses 80−30785
mammalian cellular DNA; breaks induced by accelerated heavy ions, impaired repair capacity 80−41129
material modification, conf., Budapest, Hungary (Sept. 78) 80−86038
metal, blister formation due to the ion irrad. 80−65072
metal, excitation of plasmons by ion bombardment 78−34793
metal, FCC, investigation of stage-I_E interstitial nature by TEM 78−47329
metal, FCC He ion irrad., He gas bubbles lattices obs. 79−14858
metal, He deposition and promotion of void nucleation during accelerator expts. computer simul. 79−23658
metal, He ion implanted, statistical model of low temp. blister formation 78−67754
metal, heavy ion bombard., void conc., effect of implanted He *(Russian)* 80−88213
metal, interbubble fracture mech. of blister form., He irrad. 78−6109
metal, ion and neutron irrad., low temp. defect prod. and stage 1 recovery 78−79637
metal, ion beam damage, distinguishing between models of radiation damage using TEM *(German)* 78−30680
metal, ion impact desorption cross section of H and O by light in bombardment 78−95096
metal, irrad., peak void swelling temp. 77−72608
metal, irradiated, ordered arrangement of micropores on dislocations 77−19943
metal, irradiation creep and swelling, cascade damage effect 77−19991
metal, light element implantation, radiation damage review 80−88219
metal, radiation blistering developments, review 80−44239
metal, reactive, trapping of energetic H^+ ions 78−10096
metal, wake potential for fast ion pairs, self consistent calc. 78−34792
metal atoms sputtered by light and heavy particles, velocity distrib. meas. by fluorescence spectroscopy 78−95626
metal crystal radiation defect research using field-emission microscope 78−333
metal surface, electron emission induced by low energy light ions 79−61482
metal surface, thermomechanical treatment by ionic bombardment *(French)* 78−11418
metal surface blistering due to deuterons, detection by laser light scatt. 78−26602
metals, energy loss of heavy nonrelativistic ions in matter, semiclassical theory 80−84224
metals, fraction of ions in unique sites, following ion implantation 77−15438
metals, He vacancies, random coalescence 79−51168
metals, irrad., mechanism of formation of vacancy dislocation loops *(Russian)* 80−65053
metals, irradiation creep strain, produced by vacancy loops, calc. of magnitude 78−72815
metals, mixed dumbbells, ion channelling studies 80−70277
metals, radiation effects, ion beam study, review 79−10883
metals, void swelling, depth dependent, by self-ion irradiation, generalized model 79−14856
metals and metal tritides, He behaviour 79−17981
metals irradiated, heavily, exam. of percolative mass transfer 78−79639
mica, nuclear track microfilters, prod. and props. 80−96574
mica muscovite, iron latent tracks obs. by TEM 79−73235
mica tracklengths of I and Au ions 78−38767
micropore filters, preparation by bombarding lavsan film with Ar ions 78−3305
milling, anomalous sputter yield behaviour 80−108624
minerals, thermal annealing of ion tracks 78−20604
MIS structure, radiation induced charge storage 80−6997
molecular ions, interaction with thin solid targets 78−59844
momentum transfer and damage energy gradient effects on He permeability 78−10102
MOS structure, B ion implanted, form. and annealing of radiation damage 79−56321
MOS structure, electrophysical props. after B^+ ion bombardment 77−12013
muscovite mica, annealing of latent tracks of heavy ions *(French)* 79−19290
Nimomic PE-16, equilibrium surface bombarded with high dose He^+ ions 78−95091
Nimonic PE16, He injected, bubble-void transitions in Ni ion bombard. 80−34095
Nimonic PE16, Ni ion irradiated, Ni segregation to voids 79−28020

ion beam effects continued
Nomex, fibre, mech. props., environmental effects, incl. sunlight and ionising rad. effs. 77−36560
nonmetallic crystals, collapse of tracks formed by fission fragments 80−24510
nuclear filters, prep. from polymers using Ar ions 78−86714
nucleation of defect clusters in crystalline solids 79−42051
olivine, effects of heavy ion irradiation on IR extinction, appls. to interstellar dust 79−53873
optical surface, target containing alkali metals and alkaline earths, chemical sensitisation after ion bombardment 80−3227
organic non-volatile compounds ionisation by fast heavy ions, separation by TOF mass spectrom. 77−27170
oscillatory wake, fast ion in solid, trapped electron binding energy, RPA calc. 80−96575
oxide surface, XPS exam. of chemical changes induced by Ar^+ ion bombardment 79−14993
oxides, brittle materials, swelling, blistering, p, d and He ion irrads. porosity effects 77−35603
p^+-n diode under forward bias, effects of radiation-induced deep levels on admittance 78−23157
particle accelerator target heating by ion beam, thermal characts. *(Japanese)* 80−99374
PBI fibre, mech. props., environmental effects, incl. sunlight and ionising rad. effs. 77−36560
pentamethinium cyanine dye, single cryst., effect of energetic ions on photocond. 79−51626
PET, ionizing radiation effect on life *(German)* 80−19853
phage ϕX 174 inactivation by accelerated ions, enhancement by δ-ray effect 80−36008
plasma solid interaction, surface erosion 80−38665
plasma system, ion cyclotron harmonic instabilities *(Japanese)* 78−91124
plastic detector, primary damage and secondary electron damage in heavy ion tracks 78−17514
point defects of rad. damage to construction materials, math. modelling 79−90703
polyamide fibre, sputter etching 80−21147
polyester fibre, sputter etching 80−21147
polyethylene terephthalate film, degree of crystallinity effect on particle tracks *(French)* 77−46471
polystyrene, energy losses and straggling for H^+ and He^+ beams *(Russian)* 80−84226
polystyrene, energy straggling of H^+ and He^+ ions in 0.1 to 1.2 MeV range 77−80559
polystyrol, ionizing radiation effect on life *(German)* 80−19853
pulse radiolysis, LET dependence of transient yields 80−30260
Pyrex, ion bombardment, form. of cpds., IR spectrosc. exam. *(German)* 80−88173
pyrocarbon, methane formation during p and d irrads. and thermal release of H 77−36788
pyrographite, surface struct., amorphisation, secondary electron spectra and AES 79−43077
pyrolytic C, energy depend. of methane prod. during deuteron bombardment 78−95939
quartz, bombardment by B^+ ions, waveguide layer form. 79−27454
quartz, fused, waveguide struct. form. by H_2^+ ion irrad. 78−18072
quartz, ion bombardment, extrusion, evidence for radiation-induced stress relax. of silica network 77−24335
quartz, radiation damage in birefringent samples, meas. using photoelastic modulator 78−87724
radiation blistering, fracture model, stress fields around lenticular bubble 79−86823
radiational materials, spatial distrib. of H^+, He^+, D^+ ions in solids 80−6429
rainbow scattering and orbiting of fast particles in crystals 79−99256
range and damage distributions, Sonine expansion 79−19303
range and struggle calcs. for fast ions 78−34562
rare earth-transition metal amorphous films, radiation damage 77−66398
rat embryo survival and development, RBE and OER of extended-Bragg-peak He ions 77−12961
reactor materials, radiation-induced embrittlement and swelling due to void form, ASTM research 78−13231
recoil atoms of heavy ion reactions, local lattice damage, TDPAD meas. 80−84220
recoil implantation from thin source, extension to recoil sputtering and moderately thick sources 78−95631
recoil mixing in solids by energetic ion beams 80−59531
refractories, swelling on proton, deuteron and He ion bombardment 78−67750
rhabdomyosarcoma, rat, response to Ne and He ion irrad. 79−25042
RNase, damage and energy deposition by low-energy ions 77−9172
RNase inactivation due to elastic nucl. collisions 78−28008
SAP 895 (Al-Al_2O_3) alloy containing ^4He and ^3H, tensile props. 80−34129
SAP (Al_2O_3-Al) alloy, effect of high He^+ and H_2^+ conc. on microstruct. 80−34098
sapphire, 15-keV ion bombard., chem. implantation, isotopic trapping effects and induced hygroscopicity 77−59030
saturation resistivity charges, ion and fission fragment irrad. induced 78−79643
semiconducting film, amorphous, effect of ion bombardment on cond. *(Russian)* 80−49969
semiconductor, amorphous zone accumulation under ion irrad., composite model 79−51169
semiconductor, ion implantation, radiation defect form. in presence of force fields 79−51126
semiconductor, ionisation effects in damage production 77−7772
semiconductor, ionization and subthreshold effects in defect creation and annihilation 77−84811
semiconductor, multicomponent, preferential sputtering, surface binding and mass difference effects 79−83077
semiconductor monocrystal-amorphous radiation-induced transitions 77−80554
semiconductor structure defect exposure in SEM 79−23507
semiconductor substrate, work function rel. to AES, ion beam damage *(French)* 80−50479
semiconductors, amorphisation by high-energy ion irrad. 79−51172
semiconductors, ion irradiation produced amorphisation, disorder-ion fluence functions, disorder mechanisms 80−29090

ion beam effects continued
semiconductors, radiation damage studies on implanted Te, Sb and Sn by Mossbauer spectroscopy 78−2176
silicate glasses, swelling on proton, deuteron and He ion bombardment 78−67750
solid surface analysis, ion beam sputtering 77−12477
soliton solution in the wake interaction due to virtual plasmon exchange 80−65108
solute segregation, under irradiation 78−48407
spatially correlated ions studies, background and theory 80−36024
spatially correlated ions studies, cell survival obs. using diatomic deuterium 80−36026
spatially correlated ions studies, multiple scatt., expt. facility and dosimetry 80−36025
specimen preparation for SEM, TEM and optical microscopy 78−24778
spectral reflectivity of ion bombarded surfaces 77−55308
sputter ion source, appl. to IMA analysis *(Japanese)* 79−54734
sputter profiling, depth resolution 79−33874
sputtering, cascade mixing in depth profiling 79−78811
sputtering induced topography on solids, energetics and kinetics 80−88220
stainless steel, 316, simulation of radiation damage and phase stability 78−86602
stainless steel, coated with C, surface damage by D^+ and He^+ ions irrad. 80−23146
stainless steel, machine faceted, low-energy ion erosion studies 80−80923
steady-state space charge blowup and recovery of intense ion beams 79−1323
steel, austenite, blistering after 40 keV He ion bombard. 80−39175
steel, austenite, He blistering at high irradiation doses 79−51167
steel, austenitic, 18/8, 18/12, Ni^{6+} ion irradiation, void swelling 80−11641
steel, austenitic, annealed, Ni ion bombardment, swelling temp. depend. effect of He implantation 80−29080
steel, austenitic, gas implantation effects, fusion reactor first wall damage simulation 80−29079
steel, austenitic stainless, 316, surgical implant ion beam textured, stress/strain relations, fatigue characts. 78−73297
steel, austenitic stainless, DIN 1.4970, influence of He on high temp. mech. props. 79−7636
steel, austenitic stainless, stressed state blistering 78−95085
steel, austenitic stainless, type 304 with He distrib., foil, effect of momentum transfer, damage energy gradient, on He distrib. 78−71773
steel, austenitic stainless, type 316, D-T fusion neutron and Ni^{2+} ion damage 78−14388
steel, austenitic stainless, type 316, irradiated with 46.5 MeV Ni^{6+} ions, soluble C effect on void swelling and low dose dislocation structs. 80−49280
steel, austenitic stainless, type FV 548, 20% cold worked irradiated with 22 MeV C^{2+} ions or 46 MeV Ni^{6+} ions, study of void swelling 79−37744
steel, boriding by ion bombardment with B_2H_6 *(French)* 78−60876
steel, C, ion nitriding, wear resistance *(Japanese)* 77−63828
steel, ferritic, void swelling during irradiation, suppression mechanisms 80−6441
steel, ionic nitriding, procedure and equipment, nitrided layer hardness obs. 80−45414
steel, low C, kinetic aspects of diffusion zone and compound layer formed during ion-softnitriding *(Japanese)* 79−15866
steel, mild, surface hardness improvement by dynamic recoil implantation 80−61008
steel, Mo^+ ion bombardment, phase composition and struct. change of surface layers *(Russian)* 80−24506
steel, stainless, 0Kh16N15M3B, blistering under high He^+ irradiation 80−29095
steel, stainless, 0Kh16N15M3B *(Russian)* 80−39170
steel, stainless, 304 and 316, lowering of degassing level *(French)* 79−57159
steel, stainless, 316 and 304, equilibrium surface bombarded with high dose He^+ ions 78−95091
steel, stainless, 321 and 304, D implanted, thermal desorption and bombardment induced release 78−95072
steel, stainless, absorption of O ions 79−1547
steel, stainless, blistering and exfoliation by 2 MeV He^+ beam 79−46722
steel, stainless, blistering owing to He^+ bombard., 2 MeV 80−49279
steel, stainless, cc Cr-Ni (20, 18 wt.%), effect of tensile stress on growth of He bubbles 79−55796
steel, stainless, D transport through membranes at low driving press. and 15 keV D bombardment 78−34552
steel, stainless, depth distrib. of swelling, TEM exam. 80−15165
steel, stainless, embrittlement by low energy ionic and atomic H particles 78−95809
steel, stainless, epoxide butt joints, effect of abraded and Ar ion bombarded surfaces on ultimate tensile strength 80−16638
steel, stainless, ground surface ion bombardment, in DC glow discharge 78−95098
steel, stainless, He effects on microstruct. in ion-irrad. 80−29078
steel, stainless, He induced blistering, during simultaneous sputtering 79−1808
steel, stainless, He ion bombard., in situ electron microscope examination 80−34094
steel, stainless, in-pile irrad. effect simulation by Ni ion bombardment, dislocation density, swelling 77−347
steel, stainless, ion bombardment, primary recoil energy spectra characts. 78−10103
steel, stainless, ion induced release of trapped D 78−95095
steel, stainless, ion irradiated, carbide precipitation *(French)* 77−16585
steel, stainless, solution treated, irradiated to low doses with 22 MeV C^{2+} and 46.5 MeV Ni^{6+} ions, interstitial loops 79−14855
steel, stainless, solution treated FV 548, irradiated with 22 MeV C^{2+} and 46.5 MeV Ni^{6+} ions void swelling 78−22771
steel, stainless, sputtering and chem. attack by H ions of 100 eV energy 78−95635
steel, stainless, sputtering by low energy H and D 78−95630
steel, stainless, stress corrosion cracking and microhardness, effect of bombardment by He^+, Ni^+ and Cr^+ 80−85087
steel, stainless, surface damage under high dose $^4He^+$ ion irradiation 78−95092
steel, stainless, surface morphology of H ion eroded samples 79−86968
steel, stainless, swelling, effect of free surface 78−10097

ion beam effects continued
steel, stainless, trapping and replacement of 1 to 14 keV H and D 78−95070
steel, stainless, type 304, void swelling 200 keV C^+ bombardment, dose and temp. depend. 77−55309
steel, stainless, type 316, blistering by 2 MeV He^+ ions, optical microscopy and SEM obs. 79−42119
steel, stainless, type 316, neutron irrad., Ni ion bombard. effects of injected interstitials on void volume 80−34092
steel, stainless, type 430, Ni^+-implanted, struct., comp. and electrochem. anal. of surface alloy 80−16603
steel, stainless, type EP838 ion irradiated, surface structure changes during post-irradiation heating *(Russian)* 80−75272
steel, stainless, wall and limiter material for Tokamaks, induced desorption diffusion and gas production by 100 eV electrons and ions 79−675
steel, stainless 304, secondary ion emission due to H ion bombardment 79−8216
steel, stainless 316, Fokker-Planck eqn. describing evolution of interstitial loop microstruct. during irradiation 80−107215
steel, stainless 316, ion sputtered, surface anal. by Auguer effect and SEM 78−95632
steel, stainless 316, irradiated, D trapping 78−95069
steel, stainless 316, soln. annealed, cavity alignment and precipitation during dual ion bombardment 80−70273
steel, stainless AISI 316, fast neutron void swelling simulation dose and dose rate effects 77−15457
steel, stainless AISI 316, Si and Ti effect in phase stability and swelling behaviour 79−78972
steel, stainless type 304, ion bombarded, He effects 80−29076
steel, stainless type 304, surface cleanup and sputtered ion production, AES and SIMS obs. 79−66209
steel, stainless type 316, in-situ HVEM studies under ion beam irradiation 80−103396
steel, surface cleaning in glow discharge, ion bombardment effect *(Russian)* 78−95848
steel, voids and swelling following $^{56}Fe^{3+}$ bombardment, fast neutron effects simulation 77−30651
stress wave generation in metal by electrons excited by nucl. fission fragments 79−37747
superconductor, A-15, irrad. effects on supercond. transition temp. 78−6472
superlattice thin films, sputtered, ion-bombardment-enhanced diffusion during growth 78−87882
surface, ion bombardment, equilib. at. struct. 79−56051
surface barrier detector, pulse height defects, heavy-ion detection 78−55093
surface blistering, SEM and TEM obs., ion energy, dose and target temp. depends., review 77−43261
surface coating materials in nuclear generating stations, ionising radiation protection *(German)* 80−18681
surface effects, ESCA obs. 79−33020
surface erosion, surface relief form. *(Russian)* 78−23567
surface layers, ESCA obs. 78−52612
surface modification for tribology, corrosion, catalysis, chem. synthesis and amorphous metals studies, review 77−43236
swelling during self-ion bombardment, effect of implanted interstitials 78−10099
swelling of fast reactor materials, inert gas ion irradiation 79−40999
target assembly, ultra high vacuum, for charged particle irradiations in the materials research field 78−83841
TCNQ-HMTSF, irrad. effects on resist. 21K 78−60113
Teflon, optical, elec. props., struct., ion textured surface 78−72904
Teflon, surface alteration by interaction with Ar^+ and Xe^+ beams 78−91347
thin films, ion-bombarded, simple model of dose depend. of resist. 79−42669
thin layer activation, appl. to wear and corrosion meas., surface treatment and sputtering 79−87810
thin sample, structural change obs. by transmitted fission fragment energy 78−83853
thin specimens, temp. control for mech. meas. under light ion irrad. 78−86278
tissue-equivalent gas, energy loss of H, C, N and O ions for elastic nuclear collisions 78−86759
Tokamak plasma, beam driven currents, trapped electrons effect 80−70011
toroidal plasmas, beam driven currents, trapped electrons effect 80−70011
transient magnetic field effects on particles slowing in solids 80−65106
transition metal oxide and hydroxide surfaces, chem. changes induced by Ar^+ bombardment, XPS obs. 79−83084
trapping and diffusion of particles near surface, attachment of mobile particles to non-saturable traps, theory 80−39417
trapping and gas release effects in cryst. lattices, thermal desorption spectrometry, review 77−43262
ultra cold neutron container materials, reduction of surface H by ion bombardment 80−9446
V79-spheroids, survival and kinetic response after heavy ion beam exposure 80−104651
vacancy dislocation loop microstruct. formed during heavy particle bombardment 79−99250
vacuum deposition, evaporation, ion enhanced film bonding 79−95931
Vicia faba growth reduction, RBE of d(50)-Be neutrons and 650-MeV He^{2+} 80−98025
void, and interstitial loop evolution in pulsed fusion reactors 80−84217
void swelling depth distribution produced by 5 MeV Ni ions 77−7771
void swelling simulation, effect of self ion injection 78−22772
water, heavy ion beam propag., energy loss and fragmentation of nuclei 79−54755
whisker growth, new mechanism for the blistering of surfaces in complex radiation environments 78−95093
yeast cells, dried, inactivation by accelerated heavy ions of very high LET 80−108965
Ag (111) surface, Ar ion bombardment, effect on struct. and reactivity, ellipsometry and LEED meas. 77−59192
Ag, energy losses and straggling for H^+ and He^+ beams *(Russian)* 80−84226
Ag film, electronic stopping power on irrad. by He, Li, C ions, damage-rate measurements 79−77654
Ag film, Frenkel pair prod. by light energetic ions, elec. cond., changes 77−59050
ion beam effects continued
Ag film, He^+ ion bombardment, radiation damage, ion entrapment, gas release and bubble formation 78−30679
Ag films, effect of Ar- and N-ion bombardment on texture *(Russian)* 80−107338
Ag, Frenkel defect production associated with He and light ion implantation, exam. 78−47443
Ag, ion-irradiation studies of damage function 79−37746
Ag, light ion (H, D, He, Li) irrad., defect prod. and electronic stopping power 80−34088
Ag, proton irrad., radiation-annealing effects in energetic displacement cascades, film resist. meas. 78−26603
Ag, recoil implanted ^{111}In impurities, interaction with radiation damage, TDPAC meas. 79−11362
Ag, TEM exam. of ion damage in FCC metals 78−87727
Ag thin films, spike effects of heavy ion sputtering 80−35034
Ag:^{111}Cd, hyperfine interaction, dose-rate depend. and annealing props. rel. to PAC obs. 77−27920
Ag-Au alloy, surface after sputtering, AES obs. 77−55858
Ag-Cu alloy, surface comp. after sputtering, AES obs. 77−55858
Ag-Ni supersaturated metastable solid solns. formed by ion beam mixing 80−107425
Ag-Pd alloys, inert gas ion bombardment, dynamic surface composition changes, AES obs. 80−60745
AgCl, defects induced by energetic ion implantation 78−17518
Al, 20 keV He^+ implantation, gas re-emission, critical dose, temp. effects 77−35596
Al, Al ion irradiated, void swelling and annealing of voids, electron microscopy study 80−88216
Al alloy 6061 79−675
Al and Al-Mg alloy N4, irradiation with 100 and 400 keV Al ions, obs. and analysis of damage struct. 77−4133
Al and SAP 930, 300 keV He irrad., blistering, flaking, gas reemission 77−35601
Al, annealed and powder sintered (SAP 895), sputtering under D^+ and $^4He^+$ bombardment, microstruct. effects study 80−84821
Al, barrier film growth in soln. of film promoting and aggressive ions 77−8975
Al, blistering and exfoliation by 2 MeV He^+ beam 79−46722
Al, blistering by plasma focus discharge deuterons, statistical anal., plasma diagnostics 77−35351
Al, energy losses and straggling for H^+ and He^+ beams *(Russian)* 80−84226
Al, energy straggling of H^+ and He^+ ions in 0.1 to 1.2 MeV range 77−80559
Al, film, damage production rates of 5 MeV Al^{2+} ions, exam. 78−47444
Al film, deform. under He ion bombardment 80−65073
Al film, He^+ irrad., overpressurised bubble obs. 79−51165
Al film, Pb^+ implanted, ion scatt. erosion rate, Rutherford backscatt. 79−74038
Al films, Al^{2+} irrad., increase of resist. and supercond. transition temp. 80−7027
Al films, N_2^+ and O_2^+ ion bombardment, structural and phase changes 80−2094
Al, He implanted surface deform., integrated lateral stress 77−31697
Al, ion-implanted, dechannelling by dislocations, backscatt. expts. 79−7642
Al, oxide coated, inhibitive and aggressive ion effects, secondary ion mass spectrometry 77−8974
Al, porous anodic film, ion beam thinned, electron microscopy 78−92390
Al, range of 100 keV Pr^{2+} and Tb^{2+}, M-shell X-ray cross-sections 77−35614
Al sintered powder, 100 keV He ion irrad., surface erosion due to blistering 77−35600
Al, sputtered excited Al particles, effect of O during ion bombardment on spectra 79−38703
Al, sputtering and chem. attack by H ions of 100 eV energy 78−95635
Al, surface exfoliation and blistering induced by He ion bombard. in energy range 10-80 keV 80−39173
Al, vacancy distribution, interbonding atoms, heat peaks in scattered cascades *(Russian)* 80−39169
Al:^{12}B, relax. mechanism for polarised implant 78−87693
Al-^{57}Co, implanted, Mossbauer effect obs. of annealing 80−39126
Al-Ag, dil., radiation damage by channelled and random He^+ ion beams 79−46719
Al-Cu, implanted metal system, Cu redistrib. after laser irrad. 79−69163
Al-Ge (0.1 wt.%), channelling meas. of Al interstitial atom trapping by Ge atoms 80−59537
Al-Ge alloy, Ge precip., ion irrad., dose rate and temp. depend. 78−79642
Al-Mg, Si alloy, void form. under different precip. conditions, after Al ion irrad. 80−59529
Al-Si, enhanced interdiffusion during Ar ion bombardment 79−99353
Al-Xe film, ion implanted radiation enchanced Xe outdiffusion, Rutherford backscatt. 77−76609
$Al_xGa_{1-x}As$ MBE layers, ionized beam doping, elec. and optical characts. 79−37721
Al_2O_3 *(Russian)* 80−50552
Al_2O_3, defect microstructure due to ion bombardment, TEM study 80−34100
α-Al_2O_3, ion bombard., vol. expansion, annealing compaction, surface props. 78−67748
α-Al_2O_3:Pb, implantation, lattice disorder 77−80525
^{27}Al ion damage rates in Al 77−84810
$As_{50}Te_{50}$, amorphous semicond., elec. props. after heavy-ion irrad. *(French)* 77−72639
Au, ang. distrib. of relfected keV ions 79−65127
Au, damage by ion implantation, spike threshold, TEM 79−90705
Au decoration, of individual Ag crysts. by ion bombardment *(German)* 79−69164
Au, energy losses and straggling for H^+ and He^+ beams *(Russian)* 80−84226
Au, epitaxial growth and nucleation on NaCl during ion bombardment 79−11024
Au film, discontinuous, substrate radiation damage effect on resist. and strain gauge stability 79−95520
Au film, surface craters induced by displacement cascades 80−107344
Au film on Si, use of sputtering for layer removal 79−78813
Au, heavy ion irrad., cascade energy density effect on defect cluster type 80−107340

ion beam effects continued
Au, irrad., self-interstitial type defects, combined single-double alignment channelling backscatt. 78−34561
Au nucleation on organic substrates, ion bombard. effects 78−75965
Au, proton irrad., radiation-annealing effects in energetic displacement cascades, film resist. meas. 78−26603
Au, sputtering and chem. attack by H ions of 100 eV energy 78−95635
Au, TEM exam. of ion damage in FCC metals 78−87727
Au thin films, spike effects of heavy ion sputtering 80−35034
Au-Ag (35 at.%), dechannelling of energetic He ions at dislocations 80−70275
Au-Cy alloy, surface comp. after sputtering, AES obs. 77−55858
B and B-rich borides, protective coatings, in situ prep. for controlled nuclear fusion devices 79−3238
BC, ion bombarded, chemical effects on secondary photon and ion emission 78−95637
BC, physical and chemical interaction with energetic T 79−97902
B_4C coating, erosion rates under H^+ ion bombard., fusion reactor appls. 80−39179
B_4C, sputtering yield, use as first wall material 78−95629
B_2O_3-SiO_2:Ce glasses, radiation resistance mechanism, optical absorpt. and luminesc. obs. *(Polish)* 79−86825
$BaT:O_3$, surface microrelief revealed by ion irradiation 80−54485
Be, blisters due to He irrad., proton backscatt. study 80−75273
Be coating, erosion rates under H^+ ion bombard., fusion reactor appls. 80−39179
Be, electric field gradients of recoil-implanted ^{19}F via $^{9}Be(^{12}C, np)^{19}F$ 77−8471
Be, ion bombarded, chemical effects on secondary photon and ion emission 78−95637
Be, ion bombarded, D trapping 79−19291
Be, irradiated with He^+ at 20 keV, surface damage and gas trapping profile meas. *(French)* 80−84218
Be, plasma-sprayed, response to He^+ bombardment determ. 78−86691
Be sintered powder, 100 keV He ion irrad., surface erosion due to blistering 77−35600
Be, surface morphology, effect on low energy H ion erosion yield 79−42121
BeO, radiation induced detrapping of implanted D by ^3He and proton irradiation 80−32482
BeO, sputtering by low energy H and D 78−95630
Bi:N film, ion-implanted, struct., X-ray obs. 77−76692
C, amorphous foil, electronic energy straggling of light ions, at. number depend. 77−11612
C, bombardment by Ar and ^{57}Fe ions, effects anal. by XPS 77−11769
C CVD coating, surface damage and erosion under energetic D^+ and $^4He^+$ irrad. 80−39174
C, film with random struct. growth from ion impact damage in butane plasma 79−83139
C, foil, 40-100 keV He ions, electronic energy straggling 77−15471
C foil, ion irrad., crystallographic transform. 79−55794
C foil, ion irrad., graphitisation rel. to lifetime, relevance to beam-foil spectroscopy 80−15166
C foil, ion irradiation, correlation of energy loss and crystallographic transform. 80−23215
C foil, transmitted H^+ energy loss, ang. distrib. and charge fractions 80−2102
C foils, stripping of heavy ions with energy 0.4-0.9 MeV/A, straggling, foil behaviour 78−33351
C, glassy, surface erosion by ion bombardment crystal anisotropy effect 78−23845
C, interaction with D^+ ions, 5-30 keV, temp. depend. of methane formation 78−79645
C, ion bombarded, chemical effects on secondary photon and ion emission 78−95637
C pyroceramic, sputtering and blistering from H^+ and He^+ bombardment 78−79649
C, pyrolytic, 0.6 to 3.5 MeV He^+ irrad., surface erosion, porosity effects 77−35602
C stripper foils, ethylene cracking in glow discharge, irradiation lifetimes 80−23207
C, stripper foils under 4.8 MeV Ar^{++} ion bombardment, shrinkage, rupture, lifetime 78−33352
C, swelling, blistering, 140 keV p, d and the ion irrads., porosity effects 77−35603
C thin foil, breakage times under Ar^+ bombardment 78−25753
C, thin foil, irradiation with 1.2 MeV Ar^+, electron diffraction study 80−103397
$CaCO_3$, calcite, sputtering behaviour, optical and electron microscopy 78−43968
Cd film, HCP, crystal struct. changes on ion bombard. 77−69018
CdS, defect struct. and config. produced by irrad., elastic scatt. expts. 80−84178
CdS, electron-hole pairs behaviour in energetic ion tracks 80−65457
CdS, ion irrad. damage, obs. using SEM in cathodolumin. mode 79−7633
n-CdS, photocond. film, phase memory effect and deep levels 79−82556
CdTe, laser annealing of ion bombardment damage 80−25502
Co film, HCP, crystal struct. changes on ion bombard. 77−69018
Co, HCP, heavy-ion irrad., dislocation loops, TEM obs. 77−31667
Co, magnetic permeability, effect of ion implantation 77−28414
Co-W-Cr (15,20 wt.%), surgical implant ion beam textured, stress/strain relations, fatigue characts. 78−73297
Cr film, evaporated, concurrent ion bombard. effects 80−80142
Cr film, obtained by thermo ionic precipitation, phase composition, lattice parameters *(Russian)* 80−96756
Cr, interaction with dense stream of N ions, metallography, microhardness, specific volume *(Russian)* 80−15169
Cr, thin film, chemical cpd. form. by N_2^+ and Ar^+ ion bombardment *(Russian)* 79−73225
Cr-Ni, blistering after 40 keV He ion bombard. 80−39175
Cr-Ni alloy, 01Kh18N40M5, blistering under high He^+ irradiation 80−29095
Cr-Ni alloy, He blistering at high irradiation doses 79−51167
Cr_2O_3-stainless steel system under fusion reactor first wall condition, oxide dispersoid stability 80−40374
Cu, Ar^+ ion irradiated, defects study by electron microscopy *(German)* 80−2087
Cu, Ar^+ ion irradiated, small defect clusters, electron microscopy contrast *(German)* 79−99253

ion beam effects continued
Cu, blistering by plasma focus discharge deuterons, statistical anal., plasma diagnostics 77−35351
Cu, blisters due to He irrad., proton backscatt. study 80−75273
Cu, channelling, continuum approx. calc. of scatt. yield for atom location 77−7778
Cu, crystalline reorientation following ion bombard. 80−70269
Cu, energy losses and straggling for H^+ and He^+ beams *(Russian)* 80−84226
Cu, film, Frenkel pair prod. by light energetic ions, elec. cond. changes 77−59050
Cu film, ion bombardment induced preferential orientation 79−19293
Cu, Frenkel defect production associated with He and light ion implantation, exam. 78−47443
Cu, He conc. profile meas. rel. to blistering 78−95089
Cu, He defect complexes and depth distribution, production theory 77−31686
Cu, He gas-bubble superlattice form. 80−2086
Cu, He ion irrad., 1 to 25 keV, range profiles, reemission, blistering 78−38758
Cu, impurity defect configuration, by DPAC-technique with ^{111}In 79−28021
Cu, inertial confinement fusion reactor, surface damage and thermal effects from transient thermonuclear radiation 79−648
Cu, ion bombard. by 5 keV Ar^+, sub-surface damage 80−103399
Cu, ion bombarded, cone form. and associated surface features 77−59054
Cu, ion bombarded, cone struct. initiation 79−51171
Cu, ion irrad., Frank loops, electron microscope image contrast 80−6326
Cu, ion radiation damage 78−22773
Cu, ion-irradiation studies of damage function 79−37746
Cu, irradiated, small edge dislocation loops, electron microscope image contrast, Burger's vector determ. 77−76410
Cu, irradiated with 20 keV He^+, surface damage and gas trapping profile meas. *(French)* 80−84219
Cu, irradiated with protons, α-particles and C ions, increase of elec. resist. meas. 77−84808
Cu, irradiation induced defects, electron microscope images 78−83854
Cu, irradiation with 4 to 6 kV Ar^+ ions, Ar-vacancy cluster form. and stability 77−43259
Cu, irradiation with O_2 ions, defect production and annealing 80−88214
Cu, light ion (H, D, He, Li) irrad., defect prod. and electronic stopping power 80−34088
Cu, positron source using Na^{22} ion-implantation for annihilation lifetime expts. 79−45489
Cu, proton irrad., radiation-annealing effects in energetic displacement cascades, film resist. meas. 78−26603
Cu, pyramidal structure stability on ion bombarded surface 79−51170
Cu, pyramidal structures, development on ion bombarded surfaces 80−84177
Cu, radiation damaged, temp. depend. of elec. field gradient, DPAC expt. 78−43727
Cu, range of Ni^+ ions, increase due to ion bombardment induced crystalline reorientation 78−26611
Cu, self-sputtered, secondary ion mass spectra 79−74044
Cu, sputtering, surface topography, appl. of thermodynamics of capillarity 80−20749
Cu substrate, ion induced intermixing of Au or Ag surface film 80−15420
Cu surface, poly-cryst., Ar ion bombard., regular pyramid production 78−59843
Cu, surface tension cct. cavities under Cu^+ ion irradiation, O_2 and He effects *(French)* 77−35611
Cu, surface topographical features formed by ion bombard., crystallographic depend. 80−70266
Cu, TEM exam. of ion damage in FCC metals 78−87727
Cu, thin film, sputtering yields due to Ar^+ milling, He^+ Rutherford backscattering and AES obs. 79−65969
Cu, topographical features relative stability 80−2092
Cu, vacuum deposited layer, ion bombardment induced preferential orientation 80−100290
Cu, volume change due to point defects and He bubbles, isotropic elasticity theory 78−47445
Cu, whiskers, Ar^+ ion implanted, X-ray study on lattice defects *(Japanese)* 79−99230
Cu:$^{69}Ge(^{67}Zn)$, nucl. alignment temp. depend. rel. to radiation damage during PAC obs. 77−27919
Cu-Be (0.25 at.%), cryst., Cu self-interstitial atom, trapping, nucl. reactions and ion channelling obs. 78−14384
Cu-Ga alloys, effect of ion bombardment on surface composition using differential reflectometry and AES 77−59189
Cu-Ni, clean surface, surface segregation and growth process of altered layer *(Japanese)* 80−24720
Cu_3Au, 5-100 keV Cu^+ ion bombardment, displacement cascades, TEM investig. 77−11601
Cu_3Au, displacement cascades prod. by Cu^+ bombardment 79−99251
Cu_3Au, heavy-ion or neutron bombardment, disordered zone form., TEM diffr. contrast 77−11600
CuCl, electron-hole pairs behaviour in energetic ion tracks 80−65457
Cu_5FeS_4, bornite, AES investig. of surface struct., ion sputter and electron beam effects 77−15669
Cu_2O:Cd^{2+} implanted, reson. Raman scatt., annealing effect 77−24838
$Cu_{83}Pd_{17}$, Cu^+ (Au^+) ion-bombarded, displacement cascades and disordered zones, TEM studies 80−15167
dielectric track registering media, possible new sputtering mechanism 77−392
Fe, boriding by ion bombardment with B_2H_6 *(French)* 78−60876
α-Fe, heavy ion irradiated, TEM exam. 79−7638
Fe, interaction with dense stream of N ions, metallography, microhardness, specific volume *(Russian)* 80−15169
Fe, nitriding by ion beam, SEM obs. 80−2095
Fe, pure, nitrided layers obtained by ion bombardment, microstruct. exam. *(French)* 78−15581
α-Fe, void swelling during irradiation, suppression mechanisms 80−6441
Fe:^{129}Cs, implanted atom sites and hyperfine interactions, Mossbauer obs. 77−20753
Fe:^{129}Te, implanted atom sites, Mossbauer obs. 77−20756
Fe:^{129}Tm, implantation below 15K, in situ Mossbauer obs. 77−20754
Fe:^{129}Xe, implanted atom sites, NMR/ON 77−20723
Fe:^{129}Xe, implanted atom site populations, Mossbauer, NO and NMR/ON obs. 77−20755

ion beam effects continued
Fe:^{198}Hg, combined lattice-location hyperfine-interaction expt. on implanted Hg 77−20752
Fe:^{85}Rb, implanted atom sites and hyperfine interactions, Mossbauer obs. 77−24765
Fe:Yb,^{18}O, interaction between implants 77−27921
Fe:Yb,O, interaction between impurities, perturbed ang. correlation meas. 77−1628
Fe-B amorphous alloy, fast neutron and ^{235}U fission fragment irrad. 80−100288
Fe-Cr-Ni (19, 13 wt.%), austenitic, Ni^+ ion irradiated, multiple dislocation loops *(French)* 80−65064
Fe-Cr-Ni based alloys, Ni^+ ion and neutron irradiated, γ' particle redistrib. and phase stability 79−78977
Fe-Cu-D, ion implanted, D trapping, 90-500K 80−15131
Fe-D, ion implanted, D trapping, 90-500K 80−15131
Fe-Ni-Co, magnetic permeability, effect of ion implantation 77−28414
Fe-Ni-Cr (20, 15 wt.%), fusion reactor struct. alloys, dual-ion irrad, effects 79−45403
Fe-Ni-Cr (20, 15 wt.%), single and dual ion irrad., microstruct. studies 80−29077
Fe-Ti-D, ion implanted, D trapping, 90-500K 80−15131
Fe_3Al, Cu^+ (Au^+) ion-bombarded 80−15167
$Fe_{80}B_{20}$, amorphous, fast neutron and fission fragment irrad., effect on elec. resist. 80−19846
$Fe_{78}Mo_2B_{20}$, amorphous, fast neutron and fission fragment irrad., effect on elec. resist. 80−19846
$Fe_{40}Ni_{38}Mo_4B_{18}$, amorphous, crystallization, heat treatment and irradiation effects *(French)* 79−90558
$Fe_{40}Ni_{40}P_{14}B_6$, irradiation swelling 78−30682
GaAs, disorder distrib. extraction, semiempirical method of applying dechannelling correction 78−22781
GaAs, disordered, ion implanted, elec. props. 78−84212
GaAs, electroluminescent study of irrad. induced struct. damage, athermal annealing 80−108280
GaAs, implantation disorder, flux and fluence depend., electrorefl. expts. 78−83833
GaAs, impurity gettering by ion implantation damage 77−11579
GaAs, influence of radiation damage on diffusion of implanted P and Kr atoms 78−6082
GaAs, ion bombarded, defect distrib., photolum. meas. 77−20920
GaAs, ion bombardment, composition changes, AES 78−72662
GaAs, ion damage, TEM study of laser annealing 80−88215
GaAs, ion etching, effects on optical props. and lattice disorder 78−83122
GaAs, ion-bombarded, energy band struct., electrorefl. obs. 79−19517
GaAs ion-irradiated layers switching conduction 78−34868
GaAs, laser annealing of ion bombardment damage 80−25502
GaAs, p-n junction, Zn^+ implanted, residual radiation defect influence on characts. *(Russian)* 78−84287
GaAs surface, Ar bombarded and thermally annealed, work function and photovoltage meas. 77−1446
GaAs, surface cryst. regularity by X-ray photoelectron diffr. 80−89112
GaAs, X-ray and Rutherford backscatt. yields from channelled $^4He^+$ ions 79−46730
GaAs:P^+, defect form. on P^+ implantation at various temp., He^+ backscatt. obs. 78−59828
GaAs:p^+(N^+), struct. characts. of radiation damage produced by high energy ion implantation 79−4340
GaAs:S, depth profiling using Cs^+ bombardment and negative SIMS in UH vac. 79−99232
GaAs:Se^+, TEM structural study, surface and interior damage 80−34025
GaAs:Si, film, conversion of type of conduction stimulated by ion bombardment 77−4457
GaAs:Zn MBE layers, ionized beam doping, elec. and optical characts. 79−37721
GaAs(P), ion irrad. damage, strain effect contrib., channelling meas. 78−67752
GaP, disorder distrib. extraction, semiempirical method of applying dechannelling correction 78−22781
GaP, ion-bombarded, energy band struct., electrorefl. obs. 79−19517
GaP, ion-implanted, form. and annealing of radiation damage 78−91363
GaP, ion-implanted, radiation damage, ellipsometry expts. 78−38735
GaSb film, ion bombard. effects on elemental Sb incorporation probability during sputter deposition 79−83120
GaSb-Pb junction, Ar ion bombard. effect on tunnelling props. 80−54783
$(Gd, Bi)_2$ $(Fe, Ga)_5O_{12}$ magneto-optic LPE garnet films, high-energy heavy ion irrad., props. 80−71390
$(Gd,Bi)_3(Fe,Al,Ga)_5O_{12}$ LPE film, 180° Bloch wall pinning at etched nucl. tracks 78−39376
$(Gd,Bi)_3(Fe,Ga)_5O_{12}$ magneto-optic film, ion irrad. effect on storage props. 78−52324
$(Gd,Bi)_3(Fe,Ga)_5O_{12}$ epitaxial garnet film, nucl. tracks effect on mag. props. 80−11234
Gd, energy loss and straggling of $^4He^+$ ions in vacuum-evaporated films 80−88231
Gd-Co based amorphous sputtered films, microstruct. variability and mag. anisotropy, implanted ion effects 80−88459
Gd-Co film, amorphous ferrimagnet, mag. anisotropy, effect of ion bombard. during prep. 79−1692
Gd-Co-Mo alloy film, amorphous, mag. props., ion implantation damage effects 77−89991
$Gd_3Ga_5O_{12}$, Ca, Zr and Mg substituted artificial garnets, track registration props. 78−62679
$Gd_3Ga_5O_{12}$, high energy heavy ion irrad., lattice strain 80−49278
Ge (111) surface, 500 eV Ar^+ bombard., high temp. annealing, recovery, RHEED obs. 78−87723
n-Ge accumulation layers, effect of low-energy Ar^+ ion bombardment on electron scatt. 77−66205
Ge amorphous films, self-ion bombard., electronic props. 79−28422
Ge, defect form. under radiation-accelerated diffusion conditions 80−19854
Ge, energy spikes due to heavy ion bombardment, semiempirical model 78−47453
Ge film, amorphous, ^{74}Ge ion implanted, defect struct. obs. 78−51848
Ge, ion beam irrad., defects prod. by individual displacement cascades, TEM study 80−70265
Ge, ion bombarded, radiation defect formation, atom-atom collision cascades modelling 80−10582

ion beam effects continued
Ge, ion irrad., accumulation and annealing of struct. defects, secondary emission obs. 78−2167
Ge, lattice disorder due to mol. and atomic ion implants 77−59056
Ge, low-energy heavy-ion implantation damage, spike effects 77−59055
Ge, radiation damage by 0.5 to 10 keV ions 80−100285
Ge thin films on glass substrates, annealing by Ar ion bombardment 80−80136
Ge:^{125}I(^{125}Te), implanted atom sites and quadrupole interaction, Mossbauer spectra 77−20758
Ge:Pb, ion implanted damaged layer, laser induced reorder 80−84201
Ge:Te^+, ion implanted, alignment of irrad. induced defects, TEM obs. 80−15168
Ge-Si, amorphous, freshly-evap. and ion-bombarded, struct. differences 79−55666
Ge(100) surface, Ar ion bombarded, determ. of atomic steps, LEED 78−63913
H species, on C foil, 800 keV amu^{-1}, electron loss and capture cross-sections 80−65066
H_2 gas, ^{208}Pb stopping cross-section meas. with TOF spectroscopy 77−23569
H_2O ice, erosion by H and He ions, energy depend. 80−65067
He ions, surface blister bursting, study of Nb, Nb alloy, steel, 20 keV, 700-800K 77−36349
He species, on C foil, 800 keV amu^{-1}, electron loss and capture cross-sections 80−65066
Hf film on Si substrate, ion-beam induced silicide form. 79−46718
$Hg_{0.79}Cd_{0.21}Te$, ion implanted, elec. props. 80−20184
p-InAs, surface conductance of Ar-ion-bombard. samples 79−60910
InP, recoil damage obs. by PAC with ^{111}Cd 77−89484
InSb, 300 keV Xe and Cd ions, dose rate and orientation dependence of radiation damage 77−89482
InSb film, ion bombard. effects on elemental Sb incorporation probability during sputter deposition 79−83120
InSb, ion bombard. and defect annealing, n- and p-type cond. layer prod. 78−26606
p-InSb, ion bombardment using 30-80 keV ions, isochronous annealing, elec. props. obs. 79−19295
InSb, ion implantation, anomalous radiation disordering 80−92553
InSb, ion implantation at elevated temps. 79−10870
InSb, morphological and structural changes due to ion bombardment 80−79843
InSb, recoil damage obs. by PAC with ^{111}Cd 77−89484
InSb, single crystal, chem. and ion etching, surface changes *(French)* 80−108614
InSb:Cd (Zn) (Ge), ion-irradiated, p-n conversion during heat treatment 80−96558
InSb/GaSb superlattice thin films, sputtered, ion-bombardment-enhanced diffusion during growth 78−87882
$In_{2-x}Sn_xO_{3-y}$-poly Si SIS solar cells 80−97787
Inconel-718, blistering by 2 MeV He^+ ions, optical microscopy and SEM obs. 79−42119
Li^+, amorphous target impact, 100 keV, electronic stopping power, models comparison 78−2180
LiF, high-energy particle bombard., F-centre creation, optical meas. and model 77−47497
LiF, N^+ and Ne^+ irradiation, MO X-ray intensity meas. 78−82831
LiF, thermally stimulated exoemission, radiation defects and adsorpt. centres 78−11087
$LiNbO_3$, electromigration in ion bombardment 78−26601
$LiNbO_3$, microfabrication by ion-bombardment enhanced etching 78−76779
$LiNbO_3$ surfaces, ion and electron bombard., photoelectron spectroscopy and electronic props. 80−71559
$LiNbO_3$:Ti narrow ridge optical waveguides and electro-optical, ion-bombardment-enhanced etching 80−38133
Mg, defect solute atom interaction investigation using channelling techniques 78−47442
Mg-Ag, dil., ion irradiated, interaction between Ag and defects, channelling meas. 78−38766
MgO, irrad. induced vol. changes, optical absorpt. expts. 77−59053
MgO irradiated with Li^+ and K^+ ions, optical props. of metal aggregates 79−65907
Mo alloys (MChVP and TsM10VD), erosion, effect of ion bombardment dose and previous surface treatment 80−89419
Mo, blister erosion reduction by multi-groove surface microstruct. 78−95211
Mo, blistering and surface roughening, room temp. ageing effects Ar^+ ion bombardment 78−34550
Mo, C and N ion bombard., Mo_2C and Mo_2N synthesis 78−48357
Mo cryst., radiation induced vacancies and D_2^+ implantation 80−65076
Mo, damage profile resulting from Ni^{2+} and He^+ ion bombardment 78−10100
Mo, diffusion of H(D), trapping at ion implantation induced defects 77−47622
Mo, dual beam ion bombardment 79−7634
Mo, energetic deuteron irradiated surface struct. quantitative meas. 78−95210
Mo, gas driven blister growth on He ion bombardment, SEM obs. 77−76473
Mo, H and D trapping, enhancement due to He ion damage 77−31698
Mo, H_2 diffusion enhanced by self-interstitial atoms, surface reaction const. determ. 80−75386
Mo, He implanted surface deform., integrated lateral stress 77−31697
Mo, He ion irradiated, ordered arrangement of micropores on dislocations 77−19943
Mo, He ion irradiated, TEM 77−19994
Mo, ion bombardment, damage profile, void size and density, TEM 78−47451
Mo, ion bombardment by Ni^{2+}, TEM study of damage depth distrib. 78−10101
Mo, ion irrad., dislocation loops and stacking fault tetrahedra, electron microscope image contrast 80−6326
Mo, ion irradiated, radiation-induced damage, microhardness and lattice consts. meas. 78−2170
Mo, irrad., defect anal., electron microscopy, appl. of theory of non-edge loop image contrast 80−70200
Mo, irradiated, small edge dislocation loops, electron microscope image contrast, Burger's vector determ. 77−76410
Mo, irradiated by H^+ and H_2^+ ion beams, grain ejection from surface 78−6819

ion beam effects continued
Mo, irradiation induced defects, electron microscope images 78−83854
Mo, microstruct., swelling induced by ion bombard., He injection effects 80−29083
Mo, ordered void obs. 79−86786
Mo, polycrystn., 2 keV Ne^+ ion bombard., dose and microstruct. effects on surface topography and sputtering yield 79−65124
Mo, radiation damage by 0.3-2 keV D_2^+, use of 300 eV D_2^+ as ion microprobe 77−43260
Mo, self-ion damage, influence of material purity and irradiation temp., electron microscope exam. 77−35562
Mo single crystal 78−52136
Mo single crystals, ion implanted, energy dependent channelling and backscatt. anal., $^4He^+$ ions, 1 to 2.8 MeV 79−4360
Mo surface, rolled, H_2^+ ion bombard, large blister form. 80−75274
Mo, surface blistering by 75 to 350 keV He ions, SEM study 78−72657
Mo, surface erosion, by H_2^+ bombardment 77−15464
Mo, TFTR protective plate, sputtering and surface damage by D^+ irrad. 80−18645
Mo, thin film, chemical cpd. form. by N_2^+ and Ar^+ ion bombardment *(Russian)* 79−73225
Mo, vacancy mutation to divacancies by He trapping, percolation onset 78−51601
Mo:N, single cryst., interaction of N with vacancies 79−82261
Mo-base alloy, TZM, blistering under He ion bombard. 80−92567
Mo-Ni sputter deposited, amorphous and crystn., Ni^{++} ion irradiation effects, TEM study 79−65128
Mo-Zr, heavy ion irradiated, void swelling, phase instability 80−29084
MoO_3 film, optical absorpt. after ion irrad., appl. to ion beam profile monitoring 79−26181
N^+, amorphous target impact, 800 keV, electronic stopping power, models comparison 78−2180
N^+, electronic stopping power in solids, range distrib. energy depend. 80−92575
N_2, ion pair creation by high-energy ions, meas. of average energy required 80−103105
NaCl, bi-exciton luminescence possibility 80−40167
NaCl crystal surface struct., effect of ionic bombardment *(German)* 80−24507
NaCl, Ne^+, Ar^+, Kr^+ bombard., sputtering and ionoluminescence 80−96583
NaCl(I), acoustic radiation generated by ionising particles 78−87726
NaI, Xe^+ ion bombard., sputtering processes, time of flight meas. 78−88392
Na_2O-SiO_2 glass, ion bombardment, form. of cpds., IR spectrosc. exam. *(German)* 80−88173
Nb and Nb alloys, superconductor, flux pinning under heavy ion irradiation 78−52167
Nb and Nb-Zr (1 wt.%), ion irradiated, void ordering 78−22770
Nb, blister diameter and blister skin thickness correl. under He ion irrad. SEM obs. 79−82266
Nb, blister form. on single crystal under Ne^+ ion bombardment 78−71772
Nb blistering by 5-15 keV He ions, dose rate and temp. effects 77−35595
Nb, blistering by He^+ bombardment at thermonuclear reactor energies 80−34104
Nb, blisters due to He irrad., proton backscatt. study 80−75273
Nb, channelling study of $^4He^+$ irradiation damage, effect of dissolved O_2 79−82270
Nb, channelling study of $^4He^+$ irradiation damage, effect of irradiation temp. 79−82271
Nb, diffusion of H(D), trapping at ion implantation induced defects 77−47622
Nb, effect of O ion irradiation on supercond. 78−52131
Nb film, ion bombardment with N_2^+, Ar^+, struct. changes, chemical compound formation *(Russian)* 78−95084
Nb film on Si, Ar ion bombard., $NbSi_2$ form. 80−10709
Nb, flaking and blistering due to He and Ne ion bombardment 80−29092
Nb, He blistering, large swelling meas., gas press. model 80−88218
Nb, He implanted surface deform., integrated lateral stress 77−31697
Nb, He^+ bombardment, high dose 800 to 1400°C 77−36344
Nb, ion bombard. by 5 keV Ar^+, sub-surface damage 80−103399
Nb, lattice location measurements of O using $^3He/^{16}O$ and $^1H/^{18}O$ prompt nucl. reactions, ion irrad. effects 79−86813
Nb, polycrystalline, 10 to 1500 keV $^4He^+$ irrad., blister skin thickness, meas.-calcs. correl. 77−35597
Nb, radiation blistering by $^4He^+$ ions implanted sequentially at different energies, 3 to 500 keV 77−35594
Nb, reactive, trapping of energetic 18 keV deuterons 78−10096
Nb single cryst., He ion implantation, depend. of blister deckeldicke and depth profiles on incidence angle 79−73226
Nb, stress distrib. from He ion irrad., vol. expansion, calcs. 77−35599
Nb, supercond. crit. temp. enhancement by radiation damage 78−2609
Nb superconducting amorphous film, conductivity and transition temp., ion bombardment effects *(Russian)* 80−49969
Nb, surface behaviour under ion irrad., in fusion reactor 77−57740
Nb, surface damage caused by He^+ ion bombard. 80−39177
Nb thin films on Si substrate, intermixing, ion induced silicide formation 80−34101
Nb:O, $^4He^+$ irrad.-induced lattice site change 79−99252
Nb:O, type II supercond., radiation-induced flux pinning 78−80106
Nb-Ti, superconductivity after heavy ion irradiation at low temps. and high fluence 77−69437
Nb-Ti, void volume fraction reduction, Ni^+ ion irradiation 79−51162
Nb-Zr, type II supercond., radiation-induced flux pinning 78−80106
Nb_3Ge, effect of ^{16}O and ^{32}S ion irrad. and thermal recovery on T_c, residual resist. and slope of crit. field 79−56348
Nb_3Ge supercond. thin films, He- and Ar-irradiated, X-ray diffr. studies 80−29503
$Nb_{40}Ni_{60}$, 3 MeV Ni^+ ion implantation, electron microscope exam. of ion damage 78−91365
$Nb_{40}Ni_{60}$, amorphous, produced by Ni^+ implantation, damage distrib. 80−107062
Nb_3Sn, A-15 struct. Nb based superconductors, irrad. type influence on radiation defects 80−15093
Nb_3Sn, atomic displacements induced by radiation damage, X-ray study 80−2085
Nb_3Sn, effect of O ion irradiation on supercond. 78−52131
ion beam effects continued
Nb_3Sn, low temp. irrad. with 20 MeV S ions, effect on supercond. props. 79−38223
Nb_3Sn multifilamentary composite supercond. wires, transverse sections prep., ion milling, TEM obs. of grain size 80−101000
Nb_3Sn, O^{4+} bombarded, Mossbauer studies 80−2672
Nb_3Sn, supercond. crit. temp. and transition width, 25 MeV O ion irrad. effects 77−69439
Nb_3Sn, superconducting props., effect of radiation induced atomic disorder 78−52133
NbTi films, effect of Ar- and N-ion bombardment on texture *(Russian)* 80−107338
Ni (001) surface, Ar ion bombarded, enhancement of oxidation, AES study 80−97644
Ni and alloys, heavy ion irrad., defect cluster obs. 80−107341
Ni, blistering, He^+ ion energy and irradiation temp. effects 80−34103
Ni, blistering by $^4He^+$ bombardment, temp. depend. 78−43967
Ni, blistering due to 20 keV He ion irradiation, temp. depend. 79−73228
Ni, cavity coalescence following $^4He^+$ irrad. 80−70272
Ni, cavity evolution in 500 keV $^4He^+$ irrad. 80−29082
Ni, defect cluster evolution, ion implanter adaption on 100 kV electron microscope 79−2888
Ni, diffusion of Si, ion radiation effect on redistrib. 78−34551
Ni dilute alloys, implant profiles modification by radiation enhanced diffusion and segregation 80−88217
Ni dilute alloys, mechanisms of radiation induced segregation 79−77649
Ni film, ion bombarded, porosity 77−66099
Ni film on Si substrate, ion-beam induced silicide form. 79−46718
Ni foils, 20 keV $^4He^+$ irrad., depth distrib. of bubbles 79−69166
Ni, form. of vacancy micropores during bombardment by 300 keV Ni ions 78−2172
Ni, He gas-bubble superlattice form. 80−2086
Ni, He^+ irradiated, cavity depth distrib. determ. technique 79−51161
Ni, in situ rare gas ion irrad., cluster creation obs. by electron microscopy 80−107343
Ni, irrad. with 20 and 500 keV $^4He^+$, depth distrib. of cavities and dislocation damage 80−107346
Ni, irradiated, with He^+ bubble depth distrib. meas. by TEM and blister form. mech. 78−95088
Ni, irradiated with Cu and Ni ions, depth depend. damage profile 79−14857
Ni, irradiation-induced creep, mechanism for large transient strains 78−14391
Ni light ion (H, D, He, Li) irrad., defect prod. and electronic stopping power 80−34088
Ni, magnetic permeability, effect of ion implantation 77−28414
Ni, neutron and heavy ion damage correlation, dose rate and He injection effects 79−7629
Ni, porosity depth distrib. of annealed samples following bombardment by 1 MeV Ar^+ ions 80−5333
Ni, pure, heavy ion irradiated, dendritic void growth 78−14386
Ni, self-ion irradiated, defect clusters, annealing 78−18687
Ni, self-ion irradiated, He effect on void form. 78−6112
Ni single crystal, depth distrib. of self-ion damage, TEM 77−51419
Ni, stress distrib, from He ion irrad., vol. expansion, calcs. 77−35599
Ni, TEM exam. of ion damage in FCC metals 78−87727
Ni, temp. effect on porosity of Ni irradiated with Ni ions 78−2173
Ni, thin film, chemical cpd. form. by N_2^+ and Ar^+ ion bombardment *(Russian)* 79−73225
Ni, void swelling caused by neutron and self-ion bombardment, 573 to 873K 78−14387
Ni, void swelling rates in self-ion irrad. sample 80−29081
Ni, voids and swelling following $^{56}Fe^{3+}$ bombardment, fast neutron effects simulation 77−30651
Ni:^{111}In, ion implantation damage, DPAC obs. 77−59052
Ni:^{129}Te, implanted atom sites, Mossbauer obs. 77−20756
Ni:^{83}Rb, implanted atom sites and hyperfine interactions, Mossbauer obs. 77−24765
Ni:Cr, He^+ radiation-enhanced diffusion and segregation effects of point-defect trapping 79−77824
Ni:Mn, radiation-enhanced diffusion, effect of point defect fluxes 77−89588
Ni-Al, ion irradiated, dendritic growth of voids 77−11605
Ni-Al (12.8 at.%), irradiation enhanced coarsening 79−66060
Ni-Al (12.8 wt.%). Ni^+ ion irradiation, precipitate restructuring, mechanisms and kinetics 79−77650
Ni-Al (6.35 wt.%) foil, radiation-induced precipitate redistrib. 78−30681
Ni-Al (6.35 wt.%) precipitate coarsening, redistribution and renucleation during ion irradiation 78−23709
γ,γ'-Ni-Al alloys, irrad. effects on precip. 77−8829
Ni-Al solid solns., N_2^+ irrad., void ordering 78−79644
Ni-Al(Cr)(Ti), ion irradiation induced void swelling and defect microstructs., TEM obs. 79−51164
Ni-Al(Si) foils, irrad., surface effects on precip. morphology 80−104168
Ni-base binary alloys, solute segregation and precip. under heavy-ion bombard. 79−11623
Ni-Cu, sputtering rate, radiation-induced segregation and preferential sputtering effects, kinetic model 80−40199
Ni-Mo, sputtering rate, radiation-induced segregation and preferential sputtering effects, kinetic model 80−40199
Ni-P amorphous alloy prep. by ion implantation 78−22748
Ni-Si, ion beam irradiation induced Ni_3Si surface film segregation 78−38761
Ni-Si (1 at.%), dose depend. of ion irradiation induced segregation 79−42123
Ni-Si (12.7 at.%), heterogeneous precipitation at internal and external surfaces during Ni ion irradiation 79−77647
Ni-Si (12.7 wt.%), Ni^+ ion irradiation, precipitate restructuring, mechanisms and kinetics 79−77650
Ni-Si solid solution alloys, γ phase precipitation under irrad. 77−1839
Ni-Si:Cr, He^+ radiation-enhanced diffusion and segregation effects of point-defect trapping 79−77824
Ni-ThO_2, irradiated with 5 MeV Ni^{++}, ThO_2 redistrib. 78−71771
$NiSi_2$, layer, on Si, ion implantation damage, channelling obs. 78−30676
Ni(001) surface N adsorption due to ion beam irrad., surface struct. LEED study *(Chinese)* 80−84364
O adsorbed layer on Cu (100), ejection by ion bombard 79−42373
O_2 adsorbed layer on Cu (100), ejection by ion bombard. 79−42373
O_2 chemisorption enhancement on Cu(110) during Ne^+ bombard. 80−65070

ion beam effects continued
^{16}O backscatt. appl. *(Japanese)* 79−28871
Pb, effect of O ion irradiation on supercond. 78−52131
Pb, O ion irradiated, damage rate decrease 78−26604
Pb superconducting amorphous film, conductivity and transition temp., ion bombardment effects *(Russian)* 80−49969
Pb, superconducting film, radiation induced critical temp. 79−87179
PbS epitaxial layers, ion bombardment effects on struct., and annealing 79−10882
PbS film, photosensitivity, role of surface oxide and ion bombardment 77−24631
PbS, surface defect annealing *(Russian)* 77−47658
PbSb foil production for TEM by electrolytic and ion beam thinning *(German, English)* 77−49812
PbTe film, ion-implantation-induced lattice defects 77−68985
Pd, disordered film, supercond., occurrence and crit. temp. after He^+ irrad. 79−11261
Pd film on Si, Xe ion beam induced form. of PdSi 80−10800
Pd, irradiated film, supercond. 79−78249
Pd, reactive trapping of energetic 18 keV deuterons 78−10096
Pd:^{111}Cd, radiation damage in DPAD expts., quad. interaction 77−27917
Pd-Ag, ion bombarded, surface segregation, XPES obs. 79−77885
$(Pd_{0.8}Au_{0.2})D_{0.04}$, thermal vibr. temp. depend., ion channelling exam. 78−47457
$Pd_{0.8}Si_{0.2}$, amorphous, He^{2+} ion irradiation effect on structure 79−42120
Pd_2Si layer, on Si, ion implantation damage, channelling obs. 78−30676
Pt alloy, fission-fragment-induced He blistering 78−86601
Pt film on Si substrate, ion-beam induced silicide form. 79−46718
Pt, irrad. damage, temp. depend., electron microscopy obs. of defect kinetics 80−107339
Pt, radiation damage, recovery of elec. resist., interstitial migration and clustering 77−11604
Pt, radiation damage, self-interstitials migration modes and thermal conversion 79−65126
Pt, radiation damage recovery curves, evidence for two self-interstitial configs. 77−7773
Pt, TEM exam. of ion damage in FCC metals 78−87727
Pt thin films, spike effects of heavy ion sputtering 80−35034
Pt:^{181}Ta, lattice defect induced elec. field gradient, PAC meas. 79−42878
Pt-Au, ion-irradiated, self-interstitial migration in stage II recovery, FIM obs. 77−59140
Pt-Au (4.0 at.%), ion irradiated, direct obs. of vacancy struct. of (220) platelet 78−51534
Pt-Si system, formation of Si enriched metastable cpds. using ion bombardment and post annealing 79−69143
Pt(Au), ion irradiated alloys, stage II recovery 78−47440
Pt_3Co, radiation damage profiles from low energy Ne^+, bombard. 80−70268
Pu, oxidation, binding energies, Auger and X-ray photoelectron spectra study 80−76550
RbCl(Br)(I), Xe^+ ion bombard., sputtering processes, time of flight meas. 78−88392
Re, He ion irrad., blistering, SEM obs. 78−87722
$(SN)_x$, neutron and heavy ion bombard., effect on elec. cond. along chain axis 78−56136
Sb film on NaCl, effect of ion irradiation on form., struct. and props. 77−36408
p-Se photocond. film, phase memory effect and deep levels 79−82556
Se, photoconductive film, field instability, Ar^+ ion irrad.-induced defects 78−87997
Si (111), ion bombard., struct. changes, AES obs. 80−79842
Si (111) surface, 500 eV Ar^+ bombard., high temp. annealing, recovery, RHEED obs. 78−87723
Si, amorphisation by $^{31}P^+$ ion irrad. 79−51172
Si, amorphisation by bombardment with O ions 78−10098
Si, amorphisation by ion implantation energy depend. 77−7769
Si amorphisation dependence on low-energy irrad. conditions 79−60408
Si, amorphisation due to heavy ion irradiation, ESR meas. 77−11606
Si, amorphised by ion implantation, EPR obs. of mag. ordering 79−24186
Si, amorphised by ion irrad., doping effects on cond. in hopping transport regime 79−28424
Si, amorphous, implanted, struct. transition under laser irrad. 79−50992
Si amorphous, ion bombardment, controlled hydrogenation at low temps. 79−69119
Si, amorphous, ion-implanted, hopping parameter at natural phonon freqs. 79−15152
Si, amorphous, large vacancy cluster annealing by ion bombard, EPR investig. 77−68965
Si amorphous films, self-ion bombard., electronic props. 79−28422
Si, amorphous foil, electronic energy straggling of light ions, at. number depend. 77−11612
Si amorphous layer, inhomogeneity formed by ion bombardment 77−69017
Si amorphous layer, ion-beam induced epitaxial regrowth 79−69378
Si, amorphous surface layer produced by ion bombardment, insulating props. of interfacial layer 77−59327
Si, annealing of vacancy clusters produced by ion bombardment 77−89485
Si, Ar bombarded, blistering effects, SEM obs. 78−67745
Si, B implanted layers, damage obs. by X-ray double refl. 77−15463
Si, B ion irradiated, long-range damage to crystallinity, X-ray diffr. meas. 78−2171
Si, blistering by plasma focus discharge deuterons, statistical anal., plasma diagnostics 77−35351
Si, blistering due to 400 to 1800 keV $^4He^+$ ions, modal range determ. 80−100289
Si, CF_3^+ ion bombardment, XPS and Auger study 79−70367
Si, collision cascade following ion bombard. 80−65069
Si, containing stacking faults, MeV He ion irrad., TEM obs. of defect clusters 77−89483
Si, damage profile after H_3^+-ion irradiation, proton backscatt. exam 79−60410
Si, dechannelling of H^+, generalised Fokker-Planck eqn. calc. 77−19999
p-Si, defect form. due to multiple N^+ and B^+ irrad. 79−90706
Si, defect form. under radiation-accelerated diffusion conditions 80−19854
Si, defect formation kinetics during charged particle irrad. 80−29096
Si devices, implantation damage, review 77−27899

ion beam effects continued
Si, diffusion of B,P and Sb, implantation damage effects 78−55988
Si, diffusion of Na, retarding action of radiation defects 77−1140
Si, disorder depth distrib. prod. by N^+ irrad. 79−73227
Si, disorder distrib. extraction, semiempirical method of applying dechannelling correction 78−22781
Si, displacement of group III, IV, V, and VI impurities in Si by He^+ and H^+ analysing beam 79−4330
Si, EPR of radiation defects, temp. depend. 78−15023
Si, ellipsometry of anodised layers on clean and ion bombarded Si surfaces *(Russian)* 79−24382
Si, energy depend. of amorphisation by ion implantation 78−2175
Si, energy deposition in heavy-ion path using Monte Carlo transport anal. of delta rays in track 80−39185
Si, energy spikes due to heavy ion bombardment, semiempirical model 78−47453
Si epitaxial layer growth in vacuum, Ar, Xe ion bombardment effect 80−39463
Si, etching in He-F_2 plasma, etch rates, mass spectra, direct ion sampling study 80−79510
Si, fast neutron and ion irradiation, radiative recombination centres 77−81152
Si, ferromagnetism induced by ion irrad., e.p.r. investig. *(Russian)* 77−1595
Si film, amorphous, hopping cond. control by ion bombard. induced struct. modification 80−92898
Si film, electroreflectance spectra, 2.8 to 5.0 eV, ion bombard. effects 77−1752
Si film, ion bombarded, crystalline-to-amorphous transition, defect-rich film prep. 80−65071
Si, gettering by ion damage, minority carrier lifetime and backscatt. study 80−100286
Si, H_2^+ irrad., annihilation of free excitons, inelastic scatt. by SiH_4 mols., photolum. obs. 78−19561
Si, heavily damaged ion implanted (100) and (111), development of secondary defects 79−51166
Si, heavily irrad., ESR study of annealing characts. 78−10771
Si, heavy ion induced disorder in surface and at shallow depths 80−59535
Si, high dose self-irrad., spatial correl. between primary and secondary defect profiles 80−59536
Si, implanted, complex annealing behaviour of amorphous layers, TEM obs. of defect struct. 80−107299
Si, implanted, damage struct. obs. using TEM and cross section specimens 80−107298
Si, implanted, defect struct., dislocation loops and elongated defects 80−107300
Si, implanted annealed layers, amorphised structure formation mechanism and crystallographic nature 80−29091
Si, impurities displacement by H^+ or He^+ irrad. 79−86824
Si, ion beam damaged, minority carrier lifetime distribs., electron beam meas. 79−87108
Si, ion beam irrad., defects prod. by individual displacement cascades, TEM study 80−70265
Si, ion bombard. effect on surface struct., RHEED and Au decoration 80−2096
Si, ion bombard. induced residual stress in amorphous implanted surface layers 77−35610
Si, ion bombarded, radiation defect formation, atom-atom collision cascades modelling 80−10582
Si, ion bombardment, anomalous surface damage from channelling-backscatt. meas. 80−84222
Si, ion bombardment induced buildup of disordered material, model 77−47496
Si, ion bombardment induced defect distrib., IR and electron diffr. study 80−65074
Si, ion damage TEM study of laser annealing 80−88215
Si, ion implantation, investigation of radiation damage by pendellosung topography 79−51125
Si, ion implantation damage, annealing, role of stresses 78−75679
Si, ion implantation-induced damage after Ar and P implantation, defect density and distrib. *(German)* 77−24337
Si, ion implanted, annealing of heavy ion cascade damage, channelling meas. 80−89255
Si, ion implanted, annealing by ion beam heating 80−103382
Si, ion implanted, in HF electrolyte, characterization by electrolytic reverse current 78−6078
Si, ion implanted, self implanted, self annealing using high ion current density treatment 80−89254
Si, ion implanted, voids, electron microscopy 78−67757
Si, ion implanted layers, laser annealing 78−67732
Si, ion irrad., temp. and dose depend. of defect profiles 80−29097
Si, ion irrad. damage, strain effect contrib., channelling meas. 78−67752
Si, ion irradiated, room temp., depth distrib. of disorder 79−37745
Si, ion irradiation prod. of stable vacancy-interstitial pairs 77−27925
Si, ion-excited L-shell Auger spectra, characts. 79−87533
Si, ion-implanted, cryst. to amorphous transform., ESR expts. and composite model 78−59825
Si, ion-implanted, defect struct., SEM, TEM and X-ray topography expts. 77−51399
Si, ion-implanted, secondary defects development, three-stage model 78−87725
Si, ion-implanted layers, crystalline-to-amorphous transition, radiation defect prod. 78−87696
Si, ion-implanted layers, residual defects after high temp. annealing 78−87695
Si, irrad. by 50 keV N^+ and P^+, depth distrib. of struct. defects, secondary emission obs. 78−2168
Si, irrad. with Cr^+, form. and annihilation, of defects, ESR investigation 79−90707
Si, laser annealing of ion bombardment damage 80−25502
Si, low energy Ar ion bombardment, evidence for spike-effects 79−19292
Si, low-energy heavy-ion implantation damage, spike effects 77−59055
Si, MOS capacitor, nondestructive of P^+ and He^+ induced damage, doping profiles 80−34087
Si, n-type and p-type, carrier removal rate by fission-fragment irradiation 77−51418
p-Si, Na impurity diffusion, ion irrad., defect form. effects *(Russian)* 77−43386

ion beam effects continued
Si, Ne ion implanted, oxidation expanded defects, effect on MOS parameters 78−19152
Si, oxidation induced by ion or electron bombardment, AES-SIMS study 80−108606
Si, point defect clusters identification by TEM 77−43210
Si, post-annealed amorphous layer, twinning struct. by transmission electron diffr. 77−76685
Si, postimplantation defect annealing in samples heavily damaged by 140 keV Si^{2+} ions 77−11602
Si, radiation damage by 0.5 to 10 keV ions 80−100285
Si, radiative recombination involving silane mols. 79−73998
Si, range of 100 keV Pr^{2+} and Tb^{2+}, M-shell X-ray cross-sections 77−35614
Si, reactive ion beam etching expts., selectivity, anisotropy 80−104308
Si single crystal surface, He^+ bombardment, damage production, defect diffusion 80−39181
Si, sputter cleaning using Ar^+ ions, temp. depend. of residual damage, 25 to 800°C 77−48558
Si, sputtered, cluster formation, influence of HF plasma interaction 78−64441
Si, strain meas. by Pendellosung effect after P ion bombard. 78−55773
Si substrate, implantation effects on hardening and Si_3N_4 film stress reduction 78−71748
Si substrate, ion induced intermixing of Pd or Pt film 80−15420
Si surface, interaction of oxygen gas discharge plasma 78−83840
Si surface, ion bombardment enhanced mixing of Ag layers, Rutherford backscatt. meas. 80−65034
Si, surface oxidation, after Ar^+ bombardment *(Russian)* 79−15028
Si, surface radiation damage cross sections, influence of distortions 80−6442
Si wafer, colour-banded, sheet resist. variation following high dose implantation at high dose rates 78−95074
Si:^{119}Te(^{119}Sb), implanted atom site changes with time, Mossbauer obs. 77−20757
Si:Ar, ion implanted, amorphous, epitaxial regrowth 79−10868
Si:As, 1.5 MeV H^+ and He^+ irradiations of As diffused layers 78−47447
Si:As, As implantation damage and atom location, channelling meas. 77−59032
Si:As, CW CO_2-laser annealing, comparison with thermal annealing 80−84193
Si:As, displacement effect beam energy depend., vacancy trapping 80−33996
Si:As, dual wavelength, laser ion implantation damage annealing 79−69117
Si:As, implanted, spatially varied activation during regrowth of amorphous layers, sheet resist. and backscatt. obs. 78−71749
Si:As, ion implanted, anomaly of elec. activation by additional Ne irradiation 78−84211
Si:As, ion implanted, pulsed ion beam annealing 80−103395
Si:As, ion-implanted, CW IR laser annealing 80−34022
Si:As(P), depth profiling using Cs^+ bombardment and negative SIMS in UH vac. 79−99232
Si:B, detection of atomic plane displacement in near-surface layers, ang. depend. of photoemission during X-ray Bragg diffr. 78−47207
Si:B, He^+ irradiation-induced diffuiion, effect on impurity distrib. 80−70470
Si:B, ion implanted, laser annealed, Raman scatt., Fano interactions, lattice damage 79−78711
Si:B, ion implanted, radiation defect accumulation and annealing, X-ray diffr. obs. 79−37726
Si:B, ion-implantation doped, influence of radiation dose on diffusion processes 77−1141
Si:B (0.2 wt.%) ion implanted, B atom displacement due to low temp. irrad. 80−88234
Si:B ion implanted, strain profiles from X-ray rocking curves 80−107290
Si:B^+, TEM of lateral implantation effects near mask edges in wafers 79−37724
Si:B(Be)(Li) ion implanted, channelling and random equivalent depth distrib. 80−100293
Si:B(N)(O), interstitial Si atom formation by light ion bombardment 78−47406
Si:B(P)(As), impurity diffusion from implanted layer, influence of radiation damage 77−76621
Si:Bi, implanted, channelling obs. of pulsed Q-switched ruby laser annealing 80−59542
Si:C, H^+ and He^+ beam impact phemomena, damage annealing rates 78−47450
Si:Cu(Au), recoil implantation from thin surface films, backscatt. obs. 78−63783
Si:Ga^+, impurity distrib., influence of ion damage 79−69152
Si:H, 50-250 keV H^+ irrad. damage distrib., $^4He^+$ channelling obs. 78−26587
Si:H film, amorphous, bombarded, defects, luminesc. and ESR meas. 80−34977
Si:N, struct. defects formed by 50 keV N^+ irrad., depth distrib. 78−18688
Si:Ne ion implanted, channelling anal. of disorder struct., ^4He ions, 0.7 to 2.2 MeV 79−4321
Si:Ne(Ar)(Kr), ion implantation damage, annealing, comparative study 79−10867
Si:Ne(Kr), ion implanted, amorphous, epitaxial regrowth 79−10869
Si:P, amorphised by Ne^+ implantation, high fluence P implants, plasma region obs. 79−86807
Si:P, distrib. of implanted impurity after laser annealing, e.s.r. and neutron activation analysis 77−4122
Si:P, implantation damage of channelled P ions, elec. activity recovery stages 77−59034
Si:P, implanted, two-stage laser annealing of lattice disorder 79−1452
Si:P, ion implanted, damage layer props. obs. using ellipsometric parameters *(Russian)* 77−43234
Si:P, ion implanted, subsurface damage, TEM and channelled Rutherford backscatt. study 80−107337
Si:P, ion-implanted, optical refl. obs. of damage 78−55883
p-Si:P, random and aligned implants, Rutherford backscatt. and TEM exam. 78−47454
Si:Pt, depth depend. of atomic mixing by ion beams 80−29837
Si-As(Sb) temp. depend. of irradiation-induced displacement of impurities, backscattering meas. 78−26605
Si-B, P diffusion and activity after Ar ion bombardment 78−95192

ion beam effects continued
Si-H, amorphous, H three-dimens. distrib., ion-induced AES and Rutherford backscattering 80−44132
Si-SiO_2, ion bombardment by H_2^+, D_2^+, changes in annealing behaviour 79−78185
Si-SiO_2 interface, thermal SiO_2 sputter induced roughness, Auger sputter profiling study 80−75424
Si+Ga^+ ion implantation at high current density, lattice disorder, proton backscattering 80−34085
SiC, 0.6, 3.5 MeV He^+ irrad., surface erosion, porosity effects 77−35602
SiC, 10 keV H^+ irrad., C deposition, surface swelling, surface morphology changes 77−35608
SiC, (6H), radiation damaged, luminesc. 80−25462
SiC (6H) (000$\bar{1}$), Ar^+ ion bombard., defect form., LEED obs. 79−69165
SiC, amorphisation induced by ion bombardment, Raman spectroscopy 77−80551
SiC, α- and β-types, electroreflection spectra of natural and low-energy ion-bombard. surfaces 79−61340
SiC, blistering and flaking due to light ion bombardment *(Japanese)* 80−70264
SiC distribution profiles of 30 keV Al ions using Lindhard-Scharff-Schiott model *(German)* 80−15172
SiC, energetic deuteron irradiated surface struct. quantitative meas. 78−95210
SiC, energetic ion sputtering, appl. of AES-SIMS (IMA)-FDS combined systems to physical and chemical processes 78−95636
SiC, H^+, D^+, He^+ ion bombardment, Raman scatt. and SEM anal. 77−35609
SiC, radiation damage, review 77−80553
SiC, radiation defect annealing, recovery of LEED maxima 80−65075
SiC, sputtering yield, use as first wall material 78−95629
SiC surface, H^+, D^+ and Ar^+ bombardment, 5 to 15 keV, meas. of erosion yield 78−79647
SiC, surface defects due to Ar ion bombardment, 100-1000 eV 80−6445
SiC-C, sputtering and blistering from H^+ and He^+ bombardment 78−79649
α-SiC(6H), radiation defect distrib. anisotropy near (000$\bar{1}$) surface, LEED study 80−96577
Si_3N_4, enhanced etching by ion beam, localised substrate heating effects 78−51573
Si_3N_4 film, ion beam effects on opt. props. *(Russian)* 77−48265
Si_3N_4 film, on Si, implantation effects on substrate hardening and film stress reduction 78−71748
Si_3N_4, Si(LVV) Auger spectra, ion bombardment, electron energy loss spectra 80−80911
Si_3N_4, swelling, blistering, 140 keV p, d and He ion irrads., porosity effects 77−35603
Si_3N_4:H, amorphous, ion induced H transfer from N to Si, band passivation, elec. props. 78−47439
Si_4N_4, ion-implanted, enhanced etching in buffered HF solns. 78−72903
SiO_2, amorphous anodic layer on Si, MeV light ion multiple through-scatt., backscatt. obs. 79−86828
SiO_2 amorphous film, Si(LVV) Auger spectra, ion bombardment, electron energy loss spectra 80−80911
SiO_2, etching in He-F_2 plasma, etch rates, mass spectra, direct ion sampling study 80−79510
SiO_2 film, bombardment by B^+ ions, waveguide layer form. 79−27454
SiO_2 film, ion beam effects on opt. props. *(Russian)* 77−48265
SiO_2 film, on Si, radiation damage structures, EPR obs. 78−95097
SiO_2 films, stabilised by ion bombardment and heat treatment, crystn. and phase separation 79−77931
SiO_2, fused, ion beam induced luminescence 80−40166
SiO_2 glass, ion bombardment, form. of cpds., IR spectrosc. exam. *(German)* 80−88173
SiO_2, glass, ion implanted, radiation effect on chem. stability 77−1158
SiO_2 glass, low loss optical fibre, radiation-induced IR absorpt. 80−87521
SiO_2, ion irrad., H capture, absorpt. bands *(Russian)* 78−76505
SiO_2, on Si, H_2 and D_2 ion bombardment effects 80−34086
SiO_2, reactive ion beam etching expts., selectivity, anisotropy 80−104308
SiO_2 thermal film, freon ion beam etching, IR study *(Russian)* 80−76095
SiO_2-Si, effects of processing on radiation damage 78−39223
SiO_2-Si MOS system, ion irrad. effects on struct. and electrophysical props. 80−6995
SiO_2-Si structure P^+ bombardment damage, exoelectron emission obs. 78−95383
SiO_x, amorphous, ESR and hopping cond., He^+ irrad. effects 79−61213
SiO_xN_y film, ion beam effects on opt. props. *(Russian)* 77−48265
Si(111), ion-bombard., O_2 adsorption, SIMS study 80−70522
Sn, effect of O ion irradiation on supercond. 78−52131
Sn, electric field gradients of recoil-implanted ^{19}F via $^9Be(^{12}C, np)^{19}F$ 77−8471
α-Sn, implanted with Sn, Sb or Te, impurity-defect structs., Mossbauer expts. 80−39129
Sn, oxidized surface layers, metallic layer prod. by Ar-ion bombard. 77−66572
Sn plate surface, ion-bombardment conditions effect on chem. profile 80−54287
Sn, superconducting film, radiation induced critical temp. 79−87179
^{119m}Sn, in FCC metals, isotope separator implanted, Mossbauer spectroscopy 79−24240
$SrTiO_3$, surface microrelief revealed by ion irradiation 80−54485
Ta film, ion bombardment with N_2^+, Ar^+, struct. changes, chemical compound formation *(Russian)* 78−95084
Ta ion induced continuum emission 80−89025
Ta, ion irradiated, ordered void arrays 78−34553
Ta thin film, elec. cond., strain gauge factor, ion bombardment effects 80−80417
Ta_2O_5, ion-bombarded cryst., structural and compositional changes 79−46724
Te-Au film, supercond. by ion irrad. 80−34544
Th, ion irrad., surface C and O, AES obs. 78−71775
Ti, 300 keV He^+ irrad., exfoliation, flaking, blistering, in-situ SEM obs. 77−35598
Ti, blister form. by He and H ion bombardment, target struct. effect 78−95087
Ti coated Nb, reduction of void number density and size by ion irradiation 78−51600

ion beam effects continued
Ti film, ion bombardment with N_2^+, Ar^+, struct. changes, chemical compound formation *(Russian)* 78−95084
Ti, reactive, trapping of energetic 18 keV deuterons 78−10096
Ti, sputter-erosion and impurity emission under low energy ion bombardment 78−95628
Ti, trapping coeff. of energetic H at high doses 77−31699
Ti-64, -811, 15333, fusion reactor structural alloys, dual-ion irrad, effects 79−45403
Ti-Al (14.4 at.%), void form. and solute segregation under Ni ion irradiation 79−42122
Ti-Al-V, (6,4 wt.%), single and dual ion irrad., microstruct. studies 80−29077
Ti-Al-V (6,4 wt.%), heavy ion irrad. effect on microstructure 79−10884
Ti-Al-V (6,4 wt.%), ion irradiated, microstruct. study using TEM 80−96572
Ti-Al-V alloys, 17.5 MeV Cu ion irradiation, resistance to void damage 79−55795
Ti-Fe-C-N, ion irradiated, microstruct. study using TEM 80−96572
β-Ti-Mo alloys, thinning transformation 77−44438
TiB_2 CVD coating, surface damage and erosion under energetic D^+ and $^4He^+$ irrad. 80−39174
TiB_2 coating, erosion rates under H^+ ion bombard., fusion reactor appls. 80−39179
TiB_2, swelling, blistering, 140 keV p, d and He ion irrads., porosity effects 77−35603
TiC coating, erosion rates under H^+ ion bombard., fusion reactor appls. 80−39179
TiC, sputtering yield, use as first wall material 78−95629
TiI_4:C, deep doping during ion-beam welding, microhardness meas. 79−19294
TiO_2, rutile, deuteron and alpha-particle implantation, chemical effects, optical and cond. meas. 78−67755
V, 80 keV ^4He irrad., depth profiles, migration, release, surface effects, blistering 77−35606
V, annealing after irradiation with 210 keV He at 625°C at high fluences 78−67751
V, blister behaviour during 200, 2000 keV He irrad, temp. depend. 77−35607
V, blister form and stress build-up, under the bombardment, surface prep. effects 78−95094
V, blister form. by He and H ion bombardment, target struct. effect 78−95087
V, blistering after Ar^+ ion bombard., irrad. mode effect 80−39176
V, effect of O ion irradiation on supercond. 78−52131
V, evap. layer, ion bombardment effect on superconducting transition temp. 78−52136
V, first wall material, irrad. with 40 keV ^4He ions, blistering 78−55897
V, H^+ ion bombardment, surface blistering, influence of temp. and crystallographic orientation *(Russian)* 78−95083
V, He ion bombard., blister diameter and skin thickness, SEM obs. 79−28019
V, irradiation with 2 MeV He ions, low cycle at elev. temp. 78−95086
V, oxidation during energetic particle irrad., influence of reactive gases on sputtering and secondary ion emission 78−72656
V single crystals, ion implanted, energy dependent channelling and backscatt. anal., $^4He^+$ ions, 1 to 2.8 MeV 79−4360
V, sputter-erosion and impurity emission under low energy ion bombardment 78−95628
V, void formation from 200 to 700°C following heavy-ion irradiation 78−10104
V:N, ion bombard., void form. 80−34097
V-Cr (15 wt.%), fusion reactor struct. alloys, dual-ion irrad. effects 79−45403
V-Cr (15 wt.%), radiation-induced solute segregation 80−29086
V-Cr (wt.%), 3.5 MeV $^{51}V^+$ irrad. induced void swelling and solute segregation 79−7637
$V\text{-}D_{0.01}$, enrichment of D during the ion bombardment 80−54288
V-Ni, ion bombard., void form. 80−34097
V-O (1 to 4 at.%), solid soln., void swelling, V ion beam irradiation, 550 to 905°C 78−63795
V-O alloy, temp., dose and conc. depend. of void form. following V^+ ion beam irradiation 78−10105
V-Ti, and V-Ti-Be(Zr), 4 MeV Ni^{++} irrad., He gas bubble form. 80−29085
VBe_{12} coating, erosion rates under H^+ ion bombard., fusion reactor appls. 80−39179
VO_2 film, ion bombard. effect on metal-dielec. phase transition, optical props. meas. 79−90963
VO_2 film, metal-dielec. transition, refl. after 40 keV ion bombardment 79−23899
VO_2 film, optical characts. of phase transition, ion bombardment effects 79−28281
VO_2, metal-insulator transition and electronic struct., ion bombard. effects 80−92948
VO_2 single cryst. film, ion-irrad., 'splitting' of semicond.-metal transition 80−11053
V_3Si, ^4He induced damage, channelling effect meas. 77−62570
V_3Si, He irrad., computer simulation of channelling 79−55800
V_3Si, ion irradiated, influence on struct., resist., and supercond. transition temp. 80−54823
V_3Si, low temp. irrad. with 20 MeV S ions, effect on supercond. props. 79−38223
V_3Si single crystal, radiation damage and superconductivity 78−52129
VTi alloys, blister behaviour during 200, 2000 keV He irrad. temp. depend. 77−35607
W and W alloys, ion-irradiated, recovery behaviour studied by field ion microscope 80−29074
W, electron irrad., or ion irrad., stage II, point defect struct., FIM 77−80542
W, FIM study of lattice damage caused by low-energy He ion bombardment 78−95090
W, ion irradiated, defect clusters obs. 80−2089
W, low-energy ion bombardment, depth of sputtering damage obs. by FIM 80−60734
W, oxidation during energetic particle irrad., influence of reactive gases on sputtering and secondary ion emission 78−72656
W surface, He ion bombardment damage, field ion microscope obs. 77−31701
W, trapping of He at Xe atoms, attachment of mobile particles to non-saturable traps 80−39418
W, vacancy struct. of depleted zones after ion irrad. 79−73224
W:Kr, He trapping at substitutional Kr, vacancy creation 77−43258
W-Re, ion irradiated, recovery behaviour studied by field ion microscope 80−29074
WC recoil implantation damage, PAC obs. 77−85620
WO_3 film, optical absorpt. after ion irrad., appl. to ion beam profile monitoring 79−26181
WO_3, recoil implantation damage PAC obs. 77−85620
$(Y,Sm,Lu,Cu)_3(Fe,Ge)_5O_{12}$, ion implanted, hard bubble suppression 80−11238
YAG, interrelationship between mech. props. and elec. relief on surface layer 79−23821
YIG and Ga-substituted YIG, high energy heavy ion irrad., lattice strain 80−49278
Y_2O_3, polycrystalline, high temp. O ion bombard., TEM microstruct. investig. 77−27923
Y_2O_3:Eu^{3+}, quantum yield in candoluminescence process by low energy H^+ ion bombard. 79−65930
Zn, electric field gradients of recoil-implanted ^{19}F via $^9Be(^{12}C, np)^{19}F$ 77−8471
Zn film, on Cu_2O, effect of ion irradiation on form., struct. and props. 77−36408
Zn:^{69}Ge, quad. interac., rad. damage effs. during PAC obs. 77−27918
Zn-Mn, Kondo-system, ion implantation as method for study 80−70241
ZnO film, low energy ion capture, elec. cond. increase *(Russian)* 77−12034
ZnO, multiparticle exciton complexes, luminesc. spectra *(Russian)* 80−16090
ZnO polar surfaces, H and O_2 exposed, ion irrad., and heat treated, cond., EELS study 80−71525
ZnS ion beam etching, topographic changes, amorphisation, luminescence study 80−76078
ZnS:Er^{3+}, ion-implanted, annealing, cathodolum. obs. 80−2868
Zn_2SiO_4:Mn^{2+}, quantum yield in candoluminescence process by low energy H^+ ion bombard. 79−65930
Zr, blistering and exfoliation by 2 MeV He^+ beam 79−46722
Zr, blistering by 2 MeV He^+ ions, optical microscopy and SEM obs. 79−42119
Zr, defect solute atom interaction investigation using channelling techniques 78−47442
Zr, foil bending by in situ ion irrad., neutron damage simulation, room temp. oxide growth 80−107342
Zr, irradiation induced defects, electron microscope images 78−83854
Zr, reactive, trapping of energetic 18 keV deuterons 78−10096
Zr-Au (0.3 and 0.2 wt.%), irradiated, backscattering meas. of Zr self-interstitial atom trapping by Au 77−69014
Zr_3Al, Ar^+ ion and electron irradiation, irradiation swelling, lattice parameter changes 79−65123
Zr_3Al, deformed and irrad., lattice defects obs., superlattice dislocations and defect clusters 80−107261
Zr_3Al, ion beam prod. damaged regions 79−60409
Zr_3Al, irradiation 78−6111
Zr_3Al ordered alloy, ion bombardment damage, TEM 80−100287
ZrO_2 particles, influence of ionic treatment on formation of Al coatings *(Russian)* 80−50552
$ZrSiO_4$, heavy ion irrad., metamict zircon form. 80−2088

ion beams
see also beam-foil spectra; beam-foil spectroscopy; energy loss of particles; ion beam effects; ion optics; ion-surface impact; mass spectrometers; particle accelerators; sputtering
40 kV multimegawatt neutral beam line, power flow and ion source 79−76238
aberrationless high-perveance beams, extraction from quiescent equilib. plasma 79−90472
accelerator ion beam position monitor 79−89040
alignment and energy meas. analyser 79−6781
alpha particle beams in solar wind, magnetosonic instability prod. 79−35089
applications of implantation and sputtering, book 77−31691
autoresonant acceleration, numerical simulation 78−21789
ballistic focusing of intense neutralised beam in pinched electron beam diode 78−9859
beam position location and profile measuring system for ion accelerators *(Croatian)* 77−75025
beamlet steering, linear optics theory 78−12788
beamlet steering by aperture displacement in ion sources with large acceleration-deceleration ratio 80−63430
Bevalac Minibeam facility, biomedical heavy-ion beam 77−83359
bunched proton and electron beams, longitudinal instability theory 77−83208
CAD of ion beam instrumentation systems 77−13819
calorimeter for ion implanter neutral beam component meas. 79−30605
charged particle beam focussing by cryst. film for colliding beam expt. *(Russian)* 79−67426
clinical beams, light-ion flux mixed with collimated fast-neutron beams 80−81723
cluster ion beams, mass anal. by Wien filter 80−86493
co-ordinate monitor, induced noise-like signals processing 80−102607
coherent EM radiation intensity, produced by modulated electron/ion beams in gas 78−50686
collective accelerators, ion burst accel. and prefocusing using rel. electron beam interactions 80−14008
collective ion acceleration, by temporally modulated relativistic electron beam 78−50422
collective ion acceleration by relativistic electron beam localised pinch model, simulation 78−9826
collective ion acceleration in relativistic electron beam diode, intense slow space charge generation 78−9863
collectively accelerated protons, nucl. activation, time-of-flight, and foil activation meas. 79−4195
collimating slit, edge effect on ion scatt. 79−27160
compensated ion beams, handling and expts. *(Russian)* 79−46461
conference on electron, ion and photon beam technology, Palo Alto, CA, USA (May 1978) 78−74827
conference on electron, ion and proton beam technology, conf., Boston, MA, USA (29 May-1 June, 1979) 80−67927
conical application to thin film technology *(Russian)* 80−76383

ion beams continued
consecutive microsecond pulse ion beams from reflex tetrode ion source 79−41323
current meas., microcoulombmeter for accelerated ion beams *(Czech)* 77−67476
Darmstadt heavy ion beam, research and appl. *(German)* 77−67955
deceleration across mag. fields, expt. 80−99384
deflection, in two-dimensional electrostatic quadrupole field 78−5417
detection by channel electron multiplier, counting efficiency 78−5375
detection with VELU-6 channel multiplier 77−74555
deuteron beam time-amplitude charact. in plasma focus *(Russian)* 79−82099
diode focusing, mag. insulated intense ion diode, particle diagnostics 78−9858
direct energy conversion optimisation with charged particle parabolic trajectories 80−37585
direct energy space charge based convertor, numerical simulator 77−35406
divergence, effect of preacceleration voltage 78−66743
dosimetry of ion implanted impurities using calorimeter-Faraday cup system 78−26590
dosimetry techniques, review 80−32527
doubly-ionised beams, nucl. backscatt. anal. of energy and ion impurities 77−75017
drifting gas approach cf. optical approach 79−31788
dynamic recoil implantation, two-gun ion beam system 79−14833
electrical adjustment of beam in MSKh-4 mass spectrometer 78−24884
electrochemical assay with instrument using ion-selective electrode technology and LSI technology 80−1116
electron beam ion source for multiply charged ions 79−30608
electron gas, energy loss of correlated charges 78−87729
electron microscope, HV, ion detection technique 78−45755
electron microscope specimen preparation techniques 78−32947
electron saturated plane Langmuir probe for ion beam diagnostics 79−94144
electron temp. effects for ion beam source, neutralised ion beam prod. 79−93863
electrostatic mirror for heavy ion handling 77−18136
energetic heavy ion beam model for radiobiology 80−26293
energetic neutral beams, development to MW power level of controlled thermonuclear research 79−45508
energy broadening, Boersch effect 80−69308
energy broadening analysis 80−5670
energy meas. of Van de Graaff accelerator using generating voltmeter 78−58508
energy measurement using radiative recomb. of ions in electron beam 80−74293
energy spectrum of beam from inductively coupled HF source, optical parmeter meas. of gun 78−89590
equilibrium negative charge state fractions 78−90288
expansion due to ion cyclotron wave interactions 79−31786
extraction and bunching, from spherical reflex triode, anal. 79−97471
extraction and bunching of ion beam from spherical reflex triode 80−18727
extraction from flowing plasma 80−18044
extraction from quiescent plasma, for pellet fusion 78−50326
factors affecting shape and quality 77−19160
Faraday double transmitting cup, ion optical control device 78−82556
fast, ($Z \leq 18$), semi-empirical determ. of charge states *(French)* 79−45867
fast, production technology, use in laboratory and space expts. 78−5889
fast ion beam, laser beam interaction, high-resolution obs. 77−6959
fast ion beam contamination, gas neutraliser design 78−25368
fast ion beam vel. distrib. meas. with probe 79−13890
field evaporated ions, energy spread from determ. of nanosecond high voltage pulse shapes 77−12502
fine-focused, current distrib. meas. method 77−83799
focusing and acceleration by high electron currents in betatron *(Russian)* 77−6601
focusing and prod. of intense ion beams for pellet fusion 77−83353
focusing and transport in neutralising background, for fusion expt. 78−50323
focusing by mag. insulated diodes, for inertial confinement fusion 78−50324
focusing from quadrupole mass filter using electrostatic lens 79−229
focusing in linear accelerators using magnetically hard quadrupole lenses 79−3261
fundamental constraints in various situations 77−14653
fusion reactor, TFTR, high energy heat sink, ion beam dump and calorimeter 80−99394
fusion reactor microexplosion ignition 79−18030
generation increase through moving plasma boundary 80−63439
Giessen polarisation facility, multi-detector analysing system 77−65373
Hall accelerator, four-lens, pure ion beam struct. 78−66441
handling, in vacuum system, rel. to atomic collisions in solids, review 80−54290
heavy, wide-range raction products magnetic analyser 80−86491
heavy ion beam applications in science and technology 77−55310
heavy ion beam linear energy transfer distribution calc. 79−20630
heavy ion beam prod., operational procedures 77−83436
heavy ion beams, transport of intense bursts 77−83352
heavy ion interactions with gases, measurement apparatus 79−31741
heavy ion stripping data in dilute gases and C foils, semiempirical formulas 78−33354
heavy ions, experimental methods, targets and detectors, book 79−31242
heavy ions, pellet fusion 77−83354
heavy negative ion beam prod. in range 15-90 keV by charge exchange with Mg vapour 78−25366
heavy particle beam, electron cooling 77−71713
heavy-ion beam inertial-confinement fusion, commercial power generation 79−6762
high current, from reflection triode, operating charact. *(Russian)* 80−83230
high current low-energy for plasma impulse waves generation 77−5962
high current particle beam prod. by low pressure spark discharges, accelerator 79−31247
high power beam generation, review 80−13988
high-current, prod. in triode 80−99372
high-current beams, prod. by microwave ion source 78−327
HV generator for accelerator beam control 79−26797
implantation, 400 keV heavy ion implanter 80−31943
implantation type accelerator, 400 kV, energy resolution, stability and calib. using (p,γ) react. 79−30604
impurity anal. by backscatt. meas. 78−70223
inert gas, metastable fraction determ., by W surface impact secondary electrons obs. 79−28873
inertial confinement fusion by high-energy heavy ions 79−18047
injection technique, mol. photodissoc. 77−83134
intense, production and postaccel. in magnetically insulated gaps 80−74041
intense beam production, in toroidal mag. lens, appl. to fusion ignition, X-ray laser 77−67535
intense focused ion beam, prod. in spherical magnetically insulated diode 79−85200
intense ion beam, production and focusing from self-pinched relativistic electron beam 77−24206
intense ion beams for implantation 78−66004
intense low energy ion beam transportation, space charge blow up 79−44982
intense negative ion beams from N_2 cluster ions, size specification 78−87006
intense pulsed ion beams, diagnostics 77−61160
intensity measurement, noninterceptive method *(German)* 77−387
ion acceleration from turbulent plasma by electron beam 77−10137
ion diode, dual current feed magnetically insulated for internal confinement fusion studies 79−93851
ion implantation, quantitative, current practice and appls. 79−69141
ion ring compressor, power generation in combination with subcritical fission blanket 77−23276
isotope separator implantation terminal, prep. of p-n junction particle detectors 80−34034
ISX-B neutral beam injector expt. on prototype beam line 80−74039
laser spectroscopy, high-resolution, using fast ion beams 78−86975
light ion and electron beams 80−5323
light-ion beams, prod. and focusing for fusion expts. 78−50322
light-ion beams for fusion programme at NRL 78−59042
linear accelerator development for neutron radiotherapy 79−20654
linear electron-ion beams, particle density, longit. mag. field effects 77−50597
low energy low beam system for materials studies 79−85834
low-energy high-current ion beam, production from TP-D plasms source 77−57424
magnetic focusing of proton beams by single dipole coil 79−40642
magnetically insulated diode as ion beam source 80−95491
magnetically insulated ion diode, ion beam diagnostics 80−48974
magnetically insulated vacuum diode, μs pulse insulation, ion beam generation 77−26431
mass separation in EM field, model mass separator 78−9855
mass spectrometer, beam profile display device 77−5960
mass spectrometer electrostatic analyser attachment 78−86377
material characterisation, conf., Aleria, Corsica (Sept. 1976) 79−96403
mechanical scanning, applic. to ion implantation 80−31940
mega-ampere ion beam production and focusing using self-pinched electron flow 77−24205
merged beams experiments, automatic computer-controlled beam-scanning system 77−13818
merged electron-ion beam experiment, determ. overlap integral from differential-scanning meas. 80−87282
merged electron-ion beam profile scanning system 79−35891
metal target preparation for stopping power meas. of channelled ions in low energy region 80−63431
MIN, negative ion injector, Na charge exchange cell 80−99386
molecular ion beams, mass spectrometry, absorpt. spectra, review 79−89808
moving plamsa, high current ion beam extraction 79−68361
multi-megawatt ion beam dump, design and development 77−83441
multiaperture sources, beamlet-beamlet interactions, effect on ion optics 78−46507
multiple aperture source using diverter type plasma source 77−71404
multiple charged and polyatomic ions, use in implantation accelerator 77−54017
multiply charge of beams in linear accelerator with variable-phase focusing, general soln. 80−13992
multiply-charged and polyatomic ions, use in implantation accelerator 77−74554
negative ion based neutral systems, generation, handling and acceleration 79−44981
negative ion beam, generation, transport and accel., fusion reactor appl. 78−66378
negative ion beam in gas, space-charge neutralisation 79−55048
negative ion high current beams, source plasma parameters determ. 77−83376
neutralisation in free space 78−71027
neutralisation in transverse mag. field 78−78513
neutralised, ion-acoustic instability in transverse mag. field 79−13891
neutralised plasma, LF wave dispersion *(Russian)* 79−98888
neutralizer gas evolution due to beam interaction, coupled nonlinear Euler level equations 80−47800
nuclear ion microprobe at MeV energies, production and use, review 80−7883
nuclear physics, use of heavy ion beams *(French)* 80−78182
nuclear spin polarised, generation by surface impact, optical detection use in quantum-beat expts. 77−42396
nuclear spin polarized, prod. using grazing incidence ion beam-surface interaction 80−14251
nuclear stopping power, ion beam elastic collisions with target nuclei 80−34105
overlapping, use for interial confinement fusion 80−91242
overneutralisation, by electrons in mag. field 79−10256
parametric focusing of charge- and current-neutralised proton beams 77−57421
particle-beam fusion experiments for fusion ignition, pellet compression and long solenoid approaches, breakeven experiments 80−47720
penetration switch, ion beam, for specimen thinning for TEM 78−70228
Penning ion source, ion energy charact., rel. to mode transition instabilities 77−38529
periodic transport system, K-V distrib. stability 78−50329
photofragment spectroscopy of mol. ions using fast ion beams 80−9755
pinched beam diode, geometrical focusing of intense ion beams 78−58898

ion beams continued
plasma accelerator, compensated ion beams, ion dynamics *(Russian)* 77−47274
plasma and compensated ion beam propagation, review 77−80317
plasma lens, focusing and form. of intensive beam *(Russian)* 78−21270
plasma sheath, nonequilibrium, intense ion beam extraction 77−89267
plasma triode ion beam production, anode design for reflex operation without impedance collapse 78−9862
polarised, prod. from optically pumped electron spin polarised targets 80−27851
polarised deuteron beam ionisation, beam intensity, tensor polarisation prod. in Penning discharge 77−3203
polarised ion sources and low energy collector rings, H^-, D^- beams 78−58515
positive, charge ejection system for charged spacecraft 79−12379
positive and negative ion beams nonlinear interaction, math. simulation and expt. 77−595
positive ion beam dynamic decompensation in absence of mag. field *(Russian)* 80−106993
preacceleration effects on ion beam transmission effects 78−87005
production, by relativistic electron beam, facilities at Nagoya University Plasma Physics Institute 78−5919
production, intense beam, lens system using toroidal mag. field 77−34053
production and manipulation, general considerations 79−93256
production in pulsed linear accelerator for inertial fusion 78−50325
profile, monitoring using optical absorpt. of MoO_3 and WO_3 films 79−26181
profile imaging by Ti tritide collector 78−78032
profile monitor using holed sampling disc 78−54498
propagation of highly directed high perveance ion beams across mag. fields 79−49888
propagation of pulsed beams across mag. field 79−76576
proton (antiproton) beam in storage ring, stochastic cooling anal. 80−5420
proton (antiproton) storage ring, incoherent motion damping by dissipative elements 80−5419
proton accelerating mechanisms in vacuum diodes, induced radioactivity 79−97470
proton beam, intense, space charge neutral, trapping in mag. mirror, simulation 78−9825
proton beam, radially convergent, production by cylindrical double diode 78−9856
proton beam, unidirectional, creation by reflex tetrode with second anode 78−37473
proton beam characts. control by laser-induced selective multistep processes 80−61122
proton beam formation in electron beam-plasma interaction *(Russian)* 78−29207
proton collective acceleration in intense relativistic electron beams 78−9864
protons, storage ring, NAP-M, accelerating system and beam parameters monitoring 77−65364
pulse-forming circuit, double step, for ion extraction in mass spectrometer 77−18124
pulsed charged beams, phase meas. and control 78−58523
pulseline driven neutralised linear ion accelerators, longit. instabilities 80−78459
quadrupole mass filter, transmission *(French)* 80−101877
quasineutral intense focused beam, max. current density, Coulomb interaction 77−54666
QUISTOR, ion kinetic energy calc., survey 80−78468
radioactive ions beams, for nucl. expts., review 79−97922
reflex tetrode, extracted ion beam anal. 80−23236
relativistic proton beam, energy monochromation using laser 78−90010
remote ion beam position measurement from random beam modulation 79−30606
review of ion beam utilisation for etching and film deposition 77−32522
RF ion source, ion beam extraction device 79−22513
RF modified sources of metallic ion beams 79−81111
rotating intense proton beams, extraction and propag. from mag. insulated diode 77−79195
rotating proton beam, generation and propag. 79−6217
saddle field ion source beam spectra, gas depend., at. spectroscopy appls. 78−78039
scanning, electrostatic and mechanical, high current dosimetry techniques 80−32528
scanning device for rapid meas. of emittance and brightness 78−58522
scanning systems, electrostatic 80−31939
slow proton beam spin polarisation meas. by Lamb shift 78−78031
solar flare energy spectrum simulation from monoenergetic incident proton beam 78−12786
solar wind, diffusion upstream ions origin rel. to solar wind deceleration upstream of Earth bow shock 80−98528
SOS wafer for beam profile monitoring in high-current ion implantation systems 80−13182
space charge, in intense ion beams 79−41325
space charge effects in transport, computer simulation 78−50328
space charge limited harmonic beam interceptor, increased cyclotron beam intensity 77−381
space charge neutralisation 79−45507
space charge neutralization regions for mixed positive and negative ion beams 79−27159
space limited positive charge compensation by electrons 77−71916
Space Radiation Effects Laboratory 710-MeV He ion beam, biophysical aspects 80−30871
Spacelab, use of ion beams in near-surface anal. 78−35755
spectrometer, three-dimensional quadrupole type, ion beam struct. 80−9070
spectroscopy, via laser-ion coaxial beams spectrometer 78−12775
spot analysis and ion implantation in single UV vacuum sample chamber 77−4970
steering by aperture displacement for tetrode accelerating structure 78−82075
steering of beamlets by aperture displacement in 2-stage accelerator, experimental study 80−68998
storage in vacuum by EM fields *(French)* 78−1106
storage rings, proton beam interaction with ion wake 77−83345
sub-Doppler laser spectroscopy of mol. ions in fast ion beams 80−9655
supercompression of intense ion beam, in collapsing pinch 77−80379

ion beams continued
surface crystallography, ion beam, channelling and blocking effects, double alignment backscattering 80−65350
surface topology usin Rutherford backscattering 80−47015
swept-focus scheme for ion beam laser 77−38848
synchrotron, methods of increasing heavy ion beams intensity 79−26790
telescoping beams for heavy ion fusion 79−76228
thermal particle motion effect on autoresonance acceleration process *(Russian)* 80−69007
Tokamak-trapped 26 keV beam, RF wave heating 78−59627
trajectories calc. in a 3-dimens. beam subjected to a space charge *(French)* 78−82902
transport, shape of beam envelope, beam space charge and emittance effects 80−32901
transport of low energy divergent H_2 beam at 300 eV by permanent magnets 80−69001
two component ion beam accelerator system for interactive surface effect studies 79−49880
two-beam gain saturation in an electron-ion beam without capture of electrons 78−94919
ultraintense heavy ion beam generation, by radiation cooling in long drift tube 78−58489
Van de Graaff accelerator, ion drift time measurement in gap 79−694
velocity of fast beams, meas. using Doppler shift method 80−9083
velocity-modulated, solitary quasishock compression waves *(Russian)* 80−28679
visual image produced by electron interaction on surface 78−58091
wedge type ion beam divergence profile calc. 78−82555
Ar low energy ion beam transport through apertures, source parameter depend. 77−57422
Ar, multiply charged, characts. 77−18133
Ar, plasma accelerator with closed drift of electrons for ion beam formation for surface cleaning *(Russian)* 79−38993
Ar^{+++}, prod. from RF sources 79−18070
^{40}Ar 450 MeV/amu beam microdosimetry with wall-less proportional counters 80−26370
^{10}B negative ion beam prod. with sputter source 79−93857
^{11}B negative ion beam prod. with sputter source 79−93857
C, energy loss of fast H_2^+ ions 78−79653
C ion injector, high-intensity current, using array of pulsed plasma guns 79−89512
C^+ vacuum arc source 79−21853
C^{4+}, C^{5+}, production and acceleration in cyclotron *(Japanese)* 78−5084
C^{6+}, microdosimetric measurements of pretherapeutic heavy ion beams 80−72337
C^{n+}, collective accel. in vac. diode with C tip cathode, by 180 kV, pulses 78−37104
CO^+ collective accel. in vac. diode with C tip cathode, by 180 kV pulses 78−37104
CO^+, electronic absorpt. spectrum, rot. lines, laser/ion beam reson. 77−54564
CO_2^+ collective accel. in vac. diode with C tip cathode, by 180 kV pulses 78−37104
^{12}C 400 MeV/amu beam microdosimetry with wall-less proportional counters 80−26370
CaH^-, beam prod. using Cs sputter source 77−34499
CaH_3^-, beam prod. using Cs sputter source 77−34499
^{48}Ca, and rare isotopes, beam prod. using Cs sputter source 78−29686
Cs^+ ion source, CW monoenergetic, by photoionisation 80−63910
D beam, polarised, short compression magnet for intensity increase 80−18732
D, impurity production by gas discharge source,cathode material testing 79−86592
D^-, polarised prod. in ^1H+Cs atomic collision at 40 keV, 3.1 μA 78−55078
D^-, prod. of 100 keV beam, transport, accel. and diagnostics 77−83440
D^+ beam production in relativistic electron beam oscill. diode 78−9861
H ion clusters, ioniser for accelerators 77−74551
H^- beam, intense, from Penning surface-plasma source, ion-optical characts. 79−13892
H^-, charge transfer cross sections in gases and vapours, 10 eV to 10 keV, graphs and tables 80−32824
H^-, ion beam bunching with sawtooth voltage 78−4735
H^- polarised intense beam prod. by atomic beam source 80−37674
H^-, polarised prod. in ^1H+Cs atomic collision at 40 keV, 2.9 μA 78−55078
H^- short bunch shaping at entrance of linear accelerator, calcs. 79−700
H^+ beam, 0.5 TW pulses, production with spherically focusing mag. insulated diode 79−31288
H^+, charge transfer cross sections in gases and vapours, 10 eV to 10 keV, graphs and tables 80−32824
H^+ duoPIGatron ion source, plasma studies 77−76145
H^+, energetic beam direct cryosorption pumping 80−105655
H^+, flux meas., detect. efficiency of resist. strip mag. electron multiplier particle-counting systems 77−10552
H^+, intense beam generation, appl. to controlled fusion 77−76119
H^+ ion beam generation, megavolt, 20 kA in reflex triode system 77−24203
H_2^+ beam form., selected vibr. states, by electron impact in high press. Ne 77−65547
H_2^+, energy loss of fast ions in solids 78−79652
H_2^+, fast ions, stopping power of C foil 78−79653
H_2^+, γ-ray yield curves from $^{27}Al(p,\gamma)$ 79−3530
H_3^+, ion beam prod. by coaxial electron impact ion source 80−62795
H_n^+ multispecies beam, particle species evolution in neutral-beam injection lines 79−85846
He^{2+}, microdosimetric measurements of pretherapeutic heavy ion beams 80−72337
He_2^+, ion beam prod. by coaxial electron impact ion source 80−62795
HeH^+, ion beam prod. by coaxial electron impact ion source 80−62795
^3He polarised beam, meas. with recoil deuteron polarimeter 77−34529
$^3He^+$ beam, appl. to evaluating Faraday cups for laser plasmas diagnostics 78−5941
$^3He^+(2S)$ state ion beam with nuclear polarisation, RF source 79−59602
I^- beam, duoplasmatron ion source for SIMS, Ar-I_2 medium 77−18123
I^{53+}, 40 GeV beam, propag. through fusion target chamber, stability 78−26303
^6Li tensor polarised beam prod. and calibration 78−46199
$^6Li^+$, confined ions, density distrib., laser scanning meas. 79−81303

ion beams continued
$^6Li^+$, hyperfine structure, Doppler-tuned ion beam laser spectroscopy 79−89627
MgH^-, beam prod. using Cs sputter source 77−34499
MgH_3^-, beam prod. using Cs sputter source 77−34499
N ion collective acceleration expts. at JINR 80−5406
N^{4+}, N^{5+}, production and acceleration in cyclotron *(Japanese)* 78−5084
Na beam polarisation, optimal magnetic multipole 77−30684
Ne^{+++}, prod. from RF sources 79−18070
Ne^{10+}, microdosimetric measurements of pretherapeutic heavy ion beams 80−72337
Ne^{6+}, Ne^{7+}, production and acceleration in cyclotron *(Japanese)* 78−5084
Ni film, amorphous layer covered, target prep. for channelled ion stopping power meas. 80−63431
O^{5+}, O^{6+}, production and acceleration in cyclotron *(Japanese)* 78−5084
O_2^+, predissociated $b^4\Sigma_g^-$ state, high resolution laser spectroscopy in fast ion beam 80−9656
^{16}O, acceleration in superconducting split ring resonator 77−6577
P ions, charge distrib., 72-123 MeV 80−27849
S ion charge distrib., 70-140 MeV, through C and Be foils 78−13364
SF^+_5, ion-mols. in beam, IR multiple-photon dissociation, mass spectroscopic detect. 79−89720
^{32}S 96 MeV heavy ion ps pulses, rebunching of MP Tandem pulses by spiral resonator 78−33357
^{32}S, acceleration in superconducting split ring resonator 77−6577
Si surface-barrier detectors, characts. in Xe ion beam 78−78571
T medium energy beam from α-particle fragmentation 80−27847
U, 50 keV beam prod. by charge exchange in gas and metal vapour targets 78−70675
U^+, 70 GeV beam, propag. through fusion target chamber, stability 78−26303
V_3Si, channelling, at displacements and electron phonon/defect interactions 77−84815
Xe, fast beam of metastable ions, high resolution spectra 77−42274
Xe, plasma accelerator with closed drift of electrons for ion beam formation for surface cleaning *(Russian)* 79−38993
Xe, prod. of isotope-resolved beams of highly charged ions 79−93858

ion chambers *see ionisation chambers*

ion counters *see counters*

ion cyclotron resonance heating *see plasma heating*

ion cyclotron resonance spectra *see mass spectra*

ion cyclotron resonance spectroscopy *see mass spectroscopy*

ion density
see also plasma density
air, humidified by boiling water, ion content, sensitive cell meas. 80−53913
air corona discharge ion density and mobility obs. 78−67594
air positive corona discharge between coaxial cylinders, critical density estimation 78−67595
Alcator A Tokamak, spatial profiles of light impurity ions 80−48948
arc, ion density, voltage drop, heat conduction by neutrals 77−4012
atmosphere, adiabatic evolution of trapped particle pitch angle distribs. during storm main phase 77−70949
atmosphere, ion conc. 0-85 km altitude 77−29359
atmosphere, positive ion conc. below 90 km altitude, rocket meas. 77−29539
atmosphere, surface layer, small ion number density time fluctuations 78−7730
auroral E-region, ion comp. and NO profile 77−41258
corona onset voltage in nonuniform air gap, calc. methods 77−15253
D-region, daytime solar proton event-disturbed model 78−93038
D-region, equatorial, ion and electron densities 78−36362
D-region, ion composition at midlatitude in quiet conditions, model 80−109307
D-region, ion density meas. via payload B I rocket-borne expt. package 78−45190
D-region, negative ion densities rel. to Thomson scatt. in presence of electron heating 79−16739
D-region, negative ions, Thomson scatt. detect. using Arecibo radar 79−62665
D-region, relaxation after sudden cut-off of ionisation source 77−33254
D-region, transport conditions var. and winter anomaly 79−66864
D-region nighttime ion conc., rocket meas. 77−29540
D-region plasma density measurement, rocket borne expt. 78−45126
D-region positive ions, effective recomb. coeff. vars. 77−13150
discharges in gases, pulsed, theoretical and expt. study 80−92416
E-region, midlatit. nighttime model including metallic ions 77−45249
electrochemical assay with instrument using ion-selective electrode technology and LSI technology 80−1116
electron beam, relativistic, ion accumulation caused by ion-ion interactions 80−5417
F_1-layer at nighttime, ion composition near mag. equator 80−72683
F-region, ion conc. depletion expt., thermal ion obs. 80−41620
F-region small-scale inhomogeneities, ionogram and OGO 6 satellite obs. 77−33265
flame, diffusion type, oppositely directed jets, elec. props. 78−56896
holographic interferometry system for plasma flow phenomena, Ba II ion density meas. 78−55751
HV laboratory ion density due to repetitive impulse generation 78−65913
ion sheath diagnostics using elastic surface waves *(Japanese)* 77−89266
ionosphere, calc. and obs. structure, AE-C satellite and incoherent scatter radar obs. 78−49203
ionosphere, effect of floating pot. of spherical ion trapper 79−44287
ionosphere, effective recombination coeffs. for quiet conditions and solar flare occurrence 80−12595
ionosphere, equatorial, plasma bubbles and irregularities in nighttime F-region 77−87156
ionosphere, International Reference 1978 rel. to Vertical'-6 rocket meas. 80−90285
ionosphere, ion density evolution, effects of O abundance increase 77−2300
ionosphere, ion density meas. rel. to lower hybrid reson. freq. obs. and calcs. 78−28416
ionosphere, ionization vertical lifting during mag. storms, satellite meas. of ion comp. 78−36395

ion density continued
ionosphere, lower, electron distrib. function and ion concs., Boltzmann-Fokker-Planck theory 77−78564
ionosphere, O^+/n_e relative densities at 170 km for specific heliogeophysical conditions 79−12332
ionosphere, satellite meas. appl. to low altitude incoherent scatt. interpretations 77−78568
ionosphere, topside, light ion and electron troughs rel. to plasmapause 77−87162
ionosphere effects of geomagnetic storms, OGO 6 obs. *(Japanese)* 78−85754
ionosphere-satellite interaction, ion density in wake of O^+ plasma 80−82136
JIPP-T-II Tokamak plasma, time resolved spatial profiles of impurities 80−48950
Jupiter, plasmapause theory rel. to Io as ion source 77−22133
laser ion-source, form of ion pulses depend. on plasma characts. *(German)* 77−185
laser microplasma, electron, atom and ion density determ. *(German)* 77−7588
liquid metal, surface ion density, nonmonotone, perturbative discrete ion introduction into jellium 78−72222
magnetosphere, outer, discovery of He^{2+} and O^{2+} ions of terrestrial origin 78−32295
Mars ionosphere, ion density and temps. in light of Viking obs. 78−96419
mesosphere, ion bunches form. and concs. 78−73424
mesosphere, positive and negative ions conc. meas. via payload B III instrument package 78−45194
moist air, ion content and IR absorption 80−41493
multiply-ionized species, thermal energies, in astrophysical plasmas 78−33596
negative impulse corona and sparkover, background ionisation effects 78−87540
plasma, electronic multiplication in nonuniform elec. field 79−86559
plasma, H_3^+ ion density decay, mass spectral obs. 77−3987
plasma, ion acoustic solitons, density gradients effect 77−31456
plasma, recombining, possible isotope enrichment due to reson. trapping 77−58203
plasma probe, elec. highly negative, in flowing continuum plasma, ion sheath 77−72493
plasma probe, spherical, slightly ionised continuum, current-pot. curves 77−72494
plasma rarefied flow around bodies, ion density computation accuracy 79−50849
plasma source, multifilament, mag. field effects on characts. 79−46462
plasmasphere, global morphology of light ions from ESRO-4 satellite 77−25844
protonosphere-ionosphere coupling, postsunset obs. with Arecibo radar 79−70915
pulsar magnetospheres, power-law electron and ion distributions in a strong magnetic field 79−96908
quadrupole ion store, spatial distribution of ions derived by phase space anal. 80−95185
solar corona, proton density effects on H like ions reson. lines components intensity ratio 80−101581
sporadic-E layer inhomogeneous structure influence of RF heating *(Russian)* 78−61653
storm-time ring current ions of ionospheric origin 78−28430
TFR 600, ^2H ion flux, temp., and density meas. 80−48940
thermosphere, effects of geomagnetic storms, OGO 6 obs. *(Japanese)* 78−85754
upper atmosphere, Vertical-6 rocket flight results 80−90268
Venus, dayside ion densities 80−46444
Venus ionosphere, plasma diagnostics meas. by Venus Orbiter *(German)* 79−96941
Z-pinch discharge, electron temp. and density variation obs. 78−75426
Cs plasma, in thermionic convertor, spectroscopic meas. of Cs I *(Japanese)* 77−58902
H ion sources, high current, ion species computs. 77−42209
H^+, O^+, conc. in upper atm., Aureole 2 satellite mass spectrometer obs. 78−53766
H_2 plasma, radial density and temp. profiles, using magnetoacoustic oscills. 79−19082
He^+, He_2^+ and metastable He and He_2 densities in afterglow, mass spectroscopy 77−24221
K^+ mobilities in gases *(Japanese)* 79−60101
Li^+ mobilities in gases *(Japanese)* 79−60101
Na^+ mobilities in gases *(Japanese)* 79−60101
O^+/electron density ratio in 140-200 km height range of atmosphere 80−105102

ion emission
see also field ion emission; secondary ion emission; thermionic ion emission
alkali halide, electron-ion emission due to ionisation of surface atoms 77−16474
alkali halides, cluster ions and mol. ions in salt field desorption 80−40238
conference on surface science, Cambridge, England (March 1979) 80−36773
electrolyte aqueous soln. drops, ion emission due to laser heating 78−59063
laser generated plasma, Child's law for fast ion emission 79−60163
metal, negative ion emission during microsecond laser pulse irrad. 78−2981
metal surface, photoionic emission 78−48287
negative sputtered ion emission by O_2, anomalous enhancement 79−19962
plasma, laser-generated, ion beam production from interaction with Nd:YAG laser radiation bursts 80−106939
review of recent advances in electron and ion emitters *(Japanese)* 77−63492
surface layers, photon induced ion desorption, surface atom core ionisation, Auger decay 80−59809
Al alloys, oxide-covered, characteristic emission of negatively charged particles during tensile deform. 78−92179
Al, oxide covered, tensile deform. in high vac., particle and photon emission 78−39672
$CaCl_2$, cluster ions and mol. ions in salt field desorption 80−40238
CaO:Bi surface, O_2 chemisorpt., positive ion emission determ. 80−92785

ion emission continued
Ca_2O:Bi, positive ion nonequilibrium emission in heterogeneous chemical reaction, mass spectra 80−55277
Hg vacuum arc, vapour-cone angles of neutrals and ions emanating from cathode 77−4007
LaB_6, negative surface ionisation, intense halogen ion source 79−93850
LiF, ion and electron emission following ion impact 80−100729
LiF, laser irrad., Li^+ emission, time and energy characts. 80−100710
LiF, laser-irrad., emitted electrons and positive ions delay 80−29830
NaCl, ion and electron emission following ion impact 80−100729
Ni, oxide covered, tensile deform. in high vac., particle and photon emission 78−39672
Si, ion and electron emission following ion impact 80−100729
α-U, autoionic images of dislocation struct., computer interpretation 77−62453
W (100), adsorbed O, electron stimulated desorption ion energy distrib. and surface struct. 78−75940

ion engines
see also aerospace propulsion; rockets
electron bombardment ion thruster efflux, interaction with spacecraft 80−31440
electrostatic/EM ion collection techniques, interstellar appls. 77−70974
navigation capability for comet rendezvous using ion drive 79−35096
solar power satellite engine, ion beam injection into magnetosphere 80−82149

ion etching *see sputter etching*

ion exchange
acetic acid-formic acid, 'dimer', tritium β^--decay causing H^+ transfer, ab initio MO calc. 80−3391
alkaline glass, ionic diffusion and exchange, integrated optics study *(French)* 77−88940
alkaline radioactive waste decontamination method 78−50263
aluminosilicates, isomorphous replacement theory 77−60113
anion exchange resin, for separation of B isotopes *(Japanese)* 78−33625
anion selective electrodes, using liquid ion exchangers 78−40060
aqueous-organic mixed solvent structure, solvation, cation exchange *(Dutch)* 79−83500
artificial membranes, transport regulation by environmental H^+ conc. 80−89725
bentonite, selective sorption props., thermodynamics of ion-exchange reactions 79−39203
bentonite, selectivity of ion-exchange reactions 79−34360
carboxylic acid-ethanol systems, proton exchange process kinetics, effect of H bond strength in intermediate state *(Russian)* 79−96306
cation exchange membrane, counterion interdiffusion 80−26044
cation exchangers with several groups of sites 80−3328
cellulose acetate-g-polyacrylamide membranes, radiation grafted, appl. in water desalination by reverse osmosis 80−45548
cetyl pyridinium bromide, adsorpt. on Aerosil, pH depend., mechanism 79−20466
chabazite, Cu^{2+}-exchanged, cation and water mol. positions 78−15709
cholesterol, T-labelled, prod. by catalysed exchange with T_2 *(German)* 77−90599
chromatography, appl. at NBS 80−7880
chromatography, Co and rare earth determ. in alloys for high energy magnets *(Polish)* 80−35606
chromatography, extraction, macroporous resins, use as supports for chelating liquid ion exchanger 77−90660
chromatography, inorganic ion analysis 79−83538
chromatography, on-stream, impact on energy conservation 80−55737
chromatography, significance for chemical anal. and radiochem. 77−25343
chromatography, technique and appls. 78−3411
clinoptilolite, natural zeolite, ion-exchange, struct. rel. to heating 79−39145
color developer recovery, ion-exchange method 79−49319
colour developer recovery, ion exchange method practical application 79−49320
colour positive developer comsumption, bromine ion extraction from overflow using ion exchange resins *(Russian)* 80−105733
composite membrane, anion exchanger-urease, coupling of transport and enzymic reaction 79−83510
diffusion of $^{241}Am^{3+}$ ions in ion-exchange membrane, autoradiographic method 78−35721
Dowex 50 W×8 cation exchange resin, sorption of Zn^{2+} from HCl soln., temp. depend. *(Bulgarian)* 79−87004
electrical conductivity measurement of ion exchange mats. using isocond. pt. determ. method 77−52646
electrodialysis and its applications 80−55702
electrolytic ion separation, by ion exchange membranes 78−53247
fast Ca and Zn separation by ion exchange resin *(Rumanian)* 78−23922
fibre optic multimode planar coupler device, formation using ion-exchange process 79−50429
fibre-optic planar multimode coupling structure fabrication 80−64233
fibrous ionites, ^{60}Co and ^{134}Cs sorption from water 77−56251
float glass, toughening by ion exchange, selection of technology parameters 78−84757
fluidised beds of ion exchange resins, mass transfer at low Reynolds numbers 77−68684
force-flow chromatography, alkaline earth ions detected by photometric method 80−71965
formamide dimer, tritium β^--decay causing H^+ transfer, ab initio MO calc. 80−3391
formic acid dimer, tritium β^--decay causing H^+ transfer, ab initio MO calc. 80−3391
fuel reprocessing waste ^{137}Cs, ^{90}Sr and rare earth radioisotope separation by cation exchange 78−78486
glass, Ag^+ migration for planar waveguide form. 77−27352
glass, chem. tempered, surface stress meas. using opt. waveguide effect *(Japanese)* 80−45473
glass, chemically strengthened, ion exchange temp. and time influence on stress profiles and strengths 78−31417
glass, diffusion coeffs. of Tl^+ ions meas. using ion-exchange technique 77−89583
glass, electric field controlled ion exchange, optical waveguide fabrication 78−38094
glass, refractive index gradients, form. using ion exchange diffusion 80−64227

ion exchange continued
glass, relaxation effect on ion migration during ion exchange by electrolysis 77−66759
glass cation ion exchange interdiffusion, nonidealness degree 80−39362
glass cylinder refractive index variation by field-assisted ion exchange 80−14500
glass hardening, etching in hydrofluoric acid effect by low temp. ion exchange 77−44373
glass interface with anodic electrolyte solution, simultaneous transfer of different cations in elec. fields 78−30800
glass planar optical waveguide fabricated by ion exchange, refr. index profile 80−14460
glass technology and applications, review of advances 77−66618
haemodialysis technique with dialysate regeneration by absorpt. and ion exchange *(German)* 77−48919
ice, cubic, D_2O isolated, H^+ exchange and Bjerrum defect migration, direct spectroscopic obs. 80−88356
intraparticle ion exchange mass transfer, accompanied by instantaneous irreversible reaction 78−9722
ion chromatography, method using conductimetric detection 79−16109
ion-exchanger membranes, coarse-grained, oscillatory phenomena 79−34356
ion-selective electrodes, liq. membrane, free and supported, ion transport, bulk elec. props. 79−83534
ion-selective electrodes, liq. membrane, free and supported, ion transport, interfacial kinetics, time depend. phenomena 79−83535
ion-selective liquid chloride electrodes, solvent effects *(Russian)* 79−91972
Itaya zeolite, removal of H^+, NH_4^+, Cu^{-2+}, Cd^{2+} *(Japanese)* 78−95951
kinetics, X-ray energy spectrometry 77−60111
lacustrine sediments, selective chem. extraction of CO_3^{2-} associated metals 78−65406
liquid membrane microelectrode, appl. to meas. of large extracellular Na transients 77−52949
liquid nuclear waste, simulated, ion exchange equilibration, radiotracer obs. 78−74444
meltwater, from Alpine glaciers, ion exchange influence on dissolved load 78−81228
membrane, all-round electrochem. investig. equipment 79−91970
membrane, electroosmotic energy conversion efficiency 80−61430
membrane, equilib. props. calcs. *(German)* 77−12830
membrane, neutral complexing agents basis, limiting step of ionic transport using conc. cells method *(Russian)* 79−96367
membrane, unstirred layer effects on pot. difference calcs. 77−48680
membrane, weak ion exchange, nonequilib. props., steady flow in const. elec. field 78−23966
membrane detector for liquid chromatography, characterisation appls. 79−16055
membrane selectivity w.r.t. dialysis prospects 80−45560
membranes, cation exchange, voltage against current curves 79−96365
membranes, ion diffusion studied by autoradiography 77−90637
membranes, production by electron irrad., cross linking, graft polymerisation *(Japanese)* 77−81403
membranes for ion exchange, ion and water transport eqns. 78−68930
metal and oxide surfaces, and interfaces, slow exchange processes study using SIMS 80−55653
Nafion cation exchange membranes, IR spectrum assignment 79−89818
Nafion per fluorosulphonic acid ion exchange membranes, Mossbauer spectroscopy 80−80659
neutron activation analysis using ion exchange preconc. 79−52832
nuclear class resins, radiation stability in γ field 79−43609
nuclear fuel, burn-up, chemical separation, ion exchange 80−42746
nuclear water solutions, radioactive ion removal by electrodialysis 79−36338
optical glass containing PbO, effect of Al_2O_3/Na_2O ratio on rate of ion exchange 78−44377
optical waveguide, ion-exchanged, influence on step-index profile, double alkali-effect 80−5824
optical waveguide, ion-exchanged, repeatability improved by melt dilution 80−53493
photographic process effluents, removal of haxacyanoferrate 79−54211
PMMA gels, neutralised cross-linked, selective uptake of ions 78−35719
porcelain raw material, ion exchange chromatography method, for separate determ. of Na_2O and K_2O 78−7272
preconcentration, for trace anal. of water using X-ray fluoresc. 77−12864
Pyrex glass, cation exchange and interdiffusion 80−80002
radiative waste water treatment methods *(Hungarian)* 80−18450
radioactive ion concentration using resin, river water field sampling unit 77−9532
radioactive waste, liq., treatment with chem.-treated mica and vermiculites 79−45370
radioactive waste liquid, decontamination by ion exchange and electrodialysis 79−71926
radioactive waste solidification, Sandia process 77−61551
radionuclide corrosion and fission products, ion exchange separation 80−18460
radionuclide corrosion and fission products, liquid-liquid extractions with metal diethyldithiocarbamates 80−18459
refractive index variation from field-assisted ion exchange 80−74447
resin:Cu^{2+}, interaction with ligands, EPR meas. 78−10756
resin:VO^{2+}, interaction with ligands, EPR meas. 78−10756
resin, incorporated in polyethylene or cement, ^{137}Cs leaching 77−65275
resins, comparison for use in ^{82}Rb generators for imaging studies 77−21626
sample preconcentration, for X-ray fluoresc. anal., using ion exchange filter membranes 78−7228
seawater purification, method for obtaining Si-free and PO_4-free water 78−3817
selective electrodes for dissolved gas detection *(French)* 79−100472
Selfoc lens, aberration improvement by glass composition and ion exchange process parameter choice 80−69486
silica gel, ion exchanger, isotope separation appls. 78−86961
silicate glass decomp. in alkaline aq. soln. 77−48637
soda lime glass gradient index variation by ion exchange and migration 80−14412
solid solution theory, quasi-particles method 80−24560
solid solutions, multicomponent, quasichem. variant of method of cluster components *(Russian)* 77−80622

ion exchange continued
solvent extraction processing of mixed actinide residues, air sparge batch contactor 77−46369
spinels, entropy of cation transitions 79−11812
spiral ion exchanger for rapid radiochem. separations 77−25296
steam turbine condensates, ion-exchange polishing analysis *(Russian)* 80−89487
sulphonic ion exchangers Ar selective separation of U and Th from lanthanides 78−58860
transition metal ferrocyanide selective sorbents for alkali metals, sorptive props. w.r.t. struct. 80−101051
transition metal ferrocyanides, crystal structures and ion-exchange props. 77−15362
water-sediment interface in Norwegian Sea and Intertropical Atlantic, ionic exchanges *(French)* 79−62523
waveguide, dielectric, ion exchanged, thin film overlay effect on mode props. 80−33191
waveguide, graded-index surface or buried, realized by ion exchange in glass 80−69499
waveguide fabrication in glass, optical, by low-temperature diffusion process 80−102867
waveguides, stripe, Ag^+/Na ion exchanged, propag. characts. 80−83664
zeolite, hydrated Na-Y, ^{23}Na pulsed NMR free induction decay 80−84660
5A-zeolites, cation distrib. and diffusion *(German)* 78−64828
zeolites, type Y, containg catalysts, cryst. struct., IR spectra 79−42958
$33K_2O.7Al_2O_3.60P_2O_5$, high expansion glass, chemical durability improvement by ion exchange 79−66180
^{10}B enrichment by low-temp. exchange in $BF_3.SO_2$ system *(Japanese)* 78−55251
^{10}B separation using anion exchange resin, isotopic plateau holding displacement chromatography *(Japanese)* 78−56886
$(Ca,Fe)SiO_3$, intracryst. Fe^{2+}-Ca^{2+} exchange, Mossbauer spectra 80−20548
Cs selective resin, rapid determ. of Cs in seawater 78−85609
$Cs_{12}M_{33}O_{90}(.12H_2O)$, cation exchanger with intersecting tunnel struct. *(French)* 78−20014
$CsTiMO_5$ (M=Ta, Tb), ion exchange props., synthesis and crystallographic props. *(French)* 80−28997
^{137}Cs-^{137m}Ba generator, for nucl. medicine, preparation by ion exchange chromatography 78−28071
Cu complex Cu (II) ammonia, phenanthroline complexes, ion exchanged, EPR anal. precision 77−56261
Cu(II), selective separation from rare earth elements on chelate ion exchangers 78−58861
Cu_2O-Al_2O_3-SiO_2 glasses, strengthening by alkali-Cu ions exchange 80−55467
Cu_2S-Zn_xCd_{1-x}, heterojunction, composition meas. near interface using aqueous ion-exchange 80−29465
Eu_2O_3:Gd, anal. of Gd impurity by activation anal. and cation-exchange 77−16874
Fe, high purity, prep. and recrystallisation temp. 77−55911
Fe, purification, recrystn. temp. and elec. resistivity *(Japanese)* 80−100780
Fe(III), selective separation from rare earth elements on chelate ion exchangers 78−58861
Fe^{3+}(III) water-glycerine solution-U(IV) cationic resin, inverse break through study on U isotope separation 79−41025
^{57}Fe paramagnetic ions sorbed on cation exchange resin, chem. information from relax. Mossbauer spectra 77−70332
β- and β''-Ga_2O_2-Na_2O, fast ion conductor, Na^+ self diffusion and Na-K exchange 79−28133
H^+-K^+ exchange and cell enlargement in maize coleoptile segments treated with auxin and fusicoccin 77−86469
I absorpt. on ion exchange resins in aqueous solns. 80−47610
^{131}I, separation from water by ion exchange *(Japanese)* 77−60099
$KAlSiO_4$ metastable polymorph, prep. by ion exchange with $RbAlSiO_4$, struct. 78−79585
KCl:KNO_2(KNO_3), anion exchange during tablet pressing, IR spectroscopy appl. 80−2764
KCl-CsCl solid soln., SIMS, clustering distance critical to metal dimer form. 79−72379
KNO_3 in alkali halides tablets, phase transition and ion exchange, IR spectra 80−79937
KNO_3 melts, ion exchange reaction with Na silicate glasses 80−16673
K_2O-PbO-SiO_2 glass powders, during leaching in HNO_3 79−100358
K_2O-SiO_2 glass, improvement in water resist. by ion exchange 78−85012
KOH, aqueous solution, transport parameters for cation exchange membrane 78−64883
$KTiMO_5$(M=Ta, Nb), ion exchange props., synthesis and crystallographic props. *(French)* 80−28997
La, preparation on chelate ion exchangers 79−61538
Li aluminosilicate glasses, variation of refractive index during ion-exchange diffusion from molten salts *(Russian)* 77−28539
Li-ion conductors in solid electrolytes 80−71610
$LiAlSiO_4$:Cu, β-eucryptite solid electrolyte, Cu^{2+} EPR obs. of ion exchange props. 80−108056
LiO_2-SiO_2 glass, improvement in water resist. by ion exchange 78−85012
Li_2O-Al_2O_3-SiO_2, glassy and polycryst., interdiffusion coeffs. for ion exchange 78−26738
Li_2O-Al_2O_3-SiO_2, with refractive index gradient, produced by ion exchange diffusion, exam. of refractive index and concentration changes 79−4782
Li_2O-Na_2O-B_2O_3-Al_2O_3-SiO_2 glass, Young's modulus and density, ion exchange effects 80−84982
$LiTaO_3$ optical waveguides, Ag-Li and Tl-Li ion exchange effects 80−58791
$LiTaO_3$ optical waveguide, Ag-Li ion exchange 80−91888
(Mn,Co)O⇌$(Mn,Co)Al_2O_4$, and (Mn,Co)O⇌$(Mn,Co)Cr_2O_4$, ion exchange equilib., 1100°C 77−32566
xMnO.(100−x)[19TeO_2.PbO] glasses, EPR studies of Mn^{2+} ion distribution 80−71167
^{53}Mn, preparation in cyclotron by target bombard., extraction, anal. 77−61441
$(NH_4)_{0.8}Ni_{1.1}PO_4.xH_2O$, ion exchange props., Cs^+ ion sorpt., struct., IR spectra 77−9121
(Na,Ca)-A zeolites, percolation theory rel. to exchangeable cations 78−7230
$NaNO_3$ melts, ion exchange reaction with Na silicate glasses 80−16673
NaNdX, zeolite hydrated, ion exchange of Na for Nd, cryst. structs. 80−33979
Na_2O-$2SiO_2$ high expansion glass, chemical durability improvement by ion exchnage 78−48361
Na_2O-Al_2O_3-SiO_2 glass, leaching in HCl solns., Na conc. distrib. in surface layers 80−21141
Na_2O-Al_2O_3-SiO_2 glass, interaction with aq. salt solns., alkali ions distrib. in surface layers 80−21142
Na_2O-Al_2O_3-SiO_2(-K_2) glasses, ion exchange kinetics and interdiffusion mechanisms 80−80003
Na_2O-B_2O_3-SiO_2, two-phase, stresses arising during leaching 80−81086
Na_2O-B_2O_3-SiO_2/$AgNO_3$ exam. of ion exchange equilibria 79−5178
Na_2O-CaO glass, abrasion-resistant, high strength 80−76369
Na_2O-CaO glass tube, fracture by field assisted ion exchange 78−68771
Na_2O-CaO-Bi_2O_3-SiO_2, electro-conducting glass-ceramic production by ion-exchange and reduction treatment 79−1616
Na_2O-CaO-SiO_2 glasses, ion-exchanged, mixed alkali effect rel. to elec. cond. 78−34653
Na_2O-K_2O-Al_2O_3-SiO_2, structure of modified surface layer, internal friction method 80−103258
Na_2O-SiO_2 glass, improvement in water resist. by ion exchange 78−85012
Na_2O-SiO_2/$AgNO_3$, exam. of ion exchange equilibria 79−5178
Na_2O-SiO_2/$AgNO_3$, thermodynamic characteristics of ion exchange process 79−8452
Na_2O-SiO_2-Ga_2O_3-Al_2O_3-B_2O_3-SnO_2 glasses, ion exchange reactions with $NaNO_3$ and KNO_3 melts 80−16673
Na_2O-SiO_2-Ga_2O_3-Al_2O_3 glasses in mixed $AgNO_3$-$NaNO_3$ melts, ion exchange 80−21282
$Na_2O.nAl_2O_3$, polycrystalline, Na^+ ion exchange rates with Ag^+ and K^+ ions from the molten nitrates 79−24737
$NaZr_2O_5H$ ion exchange material, use in ^{137}Cs separation from nucl. waste 80−27760
Ni(II), selective separation from rare earth elements on chelate ion exchangers 78−58861
P_2O_5-Al_2O_3-Na_2O-K_2O-Li_2O-(CaO+MgO) glass system, ion exchange effect on mech. props. 80−30229
Pu reclamation, precipitation-ion exchange scheme for actinide removal from salt waste soln. 79−49820
^{228}Ra, separation from thorium oxalate 80−45600
Rb, separation from potash salts, ion exchange methods *(German)* 78−23940
$Rb_{12}M_{33}O_{90}.(12H_2O)$, cation exchanger with intersecting tunnel struct. *(French)* 78−20014
$RbTiMO_5$ (M=Ta, Nb), ion exchange props., synthesis and crystallographic props. *(French)* 80−28997
^{82}Rb generator with alumina column, radioactive Sr adsorption 80−12257
$Sb_2O_5.nH_2O$ acid membranes, synthesis and characterisation 80−81027
SiO_2 glass, porous, adsorption of inorganic cations, in distilled water medium 79−24814
SiO_2 glass, strengthened by ion exchange and quenching brittle destruction theory 80−45398
SiO_2-Al_2O_3-B_2O_3-MgO-CaO-Na_2O, strengthened by ion exchange, exam. of internal stresses using polarising microscope 78−88549
SiO_2-Al_2O_3-CaO-MgO-Na_2O (1.58, 7.16, 3.59, 14.9 mole.%), polished sheet, strength in commercial state and after strengthening by ion exchange 79−1904
SiO_2-Al_2O_3-CaO-MgO-Na_2O, ion exchange and electrodiffusion of Li ions in surface layer 79−20227
Sr, separation from potash salts, ion exchange methods *(German)* 78−23940
^{82}Sr-^{82}Rb generator improvement using inorganic exchangers 80−17135
^{90}Sr/^{90}Y radioisotope generator, educational aid 78−78535
Ta_2O_5, hydrated, heat treatment effect on physicochem. props. 80−20966
Ta_2O_5-H_2O_n, influence of preparation on pore structure and ion exchange props. 79−1970
Th(IV), selective separation from rare earth elements on chelate ion exchangers 78−58861
$(TiNbO_5)^-$ oxide layers, intercalation of alkylammonium ions 80−64985
$Tl_{12}M_{33}O_{90}(.12H_2O)$, cation exchanger with intersecting tunnel struct. *(French)* 78−20014
$TlTiMO_5$ (M=Ta, Nb), ion exchange props., synthesis and crystallographic props. *(French)* 80−28997
U, cascade, chemical and ion exchange unit 77−34474
U determ. in natural water by ion exchange separation, delayed neutron counting 77−36847
U nuclear fuel particle prep. by ion exchange resin loading *(German)* 78−82499
U-Pu, isotope separation in HNO_3 by exchange resins 78−74782
UO_2(II), selective separation from rare earth elements on chelate ion exchangers 78−58861
^{230}U, production, tracer appls., α-spectra 77−61644
Zn^{2+}, transport in cation-exchange membranes 78−96033
Zn^{2+}-Cl^- system, complex form. studied using radiotracer, effect of macroelectrolyte cation 80−16659
$Zr(HPO_4)_2.H_2O$, Na^+ transport, gas-solid and solid-solid reaction kinetics 80−61086
$Zr(HPO_4)_2.H_2O$-Kynar membranes, struct., ion mobility 78−76915

ion exchanging *see ion exchange*

ion excited X-ray emission *see ion microprobe analysis*

ion implantation
see also semiconductor doping
10 nm layer production method and apparatus 80−19818
accelerator applications outside nuclear physics *(Polish)* 79−40641
accelerator systems for ion implantation research 80−32540
AES, energy referencing from charging samples by implanted inert gas spectra 80−40196
AES quantitative anal. of impurities *(Japanese)* 78−91356
alkali halides, implantation of ^{57}Fe, conversion electron Mossbauer spectroscopy technique 80−40012
alloys, improvement of props. by ion implantation 80−16601
alloys, ion implantation in tribology and corrosion science, overview 79−14830
alloys, ion-implanted, annealing behaviour and appls. 79−14829
alloys, ion-implanted, integral Gaussian profile determ. method 80−107313
alloys, props. and application 80−79824

ion implantation continued
alloys and compounds, recoil implantation and ion-beam-induced comp. changes 80−34021
amorphous layer formation *(Japanese)* 78−22746
amorphous metal-metalloid alloys production by ion implantation, TEM study 80−15128
amorphous metals and ion implantation, review 79−14686
amorphous semiconductors, doped, electronic props. 78−19030
amorphous target, ranges and standard deviations 78−30656
anodic oxidation, ion implanted impurities effects 77−90502
austenitic stainless steel 316, by up to 7 eV D, depth profiles 78−71751
backscattering and implantation, H and He ions, computer simulation, comparison of MARLOWE and TRIM codes 80−66350
BCC metal, heavy ion implanted, vacancy annealing stage, Mossbauer meas. 78−39463
benzene, solid, ion implantation, chem. effects 80−55635
bipolar devices, high current and medium current implanter 77−11577
blister formation after He ion irrad., mechanism involving displaced atom transport 80−39178
book 77−31691
bubble garnet, ion-implanted, gradientless propulsion for S=1 bubble 79−78470
bubble garnet film, non-implanted, surface mag. struct. 80−84628
bubble garnet film, vel. asymmetry during stripe head propag. 80−39834
carbides, technological appl. 79−28008
chemical and electrochem. aspects, review 80−100271
colour centre research, appl. of ion implantation, review 79−19272
composite implantation profiles, computer simulation 77−80528
composite ion implantation profiles, computer simulation 77−84786
computer modelling in crystals of diamond struct. 77−43235
conference, ion implantation equipment, Povo-Trento, Italy (Aug., 1978) 80−31413
conference, physics of ionised gases, Dubrovnik, Yugoslavia, (Aug.-Sep. 1976) 77−42961
conference on electron, ion and photon beam technology, Palo Alto, CA, USA (May 1978) 78−74827
conference on electron, ion and proton beam technology, conf., Boston, MA, USA (29 May-1 June, 1979) 80−67927
controlled doping profiles, angular sensitivity 79−55770
controlled implated doping profiles, angular sensitivity 78−30659
corrosion, conf., Manchester, England, (Apr. 1975) 77−8962
corrosion resistant surface alloy form. by ion implantation 78−88569
damage annealing by laser beam 77−25308
depth distrib., analytical calcs. using inhomogeneous equations 80−84203
depth distrib., secondary ion mass spectra 80−79829
depth distribution of vacancies produced by ion implantation 80−65024
depth distributions, calc. in path-length approx. 79−23626
depth profiles, influence of straggling using backscatt. and nucl. reacts. 78−47401
detector materials, Ge and Si 78−47674
developments outside semicond. technology 77−59027
diagnostic test, dosimetry 79−90690
diamond: ^{111}In, ion implanted, intrinsic limitations of doping 80−34019
diamond: Li, ion implantation doped, IR photocond. 80−20249
diamond: Sb, ion implanted, defect study using optical absorpt. and EPR 80−24480
diamond:Li, ion implantation, Hall effect and elec. cond. meas. 80−15526
diamond:Li, ion implantation, investigation of Li^+distrib. 79−77630
diamond:Sb, implanted, radiation damage and annealing study 80−100263
diamond:Sb, ion implanted under channelling conditions, depth profile, distribution tail 80−2057
diamond:Xe, quadrupole interaction of implanted Xe 79−61279
diamond, amorphisation during ^{133}Xe implantation, Mossbauer effect obs. 80−40010
diamond, amorphization process, ^{133}Cs Mossbauer spectra 79−99809
diamond, Ar ion induced struct. changes, depth profiles, from XPS 78−34554
diamond, defects and impurities 80−29017
diamond, hard conducting C ion implanted layer, resistivity 77−15974
diamond, ion implantation, heteroatom size and reactivity effect 80−44226
diamond, method for obtaining n-type ohmic contacts *(Czech)* 77−1414
diamond, natural, high conc. of implanted Si ions, He backscatt. and IR absorption 77−89466
diamond, review 78−87698
dielectric, ion implantation, space charge elec. field effect 79−82250
dielectric film, formation during ion implantation, electric field effects 78−2801
dielectric films on semiconductor devices, review of deposition techniques 78−23611
doping of channelled ion implantations, apparatus for spatial uniformity 78−51569
dosimetry techniques, review 80−32527
dynamic profiling of D, using low energy D(d,p) 78−2153
dynamic recoil implantation, two-gun ion beam system 79−14833
dynamic-implant profiling by low-energy nuclear reaction spectroscopy 77−59037
Electrochemical Society Meeting, Boston, USA, (May, 1979) 79−91959
electronic component and material improvement, ion implantation techniques *(French)* 78−18667
elemental semiconductors, group IV, Mossbauer spectroscopy of defects, radiation damage and deep levels 80−59533
energy deposition profiles from range data, simple method for calc. 77−39619
engineering component ion implantation 79−83360
enhanced diffusion mechanisms, review 78−67847
ESCA observation 78−52612
extractor accel plate, beam intensity optimisation 78−37103
ferrite garnet film, ion-implanted, hard mag. bubble suppression mechanism 80−44890
film analysis and technology applics. *(Czech)* 77−47478
films, props. and appls., review 78−71752
free carrier profile measurement on thin-layers, fast current pulse MOS deep-depletion technique 78−80075
Freeman type high current source for implantation appl. 78−66005
fusion devices, controlled, surface effects, conf., San Francisco, USA (Feb. 1976) 77−30659
fusion reactor materials, D trapping, temp. depend. 80−37577
ion implantation continued
fusion reactor materials, in-situ analysis of ion irradiation and implantation effects 79−45408
fusion reactor materials, ion implantation for radiation damage studies 77−80530
garnet, ion-implanted film, crit. curves for determining magnetisation directions 79−91263
garnet, ion-implanted film, large automotion of S=$^1/_2$ bubble 79−24203
garnet epitaxial film, damage prod. by multiple ion implantation, ferromag. reson. obs. 80−34703
garnet epitaxial films, easy magnetisation axis orientation, ion implantation effects 80−60383
garnet film, bubble, anisotropy field and nonmagnetic regions in implanted layers, ferromag. reson. study 79−99774
garnet film, ion implanted bubble circuits 79−78473
garnet film, ion-implanted, bubble collapse field, in-plane mag. field effect 77−73060
garnet film, minimum bubble drive field, ion implantation effect 77−24721
garnet film ion implanted contiguous disk structure dynamics of 1 μm bubbles 79−78474
garnet film preparation, single-crystal, for magnetic bubble domain appl. 78−60588
GCFR claddings, neutron-induced He implantation, calc. of total flux 80−42773
Ge:P, radiation-accelerated diffusion 80−6559
glass, blister formation by 150 keV He^+ irrad., effects of gas diffusivity 77−35604
glass, glass surface, inhomogeneities and defects, detection using microbubbles, implantation technique *(German)* 78−47647
graphite, pyrolytic, behaviour of implanted D and He 78−95071
graphite, surface morphology changes after irrad. with energetic He ions 78−21767
heating of target, temp. measurement 80−34032
heavy ion 400 kV accelerator of Thomson-CSF Central Research Lab. *(French)* 78−41880
heavy ion beam applications in science and technology 77−55310
heavy ion effects on properties 80−39135
heavy ion implanter, 400 keV 80−31943
heavy-dose, defect centre study, amorphous phase profile 77−80531
heavy-ions, meas. of range in solids by He ion backscatt. 77−14322
heterogeneous medium, ion implantation and energy deposition, path length approx. 78−87694
high current ion implanter with hybrid scanning 80−79826
high current low energy ion implanter, semiconductor device processing 80−31944
high throughput ion implantation systems 80−34029
highly doped, behaviour of buried O_2 implanted layers 80−59499
hydrocarbon contamination and recoil implantation 78−22747
III-V semiconductors, ion implantation, effect of implantation 78−75683
imaging for ion implantation and micromachining *(French)* 80−34027
implant ion collection with radn. enhanced diffusion and sputtering of implant 80−2055
implantation type accelerator, 400 kV, energy resolution, stability and calib. using (p,γ) react. 79−30604
impurity profile control by ion implantation 79−82258
impurity profiles at high implantation doses 80−24490
indirect recoil implantation following nuclear reactions, theory and appl. 80−75256
inert gas atoms, desorbing from solid surface, ultrahigh vacuum apparatus for detection 78−32915
inert gas crystal, lattice vibrs. and radiative transitions of implanted ions *(Russian)* 80−69098
inhomogeneous material, implanted ion distrib. 78−18663
inhomogeneous media, ion implantation range distribs. 79−23625
integrated optic devices, fabrication parameters *(German)* 78−83119
integrated optics applications 77−23781
integrated optics high quantum efficiency waveguide coupled photodetectors on Si substrate 80−58805
intense ion beams for implantation 78−66004
ion beam instrumentation systems, CAD 77−13819
ion implanted layers, complex refr. index profile, ellipsometric meas. 80−93262
ion implanted layers, strain and damage distribs., X-ray diffr. model calcs. 79−69116
ionized-cluster beam deposition and epitaxy 79−83137
isotope separator implantation terminal, prep. of p-n junction particle detectors 80−34034
Josephson junction fabrication by ion implantation, electron beam lithography and dry etching 80−88693
laser annealing, optical constants, ellipsometry observation 80−34024
laser applications in materials processing, seminar, San Diego, CA, USA (Aug. 79) 80−90609
laser-plasma ion source for ion implantation in solids 80−78474
lateral ion scattering in amorphous and polycryst. solids *(German)* 80−24508
lateral spread of implanted ions *(Japanese)* 79−4322
limits of composition achievable by ion implantation, review 79−14827
low cost 150 kV system 78−22738
low energy ion beam materials anal. with SIMS 79−49331
magnet design for high-current implanters or small isotope separators 80−68222
magnetic bubble devices, implanted disk type, domain wall energies, effective threshold anisotropy 79−78453
magnetic bubble film, uniaxial anisotropy energy, effect of ion implantation 79−78476
magnetic bubble stability in ion implanted channels, model 78−68320
magnetic bubble technology appls. 79−15329
magnetic bubbles, ion-implanted propag. patterns, cryst. symm. effects, roof-top designs 80−15768
materials modification, symposium, Yorktown Heights, USA (June, 1978) 79−14826
mechanical scanning 80−31940
metal, ^{2}H dynamic depth profiling by deuteron irradiation 78−26602
metal, corrosion mechanism and surface treatment 77−8982
metal, He deposition and promotion of void nucleation during accelerator expts. computer simul. 79−23658
metal, He ion implanted, statistical model of low temp. blister formation 78−67754
metal, heavy ion bombard., void conc., effect of implanted He *(Russian)* 80−88213

ion implantation continued
metal, heavy ion implantation, site population model 77−80518
metal, ion implanted H(D), interstitial positions and vibr. amplitudes, fast ion channelling study, review 80−79848
metal, light element implantation, radiation damage review 80−88219
metal, metastable phases, review 80−49254
metal, oxidation mechanisms study 77−8980
metal cavity, lifetime of trapped excited atom, broadening mech. for optical absorption line 79−38578
metal surface, He implantation lateral stress, role in bluster form. mech. 78−95068
metal surface, microalloy layer formation by ion implantation 80−16600
metal surface modification, metallurgical coatings, conf., San Diego, USA (23-27 Apr., 1979) 80−12848
metal-semiconductor contact junction formation by ion evaporation 77−90285
metal-semiconductor junction, deposition and post-deposition treatment effects on electrical props. 77−89853
metal-Si system, ion implanted, inert-gas-bubble form., TEM and Rutherford backscatt. anal. 79−90682
metalloid-transition metal amorphous surface alloys formed by ion implantation, TEM study 78−67730
metals, book contrib. 79−1835
metals, effects on corrosion in aqueous soln. 77−25290
metals, FCC, H implantation, lattice location and trapping, ion beam anal. 79−55769
metals, fraction of ions in unique sites, hyperfine interaction studies 77−15438
metals, H and D implantation, ion beam analysis 79−5206
metals, heavy ion implantation, site populations in case of immobile defects 79−23624
metals, heavy ion implantation, stochastic formulation of site populations 79−19271
metals, ion surface treatment 78−11415
metals, ion-implanted, friction and wear, review 80−40555
metals, ranges of $^{15}N^+$ ions, conc. distribs. meas. 79−37749
metals, technological appl. 79−28008
metals and alloys, finishing, use of ion implantation techniques, effect on wear and corrosion props. 79−34204
metastable alloy formation 79−14828
metastable alloy formation by ion implantation 80−15130
microwave ion source for high-current implanter 78−70224
MIS structure, radiation induced charge storage 80−6997
moment of implanted-ion range, energy distrib., computing methods 77−4120
momentum transfer and damage energy gradient effects on He permeability 78−10102
MOS capacitor, ion-implanted, C-V and G-V characts., effect of geometrical struct. of implanted region 77−55615
MOS capacitors, ion-implanted, temp. sensitivity 79−78181
MOS p-channel transistors, ion implantation effect on threshold voltage 78−34903
MOS structure, Ar ion effects on relax. of nonequilib. cap. 78−64140
MOS structure, B and P implantation profiles, junction depth meas. *(Japanese)* 77−39606
MOS structure, B ion implanted, form. and annealing of radiation damage 79−56321
MOS structure, effect on surface and bulk generation currents 78−47883
MOS structure, electrophysical props. after B^+ ion bombardment 77−12013
MOS structure, with ion implanted oxide layer, optically induced charge storage 77−35994
MOS structure implanted with B ions, radiation defects and impurity activation 80−103757
MOS structures, spatial position of deep levels near Si-SiO_2 interface 77−12008
MOSFETs, short channel, fabrication by ion implantation and laser annealing 80−20312
Mossbauer studies of implanted atoms 80−39913
MOST, threshold voltage shift, influence of ion implantation parameters 79−69598
multiple charged and polyatomic ions, use in implantation accelerator 77−54017
multiply-charged and polyatomic ions, use in implantation accelerator 77−74554
n^+-p-p^+ bifacial back surface field solar cells, optimisation of p^+ doping level by ion implantation 80−97784
new materials properties achievable by ion implantation doping and laser processing 79−69127
nozzle erosion, ion implantation effects, ion beam anal. 79−48011
nuclear orientation studies, below 0.5K 80−34033
p^+-n diode under forward bias, effects of radiation-induced deep levels on admittance 78−23157
p-n diode minority carrier storage effect reduction by F ion implantation damage 78−72243
p-n junction, junction termination extension technique for increasing avalanche breakdown voltage and controlling surface elec. fields 78−47866
p-n junction diode, electron-beam annealing of ion-implantation damage 79−77622
Pearson IV distrib., appl. to ion implanted depth profiles 80−88195
Permalloy film, implanted with C ions, HCP struct. formation, electron diffr. study *(Russian)* 79−82469
phase diagrams, ion beam determination of phase boundaries, exam. of techniques 79−8418
photodetector fabrication, synthesis of Si_xC_{1-x}, Si_xGe_{1-x}, $GaAl_xAs_{1-x}$, and GaP_xAs_{1-x} 79−46688
PMOS process with ion implanted threshold adjust, radiation hardening 79−46689
polyacetylene:Br(Pd), ion implantation effect on elec. props. 80−65026
profile calc. for implantation through thin film 78−18672
Pyrex, ion bombardment, form. of cpds., IR spectrosc. exam. *(German)* 80−88173
quantitative, exptl. technique and appl. 79−69141
quantitative, theoretical aspects 79−69140
quartz, effects of He ion implantation on SAW propag. 80−75421
quartz, He^+ ion implanted, SAW velocity, influence of annealing 79−14996
quartz, ion-implanted, SAW velocity 0.9 to 6K 78−84040
quartz, ion-implanted layers, total X-ray reflection investig. of clustering 78−6081
ion implantation continued
quartz, piezoelectric layer, non-crystalline characteristics after ion implantation *(French)* 77−73117
quartz, waveguide layer form. on bombardment by B^+ ions 79−27454
quartz oscillator plate, surface treatment by 100 keV B ion implantation *(Japanese)* 78−59826
radiation enhanced outdiffusion 79−73200
radionuclide, half-life meas. by ion implantation 78−70713
range parameters, nucl. stopping power, ion backscatt. determ. 80−88232
range parameters and diffusion meas. by small angle Rutherford backscatt., review 77−44108
Re-sputtering and implanting sputtered atoms during deposition 80−16137
recoil atoms, theory 80−92545
recoil density resulting from ion implantation 80−88175
recoil implantation, film thickness optimisation 77−35578
recoil implantation profile for thick film 79−1454
recoil implantation theory 80−103378
recoil mixing in high-fluence ion implantation 80−65095
remote ion beam position measurement from random beam modulation 79−30606
research appls. and new fields *(German)* 77−76439
research at Central Physical Research Institute in Hungary *(Hungarian)* 77−51395
review, ion implantation, problems and perspectives 78−75687
RF heavy ion source 80−32561
ruby, implantation temperature meas. using impurity luminesc. 79−52012
sample contamination, by sputtering, during ion implantation 80−54274
sapphire, 15-keV ion bombard., chem. implantation, isotopic trapping effects and induced hygroscopicity 77−59030
scanning, electrostatic and mechanical, high current dosimetry techniques 80−32528
scanning systems, electrostatic 80−31939
Schottky barrier height control using knock-on effect 77−76919
Schottky diodes with deep acceptor impurities, inverse square capacitance curve, theory 80−2468
secondary particle collection in ion implantation dose measurement 78−67731
semiconductor, distrib. of implemented ions near arbitrarily shaped mask edges 77−31689
semiconductor, indirect doping 80−10568
semiconductor, ion implanted, laser annealing 79−69124
semiconductor, ion implanted, ruby laser pulse effects 79−69125
semiconductor, laser annealing *(Japanese)* 80−19821
semiconductor, laser induced struct. changes related to pulse shape 79−69123
semiconductor, radiation defect form. in presence of force fields 79−51126
semiconductor, surface, effects of ion sputtering, ion implantation 78−88395
semiconductor annealing, pulsed laser and electron beam heating comparison 80−92547
semiconductor counter for neutron detection 80−69030
semiconductor device fabrication appl. 78−87692
semiconductor device processing 80−34031
semiconductor devices, ion implantation with controlled nonuniformity 80−100261
semiconductor devices, shallow doping via ion implantation 78−14371
semiconductor doping, dose measurement 78−2150
semiconductor doping by nuclear transmutation method *(German)* 78−95066
semiconductor epitaxial regrowth, ion implantation induced defects, annealing 80−24479
semiconductor epitaxial regrowth, laser annealing dynamics 80−92548
semiconductor junction, ion implanted, elec. props. correl. with n^+ region microstructure 77−76916
semiconductor layer, implanted, effectiveness of annealing by millisecond laser pulses 78−55885
semiconductor materials preparation, late 1970s innovations 80−6666
semiconductor microstructure fabrication, ion channeling effects 80−70230
semiconductor processing, survey 77−7750
semiconductor structure defect exposure in SEM 79−23507
semiconductor thin films, ion implanted, optical and luminesc. props. 80−60699
semiconductors, cryst. defects induced by radiation, review 79−55776
semiconductors, ion implanted, laser annealing 80−65023
semiconductors, ion-implanted, laser pulse annealing, TEM and channelling study 80−100264
semiconductors, laser annealing after ion implantation, temp. distrib. 80−54265
semiconductors, laser beam annealing of ion implanted layers 80−24469
semiconductors, laser processing, bibliography 79−74028
semiconductors, radiation damage studies on implanted Te, Sb and Sn by Mossbauer spectroscopy 78−2176
semiconductors, recent progress 79−14831
series III high current industrial ion implanter, performance 80−31941
shadow mask etching for ion implantation 78−6086
n-Si:B, ion implanted, rapid identification of faulted loops 79−19254
Si:O, ion implantation, SiO_2 layer form., crystallisation, structural props. rel. to annealing 78−34724
Si:P^+, ion-implanted, annealing characts., X-ray diffr. exam. 78−14372
Si, ion implanted by high energy C ions structural and optical props. 80−107292
solar cells, ion implantation and annealing technology 80−93996
solid, depth profiling of ^3He ion implantation 78−59830
solid ion source by electron bombardment *(Japanese)* 78−78035
solid state studies with Van de Graaff tandem *(French)* 79−4339
SOS, gettering effect by O implantation, Hall and Rutherford backscattering meas. 79−65103
SOS films, cryst. quality improvement by Si ion channelling, annealing 80−44222
SOS wafer for beam profile monitoring in high-current ion implantation systems 80−13182
sources, arc-discharge-type, cathode lifetime and stability problems 80−32558
sputtering process study on Au, Al, Si targets, Rutherford backscatt. technique 77−8703
state of art, review *(Italian)* 78−59829

ion implantation continued
steel, austenitic, annealed, Ni ion bombardment, swelling temp. depend. effect of He implantation 80−29080
steel, austenitic, Cr-Ni, ion-implanted N, chem. state study by AES and XPS 80−79825
steel, austenitic, gas implantation effects, fusion reactor first wall damage simulation 80−29079
steel, austenitic stainless, Cr-Ni (20, 25 wt.%), Nb stabilized, oxidation behaviour in CO_2, surface ion implantation effect 80−71791
steel, austenitic stainless, He implanted 1.4970, high temp. fracture 77−86186
steel, austenitic stainless, He role in neutron induced microstruct. evolution 80−29064
steel, bearing, M50, localised corrosion resistance, improvement by ion implantation 80−16602
steel, Cr or Ni ion implanted, corrosion behaviour 80−11840
steel, fatigue life enhancement by ion implantation 79−1910
steel, low C, type 38NCD4, fatigue life improvement by N ion implantation, dose depend. 80−76328
steel, mild, conc. profile of implanted Ni and Cr 77−81339
steel, mild, implantation of Cu(Cr), annealing and rolling behaviour of conc. profiles 78−75684
steel, mild, surface hardness improvement by dynamic recoil implantation 80−61008
steel, stainless, 304, D trapping in fusion reactor materials, temp. dependence 80−37577
steel, stainless, 304, void form., effect of sequential and simultaneous He implantation 78−71719
steel, stainless, 321 and 304, D implanted, thermal desorption and bombardment induced release 78−95072
steel, stainless, D_2^+ diffusion and permeation, ion beam meas. 80−59492
steel, stainless, D implanted, thermal desorption 78−71750
steel, stainless, deuteron trapping model, of gas sputtering 80−49398
steel, stainless, diffusion of Cs study using ion beams 77−20125
steel, stainless, Fe-Cr-Al (15, 4 wt.%) Fecralloy, oxidation behaviour, Al and Y surface ion implantation effect 80−71790
steel, stainless, He induced blistering, during simultaneous sputtering 79−1808
steel, stainless, implantation of He ions, TEM exam. of He gas bubble lattice 79−46726
steel, stainless, liner for TFR 400, D, O, and limiter material spatial and depth implantation distrib. 80−18648
steel, stainless, low energy D implanted, microstruct. 78−95073
steel, stainless, surface implantation of Y and Ce, effect on oxidation resistance at high temp. 77−8977
steel, stainless, type 304, physicomechanical and wear props., influence of ion implantation and overlay coatings 80−40603
steel, stainless, type 430, Ni^+-implanted, struct., comp. and electrochem. anal. of surface alloy 80−16603
steel, stainless 316, ion implanation produced crystalline phase transitions 80−7558
steel, stainless type 304, ion bombarded, He effects 80−29076
steel, unlubricated sliding wear, effect of N ion implantation 79−74261
steel surface hardening, ion-carbo-nitriding in CO-N_2-H_2 gas mixtures, expt. *(Japanese)* 80−71670
steels, N-implanted, surface hardness and abrasive wear resist. 80−50746
superconductivity applications 78−52134
surface alloys, metastable, prod. by ion implantation, empirical rules for substitutionality 79−14832
surface coating technology, conference, London (1978) 79−83358
surface modification for tribology, corrosion, catalysis, chem. synthesis and amorphous metals studies, review 77−43236
surface props. of metals and alloys anal. 77−68989
surface treatment process in production engineering 80−34028
surface-ion impact, luminesc. accompanied by ion implantation 80−60683
surfaces, optical examination and monitoring, review 79−67375
swelling during self-ion bombardment, effect of implanted interstitials 78−10099
target assembly, ultra high vacuum, for charged particle irradiations in the materials research field 78−83841
Teflon FEP, N implanted, TSC spectra 80−88912
thin films, ion-bombarded, simple model of dose depend. of resist. 79−42669
thin specimens, temp. control for mech. meas. under light ion irrad. 78−86278
Tokamaks, ion beam anal. of surface modifications, review 79−46457
transition metal carbides, influence of implanted ions on supercond. transition temp. 77−28276
transition metals, implantation of He^+, range profiles and thermal release 80−39138
transition metals, influence of implanted ions on supercond. transition temp. 77−28276
UH vacuum sample chamber for combined ion implantation and ion beam anal. 77−4970
V, polycrystalline, 20 keV protons penetration depth, ultrasonic meas. technique 78−30677
vacancy induced hyperfine interaction detected by γ-ray PAD 77−43913
vacuum technique problems, with modern semiconductor processes *(German)* 80−86330
vapour deposition with simultaneous ion implantation, gas impurity distrib. 79−69146
very-low-dose ion implantation by scatt. attenuation 79−77617
X-ray emission analysis in TEM, implanted ion detection 78−51575
X-ray standing wave field excitation, meas. apparatus, appls. 77−15285
$(YSmEuCa)_3(FeGe)_5O_{12}$, garnet film, ion implanted, bubble domain props. 78−88152
Si:P, sheet resistance of Gaussian n-type ion-implanted layers 79−87103
Ag film, He^+ ion bombardment, radiation damage, ion entrapment, gas release and bubble formation 78−30679
Ag, implanted Li atoms, depth profiles and sputtering anal. by optical spectra 77−35579
Ag, recoil implanted ^{111}In impurities, interaction with radiation damage, TDPAC meas. 79−11362
Ag, trapping of Cd^+ injected at various temp. 77−76436
Ag:He, implanted films, solid solutions radiation induced polymorphism 79−86810
Ag-Fe, dil., ion implanted, phase comp., Mossbauer study 80−7244
Ag-Fe, implanted, Mossbauer conversion electrons spectroscopy, rel. to dose and annealing temp. 78−52397

ion implantation continued
AgCl, colloid centres by heavy ion implantation 78−63780
AgCl, defects induced by energetic ion implantation 78−17518
Al, ^{83m}Kr implantation, low-temp. on-line Mossbauer meas. 78−35071
Al, 20 keV He^+ implantation, gas re-emission, critical dose, temp. effects 77−35596
Al and SaP 930, 300 keV He irrad., blistering, flaking, gas re-emission 77−35601
Al, corrosion, general and pitting, Mo and Ar ion implantation effects 80−71794
Al, defect structures depend. on Ca and Ga implanted species 80−59494
Al film, implanted at low temp. by H or D, critical temp. enhancement *(French)* 77−8237
Al film, Pb^+ implanted, ion scatt. erosion rate, Rutherford backscatt. 79−74038
Al film, struct. and props., effect of ion implantation 79−77936
Al films, resistance changes due to bombardment by N, C, or Ar ions 80−103670
Al granular films, self-ion implantation, supercond. transition temp. enhancement 80−103774
Al, He implanted surface deform., integrated lateral stress 77−31697
Al, heavy ion ranges, 120 keV Pb ions backscatt. obs. 80−19855
Al, hyperfine interactions of implanted Fe, conversion electron Mossbauer spectroscopy 78−52391
Al, implanted Li atoms, depth profiles and sputtering anal. by optical spectra 77−35579
Al, implanted Xe behaviour during anodic oxidation 80−71800
Al, ion-implanted, dechannelling by dislocations, backscatt. expts. 79−7642
Al, physicomechanical and wear props., influence of ion implantation and overlay coatings 80−40603
Al, polycrystalline, high dose implanted with Cu and Pb, doping profile after laser pulse irradiation 80−88194
Al, polycrystalline film, trapping of ^{3}He and ^{4}He ions at room temp. 80−84221
Al, radiation damage with radioactive probes, TDPAC meas. 77−24336
Al, ranges of ^{29}Si ions meas. by (p,γ) reson. broadening, 20-100 keV 77−69023
Al, ranges of implanted 10-30 keV D^+ 78−83858
Al, sacrificial anode dissolution, Hg effect study using ion implantation 79−39016
Al, single crystal, $^{18}O^+$ ion implantation in channelling directions, expt. conditions and range profile obs. 80−65022
Al single crystal, $^{18}O^+$ ions implantation in channelling directions, stopping power meas. from max. range 80−65078
Al:^{12}B, relax. mechanism for polarised implant 78−87693
Al:Fe(Cu), CESR, effect of ion implantation 77−20701
Al:Ga, pulsed electron-beam annealing, lattice site location improvement 80−107303
Al:Sb(Zn), ion implanted electron beam annealing, ion backscatt. and TEM meas. 80−59500
Al:Xe film, radiation-enhanced Xe outdiffusion, Rutherford backscatt. 77−76609
Al-^{57}Co, implanted, Mossbauer effect obs. of annealing 80−39126
Al-C(Si)(Ge) film, ion-implanted, enhancement of supercond. transition temp. 77−32103
Al-Cu, implanted metal system, Cu redistrib. after laser irrad. 79−69163
Al-Dy, dil., ion implanted, crystal hyperfine field interaction, Mossbauer spectroscopy study 80−44968
Al-Er, dil., lattice location of ^{169}Er ions after implantation, Mossbauer effect of ^{169}Tm 78−39460
Al-Fe, dil., Mossbauer spectra of implanted ^{57}Fe, ageing behaviour 80−7233
Al-Sb, ion-implanted, precipitation form. and evolution TEM obs. 79−55766
Al-SiO_2-Si structs., implanted B^+ ions, high-freq. CV characts. *(Russian)* 78−80056
Al-SiO_2-Si:B ions, annealing effect on energy spectrum of radiation defects *(Russian)* 78−88488
Al-Si(Ge) film, ion-implanted, percolation and superconductivity 78−26982
Al-Zn-Mg-Cu (5.6, 2.5, 1.6 wt.%), corrosion, general and pitting, Mo and Ar ion implantation effects 80−71794
AlAs-GaAs, strip heterolaser, O^+ implantation optimisation, relative threshold current density *(Russian)* 78−1230
AlAs-GaAs stripe heterojunction laser, O^+ implantation effect on threshold characts. 79−41383
$Al_xGa_{1-x}As$, solid soln., synthesis by ion implantation Al^+ ions 78−38741
$Al_xGa_{1-x}As$:N, ion implantation, in situ annealing photoluminesc. obs. 80−10567
$Al_xGa_{1-x}As:N^+$, (x=0.58), laser annealing of optically active impurities, photolum. charact. 80−20682
AlN film on Si and Ge, growth, struct. and props. 77−55468
Al_2O_3, amorphous, range of ^{29}Si meas. by (p,γ) reson. broadening 77−69023
Al_2O_3, anodic film, trapping of ^{3}He and ^{4}He ions at room temp. 80−84221
Al_2O_3, defect microstructure due to ion bombardment, TEM study 80−34100
α-Al_2O_3, ion bombard., vol. expansion, annealing compaction, surface props. 78−67748
Al_2O_3, ion implantation for radiation damage studies 77−80530
alloy, dil. metastable, produced by ion implantation, lattice location of impurities 79−51132
Au, conc. distribs. of N^+ and N_2^+ beams of 200 keV/atom and 400 keV/atom 77−80529
Au, damage by ion implantation, spike threshold, TEM 79−90705
Au, effect on dielec. function, ellipsometry, 1.8-5.5 eV 78−6697
Au lattice location in Zn, gamma-spectral study 80−80227
Au-Fe, dil., ion implanted, phase comp., Mossbauer study 80−7244
Au-Fe ion implanted alloy, Mossbauer conversion electron scatt. 80−88898
Au-Mo-Si multiple layer structure, bombarded with P ions, calc. of P ion profile in substrate *(Russian)* 79−55771
Au-ZnS electrolum. Schottky barrier diode, S^+-implanted, blue emission 80−76082
B, ionisation and beam prod. 78−843
B_4C, first-wall coating for Tokamak, H retention and release 80−18620

ion implantation continued
BP:Zn(Se)(Cd), epitaxial layers, ion implantation, defects and lattic locations, channelling obs. 80−88179
$BaTiO_3$, controlled surface layers 78−48120
Be, blistering model, correlation between blister diameter and skin thickness 78−95067
Be dilute metastable alloy formation by ion implantation 80−15130
Be, implanted D and He, interaction and radiation enhanced oxidation 80−39120
Be, ion-implanted, impurity lattice location, channelling meas., Monte Carlo calc. 80−107291
Be, metastable alloy form. by ion implantation 79−82252
Be, metastable microalloys, equilib. form. criteria 78−30762
Be, surface hardening by B ion implantation 80−16604
Be:Ar, high resolution LMM Auger spectra 79−83066
Be:Li, ion-implanted, interstitial props. 79−37876
Be:Li, lattice location of implanted ^{8}Li, ion beam channelling study 79−37730
Be:Zn, lattice location of implanted Zn, ion-beam channelling meas. 77−68992
Be-Al-Fe, phase equilibria and diffusion using high energy ion beams 77−16542
BeO, anodic film, trapping of ^{3}He and ^{4}He ions at room temp. 80−84221
BeO film, 5 keV D implantation 80−100268
BeO, radiation induced detrapping of implanted D by ^{3}He and proton irrad. 80−32482
Bi films, resistance changes due to bombardment by N, C, or Ar ions 80−103670
Bi:N film, ion-implanted, struct., X-ray obs. 77−76692
$(BiTm)_3(FeGa)_5O_{12}$ ion implanted epitaxial garnet film, bubble domains, cryst. struct. disorder 80−93150
C, amorphous, ranges of implanted 10-30 keV D^+ 78−83858
C, by 6 to 15 keV D temp. depend. and depth profile 77−30664
C, D implanted, trapping of D, calibration for particle energy meas. in plasma boundary of Tokamaks 79−98983
CC Si:B, layer resist. depend. on implanting and annealing conditions *(German)* 80−96551
(CdHg)Te, ion implanted graded gap photodiodes 78−39192
$Cd_{0.2}Hg_{0.8}Te$, ion implantation doping for realisation of IR detectors, responsivity meas., ion range straggling 80−73452
$Cd_{0.2}Hg_{0.8}Te$:B, ion implanted, B range and range straggling 80−54273
$Cd_xHg_{1-x}Te$:Hg, p-n junction photovoltaic diode, appl. as IR detector 78−86330
CdS, ion implantation effect on luminesc. and cryst. damage 78−6758
CdS:Bi film, implantation and post annealing, superlinearity 78−52028
CdS:Li lattice, location of implanted Li atoms 80−6428
$CdS:Li^+(N^+)(Ne^+)(P^+)$, ion-implanted, edge emissions 77−77274
p-CdSe layers, ion implantation prep., elec. props. 79−51699
CdSe:Ar(N)(P), implanted, electroreflection obs. 80−40089
CdTe, Cl compensated detectors, polarisation suppression methods 77−61661
CdTe, H^+ ion implanted, optical waveguiding and electrooptic modulation 77−75679
CdTe, Yb^{3+} implantation, nonstoichiometry effect 77−15440
CdTe:As(P), ion implanted, elec. props. 80−65021
CdTe:H^+, ion-implanted, optical waveguiding and electrooptic modulation 77−7197
CdTe:Xe, anomalous Xe^+ ion implantation defect introduction, cathodolum. obs. 77−62554
Co implantation in Al, replacement collision probability at 4.2K 80−70237
Cr-SiO film, elec. props., effect of P^+ and Ar^+ implantation 79−11239
^{137}Cs $T_{1/2}$ determ. using new specific activity meas. 78−70714
Cu, corrosionprotection by ion implantation of Al and Cr 80−71789
Cu dilute metastable alloy formation by ion implantation 80−15130
Cu, doubly peaked He depth profile and blistering 78−10078
Cu films, resistance changes due to bombardment by N, C, or Ar ions 80−103670
Cu, He defect complexes and depth distribution, production theory 77−31686
Cu implantation of He ions, TEM exam. of He gas bubble lattice 79−46726
Cu, implanted with Cu^+, effect on cryst. orientation, Kr penetration meas. 80−88174
Cu, in Be, low-temp. solubility meas. by ion beams 77−62646
Cu, metastable alloy form. by ion implantation 79−82252
Cu, O^+ implantation along channelling directions, stopping power 77−69021
Cu, of Ag^+ and Ta^+, metastable alloy layer form. 78−71709
Cu, radiation damage with radioactive probes, TDPAC meas. 77−24336
Cu, SOMS, effect of impurities 80−50925
Cu single crystals Au ion implanted, pulsed electron beam irrad. 80−65019
Cu substrate, ion induced intermixing of Au or Ag surface film 80−15420
Cu, thermal oxidation, influence of ion implantation 78−64768
Cu, whiskers, Ar^+ ion implanted, X-ray study on lattice defects *(Japanese)* 79−99230
Cu:^{85}Kr 80−15145
Cu:B, two site occupation by implanted ^{12}B 78−6077
Cu:In, He, lattice defect struct., PAC meas. 80−70190
Cu:O single crystal, $^{18}O^+$ ion implantation in channelling directions, expt. conditions and range profile obs. 80−65022
Cu:O single crystal, $^{18}O^+$ ions implantation in channelling directions, stopping power meas. from max. range 80−65078
Cu-Ag, ion implantation as an ultrafast quenching technique for alloy production 77−55902
Cu-Ag(Ta) metastable alloy form. by ion implantation, combined TEM and ion channelling obs. 78−34530
Cu-Fe, dil., ion implanted, phase comp., Mossbauer study 80−7244
Cu-Fe, implanted, Mossbauer effect meas. 78−31134
Cu-Fe, implanted, Mossbauer study, rel. to annealing temp. 78−31135
Cu-In, dil., point defect trapping after ion implantation, DPAC meas. 78−43728
$CuInSe_2$, Zn implantation profiles by AES 77−31692
$Cu_2O:Cd^{2+}$ implanted, reson. Raman scatt., annealing effect 77−24838
Cu_2O:He(Na)(Cd), ion-implanted, resonance Raman studies of annealing 79−55765
D trapping in C target, model 80−65025

ion implantation continued
D(d,p)T spectroscopy for studying dynamic deuteron implant effects 79−51160
Er^{3+} implanted crystals, laser active media, nonradiative losses due to $^{4}I_{11/2}$-$^{4}I_{13/2}$ transition 79−31911
$ErT_{1.8}$, ^{3}He thermal desorption, comparison of aged and ^{4}He implanted samples 77−60102
Fe, ^{155}Tb sources produced by recoil implantation, ^{155}Gd Mossbauer transition 80−40009
Fe alloys, ion-implanted, depth profile and diffusion coeff. 80−54277
Fe, conc. distribs. of N^+ and N_2^+ beams of 200 keV/atom and 400 keV/atom 77−80529
Fe, corrosion behaviour in H_2SO_4 soln., ion implantation effect 80−71793
Fe, defect trapping of ion implanted D, depth profile, diffusion eqn. calcs. 80−2047
Fe dilute metastable alloy formation by ion implantation 80−15130
Fe film, implanted with C ions, HCP struct. formation, electron diffr. study *(Russian)* 79−82469
Fe, implantation of ^{197m}Hg, NMR of oriented nuclei 77−81020
Fe, metastable alloy form. by ion implantation 79−82252
Fe, Pb implantation effect on corrosion 79−39015
Fe, pure, corrosion behaviour, effect of Ta ion implantation 78−31559
Fe surface hardening, ion-carbo-nitriding in CO-N_2-H_2 gas mixtures, expt. *(Japanese)* 80−71670
Fe:^{129}Cs, implanted atom sites and hyperfine interactions, Mossbauer obs. 77−20753
Fe:^{129}Te, implanted atom sites, Mossbauer obs. 77−20756
Fe:^{129}Tm, implantation below 15K, in situ Mossbauer obs. 77−20754
Fe:^{129}Xe, implanted atom sites, NMR/ON 77−20723
Fe:^{129}Xe, implanted atom site populations, Mossbauer, NO and NMR/ON obs. 77−20755
Fe:^{133}Xe, heavy ion implantation, recovery, Mossbauer effect meas. 78−52393
Fe:^{169}Yb, lattice location and hyperfine field of implanted Yb, annealing temp. depend. 77−48100
Fe:^{198}Hg, combined lattice-location hyperfine-interaction expt. on implanted Hg 77−20752
Fe:^{82}Rb, implanted atom sites and hyperfine interactions, Mossbauer obs. 77−24765
Fe:Ar(K), implantation perturbed ang. distrib. 78−12969
Fe:F, lattice location of implanted F rel. to mag. hyperfine fields 77−59041
Fe:N, ion implanted foil, Mossbauer effect study, nitride form. 78−27149
Fe:Xe, isotope ion implantation control *(Flemish)* 78−79623
Fe:Y, ion implanted, deep D traps due to Y-vacancy complex 80−103372
Fe:Yb,^{18}O, interaction between implants 77−27921
Fe:Yb,O, interaction between impurities, perturbed ang. correlation meas. 77−1628
Fe-Cr surface alloy formed by ion implantation, anodic polarisation 78−48561
Fe-Cr-Al-Y, oxidation resistance, heat treatment and Al^+ ion implantation 80−71785
Fe-Cr-Ni-Al alloys, 25 keV ion implanted, metallic corrosion behaviour 79−52447
Fe-Cr(Ni) surface alloys, corrosion resistant, formation by ion implantation 79−28009
Fe-Cu-D, ion implanted, D trapping, 90-500K 80−15131
Fe-D, ion implanted, D trapping, 90-500K 80−15131
Fe-Dy, dil., implanted impurity hyperfine interaction 78−68417
Fe-Ni surface alloy formed by ion implantation, anodic polarisation 78−48562
Fe-P film, amorphous, ion implanted, struct. and domain struct. obs. 79−91272
α-Fe-Ti, ion implanted, microstruct., ion beam anal. and TEM study 80−107294
α-Fe-Ti, ion implanted, with C impurity, microstruct. of TiC precips. 80−66513
α-Fe-Ti, ion-implanted and annealed, microstruct. evolution 80−15132
Fe-Ti-D, ion implanted, D trapping, 90-500K 80−15131
Fe-Ti-Sb-C alloys, Sb trapping effect on temper embrittlement, ion beam study 78−92312
$Fe_{84}B_{16}$, metallic glass, ion implanted, UPS meas. 80−97411
^{57}Fe, hyperfine interactions in implanted metals, Mossbauer spectra 80−108141
^{57}Fe implantation in metals, electric hyperfine interactions, conversion electron Mossbauer meas. 80−7241
^{57}Fe, implanted in 3d, 4d and 5d metals, conversion electron Mossbauer spectra 77−12286
GaAS, proton isolation layer, lateral spread, elec. meas. 77−80520
(GaAl)As:Be DH stripe geometry lasers with current confinement structure 80−58592
(GaAl)As:Be implanted DH stripe geometry laser 80−64044
$Ga_{1-x}Al_xAs$, Se ion implantation *(French)* 77−68986
$Ga_{1-x}Al_xAs$, solid solution, synthesized by ion implantation, Raman scattering 79−42972
$Ga_{1-x}Al_xP$:N epitaxial films, ion implanted, cathodoluminescence study 80−60684
GaAs, 40 keV N^+ implantation, disorder profiles meas. by Rutherford backscatt. and channelling 80−54270
GaAs, active layers produced by high energy Se^{++} implantation, FET appls. 77−39605
GaAs, amorphous layer formation, IR spectra 78−95063
GaAs, amorphous layers, ion-implanted, low-temp. epitaxial regrowth 80−92790
GaAs and related cpds., conference, St. Louis, MO, USA (Sept. 1978) 80−8737
GaAs, carrier removal after H_1^+, H_2^+, and H_3^+ implantation 77−8115
GaAs, developments 77−59028
GaAs device isolation with deuteron bombardment 80−75248
GaAs devices, ion implantation damage, characterisation and appl. 80−92551
GaAs diffusion of ion implanted Be, SIMS and electrical profiling 78−47605
GaAs, disordered, ion implanted, elec. props. 78−84212
GaAs, dual implantation of C^+ and Ga^+, sheet resist. and Hall effect meas. 78−67728
GaAs, effects on density of deep levels, transient spectroscopy techniques 80−2046

ion implantation continued
n-GaAs, epitaxial, thermoelec. power, temp. depend. in mm wavelength range 79−23996
GaAs epitaxial layers, surface impurity gradients, Schottky barrier capacitance meas. 80−70782
GaAs epitaxial layers, doping profile degradation due to ion implantation 80−84194
GaAs, H ion bombard., carrier removal effects 80−92542
GaAs heavily doped n-type layers, formation by multiple ion implantation 80−59491
GaAs, high-energy ion layer implanted, layer thickness and refr. indices meas. 77−24837
GaAs, implantation disorder, flux and fluence depend., electrorefl. expts. 78−83833
GaAs, implantation of Si, Al, Hf, Ta into InP and GaAs, form. of protective oxide 78−79622
GaAs, implanted amorphous layer reordering 77−76435
GaAs, implanted p-n junction form. using laser pulse annealing 77−15946
GaAs, impurity gettering by ion implantation damage 77−11579
GaAs, influence of radiation damage on diffusion of implanted P and Kr atoms 78−6082
GaAs, ion beam induced annealing effects 80−59530
GaAs, ion implantation, review 78−6080
GaAs, ion implantation, range distrib. calc. 79−55760
GaAs, ion implantation, disordered layer physical props. 79−77624
GaAs, ion implantation damage, TEM exam. of variation with ion species and stoichiometry 78−59827
GaAs ion implantation parameter determ. by microwave contactless mobility meas. 78−10527
GaAs, ion implantation review 80−88184
GaAs, ion implantation with proximity cap annealing 80−24475
GaAs, ion implanted, capless annealed and dielectrically annealed, comparison of doping profiles 80−100278
GaAs, ion implanted, diffusion of Zn and Ag, profiles 80−24681
GaAs, ion implanted, effect of channelling on elec. props. 77−8114
GaAs, ion implanted, laser annealing 79−69124
GaAs, ion implanted, laser induced damage and recrystallisation by freq.-doubled Nd:YAG laser 79−73197
GaAs, ion implanted, laser induced recrystn. and damage, ion backscatt. and Raman scatt. obs. 80−49248
GaAs, ion implanted, laser annealing 80−107296
GaAs, ion implanted, mode-locked Nd:YAG laser annealing, recrystn. 80−19817
GaAs, ion implanted and laser-annealed, photoacoustic meas. 80−47117
GaAs, ion-implantation induced damage profile, ellipsometric study, annealing 80−103400
GaAs, ion-implanted, capless anneal, effect of As partial press. 80−29038
GaAs, ion-implanted, laser pulse annealing of amorphous surface layer, TEM 80−55436
GaAs, ion-implanted layers, close contact capless annealing, elec. props. 80−84192
GaAs, ion-implanted semiconductor, annealing, crystallisation, laser pulse energy depend. 78−34528
GaAs ion-irradiated layers switching conduction 78−34868
GaAs, laser reordering of implanted amorphous layers 78−43042
GaAs, laser-induced recrystallisation and damage of ion-implanted amorphous samples 79−47557
GaAs, lateral spread of implanted ions *(Japanese)* 79−4322
GaAs, lattice location of S and Mn implanted impurities, ion channelling and ion induced X-ray meas. 79−4332
GaAs, n-type layers, heavily doped, formation by multiple ion implantation 80−88187
GaAs, O^+ implantation, effect on LPE growth and elec. props. 80−24477
GaAs, O^+ implantation, energy levels, photoluminesc. 80−24838
GaAs oxide film form., ion implantation effects 80−100266
GaAs, p-n junction, Zn^+ implanted, residual radiation defect influence on characts. *(Russian)* 78−84287
GaAs, planar ion-implanted avalanche photodiodes 80−22431
GaAs planar p-n junction fabrication by Be ion implantation 78−43470
GaAs planar p-n junctions, Be ion implantation, fabrication and characts. 78−88022
GaAs, S and Se ion implantation 78−55884
GaAs semiinsulating materials, role of substrate in elec. props. 80−59488
GaAs, Si ion implantation and annealing, damage recovery, surface carrier profile 77−4119
GaAs solar cells, ion-implanted and laser-annealed 79−79390
GaAs, stripe geometry laser, optical losses of O^+ and B^+ implanted layers 77−79827
GaAs substrate, O implanted, LPE growth of GaAs film 78−2592
n-GaAs substrates, ion implanted, compensation 78−75680
GaAs, surface segregation of implanted alkali metals, photoemitter prep. and characts. *(French)* 78−60544
GaAs technology, 1978 state of art review 79−42089
GaAs, trends 80−39132
GaAs:$^{119}In^+$, Mossbauer study of resulting ^{119}Sn impurity-defect complex 80−59486
GaAs:$^{119}Sn^m$, Mossbauer spectra 80−29667
GaAs:^{11}B, physicochem. and resistivity meas. 80−24933
GaAs:Ar^+-metal, capacitor, capacitance-voltage and current-voltage meas. assuming intermediate dielec. layer 79−56316
GaAs:B(Ge)(Mg), impurity conc. profile by glow-discharge optical spectroscopy 80−49258
GaAs:Be, deep levels 80−29358
GaAs:Be, implantation and annealing, elec. props. 79−99540
GaAs:Be, implanted, determ. of Be concentration profiles by $^9Be(p,\alpha)$ reactions and SIMS anal. 79−4335
GaAs:Be, ion implanted, elec. profiling and optical activation expts. 77−89457
p-GaAs:Be, ion implanted, annealing characts., defect cond. profiling, electron diffr. obs. 79−4318
GaAs:Be, ion-implanted, photolum. spectra, effects of implantant depth distrib. 78−27293
GaAs:Be, ion-implanted, IR refl. and transmission meas. 80−34908
GaAs:Be,Se VPE layers, ion implanted, donor-acceptor pair radiative recomb. 79−91489
p-GaAs:C, ion implantation efficiency, elec. profile and compensation level meas. 77−27880

ion implantation continued
GaAs:Cr, Be, ion-implanted, semi-insulating, carrier mobility and conc. temp. depend. 77−76808
GaAs:Cr, Be^+ implantation, atomic conc. and defect density profiles after annealing 80−39123
GaAs:Cr, bulk and epitaxial, ion implanted, Cr conc., depth distrib. and diffusion coeff. 80−49243
GaAs:Cr, ion implanted, implantation damage profiles, laser annealing, ellipsometry study 80−79819
GaAs:Cr, low dose n-type ion implantation obs. 77−39608
GaAs:Cr, Mg, ion implanted, elec. meas. and optical activation studies 79−86806
GaAs:Cr, Se implantation, carrier conc. and mobility profiles depend. on dose and annealing temp. 77−47479
GaAs:Cr, Se layers, ion implanted, ohmic contact form., contact resist. meas. 79−91158
GaAs:Cr, semi-insulating, thermal conversion suppression by arsine-controlled capless-anneal, ion implantation 80−49245
GaAs:Cr, semi-insulating, Cr redistrib. during thermal annealing as function of encapsulant and implant fluence 80−84199
GaAs:Cr, semi-insulating, damage gettering of Cr during annealing of Cr and S implants 80−107304
GaAs:Cr, Te implantation, electron conc. and mobility profiles depend. on dose and annealing temp. 77−39607
GaAs:Cr, Zn(Se) shallow impurity implantation, elec. props. after annealing 80−24465
GaAs:Cr,Se, ion-implanted, semi-insulating effects of Cr redistrib. on elec. characts. 80−59982
GaAs:Cr,Zn, implanted, doping profiles after laser annealing, elec. props. 80−2058
GaAs:Cr pulsed electron beam induced recrystallisation and damage, amorphous layer formation 80−34052
GaAs:Ge, cryst. and epitaxial layers, ion-implanted, elec. props. 79−99542
GaAs:Ge, ion implanted, elec. props., comparison with Sn, Se and Te ion implanted samples 77−39879
GaAs:Ge, ion-implanted, photoluminesc., deep emission centres 80−34965
n-GaAs:Ge epitaxial layer, ion-implantation doped, anomalous behaviour of impurities 78−18669
n-GaAs:H(D), ion implanted, carrier removal, capacitance-voltage profiling 80−84195
GaAs:Mg ion implanted, photoluminesc. and annealing characts. 77−16361
GaAs:Mg(C)(Te)(Ge), ion implanted, laser annealing, ellipsometric and Hall meas. 79−73193
GaAs:n, ion implantation, hole conc. and mobility profile meas. 78−23082
GaAs:O, annealing effects, optical absorpt. and I-V characts. 80−29037
GaAs:O, deep traps, photocapacitance meas., complementary transition energy threshold determ. 79−19550
GaAs:O, optical characterisation of deep O implants 77−55294
n-GaAs:O carrier removal profiles meas. 78−56154
GaAs:P films, epitaxial growth from melt with components introduced by ion bombardment 77−21044
GaAs:P^+, defect form. on P^+ implantation at various temp., He^+ backscatt. obs. 78−59828
GaAs:P^+, implantation profiles, backscatt. meas. 80−70238
GaAs:P^+, ion-implanted, refr. index, IR reflection and transmission meas. 77−1671
GaAs:$p^+(N^+)$, struct. characts. of radiation damage produced by high energy ion implantation 79−4340
GaAs:S, implantation depth profiles of S^+ and S_2^+ using AES 79−55774
GaAs:S, ion implantation, expt. 77−11574
GaAs:S(Se), ion-implanted, evaluation by contactless mobility meas. 79−1448
GaAs:S(Si), ion-implanted, capless anneal in As controlled vapour 79−55767
GaAs:Se, fast diffusion of elevated temp. ion implantation, SIMS meas. 78−34527
GaAs:Se, Ga, dual species ion implantation, elec. characts. 80−103377
GaAs:Se, implantation and laser annealing 80−24476
GaAs:Se, implanted, annealing with O-free CVD Si_3N_4 encapsulant 78−83834
GaAs:Se, implanted, depth profile, SIMS obs. 78−30655
GaAs:Se, implanted, multilayered encapsulation using SiO_2:As and Si_3N_4 79−11715
GaAs:Se, ion implanted, surface state study from photoreflectance 79−91465
GaAs:Se, ion implanted, Cr redistrib. during annealing, SIMS anal. 80−10570
GaAs:Se, ion implanted, laser annealing 80−24482
GaAs:Se, low dose Se^+ ions implanted, DLTS study of laser annealing 80−80204
GaAs:Se ion implanted samples, Q-switched ruby laser annealing, improvement in elec. props. 80−100460
GaAs:Se ohmic contacts, pulsed electron beam annealing donor density, mobility 80−65678
GaAs:Se^+, Cs^+-SIMS and negative ion spectrometry 79−12882
GaAs:Se^+, implanted semi-insulating, pulsed electron and laser beam annealing effects on elec. characts. 79−73196
GaAs:Se(Si), ion-implanted, capless annealing by melt-controlled ambient technique 80−75251
GaAs:Se(Te), laser annealed, donor implanted, elec. props. 79−4556
GaAs:Si, encapsulated by SiO_2 and Si_3N_4, ion-implanted As profiles 79−4319
GaAs:Si, ion implantation, thermal annealing, Hall meas., SIMS atomic profile meas. 80−75243
GaAs:Si, ion implanted, photoluminesc. 79−69887
n-GaAs:Si, ion implanted and/or annealed, As vacancy form., photolum. line 77−27875
GaAs:Si, ion implanted effect of anneal ambient and occurrence of compensated regions in Si implants 77−51394
GaAs:Si, ion-implanted, depth distrib. profiles of Si ions 77−43230
GaAs:Si, ion-implanted, elec. props. 79−46686
GaAs:Si, ion-implanted, annealing with Nd:glass laser 79−73194
GaAs:Si, pulsed laser annealing of implanted layers, defect structure and Hall effect meas. 79−69118
GaAs:Si, transferred-electron devices by low-level ion implantation 80−92543

ion implantation continued
GaAs:Si(Se), ion implanted, laser annealing, microwave device appl. 79−69139
GaAs:Si(Sn), ion implanted, laser annealed, high doping levels 80−88181
GaAs:Si(s), generation of high mobility n layers, SIMS 80−103375
GaAs:Sn, implantation, annealing, impurity-defect struct., Mossbauer study 80−54269
GaAs:Sn, proton implantation and annealing behaviour *(Chinese)* 80−44224
GaAs:Te, amorphous, ion implanted layers, optical refl., 1.5-7.0 eV 79−8152
GaAs:Te, implanted and laser annealed, surface crystallinity, refl. and channelling meas. 79−95036
GaAs:Te, ion implanted, abrupt dopant profile 77−1143
GaAs:Te, ion implanted, laser annealing 79−73192
GaAs:Te, ion implanted, surface crystallinity and stoichiometry of laser annealed samples 79−73198
GaAs:Te, ion implanted, ohmic contacts produced by laser-annealing 79−73585
GaAs:Te, ion implanted optical transitions in modulated reflectivity spectrum 79−73972
GaAs:$Te^+(Se^+)(Sn^+)(Ge^+)$, ion implanted, laser annealing effect on elec. characts. 79−73195
GaAs:Te(Cd)(Mg)(B), ion implant depth distribs., AES and glow discharge optical spectroscopy meas. 80−65028
GaAs:V, ion implanted, luminesc., level splitting 80−97338
GaAs:Zn, implanted, furnace annealed, electrical, Rutherford backscattering and TEM meas. 80−100272
GaAs:Zn, implanted, hole conc. and mobility profiles meas. 78−23081
GaAs:Zn, implanted, laser annealing, elect., Rutherford backscattering and SEM meas. 80−100273
GaAs:Zn, ion implanted, TEM study after laser and furnace annealing 80−70234
GaAs:Zn, laser annealing of implanted layers 77−55296
p-GaAs:Zn, luminescent, ion doped MBE growth 80−44436
GaAs:Zn, pulsed laser annealing, expt. 78−34828
GaAs:Zn ion implanted ionic alloy, electrophysical props., annealing 80−39133
n-GaAs:Zn substrate, ion implantation as predeposition process 79−19268
GaAs:Zn(Se), recrystn. of implanted amorphous layers, TEM and channelling obs. 77−89459
GaAs-based mixed cryst. form. by ion beam synthesis, vibr. anal. 80−103376
GaAs-C, ion implanted, obs. of localised vibrational mode absorption, effects of annealing temp. 80−16068
GaAs-GaAlAs injection lasers, narrow-stripe proton-implanted, high bit-rate modulation 80−91824
GaAs-InP heterojunction laser output wavelength control 80−74384
GaAs-Si ion implanted, impurity profiles elec. props. 80−96550
$GaAs_{0.6}P_{0.4}$:Be, implanted annealing studies, elec. resist., Hall effect meas. 78−84213
$GaAs_{0.6}P_{0.4}$:N, isoelectronic tape by ion implantation and CO_2 laser annealing 80−24464
$GaAs_{0.6}P_{0.4}$:Zn, control of Zn diffusivity by multiple implantation 78−38877
$GaAs_{0.6}P_{0.4}$:$Zn^+(Ar^+)$, ion-implanted, thermal degradation of mechanical surface perfection and surface photolum. 77−77271
$GaAs_{1-x}P_x$, diffusion of implanted Zn ions, ion microbe analysis 78−95190
$GaAs_{1-x}P_x$, N implantation, characterisation by photolum. and channelling 80−54262
$GaAs_{1-x}P_x$, N^+ implantation photoluminesc. props. 77−68987
$GaAs_{1-x}P_x$, N^+ implantation, annealing props. 77−68988
$GaAs_{1-x}P_x$, solid soln., synthesis by ion implantation P^+ ions 78−38741
$GaAs_{1-x}P_x$, solid solution, synthesized by ion implantation, Raman scattering 79−42972
$GaAs_{1-x}P_x$:N, photolum. and electrolum. study of N isoelectronic traps 80−89061
$GaAs_{1-x}P_x$:Zn implanted, Zn diffusion 77−84993
$GaAs_{1-x}P_x$-SiO_2:N,Zn ion-implanted multiple layers, ion range distribs, secondary ion microprobe meas. 79−42129
GaInSb, Be ion implantation, device appl. 80−24478
GaN, photoluminesc. characts. for 35 implanted elements 77−24884
GaN:As(P), implanted single cryst. film, cathodolum. 78−60523
GaP, complex ^{119}Sn impurity-defect, Mossbauer study 80−75898
GaP, high-energy ion-implanted, layer thickness and refr. indices meas. 77−24837
GaP, ion implantation, range distrib. calc. 79−55760
GaP, ion implanted, mode-locked Nd:YAG laser annealing, recrystn. 80−19817
GaP, ion-implanted, form. and annealing of radiation damage 78−91363
GaP, ion-implanted, radiation damage, ellipsometry expts. 78−38735
GaP, radiation defect accumulation due to ion bombardment, optical absorpt. meas. 77−76438
GaP:Mg, ion implanted, elec. profiles 79−77628
GaP:N(Te), ion implanted at 40 keV, refl. spectra, 210-2000 nm, annealing *(Russian)* 78−80386
GaP:Sn(Sb), lattice location of implanted atoms, ion backscatt. and ion-induced X-ray obs. 77−84785
GaP:Zn, implanted, elec. profiling using anodic oxidation in N-methylacetamide 80−54690
GaP(As)(Sb), site selective doping by ion implantation of radioactive nuclei 80−34023
$(Gd,Bi)_3(Fe,Ga)_5O_{12}$ magneto-optic film, ion irrad. effect on storage props. 78−52324
Gd-Co-Mo alloy film, amorphous, mag. props., ion implantation damage effects 77−89991
GdTmGa garnet bubble film, ion implanted, pot. wells under charged wells 80−34717
$Gd_{0.9}YTm_{1.1}IGa_{0.44}Fe_{4.56}O_{12}$, ion implanted, ferromag. reson. meas. 78−68385
Ge, ^{57}Co implantation, Mossbauer spectra, dose depend. 79−82899
Ge, amorphous, growth rate of crystallisation, Raman spectroscopy study 80−44227
Ge, amorphous, laser reordering of implanted amorphous layer 79−19270
Ge, amorphous, O_2^+ ion implanted, influence on electrical and optical props. 77−89891
Ge amorphous film, effects of ion implantation on structure 78−55881
ion implantation continued
Ge, amorphous film, ion-implanted, regrowth 79−15043
Ge, crystal struct., influence of implanted O ions, electroreflection method 77−84783
Ge epitaxial film, ion implantation and electron beam anneal effects on carrier conc. 80−75255
Ge film, amorphous, O implantation effects on absorpt. edge and elec. cond. 77−39970
Ge, ion implanted, cond. and valence bands study by X-ray bremsstrahlung and photoelectron spectra 80−2360
Ge, ion-implanted amorphous, epitaxial regrowth on Ge 77−35835
Ge, ion-implanted amorphous layers, melting model for pulsing-laser annealing 79−56080
Ge, lattice disorder due to mol. and atomic ion implants 77−59056
Ge, low-energy heavy-ion implantation damage, spike effects 77−59055
Ge, polarisation of implanted ^{12}B 78−43653
Ge radiation detectors, high-purity, ion implanted n-type contact 77−54416
Ge, regrowth under laser irrad. 80−24481
Ge surface ion implanted far IR composite bolometers 79−30549
Ge:^{119m}Sn, impurity lattice dynamics, Mossbauer spectra, Debye temp. 80−84262
Ge:^{125}I(^{125}Te), implanted atom sites and quadrupole interaction, Mossbauer spectra 77−20758
Ge:^{57}Co, ion-implanted, Mossbauer study, annealing effects 80−7231
Ge:Al(Sb) film, amorphous, ion implantation, effect on cond. 78−83839
Ge:B, ion implantation and depletion at low temps., radiation and DC characts. 79−60392
Ge:B,P_2, contact prod. for semiconductor counters 79−97949
Ge:B(P), ion implanted, laser-induced regrowth 79−69130
Ge:Fe, amorphous film or ion-implanted, comparison of ^{57}Fe Mossbauer data 77−40159
Ge:Fe, implanted, Mossbauer spectra, conversion electron, temp. dependence 80−40025
Ge:Fe, recoil implantation Mossbauer expt. in presence of external mag. field 80−44981
Ge:inert gas, ion implantation, UV photoemission exam. 78−80457
Ge:O ion implanted, O localisation determ. 79−95040
Ge:Pb, ion implanted, lattice reordering, channelling and sheet resist. meas. 77−35577
Ge:Pb, ion implanted damaged layer, laser induced reorder 80−84201
Ge:Sb(As)(P), implantation doping, annealing and doping profile determ. 77−19972
Ge:Sn, ion implantation of radioactive ^{119}Sn 80−59495
Ge:Te, thermally assisted Xe-flash annealing, Rutherford backscatt. meas. 79−10881
Ge:Te^+, ion implanted, alignment of irrad. induced defects, TEM obs. 80−15168
Ge-Fe, laser annealing of implanted ^{57}Co sources, Mossbauer obs. 80−39139
GeO_2:Si, optical props. IR absorpt., UV reflection spectra 78−84619
$Ge_{1-x}Si_x$, with Si implanted ions, optical and photoelec. props. 79−24014
H isotopes, nuclear reaction anal. techniques, implantation studies, appls. 78−3422
H surface layers anal., influence of ion beam bombardment 79−37731
H trapping studies in fusion first wall materials 79−45407
He, uniform concentration implantation, simulated neutron irradiation damage 78−79648
He^+ implanted stainless steel, microstructure anal. 78−82516
^{4}He stopping power, 0.15 to 1 MeV, backscatt. determ. 80−88233
Hf, RF sputter deposition, ion bombardment and ion implanation 80−25564
HfN, RF sputter deposition, ion bombardment and ion implanation 80−25564
Hg electric field gradients at different Be lattice sites, gamma-spectral study 80−80224
Hg, quadrupole interactions in Zn, lattice location, gamma spectral study 80−80227
HgCdTe epitaxial material, ion implantation, junction form. 80−100260
$Hg_{0.79}Cd_{0.21}Te$, ion implanted, elec. props. 80−20184
$Hg_{1-x}Cd_xTe$, implanted with Hg, Al, damage and lattice location study 80−103381
^{129}I impurities implanted in semiconductors, isomer shift 80−20522
In, amorphization by ion implantation 78−52135
In, film, embedded with He particles, superconductor ion implantation study of inhomogeneities 78−52181
In film, He ion implantation effects on parallel crit. field, vortex state *(Russian)* 77−69459
In, film, vac. deposited, influence of ion bombardment during condensation 79−82483
In-Mn, dil., film, ion implanted, supercond, and mag. props. 77−15987
InAs:S(Mg), ion implanted, photocond., photo-EMF, and optical absorpt. spectra 80−70763
InAsSb, Be ion implantation, device appl. 80−24478
InGaAsP, injection heterojunction laser at 1.3-1.5 μm 79−89910
InGaAsP:Be ion-implanted avalanche photodiode, struct. and characts. 79−17487
$In_{1-x}Ga_xAs_xP_{1-y}$, p-n junction diodes, fabrication by Be ion implantation 79−47156
$In_{1-x}Ga_xAs_yP_{1-y}$:Be, ion implantation, hole conc. and mobility, junction depth 79−46685
$In_{0.3}Ga_{0.7}P$, N free and implanted, photoluminescence study 80−97322
InMn, ion implanted, influence of O and lattice disorder on Kondo resist. 79−38061
InP by S and Si for n-type doping 78−91351
InP, critical implantation temp. and annealing 79−90691
n-InP, high resistivity layers produced by Fe^+ implantation 78−47404
InP, implantation of Si, Al, Hf, Ta into InP and GaAs, form. of protective oxide 78−79622
InP, ion implantation damage compensation 77−84770
InP, ion implanted, anodic oxidation and elec. carrier conc. profiles 79−70185
InP, ion-implanted layers, close contact capless annealing, elec. props. 80−84192
InP, ion-implanted n- and p-type layers, characts. 78−6075
InP, n-type, p-type and high resist. layers production 78−6076
InP, n-type conductive regions produced by ion implantation 78−10067
InP p-n junction diodes, fabrication by Be ion implantation 79−47156
n-InP, p-n junction form. by Be ion implantation 80−29474
InP planar guarded avalanche diode prod. by ion implantation 79−95473

ion implantation continued
InP:Be, ion implantation, hole conc. and mobility, junction depth 79−46685
InP:S^+(Se^+), ion-implanted VPE layers, laser annealing, elec. and struct. anal. 79−73199
InP:Se, implantation and laser annealing 80−24476
InP:Si, implantation at high temp., elec. mobilities 79−99541
InP:Si, pulse electron annealing, carrier activation and mobility 80−15124
InP:Si(Mg), ion implantation and PH_3 ambient annealing under VPE conditions 79−42085
InP(Sb)(As), site selective doping by ion implantation of radioactive nuclei 80−34023
InSb, 300 keV Xe and Cd ions, dose rate and orientation dependence of radiation damage 77−89482
InSb, charact. and phys. props., review *(Japanese)* 80−39576
p-InSb, ion bombardment using 30-80 keV ions, isochronous annealing, elec. props. obs. 79−19295
InSb, ion implantation, anomalous radiation disordering 80−92553
InSb, ion implantation at elevated temps. 79−10870
InSb, ion implanted, efficient void form., TEM obs. 80−44237
InSb, ion implanted, ellipsometric study 80−60537
InSb, ion implanted layers, amorphisation, recrystallisation 78−63782
InSb, ion irrad., isothermal annealing effects 80−6424
InSb, morphological and structural changes due to ion bombardment 80−79843
InSb n^+-p and p^+-n photodectors fabrication by S and Be ion implantation 78−49906
InSb planar p-n junction fabrication by Be ion implantation, CCD chip appls. 77−89833
InSb:S, ion implanted, Hall effect meas. 77−20342
n-InSb:Zn, Zn diffusion out of implanted layers 79−10984
InSb:Zn p-n junctions, ion implantation and diffusion spreading, elec. and photoelec. props. 79−73573
KBr, heavy metal ion implantation, mol. unit form. 80−100267
KCl, heavy metal ion implantation, mol. unit form. 80−100267
K_2MX_6 (M=Sn, Re, Os, Ir, Pt; X=Cl, Br), heavy metal ion implantation, mol. unit form. 80−100267
Kr immobilisation by incorporation into metallic matrix by ion implantation and sputtering 80−27794
Kr ion implantation using Lublin separator 79−82251
Li, liquid, trapping efficiency for 20 keV tritium ions 77−50290
LiF, alkali ion implantation, migration, segregation, effect on optical props. 80−100269
LiF:In, optical absorption effects of ion implantation 80−70239
LiF:Mg, Ti, luminesc. increase by O implantation 78−64412
$LiNbO_3$, bulk, Ti-diffused integrated optical spectrum analysers, H implantation effects, pot. uses 80−43486
$LiNbO_3$, effects of He ion implantation on SAW propag. 80−75421
$LiNbO_3$, ion implanted, acoustic model of SAW delay lines *(French)* 78−55540
$LiNbO_3$, optical waveguides by ion implantation 80−106622
$LiNbO_3$, piezoelec. layer, non-cryst. characts. after ion implantation *(French)* 77−73117
$LiNbO_3$, waveguide and modulator form. by ion implantation 80−48469
$LiNbO_3$:He, ion implantation, optical waveguide form., refr. index changes 78−46762
$LiNbO_3$:He^+, ion implanted SAW guides, air-gap Si convolver data 78−42500
$LiNbO_3$:Ti single-mode optical waveguide, fabrication by sequential combination of Ti diffusion and masked ion-implantation 80−58785
Li_2O, Ar^+ implantation, depth distrib. by proton backscatt. 78−51577
Li_2O-Al_2O_3-SiO_2 glass, crystn. aggregation and migration of ion-implanted Ag 77−55240
Mg:H, solid soln. produced by ion implantation 78−67733
Mg-Ag, ion implanted, recovery stage characterisation by electron irrad. 80−107295
MgO, implanted K aggregates, TEM and optical spectra obs. 78−83838
MgO irradiated with Li^+ and K^+ ions, optical props. of metal aggregates 79−65907
MgO, local loss of stoichiometry caused by plastic deform., cathodoluminesc. spectra 78−35209
MgO:Li^+(Na^+), precipitation rel. to dislocations *(French)* 79−51163
Mo by K^+ and by Ba^+ ions, effect on secondary electron emission 79−91544
Mo cryst., $D_2{}^+$ implantation and radiation induced vacancies 80−65076
Mo, D and ^{3}He trapping and mutual replacement 80−59493
Mo, H and D trapping, enhancement due to He ion damage 77−31698
Mo, He implanted surface deform., integrated lateral stress 77−31697
Mo single crystal 78−52136
Mo single crystals, ion implanted, energy dependent channelling and backscatt. anal., $^4He^+$ ions, 1 to 2.8 MeV 79−4360
Mo:He, accumulation and distrib., monolayer conc. by sputtering quantitative anal. 80−49253
Mo:N film, implantation effect on supercond. and struct. transform. 77−4462
Mo:Xe, BCC, heavy ion implanted, vacancy recovery, Mossbauer spectroscopy 79−82896
Mo-Ca, ion implanted, range distrib. of Ca^+ ions, work function and AES obs. 78−27365
$MoSi_2$ refractory formation by As^+ ion beam bombardment 80−107286
n-Si, ion implantation causing surface defects, electroreflectance 79−19274
Na_2O-SiO_2 glass, ion bombardment, form. of cpds., IR spectrosc. exam. *(German)* 80−88173
Nb, blistering by He^+ bombardment at thermonuclear reactor energies 80−34104
Nb, depth distrib. meas. of He 77−30665
Nb, fabrication of supercond. weak links, electron beam lithography and ion implantation 78−47913
Nb film, supercond. props., Gd ion implantation effects 77−39986
Nb, He blistering, large swelling meas., gas press. model 80−88218
Nb, He depth profile meas. by nuclear reaction methods 79−14839
Nb, He implanted surface deform., integrated lateral stress 77−31697
Nb, He implanted tensile specimens, TEM 77−51398
Nb, He trapping, temp. depend. 77−31685
Nb, ion-implanted bridge with thick Pb banks, fabrication and characterisation of film parameters 80−100569
Nb layer, ion bombarded, supercond. props. and struct. 80−88671
Nb, radiation blistering by $^4He^+$ ions implanted sequentially at different energies, 3 to 500 keV 77−35594

ion implantation continued
Nb, replacement of implanted ^{3}He by subsequent ^{4}He bombardment, and vice versa, using ^{3}He(d, α) 79−4325
Nb single cryst., He ion implantation, depend. of blister deckeldicke and depth profiles on incidence angle 79−73226
Nb, stress distrib. from He ion irrad., vol. expansion, calcs. 77−35599
Nb, supercond. T_c control by N ion implantation 78−2606
Nb, superconducting bridges by electron beam lithography and ion implantation Josephson effect 80−20355
Nb thin films on Si substrate, intermixing, ion induced silicide formation 80−34101
Nb:He, implant saturation and annealing, effect on struct. and supercond. props. *(Russian)* 78−43538
Nb:Li, depth profiling using ^{7}Li(p,n) reaction 77−80534
Nb-Ge, supercond. A-15 phase, supercond. transition temp. after ion implantation 80−49972
Nb-N system, ion-implanted, supercond. crit. temp., effect of implantation conditions 78−19176
Nb-Sn(Ge), A-15 compound formation by ion implantation 78−51572
Nb-Zr (1 at.%), He irregular bubble growth by ion implanatation, TEM investig. 80−15164
$Nb_3Al_{0.2}Si_{0.8}$, A-15 alloy synthesis by ion implantation 78−80489
NbC, C implanted, channelling crit. angle and min. yields 78−47458
$NbC_{0.89}$, implantation or diffusion of C rel. to supercond. transition temp. 77−69442
NbC_x, supercond. transition temp., light element implantation effect 80−107951
Nb_2N, supercond. props. and structural phase transform. induced by C^+ and N^+ implantation 80−107942
$Nb_{40}Ni_{60}$, 3 MeV Ni^+ ion implantation, electron microscope exam. of ion damage 78−91365
$Nb_{40}Ni_{60}$, amorphous, produced by Ni^+ implantation, damage distrib. 80−107062
Nb_3Si epitaxial layers, ion implantation synthesis, supercond. transition temp. optimization 79−38218
Nb_3Si, metastable A-15 struct. synthesis by ion implantation, supercond. transition temp. 80−55319
Nb_3Sn, produced by Sn implantation, supercond. and Mossbauer effect 79−4612
Ne depth profiling with resonant ^{20}Ne 79−7621
Ni, ^{155}Tb sources produced by recoil implantation, ^{155}Gd Mossbauer transition 80−40009
Ni absorbers, deuteron distrib., depend. on direction of implantation *(German)* 77−4123
Ni, Ar ion implantation, $1S_{1/2}O$, $1S_{1/2}C$ and $2P_{3/2}Ni$ states, X-ray photoemission spectroscopy obs. 80−16149
Ni, blistering model, correlation between blister diameter and skin thickness 78−95067
Ni by K^+ and by Ba^+ ions, effect on secondary electron emission 79−91544
Ni, conc. distribs. of N^+ and $N_2{}^+$ beams of 200 keV/atom and 400 keV/atom 77−80529
Ni, defect cluster evolution, ion implanter adaption on 100 kV electron microscope 79−2888
Ni, deuteron diffusion obs. by D(d,p)T reaction *(German)* 77−59150
Ni dilute metastable alloy formation by ion implantation 80−15130
Ni film, effect of He ion implantation on domain struct., Lorentz electron microscopy 77−20654
Ni film, implanted with C ions, HCP struct. formation, electron diffr. study *(Russian)* 79−82469
Ni, He depth profile meas. by nuclear reaction methods 79−14839
Ni, implantation of He ions, TEM exam. of He gas bubble lattice 79−46726
Ni, implanted with Dy, annealing study by Rutherford backscatt., TEM, and total current spectroscopy 79−4343
Ni, ion implantation produced crystalline phase transitions 80−7558
Ni, ion-implanted and virgin, laser irrad. effect, epitaxial lattice regrowth 80−108306
Ni, lattice defect symmetry, time differential PAC meas. 78−15069
Ni, magnetic permeability, reversible, deform. and ion implantation effects 77−48013
Ni, metastable alloy form. by ion implantation 79−82252
Ni neutron and heavy ion damage correlation, dose rate and He injection effects 79−7629
Ni, ranges of implanted 10-30 keV D^+ 78−83858
Ni, self implantation damaged, crit. behaviour, perturbed ang. distrib. meas. anal. 80−60476
Ni, stress distrib, from He ion irrad., vol. expansion, calcs. 77−35599
Ni, trapping and release of inert gases, thermal evolution mass spectrometry 78−95077
Ni:^{111}In, ion implantation damage, DPAC obs. 77−59052
Ni:^{129}Te, implanted atom sites, Mossbauer obs. 77−20756
Ni:^{83}Rb, implanted atom sites and hyperfine interactions, Mossbauer obs. 77−24765
Ni:F, lattice location of implanted F rel. to mag. hyperfine fields 77−59041
Ni:F, mag. hyperfine field, anomalous temp. depend., PAC meas. 79−4754
Ni:In, He, lattice defect struct., PAC meas. 80−70190
Ni:K^+(Ba^+), ion implantation, effect on inelastic refl. and energy losses of fast primary electrons 78−55900
Ni:Kr gas trapping and release, thermal evolution mass spectrometric study 80−34026
Ni:O, single crystal, $^{18}O^+$ ion implantation in channelling directions, expt. conditions and range profile obs. 80−65022
Ni:O single crystal, $^{18}O^+$ ions implantation in channelling directions, stopping power meas. from max. range 80−65078
Ni-Cr films implanted with N ions, electric properties *(Russian)* 80−107927
Ni-Cu(Zn)(In), implantation damaged, crit. behaviour, perturbed ang. distrib. meas. anal. 80−60476
Ni-Dy, annealing behaviour of implantation damage, Dy outdiffusion, TEM obs. 77−77505
Ni-Dy, dil., implanted impurity hyperfine interaction 78−68417
Ni-Fe films, coercivity control for single-level masking bubble devices using surface modification and intermediate layers 79−51816
Ni-H, implanted film, resistivity and TDPAC meas. 78−39229
Ni-In, ion-implanted, impurity defect interaction and diffusion, Rutherford backscatter and TDPAC expts. 80−34039
Ni-P, amorphous, prod. by ion implantation 80−75257
Ni-P amorphous alloy prep. by ion implantation 78−22748

ion implantation continued
Ni-P film, amorphous, ion implanted, struct. and domain struct. obs. 79−91272
Ni-Si:As(Sb), implanted dopant redistrib. after silicide form., appl. to ohmic contacts 79−37729
Ni-Ta(Sn)(Er)(La) ion implanted surface alloys, solid solubility and radiation-induced disorder, backscatt. obs. 79−46692
NiO, diffusion of ion-implanted ^{18}O 80−107494
NiO:Li^+(Na^+), finely divided catalyst, low-temp. doping 79−51128
$NiSi_2$, layer, on Si, ion implantation damage, channelling obs. 78−30676
P ion implantation using Lublin separator 79−82251
PLZT ceramic, proton implanted, photoferroelectric effect for image storage and display devices 80−80315
PLZT ceramics photosensitivity enhancement by H- and He-ion implantation 80−96934
Pb, ion implanted, diffusion of Co, exam. by activation analysis 78−91488
$Pb_{0.97}Hg_{0.03}Te$ photovoltaic detector produced by Sb^+ ion implantation 80−82821
$Pb_{0.8}Sn_{0.2}Te$, of S^+ and In^+ 77−19973
$Pb_{0.8}Sn_{0.2}Te$:In, implanted thin epitaxial films, laser annealing 79−65104
PbTe film, ion-implantation-induced lattice defects 77−68985
PbTe IR diode, epitaxially grown and ion implanted, minority carrier lifetimes, efficiency 77−20411
PbTe, ion implantation induced damage and reson. levels 80−49255
PbTe, ion-implanted, doping profile evaluation by Hall effect and sheet resist. meas. 78−59831
Pd film, high dose Si^+ ion implantation, silicide phases, backscatter spectra 80−19820
Pd-Si:As(Sb), implanted dopant redistrib. after silicide form., appl. to ohmic contacts 79−37729
$PdAl_xH_y$ films, ion implantation prop., supercond. crit. temp. 79−87182
$PdIn_xH_y$ films, ion implantation prop., supercond. crit. temp. 79−87182
Pd_2Si layer, on Si, ion implantation damage, channelling obs. 78−30676
Pt, polycrystalline film, trapping of ^3He and ^4He ions at room temp. 80−84221
Pt, radiation damage with radioactive probes, TDPAC meas. 77−24336
Pt:^{181}Hf, interaction of implanted impurity with radiation induced lattice defects, TDPAC meas. 80−24494
Pt-Au, amorphous struct. produced by Au implantation, spinodal decomp. TEM obs. 78−31379
Pt-Si system, formation of Si enriched metastable cpds. using ion bombardment and post annealing 79−69143
Pt-Si:As(Sb), implanted dopant redistrib. after silicide form., appl. to ohmic contacts 79−37729
PtSi, Ar bubble formation after 20 to 160 keV sputtering, TEM and backscatt. spectrometry obs. 78−64435
α-quartz, reflection and surface polariton spectra, ion implantation effect *(Russian)* 79−47451
S:P, ion implanted, defect annealing 450-800°C, deep-level transient spectroscopy 79−47042
$(SN)_x$:Br, ion implantation effect on elec. props. 80−65026
Sb, combined with Si vacuum depositiion *(Japanese)* 78−88428
p-Si, $^{49}BF_2$ ionised mols. obtained by implantation of 78−31003
Si, ^{57}Co implantation, Mossbauer spectra, dose depend. 79−82899
Si, ^{75}As implanted, comparison of effects of pulsed ruby laser and pulsed electron beam annealing 79−69135
Si, 40 keV N^+ implantation, disorder profiles meas. by Rutherford backscatt. and channelling 80−54270
Si (100), self-ion implanted, laser annealing, channelling and TEM meas. 80−24466
Si, AES examination of Ar^+ ion retention during Ar sputtering 78−56552
Si, advanced material for space solar cell 80−94007
Si, amorphisation, energy depend. 77−7769
Si, amorphisation by ion implantation, homogeneous or heterogeneous nucleation 77−11578
Si, amorphisation due to irradiation with heavy ions 77−11606
Si, amorphised by ion implantation, EPR obs. of mag. ordering 79−24186
Si, amorphised by ion implant., localised states and cond., irrad. and heat treatment, doping 80−39529
Si, amorphous, asymmetrical profile of ion implanted P 79−46693
Si, amorphous, elec. props., ion implantation effects 80−79828
Si, amorphous, implanted, recrystn. induced by scanning CW laser, reaction rates, analytical model 80−66334
Si, amorphous, implanted, struct. transition under laser irrad. 79−50992
Si, amorphous, implanted ion trajectory and spatial distrib., Monte Carlo simulation 77−11611
Si amorphous, ion bombardment, controlled hydrogenation at low temps. 79−69119
Si amorphous, ion implantation, negative magnetoresist., localised mag. states 80−70731
Si, amorphous, ion implantation method, B and P ions 80−100274
Si, amorphous, ion implanted, laser annealing, reflectivity meas. 80−29039
Si, amorphous, laser epitaxial recrystallisation threshold energy 80−70571
Si, amorphous, Si implanted, substrate-orientation depend. of epitaxial regrowth rate 78−79900
Si, amorphous, sputtered, resist. control by ion implantation 80−100262
Si, amorphous, substrate orientation effect on regrowth by laser pulses, channeling, backscatter 80−84409
Si amorphous evaporated film, doping 79−51127
Si amorphous film, heavy doping by alkali ion implantation 80−2045
Si, amorphous film, ion-implanted, regrowth 79−15043
Si, amorphous films, ion implanted, elec. and photocond. props. 80−49717
Si amorphous layer, inhomogeneity formed by ion bombardment 77−69017
Si, amorphous layer, ion-implanted, spatially controlled cryst. regrowth by laser irradiation 78−55810
Si, amorphous layer crystn., effect of ^{16}O, ^{12}C, ^{14}N and inert gases 78−14623
Si, amorphous layer prod. by ion implantation, diffusion broadening, ESR study 80−92552
Si amorphous layers, on Si substrates, deposited and ion-implanted, laser-annealing behaviour 79−69373
Si, amorphous-implanted, laser induced struct. changes related to pulse shape 79−69123
Si, and SiO_2 on Si, ranges of implanted B^+ and B^{2+} 77−31687
Si, annealed, ion-implanted, in MOSFET, defect spatial distrib. 77−11973
Si, Ar and B implantation effects on cond. 77−80779
Si, Ar bombarded, blistering effects, SEM obs. 78−67745
Si, Ar(Xe) ion bombarded, sputtering yield energy and fluence depend. 79−78805
Si, As implantation *(Japanese)* 78−38738
Si, As implantation profiles, calc. comparison with expt. 78−38748
Si, As segregation, TEM obs. 77−63674
Si, B implanted, enhanced annealing behaviour, p-n junction formation 77−43233
Si, B implanted layers, damage obs. by X-ray double refl. 77−15463
Si, behaviour of B molecular ion implants 78−47405
Si, C ion implantation, IR absorpt. of synthesised β-SiC layer 78−56492
Si, CW laser annealing 80−92550
Si, carrier lifetime depth distrib. due to Ar ion implantation 80−70232
Si, channeled B and P implantation along ⟨111⟩ and ⟨110⟩ axes 78−22739
Si, channelled-ion implantation of group III and group IV ions 78−75682
Si, complex annealing behaviour of amorphous layers, TEM obs. of defect struct. 80−107299
Si, correlations between elastic energy transferred by implanted H ions and H trapping 78−14370
Si, cryst. and amorphous surface layers, ruby laser pulse effects 79−69920
Si, crystal defects in integrated circuits, review 78−88547
Si crystals, damage profiling after heavy ion implantation, MeV region 78−75686
Si, D implanted, trapping of D, calibration for particle energy meas. in plasma boundary of Tokamaks 79−98983
Si, damage struct. obs. using TEM and cross section specimens 80−107298
Si dechannelling of MeV He ions by twinned regions 78−75700
Si, deep amorphous layer implantation, laser effects, channelling diffr. study 80−25494
Si, defect struct., dislocation loops and elongated defects 80−107300
p-Si, delineation of n-type ion implant 79−77619
Si, device fabrication techniques 77−59029
Si devices, implantation damage, review 77−27899
Si, diffusion coefficient determ. from carrier conc. depth profile 80−107566
Si, diffusion of B,P and Sb, implantation damage effects 78−55988
Si, diffusion of Na, retarding action of radiation defects 77−1140
Si, diffusion of nitrogen during annealing, effects on ion implanted layers 77−24436
Si, disorder produced by high-dose implantation, channelling meas. 77−11573
Si, dopant segregation by pulsed-laser annealing, test case for thermal melting concept 80−24489
Si doping, atomic collision theory and range-energy relations 78−71753
Si, electrodes in HF electrolyte, implanted layer characterisation method 78−6078
Si, electronic defect levels in self-implanted CW laser annealed samples 79−87053
Si, energy depend. of amorphisation by ion implantation 78−2175
Si, epitaxial layers, cryst. quality improvement by ion implantation, backscatt. and TEM obs. 79−42397
Si, furnace preannealed (111) ion implanted, laser irrad. 80−65015
Si gates, polycrystalline, ion implantation into SiO_2 insulating layer avoidance 79−7619
Si, gettering effects *(Japanese)* 79−83356
Si, H_2^+ irrad., annihilation of free excitons, inelastic scatt. by SiH_4 mols., photolum. obs. 78−19561
Si, H^+ and H_2^+ ion implantation profiles determ. by SIMS 79−4334
Si, heavily damaged ion implanted (100) and (111), development of secondary defects 79−51166
Si, heavily implanted, lattice defects and strains after high temp. annealing 78−10077
Si, heavy ion induced disorder in surface and at shallow depths 80−59535
Si, heavy ion ranges, 120 keV Pb ions backscatt. obs. 80−19855
Si, high dose self-irrad., spatial correl. between primary and secondary defect profiles 80−59536
Si, high fluence deuteron bombard. and implantation 77−59033
Si, high-current high-dose implantation visible interf. effects 77−7743
Si, high-dose Ar implantation, X-ray topographic obs. of strains and damage 80−59496
Si, implantation induced strains, X-ray interferometry and topography 78−43039
Si, implanted amorphous, comparison of laser and thermal annealing 79−70084
Si, implanted and annealed, misfit dislocations removal by laser irrad. 79−83063
Si, implanted annealed layers, amorphised structure formation mechanism and crystallographic nature 80−29091
Si, implanted Bi distrib., planar oscills. effects, low angle He^+ backscatt. obs. 78−34534
Si, implanted crystal, laser induced annealing and diffusion behaviour 80−88202
Si implanted layers, interaction of defects and impurities stimulated by induced ionisation, ESR 80−11270
Si implanted layers, utilisation coefficient of impurities after laser annealing 77−76437
Si, implanted Li atoms, depth profiles and sputtering anal. by optical spectra 77−35579
Si, implanted semiconductors, laser annealing, review 80−107301
Si implanted with ^{31}P, ^{75}As, ^{11}B, amorphous layer reordering 78−14622
Si, implanted with low solubility dopants, laser annealing, TEM study 80−70233
Si, influence on oxidation induced stacking faults wafer orientation and ion implantation effects 78−10063
Si, interstitial generation and loop form. during annealing in oxidising medium 80−107225
Si, ion bombardment induced light emission, investig. of cpd. form. 77−48257
Si, ion bombardment induced defect distrib., IR and electron diffr. study 80−65074
Si ion damage critical gettering microstructures 78−6098
Si ion damage critical gettering doses, elec. characts. 78−10085

ion implantation continued
Si, ion implantation, channelled, through metal silicide film 80−70231
Si, ion implantation, channelling, alignment effects 80−88183
Si, ion implantation, high dose, solid phase epitaxial regrowth 80−103380
Si, ion implantation and pulsed laser annealing of group III and group V dopants, supersat. alloy form. 80−54267
Si, ion implantation by laser annealing, characterisation, solar cell applications 80−70247
Si, ion implantation damage, annealing, role of stresses 78−75679
Si, ion implantation of noble gases, high fluence retention 79−23627
Si, ion implantation-induced damage after Ar and P implantation, defect density and distrib. *(German)* 77−24337
Si ion implanted, amorphous to crystalline transition due to laser irrad. 80−103451
Si, ion implanted, annealing of heavy ion cascade damage, channelling meas. 80−89255
Si, ion implanted, annealing by ion beam heating 80−103382
Si, ion implanted, colour generation model 77−85868
Si, ion implanted, damage profiles, Rutherford backscattering 80−100733
Si, ion implanted, difference between ruby and Nd:YAG laser annealing 79−37723
Si, ion implanted, dopant depend. of oxidation rate 80−89384
Si, ion implanted, dynamic behaviour of pulsed-laser annealing, time depend. optical reflectance meas. 79−60393
Si, ion implanted, EPR line shape exam. of amorphous centres 79−28587
Si, ion implanted, electron beam annealing, surface struct. study using SEM 80−70235
Si, ion implanted, extent of annealed or melted regions as function of pulsed laser irrad. energy 79−74025
Si, ion implanted, laser annealing, periodic regrowth phenomena 78−67724
Si, ion implanted, laser annealing 79−69124
Si, ion implanted, laser annealing 79−69126
Si, ion implanted, laser annealed, elec. characterization 79−69137
Si, ion implanted, laser annealed, deep levels study 79−69457
Si, ion implanted, laser annealed, elec. props. and annealing kinetics 79−69508
Si, ion implanted, laser annealed microstructure 79−74027
Si, ion implanted, laser-annealed, theoretical anal. of thermal and mass transport 78−91364
Si, ion implanted, mode-locked Nd:YAG laser annealing, recrystn. 80−19817
Si, ion implanted, pulsed electron beam annealing 79−52254
Si, ion implanted, pulsed electron and laser beam annealing, comparison 79−52256
Si, ion implanted, pulsed ruby laser annealing 79−52255
Si, ion implanted, pulsed-laser annealed, Raman obs. 79−73189
Si, ion implanted, radiation defect production at different temps. 80−103398
Si, ion implanted, scanning electron beam annealing 80−6420
Si, ion implanted, self implanted, self annealing using high ion current density treatment 80−89254
Si, ion implanted, SiO_2 antireflection coating effect on CW laser annealing 80−49242
Si, ion implanted, spin density effect on laser annealing 80−11517
Si, ion implanted, structural and elec. profiles for double damage layers 78−2169
Si, ion implanted, voids, electron microscopy 78−67757
Si, ion implanted amorphous layers, free carrier plasma effects 77−73133
Si, ion implanted and laser annealed, characterisation 80−29043
Si, ion implanted layers, laser annealing 78−67732
Si ion implanted layers, pulsed electron beam annealing, TEM and particle backscatt. meas. 79−69134
Si ion implanted p-n junction, cryst. damage influence on elec. props. 78−56219
n-Si ion implanted surface potential barriers, $LiNbO_3$ SAW obs. 77−28234
Si, ion irradiated, room temp., depth distrib. of disorder 79−37745
Si, ion penetration, computer program 80−88185
Si, ion-implantation damage, annealing using pulsed-electron-beam 79−55768
Si, ion-implantation gettering effects, crit. microstructure 77−43229
Si, ion-implanted, annealing using scanning CW laser system 80−100265
Si, ion-implanted, cryst. to amorphous transform., ESR expts. and composite model 78−59825
Si, ion-implanted, defect struct., SEM, TEM and X-ray topography expts. 77−51399
Si, ion-implanted, disorders, nature and annealing behaviour, review 78−83836
Si, ion-implanted, effect of free-carrier absorpt. on annealing by pulsed laser 79−55757
n-Si, ion-implanted, elec. characts. after laser annealing 80−88562
Si, ion-implanted, impurity activation monitoring by SAW techniques 80−65020
Si, ion-implanted, lapping and staining techniques, junction depth determ. 80−29468
Si, ion-implanted, laser annealing at 1.06 μm, computer simulation 79−47556
Si, ion-implanted, laser annealing, appls. 79−73202
Si, ion-implanted, low-fluence, primary defects, transient capacitance spectroscopy 80−44238
Si, ion-implanted, period surface struct. in laser annealing, new expt. evidence 80−29836
Si, ion-implanted, pulsed-laser annealing, dynamic behaviour by optical reflectance meas. 79−69122
Si, ion-implanted, secondary defects development, three-stage model 78−87725
Si, ion-implanted, thermally oxidised, Rutherford backscatt. analysis 78−19910
Si, ion-implanted amorphous layers, melting model for pulsing-laser annealing 79−56080
Si ion-implanted dopant redistribution under laser annealing 80−70242
Si ion-implanted laser-annealed solar cells 80−93881
Si, ion-implanted layers, crystalline-to-amorphous transition, radiation defect prod. 78−87696
Si, ion-implanted layers, crystn. by ns laser pulses, TEM and RHEED 80−100421
ion implantation continued
Si, ion-implanted layers, epitaxial regrowth by laser beam and flash annealing 80−100420
Si, ion-implanted layers, impurity profile meas. after laser annealing 78−87702
Si, ion-implanted layers, residual defects after high temp. annealing 78−87695
Si, ion-implanted layers, total X-ray reflection investig. of clustering 78−6081
Si, ion-implanted polycrystalline film, defect build-up efficiency 80−2054
Si, ion-implanted semiconductor, annealing, crystallisation, laser pulse energy depend. 78−34528
Si ion-implanted solar cells, factors controlling efficiency 80−81451
Si ion-implanted structure annealing, defect behaviour obs. *(Russian)* 80−49281
Si, ion-implanted surface, profiling method 78−95075
Si, irrad. by 50 keV N^+ and P^+, depth distrib. of struct. defects, secondary emission obs. 78−2168
Si, irrad. with Cr^+, form. and annihilation, of defects, ESR investigation 79−90707
Si junction, As-diffused, ion implantation effects on leakage current 77−62555
Si, laser annealed, charge collection microscopy, carrier lifetime determ. 79−69136
Si laser annealed, nonequilibrium solubility and segregation 80−84296
Si, laser annealed ion implanted, elec. props., melting threshold 80−10969
Si, laser annealing after ion implantation, temp. distrib. 80−54265
Si, laser annealing transient optical reflectivity study, thresholds and kinetics 79−60390
a-Si, laser induced crystallisation mechanism, epitaxial regrowth 80−84962
Si, laser irradiated, positron annihilation crystal struct. imperfection monitoring 80−11506
Si, laser pulse train shaping for polycrystal recovery in self-ion implanted samples 79−47555
Si layer, neutron activation analysis, contamination and cross-contamination 78−83837
Si layer, on buried SiO_2 layer formed by high-dose, O ion implantation, TEM, AES, and XPS obs. 80−88172
Si layers, ion implanted, pulsed electron beam annealing, He^+ backscatt. and TEM study 79−51152
Si layers amorphized by molecular ions, laser annealing 80−103379
Si, Li ion implantation, depth distrib. variation after heat treatment 79−86814
Si, Li^+ implantation, characts. for thin film solar cell use *(Korean)* 77−51812
Si, lifetime in Ar^+ ion implant damage gettered, MOS voltage ramping 80−75247
Si, low-energy heavy-ion implantation damage, spike effects 77−59055
Si, MeV region O^+ implantation, induced luminesc. spectrum 78−6788
p-Si, minority carrier lifetime, effect of low dose ion implantation *(Japanese)* 80−54715
Si, N^+ and N_2^+ ions, photon emission studies of mol. synthesis, interstellar process simulation 77−70297
Si n-p junction vertical solar cells, Al-plated, photovoltaic effect variation with impurity conc. 79−100522
Si, n-type with ^{11}B implanted ions, high-temp. treatment effect on distrib. profile *(Russian)* 77−89454
Si, Ne ion implanted, oxidation expanded defects, effect on MOS parameters 78−19152
Si, new materials properties achievable by ion implantation doping and laser processing 79−69127
Si, off-axis channelling disorder anal. 77−24325
Si, on sapphire, epitaxial, crystalline quality improvement by ion implantation and furnace regrowth 80−88452
Si, oxide layer form. by O^+ ion implantation, Rutherford backscatt. and IR transmission obs. 79−51141
Si, oxide layer formation on O_2 ion implantation, phase comp. 77−90470
Si, P implanted, low temp. annealing characts. 77−11576
Si, P implanted low pressure CVD polycryst. films, elect. characts. 80−60114
Si, P^+ implantation, induced disorders. 80−6422
Si, p^+-n junction diodes, flow fluence S implanted unequal defect densities, dynathermal obs. 80−20293
Si, p-n junction, through oxide As implantation, Ar implantation gettering 78−14802
Si piezoresistive coefficient calc. and meas. *(German)* 80−39571
Si polycryst. film, ion-implanted, pulsed laser annealing 79−77612
Si polycrystalline solar cells, ion implantation method and results 78−63784
Si position-sensitive detector production 80−23247
Si, postimplantation damage profiles, backscatt. meas. 78−47402
Si, postimplantation defect annealing in samples heavily damaged by 140 keV Si^{2+} ions 77−11602
Si prod. applications 79−51124
Si, proton irradiated, IR absorption 79−33742
Si, radiation damage, SEM electron beam absorpt. meas. 78−75696
Si, radiation damage obs. by pendellosung topography 79−51125
Si, range parameters of protons implanted at 0.5 to 300 keV 80−44242
Si, recrystallised amorphous layer, self-ion irradiated, defect structures, TEM obs. 78−75688
Si, regrowth under laser irrad. 80−24481
Si, scanning CW and pulsed laser annealing 80−92549
Si Schottky barrier metallisation characteristics 77−76922
n-Si, selective anodic oxidation after P implantation *(German)* 79−52411
Si, self implanted, and additional impurity implanted laser induced recrystn., threshold power density 79−69131
Si, self-implanted, ⟨100⟩ and ⟨111⟩, crystallised layers by laser annealing, struct. 78−47644
Si, self-implanted layer, grain size, laser irrad. energy density depend. 78−72012
Si, self-ion implanted, amorphous to polycrystalline transition induced by laser beam 77−84771
Si, Si_3N_4 film formation by N ion implantation 79−90692
Si, single crystal, depth profile of radiation damage using lattice deform. study *(German)* 77−39618
Si, single crystal solar cell manufacturing process, laser annealing of implanted area, energy saving 80−97791

ion implantation continued
Si, slip dislocation nucleation during laser annealing 80−84179
Si solar cell, effect of electrostatic drift field 77−24615
Si solar cell processing, pulsed laser techniques for annealing ion-implantation damage 80−81453
Si solar cells, fabrication using continuous or pulsed lasers *(French)* 80−61350
Si solar cells, high open circuit voltage, P implantation 80−89642
Si solar cells, implanted layers characteristics, laser irradiation effects 80−35692
Si solar cells, ion implanted, from EFG Si ribbons 80−30485
Si solar cells, ion implanted grating type 80−101102
Si solar cells, ion-implanted 80−81452
Si solar cells, ion-implanted, expt. study of efficiency controlling factor 80−93997
Si solar cells, low cost processes for fabrication 80−94013
Si, standard for TEM, EELS 80−99017
Si, strain meas. by Pendellosung effect after P ion bombard. 78−55773
Si substrate, implantation effects on hardening and Si_3N_4 film stress reduction 78−71748
Si substrate, ion induced intermixing of Pd or Pt film 80−15420
Si substrate thinness, device design, solar cell processing, empirical study of interaction 80−93995
Si surface, interaction of oxygen gas discharge plasma 78−83840
Si, surface, pulsed electron beam processing, doping, annealing 80−75254
Si, surface characterisation by Si-electrolyte interface impedance meas. 78−84291
Si, surface contamination during high dose ion implantation, AES obs. 79−70374
Si, thermal oxidation, high resolution Rutherford backscatt., implanted ions analysis 79−87911
Si thin film, polycryst., CVD, elec. props. 80−107934
Si wafer, colour-band generation during high dose ion implantation 79−1449
Si wafer, colour-banded, sheet resist. variation following high dose implantation at high dose rates 78−95074
Si wafer, ion implanted, electron beam annealing, computer simulation 80−96569
Si wafer, surface exam. of ion-implantation using SAW convolver 77−72897
Si wafer, thin surface layers, amorphous to cryst. transform., obs. technique 80−107288
Si, with Pb, channelling and RHEED anals. 78−30657
Si: As(Pb), high-dose ion implanted and annealed, implant redistribution 80−107309
Si:^{119m}Sn, impurity lattice dynamics, Mossbauer spectra, Debye temp. 80−84262
Si:^{119}Te(^{119}Sb), implanted atom site changes with time, Mossbauer obs. 77−20757
Si:^{11}B, amorphous, calc. of implanted-ion range and energy-deposition distrib. 77−7748
Si:$^{31}P^+$, implanted layers, characterisation by ellipsometry 79−90683
Si:^{57}Co, ion-implanted, Mossbauer study, annealing effects 80−7231
Si:^{57}Co(^{57}Fe), implanted, Mossbauer spectra, study of dose dependence 80−75900
Si:^{85}Kr, ion-implanted, impurity distrib. 80−15145
Si:Al(Sb) film, amorphous, ion implantation, effect on cond. 78−83839
Si:Ar, As, ion implanted, laser annealing, doping profiles, channelling 80−97506
Si:Ar, high resolution LMM Auger spectra 79−83066
Si:Ar, ion implant gettering of MOS capacitors using linear voltage ramp and N^+ backscattering 79−95502
Si:Ar, ion implanted, amorphous, epitaxial regrowth 79−10868
Si:Ar, ion-implanted, epitaxial regrowth by laser annealing, microstruct. 80−84404
Si:$Ar^+(Si^+)$. implantation effect on carrier lifetime, damage obs. by TEM 79−65493
Si:Ar(B), implantation doped, electroreflection spectra 79−51983
Si:Ar(Ne)(O)(N), ion-implanted, defect reverse annealing, 550-650°C 80−88875
n-Si:Ar(P), single cryst., positron annihilation parameters, energy-band struct. on surface in free-electron approx. 79−15555
Si:As, amorphous layers, laser induced As profile broadening 79−95045
Si:As, anomalous diffusion of As 79−14842
Si:As, anomalous tail generation, As ion channelling 80−49246
Si:As, As implantation damage and atom location, channelling meas. 77−59032
Si:As, CW CO_2-laser annealing, comparison with thermal annealing 80−84193
Si:As, CW laser annealing mechanism, annealed spot size, solid phase epitaxial regrowth 79−78798
Si:As, dislocation loops and etch pits, X-ray diffr. and TEM obs. 79−42068
Si:As, dual wavelength, laser ion implantation damage annealing 79−69117
Si:As, elec. activation of implanted As during low temp. anneal, Hall effect meas. 78−51571
Si:As, high current ion implanter system, architecture and control 80−31942
Si:As, high-dose implanted, irrad. time and subsequent heat treatment effects on laser annealing 80−29041
Si:As, implantation into polycryst. Si and diffusion into Si substrate 77−59025
Si:As, implanted, laser annealing reduction in defect conc. 77−62559
Si:As, implanted, residual defects after one- and two-step annealing 78−6083
Si:As, implanted, spatially varied activation during regrowth of amorphous layers, sheet resist. and backscatt. obs. 78−71749
Si:As, implanted, thermal diffusion of As 80−39352
Si:As, implanted As redistrib. during annealing in oxidising ambient, carrier distrib. meas. 79−19275
Si:As, implanted CW laser annealing, elec. props., cryst. struct. and limitations 80−39131
Si:As, implanted through SiO_2 films, elec. props., defect struct. 80−54264
Si:As, ion implantation system, high current, design of end station 80−34030
Si:As, ion implanted, amorphous-cryst. transition induced by multiple-pulsed ruby laser 79−90555
Si:As, ion implanted, annealing characts., elec. props. 77−19974
ion implantation continued
Si:As, ion implanted, anomaly of elec. activation by additional Ne irradiation 78−84211
Si:As, ion implanted, beam techniques 80−24474
Si:As, ion implanted, formation of As complexes 80−59511
Si:As, ion implanted, glow discharge optical spectroscopy 78−22755
Si:As, ion implanted, laser scanning apparatus for annealing 78−34526
Si:As, ion implanted, laser annealed, lattice defects, epitaxial regrowth 80−103334
Si:As, ion implanted, low temp. thermal annealing 80−96552
Si:As, ion implanted, pulsed ion beam annealing 80−103395
Si:As, ion implanted, pulsed laser annealing, partial solid-state regrowth 80−103591
Si:As, ion implanted, scanning-electron-beam annealing 79−60391
Si:As, ion implanted, two-step annealing 78−18664
Si:As, ion implanted, two-step annealing, TEM study 79−82249
Si:As, ion-implanted, CW IR laser annealing 80−34022
Si:As, ion-implanted, channelling anal. of CW Ar laser annealing 79−73186
Si:As, ion-implanted, laser annealing, channelling obs. of As cluster form. 79−69128
Si:As, ion-implanted, laser recrystallisation by freq.-doubled Nd:YAG laser 79−77613
Si:As, ion-implanted and post-annealed, dislocation loops, TEM obs. 77−84776
Si:As, ion-implanted layers, ellipsometric anal. of laser annealing 79−73190
Si:As, laser annealing, channelling, optical obs., and resist. meas. 79−1444
Si:As, laser annealing of implanted layers 77−55296
Si:As, MBE, ion implantation for n-type doping 80−15126
Si:As, MBE with simultaneous ion implant doping 80−66432
Si:As, scanning electron beam annealing, spreading resistance, junction depth 80−75267
Si:As, shallow junctions by high-dose implants 80−96694
Si:As, solid solubility of As determ. by ion implantation, CW laser annealing 80−6517
Si:As, substrate for epitaxial Si 78−6243
Si:As, time-resolved reflectivity during laser annealing 78−92086
Si:As,Sb, amorphous, damage depend. of epitaxial regrowth during annealing 78−47679
Si:As high-dose implanted single crysts., pulsed electron-beam annealing 80−103373
Si:As implanted emitters, oxidizing drive-in ambient deleterious effect 80−2044
Si:As ion implanted, laser induced diffusion modelling 80−24672
Si:As ion implanted layers, annealing by CO_2 laser, doping profile shift 80−84965
Si:As ion implanted shallow junction 80−70228
Si:As laser annealing, heat and mass transport model 80−92546
Si:As thermal diffusion retardation by inert gas ion implantation 79−77616
Si:As wafers, laser annealing, Rutherford backscatt., optical, and TEM obs. 79−1445
Si:As^+, annealing by scanning Ar ion laser, dislocation loop density comparison 78−47438
Si:As^+, implanted, CW laser annealing, electron-beam induced current 80−100709
Si:As^+ sheet resistivity rel. to isochronal annealing and defect structures 77−76443
Si:$As^+(P^+)$ ion implanted, laser annealed, correlation of struct. and elec. props 80−70855
Si:$As^+(P^+)(Sb^+)$, implantation damage removal by laser irrad. and its thermal stability, TEM study 79−74024
Si:As(B), heavy-doping effects and impurity segregation during high-press. oxidation 80−65014
Si:As(B), ion implanted, pulsed laser annealing appl. to device fabrication 79−73180
Si:As(B), ion-implanted, scanned laser and electron beam annealing 79−73182
Si:As(B)(N)(P), conc. profiles of ions and recoiled N after implantation through Si_3N_4 films 79−55764
Si:As(B)(P), ion-implanted polycrystalline films, laser annealing 79−73181
Si:As(P), ion implanted, TEM study after laser and furnace annealing 80−70234
Si:As(P)(Sb) film, implanted, elec. cond., sheet resist. as function of ion dose and temp. 79−78235
Si:As(Pb), ion-implanted, impurity redistrib. during laser irrad. 80−100280
Si:As(Sb), implanted, pulsed ruby-laser annealing, Rutherford backscatt., TEM and ion channelling study 79−86805
Si:As(Sb), ion implant lattice location after pulsed ruby laser annealing 79−73204
Si:As(Sb), ion implanted, lattice location of impurities after pulsed laser annealing 80−88196
Si:As(Sb), ion-implanted, CO_2 laser annealing 79−73183
Si:Au, autoradiographic detection of getter effect, Ar ion implantation 78−38739
Si:Au Ar ion implant gettering obs. by MOS and Rutherford backscatt. techniques 80−39119
Si:B, annealing mechanism of radiation change and dopants in pulsed laser irrad. ion implanted layers 79−46691
Si:B, anomalous B profiles prod. by BF_2 implantation 80−75252
Si:B, As, first and second order Raman scatt. by pair modes 79−65869
Si:B, conc. profile of implanted cryst., by $^{11}B(p,\alpha)$ chem. anal., annealing *(German)* 78−83843
Si:B, diffusion length, SEM-EBIC/Schottky diode 79−82605
Si:B, diffusion of As atoms from ion implanted layers, conc. profiles 77−43376
Si:B, diffusion of randomly implanted ions during high temp. processing 77−24439
Si:B, dislocation net form. during annealing 77−51385
Si:B, heavily doped, annealing characteristics obs., Ne^+ ions implantation for damage density control *(Japanese)* 78−18666
Si:B, heavily implanted wafers, secondary defect generation suppression by HCl oxidation 78−10069
Si:B, high conc. effects in ion implantation 80−75245
p-Si:B, high temp. treatment, effects on ion implanted impurity distrib. profile 78−79625

ion implantation continued
Si:B, implantation distribution determ. using ion bombardment 80−44230
Si:B, implantation energy, rel. to dose, Szabo-Bogancs effect 78−38740
Si:B, implanted, effectiveness of charged vacancies in diffusion 80−34239
Si:B, implanted, free carrier conc. and impurity location, Raman scatt. obs. 77−55295
Si:B, implanted, laser-annealed, lattice dilatation 79−46690
Si:B, implanted, oxidation induced precipitate defects, TEM 78−31556
Si:B, implanted, oxidation-induced stacking faults, EBIC and TEM expts. 78−39923
Si:B, implanted CW laser annealing, elec. props., cryst. struct. and limitations 80−39131
Si:B, implanted laser annealed, lattice strain, X-ray study 80−96554
Si:B, implemented laser annealed samples, unidirectional contraction 78−71747
Si:B, impurity range distrib. determ. by $^{10}B(n,\alpha)^{7}Li$ reaction 78−11585
Si:B, inhomogeneous surface layer, diffusion and implanted, X-ray rocking curves 80−6603
Si:B, interstitial Si atom formation by light ion bombardment 78−47406
Si:B, ion implantation, anal. of disordered regions in crystal with Promiss protonograph 80−19823
Si:B, ion implantation, channelling and random distrib. of B ions meas. 77−47473
Si:B, ion implantation using B_2O_3-B mixture, Auger spectra, channelling anal. 79−4317
Si:B, ion implanted, comparison of range and range straggling 77−55293
Si:B, ion implanted, depth and lateral profiles of B atoms, Monte Carlo simulation 77−55297
Si:B, ion implanted, ellipsometric study for low doses, cryst. damage parameter 79−65105
Si:B, ion implanted, laser annealing 78−34525
Si:B, ion implanted, laser and thermal annealing compared, TEM obs. 78−75681
Si:B, ion implanted, laser annealed, thermal annealing effect 79−73191
Si:B, ion implanted, laser annealed, IR and Raman spectra 79−73914
Si:B, ion implanted, laser annealed, Raman scatt., Fano interactions, lattice damage 79−78711
Si:B, ion implanted, localised defects, TEM study 78−87699
Si:B, ion implanted, radiation defect accumulation and annealing, X-ray diffr. obs. 79−37726
Si:B, ion implanted, SOS device struct., nonlinear impurity redistrib. 79−1625
Si:B, ion implanted, struct. of rod defects, TEM obs. 78−71744
Si:B, ion implanted, structure defects formation and behaviour under annealing in various ambients 80−65033
Si:B, ion-implantation doped, influence of radiation dose on diffusion processes 77−1141
Si:B, ion-implanted, annealing by incoherent light source 79−19267
Si:B, ion-implanted, dislocation climb, TEM obs. 78−6062
Si:B, ion-implanted, influence of US waves on charged particle channelling 79−23668
Si:B, ion-implanted, rod-like defects, TEM obs. 77−68975
n-Si:B, ion-implanted damage, positron annihilation and sheet resist. meas. 80−35003
Si:B, ionisation-assisted annealing 79−23628
Si:B, low noise avalanche photodiode fabrication by channelling implantation 79−35827
Si:B, P, first and second order Raman scatt. by pair modes 79−65869
Si:B, P, long range enhancement of B diffusivity by P diffusion 80−103386
Si:B, polycrystalline, depth profiles of implanted B atoms, meas. by secondary ion mass spec. *(Japanese)* 78−67734
Si:B, self-interstitials location by Rutherford backscatt. of channelled ions 80−2101
Si:B, sputtering influence on distrib. profile of ion-implanted impurities 79−42091
Si:B, TEM study of stacking fault form. and annealing 78−51566
Si:B,P, double implanted layer, n-p-n struct., single pulse laser annealing 80−49247
Si:B (0.2 wt.%) ion implanted, B atom displacement due to low temp. irrad. 80−88234
p-Si:B epitaxial layer, proton-implanted, annealing characts., carrier conc. profiles 77−32097
Si:B implanted wafers, ionis. assisted annealing and effects 80−100257
Si:B ion implanted, strain profiles from X-ray rocking curves 80−107290
Si:B ion implanted, X-ray topographical images at different absorption conditions 80−2052
Si:B ion implanted grating-type solar cells, var. of junction depth, collection efficiencies 80−93934
Si:B ion implanted layers, light refl. and transmission coeffs., computer program 80−66316
Si:B MOS structures, implanted laser beam irrad. effects on interface electrophys. props. 79−1627
Si:B radiation damage and minority carrier lifetime, SEM-EBIC obs. 80−96573
Si:B^+, ion implanted, lateral spread of B^+ ions through SiO_2 mask 79−51130
Si:B^+, TEM of lateral implantation effects near mask edges in wafers 79−37724
Si:BF_2^+, anomalous migration of F and electrical activity of B 78−34654
Si:BF_2^+, appl. in semicond. devices production 80−103383
Si:BF_2^+, ion implanted, arc annealing by flash lamp 80−44223
Si:BF_2^+, recrystallisation of implanted amorphous layers, F migration 79−55763
Si:BF_2^+ implanted, low-temp. annealing characts. 79−55759
Si:BF_2^+(Si^+,B^+), recrystallisation of implanted amorphous layers, elec. props. 79−55762
Si:B(Al), (P)(As)(In), ion implanted film, elec. prop. impurity depend. 80−24467
Si:B(BF_2), p^+-n junction form., ion implantation damage, leakage current 77−24334
Si:B(Be)(Li) ion implanted, channelling and random equivalent depth distrib. 80−100293
Si:B(P), ion implanted, polycryst. annealing characts. 77−24324
Si:B(P), ion implanted crystalline and amorphous laser annealing 80−97509
Si:B(P), ion implanted layers, carrier distrib. meas. precision 77−43603
ion implantation continued
Si:B(P), ion implanted processing parameters for diffusion redistribution 79−10871
Si:B(P) implanted layers as strain sensors 77−35098
Si:B(P)(As), 20-2800 keV ion implantation, obs. of X-rays produced 78−14367
Si:B(P)(As), impurity diffusion from implanted layer, influence of radiation damage 77−76621
Si:B(P)(As)(Sb), ion implanted, redistrib. of dopants by pulsed laser annealing 79−7620
Si:Be, ion implanted, correl. of atomic distrib. and implantation induced damage profiler 80−88199
Si:Bf_2^+ layers, ion-implanted, anomalous carrier tail generation mechanism 80−19819
Si:Bi, channelling obs. of pulsed Q-switched ruby laser annealing 80−59542
Si:Bi, ion-implanted, solid phase epitaxial growth during annealing, supersaturated solid soln. form. 80−103384
Si:C, disorder profiles by proton backscattering, proton bombardment annealing 78−47449
Si:C, H^+ and He^+ beam impact phemomena, damage annealing rates 78−47450
Si:C(O), photoluminescence spectra, radiation damage investig. 77−28620
Si:Co, high-temp. ion-implanted and diffused samples, Mossbauer spectra of ^{57}Co 79−51891
Si:Co, implanted, and annealed, localisation of Co atoms, Mossbauer obs. 80−39140
Si:Co, ion implanted, Co lattice location, channelling meas. 80−88201
Si:Cr, ion implanted, Cr conc., depth distrib. and diffusion coeff. 80−49243
n-Si:Cs, ion implanted, minority carrier lifetime and defect struct., annealing effect 78−6395
Si:Cu, segregation effects after laser pulse melting 79−1843
Si:Cu(Au), recoil implantation from thin surface films, backscatt. obs. 78−63783
Si:D, ion implanted, D depth distribs., SIMS meas. 80−54279
Si:D, ion implanted, struct. of impurity centre 79−7623
Si:Fe, B, Fe reaction with ion implanted B 79−77620
Si:Fe, implanted, annealing and stripping, Mossbauer expts. 80−39141
Si:Fe, implanted, Mossbauer spectra, conversion electron, temp. dependence 80−40025
Si:Fe, ion implanted, laser annealing studies using Mossbauer spectroscopy 80−79827
Si:Fe, laser annealing of implanted ^{57}Co sources, Mossbauer obs. 80−39139
Si:Fe, laser implantation, Mossbauer obs. 80−39125
n-Si:Fe 79−28312
Si:Fe(Cu)(Pt), implant redistrib. and enhanced solubility following laser irrad. 79−69129
Si:Ga, heavily damaged, channelling investigation of diffusion behaviour 79−37877
Si:Ga^+, impurity distrib. profiles using SIMS and Hall effect method 79−69152
Si:Ge, recryst. after implantation using different temp. and energy sequences 80−84196
Si:Ge, regrowth behaviour from backscatt. and channelling meas. 80−2300
Si:H, 50-250 keV H^+ irrad. damage distrib., $^4He^+$ channelling obs. 78−26587
Si:H, ion implanted Monte Carlo calcs. of profiles of H ions 78−55889
Si:H, ion-implanted, photoluminesc. spectrum 80−45129
Si:H, new IR absorpt. bands 79−87472
Si:He, B ion implantation 80−96559
Si:In, implanted, laser annealing 79−52050
Si:In, ion implanted, annealing behaviour, time differential PAC obs. 77−89455
p-Si:In, ion implanted, doping profiles from capacitance-voltage characts. 80−88203
Si:In(Sb), incorporation of implanted impurities during amorphous layer regrowth 79−55761
Si:K, ion implanted, influence of doping and annealing on carriers 78−38742
Si:Li, amorphous, elec. cond. and thermopower 79−73537
Si:Li, amorphous, interstitial doping by in-diffusion and implantation and elec. characterisation 78−26585
Si:Li(Na)(K)(F)(Cl), amorphous, implantation effects on elec. props. 80−49716
Si:Mn,Bi, standard, doubly implanted, Rutherford backscattering meas. at MeV energies, screening corrections 80−88204
Si:N, high energy ion implantation of buried insulating layers 80−88188
Si:N, interstitial Si atom formation by light ion bombardment 78−47406
Si:N, ion implantation, refractive index, IR spectra, ion range and straggling meas. 80−34020
Si:N, ion implanted, oxidation characts. 80−89385
Si:N, laser-annealed, Jahn-Teller distorted donor, EPR meas. 80−84642
Si:N, struct. defects formed by 50 keV N^+ irrad., depth distrib. 78−18688
Si:N wafers, Si_3N_4 layer growth by high dose implantation and annealing, elec. props. 80−70227
p-Si:N_2^+ implanted, anneal behaviours of lateral photovoltaic method 79−14825
Si:N(P), ion implanted, IR transmission and rel. spectra study 80−108244
Si:Na ion implanted, Hall effect temp. depend., electron surface density and mobility 80−11018
Si:Na(K)(Cs), amorphous, ion implanted, control of cond. 79−60835
Si:Ne, amorphous, implanted, cond. change 78−23097
Si:Ne ion implanted, channelling anal. of disorder struct., ^4He ions, 0.7 to 2.2 MeV 79−4321
Si:Ne(Ar)(Kr), amorphous, implanted and sputtered, epitaxial regrowth, influence of noble gas atoms 80−2289
Si:Ne(Ar)(Kr), ion implantation damage, annealing, comparative study 79−10867
Si:Ne(Kr), ion implanted, amorphous, epitaxial regrowth 79−10869
Si:O, comparision of depth profiling techniques 80−29048
Si:O, interstitial Si atom formation by light ion bombardment 78−47406
Si:O, ion-implanted between 2 and 20 MeV, range and range straggling 80−44241
Si:O, Xe, ion implanted, Xe retention, Rutherford backscatt., comparison with SiO_2+Xe 79−4320

ion implantation continued
Si:O(C), implant redistribution, annealing effects, SIMS meas. 80−96561
Si:P, amorphised by Ne^+ implantation, high fluence P implants, plasma region obs. 79−86807
Si:P, amorphous, CVD, defect compensation 80−54644
Si:P, and of P diffused layers 78−38736
Si:P, annealing after ion implantation, ellipsometric study 80−65018
p-Si:P, annealing behaviour, recovery, surface carrier density and Hall mobility meas. 77−32012
Si:P, annealing characteristics at low temp., elec. props. 78−63781
Si:P, Au gettering by P diffusion and P-induced dislocations 78−91346
Si:P, B, α-particle spectrum fabrication by ion implantation 78−33373
Si:P, BF_2^+ ion implantation, anomalous carrier profiles 80−2048
Si:P, defect annealing, ionisation effects, DLTS meas. 80−24483
p-Si:P, defect energy levels, ion implantation effects, Hall coeff., sheet resist. meas. 77−85173
Si:P, distrib. of implanted impurity after laser annealing, e.s.r. and neutron activation analysis 77−4122
Si:P, ESR-induced changes in DC resistance 78−35037
Si:P, heavily ion implanted, polycrystalline, grain growth 79−19477
Si:P, high dose implantation, outside dislocation generation 78−87672
Si:P, high fluence ion implantation, layer thickness and refr. indices, IR refl. meas. 79−82248
Si:P, implantation damage of channelled P ions, elec. activity recovery stages 77−59034
Si:P, implantation depth distrib. meas. by neutron activation anal., SIMS, junction depth method 77−31693
Si:P, implanted, pulsed electron beam annealing, Hall effect and sheet resist. meas. 80−34467
Si:P, implanted, SiO_2-film-covered, laser annealing behaviour 79−86808
Si:P, implanted, two-stage laser annealing of lattice disorder 79−1452
Si:P, implanted layers, ionisation-enhanced crystallisation 79−51151
Si:P, implanted low temp. annealed, elec. activation, damage depend. 80−88182
Si:P, impurity redistrib. by Ar ion hot implantation 77−72633
Si:P, ion implantation, effects of high dose rate 78−83835
Si:P, ion implantation defect annealing investig. by CESR 77−8404
Si:P, ion implantation doped, positron annihilation meas. 78−14380
Si:P, ion implanted, damage layer props. obs. using ellipsometric parameters *(Russian)* 77−43234
Si:P, ion implanted, ionisation enhanced annealing, resist. changes meas. 78−30667
Si:P, ion implanted, irrad. by laser of different wavelengths, annealing behaviour 79−69132
Si:P, ion implanted, lattice damage and electrical activation correlation 78−67726
Si:P, ion implanted, regrowth of damage structs. by laser annealing 80−107289
Si:P, ion implanted, resist. changes induced by ESR 78−68377
Si:P, ion implanted, sheet resistance variations at elevated temps. 78−43041
Si:P, ion implanted, subsurface damage, TEM and channelled Rutherford backscatt. study 80−107337
Si:P, ion implanted low temp. elec. cond. 79−56225
Si:P, ion implanted with small doses, defect annealing by nanosecond laser pulses 80−107297
Si:P, ion-implanted, carrier conc. reduction caused by wet O_2 oxidation 80−10565
Si:P, ion-implanted, damage-dependent elec. activation 79−55793
Si:P, ion-implanted, laser annealing 80−10564
Si:P, ion-implanted, optical refl. obs. of damage 78−55883
Si:P, ion-implanted and unimplanted, laser annealing, photoluminesc. study 80−2049
Si:P, ion-implanted layers, CESR meas., impurity distrib. inhomogeneity 78−2738
Si:P, laser and thermal annealing, elec. cond. and Hall effect meas. 79−69145
Si:P, low energy and high dose ion implantation, through SiO_2 film 77−15435
Si:P, multiscanning electron beam annealing 80−75242
Si:P, N implantation through Si_3N_4 film, depth distrib. of knock-on N, SIMS meas. 78−10066
Si:P, polycryst., channelling of implanted P during MOS device processing 80−65017
p-Si:P, random and aligned implants, Rutherford backscatt. and TEM exam. 78−47454
Si:P, secondary defect generation suppression and diffusivity restraint by HCl oxidation 79−70191
Si:P, selective annealing of amorphous layers by Nd^{3+}:YAG laser irrad. 79−14823
Si:P, thermally annealed, high dose, ion-implanted, dislocation array prevention by prior laser annealing 79−73187
Si:P, through-oxide implanted samples, anomalous residual defects after annealing 77−76432
Si:P,B, wafer, long range enhancement of B diffusivity induced by high surface conc. P diffusion 79−46687
Si:P CVD films, ion-implanted, doping effect on elec. props. 80−2495
Si:P implantation profiles, neutron activation anal. 78−7284
p-Si:P implanted films, piezoresist. stress tensors, ion dose depend., −80 to 120°C 80−100538
Si:P solar cell, minority carrier lifetime degradation during ion implanted processing, surface photovoltage 79−39305
Si:P spherical defect cluster and dislocation loop analysis 78−14356
Si:P^+, highly implanted, two step annealing effect on crystallinity 77−31683
Si:P^+, ions implanted through SiO_2 mask window, lateral spread 79−77627
Si:P^+, misfit dislocation formation mechanism, effect of implantation temp. 78−38708
Si:P^+, misfit dislocation net propagation due to osmotic forces 79−65108
Si:P^+, Zeeman energy transfer at surface layer 80−11247
Si:P^+ ion implanted single crysts., secondary defects development during annealing 80−44228
Si:P(As), conc. profiles of P (or As) and recoiled O atoms after ion implantation into SiO_2-Si, SIMS obs. 79−51138
Si:P(As)(B), nonequilibrium solid solutions obtained by heavy ion implantation and laser annealing 80−92544
Si:Pb, implanted, laser annealing 78−75685
Si:Pb, implanted and annealed, impurity redistrib. 78−75689
ion implantation continued
Si:Pb, ion-implanted and annealed, dose depend. of residual lattice disorder 77−43228
Si:Pb, low-solid solubility ion-implanted, pulsed and continuous laser annealing and furnace annealing comparison 79−73184
Si:Pb implanted layers, recrystn. on annealing, backscatt. and TEM obs. 77−51421
Si:Pt, implanted and laser annealed, segregation and increased dopant solubility 80−65016
Si:S, deep level characterisation, implantation predeposition technique 80−100444
Si:S, existence of isotope shift for S deep level, isothermal transient capacitance meas. 78−63999
Si:Sb, dopant implantation, activation analysis errors due to isotope comp. *(German)* 80−34037
Si:Sb, epitaxial regrowth of amorphous layers created by high-dose Sb implantation 78−30654
Si:Sb, high dose implanted, orientation dependent annealing effects 78−18665
Si:Sb, high dose Sb ion implantation, buried layer appls. 80−88186
Si:Sb, implantation of Sb for buried layers appl. *(French)* 77−80527
Si:Sb, ion implanted, annealing behaviour of stress 78−63778
Si:Sb, ion implanted, Sb diffusion during oxidation, snow-plough effect 80−88366
Si:Sb, ion implanted and annealed, influence of implantation temp. on dislocation generation 80−88158
Si:Sb, low energy ion implantation, profile determ. 80−88176
Si:Sb, low energy ion implantation Schottky barrier diodes and resistors 80−88177
Si:Sb, Mossbauer spectra of ^{119}Sn defect struct. 80−97174
Si:Sb, produced by ion implantation and laser annealing, Sb behaviour above solid solubility 80−88200
Si:Sb, vacuum deposition combined with ion implantation *(Japanese)* 79−28005
Si:Sb,P, double implants, residual defect reduction after damage anneal 80−88170
Si:Sb ion implantation combined with Si vacuum deposition neutron activation anal. 79−47631
Si:Sb wafers, laser annealing, Rutherford backscatt., optical, and TEM obs. 79−1445
Si:Sn, Mossbauer study of defects due to ^{119}In implantation 80−80641
Si:Te, laser annealed, lattice location of Te 78−67725
Si:Te, laser melting, surface Te atom accumulation, profiles 80−100258
Si:Te, Mossbauer spectra of ^{119}Sn defect struct. 80−97175
Si:Te implanted, laser annealing, Mossbauer obs. 80−39127
Si:Te(Sm), implanted impurity location, Mossbauer and channelling expts. 80−39128
Si:Th, ion implanted, meas. of stopping power of channeled B ions 79−28025
Si:Zn, implanted atom diffusion during laser annealing 79−37725
Si/Pd system, solid phase epitaxial growth control by C ion implantation 80−75466
Si-Au alloys, direct synthesis by inplantation of Au^+ *(Japanese)* 79−28006
Si-Au system, ion implanted induced giant gettering, annealing effects 80−88221
Si-B, diffusion-free annealing, use of scanning CW Kr laser 78−91345
Si-Cu alloys, direct synthesis by implantation of Cu^+ *(Japanese)* 79−28006
Si-H (up to 15 at.%), amorphous, ion implanted, laser annealing obs. 79−69133
Si-P, dislocation networks due to ion implantation, TEM exam. 77−35563
Si-P, excess carrier recomb., photocond. 79−65495
Si-refractory metal structs., interface modification by ion implantation 80−70475
Si-saphhire, Si ion implanted wafer, laser annealing 79−99989
n-Si-Se, ion implantation studied by deep level transient spectroscopy 78−10392
Si-SiC p-n and n-n heterojunctions, prep. by ion implantation, tunnelling cond. 77−43710
Si-SiC struct. formation on ^{12}C ion implantation in Si, optical and photoelectric props. 79−91136
Si-SiO_2, Al-implanted, low-temp. annealing effect on charge and surface state density 77−85337
Si-SiO_2, intentionally contaminated interface, transient capacitance meas. 79−33349
Si-SiO_2, ion bombardment by H_2^+, D_2^+, changes in annealing behaviour 79−78185
Si-SiO_2, ion implantation effects on charges 77−32086
Si-SiO_2, ion implantation through SiO_2 film, recoil implantation of O, EPR study 80−88180
Si-SiO_2, recoil implanted O profile after ion implantation through SiO_2 80−88198
Si-SiO_2, two layer system, P^+-ion penetration tails, expt. and computer anal. 80−75249
Si-SiO_2 abrupt interface form. by very high dose O^+ ion implantation 80−75253
Si-SiO_2 interface, effect of ^{11}B and ^{19}F ion implantation on charge density 79−10865
Si-SiO_2 interface, ion implantation induced interface states, effect of oxidation and N_2 annealing 77−39949
Si-SiO_2 interface in MIS struct., B^+ ion implanted, elec. props. due to laser irrad. 78−72272
Si-SiO_2 laminar ion-implanted systems, struct. change investig. by MSSI method *(Russian)* 80−107918
Si-SiO_2 layer formation by O_2^+ ion implantation, interface struct. and C-V charcts. 77−1142
Si-SiO_2 structures, B ions implanted, energy spectra of shallow traps at various implantation energies 80−80392
Si-SiO_2 structures, ion implanted, surface charcts. 77−80850
Si+Ga^+ ion implantation at high current density, lattice disorder, proton backscattering 80−34085
SiC, H^+, D^+ and He^+ ion implanted, Raman scatt. obs. of localised vibr. modes 78−6689
SiC ion implanted, laser induced ordering and defects 80−84754
SiC, synthesis by ion implantation of diamond, role of struct. imperfections 78−34529
α-SiC:Al diodes, ion implanted, transient charcts. of electrolum. 79−24369
SiC:Al^+ p-n junctions, elec. props., defect effects 80−15594

ion implantation continued
SiC(6H), ion-implanted, laser-induced recrystallization and defects 80−44221
α-Si_3N_4, effect of excess Si under ionic implantation of N 79−86809
Si_3N_4, enhanced etching by ion beam, localised substrate heating effects 78−51573
Si_3N_4 film, CVD, ion implanted, compressive stress buildup 77−89456
Si_3N_4 film, on Si, implantation effects on substrate hardening and film stress reduction 78−71748
Si_3N_4 film, penetration of As and P ions, 50 to 500 keV 77−76444
Si_3N_4 film formation by $^{14}N_2^+$ ion implantation into Si 79−99455
Si_3N_4 layers, prep. by N_2 ion implantation into Si, TEM and IR absorpt. obs. 79−46974
Si_3N_4 layers produced by ion implantation, oxidation inhibition and etching 80−103374
Si_3N_4-SiO_2:As, graded and stepped energy band-gap MIS struct. 80−2473
Si_3N_4-SiO_2:N,Zn ion-implanted multiple layers, ion range distribs., secondary ion microprobe meas. 79−42129
Si_4N_4, ion-implanted, enhanced etching in buffered HF solns. 78−72903
SiO, film, effect of ion implanted O_2 on optical props. 80−45027
SiO_2, Al implanted, electron traps characts. obs. 79−15226
SiO_2, Al-implanted, in MOS struct., trapped charge location, using photo I-V technique 79−15227
SiO_2, As-implanted, electron trapping and detrapping characts. 80−65692
SiO_2 coatings on SiO_2 substrate, cathodoluminescence spectra, electron irrad. 80−76085
SiO_2 film, ion bombarded, attenuated total refl. method obs. of H capture 79−95863
SiO_2 film, on GaP substrate, N ion implantation, optical refl. and EPR meas. 80−84197
SiO_2 film, on Si, range distrib. of implanted As, He^+ backscatt. obs. 77−39611
SiO_2 film, penetration of As and P ions, 50 to 500 keV 77−76444
SiO_2 film, quantitative secondary ion mass spectrometry of O isotopes and other light elements 77−9147
SiO_2 film formation, from O_2 ion implantation into Si, dielectric breakdown and I-V characts. 77−63368
SiO_2 film formed by ion implantation, dielectric props. 78−35090
SiO_2, fused, surface crystn. by Li^+ ion implantation and annealing 80−89383
SiO_2 glass, ion bombardment, form. of cpds., IR spectrosc. exam. *(German)* 80−88173
SiO_2, glass, ion implanted, radiation effect on chem. stability 77−1158
SiO_2, implanted, in MOS capacitor, direct current/voltage relns. as function of oxide doping 80−88635
SiO_2, ion implanted, fused, refr. index profiles 80−54272
SiO_2 ion implanted, radiation defects and optical props. 80−107293
SiO_2, junction microresistor prepared by double ion implantation of ^{11}B and ^4He, ^{20}Ne, ^{40}Ar, ^1H 77−15432
SiO_2 layer of MOS structs., centroid location of implanted ions by photo I-V technique 79−24079
SiO_2 layers, in MOS struct., hole trapping induced by ion implantation and annealing at room temp. 80−54792
SiO_2 layers, thermally grown, undoped and ion implanted, elec. props. 78−23187
SiO_2, prep. by O_2 implantation into Si 77−80523
SiO_2, surface pot. during ion implantation 80−19826
SiO_2:^{85}Kr, ion-implanted, impurity distrib. 80−15145
SiO_2:Al film, ion-implanted, electron trapping behaviour 78−67729
SiO_2:As^+ implanted layers in MOS struct., electron trapping and detrapping characts. 80−92982
SiO_2:Au(Ag)(Cu), XPS line broadening and extra-atomic relax. energies 80−71561
SiO_2:B, ion implanted, props. 79−65106
SiO_2:B thin films, props. *(Polish)* 80−39692
SiO_2:Cs(B) film, implanted electronic cond. mechanism in MOS struct. 77−15983
SiO_2:F-ion implanted, mobile-ion drift compensation 79−19664
SiO_2:F(BF_2), ion implanted, F influence on oxidation-induced stacking faults 80−65011
SiO_2:Xe, ion implanted, Xe retention, Rutherford backscatt., comparison with Si-O, Xe 79−4320
SiO_2-Si, P ion implantation, electrical transport props. 80−39130
SiO_2-Si MOS system, ion irrad. effects on struct. and electrophysical props. 80−6995
SiO_2-Si system, implanted with N, P, and Te ions, reflectance spectra and interference fringes 79−23629
SiO_3:B, P films doped by pyrolisis and ion implantation, IR absorpt. obs. of impurity conc. 77−72802
SiO_2film, waveguide layer form. on bombardment by B^+ ions 79−27454
Si(111):Pb ion implanted amorphous layers, recrystallisation, impurity out-diffusion model *(Chinese)* 80−88363
$(SmLuYCa)_3(FeGe)_5O_{12}$ film, ion implant profile 79−78477
$(SmTm)_3(FeGa)_5O_{12}$, small-bubble appl. 79−82845
$Sm_{0.4}Y_{2.6}Ga_{1.2}Fe_{2.8}O_{12}$, H^+ implanted film, epitaxial, mag. bubbles, walls and fine struct. 77−63241
Sn film, metastable supercond. alloys, produced by low temp. ion implantation 80−88670
Sn, film, vac. deposited, influence of ion bombardment during condensation 79−82483
α-Sn, implanted with Sn, Sb or Te, impurity-defect structs., Mossbauer expts. 80−39129
α-Sn, ion implanted, defect struct., Mossbauer spectra 80−80214
α-Sn:^{119m}Sn, impurity lattice dynamics, Mossbauer spectra, Debye temp. 80−84262
Sn-Cu film, metastable supercond. alloys produced by low temp. ion implantation 80−88670
^{119m}Sn, in FCC metals, isotope separator implanted, Mossbauer spectroscopy 79−24240
$SrTiO_3$:B layers, ion implanted, conductive props. Hall mobility, defect energy levels 79−82693
Ta, diffusion and surface distrib. of N, probed by (p,γ) resonance broadening method 78−38918
Ta, of $^{14}N^+$, target preparation 79−45501
Ta, proton implanted, anelasticity, internal friction meas. 79−24560
Ta, ranges of light ions meas. by (p,γ) reson. broadening, 20-100 keV 77−69023
Ta:Xe, BCC, heavy ion implanted, vacancy recovery, Mossbauer spectroscopy 79−82896

ion implantation continued
Ta_2O_5, amorphous, range of ^{27}Al meas. by (p,γ) reson. broadening 77−69023
Ta_2O_5, anodic film, thermally stimulated exo-electron emission 80−11546
$TaSi_2$ refractory formation by As^+ ion beam bombardment 80−107286
Te, elec. field gradient and lattice location of Sn, TDPAC and Mossbauer effect meas. 78−52395
Te, in metals, fisson reactor simulation study 80−54275
Te-Au film, metastable supercond. alloys, produced by low temp. ion implantation 80−88670
Ti, D profiles after D_3^+ implantation 80−37581
Ti, ion implantation, comparison with thermal oxidation of Zr 77−8976
Ti metal-metal interface, adhesion energy, surface treatment and ion implantation effects 80−107660
Ti, physicomechanical and wear props., influence of ion implantation and overlay coatings 80−40603
Ti, RF sputter deposition, ion bombardment and ion implanation 80−25564
Ti, trapping coeff. of energetic H at high doses 77−31699
Ti:D, implanted, deuteride imaging using scanning Auger spectroscopy 80−89092
Ti:D, implanted, nucleation and growth of TiD_2 80−97717
Ti:D, ion implanted, depth profiles, temp. depend. 80−100270
Ti:O, channelled ions, flux peaking study using protons, H_2^+ and H_3^+ ions 79−1450
Ti:Pd, ion implanted, corrosion behaviour and Rutherford backscatt. anal. 80−71792
Ti:T, depth profiling by neutron TOF spectroscopy 77−73500
Ti-Al (6 wt.%), D profiles after D_3^+ implantation 80−37581
Ti-Al-V (6,4 wt.%), D profiles after D_3^+ implantation 80−37581
Ti-Al-V (6,4 wt.%), D trapping in fusion reactor materials, temp. dependence 80−37577
Ti-Pd, dil., ion implanted, corrosion rate and electrochemical props. 79−43467
TiB_2 coatings for Tokamaks, H trapping and re-emission, annealing effects 80−37582
TiB_2, first-wall coating for Tokamak, H retention and release 80−18620
TiB_2, fusion reactor first wall material, activation energies and populations of H traps 79−45409
TiB_2, ion microanalysis and implantation applied to fusion surface research 79−45405
TiI_4:C, deep doping during ion-beam welding, microhardness meas. 79−19294
TiN, RF sputter deposition, ion bombardment and ion implanation 80−25564
TiO_2, chemical implantation of 10-keV H^+ and D^+, resist. and optical absorpt. expts. 77−59031
TiO_2, K^+ implantation, extended defects and precipitates 80−49251
TiO_2, rutile, deuteron and alpha-particle implantation, chemical effects, optical and cond. meas. 78−67755
U, D migration and trapping during D^+ implantation 80−34243
UO_2, D migration and trapping during D^+ implantation 80−34243
V, 80 keV ^4He irrad., depth profiles, migration, release, surface effects, blistering 77−35606
V, evap. layer, ion bombardment effect on superconducting transition temp. 78−52136
V, film, vac. deposited, influence of ion bombardment during condensation 79−82483
V, implanted Li atoms, depth profiles and sputtering anal. by optical spectra 77−35579
V, ion implanted with 2 MeV He under pulsed conditions, microstructure obs. 80−29088
V single crystals, ion implanted, energy dependent channelling and backscatt. anal., $^4He^+$ ions, 1 to 2.8 MeV 79−4360
V_3Si single crystal, radiation damage and superconductivity 78−52129
W (110), D^+ depth distrib., effect of surface impurities, channelling model 79−1451
W (110) surface, D depth profiles using imaging field desorption 77−59038
W, correlations between elastic energy transferred by implanted H ions and H trapping 78−14370
W, implantation effects of ^{133}Xe, annealing behaviour, Mossbauer study 80−40011
W, ion implantation, $^4He^+$ range profile and ^4He diffusivity meas. 79−33022
W:^3He, implanted ion positions, determ. using mol. deuteron beam 80−70240
W:Xe, BCC, heavy ion implanted, vacancy recovery, Mossbauer spectroscopy 79−82896
(W-Au)-SiO_2-Si:B MOS transistor, ion implantation effect on threshold voltage 78−34903
WC recoil implantation damage, PAC obs. 77−85620
WO_3, recoil implantation damage PAC obs. 77−85620
WSi_2 refractory formation by As^+ ion beam bombardment 80−107286
Xe, in metals, fisson reactor simulation study 80−54275
Xe ion implantation using Lublin separator 79−82251
Xe: ^{57}Co, solid, ion implantation for rare gas matrix isolation, Mossbauer spectroscopy study 80−54271
$^{133}Xe/^{133}Cs$, implanted in various hosts, isomer shift values, Mossbauer spectra 80−7240
$(Y,Sm,Lu,Cu)_3(Fe,Ge)_5O_{12}$, ion implanted, hard bubble suppression 80−11238
$(YEuErCa)_3(GeFe)_5O_{12}$: H, Ne, Ar, threefold symmetrical mag. bubble props. 78−64243
$Y_{2.35}Eu_{0.65}Ga_{1.2}Fe_{3.8}O_{12}$, bubble translation vel., ion-implantation effects 78−68327
$(YEuTmCa)_3(FeGe)_5$ bubble garnet films, ion-implanted, mag. susceptibility meas. 79−47311
$Y_{1.52}Eu_{0.3}Tm_{0.3}Ca_{0.88}Ge_{0.88}Fe_{4.12}O_{12}$, bubble translation vel., ion-implantation effects 78−68327
$(YEuYbCa)_3(FeGe)_5O_{12}$ bubble films, Ne^+-implanted, cryst. and mag. props., X-ray diffr. obs. 79−38362
$(YEuYbCa)_3(GeFe)_5O_{12}$ bubble film with ion-implanted layer, FMR study 80−2643
$(YEuYbCa)_3(GeFe)_5O_{12}$: H, Ne, Ar, threefold symmetrical mag. bubble props. 78−64243
YIG:La(Ga) films, ferromagnetic resonance, ion implantation effect 80−97145
$Y_{2.85}La_{0.15}Fe_{3.75}Ga_{1.25}O_{12}$ LPE films, ion implantation effect on spin waves 80−71124

ion implantation continued
$Y_{2.85}La_{0.15}Fe_{3.85}Ga_{1.15}O_{12}$ garnet, mag. props., ion implantation effect, Mossbauer study 80−97166
$Y_{1.62}Sm_{0.21}Lu_{0.27}Cu_{0.9}Ge_{0.9}Fe_{4.1}O_{12}$, implanted bubble garnet, anisotropy profile, FMR study 80−7103
$(YSmCa)_3(FeGe)_5O_{12}$ mag. bubble garnets, ion implantation induced stress influence on props. 79−91274
$Y_{3-x}Sm_xFe_5O_{12}$: ^{57}Fe film, ion implanted, Mossbauer conversion spectra study 80−80663
$Y_{2.6}Sm_{0.4}Ga_{1.2}Fe_{3.8}O_{12}$ film, ion-implanted, bubble domain behaviour 77−12177
$(YSm)_3(GeFe)_5O_{12}$: H, Ne, Ar, threefold symmetrical mag. bubble props. 78−64243
$(YSmLuCa)_3(GeFe)_5O_{12}$: H, Ne, Ar, threefold symmetrical mag. bubble props. 78−64243
$YSm_{0.5}Lu_{0.7}Ca_{0.8}Ge_{0.8}Fe_{4.2}O_{12}$ film, magnetic bubble propagation with 8 μm period ion implanted propagation patterns 79−78475
$(YSmTm)_3(FeGa)_5O_{12}$, small-bubble appl. 79−82845
Zn:Al, ion implantation, temp. and time depend. 80−65013
Zn:Al, ion implantation of Al, defect flow induced outdiffusion 78−63779
Zn-Mn, Kondo-system, ion implantation as method for study 80−70241
ZnO_x ion implantation effect on luminesc. and cryst. damage 78−6758
$ZnO:^{31}P^+$ implanted nonlinear resistor production and characteristics *(Russian)* 80−49252
ZnS, defect form. in single crysts. during implantation of Zn, S, and Ar *(Russian)* 78−14369
ZnS electroluminescent films, low energy Mn implantation system 78−30658
ZnS ion beam etching, topographic changes, amorphisation, luminescence study 80−76078
ZnS, ion implantation effects on luminesc., thermo-EMF 80−88178
$ZnS:Er^{3+}$, ion-implanted, annealing, cathodolum. obs. 80−2868
ZnS:Ne, implanted single crysts., photolum. and bombardment effect, thermolum. curve obs. 80−55166
p-ZnSe:As, ion implantation and heat treatment 78−87700
ZnSe:B(F), ion implantation, photocond. and cathodoluminesc. meas. 78−26586
ZnSe:N, ion implanted cond. type conversion on annealing *(Korean)* 78−18668
ZnTe, anomalous penetration of implanted ^{65}Zn and compensation zone build up 77−19975
ZnTe, ion implantation defect introduction, cathodolum. studies 80−75250
ZnTe ion implanted planar waveguides, refr. index profiles 77−62039
$ZnTe:B^+$ native and implant-created defects 77−76446
ZnTe:Li(Cl)(Al)(In), ion implanted and annealed, photoluminesc. meas. 78−15208
ZnTe:O, electronic and optical parameters of O related centre 77−24534
ZnTe:O, Ne or Al implantation, electronic and optical parameters of O-related centre 78−6399
ZnTe:O,Zn, dual ion implantation, luminesc. spectra obs. 78−87697
ZnTe:P(As), ion implanted, cathodoluminescence emission spectrum 80−108281
Zr, conc. distribs. of N^+ and N_2^+ beams of 200 keV/atom and 400 keV/atom 77−80529
Zr, deuteron implanted, temp. depend. depth profiles of deuterons 78−95076
Zr, H(D) implanted, superconductivity enhancement obs. 80−70884
Zr, ion implantation, comparison with thermal oxidation of Ti 77−8976
Zr, ion-implanted polycryst., thermal oxidation 80−71786
Zr, RF sputter deposition, ion bombardment and ion implanation 80−25564
Zr, ranges of implanted 10-30 keV D^+ 78−83858
ZrN, RF sputter deposition, ion bombardment and ion implanation 80−25564

ion lasers
acceleration effects in resonant interaction of laser beam and ions 80−10390
applications and laser principles *(French)* 80−83590
book, gaseous electronics and gas lasers 80−73120
book, quantum electronics 80−105442
charge transfer molecular ion lasers, excitation methods, ion-mol. processes 80−28221
commercial laser systems, design and manufacture 78−59046
confined plasma column, soft X-ray lasing action conditions 80−74346
Cu^+ hollow-cathode laser, IR output depend. on He-Ar press. ratio 80−48223
discharge, current limitation by electric double layer 78−66799
engineering aspects, colloquium, London, England (Nov. 1978) 79−31940
frequency selection using inclined Fabry-Perot etalon within cavity 79−55161
high-power ion-laser discharges, stability limits 78−37872
high-power lasers and appls., conf., Munich, Germany (June 1977) 79−964
hollow cathode discharge with variable voltage 80−59336
hollow cathode discharges for gas lasers, review 80−99717
hollow cathode discharges for gas lasers 80−83599
hollow cathode lasers, high voltage, spectroscopy appls. 79−27274
hollow cathode long life laser 77−88769
inert gas, highly ionised, vacuum UV lasing 78−63060
inert gas ion laser, high voltage-low press. discharges, stationary props. 80−92400
inert gas ion laser, wall confined, high CW power UV generation 77−19232
inert gas ion laser discharge, energy balance 78−74884
inert gas ion laser ion-acoustic wave excitation 78−74885
inert gas laser, high repetition rate operation 195 to 225 nm 78−82980
inert gas mixture, hollow cathode, CW operation and excitation mechanism 80−69363
inert gas mixture CW hollow cathode laser, internal anode system 78−9396
intracavity intensity modulated, 0.01 Hz to 1.2 GHz 79−41400
longitudinal flow, effect of flow on output power 78−58975
metal ion lasers, hollow cathode 80−99708
metal pure vapours, apparatus for stimulated emission obs. from transverse discharges 79−13954
metal vapour, hollow cathode, spectral analysis using scanning interferometer *(Japanese)* 80−9864

ion lasers continued
metal vapour laser, coherent radiation generation using transverse discharge excitation *(Russian)* 78−33727
metal vapour lasers, hollow cathode discharge, review 80−99717
metal vapour transverse separation in cataphoretic lasers 77−50659
microwave gas discharge problems in lasers *(Russian)* 80−14345
multicomponent laser plasma, soft X-ray population inversion by resonant photoexcitation 79−10680
multiply charged laser plasma, rapid cooling, possible short-wavelength radiation generation 79−41852
noise, low frequency 80−69364
plasma column, multipole confinement, radial and axial arrangement 80−83974
pulsed laser excitation source for time-resolved fluoresc. spectroscopy 80−9051
radioactive source preionisation of visible and UV discharge lasers 78−63096
rare earth ion potential vapour laser systems, spectroscopic props. 78−66812
rare earth lasers, book contrib. 80−53306
rare earths in vapour and solid phases as high intensity lasers, laser line prediction 79−3700
recombination lasers from cooled H like plasmas 77−79804
recombination lasers using elemental vap., metal ion transitions 78−17923
recombination lasers using elemental vap., stimulated emission conditions 78−17922
relativistic ion beam laser, continuously IR to X-ray tunable, in negative temp. state *(Chinese)* 80−87373
review, excitation mechanisms and characts., book contrib. 80−106512
review, neutral atom, ion, metallic vapour and mol. lasers 77−38866
review 77−7099
soft X-ray population inversion in laser plasmas, reson. photoexcitation, photon-assisted processes 80−87378
tube design, cathode fall theory studies 80−58560
UV laser *(Japanese)* 79−3686
UV metal ion lasers, spectral range 200-320 nm 78−66809
VUV and X-ray, amplification by ion accel. in plasma by steady state fields 80−28187
whitelight hollow-cathode type laser design based on cathode fall theory 79−27282
XUV lasing, gain-verification problem 78−71086
Ag, hollow cathode discharges, IR laser transitions, discharge conditions, excitation mechanisms 79−68383
Ag II, 1 W multiline output power from 800.4, 825.5, 840.4 nm transitions 78−82953
Ag II, discharge in hollow cathode, new IR transitions 77−661
Ag II, in He-Ag, Ne-Ag mixtures, unidentified laser transitions as Lyman, spectrometer ghosts 78−5464
Ag-He discharges, new ion laser transitions in near IR region, CW excitation 79−59673
Al II near IR laser transitions, large diameter hollow cathode Ne-Al discharge 80−102715
Al II slot cathode discharge, laser action 77−61943
Al ion laser, CW, in HV hollow cathode discharge 78−9371
Al, laser-produced plasma, population inversion between Al^{11+} levels, X-ray lines obs. 78−38539
Al XII, multiple photoexcitation in optically thick Si-Al plasma, lasing at 44 Å 79−3684
Ar, blue-green laser technology for ocean optics 77−78458
Ar, CW oscillation of 5062 Å line, reln. to laser Raman spectroscopy 80−1186
Ar, commercial laser systems, design and manufacture 78−59046
Ar, design suggested by determ., of Z-pinch by intrinsic stimulated emission 78−26311
Ar, endoscopic photocoagulation in human digestive tract *(German)* 78−35915
Ar, endoscopic photocoagulator for bleeding digestive lesions 78−40287
Ar, free-running, beat noise as multifreq. modulated source, for luminesc. lifetime meas. 77−57406
Ar, freq. stabilisation at 582.49 THz using saturated absorption in $^{127}I_2$ 77−79850
Ar, high power, Ti covered BeO discharge tube 78−29962
Ar high power CW laser and its problems *(Japanese)* 78−59019
Ar, high power problems 79−31944
Ar, high-power, construction of side cathode 80−99742
Ar, high-power CW ion lasers with improved service life 79−89937
Ar high-power CW laser, resonator configs. for mode selection 79−10327
Ar II, lower laser levels, natural lifetime determ. 77−6724
Ar II, magnetically confined plasma, pulsating ion laser action 78−78994
Ar II laser, square current pulse discharge excitation, waveforms *(Japanese)* 77−34873
Ar III, CW laser, short wavelength multiline performance 79−926
Ar III, CW system, high output power in visible and near UV 78−1249
Ar III, continuous high-power operation 351.1, 363.8 nm UV laser lines 77−38857
Ar III, low press. arc discharge, CW 40 W UV laser output 77−54695
Ar, internal CW parametric upconversion 78−42376
Ar, internal-mirror type air-cooled discharge tube, 5 mW output power 80−38034
Ar ion laser, CW 250 W output 79−18440
Ar ion laser, collisional radiative model and expt. 78−55338
Ar ion laser, He, Ne, impurity effects, ignition enhancement and instability suppression 79−13948
Ar, ion laser, resonator losses due to freq. selection using Fabry-Perot etalon *(Russian)* 77−38944
Ar ion laser discharge, current modulation 77−46717
Ar ion laser lines, use in Raman spectrometer calibration 79−97446
Ar ion laser plasma, collision radiation model appl. *(Dutch)* 78−29934
Ar ion laser radiation, Faraday effect, polarisation plane negative rot. 79−98424
Ar ion mode-locked laser system, temporal pulse shape, streak camera meas. 77−79799
Ar ion system, collisional radiative model 78−71080
Ar ion-laser discharges, high-power stability limits 78−37872
Ar laser, endoscopic laser photocoagulation of bleeding lesions *(French)* 79−34627
Ar laser and appls. *(French)* 80−83590

ion lasers continued
Ar laser emission under passive mode-locking conditions, temporal structure 80−9923
Ar laser holocinematography for cavitation bubble dynamics recording 79−86147
Ar laser resonator, effect of axial mag. field on loss increase 79−76716
Ar laser with passively locked modes, excitation of dye laser for picosecond pulse generation 80−95930
Ar magnetoplasmadynamic arcjet, recomb. lasing 80−48218
Ar, mode-locked pulses, second-order intensity correls., two-quantum photoeffect 79−10332
Ar, multimode, photon statistics, autocorrelation 78−9358
Ar, multiwatt, I_2 molecular beam stabilised 77−75555
Ar, possible appl. in head surgery 79−8529
Ar, pumping of CW ruby laser 78−1253
Ar, therapy of skin defects *(German)* 78−35916
Ar, treatment of haemangiomas, teleangectasia, radiodermatitis and tattoos 78−35906
Ar UHF discharge, spectral meas., Ar II lasing lines 79−99016
Ar, use of whole bandwidth analogue correlator for laser meas. 79−88983
Ar, vacuum arc discharge, lasing action 79−18402
Ar, with polarised radiation, use of three-mirror resonator 80−23712
Ar, with system for changing working gas *(Russian)* 77−88781
Ar, with wall stabilized transverse discharge 77−83849
Ar^+, 5145 nm wavelength stabilisers *(German)* 78−1247
Ar^+, 515 nm line, wavelength stabilisation for high precision length meas. 78−33766
Ar^+ and Ar^+-Kr^+ ion lasers, I_2 stabilized, beat frequency 80−95916
Ar^+, freq. stabilisation by $^{127}I_2$ absorption lines at 582 THz 78−90430
Ar^+, freq. stabilisation by saturated absorption in external $^{127}I_2$ cells 79−22965
Ar^+, high power, for pumping CW dye laser 77−7130
Ar^+ ion laser, active mode locking study 80−91827
Ar^+ ion laser, plasma instability, suppression by He admixture 79−64204
Ar^+ laser, intensity fluctuations obs. in emission 80−28197
Ar^+ laser 582 THz stabilisation by I_2 cell, improvements 80−102741
Ar^+ laser application in clinical otorhinolaryngology 77−90870
Ar^+ laser plasma, localised probe diagnostics 79−55113
Ar^+, radiation spectrum and influence of Fabry-Perot plate *(Polish)* 78−78993
Ar^+, upper laser levels collisional excitation and de-excitation, rate coeffs. 79−7112
Ar-He ion laser, population inversion radial distrib. and output characts., mag. field depend 80−19019
Ar-Kr, I_2 saturation spectroscopy for multiwavelength stabilisation 80−28282
Ar^+-Kr^+, multicolour laser light time multiplexing using rotating mirror 78−17999
As^+, CW laser oscill. on transitions in He-AsH_3 gas discharges 80−38004
Au hollow cathode laser, ion laser transitions 80−69366
Au II, ion laser transitions in He-Au mixture, 253.3 to 763.5 nm 77−7071
Au-He discharges, new ion laser transitions in near IR region, CW excitation 79−59673
Be III, X-ray lasers pumped with synchroton radiation and low-energy photons 79−41371
Br ion UV laser transitions, performance and spectroscopy 78−22111
C ion, extended plasma source for short-wavelength amplifiers 78−79447
C ion impurity in linear Z-pinch He plasma, outer 2s-shell electron excitation emission 78−22113
C VI, laser produced plasma, pumping by C VII+Ar III charge exchange 78−5462
C VI laser produced plasma, transient population inversion at 18.2 nm 79−41876
Ca XI, lasing action in far UV, 500 to 700 Å *(Russian)* 77−75491
Ca^+ cyclic laser, double-pulse excitation expts. 79−55118
Ca-Xe charge exchange system, optical gain meas. 79−10285
Cd hollow cathode laser, ion laser transitions 80−69366
Cd II, 441.6 nm, positive column He-Cd discharge, excitation mechanism 78−58983
Cd II, $4d^9 5s^2\ ^2D_{5/2}$, relax. consts. in plasma of ion laser, electron and He collisions 77−19239
Cd II, pulse excitation in discharge *(Russian)* 77−54704
Cd II laser oscillation at 5378 Å by laser-produced Cd plasma 77−3569
Cd laser produced plasma recombination laser, power output enhancement by plasma confinement 80−63989
Cd vapour laser, hollow-cathode white light, new design concept 80−87405
Cd^+ in He-CdBr, He-$CdCl_2$ and He-CdI_2 discharges, CW laser oscill. 78−50765
Cd^+, in He-halide discharge, CW oscill. 78−17913
Cd-He hollow-cathode laser, small signal gain 79−31881
CdI_2-He, hollow cathode discharge, simultaneous CW lasing by Cd^+ and I^+ 77−10951
Cl II in CuCl and $FeCl_2$ vapours, pulse generation at 5218 Å, 5221 Å 78−58990
Cl ion UV laser transitions, performance and spectroscopy 78−22111
Cl VII, transitions in laser heated plasma, intensity anomalies obs. 58 to 78 Å 78−1214
Cl^+, laser levels, radiative lifetimes meas. 78−42330
Cr vapour, laser transitions in near IR 80−99704
Cs+H_2^+, charge transfer processes with plasma gun, Lyman-α radiation exam. 78−46573
Cu, hollow cathode discharges, IR laser transitions, discharge conditions, excitation mechanisms 79−68383
Cu, hollow cathode He-Cu discharge, at. emission obs. of plasma props. 80−19021
Cu hollow cathode laser, ion laser transitions 80−69366
Cu II, 1 W continuous output from 780.8 nm transition 78−82953
Cu II, CW, hollow anode-cathode discharge 78−17963
Cu II, in Ne-Cu hollow cathode discharge, CW laser oscill. at 2703 Å 78−13689
Cu II, laser construction and performance, novel hollow cathode discharge structs. 80−38000
Cu II laser with cylindrical hollow cathodes, UV performance 80−102709
Cu^+ transitions in He-Cu halide gas discharges, CW laser oscill. 79−7116
ion lasers continued
Cu-He discharges, new ion laser transitions in near IR region, CW excitation 79−59673
CuII lasers with cylindrical hollow cathodes, performance 80−5751
Eu atoms and ions, self-terminating lasers, energy and time characts. 77−75493
F ion UV laser transitions, performance and spectroscopy 78−22111
Fe group elements, singly ionised, charge transfer, rel. to laser action 80−74246
H like ions, shock tube generated, lasing on Balmer-α line 77−58317
H-like ions, emission spectrum, depend. on electron density in laser plasma 79−27248
Hd-Cd hollow cathode laser in mag. field, Cd II stimulated emission 78−79002
He II, shock tube generated plasma ions, 1640 Å lasing on Balmer-α line 77−58317
He, nucl. pumping by fission fragments, plasma electron distrib. function 77−23653
He^+ VUV line population inversion, observed in stationary recomb. plasma 78−9836
He-Ar high voltage hollow cathode discharge, new Kr II CW laser lines new Ar II CW laser lines 79−13947
He-Ar hollow cathode discharge, laser generation on Ar II 4765 Å line 80−23671
He-As CW laser, excitation mechanism 79−3685
He-Au, UV ion laser, dominant transition at 280 nm 79−942
He-Cd, 8067 Å, He metastable atoms effect on power 78−33722
He-Cd, afterglow, Cd^+ excited state prod. by Penning and charge exchange reactions 77−15252
He-Cd, energy characts. in longit. mag. field *(Russian)* 77−50661
He-Cd, hollow cathode laser, output characts. 77−42525
He-Cd, hollow cathode laser oscillations, cathode temp. effects *(Japanese)* 79−50285
He-Cd, hollow cathode long life laser 77−88769
He-Cd, hollow cathode type, quasi-metastable state excitation 78−33721
He-Cd, intensity fluctuations meas., comparison with He-Ne laser 78−71087
He-Cd, intracavity phase modulation, spectral and time characts. 77−61988
He-Cd, long life hollow cathode laser 78−29968
He-Cd, metal ion laser, noise props. *(Japanese)* 79−64209
He-Cd, usual glow and hollow-cathode discharges, negative glow, spectroscopic obs. 77−72516
He-Cd, whitelight hollow-cathode type laser design based on cathode fall theory 79−27282
He-Cd bipolar hollow-cathode laser, 441.6, 533.7 and 537.8 nm Cd ion lines 79−50319
He-Cd cataphoretic laser discharge tube, He loss meas. rel. to tube life 79−94252
He-Cd discharge, enhancement of rate of charge exchange collisions 77−83862
He-Cd extended-life laser characts. 78−46586
He-Cd hollow cathode discharge white light laser *(Chinese)* 79−72555
He-Cd hollow cathode laser, 533.7 and 537.8 nm 77−71976
He-Cd hollow cathode laser, He singlet and triplet metastable number densities 78−29938
He-Cd hollow cathode laser, laterally emitted light 78−66810
He-Cd hollow cathode laser, axial mag. field effect on oscills. 79−59681
He-Cd hollow-cathode discharge, external cathode type, morphologic study 79−60207
He-Cd hollow-cathode laser tube, description and performance *(Bulgarian)* 79−27279
He-Cd II, 0.5378 μm oscill. spectra meas. using scanning interferometer *(Japanese)* 80−9864
He-Cd II, power interaction of laser lines 80−9862
He-Cd II hollow-cathode laser, 4416 Å pulse oscillation 79−7122
He-Cd II lasers, positive column, hollow cathode types, 4416 Å oscill. characts. *(Japanese)* 78−94392
He-Cd laser, 441.6 nm, low noise, discharge current modulation effects *(German)* 78−22117
He-Cd laser, 442 nm, high order mode crossing signals from Cd II $4d^9 5s^2\ ^2D_{5/2}$ state 79−796
He-Cd laser, drift of Cd^+ due to laser field 78−17917
He-Cd laser, freq. self-selection, transverse RF excitation *(Russian)* 77−75490
He-Cd laser, possible operation using charge-transfer excitation 77−83701
He-Cd low-power low-cost blue lasers 77−19333
He-Cd positive column laser power, effect of I_2 additive *(Japanese)* 79−7121
He-Cd positive-column laser discharge, excitation mechanisms from radial profiles 77−68205
He-Cd segmental tube laser ageing *(Bulgarian)* 79−18441
He-Cd single-mode laser, linewidth meas. and population calc. 77−14694
He-Cd vapour excitation in hollow cathode discharge 80−64815
He-Cd vapour laser, continuous wave, intensity fluctuations investig. 80−83593
He-Cd^+, cataphoretic, 441.6 nm line intensity dip due to vapour separation 77−50659
He-Cd^+, improved hollow cathode type, design and performance 80−19047
He-Cd^+, laser, cataphoretic, power noise meas. 79−36885
He-Cd^+, output radiation, influence of discharge-current fluctuations 79−10289
He-Cd^+, population densities of He excited states in positive column discharge 78−58989
He-Cd^+, positive column, power increase mechanisms by I_2 addition *(Japanese)* 79−98346
He-Cd^+, positive column laser, Cd II 441.6 nm line, effect of I_2 77−54697
He-Cd^+ cataphoretic laser, freq. fluctuations of 4416, 3250 Å lines 79−72556
He-Cd^+ hollow cathode laser, He(2^3S) densities and excitation mechanisms 80−48220
He-Cd^+ laser, exam. of Cd II 441.6 nm laser power increase by I addition 78−55344
He-Cd^+ laser, upper and lower laser states population densities, simultaneous determ. 78−87042
He-Cd^+ laser discharge, positive column, non-Maxwellian electron energy distrib., electron density determ. 77−84493

ion lasers continued
$He-Cd^+$ laser output, effects of transverse mag. field 79−86169
$He-Cd^+$ laser plasma, interferometric anal. of spectral lines 77−10892
$He-Cd^+$ positive column laser discharge, ion density 77−68885
He-Cu hollow cathode discharge, Cu II CW laser oscill. at 8096 Å 79−31878
He-Cu hollow cathode laser, three phase excitation 80−48279
He-Eu ionic gas discharge laser, increasing energy parameters *(Russian)* 77−58320
He-Eu pulsed laser, pumping rate and electron density meas. 80−9868
He-Hg laser, Hg II direct nuclear pumped gain at 7945 Å 78−5467
$He-I_2$, sequential separate multicolour output operation *(Japanese)* 80−28205
$He-I^+$, practical sealed-off laser device 77−31106
He-Kr HV hollow cathode laser, gain meas. of Kr II 4694 Å, 4318 Å CW transitions 79−45928
He-Kr high voltage hollow cathode discharge, new Kr II CW laser lines 79−13947
He-Kr hollow cathode CW laser, Kr II 4584 Å generation 80−58510
He-Kr hollow-cathode dischage, CW and pulsed lasing at Kr ion lines 79−3679
He-Kr hollow-cathode discharge, CW laser oscills. on Kr II 4694 Å, 4318 Å lines 79−3680
$He-Kr^+$, microwave-pulse-excited, spectroscopic expts. 77−71973
$He-Kr^+$ ion laser, He metastable atom concentration and time variation 79−55111
He-Kr(Ar)(Xe), ion laser transitions, hollow cathode excitation 80−1184
He-metal vapour lasers, positive column electron densities, experimental study *(Japanese)* 80−69376
He-Ne-Xe, ion laser transitions, hollow cathode excitation 80−1184
He-Se, metal ion laser, noise props. *(Japanese)* 79−64209
He-Se, vapour laser, continuous wave, intensity fluctuations investig. 80−83593
$He-Se^+$ three-colour laser engineering 78−46644
$He-Se^+$ white light laser 80−1226
He-Sr, laser plasma, double pulse excitation, singularities *(Russian)* 77−61945
He-Sr laser, possibility of nucl. pumping, 4305 Å Sr II transition 80−58518
He-Sr pulsed laser, pumping rate and electron density meas. 80−9868
He-Zn, 7588 Å, He metastable atoms effect on power 78−33722
He-Zn, coaxial type hollow cathode laser, oscillation charact. *(Japanese)* 78−13692
He-Zn, hollow cathode laser discharge, selective excitation of 5894, 7479 Å transitions by Ar 77−27280
He-Zn, hollow cathode laser, gain meas. for 7588, 4924, 7479 and 5894 Å Zn^+ transitions 77−88713
He-Zn, hollow cathode laser tube, with direct current excitation *(Japanese)* 79−76704
He-Zn, hollow cathode type, oscillation characts. improvement by inert gas additions *(Japanese)* 77−65590
He-Zn and $He-ZnCl_2$ hollow cathode laser discharges, comparison 80−28203
He-Zn hollow cathode laser, electron density, excited ions radial profiles 78−29937
He-Zn hollow cathode laser, 7588 Å in ZnII, operating characts. and upper level operating mech. 78−63071
He-Zn hollow-cathode discharge, excitation processes, rel. to Zn II laser 79−98342
He-Zn II, 0.4924 μm oscill. spectra meas. using scanning interferometer *(Japanese)* 80−9864
He-Zn laser, negative glow and positive column discharges comparison 78−1217
$He-Zn^+$, positive column laser discharge, upper and lower state densities, Penning collision 80−32964
$He^+ + Hg_0 \rightarrow He_0 + (Hg^+)^* + \Delta E$, cross sections, rate consts. 78−17785
$He^{2+} + Li$ collisions, soft X-ray emission obs. 80−83591
^{3}He-Ar nuclear pumped laser, first order model, lasing action depend. on Ar conc. 79−76668
Hg II, pulse excitation in discharge *(Russian)* 77−54704
Hg III, quasi c.w. laser action, low press. discharge 77−664
Hg ion-laser discharges, high-power, stability limits 78−37872
Hg^+, He-Hg afterglow plasma, time resolved double probe study 78−18444
I, hollow cathode, laser freq. meas. by harmonic mixing 77−83919
I I,II, radiative lifetime meas., rel. to I and $He-I^+$ laser transitions 79−54810
$^{127}I_2$ stabilised, beat freq. intercomparisons at 514.5 nm 80−74338
Kr, commercial laser systems, design and manufacture 78−59046
Kr III, CW laser, short wavelength multiline performance 79−926
Kr III, CW system, high output power in visible and near UV 78−1249
Kr IV, very strong laser emission at 195.027, 175.641 nm 78−63060
Kr, mode-locked, near UV, 50 ps pulse width 78−79030
Kr^+ ion laser, mode-locked near UV output, chem. and appls. 79−45966
Kr^+ mode-locked ion laser, pulse width and linewidth meas. 80−102696
Kr^+-He, microwave-pulse-excited, internal plasma parameters, time variation 77−38858
Li II, III, X-ray lasers pumped with synchroton radiation and low-energy photons 79−41371
Li III, shock tube generated plasma ions, 729 Å lasing on Balmer-α line 77−58317
Li ion soft X-ray laser, 199 Å, autoionising state effect 77−34876
Li plasma dynamic laser, using supersonic nozzle, population inversion, excitation cross section 78−50760
N ion impurity in linear Z-pinch He plasma, outer 2s-shell electron excitation emission 78−22113
N, travelling wave excitation 80−91774
N_2^+, charge transfer pumping, high press. pulsed glow discharge 77−14691
N_2^+ discharge laser, superluminosity, spatial-spectral struct. 79−55116
N_2^+, elec. discharge pumped 77−7069
N_2^+, gain and saturation 78−79001
N_2^+ high-pressure laser, superradiance spatial structure 79−64215
N_2^+, pumping of coumarin derivative dye lasers 78−74903
N_2^+, regenerative power amplifier operating on blue-green line 79−7139
N_2-He ion nuclear pumped lasers feasibility study and quenching 80−64001
N_2-He laser, charge transfer pumping at atm. press., in elec. avalanche discharge 79−10286
$Na + H^+$, charge transfer processes with plasma gun, Lyman-α radiation exam. 78−46573
ion lasers continued
Nd^{3+} in Nd-Al-Cl complex, vapour phase laser expts. 78−66813
Nd^{3+}:NdAlCl vapour complex, optical gain meas. 77−88708
Ne high power laser, continuous operation 79−22974
Ne II, long pulse UV laser emission, electron beam excited $Ne-NF_3$ mixture 78−78996
Ne II high-pressure supersonic flow electronic transition laser, with pulsed blowdown and electron gun facility 79−59723
Ne like ions, population inversion, gain estimate for 40 to 80 nm range transitions 77−75482
Ne like multiply charged ion transitions, stimulated emission possibility in far UV 79−10292
$Ne-Ag_I$ UV ion laser, dominant transition at 318 nm 79−942
$Ne-Al^+$, hollow-cathode laser, five Al II transitions 358 to 747 nm 77−58316
Ne-Cu, discharge processes, cathode sputtering 78−5463
Ne-Cu, UV ion laser, dominant transition at 260 nm 79−942
Ne-Cu hollow-cathode laser discharge sputtering obs. 78−66800
Ne-like multicharged ions, vacuum UV lasing action 78−1213
Ne-Tl hollow-cathode discharge, CW laser generation on Tl II 594.9 nm line 79−76675
Ne-TlCl hollow-cathode discharge, CW laser oscill. on 594.9, 695.1 nm Tl^+ transitions 80−23674
Ni I 1.3968 μm laser transition in hollow cathode discharge 79−81409
Ni II, laser oscill. at 796.24, 797.54 nm in hollow cathode discharge 79−86161
O ion impurity in linear Z-pinch He plasma, outer 2s-shell electron excitation emission 78−22113
O_2^+, $He_2^+ + O_2$ charge exchange laser 78−50759
Pb_2^+, electron collisional laser populated by recomb. 79−18405
Pb^+ high-gain laser populated by direct electron excitation, 1.159 μm transition 80−37997
Pb-He discharge, excitation process, Pb^+ emission lines 78−66803
S ion UV laser transitions, performance and spectroscopy 78−22111
Sn hollow cathode laser, emission obs. from Sn II, I transitions 80−106509
Sr vapour pulsed laser, power characts. of laser transitions in Sr I, II 79−10290
Sr^+ cyclic ion laser oscillating at 1033 and 1092 nm, single and double pulse expts. 79−22940
SrII, near IR laser transitions in hollow cathode discharge 80−1194
Tb^{3+} in $TbCl_3(AlCl_3)_x$ complex, potential vapour laser system, fluoresc. obs. 78−66812
Xe IV laser excited by long current pulse discharge, double-pulsed output 80−37993
Xe ion laser pump source for blue laser dyes 78−46621
Xe ion pumped open dye stream laser 79−81448
Xe, ionic assignment of laser lines at 3306 Å 78−1209
Xe laser pumped dye laser, construction and performance of laser and pumping source *(Japanese)* 77−58341
Xe, plasma-recombination laser, CO_2 laser prod. using periodic pumping 79−45927
Xe, pump for injection-locked dye laser 80−48280
Xe-Ne-He hollow cathode discharge, laser oscill. at 5314 Å Xe II line 79−3679
Zn^+ in $He-ZnB_2$, $He-ZnCl_2$ and $He-ZnI_2$ discharges, CW laser oscill. 78−50765
Zn^+, in He-halide discharge, CW oscill. 78−17913

ion lenses *see lenses*

ion microanalysis
see also ion microprobe analysis
14th Annual Reliability Physics Symposium, Las Vegas (1976) 77−40514
ANL HVEM-TANDEM accelerator facilities 80−101896
biological material anal. in few MeV range, review 77−81768
biological samples, irradiation chamber and sample changer 80−56198
book 77−31691
Cameca ion analyser, modifications 79−58841
channel plate, for secondary ion images obs. *(French)* 79−58840
compound semiconductors, quantitative anal. with ion microanalyser *(Japanese)* 78−7292
corrosion, conf., Manchester, England, (Apr. 1975) 77−8962
corrosion 77−8963
energy band centre, procedure for adjustment *(French)* 79−58839
flame, atm. press., ion mass spectroscopic sampling system characts. and calibr. 77−56270
heavy ion microlithography, obs. of submicroscopic structs. 80−51227
high temperature alloys, quantitative anal. by ion microanalyser *(Japanese)* 78−7291
implantation profiles meas. *(German)* 78−95978
ion beam analysis, conf., Paris, France (May 1978) 79−58837
ion bombardment thinning apparatus and its applications *(Chinese)* 79−80731
ion-bombardment Auger spectroscopy for studying surfaces of solids 79−20497
Magnox AL 80 ion beam analysis of corrosion films 77−8978
material characterisation, conf., Aleria, Corsica (Sept. 1976) 79−96403
metals, H and D implantation, ion beam analysis 79−5206
near-surface microanalysis of solids using ion beam techniques 79−24868
neutral particle beam separation, characts., anal. appl. *(Japanese)* 78−85248
PIXE, use of external beam on He filled target chamber 79−100470
plane retarding potential analyzer, effect of total transparency of field inhomogeneity 80−99003
rare earth oxide mixtures, determ. of individual rare earths *(Japanese)* 78−88683
rare-earth oxides determ. *(Japanese)* 78−23987
second-generation ion microanalyser description and performance *(French)* 80−101055
secondary ion emission, transfer optics *(French)* 79−58838
secondary ion emission phenomenon and anal. methods, review 79−96404
semiconductor design, ionic microanalysis 79−40648
semiconductor ion microanalysis, optimum exptl. conditions *(Japanese)* 77−86419
serum samples, trace element anal., automatic data acquisition, on-line method 78−48726
silicate and other natural minerals, by ion beam analysis *(French)* 77−52711

ion microanalysis continued
Spacelab, use of ion beams in near-surface anal. 78−35755
sputtered products, thermal ionisation, method of solid microanalysis *(French)* 79−61924
steel, mild, surface analysis rel. to annealing *(French)* 77−32857
steel, stainless, diffusion of Cs study using ion beams 77−20125
steel, stainless, ferritic, 430, precipitate study using ion microprobe mass analyser 79−15678
surface, composition analysis, by ion beams *(French)* 79−8467
surface, using heavy ion 400 kV accelerator of Thomson-CSF Central Research Lab. *(French)* 78−41880
surface anal. by ion scattering spectrometry and secondary ion mass spectrometry 80−103541
surface anal. tools review 80−103540
thin film analysis and characterisation, conf., Les Arcs, France (Jan. 1978) *(French)* 79−8466
Tokamaks, ion beam anal. of surface modifications, review 79−46457
Al, barrier film growth in soln. of film promoting and aggressive ions 77−8975
Al, oxide coated, inhibitive and aggressive ion effects, secondary ion mass spectrometry 77−8974
Al-Nb superimposed metallic layers, ionic movements during anodization, Rutherford backscatt. and nuclear microanal. 80−71913
BP, epitaxial growth on Si substrate, Si impurity profile, ion microanal. 78−87886
CaS, solid, tracer diffusion coefficient of S by ion microanalyser *(Japanese)* 80−34233
Co, secondary ion microanalysis for epilepsy study, use of electrostatic filter and transfer optic *(French)* 79−62414
Cu, stopping powers of 100 keV protons, meas. using ion induced X-ray emission 78−48725
GaAs:Si, quantitative anal. with ion microanalyser *(Japanese)* 78−7292
Ge, stopping powers of 100 keV protons, meas. using ion induced X-ray emission 78−48725
H profiling in Si, calibration standard, from anal. of H profiling methods using ion beams 79−5197
Nb-Al superimposed metallic layers, ionic movements during anodization, Rutherford backscatt. and nuclear microanal. 80−71913
Nb-Ge supercond. thin film characterisation by ion scatt., ion-induced X-rays, and ion resonance 77−40617
Nb-Ta superimposed metallic layers, ionic movements during anodization, Rutherford backscatt. and nuclear microanal. 80−71913
Ni, integranular precipitation after annealing, ion imaging microanalysis *(French)* 79−61594
Ni, stopping powers of 100 keV protons, meas. using ion induced X-ray emission 78−48725
^{18}O, concentration profile, secondary emission of negative or positive ions *(French)* 79−60395
Sc, stopping powers of 100 keV protons, meas. using ion induced X-ray emission 78−48725
Si, determ. of P, As by ion microanal. *(Japanese)* 78−85250
Si, thermal oxidation, high resolution Rutherford backscatt., implanted ions analysis 79−87911
Si-SiO_2-Si structures, P, As depth profiles, ion microanal. *(Japanese)* 78−85251
SiO_2 film, quantitative secondary ion mass spectrometry of O isotopes and other light elements 77−9147
Ta-Nb superimposed metallic layers, ionic movements during anodization, Rutherford backscatt. and nuclear microanal. 80−71913
Ti, and alloys, intergranular precipitation after annealing, ion imaging microanalysis *(French)* 79−61594
TiB_2, ion microanalysis and implantation applied to fusion surface research 79−45405
U, D migration and trapping during D^+ implantation 80−34243
UO_2, D migration and trapping during D^+ implantation 80−34243
W FEM tips, Pd or C adsorbed layer conc. using nucl. microanal. *(French)* 80−29860

ion microprobe analysers *see ion microprobe analysis*

ion microprobe analysis
see also ion microanalysis
absorption corrections, formula *(French)* 77−66777
accelerator applications outside nuclear physics *(Polish)* 79−40641
accuracy, basic relationships 79−43688
aerosols, proton induced X-ray emission anal., computer program for spectral anal. 77−60167
air particulate deposits, particle-induced X-ray emission anal., 2 MeV protons 80−45833
air pollution monitoring, PIXE and NRA studies using lichen indicator 80−61744
airborne particles, surface toxic elements, ion microprobe and Auger electron spectrometric anal. 78−7753
alloys, ion-implanted, integral Gaussian profile determ. method 80−107313
alpha-induced X-ray emission, thin-layer anal. 78−20132
alpha-particle backscattering, microanal. appls. 77−25324
alpha-particle induced energy dispersive soft X-ray fluorescence anal. 77−48728
apatite minerals, α-induced X-ray anal. of Y, La, Ce, Nd content 79−16084
applications, in mineralogy *(French)* 79−5628
archaeological artifacts, particle induced X-ray emission anal. 77−70398
asbestos mining area river pollution meas. by proton-induced X-ray emission 79−100556
atmospheric aerosols, composition, PIXE anal. 79−53004
atmospheric aerosols, S assessment along urban freeway, proton induced X-ray emission anal. 77−60172
atomic transport and conc. profiles 80−59723
autopsy organs, trace element levels, correl. with disease, proton induced X-ray emission anal. 77−56467
autopsy tissues, proton induced X-ray emission anal., calibration, correction methods 77−56466
backscattering, channelling surface peak role 78−43966
bielemental thick samples, atomic comp. determ., H^+ and He^+ induced X-ray anal. 79−5223
biological and medical specimens, elemental microanal. with scanning proton microprobe 80−56311
biological material, proton induced X-ray chem. anal., Fe and minor elements concs. 78−23989
biological samples, thick, PIXE anal., elimination of charging 78−88775
biological specimen elemental anal. in air 77−37116

ion microprobe analysis continued
biological specimens, elemental anal. by proton excitation of charact. X-ray emission 79−1976
Black Sea, heavy metal conc. meas. by charged particle induced X-ray anal. 78−24312
bulk material, determ. of impurity parameters from depth distrib. of foreign atoms 79−4331
calibration using matrix ion species ratios, appls. 78−61070
carbide-forming elements, K_α C line mass absorpt. coeffs. *(Czech)* 78−64905
catalyst design and evaluation using PIXE 80−61201
cataractous lenses, PIXE elemental anal. 80−21468
cereal, proton-induced X-ray emission and nuclear reactions for determ. of protein quality 78−20321
coincidence measurements between scattered particles and X-rays to obtain high depth and mass resolution 80−54278
computer control of spectrometers in microanalysis lab. *(German)* 77−52686
conference, Aarhus, Denmark, June 1979 80−41937
conference, Paris, France, (May 1977) 77−86406
conference on ion beam anal., Washington, USA (June-July 1977) 79−5194
counting rate effect elimination 79−5237
crystalline materials, investigation via low-energy proton beams, instrumentation aggregate 77−76266
crystalline solids, electronic industry, chem. anal. instrumental methods progress 80−66903
data recording and analysis system for use with scanning microprobe 80−42303
depth, effect of impurity fluoresc. by matrix X-rays 79−5224
depth profiles obtained by ion-beam sputtering, edge-effects correction 80−55757
depth profiling by ion microprobe with high mass resolution 79−46894
depth profiling by rastered beam, electronic aperture 77−18137
depth profiling of H and He using ion beam 78−7300
detector discrimination in SIMS: ion-to-electron converter yield factors for positive ions 78−73100
diamond, natural, trace element anal., genetic significance 80−55759
diffusion profiles of ^{16}O and ^{18}O in natural feldspars *(French)* 77−55400
digitally controlled scanning microprobe for trace element analysis 79−52801
electrostatic ion microprobe system 80−47144
element distributions obtained by ion microprobe, images quantification 78−73101
elemental concentration depth profiling in layered systems 78−31743
elemental concentration maps, determ. from digital secondary ion images, algorithm development 80−40761
elemental imaging errors, polarity role 78−20103
elemental mapping techniques in microscopic domain 78−24013
energy-focused atom probe design and performance 78−85276
environmental samples, proton induced X-ray anal. method appl. 77−63990
environmental samples, using low energy particle accelerator 78−85239
fracturing device for ion microprobe analyser, and appl. to grain boundary segregation 77−21341
gas density measurement, high speed, using proton-induced X-rays 79−52805
gas mixtures, kinetic studies rel. to gas lasers and pollutant detect. 79−48013
gas proportional scintillation counter, performance and applications evaluation 79−3289
geochemical applications of quantitative anal. 79−34976
glass, empirical sensitivity factor approach 79−74439
glass fibres and spheres, microscopic, production and charact. for microanal. 79−24487
glow discharge and ion-microprobe sputtering, SEM and ion-microprobe mass anal. 78−43977
grain legumes, proton-induced X-ray emission and nuclear reactions for determ. of protein quality 78−20321
graphite core, of fission reactor, impurity migration, proton microprobe obs. 79−52803
hair, human, PIXE analysis, correction factor, rel. to pollution monitoring 80−61743
hair anal. by (p, X) spectrom. 79−87916
heavy ion induced Coulomb excitation 79−79352
heavy ion induced X-ray emission anal. 77−48727
Heidelberg proton microprobe, for PIXE anal. of small, 4 μm^2, size samples 79−5239
heterogeneous materials, conc. inhomogeneities control, electron and ion probe testing 79−43505
high-intensity scanning ion probe with submicroscopic spot size 79−54225
HIXE, metal vapour targets production 78−80822
HIXE, theory and appls. 79−48006
Incoloy 800, steam oxidised, oxide coating anal. 80−89399
insulating materials, surface analysis using electron spray method 77−16887
ion analyser, appl. to natural silicates *(French)* 77−52710
ion beam monitoring using thin self-supporting reference foils 80−50911
ion excited UV lines, materials anal. appl., feasibility study using noble gas-ion impact 79−5230
ion induced optical emission for surface and depth profile analysis 79−4333
ion-induced AES 80−30305
ion-induced X-rays, review 79−96405
k-shell ionizations in proton induced X-ray emission analysis 80−101054
kidney, human, PIXE and neutron activation anal., appl. to cancer tissues 80−56199
Kirin meteorites, proton-induced X-ray emission anal. *(Chinese)* 79−40145
laser microprobe mass analyser, achievements and appls. 80−73536
laser mirror, depth concentration profile determ. by ion microprobe mass anal. 77−31126
light element anal. by 2 MeV, 150 keV proton and photon induced X-rays 78−53295
liver, bovine, PIXE and neutron activation anal. 80−56199
low energy low beam system for materials studies 79−85834
low energy proton-excited X-radiation, composition anal. appls. 79−20498
LT-1 ion microprobe mass analyser *(Chinese)* 79−30628

ion microprobe analysis continued
lubricating coating, solid, elemental anal. by proton-stimulated X-rays 78−88687
lung pathology, appl. of PIXE 80−61691
mass analyser, adaptation for liq. metals ion bombardment 77−49805
mass analyser and SEM combined depth profiling 79−74481
mass spectrometry, basic physics *(Chinese)* 80−42311
Melbourne proton microprobe 80−42302
metallurgical applications *(Japanese)* 77−25233
metallurgy, use of combined ion-, electron-beam techniques 79−43700
metals, FCC, H implantation, lattice location and trapping, ion beam anal. 79−55769
metals, ion beam analysis of light elements using nucl. reaction technique *(Japanese)* 78−31744
microbeam anal., conf., Ann Arbor, MI, USA (June 1978) 79−39258
microbeam analysis developments, application of Monte Carlo calc. method *(Japanese)* 78−3431
microbeam analysis developments, mag. contrast obs. with HV SEM, quantitative analysis by ion microprobe with quadrupole mass filter *(Japanese)* 78−3432
minerals, sputtering rates, implications for abundances of solar elements in lunar samples 80−61797
molecular noble gas ions in hot cathode ion source 80−306
monazite inclusions possessing pleochroic halos, PIXE anal. 78−69350
monolithic integrated circuits, digitised layouts and impurity profiles, particle induced X-ray fluoresc. obs. 79−52804
multielement anal., proton-induced X-ray emission 78−85272
NBS low alloy steel standard, electron induced X-ray spectrosc., detection sensitivity anal. 79−5229
NBS low alloy steel standard, PIXE detection sensitivity anal. 79−5229
nozzle erosion, ion implantation effects, ion beam anal. 79−48011
nuclear cross sections for ion beam analysis 80−45606
nuclear ion microprobe at MeV energies, production and use, review 80−7883
nuclear microprobe anal. of stable isotope tracers spatial distrib. 80−50909
particulate matter characterisation 77−60139
particulate matter concentration, moving filter technique, PIXE analysis, two hour resolution 79−92107
PESA advances in air pollution sampling 80−51023
phosphosilicate glasses, P content determ. by Rutherford backscatt., PIXE, and activation anal. *(Hungarian)* 80−85233
PIXE, absorpt. edge method of charact. filters 79−8461
PIXE, advances in air pollution sampling 80−51023
PIXE, appl. of wavelength dispersive spectrom. 77−48735
PIXE, appl. to bioenvironmental anal. 77−48976
PIXE, applications 79−48007
PIXE, atmospheric aerosol, absolute element concs., PIXE and AAS, comparison 78−85237
PIXE, biological applications 79−48008
PIXE, biomedical appls. 80−61691
PIXE, comparison of elemental composition of normal and disected tissues from biological samples 79−5364
PIXE, depth determ. using stopping foils 80−30310
PIXE, enhancement correction in high energy anal. 80−26086
PIXE, external beam elemental anal. method, sensitivity obs. for biological samples 79−5227
PIXE, impurity depth determ. 77−48725
PIXE, influence of matrix effects on absolute anal. 77−48721
PIXE, low energy mass absorpt. coeff., meas. technique 78−7309
PIXE, medium and heavy element anal. by K X-ray fluorescence, 20 to 50 MeV protons 79−57312
PIXE, method foundation, problems, precision, sensitivity *(Portuguese)* 80−45582
PIXE, procedure for thick target yield data anal. 79−8455
PIXE, sensitivity of high energy anal. in different matrix materials 79−16086
PIXE, synaptic vesicle ion content determ. 78−61166
PIXE, target preparation of aqueous samples 79−87915
PIXE, technique with external beam, and its appl. to study of valuable relics 80−61198
PIXE, thick target anal. with 30 MeV α-particles 78−31747
PIXE, trace element anal., medical appl. 77−48865
PIXE, trace element anal. with triggered beam pulsing 77−46453
PIXE, trace element determ. in bovine retina rod outer segments and disc membranes 79−48012
PIXE, uncertainties in elemental quantitative anal. 79−39254
PIXE, use of external proton beam for multielement anal. 77−48719
PIXE, use of liposomes to reduce enhancement-absorption effects 80−101053
PIXE anal., appl. to environmental samples 77−48730
PIXE anal., conc. profile determ. using beam energy variation 78−76965
PIXE anal., enhancement 77−48722
PIXE anal., review of target backings and specimen preparation 77−48979
PIXE anal., trace element detection sensitivity using external beam 80−55754
PIXE anal., trace transition elements determ. method 77−63973
PIXE anal. in viticulture and oenology 77−48733
PIXE anal. of aerosol elemental composition in particle size fractions, human respiratory uptake 77−48726
PIXE anal. of Ar implanted Al foil by heavy ion scatt. 80−45609
PIXE anal. of biological samples 77−48972
PIXE anal. of drinking water in cities of Iran 77−49096
PIXE anal. of insulating samples, reduction of bremsstrahlung background 79−20489
PIXE anal. of liquids down to ppb level 80−16755
PIXE anal. of meteoritic samples 77−49344
PIXE anal. of monazite inclusions in search for superheavy elements 77−49066
PIXE anal. of monozite inclusions, in search for superheavy elements 79−79845
PIXE anal. of S content of plant materials 77−48977
PIXE anal. of thick and thin targets of biological materials 77−48723
PIXE anal. of trace elements on liquids 77−48732
PIXE anal. on liquid samples, with external proton beam, matrix effects 79−34406
PIXE anal. with 4 MeV protons, target chamber 78−56941
PIXE analysis, MX-ray correction factors calcs., internal standard methods 80−45614

ion microprobe analysis continued
PIXE analysis of atmospheric gases, cryogenic conc. technique 79−53005
PIXE analysis of trace elements in environmental samples *(Chinese)* 79−61925
PIXE appl. to trace element anal. 77−48717
PIXE applications, conf. 77−48715
PIXE meas. at Univ. of Manitoba 77−46650
PIXE of thick samples in air, trace element analysis 79−24866
PIXE set-up for routine analyses 80−104488
PIXE spectra, wavelength dispersion anal. 77−48736
PIXE spectroscopy, trace element analysis 77−48718
PIXE system, automated anal. of environmental samples 77−48716
PIXE trace element anal., new method to determ. concentrations 78−76966
PIXE-PIGME system, automated, appl. to artefact obs. 80−61199
potential depth resolution of ion analyser, model development *(French)* 77−85867
probe using Ga EHD ion source 77−21444
protein analysis using PIXE 80−61691
proton beam diffusing system for PIXE analysis 79−85848
proton beam focusing to micrometer dimensions 77−46444
proton elastic scatt. anal. of light elements 77−48729
proton excited X-rays, appl. to thin film profiling 79−4490
proton induced γ-ray emission, interference by neutron induced γ-ray emission 78−27868
proton induced γ-ray yields 80−45608
proton induced K-shell ionisation cross sections, thin and thick target methods 80−45611
proton induced X-ray emission, K or L shell ionisation cross section meas., comparison with theory 79−5226
proton induced X-ray emission spectrometry, charging effects elimination using thin C foils 79−92024
proton induced X-ray fluoresc., anal. of lateral distrib. of trace elements in biological samples using microbeam scanner 79−5431
proton inner-shell fitted ionisation cross sections from Ca to Sn, 0.1-2.0 MeV 79−86055
proton microbeam analysis in air 77−9311
proton microprobe, feasibility study and design 79−54226
proton microprobe, X-ray and γ-ray, appls. 79−48010
proton microprobe for nondestructive trace element analysis 78−64911
proton microprobe with windowless-exit port 79−16085
proton semi-microbeam device for surface anal. 77−48720
proton-induced X-ray, human diseases and trace elements 77−70547
proton-induced X-ray emission, anal. of background radiation 77−70397
proton-induced X-ray emission, matrix effects in trace anal. 77−70396
proton-induced X-ray emission, trace element anal. 77−70438
proton-induced X-ray emission, trace element anal. 77−70548
proton-induced X-ray emission anal. for mass determ., spectrum decomp. code 79−11845
proton-induced X-ray emission anal. of single human hair roots 77−90973
proton-induced X-ray emission and proton elastic scatt., atmospheric particles anal. 77−70399
quantitative trace analysis, using ion and proton induced X-rays *(German)* 78−64900
radiation damage probing using low energy light ions 77−43260
Rutherford backscatt. standard for ion beam expts. 80−50496
Rutherford backscattering analysis, automatic ang. distrib. measuring system 77−20975
S aerosols characts. in Florida, PIXE anal. 79−21030
sampling error 78−7264
scanning high resolution probes, appl. to physics and biology 80−47156
scanning ion microprobe, improvements to give space resolution of 15 nm 78−15739
scanning ion microprobe, possible applications of a high brightness Ga source 79−2896
scanning ion microscope with field ionisation source 78−21289
scanning microprobe, digitally controlled for p and heavy ions 79−13571
scanning proton microprobe in atmospheric environment 77−70394
secondary electron imaging system for a nuclear microprobe 79−26799
secondary ion mass spectrometry at close to single-atom concentration using DC accelerators 79−48004
secondary ion microanalysis, energy selection effect on quantitative anal. 77−44539
secondary ion-ion emission, appl. to anal. of metal and alloy surfaces 77−56200
SEM-AES-IMA combination with SIM spectrometer, Si device anal. appls. *(Japanese)* 78−85249
semiconductors, surface analysis by ion beam backscattering *(Chinese)* 79−82425
sensitivity, quality assurance, and cost in automated analysis via ion induced X-rays 79−5222
serum, human, PIXE and neutron activation anal. 80−56199
SIMS ion imaging, sensitivity, lateral and depth resolutions 78−48738
small particle identification, review 78−48739
solid surface characterisation techniques, review 78−22945
sputter induced emission spectroscopy, anal. of H_2 in solids 79−5231
sputtering process, comparison with glow discharge lamp analysis 77−52730
steel, austenitic, non-oxidising, B and by secondary ion emission and X-ray microanal. *(French)* 80−11985
steel, C hot dipped aluminised, phase composition anal. of alloy layer by X-ray, electron probe and hardness meas. 79−34192
steel, carbon content in surface layers and in bulk 80−3466
steel, industrial, surface chem. characterisation by SIMS, glow discharge spectrometry and other techniques 80−66907
steel, low alloy, ion microprobe anal., sampling error 78−7264
steel, mild, conc. profile of implanted Ni and Cr 77−81339
steel, Sn (1.5 wt.%) and Mn-Mo (3, 0.4 wt.%), specimen fracturing device for ion microprobe analyser, to grain boundary segregation 77−21341
steel, stainless, D_2^+ diffusion and permeation, ion beam meas. 80−59492
surface, control and data analysis software 79−11860
surface anal., appl. of bulk H standards to calibration 80−7884
surface analysis, ion implantation and ion beam anal. in same UH vacuum sample chamber 77−4970
surface analysis, new uses of ion beams *(Japanese)* 80−90934
surface analysis, quantitative, by collision spectroscopy of backscatt. medium energy ions 77−8704
surface analysis instruments for vacuum electronics *(Czech)* 77−18145
surface and thin film analysis by high-energy ion beams 77−40320

ion microprobe analysis continued
surface bombardment, by electrons, protons and heavy ions, characterisation of materials 79−96406
surface structure anal., discussion of ion optics 79−46902
thick samples, PIXE anal., detect. limit and sensitivity 79−52802
thick specimens, proton and electron induced X-ray spectrometry, detect. sensitivities 78−20087
total ion monitoring method for correction of secondary ion intensity *(Japanese)* 77−21447
total ion monitoring method for secondary ion intensity correction 78−12796
trace element anal., comparison of PIXE and XRF methods 77−48737
trace element anal., high resolution 77−21445
trace element analysis by ion-induced X-ray fluorescence *(German)* 77−86399
trace element meas., comparison of charged particle and photon excited fluorescence 77−52716
trace element meas. in air water and organic materials by ion-induced X-ray fluoresc. *(Norwegian)* 78−53278
trace element transport meas. during haemodialysis by PIXE 80−36102
ultrahigh depth resolution surface analysis, appls. 78−71917
vacuum deposits as calibration standards for X-ray fluoresc. anal., thickness meas. 77−60177
water, elemental anal. using PIXE 78−20127
water, PIXE trace element anal. with detection limits in ppb range 79−48005
X-ray anal., conf., Denver, USA (Aug. 1976) 77−70382
X-ray analysis, appls., conf., Denver, USA (Aug 1975) 77−56307
zircaloy, nuclear microprobe methods for investigating oxidative corrosion 80−71787
α-particle induced X-ray emission, K or L shell ionisation cross section meas., comparison with theory 79−5226
γ-ray spectrometry with low-energy t and α particles, 0.1 to 100 ppm 79−8460
(pX,X) expt., partial sensitivity enhancement in trace element anal. 78−61128
Ag-Au, sputtering, ion yield depend. on alloy comp. 77−20976
AgCuAg sandwich target, proton induced K-shell X-ray yield ratios 77−48724
Al alloys, FIM and microanalysis developments 78−35782
Al film, vacuum deposited, 7 to 65 μ thick, morphology and purity determ. 77−76699
Al foil, PIXE anal. of Ar implantation by Ar ion excitation 80−45609
Al sheet surfaces, chem. characterisation by SIMS, glow discharge spectrometry and other techniques 80−66907
Al, single crystal, $^{18}O^+$ ion implantation in channelling directions, expt. conditions and range profile obs. 80−65022
Al single crystal, $^{18}O^+$ ions implantation in channelling directions, stopping power meas. from max. range 80−65078
Al, sputter deposit PIXE expt. 80−61196
Al, thick anodised films, O conc. determ. using non Coulomb H ion backscatt. 80−55753
Al, Zn and Mg impurities PIXE anal., conc. profile determ. using beam energy variation 78−76965
Al_2O_3, O conc. determ. using non Coulomb H ion backscatt. 80−55753
Al_2O_3, single cryst., O self diffusion, ion-probe meas. 80−59701
Ar ion induced X-ray fluorescence, surface anal. appl. using Ar^+ and Ar^{++} MeV ions 79−5228
C foils, impurity anal. by PIXE 80−18740
C high sensitivy meas. using nuclear microprobe 80−50908
C with Au and Al implants, Rutherford backscatt. standard 80−50496
Co, (pX,X) expt., partial sensitivity enhancement in trace element anal. 78−61128
Co, effect on surface roughness on backscattering spectra 80−47016
Cr black solar absorber surfaces, determ. of O_2 content using $^{16}O(^3He, p\ \gamma)$ 80−45610
Cr, film, sputtering yields, proton-induced X-ray meas. 80−50488
Cs^+ primary ion source for ion microprobe mass spectrometer 78−4732
Cu adhesion to Au, surface treatments and surface impurities 77−15701
Cu, sputter deposit PIXE expt. 80−61196
Cu thin layers, thickness meas. by proton-induced X-ray emission 80−4690
Cu:O single crystal, $^{18}O^+$ ion implantation in channelling directions, expt. conditions and range profile obs. 80−65022
Cu:O single crystal, $^{18}O^+$ ions implantation in channelling directions, stopping power meas. from max. range 80−65078
Cu-Zn-Sn-Pb (5, 5, 5 wt.%) alloy, analysis in glow discharge lamp and in ion microprobe, sputtering processes 77−52730
CuO surface, contaminated, cleaning treatments, ion scatt. anal. 78−53307
D, in Ti, Ti alloys, Zr, V, Nb, Ta, by ion microanalyser 78−56945
F depth profiling by $^{19}F(p, \alpha)$ and $^{19}F(p, \alpha\gamma)$ 80−45607
F in microcracked Cr plate, microanalysis by $^{19}F(p,\alpha\gamma)^{16}O$ 79−79351
Fe, and Fe-Cr, film, sputtering yields, proton-induced X-ray meas. 80−50488
Fe-Cr (9 wt.%), oxidation studied using $C^{18}O_2$ and D_2O tracers 80−71784
Fe-Mo alloy, TZM, doped, Ni activated recrystallisation, ion probe mass spectrometer obs. 77−44280
Fe-Ni-Cr (44, 17 wt.%), nuclear microprobe methods for investigating oxidative corrosion 80−71787
FeO, Fe_3O_4, identification by ion microprobe analysis *(French)* 77−86408
GaAs and GaAlAs, anal. by combined ion beam techniques with IEXE 79−7760
GaAs, anodisation, O incorporation at oxide-electrolyte interface, ion microprobe mass anal. 77−25273
GaAs oxide film, plasma-grown, analysis using Rutherford backscatt. and ion-induced X-rays 77−43438
GaAs, use of ion induced X-rays for lattice location of S and Mn implanted in single crystals 79−4332
$GaAs_{1-x}P_x$, diffusion of implanted Zn ions, ion microbe analysis 78−95190
$GaAs_{1-x}P_x$, mol. beam epitaxial growth, cryst. quality, composition investig. *(Japanese)* 77−55895
$GaAs_{1-x}P_x$, thermal oxides, elemental composition and C-V characts. 79−61772
$GaAs_{1-x}P_x$:Zn implanted, Zn diffusion 77−84993
GaP, mol. beam epitaxial growth, cryst. quality composition investig. *(Japanese)* 77−55895

ion microprobe analysis continued
H, determ. by simultaneous heavy-ion induced nuclear reacts. and at X-ray emission 78−85240
H_2^+, 6 MeV, PIXE anal. of organic materials 80−26087
$^2H(^3He, p)$, cross section meas. 80−42673
$Hg_{1-x}Cd_xTe$, implanted with Hg, Al, damage and lattice location study 80−103381
In_2O_3-SnO_2/InP junction, ion probe analysis of chemical nature 79−73411
InP, Zn diffused single-crystal, substitutional dopant and hole conc. meas. 80−75260
InSb, Cu-coated, surface contamination, ion microprobe mass analyser obs. 77−52729
Li nuclear microprobe method, appl. to in situ anal. of H-related materials problems 78−7299
^6Li induced reactions, light element anal. 77−81455
MgO, segregation of aliovalent solutes adjacent {100} surfaces 79−78979
Mo, D and ^3He trapping and mutual replacement 80−59493
$^{14}N(d, p_5)^{15}N$, cross sections determ., 0.32-1.45 MeV 80−42671
Na_2O-CaO-SiO_2 glass, SIMS anal. of aq. corrosion profile 79−66182
Nb, 14 MeV neutron sputtering, ion microprobe, SEM, He^+ backscatt. anal. 77−36317
Nb, H_2 embrittlement, microscopic obs. at low temps. 77−32666
Nb-Ga-Y system, X-ray and microprobe anal., isothermal section and supercond. transition temp. *(Ukrainian)* 79−38793
Nb-Ti films, ion beam sputtered, study by ^4He backscattering and nucl. reaction microanal. 79−42400
Ni, (pX,X) expt., partial sensitivity enhancement in trace element anal. 78−61128
Ni, energy straggling of protons 79−77652
Ni superalloy, cast, microstruct. and microanalysis 78−35393
Ni:O, single crystal, $^{18}O^+$ ion implantation in channelling directions, expt. conditions and range profile obs. 80−65022
Ni:O single crystal, $^{18}O^+$ ions implantation in channelling directions, stopping power meas. from max. range 80−65078
Ni-Cr thin film resistors, α-particle elastic scatt., and PIXE anal. 79−48022
Ni-Nb (5, 10 at.%), initial oxidation process at high temps., appl. of high energy ion backscattering anal. for O oxidation *(Japanese)* 79−24651
O_2 in thin films, determ. using $^{16}O(^3He, p\ \gamma)^{18}F$ 80−45610
Pb content in blood, PIXE determination 80−51228
Pb-Sb alloy, Sb distrib. profile as function of depth in corrosion films 80−21177
$Pt_{90}Rh_{10}$/Pt thermocouple, Inconel sheathed, MgO-insulated, decalibrations during 1200°C use, ion microprobe obs. 78−57957
S, determ. of the chemical state of particulate S in ambient aerosols, PIXE anal. 79−5225
Si, polycryst. and amorphous, sputtering with keV Ar^+ ion, meas. and Monte Carlo calc. of sputtering yield 79−95886
Si wafers, B predeposited, anal. by combined ion beam techniques and X-ray microanal. 79−5238
Si wafers, channelling dips for K and L X-ray prod., PIXE and Rutherford backscatt. anal. 79−4363
Si-SiO_2, two layer system, P^+-ion penetration tails, expt. and computer anal. 80−75249
Si(Bi), elimination of He^+ beam effect on channelling dips 80−54292
α-SiC, ^{30}Si self-diffusion, ion microprobe anal. 79−42309
SiC particles in EFG ribbon solar cells, EBIC and ion microprobe anal. 80−93838
SiC, surface characterisation by combined AES-IMA system, for first wall material of fusion devices *(Japanese)* 79−74039
Si(Li) energy dispersive X-ray spectra, computer anal. 79−1981
Sn, charged particle stopping power meas. by 100 keV proton induced X-ray emission 79−45593
Th, PIXE elemental anal. at $\mu g\ g^{-1}$ levels in ore samples 80−55758
thin film and surfaces, quantitative anal., He^{2+} induced X-ray emission technique 79−43548
U, PIXE elemental anal. at $\mu g\ g^{-1}$ levels in ore samples 80−55758
UO_2-UC_2-C microspheres, carbothermic prep., rate-controlling preps. 80−45257
V, H_2 permeability, surface impurity layer effect 77−24440
W, doped, Ni activated recrystallisation, ion probe mass spectrometer obs. 77−44280
W fibre reinforced Ni, high temp. stability 77−48372
Y, charged particle stopping power meas. by 100 keV proton induced X-ray emission 79−45593
Zr, ion-implanted polycryst., thermal oxidation 80−71786

ion microscopes
see also field emission ion microscopes; ion microscopy
aberrations and image form., study by magnetic anal. of beam from HF source 78−55293
all-metal autoionisation microscope construction and equipment 79−67433
scanning, atomic resolution capability 80−101878
surface analysis instrument for vacuum electronics *(Czech)* 77−18145

ion microscopy
see also field emission ion microscopy; ion microscopes
conference, Reston, VA., USA (Apr. 1977) 78−45683
conference, vacuum science, Jerusalem, Israel (April 1978) 79−67322
diffusible ion localization, comparison of chemically prepared and fast frozen freeze dried, unfixed liver sections 80−95189
heavy ion microradiography, of hydrated cells with SEM imaging 79−16360
heavy ions, advantages for high resolution microscopy using megawatt protons and N ions 79−2894
high-energy ion electron-loss microscopy, signal-to-damage ratio 79−25175
lithography, heavy ion, tool for object investigation and replication 80−90931
microscopic equipment, methods, appls. and related topics, bibliography 80−73124
proton scanning transmission microscopy vs. electron, ratio of elastic to inelastic cross-sections 77−22625
radioactive ion microscopy 80−101884
scanning transmission microscopy, contrast formation 77−79201
SIMS ion imaging, sensitivity, lateral and depth resolutions 78−48738
solid surface characterisation techniques, review 78−22945
three-electrode emission lens, appl. for secondary ion microscopy 79−41324

ion microscopy continued
Au, ion imaging of thin specimen 79−99035
Fe-Cr-Y, Y addition effect on high temp. oxidation resistance *(Japanese)* 79−70223
H_2^+, recombination yield on emerging from ultrathin C film below Bohr vel. 79−50108

ion mobility
see also electrolytic ion mobility; ionic conduction in solids
acetone, macroscopic model for solvated ion dynamics, cation conductance calcs. 80−65261
acetonitrile, macroscopic model for solvated ion dynamics, cation conductance calcs. 80−65261
aerosol, polydispersity, unipolar charging, charging mobility analysis 78−61059
aerosol, size distrib. determ. from mobility distrib. of charged fraction 78−61065
aerosol, unipolar diffusion charging, particle dielectric constant and ion mobility effects 78−61058
air, mobility spectra of ions created under atm. press. 77−969
air corona discharge ion density and mobility obs. 78−67594
alkali halides, shell model calc. of defect energies, crystal-independent interionic potential parameters 79−28141
alkali ion+inert gas, interaction pots., gaseous ion mobilities 77−54584
alkali polymethacrylates in alkali bromide soln., ion mobilities 79−96323
alkyl amines, plasma chromatography, reduced mobilities 79−74436
almandine garnet, Fe-Mn interdiffusion expt. meas. rel. to compositional zoning 79−77812
atmosphere, mobility spectrum, trace gases effect 77−25742
atmospheric, measurement of elec. cond. and small ion mobility, pollution aspects 78−92931
benzene, gas, liq. and crit., cation mobility 80−48842
benzene, liq., ion injection obs. 78−63870
cellulose acetate, reverse osmosis membranes, ion mobility, diffusion coeff., elec. resist. obs. 80−45550
corona discharge characts., influence of ion mobility, anal. 79−50902
critical-velocity rotating plasma interaction with neutral gas, obs. 78−75344
cyclohexane, gaseous, crit. and liq., positive ion mobility 79−37439
cyclopentane, gaseous, crit. and liq., positive ion mobility 79−37439
DC corona discharges in coaxial cylinder electrode, time variation of ionic mobility 80−33837
DC vacuum arc emitted particle flux 78−75470
trans-decalin, liq., irrad., positive charge mobility meas. by microwave absorpt. 77−20100
diatomic molecular ion mobility in gas, drift vel., resonant charge transfer 77−65832
dielectric liquids, ion mobility meas. and breakdown process, optical methods 80−84692
n-dodecane, tertiary alkylamines as sensitisers for charge injection from Se, and as charge carriers 79−91116
drift tube measurements, secondary electron effects 78−59538
drift tubes, ion time of arrival spectra determ., using CAMAC crate interfaced to microcomputer 78−93661
drift-diffusion problem with special boundary conditions, numerical soln. by integral eqns. 77−76591
electrolyte solutions, dielec. dispersion and dielec. friction 78−52436
electronegative gases, negative and positive ions, new expt. method 78−18372
ethane, positive-ion drift vels., Townsend primary ionis. coeffs. 79−55592
fluid, effect of long-wavelength fluctuations 80−49393
fluid, long wavelength fluctuations effect 79−77786
free burning arc characteristic formulae 80−70068
gas, ion transport, three-temp. theory generalisation appl. to Cs^++Ar 80−6202
gas, ion-neutral particle interaction pot. 80−23486
gas mixtures for proportional counters and drift chambers, positive ion mobility 77−27646
gaseous ion transport, three temperature theory 79−46412
gaseous ion transport theory, perturbation treatment of thermal motions 79−64820
gaseous ions transport props., data tables 80−12857
glass-forming materials, ion activation, energy parameters determ. 80−24634
n-hexane, gaseous, crit. and liq., positive ion mobility 79−37439
n-hexane, subjected to charge injection, low stress mobility, induced motion effects 79−91063
high-current free burning arcs, approximate model 80−70069
hydrogen bonded crystals, quantum theory of protonic cond. 79−90816
inert gas, diatomic ions, mobility in parent gas meas. 78−63532
inert gas ion, in parent gas, transverse diffusion coeff., reson. charge exchange effects 78−63533
inert gas ions, mobilities in He and Ne 79−90370
injected ion drift tube mass spectrometer ionic mobility data in non-parent gas 78−87428
ion+neutral neutron, ion speed effects in flow-drift tubes, Monte Carlo simulation 77−56221
ion+neutral reaction, ion speed distribution effects in flow-drift tubes 77−56219
ion+neutral reaction, ion speed effects in flow-drift tubes, statistical mechanical theory 77−56220
ion motion and charge exchange in quadrupole elec. field, Monte Carlo calcs. 77−9060
ionic mobility estimation from charge relax. 77−11719
ionisation in flames, mass spectrometric and mobility analyses for flame ionisation detector 78−40050
ionosphere, ion vels. in four-component plasma 77−13154
liquid, theories, continuum and stochastic models, comparison with conductance data 80−44345
liquid dielectric, ionic-cond. and -dissociation under low elec. field 77−8089
liquid dielectric, Sumoto effect under transient conditions 80−97198
mass identified ions in O, N, CO and CO_2, transport properties, obs. and calc. 79−50837
membranes, negative resist., current controlled, model 79−34357
MOS capacitor, TSC meas., suppression of meas. interferences from interface states and mobile ions 80−29479
negative ion mobility in O_2 and N_2, temp. depend. 79−14513
nematic mixtures, Merck 5 and 7a, EHD, ion mobility 79−33104
neutralisation escape probability, field depend. mobility effects 78−14737

ion mobility continued
neutron scattering techniques in applied research, medium-flux research reactors 79−13514
nonattaching gas, irrad., in infinite cylindrical cell, space charge and wall effects 77−68737
p-octyloxyphenyl-p′-pentyloxybenzoate, charge carrier mobility and cond. in nematic and isotropic phases 80−44347
optoelectronics, appl. in measuring gas discharge phenomena 80−107007
picrate anion active transport through organic liq. membrane 78−11556
plasma chromatograph/mass spectrometer simultaneous electron impact/chem. ionisation carrier gas mixture 79−30600
plasma chromatography, mobility and composition of hydrated positive reactant ions 79−74435
plasma in pulsed EM accelerator, time distrib. *(Russian)* 77−47267
plasma ion velocity, distrib. diagnostics by neutral particle time-of-flight spectra 78−67439
polyester, ion mobility from ionic injection current at strong diffusion 80−2210
polymer, wetted by insulating liq., under elec. field, charge transport and absorpt. 80−6534
pyridine, macroscopic model for solvated ion dynamics, cation conductance calcs. 80−65261
rarefied ionised gas, ion transport in strong elec. field 77−51155
resonant charge transfer influence, modified moment method 79−37440
RF quadrupole field trapping, collision effects on ion motion 77−75261
slags, application of activity concept to physical chemistry 78−53243
slow ion stopping power meas., multiple scatt. corrections 80−23278
solvent, ion migration and frequency-dependent dielectric loss 79−19832
spectrometer, multielectrode, for atm. elec. meas. 80−31145
Thomson model of ion conduction, steady state characts. 77−15606
Thomson model of ion conduction, transient state anal. 77−15607
toluene, gas, liq. and crit., cation mobility 80−48842
transformer, oil ion mobility and fluid motion, effect of additives and dissolved gases 78−47543
velocity and energy relaxation in drift tubes 78−9747
water vapour, ion mobilities, liq. droplet model failure 79−60097
water vapour, ion mobility, 20 to 70°C 78−75252
water vapour at saturation, droplet nucleation by ions, ion mobilities 79−46794
Ag halide grains, photographic sensitivity and response to charged particles, interstitial generation 77−10124
(Ag-Cs)Br molten mixture, transport nos. and external mobilities *(French)* 79−77787
(Ag-M)Br, (M=Na, K, Rb, Cs) molten mixtures, molar vols. and molar conductivities *(French)* 79−77788
AgCl, ionic mobility, diffusion coeffs., defect mobility energies 80−65284
AgCl(Br) emulsion, photomoment investigations of ionic and electronic props. 79−24782
AgI-PbI_2 molten mixtures, conductivity, thermodynamic excess props. 79−86914
Ag_2S and Ag_2Se melts, electrotransfer, ionic component of elec. cond., Ag ion diffusion 79−51640
Ag_3SbS_3, ionic component of conductivity *(Russian)* 78−38870
Ar^+, in Ar, transverse diffusion coeff., reson. charge exchange effects 78−63533
Ar^+ ions, mobilities in He gas at 82K 80−75023
Ar^+, mobility in Ar, spin-orbit coupling effect 78−26232
Ar^+ mobility in He gas at 82K 80−1733
As_3Se_3:Cu, glassy, broadening of electrodiffusion profiles at high elec. fields 79−55939
BaO-P_2O_5 glasses, Cu^+ ion electromigration at 400°C, luminesc. meas. 77−76610
Br^-, in He, ion reduced zero field mobility and free diffusion coeff. 77−47139
Br^-, ion mobility in Ar, flow drift tube meas. 77−72405
C^+, mobility in He, flow-drift tube meas. 80−43831
CO_2, ion drift velocities and mobilities 80−43834
CO_2^+, ion mobility in N_2, flow drift tube obs. 77−19663
CO_2^+, mobility in Ne gas 78−14125
CO^+.CO, lateral diffusion in CO, mass spectra meas. 78−91055
CaO-SiO_2-Al_2-O_3, 1500°C, ion transport coeffs., interdiffusivities 77−11718
Cl^-, in He, ion reduced zero field mobilities and free diffusion coeffs. 77−47139
Cl^-, ion mobility in Ar, flow drift tube meas. 77−72405
Cl^--Ne(Ar)(Kr)(Xe), longitudinal diffusion coeff., generalised Einstein relation 79−86552
$^{35}Cl^-$, ion mobility in inert gas, drift tube mass spectrometric obs. 79−68896
Cs^+ in He and Ne gas, ion mobility and longit. diffusion coeff. 78−67308
Cs^+, in mol. gases, ion mobility, drift tube mass spectrometer meas. 77−89228
Cs^+, ion mobility in Ar, Kr, Xe, diffusion, generalised Einstein relation 78−67298
Cs-Au, liq. alloys, ionic conductance 77−1251
Cs^+-Ar(Kr)(Xe), ion mobility and interaction pot., drift tube meas. at 300K 78−59537
Cs^++Cs, mol. ion form. rate, from mobility meas. 79−34299
D^+, mobility in He and Ne, 300K 77−11303
D^++D, thermal energy collisions, quantum mech. calcs. 80−23507
F^-, in He, ion reduced zero field mobilities and free diffusion coeffs. 77−47139
F^-, ion mobility in Ar, flow drift tube meas. 77−72405
F^- ions in Kr and Xe; mobilities and diffusion coeffs. determ. 80−100048
F^-, mobility in He, flow-drift tube meas. 80−43831
F_2-inert gas mixtures, transport and attachment processes 78−59542
H^- excess mobility in water in quartz pores, IR spectroscopic study 79−51955
H^+, calc. of mobility in He, 10 to 700K 78−66629
H^+ ion mobility in He, expt. 80−96337
H^+, mobility in He and Ne, 300K 77−11303
H_3^+, mobility in He gas 78−18371
H_2O^+, mobility in He, flow drift tube obs. 78−34257
H_3O^+, ion mobility in N_2, flow drift tube obs. 77−19663
$H_3O^+(H_2O)_n$ (n=1,2), ion mobility in N_2, flow drift tube obs. 77−19663
$H_3O^+.H_2O$, mobility in He, flow drift tube obs. 78−34257

ion mobility continued
He gas, ion mobility and longit. diffusion of Ar^+ and CH_x^+ *(French)* 79−94766
He I line profiles, ion motion effect in low electron density plasma 80−43877
He II, ion velocity shift in vortex resonance 77−35771
He, liq., impurity ion mobility 77−7921
He, liquid, solid, and dense gaseous, mobility of charges 78−2324
He, normal and superfluid phases positive ion mobility 79−4449
He, solid, diode properties 79−56021
He, superfluid, viscosity, ion mobility and λ-transition 77−72731
He, vap., positive ion mobilities, clustering 77−58837
He vapour, low-temp. positive ion mobility by absorptive model, WKB calcs. 79−77333
He^+, mobility in He gas, calc. 79−55447
He^{2+}, mobility in He gas 79−7440
He-Cd laser, drift of Cd^+ due to laser field 78−17917
$He+(H^+)(D^+)$, mobility and diffusion, runaway effect 80−33727
$He+H_2^+(H^+)(H_3^+)$, interaction pots. from ion mobility data 77−14518
$He+H^+(D^+)$, runaway mobility obs. 80−38517
He^++He, charge exchange cross section, drift-vel. meas., 0.3-8 eV 78−25694
He^{2+}+He, thermal energy collisions, quantum mech. calcs. 80−23507
HeH^+, mobility in He gas 78−18371
^{3}He, normal liq., positive ion mobility 78−22923
^{3}He, A and B phases, motion and mobility of ions 78−18861
^{3}He, containing dil. ^{4}He, shell model of positive ions 79−56007
^{3}He, ion mobilities in normal and superfluid phases 79−65280
^{3}He, liq., contamination by ^{4}He, multiple positive ionic mobility 79−46876
^{3}He, liq., ion mobility, temp. and freq. depend. 80−70493
^{3}He, liq., ion motion in normal and superfluid states 77−66054
^{3}He, liq., nagative ion mobility 79−55996
^{3}He, liq., nonlinear positive ionic motion in normal phase, equiv. of temp. and vel. depend. 79−86952
^{3}He, liq., positive ion nonlinear behaviour, expt. and parameterless theoretical prediction comparison 79−14978
^{3}He, liquid, normal and superfluid phases, NMR and ion mobility experiments 78−91505
^{3}He, mobility of positive ions 78−51773
^{3}He, negative ion mobility, theory 80−107598
^{3}He, normal and superfluid, positive ion mobility meas. 79−55995
^{3}He, normal liq., effect of ^{4}He on positive ion mobility 79−60589
^{3}He, normal liq., negative ionic mobility, absence of non-linearity at low temp. 79−28167
^{3}He, normal liq., press. and temp. depend. of positive ionic mobility 78−91504
^{3}He, normal phase liq., positive-ionic mobility 3-100 mK 78−18863
^{3}He, normal positive ion mobility 78−10244
^{3}He, superfluid, electron bubble mobility 77−43402
^{3}He, superfluid, negative ions motion, model for A, B phases 78−2326
^{3}He, superfluid A-phase, ion mobility tensor, ion-quasiparticle scatt. 80−59753
^{3}He superfluid β-phase, negative ions mobility 79−86956
^{3}He-^{4}He, tricritical normal phase liq., ion mobility 78−79850
^{3}He-^{4}He mixture, dilute solution, of ^{4}He in ^{3}He positive ion mobility 79−33151
^{3}He-^{4}He mixture, positive ion mobility 78−10244
^{3}He-^{4}He mixtures, ion trapping at crit. interface 79−65285
^{3}He-^{4}He mixtures, rotating, ion trapping on vortex lines 79−28169
^{3}He-^{4}He solutions, mobility of ions trapped on vortex lines 77−7919
^{4}He charged drops in cryogenic vap., He^+ mobility, 1.3-2.0K 79−32734
^{4}He, ion radius anomaly near lambda transition 77−76634
^{4}He, liq., phase transitions, positive and negative ion mobilities meas. 78−87833
^{4}He, liq., viscosity and positive ion mobility near melting transition 78−10240
^{4}He, pure, mobility of ions trapped on vortex lines 77−7919
^{4}He, superfluid, vortex ring transition 77−4234
^{4}He vapour, cryogenic, ion-droplet mobility 79−57308
^{4}He-^{3}He, ^{4}He impurity at. and ion interaction and mobility, in solid or liq. *(Russian)* 78−18868
I^-, in He, ion reduced zero field mobility and free diffusion coeff. 77−47139
I^-, ion mobility in Ar, flow drift tube meas. 77−72405
K^+ in Kr(Xe) gas, XX 79−10625
K^+ mobilities in gases *(Japanese)* 79−60101
K^+, mobility and clustering in Ar gas 77−84389
KBr bicrystal, Ag^+ injection transport and grain boundary mobility, electrodecoration obs. 80−2214
Kr^+, Kr_2^+, $^2P_{1/2}$ and $^2P_{3/2}$ states, mobilities in Kr, spin state depend. 77−3913
Kr^{2+}, mobility in He gas, drift-tube meas. 78−66657
Kr_2^+, mobility and clustering reaction in Kr 79−10628
Li^+, in N_2 and CO_2, obs. using injected-ion drift tube mass spectrometer 78−1784
Li^+ mobilities in gases *(Japanese)* 79−60101
Li^+, mobility and clustering in Ar gas 77−84389
Li^+ mobility in He 300K, interaction pot., drift tube meas. 77−76026
Li^++He, interaction pot., direct determ. from gaseous ion mobility 77−10720
$LiAlF_4$, struct. pot. energy surface, Li^+ migration, ab initio LCAO SCF calcs. 80−23305
LiCl-RbCl, molten, Chemla effect, mol. dynamics simulation, self exchange vel. 80−79967
Li_2O-Al_2O_3-SiO_2 glass melts, alkali ions interdiffusion coeffs., conc. depend. 79−65231
N_3^+, N_4^+, lateral diffusion in N_2, mass spectra meas. 78−91055
N_4^+ mobility in N_2 78−60985
NH_3, gas, ion mobility meas. 79−23393
N_2H^+, ion mobility in N_2, flow drift tube obs. 77−19663
NH_4NO_3, molten, countercurrent electromigration cell, isotope separation appl. 78−47547
NO^+, in CO_2, obs. using injected-ion drift tube mass spectrometer 78−1784
NO^+, mobility in CO_2 80−43834
NO^+-N_2, temp.-dependent ion mobilities 79−86553
N_2O^+, mobility in Ne gas 78−14125
Na^+ mobilities in gases *(Japanese)* 79−60101
Na^+, mobility and clustering in Ar gas 77−84389
Na^+, mobility and longit. diffusion coeffs. in Kr and Xe 80−106866
ion mobility continued
Na_2O-Al_2O_3-SiO_2 glass melts, alkali ions interdiffusion coeffs., conc. depend. 79−65231
Ne^+ ions, mobilities in He gas at 82K 80−75023
Ne^+ mobility in Ne, fine struct. splitting effect 77−39400
Ne^++Co_2, three dimens. quadrupole ion storage, ion mobility, effect of charge exchange reactions, Monte Carlo calcs. 80−55738
$NiCl_2$, aq. soln., diffusion and struct. 78−14488
O^- and O_2^- ion swarm in O_2, reactions and transport, Monte Carlo calc. 78−59539
O_2^+, in CO_2, obs. using injected-ion drift tube mass spectrometer 78−1784
O_2^+, lateral diffusion in O_2, mass spectra meas. 78−91055
O_2^+, mobility in CO_2 80−43834
O_2^+-N_2, temp.-dependent ion mobilities 79−86553
PbO-SiO_2 melts, ionic transport, tracer diffusion and chem. interdiffusion 79−77785
Rb^+, in He, Ne, Ar, H_2, N_2, O_2, CO_2 77−11305
Rb^+, ionic mobility in Ar, Kr and Xe, interaction pot. determ. 79−18991
Rb^+, longit. diffusion coeffs. in elec. field, mass spectrometric determ. 77−7502
S^+, mobility in He, flow-drift tube meas. 80−43831
SF_6, compressed, ion mobility and recombination 79−60098
SF_6-N_2 mixtures, attachment coeffs. and ionic mobilities, 1.2-4 eV 80−96338
SO_2, electron attachment processes investig. and mobility of negative ions 80−38518
SiO_2 films on Si, mobile Na ion instability 79−82503
$UO_2(NO_3)_2.2H_2O$, in n-butanol, ionic mobility determ. 78−34642
$UO_2(NO_3)_2.6H_2O$, in n-propanol, ionic mobility determ. 78−34642
Xe^+, Xe_2^+, $^2P_{1/2}$ and $^2P_{3/2}$ states, mobilities in Xe, spin state depend. 77−3913
Xe^{2+}, mobility in He gas, drift-tube meas. 78−66657
Xe^{2+}, mobility in parent gas 79−7439
$Zr(HPO_4)_2.H_2O$-Kynar membranes, struct., ion mobility 78−76915

ion-molecule collisions
see also charge exchange; ion-molecule reactions
alcohol+H_x^+, methanol to butanol, x=1-3, charge exchange ionisation *(German)* 77−83700
alcohol+H_x^+, methanol to octanol, x=1-3, charge exchange and ionisation *(German)* 77−83699
bromobenzene molecular ion+neutral atom, collisional relax., 2-photon photodissoc. 79−18258
1,3-butadienes, methyl substituted, singlet-triplet transitions, energies, relative cross-sections, $He^+(H_2^+)$ impact spectra 78−86942
charge transfer, energy disposal and reaction mechanisms 80−28103
classical differential cross-sections, anisotropic pots. 78−66627
collision spectroscopy, book 79−27065
drift tube technique in ion-neutral collisions, cross sections determ. 80−63748
elastic collision frequency, determ. by Fourier transform ICR spectroscopy 79−50105
electronic and at. collisions, conf., Kyoto, Japan (Aug.-Sept. 1979) 80−57011
electronic and at. collisions, conference, Kyoto, Japan (Aug.-Sept. 1979) 80−62394
energy transfer, modified statistical theory 79−50107
Fourier transform ion reson. spectroscopy of ions undergoing collisions with mols. 80−35598
heavy ion+atom (molecule), multiple electron loss cross sections meas. 79−45818
highly ionised ion+atom (molecule), many-electron transitions in violent encounter 78−90274
hydrocarbons+N^+, chemiluminescence, total reaction cross sections dependence on collision energy 79−47530
hydroxonium complexes, produced by collisional dissoc. method, mass spectrometric study, dissoc. energies determ. 80−95707
induced dipole-induced dipole potential, capture rate const. 79−13783
ion+permanent dipole, capture rate consts., transition state theory, summary of theories 80−28091
ion+polar molecule, perturbed rotational state approach 78−92469
ion+polar molecule collision, low-energy, rot. state approach 80−74224
ion+polar molecule collision freq., thermodynamic model 80−43145
ion induced inner shell vacancy formation 78−70926
ion-dipole capture in noncentral field, variational and trajectory investigation 80−63739
methane+X^{n+}, (X=Ar,Kr,Xe,U), Auger emission line shape after dissoc. 78−86838
molecular Λ-doublets transitions 80−14132
negative ion+molecule, electron detachment *(Russian)* 79−59566
negative ions, at. and mol. collisions electron detachment for energies near threshold 80−63797
non-reactive heavy particle collision calculations, review 79−59541
organic ring compounds, He ion stopping cross sections, ring struct., bond strain and Bragg rule deviations 79−98188
pentyl ion+methane, energy transfer, modified statistical theory 79−50107
polar mol.+ion, statistical and thermodynamic theory 80−99562
polar molecules, long range dipole interaction effect 80−102558
quasimolecules, superheavy, inner shell electronic states calc., ionisation during heavy ion collisions 79−89817
reactive and charge transfer collisions, between ions and molecules 78−62914
repulsive potential reconstruction from ion mobility in gas data 80−23486
slow collisions, K-shell excitation, impact parameter depend. 79−72388
tissue equivalent gas, stopping of heavy particles, W-values expt. results 79−7000
Ar^{6+}+H_2 collisions, ionisation and excitation resulting from electron capture 80−78683
Ar^{*+}+Kr, flowing afterglow, energy transfer reaction and quenching rates 80−23529
B^++CH_4, 200 keV, Auger spectra, single and double K-vacancy states 77−83706
B^{q+}+Ar(He)(H_2), keV electron capture cross section 80−14229
Be^++methane, autoionising core-excited Be II states, alignment prod. 80−14204
Br^-+H_2(D_2)(O_2)(N_2)(CO)(CO_2)(methane), total electron detachment cross sections for energies around threshold 80−99550

ion-molecule collisions continued
C-H, $A^2\Delta$-$X^2\Pi$, dissociative excitation, form. environment and parent mol. effects 80−78682
$C^{q+}+H(H_2)$, q=1-4, single electron capture cross sections 78−55233
$CH_4+H^+(He^+)(O^+)$, 1 MeV dissociation, kinetic energy spectra 78−94302
$C_2H_3^++HF$, interaction, struct. and stability, ab initio calcs. 80−58347
$CO+H^+$, vibr. excitation, differential scatt., low energy meas. 79−89749
$CO+X^{n+}$, X=Ar,Kr,Xe,U, Auger emission line shape after dissoc. 78−86838
$CO_2+H^+(D^+)$, vibr. excitation, isotope and time effects 80−63773
CO_2+X^{n+}, (X=Ar,Kr,Xe,U), Auger emission line shape after dissoc. 78−86838
Cl ions+Ar-methane, (isobutane), energy straggling 78−58785
$Cl^-+H_2(D_2)(O_2)(N_2)(CO)(CO_2)$(methane), total electron detachment cross sections for energies around threshold 80−99550
$^{35}Cl^{4+}$+atom (molecule), multiple electron loss cross sections meas. 79−45818
D_2+H^+, differential inelastic and reactive scatt., low energies 78−62911
$Fe^{4+}+N_2(Ar)(Kr)(Xe)(SF_6)$, 20 MeV, gaseous targets, electron loss, charge state yields 79−54957
Fe^{n+}+atom(molecule), multiple electron loss cross sections meas. 79−45818
H^++CN, perturbed rotational state approach 78−92469
$H^++CO(CO_2)(N_2O)$, electron capture into n=3 states, 2.2-8.2 keV 79−50129
H^++D_2, collisional complex form. 80−58339
H^++H_2, charge transfer into continuum 79−89765
H^++H_2, collisions at 3.7 eV, rotational transition probabilities 77−27156
H^++H_2, coupled states calcs. of inelastic collisions at 3.7 eV 77−14538
H^++H_2, elastic scatt. and rot. excitation, multistate semiclassical orbital method 79−27058
H^++H_2, electron capture, H(2s) cross section meas. 79−72386
H^++H_2, electron capture cross-section, anal. evaluation 79−36756
H^++H_2, electron capture into ground and excited s states 79−76509
H^++H_2, rot. and vibr. excitation, energy loss obs. 80−63773
H^++H_2, rot. excitation and vibr. transitions, coupled state approx. 77−61835
H^++H_2, rotational excitations, close-coupling calcs. 77−27157
H^++H_2, rotational quantum excitation, time of flight spectra 77−27154
H^++H_2, vibr. excitation, ab initio CI pot. energy surface calcs. 80−74228
H^++H_2, vibr. excitation, energy loss spectra, rot. sudden impact calcs. 77−88537
H^++H_2, vibr.-rot excitation, ab initio CI pot. energy surface calcs. 80−74229
$H^++H_2(CO_2)$, vibr. excitation, 10-30 meV 80−58358
$H^++H_2(N_2)$, 5-100 keV, secondary electron energy and ang. distrib. 80−14223
$H^++He(1s^2)$, K-shell electron capture collision, static pot. effect 80−91660
H^++methane, (Ne), (Ar), inner shell electron capture cross-sections 79−76510
H^++molecule (C-, F- or O-containing), K X-ray yields 79−45736
H^++N_2, excitation of 3914 Å band by proton impact 77−68101
H^++N_2, total ionis. cross section and stopping power for protons 80−69228
H^++N_2 collision, binary encounter calcs. of proton energy deposition 78−74746
H_2, energy dependence of $\bar{W}$ for alpha particles 79−6999
$H_2+Ar^{n+}(Kr^{n+})$, charge transfer, collision defects and dynamics, cross section meas. 80−53099
H_2+atom (ion), ionis. by one or two electron at. particles, Born approx. 79−54960
$H_2+B^{n+}(C^{n+})$, one electron capture and loss 80−18921
$H_2+C^+(N^+)(O^+)$, reactant ion electronic states, effect on charge transfer cross sections 80−63809
H_2+Cl^-, 4-11 eV, inelastic scatt. 79−98202
H_2+H^-, electron loss by 1-300 keV H^- ions 80−37857
H_2+H^+, combined rot. sudden and vibr. exact quantum treatment 78−74739
H_2+H^+ differential inelastic and reactive scatt., low energies 78−62911
H_2+He^+, 0.5-3.0 keV, direct and charge-exchange scatt. 77−75263
H_2+He^+, 25-90 keV, fast beam form, $He(2^3S)$ population 79−31740
H_2+Li^+, exponential gap relation, rot. inelasticity 80−78693
H_2+negative ion, electron-loss cross sections 80−37877
H_2+X^{Z+}, Z≥4, 1-20 keV, electron capture 80−37875
$H_2+Xe^{n+}(Ar^{q+})(Fe^{q+})$, electron capture by heavy multicharged ions at low velocities total cross sections meas. 80−99548
$H_2^++H_2 \rightarrow H_3^++H$, state-selected ion-molecule reactions threshold electron-secondary ion coincidence technique obs. 80−85166
HCO^++H_2, J=0-1 transition press. broadening, microwave absorpt. 80−52981
$H_3^+(D_3^+)+H_2(D_2)$ collisions, slow ion production, charge transfer cross sections 80−106378
H_2O vapour ionised by He^+ and He^{2+}, secondary electron emission yield obs. 80−102562
H_2O+H^+, 0.3 to 1.5 MeV, electron ejection, energy and ang. distrib. meas. 77−71851
H_2O+positive ion, inelastic scatt., 4-6 eV energy loss region 78−90277
H_2S+Ar^+, emission spectra obs. 78−50622
He^++H_2, charge transfer, appl. of atom-photon coincidence meas. 79−45829
He^++H_2, DIM approx. pot. energy surfaces and nonadiabatic coupling 80−23330
$He^++H_2(N_2)(O_2)(CO_2)$(methane)(ethane)(propane), 0.7-2 MeV, charge-changing collisions, electron capture 80−58372
He^++N_2, collisional excitation processes, visible emission, cross-sections 80−99571
$He^{2+}+H_2(O_2)$, electron capture collisions, spin conservation 78−82837
He^{2+}+methane, (Ne), (Ar), inner shell electron capture cross-sections 79−76510
$He^{2+}+N_2$, 200-600 eV, 0-20°, comparison with He^{2+}+Ne(Ar) 78−74732
$^{127}I^{5+}$+atom (molecule), multiple electron loss cross sections meas. 79−45818
Kr^++HD, kinetic isotope effect, cross sections, rot. transfer 77−9041
Kr^++molecule, $^2P_{3/2}(^2P_{1/2})$ doublet ground state reactions at 300K 80−108702

ion-molecule collisions continued
Li^++CO, 4-7 eV, final rot. state distrib., small ang. depend. 79−68300
Li^++CO_2, collisional excitation, quasiclassical trajectory calcs. 80−83467
Li^++CO_2, rot. vibr. energy transfer, 1 to 10 eV, many body theory 80−28093
$Li^++CO_2(N_2O)$, vibr. excitation, time of flight meas. 77−79682
$Li^++CO(CO_2)(N_2O)$, vibr. excitation, 70 to 1500 eV 78−82824
Li^++H_2, elastic scatt. and rot. excitation, multistate semiclassical orbital method 79−27058
Li^++H_2, quasiclassical approx. for scatt. amplitude, rot. degrees of freedom *(Russian)* 77−79676
Li^++H_2, rot. inelastic scatt., body frame partitioning approx. calcs. 80−23527
Li^++H_2 (j=0), rot. alignment, state-selected differential and integral rotationally inelastic cross sections 80−37863
Li^++H_2 (ortho, para), rot. excitation and ang. depend. transition probabilities, time of flight spectra 80−23517
$Li^++H_2(N_2)$, ion-molecule forces, generalised electron gas Drude model appl. 79−98183
Li^++methane, vibrational excitation, time of flight measurements 79−45826
Li^++N_2, rot. and vibr. inelastic collisions, trajectory calcs. rel. to previous data 78−62878
Li^{3+}+methane, (Ne), (Ar), inner shell electron capture cross-sections 79−76510
N^++H(hydrocarbons), chemiluminescence, total reaction cross sections dependence on collision energy 79−47530
N^++N_2, X-ray emission ang. distrib., MO calc. 79−54803
N^++O_2, branching ratio kinetic energy depend. 80−97703
$N^{q+}+H(H_2)$, q=1-5, single electron capture cross sections 78−55233
N_2, collisional destruction of singlet He I states in low press. glow discharge 80−49030
N_2^{n+}, Coulomb explosion following heavy ion impact, ab initio SCF calc. 79−18277
N_2+C^+ collisions, luminesc. 80−1055
$N_2+Cl^{4+}(I^{5+})$, 20 MeV, electron loss cross sections, pot. model data anal. 79−27082
N_2+H^+, energy transfer, dissoc., cross section calcs. 77−50522
N_2+H^+, spatial distrib. of excited moles. induced by 100 and 150 kev proton beams 78−58793
N_2+H^+, vibr. excitation, differential scatt., low energy meas. 79−89749
$N_2+H^+(e)$, vibrational N_2^+ excitation *(Russian)* 80−53156
N_2+He^+, K-shell ionisation, total cross-sections calcs. 79−31663
N_2+He^{x+}, energy loss straggling, ion energies of 50-500 keV per nucleon 77−46620
$N_2+N_2^+$, first negative bands, excitation cross-section calcs. 77−68100
N_2+N^+, collision, isotope exchange, ion cyclotron reson. obs. 77−52618
N_2+N^+, molecular-orbital X-rays, recoil effects 78−66645
N_2+negative ion, electron-loss cross sections 80−37877
N_2+X^{n+}, (X=Ar,Kr,Xe,U), Auger emission line shape after dissoc. 78−86838
$N_2^++O_2(H_2)$(He), $(A^2\Pi_u)$ Meinel band deactivation cross sections above thermal energies 78−66635
NH_3+X^{n+}, (X=Ar,Kr,Xe,U), Auger emission line shape after dissoc. 78−86838
NO destruction in collisions with excited molecules 80−14189
$NO+H^+$, vibr. excitation, differential scatt., low energy meas. 79−89749
$NO+H^+(He^+)(O^+)$, dissociative ionis. 79−10188
Na^++HCN, rotational excitation, Stark shifted level transitions, energy transfer calcs. 79−98059
Ne^++Co_2, three dimens. quadrupole ion storage, ion mobility, effect of charge exchange reactions, Monte Carlo calcs. 80−55738
$Ne^++D_2(H_2)$, energy-loss scaling in 0.5-3.5 keV 80−63768
O^-+N_2, electron detachment, collision with vibr. excited mols. 79−54961
O^-+O_2, electron detachment, collision with vibr. excited mols. 79−54961
$O^++N_2(O_2)$, excited ion reactions, charge transfer coeffs. at thermal energy 80−95721
$O^{q+}+H(H_2)$, q=1-5, single electron capture cross sections 78−55233
O_2+H^+, energy transfer, dissoc., cross section calcs. 77−50522
O_2+negative ion, electron-loss cross sections 80−37877
O_2+X^{n+}, (X=Ar,Kr,Xe,U), Auger emission line shape after dissoc. 78−86838
$O_2^-+N_2$, electron detachment, collision with vibr. excited mols. 79−54961
$O_2^-+O_2$, electron detachment, collision with vibr. excited mols. 79−54961
$O_4^+(O_5^+)(O_6^+)(O_2^+H_2O)$ 80−95707
$O^{+*}+O_2(N_2)$, metastable ion reactions, rate consts. and ion mobility at 300K 80−95722
reactant ion electronic states, effect on charge transfer cross sections 80−63809
$SF_6+Li^+(H^+)$, mode selective vibr. excitation 80−58351
SO_2+Ar^+, emission spectra obs. 78−50622
SiH_4+F^{n+}, X-ray emission from gaseous target, q=4-9, 1 and 2 MeV/amu 79−83060
UF_6^-+Ar, UF_6^- internal excitation 80−106386
Xe^++molecules, $^2P_{3/2}(^2P_{1/2})$ doublet ground state reactions at 300K 80−108702

ion-molecule reactions
acetaldehyde, primary and secondary photoionis. processes, ion-mol. reactions 79−36709
acetone, thermal energy charge transfer reactions 79−87828
acetone cation+ketene, proton transfer, CH_3CO^+ heat of form. 77−90592
acetyl chloride, thermal ion-mol. reactions, long-lived intermediate ion form. 79−20360
acetylene+$XH^+(X^-)$, proton transfer reactions, rate consts. meas., Average Quadrupole Orientation Theory 77−63887
acetylene cation+methane, reaction, vibr. and translational energy depend., mass spectrosc. obs. 79−47908
alcohols, α-particle impact, 0.3-2.0 MeV, O stopping cross-sections 78−17753
alcohols, chemical ionisation mass spectra 77−75273
ammoniated electron+R^{3+}, reaction kinetics meas. by ns. pulse radiolysis 79−52638
anisotropic molecular polarisability, effect on rate const. 79−15968

ion-molecule reactions continued
anisotropic molecular polarisability, effects on rates 79−15967
association, temp. depend., rate coeffs. calc. 80−16661
association density of quantum states and temp. depend. of rate coeff. 80−101015
association rate calc. for ion-molecule reaction 80−81282
association reactions, gas phase, statistical phase space theory approach 80−50839
atmosphere ion chemistry, rate consts., in situ ion comp. meas. 80−31154
atmospheric ion chemistry 80−61885
bakeable hollow cathode, ion-molecule reaction study in discharge gas mixtures 80−37117
benzene, secondary ion reactions, branching ratios 78−40035
benzene+$Li^+(Mg^+)$, relative level excitation, orbital ang. momentum quantum number depend. 78−25688
benzene+molecular ion, fragmentation and electron transfer collisions 79−79229
benzene+$Si^+(SiH^+)(SiH_3^+)(SiD_3^+)$, energy-rich collision complex form. 77−9068
benzene cation+benzene, trapped ion mass spectra 80−89470
biacetyl, thermal energy charge transfer reactions 79−87828
bimolecular positive ion reactions in interstellar clouds, comets and reducing planetary atmospheres 77−63896
binary ionic recombination, ambient gas temp. and density rate depend. 80−35522
butene, isomers, ion-mol. reactions, photoionisation mass spectra 80−81298
2-butene ion, fragmentation, angular momentum in ion-mol. reacts., RRKM calc. 80−66773
carbohydrates, reactions with hydrated electrons and hydroxyl radicals, rate constants obs. 80−50825
catalysis by polyelectrolytes 79−57217
chamber 1.5 m diameter for experiments *(Japanese)* 77−54625
chemical ionisation, using needle electron source 77−75273
chemical ionization mass spectrum *(Japanese)* 79−43669
chemical laser systems, ion-molecule reactions, thermal energy, book contrib. 77−50668
chemiluminescence, anal. of spectra 78−64832
chloromethane+Cl^-, S_N2 reaction, local orbital description, ab initio FSGO method 78−76842
1-chloropropane, formation of chlorohexanes by ion-mol. reactions in radiolysis 78−27802
cluster ion reactions in gases, review 77−81401
clusters, small, formation, struct. and props. 80−58437
collision system, pot. curves at low collision energies, beam studies 80−61088
cyanoacetylene, lab. study of ion-molecule reactions, rel. to interstellar synthesis 79−1940
cyanoacetylene, rate coeffs. for reactions with ions of interstellar significance 79−57221
cyanodiacetylene, lab. study of ion-molecule reactions, rel. to interstellar synthesis 79−1940
cyclohexane$_{(\ell)}$ solns., positive ion-solute mol. reaction rate consts. in radiolysis 77−9091
dimethyl ether-trioxane mixtures, condensation-elimination ion-mol. reactions obs. 78−23939
dimethylamine proton-bound dimers, form. in ion-mol. assoc. reactions, rates analysis 77−60054
dipole capture collisions, simple models, energy depend. of cross-section 79−91911
DNA-Au (III) interaction, rate consts., activation energies, pH, spectrophotometric obs. 80−30228
drift tube determination, selections from 1977 Comments on Modern Physics, book 79−30181
drift tube studies, buffer gas mixture choice, for ion-neutral reactions 79−57232
drift tube with hollow cathode ion source, for reaction rate consts. meas. 78−64834
electric field effect on reactions in dilute gases and solutions 80−81315
electronic states, kinetic energy, molecular beams obs. 80−30230
elementary reaction processes, fast beam studies *(Japanese)* 80−7764
endothermic reson. excited ats., optical excitation technique, radiation diffusion conditions 78−55227
entropy change, enthalpy of form., equilib. consts., thermochemistry 80−30233
equilibrium constants, determ., rel. to thermodynamics 79−5154
equilibrium constants, ion cyclotron reson. spectrometer meas. 77−56218
ethers, α-particle impact, 0.3-2.0 MeV, O stopping cross-sections 78−17753
ethyl cation+alkane reaction, temp. and kinetic energy relative rate consts. determ. 80−81299
ethyl chloride-NH_3, positive ion molecule reactions 79−24729
ethylene+$Ar^+(Kr^+)(Ne^+)(Xe^+)$, 2-stage ion beam mass spectrometric obs. 77−9061
ethylene cation+ethylene, collision complex stability, photodissoc. expts. on dimer and trimer 79−57212
ethylene oxide-d_0, -d_4, ion chemistry, photoionisation and ion cyclotron reson. obs. 77−21373
ethylene-propylene fluorinated mixtures, mol. ion reactions, cyclotron reson. spectrometer 77−21367
exothermic, rate coefficient, transition state method 80−40688
fast nucleus+molecule, atom capture, quantum calcs. 80−71911
ferrocene, proton irradiated, Mossbauer study of induced chemical changes 79−28656
fluoromethanes+$Ne^+(He^+)(Ar^+)(Kr^+)(Xe^+)(N_2^+)(CO^+)(CO_2^+)(N_2O^+)$, thermal energy charge transfer reactions mechanism 77−63889
formaldehyde+$H_3O^+(H_3S^+)(HCNH^+)(HCHO.H^+)$, proton transfer, rate and equilib. consts. 78−48636
formyl fluorides, gas phase ion-mol. reactions, comparison with H_2CO+F_2CO, H_2CO+Cl_2CO 77−63900
Fourier transform ion cyclotron double resonance, complicated ion-molecule reactions 78−80808
Fourier transform ion reson. spectroscopy of ions undergoing collisions with mols. 80−35598
gas phase reactions and high-press. mass spectrometer, review *(Japanese)* 78−64830
$H^-+H_2^+ \rightarrow H_2^*+H$ recombination react., calcs. *(Russian)* 80−55659
halocarbons, decomp. by natural tropospheric ions 77−21889
haloethylenes+$Ar^+(Kr^+)(Ne^+)(Xe^+)$, 2-stage ion beam mass spectrometric obs. 77−9061
ion-molecule reactions continued
1-5hexadiyne ion+neutral 1,5-hexadiyne, trapped-ion mass spectrometry 80−97694
hydrocarbon ions+H_2(methane), rate coeffs., ionised product. distribs. 77−44471
hydrocarbons, simple ions, reaction with simple mols. at thermal energies 77−40532
hydrocarbons $(H_2)+N^+$, rotational vibrational product excitation 79−47901
hydroocarbon chain synthesis in interstellar clouds, ion-molecule scheme 80−12786
inert gas-halogen mixture, ion form., ion-mole. reactions, mass spectra 77−61841
infrared chemiluminescence detection, vibrational product states appl. 78−88625
interstellar chemistry, implications of strongly deuterated molecules obs. 79−5891
interstellar chemistry, long-chain hydrocarbons, formation mechanism 80−46653
interstellar clouds, gas phase reactions rel. to CO isotopic abundances 77−29912
interstellar clouds, ion-molecule reactions rel. to cyanide chemistry 77 82297
interstellar clouds, ion-molecule reactions rel. to electron abundances determ. 80−41866
interstellar clouds, non-molecule reactions rel. to C chain mols. form. 80 26935
interstellar dense clouds, molecular composition 77−29892
interstellar dense molecular clouds, chem. evolution 78−28749
interstellar gas clouds, molecular synthesis, lab. meas. 78−12314
interstellar ion-molecule reactions, rel. to obs. of $N_2H^+/HCO^+/SO_2$ var. in Orion 77−26034
interstellar large molecules, deuterated species 77−53665
interstellar molecule formation in clouds from singly or multiply ionized atoms 79−17039
interstellar molecules synthesis, laboratory studies of ion-atom reactions 80−67812
interstellar reactions, appls. to relative distribs. of N_2H^+, HCO^+, HCN and CN 77−33587
interstellar shocked mol. clouds, nonequilib. chemistry 79−21377
intramolecular selectivity, stereochemistry, gas phase ionic chemistry techniques 80−35529
ion+neutral molecule, reactant internal energy, rate constants, drift tube 80−30231
ion+polar molecule collisions, average dipole orientation theory, ang. momentum conservation 78−92466
ion beam focusing from quadrupole mass filter using electrostatic lens 79−229
ion cyclotron resonance spectrometer, positive ion trapping in electron beam 78−21254
ion kinetics in high-pressure laser plasmas 80−64002
ion speed distribution effects in flow-drift tubes 77−56219
ion speed effects in flow-drift tubes, Monte Carlo simulation 77−56221
ion speed effects in flow-drift tubes, statistical mechanical theory 77−56220
ion-dipole capture in noncentral field, variational and trajectory investigation 80−63739
ion-induced dipole interaction, quantum stepwise approx. procedure 78−44376
ionic fragmentation, translational energy, phase space theory 77−9051
ionosphere, atomic processes, book contrib. 77−37482
ketene-d_0,-d_2, mol. ion reactivity, vibr. energy effects, mass spectrometric obs. 77−44470
kinetics, conf., La Baule, France (1978) 80−27043
laser excitation methods, ion-molecule processes 80−28221
low energy, dipole interaction influence 80−89475
low energy, reaction rates and cross-section determ. in drift tube 77−60052
low temperature plasmas, interstellar species form. radiative assoc., reaction types 80−31348
mass spectrometry, negative chemical ionis., ionis. techniques, review 78−325
mass spectroscopy using selected-ion flow tube 77−188
mesosphere, ion-neutral bunches charge exchange rel. to ion bunching 78−73424
metal ions interaction, with nucleic acids, nucleosides and nucleotides, review 80−3577
meteor wakes, ion-molecule reactions rel. to red afterglow 78−36536
methane+$H^- \rightarrow H^-$+methane, force decomposition anal. along reaction coord. 78−27741
methane+$Li^+(Be^+)(B^+)$, single collision, time delayed autoionisation spectra 78−1067
methane+O_2^+, reaction rate const. kinetic energy depend., 300K, 0.125-0.450 torr 78−76850
methane+$O^+_4(O_2^+)$, products, rate consts., rel. to stratosphere 77−9040
methane+$O_2^+(a^4\Pi_u)$, 0.04-1.2 eV, reaction rate consts. 79−47911
methyl cation+$H_2(N_2)(O_2)(CO)(CO_2)$, ternary assoc. reaction, rate coeffs., 100-300K 79−61845
methyl cation+NH_3, reaction kinetics, 0.04-1 eV *(French)* 80−66768
methyl chloride-NH_3, positive ion molecule reactions 79−24729
methyl ion+H_2O(He) ternary association reaction in energy range 0.04-0.1 eV 80−71896
methylamine, proton-bound dimers, form. in ion-mol. assoc. reactions, rates analysis 77−60054
molecule+fast heavy ion, dissoc. ionisation obs. 79−47899
molecule+negative ion, thermochemical data, gas phase acidity scale, mass spectroscopic techniques 80−30234
molecule+point-like charge, interaction energy, polarisation term 77−52634
naphthalene anion radical+H_2O, react., H_2 prod. 78−92460
naphthalene radical anion+TCNQ, electron transfer reactions, theory 78−15661
nitroaromatic compound+anion radical, photo-CIDNP, acid-base equilib. effects 77−75185
nucleic acid bases, protonated, anion binding, electrostatic mol. pots. 79−1999
organonitrogen molecules, synthesis in interstellar clouds, ion-molecule scheme 80−12786
pentafluoromethyl iodide, ion-molecule reactions, amongst radiolysis products, reaction rates, mechanisms, mass spectra 79−5136

ion-molecule reactions continued
perturbed rotational state approach to low energy ion+polar mol. collision 78−92469
phenyl cation, struct., ion-molecule reactions studied by trapped ion mass spectroscopy 80−102586
polar molecules, long range dipole interaction effect 80−102558
polyatomic ions, energy deposition on high-energy collision, angle-resolved mass spectrometry obs. 80−32825
polyatomic radical cations, use as probe in ion+molecule reactions 80−28055
positive ions+H_2O, reaction rate consts., product distrib., ICR obs. 79−8428
propynyl cation+propyne, reactant structure effects 80−89469
pulsed ion cyclotron resonance mass spectrometer for ion-molecule reaction studies 78−41372
radiative and ternary ion-molecule association 80−30227
rate coeffs., ions containing C and H, review 77−25260
rate constants, time resolved meas. in mass spectrometry 78−48614
rate consts., ion vel. distribs. in high field swarms, Boltzmann eqn. soln. 77−70283
reaction rate consts. meas. by ion cyclotron resonance 77−86287
reactive and charge transfer collisions, between ions and molecules 78−62914
semiclassical theory for near adiabatic photon assisted mol. collisions 79−5141
slow reactions, carbonyl addition rate consts. rel. to struct. 80−30232
slow reactions, nucleophilic displacement, rate consts. rel. to struct. 80−30232
slow reactions, proton transfer, rate consts. rel. to struct. 80−30232
slow reactions, three body assoc., rate consts. rel. to struct. 80−30232
state selected reactions, threshold electron-secondary ion coincidence method obs. 79−5190
supersonic molecular beam apparatus for ion anal. reaction studies *(Japanese)* 79−50165
symmetry selection rules for ro-vibronic states 77−81385
termolecular ionic recombination, ambient gas temp. and density rate depend. 80−35522
tetra-n-butylammonium halides in benzene, chloroform, CCl_4, far IR spectra, ion-ion, ion-mol. interactions 80−60562
tetracene anion+tetracene cation, electron transfer reaction, singlet fission 78−11502
1,1,2,2-tetrafluorocyclobutane, ion-mol. reactions, reaction pathways, mass spectra 77−21368
tetrafluoroethylene radical ion+tetrafluoroethylene, cycloaddition 78−13533
thermal, emission spectra obs. using pulsed ICR cell 77−19108
thermochemistry, flames and diagnostic techniques 80−55664
three-body ion-neutral assoc. reactions, saturation 79−39134
three-body reaction, statistical theory 79−57204
tolyl cation+alkyl nitrate, reactions and ion struct. 77−52619
transition state location from ang. momenta distribs. 78−64808
transition state theory 78−27755
translationally driven reactions, transition state theory, cross section curve 80−26000
trifluoromethoxide gas phase ion reactions with carboxylic acids, ion cyclotron reson. obs. of competitive solvation 79−79227
trifluoromethyl iodide, ion-molecule reactions, amongst radiolysis products, reaction rates, mechanisms, mass spectra 79−5136
upper atmospheres of Earth and planets, interstellar clouds, review 78−33563
vibrational energy effects on kinetics, phase space model 78−11508
vinyl fluoride, vibr. excitation effects on ion-molecule reaction pathways, photoionisation mass spectra 77−16804
water cluster ions form. in ionospheric D-region rel. to mesospheric temp. 77−21842
weakly ionised gas non-ideal behaviour, virial eqn. of state and fugacity coeffs. 80−79424
$X^+ + HD \rightarrow X + HD^+$, kinetic (orientation) isotope effect, reaction model 78−23931
$Al^+ + N_2(O_2)(N_2O)$, reaction cross sections 77−29000
$Ar^+ + (N_2)(H_2)(O_2)$, charge exchange reaction rates 77−86295
$Ar^+ + H_2$, charge transfer reactions, excited products, Ar initially metastable 78−68879
$Ar^+ + H_2$, collinear reactions, electronic nonadiabatic transitions 78−7180
$Ar^+ + H_2(N_2)(O_2)(CO)(NO)$, charge transfer cross sections 77−34751
$Ar^+ + H_2(O_2)(CO_2)$, reactions in flow-drift tube, rate consts. 78−15664
$Ar^+ + H_2(v_i=0) \rightarrow ArH^+ + H$, electronic nonadiabatic transitions, two-state model calc. 78−73035
Ar^++molecule (atom), dissociative reaction rate coeffs., in high-press. afterglow 79−87837
$Ar^+ + NO$, reaction product ratios, 300K 80−7783
$Ar^+ + O_2(N_2)(NO)(CO_2)$, reaction kinetics, mass spectrometer with selective introduction drift tube *(French)* 79−11839
$Ar^+ + O_2 \rightarrow Ar + O_2^+$, thermal energy charge transfer, energy disposal determ. 79−64099
$Ar^{2+} + O_2(CO_2)(C_2H_2)$, reactions in flow-drift tube, rate consts. 78−15664
$Ar(Ar^+) + H_2^+(H_2) \rightarrow ArH^+ + H$, electronic transitions, collinear reaction, curve crossing model, DIMZO surface 79−74373
$Ar^+(Ar^{2+}) + N_2$, reaction rate consts. 78−48613
$Ar^+(Ar^{2+}) + O_2$, reaction rate consts. 78−48613
$B^+(^3P_u) + D_2$, reactive scatt., 1-40 eV, ion products ang. and energy distrib. 79−98214
$Ba^+ + D_2 \rightarrow D + BaD^+$, sequential impulse model, prod. bond dissoc. energy and cross section 80−81295
$Be^+ + H_2(He)(Ne)(methane)$, Be Auger spectra 77−57951
Br^-+methane(fluoromethane), excitation functions, reactive scatt., eV region *(German)* 78−35677
$C + O^+$ ion-molecule reaction, 15 eV energy O^+ production system 80−84817
C^-+CO(Mg)(N_2), electron detachment cross-sections, 20-150 keV 78−25690
C^++ethylene (propylene oxide), branching ratios 78−44354
$C^+ + H_2$ in diffuse interstellar clouds rel. to CH^+ prod., role of shock waves 80−56898
$C^+ + H_2(D_2)$, $CH^+(D^+)$ $A^1\Pi$ rot.-vibr. population distribs. 80−23396
$C^+ + H_2 \rightarrow CH^+ + H$, classical trajectory anal. 78−53192
$C^+ + H_2 \rightarrow H + CH^+$, energy spectrum and prod. vibr. excitation 77−77745
$C^+ + NH_3$, role in form. of interstellar HCN and HNC 78−81672
ion-molecule reactions continued
$CD_n^+ + H_2(HD)(D_2)$, isotopic exchange, interstellar implications 80−61087
$CH^+ + H_2$, reaction products translational energies 77−86298
CH_2^+, radiative association, rate const. rel. to interstellar clouds 77−45512
$CH_2^+ + D_2$, reaction products translational energies 77−86298
CH_3^+, CD_3^+, collisional activation to form $C(H,D)_{0-3}^+$ products, energy transfer 77−44474
CH_3^+, CD_3^+, reactions with acetic acid methyl acetate, dimethyl ether and ethylene oxide 77−63901
$CH_3 + N^+$, role in form. of interstellar HCN and HNC 78−81672
$CH_3^+ + CH_4(NH_3)(H_2S)$, condensation reactions mechanism 80−25996
CH_3^++small molecules, binary and ternary reactions at thermal energies, rate coeffs., product distribs. 78−44358
CH_4^+, CD_4^+, collisional activation to form $C(H,D)_{0-3}^+$ products, energy transfer 77−44474
$CH_4^+ + CH_4(CH_2D_2)$, dissoc. charge transfer reactions, H and D atoms elimination 78−85141
$CH_n^+ + COS(H_2S)$(formamide)(methanol)(methylamine), (n=Q-4), reactions at 300K 78−44357
$CH_n^+ + H_2(HD)(D_2)$, isotopic exchange, interstellar implications 80−61087
$C_2H_2 + OH^- \rightleftharpoons C_2H^- + H_2O$, equilib. consts., ab initio SCF and CEPA calcs. 78−3361
$CO + {}^{13}C^+(HCO^+)$, isotopic exchange, interstellar implications 80−61087
$CO^+ + 2CO_2 \rightarrow 2CO_3^+$, reactions of electronically excited CO^+ 77−1915
$CO^+ + D_2$, state selected reaction cross-sections, coincidence technique obs. 80−66797
$CO^+ + H_2$, ion-molecule reaction detection of laser-induced ion spectrum, rot. components 78−74671
CO_2, positive and negative ion reactions 77−40540
CO_2, primary ionis. coeff., electron attachment coeff. rate coeff. 77−4900
CO_2^+-D_2, DCO_2^+ and DCO^+ formation 77−60056
$CO_2 + C^+(N_2H^+)$, rate coeffs. meas. at 300 and 100K in flowing afterglow 79−20346
$CO_2 + He^+(H_2^+)$, charge transfer, energy transfer, product ion excitation and fluoresc. 77−75288
$CO_2 + N_2 + He$, glow discharge positive ion species identification *(Russian)* 80−84014
$CO_2 + OH^- \rightarrow HCO_3^-$ react., MO-LCAO-SCF calcs., energy barrier 78−76846
$CO_2^+ + 2CO_2 \rightleftharpoons (CO_2.CO_2)^+ + CO_2$, reaction rates 77−36745
$CO_2^+ + CO_2$, $(CO_2)_2^+$ formation, exothermicity lower limit, photoionisation of supersonic mol. beam 78−46406
CO_2^++ethylene, rate coeffs. and product distribution determ. 80−97693
$CO_2^+ + H_2$ (D_2), HCO^+ and DCO_2^+ form., threshold form. energy 80−50844
$CO_2^+ + SO_3$, in mass spectroscopy of SO_3 mixtures 78−3415
$(CO_2)_2^+$, ion-mol. reaction product distribs. and rate coeffs. 80−50852
$CO_2^+(CO_2^{2+}) + $atom(mol.), dissoc. and charge transfer 77−65532
$(CO_2.CO_2)^+ + CO \rightarrow (CO_2.CO)^+ + CO_2$, reaction rates 77−36745
$CO_2.CO_2^+$+ethylene, rate coeffs. and product distribution determ., dissoc. energy and heat of form. 80−97693
$CO_2.CO_2^+ + SO_2$, reaction rate coeff. and product distrib. 80−3305
$C^+(^2P) + CH_4$ reaction, 0.1-10 eV, complex formation 77−9073
$C^+(^4P) + H_2$, reaction, energy and ang. distrib., energy spectra 77−1918
^{12}C+alkane (alkene), thermal energy reaction, mass spectra 77−9067
^{13}C+alkane (alkene), thermal energy reaction, mass spectra 77−9067
C (4S)+molecule, spin angular momentum conservation in proton transfer 77−16805
Ca^{2+}, interaction with bovine rhodopsin 79−100563
Ca^{2+}, interaction with bovine rhodopsin 79−100564
$Cl^- + HBr(HI) \rightarrow HCl + Br^-(I^-)$, vibr. product state distribs., IR chemiluminesc. obs. 80−81309
Cl^-+methane(fluoromethane), excitation functions, reactive scatt., eV region *(German)* 78−35677
$Cl^+ + CO \rightarrow O + CCl^+$, reaction cross section, heat of form., mass spectrometric obs. 79−61843
$Cl^+ + D_2$, inelastic and superelastic collisions, DCl^+ formation mechanisms 78−20011
$Cl^+ + H_2$, interstellar, as H ionisation source 79−40245
Cl^++molecule, reactions at room temp. 80−93749
Cl_2^-, vibrationally excited, reactions and photodestruction 77−60048
$Cl_2 + 2Br^- \rightarrow Br_2 + 2Cl^-$, aqueous soln., specific rate determ., competition technique 78−44348
$Cl_2^- + HO_2$, reaction in pulse irrad. aq. soln. containing Fe^{2+} and Cl^- 78−20036
$ClO^- + NO(NO_2)(SO_2)(CO_2)$, rate consts. at 300K 78−76829
Cs^++t-butyl chloride, reactive scatt., stripping model, ang. and energy distrib. 80−35510
$D_3O^+(D_2O)_n + H_2O(NH_3)$, binary reactions, rate coeffs. and product ion distributions determ. 80−81305
F^-+fluoromethane, S_N2 reaction, ab initio LCAO SCF calcs. 77−81402
$F^- + H_2F$, proton transfer reaction, polarisation model 79−39131
$F^- + HF$, proton transfer reaction, polarisation model 79−39131
F^-+methane, MINDO/3-FORCES study, reactant energy, products and paths 78−95926
$F^+ + H_2$, empirical and ab initio correlation diagrams, pot. energy surfaces 78−40041
$F^+ + H_2 \rightarrow FH^+ + H$, rot. effects 78−27744
Fe(III)+SCN^-, reaction kinetics, computer-controlled stopped-flow system 79−15953
H^-+BH_3, B-H bond form., kinetic energy, interference charge density changes, CNDO/2 calc. 79−57211
H^-+methane$\rightarrow$methane+H^-, nucleophilic substitution, ab initio pot. energy classical trajectory anal. 78−68886
H^-+CN, perturbed rotational state approach 78−92469
$H^+ + H_2O(N_2)$, UV and visible band emission cross-sections 77−16847
$H^+ + H_2 \rightarrow H_3$, nonadiabatic transitions, comparison of surface hopping and complex-valued time calcs. 77−9049
H^++methane$\rightarrow H_2^+$+methyl radical, quantum 80−71911
$H_2 + Cu^{2+}(Ti^{2+})$, electron capture cross-sections, 0.5-14 keV 78−42205
$H_2 + H_2O^+ \rightarrow H + H_3O^+$, reaction kinematics 78−31625
$H_2 + H^+(H_2^+)(He^+)(O^+)$, H^+ prod., from H_2^+ dissoc. states or H_2^{2+} 78−20015
$H_2 + He^+$, DIM approx. pot. energy surfaces and nonadiabatic coupling 80−23330

ion-molecule reactions continued
$H_2+N^+ \rightarrow NH^+ + H$, classical trajectory calc. 79−100337
$H_2^+ + CO \rightarrow H + HCO^+$, 1.89 eV crossed beam study 80−21287
$H_2^+ + D_2 \rightarrow {}_2H^+ + H$, product angular and vel. vector distributions meas. by crossed beam expt. 80−101012
$H_2^+ + H_2$, pot. energy surface and nonadiabatic regions, charge exchange and reaction, VB calc. 78−40027
$H_2^+ + H_2$, state selected reaction cross sections, coincidence technique obs. 80−66797
$H_2^+ + H_2 \rightarrow H_3^+ + H$, electronically excited products, merged beam apparatus meas. 78−31626
$H_2^+ + H_2 \rightarrow H_3^+ + H$, reaction dynamics, isotopic variations 78−27745
$H_2^+ + H_2 \rightarrow H_3^+ + H$, state selected, threshold electron-secondary ion coincidence method obs. 79−5190
$H_2^+ + H_2 \rightarrow H_3^+ + H$, state-selected ion-molecule reactions threshold electron-secondary ion coincidence technique obs. 80−85166
H_2^+ + methanol, dissoc. charge transfer reaction studied at rel. translational energies from 600 eV to 5000 eV 80−104432
$H_3^+ + H_2 \rightarrow H_5^+ \rightarrow H_2 + H_3^+$, ab initio GO pot. surface, C_{2v} symmetry 77−25252
H_3^+ + XCN, flowing afterglow, rate const. meas. 77−40533
$HCN + H_3O^+(H_3S^+)(HCNH^+)(HCHO.H^+)$, proton transfer, rate and equilib. consts. 78−48636
$H_3CO^+ + H_2S \rightleftarrows H_3S^+ + HCHO$, chemical equilib. consts., proton affinity of HCHO and H_2S 78−85189
$H_3CO^+ + HCN \rightleftarrows H_2CN^+ + HCHO$, chemical equilib. consts., proton affinity of HCHO and HCN 78−85189
HCl-N_2 mixture, electron swarm, Cl^-.HCl cluster formation, dissoc. attachment, drift tube mass spectra 78−68884
$HCl + O^-(O_2^-)(NO_2^-)(CO_3^-)(CO_4^-)$, rate consts. at 300K 78−76829
$HF + H^-$, reaction, ab initio pot. energy surface calcs. 79−39127
HNO_2, isomers, protonation mechanism, electrostatic pot. prediction limits 78−11506
$H_2O + Ar^+$, thermal-energy charge transfer, H_2O^+ product internal and kinetic energy 80−16654
$H_2O + H_3O^+H(H_3S^+)(HCNH^+)(HCNO.H^+)$, proton transfer, rate and equilib. consts. 78−48636
$H_2O + H^+ \rightleftarrows H_3O^+$, equilib., H_2O proton affinity calc. 78−92497
$H_2O + He^+(O^+)(N_2^+)(O_2^+)(Ar^+)$, 50 to 250 keV, OH radical form. 78−56890
H_2O^+ + diatomic (polyatomic) molecule, reaction, ICR obs. 79−8429
$H_2O^+ + H_2$, ion-molecule reaction detection of laser-induced ion spectrum, rot. components 78−74671
$H_2O^+ + NO_2(O_2)(NO)(CO)(H_2)$(ethylene)(methane), rate constants determ. as function of relative kinetic energy 80−81292
$H_3O^+(H_2O)_n + D_2O(NH_3)$, binary reactions, rate coeffs. and product ion distributions determ. 80−81305
$H_2S + H_3O^+(H_2S^+)(HCNH^+)(HCHO.H^+)$, proton transfer, rate and equilib. consts. 78−48636
$H_2S^+ + HCN \rightleftarrows H_2CN^+ + H_2S$, equilib., rate coeffs. and proton affinity, flowing afterglow 78−56885
He^+ + acetylene-d_0(-d_2), $CH^+(CD^+)$, A-X luminesc., in near-thermal charge exchange 78−50632
$He^+ + CO_2$, dissociative charge exchange kinematics 80−3318
$He^+ + H_2(D_2)$, dissociative charge transfer, 78-330K 80−61079
He^+ + methanol, dissoc. charge transfer reaction studied at rel. translational energies from 600 eV to 5000 eV 80−104432
$He^+ + N_2O$, in afterglow, N_2^+ optical emission obs. 79−68251
$He^+ + N_2O$, rate coeffs. meas. at 300 and 100K in flowing afterglow 79−20346
$He^+ + O_2$, (N_2), charge transfer reactions, product ion distribs. 77−73445
$He^+ + O_2$, metastable O^{+*} ion production 79−91933
$He^+ + O_2$, thermal energy charge transfer, O^+ product ion obs. 79−64100
He_2^+, rate coeffs. for bimol. and termol. ion-mol. reactions 78−53188
$He_2^+ + Ne(Ar)(N_2)(CO)(CO_2)(Ch_4)$, bimol. and termol. charge transfer reactions, rate coeffs. 77−1910
$HeH^+ + H_2 \rightarrow H_3^+ + He$, reaction rate. coeff. 78−18371
$I^- + CO$, endoergic ion-molecule reaction 77−25262
$I^- + COS(CS_2)(H_2S)$, endoergic reaction, time of flight mass spectral obs. 77−12786
I^- + methane(fluoromethane), excitation functions, reactive scatt., eV region *(German)* 78−35677
$I^- + SO_2$, endoergic reaction, time-of-flight mass spectral obs. 77−12785
$I_2^+ + N_2 \rightarrow I^+ + I + N_2$, 0.65-3.2 keV, dissoc. cross-section, internal excitation effects 78−64813
$K^+ + H_2$, dissociative collision, H_α, H_β emission prod. 77−75093
$Kr^+ + HD$, reactive collision dynamics, isotope effects 78−23930
Kr^+ + molecule, $^2P_{3/2}(^2P_{1/2})$ doublet ground state reactions at 300K 80−108702
$Kr^+ + SO_3$, in mass spectroscopy of SO_3 mixtures 78−3415
$Kr^{2+} + H_2(N_2)(O_2)(CO)(CO_2)$(methane), charge transfer reactions, rate coeffs. and product-ion distributions meas. 80−104431
$Kr^+ + H_2(D_2)(HD)$ reactions, temp. depend., isotope effect 78−31630
$Li^+ + H_2$, dissociative collision, H_α, H_β emission prod. 77−75093
$Li^+ + N_2$, (0.5 to 1.0 keV) energy loss spectra, ionisation, electronic and vibro-rot. transitions 77−14541
$N^+ + CO$, integral reactive cross-section calcs. 78−27750
$N^+ + CO(CO_2)$ (methane)(NO), product distribs., rate consts., ion cyclotron reson. obs. 77−52618
$N^+ + H_2$, reaction dynamics, low energy mol. beam obs. 77−9064
$N^+ + H_2$, triplet state ab inito CI pot. energy surfaces 78−74729
$N^+ + H_2$ (hydrocarbons), rotational vibrational product excitation 79−47901
$N^+ + H_2(DH)$, >6 eV reaction dynamics 77−32779
N^+ + methane, charge transfer reaction, dissoc., isotope effects, mass spectra 77−21382
$N^+ + O_2$, branching ratio kinetic energy depend. 80−97703
$N^+ + O_2$, drift tube mass spectra, rate coeffs. and prod. distrib. 77−77746
$N^+ + O_2$, $NO^+(a^3\Sigma^+)$ ion prod. 80−7784
$N_2 + H^+$, energy transfer, dissoc., cross section calcs. 77−50522
$N_2 + H^+(He^+)$, N_2^+ 3914 Å emission cross sections, 0.5-34 keV 77−54598
$N_2^+ + 2N_2 \rightarrow 2N_3^+$, reactions of electronically excited N_2^+ 77−1915
$N_2^+ + N_2$, three-body ion-neutral assoc. reactions, saturation 79−39134
$N_2^+ + N_2 + He \rightarrow N_4^+ + He$, ternary assoc., selected ion flow tube obs. 79−39128
$N_2^+ + N_2 \rightarrow N^+ + N + N_2$, with reactant $X^2\Sigma_g^+$, $A^2\pi_u$ and excited metastable states 77−29001
ion-molecule reactions continued
$N_2^+ + SO_3$, in mass spectroscopy of SO_3 mixtures 78−3415
$N_3^+ + O_2$, drift tube mass spectra, rate coeffs. and prod. distrib. 77−77746
$N_4^+ + O_2(CO_2)(H_2)(D_2)$ reactions, flow-drift tube obs. 78−60985
N_x^+, (x=1 to 4) stratospheric chemistry, reaction rate coeffs. and product distribs. 78−81305
$NH_2^- + H_2 \rightleftharpoons NH_3 + H^-$, chem. equilib., ab initio calcs. 79−34282
$NH_2^+ + H_2$, reaction products translational energies 77−86298
$NH_2^+ + H_2O$, bimolecular reactions, product. distrib., rate consts. 78−11513
NH_3 proton-bound dimers, form. in ion-mol. assoc. reactions, rates analysis 77 60054
$NH_3 + C^+(CH_n^+)$, rate coeffs., ionised product distribs. 77−40522
$NH_3 + H_2^+(He^+)$, dissociative charge transfer reactions, energy transfer depend. 77−25258
$NH_3 + N^+$, 35-200 keV, X-ray spectrum, rel. to $N^+ + N$ mechanism 78−42183
$NH_3 + OH^+(H_2O^+)(H_3O^+)$, bimolecular reactions, product. distrib., rate consts. 78−11513
NH_3 + radical ion, thermal energy charge transfer, reaction mechanism 77−16796
$NH_3^+ + H_2O$, bimolecular reactions, product. distrib., rate consts. 78−11513
$NH_3^+ + H_2O \rightarrow NH_4^+ + OH$, statistical phase space theoretical anal., vibr. depend. cross section 78−15660
$NH_3^+ + NH_3 \rightarrow NH_4^+ + NH_2$, statistical phase space theoretical anal., vibr. depend. cross section 78−15660
$NH_4^+ + LiH(H^-)$, substitution and abstraction reactions, ab initio calcs. 77−48624
NH_n^+ + molecule (n=0 to 4), reactions, selected ion flow tube obs. 80−45489
NO, interstellar, ion-molecule reactions rel. to candidate mols. form. 78−28739
NO^+ + molecule, reaction rate consts. meas. 80−7782
NO^+, stratospheric chemistry, reaction rate coeffs. and product distribs. 78−81305
NO^+, three-body reactions, rate coeffs. rel. to cluster ion form. in D-region 77−53308
$NO^+ + 2N_2 \rightleftharpoons NO^+.N_2 + N_2$, rate const., enthalpy and bond strength 77−16809
NO^+ + atmospheric gases, thermal energy reaction rates 78−92443
$N_2O_5 + CO_3^-(NO_2^-)(F^-)(Cl^-)(Br^-)(I^-) = NO_3^- + XNO_2$, rate consts. 78−56879
$N_2O_5 + H_3O^+$, rate consts. 78−56879
$N_2O_5 + NO^+ = 3NO_2^+$, $N_2O_5 + NO_2^+$, rate consts. 78−56879
$N_2O_5 + O_2^+ = NO_2^+ + NO_3 + O_2$, rate const. 78−56879
$Na^+ + HCN$, rotational excitation, Stark shifted level transitions, energy transfer calcs. 79−98059
$Ne + H_2^+$, reaction pot. energy surface, LCAO-MO-SCF energies 77−1917
$Ne^+ + H_2(N_2)(CO)(CO_2)(N_2O)(O_2)(NO)(NH_3)(SO_2)(COS)(H_2O)$, thermal energy, reaction rate coeffs. and product distrib. 79−29333
Ne^+ + methane(chloromethane)(ethylene), thermal energy, reaction rate coeffs. and product distrib. 79−29333
$Ne^+ + O_2 \rightarrow O^+ + O + Ne$, thermal energy charge transfer, energy disposal determ. 79−64099
$Ne^{2+} + H_2(N_2)(O_2)(CO)(CO_2)$(methane), charge transfer reactions, rate coeffs. and product-ion distributions meas. 80−104431
Ne_2^+ + atom (molecule), bimolecular and termolecular reaction rate coeffs. 80−81308
$Ni^+ + H_2(HD)(D_2)$, endothermic reactions, investig. 80−97692
O^+, O_2^+, stratospheric chemistry, reaction rate coeffs. and product distribs. 78−81305
O^{2+} reactions with atoms or molecules of ionospheric importance, lab. meas. 80−26004
$O^- + 2CO_2 = CO_3^- + CO_2$, reaction rates 77−60058
$O^- + CO(Mg)(N_2)$, electron detachment cross-sections, 20-150 keV 78−25690
$O^- + CO \rightarrow CO_2^+ + e^-$, vibr. chemiluminesc. 78−3340
$O^- + D_2 \rightarrow OD^- + D$, crossed beam studies product ang. and energy distrib. 78−53203
$O^- + N_2 \rightarrow N_2O + e$, N_2O ground state pot. energy surfaces 77−27175
$O^- + N_2 \rightarrow N_2O + e$, rate studies 78−40036
$O^- + O_2 \rightarrow O_2^- + O$, cross sections, 0-100 eV *(German)* 77−32785
$O^- + O_2 \rightarrow O_2^- + O$, cross section kinetic energy depend., rate consts. meas. and Monte Carlo calcs. 80−78701
O^+ + atmospheric gases, thermal energy reaction rates 78−92443
$O^+ + CO_2$, in Mars thermosphere, effects of energetically produced O_2^+ on ion temps. 79−96945
$O^+ + H_2$ in Venus, contrib. to exosphere non-thermal H budget 79−12416
O^+ + hydrocarbons, chemiluminescent reactions 79−96299
$O^+ + N_2$, atom transfer, reaction rates and cross-section determ. 77−60052
$O^+ + N_2$, in F-region, effects of soft electron precip. on N_2 vibr. energy distrib. 77−33261
$O^+ + N_2$, reaction rate coeff. in ionosphere 77−87167
$O^+ + N_2(O_2)$, reaction rates, 300-900K 79−8434
$O^+ + N_2(O)$, rate coeffs. in thermosphere, AE satellite meas. 79−48594
$O^+ + N_2 \rightarrow N + NO^+$ react., mechanism, ab initio SCF calcs. 78−60996
$O^+ + NO$, charge transfer, reaction rates and cross-section determ. 77−60052
O^{2+} + H in planetary nebula NGC 7662, effects on emission-line spectrum 80−62233
$O_2 + F^-(Cl^-)(Br^-)(I^-)$, 0.2-100 eV, reaction differential cross sections energy depend. meas., exoergicity 77−63902
$O_2 + H^+$, energy transfer, dissoc., cross section calcs. 77−50522
$O_2 + H^+(He^+)(O^+)$, dissoc. ionisation, kinetic energy spectra 78−25684
$O_2 + N^+(O^+)(C^+)$, rate coeffs. meas. at 300 and 100K in flowing afterglow 79−20346
$O_2^- + O_2$, endoergic reactions, energy depend. of cross section meas. 77−12792
O_2^+ + atmospheric gases, thermal energy reaction rates 78−92443
$O_2^+ + NO \rightarrow NO_2^+ + O$, photoionis. mass spectra, photoionis. efficiency 77−40537
$O_2^+ + O_2$, three-body ion-neutral assoc. reactions, saturation 79−39134
$O_3 + O^-(OH^-)(S^-)(SH^-)$, associative detachment, rate coeffs. 78−3325
$O_3^- + CO_2 \rightleftharpoons CO_3^- + O_2$, rate const., 200-600K in flowing afterglow 78−7193

ion-molecule reactions continued
O_3^- + molecule reactions, thermochemistry, electron affinity and rate consts. 78−40040
O_4^+, form., in O_3 photoionisation, mass spectra 77−50477
O_5^+, form., in O_3 photoionisation, mass spectra 77−50477
$O^+(^2D) + N_2$, charge exchange rate coefficient, effect of N_2^+ recomb. on aeronomic determ. 78−88954
$O^+(^2D) + N_2$, thermal rate coeff., products and branching ratios in ionosphere 80−82117
$O^+(^2D) + N_2$ charge exchange, rate coeff. temp. depend. 80−77179
OH^- + methoxybenzene (o-cresol), gas phase reaction, 299-435 K, kinetics and mechanism 78−11515
$O^+(^4S) + N_2(X^1\Sigma_g^+) \rightarrow NO^+(X^1\Sigma^+) + N(^4S)$, MCSCF potential energy surface for collinear $^4\Sigma$ pathway 80−63540
O^+* + N_2, metastable ion reactions, rate consts. and ion mobility at 300K 80−95722
$O_2^+.O_2$, reactions with CO_2, O_3 and methane rel. to stratospheric ion chemistry 79−2343
$O_2^+.O_3$, reactions with H_2O and methane rel. to stratospheric ion chemistry 79−2343
PH_3 + radical ion, thermal energy charge transfer, reaction mechanism 77−16796
S interstellar molecule formation, ion-molecule schemes inefficient 80−101632
SO_3, electron impact mass spectrometry, proton affinity, ion-mol. reactions 78−3415
SO_3^- + BrO_3^-, fast oxidation in acid medium, laser Raman multichannel spectroscopy 78−27754
SO_2XY, (X,Y=Cl,F), positive and negative ion chemistry 78−85140
SiH_4-D_2, mixture, ion-mol. reactions, cross-sections 77−60061
$T_2^+ + T_2$, charge transfer reactions rel. to vibr. states 77−9070
$U^+ + N_2(D_2)(CD_4)$, endothermic reactions, heat of formation 77−73444
$U^+ + O_2(CO)(CO_2)(COS)(CS_2)(D_2O)$, reaction cross-sections, ion beam apparatus study 80−97691
UF_6 + e^-(K)(Na)(Cs), positive and negative ion formation, electron affinity, bond dissoc. energy 77−75314
$UO^+ + O_2(CO)(CO_2)(COS)(CS_2)(D_2O)$, reaction cross-sections, ion beam apparatus study 80−97691
UO_2^{2+} + macrocyclic hexaketone, appl. to U extraction from seawater 79−92052
VO^{2+} + alkyl dinitriles, reaction, CN stretching freqs., bonding effects 77−16820
WF_6, electron and fluoride affinities, ICR spectra 79−39130
Xe^+ + molecules, $^2P_{3/2}(^2P_{1/2})$ doublet ground state reactions at 300K 80−108702
$Xe^+ + NF_3$ reaction, XeF^+ form., $Xe^+(^2P_{1/2})$ radiative deactivation 78−27737

ion optics
see also ion beams; ion microscopes; mass spectrometers
14 UD Pelletron accelerator terminal, ion optics, high energy acceleration tube 78−33321
40 kV multimegawatt neutral beam line, power flow and ion source 79−76238
acceleration, by electron beam, in gas-filled waveguide, in mag. field theory 78−9316
accelerator systems for ion implantation research 80−32540
achromatic ion prism, two-dimens. for mass spectrometer 77−54015
in air, ion trajectories due to electric field, calc. *(Slovenian)* 80−78760
axisymmetric magnetic focusing fields with foci outside the field (planar case) 80−5680
beam coasting off axis, electrostatic potential and field 77−38796
beam deviation, plasma boundary neutralisation surface depend. *(Russian)* 78−59613
beam profile determ., ion optics for display devices 77−5960
beam source, optical props., convergent iterative numerical procedure 79−3620
beam transport, phase space acceptance and emittance, appl. to tandem accelerators 77−31058
beam-beam interactions in p-p storage rings 78−78900
beamlet steering, linear optics theory 78−12788
beamlet-beamlet interaction effect on ion optics of multioperative sources 78−46507
beamlet-beamlet interaction in multiaperture sources, effect of electrode shielding 79−10254
bicylinder mirrors for appl. in multichannel mag. mass spectrometer *(French)* 78−54494
CAD of ion beam instrumentation systems 77−13819
charged particle beam-surface impact at glancing angles, reflection *(Russian)* 80−108316
charged particle energy analyser, ang. focusing with cylindrical electrostatic field 78−78896
collective field accelerator, vac. diode with relativistic electron beam operation 77−24201
collimating slit, edge effect on ion scatt. 79−27160
conference, ion implantation equipment, Povo-Trento, Italy (Aug., 1978) 80−31413
controllable ion gun with high brightness 77−87871
cyclotron extraction efficiency improvement through central region studies 79−54719
cyclotrons, superconducting, spiral electric gap effects on ion orbits, computer program calc. 80−52795
cylindrical capacitor with oblique ends, ion optical coefficients determ., first-order focusing 80−63912
cylindrical condenser, electrostatic prism appls. 77−6992
cylindrical radiofrequency mass analyser, low resolution mass filter 80−73519
double cylindrical electrostatic sector as an ion energy analyzer 80−23208
double focusing bending magnet, meas. of optical props. with thin alpha source 78−55073
drifting gas approach cf. optical approach 79−31788
duopigatron plasma generator, emission aperture shape effect on ion optics 78−5956
duoplasmatron, beam emittance as function of discharge modes 79−45511
E×B filter with improved velocity-separating capability, design 77−41728
education, electron and ion optical bench 77−45641
Eindhoven AVG cyclotron, on-line determ. of acceptances and emittances of beam guiding system 77−38515

ion optics continued
electric quadrupole lens, fringing field, conformal mapping method 79−41315
electrostatic accelerator, beam aberrations in displaced quadrupole triplet charge selector 77−38443
electrostatic accelerators, beam transmission problems during design, operation, upgrading 78−33320
electrostatic analyser, electrode geometry tolerance calcs. 77−23611
electrostatic analyser with oblique cut plates, focusing props. 77−54667
electrostatic coaxial probe forming lens suitable for high-energy ion beams 79−31787
electrostatic lenses, lens properties and computational techniques 79−44983
electrostatic lenses for control of ion or electron beams 80−32897
electrostatic mirror, ion beam focusing for low energy heavy ion accelerator 77−14654
electrostatic mirrors for heavy-ion manipulation and focusing 77−10520
EM ion separators and related ion accelerators 77−14276
energy analyzer, two-stage with cylindrical mirrors, aberration reduction 79−40640
energy spectrum of beam from inductively coupled HF source, optical parmeter meas. of gun 78−89590
factors affecting shape and quality 77−19160
field ionisation and desorption sources, for quadrupole and double focusing spectrometers 78−74092
FIM, ion trajectories for hyperboloidal and paraboloidal emitters 78−32924
focused ion beam designs for sputter deposition 79−78880
focusing electrodes shape calculation for wedge-shaped electron-ion beam 80−53202
focusing in cylindrical mirror analyser, space charge effects 78−25791
focusing of fast ion beam, in dense plasma with 100 A to 10 kA current *(Russian)* 77−7561
focusing of intense beam by wall thermonuclear microexplosion ignition 77−61611
fundamental constraints in various situations 77−14653
GANIL heavy ion accelerator facility, status report on injector, magnets and RF system 79−54630
heavy ion beam focusing, accelerated, decelerated beam, electrostatic lenses 78−89588
heavy ion toroidal collective accelerator 78−33334
heavy-ion superconducting linac, alternating phase focusing 77−3194
heavy-ion superconducting linac, design of re-entrant cavities 77−6580
high-current electrostatic scanner-deflector 77−13820
imaging for ion implantation and micromachining *(French)* 80−34027
implantation system optical props., monitoring using SOS wafer 80−13182
implanter, semiconductor device processing 80−31944
insulator coated grid with precel voltage, effect on ion optics 78−9014
ion beam diagnostics by means of electron saturated plane Langmuir probe 79−94144
ion beam extraction and bunching, from spherical reflex triode, anal. 79−97471
ion beam image transformation using magnetic quadrupole lenses 78−55071
ion beams, intense, production and postaccel. in magnetically insulated gaps 80−74041
ion implantation system, high current, design of end station, appl. to Si:As, ion implantation system, high current, design of end station 80−34030
ion linacs, permanent magnet quadrupoles, development 77−38494
ion optical props., aberration, crossed toroidal elec., mag. fields as mass spectrometer *(Chinese)* 80−82843
ionic motion, 3-D quadrupole electric field, charge exchange collisions 78−9315
ionisation chamber acceptance characts. distortion by ion source mag. field 79−21852
ISOCELE high-current on line separator development 77−26922
ISX-B neutral beam injector expt. on prototype beam line 80−74039
iteration scheme for optics of ion beams extracted from plasma 78−50693
JOSEF gas filled separator, focusing and dispersive props. 77−26426
Kiev 240 cm cyclotron facility, present status and accelerated beam characts. 79−54628
LAMPF, quadrupole field aberrations, source of emittance growth 77−38508
linac particle tracing simulations 79−71999
linear accelerator, synchronous phase focusing, standing wave continuous interaction *(Russian)* 77−38444
linear accelerator with solenoid focusing, stable particle motion 79−72000
linear transformation coeffs. charged-particle beam in mag. dipole field 80−5681
low energy ion beams, conference, Salford, Sept. 1977 78−66444
low-energy ion scattering from solid surfaces, mag. sector optics 77−40318
magnetic analyser, sector type, fringing fields and focusing 79−41328
magnetic mass analyser ion motion in rot. reference system 77−61155
magnetic quadrupole doublet, field coupling and higher order aberrations 77−38534
magnetic spectrographs for nuclear reaction studies, resolving power, kinematic broadening 79−68126
magnetic spectrometers, for heavy ion reactions, book contrib. 79−31314
magnetic vector man analyser, stigmatic focusing condition 78−70215
mass filter performance, quadrupolar field distortion effects 79−35887
mass spectrometer, double-focusing, and MIKE spectrometer, characts. 79−2871
mass spectrometer, quadrupole mass filter with flat electrodes, computer simulation 78−54492
mass spectrometer, simultaneous ion detect. with variable mass dispersion 78−78027
mass spectrometry, ion source and focusing optics, high-luminosity 79−44979
mass spectrum, second order image aberration correction by electrostatic hexapole lens 78−70216
mass-energy spectrograph, for anal. of space plasmas over energy range 0.1 to 10 keV 77−53401
MEIRA isotope separator, deflection radius and operational characteristics 77−19161
microscope aberrations and image form., study by magnetic anal. of beam from HF source 78−55293

ion optics continued
miniature slow proton source for focusing efficiency obs. 78−78538
mirror, electrostatic, transaxial, for large-incidence ang. ion beams 78−37798
misaligned beam transport elements, ion beam optics, IONBEAM program 77−65564
multiple charged and polyatomic ions, use in implantation accelerator 77−54017
multiply charge of beams in linear accelerator with variable-phase focusing, general soln. 80−13992
multistage cylindrical analyzer for simultaneous detection of several beams with different energies 79−22891
negative ion beam in gas, space-charge neutralisation and focusing 79−55048
neutral beam sciopticon 80−1117
path length and stability, in RF quadrupole ion trap 77−41722
periodic focusing of mag. channels 78−55079
pinched beam diode, geometrical focusing of intense ion beams 78−58898
plasma, ion beam collimation by ion optical system, quality determ. 77−10138
plasma ion emission, cylinder and transverse slot ion optics, theory 80−43250
plasma lens, focusing and form. of intensive beam *(Russian)* 78−21270
plasma lens, unipotential, for proton beam focusing 79−41326
plasma-optical mass separator, double focusing, 'nontransitive' cylindrical model 79−67423
plasma-optics system, temp. criterion for elec. field 77−50609
precision magnet homogenising surface coils 79−41329
proton beam, 70 GeV, channel, shaping system, for Protvino Inst. neutrino expts. 78−37476
proton beam 70 GeV, for Protvino Inst. neutrino expts., characts. 78−37475
proton beams, coherent instabilities 78−78898
proton storage ring, NAP-M, current stabilisation in guiding-field magnet supply ccts. 77−65363
proton storage rings, selection of formulae 77−83348
proton synchrotron, intense beam, bunched optimum critical energy transition 77−83346
proton synchrotron accelerator theory 77−67925
proton synchrotrons, non-linearities 78−78897
pulsed ion beam incident on mag. barrier, virtual anode form. 80−103131
quadrupole doublet, optical props., rot. of elements, effects 80−74292
quadrupole ion microprobe for secondary ion emission investigs., ion optics 79−35892
quadrupole lens, spin precession of polarised proton beam, analytic soln. 77−30692
quadrupole lenses, electrostatic and mag., ion orbit 5th order solns. 77−19159
radial focusing, using magnetic analyser with inhomogeneous field and electrostatic lens 78−78895
recoil separator, Lohengrin, ion optics, nuclear fission product spectroscopy 77−22607
review of recent work *(Japanese)* 77−58247
second-generation ion microanalyser description and performance *(French)* 80−101055
second-order coeffs. for sector mag. analyzer, compact notation 80−63911
SIN π-channel and spectrometer, technical aspects of pion scatt. facility 79−13574
SIN injector cyclotron, design of central region including ion source 77−54379
single-stage accelerated ion beams from plasma 78−1147
space charge ion optical systems, expt., theory 78−9020
space charge ion optics, influence of chromatic aberrations 78−55294
statistical phenomena in proton rings, expt. 78−78899
stored ions, in electrodynamic trap, energetic props., elastic collision effects *(French)* 78−9306
surface coils to improve magnet homogeneity 77−10829
surface multipole guide field for plasma injection, ion optics rel. to efficiency 78−14194
surface structure anal., discussion of ion optics 79−46902
synchrotron, methods of increasing heavy ion beams intensity 79−26790
tandem 1.2 MeV accelerator at Giessen polarisation facility 77−65359
tokamak, beam focusing, by aperture displacement, in two-stage acceleration system 79−46496
trajectories in any sector field in third order approx. 77−79741
trajectories in fields having straight main paths, calc. methods 78−90352
triple focusing mass separator using Wien filter 78−45748
two stage linear accelerator, H ion beam optics 79−36438
two-sector system with two dimens. H/r mag. field, ion optical characts. 78−66744
two-stage 150 keV accelerator, ion beam optics 78−9017
two-stage ion beam optics for accelerator 78−50418
vaporised metal cluster ion source, props. of ionised cluster beam 79−49337
velocity filter SHIP, efficiency for unslowed evaporation residues 80−23244
VICKSI facility, running in period and initial operating experience 79−54627
visual ion beam images, on insulator surfaces, by the coincident interaction of a rastered electron beam 79−3622
wedge type ion beam divergence profile calc. 78−82555
Wien filter, inhomogeneous field, theory and expt. of ion optics 79−45510
Ar low energy ion beam transport through apertures, source parameter depend. 77−57422
Ar^+ beam, deflection in two-dimensional electrostatic quadrupole field 78−5417
Ar^+, focused ion beam designs for sputter deposition 79−89841
Ar^+ ions moving through Ar gas in strong elec. field, energy spectrum 80−5679
Ga ionisation mechanism on W field emitter 80−76156
H^- beam, intense, from Penning surface-plasma source, ion-optical characts. 79−13892
Kr^+, and isotopes, trajectory in const. mag. field plus orthogonal sinusoidal elec. field 78−50687
ion optics continued
^{86}Kr ions accelerated in UNILAC, energy meas. by recoil proton technique 78−58527
^{238}U, single charged, numerical anal. of longitudinal motion of 9.5 GeV 79−54737

ion plating
alumina on stainless steels and Inconel, gasless ion plated films 77−40476
beam plating of surface using ion accelerator 77−90284
cemented carbide ion plating, high-speed steel tools, cost and cutting performance 80−30174
coating material deposition for steel inner vac. liner of fusion reactor 77−30669
coatings for wear and lubrication 79−19494
coatings formed by ion-beam-activated vacuum deposition, struct. and props. 80−15422
evaporation source pellet or slug feeding system 79−69996
evaporation sources, gaseous media, and transport modes 80−80984
fatty acid film, $(CH_3(CH_2)_nCOOH)$, etching in glow discharge 77−16506
field emission deposition 80−35110
filament coating, improved strength *(Japanese)* 77−90282
film deposition, ion beam techniques 80−11564
films, preparation using low pressure plasmas 77−40361
hollow cathode discharge process, mass and energy anal. for incident ions on substrate 78−23630
hollow cathode effect on film step height *(Japanese)* 77−63567
induction-heated source, arcing elimination by top coil grounding 79−47639
industrialisation, appl. of induction heating 77−8764
inert gas handling 79−69994
interface broadening during ion plating 80−65405
ion assisted deposition, review *(Japanese)* 77−73227
ion deposition techniques, AES exam. of surface cleaning methods 79−15878
ionic nitriding thermochemical process, equipment, process details and advantages and prospects *(French)* 80−108641
low-pressure, ion source for high-quality thin films deposition 80−35105
mass spectroscopic measurements, validity for pressures exceeding 10^{-4} mbar 79−85198
mechanisms and theory 78−11130
metal, RF bias ion plating process and microstruct. 78−11132
metal, surface properties improvements, using vacuum thermal process techniques 79−100283
metal coatings on steel for watch part finishing *(French)* 78−23879
metal film structure on plastic substrate 79−82501
metallurgical coatings, vapour deposition processes in vac. 80−35430
metals, ion surface treatment 78−11415
plastics, ion plating 80−16533
prep. by evap. and ion plating, AES determ. of comp. profiles 77−89675
principles and advantages review 79−74100
process features and surface film props. 79−83361
reactive ion plating *(Japanese)* 78−92202
review of ion beam utilisation for etching and film deposition 77−32522
review of technological appl. of sputtering and ion trapping 77−44107
RF plasma excitation 79−69995
ring gap discharges for high rate vac. coating 77−69991
ring gap plasmatron discharges for high rate deposition 77−44175
solid ion source by electron bombardment *(Japanese)* 78−78035
sputter ion plating technique 79−83142
surface treatment comparison *(French)* 79−57132
techniques and applications 77−70005
thin film deposition, low energy in source modification 78−52687
vacuum-arc plasma extracted ion precipitation unit 80−35106
wear resistant surface, review 78−72938
Ag film, deposited on AT-cut quartz crystal, crystallographic structure obs. 80−2280
Ag film vacuum deposition and ion plating, effects on surface topography 79−82427
Ag, ion beam plating using mass analysed ions, SIMS and AES expts. 78−19673
Ag ion plated film on permalloy, Cu and Vicalloy substrate, AES, SEM and X-ray study *(Japanese)* 78−11128
Al coating on steel, deposition conditions and props. *(Japanese)* 78−80477
Al film, deposited through mask hole, thickness nonuniformity *(Japanese)* 79−19999
Al film, ion plated, morphology exam. by SEM 79−28251
Al, film, ion plating deposition system using electron beam evaporation *(French)* 80−20802
Al, low friction wear-resist. surface form. on Ti 78−11442
Al, on C fibre, composite prep. and mech. strength 78−11165
Al-Si, ion plated contacts *(Rumanian)* 78−88029
AlN films, RF reactive ion-plating, struct. and morphology 80−104074
Au film, ion plated, defect growth structs., SEM obs. 80−24768
Au, ion beam plating using mass analysed ions, SIMS and AES expts. 78−19673
Au, process 79−66186
B film growth by phys. vapour deposition 80−16200
C, deposition processes, coating struct., for prosthetic devices 77−40374
C, on metal, deposition method, graphitic struct., and tribological props. 78−11440
Co, and alloys, ferromag. films, coercive force, ion plating prep. 77−28730
Co, ferromag. film, ion plating prep., coercive force and magnetoresist. 77−12546
Co-Ni, ferromag. film, ion plating prep., coercive force and magnetoresist. 77−12546
Cr coatings, deposition parameter influence on struct. and hardness 79−82485
Cr-C, hard coating preparation by ion beam methods 80−25579
CrN, deposition by hollow cathode discharge process, and hardness 79−24452
Cu film, ion plated, defect growth structs., SEM obs. 80−24768
Cu film, ion-plated, on stainless steel, porosity depend. on process parameters 78−84720
Cu film coating onto ABS plastics, expt. study *(Japanese)* 78−6858
Cu film on Ni, AES comparison of ion plated and vacuum evaporated films 79−28250

ion plating continued
Cu films, ion plated on polyethersulphone, structural and resistivity study 79−42411
Cu ion-plated coating, grain structure 79−28249
Cu layers, grown by ion plating method on Si wafers and glass plates, X-ray diffr. exam. *(Japanese)* 77−21039
Fe, and alloys, ferromag. films, coercive force, ion plating prep. 77−28730
Fe-Cr-Mo and Fe-Cr-Mo-Si alloys, amorphous films, corrosion resist. and ion plating use 80−89423
Fe_4N, hard coating preparation by ion beam methods 80−25579
$Fe_{32}Ni_{36}Cr_{14}P_{12}B_6$, Metglas amorphous films, corrosion resist. and ion plating use 80−89423
Ge, epitaxial and amorphous film growth, low energy ion beam deposition 77−28729
In_2O_3, reactive ion plating onto insulating substrates, and elec. and optical props. 79−87588
In_2O_3, transparent heat mirror formation by ion plating on ambient temp. substrates and props. 80−25578
In_2O_3:Sn films, pure and doped, prod. by ion plating, elec. and optical props. 80−2488
Ir, electron beam deposition and ion plating 77−44166
Mg film, deposition using low-energy ion beam, Rutherford backscatt. and SEM anal. 77−59700
Mg film, deposition using low-energy ion beam, Rutherford backscatt. and SEM anal. 77−70004
Mo ion-plated orthopaedic En58J stainless steel, corrosion fatigue 80−66694
Nb, ion plated with Pd and Ni, prep., H_2 absorption and desorption rate *(Japanese)* 80−108358
Ni, ferromag. film, ion plating prep., coercive force and magnetoresist. 77−12546
Pb film, deposition using low-energy ion beam, Rutherford backscatt. and TEM anal. 77−59699
Pb film, deposition using low-energy ion beam, Rutherford backscatt. and TEM anal. 77−70003
PbO, X-ray sensitive photoconductor 77−44174
Pd, electron beam deposition and ion plating 77−44166
Pt, electron beam deposition and ion plating 77−44166
Pt ion plating on $\alpha+\beta$ Ti alloy Ti-6242, creep property improvement 80−16408
Ru, crack-free layers, 2-3 μm thick 78−11131
Se film on brass, ESCA interface study 78−43269
Si, epitaxial and amorphous film growth, low energy ion beam deposition 77−28729
Si, polycryst. film, ion plating on Al, growth from eutectic melt 77−8765
Si:H, amorphous thin film, ion plating, IR absorpt. meas. 80−84857
SiC, film, synthesized by RF reactive ion plating, struct. 77−40391
SiC film synthesis by plasma deposition process 78−11127
Si_3N_4, hard coating preparation by ion beam methods 80−25579
Si_3N_4 protective coatings on Mo, RF reactive ion plating 78−3250
SiO_x film, durable optical, ion plating onto plastics, optical and mech. props. 80−38141
Sm, film, ion plating deposition system using electron beam evaporation *(French)* 80−20802
SnO_2, reactive ion plating onto insulating substrates, and elec. and optical props. 79−87588
Ta, ion plated with Pd and Ni, prep., H_2 absorption and desorption rate *(Japanese)* 80−108358
Ti alloy, mechanical props. at high temp., effect of Pt ion plating 79−29156
α-Ti, effect of Pt ion plating on creep behaviour 79−66123
Ti film, ion plated, morphology exam. by SEM 79−28251
Ti on steel, process parameters rel. to coating props. 77−70217
α-Ti-Al-Sn(5, 2.5 wt.%), effect of Pt ion plating on creep behaviour 79−66123
TiC coating on WC-NbC-Co, ion plating, and cutting tests 79−24678
TiC, ion plating and applics. *(Japanese)* 77−63565
TiC_x film, form. by hollow cathode discharge reactive deposition process, on mild steel sheet 79−24451
TiN coating on WC-NbC-Co, ion plating, and cutting tests 79−24678
TiN coatings on steel for watch part finishing *(French)* 78−23879
TiN decorative coating, ion plating on steel and Stellite 78−11441
TiN layers formation, on steel substrate, microchardness and structure obs. *(Hungarian)* 80−2965
TiN, reactive ion plating with auxiliary discharge deposition conditions influence on film props. 80−20801
TiN_x, deposition by hollow cathode discharge process, and hardness 79−24452
TiO_2 film, ion plated, DC cond. study 80−100457
TiO_x film, durable optical, ion plating onto plastics, optical and mech. props. 80−38141
V-Mo, effect of ion plated Mo on corrosion in liquid Na, mech. props. 78−53020
W, film, ion plating deposition system using electron beam evaporation *(French)* 80−20802
Y, film, ion plating deposition system using electron beam evaporation *(French)* 80−20802
ZnO crystalline films, deposition techniques *(Japanese)* 79−74098
ZnO piezoelectric films formed by RF reactive ion-plating 79−83140
ZnTe epitaxial growth on NaCl by ion deposition 77−32533

ion probe analysers *see ion microprobe analysis*

ion probe microanalysis *see ion microprobe analysis*

ion pumps
AC and DC ion pumping up to 30 kV 79−88969
bakeable ion-cryopumped ultrahigh vac. system 80−77802
cryopump-ion pump system, performance 78−70142
design, to accelerator specifications 79−63256
distributed sputter-ion pumps for use in low magnetic fields, electron storage ring appl. 79−67325
electron storage ring, vacuum system for synchrotron radiation source 79−63830
hydrocarbon contamination, of vacuum dependent scientific instruments 79−63259
intense pulsed neutron source, vacuum system 79−63261
ISABELLE vacuum component performance at 1×10^{-11} Torr operation 79−81105
LMFBR steam generators, safety alarm system, water leakage detection *(Czech)* 78−33268

ion pumps continued
magnetic, gas mixture pumping 77−138
orbitron device, electronic injection, ionisation phenomena and space charge influence 79−40587
orbitron device, optimum injection condition for electrons, influence of end effects 80−82784
PEP storage ring vac. system, synchrotron-radiation-induced heating effects, distributed ion pump design 79−81107
quadrupole ion pump and ionisation gauge, plasma geometry and props. 77−57337
Serpukhov proton synchrotron ion-getter pumps, operation evaluation 77−83347
single particle trajectories, through ionising regions 79−6218
Sputter ion pump *(Japanese)* 78−21152
sputter ion pumped system for annealing of metal wire, operation aspects 77−26318
sputter ion pumps, comparison of diodes and triodes 77−67454
sputter-ion pump, behaviour in 10^{-11} Torr range 77−57336
sputter-ion pumps, modified ferroresonant power supply 79−97400
TEM vacuum system, simplified low-cost design for use with ZEISS microscope 80−99012
thermal release of trapped inert gases 77−67450
triode and diode ion sputtering pumps, power supply, press. control *(Spanish)* 77−37902
ultrahigh vacuum ion pumped system, for undergraduate and postgraduate courses 79−62981
ultrahigh vacuum pumps 78−89488
ultrahigh vacuum system for ISABELLE full cell 80−77798
ultrahigh vacuum systems, ambients produced by oxygen and water vapour 78−21154
Gd small ion-getter pump 78−89487
Ti, getter pump, corrugated surface and pumping speed, fusion reactor application 78−74491

ion recombination
acetone, gas, electron-ion recombination, at 292K, three-body interaction 79−46418
(alkali atom)$^+$+(halogen atom)$^-$, recombination 78−7192
ambient gas, computer expts. on ionic recombination, coeff., binary recombination 78−22028
ambient gas, electron-ion recomb., classical theory 80−91623
ambient gas, quasiequilibrium statistical method extended to nonlinearity 78−22027
anthracene anion+dimethylaniline cation, recombination reaction in soln., time-resolved mag. field effect 80−3308
aromatic compounds, isothermal recomb. fluoresc., decay kinetics 78−29809
aromatic radical ion recomb., mag. field modulation, Liouville eqn. soln. 77−28995
atmosphere, ion-ion recombination rates 77−66972
atmosphere small ions, recomb. rates and attachment to aerosol particles 79−39817
binary ionic recombination, ambient gas temp. and density rate depend. 80−35522
η Carinae, Fe II dielectronic recomb. rel. to IR excess 78−32478
Cl, shock heated, radiative recombination under nonequilib. expansion in supersonic nozzle *(Ukrainian)* 79−37421
complex ion-electron recomb., electron energy depend., two models *(Russian)* 77−46638
complex ions, radiative recomb. 78−17782
corona discharge, gaseous ion stabilisation by H_2O drop capacitors *(Russian)* 77−62420
cosmology, recomb. lines in primordial microwave radiation 78−54097
D-region, ion recomb. studies via complementary cross modulation 77−2275
D-region recombination coefficients for normal and winter anomalous days 79−35042
diatomic asymmetric mol., vibr. self-ionisation and recomb. *(Russian)* 77−79700
dielectron recombination of electrons colliding with ions *(Russian)* 79−3564
dielectronic recomb. in plasma generalised cascade theory 80−43851
dielectronic recombination, appls. in astronomy 80−46391
dielectronic recombination, book contrib. 77−36751
dielectronic recombination and ionisation equilib., influence of autoionisation and excitation 77−15160
dielectronic recombination and resonances in excitation cross sections 78−62915
dielectronic recombination rates, ionization equilib. and radiative energy loss rates for Ne, Mg, S ions in low density plasma 79−68903
dissociative recombination, energy depend. below 0.8 eV, merged beam obs. 79−31716
E-region, coeff. at midlatitudes, determ. from daytime N_e profiles 79−5700
electrical discharge, deionisation of low press. plasma in gas discharge gap, elec. strength *(Russian)* 78−1921
electron gas, dissociative recombination 80−36940
electron impact detachment, ionisation, excitation, dissociation and recombination 80−63832
electron-ion recombination coefficient in afterglow, continuity equation, numerical solution 80−28598
ethynyl cation, dissociative recomb. cross section determ., merged beam obs. 80−78715
F_2-layer, nighttime height, influence of linear recomb. coeff. 79−8745
F-region, electron loss coeffs. calcs. 77−13156
F-region, linear recomb. coeff. rel. to neutral atmosphere parameters at fixed height 77−91346
fission fragment generated plasma, electron distrib. function, effect of collisions and diffusion 77−23653
flame, mutual ion neutralisation 80−35537
fluoromethane, gas, electron-ion recombination, at 292K, three-body interaction 79−46418
Freon 13-B1 and mixtures with Xe and Kr, saturation curve 1 to 8 atm., for ionography ionisation chambers 77−12997
galactic centre direction, low-freq. radio recomb. lines studies 78−32589
geminate recombination of radical ions in polar solvent, mag. field modulation, fluoresc. quenching 77−4912
geminate species, recomb. in presence of a scavenger, probability calcs. 79−31644
glow discharge, nonselfsustained, comp. and stability, peeling-off, ionisation and recomb. effects *(Russian)* 77−11414

ion recombination continued
H252α, recombination line emission from direction of Galactic Centre 77−45587
halide ions, recombination, exciplex or excimer form. in plasma 80−75026
heavy ion+electron radiative recombination as cooling process, dipole approx. *(Russian)* 79−3565
n-hexane, geminate ion scavenging yield, external elec. field effect 79−47909
impurity diffusion eqn., with ionisation and recombination source terms 78−30409
inert gas atomic ions with F^- in dense rare earth gas, ionic recombination 78−46574
inert gas mixtures, high-press., collisional radiative recomb. 80−63595
inert gas recombination afterglow, spectral line shapes 80−940
interstellar *(Russian)* 80−36698
interstellar ionisation fronts, narrow radio recomb. lines emission 77−29940
interstellar medium, ion recomb. rel. to fine struct. levels population ratios 79−35351
interstellar polyatomic ion-electron dissociative recomb. reactions, neutral products, statistical theory 78−57604
ion trajectories in weak electrolytes, dissociation and recomb. of ions 80−85189
ionisation, quiet nighttime, calculated and measured decay rates comparison 78−81493
ionosohere, lower, shortcomings in understanding of recomb. coeffs. 78−81492
ionosphere, charge carriers recomb. model rel. to balance eqn. 78−28369
ionosphere, effect of recomb. processes and plasma nonisothermability on thermal parametric instability 80−61967
ionosphere, N_2^+ recombination rate coeff. determ. 78−28386
ionosphere plasma clouds, deform. and striation, multilevel model with recomb. chemistry 77−25834
ionospheres, ionic reactions in lab. and planetary atmospheres 80−59168
ionospheric F_1-layer, implications of dynamical effect for dissoc. recomb. rate 79−12340
ionospheric records over Shanghai, March 1953 to June 1955, effective coefficient of recombination *(Chinese)* 80−77192
ions in low density plasma, dielectronic recomb., ionization equilib. and radiative energy loss, solar corona appl. 79−68903
large molecular ions, dissoc. recombination 79−7012
laser, recombination dynamic H plasma, freely expanding, from supersonic nozzle 77−19240
laser plasma, high press. ion kinetics 80−64002
laser produced plasma, wavelength effect on absorpt. and ionis. 77−27654
laser system, recombination processes, book contrib. 77−50663
laser using elemental vap., stimulated emission conditions 78−17922
lasers using elemental vap., metal ion transitions 78−17923
liquids, electron scavenging and ion recomb. processes, 3-dimens. continuous time random walk model 78−7216
low-conductivity fluids, dark currents, forced diffusion model 79−15182
M82, stimulated recomb. line emission obs. 77−41408
magnetic field effect 78−38449
many-electron atoms, energy levels, quantum statistical theory of recomb. continuum *(Russian)* 79−63907
meteor trails, influence of recomb. on under-dense radio-meteor data 79−80279
meteors ion-ion recombination radiation 77−74016
molecular, indirect dissociative recomb., T-matrix element, Feshbach's projection operator technique 80−58114
molecular dissociative recombination, repulsive term, states of products 77−65537
molecule, photodissociation, recomb. afterglow, quenching var., activator penetration to region inaccessible to quencher 80−64813
mutual neutralisation, rate coeff. dependence on ambient gas density 79−89740
NGC 2024, H II region, recomb. line obs. of nearby partially ionised medium 77−57077
NGC 2024 (Orion B), H II region, recomb. line obs. 77−29895
nuclear pumped lasers, population processes, ion recombination 78−9361
partially diffusion-controlled, appl. to irradiated-liq. NH_3 solvated electron yield 79−100409
neo-pentane, gas, electron-ion recombination, at 292K, three-body interaction 79−46418
photorecombination emission reaction mechs. during atomic collisions 80−18914
planetary nebulae, radio recomb. lines and mol. emission lines obs. 80−109526
planetary nebulae, recomb. and level populations of ions, resolution of ang. momentum states 77−45529
planetary nebulae, recomb. time rel. to effects of He shell flashes in nuclei 80−73021
planetary nebulae, recombination model rel. to optical spectrum and continuum 80−109522
planetary nebulae, theory of physical processes in hydrogenic recomb. spectra 80−109527
plasma, atomic ion-electron recomb. in presence molecules, appl. to HCl 80−28601
plasma, dielectron recombination, electron density effect *(Russian)* 79−98856
plasma, electron three-body recomb., Fokker-Planck theory extension 77−62332
plasma, electron-ion recombination in ambient electron and neutral gases 80−38531
plasma, ion recombination rate in boundary layer 79−1286
plasma, isotope enrichment due to reson. trapping 77−58203
plasma, low density and T_e, highly ionised, dielectronic recombination through the forbidden levels 80−43850
plasma, multicharged, heated by laser radiation, ionis. and recomb. 80−19597
plasma, multiply charged ions, collisional dielectronic recomb. rate, effect on level populations 79−1287
plasma, recomb. press. leading to compression and plasma phase change 80−64799
plasma, recombination coeff. *(Russian)* 79−50847
plasma, transient ionis. and recombination, at. physics algorithm 78−5846
plasma column in coaxial cold cathode discharge, volume recomb. coeff. meas. technique 77−51237
plasma lasers in molecular medium, thermal ionisation and recomb. *(Russian)* 78−22118
plasma-solid surface interaction, electrostatic sheath equations, inc. heating, ion mobility, and ion recomb. 80−1808
positive column, electron temp. with two- and three-body vol. recomb. 80−19645
positive column with vol. recomb., electron temp. characts. 77−84401
positive ion bunches, gas neutralisation, without mag. field *(Russian)* 79−27744
pyrene+N,N-dimethylaniline (deuterate)(3,5 dimethoxy-N,N-dimethylaniline), geminate recomb., solvent, isotope, mag. field effects 78−56888
pyrene-DMA-methanol solution, photoinduced radical ion pair geminate recombination, triplet yield 78−76879
pyrene-N,N-dimethylaniline system, radical ion pair geminate recomb., mag. field modulated, Liouville eqn. 77−86302
radiative capture and Galilean invariance 77−38730
radiative recombination in ions of astrophysical interest 77−78627
radical ion pair geminate recomb., polar solvents, mag. field modulated, stochastic Liouville eqn. 77−86302
radical pair generation, diffusion, spin motion, recombination in soln. nanosecond scale 77−77798
radiolytic spur reaction, recombination of atoms or ions 77−1940
relativistic positronium atom stimulated form. in high-intensity opposite EM wave 80−9766
review 77−30947
Rydberg atom, electron collisions 80−63833
semi-self-maintained gas discharge, ionisation instability theory 78−67511
single atom detection in particle tracks 80−9475
solvated electron+ion, in ethanol, reactivity, ion pairing effects 78−85147
spark plasma ion source effects on mass spectroscopic quantitative anal. 79−14631
spectral line broadening and radiative recombination background interferences in inductively coupled plasma-AES 80−22435
stellar winds and coronae, recomb. effects on IR and radio continua 77−29817
stratified gas discharge, binary charge layer creation recombination depend. *(Russian)* 78−22591
supernova AD 1006 optical remnant, peculiar H ion recomb. spectrum 79−21371
termolecular ionic recombination, ambient gas temp. and density rate depend. 80−35522
p-terphenyl solns., mag. field effects on scintillation pulse shape, ion pair recomb. 77−16835
three body ion-ion recombination probability, Monte Carlo simulation 80−85160
TMPD, nonpolar photoionised soln., geminate pair quantum field, recombination fluoresc. elec. field quenching 79−20389
Tokamak plasma effective charge, high electron density with impurities, X-ray obs. *(Russian)* 77−19762
universe, anisotropic, recomb. dynamics rel. to relict radiation polarisation and anisotropy 80−67917
upper atmosphere, rate of radiative recombination 78−40758
variational principle, equiv. to quasiequilib. condition, in low-density ambient gas 79−37443
vinyl cation, dissociative recomb. cross section determ., merged beam obs. 80−78715
volume recombination coeff. meas. method, in Ne positive column, ionis. role 77−51252
W35, W43, H II regions, low-freq. radio recomb. lines studies 78−32589
W49 A, struct. deduced from mol. and recomb. line obs. 77−33665
W 3, H II region, recomb. line obs. of nearby partially ionised medium 77−57077
X-ray spectra of impact excit. highly charged ions, dielectronic satellites 78−62762
Ag-electrolyte interface, enhanced Raman scatt. of adsorbed molecules, background continuum obs. 79−73926
Ar arc deviation from Saha-Boltzmann equilibrium, heavy-particle effects 78−67596
Ar arc discharge atomic excitation, effect of ion conversion *(Russian)* 79−10731
Ar, decaying arc, electron cooling, diffusion, ionisation and recombination processes 80−33841
Ar, decaying plasma arc, electron disappearance mechanism 80−38765
Ar, dissoc. recombination coeffs. in positive column 78−26367
Ar, electron pulse radiolysis, 2p levels formation and decay kinetics 78−31665
Ar, liq., α-particle excited carriers, geminate recombination 78−34876
Ar, low press. discharge afterglow, dissoc. recombination, microwave diagnostics 78−9876
Ar plasma, recombination, kinetics of stimulated atomic populations *(Russian)* 78−87436
Ar plasma jet, surrounded by Ar, He, N_2, H_2 gases, recombinations in decaying jet 78−9753
Ar plasma MHD arcjet, recombination lasing 77−65588
Ar, positive column, 4S and 4P levels populations, rel. theory with recomb. 77−10766
Ar^{2+} dissociative recombination in Ar+N_2 early afterglow 79−34305
Ar-Ti hollow cathode afterglow, energy transfer mechanisms and excited metallic ion prod. 80−43857
Ar+H_2, dissoc., recombination and inelastic scatt. pot. energy surface and cross section Monte Carlo calc. 77−27162
Ar^++Cl^-(F^-) in Ar, high press. ion-ion recomb. rate calcs. 78−31621
Ar_2^+, dissoc. recomb., total rate coeff. depend. on electron temp. 78−58817
ArH^+, dissociative recombination rates 77−86295
Ba, efficient ionis. by reson. laser pumping 80−32685
Be expanding laser-produced plasma, recombination effects 78−94935
C_2^+, dissociative recomb. cross section determ., merged beam obs. 80−78715
CH^+ ion dissociative recombination, diffuse interstellar clouds 77−53671
CH^+ $X\ ^1\Sigma^+$, dissoc. recomb. rate coeff., rel. to interstellar mol. form. 78−56884
CH_3^++e, dissociative recomb. reaction in interstellar clouds, products, statistical theory 78−57604
$C_2H_2^+$, dissociative recomb. cross section determ., merged beam obs. 80−78715
CO^+ in cometary coma, dissoc. recomb. rel. to C prod. 79−16885

ion recombination continued
CO-He-O_2-H_2O laser discharge, stability, influence of recombination and ion chem. 78−17915
CO-N_2 plasma mixture decay, effective recombination coeffs. *(Russian)* 77−47144
CO_2, gas, electron-ion recombination, at 292K, three-body interaction 79−46418
CO_2-N_2-He, vol. discharge, negative ions effect 80−14956
CO_2(-He) discharge, UV-initiated, electron ion recomb. and CO_2 dissoc. 80−44068
C252α, recombination line emission from direction of Galactic Centre 77−45587
Ca, efficient ionis. by reson. laser pumping 80−32685
Ca ions, dielectronic recombination excitation in solar X-ray lines 80−51725
$Co^+ + e^- + He \rightarrow Cs + He$, rate coeff., pulsed discharge at 625K 78−17789
Cs-N_2 plasma, collision recomb. of charged particles *(Russian)* 77−80373
D_2^+, dissociative recombination, projection operator formalism 77−3479
D_2^+, dissociative recombination cross sections 79−59568
D_2^+, electron impact, dissoc. recomb., highly excited atom form. *(Russian)* 78−33621
$F^- + Ar^+(Ar_2^+)(Kr^+)(Kr_2^+)$, in Ar, high press. ion-ion recomb. rate calcs. 78−31621
$F^- + X_2^+ \rightarrow [X_2F]^*$, 300K, 50 atm., recombination rates 78−46576
Fe IX, X, XI, effective dielectronic recombination rates in H plasma, emission time histories 80−79570
Fe XXII, XXIV, XXV, charge exchange recomb. in Princeton large torus during beam heating 80−100067
Fe XXIV, dielectronic satellite spectra, solar flares appl. 80−32646
Fe^{23+}, dielectronic recombination, Rydberg autoionising states, props. in elec. fields 79−59405
H 137β/109α intensity ratio in H II regions, interpretation 80−31344
H, Balmer recomb. lines obs. in Seyfert galaxy (NGC 4593) 80−51878
H, Balmer spectrum anal., statistically extended recomb. continuum and line dissolution 77−27006
H, decimetric recombination lines obs. in Galactic Centre direction 77−82310
H II regions, effects of dust on recomb. line temps. 77−33588
H II regions, ion recomb. initiation by shocks 77−64825
H II regions, multiple-component, radio recomb. lines press. broadening 80−4419
H, in interstellar intercloud medium, recomb. radiation rel. to ionisation 77−9782
H, isoelectronic sequence, dielectronic recomb. coeffs. 77−27172
H, on semiconductor surface, nonequilib. charge carrier generation *(Russian)* 79−91126
H, recomb. kinetics in presence of low mass primordial black holes *(Russian)* 79−17152
H^- form. by surface and vol. processes, neg. ion source appl., review 80−58375
H-like plasmas for short-wavelength lasers, population inversion 78−34277
$H^- + M^+$ (M=alkali metal atom), ion-ion recombination 78−58779
H_2 arc plasma Balmer spectrum decay and two-fluid model 78−67603
H_2^+, dissoc. following beam-foil interaction 78−70920
H_2^+, dissoc. recombination, doubly excited Rydberg states 80−83506
H_2^+, dissociative recombination, projection operator formalism 77−3479
H_2^+, dissociative recombination in low energy electron collisions 79−3563
H_2^+, dissociative recombination cross sections 79−59568
H_2^+, electron impact, dissoc. recomb., highly excited atom form. *(Russian)* 78−33621
H_2^+, electron impact, dissociative recombination 79−89796
H_2^+, electron impact dissoc. recomb. cross sections, Rydberg states form., merged-beams expt. 78−25725
H_2^+, recombination yield on emerging from ultrathin C film below Bohr vel. 79−50108
$H_2^+ + H^- \rightarrow H_2^* + H$ recombination react., calcs. *(Russian)* 80−55659
H_3^+, dissoc. following beam-foil interaction 78−70920
H_3^+ dissoc. recomb., role of H_3 excited electronic states 79−89795
H_3^+, dissociative recombination in low energy electron collisions 79−3563
H_3^+, electron impact dissoc. recomb. cross sections, Rydberg states form., merged-beams expt. 78−25725
$H_n^+ + e$, electron-ion dissoc. recomb., rate const., electron beam sustained discharge 78−50652
H_2CN^+, dissociative recomb., rel. to interstellar HCN and HNC form. 78−81672
$HCNH^+ + e$, dissociative recomb. reaction in interstellar clouds, products, statistical theory 78−57604
HD^+, dissociative recombination cross sections 79−59568
HD^+, radiative recombination rates 78−37708
HNC^+, radical cation, charge exchange mass spectrometry, HNC^+ ion recombination and ionisation pot. 78−76838
H_2O, gas, electron-ion recombination, at 292K, three-body interaction 79−46418
$H_2O + He(2^3S)$, energy transfer processes, reaction products, UV and visible obs. in flowing afterglow 78−85138
H_3O^+ (D_3O^+), plasma dissociative ion electron recomb., rate coeffs. 80−63747
$H_3O^+ + e$, dissociative recomb. reaction in interstellar clouds, products, statistical theory 78−57604
$H_3O^+.(H_2O)_n$, electron recomb., electron temp. depend. 78−82854
^AH, A=1,2,3, $\bar{p}$ radiative atomic recombination, antiprotonic atoms 80−83527
He, excited state formation from He_2^+ in afterglow, theory 79−22802
He, hollow-cathode type discharge, spectroscopic obs., laser light source appl. 80−59335
He II recombination lines, calc. intensities in UV 78−94212
He, isoelectronic sequence, dielectronic recomb. coeffs. 77−27172
He plasma, collisional-radiative recombination 77−58841
He plasma, cryogenic, recombination decay *(Russian)* 79−4104
He plasma, recombining, method of determ. of electron temp., electron density and ion density 77−84494
He plasma expansion, supersonic, population inversion 79−27755
He plasma in electron beam-excited discharge, atm. press., relax. obs. and model 79−37569
He^+, dielectronic recomb. in a mag. field 80−91662
He^+, electronic recombination in afterglow 77−62401
ion recombination continued
He^+, in galactic centre source G 0.7−0.0, interpretation of radio recomb. lines 77−17651
He^+, neutralisation, reionisation in O_2, ion pair form., differential cross sections determ. 80−53120
He^{2+} recombination in planetary nebulae, He II Ly α photons absorpt. and forbidden lines intensities 80−67833
He-CO_2(O_2) volume discharges, electron recombination and attachment 77−19799
He+CS_2, metastable atoms, energy transfer processes 80−83466
He+water (cyanomethane), afterglow, excitation and quenching reactions, optical pumping 78−35690
He_2 high press. afterglows, reviews 80−64823
He_2^+ recombination, high-temp., in plasma jet *(French)* 80−43861
HeH^+, radiative recombination rates 78−37708
HeH^+, vibrational self-ionisation of mol. and recomb. processes *(Russian)* 77−79700
^{3}He-Xe nuclear pumped laser, small signal gain coeff. and power output, theory comparison with expt. 80−63983
HgX (X=F, Cl, Br, I), three-body ion-ion recombination rates 78−63068
Hnα radio recombination lines, profile in static ion field 77−78629
K_2 excited states photorecomb., mol. ions form. *(Russian)* 79−89779
K^+, dielectronic recomb., in crossed beams, UV emission obs. *(Russian)* 79−10212
K-Kr, afterglow of laser plasma, fluoresc. spectra 79−19085
$K + Cl \rightleftharpoons K^+ + Cl^-$, chemi-ionis. and recomb. cross sections 78−33583
Kr, electron pulse radiolysis, 2p levels formation and decay kinetics 78−31665
Kr microwave afterglow, Kr_2^+ dissoc. recombination coeff., electron temp. depend. 78−30501
$Kr^+ + F^-$ and $Kr_2^+ + F^-$, ionic recomb. rates in buffer rare gases 79−8425
$Kr^+ + F^- + Ar$, three body ion-ion recombination probability, Monte Carlo simulation 80−85160
Kr_2^+ dissoc. recomb., rate coeff. and excited state prod., electron temp. depend. 78−22040
Li-like ion, in plasma, ion electron collisional radiative recomb. coeffs., bottleneck calc. 80−53942
Li-like ions, partial photoionization cross sections and radiative recomb. rate coeffs. 79−49994
Li-like ions, partial photoionis. cross-sections and radiative recomb. rate coeffs. 80−52951
Mg ions in low density plasma, dielectronic recomb., ionization equilib. and radiative energy loss, solar corona appl. 79−68903
Mg XI dielectronic recombination line, atomic parameters for reson. line satellite lines 80−78567
Mo XXXIII, dielectronic recombination rate calc. 80−14232
Mo^{29+} to $^{39+}$, photoionis. cross sections, radiative recomb. rate coeffs., rel. to plasma diagnostics 80−52953
Mo^{32+}, dielectronic recomb. rate coeffs. in plasma 80−43853
Mo^{38+}, dielectronic recomb. rate coeffs. in plasma 80−43852
N plasma, ionis. and radiation characts. 78−71459
N_2 adsorbed on W, effect of SIMS sputtering induced recomb. anal. 80−55243
N_2 arc plasma, recombination with gas glow, spectroscopic diagnostics 77−7626
N_2, high-pressure vol. discharge, stepwise ionisation processes quasi-stationary stage characts. *(Russian)* 77−27756
N_2^+, dissociative recombination rates 77−86295
N_2^+, electron impact, rate coeff. in thermosphere, AE satellite meas. 79−48594
N_2^+, electron impact dissociative recomb. coeffs. inferred from Atmosphere Explorer meas., objections 78−86957
N_2^+ recombination, effect on aeronomic determ. of $O^+(^2D) + N_2$ charge exchange rate coeff. 78−88954
N_2^{2+}, recomb. energy determ. from pot. curves 80−58335
N_2D^+, dissociative recomb., interstellar mols. appl. 79−31704
NH_3, gas, electron-ion recombination, at 292K, three-body interaction 79−46418
NH_4^+, in afterglow, electron recomb. coeffs. mass spectrometric meas. 77−6927
NH_4^+, mutual neutralisation, with simple and clustered positive (negative) ions 78−44372
$NH_4^+ + e$, dissociative recomb. reaction in interstellar clouds, products, statistical theory 78−57604
N_2H^+, dissociative recomb., interstellar mols. appl. 79−31704
$NH_4^+.(NH_3)_n$, in afterglow, electron recomb. coeffs. mass spectrometric meas. 77−6927
NO^+, dissoc. recombination, $N(^2D)$ atom quantum yield 77−63905
NO^+, electron impact, rate coeff. in thermosphere, AE satellite meas. 79−48594
NO^+ in lower thermosphere, daytime recomb. rates from Atmosphere Explorer-C meas. 77−33230
NO^+, multichannel dissociative electron recombination theory 77−83753
NO^+ recombination in mid-latitude trough and polar ionization hole 80−12575
$NO^+ + e^- \rightarrow N + O$, recombination rate const. determ. in flames 78−48632
$NO^+ + e = N + O$, in hypersonic air wake, temp. depend. meas. 79−27834
Na isoelectronic sequence, dielectronic recombination rate coeffs., 2-10^3 eV 80−10357
$Na + Cl \rightleftharpoons Na^+ + Cl^-$, chemi-ionis. and recomb. cross sections 78−33583
Ne, 2p levels prod. by dissoc. recomb. in afterglow, recomb. coeffs., level population 80−43855
Ne afterglow, recombination processes, microwave quenching 79−14624
Ne, electron pulse radiolysis, 2p levels formation and decay kinetics 78−31665
Ne ions in low density plasma, dielectronic recomb., ionization equilib. and radiative energy loss, solar corona appl. 79−68903
Ne, isoelectronic sequence, dielectronic recomb. coeffs. 77−27172
Ne, low press. discharge afterglow, dissoc. recombination, microwave diagnostics 78−9876
Ne, negative glow discharge recomb. at. excitation *(Russian)* 77−76225
Ne positive column, 3S and 3P level populations, rel. theory with recomb. 77−10766
Ne, positive column contraction under diffusion-recombination conditions 80−24293
Ne stationary discharge with diffuse recombination, limit current and multiple states 78−67498

ion recombination continued
Ne-He DC glow discharge electron density decay, microwave cavity obs. 78−91167
Ne-Ne and Ne, negative afterglows, microwave quenching and recombination processes, Mo emission 77−80307
$Ne+CS_2$, metastable atoms, energy transfer processes 80−83466
Ne_2^++e, in recombination afterglow, line intensity decay complex struct. 79−7503
O_2 electron capture rate from geminate ion recombination fluoresc. data 80−74245
O_2^+ dissociative recomb., $O(^1D)$ prod. in upper atm. 77−41251
O_2^+, dissociative recombination rates 77−86295
O_2^+, electron impact, rate coeff. in thermosphere, AE satellite meas. 79−48594
O_2^+, electron impact dissoc. recomb., pot. energy curves calcs. 80−53150
O_2^+ recomb. rate in ionosphere 77−25830
O_2-N_2 plasma mixture decay, effective recombination coeffs. *(Russian)* 77−47144
OH^+, dissociative recomb. in Venus atmosphere rel. to exosphere non-thermal H budget 79−12416
Pb^+, electron collisional laser populated by recomb., excitation and decay mechanisms 79−18405
$SF_5^-+SF_3^+$, ion recombination, flowing afterglow, cross section meas. 77−44473
SF_6, compressed, ion mobility and recombination 79−60098
SF_6 high-temp. electrical breakdown parameters 78−67567
$SF_6^-+SF_5^+$, ion recombination, flowing afterglow, cross section meas. 77−44473
$Se(^3P_1)$+inert gas, gas phase flash photolytic deexcitation obs., 1000K *(Russian)* 78−50626
Si, dielectronic recomb. and ionization equilib., autoionization and excitation influence 78−1077
Si^{2+}, interstellar, Si^+ form. by charge exchange reactions 77−9789
Sr, efficient ionis. by reson. laser pumping 80−32685
Sr-Cs mixture, laser induced collisional two-photon ionisation, fluoresc. monitoring 80−91515
$Te(^3P_1)$+inert gas, gas phase flash photolytic deexcitation obs., 1000K *(Russian)* 78−50626
Ti XX 80−100067
Xe, electron pulse radiolysis, 2p levels formation and decay kinetics 78−31665
Xe^++Cl^-+Ne, three body ion-ion recombination probability, Monte Carlo simulation 80−85160
Xe_2^+, dissoc. recomb. in afterglow, rate coeff., excited state prod. 77−46647

ion solvation *see solvation*

ion sources
see also ion emission
40 kV metal beam injector, modified duoPIGatron 79−68117
40 kV multimegawatt neutral beam line, power flow and ion source 79−76238
100 mA low emittance ion source for ion beam fusion 79−68069
180° mass spectrometer, mag. field effects on ion source 77−30216
Aarhus modified negative ion source 79−81109
active sites, effect on mass spectral fragmentation patterns 78−89581
alkali and noble gas atoms, fast on-line mass separation from high temp. carbide targets 79−22515
alkali ion source, duofilament, for undergraduate laboratory 79−40329
alkali metal solid ion source for low-energy Van de Graaff accelerator 79−31292
angle resolved mass spectrometry, ion internal energy selection 80−53164
anode layer struct. with closed Hall current, anomalous cond. effects *(Russian)* 77−46437
anode plasma, ion accel., relativistic electron beam propag. effects 80−47790
arc, for cyclotrons, thyristor current modulator 77−46438
arc discharge ion source with energy selection 77−83414
arc type for JIPP T-II injector, source and power supply system description 78−29689
arc-discharge-type ion sources, cathode lifetime and stability problems 80−32558
auto-resonant ion acceleration concept, computer simulation 77−24208
autoionisation gun, 3-electrode, for ion field source in MKh1303 mass spectrometer 77−38055
axial cold cathode ion source, change time anal. 77−83392
beam plasma source, optimum discharge parameters 78−59617
beam trajectories through einzel lens for linear accelerator ion source *(Japanese)* 80−18718
beam-plasma ion source, max. current calc. 77−11356
Berkeley multicusp ion source for use with TFTR neutral beam injector, characts. 80−54040
Berkeley multifilament, ion source, modified 79−6784
Berkeley multifilament ion source, plasma characts. 79−94807
Berkeley type ion source, long life cathode 78−66375
Bonn isochronous cyclotron, external ion sources, inject lines, description 79−54675
broad beam ion source used for sputtering and etching of Ar, Kr, O_2 and N_2 gases 80−69002
broad-beam, low-energy, high-intensity gas ion source with multiaperture extractor system 79−54217
cathode flare, fast ion emission 77−62426
charge exchange of metal atoms, ion source for twin mass spectrometer 80−106215
coaxial electron impact, H_3^+, HeH^+ and He_2^+ beam prod. 80−62795
cold cathode, for mass spectrometry 80−42293
cold cathode ion gun for sputter etching apparatus 79−34170
cold cathode ion source, floating potential of metal surface under bombardment of ions 79−41057
cold-cathode ion gun for sputter-etching, discharge characts. and improvements 80−105748
collective acceleration, rel. to relativistic radially inhomogeneous electron beams 79−50201
collective accelerator as ion source and injector for a heavy-ion cyclotron 79−54618
collective field accelerator, vac. diode with relativistic electron beam operation 77−24201
collective high-energy ion acceleration, by intense relativistic electron beam, localised pinch model 78−87460

ion sources continued
collective ion acceleration by controlled motion of virtual cathode in relativistic electron beam 77−24210
collective ion acceleration by cyclotron of space charge waves in relativistic electron beam 77−24204
collective ion acceleration by electrostatic field of mag.-confined electron beam 80−5677
collective ion acceleration following relativistic electron beam injection into low press. gas 77−24209
collective ion acceleration in relativistic electron beam diode, intense slow space charge generation 78−9863
conference on nuclear spectroscopy of fission products, Grenoble, France (May 1979) 80−77546
controllable ion gun with high brightness 77−87871
corona ion generator for removing dust and aerosol particles in rooms *(Finnish)* 77−66883
crossed-field arc discharge contraction ion source 78−86382
CRYEBIS, a multi-purpose EBIS for the synchrotron Saturne II 79−72166
Cryebis, ion source of Saturne II synchrotron *(French)* 79−41055
CRYEBIS ion sources for Saturne synchrotron *(French)* 80−63432
current trends *(Hungarian)* 80−57786
cyclotron source, pulsed ion extraction, pulse generator characts. 77−18135
DC ion beam formation with multiple electron beams, plasma boundary shape control 80−14022
DC source, neutral beam injector, Chalk River development 80−27855
design, for milling appl. 78−70222
deuteron beam generation, 1 to 5 MeV, by plasma focusing *(Russian)* 77−38537
deuteron source, laser-plasma 80−78475
diode production, mag. insulated intense ion diode design review 78−9857
direct conversion of 120 kV beam 78−54920
direct extraction H^- sources, prod. and destruction in magnetron and duoplasmatrons 77−23340
discharge chamber with volume ionisation, current distrib. 80−23227
discharge ion sources, fundamental and special physical processes 80−32559
distributed parameter ion sources, geometry, pot. profiles, ion currents 77−35365
DITE Phase II ion source, characteristics 80−83223
double plasma and other synthesised plasma devices, adjustment of ion energy distribution 80−19625
doublet III neutral beam source cryopanel system 79−76233
Doublet III noncircular Tokamak, neutral beam injection system 78−54970
drift tube ion source, for chemical ionisation mass spectrometry 78−7260
dual EI/CI ion source, for gas chromatograph-mass spectrometer *(Japanese)* 78−32919
duoPIGatron, H^+ fraction enhancement by predissoc. 77−13816
duopigatron, preacceleration effects on ion beam transmission effects 78−87005
duopigatron gas discharge ion source, perform. characts. 78−54505
duopigatron ion source, extraction electrode, hole geometry optimisation 78−32921
duopigatron ion source, modified, ion composition 78−54914
duoPIGatron ion source, optical telemetry and data transfer system 78−66443
duoPIGatron ion source, plasma studies 77−76145
duopigatron ion source for JT-60 neutral beam injector 78−54912
duoPIGatron ion source for plasma heating 77−67534
duopigatron ion source for PLT injectors 78−54913
Duopigatron metal ion source, currents and lifetime 77−18724
duoplasmatron, beam emittance as function of discharge modes 79−45511
duoplasmatron, pulsed valve for anode opening 79−68109
duoplasmatron anode plasma, ion temp. 80−6292
duoplasmatron gas discharge ion source, plasma expansion cup effects 78−58092
duoplasmatron hollow cathode bakeable source 77−6602
duoplasmatron ion source, D ion mass, energy, current density distribs. 77−23339
Duoplasmatron ion source, magnetic topography 77−57783
duoplasmatron ion source for secondary ion mass spectrometry 79−85196
duoplasmatron ion source in KEK-PS 77−83390
duoplasmatron pulsed ion source, >1 A *(French)* 77−65374
duoplasmatron source for 665 keV pre-injector for NIMROD 70 MeV injector 77−38435
duoplasmatron sputter source for multiply charged ions from solids 78−66446
ECR heavy ion source, Louvain-la-Neuve cyclotron 79−72116
ECR light ion source for Karlsruhe isochronous cyclotron 79−68012
ECR-heated plasma source, extracted multiply-charged ions charge state distrib. 80−24268
electrode power loading in high current ion sources 80−27858
electron beam ion source, charge, state distrib. of multiply charged ions, balance model 77−18726
electron beam ion source, multiply charged heavy ion prod., charge exchange expts. 78−58816
electron beam ion source for multiply charged ions 79−30608
electron beam modulator automatic control system 79−72173
electron beam type, producing low-vel. highly charged heavy ions 80−58017
electron bombardment type, for use with mass spectrom. 80−77909
electron cyclotron reson. ion source with permanent mags., plasma-wall interaction expts. 80−99378
electron cyclotron resonance ion source for CYCLONE, current status 79−54676
electron cyclotron resonance multiply charged ion sources 79−54729
electron cyclotron resonance type ion source *(Japanese)* 79−97467
electron temp. effects for ion beam source, neutralised ion beam prod. 79−93863
electron-beam superconducting ion source for high intensity multiply charged ion 77−23333
electron-bombardment ion source, accelerator system computer solns. 77−88309
electron-bombardment ion source, cylindrically symmetric, low energy spread 78−89594

ion sources continued
electrostatic, powerful oscillating electron source 77−14283
electrostatic acclerator, multiply charged ion prod. at low energy 78−66437
electrostatic electron oscillator design optimisation, ion source and vacuum gauge 78−74107
electrostatic well accumulation of multicharged ions in mag. mirror plasma by electron cyclotron reson. 79−32804
elementary discharge theory, discharge equilibrium problem, single-valued soln. 79−26801
EM ion separators and related ion accelerators 77−14276
emission current regulator for ion-cyclotron reson. mass spectrometer 77−61150
emission from laser plasma, longit. mag. field effects *(Russian)* 80−54012
energetic neutral beams, development to MW power level of controlled thermonuclear research 79−45508
energy spectrum of beam from inductively coupled HF source, optical parmeter meas. of gun 78−89590
evacuated drift tube geometry, ion acceleration 77−61637
extraction electrode cooling in long-pulse operation 80−52360
extraction element design for long pulse multi-megawatt neutral beam 80−102373
extractor electrode CAD *(Japanese)* 78−86680
extractor for large area plasma source 77−84466
fast charged particles, prod. and impact effects 79−45492
fast ion beam production technology, use in laboratory and space expts. 78−5889
FEBIAD ion source for fission fragment isotope separation 80−78483
FEBIAD source, plasma and beam characteristics 78−66002
field desorption ion source for gas chromatograph-mass spectrometer *(Japanese)* 78−32920
field emission deposition sources 79−83127
field evaporation, possible applications of a high brightness Ga source to ion microprobes 79−2896
field ionis. mass spectrometry, field desorption and field ionis. kinetics, review 78−324
field ionisation and desorption sources, for quadrupole and double focusing spectrometers 78−74092
field ionisation source, preactivated, appl. to organic compounds anal. 77−5959
field ions./electron ions. modes, of mass spectrometer, pot. distrib. calcs. 77−74553
FIM high brightness ion sources, field effect contribs. 78−32930
flowing afterglow plasma ion source, appls. 80−87955
focusing electrode improved ion source extraction system for Van de Graaff 79−76179
fragment ion kinetic energies, modified ion source and mass spectrometer 77−6958
Freeman source, electron trajectories in arc discharge 77−18722
Freeman type high current source for implantation appl. 78−66005
Freeman type ion source in low press. arc operation, discharge characteristics and beam quality 78−66006
fundamental constraints in various situations 77−14653
fusion reactor, 1000-kVa arc power supply 80−99396
fusion reactor, ASDEX, neutral beam injection, beam line design 80−99395
fusion reactor, DITE-II, neutral beam ion source particle beam identification 80−99397
fusion reactor, Heliotron E, neutral beam injector ion source power supply 80−99333
fusion reactor, long pulse high current ion source electrode cooling 80−91360
fusion reactor, MFTF, neutral beam source development 80−102368
fusion reactor, neutral beam injector mag. cusp plasma source, design and fabrication 80−99377
fusion reactor, PDX, neutral beam elec. power system, ion source supply upgrade 80−102330
fusion reactor, PDX neutral beam injector, ion accel. structural anal. 80−102375
fusion reactor, PDX neutral beam injector development 80−99375
fusion reactor, rectangular plasma generator, advanced ion source for ion injectors 80−99376
fusion reactor, Wendelstein VII A, injector design 78−54965
fusion reactor neutral beam injection, 120 keV, ion source 80−91357
fusion reactor neutral beam injection systems based on negative ions, review 80−42852
fusion reactor neutral beam source, 40 kV for TMX, engineering design 80−91358
fusion reactor PDX, ORNL prototype neutral beam injection system, ion source development 80−99391
fusion reactor stationary ion source construction 80−91359
gas and vapour sources for low-energy accelerators 78−66445
gas discharge ion source, high energy characts. 78−42772
gas discharge ion source for on line EM mass separator at heavy ion accelerator 78−17456
gas discharge ion source for on-line EM mass separator at heavy ion accelerator 78−17457
gas feed system to cyclotron ion source 79−81112
gas ion source, of mass spectrometer, ion extraction and energy discrimination 78−70226
gas mass spectrometer, ion source numerical simulation *(German)* 80−47141
gaseous discharge, for on-line isotope separators 77−23337
glow discharge source for nuclear thin film target prep. 78−55067
gun, for UHV microbalance, absolute meas. of sputtering yield *(Japanese)* 80−17951
Hall accelerator, four-lens, pure ion beam struct. 78−66441
halogen intense negative ion source 78−66001
heavy ion, postaccel., Heidelberg, first operational year review 79−72002
heavy ion beam prod., ionisation 78−843
heavy ion beam prod., operational procedures 77−83436
heavy ion beam source, high charge and intensity beam prod. 79−12884
heavy ion generator, 150 keV, for sputtering 79−697
heavy ion interactions with gases, measurement apparatus 79−31741
heavy ion linear postaccelerator for Munich MP-tandem 79−72004
heavy ion low and medium energy accelerators, recent design advances 79−67984
heavy ion source cathodes, lifetime improvements 79−72167
heavy ion source support gas mixing expts., ORIC 77−83391
heavy ion source with indirect heating 78−50427
ion sources continued
heavy ion stripping data in dilute gases and C foils, semiempirical formulas 78−33354
heavy ion supercond. linac, Argonne, initial operation and recent development 79−67985
heavy ion supercond. linac, Stony Brook, current status 79−67986
heavy ions, experimental methods, targets and detectors, book 79−31242
heavy ions, low beta linac 79−72005
heavy negative ion beam prod. in range 15-90 keV by charge exchange with Mg vapour 78−25366
heavy negative ion prod., 10-80 keV, charge exchange in Na vapour 78−33341
heavy particle beam, electron cooling 77−71713
heavy-ion beam intensity enhancement using support gas in ion source 77−34490
heavy-ion direct extraction Penning source, matching to FN-7 tandem 78−13357
heavy-ion fusion preaccelerator, 1.5 MeV, fibre-optic remote control system 80−73993
HF, proton yield increase, influence of He, Na, Ar, Kr, Xe and N_2 admixtures to H_2 obs. 80−57422
HF glow discharge source for chemical ionisation process studies *(German)* 78−70221
HF source of low-energy ions 79−36447
HICONEX 834 sputter source, negative ion test injector of Munich MP tandem 78−13363
high charge state heavy ion sources 77−83360
high current, plasma supply to extraction region, theory and expt. 80−14023
high current DC ion source development at CRNL, duoplasmatron and duoPIGatron 79−76223
high energy heavy ion acceleration, prospects 79−68010
high power beam generation, review 80−13988
high purity radioactive beams at the BEVALAC 79−72129
high temperature, for on-line isotope separation appl. 80−74063
high-aperture ratio source for MI-1309 mass spectrometer 77−13811
hollow cathode, connection of He-jet system for on-line isotope separation 77−14304
hollow cathode discharge as negative ion source 78−82072
hollow cathode discharge ion source, with drift tube, for reaction rate consts. meas. 78−64834
hollow discharge duoplasmatron H^- energy spectra 77−79490
hollow-cathode multipole boundary ion source, IBIS, plasma prod. and containment system 78−74521
hot cavity, thermal ionisation 78−70677
IBM-5, without external mag. field 80−5428
implantation type accelerator, 400 kV, energy resolution, stability and calib. using (p,γ) react. 79−30604
inert gas duoplasmatron 80−32560
inert gas ion source, highly effective 78−66003
injector for deuteron linac 79−67969
INS 176 cm sector focusing cyclotron, present status, PIG ion source 79−54648
insulator coated grid with precel voltage, effect on ion optics 78−9014
intense ion beams for implantation 78−66004
intense ion source discharge, delay of arc starvation saturation 78−79457
inverse reflex tetrode, high power ion beam generation 80−68986
inverted sputter source for heavy ion prod. 78−29687
ion beam accelerator, multimegawatt, high-voltage power system, design philosophy, for fusion reactor 78−62613
ion diode, dual current feed magnetically insulated for internal confinement fusion studies 79−93851
ion prod. in hollow cathode source 78−74525
ion pulse stacking for prod. of intense current pulses 80−23209
ion source fission product separators 80−78479
ionisation chamber acceptance characts. distortion by ion source mag. field 79−21852
ISOL novel ion source, Nielsen-type geom. 77−14286
ISOLDE as a source of neutron-rich nuclei 80−78480
ISOLDE-2 on-line isotope separator at CERN 600 MeV synchrocyclotrons 77−23330
Kaufman, appl. to low energy ion erosion expts. on fusion reactor materials 80−68942
Kyoto beam-plasma type ion source, ion extraction system 78−66007
Lamb shift polarised ion source at FN tandem Van de Graaf at Univ. of Cologne 78−55065
Lamb shift polarised ion source with spin filter proton acceleration, operating performance 78−33348
Lamb-shift polarised ion source, Sona and spin-filter polarisation schemes 77−83378
Lamb-shift polarized ion source for the tandem accelerator center, the University of Tsukuba 79−93853
Lambshift polarised H^- and $^2H^-$ source at Giessen polarisation facility 77−65372
large aperture contact ionized Cs^{+1} ion source for an induction linac for fusion 79−76229
large area DC ion beam formation with multiple electron beams 80−305
large area plasma source for ion extraction array 77−84465
large diameter source for neutral beam injection, permanent magnet and coil combination 80−74066
large vol. mag. multipole ion sources development 80−27857
laser, for MI-1309 mass spectrometer 79−21849
laser ion source, appl. in mass spectrometry 80−89564
laser ion-source, form of ion pulses *(German)* 77−185
laser ionisation source for ICR spectroscopy, metal at. ion chem. appl. 80−45597
laser irradiated targets, limitations for GeV ion generation 78−55068
laser mass-spectroscopic method, elementary comp. of solids 79−83532
laser plasma ion source, for quantitative mass spectroscopic anal. of solids 77−32863
laser plasma rel. ion yields *(Russian)* 78−59631
laser solenoid radiation test facility 77−83430
laser-plasma ion source for ion implantation in solids 80−78474
LBL 88 inch cyclotron, high charge state heavy ion source, recent developments 79−54677
light link control system 79−68093
linear accelerators [conference, Ontario, Canada (Sept. 1976)] 77−38445
linear induction accelerators made from pulse-line cavities with external pulse injection 79−76180

ion sources continued
linear plasma induction accelerator, high current ion beam source *(Russian)* 78−21272
liquid metal, analytical instrums. appl. 79−3266
liquid metal sources, emission mechanisms 79−85845
liquid metal sources, positive ion emission charact. under high electric fields 80−99369
LLL D^+ source for 14 MeV neutron prod. 77−38491
long pulse extraction from modified duoPIGatron for neutral beam fusion reactor system 80−91355
Los Alamos on-line mass anal. facility, source modification for noble gases 77−14301
low background cold cathode ion source for molecular beam detect. 78−54506
low energy, high perveance, quiescent ion source, with single electrode extraction system 79−45509
low energy (100-500 eV) high efficiency ion source, for mass spectrometer 78−62261
low energy ion beams, conference, Salford, Sept. 1977 78−66444
low-energy high-current ion beam, production from TP-D plasms source 77−57424
magnetic bubble device large-area ion milling from small sources 79−75510
magnetic multipole containment ion source 79−22510
magnetic multipole source, electron energy distrib. 80−74058
magnetic-discharge pump for pulsed H injection 77−23318
magnetically confined oscillating electron bombardment ion source, current-voltage charact., source press. determ. 77−57423
magnetically insulated diode as ion beam source 80−95491
magnetically insulated diodes for prod. of intense proton beams 80−14004
magnetically insulated ion diode 80−106213
magnetron, Penning phenomena effects on Hg ionisation in plasma 79−18069
magnetron ion source, influence of gas press. on charge comp. of emitted ion beam 79−37516
mass separators, on-line, progress in targets and ion sources 77−14300
mass spectrometer, beam profile display device 77−5960
mass spectrometer, field ion source construction and recording systems modification for field mass spectrometry 77−49803
mass spectrometer, high sensitivity for quadrupole machines 80−52353
mass spectrometer, measured- and estimated electrode voltage discrepancy 78−74098
mass spectrometer, MI-1305, cooling attachment using liquid N_2 80−105744
mass spectrometer, two-photon ionis. of mol. beam 79−27118
mass spectrometer ion source, LiF fragmentation 78−70944
mass spectrometer ion source, voltage polarity changing cct. 77−45914
mass spectrometer ion-field source emitter, influence of laser irradiation on ion current 80−101874
mass spectrometer sources, field ionisation and desorption, experimental techniques, review 79−26176
mass spectrometers, high aperture ion source with surface ionization 79−93251
mass spectrometers for van der Waals dimers 78−89585
mass spectrometers multiemitter field source of ions 77−54013
mass spectrometric analysis, high-yield laser ion source with plasma focusing 78−61097
mass spectrometry, analytical, design and construction, review 78−322
mass spectrometry, ion source and focusing optics, high-luminosity 79−44979
mass spectrometry, ionisation methods, review 78−323
mass spectrometry, negative chemical ionis., ionis. techniques, review 78−325
mass-spectrometric leak detector, heating up to 550°C, sensitivity improvement 78−78028
McClure and McIlraith type ion sources, comparison 79−67429
metal ion, gas-discharge source 79−36448
metal ion source using high power density electron impact 78−54497
metal surface-electron beam intraction, 0.4-5mA ion beam extraction 77−84456
for MI-1309 mass spectrometer in high-temp. metallurgical studies 78−24885
Micromafios, multicharged ion source, electron cyclotron resonance *(French)* 80−68997
Micromafios, multiply charged heavy ion source, radial emittance meas. 80−102365
microprobe mass analyser, adaptation for liq. metal ion bombardment 77−49805
microsecond-pulsed ion beam from Marx generator 79−49886
microwave ion source 78−327
microwave ion source for high-current implanter 78−70224
Middleton type negative ion sputter source for Van de Graaff terminal operation 78−17455
Middleton type sputter source, emittance improvement 77−10509
MIN, negative ion injector, Na charge exchange cell 80−99386
miniature slow proton source for focusing efficiency obs. 78−78538
molecular noble gas ions in hot cathode ion source 80−306
molten metal field ion sources 78−65999
monoenergetic ion beam production, sequential pulsing technique using tandem mass spectrometer 77−74548
multiaperture sources, beamlet-beamlet interactions, effect on ion optics 78−46507
multibeamlet sources, linear optics theory of beamlet steering 78−12788
multichannel, with quadrupole HF beam filtering 78−74522
multichannel source 78−21267
multicharge heavy ion emission from strong-current low induction discharge plasma *(Russian)* 80−14033
multicharged, control of the axial ion motion in Krion source 79−13575
multicusp negative ion source for high-energy neutral beam production 80−87009
multidipole source, ion beam current increase 77−79489
multiDUOPIGatron, large uniform and dense plasma for multiampere beam formation 79−49889
Multiduoplasmatron, Multiduopigatron, ion *(French)* 78−26348
multifilament, fabrication of filament chucks 80−37122
multifilament ion source at Berkeley, model 78−13332
multifilament plasma source, multipole mag. field effects on charact. 79−46462
multimode, plasma density and ion loss investigation 78−55080
multiple aperture source using diverter type plasma source 77−71404
ion sources continued
multiple charged and polyatomic ions, use in implantation accelerator 77−54017
multiple stage cluster beam ionizer 79−67425
multiple-charged metallic ion generation using TEA-CO_2 laser irradiation *(Japanese)* 77−79197
multiply charged heavy ion prod., book contrib. 79−31290
multiply charged ion interactions with Al surface, laser induced plasma 80−70007
multiply-charged and polyatomic ions, use in implantation accelerator 77−74554
multipoint field ionisation source charact. 77−22606
negative, modified Univ. of Aarhus source 80−18729
negative halogen ions source 77−41729
negative heavy ion beam production by charge exchange in metal vapour, EN tandem accelerator accessory 78−33346
negative ion based neutral systems, generation, handling and acceleration 79−44981
negative ion beam, intense, 150 kV test stand electronics system, for fusion reactor 78−54934
negative ion beam acceleration to energies up to 120 keV 78−54918
negative ion high current beams, source plasma parameters determ. 77−83376
negative ion source, nucleated boiling water cooled cathode, design and testing 80−102370
negative ion source and beam development for fusion reactor ignition 79−45411
negative ion sources, generation by sputtering in Cs plasma, recent developments, review 79−49884
negative ions, from reverse polarity field ionis. source 79−92046
negative ions from accelerated hydrogen clusters, fusion ignition appl. 80−13883
negative sources, review 78−33345
negative surface ionisation on complex emitter 77−77335
neutral beam, continuously operating, convectively cooled ion accelerator, mech. design and fabrication 80−102374
neutral beam injection system, for TFTR 78−54971
neutral beam injector, beam line studies, for fusion reactor 78−54969
neutral beam injector, continuous operation, water cooled U-tube extraction grid 80−99392
neutral beam injectors, fast, for TFR 77−76140
neutral beam injectors, for Princeton Large Torus, component design 78−54966
neutral beam injectors for the mag. fusion energy program, development and appl. 79−45404
neutral beam ion source, core snubber network design, fabrication and testing 80−102378
neutral beam lines, for Princeton Large Torus, development and testing 78−54967
neutral beam source manufacturing at Lawrence Livermore Laboratory 80−102377
neutral beam system, 120 keV, for fusion reactor ignition 78−66377
neutral beam system, for ignition Tokamak 78−54973
neutral beam transport system, for fusion reactors 78−54968
neutral beams for fusion research, review 79−45406
neutral injection system, for JAERI experimental fusion reactor 78−54972
neutralisation, multi-aperture extraction systems 80−42301
Nevis pulse synchrocyclotron ion source using single cold cathode 79−54679
Nier-Bernas type, factors affecting cathode performance 77−18723
Nier-type electron impact ion source, repeller curve interpretation 80−57421
NIRS-CHIBA isochronous cyclotron facility, status report 79−54649
nonpolar molecules, ionis. by alkali ion attachment at electrolyte surface 78−65998
NUMATRON project at INS, Tokyo Univ., heavy ion source 79−68016
organic compounds, liq., new ionis. method appl., using Penning effect and chem. ionis. *(Japanese)* 79−93255
OSIRIS, target/ion source system for isotope separation in on-line mass separator, mol. ion prod. 80−99366
OSTIS, on-line mass separator for thermically ionisable fission products 79−714
particles and radiation therapy, conference, Berkeley, USA (1976) 79−20619
PDX neutral beam injector, multi-aperture ion accel. electrodes thermal anal. 80−102371
Penning discharge ion source, ion current depend. on mag. field and anode diameter 80−54072
Penning discharge ion source with hollow cathode, HF instabilities 80−43997
Penning ion source, ion energy charact., rel. to mode transition instabilities 77−38529
Penning magnetised discharge, stabilisation, use as ion source 78−9895
Penning source for H^- and $^2H^-$ ions 77−83415
Penning type, multiply charged ions 77−83439
Periplasmatron, ion source for neutral beam injection systems 78−54915
periplasmatron ion source for intense neutral beam 80−99380
PICPAB source on Spacelab spacecraft charging problems 80−85840
PIG low power source for Frankfurt CN-Van de Graaff 77−75009
PIG source with end extraction, lifetime extension 80−78472
pinched beam diode, geometrical focusing of intense ion beams 78−58898
pinched electron beam diode, proton current density meas. using biased charge collecting probe 77−55166
Pingus type, improved version 77−6587
plasma, appearance of radial electric field, due to extraction 79−45500
plasma, flowing, efficient ion beam extraction 80−18044
plasma, ion beam collimation by ion optical system, quality determ. 77−10138
plasma accelerator, compensated ion beams, ion dynamics *(Russian)* 77−47274
plasma electron-beam ion source 78−83584
plasma emitter of ions, boundary conditions at surface 78−87432
plasma ion accelerator with closed Hall current, eqns. of motion *(Russian)* 77−47273
plasma ion emission, cylinder and transverse slot ion optics, theory 80−43250
plasma ion sources, fundamental and special physical processes 80−32559

ion sources continued
plasma neutral beam injector research and development, in USA 77−76118
plasma power absorption analysis *(Russian)* 77−75014
plasma produced by CO_2 laser, emission of multiply charged ions 80−9445
plasma source for Tokamak fusion test reactor beam lines 78−54916
plasma source of high current low energy beams 77−5962
plasma source of ions, stationary, 50 to 400 eV range 79−97469
plasma source of multiply charged ions, CO_2 laser-condensed media impact *(Russian)* 77−47236
plasma sources, cooling pattern of acceleration grids meas. by IR scanning 80−86303
plasma triode ion beam production, anode design for reflex operation without impedance collapse 78−9862
plasmatrons, mono- and duo-, anode space-charge sheath characts. rel. to ion source 79−55576
plating appl., low-pressure, high-quality thin films deposition 80−35105
polarised beam acceleration possibilities with Brookhaven AGS 79−63844
polarised deuteron beam ionisation, beam intensity, tensor polarisation prod. in Penning discharge 77−3203
polarised H^-, D^- and T^- sources for LASL tandem and LAMPF accelerator 77−34492
polarised H and D ion sources review of recent advances 79−45498
polarised high energy particle production in cyclic accel. and storage rings, possibilities 79−63843
polarised intense Li-ion source proposal 79−63853
polarised ion beam production in laser-produced plasma *(Russian)* 77−38536
polarised ion facility, LAMPF 77−83377
polarised ion sources and low energy collector rings, H^-, D^- beams 78−58515
polarised ions, acceleration by synchrotons, review 79−63840
polarised particle, production and accel., status report, Saturne 79−63847
polarised proton 200 nA variable energy beam, TRIUMF 79−63848
polarised proton beam production in high energy hyperon decay 78−58517
polarised proton beams, higher energy, conf., Ann Arbor, MI, USA, Oct. 1977 78−58514
polarised proton high energy beam from lambda decays, possibilities 79−63845
polarised protons, acceleration by 12 GeV synchrotron at KEK, possibilities 79−63846
polarised source for Saturne II proton synchrotron 77−34491
polarized ion source development at Argonne National Laboratory 79−63842
polarized source based on nuclear polarization by charge-exchange 79−22514
polarized-ion sources, production methods, review 79−63841
positive ion extraction by an anodic orifice probe 80−38712
positive ion formation energetics by negative ion charge stripping 80−78700
positive ion recovery based on mag. blocking of electrons 79−97920
positive ion source, hollow cathode design 80−99399
power supply source, 2000 V and 2×200 V, for molecules and ions collision processes obs. *(Czech)* 77−5963
power-supply block for ion source with electron bombardment 78−8467
production and manipulation, general considerations 79−93256
projector with plasma source, cold cathodes and electron focusing lens 80−22472
proton accelerating mechanisms in vacuum diodes, induced radioactivity 79−97470
proton beam heavy ion source, injector for cyclotrons, feasibility study 79−54730
proton beam heavy ion source, possible use as cyclotron injector 79−45496
proton injection into a large amplitude space charge wave 79−71990
proton intense beam production, ~1 MeV, pinched electron-beam diode 77−10521
proton linac, low energy injection 77−38470
proton pulse generation, 0.2TW 77−22618
proton source, electron loss cross section for H^- on C 79−67976
pulsed, C, N, O and Ne ions, production and acceleration in cyclotron *(Japanese)* 78−5084
pulsed intense metal ion beam from laser-produced plasma 77−26433
pulsed ion diode, self mag. insulation 77−65918
pulsed power appl. to intense neutron source development 77−83432
quadrupole ion storage mass spectrometer, cylindrical geometry and operational characts., QUISTOR comparison 80−52351
quadrupole ion storage trap, ion withdrawal studies 79−54216
quadrupole ion storage trap chemical ionisation source, for mag. sector mass spectrometer 79−12877
quadrupole ion store, of mass spectrometer, ion ejection expts. 79−89033
quadrupole ion store, of mass spectrometer, phase synchronised ion ejection study 79−89034
quadrupole mass analyser-field ionis. source interfacing, ferrite insert, repeller electrode 77−18125
quasi-DC extraction of 70 keV, 5 A ion beam 80−87010
QUISTOR, ion kinetic energy calc., survey 80−78468
QUISTOR, phase synchronised ion ejection, ejection phase width and detection pulse delay effects 79−44976
QUISTOR, phase-synchronised ion ejection from quadrupole ion storage mass spectrometer 79−44975
QUISTOR, RF mass selective excitation, resonant ion ejection 80−99363
QUISTOR, total press. mode operation with phase-synchronised ion ejection 79−44977
radio-frequency trap with semi-spherical electrodes, ion storage 80−101869
reflected beam sputter source, output improvement with CS collection techniques 79−702
reflected beam sputter source 77−34501
reflection triode, prod. of high current ion beams *(Russian)* 80−83230
reflex tetrode, extracted ion beam anal. 80−23236
reflex tetrode ion source, consecutive microsecond pulse ion beams 79−41323
reflex triode, unidirectional ion generation and geometric focusing 79−76235
reflex triode with uniform ion flow 79−98928
ion sources continued
relativistic electron beam produced, facilities at Nagoya University Plasma Physics Institute 78−5919
relativistic self focusing from laser irrad. target, MeV and GeV ion prod. 78−51323
remote ion beam position measurement from random beam modulation 79−30606
resonance ionization source for mass spectroscopy appl. isotope anal. and time of flight spectrometer 80−81380
review of ion beam utilisation for etching and film deposition 77−32522
review of sources for low energy accelerators 78−58521
RF excited ion source, for the leak detector *(Rumanian)* 80−8999
RF heavy ion source, for ion implantation 80−32561
RF ion source, 15 cm diameter, stable working conditions calcs. 78−86388
RF ion source, ion beam extraction device 79−22513
RF ion source, low energy component of extracted ions 78−55064
RF ion source, modified extraction geometry 78−33349
RF ion source, RIG 10, intense H^+ beams 80−37671
RF ion source 15 cm stable working region determ. 78−75381
RF ion source with 100 Mc/s grounded grid oscillator 78−17454
RF metal ion source, struct., operating characts. *(Chinese)* 79−22520
RF modified sources of metallic ion beams 79−81111
RF quadrupole ion trap, singly charged ion prod. 79−98224
RF sources, effect of an axial magnetic field on an improved constricted source 79−1325
RF sources, triply charged Ar and Ne beams 79−18070
RF spark ion source, multiply-charged species rel. abundance distribs. 77−61151
rod pinch diodes, intense electron-beam pinch form. and propag., ion generation 79−14589
rotating intense proton beams, extraction and propag. from mag. insulated diode 77−79195
saddle field ion source, energy distrib. 77−87873
saddle field ion source, uniform depth profiling for ESCA 78−48708
saddle-field ion source, for ion-enhanced film bonding 79−83126
saddle-field ion source, for vacuum deposition by evaporation, enhanced film bonding 79−95931
saddle-field ion source behaviour, gas depend., at. spectroscopy appls. 78−78039
saddle-field ion sources, props. and appl. 79−76239
Scandinavian low output isotope separator, upgrading to 300 kV 78−66008
scanning ion microscope with field ionisation source 78−21289
scanning laser excitation, milliprobe appls. 79−35882
self-accelerating microwave ion and plasma sources 78−66000
self-triggered channel type, with continuous dynode electron multiplier 79−17562
semiconducting channel ion sorce, secondary emission and ion feedback 80−31936
SIMS primary ion sources, selection 79−39267
SIN injector cyclotron, design of central region including ion source 77−54379
single crate CAMAC control system for negative ion source test facility 79−72216
single slit plasma source, consumption of fuel for singly charged ions 78−67379
solid ion source by electron bombardment *(Japanese)* 78−78035
SOLIS, surface ionisation integrated target-ion source 77−14303
source plasma diagnostics, via short-time pulsed probe analyser 77−15240
space charge in beam transport 79−30610
space charge ion optical systems, expt., theory 78−9020
space charge ion optics, influence of chromatic aberrations 78−55294
spark in vacuum, ion acceleration mechanisms 80−92417
spark ion source of mass spectrometer, late stage ion energy distrib. 79−55596
spark plasma ion source effects on mass spectroscopic quantitative anal. 79−14631
spark source mass spectrograph, modification of ion source to reduce residual gas effects 80−98996
spark source quadrupole mass spectrometry, development, appls. 80−62789
spark-source mass spectrometry; elemental sensitivity rel. to sparking conditions 79−57314
spherical reflex triode, extraction and bunching of ion beam 80−18727
sputter electrode preparation for multiply charged heavy ion sources 78−66009
sputter heavy ion source for tandem accelerator 78−33305
sputter ion source, low prod. of stable N^- ions, design implications for tandem for sensitive C anal. 78−33350
sputter ion source, Pt plate ioniser 79−26800
sputter negative ion sources, role of alkali metal 78−74526
sputter pig sources, improved 79−76246
sputter source design for TEM fine grained coating specimen prep. 80−99015
sputter source of negative ions, energy spread 78−29688
sputtering, appl. to IMA analysis *(Japanese)* 79−54734
sputtering apparatus, review 78−72719
sputtering apparatus for film deposition, ion source construction and performance 77−73228
stabilisation method of ion beam current 77−79491
stable ion source discharge theory 79−31278
storage in electron ring, ion-ion interaction effects 80−52796
stripped N beam ECR ion source *(French)* 80−68988
stripper foils for electrostatic accelerator, new mounting method 78−33355
strongly focused beams produced by high electron currents in betatron *(Russian)* 77−6601
superdense MeV proton beam generation in magnetically insulated diode 80−14017
surface, separation of isobar nuclei of alkali and alkaline earth elements 80−37688
surface ionisation, for on-line isotope separators 77−23337
surface ionisation integrated target-ion source for Sr, Ba 77−88314
surface ionisation type, for mass separator operating on heavy-ion beam 78−5083
surface ionization source for heavy ions 80−68999
surface plasma H^- ion source, Cs flow meas. by ionisation gauge 79−68098
surface plasma source from 90 to 500 eV H beam impact 80−38729

ion sources continued
surface-plasma Penning source, intense H^- beam production, ion-optical characts. 79−13892
Test Accumulation Ring for NUMATRON project 79−72117
tetrode, reflex, unidirectional ion flow using additional aluminised mylar anode 78−37473
Texas A&M 88-inch cyclotron, heavy ion source 79−54680
Texas A&M cyclotron, electron beam ion source, development report 79−54678
therapeutic proton and heavy ion source capabilities 79−20629
thermal negative, principle, surface mats., operating conditions *(Japanese)* 80−91350
thermionic source, for low-energy alkali ions scatt. from solid surfaces 77−40318
thermoionisation efficiency in ion source cavity 78−844
thin film deposition, low energy in source modification 78−52687
time-to-flight ion source, electron beam collimation, rel. to resolution and sensitivity 80−42294
trajectory computation, computer simulation 78−71510
triode, high current ion beam prod. 80−99372
triode extractors with large acceleration-deceleration ratio, beamlet steering by aperture displacement 80−63430
Triplemafios multicharged heavy ion source *(French)* 78−9800
TRISTAN II mass separator, ion source, beam optics, computer system 80−78481
TRIUMF 100 μA beam, achievement and control 79−54699
Triumf polarised ion source 77−34494
tubular surface ioniser, ion extraction 79−63857
two electrode ion beam formation system 78−9016
two-grid accelerator systems, ion beam divergence characts. 78−82074
two-stage 150 keV accelerator, ion beam optics 78−9017
two-stage axial accelerator, with plasma anode-layer 79−71561
two-stage discharge ion source, operational characts. 80−47797
two-stage-discharge ion source 79−90423
UNISOR integrated target-ion source 77−14302
universal negative or positive ion source 79−68077
vacuum diode, with sharp tip cathode, elective ion accel. by 180 kV pulses 78−37104
vacuum vibrator arc ion source, multiply-charged species rel. abundance distribs. 77−61151
vaporised metal cluster ion source, props. of ionised cluster beam 79−49337
VICKSI 6 MV Van de Graaff and split pole cyclotron, present status 79−67987
VICKSI facility, running in period and initial operating experience 79−54627
whisker emitters for field mass spectrometer 77−18132
XTU tandem of Lab. Nazionali di Legnaro (Padova) 78−13354
ZGS polarised ion source development activity 77−34493
Ar ion duoplasmatron source, new target ion source system for short lived nuclei meas. 78−66449
Ar low energy ion beam transport through apertures, source parameter depend. 77−57422
Ar, multiply charged beam from TRIPLEMAFIOS source, characts. 77−18133
Ar plasma bridge neutraliser operation with 10 cm beam diameter ion etching source 78−74102
Ar, using duoplasmatron, props. 78−74523
Ar^+, 30-cm multipole sputtering electron-bombardment ion source, design and characts. 77−87870
Ar^+, focused ion beam designs for sputter deposition 79−89841
Ar^{3+}, Laval 7 MV Van de Graaf accelerator, upgrading using triply charged beams 79−45476
As ion prod. in 2 MV Van de Graaff 80−14031
Au, liq., ion source fabrication and emission characts. 80−68995
B^- ion beam acceleration in EN tandem 77−26912
B^+ fraction from Freeman type high current source for implantation appl. 78−66005
^{10}B negative ion beam prod. with sputter source 79−93857
^{11}B negative ion beam prod. with sputter source 79−93857
Be^- ion beam acceleration in EN tandem 77−26912
Bi, liquid, field ion source emission characts. 80−74059
C foils, stripping of heavy ions with energy 0.4-0.9 MeV/A, straggling, foil behaviour 78−33351
C ion injector, high-intensity current, using array of pulsed plasma guns 79−89512
C, stripper foils under 4.8 MeV Ar^{++} ion bombardment, shrinkage, rupture, lifetime 78−33352
C^- ion source for radiocarbon dating using tandem accelerators 80−94620
C^+, vacuum arc source 79−21853
^{14}C, beam production for Munich tandem 78−90008
^{14}C, prod. of intense negative beam from graphite 80−102361
$^{14}C^-$ beam prod. from TaC and Ta_2C *(French)* 79−76243
^{48}Ca, and rare isotopes, beam prod. using Cs sputter source 78−29686
^{48}Ca tandem accelerated beam 77−79496
^{252}Cf fission source, ionisation characts. of electron oscillating ion source coupled to He-jet skimmer system 78−70661
Cs beam sputter ion source, T acceleration in FN tandem 78−55070
Cs, pulsed sputter negative ion source 78−33347
Cs, pulsed vapour source for ion sources in heavy ion accelerators 80−63423
Cs reflected beam sputter source, performance 78−29685
Cs sputter ion source, survey of negative ions for use with tandem accelerator 77−83412
Cs sputter source, prod. of MgH^-, MgH_3^-, CaH and CaH_3 beams 77−34499
Cs sputter source, T beam prod. 78−29684
Cs sputter source of negative ions, production mechanisms 80−27850
Cs^+, for secondary ion mass spectrometry 78−32913
Cs^+ ion source, CW monoenergetic, by photoionisation 80−63910
Cs^+ mass spectrometer quadrupole mass filter transmission 79−21851
Cs^+ primary ion source for ion microprobe mass spectrometer 78−4732
^{137}Cs sputtering negative-ion source, design and perform characts. 79−13568
D beam, polarised, short compression magnet for intensity increase 80−18732
D, magnetically insulated, pulsed, peak beam parameters 80−32548
D pressure regulation by regulating electrolyser 78−842
D^- ion source for high voltage neutral beams for fusion reactors 80−99379
ion sources continued
D^- ions, equil. charge state fractions of 3.3-39 keV D atoms and ions in Mg vapour 77−57788
D^- source using surface ionis., continuous beam prod. 78−9021
D^+, 10 kV continuous service extractor 79−45468
D^+, from externally ignited vacuum arc between ZrD electrodes 80−33845
D^+ source, performance improvement, appl. to fusion reactor neutral beam lines 79−22511
$D^+ + Rb \rightarrow D^{-,0} + Rb$, equil. fraction of D ions, charge transfer cross section 77−65375
D_2, prep. by electrolysis of heavy water using self-controlled cell 78−80752
Ga, high intensity, emission characts., atom-probe FIM obs. 80−80950
Ga, liquid, emission characts. obs. 80−62810
Ga, liquid, field ion source emission characts. 80−74059
Ga, liquid EHD source for microprobe, design 77−21444
Ga liquid metal ion source, energy distrib. meas. 80−95493
Ge^+, low energy mass analysed ion beam deposition on Ge and Si substrates 79−33946
H, cluster ion source for accelerators 77−74551
H, high current, ion species computs. 77−42209
H ion beam, intense and small emittance, formation by BPD source 77−6593
H ion source, hollow cathode device 78−54921
H molecular ions beams, appl. to prompt nucl. react. anal. 79−36452
H, plasma reaction cross sections data 77−38538
H polarised ion source, Lamb-shift type, charge exchange processes *(Rumanian)* 77−46445
H^- beam 90° bending magnet, pole face configuration study 79−68090
H^- beam source, surface-plasma type, surface Cs loss mechanism *(Russian)* 77−79196
H^-, CW plasma device, current maximisation 79−22521
H^- cluster ion beam high power injector 80−13889
H^- form. by surface and vol. processes, neg. ion source appl., review 80−58375
H^-, from ion beam surface interaction, H^- formation by reson. electron capture 80−40691
H^- injection into Zero Gradient proton synchrotron 77−83369
H^-, ion beam bunching with sawtooth voltage 78−4735
H^- ion direct extraction source 77−83393
H^- ion program at Fermilab 77−38506
H^- ion source, 50 mA for accelerator injection, beam quality and reliability 79−72172
H^- ion source for accelerators 77−83381
H^- ion yield from duoplasmatron discharge 78−75382
H^- ions, survival probability on emission from alkali-coated W and Ni surfaces 80−45187
H^-, magnetron discharge as ion source 77−38528
H^-, polarisation by spin precessor 79−68097
H^- polarised beam production by 800 MeV spin precessor 79−68096
H^- polarised intense beam prod. by atomic beam source 80−37674
H^-, polarised proton sources BNL AGS, polarised proton acceleration 79−72055
H^-, polarised proton sources, 1 to 12 GeV beam transport at ANL ZGSynchrotron 79−72056
H^-, prod. from accel. cluster ions for neutral beam plasma injection heating 77−65376
H^-, production by Hall accelerator in Cs vapour, space-charge effects 78−67375
H^-, production in laser-initiated alkali hydride arc 80−32550
H^- pulse operated polarised Lamb shift type source 77−38533
H^- source, pulsed hollow discharge duoplasmatron 77−26432
H^- source development at ANL 77−83394
H^- source for hollow beams using H_2-Cs 80−23228
H^- sources for neutral beam injection 78−54919
H^- surface ion source, plasma parameters, diagnostics 78−9849
H^-, surface plasma source, prod. by H atom backscatt. from cesiated W 77−3953
H^-, variable energy polarised proton beam for TRIUMF cyclotron 79−72059
H^+, high intensity polarised beam prod. by laser emission *(Russian)* 78−46202
H^+, intense beam generation, appl. to controlled fusion 77−76119
H^+ ion beam generation, megavolt, 20 kA in reflex triode system 77−24203
H^+ ions on Na vapour, charge transfer cross section and equilibrium fractions 80−5616
H_2 and rare gas field ion source with high angular current 80−68996
H_2^+ beam form., selected vibr. states, by electron impact in high press. Ne 77−65547
^2H, 120 keV multi-megawatt neutral beam source 77−83357
He^- high current source of 70 mA at 10.5 kV 80−95495
He^- ions fractional yield from $Rb + He^+$, 3-20 keV, vapour target 77−1919
He^-, K charge exchange vapour, Pelletron accelerator injector 78−5085
$^3He^+$, polarised source for CN Van de Graaff 79−68106
$^3He^+$(2S) state ion beam with nuclear polarisation, RF source 79−59602
I^- beam, duoplasmatron ion source for SIMS, Ar-I_2 medium 77−18123
I^{-2} ions in gas phase 79−36449
^{127}I ions, 20 MeV, emerging from gas stripper, absolute charge state yields 78−55066
Ir, gas-phase field ionisation source, ang. intensity 80−2929
Ir(110), single cryst., fine focus beam with field ionisation 78−76589
Kr ion implantation using Lublin separator 79−82251
LaB_6, hollow cathode mag. multipole ion source 80−102369
LaB_6, negative surface ionisation, intense halogen ion source 79−93850
Li ion prod., for backscatt. anal. in Al and Al_2O_3 79−3328
Li negative polarised ion beam source at Heidelberg EN-Tandem 78−33356
^6Li tensor polarised beam prod. and calibration 78−46199
^6Li vector polarised source at Heidelberg EN tandem 77−65371
Mo, extraction grid for high power ion source 80−102372
Mo, ion prod. in hollow cathode source 78−74525
N^+, acceleration by intense relativistic electron beam in spatially periodic mag. field *(Russian)* 79−10255
Na vapour charge exchange H^- ion source 77−38542
Na vapour charge exchange cell development 77−83395
Na^+, mass spectrometer quadrupole mass filter transmission 79−21851
NaCl, mol. beam, on hot W(Re), surface, Na_2Cl^+ ion form. 79−56907

ion sources continued
Nb, ion prod. in hollow cathode source 78−74525
Ne^{2+} Laval 7 MV Van de Graaff accelerator, upgrading using triply charged beams 79−45476
O, low-energy highly-stripped, double-tandem accelerator-decelerator for O^{q+}+He charge exchange measurements 80−81317
O^+ low energy ions interaction with solid C and Pt targets, preliminary study 79−34352
P ion implantation using Lublin separator 79−82251
P ions, charge distrib., 72-123 MeV 80−27849
Rb^+ mass spectrometer quadrupole mass filter transmission 79−21851
Re, ion prod. in hollow cathode source 78−74525
S ion charge distrib., 70-140 MeV, through C and Be foils 78−13364
Sb, high current, characts. 79−17561
Sb negative ion source 78−4734
Se ion prod. in 2 MV Van de Graaff 80−14031
Si, emitter for field desorpt. mass spectrometry 79−79323
Si whisker field desorption ion source, Cu, Sn, Ag, Te, Cd and Sb isotope abundance ratios 80−11975
T medium energy beam from α-particle fragmentation 80−27847
T sputter cone ion source for Minnesota MP Tandem, installation 78−29683
Ta, electron cyclotron resonance source *(French)* 78−29680
Ta, ion prod. in hollow cathode source 78−74525
U, electron cyclotron resonance source *(French)* 78−29680
Xe, high current source, operation 79−72039
Xe ion implantation using Lublin separator 79−82251
Xe, prod. of isotope-resolved beams of highly charged ions 79−93858

ion-surface impact
see also particle backscattering; sputtering
^{14}N II ground state hyperfine structure quantum beats via ion-beam surface interaction at grazing incidence 79−10233
active ion bombardment induced chemical reactions at surfaces detected by SIMS 79−16034
adhesion, surface anal. techniques appl. 80−65381
adhesion measurement, locus of failure, bond failure in adhesive joints 80−50801
adsorbate sputtering by low energy ions 77−62758
alkali halide, secondary emission, under bombard. by multiply charged Ar^+-Ar^{5+} and Kr^+-Kr^{5+} ions 78−11046
alkali halides, luminesc. induced by ion impact, −160 to 200°C 77−8654
alloy, surface composition changes 80−2913
amorphous and polycryst. surfaces, anomalous yield enhancement, for 180° He^+ scatt. 79−100008
analytic range-energy relation for light ions in materials with atomic numbers from 1 to 92 79−93895
anisotropic excitation at large inclination angles, foil angle depend. 79−45820
atom ejection studies by classical trajectory simulation 80−108311
atomic collision processes, rel. to vacuum system, review 80−54290
atomic mixing, ion-bombardment induced, diffusion model 77−90228
atomic orientation production by electron capture in beam-target interaction, semiclassical model 80−9723
Auger electron emission, appl. to surface anal. *(French)* 77−66563
Auger electrons in mol. ion+solid (gas) targets 79−45814
Auger electrons upon bombardment of solids by ions of moderate energies 80−100730
Auger spectra induced by ion impact on metals 80−71545
Auger spectroscopy, ion induced, for surface anal. 80−55756
axial shadow pattern, atomic vibr. effect on width and shape 77−39640
backscattering, material characterisation technique 79−96407
backscattering anal. of shallow surface layers 77−77338
backscattering analysis, Rutherford scattering cross section correction 80−66369
backscattering and implantation, H and He ions, computer simulation, comparison of MARLOWE and TRIM codes 80−66350
backscattering channelling surface peak calc. 79−8219
backscattering MeV spectrom., electron and ion currents rel. to accurate current integration 79−47571
backscattering of keV light ions from solid target, single collision approx. 77−1772
backscattering spectrometry and related analytical techniques 80−50505
backscattering yields, effects of correlated lattice vibrs. 79−69942
barium aluminosilicate glass coating on NbZr, d and He ion irrad., blistering 77−35605
beam-foil interaction process mechanism 80−14252
beam-foil source, non-depend. on foil temp. of emitted light intensity 78−37736
binary alloys, detection of compositional homogeneities using ion-induced Auger electron spectroscopy 80−25514
bombardment, by electrons, protons and heavy ions, characterisation of materials 79−96406
carbides, brittle materials, swelling, blistering, p, d, and He ion irrads. porosity effects 77−35603
carbonaceous surface contamination growth on ion bombard. 77−90229
channelling, 180° ion scattering, on solid targets, evidence for yield enhancement 80−70281
channelling in surface, charged particle reflection, two-wave approx. 78−6822
charge composition of light ions scattered by a metal surface 80−100724
charge exchange scatt. 78−43974
charged particle beam-surface impact at glancing angles, reflection *(Russian)* 80−108316
chemical surface analysis, low energy ISS compared with SIMS 78−64908
coating characterisation 77−31919
collision spectroscopy of backscatt. medium energy ions, quantitative surface anal. 77−8704
compositional and structural analysis of single cryst. surfaces using low energy ion scatt. review 79−87547
compound, surface composition changes 80−2913
computer simulation of ion scattering from single crystals 80−2911
conference, atomic collisions in solids, Hamilton, Canada (Aug. 1979) 80−62375
conference, physics of ionised gases, Dubrovnik, Yugoslavia, (Aug.-Sep. 1976) 77−42961
conference on inelastic ion surface collisions, Hamilton, Ontario, Canada (Aug. 1978) 80−31402

ion-surface impact continued
conference on ionised gas physics, Dubrovnik, Yugoslavia (Aug.-Sept. 1978) 80−36779
conference on solid-vacuum interface, Amsterdam, Netherlands (June 78) 79−42342
continuum electron capture and loss in ion-gas and ion-solid collisions, cusp spectroscopy of forward peak 80−14201
convoy electrons from solids, ion vel. and Z and target material depend. 78−84692
crystal surface, ion bombardment, equilib. at. struct. 79−56051
depth profiles, ion scatt. technique, digital data collection 78−56942
depth profiling techniques for thin film interdiffusion and interfacial reactions, book contrib. 79−1564
depth profiling under ion bombard., sputter broadening Monte Carlo simulation *(Japanese)* 79−83089
desorption, fission-fragment induced mechanism, time of flight obs. 77−76674
direct and recoil-induced electron emission 80−11526
double-pass cylindrical mirror analyser, for ion scattering spectroscopy, resolution factors 79−16078
drift tube measurement of ion mobility, secondary electron effects 78−59538
dynamic-implant profiling by low-energy nuclear reaction spectroscopy 77−59037
elastic ion-surface interaction, review 79−47583
elastic scattering of low-energy ions, review 80−40211
electron capture, atomic excited state polarisation, optical detection 80−58377
electron emission energy and angular spectra 80−71547
electron emission energy spectra, ion-induced, in small and large solid angles 78−2964
electron emission yields 80−71544
electronic interactions, review 78−72674
electronic material and device characterisation using surface-sensitive analytical techniques 80−65341
electronic polarization in solids probed by dissociation of fast molecular ions 80−71530
electroreflection exam., short range order in surface layers 78−6703
electrostatic deposition of thin particulate layer, resistivity meas. under ionic bombardment 80−68218
energy analysed SIMS with Auger and XPS meas. 79−4457
energy reflection coeff. during He^+ and Ne^+ bombard., depend. on target at. number 77−15470
erosion, surface relief form. *(Russian)* 78−23567
ESCA investigation 79−33020
etching, ion-induced sputtering, and ion trapping, technological appls., review 77−44107
excited states amongst sputtered particles, thermal origin 78−35238
fast charged particles, prod. and impact effects 79−45492
fast ion double collision spectroscopy, polarisation obs. of emitted photons 80−16134
fast ion excited levels produced in foil or surface collisions, orientation and alignment 80−14214
fast ion induced desorption and collective electronic perturbation at the surface 80−10789
fast molecular ion impact phenomena 80−40210
fast molecular ions, break-up on collision with solids 80−66353
fast molecular ions, collision induced fragmentation 80−66354
fast molecular ions collisionally induced dissociation, struct. determ. 80−66357
ferromagnet, ion scatt., circular polarisation of emitted light from ion 78−1072
film, backscattering spectrum edge determ., theory, and expt. for Ag on Si 77−8702
film, conducting or insulating, kinetic electron emission when penetrated by H^+ ions with 0.3 to 30 keV energy 79−91554
film, inert gas ion refl., semiempirical analysis 78−6823
film, kinetic electron emission, intermediate energy ion effects 77−28675
film growth, initial stages, ion bombardment effects 78−14639
films by elastic scatt. of ^3He, microchem. anal. 79−1975
fission fragment and alpha recoil induced secondary ion ejection 80−71533
float glass, Sn penetration depth meas. 77−76614
fluoride film, contamination by 1 MeV proton bombardment, backscatt. obs. 77−11811
fusion devices, controlled, surface effects, conf., San Francisco, USA (Feb. 1976) 77−30659
fusion reactor first-wall mat., physical sputtering model 78−80445
fusion reactor material, chem. interaction with H plasma discharge impurity ions 77−35357
glass, swelling, blistering, 140 keV p, d and He ion irrads., porosity effects 77−35603
glass/polymer interface exam. using ion scattering spectroscopy and scattered ion mass spectrometry 78−60641
graphite, chemical sputtering by H^+ ions 77−36341
graphite, D^+ bombardment, surface damage, sputtering, SEM study 80−32459
graphite, pyrolytic, N_2^+ active ion bombardment, SIMS obs. 79−16034
graphite, sputtering, physical and chemical, by H_2 and He, 600 to 7500 eV 77−36340
graphite fibres, HM, surface comp. and energetics 80−54480
grazing incidence ion beam-surface interaction, mechanism and uses 80−14251
grazing incidence obs. 80−71539
heavy ion+atom, radiative electron capture, target thickness depend. 78−58778
heavy ion collisions using GSI linear accelerator, X-ray production, appls. 77−19041
heavy ion neutralization behaviour in the 30-130 keV energy regime 80−71542
heavy ion-solid surface collision cascade theory and expt. *(Japanese)* 80−11527
heavy ions, low energy total backscattering 80−71535
heavy particle scatt. in solids, classical deflection ang. using Brinkman pot., numerical calc. 80−11525
heavy-ion impact on solid targets, mol. orbital X-rays 77−69957
ice, sputtering by MeV light ions, erosion rate 78−48268
III-V compounds, surface comp., low-energy ion scatt. spectrometry 80−100382
III-V semiconductor, and related cpds., low energy ion scattering spectrometry *(French)* 80−71551

ion-surface impact continued
implant ion collection with radn. enhanced diffusion and sputtering of implant 80−2055
impurity atom position determ. from ion-excited characteristic X-ray emission *(Russian)* 78−47408
impurity profiling with 2.5 MeV van de Graaff accelerators 79−77626
Inconel 625, electron yields under ion bombardment for clean and oxidised surfaces 80−66368
Inconel 625, plasma nitriding, hardness meas., Rutherford backscatt. surface anal. 80−45442
inelastic effects in low energy scatt. 80−71534
inelastic scattering of low-energy ions, review 80−40212
inert gas ion scattering from crystal, quasi-single collisions, calculational approach 78−27360
insulators, fission fragment sputtering 80−40207
intense pulsed ion beams, diagnostics via nuclear activation anal. 77−61160
interatomic potential functions for ion-surface scatt. phenomena *(Japanese)* 80−45192
interatomic potential screening function correction factor for computer simulation 78−23574
ion analysis, conference, Paris, France, (May 1977) 77−86406
ion Auger spectroscopy and chemical binding of atoms in a compound 80−11528
ion beam analysis and ion implantation in single UV vacuum sample chamber 77−4970
ion beam induced light emission, review 79−95850
ion beam material characterisation, conf., Aleria, Corsica (Sept. 1976) 79−96403
ion bombardment, three-dimensional surface 80−104029
ion induced optical emission for surface and depth profile analysis 79−4333
ion neutralisation spectroscopy, surface analysis, spectroscopic methods review *(Chinese)* 79−34414
ion path identification in cryst. surface channels 79−15576
ion scattering by crystalline solids, digital computer simulation 78−15270
ion scattering spectra, fine features 78−15267
ion sputtering process, model 78−88398
ion-bombardment Auger spectroscopy for studying surfaces of solids 79−20497
ion-induced X-rays, review 79−96405
ionic crystal, ion-electron mechanoemission mechanism 78−3002
irradiated solids, energy spectra of Auger electrons, possible surface diagnostic method 79−69946
K-electron ionisation probabilities by heavy relativistic particles 80−84824
kinetic electron ejection, pot. emission, semiconductors and insulators, review 77−44109
kinetic ion-electron emission, ion charge depend. 78−11045
kinetic ion-electron emission coeff., target at. no. depend., and role of recoil atoms 78−2966
layered materials, in powder form, thickness meas. by XPS and ion sputtering 79−88913
light elements (Z=15 to 28), $_5{}^{10}B$ ion bombardment, K-shell ionisation, X-ray obs. 78−95619
light exotic atoms, L-shell refilling rate, theory 77−12469
light ion sputtering in fusion reactors, discrete ordinates method calcs., ANISN code 78−92158
liquid metals ion bombardment, adaptation of ion microprobe 77−49805
(LMM) Auger electron emission by keV Ar^+ bombardment 79−95880
low energy, interaction study by ion-gun *(French)* 77−4708
low energy gas-phase and ion-surface collisions, optical emission 80−32821
low energy ion backscattering, struct. anal. 78−15271
low energy ion scattering, meas. of energy spectra of neutral particles, apparatus and expts. 80−55242
low energy ion scattering analysis of surface and thin film composition *(French)* 77−59663
low energy ion scattering for composition and struct. anal. of outer surface 79−4458
low energy ion scattering spectroscopy, UHV apparatus *(Japanese)* 80−20746
low energy light ions, anal. of interaction by Monte Carlo simulation 78−23570
low energy surface scatt., inelastic energy loss 80−70278
low-atomic-mass solids, high precision depth profiling of light isotopes 80−66902
low-energy alkali ions, apparatus for scatt. from solid surfaces 77−40318
low-energy ion scattering, appl. to surface anal. 79−95890
luminescence of solid surfaces accompanied by ion implantation 80−60683
mass spectrometer, combined ion-scatt. and secondary-ion, for ion bombardment studies 78−21259
mass spectrometer to study secondary and sputtered ions 79−83072
metal, adsorbed O and CO layers, ion impact desorption, adsorption energy depend. 80−39442
metal, corrosion anal. using ion beam and nucl. techniques 79−52448
metal, $H^+(H_2^+)(H_3^+)$ impact, backscattered H Balmer-β line intensity 77−23470
metal, ion beam induced desorption of overlayers 80−59786
metal, ion beam texturing 77−44402
metal hydride, computer simulation of H reflection and scattering 79−1806
metal surface, 10 eV ion impact, chem. modification, ESCA obs. 77−24916
metal surface, clean, ion impact, mol. effects in electron emission 78−80446
metal surface, excited atom emission, survival probabilities 78−48266
metal surface, fast ion scatt. by plasmons, theory 80−45190
metal surface, heterogeneous cluster ion bombardment, secondary electron emission 80−60742
metal surface, image force for fast particle 77−69939
metal surface, inert gas bombard., 1.05 keV, electron yields, Fermi energy estimate 78−52611
metal surface, plasmon mechanism for energy loss, dissoc. and orientation of fast ions excited by grazing collisions 80−11523
metal surface, scattered ion charge states 77−85878
metal surface treatment by ionic bombardment, new technique *(French)* 77−77643
ion-surface impact continued
metal surfaces, clean polycrystalline, ion-induced electron emission, review 80−35032
metal surfaces, H_n^+ impact, excited H form. 78−42199
metallic film, X-ray production by H^+ and H_2^+ impact, search for cluster effects 78−43961
metallic glass, bulk and surface properties, review 80−44147
metallic surface, He^+ and H^+ reflection, atomic excitation calcs. 79−87541
metallic targets, continuous emission spectra of particles ejected by ion beams *(Russian)* 78−55140
metals, 10-30 keV H ion bombardment, energy refl. meas. 78−27359
metals high density collision emission cascades following heavy ion bombard. 80−71531
microanalysis by direct obs. of nucl. reactions, material characterisation, review 79−96409
microprofile, triangular, ion bombardment at oblique incidence, sputtering erosion and growth 77−73202
molecular deexcitation radiation obs. during keV ion-solid bombard. 80−71494
molecular ions, interaction with thin solid targets 78−59844
molecular-ion beam dissociation in thin foils 77−86315
multicharge laser plasma ions, interaction with solid surface *(Russian)* 79−78817
multiple ion scattering, review 77−63517
multiple scattering, atomic chain model, surface semi-channelling *(Japanese)* 80−50501
multiple scattering at small angles, according to inverse square law *(Russian)* 77−4706
multiplet lines emitted after beam-surface interaction, polarisation calc., time development 80−14216
needle field emitter, ion bombardment effects, field emission microscope obs. 77−55869
negative ions, sputtered, characteristic electronic and vibrational temp., laser photoelectron spectral meas. 80−66346
neutralisation of ions at surfaces 78−35237
nitrided steel surface wear-related topography 78−60847
noble gas ions, low energy, backscattering from single cryst. surface, computer simulation of ang. depend. 79−19961
nonconductive materials, oscillatory scatt. ion yield, meas. for He^+ scatt. from Pb and Bi 79−4881
nonmetal, Coulomb explosion sputtering by intermediate energy multiply charged ions 80−35049
nuclear spin polarised ion beam generation 77−42396
one-electron resonant processes in presence of surface sub-monolayer 80−93445
optical emission by excited ejected atoms, effect on intensity of radiationless transitions 78−39652
optical examination and monitoring of surfaces, review 79−67375
orbital angular momentum transfer to nucl. spin polarisation in external mag. fields 80−14217
orientational effects in charge state of ions scattered by single crystal 79−52064
oxide target, MeV ion bombard., multiple inner-shell ionisation 77−8686
oxides, brittle materials, swelling, blistering, p, d and He ion irrads. porosity effects 77−35603
phase diagrams, ion beam determination of phase boundaries, exam. of techniques 79−8418
photon emission, ion-induced, quantitative analysis appl. 77−48740
plastically deformed crystal, lattice defects influence on axial shadow figure *(Russian)* 80−25508
polycrystal, heavy ion scatt., diatomic model, appl. to Cu-Ar^+ system 78−11044
polycrystal, heavy ion scatt., model 80−100731
polycrystalline materials, Ar and He ion scatt. spectra, multiple scatt. features 78−72671
polycrystalline materials, multiple scatt. feature in Ne^+ ion scattering spectra 78−43975
polycrystalline targets, double-scatt. effect 77−85875
polycrystals, double-scatt. effect 77−63514
polymer modification by plasma treatment 77−70198
proton elastic scatt. technique for depth profiling of H, He isotopes 77−24327
random solid, light ion backscattering energy spectra calcs. 78−72655
range for transmitted, reflected, and absorbed ions and electrons, phenomenological description 79−68173
recoil atom energy distrib., effect of surface atomic struct. 80−35050
recoil atoms, double scatt. effect 80−100725
recoil implantation profile for thick film 79−1454
reflected ion spatial distribs., surface semichannelling effects 79−46728
reflection coeffs. for light ion-surface interaction, review *(Russian)* 80−38663
Rutherford backscattering, small angle high resolution, ion implantation appls., review 77−44108
Rutherford backscattering spectrometry, signal overlap subtraction, surface struct. studies 80−50486
scattering, medium and high energy, two-atom model for surface blocking calc. 79−4886
scattering, two-atom model, expt. verification for Cu 77−12481
scattering by atomic chains on solid surface 79−52065
scattering from clean surface in 1 to 10 eV range, trapping probability model 77−12479
scattering peaks, displacement from predicted positions, binary collision model 79−4880
scattering spectrometry, appl. with protons, 5 to 8 MeV, and heavy ions, 15 to 25 MeV, to special anal. problems 79−5210
secondary electron acceleration by protons in vacuum, ion bombardment effects 77−52210
secondary electron emission, threshold studies 80−66360
secondary electron kinetic emission from electron and ion bombardment 80−66342
secondary ion and photon emission under medium-energy ion bombard., influence of surface plasma 79−33881
secondary ion emission mechanism, energy spectra of secondary ions 79−100013
secondary ion energy spectra 78−23573
secondary ion intensity changes, correction via new total ion monitoring method 78−12796
secondary ion yields, depend. on ionisation pot. and matrix sputtering yield 79−8214

ion-surface impact continued
secondary ion-ion emission, primary ion beam optimum current density review 77−52211
secondary-ion emission, ionisation process, review 80−35040
segregated surface, low energy Ne^+ scatt. 80−71538
SEM, in situ ion etching facility, description and appl. 77−54020
semiconducting channel ion sorce, secondary emission and ion feedback 80−31936
Si:H amorphous layers, ion bombard., AES study, $L_1L_{23}V$ Coster-Kronig transition 79−99992
simulation by classical stochastic propagator model 77−32482
single crystal surface, metal cluster form. by ion bombardment 78−92157
single scattering, ion neutralisation *(Japanese)* 80−50500
skipping motion of ion beam due to surface pot. 80−45191
slow protons, Auger neutralisation 78−72668
solid, heavy ion bombard., Mach shock electron distrib. 80−45194
solid, secondary electron emission effect of alkali and alkaline-earth ion bombardment 79−8212
solid surface, H ion backscatt. due to proton bombardment 80−99554
solid surface and thin film anal. methods, review 79−34410
solid surfaces, reflection of slow H^+ and He^+ ions 78−76572
solid target, anomalous enhancement of 180° backscatt. yields for light ions 80−45188
solid-target atoms, ejection angles of ions after double scattering 80−93446
spectrometer, ion impact, 2-100 keV, for ion-solid interaction studies 79−49338
spherical crystalline target, ion-electron emission 79−28878
spherical insulating particle, ionic charging 79−45882
spherical target, ion-electron emission 79−65966
spherical targets, ion-electron emission 79−52066
sputter profiling, depth resolution 79−33874
sputtered excited states, secondary photon emission, role of transition probability 80−102483
sputtering, atomic excitation model 78−43971
sputtering, cascade mixing in depth profiling 79−78811
sputtering, dimer ejection, statistical model 79−69948
sputtering by H^+, D^+, T^+ ions 77−36343
sputtering of fast ion beam, appl. to surface machining 80−30129
sputtering yield, absolute meas., UHV microbalance, with ion gun *(Japanese)* 80−17951
stainless steel, $H^+(H_2^+)$, energy refl. coeffs. 78−54969
stainless steel, machine faceted, low-energy ion erosion studies 80−80923
stainless steel sample, exposed to ISX and PLT plasmas, field desorption and field ion surface studies 80−34295
stainless steel surface, low energy ion scatt. of adsorbed layers *(Japanese)* 77−1774
stainless steel surface erosion under ion impact, temp. depend. 77−36350
steel, He ion irrad., 20 keV, 700-800K, surface blister bursting 77−36349
steel, ST M316, heavy ion irrad., numerical evaluation of combined self-ion injection and vacancy loop prod. 79−7635
steel, stainless, ion and electron desorption of neutral molecules from type 304 79−83507
steel, stainless, ion bombardment, primary recoil energy spectra characts. 78−10103
steel, stainless, proton and deuteron irrad., 0.5-2.5 MeV, secondary electron emission 77−63512
steel, stainless, retention and re-emission of 0.125-1 keV D^+ ions 80−66349
steel, stainless, secondary electron emission, ion-induced for cluster ions V_n^+, Nb_n^+, and $V_nNb_n^+$ 80−35035
steel, stainless, sputtering yields of 1 to 20 keV light ions 77−36339
steel, stainless, surface, roughness factor measurement, energetic D^+, He^+, Ar^+ irradiation 80−39172
steel, stainless, surface cleaning by H^+ bombard., AES study 78−53022
stopping power systematics, Z_1-oscills., in C, Al, Ni, Ag, and Au 79−65130
stopping powers determ. from backscattered ions spectra 79−97959
structure sensitive factors in molecular cluster formation by ion bombardment of single crystal surfaces 79−19964
surface (100), atomic struct., angle-resolved XPS, LEED and ISS investigation 80−10765
surface analysis, advantages and disadvantages of SIMS rel. to ion scattering spectrometry 79−12883
surface analysis, combining secondary ion mass spectrometry and ion scatt. spectrometry 77−60158
surface analysis, review of ion scattering spectroscopy 78−68948
surface analysis by ion scattering and secondary ion mass spectrometry 77−40621
surface analysis techniques and appls., symposium, Dayton, USA (Jun. 1979) 80−62363
surface analysis using double scattering effect 79−47584
surface analytical techniques, quantification, review 80−65342
surface and thin film, chemical analysis, comparative survey of methods, book contrib. 79−66393
surface composition, ion beam sputtering, spectrochem. anal. 77−48701
surface hyperchannelling, crit. angle calcs. 80−2099
surface physics, conf., Eindhoven, Netherlands (June 1976) 77−62708
surface semichannel effects on fast ion recoil energy distribs. 80−65092
surface structure, energy spectra of scattered ions, new method of surface struct. determ. 78−87854
surface structure analysis, by ion beam *(Japanese)* 80−20021
surface structure determination, in scatt. methods, review 78−71907
surface studies via ion scatt. spectrometry, high-resolution energy analyser 77−36333
surface texture effects of ion bombardment *(Rumanian)* 77−28673
surface treatment by the low-energy ions of plasma accelerators 80−97608
target, ion beam heated, soft X-ray and VUV spectra 80−2907
target thickness dependence of X-ray production 77−85846
thermal sputtering theory, thermal spike due to energetic ions 77−48293
thick target, energy spectrum of backscattered particles, multiple scatt. and ion effective charge deviation effect 77−81192
thick target, He ion backscatt., charge state distribs., target temp. depend. 79−95887
thin film, composition analysis, by ion beams *(French)* 79−8467
thin films, nature of control peak in particle distrib. in break-up of swift diatomic clusters 80−50490

ion-surface impact continued
thin films, surface anal., survey of ESCA, AES, SIMS and ISS *(Hungarian)* 80−70544
thin films, thickness meas. anal. characterisation using proton-induced X-ray emission 80−35618
thin layer thickness determ. from backscatt. ion spectrum 79−24399
thin solid target, secondary electron bremsstrahlung, directional anisotropy 77−69953
total ion monitoring method for correction of secondary ion intensity *(Japanese)* 77−21447
trajectory analysis of ions formed in field emitter inter-electrode region 77−85873
trajectory focusing effects on total reflection coeff., computer studies 80−89102
trajectory focusing in surface scatt. of channelled ions, surface struct. anal. 78−68594
transition metal film, chemical compound formation by ion bombardment 78−30846
transition metal sulphides, ion bombardment damage, XPS obs. 80−97404
two-atomic scattering ions, refl. from single cryst. 78−68591
uniform depth profiling, in XPS, using saddle field ion source 78−48708
visual ion beam images, on insulator surfaces, by the coincident interaction of a rastered electron beam 79−3622
wake-bound electron contrib. to convoy electron vel. distrib., effect of ionic field 80−60729
water clusters around alkali metal ions produced by ion bombardment, secondary emission obs. 77−63518
whisker formation by Ar ion bombardment 78−30851
X-ray MO spectra, recoil effects 80−25510
X-ray prod., solid-effects 77−77326
X-ray production by 5 MeV/amu deuterons (oxygen ions), projectile Z depend. 80−42982
yield comparison for excited neutrals and positive ions 80−71548
ALF_3, evaporated layers DC props. and α-particle scatt. 78−14845
Ag (111) surface, ionic bombardment, diffr. effects in angular distrib. of emitted secondary electrons 79−15577
Ag, clean polycryst. surface, low energy Na^+ scatt. 0.4-3.2 keV 79−87554
Ag, energy reflection coefficient for 5 to 10 keV He ions 78−95639
Ag film, inert gas ion refl., semiempirical analysis, compared with expt., 10-30 keV 78−6823
Ag film, on Si, backscatt. spectrum edge determ. theory and expt. 77−8702
Ag, H_2^+ and $^3He^+$ ion bombardment, H^+ and He^+ yields at elastic scatt. energy 78−88394
Ag, ion bombardment, sputtering, re-emitted kinetic energy ang. distrib. 80−2910
Ag, polycryst., energy spectrum of scattered Na^+ ions, double scatt. effect 78−92163
Ag polycrystal, light ion scatt. mechanism 78−11048
Ag polycrystalline surface, energetic distrib. of scatt. Na^+ ions *(Russian)* 77−12482
Ag, scatt. of 30 keV He^+, verification of formula *(Russian)* 77−4706
Ag, sputtering by heavy atomic and molecular ion bombard. 80−71532
Ag surface, production of Na Auger electrons by Na^+ bombardment 77−63515
Ag-Al polycryst. thin-film couples, interaction process 79−51443
Ag-Au, surface layer, effect of Ar^+ bombardment, AES and SIMS 80−25504
Ag-Au, surface segregation, ion scatt. spectroscopy meas. 79−82423
Ag-Au alloy, determ. of surface versus bulk composition, low energy ion scatt. spectroscopy 77−1284
Ag-Pd, surface comp. changes under ion bombardment, AES study 80−55250
AgBr:Pb, impurity distrib., ion scattering spectroscopy obs. 77−19979
Al alloy, 6061, vacuum material, desorpt. of neutral mols. by electron and ion bombardment 78−95229
Al and SaP 930, 300 keV He irrad., blistering, flaking, gas re-emission 77−35601
Al, Auger electron prod. by Ne^+ bombard. 80−7460
Al, Auger electron prod. by Ne^+ bombard., origin of Ne Auger peaks *(French)* 80−7461
Al, Auger spectra induced by 100 keV Ar^+ impact 80−84820
Al, bombard. by Ar ions, impact-parameter depend. of K- and L-X-rays 79−76501
Al, bulk and plasma-sprayed coating, D_3^+ trapping meas. 80−20754
Al, determ. of optimum depth resolution for Rutherford backscatt. anal. using ^4He 79−14840
Al film, Pb^+ implanted, ion scatt. erosion rate, Rutherford backscatt. 79−74038
Al, $H^+(H_2^+)$, energy refl. coeffs. 78−54969
Al, heavy ion ranges, He^+ backscatt. obs. 78−63796
Al, ion bombarded, photon and ion emission, simultaneous meas. 78−15276
Al, ion bombardment, sputtering, re-emitted kinetic energy ang. distrib. 80−2910
Al, ion impact excited, ang. resolved Auger emission 79−61475
Al, ion-implanted, dechannelling by dislocations, backscatt. expts. 79−7642
Al, ion-induced Auger electron emission, depend. on ion energy 79−78814
Al, ion-induced electron emission, ion charge depend. 80−108315
Al, L_{23} shell ionisation cross section under He^+ impact, Auger spectra obs. *(French)* 77−69956
Al, L_{23} shell ionisation cross-section under H^+, heavy-ion impact, Auger spectra *(French)* 79−24406
Al, proton and deuteron irrad., 0.5-2.5 MeV, secondary electron emission 77−63512
Al, proton bombarded, secondary electron bremsstrahlung, directional anisotropy 77−69953
Al, proton or α-particle bombarded, secondary electron emission 77−36346
Al, proton-excited Auger electrons, attenuation lengths of low-energy electrons 78−11058
Al sintered powder, 100 keV He ion irrad., surface erosion due to blistering 77−35600
Al, sputtering by 15 keV Ar^+ ions, microroughness 79−91556
Al surface, Ar^+ and e^- excited Ar Auger electron emission 79−47560
Al surface, H^+ beam impact, plasma form., plasma radiative and gasdynamic processes 80−53946

ion-surface impact continued
Al surface bombardment by fast H^+ 80−66376
Al, surface roughness meas. using Rutherford backscattering of protons 79−51400
Al, thin film, K X-ray production due to ^{16}O ions, 0.25-2.25 MeV/amu 79−69906
Al-Ag, dil., radiation damage by channelled and random He^+ ion beams 79−46719
Al-Cu (1 to 10 wt.%), vapour deposited films, ion scattering spectrometry characterisation 80−15386
Al+He(C)(N)(O), inner-shell multiple ionisation systematics, X-ray obs. 80−63790
AlF_3, $^4He^+$ ion scatt. spectrometry below 5 keV 80−108313
α-Al_2O_3 axial-to-planar channelling transition study using He^+ ions 79−4367
Ar^+, Au(Cu) surface-grazing scatt., 1 MeV, excited-state orientation depend. on scatt. angle 77−61847
Ar^+ bombardment, metal surface, 20-30 keV, adsorbed C^+ layer removal, in plasma 77−76103
Ar^+, kinetic energy reflection on polycryst. bombardment 77−85869
Ar-Au, polycrystalline foil, sputtering yield meas. by UHV microbalance with ion gun *(Japanese)* 80−17951
Au, 5 keV Ne ion scatt., energy spectra by TOF and electrostatic analyser methods, comparison 79−2895
Au, 70 keV ion bombardment, analysis of obs. shadow pattern 77−32488
Au, amorphous, Au ion bombarded, collision cascades, computer simulation 79−46731
Au, backscattering of H(He) positive ions, fraction reflected 80−60741
Au, discontinuous film, degradation under MeV heavy ion bombard., Rutherford scatt. and TEM obs. 79−24397
Au, energy and mass spectra of scattered 8 keV Ar^+ ions and desorbed species 77−32487
Au, energy reflection coefficient for 5 to 10 keV He ions 78−95639
Au film, inert gas ion refl., semiempirical analysis, compared with expt., 10-30 keV 78−6823
Au film, integrated condensation coeff. on NaCl cleavage faces, Rutherford ion backscatt. obs. 80−59827
Au films on Cu, oxidation exam. by ion scatt. spectra 79−79153
Au, foil, electron spectra from α-particles and fission products 77−24918
Au, H and H^+ neutralisation at solid surface 79−74043
Au, ion bombardment by Ar^+, focused ejection 80−104028
Au, L-X-ray production by 9.5 to 41.8 MeV Fl ions 77−85847
Au, sputtering, by point defects, time-of-flight spectra 79−47573
Au, surface, energy spectra of charge state fractions of backscattered H and D 77−8705
Au surface, He, Ne, and Ar ion irrad., 0.05 to 3 MeV, orientation of fast ions excited in surface collisions 79−4876
Au surface, high energy ion backscatt., computer simulation *(German)* 77−59664
Au, surface proton and electron channelling on reflection 80−39193
Au, transmission sputtering yield for 6.8 MeV Au^+ bombard. 77−1808
Au, transmission sputtering by $Ag^+(Ar^+)(He^+)$ ions 79−4885
Au, X-ray cross sections, L-shell, proton induced, 1 to 3 MeV range 79−1799
Au, X-ray production surface impact of F^{n+} and Si^{n+}, Lα X-rays 79−69907
Au-C, light ion large angle scatt. in weakly screened Rutherford region 80−84823
Au-Ni(Pd)(Pt), surface composition determ. 79−69328
Au-Pd, surface comp. changes under ion bombardment, AES study 80−55250
$Au+H^+(He)^+$ interactions, backscatt. ions energy spectrum, computer simulation of ion motion 79−43088
$BaCO_3$, excited Ba emission by Ar^+ impact 80−100727
$BaTiO_3$ ceramic surface, neutralisation of bombarding ion beam 80−71528
$BaTiO_3$, surface study using AES and ion scatt. spectroscopy 80−65339
Be, amorphous, reflection of D and T, Monte Carlo study 80−40197
Be and BeO, K X-ray spectra produced by heavy ion bombard., chem. effects 77−36314
Be, Auger spectra induced by 100 keV Ar^+ impact 80−84820
Be, oscillatory channelled $^4He^+$ ion scatt. yield 78−52610
Be, proton bombarded, Auger electron attenuation length meas., E_p=160 keV 77−44101
Be, proton-excited Auger electrons, attenuation lengths of low-energy electrons 78−11058
Be, secondary photon emission following ion bombard. 80−71493
Be sintered powder, 100 keV He ion irrad., surface erosion due to blistering 77−35600
Be, sputtered atoms, ion bombardment induced line radn. 79−91553
Be-Cu dynode, depth profiling anal. of surface layer 80−2253
Bi, L-X-ray production by 9.5 to 41.8 MeV Fl ions 77−85847
Bi, low energy $^4He^+$ scatt. yield, ang. and energy depend. 78−27361
Bi-Zn, light ion large angle scatt. in weakly screened Rutherford region 80−84823
C, determ. of optimum depth resolution for Rutherford backscatt. anal. using ^4He 79−14840
C film, deposited on Pt, H sputtering 77−69951
C, foil, electron spectra from α-particles and fission products 77−24918
C foil, He^+ and HeH^+ impact, quantum beat pattern depend. on foil thickness 80−58343
C foil, impact of $H^+(H_2^+)(H_3^+)$, H abundance in emitted beam 78−35236
C foil, ion irrad., graphitisation rel. to lifetime, relevance to beam-foil spectroscopy 80−15166
C foil, Kr^+ incident, equilib. charge state distribs. and multiple scatt. angles 80−59532
C, H and H^+ neutralisation at solid surface 79−74043
C, proton impact X-ray emission, ang. distrib. and polarisation fraction 78−56546
C, reflection of H, D and He ions 78−95640
C surface, pyrolytic, roughness factor measurement, energetic D^+, He^+, Ar^+ irradiation 80−39172
C, swelling, blistering, 140 keV p, d and the ion irrads., porosity effects 77−35603
C, trapping of 6 to 15 keV D, temp. depend. and depth profile 77−30664
$C+O^+$ ion-molecule reaction, 15 eV energy O^+ production system 80−84817

ion-surface impact continued
CH_4^+, Jahn-Teller distortion, energy and angular distrib. of collisional dissociation fragment 80−66356
CO_2^+, thin foil impact, dissoc. struct. effects in ionic fragment energy spectra 78−50631
Cd, ion bombardment, sputtering, re-emitted kinetic energy ang. distrib. 80−2910
CdS, surface energy struct. changes during ion cleaning and thermal annealing 80−92962
Co surface, electron spin polarisation, electron capture spectroscopy 78−95645
Co-Ni, surface chemical comp. changes due to ionic bombardment *(Russian)* 77−1776
$CrSi_2$ formation on Pd_2Si and PtSi, Rutherford α-particle scatt. 78−60578
Cs_2 backscattering of H(He) positive ions, fraction reflected 80−60741
Cs^+ impact on solid surfaces, energy distrib. of sputtered negative ions 77−81189
Cs^+ photon spectrum emitted from W surface 80−100726
Cu, $^4He^+$ scattered ion yields, ang. depend. 78−15272
Cu, 1035 keV Ar^+ bombarded, energy distribs. of ejected fast ionised recoils 79−47579
Cu, 4-30 keV H_1^+, H_2^+, H_3^+ impact, excited H backscatt., O_2 effect 78−15268
Cu (001) surface, with adsorbed O, Ar^+ bombarded, particle ejection ang. depend. 80−50489
Cu (100), 30 keV Ar ion scatt., spatial distribs. under blocking conditions 77−59659
Cu (100), 30 keV ion impact, scatt. ion-electron emission correlation 77−52209
Cu (100), 5-10 keV Ne^+ bombarded, time of flight meas. of ion fractions 79−47578
Cu (100), adsorbed O layer, ejection by ion bombardment of atomic and mol. species 79−42373
Cu (100), Ar^+ ion scatt., 10-35 keV 77−36348
Cu (100), clean face and with adsorbed O, ion bombard., ejected atom energy distrib., classical trajectory calc. 79−100011
Cu (100), focusing of Ar^+ ions, incident ion energy effects, E_i=15-35 keV 78−2965
Cu (110), adsorption of O_2, low energy Ne^+ ion scatt. meas. 79−51431
Cu (110), ion-electron emission, crit. energy variations 80−55246
Cu (110), ion-induced adsorption of O_2 80−54510
Cu, (110) surface struct., ion focusing effect *(Russian)* 78−26757
Cu (117), He scatt. from ordered stepped surface 78−15277
Cu (410) surface, edge atom depression, ion scatt. spectroscopy study 80−54492
Cu, amorphous, Ar^+ ion bombardment, collision cascades, computer simulation 79−46731
Cu, Ar sputtered, surface morphology influence on sputtered yield angular distribution 80−65338
Cu, Ar^+ ion bombardment, blocking effect for fast ionized recoils 79−8221
Cu, Ar^+ low energy refl., surface thermal vibrs. effect 77−16448
Cu, chain effect for fast recoils, Ar^+ ion beam impact 78−56554
Cu, cryst., ion-electron emission yield, ang. depend., atomic order effects 77−85877
Cu, Cs^+ impact, 5.5 keV, negative secondary ion emission obs., comparison with phosphor bronzes *(French)* 77−66562
Cu, determ. of optimum depth resolution for Rutherford backscatt. anal. using ^4He 79−14840
Cu, ejected particle ang. distrib., classical dynamics model 78−95643
Cu, energy depend. of surface channelling of Ar ions, 10-35 keV 77−27928
Cu, energy reflection coefficient for 5 to 10 keV He ions 78−95639
Cu film, inert gas ion refl., semiempirical analysis, compared with expt., 10-30 keV 78−6823
Cu film, on Au substrate, oxidation and interfacial behaviour, ion scatt. spectroscopy study 80−66691
Cu, grazing incidence reflection of nuclear polarised ^7Li and ^{14}Ni ions 79−64077
Cu, H and D beams impact, energy spectra negative component 79−65967
Cu, $H^+(H_2^+)$, energy refl. coeffs. 78−54969
Cu, He defect complexes and depth distribution, production theory 77−31686
Cu, inert gas ion irrad., fast ionised recoils, blocking effect 80−71550
Cu, ion bombard., energy distributions of fast ionized recoils 79−24402
Cu, ion impact phenomena, computer simulation 78−88396
Cu, ion-bombarded, particle ejection, SIMS obs. 79−78810
Cu, low energy He^+ ion bombardment, origin of autoionisation electron emission 77−20973
Cu, low energy noble gas ion refl., surface thermal vibrs. effect 77−69955
Cu, low energy noble gas ion refl., surface thermal vibrs. effect 77−73203
Cu, neutralisation and ionisation of low energy He ions scatt. from (100) face 78−23572
Cu, polycryst., 16 keV Ar^+ scatt., diatomic model 78−11044
Cu, polycryst., back sputtering of 100 to 500 eV Ne ions, computer simulation 78−60537
Cu, polycrystalline, Ar ion double scatt. 78−88399
Cu, polycrystalline target, ion-atom cross-sections for sputtering of inert-gas ion incident at low energy 79−52059
Cu polycrystals, Ar^+ double-scattered energy distrib., compared to monocryst. *(Russian)* 77−55859
Cu, scatt. of Ar ions from 10-35 keV, diatomic models *(Russian)* 77−77337
Cu, scatt. of Ar^+, orientation and alignment prod. 78−25687
Cu, scattering, two-atom model, expt. verification 77−12481
Cu, scattering of low energy He ions and atoms, elastic and inelastic effects 77−8708
Cu, secondary electron yields from ion impacts, stopping power calcs. 78−11053
Cu single crystal, surface semichannelling effects on spatial distrib. of reflected ions, computer simulation 80−35030
Cu, small angle scatt. of low energy K^+ ions 80−20752
Cu, spherical and plane surface, ion-electron emission 79−65966
Cu surface, Ar ion bombardment, fast ionized recoils, thermal lattice vibr. effects 80−100737
Cu, surface, C and H ion bombardment, secondary electron emission coeff. experimental technique 79−78804

ion-surface impact continued
Cu surface, He, Ne, and Ar ion irrad., 0.05 to 3 MeV, orientation of fast ions excited in surface collisions 79−4876
Cu surface, low energy Ar^+ ion scatt., binary collision approx., SIMS meas. 79−47582
Cu surface, secondary charge emission coeffs., low energy H^0 flux meas. 80−25509
Cu surface, surface cleaning by H^+ bombard., AES study 78−53022
Cu, surface contaminant anal. by ion-electron spectroscopy 80−54490
Cu surface+$Na^+(K^+)(Rb^+)$, elastic scatt., ang. and energy relationships, 1-3 keV *(Russian)* 79−78802
Cu target, bombardment by Ar^+-ion beam, luminosity spectrum 79−4884
Cu-Au-Cu, thin film, sandwich struct., bombarded by 3-15 keV Ar^+ at angle of incidence of 30°, sputtering yield coeff. 79−65968
Cu-Ga, ion bomard. effect on surface comp., reflectometry AES 77−81190
Cu-Ni, film, preferential sputtering due to altered layer struct., AES meas. 78−76573
Cu-Ni, surface layer, effect of Ar^+ bombardment, AES and SIMS 80−25504
Cu-Ni, surface segregation, comparison of low-energy ion-scatt. results with theory 78−38923
Cu-Pd, surface comp. changes under ion bombardment, AES study 80−55250
Cu-Pt, surface segregation, comparison of low-energy ion-scatt. results with theory 78−38923
Cu_n, cluster formation, by ion bombardment of single cryst. surface 78−92157
$CuAl_2$, Kossel interferences of proton-induced Alk_α radiation 77−43112
CuBe, electron emission following ion bombardment of electron multiplier dynode 78−23576
CuBe, secondary electron emission coeffs. for multiply charged ion bombard. 78−11051
Cu(110), Ar bombardment, fast recoil atom blocking effect 79−69172
D^+, D_2^+ and D_3^+ fragments traversing thick foils, correls. in motions, integral ang. distribs. 80−16136
D_2, solid, electron emission under bombard. by keV electrons, H and D ion beams 77−73196
D_2, solid, secondary electron emission, electron and ion induced 79−1803
D_2^+, dissociation on impact with mylar foil 80−67164
Dy, X-ray cross sections, L-shell, proton induced, 1 to 3 MeV range 79−1799
F, K-shell X-ray spectra from light ion bombard. studies 80−71518
Fe alloys, ion-implanted, depth profile, proton-induced X-ray emission study 80−54277
Fe alloys, secondary-ion emission under varying bombardment condition 77−48292
Fe, amorphous, reflection of D and T, Monte Carlo study 80−40197
Fe, diffusion and solid solubility of Sb, 773-873K, ion backscatt. anal., rel. to intergranular embrittlement 78−71880
Fe, proton and deuteron irrad., 0.5-2.5 MeV, secondary electron emission 77−63512
Fe-Cr, surface segregation of impurities (C,N and S) *(French)* 77−56192
GaAs (110), surface struct., LEED and AES study, comparison of MBE and ion bombard. surface prep. 80−54496
GaAs anodic oxide films, composition meas. by ion scatt. spectrometry, influence of current density 80−11802
GaAs, excitation by 2-4 KeV Ar^+ ions, electron energy spectra 80−11529
GaP, substoichiometric native oxide layers, $^4He^+$ backscatt. obs. 77−77610
GaP surface, Ar^+ and e^- excited Ar Auger electron emission 79−47560
GaP:Sn(Sb), lattice location of implanted atoms, ion backscatt. and ion-induced X-ray obs. 77−84785
GaSb, elastic scatt. of He^+ ions by atomic chains, screening 80−2915
GaSb-Pb junction, Ar ion bombard. effect on tunnelling props. 80−54783
GdF_3, chemically reacted film on ferroelectric-ferroelastic $Gd_2(MoO_4)_3$, characterisation 79−15057
$Gd_2(MoO_4)_3$, passivation of c surface against attack by HF by inert ion beam irradiation 78−35545
$Gd_2(MoO_4)_3$, surface passivation by He ion irrad., domain struct. obs. 78−84544
$Gd_2(MoO_4)_3$, surface study using AES and ion scatt. spectroscopy 80−65339
Ge (100), chemisorption of H, expt. results compared with pairing model calcs. for Si (100) 78−34719
Ge, amorphous, scatt. of 2 MeV He^+ 77−69954
Ge film, inert gas ion refl., semiempirical analysis, compared with expt., 10-30 keV 78−6823
Ge films, adhesion to substrates, effect of Ar^+ ion irrad. 79−11047
Ge, heavy ion impact, meas. of life-time of inner-shell vacancy in recoiled Ge atoms 77−63513
Ge, radiation piezoelec. effect, EMF generation under α-irrad. and uniaxial deform. 77−12320
Ge surface, (111), ion-bombarded and annealed, spectroscopic ellipsometry study 80−103543
Ge thin films on glass substrates, annealing by Ar ion bombardment 80−80136
H, backscatt. from Au, charge fraction ang. depend. 80−71540
H, low energy ion scattering from polycrystalline solids, computer study 77−36338
H species, on C foil, 800 keV amu^{-1}, electron loss and capture cross-sections 80−65066
H surface layer anal., influence of ion beam bombardment 79−37731
H^- production in foil breakup of H_2^+, inhibition effect 80−99549
H^+, 5 and 15 keV, energy distrib. and recoil angles 80−71537
H^+ bombardment of Si, Cu, Ge, Mo, Ta, Pt surfaces, Lyman-α emission 79−91503
H^+, H_2^+, H_3^+, 10 to 30 keV, scattering from surfaces, excited state composition and scattered H^+ flux 77−36337
H^+, H_2^+ and H_3^+ interactions with thin foils, electronic polarisation wake effects, dissoc. of mol. ions 80−16135
H^+, neutralisation in low energy surface scatt. by polycryst. graphite 80−71541
H^+, reflection from stainless steel and Nb 77−36336
H-ions neutralisation at solid surface, theory 79−74043
H_2, solid, electron emission under bombard. by keV electrons, H and D ion beams 77−73196
ion-surface impact continued
H_2, solid, secondary electron emission, electron and ion induced 79−1803
H_2^+, dissoc. following beam-foil interaction 78−70920
H_2^+, internuclear separations distrib. in 3.0 MeV collisions with C foils 80−71529
H_2^+, polarised Balmer radiation due to scatt. from Nb surface, adsorbed O_2 effects 80−99569
H_2^+, recombination yield on emerging from ultrathin C film below Bohr vel. 79−50108
H_2^+, transmission yield through thin C-foil meas. 80−100732
H_3^+, dissoc. following beam-foil interaction 78−70920
He, backscatt. from Au, charge fraction ang. depend. 80−71540
He species, on C foil, 800 keV amu^{-1}, electron loss and capture cross-sections 80−65066
He^+, isotope effects in elastic surface scatt. on sol. and liq. Ga 80−71536
He^+ reflection from Pt surface, 10 to 35 keV 80−71543
HeH^+, foil induced dissociation, H^0 prod. 80−66355
HeH^+, internuclear separations distrib. in 3.0 MeV collisions with C foils 80−71529
^4He, backscattering anal. 79−96408
Hf, RF sputter deposition, ion bombardment and ion implanation 80−25564
Hf+$H^+(He^+)$, L-subshell ionisation cross section, branching ratios, fluoresc. yield, Coster-Kronig factors 80−43166
HfN, RF sputter deposition, ion bombardment and ion implanation 80−25564
Ho, L-X-ray production by 9.5 to 41.8 MeV Fl ions 77−85847
Ho, X-ray production surface impact of F^{n+} and Si^{n+}, Lα X-rays 79−69907
In, isotope effects in ion-scattering double spectroscopy curves for He^+ 77−59658
In, X-ray cross sections, L-shell, proton induced, 1 to 3 MeV range 79−1799
InAs-GaSb superlattices, crystallography, Rutherford backscatt. and channelling obs. 80−49533
InP, excitation by 2-4 KeV Ar^+ ions, electron energy spectra 80−11529
InSb (110), ion bombard. effect on surface struct. and electronic props. 80−6923
InSb, (111) surface, anal. by low energy ion scattering spectroscopy, LEED and AES *(Japanese)* 80−20746
K^+, low energy small angle scatt. from Ni(001) 80−66367
Kr^+, kinetic energy reflection on polycryst. bombardment 77−85869
LaB_6 (100), (110), and (111), surface structs. and work functions 80−70512
LaB_6, surface (100), atomic struct., angle-resolved XPS, LEED and ISS investigation 80−10765
LiF, ion and electron emission following ion impact 80−100729
LiH+Te exothermic solid-state reaction, ion backscatt. obs. 78−20064
Mg, Auger electron prod. by Ne^+ bombard. 80−7460
Mg, Auger electron prod. by Ne^+ bombard., origin of Ne Auger peaks *(French)* 80−7461
Mg, ion-induced Auger electron emission, depend. on ion energy 79−78814
Mg, L_{23} shell ionisation cross-section under H^+, heavy-ion impact, Auger spectra *(French)* 79−24406
Mg, L_{23} shell ionisation-cross section under He^+ impact, Auger spectra obs. *(French)* 77−69956
Mg, small angle scatt. of low energy K^+ ions 80−20752
Mg surface, Ar^+ and e^- excited Ar Auger electron emission 79−47560
$Mg_{(S)}+Ne^+$, O-dependent photon emission 79−1810
MgF_2, $^4He^+$ ion scatt. spectrometry below 5 keV 80−108313
MgO film, ion induced secondary electron emission 77−44104
MgO-Ag porous layer, secondary electron emission from ion impact, gas discharge device appl. 78−68586
$MgO-Al_2O_3-SiO_2$ glass/polysulphone adhesive failure, ISS and SIMS obs. 80−55626
Mg_2SiO_4, forsterite, ion scatt. spectrometry, atom shielding effect of O 80−50493
Mo, 4-30 keV H_1^+, H_2^+, H_3^+ impact, excited H backscatt., O_2 effect 78−15268
Mo (110) surface, electron production by metastable rare gas atom impact 77−32486
Mo, amorphous, reflection of D and T, Monte Carlo study 80−40197
Mo, cryst., ion-electron emission yield, ang. depend., atomic order effects 77−85877
Mo, D^+ impact, surface blistering, SEM study 78−71774
Mo, desorption kinetics of halogens, pulsed ion beam method 80−34300
Mo, glow-discharge surface treatment, struct. defect prod. 77−63832
Mo, H, $H^+(H_2^+)$ energy refl. coeffs., surface damage obs. 78−54969
Mo, H and D trapping, enhancement due to He ion damage 77−31698
Mo, H penetration of Mo cathode in glow discharge, point defect depend. 79−41903
Mo, ion impact, radiative spectrum of sputtered particles *(Russian)* 79−91504
Mo, polycryst., $H^+(H_2^+)(H_3^+)$ impact, optical radiation emission 78−95644
Mo, proton and deuteron irrad., 0.5-2.5 MeV, secondary electron emission 77−63512
Mo, reflection of H, D and He ions 78−95640
Mo, secondary ion emission mechanism, energy spectra of secondary ions 79−100013
Mo surface, low energy ion scattering of absorbed layers 79−1807
Mo, surface erosion, by H_2^+ bombardment 77−15464
Mo, surface erosion due to H_2^+ and He^+ bombardment 79−85769
Mo, surface impurities, depend. on prep. method, ion scatt. spectroscopy 80−40200
Mo, surface structure changes due to ionic bombardment, LEED and AES obs. *(Russian)* 77−1775
Mo surfaces, backscatt. of excited H atoms in the presence of oxygen 79−3388
Mo, TFTR protective plate, sputtering and surface damage by D^+ irrad. 80−18645
MoO_3, ESCA of surface composition changes under ion bombardment 77−20974
^{14}N II, 2p3p $^1P_1$, hyperfine struct. after ion beam surface impact at grazing incidence 80−58403
N_2^++first row transition metal surface reactions 79−96363
N_2^++Group IV elements and oxides, XPS and UPS prod. determ. 78−73084

ion-surface impact continued
N_2O^+, thin foil impact, dissoc. struct. effects in ionic fragment energy spectra 78−50631
Na, Auger electron emission due to ion collisions with solid targets *(French)* 80−104031
NaCl, $^4He^+$ ion scatt. spectrometry below 5 keV 80−108313
NaCl, ion and electron emission following ion impact 80−100729
NaF, $^4He^+$ ion scatt. spectrometry below 5 keV 80−108313
Nb alloy, He ion irrad., 20 keV, 700-800K, surface blister bursting 77−36349
Nb, Ar ion surface erosion 77−36342
Nb blistering by 5-15 keV He ions, dose rate and temp. effects 77−35595
Nb, depth distrib. meas. of He 77−30665
Nb, desorption kinetics of halogens, pulsed ion beam method 80−34300
Nb, He ion irrad., 20 keV, 700-800K, surface blister bursting 77−36349
Nb, He trapping, temp. depend. 77−31685
Nb, He^+ bombardment, high dose 800 to 1400°C 77−36344
Nb, ion bombardment, sputtering, re-emitted kinetic energy ang. distrib. 80−2910
Nb, proton and deuteron irrad., 0.5-2.5 MeV, secondary electron emission 77−63512
Nb, secondary ion emission mechanism, energy spectra of secondary ions 79−100013
Nb-Zr-Ti, needle field emitter, ion bombardment effects, field emission microscope obs. 77−55869
Nd, X-ray cross sections, L-shell, proton induced, 1 to 3 MeV range 79−1799
Nd, X-ray production surface impact of F^{n+} and Si^{n+}, Lα X-rays 79−69907
Ne, Auger electron emission due to ion collisions with solid targets *(French)* 80−104031
Ne^+, isotope effects in elastic surface scatt. on sol. and liq. Ga 80−71536
Ni (001), azimuthal anisotropies of ejected dimer ions, SIMS expt. 80−60730
Ni (001) surface, Ne^+ scattering and neutralisation on first and second layers 80−35045
Ni (100), adsorption of chalcogens, orbital identification in INS and UPS spectra 77−43427
Ni (101), light emission by scattered 195 keV He^+ ions after focusing and channelling interactions 78−35240
Ni (101) surface, optical excitation of He projectiles during reflection under channelling conditions 79−47576
Ni (110), clean and S covered, atomic struct., medium energy ion scatt. 79−61483
Ni (110), struct. anal. during O_2 adsorption, low energy ion scatt. meas. 79−82424
Ni (110), surface damage induced by bombard. with 3-30 keV noble gas ions 80−60728
Ni (110), surface relax., O_2 coverage effects, medium energy ion scatt. obs. 79−28181
Ni (110) clean surface, low energy Li^+ and He^+ ion scatt. 80−104026
Ni (110) surface, Ar^+ refl. at grazing angles, computer simulation 79−87549
Ni (111), adsorption of CO and O, LEED and low-energy ion scatt. investigation 79−65324
Ni, (111) surface, scatt. of mol. and atomic H ions 79−69943
Ni {100}, adsorption of O, low energy ion scatt. study 80−39420
Ni {100} and Ni {100} with O overlayer, crystallographic effects in low energy ion scatt., local ion-atom neutralisation 80−84377
Ni, Ar^+ scatt., light emission polaris. 78−1072
Ni, binary alloy, irrad. with heavy ions, non-equilib. segregation phenomena 80−19950
Ni, blistering by $^4He^+$ bombardment, temp. depend. 78−43967
Ni, charge states of 1.5 to 15 keV backscatt. He and Ne ions 79−4882
Ni, chemisorption of O_2 and CO, ion bombard., particle ejection, SIMS obs. 79−78810
Ni, desorption of CO due to ion bombard., comparison of surface anal. methods 79−8213
Ni, H^+ beam at grazing incidence, polarised fluoresc. of reflected H atoms 79−63951
Ni, ion impact desorption of O 77−62758
Ni, ion-implanted and virgin, laser irrad. effect, Rutherford backscatt. and channelling obs. 80−108306
Ni, Li ion scatt., expt. and computer simulation 77−63511
Ni, reflection of H, D and He ions 78−95640
Ni, secondary electron emission coeffs. for multiply charged ion bombard. 78−11051
Ni, secondary electron emission under Ar^+ ion bombard. near Curie point 80−29838
Ni single crystal, H ion impact, elliptic polarisation in Balmer radiation 80−35039
Ni single crystal, surface hyperchannelling, scatt. of low energy Ar ions, computer simulation 80−34110
Ni, small angle backscattering of H_2, D_2, He and Ne from single and polycrystalline surfaces 79−24404
Ni, sputtering of adsorbed layers 77−36335
Ni, sputtering yield as function of incident ion masss 79−74042
Ni surface, electron spin polarisation, electron capture spectroscopy 78−95645
Ni surface, oxidation, structural changes, low energy ion scatt. study 80−35423
Ni target, surface layer anal. medium energy ion backscatt. expts., solid state detector 79−4456
Ni, with Te overlayer, surface sensitivity of MeV He ion scatt. 79−56904
Ni/Fe interfaces sputter profiling, by AES 79−15572
Ni_3Sn, surface composition determ. 79−69328
Ni(100), with adsorbed K^+, He^+ impact, Auger deexcitation spectrosc. 79−100010
Ni(110) surface, theory of ion scatt. 80−7458
O^+ low energy ions interaction with solid C and Pt targets, preliminary study 79−34352
OH^+, Coulomb explosion in 11.2 MeV collisions with C foils 80−66358
$PaCl_2$, thin films, reduction to Pd by Ne^+ ion irrad., 2 MeV He^+ ion backscatt. anal. 79−4493
Pb, H^-, H^+, H_2^+ and H_3^+ grazing incidence collision with surface, Balmer radiation, elliptical polarisation 78−86804
Pb, He^+ scatt., oscillatory ion yields 78−55221
ion-surface impact continued
Pb, ion bombardment, sputtering, re-emitted kinetic energy ang. distrib. 80−2910
Pb, isotope effects in ion-scattering double spectroscopy curves for He^+ 77−59658
Pb, L-X-ray production by 9.5 to 41.8 MeV Fl ions 77−85847
Pb polycrystalline surface, H ion impact, elliptic polarisation in Balmer radiation 80−35039
Pb+He^+ backscattering, emitted radiation intensity rel. to incident energy 79−89762
$PbTiO_3$, single cryst., He^+ backscatt. shoulder spectra struct., domain struct. 80−35048
$PbTiO_3$ single crystal, channelling of He^+ ions, polarisation effects 79−99258
Pd, clean and CO-covered, Penning ionisation electron spectroscopy, metastable He impact, electron energy distrib. 79−52060
Pd, H_2^+ and $^3He^+$ ion bombardment, H^+ and He^+ yields at elastic scatt. energy 78−88394
Pd, secondary electron emission, discrete levels in energy distrib., ion bombard. effects 79−87535
Pd-Ag, ion bombarded, surface segregation, XPES obs. 79−77885
Pr, L-X-ray production by 9.5 to 41.8 MeV Fl ions 77−85847
Pt (111), relax. effects, and thermal vibrs., medium energy ion scatt. 79−28182
Pt (111), surface and subsurface adsorbed O, low energy ion scatt. obs. 80−65372
Pt (111) and (100), surface struct. anal. by MeV ion backscatt. and channelling 78−71916
Pt (111) surface, 400 eV H^+ ion scatt. obs. of surface relax. 78−43972
Pt (997) surface, partial facetting, He beam scatt. and LEED study 80−103547
Pt, adsorption of O_2 on (110) surface, Ar^+ bombardment effects on reactivity 80−89099
Pt, polycrystalline, He ion refl. *(Russian)* 80−35051
Pt, surface reflection of He ions 79−87551
Pt, X-ray cross sections, L-shell, proton induced, 1 to 3 MeV range 79−1799
Pt-Cu, surface segregation, ion scatt. spectroscopy meas. 79−82423
Pt-Rh, surface composition using ion scatt. spectroscopy 79−82422
Pt-Rh alloys, surface behaviour on heating in air, XPS and SIMS *(French)* 77−40327
Pt-Rh alloys, surface comp. determ. by ion scatt. spectroscopy 80−6602
Pt(IV), reduction to Pt(II), X-ray irrad., Ar ion bombardment, XPS obs. 80−35573
Re surface, interaction with N_2^+ beam, reaction dynamics studied by XPS and thermal desorpt. spectrometry 80−93797
S to Br, $O^{2+,3+,4+,5+}$ induced K-shell ionis., 7 to 24 MeV X-ray production cross section 77−61850
Si, 1-10 keV H^+, He^+ irrad., role of Auger processes in electron emission 79−15579
Si, 3-15 keV Ar^+ induced Auger electron emission from Si and Ar 77−59654
Si, 5 keV Ne ion scatt., energy spectra by TOF and electrostatic analyser methods, comparison 79−2895
Si (001) surface struct., high energy ion scatt. study 80−59772
Si (100), N_2^+ active ion bombardment, SIMS obs. 79−16034
Si (111), O and CO sorption, ion scatt. obs. 80−59810
Si (111), surface reproducibility and impurity segregation ion neutralisation spectra and UPS obs. 78−34688
Si (111) surface, 1-3 keV He^+, Ne^+, Ar^+, Xe^+ bombard., AES obs. 79−33877
Si (111) surface, anal. by ion-electron spectroscopy 78−72670
Si, amorphous, heavy ion ranges, He^+ backscatt. obs. 78−63796
Si, amorphous, ion bombard., etch pit and ripple struct. formation mechanisms 80−66366
Si, amorphous layers, laser induced As profile broadening, MeV He scattering 79−95045
a-Si, Ar^+ bombardment induced ripple topography 77−77336
Si, Auger electron emission, ion induced and secondary ion emission 80−71546
Si, Auger electron prod. by Ne^+ bombard. 80−7460
Si, Auger spectra induced by 100 keV Ar^+ impact 80−84820
Si, axially channelled protons, transmission meas. using two-dimensional position-sensitive detector 79−1471
Si, bombardment of N_2^+ ions, form. of Si_3N_4 films 77−16705
Si bombardment with atomic and molecular noble-gas ions, secondary ion emission 80−35042
Si, epitaxial layer, growth mechanism from ion-molecular beams 80−2299
Si epitaxial layers, dechannelling by stacking faults, channelling effect technique using He^+ and D^+ ion backscatt. 79−4361
Si, H^+, H_2^+ and He^+ backscattering, energy spectra and charge fractions 80−35046
Si, ion and electron emission following ion impact 80−100729
Si, ion implanted, colour generation model 77−85868
Si, ion-implanted, period surface struct. in laser annealing, new expt. evidence 80−29836
Si, ion-induced Auger electron emission, depend. on ion energy 79−78814
Si, new materials properties achievable by ion implantation doping and laser processing 79−69127
Si, oxidation induced by ion or electron bombardment, AES-SIMS study 80−108606
Si, polycryst. and amorphous, sputtering with keV Ar^+ ion, meas. and Monte Carlo calc. of sputtering yield 79−95886
Si, proton impact, electron capture cross-section calcs. 78−95623
Si, secondary electron energy spectra due to He^+, Ar^+ ion impact 78−11049
Si, small-angle backscatt. of 350 keV protons at grazing incidence 79−83085
Si substrate, silicide formation with large bilayers of Pd-Pt, Pd-Ni and Pt-Ni 79−51444
Si surface, Ar^+ and e^- excited Ar Auger electron emission 79−47560
Si surface, N_2^+ bombardment, 500 eV chem. reactions, XPS and UPS 78−48265
Si, surface, sputter etched, damage, contamination, ion backscatt. obs. 79−33167
Si, thermal oxidation, high resolution Rutherford backscatt., implanted ions analysis 79−87911
Si, thin single crystal, MeV ion scatt. and channelling obs. of interfaces 80−50492

ion-surface impact continued
Si:As, implanted, spatially varied activation during regrowth of amorphous layers, sheet resist. and backscatt. obs. 78−71749
Si:B sputtering by Ar^+, computer simulation of sputter broadening in impurity depth profiling 80−2908
Si:Ga(As), laser-doped, impurity distrib., Rutherford backscatt. and channelling anal. 80−59507
Si-Au, (LMM) Auger electron emission by keV Ar^+ bombardment 79−95880
Si-H (up to 15 at.%), amorphous, ion implanted, laser annealing obs. 79−69133
Si-metal interface, silicide formation, interface marker technique obs. 80−59734
Si-Ni, (LMM) Auger electron emission by keV Ar^+ bombardment 79−95880
Si-Ni(Pd)(Pt) film struct., silicide form. He^+ back scatt. and X-ray diffr. obs. 79−51442
Si-Pd, (LMM) Auger electron emission by keV Ar^+ bombardment 79−95880
SiC, 10 keV H^+ irrad., C deposition, surface swelling, surface morphology changes 77−35608
SiC, (LMM) Auger electron emission by keV Ar^+ bombardment 79−95880
SiC, energetic H and Ar ion sputtering, AES-SIMS-FDS combined obs. 78−80444
SiC, of H^+, D^+, He^+ and Ar^+, combined AES-IMA system *(Japanese)* 79−74039
SiC, sputtering, physical and chemical, by H_2 and He, 600 to 7500 eV 77−36340
SiC surface, roughness factor measurement, energetic D^+, He^+, Ar^+ irradiation 80−39172
SiC, surface defect annealing, following Ar ion and electron irrad. 80−7603
SiC, surface defects due to Ar ion bombardment, 100-1000 eV 80−6445
SiH, (LMM) Auger electron emission by keV Ar^+ bombardment 79−95880
Si_3N_3, film growth by reactive sputtering, influence of electron-ion bombard. *(Russian)* 77−28717
Si_3N_4, swelling, blistering, 140 keV p, d and He ion irrads., porosity effects 77−35603
Si_3N_4:H, film, impurity profile determ. by 1.2 MeV proton-proton scatt. 80−49256
SiO surface, N_2^+ bombardment, 500 eV chem. reactions, XPS and UPS 78−48265
SiO_2 covered Si surface, scattering of keV H and He ions and neutrals 78−95638
SiO_2 film on Si substrate, Na transport caused by ion and atom impact 80−6682
SiO_2, proton induced ionisation, energy dependence of K_β/K_α intensity ratio 80−60716
SiO_2, RF sputtered, stoichiometry and atomic defects obs. 79−60647
SiO_2 surface, N_2^+ bombardment, 500 eV chem. reactions, XPS and UPS 78−48265
SiO_2, surface charge, effect of doping with P+B, differing vacuum deposition conditions *(French)* 77−85286
Si(111)-$\sqrt{3}\times\sqrt{3}$-Ag structure, atomic arrangement, low energy ion scatt. spectroscopy 80−96724
Si; Ar ion bombarded, projectile energy depend. and line shape of Ar-L AEs 80−16139
Sm, L-X-ray production by 9.5 to 41.8 MeV Fl ions 77−85847
SmB_6 (001) surface, azimuthal anisotropy in low-energy ion scatt. 79−28875
Sn, bombard. by Ar ions impact-parameter depend. of K- and L-X-rays 79−76501
Sn, isotope effects in ion-scattering double spectroscopy curves for He^+ 77−59658
Sn, X-ray cross sections, L-shell, proton induced, 1 to 3 MeV range 79−1799
Sn+He(C)(N)(O), inner-shell multiple ionisation systematics, X-ray obs. 80−63790
TZM, D^+ impact, surface blistering, SEM study 78−71774
Ta, desorption kinetics of halogens, pulsed ion beam method 80−34300
Ta, secondary electron emission coeffs. for multiply charged ion bombard. 78−11051
Ta, secondary ion emission mechanism, energy spectra of secondary ions 79−100013
Ta+H^+(He^+), L-subshell ionisation cross section, branching ratios, fluoresc. yield, Coster-Kronig factors 80−43166
TaO_n, combined SIMS, AES and XPS investigation 79−33199
Ta_2O_5, $^4He^+$ ion scatt. spectrometry below 1.0 keV 79−83088
Ta_2O_5, XPS, low energy ion backscatt. spectra 78−72660
Th, He^+(Ne^+)(Ar^+) impact, appl. of double pass cylindrical mirror analyser 78−72658
Th, L and M X-ray emission following H and O ion impact, parameter depend. 80−66327
ThO_2, H_2^+, ion beam surface interaction, H^- formation by reson. electron capture 80−40691
Ti ($10\bar{1}1$), of CO, XPS, UPS, flash desorption mass spectra, and active ion bombard. obs. 79−11822
Ti, D bombarded surface, ion fraction and energy anal. of sputtered particles 77−36345
Ti film, ion stimulated N_2 sorption, TiN_x form., sorption ratio, capture coeff. anal. 80−39411
Ti, K-shell ionisation probability, for 150 keV protons, impact-parameter depend. 79−10189
Ti oxide films, anal. by AES *(French)* 80−44440
Ti, RF sputter deposition, ion bombardment and ion implanation 80−25564
Ti, reflection of H, D and He ions 78−95640
Ti surface, Ar^+ and e^- excited Ar Auger electron emission 79−47560
Ti, trapping coeff. of energetic H at high doses 77−31699
TiB_2, coating, D^+ and $^4He^+$ irrad. effects 80−20753
TiB_2, swelling, blistering, 140 keV p, d and He ion irrads., porosity effects 77−35603
TiN, RF sputter deposition, ion bombardment and ion implanation 80−25564
TiO_2 powder, $SiO_2(Al_2O_3)$ coated, thickness meas. of coating, XPS and ion sputtering 79−88913
U, He^+(Ne^+)(Ar^+) impact, appl. of double pass cylindrical mirror analyser 78−72658

ion-surface impact continued
UF_4, condensate and ion-bombarded powder, $4f_{7/2}$ electron XPS obs., spectra of UF_3 79−45763
UO_2, (110), (100), and (111) surfaces, struct. study using He^+ ion scatt. spectroscopy 80−40206
UO_2 (111), He^+(Ne^+)(Ar^+) impact, appl. of double pass cylindrical mirror analyser 78−72658
UO_2, (111) and (553) surface struct., He^+ ion scatt. spectra 78−75917
V, blister behaviour during 200, 2000 keV He irrad, temp. depend. 77−35607
V, D bombarded surface, sputtered particles, ion fraction and energy anal. 77−36345
V, proton and deuteron irrad., 0.5-2.5 MeV, secondary electron emission 77−63512
V, secondary ion emission mechanism, energy spectra of secondary ions 79−100013
VTi alloys, blister behaviour during 200, 2000 keV He irrad. temp. depend. 77−35607
W (001), surface reconstruction and reordering by H adsorption, MeV ion scatt. 79−23835
W (001) surface structure by MeV ion backscattering, channelling 80−6605
W (100), O covered, ion scatt. spectroscopy 77−73205
W (100) single crystal, surface studies by MeV He scatt. 79−4455
W, (100) surface, scatt. of mol. and atomic H ions 79−69943
W, (110) surface, low energy ion scatt. features, inelastic loss and surface crystallography 80−66371
W {110}, chemisorption of β-N_2, underlayer mechanism 80−39432
W, amorphous, reflection of D and T, Monte Carlo study 80−40197
W, desorption kinetics of halogens, pulsed ion beam method 80−34300
W dispenser cathodes, Ba-activated, surface charact., ion scatt. spectrometry and SIMS study 80−66377
W, glancing scatt. of light ions from single cryst. surface 77−36347
W, H^+ and He^+ ion backscattering, reflection coefficients 79−43081
W, ion induced secondary electron emission, probe for adsorbed O 80−55251
W, needle field emitter, ion bombardment effects, field emission microscope obs. 77−55869
W, O_2-covered, electron emission induced by slow Ar ions 80−60740
W, polycryst., bombardment with Na and K ions, neutral component of scatt. 78−11047
W, reflection of H, D and He ions 78−95640
W, secondary electron yields from ion impacts, stopping power calcs. 78−11053
W single crysts., surface scatt. by MeV He ions 77−69952
W surface self-diffusion, ion impact induced, FIM study 80−103549
W, surface self-diffusion by ion impact, protrusion formation 78−75938
W, surface structure and topological modification during depth profiling, FIM obs. 79−78816
W, surface structure changes due to ionic bombardment, LEED and AES obs. *(Russian)* 77−1775
W+H^+(He^+), L-subshell ionisation cross section, branching ratios, fluoresc. yield, Coster-Kronig factors 80−43166
WC-Co composite, ion scatt. spectrometry and AES 77−60150
WC-Co composite, surface anal. by quantitative AES 78−76622
WC-Co composite chemical characterisation by AES and ISS 78−76621
WO_3, H^+ and He^+ ion backscattering, reflection coeff. 79−43081
Xe^+, kinetic energy reflection on polycryst. bombardment 77−85869
Y, D bombarded surface, ion fraction and energy anal. of sputtered particles 77−36345
Zn, isotope effects in ion-scattering double spectroscopy curves for He^+ 77−59658
ZnO (0001), ($000\bar{1}$) and ($10\bar{1}0$), UPS rel. to elec. struct. 78−15288
ZnO, polar ($000\bar{1}$) surface, annealing and Ar^+ bombard. effects on conductivity, LEED obs. 79−51653
ZnO surface extreme accumulation layers due to He^+ ions 77−72909
ZnS, secondary electron emission coeffs. for multiply charged ion bombard. 78−11051
Zr, RF sputter deposition, ion bombardment and ion implanation 80−25564
ZrN, RF sputter deposition, ion bombardment and ion implanation 80−25564
Zu, reflection of H, D and He ions 78−95640

ion thrustors *see ion engines*

ionic conduction in solids
see also superionic conducting materials
AC properties of ionic conductors 78−47578
acids, conc. aqueous, amorphous protonic conductors, DC cond., glass transition and elec. relax. meas. 78−2290
adsorbed salt layers, field ion emission, field desorption and ionic cond. 77−16473
$AgPS_3$-AgX (X=I, Br), glass-forming regions, struct. model *(French)* 80−100464
β-Al_2O_3-Na_2O, AE during breakdown under Na^+ transport 78−67860
β-Al_2O_3-Na_2O, diffusion and ionic cond. meas. 80−6542
β-Al_2O_3-Na_2O, mechanism of diffusion 80−2202
alkali aluminophosphate glasses, ionic cond. mechanism 80−15299
alkali glasses, rapidly quenched, alkali ion cond. 80−107559
alkali halide, cation motion energy parameters, dielectric relax. meas. 78−30784
alkali halide crystals, defect fermion properties, ionic cond. calcs. 80−59457
alkali halide crystals, inhomogeneous transport at low temp. 77−43382
alkali halide thin films, high-field electron injection, ionic cond., photocond. 80−75665
alkali halides, curvature in cond. plots as consequence of anharmonicity 77−76597
alkali halides, ion migration, barrier heights, shell model calcs. 77−35742
alkali halides, mass transport, contrib. of vacancy defects 79−46831
alkali halides, matter transport rel. to point defect parameters 80−107488
alkali halides, shell model calc. of defect energies, crystal-independent interionic potential parameters 79−28141
alkali ionic conductors with sheet structures, ion mobility and influences 80−107522
alkali metal compounds, $ASbO_3$.1/6AF, dielec. spectroscopy study, 100 Hz to 10 MHz, 238 to 417K *(German)* 80−108144
alkali metal intercalation compounds, ionicity, struct., size, intercalation amount, ion mobility anal. 80−39041

ionic conduction in solids continued
alkali metal intercalation cpds., prep. methods and cryst. struct. 79−99156
alkali metal metaphosphate glass, dielec. relax. at medium temp. 79−24257
alkali metal oxide glass, composition dependence of activated processes, mixed alkali effect 79−77525
alkali metal sheet phases, $A_x(L_xM_{1-x})O_2$, (A=Na,K; L=In,Sc; M=Ti,Zr,Hf,Sn), influence of A^+ ion environment *(French)* 79−65244
alkali perchlorates, elec. transport during struct. transforms. 78−59971
alkaline earth fluoride based solid solns., ion transport 80−107545
alkaline earth fluoride crysts., ion transport, mechanisms and energetics 77−55382
alkaline earth halide crystals, thermal transport of charged point defects 80−15293
alumina film, anodic, rel. to dielec. breakdown 77−1637
aluminophosphate glasses, alkali free, comp. effect on elec. cond. 78−26725
amorphous cation subsystem in binary cpd. by rapid cooling, ionic cond. 77−51322
amorphous semiconduction, field-depend. packet dispersion at low temps. 80−19981
anodic oxide film, open-circuit transient method, rel. to other techniques 80−24650
anodic oxide films, model 80−2197
binary ion exchange, field assisted, anal. 79−99349
Brownian motion of particle in double well potential 77−76607
cabal glass:$SiO_2(TiO_2)$, microheterogeneity, and elec. cond. 78−83997
dl-2,3-camphanedione, elec. cond., brittle-to-plastic region, cond. jump 78−39169
dl-camphor oxime, elec. cond., brittle-to-plastic region, cond. jump 78−39169
dl-camphoric anhydride, elec. cond., brittle-to-plastic region, cond. jump 78−39169
Cationic conduction and diffusion and the compensation law 78−18822
ceramic materials for ion-selective membrane electrodes development, Ag^+ and F^- based materials appl. *(Japanese)* 80−61203
ceramics, electron and ion conductivity, instrument for meas. up to 2000°C 79−96247
chalcogenide glass, elec. cond. parameters rel. to charge carriers 77−35970
coal slag, elec. props. 80−107476
cuprous halide-metal halide systems, AC cond. rel. to phase diagram 77−72712
cuprous halides, cation or anion doped, ionic cond. 79−46837
dielectric-semiconductor structures, surface ion migration, theoretical analysis 80−65700
edge and surface effects in anal. of data for ionic crysts. 78−6177
elastomer state, lattice model of ionic cond. 77−4218
electrochemical methods for determ. of kinetic props. of solids, book contrib. 79−65251
electrolyte, ionic conductivity, phenomenological theory 78−83994
electrolyte, phase transition to high ionic cond. state *(Russian)* 79−51304
electrolytes, direct current in cell with unipolar ionic cond. 78−35703
electrolytes, solid, transport modes of ions and superions *(German)* 80−15289
electrolytes, supersonic, conductivities and activation energies 79−28137
energy storage and conversion systems, characterisation 77−76596
ethyl cellulose films, secondary ion injection 79−24094
evaporated dielectrics, ion drift and diffusion numerical calc. 77−4215
excluded volume model, for superionic conduction 80−107543
fast ion transport in solids, conf., Lake Geneva, USA (May 1979) 80−57006
fast ion transport in solids, conf., Lake Geneva, USA (May 1979) 80−105427
Feynman-Hellmann theorem and oscillator strengths, force on atom in electrostatic field 80−65275
fluoride solid electrolytes 80−70464
glass, commercial, high field cond., weak electrolyte theory appl. 80−107475
glass, DC conductivity, rel. to dielectric loss peak frequency 79−78621
glass, electrical relax., Debye-Falkenhagen theory 80−108155
glass, electrothermal props. in structural transform. zones *(French)* 80−88047
glass, high-field ionic and polaronic cond., dielec. relax., Poole-Frenkel theory 80−100351
glass, ion motion and mixed alkali effect analysis 78−30793
glass, single- and mixed-alkali, high field cond. and ionic jump processes 78−38873
glass, surface layer, structure and processes *(German)* 80−38928
glasses, elec., mag., and optical props., conference, Troy, NY, USA (Aug. 1979) 80−105417
glassy polymers, elec. resist., corresponding states relationship 80−59704
$(H_3O)_{5-x}Ta_{11+x/1}O_{30}$, synthesis, non-stoichiometry, density and ionic cond. meas. *(French)* 78−52741
halide-insulator interface, interfacial polarisation, dielec. loss meas. 77−2705
hexafluoroarsenates, cryst., elec. cond. 80−34232
high field, nonsimultaneous place exchange mech. 80−70456
high field intrinsic, kinetics of growth of anodic oxide films 80−34224
hollandite, one dimensional ionic and solitary wave conduction 79−23954
hollandites, ionic cond., impedance, struct. 78−67856
homogeneous solid, small signal AC response, mobile charge recomb., theory 78−52005
hopping conductivity, freq. depend., model calcs. 80−107507
hydrogen bonded crystals, quantum theory of protonic cond. 79−90816
hydroxyapatites, elec. cond., charge carrier identification 78−67855
ice, cubic, D_2O isolated, H^+ exchange and Bjerrum defect migration, direct spectroscopic obs. 80−88356
ice, ionic cond., elec. cond. temp. depend., dielec. props., undergraduate expts. 79−35503
III-V semiconductor, anodic oxide film formation, current flow mechanism 77−90479
In_4CdI_6, ionic conductivity, Raman spectra 77−69113
interacting particle diffusion in periodic pots., two particle model, random motion 79−46828
intercalation and substitution-intercalation cpds. in dichalcogenide hosts, factors affecting ion mobility 80−59707
ionic conduction in solids continued
intercalation compound electrodes, thermodynamic and transport props. 80−66963
intercalation compounds, two dimensional, conductivity problems 79−28138
interface charge transfer, coupling to bulk tranport props. of ionic crystals 78−95183
interfacial charge transfer, coupling with bulk transport in ionic crystals 80−79986
interfacial polarisation effects in simple model ionic conductor 79−60538
ion distribution function for complex solid, appl. to cond. of glasses 78−47585
ion exchange materials, elec. cond. meas. using isocond. pt. determ. method 77−52646
ionic compounds, hopon mechanism for ion transport 79−14957
ionic crystal, space charge polarisation involving electrode reaction with surface adsorption 77−12019
ionic crystals, nonstoichiometric, equilib. with gas phase in mech. vibr. field 78−43388
ionic crystals, transport phenomena, appl. to solid state devices 78−55976
local field effects in ionic conductors 79−55918
membranes, cation exchange, voltage against current curves 79−96365
metal halides, fluorite structure, retarded ionic motion 80−88361
metal oxide thick film growth, fund. theory 80−89391
metals, electromigration, dielectric function approach using equivalence theorem 77−11733
9-methyladenine single crysts., protonic cond. 77−55388
1-methylthymine single cryst., cond. determ. using proton-injecting solution electrodes 78−18825
MIS structure, on thermal SiO_2, polarisation hysteresis, ion motion *(Russian)* 80−54793
NASICON solid electrolyte, processing and phys. props. 80−60820
natural clay permafrost, elec. props. 77−44967
NMR relaxation rates in ionic conductors, central component 80−29640
noncrystalline solids, mass transport phenomena and interpret. 78−26720
nylon 6, transient elec. conduction at high temp. 79−69513
one-dimensional ionic. conductor, site-occupancy correlation and effective interionic pot. 77−62663
oxide film, thermal and anodic, space charge effects on steady-state transport 80−11124
oxide glass, elec. cond. parameters rel. to charge carriers 77−35970
oxide glasses, elec. cond. and dielec. relax., correl. 78−79801
parchment-supported $AgPO_3$, determ. of thermodynamics of ionic diffusion processes 78−20068
perovskite type compounds, electrode catalysts for cathodic reduction of O_2 79−29371
perovskite-related oxides, oxygen-deficient, oxygen ion conductivity 77−20119
PET, ionic cond. current rel. to neutralisation at polymer-metal interface at elevated temps. 80−24664
piperazinium $Ag_{10}I_{12}$.4-dimethylformamide, exam. of electrical cond. and crystal structure 78−75871
PMMA, and related cpds., ionic charge carriers, dielec. studies 80−25291
polarisable ion, Brownian motion in periodic pot., polarizability effect on cond. 79−4427
polaritonic spectra 79−23908
6-polyamide films, cond. and relax. under very high press. 77−35748
polyamine iodide/AgI solid electrolytes, conc. depend. of elec. cond. 80−24647
polyester, ion mobility from ionic injection current at strong diffusion 80−2210
polyester polymer-C black composition, elec. cond. under press. 77−28224
polyethylene, linear, films, elec. cond. rel. to drawing, annealing *(Japanese)* 79−15817
polyethylene terephthalate, elec. cond., 120-180°C, anal. of results 79−47102
polyethylene terephthalate, TSC due to mobile ions and ionic conduction *(Japanese)* 80−54432
polyimide film, dielectric breakdown in high-temperature region 78−84522
polymer, predominant carrier species determ. using galvanic cell 77−69384
polymer film, partial discharges, HNO_3 absorption, expt. *(German)* 77−77147
polymers, book 80−7257
polypyromellitimide film, elec. cond., 120-180°C 80−60124
polystyrene-polyethylene sulphonated copolymer, ionic transport, counterion effects in membrane 77−24430
polyvinyl alcohol, ionic charge carriers, dielec. studies 80−25291
polyvinylidene fluoride, dielec. breakdown and elec. cond., room temp. to 150°C 80−60500
Portland cement clinker, elec. props. 78−59976
powder compact, appl. of van der Pauw method 78−32833
proton conductivity meas. for inorganic/organic solids for fuel cell appls. 80−16796
PVC, plasticized, humidity depend. of ion mobility, polarity reversal of applied voltage method 80−49408
PVC-metal interface, ionic carriers behaviour 79−99622
pyridine-Ag_5I_6, superionic conductor, dynamical aspects 78−79695
pyridinium pentasilver hexaiodide, freq. depend. ionic conductivity 78−2291
quadrupoles, evaluation of association parameters, in ionic cryst. 77−43365
quasi-one-dimensional solids, nomadic polarisation 77−63357
$RbBiF_4$, anionic conductivity exam. *(French)* 77−35952
refractory oxide electrolytes, elec. props. at steelmaking temps. *(German)* 77−90605
review, props. of solid electrolytes *(Czech)* 77−59142
review *(German)* 78−79795
simple ionic crystals, ion transport 78−63878
small signal electrical response theory, generation-recomb. and trapping kinetics 77−89772
solid electrolyte dielectric permeability, phase transition to superionic state *(Russian)* 80−49403
solvents adsorbed on insulating substrate, ionic conduction 79−33180
statistical theory of relaxation current and low-freq. dielectric dispersion 78−60391

ionic conduction in solids continued
styrene-sodium methacrylate (9 mol.%) copolymer cond. relax. 78−38874
sulphate based binary solid electrolytes, props., appls. 77−84971
superionic conducting oxides, review 80−49414
superionic conduction, sliding condensed-matter system model 80−44258
superionic conduction in solids, high energy density batteries appls. 79−70445
superionic conductor, chaotic states of anharmonic systems in periodic fields 80−22288
superionic conductor, scattering of light and neutrons in diffusion model 78−26719
superionic conductor, with fluorite struct., activation vol. 80−107557
superionic conductors, collective motion, AC conductivity 79−99368
superionic conductors, correlation functions theory 78−79674
superionic conductors, freq. depend. cond. 77−84973
superionic conductors, microscopic theory 78−79809
superionic conductors, review 79−55923
superionic conductors, transitions, structures, dynamics and spectra, review 79−60549
ternary fluorides, high anionic cond. of new solid electrolytes 80−107546
ternary semiconductor device applications, review 78−39207
thermally stimulated processes 78−10828
thermally stimulated relaxation in solids, transport phenomena, book 80−77553
thermocurrents in ionic crysts., review 78−60381
thermometer, high-temp., based on elec. cond. charges in ionic crystals 80−52203
$Tl_{1+\alpha}(Ta_{1+\alpha}W_{1-\alpha})O_6$, exam. of ionic conductivity *(French)* 78−51729
transient drift dominated unipolar conduction between concentric cylinders and spheres, anal. 77−8103
unipolar conduction model for solid electrolytes 79−28144
urea nitrate single cryst., elec. cond. anisotropy 78−79807
valve metal oxide-semicond. oxide, electron injection, interface reactions 77−76936
zeolite A, synthetic, with salt inclusions, elec. and thermal props. 79−55925
zeolite interface, ionic conduction bands 77−35745
zeolites, synthetic, effect of sintering on elec. cond., porosity and microstruct. 79−29009
(Ag,Na)Br, ionic transport numbers, polarization cell method 80−59705
(Ag,Na)Cl solid solns., ionic transport numbers, polarization cell method 80−59705
Ag halide microcrystals, topography of latent image centres and ionic conductivity 79−20442
Ag halides, impurity ion migration 79−19406
Ag halides, matter transport rel. to point defect parameters 80−107488
Ag^+ superionic conductors, US attenuation due to hopping of Ag^+ ions 78−22890
Ag-halide microcryst., space charge characts. 78−15097
Ag_7AsS_6, thermal, crystallographic and elec. props. *(French)* 80−40338
Ag_7AsSe_6, thermal, crystallographic and elec. props. *(French)* 80−40338
AgBr (100) microcryst., dielectric loss meas., ionic conductivity 77−43931
AgBr, Ag^+ migration vol. for vacancy and interstitial motion, influence of anharmonicity 79−14965
AgBr and AgBr:$PbBr_2$, emulsion grains, dielec. loss, ionic cond. and surface space charge 77−28038
AgBr, curvature of conductivity plots, consequence of anharmonicity 78−79800
AgBr, determ. of ionic transport processes 77−89578
AgBr emulsion grains, edge length depend. of ionic cond., space charge characteristics 80−88360
AgBr emulsions, ionic thermocurrents 79−19399
AgBr, epitaxial layer, ionic field effect 78−10588
AgBr, far IR spectra, cond., cation local motion 79−1754
AgBr, film and microcrystal, interstitials and surface conductance 79−23776
AgBr, high-temp. ionic transport processes 79−23777
AgBr, high-temp. transport anomaly from Na tracer obs., mechanism 77−62669
AgBr, ionic cond., dielec. loss meas. 79−23768
AgBr, microcrystals, activation energy for ionic cond. 80−34237
AgBr microcrystals, influence of Pb^{2+} ions on ionic conductivity and space charge characts. 79−23778
AgBr microcrystals, S sensitization effects on ionic conductivity 79−19398
AgBr, phonons at elevated temp. 78−79810
AgBr, prep. of high purity cryst. with <3 ppb I 77−69982
AgBr, thin epitaxial layer, surface ionic cond., lattice disorder, space charge region 77−11730
AgBr:Pb^{2+}, cubic microcryst., ion influence on ionic cond. and space charge characts. 79−55928
AgBr-AgCl, mixed crystals, pure and I doped, lattice defect parameters, Frenkel defect form. energy, ionic cond. 80−44359
AgBr(:Pb^{2+}), ionic conductivity, Frenkel defects 77−51542
AgBr(I) microcrystal dispersed in gelatin, effect of I^- on interstitial Ag ions 78−26726
AgCl, curvature of conductivity plots, consequence of anharmonicity 78−79800
AgCl, determ. of ionic transport processes 77−89578
AgCl, high-temp. ionic transport processes 79−23777
AgCl, ionic mobility, diffusion coeffs., defect mobility energies 80−65284
AgCl:Na^+, Frenkel defect formation energy, impurity diffusion and migration 79−99179
AgCl:Pb^{2+}, ionic cond. and dielec. loss relax. vacancy-impurity complex. form. 77−1259
AgCl(Br), enhanced defect form., mean field theory 80−107220
AgCl(Br), multivalent impurities 79−19556
$Ag_{0.85}Cu_{0.15}Br$, far IR spectra, cond., cation local motion 79−1754
$Ag_{1-x}Cu_xI$-QI, Q=NH_4, $(CH_3)_4N$, $C_5H_5NCH_3$, elec. cond., −20 to 130°C 77−55387
AgF, diffusion, elec. cond. and ^{19}F relax. $T_{1\rho}$ meas. 80−92718
$AgGa_5S_8$, galvanic cell meas. 77−47616
$AgGaS_2(Se_2)$, galvanic cell meas. 77−47616
Ag_2HgI_4, ordered and disordered phases Raman spectra temp. depend., ion hopping 78−23438
Ag_2HgI_4, Raman line shape and ionic cond., coupled mode model 80−66171

ionic conduction in solids continued
AgI, cation or anion doped, ionic cond. 79−46837
AgI, growth, elec. and optical props. 79−77805
β-AgI, ionic cond. and Frenkel pair form., dielec. loss meas. 79−33112
α-AgI, ionic motion, low freq. Raman scatt. 78−80354
α-AgI, molecular dynamics exam. of Ag diffusion 78−55981
β-AgI, piezoelectric ionic cryst., US investigation 79−77689
α-AgI, structural and dynamical behaviour 80−107544
AgI, structural model for superionic conduction 78−79797
α-AgI, superionic cond., freq. depend. cond. 77−84973
AgI, superionic conductor, dynamical aspects 78−79695
AgI type solid electrolytes, expt. props. 78−63877
AgI:Cd, polycrystalline, thermoelectric power meas. 80−59698
AgI/Ag oxysalt system, vitreous solid electrolytes, conductance mechanism 80−107560
AgI-Ag oxosalt systems, solid electrolytes with glass-like struct., thermodynamic and electrochem. props. 79−10978
AgI-Ag oxysalt ionic solids, thermoelec. power determ. 78−30947
AgI-$Ag_2Cr_2O_7$ system, solid electrolyte stability 77−15619
AgI-$Ag_2Mo_2O_7$ system, solid electrolyte stability 77−15619
AgI-$Ag_2Mo_2O_7$($Ag_2Mo_4O_{13}$), solid, intermediate compounds with fast ion transport 77−43371
AgI-Ag_2O-MoO_3, comparison of ionic conductivity between glassy and crystalline solid electrolytes 78−30786
AgI-Ag_2O-MoO_3 system, glass form. with high ionic conductivity 77−89379
AgI-Ag_2O-P_2O_5 system, glass form. and superionic cond. characts. 78−26722
AgI-$Ag_2O.B_2O_3$ system, ionic cond., struct., electrochem. prop. in galvanic cell 78−95181
4AgI-Ag_2XO_4, (X=Cr, Mo, W), ionic cond., complex admittance 77−84969
AgI-Ag_3AsO_4 system, solid electrolyte stability 77−15619
AgI-HgI_2, solid electrolyte, ionic and electronic cond., phase composition determ. 78−2296
AgI-piperazinium, (or N,N′-disubstituted piperazinium diiodides), binary salts, ionic cond. study *(French)* 78−2293
AgI-RbI films, vacuum deposited, cond. determ. 77−39689
Ag_4I_5, ionic cond., effect of press. 78−51733
$(AgI)_x(Ag_2O\ B_2O_3)_{1-x}$, amorphous superionic compound, ^{11}B lineshape and relaxation 80−108107
$Ag_{26}I_{18}W_4O_{16}$, cryst. struct. and ionic conductivity 77−80647
Ag_2O-Na_2O-B_2O_3 mixed cation glasses, electric conduction *(Japanese)* 77−24432
Ag_2O-Tl_2O-B_2O_3, mixed-cation glass, electrical cond. 79−95210
Ag_2O-Tl_2O-B_2O_3 mixed cation glasses, elec. cond. 77−80644
$AgPO_3$-AgBr(Cl)(I) system glasses, soln. calorimetry obs., thermodynamic activity correl. with ionic cond. *(French)* 79−33102
$AgPO_3$-AgX, X=I,Br,Cl, ionic conductivity *(French)* 78−79805
$AgPO_3$-AgX (X=I, Br), glass-forming regions, struct. model *(French)* 80−100464
$AgPO_3$-CdI_2 glasses, ionic conductivity and structure *(French)* 78−67854
$AgPO_3$-$HgI_2(CdI_2)(PbI_2)$ glass, elec. cond. and Raman. spectra rel. to struct. *(French)* 79−10979
$AgPO_3$-PbI_2 system, elec. conductivity as function of composition and temp. *(French)* 77−69112
$Ag_5Rb(PO_4)_2$, struct., density and elec. cond. 80−33952
β-Ag_2S, electrogalvanic and elec. props., and range of existence *(French)* 78−43175
β-Ag_2S, fast-ion conductor, Ag ion density, neutron diffr. study 80−34234
Ag_3SBr, ionic conductivity in temp. range 93-573K, X-ray diffr. and DTA 80−79988
Ag_3SI, ionic conductivity in temp. range 93-573K, X-ray diffr. and DTA 80−79988
Ag_3SI, superionic conductor, dynamical aspects 78−79695
$Ag_8S_3SO_4$, new cryst. data, elec. cond. 79−37685
$Ag_{14}Sb_{12}O_{36}F_2$, ionic conductivity, comparative study with pyrochlore phase $AgSbO_3$ *(French)* 80−103701
Ag_3SbS_3, ionic component of conductivity *(Russian)* 78−38870
Ag_3SbS_3, pyrargyrite, electronic to ionic conductivity ratio *(Russian)* 77−80818
Ag_2Se thin film, switching and Ag movement, point contact technique 80−60107
Ag_2Te, Ag movements, X-ray microanal. by SEM *(French)* 79−42304
α-Ag_2Te, diffusion of Ag^+, deviation from Einstein relation 77−76595
β-$Ag_xW_yV_{2-y}O_5$ bronzes, β-phase existence range, elec. cond. and Ag diffusion 78−35373
AgX-Ag_2O-P_2O_5 (X=I, Br, Cl), glass formation and ionic conductivity 80−65290
Al-SiO_2Si, mobile ion kinetic behaviour 79−56315
Al_2O_3, acceptor-dominated polycrystn., cond. and creep 79−78109
β-Al_2O_3 compounds, stoichiometry, phase transition and conductivity 79−23773
β-Al_2O_3, conduction and dielec. loss mechanisms, paired interstitialcy model 80−107468
Al_2O_3 polycrystalline, effects of space charge, grain-boundary segregation and mobility differences on conductivity 80−79979
α-Al_2O_3, unintentionally doped, defect struct. 79−60755
α-Al_2O_3:Mg, defect. struct., cond. and optical absorptiob 77−55279
α-Al_2O_3:Ti, defect struct., electronic and ionic cond., optical absorption meas. 78−30603
Al_2O_3-B_2O_3-RO, glass, (R=Ba,Ca,Cd,Mg,Sr,Zn), ionic and DC cond., comp. effects 77−31804
β-Al_2O_3-H_2O, H^+ and H_3O^+ conduction, dehydration effect 78−51726
β-Al_2O_3-H_3O^+, ionic conductivity at 25°C, obs. 78−22893
B-Al_2O_3-M_2O, M=Na, Ag, Rb, K, far IR absorption and ionic cond. 78−72512
Al_2O_3-MgO-H_2O fast proton conductor 78−91480
B″-Al_2O_3-Na_2O, bulk and grain boundary ionic cond. from conductance and capacitance meas. 80−2204
β-Al_2O_3-Na_2O, calculation of simultaneous ionic cond. and tracer diffusion 78−43178
β″-Al_2O_3-Na_2O, computer simulation of ionic conductivity 77−89580
β-Al_2O_3-Na_2O, conductivity dispersion in single crystal 77−28037
β-Al_2O_3-Na_2O, grain boundaries and ionic cond. 79−23620
β-Al_2O_3-Na_2O, H_2O intercalation effect on ionic cond. 79−99364
β-Al_2O_3-Na_2O, hot pressing and phys. props. 79−4940
β-Al_2O_3-Na_2O, layered material, contact free conductivity 80−2195

ionic conduction in solids continued
β''-Al_2O_3-Na_2O, Li_2O stabilized, texture conductivity relationship 79−47788
β''-Al_2O_3-Na_2O, polycryst., ionic cond., 25-800°C 77−80645
β-Al_2O_3-Na_2O, synthesis, ceramic form., sintering, cond. 79−11537
β''-Al_2O_3-Na_2O solid electrolyte, processing and phys. props. 80−60820
β-Al_2O_3-Na_2O:Ba(Ti), dopant effect on ionic cond. and phase comp. 79−65242
β-Al_2O_3-Na_2O:Mg, ionic cond., effect of microstruct. and phase composition 78−67859
β-Al_2O_3-Na_2O:Mg, with and without Co co-doping, ionic cond. and cryst. struct. 78−26723
β''-Al_2O_3-Na_2O:Na^+,Ca^{2+}, charge compensation mechanism, Na^+ and Ca^{2+} ion movement 78−22891
Al_2O_3-Na_2O-LiO_2 (8.8, 0.75 wt.%) exam. of Na^+ resistivity as function of temp. grain size model 78−80654
β''-Al_2O_3-Na_2O-MgO in Na-S batteries, blocking defects rel. to cond. loss 78−55879
β-Al_2O_3-Na_2O-SiO_2, solid electrolytes, exam. of microstruct. ionic resistivity 78−80566
Al_2O_3-P_2O_5-Mg(Ca)(Sr)O glasses, Na^+, Sr^{2+} diffusion coeffs. rel. to temp. 78−30787
β-Al_2O_3.Na_2O, ceramic tube fabrication, crystallite preferred orientation, ionic cond. 77−8781
β-Al_2O_3.Na_2O, single cryst. and polycryst., anisotropic cond., low temp. modulus spectra 77−4217
$Al(PO_3)_3$-NaF-LiF glasses, mixed-alkali effect 80−19715
As_2Se_3:Ag, amorphous, doping effect of gap states and elec. cond., dielec. relax. and DC cond. meas. 79−47098
B_2O_3-Li_2O-Li Cl(F)(I)(Br), vitreous, ionic cond. of Li *(French)* 79−90823
$BaCl_2$, molten, struct. determ. by neutron diffr. 78−42883
BaF_2, influence of O_2 on AC cond. and cation transport meas. *(French)* 77−47619
BaF_2, ionic cond., activation vols., freq. depend. cond., press. effects 80−100354
BaF_2, ionic conductivity meas., computer anal. point defect parameters 80−54429
BaF_2, NMR relax., ionic cond. and self-diffusion 78−23362
BaF_2-UF_4-CeF_3 solid soln., surface degradation, complex admittance analysis 78−55980
BaFCl, cryst., anisotropic ionic cond. 78−43171
BaFCl, luminesc. and ionic conduction 79−28829
$Ba_{1-x}La_xF_{2+x}$, enhanced ionic motion in solid solutions 80−107491
$BaMnF_4$, phase transitions review 79−78378
$BaMnF_4$, spectroscopy, ferroelectric/ferromagnetic coupling, cond. meas. 1400-3400K 79−19845
BaO-B_2O_3-SiO_2 system glass, electronic cond. of Ti ions 78−23095
BaO-BaX_2-P_2O_5 glass, X=F, Cl, Br, conductivity 78−67862
$Ba(PO_3)_2$-AlF_3-BaF_2 (SrF_2), elec. cond., density, and IR spectra 79−95215
$Ba(PO_3)_2$-AlF_3-CaF_2, glass, elec. cond. and IR spectra 80−89005
$Ba(PO_3)_2$-AlF_3-MgF_2, glass, elec. cond. and IR spectra 80−89005
$Ba(PO_3)_2$-alkaline earth fluoride and $Ba(PO_3)_2$-YF_3 glasses, pseudobinary, elec. cond. and dielec. losses 77−7890
$Ba(PO_3)_2$-BaF_2-$BaCl_2$($BaBr_2$) glasses, elec. cond., mixed anion effect 80−15300
$Ba(PO_3)_2$-fluoride glass, elec. cond., struct. 80−88056
$Ba_{1-x-y}U_xCe_yF_{2+2x+y}$, solid soln., ionic cond. 79−99356
BeF_2, vitreous, ionic transport and defect struct. 80−107472
Bi_2O_3, elec. props. of α, β, γ and δ phases 79−23771
δ-Bi_2O_3, thermoelectric power rel. to fast ionic conduction 80−107549
Bi_2O_3:MoO_3 sintered, oxide ion conduction 77−80646
Bi_2O_3-M_2O_5(M_2O_3) (where M=V,Nb,Ta,Y,Gd) ion cond. and oxide ion vacancy 79−28139
Bi_2O_3-$M2O_5$, sintered, (M=V, Nb, Ta), high oxide ion cond. 78−14503
Bi_2O_3-PbO, glass, cond. meas. using complex impedance anal. *(French)* 80−92707
δ-$(Bi_2O_3)_{1-x}(Y_2O_3)_x$, thermoelectric power rel. to fast ionic conduction 80−107549
$Bi_{1-x}Sr_xO_{1.5-x/2}$ vacancy-type solid soln., anionic cond. *(French)* 80−49407
Bi_2WO_6, ferroelectric, dielectric props., elec. cond. and relaxation phenomena obs. 80−80692
Bi_2WO_6, ionic cond. and relaxation polarisation, capacitance, losses 80−24657
CaF_2, association parameters of [Me^{3+}-Fi^-] dipoles (Me=Metal), ionic cond. meas. 78−30788
CaF_2, cond. meas. under controlled F_2 chem. pot. *(Japanese)* 78−59972
CaF_2 crystal under controlled F_2 chemical potential, cond. meas. 80−15301
CaF_2 film, ionic migration study by Rutherford scatt., defects, secondary emission *(French)* 78−55982
CaF_2, fluorite crysts., lattice O^{2-} effect on thermal, elec., and thermoelec. props. 77−76599
CaF_2, ionic cond., activation vols., freq. depend. cond., press. effects 80−100354
CaF_2, mixed cluster, doubly-doped with rare earths, elec. dipole relax. 79−82924
CaF_2, mol. dynamics studies of superionic conductors 80−107547
CaF_2, O^{2-}-F_v^- dipoles association from ionic conductivity 77−43242
CaF_2:Ce(Nd)(Dy)(Ho)(Yb), props. of ionic thermocurrents 77−7897
CaF_2:Gd^{3+}, ITC spectra of impurity aggregate 78−71883
CaF_2:O_2, absorpt., ionic cond., and thermal depolarisation 79−14960
CaF_2:O, absorption, ionic cond. and thermal depolarisation 78−14502
CaF_2:O_2^-, OH^-, ion incorporation by reaction with surrounding atm. 80−55143
CaF_2:Y^{3+}, DC cond., high Y concs. influence 78−22887
CaF_2:Y^{3+}, ionic cond. and thermal depolarisation obs. of defect clustering 80−71298
CaF_2-CaO, elec. cond. meas., CaO solubility, O^{2-} diffusion const. 78−30760
CaF_2-UF_4-CeF_3 solid soln., surface degradation, complex admittance analysis 78−55980
$CaF_{2-x}H_x$, ionic conductivity study by NMR experiments *(French)* 80−29210
$CaMoO_4$, electrical cond. and ionic transport number meas., defect struct. model 80−2388
$CaMoO_4$, exam. of electrical conductivity, absorption spectrum 79−51301

ionic conduction in solids continued
CaO-B_2O_3-Al_2O_3-V_2O_5 glass, cond. mechanism, current carriers, V_2O_5 conc. effects 77−62668
CaS, sintering method prep., ionic cond. meas., 650 to 900°C *(Japanese)* 78−75869
CaS, solid, tracer diffusion coefficient of S by ion microanalyser *(Japanese)* 80−34233
CaS-Y_2S_3 (1 wt.%), solid electrolyte, elec. cond. under low partial pressures of S *(Japanese)* 80−49409
$CaTi_{0.7}Al_{0.3}O_{2.85}\square_{0.15}$, ionic conductivity 77−20119
$Ca_{1-x-y}U_xCe_yF_{2+2x+y}$, solid soln., ionic cond. 79−99356
$Ca_{1-x}Y_xF_{2+x}$, solid anionic conducting electrolytes, struct., elec. props. 77−84977
CdF_2, electrical transport limitation by electrodes, polarisation effects 80−96689
CdF_2, ionic cond., activation vols., freq. depend. cond., press. effects 80−100354
CdF_2, ionic conducting fluoride fluorite, US velocity meas. 80−107381
CdF_2:Na(Nd), ionic cond. investigation by complex admittance method 80−100352
Cd(OH)Cl, temp. depend. of elec. cond., solid state thermal decomp. 78−19042
$Ce_{0.9}Ca_{0.1}O_{1.90}$, ionic cond. meas. 79−60543
CeO_2, rare earth doped, ionic cond. meas. 79−60543
CeO_2:$CaO(Y_2O_3)$, oxygen ion cond. and defect struct. 80−107553
CeO_2:Y_2O_3, bias sputtering, film growth and characts. 77−40366
Co-Cr-Si alloy hot corrosion and oxidation expts. for ionic conducting scale 78−11446
CsBr-TlBr, phase diagram and pt. defect parameters 79−96017
CsCl-type crystal, cation vacancies migration energies 80−2192
$CsClO_4$, electrical conductivity, frequency dependence 80−65288
CsF-BeF_2 glass, anion conductivity, transport number radiometric meas. 79−86923
CsH_2PO_4, lattice consts., temp. depend. of dielec. const. and birefringence, high temp. phase transitions 79−56746
CsI(:Na), ionic cond. temp. depend. meas., effect of Na doping 78−18829
$CuAg_3I_4$, co-ionic cond. obs. 80−34231
CuBr, cond. mechanisms and struct. at high temps. 77−84711
β-CuBr, far IR spectra, cond., cation local motion 79−1754
CuBr-AgI system, ionic cond. and phase diagram 80−2198
CuCl, effect of dispersed Al_2O_3 particles on ionic cond. 80−24649
CuCl, pure and Cu_2S doped, temp. depend., 60-370°C 77−47617
CuCl-TlCl system, phase diagram and high ionic cond. obs. 78−79802
CuCl(I), ionic mobility meas. method 77−15625
$CuGaS_2$, galvanic cell meas. 77−47616
$CuGa_5S_8(Se_8)$, galvanic cell meas. 77−47616
Cu_2HgI_4, ordered and disordered phases Raman spectra temp. depend., ion hopping 78−23438
CuI, cond. mechanisms and struct. at high temps. 77−84711
CuI, pure and CdI_2 doped, interstitial and vacancy concs. and mobilities, energies of form. and migration 77−15626
$Cu_xIn_xZr_{1-x}S_2$ system, struct. and cond. meas. *(French)* 80−88354
Cu(OH)Cl, temp. depend. of elec. cond., solid state thermal decomp. 78−19042
$CuPb_3Br_7$, ionic cond. meas. 77−47552
$Cu_{2-x}Te$, x<0.22, phase diagram, electronic and ionic cond. meas. 80−6917
CuTeCl(Br)(I), struct., partial Cu^+ ionic cond. 77−84981
Ga_2O_3:Mg(Zr) single crystals, quenched, ionic and elec. props. 78−30922
Ga_2O_3-Na_2O, β- and β''-phases, room temp. to 350°C 77−43368
Gd_2O_3, B-type monoclinic, DC(AC) elec. cond., thermoelectric power, dielectric const., temp. depends. 80−59980
$Gd_xZr_{1-x}O_{2-x/2}$, elec. cond. of ceramic solid solutions 80−107554
$Gd_xZr_{1-x}O_{2-x/2}$, fluorite and pyrochlore solid solutions, electrical conductivity meas. 80−65287
GeO_2-Na_2O, DC cond. rel. to dielectric loss peak freq. 79−78621
GeO_2-Na_2O, Na^+ partial dissociation investigated by elec. meas. 80−92716
GeO_2-Na_2O glasses, equivalent cond., temp. depend., weak electrolyte theory appl. 80−107475
GeS_{15} glass, TSD evidence for ionic cond. 77−76598
$H_3PO_4(WO_3)_{12}$ electrochemichromic cells 79−15436
$HTaWO_6$, and $HTaWO_6.H_2O$ defect pyrochlores, NMR study of proton motion 79−82889
$H_{5n-2}UO_2(IO_6)_n.4H_2O$, n=0.5 to 2.0, high proton cond. 80−107562
$H(UO_2P(As)O_4)4H_2O$, H motion, PMR obs. 78−80239
$H(UO_2PO_4)4H_2O$, solid, fast hydrogen ion diffusion, NMR relax. time meas. 80−2205
$HUO_2PO_4.4H_2O$ proton conductor applications 79−29466
$HUO_2PO_4.4H_2O$, high proton cond. 79−77809
He, solid, ion current modulation by thermal waves 78−91506
^{4}He, HCP, ion motion in strain and unstrained cryst. 79−56020
In_2ZnI_4, ionic conductivity, Raman spectra 77−69113
IrO_x anodic films, electrochromism and ionic cond., model 80−59706
K hollandite, one-dimens. ionic and solitary wave conduct. theory 79−86924
KAg_4I_5, ionic conductivity and heat capacity near T_c 78−47584
KAg_4I_5, superionic film, elec. ionic cond. and electron spectra 80−6543
$K_xAl_xTi_{8-x}O_{16}$, ionic cond., K mobility rel. to struct. and bonding *(French)* 77−76594
$K_xAl_xTi_{8-x}O_{16}$, ionic cond., rel. to struct. and chemical bonding *(French)* 78−18824
$KBiF_4$, anionic conductivity exam. *(French)* 77−35952
KBr, cation defects creation mechanism 80−75224
KBr, proton irrad., divacancies, positron capture, ionic cond. and TSC study 80−54289
KBr whisker, X-irrad., defect form., thermolum. and ionic cond. obs. *(Russian)* 78−84666
KBr:Sr, X-irradiated, first-stage F-centre production, ionic cond. meas. 77−76395
KBr-KI mixed crystals, ionic cond., 100-450°C 79−14961
K_2CO_3, study of elec. cond. and transition points 78−75873
KCl, absorption spectra exam. of H-bearing complexes 79−8167
KCl, and KCl:Ca^{2+}(Sr^{2+})(SO_4^{2-}), conductivity, self-diffusion coeffs., lattice defect props. 77−4216
KCl, cryst., colour centres, ionic cond., X-ray effects, thermoluminesc. *(Russian)* 78−6056
KCl, doped, elec. conductivity and optical absorpt., quenching from 750°C 78−2289

ionic conduction in solids continued
KCl, ionic cond., defect parameters, diffusion coeffs. 80−79978
KCl, low temp. space charge polarisation 78−43789
KCl, premelting due to thermal form. of dislocations 77−11671
KCl, room temp. X-irrad., first stage F-centre form. 78−67709
KCl, thermal hysteresis in ionic cond., dielec. loss meas. 78−34652
KCl, X-irradiated, formation of cation defects 78−91359
KCl:$BiCl_3$, electrical cond. as a function of temp., charge transport mechanism 78−83996
KCl:Eu IR laser window lattice equilibrium obs. 79−14055
KCl:Eu^{2+}, lattice defect equilib. optical absorpt. and cond. studies 80−29767
KCl:Pb^{2+}, γ-irrad., rel. to props. 78−31262
KCl:Pb^{2+}, highly doped, state of dispersion of Pb^{2+} 77−1144
KCl:Pb^{2+}, pure and doped, electrolytically coloured, elec. cond. and optical absorpt. meas. 80−100668
KCl:Sr^{2+}(SO_4^{2-}), ionic cond., defect parameters, diffusion coeffs. 80−79978
KCl:Sr^{2+}(SO_4^{2-}) 80−107487
$KClO_4$, AC electrical conductivity meas., mechanism 79−99367
$KClO_4$, electrical conductivity, frequency dependence 80−65288
$KClO_4$:CrO_4^{2-}(SO_4^{2-}), AC electrical conductivity meas. between temp. range 25-325°C, automated technique 80−59699
KD_2AsO_4, AC conduction 79−55926
KD_2PO_4, AC conduction 79−55926
KH_2AsO_4, AC conduction 79−55926
KH_2PO_4, AC conduction 79−55926
KH_2PO_4, elec. cond. and diffusion, Co dopant effects 77−72716
KH_2PO_4, single cryst., thermal depolarisation current 79−51303
KH_2PO_4:CrO_4^{2-}(CrO_7^{2-}), electrical cond., thermal depolarisation studies 79−95212
$KHSO_4$, DC electrical cond. 79−37874
$KHSO_4$, pure ionic cond., proton mobility, irreversible phase transition 77−59141
$KHSO_4$:Co^{2+}, conduction and ^3H diffusion 77−15622
$KHSO_4$:Co(II), DC conductance, extrinsic and intrinsic regions 77−59141
$KHSO_4$:Cu, DC electrical cond. 79−37874
$KHSO_4$:Fe^{3+}, DC cond. meas., mechanism 80−65285
KI:S^{2-}, photochemical reaction, F-centre production, optical absorption and ionic thermocurrent meas. 78−64861
$K_{1.54}Mg_{0.77}Ti_{7.23}O_{16}$, one-dimens. superionic cond., ionic order, defect cond. 78−87815
$K_xMg_{x/2}Ti_{8-x/2}O_{16}$, ionic cond., K mobility rel. to struct. and bonding *(French)* 77−76594
$K_xMg_{x/2}Ti_{8-x/2}O_{16}$, ionic cond., rel. to struct. and chemical bonding *(French)* 78−18824
$KNbO_3$ glass, quenched, ionic cond., appl. as solid electrolyte 79−1522
K_2O-SiO_2 system glasses, ionic cond. correl. with chem. pot. 77−89581
K_2O-SrO-SiO_2, solid glass, influence of composition on electrical conductivity 77−11723
K_2O Na_2O-B_2O_3-SiO_2, glass character of elec. cond. 80−103516
$K_2O.5Ga_2O_3$, formation and ionic conductivity 77−4351
K_2OsCl_6, impurity H^+ ion motion, ^{35}Cl NQR obs., 77 and 298K 80−60451
$KTaO_3$ glass, quenched, ionic cond., appl. as solid electrolyte 79−1522
$K_{1+x}Ta_{1+x}W_{1-x}O_6$ pyrochlore system, comp. depend. of ionic cond. 80−107517
$K_{1-x}Ta_{1-x}W_{1-x}O_6.nH_2O$, composition, struct. and ionic conductivity 80−49410
$K_xZn_{x/2}Ti_{8-x/2}O_{16}$, ionic cond., K mobility rel. to struct. and bonding *(French)* 77−76594
$K_xZn_{x/2}Ti_{8-x/2}O_{16}$, ionic cond., rel. to struct. and chemical bonding *(French)* 78−18824
$K_2[SnCl_6]$, defects determ., dipole relax. in phase transform. *(German)* 78−22711
$LaAl_{0.85}Mg_{0.15}O_{2.925}\square_{0.075}$, $LaAl_{0.8}Mg_{0.2}O_{2.9}\square_{0.1}$, $LaNb_{2.6}Zr_{0.4}O_{8.8}\square_{0.2}$, ionic conductivity 77−20119
$LaAlO_3$ perovskite electrolytes for high-temp. fuel cells 79−29467
LaF_3, ionic transport, NMR and cond. studies 80−107555
LaF_3, self diffusion studied with ^{19}F relaxation 78−6180
La_2O_3, elec. cond. and dielec. const., 400-1180K, phase transition 79−56224
La_2O_2S-AgS-Ga_2S_3, ionic conducting glasses *(French)* 78−79804
La_2S_3-Ag_2S-Ga_2S_3 glass system, prep., thermal and elec. props. *(French)* 80−89192
(Li,Na,K) (Nb,Ta)O_3, pseudo-binary and ternary systems quenched metastable glassy and cryst. phases 80−29935
Li battery solid electrolyte evaluation 79−29465
Li incorporated transition metal oxides, topochem. reactions, chem. prep. and characterisation 80−61115
Li^+-rich borate glasses, ionic cond. and activation energy 80−107561
$LiAlCl_4$, solid and liq., ionic cond., 25-180°C 77−20114
$Li_5Al(Ga)O_4$, ionic cond. depend. on moisture, potential humidity sensors 79−65248
Li_5AlO_4, ionic conduction, environment effects 77−76600
$LiAlSiO_4$, and $LiAlSi_2O_6$, freq. dispersion of cond. and capacitance 77−1256
$LiAlSiO_4$, β-eucryptite, one-dimens. Li ionic cond. 77−84982
$LiAlSiO_4$, β-eucryptite, of Li, one dimens. co-operative diffusion 78−2294
$LiAlSiO_4$ glass-ceramics, percolative ionic cond. 77−76605
$Li_{4+x}B_7O_{12+x/2}$ Cl, solid solns., ionic cond. rel. to struct. and chemical bonding *(French)* 78−2295
$Li_{4+x}B_7O_{12+x/2}$Br, solid. solns., ionic cond. rel. to struct. and chemical bonding *(French)* 78−2295
$Li_4B_7O_{12}Cl$, cryst. struct. and ionic conductivity 77−84690
LiD:Mg^{2+}, two peaks in ionic thermocurrent curves 77−31807
LiF, effect of impurity traces on physical props. 77−12450
LiF:Mg, Z_2- and associated Z-centres, elec. cond., ionic thermocurrent, and optical absorpt. meas. 80−107229
LiF:Mg,Ti, defect states, ESR and ionic cond. study 80−108058
LiF:Mg^{2+}, TLD-100, precipitation reactions and ionic cond. 77−56479
LiF:Mg^{2+}, TLD-100, precipitation during ageing, effect on thermolum. and ionic cond. 77−56480
LiF:Mg(Eu)(Co)(Si)(O), elec. cond., influence of impurity ion 79−7709
LiF-Li_2O-Al_2O_3-P_2P_5 glass, ionic cond., transport numbers determ. 79−28143
LiF-MgF_2, ionic conductivity increase rel. to point defect cone 77−72717

ionic conduction in solids continued
LiH, ionic cond., thermocurrent and photocond., defect and electronic props. 77−15621
LiH:Ca^{2+}, two peaks in ionic thermocurrent curves 77−31807
$Li_{1-x}Hf_{2-x}Ta_x(PO_4)_3$, new solid ionic conductors 77−35953
LiI complexes, ionic cond., electrochem. props. 77−60072
α-$LiIO_3$, dielectric constant and elec. cond. of single crystals *(Chinese)* 77−77134
$LiIO_3$, influence of injected protons on cond. 77−69115
α-$LiIO_3$, ion migration polarisation phenomena, current correlation function *(Chinese)* 80−6539
α-$LiIO_3$ single crystals, electrical conduction and dielectric behaviour *(Chinese)* 78−30783
α-$LiIO_3$, statistical theory of relaxation current and low-freq. dielectric dispersion 78−60391
$Li_6In_2O_6$, ionic cond. rel. to cryst. struct. 79−77810
$LiInS_2$, galvanic cell meas. 77−47616
Li_7LO_7 (L=Nb, Ta), ionic cond. rel. to cryst. struct. 79−77810
Li_8MO_6 (M=Zr, Sn), ionic cond. rel. to cryst. struct. 79−77810
Li_3N, expt. with pressed and sintered discs 78−14507
Li_3N, ionic cond., annealing, trans- and intercryst. resist. 78−43176
Li_3N, ionic conductor, single cryst. defect struct. anal. data reduction and struct. refinements, 153-678K 79−32988
Li_3N, NMR exam. of ion diffusion 79−19397
Li_3N, single cryst., electrochem. transport meas. 77−72711
Li_3N:H, ionic cond., nuclear reaction anal. 80−34454
Li_6NBr_3, $Li_{13}N_4Br$, ionic transport 79−73336
$Li_{1.8}N_{0.4}Cl_{0.6}$, fast ionic Li conduction, elec. conductivity and thermodynamic stability 79−65247
Li_2NH, ionic cond. from −30 to 105°C 79−86922
$LiN_2H_5BeF_4$, hysteresis loop, protonic cond. model *(French)* 77−32320
$LiNH_4SO_4$, DC elec. cond. 80−88603
$LiNbO_3$ glass, quenched, ionic cond., appl. as solid electrolyte 79−1522
$LiNbO_3$, OH ion incorporation, mobility and optical absorpt. 77−35583
$LiNbO_3$-SiO_2:Fe_2O_3 glasses, Li^+ ion cond. 80−107471
LiO_2-$2SiO_2$ glass, alkali motion ionic thermocurrent study, polarised impurity-vacancy dipole relaxation study 79−77806
Li_2O-$2SiO_2$ glass, ionic cond. under DC potential 79−28134
Li_2O-Al_2O_3, rapidly quenched glasses, Li ion cond., elec. cond. 80−100346
Li_2O-Al_2O_3(Ga_2O_3)(Bi_2O_3), quenched glasses, crystn. and ionic cond. 80−33899
Li_2O-B_2O_3 glass, conductivity, permittivity, and dielectric loss obs., mixed isotope effect 78−95182
Li_2O-BaO-SiO_2 glasses, elec. cond., room temp. to 450°C 80−107473
Li_2O-based mixed oxides, ionic cond., effects of moisture and LOOH on elec. and struct. props. 79−69283
Li_2O-Bi_2O_3, rapidly quenched glasses, Li ion cond., elec. cond. 80−100346
Li_2O-Ga_2O_3, rapidly quenched glasses, Li ion cond., elec. cond. 80−100346
Li_2O-LiX-B_2O_3 glass, X=halogen, high anionic cond. of new solid electrolytes 80−107546
Li_2O-SiO_2 glass, protonated, field-driven guest proton redistrib. 80−107474
($LiO_{1/2}$-$NaO_{1/2}$)-$2SiO_2$ glass, alkali motion ionic thermocurrent study, polarised impurity-vacancy dipole relaxation study 79−77806
LiOH, ionic conduction, environment effects 77−76600
$19Li_2O.19Al_2O_3.62SiO_2$ glass, ionic cond. meas. 79−33110
$LiPO_3$-$Al(PO_3)_3$:Ag glass, ionic motions, thermally stimulated depolarisation study 79−65239
$LiPO_3$-LiX(X=I, Br, Cl) glass, ionic cond. *(French)* 79−99365
Li_2S-GeS_2, glass forming region, struct. and ionic cond. 80−88358
Li_2S(O), cation diffusion NMR investigation up to 800°C 80−108092
Li_3Sb, mixed conducting electrodes, kinetic parameters determ. 78−14772
Li_3Sb(Bi), evaluation as electrode material, electrochem. expts., 360-600°C 78−11526
$Li_2Si_2O_5$, and Li_2SiO_3, freq. dispersion of cond. and capacitance 77−1256
$LiTaO_3$ glass, quenched, ionic cond., appl. as solid electrolyte 79−1522
$Li_2Ti_3O_7$, NMR data for new ionic hopping rate prefactor expression, superionic conductor 78−47559
$Li_2Ti_3O_7$, NMR data for new ionic hopping rate prefactor expression, superionic conductors 78−47560
$Li_{12}Zn_2(GeO_4)_4$ LISICON system, Li ionic conductivity *(Chinese)* 80−88350
$Li_{14}Zn(GeO_4)_4$, crystal struct. and ionic conductivity 78−51728
$Li_4Zn(GeO_4)_4$, ionic cond. 79−55922
$Li_{1-x}Zr_{2-x}Ta_x(PO_4)_3$, new solid ionic conductors 77−35953
Lu_2O_3, elec. cond. and dielec. const., 400-1180K, phase transition 79−56224
$MgAl_2O_4$, pure and Fe-doped spinel, elec. cond. 80−59702
$MgCr_2O_4$-TiO_2, porous ceramics, humidity-sensitive electrical conduction 80−107782
MgF_2:Li^+, atom transport, diffusion and ionic cond. meas. 80−107492
MgF_2:Li^+, defect struct. rel. to transport props., theory 77−47472
MgO single crystals, impurity effects on cationic cond. *(French)* 80−65286
MgO, thermoelec. props., ionic effects with $MgCl_2$ additions 78−26895
MgO:Cr, elec. cond. at high temp. in oxidising atmosphere 77−69323
Mg_2SiO_2:SiO_2, elec. and dielec. props. 400-900°C 80−104953
Mg_2SiO_4, ionic transport model 79−69285
Mg_2SiO_4:(Fe)(H), elec. cond. meas. 79−69285
$ND_4D_2AsO_4$, protonic cond. near antiferroelec. Neel temp. 80−59703
$NH_4Ag_4I_5$, ionic conductivity and heat capacity near T_c 78−47584
NH_4ClO_4, DC elec. cond. meas. 77−84984
NH_4ClO_4, elec. field effect on decomp. 79−15987
NH_4ClO_4:SO_4^{2-}(CrO_4^{2-}), thermal depolarisation, relax. parameters 78−43779
$(NH_4)_4Fe(CN)_6.1.5H_2O$, cryst. struct., and possible ionic transport mechanism 79−14758
$NH_4H_2AsO_4$, protonic conduction and electrolysis investig. 77−35749
$NH_4H_2PO_4$, elec. cond. and diffusion, Co dopant effects 77−72716
$NH_4H_2PO_4$, single cryst., thermal depolarisation current 79−51303
$NH_4H_2PO_4$:CrO_4^{2-}(CrO_7^{2-}), electrical cond., thermal depolarisation studies 79−95212
NH_4TaWO_6, rapid ionic motion, spin-lattice and spin-spin relax. times meas. 79−38396
$(NPCL_2)_3$, trimer and polymer, polycrystn., resistivity 77−51735

ionic conduction in solids continued
Na_2-β-Al_2O_3, far IR absorpt., Beevers-Ross sites, interstitials 80−66241
Na_2-S-GeS_2 system, glass formation, struct. and ionic conduction 80−54138
$Na_{1+x}Al_{1+x}Si_{1-x}O_4$, ionic cond. 79−65245
NaBr-U-centre containing cryst., X-ray radiation induced cation vacancy generation 80−39078
Na_2CO_3, elec. cond., 270-830°C, and transition points 78−10216
NaCl, low temp. space-charge polarisation 78−43789
NaCl, monocrystalline, defect struct. and intrinsic ionic cond. relationship 79−95211
NaCl, premelting due to thermal form. of dislocations 77−11671
NaCl, press. effect on ionic cond. at 300K 77−7895
NaCl single crystal-electrode interface, anomalous transient currents 78−22886
NaCl:Ba, Ba precipitation at dislocations, kinetics, ionic cond. meas. 79−60510
NaCl:Ca^{2+}, X-irrad. effects on divalent metal aggregates, ionic cond. meas. 79−82263
NaCl:Cd^{2+}, dielectric loss following plastic deform. 80−84690
NaCl:Mn, impurity-vacancy dipole aggregation, role of dimers and trimers, reanal. of dielec. and cond. data 79−1458
NaCl:Mn^{++}, Mg^{++}, doubly doped, ionic thermocurrent study of linear dimer 80−79977
NaCl:Mn^{2+}, dimer detection, EPR and ITC expts. 78−59833
NaCl:Ni single crystals, VUV spectrum, ionic conductivity, X-ray diffr. 78−92097
NaCl:Sr, dimer and trimer aggregate formation by NMR, ionic cond. and dielectric losses 80−15094
NaCl:Sr, solubility of free and assoc. Sr 77−62645
NaCl:Sr^+, ionic thermocurrent exam. 78−10833
NaCl-Ca, single crysts., load-microhardness curves, heat treatment, impurity effects obs. 78−30694
NaCl-graphite interface, elec. cond. 78−52060
NaCl-KCl mixture, electrical, electromag., and acoustic props. *(Russian)* 78−30759
NaCl-NaBr mixed crysts., ionic cond., 42-450°C, cation vacancy migration 78−59970
NaCl(Br), X-ray or UV irradiated, cation defects creation mechanism 80−75224
$Na_3Cr_2(PO_4)_3$, crystallographic data, ionic conductivity *(French)* 80−88077
$Na_3Cr_2(PO_4)_3$, $Na_3Fe_2(PO_4)_3$, $Na_3Ti_2(PO_4)_3$ and $Na_3V_2(PO_4)_3$, synthesis and cryst. struct. *(French)* 79−32964
$Na_3Cr_3(PO_4)_4$, crystallographic data, ionic conductivity *(French)* 80−88077
NaF-BeF_2 glass, anion conductivity, transport number radiometric meas. 79−86923
$Na_3Fe_2(PO_4)_3$, crystallographic data, ionic conductivity *(French)* 80−88077
$Na_3Fe_2(PO_4)_3$, polymorphism and ionic conduction *(French)* 78−67678
$NaGdSiO_4$, single cryst. data and ionic cond. 80−84158
$Na_5GdSi_4O_{12}$, ionic conductivity and struct. 78−18826
NaI, transport processes, test of validity of Arrhenius law *(French)* 79−77808
NaI:Ca^{2+}, pure and doped, ionic thermocurrents meas. 80−80677
NaI:Ca^{2+}, pure and doped, lattice defects, entropy and enthalpy of formation and migration 80−96687
$Na_xIn_xSn_{1-x}S_2$, intercalation-substitution compounds, NMR study 80−44952
$Na_xIn_xSn_{1-x}S_2$, ionic conductors, ^{23}Na NMR and complex impedance meas. 79−91314
$Na_xIn_xZr_{1-x}S_2$, ionic conduction of phases *(French)* 77−47620
$Na_2Mg_1SiO_4$, ionic cond. meas. 80−6545
$Na_4Mg_2Si_3O_{10}$, ionic cond. meas. 80−6545
$Na_2Mg_2Ti_6O_{14}F_2$, α and β forms, ionic conductivities *(French)* 77−43373
Na_2O-$2SiO_2$ glass, alkali motion ionic thermocurrent study, polarised impurity-vacancy dipole relaxation study 79−77806
Na_2O-Al_2O_3-SiO_2 glasses, elec. cond. and cation mobility 78−59973
Na_2O-B_2O_3 glass, Na and Ag diffusion, elec. cond. 79−51300
Na_2O-B_2O_3-Bi_2O_3, glass with metallic Bi granules, elec. cond. 80−84493
Na_2O-$B_2O_6$3-Bi_2O_3-SiO_2, heterophase glass, diffusion and elec. cond. 78−67858
Na_2O-CaO-SiO_2 glasses, ion-exchanged, mixed alkali effect rel. to elec. cond. 78−34653
Na_2O-GeO_2, electric cond. and dielec. relaxation *(Japanese)* 78−19905
Na_2O-K_2O-Al_2O_3-SiO_2 glass, mixed alkali effect, nonbridging O content effects 78−18827
Na_2O-NaF-B_2O_3 glass, nature of conductivity 78−63876
Na_2O-SiO_2 (96 wt.%) glasses, thermally stimulated polarisation and depolarisation current techniques for studying ion motion 80−6541
Na_2O-SiO_2 glass, conduction and dielec. loss mechanisms, paired interstitialcy model 80−107468
Na_2O-SiO_2 system glasses, ionic cond. correl. with chem. pot. 77−89581
Na_2O-SiO_2-MgO(CaO)(BaO) glasses, elec. cond., room temp. to 450°C 80−107473
Na_2O-SiO_2-SnO_2 (TiO_2) glass, exam. of Na^+ self diffusion, elec. conductivity, and viscosity 78−87819
Na_2O-Tl_2O-B_2O_3, mixed-cation glass, electrical cond. 79−95210
Na_3PO_4, pure and doped ionic cond., doping effect 78−51725
$Na_5RSi_4O_{12}$, superionic conductors, Na conductivity paths 78−91482
Na_2S-GeS_2, glass, synthesis, elec. cond., Raman spectra, temp. and composition depends. *(French)* 79−14962
Na_2S-P_2S_5, glass forming region, struct. and ionic cond. 80−88358
Na_2S-$SiS_2(GeS_2)(P_2S_5)$, synthesis, structure and ionic conduction *(French)* 80−65291
Na_2S-XS_2, X=Si, Ge, glass forming region, struct. and ionic cond. 80−88358
$Na_2S(O)$, cation diffusion NMR investigation up to 800°C 80−108092
Na_2SO_4-$Y_2(SO_4)_3$, solid solution, effect of defect concentration on ionic conductivity 78−75870
$Na_{1+x}Si_x$ Zr_2 P_{3-x} O_{12}; monoclinic to rhombohedral phase transformation 80−29950
$Na_{5-x}Ta_{11+x/5}O_{30}$, synthesis, non-stoichiometry, density and ionic cond. meas. *(French)* 78−52741
$Na_{1+\alpha}(Ta_{1+\alpha}W_{1-\alpha})O_6$, exam. of ionic conductivity *(French)* 78−51729
$Na_{1+x}Ta_{1+x}W_{1-x}O_6$ pyrochlore system, comp. depend. of ionic cond. 80−107517
Na_2UBr_6, phase transformations, elec. cond. and entropy meas., synthesis *(French)* 78−79763

ionic conduction in solids continued
Na_2WO_4, cationic transport props. and struct. 77−76601
$Na_5W_3O_9F_5$, single cryst., prep., optical and dielec. studies *(French)* 80−15994
$NaYSiO_4$, $Na_3YSi_2O_7$, $Na_3YSi_3O_9$ and $Na_5YSi_4O_{12}$, single cryst. data and ionic cond. 80−84158
$Na_5YSi_4O_{12}$, high Na^+ ion conduct. 78−91479
$Na_xY_xZr_{1-x}S_2$, ionic cond. and NMR mobility obs., comp. depend. *(French)* 80−70459
$Na_{1+x}Zr_{2-x}In_x(PO_4)_3$, three-dimens. solid soln., comp. depend. of ionic cond. *(French)* 80−34230
$25Na_20.75SiO_2$ glass, ionic cond. meas. 79−33110
Nb, anodic oxidation, open circuit transient anal., dielec. and elec. props. of oxide film 80−3245
$Nd_xZr_{1-x}O_{2-x/2}$, elec. cond. of ceramic solid solutions 80−107554
$Nd_xZr_{1-x}O_{2-x/2}$, fluorite and pyrochlore solid solutions, electrical conductivity meas. 80−65287
Ni-Si melt refining by electric fields, ionic conduction of Ni, Si *(Russian)* 80−65273
NiO, transport number and cationic cond. *(French)* 80−15297
$Pb_{1-x}Bi_xF_{2+x}$, solid anionic conducting electrolytes, struct., elec. props. 77−84977
$PbBr_2(Cl_2)(I_2)$, ionic cond. and activation volumes, high press. effects 80−100353
β-PbF_2, anion mobility from noise meas. 79−46836
PbF_2 based solid solns., ion transport 80−107545
β-PbF_2, complex impedance exam. 78−47579
PbF_2, cubic, dielec. const., ionic cond., soft modes 78−14427
PbF_2, cubic and orthorhombic, press. and temp. depends. of ionic cond. 79−95207
β-PbF_2, electrolytic props., AC cond. meas. 78−71878
PbF_2 film, ionic conduction, effect of hydrostatic press. *(French)* 79−28259
β-PbF_2 film, ionic migration study by Rutherford scatt., defects, secondary emission *(French)* 78−55982
β-PbF_2 film between metal electrodes, vac. evaporated, AC study of elec. props. 80−2207
PbF_2, ionic cond., activation volumes and high press. phase transitions 80−70461
PbF_2, NMR relax. and self diffusion 78−80236
β-PbF_2, solid electrolyte, mobile species mobility and conc., temp. depend. 77−20113
β-PbF_2, thin films, cond. mechanisms, struct. 77−84970
PbF_2:Mn, mag. tagging of ion diffusion, ^{19}F NMR meas. 80−108106
PbFBr, undoped and doped, ionic cond. 79−60545
PbFCl, ionic cond. mechanism, ^{19}F NMR meas. and struct. considerations 79−55927
PbFCl(Br), single crystal ionic cond., deviation from molecularity, effect of O_2 impurities 79−51305
$PbMoO_4$, ionic and electronic cond. 79−91107
$Pb_2Nb_2O_7$, electric cond. and dielect. props. of cathodic-sputtered films *(French)* 79−33371
PbO-B_2O_3-Bi_2O_3, glass with metallic Bi granules, elec. cond. 80−84493
PbO-SiO_2 (70 wt.%) glasses, thermally stimulated polarisation and depolarisation current techniques for studying ion motion 80−6541
PbO-SiO_2 glass, reduced channel-plate, variable range hopping conductivity 80−107466
PbO-SiO_2 glasses, elec. cond. and dielec. behaviour 80−44361
Pb(OH)Cl, temp. depend. of elec. cond., solid state thermal decomp. 78−19042
$PbSnF_4$, anionic conductor *(French)* 79−1523
$PbSnF_4$, anionic conductor, thin films and ceramics 80−107556
$PbSnF_4$, high anionic cond. of new solid electrolytes 80−107546
$Pb_{1-x}Sn_xF_2$, ionic cond. of F ion *(French)* 80−6547
$Pb_{1-x}Th_xF_{2+2x}$, solid soln., anionic cond. *(French)* 78−91481
$PbWO_4$, ionic and electronic cond. 79−91107
$Pb_{1.8}Zn_{0.15}Na_{0.05}Nb_2O_{6.95}F_{0.05}$, electric cond. and dielect. props. of cathodic-sputtered films *(French)* 79−33371
Pb(Zr, Ti)O_3-epoxy resin composite piezoelec. relax. due to ionic cond. 77−36179
$RbAg_{4-x}Cu_xI_5$, solid electrolyte, elec. cond. 77−15624
$RbAg_4I_5$, 208K phase transition, Jahn-Teller-like model 77−35694
$RbAg_4I_5$, ionic cond., effect of press. 78−51733
$RbAg_4I_5$, ionic conductivity and heat capacity near T_c 78−47584
$RbAg_4I_5$, nonequilibrium thermodynamic description, variation of ionic cond. with temp. 79−61391
$RbAg_4I_5$, solid electrolyte, cond., phase transitions 77−84972
$RbAg_4I_5$, solid electrolytes, co-ionic cond. 78−26721
$RbAg_4I_5$, superionic cond., US absorpt., ionic cond., relaxing sp. ht. 78−14505
RbCl:$CoCl_2$ system, precipitate form., ionic cond. meas. 80−96653
RbCl-CuCl, solid electrolyte, AC cond. and phase relations meas. 77−72713
RbCl(Br), cation defects creation mechanism 80−75224
$RbClO_4$, electrical conductivity, frequency dependence 80−65288
α-$RbCu_4Cl_3I_2$, solid electrolyte, cryst. struct. and anal. 79−82382
$Rb_4Cu_{16}I_7Cl_{13}$ in CuCl-CuI-RbCl system, high Cu ion cond. solid electrolyte, elec. props. and powder X-ray diffr. anal. 80−15295
$Rb_{5-x}Ga_{11+x/5}O_{30}$, synthesis, non-stoichiometry, density and ionic cond. meas. *(French)* 78−52741
RbI:Pb^{2+}, optical and elec. props. 79−15493
Rb_2O-$Nb_2O_5(Ta_2O_5)$, phase equilib. relns. and crystal chemistry, structs. useful as ionic conductors 79−20033
$Sb_2O_5.nH_2O$ acid membranes, synthesis and characterisation 80−81027
Sc_2O_3, elec. cond. rel. to defect struct. 77−80814
Si-Al-O-N system, ionic cond. from 850 to 1400°C 80−2203
SiO_2, film, drift mobilities of Na^+ and K^+ ions 78−10213
SiO_2 films on Si, mobile Na ion instability 79−82503
SiO_2, in MOS struct., thermally stimulated ionic cond. 78−10565
SiO_2 in MOS struct., room temp. cond., mobile Na^+ location 78−39217
SiO_2, mobility of K^+ ions, triangular voltage sweep technique 79−95206
SiO_2, noncryst., in MOS struct., Na ion impurities motion 78−10223
SiO_2, noncryst., MOS structure, ionic impurities motion, trapping layers 78−30999
SiO_2 RF sputtered film, Na^+ motion, small-voltage elec. response 79−90822
SiO_2-B_2O_3-Na_2O glass, high silica, conductivity behaviour, Na ion dependence 80−24652
SiO_2-K_2O, thermodynamic approach to ionic conds., statistical model of chem. potential 79−46833

ionic conduction in solids continued
SiO_2-Li_2O-Li_2SO_4, glass-forming region, struct. and ionic cond. 80−84320
SiO_2-Na_2O, thermodynamic approach to ionic conds., statistical model of chem. potential 79−46833
SiO_x, evaporated film, influence of electronic leakage current on meas. of ion polarisation 77−63014
SiO_x film, Cole-Cole diagrams of ionic hopping systems 77−66217
Sm_2O_3, B-type monoclinic, DC(AC) elec. cond., thermoelectric power, dielectric const., temp. depends. 80−59980
$Sm_2Zr_2O_7$ pyrochlore phase, O ion conduction 80−24654
$SnCl_2.2H_2O$ layered single cryst., protonic cond. and crit. behaviour 79−28136
$SnCl_2.2H_2O$, protonic cond. in layered single cryst. 80−19983
$SnCl_2.2H_2O$, quasi two-dimensional, DC protonic cond. 80−44362
SnF_2, α and γ modifications, elec. cond., $\alpha \rightarrow \gamma$ phase transitions, structs. 78−75867
SnF_2, α- and γ-phases, elec. cond. characts. determ. *(French)* 79−47093
SnF_2, SnFCl, ionic conductivity *(French)* 78−79806
$SrCl_2$, anion diffusion mechanism 80−2201
$SrCl_2$, fast ion transport 80−107558
$SrCl_2$, ionic cond., activation volumes and high press. phase transitions 80−70461
$SrCl_2$, mass and charge transport 80−100347
$SrCl_2$, point defect parameters, ionic cond. study 80−107490
$SrCl_2$, self-diffusion and ionic cond. 80−107489
$SrCl_2$:KCl, polycryst., activation energies 78−2292
SrF_2, ionic cond., activation vols., freq. depend. cond., press. effects 80−100354
SrF_2, thermo-EMF meas., ion transfer characts. 77−7892
SrF_2-UF_4-CeF_3 solid soln., surface degradation, complex admittance analysis 78−55980
$Sr_3NbO_{5.5}\square_{0.5}$, $Sr_2CaTaO_{5.5}\square_{0.5}$, $Sr_2CaNbO_{5.5}\square_{0.5}$, $SrZr_{0.8}Yb_{0.2}O_{2.9}\square_{0.1}$, $SrZr_{0.8}Mg_{0.2}O_{2.8}\square_{0.2}$, ionic conductivity 77−20119
$Sr_{1-x-y}U_xCe_yF_{2+2x+y}$, solid soln., ionic cond. 79−99356
Ta_2O_5 anodic oxide film, model for ionic cond. 80−2197
Tb_2O_3, B-type monoclinic, DC(AC) elec. cond., thermoelectric power, dielectric const., temp. depends. 80−59980
ThO_2, ^{18}O self-diffusion, isotope exchange meas. 77−11725
ThO_2 ceramics, CaO and Y_2O_3 stabilised density, elec. cond., permittivity 78−47838
ThO_2, stabilised, ionic mech. of charge transport 79−10976
ThO_2:Y_2O_3, electrochem. cell, complex impedance, temp. and freq. depends. 77−1458
ThO_2-CaO, and ThO_2-$YO_{1.5}$, solid solns., defective oxides, ionic cond. 80−107548
ThO_2-CaO electrolyte, mixed and ionic cond. regions 77−8156
TiO_2, stoichiometric single crysts., anisotropy of ion transport 80−2206
$TlBiF_4$, anionic conductivity exam. *(French)* 77−35952
Tl_4CdI_6, ionic conductivity, Raman spectra 77−69113
$TlNbO_3$, ceramics, hysteresis loops and dielec. props. 79−42885
$Tl_xNbO_{2+x}F_{1-x}$ $(0.5 \leq x \leq 1)$, heavy ion location Tl^+, and struct. refinement *(French)* 79−73144
$Tl_xNbO_{2+x}F_{1-x}$, pyrochlore phase, Tl^+ mobility 79−95209
$TlPO_3$, vitreous and polycrystalline, NMR and IR exam. of cation motion 77−66041
Tl_2SO_4, elec. cond. rel. to thermodynamic props. in phase transitions 77−39690
$TlTaO_3$, ceramics, hysteresis loops and dielec. props. 79−42885
$Tl_{5-x}Ta_{11+x/5}O_{30}$, synthesis, non-stoichiometry, density and ionic cond. meas. *(French)* 78−52741
$Tl_{1+x}Ta_{1+x}W_{1-x}O_6$ pyrochlore system, comp. depend. of ionic cond. 80−107517
$Tl_{1+x}Ta_{1+x}W_{1-x}O_6.nH_2O$, pyrochlore type, stoichiometry and ionic cond. 80−24648
$Tl_2Ti_4O_9$ ceramics, hysteresis loops and dielec. props. 79−42885
Tl_2ZnI_4, ionic conductivity, Raman spectra 77−69113
$(U_{0.3}Y_{0.7})O_{2-x}$, ionic cond. 80−6828
VO_2, from oxidation of metallic V, ionic cond. 79−51299
W, anodic oxidation, open circuit transient anal., dielec. and elec. props. of oxide film 80−3245
WO_3 thin film, partial ionic conc. of Li, appl. of AC techniques 80−70468
WO_3-P_2O_5 glass, AC cond. and dielec. props. 80−92717
Y_2O_3 film in MIM struct., electroforming and cond. 78−26969
Y_2O_3:HfO_2, elec. cond. and O ion mobility 80−34490
Zn^{++}, transport in cation-exchange membranes 78−96033
$ZnCl_2$-LiCl fused mixture, transport number determ. of Li^+ and Zn^{++} at 398°C *(French)* 79−69286
Zr, anodic oxidation, typical valve and behaviour 77−21311
ZrF_4 based glass, elec. and dielec. props. in freq. and temp. ranges 5-500 kHz and 130-280°C *(French)* 79−23772
ZrF_4 glasses, elec. props. *(French)* 78−75868
ZrF_4-BaF_2-ThF_4-$NaF(RF_3)$ (R=rare-earth) glass system, anion cond. 80−70460
ZrF_4-based glasses, elec. transport props. 80−79983
$Zr_{1-x}In_{2x}O_{2-x}$, ionic conductivity, lattice const. 80−96688
$Zr(KPO_4)_2$, cryst., ionic cond., layered struct. 80−92710
$Zr(LiPO_4)_2$ cryst., ionic cond., layered struct. 80−92710
$Zr(NaPO_4)_2$, cryst., ionic cond., layered struct. 80−92710
ZrO_2, doped, theoretical model 80−107552
ZrO_2, stabilised voltage-current-time charact. with point contact Pt electrode in Ar gas ambient 77−1461
ZrO_2:Y_2O_3, bias sputtering, film growth and characts. 77−40366
ZrO_2:Y_2O_3, low-temp. specific heat, oxygen vacancy effects 80−49376
ZrO_2-CaO, and ZrO_2-$YO_{1.5}$, solid solns., defective oxides, ionic cond. 80−107548
ZrO_2-CaO (12-19 mole%), AC elec. behaviour, 300-900°C, grain size, electrode material, and sintering effects 78−34649
ZrO_2-CaO RF sputtered film, solid electrolyte, comp., struct. and AC cond. 77−39741
ZrO_2-CaO thin film O_2 sensor, ionic transference number, cell design 77−70360
ZrO_2-Gd_2O_3, solid solution with fluorite and pyrochlore structure; exam. of elec. conductivity *(German)* 79−23766
ZrO_2-Y_2O_3, solid electrolyte, cond. maximum 78−47577
ZrO_2-$YO_{1.5}$-$TaO_{2.5}$, cubic fluorite phase, elec. cond. 80−107551
$((ZrO_2)_{0.92}(Y_2O_3)_{0.08})_{1-x}(Fe_2O_3)_x$, Fe solubility and elec. cond. 79−99354

ionic conductivity in solids *see ionic conduction in solids*
ionic thermocurrents *see thermally stimulated currents*
ionisation
see also associative ionisation; autoionisation; charge exchange; electron attachment; electron capture; field ionisation; ion recombination; ionisation of atoms; ionisation of gases; ionisation of liquids; ionisation of molecules; ionisation of solids; ionisation potential; Penning ionisation; photoionisation; surface ionisation
aerosol fine particle charging by unipolar ions, review and expt. 78−88658
aerosol particle, nonequilib. bipolar charging 78−3382
aerosol particle-small ion combination coeffs., size depend. 77−25320
automatic range-changing amplifier, ionisation current pH and vacuum measurement appls. *(French)* 79−63262
chemi-ionisation reactions of Ca, Sr, Ba, and Yb with halogens and interhalogens 77−32791
chemical ionisation mass spectrometry, simultaneous positive and negative ion form. technique 77−36806
cosmic ray ionization of Jupiter atmosphere 80−17538
V832=59 Cygni, Be star, UV spectrum vars. rel. to stellar wind ionisation balance 80−46561
fission product ionisation by He jet rapid transport technique 79−63831
flame, mass spectrometric and mobility analyses for flame ionisation detector 78−40050
galactic coronae, ionisation struct. and absorpt. line spectra 77−13448
hot cavity, thermal ionisation 78−70677
intercluster intergalactic medium, thermal, ionisation and excitation history 80−4426
intergalactic medium, temp. and ionisation struct., effect of UV stars 77−13455
interstellar dust clouds, fractional ionisation from N_2D^+/N_2H^+ abundance ratio meas. 78−16492
interstellar intercloud medium, ionisation by single O star 77−9782
interstellar ionisation fronts, comparison with phase transitions 77−33594
interstellar medium, H ionisation rate due to OB-type stars rel. to interstellar clouds form. 80−109506
interstellar medium, local, ionisation state 80−90502
interstellar medium two-phase model, fractional ionisation of intercloud medium 77−74110
interstellar molecular clouds, cosmic rays exclusion rel. to ionisation 77−13190
N-particle scatt. ionisation T matrix 79−44777
nebulae ionisation-shock fronts hydrodynamic linear theory 80−17625
NGC 6888, circumstellar nebula, spectroscopic investigations and ionisation vars. 77−57076
Nova Delphini 1967, central star props. and envelope ionisation conditions *(French)* 77−53603
nova envelopes, dust form. and ionisation theory 80−98678
nova shell ionisation, time-depend. model 79−53816
operator manifolds, expansion and completeness theorems 79−59331
planetary nebulae, ionisation models 80−109529
planetary nebulae, ionisation struct. rel. to central stars temps. determ. 79−2565
planetary nebulae ionisation, influence of He shell flashes in nuclei 80−73021
planetary nebulae ionisation structure, atomic and mol. data 80−109528
plasma, high-Z, Saha's ionisation eqn. soln., input for opacity calcs. 77−39412
plasma, rot. ternary, element separation, degrees of ionis. effects 77−15174
plasma, supplementary ionisation accompanying parametric instability development *(Russian)* 80−24150
solar flares ionisation equilib. calcs., implications of Fe XXI 1354 Å line obs. from Skylab 80−21956
solar wind, nonequilib. ionisation 79−48751
sporadic-E layer, photochemistry of Mg and Mg^+ 77−21954
stellar atmosphere in statistical equilib., effects of deviations from LTE on ionisation 80−31290
stellar winds, nonequilibrium ionisation 79−48751
Sun, ionisation phenomena rel. to use of MHD pulses as diagnostic technique 80−109405
Tycho supernova remnant, X-ray line emission rel. to plasma ionisation equilib. 80−46636
weakly bound particle ionisation, perturbation theory series convergence in alternating field 80−4575
D pellet, ionisation by Nd laser irrad. 80−43949
D pellets, ionisation by Nd laser radiation 80−70015
H II regions, effects of dust on ionisation struct. 77−33588
H II regions, statistical approach to density and ionisation fluctuations 80−77468
H II regions ionisation structure, influence of star, gas density and chemical comp. 78−61911
H plasma, ionis. in uniform elec. field *(Russian)* 80−53923
ionisation chambers
A-150 plastic-equivalent gas, dosimetry appl. 80−81745
absorbed dose determ. with ionisation chambers in e^- and photon beams, 1 to 50 MeV 80−18703
acceptance characteristics distortion by ion source mag. field 79−21852
acetylene, ionisation meas. and $\bar{W}_n$ derivation for neutron irradiation 79−36430
activity meter for nuclear medicine, ionisation chamber characts. 79−66558
air electron backscattering coeffs., 100 eV to 5 keV 80−9750
air ionisation probe for α, β, γ hand and shoe monitor 80−58084
Andersson-Braun remmeter modifications for improved directional depend. and thermal neutron sensitivity 78−53499
autoionography of beta-emitting radionuclides distrib. on thin-layer chromatograms 78−20126
avalanche 2-D position sensitive parallel plate transmission counter 78−90023
avalanche chamber, multistep gated 79−45536
avalanche counter, fast, parallel-plate, bidimensional, position sensitive 78−37487
avalanche counters, Townsend coeffs. determ. 78−78582
avalanche detector, position sensitive parallel plate with 2-D readout 78−55102
avalanche multistep chamber 79−9965
avalanche spherical fission detector with intrinsic α-discrimination 79−97945

ionisation chambers continued
Baldwin-Farmer, C_E, C_λ and effective wall material 79−22555
Baldwin-Farmer chamber response at mammographic energies 78−28040
Benjamin detectors, on-line, real-time neutron spectrum unfolding 79−59297
Bragg-Gray theory corollaries, comparison to fast-neutron cavity ionisation meas. at 14.8 MeV 80−91370
C_λ and C_E reevaluation using extended cavity ionisation theory, ferrous sulphate G-values appl. 78−92706
calibration and testing using N_2 laser beam 80−27890
calibration constants calc. for gaseous β-emitting nuclides *(Japanese)* 79−68142
calibration in absorbed dose units 78−20274
calibration methods for primary and secondary standards, in Hungary 80−5357
calibration of dose to water for ^{60}Co γ-radiation 80−74032
calibration of instruments used in radiology and radiotherapy, metrological problems *(Spanish)* 79−92377
calibration of radiation therapy machines, chamber-depend. factors 80−18704
calorimeter, segmented, hadron shower struct. meas. 79−63870
calorimeter, separation of hadrons and EM particles 77−79523
cavity chamber, model for determ. of ionisation when exposed to soft X-rays 78−17482
cavity type for absorbed dose calibration 77−40777
charged particle detector system for high rate expts., drift-proportional chambers, operating parameters 78−33379
coaxial, microprocessor based beam loss monitor system for AGS 79−72070
coaxial cables used with ionisation chambers, expt. investigation 80−78489
condenser microphone as ionisation chamber for intense α fluxes 77−79506
cosmic ray high energy interactions in emulsion stack combined with ionisation calorimeter 78−49263
cosmic ray ionisation calorimeter, fluctuations in cascade showers generated by muons 79−84618
counting gas mixtures, calc. of electron transport coeffs. 79−32727
current digitiser, 2×10^{-15} A to 2×10^{-10} A, ion chamber currents meas. appl. 77−61666
cylindrical chambers, A_c and A_{eq} factors exam. for ^{60}Co beams 79−81121
cylindrical drift chambers with delay line readout, resolution 78−33380
cylindrical gridded, ^{238}U spontaneous fission half life and fragment kinetic energy meas. 78−86555
design, maximum permissible fluence instrument 79−22556
dielectric liquid, ion collection efficiency determ. 79−85861
differential ionization chamber for the determination of small differences in decay rates of beta emitters 79−76256
directional drift chambers system, design, construction, testing 78−33378
dose equivalent measuring instrument for rapid use in mixed radiation fields 78−15901
dose from CT scan, meas. using pencil shaped ionisation chamber 79−20683
dose mapping, automated system for TRIUMF biomedical pion beam 78−73254
dose measurement, 15 to 50 MeV electron beams in graphite, compared with calorimetry 77−2052
dose meter unit for emergency operations *(French)* 80−57977
dose rate meter, use as X- and γ-ray secondary protection-level standard 77−81579
dosimeter, compared with $FeSO_4$ meas. at 6 radiotherapy centres *(French)* 77−37057
dosimeter, cylindrical, effective meas. position in electron beam dosimetry 78−9023
dosimeter, for routine meas. with X-ray therapy equipment between 10 and 250 kV 78−28084
dosimeter, low-energy, direct-reading, correction factor energy depend. 78−24144
dosimeter, pocket type, electret electrostatic generator 78−13382
dosimeter, remote-reading operational amplifier type, elec. constancy checking 78−3613
dosimeter, semiautomatic device for relative dose distrib. recording 78−85380
dosimeters, individual controlled, using capacitor chambers 78−78509
dosimetry, Ar/propane, mixed X-ray/neutron fields 79−20682
dosimetry, conversion factors for absorbed dose in water 78−40338
dosimetry for photon and electron beams, C-values 77−81575
dosimetry of high energy photons and electrons, C_λ and C_E discrepancy 77−52885
dosimetry of high energy photons and electrons, C_λ and C_E discrepancy 77−52886
dosimetry of high-energy electrons 77−40785
double cylindrical 4π ionisation chamber for γ source nuclide activity 77−10536
double ionization chamber for the differential method 79−22552
drift, time projection chamber, performance 79−68148
drift chamber, 1.5×1 m^2, operating characts., efficiency 78−5096
drift chamber, 2-D, with thin printed cct. tape delay line 77−30708
drift chamber, operation principles and appls. 77−18745
drift chamber, transition radiation detection 79−22546
drift chamber and pulse height readout systems using analog multiplexing 77−54490
drift chamber development 80−27879
drift chamber performance in supercond. mag. field, electron drift angle meas. 78−37485
drift chamber system, Dubna synchrophasotron, characts., on line operation 77−6627
drift chamber system for BNL mag. spectrometer expt., design constraints, readout electronics 78−33382
drift chamber system for K+e elastic scatt. expt. at Fermilab, efficiency, accuracy 77−57809
drift chamber with multiwire signal element and 250 mm drift gap, loading characts. 79−97937
drift chamber with multiwire signal element and large drift gap 79−97936
drift chambers, CAMAC/NIM for data acquisition and monitoring 77−88338
drift chambers, second coord. readout by charge division, optimised preamplifier system 78−33381
ionisation chambers continued
drift chambers and multiwire proportional chambers, characts. and appls. 77−14307
drift chambers for Fermilab expt. 77−10537
drift chambers of 14 m^2 hexagonal design 77−30716
drift chambers of large area with Cu strip cathode planes 77−83458
electret ionisation chamber dosimeter for long-term personnel monitoring 78−21810
electrical resistance measurement for insulating materials *(French)* 78−77929
electrical sensitivity control 78−865
electron avalanches, generated by thermionic electrons, pulse-height distrib. 79−6796
electron drift velocity in counter gas mixtures 80−28590
electron transport in air and N_2, Monte Carlo calcs. 78−90042
electrostatic relay, investigation of dosimetric characts., dosimeters IK-5B and IK-14 (USSR) 80−57966
emulsion stack connected with ionis. calorimeter for high energy cosmic ray obs. 78−25386
exposure rate and absorbed dose meas. for 6-7 MeV 79−26766
extrapolation chamber meas. of electron depth absorbed dose distribs., 77−81573
Farmer type, absorbed dose conversion factors C_λ and C_E 78−40341
Farmer type, used with Keithley electrometer for radiotherapy machine calibration 77−2055
fast electron collection ionisation chamber, principles of operation and appl. 79−68151
fast particles, mean ionising cross-section and charge produced, meas. method 78−78577
fission, ^{235}U, nondestructive assay of highly enriched spent fuel 79−89522
fission chamber, high-speed, with ^{235}U radiators and fast amplifier 77−6620
fission chamber with intrinsic suppression of α-background 78−78581
fission fragment atomic number identification using gas ionisation chamber 80−27863
fission fragments, kinetic energies and fly-off angles, ionisation method of meas., online numerical processing *(Russian)* 80−52838
fission reactor loss of coolant studies, gamma densitometer detector comparison 80−57881
focal plane, large hybrid detectors, electric field uniformity improvements 80−37684
focal plane detector for both light and heavy ions 79−18077
free air chamber for X-ray exposure standardisation at high quantum energies 80−14053
free air ionisation chamber, mean level response for α-rays 78−90024
free air parallel arid plate chambers, electrode emission effects on saturation current 78−74539
gamma ray appl. to fluid density meas., theory, practices and appl. 80−73325
gamma-ray dosimeter, KG21, features 78−74509
gamma-ray external field meas. at Vermont Yankee BWR power station 77−54368
gas analysis, isotope technique appl., ionisation detectors, review 79−20481
gas filled, fast gas mixtures 79−76279
gas proportional scintillation detectors with uniform electric fields, secondary scintillation model 80−74087
gas purity under measuring conditions, W-value determ. *(German)* 80−104489
gas radiometer, portable 80−32570
gas-filled counters, secondary electron emission, elec. field at cathode 78−17529
gas-flow, arc with position sensitive ΔE-E telescope for Z-identification 77−30726
gaseous detectors, evolutional steps 80−58041
graphite, ionisation error due to porosity 80−52829
graphite chamber with CO_2 filling, Monte Carlo anal. of fast neutron irradiation 78−82583
gridded, fission fragment angle meas. 79−85865
guarded-wall free-air, field distortion 80−83234
halide counters, time characteristics 78−863
halide detectors, discharge propag., cathode photoelectric effect and photoionis. contribs. 77−46466
heavy ion detectors, book contrib. 79−31335
heavy-ion detector system, low-energy, A≤30, TOF spectrometer and ΔE-E telescope 77−65380
hemispherical fission ion chamber designed for ≤1 μg samples 80−27900
high density projection chamber 80−58027
high resolution ionisation chamber tested with fission products of ^{235}U 79−93872
high speed trigger system for total deposited energy measurement in a liquid argon calorimeter 79−45576
high-energy photon dose meas. using exposure-calibrated ionisation chamber 78−3607
high-speed transmission avalanche counter 80−91372
high-vacuum gas-discharge electron counter 79−18086
hybrid focal plane detectors for heavy ions 79−68163
impurity monitor for liquid ionization chamber media 79−31331
in-reactor small high temp. ionisation chamber 79−18087
inert gas photoelectron counter, XUV intensity meas. 78−32842
integrating, used in medical X-ray exposure survey, performance characts. 78−853
interface ion dose distrib. meas. apparatus *(German)* 80−9464
internal-gas radioactivity-counting with pure H_2S as counting gas 78−854
ion collection efficiencies in pulsed and continuous radiation beams 78−53505
ionisation calorimeter, energy resolution calc. using cascade characts. 77−61654
ionographic imaging, saturation curve for Freon 13-B1 and mixtures with Xe and Kr, 1 to 8 atm. 77−12997
Keithley diagnostic ion chambers, energy depend. of correction factors 78−53507
large area multiwire ionisation hodoscope 77−30714
large liquid Ar shower detector for ISR expt. 79−22542
large volume MRM-3, for X, gamma rays, performance monitoring of radiation shielding 79−6797
large-area, two-dimensional position sensitive detectors 79−72202
laser induced ionisation tracks, formation and appls. 80−102393

ionisation chambers continued
liquid, current status of electron mobility and free-ion yield in high mobility liquids 79−45531
liquid, recoil electron signals, pulse height anal., indication of low energy γ and ν direction incidence 80−52823
liquid Ar cylindrical pulsed, 200 cm^3 working vol. 80−87015
liquid Ar total absorpt. detectors, electronic noise and electrode config. 77−54441
liquid ionisation chamber media, review of physical props. 79−41071
liquid ionisation detectors, design, perf. and appl. 79−68152
liquid-dielectric, appl. to ^{252}Cf dosimetry 77−13009
LMFBR high-temp. neutron detector test results 77−74909
long monitoring system for linac beam loss meas. 77−88310
low mass fast chamber as start detector in TOF meas. of ^{252}Cf spontaneous fission spectrum 79−81128
low pressure gas counters, charact. meas. *(Chinese)* 79−13590
low-energy heavy charged particle stopping power, phase effects 80−23277
LW bremsstrahlung detector, evaluation of calibration constants 79−68147
Lyman-α ion chambers, water vapour contamination 79−8731
microdosimetric results from ionisation chamber and proportional counter compared 80−9429
mixed β-γ dosimetry, ionisation and scintillation counters 80−57975
modulated molecular beam recording 79−18316
Mossbauer spectrometer design, use of resonance and selective ionisation chambers 77−48094
multi needle counter with cathode focusing 80−58039
multi-electron flame ionization detector for transient analysis of single aerosol particles 80−23246
multilayer detectors, instrument for automatic eval. of ionis. meas. 78−9033
multiplate, with intrinsic background reduction, response to photofission 80−37685
multiple plate total absorpt. ionisation spectrom. based on compressed X-e 79−36476
multistep avalanche chamber, detection of far UV photons, Cherenkov light imaging 79−93871
multistep avalanche chamber, far UV Cherenkov photon detection appl. 80−58042
multistep avalanche chamber, new family of fast high rate particle detectors 79−49904
multiwire and drift proportional chambers, design, operation, appls. 79−743
multiwire gas counters, photoelectric polling 79−68141
multiwire proportional chamber, low mass, self triggering, cathode coupled coaxial-cable delay-time readout 77−57813
multiwire proportional chamber, shift register read out system 78−86736
multiwire proportional chamber for identification of relativistic particles 80−23256
multiwire proportional chamber with anode wire winding pitch of 1 mm 80−23257
multiwire proportional chamber with short resolution time, high accuracy bidimensional readout 77−57810
muon flux measuring system for neutrino spectrum reconstruction at IHEP accelerator 78−21817
MWPC, counting gas props. at low pressure 79−85864
neutron dosimetry, basic constants and meas. principles 79−20676
neutron dosimetry, meas. standardisation for biological and biomedical appl. 80−12271
neutron ionisation chamber mean energy deposition calc., 0.1 to 20 MeV 80−9467
neutron ionization chambers, development and charact. 79−68157
neutron noise meas. technique, coupled swimming pool reactor *(French)* 77−10462
neutron sensitivity, C walled, CO_2 filled chamber 79−22557
neutron sensitivity energy dependence, C-CO_2, Mg-Ar and TE-TE chambers 79−81134
noninteractive beam position and size monitor for heavy ions 79−72149
on-line system for obs. of short lived spontaneously fissioning isotopes 78−46226
optical gas-discharge chambers in mode of pulsed proportional amplification 79−726
optimum filter responses for liq. Ar total absorpt. detectors 78−46215
orbitron, radial electronic charge distrib. 77−57827
parallel plate, saturation current determ. 78−55098
parallel plate, thin-walled, for use with photon and electron beam dosimetry 80−78490
parallel plate avalanche counter, timing props. determ. 77−88339
parallel plate avalanche counter heavy ion detectors, book contrib. 79−31335
parallel plate avalanche counters, simple accurate method for bidimens. position readout 78−21822
parallel plate avalanche counters for registration of light charged particles 80−91369
parallel plate ionisation chamber, absorbed dose meas. in polystyrene phantoms 80−72335
parallel-plate, collection efficiency in pulsed X-ray field 80−99407
particle identification statistics 79−36491
particle identifiers, ionisation loss sampling detectors, readout techniques 78−46232
particulate detector, space charge effects 77−41587
Penning mixtures, statistics of gas gain 79−45535
Penning trap, for positron detect. 78−21812
perturbation correction factor for β-radiation fields 80−37704
photon beam absorbed dose determ., cavity chamber correct. factors study 80−37703
photon dose-rate meter, MRM-3, measuring range expansion 78−879
photon dosimetry in phantoms, effective meas. point 80−78453
photon position monitors for CHESS synchrotron source, using split photoelectron detectors and ionisation chamber 80−91336
plane-parallel chamber, pulsed electron beam irrad., ion losses 80−99421
polypropylene thin stretched foils, appl. as ionisation chamber windows 80−18764
position-sensitive ionization fission chamber 79−26819
positive corona discharge, current oscills. 77−11431
positive ion mobility in gas mixtures 77−27646
pressurised, radiation monitoring at Three Mile Island 80−37637
proportional, accuracy of spatial arrangement and tension of wire electrodes 79−97938
proportional, with signal-wire spacing of 10 mm 79−97939
ionisation chambers continued
proportional counters, relativistic charged particle identification by ionisation energy loss with delta ray suppression 79−85863
pulsed ion chamber methodology appl. to full range reactor power meas. 79−13480
PWR multisection ex-core detector spatial weighting functions 79−13481
radiation exposure intercomparison with ionisation chambers 80−5363
radiation therapy, chamber factor reliability review, United States institutions 79−20685
radioisotope calibrator analysis, sensitivity 77−18738
radioisotope meas., gamma detection using 4π ionisation chambers 79−85869
radioisotope pressure transducer with linear conversion charact. from 100 to 1000 torr 79−35704
radioisotope thickness meter, increasing speed of response by optimising detector parameters 79−75494
radiometry, far UV standards comparison 77−5912
radiopharmaceutical dose calibrator performance and quality control 77−56470
Ramsauer chamber, positron scatt., optimisation study using Monte Carlo method 78−70706
reactor neutron flux meas., high temp. neutron rad. detectors and cables 79−76111
Regional Calibration Laboratory at the M.D. Anderson Hospital, Texas, USA 80−8189
REM ratemeter, for mixed radiation, using two spherical ionisation chambers 78−96100
REM ratemeter for direct reading of dose equivalent rate 78−53502
review of nucl. particle detectors 79−54740
ring imaging Cherenkov detection using multi-needle cathodic focusing detector 80−58040
saturation curves, ion densities calcs., ionisation chambers design criteria 78−37516
scatter factor determ. at depth in walls of cylindrical chambers 79−49909
secondary standard NPL ionisation chamber, calibration program 77−38584
smoke detector, ionisation type, model for response 78−88933
solid state ionisation current comparator 77−23383
spherical plate, fission cross section meas. on short lived α-emitters 77−23380
standards, American National Standards Institute quality assurance programme 77−38585
telescopes for fission fragment position and nucl. charge identification 79−36478
thin calorimeters for cosmic ray spectra meas., Monte Carlo calcs. 77−30713
time projection chamber, design, operation, appls. 79−745
time varying X-ray fields, digital acquisition system 77−57828
tissue equivalent chamber, evaluation of dose equivalent using Geiger-Muller dosimeter 80−51264
tissue-equivalent, response to 15 MeV neutrons 77−48874
tissue-equivalent gas, W-value for low energy electrons 78−15896
tissue-equivalent ionisation chamber, photon calibration for neutron dosimetry 80−56221
triaxial chamber use and experience at V.I. Lenin Leningrad nuclear power station 79−22377
tritium detection in gases and liquids, state of art *(Czech)* 77−86403
two-coordinate multiwire drift chamber, measuring 1.6×0.8 mm 80−23248
variable selectivity photoionisation analyser, hydrocarbon vapour detection 80−81511
Victoreen 570 Condenser R-Meter, energy depend. of correction factor 78−3597
Victoreen 666 Radiographic Health Survey System, energy depend. of correction factors 78−3596
W-value for ions in Ar and tissue-equivalent gas 77−35312
wall correction factors, ^{60}Co γ-ray beam standardisation, Monte Carlo calcs. 79−3288
X-ray, high-pass photocathode, for surface EXAFS 79−68164
X-ray detector, position sensitive, inductance-capacitance line encoding 78−12800
X-ray dose mean value of specific energy, variational meas. 80−12276
X-ray spectrometry, proportional counters and counting electronics *(French)* 77−74564
X-ray stopping power, cavity theory verification 80−9476
β-ray point source dosimetry using variable cavity chamber, appl. to protection instrument response 80−13942
Al chamber, air-filled, 900 l, for cosmic ray sea level meas. 79−35081
Ar liquid, drift of ionisation electrons 78−37504
Ar, liquid, drift of ionisation electrons 78−55100
Ar, liquid, Fano factor limitations on energy resolution 78−37502
Ar, liquid, high energy resolution with 4.5 cm gap 80−18761
Ar, liquid, increased time resolution using Ar-methane mixtures 80−27891
Ar, liquid, time projection, design considerations 79−63868
Ar, liquid calorimeter γ-detector, 5 to 80 MeV 79−6799
Ar purification, Li trap construction 80−47814
Ar purification system and electronegative impurity conc. meas. instrument 80−32571
Ar, solid, β and α-particle detection 77−30720
Ar/Fe liquid hadron calorimeter 78−37503
Ar-CH_4 proportional counter, light emission obs. 80−78488
Ar+10% CH_4, Fano factor determ. from α-particle pulse height distribs. 79−76284
BF_3 detector ageing, depend. of temporal distrib. function 79−63872
^{10}B, neutron cross section standards, detection techniques 79−9970
CO_2, ionisation meas. and $\bar{W}_n$ derivation for neutron irradiation 79−36430
Cl ions, charge states from (n,p) and (n,d) in liquid Ar *(Russian)* 80−9298
Fe-liquid scintillator multilayer calorimeter transition effects, muon burst rates 78−90019
He filled detector using thin foils to convert gamma rays to electrons 80−27872
He+H_2(Ar)10^{-2}%, high press. corona discharge ionisation instability impurity effects 77−11430
^3He, calibration for use with filtered neutron beams *(German)* 78−58529
^3He fast neutron detector with linear energy response 78−25393

ionisation chambers continued
^{3}He gridded fast neutron ionisation chambers, Monte Carlo calc., of energy dependent efficiency 80−99417
^{3}He, high pressure, improved time resolution in n-γ coincidence meas. 80−99416
^{3}He ionisation chamber, delayed neutron spectroscopy 77−79501
^{3}He transit time neutron spectrometry 80−63441
Kr photo-ionization proportional scintillation chamber 80−58056
^{6}Li(n,α)^{3}H reaction, as standard in neutron flux meas., instruments review 79−9969
N_2, electron backscattering coeffs., 100 eV to 5 keV 80−9750
O_2, electron backscattering coeffs., 100 eV to 5 keV 80−9750
O_2 in liquid Xe, electron capture 80−102402
Pb/liquid Ar e.m. shower detector 77−395
Rn concentration in goundwater continuous monitor 79−21068
Rn concentration measurement in groundwater and springs for earthquake prediction 78−88924
^{235}U parallel plate detector, (n,f) cross section meas. 77−23156
Xe, γ-irrad., average energy expended per ion pair *(Russian)* 80−5438
Xe, liq., ionising particle detector, signal amplification by optical pumping 79−54746
Xe, liquid, Fano factor limitations on energy resolution 78−37502
Xe-containing fast gas mixtures for gas-filled detectors, electron drift velocities 80−74089

ionisation gauges
10^{-1} to 10^{-8} Pa, automatic control *(Czech)* 80−52256
appearance pot. spectrometer design, demonstrations 80−105477
Bayard Alpert gauge, low-press. limit 77−30173
Bayard-Alpert gauge, three-grid modulated, mode B operation 80−105667
Bayerd-Alpert gauge, multi-grid modulated, concept and expt. 77−49738
cathode protection for PMI-2 manometric transducer 77−74416
collector current vs. pressure characteristic, sensitivity *(Japanese)* 79−6135
computed tomographic rotating fan-beam scanner, exptl. bench design 80−51230
flame, detector for meas. fluctuating conc., turbulent flows 80−92240
heated cathodes, emission characteristics, selection *(German)* 80−236
high pressure gauges used in standards intercomparison, 8×10^{-5}-8×10^{-2} Pa 80−86333
hot cathode type, improvement on soft X-ray limit *(Japanese)* 77−140
hot filament ionisation gauges, press. meas. limit up to 10 mm Hg *(German)* 79−17431
hot-cathode, thermal effects 80−17955
hot-filament device, electron current to anode stabilisation cct. 77−26341
ion collector current, analytical description 77−53924
JG ionisation gauge, effect of electrode voltages on elec. field distrib. 77−49737
modulated Bayard-Alpert gauge design 80−77805
multiphoton ionisation cell, balanced bias differential current amplifier cct. 80−37909
nonlinearity at upper press. limit *(Chinese)* 79−71471
orbitron device, optimum injection condition for electrons, influence of end effects 80−82784
pressure gauge and sensitive detector for investigating negative surface ionisation of UF_6 80−31781
pressure meas., extension of upper limit of gauge *(Chinese)* 79−75542
quadrupole ion pump and ionisation gauge, plasma geometry and props. 77−57337
self-modulating 80−82786
single particle trajectories, through ionising regions 79−6218
surface gauge for Cs meas. from surface plasma H^- ion source 79−68098
total pressure meas., ultrahigh vacuum, review 80−31782
ultrahigh vacuum ion pumped system, for undergraduate and postgraduate courses 79−62981
In amalgam lamp, Hg vapour partial pressure meas. 78−67488
Na ionisation detector, aerosol effects on characts. 79−49243

ionisation of atoms
see also atomic electron impact ionisation
$3d^N$ ions, free and in crystals, Slater parameters, 3d-4s excitation energy 78−33433
6p levels, two-photon excitation, time resolved fluoresc., quenching, lifetimes and photoionisation cross section 80−78587
absorbing boundary method, Golden Rule generalisation 79−97226
AC Stark splitting in doubly reson, three-photon ionisation, nonmonochromatic field 78−94220
accelerated atom+O_2, chemiionisation, crossed beam obs. 77−9085
alkali anions, autodetaching sub $^2P_{1/2}$ threshold states 79−22611
alkali atom, two-photon ionis. using elliptically polarised light 79−98052
alkali atom+alkali atom, laser-induced ionis. collisions 78−5333
alkali metal, near-resonant two-photon ionis., non-Coulomb phase shifts of photoelectron partial waves 80−106302
alkali metal, photoionisation cross sections, scaled Thomas-Fermi method 77−46549
alkali metal, quantum beats in photoionis. by fine struct. levels coherent superposition 79−6922
alkali metal, transition oscillator strengths in discontinuous and continuous spectra, review 80−52937
alkali metal, two-photon ionis. by unpolarised light, depolaris. effects 79−59409
alkali metal, two-photon ionis. via reson. intermediate state 78−42023
alkali metal, two-photon ionis. with two light beams, photoelectron polaris. 80−43011
alkali metal+N_2, thermal ionis. rate coeff. 77−30982
alkali metal +He(s^3S), Penning ionisation by slow collisions 77−50512
alkali metal anions, formation 78−5159
alkali metal atom, outer-shell photoelectron ang. distrib. 80−37797
alkali metal atom, polarised, spin-deposited photoelectrons from two-photon ionisation 79−63971
alkali metal atom, resonant multiphoton ionis. *(Russian)* 79−3401
alkali metal atoms, spin-polarised, near-reson. two-photon ionis., light polarisation effects 80−106308
alkali metals, laser three-photon absorpt., ionisation cross-sections *(French)* 78−5182
alkali metals, Rydberg states, Stark ionisation 80−52933
alkali metals, two-photon ionisation with two light beams, polarisation effects 79−81190

ionisation of atoms continued
alkaline earth atom, correl. lines, Rydberg excitations and ionisation pots. 77−6705
alkaline earth atom+inert gas ion, double ionisation, cross-section and defect energy *(Russian)* 77−83703
alkaline earth atoms, multiphoton ionisation spectroscopy 78−82703
alkaline earth metal, photoionisation cross sections, scaled Thomas-Fermi method 77−46549
approximate and exact state wavefunctions, ionisation potentials, energy difference calcs. 79−97967
atom, inner-shell photoionis., anisotropy of X-rays and Auger electrons 78−58633
atom, Schumann region absorpt. spectrum, oscill. strengths, line profiles, collisional and autoionis. broadening 77−18818
atom, two-photon ionis., time depend. model, finite bandwidth light 79−81193
atom, two-photon resonant ionis. 78−58631
atom+atom, collisional ionisation review 80−63801
atom+atom, two photon ionisation, radiative collision effect 80−106388
atom+atom, with excitation and deexcitation of atom, impulse approx. 79−59548
atom+atom collisions, 2s and 2p electrons removal, impact parameter dependence 77−65531
atom+fast nuclei collisions, multiple ionisation cross sections 77−23558
atom+H^+, emission electron angular and energy distribution 80−87222
atom+H^+, innershell ionisation 78−62930
atom+H^+, ionising central collisions and nucl. excitation 80−43164
atom+H^+, K-shell ionis., plane wave Born approx. model 77−34748
atom+H^+(He^{2+}), excitation functions rel. to ionisation *(French)* 79−31669
atom+heavy ion, inner at. shell ionisation, binary collision model, low vel. 80−5612
atom+ion, electron ejection, low electron velocity, anisotropy effect 80−37856
atom+ion, inner-shell ionisation of quasimolecular system, perturbation theory 79−31667
atom+ion collision, low energy, ionisation, total cross-section meas. 77−54606
atom+ion collision, slow, electron detachment *(Russian)* 77−30985
atom+ion collisions, ionis. or excitation, binary encounter approx. 79−22804
atom+ion collisions, KK-vacancy sharing, X-ray emission 78−42190
atom+ion collisions, L-shell Coulomb ionisation, electronic relativistic effects 77−42391
atom+ion collisions, quantum theory of ionisation in fast collisions 79−3553
atom+ion impact ionisation, inner shell alignment calcs. 80−83473
atom+ion K-shell double ionis., Kαα and Kαβ obs. 77−57918
atom+light ion, dipole transitions in K-shell ionisation 78−90281
atom+metastable atom collision, associative ionisation 78−62907
atom+metastable atom collision, Penning ionisation 78−62907
atom+molecule rot. effect on polar mol. collisional ionis. 77−83702
atom (ion)+atom, H to Fe^{25+} and H to Fe, single-electron loss, total Born-approx. cross-sections 77−83714
atom models, ionisation time depend. under intense EM fields 80−32683
atom-ion collision, X-ray cross-sections, plane wave Born approx. 77−68094
atom-ion collisions, electron loss cross section, asymptotic form 79−13807
atom-surface impact, electron tunnelling in external electric field, atomic resonant ionis. and field ionis. 77−52208
atomic inner-shell ionisation, post-collision photoelectron-Auger electron interactions 77−18870
atomic photoionisation anal. using relativistic random phase approximation and multichannel quantum defect theory 80−63602
atoms, multiphoton ionisation probability, laser pulse 78−86835
atoms, polarisation of electrons and nuclei in resonant multiphoton ionisation 80−99486
atoms, two-photon photoelectron energy spectra, AC Stark splitting 78−86834
autoionisation, astronomically oriented bibliography 78−32340
autoionisation electrons, photons emitted from collisionally aligned states, angular correl. 77−14385
autoionisation processes, review, and expt. methods 78−29763
autoionising and inner shell vacancy states, decay, time independent multichannel scatt. theory 80−47854
autoionising electronic states, Siegert eigenvalues 79−10075
autoionising resonances, density of states calc. 77−18857
autoionising states, mean-square deviation formula derivation 77−57943
autoionising states, nonexponential decay to continuum, possibility of obs. 77−42288
autoionising transitions excited in atom+ion (electron) collisions 77−42390
benzene liquid multiphoton ionisation polarisation experiments, molecular symmetry 79−98162
beta decay, K-shell internal ionisation, excitation, K-shakeoff probabilities 77−18889
beta decay, K-shell internal ionisation, many electron effect, relativistic theory 77−18890
binary collision, energy transfer and ionisation cross-section calcs. 77−50522
bound electron photon scatt., atomic ionisation, field theoretic anal. 80−23380
bound states, beam-foil excitation and decay near ionis. limit 80−9552
C O, K-shell ionis., double and single, cross section meas. by ion bombardment 78−50629
chalcogens, photoionisation cross sections and ang. distribs., outer p subshell 80−9572
charged particle excitation processes 77−71862
chemical ionisation, classical description, complex interaction pot., exponential representation 80−99570
closed-subshell atom, correl. lines, Rydberg excitations and ionisation pots. 77−6705
coherent radiation ionis. of model atom 77−38647
colliding atoms, two-photon ionisation 78−13482
collision, two-centre one-electron, nonadiabatic couplings for ionising transitions, switching functions determ. 79−22813
collision-induced three-photon ionization 80−23384
collisional inner-shell ionisation, semi-classical theory 78−62896
collisional ionisation, Penning and associative ionisation produced by laser field 80−63802

ionisation of atoms continued
collisional ionisation, Penning ionisation, laser induced, two step optical collisional perturbation sequence 80−63778
collisional ionisation in intense laser field, quasimol. state reson., quantum mechanical anal. 78−33589
collisional ionization rate coefficients 79−14518
collisions, improved impulse approx. 78−74754
collisions in intense light beams, quantum aspects *(Russian)* 79−6903
complex atoms, multiphoton ionisation cross-section calcs. 78−21888
Compton bound electron state scatt., binding and off-mass shell effects, relativistic anal. 78−17637
Compton profiles, two-electron theory 79−86012
Compton scatt., bound and free electron Compton scatt. in coherent EM field 78−94225
cooperative multiphoton ionisation, bistability effects, Bonifacio-Lugiato model 80−19010
core ionisation in 3d, 4f and 5f series, rearrangement effects 80−53065
coulomb deflection in ion-atom collisions 79−94074
Coulomb ionisation of inner shell electrons, screening effects 78−74749
Coulomb ionisation of K-shell electrons in heavy ion collisions, DWBA calcs. 78−37731
Coulombic ionisation of inner shells 78−62898
cross sections, calc. using effective Feynman diagrams, in plasma 80−38566
cross sections, positive integer spectral power moments in moment-trace calcs. 78−17729
dense metal vapour, radiation trapping, multiphoton ionisation and reson. fluoresc. 80−32654
Dirac-Slater potential, hole and exchange terms, influence on photoionisation cross-sections 80−952
direct Coulomb ionisation, origin and nature of universality 79−45791
doubly charged ion formation, 2-electron multiphoton ionisation of atoms, mechanism *(Russian)* 80−5514
education, two-electron atom, 1snl excited levels, ionisation energy calc., perturbation, Schrodinger eqn. methods 80−17728
electric field ionisation, highly excited state, linearly polarised field, freq. (amplitude) depend. 80−32630
electron polarisation produced by reson. ionisation by intense EM field *(Russian)* 78−50518
electron wavefunctions for (γ,2e) and (e,3e) processes at high energy, double Fourier transform 78−17628
electronic and at. collisions, conference, Kyoto, Japan (Aug.-Sept. 1979) 80−62394
energies, determ. from optimised one-electron wave functions 77−38599
excitation and ionisation by strong EM field, threshold features *(Russian)* 79−85940
excited atom+excited atom collision semiquantal calcs. 79−81270
excited atom ionisation due to collisions in their own gas *(Russian)* 80−91654
excited atom photoionisation by low intensity light, effective cross section 79−26946
excited atomic states in EM field, ionisation by electron diffusion *(Russian)* 78−86798
excited atoms, field ionisation mechanisms 78−70761
excited atoms, photoionisation in DC gas discharges by low intensity light 79−50904
excited state photoionisation, at. and mol. photoabsorpt. cross sections determ. 80−32783
fabrication of ionisers for electric propulsion *(French)* 79−56946
fast heavy ion+atom, and solid targets, ionis. and excitation states 78−70927
fast heavy particle collisions, radiative ionisation 77−14562
fast ion+atom, energetic electron emission as charge transfer process, Born approx. 80−53126
fast multiply charged ions, electron loss cross sections, semiempirical calcs. 79−86054
fast projectile electron loss forward peak oscill. struct. as autoionisation 80−69227
field-ionisation of Rydberg states, depend. on $|m_l|$ 78−58856
gamma-ray photoionisation cross sections, low, medium and high Z atoms 77−54544
gas atom, photoionisation cross-section, multiconfig. Hartree-Fock calc. 78−17630
gas discharge, photoionis. at low illumination intensity, nonlinearities, effective cross section 78−87517
group VI atoms, $(np)^4\ ^1S_0$-level photoionisation via autoionising levels 79−76398
H like atoms, photoionisation in homogeneous elec. field *(Russian)* 80−106309
halogen, 1s hole states, ionisation, ab initio SCF calcs. 78−17568
halogens, photoionisation cross sections and ang. distribs., outer p subshell 80−9572
heavy atom+$^4He^{2+}$2-5 MeV, inner shell ionisation cross section 79−45825
heavy atom+light ion, inner-shell ionisation, adiabatic effects 80−99561
heavy atoms, α-particle impact K-shell ionisation, 40 to 110 MeV 78−17752
heavy atoms, beam foil populations, charge-state distribs., independent-electron model 77−19035
heavy collision systems, vacancy prod. in strongly bound quasimol. states, impact parameter depend. 78−22003
heavy elements, electron config. rel. to chem. behaviour *(German)* 78−29727
heavy ion+atom, K-vacancy production, universal scaling law 79−22811
heavy ion+atom, outer shell electron emission, differential cross sections 79−45817
heavy ion+atom collisions, K X-ray transition energies, two electron-one photon mechanism 77−18828
heavy ion beam-foil spectra, ion equilib. excitation, density effect 77−19056
heavy ion collision, delta electrons as probe of high mag. fields 79−13810
heavy ion impact, inner-shell ionis., binary collision model 79−54962
heavy ion-atom collision, positron formation, calibration energy transfer for Coulombionisation 79−76506
heavy ion-atom collisions, cross sections for electron production 79−89767
heavy ion-atom collisions, inner shell ionis. X-ray emission and Auger spectra obs., appls. *(Japanese)* 78−9240
heavy particle collisions, electron spectroscopy 77−42397
heavy-ion collisions, 3dσ mol. orbital, ionisation probability 80−23538
ionisation of atoms continued
heavy-ion collisions, K-vacancy production, 1sσ excitation of transient mol. orbital 77−83718
heavy-ion collisions, K-vacancy production, 2 pσ mol. orbital, single and multiple collisions 77−83717
heavy-ion collisions, Z≥35 projectiles, 12 to 470 MeV, K-vacancy cross sections 77−19026
high angular momentum Rydberg states, autoionisation rates calcs. 79−81163
high-Z atom+H(He)(O)(F)(Cl) ions, 1sσ vacancy prod., relativistic and Coulomb deflection effects 78−58801
high-Z atoms (Z=48-104), electron impact, K-shel ionisation cross sections calcs. 80−63827
highly excited atoms, acted on by EM radiation, oscillator stochastic instability theory *(Russian)* 79−31487
hydrogen atoms, threshold behaviour of multiphoton ionisation 80−954
inert gas, atomic photoionisation, Dirac-Fock calcs., branching ratios and angular distrib. in p shells 80−63601
inert gas, field ionis. and proton capture, critical energy deficits 78−82853
inert gas, photoionis. cross sections of excited levels, quantum defect method calcs. 80−37795
inert gas atom, correl. lines, Rydberg excitations and ionisation pots. 77−6705
inert gas atom+H^+, outer S-shell ionisation cross-sections calcs. *(French)* 78−42212
inert gas atom+highly stripped ion, multiple-ionis. cross sections, Monte Carlo calcs. 79−64091
inert gas atom +H^+, electron capture, charge-state distrib. 80−32814
inert gas atom photoelectron ang. distribs., theoretical calcs. comparison 79−59412
inert gas isoelectronic sequences, positive ion p-subhsell photoionisation cross-sections calcs. 77−50374
inert gas metastable atoms, photoionisation rel. to laser development 78−13476
inert gas plasma, free-bound continuum determ. using photoionis. cross sections calc. 80−43878
inert gases, initial state wave functions for photoionisation cross-sections, multiconfigurational HF calcs. 80−47908
inert gases, inner-shell optical photon excitation, Auger, autoionisation, photoionisation processes 77−18867
inert gases, ionis. in ion+atom collisions, 200-4000 eV 77−27174
inert gases, multiphoton ionisation, by ultrashort laser pulses from tunable Nd:glass laser 77−58095
inert gases, multiple photoionisation, threshold to 280 eV, time of flight meas. 79−85939
inert gases, outer shell photoionisation, relativistic RPA calcs. 80−9571
inert gases, photoabsorption to bound state and photoabsorption to continuum state (ionisation), comparison, HF calcs. 80−47910
inert gases, photoelectron spin polarisation, ab initio calcs. 80−18833
inert gases, photoionisation cross sections of excited atoms and dimers 78−66523
inert gases, photoionisation cross-sections, multiconfig. Hartree-Fock calcs. 77−50373
inert gases, quantum defects, photoionisation cross-sections, central pot. model calcs. 77−54510
inert gases+Ar^{6+}, collisional excitation, excitation cross sections 79−98209
inner shell capture by fully stripped ions 77−54607
inner shell electron props., relativistic effects 77−18803
inner shell electron rearrangements in radioactive decay 77−18881
inner shell excitation processes in heavy ion-atom collisions, review 80−37874
inner shell ionisation, results obtained with Darmstadt electron Linac 77−83183
inner shell ionisation, semiclassical approx. method calcs. 80−43162
inner shell ionisation by electron, positron and proton impact 77−19090
inner shell ionisation by electron or proton impact, coincidence exptl. method, theory 80−1066
inner shell ionisation by heavy charged particles, semiclassical approx. 77−14559
inner shell ionisation by heavy particles, conf., Linz, Austria (May 1979) 80−41938
inner shell ionisation by nuclei, impact parameter dependence 77−23557
inner shell ionisation in electron capture decay 77−18882
inner shell ionisation phenomena, conf., Freiburg, West Germany (Mar.-Apr. '76) 77−27040
inner shell ionisation probability, multiple scatt. effects on coincidence yield 79−31670
inner shell vacancy influence on atomic props. 77−26956
inner shells, Coulomb ionisation, semiclassical description 80−42938
inner shells, multiply ionised, X-ray satellite spectra, energy levels 77−18833
inner shells, physics, quantum mech. appls., history 77−18773
inner-shell ionisation, heavy charged particles, review 78−42181
inner-shell vacancy creation, ionised fragments probability distrib. 80−83274
innershell ionisation, proton and electron impact equivalence at high vel. 77−14556
interference in two-channel two photon ionization 80−23381
interstellar H, ionisation in dense clouds by energetic secondary electrons 77−33593
ion, positively charged, photoeffect theory 78−94219
ion+atom, projectile charge dependence *(Dutch)* 79−50121
ion+atom, slow collision, K-shell ionisation, variational calcs. 78−42162
ion+atom collision, electron angular and energy distrib., first Born approx. 80−53116
ion+atom collision, electron emission, book contrib. 78−74756
ion+atom collisions, inner-shell ionisation, scaling props. 77−19048
ion+atom collisions, ionis., charge transfer, model 77−75278
ion+atom collisions, K-shell ionisation, refinement to simple ionisation theories 77−75275
ion+atom collisions, K-shell vacancy prod., impact parameter depend. 79−13803
ion induced inner shell vacancy formation 78−70926
ion induced K-shell ionisation cross-sections determ. by comparison with nuclear Coulomb excitation 79−76500
ion pair form., vibr. energy depend. 79−34287
ion pressure discharge theory in the strong ionisation regime 80−38734
ion-Rydberg atom collision cross sections, classical trajectory Monte Carlo calcs. 80−43174

ionisation of atoms continued
ionisation potentials, natural transition orbital theory, perturbation theory anal. 77−34541
ions, highly stripped, photoionisation, relativistic calcs. 79−26953
ions, photoelectric cross-section, scaled from neutral atom 78−13479
ions in low density plasma, dielectronic recomb., ionization equilib. and radiative energy loss, solar corona appl. 79−68903
K_α/K_β ratio for X-ray transitions in collisions with $e^-(H^+)(He^{2+})(D)$ 80−27972
K X-ray nuclear satellites from (p,xn) reacts. on heavy elements 80−27599
K- and L-shell ionis. by protons, plane-wave Born cross sections 80−12858
K-shell atomic ionisation by heavy particle, electronic relativistic effects, Dirac wavefunctions, semiclassical effects 78−78792
K-shell collision excitation, absolute cross section, $0<Z<11$, 40-600 keV 79−41231
K-shell collisional ionisation, at. pot. calcs., Ramsauer effect 77−10745
K-shell Coulomb ionisation, scaling parameter, relativistic correction 79−72407
K-shell hole production by light ions, hydrogenic and Hartree-Fock model of target 77−83715
K-shell internal ionisation and excitation in β decay 78−556
K-shell ionis. by charged particle impact, electronic relativistic effects 80−28099
K-shell ionis. by relativistic protons, double differential and total cross sections 78−42182
K-shell ionisation, by heavy ion impact, Magnus (sudden) approx. 77−68106
K-shell ionisation, by structureless charged particles, Coulomb deflection effect 78−17779
K-shell ionisation, light ion-induced, Coulomb deflection effects 77−71855
K-shell ionisation, PIXE meas. at Univ. of Manitoba 77−46650
K-shell ionisation, X-ray or Auger-electron prod. by ion impact, cross section tables 79−54947
K-shell ionisation by Coulomb excitation, plane-wave Born-approx. 79−18272
K-shell ionisation by H^+, electronic final states description 77−38723
K-shell ionisation by heavy particles, theoretical cross-sections and expts. 80−48076
K-shell ionisation by proton impact, semiclassical approx., projectile trajectory dependence 77−23551
K-shell ionisation by protons, semiclassical approx. 77−19039
K-shell ionisation probability by protons, E_p=100 keV-2 MeV, impact parameter depend. *(Japanese)* 78−86945
K-shell ionization in heavy-ion collisions, book contrib. 78−82834
K-shell photoionization of multielectron atomic systems 80−47949
K-shell vacancy production, by charged particles, relativistic effects calc. 78−58600
Koopman's ionis. pots., virial scaling corrections 77−65539
Koopmans atomic valence electron ionisation energy, $1/Z$ expansion method, reorganisation corrections 78−78623
L_1-shell ionisation, high-energy impact, relativistic plane-wave Born approx. 79−54970
l-shell Coulomb ionization by heavy charged particles 79−94073
L-shell ionisation by heavy charged particles, binding energy correction 77−54604
lanthanide atom+H^+, L-subshell ionisation cross-section, 150-400 keV 79−45665
lanthanides, Rydberg spectra and ionisation thresholds, time resolved resonant multistep technique 78−82701
lanthanides' ionisation pot. calc., T-value and number of 4f electrons linear correlation *(Chinese)* 80−63850
laser detection, of individual atoms 79−26950
laser ionisation, modelling 78−90133
laser radiation-matter interactions, dissertation 79−86555
laser selective detection of ultralow concentrations of atoms 78−3407
laser selective detection of ultralow concentrations of molecules 77−90669
laser-assisted excitive Penning ionisation 79−41232
laser-enhanced ionisation, appl. to anal. flame spectrometry 78−92528
laser-excited metal vapour, ion flow vel. meas. 79−82002
laser-induced selective multistep processes: impact on nuclear physics, chemistry and biology 80−61122
Li, multiphoton ionis. at ruby laser wavelength 80−9566
light atom, ionis. energy calc. 79−59382
low energy atomic collisions, ionisation processes, chemi-ionisation, review 78−22024
low energy collisions, ionisation cross sections, diffusion eqn. calcs. 77−54605
M-subshell direct Coulomb ionisation, X-ray emission, PWBA calcs. 79−45664
M-subshell ionisation cross section, by H^+ impact, binary encounter approx. 78−62890
many body perturbation calculations of photoionization 79−59406
many electron effect on K-shell internal ionisation accompanying β-decay 78−86839
many-body perturbation theory, eqns. of motion formulation 77−88373
many-electron autoionisation states, transition probability and autoionisation rate, perturbation theory Z-expansion 80−52863
metal surface, ionisation of atoms 79−68310
metal vapours, at. inner-shell optical photon excitations, Auger, autoionisation, photoionisation processes 77−18867
metastable atomic or molecular species, multiphoton transition detection 80−58231
metastable atoms in positive column, unified electron temp. characts. 77−11419
microwave ionisation of highly excited states, and excitation 79−31482
model atom in electrostatic field, ionis. dynamics 78−90311
multicharged Li-like ions, decay of metastable autoionised state *(Russian)* 78−25455
multielectron atom, correlated transitions in decay of two inner-shell vacancies 80−37799
multiphoton, doubly resonant 78−42024
multiphoton, laser temporal coherence and high laser intensity effects 78−66524
multiphoton, resonant, effective nonlinearity order 80−32688
multiphoton absorption above ionisation threshold 80−58224
multiphoton ionis., intense field, via complex dressed states 78−17629
multiphoton ionis., probability rates 79−13686
ionisation of atoms continued
multiphoton ionisation, effects of self-induced reson. 80−91519
multiphoton ionisation, Green's function method calcs. 79−89650
multiphoton ionisation, reson. cross-section, very-narrow-bandwidth source 78−55150
multiphoton ionisation, reson. effects, light coherence effects 80−58232
multiphoton ionisation, resonance peaks strengths 77−42293
multiphoton ionisation, resonant, in strong EM wave field 79−10079
multiphoton ionisation, resonant, with intense monochromatic laser 80−32689
multiphoton ionisation, short time behaviour, theory appl. 80−47951
multiphoton ionisation, short-time behaviour 79−59418
multiphoton ionisation, simple model, transition rates 80−953
multiphoton ionisation by lasers, localised and dispersive states 77−27041
multiphoton ionisation dynamics 80−91517
multiphoton ionisation from excited states 77−88433
multiphoton ionisation in gaussian beam focal space, ion generation *(French)* 77−6740
multiphoton ionisation of atoms, reson. effects, laser temporal coherence effects 80−32693
multiphoton ionisation probability, Green's function model pot. 78−25498
multiphoton ionisation processes, resonance and laser coherence effects 80−74208
multiphoton near-reson. ionisation, chaotic versus coherent light 78−33489
multiphoton resonant ionis., model calc. 78−62773
multiphoton resonant ionis. in incoherent field 79−26952
multiphoton transition amplitudes, exact summation of higher-order terms 77−18878
multiphoton transitions, continuum level shift effects 79−26956
multiphoton transitions, perturbation theory, atomic ionisation and intermediate reson., dissoc., review 79−41145
multiple electron transfer to highly charged ions, scaling of cross sections 77−83711
multiplet ratios for photoionisation and electron attachment, shell model, LS coupling and correl. 78−17636
multiply charged ion+H, electron capture, unitarised distorted wave approx. 80−63814
multiply ionised ats. prod. in ion-at. collisions 80−28098
multistage ionisation in strong EM fields, Thomas-Fermi calcs. *(Russian)* 80−58226
multistep ionisation, highly selective, by laser radiation 79−59408
Na, fluoresc. study, reson. radiation illum. 80−83314
near threshold struct. in K-shell spectra, photoionisation or fast charged particle ionisation 80−87064
nebulae, gaseous, photoionisation models for third period elements 80−46640
nebulae, N and O ionisation structs. and abundances 78−8093
negative ions, photodetachment cross-sections, crossed beam meas. *(German)* 77−42298
non-Rydberg atomic spectroscopy, review 78−90127
nonadiabatic reactions, rate const. temp. depend., influence of charact. features of elastic scatt. 80−37852
nonresonant multiphoton atomic ionisation in stochastic EM field *(Russian)* 80−99490
nuclear K-X-ray satellites, Z=50-83, by α-bombard., 17.5-22.5 MeV 80−42984
nuclear space struct. effect on ionisation energy losses in ultrarelativistic region *(Russian)* 78−46105
one electron excited atom ionisation collisions at high energy, improved impulse approx. 79−94072
one-atom detection by reson. photoionisation spectroscopy, demonstration 77−38742
one-atom detection by reson. photoionisation spectroscopy 77−79706
one-atom detection in individual ionisation tracks, heavy ion stopping in buffer gas 78−70802
one-electron ion+He(N)(Ar), sum-rule Born cross sections, excitation and ionis. contribs. 79−22812
oscillator strengths, generalised, Born approx. for ns-transitions 78−5173
parametric process, four-wave, resonant enhancement study by 4d6p autoionising resonance 77−41697
parity violating neutral currents in two-photon and autoionisation atomic transitions 80−32034
particle stripping analysers with solid and gaseous targets 79−1341
Penning collision processes, review *(Japanese)* 79−64092
Penning electron angular distrib., Born-Oppenheimer approx., probability amplitude 78−25677
Penning ionis., radiative, photoionis. cross section depend. of continuum radiation 77−19034
Penning ionisation and excitation transfer, unified treatment 78−25672
perturbation of the atomic spectrum by a strong light field 79−10073
photoabsorption, correlation effects 77−42299
photoelectron ang. distrib. and spin polarisation, theory 80−91618
photoionisation, 3d subshell absorption spectra, Kr I, Cd I, Rb I, Sr I, Cs I 77−10648
photoionisation, absolute cross-sections, expt. meas. techniques 80−63598
photoionisation, book contrib. 77−27125
photoionisation, correlation effects 78−58842
photoionisation, double, two-step autoionis. 77−50415
photoionisation, electron spectrosc. obs. using synchrotron radiation 79−31485
photoionisation, fluoresc. radiation polarisation 80−87076
photoionisation, in gas-filled photodiodes, improved detectivity for UV radn. 78−37062
photoionisation, in intense radiation and magnetic fields, quasienergy formalism 79−72284
photoionisation, inner-shell, Auger effect, post-collision interaction 77−68021
photoionisation, ion alignment, many electron correl. effect 78−74622
photoionisation, multichannel relativistic RPA calcs. 80−9570
photoionisation, multistep resonant, coherence versus incoherence 77−18859
photoionisation, one-electron excitations, local pots., many-electron effects 79−54817
photoionisation, photoelectron ang. distrib. theory 78−17730
photoionisation, polarisation of photoelectrons, review 80−78584
photoionisation, polarised electron prod., Fano effect *(Russian)* 79−26954

ionisation of atoms continued
photoionisation, post collision interactions in at. excitation processes 78−58803
photoionisation, R-matrix method 78−58833
photoionisation, R-matrix theory 78−58761
photoionisation, radiative collision-induced 78−62858
photoionisation, relativistic RPA calcs. 77−61719
photoionisation, reson. interaction of intense EM waves *(Russian)* 78−33480
photoionisation, selective, use in laser isotope separation and spectros., review 80−83332
photoionisation, single photon, AC Stark splitting of bound-continuum decay 80−5502
photoionisation, two-step laser selective method 80−23473
photoionisation cross section calc. by model pot. method 79−26951
photoionisation cross section rel. to photoelectron peak size 77−88508
photoionisation cross sections, electron correl., reson. struct., relax, effects many body perturbation calcs. 80−47852
photoionisation cross-section, intershell interactions 79−26948
photoionisation cross-section calc., absorbing boundary method 79−31623
photoionisation from low or high excited states, radial transition integrals 80−18832
photoionisation of atoms and molecules, UV photoelectron spectrosc. obs. 79−31603
photoionisation of Rydberg states, quantum beats in light absorption 78−25499
photoionisation review, expt. techniques, processes, theory 77−14402
photoionization cross-section, ground state inversion pot. method 79−31484
PIXE meas. at Univ. of Manitoba 77−46650
plasma, excited ats. population distrib., electron-density variation influence 78−87431
plasmas, low density, H to Ca, Cr, Mn, Fe, Ni, ionization equilib. 78−17768
polarised light beams two-photon ionisation rates for circ. (linear) polaris. 80−43012
polarised nuclear beam production by reson. at. ionis. 79−13576
positive atomic ions with $Z \leq 30$, photoabsorpt. cross sections 80−26727
positive ions, electron impact ionis. cross-sections 77−46642
post-collisionally Stark mixed states, autoionisation electron energy and ang. distrib. 80−18829
power broadened two-photon ionisation, reson. lineshape and photoelectron spectra 80−58229
proton induced K-shell ionisation cross sections, thin and thick target methods 80−45611
proton inner-shell fitted ionisation cross sections from Ca to Sn, 0.1-2.0 MeV 79−86055
PWBA for K shell ionisation cross sections 78−70923
quasienergy formalism, for multiphoton ionisation induced by circularly polarised radiation 78−37610
quasimolecules, superheavy, inner shell electronic states calc., ionisation during heavy ion collisions 79−89817
rare earth atoms at surface, photoionisation of 4f electrons 78−11077
rare earth elements, laser isotope separation by two-step photoionisation 78−46461
rare earth metals, photoionisation thresholds and Rydberg spectra 78−66522
recoil atoms meas. by laser spectroscopy neutron detect. possibility 79−22864
renormalized plane wave-projected and Coulomb-projected T-matrices 79−17267
resonance interaction of intense light with atoms, reviews 79−68216
resonance ionization source for mass spectroscopy appl. isotope anal. and time of flight spectrometer 80−81380
resonance ionization spectroscopy and one-atom detection 80−22441
resonance ionization spectroscopy with amplification 79−54996
resonance multiphoton processes of laser radiation interaction 80−37800
resonance region, partial cross-sections, branching ratios 77−83555
resonant and direct photoionis. 77−83553
resonant ionisation by intense EM field 77−71784
resonant ionisation spectroscopy, chem.-physics appls. 80−68259
resonant ionisation under adiabatic level inversion conditions *(Russian)* 80−32691
resonant multiphoton ionisation, influence of excitation pulse characts. 77−34598
resonant multiphoton ionisation, line profile as Fano profile with background struct. 79−72290
resonant multiphoton ionisation *(Russian)* 79−3421
resonant multiphoton ionisation by pulsed excitation, Beers-Armstrong model 78−17645
resonant multiphoton ionization by finite-bandwidth chaotic fields 79−54819
resonant phenomena, complex stabilisation method 80−78515
resonant photoionisation, nuclear polaris. *(Russian)* 79−49997
resonant two-photon ionis., polarisation effects *(Dutch)* 78−5185
resonant two-photon ionisation, time-independent rates, coherence vs. incoherence 79−54820
resonant two-photon ionisation in partially coherent radiation field 78−66525
rotated coordinate method use, rel. to stabilisation method 80−37845
Rydberg atom+atom collision, expts. 78−62908
Rydberg atom+ion, collision theory 78−62909
Rydberg atom+Rydberg atom, ionisation cross sections 79−81267
Rydberg atom+Rydberg atom, ionisation cross-section calcs. 79−31664
Rydberg atoms, expts., metastable states, multiphoton ionisation, spectroscopy, Stark struct., collisions, polarisability *(Dutch)* 78−5160
Rydberg atoms, microwave ionisation and excitation 78−94217
Rydberg atoms, selective field ionisation, 300K blackbody radiation detect. 79−58787
Rydberg states, fine struct. splitting, quantum beat and double reson. spectroscopy 78−86979
Rydberg states, spectrosc. and ionis. props. 80−23303
saturation effect in stimulated transitions between states of discrete and continuous spectra 77−42295
second-row atom, photoemission energy, rel. to homonuclear diatomics 78−86832
selective dissociation, ionis., and chem. reaction stimulation, by ultra-short pulses, isotope separation *(Russian)* 78−29825
selective photoionisation of atoms by laser radiation, appls. 78−5189

ionisation of atoms continued
singlet-triplet energy difference and singlet generalised oscillator strength, Lassettre-Dillon relation 80−63508
slow atomic collision, electron detachment, energy spectrum and isotope effects *(Russian)* 77−30984
Sn I, Sn II, Sn III, atomic partition functions and ionisation energies 77−26955
solid surface, mol. dynamic processes interaction with laser radiation 80−71943
spectral broadening, resonance ionisation under action of intense pumping wave *(Russian)* 77−42283
sputtered atoms, microscopical quantum-mech. model 79−8220
statistical model of inner-shell vacancy production in atomic collisions 79−45792
stripping cross sections, binary encounter approx. theory 78−50618
stripping in gaseous targets, equilib. charge state distrib., statistical anal., appl. to Cl, I and Br data 80−5610
strong coherent EM field ionisation, nonperturbative calc. methods 80−5512
superheavy elements, proton-induced K- and L-shell ionis. cross section estimates, comparison with actinide fission prod. X-rays in micas 77−50581
superheavy ion-atom collisions, quasiats., K-vacancy form., positron emission 80−63753
supernova remnants, electron-ion equilib. and ionization nonequilib., X-ray evidence 80−41879
surface ionisation, kinetic energy of ions 77−10751
surface layers, photon induced ion desorption, surface atom core ionisation, Auger decay 80−59809
synchrotron radiation source for atomic photoionisation studies in extreme UV and X-ray regions 80−43017
synchrotron radiation techniques for studying atomic physics 80−63583
T Tauri nebula, ionisation and emission line spectrum calc. 80−67820
thermoionisation efficiency in ion source cavity 78−844
third-row elements, at. K-shell X-ray prod. by $^{14}N^{+}$ bombardment 80−91482
three-electron atom systems with two vacancies in K-shell excited states and autoionis. state energies *(Russian)* 79−31429
three-electron atomic systems, autoionising states decay calcs. 78−78670
three-electron systems, autoionis. state widths *(Russian)* 79−49993
three-level atom, multiphoton ionisation, rate eqns., Bloch eqns. calcs. 77−83557
three-photon ionisation, reson. and non-reson., theory 79−36590
Tokamak impurity problems, atomic and mol. struct. and collision data, review 80−43959
transition functional method, ΔE SCF ionis. and excitation energies 77−88404
transition probabilities in sudden vacancy formation in electron shell 80−37788
two step reson. photoionisation, multimode and level degeneracy effects 80−78583
two-electron atom, dipole approx. for electron-electron interaction, autoionisation widths *(Russian)* 77−61691
two-electron atoms, S autoionising states, at. reson. theory appl. 80−23329
two-electron Fourier amplitudes of atomic and mol. wavefunctions using the (γ,2e) and (e,3e) processes 79−3419
two-electron multiphoton ionisation *(Russian)* 79−54822
two-hole states, one-photon decay *(Russian)* 77−79592
two-level atom, multiphoton ionisation, rate eqns., Bloch eqns. calcs. 77−83557
two-level atom, reson. pulse excitation, ionisation 78−42029
two-photon ionis., incident light polaris. effect 78−62772
two-photon ionis., sturmian expns. 79−98053
two-photon reson. ionis. with sub-ns laser pulses 78−9131
two-photon resonant ionisation saturation and Rabi oscills. 77−79589
two-photon resonant three-photon ionisation with ultrashort pulses, optical nutation effect 79−89654
two-valence electron systems, photoionisation cross sections 77−3259
unpolarised atoms, spin polarisation of ejected photoelectrons 79−45682
UV photoelectron spectra at high temp., interpretation 78−17718
vacuum spark atomic ionisation, spectroscopy *(Japanese)* 80−52911
valence shell, ionis. pots., relation between neighbours in periodic table 78−22049
very heavy ion-atom collisions, inner shell electron binding energies 80−43169
wake-bound electron contrib. to convoy electron vel. distrib., effect of ionic field 80−60729
X-ray and electron spectra excited by atomic collisions, beats mechanism *(Russian)* 79−94075
X-ray Compton and photo-effect in laser field 79−13688
X-ray production, cross-sections for inner shell ionisation by electrons, positrons, protons and α-particles 77−46643
Xalpha transition state and transition operator method calcs. 78−70743
Z=100 to 173, Dirac-Fock-Slater calcs. of energy eigenvalues and total eigenvalues 77−71739
Z=12-92, inner shell ionisation by relativistic electron impact 80−23562
Z=95 to 130, calc. of K- and L-X-rays binding energies 77−83525
(γ, e) reaction, determ. of atomic wave function, electron energy levels *(Russian)* 78−957
AR, population inversion, intershell transitions, photoionisation, from UV irradiation *(Russian)* 78−70803
Ag, ionisation energies and oscill. strengths calcs. 80−5488
Ag, K-shell ionis., X-ray prod. cross section for incident H^{+}, ^{4}He and ^{14}N ions 78−70923
Ag, loss of K-electron by proton-atom collision *(Russian)* 77−50523
Ag, photoionisation, photoelectron spectra 80−87086
Ag, polarised photoelectron yields in VUV region 80−106307
Ag, VUV absorption spectrum, autoionised level Fano parameters, photoionis. 79−49973
$Ag+H^{+}$, 1 MeV, K-shell ionisation probability, ang. depend. 77−71859
$Ag+H^{+}$, K-shell ionisation, 7-15 MeV, relativistic effects 78−82830
$Ag+H^{+}$, K-shell ionisation cross-section determ. 80−48077
$Ag+H^{+}$, L-shell ionisation at large scatt. angles 78−90283
Al I to XIII, energy levels and ionisation energies, data compilation 80−14100
Al II, energy levels, spectrum obs, 8640 to 683 Å 79−54797
Al, ion beam bombardment, $(1s^{-1}2p^{-1})^{1}P_{1}$ state nonstatistical population, X-ray spectrum 78−62894
Al, K-shell hole production by light ions, hydrogenic and Hartree-Fock model of target 77−83715

ionisation of atoms continued
Al, K-shell ionisation by ultrarelativistic electrons, density effect 80−99576
Al, laser fusion target simulation, press. ionisation 80−63374
Al+H^+, K-shell ionis., impact parameter depend., 90-200 keV 78−17775
Al+H^+, K-shell ionisation 0.5 to 40 MeV, meas. and PWBA-BEA calcs. 80−78699
Al+H^+(^{3}He) ion collisions, K-shell ionisation cross sections 77−23555
Al+H(D)(He)(Li) ions, K-shell ionis., universal cross sections 78−62895
Al+He^+(H^+), 1.9 MeV, Kα X-ray polaris. and line strengths 77−30983
Al+He(C)(N)(O), inner-shell multiple ionisation systematics, X-ray obs. 80−63790
Al+He(C)(O)(Ne), K-shell ionising collisions, average L-shell ionisation probability, K_α spectra 79−72408
Al+N^{4+}, Kα and Kβ X-ray spectra for 84 MeV incident energy 77−50517
Ar, $2p^6$ shell, oscillator strength, photoionisation cross sections, electron shell alterations determ. *(Russian)* 80−58144
Ar 3s, photoelectron ang. distrib., relativistic Dirac-Fock calc. 79−59411
Ar, 3s electron partial photoionis. cross section, branching ratios 78−29765
Ar, absolute photoionis. cross sections for VUV regions 77−46547
Ar, autoionising levels excited by heavy ion impact 79−13804
Ar, collision processes, photoionisation mass spectra obs. 79−31479
Ar, double photoionis., many-body perturbation approach 78−17634
Ar, double photoionis. cross section, calc. 77−14397
Ar, electron impact ionis., calc. for $3s^2$ subshell 79−31700
Ar, excited atom photoionisation, for sensitive UV detector 77−61122
Ar, isoelectronic sequence, many-body photoionization calcs. 78−17631
Ar, Koopmans' ionis. pot., relax. correction 79−18308
Ar, M-shell photoionis., many-body interactions 79−10081
Ar, multiphoton ionisation, EM field gradient forces 78−66608
Ar, outer 1s, 2s and 2p electron loss cross sections by multicharged ions 78−42185
Ar, photoelectron angular-distribution β parameters, resonance parameters 78−21886
Ar, photoexcited LMM Auger processes, post-collision interaction 80−32682
Ar, photoionis. cross section ratio, energies 0 to 0.05 eV above $^2P^0_{3/3,1/2}$ thresholds 78−25492
Ar, photoionisation, Auger processes, decay lifetime, line shift, profile, X-ray photoelectron spectra 80−37798
Ar, photoionisation, correl. satellites and subshell cross-sections, electron spectrosc. obs. 79−31485
Ar, photoionisation, many-body atomic transition theory 77−75111
Ar, photoionisation cross sections for excited states, rel. to KrF laser 77−75110
Ar, photoionisation cross-sections, ground state inversion pot. method 78−33481
Ar, plane polarised VUV irrad., emitted photoelectron polarisation, ang. depend. 80−47952
Ar, plasma column of hollow cathode arc, collisional model of ion system 80−38749
Ar, polarisation effects in photoionisation *(Russian)* 79−3420
Ar, radiative level lifetime, photoionisation and photoexcitation rates, in shock tube 77−34594
Ar, single-K multiple L-shell vacancy prod. in ion collisions, X-ray spectra 79−22809
Ar-Ti hollow cathode afterglow, energy transfer mechanisms and excited metallic ion prod. 80−43857
Ar+$^4He^{2+}$, ionis. cross section, Z^3 effect 78−33595
Ar+Ar^{z+}(Ne^{z+}), outer s-subshell vacancy production 79−18275
Ar+C^{2+}(O^{4+})(Si^{n+}), n=10,11,12, intense low energy autoionisation lines 79−31674
Ar+C^{4+}(C^{6+}), K-shell X-ray prod. at high energy, charge state independ. 77−6905
Ar+Cl, highly charged low vel. recoil ion time of flight spectra, cross section energy depend. 80−14222
Ar+F^-, inner-shell ionisation, X-ray cross sections 80−58369
Ar+H^+, ang. and energy distrib. of ejected electrons 79−31668
Ar+H^+, charge transfer and ionisation cross sections 79−89766
Ar+H^+, importance of d-state couplings 79−89760
Ar+H^+, ionisation, doubly differential cross sections calcs. 80−9726
Ar+H^+, K- and L-shell electron capture, 1-15 MeV 77−54607
Ar+H^+, low energy, L-shell ionisation, binding energy correction 77−54604
Ar+H^+ ions, K-Auger spectra, relative satellite line intensities, X-ray spectra 77−19066
Ar+H^+(H_2^+)(He^+), ionisation double differential cross sections 80−18913
Ar+H(H^-), 0.5 MeV $H(H^-)$ ionisation comparison 79−41230
Ar+He, Penning ionis. of Ar, He in (2^3S) state 79−41228
Ar+He^+(He^{2+}), ionisation, differential cross-sections, 0.3 to 2 MeV 79−81271
Ar+He* Penning ionisation, semiclassical descretisation procedure 78−90275
Ar+He*(1s2s,^{3}S), Penning ionis., multichannel calcs. 80−53111
Ar+$Li^{+1,2,3}$, K-shell ionisation depend. on projectile charge state 77−34743
Ar+M→Ar^++M+e^- or +M^-, (M=O_2, NO, NO_2, N_2, CO), keV energies, translational spectroscopy 78−5339
Ar^++Ar, 1-500 keV, inelastic energy loss, ionis. phenomena, theoretical model 77−34747
Ar^++Ar(He). 100-550 keV, 3s vacancy production 79−13809
Ar*+H, assoc. ionis., rovibronic struct. in electron energy spectrum 80−106380
Ar*+I_2, ion-pair form. differential cross-section, 25-133 eV, metastable Ar 78−78787
Au, L-subshell ionisation with high vel. positive ions 79−50122
Au, total L-shell photoelec. cross section ratio 77−30836
Au, VUV absorption spectrum, photoionis. cross section, Fano parameters 79−93947
Au, X-ray production cross sections for protons, fluoresc. obs. 80−102476
Au+^{3}He(^{4}He) L-subshell ionisation, Coulomb deflection effects 78−22020
Au+$^4He^{2+}$, L-shell ionis. probability, X-ray prod. 79−18276
Au+H^+, atomic K-shell ionis., X-ray emission 79−18280
ionisation of atoms continued
Au+H^+, K-shell ionisation, 7-15 MeV, relativistic effects 78−82830
Au+H^+, L-shell ionis., 0.5-3.5 MeV, X-ray emission obs. 77−54528
Au+H^+, L-subshell ionisation cross-sections, X-ray meas. 77−46520
Au+H^+, relativistic K-shell ionisation cross-section meas. 78−33593
Au+H^+ ionisation, induced L-shell alignment 80−32813
Au+H^+(D^+), L-subshell vacancy production, Coulomb deflection effects 80−9711
Au+He^{2+}, high energy ionis. probability, semiclassical approx. with relativistic Hartree-Fock function 79−6998
Au+light and heavy ions, L-shell X-ray production and subshell ionisation cross sections meas. 80−91637
B IV, ionisation rate coeff. in θ-pinch plasma, spectral meas. 77−6911
B isoelectronic sequence, ionization equilib. balance, solar and stellar atms. appl. 79−36587
B, K-shell ionis., double and single, cross section meas. by ion bombardment 78−50629
B, X-ray laser, inner-shell photoionis. pumped, practicability 77−58319
B^+, beam-foil excitation, absolute Auger yield meas. 80−14203
B^+ ions, beam foil excitation, L-Auger decays, autoionisation 77−14569
B-like ions, autoionisation states calcs. 80−43006
B+H^+(He^+), double K-shell ionis., projectile Z depend. 78−25680
B^++CH_4, 200 keV, Auger spectra, single and double K-vacancy states 77−83706
$_5^{10}B^{n+}$+Cu to Rb, 4-38 MeV, K-shell ionis., X-ray obs. 79−59549
Ba, 4d subshell spectra, strong interaction regime 79−18165
Ba, $4d^{10}$ shell, photoionisation cross sections, electron shell alterations determ. *(Russian)* 80−58144
Ba, $4d^{10}$ subshell photoionisation cross section, electron shell rearrangement 77−14400
Ba atom, laser excited, ionisation studies 80−83330
Ba, diamag. quasi-Landau spectrum near ionis. threshold, two-photon ionis. spectra obs. 78−58642
Ba, double ionisation, 20-25 eV photoionisation cross sections 80−83328
Ba, efficient ionis. by reson. laser pumping 80−32685
Ba, even-parity autoionising levels, multiphoton ionisation spectroscopy 79−59417
Ba I, 5p spectra collective excitation, rel. to double photoionis. 77−50387
Ba I, absorption spectrum, 1560 to 1770 Å 78−66487
Ba I, two-step autoionisation 80−91513
Ba, multiphoton ionis. spectroscopy of even- and odd-parity states 78−86973
Ba, multiphoton ionisation spectra of msnp^3P^0 states 77−83554
Ba, two-step autoionis., double ionis. anomaly 79−22671
Ba+Cl_2→$BaCl^+$+Cl^-, chemi-ionis. reaction, mol. beam obs. 80−104434
Be atoms, double-photoionisation cross section, core polarisation effects 78−17626
Be I, energy level calcs. term systems, convergence to Be II 2s limit 77−14354
Be II, autoionising core-excited states, alignment prod., Be^++He(methane) collision excitation 80−14204
Be, inner-shell photoionis., fluoresc. yield 77−57945
Be, ionisation energies and oscillator strengths, polarised frozen core approx. 79−36524
Be isoelectronic sequence, ionization equilib. balance, solar and stellar atms. appl. 79−36587
Be isoelectronic series, inner-shell photoionis. cross sections 78−74623
Be, K-shell ionis., double and single, cross section meas. by ion bombardment 78−50629
Be, one-particle ionis. energy, correlated wavefunction 79−45639
Be^+ ions, beam-foil excitation, L-Auger decays, autoionisation 77−14569
Be-like ions, photoionisation, 2-channel relativistic random phase approx. calcs. 79−59407
Be+H^+(He^+), double K-shell ionis., projectile Z depend. 78−25680
^{7}Be, electron capture decay, internal ionisation 77−18892
Bi+H^+, L-shell ionis., 0.5-3.5 MeV, X-ray emission obs. 77−54528
^{210}Bi→^{210}Po→^{206}Pb, decay chain, L-shell ionisation investig., X-ray emission during β, α decay 77−18891
Br II levels, NF values meas. in Ne-Br_2 mixtures 78−62753
Br, ion collisions, 12-60 MeV, K-vacancy production, multiple and single collisions in mol. orbital excitation 77−83717
Br ion+target collisions, K-X-ray yields, 1sσ excitation 77−19051
Br, ion+target collisions, X-ray yields, K-L level matching 77−19052
Br ions+target collisions, K-X-ray yields, K-vacancy sharing 77−23548
Br K-X-ray yields, 2pσ excitation 77−23549
Br, photoelectron spectra, photoionisation cross-sections 78−90131
Br+target atom, 12-60 MeV, K-vacancy cross sections, target depend. 77−19026
C, cross sections of interaction of protons 77−50538
C, electron impact, ionis. cross-section, accuracy of crossed at. beam method 79−81284
C, electron impact ionis. cross-section, accuracy of fast at. beam method 79−81283
C I photoionisation by sunlight, C II line excitation 80−58223
C III, photoionization cross sections calc. 78−17625
C, photoionisation cross section, CI calcs. 79−98050
C, photoionisation of 2s shell, photoelectron ang. distrib. 78−86833
C V, ionisation rate coeff. in θ-pinch plasma, spectral meas. 77−6911
C^+, beam-foil excitation, absolute Auger yield meas. 80−14203
C^+ ions, beam-foil excitation, L-Auger decays, autoionisation 77−14569
C+H^+, absolute C K X-ray production cross sections, 18-26 MeV 77−83719
C+H^+, K-shell ionis., impact parameter depend., 90-200 keV 78−17775
C+H^+(He^+), K-shell ionisation, impact parameter depend. 78−62891
C^{q+}+Ar, continuum electron capture and loss, 1.6-2.8 MeV/A 78−46443
Ca atom, laser excited, ionisation studies 80−83330
Ca, bound-even parity spectra, multichannel quantum defect theory anal. 77−34600
Ca, efficient ionis. by reson. laser pumping 80−32685
Ca I to XX, energy levels and ionisation energies, data compilation 80−14101
Ca, multiphoton ionis. spectroscopy of even- and odd-parity states 78−86973
Ca, multiphoton ionisation spectra of msnp^3P^0 states 77−83554
Ca, multiphoton ionisation by Nd laser radiation *(Russian)* 78−21889
Ca to Zn series, K-shell ionisation on ^{14}N-ion bombardment 77−54526

ionisation of atoms continued
Ca+H^+, K X-ray production, 0.2-0.5 MeV, ionis. cross-section 79−31459
Cd, partial photoionis. cross section 78−42022
Cd, photoionisation, alignment, linear polarisation 77−83556
Cd, photoionisation cross section, many-body perturbation theory, dipole length and vel. calc. 78−78674
Cd UV subshell photoionisation cross section, expt. and GIPM theory 78−21887
Cd^+, polarised emission of light following photoionis, Cooper-Zare model 79−81179
Cd+H^+($^2H^+$)(He^{2+}), inner-shell ionisation, Coulomb repulsion effects 80−48075
Cd+He, Penning ionisation cross section of target atom, for He(2^3S_1) 80−63777
Cl I, photoionisation cross section, calc. by many-body perturbation theory 78−62771
Cl, initial state wave functions for photoionisation cross-sections, multiconfigurational HF calcs. 80−47908
Cl, K-shell ionisation by ultrarelativistic electrons, density effect 80−99576
Cl, photoelectron spectra, photoionisation cross-sections 78−90131
Cl, photoionis. cross sections, RPA with exchange method generalisation 79−10077
Cl, photoionis. cross section of open 3p subshell 79−68213
Cl, photoionisation cross section, RPA with exchange 77−30838
Cl, photoionisation cross section and reson. theory, many body perturbation theory, 3p and 3s subshells 80−69114
Cl+He(C)(O)(Ne), K-shell ionising collisions, average L-shell ionisation probability, K_α spectra 79−72408
Cl^{n+}+Ar, K X-ray cross sections, 15 and 30 MeV, impact parameter depend. 77−19032
Cl^{n+}+Cl(Ar), branching ratio dependence on projectile velocity and nuclear charge 79−31475
Cl^{x+}+Cl(Ti)(Ni), K-shell ionization probability in energetic nearly symmetric heavy-ion collisions, 35 MeV 79−27078
Cl^{x+}+X, (X=atom with Z=11-22), K-shell ionis. cross sections 78−13596
^{36}Cl, beta decay, K-shell electron ejection 77−18888
Co+H^+, K-shell ionisation cross-sections calcs. 80−43165
Cr, K_β/K_α following K-electron capture and X-ray excitation 78−13031
Cr, $K\alpha^h$ hypersatellite spectra and double photoionisation cross-section 79−85922
Cr, Koopmans' ionis. pot., relax. correction 79−18308
Cr, multiphoton ionisation and absorpt. 80−95575
Cr+H^+, K X-ray production, 0.2-0.5 MeV, ionis. cross-section 79−31459
Cr+H^+ ion collisions, K-shell ionisation cross sections 77−23556
Cr+N^{4+}, Kα and Kβ X-ray spectra for 84 MeV incident energy 77−50517
Cs, 16^2P states, reson., 3-photon ionisation, DC Stark effect 78−42026
Cs, 2-photon and 4-photon ionisation cross-sections, absolute determ. 80−83326
Cs, $4d^{10}$ shell, photoionisation cross sections, electron shell alterations determ. *(Russian)* 80−58144
Cs, $4d^{10}$ subshell photoionisation cross section, electron shell rearrangement 77−14400
Cs, 6s-electron photoionisation, ab initio calcs. 80−91523
Cs, 7^2P excited states, photoionisation cross section meas. 77−18858
Cs arc, low-voltage hot-cathode, plasma production and props., review 77−27766
Cs, assoc. inoisation, in low press. discharge, 6P and 5D states effects 77−75284
Cs, assoc. ionisation, in low press. discharge, upper and intermediate states effects 77−75283
Cs atoms, exp. multiphoton ionisation through $9D_{3/2}$ resonant level 77−34602
Cs, cross-section meas. for four-photon ionisation 77−42297
Cs, elec. dipole approx. and elec. quadrupole resons. allowed in multiphoton absorpt. *(French)* 78−5190
Cs, electron excitation cross sections for six autoion. config., Born approx. calc. 78−25713
Cs, excited state, two-photon ionisation by ruby laser light 78−74621
Cs, excited states photoionis. cross-section, quantum defect method 78−25494
Cs, four-photon ionis., near 6F reson., rate theory 80−9568
Cs, four-photon ionis., strongly interacting resons. theory 80−52955
Cs, four-photon ionisation, new resonances 78−5187
Cs, four-photon ionisation, reson. effects 79−45689
Cs, four-photon resonant ionisation calculations 78−37613
Cs, ground state, photoionisation cross-section meas. 77−57949
Cs, He IIα $5p^{-1}$ photoelectron spectrum, config. interaction effects 80−5510
Cs I, pulsed 4-photon 6f-reson. ionis. 80−18831
Cs I, three-photon 16p reson. ionis. and DC Stark effect 80−14124
Cs, multiphoton ionis. cross sections, absolute meas. evaluation 80−14122
Cs, multiphoton ionisation, reson. shift obs. 77−445
Cs, multiphoton ionisation, reson. peak amplitude, temporal effects 78−78760
Cs, multiphoton ionisation, rel. to light statistics 79−72287
Cs, multiphoton ionisation, resonant, with intense monochromatic laser 80−32689
Cs, multiphoton ionisation spectroscopy, molecular satellites of 6^2S-7^2P doublet 78−17632
Cs, one-atom detection by reson. photoionisation spectroscopy 77−38742
Cs, oscillator strengths in principal series, Rozhdestvenskii hook obs. 80−37760
Cs, photoionis. of 6s electron, spin-orbit interaction, ab initio calc. 79−81191
Cs, polarised photoelectrons produced by circ. polarised synchrotron radiation 80−18830
Cs, reson. multiphoton ionisation by pulsed excitation, Beers-Armstrong model 78−17645
Cs, reson. multiphoton ionisation by ultrashort laser pulses, 1.06 μm 78−58630
Cs, reson. multiphoton ionis. 79−41146
Cs, reson. multiphoton ionisation near 6f reson., effective nonlinearity order 80−32688
Cs, resonant ionisation studies of proportional counter fluctuations 78−90025
ionisation of atoms continued
Cs, resonant multiphoton ionis. *(Russian)* 79−3421
Cs, resonant multiphoton ionis. 79−36589
Cs, resonant multiphoton ionisation, spatio-temporal effects 80−37794
Cs, Rydberg states collisional ionis. 79−64097
Cs, three-photon ionisation, reson. and AC Stark effects 77−68020
Cs, two photon ionisation, destructive interference effect 80−74153
Cs, two-photon ionis., profiles of $6^2S_{1/2}$-$7^2P_{1/2,3/2}$ lines 80−958
Cs, two-photon ionis. rates for linear and circular polaris. 77−50416
Cs, two-photon ionis. via $6^2P_{3/2}$ state, photoelectron spin polarisation 77−3328
Cs, two-photon ionis. via $7^2P_{1/2,3/2}$ intermediate states 77−57946
Cs, two-photon ionisation, 6s-6d quadrupole resons., ion asymmetry and spin polarisation 79−72286
Cs two-photon ionisation, effective order nonlinearity var. 80−106304
Cs, two-photon ionisation rate, time depend. 79−31622
Cs, two-photon photoionisation theory 77−6741
Cs, two-photon two-channel ionisation, laser bandwidth effect 79−59516
Cs+Ar, two-photon ionisation spectra, satellites, absorption line shape 78−82668
Cs+$H_2O(D_2O)$, ionising collisions in crossed-beam systems 78−48641
Cs+$He^m(2^3S)\rightarrow Cs^+$+He+e, reaction rate const., meas. in afterglow plasma 79−82116
Cs+I_2, ion-pair formation, energy transfer and differential scatt. 77−75272
Cs+I_2, ionising collision, trajectory surface hopping calc. 77−50509
Cs+methyl cyanide, collisional ionisation obs. 80−95716
Cs+O_2, collisional ionisation, energy spectra of forward and backward directed positive and negative ions 80−87200
Cs+UF_6, ion pair form. and atom abstraction reactions 79−1946
Cs+UF_6, ionisation reactions, absolute cross sections 80−99565
Cs+$UF_6(WF_6)$, collisional ionisation, crossed beam obs. 79−68299
Cs^++Cs^+, charge transfer, ionis., 40-280 keV, rel. to fusion scheme 80−5615
CsI, four-photon ionisation near 6f resonance 78−70801
Cu, γ-ray absorption cross-sections, 10-160 MeV 78−90136
Cu, highly ionised, spectral classifications below 55 Å 79−13658
Cu, ionisation energy, multiplet strengths, diagrammatic MBPT theory calcs. 80−9500
Cu isoelectronic series, dipole polarisability, numerical Coulomb approx. 80−43199
Cu, K_β/K_α following K-electron capture and X-ray excitation 78−13031
Cu, K-shell ionis., X-ray prod. cross section for incident H^+, ^{4}He and ^{14}N ions 78−70923
Cu, large angle K-shell ionisation probabilities, projectile charge and mass depend. 78−74750
Cu vapour, conc. determ. in hollow-cathode discharge from autoionised line intensity *(Russian)* 77−84547
Cu+H^+, atomic K-shell ionis., X-ray emission 79−18280
Cu+H^+, Cu K-shell ionis., probability ang. depend. 77−14553
Cu+H^+, K-shell ionis., Coulomb deflection effects, 0.5-2 MeV 78−17779
Cu+H^+, K-shell ionisation cross-sections calcs. 80−43165
Cu+H^+, K-shell ionisation cross-section determ. 80−48077
Cu+H^+, K-shell ionisation 0.5 to 40 MeV, meas. and PWBA-BEA calcs. 80−78699
Cu+Ni foil target, 50-65.5 MeV, K-vacancy production, impact parameter depend. 79−54958
$CuCl_4^{2-}$, core ionisation in 3d, 4f and 5f series, rearrangement effects 80−53065
^{64}Cu β^- and β^+-decays, K-shell ionisation probabilities, X-ray spectra 80−42592
D, detection by resonant three photon ionisation 78−74624
D+alkaline earth, D^- ion production, multiple charge-transfer collisions 79−89776
D+HX (X=Cl,I), HX dissociative ionisation, H^+ signal origin, mol. beam obs. 80−66778
D+He(2^1S)(2^3S), associative and Penning ionisation, autoionisation, calcs. 78−25674
D+N_2, fast collision, electron scatt. resons., ionisation, deexcitation 79−81268
Dy atom isotope separation, laser excitation, charge exchange with Cs^+ ions 80−83512
Dy atom K-shell ionisation and X-rays from ^{158}Gd(α,xn) 79−93960
Dy, atoms, prod. in nucl. reaction, K-shell ionisation cross-sections meas. 80−78687
Dy, hyperfine structure of odd isotopes, two step photoionisation, mass filtration *(Russian)* 77−46550
Dy+H^+ ionisation, induced L-shell alignment 80−32813
Er, hyperfine structure of odd isotopes, two step photoionisation, mass filtration *(Russian)* 77−46550
Eu I, 5p spectra collective excitation, rel. to double photoionis. 77−50387
Eu, laser isotope separation by two step photoionisation 77−61720
Eu+H^+, atomic K-shell ionis., X-ray emission 79−18280
Eu+H^+, two-step laser isotope enrichment using charge transfer ionisation 79−867
F ion+solid target collisions, K-shell ionisation, X-ray emission cross sections 77−19069
F ions, transient mag. field discontinuity in Fe(Co)(Ni) 80−24515
F^-+atom (Z=10-57), K-shell ionisation, X-ray prod. in transition region, collision symmetry effects 80−43163
F^{6+}+He, 10 to 40 MeV, F^{6+} K-vacancy production, role of excitation 80−37859
^{19}F, nuclear dealignment of multiply ionised 3 and 6 MeV atoms recoiling in gases 80−78267
^{19}F+Z, Z=22 to 57, 2 to 28 MeV, prod. of target atom K-shell X-rays 79−18285
Fe, highly ionised, 1s to 3p Kβ-like X-ray spectrum 77−50394
Fe, inner-shell vacancies, cascade decay, multiple ionisation and X-ray emission calcs. 80−87072
Fe, K_β/K_α following K-electron capture and X-ray excitation 78−13031
Fe, $K\alpha^h$ hypersatellite spectra and double photoionisation cross-section 79−85922
Fe, photoionis. cross section meas. 79−22674
Fe, UV photoionisation cross-section, resons. 77−14398
Fe^+, excited config. position and level struct., review 80−32621
Fe^{n+}, photoionis. cross sections, Hartree-Slater central pot. model calcs. 79−22673
Fe+H^+, K X-ray production, 0.2-0.5 MeV, ionis. cross-section 79−31459

ionisation of atoms continued
Fe+H^+, K-shell ionisation calcs. 80−23534
Fe+H^+, K-shell ionisation cross-section determ. 80−48077
Fe+H^+ ion collisions, K-shell ionisation cross sections 77−23556
Fe+I, Fe K-α X-ray emission, high-resolution meas. 80−37871
Fe+N^{4+}, Kα and Kβ X-ray spectra for 84 MeV incident energy 77−50517
Fe^{26+}+H, electron removal by collision 79−76508
Fe^{4+}+N_2(Ar)(Kr)(Xe)(SF_6), 20 MeV, gaseous targets, electron loss, charge state yields 79−54957
Gd atom, long-lived autoionisation state *(Russian)* 78−94216
Gd, ion induced K-shell ionisation cross-sections determ. by comparison with nuclear Coulomb excitation 79−76500
Gd, laser isotope separation by two step photoionisation 77−61720
Gd+H^+, K-shell ionisation, 7-15 MeV, relativistic effects 78−82830
Ge XXIV, $2p^2$-$2p^4$3s($2p^4$3d) transitions in laser produced X-ray spectra 78−13460
Ge+H^+, K-shell ionisation cross-sections calcs. 80−43165
H atom in uniform electric field, ionisation probability 79−89634
H, backscatt. from Mo in the presence of O, ion form., line emission 79−3388
H, binding energy, combined algebra for quantum description 78−8271
H, charge exchange processes in Lamb-shift type polarised ion sources *(Rumanian)* 77−46445
H, cross sections of interactions of protons 77−50538
H, dense plasma, ionisation, master eqn. analytical soln. 78−59544
H, detection by resonant three photon ionisation 78−74624
H, electron impact, ionisation, angular correls. of outgoing electrons 78−5355
H, electron impact ionis., cross-section calc. 79−76516
H, highly excited, multiphoton ionisation rates, perturb. theory calcs. 77−54542
H I, interplanetary, ionisation rate from solar H Lyman-alpha profile meas. 79−2452
H II region, extended thermal radio emission ionising agent in galactic centre 79−97059
H in anisotropic universe, ionisation history rel. to primaeval radiation polarisation 80−82552
H in quasars, photoionisation rel. to line and continuum emission 80−27003
H, interstellar, ionisation through Cl chemistry 79−40245
H, ionisation, by EM wave field, Reiss approx. calcs. 77−10647
H, ionisation, by microwave-stimulated multiphoton excitation, resons. obs. 77−68019
H, ionisation by external electrostatic field 78−13622
H ionisation coupling to acoustic instability in interstellar medium 79−97044
H, ionisation energies statistically distrib. rel. to Balmer spectrum in line merging region 77−27006
H, ionisation in AC and DC elec. fields, time depend. 80−63585
H, ionisation threshold for excited states in uniform elec. field 78−37607
H like atoms, multiphoton ionisation Pade-Sturmian approach 80−87089
H loss of K-electron by proton-atom collision *(Russian)* 77−50523
H, metastable quenching, subsequent photoionis., polarised proton prod. *(Russian)* 78−46202
H, multiphoton ionis., intense field, via complex dressed states 78−17629
H, multiphoton ionis., use of Coulomb Green's function 77−57907
H, multiphoton ionis. pot. in intense circ. polarised laser beam 80−43010
H, multiphoton ionisation, Pade approx. calcs. 79−98049
H, multiphoton ionisation, resonant, with intense monochromatic laser 80−32689
H, multiphoton ionisation potential, circularly polarized light 79−27101
H, photoionisation, two- and three-photon, calc. methods comparison 78−956
H, photoionisation cross sections elec. field-induced oscills. 80−955
H plasma, spectral intensity near series limit, taking into account sub-barrier ionisation *(Russian)* 77−31436
H, positron scatt., forming (e^+e^-)(1s)+H^+, first-order approx. 79−55006
H, resonant ionisation by laser radiation, as polarised proton source 78−78541
H, Rydberg Stark ionis. threshold scaling laws 77−6721
H, Stark effect, dispersion relation, asymptotic formulae, ionis. rate, perturbation theory calc. 80−14106
H, Stark spectrum and field ionisation, density of continuum states, normalised wavefunctions 80−83317
H, three-photon reson. photoionis. in plasma 80−58640
H, two photon ionisation in presence of one photon ionisation, cross section calc. 80−83327
H, two-photon ionis. simultaneously with one-photon ionis. 78−33484
H, two-photon ionisation, Laplace transform method 79−10084
H^- and H electron loss in plasma target 78−67371
H^-, electron loss cross sections in gases, using polarised projectiles 80−37872
H^- photodetachment, Feshbach resonances 80−37753
H^-, photodetachment cross sections, one and two electrons, multichannel J-matrix calc. 77−18860
H^-, S autoionising states, time stability theory 78−90130
H^+, and D^+, scattered from Cu, energy spectra negative component 79−65967
H^+ induced ionisation cross-sections, thick target technique 78−37726
H:He, 15 to 150 keV ionising collision, electron ang. and energy distrib. 80−53121
H-like ions, critical ionisation, by electric fields, exact classical method 78−25731
H-like ions+heavy particle, bound state effect on ionisation cross sections 78−25682
H+Ar, collisional charge production, differential scatt. calcs. 77−68107
H+Ar, collisional charge production cross-sections 77−71860
H+atom (ion), ionis. by one or two electron at. particles, Born approx. 79−54960
H+C^{6+}, collisional electron removal, cross-sections, mechanisms 78−25683
H+C^{6+}(He^{2+}), ionis. cross sections 79−22805
H+Fe^{n+}, 50-1200 keV amu^{-1}, impact ionis. and electron capture cross-sections 78−42204
H+H, excited atom ionisation collision, excitation transfer effect 79−81272
H+H collisions in laser field, excitation, charge exchange and ionis. *(Russian)* 79−94078

ionisation of atoms continued
H+H^+, 50-200 keV, excitation and ionis., U-matrix method calcs. 78−17778
H+H^+, coupled state calc., charge transfer and direct ionis. 79−22810
H+H^+, energy transfer and ionisation cross-section calcs 77−50522
H+H^+, ionis. modified second Born approx. 77−88546
H+H^+, quantum theory of ionisation in fast collisions 79−3553
H+H^+(Ar^{q+})(Kr^{q+})(B^{q+})(C^{q+})(N^{q+})(O^{q+}) charge transfer and impact ionis. cross sections calcs. 77−88555
H+H^+(He^{2+})(Be^{4+})(O^{8+}), electron capture into n, l levels, 100 keV/amu 79−22826
H+He (2^3S), pot. energy surfaces and autoionisation lifetimes calcs. 77−34740
H+He(Xe), simultaneous ionisation investig. 80−32815
H+heavy ion (highly stripped), electron loss, charge state depend. 78−70921
H+ion, charge exchange and ionis. cross sections *(Russian)* 79−50130
H+ion, collisional ionisation by fast low-charge-state ions 79−86056
H+Li(Li_2), superthermal collisions, photon and positive ion prod. 78−78788
H+N, stripping cross-sections, binary encounter approx. theory 78−50618
H+N_2(O_2), charge prod. cross sections and differential scatt. calcs. 78−94313
H+Ne*, Penning ionisation, electron energy spectrum 79−72406
H+Ne(Ar)(Kr)(Xe), free electron production, integral cross-sections determ. 79−89754
H+Ne(Ar)(Kr)(Xe)(O_2), 20-500 eV, ion pair and free electron production, integral cross sections 78−46437
H+O^{8+}, electron removal, charge transfer and impact ionisation cross-section 79−76504
H+Xe, electron-loss cross section struct., 0.05-4 MeV 78−9236
H^-+inert gas, negative ion detachment cross section determ. 80−63796
H^++Ag(Zr)(Fe)(Cu)(Ti), K-shell ionisation cross-section, 85 to 790 keV 80−106390
H^++Ar, 5-1.5 MeV, ejected-electron energy and ang. distrib., differential cross sections 77−88547
H^++atom, inner shell ionisation, electronic relativistic effects 77−23552
H^++atom, ionis. cross section, realistic vel. distrib. for target electron 78−46439
H^++atom, ionisation, proton polaris. meas. 80−9482
H^++atom, K-shell ionis. cross section for atoms, modified binary encounter model 78−46440
H^++Au(Bi)(u), L X-ray production cross sections, 0.3-1.8 MeV, expt. rel. to PWBA prediction 80−53115
H^++Cs→H^-+Cs^{2+}, proton conversion, 0.2 to 6.0 keV *(Russian)* 77−1920
H^++H, 15-200 keV, excitation and charge transfer cross sections, Sturmian expansion 77−19024
H^++H, ionisation and electron capture to continuum 80−58366
H^++He, double electron capture, close-coupling approx. calcs. 77−71868
H^++He, proton energy degradation, approx. yield spectrum 79−31643
H^++He^+, charge transfer and ionis. cross sections, coincidence meas. 78−50634
H^++He^+, fast collision, ionisation and charge transfer, cross section meas. 78−25698
H^++He^+, He^{2+} form. by charge exchange and ionis., cross sections 77−83708
H^++He^+, ionis. and charge transfer cross sections 78−42186
H^++He^+, ionisation and charge transfer using intersecting beams 77−68104
H^++He(Ar)(C), ionisation processes viewed in forward direction 77−71866
H^++He(Ne)(Ar), K-shell ionisation cross-sections, Glauber approx. calcs. 77−46629
H^++Li^+, charge transfer and ionisation, total cross sections for production of Li^{2+} determ. 80−91657
H^++Na(Mg)(Al)(Si)(Ti), K-shell ionisation cross sections for 15-65 keV protons 78−90284
H^++U(Ni)(Au)(Sn), 4.88 GeV, K-vacancy production cross sections 77−19036
H_2^+, photoionisation effective cross sections 80−43121
H_2+He(2^3S), Penning ionisation, quantum mech. scatt. calcs. rigid rotor approx. 77−34741
H_2+He(2^3S), pot. energy surfaces and autoionisation lifetimes calcs. 77−34740
H_2^++He(Ar)(C), ionisation processes viewed in forward direction 77−71866
H*+H(Li), resonant ionisation, cross section and ionisation probability 80−63785
H(1^2S)+He(2^1S), Penning ionisation, semiclassical and Born total cross-sections 78−33586
H(1s) and (2s), electron loss in passing through inert gases 79−13805
H(2s)+inert gas, electron capture, H^- form., 4-25 keV 80−9729
He, 2^1S state, two-photon ionisation, multipole interference 79−22675
He, 2^3S and 2^1S states, two-photon ionization 80−37791
He, 2^3S_1 metastable state, interactions, optical pumping investig. 80−23377
He 2S metastable state, three-photon ionis. 79−18167
He, 2S metastable states, singlet and triplet; two and three photon ionisation cross section, absolute determ. 80−83329
He (1^1S) and (2^3S), electron loss in passing through inert gases 79−13805
He, absolute photoionis. cross sections for VUV region 77−46547
He, absolute photoionisation cross section curve 78−37612
He, autoionisation of highly excited states, config. interaction 78−13445
He, autoionising resons., complex-coord. anal. 79−49992
He beam charge fraction, emerging from solid 80−9716
He, double photoionisation calcs., variational method 80−37734
He, elastic electron scatt. phaseshifts, 2s2p ^{3}P autoionisation, 1s2s ^{3}S→1sεp ^{3}P triplet continuum photoionisation 79−31480
He, electron impact, ionis. cross-section, accuracy of crossed at. beam method 79−81284
He, electron impact, secondary electron doubly differential cross-section, 50-300 eV 79−59585
He, electron impact ionis., distorted-wave model, 100-400 eV 79−45824
He, electron impact ionis. cross-section, accuracy of fast at. beam method 79−81283
He, excitation and ionisation, by instationary shock fronts 78−59540

ionisation of atoms continued
He excited atom photoionization, for UV photopreionisation CO_2 laser 78−17902
He glow discharge, low press., excitation transfer and quenching of n=3 excited states 80−38743
He II excited states in optically thin plasmas, role of direct ionisation-excitation 80−102579
He ion+Cu, neutralisation and ionisation of low energy He ions scatt. from (100) face 78−23572
He, ionisation by UV radiation from CO_2 laser produced Cu plasma 78−17624
He ions +Ti(Fe)(Cu), K-shell ionisation cross-section, 85 to 790 keV 80−106390
He, isoelectronic spectra autoionisation states n=3 hydrogenic threshold, complex rot. method 79−31477
He, Koopmans' ionis. pot., relax. correction 79−18308
He, many electron system, photoionisation and photoexcitation, at. transition strong config. interaction effect 80−47909
He, metastable, deexcitation process on Mo [110] impact 78−95642
He, metastable, multiphoton transition detection, n^3S-n^3D splitting meas. 80−58231
He, metastable, two-photon ionisation calc. for linearly and circularly polarised laser light 79−797
He, metastable, two-photon ionisation, multipole interference effects 80−23466
He, metastable $1s2s\,^1S$ state, photoionisation, perturbation theory calcs. 78−78759
He, metastable and ground state electron loss cross section, collisions with gases and metal vapours 80−53117
He metastable state, two- and three-photon ionisation 80−91518
He, metastable states, electron and proton impact ionisation, autoionisation 80−102573
He, metastable thermal atoms, interaction with solid surface, obs. of He^+ ion creation *(French)* 77−79684
He, multiphoton ionis. pot. in intense circ. polarised laser beam 80−43010
He, multiphoton ionisation potential, circularly polarized light 79−27101
He, outer 1s, 2s and 2p electron loss cross sections by multicharged ions 78−42185
He, photoabsorption, modified RPA calcs. with exchange 78−13477
He, photoionis. and photoabsorpt. cross sections for aeronomic calcs., data tables 80−41599
He, photoionis. cross-section, hyperspherical coord. method calcs. 80−102496
He, photoionisation, correl. satellites and subshell cross-sections, electron spectrosc. obs. 79−31485
He, photoionisation, frozen-core HF perturbation theory, oscillator strength, dipole length and vel. calc. 78−78672
He, photoionisation above n=2 photoionis. threshold 80−102497
He, photoionisation cross section from excited state $^4p\,^1P_1$ *(Russian)* 77−61722
He, photoionisation cross sections up to n=2 excited state, evidence of autoionisation 80−91520
He, photoionisation cross-sections, ground state inversion pot. method 78−33481
He, photoionisation cross-section, using UV laser plasma light source 79−19096
He, three-photon ionisation from metastable states, cross-sections 77−42296
He, two-electron photoionis., threshold law and photoelectron spectra 78−29767
He, two-photon ionisation cross-section calcs. 78−21888
He, two-step photoionisation via $4p\,^1P_1$ state *(Russian)* 79−59413
He^-, electron loss in passing through inert gases 79−13805
He^+, neutralisation, reionisation in O_2, ion pair form., differential cross sections determ. 80−53120
He-like ions, multiple charged, reson. photoionis. 79−54818
He-like ions, photoionisation, 2-channel relativistic random phase approx. calcs. 79−59407
He+Ar(Kr)(Xe), 2^1S and 2^3S assoc. and Penning ionisation cross sections vel. depend. 79−3551
He+atom (ion), ionis. by one or two electron at. particles, Born approx. 79−54960
$He+Cl^+$, highly charged low vel. recoil ion time of flight spectra, cross section energy depend. 80−14222
$He+e^-(H^+)$(pion), specific primary excitation by fast accelerator particles 80−23559
He+H, associative and Penning ionis. cross-sections, pot. energy curve study 79−87836
$He+H_2(He)(N_2)(Ne)(Ar)$, 25-450 keV, metastable ion beam electron loss and deexcitation cross section 77−34745
$He+H^+$, ang. and energy distrib. of ejected electrons 79−31668
$He+H^+$, determ. of He excited state populations by two-photon reson. ionisation spectroscopy 78−82707
$He+H^+$, double He ionis., polarised electron vel. distrib. effect 80−53109
$He+H^+$, double ionis. of He, binary-encounter theory 78−1066
$He+H^+$, electron ejection differential cross sections 77−46625
$He+H^+$, ionising collision, first-order Faddeev approx. 79−22827
He+He, (2^3S) and (2^1S) metastable states, direct and assoc. ionisation rate consts. in afterglow, electron energy spectra 79−13812
He+He, He^- decay cross section oscills. *(Russian)* 77−19038
He+He, ionisation mechanism, theory 77−14550
He+He, metastable atoms, collisional ionisation cross-sections 78−70911
$He+He^+$, autoionising transitions interference 77−42390
He+ion, collisional ionisation by fast low-charge-state ions 79−86056
$He+Li^+$, 2 to 5 keV, ejected electron profile variation with impact angle 78−37729
He+multiply charged ions, electron capture and impact-ionis. cross sections, Monte Carlo calcs. 79−27083
He+Xe, electron-loss cross section struct., 0.05-4 MeV 78−9236
$He^{+,2+}$+Ar, 2 MeV, ejected electron spectra, 20-450 eV, 0-10° 77−34746
He^++alkali metal atom, ionisation cross sections, binary encounter approx. with HF electron vel. distrib. 78−55225
He^++Ca(Ba), 2-1000 eV, spontaneous ionis. mechanisms 79−64090
He^++He, autoionisation electrons and scatt. ions, ang. correl. determ. 80−63792
He^++He, autoionising state excitation, ion-electron coincidence, electron azimuthal depend. 78−37734
ionisation of atoms continued
He^++He$(2p^2\,^1D)$, collisionally excited, autoionisation electron ang. distrib., interference struct. 80−32819
$He^{2+}+He^+$, ionis. and charge transfer cross sections 78−42186
He^{2+}+Li, electron capture, ionis. cross section, low-vel. $He^+(3l)$ production, X-ray production 79−22822
$He^+(He^{2+})$+He(Ar)(C), ionisation processes viewed in forward direction 77−71866
He(I), XPS relative intensity and photoionisation cross-section 80−63599
He(II), XPS relative intensity and photoionisation cross-section 80−63599
$^4He^+$+$H(H_2)$, electron loss cross section 78−22018
He*+Ar, Penning ionisation, laser modified collisional effects in electron energy spectrum 78−90278
He*+$H(H_2)$(Ar), metastable state, ionis. processes 78−62907
He*+He, collisional ionisation, cross-section meas. 77−46631
He*+He, collisional ionisation, $He_2\,^1\Sigma_g^+$ state pot. curve calcs. 77−46632
He*+He, inelastic collision, 1-5 keV, autoionising states 78−13581
$He^*+Ne^*\rightarrow He+Ne^+$+e, Penning ionisation, merging beams obs. 78−33585
$He^*(^3S)+Ar+\hbar\omega\rightarrow He+Ar^+(^2P)+e^-$, intense laser radiation assisted collisional ionis. 79−76497
$He^*(2^3S)$, $(2^1S)+O_2$, ion pair form., ion beam neutralisation reionisation spectroscopy 80−53120
$He^*(2^3S)+F$, Penning ionisation and excitation transfer, unified treatment 78−25672
$He^+(1s)$+H(1s), excitation and ionis. processes 78−42189
He$(2^3S, 2^1S)$+Ba(Y)(Ce), Penning process, double ionisation 77−3439
He$(2^3S, 2^1S)$+H, Penning ions. 79−64089
He$(2^{1,3}S)$+H, autoionising system, Siegert eigenvalues, variational calcs. 79−50106
He(2^3S)+H(D), Penning and assoc. ionis. cross sections, vel. depend. 79−22815
He$(2^3S_1)+Hg_0\rightarrow He_0+Hg^+$+e, in afterglow, rate const. meas. 78−17785
He(2^3S_1)+Na(K)(Rb)(Cs), Penning ionis. in stationary afterglow 78−42184
Hf+$H^+(He^+)$, L-subshell ionisation cross section, branching ratios, fluoresc. yield, Coster-Kronig factors 80−43166
HfI, at spectrum, g-values, Zeeman effect, LS-coupling, ionisation pot. 77−3292
Hg, four-photon resonance ionis. 77−42289
Hg, partial photoionis. cross section 78−42022
Hg-Ar, HF discharge, electron energy distrib. and atom ionisation processes 80−44048
$Hg+H^+$, L-subshell ionisation cross-sections, X-ray meas. 77−46520
Hg+He, excitation of $Hg^+(7^2P_{1/2}, 7^2P_{3/2})$ in afterglow, rate consts. *(Russian)* 78−29848
$Hg+He^{2+}$, autoionisation, 5-20 eV, electron and ion ang. distrib. 78−78795
$Ho+H^+$, relativistic K-shell ionisation cross-section meas. 78−33593
H^+(spin polarised)+atom, inner-shell ionis., subsequent radiation ang. distrib. 80−53114
I, ion collisions, 15-80 MeV, K-vacancy production, multiple and single collisions in mol. orbital excitation 77−83717
I ion+target collisions, K-X-ray yields, 1sσ excitation 77−19051
I ion+target collisions, K-X-ray yields, K-vacancy sharing 77−23548
I ion+target collisions, K-X-ray yields, 2pσ excitation 77−23549
I ion+target collisions, X-ray yields, K-L level matching 77−19052
I, partial photoionis. cross sections, rel. intensities, irreducible tensor anal. 79−98048
I, reson. UV fluoresc. and photoionis. obs., in nonlinear I_2 photodissoc. 78−37692
I+target atom, 15-80 MeV, K-vacancy cross sections, target depend. 77−19026
In I, absorption spectra, 320 to 1000 Å, intersubshell correls. 4d spectrum two-electron detachment 77−10617
In, photoionisation cross section calc. for $4d^{10}$ subshell in RPA with exchange 77−23479
In, VUV photoelectron spectra, pseudo-atomic beam technique 80−58225
$In+H^+$, inner-shell ionisation, Coulomb repulsion effects 80−48075
^{114m}In, K-shell internal conversion, $K\alpha_1$ hypersatellite line energies, intensities 77−18885
K atom beam, impact on W surface, mean residence time of K^+ and ionisation efficiency 77−73208
K, cross section depend. of many-photon ionisation on light polarisation 77−42294
K, electron excitation cross sections for six autoion. config., Born approx. calc. 78−25713
K, excited states field ionis., p states spin-orbit interaction 79−59592
K, fine-struct. intervals, polarisabilities, highly excited d states 79−27100
K II, isoelectronic series, photoionisation, multichannel CI calcs. 79−93931
K, multiphoton excitation, Rydberg transitions, ionisation detection 77−42304
K, photosensitised assoc. ionisation, excited from reson. levels 77−83710
K plasma, magnetic-mirror-trapped, heating with array of hot W wires 80−33789
K, reson. three photon ionisation, saturation effects 78−90137
K, Rydberg autoionisation state lifetime calc. 77−444
K Rydberg states, optical excitation, collision ionisation processes 80−102561
K, two-step photoionisation, triple crossed beam obs. 78−66616
K^{2+}, photoionisation cross sections calc., R-matrix theory 77−18865
K^{2+}, photoionisation cross-section, R-matrix theory 78−82702
K+Br, harpooning mechanism interactions, semiclassical optical model 79−89755
$K+Br_2$, inelastic scatt., total cross-sections, trajectory surface hopping calcs. 78−46420
$K+Cl_2\rightarrow K^+(Cl+Cl^-)$, 5.5−14.0 eV, energy loss, spectrum maxima, mechanism 77−75286
$K+Cl\rightleftarrows K^++Cl^-$, $KCl+M\rightleftarrows K^++Cl^-+M$, rate consts. in at. press. flames 77−60036
$K+Cl\rightleftharpoons K^++Cl^-$, chemi-ionis. and recomb. cross sections 78−33583
$K+D_2O\rightarrow OD^-+K^++D$, 100-200 eV, $D_2O^-(^2A_1)$, state 78−17770
$K+H_2O(D_2O)$, ionising collisions in crossed-beam systems 78−48641
$K+H_2S(DS)$, collisional ionisation, positive and negative ion energy spectra obs. 80−63775

ionisation of atoms continued
K+HCl, ion pair form., energy loss spectra 79−34286
K+I chemi-ionisation, integral cross section calc. for two state model 79−18282
K+I chemiionis. differential cross-section calc. for two-state model 79−18283
K+I_2, ion-pair formation, energy transfer and differential scatt. 77−75272
K+I_2, ionising collision, trajectory surface hopping calc. 77−50509
K+methyl cyanide, collisional ionisation obs. 80−95716
K+NO_2, ion pair form. reaction, energy loss spectra obs. 79−91921
K+O_2, collisional ionisation, energy spectra of forward and backward directed positive and negative ions 80−87200
K+O_2→K^++O_2^-, electron transfer kinematics 77−6903
K+SF_6, ion-pair form. reaction, energy loss spectra 80−55630
K+UF_6, ionisation reactions, absolute cross sections 80−99565
Kr 4s, photoelectron ang. distrib., relativistic Dirac-Fock calc. 79−59411
Kr, absolute photoionis. cross sections for VUV region 77−46547
Kr afterglow plasma, electron energy distrib. funtion 80−38748
Kr, discharge, non-self-maintained, ionis. instability of excited ats. and excimers *(Russian)* 77−84557
Kr, electron energy loss spectra, energy-depend. multichannel quantum defect theory anal. 77−61860
Kr, ion collisions, 200-330 MeV, K-vacancy production, multiple and single collisions in mol. orbital excitation 77−83717
Kr, ion+target collisions, K-X-ray yields, 1sσ excitation 77−19051
Kr ion+target collisions, X-ray yields, K-L level matching 77−19052
Kr ion+target collisions, K-X-ray yields, 2pσ excitation 77−23549
Kr ions, high energy stripping by solid foil, charge state distribs. 77−6912
Kr, Koopmans' ionis. pot., relax. correction 79−18308
Kr, photoionisation cross sections for excited states, rel. to KrF laser 77−75110
Kr, photoionisation cross-sections, ground state inversion pot. method 78−33481
Kr, population inversion, intershell transitions, photoionisation, from UV irradiation *(Russian)* 78−70803
Kr, stepwise ionis. relax., multilevel models 78−13592
Kr, twelve-photon ionis. at 10^{13} W cm^{-2} laser field 80−32687
Kr+F^-, inner-shell ionisation, X-ray cross sections 80−58369
Kr+target atom, 200-330 MeV, K-vacancy cross sections, target depend. 77−19026
^{84}Kr ions+target collisions, K-X-ray yields, K-vacancy sharing 77−23548
Kr*+Ar*, metastables, chemi-ionis,, merging beams. 0.01-10 eV 80−14198
Kr**+HCl rot. effect on collisional ionis. 77−83702
La, 4d subshell spectra, strong interaction regime 79−18165
La, ionisation cross sections for L_1 and L_2 subshells by 250-500 keV protons *(Russian)* 77−6918
Li atoms, photoexcitation and ionisation cross sections, Stieltjes-Tchebycheff procedure 78−17633
Li, Auger and autoionisation spectra, collisional excitation mechanisms 77−19042
Li, autoionisation states, config. decays and excitation energies 78−13475
Li I-like spectra, energy struct., accurate semiempirical formulae 79−49970
Li ion soft X-ray laser, 199 Å, autoionising state effect 77−34876
Li, isoelectronic sequence, photoionisation cross section, core polarisability effects 77−57944
Li isoelectronic sequence, ionization equilib. balance, solar and stellar atms. appl. 79−36587
Li isoelectronic series, dipole polarisability, numerical Coulomb approx. 80−43199
Li, laser excitation and ionisation, autoionising states obs. 77−61699
Li, photoionis., one-electron pseudopotential calc. 79−18166
Li, photoionisation, depolarisation effects 77−83663
Li, photoionisation, two- and three-photon, calc. methods comparison 78−956
Li, photoionisation cross section meas. at 2P level 78−58637
Li, saturated three-step resonance ionisation spectroscopy 79−81189
Li, selective two-step photoionisation and isotope separation 77−71783
Li, two photon ionisation in presence of one photon ionisation, cross section calc. 80−83327
Li, two-photon ionis., many-body perturbation theory 79−22679
Li, two-photon ionization spectra 80−23382
Li, vap., multiphoton absorption, space-charge ion detect. 79−54827
Li^+, autoionising, and quasibound states, Feshbach calcs. 77−54505
Li^+, doubly excited autoionis. resons., laser prod. plasma absorption spectra obs. 77−50392
Li^+, S-autoionising states, energy calcs. 79−36520
Li-like ions, partial photoionis. cross-sections and radiative recomb. rate coeffs. 80−52951
Li+$F_2(Cl_2)(NO_2)$, $4^2S_{1/2}$ excited atom crossed beam collisional ionisation 79−64087
Li+inert gas collisions, electron loss cross-section meas. *(French)* 78−86941
Li+Li*(H*), resonant ionisation, cross section and ionisation probability 80−63785
Li^++He collisions, Li-K shell excitation, autoionisation spectra meas., total cross sections 77−19053
Li^++Ne, low energy, ionisation, total cross-section meas. 77−54606
Li^{1+}+$H(H_2)$, (q=1-3), electron capture and loss cross sections 78−42187
Li(2^2S), electron loss in passing through inert gases 79−13805
Mg, inner-shell ionisation by H^+, He^+ impact, target atom ionic alignment, Born approx. 78−78789
Mg, interstellar, ionisation state rel. to existence of circumstellar clouds 80−94782
Mg ions in low density plasma, dielectronic recomb., ionization equilib. and radiative energy loss, solar corona appl. 79−68903
Mg, K-shell ionisation by ultrarelativistic electrons, density effect 80−99576
Mg, $K\alpha^n$ hypersatellite spectrum, K-shell electron double ionisation cross section, binding energy 79−36577
Mg+H^+, electron capture and impact ionisation cross sections, CI calc. 80−23343
Mg+H^+(He^+) and electron impact ionis., Auger study of collisionally induced alignment 78−90279
Mg^++H^+, Mg^{2+} form. by charge exchange and ionis., cross sections 77−83709
Mn, energy levels, Mn I to Mn XXV, review 78−21841
Mn+H^+, K X-ray production, 0.2-0.5 MeV, ionis. cross-section 79−31459
Mn+H^+ ion collisions, K-shell ionisation cross sections 77−23556
Mo, highly ionised, mean wavelength and spectral width of transition arrays 79−6913
Mo IX, energy levels, $4s^24p^4$ to $4s4p^5$ transitions obs. 77−3288
Mo XXXI-XXXIV spectra from exploded Mo wire plasmas 79−1295
Mo^{29+} to $^{39+}$, photoionis. cross sections, radiative recomb. rate coeffs., rel. to plasma diagnostics 80−52953
$Mo^{30,\ 12+}$, photoionis., relativistic RPA calc. 80−47913
Mo+Nb, K-shell vacancy prod., impact parameter depend. 80−14225
N, $^4S^0$ ground state, photoionisation calcs. 79−85909
N, cross sections of interactions of protons 77−50538
N, electron impact, ionis. cross-section, accuracy of crossed at. beam method 79−81284
N, electron impact ionis. cross-section, accuracy of fast at. beam method 79−81283
N IV, absorption spectra, 4f electron localisation effects in collapsing shell 77−3290
N, ionisation, multiphoton absorpt., spectroscopic evidence 80−63726
N, outer 1s, 2s and 2p electron loss cross sections by multicharged ions 78−42185
N, photoionis. cross section, many-channel quantum defect method 78−17638
N V, absorption spectra, 4f electron localisation effects in collapsing shell 77−3290
N V, ionis. rate meas. in theta-pinch plasma, VUV obs. 78−26254
N^-, form., by double electron transfer, cross-section meas. 78−78806
N^+, beam-foil excitation, absolute Auger yield meas. 80−14203
N+O, endoergic chemiionisation, semiclassical theory 79−98208
N^++N, 35-200 keV, K MO X-rays, production mechanism, spectral distrib. 78−42183
N^++N_2, 35-200 keV, X-ray spectrum, rel. to N^++N mechanism 78−42183
N^++$NH_3(H_2O)(Ne)$ symmetric collisions, double K-shell ionisation, two-electron-one-photon transitions 77−19067
N^{n+}+$N_2(O_2)(Ne)$(methane), K-shell vacancy prod. cross-section, charge state depend. 78−17751
N^{q+}+H_2(q=1 to 7), electron capture and impact ionisation cross sections 77−75290
NH_3+N^+, 35-200 keV, X-ray spectrum, rel. to N^++N mechanism 78−42183
Na, ^2D highly excited states, fine struct. splitting, field ionisation quantum interference 80−18835
Na (3p state), partial photoionis., cross sections $\sigma_{3p,s}$ and $\sigma_{3p,d}$, expt. separation and study 78−42020
Na, absolute photoabsorpt. cross section, 45-250 eV 77−88434
Na, Auger and autoionisation spectra, collisional excitation mechanisms 77−19042
Na, core polarisation effects, influence on photoionisation cross sections, ground and excited states 78−46308
Na, cross section depend. of many-photon ionisation on light polarisation 77−42294
Na, cross-section meas. for five-photon ionisation 77−42297
Na, detection of nF Rydberg levels by photoionisation *(French)* 77−71785
Na, diabatic field ionisation of highly excited at. states 80−43202
Na, efficiency laser ionisation via superelastic collisions and reduced ionisation pot. 77−79588
Na, electron impact excitation, L-Auger and autoionis. spectra 78−5354
Na, excited 4D and 5S state, absolute photoionisation cross-section 80−99488
Na, field ionisation of highly excited states 78−17814
Na, high-lying Rydberg states, field ionisation 79−45683
Na, highly excited d states, elec. field ionisation 77−6658
Na I, even-parity autoionising states, photoabsorpt. 350 to 400 Å, laser excitation 79−59390
Na, ionis. interference, in Ebert spectrograph with 5 kW ICP unit 80−86453
Na, ionisation and energy pooling in laser-excited vapour 79−795
Na, ionisation of high-lying states by pulsed laser field *(Russian)* 77−75113
Na isoelectronic series, dipole polarisability, numerical Coulomb approx. 80−43199
Na, K-shell ionisation by ultrarelativistic electrons, density effect 80−99576
Na, laser temporal coherence effects in two-photon resonant three-photon ionisation 80−32686
Na, multiphoton ionis., AC Stark effect 77−57948
Na, multiphoton ionisation, resonant, with intense monochromatic laser 80−32689
Na, multiphoton ionisation in third harmonic generation by mode locked Nd:YAG laser 78−94413
Na, one and two-photon ionis. of 3s and 3p states 78−50512
Na, photoionis., one-electron pseudopotential calc. 79−18166
Na, photoionis. cross section resons., time-dependent HF theory 80−32684
Na, photoionisation cross-section, electron correls. Brueckner-Goldstone calcs. 77−6742
Na, photosensitised assoc. ionisation, excited from reson. levels 77−83710
Na, quantum beats of hyperfine levels observed in photoionisation 80−32690
Na, reson. multiphoton ionisation, broadband laser AC Stark splitting 78−70808
Na, reson. two-photon ionis., photoelectron ang. distrib. and polaris., nucl. spin influence 79−10083
Na, reson. two-photon ionisation via $3p^2P_{3/2}$ state, photoelectron ang. distrib. 80−43016
Na, resonant three-photon ionis., saturation effects 78−58632
Na, Rydberg atoms, photoionisation, 300K background radiation effects 79−68271
Na, Rydberg atoms, selective field ionisation, 300K blackbody radiation detect. 79−58787
Na, Rydberg levels mm resonances detected by field ionis., quantum defects, Stark shifts 77−42262

ionisation of atoms continued
Na, Rydberg states, elec. field ionisation, sensitive detection of multiple thresholds 79−7026
Na, Rydberg states, optically pumped, electric field ionis. *(Russian)* 79−27095
Na, single atom detection by laser photoionisation *(Russian)* 78−33487
Na, Stark effect for selective stepwise ionisation by laser radiation 79−13669
Na, three-photon ionisation, laser bandwidth and intensity effects 80−52956
Na+Ar*, Penning, associative and total ionis. cross sections 77−79683
Na+Cl⇌Na^++Cl^-, chemi-ionis. and recomb. cross sections 78−33583
Na+H^+ collisions, L-Auger electron emission, autoionising states, line broadening effects 77−14568
Na+I_2, ion-pair formation, energy transfer and differential scatt. 77−75272
Na+I_2, ionising collision, trajectory surface hopping calc. 77−50509
Na+Na, crossed-beam collision, laser-induced Penning and assoc. ionisation, struct. obs. 80−83476
Na^++Ne, nonadiabatic transitions, effective ionisation cross-section calcs. 79−10195
NaI isoelectronic sequence, 3s-3p and 3p-3d transitions, ionisation energy 78−70773
Na(3^2P)+$O_2(SO_2)$, near-threshold ionis. of Na* 77−88544
Nb VIII, energy levels, $4s^24p^4$ to $4s4p^5$ transitions obs. 77−3288
^{95}Nb, beta decay, K-shell electron ejection 77−18888
^{95}Nb, K-shell autoionisation in β-decay 77−298
Ne, 1s and 2s photoionis. cross sections, L^2 calc. 80−951
Ne, 2p levels prod. by dissoc. recomb. in afterglow, recomb. coeffs., level population 80−43855
Ne 2s, photoelectron ang. distrib., relativistic Dirac-Fock calc. 79−59411
Ne, absolute photoionis. cross sections for VUV region 77−46547
Ne, atomic deexcitation effects of X-rays, X-ray preionisation in TEA lasers 79−793
Ne Auger electron decay, final charge states, beam-foil investig. 77−19060
Ne, autoionising Ne levels excited in 5-10 keV collisions 78−22017
Ne, charge-state distributions and the population of X-ray emitting states 79−68311
Ne, core ionis., single orbital relax., LCAO MO SCF calcs. 78−29739
Ne, double photoionis., many-body perturbation approach 78−17634
Ne, electron degradation spectra, inner-shell contribs. 77−3474
Ne, electron or photoionisation, electron shake-off, continuum states interaction 78−29766
Ne, electron shake-off following electron or photon bombardment, continuum states interaction 77−14403
Ne, highly-ionised, heavy ion impact, selective electron capture effects 80−14202
Ne I to Ne IV, excitation in ion-atom collisions, 100 keV region, emission spectra obs. 80−14205
Ne II, III, and IV ground state, photoionis. cross sections, close coupling calcs. 80−5513
Ne II, III, IV, photoionisation cross sections calc. 80−43014
Ne, ionisation potential, KLL Auger energies, SCF transition operator calcs. 78−41925
Ne, isoelectronic sequence, many-body photoionization calcs. 78−17631
Ne, Koopmans' ionis. pot., relax. correction 79−18308
Ne, metastable, photoionis. cross section calc. 78−33485
Ne, outer 1s, 2s and 2p electron loss cross sections by multicharged ions 78−42185
Ne, photoelectron angular-distribution β parameters, resonance parameters 78−21886
Ne, photoionis. cross-sections, L-subshells, 30-300 eV 79−31483
Ne, photoionisation, complex amplitudes at low energy singly and doubly excited resons. 78−78673
Ne, photoionisation, many-body atomic transition theory 77−75111
Ne, photoionisation, relativistic R-matrix theory 78−5184
Ne, photoionisation cross-sections, ground state inversion pot. method 78−33481
Ne, reson. free-free absorpt. by electrons in at. field, negative ion form. 77−3463
Ne, total and differential photoemission cross sections, final state approxs. comparison 77−50414
Ne VI, VII and VIII, total collisional ionis. rates in plasma 77−19102
Ne, vertical valence ionis. pot., many-body Green's functions 78−22051
Ne^- scatt. electron spectra, distinction from neutral autoionising states 80−83482
Ne^{9+} high ionisation-excitation states and mass dependent symmetric collision interactions 77−83720
Ne^{n+}-Ne, K-shell vacancy prod. cross section, X-ray and Auger electron prod. fluoresc. yield 78−13582
Ne+Al foil, projectile K-vacancy production cross section, X-ray production rel. to target thickness 77−19059
Ne+Cl^+, highly charged low vel. recoil ion time of flight spectra, cross section energy depend. 80−14222
Ne+Cl^{12+}(S^{14+}) soft X-ray emitting slow multiply charged ion prod., recoil ion spectroscopy 77−50516
Ne+e^-(H^+)(pion), specific primary excitation by fast accelerator particles 80−23559
Ne+H^+, ang. and energy distrib. of ejected electrons 79−31668
Ne+H^+(He^+)(Ne^+), multiple ionisation of Ne 2s and 2p electrons 80−18918
Ne+He^+(Li^+)(Mg^+)(Na^+)(Ne^+), autoionising level excitation, electron spectra 77−14554
Ne+heavy ion, few-electron states prod. K X-rays obs. 80−9718
Ne+ion, 100 keV, excited Ne 2s vacancy singlet/triplet population ratio, ion Z depend. 78−37733
Ne+$Li^{+1,2,3}$, K-shell ionisation depend. on projectile charge state 77−34743
Ne+Li^+(C^+)(N^+)(Ne^+)(Na^+)(Mg^+), slow collision, ionis. obs. 79−10194
Ne+Ne^+, 2s vacancy prod., coupling state calcs. in mol. basis 79−13806
Ne+Ne^+ collisions, satellite struct. of 2s-subshell ionisation of Ne 77−19065
Ne+Ne(Ne^+)(Ne^{2+}), 2s vacancy prod. 78−50623
Ne^++Ba, 2-1000 eV, spontaneous ionis. mechanisms 79−64090
Ne^++He, multiple ionisation of Ne 2s and 2p electrons 80−18918
Ne^++$NH_3(H_2O)$(Ne) symmetric collisions, double K-shell ionisation, two-electron-one-photon transitions 77−19067

ionisation of atoms continued
Ne^{n+}+Ar(Kr), (n=1, 2, 3, 4), energy spectra of electrons produced 79−45822
Ne^{n+}+$N_2(O_2)$(Ne)(methane), K-shell vacancy prod. cross-section, charge state depend. 78−17751
Ne^{n+}+Ne collisions, n=1 to 4, K-X-ray production, projectile charge state dependence 77−14570
Ne^{2+}+Ne(Ar), outer s-subshell vacancy production 79−18275
Ne*+H, assoc. ionis., rovibronic struct. in electron energy spectrum 80−106380
Ni K-shell hole production by light ions, hydrogenic and Hartree-Fock model of target 77−83715
Ni, $K\alpha^h$ hypersatellite spectra and double photoionisation cross-section 79−85922
Ni, $M_{II,III}$ spectrum, ab initio calculation 80−83276
Ni V spectrum, 990 to 1400 Å, ionisation pot. 77−30811
Ni+Cl^{n+}, 35 MeV, K-shell vacancy sharing, impact parameter depend., X-ray obs. 77−71858
Ni+H^+, K-shell ionisation calcs. 80−23534
Ni+H^+, K-shell ionisation cross-sections calcs. 80−43165
Ni+H^+($^4He^{2+}$)(O)(Li), K-shell ionis., impact parameter depend. 77−83707
Ni+H(D)(He)(Li)(C)(O)(F) ions, K-shell ionis., universal cross sections 78−62895
Ni+Mn(Pb), inner shell vacancy prod., impact parameter depend. 77−6906
Ni+N^{4+}, Kα and Kβ X-ray spectra for 84 MeV incident energy 77−50517
^{58}Ni+p, K-shell X-ray-photon proton coincidences, nucl. time delay 79−18281
$_{28}{}^{58}Ni^{n+}$+$_{25}$Mn($_{50}$Sn)($_{82}$Pb), 45, 94, and 138 MeV Ni inner shell vacancy production, impact parameter depend. 79−41130
^{237}Np electron transition excitation following K-shell photoionisation, deexcitation γ-rays 80−78196
O, autoionis., radiative emission, competition in excited state decay 77−75109
O, beam-foil spectra, multiply ionised O 80−42977
O, cross sections of interactions of protons 77−50538
O, dipole transition oscill. strengths, photoionis. cross section 78−9120
O, electron impact, ionis. cross-section, accuracy of crossed at. beam method 79−81284
O, electron impact ionis. cross-section, accuracy of fast at. beam method 79−81283
O I, photoionis. cross section 79−13685
O III, production by Auger effect, astrophysical appls. 78−20633
O IV bound states, oscillator strengths and photoionisation cross sections 80−106293
O ions, transient mag. field discontinuity in Fe(Co)(Ni) 80−24515
O, photoelectron ang. distrib. meas. 77−61721
O, photoionis. and photoabsorpt. cross sections for aeronomic calcs., data tables 80−41599
O, photoionisation absolute cross section 78−94218
O, UV photoionisation cross-section calc., 304 and 584 Å 80−43015
O VI, ionis. rate meas. in theta-pinch plasma, VUV obs. 78−26254
O^-, interstellar, ionisation and interstellar medium heating by photoelectrons 78−36666
O^+, beam-foil excitation, absolute Auger yield meas. 80−14203
O^{6+} to O, photoionis. cross sections, from ground states, Hartree-Slater model 77−57947
O^{q+}, electron loss, forward peak oscill. struct. 78−78796
$O^-/H_2O(D_2O)$, ionis. efficiency curves, Feshbach-reson. and dissoc. electron attachment 79−41246
O+H^+(He^+), double K-shell ionis., projectile Z depend. 78−25680
O^++Al, Al K-vacancy cross sections, 0.15 to 91 MeV, recoil effects and mechanisms 77−19033
O^++$NH_3(H_2O)$(Ne) symmetric collisions, double K-shell ionisation, two-electron-one-photon transitions 77−19067
O^{q+}+Ar, continuum electron capture and loss, 1.6-2.8 MeV/A 78−46443
$^{16}O^{8+}$+Au K-shell ionis., δ-ray emission 77−79557
^{191}Os, K-shell internal conversion, Kα_1 hypersatellite line energies, intensities 77−18885
^{194}Os beta decay, X-ray/gamma relative intensities, L_1 subshell yields 78−4919
P, highly ionised, beam foil radiative lifetimes and EUV spectrum 80−32671
P III, UV and vis. spectrum, ionisation limit calcs. 78−936
Pb, γ-ray absorption cross-sections, 10-160 MeV 78−90136
Pb I, interchannel interactions and series quenching in 5d and 6s spectra 77−88418
Pb, ion collisions 90-110 MeV, K-vacancy production, multiple and single collisions in mol. orbital excitation 77−83717
Pb, K-shell ionis. probability, 25- 40-and 74-MeV α particles 77−528
Pb, total L-shell photoelec. cross section ratio 77−30836
Pb, X-ray production cross sections for protons, fluoresc. obs. 80−102476
Pb+H^+, K-shell ionisation, 7-15 MeV, relativistic effects 78−82830
Pb+H^+, L-shell ionis., 0.5-3.5 MeV, X-ray emission obs. 77−54528
Pb+H^+ (L_α, L_β, L_γ) X-ray emission probability, impact parameter dependence 77−23553
Pb+H^+(D^+), L-subshell vacancy production, Coulomb deflection effects 80−9711
Pb+Pb^+, δ-electrons from K- and L-shell ionisation in adiabatic collisions 80−23541
Pb+Pb^+, inner-shell ionisation of quasimolecular system, perturbation theory 79−31667
Pb+target atom, 90-110 MeV, K-vacancy cross sections, target depend. 77−19026
^{82}Pb+H^+, L-subshell ionisation probabilities, impact parameter depend. 77−30981
^{208}Pb, 1.4 to 5.9 MeV/u, K-shell ionisation cross-section meas. 79−31671
Pd, ionisation cross sections for L_1 and L_2 subshells by 250-500 keV protons *(Russian)* 77−6918
^{208}Po, L-shell ionisation in α-decay 78−78324
^{210}Po, inner shell electron ejection in α-decay 77−79342
Pt, L-subshell ionisation with high vel. positive ions 79−50122
Pt+H^+, L-subshell ionisation cross-sections, X-ray meas. 77−46520
Rb, ejected electron spectrum of autoionis. levels excited by electron impact 77−58174

ionisation of atoms continued
Rb, electron excitation cross sections for six autoion. config., Born approx. calc. 78−25713
Rb, high lying Rydberg states, atomic beam laser spectra 79−94101
Rb, ionisation energies and oscill. strengths calcs. 80−5488
Rb, isotopically selective ionisation through Rydberg states 78−5186
Rb, multiphoton ionis. processes, fine struct., hybrid reson. 77−18877
Rb, photoionis. cross section, elec. field depend. 80−37796
Rb, photoionisation from ground state in DC elec. field, narrow resonances *(French)* 77−61718
Rb, photoionization cross-section, reson. induced by elec. field 79−13689
Rb, π-photoionisation spectra in DC field, Fano profile 79−59410
Rb, radiatively excited states, ionis. rate coeffs. in two atom collisions 80−43160
^{85,87}Rb, high Rydberg levels, press. broadening and shifts 80−52902
Rb+atom, Rb Rydberg states, collisional ionisation, rate consts. 80−32817
Rb+H^+, atomic K-shell ionis., X-ray emission 79−18280
Rb+H^+, single photon emission following double K-shell ionisation, contrib. to superheavy element search data 78−50625
Rb+H^+($^2H^+$), inner-shell ionisation, Coulomb repulsion effects 80−48075
Rb+Rb, radiatively excited states, chemi-ionisation, ionisation rate consts. determ. 80−58363
S ion+target (Z=4-40), single and double K-shell excitation, X-ray satellites, hypersatellites 77−19058
S ions in low density plasma, dielectronic recomb., ionization equilib. and radiative energy loss, solar corona appl. 79−68903
S to Br, $O^{2+,3+,4+,5+}$ induced K-shell ionis., 7 to 24 MeV, X-ray production cross section 77−61850
S V, spectral lines, 460-3604 Å 77−27011
S+F^-, inner-shell ionisation, X-ray cross sections 80−58369
S+X, (X=atom with Z=11-22), K-shell ionis. cross sections 78−13596
SF_6, valence levels, photoionisation cross-sections, MS Xα calcs. 79−54923
Sb, ionisation cross sections for L_1 and L_2 subshells by 250-500 keV protons *(Russian)* 77−6918
Sb+H^+($^2H^+$)(He^{2+}), inner-shell ionisation, Coulomb repulsion effects 80−48075
Sc^+, excited config. position and level struct., review 80−32621
Sc+H^+, K X-ray production, 0.2-0.5 MeV, ionis. cross-section 79−31459
Se I, ionisation limit determ. from reson. lines meas. 78−938
Se, loss of K-electron by proton-atom collision *(Russian)* 77−50523
Se XXVI, $2p^5$-$2p^4$3s($2p^4$3d) transitions in laser produced X-ray spectra 78−13460
Se+H^+, K-shell ionisation cross-sections calcs. 80−43165
Se+H^+, K-shell ionisation cross-section determ. 80−48077
Si, dielectronic recomb. and ionization equilib., autoionization and excitation influence 78−1077
Si, highly ionised, beam-foil lifetime obs. 80−32670
Si in astrophysical plasmas, effect of charge transfer on ionisation equilib. 80−41717
Si, K-shell ionis., X-ray prod. cross section for incident H^+, ^{4}He and ^{14}N ions 78−70923
Si^{q+} electron loss, forward peak oscill. struct. 78−78796
Si+F^-, inner-shell ionisation, X-ray cross sections 80−58369
Si+F^{q+}, q=3-9, Si K-shell ionis., electron transfer cross sections, solid targets 79−10192
Si+H^+(^{3}He) ion collisions, K-shell ionisation cross sections 77−23555
Si+He(C)(O)(Ne), K-shell ionising collisions, average L-shell ionisation probability, K_α spectra 79−72408
Si+$Li^{+1,2,3}$, K-shell ionisation depend. on projectile charge state 77−34743
$^{28}Si^{n+}$+Sc(Ti)(Cu)(Ge), K-shell ionisation, projectile charge state depend., theory 78−17786
Sm, isotope separation by two step photoionisation method 77−58205
Sm, laser isotope separation by two step photoionisation 77−61720
Sn, γ-ray absorption cross-sections, 10-160 MeV 78−90136
Sn+He(C)(N)(O), inner-shell multiple ionisation systematics, X-ray obs. 80−63790
Sr, associative ionisation of laser-excited Rydberg states, mass spectrometry obs. 78−94303
Sr, autoionisation reson. states elec. field depend., three-photon ionisation 78−33478
Sr, bound even-parity J=0 and J=2 states, multiphoton ionisation spectra 77−71789
Sr, diamag. quasi-Landau spectrum near ionis. threshold, two-photon ionis. spectra obs. 78−58642
Sr, double multi-photon ionisation *(Russian)* 77−71786
Sr, efficient ionis. by reson. laser pumping 80−32685
Sr I, Rydberg and autoionisation levels, laser ionisation spectroscopy 77−3331
Sr, multiphoton ionis. spectroscopy of even- and odd-parity states 78−86973
Sr, multiphoton ionisation spectra of msnp^{3}P^0 states 77−83554
Sr, Rydberg states, $^1D_2 \rightarrow {}^1F_3$ microwave transition meas. using selective reson. ionisation 79−72258
Sr, Zeeman effect of J=2 states, g-factor, interacting Rydberg series 78−17609
Sr-Cs mixture, laser induced collisional two-photon ionisation, fluoresc. monitoring 80−91515
Sr+H^+($^2H^+$), inner-shell ionisation, Coulomb repulsion effects 80−48075
Ta, γ-ray absorption cross-sections, 10-160 MeV 78−90136
Ta, L-subshell ionisation with high vel. positive ions 79−50122
Ta, total L-shell photoelec. cross section ratio 77−30836
Ta+H^+, K-shell ionisation, 7-15 MeV, relativistic effects 78−82830
Ta+H^+(He^+), L-subshell ionisation cross section, branching ratios, fluoresc. yield, Coster-Kronig factors 80−43166
Th, ion induced K-shell ionisation cross-sections determ. by comparison with nuclear Coulomb excitation 79−76500
Th+H^+, K-shell ionisation, 7-15 MeV, relativistic effects 78−82830
Th+H^+, L-shell ionis., 0.5-3.5 MeV, X-ray emission obs. 77−54528
Th+H^+(D^+), L-subshell vacancy production, Coulomb deflection effects 80−9711
Th+X^+, X=O, N, N_2, CO_2, charge transfer cross-section, 1-500 eV 78−82835
Ti, K_β/K_α following K-electron capture and X-ray excitation 78−13031
Ti, K-shell hole production by light ions, hydrogenic and Hartree-Fock model of target 77−83715
ionisation of atoms continued
Ti, K-shell ionis., X-ray prod. cross section for incident H^+, ^{4}He and ^{14}N ions 78−70923
Ti, K-shell ionisation probability, for 150 keV protons, impact-parameter depend. 79−10189
Ti, Kα^h hypersatellite spectra and double photoionisation cross-section 79−85922
Ti, Koopmans' ionis. pot., relax. correction 79−18308
Ti^+, excited config. position and level struct., review 80−32621
Ti+Cl^{n+}, 35 MeV, K-shell vacancy sharing, impact parameter depend., X-ray obs. 77−71858
Ti+H^+, K X-ray production, 0.2-0.5 MeV, ionis. cross-section 79−31459
Ti+H^+, K-shell ionisation calcs. 80−23534
Ti+H^+, K-shell ionisation cross-section determ. 80−48077
Ti+H^+ ion collisions, K-shell ionisation cross sections 77−23556
Ti+He^{2+}(C^{4+})(O^{5+})(N^{4+})(N^{5+}), ratio of single K-shell ionisation cross section to double K-shell ionisation cross section 80−53119
Ti+N^{4+}, Kα and Kβ X-ray spectra for 84 MeV incident energy 77−50517
Tl, ionisation limit and oscill. strength in VUV absorpt. spectra 80−74152
Tl, photoionis. cross section, spin polaris. and ang. distrib. of photoelectrons, RPA calc. 78−13478
Tl, photoionis. cross section and spin polarisation of photoelectrons 78−46307
Tl, two-photon laser spectroscopy and ionisation 78−55153
Tl, VUV photoelectron spectra, pseudo-atomic beam technique 80−58225
Tl+H^+, L-shell ionis., 0.5-3.5 MeV, X-ray emission obs. 77−54528
Tm, intense 4d-f resons., cross-sections, spectra, calcs. 79−31426
U, by Ar ion laser radiation, appl. to U laser isotope separation 78−42233
U, enrichment by two step photoionisation, laser isotope separation *(Japanese)* 79−49865
U, ion induced K-shell ionisation cross-sections determ. by comparison with nuclear Coulomb excitation 79−76500
U, L-shell photoionis., transition radn. ang. distrib. 78−33486
U, laser isotope separation, atomic spectroscopy requirements 78−33638
U, laser isotope separation by O_2 chemi-ionisation *(Japanese)* 79−13830
U, Rydberg levels, time-resolved stepwise laser photoionisation obs. 77−27038
U+H^+, L-shell ionis., 0.5-3.5 MeV, X-ray emission obs. 77−54528
U+H^+, relativistic K-shell ionisation cross-section meas. 78−33593
U+H^+(D^+), L-subshell vacancy production, Coulomb deflection effects 80−9711
U+H^+(He^+), 2-18 MeV, L-subshell ionis. cross section, projectile energy depend. 77−19031
U+Pb, K-vacancy form., rot. coupling effect in quasimol. L-shell 78−25692
U+U, K-shell ionis., classical relativistic trajectory method appl., 1, 10 GeV/n 80−43129
U+X^+, X=O, N, N_2, CO_2, charge transfer cross-section, 1-500 eV 78−82835
^{235}U, hyperfine struct. and isotope shift meas., laser separation by two-step photoionisation 78−78822
^{235}U isotope separation enhancement with RF hyperfine transitions 79−41249
^{235}U, photoionisation, isotope separation and enrichment by Ar ion laser *(Japanese)* 79−81192
^{238}U+^{238}U (^{136}Xe), nuclear Coulomb excitation, inner shell ionisation and internal conversion, quasimol. formation 78−94026
V, atomic energy levels in all stages of ionisation, data anal. 78−94207
V, K_β/K_α following K-electron capture and X-ray excitation 78−13031
V V, spectrum, 100-8500 Å, ionisation energy 77−65432
V+H^+, K X-ray production, 0.2-0.5 MeV, ionis. cross-section 79−31459
V+H^+ ion collisions, K-shell ionisation cross sections 77−23556
W, ion induced K-shell ionisation cross-sections determ. by comparison with nuclear Coulomb excitation 79−76500
W, multiphoton ionisation and absorpt. 80−95575
W, N-shell ionisation by proton impact 78−78800
W+H^+, inner-shell ionisation, Coulomb repulsion effects 80−48075
W+H^+(He^+), L-subshell ionisation cross section, branching ratios, fluoresc. yield, Coster-Kronig factors 80−43166
Xe, 11 photon ionisation probability in 1 μm beam 77−46548
Xe, 326-470 MeV, ion collisions, K-vacancy production, multiple and single collisions in mol. orbital excitation 77−83717
Xe, 4d ionis, photoelectron spectrum, post-collision interaction 77−30837
Xe, $4d^{10}$ and $3d^{10}$ shell, photoionisation cross sections, electron shell alterations determ. *(Russian)* 80−58144
Xe, $4d^{10}$ subshell photoionisation cross section, electron shell rearrangement 77−14400
Xe, 5p shell photoelectron branching ratio, energy depend. 77−88435
Xe, $5p^6$ subshell, photoelectron ang. distrib., ionisation cross section 77−14401
Xe 5s, photoelectron ang. distrib., relativistic Dirac-Fock calc. 79−59411
Xe, 5s$\rightarrow\varepsilon$p photoelectron ang. distrib., interchannel and spin-orbit coupling 77−3329
Xe, 5s$\rightarrow\varepsilon$p photoelectron ang. distrib. near Cooper minimum 80−18834
Xe, absolute photoionis. cross sections of spin-orbit components of 4d electron 77−38646
Xe, atom, photoionis., collective level existence RPA with exchange calc. 78−42025
Xe, electron energy loss spectra, energy-depend. multichannel quantum defect theory anal. 77−61860
Xe, high Rydberg state, ionis. by collision with organic mols. 78−50620
Xe, high Rydberg states, radiative lifetimes and transition probabilities 78−86817
Xe II, transition probabilities for $5p^4$6p to $5p^4$6s array 77−436
Xe, intershell correlation, double electron ejection from outer shell 78−42019
Xe, ionisation of high Rydberg states by collision with molecules 77−88545
Xe, low-energy 5s-εp photoionization, relativistic effects 78−50515
Xe, multiphoton ionisation spectrum, interatomic effects in multiphoton transitions 78−29764
Xe, photoelectron branching ratio in 4d subshell 79−18164
Xe, photoionis., $\sigma 3/2$:$\sigma 1/2$ branching ratio in $5s5p^6$6p($^1P_1$) resonance 77−42292

ionisation of atoms continued
Xe, photoionis. from excited states 79−10078
Xe, photoionisation, correl. satellites and subshell cross-sections, electron spectrosc. obs. 79−31485
Xe photoionisation, spin-polarised photoelectrons angular distrib. 80−106306
Xe, plane polarised VUV irrad., emitted photoelectron polarisation, ang. depend. 80−47952
Xe, polarisation effects in photoionisation *(Russian)* 79−3420
Xe, population inversion, intershell transitions, photoionisation, from UV irradiation *(Russian)* 78−70803
Xe, recently enhanced multiphoton ionisation and third harmonic generation 80−91526
Xe, resonantly enhanced multiphoton ionis., photoelectron energy anal. 80−63597
Xe, Rydberg atoms, field ionisation, 300K background radiation effects 79−68271
Xe, six-photon ionis., electron energy spectra 79−54824
Xe subshell photoionisation, multichannel k-matrix calc., spin orbit interactions 80−63600
$Xe+H^+$, M-subshell ionisation cross section, binary encounter approx. 78−62890
$Xe+H^+$ ionisation, induced L-shell alignment 80−32813
$Xe+NH_3(H_2S)(SO_2)(HCl)$, ionis. cross sections calc. 77−68103
Xe+target atom, 326-470 MeV, K-vacancy cross sections, target depend. 77−19026
$Xe^+ + Xe$ collisions, Auger electron ionisation, inelastic energy loss meas., multiple inner shell excitation 77−19055
$Xe^+ + Xe^+$, charge transfer and ionisation Xe^{2+} prod. 80−91659
Xe^{10+} + He(Ne)(Ar)(Kr)(Xe)(Cd)(Na)(Cs), depend. of charge transfer on ionisation pot. 79−64096
^{132}Xe, 1.4 to 5.9 MeV/u, K-shell ionisation cross-section meas. 79−31671
^{136}Xe ion+target collisions, K-X-ray yields, 1sσ excitation 77−19051
^{136}Xe ion+target collisions, X-ray yields, K-L level matching 77−19052
^{136}Xe ion+target collisions, K-X-ray yields, K-vacancy sharing 77−23548
^{136}Xe ion+target collisions, K-X-ray yields, 2pσ excitation 77−23549
^{136}Xe+Au(Pb)(Bi)(Th), 625 MeV, probability of forming 1sσ vacancies 78−25681
Xe(nf)+NH_3, at. Rydberg state further excitation by rot. transfer, field ionis. obs. 78−58795
Xe(nf Rydberg state)+NH_3, n- and l-changing and ionising collisions 80−58360
Y, XPS relative intensity and photoionisation cross-section 80−63599
Y^{10+}, spectrum and energy levels 80−32639
Yb I, high Rydberg levels of $4f^{14}$ 6snd configs., very high resolution obs. 80−106300
Yb II, III to Bi XV, XVI isoelectronic sequences, wavelengths and ionisation energies 77−429
Yb, isomers and hyperfine struct., selective detection through Rydberg states 80−52903
Yb, photoionisation cross-section of $^3P_1$ excited state, laser isotope separation *(Russian)* 78−25496
Yb, Rydberg states, optically pumped, electric field ionis. *(Russian)* 79−27095
Yb, single atom detection by selective laser excitation and field ionisation from Rydberg states 79−18159
$Yb+H^+$, K-shell ionisation, 7-15 MeV, relativistic effects 78−82830
^{169}Yb, K-shell internal conversion, $K\alpha_1$ hypersatellite line energies, intensities 77−18885
Zn, highly ionised, spectral classifications below 55 Å 79−13658
Zn I,II, excited state lifetimes, electron-photon delayed coincidence meas. 78−25478
Zn, K_β/K_α following K-electron capture and X-ray excitation 78−13031
Zn, Kβ X-ray spectra and autoionisation following β-decay of ^{64}Cu 78−13029
Zn, UV subshell photoionisation cross section, expt. and GIPM theory 78−21887
Zn XXII, $2p^5$-$2p^4 3s(2p^4 3d)$ transitions in laser produced X-ray spectra 78−13460
$Zn+H^+$, K-shell ionisation calcs. 80−23534
$Zn+H^+$, K-shell ionisation cross-sections calcs. 80−43165
Zn+He, Penning ionisation cross section of target atom, for $He(2^3S_1)$ 80−63777
ZnSe, multiphonon ionisation of deep point centres in a charged dislocation field *(Russian)* 80−100281
Zr IV, energy levels, spectrum obs. 440 to 2670 Å 80−99470
Zr V, energy levels, spectrum obs. 200 to 2670 Å 79−54798
Zr VII, energy levels, $4s^24p^4$ to $4s4p^5$ transitions obs. 77−3288
Zr, XPS relative intensity and photoionisation cross-section 80−63599
$Zr+H^+$, K-shell ionisation cross-section determ. 80−48077
$Zr+H^+(^2H^+)$, inner-shell ionisation, Coulomb repulsion effects 80−48075

ionisation of gases
see also atmospheric ionisation; electron avalanches; Townsend discharge
acetylene, ionisation meas. and $\bar{W}_n$ derivation for neutron irradiation 79−36430
air, electron impact W values and backscatt. coeffs. 80−19551
air, laser-initiated ionisation channels, form., characts. 77−89345
air, mobility spectra of ions created under atm. press. 77−969
air, photoionisation kinetics ahead of strong shock fronts 79−7438
air, stressed at high voltage, ionis. coeff. meas. using photomultiplier 78−1786
air, weakly-ionised, secondary electron distrib., produced by electron source distrib. 80−6211
air in rooms, due to physiotherapy apparatus 77−78035
alkali metal, dense vapour, anomalously large elec. cond., positive complex ions form. 80−19547
alkali metal seeded plasma, calc. of thermal nonequilib. near-electrode region 77−55186
Boltzmann eqn. method for ionis. and attachment effects on electron swarm parameters 78−5845
Bragg-Gray theory corollaries, comparison to fast-neutron cavity ionisation meas. at 14.8 MeV 80−91370
cavity ionisation, electron transport theory *(Chinese)* 80−69966
chromatography ionisation detector theory and performance, review 77−44564
cloud chamber, low-press., anal. of ionisation distribs. 80−106236
cloud chamber, low-pressure, ionisation distrib. analysis 80−9461

ionisation of gases continued
cluster ions in gases, review 77−81401
conference on ionised gas physics, Dubrovnik, Yugoslavia (Aug.-Sept. 1978) 80−36779
conference on phenomena in ionised gases, Grenoble, France (July 1979) 80−36767
corona discharge, computing process for electrons and ions distribution determ. 79−4204
critical ionisation velocity in gas mixtures, lab. expt. 78−67307
crossed magnetic field, equivalent reduced electric field concept 80−64805
cyclotron resonant gas breakdown with 1.22-mm $^{13}CH_3F$ laser 79−55549
detonation wave, gas-ionising, spatially-polarised struct., rel. to mag. viscosity *(Russian)* 77−39361
differential pumping, of gas discharge columns, ionisation enhancement 79−67330
diffusion controlled circular positive column with one and two step ionisation, charact. eqn. 80−44033
discharge, pulsed ionisation initiated, non-self-maintained, instability 79−86572
discharge, RF, gamma regime, ionis. balance and plasma characts., model 80−44022
discharge at intense current density, contraction in electronegative gases *(Russian)* 77−43096
discharge lasers, use of surface discharge for gas preionisation 79−46504
discharges between plane parallel electrodes, axial and radial development, computation 77−19794
dissociation equilibrium, phase space allocation 79−27746
effect on strength of Kh18N10T steel, test apparatus for 20-900°C 79−70252
electric arc, interaction with gaseous medium, obs. and calc. 79−77447
electric discharge, positive column, characts. rel. to diffusion and ionisation coeffs. 80−33833
electrical discharges, opto-galvanic effect with tunable gas lasers, spectroscopy appl. 78−95977
electrically excited preionisation unit with electron beam energy recuperation 78−59013
electron beam, ion density calc. partial differential eqn. *(Russian)* 77−11306
electron beam excited gas discharge, space charge and inhomogeneous ionisation *(Russian)* 77−47281
electron beam method *(Russian)* 80−10348
electron stopping model and secondary-electron distrib. in weakly ionised gas 80−6263
electron swarm with anisotropic vel. distrib. function 80−38520
electron swarms diffusion to mobility ratio, pulse meas. technique 79−55448
electronegative gases, sparking pots. and ionisation coeffs. 78−42705
electrostatic instabilities role in critical ionisation vel. mechanism 78−67355
elements, degree of ionis. determ. 77−68734
equilibrium birefringence for weakly ionised molecular gas in strong mag. field 80−83881
external photoionisation energies, comparison with liq. phase 77−90237
first Townsend coefficient, step ionisation effects, anal. 79−82117
flame, free-jet diffusion type, ionis. meas. and combustion progress 80−30238
Freon 13-B1 and mixtures with Xe and Kr, saturation curve 1 to 8 atm., for ionography ionisation chambers 77−12997
freon-N_2 low-pressure mixture prebreakdown current obs. 79−18995
gas in crossed electric and magnetic fields, elec. strength calcs. 78−87568
glow discharge, in RF sputtering system, Langmuir probe study at various freqs. 80−55294
glow discharge infinite, dense gas homogeneity, theory 77−51253
glow discharge plasma, ionization-diffusion oscills., rel. to stepwise ionization 78−1927
glow discharge sheath RF impedance, scatt. and ionisation effects 79−86630
HF discharge, EM wave ionisation instability model 78−67512
high-power non-self-sustained discharge with ionisation by repetitive electrodeless pulses in closed-cycle laser 78−71514
hypersonic boundary layer, laminar, nonequil. ionis. problem 80−59129
hypersonic flow field behind blunt body, approx. calc. and electron density in wakes *(Russian)* 79−86461
inert gas, primary specific ionisation, relativistic increase *(Russian)* 79−60102
inert gases, viscosity rel. to ionis., skin friction of wetted oscill. disc 78−34252
insert gases, primary ionisation relativistic growth 79−86554
interrupted vacuum arc, deionisation, expt. 77−27760
interstellar gas*in globular clusters, ionisation by UV radiation, evidence from OAO photometry 80−73009
interstellar H,II regions, ionization front, oblique refraction 78−54025
interstellar neutral H, weak R-type ionisation front approaching a contact discontinuity 78−49510
ionisation wave propag. in gas, turbulent diffusion effect 78−42704
ionising wave propag., appl. to air discharges 77−58918
laser, electron beam controlled, electron beam parameter optimization and choice of foil 80−48269
laser beam with retractable focus, ionis. path form. in gases 79−18992
laser pumping using self-sustained electron-photoionization discharge 80−33013
laser radiation gas breakdown at high intensity *(Russian)* 79−98853
laser radiation-matter interactions, dissertation 79−86555
laser-induced electron cascade, general eigenvalue method 77−19664
low voltage inert gas arc theory 80−38809
low-temperature plasma production by electron beam ionisation of gas mixture 80−87908
mass identified ions in O, N, CO and CO_2, transport properties, obs. and calc. 79−50837
methane, total ionization created by completely stopped H^+ ions 79−46419
methane, W-value determ. for α-particles 79−39518
microwave breakdown in gases, Schwinger variational princple 79−41788
microwave gas breakdown, ionisation pot., qualitative theory 80−43837
molecular gas, vol. discharge with UV preionisation by capillary discharge, ionis. pots. depend. 80−44065
moving gas, electric strength calcs., gas vel. effects 78−87568
multiple thermal ionisation of gaseous mixture, long range electrostatic effects 78−21065

ionisation of gases continued
optical breakdown, mol. ion reactions influence 80−96341
partial ionisation in gas dynamics, computation method 78−38447
partially ionised inert gases in travelling HF mag. field 78−75474
Penning mixtures, statistics of gas gain 79−45535
Penning-type HV discharge, ionis. average freq. in anode sheath 80−44012
photoionisation, for UV reflectivity meas. of liquids 78−294
photons, monoenergetic, microdosimetric meas. of ionisation 78−65133
plasma, low-temperature, ionisation waves excitation 78−1832
plasma generation with multiply ionised species 78−75388
positive column, of electroneg. gas, transverse stability, effect of dissoc. attachment 79−23475
positive column with two-step ionisation, var. calcs. 80−70056
power station plumes, ionisation effects on natural lightning 78−88909
powerful pulse discharge, form. and stability of fibrous struct. of current shell 77−31535
n-propanol, sparking pot. and ionis. coeffs. 80−1864
purity under measuring conditions, W-value determ. *(German)* 80−104489
QSOs, ionisation equilib., thermal equilib. and radiative accel. near radiation sources with different spectral shapes 80−41909
real gas, blast wave, effects of compressibility, vibr. excitation, dissoc. and ionisation 77−68622
residual gas in betatron, determination of ionisation by accelerating beam for measurement of parameters of electron beam 79−97915
SEM, insulating surfaces, charge neutralisation by gas ionisation 79−6235
semi-self-maintained gas discharge, ionisation instability theory 78−67511
shock wave, in transverse mag. field, theory *(Russian)* 77−89161
shock wave ionisation in transverse magnetic field, finite-difference methods 78−51249
shocks refection on end wall of shock tube, finite difference analysis *(Japanese)* 78−42629
sparking time lag statistical distribution 77−62417
stack gas in coal-fired plants, in electrostatic precipitators, using electron beams 78−57346
tissue equivalent gas, meas. of $\bar{W}$ for H^+, ^4He ions, ^{12}C ions, dosimetry appl. 80−19550
tissue equivalent gas, total ionization created by completely stopped H^+ ions 79−46419
tissue-equivalent gas, energy loss per ion pair for ions, 25 to 500 keV 77−35312
tissue-equivalent gas, radial dose, LET and energy per ion pair for ^{18}O ions 78−7452
tissue-equivalent gas, W-value for low energy electrons 78−15896
tissue-equivalent gas, W-value for pion$^-$ 77−56473
Townsend primary ionization coefficients and breakdown voltages of cyclo-paraffin vapours 80−79602
Trichel corona negative ion transit times 79−19115
vacuum science and technology, undergraduate and post-experience courses 79−62954
water, enthalpy of ionisation meas., reaction-solution rotating-bomb calorimeter 80−4717
weakly ionised gas, electron energy distrib. 79−82028
X-ray diagnostics, hot lab. and astrophysical plasma 80−59282
X-ray sources, compact, temp. and ionisation struct. rel. to X-ray spectra form. 80−22115
air, viscosity rel. to ionis., skin friction of wetted oscill. disc 78−34252
Ar, energy loss per ion pair for ions, 25 to 500 keV 77−35312
Ar gas, primary ionisation coeffs. in cross mag. field 80−83879
Ar, ionisation by energetic electrons, appl. to Mars atmosphere 77−31420
Ar, ionisation growth at high press., current growth obs. 80−38522
Ar, ionised shock wave, equilibrium zone behind shock wave *(Russian)* 77−89154
Ar, ionising shock waves, stability, H impurities effect 78−22371
Ar, low voltage arc, ionisation waves, hydrodynamical model including inelastic interaction 78−87563
Ar, positive column, progressive and regressive ionisation waves *(French)* 80−43905
Ar, preionised, CO_2 laser induced breakdown press. and pre-ionisation depend., cascade model 80−54010
Ar, restricted energy loss by ionisation of relativistic muons 77−88355
Ar, UV photoion density meas. using high press. Langmuir probe 78−51340
Ar, W-value determ. for α-particles 79−39518
Ar-CO glow discharges, positive ion spectra, ion clusters obs. 80−64807
Ar-Kr(Xe)(N_2), electron beam ionis., low temp. plasma prod. 80−87908
Ar_2*, electron impact ionisation cross sections in binary encounter approx. 79−68320
CO, ionisation growth, spatial current growth meas. 77−19665
CO-He glow discharge, positive column, ionisation processes 80−79618
CO-He-O_2 gas discharge laser plasma, positive ion generation mechanism *(Russian)* 79−99005
CO_2, electron swarm parameters for high E/N, Monte Carlo simulation 80−19548
CO_2 gas, electron mobility to lateral diffusion coeff. ratio 80−43836
CO_2, high-pressure ionization chamber for spatial growth meas. 77−46657
CO_2, ionisation and attachment coefficients 78−42706
CO_2, ionisation current growth, Townsend swarm coeffs. 78−59541
CO_2, ionisation meas. and $\bar{W}_n$ derivation for neutron irradiation 79−36430
CO_2, total ionization created by completely stopped H^+ ions 79−46419
CO_2, viscosity rel. to ionis., skin friction of wetted oscill. disc 78−34252
CO_2, W-value for pion$^-$ 77−56473
CO_2-N_2, ionisation current growth, Townsend swarm coeffs. 78−59541
CO_2-N_2-He mixture, ionisation and attachment coefficients 78−42706
Cs, dense plasma, ionisation equilib. and cond., ion clusters effects 80−75032
Cs, dense vapour, anomalously large elec. cond., positive complex ions form. 80−19547
Cs-Sr(He) mixtures, photocond. at atm. press. 80−87844
H II regions, effect of collisional ionisation time evolution 77−53664
H II regions, high-excitation, effects of inhomogeneities on ionisation profiles 78−54007
H, ionisation rates, shock tunnel meas. 80−75022
H plasma, departures of electron energy distrib. from Maxwellian rel. to ionisation 77−80274
ionisation of gases continued
H_2 clouds, ionisation by supernovae 78−69856
H_2, fast electron retardation, ionisation cascade, degradation spectra, anal. *(Russian)* 79−27741
H_2, multiple stage cluster beam ionizer 79−67425
H_2, ohmic heating, ionization meas., axial discharge 78−38511
H_2, prebreakdown current growth, ionis. coeffs. 77−80385
H_2O vapour, ionis. coeffs. and dissociative electron attachment 80−43833
$H_2(^3\Sigma_u^+)$-He(2^3S), discharge ionisation growth, diffusion coeffs. 78−83636
He, crit. pots. meas., student expt. 80−12874
He discharge, HF asymmetrical, mag. field effect on ionis. freq. *(Russian)* 78−26371
He, excitation and ionisation, by instationary shock fronts 78−59540
He, fast electron retardation, ionisation cascade, degradation spectra, anal. *(Russian)* 79−27741
He, ionisation wave, effect of electron neutral collisions 80−43846
He positive column, magnetised, temps. of charged particles, nonlinear effect of ionis. waves 80−44023
He, restricted energy loss by ionisation of relativistic muons 77−88355
He-CO glow discharges, positive ion spectra, ion clusters obs. 80−64807
He-Ne, glow discharges, AC cataphoresis meas. using light spectrometry 79−60096
He-Ne mixture, primary ionisation relativistic growth 79−86554
I_2, dissociative attachment, thermal energy electrons in equilib. with gas 78−82850
KCN, He I photoelectron spectra 79−64046
Kr discharge, secondary ionisation processes 78−59711
Kr-Cl_2 mixture, glow discharge positive column, electron energy distrib. and rates of inelastic processes, negative Cl ions form. 80−19632
Kr-H_2, ~5 torr, ionisation by Mach 15+shock waves, shock struct. and stability 77−75938
Kr-Xe, glow discharges, AC cataphoresis meas. using light spectrometry 79−60096
KrF X-ray-preionized high-pressure laser 79−18403
N, electron swarm development, Boltzmann eqn. method 80−43832
N_2, breakdown threshold using laser radiation 79−1283
N_2, electric breakdown, vol. discharge with external photoionisation, plasma focus spark channel *(Russian)* 80−38738
N_2, electron swarm parameters for high E/N, Monte Carlo simulation 80−19548
N_2, gas, in crossed elec. and mag. fields, elec. strength calcs. 78−87568
N_2, high-energy C^{6+} ions, W-value rel. to dosimetry 77−66849
N_2, ion pair creation by high-energy ions, meas. of average energy required 80−103105
N_2, ionisation current growth, Townsend swarm coeffs. 78−59541
N_2, ionisation current increase, metastable mol. induced cathode secondary electron emission 80−38830
N_2, non-self-maintained discharge, high press., ionisation instability, pulse discharge train *(Russian)* 77−47282
N_2, non-self-maintained glow discharge ionisation instability, vibr. states excitation calc. 77−19805
N_2, radial dose, LET and energy per ion pair for ^{18}O ions 78−7452
N_2, total ionization created by completely stopped H^+ ions 79−46419
N_2, viscosity rel. to ionis., skin friction of wetted oscill. disc 78−34252
N_2, W-value for pion$^-$ 77−56473
N_2-CO_2, N_2 non-self-maintained discharge, high press., ionisation instability, pulse discharge train *(Russian)* 77−47282
N_2-He-CO_2, discharge ionisation growth, diffusion coeffs. 78−83636
N_2-NO(He), discharge ionisation growth, diffusion coeffs. 78−83636
NH_3, ionis. coeffs. and dissociative electron attachment 80−43833
Na vapour, assoc. ionis. by CW dye laser and applics. *(Japanese)* 80−5515
NaCN, He I photoelectron spectra 79−64046
Ne, ionisation waves, state of electron gas 78−14124
Ne, photoionization mass spectroscopy using synchrotron radiation, reson. width meas. 79−31478
Ne-Ar, glow discharges, AC cataphoresis meas. using light spectrometry 79−60096
Ne_2*, electron impact ionisation cross sections in binary encounter approx. 79−68320
O_2, breakdown threshold using laser radiation 79−1283
O_2 discharge plasma, metastable states role, two-step ionisation, electron densities and transition pts. 80−44019
O_2 gas, electron mobility to lateral diffusion coeff. ratio 80−43836
O_2, viscosity rel. to ionis., skin friction of wetted oscill. disc 78−34252
SF_6, electrical conductivity calc., 2000 to 50000K 79−14512
SF_6, equilibrium composition calc., in 20000 to 50000K range, in dependence on pressure 79−14511
SF_6 plasma thermodynamic props. at arc extinction temp. and pressures 80−79435
SF_6, pure and mixtures, dielec. props., ionisation and attachment coeffs. 80−33726
SF_6/N_2 pressurized mixtures, electric breakdown investigation 80−14877
SF_6-N_2 mixture, electron swarm development, Boltzman eqn. anal. 80−87841
SF_6-N_2 mixtures, effective ionisation coeff. and static breakdown voltage meas. 80−19549
SO_2, electron attachment processes investig. and mobility of negative ions 80−38518
UF_6, negative surface ionisation 80−31781
Xe, ionised shock wave, equilibrium zone behind shock wave *(Russian)* 77−89154

ionisation of liquids
acid, weak, ionisation in aq. soln., rate const. meas., elec. field jump method errors 79−43611
acid-base indicators, ionisation consts. determ., spectrochem. anal. method 77−56264
dielectric, ionic-cond. and -dissociation under low elec. field 77−8089
dielectric liquid ionisation chambers, ion collection efficiency determ. 79−85861
electron slowing down in water, spatial correlation of energy deposition events 80−9473
external photoionisation energies, comparison with gas phase 77−90237
n-hexane, liq. trapped electron photoionis., photocond. 80−2418
high temperature boundary layer mass transfer, nonequilib. ionisation effects 78−93634
hydrocarbon liquid, model for thermalisation of quasifree electrons rel. to electron mobility 77−40316

ionisation of liquids continued
inert gases, liq., model for thermalisation of quasifree electrons rel. to electron mobility 77−40316
ionic fluid very long wave-length charge fluctuation spectra 77−59297
liquids, non-aqueous ionizing, review *(French)* 79−69255
organic, electrohydrodynamic ionisation, solvated ion mass spectroscopy, anal. appl. 78−73102
organic compound ionisation under atm. press. 80−86488
organic compounds liq., new ionis. method using Penning effect and chem. ionis. *(Japanese)* 79−93255
phenol, aq. soln., electron ejection, picosec. obs. 80−87187
phenolate, aq. soln., electron ejection, picosec. obs. 80−87187
photographic development rate, effect of developer ion charge 79−24753
polypeptides, in aq. poly(L-glutamic acid) soln., helix-coil transition, US relax. times 80−45849
solution, external photoionisation energies, comparison with gas phase 77−90237
solutions, induced ion pair separation, Coulomb cage pair 79−11811
N,N,N′N′-tetramethyl-p-phenylenediamine, alkane soln., charge carrier generation, elec. field depend. 80−107846
tetramethylsilane, liq., photocond., ionis. threshold 79−15191
water, electron energy deposition model, effect of 21.4 eV plasmon 77−4135
water, enthalpy of ionisation, 273 to 323K, from HCl neutralisation meas., sp. ht. changes 77−48676
water, enthalpy of ionisation meas., reaction-solution rotating-bomb calorimeter 80−4717
water, heat of ionisation, calorimetric meas. on enthalpies of reaction of I_2O_5 79−70359
water, laser-induced ionisation, quantum yield, temp. and wavelength depend. 80−11924
water ionisation energy at 298.15K 78−3364
Ar, ionisation and scintillation, application to radiation detectors, review *(Japanese)* 78−35206
Ba soln. in liq. ammonia, conductance at −62.37°C 78−91459
$Ba(ClO_4)_2$, soln. in liq. ammonia, conductance at −62.37°C 78−91459
D_2O, effect of phase density on ionisation process and electron localisation 77−89731
D_2O, liq., ionisation const., thermodynamic props. determ., 298-523K 77−32821
$KClO_4$ soln. in liq. ammonia, conductance at −62.37°C 78−91459
Kr, ionisation and scintillation, application to radiation detectors, review *(Japanese)* 78−35206
ND_3, effect of phase density on ionisation process and electron localisation 77−89731
NaCl, interpolational eqn. of state with allowance for melting, vaporis., dissoc. and ionis. processes 80−24566
Xe, γ-irrad., average energy expended per ion pair *(Russian)* 80−5438
Xe, ionisation and scintillation, application to radiation detectors, review *(Japanese)* 78−35206

ionisation of molecules
see also molecular electron impact ionisation
accelerated atom+O_2, chemiionisation, crossed beam obs. 77−9085
acetaldehyde, lowest Rydberg state, multiphoton ionisation spectra 80−83435
acetaldehyde, multiphoton ionisation mass spectra 80−83436
acetaldehyde, primary and secondary photoionis. processes, ion-mol. reactions 79−36709
acetaldehyde-d_1(-d_3), fragmentation processes, H scrambling, photoionis. mass spectra 78−42139
acetic acid vapours, clustering, effect of supersonic mol. beam sampling, mass spectrometric study 80−104481
acetone and acetone-d_6, molecular beam photoionisation 79−3504
acetylene, angular dependent photoelectron spectral meas. 80−28060
acetylene, ionis. by mol. orbital method, many-body calc. 79−36512
acetylene, photoionisation cross section at distance from threshold, chemical bond influence 80−69196
acetylene, vibr. fine struct. accompanying core ionis., STO calcs. 78−62844
acid oxalate ion in aq. soln., vibr. studies, IR and Raman spectra 80−95589
acridine, aqueous soln., laser induced two-photon ionisation investig. 80−32780
acrolein, excitation, ionisation and electron affinity, expts., HAM/3 calcs. 80−18790
alcohol+H_x^+, methanol to butanol, x=1-3, charge exchange ionisation *(German)* 77−83700
alcohol+H_x^+, methanol to octanol, x=1-3, charge exchange and ionisation *(German)* 77−83699
aliphatic compounds, alkyl substitution effects on photoionisation, photoelectron spectrosc. obs. 79−31604
alkali atom+methane derivative, collisional ionisation, nitromethane, perfluoromethyl bromide (iodide) electron affinities 78−66639
alkali dimer+halogen mol. (IBr)(ICl) thermal chemi-ionisation reactions, products, energies 77−63903
alkali metal fluoroaluminates, dissoc. enthalpies, mass spectrometric determ., heat of form. 80−97720
alkanes, polycyclic, three-photon ionisation spectra, 3s Rydberg orbital 79−68282
alkanes, saturated, ab initio LCAO MO SCF calcs., core ionis., electronic relax. 77−71745
alkyl cadmium, valence and core electron energies, photoelectron spectra, ab initio calc. 78−25613
alkyl iodides, two-photon reson . ionis. spectra 80−28071
allene, photoionisation and threshold photoelectron photoion coincidence obs. 78−21981
amines, caged, multiphoton ionisation, two-photon transition resons. 78−33558
aniline, laser two-photon ionisation in mol. beam and bulk gas phase 80−18891
aniline, photoemission for mol., polarised photoelectrons 78−66607
1,8-anilinonaphthalene sulphonate, aq. and ethanolic solns., excited singlet state decay pathway 78−17703
anthracene ion in liqs., photoelectron emission and photocond. 80−75600
approximate and exact state wavefunctions, ionisation potentials, energy difference calcs. 79−97967
aromatic compounds, two-stage photoionisation in solns., UV laser irrad. effects *(Russian)* 78−13556
aromatic higher perfluoro compounds, He(Iα) photoelectron spectra 79−31610

ionisation of molecules continued
atomic to molecular ion conversion, rate constant calc. 78−64835
autoionisation processes, review, and expt. methods 78−29763
autoionising states, mean-square deviation formula derivation 77−57943
cis-azo group, ionisation and excitation energies depend. on bond angle, ab initio MO calc. 79−72236
1-azo-bicyclo-2,2,2-octane, multiphoton ionis. spectra polaris. characts., two-photon symmetry assignment 78−74718
azulene, multiphoton ionisation, mass spectra 80−63717
benzaldehyde molecules, photoionisation mass-spectrometry with excimer KrF laser 80−95691
benzene, ^{13}C substituted, mass selective two-photon ionis., mass spectroscopy obs. 80−9651
benzene, ethylene, and fluorinated derivatives, photoelectron ang. distribs. of C-C π electrons 79−10146
benzene, multiphoton ionis. spectra polaris. characts., two-photon symmetry assignment 78−74718
benzene, multiphoton ionisation fragmentation patterns, statistical theory 80−95693
benzene, multiphoton ionisation mass spectra 80−57420
benzene, resonance-enhanced multiphoton ionis. and fragmentation of mol. beam 79−100411
benzene, Rydberg series, second ionis. process assignment, vibronic coupling 77−42333
benzene, trifluoromethyl derivatives, first ionis. pots., CF_3 group nature 79−27110
benzene, two-photon ionis. of mol. beam, mass spectrometer ion source 79−27118
benzene, UV photoelectron spectra, valence electron shake up approx. methods 80−18788
benzene, visible and UV photoionisation and fragmentation 80−69195
benzene molecules, photoionisation mass-spectrometry with excimer KrF laser 80−95691
benzene-d_6, splitting of vibrationless level in Jahn-Teller active state of D_{2h} symmetry 77−58080
Born-Oppenheimer electronic wave function, density matrices, electronic and nucl. motions separation 79−59332
bromobenzene ion fragmentation, photoelectron-photoion coincidence spectra 80−95682
bromofluorobenzens, He(Iα) and He(IIα) photoelectron spectra, assignments, ionis. energies 80−78651
bromoform and Cl substitutes, VUV photoionis. during condensation with Ar, IR spectra of $(CHX_2^+)X$ and X^--HCX_2 ions 79−13773
trans-1,3-butadiene, multiphoton ionis. spectra polaris. characts., two-photon symmetry assignment 78−74718
trans-butadiene, multiphoton transitions, multiphoton ionisation, thermal lensing spectroscopy 78−33559
butadiene, resonance-enhanced multiphoton ionis. and fragmentation of mol. beam 79−100411
butene, isomers, ion-mol. reactions, photoionisation mass spectra 80−81298
t-butyllithium, dissoc. photoionis. 79−6976
carbenes, core ionised states, singlet and triplet state binding energy, struct. changes, LCAO-SCF calc. 79−97982
carbon tetrafluoride, molecular effects in F K-shell ionisation by 0.5 to 1.5 MeV protons 77−50515
carbon tetrahalides, matrix photodissoc. and photoionisation by inert gas reson. radiation 77−83587
chloramine, HOCl, isoelectronic mols., vap. phase UV photoelectron spectra, struct. 78−66600
chlorofluorobenzenes, He(Iα) and He(IIα) photoelectron spectra, assignments, ionis. energies 80−78651
cluster beam, multiple stage ioniser, spatial potential distribution and electron trajectory calcs. *(Japanese)* 80−99596
collisional ionisation in intense laser field, quasimol. state reson., quantum mechanical anal. 78−33589
collisions in intense light beams, quantum aspects *(Russian)* 79−6903
cometary comas, positive molecular ions prod. 77−87327
comets, ionisation rate rel. to molecules collision-induced Λ-doublets transitions 80−14132
completeness theorem for operator spaces 77−34536
Compton profiles, two-electron theory 79−86012
conjugated system, potentials of twofold ionization and electron affinity calcs. 77−3287
core electron ionis., vibronic coupling, symmetry breaking, vibr. struct. 78−5279
core holes, localised-delocalised relation, ionis pot., Green's function method 77−75064
cross section by complex basis function calcs. of resolvent matrix elements 80−78662
cross section determ. in ion cyclotron resonance spectrometers 77−67527
cross sections, positive integer spectral power moments in moment-trace calcs. 78−17729
cross-section calc., absorbing boundary method 79−31623
cycloheptatriene, field ionis. to excited states 77−19002
cyclopropane-d_0, -d_6, multiphoton ionisation spectra, electronic struct. 78−82803
diatomic asymmetric mol., vibr. self-ionisation and recomb. *(Russian)* 77−79700
diatomic molecules, inner-shell ionisation, relax. effects calcs. 77−42351
diatomic mols., photoabsorpt. cross-section, photoionis. continuum 77−68029
cis-dibromoethylene, vac. UV spectrum, Rydberg transitions, ionisation limits 78−78718
dichlorobenzene+metastable inert gas atom, mol. ionis., collisional energy depend. 79−54950
dichlorodifluoromethane, matrix radiolysis, photoionis., IR spectra of CF_2Cl^+ and parent cations 78−80767
dichloroethylene+metastable inert gas atom, mol. ionis., collisional energy depend. 79−54950
diethyl ether, field ionisation, thermal energy distribution and energy deposition 80−95732
difluoromethane, ionisation energies, SCF Xα calcs. 77−14360
dimethyl ether-trioxane mixtures, condensation-elimination ion-mol. reactions obs. 78−23939
dimethylanilines, photoemission for mol., polarised photoelectrons 78−66607
diphenylethers, 1st ionisation energy, substituent effects, photoelectron spectra 77−42354
diphenylmercury, mol. photoionisation, up to 13.5 eV, formation of $HgPh^+$ 78−25633

ionisation of molecules continued
diphenylsulphides, 1st ionisation energy, substituent effects, photoelectron spectra 77−42354
doubly charged molecular ions, energy calc. by HAM/3 method 80−9512
dye proflavine bound to synthetic polynucleotides, selective laser photodamage 80−99525
dynamic symmetry breaking, mol. photoelectron ang. distrib. 79−829
electron propagator theory for mol. electron binding energies and photoionis. intensities 80−47848
electron scatt. and photoionisation, shape-resonance enhanced nuclear motion effects 80−63603
electron spectroscopy, coincidence experiments, two-parameter 78−20135
electron wavefunctions for (γ,2e) and (e,3e) processes at high energy, double Fourier transform 78−17628
electronic and at. collisions, conference, Kyoto, Japan (Aug.-Sept. 1979) 80−62394
ethane, mass spectrometric ionis., dissociation 77−3488
ethane, photoelectron spectrum below 14 eV, ab initio calc. 77−54575
ethane, photoionisation cross section at distance from threshold, chemical bond influence 80−69196
ethane, photoionisation spectra, cond. hole model 80−58326
N-ethylcarbazole, soln., laser induced ionic photodissoc., transient polyelectrolyte form. 80−53068
ethylene, π-electron system photoionisation cross-section, 2nd Born approx. calcs. 77−3424
ethylene, autoionisation and photoemitted electron ang. distrib., cylindrical mirror analyser study 80−18049
ethylene, dimer and trimer, dissoc. following photoionis. of mol. beam 79−57212
ethylene, ionisation energy, LCAO Xα calcs. 77−50353
ethylene, photoionisation cross section at distance from threshold, chemical bond influence 80−69196
ethylene, UV photoelectron spectra, valence electron shake up approx. methods 80−18788
ethylenimine, multiphoton ionisation spectra, electronic struct. 78−82803
excited state photoionisation, at. and mol. photoabsorpt. cross sections determ. 80−32783
fast molecular ions, break-up on collision with solids 80−66353
fast photoionisation processes, Dyson orbital theory 77−27122
ferrocene, multiphoton dissoc. and ionisation by tuneable dye lasers 80−99524
ferrocene, multiphoton ionis. spectra, at. Fe transitions 80−106361
first-row hydrides, correl. energy difference models 77−10600
fluorobenzene, multiphoton ionisation spectrum in one-photon wavelength region 80−63727
fluorobenzene, multiphoton reson, ionis. spectrum, 51000 cm^{-1} assignment 79−86021
fluorobenzene ions, fluoresc. quantum yields and lifetimes, meas. method ion form. 77−6815
fluoromethanes, ionisation pots., SCF-multiple scatt.-Xα calcs. 78−5141
forced ionisation, appl. in secondary batteries 79−43755
formaldehyde, core ionisation, valence orbital relax. calcs. 78−5135
formaldehyde, orbital contribs. to relax. energies accompanying core ionis., ΔSCF HF calcs. 78−82642
formaldehyde, two-step photoionisation, $^1A_2$ state lifetime 77−10711
formamide, CI calc. of vertical ionisation and excitation energy 78−78836
formamide, valence ionisation energy and electron affinity, HAM/3 calc. and photoelectron, UV spectra 79−50081
formic acid, ionis. and photoelectron spectra, inner valence electrons 78−82784
formic acid+Ar($^3P_{2,0}$), ionisation in crossed mol. beams, energy depend. 79−52669
formic acid dimer-t_1, H bonding, β^--decay effects, ab initio calcs. 79−54763
formic acid ions, fragmentation, energy selected, photoelectron-photoion spectra 80−95676
Freon, matrix radiolysis, photoionis., IR spectra of CF_2Cl^+ and parent cations 78−80767
fumaronitrile exciplexes, photoisomeris. and photoionis, dissolved O_2 effect 78−27789
furan, resonantly enhanced multiphoton ionisation 80−106362
furan, trifluoromethyl derivatives, first ionis. pots., CF_3 group nature 79−27110
gas mixture, self sustained volume photoionisation discharge existence conditions 80−79610
geometry changes on ionisation 77−34573
glow discharge instability in N_2-CO_2 non self sustained ionisation source, mechanism 80−38819
graphite-AsF_5 intercalated species, fractional ionisation and identification 80−97397
Green's function method for vertical ionis. pots. calc., CNDO adapted approx. 80−18799
H_2^+, negative surface ionisation on ThO_2, plasman diagnostics appl. 80−6280
halogen diatomic molecule, 1s hole states, ionisation, ab initio SCF calcs. 78−17568
heavy ion collisions, 3dσ mol. orbital ionisation 78−94311
1-heptene, field ionisation mass spectra, surface processes 79−11503
heteroaromatic compounds, two-stage photoionisation in solns., UV laser irrad. effects *(Russian)* 78−13556
1,5-hexadiyne, time-depend. mass spectra, ionisation efficiency and breakdown curves 80−95747
hexafluorides, MF_6, M=S,Se,Te,Mo,W,Re,Ir,Pt, ionisation 78−55226
hexafluoroethane, molecular effects in F K-shell ionisation by 0.5 to 1.5 MeV protons 77−50515
hexanes, isomeric, 80−95732
hexanes, isomeric, unimol. decomp. processes following field ionisation, temp. depend. 80−95733
trans-hexatriene, multiphoton ionization spectrum in 6.2 eV region 77−27133
1,3,5-hexatriene radical cation, in Ne matrix, laser induced fluoresc. and emission spectra 80−87163
hydrocarbon, (C_nH_{2n+2}, n=1-4)+H^+, electron capture and loss cross-sections 1-20 keV *(French)* 77−38728
hydrocarbons, cyclic, ionis. pot., electron affinity, semiempirical MO theory 77−50365
hydrocarbons, saturated and unsaturated, ionisation spectral intensities, correlation effects 78−90234
hydroxonium complexes, produced by collisional dissoc. method, mass spectrometric study, dissoc. energies determ. 80−95707
inert gas+diatomic (triatomic) mol., Penning ionis. process from electron spectroscopy 77−14555
inert gas+H_2^{**}, ionising or deactivating collisions 79−100338
inert gas-halide lasers, halide mol. negative ion prod. rates 80−18938
inert gas-halogen mixture, ion form., ion-mole. reactions, mass spectra 77−61841
inner shell spectra anal., rel. to electron impact vibr. excitation 80−5629
inner-shell photoabsorpt., shape resonances, extended X-ray absorpt. fine struct. 77−18979
interstellar matter, ionisation rate rel. to molecules collision-induced Λ-doublets transitions 80−14132
3-iodoaniline, photoemission for mol., polarised photoelectrons 78−66607
ion induced inner shell vacancy formation 78−70926
ion pair form., vibr. energy depend. 79−34287
ionisation potential, SAMO-ZDO method 78−41947
ionisation potentials, natural transition orbital theory, perturbation theory anal. 77−34541
ketene, photoionis., ion fragmentation kinetic energy 78−9206
laser ionisation, modelling 78−90133
laser-assisted excitive Penning ionisation 79−41232
laser-induced selective multistep processes: impact on nuclear physics, chemistry and biology 80−61122
liquid, electron-hole interactions and double proton transfer, picosec. laser obs. 79−45773
localisation and local phenomena in excited and ionisation stationary states 77−34563
localisation approach 77−30806
malachite green leucocyanide, photoionization in polar solvents, mechanism 77−25295
many-body perturbation theory, eqns. of motion formulation 77−88373
many-electron systems, ionis, pot., excitation energy, cluster expansion direct calcs. 79−26912
mass spectroscopy, ion registration, stepwise selective photoionisation technique *(Russian)* 78−21262
metal hexafluorides, MF_6(M=W,Re,Os,Ir,Pt), ionisation energies and optical spectra in Dirac-Slater model 77−83488
metastable atomic or molecular species, multiphoton transition detection 80−58231
methane, core ionis., single orbital relax., LCAO MO SCF calcs. 78−29739
methane, ionis. by mol. orbital method, many-body calc. 79−36512
methane, orbital relax. energy for single and double ionis. from valence shells 80−106253
methane, photodissoc. ionis., 16-41 eV 77−18995
methane, photoelectron ang. distrib., near threshold to 30 eV, photon energy depend. 80−53045
methane, photoionis., ion fragmentation kinetic energy 78−9206
methanol, field ionisation, geometry changes, INDO-SCF-MO calc. 77−38614
methanol, ionic dissoc., photoelectron-photoion coincidence spectroscopy 80−66774
methanol-d_4, dissoc. following photoionis., using coincidence spectrometer 79−54998
methanol-O_2 flame, combustion and ionisation 79−20357
N-methyl pyrrole, resonantly enhanced multiphoton ionisation 80−106362
methyl radical and anion, electron affinity determ., ab initio SCF and CI calcs. 78−5149
2-methylaniline, photoemission for mol., polarised photoelectrons 78−66607
methylbenzenes, 3p Rydberg transitions, multiphoton ionis. spectrosc. obs. 80−95644
methylchloramines, CH_3NHCl, CH_3NCl_2, $(CH_3)_2NCl$, UV photoelectron spectra, assignments 78−86911
molecular orbital methodology 79−36512
molecular photoionisation cross sections, at. extrapolation, ground state inversion method appl. 80−18787
molecular photoselected excited states, dynamics, advances using synchrotron radiation 80−37836
molecule+fast heavy ion, dissoc. ionisation obs. 79−47899
monohalobenzenes, inner shell excitation and ionis., electron energy loss spectra, XPS, assignments 78−62934
mucopeptide N-acetylmuramoyl hydrolase, hen egg-white lysozyme, ^{13}C n.m.r., carboxyl ionisation consts. 77−1978
multiphoton ionisation, laser-induced, detection using balanced bias differential current amplifier cct. 80−37909
multiphoton ionisation, reson. effects, light coherence effects 80−58232
multiphoton ionisation, resonance peaks strengths 77−42293
multiphoton ionisation and fragmentation, UV laser induced, time of flight mass spectra 79−31625
multiphoton ionisation by spontaneous emission absorpt. 78−74721
multiphoton ionisation dynamics, rate eqn. modelling 80−48046
multiphoton ionisation in gaussian beam focal space, ion generation *(French)* 77−6740
multiphoton ionisation spectroscopy, sequential, appl. to I_2 79−50163
multiple electron transfer to highly charged ions, scaling of cross sections 77−83711
multiplet ratios for photoionisation and electron attachment, shell model, LS coupling and correl. 78−17636
naphthalene, multiphoton ionisation, mass spectra 80−63717
naphthalene, photoionis., negative ions role in photoionis. plasma 79−27048
naphthalene, stepwise photoionisation process 78−82791
naphthalene, trifluoromethyl derivatives, first ionis. pots., CF_3 group nature 79−27110
nickelocene, multiphoton dissoc. and ionisation by tuneable dye lasers 80−99524
p-nitroaniline, adsorbed layer, core ionisation, negative shake-up energy 79−56913
p-nitroaniline, core ionisation negative shake up energy, ab initio SCF CI calc. 79−64041
nitrobenzene$^-$, positive ion formation energetics by negative ion charge stripping 80−78700
nitrobenzene, collision-induced dissoc., ionisation characts. in corona discharge 77−60156
nitrogenous bases of nucleic acids, ionisation pots. 77−29094
nitromethane, IR laser mutliple photon ionis. 79−74403

ionisation of molecules continued
nonpolar molecules, ionis. by alkali ion attachment at electrolyte surface 78−65998
nucleic bases, interactions and self-organisation, ionisation and solvent salt comp. effects 80−55985
nucleotides, interactions and self-organisation, ionisation and solvent salt comp. effects 80−55985
open shell systems, orbital energies, semiempirical calcs. 77−3272
organic ion, excited electronic state correlation with mass-spectral fragmentation pattern 80−45482
organic molecules, core ionisation and electronic redrganisations, LCAO MO SCF calcs. 79−18115
organic molecules, multiphoton ionisation mass spectra by ArF excimer laser 80−81381
organic non-volatile compounds ionisation by fast heavy ions, separation by TOF mass spectrom. 77−27170
organic seedants for UV preionised lasers, photoionisation and photoabsorpt. characts. 78−13688
orthogonalised-plane-wave approximation, cross-section 79−41202
oxalic acid in aq. soln., vibr. studies, IR and Raman spectra 80−95589
oxirane cation, struct. rearrangement following vertical ionisation, ab initio CI calc. 80−58191
Penning collision processes, review *(Japanese)* 79−64092
Penning ionisation processes investig. by electron spectroscopy 80−58364
peptides and derivatives, mol. electron acceptor groups 80−30637
phenol, aq. soln., electron ejection, picosec. obs. 80−87187
phenol, field ionis. to excited states 77−19002
phenolate, aq. soln., electron ejection, picosec. obs. 80−87187
photoelectron angular distribs., oriented or rot. resolved unoriented mols., dynamic and struct. data 78−37682
photoelectron recoil effects in light atom mols., X-ray photoelectron vibr., rot. excitation 78−42129
photofragment spectroscopy of mol. ions using fast ion beams 80−9755
photoionisation, ground and selectively excited states, by vac. UV laser *(Russian)* 78−9205
photoionisation, linear mols., selection rule, parity unfavoured transitions 77−83662
photoionisation, multiple, infrared laser 80−69194
photoionisation, photoelectron ang. distrib. theory 78−17730
photoionisation, shape-reson. enhanced nucl. motion effects 80−1031
photoionisation, vibrationally-excited ions form. in Franck-Condon gaps, threshold photoelectron spectra obs. 79−68262
photoionisation ang. distrib. asymmetry, parity favouredness 78−50600
photoionisation cross section, modified plane wave model 77−88509
photoionisation cross section rel. to photoelectron peak size · 77−88508
photoionisation in mass spectrometer, using H_2 vac. UV laser 77−88606
photoionisation mass spectroscopy, reson. peak shapes 80−42295
photoionisation of atoms and molecules, UV photoelectron spectrosc. obs. 79−31603
photoionisation review, expt. techniques, processes, theory 77−14402
photoionization cross-section, ground state inversion pot. method 79−31484
photosynthetically relevant mols., electronic structural props. 80−16902
pigments, photochemical ionisation reactions in soln., automatic conductimetric instrument for kinetic studies 77−4971
plasma lasers in molecular medium, thermal ionisation and recomb. *(Russian)* 78−22118
poly N-vinylcarbazole, soln., laser induced ionic photodissoc., transient polyelectrolyte form. 80−53068
poly-ynes, struct., vibr. freqs., ionis. energies, MNDO calc. 77−88390
polyatomic molecule, multiphoton absorpt. resons., dynamic Stark splitting 80−9670
polyatomic molecules, multiphoton ionisation spectroscopy 79−41203
polyatomic molecules, new method, laser photoionisation in a mass spectrometer 78−78840
polyatomic molecules, photoionisation cross section and efficiency, doubie ion chamber meas. 80−91613
polyatomic molecules, visible and UV photoionisation and fragmentation 80−69195
polynucleotides, interactions and self-organisation, ionisation and solvent salt comp. effects 80−55985
POPOP, dye vapour, intense multistep photoionisation 79−10298
positive ion formation energetics by negative ion charge stripping 80−78700
preionis. and predissoc., rel. to spectral line shape 80−63724
propynyl cation+propyne, reactant structure effects 80−89469
protein, radical limiting conc. on UV irrad. at 77K, effect of luminesc. quenchers 80−30662
pyrazine, multiphoton ionisation spectra, circular to linear polarisation ratios, lowest ionisation pot. 78−74716
pyrazine, multiphoton ionisation spectra, of three-photon ionisation region 78−37689
pyrene, in alcohol solns., polar fluid electrons optical absorption coeffs., ns laser ionis. obs. 78−84600
pyrene, laser-induced two-photon photoionisation, simulation, double pulse investig. 78−37690
pyrene, mol. ionisation pot., two photon ionisation, micellar interface effects on ionisation threshold 80−91609
pyridine, multiphoton ionisation spectra, circular to linear polarisation ratios, lowest ionisation pot. 78−74716
pyridine, multiphoton ionisation spectra, of three-photon ionisation region 78−37689
pyridine, on hot W filament, mass spectrometric obs. 79−81302
pyridine-N-oxides, substituted, absolute energy levels in gas and condensed media, ionis. energy, electron affinity 77−67995
pyrrole, multiphoton ionisation, photoionisation threshold meas. 79−27047
pyrrole, resonantly enhanced multiphoton ionisation 80−106362
quark influence on ionis. pot., ab initio SCF calcs., appl. to H_2O and SO_2 79−10058
quasimolecules, electron spectra on autoionisation *(Russian)* 77−79690
rare earth oxides, XPS, 4f-electron ionisation 77−14493
rare earth tris-dipivaloylmethide chelates, XPS, 4f-electron ionisation 77−14493
resonance multiphoton processes of laser radiation interaction 80−37800
resonant ionisation spectroscopy, chem.-physics appls. 80−68259
resonant phenomena, complex stabilisation method 80−78515
resonant two-photon ionisation, time-independent rates, coherence vs. incoherence 79−54820
Rydberg transitions, term value-ionisation energy correls. 78−70738
ionisation of molecules continued
saturation effect in stimulated transitions between states of discrete and continuous spectra 77−42295
second-row homonuclear diatomics, photoemission energy, rel. to atoms 78−86832
second-row hydrides, correl. energy difference models 77−10600
selective dissociation, ionis., and chem. reaction stimulation, by ultra-short pulses, isotope separation *(Russian)* 78−29825
shake-up and UV charge transfer transitions, comparison 80−102567
singlet-triplet energy difference and singlet generalised oscillator strength, Lassettre-Dillon relation 80−63508
sublesion combination probability, molecular ion expt. 80−26285
superheavy quasimolecules, inner-shell ionisation, scaling behaviour 78−25691
superheavy quasimolecules, inner-shell vacancy formation, coupled channel anal. 80−48116
surface ionisation, kinetic energy of ions 77−10751
tetracyanoethylene molecule with high electronegativity on field polarisation, electron affinity determ. 79−27111
thiophosphoryl compounds, bond ionisation energies, mol. struct. from UV photoelectron spectra 78−82782
threshold photoion-photoelectron coincidences method for ion state selection 80−63718
Tokamak impurity problems, atomic and mol. struct. and collision data, review 80−43959
toluene, field ionis. to excited states 77−19002
toluene, two-photon ionisation spectrum, of $^1L_b \leftarrow S_0$ transition 80−14180
trans-hexatriene, 6.2 eV Rydberg state symmetry, multiphoton ionis. spectrum polaris. assignment 78−70759
transition functional method, ΔE SCF ionis. and excitation energies 77−88404
triatomic ions, fluoresc. quantum yields and lifetimes, meas. method, ion form. 77−6815
trichlorofluoromethane, matrix radiolysis and photoionis. at 15K,IR spectrochem. anal. 78−76893
triethylenediamine, multiphoton ionis. and two-photon fluoresc. excitation spectra 79−98164
tropomyosin, isotopic H exchange as function of state of ionisation of side groups 78−68979
tryphoton, aqueous, one and two photon ionisation by Na laser harmonics 80−69193
l-tryptophan, gas, UV photoelectron spectrum, photoionisation threshold 79−86004
tryptophanyltryptophan, laser flash photolysis, photoionis. mechanism 77−90619
tryptophanyltyrosine, laser flash photolysis, photoionis. mechanism 77−90619
two-atom system, with weakly bound electron, s-term passing through continuum parabolic boundary 79−72392
two-electron Fourier amplitudes of atomic and mol. wavefunctions using the (γ,2e) and (e,3e) processes 79−3419
tyrosine, UV absorpt. in aq. soln. of trypsin, photoluminescence after UV irradiation *(German)* 79−92137
UHF orbitals, ionisation energy calcs. appls. 80−58141
unimolecular decomposition, photon catalysed, first-order rate constant 80−99528
valence and core photoionisation, spectral lines, many body effects 80−47853
vertical valence ionisation potential, many-body Green's functions 78−22051
X-ray photoionisation cross section calcs., at. and mol. levels, HF rel. to OPW method 77−42353
Xalpha transition state and transition operator method calcs. 78−70743
zinc octaethyl porphin, soln., photochem. ionogenesis 80−61116
$Ar^+ + H_2$, charge transfer kinematics 78−9242
Ar_2 $^1\Sigma_u^+$ excimer state, photoionis. cross section 78−70882
Ar_2, photoionisation 77−54578
Ar_2^+, vibr. excited, form. by assoc. ionisation, photodissoc. 79−68279
BF_3, molecular effects in F K-shell ionisation by 0.5 to 1.5 MeV protons 77−50515
BF_3, threshold photoelectron, photoionisation and coincidence ion-threshold photoelectron spectra 79−820
$Ba + Cl_2 \rightarrow BaCl^+ + Cl^-$, chemi-ionis. reaction, mol. beam obs. 80−104434
Ba+HCl, beam-gas reaction, multiphoton ionisation, product identification 78−23946
Br_2+K, inelastic scatt., total cross-sections, trajectory surface hopping calcs. 78−46420
C_2, pot. curves, binding and ionisation energies and config. variational cellular method 80−32597
CH, photoionis. and photodissoc. near ionis. threshold, SCF MO CI and Steltjes imaging 78−58749
CLi_3, desorption from graphite expt., ionis. pot. 79−34392
CN^-, ionisation pot., CI and perturbation methods 79−31734
CO, $^1\Sigma^+$ state, ionisation pots., dissoc. energy, atoms-in-mol. calcs. 77−88410
CO, adsorbed layer, electron impact, electron impulsive ionisation spectroscopy obs. 80−60720
CO, C_{1s} ionis., CI calcs. of satellite peaks 78−916
CO, core ionis., electric field depend. 78−13424
CO, core ionisation and single orbital relax. calcs. 78−5133
CO, core ionisation single orbital relax. energy, LCAO-SCF basis set depend. 79−89604
CO, dissociative ionisation 77−54616
CO, field ionis. to excited states 77−19002
CO, inner-shell ionisation, relax. effects calcs. 77−42351
CO, inner-shell ionisation, vibr. struct., sudden approx. calcs. 79−50002
CO, inner-valence ionisation, correl effects calcs. 78−9198
CO, orbital contribs. to relax. energies accompanying core ionis., ΔSCF HF calcs. 78−82642
CO, partial photoionisation cross-section determ. using synchrotron radiation 77−75243
CO, photoabsorption, photoionisation cross section, separated channel static exchange Stieltjes-Tchebycheff calc. 79−3502
CO photodissoc. ionis., 16-41 eV 77−18995
CO, photoelectric cross section and angular distribution calcs. 80−58323
CO, photoionis., vibr. intensity distrib., shape reson. effects 79−98167
CO, pot. curves, binding and ionisation energies and config. variational cellular method 80−32597
CO^+, fluoresc. and production cross-sections by photoionis. of CO 78−9204

ionisation of molecules continued
$CO^+ + D_2$, state selected reaction cross-sections, coincidence technique obs. 80−66797
CO_2, core electron ionis., vibronic coupling, symmetry breaking, O1s line vibr. struct. 78−5279
CO_2 dimer, photoionisation efficiency curve, supersonic mol. beam expt. 78−46406
CO_2, double ionis. by photon impact 77−88506
CO_2, ionisation energy, LCAO Xα calcs. 77−50353
CO_2 laser, atmospheric pulsed photoionisation, active medium optical homogeneity 80−58508
CO_2, negative ion form., photodissoc., mass spectrometric obs. 78−13558
CO_2, partial photoionisation cross-sections, branching ratios, synchrotron radiation meas. 78−42141
CO_2, partial photoionisation cross-sections meas. 20 to 60 eV 79−31624
CO_2, photodissoc. ionis., 16-41 eV 77−18995
CO_2, photoionisation, nuclear motion effects 80−58324
CO_2, photoionisation efficiency curve, supersonic mol. beam expt. 78−46406
CO_2, pulsed laser characts., UV preionisation 77−7059
CO_2, valence shell ionic photofragmentation, oscill. strengths, EELS and electron-ion coincidence meas. 80−37879
CO_2^+, electron impact ionisation, cross section obs. 80−58397
CO_2-Ar(He), stepwise pulsed photoionisation 77−50479
CO_2-H_2O-O_2, gas mixture, photodetachment and photodissoc., mass spectra meas. 77−500
CO_2-O_2, negative ion form., photodissoc., mass spectrometric obs. 78−13558
CO_2+He, Penning ionisation of target mol., for He(2^3S) 79−41228
$CO_2^+(C^2\Sigma_g^+)$, formation and predissoc., photoelectron spectra 78−5300
COH^+, orbital contribs. to relax. energies accompanying core ionis., ΔSCF HF calcs. 78−82642
COS, dissoc. photoionisation, mass spectrometric obs. 79−72366
COS^+, photoionis. reson. study of ($^2\Pi$) and ($^2\Sigma^+$) states, vibr. freqs., ionis. pot. 78−29821
CS molecule, calc. of HeI photoelectron spectrum, ionisation pot., vibr. struct. 77−3415
CS, valence electron photoionisation, ionisation pot. and spectral intensities 78−70883
CS_2, absorpt. spectra, Rydberg series converging to $A^2\Pi_u$ states of CS_2^+ 78−90182
CS_2, dissoc. photoionisation, mass spectrometric obs. 79−72366
CS_2, ionisation and fragmentation by monoenergetic electron impact, mass spectrometric study 80−102581
CS_2, photoionisation and dissociative ionisation due to 60-129 nm light, mass spectra study 79−94044
CS_2^+, and $(CS_2)_2^+$, photoionis. in supersonic mol. beam 79−98165
CS_2^+, electronic transitions, solid phase UV spectra 77−3380
CS_2^+, photoionis. reson. study of ($^2\Pi$) and ($^2\Sigma^+$) states, vibr. freqs., ionis. pot. 78−29821
CS_2+Ar*, Penning ionisation and dissoc. fluoresc, collisional energy depend. 78−33584
CSe_2, photoionis. mass spectrum, Rydberg states props., heat of form., CSe dissoc. energy and ionis. pot. 77−46604
Cl_2, ground and ionised states, Koopman's theorem and Mo relax. in ab initio calcs. 78−1035
$ClF(ClF_2^-)(ClF_3)$, ground and ionised states, Koopman's theorem and Mo relax. in ab initio calcs. 78−1035
CoO, ionisation, electron density relax. effects. ab initio calcs. 78−50466
CoO_6^{10-}, ionisation, electron density relax. effects. ab initio calcs. 78−50466
$Cr(CO)_5$, multiphoton ionisation, mol. cooling in pulsed supersonic beam 80−28070
$Cr(CO)_6$, photoionisation reson., 30 to 100 eV 79−76473
$CrOCl_3$, electronic structure and valence ionisation energies, obs. by ab initio and SW-Xα methods 80−69073
$CrOCl_3$, ionisation energy, CI and ΔSCF methods 79−68194
Cs+$H_2O(D_2O)$, ionising collisions in crossed-beam systems 78−48641
Cs+I_2, ion-pair formation, energy transfer and differential scatt. 77−75272
Cs+UF_6, ion pair form. and atom abstraction reactions 79−1946
Cs_2, $\tilde{a}^3A_2$-state detect. by reson. enhanced multiphoton ionis. spectrosc. 80−95551
Cs_2, ion-pair form. in two-photon absorpt. 77−88507
Cs_2^+, form. by Cs+Cs assoc. ionisation, dissoc. energy 78−58804
Cs_2+halogens($SnCl_4$)(MoF_4)(UF_6), ionisation reactions, absolute cross sections 80−99565
CsCl(Br)(I), He II photoelectron spectra, ionisation energy 77−18977
$CsCl(Cs_2Cl_2)$+Ar(Kr)(Xe), collision-induced ion-pair form., absolute cross sections 78−73029
D I, ionisation pot. photoionisation mass spectra 78−25632
D_2+He^+, dissociative ionisation, D^+ energy spectra 77−58154
DF, threshold photoelectron spectra, photoionis. threshold, resonant autoionis. 77−499
D_2O, collisionless multiphoton ionis. energy depend. by TEA-CO_2 laser 78−46405
D_2O+He(Ne), metastable, chemi-ionisation and secondary ion reactions 77−40531
F_2, ground and ionised states, Koopman's theorem and Mo relax. in ab initio calcs. 78−1035
F_2, pot. curves, binding and ionisation energies and config. variational cellular method 80−32597
F_2, threshold photoelectron spectra, photoionis. threshold, resonant autoionis. 77−499
$FO(X^2\Pi_i)$ radical from F+O_3 reaction, VUV photoelectron spectra 80−104455
$Fe(CO)_5$, multiphoton ionisation, mol. cooling in pulsed supersonic beam 80−28070
$Fe(CO)_5$, multiphoton ionis. spectra, at. Fe transitions 80−106361
H containing mixture extraction from D compounds, ionis. radiation effects *(Russian)* 77−6961
H I, ionisation pot. photoionisation mass spectra 78−25632
H-bonded systems, core and valence ionis., nonempirical LCAO MO SCF calcs. 77−67973
H+$Li(Li_2)$, superthermal collisions, photon and positive ion prod. 78−78788
H+$N_2(O_2)$, charge prod. cross sections and differential scatt. calcs. 78−94313
H_2, autoionising states, complex scaling method calcs. 80−9527
H_2, chemiionisation by He(2^3S) and He(2^1S), pot. surfaces, autoionisation widths, cross sections 77−36739
ionisation of molecules continued
H_2, D_2, photoionisation, body-frame Hund's case b description 78−94295
H_2, diabatic and reson. states, dissociative photoionisation calcs. 80−47883
H_2, dissociative photoionis. at 26.9 eV 77−3423
H_2, dissociative photoionisation, 19.8-40.8 eV, proton kinetic energy spectra 79−68273
H_2, electron impact, energy deposition and energy degradation, 2, 10 and 30 keV 79−31709
H_2, electron impact dissoc. ionisation, energetic protons for autoionising states 78−25728
H_2, field ionis. to excited states 77−19002
H_2, field ionisation under nonequilibrium conditions 80−74244
H_2, interstellar, ionisation, dissociation and heating efficiencies of cosmic rays 78−28454
H_2, photoabsorption, photoionisation, predissoc., high resolution obs. 77−477
H_2, photoelectron ang. distribs., oriented or rot. resolved unoriented mol., dynamic and struct. data 78−37682
H_2, photoelectron ang. distrib., 304 Å line, vibr. state depend. 79−45764
H_2, photoelectron angular distrib. and intensity, vibr.-rot. struct. 78−46393
H_2, photoionisation, ang. distrib. of photoelectrons 80−37834
H_2, photoionisation, dissociative, at 304 Å, photoion ang. distribs. photoelectron channels 78−82792
H_2, photoionisation, resonant, dissociative 79−68272
H_2, photoionisation cross sections, photoelectron ang. distribs. 78−5299
H_2, photoionisation cross-section, calc. for vibr. excited mol. 78−17732
H_2, photoionisation cross-sections, involving vibr. states, data tables 79−18242
H_2, photoionisation cross-sections, ang. distrib. and intensity, vibr.-rot. struct. 79−50091
H_2, photoionised continuum states, electron scatt. eqns. convergence 78−66663
H_2, pot. curves, binding and ionisation energies and config. variational cellular method 80−32597
H_2, preionis. and predissoc., rel. to spectral line shape 80−63724
H_2, statistical fluctuations in ionisation yield, rel. to electron degradation spectrum 80−99581
H_2, vibr. autoionisation and H_2^+ vibr. state distrib. depend. 77−48628
H_2^+, autoionising states, complex scaling method calcs. 80−9527
H_2^+ and D_2^+, scattered from Cu, energy spectra negative component 79−65967
H_2^+, ionisation energy, internucl. separation in intense mag. fields, var. calcs. 77−57898
H_2^+, ionisation energy in strong mag. field, variational calcs., equilib. internucl. separation 77−46654
H_2+ He (metastable), Penning ionisation *(French)* 80−1060
H_2+Ar^{6+}, collisions, ionisation and excitation resulting from electron capture 80−78683
H_2+atom (ion), ionis. by one or two electron at. particles, Born approx. 79−54960
H_2+Fe^{n+}, 262-1100 keV amu^{-1}, electron capture and impact ionis. cross-sections 78−42204
H_2+$H_2(N_2)$ cross sections for electron stripping of fast H_2 meas. 77−83705
H_2+H^+, 5-100 keV, secondary electron energy and ang. distrib. 80−14223
H_2+$H^+(H_2^+)(He^+)(O^+)$, H^+ prod., from H_2^+ dissoc. states or H_2^{2+} 78−20015
H_2+He^+, dissociative ionisation, H^+ energy spectra 77−58154
H_2+He*, Penning ionisation, singlet interaction pot. anomalous struct. 77−75274
H_2+He(2^3S_1) mol. ionis., optical atom orientation method *(Russian)* 78−13591
H_2^++H_2, state selected reaction cross sections, coincidence technique obs. 80−66797
H_2^++He, 10 keV, dissoc. excitation, ionis., energy distrib. 77−61849
H_3, correl., ionis. and attachment operators, diagrammatic method calcs. *(French)* 79−22607
H_3^+, correl., ionis. and attachment operators, diagrammatic method calcs. *(French)* 79−22607
HCN, HNC, electronic reorganisation, with core ionisation 78−94196
HCN, ionis. and photoelectron spectra, inner valence electrons 78−82784
HCN, ionis. by mol. orbital method, many-body calc. 79−36512
HCN ionisation potential, Green's function method 77−3260
HCN, K-shell excitation by electron energy loss spectroscopy 79−31712
HCN, vibr. fine struct. accompanying core ionis., STO calcs. 78−62844
HCO^+, orbital contribs. to relax. energies accompanying core ionis., ΔSCF HF calcs. 78−82642
HD, ionisation, Franck-Condon factors calcs. 77−58102
HF, core ionis., single orbital relax., LCAO MO SCF calcs. 78−29739
HF, ionisation energy, LCAO Xα calcs. 77−50353
HF, orbital relax. energy for single and double ionis. from valence shells 80−106253
HF, threshold photoelectron spectra, photoionis. threshold, resonant autoionis. 77−499
$(HF)_2$, photoionis., HF proton affinity 78−17731
$H^+(H_2O)_c$ ion-induced water clusters, mass spectra, IR continuum absorpt. 80−87257
HN_3, decomposition and ionisation in shock tube *(Russian)* 78−7182
HN_3, photodissoc. ionis., 16-41 eV 77−18995
HNC ionisation potential, Green's function method 77−3260
HNO, HON, electronic reorganisation, with core ionisation 78−94196
HO^-/H_2O and DO^-/D_2O, ionis. efficiency curves, Feshbach-reson. and dissoc. electron attachment 79−41246
H_2O, binding energy, MO momentum distrib., electron impact coincidence spectrometer obs. 77−61869
H_2O, collisionless multiphonon ionis. 77−65517
H_2O, core ionis., single orbital relax., LCAO MO SCF calcs. 78−29739
H_2O, core ionis. pot. of O, basis set depend. 78−17821
H_2O, D_2O, fragment ion formation on photoionisation, energetics and mechanism 77−501
H_2O, dipole oscillator strengths, 10-60 eV, for photoabsorpt., photoionis. and fragmentation 78−42133
H_2O, mol., ionisation pot., CI and perturbation methods 79−31734
H_2O, orbital relax. energy for single and double ionis. from valence shells 80−106253
H_2O, photodissoc. ionis., 16-41 eV 77−18995

ionisation of molecules continued
H_2O, photoionis. cross section by atomic extrapolation method 79−81242
H_2O, radiolysis, excitation, ionisation processes *(Rumanian)* 77−48666
H_2O vapour ionised by He^+ and He^{2+}, secondary electron emission yield obs. 80−102562
$H_2O+Ar(^3P_{2,0})$, ionisation in crossed mol. beams, energy depend. 79−52669
H_2O+H^+, 0.3 to 1.5 MeV, electron ejection, energy and ang. distrib. meas. 77−71851
$H_2O+He(Ne)$, metastable, chemi-ionisation and secondary ion reactions 77−40531
H_2O_2, ionisation energy, LCAO Xα calcs. 77−50353
$(H_2O)_2$, photoionis., H_2O proton affinity 78−17731
HOCl, chloramine, isoelectronic mols., vap. phase UV photoelectron spectra, struct. 78−66600
H_2S, inner valence electron ionisation calcs., photoelectron spectra obs. 78−82619
H_2S, S K-LL Auger energies and chemical shifts 80−28069
H_2S, valence shell binding energy spectrum, 8-34 eV, electron scatt. simulation of photoionis. 79−10213
$H_2S+O^+(Cl^+)$, S highly stripped core ion outer shell rearrangement, Kα X-ray spectra 77−3451
H_2SO_2, S K-LL Auger energies and chemical shifts 80−28069
H_2SO_4, S K-LL Auger energies and chemical shifts 80−28069
H_4SO_2, S K-LL Auger energies and chemical shifts 80−28069
$H^*_2+H_2O(SF_6)$, ionis. collisions 79−64088
He $(2^3S_1)+H_2$, ionis., interaction pot. at thermal energies *(Russian)* 79−94077
He_2^{2+}, autoionising states, adiabatic pot. energy curves calcs. 78−42140
HeH^+, vibrational self-ionisation of mol. and recomb. processes *(Russian)* 77−79700
$He(2^3S)+H_2O(H_2S)$, energy transfer processes, reaction products, UV and visible obs. in flowing afterglow 78−85138
$He(2^3S$ and $2^1S)+H_2(D_2)$, Penning, rearrangement and total ionis. cross sections, vel. depend. 79−22816
HgPh, photoionisation effectiveness curves 78−25633
I_2, coherent multiphoton transitions, nonlinear resonant photoionis. 77−61814
I_2, multiphoton ionis. and dissoc. vibronic/mass spectra method 79−3507
I_2, multiphoton ionis. spectroscopy, sequential 79−50163
I_2, multiphoton reson. ionis. bands, 360-600 nm 78−90233
I_2, resonance-enhanced multiphoton ionis. and fragmentation of mol. beam 79−100411
I_2+Ar^*, ion-pair form. differential cross-section, 25-133 eV, metastable Ar 78−78787
$I_2+Cs(Na)(K)$, ionising collision, trajectory surface hopping calc. 77−50509
K+Br, harpooning mechanism interactions, semiclassical optical model 79−89755
$K+Cl_2 \rightarrow K^+(Cl+Cl^-)$, 5.5−14.0 eV, energy loss, spectrum maxima, mechanism 77−75286
$K+D_2O \rightarrow OD^-+K^++D$, 100-200 eV, $D_2O^-(^2A_1)$, state 78−17770
$K+H_2O(D_2O)$, ionising collisions in crossed-beam systems 78−48641
$K+I_2$, ion-pair formation, energy transfer and differential scatt. 77−75272
$K+NO_2$, ion pair form. reaction, energy loss spectra obs. 79−91921
$K+O_2 \rightarrow K^++O_2^-$, electron transfer kinematics 77−6903
K_2, beam, multiphoton ionisation mass selective laser spectroscopy, vibronic, gyrovibronic states, clusters 78−21985
K_2, supersonic mol. beam, isotope selective two-step photoionisation study 80−74203
K_2^+, form. by electron impact in elec. discharge, low-press. vap. 79−10738
$K_2+Br_2(Cl_2)$, collisional ionisation reactions 77−50508
K_2+halogens$(SnCl_4)(MoF_4)(UF_6)$, ionisation reactions, absolute cross sections 80−99565
KCl, beam, surface ionisation on W ribbon, mass spectra 77−27173
KCl(Br)(I), He II photoelectron spectra, ionisation energy 77−18977
Kr_2, in non-self-maintained high-press. discharge, ionis. instability *(Russian)* 77−84557
Kr_2, photoionisation 77−54578
KrAr, photoionisation spectra of ground and excited states 78−5297
KrF, electric discharge pumped laser, model for UV preionisation 77−23658
Li^++N_2, (0.5 to 1.0 keV) energy loss spectra, ionisation, electronic and vibro-rot. transitions 77−14541
Li_2, isotope separation, by two-photon ionisation, ionisation pot. determ. 78−70950
Li_2, isotopes fractionation in two step photoionization, due to Ar laser beam 78−25631
LiF, N^+ and Ne^+ irradiation, MO X-ray intensity meas. 78−82831
LiH_2 and LiH_2^+ binding energies, LiH_2 ionis. pot. and form. heat 79−94042
Li_2H, Li_2H^+, binding energies, ionisation pot., mass spectrometric determ. 77−65546
$Mo(CO)_6$, multiphoton ionisation, mol. cooling in pulsed supersonic beam 80−28070
$N+O(^3P)$, endoergic assoc. ionisation, merged beam obs. 79−100348
$N^{n+}+N_2(O_2)(Ne)$(methane), K-shell vacancy prod. cross-section, charge state depend. 78−17751
N_2, $3\sigma_g$ photionis., shape-reson.-induced non-Franck-Condon vibr. intensities 80−43120
N_2, collisional destruction of singlet He I states in low press. glow discharge 80−49030
N_2, core ionisation, single orbital relax. energy contrib. calcs. 78−82637
N_2, core-ionised, core-valence excited and shake-up states, all electron MRD CI calc. 78−21858
N_2, electron impact ionis., rot. energy distrib. of $N_2+(X^2\Sigma_g^+)$ 79−76520
N_2, inner-shell ionisation, relax. effects calcs. 77−42351
N_2 inner-valence ionisation, correl effects calcs. 78−9198
N_2, ionisation by UV radiation from CO_2 laser produced Cu plasma 78−17624
N_2, ionisation potential, Green's function-eqns. of motion calcs., third order terms 78−41926
N_2, K-shell photoabsorpt. spectra using synchrotron radiation 78−74711
N_2, K-shell photoionis. cross section 77−88505
N_2, K-shell photoionisation, symmetry breaking hole localisation 79−829
N_2, multiphoton absorpt., spectroscopic evidence 80−63726
N_2, multiphoton ionisation, EM field gradient forces 78−66608

ionisation of molecules continued
N_2, multiphoton ionization, nonlinear interaction order and kinetic energy 79−45771
N_2, oscillatory-dissoc. relax. in hypersonic shock layer at moderate Reynolds number *(Russian)* 77−39311
N_2, partial photoionisation cross-section determ. using synchrotron radiation 77−75243
N_2 photodissoc. ionis., 16-41 eV 77−18995
N_2, photoionis., shape-reson. enhanced nucl. motion effects 80−1031
N_2, photoionis., transition probabilities at threshold, to $X(^2\Sigma_g^+)$, $A(^2\Pi_u)$ and $B(^2\Sigma_u^+)$ vibr. levels 78−94294
N_2, photoionis. and photoabsorpt. cross sections for aeronomic calcs., data tables 80−41599
N_2, photoionisation of π-shell, π-π^* transition, modified static-exchange calcs. 79−98163
N_2, pot. curves, binding and ionisation energies and config. variational cellular method 80−32597
N_2, preionis. and predissoc., rel. to spectral line shape 80−63724
N_2, total and partial photoionis. cross sections, threshold to 100 Å 77−58092
N_2^+, 1s hole satellite spectrum, large-scale CI calc. 77−65428
N_2^+, fluoresc. and production cross-sections by photoionis. of N_2 78−9204
N_2^+, fluoresc. quantum yields and lifetimes, meas. method, ion form. 77−6815
N_2^+, partial photoionisation cross section and photoelectron angular distribution for $X^2\Sigma_g^+$ state determ. 80−83429
N_2^{n+}, Coulomb explosion following heavy ion impact, ab initio SCF calc. 79−18277
$N_2+CO(N_2)(O_2)(NO)(CO_2)$(methane), ionis. at low energy 78−58791
$N_2+H_2^+ \rightarrow N_2^++H_2$, rot. energy distrib., 10 and 25 keV 79−76507
N_2+H^+, 5-100 keV, secondary electron energy and ang. distrib. 80−14223
N_2+H^+, electron capture and loss cross-sections, 1-20 keV *(French)* 77−38728
N_2+H^+, electron ejection, energy distrib. binary encounter approx. calcs. 77−30971
N_2+H^+ collision, total ionis. cross section and stopping power for protons 80−69228
$N_2+H^+(He^+)$, 1 MeV, dissoc. ionis., time-energy spectra 77−34744
$N_2+H^+(He^+)$, N_2^+ 3914 Å emission cross sections, 0.5-34 keV 77−54598
N_2+He_2, Penning ionisation of target mol., for $He(2^3S)$ 79−41228
N_2+He^+, K-shell ionisation, total cross-sections calcs. 79−31663
N_2+He^*, Penning ionisation, ejected electron spectra obs. 80−48074
N_2F_2, trans- and cis-isomers, photoelectron spectra, Green's function calc. 77−83650
NH_3, and ND_3, new electronic state, multiphoton ionis. obs. 78−74717
NH_3, $\tilde{C}'$-state, 3-photon gas phase spectroscopy obs. 79−89715
NH_3, core ionis., single orbital relax., LCAO MO SCF calcs. 78−29739
NH_3, electron impact ionisation, total and partial cross sections meas. 80−95729
NH_3, field ionis., critical energy deficits, field depend. 78−82852
NH_3, Franck-Condon factors calcs. 78−17723
NH_3, orbital relax. energy for single and double ionis. from valence shells 80−106253
NH_3, photoionisation branching ratios and partial oscill. strengths 78−5303
NH_3^+, ionisation pot. of ^2E state, Jahn-Teller effect 78−62948
NH_2Cl, $NHCl_2$, NCl_3, UV photoelectron spectra, assignments 78−86911
$NH_2(X^2B_1)$ radical, and ND_2, ionisation pot., vibr. anal., ab initio calcs. and vacuum UPS obs. 80−53047
NO, 4-photon ionis. spectrum 2- and 3-photon resons., low temp. assignments 78−70887
NO, adsorbed layer, electron impact, electron impulsive ionisation spectroscopy obs. 80−60720
NO, autoionisation struct. at first ionisation limit, photoionis. data 78−58748
NO, high resolution absorpt. spectrum in region of first ionization limit 77−461
NO, ionis. pot. and electron affinity, overlapping sphere MS Xα calc. 78−41948
NO, multiphoton ionis. spectrum 79−10157
NO, photodissoc. ionis., 16-41 eV 77−18995
NO, photoionis. resonant processes, preionis. and predissoc. 77−65516
NO, photoionisation and ionisation pot., mol. beam meas. 77−10709
NO, resonance-enhanced multiphoton ionis. and fragmentation of mol. beam 79−100411
NO, selectively excited rovibrational states, multiphoton ionisation spectra 80−69202
NO, state selective step-wise photoionis. with mass spectroscopic ion detect. 80−43119
NO, UV absorpt. spectra, 600-1000 Å, Rydberg series, ionisation energy 77−75180
NO, UV irrad. photoionisation, NO^+ high vibr. excitation, photoelectron spectra 77−71830
NO $X^2\Pi(\nu''=0)$, ionis. energies to NO^+ $X^1\Sigma^+(\nu=0\text{-}34)$, NO^+ mol. consts., UPS obs. 80−14177
NO+He, multiphoton ionisation spectra in supersonic expansion, laser entranced collisional effects 80−83459
NO+He, Penning ionisation of target mol., for $He(2^3S)$ 79−41228
$(NO)_2$, photoionisation efficiency curve, bound vibr. states 77−61811
NO_2, single and double ionisation by electron impact, ionisation pot. determ. 80−95730
N_2O, ionis. by low-energy electrons and near thermal inert gas ions, emission obs. 79−31707
N_2O, K-shell photoabsorpt. spectra using synchrotron radiation 78−74711
N_2O, partial photoionisation cross-sections meas. 20 to 60 eV 79−31624
N_2O, photoelectron spectrum, vibronic interaction and autoionis. effects 80−95680
N_2O, photoionisation, partial oscill. strengths 79−6973
N_2O, photoionisation and ion dissoc., isotope effects, mass spectra 78−9203
N_2O, preionis. and predissoc., rel. to spectral line shape 80−63724
N_2O, valence shell ionic photofragmentation, oscill. strengths, EELS and electron-ion coincidence meas. 80−37879
N_2O^+, fluoresc. and production cross-sections by photoionis. of N_2O 78−9204
N_2O+He, Penning ionisation of target mol., for $He(2^3S)$ 79−41228
N_2O_4, ionis. by mol. orbital method, many-body calc. 79−36512

ionisation of molecules continued
N_2O_4, second ionis. pot. by CI wavefunction 79−31732
$NO_2(NO_2^-)$, ionis. pot. and electron affinity, overlapping sphere MS Xα calc. 78−41948
$NO_3(NO_3^-)$, ionis. pot. and electron affinity, overlapping sphere MS Xα calc. 78−41948
$N_3P_3Cl_6$, ionisation energy and electronic struct., UV photoelectron spectra and Xα calcs. 78−94281
NS, ground ionic state, photoelectron spectra determ. 77−46596
$Na+I_2$, ion-pair formation, energy transfer and differential scatt. 77−75272
Na_2, 2-photon ionisation by Ar laser 78−55204
Na_2, beam, multiphoton ionisation mass selective laser spectroscopy, vibronic, gyrovibronic states, clusters 78−21985
Na_2, supersonic mol. beam, characterisation by multiphoton ionisation 78−23946
Na_2^+, form. from Na beam, resonance fluorescence 79−98215
Na_2^+, photodissoc. and photoionisation in Na_2 multiphoton absorpt. 79−31628
$Na_2+Br_2(Cl_2)$, collisional ionisation reactions 77−50508
NaCl+Ar, dissoc.-ionis. process rates in shock tube 78−35674
$Ne^{n+}+N_2(O_2)$(Ne)(methane), K-shell vacancy prod. cross-section, charge state depend. 78−17751
Ne_2^+, formation and destruction in Townsend discharges 80−38747
O_2, ab initio CI STO calc., photoelectron spectra 78−74585
O_2, ionisation, photodissoc. of positive and negative ions, mass spectrometric obs. 78−13559
O_2, multiphoton ionisation, electron energy spectra 77−6865
O_2, photoabsorpt., photoionis, and photodissoc., dipole oscill. strengths in UV 79−76468
O_2, photodissoc. ionis., 16-41 eV 77−18995
O_2, photoexcitation and photoionisation cross sections, HF Gaussian method 80−53064
O_2, photoionis. and photoabsorpt. cross sections for aeronomic calcs., data tables 80−41599
O_2, photoionisation, partial channel cross-sections calcs. 80−53061
O_2, photoionisation, producing $O_2^+(A^2\Pi_\mu \rightarrow X^2\Pi_g)$ and $O_2^+(b^4\Sigma_g^- \rightarrow a^4\Pi_u)$ emissions 79−94041
O_2, photoionisation angular distribution of photoelectrons 78−90235
O_2, photoionisation cross-sections, 100-800 Å 78−5302
O_2, soft X-ray photoionisation cross-sections, 6 to 22 Å 77−14499
O_2^+, photoelectron spectra, vibronic transition ionisation energies, ground state mol. consts. 79−89710
O_2^+, symmetric charge transfer reactions, selected states, photo-ion, electron coincidence 78−73028
$O_2+H^+(He^+)(O^+)$, dissoc. ionisation, kinetic energy spectra 78−25684
O_2+He, Penning ionisation of target mol., for He(2^3S) 79−41228
O_2+He*(2^3S), (2^1S), ion beam neutralisation reionisation spectroscopy 80−53120
$O_2^+ + NO \rightarrow NO_2^+ + O$, photoionis. mass spectra, photoionis. efficiency 77−40537
O_3, radiative electron attachment spectra, vibr. stretching, electron affinity, theory 77−54617
O_3^-, photoelectron, photodetachment and photodestruction spectra 79−64042
OF_2, photoelectron spectra, ionisation energies, ab initio many-body Green's function calc. 79−89709
OH_n, ab initio LCAO SCF calcs. of ionisation pot., electron, proton, H and hydride affinities 77−88387
$O_4^+(O_5^+)(O_6^+)(O_2^+H_2O)$ 80−95707
P_2, valence electron photoionisation, ionisation pot. and spectral intensities 78−70883
PH_3, inner valence electron ionisation calcs., photoelectron spectra obs. 78−82619
PN, valence electron photoionisation, ionisation pot. and spectral intensities 78−70883
RbCl(Br)(I), He II photoelectron spectra, ionisation energy 77−18977
SF_2, photoelectron spectra, ionisation energies, ab initio many-body Green's function calc. 79−89709
$SF_4+O^+(Cl^+)$, S highly stripped core ion outer shell arrangement, Kα X-ray spectra 77−3451
SF_6, absorpt. structs. in VUV region, ionisation efficiencies 79−3458
SF_6, ionisation pot., discrete variational Xα calc., Slater-type orbitals in Hartree-Fock basis 78−78837
SF_6, molecular effects in F K-shell ionisation by 0.5 to 1.5 MeV protons 77−50515
SF_6, multiphoton-excited in mol. beam, photoionsation probe of vibr. energy distrib. 79−76476
SF_6, partial photoionis. cross-sections, 20-54 eV, photoelectron spectrum 79−13769
SF_6, photoabsorption and ionic fragmentation, 5-63 eV, absolute oscill. strengths 79−72367
SF_6, photoionisation spectra in XUV region 80−37837
SF_6-hydrocarbon mixtures, IR laser induced ionis., mechanism 77−81415
$SF_6+H^+ \rightarrow SF_6^+ + e^- + H^+$, 0.3-1.8 MeV, electron energy and ang. distrib. 78−22015
SF_6+K, ion-pair form. reaction, energy loss spectra 80−55630
$SF_6+X^- \rightarrow SF_5^- + F + X$ (X=O, S, F, Br, I), electron affinity of SF_5 radical 80−45495
SO_2, radiative electron attachment spectra, vibr. stretching, electron affinity, theory 77−54617
SO_2, S K-LL Auger energies and chemical shifts 80−28069
SO_2^+ radical-ion formation 77−25285
SO_2+He, Penning ionis. due to He(2^3S), SO_2^+ fluoresc. 79−13758
SO_2+He(2^3S), Penning ionisation, mol. ion fluores., vibr. and bending freqs. 77−50507
S_2O, photoionis. mass spectrum, heat of form., dissoc. energy 77−46605
SbF_5+benzyl chloride, chemi-ionis. reaction, temp. depend., flow tube investig. 80−108701
$SiF_4+O^+(Cl^+)$, Si highly stripped core ion outer shell rearrangement, Kα X-ray spectra 77−3451
$SiH_4+O^+(Cl^+)$, Si highly stripped core ion outer shell rearrangement, Kα X-ray spectra 77−3451
SiO molecule, true potential energy curves, dissoc. energy, ionisation potential 77−6704
TeF_6, molecular effects in F K-shell ionisation by 0.5 to 1.5 MeV protons 77−50515
$TeF_6+H^+ \rightarrow TeF_6^+ + e^- + H^+$, 0.3-1.8 MeV, electron energy and ang. distrib. 78−22015
TiO^+, interstellar, prod. by associative ionisation 77−29893

ionisation of molecules continued
UF_6, electronic struct., relativistic MS Xα calc. 79−85911
UF_6 on C-coated Pt(Pt-W), mol. negative surface ionisation 78−56913
UF_6, strong UV-visible emission and weak ionisation induced by focused KrF laser 79−64034
UF_6+e^- (K)(Na)(Cs), positive and negative ion formation, electron affinity, bond dissoc. energy 77−75314
XeAr(XeKr) photoionisation spectra of ground and excited states 78−5297
XeF, electric discharge pumped laser, model for UV preionisation 77−23658
XeF_6 seeded mol. beam, transverse ionisation, space charge, mass spectra and vel. 80−78725

ionisation of solids
anthracene, crystal-electrolyte interface, ionis. energy of uppermost cryst. mols. 78−27764
avalanche ionisation, multiphoton ionis. *(Russian)* 79−51906
chrysene, crystal-electrolyte interface, ionis. energy of uppermost cryst. mols. 78−27764
dielectric ionization density distrib. meas. during pulsed electron beam irradiation 77−20810
electron wave function pair Fourier transforms, at., mol. and solids, by (γ,2e) and (e,3e) *(Russian)* 77−71878
fast electron distribution after ionisational energy loss 78−2177
naphthalene, crystal-electrolyte interface, ionis. energy of uppermost cryst. mols. 78−27764
perylene, crystal-electrolyte interface, ionis. energy of uppermost cryst. mols. 78−27764
phenanthrene, crystal-electrolyte interface, ionis. energy of uppermost cryst. mols. 78−27764
polystyrene latex sphere beams, secondary electron emission 77−24914
pyrene, crystal-electrolyte interface, ionis. energy of uppermost cryst. mols. 78−27764
semiconductor, ionization and subthreshold effects in defect creation and annihilation 77−84811
semiconductors, impact ionisation, Auger recombination involving traps 80−80912
spatial distrib. for 0.5 to 500 keV electron bombarded solids, empirical eqns. 79−19956
transparent dielectrics, cumulative ionisation by strong light pulse, numerical soln. *(Russian)* 77−28667
X-ray K-shell prod. cross-sections of Sc, Ti, V, Mn, Fe, Co, Ni for 4-38 MeV B ions 77−69958
GaP:Cs-O simultaneous adsorption, oxidation interface chemical struct. 80−103584
Si (100), oxides formed in Cs-O adsorbed films, ionisation loss spectra, Auger spectra 79−69365
Si, SiO, SiO_2, N^+ bombard., 500 eV chem. reaction, XPS and UPS 78−48265
Si:B implanted wafers, ionis. assisted annealing and effects 80−100257
Xe, γ-irrad., average energy expended per ion pair *(Russian)* 80−5438

ionisation potential
see also work function
acetic acid, monomer and dimer, photoelectron spectrosc. 80−87172
acetone and acetone-d_6, molecular beam photoionisation 79−3504
acetones, halogen substituted, photoelectron spectra 77−14490
acetophenones, mono substituted, semi empirical Π-electron calcs. 80−74131
acetylene, and $C_2H_2^+$, ionis. pots., photoelectron spectra, ab initio VB calcs. 77−88396
acetylene, core ionised, core-excited and shake-up states, ab initio MRD-CI methods 80−42950
acetylene, electron ionisation efficiency curves, fragment ion appearance pot. 78−86959
acetylene, ionis. efficiency curves by electron impact, $CH_2^+(C_2H^+)$ form., ~10 eV 78−62935
acetylene, vertical ionisation pots., CI calcs. 79−13645
aldehydes, conjugated, ethylenic, UV photoelectron spectra *(French)* 78−90215
alkali hydroxides, dissoc. energies and bond lengths, ion props. depend. 78−86801
alkali metaborates, dissoc. energies and bond lengths, ion props. depend. 78−86801
alkaline earth atom, correl. lines, Rydberg excitations and ionisation pots. 77−6705
alkaline earth fluorides, orbital binding energy and ionicity relations, XPS meas. 80−97399
n-alkenes, photoelectron spectra, MINDO/1, MINDO/3 and Fenske-Hall calcs. 78−5285
alkyl iodide-$I_{(atom)}$ complex, multiple charge-transfer bands in liquid-phase 77−32776
allene, ionis. pots., Green's function method 77−14608
allene, photoionisation and threshold photoelectron photoion coincidence obs. 78−21981
allene, vertical valence ionis. pots., ab initio UB calcs. 79−85917
allyl radical, ionisation potential, ab initio valence bond calcs. 79−31407
18-annulene, geometrical parameters, STO-3G ab initio calc. 80−52867
aromatic higher perfluoro compounds, He(Iα) photoelectron spectra 79−31610
aromatic hydrocarbons, catacondensed, photoelectron spectra, correlations with UV absorpt. spectra 77−34690
atmospheric thermal plasma, continuous emission, ionisation potential lowering and total excitation cross section 80−38705
atom, ionis. energy calc. 79−59382
atom, Koopman's ionis. pots., virial scaling corrections 77−65539
atom, Li to Ar, CI calcs. in spin density functional formalism 79−18122
atom, many-electron, using Slater's value of at. screening parameters 80−912
atom, s-electron binding energy regularities in $^1S^M$ configs. 78−62731
atom-ion core level shifts, ΔSCF calcs. 80−87176
atomic and mol. systems breakdown of quasiparticle picture, inner valence electrons 78−5112
atomic chemical and ionisation potentials 80−99584
atomic electronegativity scale rel. to work function 78−64096
atomic ionisation potential, X_α eigenvalues and Slater transition state 79−31394
atomic ionisation pots. in EM field, Kramers-Henneberger transformation, QED and semiclassical 77−23481
atomic ionization potentials, relation between neighbours in periodic table 78−22049

ionisation potential continued
atoms, approximate and exact state wavefunctions, ionisation potentials, energy difference calcs. 79−97967
atoms, first ionis. potential, Slaters transition-state method 78−46269
atoms, ionisation pots., electron affinities, Rayleigh-Schrodinger and Green's function calcs. 77−75075
atoms and ions, valence shell electronic energies from nucl.-electronic interaction energy 79−3347
azobenzene, derivatives, photoelectron spectra, ionisation pot., electronic struct. determ. 80−1024
azomethine compounds, nonaromatic, photoelectron and far UV absorpt. spectra 77−58079
benzaldehyde, proton affinity, MINDO/3 results compared to ICR obs. 78−1103
benzene:I_2, charge transfer spectra line shape 79−78700
benzene, and substituted forms, thermodynamic ionis. energy, rel. photoionis. energy 77−16858
benzene, correl. problem, open-shell coupled-cluster approach, PPP calc. 79−81157
benzene, ground, singlet and triplet states, ab initio VB STO, GTO calcs. 77−75060
benzene, trifluoromethyl derivatives, first ionis. pots., CF_3 group nature 79−27110
benzene, visible and UV photoionisation and fragmentation 80−69195
benzenes, substituted, electronic struct., ab initio calcs., photoelectron spectra 80−58314
benzenoid aromatic hydrocarbons, ionisation pot. and electron affinities, semiempirical MO theory 79−6843
bibliography at. energy levels and spectra, (July 1971-June 1975) 77−71764
binding energies, ionic, rel. to nonrelativistic neutral atom 78−90054
1,2-bromochloroethane, photoelectron spectra, trans- and gauche-conformers 79−27034
bromoethylene, vac. UV spectra 77−23507
bromomethane, ab initio SCF MO calcs., ionis. pots., dipole moment, config., electronic props. 78−1104
trans-butadiene, correl. problem, open-shell coupled-cluster approach, PPP calc. 79−81157
butadiene, electron momentum distribs. in π orbitals from (e,2e) expts. 80−14239
butadienes, cis- and trans-, ionisation potential, ab initio valence bond calcs. 79−31407
butatriene, ionis. pots., Green's function method 77−14608
butatriene, vertical valence ionis. pots., ab initio UB calcs. 79−85917
trans-2-butene, charge transfer mass spectra and photoelectron spectra 80−40778
t-butyl radical, VUV photoelectron spectrum, geometry, vibr. struct. and ionisation pots. 78−50577
carbenes, bond angles, inversion barriers, singlet-triplet energy differences, struct. fragments method 77−10782
carbenes, unrestricted HF calcs. of electronic structure 77−6683
carbon tetrachloride, low-energy X-ray emission spectra, MO anal., ionis. pot., rel. to CH_4 and $CHCl_3$ 79−85975
cationic dyes, adsorbed, local environment effects 79−34337
chemical ionisation, classical description, complex interaction pot., exponential representation 80−99570
chemical potential and ionisation potential, fundamental difference 80−907
chloramine, HOCl, isoelectronic mols., vap. phase UV photoelectron spectra, struct. 78−66600
chlorofluoromethane negative ion products, in 0-10 eV near-monoenergetic electron impact 79−41245
chlorofluoromethanes, MS Xα calcs., ionis. pots., electron affinities 77−79540
chloromethane, mol., valence and core ionis. energy, RHF-SCF and PNO-CEPA calc. 79−85890
closed shell systems, theory including electronic relax. and correlation 78−906
closed-shell configurations of isoelectronic ions and atom, SCF and STO energies 79−89598
closed-subshell atom, correl. lines, Rydberg excitations and ionisation pots. 77−6705
conjugated system, potentials of twofold ionization and electron affinity calcs. 77−3287
core holes, localised-delocalised relation, ionis pot., Green's function method 77−75064
cyanoacetylene, photoelectron spectra, electronic states of radical cations 79−22756
cyclobutenedione derivatives, photoelectron spectra, 2p lone pair delocalisation 78−46392
cyclopentadiene, HAM/3 calc. of ionis. and excitation energy and electron affinity 79−26894
cyclopentadienone, photoelectron spectra, ionisation pot., PERTCI method and obs. *(German)* 78−42130
cyclopropane, ionis. pot., many-body Green's function method 77−67972
diatomic homonuclear molecule, of 1st row, canonical exchange energy modulation parameters, MTXα calc. 79−97997
diatomic mol., Hellman pseudopot. calcs., dissoc. energy, ionis. pot., bond length 77−10577
1,2-dibromoethane, gauche and trans conformers, photoelectron spectra 78−50574
trans-dibromoethylene, VUV and photoelectron spectra, Rydberg series, vibr. fine struct. 77−6799
dibromoethylenes, vac. UV spectra 77−23507
dicyanodiacetylene radical cation, photoelectron and emission spectra 80−5558
diene-iron tricarbonyl complexes, π-orbital perturbation energies, ionisation energies; UV photoelectron spectra 80−32775
p-difluorobenzene, electronic struct., many-body calc., photoelectron spectrum assignment 77−23421
difluorobenzenes, X-ray and UV photoelectron spectra, ionis. pots., ab initio GO calcs. 77−61795
difluoromethane, binding energy, ionisation pots., overlapping sphere MS Xα 77−83499
difluoromethane, ionisation energies, SCF Xα calcs. 77−14360
dimethyl ether-trioxane mixtures, condensation-elimination ion-mol. reactions obs. 78−23939
dimethyl zinc, valence band and Zn 3d levels, electric field gradients 77−88495
diphenylmercury, mol. photoionisation, up to 13.5 eV, formation of $HgPh^+$ 78−25633
ionisation potential continued
diynes, acyclic, non-conjugated, UPS comparison, obs. and calc. 80−32772
doublet state, ionis. pots., electron affinities, using electron propagator, appl. to Li, Na, and BeH 79−63933
empirical calculation formula, new *(Chinese)* 78−70956
equations of motion Green's function methods, higher order terms, ionisation pots. 80−52891
equations of motion Green's function methods, higher order terms, ionisation pots., CI comparison 80−52892
ESCA chemical shift, indirect evaluation of Coulombic contribution to ionis. pots. for nonbonding electrons 78−92572
ethane, (e,2e) spectroscopic obs., valence electron momentum distribs. and separation energies 77−3480
ethane, ab initio MRD-CI calc., 14-25 eV PES region, Rydberg states 78−41962
ethane, electron ionisation efficiency curves, fragment ion appearance pot. 78−86959
ethane, ionis. efficiency curves by electron impact, fragment appearance pots. 77−61863
ethane, mass spectrometric ionis., dissociation 77−3488
ethyl radical, photoelectron spectra, first ionis. pot. 77−58078
ethylene, and perfluoro derivatives, negative ion states, electron affinities, ionisation pots., overlapping spheres Xα calc. 79−26885
ethylene, benzene, and fluorinated derivatives, photoelectron ang. distribs. of C-C π electrons 79−10146
ethylene, core ionised, core-excited and shake-up states, ab initio MRD-CI methods 80−42950
ethylene, electron ionisation efficiency curves, fragment ion appearance pot. 78−86959
ethylene, ionis. pot., Green's function method and CI calcs. 79−13839
ethylene, ionis. pots., Green's function method 77−14608
ethylene, ionisation potential, ab initio valence bond calcs. 79−31407
ethylene, ionisation pots. and excitation energies, correl. calcs. 77−26986
ethylene imine, ionis. pot., many-body Green's function method 77−67972
ethylene oxide, ionis. pot., many-body Green's function method 77−67972
exciplexes and excited aromatic molecules, donor-acceptor props., comparison of fluorescence quenching 80−69174
fast photoionisation processes, Dyson orbital theory 77−27122
ferricytochrome c and c_3, ionis. pot. from VUV photoelectron spectra 79−43821
ferrocytochrome c_3, anhydrous, ionisation pot., UV photoelectron spectrosc. obs. 80−85328
ferrocytochrome c, ionis. pot. from VUV photoelectron spectra 79−43821
first-row atoms, atomic X_α calcs. 80−83280
fluoroethylenes, variable angle photoelectron spectra, ionisation pot. asymmetry parameter 80−28064
fluoromethane, binding energy, ionisation pots., overlapping sphere MS Xα 77−83499
fluoromethanes, ab initio calcs. of K-shell ionisation potentials 77−18784
fluoromethanes, ionisation pots., SCF-multiple scatt.-Xα calcs. 78−5141
fluorophenol cations, emission and photoelectron spectra in gaseous phase 80−58316
formaldehyde, O and C 1s ionis. pots., shakeup XPS spectra electron spin coupling depend. 77−30925
formamide, CI calc. of vertical ionisation and excitation energy 78−78836
formamide, photoelectron spectrum, Green's function calcs., satellite lines 80−28061
formic acid, fragmentation, fragment structs. and energies calcs. 80−74124
formic acid, ionis. and photoelectron spectra, inner valence electrons 78−82784
formic acid, valence and Rydberg state empirically adjusted ab initio calcs. 77−10609
formyl chloride, photoelectron spectrum, vibr. struct., ionis. pots., assignments 78−9195
formyl radical, $-d_0$, $(-d_1)$, first ionis. pot., photoelectron spectrosc. determ. 80−48039
freon-N_2 low-pressure mixture prebreakdown current obs. 79−18995
fulvene, correl. problem, open-shell coupled-cluster approach, PPP calc. 79−81157
furan, HAM/3 calc. of ionis. and excitation energy and electron affinity 79−26894
furan, transition operator calcs. 77−30771
furan, trifluoromethyl derivatives, first ionis. pots., CF_3 group nature 79−27110
Green's function method for vertical ionis. pots. calc., CNDO adapted approx. 80−18799
haloacetylenes, photoelectron spectra, electronic states of radical cations 79−22756
heavy elements, electron config. rel. to chem. behaviour *(German)* 78−29727
heterocyclic conjugated compounds, electronic struct., spectra, ionisation pot., INDO-CI LACO-MO-SCF calcs. 79−54834
heterocyclic molecules, ionisation pot. and heat of form., IOC-ω method 79−31733
trans-hexatriene, correl. problem, open-shell coupled-cluster approach, PPP calc. 79−81157
hydride ions, XH^+, X=first and second row elements, PNO-CI and CEPA studies of electron correlation effects 77−34561
hydrides, second row, ab initio calcs. using FSGO basis, mol. parameters correlation 78−901
hydrocarbons, cyclic, ionis. pot., electron affinity, semiempirical MO theory 77−50365
hydrocarbons, ionisation pots. calc., PPP method 78−58592
hydrocarbons, nobenzoid, ionisation pot. and heat of form., IOC-ω method 79−31733
hydrocarbons, saturated, topological orbitals, graph theory and ionis. pots. 78−82615
hydronaphthyl radicals embedded in naphthalene cryst., optical transition energies and ionisation energies 80−78595
inert gas atom, correl. lines, Rydberg excitations and ionisation pots. 77−6705
inert gas mixtures, high-press., collisional radiative recomb. 80−63595
inorganic binary iono-covalent compounds, cryst., inorganic static effective charge calcs. *(French)* 80−2331

ionisation potential continued
inorganic molecules, UV photoelectron spectroscopy, spectral assignment criteria, bonding 78−17717
ions, ionisation potentials, electron affinities, perturbation theory-CI calcs. 78−9084
ions emerging from C foils, mean charge, inner-shell vacancy effects 80−87219
ketene, vertical ionis. pot., Koopmans' theorem perturbation corrections 79−76336
ketones, conjugated, ethylenic, UV photoelectron spectra *(French)* 78−90215
Koopman's ionisation potential, virial scaling corrections, appl. to He, Ne and Ar series 79−45655
lanthanides, 4f-screening, ionisation pots. by modified Slater method *(Chinese)* 79−97977
liquids, nonpolar, b.p. calc. as function of mol. polarisability, ionisation energy, and size 79−95148
LNDO/S, semiempirical SCF-CI method for calc. ionis. pot. and electronic transition energies 79−18117
many-electron systems, ionis, pot., excitation energy, cluster expansion direct calcs. 79−26912
metal hexafluorides, MF_6(M=W,Re,Os,Ir,Pt), ionisation energies and optical spectra in Dirac-Slater model 77−83488
methane, ionisation pot., quasidegenerate many-body perturbation theory calcs. 77−50346
methane, low-energy X-ray emission spectra, MO anal., ionis. pot., rel. to CCl_4 and $CHCl_3$ 79−85975
methane, orbital relax. energy for single and double ionis. from valence shells 80−106253
methanol, ab initio calcs. of K-shell ionisation potentials 77−18784
methanol, dissoc. ionisation mechanism, correlation diagram approach, mass spectra obs., metastable processes 80−95728
methanol, processes of photoionisation studied using ion-electron coincidence method 80−74204
methyl ethyl ketone, processes of photoionisation studied using ion-electron coincidence method 80−74204
methylchloramines, CH_3NHCl, CH_3NCl_2, $(CH_3)_2NCl$, UV photoelectron spectra, assignments 78−86911
methylene, photoelectron spectra, singlet and triplet state calcs. 78−42127
4-methylene-cyclohexadiene-2,6-one-1, proton affinity, MINDO/3 results compared to ICR obs. 78−1103
microwave gas breakdown, ionisation pot., qualitative theory 80−43837
MNDO semiempirical calcs. accuracy rel. to current MO methods 80−47893
molecular and fragment ions, difluoroethylene decay 79−59514
molecular open shell systems, orbital energies, semiempirical cals. 77−3272
molecule, CNDO-MO calcs. 78−912
molecule, influence of quarks, ab initio SCF calcs., appl. to H_2O and SO_2 79−10058
molecule, optical transition energies, Koopman's theorem, ionis. pot. 77−18908
molecules, approximate and exact state wavefunctions, ionisation potentials, energy difference calcs. 79−97967
molecules, ionisation potentials, electron affinities, perturbation theory-CI calcs. 78−9084
molecules, ionisation pots., electron affinities, Rayleigh-Schrodinger and Green's function calcs. 77−75075
molecules, MNDO semi-empirical SCF-MO calcs. 78−74578
molecules, SAMO-ZDO method 78−41947
molecules, truncated CI calcs. 80−27954
molecules, vertical valence ionis. pot., many-body Green's functions 78−22051
molecules containing C, N, O and H atoms, electron affinities and ionisation pot., semiempirical calcs. 80−78535
naphthalene, trifluoromethyl derivatives, first ionis. pots., CF_3 group nature 79−27110
naphthalene and fluoro derivations, CNDO calcs., σ core effect 79−41107
natural transition orbital theory, perturbation theory anal. 77−34541
nitrogenous bases of nuclei acids 77−29094
nitromethane, ab initio SCF MO calcs. of geom. and bond energies 79−31381
nitromethyl anion, ab initio SCF ab initio MO calcs. of geom. and bond energies 79−31381
nitronaphthylamines, ESCA and UV photoelectron spectra, assignments 78−50588
nonperturbative open shell theory, mol. ionisation pot. and excitation energies, HF multiple cluster expansion 79−22599
open shell systems, coupled cluster approach 78−58595
open-shell systems, ionisation pots. and dissoc. energies, correl. energy calcs. 79−31413
organic compounds, photoelectron spectroscopy, ionis. pots., MO models 78−17716
organic molecules, improved IOC-ω technique 77−14336
parabenzoquinone, and perfluoro derivatives, negative ion states, electron affinities, ionisation pots., overlapping spheres Xα calc. 79−26885
pentafluoroethyl iodide, electron impact, time of flight mass spectrometry 77−42424
periodic regularities, relativistic corrections calcs. 79−49950
photoionisation, expt. techniques, processes, theory, review 77−14402
photosynthetically relevant mols., electronic structural props. 80−16902
piezoelectric semiconductors, US ionisation of shallow impurities 77−43588
planetary probe atmospheric entry calcs., reduction-of-ionisation-pot. model 77−9651
poly-ynes, struct., vibr. freqs., ionis. energies, MNDO calc. 77−88390
polyatomic molecules, visible and UV photoionisation and fragmentation 80−69195
polycyclic aromatic ring systems, localised MOs and wave functions 79−31398
polyethylene, one-, three-dimensional, energy band struct., ab initio calcs. 79−95330
propane, vertical electronic spectrum, ab initio MRD-CI calcs. 78−70810
propane mol. ion, competing slow metastable processes, tunnelling mechanism, tandem-ICR obs. 77−28976
propylene, electron impact ionisation and dissoc. 80−37894
pyrazine, multiphoton ionisation spectra, circular to linear polarisation ratios, lowest ionisation pot. 78−74716
pyrene, mol. ionisation pot., two photon ionisation, micellar interface effects on ionisation threshold 80−91609
pyridine, multiphoton ionisation spectra, circular to linear polarisation ratios, lowest ionisation pot. 78−74716
pyridine-N-oxides, substituted, absolute energy levels in gas and condensed media, ionis. energy, electron affinity 77−67995
pyrrole, HAM/3 calc. of ionis. and excitation energy and electron affinity 79−26894
rare earth elements, atomic energy levels, data tables 78−86805
rare earth metals, photoionisation thresholds and Rydberg spectra 78−66522
Rydberg transitions, term value-ionisation energy correls. 78−70738
screening loss, penetration, ionic charge effects and the calculation of ionization potential *(Chinese)* 79−94102
second-row atoms, atomic X_α calcs. 80−83280
secondary ion yields, depend. on ionisation pot. and matrix sputtering yield 79−8214
self-consistent-charge Hartree-Fock-Slater calcs. 77−6687
semiconductors, ionisation coeffs. of electron and hole multiplication, empirical fit to Baraff's curves 80−96897
solutes, ionisation threshold energies and excess electron ground state energies 77−83508
sum rule, Manne Åberg theorem connection, many body Green's function formalism 80−27930
surface ionisation density, calc. in a material due to electron beam irradiation 80−55234
Tamm-Dancoff approximation, 2p-h, rel. to other self energy approximants 80−83243
ten-electron positive ions, ionic size rel. to Koopmans' ionisation pot. 79−85892
11,11,12,12-tetracyanonaphthoquinodimethane, XPS of solid and mol., ionis. pot. 79−31593
3,3,4,4-tetramethyldiazetine, photoelectron spectra, ring size effects on azo group ionis. pots. 77−61793
thioacetamides, CNDO calcs., internal rot., ionisation pots., photoelectron spectra 78−5143
Thomas-Fermi positive ions in extremely strong mag. field, 1/Z expansion for total energy 80−52855
trans-butadiene, ionis. pot., π-π^* energies, open shell many-body formalism calc. 77−46508
transition metal atoms, electron impact expts. 79−45849
transition metal compounds, reduced ionisation potentials as parameters in superconducting transition temp. calcs. 80−75671
transition metal hydrides, electron affinities and ionis. pots. MS Xα calcs. 79−10031
transition metal pentachlorides, photoelectron spectra 79−821
transition metal trifluorides, mol. and electronic structs., ab initio restricted Hartree-Fock calcs. 79−63900
transition metals, third row, by vertical anal. 78−41964
triallyl orthoformate, photoelectron spectra, ionisation pot. bands, conformation, SPINDO calc. 78−9194
trichloromethane, low-energy X-ray emission spectra, MO anal., ionis. pot., rel. to CCl_4 and CH_4 79−85975
trifluoroacetic acid, monomer and dimer, photoelectron spectrosc. 80−87172
trifluoroiodomethane, liquefied gas solns. bound exciton model for Rydberg bands 78−31214
trimethyl orthoformate, photoelectron spectra, ionisation pot. bands, conformation SPINDO calc. 78−9194
tropone, proton affinity, MINDO/3 results compared to ICR obs. 78−1103
UV photoelectron spectra at high temp., interpretation 78−17718
valence ionisation pots., SCF-MS-Xα calcs., mol. space partitioning 79−36529
vertical ionisation energies, finite order perturbation theory 78−33630
vertical ionisation potential, inner and valence shells, ab initio SCF MO CI perturbation calc. method 78−74800
vinyl isocyanate, microwave and photoelectron study of cis- and trans-forms 78−70819
X-ray elastic scatt., electron density and ionisation pots., Thomas-Fermi and Hartree Fock anal. 79−52041
Ag cluster 78−33646
Ag I, absorption spectrum, 1540-1850 Å 78−13453
Ag latent image particles, electronic effects 80−82840
Al I to XIII, energy levels and ionisation energies, data compilation 80−14100
$AlAs_3$ gas phase dissoc. energy, mass spectrometric determ. 79−81301
AlF_6^{3-}, octahedral complex, ionis. energy, SCF-Xα study 78−70967
AlF_6^{3-}, SCF Xα SW calcs., ionis. pot. 79−26887
Ar ions, electron impact ionisation, trapped ion cyclotron resonance spectroscopy 80−53140
Ar, Koopmans' ionis. pot., relax. correction 79−18308
Ar_2, photoionisation 77−54578
AuH, AuCl, relativistic effective core potentials, ab initio calcs. 78−86767
AuV, gas, bond dissoc. energy, from high-temp. mass spectra of V-Nb-Mo-Au 79−45860
B-containing mols., MNDO calcs. for ground-state 77−88391
BF, isoelectronic sequence, Rydberg transitions, term value-ionisation pot. correl. 80−58276
BF_2 radical, thermomechanical studies by mass spectrometry, enthalpy of form. and ionisation pot. determ., chem. bonds 80−81382
B(I) hydrides, ab initio calcs., proton and hydride affinities 79−10029
BO^-, ionisation pot. calcs. 77−75076
$BaTiO_3$ crystals, octahedral TiO_6^{8-} cluster atomic population, ionisation energy, SCF MS Xα calcs. 79−72244
Be, one-particle ionis. energy, correlated wavefunction 79−45639
Br^{7+}, ionisation pot., periodic regularities, relativistic corrections calcs. 79−49950
BrF_3, electronic struct. and ionisation pot., SCF DV Xalpha method 80−69057
BrF_5, electronic struct. and ionisation pot., SCF DV Xalpha method 80−69057
$BrO(X^2\Pi_i)$ radical, ionisation potential, photoelectron spectroscopic determ. 78−25612
C, theoretical ionis. energies and oscill. strengths, excited s-, p- and d-levels 78−86823
C-containing mols., MNDO calcs. for ground state 78−911
C_2, pot. curves, binding and ionisation energies and config. variational cellular method 80−32597

ionisation potential continued
CH_2 and CH_2^+, valence states, ab initio calcs. 79−6859
C_3H_5NH radical, valence shell ionis. pot. determ. 77−31014
CLi_3, desorption from graphite expt., ionis. pot. 79−34392
CN^-, ionisation pot., CI and perturbation methods 79−31734
CN^-, ionisation pot. calcs. 77−75076
CO, $^1\Sigma^+$ state, ionisation pots., dissoc. energy, atoms-in-mol. calcs. 77−88410
CO and $(CO)_6$, electronic struct. and bonding, SCF-Xα-MSW calcs. 78−25431
CO, inner-valence ionisation, correl effects calcs. 78−9198
CO, isoelectronic sequence, Rydberg transitions, term value-ionisation pot. correl. 80−58276
CO, pot. curves, binding and ionisation energies and config. variational cellular method 80−32597
CO, single and double ionisation by electron impact, energy depend. and ionisation pot. 79−13827
CO_2, electron impact single and double ionisation cross-sections 79−3584
CO_2 laser self-sutained discharge, effect of low-ionisation-potential additives 78−71616
CO_2^+, photoionisation reson. spectra and threshold electron-ion coincidence meas. of fragmentation 77−38700
CO_2-N_2-He laser mixtures, self-sustained glow discharges, low ionisation pot. organic additives effects *(French)* 77−88694
COS^+, photoionis. reson. study of ($^2\Pi$) and ($^2\Sigma^+$) states, vibr. freqs., ionis. pot. 78−29821
CS molecule, calc. of HeI photoelectron spectrum, ionisation pot., vibr. struct. 77−3415
CS, valence electron photoionisation, ionisation pot. and spectral intensities 78−70883
CS_2, liquefied gas solns. bound exciton model for Rydberg bands 78−31214
CS_2, thermodynamic ionis. energy, rel. to benzene and photoionis. energy 77−16858
CS_2^+, and $(CS_2)_2^+$, photoionis. in supersonic mol. beam 79−98165
CS_2^+, electronic transitions, solid phase UV spectra 77−3380
CS_2^+, photoionis. reson. study of ($^2\Pi$) and ($^2\Sigma^+$) states, vibr. freqs., ionis. pot. 78−29821
C_3S_2, electronic struct., optical and photoelectron spectra 78−70745
C_3S_2, electronic struct., optical and photoelectron spectra 78−70982
CSe, from CSe_2 photoionis. mass spectrum 77−46604
Ca I to XX, energy levels and ionisation energies, data compilation 80−14101
CdS(Se)(Te):Co^{2+}, IR luminesc. quenching, Co^{2+} level position, ionisation energy 80−16079
CeF_3, CeF_3+, MS Xα electronic struct. calc., inner shell photoelectron spectra 77−10594
Cl_2, ground and ionised states, Koopman's theorem and Mo relax. in ab initio calcs. 78−1035
$ClF(ClF_2^-)(ClF_3)$, ground and ionised states, Koopman's theorem and Mo relax. in ab initio calcs. 78−1035
ClO_4^-, ionisation energies, SCF-Xα transition state calcs. 80−74115
Cl_2O, ab initio vertical ionis. pot., corrections to Koopmans' theorem 78−25749
ClO($X^2\Pi_i$) radical, first ionis. pot., photoelectron spectrosc., vibr. struct., bond length 77−14495
Cr I to XXIV, energy levels, ionis. pots., g-factors, from spectral data review 77−79556
Cr, Koopmans' ionis. pot., relax. correction 79−18308
$Cr(CO)_6$, electronic struct. and bonding, SCF-Xα-MSW calcs. 78−25431
$Cr(CO)_6$, LCAO-HFS-STO calc., basis set effects 80−52882
$Cr(NO)_4$, XPS and UV photoelectron spectra, compared to NO data 80−58317
Cs, applicability in MHD generation *(Hungarian)* 80−3526
Cs, atom, XPS, free atom core binding energy 78−74699
Cs I, $n^2S_{1/2}$ and $n^2D_{3/2,5/2}$ states, energies 80−87066
Cs^+ and Cs, analytic SCF HF ground state wave function, ionis. pot., mag. props. 77−18785
CsX,(X=F,Cl,Br,I), ionis. energy, relativistic Dirac-Slater and nonrelativistic HF-Slater calcs. 77−26983
Cu IV, wavelength region 700-1200 Å, extended analysis 80−99473
Cu, isoelectronic series, semi-empirical oscillator strengths, lifetime, transition probability 80−32672
D I, ionisation pot. photoionisation mass spectra 78−25632
EuO(g), thermochem. props. 77−14604
F compounds, ground states, mol. parameters, MINDO calcs. 78−41955
F_2, correlated wavefunctions, ionisation pot. 77−67986
F_2, ground and ionised states, Koopman's theorem and Mo relax. in ab initio calcs. 78−1035
F_2, pot. curves, binding and ionisation energies and config. variational cellular method 80−32597
F_2O, geometry, electron spectrum, vert. ionis. pot. ab initio calc. 80−58187
FOCl, ab initio vertical ionis. pot., corrections to Koopmans' theorem 78−25749
Fe complex, $[Fe(CN)_6]^{3-}$, electronic struct., optical transitions, XPS, Mossbauer isomer shift, valence ionisation pot., SCF-MSX calc. 79−6864
Fe XVII, ionisation pot. in Ne isoelectric sequence 78−5363
$FeBr_2$, transient species, He(I) photoelectron spectrosc. calcs., relativistic corrections 80−95677
Ge, acceptor levels, ionis. energy and IR absorpt. 79−78033
GeO, mol., VUV photoelectron spectra, $X^2\Sigma^+$ state 79−72358
H atom, energy level calcs. in superstrong mag. field 80−37737
H I, ionisation pot. photoionisation mass spectra 78−25632
H ionisation potential and energies in mag. field 80−99585
H, multiphoton ionis. pot. in intense circ. polarised laser beam 80−43010
H, multiphoton ionisation potential, circularly polarized light 79−27101
H-containing mols., MNDO calcs. for ground state 78−911
H_2, pot. curves, binding and ionisation energies and config. variational cellular method 80−32597
H_2 vertical ionis. pot., many-body Green's function calcs. 80−102439
HCN, Green's function method 77−3260
HCN, ionis. and photoelectron spectra, inner valence electrons 78−82784
HCN, vertical ionisation pots., CI calcs. 79−13645
HCNH radical, valence shell ionis. pot. determ. 77−31014
H_2CNH_2 radical, valence shell ionis. pot. determ. 77−31014
ionisation potential continued
H_3CNH_3 radical, valence shell ionis. pot. determ. 77−31014
HCNO, vertical ionisation pot., Koopmans' theorem, perturbation connections calcs. 80−42966
H_2CS, ionis. pot., many-body Green's function method 77−67965
HF, highly excited, ionis. pot., mass spectrometric meas. 78−58603
HF, orbital relax. energy for single and double ionis. from valence shells 80−106253
HN_3, vertical ionisation pot., Koopmans' theorem, perturbation connnections calcs. 80−42966
HNC, Green's function method 77−3260
HNC^+, radical cation, charge exchange mass spectrometry, HNC^+ ion recombination and ionisation pot. 78−76838
HNCO, vertical ionisation pot., Koopmans' theorem, perturbation connections calcs. 80−42966
HNF_2 and DNF_2, photoelectron spectra, vibr. struct. obs, ionisation pot. determ., ab initio calcs. of ionic geometry 80−83418
HNF_2, vertical ionisation pot. calc. by perturbation corrections to Koopmans' theorem 80−83520
HNO, isomerism, low lying electronic states, ab initio MRD-CI calcs. 80−83291
H_2O, 78−82616
H_2O, D_2O, fragment ion formation on photoionisation, energetics and mechanism 77−501
(H_2O), electron affinity, ab initio SCF calcs. 79−76343
H_2O, ground state ionis. pots., generalized Mo theory 80−52907
H_2O, ionisation pot., quasidegenerate many-body perturbation theory calcs. 77−50346
H_2O, many-body Green's function, electronic mol. props. 78−25417
H_2O, mol., ionisation pot., CI and perturbation methods 79−31734
H_2O, orbital relax. energy for single and double ionis. from valence shells 80−106253
H_2O, relative ionisation energies, Tamm-Dancoff approx. calcs. 80−83243
H_2O, vertical ionis. pot. calc. from one-body Green's function 77−42440
H_2O, vertical ionis. pot., many-body Rayleigh-Schrodinger perturbation theory 78−9063
H_2O, vertical ionisation pots., CI calcs. 79−13645
H_2O, vertical valence ionis. pot. calc. by perturbation, CI and CPA techniques 80−69263
$(H_2O)_n$, n=2 to 8, correlation energies, ab initio and SCF calcs. semiempirically corrected 80−43223
HOCN, vertical ionisation pot., Koopmans' theorem, perturbation connnections calcs. 80−42966
HOCl, ab initio vertical ionis. pot., corrections to Koopmans' theorem 78−25749
HOCl, chloramine, isoelectronic mols., vap. phase UV photoelectron spectra, struct. 78−66600
H_2S, gas-phase, states in valence photoelectron spectrum 78−94284
H_2S, ionis, pot., many-body Green's function method 77−67965
H_3SiCl, mol., valence and core ionis. energy, RHF-SCF and PNO-CEPA calc. 79−85890
He, crit. pots. meas., student expt. 80−12874
He, field-ion appearance pot., theory 77−545
He, Koopmans' ionis. pot., relax. correction 79−18308
He, multiphoton ionis. pot. in intense circ. polarised laser beam 80−43010
He, multiphoton ionisation potential, circularly polarized light 79−27101
HfI, at spectrum, g-values, Zeeman effect, LS-coupling, ionisation pot. 77−3292
HfX_4, (X=Cl,Br,I), He I and He II photoelectron spectra, ionis. energy, chem. bonding 78−46394
HgH, $HgCl_2$, relativistic effective core potentials, ab initio calcs. 78−86767
HgPh, photoionisation effectiveness curves 78−25633
I VI, beam-foil spectrum, 400 to 1300 Å 79−86059
I VII, beam-foil spectrum, 400 to 1300 Å 79−86059
I_2, $M_{4,5}N_{4,5}X$ Auger electron spectra, many-body effects 79−59415
I_2+Na(K)(Cs), ion-pair form. cross section, 15-120 eV, mol. props. depend. 77−28996
In^{2+}, emission spectrum, 340 to 6500 Å, ionisation pot. and dipole polarisability 78−78654
InCl, InBr, InI, UV photoelectron spectra of valence d shells, gas-phase 78−62845
$InSb_{1-x}Bi_x$ disordered solid solns, ionisation energy of fluctuation levels 78−72116
K, atom, XPS, free atom core binding energy 78−74699
K I to K XIX, energy levels, tabulated data 80−51966
K, vapour, absorpt. spectra 79−21509
K_x, $(KNa)_x$, prep. and photoionisation pots. 78−55268
KLi, appearance pot., dissoc. energy, ionis. pot., mass spectra obs. 78−25750
Kr, Koopmans' ionis. pot., relax. correction 79−18308
Kr VIII, excited state energies and lifetimes, beam foil spectra 80−63591
Kr_2, photoionisation 77−54578
LaF_3, MS Xα electronic struct. calc., inner shell photoelectron spectra 77−10594
Li I-like spectra, energy struct., accurate semiempirical formulae 79−49970
Li isoelectronic series, ionisation pot. relativistic corrections calcs. 77−46484
Li, vapour, absorpt. spectra 79−21509
Li_2, core-excited states, UV photoabsorpt. and ejected electron spectra 78−37655
Li_2, isotope separation, by two-photon ionisation, ionisation pot. determ. 78−70950
Li_{2n}, (n=1, 2, 3), stable cluster configs., ionisation pots., binding energies, vibr. freqs., al initio SCF and CEPA calcs. 80−14265
Li_2Br_2, UPS of dimeric mol., expt. and Xα calc. 80−9640
Li_2Cl_2, UPS of dimeric mol., expt. and Xα calc. 80−9640
LiF and dimer, Li 1s ionisation pot. calc., Li 1s XUV absorpt. spectrum 77−23443
Li_2F_2, UPS of dimeric mol., expt. and Xα calc. 80−9640
LiH, many-body Green's function, electronic mol. props. 78−25417
LiH_2 and LiH_2^+ binding energies, LiH_2 ionis. pot. and form. heat 79−94042
Li_2H, Li_2H^+, binding energies, ionisation pot., mass spectrometric determ. 77−65546
Li_2I_2, UPS of dimeric mol., expt. and Xα calc. 80−9640
LiO, struct., spectra, SCF MO calcs. 78−17559

ionisation potential continued
Li_2O (LiOLi, LiLiO), struct., spectra, SCF MO calcs. 78−17559
Li_2O_2, ab initio geometry, vibr. freqs., ionis. pots., and force consts. 77−65421
LiOO, struct., spectra, SCF MO calcs. 78−17559
Li_3(g), thermochem. props. 77−21410
Mg, atom, XPS, free atom core binding energy 78−74699
Mg, I-XII, energy levels and optical spectra 80−87065
Mg, vertical ionis. pot. calc. from one-body Green's function 77−42440
Mn I, absorpt. spectrum, 1305-2040 Å, ionis. energy 79−26921
N^-, appearance pot., form. by electron impact ionisation, mass spectra 77−75320
N-containing mols., MNDO calcs. for ground state 78−911
N_2, calc. by equations-of-motion, Green's function method, critical analysis 77−30762
N_2, ground state ionis. pots., generalized Mo theory 80−52907
N_2 inner-valence ionisation, correl effects calcs. 78−9198
N_2, ionisation potential, Green's function-eqns. of motion calcs., third order terms 78−41926
N_2, ionisation pots. and excitation energies, correl. calcs. 77−26986
N_2, isoelectronic sequence, Rydberg transitions, term value-ionisation pot. correl. 80−58276
N_2, Koopman's theorem, corrections using energy shifted perturbation theory 79−6845
N_2, photoelectron spectra, valence region strong shake-up bands, Koopman's theorem breakdown 79−72354
N_2, pot. curves, binding and ionisation energies and config. variational cellular method 80−32597
N_2 relative ionisation energies, Tamm-Dancoff approx. calcs. 80−83243
N_2, vertical ionisation pots., CI calcs. 79−13645
N_2, vertical valence ionis. pot. calc. perturbation, CI and CPA techniques 80−69263
NF_2, ionis. pot., many-body diagrammatic RSPT calc. 79−31378
NH_3, electron impact ionisation, threshold to 180 eV, mass spectrometric obs. 78−13615
NH_3, ionisation pots. and excitation energies, correl. calcs. 77−26986
NH_3, orbital relax. energy for single and double ionis. from valence shells 80−106253
NH_3^+, ionisation pot. of ^2E state, Jahn-Teller effect 78−62948
NH_3-ND_3, electron impact ionisation, threshold to 180 eV, mass spectrometric obs. 78−13615
N_2H_2, isomers, photoelectron spectra, vibr. struct., ionisation pots., Green's function calcs. 77−75213
N_2H_2, $N_2H_2^+$, ab initio calcs., electronic struct., geometries relative energies 77−46487
N_2H_4, heat of form. determ. by electron impact dissoc. 78−61040
NH_2Cl, $NHCl_2$, NCl_3, UV photoelectron spectra, assignments 78−86911
$NH_2(X^2B_1)$ radical, and ND_2, ionisation pot., vibr. anal., ab initio calcs. and vacuum UPS obs. 80−53047
NO, ionis. pot. and electron affinity, overlapping sphere MS Xα calc. 78−41948
NO, photoionisation and ionisation pot., mol. beam meas. 77−10709
NO, UV absorpt. spectra, 600-1000 Å, Rydberg series, ionisation energy 77−75180
NO $X^2\Pi(v''=0)$, ionis. energies to NO^+ $X^1\Sigma^+(v=0\text{-}34)$, NO^+ mol. consts., UPS obs. 80−14177
NO^+, pot. energy curves, dissoc. energy 79−22623
NO_2, ionis. pot., many-body diagrammatic RSPT calc. 79−31378
NO_2, single and double ionisation by electron impact, ionisation pot. determ. 80−95730
N_2O, X-ray fluoresc. obs., ionis. pot., fine struct., LCAO SCF calc. 77−68055
N_2O_4, second ionis. pot. by CI wavefunction 79−31732
N_2O_4, UV photoelectron spectrum, variable temp./fast pumping technique, ionis. pots. 77−30926
NOH isomerism, low lying electronic states, ab initio MRD-CI calcs. 80−83291
$NO_2(NO_2^-)$, ionis. pot. and electron affinity, overlapping sphere MS Xα calc. 78−41948
$NO_3(NO_3^-)$, ionis. pot. and electron affinity, overlapping sphere MS Xα calc. 78−41948
$N_3P_3F_6$, ionis. energies, Xα scatt. wave calcs. 77−42242
NS, ground ionic state, photoelectron spectra determ. 77−46596
Na, atom, XPS, free atom core binding energy 78−74699
Na, efficiency laser ionisation via superelastic collisions and reduced ionisation pot. 77−79588
Na, excited states ionis. pot. calc., improved virtual orbitals 77−46491
Na particle, consisting of ats., metallic Na, model, electronic levels 78−50673
Na, quantum defects and ionis. pots., graphical procedure for students 80−7
Na, vapour, absorpt. spectra 79−21509
Na_3, electronic struct., pot. energy surface, ab initio CI study 78−70996
Na_n ($n\leq 8$), equilibrium geometries and ionization energies calcs. 80−1099
Na_x, $(NaK)_x$, prep. and photoionisation pots. 78−55268
NaK, appearance pot., dissoc. energy, ionis. pot., mass spectra obs. 78−25750
NaLi, appearance pot., dissoc. energy, ionis. pot., mass spectra obs. 78−25750
Ne, atom, calculation from optimised potential model 79−6895
Ne, atomic structure determ. by model pot. method 78−86777
Ne, electron impact K-shell excitation, EELS 80−106396
Ne, ionisation potential, KLL Auger energies, SCF transition operator calcs. 78−41925
Ne, isoelectronic series, ionisation pots., Ritz law and Edlen formula 80−32854
Ne, Koopmans' ionis. pot., relax. correction 79−18308
Ne, vertical ionis. pot., many-body Rayleigh-Schrodinger perturbation theory 78−9063
Ne, vertical ionis. pot. calc. from one-body Green's function 77−42440
Ne, vertical valence ionis. pot., many-body Green's functions 78−22051
Ne, vertical valence ionis. pot. calc. by perturbation, CI and CPA techniques 80−69263
Ni, UV matrix freq. shifts, ionis., pot., assignments, appl. to Ni_2, Ni_3 77−75178
$Ni(CO_4)$, approx. SCF Hartree-Fock-Slater calcs. 77−75334
Np I, first ionisation pot., radiative lifetimes, high-lying energy levels, laser spectroscopy 79−76370
Np, ionisation potentials, 2nd-6th, thermochemical calcs. 79−98248
O-containing mols., MNDO calcs. for ground state 78−911
ionisation potential continued
O_{2_g}, ionisation pots. and excitation energies, correl. calcs. 77−26986
O_2^+, vibr. energy levels, dissoc. energy, photoelectron spectra 77−83651
O_3, CI calc., ground and excited states, energy locations, transition probabilities 78−74584
O_3, photoelectron spectrum, vibr. struct., ionos. pot. 77−75217
OH_n, ab initio LCAO SCF calcs. of ionisation pot., electron, proton, H and hydride affinities 77−88387
OH(OD) radical, photoelectron spectra 77−27113
OsO_4, MS Xα calc., ionis. pots., energy levels, atomic spheres radii effect 77−18789
P IV, 200-9800 Å, spectral line classification and term system 77−79564
P^+, ionisation pot., periodic regularities, relativistic corrections calcs. 79−49950
P_2, valence electron photoionisation, ionisation pot. and spectral intensities 78−70883
P_2^+, electronic states pot. energy curves, dissoc. energy, ionisation pot., curve fitting 80−32796
P_3, from P_4 photoionisation mass spectra 77−30935
PF, pot. energy curves and dissoc. energy, Hulbert-Hirschfelder calc. 80−30210
PF_6^-, octahedral complex, ionis. energy, SCF-Xα study 78−70967
PH_3, X-ray K-fluoresc. obs. of electronic struct. 80−37818
PN, photoelectron spectra, ionisation pot., vibr. struct., Green's function method 77−61799
PN, valence electron photoionisation, ionisation pot. and spectral intensities 78−70883
$PN(X^1\Sigma^+)$, VUV photoelectron spectrum 78−1024
PO_4^{3-}, ionisation energies, SCF-Xα transition state calcs. 80−74115
$POCl_3$, He I(II) XPS spectra comparison, ion states assignments, pseudopot. calcs. 77−61794
$PbCl_2$, $PbBr_2$, PbI_2, UV photoelectron spectra of valence d shells, gas-phase 78−62845
$PtCl_4^{2-}$, electronic struct., SCF Xalpha ESCA spectrum assignment 80−23339
$PtCl_2(NH_3)_2$, cis- and trans-isomers, electronic struct., SCF-Xα study 80−18795
Pu, ionisation potentials, 2nd-6th, thermochemical calcs. 79−98248
Rb applicability in MHD generation *(Hungarian)* 80−3526
Rb, atom, XPS, free atom core binding energy 78−74699
Re_3Cl_9 metal cluster complexes, He(I) photoelectron spectrum, SCC DV Xα calcs., $Re_2Cl_8^{2-}$ comparison 80−28063
S VI, spectrum, 100-8000 Å, ionis pot. 79−93946
S^+, ionisation pot., periodic regularities, relativistic corrections calcs. 79−49950
S_2 ionisation pot. determ. from CS_2 photoionisation mass spectra determ. 79−94044
S_2, v.u.v. absorpt. spectrum, Rydberg transitions 77−3382
S_n, properties of small aggregates rel. to metallic character of Te_n 78−86985
SBr_2, transient species, He(I) photoelectron spectroscopy, discrete variational HFS calc. 79−31594
SF_6, ab initio electronic struct., and photoelectron spectral assignment 79−54764
SF_6, ionisation pot., discrete variational Xα calc., Slater-type orbitals in Hartree-Fock basis 78−78837
SF_6, octahedral complex, ionis. energy, SCF-Xα study 78−70967
SH, ionis. pot. of $(X^2\Pi_i)$ radical, ab initio ΔSCF calc. with electron correl. 79−98153
SO_2, photoelectron spectrum, vibr. struct., ionos. pot. 77−75217
SO_3, photoelectron spectrum assignment, ionisation pot. and electron affinity, Green's function method 77−54576
SO_4^{2-}, ionisation energies, SCF-Xα transition state calcs. 80−74115
Sb_xSe_y (x=0 to 4; y=1 to 4) molecular species formed in vaporisation of solid $SbSe_3$, thermodynamic props. 80−11943
Se VI, 2400 to 90 Å spectrum anal. 78−58616
Se^+, ionisation pot., periodic regularities, relativistic corrections calcs. 79−49950
Se_n, properties of small aggregates rel. to metallic character of Te_n 78−86985
$SeBr_2$, He I photoelectron spectra, ionis. pots. calcs. 79−50080
$SeCl_2$, He I photoelectron spectra, ionis. pots. calcs. 79−50080
SeF_2, He I photoelectron spectra, ionis. pots. calcs. 79−50080
SeH, isotope effects, Rydberg levels-ground state transitions, rot. const., VUV spectra obs. 80−58279
Si (111) surface, relax. of surface atoms, Si_4H_9 clusters 77−8171
Si (111) surface, relax. of surface atoms, Si_4H_9 clusters 77−35980
n-Si, A-centre ionisation energy change due to uniaxial deform. 78−71733
Si, acceptor levels, ionis. energy and IR absorpt. 79−78033
Si phthalocyanine, monomer and dimer, UV photoelectron spectra, valence level splitting 77−38695
SiF_4, photoelectron spectra, bonding, MS Xα calcs. 79−18116
SiF_6^{2-}, octahedral complex, ionis. energy, SCF-Xα study 78−70967
SiF_6^{2-}, SCF Xα SW calcs., ionis. pot. 79−26887
SiH_4, ab initio Hartree-Fock SCF-LCAO-MO method 78−94195
SiH_4, mol., valence and core ionis. energy, RHF-SCF and PNO-CEPA calc. 79−85890
SiH_4, photoelectron spectra, bonding, MS Xα calcs. 79−18116
SiH_3Br, mol. ionis. and excitation energy, Xalpha calc. 79−41105
SiH_3Cl, mol. ionis. and excitation energy, Xalpha calc. 79−41105
SiH_2F_2, ab initio Hartree-Fock SCF-LCAO-MO method 78−94195
SiH_3F, ab initio Hartree-Fock SCF-LCAO-MO method 78−94195
SiH_3F, mol. ionis. and excitation energy, Xalpha calc. 79−41105
$SiH_{4-n}F_n$ (n=1 to 3), photoelectron spectra, bonding, MS Xα calcs. 79−18116
SiH_3I, mol. ionis. and excitation energy, Xalpha calc. 79−41105
Si_2H_6O, geom. and electronic struct., ab initio MO calc. 79−97972
SiO molecule, true potential energy curves, dissoc. energy, ionisation potential 77−6704
SiO, VUV absorpt. spectra of mol., Rydberg, series and ionis. pot. 79−81213
SiO_2, valence ionis. energy, calc. including correl. effects 79−68185
SiO^+, vac. UV photoelectron spectra, ab initio mol. orbital and Xα calcs., $(X^1\Sigma^+)$ state 78−46395
$SnCl_2$, $SnBr_2$, UV photoelectron spectra of valence d shells, gas-phase 78−62845
Te_n, small aggregate, metallic character 78−86985
$TeCl_2$, transient species, He(I) photoelectron spectrosc. calcs., relativistic corrections 80−95677

ionisation potential continued
Ti, atomic energy level data tables, Ti I to Ti XXII 79−59385
Ti, Koopmans' ionis. pot., relax. correction 79−18308
$TiO_{(g)}$, $TiO_{2(g)}$, electron impact threshold determ. 77−16857
TiX_4, (X=Cl,Br,I), He I and He II photoelectron spectra, ionis. energy, chem. bonding 78−46394
TlCl, TlBr, TlI, UV photoelectron spectra of valence d shells, gas-phase 78−62845
U, ionisation potentials, 2nd-6th, thermochemical calcs. 79−98248
UF_5, thermochem., heat of formation, dissoc. energy, ionis. pot. 77−70326
UF_6, electronic struct., non-relativistic Hartree-Fock-Slater method 78−50469
UF_6, electronic struct., relativistic MS Xα calc. 79−85911
UH_4, thermochem., heat of formation, dissoc. energy, ionis. pot. 77−70326
UO_2, ionisation potential, cohesive, electronic and redox props. 79−47916
UO_2^{2+}, electronic struct., secondary ligands effects, Dirac-Slater model 77−411
Xe, autoionising reson., Stark effect 80−58198
Xe III, $5s^25p^3(^4S)nl$ levels, ionis. pot., from spectral data 80−47920
Xe VIII, one-electron spectrum in theta pinch discharge, line identification 80−32640
$Xe^{2+}(Xe^{3+})(Xe^{4+})(Xe^{5+})$, molecular electron impact ionisation 80−102582
YIG target and DC glow discharge sputtered film compositions compared 77−55886
YbF_3, MS Xα electronic struct. calc., inner shell photoelectron spectra 77−10594
ZnS(Se)(Te):Co^{2+}, IR luminesc. quenching, Co^{2+} level position, ionisation energy 80−16079
ZnTe, elec. field and impurity conc. effects on ionisation energy of impurities, appl. to acceptors 80−88514
ZrX_4, (X=Cl,Br,I), He I and He II photoelectron spectra, ionis. energy, chem. bonding 78−46394

ionisation time *see ionisation*

ionogen *see electrolytes*

ionoluminescence
alkali halide: CN radical, impurity effects on ion induced luminesc. 77−16402
bombardment induced light emission, chem. effect 77−28672
bombardment-induced photon emission, spectral fractures, mechanisms band struct. depend., review 77−44072
conference on inelastic ion surface collisions, Hamilton, Ontario, Canada (Aug. 1978) 80−31402
excited state lifetimes, differential meas. 79−13672
inert gas ion excitation of solids, vac. UV continua 80−25468
ion beam induced light emission, review 79−95850
low energy gas-phase and ion-surface collisions, optical emission 80−32821
Lyman-α emission from proton bombard. of Si, Cu, Ge, Mo, Ta, Pt surfaces 79−91503
molecular deexcitation radiation obs. during keV ion-solid bombard. 80−71494
obsidian, hydration profiles meas. by sputter-induced optical emission, rel. to dating technique 79−24871
optical emission from low energy particle-surface collisions 77−36300
oxide glasses, ion-bombarded, optical line intensities 80−35037
photon emission from sputtered atoms, obs. of apparent local thermodynamic equilib. in excitation 78−72673
pulsed proton radioluminescence in binary liquid scintillators 79−52731
solid surface, energetic particle irrad.,, collision cascade 80−45186
sputtered excited states, secondary photon emission, role of transition probability 80−102483
sputtering, photon yield relation to population distribution and excitation function 80−34989
steel, stainless, photon emission from sputtered atoms, apparent local thermodynamic equilib. in excitation 78−72672
surface analysis, quantitative, using ion-induced secondary ion and photon emission 77−86423
surface-ion impact, luminesc. accompanied by ion implantation 80−60683
Ag film, sputtering, photon emission enhancement compared with sputtering rate 79−78815
Ag, implanted Li atoms, depth profiles and sputtering anal. by optical spectra 77−35579
Al,Ar^+ ion bombard., photon and secondary ion emission, single cryst. struct. effect 77−59660
Al, continuous UV emission under inert gas bombard. 78−84664
Al, implanted Li atoms, depth profiles and sputtering anal. by optical spectra 77−35579
Al, ion bombarded, photon and ion emission, simultaneous meas. 78−15276
Al, sputtered excited Al particles, effect of O during ion bombardment on spectra 79−38703
Al-Mg-Zn, O_2^+ ion bombard., SIMS and photon emission spectra, local thermodynamic equilib. model 80−20751
Au, ion bombardment-induced photon emission as function of target temp. 80−100698
Be, foil, ion bombardment, secondary photon emission, ion energy depend. 80−97346
Be, secondary photon emission following ion bombard. 80−71493
Be, sputtered atoms, ion bombardment induced line radn. 79−91553
$CaSO_4$:Mn, phosphor, thermoluminesc., low energy ion excitation 77−55838
CdS, luminesc. from heavy ion tracks 78−88365
Cr, ion bombard. induced photon and secondary ion emission in O_2 atmosphere 77−90231
Cr, photon emission due to Ar^+ ion bombard., adsorbed and recoil-implanted O effect 80−80872
CsI:Tl(Na), light yield under charged-particle bombardment 80−93409
Cu, exited state formal by B^+ impact, light emission coeffs. 78−64417
Cu, ion bombardment-induced photon emission as function of target temp. 80−100698
Cu, photon emission from inert gas surface impact 78−11059
Cu target, bombardment by Ar^+-ion beam, luminosity spectrum 79−4884
CuCl, H^+ irrad., luminesc., high density excitons in particle tracks 79−47020

ionoluminescence continued
GaAs surface, Ar ion bombardment induced photon emission, rel. to target temp. 78−72612
GaAs:Te(Cd)(Mg)(B), ion implant depth distribs., AES and glow discharge optical spectroscopy meas. 80−65028
GdF_3:H films, H and F profiles meas. by sputter-induced optical emission 78−47407
Ge, ion bombardment-induced photon emission as function of target temp. 80−100698
K salts, spectral refl. changes and luminesc. during 2-10 keV proton bombardment, implications for Io 79−96950
KBr, decay and time resolved emission spectra from σ-excitons produced by heavy-ion irradiation 80−89071
KBr, heavy ion irrad., σ and π exciton emission spectra, 4.2 K 78−76534
Mg, photon emission from inert gas surface impact 78−11059
MgO-Al_2O_3-SiO_2:Ce^{3+} glass scintillator, energy transfer, luminesc. efficiency under UV and charged-particle excitation 79−95821
Mo, bombardment by 1 to 30 keV use, emitted radiation sepctral comp. *(Russian)* 77−81159
Mo, broadband optical emission for heavy ion bombard. 77−28635
Mo, excited state formal by B^+ impact, light emission coeffs. 78−64417
Mo, ion bombard., ion and photon yields, CO adsorption effect 80−89098
Mo, ion impact, radiative spectrum of sputtered particles *(Russian)* 79−91504
Mo, photon emission from inert gas surface impact 78−11059
Mo, visible emission from excited ats. emitted from 40 keV Ar^+-bombarded surface 80−11481
Na salts, spectral refl. changes and luminesc. during 2-10 keV proton bombardment, implications for Io 79−96950
NaCl, bi-exciton luminescence possibility 80−40167
NaCl, electron and ion beam excited luminesc. spectra 79−52026
NaCl, Ne^+, Ar^+, Kr^+ bombard., sputtering and ionoluminescence 80−96583
NaI:Tl, and inactivated NaI, scintillation response to random and channelled ions 77−48255
Nb, broadband optical emission for heavy ion bombard. 77−28635
Ni, bombardment by 1 to 30 keV use, emitted radiation spectral comp. *(Russian)* 77−81159
Ni, ion bombard., ion and photon yields, CO adsorption effect 80−89098
Ni, photon emission due to Ar^+ ion bombard., adsorbed and recoil-implanted O effect 80−80872
Pb, ion bombardment-induced photon emission near melting point 80−100699
RbI, luminesc. spectra induced by pulsed Ne^+ and electron beams and X-rays 80−80851
Si,IR emission under α-irrad. *(Russian)* 77−85811
Si,Si_3N_3, and SiC, ion bombard. induced light emission 77−48257
Si, implanted Li atoms, depth profiles and sputtering anal. by optical spectra 77−35579
Si, MeV region O^+ implantation, induced luminesc. spectrum 78−6788
Si, nonradiative deexcitation in O_2 atm., using differential meas. of excited state lifetime 78−2920
Si, photon emission due to Ar^+ ion bombard., adsorbed and recoil-implanted O effect 80−80872
Si, sputtering by Ar^+ ions, energy depend. of excitation 79−56906
SiO_2, fused, ion beam induced luminescence 80−40166
Sn, ion bombardment-induced photon emission near melting point 80−100699
SrO-Li_2O-Al_2O_3-SiO_2:Tb^{3+} glass, energy transfer, luminesc. efficiency under UV, neutron and charged-particle excitation 79−95822
Ta, bombarded by Cs^+, transient emission of continuous photon spectrum by cathodic sputtering products 79−74046
Ti, photon emission due to Ar^+ ion bombard., adsorbed and recoil-implanted O effect 80−80872
V, implanted Li atoms, depth profiles and sputtering anal. by optical spectra 77−35579
W, bombardment by 1 to 30 keV use, emitted radiation spectral comp. 77−81159
W, broadband optical emission for heavy ion bombard. 77−28635
Xe, liq., α-particle and electron excited luminesc., time depend., specific ionisation density effect 80−71495
Zr, photon emission due to Ar^+ ion bombard., adsorbed and recoil-implanted O effect 80−80872
Zr, photon emission from inert gas surface impact 78−11059

ionosondes *see ionospheric measuring apparatus*

ionosphere
see also D-region; E-region; F-region; ionospheric electromagnetic wave propagation; ionospheric techniques; sporadic-E layer
100 to 500 kHz noise, rel. to auroral arcs and field aligned currents and auroral electrons accel. 79−66859
acceleration mechanism, satellite obs. 77−21975
acceleration mechanism producing energetic ions perpendicular to geomag. field 77−87168
acoustic waves generation by LF radiowaves 78−69581
acoustic-gravity waves, theoretical props. rel. to travelling ionospheric disturbances 77−33270
acoustogravity waves from earthquakes and explosions 80−36451
acoustogravity waves generation mechanism 79−66776
albedo electron flux for artificially injected electron pulses 79−62664
albedo particles ionization losses calc. with allowance for geomag. field 79−53621
Alfven wave at ATS 6, soln. with finite ionospheric conductivity 79−12346
Alfven waves, axisymmetric, dipole field model with finite ionospheric cond. 79−29941
Alfven waves in ionosphere, boundary condition 79−53611
anisotropic irregularities in geomagnetic field, diffuse spread *(Russian)* 77−64518
anomalous equatorial elec. fields assoc. with northward turning of interplanetary mag. field 79−70914
anomalous resistivity, review 77−64528
Antarctic ionosphere, working group of Antarctic and Southern Hemisphere Aeronomy Year (ASHAY) 77−87210
antisymmetric S_q-variations, appl. of plasmasphere dynamo electric field-aligned currents theory 78−81499
ARAKS Project 79−21021

ionosphere continued
Arctic ionosphere, study by European Incoherent Scatter (EISCAT) project *(French)* 79−2437
artificial aurora, conjugate to a Hawaiian launched electron accelerator 80−82124
artificial aurora prod. by electron beam injection 79−62638
artificial Ba clouds, laser scatt. by metallic particles in two-phase nozzle flow into vacuum 77−35194
S.Atlantic geomagnetic anomaly, ionization rates during total eclipse 80−12608
S.Atlantic Ocean, shipborne ionosonde obs. 78−81505
atmospheric dynamo, rel. to low latit. geomag. daily var. 78−36098
atmospheric-ionospheric disturbances, seasonal vars. 77−53289
atom and ion radiative recombination, rate coeffs. 78−40758
atomic and molecular ions, transverse motions generated by elec. fields and neutral winds 77−13155
atomic ions composition, reaction to rapid changes in large-scale elec. fields 77−91350
atomic processes, book contrib. 77−37482
ATS-6 radio beacon studies, review 80−56677
Auger electrons and photoelectrons, fluxes and spectra comparison 78−45094
Auger electrons in upper atmosphere, fluxes and spectra 78−28376
aurora, detached arcs in trough region 78−88965
aurora, electron flux meas. and ionosphere elec. props. 77−9592
aurora, pulsations of electron and ion intensity 80−61934
aurora, time-depend. model, precip. effects on ionospheric props. 78−4021
aurora irregularities, overnight north-south movements obs. at 42 MHz 80−67449
aurora modelling, time-depend. study 80−72672
aurora-generated gravity waves dynamic effects on midlatit. ionosphere 80−17438
auroral acceleration regions, energetic particle meas. 79−53644
auroral and equatorial two-stream irregularities, nonlinear states 78−28403
auroral arc, energy source for electron accel. and field-aligned currents 77−9593
auroral arc, relation with field aligned currents carried by suprathermal electrons 78−28362
auroral arc electric fields, radar obs. 80−72692
auroral arcs, plasma transverse Kelvin-Helmholtz instability rel. to electrostatic turbulence 77−53287
auroral arcs global formation, numerical simulation in three-dimensionally coupled ionosphere magnetosphere 80−67446
auroral Birkeland current systems, anomalous resistivity effects 77−9591
auroral breakup and westward current flow 80−51593
auroral bulge expansion features during substorms 80−41597
auroral circle, poleward boundary of quiet auroral belt 77−33244
auroral current system oscillations, Earth induction effects on Pc 5 pulsations vertical polarisation 79−12355
auroral currents, magnetometer array and radar backscatt. joint obs., N.Scandinavia 78−85768
auroral elec. field, non-neutral field-aligned current sheet, theory 80−77196
auroral electric field, model 79−53608
auroral electric field obs., comparative rocket obs. 80−85789
auroral electrojet, gravity waves and infrasound generation, Joule heating and Lorentz force 79−66866
auroral electrojet, magnetostatic model 77−13163
auroral electrojet, parameters from mag. vars. along meridian 79−25395
auroral electrojet events, simultaneous magnetosphere dynamics from energetic electron obs. at synchronous orbit 79−66882
auroral electrojet region, elec. fields and mag. effects of solar flares 78−69576
auroral electrojets, movements during high-latit. substorms 80−109315
auroral electron accel. by electrostatic double layers, discrete auroral forms prod. 77−25809
auroral electron beam, electrostatic noise generation 78−85759
auroral electron bunching near artificial electron beam 80−98511
auroral electron energy distrib., secondary peaks driving instability 80−82135
auroral electron flux, rel. to field aligned elec. pot. difference 80−72684
auroral electron flux obs. 80−67466
auroral electron transport and energy degradation 80−77219
auroral electrons, accel. in array of auroral arcs 78−36357
auroral electrons, large-scale longit. intrusions 77−64510
auroral electrons modulation by electrostatic waves, freq. anal. of 4-6 keV electrons 78−45086
auroral energy input, effect on neutral and ion drifts 78−65446
auroral field lines, region of intense plasma wave turbulence 77−45228
auroral hiss, nearly reson. whistler amplified Cherenkov radiation, limitations 80−101482
auroral infrasonic wave emissions, temporal and spatial changes rel. to polar substorms 79−100996
auroral ion composition and energy spectrum vars. 77−64509
auroral ionosphere, collisional ion cyclotron waves 77−29574
auroral ionosphere, E_s-layer large-scale inhomogeneities 80−4171
auroral ionosphere, effect of ion-neutral collisions on ion vel. distrib. 77−29565
auroral ionosphere, electric fields and conductivity in quiet periods 77−53280
auroral ionosphere, field-normal plasma-line scatt. detect. expt. 78−73680
auroral ionosphere, heating during aurora 77−21973
auroral ionosphere, large parallel elec. fields obs. 77−9595
auroral ionosphere, radio investigations via VHF bistatic Doppler system 78−28387
auroral model with comp. meas. 80−12609
auroral $O(^1S)$ production sources determ. from rocket and satellite meas. 80−26662
auroral oral size diurnal var. assoc. with geomag. pole precession 80−26661
auroral oval, dayside, elec. fields meas. 80−98501
auroral oval, dayside, evidence for parallel elec. field particle accel. 80−98503
auroral oval, dayside, rocket-borne VLF and ELF waves meas. 80−98504
auroral oval, dayside, ULF elec. field fluctuations obs. 80−98505
auroral oval, morning, solar wind ion injections 80−98502

ionosphere continued
auroral oval and polar cap mag. field perturbs., rel. to charged particles and interplanetary mag. field 78−45160
auroral oval compression, convection reversal at subauroral latits. 77−60528
auroral oval size, effect on mag. substorm occurrence probability 78−32298
auroral particle distrib., parallel electric field acceleration 80−12602
auroral particle distrib. rel. to mag. field perturbations assoc. with field-aligned currents 80−41596
auroral particles, stratified precip. struct. development during magnetospheric convection 78−28377
auroral phenomena, role of mag. mirroring in magnetosphere-ionosphere current system 78−20572
auroral plasma, stability, parallel and perpendicular propag. of electrostatic waves 79−35040
auroral processes, IAGA/IAMAP symposium (Seattle, August 1977) 79−88521
auroral proton bursts struct. during mag. quiet times and substorms 77−29531
auroral protons energy and pitch angle spectra vars. in upper atm. 79−75032
auroral pulsations, harmonic anal. rel. to wave-particle interactions 79−8736
auroral region, electric field and conductivity meas. during substorms 79−80073
auroral region, self-consistent particle and parallel electrostatic field distrib. 78−45120
auroral regions, electric fields from ion and electron distribs. 77−87155
auroral substorm expansion phase, ionospheric currents and elec. field vars. assoc. with absorpt. spikes 79−35039
auroral X-ray bremsstrahlung rel. to VLF emissions 78−45106
auroral zone, elec. currents induction in Alaska pipeline 79−39645
auroral zone, electrodynamic struct. of evening sector 80−72691
auroral zone, joule and particle heating 77−45218
auroral zone, nighttime scintillation localised enhancements struct. 80−98506
auroral zone, Pi 2 pulsations spectral components latit. var. 77−64546
auroral zone current system, fluctuations rel. to geomag. pulsations 77−87188
auroral zone currents, obs. in morning sector pass 80−98510
auroral zone electric fields, conductivities and currents, latitudinal distrib. 78−77399
auroral zone electric fields rel. to interplanetary magnetic field vars. 78−77431
auroral zone energy dissipation due to ionospheric currents, high-resolution altitude profiles 78−88978
auroral zone ionosphere irregularities, simultaneous rocket probe, scintillation and incoherent scatter radar obs. 80−94640
auroral zone physics, review 77−17268
auroral zone precipitation and convection reversal, satellite obs. 80−101479
axisymmetric toroidal Alfven wave resonances effect of finite ionosphere conds. 79−75035
balloon and rocket programs, conf. Bournemouth, England (1980, Aug.) 80−105433
baselevel trough, struct. 78−28402
bay phenomena, theory of equivalent current systems including ground induction 80−41610
beam-plasma discharge, near Zarnitsa-2 rocket, parameter estimation *(Russian)* 78−26357
Birkeland currents, primary sources 80−31176
Birkeland currents and auroral structure 80−77209
Birkeland currents occurrence during aurora *(Norwegian)* 80−31158
bottomside ionogram analysis, valley problem 77−33268
bubbles detect. by Faraday rot. and scintillation obs. at Natal, Brazil 79−88524
bubbles in equatorial region, obs. by radiowave propag. 80−41621
bubbles in equatorial spread F, nonlinear evolution 80−85801
bubbles seen in topside soundings of spread F, characts. 80−85800
C-layer, electron conc. profiles, generalised exponential model 77−67005
C-layer, props. from ULF field obs. 77−25816
characteristics variations during stratospheric winter warmings 77−29550
charged particle-beam interactions, space and laboratory plasma workshop 78−7821
charged particles precip. by parallel elec. field, model 78−65459
Chatanika incoherent scatter radar obs. of field-aligned currents 78−57387
chemical modification, use as lens for refracting radiotelescope 77−45312
chemical processes 80−17431
chemistry, implications for radio communication 77−17267
chemistry and transport processes, numerical modelling 78−49202
Cherenkov, radiation from artificially injected electron beam 79−84571
cleft currents determined from magnetic and electric fields 79−35036
coherent anomalous resistivity, in region of electrostatic shocks 80−4189
coherent parametric instabilities excited by two or more pump waves, theory 78−57381
collapsing post-sunset ionosphere and protonosphere, induced proton flow 78−49222
collision frequencies, recomb. coeffs., rel. to resistivity of semiconductors and metals 79−8742
collisionless electrostatic drift waves, linear theory, space plasma appls. 79−1305
combined ground and satellite measurements, IRI model extension 80−61911
conductivity, elec. fields and electron density during 1972 August 4-7, incoherent scatt. radar obs. 77−45248
conductivity of high-latit. ionosphere, determ. from auroral electrons 79−12334
conductivity of lower ionosphere, effects on Schumann reson. freqs. and ELF attenuation 80−31099
conductivity rel. to Pi 2 pulsations attenuation 78−45101
conf. Tokyo, Japan, 1978, AEROS and TAIYO satellite results 80−46340
conjugate electron precipitation from magnetosphere, high time resolution riometer and X-ray meas. 80−41666
conjugate photoelectron fluxes obs. on AE-C satellite 77−45224
conjugate photoelectrons in predawn ionosphere, rocket obs. 79−29931

ionosphere continued
conjugate photoelectrons influx rel. to predawn 630 nm airglow, direct meas. 78−49196
continuum momentum eqns. applied to lower ionisophere, collision freqs. 77−87171
cosmic rays, ionospheric effects on neutron intensity 79−84604
Cosmos 490 meas. of charged particle streams 79−88522
counter electrojet caused by vertical wind, equator region 80−85795
counterelectrojet, search for correl. with interplanetary mag. field 78−88983
coupling between neutral and ionized atmosphere, NATO conf. proceedings (Spatind, Norway, 1977 April 12-22) 80−27036
critical frequency data analysis, Ionosphere Sounding Satellite appl. to topside *(Japanese)* 79−16750
critical frequency determination, radio sounding method 80−46286
critical ionization vel., Spacelab expt. 79−44289
current and wind systems, generation by motion of plasmasphere material 77−13161
current convective instability in auroral F-region 80−72680
current distribution quantitative modelling 78−88988
current model rel. to quiet time vertical magnetic field component over India 78−61326
current system, steady state, for high-latit. mag. activity, comprehensive model 79−92636
current systems during magnetic storms 79−12349
current systems in polar ionosphere, computation 78−45090
currents, EM induction at S.American geomagnetic equator 79−75021
currents, night-time induced effects on geomag. regular daily var. 77−9627
currents during polar magnetic substorm observed in the evening sector with a two-dimensional magnetometer array 79−8776
currents from Arecibo radar obs., rel. to mag. vars. and elec. fields 77−87166
cusp region on dayside, field line topography, precipitation implications 80−85822
cusplike electron precipitation regions during 1977, September 19 to 21 event, DMSP-F2 obs. 79−35056
daily mag. variations meas. in Alaska, atmos. current system 80−85590
day-night conductivity gradient effect on polar cap convective flow 78−45121
dayside aurora, rocket-borne meas. of particles and ion convection 78−77391
dayside auroral arcs and convection 78−81484
dayside cleft aurora and ionosphere effects, review 80−94633
dayside cleft field lines, assoc. Pi 1-2 activity 77−87206
dayside polar cusp, ionospheric and field-aligned currents relationship 79−35058
dayside south polar cusp, field-aligned currents rel. to interplanetary mag. field 79−35059
daytime positive storm effects at middle latits., prod. by travelling atmospheric disturbances 79−25394
daytime slab thickness depend. on geomag. activity 77−21992
density gradients effect on VLF propag. at low latits. 79−88530
detached plasma region detect. 78−7836
differential charging and sheath asymmetry of nonconducting spacecraft due to plasma flows 79−12378
diffuse aurora equatorward boundary, electron precipitiation interpretation 80−72668
diffuse auroral zone, form. and dynamics of polar edge of ionospheric trough 79−8743
diffusion inhomogeneities, small-scale, dissipative parametric generation 78−69580
discharge around rocket following injection of electron beam 77−78570
disturbance, 1960, April 1, electrodynamic interaction between ionosphere and magnetosphere 78−28372
disturbance caused by magnetosphere substorm, location and development study 80−4185
disturbance dynamo, caused by thermospheric wind 80−82134
disturbances, day-night terminator temperature gradient study 80−4186
disturbances due to energy transfer from lower atm. 78−28381
disturbances due to gravity waves generated by 1973 June 30 solar eclipse 77−21993
disturbances during 1976 December 8 substorm 80−4201
disturbances effects on mag. pulsations propag. 77−25819
disturbances in lower ionosphere, during Soyuz-Apollo expts. 78−45110
disturbances in mid-latitudes, magnetospheric convection intensification effects 80−105122
Doppler spectra of current-driven plasma instabilities 79−58163
downward flowing ions and ionospheric ions injection into plasma sheet 80−26694
DP-2 current system, rel. to pulses in interplanetary mag. field B_z-component 78−73583
drift analysis, correlation ellipse physical significance 77−13179
drift meas. of mesopause wind, geomagnetic storm effects 79−35025
drift measurements, rel. to upper mesopause region wind systems behaviour 79−44220
drift waves, instability in AC elec. field, wave growth rate and dispersion relation 80−48886
drift waves, solitary, excitation and propag. *(Russian)* 77−70915
drifts, rel. to polarisation elec. field prod. by solar tidal dynamo 78−36391
drifts, review 78−36364
dynamo, contrib. to O_1 tidal component of geomag. lunar daily var. at Alibag 80−56355
dynamo, small scale, multiple layer model 79−53612
dynamo calculations with semidiurnal winds 77−91366
dynamo currents from EMFs at different latitudes 77−64524
dynamo region, long-period winds, effects on surface geomag. field elements 77−2090
dynamo region, wind systems rel. to mag. vars. during reverse equatorial electrojet events 78−36368
dynamo regions, auroral and equatorial, global scale electrodynamic coupling 79−44297
E- and F-regions, vars. due to solar EUV flux changes, calcs. 79−44293
E-region/F-region coupling, effects on Perkins spread-F instability 78−40755
Earth-ionosphere cavity, resonance phenomena *(Russian)* 77−73801
Earth-ionosphere cavity, Schumann resonance problem, convergence of zonal harmonic series 79−2348
Earth-ionosphere waveguide, VLF signal variations, spectral anal. *(Russian)* 77−78305
ionosphere continued
Earth-ionosphere waveguide parameter determ. by VLF transitional route meas. 77−91234
eastward electrojet and field-aligned current flow at dusk meridian 79−80076
eastward electrojet coupling with asymmetric ring current 78−7823
eastward electrojet over auroral arc, rocket obs. of N.edge 80−101481
eastward electrojet position rel. to energetic electrons trapping boundary and aurora 77−25822
Echo IV electron beam-emitting rocket, neutral N_2 cloud effect on elec. charging in ionosphere 79−75017
effective recombination coeff. of lower ionosphere 77−49223
effective recombination coeffs. for quiet conditions and solar flare occurrence 80−12595
elect. heating and cooling rates discrepancy, Atmosphere Explorer-C meas. 77−29564
electric and mag. fields rel. to magnetosphere-ionosphere coupling 79−66870
electric current, of polar cap and sunlit cleft, obs. and theory 80−41615
electric current and atmospheric motion in lower thermosphere, symposium, Seattle, Washington, 1977 August to September 80−62371
electric current collection, by long wire in near-Earth orbit 79−25438
electric current sources, field-aligned, in high-latit. ionosphere 80−72674
electric current system inferred from S_q^p obs. in Alaska 80−85813
electric currents, obs. by S-310-5 rocket *(Japanese)* 80−94635
electric currents, rel. to magnetotelluric investigations at Ronde *(Danish)* 80−8250
electric currents and fields due to field-aligned auroral currents 78−96339
electric currents and magnetic var. induced on the ground 77−70594
electric currents in cosmic plasmas 78−12094
electric currents in late evening plasma flow reversal 80−26675
electric currents over auroral arc, theory 77−33296
electric currents to explain daily geomag. variation patterns, Alaskan 1978 obs. 80−41374
electric currents variations during 23 October 1976 solar eclipse, mag. obs. in Australia 78−81498
electric field, balloon meas., SAMBO-1 expt. 79−66738
electric field, midlatitude obs. of ALADDIN rocket 80−101488
electric field, plasma density and temp., field-aligned currents, S3-3 satellite obs. 80−26699
electric field and currents in high-latit. region 79−80075
electric field at high latitudes, ULF oscills. 79−75025
electric field configuration, Ps 6 mag. distrubances seasonal and diurnal var. 80−67477
electric field induced drifts, incoherent scatt. radar obs. 77−29576
electric field observations, indicating magnetosphere electricity at mid-latitude 80−77230
electric field power spectra, double probe meas., Doppler shift effects 80−26634
electric field spreading, two-dimensional and three-dimensional mapping comparison 79−66861
electric field structure in disturbed zone behind cylinder streamlined by rarefied plasma 79−53623
electric field turbulence, high latit., polarization determ. from satellite data 80−26679
electric field wavelike fluctuations obs. at Ft. Churchill, Canada 77−21982
electric fields, high-latit., empirical models 77−45255
electric fields, incoherent scatter radar studies 77−22001
electric fields, latitudinal struct. on November 21, 1975, Chatanika obs. 77−87160
electric fields, poleward-directed, near ionospheric projection of plasmapause 78−20574
electric fields, prod. by polar field-aligned currents 78−65455
electric fields and currents, global distrib. produced by magnetospheric field-aligned currents 80−109303
electric fields and currents, origin and structure *(German)* 78−32196
electric fields and currents assoc. with auroral arcs, radar obs. 78−28396
electric fields and currents in quiet periods, simulation 80−12600
electric fields and currents in substorms, simulation 80−12601
electric fields and currents in the ionosphere generated by field-aligned currents observed by TRIAD 79−40013
electric fields at auroral latitudes, balloon meas. 78−57408
electric fields generated by gravity wave winds in equatorial regions 77−53283
electric fields generated during magnetosphere substorms, determ. from Doppler sounding 80−4169
electric fields in equatorial ionosphere, rel. to geomag. vars. during mag. storms 77−78578
electric fields induced by ion drag and substorms 80−77199
electric fields of magnetospheric origin, simulation 79−62655
electric fields of magnetospheric origin, simulation 80−4177
electric fields penetration along geomag. force lines, electrostatic approach applicability 80−4178
electrical conductivity, enhancement by particle precip. rel. to magnetosphere convection 79−25400
electrical conductivity, rel. to hot plasma role in magnetosphere convection 78−32297
electrical conductivity and drifts, theory 78−36366
electrical conductivity of lower ionosphere, profiles evaluation from expt. Schumann reson. data 80−36360
electrical coupling to lower atmos., quasi-static model 80−61865
electricity, differences between regions of upflowing and outflowing current 79−100999
electrodynamic coupling, global scale of high and low latit. regions 80−77194
electrojet boundary definitions using energetic electron spectra and magnetometer data 79−75026
electrojet during isolated substorm event 80−105132
electrojet model involving field-aligned currents 77−9600
electrojets, model with allowance for field aligned currents 77−21974
electron accelerator expt. on POLAR-5 sounding rocket, evidence of elec. charge accumulation 80−77213
electron accelerator expt. on POLAR-5 sounding rocket, for use within aurora 80−77170
electron and ion drift motions, in situ meas. technique 79−29893
electron and ion temperatures, ground-based incoherent scatt. and AE-C satellite meas. 77−29575
electron and ion temps., correl. meas. 77−25820
electron beam expansion and propag., space shuttle expt. 78−7830

ionosphere continued
electron beam injection, beam-plasma discharge at low press. and mag. field strengths 78−42769
electron beam injection into plasma causing HF emission 80−56670
electron beam interaction expts. planned for space shuttle 78−9796
electron beam scattering in atoms, sounding rocket expt. (POLAR-5) 80−77212
electron beams, artificially injected, 3914 Å light prod. and electron scatt. meas. 77−21983
electron collision frequency profiles vars., multiple-freq. meas. of radio wave absorpt. 77−91347
electron conc. and collision freq., rocket meas. 79−80074
electron conc. distrib. models for quiescent atmosphere 80−41600
electron conc. irregularities, Kosmos 381 meas. 78−16228
electron concentration profile, vert. struct. 80−61936
electron concentration var. with height, improved model 78−49214
electron concentration variations rate use 80−12598
electron content, lunar perturbations, and dynamo electrostatic fields interpretation 77−29570
electron content and peak electron conc. appl. to thermospheric quantities determ. 77−53268
electron content and slab thickness meas. near equatorial anomaly 79−84574
electron content data, mixing freq. components identication by multiplicative homomorphic filtering 79−29929
electron content during ionospheric storms, behaviour during positive phase 77−37480
electron content in S.Atlantic geomag. anomaly region, east-west asymmetry 79−21097
electron content quasiperiodic fluctuations during 1976 April 29 partial solar eclipse 78−24407
electron content-latitude profiles at low latitudes, development and decay 78−36374
electron cyclotron harmonic waves excitation, lab. expt., rel. to topside ionosphere RF sounder expt. 78−93042
electron densities and temperatures, results from Intercosmos-10 Langmuir probe expts. *(German)* 79−2469
electron densities at 1000 km, Kosmos 381 obs. during calm and disturbed conditions 77−64513
electron density, daily vars. at 100-200 km at middle latits. 77−64515
electron density, inhomogeneities in ionospheric valley rel. to internal gravity waves 77−91348
electron density and collision rate, rocket meas. 80−41601
electron density and temp. meas. by sounding rockets 79−8760
electron density comparison with meteor wind profile 77−9587
electron density depletion due to mag. storm 80−85784
electron density determ. from ionograms, true height calc. technique 80−8486
electron density disturbance spatial struct. affected by magnetosphere convection 80−41606
electron density during winter anomaly, 70-100 km 80−36441
electron density equatorial anomaly, dissimilar forms in E.Asia and India 80−109301
electron density fluctuations, rel. to gravity wave spectra propag. in thermosphere 79−66848
electron density in lower ionosphere, rocket meas. by VLF waves propag. characts. 78−49219
electron density in S hemisphere middle latits., Universal Time effect model 79−25396
electron density in South Atlantic Anomaly region 80−12611
electron density increase during stratospheric warming 77−91356
electron density irregularities, Fresnel diffraction patterns 77−9614
electron density latit. vars. from Alouette-2 data, internal gravity waves 78−32269
electron density model distribs. over Delhi 79−88536
electron density models, review 79−48617
electron density profile, field-aligned currents effect 79−62651
electron density profile analyses of ionograms, model starting heights 79−66869
electron density profile in lower ionosphere, estimates from Hollingworth patterns in VLF range 77−64516
electron density profile parameters estimation from VLF propag. data, effectiveness 79−53614
electron density profiles, calc. from ionograms via simplified inversion procedure 77−41263
electron density profiles, determ. from transionospheric sounding data 78−28371
electron density rel. to whistler dispersion 78−93050
electron density spatial distrib. in nighttime polar ionosphere 78−73570
electron density troughs and equatorial plasmapause, coincident satellite obs. 77−17291
electron distrib. in lower ionosphere, rel. to electron production and heating 80−41605
electron distrib. rel. to production rate and heating 80−105103
electron distribution function and ion concs. in lower ionosphere, Boltzmann-Fokker-Planck theory 77−78564
electron flux, energy spectrum and latitude depend., Kosmos 490 meas. 79−2424
electron flux in topside region, excitation of SAR arc event 80−77217
electron flux measurements at altitude 250-500 km 79−2425
electron gas effective energy reception per created ion electron pair 80−67463
electron heat budget 77−53276
electron heating by EM emission of vertical lightning discharges 77−25818
electron injection, Feyerverk expt., optical 77−13160
electron kinetics in disturbed ionosphere above 100 km, approx. calc. method 77−64512
electron kinetics in lower ionosphere (100 to 260 km) *(Russian)* 78−77395
electron microburst precipitation at L∼4 77−33260
electron precipitation, quiet time, effects of localised scatt. sources 77−87157
electron precipitation and VLF emissions, modulation temporal-spectral anal. from Interkosmos 5 data 77−64511
electron precipitation daily vars., rocket meas. 78−69575
electron precipitation during substorm, modulation by hydromagnetic waves 80−105113
electron precipitation in auroral zone, field-aligned suprathermal fluxes below 270 km 77−33278
ionosphere continued
electron precipitation in slot region, time persistence of features 78−28395
electron precipitation pulsating aurora 80−85794
electron precipitation stimulated by Cs doped explosion 80−17436
electron production and loss rates, satellite meas. 79−35047
electron temp. and density, calc. technique for ground and satellite obs. 80−90275
electron temp. and density fluctuations meas. by Aeros-B, global distrib. 79−58160
electron temp. enhanced by suprathermal electron beam passage, auroral zone 80−85803
electron temp. profile, local characts. 77−78577
electron temp. profile over S.Atlantic geomag. anomaly *(Japanese)* 78−28368
electron temp. var. with solar activity satellite meas. 80−26678
electron temperature distribution, approx. expressions using vertical rockets data 80−12599
electron temperature in ionosphere main valley, behavioural charact. from satellite meas. 80−4170
electron temperature in topside ionosphere, models for low and medium solar activity conditions 80−67460
electron temperature profiles, satellite meas. up to 800 km altitude in late afternoon sector 79−70917
electron temperatures at trough latits., obs. concerning relationship to quiet-time ring current 79−101015
electron-ion collisions, cross-section 80−26666
electron-ion conc. and electron temp., Vertikal' 4 rocket meas. 79−84566
electrons, thermal, in winter ionosphere, energy distrib. obs. by S-310-5 rocket *(Japanese)* 80−94636
electrons collision freq. and transport props. 79−80079
electrons responsible for auroral absorpt., onset latit. of precip. 77−91357
electrostatic double layers, review 78−67368
electrostatic field, struct. in wake of body in rarefied plasma flow 77−91402
electrostatic field structure in wake of disc, external mag. field effect 79−10648
electrostatic fields, perturbation theory 78−36387
electrostatic fields generated by ionospheric dynamo region, penetration into lower atm. *(Russian)* 77−9606
electrostatic ion cyclotron waves, modulational instability, auroral plasma 79−62643
electrostatic ion cyclotron waves, optical detect. in auroral plasma 77−73900
electrostatic lower hybrid wave, nonlinear decay to whistler and Alfven wave pair 78−26275
electrostatic shock waves assoc. with auroral electron precip., model 77−9616
electrostatic wave generation near lower hybrid reson. by LF EM wave 77−29557
electrostatic wave propag. near lower hybrid resonance at ionospheric heights 77−58856
electrostatic waves, obs. in unstable polar cap ionosphere 79−29927
electrostatic waves assoc. with intense vel. shear near auroral arc 77−70911
ELF and VLF noise, diurnal var. observed on low-altitude satellite at latit. of Sanae 77−87181
ELF emission, spatial distrib. 80−4174
ELF ion plasma oscills. in Nike-Apache rocket apogee region 79−40012
ELF radio signals is auroral ionosphere, generation by LF and MF transmissions nonlinear demodulation 80−94639
EM induction in thin two-dimens. anisotropic conducting ionosphere *(German)* 77−70917
EM wave field, representation in spherically symmetric ionosphere 77−13152
EM wave propagation, evidence for reflecting layer below classical D-region 80−98508
energetic electron efflux, caused by plasma jet injection from rocket *(Russian)* 79−5701
energetic ions and EM radiation in auroral regions 78−81490
energetic ions of ionospheric origin in magnetosphere 79−66874
energy dissipation rel. to interplanetary quantity ϵ, influence on ring current growth 79−75057
equatorial, electric field meas. 77−87177
equatorial, electron production by energetic particle precipitation 77−33255
equatorial, meridional currents detect. 78−85767
equatorial, modelling of H_2 gas release effects 79−16741
equatorial, vars. rel. to interplanetary mag. field vars. 79−84572
equatorial anomaly and interplanetary mag. field sign reversal 79−2430
equatorial bubbles, model computations of assoc. radio wave scintillation 80−94641
equatorial bubbles, topside sounder obs. 79−16737
equatorial counter-electrojet, afternoon events occurrence characts. in Indian region 80−56672
equatorial counter-electrojet, electron drift vel., radar obs. 80−82126
equatorial counter-electrojet, geomag. aspects review 78−36367
equatorial daytime topside, plasma temps. and ion dynamics 79−84584
equatorial electrojet, irregularity drift vels. observed by close-spaced antenna technique and Doppler radar 78−36365
equatorial electrojet, multifreq. HF radar studies of plasma instabilities in Africa 78−36370
equatorial electrojet, storm-time obs. 77−33276
equatorial electrojet, strength rel. to SSC magnitudes equatorial enhancement 80−31174
equatorial electrojet, three metre irregularities depend. on Zenith angle, radar obs. 80−105109
equatorial electrojet, type 1 radar echoes with double-peaked Doppler spectra 80−67458
equatorial electrojet, westward, emergence 80−26663
equatorial electrojet and assoc. plasma instabilities 79−8750
equatorial electrojet control of total electron content 80−56673
equatorial electrojet irregularities, parallel wave propag. effects 77−2302
equatorial electrojet models, comparison 78−36372
equatorial electrojet theory 78−69607
equatorial electron densities, seasonal and solar cycle changes 78−36378
equatorial field and ionosphere, interplanetary magnetic field polarity effects 78−36416
equatorial hiss in topside ionosphere, obs. 80−61939
equatorial horizontal plasma waves, HF radar obs. 79−29930

ionosphere continued
equatorial ionosphere, effects of atmospheric waves 78−36232
equatorial ionosphere, EM state rel. to interplanetary mag. field vars. 78−77413
equatorial ionosphere, features assoc. with radio scintillations 80−77191
equatorial ionosphere, long-term 1.5 GHz amplitude scintillation meas. 80−85792
equatorial ionosphere holes and spread-F, ion chemistry and transport 78−88982
equatorial ionosphere plasma density bubbles, ESRO-4 obs. 80−4194
equatorial irregularity belt movement during magnetic storm 78−40757
equatorial irregularity experiment (Equion) for spread-F obs. 77−33266
equatorial irregularity patches, form., motion and decay 80−67456
equatorial Mg^+ ion distrib. from Mg II 2800 Å airglow obs. 80−26673
equatorial topside region, ion temp. troughs, OGO-6 obs. 77−64526
escape of ions to space, ion chem. and low altitude accel. effects 80−85798
W.Europe, ion production obs., 50-120 km altitude, 1975/6 winter anomaly 80−36439
evolution, with increase of O content 77−2300
excess radiation flux at heights of 200-300 km meas. 77−53278
F-lacunae, geographical distrib. and simultaneity of occurrence 80−4193
field aligned current above auroral arc, e^- and H^+ precipitation obs. 80−77215
field aligned currents driven by ionospheric dynamo 77−87178
field-aligned current closure and Joule heating near Harang discontinuity 80−72682
field-aligned current flow during moderate geomag. activity periods 77−70943
field-aligned currents and auroral electrojets, spatial relationship to night-side auroras 78−32267
field-aligned currents and ionospheric electric fields 77−53282
field-aligned currents and plasma drift vels., simultaneous obs. by Atmosphere Explorer C 80−72681
field-aligned currents at subauroral latitude, assoc. with convection elec. fields 80−90278
field-aligned currents in morning sector, rel. to auroral electrojet 77−29573
field-aligned currents meas. by Spacelab incoherent scatter radar 77−21946
field-aligned currents role in mag. disturbances generation 80−41631
field-aligned high-latit. current sources and induced elec. fields 80−26669
field-aligned ionisation irregularities rel. to HF-induced plasma line 78−88979
fine structure at low latitude from impedance obs. at 406 kHz 80−67468
fine structure cooling rate calc. 77−5387
flight conditions simulation 79−16796
formation of high-latitude ionosphere, role of elec. fields 78−28370
from spectral characts. of geomag. field vars. 77−87179
gas analysis, high-resolution high-pressure mass spectrometer 79−87906
general circulation above 100 km, empirical model 78−73558
general circulation at altitudes >100 km, empirical model 78−61664
general study of upper atm. *(Chinese)* 79−75039
geomagnetic crochet, two-layer current model 79−44300
geomagnetic daily variations influenced by interplanetary field 80−85591
geomagnetic field elements annual line, ionospheric source component 79−20752
geomagnetic field line forced oscills. due to ionospheric cond. change 79−48623
geomagnetic field meas. from near-Earth orbit, review of obs. 80−56347
geomagnetic H-component regular daily var. at Alibag, solar cycle depend. 79−8593
geomagnetic lunar daily var. at Alibag, oceanic and ionospheric dynamos contrib. 80−26444
geomagnetic pulsations, damping by ionosphere 78−49218
geomagnetic solar-flare effect and ionospheric induction 79−53632
geomagnetic Sq var. effect at satellite altitudes, correction for Magsat data analysis 79−75015
geomagnetic storm effects, OGO 6 obs. *(Japanese)* 78−85754
geomagnetic storm sudden commencement, uniform ionosphere transient response rel. to preliminary reverse impulse 80−8477
geomagnetic variations and equivalent current systems, UT and diurnal variation 80−51330
global electricity quasi-static model, coupling with lower atmosphere 79−96799
global morphology of light ions from ESRO-4 satellite 77−25844
gravity wave assoc. with sudden commencement, ionospheric effects 78−57385
gravity wave detect. from periodic fadings in VHF satellite transmissions during solar eclipse 77−33277
gravity wave-plasma interaction, elec. field and current prod. 80−61957
gravity waves, density response of layer structs. 78−81290
gravity waves, obs. at S. hemisphere station using total electron content technique 79−21096
gravity waves assoc. with Hurricane Eloise 79−66872
gravity waves revealed by radar obs. of electron density 80−77182
gravity-acoustic waves, self-localisation, non-linear effect in non-uniform atmosphere 79−8761
handbook, of upper atmosphere, ionosphere and magnetosphere 78−73557
Harang discontinuity, elec. current continuity 78−49220
Harang discontinuity, electron flow and visual aurora 80−8475
Harang discontinuity and substorm injection boundary relation 78−20576
Harang discontinuity electric field, auroral radar and rocket double-probe obs. 78−88971
heating at night, contribution of $O(^1D)$ 79−44288
heating by artificially injected 40 keV electron beam 78−40746
heating by radio waves, predictions for Arecibo and satellite power station 78−77403
heating by solar radiation in Schumann-Runge continuum and by chem. reactions 79−62653
heating by strong radiowave, geomag. pulsations artificial generation 77−29541
heating effects of conjugate photoelectrons 79−62670
heating experiments, effects of HF-induced plasma instabilities on electron temps. 78−40756
height changes in low latitude rel. to substorms 78−36377
ionosphere continued
height random changes calc., based on VLF signals phase fluctuations *(Russian)* 77−91358
height rises, relationship with polar mag. substorms and spread-F occurrence 78−81494
heterogeneous structure of the low-latitude ionosphere 78−96338
HF Doppler sounding of infrasound, due to earthquake-generated oceanic Rayleigh waves, group vel. dispersion curve determ. 79−70756
HF heating enhancing plasma line 80−82140
HF radio wave backscatter by artificial ionised clouds 77−56788
HF-induced parametric decay in presence of field-aligned irregularities 80−41613
high latitude topside sounding, Bernstein modes propag. trajectories *(Russian)* 77−33258
high-latit. ionosphere, average parallel elec. field from perpendicular elec. field vars. below 8000 km 80−72706
high-latitude electrostatic turbulence, polarisation, freq. and wavelengths 78−88981
high-latitude ionosphere, currents prod. by vars. of asymmetric ring current 77−21971
high-latitude ionosphere, energy spectra of 1 to 500 eV electrons, Atmosphere Explorer C obs. 77−29568
high-latitude ionosphere, obs. during near-steady state conditions 79−40000
high-latitude ionosphere-atmosphere interactions 77−22000
hiss associated with active auroral arcs, sounding rocket obs. 80−98512
holographic interpretation of radiowave sounding data 80−77200
horizontal drift meas. using closely-spaced receiver technique 78−40743
horizontal electric currents, rel. to plasmasphere elec. fields and whistler ducts form. 78−57407
hot electron layer, electron heating near Sq focus anomaly 80−51599
hydromagnetic dynamo 78−96335
in situ irregularity spectra, appl. to ionospheric scintillation calcs. 78−28415
Indian equatorial region, lunar magnetic tides 77−87154
induced elec. fields in ionosphere-magnetosphere system, review 80−94647
inhomogeneities drift, in presence of geomagnetic field, ionospheric wind influence *(Russian)* 79−29926
inhomogeneities drift in geomagnetic field 79−88546
inhomogeneities revealed by VLF propag., auroral zone 80−105107
inhomogeneity diffusion affected by geomag. field 80−41607
inhomogeneity formation, influence of elec. field temporal variation 80−105105
internal gravity waves, generation of inhomogeneities, effects on geomag. pulsations 78−45143
internal gravity waves, generation of small-scale inhomogeneities 78−45100
international model, appl. to O I 6300 Å emission nighttime vertical distrib. 79−53602
International Reference Ionosphere, descriptive empirical model, intentions and build-up 79−58173
International Reference Ionosphere, goals and status 79−5714
International Reference Ionosphere 1978 rel. to Vertical'-6 rocket meas. 80−90285
interplanetary magnetic fields influencing atmos. elec. currents 80−105126
inverted V event, electron flux fluctuations, Nov. 5 1975 obs. 80−41618
ion beam creation of dense plasma 78−5889
ion convection, momentum sources obs. in thermosphere neutral comp. 78−77380
ion cyclotron waves, critical-level behaviour 80−6238
ion cyclotron waves, generated by ionospheric Ba injection 79−53648
ion densities, response to mag. storm, OGO 6 in situ meas. 77−9588
ion density, effect of floating pot. of spherical ion trapper 79−44287
ion depletion in AE-C satellite wake, electron temp. and relative ion comp. influence 79−62667
ion drag, influence on winds in N Polar Cap thermosphere 80−67445
ion exchange with solar wind 79−40050
ion formation, nonstationary effects of gravity waves in lower ionosphere 78−73567
ion formation at high latits. during mag. quiet periods 78−69582
ion heating in auroral zone, by electrostatic ion cyclotron waves 80−72686
ion photochemistry, from Atmosphere Explorer C meas. 78−32261
ion production, density and composition in lower ionosphere during auroral absorpt. event 80−36443
ion production at high latit. by auroral electrons and short-wave solar radiation 77−60518
ion temp. troughs and interhemispheric plasma transport 78−96340
ion velocities, in four-component plasma 77−13154
ion velocity distribs. in high-latit. regions 79−101018
ion-cyclotron noise excitation in topside, Intercosmos 14 obs. 79−8755
ion-cyclotron noise in topside 80−101470
ion-molecule reactions, exothermic, review 78−33563
ionic concentrations, satellite meas. appl. to low altitude incoherent scatt. interpretations 77−78568
ionic reactions in lab. and planetary atmospheres 80−59168
ionis. struct. and composition, winter anomaly conditions 80−36442
ionisation, density profiles rel. to ELF propag. in Earth-ionosphere transmission line 78−36234
ionisation, effects of solar flares Fe XXV 1.87 Å line emission 78−65588
ionisation, rel. to quiet Sun EUV and soft X-ray fluxes 77−13307
ionisation irregularity drift motion from spaced fading and scintillation obs. 80−82133
ionisation profiles, from oblique sounding data inversion 77−41265
ionisation structure, fluctuations rel. to SHF refr. scatt. and scintillations 79−48615
ionisation waves, reson. coupling with acoustic gravity waves in mag. field 77−25832
ionization due to low energy solar and magnetospheric particles 79−53625
ionization inhomogeneities advected neutral gas motions, geomag. field effects 80−26677
ionization vertical lifting during mag. storms, satellite meas. of ion comp. 78−36395
ionosphere total electron content, nighttime enhancements at low latits. 80−72677
ions, transverse acceleration as source of hot magnetospheric ions 80−12604

ionosphere continued
IPDP pulsations, ionospheric propag. and assoc. source movements 79−25404
IRI lower ionosphere model compared to radiowave propagation data 80−61948
irregularities, characts. from Faraday fading of 40 MHz signals 77−13166
irregularities, drift vels. from ATS-6 140 MHz Faraday rot. records 78−69599
irregularities, formation and evolution by mag. flux tubes interchange 80−21876
irregularities determ. by radiosource scintillation obs. 79−84579
irregularities effects on radio waves, group path changes 77−53291
Kelvin-Helmholtz instability and ionospheric phenomena 77−29558
Kelvin-Helmholtz instability in magnetoplasma 79−23407
Lamb waves originating in nongeostrophic disturbances, a case study 77−45085
Landau nonlinear damping 80−8474
Langmuir envelope solitons in turbulent plasma 78−67334
Langmuir probe expts. on Intercosmos 10, results, rel. to VLF emissions *(German)* 77−70939
large-scale electric field, rel. to geomag. activity and terrestrial kilometric radiation 77−87159
large-scale horizontal winds, flow in presence of vertical vels. 77−78561
large-scale plasma stratification during vertical ionospheric sounding 77−17273
latitudinal total electron content, gradients over midlatit. stations 77−33251
latitudinal variation of auroral ionization, radar meas. 77−5385
LF noise induced in dipole antenna in ionospheric plasma 79−80072
LF sound waves relax. absorpt. *(Russian)* 78−65356
low altitude ion acceleration, rocket obs. 78−45115
low latitude interlayer ionisation variations during max. and min. solar activity *(Russian)* 77−73902
low-energy charged particle ring around equator in 400-1100 km altitude range 77−49213
low-latitude VLF emissions, prod. by incoherent Cerenkov process 79−75036
lower, current and wind systems, influence of magnetospheric convection 77−5386
lower, electron density space-time vars. 77−17282
lower, total cond. vars. effect on long-period MHD pulsations propag. 78−40730
lower daytime ionosphere, model for VLF field forecasting 77−49216
lower hybrid drift instability 80−46343
lower hybrid resonance (LHR) frequency, VLF receiver obs. and calcs. from ion density meas. 78−28416
lower ionosphere, electron density profile from radiowave data 80−67462
lower ionosphere, shortcomings in understanding revealed by radiowvave absorpt. meas. 78−81492
lower ionosphere, solar soft X-rays effects anal. rel. to nature of solar flares 79−8740
lunar tides, rel. to monthly mean lunar daily geomag. vars. in Japan (1958-1973) 79−96739
lunar tides, theory 78−77382
magnetic disturbances, 1972, February 24 and 1970, November 21, elec. fields and particle fluxes 77−21970
magnetic field aligned electric fields, mechanisms 77−9618
magnetic field aligned pot. diff. meas. from photoelectron energy spectra 78−7825
magnetic field line merging and slippage in auroral arcs 78−77393
magnetic field var. at low and equatorial latitudes, spectral characts. 78−36379
magnetic field variations due to quiet-time electrojets 80−30985
magnetic storm, 1972, August 4-5, in Asia-Australia-Pacific sector 77−33269
magnetic storm, Injun 5 low-energy plasma obs. 78−88987
magnetic storm sudden commencements and Pc 5 event, ionospheric response 77−33264
magnetically active quasistationary ionosphere, decametric freq. shift of magnetoionic component 80−105104
magnetosphere boundary layer, model involving interaction with ionosphere 80−85808
magnetosphere interaction, elec. convection field at ionospheric heights 78−89004
magnetosphere-ionosphere coupling during mag. storm 80−85821
magnetosphere-ionosphere coupling flux, VLF whistler obs. 80−77239
magnetosphere-ionosphere current system, generating Pi ULF waves 80−85819
magnetosphere-ionosphere electrical coupling, two-dimens. model 80−61938
magnetospheric substorms at night, ionospheric effects 79−62656
magnetotelluric apparent resistivity, effect of localised source 80−72429
mesopause temperature, determ. from $[NO^+.H_2O]/[NO^+]$ ratios 79−96849
mesoscale travelling disturbances, generated in tropopause gap region *(French)* 79−84346
mesoscale waves in D-region and F-region, temporal vars. 80−8483
metallic tethers in ionospheric plasma, electrodynamics 78−69652
meteor trail diffusion, radio refl. determination 80−46329
meteor trial, diffusion of weakly ionised plasma filament forming angle with mag. field 79−53610
MHD modes in plasmasphere, lower ionosphere effect 79−35055
MHD wave propag. characts. 77−2298
MHD waves, absorpt. rel. to neutral upper atmosphere heating 79−53588
mid-latitude, response to solar mag. sector crossing 79−35030
mid-latitude charged particle precipitation, optical evidence 79−44291
mid-latitude disturbance of corpuscular origin, coordinated international meas. 78−28374
mid-latitude trough, discovery in bottomside ionosphere 80−109300
mid-latitude trough, rel. to Pc 3 pulsations spatial distrib. at Earth surface 79−53659
mid-latitude trough, scintillation of extraterrestrial radio noise sources signals 78−73574
mid-latitude trough location, noon and midnight obs. by Ariel 4 78−85765
middle-latitude ionosphere, mathematical model of photoelectron fluxes 77−67009
midlatitude, dynamical model for 100-1000 km altitude range 78−53768
midlatitude, effective recomb. coeff., model 79−62652
ionosphere continued
midlatitude, reaction to neutral atm. disturbances 77−25805
midlatitude disturbances caused by high energy particles 77−60517
midlatitude electric fields at ionospheric heights, magnetospheric effect 79−2433
midlatitude ionosphere, relative ion comp. model 79−21094
midlatitude upper, parameters during high solar activity 79−62649
mixed mode echo of vertical-incidence ionogram, mixed-path mechanism 80−61942
mixed-mode echo obs. during vertical sounding 80−61943
model of midlatitude ionosphere and plasmasphere 80−105120
modelling, for use in administration of HF radio transmission networks *(French)* 79−58175
modification, initial report on artificially created equatorial spread-F 78−88972
modification by intense radiowaves, mag. field effects on electrons 77−60531
modification by release of highly reactive molecules, diffusion aspects 77−21988
modification experiments, electron flux vars. induced by HF waves *(Portuguese)* 80−41592
molecular ions conc. reaction to large-scale elec. field vars. 79−62654
moving current systems, EM induction in Earth 79−16370
multi-region electron density profiles, fitting to analytic function of height 77−60537
multilayer model, electrodynamic state, horiz. mag. field component influence *(Russian)* 78−73556
multiple auroral arcs, electron meas. 77−49210
multispecies flows, transport eqns. mathematical struct. 78−47084
negative ion hydration in stratosphere and lower ionosphere 79−100909
negative storms, numerical simulation using observed neutral comp. data 79−25393
Netherlands research, ionospheric features *(Dutch)* 78−4029
neutral composition vars. during 1974 Feb. mag. storm, ionospheric effects 77−87142
neutral gas diffusion rel. to ionospheric depletions, three-dimensional time-depend. modelling 79−66846
nightime ionosphere, current channelling rel. to transient dusk to dawn magnetospheric elec. field 79−96863
nighttime disturbances, rel. to VLF propag. anomalies 78−28414
nighttime equatorial atmosphere, Rayleigh-Taylor and wind-driven instabilities 79−96855
nighttime field aligned O^+ and H^+ fluxes in mid-latit. mag. field tube 77−33273
nighttime global zones of energetic particle precipitation 80−61947
nighttime ionospheric intermediate layer obs. by rocketborne impedance probe *(Japanese)* 78−61646
NO height distribution from rocket ion comp. results 80−26674
nocturnal topside, midlatit. electron density enhancements, longit. inequalities 79−16746
nonlinear sounding, resonant wave-wave interaction 78−28385
obstacle waves, steady-state soln. 77−49215
operational physical models 79−58172
outer plasmasphere hot zone, Prognoz ion temp. meas. 77−25845
palaeofield weak dipole epochs, nondipole component effect on auroral zone config. 80−105098
parallel electric field, signature in ion and electron distribs. in vel. space 78−89005
partial reflection drifts, comparison with winds determined by rocket techniques 77−87019
particle precipitation, effects of pitch-angle diffusion with asymmetric loss cones 77−13162
particle precipitation, latitudinal struct. on November 21, 1975, Chatanika obs. 77−87160
particle precipitation rel. to convection in plasma sheet 79−88544
pattern motion, spaced sensor obs. 79−25427
Pc1 ducted propagation in upper ionosphere 77−17292
Pc5 pulsation theory, consequences of ionosphere Hall current 80−105129
Pc5 pulsation theory, consequences of N. and S. hemispheres ionosphere electricity 80−109316
Pc5 pulsations, model of magnetosphere and ionosphere elec. and mag. fields 80−77234
Pc 1 pulsation signal, horizontal propag. 80−51604
Pc 4 pulsation event in plasmasphere, meridional characts. 79−5716
Pc 5 geomagnetic pulsations, Stare auroral radar obs. 79−96862
Pc 5 pulsation power depend. on cond. vars. in morning sector 79−62687
penetrating radiation composition, Cosmos 721 obs. 77−53279
perturbation magnetic fields and current systems associated with eastward drifting auroral structures 79−75009
perturbation of collisional plasma by opposing EM wave, anal. *(Russian)* 77−9605
perturbations caused by mag. storms, review of obs. 80−98495
photoelectron current, general, meas. technique 80−12636
photoelectron daytime energy distrib. meas. by AE-E satellite 78−88953
photoelectron distrib. determ. from plasma line intensity meas. 77−41259
photoelectron distrib. with interhemispheric coupling, two-stream methods 79−62669
photoelectron flux, calcs. 79−21103
photoelectron flux, low-altitude plasma line anisotropy theory 78−77414
photoelectron flux determination from plasma line obs. by radar 80−105117
photoelectron flux near photoionization peak energies 79−16738
photoelectron fluxes, calcs. compared with meas. from Atmosphere Explorer C and E 78−28400
photoelectron fluxes in ionosphere and plasmasphere, solar activity effects 78−16374
photoelectron spectra allowing for Auger effect 78−69557
photoelectron thermalisation and transport, isotropic scatt. 77−70933
photoelectron transport analytic approach 77−70932
photoelectrons, Coulomb-collision induced trapping by geomag. field rel. to plasmasphere electron gas heating 79−8739
photoelectrons and secondary electrons, kinetic theory 77−13148
photographic investigation by Salyut-6 *(French)* 79−40059
photoionisation and photoabsorption cross sections of He, O, N_2 and O_2 for aeronomic calcs., data tables 80−41599
Pi 2 micropulsations, harmonics in power spectra assoc. with plasmapause 77−25885
planetary wave vertical penetration into lower ionosphere 79−58142

ionosphere continued
plasma, acoustic wave propagation, quasihydrodynamics approx. *(Russian)* 77−82079
plasma, Debye screening and electron conc. nonuniformity effects on cylindrical antenna on satellite 78−69563
plasma, effect on obs. of solar type III radio bursts 80−72904
plasma, electrostatic cyclotron oscillation, photoionisation *(Russian)* 78−63552
plasma, HF radio wave-heated, with non-Maxwellian vel. distrib., electron oscills. *(Portuguese)* 78−83557
plasma, ionospheric ions population in open model magnetosphere 80−90295
plasma, lower hybrid drift instabilities, electron collisional effects 80−101484
plasma, nonlinear mixing of EM waves 78−77406
plasma and ion-acoustic waves parametric excitation by strong radiowave 77−17283
plasma bubbles, spatial relationship with 1 m equatorial spread-F irregularities 80−67457
plasma bubbles in nighttime equator region, field-aligned characts. 80−109308
plasma clouds, deform. and striation, multilevel model with recomb. chemistry 77−25834
plasma clouds, late time striation spectra 77−25836
plasma clouds, nonlinear stabilization of E×B gradient drift 79−58162
plasma conductivity, kinetic theory 79−53609
plasma conductivity, limits of applicability of formulae of mean path theory 77−60512
plasma convection, high-latit., and ionospheric depletion, effect of displaced geomag. and geographic poles 80−26680
plasma convection at high latitude, using 80−41612
plasma convection at high latitudes, model rel. to incoherent scatter obs. 80−72687
plasma disturbance due to earthquakes and volcanic eruptions 80−36453
plasma disturbances created by probes, impact on Spacelab proposed low-energy meas. 78−77458
plasma drift in polar region, meas. at Ny Alesund, Spitsbergen 77−45245
plasma energy balance eqns. analytical soln., midlatit. ionosphere and plasmasphere 77−17287
plasma f_H resonance, relax. sounding rocket expt. and interpretation 78−45129
plasma flow, var. in topside and F-layer, ionospheric-protonospheric interaction model calcs. 80−4180
plasma fluxes between ionosphere and protonosphere, ATS-6 obs. 78−28409
plasma heating by photoelectrons from ionization by solar UV radiation 79−53622
plasma inhomogeneities, diffusion spreading according to electrostatic approx. 80−4187
plasma instabilities, obs. in multiple pump ionospheric heating expt., 78−57382
plasma instability, prompt striation of Ba cloud 80−72685
plasma line, meas. at Chatanika with high-speed correlator and filter bank 80−98507
plasma line intensity, aeronomical diagnostic, suprathermal electrons, solar EUV, electron-gas thermal balance 78−32271
plasma line intensity meas. in terms of photoelectron fluxes, inversion problem 79−62668
plasma line shifts induced by HF wave at Arecibo 79−101012
plasma measurements, during Western European Winteranomaly Campaign 78−45125
plasma motion, rel. to magnetosphere convection and neutral upper atmosphere dynamics 77−29525
plasma motion in depleted regions at equator 80−12605
plasma oscillations, parametric generation during EM sounding from Alouette and Isis satellites 77−60510
plasma parameters, incoherent scatt. of EM waves, EISCAT project *(French)* 80−82142
plasma physics, book 79−84625
plasma processes in lower ionosphere, rel. to atmosphere mass distrib. by latitude 80−90115
plasma props. around S. Atlantic geomagnetic anomaly region *(Japanese)* 80−72695
plasma resonance characteristics of sounding rocket impedance *(Japanese)* 77−17271
plasma thermal response to electron and ion heat sources 77−45239
plasma turbulence, velocity shear driven 77−9608
plasma turbulence with two characteristic wavelength scales 77−80305
plasma wave spectrum, meas. via satellite-borne cross-power spectrum analysers 80−94621
plasma wave trajectories near resonance at upper hybrid freq. *(Russian)* 77−73903
plasma waves, parallel propag., stability of electron shell distrib. 78−4032
plasma waves, parametric generation by extraordinary radiowave 77−13153
plasma waves, stimulated by RF topside sounders, review 78−45128
plasmapause, correlated electron precipitation and magnetic IPDP events 78−28388
plasmapause, electron density profile meas. stimulated plasma wave results *(Japanese)* 80−94650
plasmapause, fluctuations of drift wave type 80−82137
plasmapause, Kelvin-Helmholtz instability to hydromagnetic pulsations 78−73584
plasmapause, MHD surface wave rel. to mini-substorm and long-period Pi 2 event *(Japanese)* 80−94653
plasmapause, position obs. by (Explorer 45) 77−53285
plasmapause, refr. of whistler precursors 77−25869
plasmapause, shocks and solitons 77−25840
plasmapause, VLF ground based obs. 77−25851
plasmapause afternoon sector, simultaneous ULF and strong riometer absorption events 77−25849
plasmapause and BDI positions during magnetic storm of 1972, Feb. 13-17th 80−56666
plasmapause as plasma sheath, min. thickness 77−25842
plasmapause crossing by JIKIKEN (EXOS-B) satellite, detect. by VLF Doppler shift crossing *(Japanese)* 80−94651
plasmapause displacements, recording technique 77−22034
plasmapause electric field variation from pulsation-pearl method, effect of substorm phases 77−25848
ionosphere continued
plasmapause location and H^+ density decreases, correl. 78−81500
plasmapause physics, conf., Grenoble, 1975, Aug. 77−25838
plasmapause props. and struct. rel. to micropulsations 77−25846
plasmapause signatures in ionosphere and magnetosphere 78−57391
plasmapause steady state positions from McIlwain's electric field models 77−25839
plasmas, field aligned distrib. rel. to plasma mantle 78−57406
plasmasphere, characteristic size determ. from solar wind meas. 77−49224
plasmasphere, columnar electron content 77−60533
plasmasphere, corotation electric field 77−25841
plasmasphere, diffusion of monoenergetic photoelectron fluxes 79−75018
plasmasphere, electron content and scintillations, deduced from study of ATS-6 radio beacon signals *(French)* 79−58184
plasmasphere, gyroresonance interactions 77−25850
plasmasphere, large scale elec. fields and currents, related geomag. vars., review 80−105121
plasmasphere, magnetospheric and ionospheric elec. field simultaneous obs. 80−105110
plasmasphere, mid-latit., He ions behaviour 80−41630
plasmasphere, mid-latitude, nighttime electron content, geophysical disturbance effects, 1974 August to November 80−94642
plasmasphere, parameter determ. from geomagnetic pulsation amplitudes 77−25847
plasmasphere, radio beacon studies 77−45229
plasmasphere, simulated plasma wave expts. by JIKIKEN (EXOS-B) satellite *(Japanese)* 80−94649
plasmasphere asymmetry in noon-midnight direction from Prognoz satellites 77−25843
plasmasphere ELF hiss during substorm activity, local time var. 77−53328
plasmasphere hot H^+ ions, charge exchange rel. to H escape rate 77−37469
plasmasphere of Earth, review 79−12329
plasmasphere origin, dimensions and particle precip. 78−69584
polar cap and low latitude bays during substorms, ionospheric current systems 77−17300
polar cap elec. field orientation and field aligned currents 80−41616
polar cap electric field, simplified model 78−12046
polar cusp, turbulent, temps. and low-energy particles obs. rel. to Kelvin-Helmholtz instability 78−96343
polar electric field, horizontal transmission to equator 80−8478
polar electric fields, transmission to Equator 78−65456
polar ionization hole, NO^+ recombination in mid-latitude trough 80−12575
polar ionosphere structure, dynamics and interrelations with magnetosphere convection struct. 80−4176
polar magnetic substorm development, two-dimensional magnetometer array study 77−91368
polar region, elec. field distrib. from crochet type mag. disturbances 78−40733
polar region, EM resonances for diagnosis and modification expts. 80−56676
polar region, struct. rel. to magnetospheric convection behind plasmapause 78−40731
polar region, three-dimens. current system reconstruction from ground-based geomag. meas. 78−45103
polar regions, adiabatic potential transitions properties 79−5713
polar regions, small-scale transverse magnetic disturbances 78−77423
polar substorms, equatorial-auroral ionosphere coupling 78−32291
polar wind morphology in mag. quiet conditions 80−72713
polar wind profiles latit. var., Alouette II data 78−69588
polar-equatorial electrical coupling during magnetically active periods, theory 78−93029
polarisation electric field vert. distrib. in topside 80−61935
positive ion concentration below 90 km altitude, rocket meas. 77−29539
positive ionospheric storms, worldwide distrib. 79−44290
positive ions, photodissociation, 3500-8600 Å 79−24763
potential double layers and discrete aurora 80−12607
potential equation separation *(German)* 77−70916
precipitating electrons energy spectrum effects on bremsstrahlung X-ray flux 78−40744
precipitating particle flux instability and geomag. pulsations generation 77−49232
pressure oscillations, generation of atmospheric acoustic-gravity waves 78−77296
pressure oscillations during substorms, transfer to neutral atmosphere 79−58158
primary ion-electron prod. rates, change with solar EUV flux 80−72675
primitive ionosphere, thermal struct. 78−40754
processes in neutral and ionized atmosphere in 60-150 km altitude range, problems 77−21961
profile inversion of simple plasmas and nonuniform regions, three-pole reflection coeff. 77−3984
propagation parameters, diurnal and seasonal vars. studied by vertical sounding at Surlari station *(Rumanian)* 80−51605
proton flux precipitating in equatorial ionosphere, estimation of energy release 78−32268
protonosphere interaction, dynamic model 77−45220
protonosphere interaction, rel. to protonosphere electron content meas. from American and European sectors 78−45151
protonosphere-F-region nighttime proton fluxes 78−93034
protonosphere-ionosphere coupling, postsunset obs. with Arecibo radar 79−70915
protonosphere-ionosphere thermal plasma flow, convection elec. field effects 79−62672
protonospheric-ionospheric modelling of magnetospheric VLF ducts 78−28446
Ps 6 pulsation assoc. with magnetospheric substorm, obs. polarization, two-snake model 79−66887
pulsating aurora, the importance of the ionosphere 80−85787
pulsed RF waves, proton cyclotron echoes, generating mechanism 78−77407
quasiperiodic disturbances, effect on guided MHD waves 78−73568
quasitrapped electrons, 100 MeV, in geomag. field 200-250 km above equator *(Russian)* 78−49223
quiet auroral arcs, feedback instability in ionosphere-magnetosphere system 78−57379
quiet dayside cusp, AE-C and -D low-energy particle obs. 78−28390

ionosphere continued
quiet night ionosphere, calculated and measured decay rates comparison 78−81493
radio aurora, ion-acoustic plasma waves and two-stream instability 78−36355
radio aurora (diffuse), rel. to field-aligned currents and particle precipitation 80−105119
random and anisotropic irregularities at low latits. 79−88532
random inhomogeneities rel. to diffusion of limited radio beam 77−91349
Rayleigh-Taylor bubbles in equatorial ionosphere 78−77409
Rayleigh-Taylor gravitation-induced instability, rel. to equatorial spread-F 78−69595
Rayleigh-Taylor instability of equatorial region, linear theory 80−41619
rays calculation in inhomogeneous magnetoactive ionosphere by perturbation method 80−21874
records over Shanghai, March 1953 to June 1955 *(Chinese)* 80−77192
response to sudden storm commencements *(Japanese)* 80−101490
responses during August 1972 mag. storms, review 77−25858
ring current proton interaction with electron cyclotron emissions 77−25853
ringing irregularities, meteor hypothesis 79−84581
riometer sounding, absorption data appls. to ionospheric study *(French)* 77−53216
rotational electric field of auroral origin 78−45102
S_q variation, magnetosphere or ionosphere dynamo? 80−109090
S_q variation currents, day to day variability over Europe 79−44299
S_q-field, seasonal and latit. vars. deduced via natural nonorthogonal functions method 78−36359
S polar cusp, low energy electrons obs. by AE-C during 1977, September 21 geomag. storm 79−35076
satellite gyroharmonic resonance obs., interpretation 79−48614
satellite wake, assessment of ion current distrib. in wake 80−101527
satellite wake, struct. of electrostatic field 77−60509
satellite wake ion density, for probe meas. in O^+ plasma 80−82136
Schumann resonance in ionosphere-Earth waveguide, line splitting detection, chirp-z transform 78−3861
scintillation-producing irregularities in southern mid-latits., horizontal struct. 79−12339
SEA rel. to X-ray radiation and active areas, statistical study *(French)* 78−20788
semiannual variations of n(O), 120-500 km heights 77−49214
semidiurnal winds seasonal var. in dynamo region 78−93033
sheet-like auroral ionospheric irregularities 79−35033
SID phenomena, peculiar events of non-XUV origin 80−109309
SITEC disturbances (1966-1977), rel. to solar flare occurrence 80−90276
slab thickness during geomagnetic storms 79−88538
slow MHD waves, dispersion relations and speed 78−45093
small-scale irregularity structs. assoc. with subtrough density gradients, Ogo 6 obs. 78−40753
small-scale stratification in upper ionosphere, influence of strong radio wave with amplitude modulation 79−12330
solar eclipse, 1973, June 30, ionospheric disturbance obs. 77−53302
solar eclipse effect upon effective height *(Russian)* 78−49201
solar particle absorption event, atmospheric electricity supply current modulation 80−17329
sound generation in nonadiabatic ionosphere, theory 80−41604
sounding rocket expts., during 1979 February 26 total solar eclipse 79−58145
space and time dependent media, problem of nonreproducible data, ionosphere appl. *(German)* 77−64464
Space Experiments with Particle Accelerators (SEPAC), program for first Spacelab mission 79−48650
space sciences, conf., Trivandrum, India (Jan. 1977) 78−69586
space simulation plasma chamber, elec. field meas. with double probes, atm. appl. 79−64909
space vehicle obs. (1966-76) *(Japanese)* 78−24402
spacecraft charging in ionosphere due to positive ion emission 79−84633
spatial resonance mechanism, rel. to equatorial spread-F drifting patches 79−21095
Sq at low latitude, hourly study of secondary effect 80−56362
Sq current system during International Geophysical Year 77−45219
Sq current variability affecting magnetosphere ring current 80−72714
Sq currents of N. and S. hemispheres affecting equator mag. variations 80−76904
stable auroral red arc formation, proton obs. supporting ion cyclotron wave heating theory 78−49197
stationary and non stationary conditions, semi empirical model 80−4181
storm initiation and propag. from solar flares *(Korean)* 77−53335
storm time auroral ionosphere, anomalous transport coeffs. effect on thermal struct. 79−16743
storm-time magnetic field changes, ionospheric-magnetospheric contribs. 80−12612
stratosphere-ionosphere-magnetosphere coupling at midlatitudes, 1969-74, southern hemisphere 77−9471
striations produced in radiowave heating expts., theory 80−41625
structure, calc. and obs., AE-C satellite and incoherent scatter radar obs. 78−49203
structure, from satellite radio beacon signals 78−12050
structure, model effects on thermospheric calcs. 78−36345
subauroral ionosphere, persistent scintillation enhancement obs. rel. to irregularities struct. 78−20573
subauroral ionosphere, rapid ion drifts obs. by Atmosphere Explorer C 80−4188
subauroral zone, electron content and f_0F_2 latit. var. 77−13164
subsatellites launched from Spacelab, for atm., magnetospheric and plasma physics research 77−21944
subsonic wave-ionised plasma interaction, electron density study 80−4183
substorm and auroral activity, development after southward turning of interplanetary mag. field 78−28435
substorm associated field-aligned currents large-scale characts. 78−45156
substorm development in postmidnight sector, electron density vars. 77−60525
substorm inhomogeneities affected by ionosphere, experimental verification proposed 80−4199
substorms, comprehensive model current system for high-latit. mag. activity 79−92640
substorms, role of ionosphere, field-aligned currents generation 78−88998
substorms, ULF mag. vars. assoc. with ionospheric cond. changes 78−88994
substorms in subauroral ionosphere 77−49217
sudden frequency deviations during solar flares, character of depend. on operating freq. 78−28373
sudden phase anomalies, correl. to solar X-ray bursts 80−98513
suprathermal particle obs. in low latit. nighttime ionosphere 77−53281
synthesised trough ionogram 79−8759
techniques and phenomena, book 79−75040
temperature, numerical soln. of magnetosphere time-dependent heat energy eqns. 80−21875
temperature domains, nonlinear stationary 79−35052
tensor conductivity 77−13172
thermal electrons energy distrib. distortion near focus of S_q current vortex 79−35053
thermal parametric instability, effect of recomb. processes and plasma nonisothermability 80−61967
thermal parametric instability in ionospheric plasma at freqs. close to electron gyrofreq. 80−46344
thermal proton outflow, convection elec. field influence 77−45243
thermosphere, lower, ionospheric sublayers form. 80−61956
thermosphere neutral winds, seasonal var. rel. to ionosphere struct. and behaviour 77−53267
tidal wind variations, upper mesopause region, ionospheric reflection height *(German)* 77−87139
topside, anomalous resistivity of auroral plasma 77−5389
topside, effects of magnetic and sunspot activities 77−70918
topside, electron heating rates during medium solar activity 77−70919
topside, ion composition changes during 13 Sept. 1967 storm 78−16232
topside, ion heating by electrostatic ion cyclotron waves 80−12606
topside, large scale wave-like struct. at low and middle latits. 77−21985
topside, light ion and electron troughs rel. to plasmapause 77−87162
topside, low density regions at high altitudes, rel. to equatorial spread-F 79−62671
topside, low-energy plasma, Injun 5 Lepedea obs. 78−77408
topside, midlatit. trough position from ESRO 4 obs. 77−64525
topside, midlatitude, diffusion and heat flow eqns. 78−4030
topside, midlatitude, effects of relative ion flows on thermal struct. 77−91367
topside, midlatitude, relative flow of H^+ and O^+ ions 78−4031
topside, postsunrise flux tube refilling at low latitudes 80−8476
topside, static elec. cond., geomag. field effect on charged particle collisions 78−40728
topside, thermal plasma enhancements rel. to auroral electrojets 77−9617
topside, transient response to precip. 77−78566
topside, turbulent transport and heating of auroral plasma 79−35054
topside at high latitudes, diffusion-thermal heat flow effects 78−49217
topside ion composition from VLF hiss obs. near plasmapause *(Japanese)* 77−21999
topside ion transport, obs. of H^+ and O^+ ions 80−61940
topside ionosphere, comp., temps. and electron loss coeff. over Arecibo 78−36386
topside ionosphere, diffusion and heat flow eqns. with large temp. differences between interacting species 79−66857
topside ionosphere, features of pararesonance whistlers 80−67455
topside ionosphere, low-freq. emission pulsations spectra rel. to surface geomag. SPP spectra 79−58157
topside ionosphere, O^+ to H^+ transition level height rel. to very low dispersion whistlers 79−44301
topside ionosphere, plasma bubbles near dawn terminator 79−101016
topside ionosphere model, O^+ and H^+ continuity and momentum eqns. 80−51603
topside ionosphere trough morphology, occurrence freq. and diurnal, seasonal and altitude vars. 79−53645
topside irregularities in equatorial region 78−36384
topside magnetospheric cleft ionosphere, Isis 2 spacecraft obs. 77−29571
topside of nocturnal equatorial ionosphere, diffusion-thermal effects 78−40751
Tordo 1, polar cusp Ba plasma injection expt., obs. 78−77402
total electron content, ATS-6 radio beacon expt. meas. 77−2303
total electron content, ATS-6 radio beacon obs. over Europe and USA 80−77201
total electron content, effect of elec. fields and vertical neutral-gas drifts 78−45089
total electron content, equatorial electrojet control 79−88539
total electron content, low latit., numerical model 79−88531
total electron content, lunar var. at Lunping 79−21100
total electron content, mag. storm effects, Indian region 79−84576
total electron content, storm-time changes at nearby mid-latit. locations 80−31164
total electron content and F-region electron density distrib. near mag. equator 79−75028
total electron content at equator, fluctuations due to atmospheric waves 78−36360
total electron content at Sagamore Hill, solar cycle var. 78−81496
total electron content determ. from Faraday rot. 77−33249
total electron content determ. in transverse zone, new methods 77−33250
total electron content diurnal and seasonal trends, obs. at Waltair 78−69596
total electron content during 1971-4 period above Melbourne 79−5712
total electron content during magnetic storms over Hawaii 78−16238
total electron content during nonstorm times, Arecibo meas. 77−25829
total electron content equinoctial variations 77−60542
total electron content from group delay meas. at Ootacamund 79−101006
total electron content meas. at Gauhati, using ATS-6 140 MHz transmissions 78−69598
total electron content meas. by SHF differential phase shift method 78−36304
total electron content meas. during 1976 Oct. 23 solar eclipse over Australia, rel. to induced gravity waves 78−49210
total electron content models, for European and Mediterranean regions 80−98516
total electron content nighttime increases, ATS-6 radio beacon obs. 79−75020
total electron content numerical model, corrections for satellite tracking systems 78−69587

ionosphere continued
total electron content obs. at Kurukshetra, suing ATS-6 140 MHz transmissions 78−69597
total electron content obs. at low and mid latitude during mag. storms 78−77396
total electron content over Hawaii, secondary maxima 77−70925
total electron content over Indian subcontinent, electrojet effects 77−64523
total electron content over mag. equator rel. to solar cycle during 1964-69 period 79−53636
total electron density nighttime behaviour 78−69570
transitional electrodynamic processes, rel. to geomag. disturbances 77−60515
transport eqns. for low speed thermal proton flows 79−44304
transverse electric fields rel. to field aligned currents, model 78−77397
transverse electrical conductivity 77−49227
travelling disturbances, effect on statistical characts. of refl. signals 78−45092
travelling disturbances, electron density spectra 78−77398
travelling disturbances, medium-scale, diurnal and seasonal var. modelling 79−58181
travelling disturbances, possible correl. with jet stream activity 78−69601
travelling disturbances, spectral comp. meas. 77−25824
travelling disturbances characts. over Thumba 78−69590
travelling disturbances effect on radio noise from discrete sources 77−91353
travelling disturbances in equatorial ionosphere, assoc. with penetrative cumulus convection 78−36361
travelling disturbances study using multistation rapid-run ionosondes 78−93041
travelling ionospheric disturbance, $1F_D$ propag. obs. *(French)* 78−12043
travelling ionospheric disturbance effects on ionograms 77−45232
travelling ionospheric disturbances, detec. by auroral zone incoherent scatter radar 79−48610
travelling ionospheric disturbances, Faraday rot. modulation obs. 79−21101
travelling ionospheric disturbances, rel. to thermosphere storms 77−9583
travelling ionospheric disturbances, Tromsoe-Valensole propag. *(French)* 78−12041
travelling ionospheric disturbances (TIDs), wave-normal depression and disturbance amplitude height depend. 79−40006
travelling ionospheric disturbances and assoc. internal gravity waves, obs. via electron density power spectra 78−28394
tropical waves 79−74945
troposphere-ionosphere coupling during 1973 November 20 isolated tornadoes 79−70851
turbulent fluctuations, rel. to strong turbulence in partially ionised plasmas 80−79499
uniform-conductivity, ground magnetic effect of vertical currents connected with Pedersen currents 77−29579
upper, perturb. assoc. with magnetospheric cleft in local summer *(French)* 78−4022
upper atmosphere tidal effects on geomagnetic and ionosphere variations 77−87137
upper boundary conditions, effect on simulated ionospheric parameters 77−17272
upward flowing energetic ions, latit., diurnal and altitudinal distribs. 78−49199
UV fluoresc. excited by electron beam, POLAR-5 rocket expt. at 391.4 nm 80−77214
vertical ionisation gradient max. identification from ionogram trace derivatives 77−60522
Vertical-6 rocket flight results 80−90268
viscosity spatial inhomogeneity and dynamic effects 79−53590
VLF emission, mid-latit. modulation theory 79−12335
VLF hiss from auroral zone, direction find method and obs. 80−85777
VLF plasma wave excitation due to electron beam injection 80−12603
VLF waves, natural and electron-beam produced, rocket obs. 78−7829
VLF waves, nonlinear effects on magnetosphere/ionosphere plasma *(Russian)* 78−32287
near-wake structure of Atmosphere Explorer C (AE-C) satellite, parametric investigation 79−53647
wave spectrum measurements using cross-power spectrum analyzer on space shuttle *(French)* 79−70912
waveguide disturbances, Pc 1 pulsations intensity modulation 77−49233
weak global magnetic disturbances, characts. and origin 79−53660
whistler mode radiation, generation by parametric decay of Berstein waves 77−76095
whistlers, group vel. in two-ion plasma 78−87452
wind field disturbances, 90-100 km altitude, rel. to stratospheric warmings *(German)* 77−70894
wind in lower ionosphere, obs. by Kyoto meteor radar 80−67444
winter lower ionosphere, influence of interplanetary mag. field sector struct. 80−8510
winter nighttime ionosphere distortions at L=4 77−87165
winter polar ionosphere, Isis 1 and 2 meas. 78−77400
X-ray microbursts in auroral zones, power spectra rel. to primary electron transient times 77−78556
Zarnitsa.2 electron injection expt., circumrocket glow spectral obs. *(Russian)* 80−12596
zonal and meridional elec. fields effects in evening sector 78−69571
zonal electric field effects in daytime winter midlatit. ionosphere 78−28379
zonal electrostatic potential 78−36393
zonal electrostatic potential distrib. 78−7824
0 I, 63 μm emission as cooling mechanism in thermosphere and ionosphere 79−16732
Ba clouds in inhomogeneous ionosphere, assoc. striation form. 77−9607
H^+ distribution in equatorial anomaly, empirical model 79−8768
H^+ field-aligned downward vels. at mid-latitudes 79−40015
H^+ midlatitude trough location from Oreol 2 data 80−8473
H^+, O^+, conc. meas., Aureole 2 satellite mass spectrometer obs. 78−53766
H_2O^+ density, contrib. from H-implanted interplanetary dust grains 78−65445
He^+, Atmosphere Explorer-C abundances rel. to solar EUV flux 79−16919
He^+ escape fluxes from polar ionospheres, calcs. 79−35037
He^+, outflow from terrestrial ionosphere 78−49221
MgO, wavelengths and relative intensities of IR bands 79−2407

ionosphere continued
N and O radiative recomb., source of NO γ and δ bands auroral emission 77−91343
N_2^+ 4278 Å emission and electron flux comparison in auroral zone 77−87151
N_2^+, dissociative recombination in ionosphere, rate cont. 80−17435
N_2^+ recombination rate coeff. determ. 78−28386
N_2^{2+}, auroral ionosphere spectral emission process 80−41577
N_2^++O reaction, rate coeff. determ. 77−53288
NO^+, daytime chemistry from Atmosphere Explorer-C meas. 77−33230
NO^+, form. by $N(^2D)$+O associative ionisation 80−4161
N_2O^+, pot. energy hypersurface characts. calc. in $O^+ + N_2 \rightarrow N + NO^+$ react. 78−60996
$NO^+.N_2$ formation rate consts. at low temps. 77−60538
O, conc. in lower ionosphere, fluorescence spectra 80−36434
O I 6300 Å forbidden emission at mag. equator, rel. to vertical E×B plasma drift vel. 80−36435
O I EUV and far UV emissions obs. in tropical ionosphere 77−2297
O^+ and H^+ equal ionisation level, during max. of solar activity 80−90280
O^+ ions, presence in magnetotail lobe plasma 78−32299
O^+ reactions with N_2, O_2, and NO, nonthermal rate coeffs. 78−57375
O^+, upward fluxes rel. to O^+ obs. in magnetotail 77−33284
O^{2+} ions in disturbed ionosphere 79−62647
O^{2+} reaction rates with O_2 and N_2, ionospheric implications 79−16726
O^{2+} reactions with atoms or molecules of ionospheric importance, lab. meas. 80−26004
O^+/electron density ratio in 140-200 km height range 80−105102
O^+/n_e, relative densities computation at 170 km for specific heliogeophysical conditions 79−12332
$O+N_2$, excitation and deactivation at above-thermal energies 80−43171
$O^+ + N_2$, charge exchange collision, rate coeff. and ionosphere implications 80−87224
$O^+ + N_2$, reaction rate coeff. 77−87167
$O^+ + O_2$, charge exchange collision, rate coeff. and ionosphere implications 80−87224
O_2, electron impact vibr. excitation, direct and stepwise, rate coeffs. 80−5630
O_2^+ recombination rate 77−25830
O_2^{2+}, auroral ionosphere spectral emission process 80−41577
$O_2+N^+(N_3^+)$, drift tube mass spectra, rate coeffs., prod. distrib. 77−77746
$O^+(^2D)$, quenching by electrons 80−94630
O^1D 6300 Å photoelectron induced predawn enhancement, altitude profiles 77−17290
$O^+(^2D)+N_2$, charge exchange rate coefficient, effect of N_2^+ recomb. on aeronomic determ. 78−88954
$O^+(^2P)$, ionisation freq. vars. during solar cycle 21 from airglow meas. 80−77195

ionospheric electromagnetic wave propagation
see also atmospherics
A1 absorption measurements at 2.4 and 5.6 MHz 80−82132
absorption, global meas. on board ships 80−98500
absorption, mid-latitude rel. to zero and maximal vel. contours in equatorial ionosphere 80−12597
absorption, solar X-ray control, sweep freq. method meas. 79−84582
absorption, vars. rel. to geomag. influence on atmospheric press. geopotential 80−4067
absorption and geomag. activity rel. to solar electron fluxes increase after flares 79−75175
absorption effects of wind and temperature, 1975/6 winter anomaly obs. 80−36438
absorption events at high latits. 77−21987
absorption meas. using sweep freq. technique 79−75029
absorption studies by riometer technique at magnetic equator 77−53275
acoustic gravity waves role in generation of spread-F and ionospheric scintillation 79−66868
aerospace propagation environment operational modelling conf., Ottawa, Canada, 1978, April 79−53651
airborne soundings over Kazakhstan, surface topography effects on electron density 78−69579
amplitude scintillation at 1.5 GHz, long-term meas. at mag. equator 80−85792
amplitude scintillations, multifreq. spectra 77−87161
Amsat-Oscar 7 subhorizon ratio signals beacon, above F2 layer, 30 MHz 77−70937
anomalous radiowave absorpt. due to heating effects 77−25857
ARAKS expt., EM wave meas. 79−21071
Arctic ionosphere, European Incoherent Scatter (EISCAT) project *(French)* 79−2437
artificial quasiperiodic inhomogeneities formation due to powerful radiowave 79−84585
astronomical radio sources, phase stability meas. by radio-link interferometer 77−5452
asymmetry between N. and S. hemisphere radiowave absorpt. in winter 80−101485
atmospherics, sweepers modulation struct. in HF and VHF bands 79−5707
atmospherics noise variation with sunspot number during 1600-2000 hours at Delhi 78−49083
ATS-6 140 MHz Faraday rot. records, irregularities drift vels. determ. 78−69599
ATS-6 radio beacon data, rel. to geophysical disturbance effects on mid-latit. plasmasphere nighttime electron content 80−94642
ATS-6 radio beacon obs. of total electron content nighttime increases 79−75020
ATS-6 radio beacon signals, Faraday rot. modulation rel. to travelling ionospheric disturbances 79−21101
attenuation determination, errors for signals with small arrival angles 79−58155
aurora, radar Doppler data interpretation rel. to auroral electrojet curvature 77−41266
aurora, small scale absorpt. events assoc. with substorms 77−56791
aurora irregularities, overnight north-south movements obs. at 42 MHz 80−67449
aurora large scale structure, by riometer radiowave absorpt. 80−72670
auroral absorption event, lower ionosphere ion prod., density and comp. 80−36443
auroral absorption regions poleward expansion triggered by SSC 78−57403

ionospheric electromagnetic wave propagation continued
auroral absorption spikes, currents and elec. fields vars. during substorm expansion phase 79−35039
auroral D-region, unusually strong partial refls. obs. during absorpt. event 78−36388
auroral E-layer, plasma lines meas. 79−25386
auroral E-region fine structure obs. in substorm 80−36452
auroral electrojet, Chatanika radar meas. compared with Anchorage VHF backscatt. obs. 78−12048
auroral electrojet, nonpotential waves 77−49212
auroral electron beam, assoc. EM radiation bursts during substorms 79−88557
auroral ionosphere, field-normal plasma-line scatt. detect. expt. 78−73580
auroral ionosphere, radio turbidity coeff. 78−45112
auroral kilometric radiation, ISIS 1 obs. at source 79−84558
auroral kilometric radiation coherent generation by nonlinear beatings between electrostatic waves 80−26691
auroral kilometric radiation correl. with inverted-V electron precip. 80−26692
auroral oval, dayside, rocket-borne VLF and ELF waves meas. 80−98504
auroral oval, VHF amplitude scintillation 78−61660
auroral propagation condition anticipation for radio amateurs 77−64529
auroral radio absorption obs. by riometers rel. to 10-80 keV electron precip. at geosynchronous orbit 79−48606
auroral radio backscatter at 42 MHz, amplitude rel. to Doppler shift 80−61955
auroral radio echo, ion-acoustic, short term characts. 78−45080
auroral substorm expansion riometer absorpt. of spikes obs. 80−85799
auroral zone, nighttime scintillation localised enhancements struct. 80−98506
auroral zone activity coupled to mid-latitude radiowave absorpt. 80−61945
auroral zone riometer meas., day/night absorpt. ratio 77−91365
autumn-winter transition in mid-mesosphere, ionospheric absorpt. at 25 kHz 79−62644
backscatter echo spectral analysis and radio transmission forecasts *(French)* 79−29912
backscatter inversion is spherically asymm. ionosphere 80−36446
backscatter obs. at 3 m wavelength rel. to F-region irregularities 79−12338
backscatter radar data rel. to O I 6330 Å nightglow intensity 78−77401
backscatter sounding method using spatial and spectral sampling, for investigation of plasma inhomogeneities *(French)* 79−29911
backscatter sounding technique *(Spanish)* 79−100998
blanketing E_s-layers in equatorial electrojet, VHF radar obs. of assoc. gradient instabilities 77−29577
bottomside, fictitious surface admittance for arbitrary geometric field 79−84565
bottomside ionogram analysis, valley problem 77−33268
bounded beams dispersion due to anisotropic heterogeneity *(Russian)* 79−12341
bounded inhomogeneous isotropic media, generalized charact. functions appl. to propag. 79−72462
broad-band wave meas. in ARAKS expt. 79−21072
bubbles in equatorial region, obs. by radiowave propag. 80−41621
C-layer, props. from ULF field obs. 77−25816
channel lower hybrid resonance excitation by superthermal particle streams *(Russian)* 78−4025
Cherenkov radiation, prod. by unstable plasma wave coupling 79−40003
circumglobal signals in Atlantic equatorial zone *(Russian)* 78−69585
circumterrestrial plasma faraday inverse effect *(Russian)* 80−4190
cold lossless plasma half-space, transient response in presence of transverse static mag. field 78−67361
cold lossy plasma half-space in transverse mag. field, transient response 79−77388
combination frequency radiation generation in region of auroral electrojet *(Russian)* 77−41268
complex refractive index, application of Appleton-Hartree formula *(Chinese)* 80−105100
condition forecasting and prediction, long- and short-terms 78−93046
conductivity anal., electron motion 80−46335
correlation ellipse physical significance in ionospheric drift anal. 77−13179
corrugated reflector model for one-hop oblique propagation 79−35041
cosmic noise absorption, F-lacuna and slant-E condition rel. to E-region Farley-Buneman instability 78−73563
cosmic noise absorption produced by magnetosphere conjugate electron precip., high time resolution meas. 80−41666
cosmic radio noise 'absorbed' by E-region plasma waves 80−82139
cosmic radio noise absorpt. events meas. on riometers, due to backscatt. by E-region irregularities 77−25831
cosmic radio noise absorpt. over Delhi, calc. and obs. 77−64521
cosmic radio noise absorpt. rel. to mag. storms at Delhi 78−69589
cosmic radio-noise absorpt., impulsive quasi-periodic variations 80−105116
critical frequencies, diurnal and seasonal vars. studied by vertical sounding at Surlari station *(Rumanian)* 80−51605
critical frequency determination, radio sounding method 80−46286
critical ionosphere layer, double reson. excitation 80−36444
cross-modulation of radio cosmic noise 77−70936
cross-modulation of radio signals between two nearby stations 78−93048
D-region, anomalous radiowave absorpt. during sudden disturbances, solar zenith angle depend., electron loss coeff. 78−69568
D-region, diurnal vars. during storm after-effect 78−65451
D-region, electron densities vars. from radiowave propag. 77−33267
D-region, electron density diurnal var. at midlatit., from VLF meas. 77−64520
D-region, electron density profiles from gyrowave interaction expt., error anal. 79−5705
D-region, enhanced electron conc. at mid-latitude, positive-ion model 80−105115
D-region, irregularities responsible for partial reflection 80−41629
D-region, long radiowave absorption observations, morphological scheme of post-storm event 79−88523
D-region, lower, Faraday rot. and absorpt. calcs. rel. to electron density meas. 80−31162
D-region, mid-latit., energetic particles precip. during baylike absorpt. disturbance 79−12333

ionospheric electromagnetic wave propagation continued
D-region, negative ions, Thomson scatt. detect. using Arecibo radar 79−62665
D-region, negative ions effects on collision-dominated Thomson scattering 78−45118
D-region, partial reflections, sensitivity to irregularity comp. 78−81495
D-region, partial refls. ang. and temporal characts. 79−66858
D-region, partially refl. radiowaves ang. distrib. meas. 78−49204
D-region, polar electron density profiles during solar proton event, from VLF refl. height vars. 79−8764
D-region, quiet polar region characts. using partial refl. method 78−49215
D-region, radiowave absorpt. diurnal var. at high latit., riometer data 77−53294
D-region, radiowave absorpt. rel. to interplanetary mag. field polarity changes 77−33272
D-region, radiowave absorption during solar minimum, 2.5-4.1 MHz 80−41628
D-region, radiowave heating at HF, consequent MF absorpt. effects 80−94646
D-region, radiowave propag. rel. to plasma density meas. 78−45126
D-region, radiowave propag. results during Western European Winter Anomaly Campaign (1975/76) 78−45123
D-region, radiowaves self-action effect *(Russian)* 77−41254
D-region, southern hemisphere, radio wave scatt. obs. 78−36363
D-region, steerable beam radar obs., angular variation obs. 80−101487
D-region absorption, effect on forward scatter radiometeor amplitude distrib. index 78−65552
d-region absorption and forward-scatter radio-meteor data 79−75033
D-region anomalous radiowave propag. rel. to relativistic electron precip. events 77−25827
D-region electron density during W.Europe 1975/6 winter anomaly 80−36440
D-region HF wintertime absorption, O I airglow emission as precursor 79−58148
D-region ion chemistry during intense radiowave heating 80−61952
D-region partial reflection experiment, appl. phase switched correlation polarimeter, 77−87169
D-region partial reflections, filtering effect on drift parameters determined by full correl. anal. 78−65450
D-region short-wave radio absorpt. vars., transient coupling with tropospheric planetary press. waves 77−33162
day to night absorpt. ratio in auroral zone riometer meas. 78−20580
daytime absorption surges, as function of substorm phase and interplanetary mag. field direction 78−73575
daytime effect on radioastronomical intensity meas. and interferometry 80−67450
daytime satellite radio scintillation rel. to sporadic-E layer near mag. equator 77−45225
daytime scintillation assoc. with geomagnetic storm 77−78563
daytime sky wave component in Calcutta-C MF signals 78−16239
decametric freq. shift of magnetoionic component in quasistationary ionosphere 80−105104
decametric wave propagation, ionosphere conditions forecasting by CNET, in France *(French)* 80−85790
deuteron whistlers in topside ionosphere, trans-equatorial propag. 80−77203
differential equation, generalised, inc. anisotropy, inhomogeneity and fluctuations 78−53770
diffraction trapping of HF waves by ionospheric waveguide 78−53772
diffuse radio aurora at high aspect angle, radar obs. 80−41623
directional ionosonde, aerial pairs interferometry technique, ionogram display 77−29496
dissipative parametric generation of small-scale diffusion inhomogeneities 78−69580
distant HP propagation, role of near-critical rays 79−53619
diurnal radiowave absorption variation asymmetry, seasonal variation 77−87175
DNA Wideband satellite expt., complex signal scintillation 78−45133
Doppler fluctuations and angle-of-arrival var. caused by ionospheric scintillation 78−77411
Doppler processing of HF backscatter radar and mode structures of ionospheric propagation 79−16753
Doppler shift meas. with rot. antenna, ordinary and extraordinary modes 80−17426
ducting at high-frequency, review 80−21872
duroral zone ionospheric modification, incoherent scatter radar obs. 77−82083
Dynasonde virtual height meas. methods, comparisons, accuracy and interpretation 80−94643
E_s-layer, behaviour in EM field during oblique irradiation by radio waves 78−73566
E_s-layer, critical freq. integral distrib. patterns 77−60524
E_s-layer, h-type, at Uppsala, features 78−81497
E_s-layer, Langmuir wave propag. and enhanced plasma line 79−29928
E_s-layer, meteors propag. 77−25837
E_s-layer, oblique incidence propag. and ionospheric attenuation 78−73578
E_s-layer, props. at Sodankyla, Finland 77−87183
E_s-layer, reflection coefficient at high latitude 80−61922
E_s-layer, relationship of class 1 E_m to meteors 77−29572
E_s-layer, temperate zone, maps of $f_0E_s > 7$ MHz 78−73579
E_s-layer in Brazilian geomag. anomaly, fbE_s values rel. to particle ionisation source 77−78558
E_s-layer parameters determ. from refl. coeffs. 79−53626
E-layer critical penetration freq. var. 78−7828
E-region, appl. of group and phase height meas. to electron density profile distortion meas. 80−109299
E-region, critical freq. computation 78−45109
E-region, deviative radio wave absorpt. rel. to effective electron collision frequency 79−58153
E-region, electron densities vars. from radiowave propag. 77−33267
E-region, mag. disturbance effects on daytime critical freq. 77−64527
E-region, radiowave absorpt. correl. with O I green line airglow emission 78−45075
E-region, sounding techniques rel. to drift obs. at low and mid-latits. 77−53303
E-region, unstable polar cap, rocket-borne wave, field and plasma obs. 77−21978
E-region, vertical drift effect on absorpt. and phase height change of refl. 79−101003

ionospheric electromagnetic wave propagation continued
E-region critical frequency changes during 1968 Sept. 22 solar eclipse *(Chinese)* 77−22154
E-region critical penetration freq. prediction methods, accuracy *(Japanese)* 79−40017
E-region drift and anisotropy parameters of small-scale irregularities at Waltair, India 77−13176
E-region irregularities meas. by spaced receiver technique 79−53633
E-region reflections at 2.2 MHz rel. to phase height var. and vertical drift 78−40747
Earth-ionosphere channel excitation by LF sources in inhomogeneous ionosphere *(Russian)* 78−85757
Earth-ionosphere waveguide, geomag. disturbances propag. 77−17157
Earth-ionosphere waveguide, mode conversion coeffs. for VLF propag. below stratified anisotropic ionosphere 77−53143
Earth-ionosphere waveguide, program to compute EM fields in irreg. spheroidal model 80−94638
Earth-ionosphere waveguide, VLF radio signal refl. from day-night transition region 79−96859
Earth-ionosphere waveguide excitation by low-freq. sources in inhomogeneous ionosphere 79−66873
echo signals propag. characts., 10 and 15 MHz 78−69574
EISCAT project, plasma parameter determ. *(French)* 80−82142
electron densities meas. by radio wave scattering, by artificial plasma inhomogeneities *(Russian)* 79−5636
electron density and recomb. coeff. profiles calc. rel. to absorpt. and rocket meas. 78−69559
electron density over Delhi and latitudinal depend., INTASAT Faraday fading obs. 80−109293
electron density profile determ. from rocket-based 40 kHz propag. obs. *(Japanese)* 78−24403
electron density profile from rocketborne meas. of VLF propagation in lower region 77−82082
electron wave, transform. into ion wave in multicomponent plasma during quasilongit. propag. 78−73572
electrons heating in lower ionosphere by horizontal lightning discharges 80−90283
electrostatic plasma wave growth, echoes, noise bands 77−80308
ELF band, sporadic-E affecting nighttime propag. 80−77202
ELF Earth-ionosphere waveguide daytime propag. parameters, 5 to 2000 Hz 79−92637
ELF eigenvalues approx. determ. in Earth-ionosphere waveguide 79−8763
ELF mode theory for Earth-ionosphere cavity 78−45131
ELF normal mode reflection and absorption, nighttime ionosphere effects 79−8754
ELF propag. in nonstratified Earth-ionosphere waveguide, integral eqn. method 80−61959
ELF propagation and midlatit. localized nighttime D-region disturbances 77−21989
ELF propagation in Earth-ionosphere cavity, flat Earth approx. 77−13178
ELF radiation, from New Zealand power system, in Earth-ionosphere waveguide 79−48609
ELF radiation flux during 1971 December 16 magnetic storm 78−69564
ELF radio waves, effect of sporadic-E on nocturnal propag. 78−36392
ELF resonance mode splitting in Earth-ionosphere cavity during high solar activity 78−77416
ELF sferics in polar region during solar proton event, June 1968 Antarctic obs. 80−90291
ELF transmission anomalies and energetic particle precip. 78−93040
ELF waves assoc. with equatorial spread-F, satellite obs. 79−35051
ELF waves in Earth-ionosphere cavity, field eqn. for inhomogeneous ionosphere 80−61950
ELF-LF radiowave reflection from lower ionosphere, mechanism 78−49224
engineering problems from ionospheric effects in VLF to VHF bands 79−16751
equatorial bubbles, echo signatures in topside sounder obs. 79−16737
equatorial counter-electrojet, two-stream instability, HF radar meas. 80−26671
equatorial electrojet, type 1 radar echoes with double-peaked Doppler spectra 80−67458
equatorial ionosphere, dissimilar forms of electron content anomaly in E.Asia and India from Faraday rot. 80−109301
equatorial ionosphere, scintillation obs. rel. to irregularity patch form., motion and decay 80−67456
equatorial ionosphere spread-F echoes in HF and VHF bands, theoretical model 78−85764
equatorial scintillation at 40, 140, 360 and 860 MHz simultaneous obs. 78−57393
equatorial scintillation rel. to irregularities, review 78−36380
equatorial sporadic-E, plasma instabilities and echo layer splitting, multifreq. HF radar obs. 78−36370
equatorial spread F, radar backscatter obs. 77−29566
equatorial spread-F, artificial control technique 78−69602
equatorial spread-F, nonlinear Rayleigh-Taylor instability 79−16748
equatorial spread-F, onset during post-midnight period 80−4166
equatorial spread-F, VHF and UHF backscatter from high freq. drift waves 78−88973
equatorial spread-F, VHF scattering 78−61661
equatorial spread-F irregularities, spatial relationship with plasma bubbles 80−67457
equatorial spread-F irregularities drifting patches, support for ionospheric spatial reson. mechanism 79−21095
equatorial spread-F irregularities from spaced fading records, Thumba, India 79−88543
equatorial spread-F meas. by Altair incoherent scatter radar 80−61927
equipment calibration using standard frequency broadcasts 79−67258
exact time signal transmission using artificial satellites 77−79069
extraordinary wave, plasma disturbance in refl. region 77−29542
f0E, geomag. storms effect at mid-latits. 79−44294
f0E, storm time var. at low latit. station 79−44295
F2 critical frequency, solar influence 79−2423
f_0F2, relationship to O I 6300 Å airglow 78−36354
f_0F_2, correl. with S. hemisphere mid-latit. gravity waves obs. 79−21096
f_0F_2, geomag. activity effects 80−8480
f_0F_2, lunar daily var. correl. with ionosphere total electron content var. 79−21100
f_0F_2, median values obs. over S.Atlantic Ocean 78−81505
f_0F_2, spectral components temporal and spatial distrib. 78−49211

ionospheric electromagnetic wave propagation continued
f_0F_2, vars. rel. to thermospheric storms 77−9583
f_0F_2 and electron content latit. var. in subauroral zone 77−13164
f_0F_2 determ. from satellite obs. of HF noise 77−53292
f_0F_2 diurnal var. at equatorial latitudes and counter electrojet 79−48600
f_0F_2 monthly median values, verification of long-range forecast 77−60513
f_0F_2 variations correl. with stratospheric O_3 content vars. 78−45098
F_2 layer seasonal anomaly rel. to composition changes 77−33252
F_2-layer, analytic description of geometric parameters maps by spherical functions 79−53616
F_2-layer, critical freqs. rel. to nighttime ionisation latit. depend. var. in solar cycle 79−53617
F_2-layer, electron density long-period variation f_0 evidence 80−56667
F_2-layer, hemispherical f_0F_2 differences rel. to neutral atmosphere 78−69603
F_2-layer, mid-latit., internal gravity waves day and night effects on radiowave propag. 79−58150
F_2-layer, night-time, over Arecibo, incoherent scatter obs. rel. to seasonal mean struct. 80−31163
F_2-layer, peak electron densities in main trough region rel. to radiowave propag. 78−28417
F_2-layer, seasonal difference in ionisation and height due to neutrals 80−61951
F_2-layer, temporary vars. in critical freq., rel. to solar activity 77−67008
F_2-layer critical frequency, forenoon bite-out characts. 78−65453
F_2-layer ionisation through a solar cycle, SW radiocommunication appl. 80−41626
F_2-layer noontime critical frequency variation through a solar cycle, SW radio communication appl. 79−21102
F_2-layer vertical sounding, radio signal Doppler spectrum and arrival angle meas. *(Russian)* 78−61651
$f_{min}F$ in mid-latit. nighttime ionosphere, effect of interplanetary mag. field 79−58151
F-lacuna events rel. to state of ionosphere 78−93036
F-lacunae, geographical distrib. and simultaneity of occurrence 80−4193
F-layer, large-scale artificial inhomogeneity spectrum 80−98515
f-min at southern latitudes, correl. with stratospheric temp. 77−9469
F-region, $1F_D$ propag. obs. of travelling ionospheric disturbance *(French)* 78−12043
F-region, absorpt. separation from cosmic radio noise absorpt. 78−85769
F-region, critical freq. rel. to ionosphere global scale electrodynamic coupling of high and low latit. regions 80−77194
F-region, drift instability, generation by action of strong radio wave 77−91344
F-region, electron density disturbances nonlinear saturation, strong radiowave effects 78−28378
F-region, equatorial, irregularity patches obs. rel. to localised origin 78−77404
F-region, equatorial, plasma bubbles and irregularities rel. to VHF radar propag. 77−87156
F-region, equatorial f_0 affected by strong mag. storms 80−77197
F-region, equatorial irregularities and electron density, radar obs. 80−77222
F-region, equatorial spread-F, 3-metre irregularities due to plasma instability 80−41624
F-region, equatorial spread-F irregularities and electron depletion, radar obs. 80−41611
F-region, generalized magnetoionic formulae for radiowave propag. 80−61963
F-region, n_2F_2 annual vars. with latit. and solar activity level 78−69577
F-region, nighttime, incoherent scatt. obs. rel. to neutral atmosphere parameters var. *(Portuguese)* 80−41584
F-region, nighttime equatorial, coexistence of km and m scale irregularities, radar and scintillation obs. 79−2427
F-region, plasma interactions *(Russian)* 78−32277
F-region, radiowaves modulation instability 77−25814
F-region critical frequency small scale fluctuations at Kodaikanal 79−16745
F-region equatorial scintillations model from in situ meas. 77−13180
F-region field-aligned irregularity excitation and thermal parametric instability 78−77419
F-region heating, caused by powerful radiowaves, calc. *(Russian)* 78−32278
F-region HF phase path records, anomalous var. over daytime Waltair 77−70924
F-region irregularities and scintillations in equatorial region, VHF radar maps 78−36382
F-region irregularities from plasma reson. phenomena obs. by rocket-borne relax. sounding expt. 79−8767
F-region scintillation, rel. to aurora 77−87158
F-region temp. meas. by satellite and incoherent scatter radar 78−36394
fading, obs. E- and F-regions 80−101478
fading from spaced receiver obs. at Thumba 80−109296
fading obs. in E-region refl. near equatorial electrojet 80−101473
Faraday effect, meas. at 140 MHz using two-channel polarimeter, first results 80−61912
Faraday fading records, mean field height determ. using Q-T position 80−8482
Faraday rotation and scintillation obs. at Natal, Brazil, ionospheric bubbles detect. 79−88524
Faraday rotation measurements at Ootacamund 79−88533
Faraday tarotion, effects of pulsewidth 78−71540
field aligned radiowave scattering, artificial small scale irregularities, field aligned scattering *(Russian)* 78−32274
field strength near caustic and cusp in isotropic ionosphere 77−21986
field strength variation for WWV, 15 MHz SW cct. at Hiraiso, Japan, rel. to mag. storms 79−53650
fixed frequency sounding, appl. to gravity waves obs. in high latit. F-region 79−25390
fluctuating component of scattered field in far-field zone 80−36456
frequency depend. of ang. wave fluctuations in plane-stratified isotropic medium 79−53627
frequency method of signal averaging 79−53628
Fresnel diffraction patterns for ionospheric irregularity modelling 77−9614
geostationary satellite signals, mid-latit. ionospheric scintillation at 137 MHz 79−25388
geostationary satellite VHF Faraday rotation mea. for ionospheric electron content 78−61599

ionospheric electromagnetic wave propagation continued
geostationary satellites signals, severe scintillation of VHF and GHz waves during mag. storm 80−109302
global radiowave absorpt., temporal and spatial variation by empirical formula 80−77204
ground diffraction pattern parameters assoc. with D-region partial reflections 77−60534
group delay meas. at Ootacamund, total electron content determ. 79−101006
group delay var. at oblique incidence rel. to TIDs 78−45132
guiding properties of a smoothly inhomogeneous layer and diffraction excitation of ionospheric waveguides 80−36449
gyrowave interaction expt., diurnal var. of impressed modulation 79−5706
H_E scatter signals power calc. 77−60520
heating by radiowaves, theory of striation form. 80−41625
heating due to parametrically excited Langmuir waves, short-scale field-aligned density striations form. 79−8766
heating experiment, coherent parametric instabilities excited by two or more pump waves 78−57381
heating experiments, effects of HF-induced plasma instabilities on electron temps. 78−40756
HF, in horizontally inhomogeneous ionosphere, anal. *(Russian)* 77−5391
HF, seasonal and daily vars. of multiple rays 77−21972
HF (14-17 MHz) band echo signals, between Khabarovsk and Irkutsk *(Russian)* 78−32281
HF absorption at low latits., solar particle effects 78−69594
HF and MF bands, Doppler meas. accuracy 78−77417
HF and MF signals refl. from spread-F, fading anal. 79−101005
HF and VHF refl. from E_s-layer on 1050 km path, M factor determ. 77−17281
HF and VHF signals amplitude fluctuations due to scatt. and E_s-layer refl. 78−45105
HF backscatter curtains rel. to plasmapause location 79−58165
HF communication at low latitudes, problems and solns. 77−70921
HF Doppler method studies of high-latitude ionospheric dynamics 78−73569
HF Doppler obs., realtime display system 77−73887
HF Doppler obs. over S.E. Australia during 1976 Oct. 23 total eclipse 78−61662
HF Doppler observations associated with spread-F 79−70918
HF Doppler observations at Chubu Inst. Tech. (Japan) *(Japanese)* 80−31165
HF Doppler sounder array obs. of travelling ionospheric disturbance 79−48619
HF excited plasma instabilities 78−45130
HF fading ionospheric reflection channel, delay and Doppler power spectra 79−8765
HF group path vars., modulation envelope meas. 80−51597
HF heating of ionosphere, enhancing of plasma line 80−82140
HF high power radio wave, effect on vertical distrib. of inhomogeneities, meas. *(Russian)* 77−78555
HF induced plasma waves, time vars. 78−45119
HF long-range propag. in ionospheric ducts 77−78569
HF max. usable freq. prediction algorithm, MINIMUF-3 79−25372
HF mode predictions using simple method with approximation 79−16754
HF multiray propag. during equinoctial periods 77−49220
HF oblique direct and oblique-backscatter sounding on multihop paths, signal intensities 78−45113
HF oblique radar obs. of plasma instabilities in equatorial electrojet over Africa 78−49205
HF oscillating echoes from polar E-region 78−57390
HF peculiar lunar echoes, guided wave propag. in ionosphere and magnetosphere 78−93032
HF phase path records of short period oscills. in F-region rel. to cyclonic weather 78−16234
HF phased array radar for ionospheric and diagnostic appls. 79−5639
HF propag., freq. standard utilisation 78−93027
HF propag. in ionosphere in minimum sunspot cycle, records 79−25397
HF pulse, reflection by a randomly dispersive and absorbing ionosphere 79−84568
HF pulsed signals, oblique propagation, dispersion coeffs. calc. 77−13181
HF radar obs. of horizontal plasma waves, in equatorial ionosphere 79−29930
HF radio communication, recurrent storms causes, effects and occurrence probability 78−4028
HF radio signals, artificial disturbances effects, expt. *(Russian)* 77−56789
HF radio wave absorption at mid-latits., temporal vars. 77−53305
HF radio waves, power losses and Doppler shifts rel. to bottomside mid-latit. trough 80−109300
HF radioemission during ARAKS expt., ground-based obs. 79−21078
HF radiowave absorption variation in ionosphere *(Spanish)* 79−16735
HF radiowave forecasting scattering by induced ionospheric irregularities, expt. *(Russian)* 77−29553
HF radiowave propag. at oblique incidence, anal. 78−93045
HF radiowave propagation, calculation of max. usable freq. in presence of steep electron density distrib. gradients *(French)* 79−58177
HF radiowave propagation at high latitudes, geomagnetic activity influence *(Russian)* 77−29551
HF radiowaves, 6300 Å airglow enhancement *(Portuguese)* 80−41592
HF radiowaves, plasma heating, electron oscills. *(Portuguese)* 78−83557
HF range, noise intensity distrib., empirical laws approx. 77−9603
HF reflected waves, freq. var. *(Chinese)* 80−56665
HF reflection and transmission coeffs. for horiz. polarised waves, sporadic-E layer 78−32290
HF signal envelopes, spatial correlation coeff. 79−62663
HF signal fluctuation spectra in auroral zone, geophys. conditions effects 77−25821
HF signal fluctuations energy spectra in auroral zone 77−17284
HF signal reflection obliquely from ionosphere, trajectories 77−21996
HF signal strength, triangular enhancements rel. to TIDs 78−16236
HF signal trajectory parameters for single-hop path in auroral zone 77−25823
HF signals, allowance for fadings in computation of single-hop paths 77−91352
ionospheric electromagnetic wave propagation continued
HF signals, arrival angles meas. on paths between Moscow and Indian and Atlantic Oceans 77−91351
HF signals, freq. shift during solar eclipse (1976, April 29) 78−45111
HF signals and oblique sounding charcts. 79−62658
HF signals statistical charcts. during auroral substorms 78−69583
HF signals statistical charcts. on auroral radio paths during equinox 77−60526
HF signals transmitted along high-latitude path 80−41609
HF sky wave radar remote sensing of sea state, minimisation of ionospheric disturbance 80−21857
HF sky-wave field strengths, developments in prediction techniques 79−58132
HF sky-wave received signal level determination for communication link 78−85758
HF transionospheric long range propag. from satellite, obs. at Florence 78−36396
HF wave at Arecibo, induced plasma line shifts 79−101012
HF waves nonlinear interactions 77−13175
HF-enhanced plasma-line height above Arecibo 78−28392
HF-induced parametric decay in presence of field-aligned irregularities 80−41613
HF-induced plasma line rel. to field-aligned ionisation irregularities 78−88979
HF/VHF absorption in disturbed D-region, meas. 77−53286
high latitude absorption, riometer meas. 80−8488
high latitude topside sounding, Bernstein modes propag. trajectories *(Russian)* 77−33258
holographic interpretation of reflected radiowave data 80−77155
hydromagnetic wave rotation between magnetosphere and ground 80−61969
incoherent radiowave scattering, nonlinear effects 78−40729
incoherent scatter data, analytic partial derivatives for least-squares fitting 78−73581
incoherent scatter measurement complex, Kharkov Poly. Inst. 77−9555
incoherent scatter radar, correlation function meas. 77−73888
incoherent scatter radar, for correl. meas. of electron and ion temps. 77−25820
incoherent scatter radar spectrum, plasma line intensity as aeronomical diagnostic 78−32271
incoherent scattering, physical processes *(Portuguese)* 79−2417
incoherent scattering, total cross section 80−72690
incoherent scattering of radio waves by whistler mode oscills. 78−45135
inhomogeneous isotropic ionosphere, propag. parameters of VLF radio waves during sunrise period 80−31166
Intelsat transmissions, determ. of electron content and slab thickness near equatorial anomaly 79−84574
International Reference Ionosphere, descriptive empirical model, intentions and build-up 79−58173
intersatellite wave propagation expts. at medium freqs., general results 78−69604
intersatellite wave propagation expts. at medium freqs., whistler-mode pulses 78−69605
ion cyclotron whistlers, topside ionosphere, complex ray tracing study 78−96346
ion-cyclotron noise excitation in topside, Intercosmos 14 obs. 79−8755
ionization irregularities drift meas. from first and second order refl. 79−53642
ionization var. caused by powerful radiowaves *(Russian)* 78−32273
ionograms, multi-parameter, from universal digital ionosonde 78−73577
ionograms, vertical incidence, simulation by ray tracing with replacement layer and ionospheric trough 77−78559
ionosonde, high resolution, equipment and preliminary results 77−9542
ionosonde observations of northern magnetospheric cleft 77−29595
ionosonde resolution, improvement via pulse synthesis technique 78−28411
ionospheric radio lenses, satellite to ground signal fading, investigation 78−7833
joint Gaussian statistics 78−42265
L-band signals coded by phase reversal, signal degradation 80−41632
layered plasma, use of Fuchsian differential eqns. 80−75060
LF, relation between seasonal absorpt. course and winds in stratomesosphere 79−62645
LF absorption at midlatits., interplanetary mag. field sector struct. effects 77−29546
LF absorption events during meteor showers, rel. to meteoric constituents ionization 78−40736
LF and MF very strong radiowaves cross-modulation 77−17285
LF atmospheric data anal. with PDP computer 77−82014
LF band, noise field and skywave propag. 79−5708
LF broadcasting, sky-wave propag. in daytime 78−61648
LF field strength meas. on single-hop path 77−29547
LF propag. in Earth-ionosphere waveguide, model *(Russian)* 77−41257
LF propagation, contrib. of low level meteors to ionization, obs. system 79−84514
LF propagation, refl. coefficient determ. via modulation method 78−45114
LF radiation generation by HF transmitter, nonlinear currents height meas. *(Russian)* 77−41256
LF radio propag. at high altitudes 79−16752
LF radio wave absorpt. temp., seasonal variation 79−48602
LF radio waves, signal vars. over sunspot cycle 77−78560
LF radiowave absorpt., variation during solar cycle 80−77193
LF radiowave absorpt. events rel. to meteoric ionization 79−48608
LF signals attenuation due to meteor trains 78−40726
LF signals knife-edge type field strength depression during mag. storms 78−40740
LF signals nocturnal amplitude correl. with neutron monitor count 78−40741
LF signals transmission, electrons effective collision freq. determ. 78−40683
LF sky wave, atm. refr. effects *(Chinese)* 80−4165
LF strong signal demodulation in subauroral ionosphere, geomag. oscill. freq. range *(Russian)* 77−41267
LF waves, acoustic waves generation 78−69581
LF waves, electrostatic wave generation near lower hybrid reson. 77−29557
LF/MF radio transmissions, non-linear demodulation in auroral ionosphere rel. to ELF signals generation 80−94639
LF/VLF propag. below nonuniform isotropic ionosphere 79−44224
LF/VLF radiowave propag. charcts. anal. 78−93049

ionospheric electromagnetic wave propagation continued
lightning location and ionospheric refl. heights from two-station mag. field meas. 79−70845
linear interaction of EM waves in inhomogeneous magnetoactive plasma 79−94802
linear wave transformation in ionosphere and ion whistler formation *(Russian)* 78−65449
local absorption in dense plasma, geometrical optics approx. 77−5396
long-delay echoes, 28 MHz amateur band obs. 80−90277
longitudinal mode coupling, analysis using dielectric tensor 78−16242
longitudinal wave trajectories in inhomogeneous magnetoactive plasma near Langmuir freq. *(Russian)* 77−64517
Loran-C 100 kHz signals, possible effect of atmospheric gravity waves 80−109304
Loran-C in polar regions, amplitude and time-delay computations, full wave analysis 78−7834
lossy channel, band limited impulse response 79−84569
low latitude whistlers, lower and upper freq. cut-off explanation 80−82131
low-frequency emission pulsations in topside ionosphere, spectra rel. to surface geomag. SPP spectra 79−58157
low-latitude VLF emissions, prod. by incoherent Cerenkov process and raypaths 79−75036
low-latitude whistlers charact. observed at Okinawa, Japan 78−73576
lower daytime ionosphere, model for VLF field forecasting 77−49216
lower hybrid drift instability 80−46343
lower ionosphere, 164 kHz propag. rel. to ionisation, correl. with interplanetary mag. field sector struct. 80−4167
lower ionosphere, electron density profile from radiowave data 80−67462
lower ionosphere, IRI model compared to radiowave propagation data 80−61948
lunar tides in equatorial ionospheric absorption 79−44286
magnetic field effects 78−96332
magneto-active plasma, group-vel. direction 80−59201
magnetoactive collisional plasma, dielectric tensor, refl. index and attenuation 80−59202
magnetoactive collisional plasma, nonlinear energy repump *(Russian)* 78−34319
magnetoplasma, refr. index profiles in layered media, extraordinary mode 80−77223
maximum usable frequency for distant radio lines, comparison of calc. methods *(Russian)* 78−32282
maximum usable frequency predictions, real-time updating 79−58179
medium wave broadcasting, interference fading *(Russian)* 79−40018
meteor burst data communication system 78−69608
meteor trail diffusion, radio refl. determination 80−46329
meteor trail radar refl., maximum ionization height detect. method 80−8487
MF, combined terrestrial diffraction/ionospheric reflection effects 78−28410
MF absorption nocturnal var. and nighttime E-region 77−29563
MF broadcasting waves, long-distance propag. characts., round-Pacific mobile expt. *(Japanese)* 77−21997
MF closely-spaced receiver technique for horizontal drift meas. 78−40743
MF obs. of E-region drift meas. over Udaipur 78−16233
MF pulsed transmissions, method for separating D- and E-region contribs. to toal absorpt. 78−69593
MF skywave attenuation, polarisation coupling loss and sea gain effects 79−5709
MF wave propagation expts. between two ionospheric satellites, Z-mode pulses 79−53646
MF waves, cross-modulation phenomenon 77−13167
MF waves generated by 8-40 keV electron beam 78−40750
MF waves over strong aurora, rocket obs. 78−45082
micropulsations, obs. at ground, ionosphere control 80−77207
microwave propagation under multipath conditions, expt. investigation *(Russian)* 77−5392
microwave radiation from solar power satellite, theoretical anal. of nonlinear interaction with ionosphere *(Japanese)* 80−94634
mid-latitude scintillations, rel. to plasma instabilities assoc. with subtrough density gradients 78−40753
mid-latitude trough, scintillation of extraterrestrial radio noise sources signals 78−73574
Mitra-type fading near travelling ionospheric disturbances, cross spectral anal. 80−82128
mixed mode echo of vertical-incidence ionogram, mixed-path mechanism 80−61942
mixed-mode echo obs. during vertical sounding 80−61943
modelling of ionosphere, for use in administration of HF radio transmission networks *(French)* 79−58175
modification studies, complementary cross modulation technique 77−2275
molecular rotation amplification of intersecting radiowave modulation *(Russian)* 77−41255
multicomponent HF skywave arrival elevation angle meas. 78−24408
multiple pump ionospheric heating expt. plasma instabilities obs. 78−57382
MW broadcast field strength meas., sunset, night 77−67010
natural noise, Interkosmos-Copernicus 500 satellite obs. 77−53503
natural radio noise, Bernstein mode, excited by solar electron streams 79−62646
negative ions effect 80−4164
nighttime equatorial F-region, radiowave scintillation 80−26681
nonlinear VHF/UHF wave mixing, sounding, theory 80−36445
oblique sounding signals Doppler freq. shift in disturbed region 79−53630
oblique-backscatter sounding signal fluctuations and accumulation method of reception 77−60521
OMEGA, navigational transmission, polar region ionospheric disturbance 78−7835
one-dimensional inverse scattering problem, review 80−46346
operational physical models 79−58172
ordinary EM waves scatt. by electrostatic ion cyclotron waves 79−70916
parametric decay of non-ducted whistler-mode signal 80−6239
parametric instabilities and modification 79−101019
pararesonance (PR) whistlers, features 80−67455
partial reflection sounder, limited height resolution effect in differential phase meas. 77−21991
partially coherent radiation by charged particle beams in ionosphere 78−28407
ionospheric electromagnetic wave propagation continued
partially reflected radio signals *(Russian)* 79−48603
Pederson ray effect on direction finding accuracy 77−91355
perturbation of collisional plasma by opposing EM wave, anal. *(Russian)* 77−9605
perturbations in auroral zone, SW radio noise level variation obs. *(Russian)* 77−91359
phase scintillation of 40 MHz signals rel. to ionization irregularities in equatorial ionosphere 79−44303
physical model and profile reconstruction, for inhomogeneous ionised regions 80−1109
planetary waves at 20-80 km altitude rel. to ionospheric absorpt. winter anomaly 80−36359
plasma line, low-altitude anisotropy theory 78−77414
plasma line, meas. at Chatanika with high-speed correlator and filter bank 80−98507
plasma shortwave drift-dissipative instability, caused by powerful EM wave *(Russian)* 77−47179
plasmapause, displacements meas. via radiowave phase shifts 77−22034
plasmapause, sounder design using ray tracing studies from geostationary satellite 80−4191
plasmapause, VLF ground based obs. 77−25851
plasmasphere, radio beacon propag. and obs. technique 77−45229
polar cap absorption, recording using ULF meas. 79−53620
polar cap absorption event, August 1972, optical aurora diagnostics 77−29567
polar cap absorption intensity and solar cosmic rays north-south asymm., riometer data 78−69629
polar cap riometer absorpt. and solar protons, night and day relationships 78−28413
polar electrojet, modulation by powerful HF waves 77−70929
polar slant-E condition, rel. to polar cap plasma flow entry region longit. position 80−67472
powerful radiowaves, excitation of sound waves, heating effect investigation *(Russian)* 77−78554
probing at dm wavelengths, aspect depend. characts. 79−88547
PROPHET, real-time propagation assessment system, operational environmental models 79−58170
pulsation excitation by 4.61 MHz transmitter action on ionosphere *(Russian)* 78−4026
pulse, mean arrival time and mean pulse width, dispersive and random medium 77−82080
pulse time dispersion, Earth's mag. field effects 78−45116
pulse-long distance propagation measurements in HF region, results *(German)* 80−41637
quadrature components of narrowband signal, statistical props. 79−75038
quasiperiodic scintillations, morphological and ionospheric aspects 77−91361
radar aurora, per-unit-vol. RF scatt. cross section calc. 78−45079
radar echoes from E-region, height shift around morning and evening electrojet reversals 79−66871
radar measurement, incoherent scatter, systematic error due to noise contamination 78−49225
radiation fields and losses below upper hybrid freq. *(Russian)* 78−4024
radio and optical, conf., Oslo, Norway (May 1978) 78−93044
radio aurora, 398 MHz echoes, depend. on electron density and elec. field 79−66854
radio aurora (diffuse), rel. to field-aligned currents and particle precipitation 80−105119
radio aurora dynamics as seen by Doppler radar 79−62639
radio beacon expt., ATS-6, results 78−69592
radio beacon expt., ATS-6, temporal amplitude and phase spectra 77−45251
radio beacon signals, ATS-6, plasmaspheric electron content and scintillations *(French)* 79−58184
radio beacon signals from ATS-6 satellite, ground refl. effects on polarization 78−40612
radio beacon signals of amplitude scintillations 77−29578
radio communication and ranging pulses, dispersion and scattering effects 80−26667
radio drift meas. simulation and analysis by correlation methods 78−45033
radio lens in ionosphere, UHF and VHF fading patterns 77−53299
radio noise from discrete sources, travelling disturbances effects 77−91353
radio noise propagation through sporadic-E layer in equatorial region 79−84575
radio noise vars. at Ping-Cheng, Taiwan 77−45246
radio propag., weak large-scale inhomogeneities effect of auroral ionosphere 79−101017
radio pulse dispersion and virtual height determ. 80−61954
radio pulse reflection from ionospheric model, distortion, compression, approximate theoretical solution 77−21969
radio pulses, nonlinear phase distortion of partially refl. signal 78−69573
radio signal transmission, long-delay echoes generation, models 80−26670
radio signals, meteor trail ionization effects on propag. 79−101001
radio signals Faraday rot. obs. for total electron content determ. 77−33249
radio source scintillation from artificial ionosphere inhomogeneities at 25, 240 and 290 MHz 80−36454
radio time signals, Tokyo reception accuracy 78−69606
radio transmission in Earth-ionosphere waveguide, concise theory 79−48616
radio wave absorption, riometer meas. 78−85763
radio wave echo from ionospheric sublayers in lower thermosphere 80−61956
radio wave propag. model, teaching 79−97159
radio wave scattering from artificial plasma inhomogeneities, ionospheric electron density meas. appl. 79−75074
radio wave scintillation caused by equatorial ionospheric bubbles, model computations 80−94641
radio waves, diffr. from discrete and homogeneously structured irregularities 79−48612
radio waves, envelope distrib. functions and phase of periodically nonstationary process 80−4173
radio waves, forecast chart for periods of high solar activity, amateur radio appl. 80−26664
radio waves, limited beam diffusion due to scatt. on random ionospheric inhomogeneities 77−91349

ionospheric electromagnetic wave propagation continued
radio waves, nonlinear effects during partial refls. 77−60516
radio waves, nonlinear thermal focusing in lower ionosphere 77−60511
radio waves, phase path changes due to gravity waves 79−35043
radio waves, time struct. of transionospheric signals scintillation 80−90281
radio waves absorption in equatorial ionosphere, seasonal var. 78−85762
radio waves anomalous absorpt. during sudden ionospheric distrubances rel. to solar X-ray radiation intensity 79−96857
radio waves interaction in plasma, nonstationary processes *(Russian)* 78−93028
radio waves reflection from E-region arrival direction meas. system 79−25387
radio waves scattered by meteor trails, trapping by ionospheric ducts 80−4172
radio waves self action in ionospheric plasma, nonstationary theory *(Russian)* 79−48604
radio waves transionospheric propag., appl. to total electron content comparative study 80−98516
radio waves winter absorption, correl. with Na nightglow 77−33239
radio window theory, transmission coeff. 80−61953
radio-aurora, rocket borne radar study of ion-acoustic waves 79−100995
radio-wave propag., nonlinear effects 77−60544
radiowave, derivation of WKB soln. for coupled eqns. 77−13177
radiowave, extraordinary, parametric generation of plasma waves 77−13153
radiowave, implications of ionospheric chemistry 77−17267
radiowave, magnetoionic components lateral deviations during vertical sounding 79−8747
radiowave, parametric excitation of plasma and ion-acoustic waves 77−17283
radiowave, strong obliquely incident, ionospheric irregular struct. 79−62648
radiowave absorpt. in ionospheric cosmic ray layer 77−22024
radiowave absorption, coherence with 30 mb temp., five-day wave 77−33275
radiowave absorption, effects of solar X-ray and Lyman α radiation 78−40737
radiowave absorption, Gauhati, India 77−41261
radiowave absorption, general formulae 79−58166
radiowave absorption, meas. at Waltair, India, D- and E-region models 77−13173
radiowave absorption, multiple-freq. meas. rel. to vars. of effective electron collision freq. 77−91347
radiowave absorption, peak amplitude recording system 78−3979
radiowave absorption, seasonal pattern of freq. depend. 77−49221
radiowave absorption and Pc 1 pulsations following enhanced geomag. activity 77−53332
radiowave absorption azimuthal patterns for circumterrestrial signals 77−49222
radiowave absorption freq. var. in model D- and E-regions 77−13169
radiowave absorption in D-region, winter anomaly 79−58176
radiowave absorption mag. equator, obs. using A_2-technique 79−21099
radiowave absorption meas., differences between sporadic-E and normal E-layer refls. 78−40734
radiowave absorption measurements, anal. rel. to shortcomings in understanding of lower ionosphere 78−81492
radiowave absorption near 100 km height, travelling (wave) disturbances 79−25392
radiowave absorption rel. to solar activity 78−69591
radiowave absorption vars. at 2.5 MHz at Ahmedabad, India 77−13165
radiowave attenuation meas. by oblique pulsed sounding method 78−28380
radiowave causing ionospheric heating, geomag. pulsations artificial generation 77−29541
radiowave fluctuations during multiple refl. 78−45104
radiowave incoherent scattering by plasma, Nyquist theorem appl. 79−75024
radiowave influence on nonhomogeneity appearance connected with current instability *(Russian)* 78−49200
radiowave penetration of quasi-parabolic layer, path integrals calc. 78−49208
radiowave phase and amplitude meas. interpretation *(Russian)* 78−77394
radiowave polarisation fading records, spectra interpretation 77−60527
radiowave propag., prediction and extrapolation of ionospheric effects 79−58168
radiowave propag., user requirements of aerospace propag. environment modelling and forecasting 79−58169
radiowave propag. errors during geomag. storms 80−4077
radiowave propag. studies by International Radio Consultative Committee 78−77311
radiowave propagation, disturbance effects and their predictability 79−58171
radiowave propagation, foreshortened scatt. by auroral inhomogeneities *(Russian)* 77−64519
radiowave propagation, prediction techniques for ionospheric structure 79−58178
radiowave propagation, ray trajectory props. in irregular ionospheric waveguide 80−90284
radiowave propagation, satellite expt. using Doppler effect in presence of wave perturbs., modelling 79−8744
radiowave propagation above 30 MHz, role of sporadic-E layer and troposphere 80−41636
radiowave propagation conditions at decimetre wavelength 78−45136
radiowave propagation in E-region, quasi-periodic artificial inhomogeneities formation *(Russian)* 79−21093
radiowave reflection, large-scale screen speed determ. 77−9602
radiowave reflection from ionosphere, multimode signal operation, propag. direction fluctuations 77−53309
radiowave scatter communications, review 79−34935
radiowave scattering amplitude distrib. and focusing effect of large-scale inhomogeneities 77−91354
radiowave scattering by superexcited atoms, quantum model 80−32677
radiowave scattering on artificial inhomogeneities, trapped energy escape from interlayer duct 77−9601
radiowave scattering signals, incoherent, computerised spectral analysis *(Russian)* 79−5621
radiowave scintillation, calc. by thin phase screen approx. 77−53298
radiowave scintillation by ionosphere, statistical study 80−109306
ionospheric electromagnetic wave propagation continued
radiowave scintillation enhancements rel. to sheet-like auroral ionospheric irregularites 79−35033
radiowave scintillation produced in F-layer, signal-statistical and morphological model 79−58185
radiowave scintillation studies using ATS-6 radio beacons at Delhi 78−69600
radiowave self-focusing instability in oblique ionosonde meas. 80−105101
radiowave studies of ionosphere, incoherent scatter technique development, review 78−81503
radiowave trajectories in horizontally inhomogeneous ionosphere 78−73571
radiowaves, asymptotic distrib. law of scatt. field amplitude and phase 77−29548
radiowaves, ATS-6 signals diffr. by isolated irregularities 79−35049
radiowaves, ATS-6 signals equatorial scintillations, freq. depend. 79−35050
radiowaves, effects on communication systems 78−92954
radiowaves, Faraday fading of 40 MHz signals, ionospheric irregularities characts. 77−13166
radiowaves, focusing at boundary of zone of silence 77−13158
radiowaves, group refr. index for propag. over Rio de Janeiro 77−13171
radiowaves, ionospheric irregularities and associated VHF/UHF scintillations 80−46345
radiowaves, irregularities effects on group path 77−53291
radiowaves, long-distance propag. and relationship with processes in Earth's crust 80−26682
radiowaves, medium and short, seasonal absorpt. courses, rel. to stratomesosphere dynamics 79−58149
radiowaves, multiple scattering, iterative treatment method 79−8709
radiowaves, pulse delay and distortion by random scattering 79−29934
radiowaves, quasioptical approx. isotropic absorbing medium 77−75377
radiowaves, spatial dependencies of props. of wavelike inhomogeneities, anal. of diffraction patterns 80−36448
radiowaves, theoretical soln. of Helmholtz eqn. in statistically inhomogeneous medium 79−92638
radiowaves, trans-ionospheric, scattering due to equatorial F-region irregularities 79−29933
radiowaves anomalous absorpt. during disturbance due to strong radio emission 79−53624
radiowaves causing ionospheric modification, mag. field effects on electrons 77−60531
radiowaves from Cassiopeia A by artificial ionospheric irregularities *(Russian)* 77−29552
radiowaves hysteresis effect on artificial excitation of inhomogeneities 80−36450
radiowaves oblique incidence, self-focusing instability 77−49218
radiowaves partial refl. expt., quasi-longit. approx. to generalized magnetoionic formula 77−13170
radiowaves refl. or scatt. by ionosphere, automatic processing device 77−49179
radiowaves through chemically modified ionosphere, use as lens for refracting radiotelescope 77−45312
rain attenuation distribution estimation method *(Japanese)* 79−100891
rain attenuation estimation formulae, worst-month, worst-year, satellite communications in Japan appl. *(Japanese)* 79−100890
randomly inhomogeneous collisionless magnetoactive plasma, anomalous EM absorption *(Russian)* 77−27683
ray path eqns., multisegment quasi-parabolic ionosphere 80−41633
ray statistics, in medium with ellipsoidal inhomogeneities and regular refr. 78−25773
ray statistics in plane stratified isotropic medium with isomeric inhomogeneities *(Russian)* 78−53773
ray tracing study, ionospheric irregularities effects on HF and VHF radio waves 77−91362
ray trajectories in ionospheric waveguide, influence of inhomogeneities 80−61966
ray-tracing calc., computer-aided, through Bradley/Dudeney ionospheric model 78−7826
reflected monochromatic wave for parabolic layer, phase and dispersion signal blurring *(Russian)* 77−17293
reflected signal, sum phase random props. investigation 79−53615
reflected signals statistical characts., effect of travelling disturbances 78−45092
reflection, evidence for reflecting layer below classical D-region 80−98508
reflection, meas. of fluctuations in angle of arrival and amplitude of reflected signals 80−17439
reflection and transmission coeffs. determ., low freq., using 4×4 matrices 78−53769
reflection drift data, internal consistency analyses 79−53539
reflection height estimation from Doppler measurements 77−21979
reflection of 10-10^3 Hz and 15-80 kHz waves normally incident on inhomogeneous anisotropic ionosphere 78−28375
refractive index determ. using GEOS-3/ATS-6 satellite-to-satellite tracking data 78−93039
refractive influence on geodetic measurements using artificial satellites *(French)* 79−58133
regular absorption, latit. differences in daily vars. and annual pattern in N.hemisphere 78−45091
research projects at IROE Institute (Firenze) *(Italian)* 80−56668
resonant EM oscillations in polar region, for modification expts. 80−56676
RF frequency standard transmission, phase instability due to effect of ionosphere 78−41279
round-the-world echo signals, height factor estimate from expt. results 77−13159
round-the-world signal group delay, frequency dependence calc. *(Russian)* 78−61654
SARSAT, search and rescue satellite, ionospheric effects on Doppler frequency 79−58183
satellite links, ionospheric wave disturbances effect on polarisation fading freq., simulation 78−69572
satellite loss angle transmission effects, VHF and UHF 78−7747
satellite navigation systems, ionospheric and plasmaspheric effects 77−82100
satellite radio beacon signals, ionospheric struct. determ. 78−12050
satellite radio signals amplitude scintillations rel. to spread-F and sporadic-E over Brisbane 78−49209
satellite-referenced propagation correction for USAF SPACETRACK radar systems 79−58131

ionospheric electromagnetic wave propagation continued
satellite-to-satellite tracking, range-rate effects 79−58174
scattering, appl. to ionospheric props. meas. at Arecibo Observatory 78−81488
scattering by E-region anisotropic inhomogeneities oriented along geomag. field 78−53771
scattering in linear layers with ellipsoidal inhomogeneities 79−62662
scattering in whispering gallery type mode 80−98514
scintillation, calcs. based on in situ irregularity spectra 78−28415
scintillation, critical propag. freq. up to 1 GHz 78−7827
scintillation, effect of VHF/UHF satellite communications 77−41264
scintillation, effects on received signal level 78−93047
scintillation, model review 77−21995
scintillation, multifreq. data from ATS-6 radio beacon expt. 77−45250
scintillation, power law phase screen model, strong scatt. 80−61962
scintillation, power law phase screen model, weak scatt. 80−61961
scintillation, thin screen theory for spherical wave 78−13645
scintillation in equatorial region, 100 MHz to 10 GHz, theory 80−61946
scintillation irregularities at VHF, instrumentation for investigation using satellite radio beacon 80−56639
scintillation meas. at 1.5 and 4 GHz 77−29581
scintillation meas. at 1.7 GHz at midlatitude 79−2434
scintillation observations in southern mid-latits., horizontal struct. 79−12339
scintillation of solar bursts at 30 and 60 MHz, STEREO-5 obs. 78−61822
scintillation probability distrib. function 80−41598
scintillation theory, mini-review 77−5393
scintillations, assoc. with features of equatorial ionosphere 80−77191
scintillations, night-time, at mag. equator, obs. 79−44292
scintillations at 4 and 6 GHz using INTELSAT programs 79−5715
scintillations at GHz freqs. power spectra model comp. 77−45233
scintillations induced by cloud of sporadic-E layer 77−37477
scintillations obs., at Lunping Observatory, geomagnetic activity influence 79−88545
scintillations of ISIS-1 VHF beacon signals 79−8752
sea echo radar spectra resolution limitation inferred from ionospheric Doppler broadening 78−81489
seasonal variation of radiowave absorpt. over Europe 80−31161
self-focusing of HF EM waves, striations 78−96347
SHF differential phase shift method for total electron content meas. 78−36304
SHF scintillations, refr. scatt. explanation 79−48615
short radiowaves, horizontally inhomogeneous, adiabatic mode constriction *(Russian)* 77−78553
short radiowaves, refl. freqs. during vertical and oblique sounding 78−45099
short radiowaves ducted propag., large-scale inhomogeneities effects 79−62657
short wave radio absorpt. in winter, rel. to O airglow 80−77184
short-wave echo azimuthal variation obs. over 2300 km *(Russian)* 78−4027
signal level fluctuations on long-distance radio paths, energy spectra 79−53629
single-hop high-latit. path propag., upper and lower rays signal levels ratio 79−8748
singly scatt. wavefields, angle depend. 77−87174
skywave field strength prediction, North America, new method 77−73904
solar activity implications, historical account and predictions *(Italian)* 78−24496
solar bursts, night-time reception due to anomalous propag. in E-region 77−56790
solar eclipse, 1973, June 30, soundings disturbances rel. to atmospheric waves 77−53302
solar EM radiation and terrestrial effects *(Japanese)* 80−51600
solar energy flux determ. in 770-80 Å region 78−28605
solar radio bursts at 26 MHz, obs. brightness distrib., possible ionospheric effects 80−41806
solar X-rays, intensity in E-region meas. by rocket-borne proportional counters 78−45072
solar-terrestrial environment monitoring and forecasting system, SELDADS, for radiocommunication appls. 79−58097
sounding, Dynasonde software, real-time data acquisition and display 80−36405
sounding using frequency shift method 78−40742
soundings, unresolved spread-F as result of pulse spreading 77−78557
soundings from Alouette and Isis satellites, parametric generation of oscills. 77−60510
space sciences, conf., Trivandrum, India (Jan. 1977) 78−69586
space sciences, conf., Waltair, India (Jan. 1978) 79−101000
spaced fading for D-region drift, obs. interpretation methods 80−41627
spaced fading records, correlation analysis, occurrence of negative V_c^2 79−88540
spaced receiver drift experiments, triangle size effect 79−53635
spaced receiver drift expt., triangle size effect, ground diffr. pattern estimation errors 79−88525
spaced receiver fading records, nature of ionospheric irregularities determ. 79−88532
spatial and temporal variation meas., differential Doppler technique using satellite 79−12311
spatial phase structure meas. of ionospherically reflected waves using HF array 79−84505
sporadic-E, midlatit., obs. using HF Doppler technique 79−66867
sporadic-E (E_3) layer over Japan, sky-wave backscatter obs. 79−44298
sporadic-E at high latitude, occurrence, f_0E_s and $h'E_s$ 80−51595
sporadic-E layer, VHF fading evidence for F-region disturbances 80−101475
sporadic-E layer behaviour in EM field of strong decametric waves 78−69569
sporadic-E layer inhomogeneous structure influence of RF heating *(Russian)* 78−61653
sporadic-E layer radiowave reflection, full-wave anal. 77−87176
sporadic-E modes, directional dispersion between 9 and 14 MHz 78−28412
spread-F, equatorial, seasonal and solar cycle vars. in American zone 80−109298
spread-F, lunar tidal effect 79−80070
spread-F, range and frequency spread occurrence at Kodaikanal 80−72676
spread-F and magnetic activity at Kodaikanal, India 79−88542

ionospheric electromagnetic wave propagation continued
spread-F in equatorial ionosphere, assoc. with radio scintillations 80−77191
spread-F obs. rel. to plasma density profile 78−36383
spread-F occurrence, sunspot cycle vars. rel. to F-region irregularity model 77−41262
spread-F occurrence following geomag. activity, time delay latit. depend. 80−8481
spread-F parameters, related to geomag. disturbance index 80−8471
standard transmissions stability on transionospheric paths 79−84577
stimulated Brillouin scatt. and incoherent backscatter 77−78552
stimulated Brillouin scattering, detect. by Jicamarca radar 78−77412
stimulated Brillouin scattering, theory 77−37478
stimulated resonance line scattering with Eiscat radar 78−57389
strong radio wave, modulation trough of small-scale plasma scatt. intensity 79−58159
strong radio wave with amplitude modulation, upper ionosphere disturbance 79−12330
strong radio waves, effect on form. of mid-latit. E_s-layer 77−60514
strong radio waves, effects of induced and combination scatt. 77−91345
strong radio waves, self-focusing instability near caustic 78−45107
strong VLF waves action on ionosphere, obs. 79−48613
subauroral scintillation enhancement, obs. in Alaska 78−20573
sudden commencement absorpt. events at polar cap edge 77−70935
sudden commencement absorption events at S. pole, rel. to lower cleft boundary 78−77437
sudden cosmic noise absorpt., solar Zenith angle depend. 78−12047
sudden frequency deviations, solar flare UV radiation spectral energy distrib. calc. 78−69771
sudden frequency deviations (SFD), appl. as detectors of solar flares EUV radiation 80−8484
sudden frequency deviations and phase anomalies in F-region due to solar flares *(Italian)* 78−96345
sudden frequency deviations during solar flares, character of depend. on operating freq. 78−28373
sudden ionospheric disturbance, mid-latit., of corpuscular origin 78−28374
sudden ionospheric disturbance, VLF phase shifts and amplitude variations 77−91363
sudden phase anomalies, correl. to solar X-ray bursts 80−98513
super distant trajectories, 10-15 MHz signal transmission, amplitude charcts. *(Russian)* 78−32280
SW night propagation, above Earth-waveguide channels, through polar and subpolar ionosphere *(Russian)* 78−32279
SW propag. over long distances, predictions and observations 79−70919
SW radio transmissions, proportional effect of ionospheric damping, solar activity *(Hungarian)* 80−56675
SW radio waves, polarisation on slant path 78−73573
SW reception effects 80−67451
SW scattering by periodic artificial irregularities *(Russian)* 78−32276
SW transmission and disturbed artificial irregularity spectra *(Russian)* 78−32275
sweepers in HF and VHF bands 78−16231
synchronisation by JJY signal reception via the E-region 78−65910
thermal instability of ionosphere due to power transmitting satellite 77−25826
Thomson scattering in presence of electron heating, effect of negative ions 79−16739
time dispersion of EM pulses 80−94645
time signals transmission times meas., dynamics of seasonal variations obs., in SW and VLW ranges 77−79061
time varying medium, transmission and refl. of EM wave 79−81341
time-varying medium, EM wave reflection anal. 79−25385
TM mode-conversion at terminator for anisotropic ionosphere, param. study *(German)* 80−46333
topside HF noise meas. for F_2 critical freq. determ. 79−8756
topside RF sounder extp. rel. to lab. excitation of electron cyclotron harmonic waves 78−93042
topside temporal variation of intensity measurements, Ionosphere Sounding Satellite appl. *(Japanese)* 79−16750
trajectory characteristics, of rays in inhomogeneous ionosphere, effect of magnetic field *(Russian)* 78−32286
trajectory in Earth-satellite transmission, electron density determ. in ionosphere 80−72679
transequatorial propag. in 144 MHz amateur radio band, forward scattering at rising plasma bubbles 79−35057
transequatorial radiowave propag. in freq. range 28 to 432MHz, amateur bands, obs. and expts. 80−101491
transequatorial radiowave propag. over 21 year period, VHF/UHF signals, theories 80−109311
transhorizon radiocommunication by short-wave ionospheric refraction 79−84567
transionospheric propagation from a satellite, observations on the beyond-the-horizon statistics 77−25825
transionospheric radio signal time delay spatial correlation 78−45117
transionospheric radio signal time delays at widely separated locations 79−58186
transionospheric sounding signals, group delays rel. to electron density profiles determ. 78−28371
TRANSIT, satellite observations, phase fluctuations, and ionospheric irregularities 78−7832
travelling ionospheric disturbance effects on ionograms 77−45232
travelling ionospheric disturbances, in F1 region, phase path technique obs. 80−36436
travelling ionospheric disturbances, Tromsoe-Valensole propag. *(French)* 78−12041
turbulence diagnostics, by EM wave propag. obs. 78−45032
turbulent layer scintillation, phase and frequency spectra, after nuclear explosion 78−24405
tweek atmospherics propag. mechanism 78−49213
UHF and VHF scintillation in equator region, signal from geostationing satellite 80−56674
UHF waves reflected from ionosphere, angle-of-arrival fluctuations 80−109291
ULF noise emission, ion-cyclotron waves 80−101470
ULF signal conversion coeffs. seasonal depend. on ionospheric height in sunrise zone 77−25817
ULF wave, propag. in plasmapause vicinity 80−6238
vertical incidence absorption during winter anomaly, calcs. using electron density profiles 79−21098

ionospheric electromagnetic wave propagation continued
VHF, UHF and SHF equatorial scintillations calc. using disturbed ionosphere model 77−17289
VHF absorpt. winter anomaly over Delhi 77−64522
VHF and L-band scintillation over Huancayo 78−36381
VHF and SHF scintillations and F-region irregularities correl. meas. 77−21977
v.h.f. and u.h.f. ATS-6 radio beacon meas. of total electron content 77−2303
VHF backscattering from E/region irregularities near mag. equator 77−33248
VHF daytime scintillations and electrojet irregularities 78−28406
VHF double-peaked spectra at negative Doppler shifts in the morning sector of radio aurora 79−40014
VHF duty cycle diurnal and seasonal vars. due to meteor forward scatt. 79−88534
VHF Faraday rotation meas. of total electron content at low latitudes 79−16749
VHF forward scattering, role of metallic ions of meteor origin effect, also contrib. as sporadic-E form. 80−67461
VHF ionosphere forward scattering, effect of meteors *(Japanese)* 78−81504
VHF multi-satellite scintillations correl. with spread-F and sporadic-E increase over Brisbane 77−53297
VHF noise field strength at 95 MHz over India, meas. techniques and obs. 80−109294
VHF periodic fadings from satellites during solar eclipse 77−33277
VHF propagation through ionosphere equatorial plasma bubbles, transequatorially 80−41635
VHF radar aurora and strong HF backscatt. comparison 80−61960
VHF radar echoes from equatorial E-region irregularities, sudden disappearance 78−40738
VHF radar partial reflections from equatorial E-region plasma density gradients 77−25828
VHF satellite signals, 40 MHz, ionospheric characts. determ. 79−88529
VHF satellite signals, 40 MHz, scintillations obs. at Kurukshetra 79−88527
VHF scintillation, assoc. with reversal of horiz. elec. field 80−101489
VHF scintillation at high-latitude, analytical formulas 80−77224
VHF scintillation at high-latitude near 70°W 80−77221
VHF scintillation late evening enhancements at low latits. 79−75031
VHF scintillation rel. to peculiar Faraday rotation fluctuations 78−61663
VHF scintillations, equatorial, nature and dynamics of irregularities 79−48601
VHF signal scintillation, from ETS-2 satellite, obs. of Waltair and Calcutta 80−109295
VHF signals, ionospheric radio fluctuation obs. from geostationary satellite 79−21091
VHF signals from satellite radio beacons, ionospheric scintillations 79−53634
VHF SIRIO satellite link telemetry emission, use for ionospheric meas. 78−69553
virtual height-freq. curves, nocturnal, reduction method using ionisation models *(Chinese)* 80−105099
VLBI, correction for effects of troposphere, ionosphere and Earth crustal tide *(Japanese)* 80−21926
VLF, anisotropic 3-layer model *(German)* 78−36358
VLF, at sunrise and sunset, spatial phase-difference vars. *(Russian)* 77−5390
VLF, Hollingworth patterns rel. to electron density profile in lower ionosphere 77−64516
VLF, over Greenland Ice Cap, mode conversion coeff. calc. 79−25398
VLF, sunrise modal interference over west-east paths 77−53296
VLF amplitude-phase vars. and AA-type absorpt. 77−60519
VLF and LF propagation and eigenmode scatt. relations 80−61944
VLF atmospherics anomalies, rel. to rainy days over Calcutta 80−82127
VLF bursts, daily vars. in number, synchronous obs. 77−29549
VLF bursts synchronous obs. in Schumann reson. freq. range 77−17286
VLF cross meridian refraction at 500-600 km height, electron density 80−46339
VLF direction-finding techniques comparison for determ. whistlers exit point at ionosphere 80−26631
VLF emissions triggered by unducted VLF energy from tropical lightning 77−21980
VLF focusing during solar eclipse 80−61965
VLF guide over Atlantic Ocean, obs. of shadow of mesosphere O_3 on D-region 79−58161
VLF hiss propag. characts. obs. at low latit. ground stations 78−69561
VLF long-distance transmission at middle latit., lower ionospheric disturbances obs. 80−8485
VLF nighttime propagation anomalies, comparison at 10.2 and 13.6 kHz 78−28414
VLF non-ducted whistler-mode signals at low latitudes 78−61658
VLF phase deviation, quantitative relationship to 1-8 Å solar X-ray fluxes during flares 77−87170
VLF phase disturbances and energetic electron precip. following 1971 Dec. 16 mag. storm 77−53284
VLF propag., X-ray star effects 79−53649
VLF propag. during sunrise 78−93030
VLF propagation, revealing inhomogeneities in auroral zone 80−105107
VLF propagation, theory of rays and foci in magneto-ionic medium 80−105135
VLF propagation at low lattis., density gradients effect 79−88530
VLF propagation data, appl. to electron density profile parameters estimation 79−53614
VLF propagation in auroral zone, essential height determ. 79−53631
VLF propagation in lower ionosphere, solar flares soft X-ray affects 79−8740
VLF radio waves phase anomalies in midlatitudes, assoc. with geomag. disturbances 80−56671
VLF signal phase and amplitude vars. over transequatorial path, Australia-New Delhi 79−5703
VLF signal phase velocity calc., curvature correction/frequency relationship 77−60543
VLF signal propagation, multi-mode, statistical characts. *(Russian)* 79−5702
VLF signals, differences in diurnal phase and amplitude vars. 78−49212
VLF signals in ionosphere-Earth waveguide, geomag. activity effects *(Russian)* 79−2426

ionospheric electromagnetic wave propagation continued
VLF signals phase fluctuations, ionosphere height random changes calc. *(Russian)* 77−91358
VLF subionospheric propag., whistler-induced anomalies 80−26668
VLF sudden phase anomalies correl. with solar microwave burst energies 78−77418
VLF sudden phase anomalies during 1972 Aug. 2-4 solar flares 78−40739
VLF triggered emissions, beam-plasma instability appl. 79−14564
VLF waves, nonlinear effects on magnetosphere/ionosphere plasma *(Russian)* 78−32287
VLF waves generated by ground transmitter, mag. field intensity world wide mapping 77−78567
VLF waves in Earth-ionosphere waveguide near eigenvalues degeneration points 77−49219
VLF waves observed on ground, props. characts. after emerging from ionosphere ducts 79−8741
VLF waves polar disturbances obs. at Inubo, Japan *(Japanese)* 77−21998
VLF waves propagation, rocket meas. rel. to lower ionosphere electron density 78−49219
VLF waves self-interaction 78−28382
VLF/ELF noise, amplitude-probability distribution model 78−32288
waveform distortion by microwave scatt. 79−50859
waveguide propagation rel. to Pc 1 source regions 77−25881
waveguides, excitation by ground based sources *(Russian)* 78−32283
waveguides, excitation of electromagnetic modes, using Lorentz lemma method *(Russian)* 78−32284
waveguides, excitation problem, using asymptotic method *(Russian)* 78−32285
whistler, occurrence rate variation with geomagnetic latitude 79−40010
whistler banded struct. origin, on refl. from ionosphere 80−101476
whistler detection, multichannel filter and shift register obs. system 78−93031
whistler dispersion, automatic meas. by phase locked loop discriminator *(Japanese)* 77−91312
whistler dispersion, group delay automatic meas., ionosphere and magnetosphere electron density 78−93050
whistler mode, interpretation of 6-component measurements 80−83921
whistler mode signals, initial results from tracking receiver direction finder 78−77429
whistler propag. theory 77−45261
whistler propagation, theory, ray-tracing 78−49216
whistler propagation affected by equatorial anomaly, ground reception study 80−51601
whistler propagation at low latits., review 78−73586
whistler pulse, self-distortion in plasma 79−46456
whistler range in plasma, wave radiation *(Russian)* 78−36400
whistler-mode signals, man-made, spacecraft obs. near electron gyrofrequency 78−28418
whistlers, absence at equatorial Earth surface 80−77216
whistlers, anomalous dispersion, ray propag. in middle latits. 77−33253
whistlers, effect of Earth-ionosphere waveguide propag. on polarisation and arrival angles 79−100924
whistlers, effect of Earth-ionosphere waveguide propagation on polarisation and arrival angles 80−36457
whistlers, low-latit., clouds distrib. in conjugate area rel. to whistler propag. 77−2309
whistlers, measurement of wave normal directions of low latitude types in the ionosphere 78−4023
whistlers, propag. characts. at low latitudes 79−80078
whistlers polarisation and arrival direction meas. at low latit. 77−45240
whistlers with very low dispersion, non-ducted low latit. VLF path model 79−44301
winter absorption, 1975/76, obs. at about 52°N, 9°E 78−45124
winter absorption anomaly, implications of eddy diffusion models for mesosphere and lower thermosphere 80−109198
winter absorption anomaly, influences of NO conc. and H_2O dissoc. 79−58152
winter absorption anomaly at middle latits., morphological features 80−67459
winter absorption anomaly rel. to D-region electron density 77−21990
winter anomaly absorption events and E_s-layer form. due to metallic ion drifts 77−9599
wireless transmission, 1900-1935, early ionospheric research 79−9070
O I, red line luminesc. amplification by radiowave anomalous absorpt. *(Russian)* 79−29925
O_2^-, affecting EM wave propag. 79−8762

ionospheric measuring apparatus
aerial pairs, interferometry technique, directional results, ionogram display, receiver modifications 77−29496
aerials, receiving and transmitting, for vertical soundings *(Polish)* 77−45252
Altair incoherent scatter radar for equatorial spread-F meas. 80−61927
Arecibo Observatory, ionospheric props. meas. without rockets 78−81488
Aryabhata satellite aeronomy expt. 79−84637
Atmospheric Explorer, low perigee aerodynamic heating during orbital flight 77−45290
cross-power spectrum analysers, satellite-borne, appl. to ionospheric plasma wave meas. 80−94621
D-region plasma density measurement, rocket borne expt. 78−45126
Digisonde 128PS, universal digital ionosonde 78−73577
Dynasonde software, real-time data acquisition and display 80−36405
Eiscat radar, appl. to stimulated Brillouin scatt. prod. in ionosphere 77−37478
electric potential of rocket, and electron beam injection expts. *(Russian)* 78−93069
electron accelerator expt. on POLAR-5 sounding rocket, for use within aurora 80−77170
electron energy analyser, experimental data components isolation via Fourier transforms 78−36434
ELF antenna, ferrite rod, for Magion satellite for 0.1 to 16 kHz freq. range *(Czech)* 80−85775
F_2-layer vertical sounding, radio signal Doppler spectrum and arrival angle meas. *(Russian)* 78−61651
geostationary satellite VHF Faraday rotation mea. for ionospheric electron content 78−61599
gridless retarding potential analyser for use in very-low-energy charged particle detection 77−5343
gyrowave interaction experiment, pulsing and timing circuits 77−45191

ionospheric measuring apparatus continued
Hadamard energy spectrometer, appl. to F-region energetic electrons spectra meas. *(Japanese)* 80−94637
HF Doppler obs., realtime display system 77−73887
HF phased array radar for ionospheric and diagnostic appls. 79−5639
high-gain, narrow-band, amplifier using active filters for ionosphere measurement 77−56760
incoherent scatter measurement complex, Kharkov Poly. Inst. 77−9555
ion measuring device, for three-dimens. vel. and mass distrib. 80−41620
ion temperature probes, boarded on space sounding rockets, system designs *(Japanese)* 80−85838
ionic drift, logarithmic instrument for small differential difference meas. in flat traps 80−41558
ionosonde, high resolution, equipment and preliminary results 77−9542
Ionosphere Sounding Satellite, operation planning and data analysis ground support system *(Japanese)* 79−16799
Ionospheric Sounding Satellite, automated control system *(Japanese)* 77−78607
Ionospheric Sounding Satellite, command system *(Japanese)* 77−78609
Ionospheric Sounding Satellite, control centre tracking system *(Japanese)* 77−78608
Ionospheric Sounding Satellite, summary of control centre *(Japanese)* 77−78606
Ionospheric Sounding Satellite, telemetry receiving system *(Japanese)* 77−78610
Ionospheric Sounding Satellite control, data recording and anal. system *(Japanese)* 77−78611
KYOKKO (EXOS-A), ionospheric and auroral research satellite, instrumentation 79−48648
Langmuir double modulation probe, current ratio optimisation 79−48576
Langmuir probe, control system for maintaining prone at plasma potential 78−5943
Langmuir probe, technique for accurate electron temperature 79−2379
LF real-time spectral analyser design and operation *(French)* 78−20538
mass spectrometers, mass discrimination in ion and neutral extraction under spacecraft conditions 80−4230
mass-energy spectrograph, for anal. of space plasmas over energy range 0.1 to 10 keV 77−53401
MF radiowave field strength digital measurement equipment *(Japanese)* 77−82051
particle telescopes, anisotropies meas. by multiple telescope system 77−82103
payload B I, compact D-region expt. package for use on small sounding rockets 78−45190
phase switched correlation polarimeter, new approach to D-region partial refl. expt. 77−87169
planar retarding potential analysers, for plasma meas. during Western European Winteranomaly Campaign 78−45125
plasma gun, rocket-borne, use in controlled ionospheric experiment 78−57424
plasma line filter bank and high-speed correlator appl. to plasma line meas. at Chatanika 80−98507
plasma probe and ionospheric structure studies by space vehicle obs. 79−53540
plasma resonance characteristics of sounding rocket impedance *(Japanese)* 77−17271
plasma resonance probe applications *(Chinese)* 80−90226
Platteville ionospheric modification expt., enhanced O I 6300 Å regions 77−33263
polarimeter, two-channel, for ionospheric Faraday effect meas. at 140 MHz, first results 80−61912
positive ion detection, with rocket-borne mass spectrometer, Monte Carlo flow simulation 80−8459
radar auroragraph, for auroral radar echoes drift meas. 78−65436
radio and optical system for meas. meteoric contrib. to LF propag. 79−84514
radiospectrograph for 25-50 MHz range 79−21077
radiowave absorption measurement, peak amplitude recording system 78−3979
radiowaves refl. or scatt. by ionosphere, automatic processing device 77−49179
recording pulse expander IC 79−70892
riometers, cosmic radio noise absorpt. events due to backscatt. by E-region irregularities 77−25831
rocket expt. high-power electron gun *(Japanese)* 78−61566
SEPAC for ionosphere and magnetosphere studies from Space Shuttle/Spacelab 77−73925
SIRIO VHF telemetry emission, use for ionospheric meas. 78−69553
space probe, automatic setting of range of amplifying path 77−67019
space shuttle-tethered balloon subsatellite, current collection by long wire 77−25859
space shuttle-tethered balloon subsatellite for ionospheric plasma studies and power generation 77−25912
spherical ion trapper, floating pot. effect on ion density meas. 79−44287
triple probe method for meas. plasma parameters in low-density flowing collisionless plasma 78−1898
UV fluoresc. excited by electron beam, POLAR-5 rocket expt. at 391.4 nm 80−77214
vertical ionosonde receivers, interference suppression *(Polish)* 78−88950
VHF 15 W transmitter design, covering 6 metre band *(Spanish)* 77−53310
VHF bistatic Doppler system, for radio investigations of auroral ionosphere 78−28387
VHF noise field strength at 95 MHz over India, meas. techniques and obs. 80−109294
VHF system for spaced-receiver meas. of scintillation irregularities 80−56639
whistler detection, multichannel filter and shift register obs. system 78−93031
whistler routine observation control with microprocessor *(Japanese)* 80−31144
whistlers, measurement of wave normal directions of low latitude types in the ionosphere 78−4023

ionospheric measuring instruments *see ionospheric measuring apparatus*

ionospheric propagation *see ionospheric electromagnetic wave propagation*

ionospheric techniques
see also electron density; ion density
antipodal focusing, simple correction formula *(German)* 78−4034
ARAKS expt., EM wave meas. 79−21071
ATS-6 radio beacon studies, review 80−56677

ionospheric techniques continued
attenuation determination, errors for signals with small arrival angles 79−58155
aurora initiated by electron injection from rocket, optically observed from ground 80−41559
auroral electric fields, meas. from E-region irregularity drifts via backscatter radars 77−33262
auroral radar echoes drift meas. using radar auroragraph 78−65436
automated mapping technique for representing hourly behaviour 77−5344
automatic analysis of digital diurnal ionograms *(Italian)* 78−85699
book, ionospheric techniques and phenomena 79−75040
bottomside ionogram analysis, valley problem 77−33268
broad-band wave meas. in ARAKS expt. 79−21072
chemical releases in the ionosphere, review 79−101049
chirp radar, transmit receive switching, effect on ambiguity function 79−84504
combined ground and satellite measurements, IRI model extension 80−61911
complementary cross modulation, new technique for ionospheric modification studies 77−2275
correlation function meas. for incoherent scatter radar 77−73888
critical frequency determination, radio sounding method 80−46286
current determ. from surface geomagnetic obs. *(Japanese)* 78−24406
D-region electron density, intercomparison of groundbased techniques, wave interaction and partial reflection 77−45235
D-region negative ions, detect. via Thomson scatt. in presence of electron heating 79−16739
D-region partial reflection experiment, appl. phase switched correlation polarimeter, 77−87169
D-region partial reflections technique, sensitivity to irregularity comp. 78−81495
D-region plasma density measurement, rocket borne expt. 78−45126
D-region thermal phenomena, investigation by cross modulation tech. *(Russian)* 78−24404
direct reception method of swept-frequency topside sounder signals from ISIS-II 77−21923
disturbance forecasting through solar radiation measurements from NRL SOLRAD satellites 79−58134
Doppler shift meas. with rot. antenna, ordinary and extraordinary modes 80−17426
Doppler sounding, determ. of electric fields generated during magnetosphere substorms 80−4169
drift measurement of Ba cloud, spaced receiver technique 80−72678
drift parameters determination by full correl. anal., effect of filtering 78−65450
duroral zone ionospheric modification, incoherent scatter radar obs. 77−82083
Dynasonde virtual height meas. methods, comparisons, accuracy and interpretation 80−94643
E_s-layer, method to meas. refl. coeff. 80−61922
E-region, sounding techniques rel. to drift obs. at low and mid-latits. 77−53303
E-region critical frequency computation, comparison of formulae 78−45109
E-region critical penetration freq. prediction methods, accuracy *(Japanese)* 79−40017
E-region nighttime neutral conc. vars. meas., expt. method 77−45200
E-region reflected radiowaves arrival direction, meas. technique 79−25387
electric field double probe meas., Doppler shift effects on power spectra 80−26634
electric field spreading, two-dimensional and three-dimensional mapping comparison 79−66861
electric potential of rocket, and electron beam injection expts. *(Russian)* 78−93069
electron accelerator expt. on POLAR-5 sounding rocket, evidence of elec. charge accumulation 80−77213
electron accelerator expt. on POLAR-5 sounding rocket, for use within aurora 80−77170
electron and ion drift motions, in situ meas. technique 79−29893
electron beam emission, laboratory studies of rocket payload charge neutralisation 80−77258
electron beam injection, dynamics study 80−4179
electron beam scattering in atoms, sounding rocket expt. (POLAR-5) 80−77212
electron beams, results for thin field-aligned beam in plasma 77−76124
electron collision freq. profile determ., Volterra eqn. analytical method 78−73525
electron conc. determ. by regularisation method 80−72679
electron conc. rocket meas., improved Faraday rotation expt. 77−9543
electron concentration variations rate, possible utilisation 80−12598
electron content, determ. via galactic linear polarised radio emission obs. 77−17709
electron content data, mixing freq. components identication by multiplicative homomorphic filtering 79−29929
electron content data digital processing methods 80−56629
electron content during storms, data presentation rel. to storm positive phase 77−37480
electron densities meas. by radio wave scattering, by artificial plasma inhomogeneities *(Russian)* 79−5636
electron density, determ. of daily vars. at 100-200 km from experimental rocket data 77−64515
electron density and temp. meas. by sounding rockets 79−8760
electron density determ. from topside ionograms, comparison of methods 79−39978
electron density in lower D-region, meas. via Faraday rot. and absorpt. 80−31162
electron density meas., using radio wave scattering, from artificial plasma inhomogeneities 79−75074
electron density profile parameters estimation from VLF propag. data, effectiveness 79−53614
electron density profiles, calc. from ionograms via simplified inversion procedure 77−41263
electron density profiles, determ. from transionospheric sounding data 78−28371
electron energy analysis, experimental data components isolation via Fourier transforms 78−36434
electron temp. and density, calc. technique for ground and satellite obs. 80−90275
electron temp. meas. by HF probe method 79−92632

ionospheric techniques continued
electron temperature, cylindrical Langmuir probe techniques 79−2379
electron-ion turbulence in collision dominated regime, ionospheric turbulence meas. appl. 79−48605
electrons effective collision freq. determ. from LF signals transmission 78−40683
EM absorption meas. using sweep freq. technique 79−75029
EM sounding method using spatial and spectral sampling, for investigation of inhomogeneities in ionospheric plasma *(French)* 79−29911
equatorial spread-F, artificial control technique 78−69602
European Incoherent Scatter (EISCAT) project, for Arctic ionosphere obs. *(French)* 79−2437
exploration by radar 78−73663
F_2-layer, analytic description of geometric parameters maps by spherical functions 79−53616
F_2-layer, mid-latit. trough boundary determ. from radio sources signals scintillation 78−73574
F-region, absorpt. separation from cosmic radio noise absorpt. 78−85769
F-region, equatorial, motions deduction from Sq currents 78−96344
F-region, O^+-O reson. transfer charge cross-section from incoherent scatt. meas. 77−45231
F-region, photoelectron energy loss and spectral features deduced by plasma line technique 77−45227
Faraday rotation technique, mean field height determ. using Q-T position on fading records 80−8482
fixed frequency sounding, appl. to gravity waves obs. in high latit. F-region 79−25390
frequency method of signal averaging 79−53628
GEOS-3/ATS-6 satellite-to-satellite tracking data for ionospheric refr. index determ. 78−93039
gravity wave induced wind field determ. using phase path meas. 78−16178
heat nonlinearity meas. by partial reflection method *(Russian)* 78−24379
heating by radio waves, predictions for Arecibo and satellite power station 78−77403
heating experiment, coherent parametric instabilities excited by two or more pump waves 78−57381
HF Doppler method studies of high-latitude ionospheric dynamics 78−73569
HF Doppler sounding of infrasound, due to earthquake-generated oceanic Rayleigh waves, group vel. dispersion curve determ. 79−70756
HF max. usable freq. prediction along foF2 line, MINIMUF-3 algorithm 79−25372
HF signals single-hop paths computation, allowance for signal fadings 77−91352
HF sky-wave field strengths, developments in prediction techniques 79−58132
HF vertical sounding, Alfven waves stimulated excitation in magnetosphere 79−58192
holes created artificially by H_2 or H_2O releases 78−40752
holographic interpretation of radiowave sounding data 80−77200
holographic interpretation of reflected radiowave data 80−77155
horizontal drift meas. using closely-spaced receiver technique 78−40743
incoherent scatter data, analytic partial derivatives for least-squares fitting 78−73581
interferece suppression for vertical ionosonde receivers *(Polish)* 78−88950
inverse problem solution by simplex method 80−26619
ion temp. estimation with ion trap data from rockets and satellites 78−16237
ionogram analysis, increased accuracy with simple methods 79−53538
ionograms, true height calc. technique 80−8486
ionograms, vertical incidence, simulation by ray tracing with replacement layer and ionospheric trough 77−78559
ionosonde, high resolution, equipment and preliminary results 77−9542
ionosonde, high resolution, technique and analysis methods 77−9541
Japanese satellite, Ume-2, ionosphere-sounding *(Japanese)* 79−88564
Langmuir double modulation probe, current ratio optimisation 79−48576
Langmuir probes appl. to D-region electron density and energy distrib. meas. 77−82078
least squares polynomial analysis appl. to topside ionograms 77−78476
LF radiation generation by HF transmitter, nonlinear currents height meas. *(Russian)* 77−41256
low-energy measurements by Spacelab, effects of probe-created plasma disturbances 78−77458
lower ionosphere research, Dive and Ascent Satellite programme 80−77252
lunar dynamo electrostatic fields, determ. from perturbations in columnar electron content 77−29570
magnetotelluric methods, methods to study crust cond. beneath magnetometer array, review 80−98486
mass spectrometers ion and neutral extraction, mass-discrimination effects under spacecraft conditions 80−4230
maximum entropy spectral anal. of radar auroral echoes 78−93006
meteor bursts, forward scatt. technique, obs. over India 78−89132
modification, initial report on artificially created equatorial spread-F 78−88972
modulation method, for ionosphere LF propag. investigation 78−45114
multiple pump heating experiment, plasma instabilities obs. 78−57382
multistation rapid-run ionosondes for study of travelling disturbances 78−93041
oblique direct and oblique-backscatter sounding on multihop paths, relation of HF signal intensities 78−45113
oblique sounding data, inversion method 77−41265
partial reflection experiment using FM-CW technique 77−29580
peak electron densities of F_2-layer, comparison of CCIR predictions with in situ meas. 78−57394
photoelectron current, general, meas. technique 80−12636
plasma f_H resonance, relax. sounding rocket expt. and interpretation 78−45129
plasma probe and ionospheric structure studies by space vehicle obs. 79−53540
plasma probe measurements, commutable source of ref. voltages 80−31192
plasma resonance probe applications *(Chinese)* 80−90226
plasmapause displacements, recording technique 77−22034
plasmasphere, electron content determ. via radio beacon studies 77−45229
polar cap absorption, recording using ULF meas. 79−53620
ionospheric techniques continued
positive ion detection, with rocket-borne mass spectrometer, Monte Carlo flow simulation 80−8459
pulse synthesis technique, for improving ionosonde resolution 78−28411
pulsed oblique sounding, upper and lower rays signal levels ratio 79−8748
pulsed sounding, historical review 77−5395
radar and optical simultaneous meas. of E-region neutral winds 78−32272
radar measurement, incoherent scatter, systematic error due to noise contamination 78−49225
radar sounding, appl. to studies of equatorial electrojet longit. differences 78−36371
radio drift meas. simulation and analysis by correlation methods 78−45033
radio sounding, envelope distrib. functions and phase of periodically non-stationary process 80−4173
radio transmission forecasts, backscatt. echo spectral anal. appl. *(French)* 79−29912
radiowave phase and amplitude meas. interpretation *(Russian)* 78−77394
radiowave propag. condition forecasting and prediction, long- and short-terms 78−93046
radiowave propagation, maximum usable frequency predictions, real-time updating 79−58179
radiowave studies of ionosphere, incoherent scatter technique development, review 78−81503
reflection height estimation from Doppler measurements 77−21979
resonant EM oscillations in polar region, for modification expts. 80−56676
riometer sounding, absorption data appls. to ionospheric study *(French)* 77−53216
riometer technique for absorption studies at magnetic equator 77−53275
rocket observational methods, comparison for aurora elec. field meas. 80−85789
S_q-field, seasonal and latit. vars. deduced via natural nonorthogonal functions method 78−36359
satellite obs. of plasma, data analysis *(Spanish)* 78−16270
satellite radio beacons, effects of ground refls. on ATS-6 expt. 77−53144
satellite sounding, gyroharmonic reson. obs. interpretation 79−48614
satellite universal telemetering system for magnetospheric and ionospheric research *(German)* 77−73924
satellite wake ion density, for probe meas. in O^+ plasma 80−82136
satellite-referenced propagation correction for USAF SPACETRACK radar systems 79−58131
simulation of satellite flight using synthesised plasmas *(French)* 78−16269
sounding, nonlinear VHF/UHF wave mixing, theory 80−36445
sounding techniques improved by digitization 80−36427
sounding using frequency shift method 78−40742
sounding using spaced ground receiving array Dynasonde system 80−36406
soundings using small spaced receiving array with Dynasonde system 80−36406
space science without rockets, ionospheric props. meas. at Arecibo Observatory 78−81488
spaced fading records, correlation analysis, occurrence of negative V_c^2 79−88540
spaced receiver drift experiments, triangle size effect 79−53635
spaced receiver drift expt., cause of triangle size effect 80−41557
spatial and temporal variation meas., differential Doppler technique using satellite 79−12311
structure prediction techniques, for radiowave propagation 79−58178
time series, rest frame spectra deduction from spectra computed in moving frame 77−25795
topside profile determ. by single meas. 77−56739
topside sounding and determination of electron profiles, review 80−56669
total electron content determ. in transverse zone, new methods 77−33250
trajectory characteristics, of rays in inhomogeneous ionosphere, effect of magnetic field, calc. method *(Russian)* 78−32286
TRANSIT, satellite observations, phase fluctuations, and ionospheric irregularities 78−7832
travelling ionospheric disturbances, detec. by auroral zone incoherent scatter radar 79−48610
tsunami-generating earthquakes, ionosphere detect. method 79−44681
turbulence diagnostics, by EM wave propag. obs. 78−45032
ULF wave generation by peninsular loop currents 80−90247
UV fluoresc. excited by electron beam, POLAR-5 rocket expt. at 391.4 nm 80−77214
vertical electron density profile comp. from single magnetoionic ionogram component 77−45222
vertical sounding by radiowaves, magnetoionic components lateral deviations 79−8747
vertical soundings, diurnal and seasonal ionisation of critical freq., min. virtual heights at Surlari *(Rumanian)* 80−51605
VHF noise field strength at 95 MHz over India, meas. techniques and obs. 80−109294
virtual height radio pulse dispersion, computer simulation 80−61954
virtual height-freq. curves, nocturnal, reduction method using ionisation models *(Chinese)* 80−105099
VLF direction-finding techniques comparison for determ. whistlers exit point at ionosphere 80−26631
VLF hiss from auroral zone, direction find method and obs. 80−85777
wave measurement, via satellite-borne cross-power spectrum analysers 80−94621
wave spectrum measurements using cross-power spectrum analyzer on space shuttle *(French)* 79−70912
whistler dispersion measurement using five channels phase-locked loop discriminator *(Japanese)* 80−31143
whistler routine observation control with microprocessor *(Japanese)* 80−31144
whistlers, spectral-temporal anal. by digital methods 80−4175
O content of lower thermosphere, 100-160 km, new spectral method 80−41578
O I 130 nm fluorescence technique, appl. to O conc. determ. in lower ionosphere 80−36434

ionotophoresis *see electrophoresis*
ions
see also atoms; electrolytic ions; hydrogen ions; negative ions
central analytic potential with three parameters 77−71737
electron density, semi-statistical model 78−21850
multiply charged, two-electron, parity nonconservation in spectra 79−10087
parity nonconservation effects in ats. and ions 79−10086
Thomas-Fermi-Dirac model, mag. susceptibility and binding energy 77−67981
H-like ions, scaled Coulomb-Born-Oppenheimer collision strengths 79−22839
i.r. astronomy *see infrared astronomy*
i.r. detectors *see infrared detectors*
IR drop *see electric potential*
i.r. imaging *see infrared imaging*
i.r. sources *see infrared sources*
irasers *see lasers*
iridium
see also nuclei with .....
absorption of H_2, influence of surface steps and clusters, field emission investig. 77−28698
adatom, on W (110), dipole moment, field emission meas. 77−47674
adatom on Pt, surface diffusion, FIM expts. and Morse potential calcs. 78−34717
adatom on Pt, surface diffusion energies 79−77923
adsorbed O on (110), surface struct. anal. using hybridisation model 80−44423
adsorption and condensation of Sm, thermal desorption mass spectra and thermionic emission meas. 79−69362
adsorption of benzene and pyridine on (111), electronic transitions sensitivity to molecule-surface orientation, energy loss spectra 80−45184
adsorption of CO, AES obs. 77−35818
adsorption of CO, O_2, H_2, N_2, ethylene and benzene on (110) surface 78−38961
adsorption of CO and reaction with O_2 on (100) surface, transient study 80−30284
adsorption of CO on evaporated films, IR refl.-absorpt. spectroscopy 80−34925
adsorption of N_2, field emission exam. of effect of steps on surface potential 78−30829
adsorption of N_2 and Xe, field emission meas. 77−24479
adsorption of O, structure of c(2×2)O overlayer 79−19463
adsorption of Xe on (100) surface, local surface struct., UPS study 80−39429
adsorption on W (100), effect on surface reson. 79−65983
atom, even config., parametric calcs. 78−82631
atom, hyperfine interaction parameters, effect of local exchange, Xα and HF calcs. 78−78622
atom, magnetic hyperfine struct. 78−934
Auger spectra, $N_{4,5}N_{6,7}N_{6,7}$ and $N_{4,5}N_{6,7}O_{4,5}$ 80−89094
brittle fracture, impurity segregation to grain boundary effects 78−64637
with C adsorbed layer, effects on NaCl mol. beam condensation 77−66593
catalyst, CO oxidation by NO, XPS and UPS 78−15702
catalysts, supported, Cl determ. by X-ray photoelectron spectroscopy 77−9146
catalytic film, evaporated, ethane hydrogenolysis mechanism and kinetics 79−100436
catalytic gasification of graphite, small bimetallic particle identification by controlled atm. electron microscopy 79−83502
chemisorption, clean normal and reconstructed (100) surfaces, multiplets role 77−15694
chemisorption, of CO, on (111) surface, XPS and UPS 77−16450
chemisorption of acetylene, benzene and ethylene, geometric and electronic effects 77−55457
chemisorption of CO, coverage dependent interaction, UPS 77−85897
chemisorption of CO, preexponential factor and desorption energy 78−71963
chemisorption of CO and O on (100) and (110) faces, electron states, electron field emission 78−84704
chemisorption of CO on (100) surface, chemisorptive bonding and dissociation 77−59212
chemisorption of H_2, adsorption and desorption kinetics, struct. of overlayer 80−84367
chemisorption of H_2 and hydrocarbons, LEED, AES and thermal desorption meas. 77−1297
chemisorption of NO, chemisorptive bonding and reaction 77−51596
chemisorption of O_2 on (110) surface, sorption and dissoc. kinetics 79−33186
chemisorption of O_2 on (111) surface, dynamics 77−59211
chemisorption on clean and oxidised Ir (110) surfaces, kinetics obs. 79−11015
chemisorptive bonding of CO on (100) surface, photoemission investig. using synchrotron radiation 77−12498
coating, electron beam deposition and ion plating 77−44166
desorption, from Ir (111) textured surface, of O^+, electron stimulated 300-1085K *(Russian)* 77−47672
desorption of CO, coverage dependence of kinetic parameters 79−19462
diffusion in liquid Cu *(Japanese)* 78−59962
diffusion of C from surface into bulk 80−6562
dispersed metal catalyst clusters, EXAFS obs. 79−91530
electrode, evaporation rate from cathode spot in vac. arcs. 80−49024
electrodeposition, from molten chloride and cyanide 79−24640
electronic struct. determ. from optical refl. meas. 77−62812
energy band structure, X-ray emission spectra, APW calc. 80−92811
epitaxial growth on (001)W and (001)Mo 79−99450
EPR, quadrupole interaction 78−48027
evaporation/oxidation kinetics 77−36691
field emission spectrosc. from (111) flat and stepped planes 80−76157
field evaporation end form at 4.2K 77−1790
field ion emitter, calibration using energy distrib. of free space field ionisation 77−69971
field-ion emitter, determ. of precise geometry from field-ion image 80−2930
filament for electron gun, ThO_2 coated poisoning resistant 78−54493
film, CO oxidation, IR absorpt. spectroscopy 80−71398
fracture mechanisms, and cleavage criteria 79−74253

iridium continued
gas-phase field ionisation source, ang. intensity 80−2929
Kambalda (W.Australia) komatiite sequence, Au, Pd, Ir and Ag in interflow sedimentary rocks 79−20830
L_{III}-edge X-ray absorpt. reson., chem. environment effects 79−72256
lattice dynamics, phonon/wave vector dispersion relations, Debye temp., modified axial symmetric model 80−70339
lattice parameters, densities and atomic vols., tabulation for Pt metals 79−65033
in mafic and ultramafic rocks from Mid-Atlantic Ridge, Pd, Ir, and Au contents 77−91073
oxidation of (111) surface, combined LEED/UPS obs. 78−19955
oxidised surface, adsorbed amines and hydrazines identification by surface ionis. 77−21456
particles, nucleation centres in polyethylene terephthalate crystn. 79−15658
reconstructed (110)-(1×2) surface, LEED expts., test of struct. models 79−56050
reconstructed surfaces, reorganisation of (100) 78−95214
recovery from laboratory residues 78−81957
spectrophotometric methods of determination, review 78−61115
superconducting film, props. 79−56444
superconductive device to provide reference temps. below 0.5K 79−63220
surface, (100), adsorbed Xe layer, 5p photoemission, local surface struct. influence 80−2920
surface, (100), reconstruction, superstruct., model 80−103551
surface, (100)-1×1 struct. and reconstruction kinetics, LEED, UPS and work function meas. 79−90851
surface, (110), chemisorption of O_2, AES, LEED, thermal desorption mass spectra, and contact pot. difference meas. 79−77901
surface, (110), surface diffusion of W adatoms by atomic exchange mech. 80−49508
surface, (110), unreconstructed, determ. of atomic arrangement by LEED 79−14990
surface, (110)-(1×2) reconstructed, adsorption, of S, AES study 79−42384
surface, (111), chemisorbed NH_3, mol. adsorbate structs. from angular-resolved photoemission 80−76141
surface, (111), decomp. of hydrazine, N_2 emission, ang. depend. 80−97731
surface, (111), electron field emission, step effects on total energy distrib. 79−100026
surface, (111), kinetics of CO oxidation reaction, appl. of XPS 77−31886
surface, (111), LEED structural anal. of (2×2) O overlayer 80−2264
surface, (111), phase state of adsorbed Ba(C-Ba), thermionic emission obs. 77−85881
surface, adsorbed gases, field desorption from field ion tips 80−59793
surface, clean (001), electronic props. 77−72901
surface, clean and adsorbate covered, field emission energy distrib. spectra 80−25535
surface, CO chemisorpt., mol. cluster calc. 80−100407
surface, field depend. of spectral line energy of H_2-He adsorbate 79−78853
surface, field ionisation of ozone 78−35273
surface, superstructure from LEED meas. 79−73259
surface, tracer studies on reaction path and kinetics of CO oxidation 80−7857
surface (100), chemisorpt. and reaction of acetylene, ethylene and benzene, geometric and electronic effects 77−21421
surface (110), unreconstructed and reconstructed, LEED obs. 79−77880
surface (110) 1×2, reconstructed, struct. study by LEED, reliability factor anal. 80−39399
surface (111), $(\sqrt{3}\times\sqrt{3})$R30° S overlayer struct., LEED obs. 80−15365
surface (111), chemisorption of CO, UPS and XPS obs., comparison with Pt 78−38942
surface (111), chemisorption of O_2, LEED-Auger expts. 77−20191
surface (111), flash desorption spectra of NO, recombined mol. identification 79−86996
surface (111), O_2 chemisorption, XPS obs. 77−20190
surface (111) with pre-adsorbed O, titration by CO, XPS investigation 79−91994
surface electron density crimping, Ashcroft potential, density functional calcs. *(Russian)* 79−82653
surface electronic props. 78−95332
surface reconstruction, physical realisation of two-dimensional Ising and X-Y model 80−15351
surfaces (100) and (111), chemisorptive bonding and reaction of NO, UPS obs. 77−72786
surfaces (110) and (111), Debye temps., LEED meas. 79−60619
surfaces (111), (100)-(5×1) and metastable (100)-(1×1) struct. depend. 4f-core-level binding energies for surface atoms 80−44406
thermal expansion, 440-2220°C, improved empirical formula 77−11709
thermophysical props. at temps. up to 7000K 80−103497
thin film, electrographic investigation of interaction with atmospheric O_2 *(Russian)* 77−25196
wear coefficients determ. using pin-on-cisc apparatus 80−76366
work function, absolute value determ. 77−28697
work function changes rel. to O_2 adsorption, continuous meas. method 79−33328
work function meas. rel. to O_2, H_2 adsorpt. 77−66094
Al-Al_2O_3-Ir, tunnel junction, supercond. props. of Ir film 79−56444
CaO:Ir, quadrupole interactions and static Jahn-Teller effect in EPR spectra 77−72842
$CdCr_2Se_3$:Ir, mag. props., near Curie temp. *(Russian)* 77−63234
^{114m}In, K-shell internal conversion, Kα_1 hypersatellite line energies, intensities 77−18885
Ir I, radiation lifetimes, beam-sputtering technique meas. 79−18142
Ir II, term anal. of spectrum 79−6902
Ir/Ir-Rh alloy, appl. to temp. meas. in atm. press. flame 77−86314
Ir-C, adsorption and initial stages of condensation of Sm 79−69366
^{192}Ir, dose calc. system, interstitial radiation therapy 79−16268
^{192}Ir, estimation of long-term biological elimination 79−70642
^{192}Ir ground state spectroscopic quadrupole moment, g-factor, hyperfine quadrupole splitting 79−89235
^{192}Ir radioactive sources, field determ. of output and effective size 80−30193
^{192}Ir source for radiographic inspection method 80−71861

iridium continued
^{192}Ir, tongue carcinoma, dose and dose rate for interstitial irradiation 79−16267
MgO:Ir^{2+}, quadrupole interactions and static Jahn-Teller effect in EPR spectra 77−72842
MgO:Ir^{2+}, superhyperfine struct. of ^{25}Mg in EPR spectra of Ir^{2+} 77−69683
Mo, C and Ir impurities in single cryst. growth, effect on fine struct. *(German)* 77−28714
$NaCl_4$ on Pt and Ir surfaces, adsorption kinetics 80−84393
Nb-Ga-Ir system, phase equilib. at 1000°C and supercond., Nb-rich portion 77−36480
$NiFe_2O_4$:Ir^{4+}, mag. anisotropy, single ion contrib., octahedral sites 77−4511
Re:Ir, electric quadrupole orientation of $^{186,188-190}$Ir 80−78140
Si:Ir, Ir diffusion and solubility 77−15448
Si:Ir, magnetosensitive diodes, characts. 79−24069
Si:Ir, precipitation of solid soln., photocapacitance, electrical resistivity meas. 78−47833
Si:Ir S-type diodes, characts. 78−56224
YIG:Ir, Ir on tetrahedral sites, contrib. to mag. anisotropy, optical absorpt. meas. 77−69867

iridium alloys
see also iridium compounds
neutron activation determ. of microcomponents Pt, Pd, Ir, Rh, in noble metal alloys *(Russian)* 77−32858
rare earth alloys, RIr_2X_2 (X=Si,Ge), cryst. struct. 80−1964
rare earth intermetallics, RIr_2, (R=Y, La, Ce, Lu), ESR of Nd^{3+} and Gd^{3+} 77−85564
rare earth-Sn-X, X=Rh, Ir, Ru, Co, cryst. growth and cryst.-chem. invest, supercond./mag. ternary cpds. 80−100777
transition metal iridium intermetallics, enthalpies of form. 77−12595
Al-Ir, composite, paramagnetic resonance and electron-positron annihilation *(Russian)* 79−87314
Al-Zn-In-Mg, substitution for Mg in Mg-MnO_2 short-circuited cell, performance 79−61964
Be-Ir, dil., elec. field gradient, Mossbauer meas. 80−80665
$CeIr_2$:Nd^{3+}, ESR investigation 79−78514
CoIr, mag. susceptibility, 77-500K *(Russian)* 77−80911
Cr-Ir, magnetic transformations, triple point *(Russian)* 80−88747
Cu-Ir, dil., impurity diffusion, temp. depend. *(Russian)* 78−67851
Dy_5Ir_2, cryst. struct. 80−96473
Er_5Ir_2, cryst. struct. 80−96473
$EuIr_2$, superconductivity 79−78248
Fe-Ir, hyperfine field distrib., spin echo NMR meas. 78−76351
Fe-Pt-Ir, Mossbauer effect of ^{193}Ir and ^{57}Fe, hyperfine field, isomer shift 78−15072
Ga-In-WSe_2 eutectic alloy, self-lubricating, struct. and props. 79−100267
$Gd(Co_xIr_{1-x})_2$, C15 Laves phase struct., g shift, linewidth EPR meas., Fermi level movement interpretation 79−61210
$Gd(Co_xIr_{1-x})_2$, struct. and mag. moments, comp. depend. 79−86743
$Gd_{0.5}Dy_yY_{0.5-y}Ir_2$, effect of dil. Dy substitution on Gd ESR 79−82868
$GdIr_2$, H_2 sorption props. 79−86980
Gd_5Ir_2, cryst. struct. 80−96473
$Gd_xY_{1-x}Ir_2$, ESR meas., bottleneck and relax. rates 79−38369
Hf-Ir, dil., elec. field gradient at ^{193}Ir, Mossbauer meas. 80−66090
Ho_5Ir_2, cryst. struct. 80−96473
Ir-Al, transition metal group VIII aluminide, NMR near equiatomic composition *(Russian)* 80−20479
Ir-Ce (0.4 wt.%), field emission characts., crystallography and heat treatment effects 78−2994
Ir-Fe, dil., local magnetisation, Mossbauer meas. 80−66091
Ir-Fe, spin fluctuation alloy, thermopower peak diffusion origin 80−88542
Ir-Rh/Ir alloy, thermocouple, appl. to temp. meas. in atm. press. flame 77−86314
Ir-Sn-M, M=Mg, Ca, Sr, Sc, Y, Zn, Cd, In or Tl, cryst. growth and cryst.-chem. invest, supercond./mag. ternary cpds. 80−100777
Ir-W (0.3 wt.%), grain growth, temp. and time effects 79−100186
Ir-W (0.3 wt.%), P segregation to grain boundaries, effect on high temp. ductility 78−95754
Ir-W (0.3 wt.%), polycrystn., brittle fracture TEM study 79−61715
Ir-W (0.3 wt.%): Al(Fe)(Th)(Ni)(Rh), effect of additions on grain boundary composition 79−83309
Ir-W (0.3%), grain boundary comp., trace element additions effect 80−66661
Ir-Y eutectic alloy, supercond. transition enhancement due to lattice softening 80−103775
Ir_3Cr, yield stress and saturisation magnetisation 80−16389
IrLi and Ir_3Li, cryst. struct. 77−11506
$Ir_{1.07}Mn_{1.07}Sn_{0.88}$, ferromag. Heusler alloy, ^{193}Ir and ^{119}Sn hyperfine fields 79−78581
$IrSi_x$, formation, Ir films on Si, He ion backscatt. X-ray diffr. study 79−82471
Ir_5Sn_7, cryst. struct. determ. *(German)* 79−27952
α-IrV, internally deformed struct. as source of homogeneous linear struct. 78−26497
$LaIr_2$, H_2 sorption props. 79−86980
$LaIr_2$:Nd^{3+}, ESR investigation 79−78514
LaIr(g), thermodynamic stability, high-temp. mass spectra obs. 80−7781
LiIr, struct. and props. exam. 78−92245
Lu-Ir, dil., elec. field gradient at ^{193}Ir, Mossbauer meas. 80−66090
Nb-Al-Ir A-phase, crystal struct. determ., $MgZn_2$-Laves C14 type 77−1099
Nb-Ga-Ir, phase equilib. at 1000°C, cryst. data for intermediate phases 78−52763
Nb-Ge-Ir, A15 cpds. prod. by liq. quenching, phase stability and supercond. props. 79−95538
Nb-Ir, A 15- and σ-phases, supercond. 79−73645
Nb-Ir-O, H-phase, cryst. struct. 78−38664
Nb-Ir-O, phase struct., supercond. H-phase 78−39246
Nb-Si-Ir, A15 cpds. prod. by liq. quenching, phase stability and supercond. props. 79−95538
$Nb_{0.55}Ir_{0.45}$ metallic glass, Young's modulus meas. by impulse induced resonance technique 80−40411
Nb_3Ir, A-15 struct. supercond., microhardness, bonding 78−76199
Nb_3Ir, polycryst. substrate for epitaxial growth of Nb_3Ge films 77−63015
Nd_5Ir_2, cryst. struct. 80−96473

iridium alloys continued
$NpIr_2$, itinerant antiferromagnetism 79−61154
$PrIr_2$, hyperfine sp. ht. and magnetisation meas. at 4.2K 80−75775
$PrIr_2$, sp. ht., differential susceptibility and elec. resist. meas., 1.4-40K 80−71063
Pr_5Ir_2, cryst. struct. 80−96473
Pt-Ir, Au covered, spectral characts. of VLF noise, allowing for logarithmic creep *(Russian)* 77−85301
Pt-Ir, catalytic behaviour on graphite-O_2 reaction, small bimetallic particle identification by controlled atm. electron microscopy 79−83502
Pt-Ir, cleaning and polishing by low press. high frequency induction plasma *(Russian)* 78−35578
Pt-Ir, structural phase transform., ion field emission microscopy obs. *(Russian)* 80−50628
Pt-Ir alloys, surface composition 79−19433
Pt-Ir coated Ti anode, corrosion and passivation behaviour in Cu electrowinning appl. 80−55573
Pt-Ir coating electrodeposition, from molten chloride and cyanide 79−24640
Pt-Ir solid solutions, investigation of field-ion micropattern contrast, selective evaporation and ionisation models 79−69962
$Pt_{90}Ir_5Au_5$, $Pt_{80}Ir_{10}Au_{10}$, low temp. sp. ht. 79−73320
Pu_5Ir_3, cryst. struct. 77−58975
Pu_5Ir_4, cryst. struct. 77−19909
Re-Ir (1 wt.%), positron annihilation, photon ang. distrib. meas. effect of deformation, annealing temp. *(Russian)* 78−35220
Rh-Ir, local environment and mag. props. effect of disorders 77−63085
Sc-Ir, dil., elec. field gradient at ^{193}Ir, Mossbauer meas. 80−66090
ScIr, electronic struct., NMR relax. times meas. 79−51871
ScIr, UPS exam. 78−48276
$ScIr_3C_{1-x}(B_{1-x})$, stabilising effect of C and B on alloying behaviour of Sc 77−36454
n-Si-$IrSi_x$, Schottky diode, rectifying barrier height meas. 79−99619
Sm_5Ir_2, cryst. struct. 80−96473
Ta-Ir (1 wt.%), positron annihilation, photon ang. distrib. meas. effect of deformation, annealing temp. *(Russian)* 78−35220
Tb_5Ir_2, cryst. struct. 80−96473
Th-Ir system, phase diagram and thermodynamic props. *(German)* 79−47958
Ti-Ir, dil., elec. field gradient at ^{193}Ir, Mossbauer meas. 80−66090
Ti-Ir, Ti-rich, thermodynamic study at high temp. using Knudsen cell mass spectrometry 80−45539
Ti-Ir system, high temp. thermodynamic investig. of Ir-rich portion by Knudsen cell mass spectrometry 77−12595
UIr_3, (100) surface reconstruction, LEED, AES, electron energy loss spectra study 78−75918
UIr_3, de Haas-van Alphen effect, Fermi surface obs. 77−28099
V_xIr_{1-x}, nuclear spin-lattice relax. time, electronic density of states 77−59354
$V(Ir_{1-x}Pt_x)_3$, mag. props., ferromagnetism, comp. depend. 77−77039
W-Ir (1 wt.%), positron annihilation, photon ang. distrib. meas. effect of deformation, annealing temp. *(Russian)* 78−35220
Y-Ir, dil., elec. field gradient at ^{193}Ir, Mossbauer meas. 80−66090
$Y(Fe_{1-x}Ir_x)_2$, magnetisation, mag. hyperfine field 80−20531
YIr_2:Nd^{3+}, ESR investigation 79−78514
Y_5Ir_2, cryst. struct. 80−96473
Zr-Ir, $\alpha \rightleftarrows \beta$ transform. *(Russian)* 78−80540
Zr-Ir, dil., elec. field gradient at ^{193}Ir, Mossbauer meas. 80−66090
Zr-Ir, high temp. modification, X-ray diffr. obs. *(Ukrainian)* 79−32947
Zr-Ir hardened alloys, metastable phases *(Ukrainian)* 79−34000

iridium compounds
see also iridium alloys
(111) surface states, surface Umklapp effects, photoelectron spectra 80−93457
borides, MIr_3B_2 (M=La, Th, U), supercond. and mag. props. 80−97028
π-cyclopentadienyl (carvone) iridium (I), synthesis and protonation 77−60062
rare earth iridium borides, RIr_4B_4, supercond., magnetism and metastability 80−29501
tetraethylene iridium chloride, ligand-ligand interactions; low freq. vibr. obs. 78−94255
tetraethylene iridium chloride dimer, ligand-ligand interactions, low freq. vibr. obs. 78−94255
Hf-Ir-B system, phase equilib. and cryst. structs. 80−15072
$Ho(Ir_xRh_{1-x})_4B_4$ pseudoternary system, supercond. and mag. ordering 80−70876
InGaAs on (100) InP substrate, VPE 80−40267
InP, LPE, solvent choice, equilib. in In-Ga-P system 79−87589
Ir complexes with adenosine, xanthosine, prep., elec. cond., IR spectra, characterisation 78−92065
Ir IV hexahalides, hyperfine spectra of mag. ordered state at very low temp., Mossbauer meas. 77−69744
$Ir_4(CO)_{12}$ EELS, AES, comparison with XPS and UV absorpt. spectra obs. 80−35021
$IrBr_6^{2-}$, complex Raman tensors, irreducible tensor method, antisymmetric scatt. 78−37623
$IrBr_6^{2-}$, Raman tensor patterns, vibr. reson. Raman scatt., group theoretical calcs. 78−986
$IrBr_6^{2-}$, resonance spectra, vibrational and electronic Raman effects 79−47437
$Ir_4(CO)_{12}$, Ir-C-O deformation modes, group theoretical anal., for teaching 78−11
$IrCl_6$, reduction by BH_4^- 78−76854
$IrCl_6^{2-}$, circularly polarised Raman spectra, spin-orbit induced vibr. antisymmetry 78−5232
$IrCl_6^{2-}$, complex Raman tensors, irreducible tensor method, antisymmetric scatt. 78−37623
$(IrCl_6)^{2-}$, electronic Raman spectra, spin-orbit components of ground state, vibr. 78−5231
$IrCl_6^{2-}$, ground state Zeeman splittings, reson. Raman spectra and mag.-optical activity 80−5579
$IrCl_6^{2-}$, resonance spectra, vibrational and electronic Raman effects 79−47437
IrF 6, $\Gamma_{8g}(^2T_{1g})$ state, electronic Raman scatt. and absorption spectra at 1.6 μ, resolution of Jahn-Teller problem 79−36648
IrF_6, electron affinities from collisional ionisation with alkali atoms 78−55226
IrF_6, in mixed crysts., Jahn-Teller effect, $\Gamma_{8g}(t_{2g})^3$ state, 6800 Å 78−76032
IrF_6, ionis. energies, optical spectra, Dirac-Slater model 77−83488

iridium compounds continued
IrF_6, ligand field theory analysis of spectra 79−72248
IrF_6, neat and mixed cryst., Raman scatt., Jahn-Teller interaction in ground state 79−38540
$IrGe_{1.5}S_{1.5}(Se_{1.5})$, new skutterudite relation compounds, prep. and charact. 78−52700
Ir(III) complex, cis-dichlorobis(4,4′-dimethyl 2,2′-bipyridine) iridium chloride 80−97319
IrO, ground state, matrix isolation spectra 78−46352
IrO reactively sputtered electrochromic films, electrocatalytic O_2 evolution 80−26125
IrO_2 anodic amorphous film, electrochromism isotherms, internal entropy 80−50300
IrO_2 anodic films, electrochromium, on transparent substrates 79−19861
IrO_2 anodic films, electrochromism, anion mechanism 80−100647
IrO_2, electrochromic film, prep. by reactive sputtering 80−29876
IrO_2, electronic struct., XPES obs., rel. to TiO_2, RuO_2 78−52632
IrO_2 film, A-C response 80−107926
IrO_2 heat-treated anodic films, pH depend. of electrochromism 79−8120
IrO_x anodic film electrochromics in nonaqueous acid soln. 80−2722
IrO_x, anodic film electrodes in electrochromic cell 80−7329
IrO_x anodic film electrochromic cell, fabrication and display device use 80−61320
IrO_x, anodic films, electrochem. characts., electrochromic system 78−80316
IrO_x anodic films, electrochromism and ionic cond., model 80−59706
IrO_x anodic films, electrochromic props. and device uses 80−61319
IrO_x anodically grown film as electrochromic material 80−71377
IrO_x, electrochromic, oxidation state changes and struct. 80−100950
IrO_x film, anodic, electrochromism, pH effects on corrosion stability, coloration and bleaching mech. 80−2726
IrP_2, prep. and characterisation 78−39679
IrS_2, thermodynamic props. by effusion technique 77−40570
IrSi, Schottky barrier height meas. 79−47160
$IrSn_{1.5}S_{1.5}$, new skutterudite relation compounds, prep. and charact. 78−52700
$La_3Ir_3O_{11}$, prep. and cryst. struct. *(French)* 79−51084
Li_4IrH_4, and Li_4IrH_6, struct. and props. exam. 78−92245
Sc-Ir-B system, phase equilib. and cryst. structs. 80−15072
Si-IrSi interface microstructure and Schottky barrier height 80−34508
Xe-MF_6, M=W, Mo, U, Re, Ir, charge transfer interactions, VUV and IR obs. 78−50664
$Y_xLu_{1-x}Ir_4B_4$, supercond., magnetism and metastability 80−29501
Zr-Ir-B system, phase equilib. and cryst. structs. 80−15072
$ZrIr_3Br_{\sim 4}$, cryst. struct. 78−42963

iron
see also nuclei with .....
^{59}Fe fixation in solid/liquid systems 79−13530
Abel 1060 galaxy cluster, Fe X-ray emission feature obs. and abundance 80−82518
abrasion, low speed, strain rate effects 79−20208
abundance in red giant star ε Virginis, differential model atmosphere analysis 79−25604
abundance in solar system rel. to nucleosynthesis 77−53435
abundance in stars, Utrecht UV spectrophotometer obs. 78−69793
abundance in X-ray galaxy clusters 79−12530
acidic corrosion, effect of aromatic and arylaliphatic sulphides 78−35560
acoustic velocity, shock-compressed uniform solid, lateral discharge ang. semiempirical formula *(Russian)* 78−55910
activated silicate glass, diffraction grating recording by UV laser 80−5842
addition to Si, effect on nitridation 79−57129
adsorbed on W (100) surface, field emission microscopy study 79−15015
adsorption, of N_2 and NH_3, 80-290K, XPS and UPS obs. 77−31901
adsorption, of O_2, oxidation 80−108730
adsorption, segregation and reactions of non-metal atoms, LEED and AES obs. 80−59783
adsorption and condensation on W foil, meas. by thermal desorption in pulse time-of-flight mass spectra 79−15023
adsorption and desorption of CO and H_2 on (100), C, O, S and K adlayer effects 80−71573
adsorption and surface reaction of formic acid 80−40741
adsorption of acetic acid and ethylenediamine, XPS study 80−76132
adsorption of Br_2 on (100) surface, AES, LEED, work function, and thermal desorption study 80−15375
adsorption of C, N, O, S, CO, NO and C_2H_2 on (110), UPS and LEED/Auger meas. 77−72773
adsorption of C(O)(S)(K), on (100) surface, adsorbate coverage determ. by LEED, AES and XPS 80−103566
adsorption of carbon tetrachloride on (100) surface, AES, LEED, work function, and thermal desorption study 80−15376
adsorption of Cl_2 on (100) surface, AES, LEED, work function, and thermal desorption meas. 79−82465
adsorption of CO, random occupation of adsorption sites, LEED exam. 78−63930
adsorption of CO, resistance changes, work function change and thermal desorption meas. 79−19450
adsorption of CO and O_2 obs., core-level photoemission and LEED methods appl. 79−15003
adsorption of CO on polycryst., SIMS 78−14585
adsorption of ethoxysilanes, XPS 77−89639
adsorption of I_2 on (100) surface, AES, LEED, thermal desorption, and work function study 80−15374
adsorption of K on Fe(110), UPS and XPS meas. 80−95675
adsorption of NO, anal. at low press., XPS, UPS 77−7970
adsorption of O_2, oxide formation, XPS/UPS obs. 77−85074
adsorption of SO_2, X-ray photoelectron spectra 78−27370
adsorption of tetrabromomethane on (100) surface, AES, LEED, work function, and thermal desorption meas. 80−39422
adsorption of water under the influence of 2.5 keV electrons 79−28199
adsorption on W, work function and field emission obs. *(Japanese)* 78−91536
aerosol powders, oxidised, nucl. gamma reson. study *(Russian)* 79−1725
aerosoled fine particles, Mossbauer spectra 80−7223
aerosoled ultrafine Fe particles, oxidation 80−21183
AES meas. 77−36323
air pollution neutron activation anal. using 14 MeV neutrons 77−91257
alloy systematics, rel. to the long periodic table, allotropy of Fe and Mn 79−37649

iron continued
alpha phase, vacancy, lattice vibrs., reson. and localised modes 80−39236
alum:Fe^{3+}, forbidden EPR transitions, theory 78−31106
aluminising coating 78−11430
amethyst, Fe^{3+} diffusion, associated phenomena 77−36269
amorphous, elec. cond. calc., t-matrix approach 77−55510
amorphous, radiation damage simulation 80−34045
amorphous, realistic structural model, search for Bernal holes 78−83734
amorphous, reflection of D and T, Monte Carlo study 80−40197
amorphous, relaxed Bernal structure, model 78−2007
amorphous, sputtering mechanism for light ions, computer simulation 79−56901
amorphous, struct. model, polyhedron and cavity anal. 79−50994
amorphous, struct. relax. of dense random packing model 78−30540
amorphous, tensile deform., three-dimens. computer simulation 79−43350
amorphous and liq., electronic struct., dense random packing model 79−51476
amorphous andliquid state, electronic states and transport 79−99474
amorphous film, getter sputtering at 25K 79−38741
amorphous film, Hall effect and magnetisation *(Russian)* 77−35922
amorphous structure, chain of Bernal holes, dislocation model 79−4249
amorphous structure obtained by liq. state quenching 79−46573
analysis in ore using prompt gamma-ray from 3.29 MeV neutron inelastic scatt. 77−36832
annealed, and deformed, exam. of immobile dislocation distrib. *(Russian)* 79−32995
anodic behaviour, in acidic solns. of liq. NH_3 78−27671
anodic behaviour in 1M H_2SO_4, influence of straining 80−97612
anodic dissolution, electrochem. noise generation, interface stochastic behaviour 77−25277
anodic dissolution in acidic chloride solns., exam. 78−92389
anodic dissolution model, passivation 80−35545
anodic oxidation, two phase film form., overpot. anal. 77−16737
anodic polarisation in H_2SO_4, current and potential oscillation *(Japanese)* 78−11412
antiferromagnetism of FCC Fe and its alloy 78−88124
Arabian Sea, DSDP Site 220, Fe, Mn and Ti distrib. 77−73708
Armco, α-phase, determ. of H solubility 80−54390
Armco, adsorpt. of Hg, effect on mech. strength, creep, fatigue, embrittlement *(Russian)* 79−29267
Armco, Bauschinger effect, computerised evaluation method 80−93625
Armco, boride coatings, under elec. heating conditions, hydroabrasion wear resist. 80−55543
Armco, borided surface layers, Mossbauer and metallographic anal. 80−50769
Armco, carburising kinetics, in endothermal atm. 80−76410
Armco, coated and uncoated, laser interferometric obs. of corrosion 79−47810
Armco, coating with NbC, deposition technique, struct. and props. 79−52462
Armco, cold-rolling cavity formation, TEm study 78−6947
Armco, corrosion and mechanical behaviour in liquid Li 78−53036
Armco, crack and slip band form. during US fatigue 78−56723
Armco, cumulative fatigue damage at US freqs., thermal activation 77−70181
Armco, cyclic deform. in presence of H_2 *(Russian)* 77−16728
Armco, cyclic loading and fracture toughness 80−35298
Armco, D penetration, mass spectrometric obs. 78−47606
Armco, deform. strengthening during low-cycle fatigue in H gas *(Russian)* 77−52460
Armco, discontinuous laser beam effect on mass transfer *(Russian)* 79−33109
Armco, dislocation struct. after hot and cold rolling *(Russian)* 77−8847
Armco, dislocation struct. effect on creep *(Russian)* 78−39841
Armco, dyuamic $\alpha \rightleftarrows \varepsilon$ transform., stress gauge meas. 80−96594
Armco, electron microscope object prep. method 80−50789
Armco, exam. of pore formation mechanism 78−85120
Armco, fatigue crack propag., influence of specimen thickness *(German)* 80−66669
Armco, fatigue cracking under 23 kHz loading at 23°, 60° and 100°C 78−60763
Armco, fatigue micromechanism *(Russian)* 78−23818
Armco, flat-rolled and annealed, dislocation struct. and mech. props. *(Russian)* 79−20062
Armco, fracture in liq. metals, Rebinder effect *(Russian)* 79−29266
Armco, fracture stress, effect of Pb melts *(Russian)* 77−21246
Armco, fracture toughness characts. under cyclic loading 79−11703
Armco, friction in vac. at elevated temps. 80−55542
Armco, friction pair with Cu, bronze or C steel *(Russian)* 77−70185
Armco, grain size and strength depend. on nonmetallic inclusions *(Russian)* 80−100894
Armco, H_2^+ diffusion 0 to 300°C, effect on elongation tension *(Russian)* 77−66044
Armco, impact strength, exam. with pulsed drop impact loading 78−84944
Armco, inelasticity when under cyclic strain, in active media 78−80613
Armco, inter- and intragranular sulphidation 80−55570
Armco, ion bombardment thermochemical treatment *(French)* 77−86229
Armco, kinetic singularities of plastic deform. during $\gamma \rightarrow \alpha$ transform. *(Russian)* 78−92262
Armco, long-term strength, H effect 80−55581
Armco, low-cycle fatigue, electric field effects 77−1868
Armco, membrane, superpermeability to D 79−24830
Armco, microstruct., effect of strain rate on change, due to tension-compression 78−80614
Armco, microstruct. and hardness after electron bombardment 79−38956
Armco, microstructure in quasibrittle and plastic fracture 77−1863
Armco, Nd^{3+}-glass laser light interaction in high press. N_2 medium 79−99990
Armco, oxide films, passivating, transient growth kinetics 80−93672
Armco, phosphate coating, Fourier transform IR absorpt.-reflection spectra 80−71500
Armco, pitting corrosion in Na_2SO_4 78−35559
Armco, plastic deform., surface dissolution effect 77−8883
Armco, plastic zone around fatigue crack, vac. effect 80−100914
Armco, recrystallisation, structural inheritance characts., X-ray and internal friction obs. 79−57017
Armco, rupture onset during cold rolling *(Russian)* 77−8904

iron continued
Armco, SCC in phosphate soln. 79−96184
Armco, screw dislocation effect on mech. props. *(Russian)* 78−60704
Armco, siliciding with Si-SiO_2 mixture, exam. of corrosion resistance 80−16584
Armco, sleeve, deformed by cold drawing, exam. of surface and texture *(Russian)* 79−34057
Armco, strength, fracture, effect of H_2 *(Russian)* 77−25129
Armco, stress relaxation expt., significance under strain ageing cond. 79−57039
Armco, struct. and mech. props., effect of hydrostatic extrusion *(Russian)* 77−56022
Armco, texture role in prestrain embrittlement 78−60796
Armco, thermal diffusivity meas. using new apparatus 77−67429
Armco, transform. of observed crack traces on section to true crack density for fracture calcs. 79−10533
Armco, wear resistance in liquid Sn and Bi *(Russian)* 77−59941
Armco, Young's modulus of Fe_3C phase *(Russian)* 80−76297
Armco and Ferrovac E, strength differential effect, temp. and strain rate sensitivity in saturation cycling 79−66094
Armco Fe, ground, residual stresses, X-ray evaluation 80−79863
Armco Fe, microflow and strain hardening under cyclic loading 80−104182
armco Fe, X-ray diffractometrical sub-structure analysis *(German)* 77−68894
Armco iron, effect of low temps. and heat treatment on growth rate of fatigue cracks 79−57027
Armco iron specimen, elastic const. meas., X-ray diffr. technique 78−5714
Armco nitriding characts. at low atmos. press. of NH_3, thermodynamic *(Russian)* 78−15573
atmospheric Fe aerosol source determ. by gamma-ray spectroscopy 77−41235
atom, $3d^64s^2$ and $3d^74s$ configs., Rayleigh and Compton scatt., differential cross sections 80−52912
atom, Auger transitions, two-electron-one-photon radiative rate calc. 77−18869
atom, beam foil spectra, 20 to 350 nm wavelength, 16 to 110 MeV beam energy 78−78655
atom, Compton profile asymmetry obs., Al, Ti, Fe, Cu, using Kα fluoresc. 77−57937
atom, double K-shell ionisation by electron impact, X-ray spectra 78−62928
atom, double K-shell ionisation by electron impact 78−62929
atom, elastic electron scatt., 1-8 keV, differential shielded cross section calc. 79−13824
atom, electron bombard., 300 to 600 keV, K_α/K_β X-ray intensity ratios, K-shell ionis. cross sections 78−37747
atom, fine struct. levels fitting, config. interaction effect, spin-orbit and electrostatic interaction parameters 80−69248
atom, from $Fe(CO)_5$+inert gas, chemiluminesc. 80−55647
atom, highly ionised, 1s to 3p Kβ-like X-ray spectrum 77−50394
atom, hyperfine interaction parameters, effect of local exchange, Xα and HF calcs. 78−78622
atom, incoherent γ-ray scatt. by K-shell electrons 77−83560
atom, inner-shell vacancies, cascade decay, multiple ionisation and X-ray emission calcs. 80−87072
atom, ionisation potential, term value, correlation energy by vertical anal. 78−41964
atom, K_α X-ray line, natural width at energy threshold meas. 78−41992
atom, $K\alpha^n$ hypersatellite spectra and double photoionisation cross-section 79−85922
atom, $K\alpha^n$ hypersatellite spectra and K-shell double photoionisation cross-section 78−21874
atom, $K\alpha\alpha^n$ emission, method for L-shell config. calc. 77−42269
atom, Kα and Kβ X-ray spectra induced by 84 MeV N^{4+} 77−50517
atom, Kα satellite lines following electron bombardment 80−69097
atom, Kβ/Kα ratio anomalies, K-capture rel. to bremsstrahlung excitation 77−18825
atom, K-shell ionisation cross sections, proton induced 77−23556
atom, L-shell internal excitation accompanying L-capture 80−95726
atom, $O^{2+,3+,4+,5+}$ induced K-shell X-ray production cross section, 7 to 24 MeV 77−61850
atom, orbital calc., model potential method 79−36513
atom, photoionis. cross section meas. 79−22674
atom, rel. at. transition probabilities, by flame at absorption spectroscopy 79−89642
atom, revised lifetimes of energy levels 77−65440
atom, Sternheimer shielding functions calcs. 79−76352
atom, two-electron one-photon transition rate 77−71772
atom, UV photoionisation cross-section, resons. 77−14398
atom, valence electronic struct., pseudopot. method 79−68184
atom, X-ray fluorescence, Kα hypersatellites 77−18830
atom, X-ray production by protons by 0.5 to 2.0 MeV energy 78−66646
atom, X-ray spectra, chemical bonding and multiple ionis. effects 78−50630
atom, X-ray spectra in Tokamak-10 facility plasma *(Russian)* 78−9837
atom+ion collisions, K X-ray transition energies, two electron-one-proton mechanism 77−18828
atomic and metallic 3p excitation 79−22633
atomic layers, Pauli paramagnetism to band ferromagnetism transition thickness depend. 78−72377
atomic magnetic moments comparison to values of ferromagnetic metal 78−52244
atomised powder, props. 80−25600
atomised powder, sintering effect on recrystn., mech. props. 80−40292
atomised powder compacts for mag. cores, oxidation, compressibility, heat treatment *(Japanese)* 78−72752
atomised-Fe powder, friction of compaction process *(Japanese)* 77−59716
atomized powder compacts for mag. cores, mag. props. *(Japanese)* 78−72751
atoms, in strong mag. fields, var. calc. of ground-state energy 77−75046
atoms, metastable states, hyperfine struct. meas. by laser RF double-resonance 80−58404
attenuating shock waves, following meteoroidal impact *(Russian)* 77−71068
Auger analysis of passive film in neutral aqu. soln. 80−16605
austenite formation kinetics during accelerated heating model, kinetic curves *(Russian)* 79−70058
band electron momentum distributions calc. 78−18950

iron continued
band structure, parametrisation via Hubbard's scheme 77−31938
band theoretic interpretation of neutron scatt. expts., spin wave modes 80−44791
Barkhausen effect, grain size depend. at 300K and 77K *(German)* 77−16113
BCC, α-phase, divacancy binding energy, appl. stress effect, computer simulation 77−15408
BCC, anharmonicity and Debye-Waller factors 77−47533
BCC, atomistic studies of H_2 enhanced crack propag. 78−31538
BCC, computer simulation of entropy of $^1/_2\langle111\rangle\{110\}$ edge dislocation 78−67716
BCC, cyclic cleavage crack growth model for fatigue 80−55519
BCC, diffusion of C and N 77−4222
BCC, high field Knight shift and hyperfine anisotropy of ^{57}Fe 80−71205
BCC, low energy interband absorption, electronic struct. exam. 79−73930
BCC, migration of vacancies near twin boundaries in α-phase 78−51535
BCC, neutron-irradiated, Frenkel defect spontaneous recomb. volumes 79−60355
BCC, one-dimens. Morse function cryst. stability anal., for teaching 78−54134
BCC, shock wave simulation using Morse pot. 78−2196
BCC, strain hardening and recovery by pure metal mode, high temp. deform. *(Japanese)* 78−52843
BCC, stress-induced interaction and ordering 79−42057
BCC, void nucleation following electron irrad. 80−29054
BCC α-irons, LEED intensity spectra of (100), (110) and (111) surfaces *(German)* 77−31854
BCC and FCC struct., X-ray absorption spectra, Mossbauer spectra, comparison *(Russian)* 78−64299
BCC containing impurity atoms, Peierls energy of $1/2\langle111\rangle\{110\}$ edge dislocation, temp. effect 77−84751
BCC crystal, anisotropic spin-pair correlation function, neutron mag. crit. scatt. cross-section 80−60194
BCC surface ledge simulation, dislocation-like relaxation 78−30620
bicrystal, vapour grown, statistical analysis of grain boundary angles 77−47470
biological material, proton induced X-ray chem. anal., Fe and minor elements concs. 78−23989
biomedical meas., Fe stored in human tissue, in vivo, using susceptometer 80−101245
biomolecules, Fe-containing, appl. of spectroscopy 79−24956
Bloch wall, zig-zag 90°, magnetoelastic problem 77−4526
blood cell, red, Fe content anal. by electron microprobe and scanning electron microscopy 79−53065
blood plasma total Fe-binding capacity meas. by EPR 77−17003
bonding of Al, growth of intermediate phases, effect of O and N impurities 78−27680
borate glass:Fe^{3+}, EPR spectra 77−8394
boride films, produced by ion bombardment on Fe and plain steel, X-ray struct. anal. *(French)* 79−73413
boriding by ion bombardment with B_2H_6 *(French)* 78−60876
boriding of high purity Fe with cryst. B powder 80−84951
Bremsstrahlung distrib. from 22 MeV electron irradiation 78−59840
Brillouin-Mandelstam scattering from thermal and excited magnons 80−70980
brittle fracture, quantitative determ. of transcryst. and intercryst. portions by opt. and SEM fractography 77−52464
brittle fracture mech., review *(Russian)* 79−34139
bulk modulus and thermal expansion coefficient, mag. contributions 79−8039
burning particles, flashes, spectrographic obs. 80−89078
carbonyl, kinetic singularities of plastic deform. during $\gamma\rightarrow\alpha$ transform. *(Russian)* 78−92262
carbonyl iron microspheres, charge reversal during impact on charged conductor, surface oxidation effects 77−12042
carbonyl iron microspheres, semi-elastic impact on diamond-polished metal targets 77−11124
carbonyl pore struct. orientation, shrinkage anisotropy effect 80−20845
carbonyl powder, kinetics of phosphatizing reaction 79−96218
carbonyl powder, magnetic material 77−12160
carbonyl powder, particle size distrib. anal. by microscopy with statistical anal. of results 78−19691
carbonyl powder, specific elec. conductivity, 5 to 200 MPa *(German)* 80−70664
carboxylic acid surface film struct. 79−74294
carburisation rel. to interstitial penetration 77−12737
carburised sintered and pressed specimens, wear resistance 77−77590
carburization, methane gas$\rightarrow$C(dissolved)+$2H_2$ (gas), kinetics 80−55712
η Carinae, IR Fe II lines and interpretation of IR excesses 78−32478
cast, ferritic, ductile fracture initiation and propag. 78−84966
cast, low-cycle fatigue 80−16474
cast, molten, design and field test of radiation pyrometer *(Japanese)* 80−98917
cast, white, superplasticity parameters 77−56042
cast iron with lamellar graphite, tensile strength, reactor appl. 77−57718
cast iron-steel mixture, interaction of Zr, formation reaction thermodynamics *(Russian)* 80−55645
cast with spheroidal graphite, fine cryst. struct. on tempering *(Russian)* 80−96476
casting, fatigue strength, section size and surface struct. effect *(Japanese)* 79−20170
casting in metal mould, strength before, after heat treatment *(Japanese)* 77−48461
catalyst, decomposition of NH_3, kinetics, IR obs. 79−11792
catalyst, gasification of graphite, electron, microscopy 80−104358
catalytic synthesis of NH_3 on Fe, promoter action of K 79−29390
cathodic charging effect, on creep and tensile deformation 80−76320
cathodic electrodeposition, electrolyte acidity effect 79−61522
cavitation erosion, exam. of mechanism and rates 79−5063
cavity formation at grain boundary-subboundary interactions in α-Fe 77−86040
cementation, of Cu, deposit struct., reaction rates, SEM 80−104421
cementation of Cu on surface *(Japanese)* 79−70002
Centaurus galaxy cluster, Fe X-ray emission feature obs. and abundance 80−82518
centrifugal casting method, and high frequency induction melting, sample prep., emission spectral anal. 77−48367

iron continued
chalcogenide glass, Fe, doped in equil. conditions, impurity cond. and Mossbauer effect 80−49726
characterisation in environmental samples by Mossbauer technique 79−66433
chemically induced grain boundary motion in Zn atmos. 78−38724
chemisorbed CO, low energy vibr. modes studied by tunnelling spectroscopy 80−78590
chemisorption, competitive, on metallic films, IR spectra, oil matrix technique 77−9118
chemisorption, dissoc. of $CO(H_2)(N_2)$, on cryst. surface *(German)* 78−53257
chemisorption, equilibration and replacement reactions between H_2 and D_2, anisotropies 77−24482
chemisorption of benzene and methyl derivatives, MO LCAO calcs. 77−52674
chemisorption of CO, CO_2, acetylene, ethylene, H_2 and NH_3 on clean (100) and (111) surfaces 78−71996
chemisorption of CO, H_2 on fine Fe particles, Mossbauer study 80−39415
chemisorption of CO, surface deactivation effects 77−76669
chemisorption of CO on (100) surface, chemisorptive bonding and dissociation 77−59212
chemisorption of H_2, LEED, UPS, thermal desorption spectroscopy, work function meas. 78−14566
chemisorption of N_2, NH_3 and H_2, photoelectron spectra and LEED meas. 77−66087
chemisorption of O, molecular orbital theory of bonding 77−85059
chemisorption on α-Fe(111) of CO at 300K, photoelectron spectroscopy study 77−62739
chemisorption on α-Fe(111) single crystal surface, of ethylene, halogeno-substituted alkenes, photoelectron spectroscopy study 77−62740
chromised layers, fatigue fracture kinetics study by reverse bend tests *(Russian)* 78−31511
circumstellar Fe grains, form. around Wolf-Rayet star (HD 193793) 80−31301
close-packed phases, eqns. of state and implications for Earth core 79−20780
clusters, electronic struct. and mag. props., MO calc. 77−20219
clusters, supported, Mossbauer spectra 80−7220
coadsorption of CO and H, effect of preadsorption of one on adsorption of other 79−19451
coadsorption of K and O_2 on (110) surface, XPS, UPS, AES, and LEED study 80−80084
coatings for corrosion protection, data sheet 79−70211
coercive force measurement method of quality inspection of heat and thermomechanically treated parts 79−5113
cold rolled, struct., transmission Kossel patterns obs. 77−48451
cold work stored energy effect on mag. moment vs. temp. curve 78−95419
colloidal dispersion, mag. props., struct. and oxidation 80−34699
commercial, deformability, containing H_2 77−90411
commercial, ductile-brittle transition temp., variation with grain size 78−27640
commercial deformability at 600 to 950°C 77−70117
commercially pure, time-temp.-austenization diagram *(Japanese)* 78−6900
compact, form. and growth of metal bridges during short sintering periods 77−1827
compact, on H_2 permeated backing, precipitation *(Russian)* 78−27520
compacts, porous, dynamic hot pressing, press. rel. to density, time 78−60599
compacts, sintered, prod. directly from Fe_3O_4 powder *(Slovak)* 79−15626
compressed, recrystallisation, transmission Kossel study of struct. 78−19776
compression deformed single cryst., induced uniaxial anisotropy 78−52336
Compton profile of mag. electrons meas. 77−32461
concentration determ. in atm. and rainwater in Vizcaya, Spain *(Spanish)* 78−57264
configuration in Sn, Mossbauer effect measurements 78−47333
contact interaction with graphite at high press. and temp. *(Russian)* 79−11722
contact reactions with Al base melt 78−60879
contact to GaAs, effect on minority carrier diffusion length 78−72260
contamination of powdered quartz, thermal effects on DTA 79−100161
conversion electron meas. of core polarisations 80−20530
conversion spectrum anal., outer-shell s-electron density, ACSEMP program 80−7208
in cores of planets rel. to formation from dust grains in early solar system 78−85869
corrosion, and passivation in presence of halide ions in aq. solns. 80−50758
corrosion, colloid chem. appls. 80−89541
corrosion, effect of Pb ion implantation 79−39015
corrosion, Fe_3O_4 film formed in caustic electrolyte, deform. 77−25181
corrosion, indoor, rate meas. 80−76404
corrosion, inhibition and monitoring techniques 80−30132
corrosion, inhibition by Pb azelate, uptake and distrib. of azelate and Pb ions 77−56137
corrosion, monitoring using polarisation resistance meas., techniques and correlations 77−16711
corrosion, oxidation, combined ion-, electron-beam techniques appl. 79−43700
corrosion, substituted methylamines as inhibitors 79−83384
corrosion and conservation of unearthed objects *(Japanese)* 79−79161
corrosion and electrochem. behaviour in NaOH soln. containing ClO_3^- *(Japanese)* 78−72928
corrosion and oxidation, new technique for simultaneous acquisition of Mossbauer spectra and microbalance data 78−44252
corrosion and passivation in LiCl soln., peripheral velocity effect 80−61000
corrosion behaviour, effect of Ta ion implantation 78−31559
corrosion behaviour in distilled water, velocity and dissolved O_2 influence 80−35375
corrosion behaviour in H_2SO_4 soln., ion implantation effect 80−71793
corrosion behaviour of borided and nitrided steels in aqueous media 78−95837
corrosion by molten alkali metal hydroxides and liquid Li 77−44414
corrosion due to V_2O_5 melts *(Japanese)* 80−93691
iron continued
corrosion in acids, inhibition by thiourea and its derivatives 79−20262
corrosion in aq. H_2S, FeS polymorph form. 80−81231
corrosion in H_2SO_4, substituted purine effect 80−30148
corrosion in H_2SO_4 soln., inhibiting effect of Mn, Cd, and Zn ions, H_2 evolution 79−47803
corrosion in HCl, inhibition by thiourea and derivatives 78−7097
corrosion in hot conc. caustic soda soln. *(Japanese)* 79−43473
corrosion in Na loop systems 77−48576
corrosion in O_2 free water, catalytic effect of certain metals 79−47804
corrosion in phosphoric acid, kinetics and mechanisms 79−96188
corrosion inhibition in Na_2SO_4 soln. containing aliphatic acids, electrochemical and ellipsometric study 79−74309
corrosion inhibition in pH range 9.3 to 12.6, tartrate ion effect on oxide film thickening 78−44251
corrosion inhibitor, acid Na_2PO_4 soln. in tap water 80−45424
corrosion of tubes in air saturated soln. under turbulent flow conditions *(Japanese)* 79−61783
corrosion pitting in acid, alkaline solution, gelatin effect 78−95838
corrosion product analysis by Mossbauer spectroscopy 77−28927
corrosion products, Raman spectroscopic detect. 79−16063
corrosion protection 80−30173
corrosion protection by organic coatings, qualitative ellipsometric-electrochem. approach 80−104344
corrosion resistant surface alloys, form. by ion implantation 78−88569
cosmic, dust grains formation, influence of Fe condensation 80−26927
cosmic ray FE peak isotopic resolution, Lexan detectors from Apollo 17 mission 77−56801
cosmic-ray showers in Pb and Fe, hadron-induced 77−60561
cracking, H_2 induced, stress state effect 79−20147
creep, effect of H_2 on struct. 77−16652
creep at 77, 295K, formation of five struct. 80−60926
crevice corrosion in chloride solns. by chromate 79−91847
critical behaviour of thermal cond., elec. resist., Lorenz number and magnetisation 77−4521
crystal grain analysis, using SIMS utilising digital image processing 79−43684
crystal hyperfine fields and neutron scatt. 79−56172
crystallites, vacancy diffusion and vacancy lattices, semi-empirical mol. orbital calcs. 77−1121
Curie point and A-γ transition to 53 kbar, re-examination 79−56529
Curie temperature calc. using model containing five bands 79−56536
cyclically deformed, α-single crystals, mag. props. 77−28412
Cygnus X-3, evidence for X-ray Fe line emission obtained with cryst. spectrometer 78−8153
cytochrome $P\text{-}450_{cam}$, Fe^{3+} zero-field splitting, Orbach relax. rates 77−21483
damping during and after deformation 79−43344
de Haas-van Alphen effect and exchange splitting, effect of pressure *(Russian)* 78−95252
Debye-Waller factors, extended de Launay model calcs. 80−70352
decarburisation of white and malleable in H_2 atmosphere *(Russian)* 77−70210
defect creation anisotropy in electron irradiated samples 77−31994
defect trapping of ion implanted D, depth profile, diffusion eqn. calcs. 80−2047
defects, thermal relaxation, positron experiments *(German)* 80−50455
deformation, influence of crystallographic lattice type *(Russian)* 79−34106
deformation twin form. during high temp. creep *(Russian)* 79−24573
deformed, deep trapping states for H_2 80−29045
deformed, internal friction, dislocation relax. and dislocation-defect interactions 79−29125
deformed single crystal, dislocation distrib. 77−59880
degree of charging of surfaces polished by TiC and synthetic diamond micropowders 78−60880
densification of particulate materials, general law 78−19692
density and thermal expansion in liq. and solid states 80−96668
density of states, photoemission expts. above and below T_c, rel. to magnetism model 77−20536
deoxidation by H_2 during plasma arc heating *(Russian)* 78−15703
deoxidation by V, phase equilibrium with V_2O_3 *(Russian)* 80−16275
deoxidation of liq. by Al, Mossbauer meas. 80−20553
deposition of layers from carbonyl vapour 77−4727
desorption, of $O_2(N_2)$, surface anal., XPS appl. 79−24875
desorption of H into ultrahigh vac. system, using permeation cell 80−86326
determ., in seawater, graphite furnace atomic absorption spectroscopy 80−40768
determ. in water and organic materials, flameless atomic absorpt. spectrometry with wire loop atomiser 80−45586
determination, in flux-grown magnetic garnets, by AAS 78−92585
determination, in radioactive soln., sub- and super-equivalence isotope dilution anal. 78−95984
determination, in salt, spectrochem. method *(Russian)* 79−29440
determination, in silicate materials, by flame emission and absorpt. spectrometry, additive method *(German)* 79−39235
determination, in Venezuelan laterites, interference-free at. absorpt. method 78−31728
determination, in waters, colorimetric-acid digestion method 78−61088
determination by proton-induced X-ray emission anal. in blood and liver tissue 79−53291
determination in atmospheric aerosols by Mossbauer technique 79−79442
determination in bauxite by neutron activation anal. 79−24858
determination in blood serum using AAS 1 at absorpt. spectrophotometer 77−48706
determination in natural waters 79−84550
determinations, effect of surface changes in Pt crucibles 80−61192
diffusion, in HgTe single crystals 79−77818
diffusion, in Ti, under plastic deformation *(Russian)* 79−28146
diffusion, of H, coeff. meas. at low temps. by electrochem. alternating method *(Japanese)* 80−39354
diffusion and electrotransport in Th, 965-1625°C 79−90828
diffusion and permeability of H_2 and D_2 at 49 to 506°C 78−59977
diffusion and solid solubility of Sb, 773-873K, ion backscatt. anal., rel. to intergranular embrittlement 78−71880
diffusion and solubility of Cu, 690-1050°C 77−59146
diffusion bonding with Al 77−62687
diffusion chromising with sintering, effect on porous struct. of Fe-based powder Pzh2K 79−66219

iron continued
diffusion coating by Cr and Pb melt bath, kinetics *(Korean)* 78−60873
diffusion coating of steel, fatigue fracture, microstruct. investigation *(Russian)* 79−52446
diffusion impregnation enhancement by Fe powder addition to impregnant mixtures 77−28044
diffusion in Ag single crystals 78−10225
diffusion in AgBr, vacancy migration evidence 78−47603
diffusion in Au, 700-1050°C *(Russian)* 77−80651
diffusion in Cu, resistometric technique 78−38880
diffusion in Cu, study at high temp. using molten salt electrochemistry 77−84997
diffusion in Fe, Ni and Fe-Ni alloy, effect of plastic deform. and martensitic transformation *(Ukrainian)* 78−55974
diffusion in Mn steel with varying Mn content *(Czechoslovakian)* 77−35743
diffusion in Nb, effect on self diffusion 77−84992
diffusion in Nb, radiotracer and electron microprobe meas. 77−76615
diffusion in Th at 500 to 800°C *(German)* 79−28157
diffusion in Y, Mossbauer exam. 78−27138
diffusion mechanism in Nb 78−47590
diffusion melting in Fe-C melts, heat transfer correl. 80−54348
diffusion of C, coeff. meas. by mag. aftereffect 78−29129
diffusion of C, under US vibrs., initial struct. effect *(Russian)* 78−38876
diffusion of C and Cr, US effects *(Russian)* 77−59144
diffusion of H, 230 to 300K 79−95220
diffusion of H, book contrib. 79−82390
diffusion of Mo, rel. to transforms. 77−4214
diffusion of positive muons 79−56688
diffusion of S in γ-Fe, grain size effect 79−86930
diffusion process acceleration, accompanying US treatment *(Russian)* 80−19976
diffusion saturation with Cr in closed reaction space, kinetics and mechanisms 79−52458
dilute impurity hyperfine fields, comparison with model 78−14954
discharge, hollow cathode in pulse mode, spectral lines and intensities 78−34376
discontinuous film, Mossbauer effect exam. of magnetic state 77−24769
dislocation cores of screw and 71° dislocations, kinks and constrictions *(German)* 77−24316
dislocation density determ. after quenching, internal friction meas. 78−18658
dislocation dynamics, HVEM in situ obs. 78−83822
dislocation mobility and internal friction of α-phase, effect of alloying *(Russian)* 77−31671
dislocation relaxation peaks under low temp. deform., pure specimen *(French)* 80−100867
dislocation struct. around fatigue cracks, exam. *(Japanese)* 78−64623
dislocation struct. at tip of fatigue crack 77−4107
dislocation struct. round fatigue cracks 78−48519
dislocation structure determ. from magnetic props. 78−55874
dislocation velocity, thermal activation exam. of applied stress and temp. depend., expt. methods *(French)* 80−59474
dislocation-magnetic domain wall interaction, magnetomechanical damping expts. 78−39360
dispersed particles, in lunar matter, FMR study, effective linewidth method 78−95523
dispersion strengthened, thick condensates, struct., mech. props. 77−90361
displacement energy, high voltage electron microscope obs. 77−76464
dissociative diffusion in β-Sn, Mossbauer expts., 90-462K 79−7714
dissolution, morphology of differently oriented single crystal surfaces, dislocation effects *(German)* 77−9002
dissolution and passivation, effect of phosphate and chromate corrosion inhibitors 80−21152
dissolution and passivation kinetics in solns. containing O 80−76547
dissolution kinetics, and passivation depend. on temp. and ionic strength 80−97626
dissolution kinetics and diffusion coefficients in molten Al 80−59666
dissolution kinetics in liq. Al, 700-900°C *(Russian)* 77−59119
dissolution rate into molten Al, convection mass transfer *(Japanese)* 78−71858
dissolution under cathodic polarization 80−25899
dissolved, groundwater component indicator of streams draining granite terrain 80−12444
dissolved Fe in rivers, removal during estuarine mixing 79−34830
dissolved organic Fe, determ. in seawater 78−81208
distribution function in interplanetary corotating energetic particle streams 79−70938
distribution in olivine and lunar basaltic liquids 79−35158
distribution in Sn melt when in contact, thermal cycling effect *(Russian)* 80−16562
domain walls, 90°, stable orientations, theory and X-ray observations *(Japanese)* 80−60359
double critical magnetic scattering in polarised neutron expts. 79−65652
droplets in oxidizing slag, decarburization, rate limiting step 79−56944
ductile, influence of crack tip sharpness and morphology of graphite on K_{1c} *(Chinese)* 80−81144
ductile, with different secondary struct., abrasive wear *(German)* 80−25871
ductile fracture, effect of nonmetallic inclusions 78−64660
ductile fracture, fractographic characts. SEM exam. of fracture surface necking obs. 78−35506
ductile fracture analysis, allowance for discontinuity *(Russian)* 77−25133
dust particles, respirable, meas. of mass and thickness by SEM backscattered electron imaging 79−21707
dynamic exponent, crossover obs., TDPAC meas. 80−108021
dynamic hot densification of porous blanks, degree of deformation 77−63585
in early type peculiar stars, abundances 77−78803
eddy current and hysteresis losses anal., simulation of saturation and hysteresis characts. 77−12153
eddy currents in saturable solid, calc. methods *(German)* 77−54644
edge dislocation modelling, flexible boundary conditions and nonlinear geometric effects in α-phase 78−75667
elastic constants, third-order 79−51184
elasticity modulus variation, depend. on external mag. field for single crysts. in trigonal direction (111) *(Russian)* 79−82849
iron continued
elastoresistivity effect, meas. of resistance at 4.2K and 300K, using mag. field method 78−72132
electrical resistivity between 2 and 30K, deviations from Matthiessen's rule 80−10944
electrical resistivity of pure Fe, temp. depend., 1.6 to 298K 78−84194
electrocapillary curves in liq. sodium tetraborate 79−91968
electrochemical behaviour, in molten V_2O_5 *(Japanese)* 80−89498
electrochemical displacement reactions, electron microscope obs. of nucleation and growth, comparison of Cu/Fe and Cu/Al cementation systems 79−47939
electrochemical dissolution, steps and kinks quantitative anal. 79−74103
electrochemical nucleation and growth, of Cu, TEM 80−104451
electrode, electrochem. behaviour in liq. NH_4 solns., effects of added impurities 80−50857
electrode, evaporation rate from cathode spot in vacuum arcs 79−37566
electrode, passive layer, semiconductor model, appl. to electrochem. reactions, review 80−26022
electrode porous, discharge capacity, importance of physical struct. 80−26123
electrode reactions with molten glass 80−85186
electrodeposited coatings, microhardness, Ha_5 design appl. 79−39069
electrodeposition in molten LiF-BeF_2-ThF_4 at electrode, voltammetric and chronopotentiometric exam. 77−1930
electrodes, in (Na, H)ClO_4 solns., complex formation meas. 80−55569
electrolytic, effect of dissolved H precip. on flow stress *(Japanese)* 78−39848
electrolytic, flow stress, effect of cathodic, H_2 charging *(Japanese)* 79−52313
electrolytic, oxidation in melting *(Korean)* 78−19946
electrolytic coated medium C steel, distrib. of bounded fatigue limits 80−81198
electrolytic Fe based composite metal-powder coating structure *(Russian)* 79−83170
electron beam irradiated, influence of created pulsed press. on struct. and props. *(Russian)* 78−34539
electron damage, appl. of KUR LINAC 78−71760
electron irrad., mag. aftereffect 80−88838
electron irradiated pure Fe, annealed, magnetoresistance at 20K *(French)* 80−103677
electron irradiation damage, elec. resist., 20K *(French)* 78−2160
electron spin polarisation in field emission, surface magnetism 78−68607
electron stopping power, continuous slowing down approx., range difference for 0.2 to 10 MeV electrons 80−39187
electron tunnelling into ferromagnetic metals 80−60104
electron-phonon coupling, point contact spectroscopy obs. *(Russian)* 80−70342
electronic band struct., generalised k.p. interpolation method 80−6709
electronic specific heat calculations 79−73323
electronic structure, bulk d-band densities of states calc., optimisation of local orbitals 77−47711
electronic structure, influence of temp. X-ray photoelectron study 77−28681
electronic structure, positron annihilation meas. 79−91524
electronic structure of nontransition element impurity atoms 77−73023
electroplastic effect 79−24589
electroplated with soft Fe coating 80−55524
electropolishing in alcoholic soln. of H_2SO_4 77−16718
EM cascades caused by electrons and photons, 10-100 GeV, longit. development 79−21120
emulsion, magnetic and dielectric, prep., as rubbing sludge *(German)* 78−3376
energy band dispersion and mag. exchange splitting, angle-resolved photoemission meas. 80−71567
energy bands, tight binding calc. *(Korean)* 79−51479
energy loss of heavy nonrelativistic ions in matter, semiclassical theory 80−84224
entropy of fusion, local spin disorder 77−47601
epitaxial film, Mossbauer effect, depth profiling of mag. hyperfine field 80−11295
epitaxial film, Mossbauer effect, interface magnetism 80−11297
epitaxial film on Sb, ultrahigh vac. deposition 78−56572
epitaxial films, even magneto-optical effects 80−76007
epitaxial growth, on alkali halide substrates, role of phase interaction, TEM study 79−46979
epitaxial growth on Au platelets, dislocations 80−96760
epitaxial growth on Au single crystals, substrate temp. effect on morphology 78−26798
epitaxial growth on Cu(111), supersaturation and mode of growth, LEED and AES exam. 78−18929
epitaxial growth on W tip, FIM obs. 78−79904
epitaxial layer on Au(111), misfit dislocation obs. 79−73415
epitaxial layers on Cu (111) mag. props. 78−31098
epitaxy on Au, growth processes, ultra high vac. in situ electron microscopy 78−30842
equation of state of ε phase under static press. conditions, rel. to Earth core-mantle models 80−19904
erosion by laser beam, in self-consistent mode *(Russian)* 77−69945
estuarine river water, particulate heavy metal content, Cochin backwater, India 80−7964
eutectic grain in grey Fe, method of size determ. 77−72529
EXAFS Debye-Waller factors 80−45168
exploded wire, X-ray line emission and plasma conditions 78−59670
exploding wire, elec. resist. at high temp., submicrosec. pulse heating meas. 77−89747
explosive compaction of metal powders 78−64501
extrinsic grain boundary dislocations, study in thin foils, C content influence 80−107273
fast neutron albedo for Fe, concrete and Fe-covered concrete radiation shields 79−76151
fast neutron irradiated at high temps., mech. props. 79−51157
fast neutron penetration, cross section characts. effect, Monte Carlo study 77−23216
fast neutron spectra, an assessment of ENDF/B-IV based on integral meas. 77−50194
fast reactor structural material, integral expts. 80−13612
fast reactor structural materials, activation, (n,p), (n,α) cross sections 80−13624
fast reactor structural materials, meas. and calcs. of integral capture cross-sections 80−13613
fast reactor structural materials, nuclear data 80−13611

iron continued
fatigue, effect of active liquid media on struct. and stress condition *(Russian)* 77−28929
fatigue, push-pull in [110] and [410] single crysts., TEM fracture surface obs. 79−74257
fatigue crack direct obs. by SEM, propag. mechanism *(Japanese)* 79−20164
fatigue crack propag., crack closure, dislocation struct., electron microscopy obs. *(Japanese)* 80−25845
fatigue crack propag., environmental effects in large crystals *(French)* 77−66711
fatigue crack propag., low temp. 78−72876
fatigue crack propag., low temp. 80−35311
fatigue cracking in air and vacuum, optical and SEM obs. *(Japanese)* 79−8387
fatigue fracture kinetics at various deform. amplitudes, vacuum effects 77−4851
fatigue fracture strength and failure, at 77K after cyclic loading at room temp. 78−84996
FCC, electronic struct. at Earth core press. 77−1356
FCC, grain boundary struct. and energy, computer expt. 78−30643
FCC film, epitaxial growth on CuAu (111) surfaces, strong ferromagnetism 80−70557
α-Fe, mag. ordering affecting homodiffusion coeff., 511-1200°C 79−73711
Fe-Cr-Co-Si-Mo, plastic deform. influence on structure and mag. props. *(Russian)* 79−70176
Fermi surface under press., de Haas-van Alphen effect meas. 80−75499
ferrite/austenite interface, prep. and charact. *(French)* 79−95272
δ-ferritic, plastic deform. at intermediate strain rate 77−36592
ferromag., magnetostatic theory of response functions, appl. to Brillouin scatt. 79−61083
ferromagnet, dynamic susceptibility calc. 80−80488
ferromagnet, static and dynamic magnetoelastic coupling 77−20665
ferromagnetic, calc. hyperfine fields and their press. derivations 80−6796
ferromagnetic, chemisorption of H, spin-spin interactions, UPS spectra calc. 80−6630
ferromagnetic, cluster method, environmental effects 78−95405
ferromagnetic, cold work aftereffects 80−88830
ferromagnetic, Compton profile meas. with circularly polarised gamma rays from oriented nuclei *(Japanese)* 78−23548
ferromagnetic, effect of pressure on electron struct. *(Russian)* 79−77987
ferromagnetic, EMF generation by pulsed laser irrad. 78−68021
ferromagnetic, evidence for itinerant electron model, angle resolved photoemission from surface 79−24414
ferromagnetic, hyperfine fields at positive muons 78−43758
ferromagnetic, hyperfine mag. fields at ^{67}Ge, TDPAC meas. 78−43701
ferromagnetic, itinerant, Fermi surface and single particle excitations 80−34350
ferromagnetic, non-mag. impurities, size effects on mag. hyperfine fields 78−43586
ferromagnetic, nonrelativistic LCAO energy band calc. 78−10343
ferromagnetic, partial circular polarisation of thermal emission in mag. field 80−71387
ferromagnetic, spectral thermal emission, partial circular polarisation 78−18806
ferromagnetic, spectral thermal emission, partial circular polarization 79−23751
ferromagnetic, spin wave energies and intensities calc. 77−8293
ferromagnetic, temp. depend. of hyperfine fields for F 80−20141
ferromagnetic, transient mag. field for ^{13}C 79−47362
ferromagnetic γ-phase, Stoner theory support for two-state hypothesis 77−69477
ferromagnetic domain struct., small-angle neutron scatt. 77−66382
ferromagnetic domain theory, quasi-dislocation theory appl. *(Japanese)* 80−60358
ferromagnetic film, surface states, surface magnetisation and electron spin polarisation 80−65648
ferromagnetic films, coercive force, ion plating prep. 77−28730
ferromagnetic liquid, Fe particles in Hg, mag. props., ageing effects 77−12154
ferromagnetic metals, spin fluctuation theory, Curie temp., mag. susceptibility 80−65937
ferromagnetic micropowder, cryst. struct., coercivity, remanence, saturation 80−65967
ferromagnetic properties, book contrib. 80−75724
ferromagnetism, itinerant electron model, spin quantization direction fluctuations, short range order. 80−34582
ferromagnetism, Stoner model, mol. field coeff., temp. and field depends. 77−72975
ferromagnetism, transition metal valence electron struct. explanation 78−47932
FFHR, tailoring the breeding-fission ratio by neutron moderation with iron 78−21677
fibre porous material, props. 79−98798
fibre texture of filaments produced by glass coated melt spinning 77−85966
fibres, extruded, heat treatment 78−35414
field emitted electrons, spin polarisation 77−40337
field-emitted electron spin polarisation by tunnelling through surface pot. 80−29861
filament produced by glass-coated melt spinning, tensile strenght 77−48508
film, amorphous and polycrystalline, Hall effect, resistivity and mag. moment 78−91786
film, amorphous-polycrystalline resistivity transform. temp. of codeposited N_2 78−6461
film, antiferromagnetic ordering, Mossbauer spectroscopy 78−14990
film, asymmetric 180° Bloch walls, Lorentz electron microscopy obs. 78−27063
film, bounded by dielec. layers, surface polariton in ATR angular spectra 79−15545
film, chemisorption induced mag. dead layers, ferromag. reson. obs. 79−91261
film, chemisorption of O_2 and water vapour, XPS obs. 77−48587
film, coated, interface magnetism by Mossbauer spectroscopy 80−75890
film, columnar grain struct. 77−11808
film, core electron polarisation measurement 79−4756
film, domain wall struct. obs. by Lorentz electron microscopy 77−85527
film, EELS, anomalous L_3/L_2 white-line ratios 80−93444
iron continued
film, effect of tensile stress on mag. domain struct. 78−68332
film, electron beam evaporator for in situ deposition studies in UHV electron microscope 80−40264
film, enriched, NMR obs. 78−39443
film, epitaxial, γ-phase, ferromagnetism, spontaneous magnetisation and Curie temp. determ. 78−2711
film, evaporated, adsorbed acetylacetone, XPS study 80−76133
film, evaporated, oxidation resistivity change meas. *(Japanese)* 79−11723
film, evaporated at oblique incidence, columnar and textural struct. *(Japanese)* 77−62776
film, evaporated at oblique incidence, columnar grain struct. using anisotropy-field meas. 77−59231
film, evaporated at oblique incidence, columnar grains inclination angle 80−75468
film, evaporated at oblique incidence, optical and mag. anisotropies 80−7134
film, even magneto-optical transmission effects 77−32354
film, exchange coupled with Fe-Ni film, mag. reversals, hard layer thickness effects *(Russian)* 78−56359
film, FCC, antiferromag. ordering, Mossbauer expts. 77−85508
film, ferromag., magnetoresistance parameter meas. *(Spanish)* 80−2485
film, ferromag. reson., thermodynamical anal. 79−42840
film, ferromagnetic, transverse Kerr magneto-optical, effect, thickness depend. 77−59559
film, five atomic layers, electronic band struct. using linearised APW method 79−69393
film, Hall resist., effect of N impurity codeposition 78−64146
film, high rate deposition by sputtering from two facing targets 77−85938
film, implanted with C ions, HCP struct. formation, electron diffr. study *(Russian)* 79−82469
film, ion beam sputtering prep., struct. and mag. props. 80−35085
film, linear mag. birefr. dispersion 77−69807
film, low-angle grain boundary struct. *(Russian)* 79−42807
film, magnetoelastic excitations, phonon spectroscopy and forbidden transitions 79−82853
film, nuclear magnetisation relax., at 77 to 500K 78−60352
film, nuclear spin system dynamics Mossbauer study in FMR conditions *(Russian)* 80−80651
film, on Cu and Ag substrates, mag. props., Mossbauer spectra meas. 80−11233
film, on NaCl, preferential epitaxy induced by electron bombard. or elec. field 80−10824
film, on PMMA, mag. behaviour during mech. stress cycles *(German)* 80−80581
film, polycryst., heat of adsorpt. of H_2 and D_2 78−91530
film, single crystal, less than 1000 Å thick, inclined 90° walls 78−72384
film, spin polarised photoemission, surface magnetism 79−52083
film, sputtering yields, proton-induced X-ray meas. 80−50488
film, thermally evaporated, contamination effects obs. 80−49545
film, transverse Kerr magneto-optical effect enhancement by surface magnetoplasma waves 77−52056
film, ultra-thin Mossbauer spectroscopic studies of mag. props. 80−44970
film, ultrathin, mag. hyperfine field, temp. and thickness depend. 78−39478
film, vacuum deposited, resist. minimum 80−44741
film, vacuum deposited on Au (111), interaction layer formation mechanism 80−54559
film, vacuum-evaporated contamination, conversion electron Mossbauer spectroscopic obs. 78−23985
film, work function changes upon water contamination 80−44705
film coated by MgO, Mossbauer spectra, mag. hyperfine field 80−7221
film coated with MgO, MgF_2 and Sb, surface mag. 80−7196
film on Fe foil, EM excitation of sound, Mossbauer study *(Russian)* 79−99795
film pulse biased sputter deposited, Kr entrapment 79−28255
films, ferromagnetic reson., photoacoustic detection 80−80613
films, thickness variations in extraordinary and spontaneous Hall coeffs. 80−97013
films, vacuum evaporated, exam. of texture for various vapour beam incidence angles *(Japanese)* 78−48318
fine particle dispersions, shock induced mag. effects 79−82832
fine particles, prep. by gas evaporation technique, crystal habit 77−52239
fine particles formed by gas-evap. technique, cryst. struct. and habit 79−27935
fine particles in matrices, lattice vibr., Mossbauer effect 80−15924
fine particles prepared by vacuum evaporation, mag. props. 78−35007
fine particulate Fe in lunar regolith *(Russian)* 78−89089
fission reactor structural material, resonance data eval. below 300 keV, Doppler effect calc. 80−13618
fission reactor structural material, resonance parameters below 650 keV, self shielding coeffs. 80−13619
fission reactor structural material data eval. for JENDL-1 80−13617
flakes, light flashes, tribo-induced discharge luminesc. rel. to astrophys. 80−25471
flameless atomisation, effect of interfering metals on absorption 77−90675
flow stress, effect of mag. field 77−20673
flow stress during cutting 77−59881
foil, electrodeposited, phys. and mag. props. 79−91275
foil, fatigue crack, low growth rate, microstruct. round tip 77−16674
foil, ferromag. domain-wall width, anisotropy depend. 78−19269
foil, ferromagnetic resonance detection by photoacoustic effect 80−20463
foil, hyperfine interactions of implanted reaction products 78−48093
foil, Lamb-Mossbauer factor at 4.2K 80−20561
foil, Mossbauer spectra, demagnetising field effect on magnetic splitting 80−39932
foils, electrodeposited, microstruct., internal stress and mech. props. 80−20807
fracture mechanism in various temperature and stress intervals *(Russian)* 79−24600
fracture surface singularities under single loading conditions *(Russian)* 80−50696
fracture under influence of high power US waves *(Russian)* 79−5034
fracture-mechanisms, tensile specimens 80−85039
friction at elevated temps. 78−15548

iron continued
friction behaviour in oxygen, development of wear-protective oxides and influence on sliding friction 80−30111
friction in liq. Sn, Rebinder effect *(Russian)* 79−29269
friction props. of surface films in air and high vacuum 78−60850
frictional behaviour, effect of mechanical properties 80−55548
fusion reactor materials, neutron experiments for data testing 78−5023
g-factor, in pure polycryst. Fe 77−24748
GaAs:Fe, superparamagnetism, spontaneous magnetization 79−11285
galactic cosmic rays, isotopic composition, balloon meas. 78−89024
gamma fields induced by ^{252}Cf neutrons 78−50240
gamma photon backscattering, energy dependence *(Rumanian)* 79−76316
gamma point source building factors, moments method code 80−27828
gamma to alpha transform. 79−29051
gamma-ray buildup factors 80−27822
gamma-ray impact, absolute pair production cross-section meas. 78−43958
garnet:Fe^{3+}, spin Hamiltonian parameters, g-factors, temp. depend. EPR obs. 77−48038
gas phase abundances in planetary nebulae 78−28744
geochemistry of Fe in Puget Sound 78−69370
Gibbs energy in BCC and liquid states rel. to FCC, Fe-C and Fe-N phase diagrams 80−60846
glass:Fe^{3+}, EPR line shape, H to g transforms. 77−12193
glass:Fe, thermally detected EPR meas. 77−63273
glass, realistic relaxed struct. model, pair distrib. function 78−30544
glassy, heat of crystn., and bulk modulus, calc. using struct. model 78−51428
grain boundaries, electron microscope obs. *(Russian)* 79−4311
grain boundary diffusion of Ni *(Japanese)* 78−18837
grain growth, abnormal, kinetics 79−24537
grain growth, normal and abnormal, statistical distrib. of linear grain sizes 80−93581
grain growth kinetics under 2 to 10% tensile deform. 77−40435
granular deposits, plasma reson., rel. to interstellar dust extinction curve 79−21387
granular film, microstructure using X-ray, electron diffr. and TEM 79−65344
graphite and cast Fe dissolution during sintering 79−33969
grey cast, in ethanediol/water, inhibition of corrosion by benzoate/benzotriazole mixture, synergistic effect 80−45425
group consts., neutron spectra of small pile surrounded by Pb reflector 79−6738
Gruneisen parameter, behaviour at high press. 78−83899
guanidine aluminium sulphate hexahydrate type ferroelectrics, ESR of Fe^{3+} exchange pairs 77−90022
guanidinium aluminium sulphate hexahydrate:Fe^{3+}, EPR spectra, angular var. calc. 80−54940
hardening and softening during adsorption fatigue in surface active medium, governing laws 77−86230
heart tissue, thalassaemic, Mossbauer spectra of Fe deposits 78−73202
heat capacity temp. depend. meas., internal energy and entropy, anharmonic theory calcs. *(Russian)* 80−54402
heat treatment to produce graphite *(German)* 77−59818
heavy ion irradiated, TEM exam. 79−7638
Hercules X-1, Fe line emission discovery in low-state spectrum by (HEAO-1) 79−5922
hexavalent, ZPS, binding energies calcs. 80−43013
high C, interfacial tension in phase boundary with MnO-TiO_2-SiO_2(Al_2O_3) *(Czech)* 78−63907
high dispersion ferromagnet, magnetic powder defectoscopy material 80−35137
high purity, H induced softening *(Japanese)* 79−78988
high purity, large single crystal sheet prep. method *(French)* 77−77375
high purity, prep. and recrystallisation temp 77−55911
high purity prep. by electron beam floating zone melting under ultra high vacuum 77−28751
high purity single crystals, dislocation density rel. to work hardening *(German)* 77−32590
hollow-cathode emission spectra, 200 to 430 nm 79−72263
hot dip galvanising, texture of δ-Fe-Zn layer formed 77−9001
hot galvanising with liquid Zn, Fe-Zn compound form. *(French)* 79−20275
hot shortness, high-temp. embrittlement, residual and trace elements influence 80−66644
human body Fe stores meas. technique, nuclear resonant scatt. 79−83914
hydrogen, induced cracking, crystallographic and fractographic studies 79−5052
hydrogen adsorption at dislocations and cracks 79−20146
hydrogen embrittlement, fracture mode transition as function of grain boundary sulphur 80−55520
hydrogen embrittlement and H_2 adsorption 80−89401
hydrogen permeation, rel. to embrittlement, organic inhibitors, surface treatment 80−108635
hydrostatic compression of Fe and related compounds, overview 78−83862
hyperfine field and diffusion of μ^+ 77−52006
hyperfine field at nonmagnetic impurities 80−25129
hyperfine field at positive muon 80−40029
hyperfine fields at impurities in ferromag. metal 78−52244
hyperfine fields of ^{57}Fe nucleus isolated in solid Xe 78−43749
hyperfine interactions, for ^{238,240}Pu and ^{248}Cm, PAC obs. *(Russian)* 77−4593
hyperfine interactions in implanted metals, Mossbauer spectra 80−108141
implantation in metals, electric hyperfine interactions, conversion electron Mossbauer meas. 80−7241
implanted, ^{155}Tb sources produced by recoil implantation, ^{155}Gd Mossbauer transition 80−40009
implanted into Al, hyperfine interactions, conversion electron Mossbauer spectroscopy 78−52391
implanted with heavy impurity, relation between hyperfine field and lattice-location meas., influence of radiation damage 80−6794
impure, Snoek peak figures in various strain amplitude ranges 80−66562
impurity, in Pd-H, Mossbauer study of local environment of substitutional impurities 80−60475
impurity concentrations on wall during Tokamak discharges, laser probing technique 80−49013
impurity hyperfine fields 79−99518
iron continued
impurity in Al nuclear reactor fuel tubes, proton activation determ. 80−27741
impurity in Ni substrate, effect on depassivation 79−61777
impurity in rare earth oxides, determ. by at. absorpt. 79−87905
impurity segregation, physico-chemical aspects *(Czech)* 80−60866
industrial catalysts for NH_3, XPS studies 79−70370
inelastic deformation, mech. eqn. of state, stress relax. 77−56047
inelastic deformation mechanism, fatigue testing in air and corrosive environments *(Russian)* 79−52432
inner level ESCA spectra, many particle effects *(Russian)* 79−91560
interaction with dense stream of N ions, metallography, microhardness, specific volume *(Russian)* 80−15169
interatomic potentials from phonon spectra 80−19744
interband optical conductivity, self energy correction 80−2792
intercalation compound with TaS_2, NbS_2, microstructure 77−84729
intercell exchange energy, Hartree-Fock approx. 80−60239
intergranular brittleness, effect of O and S 77−36650
intermediate layer in Zircaloy-4/stainless steel diffusion couple 79−10987
internal fields, positive muon investigation 78−68438
internal friction, H-dislocation interactions, varying purity 77−52377
internal friction and elastic constants, reson. vibrs. of metal spheres 78−15443
internal friction in plastic deformation process *(Chinese)* 80−88259
internal friction near Curie point 79−24567
internal magnetic pressure and compressibility anomalies, itinerant model 77−16034
internal stress meas. by decremental unloading technique 78−64576
interstellar Fe, depletion derived from S 59 obs. of 67 stars 79−2563
interstellar gaseous Fe depletion from Fe II resonance line UV obs. toward early-type stars 79−44584
interstitial site determ., μSR technique 80−71287
intracluster Fe mass and distrib. between rich clusters of galaxies 79−5895
ion fine structure in haemoprotein 80−30661
ion resonance-line intensity meas. for Tokamak plasma spectroscopic diagnostics 80−48993
ions, $2s^22p^53l$ and $2s^22p^63l$ configs., excited state energy levels 79−54781
ions, Li-like Auger contribs. to electron impact ionisation 80−87231
ions, multiply charged, solar wind spectrum, ion frequencies and velocities *(German)* 80−51636
ions, two vacancies in K shell, 2 electron 1 photon, and hypersatellite transition probabilities 78−46294
ions in Tokamak plasmas, spectroscopy and atomic physics 80−53938
irradiation softening in single crystal, temp. and orientation depend. 77−86113
isochronous annealing recovery, in cold rolled and explosively formed samples 79−100166
isotopic composition of primary cosmic rays 79−70937
itinerant electron ferromagnet, magnetovolume effects 80−60397
itinerant electron ferromagnetism, local exchange model 77−72994
itinerant electron ferromagnetism, press. effects on mag. props. 77−66241
itinerant ferromagnet, neutron inelastic scatt. 79−7970
itinerant ferromagnet, spin-wave dispersion and linewidth 79−4668
K shell photoelectric cross section, at 74.409 keV 79−72288
K shell prod. cross section of Ti, Cr, Fe, Ni, Cu, Zn for 75 to 150 keV p and e excitation 79−47552
kinetic friction re-examination using modified pin and disc machine 80−55547
$L\alpha_{1,2}$ and $L\beta$ X-ray emission spectrum, determ. using modified photoelectron spectrometer 78−50557
laser, pumping using KrF laser, vap. form. by flash and discharge decomp. of $Fe(CO)_5$ 78−74890
laser irradiated α-Fe, Mossbauer effect and positron annihilation *(Russian)* 78−19390
laser microprobe emission spectroscopy, matrix effects 77−16870
laser radiation absorptance at 1.064μm 79−87528
lattice atom displacements near end of implanted μ^+ tracks 78−55890
lattice defects, relax. studies, computer simulation 78−79604
lattice diffusion and grain boundary diffusion of Cu *(Japanese)* 78−18836
lattice dimensions, difference between vacuum condensates and massive specimens *(Russian)* 77−31912
lattice distortions due to H, X-ray diffr. exam. 78−79629
lattice hardening and anomalous softening caused by electrolytic H_2 charging *(Japanese)* 79−43398
lattice hardening due to dissolved H_2 77−8952
lattice hardening due to dissolved H_2 in Fe, and ferritic steel 78−76656
lattice hardening/softening due to dissolved H_2 77−77581
lattice isolation of impurities from hyperfine interaction and channelling results 78−43731
lattice parameter determ. ratio method 77−43106
lattice parameters, 293 to 1273K, α to γ phase transform., X-ray diffr. exam. *(Russian)* 80−50625
lattice vibrations, temp. depend. 78−95124
layers formed by reaction with molten Al, X-ray, EPMA and hardness meas. *(Japanese)* 78−72926
LEED analysis of clean (001) surface 77−43411
LEED from ferromagnets, spin polarisation effects, calc. 79−99686
light scattering by spin waves 80−45086
light scattering from surface and bulk thermal magnons 80−45087
liquid, absorption of gaseous O_2 78−51686
liquid, alloying element effect on H_2 diffusion *(Russian)* 79−69270
liquid, asymptotic form of structure factor 77−7651
liquid, at Earth outer core conditions, Gruneisen γ function determ. 79−84186
liquid, C saturated, decarburization by CO_2, effect of S 79−11726
liquid, C saturated, interfacial tension determ. between graphite by buoyancy meas. *(German)* 80−34273
liquid, C solubility, donor-acceptor mechanism 80−49365
liquid, coordination numbers, calc. in microinhomogeneous struct. model *(Russian)* 80−38902
liquid, CPA theory of excitations, lattice model 79−87030
liquid, density of states and effective medium approach 77−76717
liquid, diffusion of O_2, Ar, H_2 *(Russian)* 77−55369
liquid, electrical transport 79−38040
liquid, eqn. of state in Earth's core conditions 77−73694
liquid, H_2 diffusion *(German)* 78−14487
liquid, Hall effect, band struct. and exchange scatt. 80−80250

iron continued
liquid, homogeneous nucleation of CO bubbles 77−60106
liquid, in heterogeneous equilib. with CaO, MgO, Al_2O_3, SiO_2, calcs. *(Russian)* 77−59093
liquid, multiple scatt. calcs. of resist. 78−76039
liquid, N activity coeff. 77−72699
liquid, N solubility and AlN precipitation 79−11630
liquid, N solubility depend. on added elements, mechanism *(Russian)* 80−65223
liquid, O_2 diffusivity, meas. by EMF method 78−14494
liquid, reactions of CO, CO_2, with dissolved O and C, equilibria 78−44397
liquid, short-range order struct., O impurity influence *(Russian)* 80−38901
liquid, soft X-ray band spectra 77−52199
liquid, sp. ht. eqn. for high temp. 77−51510
liquid, struct. factor and isothermal compressibility 77−11462
liquid, struct. factor and radial distrib. curves, X-ray determ. *(Russian)* 77−31580
liquid, struct. model, mol. dynamics calc. 79−50994
liquid, structure factor near MP, X-ray diffr. anal. *(Russian)* 77−31579
liquid, surface tension meas. with levitated metal droplets, influence of oscill. amplitude 78−51798
liquid, thermodynamic data *(German)* 80−40328
liquid, thermoelec. power meas. 77−35928
liquid, viscosity, effect of C, O, S, P additions *(Russian)* 77−59134
liquid, viscosity, up to 2100K, vibr. method 78−38866
liquid, viscosity calc. using microinhomogeneous struct. model *(Russian)* 80−15284
liquid, viscosity meas., temp. depend. *(German)* 77−55377
liquid and amorphous states, short-range order comparison 77−1069
liquid impact erosion and cavitation erosion comparison 80−104302
liver overloaded with iron diagnosis, SQUID biomedical appl. 80−101244
liver tissue and tumour proton mag. relaxation rel. to Fe content 79−39355
localised moments, detection by electron energy loss spectra 77−69949
long-time strength, in alpha phase *(Russian)* 77−44330
loss from asbestos fibres in pulmonary tissue, obs. 79−74825
low temperature deform., strain-rate cycling and stress relaxation tests *(Japanese)* 78−52876
Luder's band form. high speed camera obs. 80−16410
Luders band formation, and plastic instability model related with strain softening due to Johnston-Gilman-Hahn theory 79−61676
lunar drill sample, neutron activation and radiochemical anal. *(German)* 80−51673
lunar mare basalts, Fe^{2+} reduction by S loss 77−9681
lunar regolite, Fe reduction on heating in vacuum, XPES spectra 80−41740
lunar regolith, metallography of Fe particles *(Russian)* 78−16321
lunar regolith, reduction of Fe, Ti, Si in H atom., X-ray photoelectron spectra 79−25527
lunar samples, metallic Fe prod. by preferential sputtering 77−29666
lunar soil, Fe and Ti bands in glass fraction 77−49320
lunar soil grains, surface related component of Fe metal 79−16851
lunar soil samples Fe content via Mossbauer studies, Luna 16 and 20 samples 77−22124
macrosegregation of S and form. of equiaxed crystals, autoradiographic study, cast struct. effect 77−63658
magnetic 90° domain wall-dislocation tangle interaction, magnetomechanical damping expts. in high purity samples 79−78496
magnetic aftereffect, phenomenological description 80−88835
magnetic aftereffect correlations with internal friction after low temp. neutron irradiation 78−10733
magnetic aftereffect in α-phase, neutron irrad. at 77K 78−2705
magnetic aftereffect of interstitial O 78−91903
magnetic aftereffect spectrum after low temp. neutron irradiation 78−10732
magnetic aftereffect spectrum of α-phase low temp. electron irrad. 78−2704
magnetic aftereffects of H isotopes, book contrib. 79−82835
magnetic anisotropy energy, band calcs. *(Russian)* 77−20583
magnetic anisotropy in crit. region, neutron polarisation-vector analysis 78−31065
magnetic breakdown and Hall resist. theory and model calcs. 80−75552
magnetic disaccommodation, low temp., in neutron-irrad. sample, Bordoni relax. 77−4542
magnetic domain structure, neutron small-angle scatt. from dynamical theory of diffr. 79−24189
magnetic domain wall mass, press. due to eddy currents 77−12144
magnetic domain wall-dislocation interaction, magnetoelastic damping 78−14980
magnetic ground state props., simple one-electron theory 77−63063
magnetic hyperfine field at ^{129}I, press. depend., nucl. gamma reson. 80−71256
magnetic hyperfine field of K, Ca and Ti in Fe, TDPAD meas. 78−52389
magnetic hyperfine fields, SCF calcs. 77−8061
magnetic hyperfine fields of Zr, DPAD meas. 80−39901
magnetic impurity in β'-NiAl, self consistent embedded cluster model 80−2549
magnetic ink, prep. 77−9128
magnetic moment var. during plastic deform. *(Russian)* 77−66401
magnetic moments, local short range order, high temp. effects 80−65902
magnetic powder, particle deformation effects on mag. props. 77−63236
magnetic relaxation below 30K, permeab. after thermal ageing and demagnetisation, in high-purity Fe 77−85502
magnetic relaxation of H and D 78−64228
magnetic resonance, singleand multiple-pulse of oriented ^{60}CO nuclei pulse, of oriented ^{60} nuclei, radiative detection 77−66437
magnetic structure of γ-phase, Mossbauer studies 80−39917
magnetic surface props., Mossbauer effect 77−69757
magnetic susceptibility, lineshape and moment analysis, magnon excitations 79−99693
magnetic susceptibility, orbital, calc. for paramagnetic Fe 80−7075
magnetic transient fields at N and O nuclei recoiling in external mag. field 77−12263
magnetic transitions, first order, shock induced, characts. and discrimination from TRM 78−64205
magnetic viscosity of high purity samples 78−19282
magnetisation, spin wave and Stoner contribs. 77−73017
iron continued
magnetisation curves in high mag. fields above Curie point 77−66386
magnetisation process in high mag. fields in crit. region 77−85498
magnetised, ^{13}C recoil, spin precession for $5/2^+$ state, transient field 77−2904
magnetised, nature of dynamic mag. fields acting on ^{82}Se, ^{56}Fe and ^{28}Si, gamma-ray spectra meas. 78−43697
magnetised foils, ^{56}Fe recoil, enhanced transient fields 77−15802
magnetised to saturation, props., positive-muon study 78−6619
magnetism, mol. Jahn-Teller reson. states as possible antecedents 80−75701
magnetism, randomised exchange field theory 80−39733
magnetism at high temps. 80−75721
magnetism theory 79−78299
magnetization self-reversal in circular magnetic field 78−14982
magneto-optical effects and current operator form, appl. of theory for ferromagnet. *(Russian)* 77−81084
magneto-optical near UV reflection-spectra, meridional and polar intensity effects *(Russian)* 78−39572
magneto-volume effects calc., rel. to itinerant electron model 78−43621
magnetoelastic damping at low shear stress amplitudes *(French)* 77−59441
magnetoelastic excitations and ferromagnetic resonance 79−82879
magnetomechanical acoustic emission for residual stress NDT 80−71149
magnetomechanical damping, magnetic field variations 80−93156
magnetoresistance, grain-oriented mag. steel sheet *(German)* 78−68020
magnetostatic field prod. by toroidal conductor 80−1104
magnetostriction sign change under compressive stress for polycryst. samples 80−29596
making industry, evolution, review 77−73431
martensite, molecular cluster theory for electronic struct. 77−55497
martensitic transform., induced by H_2 *(Russian)* 77−66643
martensitic transformation, morphology and transition temp. 80−3042
martensitic transformation at high temp., transform. temp., growth rate, stress relaxation 78−56636
mechanical properties of low temps. 78−44219
melt, treatment by high-temp. gas stream, math. model, applic. to nitriding *(Russian)* 78−53016
melt, wettability of CaO-MgO refractory *(Russian)* 78−10257
melt, wettability of ZrO_2 melt 77−89619
melt, wetting of MgO-Al_2O_3 ZrO_2 refractory 78−22936
melting and adiabatic temp. distribs. in outer Earth core 77−70626
melting temperatures, depend. on interatomic pots. choice 79−74863
melting under Earth core conditions in shock wave expt. 80−104931
melting without crucible, with EM levitation *(Polish)* 80−89130
membranes, effect of electrodeposited metals on H permeation, proposed catalytic mechanism 78−53252
metallic adhesion, use of fracture mechanics and contact resistance meas. 77−70271
metallic coated, produced by electrospark alloying, corrosion behaviour in Cl saturated NaCl solns. *(Russian)* 79−39026
metallised pellet, factors influencing crushing strength after H_2 reductions 79−11531
meteorite fusion crusts and ablation debris 78−61819
microcracks formed by H_2 precipitation, SEM and TEM obs. *(Japanese)* 79−70071
microcrystal, Mossbauer Debye-Waller factor size and temp. depend. 78−15065
microcrystal, Mossbauer effect 79−1736
microcrystals, dislocation struct. singularities in early deform. stage *(Russian)* 77−55284
microhardness of single crysts. effect of temp. on dislocation structure *(German)* 79−52357
microparticle, trigger discharges and impact damage in HV vacuum insulated gap 77−24227
microspheres, impact on mech. polished electrodes, contact pot. influence on charge transfer *(French)* 78−47198
microvoid form., gaseous impurity atom effects, positron annihilation study 80−49275
migration of C to the surface of cast Fe, solubility *(Russian)* 80−92720
minerals and concretions origin from Hepworth carboniferous sediment, geochemistry 80−17262
mitochondria of bovine heart, EPR investigation of two forms of Fe-S centre N-2 78−69014
molecular adsorption and dissociative chemisorption of N_2, XPS obs. 79−99427
molten, Ce-S-O equilibrium *(Chinese)* 80−104423
molten, contact reaction with graphite 80−15342
molten, diffusion of V, Co, Mb *(Japanese)* 77−51531
molten, gases O_2 absorption 80−11836
molten, impurities effect on viscosity 78−95172
molten, mag. neutron scatt. at small momentum transfer caused by spin fluctuations 77−47968
molten, mag. small-angle scatt., persistent spin fluctuations 79−11288
molten, near-order struct., X-ray scatt. meas. 77−55231
molten, transfer of Si from gas phase to molten Fe in blast furnace 77−4930
monomers and dimers in solid Ar, EXAFS study 80−97381
Moon, Fe and Ti surface distrib., orbital γ-ray spectra 80−94727
Moon, Mg/Fe large-scale var. from orbital gamma-ray data 78−12123
Morse potential, equation of state determ., high temp. and pressure, computer expt. 78−75800
Mossbauer absorpt. spectrum, domain struct. effect 79−69758
Mossbauer effect at high press. in α-, ε- and γ-phases 80−15858
Mossbauer energy shift near Curie temp. 78−52388
Mossbauer observations of critical fluctuations 78−43724
Mossbauer spectrometry of Fe in hepatic and splenic tissues 80−81544
Mossbauer spectrum linewidth, influence of dislocations 79−99806
multilayer films stability, Mossbauer spectra 80−29651
muon$^+$, 40 MeV, traversing magnetised plates, dynamic mag. fields 79−38422
muon$^+$ diffusion, spin rotation, effect of impurities 80−7249
muon$^+$ hyperfine field and relaxation, temp. depend. 78−95538
muon$^+$ rotation meas., local hyperfine field temp. depend. 77−63349
muon$^+$ spin precession and relax., hyperfine field temp. depend. 77−63350
muon$^+$SR, theory of spin depolarisation rate 78−80271
muon diffusion, spin relax. 79−78599
muon probe diffusion studies 80−75913
muon quantum diffusion 79−78598
muon spin rotation; freqs., and relax. rates 80−55006

iron continued
myoglobin-Fe^{3+} compounds, Mossbauer and suscept. expts. 78−24019
n=2-2 transitions in XUV spectra, anal. 80−102472
natural, neutron total cross section minima 78−37387
neutron critical scatt., above T_c, polaris. asymmetry 78−34994
neutron critical scattering, temp. shift 78−38589
neutron critical scattering anisotropy in monocryst. 77−66327
neutron critical scattering max., temp. shift, polycryst., test of dynamic scaling theory 79−50953
neutron group constants, meas. of energy and space distribs. 77−26829
neutron irrad., mobile C atom trapping, anelastic and mag. relax. 80−100306
neutron irrad. and H_2 absorption effects on mech. props. 78−34546
neutron irradiated, low temp. mag. relaxation 79−8022
neutron irradiation damage simulation, reliability of use of fission fragments 79−42113
neutron magnetic critical phenomena, review of new effects 79−56534
neutron ns. slowing down time, expt. obs. 78−58319
neutron number and dose albedo 79−93681
neutron slowing-down equation, with inelastic scatt. 79−26465
neutron yield calcs., electron beam incidence 78−95622
Ni_2SiO_4, reaction with Fe to produce Ni gamma resonance spectroscopy *(Russian)* 78−15332
nitrided, X-ray and Mossbauer study of surface 78−48568
nitrided layers obtained by ion bombardment, microstruct. exam. *(French)* 78−15581
nitrided wire, magnetic charact. and microstruct. *(Korean)* 78−19277
nitriding, thermodynamic considerations *(German)* 78−60874
nitriding by ion beam, SEM obs. 80−2095
NMR of oriented nuclei on ^{197m}Hg implanted at T<0.5K 77−81020
noncrystalline, electronic density of states, multiple scatt. calcs. 78−91578
noncrystalline, mag. hyperfine data from Mossbauer spectra 78−39477
nonlinear magnetostatic problem soln. *(Russian)* 79−64138
notch toughness of high-purity iron 77−44353
nuclear inelastic channel suppression in ^{57}Fe, nuclear reson. and electronic scatt. of γ-quanta, hyperfine transitions 78−60361
nuclear material, neutron capture cross sections in intermed. energy region, method and exptl. facility 78−21637
nuclear orientation and NMR/ON on implanted ^{114m}In 79−47345
nuclear orientation-mag. reson. of ^{48}V 79−61288
in oceanic phosphorites, Fe, Ti and Al behaviour during initial form. stages 80−31029
optical and electronic properties, temp. depend., 20, 1400 and 1600°C 79−87412
optical constant dispersion and emissivity, up to 900K 78−52464
optical constants 12 to 24 μm, anomalous skin effect region 77−20842
ore, leaching, effects of ultrasonics and their appls. 78−92214
ore, texture anal. of Ca ferrites in sinters 80−18009
ore, wet sieving in fine grain range *(German)* 80−93515
ore band associated with meta- acidic intrusive, Himalayas, Mossbauer meas. 79−79821
ore concentrate, sinter quality improvement *(Chinese)* 80−104089
ore deposit integral charact. determ. from magnetic anomalies *(Russian)* 79−62621
Orion Nebula, Cl and Fe abundances from forbidden Cl II and Fe II near IR mapping 80−62217
oxidation, combination anal. using ESCA, AES and SIMS 78−72924
oxidation, conversion electron Mossbauer spectroscopy, appl. to surface props. and reactors 78−60359
oxidation, core and valence level photoemission studies of Fe oxides 78−15290
oxidation, electron re-emission Mossbauer spectroscopy 77−16752
oxidation, FIM obs. 80−89388
oxidation, in hostile environment, in situ meas. method 78−44277
oxidation, reflectance IR study rel. to component of stainless steel 79−47811
oxidation, scanning electron diffr. appl. 77−25178
oxidation, thickness of oxide layers 77−77640
oxidation, under low O_2 partial press., wustite whisker form. obs. 79−77972
oxidation and domain structure, electron microscope exam. *(Russian)* 79−1437
oxidation and reduction kinetics in O_2-H_2 atmosphere *(Korean)* 80−71906
oxidation at 300°C 79−61792
oxidation at Curie temp. 79−29279
oxidation at elev. temp., scale/metal interface charact. 79−74286
oxidation in CO_2, early stage obs. by AES 78−48570
oxidation in CO_2 at 1330°C 79−5077
oxidation in NaCl soln., ferric oxide film form. 80−25898
oxidation in O_2 and CO_2 at 550°C, growth and struct. of oxide films 77−52549
oxidation in pure O_2 at 973 to 1173K, morphological study of oxide scale 78−15595
oxidation in SO_2 atmospheres, study by means of ^{35}S radioisotope 77−52550
oxidation kinetics near Curie temp. 79−66218
oxidation kinetics using proton-induced X-ray emission 80−35618
oxidation mechanism in composite atmos. *(Polish)* 79−79142
oxidation of (001) surface, first monolayer at. struct. 78−34706
oxide film thickness determ. by electron backscatt. Mossbauer spectroscopy 78−72933
oxide overlayer thickness determ. by ^{57}Fe conversion elec. Mossbauer spectroscopy 79−57142
oxide scale fracture on substrate deform. 78−11407
oxide surface layer, TOF atom probe anal. 78−64766
oxidised powder in prod. of soft mag. mat. 77−63813
paramagnetic mag. entropy 77−63081
paramagnetic state, itinerant electron model 80−65769
partial densities of states, electron-phonon interaction 78−51869
particle, motion as graphite surface 79−90850
particle formation, ultrafine, via pulsed laser breakdown of $Fe(CO)_5$ 80−84881
particle formation by evap., electron microscopy obs. of interaction processes 80−104053
particle motion effect on Mossbauer spectra 80−84671
particles, dispersed in Hg, mag. props., aggregate form. 80−60375
particles, spin collinearity, Mossbauer spectra study 80−71114
particles, sulphuration, FeS hollow particle growth 77−68934
particles in glass-like C matrix, identification and props. 80−11229
iron continued
particles in Hg, ferromagnetic liquid, resistivity 79−1591
particles in Hg liq., time depend magnetisation 80−44877
partition patterns in recent sediments of Indian continental shelf 77−73710
passivated, Fe_3O_4-Fe_2O_3 thin film, electron diffr. study *(German, English)* 80−89418
passivation, by O_2, mechanism of action of weak acids and their salts 80−50886
passivation, film form., stability and breakdown 78−19937
passive, interfacial impedance *(Japanese)* 77−48581
passive film AC electroreflectance and impedance obs. 78−7093
passive film form. in phosphate soln., intensity-following ellipsometry study 80−104345
passive films and phosphate layers, sputtering rate evaluation in glow discharge lamp 80−45443
passive films studied using AES combined with ion sputtering technique 80−35378
passivity, electrochem. exam. *(Japanese)* 78−39946
passivity in aq. soln., correlation with mol. struct. 80−16541
passivity in aqueous soln., correlation with molecular struct., electrostatic hypothesis 79−91831
permeability, diffusivity, and solubility, of H and D at 10 to 60°C 78−75887
permeability, solubility and diffusion of H and D, 9 to 73°C 77−76560
permeability to H_2, influence of microstruct. changes induced by cold working *(Russian)* 77−20182
permeation by H in fusion reactor 80−34242
phase diagrams, use in production 79−11572
phase transformations and vacancy form. by positron annihilation 80−2155
phase transition thermodynamics 78−18769
phonon dispersion relations, modified tensor force model 80−103428
phonon spectrum of α-phase, slow neutron inelastic scatt. meas. 77−80592
photoelectron spin polarisation and itinerant magnetism 78−68602
photoemission, exchange-split energy-band dispersions 80−35059
photoemission and electronic spectra, exchange splitting 77−4717
photoemission study of (100), (110) and (111) surfaces, ferromag. band struct. 79−38714
photon absorption and photoelectric cross-sections calcs. 79−31486
photon penetration, photon backscatt. incidence angle depend. 80−104008
photoneutron yields released by incident electrons, improved calc. 80−27630
physiological kinetics, erythropoietic activity clinical assess., distrib. model 79−100587
pinned domain wall motion, magnetic damping studies 80−65956
pion$^-$ absorpt. length in Fe in range 15<E<140 GeV 80−894
pionic atom, 2p level shifts and widths 78−46469
pitting in Na_2SO_4-NaCl solns. *(Japanese)* 78−85042
plagioclase:Fe^{3+}, ligand field bands of impurity luminesc. centres and their site occupancy 78−88350
planetary nebulae, Fe condensation and nebula form. models 79−40238
plasma, Fe-H mixture, confined atom-, and Debye Huckel-, Thomas-Fermi-Dirac models 77−24053
plasma, laser prod. study by UV spectroheliography 78−22529
plasma, laser produced, extreme UV line profiles of expansion velocities 78−14199
plasma, simplified spectra obtained by electro-optic gating of radiant emission 78−22561
plasma, Tokamak-produced, $2s^22p^k$-$2s2p^{k+1}$ transitions in F I to Be I isoelectronic sequences 80−37765
plasma impurity, flux on wall of DITE Tokamak 80−28688
plasma impurity, high-temp. ionis. equilib. and radiative cooling 78−42712
plasma impurity, in PLT, charge-state determ. by Bragg cryst. X-ray spectroscopy 79−68956
plasma impurity, radiation loss effects on Tokamak expts. 78−22465
plasma impurity, radiation losses 77−19678
plasma impurity, radiative cooling processes 77−19677
plasma impurity, screening effect of divertor in T-12 Tokamak 80−28844
plasma produced by 250 ps laser pulse, X-ray spectra 77−19769
plasma Tokamak discharge, impurity emission spectra for diagnostics 77−11403
plastic deform. and fracture, H_2 effect, studied by electron microscopy and Auger spectroscopy *(French)* 77−77545
plastic deform. of single crystal with shear tests in {110}⟨111⟩ and {112}⟨111⟩ slip system 77−48509
plastic deformation, homogeneous, yield point behaviour *(German)* 80−35248
plastic deformation mechanism, meas. of microplasticity 78−60720
plastic flow props. of single crysts., hydrostatic press. effects 79−38887
plastic strain, thermoactivation anal. exam. of method *(Russian)* 79−57164
plastically deformed, dislocation arrangement exam. by ferromag. techniques 78−63774
plastically deformed, high field suscept. anisotropy and domain struct. 78−15002
plastically deformed by pulsed mag. field, mobility of Fe atoms, radiotracer profiles 79−28584
plastically deformed grads EA, magnetoelastic props. *(Russian)* 80−44893
plasticity, athermal and thermal *(Russian)* 79−11685
plasticity, temp. and rate dependence for different rigidities of stressed state *(Russian)* 79−29139
plated with Ni, surface film softening in single slip orientation 77−32719
plating cathode current distrib. influences *(Russian)* 79−96197
point contacts between ferromag. metals, singularities depend. in d^2V/dI^2, phonon spectra 79−60457
point defect estimation from specific heat and volume in plastically deformed pure metals *(Russian)* 80−54223
polarised, ferromag., evidence for K-shell polarisation of ^{12}C ions via mol. orbital promotion 80−71273
polarised, high vel. ion recoil, transient mag. fields 77−43910
polarised, precession meas. on nucl. excited C-, O- and F-ions recoiling 78−37285
pole pieces, in electromagnets, mag. anisotropy effect on mag. field homogeneity *(Japanese)* 80−93111

iron continued
polishing in H_2SO_4+methanol, H_2PO_4 and $HCLO_4$+methanol, polarisation curves 78−56851
polyacrylic acid:Fe^{3+}, electron state of Fe^{3+}, Mossbauer and magnetisation obs. 79−73872
polycrystalline, exam. of Luders deformation 78−84893
polycrystalline, H_2 adsorpt. and embrittlement, work function changes 80−96741
polycrystalline, influence of α-γ transform. on creep *(Russian)* 80−89289
polycrystalline, spectral thermal emission circular polarisation 79−77784
polycrystalline, two ferromag. methods for eval. of fatigue limit 80−89438
polycrystals, grain misalignment, electron microscope determ. *(Russian)* 80−103358
polyethylene based compositions, filled with Fe, Al_2O_3 powder, effect of filler particle size on wear resistance 78−44226
polyethylene-Fe, wear resistance on steel counterbody, exam. 78−68826
polymorphism effect on failure accompanying electrospark action *(Russian)* 79−74236
porous, density, elec. cond., Young's modulus, toughness 78−64645
porous, sintered, deform. diagram based on theory of plasticity *(Russian)* 78−88494
porous, volume strained, correlation between strength and acoustic props. 77−16770
positive muon diffusion, press. depend 80−75907
positive muon spin precession, effect of press. 80−40030
positive muons as light isotopes of H, book contrib. 79−82907
positron annihilation, Doppler broadened lineshapes, prevacancy lattice expansion 78−27349
positron annihilation, lifetime meas. in electron irrad. Fe and Fe-C 80−93431
positron annihilation, temp. depend. 78−56540
positronium form. in two-photon positron annihilation 79−61462
powder, acid dissolution inhibition by aniline and thiourea, iodide effect 79−79181
powder, air-atomised, manufacture with predetermined characts. 80−100808
powder, atomised, processing props., particle size distrib. effect, with and without Zn stearate additions 79−100077
powder, BH_4 reduced, coercive force and remanence ang. variation 80−44879
powder, carbonyl, R10 and R20, manufacturing effects on magnetic permeability 78−35009
powder, consolidated, exam. of mech. and electrical props. 78−56599
powder, Debye-Waller factor by neutron diffraction 79−95113
powder, density distrib. in rolling deformation region 80−40288
powder, electroless Ni plating 80−61026
powder, electrolytic Ag plating 79−66017
powder, exam. of consolidation process based on electronic structure of solid 80−20842
powder, final reduction annealing in vibrating bed 80−84883
powder, fine reduced, mean normal contact stress in rolling 77−12571
powder, hot pressing on steel substrate, densification kinetics 80−40290
powder, mag. susceptibility meas. by high frequency pulse technique 78−93739
powder, Mossbauer spectra, demagnetising field effect on magnetic splitting 80−39932
powder, Mossbauer spectra parameter calc. with aid of computer *(Russian)* 78−76361
powder, NMR excitation function, drumhead model of Bloch walls 80−15810
powder, oxidation, magnetically soft material form., elec., mag. props. 77−8778
powder, passivating oxide layer comp. 78−31558
powder, prep. by reducing iron phthalate in mag. field, mag. props. 77−40090
powder, recryst. annealing effect on struct. and technological props. *(Czech)* 80−89250
powder, reduced, manufacture, collision speed effect 80−84884
powder, reduction annealing, comminution of sintered cakes 80−66456
powder, reduction annealing, thermodynamic anal. 78−60597
powder, resist.-sintability *(Japanese)* 80−16228
powder, sintered and hot pressed, effect of porosity, grain size on magnetic props. 79−96159
powder, sintering, effect of repeated allotropic transform. 77−40406
powder, sponge and atomized types, steam oxidation, pore closure and surface hardness 80−45441
powder, supersonic vibration effect on pressing *(German)* 78−64500
powder, vibratory densification in vibratory press 77−12576
powder, ZhGr1.0, optimisation of heat treatment in salt bath 77−28756
powder based sintered porous permeable materials, diffusion chromising 80−100958
powder compact, apparent density, mixing, and friction, zinc stearate lubricant effect 80−45403
powder compaction, elect. cond. changes 79−66175
powder compacts, pressed under static or vibr. load, shrinkage anisotropy during sintering 80−50574
powder forged, impact and fatigue strengths, slag inclusion effects 77−21271
powder layers, on sinter-bonded, hot-pressed, on steel, struct. and props. 79−95976
powder preforms., hot consolidated rolled strip, mech. props. 78−15338
powder production, water jet atomisation of Fe-C melts 79−100090
powder sintered compacts, mech. props. effect of powder type and processing conditions *(Czech)* 77−59830
powder-forged, elastic consts., density depend. 80−84987
powder-plastic composite, soft mag. material, mag. and mech. props. 80−75812
powdered compacts and Armco, electrolytic boriding 79−39044
powders, Co- or Cu-plated, prep. by rad. and chem. plating, mag. props. 80−44867
powders, cold-pressed, props., effect of air 80−100810
powders, exam. of production, props. and testing methods *(German)* 79−4927
powders, from Fe-C melts, atomisation, props. 79−70013
powders, packed, complex mag. permeability calcs. 80−29583
powders, prepared by BH_4 process, comp. and stability 80−44878
powders, rapidly solidified, nucleation, undercooling and homogeneous structs. 78−52708

iron continued
precipitation, reaction with methane at 750 C, micro Auger anal. 80−104020
precipitation as Jarosite from $Fe_2(SO_4)_3$ soln. *(Korean)* 79−87842
precipitation in Vellar estuary, conc. determ. 80−77015
propane-(1,2)diol:$^{57}Fe^{2+}$, dil. solution, Mossbauer exam. of struct. relax. at glass transition 77−66016
protective coating on Al powder *(Russian)* 78−60881
proton beam dosimetry, miniature Si dosimeter 80−47733
proton irradiation, 10 to 16 MeV, isochronal annealing meas. 80−2083
proton irradiation, 10-16 MeV, neutron damage simulation 80−34089
proton irradition, 10 to 16 MeV, resistivity changes 80−2082
pseudo-brittleness, aspect of impact testing 79−79111
pure, cubic, single cryst. elastic constants from mech. and X-ray elastic constants of polycryst. *(German)* 80−10591
pure, hydrogen-charged, initial cracking obs. 80−108580
pure, Sn and Cr diffusion, effect of boundary struct., autoradiography study *(Japanese)* 80−49419
pure, tensile deformation, behaviour under high pressure *(Japanese)* 80−16381
pure AISI, flow stress, temp. and strain rate sensitivities 77−90421
purification, recrystn. temp. and elec. resistivity *(Japanese)* 80−100780
purification, removal of C, N, and O by dry H_2 method *(Japanese)* 78−11234
PVC:Fe film, struct. and optical props., soln. growth technique 78−51837
PVC film, Fe doping effect on chain vibrs. 79−95868
pyrophoric powders, stabilising layer form. during passivation, saturation moment meas. 80−44865
quanidinium aluminium sulphate hexahydrate:Fe^{3+}, EPR, zero-field splitting 77−8395
quantum diffusion of positive muons, 3 to 300K 80−75909
α-quartz:^{57}Fe, anomalous hyperfine splitting 80−103650
quartz:Fe^{3+}, crystalline, absorpt. spectra and structural state 80−16071
quartz:Fe^{3+}, EPR for phase transform., reduced signal above 670K 77−90016
quartz, single-cryst., Fe^{2+} absorpt. spectra in polarised light and struct. position 79−43007
quenched-in hydrogen, yield stress decrease of prestrained specimens 80−16454
quenching from high temps. of α-phase, form. of C atom pairs 77−36540
radiation effects at 20K, fast neutrons and ^{235}U fission products, elec. resist. *(French)* 79−51159
radiation energy loss of impurity atoms in hot plasma 78−18441
radiation induced defects, annealing exam. using channelling tech. 78−47316
radiation shielding, computational benchmark for deep penetration 80−47738
radiation shielding, TRD meas. of neutron and gamma-ray energy deposition 80−23163
radiation-induced swelling in BOR-60 reactor 79−97814
radioactivation of shielding materials Fe, Benelex by fast neutrons, γ-ray spectra, decay rates 79−682
range distributions for 25-200 keV $^{14}N^+$ ions 80−103405
rapid melting and solidification of surface layer, exam. using computer heat flow model 78−83228
re-oxidation of porous metallised Fe pellets, needle-like haematite crystal growth 80−35431
reaction kinetics of liquid with B_4C 80−84344
reaction with liquid Zn, interdiffusion exam. *(Japanese)* 78−39944
reaction with sodium disilicate glass, Mossbauer effect 78−11190
reactor structural material s-wave resonance parameters from capture cross section data 80−13629
recrystallisation, single cryst. growth, twinning *(French)* 77−12523
red blood cells of thalassemia, sickle-cell anaemia, and haemoglobin Hammersmith, ferritin-like Fe, Mossbauer study 80−8018
relaxation, effect of H_2 77−52391
relaxation process effect on initial stages of flow *(Russian)* 79−74189
remagnetisation processes, temp. and grain size depend. *(German)* 78−14987
residual stress evaluation by X-rays *(German)* 80−40670
residual stress induced by uniaxial deform., mag. meas. 77−73390
resistivity anomalies at mag. transitions, sp. ht. 80−39785
resistivity recovery at low temps. of high-purity, H_2 charged Fe 78−26729
river water solution with Mn and organic material, estuarine mixing implications 80−17296
rivers, 'dissolved' Fe removal mechanism in estuaries 78−20437
rod, spontaneous vibr. modes excited by reversible magnetostriction 79−56587
rolled sheet, magnetic film form. at metal/calamine interface after ferrous products cooling *(French)* 79−43274
rolling texture in pure Fe *(German)* 77−86054
rotating disc electrode, corrosion in acidic chloride soln., O_2 and benzotriazole effects 78−35564
rotational hysteresis 78−91889
scattering and radiation damage for 14 MeV neutrons and 10 to 20 MeV protons 77−15458
screening of non-transition element impurities, model 77−4312
screw dislocation motion, orientation depend., tight-binding type electronic theory 79−51109
seafloor around Vulcano Island, Fe mineralisation in volcanic and hydrothermal sediments *(French)* 79−62482
secondary electron emission, on proton and deuteron irrad., 0.5-2.5 MeV 77−63512
secondary electron emission 2-12 MeV electron impact, Monte Carlo calc. 79−28868
secondary ion emission, effects of initial ion bombardment and oxidation 77−1777
secondary ion emission, energy spectra, 0-55 eV, contamination levels 79−15573
sedimentary distrib. rel. to O_2 in Precambrian atmosphere 77−5272
sediments, Fe formations, REE data rel. to seawater 79−66715
segregation and adsorption of S, influence on carburisation and nitrogenation 80−66701
segregation behaviour, of S, O and P at (100) surface 80−100841
segregation of ^{119m}Sn at grain boundaries, Mossbauer effect 78−15414
segregation of C or N, equilib. and struct. *(German)* 79−47690
segregation of S, O_2 and P at (100) surface in single crystal *(Japanese)* 79−61591

iron continued
self-diffusion, laser irrad. effects on atom mobility *(Russian)* 77−59139
shear transformations, (twinning, martensitic), correspondence matrices *(German)* 78−31406
sheet, surface magnetisation, ferromag. nucl. reson. meas. 78−60348
sheet metal, texture heterogeneity, numerical simulation *(French)* 78−92274
shielding, two dimens. cross section sensitivity anal. of Fe in concrete 77−23311
shielding of 14 MeV neutrons using iron-water combination 77−61614
shock adiabatics at ultrahigh press. *(Russian)* 77−27941
shock compressed, thermal energy relaxation 77−69043
shock wave compression, reduced Hugoniot curve and eqn. of state *(Chinese)* 80−44259
Shockley surface states, three faces of BCC cryst. 78−76126
single component, powder, compressibility and elec. resistivity in cold pressing under low press. 77−77444
single crystal, muon spin rotation expt. results 77−12294
single crystal frames, use in transient field meas. 79−59324
single crystal prep., high purity, by strain-anneal technique *(German)* 77−48326
single crystals, absorbed H, strain anal., X-ray divergent beam method 78−15463
single crystals, spherical, recrystallisation annealing 79−74086
sintered, austenitic nitriding and bainitic hardening 80−85084
sintered, effect of represssing and double sintering on impact strength *(Japanese)* 78−92217
sintered, fatigue, metallographic obs. 78−64646
sintered, fracture behaviour, microscopic obs. 79−47771
sintered, fracture mechanics *(German)* 77−8948
sintered, friction and wear 77−59946
sintered, hot forging and chemicothermal treatment, wear resistance 80−25606
sintered, influence of metallographic treatment on pore analysis 80−76417
sintered, metallographic meas. of pore size, effect on mech. props. 78−19685
sintered, plastic deform., porosity effects 78−23801
sintered, porosity estimation by screen image of brittle fracture 77−52585
sintered, porous, yield point *(Czechoslovakian)* 77−28748
sintered, produced by dynamic hot pressing, recrystn. diagram 79−70017
sintered, steam oxidation effect on porosity 77−59997
sintered, strength and elongation, rel. to density, 80−30047
sintered and pressed, props., effect of atomised Fe powder particle size distrib. 80−11601
sintered compact, shrinkage and mech. props., admixed zinc stearate lubricant effect 80−45402
sintered friction material, wear rate, depend. of phase struct. 79−15801
sintered material, operating performance, effect of polymer and graphite lubricant additives 80−11785
sintered parts, densification in burnishing process by rocking die method 78−35331
sintered parts, struct. stabilisation with C potential control of protective atmosphere 78−60614
sintered powder, plastic deformation, constitutive eqns. 79−61667
sintered PZh1M, fracture resistance subject to thermomechanical treatment 77−77517
size effect on slip deformation ability at very low temps., in single crysts. 80−21049
slag interface, interaction under diffusion conditions, impurity oxidation *(Russian)* 80−35390
slip, influence of H *(French)* 78−6965
slip deformation high purity single crysts., between 4.2 and 300K 80−25801
slip-initiation phenomenon by fatigue, appl. to stress meas. 80−45342
small particles, magnetisation-pressure isotherms for H_2 and SO_2 78−39949
small particles, Mossbauer effect study of lattice vibr. 80−44963
smoke-particle aggregates, long-range correlations 79−46369
soft, solid cylinder, annealed, dynamic forming by compression *(Japanese)* 77−70267
soft magnetic mat. prep. by precip. of insulating film on Fe powder in polishing bath 78−23637
soft magnetic materials, powder-based, phase comp., thermal analysis 77−51928
softening and hardening by H_2 charging during tensile deformation 80−16453
softening caused by electrolytic H charging *(Japanese)* 80−35197
softening effect, tensile test at low temps. *(French)* 77−63875
softening of H_2 charged Fe, depend. on specimen size, charging current density and strain rate 80−16455
solar abundance, determ. from 300 to 900 nm Fe I lines using precise oscillator strengths 79−40155
solar central Fe-H plasma, limited solubility of Fe 78−89149
solar coronal abundance, determ. from XUV emission lines 78−4180
solar flare energetic particles Fe charge states meas. 77−2418
solar flares, Fe Kα fluoresc. 80−17569
solar interior, Fe coalescence in centre of Sun 80−77373
solar interior, Fe segregation from H, ionic mixtures phase separation theory 80−77279
solar photosphere, Fe abundance determ. from weak Fe I Fraunhofer lines *(Russian)* 80−12720
solar photosphere Fe abundance, curve of growth and fine anal. 77−56883
solid, Kα hypersatellite spectrum, double K ionis. 77−18829
solid, reaction with Zn vapour, Zn chem. potential effect on interaction layers 78−11416
solubility in β-Na_2O-Al_2O_3 rel. to isomorphous replacement of Al^{3+} 77−85926
solubility in liq. Li, impurity effects of O_2, N_2 and C 79−77760
solubility of H_2 at press. up to 67 kbar *(Russian)* 79−51260
solubility of H_2 in 600-1500°C temp. and 0.1000 atm. pressure ranges *(Russian)* 78−59948
solubility of P, alloying element effects *(Russian)* 79−69248
solute segregation to grain boundaries 78−72780
solution mechanism in fused KNCO 79−39271
sorption of water, visualisation using THO and autoradiography 78−26761
spark-source mass spectrometry, relative sensitivity coeffs. 79−92045
specific heat, electronic heating in modulation meas. method 80−24609
iron continued
spectral line wing shapes in solar spectrum 80−4317
spectrochemical analysis, atomic-absorption, tubes design with hollow cathode *(Bulgarian)* 80−85232
spectrochemical analysis of biological solns. using wall stabilised arc source 80−41343
spectroscopic flame temperature measurements, role of transition probability factors 77−1925
spherical microparticles in elec. discharge, impact on polished electrodes, mech. effects *(French)* 78−22595
spin correlation function 79−78334
spin dependent momentum distrib., APW calc. 78−2416
spin fluctuations above Curie temp., diffuse mag. neutron scatt. obs. 80−50102
spin polarisation of field emitted electrons, itinerant model 78−95685
spin polarised electron tunnelling results 79−28417
spin polarised low energy electron scatt., elastic and magnon-inelastic 78−34970
spin susceptibility, high-field, spin-density functional formalism 80−70959
splat-quenched, martensite morphology, SEM study 80−7547
splat-quenched, microhardness and martensite 80−76359
sponge, heat of adsorpt. of pyridine and ethyl pyridine, flow microcalorimetry 78−85193
sponge Fe, oxidation kinetics by nuclear γ-resonance method *(Russian)* 80−40681
spontaneous magnetisation, temp. depend. 77−63141
spontaneous magnetisation data up to 0.98 T_c, reanalysis 78−47959
spontaneous volume magnetostriction 80−65989
spreading behaviour of Al-Si melts 80−84345
sputtered film, amorphous, Mossbauer study and electron diffr. obs. 80−75897
sputtering, under N_2^+ and O_2^+ bombardment, theory and expt. test 77−85864
sputtering by fast electrons 77−90226
sputtering in inert atm., with uncooled cathode, oxidation of metallic coatings, X-ray diffr. obs. 78−3041
stable levitation using superconductors 77−38799
static loading over wide deform. and temp. range, acoustic emission, plastic flow, fracture 77−90424
static loading over wide deform. and temp. range, acoustic emission, fracture, plastic flow 77−90425
stellar spectra, Fe lines equivalent widths in cool standard stars for spectral anal. 77−78771
stimulated spin echo obs. of oriented ^{60}Co nuclei 79−65780
stopping of 3-7 MeV α-particles *(Russian)* 79−51181
stopping power for 28 MeV α-particles, re-evaluation 78−79651
stopping power meas. of 0.3 to 2.6 MeV ^{4}He ions 79−3329
stopping power nucl., in ferromag. Gd, transient mag. field 78−34555
stopping powers, projectile range for Z=8-20, 0.0125-12.0 MeV/nucleon 78−83856
stopping powers for 28.8 MeV α-particles 77−80556
strain ageing and fatigue *(Japanese)* 79−20161
strain enhanced corrosion in caustic 77−16715
strain hardening and rate sensitivity, effect on ductile-brittle transition temp. 78−39900
stray grains, on surface, optical microscopy study 80−70509
stray mag. fields above stripe domains, electron microscope and μ^*-tensor determ. 80−71089
strengthening in H_2S04, H_2 hardening rel. to struct., anodic behaviour *(Russian)* 79−15855
stress fields and strains energies associated with closure domains 77−1563
stress relaxation in high purity single crystal with controlled amounts of C *(French)* 79−70105
stress strain anal. of single crystal induced by absorbed H_2 *(Japanese)* 78−11276
structural stabilisation, influence of C interstitials, HF calc. 79−11611
subharmonic generation, transmission reson. expt. 77−20709
submitochondrial particle succinic dehydrogenase, interaction of ubisemiquinone with Fe-S centre, EPR 78−69016
substrate for epitaxially grown Au bicrystal interfacial dislocation behaviour 77−51622
substrate surface contamination from dark-space shielding during sputter cleaning 77−8968
substrate with epitaxially grown Ag, interface struct. 77−55470
superconductivity in ϵ-phase, low temp., transition temp. estimated 80−34540
supercooling by method of microvolumes *(Russian)* 77−21092
surface, {001}, determ. of c(2×2) structure of S, LEED 77−85063
surface, (001), initial reaction with water vap. 77−69173
surface, (110), adsorption and decomposition of ammonia 79−69345
surface, (110), adsorption of Xe, UPS obs. 79−33897
surface, (111), (100) and (110), UPS obs. 79−38712
surface, (111), interaction with hydrazine 79−46956
surface, (111), S segregation, LEED, AES and work function changes 80−15350
surface, (111) and (100), adsorpt. and decomp. of NH_3 78−40077
surface, adsorbed O_2 effect on chem. reaction kinetics 80−55572
surface, adsorbed S effects on surface reaction kinetics and surface self-diffusion 78−7234
surface, adsorption of K, LEED, AES, UPS and XPS meas. 79−77919
surface, Cl_2, CO_2, NH_3 and alkanes thermal accommodation coeffs., translational (internal) gas-solid energy exchange 78−92506
surface, contamination in vac. depth selective conversion electron Mossbauer spectroscopy 80−2671
surface, form. and decomp. of nitrides 79−24831
surface, interacting mechanisms with organic sulphides rel. to friction and lubrication behaviour 80−45546
surface, laser doping with V *(Russian)* 78−95065
surface, luminesc. accompanied by ion implantation 80−60683
surface, magnetic order 78−95439
surface, N atom recomb., vibr. energy of desorbing N_2, electron beam induced fluoresc. 80−61149
surface, newly generated, occurrence of salt films during repassivation 79−15860
surface, nitride layer formation, activated surface passivation 80−16577
surface, O_2 layer thickness, reson. α-scatt. from ^{16}O 78−64778
surface, purposeful modification by gas adsorption, charact. by photoemission 78−71955

iron continued
surface, spin orientation effect of shallow electrons by magnetization 79−65881
surface, X-ray prod. by 5 MeV/amu deuterons (oxygen ions), projectile Z depend. 80−42982
surface 78−60553
surface {110}, atomic struct., LEED anal. 80−88410
surface (001), ang. resolved Auger emission, model 78−39635
surface (001), ferromag., spectral density of states, transfer matrix formalism 78−39185
surface (110), adsorption and decomposition of NH_3, identification of surface species using SIMS 79−90862
surface (110), complexes with PF_3, CO and cyanomethane, UV photoelectron obs. 78−19629
surface (110), K promoted, adsorption of CO, UPS, XPS, AES, and flash desorption obs. 79−82463
surface (111), spin polarised photoemission 80−45221
surface (111) adsorption of N_2, temp. controller for filament heating appl. *(Japanese)* 77−51603
surface atom electron binding energy depend. on composition, Auger spectra, APS spectra 80−39655
surface catalyst for CO hydrogenation to methane and higher mol. wt. compounds 78−73034
surface chemistry during annealing of soft magnet 78−48546
surface cleanliness control by glow discharge emission spectroscopy anal. *(French)* 79−87923
surface contamination due to polishing, determ. by luminescent-discharge spectrometry *(French)* 79−52839
surface covered with C, O, N, S, CO adsorption, photoemission spectroscopy study 80−54527
surface crater form., by laser pulse, frontal method, approx. soln. 77−77327
surface density of states, continued fraction method 77−20388
surface electronic structure, role of self-consistency in evaluation, tight-binding calcs. 77−39908
surface films formed in inhibitive solns., optical props., protective quality 79−20260
surface hardening, ion-carbo-nitriding in CO-N_2-H_2 gas mixtures, expt. *(Japanese)* 80−71670
surface lattice dynamics 78−95224
surface oxide effect on acid corrosion inhibition 78−11384
surface props. rel. to adsorbed O_2, H_2O vapour, work function determ. 78−60187
surface relaxation, lattice statics calc. in α-phase 78−63925
surface segregation of Sn, AES obs. 77−20172
surface sliding damage, no lubrication, materials depend. *(Japanese)* 78−56780
surface subjected to friction, wear, exoelectron emission, rel. to O_2, H_2O, gaseous adsorpt. 79−1816
surface treatment by N_2 of atomically clean surface, corrosion inhibition 78−19954
surface treatment process in nontoxic salt bath 79−83398
surfaces, adhesion, effect of adsorbed atoms, AES study 80−39456
Swift effect, dynamic and static response to simple compression, tension and torsion 77−28858
Swift effect, in twisted tubes 77−28859
Swift effect, rel. to stress/strain behaviour in simple compression, tension and torsion 77−28860
tektites-irgizites, Fe ions state rel. to form. conditions 78−61420
tensile deform., sources of acoustic emission 78−19814
tensile strength and cyclic tensile fatigue strength at high temp. in vacuum, BCC and FCC phases *(Japanese)* 79−100251
terrestrial planets interiors, Fe condensed matter physics 80−77307
tetrahedral site occupation by C, study of possibility *(French)* 77−51508
texture, recryst. annealing effect *(Czech)* 80−89249
textures, annealing and cold rolling, initial grain boundaries effect *(Japanese)* 80−35205
TGS:Fe^{3+}, crysts. and their aq. solns., ESR 80−39862
TGS:Fe^{3+}, thermal diffusivity, 25°C 79−90833
TGS:Fe^{3+} and aq. solns., optical absorpt. spectra 79−82997
thermal acoustic magnons, Brillouin scatt. meas. 78−95424
thermal diffusivity by pulse method 80−15497
thermal emission, magneto-optic circular polarisation obs. 80−70435
thermal emissivities and diffusivities, expt. transient technique and theory for foils 78−43353
thermal energy storage in a packed bed of iron spheres with liquid sodium coolant, thermocline broadening 80−45762
thermal properties at high-press. (150 GPa), from shock wave data, Earth core 80−21683
thermally activated slip deformation, 0.7 to 77K 79−91755
thermobalance for studying high-temp. sulphidation kinetics of metals 78−23876
thermodynamic data *(German)* 80−40328
thermodynamical Gruneisen function for pure Fe in Earth's core 78−61361
thiazine dye-Fe photoelectrochem. cells for H_2 production, cell instabilities 80−16814
thick probes, subthermal neutron transmission curves for grain size and texture eval. *(German)* 80−71667
thin film, Brillouin scattering from spin waves 80−65843
thin films, surface demagnetisation due to chemisorption, ferromagnetic reson. study 80−80616
Tokamak impurity in fusion reactor, at. (mol.) struct. and collision data, review 80−43959
transient mag. field, vel. and atomic number depend. 78−91999
transient magnetic field discontinuity seen by O(F) ions 80−24515
transient magnetic field velocity and Z depend. 80−39904
transient magnetic low velocity field 80−80642
transition metal dichalcogenides:^{57}Fe, Mossbauer spectra, isomer shift 80−15885
trapping of H, average trapping depth and trapping sites density 80−84297
triboelectric charging, effects of fluorinated compounds 78−60188
tribothermoluminescence of flakes in grinding wheel, rel. to solar coronal dust radiation 78−68570
tunnelling electron spin polarisation rel. to band struct. 78−68095
twin and stacking fault energies calc. 80−2038
twin boundary and twinning dislocation struct., computer simulation 78−30644
twinning under influence of plane shock wave *(Russian)* 80−92538

iron continued
ultrafine particles, Fe_3O_4/γ-Fe_2O_3 surface layers, Mossbauer expts. 79−8081
ultrafine particles prepared by vacuum evap. on running oil substrate, mag. behaviour 79−28565
US attenuation at large strain amplitudes 77−1182
US hardening kinetics rel. to dislocations 80−50644
US oscillatory stress superimposition effects on deformation 80−35287
US velocity anomalies, at elevated temp., α-γ transition 78−75830
US vibrations, damping under high hydrostatic press. 77−55324
vacancies, formation entropy, diffusion const. by determinant and Green's function methods 79−77595
vacancy diffusion along single edge dislocations, computer modelling *(Russian)* 77−47612
vacancy form. by positron annihilation in thermal equilibrium 78−10041
vacancy formation energy by positron annihilation 78−51531
vacancy mobility determ., HVEM expts. 80−33993
vacancy recovery stage, radiation doping, elec. resistivity meas. 79−51102
vacuum deposited, epitaxially grown double layers of Au, interfacial dislocations 78−30847
vacuum deposits on Ni(Cu)(Ag) (111) FCC substrates, orientation relationships 80−59836
vapour deposition, columnar struct. rel. to deposition conditions 78−52675
vapour growth of small particles on Al_2O_3 substrate 78−75958
vapour laser, 4529 Å emission 79−10282
vapour laser, operation by dissoc. of metal complex 77−54702
vapour press. above different crystallographic planes *(Russian)* 78−18762
vibrational spectrum with interstitial C atoms 78−67796
viscoelasticity under transformational superplasticity *(Japanese)* 77−52416
volume changes and defect healing due to plastic deform. *(Russian)* 80−81139
VPE on W tip, depositing direction depend. 80−10812
waisted cylinders, fatigue, exam. of Miner's rule 78−64689
water, natural, trace metals, energy dispersive X-ray fluoresc., at absorpt. anals., comparison 77−60175
weakly inductive vacuum discharge, multiply ionised Fe ion spectra *(Russian)* 77−76224
wear measurement by thin layer activation technique 78−72945
wear of surface due to friction, surface hardening 78−44227
wear resistance, surface hardening processes, review 78−72894
wear sliding track, deformation 77−12707
whisker, domain wall interaction with mobile impurities 77−12145
whisker, H_2 effect on deform. 78−68755
whisker, mag. memory function at crit. temp. 77−24714
whisker, magnetic aftereffect in 180° mag. bowed Bloch walls 79−78432
whisker, magnetisation curve meas. using SQUID system 80−86347
whisker, magnetoresistance, deviations from Kohler's rule 80−70673
whisker, optimisation of magnification of magneto-optic Kerr effect by interference layers 79−51808
whisker, polycryst., FIM obs. of struct. 78−84111
whisker, polycryst., microstruct., SEM and TEM 77−39755
whisker, [111] oriented, mag. domain struct. and approach to saturation 79−82814
whisker crystals, domain walls, interaction with dislocation bundle, X-ray topography obs. 79−87282
whisker growth, added C black effect 78−30852
whisker growth, on wustite, Wagner's mechanism 80−10847
whisker single crystals, ferromag. reson. and surface anisotropy 80−71187
whiskers, ⟨100⟩, inverse Wiedemann effect 77−90001
whiskers, AC susceptibility, critical slowing down of mag. fluctuations 77−69594
whiskers, cryst. morphology and dislocation struct. study using optical and SEM, X-ray diffr. topography 79−23876
whiskers, dynamics of mag. freq. response near Curie point 80−34648
whiskers, elastically and plastically deformed, mag. domain structs. 80−15752
whiskers, elongation induced struct. distortion, X-ray topographic investig. 77−85121
whiskers, galvanomag. size effects 78−14709
whiskers, H_2 effect on mech. props. 80−108556
whiskers, high strength, polycrystalline, microstruct. obs. 79−33214
whiskers, inverse Wiedemann effect, torsional strain and azimuthal mag. field influence 80−108045
whiskers, mag. anisotropy, magnetisation and temp. depend. near T_c 80−39766
whiskers, mag. crit. phenomena, size effects 78−68258
whiskers, magnetisation in small mag. fields, investigation using Kerr magneto-optic effect 80−2603
whiskers, polycrystn., H_2 embrittlement 79−100259
whiskers, soft magnetic metals, ideal, AC response 78−64223
whiskers, struct., dislocations, mag. domains *(Polish)* 79−33210
whiskers, undeformed, X-ray topographic study 77−80716
wire polarised, elongation in presence of acetylene type acid corrosion ihibitors 80−55590
wires, catalytic, electrically heated, steady state temp. multiplicity, resist. meas. 77−32828
work hardening, and behaviour and dislocation struct. in single crystals during simple shear tests 78−95762
X-ray absorpt. spectra, effective co-ordination charges 80−84805
X-ray absorption, heat treatment effects 80−84806
X-ray absorption spectra, far fine struct., multiple scatt. terms contrib. 80−40184
X-ray Compton line shape, effect of valence state 77−8682
X-ray emission spectra, L_l and L_n 78−39631
X-ray emission spectra, low energy plasmon satellites 79−65957
X-ray emission spectra in PbO-B_2O_3 glass 77−44089
X-ray K absorpt. discontinuities 78−60532
X-ray K-absorpt. spectra, depend. on composition and temp. changes *(Russian)* 80−55226
X-ray K-emission satellites, quasi-stationary states and origin 80−80903
X-ray resonant Raman scatt. and fluoresc. near K-absorpt. edge 79−52042
X-ray topography and double-crystal diffraction of high-purity single crystals 80−92534
XPS, electron level binding, energy determ., and spectrometer calibration method 77−16458

iron continued
XPS, excitation of 1s core-level photoelectrons with synchrotron radiation 78−19632
XPS, valence bands 78−35249
XPS escape depths and relative photoionisation cross section for 3p subshell 77−73212
XPS line intensity ratios for outer electron shells 79−100018
XPS obs. of Fe 2p states 78−52625
yield, H_2 effects 78−15474
yield condition for isotropic hardening 79−61653
yield stress, temp. depend. *(Russian)* 78−56691
Z dependence of thick target β-ray backscattering 80−76118
Zeeman tuned mag. confined arc lamp, appl. to U 78−17593
zone melted, H_2 charged, reversible dilation of lattice, interstitial diffusion 77−11732
zone refined, strained, substructural changes during annealing *(Slovenian)* 78−84845
zone-refined, positive muon diffusion at room temp. 79−47377
n backscattering, emergence of secondary gamma rays *(Japanese)* 80−18595
adsorption of acetylene on Fe containing segregated C, hydrogenation, C-1s XPS spectra obs. 80−84366
Ag-Pd-Fe, mag. susceptibility, effect of Fe impurities 79−73677
$AgGaS_2$:Fe, EPR of Fe-associated defect 80−60412
Al:Fe, CESR, effect of ion implantation 77−20701
Al-Cu-Mg(:Fe,Si) alloys, double-ageing, resist., hardness meas. 77−28822
Al-Fe bimetal, O_2 effect on diffusion inhibition 77−89597
$Al(NO_3)_3.9H_2O$:Fe^{3+}, nucl. level hyperfine struct., reson. RF field effect, Mossbauer effect *(Russian)* 77−77133
Al_2O_3:Fe, gamma-irrad., low temp., induced absorpt. spectra 79−56820
Al_2O_3:Fe, pore form. during oxidative annealing, grain growth slowing 80−100856
Al_2O_3:Fe^{2+}, hyperfine splitting and magnetoelastic consts., freq. crossing spectroscopy 80−107392
Al_2O_3:Fe^{2+}, phonon spectroscopy using superconducting tunnel junctions 78−91389
Al_2O_3:Fe^{3+}, dynamic nuclear polarisation, correl. ESR and NMR strain-broadening effects 77−48090
Al_2O_3-Fe cermet, microstruct. and physical props. 79−42279
β-Al_2O_3-Na_2O:Fe, coordination site, oxidation state, Mossbauer, absorpt., emission spectra, mag. susceptibility meas. 78−68431
$AlPO_4$:Fe^{3+}, EPR, α-β phase transition 77−90016
$AlPO_4$:Fe^{3+}, luminesc. emission and excitation spectra 79−69873
Al_2SiO_5:Fe^{2+}, andalusite travelling wave maser in 40 to 46 GHz freq. range *(Ukrainian)* 80−53246
Al_2SiO_5:Fe^{3+}, spin lattice relax. 77−73076
Al_2SiO_5:Fe^{3+} appl. of sensitive EPR spectrometer to zero field splitting determ. *(Russian)* 77−57372
Al_2SiO_5:Fe^{3+} crystals, andalusite, spin-lattice relaxation, lattice oscillator heating 78−23329
$Al_6Si_2O_{13}$:Fe^{3+}, mullite:Fe^{3+}, Mossbauer exam. of relaxation behaviour of Fe^{3+} 77−1620
As_2S_3:Fe glass, photolum. and ESR, Fe impurities as non-radiative recomb. centres 80−29788
$AsSe_{1.2}$:Fe, Fe effect on physiochem. props. of glass 80−24370
As_2Se_3:Fe, glassy, mag. susceptibility investig. of doping effect 77−77024
$AsSe_{1.1}Te_{0.2}$:Fe, Fe effect on physiochem. props. of glass 80−24370
Au/Fe/Au superimposed layers, influence of O_2 on interdiffusion, controlled-atmosphere electron microscopy 77−51552
BCC, mag. relax. due to C and N meas., 210 to 410K 77−36102
$Ba_2NaNb_5O_{15}$:Fe,Mo, photorefraction mechanism and photoelec. props. 80−71381
$BaTiO_3$:Fe, annealed in H_2 and O_2, valence change in phase stability 80−20600
$BaTiO_3$:Fe, antireson. in EPR spectra of Fe^{3+} ions *(Russian)* 80−11257
$BaTiO_3$:Fe, photoinduced Rayleigh scatt. and bulk photovoltaic effect 79−38554
$BaTiO_3$:Fe, short circuit photocurrent, depend. on polarization 79−38121
$BaTiO_3$:Fe, switching and electrolum. 80−76079
$BaTiO_3$:Fe, X-ray induced luminesc. 79−69885
$BaTiO_3$:Fe ceramic, dopant distrib., STEM obs. 79−82255
$BaTiO_3$:Fe^{3+}, local position of Fe^{3+} in ferroelec. phases, EPR study 80−25196
$BaTiO_3$:Fe^{3+}, local position determ. by EPR 80−108057
$BaTiO_3$:Fe^{3+} bulk photovoltaic effect and photoinduced Rayleigh scatt. 77−77226
$BaVS_3$:Fe, Mossbauer and mag. studies, electronic state of Fe 80−108130
Br-Ca-Fe H_2O-decomposition cycles for thermochem. H prod. 80−35784
C content determ., isotope-spectral method *(Russian)* 80−55766
C diffusion in γ-phase high temp. vacuum metallography investigation *(Russian)* 77−72718
$CaCO_3$:Fe^{2+}, electronic spin relax., effect of second-order spin-orbit coupling 80−10935
$CaCO_3$:Fe^{2+}, Mossbauer spectra 80−108138
CaF_2:Fe, X-irrad., impurity effects on defect prod. 80−92525
CaF_2:Fe^{2+}, electronic props., Mossbauer and far IR spectroscopy 79−99803
CaF_2:Fe^{2+}, relax. meas., Mossbauer spectroscopy, 10-30K 80−44977
$CaMoO_4$:Fe^{3+}, single crystals, structure and kinetics, EPR meas. 79−99760
CaO:Fe^{2+}, octahedral symm., vibronic effects from Zeeman field induced Mossbauer spectra 77−8477
CaO-Al_2O_3, binary slag, reduction of Al_2O_3 by C saturated Fe *(Japanese)* 79−24733
$CaWO_4$:Fe^{3+}, EPR, spin Hamiltonian parameters from anal. of Kramers' doublets 79−28595
$CdBr_2$:Fe^{2+}, charge transfer near UV spectra, 4.2K, mag. circular dichroism 78−80378
$CdCO_3$:Fe^{2+}, Mossbauer spectra 80−108138
$CdCl_2$:Fe^{2+}, charge transfer near UV spectra, 4.2K 78−80378
$CdCl_2$:Fe^{2+}, magneto optical study, ferromagnetically coupled Fe(II) pairs 78−6711
$CdCo_3$:Fe^{2+}, electronic spin relax., effect of second-order spin-orbit coupling 80−10935
CdI_2:Fe^{2+}, polarised electronic Raman scatt. 80−29733
CdSb:Fe, self absorpt. edge, impurity effect *(Russian)* 80−97316
CdSe:Fe, exciton electroreflectance spectra, impurity effects 77−16335
iron continued
CdTe:Fe, annealed, magnetically ordered, Hall effect and photocond. 78−19060
CdTe:Fe, dopant solubility 77−90334
CdTe:Fe, exciton refl., photoluminesc. and mag. suscept. meas., influence of impurities 77−39787
CdTe:Fe introduction of elec. active defects 80−103647
CdTe:Fe^{2+}, reson. relax. time for impurity electrons and localised phonons interaction, appl. to thermal cond. 80−59590
CdTe:Ni, luminesc. and refl. spectra, high temp. annealing effects 80−24472
CdY_2S_4:Fe, superhyperfine interaction of Fe, ESR spectra 77−63271
CeSe:Fe, long-wavelength fundamental absorpt. edge formation, role of Fe 77−16351
Co complex, bis-(β-diketonato) Co(II) dihydrate, Fe chem. states, Mossbauer emission 80−15917
Co-Fe system, interdiffusion zone growths *(Czech)* 78−84009
Co-Ni-Fe, semi-hard magnet, irreversible magnetisation changes, directional distrib. 79−24196
Co_2SiO_4, reaction with Fe to produce Co, gamma resonance spectroscopy *(Russian)* 78−15332
CoV_2O_4:Fe, spinel, prep. and Mossbauer spectra 79−28660
^{57}Co:Fe Mossbauer source linear polarisation rate meas. *(French)* 79−30633
Cr powders (60 to 70%), spectral determination of Al and Fe 77−90679
$CsCdF_3$:Fe^{3+}, ENDOR meas. on Fe^{3+}-F^--Cd^{2+} struct. 78−31122
$CsCdF_3$:Fe^{3+}, ligand polarisation and transferred hyperfine interactions 79−51535
CsCl:Fe, defect struct., Mossbauer spectra and X-ray diffr. obs. 80−7237
Cu:Fe, NMR satellite data rel. to impurity struct. 78−35052
Cu-Fe, composite, fibre and layer structs., anomalous props. caused by internal phase boundaries 78−72754
Cu-Fe, interface, ferromagnetic and cond. spin reson. mode coupling 79−78521
Cu-Fe (1 wt.%), stress induced martensitic transformation of spherical Fe particles, exam. 78−52803
Cu+Fe+Cd, nuclear target proparation by evaporation and rolling 80−23224
Cu+Fe+Sn, nuclear target preparation by evaporation and rolling 80−23224
$CuGaS_2$:Fe, effect of Fe content and stoichiometry on coloration 78−88336
Cu_2O:Fe, impurity scatt. effect on cyclotron reson. 79−56614
D NaCl:Fe, defect struct., Mossbauer spectra and X-ray diffr. obs. 80−7237
F+Co(Fe) recoil, transient mag. field 78−29838
α-Fe, 0.14 wt.% P addition effect on creep 77−90420
α-Fe, (001), surface relax. and thermal expansion calcs. 79−23820
Fe, (100) surface, S segregation and 2D compounds precipitation *(Japanese)* 80−35188
α-Fe, $(\bar{1}\bar{1}2)$ $[\bar{1}\bar{1}\bar{1}]$ anti-twinning slip system, low temp. strengthening, dislocation struct. 77−21164
α-Fe, ⟨111⟩ screw dislocation−vacancy interaction energy 77−15415
α-Fe, a/2 ⟨111⟩ {110} edge dislocation, at. simulation 77−89435
α-Fe, acoustic emission signals in plastic deform., amplitude distrib. *(Japanese)* 78−6978
Fe, Armco, fracture in liq. metals, Rebinder effect *(Russian)* 79−29266
γ-Fe, atomic mag. moment in FCC lattice of transition d-metals *(Russian)* 78−72337
α-Fe, BCC, ⟨111⟩ screw dislocations, displacements of atoms 77−15414
α-Fe, BCC, interaction energy between self-interstitial and screw dislocation, calc. 80−70248
Fe, BCC, vib. entropy of $^1/_2$ ⟨111⟩ {110} edge dislocations 78−63768
α-Fe, BCC metal, vacancy-edge dislocation interactions, computer simulation 78−83845
α-Fe, BCC metals, stressed, computer simulation of vacancy and divacancy migration 78−47573
Fe based ternary solutions, liquid, exam. of thermochemistry 78−80782
α-Fe, C, electromigration, current density and temp. effects 77−59145
α-Fe, C drift velocity for electromigration temp. depend. in paramag., ferromag. phases 78−18835
α-Fe, carburisation and decarburisation kinetics in methane/H_2 mixture *(German)* 79−1949
α-Fe, cavitation and sliding distrib. changes during creep at 500°C 78−6991
α-Fe, chem. interaction with aluminophosphate and alumino-chromophosphate adhesives, Mossbauer obs. 80−40596
α-Fe, chemisorption of acetylene, (ethylene) struct., bonding, dissoc., UPS obs., MO calcs. 78−84050
α-Fe, cold rolled, hydrostatic press. effect on microstructural changes during creep 78−39871
Fe, Compton profile from 662 keV γ-ray spectroscopy 78−56539
α-Fe, crack initiation study at low-cycle fatigue using slip bands *(Slovak)* 79−38949
α-Fe, creep and fracture between 77 and 673K 79−7649
α-Fe, creep behaviour, static and cyclic, influence of C and ZrH_2 78−39856
α-Fe, creep life, meas. by microstruct. changes 78−35443
α-Fe, cryst. equilib. lattice dynamical model 78−22811
α-Fe, Debye-Waller factors, temp. depend. calc. 78−22807
α-Fe, Debye-Waller factors, temp. variation, lattice dynamical calc. 78−55925
α-Fe, deformation induced intergranular creep cavitation 78−31473
α-Fe, deformed, changes in dislocation density, mech. props., dependence on deformation temp. *(Russian)* 79−20130
Fe, diffusion of alloying elements *(Russian)* 78−79791
γ-Fe, diffusivity of N_2 79−46845
α-Fe, dislocation loops, equilib. shape under shear stress 79−7608
α-Fe, distrib. of dislocations in intersecting pile-ups *(Russian)* 78−87668
α-Fe, edge dislocation interaction with interstitial atoms, influence on Peierls stress 78−34537
Fe, effect on nitriding of Si powder 79−33985
Fe, electrolytic particle morphological characterisation derived from Walsh coeffs. 80−50816
α-Fe, electron irradiated, vacancy annealing 79−55785
α-Fe, exam. of structural defects due to shock waves, and induced hardness 78−48427
α-Fe, FIM specimens annealed at 0.5T_m, surface energy anisotropy 77−20181

iron continued
2-Fe, ferromagnetic self-diffusion 78−6176
α-Fe film, deform. in electron microscope, dislocation mechanism 79−82227
α-Fe film, mag. mechanism, at. mag. moment *(Korean)* 79−7973
α-Fe, Frenkel defect recombination zone, effect of uniaxial compression 78−6987
α-Fe, freq. spectra, sp. ht., Debye temp., Clark-Gazis-Wallis ang. force model 78−22799
γ-Fe, grain boundary diffusion of Ni 79−23787
α-Fe, grain boundary segregation of C, N_2 and C Auger spectroscopy 78−72778
Fe group elements, singly ionised, charge transfer, rel. to laser action 80−74246
α-Fe, growth rate of γ-phase 79−20049
α-Fe, H ordering 79−7597
α-Fe, He atom clustering at $^1/_2\langle 111\rangle\{110\}$ edge dislocation, calc. 78−2154
α-Fe, high purity, neutron and electron-irrad., interstitial migration at 200K 79−55920
α-Fe, high temp. deform., Cottrell-Stokes law 79−83274
α-Fe, high temp. deform. and substruct. *(Japanese)* 77−21226
α-Fe, hydrostatic pressure effect on creep rate and failure time 78−92306
Fe I, a^3F_{2-4} levels, relative oscillator strengths 80−63572
Fe I, excited levels measured lifetimes compared with calcs. from oscillator strengths 79−36586
Fe I, gf-values rel. to metal-poor dwarf stars abundance anals. 79−92760
Fe I, isoelectronic sequence, abnormal intensities in multiplets 79−22635
Fe I, new levels and classification for 1.3-2.5 μm range 77−18819
Fe I, precision oscillator strengths from levels a^5F_{1-5} and a^5D_{0-4}, comparison 79−36584
Fe I, relative oscillator strengths for transitions from $a^5D_{0,1,2}$ levels, precision meas. 77−438
Fe I 3719.94 Å line broadening by He, line width and shift meas., astrophys. significance 77−73942
Fe I 3737 Å emission line studies of prominences and flares *(Russian)* 80−51717
Fe I 5250 Å line magnetic field meas. of polar regions of Sun *(Russian)* 77−64724
Fe I 5383 Å line width, Stark broadening 79−31463
Fe I even-odd and odd-even transitions, difference in curves of growth 77−25996
Fe I in Ap stars, photoionisation spectrum causing UV absorpt. 80−109437
Fe I in solar photosphere line broadening, Smirnov Roueff pot. calcs. 80−98632
Fe I Kα fluorescence in solar flares, photospheric Fe abundance probe 79−75192
Fe I levels, mean radiative lifetimes determ. 79−49987
Fe I line profiles and magnetic field in quiet network regions of solar photosphere 78−69758
Fe I lines, equivalent widths and microturbulent vels. determ. for solar photosphere *(Russian)* 80−51719
Fe I lines in solar spectrum, statistical anal., mag. line broadening 77−74028
Fe I lines in solar spectrum, damping const. determ. preliminary results *(Russian)* 80−72900
Fe I lines limb shift in solar atmosphere, pressure shifts effect 78−89150
Fe I low excitation lines, collisional broadening 80−37778
Fe I oscillator strengths, comparison of calc. and meas. 77−3310
Fe I solar spectrum, 300 to 900 nm, microturbulence, Fe abundance, damping, oscillator strengths 77−5516
Fe I transition from levels a^5F_{1-5}, relative oscillator strengths precision meas. 79−36585
Fe I transitions from levels a^5D_{0-4}, relative oscillator strengths precision meas. 79−36583
Fe I weak Fraunhofer line profiles rel. to absorption coeff. *(Russian)* 78−20783
Fe II, 3000-12000 Å, forbidden transitions, excitation pot. and transition probability 77−79563
Fe II, Fe III, lifetimes, VUV beam-foil spectroscopy 79−22657
Fe II, Fe III, line emission in optical and UV spectra of peculiar stars 77−13364
Fe II, IR spectral lines identification in η Carinae 77−45463
Fe II, intense emission lines discovery in narrow line quasar (PHL 1092) 80−77508
Fe II, oscill. strengths, astrophys. appl. 79−59398
Fe II, oscillator strengths derived from solar spectrum, choice of solar model atmosphere 80−56791
Fe II, spectrum, term system 79−778
Fe II emission line spectra in Be-stars 77−56978
Fe II emission lines in supergiant star α Orionis 79−101144
Fe II lines, permitted, in type 1 Seyfert galaxies and quasars, form. and relative intensities 80−62278
Fe II lines in quasars and Seyfert galaxies, excitation and line strength 80−67896
Fe II newly identified lines in solar limb spectrum 77−33442
Fe II permitted emission, excitation mechanism in Seyfert 1 galaxies and QSOs 79−21412
Fe II permitted emission in Seyfert 1 galaxies and QSOs, obs. 79−35361
Fe II permitted lines in spectra of type 1 Seyferts and quasars 79−44602
Fe II UV lines in QSOs, spectrophotometry obs. 80−73063
Fe III, Fe VI, electron impact excitation cross sections and gaseous nebulae Fe abundances 78−53806
Fe III, high-spin, in cancer, EPR 78−53466
Fe III, metastable states in Be star φ Persei rel. to mass loss 79−5832
Fe III, UV spectral lines as stellar classification criterion 78−16404
Fe III in astronomical sources, multiplet table 80−41732
Fe III-VI, struct. and transition probabilities, ab initio calc. using Thomas-Fermi central pot. 79−3360
Fe IV, spectrum, term anal., rel. to RR Telescopic 78−82677
Fe IX, autoionising transitions $ns^2np^6-nsnp^6mp$ 77−88419
Fe IX, Fe X, forbidden transitions, solar coronal spectrum appl. 78−77537
Fe IX, X, XI, dielectronic recomb. rates in θ-pinch plasma 78−71525
Fe IX, X, XI, effective dielectronic recombination rates in H plasma, emission time histories 80−79570

iron continued
Fe IX lines in solar corona, appl. as plasmas density indicators 79−44429
Fe IX radiative and collisional data rel. to solar coronal emission spectrum 77−49350
Fe, in chloride solns., role of Mo as localised corrosion inhibitor 79−20255
α-Fe, interaction of foreign interstitial atoms with vacancies 78−6052
α-Fe, interaction of He with C impurities, computer simulation calc. 79−99235
Fe, intergranular corrosion in NO_3 solns., electrochem. and AES study 80−50751
α-Fe, internal friction for low temp. deform. 80−40420
α-Fe, internal friction peaks from dislocation relax. in plastically deformed and/or neutron irrad. sample 78−48438
Fe ion+Fe (Ni) collisions, X-ray spectra, two-electron transitions 77−19050
Fe ions, transition energies, inner-shell electron effects 77−42259
α-Fe, irradiation induced void swelling, Cr additions effect 80−55408
γ-Fe, kinetics of carburisation in CO-He and CO-H_2 atmospheres at 920°C *(German)* 78−85024
α-Fe, lattice and force consts., pairwise atomic repulsions in cluster model 79−32939
α-Fe, lattice wave dispersion, lattice consts., elastic consts. 80−24545
α-Fe, low cycle deform., strain rate and depressed temp. effect 79−61660
α-Fe, magnetic aftereffect disaccommodation between 30 and 300K after low-temp. neutron-irrad. 80−29585
α-Fe, μ^+ diffusion 79−56687
α-Fe, nitrided, aging at room temp. 80−71679
Fe, nitrogen, impurity defect interaction influence on radiation hardening and embrittlement 80−35199
α-Fe, O_2 potential effect on surface self-diffusion coeff. 80−15353
R-Fe octagonal transducer 80−74684
α-Fe particles, in fused SiO_2, g-values and anisotropy consts., FMR study 79−82876
α-Fe particles supported on silica, investigation using in situ Mossbauer cell 79−49357
α-Fe, phonon dispersion curves, extended de Launay model 77−4162
α-Fe, phonon spectrum, cold neutron inelastic scatt. obs. 77−7811
α-Fe, plastic deform. in neck leading to fracture 78−64655
αFe, plastically deformed and/or irrad., high purity, internal friction peaks due to dislocation relax. 77−86075
α-Fe, point defects short term annealing, computer simulation 80−54282
α-Fe, polycrystalline, shear modulus, H_2 effects 77−36561
γ-Fe precipitates, antiferromag. ordering, press. depend., Mossbauer meas. 79−73861
α-Fe, quench ageing of N_2, effect of soln. heating and quenching temps. *(German)* 77−55991
α-Fe, S and C diffusion, AES obs. 77−51543
α-Fe, screw dislocation with nonplanar core, model 77−1126
Fe series atoms and ions, LSD approx., density functional calcs. 80−78720
α-Fe, single crystal, Sb diffusion induced dislocations 78−30798
α-Fe single crystal whiskers, controlled growth by H reduction of ferrous halides, X-ray and SEM exam. of crystals 78−60554
α-Fe, single crysts., work hardening *(German)* 80−50652
α-Fe, slip, rel. to screw dislocation core struct. in BCC lattice 79−82211
Fe, sponge, particle profiles, morphological characterisation derived from Walsh coeffs. 80−50816
α-Fe, strengthening kinetics due to deformation ageing, impurity atom sources *(Russian)* 80−55435
α-Fe, stress induced interaction of point defect pairs, in BCC solutions 78−79608
α-Fe, struct. after polymorphic transform. under press. *(Russian)* 80−29946
Fe, surface phonon spectra 78−71934
α-Fe, TEM on struct. round fatigue cracks 77−12699
α-Fe, twin boundary struct., plane translations 79−69113
Fe, UPS, density of states determ. 78−52623
α-Fe, uniaxial stress effect on Mossbauer spectrum 80−71244
Fe utilisation studies by stable tracer ^{58}Fe technique 80−61734
Fe V, VI, beam-foil level populations, charge state fractions 80−52913
Fe VI, forbidden emission under nebular conditions 79−8970
Fe VI spectrum $3d^3$-$3d^24p$ transition, wavelengths and energy levels 77−42264
Fe VIII to Fe XXVI, wavelength tables *(Japanese)* 79−13661
α-Fe, vacancy migration, annealing expt. study, irradiation induced defects 78−6956
Fe vapour, line strengths, energy-level structure for 3p-edge absorption spectrum 79−45673
α-Fe, vibrational states, phonon dispersion, phonon softening 80−88289
α-Fe, void swelling during irradiation, suppression mechanisms 80−6441
α-Fe, void swelling response after fast reactor irradiation 80−6437
Fe, whiskers, polycrystn., Mossbauer study 80−20571
α-Fe whiskers, pure, ductile fracture initiation, macroscopic obs. of deform. history and failure 80−85043
α-Fe whiskers, pure, ductile fracture, microscopic obs. of initiation mechanism 80−85044
Fe whiskers grown from $FeCl_2.4H_2O$, exam. of growth morphology 78−72051
Fe X, $3p^44s$ levels, population processes 80−47926
Fe X, Fe XIV, unsuccessful search for forbidden emission in HD 153919 (3U 1700−37) 80−4358
Fe X (XI), energy levels and oscill. strengths, Slater radial integrals 77−79583
Fe X and XIV, solar line intensity ratio and coronal temp. determ. 78−73697
Fe X and XIV forbidden line emission from supernova remnants 79−44580
Fe X and XIV forbidden line emission in Cygnus Loop, radial distrib. 80−51828
Fe XI, XII and XV solar line intensities, OSO-7 obs. of limb brightening 78−69759
Fe XII, in solar corona, excitation of spectrum 77−17458
Fe XII and XIII, energy levels and oscillator strengths for XUV transitions 78−46277
Fe XIII, IR lines of solar corona, polarisation degree calc. 77−45373
Fe XIII and XIV emission lines in solar corona 77−13299
Fe XIII coronal emission line polarization from mag. sublevels statistical equilib. 77−53492

iron continued
Fe XIV 5303 Å coronal emission line polarisation obs. during 1973, June 30 eclipse 77−49352
Fe XIV 5303 Å forbidden line emission from Puppis A SNR 80−26962
Fe XIX, Fe XX, Fe XXI, forbidden lines obs. in solar flares 78−57519
Fe XIX, XXI, spectral energy levels, relativistic corrections, config. superposition method 80−32616
Fe XIX and isoelectronic ions $2p^4$-$2p^3$3d transition array 77−42267
Fe XIX-XXII blend at 1.9 Å in flare X-ray spectra 79−96979
Fe XV, line intensity and linewidths at high electron density, generalised population ratio 80−99481
Fe XV, transition probabilities and collision strengths 80−78562
Fe XV 284 Å spectroheliograms and rot. characts. of EUV coronal holes 77−53547
Fe XV solar coronal EUV line intensities 80−51731
Fe XVI, autoionisation contrib. to total ionisation rates 80−9738
Fe XVI, electron impact excitation, transition probabilities, oscill. and collision strengths 78−25718
Fe XVI, L-series satellite spectra 79−98012
Fe XVII, ionisation pot. in Ne isoelectric sequence 78−5363
Fe XVII, mag. quadrupole lines, in TFR600 Tokamak plasma, 10-20 Å 79−13662
Fe XVII, X-ray spectra due to n=3 and 4 quantum nos. 79−22641
Fe XVII to Fe XXI spectra, 8 to 18 Å, emitted from plasma after laser heating 78−25464
Fe XVII-XXIV X-ray line complex obs. of M87 galaxy halo 79−21425
Fe XVIII, Fe XXII, forbidden transitions in solar flares, fine struct. 79−22634
Fe XVIII, spectra and energy levels of F isoelectronic series 79−93948
Fe XVIII and XIX $2s^22p^n$-$2s^22p^{n-1}$4d classification, for laser produced plasmas and solar spectra 77−42268
Fe XVIII-Zn XXII, transitions between $1s^22s^22p^5$-$1s^22s^22p^4$3d and $1s^22s^22p^5$-$1s^22s^22p^4$3s configs. 79−26925
Fe XX and isoelectronic ions, $2p^3$-$2p^2$3d transition array 77−65434
Fe XXI, Fe XVII, identifications in solar flares XUV spectra 78−49406
Fe XXI, relativistic energy levels, Dirac-Fock multiconfig. calc., triplet state fine struct. and Lamb shift 80−23315
Fe XXI, transition probabilities, energy spectra calcs. 78−70791
Fe XXI 1354 Å in solar flares, line width obs. from Skylab rel. to ionisation equilib. calcs. 80−21956
Fe XXI and isoelectronic spectra $2p^2$-2p3d transition array 77−38632
Fe XXI as electron density diagnostic in solar flares 79−44435
Fe XXII, allowed transition CI wave functions, oscill. strengths and transition probabilities 80−32664
Fe XXII, coupling energy levels, oscillator strengths, electron collision energies 80−69068
Fe XXII, intercomb. transitions, oscill. strengths, transition probs., rel. to solar spectra 80−52935
Fe XXII, XXIV, XXV, charge exchange recomb. in Princeton large torus during beam heating 80−100067
Fe XXII,XXIII, Be I and B I like spectra from laser-produced plasma, classification 78−67410
Fe XXIII, $2s2p(^3P_1{}^o)\rightarrow 2s^2(^1S_0{}^e)$ transition probabilities, CI calcs. 79−36544
Fe XXIII, energy levels and transition 79−59383
Fe XXIII, Fe XXIV, new line obs. in laser-produced spectra 79−81175
Fe XXIII, wavefunctions and oscill. strengths, CI calcs. 80−23317
Fe XXIII and XXIV, reson. and intersystem transitions, oscill. strength, lifetime, beam-foil spectra 78−82685
Fe XXIII and XXIV resonance lines in Tokamak discharges 79−68941
Fe XXIV, dielectronic satellite spectra calc., solar flare spectra appl. 79−35123
Fe XXIV, dielectronic satellite spectra, solar flares appl. 80−32646
Fe XXIV, oscillator strengths, electron impact excitation collision strengths, solar flare spectra appl. 80−32647
Fe XXIV, spectra, radiative corrections 79−98015
Fe XXIV, wavelength, for line identification in solar corona radiation 77−79569
Fe XXIV, XXV, line wavelengths in 1.85 to 1.87 Å region in solar flare X-ray spectra 80−21973
Fe XXIV solar flare spectra, high dielectronic satellite lines analysis for plasma props. calc. 80−12728
Fe XXV, dielectronic satellite line spectra as measure of nonthermal electron energy distribs. 80−21911
Fe XXV, Fe XXVI, astrophysical X-ray and gamma-ray lines prod. by nonthermal ions 78−36725
Fe XXV, He-like, dielectronic satellite spectrum, electron temp. diagnostics in plasma 79−82098
Fe XXV, He-like ion, oscillator strengths of transitions between low-lying S and P states 78−13470
Fe XXV, He-like ion resonance line satellites 79−10064
Fe XXV, X-ray spectra from laser plasma 78−17596
Fe XXV, XXVI, X-ray spectral lines profile evolution due to Comptonisation, Monte Carlo computations 79−66916
Fe XXV and FE XXVI emission lines in SC 0627−544 galaxy cluster 79−48941
Fe XXV and XXVI, line emission from Alfven shell in X-ray binary stars 80−98737
Fe XXV-XXVI resonance lines region, laboratory reproduction of solar flare X-ray spectra 80−18819
Fe XXVI, and isoelectronic ions, electron impact excitation cross section calcs. 78−9257
α-Fe, yield point behaviour for extremely inhomogeneous deformation *(German)* 80−55453
Fe^-, electron affinity, nonstatistical fine-struct. detachment intensities at 488 nm, laser electron spectra 79−41144
Fe^+, at. spectra, laboratory determ. of gf values for solar studies 80−42994
Fe^+, excited config. position and level struct., review 80−32621
Fe^+, Fe^{++}, synthetic spectra rel. to radioactive excitation source model for late time spectra for Type I supernovae 80−105264
Fe^+, generation by laser ionis. source for ICR spectroscopy, chem. appls. 80−45597
Fe^+ ions in high latitude F-region, distrib. 79−16736
Fe^{11+} ground configuration, proton collisional excitation 78−33582
Fe^{12+}, forbidden lines collisional excitation, importance of short-range pot. 77−17457
Fe^{14+}, Fe^{15+}, electron impact ionis. from 3s sub-level 78−90297
Fe^{16+}, Na like ions, dielectronic recombination rate, scaling props. 80−32668
Fe^{19+}, forbidden line in UV, Tokomak plasma diagnostics 78−83602
iron continued
Fe^{19+}, new atomic data rel. to solar phase spectra 80−67545
$Fe^{2+,3+}$, fluoresc. quenching of organic excited singlet states, rate meas., mechanism 77−38685
Fe^{2+} electroactive species, electrolysis, conc. polarisation at electrode, interferometric investig. 78−68896
Fe^{2+}, in octahedral symm., vibronic effects from Zeeman field induced Mossbauer spectra 77−8476
Fe^{2+}, irreducible Raman scatt. tensor operator for 32 cryst. point groups 77−8572
Fe^{2+}, mag. form factors, spherical and aspherical parts 79−78315
Fe^{2+}, magnetostriction effects in garnets and ferrimagnetic spinels 79−91277
Fe^{2+}, nuclear quadrupole interaction, theory, including many-body effects 78−34813
Fe^{2+} partitioning in olivine and silicate melts 79−66683
Fe^{2+}, singlet ground state high-spin, in complexes with rhombic distortions, spectroscopic props. 77−51861
Fe^{2+}, Sternheimer valence shielding antishielding factor including exchange 77−85182
Fe^{23+}, dielectronic recombination, Rydberg autoionising states, props. in elec. fields 79−59405
Fe^{23+}, electron impact excitation, relativistic Coulomb-Born approx. 79−68318
Fe^{23+}, partial photoionis. cross-sections and radiative recomb. rate coeffs. 80−52951
Fe^{25+} line emission in Hercules X-1 (HZ Herculis), theory of emission during X-ray source low state 80−105393
Fe^{3+} bound to serum transferrin during rat lymphosarcoma development, EPR 77−77878
Fe^{3+} clusters in mol. complexes, interference effects in neutron scatt. 77−85544
Fe^{3+}, crystalline spherical pot., effect on Fermi-contact term 80−20140
Fe^{3+}, cubic spin-Hamiltonian parameters in inorganic compounds, superposition model anal. 80−20367
Fe^{3+} electron transfer quenching, Ru bipyridine ion, limiting efficiency and rate const. meas. 79−91929
Fe^{3+} in crystals, quadrupole hyperfine struct., screening coeffs., Mossbauer spectra 77−52000
Fe^{3+} ion compounds, effect on Mossbauer spectra of thermal vibrs. rel. to covalently populated 4S shell nucleus 78−72444
Fe^{3+} ions, in frozen aq. solns., spin-spin relax., Mossbauer obs. of effect of paramag. impurity ions 79−33573
Fe^{3+} ions in ferroelectrics, Mossbauer spectrum parameters, covalency occupied 4s shell polarisation 79−56648
Fe^{3+} isoelectronic series, radial charge distrib. calc. 80−9507
Fe^{3+} molar extinction coeffs., determ. by Fricke dosimetry 80−13949
Fe^{3+}, quadrupole antishielding factors, Hartree-Fock perturbation theory 78−62723
Fe^{3+}, spin-Hamiltonian parameters, superposition model analysis 77−15798
Fe^{3+}, zero-field splittings, correl. with axial site distortions, superposition model 80−93168
Fe^{n+}, n=8-13, in plasma, collisional dielectronic recombination rate, effect on level populations 79−1287
Fe^{n+}, photoionis. cross sections, Hartree-Slater central pot. model calcs. 79−22673
Fe^{n+}, Tokamak plasma spectra, forbidden lines for plasma diagnostics 79−98958
Fe^{n+}, valence electronic struct., pseudopot. method 79−68184
Fe: ^{119}Sn, pressure dependence of effective magnetic fields 78−52382
Fe: ^{103m}Rh, γ-detected NMR of 40 keV metastable state, 0.5 to 14 kG external fields 77−59499
Fe: ^{105}Rh(^{95}Tc), nuclear orientation of nuclei, anisotropy of gamma-ray emission 77−46111
Fe: ^{106}Rh, nuclear orientation and mag. moment 77−85623
Fe: ^{110}In, nucl. orientation, nucl. mag. moment, γ-ray spectra 77−28485
Fe: ^{116}Er, hyperfine interaction of impurities, Mossbauer spectra 77−48105
Fe: ^{119m}Te, mag. moment, nucl. orientation, γ-ray spectra 77−28486
Fe: ^{129m}Xe, mag. hyperfine field determ. by Mossbauer effect 77−8460
Fe: ^{129}Cs, implanted atom sites and hyperfine interactions, Mossbauer obs. 77−20753
Fe: ^{129}Te, implanted atom sites, Mossbauer obs. 77−20756
Fe: ^{129}Tm, implantation below 15K, in situ Mossbauer obs. 77−20754
Fe: ^{129}Xe, implanted atom sites, NMR/ON 77−20723
Fe: ^{129}Xe, implanted atom site populations, Mossbauer, NO and NMR/ON obs. 77−20755
Fe: $^{12}C(2_1{}^+)$, PAC meas. of transient mag. fields 79−99800
Fe: ^{131}Xe, negative parity states, nucl. orientation, γ-ray spectra 77−28487
Fe: ^{133}Xe, heavy ion implantation, recovery, Mossbauer effect meas. 78−52393
Fe: ^{169}Tm(^{175}Lu), radiation-damage evolution influence on hyperfine interaction 80−6793
Fe: ^{169}Yb, lattice location and hyperfine field of implanted Yb, annealing temp. depend. 77−48100
Fe: ^{172}Yb, hyperfine mag. field, TDPAC meas. 78−52394
Fe: ^{198}Hg, combined lattice-location hyperfine-interaction expt. on implanted Hg 77−20752
Fe: ^{199}Au, quad. interaction, orbital mag. hyperfine field by NMR/ON 77−12250
Fe: ^{220}Rn(^{222}Rn), combined elec. quad. and mag. interaction, PAC 77−16214
Fe: ^{57}Fe, suppression of nuclear reaction in direct γ-quantum beam 77−20780
Fe: ^{60}Co, nucl. orientation-pulsed NMR obs., γ-radiation anisotropy 77−59490
Fe: ^{60}Co, elec. quad. interaction, single passage NMR/ON 77−16204
Fe: ^{60}Co, nucl. spin-lattice relax. meas. method 77−85596
Fe: ^{71}As(^{72}As), nucl. mag. moment by NMR/ON 77−12251
Fe: ^{82}Br, nucl. orientation 77−59486
Fe: ^{83}Rb, implanted atom sites and hyperfine interactions, Mossbauer obs. 77−24765
Fe: ^{93,94}Tc, γ-ray spectra, nucl. mag. moment determ. 77−28484
Fe: ^{95}Nb NMR 77−59482
Fe:Ar(K), implantation perturbed ang. distrib. 78−12969
α-Fe:B(C)(N)(O), valency effect of interstitials 80−65502
Fe:Bi, impurity site distrib., channelling and nucl. orientation obs. 77−15447

iron continued
Fe:C, decarburisation by H_2, conversion electron Mossbauer obs. 78−85198
α-Fe:C, electron irrad., vacancy-C interaction, positron lifetime meas. 80−75264
α-Fe:C, electronic struct., Hartree-Fock calc. 78−14692
Fe:C, neutron irradiated at low temp., mag. disaccommodation 80−44881
Fe:C(N), small concs. determ., mag. and mech. relax. methods 80−7879
Fe:F, lattice location of implanted F rel. to mag. hyperfine fields 77−59041
Fe:He, BCC, process of interstitial trapping by impurities 79−46697
α-Fe:He, impurity clustering in vacancies bound to edge dislocations 78−91358
α-Fe:He, interaction of He with small self-interstitial platelets 79−60399
Fe:I, ^{131}I NMR, vacancy associated impurity sites 78−91964
Fe:K(Ar), mag. hyperfine interaction, temp. depend. 78−68420
Fe:Lu, nuclear orientation meas., hyperfine field 77−32308
Fe:N, difference in conc. distribs. between implanted N^+ and N_2^+ ions 77−80529
Fe:N, ion implanted foil, Mossbauer effect study, nitride form. 78−27149
α-Fe:N, mag. field depend. of reverse permeability 77−80969
Fe:Ra, hyperfine field determ. 77−85622
Fe:Ti, C induced amorphous surface layers 80−107287
Fe:Xe, gyromagnetic ratios of first 2^+ states in Xe, implantation PAC 78−12966
Fe:Xe, isotope ion implantation control *(Flemish)* 78−79623
Fe:Xe(Te), interaction of impurities with point defects, Mossbauer spectroscopy exam. 78−47414
Fe:Y, ion implanted, deep D traps due to Y-vacancy complex 80−103372
Fe:Yb, ^{18}O, interaction between implants 77−27921
Fe:Yb,O, interaction between impurities, perturbed ang. correlation meas. 77−1628
Fe:Yb(Au), radiation-damage evolution, influence on lattice-location meas. 80−6426
Fe^{3+}:TiO_2, low noise travelling wave maser, noise temp. 80−32945
Fe^{3+}:TiO_2 86-88 GHz low-noise TW maser 80−69354
Fe/'FeO', relative chemical potential of oxygen *(German)* 78−31642
Fe/Al_2O_3 composite film, optical props., rel. to solar collector appls. 78−72622
Fe/Cu (100), metastable 2D condensations, epitaxy, growth modes, exp. techniques, book contrib. 80−49558
Fe/Cu composite, prop. of fatigue crack crossing interface under residual thermal stress effect 80−45371
Fe/Cu_2O displacement reaction kinetics at temps. between 800 and 1050°C 80−21278
Fe/Fe-Cu composites, microplastic deformation development 78−39877
Fe/Fe-Ni bimetal film, exchange const. determ. from hysteresis loops *(Russian)* 77−48015
Fe/H abundance determ., catalogue for 515 stars 77−29815
Fe/H abundance in 628 stars, catalogue 80−98579
Fe/H abundance ratio in giant stars of G and K type 79−16944
Fe/H abundances of extreme Population II stars in globular and dwarf galaxies 78−40939
Fe/H determ. catalogue for stellar atmospheres, comments 77−29806
Fe/MgO composite film, optical props., rel. to solar collector appls. 78−72622
Fe/Ti battery system, soluble, discharge characts. 79−92070
Fe/ZrB_2, metal-like cpd. form. in diffusion layer during solid phase saturation 80−19994
Fe-air batteries, bifunctional air electrode 80−72028
Fe-Al interface, O_2 content, reson. α-scatt. from ^{16}O 78−64778
Fe-Al_2O_3 granular film, interface props., Mossbauer spectroscopy 80−34336
Fe-Al_2O_3 granular films, superparamagnetism and relax. effects 80−71118
Fe-Al_2O_3-Al superconductor, spin polarisation of tunnelling electrons, band model 77−72947
Fe-Ar low press. flow discharge, axial density profiles of sputtered cathode atoms 80−49029
Fe-Au (111) bicrystal films, misfit dislocations obs., for 500°C substrate temp. 77−51624
Fe-Au (111) interface, nature of interaction layer 79−99433
Fe-Au bimetal epitaxial films, examination of interaction at temps. ≥600°C 80−75482
Fe-C reactively sputtered, solar absorbing surface, struct. and optical props. 79−79407
Fe-C-O, sintered, ferritic struct. obtained by Ar_3 transform. *(Japanese)* 78−6874
Fe-C(0.001 to 0.44 wt.%), C effect on low temp. brittleness *(Japanese)* 80−50711
Fe-Cl thermochem. cycle for H_2 prod. by H_2O pyrolysis 80−97811
Fe-Co laminated mirror, with Ti-Gd sublayer, in polarising neutron guide 78−9012
Fe-Co(Ni)(Cu), bimetallic molecule, matrix isolated, Mossbauer spectrum 78−68425
Fe-Co(Ni)(Cu), bimetallic molecule, matrix isolated, Mossbauer spectrum 78−88233
Fe-Cr diffusion couple, tracer diffusion meas. using tracer anal. 79−7716
Fe-Cu composite plates, vol. fraction and residual stress, effect on fatigue strength *(Japanese)* 79−8349
Fe-Fe_2C, cavity nucleation, by plastic deform. 79−29127
Fe-Fe_2O_3 composite mixture, preferential sputtering, XPS expts. 79−87544
Fe-FeS, Mars core formation, radioactive element diffusion, thermal history 79−84724
Fe-glass couples, seals, Auger spectroscopy study of interface 80−76587
Fe-glass porous material, wear resist. under dry friction 80−25876
Fe-graphite porous sintered, determ. of impregnation depth with polycaprolactam-finely divided Cu metallic polymer 79−70272
Fe-group, atoms and singly ionised, f-value meas., review 78−17617
Fe-H, deformed, internal friction 79−57041
Fe-H, recovery of hydrogenated and quenched alloy, solute diffusion 77−77510
Fe-H_2O laminated radiation shield, fast neutron transport 80−13931
Fe-I system, photochemical conversion efficiency 80−71923
Fe-like ions, multiply charged, laser plasmas, 1.5-15 Å 78−13462
Fe-Mn deposits on abyssal sea floor, geochem. 79−12107

iron continued
Fe-Mn diffusion pair, mutual diffusion coeffs. calc. by computer 79−69299
Fe-Mn interdiffusion in almandine garnet, expt. meas., rel. to compositional zoning 79−77812
Fe-Mn powders, reactions with NH_4Cl and $(NH_4)_2CO_3$ 80−11597
Fe-MoS_2, exam. of props., using differential thermal analysis, and metallography *(Russian)* 79−15653
Fe-Ni film thermocouple, fabrication and calibration 77−37885
Fe-Ni system, interdiffusion zone growths *(Czech)* 78−84009
Fe-P-S composite sintered bearing materials manufacture, wear intensities 80−20881
Fe-refractory compound condensate, struct. and mech. props., disperse particle content depend. *(Russian)* 78−19772
Fe-SiO multilayer film, interface magnetisation, neutron Bragg refl. 78−56355
Fe-SiO multilayer film, interface magnetisation 80−7135
Fe-SiO multilayer films, interface magnetisation 80−88858
Fe-SiO_2, granular compund, superpara- to ferromag. transition temp. meas. 77−69633
Fe-SiO_2 cermet film, solar absorbing, production by dual cathode DC magnetron sputtering 80−16186
Fe-SiO_2 granular film, interface props., Mossbauer spectroscopy 80−34336
Fe-SiO_2 supported catalysts, Mossbauer spectra 80−11296
Fe-SiO_2(Al_2O_3)(ZrO_2) granular films, superparamag., Mossbauer effect 80−7131
Fe-water multilayer radiation shielding design optimisation, conversational procedure 77−14273
Fe-ZrO_2 granular film, interface props., Mossbauer spectroscopy 80−34336
Fe^{3+}-doped crystals, mag. susceptibility, cryst. field calc. 78−76035
Fe^{3+}-F^-, overlap and covalency contrib. to zero field splitting, LCAO-MO calc. 80−24850
Fe^{3+}-O^{2-}, overlap and covalency contrib. to zero field splitting, LCAO-MO calc. 80−24850
$Fe + {}^1/_2O_2 + V_2O_3 = FeV_2O_4$ react., free energies of form., 1400-1750K, electrochem. method determ. 79−43613
Fe+Ar, Fe I reson. line, collisional broadening at high temp. *(German)* 80−106298
$Fe + F^{q+}$, (q=6, 8, 9), target and projectile cross-sections, X-ray prod. yields 79−81269
Fe+Fe, symmetric collisions, MO-2pσ radiation anisotropy, quasimolecular nature 78−70924
Fe+Fe symmetric collisions, molecular-K-X-ray anisotropy spectra, discrete struct. 77−14560
Fe+H in type 1 Seyfert galaxies and quasars, collisional ionisation rel. to permitted Fe II lines 80−62278
Fe+H shield, neutron flux meas., comparison with Monte Carlo calcs. 77−23349
$Fe + H_2O$, clean surface oxidation and passivation by H_2O vap., XPS 77−81424
$Fe + H^+$, K X-ray production, 0.2-0.5 MeV, ionis. cross-section 79−31459
$Fe + H^+$, K-shell ionisation calcs. 80−23534
$Fe + H^+$, K-shell ionisation cross-section determ. 80−48077
$Fe + H^+$(He ions), K-shell ionisation cross-section, 85 to 790 keV 80−106390
Fe+I, Fe K-α X-ray emission, high-resolution meas. 80−37871
$Fe + N_2(NH_3)$ interaction, chemical species formed studied by Mossbauer effect 80−43080
$Fe + N^+$, X-ray production cross section, Kβ/Kα ratio, 0.5-2.5 MeV/amu 77−54526
$Fe + Ne^+$, charge exchange obs. through spectral line enhancement 79−7005
Fe+Ni, two electron one-photon X-ray transitions, Dirac-Fock calcs. 78−17600
$Fe + O_2$, cyclic complex form., matrix isolated IR spectra assignments 77−88449
Fe^+ + Fe(Ni), 25, 40 MeV K-shell double ionis., Kαα and Kαβ obs. 77−57918
$Fe^{20+} + H^+$, collisional excitation of fine struct. transitions in ground state 77−19017
$2Fe^{2+} + I_3^-$, solar photochemical decomposition for H_2 prod. 80−16822
$Fe^{4+} + N_2(Ar)(Kr)(Xe)(SF_6)$, 20 MeV, gaseous targets, electron loss, charge state yields 79−54957
$Fe^{n+} + H$, electron transfer cross-section meas. 78−17787
$Fe^{n+} + H$, single electron capture cross-section 79−59560
$Fe^{n+} + H_2$, single electron capture cross-section 79−59560
$Fe^{n+} + H(H_2)$, 50-1200 keV amu^{-1}, impact ionis. and electron capture cross-sections 78−42204
$Fe^{q+} + H$, ($^1_2H_2$), electron capture by heavy multicharged ions at low velocities total cross sections meas. 80−99548
Fe^+(Fe^{2+}), Rayleigh and Compton scatt., differential cross section determ. 80−52912
Fe(III), selective separation from rare earth elements on chelate ion exchangers 78−58861
$Fe(III) + SCN^-$, reaction kinetics, computer-controlled stopped-flow system 79−15953
$Fe_{40}Ni_{40}P_{14}B_6$, amorphous, thermal stress effect on mag. easy axis 77−80928
Fe^{3+}(^6S) paramagnetisations, spin lattice relaxation Mossbauer study, dynamic spin Hamiltonian formalism 80−97173
FeV and VI, beam-foil lifetime meas., 1100-1900 Å 80−23532
FeVIII-XXVI energy level tables and Grotrian diagrams 80−74142
^{52}Fe, production for use in a radionuclide generator system, medical appls. 80−51253
^{52}Fe, recovery of uptake in erythropoietic bone marrow following large field radiation therapy 79−20616
^{55}Fe and stable Fe forms and availability in oceanic aerosols 79−12241
^{55}Fe, appl. to determ. of Ti in laterite samples using energy dispersive XRF 78−76955
^{55}Fe, susceptibility of haematopoietic stem cells to radiation damage 79−11975
^{56}Fe, possible fusion reactor material, gamma-rays from 14 MeV neutron scatt. in extended samples 77−57739
^{57}Fe, configuration interaction, SL-dependent, effect on hyperfine structure 80−37749
^{57}Fe conversion electron Mossbauer spectroscopy at low temps., proportional counter 77−10542

iron continued
^{57}Fe, implanted in 3d, 4d and 5d metals, conversion electron Mossbauer spectra 77−12286
^{57}Fe, isomer shift calibration const. rel. to biological cpds. 80−7227
^{57}Fe isomer-shift calibration by lifetime variations in electron capture decays of ^{57}Fe 80−75902
^{57}Fe, Mossbauer, isomer shift, book contrib. 79−87354
^{57}Fe, Mossbauer absorpt. and emission spectra, hyperfine struct. and relax. effects 80−71279
^{57}Fe, Mossbauer effect-time dependent PAC technique, theory of combined method 79−28645
^{57}Fe, Mossbauer isomer shift calibration scheme, matrix isolation of atoms and ions, book contrib. 79−85924
^{57}Fe Mossbauer level excitation using synchrotron radiation 80−7204
^{57}Fe Mossbauer spectroscopy, possible appl. to geochronology 80−41416
^{57}Fe nuclei, spin-echo signal recording by pulse generator and fast signal averager 78−21188
^{57}Fe paramagnetic ions sorbed on cation exchange resin, chem. information from relax. Mossbauer spectra 77−70332
^{57}Fe resonant absorber, anomalous γ-ray transmission, energy spectrum *(Russian)* 77−28501
^{57}Fe, variation of hyperfine splitting consts. with interatomic distance for $3d^5$ ions 80−97133
^{59}Fe, sediment-bound, absorpt. through digestive tract of marine demersal fish 79−92400
^{59}Fe sorption on natural sorbents clinoptilolite and vermiculite *(Russian)* 77−38370
^{59}Fe uptake in marrow, rel. to ^{239}Pu deposition in bone, mouse 78−85395
^{59}Fe uptake in normal and splenectomised rats, marrow dose estimation, 1000 kVp X-irrad. 78−15894
^{59}Fe, uptake of gamma-emitting activation products in plants 80−30614
^{59}Fe/^{55}Fe activity ratio of blood, meas. using semicond. detector 80−17062
^{67}Fe, uptake in human melanoma cells 79−62217
GaAS:Fe,O_2 effects on opt. props. 77−16350
GaAs:^{56}Fe(^{57}Fe), paramag. centres, identification from ESR and ENDOR spectra 80−80600
n−GaAs:Fe, diffusion doped compensated layers 80−15125
p-GaAs:Fe, ESR line width, temp. depend., 4.2-330K 77−12195
GaAs:Fe, exchange-coupled pairs, ESR 79−11343
GaAs:Fe, for FET, VPE and characterisation 78−19672
GaAs:Fe, impurity atom charge exchange, Mossbauer spectroscopy 79−47050
GaAs:Fe, ordering of Fe impurity, NMR anomalous line shift obs. 78−27102
GaAs:Fe, p-π-ν-n struct., photoelec. props. 80−107862
GaAs:Fe, photoionisation cross section meas. of deep levels 77−8042
GaAs:Fe, profile of impurity optical absorption bands 78−56509
GaAs:Fe, static magnetis. rel. to doping method and heat treatment conditions 77−36092
GaAs:Fe, substitutional impurity elec. struct. 80−88513
GaAs:Fe LPE layers, negative resist. effects and deep acceptor model 77−72929
GaAs:Fe p^+-n junction minority carrier trap meas. by photo-excited DLTS 80−96816
GaAs:Fe reverse biased π-ν-n struct., switching effect 80−88628
GaAs:Fe^+, EPR assessment of $3d^7$ transition metal impurity state 78−48031
GaAs:O, Fe, temp. depend. of ionisation energies of O and Fe levels, electroabsorption meas. 78−47736
GaN:Fe, lattice parameters, variation with stoichiometry and doping 79−73153
GaP:^{56}Fe(^{57}Fe), paramag. centres, identification from ESR and ENDOR spectra 80−80600
GaP:Fe, current-voltage characteristics, p-i-n diodes, luminescence, absorpt. double injection methods 79−65407
GaP:Fe, diffusion, solubility, elec. activity and energy levels 77−55395
GaP:Fe, double electron trap state, ESR identification 77−36124
GaP:Fe, double Fe-thermal acceptor centre, energy states 80−96823
GaP:Fe, electron exchange via val. band between Fe acceptor centres, Mossbauer spectra 77−55741
GaP:Fe, heat treated, EPR spectra, struct. defects 80−7158
GaP:Fe, impurity atom charge exchange, Mossbauer spectroscopy 79−47050
GaP:Fe, multivalence impurity, EPR and optical absorpt. meas. 80−75844
GaP:Fe, optical absorption spectrum and Faraday effect 80−108245
GaP:Fe, photo-ESR of annealed crysts. 80−15795
p-GaP:Fe, photoionisation spectrum of acceptor level 77−55810
GaP:Fe, profile of impurity optical absorption bands 78−56509
GaP:Fe n-i-n epitaxial struct., photoconductivity, recombination scheme *(Russian)* 80−15569
GaP:Fe^+, EPR assessment of $3d^7$ transition metal impurity state 78−48031
GaP:Fe^{2+}, absorpt. and luminesc. spectra 77−16388
GaP:Fe^{2+}, d→d luminesc. spectra 80−7414
GaP:Fe^{3+}, deep impurity states investig. 77−15794
GaP:Fe^{3+} ESR spectrum, elec. field, uniaxial compression influence 80−103882
GaSb:Fe, shallow acceptor level, electrical meas. 79−11087
Ge:Fe, amorphous film or ion-implanted, comparison of ^{57}Fe Mossbauer data 77−40159
Ge:Fe, implanted, Mossbauer spectra, conversion electron, temp. dependence 80−40025
Ge:Fe, polycrystalline film, electron transport props. 79−99642
Ge:Fe, recoil implantation Mossbauer expt. in presence of external mag. field 80−44981
Ge-Fe, laser annealing of implanted ^{57}Co sources, Mossbauer obs. 80−39139
$Ge_{2.33}SbSe_5$:Fe, Fe effect on physiochem. props. of glass 80−24370
H charging, softening vs. hardening effects 79−74172
H diffusion, and solubility 80−49422
H martensite production *(Ukrainian)* 77−52321
H_2 charging, lattice hardening, during tensile testing 79−66156
H_2, effect on phys. and mech. props. 80−101657
H_2 penetration rate, effect of anion and organic corrosion inhibitors 80−100938
H_2+Fe^{+q} collisions, 3.4 MeV/nucleon single electron capture and loss cross sections 77−83726
iron continued
H_2+Fe(001), gas-surface reactions, semiempirical generalised LEPS pot. 78−68923
HIO_3:Fe, growth and struct. perfection, effect of impurity ions 77−12514
H_2SO_4:Fe^{2+}, frozen aq. soln., photolysis, H form., distrib. and diffusion 78−20044
H_2SO_4:Fe^{2+}, frozen soln., photo- and radiation-produced H-atoms obs. 79−39162
I_2:Fe, doping effect on elec. cond., semicond. props. 80−49732
InP:Fe, deep acceptor levels, photocond. meas. 80−20116
InP:Fe, deep levels 79−56166
InP:Fe, diffusion, solubility and elec. activity of Fe 77−43240
InP:Fe, electroabsorption spectra obs. 80−50301
InP:Fe, Fe acceptor charge states, photolum., absorpt. and ESR meas. 77−36123
InP:Fe, Hall and resistivity meas., optical absorpt. 80−10990
InP:Fe, influence of covalence on EPR spectra 78−26827
n-InP:Fe, oscill. intrinsic photocond. 79−60871
InP:Fe, photocond., Fe^{2+} intracentre excitation model 80−29436
InP:Fe, precipitate mixture 77−77485
InP:Fe, resonance photocond. 80−44651
InP:Fe shallow trap thermally stimulated cond. spectroscopy, photocond. spectrum under DC conditions 80−65585
InP:Fe^+, EPR, symm., spin Hamiltonian parameters 78−10759
InP:Fe^+, EPR assessment of $3d^7$ transition metal impurity state 78−48031
ingot, cast, exam. of nonmetallic inclusions, size freq. distrib. 78−39989
KD_2PO_4:Fe^{3+}, ESR, anomalous temp. depend. of D tensor 79−61205
KH_2PO_4:Fe^{3+}, ESR, anomalous temp. depend. of D tensor 79−61205
$KHSO_4$:Fe^{3+}, DC cond. meas., mechanism 80−65285
$KHSO_4$:Fe^{3+}, impurity effect on growth babit from saturated soln. 77−4059
KM_gF_3:Fe^{2+}, US relax. absorpt., acoustic wave-impurity coupling, spin-orbit splitting 79−4375
$KMgF_3$:Fe, EPR temp. depend. 78−80202
$KMgF_3$:Fe^{2+}, 3d→4d absorpt. band exam. 77−63435
$KMgF_3$:Fe^{2+}, anomalous acoustic relax. absorpt. and APR 80−88864
$KMgF_3$:Fe^{2+}, Jahn-Teller quenched spin-orbit, splitting of $^5T_{2g}$ state 77−63442
$KMgF_3$:Fe^{2+}, octahedral symm., vibronic effects from Zeeman field induced Mossbauer spectra 77−8477
$KMgF_3$:Fe^{2+}, super hyperfine struct., Zeeman splitting and dynamic Jahn-Teller effect 77−85555
$KMgF_3$:Fe^{2+}, transferred hyperfine interactions, EPR exam. 78−31105
$KMgF_3$:Fe^{2+} high energy absorption spectra interpretation 78−6716
$KMgF_3$:Fe^{3+}, superposition-model anal. of second- and fourth-order spin Hamiltonian parameters, EPR study 79−87311
$KNbO_3$:Fe, ferroelec. semiconductor, anomalously high photovoltage 77−69378
$KNbO_3$:Fe, ferroelec., anomalous photovoltaic effect and photocond. 78−52449
$KNbO_3$:Fe, optically induced refractive index changes 77−4612
$KNbO_3$:Fe, orthorhombic, EPR of Fe^{3+} 80−39861
$KNbO_3$:Fe, photorefr. effects and photocurrents 78−43434
$KNbO_3$:Fe, photovoltages, photocurrents and photorefractive effects 79−42580
$KNbO_3$:Fe, single crystals, exam. of crystal preparation 78−60564
$KNbO_3$:Fe photorefraction and photocurrent effects *(Russian)* 79−7091
K_2SO_4-$ZnSO_4$ glass:Fe^{2+}, visible spectra 79−51990
$KTa_{1-x}Nb_xO_3$:Fe^{3+} ($0 \le x \le 0.16$), ferroelec., EPR meas. *(French)* 79−11337
$KTaO_3$:Fe^{3+}, EPR, elec. field effect, local fields *(Russian)* 79−8048
$KTaO_3$:Fe^{3+} local phase transition, EPR line temp. broadening *(Russian)* 80−54944
$KZnF_3$.(Fe^{3+}-O^{2-}), overlap and covalency contrib. to zero field splitting, LCAO-MO calc. 80−24850
$KZnF_3$:(Fe^{3+}-$V(K)^+$), overlap and covalency contrib. to zero field splitting, LCAO-MO calc. 80−24850
$LiBaF_3$:Fe^{3+}, EPR, spin Hamiltonian parameters 79−65718
LiCl:Fe, defect struct., Mossbauer spectra and X-ray diffr. obs. 80−7237
LiCl:Fe, electron transfer absorption bands 79−95810
LiCl(Br):Fe^{2+}, optical absorpt., charge transfer spectra 80−2797
LiF:Fe, dispersed ions, absorber Mossbauer spectra 78−15077
LiF:Fe, Mossbauer study of Fe precipitates 79−91327
LiF:Fe^{3+}, optical absorpt., 200-750 nm 78−39576
$LiGaO_2$:Fe, phosphor, luminesc. 78−92108
$LiGaO_2$:Fe IR emitting phosphor preparation and props. 78−6789
α-$LiIO_3$:Fe^{3+}, EPR of impurity ion and radn. induced defects *(German)* 78−84480
α-$LiIO_3$:Fe^{3+}, hyperfine interactions, RF discrete saturation of EPR lines 78−48032
α-$LiIO_3$:Fe^{3+}, local environment and superhyperfine interactions by RF discrete saturation 77−85554
α-$LiIO_3$:Fe^{3+}, zero-field splitting const. calc. 77−51709
$LiNbO_3$:$^{57}Fe^{2+}$, Mossbauer spectroscopy 77−20782
$LiNbO_3$:$^{57}Fe^{2+}$ Mossbauer spectra, EFG axis 77−20760
$LiNbO_3$:Cu(Fe), light induced charge transport, photovoltaic effects, impurity states 80−80317
$LiNbO_3$:Fe, anomalous photovoltaic effect in polarised light *(Russian)* 80−34484
$LiNbO_3$:Fe, bulk photovoltaic effect in ferroelecs. 79−15181
$LiNbO_3$:Fe, calc. of photorefraction *(Russian)* 78−90474
$LiNbO_3$:Fe, charact. for holographic storage appls. 77−23630
$LiNbO_3$:Fe, dynamic optical storage 78−33706
$LiNbO_3$:Fe, effect of external elec. field and light intensity on photorefraction *(Russian)* 79−56766
$LiNbO_3$:Fe, efficient hologram recording using Nd:YAG laser pulses 79−55081
$LiNbO_3$:Fe, elec. resist., temp. and conc. depend. 80−80275
$LiNbO_3$:Fe, electro-optic cryst., light induced charge transport, holographic obs. 80−70747
$LiNbO_3$:Fe, electron irrad., photoinduced charge transfer and hologram recording 79−36859
$LiNbO_3$:Fe, electron spin relaxation study, Mossbauer effect, mag. and crystal field effects 80−39902
$LiNbO_3$:Fe, exoelectron emission in pyroeffect regime 80−76158
$LiNbO_3$:Fe, ferroelec. semiconductors, anomalously high photovoltage 77−69378
$LiNbO_3$:Fe, ferroelectric, treated in Li_2CO_3, formation of Fe^{2+} state, Mossbauer effect 78−92003

iron continued
LiNbO$_3$:Fe, hologram recording, photorefr. effect time depend. *(Russian)* 77−7032
LiNbO$_3$:Fe, hologram writing, beam coupling and transport length in bulk photovoltaic effect 79−94190
LiNbO$_3$:Fe, hologram nondestructive readout using different recording and readout wavelengths 80−14302
LiNbO$_3$:Fe, holographic storage, effects of nonstoichiometry 80−69344
LiNbO$_3$:Fe, holographic recording and thermal fixing, invest. of mechanisms 80−78810
LiNbO$_3$:Fe, IR induced acousto-photorefractive memory effect 80−80746
LiNbO$_3$:Fe, impurity valence state charge on X-ray irrad., Mossbauer meas. 80−7235
LiNbO$_3$:Fe, impurity charge states after UV irradiation 80−60462
LiNbO$_3$:Fe, induced optical inhomogeneity, refr. index and short-circuit photocurrent meas. 79−69806
LiNbO$_3$:Fe, influence of anomalous photovoltaic effect on exoelectron emission 79−28374
LiNbO$_3$:Fe, intensity enhanced bulk photovoltaic effects 79−19616
LiNbO$_3$:Fe, lattice-strains induced by light, X-ray topography 77−76458
LiNbO$_3$:Fe, local photodeformation 79−42932
LiNbO$_3$:Fe, local photodeform. and photorefraction 80−16003
LiNbO$_3$:Fe, Mossbauer spectra quadrupole doublet asymmetry 80−44960
LiNbO$_3$:Fe, nonlinear image processing in 3-dimens. hologram 80−14303
LiNbO$_3$:Fe, optical damage induced by laser light, X-ray irrad., carrier mobility effects 79−33657
LiNbO$_3$:Fe, optical damage, Fe ion conc., EPR and optical spectra evaluation 79−42933
LiNbO$_3$:Fe, optical damage depend. on temp., press., and applied elec. field *(Japanese)* 79−81498
LiNbO$_3$:Fe, origin of photoelectrons and conc. of point defects 77−43645
LiNbO$_3$:Fe, photocond. and photorefractive effects 79−38124
LiNbO$_3$:Fe, photocond. and dark cond. 80−29439
LiNbO$_3$:Fe, photoinduced Rayleigh scatt. and bulk photovoltaic effect 79−38554
LiNbO$_3$:Fe, photoinduced scatt. and bleaching effect 80−95959
LiNbO$_3$:Fe, photorefractive recording of vol. holograms 77−637
LiNbO$_3$:Fe, photorefractive effects under external elec. field 77−23723
LiNbO$_3$:Fe, photorefraction kinetics under irradiation and heating 79−42934
LiNbO$_3$:Fe, photorefr., surface recombination 79−56759
LiNbO$_3$:Fe, photorefraction, γ-irrad. influence, polarisation-optic and holographic obs. 80−11359
LiNbO$_3$:Fe, photorefraction, temp. and light intensity depend. 80−50288
LiNbO$_3$:Fe, photovoltaic effect and charge transport mechanism 79−38123
LiNbO$_3$:Fe, pure and doped, nonlinear excitation, multiphoton photorefractive process 79−36950
LiNbO$_3$:Fe, recording dynamical holograms in crystals with photovoltaic effect, nonstationary energy exchange *(Russian)* 79−31842
LiNbO$_3$:Fe, refractive index change induced by light irrad. *(Japanese)* 79−65824
LiNbO$_3$:Fe, SHG, phase-matching temp., impurity influence 80−69463
LiNbO$_3$:Fe, spontaneous polarisation reversal and photorefractive effect 78−31163
LiNbO$_3$:Fe, state of impurity Fe cation, nucl. gamma reson. study 80−40014
LiNbO$_3$:Fe, temp. depend., electron cond., holography appl. 78−14731
LiNbO$_3$:Fe, thermally activated trapping caused by small polaron formation 77−20259
LiNbO$_3$:Fe, two-photon photorefractivity 80−80753
LiNbO$_3$:Fe, unipolar Malter emission under pyroelectric effect conditions 80−29862
LiNbO$_3$:Fe, X-ray and γ-ray irradiation effects on Fe charge state, Mossbauer study 80−40013
LiNbO$_3$:Fe crystal conductivity and photoinduced birefringence obs. *(Russian)* 78−60151
LiNbO$_3$:Fe crystals, reflection hologram recording 79−10272
LiNbO$_3$:Fe electro-optic crystal holographic storage data error probability 80−43304
LiNbO$_3$:Fe monocrystal, pulsed holographic recording *(Russian)* 77−629
LiNbO$_3$:Fe^{3+}, electrooptical effect, charge transfer mechanism, defect. pair form. 79−38519
LiNb0$_3$:Fe, anomalous photovoltaic effect and diffraction efficiency *(Russian)* 79−15190
LiScO$_2$:Fe^{3+}, Mossbauer exam. of relaxation behaviour of Fe^{3+} 77−1620
LiTaO$_3$:Cu(Fe), light induced charge transport, photovoltaic effects, impurity states 80−80317
LiTaO$_3$:Fe, electro-optic cryst., light induced charge transport, holographic obs. 80−70747
LiTaO$_3$:Fe crystal, holographic storage process 80−32942
Mg^{2+}-Fe^{2+} partitioning in garnet lherzolite, rel. to high-press. phase equilibria 79−66687
MgAl$_2$O$_4$:Fe, spinel, elec. cond. 80−59702
MgF$_2$:Fe^{2+}, γ-irrad., F-centres, Fe^{2+} ion hole traps, absorpt. and EPR meas. 79−7598
MgO, Fe^{2+} and Fe^{3+} conc. and valency, optical density, EPR and MCD obs. 77−89462
MgO:Fe, Fe^{2+} oxidation and Fe^{3+} reduction kinetics, EPR obs. 79−70399
MgO:Fe, X-ray stimulated luminesc. 79−28802
MgO:Fe crysts., oxidised and reduced, optical absorpt. spectrum at low temps. 77−63436
MgO:Fe^{2+}, $^5T_{2g}\rightarrow{}^5E_g$ adsorption, Zeeman effect meas. 77−12405
MgO:Fe^{2+}, far IR absorpt. meas. by Fourier transform, apparatus 77−177
MgO:Fe^{2+}, impurity electron-phonon reson. relax. time, thermal cond. 77−59085
MgO:Fe^{2+}, intrinsic spin-lattice relaxation rates, nonresonant US meas. 78−80203
MgO:Fe^{2+}, Jahn-Teller effect in ^5E_g state, tunnelling splitting obs. 78−19517
MgO:Fe^{2+}, lifetime of coupled spin-phonon excitations 77−69053
MgO:Fe^{2+}, microwave acoustic relaxation losses 78−43635

iron continued
MgO:Fe^{2+}, phonon-induced transition interf. in EPR and IR spectra, ion-lattice coupling 77−51945
MgO:Fe^{2+}, redox behaviour, ESR and X-ray diffr. 78−52341
MgO:Fe^{2+}, reson. relax. time for impurity electrons and localised phonons interaction, appl. to thermal cond. 80−59590
MgO:Fe^{2+}, shock compressed absorpt. spectrum, appl. to Earth mantle 80−90039
MgO:Fe^{2+}, thermal magnetoresist. calc. 79−10994
MgO:Fe^{3+}, clustering, EPR meas. 78−56372
MgO:Fe^{3+}, defect struct., shell model calcs. 79−99180
MgO:Fe^{3+}, defect structure, and oxidation reduction behaviour of Fe 79−99181
MgO:Fe^{3+}, EPR, 94-600K, temp. depend. of cubic spin Hamiltonian parameter 78−60332
MgO:Fe^{3+}, EPR of Fe^{3+} in orthorhombic symmetry sites 77−20689
MgO:Fe^{3+}, EPR spectra obtained at room temp. and 1200°C 80−68233
MgO:Fe^{3+}, Mn^{2+}, X-irrad. induced anion Frenkel defects, stabilisation by Fe^{3+}, optical and ESR obs. 77−68969
MgO:Fe^{3+}, point defect complex-edge dislocation interaction energies, atomistic calc. 80−107314
MgO:Fe^{3+}, spin-lattice relax. 77−90037
MgO:Fe^{3+}, spin-lattice relax. time, meas. 80−66020
MgO:Fe^{3+}, valence conversion in single crysts., by UV irradiation *(German)* 78−84620
MgO:Fe^{3+} single cryst., exchange energy 80−96834
MgO:Li, Fe, charge compensation before and after ionising irrad. and light excitation 79−77598
Mg(OH)$_2$:Fe, crystal field properties, Mossbauer spectra, isomer shift and quadrupole splitting 79−61278
Mg$_2$SiO$_4$:Fe, forsterite, ionic transport 79−69285
Mg$_2$SiO$_4$:Fe^{3+}, elec. field gradients, asymmetry parameters 80−54660
MgTiO$_3$:Fe, ESR study of Fe^{3+} 80−50173
MgTiO$_3$:Fe^{3+}, EPR spectra 79−91285
MgWO$_4$:Fe^{3+}, effect of electric field on ESR of Fe^{3+} ions 78−88176
MnF$_2$:Fe^{2+}, temp. depend. of magnon pair-mode energies, Raman scatt. meas. 77−20577
Mo, arc, steady, vac., plasma ion mass and energy diagnostics 78−51385
Mo, recrystallisation kinetics, deform. degree effects *(Russian)* 78−6943
N_2+Fe (atomic), interaction mechanism via clusters 77−25263
NH$_4$Al(SO$_4$)$_2$.12H$_2$O:Fe^{3+}, spin-lattice relax. of paramag. ions, Mossbauer effect 79−95688
NH$_4$H$_2$PO$_4$:^{57}Fe, Mossbauer study, Fe^{3+} effect in habit 80−100627
NH$_4$H$_2$PO$_4$:Fe^{3+}, mechanism of habit change due to Fe^{3+}, Mossbauer study 79−19821
(NH$_4$)$_2$InCl$_5$:Fe^{3+} EPR, site g-tensor, spin Hamiltonian factors 77−63270
Na$^+$+Ti(Ni)(Zn)(Fe), 0.2-3.0 MeV, united-at. limits, mol.-orbital continua 77−19030
NaCl:Fe, nucleation of Au, surface imperfection effects 77−15699
NaClO$_4$:Fe^{2+}, frozen soln., photo- and radiation-produced H-atoms obs. 79−39162
NaF:Fe, dispersed ions, absorber Mossbauer spectra 78−15077
NaF:Fe, Mossbauer study of Fe precipitates 79−91327
NaF:Fe$^+$, ENDOR associated with Na$^+$ vacancy 79−61264
Na$_2$O-3SiO$_2$:Fe^{2+}, Fe^{3+} glasses, Mossbauer and ESR spectra and internal friction 80−100865
Na$_2$O-B$_2$O$_3$-SiO$_2$-Fe glass, near IR optical absorption of Fe (II) 78−84616
Na$_2$O-CaO-SiO$_2$ glass:Fe, Mossbauer spectra of Fe^{2+}, Fe^{3+} impurities *(French)* 79−51893
Na$_2$O.2Al$_2$O$_3$.5SiO$_2$:Fe^{3+}, Mossbauer effect and magnetometric exam. 78−6613
NbSe$_2$:Fe, local moment form., mag. susceptibility meas. 79−82756
NbSe$_2$:Fe (2H), layer supercond., anisotropy and temp. depend. of H_{c2} 77−51857
NbSe$_2$:Fe (2H), magnetoresist. and elec. resist. temp. depend. rel. to CDW form. 80−44574
NbSe$_2$(2H) layered supercond., effect of Fe impurities on sp. ht. 79−60972
Ni, film deposit on (001)Fe substrate, misfit twin crystals 77−4273
in Ni, paramag. region, impurity effects on susceptibility, Faraday obs. *(Russian)* 80−88731
Ni plated Fe single crystal, deformed at 77K, surface obs. 78−19916
Ni/Fe interfaces sputter profiling, by AES 79−15572
Ni/Fe layers, interdiffusion, Auger sputter profiling obs. 79−46848
Ni-coated, heat resistance assessment at varying temps. *(Russian)* 77−25189
Ni-Fe thermocouple, appl. to surface temperature measurement 80−62668
NiCr$_2$O$_4$:Fe, Mossbauer effect 80−15874
NiO:Fe, estimation of 4s covalent bonding of Fe^{2+} and Fe^{3+} ions, Mossbauer spectra 78−72441
NiO:Fe, exchange anisotropy of Ni-ferrite precipitates 79−28520
P determination by at. emission spectroscopy using steeloscope 79−57330
PLZT:Fe, enhancement of photochromic effect by multi-reflection scatt. 77−75632
Pb-Fe multilayers, zero pair pot. verification by supercond. tunnelling 80−54841
Pb+Pb quasimolecules ab initio calc. of K X-ray spectra 78−21941
Pb$_5$Ge$_3$O$_{11}$:Fe^{3+}, ESR 79−95639
PbMoO$_4$:Fe^{3+}, ESR, effective g-factors, Fe^{3+} sites 77−51947
PbMoO$_4$:Fe^{3+}, single crystals, structure and kinetics, EPR meas. 79−99760
PbMo$_6$S$_8$:Fe, elec. cond. anomalous temp. depend., mag. moments *(Russian)* 80−92878
PbMo$_6$S$_8$:Fe, influence on supercond. transition temp., and mag. props. *(Russian)* 79−42686
PbO-SiO$_2$:Fe^{3+} glasses, high temp. ESR 80−60410
PbTe:Fe, single crystals, state and behaviour of Fe, mag. props. 80−93080
Pb(Zr,Ti)O$_3$:Fe(Nb) ceramic, elec. and electromechanical props., depend. on dopants 80−81212
PdH$_{0.97}$:Fe, supercond. transition temp. depression, coexistent mag. behaviour 80−49976
PdH$_x$:Fe, diffusion and interstitial site occupancy, Mossbauer spectra 80−20555
Rb$_2$CoF$_4$:^{57}Fe, Ising antiferromag., Mossbauer spectra, critical dynamics 80−15884

iron continued
Rb_2CoF_4:^{57}Fe, Mossbauer spectra, critical region anal. 80−15888
$Rb_2Co_{0.95}Mg_{0.05}F_4$:^{57}Fe, Mossbauer spectra, critical region anal. 80−15888
$RbIn(MoO_4)_2$:Fe^{3+} monocrystals, EPR spectrum in the phase transition neighbourhood 80−2624
$RbMnF_3$:Fe, thermal cond., spin wave and mag. impurity contribs. 77−40046
$RbMnF_3$:Fe^{2+}, high-temperature EPR linewidth, impurity fast relax. effects 77−85556
Si contaminant, effects on nitridation, mechanism 78−80496
Si, nitridation, effects of Fe and Al additions 77−16708
Si:^{57}Fe, implanted, Mossbauer spectra, study of dose dependence 80−75900
p-Si:B, Fe, 0.45 eV majority carrier trapping level after quenching 78−18990
Si:Fe, anisotropic broadening of linewidth in EPR spectra of Fe^0 77−66417
Si:Fe, B, Fe reaction with ion implanted B 79−77620
Si:Fe, B thermally activated Fe interstitial, elec. and kinetics props. *(German)* 80−34035
Si:Fe, compensated substrates for solar cells, effects of Fe and Al 80−94009
Si:Fe, diffusion mechanism of fast impurities, distrib. in surface layers 77−11735
Si:Fe, dopant profile changes induced by laser irrad. using SIM and backscatt. meas. 79−69148
Si:Fe, EPR and neutron activation anal. of thermal defects 78−91355
Si:Fe, EPR line intensity and widths, temp. depend. 79−28604
Si:Fe, ESR, cryst. field under stress, C_{11} and C_{44} meas. 77−12194
-Si:Fe, effect of γ-irradiation, photocapacitance meas., impurity centre conc. 78−18993
Si:Fe, implant redistrib. and enhanced solubility following laser irrad. 79−69129
Si:Fe, implanted, annealing and stripping, Mossbauer expts. 80−39141
Si:Fe, implanted, Mossbauer spectra, conversion electron, temp. dependence 80−40025
Si:Fe, impurity segregation and microstructural changes by pulsed laser irrad. 79−82254
Si:Fe, impurity states, localised orbital approach 80−92851
Si:Fe, interstitial form., Au dopant effect 80−29611
Si:Fe, ion implanted, doping profile, pulsed laser annealing effects 80−88197
Si:Fe, ion implanted, laser annealing studies using Mossbauer spectroscopy 80−79827
Si:Fe, laser annealing of implanted ^{57}Co sources, Mossbauer obs. 80−39139
Si:Fe, laser implantation, Mossbauer obs. 80−39125
Si:Fe, photoconductivity and Hall effect 79−4579
Si:Fe, photoionisation cross-sections and energy levels 79−87060
Si:Fe, solubility study by EPR and neutron activation anal. 80−75361
Si:Fe, thermally induced donors due to heat treatment and Fe contamination 79−78035
n-Si:Fe 79−28312
Si:Fe amorphous films, ESR and elec. cond. 80−50171
Si:Fe contaminated solar cells, $POCl_3$ gettering 80−94010
Si:Fe^0, solid soln. decomp., Fe deposition on dislocations 77−51943
Si:Fe^0, spin relax. rate ang. depend. for pulsed saturation of inhomogeneously broadened ESR line 79−65721
Si:Fe^0 interstitial localisation, EPR spectrum 79−1582
Si-Fe-H_2-N_2, combined effect of Fe and H_2 78−95722
Si+Co(Fe) recoil, transient mag. field 78−29838
Si_3N_4:Fe, α- and β-phases, Mossbauer and Raman obs. of state of Fe 79−33572
Si_3N_4-MgO, reaction with Fe to produce surface pitting 78−76778
SiO_2, vitreous, Fe^{2+} absorpt. spectra in polarised light and struct. position 79−43007
SiO_2:Fe, vitreous and cryst., with or without Al_2O_3, Na_2O additions, exam. of Fe^{2+} coordination, IR spectroscopy 78−88344
SiO_2:Fe^{3+}, vitreous silica, absorpt. spectra and structural state 80−16071
SiO_2-Al_2O_3-CaO-Na_2O:Fe^{3+}, optical absorpt. due to Fe^{3+} ligand field and charge transfer 80−89020
SiO_2-MgO-CaO-Al_2O_3:Ce,Fe, redox equilib., expt. 80−85171
SiO_2-Na_2O-CaO:Fe(As)(Cr) glasses, optical absorpt. changes on heat treatment 78−31224
Sn melt in contact with Fe, Fe distrib. on thermal cycling *(Russian)* 80−16562
SnO_2:Sb,Fe, CVD thin film, resist. temp. coeff. 79−38198
$Sr_{0.5}Ba_{0.5}Nb_2O_6$:Fe, ceramic, additive effects on ferroelec. and pyroelec. props., EPR 77−16256
$SrCl_2$:Fe^{2+}(Co^{2+}) electronic absorption spectra in far and middle infrared 78−68537
$SrCl_2$:Fe^{3+}, EPR spectra of Fe^{3+}($^6S_{5/2}$), 4-100K 78−95512
$SrCoO_3$:Fe^{4+}, ferromag., sign of Fe^{4+} hyperfine field, spin struct., Mossbauer study 80−39933
SrO_2:Fe^{2+}(Fe^{3+}), EPR spectra, evidence for off-centre displacement of Fe^{2+} 78−72398
$SrTiO_3$:Fe, EPR, of Fe^{3+}-rhombic, Fe^{2+}-V_O and Fe^{1+}-V_O complexes 78−76302
$SrTiO_3$:Fe, photochromic Fe^{5+} in non-cubic local fields, EPR spectra of $S=^3/_2$ centre obs. 77−40127
$SrTiO_3$:Fe^{3+}, order-disorder and central peak behaviour, EPR study 80−75970
$SrTiO_3$:Fe^{4+}, opt. absorpt. 77−16349
TaS_2:Fe, local moment form., mag. susceptibility meas. 79−82756
$TaSe_2$:Fe, competition between charge and spin density waves, Landau-Ginzburg theory 79−95352
$TaSe_2$:Fe, local moment form., mag. susceptibility meas. 79−82756
Tc:^{51}Fe, dilute, quadrupole splitting and isomer shift, Mossbauer spectrum 78−48096
in α-Ti, recrystallised commercial purity, Fe-rich precipitates obs. *(French)* 80−50637
TiAl, Ti_3Al, ordered alloys, Fe impurity atoms distrib. *(Russian)* 77−35584
TiO_2:Fe, impurity levels, photocurrent and ESR meas. 80−29346
TiO_2:Fe, Mossbauer effect exam. of impurities 78−31140
TiO_2:Fe, rutile, ESR meas. 80−54945
TiO_2:Fe^{3+}, microwave second harmonic generation and freq. conversion 80−50166
iron continued
TiO_2:Fe^{3+}, rutile, temp. depend. of spin Hamiltonian parameters, ESR meas. 77−32251
TiO_2:Fe^{3+}, uniaxial stress method for determ. of spin-lattice coeff. for Fe^{3+} 77−90018
TiO_2:Fe^{3+}. appl. of sensitive EPR spectrometer to zero field splitting determ. *(Russian)* 77−57372
TiO_2:Si(Fe)(Ni)(Mn)(Cr), anodes, performance in photoelectrolysis of water 79−74407
$TiO_{1.95}$iFe, quenched near melting point, transverse composition waves 79−99220
V-Fe interface, diffusion above 500°C *(German)* 79−28156
VO_2:Fe, phase transforms., influence of nonstoichiometry 77−85274
V_2O_5:Fe^{3+}, EPR, 5-300K 77−81002
V_5S_8:Fe, Mossbauer and mag. studies, electronic state of Fe 80−108130
$(V_{1-x}Ti_x)_2O_3$:Fe, metallic antiferromagnetism, Mossbauer spectra 80−15881
W fibre reinforced, high temp. strength 79−70021
YAG:Fe^{3+}, ESR absorption spectra, line broadening 78−91940
$Y_3Ga_5O_{12}$:Fe^{3+}, impurity absorpt. spectra to 5.5 eV 77−20892
YIG:Fe^{2+}, magnetocrystalline anisotropy, effect of high hydrostatic press. 77−43831
YIG:Fe^{2+}, magnetostriction const. temp. depend., ferromag. reson. meas. 77−40103
Y_2O_3:Fe^{3+}, EPR obs. of non-cubic phase 78−19316
$Y_{3-x}Sm_xFe_5O_{12}$:^{57}Fe film, ion implanted, Mossbauer conversion spectra study 80−80663
Zn electrodeposited, reaction rate in solid state *(Japanese)* 78−15322
$ZnAl_2S_4$:Fe_3 superhyperfine interaction of Fe, ESR spectra 77−63271
$ZnCO_3$:Fe^{2+}, electronic relaxation, Mossbauer effect 78−19385
$ZnGa_2O_4$:Fe^{3+}, EPR, spin Hamiltonian parameters 80−25195
ZnO:Cu, O:Fe, photocond., electron escape probabilities and trap depths 77−32041
ZnS, Fe^{3+}-Cu^+ complexes and A-centres, g-factor anisotropy *(Russian)* 77−20271
ZnS:Cr^+, Fe^{3+}, luminesc., cond. and paramag. centre conc. parameters 78−6724
ZnS:Cu, O, Fe, photocurrent spectral distrib., killer impurity effects 77−8135
ZnS:Cu, O, Fe photoconductors, killer impurities effect on electron escape probabilities and trap depths 77−4392
ZnS:Fe, impurity-induced Raman scatt., central force const. reduction 77−32379
ZnS:Fe, luminesc. and ESR investigations 80−2822
ZnS:Fe, piezospectroscopic effect on electron-vibr. lines of Fe^{2+} 78−27269
ZnS:Fe, Raman spectra, impurity induced first order transitions 78−88310
ZnS:Fe, vibr. modes of transition element impurities 78−76472
ZnS:Fe^{2+}, impurity electron-phonon reson. relax. time, thermal cond. 77−59085
ZnS:Fe^{2+}, low temp. Mossbauer spectra, in source and absorber expts. 77−28500
ZnS:Fe^{2+}, relax. meas. from Mossb auer absorber and source expts. 80−39956
ZnS:Fe^{2+}, reson. relax. time for impurity electrons and localised phonons interaction, appl. to thermal cond. 80−59590
ZnS:Fe^{2+}, thermal expansion and heat capacity, effect of Fe^{2+} 77−31782
ZnS_xSe_{1-x}:Fe_3 photolum. meas. 79−19921
ZnSe:Cr^+, Fe^{3+}, luminesc. cond. and paramag. centre conc. parameters 78−6724
ZnTe:Fe, exciton refl. spectra 80−2806

iron alloys
see also Elinvar; Invar; iron compounds; Permalloy; steel
actinide intermetallics, $AnFe_2$, (An=U, Np, Pu, Am), magnetisation, neutron diffr. and Mossbauer expts. 77−63137
additions to Si, effect on nitridation 78−48650
Alinco 5, thermal treatment in mag. field, mag. props. 78−91905
alloying elements, distribution ability *(Czech)* 80−29047
Alnico, domain struct., variation under influence of heat treatment *(Russian)* 78−23292
Alnico, high-energy magnetic materials technology developments and props. *(Italian)* 80−54914
Alnico, hot worked, properties *(German)* 77−52352
Alnico, interaction domains after heat treatment in mag. field *(Russian)* 78−68286
alnico, thermal magnetic hysteresis *(Russian)* 77−16119
Alnico 5, two-phase separation during ageing, Mossbauer study 80−7533
Alnico 5 alloy, S and Ti additions effect rel. to non-metallic inclusions, coercive force and grindability 80−89375
Alnico 8 permanent magnet, magnetic props. rel. with crystallographic texture 78−95483
Alnico alloy, C addition effects on struct. and mag. props. 78−23835
Alnico alloys, effect of Ce addition on mag. props. 78−2699
amorphous, corrosion characteristics, book contrib. 79−66225
amorphous, effects of metalloids on mag. props. 80−75738
amorphous, ferromag., sputter-deposited, soft mag. props., magnetostriction 80−34696
amorphous, liq. quenched, struct., thermal stability and mech. props. 80−88059
amorphous, saturation magnetisation, Curie temp. and size effect 80−65815
amorphous Fe base, Ni addition effect on corrosion resistance 77−4869
amorphous metal-metalloid alloys production by ion implantation, TEM study 80−15128
amorphous ribbon, saturation magnetostriction, and electronically controllable delay line 79−1700
anisotropic precipitation struct. in external mag. field *(German)* 78−72785
Armco, shock front phase transition kinetics 78−10122
Armco Fe, constitutive eqn. covering wide range of strain rates *(Japanese)* 80−79862
Armco iron, kinetics of form. and struct. of thermodiffusional protective coatings 77−56158
austenite formation kinetics during accelerated heating model, kinetic curves *(Russian)* 79−70058
BCC and FCC struct., X-ray absorption spectra, Mossbauer spectra, comparison *(Russian)* 78−64299
binary, magnetic resist. anisotropy, two-current model 77−20295

iron alloys continued
binary ferro alloys, crystallisation under forced mixing in ingot mould *(Russian)* 79−52192
brass leaded, effect of Al, Sn, Fe on solidification, differential thermal analysis exam. *(Russian)* 79−29041
brittle fracture, quantitative determ. of transcryst. and intercryst. portions by opt. and SEM fractography 77−52464
Carpenter 20 Cb-3 alloy, pitting resist. in low salinity geothermal brines 80−93681
case Fe, Ni resist alloy, austenitic type ChN15D7Kh2, struct. stability 79−87633
cast, austenitic grain size determ. 80−81255
cast, boride coatings, technology, props., book contrib. 78−48574
cast, developments in comp., prod. and applic. 78−48347
cast, ductile, strain rate and temp., influence on strength, elongation and deformation *(Japanese)* 80−45356
cast, EM wave propagation, penetration depth calc. *(Bulgarian)* 78−50679
cast, Fe, ferritic, spheroidal, graphite nodule size and distrib. effect of fracture *(French)* 79−20176
cast, Fe, ferritic grey, exam. of ordering kinetics by elastic modulus meas. 79−100136
cast, Fe, graphite nodule form., ion microprobe mass anal. appl. 79−43295
cast, Fe, with uniaxial loading, changes in ultrasonic waves vel. and attenuation 79−15756
cast, fracture toughness prediction 79−5045
cast, fracture under proportional straining 77−35091
cast, grey, Cr-Mo pearlitic, isothermal transform. of austenitic in bainitic range *(Rumanian)* 78−23698
cast, grey, pearlitic Fe, relationship of magnetic props. to condition of C 78−56353
cast, grey, surface hardening by continuous laser emission *(Russian)* 77−70212
cast, high tensile, with spheroidal graphite, depth length relationship of fatigue crack developing in circular specimens during bending 79−11705
cast, high-chrome, corrosion resistance increase by Pd electrospark coating *(Russian)* 78−27669
cast, nodular, solidification *(Japanese)* 78−11217
cast, spheroidal graphite, cooling velocity and C effect on matrix struct. *(Korean)* 78−19789
cast, Ti diffusion coated, wear resistance 79−52459
cast, US flaw detection by boxcar integration 80−89437
cast, white, comp. development 78−48347
cast, white, graphitisation, effect of hot impact deform. 78−19780
cast, white Fe-Cr, effect of C on austenite and martensitic transformation 78−44124
cast, white freezing rate and Si content effect on graphitisation *(Japanese)* 77−56009
cast, with spherical graphite, SiC-Q apparatus for tensile strength meas. *(German)* 80−76450
cast Fe, abrasive wear rel. to lamellar or spheroidal graphite content *(German)* 78−85000
cast Fe, alloyed, struct., props., heat treatment 77−16623
cast Fe, alloyed and unalloyed, microsegregation thermodynamics 80−76261
cast Fe, anodic polarisation in slag melt *(Russian)* 80−45513
cast Fe, anodic protection under boiling H_2SO_4 in industrial conditions 79−20245
cast Fe, atomised powder, reduction and decarburisation annealing in converted gas 79−24463
cast Fe, atomised powder, reduction-decarburisation annealing with converted gas, optimum conditions 79−24465
cast Fe, atomised powders, particle size effect on purification in US pickling 79−28985
cast Fe, C and Si effect on spheroidal graphite *(Korean)* 79−38839
cast Fe, cam-roller pair, wear resistance after strengthening treatment *(Russian)* 78−31542
cast Fe, cast, thermal treatment influence on mechanical props. *(German)* 80−29980
cast Fe, cavitation erosion rate, effect of stress level 78−15545
cast Fe, Ce hypoeutectic, new phase formation sequence during crystallisation, X-ray obs. *(Russian)* 78−95731
cast Fe, compact graphite inclusions, surface hardening by continuous action laser emission *(Russian)* 78−15567
cast Fe, contact deformation, reverse slipping effect *(Russian)* 80−97591
cast Fe, corrosion in uninhibited alcohol/water coolants, and graphitization 78−44248
cast Fe, craze crack form. 78−44221
cast Fe, crazing with directionally arrayed flake graphite 77−59935
cast Fe, dispersed with interdendritic graphite, eutectoid transformation of austenite during cooling 78−84800
cast Fe, ductility under tension or compression at high press. *(Japanese)* 78−35617
cast Fe, dynamic tear charact. 77−44448
cast Fe, effect of heat treatment, on wear resistance, 78−44148
cast Fe, eutectic cells microstruct., crystallisation kinetics *(Polish)* 79−52186
cast Fe, eutectic solidification, expt. study by quantitative metallography 79−24516
cast Fe, fatigue strength, effect of notches and effective sectional area, for cast Fe with various graphite sizes *(Japanese)* 78−64626
cast Fe, ferritic, Ce addition effect on impurity distrib. Mossbauer study *(Russian)* 78−18673
cast Fe, ferritic SG ductile fracture initiation and propagation 78−64661
cast Fe, flake and nodular, heterogeneous nuclei and graphite chemistry 79−55896
cast Fe, flaky graphite, damping capacity 77−8869
cast Fe, form. of surface graphitisation centres *(Russian)* 79−11720
cast Fe, fracture mech. and fractography *(Japanese)* 78−7031
cast Fe, fused metal, solidification enhancement using Bi and Te *(Italian)* 80−7540
cast Fe, graphite content determ. by X-ray diffr. method 80−100977
cast Fe, graphite spheroidization, Mg residue effects *(Korean)* 79−43286
cast Fe, gray, relationship between cutting conditions and reaming precision 79−61801
cast Fe, grey, abrasive wear rate rel. to fracture toughness and microstructure *(German)* 79−29232
iron alloys continued
cast Fe, grey, carbide-free Cr diffusion coating 79−96205
cast Fe, grey, chromisation, influence on surface roughness *(German)* 79−11729
cast Fe, grey, corrosion in water at 50°C dissolved O_2 conc. effect 80−11820
cast Fe, grey, density variation during slow crystallisation *(Russian)* 78−95737
cast Fe, grey, eddy current test for hardness certification 80−7733
cast Fe, grey, effect of quenching conditions, on elastic modulus 78−56675
cast Fe, grey, electric arc sprayed coating on wire, elastic and elastic-plastic props. *(German)* 79−34089
cast Fe, grey, eutectic transform. mechanism *(Russian)* 80−20924
cast Fe, grey, fracture kinetics, surface hardening effect 80−76354
cast Fe, grey, fracture surface after dynamic fracture, Mg conc. effect 80−100909
cast Fe, grey, pipe, resist. to fracture under hydraulic pressure 79−96124
cast Fe, grey, solidified in oscillating and rotating moulds, metallographic study 80−89213
cast Fe, grey, tensile strength, surface area to volume ratio effect *(Japanese)* 80−45389
cast Fe, grey, wear of plasma-sprayed TiO_2 coating 79−34155
cast Fe, grey *(Japanese)* 80−7728
cast Fe, grey Al-Si eutectoid decomp. of austenite 80−29951
cast Fe, grey and ductile, subsurface defects, SEM and EDAX study 80−44400
cast Fe, grey brittle, strength in three axial stress state 79−66134
cast Fe, H_2 charging effect on nodularizing efficiency of Ce-La additions 78−27544
cast Fe, hardness, wear resist. and struct., electron irrad. effects 79−96126
cast Fe, heated in CO atm., obs. cracks around graphite flakes *(Japanese)* 78−84974
cast Fe, high Cr, hardfacing of roll, wear resistance and thermal durability 80−7686
cast Fe, high Cr, phase composition, mech. props. rel. to heat treatment 79−29108
cast Fe, high Mg content (0.33%), exam. of phase composition characts. 78−84780
cast Fe, high strength, wear resist., electrocontact surface facing influence *(Russian)* 79−52385
cast Fe, high-strength bainitic with spheroidal graphite, mech. props., isothermal transform. 79−96023
cast Fe, homogenization of property difference due to mass effect by repeated heat treatment *(Japanese)* 79−38857
cast Fe, hypoeutectic, Ce distrib. in graphite grains 80−100279
cast Fe, hypoeutectic, primary crystn. features by means of apparent viscosity meas. in early stages of solidification *(Japanese)* 79−43231
cast Fe, increase in yield strength, after phase transformations 78−44125
cast Fe, influence of interfacial energy on shape of graphite 80−16360
cast Fe, inoculated with Ce, exam. of phase composition 78−56620
cast Fe, instrumental dynamic tear tests 77−44447
cast Fe, interdendritic dispersed graphite, dissolution kinetics on heating, excess time *(Russian)* 77−52360
cast Fe, internal notch effect on abrasive wear in martensitic, lamellar, grey Fe *(German)* 79−29231
cast Fe, liquid metal embrittlement, eval. by quasistatic crack propag. technique 79−29262
cast Fe, low-cycle fatigue, theory 80−89349
cast Fe, malleable with divorced pearlite structural strength improvement by annealing 79−96049
cast Fe, mech. charact. in plane stressed state of type SCh15-32 79−57072
cast Fe, mech. props., demodification influence of isothermal holding and Mg addition *(Bulgarian)* 79−15707
cast Fe, mech. props., effect of repeated heating and cooling *(Japanese)* 77−59907
cast Fe, mechanism of boundary lubrication with zinc dithiophosphate 79−79120
cast Fe, Mg, austenite isothermal transform., Sn addition effect 79−87611
cast Fe, Mg, high strength bainitic transform. in C-shape diagram *(Russian)* 79−1860
cast Fe, Mg effect of Pb impurities on struct. and mech. props. 79−96089
cast Fe, Mg microdistrib., microprobe anal., electron fractography 77−70373
cast Fe, Mg treated, fading behaviour *(Japanese)* 78−11152
cast Fe, Mg treated, graphite modularisation by Mg gas bubbles 78−52867
cast Fe, Mg-modified, scale for shapes eval. of graphite inclusions 78−35609
cast Fe, Mg-Sb, despheroidising composition and distribution of phases, X-ray obs. *(Russian)* 78−95732
cast Fe, Mn, wear resist. and hardening, struct. effect 79−87734
cast Fe, Mn-Si-C, Mn effect on struct. during solidification 79−83191
cast Fe, Mo distribution 78−92269
cast Fe, nitrided, wear resistance *(Korean)* 80−21178
cast Fe, nodular, hardenability, isothermic bainitic transforms. *(Czech)* 77−59778
cast Fe, nodular, high strength, low cycle fatigue 79−57112
cast Fe, nodular, transition from quasistatic to fatigue fracture under low cycle loading 79−66167
cast Fe, nodular graphite, annealed, fracture behaviour at low temps. 78−72875
cast Fe, nodular graphite, welded, struct. exam., heat treatment effects 78−80703
cast Fe, nodular graphite form., Ce effect *(Japanese)* 77−56000
cast Fe, nodular graphite form. by Ar, N_2 or CO_2 gas bubble suspension *(Japanese)* 77−63694
cast Fe, nodular graphite form. by Bi and Pb additions *(Japanese)* 77−63693
cast Fe, nodular graphite formation, Mg and S effects *(Japanese)* 77−56001
cast Fe, nodularisation of graphite by Ce, Y, La, Ti, and Zr additions *(Japanese)* 77−55999
cast Fe, nodularization efficiency of rare earth alloy treatment, charging effect 79−91714

iron alloys continued
cast Fe, noise reduction by electrolytic coating 78−80681
cast Fe, notch strength, non-uniform stress distrib. effect *(Japanese)* 79−79090
cast Fe, P and Ce effect on struct. *(Russian)* 79−52224
cast Fe, parts inspection of unmachined surfaces using fluorescent penetrant method 79−11754
cast Fe, pearlitic, nodular graphite type, struct. evolution *(French)* 80−93551
cast Fe, pearlitic, residual compressivel stress distrib. effect on resultant stress conc. in notched samples 78−92336
cast Fe, photometric determ. of Ce *(German)* 78−68955
cast Fe, powder, exam. of reaction between C and O, before and after annealing in converted gas 79−33973
cast Fe, quantitative metallography, study by image anal. 78−31492
cast Fe, rare earth-Mg, metallurgical and technological features, appl. in China *(Chinese)* 78−84851
cast Fe, rare-earth-Mg nodular, fracture toughness and fatigue *(Chinese)* 78−95791
cast Fe, rod, breakdown charact. by longitudinal stress waves 78−38773
cast Fe, rod, torsion, St. Venant's problem 77−70135
cast Fe, Si ferrite heterogenisation, phase separation and embrittlement, Si effects 79−96125
cast Fe, spatial dispersion of graphite particles, metallographic study 78−92419
cast Fe, spherical mech. behaviour, continuous theory of dislocations appl. 78−67717
cast Fe, spheroidal graphite, degree of normalization effect on mech. props. *(Korean)* 79−87664
cast Fe, spheroidal graphite, graphite size effect on mech. props. *(Korean)* 78−11278
cast Fe, spheroidal graphite, hydrostatic pressure effects on ductile fracture 78−60779
cast Fe, spheroidal graphite, Mn effects *(Korean)* 77−8841
cast Fe, spheroidal graphite, rare earth treated, nodularizing element distrib. *(Chinese)* 80−11653
cast Fe, spheroidal graphite effects of Si and C on mechanical props. *(Korean)* 79−66114
cast Fe, spheroidal graphite form., role of interphase boundary adsorption 77−63657
cast Fe, spheroidal graphite pipe, fatigue strength 80−16419
cast Fe, spheroidal segregation investigation by X-ray spectral analysis *(German, English)* 77−63993
cast Fe, spheroidizing effect of Mg and Ce modifiers 80−35193
cast Fe, strength and plasticity under hydrostatic pressure 78−56694
cast Fe, structural changes, due to pulsed action of high temps. and pressures *(Russian)* 80−7554
cast Fe, surface hardening using CO_2 laser beam 77−90490
cast Fe, surface temperature effect on dry sliding wear 80−60983
cast Fe, tensile strength, Al addition effects *(Korean)* 80−71736
cast Fe, thermal diffusivity meas. 293 to 873K, exam. of thermal cond. *(Japanese)* 78−47763
cast Fe, thermoelec. method of Si, Mn, C content monitoring, thermo EMF meas. 77−73490
cast Fe, turning, wear of cemented carbide tools 79−43442
cast Fe, unalloyed and alloyed, addition effects on struct., thermodynamics of microsegregation 79−8305
cast Fe, u.s. detection of spongeosis in pipes *(German)* 77−4879
cast Fe, US study of sections undergoing deform. or thermal cycling 80−104285
cast Fe, vermicellular, eutectic cell struct. *(Rumanian)* 79−74167
cast Fe, wear, effect of vibrations 79−52389
cast Fe, wear exam. 79−87738
cast Fe, wear mechanisms, metallographic obs. 77−59942
cast Fe, wear resist., effect of rolling friction strengthening, oil abrasive environment *(Russian)* 79−15799
cast Fe, white, Cr alloyed, wear resistance, effect on abrasive hardness 78−64722
cast Fe, white, fracture toughness testing by double torsion bend test 78−27705
cast Fe, white, graphitisation during heat treatment *(Russian)* 80−20971
cast Fe, white, high Cr, phase composition, B effect 80−104172
cast Fe, white, prep. and morphological obs. *(French)* 79−43168
cast Fe, with Mn, high S, exam. of sulphide phases, cocrystallisation during solidification 78−56646
cast Fe, Y effect on struct. 80−29967
cast Fe, Young's modulus of Fe_3C phase *(Russian)* 80−76297
cast Fe (3% C), erosion in cavitating venturi 80−108602
cast Fe alloys, Young's modulus and microstructure *(German)* 77−25090
cast Fe friction couples, wear mechanism 79−83329
cast Fe influence of Y and Sb on microhardness and lattice spacing of ferrite *(Russian)* 80−19748
cast Fe innoculated with Ce-Mg-Fe master alloy, struct. and props. 80−100843
cast Fe sintered, friction and wear 79−91806
cast Fe with spheroidal graphite, crystn. *(German, English)* 80−97473
cast Fe-C-Si, graphite nodularization during annealing, Mg and S effects *(Japanese)* 80−81087
cast Fe-Mg, effect of Cu, Ni and Sn on grain growth 78−44149
cast Fe-Ni austenitic, struct. and props., review 78−44086
cast Fe-P powder, H annealing 79−66025
cast Fe-steel friction couple, adsorption effect in oil-abrasive medium 80−55546
cast grey Fe, friction and wear, phosphating effect 77−70190
cast iron, air-atomized powder, effect of particles on C and O content 78−15340
cast iron, electron probe determ. of traces of modifying agents in spheroidal graphite 79−52814
cast iron, growth of graphite crysts. from δ-containing Fe-C melt *(German)* 78−3148
cast iron, hypereutectic, transform. of cementite to austenite 77−52318
cast iron, kinetics of form. and struct. of thermodiffusional protective coatings 77−56158
cast iron, white, high Cr-Mo, fracture toughness 80−50726
cast modified with Al and S, nonmetallic inclusion effects, electron microscope obs. *(Russian)* 77−65987
casting surface alloy layer by flame spraying technique *(Japanese)* 77−48586
cementite, in white pig Fe, deform. and fracture 77−4827

iron alloys continued
chromindur, origin of coercivity, Lorentz microscopy, magnetisation and Mossbauer effect 78−64219
chromindur, phase separation, Mossbauer obs. 78−88116
Cl $(Co_{100-x}Fe_x)_{83}B_{17}$, $1 \leq x \leq 30$, annealing embrittlement and crystn. 80−45329
Colmonoy, friction behavior in high temp. Na environment *(Japanese)* 80−40546
Colmonoy, self-weldability in high temp Na *(Japanese)* 80−89392
Colmonoy hardfacing materials, friction charact. in high temp. Na *(Japanese)* 80−89356
compacts, sintered, prod. directly from Fe_3O_4 powder *(Slovak)* 79−15626
compatibility with Si_3N_4, solid-solid reactions 79−28151
component interaction parameters, enthalpy and mixing energy *(Russian)* 80−54382
composite material, sintered, microstrained state, opt. polarisation investig. 78−11476
containers for liquid Li, corrosion resistance properties 79−47815
correl. between void swelling and thermodynamic stability 80−641
corrosion, monitoring using polarisation resistance meas., techniques and correlations 77−16711
corrosion inhibition, chem. nature and struct. of protective films 77−60001
corrosion potential/time, and potentiostatic polarisation curves as a method of predicting corrosion 80−45419
Coulomb and exchange scatt. amplitudes, spin dependent residual resistivities 78−64033
crevice corrosion by water vapour, CO, methane in HTR coolants, model 77−25202
cyclic oxidation, static and dynamic, high temp. alloys 78−88576
design, fundamental aspects, phase transformation utilization *(Korean)* 79−66058
diffusion impregnation enhancement by Fe powder addition to impregnant mixtures 77−28044
dilute, charge transfer and alloy binding, Thomas-Fermi-Dirac aprox. 77−76775
Dilute, Fe-X-Sn, Mossbauer meas. of Sn interaction with solute atoms 80−15856
dilute, hyperfine field at positive muon 80−40029
dilute, hyperfine fields at impurity sites 77−66297
dilute, hyperfine fields for transition metal impurities 80−80237
dilute, itinerant 3d electron spin density oscills. around solute atoms 77−72978
dilute, residual resist. in two-current model, impurity mag. moments 77−15818
dilute alloys, amorphous, exhibiting Mossbauer effect, mean mag. props. *(French)* 80−80489
dilute metastable alloy formation by ion implantation 80−15130
dispersion strengthened, thick vacuum condensate, control of struct. and mech. props. 80−16324
ductile, RE inoculated, black spots *(Chinese)* 77−72628
ductile, stress corrosion cracking theory based on model for anodic dissolution reactors 77−56133
elastic props., texture correction formulae *(German)* 78−15439
electrical resistivity and specific heat anomalies, comparison with Co, Co, alloys 80−6809
electrodes, rolled from powders, sintering problems 80−25608
fast neutron irradiated at high temps., mech. props. 79−51157
FCC, Invar effect, model 80−25105
$Fe_{40}Ni_{40}P_{14}B_6$, amorphous, tape wound core, fluctuations of driving field 78−10726
$Fe_{40}Ni_{40}P_{14}B_6$, $Fe_{32}Ni_{36}Cr_{14}P_{12}B_6$, amorphous Hall effect, press. and temp. depends. 77−66155
Fe-W(Co)(Ni)(Mo)(Nb)(Cr)(V), for working curves, HF induction melting and centrifugal casting 80−22340
ζ-Fe-Zn layer formed during hot dip galvanizing, texture 79−29287
ferrite, transform. kinetics, grain size, alloying element effect, carbide precip. 80−93560
ferrite-austenite transition, C diffusion const. determ., rate const. of carburization and decarburization 78−48396
ferrite-pearlitic grey Fe, tensile testing of mechanical props., from room temp. to liquidus *(Japanese)* 80−7728
ferritic, reinforced by dispersed oxide, mech. props. modification by recovery heat treatment *(French)* 77−59837
ferritic grey Fe, tensile testing of mechanical props., from room temps. to liquidus *(Japanese)* 80−7728
ferromagnetic, EMF generation by pulsed laser irrad. 78−68021
ferromagnetic, hyperfine fields of 4d and 5d impurities 78−31133
ferromagnetic, thermodynamic analysis of solubility and miscibility gap, in α-phase 79−60508
ferromagnetic domain wall, freq. const. for thermal activation 77−89976
ferromagnetic films, coercive force, ion plating prep. 77−28730
ferromagnetic metallic glass, hyperfine field and spin wave excitations, $T^{3/2}$ depend. 78−10672
ferromagnetic wire, torsion stress influence on magnetisation *(Slovak)* 77−90468
ferromagnetism, Stoner model, mol. field coeff., temp. and field depends. 77−72975
ferrous, FCC, anomalous thermal expansion in paramagnetic temp. range 77−35724
ferrous martensites, trace analysis of (112) transform. twins 77−86030
ferrous material fractured surface exam., oxide scale removal 78−95886
filamentary crystal prep. from brittle high-strength mats., mech. props. *(Russian)* 77−59712
fracture mechanism in various temperature and stress intervals *(Russian)* 79−24600
fracture toughness of cryogenic temp. 78−72878
free surface and grain boundary O_2 and S chemistry 80−75410
Gentalloy, in Fe-W system, damping capacity *(Japanese)* 79−20094
glassy, continuous-biased sputter-deposited Kr entrapment 80−24603
glassy wire, shape, energy, eddy current loss and relax. damping of mag. domain walls 77−89975
granule reinforced Cu, friction in vacuum 80−25880
granule reinforced Cu M2, wear resistance in rubbing with lubrication 80−16490
gray, Mg bearing, high strength, eutectic grain determ. by Si reverse liquation 79−15886
grey cast, corrosion resist., Cu alloying additions effect *(Russian)* 78−56807
grey cast Fe, P effect on distrib. of alloying elements 77−12634

iron alloys continued
grey cast iron, deform. and fracture regions in microzones *(Russian)* 78−80585
Hastelloy, C-276, H-induced crack growth 80−71747
Hastelloy, H_2 embrittlement in H_2S environments, impurity segregation effects 80−71724
Hastelloy C, stress corrosion cracking in high temp. caustic soln. 77−59964
Hastelloy C-276, cold worked, annealed, surface segregation, Auger spectroscopy study 79−83204
Hastelloy C-276 and C-4 cold worked high alloy material, factors affecting H_2 embrittlement in H_2S environments 78−31502
Hastelloy C-276 and G, accelerated H_2 charging in aq. H_2SO_4 at 0.2% yield stress 80−30144
Hastelloy C-276/Bi_2Te_3 contacts, elevated temp. compatibility, appl. to radioisotopically powered thermoelec. generator 79−49680
Hastelloy N, air contamination effect on compatibility with liquid Li in stainless steel vessels at 600°C 78−25285
Hastelloy N, Si additions, comp. of eta carbide after ageing 78−52816
Hastelloy X, carburisation and dimens. stability in HTGR, He environment 80−45366
Hastelloy X, corrosion behaviour in simulated HTGR He environment 79−54495
Hastelloy X, creep, effect of He environment and grain size *(Japanese)* 77−48488
Hastelloy X, creep and creep rupture props. in air and helium at 900°C *(Japanese)* 77−52405
Hastelloy X, creep props. and appl. to structural design *(Japanese)* 77−59862
Hastelloy X, grain size effect. creep and creep-rupture *(Japanese)* 80−16382
Hastelloy X, heat resistant superalloys, for nuclear plants in He, creep props. *(Japanese)* 79−83263
Hastelloy X, high temp. low cycle fatigue strength *(Japanese)* 77−59910
Hastelloy X, high temp. low cycle fatigue tests, ductility, fracture 77−90523
Hastelloy X, thermal fatigue props. 80−21071
Hastelloy X-R, reaction with sintered Li_2O pellets 79−39137
Hastelloy-X, fatigue crack propag. at elevated temps. in solid solution strengthened superalloys 78−39895
Hastelloy-X, low cycle fatigue crack propagation at 25°C and 760°C 80−104270
Hastelloy-X, Ni-Cr-Fe-Mo, cyclic oxidation resist. improvement by high temp. etching treatment 80−97627
Hasteloy B, equilibrium surface bombarded with high dose He^+ ions 78−95091
Hayes alloy no.716, Fe-Cr-Ni-Co-W-Mo-Si-C-B (26, 22, 12, 3.5, 3, 1.2, 1.1, 0.4 wt.%), hardfacing alloy 80−100802
Haynes alloy 188, fatigue crack propag. at elevated temps. in solid solution strengthened superalloys 78−39895
Haynes alloy 188, H_2 permeability 77−46399
Haynes alloy 188, SEM exam. of fracture surface, due to low cycle fatigue at 700°C *(Japanese)* 78−52963
Haynes alloy 20 Mod, pitting resist. in low salinity geothermal brines 80−93681
heat-resistant composite materials, creation of matrices with operating temp. of 1100°C *(Russian)* 77−55913
high heat resistant, industrial appl. and comp. *(Korean)* 79−24716
hydrogen embrittlement of Fe and alloys, review of embrittlement mechanisms 78−72853
Iconel, oxide film quantitative anal. by XPS and rastered ion bombardment 77−40604
implanted Fe in metals, residence sites of Fe, Mossbauer data 80−39299
Incaloy 623, cold worked, factors affecting embrittlement in H_2S 78−31502
Incaloy 800, for LMFBR steam generators 77−3108
Incoloy, 800 and 807, heat resistant superalloys, for nuclear plants in He, creep props. *(Japanese)* 79−83263
Incoloy, 800 intergranular precipitation, predicted behaviour 79−100148
Incoloy, alloy 800, $M_{23}C_6$/austenite phase boundary defect struct. resolution by weak beam microscopy 80−3046
Incoloy, evaluation for use in nuclear process heat appl. 78−13234
Incoloy, oxide-dispersion-strengthened, pulsed YAG laser welding 79−70075
Incoloy, stress corrosion cracking in high temp. caustic soln. 77−59964
Incoloy 600, H_2SO_4 vapour corrosion, in general atomic S-I thermochem. water-splitting cycle 80−45449
Incoloy 600 and 800, surface film in hot conc. NaOH, XPS study 80−11824
Incoloy 600 vacuum heat treatment for improved corrosion resistance of PWR steam generator tubing 80−5246
Incoloy 800, 600 and 718, press. vessel, fatigue design criteria 78−60758
Incoloy 800, and 800 H, low cycle fatigue behaviour comparison 79−43438
Incoloy 800, and 800H, proposed specification changes 79−43298
Incoloy 800, appl. 79−43553
Incoloy 800, austenitic, creep fatigue interaction at 600°C 78−64672
Incoloy 800, austenitic, fatigue at elevated temps., second phase form. effect 77−36637
Incoloy 800, cast, microstruct. evolution during creep, TEM obs. 79−43366
Incoloy 800, chem. behaviour and mech. performance in HTR He at high temps. 79−47842
Incoloy 800, clean and steam oxidised, T_2 permeation 80−88364
Incoloy 800, contamination and decontamination of samples from KFA experimental duct of DRAGON reactor 79−45600
Incoloy 800, corrosion and carburization in liquid Na up to 973K 79−47841
Incoloy 800, corrosion fatigue crack propagation in pure water at 85°C *(Japanese)* 79−43472
Incoloy 800, corrosion resist. props. in high temp. steam, review 79−47839
Incoloy 800, cracking in NH_3 at 600°C 79−70207
Incoloy 800, creep and fatigue props. in high temp. gas cooled reactor He environment 79−47776
Incoloy 800, creep crack growth, age hardening effect 79−43436
Incoloy 800, creep rupture, creep strength and tensile data, 500 to 800°C 79−43371
Incoloy 800, creep rupture ductility, 500 to 600°C, hardness and metallurgic exam. 79−43435

iron alloys continued
Incoloy 800, creep rupture props. at 525°C 79−43437
Incoloy 800, design codes and lifetime prediction aspects for nuclear and non nuclear appls. 79−47778
Incoloy 800, design problems in steam generators of high temp. reactors 79−45352
Incoloy 800, eddy current testing *(German)* 79−96257
Incoloy 800, effect of liquid Na on creep and rupture props. 79−47775
Incoloy 800, exam. of caustic stress corrosion cracking, comparison with type 304 stainless steel 79−29261
Incoloy 800, exam. of mech. and microstructural props. 79−5022
Incoloy 800, fatigue crack behaviour in bending and pull-push modes 77−81315
Incoloy 800, from KFA experimental duct at 700°C and 480 d in DRAGON reactor, mech. props. before and after contamination 79−47777
Incoloy 800, high temp. corrosion and mech. props. in Na environment 79−47840
Incoloy 800, high temp. gaseous corrosion in sulphidising environments 79−47838
Incoloy 800, high temp. oxidation in low O_2 pressures, SEM obs. of oxide morphologies 79−47844
Incoloy 800, mech. props. above 600°C 79−43370
Incoloy 800, mechanical props., heat treatment and appl., conf., Petten, Netherlands (March 1978) 79−43296
Incoloy 800, mechanisms of corrosion in He 79−47843
Incoloy 800, microstruct. effect on mech. props. 79−43367
Incoloy 800, oxidation resistance, alloy depletion effect 77−8989
Incoloy 800, pretreatment potential effect on pit generation *(Japanese)* 79−43474
Incoloy 800, reaction with sintered Li_2O pellets 79−39137
Incoloy 800, review of mech. props. up to 600°C 79−43368
Incoloy 800, review of structural charact., heat treatment and comp. effects 79−43297
Incoloy 800, review on high temp. gaseous corrosion in carburising and oxidising environments 79−47837
Incoloy 800, sensitisation and intergranular corrosion 79−47721
Incoloy 800, solution annealed, low and high cycle fatigue correlation 79−43439
Incoloy 800, steam oxidised, oxide coating anal. 80−89399
Incoloy 800, stress corrosion cracking and anodisation during straining in boiling NaOH soln. 80−30140
Incoloy 800, stress corrosion cracking in contaminated aq. media at high temp. *(French)* 79−20273
Incoloy 800, stress corrosion cracking in NaOH solns., electrochem. aspects, peening treatment 80−97618
Incoloy 800, thin wall tubing, creep-rupture testing in steam under constant and cyclic load 79−47774
Incoloy 800, use up to 550°C, creep ductility 79−43369
Incoloy 800 Fe base heat resistant alloy oxidation 77−86231
Incoloy 800 for HTR appls., correlation of carburization behavior, mechanical property degradation, and exposure conditions 80−5244
Incoloy 800H, carburisation and dimens. stability in HTGR, He environment 80−45366
Incoloy 800H, H_2SO_4 vapour corrosion, in general atomic S-I thermochem. water-splitting cycle 80−45449
Incoloy 800H, high temp. low cycle fatigue, ageing and cold working effect 79−43277
Incoloy 800H, high temp.-low cycle fatigue, ageing and cold working effect on initial stress/strain curve 79−47720
Incoloy 825, corrosion resistance as structural material for denitrification vessel 77−36685
Incoloy 901, foil prep. for TEM exam. 80−88001
Incoloy 903, H_2 permeation and diffusion 78−26730
Incoloy 903, microstruct. and effect of H_2 charging 77−86143
Incoloy MA956E, mechanical alloying for high temp. appl. 78−44046
Incoloy-800, annealed, mech. behaviour anal. for elevated-temp. LMFBR appl. 80−18428
Incoloy-800, creep-fatigue interaction 77−70113
Incoloy-800, meas. of H and D permeation for reactor safety anal. 79−77822
Inconel, 617 and 625, heat resistant superalloys, for nuclear plants in He, creep props. *(Japanese)* 79−83263
Inconel, caustic stress corrosion cracking resistance, processing variables effect 80−71796
Inconel, chloride corrosion in hot acidic media 78−35552
Inconel, compact ductile fracture toughness specimens, load line displacement measurement method at elev. temps. 78−27700
Inconel, fatigue crack growth rate in high temp., high purity oxygenated water 80−40622
Inconel, ion plating using alumina 77−40476
Inconel, steam generator tubing, mag. probe inspection 80−85119
Inconel, stress corrosion cracking in high temp. caustic soln. 77−59964
Inconel, type 600, Li corrosion inhibitions by Al additions 80−108646
Inconel, type 706, precipitation and creep rupture behaviour, optical and TEM study 79−74158
Inconel 600, atomic S diffusion *(French)* 79−74307
Inconel 600, corrosion fatigue crack propag. at 85°C in 50% NaOH, potential effect *(Japanese)* 80−11834
Inconel 600, corrosion fatigue crack propagation in pure water at 85°C *(Japanese)* 79−43472
Inconel 600, Cr diffusion 77−20110
Inconel 600, effects of ageing and misorientation on intergranular corrosion *(Japanese)* 79−79158
Inconel 600, equilibrium surface bombarded with high dose He^+ ions 78−95091
Inconel 600, exam. of caustic stress corrosion cracking, comparison with type 304 stainless steel 79−29261
Inconel 600, fusion reactor vac. vessel, air, N, adsorpt., thermal desorpt., heat treatment effects 78−54880
Inconel 600, oxide layer, mechanical impedance meas. method 80−45444
Inconel 600, PWR primary corrosion products 80−13578
Inconel 600, reaction with sintered Li_2O pellets 79−39137
Inconel 600, S penetration leading to sulphide form. *(French)* 79−74306
Inconel 600, small bore tubing, crevice corrosion 80−60999
Inconel 600, stress corrosion cracking and anodisation during straining in boiling NaOH soln. 80−30140
Inconel 600, stress corrosion cracking in NaOH soln. 79−66196
Inconel 600, stress corrosion cracking in NaOH solns., electrochem. aspects, peening treatment 80−97618

iron alloys continued
Inconel 600, stress corrosion cracking in primary water 79−93728
Inconel 600, surface composition depend. on H atom influx, AES 79−5192
Inconel 600, thermal outgassing after various surface preparations 79−67952
Inconel 600, thermal treatment, grain boundary microstruct. and SCC resistance 80−71675
Inconel 600, XPS exam. of initial growth of oxide films 79−20240
Inconel 600 alloys, stress corrosion cracking, prediction in 10% NaOH soln. at 315°C 80−97616
Inconel 600 and 718, gas desorption coeffs., electron- and ion-induced, bakeout temp. effect 79−65329
Inconel 600 and 718 in liquid Na environment, fatigue crack propag. 80−40624
Inconel 600 safe-end cracking failure at Duane Arnold reactor 80−104295
Inconel 617, 800, corrosion behaviour in simulated HTGR He environment 79−54495
Inconel 625, accelerated H_2 charging in aq. H_2SO_4 at 0.2% yield stress 80−30144
Inconel 625, creep rupture behaviour in Ag environment 80−25853
Inconel 625, electron yields under ion bombardment for clean and oxidised surfaces 80−66368
Inconel 625, nitriding in N_2-H_2 glow discharge 80−16590
Inconel 625, organic contamination removal by plasma cleaning and etching 80−97645
Inconel 625, plasma nitriding, hardness meas., Rutherford backscatt. surface anal. 80−45442
Inconel 625, secondary ion emission due to H ion bombardment 79−8216
Inconel 625, surface treatment of plane and hollow components in glow discharges 79−1923
Inconel 675, wall and limiter material for Tokamaks, induced desorption diffusion and gas production by 100 eV electrons and ions 79−675
Inconel 718, blistering by 2 MeV He^+ ions, optical microscopy and SEM obs. 79−42119
Inconel 718, environment effect on high temp. fatigue crack growth 80−30090
Inconel 718, grain growth during sintering 80−97449
Inconel 718, H_2 permeation and diffusion 78−26730
Inconel 718, H plasma effects on fusion device vacuum vessel 80−21111
Inconel 718, heat capacity 313 to 1053K 79−10964
Inconel 718, high temp. fretting fatigue, fatigue and fretting wear 80−3197
Inconel 718, low cycle fatigue at 298 and 823K 77−86151
Inconel 718, plastic deform., accelerated evolution of H_2 77−36594
Inconel 718, superalloy, wear of superhard tool during cutting, SEM and metallographic obs. 78−64720
Inconel 738, SEM and electron beam analyser study *(German)* 79−20056
Inconel 750, volatilisation of oxides during oxidation at 1200°C 78−23873
Inconel 800, simulated, steam oxidation 80−76405
Inconel alloy 600, precipitation effect on corrosion 77−25180
Inconel alloy 600 in 10% NaOH soln. at 315°C, influence of thermal treatment 79−91841
Inconel alloy 718, exam. of struct., properties and continuum synthesis of ductile fracture 78−76736
Inconel hardfacing materials, friction characts. in high temp. Na *(Japanese)* 80−89356
Inconel MA754, mechanical alloying for high temp. appl. 78−44046
Inconel X750, positron annihilation study of ageing and creep 80−29824
Inconel X750 springs, in-reactor stress relaxation 78−11256
Inconel X, X-ray study of stress meas., elastic const. *(Japanese)* 79−66092
Inconel X-750 foil, surface pretreatment for improved coating adherence 79−15877
Inconel-625, hydrogen permeation characts. 79−69295
Inconel-718, blistering and exfoliation by 2 MeV He^+ beam 79−46722
Inconel-sheathed MgO-insulated $Pt_{90}Rh_{10}$/Pt thermocouple, decalibrations during 1200°C use, ion microprobe obs. 78−57957
Kh20N40 alloys, phase composition after quenching, tempering 78−60650
Kovar, effect of magnetic electrons on atomic interactions 77−43820
Kovar, thermostress treatment of thin-rolled sheets 79−52273
Kovar substrate, TiB_2 coating prep. by CVD and interaction with substrate 79−24680
Kovar-silicon oxynitride-aluminium cathode, local electron emission and electroluminescence patterns obs. 80−108327
laminates, superplastic bonding 80−25981
liquid, complex, diffusivity and solubility of N_2 at 1600°C 77−39684
liquid, diffusion of N 78−75862
mag. props. after isothermal thermomag. treatment *(Russian)* 80−25159
mag. props. from Mossbauer effect obs. *(Japanese)* 80−15933
magnetic, YuNDK35, brittle, strength in three axial stress state 79−66134
magnetic alloy YuNDK35T5 solidification, direct elec. current effect 79−78954
magnetic sp. ht., Curie temp., alloying effects model 79−61116
magnetically-soft materials, mag. characts. determ. methods, review 79−40593
magnetoelastic effects, effect of alloying additions 78−43624
Magnico alloy, with Si, Nb, Ti and La, low-temp. thermomag. treatment 77−63812
Magnico alloy, with Si, Nb, Ti effect of Ub on mag. props. and grindability 77−63811
martensitic $\gamma \rightleftharpoons \varepsilon$ transformation, dislocation pile-ups, ε phase nucleation in type G18 alloy *(Russian)* 80−55396
martensitic transform., critical driving force, effect of alloying elements 77−48437
melt, thermodynamic props. *(Russian)* 77−55363
metallic coating, oxidation effects, wetting, adherence 78−7085
metallic glasses, Curie temp., struct. relax. effect 77−8313
metallic glasses, delayed fracture in atmosphere, effect of alloying additions *(Japanese)* 79−96212
metallic glasses, ductile-brittle transition 77−4847
metallic glasses, effect of metalloidal elements on thermal stability, crystn. temp. *(Japanese)* 79−94909
metallic glasses, elastic const. 77−66671

iron alloys continued
metallic glasses, Invar and Elinvar characts. 80−29592
metalloid-transition metal amorphous surface alloys formed by ion implantation, TEM study 78−67730
metastable alloy form. by ion implantation 79−82252
metastable alloy formation by ion implantation 79−14828
Metglas 2605, and 2605 A, transport props., resist. and magnetoresist. 79−1590
Metglas 2605 ribbon, saturation magnetostriction meas. by small-angle magnetisation rot. 80−60391
Metglas 2826 ribbon, saturation magnetostriction meas. by small-angle magnetisation rot. 80−60391
Metglas 2826 ribbon, voids formation during crystallisation 80−108428
Metglas 2826-A, anomalous magnetisation, critical effects, superparamagnetism 77−8328
Metglas 2826A, direct meas. of decomp. on crystn. by X-ray microanal. in STEM 79−48025
Metglas type, ohmic and Hall resist., 100-700K, mag. behaviour obs. 80−80254
mischmetal-Co-Cu-Fe-Mg, mag. props. 80−35353
$Mn_{1.98-x}Cr_xFe_{0.02}Sb$, Mossbauer effect exam. 78−68432
modular cast Fe, probability prediction of spheroidisation by parametric diagram of chem. bond *(Chinese)* 80−66543
molten, N_2 diffusion, effect of Si, P, Al and B *(German)* 77−20099
Monel, Ni-Cu-Fe-Mn, resistance spot weld quality evaluation, using stress wave emission technique 78−53066
Monel 400, corrosion susceptibilities in synthetic geothermal brines 77−86223
Monel 400, stress corrosion cracking in high temp. caustic soln. 77−59964
Mossbauer isometric effects *(Dutch)* 79−1731
Mossbauer spectra, local mag. moments in BCC alloys 80−15861
Mossbauer spectroscopy, effect of neighbours on hyperfine field 80−39931
Mossbauer spectroscopy of phase transformations in ferrous alloys 77−12619
Multimet, fatigue crack propag. at elevated temps. in solid solution strengthened superalloys 78−39895
Mumetal, magnetization curve and Gaussian error function *(German)* 80−50137
N31, martensitic point lowering by microplastic deform. and room temp. ageing *(Russian)* 77−25049
Ni-Fe atomic and mag. ordering, cluster variation calc. *(Russian)* 78−15391
nickeliferous materials, properties and appls. *(German)* 79−79182
Nilomag alloy 771 coloured, X-ray photoelectron spectroscopy of surface film 78−64899
Nimonic alloy, effect of annealing on hardness, carbide phase strengthening *(Russian)* 79−34137
Nimonic PE16, creep rupture props. in CO_2, air and vacuum environments at 700°C 79−74248
Nimonic PE-16, electron irrad. in HVEM, void growth, vacuum environment influence 80−107323
nodular castings, comparison of sonic-resonance and US velocity techniques for quality control 80−97654
oxide dispersed, mech. alloying, microstruct. 77−25063
oxide dispersion strengthened sheet alloy MA-956E, tensile and creep props. at 1365K 78−48470
oxide spallation, influence of ΔT (oxidising temp. minus cooling temp.) 77−52551
particle erosion meas. 77−66703
Pd_3Fe, ferromag. spin wave meas., inelastic scattering of polarised neutrons 78−2665
Permalloy-type sputtered film, structuring rel. to laser sputtering method *(Russian)* 77−59689
Permendur, 50KF, magnetostrictive props., compression effcts 77−40109
Permendur 49, ordered and disordered, clean mild wear 80−16508
phosphor bronzes, surface Cs^+ impact, 5.5 keV negative secondary ion emission obs., rel. to Cu *(French)* 77−66562
pig, white, mech. props. meas. *(French)* 80−104370
pig Fe, liquid gas bubble form. at nozzles, acoustic exam. 78−52723
pipe, commercial, corrosion under flow conditions, SO_4 ion effect 80−97629
polymorphism effect on failure accompanying electrospark action *(Russian)* 79−74236
porous powder metallurgical components, gamma nitriding 79−20088
quench-condensed thin film, annealing effect on resistivity 78−43488
rare earth alloys, magnetoelasticity and moment rot., US vel. calc. and neutron scatt. meas. 80−65992
rare earth alloys, $R(Fe_xRh_{1-x})_2$, mag. props., Mossbauer spectra 80−25108
rare earth alloys, RFe_2, (R=Gd, Tb, Dy, Ho, Er, Tm, Lu), electronic heat capacity coeffs. 80−39787
rare earth alloys, RFe_2, magnetostriction studies, book contrib. 80−39846
rare earth alloys, RFe_4Al_8, cryst. struct. mag. props. and hyperfine interactions 78−87648
rare earth alloys, RFe_4Al_8, mag. props., Mossbauer spectra, ordering effects 77−63179
rare earth germanide, RFe_2Ge_2, magnetisation and Neel temp. 77−8310
rare earth intermetallic, amorphous film, cosputtered, struct. and mag. props. 78−60323
rare earth intermetallic, O-stabilised, $R_{12}Fe_{32}O_2$, prep., struct. and mag. props. 77−8956
rare earth intermetallic, $R(Fe_{1-x}Mn_x)_2$, phase struct., mag. and Mossbauer meas. 77−20563
rare earth intermetallics, elastic vs. magnetoelastic anisotropy 78−68347
rare earth intermetallics, R_2Fe_{17} and $R_2Fe_{17-x}Ni_x(Co_x)$, mag. anisotropy and hyperfine interactions 77−8298
rare earth intermetallics, R_xFe_{1-x} amorphous film, crystn., TEM obs. 79−87019
rare earth intermetallics, R_xFe_y, conc. depend. of Fe moments 78−56413
rare earth intermetallics, RFe_2, spontaneous magnetoelastic distortion, X-ray diffr. expts. 77−63253
rare earth intermetallics, RFe_2 and $R(Co_{0.98}\ Fe_{0.02})_2$, magnetostrictive material, changes in vibr. modes near mag. phase transition 79−90736
rare earth intermetallics, $RFe_{5-x}Ni_x$, giant intrinsic mag. hardness 78−56354
rare earth iron intermetallics, RFe_2, (R=Sc, Lu, Y), mag. props., 80-1300K *(Russian)* 80−75750

iron alloys continued
rare earth iron intermetallics, RFe_2 type, magnetostriction in polycryst. samples 77−73065
rare earth iron silicides, $R_2Fe_4Si_9$ and $RFeSi_3$, cryst. struct. and mag. suscept., temp. depend. *(Russian)* 78−34957
rare earth silicides, RFe_2Si_2, mag. props. 4.2 to 950K 77−20544
rare earth ternary alloys, RT_6Al_6, T=Cr, Mn, Fe, Cu, cryst. struct. 80−107110
rare earth-Fe_2, mag. props. changes due to H_2 absorption, unit cell vol. 77−63178
rare earth-Fe_2, magnetomech. coupling and Young's modulus 78−84472
rare earth-Fe_2 compounds, magnetostrictive, book contrib. 80−75838
rare earth-Fe_2 high anisotropy powder, magnetic and hysteresis props. *(Russian)* 79−42800
rare earth-Fe_2 Laves phase compounds, magnetostriction anisotropy 77−63250
rare earth-Fe_2 Laves phase intermetallics, mag. ordering temps. by DTA 79−47283
rare earth-Fe, amorphous, random anisotropy model, generalised mol. field calcs. 77−28345
rare earth-Fe, intermetallic compounds, mag. props. *(Rumanian)* 78−92007
rare earth-Fe alloys, highly magnetostrictive, isotropy breaking magnetoelastic behaviour 78−72386
rare earth-Fe alloys, magnetoelastic props. *(Japanese)* 78−23316
rare earth-Fe alloys, magnetostrictive, elastic props. 78−84469
rare earth-Fe alloys, RFe_2, temp. depend of coercivity 79−61185
rare earth-Fe Laves phase alloys, sintering, magnetostrictive props. 77−16139
rare earth-Fe rod, US resonance with large eddy currents 80−54933
rare earth-Fe-Al alloys, RFe_4Al_8, mag. props. 78−52250
rare earth-Fe-Si(Ge), $ThCu_2Si_2$ type, lattice parameters 78−51469
rare earth-iron, RFe_2, Laves phase intermetallics, ordered and paramagnetic phases, mean field exchange consts. 80−50084
rare earth-Tb-Fe alloys, $R_xTb_{1-x}Fe_2$, Laves phase type, magnetostriction *(Russian)* 77−51932
Recalloy, Fe-Nb, semihard magnetic alloy, magnetic props., hardness, microstruct. 78−56660
Rene 41, Ni-Cr-Co-Mo-Ti-Al-Fe (18.96, 11.09, 9.65, 3.06, 1.59, 0.89 wt.%) formation of Cr_2O_3 monocrystals on heat treatment 79−52455
resistivity, effect of sp-3d impurity interactions 79−46696
resistivity magnetoresistance, s,p impurities in ferromag. host 78−68008
rolled repetitive sections, ultrasonic quality inspection 79−87770
Sanicro 30, stress corrosion cracking in NaOH soln. 79−66196
Sanicro 31, T_2 permeation 80−88364
secondary-ion emission under varying bombardment condition 77−48292
Sendust alloy, magnetic head wear resistance and surface charact. against mag. tape *(Japanese)* 80−35335
Sendust ribbon, mag. props. 80−15761
sintering, physical and chemical phenomena *(Italian)* 79−83147
slip band theory, model for creep based on dislocation climb at grain boundaries, comparison with expt. data 79−37756
Snoek-Koester relaxation and impurity-dislocation interactions *(Russian)* 78−59834
softening effect, tensile test at low temps. *(French)* 77−63875
solidification, method for evaluating influence of each element on microsegregation *(French)* 79−74159
solute segregation to grain boundaries 78−72780
spheroidal graphite, deformation under compression rel. to ductility 77−16639
spin glass-ferromag. alloys, high-field magnetisation 79−33488
sputtering, alloy surface topography obs., Stewart-Thompson theory 78−43977
steel, alloy, Fe-Ni-Mn-Si-Cr-Ni-Mo, effect of metallurgy on stress corrosion cracking, and hydrogen embrittlement 78−60885
steel, Fe-Cr-Al, sulphidation behaviour, 750°C, preoxidation effect *(French)* 78−15566
steel, Fe-Mo-C low-alloy, photoelectron microscopy of diffusional transformations 77−44242
steel, galvanized, Fe-Zn phases, Mossbauer study 80−50233
steel, Ni-Cr, (4,1, wt.%), isothermal embrittlement, AES exam. of grain boundary segregation 78−60814
Stellite 6B, volatilisation of oxides during oxidation at 1200°C 78−23873
stress corrosion cracking test machine, design and construction, appl. to Fe-Cr-Ni alloys 80−97649
superalloy, PHACOMP appl. to σ-phase estimation of various heats *(Chinese)* 79−100109
superalloys, Al-based coatings for high temp. appl., process development and props. 80−40614
superalloys, FCC base hard materials, low temp. toughness *(Japanese)* 80−100916
Supermalloy, 24 GHz ferromagnetic antiresonance transmission 77−51957
Supermalloy, 9, 24 and 38 GHz ferromagnetic reson. absorpt., line shapes 77−51958
supermalloy, foil, microwave transmission, parallel RF and mag. fields 77−59462
supersaturated solid solution, recrystallisation inhibition by cold rolling 77−73286
surface defect detection by portable EM inductors *(French)* 78−35616
surface layer refining by electric fields in vacuum, surface active impurity elimination *(Russian)* 80−55563
surface layers examination, X-ray method 78−35606
susceptibility meas., initial, temperature-time instability, using bridge instrument with electronic demagnetiser *(Slovak)* 78−57989
swelling, correlation with number of bonding d electrons 77−47491
systematics, rel. to the long periodic table 79−37649
taenite, cloudy, origin in meteorites, TEM study of Santa Catharina anomalous Fe meteorite 79−66968
ternary soln., containing interstitials and substitutional solutes, thermodynamic and kinetic props. 78−2297
texture development by recrystallisation and normal grain growth 78−27539
texture development by recrystallization and normal grain growth 77−32594
textured low alloy Fe, (110)[001] oriented, mag. charact. 77−1879
Th_6Mn_{23} type struct., mag. susceptibility *(Russian)* 79−42736
thermal expansion, low at elev. temps. *(Chinese)* 77−72704
thermoelectric force caused by internal adsorption *(Russian)* 78−95288
iron alloys continued
thermomagnetic treatment of YuNDK35T5BA, post-decomp. processes 79−87668
Ticonal, domain struct., variation under influence of heat treatment *(Russian)* 78−23292
Ticonal, effect of rare earth metals on mag. props., struct., and phase transformations 79−99732
ticonal, grindability improvement, thermomagnetic and heat treatments 77−16625
Ticonal, interaction domains after heat treatment in mag. field *(Russian)* 78−68286
Ticonal, two- and one-dimens. modulated struct. after thermomag. treatment and water quenching *(Russian)* 80−29983
Ticonal strength, effect of thermal stresses and phase transforms. 79−87721
Ticonal with magnetic texture, struct. damages during ageing 77−16626
Ticonal with Sm, magnetic props., phase transform. after thermomagnetic treatment 78−3155
Ticonal-type alloys, struct. after quenching from 800-850°C *(Russian)* 77−59822
Trafoperm N2, magnetization curve and Gaussian error function *(German)* 80−50137
transition metal alloy, ferromag., H-impurity complex obs. by magnetic aftereffect 78−72373
transition metal alloys, AFe_2 and ACo_2, Invar effect, magnetovolume meas. 79−56592
twinned martensite structure, influence of plastic deform. *(Russian)* 78−88493
TZM, air contamination effect on compatibility with liquid Li in stainless steel vessels at 600°C 78−25285
universal diags. of cohesive strength *(Russian)* 78−56733
US attenuation, meas. at large strain amplitudes 77−1182
V-Fe (29-35 at%), ferromag., mag. props. near crit. conc. for ferromagnetism 78−19225
Vicalloy 1, dilatometric anomalies and α to γ transform., effect of heating rates *(Russian)* 78−39762
vicalloy-2, high heating rate effect on mag. props. *(Russian)* 77−81328
VT22, hot deform., microstruct. form. and mech. props. *(Russian)* 77−28830
wear resistance, struct. effect 79−29229
wear resistance, surface hardening processes, review 78−72894
wear resistance improvement in high Cr cast Fe 77−70186
white cast Fe, abrasive wear 80−108587
white cast iron, plasticity in impact toughness, bending angle tests 77−56039
white Fe castings, morphology of eutectic M_3C and M_7C_3 80−108427
Zircaloy, H absorption, Sn(Fe)(Cr)(Ni) effect 80−49527
Zircaloy-2, tritium diffusion 80−32341
Zircaloy-4, quenched and annealed, strain ageing 77−25071
Ag-Fe, dil., estimate of Kondo temp. from static mag. susceptibility meas. 78−19214
Ag-Fe, dil., ion implanted, phase comp., Mossbauer study 80−7244
Ag-Fe, implanted, Mossbauer conversion electrons spectroscopy, rel. to dose and annealing temp. 78−52397
Ag-Fe, Kondo system, magnetisation, Mossbauer expts. 77−77028
Ag-Fe, local moment system, low temp. susceptibility, Mossbauer effect meas. 77−43810
Ag-Fe alloy film, mag. susceptibility max. 79−24173
Al determination, in presence of V *(Polish)* 80−35605
Al-Al_3Fe, anodic film struct. and stability 78−48564
Al-Al_6Fe, fibre reinforced eutectic, deformation behaviour by rolling, TEM and SEM study 79−29129
Al-Al_6Fe eutectic, thermal stability rel. to soaking times 77−21131
Al-Cu-Fe, liquid, mag. moment and transition from mag. to nonmag. state 79−24132
Al-Cu-Fe alloys, solid and liquid, exam. of constitution and mag. props. *(German)* 78−52206
Al-Cu-Mg-Fe-Ni, Hiduminium RR58, crack propag. rates in air and salt soln. 80−21063
Al-Cu-Mg-Mn-Fe-Si, alloy D16, effect of mechanisothermal treatment on mech. props. 78−56674
Al-Cu-Mg-Mn-Si-Fe, endurance with cyclic bending, effect of loading conditions 80−50724
Al-Cu-Mg-Mn-Si-Fe, subcritical crack growth under static plane stress 80−55528
Al-Cu-Mg-Mn-Si-Fe, torsional vibrations decrement, deformed vol. effect 80−76326
Al-Cu-Mg-Ni-Fe alloy RR 58, creep resistance at elevated temps., thermomechanical treatment effects 77−59836
Al-Cu-Mg-Si-Fe-Mn-Ti, Si, Fe, Mn and Ti effect on precipitation in solid soln. *(Korean)* 79−66064
Al-Cu-Mn-Mg-Fe-Si, corrosive environment effect on fatigue crack growth rate 80−55584
Al-Cu-Mn-Mg-Fe-Si (4.48, 0.66, 1.55, 0.43, o.23 wt.%), alloy D16, relationship between intercrystallite corrosion depth, and elec. cond. 79−20220
Al-Cu-Mn-Mg-Fe-Si-Zn alloy D16, surface layers chem. composition rel. to fatigue resist., corrosion-fatigue resist. 79−29275
Al-Cu-Mn-Zr-Fe-Si (6,0.3,0.18,0.3,0.1 wt.%) experimental evidence of Mn enrichment in Al_2Cu precipitates by EDS in TEM 78−15415
Al-Fe, alloy with mixed types of order, uniform mag. phase diagram 79−78368
Al-Fe, cast, influence of Zr on precipitation, solidification and grain size *(Rumanian)* 78−84813
Al-Fe, dil., annealing after cold working, impurity-vacancy interactions, Mossbauer meas. 80−7236
Al-Fe, dil., defects and phases, Mossbauer studies 80−40004
Al-Fe, dil., electronic states, XPS meas. 77−44117
Al-Fe, dil., Mossbauer spectra of implanted ^{57}Fe, ageing behaviour 80−7233
Al-Fe, dil., phase analysis by Mossbauer spectra 80−15922
Al-Fe, dil., quenched secondary defects, Mossbauer spectroscopy 77−28491
Al-Fe, dil., screening charge around 3d impurities, NQR meas. 77−32287
Al-Fe, dil. solid soln., vacancy-trapped Mossbauer impurity Debye Waller factor 80−60468
Al-Fe, electron irradiated, interstitial-solute complexes, internal friction spectra 78−92289
Al-Fe, liq., dissoln. and diffusion of alloying components, 700-1000°C *(Russian)* 80−15275

iron alloys continued
Al-Fe, liquid alloys, thermodynamic charact. calc. *(Russian)* 78−27475
Al-Fe, spectrophotometric determ. of Al content *(Polish)* 80−35604
Al-Fe (0.02 at.%), rapidly quenched, ^{57}Fe Mossbauer spectrum associated with vacancy 78−23378
Al-Fe (0.02 wt.%), Mossbauer spectrum of ^{57}Fe associated with vacancies 77−85636
Al-Fe (0.5 wt.%)-Ti-Cr, Ti, Cr addition effects on toughness/microstruct. relationship *(Japanese)* 77−48525
Al-Fe (1 wt.%), depth resolved ^{57}Fe conversion electron Mossbauer spectra 79−38413
Al-Fe (49 at.%) quenched alloy, neutron diffuse scatt., diffuse ω phase obs. 80−84141
Al-Fe alloys containing dispersed Al_3Fe phase, anodic film structure and stability 78−11449
Al-Fe dil. alloy, bamboo struct., grain boundary internal friction peak 79−43306
Al-Fe-Ni, influence of strain path on mech. props., orthogonal tensile paths 80−30035
Al-Fe-Ni, oxidation in hot water, electron microscope obs. of initial stages 79−11718
Al-Fe-Si, eutectic alloy growth, by twinning plane propagation *(French)* 78−60667
Al-Fe-Si, Fe phase form., solidification condition effects *(French)* 77−70030
Al-Fe-Si commercial alloy, elevated temp. low cycle fatigue behaviour under rotating bending 79−47766
Al-Fe-Si(0.5, 0.2 wt.%), cast, phase determ. 77−70032
Al-Fe-X-Si (X=transition metal), struct. and comp. by electron microscopy 80−88093
Al-$FeAl_3$, unidirectionally solidified eutectic, α-liq. interface stability 77−63650
Al-Mg-Fe-Mg-Si-Cr, alloys, dendritic segregation with Fe, Mg, Si and Cr additions *(Polish)* 79−56980
Al-Mn-Fe, permanent magnetic materials, grain struct. effect *(Rumanian)* 79−73773
Al-Ni(Cd)(Fe)(Si), cold worked, struct. and props. 80−71666
Al-Pr (16 wt.%), resist. depend. on temp. and hot rolling *(Polish)* 80−39555
Al-Ti-Fe, ternary phase diagram, computer calculations 80−45274
Al-Zn-Fe, dil. alloy, ^{65}Zn diff. 77−51540
Al-Zn-Fe-Si, Fe and Si effects on precip., TEM and X-ray diffr. obs., ageing at 90°C 77−48439
Al-Zn-Mg-Mn, correlation of microscopic features, with macroscopic crack propagation 78−60800
α-AlFeSi, crystal struct., anomalous dispersion methods 78−9998
$AmFe_2$, crystal structure and mag. props. of Laves phases 77−27851
$AmFe_2$, high temp. mag. props., 300 to 1100K 79−51757
Au-Cu-Fe spin glass alloys, impurity mag. resist. meas. 80−59972
Au-Fe, alloy with mixed types of order, uniform mag. phase diagram 79−78368
Au-Fe, anomalous Hall effect, asymm. scatt. of itinerant electrons 77−43569
Au-Fe, competing interactions in FCC alloys 78−95453
Au-Fe, conc. spin glasses, thermopower 80−65538
Au-Fe, dil., approach to saturation of magnetisation 78−56293
Au-Fe, dil., conduction electron-local moment interactions using dHvA waveshape anal. 79−77981
Au-Fe, dil., contact charge density, internal conversion meas. 79−56630
Au-Fe, dil., crit. dynamics 80−60325
Au-Fe, dil., in supercond. proximity, localised bands 78−10613
Au-Fe, dil., ion implanted, phase comp., Mossbauer study 80−7244
Au-Fe, dil., local mag. moments, neutron scatt. study 79−61058
Au-Fe, dil., local moments, third harmonic de Haas-van Alphen wave shape anal. 78−84127
Au-Fe, dil., spin glass state and Kondo effect nucl. orientation of ^{54}Mn 78−6514
Au-Fe, dil., thermopower, interconfig. fluctuations 79−65412
Au-Fe, dil., valence and core level spectra, XPS study 80−84838
Au-Fe, dil. alloy, transverse magnetoresist. in spin glass regime 80−34417
Au-Fe, dil. alloys, spin glasses, modified bond model calcs. 79−33489
Au-Fe, finite mag. clusters near percolation conc. 78−72371
Au-Fe, impurity spin dynamics in magnetic glasses at low frequencies *(French)* 78−88126
Au-Fe, Kondo system, magnetisation, Mossbauer expt. 77−77028
Au-Fe, liq., thermodynamic mixing effects, mass spectrometric meas. eval. *(German)* 77−59123
Au-Fe, long range mag. order 77−63215
Au-Fe, mictomagnet, freq. depend. of susceptibility max. 78−95445
Au-Fe, polygonisation, recrystallisation, precipitation microstruct. without external plastic deform. 79−43276
Au-Fe, spin glass, anomalous Hall effect 78−30908
Au-Fe, spin glass, mag. moment dynamics, neutron diffuse scatt. meas. 77−69584
Au-Fe, spin glass, quench-condensed film, reduced MFP influence on elec. resist. 77−69306
Au-Fe, spin glass, residual resistivity conc. depend. 80−2382
Au-Fe, spin glass, spin relaxation rates, neutron scatt. study 79−47235
Au-Fe, spin glass, transition temp., freq. depend. 80−97113
Au-Fe, spin glass behaviour in low DC field 77−66373
Au-Fe, spin glass in low DC field, mag. viscosity, time decays of remanences 78−64209
Au-Fe, spin glass transition and anomalous Hall effect 79−61162
Au-Fe, spin glasses, alternating susceptibility 80−65912
Au-Fe, spin-glass, characteristic temps. 79−38348
Au-Fe, spin-orbit coupling and electron scatt. 80−2370
Au-Fe, spin-orbit electron scatt. near percolation limit, anomalous Hall effect meas. 79−73492
Au-Fe, UPS study, localised states 80−93449
Au-Fe, very dil. alloy, Kondo temp. 78−91688
Au-Fe (1 at.%), spin glass, specific heat 80−60355
Au-Fe (1-7 at.%), extraordinary Hall effect, near ferromag. percolation limit 79−19575
Au-Fe (14.5 at.%), spin dynamic exam. by diffuse magnetic neutron scatt. 77−8320
Au-Fe (15 at.%), small angle neutron scatt. study 79−47293
Au-Fe (16.2 at.%), cluster glass, mag. small angle neutron scatt. 80−50111
Au-Fe (17 at.%) alloy, fission fragment irrad., simulation of neutron effects 77−80549

iron alloys continued
Au-Fe (20 at.%), mag. virtual bound state alloys, XPS of core states 79−47588
Au-Fe (22 at.%), ferromag. phase, AC susceptibility near T_c 78−43575
Au-Fe (3.1-10.4 at.%) spin glass alloys, high field magnetisation curves 80−11213
Au-Fe (4 at.%), spin glass energy relaxation of remanent magnetisation at low temp. 79−87271
Au-Fe (4 at.%), spin glass, magnetisation and energy relax. below T_g 80−65921
Au-Fe (40 at.%), discontinuous precipitation reaction at grain boundaries 79−87642
Au-Fe (4.2 at.%), spin glass, DC magnetisation, field depend. 80−97103
Au-Fe (4.4 and 4.8 at.%), isotropic spin glass behaviour and transverse magnetoresist. 77−15830
Au-Fe alloy, dil., Mossbauer exam. in spin glass regime 79−61289
Au-Fe alloy, spin glass, neutron scatt. 78−68265
Au-Fe alloy film, mag. susceptibility max. 79−24173
Au-Fe alloys, magnetism and atomic clustering 80−103810
Au-Fe alloys, spin correlations, neutron diffr. meas. 80−80482
Au-Fe dil. spin glass alloy, impurity-impurity interaction press. depend., resistivity meas. 77−20308
Au-Fe film spin glass, low temp. resistivity, mean free path effects 78−80163
Au-Fe ion implanted alloy, Mossbauer conversion electron scatt. 80−88898
Au-Fe solid soln., diffusion coeffs., Mossbauer spectra 77−12260
Au-Fe solid soln. alloys, reson. and relax. effects 79−82865
Au-Fe spin glass, energy flux associated with remanent magnetization relaxation *(French)* 80−7110
Au-Fe spin glass, long-time relax. processes, heat capacity expts. 77−66374
Au-Fe spin glass, susceptibility cusp, influence of Fe clusters 79−61163
Au-Fe spin glass alloy, neutron scatt. study 79−61179
Au-Fe spin glasses in low DC fields, susceptibility and thermoremanence 77−77063
Au-Fe-Ni layer coating, Fe and Ni conc. meas. by X-ray diffr. *(German, English)* 80−34330
$Au_{1-x}Cu_x$-Fe, dil., resistance maximum 79−61056
AuFe alloy films, mag. susceptibility, Fe concentration and annealing depend. 79−61119
AuFe, Ising spin glass, calc. of wavevector depend. susceptibility 77−63223
AuFe, spin glass, anomalous magnetoresistance 79−78077
AuFe spin glass, μ^+ zero-field spin relax. probe for spin dynamics 80−97177
AuFe, spin glass freezing above ferromag. percolation limit 78−52264
$Au_{1-x}Fe_x$, $0.14<x<0.28$, ferromagnetism study by specific heat meas. 80−7121
$Au_{85}Fe_{15}$, and $Au_{82}Fe_{18}$, mag. props. 80−84592
$Au_{92}Fe_8$, apparatus for measurement of initial paramagnetic susceptibility 79−54160
$(Au_xPb_{1-x})_{1-c}Fe_c$, ferromag. and spin glass ordering 78−56335
$Au_{75}Si_{19}Fe_6$, apparatus for measurement of initial paramagnetic susceptibility 79−54160
B-Fe (16 at.%), magnetisation in high mag. field, Arrott-Noakes plot 80−54919
Be-Al-Fe, phase equilibria and diffusion using high energy ion beams 77−16542
Be-Al-Fe system, phase equilibria using high energy ion beams 79−43203
$Be_5(Fe_{1-x}Mn_x)$, mag. and calorimetric props. 77−63083
$Be_2Mn_{1-x}Fe_x$, mag. props., giant moment clusters 79−28508
CC Fe-Ni-Cr (35, 15 wt.%): Nb(Ti)(Mo), corrosion in HTGR He environment 80−61021
cast Fe, with Mg despheroidising effect of Bi, Sn on graphite in alloy 78−56670
cast Fe 78−53032
Cd-Fe powders, predetermined comp., electrodeposition 79−70014
Ce-Co-Cu-Fe-Ti, sintered magnet, prep. and mag. props. 77−73043
Ce-Fe-Si, thermoelectromotive force and electrocond. *(Ukrainian)* 80−54670
Ce-Fe-Si system, mag. props. in 77-300K range *(Russian)* 78−56290
Ce-Mg-Fe master-alloy innoculated cast Fe, struct. and props. 80−100843
Ce-Mn-Fe, cryst. struct. determ. 77−11508
Ce-Sm-Co-Fe-Cu, permanent magnet props. 79−8013
$CeFe_2$, ferromagnetic cpds., mean field exchange consts., Stoner itinerant model calcs. 80−50084
$CeFe_2$, H_2 absorption effect on mag. props. and struct. 77−40045
$CeFe_2$, magnetostriction and magnetisation 80−39844
$Ce_{8.5}Fe$, absorpt. of D, heats of reaction and equilib. press., T-getters for CTR 78−51683
$Ce(Mn_{1-x}Fe_x)Si_2$, mag. props. 80−25134
$(Ce_xY_{1-x})Fe_2$, mag. susceptibility and Mossbauer meas., lattice parameters 80−97068
$(Co, Cu, Fe)_5Ce$, sintered permanent magnets, magnetic charact. 78−60608
$(Co,Cu,Fe)_5Ce$, sintered, mag. props. 78−68302
$(Co,Fe,M)_{78}Si_8B_{14}$ amorphous alloys (M=V,Nb,Ta,Cr,Mo,W,Mn or Ni), zero magnetostriction and low field mag. props. 80−34741
$(Co,Fe)_{0.75}B_{0.25}$ metallic glasses, annealed, equilib. crystalline phases 80−3019
$(Co,Fe)_{80}B_{20}$ glass, induced anisotropy and time changes of permeability 80−75815
Co-Cr-Mo-Ni-Fe-Si-Mn-C, protective coatings by B diffusion, microstruct. and mech. props. 78−11427
Co-Cu-Fe-Ce, mag. characteristics of sintered permanent magnets 78−60312
Co-Cu-Fe-Ce alloys, sintered permanent magnets, mag. charact. 77−43855
Co-Cu-Fe-Sm magnet, microstruct. exam. after ageing, TEM meas. 77−48555
Co-Fe, dendritic segregation 80−76260
Co-Fe, dil., effective mag. field at ^{59}Co, impurity conc. depend., spin echo expts. 78−48080
Co-Fe, dil., hyperfine mag. fields, press. effect, Mossbauer meas. 80−71277
Co-Fe, dil., magnetocrystalline anisotropy anomalous temp. depend. 80−71007

iron alloys continued
Co-Fe, double hexagonal alloys, crystalline and mag. props. *(Japanese)* 79−73132
Co-Fe, film, mag. and hyperfine field exam. of uniaxial anisotropy 77−66391
Co-Fe, internal friction anomalies in spin reorientation temp. range *(Russian)* 80−49299
Co-Fe, magnetic anisotropy induced by magnetic and stress annealing 78−35010
Co-Fe, morphology and certain props. of α-and η-phase martensite *(Russian)* 77−1838
Co-Fe, neutron radiation stimulated diffusion, electrical resistivity exam. *(Russian)* 79−14959
Co-Fe, soft mag. props. rel. to metallurgical aspects 80−88810
Co-Fe, temp. depend. of asphericity of mag. moment distrib. 77−20538
Co-Fe, transformation matrices, electron diffraction patterns 77−59779
Co-Fe (2.92 to 30.05 wt.%), determination of phase equilibrium diagram *(Japanese)* 78−48374
Co-Fe (30%) effect of annealing on magnetostrictive vibrs. 78−6558
Co-Fe (6 wt.%), magnetic properties, 850 to 1000°C range *(Slovak)* 79−4698
Co-Fe (6.25 wt.) FCC to HCP transform., model and expt. evidence 77−44243
Co-Fe alloy, HCP and DHCP, magnetostriction consts. determ. 78−80184
Co-Fe alloy, Invar characts. 77−1550
Co-Fe alloy, plastic deform. effects on phase comp. *(Russian)* 78−19743
Co-Fe alloy films, magnetostriction and orientation of easy magnetisation axes *(Russian)* 79−19756
Co-Fe alloys, FCC structure, average mag. moment, conc. depend. 78−88099
Co-Fe alloys, mag. anisotropy induced by mag. annealing through to double h.c.p. 77−1552
Co-Fe alloys, transformation induced microstructs. extended total dislocations, TEM study 79−42073
Co-Fe amorphous alloys, high permeability props. *(Japanese)* 77−51927
Co-Fe amorphous alloys, worked, perminvar type mag. hysteresis loop, longit. Kerr effect obs. 80−65958
Co-Fe epitaxial films, singularities of $\gamma \rightarrow \alpha$ transform., X-ray diffr. obs. *(Russian)* 79−52198
Co-Fe-B, amorphous, crystn. and thermal stability 80−107057
Co-Fe-B films, amorphous, mag. annealing behaviour 79−73782
Co-Fe-B sputtered amorphous films, mag. props. and corrosion resist. 79−28567
Co-Fe-Cr-P-B sputtered amorphous films, mag. props. and corrosion resist. 79−28567
Co-Fe-Mn, dil. ferromag. alloy, mag. moment, saturation magnetisation meas. 78−64195
Co-Fe-Nb, heavily cold worked, magnetic hardening 79−20073
Co-Fe-Nb (12, 3 wt.%), semihard magnetic alloy, relationship between precipitation and coercivity 77−8839
Co-Fe-Nb alloy, mag. precipitation-hardening and Bloch wall pinning 78−80173
Co-Fe-Nb alloys, effect of cold working on mag. props., and precipitation morphology 78−39803
Co-Fe-Nb semihard mag. alloy, mag. precip. hardening 77−8960
Co-Fe-Nb-Mo, semihard magnetic alloy, magnetic props. 78−95469
Co-Fe-Ni semi-hard mag. alloy, 3-D Barkhausen effect meas. 77−69623
Co-Fe-Ni semihard magnetic alloy, directional distrib. of magnetisation changes connected with Barkhausen effect 78−14985
Co-Fe-Ni-Si-B glasses, soft mag. props. 79−73774
Co-Fe-P film, ferromag., coercive force meas. 78−10737
Co-Fe-Si-B, amorphous alloys, substitution effect on mag. props. 79−69695
Co-Fe-Si-B, decomp. of amorphous state during annealing below recryst. temp., electron microscope study *(Russian)* 80−75164
Co-Fe-Si-B, ferromag., magneto-optical spectra in amorphous and cryst. states *(Russian)* 80−84749
Co-Fe-Si-B amorphous alloys, mag. props. 77−16055
Co-Fe-Ti (12,6 wt.%), semihard permanent magnet, magnetic precipitation hardening 78−52830
Co-Fe-Ti alloy, precipitation hardened, rel. between struct. and mag. props. 78−95470
Co-Fe-V-Ni, mag. and mech. props., heat treatment and stress effects 80−60363
Co-Fe(70 wt.%) alloy oxidation, diffusional scale growth at 1200°C 77−16748
Co-Ga-Fe, small-angle mag. neutron scatt., states of mag. order study rel. to Mn and Fe substitution 79−11292
Co-Mn-Ni-Fe-Si-B amorphous alloys, mag. props., low magnetostriction 80−75832
Co-Ni-Fe, metallic glasses, mag. props. *(German)* 79−51813
Co-Ni-Fe, semi-hard magnet, irreversible magnetisation changes, directional distrib. 79−24196
Co-Ni-Fe-Si(B), amorphous ribbon, magnetostriction meas. 80−15778
Co-Si-B-Fe alloy magnet, Al_2O_3 particle embedded surface, amorphous mag. anal. using electron diffr. 79−56568
Co-Ti-Fe (3, 1 to 2 wt.%), spinodal decomposition 80−100839
$Co_{0.91}Fe_{0.09}$, X-ray scatt. factor 79−41907
$Co_{0.92}Fe_{0.08}$, lattice dynamics by neutron scatt., FCC phase 77−51463
$Co_{0.92}Fe_{0.08}$, phonon dispersion and Debye temp. temp. depend., neutron inelastic scatt. 79−33047
$(Co_{1-x}Fe_x)$-B-Si, amorphous mag. props. *(Japanese)* 77−85433
$Co_{92}Fe_8$, FCC, electronic struct., ang. correlation of positron annihilation γ-quanta, meas. 80−10864
Co_xFe_{1-x}, ferromagnetism and spatial long-range order 80−60159
$(Co_{1-x}Fe_x)B$, ferromag., internal fields meas. by NMR spin echo 80−29646
$(Co_{1-x}Fe_x)B$, paramag., spin echo NMR spectra, ferromag. transition, spin-lattice relax. 80−29645
$Co_{74}Fe_6B_{20}$, metallic glass, zero magnetostriction, magnetisation characts. 77−12158
$Co_{79}Fe_{6.5}B_{14.5}$ amorphous thin films, zero magnetostriction, high magnetisation 80−34708
$(CoFeB)_{100-x}Cr_x$ thin films, magnetic props. and corrosion resist. 80−34709
$(Co_{0.93}Fe_{0.07})_{75-x}Cr_xSi_{15}B_{10}$ amorphous alloy, thermal stability, Cr conc. effects, DTA expts. 80−59395
Co_2FeGa, alloy, site preference of Co and Fe, Mossbauer and neutron study 79−78577

iron alloys continued
$(Co_xFe_{1-x})_5Ge_3$, Mossbauer investig. of hyperfine field at Fe nuclei 77−20776
$(Co_{0.89}Fe_{0.11})_{72}Mo_3Si_{15}B_{10}$, metallic glass, strain- and field-induced mag. anisotropy 80−108004
$Co_{57}Fe_5Ni_{10}(Si,B)_{28}$, amorphous, soft mag. props., switched-mode power supply appls. 80−88850
$(Co_{1-x}Fe_xNi_y)_{80}(Si_{1-z}B_z)_{20}$, amorphous films, spin wave spectra 80−34777
$Co_{1-x}Fe_xSi$, solid solution, optical props. 78−72556
$Co_{70}Fe_5Si_{15}B_{10}$, amorphous, crystn. and thermal stability 80−107057
$Co_{70.4}Fe_{4.6}Si_{15}B_{10}$, amorphous, mag. aftereffect spectra and annealing props. 80−88831
$Co_{75-x}Fe_xSi_{15}B_{10}$, quenched ferromag. ribbon, Brillouin spectra 80−2776
$(Co_{1-x}Fe_x)_2Y$, substitutional Fe atoms effect on mag. and elec. props., paramagnon scatt. 77−36054
$Co_2Ga_{2-x}Fe_x$, mag. props. and order 77−12093
$Co_2Ga_{1.95}Fe_{0.05}$, mag. behaviour, Mossbauer effect and DC magnetisation meas. 80−50244
$Co_2Ga_{2-x}Fe_x$, elec. resist. anomalies 79−38044
$Co_2Ga_{2-x}Fe_x$, elec. resist., temp. and mag. field depend., mag. contrib. 80−96846
$Co_2Ga_{2-x}Fe_x$, mag. field depend. of resist., 5.80K 80−70676
Co_2HfSn-Fe, dil., Heusler alloy, Fe hyperfine fields, Mossbauer obs. 78−68424
$Co_{1-x}M_xSi$ (M=Fe, Ni), elec. field gradient, quadrupole splitting of ^{59}Co 80−29641
$Co_2Mn_xFe_{1-x}M$, (M=Ga,Ge,Si,Sn), hyperfine fields of Fe impurities, Mossbauer effect meas. 78−31130
$Co_{2-x}(Ni,Fe)_xTiSn$, Heusler alloy, positive contribs. to hyperfine fields, magnetisation and NMR meas. 78−43654
$Co_{50}Ni_{20}Fe_6Si_{12}B_{12}$, amorphous, mag. props., effects mech. deform. 80−39840
Co_2TiSn-Fe, dil., Heusler alloy, Fe hyperfine fields, Mossbauer obs. 78−68424
Co_2ZrSn-Fe, dil., Heusler alloy, Fe hyperfine fields, Mossbauer obs. 78−68424
Cr-Co-Fe, chromindur alloy, field heat treatment, and mag. props. 80−35354
Cr-Co-Fe, for telephone receiver mag. use 80−45318
Cr-Co-Fe, low Co, phase separation, TEM and Mossbauer spectra obs. 80−71269
Cr-Co-Fe cold formable mag. alloys for use in telephone receiver 79−52227
Cr-Co-Fe permanent magnet anisotropic alloys, plastic deform., ageing, particle alignment temp. 80−35254
Cr-Fe, alloy with mixed types of order, uniform mag. phase diagram 79−78368
Cr-Fe, antiferromag., elec. resistivity, Kondo effect 79−60812
Cr-Fe, antiferromag. phase boundary, neutron diffr. meas. 78−95437
Cr-Fe, antiferromag. sp.ht. around Neel point 79−73750
Cr-Fe, antiferromagnetic, effect of press. on hyperfine mag. fields at Fe nuclei *(Russian)* 80−15936
Cr-Fe, Ar ion bombard., O_2 flooded, secondary ion yield as function of original conc. *(French)* 78−39643
Cr-Fe, dil., antiferromag., mag. incoherent elastic neutron scatt. 79−73678
Cr-Fe, dil., antiferromag., elec. resist. min., press. and impurity effects 80−59970
Cr-Fe, dil., exchange interactions 77−47986
Cr-Fe, dil., latent heat exam. of magnetic transitions 79−61156
Cr-Fe, dil., magnetisation, Fe local moments 80−60215
Cr-Fe, dil., spin correlations and neutron scatt. near crit. conc., theory 80−60327
Cr-Fe, dilute, localised moment cluster model, ferromagnetic exchange coupling 80−39774
Cr-Fe, disordered, polarised neutron diffuse scatt. meas., 4.6-110K 80−34592
Cr-Fe, elastic moduli, electron conc., pulse echo overlap meas. 80−59550
Cr-Fe, electronic struct., Mossbauer and positron annihilation study 79−82518
Cr-Fe, low conc. alloys, coexistence of itinerant antiferromagnetism with paramagnetism 78−84386
Cr-Fe, mag. moment of Fe, mag. suscept. meas. 79−61079
Cr-Fe, mag. phase transition, sp. ht. meas. 77−12120
Cr-Fe, magnetically insensitive Invar-type alloys *(Japanese)* 79−8034
Cr-Fe, polycrystalline, antiferromag., elastic moduli and thermal expansion meas. 77−43860
Cr-Fe, spin-glass phase, magnetisation curve test for mag. ordering 80−11201
Cr-Fe, superparamagnetism and mag. order charact. near critical conc., neutron scatt. study 79−11293
Cr-Fe, with Si and Ta additions, metallurgical and mechanical characterisation *(Italian)* 77−66674
Cr-Fe (0.6 at.%), antiferromag., anomalous press. effect on resist. minimum 79−15138
Cr-Fe (0.8-8 at.%), mag. phase transforms., sp. ht. obs. *(Russian)* 77−80941
Cr-Fe (1 wt.%), fracture during electrospark cutting *(Russian)* 79−87719
Cr-Fe (14 wt.%), spin density wave and spin glass ordering coexistence at low temps. 79−61059
Cr-Fe (20 to 30 at.%), Mossbauer spectra temp. var. and ferromag. props. 77−81037
Cr-Fe (30 wt.%) alloys, refined fine comminution 78−60598
Cr-Fe (6.5 wt.%), atomic clustering and mag. defects, mag. moments 80−60246
Cr-Fe alloy (up to 50%), hardness, oxidation and electronic constitution 80−30154
Cr-Fe itinerant antiferromag. effect of mag impurities 77−32186
Cr-Fe microstructural changes, heating and cooling cycles 79−78956
Cr-Fe_x (x=0.5, 1.5 and 3.5 at.%), antiferromag., Kondo anomaly 80−11163
Cr-Fe-C (28.4, 9.1 wt.%) prep. from $FeCr_2O_4$ chromite 80−100804
Cr-Fe-Co dilute alloys, Neel temp., thermal expansion rel. to Co content 79−47281
Cr-Fe-Ga system, phase obs. at 800 and 820°C *(Russian)* 78−23662
Cr-Fe-Ni, cryst. struct. and defects, high resolution electron microscopy obs. 79−94961
Cr-Fe-Ni, γ-solid soln., thermodynamic activity determ. at 1500K 80−108397

iron alloys continued
Cr-Fe-Ni, phase diagram calc. 79−1848
Cr-Fe-Ni alloys, claddings, chemical compatibility with UC nuclear fuels, thermodynamic model 80−63263
Cr-Fe-Ni alloys, interface with Th carbide fuels, basic chemical compatibility, thermodynamic calcs. 79−93727
Cr-Fe-Ni-Si, ternary phase equilibria for Cr-Fe-Ni rich portion, lattice stabilities 80−71628
Cr-Fe-Si, mag. excitation, neutron spectrometry 79−4654
Cr-Fe-Si, sp. ht., 1.4-4.2K 77−20079
Cr-Fe-Si, spin density wave, neutron diffraction studies 79−1664
Cr-Fe-V, calc. of phase equilibria using thermodynamic values from different models 78−60646
Cr-Fe-V, dil., V effect on para- to incommensurate and commensurate transitions 78−68260
Cr-Fe-V, effects of V on mag. transition, elec. and mag. props. 77−69554
Cr-Fe(2.8 at%), antiferromag., meas. of incoherent elastic neutron scatt. cross section 79−19723
Cr-Mo-Fe, dil., behaviour of mag. impurities 79−4672
Cr-Mo-Fe (2, 14 wt.%), spin density wave and spin glass ordering coexistence at low temps. 79−61059
Cr-Ni-Fe, Inconel 625, plasma chamber material for power generating Tokamak, suitability tests 80−32449
Cr-Ni-Fe, ternary phase diagrams, interactive computer program 80−71629
Cr-Si-Fe, mag. moment of Fe, mag. suscept. meas. 79−61079
Cr-V-Fe, mag. moment of Fe, mag. suscept. meas. 79−61079
Cr-V-Fe alloy, resistivity minimum, press. effect 79−38043
CrFe, mag. correls. and onset of ferromag., neutron scatt. study 80−50105
$Cr_{1-x}Fe_x$, Mossbauer spectra, mag. behaviour 80−20532
$(Cr_{1-x}Fe_x)_{1+\delta}Sb$, interstitial occupancy, Cr:Fe distrib., X-ray and neutron diffr. study 79−42012
$(Cr_{98}Mo_2)_{90}Fe_{10}$, spin glass behaviour obs. 79−61157
$Cr_{2.8}V_{0.7}Fe_{3.4}C_3$, stacking fault study, morphology, comp. and struct. 80−84190
Cu-Al-Fe, dil. liq. alloy, localised mag. state interactions *(German)* 77−1539
Cu-Al-Fe, mech. props. rel. to heat treatment 80−50682
Cu-Al-Fe, strength increase from intermediate annealing determ. of annealing temp. by recrystallisation 78−44136
Cu-Al-Fe (11, 2 and 1 wt.%), Fe effects on microstruct. and mech. props. *(Korean)* 77−28807
Cu-Al-Fe-Mn, phase transform. during continuous cooling *(German, English)* 79−70044
Cu-Al-Fe-Mn (10,3,2 wt.%), phase comp. struct., continuous cooling from β-phase effect 79−24499
Cu-Al-Ni-Fe, (10, 5, 5 wt.%), cast microstruct. 78−80535
Cu-Al-Ni-Fe system, corrosion behaviour in sea water 80−45421
Cu-Al-Ni-Fe-Mn, cast Ni-Al bronze, fracture metallography 78−27597
Cu-As-Fe, Mossbauer effect of Fe impurities 78−31131
Cu-Au-Fe, ferromag. ordering in FCC γ-Fe precipitates, Mossbauer study 80−71267
Cu-Bi-Fe, Fe effects on embrittlement 77−28900
Cu-Co-Fe, dil. alloy, low temp. resistivity maxima *(Russian)* 79−87091
Cu-Fe, biphase material X-ray stress determ. *(Russian)* 79−5097
Cu-Fe, classical Kondo system, impurity spin dynamics, NMR relax. of impurity neighbour nuclei 77−36056
Cu-Fe, cluster form., Fe solubility determ., 450 to 1000°C, Mossbauer spectra obs. *(German)* 79−29021
Cu-Fe, composite, simulation of tensile behaviour and fracture void initiation *(Japanese)* 78−52948
Cu-Fe, dil., diffusion and ageing processes, Mossbauer study 80−7245
Cu-Fe, dil., in supercond. proximity, localised bands 78−10613
Cu-Fe, dil., interaction between local mag. moments 77−1540
Cu-Fe, dil., internally oxidised mag. and electrical prop. 77−12100
Cu-Fe, dil., ion implanted, phase comp., Mossbauer study 80−7244
Cu-Fe, dil., Kondo system, host NMR exam. 78−80246
Cu-Fe, dil., local mag. moments, neutron scatt. study 79−61058
Cu-Fe, dil., local mag. moments and Kondo effect, theoretical model 79−69651
Cu-Fe, dil., local susceptibility, Mossbauer meas. 78−19400
Cu-Fe, dil., NMR data, ionic model and Kondo temp. 78−68399
Cu-Fe, dil., NMR satellite data, rel. to electronic struct. 78−68398
Cu-Fe, dil., powder, transferred orbital hyperfine field on near neighbours, NMR meas. 78−27098
Cu-Fe, dil., thermopower, interconfig. fluctuations 79−65412
Cu-Fe, dil., transmission ESR meas. 2 to 40K 78−68364
Cu-Fe, dil., valence and core level spectra, XPS study 80−84838
Cu-Fe, dil. alloy, anomalous thermoelec. power, sensitivity to defects, annealing effect 77−51728
Cu-Fe, dil. alloy, quench-condensed thin film, annealing effect on resistivity 78−43488
Cu-Fe, dil. alloy, spin relaxation rates, neutron scatt. study 79−47235
Cu-Fe, dil. alloy solubility and diffusion of Fe 78−43170
Cu-Fe, dil. mag. alloy, NMR of ^{63}Cu around impurities 77−16187
Cu-Fe, dilute, low temp. heat capacity in mag. field, superparamagnetism 80−39804
Cu-Fe, dilute solid soln., exam. of recrystallisation and stored energy 78−52836
Cu-Fe, explosive plasma sputtered coatings, struct. and props. *(Russian)* 80−100783
Cu-Fe, force constant change with pressure, relative Mossbauer fraction 80−34163
Cu-Fe, growth kinetics and interfacial energy of coherent γ-Fe particles *(Japanese)* 78−19765
Cu-Fe, highly dil., mag. impurity scatt., and deviations from Matthiessen's rule 78−43371
Cu-Fe, implanted, Mossbauer effect meas. 78−31134
Cu-Fe, implanted, Mossbauer study, rel. to annealing temp. 78−31135
Cu-Fe, Kondo system, Cu-Fe, static and dynamic susceptibilities, hyperfine studies 77−63090
Cu-Fe, Kondo system, magnetisation, Mossbauer expts. 77−77028
Cu-Fe, liq., thermodynamic props. *(Polish)* 80−89199
Cu-Fe, liquid, surface tension *(Japanese)* 79−19431
Cu-Fe, local moment system, low temp. susceptibility, Mossbauer effect meas. 77−43810
Cu-Fe, metastable solid solutions, production by explosive plasma compressor *(Russian)* 77−90289

iron alloys continued
Cu-Fe, microconductors, cast, struct. and physical props. exam 78−44232
Cu-Fe, mixed cryst., Debye-Waller factors, Mossbauer spectra obs. *(German)* 78−52412
Cu-Fe, Mossbauer studies of ageing and precip. 79−38415
Cu-Fe, precipitation kinetics study by thermoelectric power measurement *(French)* 79−20050
Cu-Fe, precipitation processes during aging, TEM, resistivity, hardness study *(Japanese)* 80−35221
Cu-Fe, preferred crystallographic orientation of unidirectionally solidified polycrystals *(Czech)* 79−43233
Cu-Fe, single crystal with coherent γ-Fe particles, precipitation hardening 78−31416
Cu-Fe, supersaturated, spontaneous magnetisation region development, Mossbauer obs. *(German)* 78−64306
Cu-Fe, thermal treatment effect on thermoelec. power *(French)* 77−32000
Cu-Fe, vapour deposited, electron irrad., resistance behaviour *(German)* 78−47779
Cu-Fe (0.04 to 0.9 at.%), film, resistivity temp. depend., 1.5 to 17K, impurity interactions 77−63007
Cu-Fe (0.2 at.%), clustering, precipitation, and oxidation, 298 to 919K, Mossbauer study 80−7242
Cu-Fe (0.2 at.%), quenched, Fe dimers and defects 80−40007
Cu-Fe (0.2 at.%), surface oxidation, Mossbauer obs. 80−55564
Cu-Fe (1 wt.%), stress induced martensitic transformation of spherical Fe particles, exam. 78−52803
Cu-Fe (1.2 at.%), Fe moment and lattice distortion, neutron scatt. meas. 79−24133
Cu-Fe (1.5 wt.%), precipitation-effect on void formation during electron irradiation 80−84211
Cu-Fe (1.5 wt.%), void form. during irrad. in HVEM, reactor irrad. simulation and ageing effects 80−107327
Cu-Fe (2.46 wt.%), reversion phenomena and cold-working effect *(Japanese)* 80−35204
Cu-Fe (<4 wt.%), solubility determ. by thermoelectric power meas. *(French)* 77−62644
Cu-Fe alloy film, mag. susceptibility max. 79−24173
Cu-Fe binary system, high-temp. phase relations in Fe-rich region 77−81249
Cu-Fe clusters, electronic states and mag. props., MO calc., appl. to Kondo problem 77−20219
α-Cu-Fe dil. alloys, Al ion charge screening, elec. resist. obs. 77−4500
Cu-Fe dilute alloy, host NMR spin lattice relaxation 79−51873
Cu-Fe group, dil., NMR satellite data calc., struct. of mag. impurities 80−103894
Cu-Fe phase diagram, 650 to 1050°C *(German)* 78−60658
Cu-Fe system, ageing and reversion phenomena study 80−89274
Cu-Fe-O system, distrib. of Fe between Cu and Cu_2O *(Russian)* 77−16540
Cu-Fe-P alloy, CA 196, flat spring, mechanical props. in bending, stress relax. test, 23 to 232°C 78−72806
Cu-Fe(2.5 wt.%), isothermally reacted austenite stability in very small particles 77−48432
Cu-ferrous alloy, hard inclusion composite exam. of wear resistance props. 79−34153
Cu-Ga-Fe, Mossbauer effect of Fe impurities 78−31131
Cu-Ge-Fe, Mossbauer effect of Fe impurities 78−31131
Cu-Ni alloys, alloying additions effect on thermal conductivity, 20-400°C *(Russian)* 77−59159
Cu-Ni-Fe, age hardenable, dislocation interactions with internal coherency stresses 77−36528
Cu-Ni-Fe, age hardened, yield strength correlation with internal coherency strains 77−44254
Cu-Ni-Fe, alloy pre-form prep. through reduction of sintered oxides 80−40284
Cu-Ni-Fe, cast, strength and hot ductility, Fe effect 80−66595
Cu-Ni-Fe, corrosion resistant, SCC, crevice corrosion in seawater 79−96177
Cu-Ni-Fe, magnetic properties, heat treatment and compressive stress effects 80−60367
Cu-Ni-Fe, permanent magnet, temp. effect 80−34701
Cu-Ni-Fe, spinodal alloy, heat treatments for improved mech. props. 79−5024
Cu-Ni-Fe, spinodally decomposable, densification using four different powder methods 80−40283
Cu-Ni-Fe, synergistic effect of Ni and Fe on sea water corrosion 78−35561
Cu-Ni-Fe (14, 7 wt.%), solid soln., decomposed, magnetostatic interaction between ferromag. particles *(Russian)* 77−80967
Cu-Ni-Fe (26,8 wt.%), microduplex struct. form., hardness meas., optical and electron microscopy *(Japanese)* 78−76659
Cu-Ni-Fe alloys superparamag. early stages of decomp. *(Russian)* 78−6890
Cu-Ni-Fe solid solution, after precip., susceptibility of interacting superparamag. grains 79−99733
Cu-Ni-Fe tube, stressed, corrosion failure caused by cooling water, denickelation *(German)* 79−29286
Cu-Sn-Pb-Fe-graphite, bronze-based, sintered alloy, silica additions effect 77−63807
Cu-Ti-Fe, internally oxidised, morphology, struct., particle precipitation singularities *(Russian)* 79−70067
Cu-Ti-Fe, struct. and coalesc. of oxide particles during internal oxidation *(Russian)* 79−90781
Cu-Ti-Fe (0.7, 0.9 wt.%) film, dispersion-strengthened, form. by high rate magnetron/plasmatron sputtering, and props. 80−25715
Cu-Zn-Fe, Mossbauer effect of Fe impurities 78−31131
CuFe, dil., anisotropic hyperfine coupling, NMR study 80−65784
CuFe film, metastable polycrystalline optical props. 79−83044
CuFe solid solns., quenched from vap. phase, mag. props. 80−60307
$D\text{-}_{12}Fe_{32}O_2$, anomalous magnetisation, compensated to uncompensated mag. arrangement transition 78−52254
dilute, with s-p elements of third or fourth periods, Mossbauer spectra meas. 77−63344
Dy-Fe, amorphous, random anisotropy effects 78−68223
Dy-Fe, amorphous ferrimag. film, mag. props. and Curie point writing 77−12164
Dy-Fe, amorphous film, Kerr readout charact. 79−15439
Dy-Fe film, amorphous, contact printing 77−73061

iron alloys continued
Dy-Fe_xNi_{1-x} system, mag. hyperfine field, influence of lattice struct. and substituent 77−8058
Dy-Fe-Al, pseudobinary alloy, struct. exam. 77−58979
Dy-Fe-Al, pseudobinary alloys, mag. props. 77−59397
$Dy(Fe,Al)_2$, saturation and remanent magnetostriction meas. 77−63256
$Dy_2(Fe,Co)_{17}$, mag. anisotropy fields by singular pt. detection 79−24156
$Dy_2(Fe,Co)_{17}$, magnetic anisotropy meas. by singular point detection method 77−63170
DyFe amorphous film, Mossbauer and mag. meas. 80−15844
$DyFe_2$, amorphous, mag. struct., US meas. 79−99683
$DyFe_2$, amorphous, struct. determ. EXAFS exam. 78−51421
$DyFe_2$, amorphous, ultrasonic exam. below T_c 79−73793
$DyFe_2$, H_2 absorpt., Mossbauer study 80−44987
$DyFe_2$, high field magnetostriction and magnetisation 78−84473
$DyFe_2$, highly magnetostrictive props. 77−12180
$DyFe_2$, hyperfine interactions 80−44549
$DyFe_2$, magnetisation and magnetic anisotropy 78−91862
$DyFe_2$, phonon softening below Curie temp., Mossbauer effect 77−4589
$DyFe_3$, amorphous, mag. struct. and moments 77−66260
$DyFe_3$ and Dy_6Fe_{23}, magnetostriction, room temp. to 80K 80−65993
$DyFe_3$, effect of adsorbed H on mag. props. 77−63129
$DyFe_3$ hydrides, desorption isotherms 80−103565
$DyFe_3$, Mossbauer spectra, easy magnetisation axis temp. rot. 80−15859
$DyFe_{3.4}$, amorphous, mag. props. 77−72985
$DyFe_{3.4}$, magnetisation data 77−32177
$Dy_{1-x}Fe_x$, mean mag. moment calc. 79−82761
Dy_2Fe_{17}, domain structures and anisotropy constant. 80−93136
Dy_2Fe_{17}, hyperfine interactions and cryst. field effects, Mossbauer spectra 80−2369
$Dy_2(Fe_{1-x}Co_x)_{17}$, hyperfine interactions, Mossbauer spectra 78−2780
$DyFe_2H_x$, thermodynamic props., H_2 desorption isotherm meas. 80−89516
$Dy(Fe_xNi_{1-x})$, mag. interactions, mol. field model 77−73010
$Dy(Fe_xNi_{1-x})_2$, mag. behaviour, susceptibility and Mossbauer expts., 4.2-1300K 78−52235
$Dy_2(Fe_{1-x}Ni_x)_{17}$, Mossbauer spectra, hyperfine field interactions 78−6614
$DyFe_2Si_2$, Mossbauer spectra 80−20558
$Dy_{0.7}Tb_{0.3}Fe_2$, magnetostrictive material, liq. phase sintering 78−64493
$Dy_xTb_{1-x}Fe_2$, and $Ho_xTb_yDy_{1-x-y}Fe_2$, high magnetostriction cpd., mag. anisotropy origins 78−68217
$Dy_xTb_{1-x}Fe_2$, single cryst., torque meas. 80−65877
Er-Fe amorphous alloys, mag. props. 79−90557
Er-Fe-Al(Mn)(Co), cryst. struct. and H_2 capacity 77−89543
$Er_2(Co_{1-x}Fe_x)_{17}$, mag. anisotropy and intersublattice exchange interactions 78−31066
$Er_2Co_{17-x}Fe_x$, magnetisation, Curie temp., anisotropy 77−89947
$Er_2Co_{17-x}Fe_x$, saturation magnetisation, Curie temp., easy direction, and anisotropy field 77−8304
$ErFe_2$, crystal field interaction contribution to specific heat 80−39788
$ErFe_2$, Czochralski growth, and cryst. quality determ. 77−8742
$ErFe_2$, effect of H on sublattice magnetization, elastic neutron scatt. obs. 79−78327
$ErFe_2$, excited state spin waves inelastic scatt. meas. 78−76234
$ErFe_2$, highly magnetostrictive props. 77−12180
$ErFe_2$, lattice dynamics, Mossbauer spectra 80−19888
$ErFe_2$, Laves phase, cryst. field effects on spin wave dispersion relations 78−84408
$ErFe_2$, mag. excitations, RPA theory 80−65830
$ErFe_2$, spin excitations, neutron scatt. obs. 77−63153
$ErFe_2$, spin waves, exchange interaction, neutron scatt. study 79−47267
$ErFe_2$ surface, effect of H and O adsorption, spin polarised photoemission study 80−29854
$ErFe_2$-YFe_2, and $ErFe_2$-$LuFe_2$, mag. props., 80-1300K *(Russian)* 80−75750
$ErFe_3$, 47K magnetic anomaly, point charge crystal field model 77−20517
$ErFe_3$ and Er_6Fe_{23}, magnetostriction, room temp. to 80K 80−65993
$ErFe_3$, H_2 sorption, mag. and struct. props. of hydrides 80−34831
$ErFe_3$, mag. anomalies at 47 and 131K 77−63134
$ErFe_3$, mag. struct., powder neutron diffr. meas. 78−2651
$ErFe_3$, Mossbauer and magnetisation investig. of 47K mag. anomaly, atomic rearrangement 77−20766
Er_6Fe_{23}, lower critical field 80−20414
Er_6Fe_{23}, magnetostriction, temp. depend., 20 to 350K 80−65994
$ErFe_4Al_8$, neutron diffr. exam., mag. struct. 78−10656
$(Er_{65}Fe_{35})_{100-x}B_x$ glasses, mag. props. 79−73693
$Er(Fe_{1-x}Co_x)_3$, spin reorientation, easy axis of magnetisation 80−25144
$Er_2Fe_3Co_{14}$, Kerr effect determ. of domain structure, Bloch wall energy 80−39805
$ErFe_2H_{3.9}$, mag. props. and lattice consts., effect of hydrogen absorpt. 77−20561
$ErFe_2H_x$, multiplateau absorpt. isotherms, theory 80−103564
$ErFe_2H_x$, thermodynamic props., H_2 desorption isotherm meas. 80−89516
$Er(Fe_{1-x}Mn_x)_2$, struct. determ. by X-ray diffr. *(Russian)* 77−76358
$Er_6(Fe_{1-x}Mn_x)_{23}$, mag. props. and mol. field coeffs. 78−39319
$EuFe_4Al_8$, mag. ordered, mixed valency of Eu, X-ray, susceptibility and Mossbauer spectra studies 79−19728
FE-Si, ordering studied by Mossbauer effect 77−63342
FE-Zn, prep. and phase diagrams *(French)* 80−76231
(Fe,Co,Ni)-Si(B), amorphous mag. alloy, magnetostriction rel. to soft mag. props. 80−84633
$(Fe, Co, Ni)_3V$, control of ordered struct. and ductility 80−21029
(Fe,Co)PBAl, metallic glass, viscous flow, alloying effect 78−79793
$(Fe,Mo)_{80}B_{20}$, glassy alloy, Curie temp. and crystn. temp., Mo additions effect, Mossbauer spectra 78−68428
(Fe, Ni, Co)-Si-B, amorphous, compositional effect on struct. changes, after heating up to 700°C, exam. *(Japanese)* 78−48433
$(Fe,Ni,Co)_3V$, long-range ordered alloy for fusion reactor appl. 80−32481
$(Fe,Ni)_{83}B_{15}C_2$, amorphous alloy, mag. props., possible appl. to power transformers 79−28558
$(Fe,Ni)_{80}(P,B)_{20}$, quenched alloy ribbon, mag. moments, Curie temp. 77−40041
$(Fe,Ni)_{80}P_{14}B_6$ amorphous alloy, mag. props., possible appl. to power transformers 79−28558
Fe alloy electrodes, rolled from powders, sintering problems 80−25608
Fe alloy granules in Cu binder, exam. of wear characteristics without lubrication 79−96154

iron alloys continued
Fe base amorphous alloys, magnetoelastic props. *(Japanese)* 78−23316
Fe base amorphous alloys, alloying element role in improving corrosion resist., ESCA study 80−50754
Fe base composite, sintering, damping props. 77−21061
Fe base superalloy, type A-286, elevated temp. fracture toughness testing of thin section irrad. materials 80−61063
Fe based amorphous alloy, mag. ordered, hyperfine field distribs., NMR meas. 78−68409
Fe based binary and ternary alloys, intercrystalline internal adsorption exam. by electrolytic dissolution *(Russian)* 78−35390
Fe based porous metals, exam. of volume change under high pressure 78−52906
Fe, cast, hardness, wear resist. and struct., electron irrad. effects 79−96126
Fe, cast, P, powder, H annealing 79−66025
Fe, cast, white martensitic, centrifugally cast metallurgical coatings for wear resistance in plastics molding machines 79−29285
Fe, cast flake and nodular, rupture strength, circumferential notch *(Japanese)* 80−93649
α-Fe, interstitial or substitutional sp impurity doped, electronic struct. 80−34384
Fe solid solution, substitution strengthening by Cr and Mo *(Czech)* 80−30080
Fe/Fe-Cr composite powder, X-ray diffr. exam. of densification during rolling 80−40289
Fe/Fe-Cu composites, microplastic deformation development 78−39877
solid Fe/liquid Zn, interdiffusion reaction 79−77845
Fe-^{48}V, nucl. orientation of ^{48}V, γ-ray anisotropy obs. and NMR meas. 80−97169
Fe-(Co)-B, amorphous, crystn. 80−79704
Fe-(Cr)-C, sintered, successive impregnation with C and Cr 79−95979
Fe-(Cu)-C, sintered parts, struct. stabilisation with C potential control of protective atmosphere 78−60614
Fe-(Mo)-CaF_2, sintered, friction and corrosion props. for frictional units of nuclear plants 78−60845
α-Fe-(Ni,Mn,Cr,Mo,W)-P (1 wt.%). grain boundary segregation, temper brittleness, AES study *(Japanese)* 79−78981
Fe-(Ni), cast, influence of Ni content on corrosion props. *(German)* 80−35370
Fe-(Ni)(Si)-C, cast, spheroidal graphite, metallography of solidification 78−19737
Fe-Ag, three-dimensional microstruct. analysis, appl. of basic topological concepts 77−59739
Fe-Ag (50 vol.%), two-phase system, plastic deformation *(French)* 78−39831
Fe-Ag (50 wt.%), plastic behaviour in compression, deform. rate effect *(French)* 80−71711
Fe-Ag-Cu melts, phase interface props., Cu influence *(Russian)* 79−51261
Fe-Al, Al effect on softening in solid soln. *(French)* 79−52226
Fe-Al, antiphase boundary motion, microscopic diffusional theory, appl. to domain boundary coarsening 79−61563
Fe-Al, atom-probe field ion microscopy obs. *(French)* 78−86389
Fe-Al, band struct. and density of states, KKR method and X-ray meas. 80−10863
Fe-Al, chemical emission by Ar^+ ion bombardment *(French)* 77−86410
Fe-Al, cold-worked, Mossbauer study of recovery 80−7593
Fe-Al, conduction band states, X-ray spectra obs. *(Russian)* 80−29317
Fe-Al, couple phase diagrams and thermochemical data 79−66037
Fe-Al, deformed, low temp. recovery of elec. resist. *(Russian)* 80−7697
Fe-Al, dil., film, NMR spin echo, rel. to struct. inhomogeneities *(Russian)* 80−29644
Fe-Al, dil. alloy, temp. depend. of ^{27}Al hyperfine field 78−47972
Fe-Al, directional Compton profiles, self-consistent APW band struct. calc. 80−25476
Fe-Al, domain struct. and magnetostriction, heat treatment effect 80−60398
Fe-Al, electron density distrib. vs. at. order 79−60309
Fe-Al, electron-beam-induced surface oxidation, HVEM obs. 80−14978
Fe-Al, equilibria of Fe, Al ordered phase *(Japanese)* 79−70042
Fe-Al, ferromag.-mictomag. transition, intermediate superparamag. 77−12140
Fe-Al, high temp. Mossbauer study of order-disorder transform. 79−100137
Fe-Al, hot- and cold-rolled, texture form., pole figures method *(Russian)* 80−45317
Fe-Al, hyperfine field meas. using muon-spin-rotation method 80−10933
Fe-Al, ion-implanted, depth profile and diffusion coeff. 80−54277
Fe-Al, liq., thermodynamic characts. calc. *(Russian)* 80−15264
Fe-Al, local ordering, neutron scatt. study 78−64193
Fe-Al, low energy Stoner excitations, spin wave obs. in neutron scatt. study 79−51770
Fe-Al, magnetic moment determ. from neutron scatt. 77−73011
α-Fe-Al, migration of C, mag. permeability disaccommodation meas. 77−36100
Fe-Al, morphological stability study, phase transformations, two phase structure 78−11231
Fe-Al, Mossbauer spectra, local mag. moments 80−15861
Fe-Al, Mossbauer study of ordering *(Japanese)* 79−19822
Fe-Al, optical props., comp. and order-disorder transform. depend. *(Russian)* 79−28852
Fe-Al, optical props. rel. to order-disorder transformations 80−29736
Fe-Al, ordered, superlattice fringe images, computer simulation 80−103296
Fe-Al, ordering and phase separations *(Japanese)* 80−50595
Fe-Al, ordering studied by Mossbauer effect 77−63342
Fe-Al, paramag. props., T_c to 1500K 78−68153
Fe-Al, planar faults, faint electron microscopic image contrast obs. 80−107283
Fe-Al, positron lifetime and angular correl. curves 79−47538
Fe-Al, rate of form. and thickness of diffusion layer, 200 to 600°C 80−15315
Fe-Al, residual elec. resist., contrib. from static lattice distortions and short-range parameters *(Russian)* 79−51548
Fe-Al, short range order, neutron scatt. meas. 77−19907
Fe-Al, single crystal, twinning and pseudoelasticity 79−15718
Fe-Al, single crystals, deform. at high temps. 80−81125
Fe-Al, sintered and worked alloy, nonmetallic inclusion identification by quantitative metallography 77−77701
Fe-Al, soft X-ray emission 77−32471

iron alloys continued
Fe-Al, spin glass transition, Monte Carlo study 80−39801
β-Fe-Al, struct. defect obs. 78−14337
Fe-Al, transition metal group VIII aluminide, NMR near equiatomic composition *(Russian)* 80−20479
Fe-Al, vacancy formation energy 78−18638
Fe-Al, variation in absolute thermoelec. power under heat/treatment *(Ukrainian)* 79−38051
Fe-Al, X-ray emission spectra 80−25489
Fe-Al (0.069 and 0.158 wt.%), internally oxidised, low temp. deform. *(Japanese)* 78−52876
Fe-Al (0.27 to 0.50 at.%), spin glass behaviour, microscopic model, Ising lattice, exchange and superexchange 80−39800
Fe-Al (1 to 4 wt.%), effect of nitriding on surface structure and props., and on diffusion layer *(Russian)* 79−34197
Fe-Al (12 wt.%) alloy 23 kHz US transducer piezomagnetic props. 78−59240
Fe-Al (15 at.%), short range order form. kinetics *(Russian)* 78−3146
Fe-Al (16 wt.%), improvement of certain props. discussion *(Chinese)* 78−84826
Fe-Al (16 wt.%), prop. improvement *(Chinese)* 77−73280
Fe-Al (25 at.%), anomalous magnetic behaviour *(Japanese)* 77−48011
Fe-Al (25 at.%), double Curie point phenomena 77−73030
Fe-Al (25 at.%), long-range ordered, compression induced mag. anisotropy 77−69546
Fe-Al (30 or 45 at.%) film, elec. resist. and magnetoresist., atomic ordering effects *(Russian)* 77−80853
Fe-Al (38.5-47 at.%), type B_2 ordered alloys, elec. resist. recovery stages after neutron irrad. *(French)* 77−69010
Fe-Al (4 wt.%), mag. anisotropy induced by cold rolling *(Russian)* 80−84595
Fe-Al (4 wt.%) single crystals, rolling induced mag. anisotropy and its removal by annealing treatment *(Russian)* 79−61746
Fe-Al (40 at.%), ordered, plastically deformed, neutron irrad. damage and recovery, resist. meas. 77−19993
Fe-Al (40 at.%) and Fe-Al (50.5 at.%) ordered alloys, 20K neutron irrad. effects, stoichiometry depend., resist. obs. *(French)* 80−84215
Fe-Al (40 at.%) B_2 type ordered alloy, C migration, resistivity meas. *(French)* 78−52868
Fe-Al (40 wt.%), defect elimination by laser irradiation *(French)* 79−65960
Fe-Al (45%), ordered and disordered states, optical and elec. props. 77−85826
Fe-Al (50.5 at.%), ordered, neutron irrad. enhanced defect diffusion, resist. meas. 77−11598
Fe-Al (51 at.%), crystal vacancies, dilatometric and field ion microscopy exam. 78−47346
Fe-Al (8 at.%), XPS investig. of cond. band region 77−16456
Fe-Al (up to 7.2%), oxidation process 78−85022
Fe-Al alloy, antiphase boundary energies 77−36460
Fe-Al alloy, B_2-type, electrical resist. meas. 78−30917
Fe-Al alloy, C saturated, at 1873K, activity meas. with Knudsen cell-mass spectrometer 78−39745
Fe-Al alloy, γ-ray effect on resistivity and configuration struct. *(Russian)* 78−43049
Fe-Al alloys, pairwise interaction energy 77−36461
Fe-Al alloys, powdered composites, metastable gamma-phase decomp. *(Russian)* 77−59741
Fe-Al alloys, rapidly quenched, mag. props. 80−29579
Fe-Al alloys, X-ray fluoresc. spectra, cond. electron wave function, lattice symm. depend. 77−85844
Fe-Al alloys with Fe_3Al order, phase separation 77−73258
Fe-Al α phase solid solution, interdiffusion coeff. depend. on ordering *(Russian)* 79−99373
Fe-Al compounds, X-ray emission investig. of electron localisation in valence zone *(Russian)* 77−48277
Fe-Al eutectic alloy, duplex crystals, unit cell parameters, appl. of Weissenberg technique 78−67684
Fe-Al liquid alloys, apparatus for viscosity meas. *(Czech)* 80−29103
Fe-Al powder composite, phase composition, produced in low-temp. plasma 77−90295
Fe-Al powder cpds., prep. in low-temp. plasma, struct. props. 77−44192
Fe-Al systems, band struct. and cluster calcs. 79−51480
Fe-Al-C, gamma irrad., crystal lattice parameter reversible changes *(Russian)* 80−10576
Fe-Al-C, low C, precip. of carbides and cementite after quenching and ageing 78−52814
Fe-Al-C, mag. permeability disaccommodation 78−88141
Fe-Al-C alloys, C migration and mag. aftereffect, mag. permeab. disaccommodation and long-range order meas. 79−8020
Fe-Al-Co-Ni, Alnico alloys, irreversible remagnetisation processes in rotating fields *(Russian)* 79−8015
Fe-Al-Cr (10, 5 to 10, wt.%), corrosion by coal char, SEM and X-ray diffr. exam. 78−88573
Fe-Al-Fe, phase diagram, microscopic model 80−34630
Fe-Al-N alloy, precipitation and coarsening of AlN *(Korean)* 79−91652
Fe-Al-Ni-Co-Cu alloys, Ti alloying and deoxidising addition *(Russian)* 78−80181
Fe-Al-Si, bending test, mech. props. under high press. and temp. *(Japanese)* 78−76711
Fe-Al-Si (6.22, 9.63 wt.%), bending test under high press., high temp. 80−85057
Fe-Al-Si alloy, order-disorder transform. exam. by Mossbauer spectroscopy 77−63334
Fe-Al-(Nb), fatigue deform. 77−44350
Fe-Al(Cr), gas corrosion, in composite atmospheres *(Polish)* 79−79142
Fe-Al(Cr)(Mn)(Pt)(V), X-ray exam. of dynamic characts. *(Russian)* 77−62608
Fe-Al(Cr)(V)(Ti), hardness after nitriding, metallographic, electron microscopic and microprobe anal. 78−51608
Fe-Al(Si), disordered, obs. of Kohn singularities in X-ray diffuse scatt. 79−27874
Fe-Al(Si)(Ga)(Ge)(As)(Sn)(Sb) dil., mag. hyperfine fields, Curie temps. and Mossbauer meas. 77−63190
Fe-Al(Si)(Ga)(Ge)(As)(Sn)(Sb), dil., XPS meas. 77−63538
Fe-Al(Ti), O containing, mag. aftereffect and disaccommodation meas., time depend., activation energy, and ageing props. 80−88836
Fe-Al(V)(Ti), nitrided, struct. and props. 78−19950
α-Fe-Al(Zn), ⟨111⟩ fibre texture development through diffusion process without α-γ transform 79−100170

iron alloys continued
Fe-Al(16 wt.%), ordered, antiphase region obs. cooling rate effects *(French)* 77−59834
Fe-Al(24.3 at.%)-C alloy, magnetic permeability disaccommodation, 260-400K 80−93144
Fe-Al(25 at.%), mag. anisotropy induced by plastic deform., dislocations, long-range order 77−4544
Fe-Al(4 wt.%), ferromag. alloy, mag. anisotropy induced by cold rolling 80−30114
Fe-As, liquid alloy, density and surface free energy *(Russian)* 78−11204
Fe-As (0.22 to 1.68 wt.%), martensitic transform., struct. features 77−36499
Fe-As melts, influence of Sn, Si, Mn and Cr additions on surface tension and density *(Russian)* 80−15337
Fe-As melts, surface tension, density, adsorption *(Russian)* 80−92757
Fe-As system, mag. props., Mossbauer study 80−88897
Fe-As-Su-Si (Cr)(Mn) melts, As and Sn distrib., Si, Cr, and Mn influence *(Russian)* 80−16274
Fe-Au layers, amorphous ferromag., elec. transport phenomena and reson. scatt. *(German)* 77−72847
Fe-B, (16.3 at.%) amorphous, coercive force temp. depend. 80−25158
Fe-B, amorphous, anomalous thermal expansion, ΔE effect, Invar and Elinvar characts., delay time 80−80589
Fe-B, amorphous, crystn., metal or metalloid exchange influence 80−75172
Fe-B, amorphous, elec. resist., temp. depend. 80−44563
Fe-B, amorphous, induced anisotropy, development by mag. annealing and under applied mech. stress 80−65868
Fe-B, amorphous, induced anisotropy by heat treatment in mag. field and under applied mech. stress 80−75758
Fe-B, amorphous, Invar-type alloy, mag. moment and high field susceptibility 78−34965
Fe-B, amorphous, mag. aftereffect, initial susceptibility time depend. 80−88829
Fe-B, amorphous, short-range order, Mossbauer meas. 80−44986
Fe-B, amorphous alloy, mag. props. 80−84618
Fe-B, amorphous alloys, compositional study on short-range struct. 80−84095
Fe-B, amorphous alloys, phase diagram 79−96002
Fe-B, amorphous ferromag., Invar type, magnetisation, elec. resist. and thermal expansion meas. 78−2663
Fe-B, amorphous ferromag., temp. depend. of resist., appl. of extended Ziman theory 80−59950
Fe-B, amorphous metallic glasses, high-temp. mag. anal. 78−91258
Fe-B, amorphous paramag. alloys, hyperfine field distrib., Mossbauer study 80−39958
Fe-B, binary alloys, giant ΔE effect and Elinvar characts. 78−76291
Fe-B, columnar alloys, metallographic obs. of eutectic struct. *(Russian)* 78−27469
Fe-B, eutectic, crystallisation *(Russian)* 79−70087
Fe-B, for infiltration of Fe compacts 80−60806
Fe-B, liq., mag. susceptibility meas. 80−75740
Fe-B, metallic glass, Mossbauer investigation of electronic struct. 78−92009
Fe-B, metallic glass, theoretical studies on structural models 79−37633
Fe-B, metallic glasses and vapour deposited films, amorphous to cryst. transition 80−88048
Fe-B, rapidly quenched, metastable phases 80−76234
Fe-B, rapidly quenched metastable solid solns., prop. and mag. props. 78−92218
Fe-B, rapidly solidified, metastable phases *(German)* 79−29045
Fe-B, sputtered amorphous film, strong stripe domains, Kerr effect obs. and theory 79−91265
Fe-B (14-25 at.%), amorphous, saturation magnetisation, temp. and comp. depend. 77−85430
Fe-B (15-25 at.%) glass, quasicryst. struct. Mossbauer expts. 79−4255
Fe-B amorphous, crystallisation, activation energy conc. depend., DTA calcs. 79−60284
Fe-B amorphous alloy, annealed, microstruct. and mag. domain changes 80−75790
Fe-B amorphous alloy, crystallisation kinetics 78−83736
Fe-B amorphous alloy, fast neutron and ^{235}U fission fragment irrad. 80−100288
Fe-B amorphous alloy, mag. anisotropy temp. depend. 80−15846
Fe-B amorphous alloys, mag. aftereffect 80−65970
Fe-B amorphous alloys, Mossbauer spectra, soft ferromag. props. 80−11302
Fe-B amorphous alloys, Mossbauer spectra, mag. moment conc. depend. 80−15847
Fe-B amorphous alloys, valence band spectrum, XPS study 80−50534
Fe-B amorphous metallic glasses, low-temp. resistivity in mag. field 78−91667
Fe-B amorphous ribbons formation, high-speed photography investigation 80−76216
Fe-B based alloys, amorphous, amorphous, thermopower meas., Nordheim-Gorter relations 79−99535
Fe-B ferromag. film, props. 79−4709
Fe-B films, amorphous, mag. annealing behaviour 79−73782
Fe-B glass, crystallisation kinetics, elec. resist. meas. 78−83741
Fe-B glass, crystallisation kinetics, elec. resist. meas. 79−4254
Fe-B glass, X-ray obs. of struct. 79−1399
Fe-B metallic glass, hardness, elastic moduli, density, cryst. temp., mech. props., for flywheel appl. *(Dutch)* 78−52878
Fe-B metallic glass, role of Fe_3B in crystn., mag. and Mossbauer expts. 78−94997
Fe-B metallic glass, struct. and crystallisation, Mossbauer spectra, calorimetry and magnetisation meas. 79−23528
Fe-B metallic glass, X-ray diffr. meas., semi-empirical struct. model 80−107059
Fe-B metallic glasses, crystn. kinetics by differential scanning calorimetry 78−91257
Fe-B metallic glasses, density, mech. and thermal props. 78−31432
Fe-B metallic glasses, diffusion coeffs. from primary crystn. data 80−100345
Fe-B metallic glasses, short-range orders 79−65002
Fe-B metallic glasses, short range order 79−77528
Fe-B metallic glasses, struct., stability and crystn. 80−75173
Fe-B metallic ribbons, correl. between quenching temp. and mech. and mag. props. 80−89373

iron alloys continued
Fe-B metastable alloys, Mossbauer spectroscopy and electron microscopy 79−28653
Fe-B phase ferromag. amorphous alloys, stiffening below Curie temp., pole effect *(Japanese)* 80−84632
Fe-B ribbon, microhardness, and static coercive force, melt overheating effect 80−84978
Fe-B_4C powder mixtures, phase changes and struct. of sintered materials *(Russian)* 78−6872
Fe-B_4C sintered material, mech. props. and struct. charcts. 79−100084
Fe-B-C, amorphous, effects of replacement of B by C on mag. props. 80−84621
Fe-B-C alloys, amorphous, temp. depend. of magnetisation 79−73690
Fe-B-C amorphous alloy, formation, mag. props., thermal stability and density 80−75796
Fe-B-C amorphous alloys, room-temp. saturation induction over 17.5 kG 79−47300
Fe-B-C amorphous alloys, atomic struct., energy dispersive X-ray diffr. meas. 79−73100
Fe-B-C amorphous alloys, effect of Si addition on mag. props. 80−34694
Fe-B-C amorphous alloys for use in power transformers 80−88808
Fe-B-C amorphous alloys with high saturation induction 80−84617
Fe-B-C system, phase composition, morphology after heat treatments, $Fe_{23}B_5C$ struct. 77−28779
Fe-B-Cr(Mo), metallic glasses, mag., struct., and elec. props. 80−88751
Fe-B-Cr(Si) thin film glasses, mag. props. and corrosion resist. 80−80576
Fe-B-Mo-Cr, amorphous, Mo and Cr addition effect on corrosion behaviour 80−16568
Fe-B-Si, amorphous ferromag. alloys, mag. struct., Mossbauer study 80−39746
Fe-B-Si amorphous alloy, liq. quenched, elec. resist. and cyclic deform. 80−59949
Fe-B-Si amorphous alloys, crystallisation temp., Curie temps., saturation magnetisation 79−82820
Fe-B-Si amorphous ribbon, strain induced anisotropy, and toroid diam. effect on mag. props. 80−34623
Fe-B-Si amorphous ribbons, effect of annealing conditions on magneto-mechanical props. 80−34740
Fe-B-Si-C amorphous alloys, prep. and props. 80−88748
Fe-B(-Co), two amorphous phases form. and crystallisation 79−27924
Fe-B(-Si), glassy, field-induced mag. anisotropy near eutectic comp. 80−93110
Fe-B(-Si) alloy filaments produced by glass-coated melt spinning 80−76213
Fe-B(-Si)(-Ni), amorphous alloy, anelastic relaxation 79−4997
Fe-B(C), amorphous phase form. by rapid quenching from melt *(Russian)* 77−66664
Fe-B(Si) amorphous alloys, Mossbauer spectra, struct. 80−15840
Fe-B(−Ni), chemical ordering, crystallisation and glass transition temp. 79−90563
Fe-base amorphous alloys, embrittled by H and heat-treatment 80−55518
Fe-base wear resistant dispersion hardened electrolytic coating, annealed and sintered 78−35593
Fe-based alloys, volume interactions between substitutional sp and 3d solutes 79−78069
α-Fe-based dil. solid solutions, electronic struct., hyperfine interactions 78−79968
Fe-based system, concentration ferro-antiferromag. transitions *(Russian)* 79−99699
Fe-Be, formation of quasi-periodic distrib. of precipitates during ageing *(Russian)* 78−56642
β-Fe-Be, pseudotwinning and pseudoelasticity 79−96056
Fe-Be (16.5 or 19.5 at.%), four-phase model of struct. in initial ageing stages *(Russian)* 78−48430
Fe-BeO, dispersion hardened alloy, struct.-props. relationships 77−66652
α-Fe-Be(P)(Mo)(W)-Co, effect of Co on solubility anomaly due to mag. transition *(Japanese)* 79−42257
α-Fe-Be(Ti)(Mo)(P)(Sb), effect of mag. transition on solubility of alloying elements *(Japanese)* 79−42256
Fe-bearing binary, substitutional liq. and solid solns., statistical thermodynamics 80−11630
Fe-C, (0.8 wt.%), sintered, hot forging and chemicothermal treatment, effect on wear resistance 80−25606
Fe-C, ageing late stages, diffusional coalescence of precip. along dislocation lines *(Russian)* 77−25060
Fe-C, binary, solidification, predicted volume change 77−28802
Fe-C, coupled phase diagrams and thermochemical data 79−66036
Fe-C, diffusion of Sn, microprobe anal. of intermediate phases *(French)* 80−50596
Fe-C, dil., Hall-field electrotransport of C, effective valence numbers 79−28148
Fe-C, dil. alloys, softening, conventional and in situ expt. 79−47744
Fe-C, dilute alloys, softening, conventional and in situ expt., HVEM obs. 79−47743
Fe-C, effect of H on elastic props., due to internal microcracking *(Russian)* 79−24561
Fe-C, electromigration of C, effect of Ni and Cr addition 78−6184
Fe-C, electron-irradiated, positron lifetime meas. 80−93431
Fe-C, electronic structure of interstitials 79−1583
Fe-C, exam. of phase equilbria, at high temp. and pressure 78−52759
Fe-C, ferromag., prep. by splat-quenching, obs. of electronic struct. of interstitial C 77−62868
Fe-C, graphitisation, interfacial segregation effects 77−52373
Fe-C, interstitial diffusion in presence of chem. conc. gradient 77−76612
Fe-C, lamellar eutectoid, calorimetric determ. of interfacial enthalpy 78−60668
Fe-C, lenticular martensite growth by transformation wave propag. 80−81055
Fe-C, levitated drops, carburisation and decarburisation in CO-CO_2 gas mixture, exam. of reaction kinetics 78−85053
Fe-C, liq., C solubility, donor-acceptor mechanism 80−49365
Fe-C, liq., struct., neutron and X-ray diffr. meas. 77−51306
Fe-C, liquid, C content effect on short-range order struct., X-ray diffr. obs. 80−6351
Fe-C, martensite, struct., Mossbauer meas. 80−40000
Fe-C, martensitic transformation, thermodynamical study *(Chinese)* 80−55395

iron alloys continued
Fe-C, optical emission spectrographic analysis of some binary alloys by a glow discharge of Grimm lamp *(Japanese)* 79−99015
Fe-C, oxidation at 700°C, electron diffr. obs. 79−61790
Fe-C, pearlite, eutectoid alloy, efficiency of directional transformation on orientated growth 78−76642
Fe-C, proeutectoid ferrite nucleation kinetics at austenite grain boundaries 80−55405
Fe-C, softening by C in solid soln. *(French)* 77−36660
Fe-C, softening of high purity Fe, by C, due to double kink nucleation *(French)* 78−84949
α-Fe-C (0.03 wt.%), structural singularities of transition from thermally activated to force-induced fracture *(Russian)* 78−56731
Fe-C (0.11, 0.23, 0.42 wt.%), grain boundary ferrite allotriomorphs, growth kinetics 77−44244
Fe-C (0.16 wt.%) hardness-flow stress rel. during strain-controlled bending fatigue 79−74245
Fe-C (0.25 wt.%), austenitising temp. effect on proeutectoid ferrite reaction kinetics, scanning Auger microprobe exam. 78−44144
Fe-C (0.52 wt.%), FCC structure, exam. of electromigration of C by steady state method 78−75865
Fe-C (0.64 wt.%), fatigue crack bifurcation 80−71748
Fe-C (0.64 wt.%), quasicleavage during fatigue crack propag., pearlitic microstruct. effect 79−11702
Fe-C (0.8-4.2 wt.%), eutectoid transform., effect of heat treatment in H_2 *(Russian)* 79−4947
Fe-C (1.0 wt.%), mixed powder compact, sintering, C diffusion meas. 77−90293
Fe-C (1.2 wt.%), Mossbauer study of early stages of tempering 80−16342
Fe-C (1.6 wt.%) martensite habit plane poles, statistical TEM trace anal. 80−97494
Fe-C (1.86 wt.%), exam. of C clustering in martensite, using Mossbauer spectroscopy 78−84821
Fe-C (2. wt.%), sintering shrinkage kinetics 80−20829
Fe-C (30 at.%), production of Fe_7C_3 at high press., morphology and microstruct. *(Russian)* 79−38828
Fe-C (4 at.%), dislocation-C atom relax. 77−70074
Fe-C (4.3 wt.%), splat cooled, amorphous phase form. and crystn. 77−15323
Fe-C (graphite, 0.3 wt.%), powder-forged, elastic consts., density depend. 80−84987
Fe-C (graphite), adhesion and wettability of graphite *(Russian)* 80−20008
Fe-C (synthetic diamond) role of diffusion of graphitisation in phase interaction 77−36449
Fe-C alloy, oxidation at 500°C cold work and annealing effects 78−44276
Fe-C alloys, thermodynamics of proeutectoid ferrite transform. re-exam. 78−84763
Fe-C alloys abrasion resist. materials, review 80−108586
Fe-C amorphous alloys, corrosion resistance improvement by Cr and/or Mo addition 79−66211
Fe-C eutectic, irregular. branching limited growth 80−81042
Fe-C eutectic, solidification cycle, thermal anal. 80−29945
Fe-C hypoperitectic, solidification cycle, thermal anal. 80−29945
Fe-C interstitial alloys, electronic structure and ordering of sp defects 78−91639
Fe-C interstitial solid solutions, self-diffusion activation energy rel. to partial molar energy 80−15291
Fe-C liquid alloys, Si and C transfer from SiO-CO gas phase 80−55655
Fe-C martensite, crystal struct. and morphology of ordered phase 79−42011
Fe-C melt, graphite cryst. growth rate rel. to supersaturation *(German)* 77−55940
Fe-C melt, mag. susceptibility and short range order, 900-1800°C 78−84382
Fe-C melt structure, X-ray diffr. study *(Russian)* 80−19685
Fe-C melts, C oxidation by CO_2, kinetics *(Russian)* 80−40680
Fe-C melts, short-range order, neutron scatt. obs. *(German)* 78−71669
Fe-C molten alloy, short range order *(Russian)* 79−90521
Fe-C single crystals, effect of heat treatment prior to cold rolling on recrystn. texture 79−83232
Fe-C solid solns., surface graphite layer form., high-temp. metallography investig. 79−29306
Fe-C solid solution, martensite, carbide decomposition, electron microscopy and X-ray diffr. obs., review *(Russian)* 79−33998
Fe-C solid solution, volume effects on enthalpy and internal energy 78−75839
Fe-c sputtered amorphous films, mag. props. and corrosion resist. 79−28567
Fe-C system, effect of microstruct. on fatigue crack propagation 79−79097
Fe-C system, FCC, austenite field thermodynamics, re-anal. 80−89201
Fe-C system, liq.-solid equilib. at high press., influence of graphitising elements *(Russian)* 78−56613
Fe-C system, mixing variables, activities and entropies calc., short range order model *(German)* 80−25655
Fe-C-B, amorphous, room-temp. saturation induction 78−95476
Fe-C-B, exam. of phase diagram using neutron autoradiography 79−8279
Fe-C-Cr, pearlite reaction kinetics 80−3006
Fe-C-Cr, thermodynamics and phase equilibria near eutectoid temp. 80−3005
Fe-C-Cr-Mn-Si-Ni (4.6, 38.7, 1.1, 2.0, 1.58 wt.%) alloy US-25, powder, compressibility and elec. resistivity in cold pressing under low press. 77−77444
Fe-C-Cr-Mo(Ni)(V), white cast, effect of abrasion on carbide microstructure *(German)* 78−88540
Fe-C-Cr(Al), electronic structure, thermodynamics of structure formation 79−99475
Fe-C-Cu (0.21, 0.2 wt.%), neutron-irradiated, resolution of C atoms, internal friction meas. 78−31442
Fe-C-Cu (0.21, 0.2 wt.%), neutron irradiated, torsional props. effect of Cu additions and annealing temp. 78−56699
Fe-C-Fe_xO_y, cleavage initiation by ductile tearing 78−64656
Fe-C-H phase diagram, effect of H on eutectoid equilib. *(Russian)* 79−15648
Fe-C-Mg, cast iron, graphite phase obs. *(Russian)* 77−59744
Fe-C-Mn (0.5, 0.6 wt.%), powder forged, mech. props. 80−21096

iron alloys continued
Fe-C-Mn-Si (4, 2, 1.5 wt.%), cast wire, influence of B addition on struct. and elec. cond. *(Russian)* 80−55391
Fe-C-Mn-V, austenite microstruct. memory *(German)* 80−84977
Fe-C-Mo-Nb-Al-Ti-B (0.015, 5.75, .7, 1.6, 2.5, 0.1 wt.%), TZM sheet, wear resistance, effect of surface hardening 77−59985
Fe-C-N, annealing in dry H_2, below 1180K, to purify to low C and N concs. 78−3072
Fe-C-N, BCC, Snoek type reordering during strain ageing *(French)* 79−8312
Fe-C-Ni-Cr, athermal alloy, exam. of martensite transformation kinetics 78−80545
Fe-C-Ni-Cr(Cu), dynamically hot pressed, mech. props., additives effect 78−60620
Fe-C-O, deoxidation when cooled and frozen, appl. of quasiequilib. two-phase zone model *(Russian)* 80−16222
Fe-C-Pb, sintered, antifriction props., Pb introduction effect 79−96155
Fe-C-S-Mg melt, S and Mg effect on graphite growth shape 79−38817
Fe-C-Si, effects of Si on matrix struct. of spheroidal graphite cast iron *(Korean)* 78−60666
Fe-C-Si, high purity, vacuum melted, nodular graphite form. 80−108452
Fe-C-Si, S effect on graphite morphology, formed during annealing *(Japanese)* 78−15434
Fe-C-Si, spheroidization 77−66665
Fe-C-Si, struct. and constitution on quenching from liquid state *(Russian)* 77−52309
Fe-C-Si (0.62, 2.0 wt.%), interfacial struct. of broad faces of ferrite plates 79−46660
Fe-C-Si alloy, lattice parameters of cementite after quenching 78−11198
Fe-C-Si-Mn, cast, high C, K_1 phase formation due to peritectoid transitions *(Russian)* 79−11548
Fe-C-Si-Mn (1.5-2.9, 2.4-3.4, 0.54-31.7 wt.%), discontinuous decomp. of supersaturated austenite *(Ukrainian)* 79−38788
Fe-C-Si(Co), eutectoid alloy, Si and Co addition effects on pearlite growth rate 77−16575
Fe-C-Ti (0.2 to 1.8, 0.1 to 1.7 wt.%), crystallisation and microstruct. *(Russian)* 77−66632
Fe-C-X, glasses and metastable cryst. phases, third element effect 80−75171
Fe-C-(P)(S), drops, oxidation kinetics in oxidizing slags 78−11153
Fe-C-(Si), splat quenched, electron diffr. and Mossbauer study of retained ε-phase 77−52354
Fe-C-(Si)(s), graphitisation during heat treatment *(Russian)* 80−20971
Fe-CR, ion-etched, surface comp., effect of adsorbed CO, AES obs. 79−46896
Fe-CR (26 wt.%), role of C and N in brittle fracture 80−16456
Fe-C(C-B)(C-Si), splat cooled, formation of metastable crystalline phases and glasses 78−88461
α-Fe-C(N), containing substitutional atoms, mag. permeability disaccommodation *(Polish)* 79−95612
Fe-C(Si)(Mn)-S melt, S evaporation *(Russian)* 78−19716
Fe-C(1.54 wt.%), electrocapillary curves in liq. sodium tetraborate 79−91968
Fe-Ci, high permeability, mag. props., applied stress effects 80−34726
Fe-Ci (3 wt.%), commercially produced, grain-oriented, mag. props., stress coating effects 80−34727
Fe-Ci (3 wt.%), local magnetisation losses, grain orientation effect 80−88817
Fe-Co, 3d ferromagnet nuclear spin-lattice relaxation 80−80627
Fe-Co, amorphous alloy, stress effect on mag. domain struct. 79−33502
Fe-Co, annealing of point defects produced by plastic deform. *(French)* 78−72829
Fe-Co, atomic ordering phenomena, neutron diffr. obs. *(Russian)* 77−81254
Fe-Co, atomic valence states, ferromag. props. *(Ukrainian)* 78−2656
Fe-Co, BCC, ferromag., spin wave stiffness constant 78−91851
Fe-Co, damping capacity of Gentalloy, internal friction meas., mech. and mag. depend. *(Japanese)* 78−52875
Fe-Co, dil., ensemble rotation concept in NMR on oriented nuclei 77−90061
Fe-Co, dil., film, NMR spin echo, rel. to struct. inhomogeneities *(Russian)* 80−29644
Fe-Co, dil., Mossbauer source, self-absorption effects *(French)* 79−24246
Fe-Co, electrodeposit, struct. *(Russian)* 79−56079
Fe-Co, electron energy spectrum calc. by Green function method *(Russian)* 77−35860
Fe-Co, equiatomic, atomic order, Mossbauer study *(French)* 78−27135
Fe-Co, ferromagnetic micropowder, cryst. struct., coercivity, remanence, saturation 80−65967
Fe-Co, film, magnetisation induced uniaxial anisotropy, dislocations effects 78−43618
Fe-Co, free enthalpy data, thermodynamic activity determ. at 1500K 77−59751
Fe-Co, Hall effect, anomalous, residual coeff. calcs. using coherent pot. method *(Russian)* 80−80249
Fe-Co, hyperfine field distrib., temp. and press. depend. 78−91651
Fe-Co, isothermal compression and BCC→HCP phase transition, up to 300 kbar, at room temp. 77−90346
Fe-Co, liq., X-ray diffr., struct. determ. *(Russian)* 77−80409
Fe-Co, liquid, solubility of H, 1400 to 1800°C 77−1231
Fe-Co, local environment effect on atomic moments, itinerant model 78−68188
Fe-Co, local environment effect on at. mag. moment 79−82763
Fe-Co, long range order, neutron powder diffr. meas. 79−42243
Fe-Co, mag. moment of Cr and Mn atoms, polarised neutron scattering 79−11290
Fe-Co, magnetised, circ. polarised γ-ray Rayleigh scatt., spin depend. 77−59637
Fe-Co, mech. behaviour in microplastic strain region *(Russian)* 78−39838
Fe-Co, Mossbauer investig. of order-disorder and α-γ transitions 77−48110
Fe-Co, order-disorder transformation, metallography, ordering kinetics 80−3026
Fe-Co, partially ordered, elec. cond. 78−91663
Fe-Co, surface comp. and surface segregation 80−34280
Fe-Co, surface excitations 80−25179
Fe-Co (25-35%), ordering, Cr addition effects, Mossbauer expts. *(Russian)* 78−19741

iron alloys continued
Fe-Co (30-70 at.%), order-disorder transition, comp. depend., neutron diffr. expts. 78−15393
Fe-Co (33 wt.%), oxidation and domain structure, electron microscope exam. *(Russian)* 79−1437
Fe-Co (35 wt.% and 52 wt.%), heat treated, decrease in sensitivity of mag. props. to mech. stresses *(Russian)* 78−56363
Fe-Co (46%) film, evaporated, uniaxial mag. anisotropy 77−51929
Fe-Co (5 to 25 wt.%), exam. of damping capacity of Gentalloy 78−72800
Fe-Co alloy, diffusion of H_2, diffusion coefficient and permeability *(Russian)* 78−79819
Fe-Co alloy, electrodeposited, comp. and struct. effects on H_2 diffusion and evolution overpot. 77−43377
Fe-Co alloy, optical characts., 0.073-4.92 eV, quantum absorption 79−56814
Fe-Co alloy, order-disorder and α-γ transitions 77−25042
Fe-Co alloy, V addition effect on atomic order parameters, dislocation struct., mechanical props. 79−91762
Fe-Co alloy particles for mag. tapes, mag. props. 78−95479
Fe-Co alloy ring samples, force fitting effect on mag. props. 77−40083
Fe-Co alloys, optical and spectrosc. props. *(Russian)* 78−72529
Fe-Co amorphous ribbon, mag. props. in low fields 79−73777
Fe-Co based alloys, redistrib. of elements, combined appl. of emission and absorption Mossbauer spectroscopy *(Russian)* 78−6031
Fe-Co based alloys (52KF, 35KKh, 35KFN), effect of heat treatment and mech. working, on sensitivity of mag. props. to mech. stresses *(Russian)* 79−34161
Fe-Co based amorphous alloys, mag. props. *(Japanese)* 79−95971
Fe-Co film, magnetisation induced uniaxial anisotropy 77−48016
Fe-Co films, optical props. order-disorder transformation influence, absorpt. band existence *(Russian)* 79−65942
Fe-Co films, ordered and disordered, Mossbauer study 79−24241
Fe-Co heterogeneous alloys, fabrication by powder metallurgy, tensile strength 77−63600
Fe-Co melt, volumetric characts., molar volume conc. depend. density *(Russian)* 80−33873
Fe-Co ordered alloys, enthalpy of form. 78−48376
Fe-Co-Al-Cu-Ti (40, 14, 7.5, 4.5 wt.%), metastable equilibrium, high coercive state *(Russian)* 80−66476
Fe-Co-B, metallic glass, Mossbauer investigation of electronic struct. 78−92009
Fe-Co-B powders, synthesis and mag. props., appl. to mag. recording 80−20432
Fe-Co-C (0.8 wt.%), unidirectional transformation process per struct. relationship, pearlite interlammellar spacing meas. 77−70045
Fe-Co-C-B, amorphous, room-temp. saturation induction 78−95476
Fe-Co-C(0.8 wt.%), unidirectional transformation, eutectoid reaction kinetics 77−70029
Fe-Co-Cd(Sn), mag. hyperfine fields at Fe, Cd and Sn sites, Mossbauer and TDPAC meas. 78−60363
Fe-Co-Cr, 25KKh15 alloy, nuclear γ-reson. investig. of atomic redistrib. during annealing *(Russian)* 77−12640
Fe-Co-Cr, alloy K25Kh15, phase tranforms., nucl. gamma reson. and X-ray diffr. meas. *(Russian)* 77−44241
Fe-Co-Cr, atomic mag. moment, magnetisation, Mossbauer spectra and NMR spin echo spectra 77−63127
Fe-Co-Cr, Cr effect on struct. *(Russian)* 78−27535
Fe-Co-Cr, Cr effect on struct. of ordering 78−35407
Fe-Co-Cr, heats of form. adiabatic calorimeter determ. 78−35713
Fe-Co-Cr, magnetic, phase transform. obs. *(French)* 79−47676
Fe-Co-Cr, solid state phase equilib., isothermal sections determ. 800-1300°C 79−91623
Fe-Co-Cr (27, 0.5 wt.%), internal stress and brittleness in ordered state *(Russian)* 79−61698
Fe-Co-Cr (50, 0.4 wt.%), ordering and recrystallisation 79−34029
Fe-Co-Cr film RF sputtering for magnetic recording 80−2947
Fe-Co-Cr-Mo (20, 15, 5 wt.%), maraging, stainless alloy fracture toughness 77−73326
Fe-Co-Cr-Si, structural transform. and mag. props. following heat treatment *(Russian)* 77−81274
Fe-Co-Mn, BCC, atomic mag. moments determ. 77−59396
Fe-Co-Mn, BCC, atomic mag. moment, magnetisation, Mossbauer spectra and NMR spin echo spectra 77−63127
Fe-Co-Mn, BCC, mag. state of Mn, NMR and saturation magnetisation meas. 78−39442
Fe-Co-Mn, dil. alloys, NMR freq. temp. depend., spin echo meas. 78−64296
Fe-Co-Mo, phase relations in system at 1100°C 80−108392
Fe-Co-Mo ternary system, phase diagram *(Russian)* 80−16269
Fe-Co-Mo-C, amorphous alloys, med. props. and thermal stability *(Japanese)* 80−85049
Fe-Co-Mo-Nb(Ta) semihard mag. alloy, mag. props., thermal expansion, elec. resistivity and hardness *(Japanese)* 80−88789
Fe-Co-Ni, at. mag. moments, neutron scatt. and Mossbauer meas. 79−42744
Fe-Co-Ni, liquid, solubility of H, 1400 to 1800°C 77−1231
Fe-Co-Ni Perminvar, mag. props. singularities in region of mag. anisotropy *(Russian)* 80−84614
Fe-Co-Ni powder, video recording appl. *(Russian)* 77−55910
Fe-Co-Ni-Al, Si alloying of mag. hard alloys *(Russian)* 79−73765
Fe-Co-Ni-Al (35, 14.5, 7.2 wt.%), high-coercivity, substructure and texture change during bending and upsetting 80−21037
Fe-Co-Ni-Al-Cu, polycryst. hard mag., C diffusion 79−77827
Fe-Co-Ni-Al-Nb (15-20, 14, 9, 0.1-5.5 at.%), Nb effect on magnetic props., lattice parameter *(Russian)* 77−55689
Fe-Co-Ni-Al-Zr magnetically hard alloys, reduction *(Russian)* 78−43614
Fe-Co-Ni-C, activity coeff. of C at 1273K 80−96667
Fe-Co-Ni-Si-B amorphous alloy, magnetostriction and permeability, effect of annealing 79−1701
Fe-Co-Ni-W alloy, 45KKhVN, plastic deform., electron microscope obs. *(Russian)* 78−80584
Fe-Co-P-C amorphous alloys, mag. props. 77−16055
Fe-Co-Si, BCC solid soln. interchange energies, high temp. neutron diffr. 80−29166
Fe-Co-Si (4,1.5 wt.%), textured, mag. props. 80−35200
Fe-Co-Si solid solutions, BCC, atomic configs., Mossbauer study 80−39006
Fe-Co-Si-B, amorphous, rapidly quenched, mag. heads appl. *(Japanese)* 80−54922

iron alloys continued
Fe-Co-Si-B, amorphous soft ferromagnet with high mag. induction 80−84619
Fe-Co-Si-B, zero magnetostrictive amorphous alloy with high saturation induction, mag. annealing 80−60362
Fe-Co-Si-B sputtered amorphous thin film, coercivity, galvanomagnetic props., resistivity 80−29578
Fe-Co-Si(B), amorphous ferromagnet, mag. after effect on soft mag. props. 80−84626
Fe-Co-Ta for semipermanent magnets *(French)* 79−47675
Fe-Co-Ti-Al alloy type YuNDK magnets, metallographic method of distinguishing cracks 80−85096
Fe-Co-Ti(V)(Cr)(Mn), sp. ht. in ordered and disordered phases 80−71061
Fe-Co-V, anelastic phenomena, related to atomic order, exam. of magnetostriction *(French)* 78−80579
Fe-Co-V, neutron irradiated, damage rates 79−77646
Fe-Co-V, ordered and disordered, dynamic ageing *(French)* 80−16355
Fe-Co-V, Vicalloy, $\alpha \rightarrow \gamma$ transform. under plastic deform., morphological singularities *(Russian)* 77−32576
Fe-Co-V, Vicalloy, magnetisation reversal by stretching and twisting 80−34733
Fe-Co-V, Vicalloy 1, γ-phase morphology and structural inheritance depend. on heating rate *(Russian)* 79−70059
Fe-Co-V (2 wt.%), gamma phase 77−36514
Fe-Co-V (2%), annealing of point defects produced by plastic deform. *(French)* 78−72829
Fe-Co-V (33, 33 at.%), BCC β phase, high temp. creep, existence of master curve 80−55473
Fe-Co-V alloy, Remendur, heat treatment effects on mech. and struct. props. 77−8846
Fe-Co-V alloys, effect of V on struct., electron diffr. and Mossbauer meas. *(Russian)* 77−77507
Fe-Co-V wire for high-speed matrix printers, wear resistivity obs. *(Japanese)* 80−55540
Fe-Co-V-Cr alloys, struct. transform., appl. of mag., thermomag. methods *(French)* 79−20318
Fe-Co-V(-Ni), annealing effect on microstruct. rel. to mag. and mech. props. 80−89267
Fe-Co-V(2%) alloy, correl. of resistivity with microstructure 78−72896
Fe-Co-X alloys, semihard wires, creeping magnetisation reversal 77−16106
Fe-Co-2 V, (49, 2 wt.%), solid soln., rheological study of crystallographic order on creep *(French)* 80−97548
Fe-Co(-V), neutron irradiated, influence of dislocation doping on recovery 79−46715
Fe-Co(-V), plastic flow, order-disorder transform. effect on creep, traction and relaxation *(French)* 80−35180
Fe-Co(Al), B_2 superlattices, point defect investigations 78−47357
Fe-Co(Cr), compositional diffusionally bonded alloy, mass transfer investigation *(Russian)* 80−39342
Fe-Co(Cr), M_s calc. 77−8824
Fe-Co(Ni)(Cr), liquid, N activity coefficient 77−72699
Fe-Co(Si), determ. of chem. and magnetic interchange energies 77−80925
Fe-Cr, alloy, composition determination using secondary ion emission *(French)* 77−86409
Fe-Cr, amorphous alloy, effect of metalloidal impurities on corrosion resistance and electrochem. behaviour 78−72925
Fe-Cr, Auger electron and appearance pot. spectroscopic study of surfaces 80−11520
Fe-Cr, BCC, ferromag., spin wave stiffness constant 78−91851
Fe-Cr, BCC, local moments in Mossbauer study 80−108125
σ-Fe-Cr, brittle fracture stresses under high hydrostatic press. and high temp. *(Japanese)* 79−43397
Fe-Cr, corrosion in hot conc. caustic soda soln. *(Japanese)* 79−70225
Fe-Cr, crit. mag.-props. near ferromag. Curie points 77−63216
Fe-Cr, crystallisation temp., overcooling temp. *(Russian)* 80−97472
Fe-Cr, damping capacity *(Japanese)* 79−70104
Fe-Cr, decomposition Mossbauer study *(French)* 77−63678
Fe-Cr, diffusion of C 77−7907
Fe-Cr, dil., spin density wave under high press., neutron diffr. study 80−65798
Fe-Cr, dislocation mobility and internal friction, effect of alloying in α-Fe *(Russian)* 77−31671
Fe-Cr, disordered, mag. order, Mossbauer study 80−39992
Fe-Cr, electron state density and elec. resist. 80−39558
Fe-Cr, ellipsometric study of films formed in orthophosphoric acid 79−74290
Fe-Cr, Fe-Cr-Al(Si) film heaters, lifetimes for 800 to 1000°C temp. range 78−215
Fe-Cr, feasibility of electrochem. corrosion protection 79−70220
Fe-Cr, flow stress, effect of cathodic, H_2 charging *(Japanese)* 79−52313
Fe-Cr, friction and wear in controlled environment, effect of sliding mode and specimen geometry 78−15542
Fe-Cr, friction at elevated temps. 78−15548
Fe-Cr, friction behaviour in oxygen, development of wear-protective oxides and influence on sliding friction 80−30111
Fe-Cr, from ore reduction, metallographic investigation, optical miroscopy and SEM *(French)* 78−68648
Fe-Cr, grain-boundary segregation of carbon, electrochemical study 79−100147
Fe-Cr, high purity binary alloy, isothermal decomp. of austenite 78−64525
Fe-Cr, high temp oxidation studies using $^{18}O(p,\alpha)^{15}N$, ^{18}O distrib. determ. 79−87912
Fe-Cr, high temp. oxidation, internal stable nitride and oxide dispersion 79−39017
Fe-Cr, high-C, sulphide inclusion distrib. obs. 79−74168
Fe-Cr, high-temp. oxidation, borate inhibitors 80−66705
Fe-Cr, hyperfine magnetic fields, Mossbauer spectra 80−97165
Fe-Cr, impact strength, rel. to '475°C brittleness' *(Russian)* 78−92323
Fe-Cr, influence of annealing on hyperfine interaction parameters, Mossbauer effect 80−71263
Fe-Cr, Invar alloy, explanation of phys. anomalies *(Russian)* 78−88112
Fe-Cr, ion-implanted, depth profile and diffusion coeff. 80−54277
Fe-Cr, irradiation induced void swelling, Cr additions effect 80−55408
Fe-Cr, lattice parameters, 293 to 1273K, α to γ phase transform., X-ray diffr. exam. *(Russian)* 80−50625

iron alloys continued
Fe-Cr, mag. moments and Fe site hyperfine fields, magnetis. obs. 78−76276
Fe-Cr, mag. props. of Fe, local coupling with spin modulation of matrix 79−15299
Fe-Cr, mechanically polished, XPS determ. of comp. of surface and surface oxide 78−7074
Fe-Cr, microstructural study of oxidation, selective etching 78−44245
Fe-Cr, nondestructive in-depth surface anal. by XPS with different excitation X-ray energies 79−20328
Fe-Cr, oxidation, in H_2/H_2O vapour mixtures, epitaxial oxide phase formation, effect on oxidation 78−88568
Fe-Cr, oxidation, in hostile environment, in situ meas. method 78−44277
Fe-Cr, passivation films, modulation spectroscopy study 80−3244
Fe-Cr, passivity in H_2SO_4, XPS study 78−44256
Fe-Cr, random ferromag. alloys, local mag. moment calc. 80−70974
Fe-Cr, role of C in transform. by heating in $(\alpha+\gamma)$ phase *(French)* 78−52798
Fe-Cr, segregation of ^{121}Sb, Mossbauer spectroscopy 79−47698
Fe-Cr, single and two component, powder, compressibility and elec. resistivity in cold pressing under low press. 77−77444
Fe-Cr, specific heat enhancement and electron-phonon interaction 80−65242
Fe-Cr, spin waves by neutron spectrometry 80−44819
Fe-Cr, surface and bulk alloys, oxidation at 300°C 79−61792
Fe-Cr, surface atom electron binding energy depend. on composition, Auger spectra, APS spectra 80−39655
Fe-Cr, surface composition change caused by heating in high vacuum, XPS obs. 78−44254
Fe-Cr, surface covered with anodic oxide film, in-depth composition profiles 80−10763
Fe-Cr, surface segregation of impurities (C,N and S) *(French)* 77−56192
Fe-Cr, thermodynamics of chlorination *(Russian)* 79−52168
Fe-Cr, tracer diffusion meas. using tracer anal. 79−82376
Fe-Cr (Mn)(Ni)(Si), liquid diffusion of H_2 *(German)* 78−14487
Fe-Cr (10 to 70 at.%), ferromag. reson., anisotropy const., and saturation magnetisation *(Russian)* 77−81013
Fe-Cr (12 wt.%), corrosion in o-phosphoric acid 80−97622
Fe-Cr (13 wt.%)+polycarbosilane, powder metallurgy, charact. 77−85962
Fe-Cr (17.3 wt.%), oxidation at 1000°C, alloy grain growth effect 78−7075
Fe-Cr (1.20, 3.63, 7.98 wt.%), Mossbauer spectra shape depend. on deformations 79−61272
Fe-Cr (2 at.%), plastic flow enhancement during massive transformations 78−48468
Fe-Cr (20 wt.%), high temperature oxidation resistance, effect of rare earth and reactive element additions *(Japanese)* 79−20271
Fe-Cr (20 wt.%), role of rare earths and reactive elements in high-temp. oxidation 79−79178
Fe-Cr (20 wt.%) high temp. oxidation behaviour with small La additions (0 to 1.3 wt.%) *(Japanese)* 78−85039
Fe-Cr (24 wt.%), low temperature oxidation, kinetics, oxide morphology 80−11838
Fe-Cr (25 wt.%), vaporisation kinetics in vacuum *(Russian)* 77−72683
Fe-Cr (25wt.%), continuously cooled, embrittlement 77−36636
Fe-Cr (25wt.%), surface comp. rel. to passivation phenomena *(French)* 79−43479
Fe-Cr (26 wt.%) effect of Ni content and austenite phase, on low temp. toughness and embrittlement 78−60754
Fe-Cr (27.4 wt.%), oxidation, alloy depletion profiles resulting from preferential removal of less noble metals 79−11728
Fe-Cr (28 wt.%), intergranular corrosion and anodic polarization at grain boundary groove *(Japanese)* 79−15869
Fe-Cr (5, 10 and 20 wt.%), microcrack generation, healing of oxide scale 79−20280
Fe-Cr (5 to 30 wt.%), transpassive behaviour in acidic sulphate soln. 78−15565
Fe-Cr (5 to 40 wt.%), breakdown and healing of oxide scale during oxidation 77−63836
Fe-Cr (5 wt.%), friction and wear in controlled environments, oxide film effect 78−15546
Fe-Cr (70-92 at.%), coexistence of ferro- and antiferromagnetism *(Russian)* 78−47955
Fe-Cr (9 wt.%), extrinsic grain boundary dislocations, low C content influence 80−107273
Fe-Cr (9 wt.%), oxidation studied using $C^{18}O_2$ and D_2O tracers 80−71784
Fe-Cr alloy, Cr rich, solubility of S *(French)* 78−30761
Fe-Cr alloy, N solubility investigation *(Russian)* 80−92675
Fe-Cr alloy, sputter etching oxide film, comp. profile, quantitative AES 80−81383
Fe-Cr alloys, cold worked, internal friction due to H *(Japanese)* 80−70305
Fe-Cr alloys, corrosion, oxidation, combined ion-, electron-beam techniques appl. 79−43700
Fe-Cr alloys, damping capacity 79−100206
Fe-Cr alloys, in acid and neutral solns., thickness and optical constants of passive and transpassive films 80−66698
Fe-Cr alloys, M_s calcs. 77−8824
Fe-Cr alloys, mixed ferro-/antiferromag. interactions *(Russian)* 77−32173
Fe-Cr alloys, $NaClO_3$ and NaCl effects on corrosion behaviour in hot NaOH soln. *(Japanese)* 80−35407
α-Fe-Cr alloys, recrystallised, C segreg. effects, TEM *(French)* 77−28828
Fe-Cr based coatings, hot corrosion resist. 79−24674
Fe-Cr film, sputtering yields, proton-induced X-ray meas. 80−50488
Fe-Cr melts, ultrasonic propag. and isothermal compressibility using pulse-phase method *(Russian)* 79−51202
α-Fe-Cr solid soln., thermodynamic activity of components 79−38797
Fe-Cr surface alloy formed by ion implantation, anodic polarisation 78−48561
Fe-Cr-Al (14, up to 2 wt.%), Al effects on high temp. oxidations *(Japanese)* 79−15865
Fe-Cr-Al, Al addition effect on oxidation, 900 to 1200°C 79−66222
Fe-Cr-Al, Al effect on high temp. oxidation in wet O_2 79−66223
Fe-Cr-Al, attenuation and vel. of acoustic shock waves, amplitude depend. 78−63810

iron alloys continued
Fe-Cr-Al, blackness change in air, 1-8 micron, 1200°C, film props. depend. 77−66033
Fe-Cr-Al, elec. heating alloy, effect of rare earth additives on quality *(Chinese)* 78−84825
Fe-Cr-Al, electrical heating material, SEM obs. and surface analysis of oxide films formed at high temps. 77−16738
Fe-Cr-Al, HOS 875, oxidation, cyclic, role of thermal shock 80−97640
Fe-Cr-Al, Kanthal films, vac. deposited, evaporation characts., comp., struct. and elec. props. 80−88646
Fe-Cr-Al, kinetics and mechanism of high temp. S corrosion 80−25911
Fe-Cr-Al, scale and spalling resist. determ., appl. of cyclic oxidation method 77−77695
Fe-Cr-Al, scales, α-Al_2O_3, early stages development at high temp. 80−89413
Fe-Cr-Al, thermodynamic predictions in coal gasifier environment 79−38799
Fe-Cr-Al (0.3 wt.%), oxidation behaviour at high temps. *(Japanese)* 80−35404
Fe-Cr-Al (12, 3 wt.%), internal friction and rigidity modulus, strain amplitude depend. *(Japanese)* 80−92606
Fe-Cr-Al (14, 0.1 to 2 wt.%), oxidation at high temps. *(Japanese)* 78−60872
Fe-Cr-Al (17, 4 or 6 wt.%), high temp. corrosion in S vapour 80−40591
Fe-Cr-Al (7, 5 wt.%), expt. stainless alloys, phys. and mech. props. 80−97637
Fe-Cr-Al alloys, localised mag. moment determ. and electron struct. 77−66268
Fe-Cr-Al alloys, low temp. sp. ht., resistivity and coercive force 78−63866
Fe-Cr-Al-Ce, Ce effect on high temp. oxidation 79−100301
Fe-Cr-Al-Ce, high temp. oxidation *(Japanese)* 78−11413
Fe-Cr-Al-TaC (13.5, 3.7, 9 wt.%) eutectic alloy, directionally solidified, thermal cycling effects on microstruct. 77−32686
Fe-Cr-Al-Ti-Y_2O_3 (20, 4.5, 0.5, 0.5) type MA956, strain rate effect on fracture behaviour at 1366K 80−16458
Fe-Cr-Al-Y, high temp. corrosion depend. on Y, oxidation, stress growth *(Russian)* 80−40588
Fe-Cr-Al-Y, influence of Y additions on oxide-scale adhesion 77−8993
Fe-Cr-Al-Y, oxidation resistance, heat treatment and Al^{+} ion implantation 80−71785
Fe-Cr-Al-Y, scales, α-Al_2O_3, early stages development at high temp. 80−89413
Fe-Cr-Al-Y (Y-Al_2O_3)(Y_2O_3), preparation and exam. of mech. props. 78−52720
Fe-Cr-Al-Y-C, GE-1541, volatilisation of oxides during oxidation at 1200°C 78−23873
Fe-Cr-Al(-Y), isothermal oxidation behaviour at 1200°C, SEM 80−50755
Fe-Cr-Al(-Y), oxide grain morphology and growth mechanism 80−3239
Fe-Cr-Al(-Y), thermal cycling influence on oxidation behaviour at 1200°C, SEM 80−50756
Fe-Cr-Al(Ni), corrosion by coal char at 871° and 982°C 80−3237
Fe-Cr-B, amorphous, Elinvar and Invar charact. *(Japanese)* 80−11832
Fe-Cr-B, B inhibition of oxidation, AES study 79−61785
Fe-Cr-B amorphous alloys, corrosion resistance, Invar and Elinvar charcts. *(Japanese)* 79−96213
Fe-Cr-C, austenite to ferrite+precipitate reaction, TEM/STEM study 80−3075
Fe-Cr-C, crystallography of austenite-ferrite/carbide transformation 80−16303
Fe-Cr-C, isothermal transformations 80−16302
Fe-Cr-C, lattice parameters of cementite, annealing effect 80−29007
Fe-Cr-C, lqiuid, reduction of Cr_2O_3 by dissolved C 78−6877
Fe-Cr-C, self-diffusion processes during homogenisation of heterogeneous systems *(Russian)* 79−60539
Fe-Cr-C, steel carbide formation during chromising, exam. in terms of ternary phase diagrams 78−56818
Fe-Cr-C (10,0.2 wt.%), isothermally transformed, precipitate orientations 80−50640
Fe-Cr-C (10,0.2 wt.%) isothermally transformed, carbide distrib., microstruct. development 80−3076
Fe-Cr-C alloy, bainitic struct. morphological changes, due to external stress, plastic deform. 78−44120
Fe-Cr-C alloys, equilibrium partition coeffs. for ferrite/liquid, austenite/liquid 78−39744
Fe-Cr-C solid solns., ordering and γ to α transforms, effect of heat treatment *(Russian)* 79−24520
Fe-Cr-C system, isothermal sections, 873 to 1373K, computer plotting 78−6894
Fe-Cr-C system at 870°C 77−28782
Fe-Cr-Co, anisotropic, spinel type permanent magnet, magnetic aftereffect 77−16118
Fe-Cr-Co, BCC, atomic mag. moments determ. 77−59396
Fe-Cr-Co, ductile magnet alloys, mech. props. 80−85001
Fe-Cr-Co, effect of heat treatment on strain gauge factor 78−72802
Fe-Cr-Co, elastic props. anisotropy at room temp. *(Russian)* 80−89279
Fe-Cr-Co, heat treatment effect on strain gauge factor *(Japanese)* 78−6954
Fe-Cr-Co, mag. alloys, Mossbauer spectra 78−19386
Fe-Cr-Co, mag. props., heat treatment effects *(Russian)* 78−39365
Fe-Cr-Co, mag. props. of ductile permanent ductile alloys *(Chinese)* 79−19746
Fe-Cr-Co, magnetic domain walls, Lorentz microscopy 80−103854
Fe-Cr-Co, mechanism of coercive force 80−34674
Fe-Cr-Co, metallic magnets investigation, present state *(Polish)* 80−107987
Fe-Cr-Co, permanent magnet, temp. effect 80−34701
Fe-Cr-Co, spinodally decomposed magnetic alloy, magnetic flux temp. coeff. *(Japanese)* 78−35006
Fe-Cr-Co (28, 10.5 wt.%) ductile magnet alloy, humidity-induced H_2 embrittlement 80−89406
Fe-Cr-Co (31 wt.%, 23 wt.%), microstruct. and mag. props., ageing and thermomag. treatment effects 78−76769
Fe-Cr-Co alloy, coercive force mechanism 80−71103
Fe-Cr-Co alloy, Mossbauer exam. of spinodal decomposition 77−69742
Fe-Cr-Co alloy, spinodally decomposed, micro-twinning 80−92537
Fe-Cr-Co alloys, (5-9 wt.% Co), obtained by slow cooling under mag. field, permanent magnet props. 80−75797
Fe-Cr-Co alloys, permanent magnet material development 78−91895
iron alloys continued
Fe-Cr-Co alloys, permanent magnets, magnetic props. and heat treatment *(Russian)* 79−91809
Fe-Cr-Co ductile magnet, with high $(BH)_{max}$, processing, mag. props., and microstruct. 77−8957
Fe-Cr-Co ductile magnet alloys, phase diagram and mag. props., V or V+Ti addition effects 77−8959
Fe-Cr-Co hard-mag. alloys, fine cryst. struct. *(Russian)* 77−66706
Fe-Cr-Co martensite, ordering and segregation *(Russian)* 79−20052
Fe-Cr-Co permanent magnet system, miscibility gap, microstruct. and mag. props. obs. 80−76228
Fe-Cr-Co phase diagram, lamination region, resist. meas. *(Russian)* 78−27479
Fe-Cr-Co-Al (27.5, 17.5, 0.5) alloy, magnetic props. and microstructure 78−72367
Fe-Cr-Co-Al (27.5, 17.5, 0.5 wt.%) alloy, induced anisotropy 78−76239
Fe-Cr-Co-Al(V)-(Nb)(Ti), phase equilib., X-ray diffr. meas. *(Russian)* 79−47658
Fe-Cr-Co-Mo, melted in open induction furnace, microstruct. and magnetic props. 79−61626
Fe-Cr-Co-Mo, microstruct., hardness, mag. props., influence of isothermal tempering and heat treatment 79−79129
Fe-Cr-Co-Mo alloys, struct. transform. and mag. props. *(Russian)* 77−76543
Fe-Cr-Co-Mo high energy permanent magnets, mag. props. 80−97119
Fe-Cr-Co-Si alloy, interaction domains after heat treatment in mag. fields *(Russian)* 78−68286
Fe-Cr-Co-V alloy, microstruct. and mag. props. 78−68221
Fe-Cr-Co-V-(Ti) hard magnets, V and V-Ti effects on mag. and mech. props. 79−91810
Fe-Cr-La(Y)-Al, La or Y with Al addition effect on high-temp. oxidation 79−100302
Fe-Cr-Mn, Cr and Mn effect on N_2 solubility above 1000°C *(Bulgarian)* 79−65203
Fe-Cr-Mn, influence of alloying with Ni, Mo, N on defect conc. energy *(Russian)* 80−54241
Fe-Cr-Mn alloys, Mn content effect on Cr distrib. in suboxide layers *(Russian)* 77−12732
Fe-Cr-Mn-C, high temp. oxidation, X-ray and weight gain meas. *(Russian)* 78−15571
Fe-Cr-Mo, (30,2 wt.%) Bridgman-type, unexpected embrittlement phenomena, hydrostatic tensile test *(Japanese)* 80−55517
Fe-Cr-Mo, sputtering effect on surface comp., AES obs. 80−6601
Fe-Cr-Mo, white cast, optimising fracture toughness and abrasion resist. 80−85042
Fe-Cr-Mo (26, 1 wt.%), single crysts. and polycrysts. strain rate influence on low cycle fatigue props. 80−3126
Fe-Cr-Mo alloy castings, thick-section, factors affecting 80−108374
Fe-Cr-Mo and Fe-Cr-Mo-Si, amorphous films, corrosion resist. and ion plating use 80−89423
Fe-Cr-Mo sintered, damping capacity and mech. props. 78−44161
Fe-Cr-Mo-C, X-ray investigation after friction and oxidation 78−52997
Fe-Cr-Mo-Ti (13, 1.5, 3.5 wt.%), equilibrium studies on chi-phase strengthening 79−24496
Fe-Cr-Mo(Ni)(Mo-NI), AES using peak-to-peak value *(Japanese)* 79−20485
Fe-Cr-N (5.9, 0.5 wt.%), martensitic, tempered, fine struct. 77−25079
Fe-Cr-N system, distrib. of Er between austenite and ferrite at 1200°C 79−43205
Fe-Cr-Nb-C, X-ray microanal. of carbide phases rel. to Nb conc. *(Russian)* 78−88467
Fe-Cr-Ni, AES investigation of corrosion and growth nature of surface layers 77−77330
Fe-Cr-Ni, analysis and synthesis of phase diagrams 79−11563
Fe-Cr-Ni, appl. of computational techniques for treatment of thermodynamic data, phase diagram calc. 78−10172
Fe-Cr-Ni, austenitic, oxidation behaviour on addition of Si 77−12740
Fe-Cr-Ni, austenitic, self-diffusion and swelling under irradiation 80−39343
Fe-Cr-Ni, α-particle induced precip. and phase instability 79−1470
Fe-Cr-Ni, BCC, atomic mag. moments determ. 77−59396
Fe-Cr-Ni, cold-rolled foils, dilatometric study 80−21033
Fe-Cr-Ni, corrosion behaviour in hot conc. NaOH soln. *(Japanese)* 80−85082
Fe-Cr-Ni, electron irradiated, resistivity during annealing, 4.2-1300K 78−87962
Fe-Cr-Ni, Fe-rich, melting equilibria *(German)* 77−52282
Fe-Cr-Ni, foil, in situ oxidation in HVEM 80−104354
Fe-Cr-Ni, irradiated, Ni segregation to sinks 78−91472
Fe-Cr-Ni, mag. state at low temps. *(Russian)* 78−56298
Fe-Cr-Ni, melting and solidification *(French)* 77−66635
Fe-Cr-Ni, neutron irradiated, rel. between irradiation induced swelling and shear modulus 80−15157
Fe-Cr-Ni, shock loading effect on phase equilib. *(Russian)* 79−29017
Fe-Cr-Ni, single crystal anomalies in curve of critical shear stress versus temp. at low temps. 77−16656
Fe-Cr-Ni, solid soln. strengthened and precipitation hardened, in-reactor creep 79−43327
Fe-Cr-Ni, spin system, relaxation props. at low temp. 79−82758
Fe-Cr-Ni, stable and metastable, thermal expansion, 4.2-290K *(Russian)* 78−47537
Fe-Cr-Ni, stress corrosion cracking in high temp. caustic soln. 77−59964
Fe-Cr-Ni, textured (α+γ) alloy, α' lath martensite formation 78−95749
Fe-Cr-Ni, thermodynamic prediction in coal gasifier environment 79−43206
Fe-Cr-Ni, two phase (α+γ) alloys, transformation-induced plasticity 77−63721
Fe-Cr-Ni, two-phase (α+γ), and metastable austenitic, uniform elongation peak 77−77547
Fe-Cr-Ni (12, 15 wt.%) austenitic alloy, Ni^{6+} irradiated, void swelling and phase stability, Si and Ti effects 80−65055
Fe-Cr-Ni (18, 14 wt.%), single strain induced γ to α' cryst. transform. *(Japanese)* 78−11221
Fe-Cr-Ni (18,14 wt.%), γ to ε to α martensitic transform., external stress effect, double tensile deform. exam. 80−108438
Fe-Cr-Ni (19, 13 wt.%), austenitic, Ni^{+} ion irradiated, multiple dislocation loops *(French)* 80−65064
Fe-Cr-Ni (20,15 wt.%), low cycle fatigue life under hold time conditions, grain size effect 77−77577
α+β-Fe-Cr-Ni (23.19, 4.91 wt.%), orientation relationship between austenite and lath martensite 78−39775

iron alloys continued
Fe-Cr-Ni (25, 20 wt.%), single crystal, stress corrosion cracking 78−35553
Fe-Cr-Ni alloy, austenitic, Neel temp. and max. susceptibility predictions comp. effects 77−43833
Fe-Cr-Ni alloy, deforming stresses anomalous temp. depend. *(Russian)* 77−81296
Fe-Cr-Ni alloy, dual-ion-irradiated, swelling anal. 78−86600
Fe-Cr-Ni alloy, quantitative anal. method based on ion bombardment induced secondary ion and photon emission 79−19963
$\alpha+\gamma$Fe-Cr-Ni alloy, stress-induced α'-martensite occurrence 78−23704
Fe-Cr-Ni alloy 800, sensitization times for intergranular corrosion 77−16746
Fe-Cr-Ni alloys, linear expansion, 4.2-300K rel. to antiferromag. rearrangement 78−43146
Fe-Cr-Ni alloys, oxidation-sulphidation in gas mixture, parabolic kinetics, thermochem. diagram 78−72932
Fe-Cr-Ni austenitic alloys, environment sensitive cracking, metallurgical variables effect 80−35391
Fe-Cr-Ni austenitic alloy, cold deformed, α-γ transition, calorimetric study *(Russian)* 80−55390
Fe-Cr-Ni based alloys, Ni^+ ion and neutron irradiated, γ' particle redistrib. and phase stability 79−78977
Fe-Cr-Ni based alloys, surface oxides at high temps., backscattering Raman spectroscopy 80−93291
Fe-Cr-Ni liquid alloy, N_2 soln. and TiN precipitation 78−6931
Fe-Cr-Ni melts, S solubility and solid soln. precipitation *(Russian)* 80−15251
Fe-Cr-Ni system, austenitic, energetic particle bombardment, thermodynamic and dimensional stability 77−27904
Fe-Cr-Ni system, diffusion coeff. consts. calcs. for multi-component systems *(Russian)* 79−90815
Fe-Cr-Ni system, isothermal diffusion *(Russian)* 79−69300
Fe-Cr-Ni-Al alloys, 25 keV ion implanted, metallic corrosion behaviour 79−52447
Fe-Cr-Ni-C (17.2, 7.34, 0.2 wt.%), twin related laths, fracture elongation, TEM study 79−29192
Fe-Cr-Ni-C (23.19, 4.91, 0.025 wt.%), two phase alloy, effect of prestrain above Md temp. on Ms temp. 78−80543
Fe-Cr-Ni-Cu-Sn, Cu and Sn effect on Cr and Ni segregation *(German)* 78−72777
Fe-Cr-Ni-Mn-Mo, liquid, N_2 solubility 78−44087
Fe-Cr-Ni-Mo-V, Mo and V effects on segregation *(German)* 77−55942
Fe-Cr-Ni-P-C, amorphous, stress corrosion cracking 77−25123
Fe-Cr-Ni-Si, sintered, carbide coated, crack propag. energy in impact bending 79−66162
Fe-Cr-Ni-Ti-Al, superalloy, Ti, Ni, Al, H_2 variations effect on mech. props. 78−3188
Fe-Cr-Ni(Mn)(Ni-Mn)-C alloy, carbide-austenite equilibria, 1173 to 1373K, microscopic and X-ray obs. 78−44085
Fe-Cr-O system, phase relations at 1200°C using diffusion couple technique 80−89205
Fe-Cr-O-C, stability diagrams, characteristics and calc. 79−10917
Fe-Cr-P-C, amorphous, corrosion resist. in 1N HCl 78−80678
Fe-Cr-P-C amorphous alloys, mag. props. 77−16055
Fe-Cr-P-C sputtered amorphous films, mag. props. and corrosion resist. 79−28567
Fe-Cr-Pd, electrospark coating on alloys, corrosion resist. increase *(Russian)* 78−27669
Fe-Cr-Pd, Pd alloying effects on passivation 80−35373
Fe-Cr-Si, heat resistive films prepared by sputtering, lifetime meas. 80−80132
Fe-Cr-Si, oxidation resist. in high pressure CO_2, Si effect 80−66704
Fe-Cr-SiC-B_4C powder mixture, compressibility and elec. cond. in cold pressing under low press. 78−60609
Fe-Cr-Ta, eutectic alloy, exam. of eutectic temp., composition, and oxidation resistance 78−52767
Fe-Cr-Ti (18, 0.1-0.9 wt.%), high temp. oxidation *(Japanese)* 80−71806
Fe-Cr-Ti-Mo, sintered, mech. props. *(French)* 79−91726
Fe-Cr-Ti-Mo ferritic alloy, annealed, cold rolled, fast reactor material, mech. props. 78−21646
Fe-Cr-Ti-Mo-TiO_2 (13, 3.5, 1.5, 2 wt.%) dispersion hardened, void swelling 80−65046
Fe-Cr-Ti-TiO_2 (13, 2.5, 2 wt.%), dispersion hardened, ferritic alloy DT02, oxidation, 823 to 1123K 79−61803
Fe-Cr-Ti(Al) liquid alloy, thermodynamical anal. of O_2 solubility *(Russian)* 80−92676
Fe-Cr-V-C, X-ray microanal. of carbide phases rel. to V conc. *(Russian)* 78−88467
Fe-Cr-W-C, carbide/austenite equilibria, expt. and thermodynamic study 77−36459
Fe-Cr-Y, Y addition effect on high temp. oxidation resistance *(Japanese)* 79−70223
Fe-Cr-(C), oxidation, grain size and growth effects *(Japanese)* 77−48583
Fe-Cr-(Co), decomposition of solid soln. in mag. field, neutron and X-ray diffr. study *(Russian)* 78−68694
Fe-Cr(-Mo), passivated single crystal, selective dissolution and surface enrichment 80−16543
Fe-Cr(Cr-Ni)(Cr-Ni-Mo)-Al, liquid, N solubility, AlN precipitation 79−11630
Fe-Cr(Ni), use of electrochemistry in understanding $\alpha\rightleftarrows\gamma$ transform., interstitials role *(French)* 77−63662
Fe-Cr(Ni) surface alloys, corrosion resistant, formation by ion implantation 79−28009
α-Fe-Cr(V)(Ti)(Mo)(W), morphology and growth kinetics of δ-eutectoid produced by carburisation 77−16618
Fe-Cr(W)-M, (M=Si,Mo,Ni,Mn,P,Cr), cellular growth of S-pearlite formed by carburisation 80−108486
Fe-Cr(100) and (110) surfaces, lateral lattice spacings, simultaneous LEED and AES 77−20174
Fe-Cr(100) and (110) surfaces, initial oxidation stages, simultaneous LEED and AES obs. 77−20175
Fe-Cr(6 to 9 wt.%), transform. study during ($\alpha+\gamma$) region reversion *(French)* 77−59780
α-Fe-Cu, coordination fields of crystal struct., rigid-sphere model 78−47266
Fe-Cu, dilute, coercive field, initial permeability and relax. loss, non-mag. impurity effect 77−69628
Fe-Cu, generation of self-consistent Gibbs energy functions 79−11565
Fe-Cu, lath martensite habit planes, TEM study 80−84942

iron alloys continued
γ-Fe-Cu, lattice and grain boundary diffusion of Cu 79−23765
Fe-Cu, liq., thermodynamic characts. calc. *(Russian)* 80−15264
Fe-Cu, liquid phase sintering 80−16232
Fe-Cu, mag. moment distrib., elastic neutron scatt. obs. 79−78340
Fe-Cu, modulated microstruct., continuous cooling effect, hardness and electron microscope obs. 79−87665
Fe-Cu, precipitation hardening of α-Fe containing weak and strong particles 80−20946
Fe-Cu, protective coating on Al powder *(Russian)* 78−60881
Fe-Cu, sintered compacts, cooling effect on strength 77−73293
Fe-Cu, thermodynamic analysis of phase relationships 77−73260
Fe-Cu, vapour-deposited struct. and thermal stability 78−43265
Fe-Cu (0.34 wt.%), neutron irradiated, field-ion microscope detection of ultra-fine defects 79−42116
Fe-Cu (1.2 wt.%) effect of precipitation on recrystallisation, texture 78−88476
Fe-Cu (1.77%) alloy, influence of neutron irrad. on electric resist. *(Russian)* 79−38041
Fe-Cu (2 wt.%), furnace cooled, ageing and steam oxidation 78−23744
Fe-Cu (30 wt.%) alloy, dendrite remelting during isothermal holding, microspin obs. *(Japanese)* 78−71836
Fe-Cu (4.54 wt.%) alloy, scaling behaviour, 700-1000°C, 1 atm. O_2 80−93679
Fe-Cu (75 ppm), internal oxidation, local struct. determ. by EXAFS 80−25916
Fe-Cu alloy, effect of ε-Cu phase on strain ageing *(Japanese)* 80−7582
Fe-Cu alloys, transform. substruct., lath microstructure after quenching 80−16298
Fe-Cu clusters, mag. interaction, Mossbauer study 79−82895
Fe-Cu liquid alloy, heats of mixing, mixing entropies *(Russian)* 80−65224
Fe-Cu metastable dil. alloy film, hyperfine interactions 78−52398
Fe-Cu pseudoalloy, contact corrosion in tropical marine environment 78−11422
Fe-Cu-C, mixed powder compact, sintering mechanism 78−15343
Fe-Cu-C, phase equilibria, 950 to 1500°C 80−60836
Fe-Cu-C sintered porous materials, machinability 80−66457
Fe-Cu-C sintered with added S, thermophys. props. 79−61541
Fe-Cu-C-O(-Ni) powder, atomized, reduction and decarburizing annealing parameters 80−25603
Fe-Cu-D, ion implanted, D trapping, 90-500K 80−15131
Fe-Cu-Ni, austenite to ferrite+precipitate reaction, TEM/STEM study 80−3075
Fe-Cu-Ni, Ni effect on austenite decomposition 80−3048
Fe-Cu-Ni (2, 5 wt.%), interphase precipitation obs. in assoc. with Widmanstatten ferrite lateral growth 80−40365
Fe-Cu-Ni (2,2 wt.%), isothermally transformed, precipitate orientations 80−50640
Fe-Cu-Ni-Cr_3C_2-C based sintered friction material, wear, surface geometry and struct. effects 80−25875
Fe-Cu-Ti, improvement of irradiation-enhanced Cu embrittlement by Ti addition 79−43393
Fe-Cu-Zn, high-temperature phase diagrams *(German)* 80−108390
Fe-Cu(-C), alloyed with graphitising elements, geometrical thermodynamics *(Russian)* 79−52261
Fe-Cu(Al,Si,Sr,Ni,Mo,W) powder based composite, high temp. strength of W reinforcing fibres 79−70021
Fe-Cu(Zn)(Sn)(Sb)(Au), dil. size effects on mag. hyperfine fields at non-mag. impurities 78−43586
Fe-Cu(2, 4 and 6 wt.%), sintered, precipitation hardening 77−66653
Fe-D, ion implanted, D trapping, 90-500K 80−15131
Fe-Dy, dil., implanted impurity hyperfine interaction 78−68417
Fe-Eu, dil., hyperfine interaction of ^{153}Eu, Mossbauer effect meas. 78−43703
α-Fe-Fe_3C alloys, ground surface layer exam. of props. 78−84840
Fe-Fe_xSb, directionally crystallised eutectic, influence of prolonged annealing on microstructs. and props. *(Russian)* 79−74182
Fe-Ga, constitution between 10 and 50 at.% Ga, heat treatment depend., BCC phases *(German)* 77−90325
Fe-Ga, Mossbauer effect for phase transitions, 20-720°C, 25.7-28.3 at.% Ga *(German)* 78−68437
Fe-Ga, phase constitution depend. on heat treatment, phase diagram *(German)* 78−39748
Fe-Ga, solid soln., order-disorder transform. *(French)* 78−3121
Fe-Ga, volume change during solid state transformation *(German)* 78−84802
Fe-Ga (25 at.%), precipitation *(French)* 77−70057
Fe-Ga (up to 50 at.%), liq., elec. resist., 1200-1800°C *(Russian)* 78−6341
Fe-Ga-C melts, thermodynamics and C solubility *(Russian)* 80−39292
Fe-Gd amorphous film, struct. and mag. props. 80−20439
Fe-Gd amorphous films with comp. gradient, volume and surface hysteresis *(Russian)* 78−88148
Fe-Gd film, amorphous, mag. props., mean field analysis 78−64236
Fe-Gd film, amorphous, O_2 contamination effects on mag. props. 78−64231
Fe-Gd film, magneto-optic coeff., and refr. index, ellipsometric determ. 80−71501
Fe-Gd films, crystallisation, electron microscope obs. 79−15034
Fe-Ge, amorphous, atomic struct., neutron diffr. study 80−59392
Fe-Ge, characteristic energy losses and optical props. 80−29834
Fe-Ge, liquid alloy, thermodynamic mixing function determ. by mass spectrometric meas. 79−29025
β-Fe-Ge, mag. props. from X-ray, magnetisation and Mossbauer meas. 79−42755
Fe-Ge (10 to 50 at.%), phase diagram rel. to heat treatment, supercooling diagram *(German)* 78−92240
Fe-Ge amorphous alloys, radial distrib. funct., electron diffr. exam. 77−68922
Fe-Ge amorphous films, conversion electron Mossbauer spectra, mag. moments 77−16231
Fe-Ge melts, struct. determ. 79−41940
Fe-Ge system, cryst. growth forms and interface struct. 79−61515
Fe-glass-Cu sintered material, Cu effects on strength 77−77443
Fe-H, recovery of hydrogenated and quenched alloy, solute diffusion 77−77510
Fe-H, Snoek-Koster peak of internal friction, Schoeck model *(Polish)* 79−96076
Fe-H system, cold work internal friction peak, appl. of Schoeck's model 78−95771

iron alloys continued
Fe-H system, influence of H press. on Fe crit. points and H solubility 78−52758
Fe-H system, specific heat 7 to 60K 79−99332
Fe-Hl (Si) (Ti) (V), molten, gaseous O_2 absorption 80−11836
Fe-In, dil., hyperfine field of In, clustering effect, nucl. orientation obs. 77−16188
Fe-In, superconducting Kondo alloys and alloys with strong electron-magnetic impurity interaction, EM absorpt. of light 80−39711
Fe-Ir, hyperfine field distrib., spin echo NMR meas. 78−76351
Fe-K(Ca)(Ti), dil., mag. hyperfine field, TDPAC meas. 78−43699
Fe-La, Fe-rich alloys, mag. props. for bulk amorphous deposits *(Japanese)* 79−95971
Fe-La(Zr) amorphous films, mag. props., Mossbauer effect and magnetisation meas. 79−69701
Fe-M, (M=Cr,W,Mo,V,Ti), morphology and growth kinetics of δ-pearlite formed by carburisation 80−108485
Fe-M, dil., M=transition metal, impurity electronic struct., multiple scatt. approach 80−92856
Fe-M-SiO_2 (M=Ru,Pt), supported catalysts, Mossbauer spectra 80−11296
Fe-M-(I) (M≡Ni, Cr, V, Ti, Mo; I≡Sb, P), co-segregation at free surfaces studied by Auger spectroscopy 80−59767
Fe-Mg, Burgers vector determ., crystal defect observation by weak beam image *(Japanese)* 79−82130
Fe-Mg, cast ferrite-based, graphite nucleation on surface *(Russian)* 80−40360
Fe-Mn, annealed, α-γ phase transformation obs. 78−75831
γ-Fe-Mn, antiferromag., mag. and crystallographic transformations 77−55964
Fe-Mn, as cast, pseudo-composite struct. resulting from interdendritic segregation, cryogenic materials appl. *(French)* 80−93556
Fe-Mn, BCC, ferromag., spin wave stiffness constant 78−91851
Fe-Mn, dil. alloy, mag. moment distrib., temp. depend., diffuse polarised neutron scatt. study 79−47250
Fe-Mn, dilute, short-range ordering and segregation ascending diffusion *(Russian)* 77−24406
Fe-Mn, dislocation mobility and internal friction, effect by alloying in α-Fe *(Russian)* 77−31671
Fe-Mn, effect of N on cryst. lattice parameter of austenite *(Russian)* 78−67683
Fe-Mn, electron redistrib. and BCC struct. stability, Mossbauer meas. *(Russian)* 79−42873
Fe-Mn, electron state density and elec. resist. 80−39558
Fe-Mn, ε-martensite, preferred orientation and constitution, reverse pole figures *(Russian)* 80−104178
Fe-Mn, FCC to HDP transform. 79−61581
Fe-Mn, γ to α transition on cooling, struct. and microhardness investig. *(Russian)* 77−44246
Fe-Mn, γ to ε phase transform. induced by high press. and plastic deform. 78−68686
Fe-Mn, high-temp. sulphidation, scale struct., corrosion kinetics 80−50777
Fe-Mn, jump stress relaxation obs. during cooling before martensitic transform. *(Russian)* 79−38884
Fe-Mn, mag. susceptibility and conc. depend. of Neel point *(Russian)* 79−47279
Fe-Mn, martensitic FCC→BCC transform., orientation relation, diffractometric determ. *(Russian)* 77−44240
Fe-Mn, mechanical twinning of close-packed hexagonal ε-phase during plastic deform. *(Russian)* 80−60909
Fe-Mn, Mossbauer spectroscopy of temp. hysteresis of phase transformations *(Czech)* 80−29949
Fe-Mn, Mossbauer study near martensitic transform. temp. 78−3128
Fe-Mn, plastic deformation mechanism, meas. of microplasticity 78−60720
α-Fe-Mn, singularities of martensite struct. *(Russian)* 80−28948
Fe-Mn, splat-quenched, martensite formation obs. 77−44247
Fe-Mn, stacking fault energy, Mn conc. depend. *(Russian)* 77−1836
Fe-Mn, struct. and props., effect of Nb, C and Si alloying *(Russian)* 77−90360
Fe-Mn, thermodynamic props. *(Czech)* 77−85990
Fe-Mn, warm rolled, rel. contribs. of texture and grain shape to props. 79−91705
Fe-Mn 8%, type K1525 thermal cycling, effect on impact toughness 80−7608
Fe-Mn (-C), Mn influence on martensitic transform in presence of strain *(Russian)* 80−20934
Fe-Mn (0.5 wt.%), Burgers vector of dislocation determ. by weak-beam image in HVEM 80−103351
Fe-Mn (1 at.%), strain age hardening 80−108472
Fe-Mn (10 to 14 at.%), martensitic transforms., dilatometric effects and X-ray diffr. meas. *(Russian)* 78−6922
Fe-Mn (12% Mn), decomposition during plastic deform., Mossbauer parameters *(Russian)* 77−36166
Fe-Mn (14.1 wt.%), G14, α-martensite formation in mag. field 79−91648
Fe-Mn (15(24)(30)wt.%), high hydrostatic pressure influence on stress-strain curve 80−25805
Fe-Mn (18.6 wt.%), HCP-FCC martensitic transform., Mossbauer effect meas. 78−44121
Fe-Mn (2 to 8 wt.%) alloys, phase transformations, tempering influence *(Russian)* 80−25735
Fe-Mn (22 wt.%), ε→γ transformation, effect of H_2 pressure up to 23 kbar on transition temp. *(Russian)* 79−24517
Fe-Mn (3 wt.%), Sn diffusion along grain boundaries, micro-Auger spectroscopy 77−11740
Fe-Mn (8 wt.%), quenched, exam. of intergranular embrittlement 78−76745
Fe-Mn (8.25 wt.%), irreversible temper embrittlement, Mossbauer spectra, impact strength depend. on interstitials *(German)* 79−74235
Fe-Mn (9 to 20 wt.%), ^{57}Fe Mossbauer spectroscopy in phase transformations 80−29948
Fe-Mn (up to 8 wt.%), microstructure, mech. props. and fracture *(Japanese)* 80−35304
Fe-Mn alloy, magnetovolumetric anomaly *(Russian)* 78−64248
Fe-Mn alloys, α, ε and γ, brittleness 80−35314
Fe-Mn alloys, elasticity modulus anomaly and magnetoelastic effect *(Russian)* 79−28578
Fe-Mn alloys, high-purity, martensitic transform., heat treatment effect 79−56979

iron alloys continued
Fe-Mn alloys, quantitative phase anal., correction factor for texture 79−52528
Fe-Mn base alloy, mag. preferred directions 78−39370
Fe-Mn cast alloys, homogenisation annealing and chemical diffusion *(Czech)* 80−66551
Fe-Mn mag. contributions to γ→ε phase transformations 80−25694
Fe-Mn-As, crystal struct. and magnetic props. of intermetallic cmpds. with Cu_2Sb type struct. *(Japanese)* 78−59785
Fe-Mn-B, B effect on intergranular embrittlement 80−108555
Fe-Mn-C, anomalous changes in austenite and martensite lattice parameters 80−50636
Fe-Mn-C, atomic interaction structure in carbides 78−42955
Fe-Mn-C, austenitic, strain induced γ to ε transform., active slip systems 77−48427
Fe-Mn-C, cast iron and steel, Mn effects on struct. 78−23696
Fe-Mn-C, γ→ε→α′ martensitic transform. 79−24523
Fe-Mn-C, lattice parameters of cementite, annealing effect 80−29007
Fe-Mn-C, martensitic transform., Mossbauer obs. *(Russian)* 78−6927
Fe-Mn-C, struct. superplasticity 80−76317
Fe-Mn-C, structural var. during warm deform. in γ→ε transform. region *(Russian)* 77−81293
Fe-Mn-C, thermodynamic analysis 77−32563
Fe-Mn-C, variation of martensite morphology with Mn and C composition 80−50635
Fe-Mn-C (0.7, 0.9 wt.%), pearlitic, deform. 77−86095
Fe-Mn-C (11.5, 0.2 to 1.6 wt.%), water quenched, effect of C on phase composition, abrasion, plasticity *(Russian)* 78−35445
Fe-Mn-C system, Gibbs energy, high temp. phase relations 78−80779
Fe-Mn-C system, isothermal sections, 873 to 1373K, computer plotting 78−6893
Fe-Mn-C-Si alloy, G20 type, vol. effects during γ→ε transform., lattice parameters of γ-and ε-phases, Si and Mn effects *(Russian)* 78−6918
Fe-Mn-C-Si alloy G20, effect of Si and Mn additions on phase composition in multiple γ⇄ε transitions *(Russian)* 78−95743
Fe-Mn-Co-Ni-Cr, antiferromag. props., Neel temp. determ. 78−88124
Fe-Mn-Cr-C, twinning and strain induced FCC to HCP transform. 77−44248
Fe-Mn-Cr(Ni), mag. and crystallographic transformation depend. on Cr-Ni addition *(Russian)* 79−83334
Fe-Mn-Cu-C, Cu effect on ε′-martensite, X-ray obs. of heating effects *(Russian)* 79−87667
Fe-Mn-Mi, martensitic, morphology and substruct. study 77−70059
Fe-Mn-Nb-V, high Mn, dispersion strengthening 77−16602
Fe-Mn-Ni, age hardenable, struct. and strength 77−52339
Fe-Mn-Ni, fracture toughness, thermomechanical treatment effects 78−60794
Fe-Mn-Ni antiferromag. alloy, neutron scatt. exam. of antiferromagnons 77−66283
Fe-Mn-Ni base maraging alloys, age hardening 79−74170
Fe-Mn-Ni-C, age hardenable, struct. and strength 77−8844
Fe-Mn-Ni-V-C (0.5, 3.0, 1.0, 0.2 wt.%), austenite decomp., isothermal transform. characts. 80−97477
Fe-Mn-O, phase equilibrium diagram *(German)* 78−15355
Fe-Mn-O melts, formation of oxide inclusions, cryst. pulling, Bridgeman tests *(German)* 80−35074
Fe-Mn-P-B-Al metallic glass, exchange anisotropy 77−16068
Fe-Mn-PBAl, amorphous mixed mag. system, resist. minima 79−60784
Fe-Mn-S, thermodynamics, activity of FeS-MnS solid soln., 1100 to 1400°C 78−6902
Fe-Mn-S, thermodynamics, solid/liquid phase equilibria, 1100 to 1300°C 79−47663
Fe-Mn-S, thermodynamics, solubility of S and Mn in γ-Fe, 1100 to 1300°C 79−47662
Fe-Mn-Sb, phase comp. 80−16267
Fe-Mn-Ti alloys, austenitic, precipitation strengthened 80−25714
Fe-Mn-Ti-Al, magnetic texture rel. to annealing temp., Mossbauer investig. 77−28499
Fe-Mn-V-C (0.5, 1.0, 0.2 wt.%), austenite decomp., isothermal transform. characts. 80−97477
Fe-Mn-V-C austenitic steel, discontinuous precipitation, morphological changes 80−3078
Fe-Mn-Zn, high-temperature phase diagram *(German)* 80−108390
Fe-Mn(Ni) systems, struct. defects effect on interdiffusion 80−15314
Fe-Mn(Sb)(Sn), additive effect, on eutectoid transformation of Fe 78−52799
Fe-Mn(0 to 80 wt.%), paramagnetic susceptibility by Faraday method, band model interpretation *(Russian)* 77−20545
Fe-Mo, carburised, austenite-carbide colonies struct. *(Russian)* 79−52449
Fe-Mo, cryst. struct. and defects, high resolution electron microscopy obs. 79−94961
Fe-Mo, damping capacity 77−86082
Fe-Mo, damping capacity *(Japanese)* 78−11259
Fe-Mo, dislocation mobility and internal friction, effect of alloying in α-Fe *(Russian)* 77−31671
Fe-Mo, ferritic, thermodynamics and solubility of C and ferrite 77−36456
Fe-Mo, hyperfine field distrib., spin echo NMR meas. 78−76351
Fe-Mo (0 to 6 wt.%), in chloride solns., role of Mo as localised corrosion inhibitor 79−20255
Fe-Mo (0.54 to 2.50 wt.%) ferromag. ordering effect on Fe diffusion *(Czech)* 77−62665
Fe-Mo (13-20 at.%) binary alloys, spinodal decomp. on ageing, TEM and X-ray diffr. study 80−97503
Fe-Mo (15.5 and 19.5 at.%), modulated struct., heat treatment effects, TEM obs. 79−100192
α-Fe-Mo (1.5 and 1.8 at.%), deform., testing mode effect at stages prior to steady states 77−66721
Fe-Mo (1.8 at.%), high temp. creep mech., use of stress exponent 79−5025
Fe-Mo (1.8 at.%), recovery creep theory estimation using high temp. creep data 79−15747
Fe-Mo (1.8%), creep, absence of instantaneous plastic strain upon stress changes 78−75718
Fe-Mo (3 wt.%), substitutional solid soln. with cubic faced symmetry, Portevin-Le Chatelier effect *(French)* 78−23785
Fe-Mo (3at.%), internally nitrided, precipitate, morphology and chemistry 78−44128
Fe-Mo (4.1 wt.%), substructs. developed during steady state creep at 1100-1200K, TEM obs. *(Japanese)* 79−38900

iron alloys continued
Fe-Mo (5 wt.%), Auger anal. of passive films in neutral aqu. soln. 80−16605
Fe-Mo alloy, TZM, doped, Ni activated recrystallisation, ion probe mass spectrometer obs. 77−44280
Fe-Mo alloys, pitting 80−16549
Fe-Mo alloys, spinodal decomp. and modulated struct. form. on ageing *(Japanese)* 79−100184
Fe-Mo austenite, thermodynamics of C 77−36457
Fe-Mo catalyst, Mossbauer spectra 80−7222
Fe-Mo doping surfaces of Fe with Mo under laer emission *(Russian)* 77−70211
Fe-Mo quenched alloy, electron microscope exam. of planar defects 79−79000
Fe-Mo system, self-diffusion 77−4214
Fe-Mo system, thermomech. props. 80−89208
Fe-Mo systems, galvanic cell meas., 1160 to 1366K 78−61042
Fe-Mo-Au, orienting of precipitating Au particles by external elastic stress 77−73279
Fe-Mo-B metallic glass ribbons, tensile strength, crystn. temp. 80−89173
Fe-Mo-C, eutectoid transform. of δ-ferrite 77−16570
Fe-Mo-C, lattice parameters of cementite, annealing effect 80−29007
Fe-Mo-C (0 to 4, 1 wt.%), phase equilibria at 1143, 1198 and 1253K 80−60835
Fe-Mo-C alloy, splat cooling, microstruct. changes 78−84855
Fe-Mo-C amorphous alloys, Mo effect corrosion resistance in HCl *(Japanese)* 79−96214
Fe-Mo-C system, isothermal sections, 973 to 1273K, thermodynamic analysis 78−6895
Fe-Mo-CaF_2 sintered composite, struct. and mech. props., heat treatment effect 80−66526
Fe-Mo-Cr alloys, creep tests *(German)* 79−61648
Fe-Mo-Cr(Ni)(Mn)-C, carbide-austenite equilibria, 1173 to 1373K, microscopic and X-ray obs. 78−44085
Fe-Mo-P, P-induced temper embrittlement, Mo role 80−35316
Fe-Mo-P-C, amorphous, corrosion resist. in 1N HCl 78−80678
Fe-Mo-P-C, amorphous, XPS study of passivity 79−96185
Fe-Mo-Ta, ternary Laves phase strengthening 80−108466
Fe-Mo-(C)-(Ni), sintering 78−35333
Fe-Mo(V), nitrided by const. activity ageing, X-ray studies 77−32720
Fe-Mo(W), semihard magnetic alloys, magnetic, elec. mech. props. *(Japanese)* 79−70078
Fe-Mo(4.1 wt.%), steady state creep at high temps. 80−89316
Fe-MuS eutectics, unidirectional solidification *(German)* 80−100827
Fe-N, BCC, solution hardening and softening 77−12635
Fe-N, hexagonal, ferromag. Mossbauer spectroscopy 77−63331
Fe-N, neutron irrad. effects on mech. props. 79−4338
Fe-N, nucleation and precipitation growth on dislocations, electron microscope studies 80−3064
Fe-N, precipitated $Fe_{16}N_2$ nitride distrib. during isothermal ageing 77−21143
Fe-N, single cryst., solid soln. softening, effect of interstitial N 80−97496
α-Fe-N, supersaturated solid solns., N atom precip. kinetics, resist. meas. 80−60864
Fe-N (0.022 wt.%), quenched, N precipitation during isothermal ageing 77−28820
Fe-N (0.03 at.%), single cryst., stress distrib. around spherical inclusion, TEM study 79−34038
Fe-N (10 at.%), structural transforms., expt. investig. *(Russian)* 77−12613
Fe-N alloy, dil., galvanomag. effects, 4.2-250K 78−87964
Fe-N alloys, secondary ion emission, phase transforms. effect *(Russian)* 80−66347
Fe-N single crystals, plastic deform. in temp. range 4.2 to 300K 80−76321
Fe-N single crystals, solid soln. stress assisted nucleation of α″ precipitates 78−52810
α-Fe-N solid soln., N precipitation kinetics, defects effect 77−59789
Fe-N system, spattering phenomenon during arc melting 79−39053
Fe-N(C), solid soln., metastable and stable, interstitial atom config. 77−36512
Fe-N(0.013 wt.%), effect of electron irradiation on precipitation 79−52221
Fe-Nb, mag. and Mossbauer meas. 77−63133
Fe-Nb (3.1 wt.%), semihard mag. alloy, Recalloy, mag. props., elec. cond. *(Japanese)* 78−10723
Fe-Nb creep resistant alloy, precipitate free zones elimination 80−16312
Fe-Nb-C (0.04, 0.02 wt.%), strengthening, hot rolling *(Chinese)* 79−100154
Fe-Nb-V-C-N, equilibrium comp. and solubility in steels, model of ideal solns. *(Russian)* 80−60832
Fe-NbC, exam. of phase diagram, and mech. props. *(Russian)* 79−20028
Fe-Nb(Ta)-Co, Recalloys, semihard mag. alloys, mag. and elec. props., hardness, thermal expansion *(Japanese)* 79−5066
Fe-Ni, (10 at.%), magnetisation in high mag. field, Arrott-Noakes plot 80−54919
Fe-Ni, alloy, composition determination using secondary ion emission *(French)* 77−86409
Fe-Ni, alloy 20N24, martensitic, exam. of structure after laser treatment, and recrystallisation *(Russian)* 79−11608
Fe-Ni, and Fe-Ni-Cr alloys, preferential sputtering, XPS expts. 79−87544
Fe-Ni, arc electrode processes, thermodynamic approach *(Russian)* 77−27755
Fe-Ni, atomic valence states, ferromag. props. *(Ukrainian)* 78−2656
Fe-Ni, austenite formed from martensite during annealing in (α+γ) region, crystallographic study 78−19782
Fe-Ni, α to γ transformation, changes in Young's modulus and electrophysical props. *(Russian)* 79−20042
Fe-Ni, α→γ conversion, electron microscope and X-ray spectral microanal. 79−78966
Fe-Ni, α→γ transform., role of grain boundary diffusion, Mossbauer obs., homogenisation effect *(Russian)* 79−52197
Fe-Ni, BCC, cyclic cleavage crack growth model for fatigue 80−55519
Fe-Ni, BCC, ferromag., spin wave stiffness constant 78−91851
Fe-Ni, brittle transgranular and intergranular fatigue crack growth rate, yield strength effect 78−68786
Fe-Ni, carburization, methane gas→C(dissolved)+$2H_2$ (gas), kinetics 80−55712

iron alloys continued
Fe-Ni, coercive force depend. on grain struct. and inclusions 77−20635
Fe-Ni, cryst. growth from melt, distrib. of growth directions 79−33924
Fe-Ni, crystallisation temp., overcooling temp. *(Russian)* 80−97472
Fe-Ni, crystallization texture, rolling, effect of impurities 78−15425
Fe-Ni, DC arc plasma, meas. of conc. ratio of component atoms *(Russian)* 77−27754
Fe-Ni, deposition of layers from carbonyl vapour 77−4727
Fe-Ni, dil., point defect relax. after low temp. neutron irrad. 78−52316
Fe-Ni, dilute, irradiation softening effect on yield stress 80−76319
Fe-Ni, effect of electron irradiation and deform. on martensitic transform. 77−16581
Fe-Ni, effect of plastic deform. and martensitic transformation on Fe atom mobility *(Ukrainian)* 78−55974
Fe-Ni, elect. phenomena rel. to martensitic avalanche *(French)* 78−68691
Fe-Ni, electrical resist., 1000 to 1700°C *(Russian)* 77−85193
Fe-Ni, electrodeposition, mag. props. *(French)* 78−64488
Fe-Ni, electrolytic film, coercive force depend. on electroplating conditions *(French)* 77−55691
Fe-Ni, electronic struct., XPS study 80−29842
Fe-Ni, electronic struct. calc., effects of chemisorption; contact pot. and surface magnetisation 80−103734
Fe-Ni, elinvar comp., props. of materials used in electromechanical filter resonators *(Czech)* 80−76318
Fe-Ni, enthalpy of transform. of $\bar{\gamma}$ to α' and α' to γ transforms. *(French)* 79−47683
Fe-Ni, exam. of mech. adhesion, with vitreous coating 79−20336
Fe-Ni, FCC, anomalous props. at high temp. and new phase *(Japanese)* 78−80520
Fe-Ni, FCC, elastic props. and stability near martensitic transform. temp. *(Russian)* 78−6921
Fe-Ni, FCC alloy, magnetovolume instability 79−8031
Fe-Ni, FCC alloy, thermoelec. power, anomalous conc. depend. at high temp. 79−4548
Fe-Ni, FCC and BCC lattices, X-ray characteristic temp. *(Russian)* 78−67797
Fe-Ni, fatigue crack propag., low temp. 80−35311
Fe-Ni, fcc alloys, spin wave energy calc. 79−87247
Fe-Ni, $Fe_{65}(Ni_{1-x}Cr_x)_{35}$, low-temp. elec. and galvanomag. props. rel. to mag. boundaries *(Russian)* 77−35910
Fe-Ni, ferro-nickel oxidation, appl. of mag., thermomag. methods *(French)* 79−20318
Fe-Ni, ferromagnetic films, domain boundary creep relaxation effects *(Russian)* 79−82840
Fe-Ni, film, depth profiles, sputter etching obs. 79−83079
Fe-Ni, first order displacive transformations, localized soft modes and US effects 79−73281
Fe-Ni, fracture toughness of cryogenic temp. 78−72878
Fe-Ni, grain boundary segregation, X-ray microanal. by STEM 80−66740
Fe-Ni, Hall effect, anomalous, residual coeff. calcs. using coherent pot. method *(Russian)* 80−80249
Fe-Ni, hardening by plastic deform. during polymorphic transform., struct. mechanics for γ-phase form. *(Russian)* 77−90344
Fe-Ni, hardening by plastic deform. during polymorphic transform., mechanical props. *(Russian)* 77−90345
Fe-Ni, hot shortness *(Japanese)* 78−84998
Fe-Ni, hydrogenated, Mossbauer effect meas. 78−92002
Fe-Ni, hyperfine field distrib., temp. and press. depend. 78−91651
Fe-Ni, influence of hydrogen press. on temp. of martensitic transform. *(Russian)* 78−27514
Fe-Ni, interference microscopy, for colour development and phase separation 80−100976
Fe-Ni, internal friction study, tempering effects *(French)* 77−81286
Fe-Ni, Invar alloy, explanation of phys. anomalies *(Russian)* 78−88112
Fe-Ni, ion-implanted, depth profile and diffusion coeff. 80−54277
Fe-Ni, lenticular martensite growth by transformation wave propag. 80−81055
Fe-Ni, liq., thermodynamic characts. calc. *(Russian)* 80−15264
Fe-Ni, liq. alloy, electrochem. meas. of O, thermodynamic props. at 1873K 80−30244
Fe-Ni, liquid, solubility of H, 1400 to 1800°C 77−1231
Fe-Ni, liquid and solid, thermochem. props. 77−59755
Fe-Ni, local environment effect on at. mag. moment 79−82763
γ-Fe-Ni, local magnetisation of Fe atoms, Mossbauer effect meas. 80−75891
Fe-Ni, local ordering, neutron scatt. study 78−64193
Fe-Ni, low frequency power losses 78−95466
Fe-Ni, low-noise, for cores of ferromag. probes and mag. modulators 79−8017 .
Fe-Ni, magnetic ordering, effect on diffusibility, penetrability and solubility of H_2 *(Russian)* 77−24435
Fe-Ni, magnetisation calc. method based on moments of density of states 80−65770
Fe-Ni, martensite burst transformation, supercooling 78−84806
Fe-Ni, martensitic transform. dynamic, quasi-static atomic displacements, NGR, X-ray and electron scatt. meas. *(Russian)* 78−68688
Fe-Ni, martensitic transformation, microscopic mechanism *(Russian)* 79−34036
Fe-Ni, mechanisms of EM generation and detection of US Lamb waves 78−39382
Fe-Ni, metallic glass, mag. props. *(German)* 79−51813
γ-Fe-Ni, Mossbauer exam. 79−56640
Fe-Ni, N27T2 and N28, internal friction peaks after reverse martensitic transform. *(Russian)* 78−92287
Fe-Ni, optical and electronic characts., 20-1750°C, comp. depend. *(Russian)* 78−84601
Fe-Ni, ordered, low temp. α→γ transform. *(Russian)* 78−19740
Fe-Ni, ordered, tetragonal, identification with clear taenite in meteorites 80−8604
Fe-Ni, ordered phase, Llo superstruct., Mossbauer spectrum, Debye-Scherrer pattern from LL-chondrite 80−50241
Fe-Ni, oxidation, Mossbauer spectroscopy, metallography, SEM and X-ray diffr. anal. 78−15577
Fe-Ni, permeability and coercive force, effect of thermomag. treatment in rotating field *(Russian)* 77−21294
Fe-Ni, point defect form. at high temps. *(Russian)* 79−86787
Fe-Ni, quenched irreversible alloy, zero or negative thermal dilatation 79−4419

iron alloys continued
Fe-Ni, reactive metal alloy, effects of thermomechanical processing on strength and toughness 79−70112
Fe-Ni, reference material for determ. of C activity, interaction parameter *(Czech)* 79−42278
Fe-Ni, reverse martensitic transform., prior deform. effect 77−63668
Fe-Ni, reverse martensitic transform., shape deform. reversibility 80−66506
Fe-Ni, reversibility of crystal orientation in reverse martensitic transformation 79−83199
Fe-Ni, secondary recrystallization *(Czech)* 79−70080
Fe-Ni, secondary recrystallisation singularities *(Russian)* 80−66528
Fe-Ni, secondary recrystn. and mag. props. 80−89247
Fe-Ni, segregation of ^{121}Sb, Mossbauer spectroscopy 79−47698
Fe-Ni, segregation of inhomogeneities during crystallisation *(Russian)* 78−27521
Fe-Ni, sintered, porosity determ. by US attenuation and sound vel. meas. *(German)* 80−76437
Fe-Ni, slip and twinning, SEM and optical obs. 79−71209
Fe-Ni, solid and liquid, determ. of activities for temp. range 1500-1900K, using mass spectroscopy 79−11558
Fe-Ni, sputtered using Hg^+ and Ar^+ beams, variation as function of ejection angle, AES exam. 77−44105
Fe-Ni, strain energy controlled shape of cryst. forming due to martensite transform. or decomposition 78−38648
α-Fe-Ni, struct. after polymorphic transform. under press. *(Russian)* 80−29946
Fe-Ni, surface comp. obs. by AES 78−10266
Fe-Ni, taenite, superstruct. in Fe meteorites 78−61820
Fe-Ni, thermal conductivity, data anal. and synthesis 78−95284
Fe-Ni, thermal diffusivity during martensitic and austenitic transform. *(French)* 77−59781
Fe-Ni, thermal expansion, ferromagnetic-paramagnetic transition *(Russian)* 80−54412
Fe-Ni, thermodynamic props., anomalous 80−39313
Fe-Ni, XPS obs. of Fe 2p states 78−52625
Fe-Ni, XPS of valence electrons *(Russian)* 77−77340
Fe-Ni, yield stress, temp. depend. *(Russian)* 78−56691
Fe-Ni (1 to 5 at.%), mech. props. below 300K *(French)* 79−8314
Fe-Ni (1 wt.%), machine induced residual stress contrib. to pitting susceptibility 79−61784
Fe-Ni (15, 25 at.%), longitudinal forces in the hot torsion test *(German)* 79−38889
Fe-Ni (18 wt.%), martensitic transform., external stress effect *(French)* 78−23707
Fe-Ni (19wt.%), oxidation in CO_2, 700 to 1000°C, kinetics study 78−72931
Fe-Ni (20 to 100 wt.%), exam. of C diffusion coeff., in temp. range 950 to 1100°C 78−51747
Fe-Ni (20 to 31 wt.%), exam. of martensitic transform. and reverse transform. using differential and thermomagnetic resistance analysis *(French)* 79−52214
Fe-Ni (23 wt.%), struct., composition changes during α to γ transform., martensite plastic deformation influence *(Russian)* 80−11642
Fe-Ni (23-35 at.%), cooled below 70K in mag. field, uniaxial anisotropy *(Russian)* 78−19244
Fe-Ni (23.1 wt.%), α to γ transformation, struct., conc, changes, heating rate, residual austenite influence *(Russian)* 79−83194
Fe-Ni (24 wt.%), isothermal decomp., mag. determ. of austenite content 80−20886
Fe-Ni (25 to 50%), FCC, meteorites and thermodynamic equilib., Mossbauer and X-ray diffr. study 80−88087
Fe-Ni (25 wt.%), and single phase, solidified from undercooled melt, mech. props. 77−48540
Fe-Ni (25%), solidification of powder or large ingot, heat losses 77−12612
Fe-Ni (28 at.%), martensitic transformations, Mossbauer scattering evidence of soft modes 80−93223
Fe-Ni (28 wt.%), martensitic reversion, effect of internal stresses *(French)* 77−21142
Fe-Ni (29 at.%), calc. of elastic interaction between locally transformed regions with screw and edge dislocations 78−83844
Fe-Ni (29 wt.%), martensite nucleation at dislocations, elasticity model 80−55393
Fe-Ni (29.3%), N29, martensitic tranform. kinetics and morphology, ordering role 77−63673
Fe-Ni (29.58 wt.%), acoustic absorpt. and emission associated with martensitic transform. 79−34035
Fe-Ni (29.5at%), martensitie transform., pisition lifetime spectra meas. 77−36498
Fe-Ni (3 wt.%), embrittled, microanalysis of grain boundary segregation using STEM 78−35633
Fe-Ni (3 wt.%), grain boundary segregation of Sn and P embrittling additions, STEM microanal. 78−76654
Fe-Ni (3 wt.%), grain boundary segregation microanal. using X-ray (STEM) and AES 78−87685
Fe-Ni (3 wt.%), influence of temper embrittlement, on stress corrosion susceptibility 78−85023
Fe-Ni (3 wt.%), low temp. softening *(German)* 79−29081
α-Fe-Ni (3-12 wt.%), structure and $\gamma \rightarrow \alpha$ polymorphic transform. kinetics 80−71645
Fe-Ni (30 wt.%), Ni segregation singularities during dendrito-cellular solidification *(Russian)* 80−7542
Fe-Ni (31 at.%), austenitic, ageing, absence of at. order 77−11502
Fe-Ni (31 wt.%), thermoelastic martensite obs. 80−3052
Fe-Ni (31 wt.%) alloy, Bridgman grown, cellular to dendritic crystn. transition, morphology and microstruct. *(Russian)* 79−14709
Fe-Ni (31%), deformed by slip, misaligned zones in $\{259\}_A$-martensite crysts. *(Russian)* 77−59850
Fe-Ni (32 at.%), exam. of streaming due to intrinsic fluctuations 79−11602
Fe-Ni (32 wt.%), EMF appearance during $\gamma \rightarrow \alpha$ transform. *(Russian)* 80−89215
Fe-Ni (32 wt.%), electrohydraulic effect and struct. changes *(Russian)* 78−23783
Fe-Ni (32 wt.%), martensitic transform., study by fast electronic amplification *(French)* 77−86028
Fe-Ni (32.3 at.%), mag. struct. in commensurable approx., neutron diffr. study 80−60212
Fe-Ni (32.86, 30.65 wt.%), characts. of quenched struct. formed in textured sheets, TEM and optical microscopy study 79−34084

iron alloys continued
Fe-Ni (33-38 at.%), low-angle neutron diffr., anomalous crit. scatt. *(Russian)* 80−60193
Fe-Ni (33.7 wt.%), γ-phase stability near martensitic transform., shear modulus obs. *(Russian)* 79−4966
Fe-Ni (35 at.%), fine coherent effects, neutron diffr. study *(Russian)* 78−75502
Fe-Ni (35 to 100%), magnetoelastic attenuation of torsional vibr. and shear modulus defect *(Russian)* 77−80982
Fe-Ni (4 wt.%), extrinsic grain boundary dislocations, low C content influence 80−107273
Fe-Ni (47 to 65 wt.%), soft magnetic alloy with crystallographic texture and field induced anisotropy, pulse permeability and excursion rate *(German)* 79−73779
Fe-Ni (50 to 94 wt.%), FCC, form. and migration energy of vacancies, induced magnetic anisotropy *(French)* 78−2110
Fe-Ni (50 wt.%), obs. in Santa Catharina meteorite 79−30024
Fe-Ni (50 wt.%), surface comp. and oxide film thickness after various surface treatments, AES study 80−66693
Fe-Ni (6-8 wt.%), solution of ^{119}Sn, study by Mossbauer spectroscopy 80−75888
Fe-Ni (8 wt.%), monocrystal, thermodynamics of growth, model *(French)* 78−87635
Fe-Ni (9.21 wt.%), oxidation in CO_2 at 700-1000°C 78−44265
Fe-Ni alloy, anisotropic hyperfine interactions, Mossbauer spectra 80−15854
Fe-Ni alloy, anodic oxide film formed in H_3BO_3-$Na_2B_4O_7$ soln., exam. of in depth profile by AES and sputter etching 79−20247
Fe-Ni alloy, α to γ slow transformation mechanism, Ni content influence *(Russian)* 80−7569
Fe-Ni alloy, cellular-dendrite struct., effect of temp. gradient and crystallisation rate on morphological singularities *(Russian)* 78−3115
Fe-Ni alloy, cold work stored energy effect on mag. moment vs. temp. curve 78−95419
Fe-Ni alloy, detection in Santa-Catharina meteorite *(French)* 79−16895
Fe-Ni alloy, diffusivity, heat capacity and thermokinetic behaviour, simultaneous meas. *(French)* 77−1235
Fe-Ni alloy, disordered, short-range order study by time-depend. PAC method 78−6618
Fe-Ni alloy, distillation deoxidation during electron beam melting *(Russian)* 79−70306
Fe-Ni alloy, electropolishing in alcoholic soln. of H_2SO_4 77−16718
Fe-Ni alloy, FCC, high-field susceptibility and spin wave spectrum 79−56493
Fe-Ni alloy, martensitic transform., influence of thermal and electron irrad. treatment of austenite *(Russian)* 80−66509
Fe-Ni alloy, positron lifetime 80−2891
Fe-Ni alloy, rod-shaped martensite→austenite transform, struct. mech. *(Russian)* 77−66636
Fe-Ni alloy, solid solution, vibr. analogue of Bain deform. and morphology of martensite in 78−2224
Fe-Ni alloy, surface decarburisation rate in dry H_2, soft mag. material manufacture 78−60882
Fe-Ni alloy, X-ray microanalysis in scanning transmission electron microscope, limitations 78−20122
Fe-Ni alloy near crit. conc., Mossbauer γ-rays small angle scatt. 80−7217
Fe-Ni alloy toroidal core, magnetic noise *(Russian)* 78−60308
Fe-Ni alloy type YuNDK25B, anomalous magnetocaloric effect 80−60278
Fe-Ni alloys, cold rolled, exam. of phase composition using Mossbauer spectroscopy 80−21204
Fe-Ni alloys, diffusivity of N_2 79−46845
Fe-Ni alloys, electrodeposit on Cu, texture investig. 77−11818
Fe-Ni alloys, electronic struct. by XPS obs. 79−33226
Fe-Ni alloys, FCC, mag. props. calc. 79−65659
Fe-Ni alloys, graim growth texture 79−91687
Fe-Ni alloys, γ- and α-phase struct. in supercooled austenite *(Russian)* 77−66642
Fe-Ni alloys, heat treatment variations effect on surface conditions and on Hg wetted switch behaviour 80−66547
Fe-Ni alloys, influence of hydrostatic press. on γ to α' transform. during plastic deform. *(Russian)* 79−15663
Fe-Ni alloys, mag. state of austenite and $\gamma \rightarrow \alpha$ transform. *(Russian)* 80−40350
Fe-Ni alloys, qualitative analysis of order-disorder structure by secondary ion-ion emission *(Ukrainian)* 77−69950
Fe-Ni alloys, reverse martensite start temp., heating rate effects *(Russian)* 78−6924
Fe-Ni alloys, shape memory effect, martensite fine struct. effect *(Russian)* 79−52215
Fe-Ni alloys, struct. of γ and α-phases near martensitic transform. point *(Russian)* 78−64541
Fe-Ni alloys, thermal expansion rel. to X-ray emission spectra *(Russian)* 77−32470
Fe-Ni alloys, thermal props., let. review *(Russian)* 78−18805
Fe-Ni austenite, $\alpha \rightarrow \gamma$ transform and stabilisation, Mossbauer and electron microscopy obs. *(Russian)* 78−23703
Fe-Ni austenite, precipitation hardened, transform. strengthening 79−24531
Fe-Ni austenitic, effect of Al and Ti on relaxation resist. 80−20993
Fe-Ni base alloy, precracked specimen, K_{Ihcc} threshold value under const. load at high temp. *(Chinese)* 78−31499
Fe-Ni base amorphous alloy, crystallisation 77−84660
Fe-Ni base amorphous alloys, effect of annealing on Curie temp. 80−34632
Fe-Ni base metallic glass, annealing embrittlement 78−64635
Fe-Ni base metallic glasses, microhardness charact. of stability under annealing 79−57011
Fe-Ni based alloy, amorphous rapidly quenched, mag. props. 77−66269
Fe-Ni based alloys, amorphous, amorphous, thermopower meas., Nordheim-Gorter relations 79−99535
Fe-Ni based amorphous alloys, Hall and ohmic resistivities 79−91013
Fe-Ni based metallic glasses, hydrostatic press. effect on mag. props. 78−19300
Fe-Ni based metallic glasses, nonisothermal crystallisation kinetics, DSC anal. 79−27927
Fe-Ni based metallic glasses, search for Invar-like magnetoelastic behaviour 79−56596
Fe-Ni based metallic glass, Metglas 2826 MB, Mossbauer study 80−75897

iron alloys continued
Fe-Ni binary alloy, specific heat temp. depend., α to γ transformation *(Russian)* 79−83198
Fe-Ni electrodeposit, sectional analyses and impurities *(Japanese)* 80−21350
Fe-Ni electrodeposited coatings, packing defects 79−60662
Fe-Ni evaporated films with perpendicular anisotropy, magnetoresistance obs. 78−2585
Fe-Ni film, amorphous, martensite form. time and struct. 80−104159
Fe-Ni film, $\alpha \rightarrow \gamma$ transition, Mossbauer effect *(Russian)* 77−40154
Fe-Ni film, mag. and struct. props., effect of O_2 partial press. during deposition 79−90903
Fe-Ni film, vacuum-deposited, internal stresses, thickness and comp. effects *(Russian)* 77−80713
Fe-Ni films, dynamic domains and pulse mag. reversals *(Russian)* 79−28571
Fe-Ni films, lattice constants rel. to mag. moments *(Russian)* 77−32218
Fe-Ni films, on glass substrate, thermoelec. effect 80−107769
Fe-Ni films, scatt. of homogeneous spin waves by anisomeric oriented plane, ferromag. reson. 78−19336
Fe-Ni fluorination kinetics and fluoride film form., chem. nature obs. 80−101035
Fe-Ni heterogeneous alloys, ferrite, martensite and austenite phase distrib., effect on mech. props. 80−45363
Fe-Ni liquid alloy, physical and chemical props. deviations from Raoult's law *(Russian)* 78−95729
Fe-Ni martensite, TEM of passivity layer 77−36689
Fe-Ni martensite, twin struct. 79−77607
Fe-Ni martensites, deform. twinning for crystals with transform. twin microstruct. 77−31677
Fe-Ni martensitic alloys, age hardening 79−47736
Fe-Ni melt, short-range order, m.p. to 1750°C *(Russian)* 78−94966
Fe-Ni metallic glass wide strips, low-field mag. props. 79−51822
Fe-Ni metallic glasses, crystallisation 77−43157
Fe-Ni Metglas type, ohmic and Hall resist., 100-700K, mag. behavour obs. 80−80254
Fe-Ni mixed powders, effect of Ni particle size and unequal interdiffusion, on sintering process *(Japanese)* 78−84728
Fe-Ni ordered phase in meteorites, Mossbauer studies 80−41776
Fe-Ni ordering on annealing and electron irrad., mech. props. change *(Russian)* 80−29981
Fe-Ni powder, Ni clad Fe grains, exam. of electrochemical formation process 79−33974
Fe-Ni single crystal, lattice strain induced by anisotropic distrib. of M_2 *(Japanese)* 80−35262
Fe-Ni single crystal, pseudo-Kossel study of fibrous substruct. 77−1835
Fe-Ni single crystals, stress induced martensite 77−8827
Fe-Ni solid soln., thermodynamic study 78−6904
Fe-Ni solid solution, deformation mechanism, softening phenomena, dislocation-solute atom interactions *(French)* 80−45344
Fe-Ni superstructure in metal particles in chondrites 80−12713
Fe-Ni surface alloy formed by ion implantation, anodic polarisation 78−48562
Fe-Ni system, constant modulus alloys for mech. oscillators 79−61641
Fe-Ni system, ferro-antiferromag. transition, γ phase mag. struct. 79−91231
Fe-Ni system, Ni addition effects on activated sintering of Fe powder compacts 77−4756
Fe-Ni two-phase films, alloy component redistrib. during annealing, electron diffr. anal. *(Russian)* 79−20053
Fe-Ni/Fe, bimetal film, exchange const. determ. from hysteresis loops *(Russian)* 77−48015
$Fe\text{-}Ni_3$, hyperfine field, variation with atomic order 79−7953
$Fe\text{-}Ni_3S_2$ reaction couple solid-state displacement reactions 79−77841
Fe-Ni/pure Fe exchange coupled films, mag. reversals, hard layer thickness effects *(Russian)* 78−56359
Fe-Ni-Al, correlation of microscopic features, with macroscopic crack propagation 78−60800
Fe-Ni-Al, Curie temp. depend. on ordering, antiferromag. ordering *(Russian)* 79−61101
β_2-Fe-Ni-Al, diffusion 77−24449
Fe-Ni-Al, liq. alloys, N solubility and AlN precipitation 80−11648
Fe-Ni-Al, magnetic anisotropy form. and struct. changes by annealing, Mossbauer obs. 80−39994
Fe-Ni-Al, Mossbauer spectra, strong elastic stress effects 77−90084
Fe-Ni-Al, oxidation in O_2 at 600 to 800°C 79−83376
Fe-Ni-Al, struct. of aged austenite *(Russian)* 77−52357
Fe-Ni-Al, type YuN14DK25BA, thermomag. treatment 80−16512
Fe-Ni-Al (10, 0.1 wt.%), clustering of Al_2O_3 inclusions 79−83205
Fe-Ni-Al (18.2 wt.%) aged, fracture toughness and mode, grain size depend. 77−12700
Fe-Ni-Al (30, 4wt.%), ageing, peculiarities of struct. state *(Russian)* 79−57008
Fe-Ni-Al alloy, metastable equilib. in its high-coercivity state *(Russian)* 79−52161
Fe-Ni-Al alloys, ordering X-ray and neutron diffr. obs. *(Russian)* 79−20038
Fe-Ni-Al alloys, phase diagram, miscibility gap, DTA meas. 78−92237
Fe-Ni-Al system, multiphase diffusion at 1000°C, diffusion structs. and props. 80−19995
Fe-Ni-Al system, multiphase diffusion at 1000°C, interdiffusion coeffs. for β and γ alloys 80−24684
Fe-Ni-Al-Co-Cr-Ti, YuNDK35T5BA, exam. of hypodissociation process *(Russian)* 79−11547
Fe-Ni-Al-Co-Cu alloy, sintered single-crystal mag. prod., props. 77−66709
Fe-Ni-Al-Co-Cu-Sn alloy YuNDK35T5, Sn addition effects on physicomechanical and magnetic props. and workability *(Russian)* 77−70101
Fe-Ni-Al-Co-Cu-Ti, 38 to 40 wt.% Co, 8 to 8.5 wt.% Ti, alloy YuNDKT tempering and thermomagnetic treatments 78−3154
Fe-Ni-Al-Co-Cu-Ti alloy YuNDKT, nature of X-phase heat treatment effect on microstruct. 77−90380
Fe-Ni-Al-Co-Cu-Ti magnetic alloy electrolytic treatment with programmed pulse current *(Russian)* 79−100282
Fe-Ni-Al-Co-Cu-Ti YuNDK type, S effect on mech. props. 80−60927
Fe-Ni-Al-Co-Ti base alloys, highly coercive, phase comp., Mossbauer meas. 80−39996
Fe-Ni-Al-Cu (25, 14, 4 wt.%), alloy YuND4, effect of Ti addition on structure, mag. props. 80−15714

iron alloys continued
Fe-Ni-Al-Ti, N27Yu2T2, aged austenite, diffuse electron scatt. distrib. during martensitic deform. *(Russian)* 78−60669
Fe-Ni-Al-(Cu) (12, 0.5, 0.5 to 3 wt.%), Cu addition strengthening at 77K, mech. props. 80−60875
Fe-Ni-Al(Ti)(Nb)(V), cryogenic toughness, strength, rel. to reactive metal addition 78−39885
Fe-Ni-Al(2.5, 7.5 at.%), fracture surface morphology, ageing temp. effects 77−16600
Fe-Ni-B, metallic glass, Mossbauer investigation of electronic struct. 78−92009
Fe-Ni-B glassy ribbons melt spinning, gas boundary layer effects 80−76217
Fe-Ni-B metallic glass, X-ray diffr. meas., semi-empirical struct. model 80−107059
Fe-Ni-B-Mo, crystn. temp. and elec. cond. correl., Mo effect 80−75179
Fe-Ni-B-Si, amorphous, mag. props., heat treatment effects 80−89370
Fe-Ni-B(-P), ferromag., magneto-optical spectra in amorphous and cryst. states *(Russian)* 80−84749
Fe-Ni-B(-P) amorphous alloys, mag. annealing mechanism, induced anisotropy 78−95484
Fe-Ni-B(P), amorphous, crystn. 80−79704
Fe-Ni-C, atomized, O/C ratio effect, particle size on annealing kinetics, physicotechnological props. 80−20832
Fe-Ni-C, ausformed, ductility of martensite *(Japanese)* 77−48490
Fe-Ni-C, austenite cryst. volume effect on martensitic transformation temp. 80−40352
Fe-Ni-C, C effect on recrystallisation and reversion *(French)* 77−81282
Fe-Ni-C, calc. of activity data, and exam. of phase equilibria 79−10912
Fe-Ni-C, couplings of thin plate martensites 79−24492
γ-Fe-Ni-C, electromigration of C, effect of Ni 78−6184
Fe-Ni-C, FCC, effect of two gamma states on C activity 78−6897
Fe-Ni-C, Fe rich portion of phase diagram determ. 79−24497
Fe-Ni-C, HVEM study of strain induced martensite 79−20047
Fe-Ni-C, intercrystalline embrittlement in tempered martensite, elimination by reaustenitization *(Slovak)* 80−108548
Fe-Ni-C, internal friction anomaly with reheat transform. 79−100204
Fe-Ni-C, lattice parameters of cementite, annealing effect 80−29007
Fe-Ni-C, lenticular martensitic alloy, fractured at liquid N_2 temps., crack propag. mode *(Japanese)* 77−48524
Fe-Ni-C, martensite nucleation, tensile prestraining effect 77−8828
Fe-Ni-C, martensitic, deformed, stress induced C distrib. *(Czechoslovakian)* 77−32641
Fe-Ni-C, martensitic, H_2 effect on fracture charact. *(Czech)* 78−60746
Fe-Ni-C, martensitic, internal friction 77−16633
Fe-Ni-C, martensitic, mech. charact., effect of ageing and tempering *(Slovak)* 78−19791
Fe-Ni-C, martensitic, mech. and fracture charact., effect of starting austenite heterogeneity *(Slovak)* 78−19792
Fe-Ni-C, martensitic, modulation of local C atom cumulation during ageing *(Slovak)* 78−19790
Fe-Ni-C, martensitic delayed fracture *(Slovak)* 79−43401
Fe-Ni-C, martensitic transform., Mossbauer obs. *(Russian)* 78−6927
Fe-Ni-C, martensitic transform., new investigation method *(French)* 79−91881
Fe-Ni-C, mech. and structural props. under cathodic H_2 at elevated temps. *(French)* 77−59920
Fe-Ni-C, model alloy, intercrystalline brittleness caused by segregation and precipitation in austenite *(Slovak)* 79−70073
Fe-Ni-C, N31, austenite state in premartensitic temp. interval *(Russian)* 78−56634
Fe-Ni-C, phase diagram determ. 79−24495
Fe-Ni-C, plastic deform. effect on austenite stabilisation *(Korean)* 80−21021
Fe-Ni-C, quenched martensite, annealing during cathodic hydrogenation, 200°C *(French)* 80−93573
Fe-Ni-C, Redlich-Kister eqns., activity coeffs., phase equilib. 78−23664
Fe-Ni-C, role of strain in deform. induced martensitic transform. *(Japanese)* 78−92263
Fe-Ni-C, self-diffusion processes during homogenisation of heterogeneous systems *(Russian)* 79−60539
Fe-Ni-C, single crystal, form. and strength of strain-induced martensite 79−100225
Fe-Ni-C, splat-quenched martensite formation obs. 77−44247
Fe-Ni-C, thin foil, high voltage TEM exam. of martensitic form. 78−92264
Fe-Ni-C (0.15, 0.05 wt.%) pore formation kinetics during crystallisation, FORTRAN study *(Russian)* 80−54158
Fe-Ni-C (10, 0.6 wt.%), effect of austenite yield strength on martensitic transformation 78−39772
Fe-Ni-C (19 to 30, 0.04 to 0.8 wt.%) alloys, transformation of martensite in austenite, optical and electron microscopic exam. *(Russian)* 78−35382
Fe-Ni-C (19.5, 0.73 wt.%), banded struct. formed by deform., TEM and optical obs. 78−39869
Fe-Ni-C (21, 0.6 wt.%), stress assited and strain induced martensite morphologies 78−3187
Fe-Ni-C (23, 0.39 wt.%), austenitic or martensitic structs., corrosion faces anal. *(French)* 80−21181
Fe-Ni-C (24, 0.45 wt.%), martensites, TEM observation of double twinning 78−76651
Fe-Ni-C (24, 0.45 wt.%), single crystal, plastic deform. effect on martensitic burst transform. 79−15695
Fe-Ni-C (24, 0.5 wt.%), struct. of burst and isothermal martensites 79−38825
Fe-Ni-C (25, 0.02 wt.%), thermal stabilisation role in martensitic transformations 80−25697
Fe-Ni-C (25, 0.2 wt.%), strain-induced martensite *(Korean)* 80−71646
Fe-Ni-C (26.4, 0.24 wt.%) martensite, partially twinned, slip lines obs. 78−84913
Fe-Ni-C (26.4, 0.24 wt.%), austenitic single crysts., effect of prior deformation on martensite burst transformation, SEM obs. 79−38823
Fe-Ni-C (27, 0.23 wt.%), work hardening and martensitic transform. at 263K 79−100143
Fe-Ni-C (30, 0.5 wt.%) single cryst., stress induced martensitic transform. 80−60860
Fe-Ni-C (30.59, 0.02 wt.%), effect of loading on transformation of retained austenite to martensite 79−47686
Fe-Ni-C (31, 0.1 wt.%), kinetics of deform. induced martensite, shock loading and grain refinement effects 78−15395
Fe-Ni-C (31, 0.1 wt.%), metastable austenite, fractography 77−59919

iron alloys continued
Fe-Ni-C (31, 0.1 wt.%), pre-deformation and temp. effect on transformation-deformation behaviour 80−3127
Fe-Ni-C (31, 0.28 wt.%), crossings of thin plate martensites, TEM obs. 80−25756
Fe-Ni-C (31.1, 0.02 wt.%), coarse grained, microstructural aspects of martensitic transform. 79−56978
Fe-Ni-C (31.1, 0.02 wt.%), kinetics analysis of temp. rate of nucleation of a thermal martensitic transformation 79−78965
Fe-Ni-C (31.24, 0.21 wt.%) effect of deformation and ageing after deformation, on martensitic transformation temp. 78−76650
Fe-Ni-C (31.9, 0.02 wt.%), metallographic study of austenite grain size effect on martensite kinetics 79−1863
Fe-Ni-C (31.9, 0.02 wt.%) alloy, hardness of martensite-austenite mixtures 80−60959
Fe-Ni-C (31.9,0.02 wt.%), determ. of number and size distrib. of martensitic plates 80−76255
Fe-Ni-C (32.7, 0.01 wt.%), athermal marrtensitic transition investigation by acoustic emission *(Russian)* 79−91645
Fe-Ni-C alloy, external stress effects on equilibrium morphology, thermodynamic model *(Russian)* 78−52804
Fe-Ni-C alloy with single-component martensite texture, $\alpha \rightarrow \gamma$ transform., changes in shape *(Russian)* 80−104152
Fe-Ni-C alloys, obs. of banded struct. formed by deformation 79−79050
Fe-Ni-C austenite, effects of strain rate grain size, temp., on yield stress 78−72821
Fe-Ni-C austenite, metastable, influence of prior deform. on yield stress 78−15461
Fe-Ni-C austenitic alloy, banded struct. formed by deform. 80−71713
Fe-Ni-C austenitic single crysts., deform. props., martensitic transformation, SEM study 79−29143
Fe-Ni-C martensite, autoradiographic evidence of C clustering 79−83203
Fe-Ni-C martensite morphology, butterfly-lenticular transition temp., Cr addition effect *(Japanese)* 80−81053
Fe-Ni-C-B, and Fe-Ni-Co-B-C-Si, amorphous, room-temp. saturation induction 78−95476
Fe-Ni-C-Mn (3.56, 3.25, 0.6 wt.%), solid soln., quenched, changes during annealing to crystal structure, mech. props. *(Russian)* 79−34076
Fe-Ni-C-Sb, Sb additions effect on fracture charact. of martensite *(Czech)* 77−70162
Fe-Ni-Co, diffusion controlled phase growth 78−30782
Fe-Ni-Co, magnetic permeability, effect of ion implantation 77−28414
Fe-Ni-Co, phase diagram redeterm., Fe-rich portion 77−44219
Fe-Ni-Co, rel. between induced uniaxial anisotropy and coercive force 78−91904
Fe-Ni-Co, texture form. after cold working and annealing *(German)* 80−3089
Fe-Ni-Co alloys, struct., appl. of mag., thermomag. methods *(French)* 79−20318
Fe-Ni-Co base alloys, composition changes during electron radiation melting *(Russian)* 78−19718
Fe-Ni-Co coating electrodeposition optimum conditions *(Russian)* 79−83292
Fe-Ni-Co film, electron-nucl. mag. reson. 78−35063
Fe-Ni-Co foils, mag. reversals of mag. domains in low-coercivity channels *(Russian)* 79−42813
Fe-Ni-Co-B-P soft magnetic metallic glasses, status report 78−64226
Fe-Ni-Co-C, substruct. effect in mech. props. 80−30086
Fe-Ni-Co-C (29.6, 10.7, 0.009 wt.%), thermal stabilisation role in martensitic transformations 80−25697
Fe-Ni-Co-Cu-Ti YuNDKT alloys, impaired mag. props. with C and S additions 80−60368
Fe-Ni-Co-Mo alloys, struct. transform. produced during tempering 77−86058
Fe-Ni-Co-Mo phase diagram and structure *(Russian)* 80−20899
Fe-Ni-Co-Mo-Ge alloy 40NKM, excess mag. noise after various thermomag. treatments *(Russian)* 80−29575
Fe-Ni-Co-Ti, coherent particles effect inherited by martensite on $\alpha \rightarrow \gamma$ transformation *(Russian)* 80−108443
Fe-Ni-Co-Ti, martensite cryst. lattice tetragonality, $\gamma \rightleftharpoons \alpha$ transform. *(Russian)* 79−61587
Fe-Ni-Co-Ti, shape memory effect after appl. of bending moment *(Russian)* 80−45305
Fe-Ni-Co-V, effects on fusion reactor neutronics performance 80−47705
Fe-Ni-Co-W(Mo) (18.65, 8.99, 4.87 wt.%), ageing charact., 380-530°C 80−60876
Fe-Ni-Co(Cu) alloy components, dynamics of arrival to arc discharge during roasting *(Russian)* 77−16895
Fe-Ni-Cr, at. distrib. effect on mag. props. *(Russian)* 78−2657
Fe-Ni-Cr, austenitic, creep strength and ductility, effect of γ' precipitation 77−36597
Fe-Ni-Cr, austenitic, dispersion-hardened alloys, thermomechanical working *(Russian)* 77−66659
Fe-Ni-Cr, austenitic with dispersed phases, oxidation 80−16540
Fe-Ni-Cr, carbide form. by C diffusion, precip. distrib. and morphology 80−104164
Fe-Ni-Cr, compatibility with Li_2O pellets, mass spectrometric study of Li_5FeO_4 evaporation 79−8385
Fe-Ni-Cr, diffusion in Th at 500 to 800°C *(German)* 79−28157
Fe-Ni-Cr, heavy ion irrad., defect cluster obs. 80−107341
Fe-Ni-Cr, high Ni content, intergranular corrosion, effect of Cr *(French)* 80−7708
Fe-Ni-Cr, mag. props. in weak mag. fields *(Russian)* 80−75771
γ-Fe-Ni-Cr, mag. struct., neutron scatt. study *(Russian)* 78−68160
γ-Fe-Ni-Cr, magnetic phase diagram *(Russian)* 78−39292
Fe-Ni-Cr, oxide film form., combination anal. using ESCA, AES and SIMS 79−16092
Fe-Ni-Cr, pulsed HVEM irrad., effect on microstruct. evolution 80−34053
Fe-Ni-Cr, vapour-deposited film, effect of condensation temp. on form. of metastable phases and mag. props. 79−65700
Fe-Ni-Cr (10, 6 to 14 wt.%), electrochemical polarisation in high temp. water *(Japanese)* 79−15868
Fe-Ni-Cr (20, 15 wt.%), fusion reactor struct. alloys, dual-ion irrad, effects 79−45403
Fe-Ni-Cr (20, 15 wt.%), single and dual ion irrad., microstruct. studies 80−29077
Fe-Ni-Cr (23, 5 wt.%), martensite orientation formed under uniaxial stress alloy [001] 77−77475

iron alloys continued
Fe-Ni-Cr (25, 15 wt.%), high temp. creep, dispersed γ'-Ni_3(Al, Ti) effects *(Czech)* 78−64590
Fe-Ni-Cr (25, 15 wt.%), mobile dislocation density in steady state creep, strain transient dip test, TEM exam. 80−7650
Fe-Ni-Cr (30.6, 21.3 wt.%), Alloy 800, high temp. oxidation at low O_2 press., SEM, AES and electron probe microanal. study 80−93688
Fe-Ni-Cr (35, 15 wt.%), high temp. alloys, for HTR primary components, alloying additions for carburisation protection 80−5243
Fe-Ni-Cr (35, 15 wt.%) superalloy, stress rupture and tensile props., C and B additions effect *(Chinese)* 80−104244
Fe-Ni-Cr (40, 15.8 wt.%), precipitation and creep ruputure behaviour, optical and TEM study 79−74158
Fe-Ni-Cr (44, 17 wt.%), nuclear microprobe methods for investigating oxidative corrosion 80−71787
Fe-Ni-Cr (45,25 wt.%), surface oxide layers, compar. study of comp. and struct. by secondary ion emission and electron microprobe *(French)* 77−56286
Fe-Ni-Cr alloy, cast, etching methods for determ. of primary struct. 78−23888
Fe-Ni-Cr alloy 800, creep ductility decline 77−48502
Fe-Ni-Cr alloy 800, minor alloying element effect on creep, ageing microstruct. 78−27572
Fe-Ni-Cr alloy electrodeposition from sulphate electrolyte with cystine and Na citrate additives *(Russian)* 78−48336
Fe-Ni-Cr alloys, stacking fault energies calc. 79−60387
Fe-Ni-Cr alloys, X-ray fluorescence anal., interelement correction, models, computer program 77−56315
Fe-Ni-Cr austenitic alloy, homogeneous and dispersion strengthened, internal stresses and high temp. creep 78−19841
Fe-Ni-Cr base alloy, oxidation and hot corrosion *(Chinese)* 80−21149
Fe-Ni-Cr based alloy, KhN35VTYu, temp. depend. of energy of fracture, influence of γ' phase *(Russian)* 80−81147
Fe-Ni-Cr coating, electrodeposited, exam. of passivity 78−80655
Fe-Ni-Cr corrosion protective coating on steel 78−48572
Fe-Ni-Cr film, ferromag. reson. meas. *(Russian)* 77−1601
Fe-Ni-Cr melts, O solubility *(Russian)* 80−15250
γ-Fe-Ni-Cr solid soln., thermodynamic activities determ. in Ni rich corner at 1500K 77−32561
Fe-Ni-Cr system, absolute partial pressures and chem. activities of component metals 80−50600
Fe-Ni-Cr vapour deposited film metastable phase formation *(German)* 78−38984
Fe-Ni-Cr-Al-Ti-W-Mo (35, 15, 2.4, 2.3, 2.2 wt.%) wrought superalloy, freckles *(Chinese)* 80−104137
Fe-Ni-Cr-Al-Y, oxidation mechanism, Y addition effect on kinetics and oxide adherence 80−97623
Fe-Ni-Cr-B, X-101 centrifugally cast cylinder lining alloy, compatibility with hardfacing alloys 77−32726
Fe-Ni-Cr-C, effect of austenite yield strength, stacking fault energy, on martensite morphology 78−80546
Fe-Ni-Cr-C, ferritic, P segregation to free surface, 723 to 823K, AES 78−48411
Fe-Ni-Cr-C, martensitic transform. effect of austenite prestrain above M_d temp. 78−15398
Fe-Ni-Cr-Mn-Al-Ti Incoloy 800, exam. of scale morphology, alloying element distrib. after oxidation 78−80677
Fe-Ni-Cr-Mo superalloy, mech. props., η-phase form. effect *(Chinese)* 80−20925
Fe-Ni-Cr-P-B, Metglas 2826A, TEM of shear bands 78−48483
Fe-Ni-Cr-P-B, Metglas 2826A, hardness, elastic moduli, density, cryst. temp., mech. props., for flywheel appl. *(Dutch)* 78−52878
Fe-Ni-Cr-P-B amorphous alloy, localized corrosion 80−16559
Fe-Ni-Cr-S, phase relations rel. to sulphidation of austenitic stainless steel 79−38800
Fe-Ni-Cr-Si, superalloy, Cr and Si effect on mech. props. and microstruct. *(Chinese)* 79−100207
Fe-Ni-Cr-Si (35, 18, 2 wt.%), heating element wire, failure and oxidation 79−83378
Fe-Ni-Cr-Si alloy 800, Si effect on creep and age hardening 77−48444
Fe-Ni-Cr-Ti, superalloy A286, powder, exam. of microstruct. and mech. properties 78−52979
Fe-Ni-Cr-Ti based alloy, 36 NKhTYu, high temp. deform. charact., superplastic behaviour *(Russian)* 77−63719
Fe-Ni-Cr-Ti-Al, ausaging alloy, cellular precipitate indentification *(Chinese)* 78−11225
Fe-Ni-Cr-Ti-Al, Ti and Al effect on microstruct. and mech. props. *(Chinese)* 79−74130
Fe-Ni-Cr-Ti-Al, with thermoelastic control coeff., comp. and heat treatment influence on props. *(French)* 80−81074
Fe-Ni-Cr-Ti-Al Elinvar alloys, dispersion-hardened, structural transform. *(Russian)* 79−1872
Fe-Ni-Cr-Ti-Mn-Mo, (25.8, 14.04, 2.17, 1.27, 1.30 wt.%), superalloy A-286, precipitation hardening, exam. of fracture toughness and mech. props. 78−92355
Fe-Ni-Cr-Y, oxidation at 800 to 1300°C, Y addition effects, comparison with Ni-Cr-Y alloy *(French)* 79−43481
Fe-Ni-Cr-Y, Y addition effect on selective oxidation/diffusion phenomena relationship *(French)* 80−108623
Fe-Ni-Cr-base superalloys, characterization for PNP components 80−5242
Fe-Ni-Ge, liquid alloy, H_2 thermodynamic interaction, solubility *(Russian)* 78−11202
Fe-Ni-M alloys, (M=C, Ti,Mn), habit plane and morphology of lath martensites 77−8823
Fe-Ni-Mn, BCC, atomic mag. moments determ. 77−59396
Fe-Ni-Mn, BCC, mag. state of Mn, NMR and saturation magnetisation meas. 78−39442
Fe-Ni-Mn, dil. alloys, NMR freq. temp. depend., spin echo meas. 78−64296
Fe-Ni-Mn, martensite, aged, grain boundary embrittlement 79−96144
Fe-Ni-Mn, martensitic transforms., expt. investigation *(French)* 78−84803
Fe-Ni-Mn, temp. coeff. of linear expansion *(Russian)* 77−80634
Fe-Ni-Mn (20, 5 wt.%), rel. orientation between adjacent martensite laths 80−76254
Fe-Ni-Mn (20, 5 wt.%), surface martensite, crystallography and morphology 80−40354
Fe-Ni-Mn alloy, martensitic transform. kinetics *(Russian)* 77−81262
γ-Fe-Ni-Mn alloys, spin glass state, short and long range order investigation 80−65808

iron alloys continued
Fe-Ni-Mn martensitic alloy, precipitation 77−12630
Fe-Ni-Mn melt, thermodynamic dissolution of O_2 *(Russian)* 78−27473
Fe-Ni-Mn-C (5.9, 4.4, 0.48 wt.%) alloy, elastic moduli near martensitic transform. 80−7619
Fe-Ni-Mn-H, ferromag., magnetisation curves 78−88144
Fe-Ni-Mn(Mo) alloys, two-stage martensitic transformation kinetics, depend. on austenite initial state *(Russian)* 79−74151
Fe-Ni-Mo, ferrite plus martensite structures, exam. of mech. props. 78−56709
Fe-Ni-Mo, high-strength ferritic, for cryogenic service, mech. characteris. 77−70143
Fe-Ni-Mo, inhomogeneous solid solns., annealed and work hardened states, X-ray K-absorption spectra *(Russian)* 78−56544
Fe-Ni-Mo, martensitic transformation, annealing, influence on struct. of austenite *(Russian)* 80−81057
Fe-Ni-Mo, phase relations in system at 1100°C 80−108392
Fe-Ni-Mo, small angle X-ray scatt. study, pre-precipitation phenomenon obs. *(French)* 78−19757
Fe-Ni-Mo (16.4, 8.1 wt.%), effect of substituting Mo by W during ageing 80−29991
Fe-Ni-Mo-C, amorphous alloys, med. props. and thermal stability *(Japanese)* 80−85049
Fe-Ni-Mo(Si), austenite, annealing effect on atom redistrib., Mossbauer anal. *(Russian)* 80−66529
Fe-Ni-Mo(Ti)(Si), ordered, low temp. $\alpha \rightarrow \gamma$ transform. *(Russian)* 78−19740
Fe-Ni-Mo(13,3wt%), welded alloy, fracture and strength for cryogenic service 79−38930
Fe-Ni-P, interface composition during diffusion controlled precipitate growth 77−36513
Fe-Ni-P, segregation kinetics, theory, and temper brittleness 80−11649
Fe-Ni-P-B, amorphous, crystn. and struct. 80−75175
Fe-Ni-P-B, amorphous, magnetically induced anisotropy 77−89948
Fe-Ni-P-B, amorphous ferromag. alloys, mag. struct., Mossbauer study 80−39746
Fe-Ni-P-B, amorphous paramag. alloys, hyperfine field distrib., Mossbauer study 80−39958
Fe-Ni-P-B, metallic glasses, fracture toughness, shear rupture failures, critical thickness 79−52365
Fe-Ni-P-B, metallic glasses, struct. relax., annealing effects on mag. props. 80−89261
Fe-Ni-P-B amorphous ribbons, form. by melt spin technique 80−76215
Fe-Ni-P-B metallic glass, crystallisation temperature values from isothermal transformation times 80−59397
Fe-Ni-P-B(C), amorphous alloy, anelastic relaxation 79−4997
Fe-Ni-Pt system, ordered phase fields of equilibrium diagram 78−48373
Fe-Ni-S, exam. of liquidus surface and tie lines, using electron probe analysis 79−11557
Fe-Ni-Sb (4, 0.0087 at.%), surface segregation 79−96031
Fe-Ni-Sb-S, S/Sb surface site competition in segregation 80−40366
Fe-Ni-Si, double spontaneous reversible deformation during thermal cycling 78−84942
Fe-Ni-Si-B, amorphous paramag. alloys, hyperfine field distrib., Mossbauer study 80−39958
Fe-Ni-Si-Mn-Cr(Co-Mo), effect of prolonged aging on mag. props. 80−16513
Fe-Ni-Ta (-Co), alloys, Co effect on martensite ageing at 300-600°C *(Russian)* 80−20972
Fe-Ni-Te alloy system, first-order phase transformation obs. 78−64533
Fe-Ni-Te alloys, magnetisation 79−7975
Fe-Ni-Ti, ageing mechanism, neutron diffr. expts. *(Russian)* 78−48403
Fe-Ni-Ti, martensite, tetragonality, X-ray obs. 77−63665
Fe-Ni-Ti, preaged martensite, shear strain magnitude, X-ray diffr. method 80−93592
Fe-Ni-Ti, shape recovery depend. on hardening *(Russian)* 79−83259
Fe-Ni-Ti, undeformed metastable alloy, cellular decomposition of austenite during ageing *(Russian)* 79−100178
Fe-Ni-Ti (25.9, 2.15 wt.%), exam. of effect of inhomogeneous solid soln., on martensitic transformation *(Russian)* 79−34034
Fe-Ni-Ti (27.4, 2 to 3 wt.%), aged, stress induced martensitic transform., mech. props. *(Russian)* 79−87632
Fe-Ni-Ti (30, 3 wt.%), reverse martensitic transform. and memory effect *(Russian)* 79−87627
Fe-Ni-Ti (30, 6 wt.%), austenitic, discontinuous coarsening of lamellar cellular precipitates, morphology 79−78967
Fe-Ni-Ti (30, 6 wt.%), austenitic, discontinuous coarsening of lamellar cellular precipitates, growth kinetics 79−78968
Fe-Ni-Ti (31.2, 5.3 wt.%), γ-phase ageing effect on martensitic transform. *(Russian)* 77−28814
Fe-Ni-Ti alloys, high pressure effect on martensite crystal nucleation and growth *(Russian)* 78−39769
Fe-Ni-Ti martensitic alloy, γ' particle effect on crystallisation struct. *(Russian)* 78−44129
Fe-Ni-Ti-Al, martensite, nature of tetragonality 79−32936
Fe-Ni-Ti-Al-Nb, struct. mechanism for inverse $\alpha \rightarrow \gamma$ transform. *(Russian)* 80−40351
Fe-Ni-Ti-C (31, 4, 0-18 wt.%), coherent precipitates in austenite, effect on martensite substruct. 77−52327
Fe-Ni-Ti-(Cu) (12, 0.25, 2 wt.%), Cu addition strengthening at 77K, mech. props. 80−60875
Fe-Ni-V, austenite, martensite elec. cond. depend. on heating *(Russian)* 79−70177
Fe-Ni-V, effect of low temp. ageing on props. during high temp. ageing *(Russian)* 78−39811
Fe-Ni-V, nitrided austenitic alloys, modulated substitutional interstitial solute atom clustering 79−74160
Fe-Ni-V alloy, ageing of martensite *(Russian)* 78−39808
Fe-Ni-V-C alloy, reverse α to γ transformation, previous deformation influence on struct. and props. *(Russian)* 79−100139
Fe-Ni-V-Co, Co influence on age hardening *(Russian)* 78−68703
Fe-Ni-V-(CO) alloy, lattice parameter variation during ageing *(Russian)* 78−39812
Fe-Ni-V-(Cu) (12, 2, 2 wt.%), Cu addition strengthening at 77K, mech. props. 80−60875
Fe-Ni-WC hard alloy, struct. and props. 79−79007
Fe-Ni-(C), substruct. of ausformed martensite 77−36548
Fe-Ni-(C), thin foil martensite, TEM obs. 77−51378
Fe-Ni-(Cr)(Ti)(Al) austenite, high N content, cryst. struct. electron diffr. and electron miscroscope anal. *(Russian)* 79−24490

iron alloys continued
Fe-Ni-(Cu) (12, 0.5 to 3 wt.%), Cu addition strengthening at 77K, mech. props. 80−60875
Fe-Ni-(P), phase diagram determ., 700 to 300°C 80−108399
Fe-Ni(-Mn)(Cr)(V), concentration ferromag. antiferromag. phase transition and mag. state diagram. *(Russian)* 80−20401
Fe-Ni(-Mo), formation of austenite structure in relation to α to γ transformations 79−100142
Fe-Ni(Al), mag. aftereffect meas., phenomenological description 80−88835
Fe-Ni(Co), liquid, activity meas. by transportation method *(Japanese)* 79−4949
Fe-Ni(Co), powder mixture, effect of granulometric distrib. on importance of Kirkendall effect during calcination *(French)* 77−11721
Fe-Ni(Co), solid and liq., paramag. susceptibility and electron struct., 800-1800°C *(Russian)* 80−25081
Fe-Ni(Co)(V), BCC, ferromag., high-field susceptibility 80−7083
Fe-Ni(Mn) alloy, shape memory effect *(Russian)* 78−38771
Fe-Ni(Mn)-Al-C, form. of ductile Ni_3Al by split quenching, mech. props. 79−100197
Fe-Ni(Mo), solid soln., cyclic stress-strain props., depend. of fatigue crack growth rate 77−4853
Fe-Ni(Si), precipitation of AlN *(French)* 78−23711
Fe-Ni(Si), strain hardening and rate-sensitivity, effect on ductile-brittle transition temp. 78−39900
Fe-nonmagnetic impurity, transferred hyperfine field using volume overlap model 79−78054
Fe-O-V melts, phase equilib. *(Russian)* 80−16273
Fe-P, amorphous, anomalous thermal expansion, ΔE effect, Invar and Elinvar characts., delay time 80−80589
Fe-P, amorphous, temp. depend. of saturation magnetisation 78−19223
α-Fe-P, grain boundary adsorption of P, internal friction *(Russian)* 77−32609
Fe-P, metallic glass, theoretical studies on structural models 79−37633
Fe-P, P equilib. grain boundary segregation 79−38835
Fe-P, sintered frictional material, friction and wear rubbing pair under moderate load 77−21208
α-Fe-P, static strain ageing 77−70079
Fe-P (0.14 wt.%), cavity formation at grain boundary-subboundary interactions 77−86040
Fe-P alloys, amorphous, Mossbauer spectra 79−51886
Fe-P alloys, X-ray exam. of amorphous structure *(Japanese)* 77−84661
Fe-P amorphous alloys, electrodeposited, mag. anisotropy 80−15713
Fe-P amorphous alloys, initial permeability, time depend. 80−15759
Fe-P electrodeposited foil, amorphous, mag. domains 80−75821
Fe-P film, amorphous, ion implanted, struct. and domain struct. obs. 79−91272
Fe-P-Al(Si)(B), amorphous alloy, anelastic relaxation 79−4997
Fe-P-B, amorphous alloy, Mossbauer effect and short-range order 80−2675
Fe-P-B, amorphous alloys, mag. props., conc. depend. 77−8314
Fe-P-B-Al, amorphous, magnetostriction as function of glass formers 78−19299
Fe-P-C, amorphous, crystn. and struct. 80−75175
Fe-P-C, amorphous, internal friction and shear modulus 77−25085
Fe-P-C, amorphous, struct. and mag. props., Mossbauer, X-ray diffr. and elec. resist. meas. 78−2009
Fe-P-C, amorphous alloy, crystallisation 79−100112
Fe-P-C, amorphous alloy, Mossbauer effect and short-range order 80−2675
Fe-P-C, embrittlement by crystallisation *(Japanese)* 78−48513
Fe-P-C, viscoelastic behaviour of amorphous alloys *(Japanese)* 77−86110
Fe-P-C alloys, amorphous, mag. anisotropy, Mossbauer obs., prior cooling effects *(Russian)* 77−32300
Fe-P-C amorphous alloy, small angle X-ray scattering study of struct. and crystallisation 79−50999
Fe-P-C amorphous alloys, corrosion resistance by alloying with metallic elements 79−66212
Fe-P-C amorphous alloys, Mossbauer spectra, struct. 80−15840
Fe-P-C amorphous alloys with metalloid elements, embrittlement/crystn. relationship *(Japanese)* 79−96134
Fe-P-Cu-SiO_2-$FeAl_3$-asbestos composite, thermal and elec. conds., temp. and composition depends. 77−66609
Fe-P-Si alloys, electrothermal-grade, thermoelec. characts. in region 273 to 573K 78−23834
Fe-P(Ga)(As)(Sb), dil., short range order, NMR study 80−71237
Fe-P(S) sintered materials, antifriction props. 79−24626
Fe-Pd, anomalous elec. cond. near mag. phase transition point, α to γ phase transition 80−15722
Fe-Pd, diffusion coeffs. of ^{59}Fe and ^{103}Pd meas. *(French)* 77−15617
Fe-Pd, FCC, ferromag., spin wave stiffness constant 78−91851
Fe-Pd, mag. moment, comp. depend. *(Russian)* 78−47280
Fe-Pd, magnetic after-effect of H isotopes 80−75817
Fe-Pd, magnetic struct. changes assoc. with crystallite thickness increase *(Russian)* 77−80913
Fe-Pd, residual resist., s-d hybridisation effect 80−39559
Fe-Pd (1•2 wt.%), solution of ^{119}Sn, study by Mossbauer spectroscopy 80−75888
Fe-Pd (31.2 wt.%), thermoelastic FCC-FCT martensitic transformation 80−104156
Fe-Pd (47 at.%) alloy, powders and powder compacts, mag. props. rel. to heat treatment *(Russian)* 79−15816
Fe-Pd (50 at.%), ordering under load, nuclear gamma reson. obs. *(Russian)* 78−92258
Fe-Pd (50 at.%), structural changes during ordering *(Russian)* 77−77471
Fe-Pd alloy, mag. struct. determ., neutron scatt., Mossbauer and mag. meas. *(Russian)* 78−2648
Fe-Pd alloy, uniaxial ferromag., anisotropic component of localised mag. field, Mossbauer meas. *(Russian)* 79−15382
Fe-Pd alloys, spin density radial distrib. determ. 79−73685
Fe-Pd crystalline alloy, positive large linear magnetostriction 80−25173
Fe-Pd film, depth profiles, sputter etching obs. 79−83079
Fe-Pd-Pt alloy powders, coercive force and specific remanence *(Russian)* 79−47302
Fe-Pt, austenite ordering effect on mode of reverse transform 79−61588
Fe-Pt, crystallography and morphology studies, lenticular thin plate transition, thin plate morphology 79−1862
Fe-Pt, high mag. field phase transition 77−66301
Fe-Pt, Invar type, charact. magnetovolume effects 79−82855

iron alloys continued
Fe-Pt, Invar type, strong ferromagnetism, mag. props. 78−64197
Fe-Pt, magnetic struct. changes assoc. with crystallite thickness increase *(Russian)* 77−80913
Fe-Pt, Mossbauer exam. 79−56639
Fe-Pt, nearly thermoelastic, irreversible lattice defects formed by martensitic transform. cycles 78−60671
Fe-Pt, ordered, anisotropy of mag. props. *(Russian)* 78−60280
Fe-Pt, ordered single cryst., magnetisation in strong mag. field *(Russian)* 78−47954
Fe-Pt, plastic deform. effect on struct. singularities and mag. props. *(Russian)* 80−44892
Fe-Pt, solubility of H_2 at press. up to 67 kbar *(Russian)* 79−51260
Fe-Pt (Ni), itinerant electron ferromagnet, magnetovolume effects 80−60397
Fe-Pt (22-24 at.%) austenite, long range order parameter, temp. depend. 80−40353
Fe-Pt (23,24,25 at.%), effect of austenite ordering on some thermoelastic transform. factors 78−88466
Fe-Pt (24 at.%), colour metallographic technique, for studying microstructural reproducibility, in martensitic transformations 78−72954
Fe-Pt alloy, diffusion of ^{197}Pt and ^{59}Fe *(Czech)* 79−77804
Fe-Pt films, mag. and magneto-optic props., appl. to holographic and bit-by-bit storage 79−33512
Fe-Pt-Ir, Mossbauer effect of ^{193}Ir and ^{57}Fe, hyperfine field, isomer shift 78−15072
Fe-Pu, dil., effective mag. fields, temp. depend. *(Russian)* 78−43587
Fe-R alloys, mag. elastic properties 78−52331
Fe-rare earth, amorphous thin film, crystallisation, TEM obs. 79−19483
Fe-rare earth, dil., contact contribution to mag. hyperfine interaction of rare earth impurities 77−80932
Fe-Rh, ferromag., spin wave stiffness constant calc. 79−38307
Fe-Rh, hyperfine field distrib., spin echo NMR meas. 78−76351
Fe-Rh, mag. phase transitions, triple point 79−1672
Fe-Rh, spin wave spectrum in antiferromag. and ferromag. phases, inelastic neutron spectrometry 77−63158
Fe-Rh alloy, nonmag. and mag., band theory 79−37973
Fe-Rh(Os), mag. hyperfine interactions Mossbauer effect meas. 77−66442
Fe-Ru (30-60 at.%) mag. ordering, Mossbauer obs. 77−4585
Fe-Ru(Os), CC hexagonal phase, ^{57}Fe Mossbauer study 79−91321
Fe-Ru(Os) alloys, antiferromag. ordering, hyperfine fields 80−15867
Fe-S system, segregation kinetics *(Japanese)* 79−61592
Fe-S-C (1,3 wt.%), sulphidised Fe-graphite bearing materials, sintering, struct. form. 78−60601
Fe-Sb amorphous films, Mossbauer effect study 80−75896
Fe-Sb system, α-phase, interdiffusion 79−73349
Fe-Sb-Ni(Cr), dil., short range order, NMR study 80−71237
Fe-Sb-Ti(V)(Cr)(Mn)(Co)(Ni), dil., interactions and precip., Mossbauer study 80−39997
Fe-Sb-Ti(V)(Cr)(Mn)(Co)(Ni), interactions and segregations, Mossbauer and X-ray diffr. study 80−70415
Fe-Sb(Sn), dil., spontaneous magnetoresistance anisotropy and deviations from Mattheissen's rule 79−51553
Fe-Se, low conc. binary system, Mossbauer spectroscopy meas. 79−24239
Fe-Si, 180° Bloch wall motion, Barkhausen jumps *(French)* 78−23294
Fe-Si, 6.3-25 at.% Si, single crysts., adiabatic elastic consts., room temp. US pulse echo meas. 77−48467
Fe-Si, (110) [001] oriented, mag. props., compressive stress effects 80−60392
Fe-Si, (3 wt.%), nonuniform elastic deform. in grains *(Russian)* 78−35415
Fe-Si, (3wt.%) alloys, grain boundary anal.,, scanning AES 79−43256
Fe-Si, amorphous film, mag. props. 77−1575
Fe-Si, BCC, cyclic cleavage crack growth model for fatigue 80−55519
Fe-Si, Bloch wall motion, irreversible processes 79−78431
Fe-Si, Bloch wall motion self-similarity *(French)* 79−82810
Fe-Si, coated, effective domain and grain obs. methods and Fe losses 80−34675
Fe-Si, crack propag. kinetics, effect of current pulses 78−31531
Fe-Si, determ. of Si by X-ray fluorescence spectrometry *(Japanese)* 79−57324
Fe-Si, dil., Mossbauer spectra meas. 77−63344
Fe-Si, dilute, irradiation softening effect on yield stress 80−76319
Fe-Si, dislocation struct. of plastic relax. zone at tip of brittle crack 77−77582
Fe-Si, dislocation wall form. in contact with surface active melt, stacking fault energy *(Russian)* 77−72626
Fe-Si, domain struct., influence of insulating coating, high voltage SEM obs. 77−1565
Fe-Si, domain struct. obs. by high voltage SEM 77−1564
Fe-Si, domain structure of Neel oriented samples 77−69601
Fe-Si, dynamically strained, temp. depend. of twinning characts. *(Russian)* 79−46673
Fe-Si, elastic consts., temp. depend., 77 to 300K 77−70089
Fe-Si, electron density distrib. vs. at. order 79−60309
Fe-Si, etch figure method appl. *(Chinese)* 80−21194
Fe-Si, fatigue crack propag., low temp. 80−35311
Fe-Si, fatigue fracture fractography in broad strain-amplitude range, in air and vacuum 80−81186
Fe-Si, ferromag., magnetisation in high fields, influence of internal field nonuniformity 79−51819
Fe-Si, glissile and twinning dislocation motion temp. depend., influence of grain boundaries *(Russian)* 77−47452
Fe-Si, grain oriented, core losses *(Japanese)* 78−60303
Fe-Si, grain oriented, effect of tensile stress on domain struct. 78−95462
Fe-Si, grain oriented, fatigue crack direct obs. by SEM, propag. mechanism *(Japanese)* 79−20164
Fe-Si, grain oriented, misorientation effects on mag. props 80−88792
Fe-Si, grain oriented, phosphate coating anal. by IR spectroscopy 80−89570
Fe-Si, grain oriented, with unique inhibition system for texture development 77−90366
Fe-Si, grain oriented sheet, grain struct. by computer mapping 80−88168
Fe-Si, grain oriented sheet, AC hysteresis, surface struct. and elastic stress effects 80−88791
Fe-Si, grain oriented transformer sheets, permeability and magnetostriction, tensile stress effects 80−88843

iron alloys continued
Fe-Si, grain-oriented, AC magnetostriction at high temp., mag. annealing effects 77−20672
Fe-Si, grain-oriented, magnetostriction, and domain struct. 79−1703
Fe-Si, grain-oriented, surface coating effect on transverse magnetostriction 77−66402
Fe-Si, grain-oriented sheets, high permeability, low losses, review 80−88790
Fe-Si, H_2, induced cracking, crystallographic and fractographic studies 79−5052
Fe-Si, hyperfine fields, Mossbauer meas. 80−40024
Fe-Si, hysteresis loops described by 180° Bloch wall *(French)* 79−15322
Fe-Si, influence of stress on rotational loss, lamination appl. 78−35384
Fe-Si, internal friction, domain boundary area *(Russian)* 79−24562
Fe-Si, internal friction anisotropy, dynamic magnetostriction *(Russian)* 78−2194
Fe-Si, irreversible Barkhausen jumps *(French)* 77−1568
Fe-Si, liq., thermodynamic characts. calc. *(Russian)* 80−15264
Fe-Si, liq. alloys, surface tension, sessile drop method meas. *(French)* 78−84029
Fe-Si, liquid, surface tension model using surrounded atom concept 77−15665
Fe-Si, loss meas. at high flux densities 80−88799
Fe-Si, low frequency power losses 78−95466
Fe-Si, low-temperature fatigue crack propagation 78−72876
Fe-Si, mag. losses, depend. on stress and orientation 77−1882
Fe-Si, mag. method for rapid analysis 77−44540
Fe-Si, mag. props., stress and reannealing effects 80−88844
Fe-Si, magnetic domain obs. by SEM 77−69606
Fe-Si, magnetic props., material for electrical engineering *(German)* 77−21293
Fe-Si, magnetostatic couplings between 180° Bloch walls 77−69613
Fe-Si, maze domains upon appl. of horizontal mag. field or mech. tension 80−11218
Fe-Si, microflow and strain hardening under cyclic loading 80−104182
Fe-Si, microplastic deform. and amplitude depend. of internal friction *(Russian)* 80−45349
Fe-Si, Mossbauer study of mag. ordering 79−24245
Fe-Si, non-oriented sheets, production and props. 80−88797
Fe-Si, plastic deform., synchrotron X-ray topography dynamic expts. 78−67621
Fe-Si, plastic deformation mechanism, meas. of microplasticity 78−60720
Fe-Si, polycrystalline, domain struct. at grain boundaries *(Russian)* 77−51917
Fe-Si, polycrystalline, exam. of stress-strain state of individual grains 78−80580
Fe-Si, power loss and permeability meas. by means of Hall probes and stochastic ergodic correl. 80−86350
Fe-Si, rapid cracks self-arrest potential, −196-0°C 80−100911
Fe-Si, recrystallisation study 79−91275
Fe-Si, recrystallization, in situ studies, appl. of X-ray synchrotron topography 78−35610
Fe-Si, ribbon, prep. by rapid quenching 79−33957
Fe-Si, ribbon-form material, rapid quenching from melt *(Japanese)* 78−92210
Fe-Si, simple domain structs., magnetisation jumps 77−69624
α-Fe-Si, single cryst., ^{59}Fe diffusion coeffs., 1013 to 1373K 77−69110
Fe-Si, single cryst., lattice parameter determ., ratio method 77−43106
Fe-Si, single cryst., mag. domain wall motion, X-ray topography study 80−65953
Fe-Si, spin- and charge-density oscillations 77−11886
Fe-Si, spreading behaviour of liq. Al 80−84345
Fe-Si, stator core, grain-oriented and non-oriented, magnetic flux and loss distrib. 80−88798
Fe-Si, stress and plastic deform. effect on Barkhausen effect, instrumentation 78−52313
Fe-Si, strips and rods, spatial extent of flux due to irreversible changes of mag. polarisation 79−33506
Fe-Si, temp. depend. of twinning intensity, development of deform. *(Russian)* 79−51116
Fe-Si, temperature dependence of the twin growth rate *(Russian)* 79−27999
Fe-Si, thermally activated motion of 180° Bloch wall 78−95457
Fe-Si, thin cryst., domain struct. behaviour during magnetisation *(Russian)* 78−2697
Fe-Si, transformer steel, high-temp. heat treatment, resist. of refractories in contact 80−66554
Fe-Si, twinned annealing, plastic deform., and recrystallisation *(Russian)* 77−28829
Fe-Si, type B_1 domain struct., Mossbauer exam. 77−51931
Fe-Si, yield stress, temp. depend. *(Russian)* 78−56691
Fe-Si (0-25 at.%), composition depend. of elastic consts. at 0K 77−84830
Fe-Si (0-6 wt.%) melts, viscosity *(Russian)* 80−15285
Fe-Si (1-5 wt.%), optimum sintering conditions and mag. props. 77−85958
Fe-Si (1%), LEED-Auger exam. of $(1\bar{1}0)$ surfaces 78−71915
Fe-Si (10 wt.%), effect of short range order on yield stress *(German)* 78−52932
Fe-Si (110)[001] sheet, normal stress effect on magnetostriction 77−40102
Fe-Si (2-8 wt.%), single crysts., growth striations, X-ray studies 80−79774
Fe-Si (2.35 wt.%), misorientation dependence of grain boundary segregation, Auger spectroscopy exam. 78−76629
Fe-Si (2.4 wt.%), ductile fatigue crack growth mechanism in single crystals, in situ SEM obs. 79−61695
Fe-Si (2.4 wt.%), simulation of X-ray topographies of ferromag. domains *(French)* 77−77070
Fe-Si (2.5%), Bloch wall zig-zag struct., neutron small angle scatt. 77−16099
Fe-Si (2.5%), mag. stray fields above stripe domains, electron optic meas. 80−15755
Fe-Si (2.6 wt.%) single cryst., crack propag., controlled plastic crack tip opening rate 80−60943
Fe-Si (2.9 wt.%), spatial orientation of grain boundaries *(Russian)* 77−11567
Fe-Si (3 at%), deformation and electron bombardment, influence on dislocation struct., 20-500°C *(Russian)* 80−92536

iron alloys continued
Fe-Si (3 at.%), acoustic emission response 79−87801
Fe-Si (3 to 5 wt.%) sinters, mag. props., Si and Fe-Si additions effect 80−71104
Fe-Si (3 wt.%), (110)[001] oriented single crystal, form. of rolling and annealing texture 77−16608
Fe-Si (3 wt.%), Al-bearing, grain-oriented, N_2-H_2 annealing effect on texture, mag. props. 77−12714
Fe-Si (3 wt.%), AlN-inhibited, Se effect on primary grain recrystallisation 77−12715
Fe-Si (3 wt.%), anisotropy induced by rolling in (001) and (111) planes *(Russian)* 77−80931
Fe-Si (3 wt.%), BCC, crystallographic depend. of fatigue crack propag. *(Japanese)* 77−48528
Fe-Si (3 wt.%), BCC, transcrystal fatigue crack propag. mechanism *(Japanese)* 77−48529
Fe-Si (3 wt.%), Barkhausen effect meas. 77−85492
Fe-Si (3 wt.%), behaviour of disperse inclusions, influence of recrystn. processes *(Russian)* 80−66519
Fe-Si (3 wt.%), breaking stress grain size and grain boundary energy during onset of reversible temper brittleness *(Russian)* 77−32673
Fe-Si (3 wt.%), chemical comp. and hot rolling effect on brittleness *(Czech)* 80−50712
Fe-Si (3 wt.%), cold rolled, effect of primary recrystallisation texture, on behaviour of secondary recrystallisation 78−39802
Fe-Si (3 wt.%), containing B, grain boundary segregation, AES evidence 77−86046
Fe-Si (3 wt.%), cube-on-edge oriented, high permeability, mill processing and mag. props. 77−86045
Fe-Si (3 wt.%), current pulse effects on structure at crack tip *(Russian)* 77−44332
Fe-Si (3 wt.%), deform., effect of superimposed US oscillatory stress *(Japanese)* 78−31461
Fe-Si (3 wt.%), degeneration of slip on $(\bar{2}11)$ planes *(Russian)* 78−80587
Fe-Si (3 wt.%), directional, power loss anomalies temp. depend., effect of intrinsic parameters 77−12156
Fe-Si (3 wt.%), domain struct. rel. to cryst. size *(Russian)* 80−29568
Fe-Si (3 wt.%), domain wall spacing and losses, orientation depend. 78−56343
Fe-Si (3 wt.%), domain wall drift due to nucleation during cyclic magnetisation 78−95461
Fe-Si (3 wt.%), domain wall spacing and core loss, forsterite and stress coatings effect 80−88780
Fe-Si (3 wt.%), EM losses, effect of bending of 180° domain boundaries *(Russian)* 78−39357
Fe-Si (3 wt.%), eddy current and hysteresis losses, role of domain struct. *(Russian)* 77−80961
Fe-Si (3 wt.%), eddy current losses, domain structure influence obs. and calc. *(Slovak)* 79−4693
Fe-Si (3 wt.%), effect of heating rate during primary recrystn. on props. after secondary recrystn. 78−84837
Fe-Si (3 wt.%), elec. field gradient by trigonal and tetragonal distortions 77−8474
Fe-Si (3 wt.%), electron irradiated, yield strength and elongation 80−76325
Fe-Si (3 wt.%), exam. of plastic deformation, slip band dislocation, under hydrostatic pressure 78−56695
Fe-Si (3 wt.%), fatigue crack propag. work coeff. 80−16422
Fe-Si (3 wt.%), ferromag. domains, imaging by neutron interferometry 80−71087
Fe-Si (3 wt.%), Goss oriented, stress effects 78−91916
Fe-Si (3 wt.%), grain growth inhibition by MnS spherical particles with size distrib. 80−35218
Fe-Si (3 wt.%), grain oriented tape-wound core, dynamic domain size var. and Fe losses 77−12146
Fe-Si (3 wt.%), grain oriented, MnS-AlN-inhibited, precipitate morphology 77−12648
Fe-Si (3 wt.%), grain oriented, lowest core loss 78−91887
Fe-Si (3 wt.%), grain orientated, negative magnetostriction, theory 78−91917
Fe-Si (3 wt.%), grain oriented, domain wall variation throughout magnetisation cycle 78−95459
Fe-Si (3 wt.%), grain oriented, power loss depend. on domain wall bowing 78−95460
Fe-Si (3 wt.%), grain oriented, MnS precipitate distribution, electron microscope observation *(Chinese)* 78−95751
Fe-Si (3 wt.%), grain oriented, mag. domain movements 79−82815
Fe-Si (3 wt.%), grain oriented, mag. props., effect of decarburizing *(Chinese)* 80−103821
Fe-Si (3 wt.%), grain-oriented, effect of forsterite coatings in domain struct. 78−23293
Fe-Si (3 wt.%), grain-oriented, domain struct. regulation and power loss reduction 80−88779
Fe-Si (3 wt.%), grain-oriented, domain wall profiles throughout magnetisation cycle 80−88781
Fe-Si (3 wt.%), grain-oriented, stacking effect on power loss, mag. props. 80−88795
Fe-Si (3 wt.%), grain-oriented, power loss and domain wall variation with lamination thickness 80−88814
Fe-Si (3 wt.%), grain-oriented, energy loss reduction by lowering sheet thickness 80−88816
Fe-Si (3 wt.%), high induction grain oriented, metallurgical treatment and mag. props. 77−86044
Fe-Si (3 wt.%), high permeability, use in transformer cores 80−88793
Fe-Si (3 wt.%), hot rolled sheet steel, ductile-brittle transition temp. *(Chinese)* 78−31498
Fe-Si (3 wt.%), hysteretic losses, domain struct. and cryst. defects 79−19747
Fe-Si (3 wt.%), internal friction, instantaneous, depend. on phase of torsional oscills. *(Russian)* 80−71142
Fe-Si (3 wt.%), loss contribs. from correlations among irreversible movements of Bloch walls 77−85483
Fe-Si (3 wt.%), loss prediction, from distorted waveforms 78−76273
Fe-Si (3 wt.%), losses, demagnetisation freq. and grain orientation depend. 80−88796
Fe-Si (3 wt.%), mag. anisotropy induced by rolling in (110) plane *(Russian)* 78−34978
Fe-Si (3 wt.%), mag. anisotropy induced by cold rolling *(Russian)* 80−84595

iron alloys continued
Fe-Si (3 wt.%), mag. domain wall contrast in synchrotron X-ray topographs 80−75792
Fe-Si (3 wt.%), mag. loss and magnetostriction, DC flux alternation effects 80−88794
Fe-Si (3 wt.%), mag. props., stress coating effects 80−34728
Fe-Si (3 wt.%), magnetisation variation during bending oscills., rel. to ΔE effect *(Russian)* 80−65983
Fe-Si (3 wt.%), Mossbauer spectra, domain magnetisation vector rotations, domain struct. 79−69761
Fe-Si (3 wt.%), nonoriented sheets, magnetisation, tensile stress effects 80−88845
Fe-Si (3 wt.%), orientation distrib. in primary recrystallised textures, mag. permeability 77−12712
Fe-Si (3 wt.%), orientation development during secondary recrystallisation, primary matrix effect, magnetic props. *(Czech)* 78−60679
Fe-Si (3 wt.%), oriented, losses and domains, mech. stress effects 80−88852
Fe-Si (3 wt.%), polycryst. (110), synchrotron radiation topographs and mag. domain obs. 78−67620
Fe-Si (3 wt.%), polycrystal in mag. field, stress induced magnetisation, synchrotron Bragg refl. topography obs. 80−50139
Fe-Si (3 wt.%), power losses at extremely low freqs. 80−88815
Fe-Si (3 wt.%), prediction of magnetisation hysteresis loops for distorted waveforms 79−47303
Fe-Si (3 wt.%), pulsed laser induced deform. 77−36605
Fe-Si (3 wt.%), recrystallisation along grain boundaries *(Russian)* 78−6942
Fe-Si (3 wt.%), rotational power losses, freq. depend. 78−91888
Fe-Si (3 wt.%), scratching effects on mag. losses in single crysts. with orientation near (110)[001] 79−51802
Fe-Si (3 wt.%), secondary recrystn., struct. inhibition, permeability improvement 77−12713
Fe-Si (3 wt.%), secondary recrystn., role of solutes 77−86043
Fe-Si (3 wt.%), secondary recrystallisation, effect of composition and original orientation 78−68707
Fe-Si (3 wt.%), single crystal, colour etching of striations 77−70253
Fe-Si (3 wt.%), single crystal, plastic deform., 473 to 1000K 77−73310
Fe-Si (3 wt.%), single crystal growth by floating zone melting at various rates, growth striation obs. 79−95914
Fe-Si (3 wt.%), single crystals, cyclic deformation oriented for single glide 79−100224
Fe-Si (3 wt.%), single crysts. and polycrysts. strain rate influence on low cycle fatigue props. 80−3126
Fe-Si (3 wt.%), singularities in geometry of slip, point temp. depend. *(Russian)* 79−24574
Fe-Si (3 wt.%), solubility of MnS, 950-1200°C *(Russian)* 77−16541
Fe-Si (3 wt.%), square etch pit characts., subgrain misorientation and mag. domain patterns 77−25199
Fe-Si (3 wt.%), strain aged polycrystalline samples, AE study of deform. 77−63696
Fe-Si (3 wt.%), strain distribution near notch tip under mixed plane stress-plane strain condition *(Japanese)* 77−8891
Fe-Si (3 wt.%), stripe domain structure, dynamic behaviour at high max. induction values *(Russian)* 80−80553
Fe-Si (3 wt.%), struct. and preferred orientation, annealing parameters influence *(Czech)* 80−89248
Fe-Si (3 wt.%), temp. depend. of migration rate of secondary recrystallisation grain boundaries *(Russian)* 79−1436
Fe-Si (3 wt.%), tertiary products from deoxidation, electron emission microscope study *(Russian)* 78−11214
Fe-Si (3 wt.%), texture, Mossbauer expts. 80−71262
Fe-Si (3 wt.%), texture form., plastic strain effect, hot rolled 79−79002
Fe-Si (3 wt.%), total losses under tensile stress, rel. to orientation near (110)[001] 78−76272
Fe-Si (3 wt.%), transformer steel, grain-oriented, magneto-optical domain obs., magnetisation mechanism 77−12364
Fe-Si (3 wt.%), transformer laminations, processing and props. 78−52325
Fe-Si (3 wt.%), triaxial ferromagnets, spontaneous magnetisation distrib., plane stress state influence *(Russian)* 79−61071
Fe-Si (3 wt.%), US oscillatory stress superimposition effects on deformation 80−35287
Fe-Si (3 wt.%), yielding phenomena at high temp. *(Japanese)* 77−48489
Fe-Si (3 wt.%) (001) [100] single crystal, cold rolled texture *(Japanese)* 77−21169
Fe-Si (3 wt.%) (110), domain size depend. on crystal thickness *(Russian)* 79−69692
Fe-Si (3 wt.%) alloy, H containing, H influence on internal friction *(Russian)* 79−38877
Fe-Si (3 wt.%) alloy, mag. domain movements prod. by mech. stress 79−87284
Fe-Si (3 wt.%) BCC single crystals, low cycle fatigue *(French)* 79−20177
Fe-Si (3 wt.%) cores with insulative coatings, morphological and struct. SEM characteris. 78−23881
Fe-Si (3 wt.%) domain struct., tensile load effects *(Russian)* 78−47995
Fe-Si (3 wt.%) grain-oriented transformer sheet, effect of phosphate coating containing Cr_2O_3 and CaO 77−16135
Fe-Si (3 wt.%) high-permeability grain-oriented steel, quenching effect on primary recrystn. texture development 80−84956
Fe-Si (3 wt.%) laminations, orientation and stacking influence on losses obs. *(Slovak)* 79−4696
Fe-Si (3 wt.%) laminations, isotropic and cube-on-face, magnetostriction behaviour 80−39843
Fe-Si (3 wt.%) laminations, magnetostriction behaviour associated with closure domain spikes 80−75834
Fe-Si (3 wt.%) laminations, grain oriented, plastically deformed, anomalous losses 80−88853
Fe-Si (3 wt.%) layers, with ceramic coating, interface struct., electron microscopy and Mossbauer obs. *(Russian)* 79−28216
Fe-Si (3 wt.%) locally deformed, EM loss depend. on cryst. struct. and orientation *(Russian)* 80−7694
Fe-Si (3 wt.%) mag. domain motion quasi-lifetime topography using white synchrotron radiation, mag. field effects 79−42797
Fe-Si (3 wt.%) sheet, obs. through surface coating of domain struct., SEM 77−85482
Fe-Si (3 wt.%) single crysts., rolling-induced mag. anisotropy *(Russian)* 78−19243
Fe-Si (3 wt.%) steel, high permeability, grain oriented 78−91886

iron alloys continued
Fe-Si (3 wt.%) steel, high permeability, magnetostriction, stress inducing coating effects 80−34730
Fe-Si (3 wt.%) steel, oriented, stress depend. mag. props., coating effects 80−34729
Fe-Si (3 wt.%) struct. and texture changes during repeated deform.-recrystn. *(Russian)* 78−88474
Fe-Si (3% wt.) polycrystalline, short-range order and induced anisotropy *(Russian)* 79−51772
Fe-Si (3%), power loss, domain wall motion depend. 77−16100
Fe-Si (3%), spikn related contrast effect, visibility of 180° ferromag. domain walls 78−43612
Fe-Si (3%wt.), dynamics of 180° domain boundaries and electromag. losses *(Russian)* 79−51801
Fe-Si (3.1 wt.%), anisotropy of electromigration of substructure of polygonisation *(French)* 77−28047
Fe-Si (3.1 wt.%), solubility product of BN 79−10955
Fe-Si (3.12 wt.%), brittle fracture, work hardening effect at notch tip 78−44220
Fe-Si (3.2 wt.%), single cryst., prism-shaped closure domains on (110) surface 79−69690
Fe-Si (3.22 wt.%), topographic and type-2 magnetic contrast, effect of collector position in SEM 79−12909
Fe-Si (3.25 wt.%), Burgers vector identification from electron microscope images 80−2030
Fe-Si (3.25 wt.%), dislocations in twin boundaries, electron microscopic images 80−34006
Fe-Si (3.25 wt.%), mag. props., influence of struct. and chemical composition of surface oxide layer 78−2700
Fe-Si (3.25 wt.%), single crystals and polycrystals, cutting surface texture 79−20291
Fe-Si (3.25 wt.%), single cryst. with (007) planes, domain struct. influence on mag. torque 80−108034
Fe-Si (3.5 wt.%), Barkhausen noise, strain depend., interaction of dislocations and domain walls 77−12155
Fe-Si (3.5 wt.%), cutting of bicrystal to compare mechanism for large crystals and polycrystals *(Japanese)* 78−60871
Fe-Si (3.5 wt.%), dynamic neutron depolarisation meas. of ferromag. domain struct. 79−82812
Fe-Si (3.5 wt.%), magnetisation reversal and domain walls 78−84451
Fe-Si (3.5 wt.%), static neutron depolarisation meas. of ferromag. domain struct. 78−14978
Fe-Si (3.5 wt.%) picture frame cryst., domain wall bowing dynamic neutron depolarisation 78−56344
Fe-Si (3.5 wt.%) picture frame, domain wall bowing, time-depend. neutron depolarisation 78−95458
Fe-Si (3.5 wt.%) plastic deform., slip initiation, X-ray topography study 79−47750
Fe-Si (3.72 wt.%) fatigue failure in vacuum and air 78−68789
Fe-Si (3wt.%), grain-oriented, secondary recryst., grain growth inhibition 80−89245
Fe-Si (3wt.%), hardening under dynamic load, grain boundary effect 77−12674
Fe-Si (3wt.%), notched sheet under tensile loading, notch tip opening/contraction, J-integral relationship *(Japanese)* 77−4840
Fe-Si (3wt.%), quantitative determ. of grain orientation and textile by etch figure method *(Chinese)* 78−11233
Fe-Si (4 at.%), Bloch wall thickness determ. by neutron small-angle scatt. 80−15754
Fe-Si (4 wt.%), coercive force, influence of stabilisation of domain struct. on temp. depend. *(Russian)* 77−52513
Fe-Si (4 wt.%), freq. depend. of Fe losses in single crysts. with (100) [001] 79−51803
Fe-Si (4 wt.%), neutron crit. scatt., experimental anisotropy 78−38590
Fe-Si (4%), (110)[001] and (100)[001], dynamic domain struct., AC excitation 77−16097
Fe-Si (5.8 at.%), mech. behaviour in microplastic strain region *(Russian)* 78−39838
Fe-Si (6.5 wt%) filament, formation by modified Taylor technique, and mag. props. 80−75795
Fe-Si (6.5 wt.%), ductility and mag. props., Ni and Mn addition effects 78−76704
Fe-Si (6.5 wt.%), effect of ordering on mag. props. 79−51833
Fe-Si (6.5 wt.%) ribbon, splat-cooled, mag. props. 80−88805
Fe-Si (6.5%), struct. and rolling texture 79−79006
Fe-Si (7.5, 14.3 at.%), mag. moments and form factors, neutron diffr. obs., d-band electron redistrib. 79−51751
Fe-Si (up to 8 wt.%), magnetostriction temp. and comp. depend. 77−66405
Fe-Si alloy, deformed by slip, polygonal boundary form. *(Russian)* 79−24534
Fe-Si alloy, Si content determ. from Seebeck coeff. 77−56269
Fe-Si alloys, kinetics of spinodal decomposition in 2-phase region of B_2+DO_3 77−28806
Fe-Si alloys, liq., refractive index, absorpt. coeff., elec. cond. 78−43830
Fe-Si alloys, recrystn. while carburising, interphase boundaries movement 79−52208
Fe-Si amorphous film, conversion electron Mossbauer effect 78−72440
Fe-Si amorphous film, crystallisation, Mossbauer studies 80−33900
Fe-Si amorphous film, Hall const. and magnetoresistive effect 78−52105
Fe-Si amorphous film, struct. and crystallisation, Mossbauer study 80−11300
Fe-Si amorphous films, mag. and magnetoelastic props. 79−99746
Fe-Si as grown crystal, dislocation study by etching and X-ray topography 78−47377
Fe-Si binary alloys, anodic behaviour using cyclic voltammetry 79−52417
Fe-Si cast alloy with spheroidal graphite, transform. investigation during tempering *(Russian)* 80−97479
Fe-Si crystal, neutron depolarisation studies of ferromagnetic domain structures 80−25155
Fe-Si ferromag. film, props. 79−4709
Fe-Si film, amorphous, conversion electron Mossbauer study 78−84507
Fe-Si gas-flame spray deposited protective coating, for C steel heat exchanger 80−61025
Fe-Si layer, growth kinetics and morphology 78−95700
Fe-Si melts, high Si, O solubility *(Russian)* 80−15252
Fe-Si plate, ferromag. domain structure obs. by neutron diffr. topography 77−69645
Fe-Si protective oxide film form. 80−11818

iron alloys continued
Fe-Si sheets, grain oriented, with insulating coating, nondestructive grain identification methods *(Slovak)* 79−5090
Fe-Si single crystals with cube-on-edge orientation, iron-loss-domain-struct. correls. *(Japanese)* 80−7534
Fe-Si single crysts., interaction of {110} 90° walls with lattice imperfections 80−39807
Fe-Si steel, high permeability, processing effect on recrystn. and deform. 77−12716
Fe-Si system, melting equilibria study *(German)* 80−66473
Fe-Si-Al, high temp. oxidation resist., comp. depend. 77−12739
Fe-Si-Al, Sendust, 12 μ thick film prep. by sputtering, mag. and other props. 77−55888
Fe-Si-Al, Sendust, ribbon-form, prep. by rapid quenching, mech. and mag. props. 80−71611
Fe-Si-Al, surface oxide layer struct., AES study 80−89396
Fe-Si-Al (2.8-3.4, 0-0.86 wt.%) oxidation, annealing 80−89395
Fe-Si-Al (5,10 wt.%) struct. anal. by electron microscopy and electron diffr. *(Chinese)* 79−11618
Fe-Si-Al (6,4 wt.%), Sendust alloy, effect of Ni content on mag. props. 78−72897
Fe-Si-Al (6.5 wt.%, up to 0.5 wt.%), elongation, cold workability and mag. permeability meas. 77−12667
Fe-Si-Al (9.6, 5.4 wt.%), ribbon-form Sendust alloy, mag. props., annealing effects 80−88800
Fe-Si-Al alloy, cryst. lattice deform. at antiphase boundaries, theoretical electron images exam. 77−11448
Fe-Si-Al ribbon-form Sendust alloy made by rapid roll quenching, mag. props., recording head appls. 80−81001
Fe-Si-Al Sendust alloy ribbon form, rapid quench prepared, elec. cond., coercive field, permeability 79−83151
Fe-Si-Al sendust type alloys, Co preferred substitution sites, Mossbauer spectra 79−91328
Fe-Si-Al-Ni alloy, Super Sendust, Ni content and thermomag. treatment effects 77−4861
Fe-Si-B, embrittlement by crystallisation *(Japanese)* 78−48513
Fe-Si-B, high induction, hot rolling treatment 80−89266
Fe-Si-B, high induction alloy, improving mag. props. by adding B to coating 79−83338
Fe-Si-B, magnetic metallic glasses, mag. props. 80−84620
Fe-Si-B, melt C content effect on grain growth and induction 80−35351
Fe-Si-B, surface tension, density, and oxidation kinetics 80−20028
Fe-Si-B amorphous alloys, metalloid content effects on Curie temp. and mag. moments 78−14956
Fe-Si-B amorphous alloys, Mossbauer spectroscopy *(French)* 80−80653
Fe-Si-B amorphous alloys with metalloid elements, embrittlement/crystn. relationship *(Japanese)* 79−96134
Fe-Si-B amorphous films, mag. props. 80−34710
Fe-Si-B amorphous powder, production by spark erosion, and mag. props. 77−90290
Fe-Si-B ferromagnetic amorphous alloys, Young's modulus and delay time characts. *(Japanese)* 77−85543
Fe-Si-B glassy alloys, mag. props., comp. effects 80−88752
Fe-Si-B magnetic powder, amorphous, prep. by atomisation technique 78−92213
Fe-Si-B metallic glass, magnetisation meas. 78−23252
Fe-Si-B metallic glasses, mag. props., depend. on metalloid content 77−85485
Fe-Si-B metallic glasses, crystn., differential scanning calorimetry obs. 79−82160
Fe-Si-B sputtered amorphous films, mag. props. and corrosion resist. 79−28567
Fe-Si-B-N-S, B, S, N effects on grain boundary segregation and grain growth inhibition, review 80−3047
Fe-Si-B-S, grain-oriented, high induction, B and S addition effect on magnetic props. *(Slovak)* 79−4697
Fe-Si-C, austenitic, C diffusivity *(German)* 80−92705
Fe-Si-C, liquid alloy, activity of Si and C *(Russian)* 78−11203
Fe-Si-C (2.86, 0.07 wt.%), internal friction peak at about 300°C *(Russian)* 77−81284
Fe-Si-C melt, Si and C activity *(Russian)* 77−55364
Fe-Si-C mixed powder, cast Fe powder sintering study *(Japanese)* 80−108373
Fe-Si-Cr magnetic films, sputtered, corrosion reduction, effect of Cr obs. 80−80573
Fe-Si-Mg, Mg residue effects on graphite spheroidization in cast Fe *(Korean)* 79−43286
Fe-Si-Mn, effect of Mn addition on mag. props. and elec. resist. 78−91890
Fe-Si-Mn (3, 0.004 to 0.1 wt.%), Mn effect on oxidation in H_2O-H_2 atmos. 78−31560
Fe-Si-Mn (6.5 wt.%, up to 0.12 wt.%), elongation, cold workability and mag. permeability meas. 77−12667
Fe-Si-Mn-C, east, Ce additions, nonmetallic inclusions *(Russian)* 78−19710
Fe-Si-MnS-Al, Al effect on hot rolling struct., recrystallization, texture magnetic props. *(Chinese)* 78−11237
Fe-Si-N alloy, BCC→FCC transform., martensitic character obs. *(Russian)* 78−48397
Fe-Si-Ni (6.5 wt.%, up to 2 wt.%), elongation, cold workability and mag. permeability meas. 77−12667
Fe-Si-Ti(Zr)(V)(Nb), eutectic alloy, exam. of eutectic temp., composition, and oxidation resistance 78−52767
Fe-Si-Zn, influence of trace elements on morphology *(German)* 80−108390
Fe-SiO_2, slowly and rapidly solidified, coarsening of SiO_2 77−86023
Fe-Si(Al), oxide layer form. during annealing, AES in-depth anal. *(German)* 80−16576
Fe-Si(Cr)(Ni)(Mn)(C), alloy layers formed by reaction with molten Al, X-ray, EPMA anal., hardness meas. *(Japanese)* 78−72926
Fe-Si(Ge)(Al), solid and liq. paramag. props. *(Russian)* 77−66247
Fe-Si(Mn)(C), atomisation of melt, charact. of metal powder 78−19688
Fe-Si(Ni)(Cu)(Mn)(C), dissolution rate into molten Al, convection mass transfer *(Japanese)* 78−71858
Fe-Si(3 wt.%), ferromag. alloy, mag. anisotropy induced by cold rolling 80−30114
Fe-Si(3.25 wt.%), crack nucleation depend. on twins during intense slip *(Russian)* 79−100239
Fe-Si(4 wt.%), (110) and (100)[001] oriented, simulation of domain wall bowing 80−44854

iron alloys continued
Fe-Si(6.5 wt.%) ribbon, prep. by rapid quenching and mag. props. 80−45251
Fe-Sn, dil., ferromag., temp. anomalies of Sn mag. hyperfine field and thermal expansion 79−33270
Fe-Sn, grain boundary embrittlement by Sn segregation, Mossbauer study 80−7239
Fe-Sn, segregation of Sn, kinetics, theory 80−11649
Fe-Sn, thermodynamic assessment, phase diagram 79−91618
α-Fe-Sn alloy, grain boundary hardening and segregation 80−55417
Fe-Sn compounds, type of binding *(German)* 77−35503
Fe-Sn liquid alloy, conc. depend. of enthalpy of form., conc. depend. *(Russian)* 78−44081
Fe-Sn system, Sn binding state, using segregated ^{119m}Sn, Mossbauer anal. *(Japanese)* 80−20525
Fe-Ta, nuclear mag. moment of ^{182}Ta NMR-ON study 80−78139
Fe-Ta alloy, mech. drawn and aged, exam. of electrical resistivity, hardness, microstruct., and mag. props. *(Japanese)* 78−48545
Fe-Tb, magnetoelastic hysteresis, elastic stress and mag. field depend. *(Russian)* 80−65982
Fe-Tb dilute alloy, amorphous, small angle mag. scatt. 78−27021
Fe-Tb film, magneto-optic coeff. and refr. index, ellipsometric determ. 80−71501
Fe-Ti, BCC, mag. moment distrib. 79−47240
Fe-Ti, D storage, desorption isotherm and struct. study by neutron diffr. 79−1549
Fe-Ti, dislocation mobility and internal friction, effect of alloying in α-Fe *(Russian)* 77−31671
Fe-Ti, H_2 storage appl., alloy bonding theory approach 78−18786
Fe-Ti, industrial hydride reservoir, charact., technological aspects 80−45792
α-Fe-Ti, ion implanted, microstruct., ion beam anal. and TEM study 80−107294
α-Fe-Ti, ion implanted, with C impurity, microstruct. of TiC precips. 80−66513
α-Fe-Ti, ion-implanted and annealed, microstruct. evolution 80−15132
Fe-Ti, mag. moment distrib. and environmental effects around Ti impurity 80−7092
Fe-Ti, mag. permeability disaccommodation rel. to dissolved N migration *(Polish)* 79−95611
Fe-Ti, magnetic aftereffects of H isotopes, book contrib. 79−82835
Fe-Ti, magnetism and H_2 storage 80−70941
Fe-Ti, multiphase binary diffusion couple, layer growth rate of intermediate phase, numerical calc. *(Japanese)* 78−14513
Fe-Ti, precipitation hardening of α-Fe containing weak and strong particles 80−20946
Fe-Ti, solubility and diffusivity of H and D in mixed crystal phase, elec. cond. meas. *(German)* 80−107575
Fe-Ti, Ti as H trap for embrittlement control 80−66662
Fe-Ti (V)(W), dil., thermophysical props. and elec. cond., temp. depend. 80−96842
Fe-Ti (0.056 at.%), mobile dislocations during stress relaxation 78−68721
Fe-Ti (0.056 at.%), mobile dislocations during stress relaxation 78−68722
Fe-Ti (0.056 at.%), stress relaxation curves, anal. interpretation 77−59847
Fe-Ti (0.056 at.%) alloy, mobile dislocations during stress relax. 77−7729
Fe-Ti (0.056 wt.%), mobile dislocations during stress relaxation, comment 79−74193
Fe-Ti (0.056 wt.%), mobile dislocations during relaxation, reply to comment 79−74194
Fe-Ti (0.15 wt.%), H trapping obs. by high resolution autoradiography 79−73205
Fe-Ti (0.15 wt.%), Ti distrib., segregation, FIM anal. 80−84200
Fe-Ti alloys, kinetic trapping model for H_2-induced grain boundary cracking 79−29164
Fe-Ti metal hydrides, numerical physical property data for H storage 80−40929
Fe-Ti multiphase, binary diffusion couple, layer growth rate of intermediate phase *(Japanese)* 78−14514
Fe-Ti:H(D), isotope effects of diatomic TiH and TiD complexes 79−47259
Fe-Ti-C, quantitative anal. of H trapping 79−23622
Fe-Ti-C, rapidly quenched by splat-cooling 80−84923
Fe-Ti-D, ion implanted, D trapping, 90-500K 80−15131
α-Fe-Ti-N, mag. migrational relax., −60 to +200 degrees C 77−36099
Fe-Ti-S-(C), sulphide phases *(Russian)* 77−25017
Fe-Ti-Sb-C alloys, Sb trapping effect on temper embrittlement, ion beam study 78−92312
Fe-Ti-Si-Ni-P-C-S, H_2 segregation kinetics *(Russian)* 78−18832
Fe-Ti-V-C-N, equilibrium comp. and solubility in steels, model of ideal solns. *(Russian)* 80−60832
Fe-Ti-(Mn)(O), exam. of interrelations between phase diagrams and hydriding props. 79−8277
Fe-TiB_2, eutectic alloy, high temp. props. 78−84931
Fe-TiB_2, phase composition, secondary ion-ion emission study *(Russian)* 80−20896
Fe-TiC pseudofused composite magnetoabrasive powders, props. 80−100926
Fe-Ti(Nb), internally nitrided, mech. props. 77−44307
γ-Fe-transition metal alloy, mag. moment in FCC d-metal lattices *(Russian)* 78−72337
Fe-V, ^{59}Fe self-diffusion *(Czech)* 80−88352
Fe-V, conc. depend. of mag. moment distrib., polarised neutron diffr. meas. 78−19218
Fe-V, Curie temp. determ. using deviation from Mattheisen's rule 79−15306
Fe-V, dilute, irradiation softening effect on yield stress 80−76319
α-Fe-V, dilute alloy, Mossbauer diffusion line broadening, exponential fitting evaluation 78−52379
Fe-V, dislocation mobility and internal friction, effect of alloying in α-Fe *(Russian)* 77−31671
Fe-V, elec. resist. between 78 and 1200K 77−8065
Fe-V, ferromag. struct. in nucl. spin echoes 80−60453
Fe-V, H permeability, 300-700°C *(Russian)* 77−15627
Fe-V, local environment effect on atomic moments, itinerant model 78−68188
Fe-V, order-disorder transition and σ-phase form. 80−7555
Fe-V, polarised neutron diffr., appl. of multiband CPA theory 77−77033

iron alloys continued
Fe-V, with atomic short range order, local environment effects on electronic struct. 78−67936
Fe-V (1 wt.%), nitrided and annealed, struct. 77−8998
Fe-V (10 to 50 at.%), solid soln., tempered, exam. of long and short range order, using Mossbauer effect *(Russian)* 79−29105
Fe-V (1.06, 5.23, and 15.55 wt.%), nitriding 78−3253
Fe-V alloys, hyperfine fields at solute and solvent sites rel. to mag. moments 77−8461
Fe-V alloys, Mossbauer study, hyperfine field effect on formation of local moments 78−27134
Fe-V solid solution, diffusion of V 79−90817
Fe-V-C, austenite to ferrite+precipitate reaction, TEM/STEM study 80−3075
Fe-V-C (0.3, 0.05 wt.%), interphase precipitation obs. in assoc. with Widmanstatten ferrite lateral growth 80−40365
Fe-V-C melts, electron struct., mag. susceptibility meas. *(Russian)* 78−47729
Fe-V-S-(C), sulphide nature exam. by X-ray spectral anal., solidification effects *(Russian)* 79−52191
Fe-VC alloys, struct. and mech. props. 79−52171
Fe-VC-WC(TiC), sintering, densification 80−25615
Fe-VN(NbN)-(C), dispersion hardening effect on mech. props. 78−3137
Fe-V(Cr)(Mn), dil., local mag. moments, polarised neutron elastic diffuse scatt. 80−50088
Fe-V(Cr)(Mn)(Ni), unlimited component solubility, intercrystallite internal adsorption *(Russian)* 80−39294
Fe-V(Cr)(Mo)(W)(Ti)(Nb) alloys, split bands evidence from sp. ht. and elec. transport data 77−24515
Fe-V(Nb)-N, precipitation study, 550 to 600°C *(German)* 77−90350
Fe-W, dislocation mobility and internal friction, effect of alloying in α-Fe *(Russian)* 77−31671
Fe-W, Gibbs energy of form. of phases *(German)* 80−97724
Fe-W (5%), internal friction, mag. and nonmag. components *(Russian)* 78−48018
Fe-W system, damping capacity of Gentalloy, internal friction, mech. and mag. props. 79−77679
Fe-W-C, eta carbides at 1250°C 77−36506
Fe-W-C-Cr, eta carbides at 1250°C 77−32581
Fe-W-Cr-Mo system, mag. and mech. props. rel. to production methods *(Japanese)* 80−71107
Fe-W-Cr-Mo-Co (18,12,3,x wt.%) magnetisation and hardness, cold working effect obs. *(Japanese)* 77−40428
Fe-W-Cr-Mo-Co with austenitic phase, magnetic and mech. props., cold working and ageing effects *(Japanese)* 78−60678
Fe-W-P-C, amorphous, corrosion resist. in 1N HCl 78−80678
Fe-WC-VC(TiC), sintering, densification 80−25615
Fe-W(Ni), recrystallisation under laser irradiation *(Russian)* 78−35396
Fe-X-C (X=Cr, Mo, W), quenched rapidly from melts, nonequilib. phases *(Japanese)* 80−71630
Fe-X-MoS_2 (X=WC, HfC, Al_2O_3, ZrO_2, HfB_2, ZrB_2), self lubricating coatings, exam. of props. 79−96217
Fe-Y, amorphous, resist. and magnetoresist. meas., local moment system 78−68018
Fe-Y, dil., hyperfine interactions, $^{87}Y^m$ nuclear orientation meas. 78−43715
Fe-Y(Lu) amorphous films, mag. props., Mossbauer effect and magnetisation meas. 79−69701
Fe-Y(Th)(Zr), amorphous, charge transfer and mag. props., ^{57}Fe Mossbauer spectra 79−19719
Fe-Zn, chemically induced grain boundary motion 78−38724
Fe-Zn, coercive force anisotropy after cold plastic deform. *(Bulgarian)* 80−75809
Fe-Zn, crystallographic relations by X-ray diffr. 80−24408
Fe-Zn, diffusion coefficients in δ_1 phase *(Japanese)* 78−14512
Fe-Zn, δ-phase, X-ray analysis 77−59758
Fe-Zn, galvanised coating appl., metallurgy review 79−96199
Fe-Zn, galvanization study *(French)* 80−66447
Fe-Zn, homogeneous intermetallic cpd., synthesis and charact., ξ-phase 79−83177
Fe-Zn, homogeneous intermetallic cpd., synthesis and charact., δ_1-phase 79−87616
Fe-Zn, homogeneous phases, Gibbs free energies of form., Knudsen effusion method 80−66481
γ-Fe-Zn, inversion antiphase domains, formation and stabilisation, electron conc. effect 78−14363
Fe-Zn, layer formed in diffusion couple, effect of small alloying element addition *(French)* 77−43388
Fe-Zn, liquid-solid reaction in Zn bath, effect of Fe concentration, alloy layer growth, exam. *(Japanese)* 78−85037
Fe-Zn, multiphase diffusion 78−79822
Fe-Zn, phase diagram, DTA, EDAX, X-ray diffr. study 80−50602
Fe-Zn, phase diagram, ferrite-austenite phase boundaries, X-ray diffr. exam. *(German)* 78−80510
Fe-Zn, phase diagram Zr aggregated effect on Fe corrosion *(Dutch)* 78−48571
Fe-Zn, physical-chemical metallurgy *(German)* 80−108390
Fe-Zn, quenched, martensite struct. and hardness, electron microscope exam. *(Russian)* 80−66619
Fe-Zn, stable and metastable alloys, order-disorder, mag. interactions and corrosion behaviour 78−68422
Fe-Zn alloys, electrochem. corrosion of ζ, δ_1 phases *(French)* 79−20274
Fe-Zn compound form. after hot galvanising Fe with liquid Zn and by diffusion *(French)* 79−20275
Fe-Zn couple, Zn electrodeposited on polished Fe, reaction rate in solid state *(Japanese)* 78−15322
Fe-Zn intermetallides, initial stages of form. *(Russian)* 80−20889
δ-Fe-Zn layer formed on hot dip galvanising, texture 77−9001
Fe-Zr, amorphous phase form. in Zr-poor region, hardness and fracture strength *(Japanese)* 80−84914
Fe-Zr, dilute solid solution, surface segregation, AES exam. 77−43413
Fe_2-Mn-Al alloys, Fe-rich, disordered, local moments on Fe and Mn 77−43811
Fe_2-rare earths, H_2 reaction, thermal anal. 79−100434
Fe_3, effect of adsorbed H on mag. props. 77−63129
Fe_3-Al, solid soln., rheological study of crystallographic order on creep *(French)* 80−97548
Fe_{40} $Ni_{40}B_{20}$, amorphous alloy, ductile-brittle transition temp., relation to composition 78−52972
$(Fe\text{-}Co\text{-}Ni)_{78}Si_8B_{14}$, amorphous, low coercivity and zero magnetostriction 78−23299

iron alloys continued
$(Fe\text{-}Ni\text{-}Mo)_{80}(P\text{-}B)_{20}$, amorphous, mag. aftereffects and struct. instabilities 80−88833
$(Fe\text{-}Ni)_{1-x}(SiO)_x$, cermet film, internal strsses *(Russian)* 78−75951
FeAl B2 struct., band struct. and density of states, KKR calc. 78−63969
FeAl, bonding, self-consistent energy bands 78−91610
FeAl, electronic struct., cluster calc. 77−69209
ε-FeAl, eutectoid, directional decomp. rate rel. to lamellar period 77−4773
ε-FeAl, eutectoid, directional decomp. rate, reply to comments 77−4775
ε-FeAl, eutectoid directional decomp. rate, comment 77−4774
FeAl intermetallic, constitutional vacancies, lattice parameter and thermal vacancy conc. obs. 79−23599
FeAl, isomer shift, electronic charge density 78−80264
FeAl, order parameter, atomic scattering factor, thickness fringes in electron micrographs 79−10832
FeAl, positron localisation in metallic alloys 78−79962
FeAl single crystal, compressed, dislocation arrangement 78−14354
FeAl, X-ray spectra, electronic structure 79−78793
$FeAl_x$, ferromag. to mictomag. transition, Mossbauer meas. 77−24692
$Fe_{0.7}Al_{0.3}$, local environment effects and magnetic clustering 78−10658
Fe_2Al, mag. moment determ., role of local environment, self consistent calcs. 80−44815
Fe_3Al, alloys, superlattice-fringe imaging theory, images formed from two beams 80−79649
Fe_3Al, computer simulation of energy dissipation from near threshold knock-ons 78−30666
Fe_3Al, containing C in solid solution., mag-permeability disaccommodation *(Polish)* 79−95613
Fe_3Al, Cu^+ (Au^+) ion-bombarded 80−15167
Fe_3Al, elec. resist. due to crit. fluctuations near order-disorder temp., theory 77−40071
Fe_3Al, electrical resistivity and LRO, energy gap formation in Fermi surface 80−88533
Fe_3Al, electronic structure, X-ray spectra comparison with band struct. calcs. 80−97383
Fe_3Al, electronic structure, magnetic moments 80−107695
Fe_3Al, exam. of hyperfine field variations with order state 80−6800
Fe_3Al, long-range order parameter from electron micrograph thickness fringes 77−65938
Fe_3Al, magnetic form factor 78−76222
Fe_3Al, magnetoresistance tensor depend. on degree of ordering, −196 to 650°C *(Russian)* 77−31997
Fe_3Al, order-disorder transform. effect on optical and elec. props. *(Russian)* 77−39820
Fe_3Al, order-disorder transition, elec. resistance meas. 79−42518
Fe_3Al, order-disorder transition effect on low energy spin waves 79−47271
Fe_3Al, ordered, magnetostriction and thermal expansion 80−39842
Fe_3Al, ordered alloys, atomic order parameters from topology of electron-microscope diffr. contrast from antiphase boundaries, quantitative determ. 78−95016
Fe_3Al, ordered binary alloy, computer simulation of radiation effects 78−87709
Fe_3Al, partly disordered B2 struct., spin wave dispersion relation 78−64201
Fe_3Al, phase separation 77−63664
Fe_3Al, roll magnetic anisotropy and dislocations *(Japanese)* 77−80930
Fe_3Al, slip geometry and pseudoelastic behaviour, effect of crystal orientation *(French)* 78−87681
Fe_3Al, super-lattice, band theory 77−15758
Fe_3Al, vacancy conc. and ordering conc. 78−18639
Fe_3Al-M, ternary ordered solid solns. with M=Ti, Mn, Ni, Cu, Ge substituent 77−43177
$Fe_{49.7}Al_{50.3}$, Compton scatt., 59.54 keV γ-rays, charge transfer study 78−68578
$Fe_{70.8}Al_{29.2}$, meas. of ordering instability 79−38818
$Fe_3Al_xSi_{1-x}$, DO_3 structured, ferromag., lattice parameters 79−42010
$Fe_{73}Al_xSi_{27-x}$, DO_3 structured, ferromag., lattice parameters 79−42010
FeAs, Mossbauer spectra of paramag. and ferromag. states, helimagnetic spin ordering 80−7197
$Fe_{1-x}Au_x$, amorphous, elec. resist., temp. depend., spin wave contrib. and resist. minimum 78−51961
FeB and Fe_2B, multiplet splitting of ESCA Fe 3s core levels 80−29847
$Fe_{0.8}B_{0.2}$ alloy amorphous thin films, anisotropic mag. and microstruct. props. 78−95487
$Fe_{1-x}B_x$, amorphous, hyperfine fields and local mag. moments, Mossbauer study 80−75895
$Fe_{1-x}B_x$ amorphous film, crystn., TEM obs. 79−87019
$Fe_{1-x}B_x$ amorphous films, mag. props. and thermal stability 79−78446
$Fe_{1-x}B_x$ film, optical and magneto-optical characts., mag. preps. 79−82956
$Fe_{1-x}B_x$ metallic glasses, struct. and cryst., Mossbauer spectra, DSC, and magnetisation meas. 79−94906
$Fe_{1-x}B_x$, polycrystalline and amorphous sputtered films, Brillouin spectra 80−2775
$Fe_{100-x}B_x$ ($11.5 \leq x \leq 22$), magneto-volume effect 78−91922
$Fe_{100-x}B_x$, amorphous, effect of metalloids on mag. props. 79−11304
$Fe_{100-x}B_x$, amorphous, mag. saturation, spin wave stiffness, temp. depend. 80−75741
$Fe_{100-x}B_x$, amorphous, mag. struct., mag. susceptibility meas. 80−80485
$Fe_{100-x}B_x$ amorphous alloys, magnetostriction meas. 79−19760
$Fe_{100-x}B_x$, amorphous alloys, saturation magnetostriction and annealing behaviour 80−34739
$Fe_{100-x}B_x$, crystalline and glassy, low temp. magnetisation study 79−95608
$Fe_{100-x}B_x$ glass, magnetostriction meas., temp. depend. 79−73792
$Fe_{100-x}B_x$, mag. and struct. props., comp. depend. 78−60314
$Fe_{100-x}B_x$ metallic glass, magnetisation meas. 78−80134
$Fe_{100-x}B_x$, quenched ferromag. ribbon, Brillouin spectra 80−2776
$Fe_{100-x}B_x$ ribbon, magnetostriction exam. 79−73794
Fe_3B, distinctness of magnetic hyperfine fields associated with structurally unique Fe sites 77−63330
Fe_3B, mag. props., ^{57}Fe Mossbauer spectra meas. 79−95693
$Fe_{75}B_{25}$ metallic glass, nonisothermal meas. evaluation, non-existence of dynamic correction term 80−107406
$Fe_{80}B_{20}$, absolute thermoelectric power between 300 and 1000K 79−19579
$Fe_{80}B_{20}$, amorphous, Brillouin scatt. from magnons, ferromag. reson. 80−65844
iron alloys continued
$Fe_{80}B_{20}$, amorphous, cold neutron scatt., local and extended defects 80−84089
$Fe_{80}B_{20}$, amorphous, crystallization 78−42917
$Fe_{80}B_{20}$, amorphous, crystn. temp. under press. 79−23523
$Fe_{80}B_{20}$, amorphous, crystn. 80−75187
$Fe_{80}B_{20}$, amorphous, deform. and annealing effects on mag. and mech. props. 77−12717
$Fe_{80}B_{20}$, amorphous, elec. and mag. hyperfine field distribs., Mossbauer study 80−39964
$Fe_{80}B_{20}$, amorphous, evaluation of complex Mossbauer spectra 78−43755
$Fe_{80}B_{20}$, amorphous, fast neutron and fission fragment irrad., effect on elec. resist. 80−19846
$Fe_{80}B_{20}$, amorphous, mag. permeability aftereffect during annealing 80−88834
$Fe_{80}B_{20}$, amorphous, transverse magnetoresist., stress effect 80−15501
$Fe_{80}B_{20}$ amorphous alloy, low field magnetic props. 77−55690
$Fe_{80}B_{20}$ amorphous alloys, domain struct. exam., magneto-optic Kerr effect 79−28550
$Fe_{80}B_{20}$, amorphous ferromag., temp. depend. of hyperfine field distrib. 78−43756
$Fe_{80}B_{20}$, amorphous ferromag. metallic glass, stress-induced rot. of magnetisation, Mossbauer study 80−20445
$Fe_{80}B_{20}$, amorphous ferromagnet, Mossbauer hyperfine fields, mag. struct. 80−75894
$Fe_{80}B_{20}$ amorphous ribbons, magnetomechanical coupling constant and Young's modulus, mag. annealing 79−15333
$Fe_{80}B_{20}$ amorphous ribbon, initial susceptibility time lag 80−100579
$Fe_{80}B_{20}$, amorphous struct., Mossbauer spectroscopy investigation 80−84677
$Fe_{80}B_{20}$, amorphous to cryst. transorm. 80−34188
$Fe_{80}B_{20}$ amorphous wire, crystn. by annealing at 780°C 80−100177
$Fe_{80}B_{20}$, crystallisation of amorphous alloys, TEM and X-ray diffr. exam. of struct., growth characts. 78−79539
$Fe_{80}B_{20}$, elastic, magnetoelastic and thermal props. 79−19759
$Fe_{80}B_{20}$, evaluation of complex Mossbauer spectra 78−60370
$Fe_{80}B_{20}$, $Fe_{78}Mo_2B_{20}$ glasses, internal friction and shear modulus 79−52287
$Fe_{80}B_{20}$, ferromagnetic metallic glasses, Brillouin scattering 78−92085
$Fe_{80}B_{20}$ film, amorphous metallic, standing spin waves, Brillouin scatt. obs. 80−97291
$Fe_{80}B_{20}$ glass, low-field mag. props. 77−8380
$Fe_{80}B_{20}$ glass, magnetisation reorientation, Mossbauer effect 80−66092
$Fe_{80}B_{20}$ glass, temp. depend. of magnetostriction 77−59443
$Fe_{80}B_{20}$, glassy, ferromag. anisotropy of resistivity 79−23939
$Fe_{80}B_{20}$, hardness, elec. cond., photo emission, and mag. props. *(Norwegian)* 79−32909
$Fe_{80}B_{20}$, METGLAS 2605, mag. anisotropy and electronic struct., Mossbauer meas. 77−28384
$Fe_{80}B_{20}$, magnetostriction, temp. depend. 78−91921
$Fe_{80}B_{20}$, metallic glass, ferromag. props. 77−16107
$Fe_{80}B_{20}$, metallic glass, elec. resist., 78 to 1000K, probe of crystn. process 77−76787
$Fe_{80}B_{20}$, metallic glass, Mossbauer spectroscopy 78−60365
$Fe_{80}B_{20}$ metallic glass, spin texture determ. 80−15842
$Fe_{80}B_{20}$, metallic glass, high-resolution XPS study, electronic state struct. 80−29846
$Fe_{80}B_{20}$, metallic glass, low temp. specific heat, metalloid effects 80−34654
$Fe_{80}B_{20}$, metallic glass, triplet correlation, field-ion microscopy study 80−38921
$Fe_{80}B_{20}$, metallic glass, Doppler broadening of positron annihilation γ-radiation and elec. resist. 80−66321
$Fe_{80}B_{20}$ metallic glass, crystn. and struct. relax., Mossbauer effect study 80−75182
$Fe_{80}B_{20}$ metallic glass, crystn. kinetics 80−84083
$Fe_{80}B_{20}$, metallic glass, optical and magneto-optical props. 80−84728
$Fe_{80}B_{20}$ metallic glasses, stability and transforms. 80−75174
$Fe_{80}B_{20}$, Metglas 2605, amorphous ferromag., resistivity down to 60 mK 79−60783
$Fe_{80}B_{20}$, Metglas 2605, amorphous ribbon, power loss variation with freq. and applied stress 80−88849
$Fe_{80}B_{20}$, Metglas 2605, Young's modulus meas. using piezoelectric US composite oscillator technique 80−108656
$Fe_{80}B_{20}$ Metglass, Mossbauer spectra line broadening 78−52400
$Fe_{80}B_{20}$, sputter deposited amorphous, low field mag. props. 78−68335
$Fe_{81}B_{19}$ amorphous alloy, mag. anisotropy temp. depend. 78−14953
$Fe_{83}B_{17}$ metallic glass, struct. from neutron diffr. study 80−6363
$Fe_{83.4}B_{16.6}$, amorphous, mag. props. and microstruct., cooling rate and melt overheating effects 80−65965
$Fe_{83.4}B_{16.6}$ amorphous, mag. props., melt overheating and cooling rate effects 80−89371
$Fe_{84}B_{16}$, amorphous, struct., X-ray diffr. meas. 79−4252
$Fe_{84}B_{16}$, metallic glass, electrical resistivity and crystallisation 80−88526
$Fe_{84}B_{16}$, metallic glass, ion implanted, UPS meas. 80−97411
Fe_xB_{100-x}, amorphous, mag. props., ^{57}Fe Mossbauer spectra and magnetisation meas. 79−95693
Fe_xB_{100-x}, amorphous, stress relax. after annealing 80−55447
$Fe_{80}(B_xC_{1-x})_{20}$, amorphous, saturation magnetostriction, comp. effects 80−34735
$Fe_{84}B_{16-x}C_x$, amorphous, hyperfine interaction and Curie temps., Mossbauer meas. 79−73858
$Fe_{84}B_{16-x}C_x$, amorphous, mag. saturation, spin wave stiffness, temp. depend. 80−75741
$Fe_{84}B_{16-x}C_x$, amorphous alloys, short range order, Mossbauer and DSC study 80−39960
$FeB_5C_{15}SSi_{15}Cr_5$, amorphous, exam. of metalloid atom mobility by Auger spectroscopy 78−47575
$Fe_{80}B_{20-x}Ge_x$, amorphous, mag. saturation, spin wave stiffness, temp. depend. 80−75741
$Fe_{80}B_{20-x}M_x$ (X=Al, Si, Ge, C, P) and $(FeCo)_{80}B_{20}$ glass, magnetisation, Curie and crystn. temps. 79−87289
$Fe_{80}(B_{1-x}P_x)_{20}$ amorphous alloys, isothermal crystallisation kinetics 80−33895
$Fe_{40}B_{40}P_{14}B_6$, Metglas 2826, amorphous ribbon, power loss variation with freq. and applied stress 80−88849
$Fe_{78}B_{12}Si_{10}$, amorphous, continuous versus discrete hyperfine field distrib., Mossbauer spectra 79−33583
$Fe_{78}B_{12}Si_{10}$, amorphous, Mossbauer study of hyperfine interaction and mag. anisotropy 80−40027

iron alloys continued
$Fe_{78}B_{12}Si_{10}$, amorphous ferromagnet, long and short range exchange interactions, Mossbauer spectra and interpretation 79−56526
$Fe_{80}B_{15}Si_5$ metallic glass, large uniaxial magnetostrictive anisotropy, magnetisation reversal 80−34736
$Fe_{80}B_{20-x}Si_x$, amorphous, mag. saturation, spin wave stiffness, temp. depend. 80−75741
$Fe_{80}B_{20-x}Si_x$, metallic glass, mech. and mag. props., depend. on metalloid content 79−91213
$Fe_{80}(B_ySi_{1-y})_{20}$, amorphous, saturation magnetostriction, comp. effects 80−34735
$Fe_{81.5}B_{14.5}Si_4$, amorphous metal ribbon, stresses, magnetoelastic anisotropy and zero-field mag. domain struct. 80−44896
$Fe_{82}B_{15}Si_3$, metallic glass, low temp. specific heat, metalloid effects 80−34654
$Fe_{82}B_{18-x}Si_x$ glasses, soft mag. props. 79−73774
$Fe_{83}B_{16.5}Si_{0.5}$, amorphous, spin waves, inelastic neutron scatt. meas. 79−73701
$Fe_{84}B_{13}Si_3$, metallic glass, electrical resistivity and crystallisation 80−88526
$Fe_{100-x}Be_x$, amorphous ribbon, saturation magnetostriction, and electronically controllable delay line 79−1700
FeC_x ($x \leq 0.05$), splat-quenched, struct., elec. and mag. props. 77−21187
Fe_3C, alpha-particle irrad., Mossbauer study of nucl. reaction aftereffects 80−40015
Fe_3C, cementite, modified by rare earth metal and alloying additions, thermal stability *(Russian)* 78−56663
Fe_xC_{1-x} amorphous sputtered film, mag. props. 78−68311
$Fe_{80}(C_{1-x}B_x)_{20}$ amorphous alloy, α-Fe crystn., morphology 80−70129
α-FeC(P) solid soln., deform. interaction of atoms, pseudopot. calc. *(Russian)* 78−18636
FeCo, BCC alloy, order-disorder transform., three-body interaction effects 80−39257
FeCo disordered alloys, Mossbauer spectra, hyperfine mag. field distrib., Curie temp. 80−7198
FeCo, electronic structures, order effect 79−90938
FeCo, ferromag., surface spin waves, cluster Bethe lattice approach 80−70983
FeCo, isothermal annealing effect on lattice const. *(Japanese)* 79−20076
FeCo molecules, matrix-isolation Mossbauer spectra 80−23448
FeCo, neutron irradiated, damage rates 79−77646
FeCo, ordered alloy, 550°C change, study through elec. cond. and specific heat meas. 78−56633
FeCo, ordered and disordered alloy, annealing of point defects created by neutron irrad. at 20K *(French)* 79−1467
FeCo, planar faults, faint electron microscopic image contrast obs. 80−107283
$(Fe_{0.06}Co_{0.94})$-B, amorphous, ferromag., mag. instability rel. to struct. 79−99729
$Fe_{50}Co_{50}$, disordering by laser irradiation, Mossbauer transmission spectroscopy and electron microscopy study *(French)* 79−23639
$Fe_{50}Co_{50}$, neutron irradiation, close pair recombination *(French)* 80−39162
$Fe_{68}Co_{32}$, ferromagnet, magnon heat cond. and lifetimes, 1-2 to 4.5K 77−16066
$Fe_{1-x}Co_xAl$, Knight shift and mag. susceptibility study, electron struct. peculiarities *(Russian)* 80−15814
$Fe_{3-x}Co_xAl$, site preference and local environment effects, Mossbauer and NMR meas. 80−71264
FeCoB, corrosion-resistant amorphous mag. thin films 80−54923
$(FeCo)_{80}B_{20}$, glass, elastic consts. 79−83249
$(FeCo)_{80}B_{20}$, metallic glass, saturation moments and Curie temp. 77−1542
$(Fe_{0.5}Co_{0.5})_{1-x}B_x$, amorphous, hyperfine fields and local mag. moments, Mossbauer study 80−75895
$(Fe_{0.65}Co_{0.35})B$, crystalline disordered, evaluation of complex Mossbauer spectra 78−43755
$Fe_{0.65}Co_{0.35}B$, crystalline disordered, evaluation of complex Mossbauer spectra 78−60370
$Fe_5Co_{75}B_{20}$, amorphous, magnetisation reversal and domain boundary configs. 80−88809
$Fe_{71}Co_9B_{20}$, glassy ribbon, magnetostatic effects 79−73790
$Fe_{80-x}Co_xB_{20}$, ferromag. metallic glass saturation magnetostriction meas. 77−36108
$Fe_{80-x}Co_xB_{20}$, spontaneous Hall effect and resistivity 79−19576
$Fe_xCo_{80-x}B_{20}$, amorphous, mag. after-effect 79−61189
$Fe_{35}Co_{32}B_{20}Si_{10}Al_3$, stress-induced variation in magnetisation and dynamic magnetostrictive charact. 80−88855
FeCoC, unidirectionally transformed eutectoid, crystallography of herringbone pearlite, TEM obs. 78−31399
$Fe_{0.5}Co_{0.5-x}Cr_x$ films, vacuum-deposited cryst. and mag. struct. *(Russian)* 80−93081
$(Fe_{0.07}Co_{0.93})_{75-x}Cr_xSi_{15}B_{10}$, amorphous, disaccommodation of mag. permeability and induced anisotropy 80−88741
Fe_2CoGa, alloy, site preference of Co and Fe, Mossbauer and neutron study 79−78577
$(FeCoNi)_8B_{20}$, glass, evidence supporting split-band model from magnetostriction 78−95509
$(Fe_xCo_yNi_{1-x-y})_{78}Si_8Bi_{14}$ amorphous ribbons, saturation magnetostriction and vol. magnetostriction 77−85538
$(Fe_{0.2}Co_{0.8})_{80}P_{17}Al_3$, Mossbauer spectra, isomer shift, mag. hyperfine field 80−11301
$(Fe_{100-x}Co_x)_{79}P_{13}B_8$, amorphous, hyperfine field distrib., ^{59}Co NMR spin-echo meas. 80−34818
$(Fe_{1-x}Co_x)_yPBAl$ metallic glasses, influence of composition and ageing on Curie temps. 77−85445
$(Fe_{1-x}Co_x)_{80}P_{13}C_7$ amorphous alloy, soft mag. material, props. 77−4533
$FeCo_2Si$, Heusler type materials, mag. props. 77−40042
$(Fe_{0.5}Co_{0.5})Si$, weak itinerant ferromag., polarised neutron scatt. exam. 77−4503
$Fe_{1-x}Co_xSi$, mag. props., sp. ht., n.m.r. and Mossbauer effect meas. 77−12129
$(Fe_{1-x}Co_x)_3Si$, order distrib., hardening effect *(Russian)* 77−89410
$Fe_{3-x}Co_xSi$, structural, mag. moment, and hyperfine field behaviour, local environment model 79−65762
$Fe_xCo_{1-x}Si$ alloys, disordered, hydrostatic pressure effects on mag. props. 77−32175
$Fe_xCo_{1-x}Si$, mag. props., effect of hydrostatic press. 77−12101
$Fe_xCo_{1-x}Si$, mag. props. 79−56532

iron alloys continued
$(Fe_{0.05}Co_{0.95})_{78}Si_8B_{14}$ amorphous ribbon, anomalous mag. aftereffect 80−100602
$(Fe_{0.9}Co_{0.1})_xSi_yB_2$, $(Fe_{1-x}Co_x)_{78}Si_8B_{14}$ amorphous ribbons, magnetomech. coupling and saturation magnetostriction 78−68353
$(Fe_{1-x}Co_x)_{75}Si_{15}B_{10}$ amorphous alloy, soft mag. material, props. 77−4533
$(Fe_{1-x}Co_x)_{77}Si_{10}B_{13}$ alloys, amorphous, induced mag. anisotropy by mag. annealing 79−4671
$(Fe_{1-x}Co_x)_{77}Si_{10}B_{13}$, amorphous, mag. moments at 0K, Curie temp., mag. interactions 79−4670
$(Fe_{1-x}Co_x)_{77}Si_{10}B_{13}$, amorphous magnetic alloys, density meas. 80−1934
$(Fe_{1-x}Co_x)_{78}Si_{10}B_{12}$, amorphous, Hall effect and magnetoresist. *(Japanese)* 77−85199
$(Fe_{1-x}Co_x)_{78}Si_{10}B_{12}$, amorphous alloys, magnetic anisotropy meas. 80−2570
$(Fe_{1-x}Co_x)_{78}Si_{10}B_{12}$, amorphous, roll mag. anisotropy 80−75757
$(Fe_{1-x}Co_x)_{78}Si_8B_{14}$ ribbon, magnetostriction exam. 79−73794
$Fe_{4.7}Co_{70.3}Si_{15}B_{10}$, amorphous ferromag., roll mag. anisotropy 79−51773
$Fe_5Co_{70}Si_{10}B_{15}$ amorphous magnetic alloy, decrease of permeability after demagnetisation, disaccommodation 80−39814
$Fe_5Co_{70}Si_{15}B_{10}$, amorphous ribbon, zero magnetostriction, low residual mag. loss 77−12157
$Fe_5Co_{70}Si_{15}B_{10}$, amorphous ribbon, HF mag. characts., magnetostriction role 77−66408
$Fe_5Co_{70}Si_{15}B_{10}$ amorphous ferromag. ribbons, change of permeability by heat treatment 77−85493
$Fe_5Co_{70}Si_{15}B_{10}$, amorphous, change of mag. props. by low temp. annealing 78−27058
$Fe_5Co_{70}Si_{15}B_{10}$, amorphous toroidal core, switching characts. and domain structs. 78−95477
$Fe_5Co_{70}Si_{15}B_{10}$, amorphous ferromagnetic alloy, isothermal annealing effect on static magnetic props. *(Japanese)* 79−52398
$Fe_5Co_{70}Si_{15}B_{10}$, amorphous, crystn. effect on mag. props. *(Russian)* 80−44858
$(Fe_xCo_{1-x})_{100-y}(Si_{0.4}B_{0.6})_y$ amorphous alloy zero magnetostrictive, mag. props. 79−99743
$(Fe_xCo_{1-x})_{78}Si_8B_{14}$, amorphous, saturation magnetostriction, strain modulated FMR obs. 80−75863
$(Fe_xCo_{100-x})_{100-(y+z)}Si_yB_z$ amorphous ribbon, mag. moment and Curie temp., comp. depend. 78−95421
$Fe_xCo_{1-x}Si(Ti)$, magnetic props., sp. ht. and resist. meas. 79−61120
$Fe_{1-x}Co_xSn$, transferred hyperfine fields at ^{119}Sn, Mossbauer spectroscopy 79−33582
$Fe_xCo_{1-x}Ti$, ferromag., high-field and high-press. mag. behaviour 78−91919
$Fe_xCo_{1-x}Ti$, high press. mag. props. 78−23271
$Fe_xCo_{1-x}Ti$, mag. props. 79−56532
$Fe_{0.5}Co_{0.5}TiH_x$, transmission Mossbauer spectra 80−44964
$FeCo_2V$, ordered and disordered alloys, annealing of point defects created by neutron irrad. at 20K *(French)* 79−1467
$Fe_{49}Co_{49}V_2$, neutron irradiation, close pair recombination *(French)* 80−39162
$Fe_{1-x}Cr_x$, Mossbauer exam. 77−16222
$(Fe_{1-x}Cr_x)$-P-C, amorphous mag. props. *(Japanese)* 77−85433
Fe_xCr_{1-x}, spin-wave evolution crossing from ferromag. to spin-glass regime 80−97080
$Fe_{65.4}Cr_{20.5}Al_{10.7}V_{3.4}$, effect of Al and V on form. of $L2_1$ superstructure and stratification 77−77474
$Fe_{85-x}Cr_xB_{15}$ metallic glass, Curie temp., crystn. temp. and room temp. elec. resist., Cr content effect 79−91229
$Fe_{36}Cr_{32}Ni_{14}B_{12}B_6$, amorphous X-ray absorpt. spectra, effective coordination charges 80−84805
$(Fe_{98}Cr_2)_{79}P_{13}B_8$ and $(Fe_{96}Cr_4)_{79}P_{13}B_8$, amorphous, low temp. sp. ht., mag. contribs. 80−80552
$Fe_{36}Cr_{12}Ti_7Mo_3$, high temp. precipitation kinetics, internal friction study 79−43254
$Fe_5(Fe_{1-y}Co_y)$, mag. and calorimetric props. 77−63083
Fe_3Ga, Ll_2 ordered alloy, positive temp. depend. on strength, phase destabilization 80−81203
FeGd, H_2 and N_2 contaminated amorphous films, mag. props. 79−1690
Fe_xGd_{1-x}, $0.5 > x > 0.65$, amorphous film, FMR, spin wave spectra 77−16181
FeGe, cubic, spin reson., 4.2-300K, 3-35 GHz 79−38384
FeGe, hexagonal, low-temp. mag. struct., neutron diffr. meas. 78−95418
FeGe, hyperfine interactions of ^{119}Sn atoms, Mossbauer spectra *(Russian)* 80−29665
$FeGe_2$, amorphous film, annealing effects on struct. and elec. resist. 77−85099
$FeGe_2$, antiferromag., Fermi surface, stress effects, oscillatory magnetostriction and torque meas. 80−103616
$FeGe_2$, antiferromagnet, de Haas-van Alphen effect 79−4505
$FeGe_2$, collinear and canted antiferromag. structures 77−51887
$FeGe_2$, Fe_2Ge, optical consts., electron energy loss spectra meas. 77−90121
$FeGe_2$, Fermi surface press. depend., de Haas-van Alphen method 77−43478
$FeGe_2$, interface struct. and growth mechanism from melt 79−14715
$FeGe_2$, mag. struct., Mossbauer method 78−60268
$FeGe_2$, single cryst. perfection depend. on growth rate and direction 80−55284
$Fe_{1.67}Ge$, Mossbauer and X-ray expts. 79−1734
$Fe_{1.76}Ge$, interface struct. and growth mechanism from melt 79−14715
Fe_3Ge, ^{119}Sn mag. hyperfine interaction, Mossbauer spectra *(Russian)* 79−38420
Fe_3Ge amorphous films, short-range struct., electron diffr. obs. 77−24267
Fe_3Ge, mag. props. of cubic and hexagonal phases 77−8475
Fe_5Ge_3, collinear mag. struct. from Mossbauer effect meas. 77−63343
Fe_5Ge_3 film, electron diffr. study of struct. and microheterogeneity 77−85108
β-Fe_5Ge_3 formation in isothermal sintering, phase transition kinetics 80−89197
Fe_xGe_{1-x}, amorphous, conversion electron Mossbauer spectra down to 4.2K 80−7205
Fe_xGe_{1-x}, amorphous, mag. behaviour, rel. to Fe_xSi_{1-x} and Fe_xSn_{1-x} amorphous alloys 78−95478
Fe_xGe_{1-x}, amorphous alloy, short range order anal. 77−80423
Fe_xGe_{1-x} amorphous alloys, conversion electron Mossbauer spectroscopy 78−84504
Fe_xGe_{1-x} amorphous alloys, high field mag. meas. 79−82765

iron alloys continued

Fe_xGe_{1-x}, amorphous film, FMR meas. of mag. props., temp. and comp. depend. 77−69636
Fe_xGe_{1-x} amorphous film, low temp. conversion electron Mossbauer spectroscopy 78−48101
Fe_xGe_{1-x} amorphous film, XPS and Mossbauer exam. 79−56577
Fe_xGe_{1-x}, liq., ang. distrib. of positron annihilation 77−55848
Fe_2Hf, ferromagnetism in hexagonal and cubic compounds 77−36074
$Fe_{83-x}M_xB_{17}$ and $Fe_{78-x}M_xSi_{10}B_{12}$ (M=refractory metal), glass form. and thermal stability 80−79703
FeMn, dil., diffuse scatt. cross sections, polarized neutrons 78−43567
γ-FeMn, itinerant antiferromag., spin dynamics, neutron scatt. meas. 77−12105
$Fe_{1-x}Mn_x$, elec. resist., anomalies in temp. depend. 79−23942
Fe_3Mn-Fe_3Si, slow neutron polariser, by single cryst. (111) refl. 80−49052
$(Fe_{1-x}Mn_x)_3Al$ alloys, disordered, mag. moments and distrib. on lattice sites 77−63112
$(Fe_{1-x}Mn_x)_3Al$, local Mn moment distrib., neutron scatt., nucl. spin echo *(Russian)* 77−12091
$(Fe_{1-x}Mn_x)_3Al$, mag. moments determ. from magnetisation and neutron and electron diffr. expts. 79−56520
Fe_2MnAl, dislocation structure, antiphase boundary energies, deformation behaviour prediction *(Russian)* 79−65085
Fe_2MnAl, plastically deformed, domain struct., X-ray diffr. and electron microscope obs. *(Russian)* 79−20110
$Fe_{3-x}Mn_xAl$, ordering of Fe atoms, X-ray diffr. meas. and mid gamma reson. anal. *(Russian)* 80−96469
$Fe_{2.1-x}Mn_xAs$, $0 \leq x \leq 2.1$, mag. phase transitions 78−2679
$(Fe_{1-x}Mn_x)_{75}P_{16}B_6Al_3$, amorphous, spin-glass-ferromag. multicritical point, AC susceptibility meas. 80−50117
$(Fe_xMn_{1-x})_{75}P_{16}B_6Al_3$, amorphous, mag. ordering temp., hyperfine field distrib., elec. resist. 80−34633
$(Fe_{1-x}Mn_x)_{75}P_{15}C_{10}$, amorphous, mag. ordering, Mossbauer study 80−39747
$(Fe_{1-x}Mn_x)_{75}P_{15}C_{10}$, amorphous pair radial distrib. functions, neutron scatt. study 80−49128
$Fe_xMn_{1-x}Pt_3$, ferro-antiferromag. transform. at 4.2K *(Russian)* 78−88117
$(FeMn)_3Si$ alloys, mag. and crystallographic props. by diffr., resist. and magnetisation meas. 77−59393
$(Fe_{1-x}Mn_x)Si$, US vel. rel. to mag. struct. and phase transforms *(Russian)* 77−47976
$(Fe_{1-x}Mn_x)_3Si$, mag. phase diagram determ. 77−24697
$(Fe_{1-x}Mn_x)_3Si$, order distrib., hardening effect *(Russian)* 77−89410
$(Fe_{1-x}Mn_x)_3Si$, sp. ht. at low temps., mag. transitions *(Russian)* 77−32189
Fe_2MnSi, antiferro- and ferromag. props. 77−12104
$Fe_{3-x}Mn_xSi$, evidence for the ang. depend. of the hyperfine interactions 78−76241
$Fe_{3-x}Mn_xSi$, Mossbauer and NMR exam. of site substitution and mag. struct. 77−12092
$Fe_{3-x}Mn_xSi$, struct., magnetisation, and spin echo expts., rel. to local environment model 77−20518
$Fe_{1-x}Mn_xSn$, spin reorientation, Mossbauer study, 77 to 400K 80−97172
$Fe_{1-x}Mn_xSn$, transferred hyperfine fields at ^{119}Sn, Mossbauer spectroscopy 79−33582
$Fe_{0.49}Mn_{0.01}Ti_{0.5}H_x$, localised vibrs., sp. ht. obs., room temp. 80−65248
$(Fe_{1-x}Mn_x)_2Y(B)$, Mn effect on Fe mag. moments, Mossbauer and mag. meas. 80−71016
Fe_2Mo, standard Gibbs energies, enthalpies, entropies of formation 78−61042
Fe_3Mo_2, standard Gibbs energies, enthalpies, entropies of formation 78−61042
$Fe_{76}Mo_4B_{20}$, quenched ferromag. ribbon, Brillouin spectra 80−2776
$Fe_{78}Mo_2B_{20}$, amorphous, transverse magnetoresist., stress effect 80−15501
$Fe_{78}Mo_2B_{20}$, amorphous, fast neutron and fission fragment irrad., effect on elec. resist. 80−19846
$Fe_{78}Mo_2B_{20}$, amorphous ferromag., $T^{3/2}$ depend. of hyperfine field 78−39474
$Fe_{78}Mo_2B_{20}$, amorphous ferromag., mag. props. 79−38309
$Fe_{78}Mo_2B_{20}$ amorphous ribbons, magnetoelastic effects in as-quenched and stress-relieved states 80−80588
$Fe_{78}Mo_2B_{20}$, exam. of mag. props. between 300 and 900K 78−85010
$Fe_{78}Mo_2B_{20}$ glass, thermal expansion, glass transform. and crystn. temps. 80−2183
$Fe_{78}Mo_2B_{20}$, glassy, ferromag. anisotropy of resistivity 79−23939
$Fe_{78}Mo_2B_{20}$, metallic glass, elec. resist., 78 to 1000K, probe of crystn. process 77−76787
$Fe_{78}Mo_2B_{20}$, metallic glass, triplet correlation, field-ion microscopy study 80−38921
$Fe_{78}Mo_2B_{20}$, metallic glass, Doppler broadening of positron annihilation γ-radiation and elec. resist. 80−66321
$Fe_{78}Mo_2B_{20}$, Metglas 2605 A, amorphous ferromag., resistivity down to 60 mK 79−60783
$Fe_{80-x}Mo_xB_{20}$ metallic glasses, Curie temp., crystn. temp., elec. cond. as function of composition 79−60285
$(Fe_{93}Mo_7)_{80}B_{10}P_{10}$, amorphous, neutron scatt. investig. of spin waves, magnetisation 77−47984
$(Fe_xMo_{1-x})_{75}P_{16}B_6Al_3$, amorphous, effects of Mo on mag. props., Mossbauer meas. 79−73859
FeN alloy, coercive force, effect of $Fe_{16}N_2$, anisotropic model 77−85501
γ′-Fe_2N film, mag. mechanism, at. mag. moment *(Korean)* 79−7973
Fe_4N growth kinetics in Fe-N system *(Korean)* 80−93540
FeNi amorphous films, fast phase transition investigation by TEM method 80−107029
FeNi, enrichment to 90% Ni 77−28749
FeNi, itinerant electron model, spin wave stiffness const. calc. 80−34613
FeNi-Cu, composite fibre and layer structs., anomalous props. caused by internal phase boundaries 78−72754
$(Fe_{0.5}Ni_{0.5})$-Co, solid and liq., paramag. susceptibility and electron struct., 800-1800°C *(Russian)* 80−25081
$Fe_{1-x}Ni_x$ (x<29at.%), γ-phase dispersion, Mossbauer spectra 78−52399
$Fe_{1-x}Ni_x$, elec. resist., anomalies in temp. depend. 79−23942
$Fe_{1-x}Ni_x$, FCC, anomalies in sp. ht. and thermal expansion 79−19739
$Fe_{40}Ni_{38}Mo_4B_{18}$ amorphous alloys, compatibility of DC and AC mag. props. 80−34695
$Fe_{65}Ni_{35}$, mag. cluster structs., 25-422°C 77−69493
$Fe_{65}Ni_{35}$, quasi-localised spin system, neutron scatt. 78−68194
Fe_xNi_{1-x} amorphous film, growth stress and structure factor, stabilisation by conduction electrons 80−38920
Fe_xNi_{1-x}, amorphous films, crystallisation, effect of codeposited O_2, N_2 or Kr gases 80−10807
$Fe_{1-x}Ni_xAl$, Knight shift and mag. susceptibility study, electron struct. peculiarities *(Russian)* 80−15814
FeNiB, amorphous alloy, high resolution imaging by electron microscopy 79−99039
$(FeNi)_{80}B_{20}$, glass, elastic consts. 79−83249
$(FeNi)_{80}B_{20}$, metallic glass, saturation moments and Curie temp. 77−1542
$(Fe_{0.6}Ni_{0.4})_{100-x}B_x$ and $(Fe_{100-x}Ni_x)_{80}B_{20}$ amorphous alloys, X-ray diffr. struct. determ. 80−64906
$(Fe_{1-x}Ni_x)_{75}B_{25}$, amorphous and cryst., short range order, Mossbauer study 80−39961
$(Fe_{1-x}Ni_x)_{83}B_{17}$, amorphous alloys ferromagnetic resonance 80−108080
$(Fe_{100-x}Ni_x)_{100-y}B_y$, metallic glass, embrittlement and crystn. 80−7685
$(Fe_{100-x}Ni_x)_{83}B_{17}$, amorphous, crystn. 80−75176
$(Fe_{100-x}Ni_x)_{83}B_{17}$ glassy alloys, Ni content influence on crystn., and bend ductility changes, during annealing 79−73103
$Fe_{38}Ni_{38}B_{24}$, amorphous, magnetisation and FMR expts. 79−95607
$Fe_{40}Ni_{20}B_{20}$, metallic glassy ribbon, casting conditions *(Japanese)* 80−55386
$Fe_{40}Ni_{40}B_{20}$ alloys, crystalline and amorphous, resistivity minimum, X-ray, Mossbauer studies 79−73489
$Fe_{40}Ni_{40}B_{20}$, amorphous, induced mag. anisotropy, reorientation kinetics 77−43829
$Fe_{40}Ni_{40}B_{20}$, amorphous, hyperfine field distrib., Mossbauer effect meas. 79−4755
$Fe_{40}Ni_{40}B_{20}$, amorphous, hyperfine field distrib., Mossbauer study 79−28657
$Fe_{40}Ni_{40}B_{20}$, amorphous, anomalous thermal dilatation 79−55668
$Fe_{40}Ni_{40}B_{20}$, amorphous, resist. min. disappearance on annealing 79−60786
$Fe_{40}Ni_{40}B_{20}$, amorphous, processing conditions effect on mag. props. 79−73775
$Fe_{40}Ni_{40}B_{20}$, amorphous, mag. loss meas. 79−73776
$Fe_{40}Ni_{40}B_{20}$, amorphous, high-field magnetisation curve, spin wave spectrum and microstructural inhomogeneities 80−15702
$Fe_{40}Ni_{40}B_{20}$, amorphous, casting conditions effect on mag. props. *(Japanese)* 80−34698
$Fe_{40}Ni_{40}B_{20}$, amorphous, mag. props., effects mech. deform. 80−39840
$Fe_{40}Ni_{40}B_{20}$, amorphous, phase transforms., resistometric anal. 80−75538
$Fe_{40}Ni_{40}B_{20}$, amorphous, RF annealing effects 80−108037
$Fe_{40}Ni_{40}B_{20}$, amorphous ribbon prod., apparatus parameters effect on dimens. 77−12570
$Fe_{40}Ni_{40}B_{20}$, amorphous ferromag., resist. and galvanomagnetic props., rel. to magnetisation 78−14712
$Fe_{40}Ni_{40}B_{20}$, amorphous and crystalline, resist. minimum 79−47079
$Fe_{40}Ni_{40}B_{20}$, amorphous ferromag., resistivity down to 60 mK 79−60783
$Fe_{40}Ni_{40}B_{20}$, amorphous ribbon, anal. of casting conditions 79−95965
$Fe_{40}Ni_{40}B_{20}$, amorphous ribbon, power loss variation with freq. and applied stress 80−88849
$Fe_{40}Ni_{40}B_{20}$ and $Fe_{40}Ni_{40}P_{14}B_6$, amorphous, mag. aftereffect spectra and annealing props. 80−88831
$Fe_{40}Ni_{40}B_{20}$ glass, ^{10}B self-diffusion, meas. by SIMS 80−49406
$Fe_{40}Ni_{40}B_{20}$, metallic glass, embrittlement kinetics and crystn., quenching influence 78−68766
$Fe_{40}Ni_{40}B_{20}$, metallic glass, low temp. specific heat, metalloid effects 80−34654
$Fe_{40}Ni_{40}B_{20}$, molten, jet streaming, planar and cylindrical, instabilities rel. to glassy alloy casting 80−35129
$Fe_{50}Ni_{30}B_{20}$, crystallisation of amorphous alloys, TEM and X-ray diffr. exam. of struct., growth characts. 78−79539
$Fe_{80-x}Ni_xB_{20}$ and $Fe_{80-x}Ni_xP_{14}B_6$ amorphous alloys, microhardness correl. with mag. props. 80−88826
$Fe_{80-x}Ni_xB_{20}$, $Fe_{80-x}Ni_xP_{14}B_6$, amorphous, microhardness meas., dependence on mag. props. *(Croatian)* 79−11688
$Fe_{80-x}Ni_xB_{20}$, ferromag. metallic glass, saturation magnetostriction meas. 77−36108
$Fe_{80-x}Ni_xB_{20}$, spontaneous Hall effect and resistivity 79−19576
$(Fe_{1-x}Ni_x)_{80}B_{20}$ amorphous soft magnetic films 79−82836
$(Fe_xNi_{1-x})_{80}B_{20}$, $(Fe_xNi_{1-x})_{80}P_{14}B_6$, new soft amorphous ferromagnetic glasses *(Croatian)* 79−11298
$(Fe_xNi_{1-x})_{80}B_{20}$, amorphous alloys, engineering mag. props. 79−51832
$(Fe_xNi_{1-x})_{80}B_{20}$, amorphous, Mossbauer spectra, mag. props. 80−15843
$(Fe_xNi_{100-x})_{80}B_{20}$, glassy, elec. resist. at elevated temp. 79−73484
$Fe_xNi_{80-x}B_{20}$, amorphous ferromag., low temp. resistivity 79−56181
$Fe_xNi_{80-x}B_{20}$ and $Fe_xNi_{80-x}P_{14}B_6$ metallic glasses, low temp. resist. and galvanomag. effects, mag. state influence 80−84461
$Fe_xNi_{80-x}B_{20}$, $Fe_xNi_{80-x}P_{14}B_4$, amorphous Hall effect voltage meas. *(Croatian)* 79−11102
$Fe_xNi_{80-x}B_{20}$, $Fe_xNi_{80-x}P_{14}B_6$, amorphous ferromag., galvanomag. props. 79−56196
$Fe_xNi_{80-x}B_{20}$ glass, resist., magnetoresist., and thermoelec. power 80−70681
$Fe_xNi_{80-x}B_{20}$, quenched ferromag. ribbon, Brillouin spectra 80−2776
$(Fe_yNi_{1-y})_{80}B_{20}$, mag. anneal anisotropy in amorphous alloys 77−16069
$(Fe_{1-y}Ni_y)_{0.8}B_{0.2-x}P_x$, amorphous, hyperfine fields and local mag. moments, Mossbauer study 80−75895
$Fe_{1.6}Ni_{78.4}B_{10}P_{10}$ metallic glass, superparamag. behaviour, chem. inhomogeneities role 80−84625
$Fe_{20}Ni_{60}B_{19}P_1$, amorphous, spin waves, inelastic neutron scatt. meas. 79−73701
$Fe_{40}Ni_{40}B_{20-x}P_x$, amorphous, mag. saturation, spin wave stiffness, temp. depend. 80−75741
$Fe_{40}Ni_{40}B_{20-x}P_x$ metallic glasses, local struct. and dynamic disorder of Fe and Ni, EXAFS obs. 80−89088
$Fe_{80-x}Ni_xB_{20-y}P_y$, amorphous, Rayleigh region and coercive force 80−88806
$(FeNi)_{80}Bi_{17.5}Al_2Si_{0.5}$, stress-induced variation in magnetisation and dynamic magnetostrictive charact. 80−88855
$(Fe_{0.5}Ni_{0.5})_{1-x}Co_x$, paramag. susceptibility, solid and liq. phases 1000-1800°C *(Russian)* 77−16040
$Fe_{65}(Ni_{1-x}Cr_x)$, microhardness and specific heat, depend. on Cr content *(Russian)* 79−100240
$Fe_{65}(Ni_{1-x}Cr_x)_{35}$, mag. viscosity and anomalies near Curie temp. 79−73781
$Fe_{65}(Ni_{1-x}Cr_x)_{35}$, remanent magnetisation, temp. depend., anomalies near Curie temp. *(Russian)* 78−60310

iron alloys continued
FeNiCrAlLi alloy, γ' hardened, noncellular mech. for form of lamellar η phase morphology 77−28824
$Fe_{32}Ni_{36}Cr_{14}P_{12}B_6$, Metglas 2826 A, ferromag. reson. for g-values and relax. parameters, 77 to 430K 77−63289
$Fe_{32}Ni_{36}Cr_{14}P_{12}B_6$, metallic glass, changes in Curie temp., physical dimensions and mag. anisotropy during annealing 77−85446
$Fe_{32}Ni_{36}Cr_{14}P_{12}B_6$, Metglas 2826A, Hall resistivity, effect of thermal cycling and annealing 78−56125
$Fe_{32}Ni_{36}Cr_{14}P_{12}B_6$, shear band form. 78−68756
$Fe_{32}Ni_{36}Cr_{14}P_{12}B_6$ metallic glass, dynamic mechanical props. 79−10894
$Fe_{32}Ni_{36}Cr_{14}P_{12}B_6$, elastic, magnetoelastic and thermal props. 79−19759
$Fe_{32}Ni_{36}Cr_{14}P_{12}B_6$, glassy, ferromag. anisotropy of resistivity 79−23939
$Fe_{32}Ni_{36}Cr_{14}P_{12}B_6$, METGLAS 2826A, metastable crystallization phases, TEM obs. 79−55671
$Fe_{32}Ni_{36}Cr_{14}P_{12}B_6$, amorphous ferromagnet, long and short range exchange interactions, Mossbauer spectra and interpretation 79−56526
$Fe_{32}Ni_{36}Cr_{14}P_{12}B_6$, amorphous mag. solids, Mossbauer exam. 79−61281
$Fe_{32}Ni_{36}Cr_{14}P_{12}B_6$, Metglass 2826A, mag. props. under high press., Mossbauer meas. 79−73860
$Fe_{32}Ni_{36}Cr_{14}P_{12}B_6$, Metglas 2826A elec. resist. during crystn. 79−91014
$Fe_{32}Ni_{36}Cr_{14}P_{12}B_6$ glass, thermal expansion, glass transform. and crystn. temps. 80−2183
$Fe_{32}Ni_{36}Cr_{14}P_{12}B_6$, metallic glass, high-resolution XPS study, electronic state struct. 80−29846
$Fe_{32}Ni_{36}Cr_{14}P_{12}B_6$, metallic glass, Doppler broadening of positron annihilation γ-radiation and elec. resist. 80−66321
$Fe_{32}Ni_{36}Cr_{14}P_{12}B_6$ metallic glass, crystn. kinetics by TEM 80−75186
$Fe_{32}Ni_{36}Cr_{14}P_{12}B_6$, Metglas 2826A, EPR at 20 GHz 80−75848
$Fe_{32}Ni_{36}Cr_{14}P_{12}B_6$ Metglas, bending deform., shear band form., high-speed cinematographic obs. 80−89322
$Fe_{32}Ni_{36}Cr_{14}P_{12}B_6$, Metglas amorphous films, corrosion resist. and ion plating use 80−89423
$Fe_{32}Ni_{36}Cr_{14}P_{12}B_6$ metallic glass, effect of pre-ageing on glass transition temp. 80−100326
$Fe_{0.5}(Ni_xMn_{1-x})_{0.5}$, elec. resist., anomalies in temp. depend. 79−23942
$Fe_{0.5}(Ni_xMn_{1-x})_{0.5}$, FCC, anomalies in sp. ht. and thermal expansion in paramag. temp. range 79−19739
$Fe_{65}(Ni_{1-x}Mn_x)_{35}$, anomaly of subcrit. neutron scatt. and depolarisation effects at antiferro- to ferromag. transition *(Russian)* 77−47996
$Fe_{65}(Ni_{1-x}Mn_x)_{35}$, magnetic struct. and inhomogeneities by neutron scatt. and Mossbauer effect *(Russian)* 77−63122
$Fe_{65}Ni_{28}Mn_1$, disordered, mag. struct. near ferro-antiferromagnetic transition 80−60211
$Fe_{40}Ni_{40}(Mo,Si,B)_{20}$, amorphous, soft mag. props., switched-mode power supply appls. 80−88850
$Fe_{0.49}Ni_{0.415}Mo_{0.095}$, Vibralloy, high-temp. vibrating reed meas. 79−55811
$Fe_{40}Ni_{38}Mo_4B_{18}$ amorphous ribbons, magnetoelastic effects in as-quenched and stress-relieved states 80−80588
$Fe_{40}Ni_{38}Mo_4B_{18}$, amorphous, crystallization, heat treatment and irradiation effects *(French)* 79−90558
$Fe_{40}Ni_{38}Mo_4B_{18}$, amorphous, mag. anisotropy, Mossbauer study 80−65864
$Fe_{40}Ni_{38}Mo_4B_{18}$, amorphous, reversible enhancement of mag. directional ordering rate 80−103829
$Fe_{40}Ni_{38}Mo_4B_{18}$ glassy alloy, high permeability, low field mag. characts. 78−68301
$Fe_{40}Ni_{38}Mo_4B_{18}$ metallic glass, reorientation kinetics of magnetization 79−24155
$Fe_{40}Ni_{38}Mo_4B_{18}$, metallic glass, mag. and transport props. 80−39752
$Fe_{40}Ni_{38}Mo_4B_{18}$ ribbon, magnetic characterisation 80−34680
$(Fe_{1-x}Ni_x)_2P$, mag. props. 78−23248
$(Fe_{1-x}Ni_x)_{80}P_{20}$, amorphous, ferromagnetic alloys, mag. anomalies of Invar type *(Russian)* 80−93089
$Fe_{40}Ni_{40}P_{20}$, amorphous alloy, ductile-brittle transition temp., relation to composition 78−52972
(FeNi)PB amorphous wires, surface oxidation and annealing influence on induced anisotropy 80−100957
$(Fe_{0.04}Ni_{0.96})_{80}P_{10}B_{10}$, amorphous, mictomagnetic to ferromag. transition 78−34981
$(Fe_{0.04}Ni_{0.96})_{80}P_{10}B_{10}$, amorphous magnetisation, field and temp. depend. 80−39755
$(Fe_{1-x}Ni_x)_{80}P_{10}B_{10}$, amorphous, magnetostriction meas. by ferromag. reson., induced anisotropy 77−32232
$(Fe_{1-x}Ni_x)_{80}P_{10}B_{10}$, amorphous microwires, magnetisation reversal and anisotropy 78−91885
$Fe_{20}Ni_{60}P_{14}B_6$, $Fe_{30}Ni_{50}P_{14}B_6$, amorphous ferromags., thermoelec. power and resistivity near Curie temp. 79−56200
$Fe_{27}Ni_{53}P_{14}B_6$, amorphous, Hall resist. and mag. props., short range order effects 80−34422
$Fe_{27}Ni_{53}P_{14}B_6$, metallic glass, changes in Curie temp., physical dimensions and mag. anisotropy during annealing 77−85446
$Fe_{40}Ni_{40}P_{14}B_{06}$, amorphous, strip domains, anisotropy const. effects 80−29571
$Fe_{40}Ni_{40}P_{14}B_{20}$, Metglas 2826, amorphous ferromag., resistivity down to 60 mK 79−60783
$Fe_{40}Ni_{40}P_{14}B_6$, (Metglas 2826), ferromag. Curie temp. determ. 78−64206
$Fe_{40}Ni_{40}P_{14}B_6$, amorhpous ribbon, influence of torsion on mag. props. 80−7138
$Fe_{40}Ni_{40}P_{14}B_6$, amorphous ribbon, cold rolling, annealing mag. props. 77−8958
$Fe_{40}Ni_{40}P_{14}B_6$, amorphous, deform. and annealing effects on mag. and mech. props. 77−12717
$Fe_{40}Ni_{40}P_{14}B_6$, amorphous, magnetoelastic props. 77−16136
$Fe_{40}Ni_{40}P_{14}B_6$, amorphous alloy, small angle X-ray scattering 77−65953
$Fe_{40}Ni_{40}P_{14}B_6$, amorphous, domain struct. 78−10719
$Fe_{40}Ni_{40}P_{14}B_6$, amorphous tape wound cores, mag. props. *(German)* 78−10727
$Fe_{40}Ni_{40}P_{14}B_6$, amorphous, mag. props. 78−10728
$Fe_{40}Ni_{40}P_{14}B_6$, amorphous alloy, structural relaxation kinetics, X-ray diffr. exam. 78−38627
$Fe_{40}Ni_{40}P_{14}B_6$, amorphous alloy, ductile-brittle transition temp., relation to composition 78−52972
$Fe_{40}Ni_{40}P_{14}B_6$ amorphous ribbon, mag. anisotropy distrib. near surface 78−95430
$Fe_{40}Ni_{40}P_{14}B_6$, amorphous toroidal core, switching characts. and domain structs. 78−95477
$Fe_{40}Ni_{40}P_{14}B_6$, amorphous, energy dispersive X-ray diffr. study of structural relaxation 79−14689

iron alloys continued
$Fe_{40}Ni_{40}P_{14}B_6$, amorphous, annealed and unannealed, temp. depend. of flow stress and ductility 79−29119
$Fe_{40}Ni_{40}P_{14}B_6$, amorphous alloy sheet, fabrication by gas melt spraying method 79−24466
$Fe_{40}Ni_{40}P_{14}B_6$, amorphous ferromagnet, domain struct., Rayleigh region and coercive field 79−28559
$Fe_{40}Ni_{40}P_{14}B_6$, amorphous, continuous versus discrete hyperfine field distrib., Mossbauer spectra 79−33583
$Fe_{40}Ni_{40}P_{14}B_6$, amorphous, transverse magnetoresist., stress effect 80−15501
$Fe_{40}Ni_{40}P_{14}B_6$, amorphous, mag. props., effects mech. deform. 80−39840
$Fe_{40}Ni_{40}P_{14}B_6$, amorphous, resistometric study of short-range ordering rel. to heat treatment 80−70140
$Fe_{40}Ni_{40}P_{14}B_6$, amorphous ferromagnet, Mossbauer hyperfine fields, mag. struct. 80−75894
$Fe_{40}Ni_{40}P_{14}B_6$ amorphous alloy, temper embrittlement 80−76295
$Fe_{40}Ni_{40}P_{14}B_6$, amorphous, mag. polarisation in approach to ferromag. saturation 80−80560
$Fe_{40}Ni_{40}P_{14}B_6$, amorphous, steady-state creep rate, cryst. effect 80−81102
$Fe_{40}Ni_{40}P_{14}B_6$, amorphous, mag. permeability aftereffect during annealing 80−88834
$Fe_{40}Ni_{40}P_{14}B_6$, amorphous ferromag., spin wave excitations 80−97079
$Fe_{40}Ni_{40}P_{14}B_6$ amorphous ribbon, mag. domains and anisotropy distrib. 80−108029
$Fe_{40}Ni_{40}P_{14}B_6$, elastic, magnetoelastic and thermal props. 79−19759
$Fe_{40}Ni_{40}P_{14}B_6$, $Fe_{29}Ni_{49}P_{14}B_6Si_2$ glasses, internal friction and shear modulus 79−52287
$Fe_{40}Ni_{40}P_{14}B_6$, $Fe_{35}Ni_{32}Cr_{15}P_{12}B_6$, amorphous ferromagnets, Barkhausen noise and core losses 77−69618
$Fe_{40}Ni_{40}P_{14}B_6$, ferromagnetic metallic glasses, Brillouin scattering 78−92085
$Fe_{40}Ni_{40}P_{14}B_6$ glass, ferromagnetic, low temp. heat capacity meas., electronic, phonon contributions exam. 78−10689
$Fe_{40}Ni_{40}P_{14}B_6$ glass, crystn. kinetics, DSC expts. 78−26444
$Fe_{40}Ni_{40}P_{14}B_6$ glass, positron lifetimes in as-received, cold-rolled, embrittled and crystallized samples 79−74177
$Fe_{40}Ni_{40}P_{14}B_6$ glass, struct. relax., ferromag. reson. and X-ray scatt. 79−90566
$Fe_{40}Ni_{40}P_{14}B_6$ glass, thermal expansion, glass transform. and crystn. temps. 80−2183
$Fe_{40}Ni_{40}P_{14}B_6$ glass, viscosity near T_g, using rapid heating, and fusion characts. 80−70438
$Fe_{40}Ni_{40}P_{14}B_6$, glassy metal fabric for mag. shield 77−8347
$Fe_{40}Ni_{40}P_{14}B_6$, glassy, mag. props. and hyperfine interactions, Mossbauer obs., 4.2-1000K 78−10812
$Fe_{40}Ni_{40}P_{14}B_6$, glassy, ferromag. anisotropy of resistivity 79−23939
$Fe_{40}Ni_{40}P_{14}B_6$, hardness, elec. cond., photo emission, and mag. props. *(Norwegian)* 79−32909
$Fe_{40}Ni_{40}P_{14}B_6$, high-field suscept. and spin wave spectrum 78−10662
$Fe_{40}Ni_{40}P_{14}B_6$, induced anisotropy energy and saturation magnetisation temp. depend., torque magnetometer meas. 78−10680
$Fe_{40}Ni_{40}P_{14}B_6$, irradiation swelling 78−30682
$Fe_{40}Ni_{40}P_{14}B_6$, metallic glass, acoustic emission generated during viscous flow 78−39853
$Fe_{40}Ni_{40}P_{14}B_6$, metallic glass, cryst., isothermal annealing behaviour 80−6367
$Fe_{40}Ni_{40}P_{14}B_6$ metallic glass, ferromag. reson., spin waves, thermal ageing and long-range order effects 80−25214
$Fe_{40}Ni_{40}P_{14}B_6$, metallic glass, high-resolution XPS study, electronic state struct. 80−29846
$Fe_{40}Ni_{40}P_{14}B_6$ metallic glass, isothermal viscosity and crystn. 80−49395
$Fe_{40}Ni_{40}P_{14}B_6$ metallic glass, crystn. 80−70127
$Fe_{40}Ni_{40}P_{14}B_6$, metallic glass, glass transition, viscous flow and differential scanning calorimetry meas. 80−96635
$Fe_{40}Ni_{40}P_{14}B_6$, metallic glass, bending tests, evidence of ideal elastic-plastic deform. 80−97543
$Fe_{40}Ni_{40}P_{14}B_6$, Metglas 2826, ferromag. reson. for g-values and relax. parameters, 77 to 430K 77−63289
$Fe_{40}Ni_{40}P_{14}B_6$, Metglas 2826, ferromag. antireson. transmission at 24 GHz, 26 to 270°C 77−69696
$Fe_{40}Ni_{40}P_{14}B_6$, Metglas 2826, magnetising processes 78−10725
$Fe_{40}Ni_{40}P_{14}B_6$, Metglas 2826, acoustic emission during viscous flow 78−42915
$Fe_{40}Ni_{40}P_{14}B_6$, Metglas 2826, stability, crystallisation, ductility meas. 78−47246
$Fe_{40}Ni_{40}P_{14}B_6$, Metglas 2826, amorphous ribbon core, appl. in force transducer 78−93669
$Fe_{40}Ni_{40}P_{14}B_6$, metglas 2826, amorphous, Hall resistivity, thermal cycling and annealing effects 79−38050
$Fe_{40}Ni_{40}P_{14}B_6$ Metglass, spontaneous vibr. modes excited by reversible magnetostriction 79−56587
$Fe_{40}Ni_{40}P_{14}B_6$, Metglas 2826, hot forming 80−84980
$Fe_{40}Ni_{40}P_{14}B_6$, Metglas 2826, amorphous ribbon under tension, mag. domain walls and pulsed magnetisation reversal 80−88825
$Fe_{40}Ni_{40}P_{14}B_6$, quenched amorphous, high field susceptibility and microstructure 77−69506
$Fe_{40}Ni_{40}P_{16}B_6$, amorphous, kinetics of induced mag. directional order 80−44824
$Fe_{40}Ni_{40}P_{20-x(B)}B_{x(B)}$, ferromagnetic metallic glass, thermal and mech. stability 77−66698
$Fe_{40}Ni_{40}P_yB_{20-y}$, amorphous, mag. props. effect of metalloid elements 79−28658
$Fe_{44}Ni_{40}P_{14}B_6$, homogeneous deformation effect on crystn. and Curie temp. 80−21045
$Fe_{46}Ni_{40}P_{16}B_6$, ferromagnetic amorphous alloy, even magneto-optic effects 77−55776
$Fe_cNi_{80-c}P_{14}B_6$, amorphous, annealing effects on mag. props. 79−78383
$Fe_xNi_{1-x}P_{14}B_6$, amorphous, spin-glass regime, magnetoresist. meas. 80−34418
$(Fe_xNi_{1-x})_{80}P_{10}B_{10}$, amorphous, weak itinerant ferromag., Arrott plots 77−73007
$(Fe_xNi_{1-x})_{80}P_{10}B_{10}$, amorphous, magnetisation reversal and domain boundary configs. 80−88809
$(Fe_xNi_{1-x})_{80}P_{14}B_6$, Mossbauer spectroscopy, mag. hyperfine interaction, Curie temps. 78−6617
$(Fe_xNi_{100-x})_{80}P_{10}B_{10}$, amorphous, elec. resist., 2 to 300K, composition depend. 80−44562
$Fe_xNi_{80-x}P_{14}B_6$ (x=0, 20, 40, 60, 80), metallic glass, low temp. sp. ht. 80−2588

iron alloys continued
$Fe_xNi_{80-x}P_{14}B_6$, amorphous, sp. ht. and susceptibility meas., spin glass and mictomag. props. 78−68274
$Fe_xNi_{80-x}P_{14}B_6$, amorphous ferromag., resistivity, mag. contrib., 1.5-50K 79−56182
$Fe_xNi_{80-x}P_{14}B_6$, amorphous ferromag., T^2 saturation in resist. below 0.3K 79−60785
$Fe_xNi_{80-x}P_{14}B_6$, and $Fe_xNi_{80-x}B_{20}$ glass, microhardness, correl. with mag. props. 79−57085
$Fe_xNi_{80-x}P_{14}B_6$ glass, resist., magnetoresist., and thermoelec. power 80−70681
$Fe_xNi_{80-x}P_{14}B_6$ metallic glasses, low temp. resistivities 78−91659
$Fe_xNi_{80-x}P_{14}B_6$, metallic glass, low temp. sp. ht. for spin-glass and spin-cluster-glass regime 80−71071
$(Fe_yNi_{100-y})_{79}P_{13}B_8$, metallic glass, low temp. sp. ht. for spin-glass and spin-cluster-glass regime 80−71071
$(Fe_{0.3}Ni_{0.7})_{0.75}P_{0.16}B_{0.06}Al_{0.03}$, amorphous, spin wave spectrum, neutron scatt. 77−16064
$(Fe_{0.5}Ni_{0.5})_{75}P_{16}B_6Al_3$ glass, struct. relax. as origin of Curie temp. ageing 78−84418
$(Fe_{1-x}Ni_x)_{75}(PBAl)_{25}$, amorphous, high-field magnetoresist. meas. 80−34423
$(Fe_{1-x}Ni_x)_{75}P_{16}B_6Al_3$, amorphous alloy, low temp. elec. resist. saturation 78−68005
$(Fe_{1-x}Ni_x)_{75}P_{16}B_6Al_3$, amorphous, low temp. elec. resist. 79−56183
$(Fe_{1-x}Ni_x)_{75}P_{16}B_6Al_3$, amorphous, saturation magnetisation, temp. depend., ferromag. reson. meas. 79−73818
$(Fe_{65}Ni_{35})_{75}P_{16}B_6Al_3$, amorphous ferromag., high temp. spin dynamics 78−47965
$(Fe_{65}Ni_{35})_{75}P_{16}B_6Al_3$, mag. excitations 79−7984
$(Fe_{65}Ni_{35})_{75}P_{16}B_6Al_3$, amorphous, crystn. temp., press. and heating rate depend. 80−70132
$(Fe_xNi_{1-x})_{0.75}P_{0.16}B_{0.06}Al_{0.03}$, metallic glass, thermal expansion 78−43151
$(Fe_xNi_{1-x})_{75}P_{16}B_6Al_3$, amorphous, spin wave excitations and low temp. magnetisation 79−33468
$(Fe_xNi_{1-x})_{75}P_{16}B_6Al_3$, magnetisation temp. depend., spin wave theory 80−44927
$Fe_xNi_yP_{14}B_6(S_2)$, coiled ribbons, stress relaxation 79−29120
$Fe_{29}Ni_{49}P_{14}B_6Si_{12}$, Metglas fibre reinforced mortar, fracture props. 79−70159
$Fe_{29}Ni_{49}P_{14}B_6Si_2$ glass, crystn. kinetics, DSC expts. 78−26444
$Fe_{29}Ni_{49}P_{14}B_6Si_2$, Metglas 2826 B, paramag. reson. for g-values and relax. parameters, 77 to 430K 77−63289
$Fe_{29}Ni_{49}P_{14}B_6Si_2$, metallic glass, changes in Curie temp., physical dimensions and mag. anisotropy during annealing 77−85446
$Fe_{29}Ni_{49}P_{14}B_6Si_2$, Metglas 2826B, Hall, elec. resist., magnetisation and heat capacity meas. 78−68019
$Fe_{29}Ni_{49}P_{14}B_6Si_2$, Metglass 2826B, saturation magnetisation, temp. depend., ferromag. reson. meas. 79−73818
$Fe_{72}Ni_8P_{13}C_7$ glass, erosion craters produced by spark machining, scanning microscopy obs. 78−44268
$(Fe_{1-x}Ni_x)_{80}PyB_{20-y}$, local struct. disorder and crystallisation, Mossbauer exam. 79−1728
$(Fe_{1-x}Ni_x)_{77}Si_{10}B_{13}$, amorphous magnetic alloys, density meas. 80−1934
$(Fe_{1-x}Ni_x)_{77}Si_{10}B_{13}$ amorphous alloy system, saturation mag. moment, Curie temp., mag. susceptibility 80−39753
$(Fe_{1-x}Ni_x)_{77}Si_{10}B_{13}$, amorphous, Landau-Ginzburg theory, magnetisation and Curie temp. 80−75700
$(Fe_{1-x}Ni_x)_{78}Si_{10}B_{12}$, amorphous, Hall effect and magnetoresist. *(Japanese)* 77−85199
$(Fe_{1-x}Ni_x)_{78}Si_{10}B_{12}$ amorphous alloys, cold rolled and as-quenched, mag. anisotropy 80−97089
$Fe_{62.4}Ni_{15.6}Si_7B_{15}$ amorphous ferromagnetic alloy, anomalous magnetisation possible reasons, Mossbauer spectra *(Russian)* 79−78441
$Fe_{1-x}Ni_xSn$, transferred hyperfine fields at ^{119}Sn, Mossbauer spectroscopy 79−33582
FeNiTe alloys, disordered, polycrystalline, elec. resist., temp. depend. 80−49692
$Fe_{1-x}(P,B)_x$, amorphous and crystalline, photoemission and band structure 80−60754
$Fe_{1-x}P_x$ dilute alloys, electronic struct., mag., elec. and struct. props. 79−37971
$Fe_{100-x}P_x$, structural analysis of models for amorphous metallic alloys 80−103249
Fe_2P, spin wave excitations meas. 80−65831
$Fe_{75}P_{25}$ amorphous alloy, atomic struct., computer simulation 80−88043
$Fe_{76}P_{24}$, amorphous alloy, electronic struct., KKR calc. 80−96775
$Fe_{80}P_{20}$, binary amorphous ferromagnet, Mossbauer study 80−34829
$Fe_{80}P_{20}$ glass, mag. props. 77−63125
$Fe_{82}P_{18}$, amorphous, uniaxial mag. anisotropy 78−19246
$Fe_{79}P_{13}B_8$ amorphous alloys, splat cooled, Mn, Cr and V substituted, mag. and transport props. 80−84593
$Fe_{80}P_{14}B_6$ glass, ferromagnetic, low temp. heat capacity meas., electronic, phonon contributions exam. 78−10689
$Fe_{83}P_{17-x(B)}B_{x(B)}$, ferromagnetic, metallic glass thermal and mech. stability 77−66698
$Fe_{75}P_{16}B_6Al_3$, aged metallic glass, Mossbauer effect 79−91318
$Fe_{80}P_{16}B_1C_3$, ferromag. metallic glass, Mossbauer spectra, crystn. 77−12276
FePC molten and amorphous alloys, struct. factors 80−79674
$FeP_{13}C_7$, amorphous, exam. of metalloid atom mobility by Auger spectroscopy 78−47575
$Fe_{0.75}P_{0.15}C_{0.10}$, amorphous, mag. excitations and static struct., neutron scatt. obs. 78−68204
$Fe_{75}P_{15}C_{10}$, amorphous, magnetoelastic props. 77−16136
$Fe_{75}P_{15}C_{10}$, amorphous, mag. excitations, inelastic neutron scatt. 78−10674
$Fe_{75}P_{15}C_{10}$ amorphous foil, ferromag. domain orientation, Mossbauer exam. 78−52402
$Fe_{75}P_{15}C_{10}$, ferromagnetic, amorphous, spin echo NMR of ^{31}P 78−2770
$Fe_{75}P_{15}C_{10}$ foils, amorphous, ferromag. domain orientation, Mossbauer study 78−15000
$Fe_{75}P_{15}C_{10}$, glassy ferromag., crit. sp. ht. meas. 78−10716
$Fe_{75}P_{15}C_{10}$, temp. depend. of the ΔE-effect 78−80188
$Fe_{80}P_{13}C_7$, amorphous, mag. domain struct. obs. 77−36091
$Fe_{80}P_{13}C_7$, amorphous, mag. anisotropy 79−65670
$Fe_{80}P_{13}C_7$, amorphous, rapidly quenched, magnetic props., effect of annealing 77−16701
$Fe_{80}P_{13}C_7$, amorphous ferromag. ribbons, US rel. meas. 77−80582
iron alloys continued
$Fe_{80}P_{13}C_7$ amorphous ferromag. ribbons, change of permeability by heat treatment 77−85493
$Fe_{80}P_{13}C_7$, amorphous ferromagnetic alloy, isothermal annealing effect on static magnetic props. *(Japanese)* 79−52398
$Fe_{80}P_{13}C_7$, amorphous ribbon, giant ΔE effect, magnetomech. coupling factor 77−8379
$Fe_{80}P_{13}C_7$, amorphous ribbon, HF mag. charcts., magnetostriction role 77−66408
$Fe_{80}P_{13}C_7$, amorphous toroidal core, switching charcts. and domain structs. 78−95477
$Fe_{80}P_{13}C_7$, metallic glass, crystallisation kinetics 77−66637
$Fe_{80}P_{16}C_3B_1$ amorphous filament, produced by glass coated melt spinning, mech. props. 78−15483
$Fe_{80}(P_{13}C_7)_{20-y}B_y(Si_y)$, density, microhardness, and crystn. temp., comp. depend. 80−84093
$Fe_{80}P_{20-x}C_x(Si_x)(Ge_x)$, amorphous, size effect of metalloids on mag. props. 80−84594
FeP(Ga)(As)(Sb), dil., short-range order, neutron diffuse scatt. and spin echo NMR 80−50106
$Fe_{75}P_{15}O_{10}$, amorphous, ferromag. domain-wall width, anisotropy depend. 78−19269
Fe_3Pb, reversible shape memory effect, rel. to microstruct. memory and residual stresses 77−90419
FePd epitaxial film, vacuum-deposited, for thermomag. recording, mag. and magneto-optical props. *(Russian)* 78−60319
$FePd_{1-x}Pt_x$, permanent magnet, coercive force increased by Pt 79−24157
$Fe_{1-x}Pd_x$ film, air-exposed, comp. profiles by AES, ESCA and ion sputtering 78−95245
$Fe_{1-x}Pd_x$ film, UHV deposited, effects of applied stress on B-H loops 78−64239
$Fe_{1-x}Pd_x$ film, vac. deposited, oxidation and corrosion, AES, XPS and STEM obs. 79−100286
$Fe_{1-x}Pd_x$ films, vacuum deposited, mag. and corrosion props. 79−56574
Fe_3Pd, quenched, or annealed exam. of magnetostriction, galvano- and thermomagnetic props. *(Russian)* 79−19757
$Fe_{50}Pd_{50}$, order-disorder transition, Mossbauer study 80−71268
$Fe(Pd_{1-x}Au_x)_3$, mag. struct. ferro-antiferromagnetism coexistence *(Russian)* 79−82759
$Fe(Pd_{1-x}Au_x)_3$ ordering alloys, mag. props., 4.2 to 500K *(Russian)* 79−47301
$Fe_{25}Pd_{50}Au_{25}$, atomic ordering influence on mag. props. and elec. resistance *(Russian)* 80−7551
$Fe_{34}Pd_{46}P_{20}$, amorphous, sp. ht. and resist. near ferromag. phase transition 78−56333
$Fe_xPd_{80-x}Si_{20}$, amorphous, structural and mag. heterogeneities 80−80484
$Fe_xPd_{80-x}Si_{20}$, low field susceptibility near transition temp. 77−66359
$Fe_xPd_{82-x}Si_{18}$, amorphous, magnetisation, magnetoresist., spin glass and ferromag. phases 80−34697
$Fe_xPd_{82-x}Si_{18}$ metallic glass, long range interaction and spin wave interactions 80−65949
$Fe_xPd_{82-x}Si_{18}$ metallic glass, mag. transitions, weak ferromagnetism 80−100583
FePt epitaxial film, vacuum-deposited, for thermomag. recording, mag. and magneto-optical props. *(Russian)* 78−60319
FePt lattice, symmetry, state of order, vibration, temp. effects *(German)* 77−4067
$FePt_3$, metamagnetic transitions in external fields 80−60272
$FePt_3$, neutron scattering study of spin waves 78−91856
Fe_3Pt, atomic thermal vibr. anisotropy, martensitic transform. model *(French)* 80−70355
Fe_3Pt austenite, long range order parameter, temp. depend. discussion 80−97481
Fe_3Pt austenites, ordering kinetics 80−104155
Fe_3Pt austenitising conditions on M_s temp. 80−81088
Fe_3Pt, interface struct. of martensite 78−48400
Fe_3Pt, Invar alloy, elastically stressed, ^{57}Fe effective field, anomalous behaviour, Mossbauer obs. *(Russian)* 77−8485
Fe_3Pt, Invar alloy, theory of elastic-anomalies 78−95505
Fe_3Pt, martensite austenite interface, twin thickness in martensite 77−32579
Fe_3Pt, martensitic transform., change from nonthermoelastic to thermoelastic type 78−19755
Fe_3Pt, off stoichiometric, austenite ordering and martensite tetragonality 77−36501
Fe_3Pt, plastically deformed, struct. inhomogeneities, positron annihilation meas. 79−33859
Fe_3Pt, premartensitic phenomena *(French)* 79−8297
Fe_3Pt, quasi-localised spin system, neutron scatt. 78−68194
Fe_3Pt, stoichiometric composition, internal friction, microdeform. and memory effect, rel. to martensitic transform. *(French)* 77−52323
$Fe_{3-x}Pt_{1+x}$, ordered and disordered, mag. props. at low temp. 79−56517
$Fe_{72}Pt_{28}$, ferromagnetic Invar alloy, lattice vibrations 78−91403
$Fe_{72}Pt_{28}$ Invar alloy, low temp. thermal expsn. 79−65221
$Fe_{76}Pt_{24}$ Invar alloy, ferromag., fine-powdered, Mossbauer effect 79−56634
$Fe_2Pu(Np)(U)(Zr)(Tm)$, Mossbauer diffr., combination type maxima, hyperfine interactions on nuclei 80−25263
FeRh, antiferromag., band structure and effect of Fe impurity on mag. props. 77−28377
FeRh, antiferromag., band struc., off-stoichiometry effects 78−10341
FeRh, antiferromag.-ferromag. transition, appl. of interacting virtual bound state picture 77−69464
FeRh, transition mechanism, interacting virtual state approach 77−72987
$Fe_{1-x}Rh_x$, press. effects on mag. phase transition, resist. meas. 77−4516
$Fe_{48}Rh_{52}$, hyperfine mag. field at ^{57}Fe and ^{119}Sn nuclei, press. depend. *(Russian)* 78−80266
$FeSb_2$, phase structure, X-ray crystallography *(French)* 78−91305
$Fe_{1+x}Sb$, Mossbauer meas. of lattice and interstitial Fe atom mag. ordering 79−99807
$Fe_{1+x}Sb$, phase structure, X-ray crystallography *(French)* 78−91305
FeSe-MnSe phase relationships in presence of excess Fe 77−52291
FeSi, (110), Neel cryst., refr. of neutrons in Bloch walls using double cryst. arrangement 79−24191
FeSi, domain struct. and magnetisation reversal, time depend. neutron depolarisation 80−50138
FeSi, hyperfine fields about μ^+ 79−56664
FeSi, NMR and μSR, microscopic mag. props. *(Japanese)* 78−52368

iron alloys continued
FeSi, nearly ferromag. semicond. mag. and thermal props., spin fluctuation theory 79−65687
FeSi picture frame single cryst., domain wall motion and magnetisation reversal, time-depend. neutron depolarisation study 80−88782
FeSi, single cryst., orientation of pieces of zigzag Block walls, neutron small-angle scatt. determ. 79−24190
FeSi, single crysts., domain struct., temp. and field depend. 80−71085
FeSi-Ca-V complex alloy oxidation of steel, nonmetallic additions *(Russian)* 80−93685
FeSi-Fe_2Si_5 eutectic, $FeSi_2$ formation, annealing temp. and time effects 79−24512
FeSi-graphite-SiC refractory, oxidation loss and wettability of inorganic fluxing materials *(Japanese)* 78−84755
$FeSi_2$, effect on nitriding of Si powder 79−33985
$FeSi_2$ films, Mossbauer investig. of struct. 79−87341
$FeSi_2$ films, structural and Anderson transitions, cond. and IR reflectance meas. 79−15200
α-$FeSi_{2.33}$, interface struct. and growth mechanism from melt 79−14715
α-$Fe_{1-x}Si_2$, many-body atomic correlations, Mossbauer spectroscopy study 80−15934
α-$Fe_{1-x}Si_2$, vacancy ordering, cryst. stabilisation energy aspects 80−103325
$Fe_{1-x}Si_x$ film, optical and magneto-optical characts., mag. preps. 79−82956
$Fe_{100-x}Si_x$ ribbon, magnetostriction exam. 79−73794
Fe_2Si-transition metal alloys, Heusler type materials, mag. props. 77−40042
α-Fe_2Si_5-ε-FeSi eutectic, orientation relationships 78−31397
Fe_3Si, 3d transition metal substituted, limits of solubility, mag. props. and electron conc. 78−10670
Fe_3Si, elastic consts., elec. resist. 77−39815
Fe_3Si, electronic structure, X-ray spectra comparison with band struct. calcs. 80−97383
Fe_3Si, electronic structure, magnetic moments 80−107695
Fe_3Si, etching of slip produced antiphase domain boundaries 78−63769
Fe_3Si hardening and softening during absorption fatigue in surface active medium, governing laws 77−86230
Fe_3Si, ordering energy, electron micrography determ. 78−14353
Fe_3Si, transition metal impurities, hyperfine fields 77−59365
Fe_3Si-based alloy, dil., cond. electron polarisation and moment perturbations 78−68224
Fe_3Si-based dil. alloys, conduction electron polarisation, moment perturbations 78−68225
$Fe_{3+x}Si_{1-x}$, electron transport 78−91669
$Fe_{95}Si_5$, thermal and elec. cond., heat transport by spin waves 79−38047
Fe_xSi_{1-x}, amorphous, high field magnetisation meas. 78−39367
Fe_xSi_{1-x}, amorphous, mag. behaviour, rel. to Fe_xSn_{1-x} and Fe_xGe_{1-x} amorphous, alloys 78−95478
Fe_xSi_{1-x}, amorphous, struct. and mag. props., giant moment form. at mag. ordering 78−68192
Fe_xSi_{1-x} amorphous alloys, magnetisation meas. showing crit. conc. at $x=0.4$ 77−59429
Fe_xSi_{1-x}, amorphous film, magneto-optic Kerr effect 80−66158
Fe_xSi_{1-x}, struct. exam. by electron diffr. and resist. meas. 77−89409
$Fe_3Si_{1-x}Al_x$, hyperfine interactions and structural disorder, spin echo, X-ray and magnetisation meas. 77−32289
$Fe_3Si_{1-x}Al_x$, hyperfine-field distrib. 79−69732
$Fe_3Si_xAl_{1-x}$-Co, dil., site preference of ^{57}Co impurities, Mossbauer study 80−39999
$Fe_xSi_yAl_z$ ribbon, magnetostriction exam. 79−73794
Fe_5SiB_2, Mossbauer spectra, 140-784K, spin rotation 78−52409
$Fe_{75}(Si_{0.5}B_{0.5})_{25}$ film, amorphous, sputtered, ferromag., thermal stability 78−76280
$Fe_{75}Si_{15}B_{10}$, amorphous ferromag. ribbons, US rel. meas. 77−80582
$Fe_{75}Si_{15}B_{10}$, amorphous ferromagnetic alloy, isothermal annealing effect on static magnetic props. *(Japanese)* 79−52398
$Fe_{75}Si_{15}B_{10}$, duplex ferromag. alloy, thermoremanent magnetization 79−73778
$Fe_{75}Si_{15}B_{10}$, mag. behaviour rel. to magnetostatic interactions 80−11224
$Fe_{78}Si_{10}B_{12}$ amorphous ferromag. ribbons, change of permeability by heat treatment 77−85493
$Fe_{78}Si_{10}B_{12}$, amorphous alloy crystallisation study *(Japanese)* 78−9959
$Fe_{78}Si_{10}B_{12}$, amorphous toroidal core, switching characts. and domain structs. 78−95477
$Fe_{78}Si_{10}B_{12}$ amorphous ribbons, magnetomechanical coupling constant and Young's modulus, mag. annealing 79−15333
$Fe_{79.5}Si_{1.5}B_{19}$, evaluation of hyperfine parameter distribs. from overlapped Mossbauer spectra at room temp. 79−99804
$Fe_{80}Si_5B_{15}$, amorphous, soft mag. props. and potential uses 80−88807
$Fe_xSi_yB_z$, $(Fe,Ni)_{78}Si_{10}B_{12}$ and $(Co,Fe)_{78}Si_{10}B_{12}$ ternary and quaternary amorphous alloys, effect of comp. on crystn. *(Japanese)* 79−94910
$(Fe_{1-x}Si_x)_{1-y}By$, metallic glass, mag. props., crystallisation 80−65885
$FeSn_2$, hyperfine mag. fields at ^{57}Fe, ^{119}Sn nuclei, under press. *(Russian)* 78−39486
Fe_3Sn_2, magnetic properties, ^{119}Sn Mossbauer study 79−91323
Fe_3Sn_2, Mossbauer effect and magnetisation meas. 78−31132
Fe_xSn_{1-x}, amorphous, mag. behaviour 78−95478
Fe_xSn_{1-x} amorphous alloy films, magnetisation meas. and Mossbauer spectra 78−95489
Fe_xSn_{1-x} amorphous alloy, elec. resistivity, Ziman's formula 79−15130
Fe_xSn_{1-x}, amorphous alloy stability, comp. and temp. depend. 79−19156
Fe_xSn_{1-x}, amorphous alloy, Mossbauer spectra, charge transfer and atomic vol. effects 80−39959
Fe_xSn_{1-x} amorphous alloy, elec. resist. 80−80246
Fe_xSn_{1-x}, amorphous film, struct. and mag. props. 80−65972
$Fe_2(Tb_{0.2}Dy_{0.22}Ho_{0.58})$, highly magnetostrictive alloy, vibrating-reed meas. of ΔE effect and internal friction 79−42819
$FeTe_2$, Mossbauer spectroscopy and nonstoichiometry 78−31125
$Fe_{1.2}Te$-MnTe phase relations in presence of excess Fe 77−52292
FeTi alloy, elec. and mag. props. near order-disorder transition 79−82576
ε-FeTi, Ce addition effect on H_2 absorption capacity 79−61899
FeTi crystals, use in storage and production of superpure H_2 *(German)* 78−53184
ε-FeTi, effect of Ce on H_2 absorption 79−73315
FeTi, H storage alloy, prep. for TEM *(German, English)* 80−30197
FeTi hydrides, struct., heat of soln., diffusion and hydriding kinetics for H storage 80−40930
FeTi, hydrogen energy storage, surface segregation *(German)* 79−77872
FeTi, hydrogen storage, annealing effects *(Japanese)* 79−100542

iron alloys continued
FeTi, hydrogenation, effect of surface segregation on mag. props. 78−84819
FeTi, positronium form. after hydrogenation-dehydrogenation cycling and annealing 80−18947
FeTi, surface and mag. props., heat treatment and hydrogenation effects 80−75447
FeTi, surface segregation and catalytic effect on hydrogenation, AES and XPS study 79−11626
FeTi, surface segregation, catalytic effect on hydrogenation 80−45814
FeTi-H system, TEM study 79−58850
$Fe_{1-x}Ti_{1+x}$, Mossbauer study, superparamag. clusters 77−85633
$Fe_{1-x}Ti_x$, ferromag. props., Ti conc. effect 80−54872
Fe_2Ti-Fe eutectic alloy, directional solidification singularities *(Russian)* 78−68678
FeTiB, corrosion-resistant amorphous mag. thin films 80−54923
β-FeTiD, neutron diffr. exam. of struct. 78−47282
α-$FeTiD_{0.057}$, solid soln., interstitial D, neutron diffr. study 80−39071
$FeTiD_x$ $(0\leq x\leq 1.9)$, structural phase transitions, absorpt. and desorpt. isotherms 80−19948
FeTiH, H storage material, H diffusion, neutron diffr. obs. 80−51013
FeTiH, solar energy storage by metal hydride 80−61455
FeV (2 at.%), NMR spin echoes, domain wall effects 80−75883
$Fe_{0.85}V_{0.15}$ film, ^{51}V NMR, spin echo expts., 77 and 300K 77−69728
$(Fe_{1-x}V_x)_3Ge$, magnetic and X-ray studies 80−1966
$Fe_{3-x}V_xSi$, Fe hyperfine fields 79−78055
$Fe_{3-x}V_xSi$, selective site substitution and spin polarisation 79−78583
$Fe_{3-x}V_xSi$, struct., magnetisation, and spin echo expts., rel. to local environment model 77−20518
Fe_4Zn_9, γ-brass with J cell, ordering 77−24290
$Fe_{80}b_{20-x}C_x(Si_x)(Ge_x)$, amorphous, size effect of metalloids on mag. props. 80−84594
Fo-Fe-Nb, cold-worked and aged, mag. props. and microstruct. 80−34690
Fw-W(Co)(Ni)(Mo)(Nb)(Cr)(V), dil. system, high freq. induction melting and centrifugal casting, working curve sample prep. photoemission anal. *(Japanese)* 78−53050
GCFR fuel pin claddings, oxidation behaviour in He environment 80−16594
Ga-Fe dilute alloy, Mossbauer spectrum 77−90080
Gd-Co-Fe film, amorphous, bias-sputtered, uniaxial perpendicular anisotropy 78−64234
Gd-Fe, amorphous film, galvanomag. effects, Hall detector 77−89882
Gd-Fe, amorphous film, Kerr and Hall effect meas. 77−24722
Gd-Fe, amorphous film, Kerr readout characts. 79−15439
Gd-Fe, amorphous film, stress induced anisotropy 77−89989
Gd-Fe, amorphous film, thermomagnetic writing 78−84428
Gd-Fe, amorphous sputtered film, magnetostriction 79−47320
Gd-Fe, CPA calcs., moments and transition temps. 78−52252
Gd-Fe, co-evap. amorphous film, anomalous hysteresis loop, domains obs. 77−89995
Gd-Fe, DC bias RF sputtered film, mag. props. 77−16124
Gd-Fe, disordered, saturation mag. moment calc., CPA 77−20515
Gd-Fe, LV multitarget sputtered film, substrate bias effect on anisotropy 77−16125
Gd-Fe, mag. moment of Fe, multiplet splitting in photoemission 79−78846
Gd-Fe, splat-cooled, internal friction exam. 77−20012
Gd-Fe, thin amorphous system, resistance and hardness, chemical comp. and temp. effect 80−15625
Gd-Fe alloy amorphous thin films, anisotropic mag. and microstruct. props. 78−95487
Gd-Fe amorphous alloys, mag. props. and crystn. 79−90557
Gd-Fe amorphous film, atomic diffusion of deposited Co 79−73346
Gd-Fe amorphous film, prep. by dual-source evaporation, mag. props. 77−89988
Gd-Fe amorphous films, anisotropy dispersion, FMR meas. 79−73824
Gd-Fe amorphous films, O_2 adsorption, effect on perpendicular anisotropy 80−34713
Gd-Fe amorphous films, stress contrib. to perpendicular anisotropy 80−75819
Gd-Fe amorphous films with CeO_2 coatings, Kerr magneto-optical effect enhancement 79−19866
Gd-Fe amorphous sputtered films, magnetoelastic contrib. to perpendicular anisotropy, internal stress meas. 78−95490
Gd-Fe film, amorphous, contact printing 77−73061
Gd-Fe film, amorphous, in-situ ion beam sputtered, microstruct. and Lorentz mag. struct. 78−63947
Gd-Fe film, amorphous, mag. props., annealing effects 78−64235
Gd-Fe film, amorphous, microstruct. and magnetism 78−64230
Gd-Fe film, amorphous, preferential resputtering effect induced anisotropic distrib. of atomic pairs 78−63950
Gd-Fe influence of gaseous phase on mag. props. *(Polish)* 80−39820
Gd-Fe-B ternary systems, phase equilibria and cryst. struct. *(Ukrainian)* 80−11626
Gd-Fe-Si, phase diagram 79−52158
Gd-Fe-Y, amorphous film, thermomagnetic writing 78−84428
$Gd(Al_xFe_{1-x})_2$, intermetallic compounds, pseudobinary, Mossbauer studies 80−75887
$Gd(Co_xFe_{1-x})_2$, mag. props., composition and temp. depend. 79−15289
$Gd_2(Fe,Co)_{17}$, mag. anisotropy fields by singular pt. detection 79−24156
$Gd_2(Fe,Co)_{17}$, magnetic anisotropy meas. by singular point detection method 77−63170
GdFe amorphous film, Mossbauer and mag. meas. 80−15844
GdFe, amorphous film, XPS meas. 79−87295
GdFe, amorphous films, thermal stability of mag. props. *(Japanese)* 79−47307
GdFe film structure, dependent on substrate type *(Russian)* 80−24747
GdFe homogeneous amorphous films, compensation point switching, magneto-optical Kerr signal anal. 80−15726
$GdFe_2$, amorphous, small angle neutron scatt. study of mag. order and mag. microstruct. 79−15283
$GdFe_2$, amorphous alloys, atomic order, mag. behaviour 78−19221
$GdFe_2$, easy direction of magnetisation 80−20535
$GdFe_2$ films, electron beam deposited, amorphous and cryst., mag. and struct. props. 79−4710
$GdFe_2$, H_2 sorption props. 79−86980
$GdFe_2$, Mossbauer sample, X-ray diffr. obs. 78−22737
$GdFe_x$, mag. interactions, exchange fields, mol. field model 77−4498
$Gd_{1-x}Fe_x$, temp. depend. of magnetisation 77−77043
$Gd_{1-x}Fe_x$, CPA calcs., mean mag. moments 77−72997

iron alloys continued
Gd_2Fe_{17}, Mossbauer effect 77−85635
Gd_xFe_{1-x} amorphous films, microstruct. and mag. anisotropy 79−82838
Gd_xFe_{1-x} amorphous foil, EELS as analytical tool, data handling and processing 80−81407
Gd_xFe_{1-x} film, mm-wave ferrimag. reson. using optically pumped waveguide laser source 77−55710
$Gd(Fe_{1-x}Al_x)_2$, magnetisation, Curie temps., and mean mag. moments 79−51817
$Gd(Fe_xAl_{1-x})_2$, magnetic behavior 80−108079
$(Gd_{65}Fe_{35})_{100-x}B_x$ glasses, mag. props. 79−73693
$(Gd_{65}Fe_{35})_{90}B_{10}$, amorphous, mag. props., Mossbauer study 80−93093
GdFeBi, amorphous ferrimag. films, magneto-optical props., optical spectra 80−76008
$(Gd_{1-x}Fe_x)_{1-y}Bi_y$ amorphous films, saturation magnetisation, Kerr and Faraday rotation 80−40093
$Gd(Fe_xCo_{1-x})_2$, ferromag. reson. of pseudobinary cubic compounds 78−91961
$Gd(Fe_xCo_{1-x})_2$, Mossbauer effect at 78 and 300K, ^{57}Fe hyperfine fields 80−2677
$Gd(Fe_xCo_{1-x})_2$, paramag. behaviour, itineracy 78−39289
$Gd_2(Fe_{1-x}Co_x)_{17}$, hyperfine interactions, Mossbauer spectra 78−2780
$Gd_x(Fe_{1-y}Co_y)_{1-x}$, evap. amorphous film, mag. anisotropy due to pair ordering 77−32219
$Gd_{18}Fe_{82-x}Ni_x$, amorphous film, mag. and galvanomag. props. 77−24715
$Gd_2(Fe_{1-x}Ni_x)_{17}$, Mossbauer spectra, hyperfine field interactions 78−6614
$Gd(Fe_xT_{1-x})_2$, Mossbauer spectra, mag. props. 80−20563
$Gd_{0.99}Ho_{0.01}(Rh_{1-x}Fe_x)_2$, spin echo meas. on ^{165}Ho, quenching effect of Fe substitution 78−48079
$(Gd_{1-y}Nd_y)_{1-x}Fe_x$ amorphous bubble films with good temp. characts. 79−95616
$Gd(Rh_{1-x}Fe_x)_2$, $x \leq 0.15$, magnetisation and EPR studies 80−34767
$Gd_xY_{1-x}Fe_2$, effective g-values, ferromag. reson. meas. 77−20720
$(Gd_xY_{1-x})Fe_2$, Fe mag. behaviour, FMR measurements, mag. props., Vangsness relation anal. 79−78336
$(Gd_xY_{1-x})Fe_2$, high temp. mag. behaviour 77−1538
$Gd_xY_{1-x}Fe_2$, s-d exchange interaction integral, change due to hydrostatic compression 78−88199
$Gd_xY_{1-x}Fe_3$, saturation magnetisation, magnetostriction, Curie temp., ferrimag. ordering, exchange field *(Russian)* 78−68343
$GdZrFe_2$, hyperfine field at Gd, TDPAC meas. 80−93214
$Gd[Co_xFe_{1-x}]_2$, NMR, hyperfine fields, conc. depend. 77−43902
Ge-Fe, liq., enthalpy of formation meas. 80−30267
Ge-Fe, sputter deposited amorphous alloy, substrate bias, magnetic anisotropy, annealing 78−48006
Ge-Fe amorphous film, sputtered, stress induced anisotropy 79−73706
Ge-Fe film, codeposited, amorphous and polycryst., struct. and elec. props. 80−24766
Ge-Fe film, polycryst., struct. props. determ. 79−4494
Ge-FeS, GeS-FeS, density of alloys, volume changes on melting 77−51473
Ge-Sb, chemical diffusion *(Japanese)* 78−14515
Ge-Se-Fe films, metallic and semicond., amorphous, mag. and elec. props. 78−52319
Ge_2FeGa, and Fe_2CoGa, site preference and local environment effects, Mossbauer and NMR expts. 78−43710
H related failures study 78−11322
H solubility in binary alloys, 850-1150°C, conc. depend. *(Russian)* 77−59120
H_2 embrittlement, rel. to metallurgical microstruct. 80−55539
H_2 trapping, electrical analogue model 79−46841
Hf-Fe, amorphous, thermal stability, crystn., DSC and elec. resist. study 80−107060
Hf-Fe, oxidation of intermetallic phases 79−100298
Hf-Fe alloys, oxidation 79−52460
Hf-Ge-Ga, X-ray microanalysis of phase equilibria *(Ukrainian)* 78−6898
$Hf_{1-x}Fe_x$ amorphous alloys, formation, crystallisation and electrical resistivity 80−96838
Hf_2Fe, moment form. on H_2 absorpt. 79−87343
$Hf(Fe_{1-x}Co_x)_2$, mag. props., Mossbauer spectra and magnetisation meas. 80−39948
$HfFe_{2-x}Si_x$, Laves pseudo-binary compound, cubic C15 phase stabilisation 77−39559
$HfFe_{2-x}Si_x$, Mossbauer spectra, hyperfine interactions 80−15862
$HfFe_2Si_2$, cryst. struct. 77−31633
$HoCo_{5.5-x}Fe_x$, cryst. struct. and mag. props. 80−75800
$Ho_xDy_yTb_{1-x-y}Fe_2$, Laves phase cpds., anisotropy and magnetostriction 77−63167
$HoFe_2$, amorphous, small angle neutron scatt. study of mag. order and mag. microstruct. 79−15283
$HoFe_2$, amorphous, struct. determ., EXAFS exam. 78−51421
$HoFe_2$, amorphous, ultrasonic exam. below T_c 79−73793
$HoFe_2$, crystal field interaction contribution to specific heat 80−39788
$HoFe_2$, Czochralski growth, and cryst. quality determ. 77−8742
$HoFe_2$, effect of H on sublattice magnetization, elastic neutron scatt. obs. 79−78327
$HoFe_2$, mag. struct., polarized neutron diffr. study 79−78326
$HoFe_2$, magnetostriction and magnetisation temp. depend. 79−73795
$HoFe_2$, spin wave and cryst. field excitations, neutron scatt. 78−68196
$HoFe_3$ and Ho_6Fe_{23}, magnetostriction, room temp. to 80K 80−65993
$HoFe_3$, effect of adsorbed H on mag. props. 77−63129
Ho_6Fe_{23}, magnetostriction, temp. depend., 20 to 350K 80−65994
$Ho_2Fe_3Co_{14}$, Kerr effect determ. of domain structure, Bloch wall energy 80−39806
$HoFe_2H_{4.5}$, mag. props. and lattice consts., effect of hydrogen absorpt. 77−20561
HoFeMn, Laves phase, mag. moment on Ho, neutron diffr. obs. 77−63107
$Ho(Fe_xNi_{1-x})$, mag. interactions, mol. field model 77−73010
$Ho(Fe_xNi_{1-x})_2$, mag. behaviour, susceptibility and Mossbauer expts., 4.2-1300K 78−52235
$Ho_{0.58}Tb_{0.20}Dy_{0.22}Fe_2$, magnetoelastic surface wave propagation, mag. field depend. 77−85535
$(Ho_{0.58}Tb_{0.2}Dy_{0.22})Fe_2$, microwave mag. props. 80−65860
$Ho_xTb_{1-x}Fe_2$, and $Ho_xTb_yDy_{1-x-y}Fe_2$, high magnetostriction cpd., mag. anisotropy origins 78−68217
$Ho_xTb_{1-x}Fe_2$, Laves phase, mag. anisotropy meas., cubic harmonic anal. 78−84410
$Ho_xTb_{1-x}Fe_2$, single cryst., spin orientations 78−84425
iron alloys continued
$Ho_xTb_{1-x}Fe_2$, single crystals, continuous spin orientations, magnetisation easy direction 78−84453
$Ho_xY_{1-x}(Fe_{0.1}Co_{0.9})_2$, ^{57}Fe hyperfine interaction, mag. props., Mossbauer study 80−39951
In-Fe film, dil., supercond., Raman scatt. of light 79−73634
Ir-Fe, dil., local magnetisation, Mossbauer meas. 80−66091
Ir-Fe, spin fluctuation alloy, thermopower peak diffusion origin 80−88542
La-Fe, amorphous alloy film, spin reson. meas. 78−68389
La-Fe, FCC, Mossbauer spectra, Fe atom position 80−20549
La-Fe, liquid quenched, X-ray diffr. and Mossbaeur effect exam. of structure 78−76678
La-Fe alloy, amorphous, sputtered at high rate, mag. props. 80−75753
La-Fe amorphous alloy film, mag. props. 77−16121
La-Fe bulk amorphous alloys, mag. props. *(Japanese)* 79−95588
$LaNi_4Fe$, H_2 absorpt. cracking, acoustic emission characts. *(Japanese)* 80−66631
$LaNi_{5-x}Fe_x$, Fe effect on hydride form. *(Japanese)* 79−43202
Lu-Fe, amorphous alloy film, spin reson. meas. 78−68389
Lu-Fe amorphous alloy film, mag. props. 77−16121
$LuFe_2$, crystal field interaction contribution to specific heat 80−39788
$LuFe_2$, ferromag., magnetisation density, neutron diffr. study 80−60217
$LuFe_2$, ferromagnetic cpds., mean field exchange consts., Stoner itinerant model calcs. 80−50084
$LuFe_2$, mag. props. changes upon H_2 absorpt. 80−71270
Mg cast Fe, isothermal dissociation of supercooled austenite, exam. of kinetics *(Russian)* 79−29013
Mg cast iron, effect of heating temp. on microstruct. and mech. props. 77−56005
Mg cast iron, effect of heat treatment on phase comp., microstruct., wear resistance 77−56006
Mg cast iron, microstruct. of spheroidal graphite, rel. to polishing and annealing treatments 77−56160
Mg-Fe, dil. alloy, single impurity Kondo behaviour in elec. resist. *(French)* 79−60815
Mg-Fe, unidirectional solidification, method for determ. of diffusion and thermal diffusion coeffs. in molten Mg 78−30772
Mg-Fe alloy film, quench-condensed, resistance meas. 79−15235
Mg-Fe film, defect energy distrib., elec. resist. meas. during annealing 80−54808
Mi-Mn-Fe, low temp. anomalies of elec. resist. *(Russian)* 79−60788
Mn cast Fe, W effect on transform. in thin surface layers during dry sliding friction 77−21289
Mn content determination *(Polish)* 80−31889
Mn determ. by neutron activation anal., nondestructive, destructive methods 77−63987
γ-Mn-Fe, FCC→FCT transform. temp. and Neel temp., X-ray and neutron diffr. expts. *(Russian)* 78−84797
α-Mn-Fe, influence of Fe and Cr on Neel point *(Russian)* 77−1554
γ-Mn-Fe, Mn rich, damping capacity 79−83252
Mn-Fe, spin fluctuations effect on sp. ht. 79−82788
Mn-Fe-Al, phase stability 77−48397
Mn-Fe-C, melts, activities of Mn at 1673K 80−50597
Mn-Fe-C, phase instability 80−11628
Mn-Fe-Si-C, activity determ. by vapour press. meas. *(Japanese)* 77−63631
Mn-Fe-Si-C, melts, activities of Mn at 1673K 80−50597
β-Mn-Fe-Sn, weak itinerant electron antiferromagnetism, Mossbauer spectra meas. 77−36158
Mn-Ti-Fe, ternary phase diagram, computer calculations 80−45274
$Mn_{0.97}Fe_{0.03}As$, field induced ferromag. phase *(Russian)* 77−36070
$Mn_{1-x}Fe_xAs$, high-pressure phase, magnetic properties 78−52247
$Mn_{1-x}Fe_xAs$, mag. props., phase diags. 77−66300
$Mn_{1-x}Fe_xAs$, mag. props. in ground state *(Russian)* 78−56294
$Mn_{1-x}Fe_xAs$, magnetic transition under high press., exchange striction model calcs. *(Russian)* 80−50096
$(Mn_{1-x}Fe_x)B$, Invar charact. 77−15602
$Mn_{1-c}Fe_cPt_3$, noncollinear mag. structs., neutron diffr. anal. *(Russian)* 80−25087
$Mn_{2-x}Fe_xSb$, mag. struct. and spin flop transition, ^{57}Fe Mossbauer expts. 77−66261
$Mn_{2-x}Fe_xSb$, Mossbauer effect exam. 78−68432
$Mn_{1-x}Fe_xSi_{1.7}$, solid soln. system, temp. depend of conductivity and thermo-EMF, conc. depend of Hall const. 77−11913
$Mn_{5-x}Fe_xSi_3$, elec. resist. and mag. susceptibility, ferromag. to antiferromag. transition 80−80504
$Mn_{77}Fe_8Si_{19}$, cryst. struct. and superstruct. 77−35511
Mo-B-Fe, microalloying influence on mechanical props., cold rolling, plasticity *(Russian)* 80−40502
Mo-Fe, dil., Kondo effect of RKKY interaction 78−31052
Mo-Fe, Kondo system, magnetisation, Mossbauer expts. 77−77028
Mo-Fe, local magnetisation from Mossbauer meas. 77−20549
Mo-Fe, local moment system, low temp. susceptibility, Mossbauer effect meas. 77−43810
Mo-Fe, spin glass and mictomag. regimes, sp. ht., resist. and susceptibility meas. 77−69581
Mo-Fe alloy powders, densification and alloy formation on sintering 77−63597
Mo-Fe metalloceramic alloy, brittle fracture investigation, segregation, morphology, struct. *(Russian)* 80−55503
Mo-Fe-O-H system, thermodynamic equilib. 78−60657
Mo-Mn-Fe-Si/Al_2O_3 ceramic seal, interfacial phases 78−72011
Mo-Ni-Fe-Co-Zn alloys, Ni, Fe, Co and Zn distrib. using neutron-activation anal. 79−52531
MoFe, occurrence of spin glass and mictomagnetic regimes, props. meas. 77−16085
$(Mo_{0.6}Ru_{0.4})_{0.8}G_{0.2}$-Fe (G=P,B), amorphous supercond., upper crit. field as function of temp. 79−73646
Na_3AlFe_6 coatings, transmission and refraction dispersion spectra *(Russian)* 77−48264
Nb-Fe, alloying element influence on strength, ductility, surface and grain boundary energies *(Russian)* 79−74234
Nb-Fe, formed on laser irradiation of Nb-Fe interface, Mossbauer spectra *(Russian)* 79−60560
Nb-Fe, X-ray emission spectra study of electron struct. of Laves phases *(Russian)* 78−23555
Nb-Ga-Fe ternary system, phase equilib. at 1000°C, supercond. transition temp. 80−35158
Nb-Ge-Fe, effect of Fe on supercond. and mag. props. 79−56351
Nb-Mo-Fe, dil., local environment and mag. props. 78−64187

iron alloys continued
Nb-Mo-Fe, dil., local moment formation 78−43562
Nb_3Al-Fe, mag. impurities effect on supercond. props. 77−1524
$NbFe_2$ layers form. by diffusion during Nb wire drawing 79−28153
$Nb_{40}Fe_{40}P_{14}B_6$, metallic glass, explosive compaction, mech. props. 80−89176
$NbFe_{2-x}Si_x$, crystalline struct., electron microscopy determ. *(French)* 80−54174
$Nb_{78}Fe_{40}Si_{80}$, X-ray cryst. struct. determ. *(French)* 80−15048
$Nb_{78}Gn_{22-x}Fe_x$, $Nb_{80}Ga_{20-x}Fe_x$, A15 phase supercond. 79−87181
$Nb_{50}Ni_{50-x}Fe_x$, amorphous, mag. ordering and local random anisotropy 78−68273
$Nb_{50}Ni_{50-x}Fe_x$, amorphous alloy, mag. interactions 78−95432
$Nb_{50}Ni_{50-x}Fe_x$, magnetically dil. glass, 3d moments, mag. susceptibility and magnetisation meas. 79−95574
$NbSe_2$-Fe, dil. alloy, magnetotransport and superconductivity 77−55516
Nb_3Sn-Fe, mag. impurities effect on supercond. props. 77−1524
Nd-Fe-B ternary systems, phase equilibria and cryst. struct. *(Ukrainian)* 80−11626
$NdFe_2$, amorphous, magnetization and neutron scatt. meas. 79−78314
$NdFe_2$, amorphous, small angle neutron scatt. study of mag. order and mag. microstruct. 79−15283
$NdFe_2$, Curie temp., elec. quadrupole couplings, Mossbauer study 80−39949
$NdFe_2$, high field Mossbauer study 80−75893
$NdFe_2$, preparation and mag. props. 80−25259
Nd_xFe_{1-x} film, amorphous, mag. props. meas. 78−68312
$(Nd_xSm_{(1-x)})_2(Co_{0.7}Fe_{0.3})_{17}$, mag. anisotropy 80−34622
$(Ni,Fe)_3Ga$, magnetovolume effects near crit. conc. for ferromag. 79−56591
Ni/Cr-Fe-C, Inconel, dislocation intersection and solution strengthening, effect of solute on obstacle profiles 80−7590
Ni-Al bronze, fracture toughness 77−81312
Ni-Al-Fe, electrical and mag. anomalies due to substitutional atoms 77−15839
β'-Ni-Al-Fe, mag. impurity states, resist. meas. 77−55519
Ni-Al-Fe system, order-disorder phase transform., Gorskii-Bragg-Williams approx. *(Russian)* 79−29048
Ni-Au-Fe, liq., activity of iron at 1573K 77−70328
Ni-Be bronze, Fe and Si alloying addition effect on phase composition *(Russian)* 78−15360
Ni-Ce-Fe-Ti (77, 20, 4, 2.5 wt.%), long-term strength in H at high pressure 80−55485
Ni-Co, film, magnetisation induced uniaxial anisotropy, dislocations effects 78−43618
Ni-Cr-B-Si-Fe alloy, Cr content by X-ray fluoresc. 79−43654
Ni-Cr-Co-Fe, oxidation resistance 77−21320
Ni-Cr-Fe, blackness change in air, 1-8 micron, 1200°C, film props. depend. 77−66033
Ni-Cr-Fe, high temp. corrosion and creep in carburizing and oxidising atmos. 79−11727
Ni-Cr-Fe, Inconel, effects of heat treatment on surface segregation, Auger spectroscopic exam. 80−7602
Ni-Cr-Fe, Nimonic-75, electroless siliconization 78−27679
Ni-Cr-Fe, radiation enhanced precip. and dissolution of precipitates, point defect kinetics and dislocation obs. 80−108467
Ni-Cr-Fe, stress corrosion cracking, factors influencing susceptibility 80−97617
Ni-Cr-Fe (15.7, 7.63 wt.%), Inconel 600, anal. of pit generation by 3.5% NaCl, by stochastic theory *(Japanese)* 78−85038
Ni-Cr-Fe (75, 35, 12 wt.%), electron and α-particle irrad., positron annihilation and elec. resist. meas. 79−83054
Ni-Cr-Fe Alloy 600, acid intergranular corrosion rel. to caustic stress corrosion cracking stress relieving effect 77−66712
Ni-Cr-Fe Alloy 600, stress corrosion cracking in high purity water, effect of microstruct. 77−66713
Ni-Cr-Fe steam generator tubes, stress corrosion susceptibility, heat treatment effect 79−20258
Ni-Cr-Fe-Mo-Co (21.41, 19.28, 8.64, 2.16 wt.%), Hastelloy alloy X, exam. of thermal stability 78−84865
Ni-Cr-Fe-Si-B wear-resist. and corrosion-resist. coatings by furnace melting 80−35428
Ni-Cr-Fe-W, type EHI868, loading history effect on resist. to cyclic elastoplastic strain 80−16398
Ni-Cr-Mn-Fe-Nb (20,3,3,2.5 wt.%), short-range order effects on tensile behaviour 80−25793
Ni-Cr-Mo-Fe-Mn, Kh12M23, intermetallic phases exam. *(Russian)* 78−39740
Ni-Cr-Ti-Al-Fe-Co (19.65, 2.40, 1.37, 0.78, 0.52 wt.%), strength of γ' hardened alloy, ageing exam. 78−88501
Ni-Cr-Ti-Al-Mo-Nb-Fe (13-16, 2.35-2.75, 1.3-1.7, 2.8-3.2, 1.8-2.2, 2.0 wt%), heat resistant props, mech props. struct., stepwise ageing effects *(Russian)* 78−76666
Ni-Fe, 79 NM alloy, gamma and neutron influence on mag. susceptibility comparative study *(Russian)* 80−39751
Ni-Fe, (100) surface, O interaction, LEED and XPS studies 79−82437
Ni-Fe, activity of iron at 1573K 77−70328
Ni-Fe, adsorption of O_2, oxidation 80−108730
Ni-Fe, alloy pre-form prep. through reduction of sintered oxides 80−40284
Ni-Fe, Ar ion bombard., O_2 flooded, secondary ion yield as function of original conc. *(French)* 78−39643
Ni-Fe, chemical emission by Ar^+ ion bombardment *(French)* 77−86410
Ni-Fe, Curie points, mag. props. of H solutions FCC metal sublattice parameter behaviour 79−69671
Ni-Fe, dil., hyperfine mag. fields, press. effect, Mossbauer meas. 80−71277
Ni-Fe, dil., impurity effects on grain boundary mobility *(Polish)* 79−96073
Ni-Fe, dil., optical absorpt., electronic struct. 80−108227
Ni-Fe, dil., temp. depend. of Mossbauer absorpt. near Curie point *(French)* 80−11305
Ni-Fe, disordered alloy, CPA treatment, elec. resist. 77−1408
Ni-Fe, disordered FCC, local densities of states calc. 77−59244
Ni-Fe, elementary excitations, exchange stiffness const., inelastic neutron scatt. study 79−47294
Ni-Fe, epitaxial thin film, mag. structures and stresses, ferromag. resonance 78−72375
Ni-Fe, FCC, H_2 embrittlement *(Japanese)* 77−48526
Ni-Fe, FCC, Invar behaviour, spin waves stiffness consts., neutron scatt. study 79−51769

iron alloys continued
Ni-Fe, fatigued, struct. and cyclic stress strain, influence of stacking fault energy and atomic size-module-interactions *(German)* 79−42082
Ni-Fe, ferromag., influence of local ordering on spin wave stiffness const. 77−89937
Ni-Fe, film, anomalous Hall and Nernst-Ettingshausen effect, contribution of phonon and impurity scatt. *(Russian)* 78−64145
Ni-Fe, film, domain struct., effect of biaxial stresses 78−88153
Ni-Fe, film, magnetisation induced uniaxial anisotropy, substrate temp. depend. 77−8367
Ni-Fe, film, magnetisation reversal, magnetoresistance meas. 77−16132
Ni-Fe, high-field susceptibility, spin-wave spectrum, CPA calc. 80−65818
Ni-Fe, high-permeability alloys developments *(Slovak)* 79−4694
Ni-Fe, IR spectra, cond. electron charact. *(Russian)* 77−48173
Ni-Fe, influence of atomic ordering on spin waves 79−7987
Ni-Fe, magnetic aftereffects of H isotopes, book contrib. 79−82835
Ni-Fe, magnetisation curling in superparamagnetic spheres 77−8363
Ni-Fe, magnetostrictive vibr. meas., appl. of laser interferometric technique 80−37059
Ni-Fe, matrix effect in SIMS anal. using O_2^+ primary beam 80−76576
Ni-Fe, neutron irradiated, thermally activated deform. 80−6438
Ni-Fe, new soft magnetic material for pulse transfer and choking in power electronics *(German)* 79−28555
Ni-Fe, orientation aftereffect 80−88830
Ni-Fe, power losses at extremely low freqs. 80−88815
Ni-Fe, residual resist., CPA calc. to muffin tin pot. 77−62892
Ni-Fe, soft mag. props. rel. to metallurgical aspects 80−88810
Ni-Fe, spin polarised tunnelling expts. 78−39372
Ni-Fe, spin wave stiffness consts., RPA CPA band model 79−61088
Ni-Fe, split bands rel. to sp. ht., g-factor and magnetostriction data 77−72977
Ni-Fe, thermal fluctuation aftereffect meas. by pulse field method 80−88837
Ni-Fe, W-fibre reinforced, fabrication, heat treatment, and mag. and mech. props. 77−40408
Ni-Fe, X-ray study of occluded H_2 77−16586
Ni-Fe (15%) film, evaporated, uniaxial mag. anisotropy 77−51929
Ni-Fe (19 wt.%), mag. anisotropy induced by cold rolling *(Russian)* 80−84595
Ni-Fe (2 wt.%) oxidation, 800 to 1000°C 77−36686
Ni-Fe (20 wt.%), thin film ferromagnetic band, magnetisation under domain creep conditions *(Russian)* 79−91262
Ni-Fe (20%) film, condensed, struct. from electron diffr. 77−59222
Ni-Fe (20at.%), vacancy-C interaction, Lomer's model insufficiency *(French)* 77−76456
Ni-Fe (36 to 50 wt.%), initial permeability, domain struct. model 80−88811
Ni-Fe (40%), Mn coating, mag. interface effects 77−69638
Ni-Fe (40%) (111) film with C coating, surface magnetism 77−73056
Ni-Fe (50%), slow mag. domain wall motion 77−69597
Ni-Fe (67.7 at.%), noncommensurate atomic struct., neutron diffr. exam. *(Russian)* 77−84701
Ni-Fe alloy, continuous electrodeposition 80−16208
Ni-Fe alloy, extraordinary viscous magnetic wall motion 78−84465
Ni-Fe alloy, FCC, density, lattice parameters, X-ray diffr. and hydrostatic weighing 78−55904
Ni-Fe alloy, local ordering effect on spin wave stiffness const. 77−66282
Ni-Fe alloy, Ni base cathodes, powder metallurgy technique 80−29903
Ni-Fe alloy, oxidation, diffusion enthalpy and entropy 78−7084
Ni-Fe alloy film electrodeposition, modification of soln. composition 80−16209
Ni-Fe alloys, electrodeposited, electron microscope investig. *(Russian)* 77−43442
Ni-Fe alloys, pulse permeability and loss in toroidal core pulse current transformers 78−43615
Ni-Fe based metallic glasses, Curie pt. anomalies 80−60256
Ni-Fe conductor, EM pulse shielding, magnetisation curves 80−28143
Ni-Fe epitaxial films (110), uniaxial anisotropy, expt. 77−20648
Ni-Fe film, anal. of main component by atomic absorpt. spectrophotometry 77−70381
Ni-Fe film, Barkhausen noise spectra meas. 77−16131
Ni-Fe film, differential susceptibility, struct. const. and losses 79−91271
Ni-Fe film, domain struct., uniaxial stress effects 78−10740
Ni-Fe film, effect of tensile stress on mag. domain struct. 78−68332
Ni-Fe film, electrodeposition, role of buffers and anions 80−25583
Ni-Fe film, electron spin polarisation, meas. using supercond. tunnel junction 77−69637
Ni-Fe film, ferromag. reson. under weak influence of eddy currents *(German)* 77−8412
Ni-Fe film, Kerr magnetooptic effect, appl. to waveguide type optical modulator, theory 77−11015
Ni-Fe film, low field domain wall mobility 80−25167
Ni-Fe film, mag. and hyperfine field exam. of uniaxial anisotropy 77−66391
Ni-Fe film, oligatomic, ferromag. reson. and torsion magnetometry, 123-373K 77−59461
Ni-Fe film, relax. effects in domain boundary creep *(Russian)* 77−24723
Ni-Fe film, thermally activated domain wall motion 80−88777
Ni-Fe film, unidirectional anisotropy by exchange coupling, appl. to biasing of magnetoresist. read head 78−91907
Ni-Fe films, coercivity control for single-level masking bubble devices using surface modification and intermediate layers 79−51816
Ni-Fe films, energy change of Bloch wall with angle to easy axis, calc. *(Slovak)* 80−103863
Ni-Fe films, in state of undersaturation in perpendicular fields, micromagnetic struct. *(Russian)* 79−61193
Ni-Fe films, magnetisation reversal in narrow strips, TEM study 80−34720
Ni-Fe films, US generation by ferromag. reson. 78−88155
Ni-Fe films, viscous magnetic domain wall motion anal. 79−95617
Ni-Fe metallic glass, METGLAS 2826, creep props. 79−15746
Ni-Fe microelectrode array probe for electrophysiology 79−84049
Ni-Fe multilayered films, mag. domain structures 79−82847
Ni-Fe narrow stripes, mag. props. and domain struct. 79−82843
Ni-Fe overlay, influence on bubble device performance 79−78466
Ni-Fe oxidised film, extraordinary viscous wall motion at extreme vel. 78−14997
Ni-Fe oxidised films, easy-axis switching 79−91266

iron alloys continued
Ni-Fe polycrystalline film cross-tie memory for shipborne radar/sonar 80−42204
Ni-Fe powder, effect of vibration and current pulses on shaping 79−95973
Ni-Fe protective coatings on Al powder *(Russian)* 78−60881
Ni-Fe reed contact, Au-plated, submicron Auger spectroscopy exam. 79−15027
Ni-Fe soft magnetic alloys, developments and components *(Hungarian)* 78−48000
Ni-Fe solid soln., precip. hardened, paramag.-ferromag. transition on ageing 78−52255
Ni-Fe wire, hard-drawn, increased Barkhausen noise at low temps. 77−16114
Ni-Fe/Mn interface, mag. surface effects, dead layers and exchange anisotropy 77−24718
Ni-Fe-Al type B2 lattice alloys, Fe atom distribution, Mossbauer study *(Russian)* 79−99796
Ni-Fe-C, 20 at.% Fe, vacancy-C interaction, induced mag. anisotropy *(French)* 79−55775
Ni-Fe-Cd, ternary alloy, electrodeposition from acetate bath 79−95950
Ni-Fe-Ce superalloy, vacuum melted, Ce effects on microstruct. 77−36552
Ni-Fe-Co, alloy with step hysteresis loops *(German)* 79−42806
Ni-Fe-Co (17,3 wt.%), thin film ferromagnetic band, magnetisation under domain creep conditions *(Russian)* 79−91262
Ni-Fe-Co film, domain wall energy meas., by domain tip propag. method 77−55692
Ni-Fe-Co film, magnetoelastic vibr. generation during high freq. mag. reversals *(Russian)* 78−60320
Ni-Fe-Co film, nonmagnetostrictive, mag. props., effect of deposition parameters of Al underlayer 77−77078
Ni-Fe-Co films, for logic devices, mag. switching vel., anisotropy field and coercive force *(Korean)* 77−51930
Ni-Fe-Co films, nonmagnetostrictive, magnetoresistance effects 78−35013
Ni-Fe-Co films, saw tooth magnetic domains investigated 78−14994
Ni-Fe-Co-Ti, electron microscopy and mag. meas. 80−71097
Ni-Fe-Co(Mo) films, anal. of main component by atomic absorpt. spectrophotometry 77−70381
Ni-Fe-Cr, extraordinary Hall effect, elec. and mag. meas. at 77 and 300K 80−34421
Ni-Fe-Cr, PE 16, thermally activated domain wall motion 79−95603
Ni-Fe-Cr (18, 18 wt.%) superalloy, mech. props., 4-295K 77−44327
Ni-Fe-Cr alloy, PE 16, coercivity of picture frame cryst. 78−14988
Ni-Fe-Cr base superalloy, addition effect on mech. props. *(Chinese)* 80−20998
Ni-Fe-Cr film, hysteresis loop meas. using magnetooptical system 79−69707
Ni-Fe-Cr soft magnetic film plating bath 79−43465
Ni-Fe-Cr superalloy type 718, heat treatment effect on room temp. and elevated temp. fracture toughness response 80−100922
Ni-Fe-Cr-Mo-Ti-Al, PE 16, thermally activated domain wall motion 80−88777
Ni-Fe-Cr-Nb-Ta-Mo alloy, fatigue crack growth, stress ratio and hold-time effects 80−40531
Ni-Fe-Cu, Mu-metal, mag. aftereffects, dynamic neutron depolarisation study 80−50147
Ni-Fe-Cu, thermodynamic activities of components in pseudobinary section Ni_3Fe-Cu at 1520K 77−59752
Ni-Fe-H, hydride formation in high press. range 80−65235
Ni-Fe-Ho film strips, domain struct. and new rot. processes 77−85533
Ni-Fe-Mn, ferromag. reson. linewidth and saturation magnetisation 78−72418
Ni-Fe-Mn alloy, NMR signals due to Mn atoms with antiparallel moments 78−27113
Ni-Fe-Mn ferromagnetic alloy, magnetic state of Mn atom, local environment effect 77−66298
Ni-Fe-Mo, K-effect, Mossbauer study 80−39998
Ni-Fe-Mo-Cu (79, 16, 4.3, 0.7 wt.%) K-state formation, physical props. exam. 78−47761
Ni-Fe-Mo(Cr), determ. of preferential locations of Mo or Cr on Fe and Ni sublattices, by X-ray intensity study 79−37662
Ni-Fe-Nb, Hardperm, origin of high magnetic permeability 77−8362
Ni-Fe-Nb, hardperm alloy, effect of sheet thickness and heat treatment on magnetic props. *(Japanese)* 78−31095
Ni-Fe-Nb, Hardperm alloy, sheets, effect of sheet thickness, and annealing, on mag. props. 78−76772
Ni-Fe-Nb, mag. props. and struct. *(Chinese)* 78−84450
Ni-Fe-Nb (Mo), magnetic alloy, TEM and X-ray obs. *(Chinese)* 80−24401
Ni-Fe-Nb-Al, mag. props. and struct. *(Chinese)* 78−84450
Ni-Fe-Nb-Al (11.2, 8.09, 79.66 wt.%), modulated struct. growth process rel. to ageing *(Chinese)* 80−66541
Ni-Fe-Nb-Al(-Mo), wear resisting mag. head material, mag. props. and struct. 80−35350
Ni-Fe-Nb-Mo (11.42, 6.92, 1.54 wt.%), Hardperm, high magnetic permeability alloys 77−8361
Ni-Fe-Nb-Mo-Al, head material for mag. recording, DC and AC mag. props. 80−88812
Ni-Fe-Nb(Ta)-W, high magnetic permeability alloys, Hardperm 77−48012
Ni-Fe-Pd thin films, mag., surface and corrosion props. 80−34707
Ni-Fe-Rh films, mag. and corrosion props. 80−34702
Ni-Fe-W alloy, electrodeposition, SEM and optical obs. 79−66018
Ni-Ta-Al-Fe, Al and Fe effect on precipitation kinetics 79−20054
Ni-Zn-Mn-Fe spinel, crystn. from soln. in melt 80−2945
$Ni_{0.95}$ S Fe, spin glass, spin flop in exchange field 80−34640
Ni_3Al-Fe, Fe effect on Mossbauer effect study 77−32298
Ni_3Al-Fe, powder, X-ray spectral analysis exam. 80−16239
Ni_3Al-Fe (10 at.%), activation anal. of plastic deform. 79−1900
γ'-Ni_3Al-Fe (10 at.%) alloy, steady-state creep 78−15460
Ni(Fe,Cr), electron states density model and mag. characts. calcs. *(Russian)* 80−92804
Ni_3(Fe,Cr), electron states density model and mag. characts. calc. *(Russian)* 80−92804
Ni_3(Fe,M), M=Cr,Mo,W, elec. resist., temp. depend. anomalies, Hall and Nernst-Ettinghausen effects *(Russian)* 80−10942
Ni_3(Fe,M), M=Cu, Cr, Mo, W, kinetic phenomena rel. to ordering and electron struct. *(Russian)* 78−76043

iron alloys continued
NiFe alloy, ion-beam sputtering, excitation efficiency of atoms 78−19623
NiFe alloys, spin-wave exchange stiffness const. calcs., weak ferromagnetism 77−4510
NiFe disordered alloys, Mossbauer spectra, hyperfine mag. field distrib., Curie temp. 80−7198
NiFe film, domain wall mass and relax. time from forced oscills. 80−71133
NiFe film, ferromag. reson., thermodynamical anal. 79−42840
NiFe film, sputtered, physical props. 79−77938
NiFe film, stationarity and behaviour of Barkhausen noise 79−24198
NiFe, film deposition, sputter gun system, bubble device appls. 77−12532
NiFe, grain oriented, mag. domain wall slow motion, tunnelling mechanism 77−32210
NiFe, itinerant electron model, spin wave stiffness const. calc. 80−34613
NiFe, mag. hysteresis, departure from Rayleigh law in low mag. fields 77−40086
NiFe, magnetic surface anisotropy of transition metals, model calc. 80−34625
NiFe, magnetising energy, anisotropic effects 80−88743
NiFe, single and multilayer thin films, strip domains, inplane magnetisation 80−103866
NiFe soft magnetic alloys, magnetic props., effect of annealing and fabrication *(German)* 78−53004
NiFe, sputter etching in Ar-O plasma, implications for mag. bubble device fabrication 79−83347
NiFe stripes, mag. props. and domain struct. 80−44886
NiFe tape, rapid surface and vol. magnetisation, eddy-current-limited domain wall motion 77−12159
NiFe thin films, magnetoresistance, quasi-static characts. 80−107766
NiFe, US induced mag. reversals, stroboscopic electron microscope obs. 77−48026
NiFe-Ho film strips, curling-type mag. domains 77−48020
$Ni_{0.75}Fe_{0.25}$, influence of atomic ordering on spin waves, inelastic neutron scatt. 77−69516
$Ni_{0.83}Fe_{0.17}$ films, reson. oscills. of mag. domain walls and Bloch lines, stroboscopic electron microscopy 80−54931
$Ni_{1-x}Fe_x$, short range order exam. allowing for formation of structural domains *(Russian)* 78−6888
Ni_3Fe alloy, step-like deformation *(Russian)* 78−27559
Ni_3Fe, atomic order, Mossbauer effect obs. 77−69736
Ni_3Fe, change of H_2 diffusivity with order-disorder transformation 80−59729
Ni_3Fe, compression induced mag. anisotropy and superlattice dislocations, annealing effect 78−31067
Ni_3Fe, compression induced magnetic anisotropy, annealing effect 80−93112
Ni_3Fe, Debye temp. determ. from elastic consts. and X-ray meas., effect of configurational order 78−30727
Ni_3Fe, disaccommodation meas. after low temp. electron and neutron irrad. 80−88832
Ni_3Fe, dislocations, rate of piling up, rel. to average length of slip lines *(Russian)* 77−76416
Ni_3Fe disordered alloys, Mossbauer spectra, hyperfine mag. field distrib., Curie temp. 80−7198
Ni_3Fe, disordered single crysts., thermo-activated mechanism of plastic deform. *(Russian)* 78−84909
Ni_3Fe, domain struct. after tensile deform., dislocation effects 80−71083
Ni_3Fe, electronic structures, order effect 79−90938
Ni_3Fe, influence of order on Mossbauer spectra of ^{119}Sn 79−42876
Ni_3Fe, low-temperature specific heat, long and short range order effects 80−100339
Ni_3Fe, magnetocryst. anisotropy, annealing temp. depend. 80−103828
Ni_3Fe, mono- and polycrysts., strain hardening, test temp. effects *(Russian)* 80−66531
Ni_3Fe, Mossbauer spectra, long range order 78−10810
Ni_3Fe, Mossbauer spectra, order-disorder transition 78−10811
Ni_3Fe, non-linear local environment effect, Mossbauer effect of ^{57}Fe 80−39909
Ni_3Fe, nondislocation origin friction stress in alloys, deformation hardening 80−21050
Ni_3Fe, order-disorder transition phase diagram, Mossbauer meas. 80−39995
Ni_3Fe, ordered, monocrystals, thermally activated deform. processes 80−50684
Ni_3Fe, ordered and disordered states, strain hardening characts., temp. depend., multiple slip case *(Russian)* 78−15421
Ni_3Fe, polycrystalline alloy evolution of slip-line pattern during straining 80−107362
Ni_3Fe, roll magnetic anisotropy and dislocations *(Japanese)* 77−80930
Ni_3Fe, short range order determ. after heat treatments 79−96044
Ni_3Fe, short-range order, diffusive elastic neutron scattering 80−24400
Ni_3Fe, short-range order parameter calc. in pseudopot. approx. *(Russian)* 80−49183
Ni_3Fe, single cryst. ordered and quenched, stress relax. *(Russian)* 77−44282
Ni_3Fe single crystals, longitudinal magnetoresist. meas. 80−70675
Ni_3Fe, single crysts., long range order degree influence on strain hardening *(Russian)* 80−11660
Ni_3Fe, superlattice dislocations, compression induced mag. anisotropy 77−85442
Ni_3Fe, superlattice dislocations, compression induced mag. anisotropy 77−85443
Ni_3Fe, transport props. and magnetisation, effect of alloying with Cr, Mo, W or Cu *(Russian)* 78−39095
Ni_3Fe, X-ray diffraction investig. of order-disorder transform. *(Russian)* 77−70043
Ni_3Fe:C, mag. anisotropy depend. on C content, magnetometric study *(Russian)* 80−54887
Ni_3Fe-Sn, dil., atomic order detection by ^{119}Sn spectroscopy 80−39993
$Ni_{73}Fe_{27}$, order-disorder transition, Mossbauer study 79−95163
$Ni_{1-x}Fe_xAl$, self-consistent embedded-cluster model for mag. impurities 78−67973
$Ni_{40}Fe_{40}B_{20}$ glass alloy, rapidly quenched, explosive welding to A516-70 steel and to itself 78−39954
$Ni_{50}Fe_{30}B_{20}$, magnetostriction, temp. depend. 78−91921
$Ni_xFe_yCr_{1-x-y}$ films, struct., mag. props., and corrosion resist. 80−34706

iron alloys continued
$Ni_{35}Fe_{30}Cr_{15}P_{14}B_6$, amorphous, anodic polarisation and localised corrosion 77−21310
$Ni_{36}Fe_{32}Cr_{14}P_{12}B_6$, metallic glass, crystallisation 79−77520
$Ni_{36}Fe_{32}Cr_{14}P_{12}B_6$, amorphous, electrochem. corrosion in chloride solns. 80−50763
$Ni_{36}Fe_{32}Cr_{14}P_{12}B_6$ metallic glass, mech. props. and thermal stability 80−76362
$(Ni_{1-x}Fe_x)_{99}Mn$, ferromagnetic, NMR study of local environment effect, relaxation mechanism 80−7193
$Ni_3(Fe_{1-x}Nb_x)$, temp. and conc. depend. of anomalous Hall effect *(Russian)* 80−70674
$(Ni_{100-x}Fe_x)_{79}P_{13}B_8$, amorphous dil. alloys, spin glasses, magnetisation meas. 79−61178
$Ni_{40}Fe_{40}P_{14}B_6$, amorphous alloy, microstruct. study of crystallisation 77−86062
$Ni_{40}Fe_{40}P_{14}B_6$ metallic glass alloy, US spot welding to Cu 79−21730
$Ni_{80-x}Fe_xP_{14}B_6$, amorphous alloy, resistivity variations near critical temp. 79−73488
$(Ni_{99}Fe_1)_{79}P_{13}B_8$, amorphous, low temp. sp. ht., mag. contribs. 80−80552
$(Ni_xFe_{1-x})_{80}P_{10}B_{10}$, amorphous, Curie temp., press. effect 80−75833
$Ni_{49}Fe_{29}P_{14}B_6Si_2$ glass, flow and failure 80−40438
NiFr, mag. film, pulse switching at low temp. 80−103868
Ni_3Ge-Fe_3Ge solid soln., flow stress, transition from positive to negative temp. depend. 80−60906
$Ni_2Mn_{0.9}Fe_{0.1}Sn$, Fe site hyperfine field and mag. moment, Mossbauer effect meas. 78−76365
$Ni_{65}Mo_2Fe$, O_2 effect on secondary recrystallisation and mag. props. 80−35201
$NpFe_2$, high temp. mag. props., 300 to 1100K 79−51757
$NpFe_2$, lattice distortions in ferromag. phase, X-ray obs. 80−15774
Np_6Fe, existence and cryst. chemistry 77−51349
$NpFe_{2-x}Co_xSi_2$, mag. and hyperfine props. 79−51887
$NpFe_{2-x}Co_xSi_2$, mag. and hyperfine props. 80−7247
$NpFe_2Si_2$, itinerant magnetism obs. 77−28406
$NpFe_2Si_2$, Mossbauer and magnetisation expts. 78−31138
$(Np_{1-x}U_x)Fe$, Mossbauer spectra, magnetism and hyperfine interactions 80−20529
Pb-Fe, liq., thermodynamic props. *(Polish)* 80−89199
Pb-Fe, supercond. films, modification of props. by Fe grains *(French)* 79−60957
Pd-Ag-Fe, (0.5, 1.0, 2 at.% Fe), elec. resist. reduction near ferromag. and spin glass ordering 77−69299
Pd-Fe, del. alloy, Mossbauer obs., 0.018-300K 77−69740
Pd-Fe, dil., anisotropy of neutron polarisation near ferromag. phase transition 77−32234
Pd-Fe, dil., anomalous lattice parameters and H_2 solubilities 79−33091
Pd-Fe, dil., depend. of neutron small-angle scatt. intensities on appl. mag. field and temp. 79−11291
Pd-Fe, dil., ferromag., magnetoresist. 78−91665
Pd-Fe, dil., ferromag. and spin-glass states, cond. electron polarisation studied by positive muons 77−28397
Pd-Fe, dil., plastically deformed, positron annihilation study of recovery of crystal, imperfections *(German)* 77−85835
Pd-Fe, dil., spin polarisation effect on hyperfine interactions, anal. of Mossbauer meas. *(Russian)* 79−47055
Pd-Fe, dil., transport props. at low temp. 0.05 to 5K 79−38046
Pd-Fe, dil. alloy, conduction electron polarisation at 0.1K, μ^+SR 77−20784
Pd-Fe, dilute, muon$^+$ Knight shift, cond. electron polarisation 77−66450
Pd-Fe, dilute ferromagnets, press. effect on Curie temp. 80−65873
Pd-Fe, disordered FCC, exchange stiffness consts., temp. depend. of magnetisation 77−69528
Pd-Fe, highly dil., mag. behaviour, 0.06-300K, Mossbauer expt. 78−43711
Pd-Fe, hydrogenated and unhydrogenated, EPR and demagnetisation field 77−32250
Pd-Fe, mag. ordering phenomena, neutron scatt. obs. 80−44812
Pd-Fe, magnetic anisotropy near Curie point, quasi domain struct. *(Russian)* 80−65867
Pd-Fe, magnetoresist., rel. to dil. ferromag. model 78−30907
Pd-Fe, molecular field distribution function in disordered Ising model *(Russian)* 80−54859
Pd-Fe, Mossbauer effect under press. for ^{119}Sn impurity atoms and hyperfine mag. field model *(Russian)* 77−55742
Pd-Fe, Mossbauer spectra, scatt. and transmission geometries, differences in crit. behaviour near T_c 78−76367
Pd-Fe, NMR of ^{27}Al meas. 77−12215
Pd-Fe, normal Hall effect, temp. and conc. depend. *(Russian)* 77−80763
Pd-Fe, normal Hall effect *(Russian)* 80−103676
Pd-Fe, onset of ferromagnetism 78−23270
Pd-Fe, Pd-Fe-H and Pd-Fe-D, Mossbauer effect, internal hyperfine field temp. depend. 77−12283
Pd-Fe, resist. min. 80−11050
Pd-Fe, scatt. and transmission Mossbauer spectra near Curie temp. 80−15864
Pd-Fe, very dil., Mossbauer emission spectra, relax. effects 80−66084
Pd-Fe, very dilute, very low temp., spin glass-like behaviour 79−99708
Pd-Fe (0.54-8.0 at.%), thermo EMF at 4.2-300K *(Russian)* 80−92881
Pd-Fe (1 wt.%), alloy component surface conc. changes kinetics under vac. sputtering and volatilisation *(Russian)* 79−60608
Pd-Fe (25-55 at.%) ^{57}Fe effective field and mag. struct., Mossbauer and magnetisation expts. *(Russian)* 77−90085
Pd-Fe alloy, IR absorpt. characts., 0.9 to 19 μm, mag. order effect 78−84577
Pd-Fe alloys, H_2 absorption and mag. behaviour 78−35012
Pd-Fe disordered alloy, Landau model for mag. props. 77−66276
Pd-Fe type dil. ferromag. alloys, spin wave propag. *(Russian)* 77−12110
Pd-Fe-H, elec. resistivity, 4.2 to 300K *(Russian)* 79−7814
Pd-Fe-H alloy, Mossbauer line shift with H conc. *(Russian)* 77−40165
Pd-Fe-Mn, differential susceptibility, spin glass and ferromag. transition 79−61169
Pd-Fe-Mn, dil. alloy, high press. study 80−34600
Pd-Fe-Mn, ferromag. and spin-glass props; comment 80−2591
Pd-Fe-Mn, ferromagnet-spin glass, thermal expansion forced, magnetostriction and magnetisation under high press. 80−65255
Pd-Fe-Mn, ferromagnetic-spin glass transition 78−39339

iron alloys continued
Pd-Fe-Mn alloy, spin glass-ferromagnetic systems, differential susceptibility 78−88131
Pd-H-Fe, Mossbauer effect, hyperfine field, effect of changing spin susceptibility 77−20494
Pd-Si-Fe amorphous alloy, Mossbauer spectra, struct. and bonding 80−7224
PdAgFe, ferromag., Curie temp. depend. on susceptibility, non-mean field theory 80−44829
PdAl-Fe, phase diagrams, eutectic points and solubility *(Russian)* 80−40333
$(Pd_{80}Au_7Si_{13})/Fe_{30}$, compositionally modulated amorphous film, diffusion, struct. relax. 80−103518
PdFe (4.7 at.%), effect of alloying on activation energy of H_2 diffusion 80−107571
PdFe alloy, magnetoresistance meas. below 295K 79−78070
$Pd_{0.5}Fe_{0.5}$, disordered, spin wave dispersion relation, neutron inelastic scatt. 79−61090
$Pd_{0.98}Fe_{0.01}$ $Gd_{0.01}$, Pd-Gd exchange const., neutron diffuse scatt. meas. 80−71002
Pd_3Fe, ferromag., spin wave spectrum 77−69515
Pd_3Fe foil, $L1_2$ superstructure, antiphase boundary orientation and energy 80−39112
Pd_3Fe, hyperfine interactions during atomic ordering, Mossbauer obs. *(Russian)* 78−56630
Pd_3Fe, itinerant ferromagnet, neutron inelastic scatt. 79−7970
Pd_3Fe, spin wave dispersion relation at 4.2K, neutron inelastic scatt. meas. 77−63157
Pd_3Fe, spin wave dispersion, neutron inelastic scatt. meas. 78−14943
Pd_3Fe, X-ray and electron microscope obs. of antiphase domains and superdislocations *(Russian)* 77−86017
$(Pd_{0.67}Fe_{0.33})_{1-x}Au_x$, ordering effects on mag. props. *(Russian)* 78−47942
$Pd_{50}Fe_{37.5}Co_{12.5}$, elec. resist., cond. electron scatt. and heterogeneities of spin system *(Russian)* 79−56189
$PdFe_{1-x}Cr_x$ ordering alloys, elec. resist., temp. depend. *(Russian)* 80−24866
$Pd_{0.98}Fe_{0.01}Gd_{0.01}$, ferromag., Pd-Gd exchange const. and Pd polarisation, neutron scatt. meas. 80−25122
$(Pd_{0.9965}Fe_{0.0035})Mn_{0.05}$, ferromag. and spin-glass props. 80−2590
$(Pd_{0.9965}Fe_{0.0035})_{1-x}Mn_x$, mag. behaviour at Fe sites, Mossbauer effect meas. 80−66085
PdFeRh, ferromag., Curie temp. depend. on susceptibility, non-mean field theory 80−44829
$Pd_{70}Fe_{10}Si_{20}$ alloy, amorphous to cryst. transition, 350 to 450°C, Mossbauer spectra 78−59758
PdH_x-Fe, dil., Kondo system, local moment hyperfine studies, Mossbauer expt. 80−39908
$PdH_xFe_{0.003}$, Kondo system, local moments, hyperfine fields, Mossbauer study 80−80478
$PdH_x(\alpha')Fe_{0.003}$, Kondo effect and RKKY coupling, Mossbauer spectra 79−61054
$(Pd_{1-y}M_y)_{100-x}Fe_x$, M=Ag, Rh, exchange-enhanced alloys, mag. ordering 79−61050
$(Pd_xPt_{1-x})_3Fe$ atomically ordered alloy, thermoelectric power, carrier energy spin shift, mag. props. 80−29394
$(Pd_xPt_{1-x})_3Fe$, magnetisation intensity and coercive force, antiferro- to ferromag. transition *(Russian)* 77−48008
$(Pd_{86}Si_{15})_{61}/(Fe_{85}B_{15})_{39}$, compositionally modulated amorphous film, diffusion, struct. relax. 80−103518
$Pd_{100-x-y}Si_xFe_y$, amorphous, ^{57}Fe Mossbauer spectra, X-ray diffr., ageing behaviour 79−28651
$Pd_{80-x}Si_{20}Fe_x$, amorphous, low x, hyperfine interactions and mag. ordering temp. 79−15303
$Pr_2(Co_{1-x}Fe_x)_{17}$, hard direction magnetisation, 5-300K, and anisotropy field 77−12114
$PrFe_2$, Curie temp., elec. quadrupole couplings, Mossbauer study 80−39949
$PrFe_2$, high field Mossbauer study 80−75893
$PrFe_2$, Laves phase, mag. props., Mossbauer spectra, crystalline field mag. anisotropy 80−65851
$PrFe_2$, preparation and mag. props. 80−25259
Pt-Fe, competing interactions in FCC alloys 78−95453
Pt-Fe, dil., breakdown of ferromag. order, magnetoresist. obs. 80−71046
Pt-Fe, dil., skew scatt. Hall effect, magnetoresist. and mag. anisotropy, orbital magnetism of impurity 80−70678
Pt-Fe, dil., surface segregation, equilib. surface compositon, AES meas. 77−85039
Pt-Fe, dilute ferromagnets, press. effect on Curie temp. 80−65873
Pt-Fe, supported, mag. prop. meas. in H_2 and O_2, 77 to 700K 79−91257
Pt-Fe, very dil., Mossbauer emission spectra, relax. effects 80−66084
Pt-Fe alloy, low field AC susceptibility 79−73698
Pt-Fe alloy, ordered, T-c phase diagram, antiferro- and ferromagnetism *(Russian)* 80−65871
Pt-Fe alloy foils prep. by electrodeposition of Fe 80−35113
Pt-Fe ordered alloy, multiply mag. phase transitions 80−60264
$Pt_{0.72}Fe_{0.28}$, isomer shift and effective mag. field at ^{57}Fe, press. depend. 77−16232
Pt_3Fe, collision cascades, neutron induced superparamagnetism *(Russian)* 78−2166
Pt_3Fe, transport and mag. props. near Neel temp. 79−7976
$Pt_{50}Fe_{12.5}Co_{37.5}$, elec. resist., cond. electron scatt. and heterogeneities of spin system *(Russian)* 79−56189
$Pt_{0.7}Ni_{0.3}Fe$, magnetically hard, cryst. morphology and mag. domain struct. 77−69615
$Pt_{12.5}Pd_{37.5}Fe_{50}$, elec. resist., cond. electron scatt. and heterogeneities of spin system *(Russian)* 79−56189
$PuFe_2$, ferromag. mag. cross section, form factors, saturation magnetisation values, polarized neutron study 79−47245
$PuFe_2$, high temp. mag. props., 300 to 1100K 79−51757
$PuFe_2$, Laves phase cpds., thermodynamic props. 77−20092
RFeAl, scatter order cpds., mag. props. 77−51891
rare earth-Tb-Fe alloys, $R_xTb_{1-x}Fe_2$, (R=Gd, Sm, Dy, He, Zr), props. of near magnetostrictive materials 77−51934
Re-Fe-Al, physical-chemical investigation *(Russian)* 78−15362
Rh-Fe, competing interactions in FCC alloys 78−95453
Rh-Fe, dil., anti-Kondo effect, de Haas-van Alphen obs. 79−73427
Rh-Fe (25, 20 at.%), mag. virtual bound state alloys, XPS of core states 79−47588
Rh-Pd-Fe, dil., local environment and mag. props. 78−64187
Rh-Pd-Fe, dil. alloy, mag. moment 78−95416

iron alloys continued
Rh_2FeSn, ferromag., mag. hyperfine fields of ^{119}Sn, Mossbauer meas. 78−10816
Rh_2FeSn, ferromag. Heusler alloy, hyperfine fields, spin echo meas. 77−63314
Rh_2FeSn, Heusler alloy, Sn and Fe hyperfine field, Mossbauer exam. 77−43920
Rh_2FeSn, hyperfine mag. fields at ^{119}Sn and ^{57}Fe, under press., Mossbauer expts. 79−99812
Rh_2FeSn, metallic ferromagnet, hyperfine mag. field temp. depend. *(Russian)* 78−80265
Ru-Fe, dil., local magnetisation, Mossbauer meas. 80−66091
Ru-Fe, dil., localised spin fluctuation system, supercond. transition temp., conc. depend. 78−56253
Ru_2FeSn, ferromag. Heusler alloys, hyperfine fields at nonmagnetic atoms in various sites, Mossbauer effect and NMR meas. 80−66089
Ru_2FeSn, hyperfine mag. field, Mossbauer spectra 80−15865
S-Cu-Fe, phase diagram calc. 78−10172
Sc-Fe, dil., elec. field gradient, Mossbauer meas. 80−80665
Sc-Fe, electrotransported, low temp. sp. ht. meas. 77−7872
Sc-Fe system phase diag. *(Ukrainian)* 78−84773
Sc-Fe-Si system, phase obs. at 800°C *(Russian)* 78−23661
$ScFe_2$, Mossbauer effect of ^{57}Fe 80−75903
$ScFe_{2-2x}Al_{2x}$, mag. props., composition depend. 77−20593
$Sc(Fe_{1-x}Co_x)_2$, magnetic saturation moment, Co conc. depend., NMR exam. 78−15037
$ScFe_2H_2$, Mossbauer effect of ^{57}Fe 80−75903
Si-Fe, domain and grain obs. using ferromag. colloid technique 80−11219
Si-Fe, ferromagnetic domains and their junctions, simulation of X-ray topographs 79−78434
Si-Fe, freq. spectrum of Barkhausen noise of moving 180° domain wall 77−16115
Si-Fe, liquid alloys, thermodynamic charact. calc. *(Russian)* 78−27475
Si-Fe-W, dil. alloy, compositional changes on sputtering, projectile energy depend. 80−66362
SiFe sheets, grain-oriented, stray field meas. 80−88775
Si_xFe_{100-x} polycryst. ribbon, prep. by rapid quenching, and props. 80−75803
Sm-Co-Cu-Fe, single phase 2-17 sample, hard mag. props. 77−8349
Sm-Co-Cu-Fe-Ti magnets, comp. and sintering effects on coercivity 79−15326
Sm-Co-Cu-Fe-Zr, reversible changes in coercive force and struct. state during heat treatment 400-800°C *(Russian)* 80−29574
Sm-Co-Cu-Fe-Zr magnet, production and mag. props. 77−40085
Sm-Fe, dil., valence impurity state, inference from mag. susceptibility 78−95270
Sm-Fe-B ternary systems, phase equilibria and cryst. struct. *(Ukrainian)* 80−11626
$Sm_{1-u}Ce_u(Co_{1-x-y-w}Fe_xCu_yCr_w)_z$, permanent mag., improved mech. props. 79−87593
$Sm_2(Co, Cu, Fe, M)_{17}$, M=Nb, V, Ta, Zr, effect of M on mag. props. 77−89978
$Sm_2(Co,Fe)_{17}$, exchange and crystal field parameters, anisotropy meas. 77−69535
$SmCo_x$-Fe composite permanent magnet material, mag. props. 77−40089
$Sm(Co_{0.81}Cu_{0.15}Fe_{0.04})_{6.9}$ powders, mag. props. *(Russian)* 80−20434
$Sm(Co_{0.86-x}Cu_{0.14}Fe_x)_7$, permanent magnet, sintering and heat treatment effects 80−39817
$Sm_2(Co_{1-x}Fe_x)_{17}$ 77−40054
$Sm_2(Co_{1-x}Fe_x)_{17}$, anisotropy consts., conc. and temp. depend. *(Russian)* 78−64202
$Sm_2(Co_{1-x}Fe_x)_{17}$, bulk magnetisation and magnetocryst. anisotropy, interpretation 77−40055
$Sm_2(Co_{1-x}Fe_x)_{17}$, magnetocryst. anisotropy, Tb, Mn or Cr substituent effects 77−8297
$Sm(Co_{0.85}Fe_{0.05}Cu_{0.10})_z$, coercive force meas. 77−4530
$Sm(CoFeCuMn)_7$, coercive force and anisotropy temp. depend. 78−68297
$Sm_2(Co_{0.8}Fe_{0.14}Mn_{0.04}Cr_{0.02})_{17}$, sintered, hard mag. props. 77−8340
$Sm_2Cu_{1.6}Zr_{0.16}Fe_{3.3}Co_{12}$, enhancement of mag. props. 79−82825
$SmFe_2$, ferromagnetic-ferrimag. cpds., mean field exchange consts., Stoner itinerant model calcs. 80−50084
$SmFe_2$, highly magnetostrictive props. 77−12180
$SmFe_2$, hyperfine field exam. by NMR spin echo 78−23365
$SmFe_2$, hyperfine interactions and exchange fields acting on Eu^{3+}, Mossbauer obs. 77−63338
$SmFe_3$ and Sm_6Fe_{23}, magnetostriction, room temp. to 80K 80−65993
$Sm_{1-w}MM_w(Co_{1-x-y}Cu_xFe)_z$, (MM-mischmetal), mag. meas. and metallographic exam. 77−56119
$Sm_6Mn_{23-x}Fe_x$, magnetic behaviour, temp. and comp. depend. 80−93090
$SmNi_4Fe$, intrinsic mag. hardness 77−85506
$Sm_{0.91}Zr_{0.09}(Co_{0.68}Cu_{0.10}Fe_{0.22})_{6.7}$, alloy permanent magnet, coercive force *(Russian)* 80−65966
stabilisation of α and γ phase of Fe by transition impurities 77−76552
Ta-Fe, X-ray emission spectra study of electron struct. of Laves phases *(Russian)* 78−23555
TaS_2-Fe, dil. alloy, magnetotransport and superconductivity 77−55516
$TaSe_2$-Fe, dil. alloy, magnetotransport and superconductivity 77−55516
(Tb,Dy)-Fe amorphous films prep. by cosputtering, magnetoelastic props. 80−97429
$(Tb,Dy)Fe_2$ alloys, giant magnetostriction *(Chinese)* 79−51830
Tb-Fe, amorphous, random anisotropy effects 78−68223
Tb-Fe, amorphous ferrimag. film, thermomag. writing using He-Ne laser 77−12163
Tb-Fe, amorphous ferrimag. film, mag. props. and Curie point writing 77−12164
Tb-Fe, amorphous film, Kerr and Hall effect meas. 77−24722
Tb-Fe, amorphous film, Kerr readout charact. 79−15439
Tb-Fe, amorphous magnetism in bulk samples 77−66278
Tb-Fe, amorphous sputtered film, magnetostriction 79−47320
Tb-Fe amorphous film, sputtered, stress induced anisotropy 79−73706
Tb-Fe amorphous film, thermomag. contact printing 77−89986
Tb-Fe amorphous films of rare earth transition metal system, preparation by co-sputtering 79−56928
Tb-Fe amorphous magnetic films, domain wall obs. by Lorentz electron microscopy 77−80979
Tb-Fe amorphous thin films, magnetic after-effect, Kerr magneto-optic effect obs. 80−97123
Tb-Fe film, amorphous, contact printing 77−73061

iron alloys continued
Tb-Fe film, undoped and O-doped, amorphous, microstruct. and mag. props. 79−91273
Tb-Fe sputtered films, amorphous, mag. aftereffect due to domain wall motion 79−73780
$Tb_{0.24}Dy_{0.73}Fe_{1.95}$, magnetostrictive underwater sound transducer 78−13881
$Tb_{0.26}Dy_{0.74}Fe_2$, temp. depend. of magnetomechanical coupling factor 77−90002
$Tb_{0.27}Dy_{0.13}Fe_{1.98}$, grain-oriented, permeability, magnetomechanical coupling and magnetostriction 79−78491
$Tb_{0.27}Dy_{0.73}Fe_2$, anomalous thermal expansion and magnetostriction 77−90003
$Tb_{0.27}Dy_{0.73}Fe_2$, domain configurations, obs. by Kerr effect and synchrotron radiation topographs 78−64215
$Tb_{0.27}Dy_{0.73}Fe_2$, LF magnetoelastic effects 78−68348
$Tb_{0.27}Dy_{0.73}Fe_2$, magnetisation and magnetic anisotropy 78−91862
$(Tb_{0.27}Dy_{0.73})Fe_2$, magnetisation, ferromag. domains 80−25162
$Tb_{0.27}Dy_{0.73}Fe_2$, perpendicular suscept., magnetomechanical coupling and shear modulus 78−91918
$Tb_{0.27}Dy_{0.73}Fe_2$, vertically zoned, magnetomechanical coupling and magnetostriction 80−65999
$Tb_{0.3}Dy_{0.7}Fe_2$, elastic vs. magnetoelastic anisotropy 78−68347
$Tb_{0.3}Dy_{0.7}Fe_2$, magnetoelastic coupling meas. by US method 77−69652
$Tb_{0.3}Dy_{0.7}Fe_2$, magnetostrictive, resonant coupling of shear waves 79−33517
$Tb_{0.3}Dy_{0.7}Fe_2$, prep. by powder metallurgy, magnetostrictive props. 80−75826
$Tb_{0.3}Dy_{0.7}Fe_2$, sound velocity mag. field and temp. depend. elastic moduli calcs. 80−39839
$Tb_{0.3}Dy_{0.7}Fe_2$, US velocity and attenuation obs. 77−28423
$Tb_{1-x}Dy_xFe_2$, pseudobinary Laves cpds., spin-orientation diagram, Mossbauer effect meas. 77−55739
$Tb_xDy_{1-x}Fe_2$, Laves phase alloy, magnetostriction depend. on powder orientation before sintering 78−76284
$Tb_{0.20}Dy_{0.22}Ho_{0.58}Fe_{1.95}$, grain-oriented, permeability, magnetomechanical coupling and magnetostriction 79−78491
$Tb_xDy_yHo_zFe_2$, temp. depend. of magnetomechanical coupling factor 77−90002
$TbFe_2$, amorphous, mag. struct., US meas. 79−99683
$TbFe_2$, amorphous, Mossbauer spectra *(French)* 80−25261
$TbFe_2$, amorphous, struct. determ., EXAFS exam. 78−51421
$TbFe_2$, amorphous, temp. depend. of mag. hystersis props. 79−61186
$TbFe_2$, amorphous and crystalline, small angle neutron scatt. study of mag. order and mag. microstruct. 79−15283
$TbFe_2$, domain configurations, obs. by Kerr effect and synchrotron radiation topographs 78−64215
$TbFe_2$, high field magnetostriction and magnetisation 78−84471
$TbFe_2$, highly magnetostrictive props. 77−12180
$TbFe_2$, magnetisation, ferromag. domains 80−25162
$TbFe_2$, magnetisation and magnetic anisotropy 78−91862
$TbFe_2$, magnetoelastic props., magnetostriction hysteresis *(Russian)* 80−29590
$TbFe_2$ monocrystalline (111), under elastic compressive stresses, domain structure *(Russian)* 79−91247
$TbFe_2$, X-ray obs. of low temp. modifications of crystal struct. *(Russian)* 78−75632
$TbFe_3$ and Tb_6Fe_{23}, magnetostriction, room temp. to 80K 80−65993
$TbFe_3$, ferrimag., mag. struct., powder neutron diffr. determ. 79−78328
$Tb_{0.018}Fe_{0.982}$, amorphous, small angle neutron scatt. study of mag. order and mag. microstruct. 79−15283
Tb_xFe_{1-x} film, amorphous, magnetostriction and magnetisation 78−68305
$TbFe_{1.5}Al_{0.5}$, crystalline, small angle neutron scatt. study of mag. order and mag. microstruct. 79−15283
$TbFe_4Al_8$, commensurate-incommensurate modulated mag. struct., neutron diffr. obs. 79−95576
$TbFe_4Al_8$, neutron diffr. exam., mag. struct. 78−10656
$Tb(Fe_{1-x}Rh_x)_2$, Fe sublattice spin reorientation possibility, Mossbauer spectra *(Russian)* 79−78335
Tc-Fe, dil., effect of Fe impurities on superconductivity 79−61007
Tc-Fe, dil., local magnetisation, Mossbauer meas. 80−66091
Tc-Fe alloy, Mossbauer spectra, hyperfine field 80−20526
Tc-Fe dilute alloys, supercond. and mag. props. 80−29494
Th-Fe (20 to 70 at.%), amorphous alloy, electrical resistivity and thermal stability 80−33901
$ThFe_3$, H_2 absorption effect on mag. props. and struct. 77−40045
$ThFe_5$, mag. props., ferrimag. moment arrangement 79−33475
$Th_{1-x}Fe_x$ amorphous alloys, mag. props. and Mossbauer spectra 79−91326
Th_7Fe_3, H induced change from supercond. to mag. ordered state 79−28525
Th_7Fe_3, Mossbauer spectra, mag. props. 80−15852
Th_7Fe_3, spin-pairing state investig. via Josephson current between weakly-coupled superconductors 77−47942
$ThFe_{5-x}Al_x$, homogeneity regions, X-ray powder diffr. study 79−77554
$Th_{1-x}Y_xCo_{5-y}Fe_y$, lattice consts., magnetisation, and anisotropy fields 79−78364
Ti alloy VT3-1, large forgings, heat treatment, struct. and mech. props. 78−52864
α-Ti/Fe, retrograde solid solubility 80−79950
Ti-Al-Cr-Fe-Si alloy AT6, and weldments, mech. and corrosion props. 77−90409
Ti-Al-Cr-Mo-Fe, effect of structure and heat treatment on tensile strength, ductility, fatigue limit and notch sensitivity 78−56711
Ti-Al-Fe, thermomechanical treatment effect on mech. props., strengthening mechanisms 80−55441
Ti-Al-Mo-Cr-Fe, distrib. of Sn, Zr between phases, temp effect. 80−55357
Ti-Al-Mo-Cr-Fe, effect of heating on thermal stability of phases, lattice constants and chem. comp. 78−56672
Ti-Al-Mo-Cr-Fe (6.4, 2.7, 1.6, 0.4 wt.%), quenched VT3-1, decomposition kinetics of α'' and β in annealing *(Russian)* 77−66662
$(\alpha+\beta)$-Ti-Al-Mo-Fe alloy VT-22, behaviour during creep testing, solid soln. dissoc. *(Russian)* 80−40346
Ti-Al-V-Cr-Zr-Mo-Fe (3.4, 8.3, 5.8, 3.9, 4.2, 0.06 wt.%), shock loaded, residual strength 77−36589
Ti-Al-V-Fe-Cu, melt-extracted polycryst., mech. props. 80−76360
β-Ti-Fe, (7.1 wt.%) exam. of ω phase formation, by X-ray diffr. and Mossbauer spectroscopy 78−52800

iron alloys continued
Ti-Fe, corrosion, effect of microstruct. caused by casting, annealing, beating *(Russian)* 79−57140
Ti-Fe, diffusion of H_2 *(Korean)* 78−18838
Ti-Fe, diffusion of stored H, Mossbauer study 80−34838
Ti-Fe, dil., phase analysis by Mossbauer spectra 80−15922
Ti-Fe, equiatomic, heats of form., influence of short-range order *(Russian)* 80−81354
Ti-Fe, eutectoid decomposition 79−24491
Ti-Fe, force constant change with pressure, relative Mossbauer fraction 80−34163
Ti-Fe, H storage material, Mossbauer surface studies, Fe clusters 80−97167
Ti-Fe, magnetic susceptibility depend. on phase composition *(Russian)* 80−54875
Ti-Fe, oxidation of intermetallic phases 79−100298
αTi-Fe, plastically deformed, $\alpha \rightarrow \omega$ transform. 78−3095
α-Ti-Fe, solubility, resistivity variation rel. to quenching temp. 79−99324
β- Ti-Fe (1 to 6 wt.%) alloys, H diffusion *(Korean)* 79−42312
Ti-Fe (1.4 wt.%), polymorphic transform. due to plastic deform., positron annihilation 80−79939
Ti-Fe alloys, elec. and thermal props. *(Russian)* 78−19020
Ti-Fe corrosion resistant coating on Cu, obtained by contact eutectic fusion 80−50772
Ti-Fe microprobe anal. of alloying addition distrib. 80−55358
Ti-Fe-Al(Mn), homogeneity and lattice parameters, Mn and Al effect on hydriding cmpd. FeTi 80−108400
Ti-Fe-C-N, ion irradiated, microstruct. study using TEM 80−96572
Ti-Fe-H(D) system, struct. phase diagram, thermodynamics and diffusion *(German)* 79−56963
Ti-Fe-Ni (67, 30, 3 wt.%), reversible shape alteration *(Russian)* 80−71647
α-Ti-Fe(0.22 wt.%), ω phase form. during ageing 77−52355
Ti-Mo-Fe (3, 0.13 at.%), metastable phases, Mossbauer study 80−7243
Ti-Mo-Fe-Cr-Al, alloy VT3-1, influence of constitution on fracture toughness *(Russian)* 77−77559
Ti-Mo-V-Al-Cr-Fe (4.8, 4.7, 5.2, 1.1, 1.0 wt.%), structural changes during heating up to 1000°C, DTA study *(Russian)* 80−93552
β-Ti-Mo-V-Fe-Al (8, 8, 2, 3, wt.%), exam. of stress induced H_2 migration 78−87823
Ti-Mo-V-Fe-Al (8,8,2,3, wt.%), exam. of stress controlled fatigue response 79−61734
β-Ti-Mo-V-Fe-Al (8,8,2,3 wt.%), metastable, high cycle fatigue crack initation, grain size effect 77−86145
β-Ti-Mo-V-Fe-Al (8,8,2,3 wt.%), metastable alloy, microstruct. and mech. props. ageing time and temp. effect 78−64569
Ti-Mo-V-Fe-Al (8823 wt.%), heavy section extrusion, fabrication and mech. props. 78−6985
β-Ti-Mo-V-Fe-Al(8,8,2,3 wt.%), metastable factors affecting stress corrosion cracking 77−28928
Ti-Mo-Zr-Sn-Fe-C-Si alloy, β-III, cold deform. and annealing, effect on struct. and mech. props. *(Russian)* 79−24533
Ti-Nb alloys, Fe, Mo, V, Ta alloying additions on microstruct. after combined treatment *(Russian)* 77−59826
Ti-Nb-Zr-Fe, supercond. and paramag. props., effect of Fe additions *(Russian)* 80−65730
Ti-Nb-Zr-Fe-Mo-V, cold worked, struct. and phase transform. during ageing 78−3153
Ti-Ni-Fe, multiplicity of structural transitions, phase diagrams, elec. cond. meas. 80−71649
Ti-Ni-Fe, plasticity, tensile stress-strain diagrams, ultimate tensile strength, elec. resist. depend. on temp. *(Russian)* 79−61652
Ti-Ni-Fe, shape memory temp., alloying effect 79−38912
Ti-V-Fe-Al (10, 2, 3 wt.%), fracture toughness and stress corrosion resistance 80−100904
Ti_3Al, Cu, Fe, Mo (1 at.%) additions, oxidation resistance, 700 to 800 degrees C 77−12744
$Ti(Al_xFe_{1-x})_2$, $0<x<0.4$, influence of Al on H sorption props. X-ray cryst. struct. determ. 79−28198
TiC-Fe-Cr powder mixture, exam. of milling condition effects 80−16237
Ti(Fe, Co), itinerant ferromagnet, magneto-volume expts. 77−66404
Ti(Fe,Co), magnetovolume effects near crit. conc. for ferromag. 79−56591
Ti(Fe, Co), off-stoichiometric alloy, inverse mag. susceptibility rel. to defect conc. 80−60216
$Ti(Fe,Co)H_y$, mag. and ^{57}Fe Mossbauer studies 80−71272
TiFe hydrides for bulk H_2 storage 80−61463
$TiFe_2$, mechanism of mixing and reactive diffusion 79−7706
$Ti_{1-x}Fe_x$ alloys, $(0<x\leq0.2)$, nonmetallic resistivity and simultaneous superconductivity *(Russian)* 77−36005
$Ti(Fe\text{-}Co)_2$, itinerant electron ferromagnet, magnetovolume effects 80−60397
$Ti_{70}Fe_{20}B_{10}$, amorphous alloys, crystn. behaviour, TEM study *(Japanese)* 80−84087
$TiFe_{0.8}Be_{0.2}$ alloys for H_2 storage 80−97817
$Ti(Fe_{1-x}Co_x)$, density of states estimation from magnetisation and resistivity meas. 78−84119
$TiFe_{1-x}Co_x$, electronic struct. and mag. moment calcs. 80−65821
$Ti(Fe_{1-x}Co_x)$, ferro- to paramag. transition, press. depend. 77−73028
$TiFe_{1-x}Co_x$, mag. props., under high press. and in high mag. fields 78−95423
$TiFe_xCo_{1-x}$, thermal expansion and magnetoelastic effects 80−80585
TiFeD, cryst. struct., Mossbauer and neutron diffr. obs. 80−34839
$TiFeH_x$, metallurgical and electronic struct., Mossbauer effect meas. 77−16223
$Ti_{50}Ni_{47}Fe_3$, premartensitic phases, neutron scatt., sp. ht. and electron microscopy obs. 79−96025
TmF_2, ^{169}Tm Mossbauer effect 80−71261
TmFe, Mossbauer expt. in ^3He-^4He dilution refrigerator 78−27127
$TmFe_2$, amorphous, neutron scatt. at transition, spin diffusion, magnetisation meas. 78−68174
$TmFe_2$, amorphous, small angle neutron scatt. study of mag. order and mag. microstruct. 79−15283
$TmFe_2$, low temp. magnetisation and magnetostriction 78−64249
$TmFe_2$, magnetisation and magnetic anisotropy 78−91862
$TmFe_3$ and Tm_6Fe_{23}, magnetostriction, room temp. to 80K 80−65993
$Tm_2Fe_{17-x}Co_x$, and related cpds., easy magnetisation direction, Mossbauer spectra 77−63169
$TmFe_2H_{4.3}$, mag. props. and lattice consts., effect of hydrogen absorpt. 77−20561
U-Fe metallic glasses, glass form. and thermal stability 80−75183

iron alloys continued
U-Fe-B, isothermal section of phase diagram, X-ray obs. 79−52157
$U(Co_{1-x}Fe_x)_2$, ferromag. onset, susceptibility and resist. meas. 80−70967
UFe_2, giant magnetoelastic deform. of cryst. struct. mag. props. *(Russian)* 80−93159
UFe_2, mag. anisotropy of single crysts. 79−56527
UFe_2, magnetisation meas. 79−51756
UFe_2, nonstoichiometry effects on Curie temp., susceptibility obs. 80−25131
UFe_2, thermodynamic props., agreement with Campbell correlation of laves phase compounds 78−15370
U_6Fe, spin-pairing state investig. via Josephson current between weakly-coupled superconductors 77−47942
$U_6Fe_{0.98}$ supercond. transition temp. reduction by neutron irradiation 77−63020
UMn_2-UFe_2, mag. props., ferromag. transition *(Russian)* 78−68148
$(V,Fe)_3M$, M=Si, Ge, Ga, solid soln. form. and supercond. T_c *(Russian)* 78−80512
V-Fe, diffusion in H_2 *(Japanese)* 78−10221
V-Fe, ferromagnetism to mictomagnetism at low Fe conc. 78−91878
V-Fe, force constant change with pressure, relative Mossbauer fraction 80−34163
V-Fe, mag. ordering temp. depend. on atomic short-range order from susceptibility meas. 79−61159
V-Fe (5.0 at.%), stress relaxation test, appl. to discerning frictional and internal stresses 77−63712
V-Fe (5.0 at.%), work softening at elevated temps. *(Japanese)* 77−52347
$V_3(Fe,Ge)$, struct. and supercond. transition temp. *(Russian)* 79−7920
$V_{1-x}Fe_x$, low temp. sp. ht. and mag. props. 80−2548
$V_{3-x}Fe_xCo$, cryst. struct. and microhardness meas. 79−86740
$V_{75-x}Fe_xGa_{25}$, Mossbauer exam. 77−90078
$V_{75-x}Fe_xGa_{25}$, supercond. transition temp. and electron-phonon coupling parameter 79−60952
$V_{1-x}Fe_xH_n$, low temp. sp. ht. and mag. props. 80−2548
V_3Si-Fe, mag. impurities effect on supercond. props. 77−1524
Ve-Fe-Ga system, phase obs. at 800 and 820°C *(Russian)* 78−23662
W-Fe, dil., excess resistivity, temp. depend. 78−68011
W-Fe, dil., spin glass props., DC mag. susceptibility meas. 78−68283
W-Fe, electronic transport below 1K 80−2377
W-Fe, spin glass props., DC susceptibility and remanence meas., 1.6 to 295K 80−29560
W-Fe spin glass, optical props. and electronic states 80−20412
W-Fe-Co, sintering and mechanical props. *(Japanese)* 80−21086
W-Ni-Fe, liquid phase sintered, interfacial embrittlement 79−57101
W-Ni-Fe, structural characterisation *(French)* 77−56074
W-Ni-Fe, W-Ni-Fe-Mo (Mn), sintering and mechanical props. *(Japanese)* 80−21086
W-Ni-Fe (5(2), 5(2) wt.%) pore formation, effect on mech. props. 80−45396
W-Ni-Fe system, reduction kinetics and alloy form. 80−60801
$W_{50}Fe_{50}$ glassy alloy, refractory, triode sputtered 80−75185
Y-Fe, amorphous, thermal stability, crystn., DSC and elec. resist. study 80−107060
Y-Fe, evap. amorphous alloys, thermomag. history effects 77−66389
Y-Fe alloy amorphous thin films, anisotropic mag. and microstruct. props. 78−95487
Y-Fe alloys, mag. interactions, effects on moments *(Rumanian)* 79−15296
Y-Fe amorphous alloy film, mag. props. 77−16121
Y-Fe film, amorphous, microstruct. and magnetism 78−64230
Y-Fe-Si alloys, phase diagrams 79−52158
$Y(Co_{1-x}Fe_x)_5$, magnetocryst. anisotropy. different contribs. of two Co sites 77−8301
$Y_2(Co_{0.31}Fe_{0.69})_{19.2}$, statistical site occupancy deviations, neutron diffr. investig. 77−7717
$Y_2(Co_{1-x}Fe_x)_{17}$, bulk magnetisation and magnetocryst. anisotropy, interpretation 77−40055
$Y_2(Co_{1-x}Fe_x)_{17}$, magnetocryst. anisotropy 77−40054
$Y_2(Co_xFe_{1-x})_{17}$, mag. anisotropy assoc. with Fe substitution 78−76240
$Y_2(Fe,Co)_{17}$, mag. anisotropy fields by singular pt. detection 79−24156
$Y_2(Fe,Co)_{17}$, magnetic anisotropy meas. by singular point detection method 77−63170
$Y_6(Fe, Mn)_{23}$, itinerant ferromagnet, magneto-volume, expts. 77−66404
YFe_2, amorphous, mag. order, cluster phenomena, hyperfine struct. 77−16079
YFe_2, amorphous, small angle neutron scatt. study of mag. order and mag. microstruct. 79−15283
YFe_2 amorphous, spin-glass and mag. blocking transitions, low field DC susceptibility meas. 79−61141
YFe_2, amorphous, surface ferromag. layer, spin wave reson. Rutherford backscatt., and magnetisation meas. 79−73819
YFe_2, amorphous concentrated spin glass, susceptibility, Mossbauer and neutron scatt. meas. 80−39783
YFe_2, density of states, mag. props. 79−90936
YFe_2, ferromagnetic cpds., mean field exchange consts., Stoner itinerant model calcs. 80−50084
YFe_2, phonon softening below Curie temp., Mossbauer effect 77−4589
YFe_x film, $(x\simeq2)$, magnetoelastic excitations obs. 78−68307
YFe_x, mag. interactions, exchange fields, mol. field model 77−4498
$Y_{1-x}Fe_x$, amorphous, Mossbauer spectra, appearance of magnetism 78−52401
$Y_{1-x}Fe_x$, amorphous, spin resonance exam. 79−51860
$Y_{1-x}Fe_x$, mean mag. moment calc. 79−82761
Y_2Fe_{17}, hyperfine interactions, Mossbauer effect, 5 to 300K 77−85634
Y_6Fe_{23}, magnetostriction, temp. depend., 20 to 350K 80−65994
Y_xFe_{1-x} amorphous films, microstruct. and mag. anisotropy 79−82838
$Y(Fe_{1-x}A_x)_2$, A=Al or Ni, Laves phase, mag. props. and Mossbauer effect 77−85632
$Y(Fe_{1-c}Al_c)_2$, local model for mag. behaviour 77−63135
$Y(Fe_{1-c}Al_c)_2$, mag. and Mossbauer study, local environment effects 78−27033
$YFe_{2-x}Al_x$, magnetisation behaviour, mag. scatter order 77−28373
$Y(Fe_cAl_{1-c})_2$, mag. props. 79−38308
$Y(Fe_xAl_{1-x})_2$, mag. order in pseudobinary systems down to millikelvin temps. 78−19251
$Y(Fe_xAl_{1-x})_2$, Mossbauer spectra and mag. props. 80−39950
$Y_6(Fe_{1-x}Al_x)_{23}$, cryst. struct. and mag. props. 79−82180
$(Y_{65}Fe_{35})_{100-x}B_x$ glasses, mag. props. 79−73693
$Y(Fe_xCO_{1-x})_2$ model, Co, mean mag. moment composition depend.; reciprocal susceptibility, thermal var. 78−47945

iron alloys continued
$Y(Fe_{0.022}Co_{0.978})_2$, ferromag. relax. model, Mossbauer spectra 80−15853
$Y(Fe_{0.022}Co_{0.978})_2$ mag. props., Mossbauer expts., 0.15-4.2K 78−43712
$Y(Fe_{1-x}Co_x)_2$, mag. hyperfine field, conc. depend., Mossbauer expts. 77−63337
$Y(Fe_{1-x}Co_x)_2$, mag. saturation moment, Co conc. depend., NMR exam. 78−15037
$Y(Fe_{1-x}Co_x)_2$, NMR study 80−75882
$Y(Fe_xCo_{1-x})_2$, $0.5 \geq x \geq 0.2$, Mossbauer effect meas., 5 to 300K *(German)* 77−24771
$Y(Fe_xCo_{1-x})_2$, compositional dependence of Co's mean mag. moment, local environment model anal. 78−43560
$Y(Fe_xCo_{1-x})_2$, ferromag. reson. of pseudobinary cubic compounds 78−91961
$Y(Fe_xCo_{1-x})_2$, Mossbauer effect at 78 and 300K, ^{57}Fe hyperfine fields 80−2677
$Y(Fe_xCo_{1-x})_2$, $x \leq 0.2$, mag. props. and Mossbauer meas. 80−75798
$Y_2(Fe_{1-x}Co_x)_{17}$, hyperfine interactions, Mossbauer spectra 78−2780
$Y(Fe_{1-x}Ir_x)_2$, magnetisation, mag. hyperfine field 80−20531
$Y(Fe_{1-x}Mn_x)_2$, mag. order onset 80−25135
$Y(Fe_{1-x}Mn_x)_2$, Mossbauer spectra and mag. props. 80−39952
$YFe_{2x}Mn_{2-2x}$, mag. props. and FMR 79−95581
$Y_6(Fe_{1-x}Mn_x)_{23}$, ferro- to paramag. transition, press. depend. 77−73028
$Y_6(Fe_{1-x}Mn_x)_{23}$, Mn-rich compounds, Mossbauer effect study 80−71276
$Y_6(Fe_{1-x}Mn_x)_{23}$, struct. and mag. props. 80−25083
$Y_6(Fe_xMn_{1-x})_{23}$, mag. order in pseudobinary systems down to millikelvin temps. 78−19251
$YFe_{3-x}Ni_x$, electronic sp. ht., saturation magnetisation and lattice parameter meas. 78−68261
$Y_2(Fe_{1-x}Ni_x)_{17}$, Mossbauer spectra, hyperfine field interactions 78−6614
YFe_2Si_2, mag. props. 4.2 to 950K, diamag. Fe atoms 77−20544
$Y(Fe_xT_{1-x})_2$, Mossbauer spectra, mag. props. 80−20563
$Y(Fe_{1-}xCo_x)_2$, electronic sp. ht. meas., rel. to mag. props. 77−63197
$Y_6(Mn_{0.75}Fe_{0.25})_{23}$, mag. scatter state, hysteresis loops 78−56350
$Y_6(Mn_{1-x}Fe_x)_{23}$, hydriding characts. and mag. props. 77−69527
$YMn_{2-x}Fe_xH_z$, mag. props., ordering temps. 80−71028
$Y_{1-x}Th_xFe_3$, saturation magnetisation, fields up to 120 kOe, comp. depend. 77−8283
$Y_{1-x}Th_xFe_3$ system, elec. resist. meas., 77-300K 80−34413
$Yb_2Co_{17-x}Fe_x$, magnetisation, Curie temp., anisotropy 77−89947
$YbFe_2$, cryst. elec. field and exchange interac., ^{170}Yb Mossbauer obs., magnetostriction contrib. 80−108124
$YbFe_2$, Curie temp., elec. quadrupole coupling, Mossbauer study 80−39949
$YbFe_2$, high field Mossbauer study 80−75893
$YbFe_2$, Laves phase compounds, synthesis, mag. props., ^{57}Fe Mossbauer effect 78−10807
$YbFe_2$, Mossbauer spectra, cryst. elec. field and exchange interaction 79−47368
$YbFe_2$, preparation and mag. props. 80−25259
Yfe_3, NMR investig. of Y hyperfine field temp. depend. 77−4567
Zircaloy-4, deformation behaviour between 77 and 900K 80−71686
Zircaloy-4, vapour transport of Zr and Si 80−55437
Zn-Cd liquid/Fe-Ni-Al mag. powder, effective viscosity of composites *(Russian)* 80−54424
Zn-Fe, dil., ^{57}Fe Mossbauer effect meas. 78−95534
Zn-Fe alloys, dil., positron-electron annihilation spectra, Doppler broadened 79−65953
$Zn_{13}Fe$, ^{57}Fe Mossbauer effect meas. 78−95534
$(Zr,Hf)Fe_2$, mag. hyperfine field at Hf sites, TPDAC meas. 79−82901
Zr-Al-Fe (8.9, 0.001 to 0.006 wt.%) Fe partitioning to Zr_2Al during peritectoid transformation 78−39784
Zr-Al-(Fe,Co), H sorption props. for H storage, influence of Al 80−45794
Zr-Cr-Fe, irradiation damage, metallurgical struct. effect 77−51412
Zr-Fe, amorphous alloy film, spin reson. meas. 78−68389
Zr-Fe, amorphous alloy quenched by levitation method, crystallisation 79−55669
Zr-Fe, Mossbauer spectra parameters of Zr_2Fe particles *(Russian)* 80−29654
Zr-Fe, oxidation of intermetallic phases 79−100298
Zr-Fe, role of oxide plasticity in oxidation behaviour 77−36680
Zr-Fe metallic glasses, glass form. and thermal stability 80−75177
Zr-Fe-Cu-W, Mossbauer spectra parameters of Zr_2Fe particles *(Russian)* 80−29654
Zr-Fe-H, catalytic props. 80−30274
Zr-Fe-H, synthesis at high H pressure exam. of props. 80−29924
Zr-Nb-Fe (13 wt.%, 5 wt.%), struct. changes during decay of BCC β solid solution 79−15669
Zr-Nb-Fe alloys, decomp. of β solid soln., metastable and equilib. phases 79−11632
Zr-Nb-V-Fe (12 wt.%, 6 wt.%, 4 wt.%), struct. changer during decay of BCC β solid soln. 79−15669
Zr-Sn-Fe-Ni (1.5, 0.1, 0.15 wt.%), electron irradiation damage, direct obs. 80−84212
Zr-Sn(Fe)(Ni) (0.15 wt.%), electron irradiation damage, direct obs. 80−84212
$Zr(Al_xFe_{1-x})_2$, Laves phase, H_2 absorption capacity meas. 78−87866
$Zr_3Co_{1-x}Fe_x$, phase stability and supercond. T_c 78−80519
$Zr(Cr_xFe_{1-x})_2$, Laves phase, phenomenological model for H_2 absorption capacity 77−84935
$Zr(Cr_xFe_{1-x})_2$, mag. props. H absorpt. effect 80−88821
$Zr_{40}Cu_{50}Fe_{10}$, magnetically dil. glass, 3d moments, mag. susceptibility and magnetisation meas. 79−95574
$Zr_{40}Cu_{60-x}Fe_x$, amorphous, mag. ordering and local random anisotropy 78−68273
$Zr_{40}Cu_{60-x}Fe_x$, amorphous alloy, mag. interactions 78−95432
$Zr_{40}Cu_{60-x}Fe_x$, electronic and mag. props. 77−8271
$Zr(Fe,Al)_2$, weak itinerant ferromag., mag. anisotropy effects on mag. isotherms 80−11187
$Zr(Fe, Co)_2$, itinerant ferromagnet, magneto-volume expts. 77−66404
$ZrFe_2$, lattice dynamics, Mossbauer spectra 80−19888
$Zr_{70}Fe_{30}$ amorphous alloys, struct. factors and radial distrib. functions 80−84096
$Zr(Fe\text{-}Co)_2$, itinerant electron ferromagnet, magnetovolume effects 80−60397
$Zr(Fe_{1-x}A_x)_2$, A=Al or Ni, Laves phase, mag. props. and Mossbauer effect 77−85632
$Zr(Fe_{1-x}Al_x)_2$, Curie temp., magnetisation, and cryst. struct., conc. depend. 80−75730

iron alloys continued
$Zr(Fe_{1-x}Al_x)_x$, transition region, spin glass or long range mag. order 80−44841
$Zr(Fe_{1-x}Co_x)_2$, density of states estimation from magnetisation and resistivity meas. 78−84119
$Zr(Fe_{1-x}Co_x)_2$, ferromag. and mictomag., thermal expansion and forced volume magnetostriction 80−75830
$Zr(Fe_{1-x}Co_x)_2$, low temp. sp. ht. and mag. props. 79−61153
$Zr(Fe_{1-x}Co_x)_2$, mag. props. and Mossbauer effects 79−91322
$Zr(Fe_{1-x}Co_x)_2$, mag. saturation moment, Co conc. depend., NMR exam. 78−15037
$Zr(Fe_{1-x}Co_x)_2$, magnetovolume effects, thermal expansion and forced vol. magnetostriction meas. 80−29595
$Zr(Fe_{1-x}Co_x)_2$, mictomagnetism 80−15863
$Zr(Fe_{1-x}Co_x)_2$, NMR study 80−75882
$Zr(Fe_{1-x}Co_x)_2$, press. effects on ferromag. to paramag. transition 77−66302
$Zr(Fe_{1-x}Co_x)_y$, transition region, spin glass or long range mag. order 80−44841
$Zr(Fe_xCo_{1-x})_2$, mag. order in pseudobinary systems down to millikelvin temps. 78−19251
$Zr(Fe_xM_{1-x})_2$, (M=V,Cr,Mn), H absorption and desorption props. 77−55448
$Zr(M_xFe_{1-x})_2$ (M=V, Cr, Mn), H_2 absorpt. capacity 80−88433
$Zr(Mn_xFe_{1-x})_2$, Laves phase, phenomenological model for H_2 absortion capacity 77−84935
$(Zr_{1-x}Nb_x)Fe_2$, antiferromag. spin struct., Mossbauer effect study 80−66086
$(Zr_{1-x}Nb_x)Fe_2$, magnetovolume effects and Invar characters 80−15773
$Zr_xTb_{1-x}Fe_2$, Laves phase alloys, magnetostriction *(Russian)* 77−51932
$Zr(V_xCo_{1-x})_2$, Laves phase, phenomenological model for H_2 absorption capacity 77−84935
$ZrZn_2$: ^{57}Fe mag. props. from Mossbauer effect obs. *(Japanese)* 80−15933

iron compounds
see also ferrites; iron alloys
Auger radiative transition, $K \rightarrow M^2$, weak X-ray emission lines 78−33556
bauxite, Fe-containing, Mossbauer analysis 78−44806
behaviour during RBMK reactors start up and shutdown, investigation 79−9822
(2,2′-bi-2-thiazoline) iron thiocyanate, high spin to low spin transition, X-ray diffr. and Mossbauer obs. 79−38418
biological systems, electronic and mag. struct., semiempirical MO cluster calc. 78−62733
biotite, Mossbauer and optical spectra, Fe^{2+}-Fe^{3+} interactions 80−60470
biotites, optical absorpt. bands 80−7371
boiling in steam generating pipe with Fe oxide deposits on wall, steam bubble growth 79−76947
boulangerite, cryst. struct., superlattice variations, order-disorder struct. 79−86770
carbides, oxidation of H_2 80−104462
chalcogenide spinels, thermal stability, thermochemical, thermodynamic and crystallochemical props. 77−51519
chloride layered compound with graphitised PAN fibre, struct. and elec. cond. 79−91600
chloritoid, topotactical dehydration, X-ray diffr. and TEM study 79−51057
complex, binuclear ferricyanides, Mossbauer effect 79−78576
complexes, cyanides, mag. susceptibility and optical reflection spectra 77−59382
complexes, Mossbauer isomer shift and core electron binding energies of Fe 78−82620
crystal growth from fused oxides, flow method, simple and economical apparatus *(Italian)* 80−80960
dimethylammonium iron tetrachloride, Mossbauer study of struct. phase transition 80−39278
electronic props. CC $Fe_xCo_{1-x}S_2$, ferromagnetic solid soln. 79−7990
Fe-N system, fine particles growth, prep. by reactive gas evaporation technique, lattice consts. and habit study 79−56919
$FeCl_3$-graphite intercalation compound prep. *(French)* 78−27445
δ-FeOOH (feroxyhyte), possible occurrence on surface of Mars 80−85879
ferric haeme complex of low spin, Mossbauer spectra, crystal field parameters 80−26203
ferricyanides, reduction on Au electrodes partially covered with photoresist. layer 78−85236
ferrite, spinel type catalytic oxidation of CO, role of mag. exchange interactions 78−56916
ferritin, iron core particle size distrib., Mossbauer determ. 78−92696
ferrocene, cryst., stable low-temp. phase 80−34185
ferrocene, cryst. and soln., dynamic struct., NMR expts. 77−15328
ferrocene, mol. struct., ordered phase, 130K *(French)* 79−51093
ferrocene, ordered, disordered phases, structs. *(French)* 78−63749
ferrocene, triclinic, struct. anal. at 101, 123 and 148K 80−19785
ferrographite, sintered, porous, electrolytic preparation 79−52530
ferrous complexes, Mossbauer quadrupole splitting calcs. using cryst. field model 77−32301
ferrous formate dihydrate, mag. sp. ht. 79−91235
ferrous nitrosylhaemoglobin, NO binding, spin distrib., orbital model and mag. props. 80−81534
ferrous oxalate dihydrate, Mossbauer spectrum, hyperfine fields 78−39483
ferrous oxalate dihydrate, reaction with sodium disilicate glass 78−11191
ferrous porphyrin, intermediate spin, reson. Raman spectra 79−69820
ferrous porphyrins, 4-coordinated, PMR 77−58044
ferrous sulphamate radiolytic instability in nuclear process solns. 77−70314
ferrous tetrakis thiophenolate, powder, far IR mag. reson., zero field splitting 77−81000
ferrous tetraphenylporphyrin, Mossbauer effect, mag. hyperfine interaction 79−24236
ferrous-formate dihydrate, mag. system model, mag. sp. ht. *(Japanese)* 78−31091
FeS_2, thin films, prep. and charact. 80−16178
formate dihydrate, mag. sp. ht., S_z^4-term 79−61127
formate dihydrate, mag. sp. ht., S_z^4-term 80−60289
formate dihydrate, paramagnetic specific heat, decoration iteration transformation anal. 80−70938

iron compounds continued
garnet, Bi substituted, epitaxial film, magneto-optical controlled transparencies 78−50932
garnet epitaxial film, thermomag. data recording by electron beam heating 78−27066
garnet film in mag. field, domain dynamics *(Russian)* 79−4711
garnets, low-freq. excitation spectra, mobility of domain boundaries 79−42815
Geothite synthesis by ammoniacal method, prep. of Fe_2O_3 77−28741
germanate glass, ion-beam sputtering, excitation efficiency of atoms 78−19623
glass-ceramics, Fe-containing, effect of Mn_2O_3 on strength 77−48380
graphite-$FeCl_3$ intercalation complex, IR and Raman spectra study of optical modes 79−56797
ground state Zeeman splittings, reson. Raman spectra and mag.-optical activity 80−5579
haematite, degree of reduction, potential relaxation due to cracks *(Russian)* 80−66770
haematite, grain size and coercive force from high temp. AF demag. 77−37189
haematite, importance of convective mass transfer during reduction 79−52769
haematite, neutron diffr. exam. of texture, comparison with magnetite 78−52849
haematite, reduction to magnetite, HVEM 78−6892
haematite, reduction to magnetite under natural and laboratory conditions 78−65277
haematite, sintered granules, onset of stresses of first kind, mechanism *(Russian)* 78−80485
haematite, textures and topotactical relationships, neutron diffr. study 79−83229
haematite reduction to magnetite, stress development mechanism *(Russian)* 80−93553
haematite-magnetite two-phase porous bodies, internal stresses *(Russian)* 80−16319
halides, electronic charge and spin distrib. from interpretation of hyperfine interactions 79−60776
halides, matrix isolated, Mossbauer effect, isomer shift and quadrupole splittings obs. 78−46377
hematite, multiple orientation relationships between magnetite, TEM study 79−60298
hematite, reduction by C 77−48687
hematite pellet, reduction with CO-H_2 mixture 77−4935
hexacyanoferrates, $M_4Fe(CN)_6.nH_2O$, Mossbauer and IR spectra 80−2739
hydrazinium iron tri(hydrazoformate) monohydrate single cryst., effective EFG tensor, Mossbauer spectra obs. 79−56628
hydride, computer simulation of H reflection and scattering 79−1806
hydrostatic compression of Fe and related compounds, overview 78−83862
hydroxides, crystallogenesis, Mossbauer study 79−31564
ilmenite, cryst. struct. at various compositions 79−86769
ilmenite, idealized, chlorination in presence of excess C 78−7226
ilmenite, roasted ore, Fe chlorination kinetics in fluidized bed reactor 79−47979
ilmenite, solid soln., phase transform. during reduction *(Russian)* 78−44042
ilmenite ore, liquid, behaviour above 1500°C, X-ray obs. *(French)* 79−70100
ilvaite, Fe temp. depend. oxidation states, electron hopping, Mossbauer spectra, X-ray diffr. obs. 78−2779
ilvaites, Mossbauer spectra and mag. features 80−7248
intercalation, electron microscopy 80−84164
internal motion, mol. vibr. calcs. 80−106323
(iron, chromium) carboxylates, heteronuclear trimer exchange clusters, ESR spectra 80−80603
iron tetraphenylporphyrin chloride, electron spin pairs, low and ultralow temps. 77−77092
iron-transition metal oxinates, Mossbauer spectra 77−90082
jamesonite, cryst. struct., superlattice variations, order-disorder struct. 79−86770
K-absorption edge energy shift 79−4870
magnetite, electrode, polycrystn., differential capacitance 80−66136
magnetite, multiple orientation relationships between hematite, TEM study 79−60298
magnetite, neutron diffr. exam. of texture, comparison with haematite 78−52849
magnetite, spin polarisation, effect of temp. and photon energy 80−45221
magnetite, textures and topotactical relationships, neutron diffr. study 79−83229
magnetite nodules, from superconcentrates, strengthening annealing and reduction *(Russian)* 80−16333
magnetites, cond. mechanisms *(Russian)* 79−42539
mantle related, thermodynamic props. at high press. and temp. 80−81874
$Mg_{1.34}Fe_{0.16}Al_{0.12}Ti_{0.38}OBO_3$, warwickite, cation distrib. from X-ray struct. and Mossbauer spectra anal. 79−1424
mica, Fe^{3+} localisation determ. by EPR *(French)* 77−43196
Mossbauer ^{57}Fe spectra, ferrous charact., cryst. field interactions 80−108133
Mossbauer spectra of Fe^{3+} cpds., temp. depend. of isomer shift *(Russian)* 78−39479
Mossbauer spectroscopy, effect of neighbours on hyperfine field 80−39931
myoglobins, Fe-substituted, O_2 binding, comparison with Co-substituted myoglobins, thermodynamic investig. 80−67030
$Na_2[Fe(CN)_5NO]$, valence levels, X-ray photoelectron and X-ray spectra 77−88500
nitrides, thermodynamic considerations of nitriding of Fe *(German)* 78−60874
ore, water bearing mineral effects on X-ray fluorescence analysis 77−12866
ore concentrates, two-layer charge, sintering conditions *(Russian)* 80−45248
ore super-concentrate, deep drawing props. by integrated powder technology route 80−100806
ores, sintering, agglomeration charge layer shrinkage *(Russian)* 80−16224
organometallics, interaction of naked Fe atoms with small mols., Mossbauer study of bonding in products 80−43080
oxalate, quadrupole splitting, Mossbauer spectroscopy 79−11365
oxalates, γ-ray and neutron irrad. effects, Mossbauer spectra obs. 79−65778
oxide deposition, surface modification of Teflon, contact angle meas. 77−51574
oxide film-Fe composite material, magnetically soft, preparation, elec., mag. props. 77−8778
oxide films, anodically formed, compositions 79−90898
oxide films, semicond. electrode props. 79−91093
oxide reduction by electron cyclotron reson. plasma of H, model study on discharge cleaning 80−76548
oxide reduction in V slag enrichment during plasma melting *(Russian)* 78−52716
oxide reduction processes by gases, mathematical modelling *(Russian)* 80−93742
oxide scale fracture on substrate deform. 78−11407
oxide surface layer, TOF atom probe anal. 78−64766
oxides, AES meas. 77−36323
oxides, core line X-ray photoelectron spectra 78−7263
oxides, disperse, reduction in electrical arc discharges *(Russian)* 78−95915
oxides, effective atomic charge rel. to chemical shifts in transition metal compound XAS 79−78788
oxides, haematite and wustite, structural changes during reduction by CO-CO_2 mixtures 77−60140
oxides, interatomic interaction by XPS 80−7474
oxides, magnetic, in first American civilisation 77−60886
oxides, Mossbauer and mag. susceptibility studies of soils from archaeological sites 77−30224
oxides, phase equilibrium and microstructure interpretation 80−60847
oxides containing V as NO_x reduction catalysts 79−12285
oxides in soils and sediments, Co and actinide adsorption 79−66422
oxides on Fe powder, passivating oxide layer comp. 78−31558
pearlite in C steels (0.08 to 1.6 wt.%), exam. of temp. depend. of mag. coercivity 78−52304
pentlandite, prep., H_2 reduction with lime, to yield Fe-Ni alloy 78−85018
periodic regular texture 79−99328
phosphites, polycryst. EPR and Mossbauer spectra 78−76369
phthalate, reduction, prep. of Fe powder 77−40090
phthalocyanine, valence band studies, UPS meas. 77−52221
potassium iron tri(hydrazoformate), Debye-Waller factor, Mossbauer spectra obs. 79−56627
pyrite-solvent boundaries, two-layer capacitance meas. *(Russian)* 78−10551
pyroxenes, high Ca_2 of diopside-hedenbergite series, change in struct. geometry with Fe^{2+} content 79−14783
pyrrhotite, complex refractive indices rel. to comp. of Saturn's rings 77−29716
pyrrhotite ($Fe_{1-x}S$) in sulphide ores from Kambalda, W.Australia, sulphide fabrics 78−77229
rare earth gallium garnet, growth of crystals from $50PbO.40PbF_2.10B_2O_3$ flux 77−21014
rare earth iron silicides, $R_2Fe_3Si_5$, superconductivity 80−49968
red ochre, chem. anal. by Mossbauer spectroscopy, and superparamagnetism 78−20397
salicylates, Mossbauer and IR spectra, mag. susceptibility 80−50242
schorl tourmaline, elastic const. 78−68718
silicate glasses, local order around Fe, exam. using X-ray absorpt. spectrometry 80−79701
silicate glasses containing iron, switching and memory effects 77−8155
sodium iron fluorophosphate glasses, EPR and Mossbauer resonance study 80−39968
soft magnetic materials, powder-based, phase comp., thermal analysis 77−51928
solid solns., determ. of degree of imperfection 77−80624
spin 3/2, in strong crystal field, axial and rhombic symmetry, EPR parameters 79−28591
spinels, ligand field stabilisation evaluation using Mossbauer determ. cation distrib. 78−31126
spinels containing Fe^{3+} and Sb^{5+}, $M_4^{2+}Fe^{3+}Sb^{5+}O_8$, Mossbauer spectra 80−15892
sulphides, reduction by H_2 78−61053
tetrabutylammonium iron tetraiodide, structural and mag. props., ^{57}Fe and ^{129}I Mossbauer spectra 79−61282
tetraethylammonium iron tetraiodide, structural and mag. props., ^{57}Fe and ^{129}I Mossbauer spectra 79−61282
tetramethylene bridged ferrocene derivatives, mol. struct., Mossbauer expt. 78−60372
titanomaghemite, synthetic, cation distrib. 78−55856
titanomagnetite, monodomain behaviour in multiphase oxidised material 77−60366
titanomagnetites, temp. depend. cation distrib., mag. prop. obs. 80−85647
tourmaline, microwave acoustic relax. absorpt. 78−22791
troilite, complex refractive indices rel. to comp. of Saturn's rings 77−29716
vermiculite, electric field gradient, Mossbauer absorption 79−73865
wustite, intrinsic rates of reduction and mechanism 79−83153
X-ray $K\beta$ spectra of Fe atoms in chem. compounds, struct. similarities 77−28655
yellow ochre, chem. anal. by Mossbauer spectroscopy 78−20397
zeolite-A, reduction, mag. and Mossbauer study 80−71115
Zircon ceramic, exam. of development and fabrication 80−11608
Fe_2O_3-Bi_2O_3 sintered material, elec. switching effects due to thermal ionic breakdown *(Korean)* 80−70776
$AgFeSe_2$, thermographic investigation of phase transitions *(Russian)* 80−10661
$AgFeSe_2(S_2)(Te_2)$, elec. props., band gap *(Russian)* 79−11116
$AgFeTe_2$, Mossbauer parameters in phase-transition region 80−11308
$AgFeTe_2$, thermographic investigation of phase transitions *(Russian)* 80−10661
$Al/AlCl_3$-NaCl/FeS_2 secondary cell, preliminary study 80−108793
Al-Fe_2O_3-Al, space charge limited current, current density as function of elect. field and temp. 79−51688
Al-Fe_3O_4 binary thermite powder mixture, compaction 79−74125
Al_2O_3-Fe_2O_3:Cr^{3+}, dil. paramag. system, Cr^{3+} conc., effect on cross relax. 79−15387
Al_2O_3-Fe_2O_3(:Cr^{3+}) paramag. system, cross relax. temp. and mag. field effects on Mossbauer spectra 79−33576

iron compounds continued
Al_2O_3-SiO_2-Fe_2O_3-CaO-MgO-TiO_2, refractory, corrosion and mech. behaviour correlations 80−40563
Al_2O_3-SiO_2-MO-Fe_2O_3 glass, M=Ca, Mg, Ba, Sr, UV and EPR absorpt. spectra 80−89018
Al_2O_3-SiO_2-TiO_2-B_2O_3-Fe_2O_3, exam. of porous structure, using a combinational method 79−29303
$(Al_2O_3$-$Fe_2O_3):Cr^{3+}$, (0.04 mol.% Fe_2O_3), paramag., cross relax., annealing temp. effect from Mossbauer meas. 80−44983
B_2O_3-CaO-Fe_2O_3 glasses, semicond., cond. models, electronic props., 77-800K 80−54688
B_2O_3-Li_2O-Fe_2O_3, prep. by quenching methods, exam. of microcrystalline precipitates of Li_2O-Fe_2O_3 *(French)* 79−20019
B_2O_3-Na_2O-Fe glass, mag. susceptibility 79−42733
B_2O_3-PbO-GeO_2-Fe_2O_3 glasses, mag. props. and Mossbauer spectra, speromag. order at low temps. 80−80530
$Ba_x(Ba_{1-x}Al_x)Fe_2S_6[S_{1-y}(S_2)_y]$, cryst. struct., Mossbauer and mag. behaviour 77−55273
BaF_2-MnF_2-FeF_3 system, X-ray investigation, struct. relations, liquid-solid equilibria diagram, study by DTA *(French)* 79−34017
$BaFe_2O_4$-Fe_2O_3-$ZnFe_2O_2$ system, phase relations at 1200°C 78−72767
Ba_2FeReO_6, new seignettomagnets and ferroelectrics 78−19425
$Ba_2Fe[Ge_2O_7]$, hydrothermal growth, struct. and opt. props. 77−65971
BaO-B_2O_3-V_2O_5-$(Fe_2O_3)(Cu_2O)$, glass, resist. and activation energy, reduced valency 77−51749
BaO-Fe_2O_3, splat quenching struct. and crystn. mechanism *(French)* 78−51426
BaO-Fe_2O_3-B_2O_3 glass system, mag. struct., Mossbauer study 78−39485
BaO-Fe_2O_3-B_2O_3 glass, Mossbauer study of struct. and mag. props. 79−47369
BaO-Fe_2O_3-B_2O_3 glass, struct. and mag. props., Mossbauer spectra 80−7226
BaO-Fe_2O_3-B_2O_3 glass, splat cooled, low temp. micromagnetism 80−34660
BaO-Fe_2O_3-B_2O_3(Na_2O) glasses, high Fe_2O_3 content, mictomagnetic props. 80−65916
BaO-Fe_2O_3-Na_2O glass, mag. props. 78−88123
BaO-Fe_2O_3-(Na_2O) glass, rapidly quenched, mag. and ferrimag. props. 80−75744
BaO.$6Fe_2O_3$, solubility of CaO 80−100333
$BaTiO_3Fe_2O_3$, photoacoustic effect, first order phase transitions at increasing and decreasing temp. 80−70320
$Ba[Fe(CN)_5NO]_2.2H_2O$, NMR, H_2O orient. *(French)* 78−52366
$Bi_2Fe_4O_9$, antiferromag., mag. glass props. *(Russian)* 77−4519
$(BiTm)_3(FeGa)_5O_{12}$ ion implanted epitaxial garnet film, bubble domains, cryst. struct. disorder 80−93150
$C_{6.6}FeCl_3$ intercalation compound, charge transfer, acceptor sites, XPS study 80−49218
C_8FeCl_3, behaviour with H_2 and CO, effect of activation 79−43623
$(Ca,Fe)SiO_3$, intracryst. Fe^{2+}-Ca^{2+} exchange, Mossbauer spectra 80−20548
$CaFe_2^{2+}Fe^{3+}Si_2O_8(OH)$, Mossbauer spectra, temp. depend. electron delocalisation 80−20567
$CaFe^{3+}Fe_2^{2+}(Si_2O_7)O(OH)$, ilvaite, electronic struct., press. and temp. depend. of ^{57}Fe Mossbauer spectrum 80−108129
$Ca_3Fe_2Ge_3O_{12}$ garnet, light absorpt. spectral study 80−93322
$CaFeSbAs_2O_7$, stenhuggarite, cryst. struct. 77−58983
$(Ca_{0.15}Mn_{0.8}Fe_{0.05})SiO_3$, rhodonite lattice imaging of struct. defects 80−49240
CaO-Al_2O_3-B_2O_3-SiO_2-FeO, glass, IR spectra at room and melt temp. 80−88986
CaO-Al_2O_3-Fe_2O_3-SiO_2, phase relations 77−12610
CaO-B_2O_3-Fe_2O_3 glasses, effect of heat treatment on electronic props. 78−2480
CaO-B_2O_3-Fe_2O_3 glass, dielec. relax., AC and DC cond., dielec. const. and loss 78−23393
CaO-Fe_2O_3-Al_2O_3 system, solid soln. of $Ca_2Fe_{2(1-x)}Al_{2x}O_5$ *(Russian)* 80−16284
CaO-Fe_2O_3-SiO_2 glass, struct. behaviour at melting, Mossbauer exam. 79−10802
CaO-MgO-Al_2O_3-Cr_2O_3-Fe-O_2-SiO_2 system, exptl. determ. of periclase and spinel comps. 78−6906
CaO-Nd_2O_3-Fe_2O_3-Al_2O_3 system, solid-state reactions 80−35173
CaO-SiO_2-Al_2O_3-Fe_2O_3 mix, liquid phase sintering 79−91610
CaO-SiO_2-Fe_2O_3, melt, CaO dissolution *(Japanese)* 78−6909
CaO-SiO_2-Fe_2O_3 glass, Mossbauer spectra 80−15850
CaO-SiO_2-Fe_xO system, liq., steel making slag, Ca and Fe tracer diffusivities, O_2 press. depend. 78−38863
CaO-V_2O_5-Fe_2O_3-PbO, crystallisation field of Ca-V ferrogarnet 77−16548
Ca_2SiO_4-FeO, conditions and mechanism in cryst.-chemical stabilisation of unstable phases 80−39302
Ca_3SiO_5-Fe_2O_3 solid soln., elec. cond., 800-1000°C, hydration 80−54683
$Ca_3Ti_2V_{1.5-x}Fe_{3.5-x}O_{12}$, garnet, mag. and neutron diffraction investigation 77−16044
$Cd_{1-x}Fe_xCr_2S_4$, Fe II electronic struct., Mossbauer spectra 80−15876
$Cd_{1-x}Fe_xCr_2S_4$ series of magnetic semiconductors, magneto-optical effects, expt. *(Japanese)* 77−40212
$Cd_{1-x}Fe_xCr_2S_4$, single cryst., mag. semicond., spinel-type, magneto-optical effects *(Japanese)* 79−47415
$Cd_{1-x}Fe_xCr_2S_4$:Cu, effect of doping on elec. props. and Curie temp. 78−84214
$Cd_xFe_{3-x}O_4$, cond. mechanism, collective electron description 77−4588
$CdFeTi(PO_4)_3$ cryst. struct., and prep., rhombohedral lattice *(French)* 77−27856
CdO-ZnO-Al_2O_3-Fe_2O_3-SiO_2 system glass, ESR spectra 79−65711
$CeFe_2Si_2$, charge state of 3d shell, state of Fe atoms, atomic bonds *(Russian)* 80−47884
Co^{2+} $[Fe(CN)_6]^{3-}$, time depend. phenomena caused by EC decay, Mossbauer study 80−44978
$Co_xFe_{1-x}Cl_2.2H_2O$ solid soln., mag. props. and phase diagram 79−78346
$Co_{1-x}Fe_xCr_2S_4$, ferrimag. spinel semicond., Curie temp. variation with composition and elec. props. 77−15849
$Co_x^{2+}Fe_{1-x}^{2+}Fe_2^{3+}O_4$, Mossbauer parameters, effect of Fe^{2+}, Zeeman patterns 79−28647
$CoFe_2Se_4$, low-temp. thermal expansion anomalies and isothermal compressibility, mag. ordering and magnetorestriction 79−38363
$Co_{1-x}Fe_xSi$, elec. and optical props. 80−49740
CoO-Fe_2O_3, isoelectric point meas. 80−88609
CoO-MgO-Cr_2O_3-Fe_2O_3-TiO_2, form. and colour of spinel solid soln. *(Japanese)* 80−16059

iron compounds continued
Cr-Fe-O, rutile type oxides, obtained from thermal decomp. of $Cr_{1-x}Fe_x$-OOH, Curie temp. and saturation magnetisation 79−24740
$Cr_xFe_{2-x}CaO_4$ mag. phase transitions meas. *(Russian)* 79−75556
$Cr_xFe_{3-x}O_4$, spin and charge density oscillations due to impurities *(Korean)* 80−20565
$Cr_{1-x}Fe_xOOH$, $0 \leq x \leq 10$, prep., Mossbauer effect, Neel temp. 80−108134
$Cr_{1-x}Fe_xS$, metal-dielec. transition, X-ray, thermal anal., elec. cond. temp. depend. 78−67942
$Cr_{1-x}Fe_xSi_2$, prep., elec. cond. and thermoelec. props. 80−49697
Cr_2O_3 X-ray diffr. studies, crystallite size, phase transformation 77−21138
Cr_2O_3/γ-Fe_2O_3/Pt electrode, two layer oxide surface film anal. by modulation spectroscopy *(Japanese)* 80−11491
Cr_2O_3-Fe_2O_3 solid soln., completely annealed, reclustering of Fe^{3+} ions 79−33578
$(1-x)Cr_2O_3$-$x\alpha Fe_2O_3$, influence of Fe^{3+} on phase transition *(Russian)* 79−28522
$(1-x)Cr_2O_3$-$x\alpha Fe_2O_3$, mag. phase diagram, EPR method *(Russian)* 79−28521
CrS-FeS, sulphorspinel, struct. and elec. props. 80−49834
$CsFeCl_3$, linear chain cryst., quadrupole and mag. reson., rel. to $RbFeCl_3$ 79−38403
$CsGa_{1-x}Fe_xS_2$, tetrahedrally coordinated Fe atoms in low spin state, mag. props. and neutron diffr. study *(German)* 80−88714
$CsLi_{0.5}(Al,Fe)_{1.5}F_6$ pyrochlore, Mossbauer contrib. to exam. of cationic order *(French)* 80−93224
$CsLi_{0.5}Fe_{1.5}F_6$ pyrochlore, Mossbauer contrib. to exam. of cationic order *(French)* 80−93224
$Cs_2NaFe(CN)_6$, structural phase transformations 79−19178
$CsNiFeF_6$ pyrochlore, Mossbauer contrib. to exam. of cationic order *(French)* 80−93224
Cu-Fe-O system, ternary phases, activities in spinel solid soln., phase equilibria and thermodynamic props. 78−6910
Cu-Fe-S-O matte, appl. of Gibbs-Duhem eqn. 77−4923
$CuAl_{1-x}Fe_xS_2$ system, delocalisation of d-electrons, mag., elec. and optical obs. 78−34804
$CuFeO_2$-Fe_2O_3, decomposition kinetics and mechanism of spinel solid soln., composition and precipitation effects *(Japanese)* 77−77489
$Cu_{1-x}Fe_{2+x}O_4$, cation distrib. and valence state 78−63732
$Cu_{1-x}Fe_{2+x}O_4$, elec. resist., Seebeck coeffs., 20 to 900°C, cation distrib. 79−4575
$CuFeS_2$, chalcopyrite, electrode surface reduction kinetics 78−56897
$CuFeS_2$, chalcopyrite, ionic diffusion obs., use of cathodolum. and AES 80−71497
Cu_2FeS_3, pseudocubic mineral, twinning obs. in point electron-diffr. photographs 77−43225
Cu_5FeS_4, bornite, cathodolum. and AES, ionic diffusion obs. 80−71497
$Cu_3FeTl_2Se_4(Cu_3FeTl_2Te_4)$, crystallographic studies 77−31640
CuO-Fe_2O_3, isoelectric point meas. 80−88609
Cu_2S-Fe S mattes equilibration with Fe-O-SiO_2 slags under controlled partial pressures of SiO_2 79−83152
$DyFe_2H_2$, mag. props., ^{57}Fe and ^{161}Dy Mossbauer spectra and magnetisation meas. 79−78579
$DyFeO_3$, orthoferrite, domain struct. and hysteresis props. 77−77071
$Dy_2Fe_3Si_5$, cryst. struct. determ. 78−18620
$ErFe_2H_{3.65}$, $ErFe_2H_{4.12}$, Mossbauer spectra, electronic and structural studies 80−15860
$ErFe_2H_n$, pressure-composition-temperature phase diagram 80−3010
Eu-Fe garnet, light mag. linear birefringence and dichroism near absorption band *(Russian)* 80−55063
EuIG:Sb(Ca)(Ti), growth from PbO-B_2O_3 based flux, prop. depend. on Pb content 80−39824
EuYIG:Sb, growth from PbO-B_2O_3 based flux, prop. depend. on Pb content 80−39824
β-FEOOH, Mossbauer spectra obs., chemical and thermal anal., X-ray diffr., saturation magnetisation 80−88896
$F_{1-x}O$, wustite, X-ray struct. anal. *(French)* 80−70175
α-F_2O_3:alkali metal hydroxides, reduction, Mossbauer spectra 80−16672
$(Fe,Cr)_3C$, reln. between bond energy and X-ray emission line shifts 78−50555
(Fe, Mn)-V spinels, complex, oxidation, effect of Cr_2O_3, TiO_2, MgO additions 79−43453
(Fe, Mn)B and $(Fe, Mn)_2B$, lattice constants of solid solns. *(Italian)* 77−48402
$(Fe,Mn)_3C$, crystallochemical struct. *(Russian)* 77−55271
$(Fe,Mn)_5C_2$, crystallochemical struct. *(Russian)* 77−55271
$(Fe,Mn)_7C_3$, crystallochemical struct. *(Russian)* 77−55271
(Fe, Mn)O_x, thermodynamic characts. deduced from Wustite reaction *(Italian)* 77−48401
$(Fe,Mn)WO_4$, mixed cryst., magnetically disordered system, Mossbauer and neutron diffr. meas. 77−16225
(Fe, Ti) silicate glasses, optical absorption and Mossbauer spectra 80−55136
$(Fe,X)O_4$, (X=Ti, Co, Mg, Mn, Ni), magnetostriction calcs. *(Dutch)* 80−2619
Fe $(H_2O)_6^{2+}$, in crystals and aqueous soln., asymmetrical quadrupole spectra 80−44974
Fe (III) gels, magnetisation vector diffusion coeff., anisotropy energy, vol. distrib. of particles by Mossbauer effect 78−48099
Fe (III)M (II)$F_5.7H_2O$, M=Fe, Co, Ni, Zn, antiferromagnetism 77−59395
Fe $(NO_3)_3.9H_2O$, spin-spin relax., Mossbauer effect studies, 4.2K 78−31128
Fe complex, ^{57}Fe Mossbauer spectra, temp. depend. 77−12262
Fe complex, ^{57}Fe(2-aminomethylpyridine)$_3Cl_2.C_2H_5OH$, temp. depend. spin state, ^{57}Fe Mossbauer emission spectroscopy 80−39980
Fe complex, 1-(2-thiazolylazo)-2-naphtholato Fe (II), cryst. struct. 77−11536
Fe complex, 2,2′-bipyridine, visible spectra of cryst. 79−47424
Fe complex, $[Fe^{3+}(EDTA)]_2$, effect of mag. field on decomposition rate of H_2O_2 79−52631
Fe complex, $[Fe(CN)_6]^{3-}$, electronic struct., optical transitions, XPS, Mossbauer isomer shift, valence ionisation pot., SCF-MSX calc. 79−6864
Fe complex, $[Fe(S_2C_2O_2)_2X]^{2-}$, (X=Cl,Br,I), Mossbauer effect, EPR, mag. susceptibility 79−11366
Fe complex, $[Fe(2\text{-pic})_3]Cl_2.EtOH$, struct. changes, spin phase transition mechanism 79−78380
Fe complex, anomalous spin states, Mossbauer spectra 77−12261

iron compounds continued
Fe complex, bis(N,N-dialkyldithiocarbamato) iron III halides, short range antiferromag. coupling, Mossbauer spectra 77−90076
Fe complex, bis(N,N-diethyldithiocarbamato)-iron chloride, ferromag., sp. ht. meas., 0.4-20K 78−19258
Fe complex, bis[2-(2-pyridylamino)−4-(2-pyridyl)thiazole]Fe(II) complexes, high spin-low spin transitions 77−8456
Fe complex, carboxylate-Fe (III), surface alignment of liq. cryst. 80−1924
Fe complex, cis-dichlorotetrakis (dimethylformamide) iron (III) tetrachloroferrate, cryst. struct. 79−32981
Fe complex, dithiocyanato bis(4-methyl-1, 10-phenanthroline) iron, Mossbauer effect and magnetism down to 0.98K 77−28490
Fe complex, electronic and mag. struct., semiempirical MO cluster calcs. 78−62733
Fe complex, FE II cyclohexanone thiosemicarbazone, Mossbauer spectrum, quadrupole splitting 79−28641
Fe complex, Fe (III) acetylacetonate, solvent effects on oscillator integrated strength, IR absorpt. bands 78−84575
Fe complex, Fe (II) pseudo-tetragonal high-spin cpds., paramag. susceptibility amd Mossbauer quadrupole splitting 78−26834
Fe complex, Fe (alkyldithiocarbamate)$_2$X, X=Cl, I, mol. orbital calc., hyperfine fields, elec. field gradient 80−39981
Fe complex, Fe II- and Fe III-porphyrins, metalloporphyrin triplet state quenching 78−76992
Fe complex, $Fe_4[Fe(CN)_6]_3$, $Fe_3[Fe(CN)_6]_2$ and oxidised $Fe[Fe(CN)_6]$, electron structs. and refl. spectra 77−55813
Fe complex, Fe_xM_{1-x}(1,10-phenanthroline)$_2$(NCS)$_2$, M=Mn,Co,Ni, spin crossover, Mossbauer and magnetism study 80−44980
Fe complex, Fe^{2+} chelate of hydrazinecarboxylic acid, Mossbauer effect, cryst. field splitting 79−78591
Fe complex, $FeCl_3$-tetraphenylporphyrin in PVC matrix, excited state props., electrochromism obs. 80−37815
Fe complex, $FeCl_3L_3$ type, L=ligand, Mossbauer study 78−2783
Fe complex, $FeCl_4^-$, effective charge, from IR and Raman scatt. intensity obs. 78−62809
Fe complex, FeOCl[(ethyltetramethylcyclopentadienyl)$_2$Fe]$_{0.16}$ synthesis and struct. 80−44176
Fe complex, Fe(Br)[$S_2CN(C_2H_5)_2$]$_2$, 3-D Ising ferromag., cryst. susceptibility, 1.5-20K 80−20390
Fe complex, Fe(Cl)[$S_2CN(C_2H_5)_2$]$_2$, single cryst. susceptibilities 78−31057
Fe complex, Fe(Cl)[$S_2CN(C_2H_5)_2$]$_2$, susceptibility near critical pt. 79−24147
Fe complex, Fe(Cl)[$S_2Cn(C_2H_5)_2$]$_2$, 3-D Ising ferromag., cryst. susceptibility, 1.5-20K 80−20390
Fe complex, Fe(III) Schiff-base complexes, mag. relax., Mossbauer spectra 80−15897
Fe complex, Fe(III) tris diseleno chelates, sextet doublet Boltzmann equilib. Mossbauer spectra 78−60366
Fe complex, Fe(II), 2,2′-bipyridyl complexes, reson. Raman spectra, vibr. anal. 79−61363
Fe complex, Fe(II) and Fe(III) cyanides-3d transition metal, mag. suscept., reflectivity spectra, cryst. field 79−56808
Fe complex, Fe(II) oxalato-bridged chain compounds, Mossbauer spectra 80−15890
Fe complex, Fe(1,2,4-triazole)$_2$(NCS)$_2$, quasi-2-dimens. S=$^1/_2$ antiferromag., mag. props., hidden canting 80−107986
Fe complex, Fe(5-methylpyrazole)$_4X_2$, X=Cl, Br, I, mag. susceptibility, mag. saturation; Mossbauer and ligand field spectra, single model interpretation 78−23064
Fe complex, Fe(acac)$_3$, paramag. relax. reagent, effect on ^{15}N NMR chem. shifts in pyridenes 78−15042
Fe complex, Fe(dithiocarbamate)$_2$X, X=NCS,Cl,Br,I,NO, elec. field gradient, HMO calc. 80−39543
Fe complex, Fe(papt)$_2$, high spin $^5T_2$⇌low spin $^1A_1$ transition, Debye-Waller factors and magnetism 78−80259
Fe complex, Fe(pyrazole)$_4X_2$, X=Cl, Br, I, mag. susceptibility, mag. saturation; Mossbauer and ligand field spectra, single model interpretation 78−23064
Fe complex, ferrous pseudo-tetrahedral compounds, paramag. relax., Mossbauer spectra 80−15869
Fe complex, haemoglobin in salt. soln., diffusion rel. to intermol. interactions, light scatt. investig. 77−44585
Fe complex, halobis(morpholyldithiocarbamato)Fe(III), solvation effects, mag. susceptibility and Mossbauer spectra 78−27129
Fe complex, halobis(morpholydithiocarbamato)Fe(III), Mossbauer HFS spectra, mag. relax. and cooperative transitions 78−27130
Fe complex, hexa(pyridine-N-oxide)$(ClO_4)_2$, sp. ht., comparison with simple cubic S=1/2 Ising magnet 78−23290
Fe complex, iodobis(morpholyldithiocarbamate), allotropes, intermol. exchange interactions 77−8455
Fe complex, $K_3[Fe(SCN)_6].4H_2O$, optical reflection spectrum, mag. suscept., permittivity, dehydration temp. 79−56809
Fe complex, ligand-bridged binucl. complex anions, reson. Raman spectra 78−42067
Fe complex, $N_2H_5[Fe(N_2H_3COO)_3].H_2O$, elec. field gradient at Fe^{2+}, perturbation theory calcs. 78−19002
Fe complex, nitrile nonacarbonyl, cryst., mol. structs. 80−64967
Fe complex, nitrile nonacarbonyl cryst., mol. struct. 80−64968
Fe complex, octahedrally coordinated Fe(II), Jahn-Teller induced high spin-low spin transitions 79−69676
Fe complex, perchlorato(meso-tetraphenylporphinato) iron (III), mag. props., Mossbauer study 79−99802
Fe complex, pyridine-n-oxide perchlorate, Mossbauer spectra, site distortions enhanced by grinding 80−15883
Fe complex, redox enzyme, electron transfer peculiarities 80−16896
Fe complex, tetraphenylporphynate iron III bromide, mag. props., zero-field splitting 80−34584
Fe complex, tris (1,10-phenanthroline) iron(II), transient bleaching, excitation wavelength absorpt. 78−73060
Fe complex, tris-(4-morpholinecarbodithioate-S,S′)Fe(III), and dichloromethane solvate, Mossbauer and EPR spectra, spin 3/2 state 78−9169
Fe complex, tris(1-pyrrolidinecarbodithioato)iron(III), and related cpds. mag. props., struct. 77−89933
Fe complex, tris(monothio-β-diketonato) Fe (III), spin equilib., Mossbauer spectra 80−15910
Fe complex, ubiquinone-Fe, bacterial photosynthesis primary electron transfer processes, psec. dynamics 78−80841
Fe complex, with 1,2,4-triazole, mag. susceptibility, 2-300K, struct. 77−77045

iron compounds continued
Fe complex (2, 9-dimethylphenanthroline) sulphate, mag. props., Mossbauer spectra 80−66081
Fe complex Fe(NO)[$S_2CN(C_2H_5)_2$]$_2$ in frozen toluene, for dynamically proton polarised target 78−52378
Fe complexes, 1-(2-pyridylazo)-2-naphthol and 1-(2-pyridylazo)-2-phenanthrol, back co-ordination, Mossbauer study 80−20572
Fe complexes, 2- or 3-pyridyl imine complexes of $FeCl_2$, Mossbauer and mag. props. 80−15896
Fe complexes, Fe (III) bis(dithiocarbamato) iodides, transferred hyperfine interactions and mag. ordering 77−20759
Fe complexes, FeOCl[Co(cyclopentadienyl)$_2$]$_{0.16}$ and FeOCl[Fe(cyclopentadienyl)$_2$]$_{0.16}$, Mossbauer and mag. susceptibility meas. 80−44176
Fe complexes, high spin ionic with halogen ligands, Mossbauer isomer shift calibration 77−16210
Fe complexes, $M[Fe(C_2O_4)_3].XH_2O$, M=Li, Na, K, Rb, Cs, NH_4, Mossbauer studies of electronic relax. phenomena 80−44973
Fe complexes, mag. susceptibility, Mossbauer spectra 78−15071
Fe complexes, paramag., XPS, temp. depend. 79−15582
Fe complexes, rhombic, g-values and zero-field splitting 79−78061
Fe complexes, S-bridged binuclear, orbitally dependent exchange 77−24688
Fe complexes, tetraphenylporphyrins, mag. susceptibility, hyperfine mag. field value Mossbauer spectra 80−37824
Fe complexes, tris and bis dithiocarbamates, quad. splitting, Mossbauer obs. 77−59489
Fe complexes with dimethylformamide, dimethylthioformamide, Mossbauer and mag. props. 80−39974
Fe F2 (Fe F3), electronic struct., binding energy, X-ray emission and photoelectron spectra obs. 80−35008
Fe garnets, sublattice magnetisation curves, Mossbaeur study 80−75808
Fe hydroxylboracite, hydrothermal crystallisation 77−85917
Fe III low-spin complexes, nucl. spin-lattice relax., electron spin density matrix theory 78−13521
Fe one raw material, sintered, ionic etching as new method of struct. investigation 77−52588
Fe ore, cold bound pellets, reduction using H_2 gas, 700 to 900°C *(Japanese)* 80−71907
Fe ore, reduction degree, chemical anal. calcs. *(Russian)* 80−66769
Fe $SiF_6.6H_2O$, phase transform., temp. depend. of Mossbauer parameters 77−73102
Fe^{2+} and Fe^{3+} hydrate clusters, aq. electron exchange reaction, ab initio RHF MO calc. of inner shell reorganisations, vibr. freq. 80−102564
Fe^{2+} compounds, Mossbauer spectra, spin-lattice relax. effects 80−50239
Fe^{2+} d^6-complexes and oxides, spin-state transitions, PES study 79−100014
Fe^{2+} ions influence on $PbSO_4$ flotation, with sodium hexadecyl sulphate, metallurgical waste treatment appl. *(Japanese)* 80−55701
Fe^{3+} ions, in frozen aq. solns., spin-spin relax., Mossbauer obs. of effect of paramag. impurity ions 79−33573
Fe^{3+} ions influence on $PbSO_4$ flotation, with sodium hexadecyl sulphate, metallurgical waste treatment appl. *(Japanese)* 80−55701
Fe^{3+} solutions, UV absorption spectrosc. obs. of equilib. 80−93812
Fe^{3+} transferrin, EPR spectrum analysis, polynomial regression and non-derivative search technique 77−14461
Fe/'FeO', relative chemical potential of oxygen *(German)* 78−31642
Fe^{3+}/Fe^{2+} in frozen solns., stabilisation on ^{57}Co decay, electron scavenger effects, Mossbauer obs. 77−40562
Fe^{3+}/Fe^{2+} ratio, quantitative Mossbauer spectra 80−7209
Fe-Al oxide system, depth profile anal. by secondary ion mass spectra *(Japanese)* 78−7290
Fe-As, phase equilib. diagram *(German)* 80−16280
Fe-C phase diagram, thermodynamic anal. 80−60846
Fe-C reactively sputtered, solar absorbing surface, struct. and optical props. 79−79407
Fe-CaF (6 and 9 wt.%), sintered, elevated temp. mech. props. 77−28878
Fe-Co-Ni-O, mag. powder prod. by reduction of oxalates 77−63582
Fe-complex, Fe^{2+}-thionine photoelectrochem. cells, power output 80−45711
Fe-complex, Fe^{2+}-thionine electrochem. cells 80−50993
Fe-complex, Fe-thionine in homogeneous-type photoelectrochem. cells, photogalvanic effect 80−45710
Fe-Cr oxide, quantitative depth profile, by AES *(Japanese)* 80−16751
Fe-Cr-O, computer-assisted anal. and calcs. of phase diagrams 80−25667
Fe-Cr(55 wt.%), phase decomp. early stages and clustering *(Japanese)* 80−55403
Fe-Cu: graphite-$BaSO_4$-$CuSO_4$, friction material, solid state sintering kinetics 80−104096
Fe-Fe_2O_3 composite films, structural props., microhardness, 250 to 700K 78−84095
Fe-Fe_2O_3-$NaFeO_2$, study of Na-containing wustite region *(French)* 77−73264
Fe-Fe_2O_3-SiO_2-Si melt, interacting system, oxidation products *(Russian)* 78−19728
Fe-Fe_3C system, cavity nucleation, by plastic deform. 79−29127
Fe-FeS, Mars core formation, radioactive element diffusion, thermal history 79−84724
Fe-FeS-MnS-Mn reciprocal system, interaction between three liq. miscibility gaps 77−7865
Fe-Ge intermetallides, melt struct. rel. to growth mechanism 77−84681
Fe-graphite, intercalate, prod. by slow electrochemical reduction *(French)* 78−27437
Fe-graphite, sintered, diffusion layer form. 79−100299
Fe-I boracite, pyroelec. coeff. meas. 80−75951
Fe-lanthanid-O systems, thermodynamic props., composition and lattice constants 78−31390
Fe-MgO system, decomp. reactions, ferromag. reson. obs. 77−9058
Fe-Mo/SiO_2 oxide catalyst for methanol oxidation 79−100440
Fe-Mo-CaF (15, 9 and 6 wt.%), sintered, elevated temp. mech. props. 77−28878
Fe-N crystal, orienting $Fe_{16}N_2$ particles by external magnetic field *(German)* 77−25058
Fe-N phase diagram, thermodynamic anal. 80−60846
Fe-Ni sulphides in Murchison meteorite, props. and rel. to phase Q1 79−58303
Fe-Ni-Cr-S-O compounds, occurrence in Allende chondrite *(French)* 78−32411
Fe-Ni-O, computer-assisted anal. and calcs. of phase diagrams 80−25667

iron compounds continued
Fe-O, exam. of thermodynamic data, using a computer aided strategy 79−11592
Fe-O compounds, MO cluster calc. of charge densities and elec. field gradients 77−76783
Fe-O noncrystalline RF sputtered film, vapour species control 78−60575
Fe-O system, thermodynamics of viustite-haematite alloy melt *(Russian)* 80−65249
Fe-O-Ca-Al system, inclusion precipitation diagram 80−108415
Fe-P base frictional material, sintered, friction and wear under moderate load 77−12704
Fe-S (34.0-41.0 wt.%), Mossbauer investigations 79−47376
Fe-S eutectic, Lindmann's melting law, solid-liquid core boundary, core mantle boundary 78−18743
Fe-S liquid, K solubility and silicateK-(Fe-S liq.) equilibria, planetary implications 78−11843
Fe-S phase diagram, thermodynamics 79−56966
Fe-S system, chemical transport of non-stoichiometric phase 79−69972
Fe-S system, solubilities in aqueous H_2S and mass transport role in girdler-sulphide heavy water plants 78−83963
Fe-S-O, equil. cond. *(Rumanian)* 79−29029
Fe-SO_4-H_2O suspension system at 90°C, potential-pH diagram 78−61068
Fe-Si intermetallides, melt struct. rel. to growth mechanism 77−84681
Fe-SiO_2-Al_2O_3 Lisakovskii concentrate mixture, sintering process, temp. thermal treatment *(Russian)* 80−55317
Fe-thiamine solution, modified, photogalvanic effect 78−91722
Fe-thiazine photogalvanic cell, blue sensitization, photoredox reaction, insolation spectrum match 77−90628
Fe-thionine, photogalvanic cell, photostationary state comp., current depend. 77−90629
Fe-Ti oxide minerals from Asama volcano, Japan, in 1973 eruption 77−17065
Fe-W-O system, phase relations in dioxide-trioxide region, 1373K 78−11212
Fe-W-O(C), Gibbs energy of form. of phases *(German)* 80−97724
Fe-WO_3 system, struct. phase exam. by optical microscopy and X-ray diffr. 78−31389
Fe^{3+}-Fe^{3+} distances, in aq. NO_3^- and ClO_4^- solns., from small-ang. X-ray diffr. maxima 78−42880
Fe+H_2O, clean surface oxidation and passivation by vapour, XPS, FeOOH formation 77−81424
$Fe_{0.394}$-$Ti_{0.606}$-O-S subsystem, equil. phase data under reducing conditions rel. to ilmenite upgrading 80−76240
$FeAl_{2-x}Cr_xO_4$, spinel, elec. cond. behaviour during oxidation 79−19593
γ-$(Fe_{1/3}Al_{2/3-y}Cr_y)_2O_3$, lacunar spinels, elec. cond. behaviour during oxidation 79−19593
$(Fe_{1-y}^{3+}Al_y^{3+})_2O_3^{2-}$, γ to α transform. elec. cond. study, oxidation initial stage kinetics, lacunar spinel form. 78−92384
$Fe_{3-x}Al_xO_4$, cation distrib., mag. and other phys. props. 77−43818
$(Fe_{6-y}Al_y)O_9$, IR spectra, lacunar γ-phase to corundum α-phase transform. 80−108199
$Fe_{1-x}Al_xOOH$, Mossbauer study, determ. of Al content and mag. props. 80−39938
Fe_2As, antiferromagnet, Mossbauer spectra determ. 77−8480
$FeAsO_4$, XPS of cryst., inner shell binding energies of elements 79−43092
FeB and Fe_2B, ESCA and mag. spin data, electronic struct., isomer shifts, valence bands and chemical bonding 80−75489
FeB coating on steel, formed by B diffusion, pack cementation process, microstruct. and mech. props. 78−15592
FeB, thermophysical props., 296-2000K 78−14477
Fe_2B coating on steel, formed by B diffusion, pack cementation process, microstruct. and mech. props. 78−15592
Fe_2B_6, UV-visible absorpt. spectrum 78−13512
$Fe_{80}B_{20}$, binary amorphous ferromagnet, Mossbauer spectra 79−4749
$Fe(BF_4)_2.6H_2O(6D_2O)$, phase transition, mag. susceptibility and anisotropy and permittivity meas. 79−23718
$FeBMO_4$, M=Mg, Cu, Co, Ni, mag. props. meas. 80−34607
$FeBO_3$, antiferromag., vibr. spectra, 6000-30 cm^{-1} 78−19473
$FeBO_3$, antiferromag., optical absorpt. spectra, role of local mag. mode 79−28785
$FeBO_3$, antiferromag., two magnon reson. Raman scatt. 79−33703
$FeBO_3$, basal mag. anisotropy, antiferromag. reson. *(Russian)* 79−47338
$FeBO_3$, Brillouin scatt. from parametrically excited phonons 79−73956
$FeBO_3$, Brillouin-Mandelstam scattering from thermal and excited magnons 80−70980
$FeBO_3$, crit. behaviour, Mossbauer and magnetisation meas. *(Russian)* 79−61106
$FeBO_3$, Curie temp. displacement under press. up to 3 kbar 77−20603
$FeBO_3$, dynamic NMR frequency shift for ^{57}Fe *(Russian)* 78−43677
$FeBO_3$, dynamical diffraction of gamma rays, enhanced nuclear reson. scatt. 80−108127
$FeBO_3$, Faraday effect, polaris. ellipse rot. 77−20834
$FeBO_3$, $FeBO_6$, magneto-optical materials, single cryst. growth *(Japanese)* 79−47612
$FeBO_3$, Laue refl. of Mossbauer radiation, depend. on mag. field direction 80−40020
$FeBO_3$, mag. linear dichroism and absorpt. spectra, Jahn-Teller effect 80−54662
$FeBO_3$, mag. linear dichroism and absorpt. spectra, exciton-magnon absorpt. mechanism 80−66160
$FeBO_3$, magnetically tunable ultrasonic transducers for shear waves 80−74682
$FeBO_3$, magnetisation near crit. temp., up to 3 kbar hydrostatic press., scaling theory 77−8316
$FeBO_3$, magnetoelastic coupling, antiferromag. reson. deform. depend. meas. 77−73069
$FeBO_3$, magnon dispersion by light scatt. and ferromag. reson. 77−55668
$FeBO_3$, Mossbauer coherent scatt. polaris., rel. to cryst. mag. struct. *(Russian)* 79−11368
$FeBO_3$, nuclear reaction suppression, Mossbauer spectra for Laue diffr. *(Russian)* 80−66093
$FeBO_3$, parametric echo, magnetoelastic NMR excitation *(Russian)* 80−66072
$FeBO_3$, parametric effects in nucl. spin echo *(Russian)* 78−56404
$FeBO_3$, photoinduced linear birefringence *(Russian)* 78−52469
$FeBO_3$, polycrystalline, ferromagnetic resonance, crystallite orientation 78−15027

iron compounds continued
$FeBO_3$, size effect during parametric spin wave excitations *(Russian)* 80−103824
$FeBO_3$, spin wave dispersion at small wavevectors, Brillouin scatt. and ferromag. reson. 78−47962
$FeBO_3$, spin waves, Brillouin scatt. studies 79−99696
$FeBO_3$, spin-reorientation phase transition *(Russian)* 80−93122
$FeBO_3$, suppression effect under hyperfine quadrupole splitting, Mossbauer study *(Russian)* 80−75906
$FeBO_3$, weak ferromag., mag. field influence on crit. behaviour of susceptibility 78−14942
$FeBO_3$, weak ferromag., FMR instability, parametric excitation of phonons, Brillouin scatt. obs. 79−78529
$FeBO_3$, weak ferromagnet, spin wave band struct. and microwave props. 79−1661
$^{57}FeBO_3$ single cryst., weakly ferromag., diffr. of Mossbauer emission *(Russian)* 77−81038
$FeBO_3$-MBO_3 solid soln., (M=Mn, Cr, Al, Ga, In), synthesis, crystal chem. and mag. props. 78−31058
$FeBO_6$, critical indices splitting of sublattice magnetisation *(Russian)* 78−60299
Fe_3BO_6, canted mag. struct. near Neel point, Mossbauer meas. 78−35073
Fe_3BO_6, Faraday rotation and birefringence 80−100650
Fe_3BO_6, MOssbauer spectra in spin reorientation region 77−52002
Fe_3BO_6, Mossbauer exam. of electric field gradients 77−40163
Fe_3BO_6, orthorhombic cryst., birefr. and refr. index determ., refl. method 80−86380
Fe_3BO_6, polarised absorpt. spectra in range of $^6A_1 \rightarrow {}^4T_1$, $^4T_2$ transitions 77−52092
Fe_3BO_6, spin reorientation by mag. field, Mossbauer meas. 78−35074
Fe_3BO_6, spin-reorientation, elec. resist. and microwave absorption 78−14751
Fe_3BO_6, weak ferromag., growth of bulk single crysts. by vapour phase reaction 77−24939
Fe_3BO_6, weak ferromag. state, Mossbauer determ. of mag. struct. 77−40164
Fe_3BO_6, weak ferromag. and antiferromag. reson. modes obs. 77−69706
Fe_3BO_6, weak ferromagnetism and spin reorientation, antiferromag. reson. spectra 78−6580
$Fe_3B_7O_{13}Br$, $Fe_3B_7O_{13}Cl$, polydomain ferroelec., magnetoelec. effect below Neel temp. 78−10745
$Fe_3B_7O_{13}Br(Cl)(I)$, boracite, single cryst. prep. and phys. props. 80−100763
$Fe_3B_2O_{13}I$, boracite single cryst., nucleation control density growth 80−80955
$Fe_3B_7O_{13}I$, cubic, approx. nonlinear optical susceptibility 80−78904
$Fe_3B_7O_{13}I$, ferroelec., mag. ordering, neutron diffr. meas. 78−72331
$Fe_3B_7O_{13}I$, ferroelec. 43m-mm2 phase transition, molar heat capacity meas. 80−93249
$Fe_3B_7O_{13}I$, improper ferroelectric, electro-opt. props. 78−76426
$Fe_3B_7O_{13}I$, improper ferroelectric, dielectric props., IR radiation pyroelectric detection 80−80711
$Fe_3B_7O_{13}I$, spontaneous polarisation, dielec. const., d.c. resist., sp. ht. 77−1643
$Fe_3B_7O_{13}I$, twinning in orthorhombic phase, ferroelec. domain struct. with switching 78−19434
$Fe_3B_7O_{13}X$, X=Cl, Br, I, ferromag. ferroelectrics *(Japanese)* 79−65804
$Fe^{2+}BSi_2O_6$, B=Mg, Fe^{3+}, Al, pyroxenes, order-disorder interpretation 80−38987
$FeBr_2$, dynamic Jahn-Teller system, Raman scatt. from electronic excitations and phonons 78−56474
$FeBr_2$, electron diffr. determ. of mol. struct., evidence for Fe_2Br_4 species 78−37767
$FeBr_2$, far IR antiferromag. reson., two-sublattice model 77−36138
$FeBr_2$, Faraday rot., optical absorption, multicrit. behaviour 77−4627
$FeBr_2$, Faraday rotation in pulsed mag. field, linear absorpt. const. 80−45041
$FeBr_2$, hyperfine interaction, ^{57}Fe Mossbauer expts., mag. transition obs. 78−43720
$FeBr_2$ metamagnet, unusual phase diagram, theory 80−93119
$FeBr_2$, metamagnetic, optical study of mag. phase diagram 78−56312
$FeBr_2$, optical props. around Neel temp. 79−78658
$FeBr_2$, UV-visible absorpt. spectrum, vaporisation thermodynamics 78−13512
$FeBr_2$, XPS, satellite of Br 4s line 78−56556
$^{57}FeBr_2$, matrix isolation Mossbauer spectra, isomer shift, quadrupole splitting 78−42104
$FeBr_2$:Mn^{2+}, antiferromag., impurity spin reson. 77−43876
$FeBr_2$:Mn^{2+}, layered antiferromag., infinity mode NMR study 79−38390
$FeBr_2$:$MnBr_2$, magnon modes and impurity spin reson. 79−15501
$FeBr_3$ aqueous soln. photogalvanic effect 79−24902
$FeBr_3$, UV-visible absorpt. spectrum 78−13512
$FeBr_4^-$, circularly polarised Raman spectra, spin-orbit induced vibr. antisymmetry 78−5232
$FeBr_4^-$, complex Raman tensors, irreducible tensor method, antisymmetric scatt. 78−37623
$FeBr_4^-$, in various solvents, $^4A_1$ ^4E d-d band reson. Raman spectra, solvent depend. 80−55085
Fe_2Br_4, UV-visible absorpt. spectrum 78−13512
$Fe_x(C,N)$, obtained by ion bombardment thermochemical treatment of Armco Fe *(French)* 77−86229
FeC form. in ferrite, Monte Carlo simulation *(German)* 78−39779
FeC_2^+, electron impact appearance pot. in dissoc. of $Fe(CO)_5$ 79−34281
FeC_x-CrC_y-NiC_z, stainless steel carbide, solar selective surface, fabrication, magnetron sputtering system description 80−80967
FeC_y-CrC_y-NiC_z, stainless steel carbide, graded solar selective surface, magnetron sputtered 80−81485
FeC_x-CrC_y-NiC_z, stainless steel carbide, sputtered solar selective surface, grading profile 80−81486
α-Fe_2C_3, anisotropic linear mag. birefr., light modulation 77−8548
Fe_3C (cohenite), interstellar, condensation rel. to astrophysical dust grains form. 80−26927
Fe_3C, cementite spherol crystals, morphology and growth 78−18567
Fe_3C, in Fe and its alloys, Young's modulus *(Russian)* 80−76297
Fe_3C melts, measuring C content using automatic device 79−39252
Fe_3C, microhardness and charact. hardness 79−52376
Fe_3C, modulation operations and derived structs. 79−94930
Fe_5C_2, modulation operations and derived structs. 79−94930

iron compounds continued
$Fe_pC_n^+$, p=1 to 4, clusters, electronic props., mass spectra obs. *(French)* 79−45877
$Fe(CN)_6$, adsorbed on Al_2O_3, tunnelling spectra, isotope shifts 80−29262
$Fe(CN)_6$, Mossbauer isomer shift const., ab initio SCF calcs. 78−43751
$Fe(CN)_6^{3-/4-}$, redox reaction on CdTe and ZnTe electrodes *(French)* 80−89482
$Fe(CN)_6^{3-}$, binding sites on lecithin liposomes 79−79481
$Fe(CN_6)^{3-}$, effects on chlorophyll a fluoresc. duration in chloroplasts 77−25393
$Fe(CN)_6^{3-}$, mass transfer rates at spheres, moving on circular path 77−3890
$Fe(CN)_6^{3-}$, transfer characteristics at conical surfaces under axisymmetric impinging jets 77−3889
$FeCN_6^{4-}$, triplet state quenching agent, in ZnO electrode dye sensitisation obs. 78−76869
$Fe(CN)_6^{3-}/Fe(CN)_6^{4-}$, ionic mass transfer in narrow rectangular conduits 80−61105
$Fe(CN)_6^{3-}$-$Fe(CN)_6^{4-}$, electrochem. behaviour on $La_{1-x}Sr_xCoO_{3-y}$ rot. disk electrodes 79−79257
$Fe(CN)_6^{4-}-Fe(CN)_6^{3-}$, redox reactions, mass transfer at vibr. spheres 80−57220
$Fe(CN)_6^{4-} \leftrightharpoons Fe(CN)_6^{3-}$, redox pot. in nonaqueous-water mixtures 79−52654
$FeCO_3$, antiferromag., siderite, Raman spectra obs. 77−85708
$Fe(CO)_3$, bond angles, hybrid bond orbital calcs. 78−94188
$FeCO_3$, mag. field drawn destruction of antiferromag. destruction, light depolarisation at mag. transform. *(Russian)* 78−23432
$FeCO_3$, mag. neutron scatt., spin orbit coupling effects 77−85419
$FeCO_3$, metamagnetic insulator Neel temp. anal. by model including spin fluctuations *(Russian)* 80−15715
$FeCO_3$, Mossbauer quadrupole splitting of ^{57}Fe, vibronic effects 79−19813
$FeCO_3$, siderite, Fe^{2+} Mossbauer spectrum, ligand field theory 77−16212
$FeCO_3$, siderite, powder, Mossbauer spectra, acoustic-excitation-induced asymmetry of quadrupole splitting 78−27145
$FeCO_3$, vibronic coupling at Neel temp. 80−15491
$FeCO_3$:Mn^{2+}, far IR host and impurity excitations, antiferromag. and paramag. temp. ranges 77−52140
$Fe(CO)_4$, IR laser induced isomerisation, non-Berry pseudorotation 78−31658
$Fe(CO)_4$, IR spectra and laser photochem., matrix isolated at 20K 78−74651
$Fe(CO)_4$, in N_2, Ar low temp. matrix, IR laser photochemistry, orientational and site selectivity 78−23954
$Fe(CO_4)^{2-}$, Raman spectra 77−59571
$Fe(CO)_5$, chem. thermodynamics 78−18799
$Fe(CO)_5$, electron impact appearance pots. for ion fragments, mass spectra obs. 79−34281
$Fe(CO)_5$, Fe-C-O deformation modes, group theoretical anal., for teaching 78−11
$Fe(CO)_5$, gas phase collisions, negative ion form., struct. 77−6945
$Fe(CO)_5$, matrix isolated species, MCD spectrosc. appls. 78−46378
$Fe(CO)_5$, microwave dielec. relax., fluxional mechanism 78−94235
$Fe(CO)_5$, multiphoton ionisation, mol. cooling in pulsed supersonic beam 80−28070
$Fe(CO)_5$, multiphoton ionis. spectra, at. Fe transitions 80−106361
$Fe(CO)_5$ photodissociation laser 78−74886
$Fe(CO)_5$, solns. with dissolved NO, photolysis, $Fe(NO)_3CO$ form. 80−53024
$Fe(CO)_5+Ar^*$,(Ne*) chemiionisation and chemiluminescence reactions, Penning ionisation and fluoresc. obs. 80−97689
$Fe(CO)_5+Ar^*(^3P)$, chemiluminesc. 78−61014
$Fe(CO)_5$+inert gas, dissoc. energy transfer, chemiluminesc. 80−55647
$Fe(CO)_5+O_3$, modulated chemiluminesc. by CO addition 80−40692
$Fe_2(CO)_9$, solid, Raman and IR spectra, vibr. exam. 78−27214
$Fe_2(CO)_6(HC_2R)_2$, R=H, Bu^t, Ph, binuclear complexes, isomer identification and stability *(Italian)* 77−54620
$Fe(CO)_2(NO)_2$, vib. assignment using ^{15}N isotopic substitution, solid, liq. and soln. spectra 77−48152
$Fe(CO)_2(PF_3)_3$, ^{31}P and ^{19}F NMR, 25 to −100°C axial and equatorial ligand interchange 77−73091
$Fe(CO)_3(PF_3)_2$, ^{31}F and ^{19}F NMR, 25 to −100°C, axial and equatorial ligand interchange 77−73091
$Fe_4Ca_3S_3O_6$, struct. and phase analysis *(Russian)* 77−58995
$Fe_2Ca_3Si_3O_{12}$ glass, mag. ordering effects at low temps., Mossbauer and neutron diffr. meas. 77−16047
$FeCl_2$, adsorbed monolayers, gamma-ray reson. 77−8478
$FeCl_2$, anisotropic ferromag., temp. depend. of one-magnon light scatt. 77−90161
$FeCl_2$, antiferromag., magnon-phonon interactions in thermal cond. 80−65315
$FeCl_2$, antiferromag. reson., temp. depend. 78−68384
$FeCl_2$, antiferromag. reson., 2-D Ising model interpretation 79−47323
$FeCl_2$, collinear metamag., mag. phase diagram 80−71035
$FeCl_2$, cryst., self-consistent band struct., intersecting spheres model 80−75505
$FeCl_2$, dynamic Jahn-Teller system, Raman scatt. from electronic excitations and phonons 78−56474
$FeCl_2$, EXAFS amplitudes, many-body effects 80−97379
$FeCl_2$, electron diffr. determ. of mol. struct. 78−37767
$FeCl_2$, electron-phonon coupling, temp. depend. Raman scatt. obs. 79−15451
$FeCl_2$, epitaxial relationships studied by RHEED and Auger emission spectra *(French)* 78−22990
$FeCl_2$, far IR absorpt. meas. by Fourier transform, apparatus 77−177
$FeCl_2$, far IR antiferromag. reson., two-sublattice model 77−36138
$FeCl_2$, ferromag., one-magnon light scatt., temp. depend. 77−52063
$FeCl_2$, in transverse mag. field, magnetoelastic coupling effect on mag. props. 79−28582
$FeCl_2$, interlayer force constants 78−14406
$FeCl_2$, internal motion, mol. vibr. calcs. 80−106323
$FeCl_2$, light scatt., metamagnetic transition effects 77−4513
$FeCl_2$, logarithmic corrections to tricritical scaling 80−65940
$FeCl_2$, magnetic excitation in presence of transverse field, ferromag. reson. 78−19335
$FeCl_2$, magnetic materials, transparent, optical studies of phase transitions 77−66481
$FeCl_2$, magnetic phase diagram, optical studies 78−88121

iron compounds continued
$FeCl_2$, magnetic transition and sublattice mag. moment rotation nonequivalence *(Russian)* 80−100586
$FeCl_2$, magnetic tricriticality nonuniversality 79−78392
$FeCl_2$, magnon-phonon hybridisation, inelastic neutron scatt. study 79−47272
$FeCl_2$, metamagnet, one-magnon light scatt., effect of anisotropy 79−33678
$FeCl_2$, metamagnet, optical determ. of thermodynamic phase diagram 78−60285
$FeCl_2$, metamagnet, scaling props. of magnetisation and heat capacity, test of tricritical scaling 80−60336
$FeCl_2$, metamagnetic, phase diagram determ. 78−68254
$FeCl_2$, metamagnetic, sound propag. near tricritical point 78−48024
$FeCl_2$, metamagnetic hysteresis, magnetooptical rot. meas. 77−40057
$FeCl_2$, mixed antiferromag.-paramag. state, light scatt. in mag. field 77−40069
$FeCl_2$, one-magnon Raman scatt. 78−43877
$FeCl_2$, optical props. around Neel temp. 79−78658
$FeCl_2$, phase diagrams of magnets with two-sublattices *(Russian)* 78−23268
$FeCl_2$, pulse generation of Cl II at 5218 Å, 5221 Å 78−58990
$FeCl_2$, reorientation of mag. moments under mech. stresses at 0K 80−93153
$FeCl_2$, soln., activity coeffs., osmotic coeffs., water activity, Gibbs energy, molality depend. 80−51963
$FeCl_2$, spin orientation of mag. impurity atom 77−59403
$FeCl_2$, thermodynamic phase diagram determ., using pulsed dye laser, piezoelectric modulator, and gated amplifier 79−7991
$FeCl_2$, tricritical dynamcis, model 77−39719
$FeCl_2$, vibrational excitations, polarised Raman spectra 79−19888
$^{57}FeCl_2$, matrix isolation Mossbauer spectra, isomer shift, quadrupole splitting 78−42104
$FeCl_2$-graphite, intercalation compound, formation by reduction of Fe(III) compounds with $Fe(CO)_5$ 78−63721
$FeCl_2$-graphite intercalation cpd., lattice dynamics, Mossbauer spectra 80−15925
$FeCl_3$ aq. soln., quasi-elastic neutron scatt. 79−37607
$FeCl_3$, Fe_2Cl_6, matrix isolation Raman spectra, assignments 77−65480
$FeCl_3$ intercalated with graphite, vibrational excitations, polarised Raman spectra 79−19888
$FeCl_3$ intercalated with graphite, stage 1, dielec. response and intraband plasmon dispersion 80−59902
$FeCl_3$, intercalation in graphite, form. kinetics and microstruct. *(German)* 79−43560
$FeCl_3$, internal motion, mol. vibr. calcs. 80−106323
$FeCl_3$, intramolecular force fields, compliance consts. and vibr. amplitudes 80−58234
$FeCl_3$, matrix isolation Raman spectra, mol. config., thermodynamic props. 78−46346
$FeCl_3$, nonaq. solns., solvent-solute interactions, Mossbauer investig. of equilib. consts. 79−1729
$FeCl_3$ pyrolysis, effect of CO presence 79−43623
$FeCl_3$, solns. and hydrated melts, complexes form., X-ray diffr. obs. 80−24342
$FeCl_3$-graphite, intercalaton kinetics, of $FeCl_3$ yapour 78−31354
$FeCl_3$-graphite, intercalation compound, Fermi level lowering and core exciton spectrum, EELS study 79−74036
$FeCl_3$-graphite intercalation compound, struct., expt. data for domain theory 78−30596
$FeCl_3$-graphite intercalation compound form., effect of added O, Cl, and water vapour *(German)* 79−52634
$FeCl_3$-graphite intercalation cpd., lattice dynamics, Mossbauer spectra 80−15925
$FeCl_3$-graphite intercalation compound, Mossbauer spectra 80−20538
$FeCl_3$-graphite intercalation cpd., electronic excitation spectrum, high resolution EELS meas. 80−45182
$FeCl_3$-graphite intercalation compound, dielec. function, band struct. EELS study 80−49643
$FeCl_3$-graphite layered compound, lattice modes, Raman spectra 79−95785
$FeCl_3$-intercalated graphite, plasmon spectra 79−38011
$FeCl_4$ on Dowex 1×2, Mossbauer study of Fe complexes and Cl^- soln. effects *(Russian)* 79−19817
$FeCl_4^-$ in organic solvents, dilute, ESR linewidths *(German)* 80−11258
$FeCl_n$, electronic struct., INDO theory 80−42948
$Fe_{1-x}Cl_2$:Cd_x, randomly disordered, tricrit. behaviour, light scatt. 78−68255
Fe_2Cl_4, internal motion, mol. vibr. calcs. 80−106323
Fe_2Cl_6, matrix isolation Raman spectra, mol. config., thermodynamic props. 78−46346
$^{57}Fe_2Cl_6$, matrix isolation Mossbauer spectra, isomer shift, quadrupole splitting 78−42104
$FeCl_5(Br_2)$, polymorphic phase changes of adsorbed NO 77−31900
$FeCl_2(Br_2)(I_2)$, prep. using chem. transport via gas complexes *(German)* 79−15599
$Fe(ClO_4)_2$, frozen aq. soln., Mossbauer spectra, ligand field calc. for $Fe(H_2O)_6^{2+}$ complex 80−39971
$Fe(ClO_4)_3$, soln., struct., X-ray scatt. obs. 78−34421
$Fe(ClO_4)_3$-DMSO, solvation spheres, exchange kinetics, PMR *(French)* 77−58045
$Fe(ClO_4)_2.6H_2O$, paramag., Mossbauer absorpt. in external mag. field, polarisation effects 77−48099
$Fe(ClO_4)_2.6H_2O$, single cryst. polarised opt. spectra 77−48188
$FeCl_2.2D_2O$, magnon-phonon coupling 78−72530
$FeCl_2.2D_2O$, metamagnetic, excitonic Davydov splitting in Raman spectrum 79−33704
$FeCl_2.2H_2O$, also deuterated, electronic transitions in Raman spectra 78−80337
$FeCl_2.2H_2O$, and $FeCl_2.2D_2O$, Raman scatt. at metamagnetic phase transitions, mag. hysteresis 78−14958
$FeCl_2.2H_2O$, antiferromag. metastable state obs. in metamag. transition 77−66314
$FeCl_2.2H_2O$, linear chain metamag. system, phonon and magnon widths 77−36065
$FeCl_2.2H_2O$, magnon-phonon interactions and two-magnon Raman scatt., magnetoelastic waves and selection rules 80−34917
$FeCl_2.2H_2O$, metamagnetic, resonant magnon-optical phonon coupling 79−28773
$FeCl_2.2H_2O$-$CoCl_2.2H_2O$ random mixture, phase diagram 79−73748

iron compounds continued
$FeCl_2.2H_2O$-$CoCl_2.2H_2O$, random mixture with competing spin anisotropies, tetracrit. transition, neutron diffr. obs. 80−2575
$FeCl_2.2H_2O(2D_2O)$, phonons and electronic transitions, Raman spectra 79−28761
$FeCl_2.4H_2O$, antiferromag., Mossbauer exam. 77−16221
$FeCl_2.4H_2O$, finite thickness cryst., Mossbauer spectra evaluation 77−43912
$FeCl_2.4H_2O$, frozen solns., isotope effect of Mossbauer parameters 80−34835
$FeCl_2.4H_2O$, polarisation effects in Mossbauer absorption in external mag. field 78−31137
$FeCl_2.4H_2O$, pressure effects on hyperfine interaction in single crysts. in mag. field 77−16211
$FeCl_2.4H_2O$, proton radiation effects, Mossbauer spectra meas. 77−11603
$FeCl_2.nH_2O$, cryst. struct. *(German)* 80−1987
$1.5Fe_2Cl_6(g)+GdCl_3(s)=GdFe_3Cl_{12}(g)$, entrainment, quenching and chem. transport, rel. to appl. for GdIG CVD 80−24750
$FeCl_2$(pyrazole)$_2$, linear-chain cpd., low-temp. mag. behaviour 80−71253
$Fe_{1-x}Co_xCl_2$, mag. phase diagram 80−11198
$Fe_xCo_{1-x}Cl_2$, metamagnet, mag. phase diagram by mag. induced light scatt. 80−65883
$Fe_{1-x}Co_xCl_2.2H_2O$, random mixture with competing spin anisotropies, tetracrit. behaviour 80−60324
$Fe_{(1-x)}Co_xCl_2.2H_2O$, random mixture of anisotropic antiferromags., isotropic state obs. 78−84396
$Fe_{(1-x)}Co_xCl_2.2H_2O$, antiferromag. random mixture, sp. ht. meas. 79−65678
$FeCoCrO_4$, ^{57}Fe Mossbauer spectra, cation distrib. 80−15879
$FeCoCrO_4$, Mossbauer study, cation distrib. and Neel temp. determ. 79−33571
$FeCoCrO_4$ spinel, elec. resistivity, temp. var. 79−38065
$FeCoF_5.2H_2O$, ferrimag. props., suscept. and transitions, 3-296K 79−87240
$FeCoF_5.7H_2O$, Mossbauer spectra, thermal decomposition products 78−80258
$Fe_{1-x}Co_xGe_2$ solid solns., mag. susceptibilities, multiple stages in mag. transitions, effective mag. moment 77−8286
$FeCo_2O_4$, spinel, cation distrib., Mossbauer spectra meas. 78−31127
$Fe_{0.5}Co_{2.5}O_4$, spinel, cation distrib., Mossbauer spectra meas. 78−31127
$Fe_{3-x}Co_xO_4$, charge transfer, ion distribs., Mossbauer effect 77−20767
$Fe_{3-x}Co_xO_4$, effect of Fe^{2+} content on coercivity instability 79−51820
$Fe_{3-x}Co_xO_4$, Mossbauer spectra, effect of Fe^{2+} conc. 77−69754
$(Fe_{1-x}Co_x)_2P$, magnetisation, susceptibility, thermal expsn. 79−11302
$(Fe_{1-x}Co_x)_3P$, cryst. struct. and mag. props. 78−19222
$Fe_{2-x}Co_xP_{1-y}As$, mag. props., Mossbauer effect 77−40156
$Fe_xCo_{1-x}Rh_2S_4$, spinel struct., X-ray, mag., elec. and Mossbauer spectra meas. 77−12278
$Fe_{0.2}Co_{0.8}S_2$, narrow-band ferromag., high press. effect on anomalous elec. resist. 80−70698
$Fe_{1-x}Co_xSi$ solid solution, semiconductor-metal transition 80−103627
$Fe^{2+}Cr_x^{3+}Al_{2-x}^{3+}O_4^{2-}$, finely divided, oxidation kinetics 80−50848
$(Fe_2Cr_{4-y}Al_y)O_9$, IR spectra, lacunar γ-phase to corundum α-phase transform. 80−108199
$Fe_{1-x}Cr_xBO_3$, magnetisation, 4.2-600K 78−68187
$FeCr_{2-x}In_xSe_4$, struct. and mag. props., comp. depend. 77−66262
$FeCr_2O_4$, $FeAl_2O_4$, solid solns. and oxidation products (lunar spinels), IR spectra 77−81099
$FeCr_2O_4$, Mossbauer spectra and cryst. struct. determ. 79−56637
$FeCr_2O_4$, reduction by C *(Japanese)* 77−48682
$(Fe_{1-x}Cr_x)_2O_3$, Mossbauer exam. of mag. struct. 77−24694
$(Fe_{1-x}Cr_x)_2O_3$, yH_2O crystal growth, characterisation by Mossbauer spectroscopy, mag. meas. and electron microscopy *(French)* 80−80655
$(Fe_{1-y}^{2+}Cr_y^{3+})_2O_3^{2-}$, γ to α transform. elec. cond. study, oxidation initial stage kinetics, lacunar spinel form. 78−92384
$Fe_2(CrO_4)_2\ Cr_2O_7.4H_2O$, synthesis and struct. determ. Patterson and electronic density functions *(French)* 77−27853
$Fe_{2-x}Cr_xO_3$, elec., optical and photocond. props. 79−56262
$Fe_{3-x}Cr_xO_4$, electron transfer and spin density distribs., Mossbauer spectra 79−24243
$Fe_{3-x}Cr_xO_4$, Mossbauer study above Verwey transition 78−43750
$(Fe_{6-y}Cr_y)O_9$, IR spectra, lacunar γ-phase to corundum α-phase transform. 80−108199
$(Fe_xCr_{1-x})_2O_3$ corundum-type solid solution single crystal growth, chem. vapour transport 80−93465
α-$Fe_2(CrO_4)_3.3H_2O$, cryst. struct. *(French)* 78−42960
$Fe_{2-x}Cr_xP_{1-y}As_y$ mag. props., Mossbauer obs. 77−40156
$FeCr_2S_4$, elec. and galvanomag. props. 78−23111
$FeCr_2S_4$, excess entropy terms 79−86905
$FeCr_2S_4$, ferrimag. semicond., elementary step growth on surface of vapour grown cryst. 77−76649
$FeCr_2S_4$, ionic distrib. and band struct., Mossbauer study 80−80646
$FeCr_2S_4$, Mossbauer spectra, second order phase transition 80−20539
$FeCr_2S_4$, normal ferrimag. spinel, NMR studies 2-77K *(Russian)* 79−19785
$FeCr_2S_4$, pure and doped, CVD grown, surface struct., elec. props. and band struct. 79−4905
$FeCr_2S_4$, single crysts., vapour grown, growth of triple unit cell steps on surface 79−19984
$FeCr_2S_4$, vapour grown, step growth by elementary steps and multi-steps 78−27392
$FeCr_2S_4$, vapour grown, growth mechanism of multisteps on surface 78−75605
$FeCr_2S_4$, vapour grown, struct. and stoichiometry, X-ray fluoresc. anal. 79−4263
$Fe_xCr_{3-x}S_4$, x=1, 1.2, specific heats 79−11315
$FeCr_2S_{4-x}Se_x$ chalcospinels, ESR spectrum and paramag. susceptibility 80−15789
$FeCr_2S_{4-x}Se_x$, elec. props. 78−23083
$Fe^{2+}{}_{1+x}Cr_{2-2x}Ti_xO_4$ spinel, low temp. crystallographic transitions 77−15589
$FeCs_2(SO_4)_2.6H_2O:Mn^{2+}$, EPR, 298K, spin-Hamiltonian parameters, cryst. fields 78−27086
$FeCs_2(SO_4)_2.6H_2O:VO^{2+}$, EPR, spin Hamiltonian parameters 79−19771
$Fe_{0.5}Cu_{0.5}Cr_2S_4$, ESR spectra, elec. and mag. props., Curie temp. 80−97137
$Fe_{1-x}Cu_xCr_2S_4$, Hall effect and magnetoresist. 79−78119
$Fe_{1-x}Cu_xCr_2S_4$, mag. semicond., mag. props. and elec. cond. *(Japanese)* 79−47111
$Fe_xCu_{1-x}Cr_2Se_4$, crystallographic and image props. 80−39049

iron compounds continued
$(Fe_{1-x}Cu_x)_2O_3$, yH_2O crystal growth, characterisation by Mossbauer spectroscopy, mag. meas. and electron microscopy *(French)* 80−80655
$Fe_xCu_{1-x}Rh_2S_4$, mag. tetrahedral intrasublattice interaction, X-ray, magnetisation and Mossbauer expts. 78−52241
FeF, electronic states, ab initio calcs., UV spectrum elucidation 78−74570
FeF, electronic states, anal. of rot. struct. 78−74674
FeF_2 (rutile), high press. phase transform. 78−79761
FeF_2, absolute first order Raman polarisabilities 78−64369
FeF_2, amorphous, magnetic props. *(French)* 80−80490
FeF_2 antiferromag., anomalous anti-Stokes/Stokes Raman scatt. intensity ratio 80−66177
FeF_2, antiferromag. reson. relax., multimagnon processes 77−4564
FeF_2, antiferromag. spin flop boundary 78−84419
FeF_2, antiferromagnet, fourth-order spin Hamiltonian terms for Fe^{2+} 78−10628
FeF_2, dielectric properties, IR spectra, lattice dynamics *(French)* 80−76026
FeF_2, EXAFS at high press., bond compressibility, at. spacings 78−39628
FeF_2, electronic and mag. struct., semiempirical MO cluster calcs. 78−62733
FeF_2, electronic struct., charge density and elec. field gradient, MO cluster calc. 77−51704
FeF_2, IR reflectivity spectrum 79−51952
FeF_2, interacting phonon-magnon states, theory of Raman scattering and IR obs. 80−71426
FeF_2, long-wavelength lattice vibr. modes, symmetry coordinates 78−43081
FeF_2, mag. sp. ht. near Neel temp. mag. susceptibility meas. 80−60341
FeF_2, magnon-acoustic phonon hybridisation in far IR absorpt. spectra 78−60271
FeF_2, Mossbauer effect at high press. 80−15858
FeF_2, one-magnon Raman scatt., anomalous behaviour of anti-Stokes-Stokes intensity ratio 80−40115
FeF_2, Raman spectra, cross section determ. 78−56471
FeF_2, theory of Raman scattering, coupled phonon-magnon excitations 78−72531
FeF_2, valence-electron density of states, XPS meas. 77−69963
FeF_2:Co^{2+}, impurity-induced magnon, influence of localisation 80−11182
FeF_2:Mn, antiferromag., NMR relax., impurity bonding 80−66061
FeF_2:Mn, antiferromag. reson. and local magnon mode, FIR laser study 80−66042
FeF_2:Mn, Heisenberg antiferromagnet, impurity thermodynamics, NMR meas. 79−61098
FeF_2:Mn, Heisenberg antiferromag., impurity banding and mag. reson., theory 80−93181
FeF_2:Mn, Heisenberg model, impurity band resonance at 0K, theory 80−66041
FeF_2:Mn, mag. polariton, impurity mode enhancement and superradiance effects 79−28622
FeF_3, amorphous, mag. props. and Mossbauer spectra, speromagnetism and mictomagnetism 80−75778
FeF_3, amorphous, noncryst. magnet with antiferromag. interactions 79−91228
FeF_3, amorphous, struct. and mag. props., computer model 80−96446
FeF_3, antiferromag. Mossbauer spectrum, effect of mag. hyperfine struct. at low temps. 79−28662
FeF_3, antiferromagnetic, press. depend. of effective mag. fields on ^{57}Fe nuclei 78−52383
FeF_3, canted antiferromag., spin echo spectra of ^{57}Fe and ^{19}F nuclei 80−2662
FeF_3 film, elec. cond. mechanisms 79−99649
FeF_3 film, localised electronic states effect on elec. cond., MIM struct. meas. 80−20328
FeF_3 isomer shift, using LCAO form of molecular orbital method 78−62856
FeF_3, L_l and L_η X-ray emission spectra 78−39631
FeF_3, magnetic susceptibility near Neel point 77−55670
FeF_3, muon Coulomb capture ratio 78−62959
FeF_3, overlap contribution to $^{57}Fe^{3+}$ isomer shifts, nuclear size change 80−39903
FeF_3, single crysts., vapour phase chem. transport prep. *(French)* 79−69971
FeF_3, thin film, optical absorpt. meas. 79−15546
FeF_3 thin film, polarisation mechanism, AC and TSC study 80−66104
FeF_3 thin film prep. and charact., *(French)* 78−64470
FeF_3, weak ferromag., NMR of ^{57}Fe nuclei 79−95676
FeF_6, Mossbauer isomer shift const., ab initio SCF calcs. 78−43751
$Fe_2F_5.2H_2O$, ferrimagnetism, susceptibility obs. 5-300K, phase transition 79−4658
$FeF_3.3H_2O$, α and β phase, ^{57}Fe Mossbauer study of local struct. 80−39973
$Fe_2F_5.7H_2O$ and oxidation products, ^{57}Fe Mossbauer study of local struct. 80−39973
$Fe_2F_5.7H_2O$, Mossbauer spectra, thermal decomp. products 78−80258
$Fe_2F_5.7H_2O$, thermal decomp. 77−81394
$Fe^{2+}Fe_{0.2}^{3+}Cr_{1.8}^{3+}O_4$, acoustic props. rel. to cooperative Jahn Teller effect and structural phase transform 80−24538
$(Fe^{2+}Fe_{2-x}^{3+}M_x^{3+})O_4^{2-}$, ($M^{3+}=Cr^{3+}$ or Al^{3+}), elec. cond., Verwey transition temp. *(French)* 79−60878
$(Fe^{2+}Fe_{2-x}^{3+}M_x^{3+})O_4^{2-}$ ($M^{3+}=Al^{3+}$, Cr^{3+}), oxidation to γ lacunar spinels, rate law vs. O_2 press. 80−50849
$Fe_{0.95}^{2+}Fe_{2.05}^{3+}O_4^{2-}$, magnetite, elec. resistivity above 300K 79−78099
$FeGa_2O_4$, magnetic props. by Mossbauer effect, neutron diffr. and magnetisation meas. 77−43918
α-$FeGa_2S_4$, 1T polytype, cryst. struct. refinement *(French)* 80−103304
$FeGa_2Se_4$, elec. cond., mag. susceptibility 80−88301
$FeGe_2$, antiferromag., biquadratic exchange 80−2371
$FeGe_2$ canted antiferromagnet, mag. susceptibility anisotropy and temp. dependence 80−25112
$FeGeO_3$, HP phase transform. 80−19941
$Fe_3Ge_2O_8$, crystal struct. determ. 80−49207
FeH and FeH_2 formation in interstellar clouds 80−98704
FeH, FeD, matrix isolated IR spectra, mol. vibr. 79−93992
FeH, identification in spectra of sunspots and cool stars 78−7952
FeH, identification in S-type stars 79−21280
FeH, partition function and equilib. const. 77−38626
FeH, proposed identification in M dwarfs and S stars 77−45418

iron compounds continued
FeH, wavelengths and line intensities for 4920 Å, 5320 Å and 8690 Å bands 77−10680
FeH^+, valence electronic struct., pseudopot. method 79−68184
FeH_4, electronic structure, ab initio calcs. 79−89601
$Fe_3(HCOO)_6(OH)_2HCOO.4H_2O$, thermal decomp. 78−80741
$Fe(HCOO)_2.2H_2O$, heat capacity 78−22865
$Fe(H_2O)_6^{3+}$, in frozen aqueous soln., Mossbauer spectrum, hyperfine struct. 77−77130
$Fe(H_2O_6)^{3+}$ ion, amorphous frozen soln., Mossbauer study, hyperfine struct. 80−80644
$Fe(H_2)_{6-n}(OSO_3)_n$ complex., form. in $Fe_2(SO_4)_3$ aq. soln., X-ray diffr. 79−32875
$Fe(H_2O)_6SiF_6$, Raman spectra, vibr. modes 79−61369
$Fe(H_2O)_6.SiF_6$, pressure-induced orbital ground state inversion, Mossbauer study 80−39979
$Fe(H_2PO_2)_2$, γ-ray and electron radiolysis, Mossbauer study 80−7816
$FeH_2P_3O_{10}.H_2O$, cryst. struct. determ. *(French)* 77−47418
$Fe^{II}(H_2PO_4)_2.2H_2O$, cryst. and powder diffr. data *(French)* 80−24419
$FeH(SO_4)_2.4H_2O$, cryst. parameters and X-ray powder diffr. data *(French)* 79−14765
FeI boracite single crystals, dielectric, pyroelectric props., vapour phase transport growth 80−80673
FeI, magnon energies, phase transitions of eight sublattice model 77−59463
FeI, self-absorption-free spectral lines for temp. meas. in DC C-arc 80−87965
FeI_2, antiferromag. struct., four spin exchange interaction 78−14948
FeI_2, eight sublattices model, antiferromag. reson. uniform modes and metamag. behaviour 77−69498
FeI_2, far IR antiferromag. reson., two-sublattice model 77−36138
FeI_2, far IR magnetoabsorption, excitation of two spin deviations 78−80339
FeI_2, first order mag. phase transition, neutron scatt. study 80−50090
FeI_2, hyperfine interaction, ^{57}Fe Mossbauer expts., mag. transition obs. 78−43720
FeI_2, magnetic phase transitions, Mossbauer spectra in high mag. fields 80−39936
FeI_2, Mossbauer spectrum, electronic and mag. props. 77−32302
FeI_2, neutron inelastic scatt. from mag. excitations 80−50078
Fe_xI_y cyclodextrin, quasi-one-dimens. cpd., synthesis, elec. and mag. props. 80−2380
Fe_xI_y, vapour phase, UV-visible absorpt. spectra, absorbance peaks 80−994
Fe(II) complexes, high spin-low spin transition, phenomenological thermodynamic model 79−69675
Fe(III) compounds, $A_2FeX_5.H_2O$, (A=alkali ion, X=Cl or Br), antiferromag. props. and struct. 78−31056
Fe(III) Laeme complex, EPR g-value anal. 80−30657
Fe(III) salt soln., hydrolysis products, Mossbauer spectra 80−16671
$Fe_{3-x}In_xO_4$, ferrospinels, cation distrib., Curie point and magnetisation meas. 79−42095
$FeIn_2S_4$, indite, thiospinel, cation ordering in tetrahedral sites, X-ray diffr. meas. 78−95028
$FeK_2(SO_4)_2.6H_2O:Mn^{2+}$, EPR spectra, spin-Hamiltonian anal. 77−77088
Fe_5LiO_8, magneto-crystalline anisotropy, magnetoelectric effect interpretation *(French)* 79−47316
Fe_5LiO_8, magnetoelec. effect interpretation by magneto-cryst. anisotropy *(French)* 79−33515
Fe_5LiO_8, magnetoelectric-effect and magnetisation process 79−1688
$FeLu_2S_4$, structural study, X-ray diffr., Mossbauer spectroscopy 80−107159
$Fe_{1-x}M_xCl_2$, disordered, Mn spin excitations by microwave absorption at high freqs. 80−34759
$Fe_{2-x}M_xO_4$, M=Al,Cr, time dependence of oxidation, elec. cond. obs. *(French)* 77−66710
$FeMO_2S_4$, Mossbauer investigation, Neel point, superparamag. effects 80−97170
$(Fe_{1-x}M_x)_3P$, cryst. struct. and mag. props. 78−19222
$Fe_{2-x}M_xP_{1-y}As_y$, (M=Mn,Fe, Co,Ni), band model of mag. props. 77−40029
$FeMgBO_4$, and $FeMg_2MO_5$, imperfect 1D mag. systems, Mossbauer expts. 80−60466
$FeMgBO_4$, mag. props., spin glass behaviour 79−61145
$FeMg_2BO_5$, mag. props., spin glass behaviour 79−61145
$Fe_{1-p}Mg_pCl_2$, magnetic excitations 78−91852
$Fe_pMg_{1-p}Cl_2$, Ising metamagnet, dilute, tricritical point calcs. 80−50099
$Fe_xMg_{1-x}Cl_2$, metamag. percolation, Ising model calc. 79−28542
$Fe_xMg_{1-x}Cl_2$, metamagnetic transition, magnetooptic exam. of mag. phase diagram 77−63175
$Fe_xMg_{1-x}Cl_2$, metamagnet, mag. phase diagram by mag. induced light scatt. 80−65883
$(Fe_{0.19}^{2+}Mg_{0.56}^{2+}Mn_{0.25})$ $[Fe_{1.87}^{3+}Al_{0.13}^{3+}]O_4^{2-}$, influence of Fe^{2+} ion substitution on electron hopping, Mossbauer study 80−71247
$(Fe_{0.55}^{2+}Mg_{0.32}^{2+}Mn_{0.03}^{2+}Cu_{0.10}^{2+})$ $[Fe_{1.74}^{3+}Al_{0.26}^{3+}]O_4^{2-}$, influence of Fe^{2+} ion substitution on electron hopping, Mossbauer study 80−71247
$Fe_{3-x}Mg_xO_4$, Verwey transition, Mossbauer study 80−39942
$Fe_xMg_{1-x}SO_4.7H_2O$, EFG tensor evaluation, ^{57}Fe single crystal Mossbauer meas. 78−88237
$Fe_{0.55}Mg_{0.47}SiO_3$, orthopyroxene, electron irrad. effects, Mossbauer study 80−40016
$Fe_{0.2}Mg_{1.9}Ti_{0.9}O_4$, Mossbauer parameters temp. depend. 78−23381
$Fe_{0.4}Mg_{1.8}Ti_{0.8}O_4$, Mossbauer parameters temp. depend. 78−23381
$(Fe_{0.5}Mg_{0.5})Ti_2O_5$, armalcolite, stability as function of press. and O_2 fugacity 77−64275
$Fe_{1.2}Mg_{1.4}Ti_{0.4}O_4$, mag. ordering, Mossbauer effect in external mag. fields 80−71257
$Fe_{2(1-y)}Mg_{1+y}Ti_yO_4$ spinel, incomplete mag. ordering, static magnetisation and Mossbauer meas. 77−16056
$Fe_{2(1-y)}Mg_{(1+y)}Ti_yO_4$, Mossbauer spectra anal., model 80−20560
$Fe_{1.4}Mg_{1.3-x}Zn_xTi_{0.3}O_4$ spinel system, X-ray diffraction, Fe Mossbauer effect 80−88900
FeMn hydrated oxides, ferromanganese freshwater nodules, antiferro- to speromag. order 77−70649
FeMn, matrix isolated Mossbauer spectra, ground state determ. 79−45740
$(Fe_xMn_{1-x})_3C$ in steel, X-ray K-absorpt. spectra *(Russian)* 78−6813
$Fe_{1-x}Mn_xCl_2$, disordered, Raman scatt. from Fe^{2+} and Neel temp. 80−60579

iron compounds continued
$Fe_{1-x}Mn_xCl_2$, low-lying electronic excitations in antiferromag. and paramag. phases Raman scatt. study 80−71414
$FeMnGaO_4$, X-ray study of cryst. struct. and ionic config. 78−55851
$(Fe_{1-x}Mn_x)_3P$, cryst. struct. and mag. props. 78−19222
$Fe_{2-x}Mn_xP_{1-y}As_y$, mag. props., Mossbauer obs. 77−40156
$FeMoO_3$, standard Gibbs energies, enthalpies, entropies of formation 78−61042
$FeMoO_4+TeO_2$, solid state reaction 80−108709
Fe_2MoO_4, ^{57}Fe Mossbauer spectra, cation distrib. 80−15879
Fe_2MoO_4, electron exchange between $Fe^{2+}-Fe^{3+}$ ions on tetrahedral and octahedral sites, Mossbauer spectra 79−78585
Fe_2MoO_4, magnetic struct. of low and room temp. by neutron diffr. 77−63100
$Fe_2(MoO_4)_3$, ^{57}Fe Mossbauer effect obs. 77−48108
$Fe_2(MoO_4)_3$, cryst. struct. and twinning behaviour 80−33967
$Fe_2(MoO_4)_3$, paramag. props., 90-800K *(French)* 80−39734
$Fe_2(MoO_4)_3$, polymorphism 77−84691
$Fe_2(MoO_4)_3$, pure and Bi-doped, chem., struct. and catalytic modifications 77−86362
$FeMo_2Re_2S_8$, cubic structure, mixed tetrahedral cluster *(French)* 77−15372
$Fe(Mo_2Re_2)S_8$, synthesis and electrical props. of mixed tetrahedral cluster phases 80−2971
$FeMo_2S_4$, cryst. struct., mag. struct. and props., neutron diffr. meas. *(French)* 77−47971
$FeMo_2S_4$, Mossbauer spectra, 79-300K, Neel pt. determ. 78−60360
$FeMo_3S_4$, triclinic, containing Fe pairs, X-ray cryst. struct. anal. 80−54193
$FeMo_6S_8$, mixed Chevrel phases, crystallography 80−39038
FeN alloy, coercive force, effect of $Fe_{16}N_2$, anisotropic model 77−85501
FeN_2 complexes, electronic configuration calc. using SCCC-LCAO-MO method *(Chinese)* 80−1082
$Fe(N_3)_5^{2-}$, paramag. relax. in trigonal bipyramidal environment, Mossbauer spectra 80−15871
Fe_4N, hard coating preparation by ion beam methods 80−25579
Fe_xN_y, prep. by reactive sputtering, struct. and props. *(Japanese)* 78−92190
$^{57}FeNH_3$, Mossbauer study of iron bonding to solid ammonia and its photofragments 80−15833
$Fe(NH_2)SO_3$, nuclear fuel processing solutions 78−78487
$Fe(N_2H_5)_2(SO_4)_2$:Co, Mossbauer effect and paramag. relax., superparamag. behaviour of correl. spin domains 77−69756
$FeNH_4(SO_4)_2.12H_2O$, Mossbauer study mag. transition in region 0.024-0.029K 79−38417
$Fe(NH_4)_2(SO_4)_2.4H_2O$, rehydration kinetics, Mossbauer effect study 80−61081
$Fe(NH_4)_2(SO_4)_2.6H_2O$, complex with rhombic distortion, spectroscopic props. of high spin Fe^{2+} 77−51861
$Fe(NH_4)_2(SO_4)_2.6H_2O$, Fe^{3+} EPR, tetragonal cryst. field 77−51946
$Fe(NH_4)_2(SO_4)_2.6H_2O$, Mohr salt, elec. field gradient determ., appl. of intensity tensor to thick single cryst. 80−44966
$Fe(NH_4)_2.(SO_4)_2.6H_2O$, $K\beta'$ satellite of $K\beta_1$ X-ray emission line, plasmon oscill. theory 78−23556
$Fe(NO_3)_3$, aq. soln., Fe (III) hydration shells, X-ray diffr. 79−29337
$Fe(NO_3)_3$ conc. aq. solns., and nonahydrate melt, struct., X-ray scatt. investig. 77−31576
$Fe(NO)_3CO$ radical, form. by $Fe(CO)_5$ photolysis in NO soln., EPR spectrum 80−53024
$Fe_2NaBa_6Ge_8O_{24}.4(OH,H_2O)$, growth and struct. 77−65971
$FeNa_6(SO_4)_4$, vanthoffite cryst. struct. lattice parameters and thermal behaviour 77−19929
$FeNb_2O_6$, bonding characterisation 78−38680
$FeNb_2O_6$, flux growth 77−21015
$FeNb_2O_6$, low temp. Mossbauer exam. 79−28659
$FeNb_2O_6$, magnetisation, 1.4-80K, antiferromag. ordering 78−10666
$(Fe_{0.45}Nb_{0.53})O_2$, rutile, cation distrib. and mag. ordering *(German)* 80−107116
$Fe_{0.33}NbS_2$, intercalation compound, struct. and photoemission meas. 77−16453
$Fe_{0.33}NbS_2$, lattice dynamics and hyperfine interactions, Mossbauer spectra study 80−108135
$Fe_{1/3}NbS_2$, intercalate, metallic cond., Hall effect and mag. props. 77−76789
Fe_xNbS_2, ordering of Fe atoms 78−38650
$Fe_{1/4}NbSe_2$, Hall coefficient and resistivity 80−39610
$Fe_{1/4}NbSe_2$, magnetic susceptibility, function of temp. 80−39756
Fe_xNbSe_2 (2H), mag. susceptibility meas., 1.3-300K 80−39740
Fe_xNbSe_2, transport props. and mag. ordering 80−65527
$Fe_xNb_xV_{2-2x}O_4$ complex solid solns., synthesis and phase diagram, semicond.-metal transition temp. 79−43214
$Fe_xNb_xV_{2-2x}O_4$, NMR analysis of semiconductor transitions 78−52367
$Fe(Nb_{1-x}W_x)O_4$, mag. and elec. props. and Mossbauer effect 79−78590
$Fe_{40}Ni_{40}B_{20}$ glass, phase transform. during isochronal annealing 78−14451
$FeNiBO_4$, $FeNi_2BO_5$, Mossbauer spectra, mag. relax. 80−15889
$FeNiBO_4$, mag. and Mossbauer studies 79−65661
$FeNi_2BO_5$, mag. and Mossbauer studies 79−65661
$Fe_{40}Ni_{40}C_{14}P_6$ amorphous film, dislocation and mag. struct., neutron diffr. study 80−70956
$(Fe_{1-x}Ni_x)_2O$, yH_2O crystal growth, characterisation by Mossbauer spectroscopy, mag. meas. and electron microscopy *(French)* 80−80655
$Fe_{3-x}Ni_xO_4$, low temp. Mossbauer spectra, electron transfer and spin density distribution 78−52404
$Fe_{3-x}Ni_xO_4$, Mossbauer spectra, effect of Fe^{2+} conc. 77−69754
$(Fe_{1-x}Ni_x)_2P$, Curie temp., press. depend. meas. 80−97091
$(Fe_{1-x}Ni_x)_3P$, cryst. struct. and mag. props. 78−19222
$Fe_{2-x}Ni_xP_{1-y}As_y$, mag. props. Mossbauer obs. 77−40156
$(Fe_xNi_{1-x})_{80}P_{14}B_6$, amorphous, hyperfine field distrib., ^{57}Fe Mossbauer spectra 79−11367
$FeNi_2S_4$, violarite, mag. and elec. props., struct. determ. 77−43633
$Fe_{0.5}Ni_{0.5}S_2$, hyperfine field at ^{57}Fe, Mossbauer effect *(Japanese)* 77−43916
FeO, absorption spectra, 0.1-6 eV, one electron energy level diagram 78−52487
FeO based pigments, willemite struct., synthesis 80−20855
FeO based slag, thermophysical props., effect of basicity, rate of heating *(Russian)* 77−25009
FeO compacted powder, powder wall friction against WC, effect of wall groove orientation and wall lubricants 78−23831

iron compounds continued
FeO content of Venus, determ. from oxidation state of atmosphere and crust 80−98586
FeO, data base development for phase diagram calc., quasibinary and quasiternary oxide systems 79−96006
FeO, electronic polarisability of ions 77−40175
FeO, electronic struct. calc. 78−43297
FeO, eqn. of state at high press., appl. to Earth core and mantle 80−109122
FeO, Fe_3O_4, identification by ion microprobe analysis *(French)* 77−86408
FeO→Fe_3O_4, in-situ AES using galvanic cells 78−19615
FeO, gas, thermochem. props., mass spectrosc. meas. 80−101034
FeO inhibitor film on Fe, passivation and inhibitor props., X-ray photoemission spectroscopy exam. 78−88561
FeO, interstellar grains, IR absorption features 78−49509
FeO, lattice dynamics, coherent inelastic neutron scatt. 78−59899
FeO, matrix isolated IR spectra, ground state vibr. freqs. 80−28015
FeO, molten, reduction mechanism by solid C 77−48636
FeO, phonon dispersion, extended three-body force shell model 79−90743
FeO, reactions with mullite-corundum refractories in different media 77−24994
FeO, reduction rate by C 77−73468
FeO, self consistent energy band calc. 78−23022
FeO, solubility in NiO at 1273K *(French)* 79−33089
FeO ultrathin homogeneous absorbing films, ellipsometric nucl. microanalysis data analysis, opt. consts. *(French)* 78−11011
FeO, valence band XPS and UPS, LCAO-MO calcs. 80−45197
FeO, vibr. IR spectra, $X(^3\Delta)$ and the ground state 79−63998
FeO, wustite, invariant points between stable and metastable phases, T-P-X diagram *(French)* 80−29938
FeO, wustite, lattice dynamics, inelastic neutron scatt. meas. 77−84867
FeO, wustite, simultaneous solubilities of Na and Ca *(French)* 78−31392
FeO, XPS and UPS 79−91565
FeO^-, UV photoelectron spectra, FeO electron affinity, new ground state assignment, vibr. 77−75212
FeO-aluminosphosphate melt, resistivity, 800-1200°C 77−39903
FeO-Cr_2O_3, melt, exam. of viscosity and self-diffusion 79−95198
FeO-Fe_2O_3, evaporation curve struct. from AC arc electrodes *(Russian)* 78−3051
FeO-Fe_2O_3-SiO_2 -Al_2O_3-$CuO_{0.5}$/Cu slag-metal system, distrib. equilib. of Sn, Se, Te 78−44111
FeO-Fe_2O_3-SiO_2 system, molten, struct. using high temp. X-ray method *(Japanese)* 80−14992
FeO-Fe_2O_3-SiO_2 system, molten, struct. by high temp. X-ray diffr. 80−49084
FeO-Fe_2O_3-SiO_2-Al_2O_3-$CuO_{0.5}$ slag, and Cu, distribution equilibria of Sn, Se, Te 77−51502
FeO-FeS, mag. susceptibility, eutectic phase diagram *(Russian)* 80−15682
FeO-MnO-SiO_2 system, melts, viscosity rel. to temp., composition *(Czech)* 79−19387
FeO-P_2O_5 glass, elec. props. effect of high energy γ-radiation 79−11173
FeO-SiO_2, molten, viscosity and density 78−59965
FeO-SiO_2, molten, X-ray diffr. exam. of struct. 79−46543
FeO-SiO_2 melt, viscosity and polymerisation *(Russian)* 78−26712
FeO-SiO_2 system, high press. phases stability and MO-SiO_2 systems phase diagrams code 79−90779
FeO_2, matrix isolated IR spectra, cyclic complex struct. 77−88449
FeO_4, normal vibr. freqs., force consts. calc. *(Russian)* 77−6759
FeO_4^{2-} ion, electronic struct., hyperfine interactions, SCF Xα calcs. 79−37951
FeO_x, O(1s) XPS energies, oxidised metal surfaces, powders 77−16457
FeO_x, struct. and coalescence of oxide particles, during internal oxidation of Cu-Ti-Fe *(Russian)* 79−90781
FeO_x, work function, high temp. meas. using dynamic condenser 78−64097
FeO_x, wustite field, thermodynamic props. and subphases, thermogravimetry, 1100-1300°C 80−76239
FeO_x-P_2O_5 glass, semicond., dielec. props., thermally stimulated depolarisation meas. 79−95704
FeO_x-valve metal oxide interface, electron injection and reactions 77−76936
$Fe_{0.91}O$, photothreshold changes below mag. ordering temp. 80−97406
$Fe_{0.925}O$, wustite, kinetics of reduction at moderate temps. 79−83154
$Fe_{1-x}O$, IR reflectivity obs. 77−43996
$Fe_{1-x}O$, low-energy mag. excitation dispersion curves 79−4665
$Fe_{1-x}O$ powder, wustite, AES study, ion and electron bombard. effects 80−76114
$Fe_{1-x}O$, precipitation of Fe_3O_4 during decomposition 78−84823
$Fe_{1-x}O$, quenched, decomposition and ordering, electron diffr. and microscopy 77−31635
$Fe_{1-x}O$, single cryst. growth by skull melting 80−84844
$Fe_{1-x}O$, surface struct., XPS study 80−20759
$Fe_{1-x}O$, thermodynamic props. of wustite phase of iron-oxygen system, review 78−79780
$Fe_{1-x}O$, wustite, cryst. dynamics, mag. excitations, neutron scatt. study *(French)* 79−51740
$Fe_{1-x}O$, wustite, crystals of various stoichiometries, growth in arc furnace 80−25545
$Fe_{1-x}O$, wustite, defect struct. 80−107216
$Fe_{1-x}O$, wustite, modulated struct., struct. refinement 79−94966
$Fe_{1-x}O$, wustite, phonon and magnon props., inelastic neutron scatt. 78−52236
$Fe_{1-x}O$, wustite, thermoelec. power coeff. rel. to O_2 press. at high temp. *(French)* 77−76850
$Fe_{1-x}O$, wustite, vacancy and interstitial ion order, equilib. conditions, neutron diffr. obs. *(French)* 78−14336
$Fe_{1-x}O$, wustite, vaporisation, mass spectrometric analysis of gaseous phase 78−48652
$Fe_{1-x}O$, wustite decomposition, coherent magnetite precipitation, electron diffraction study *(Russian)* 80−16318
$Fe_{1-x}O$, wustite disc reduction with CO, 573 to 845°C 78−53253
$Fe_{1-x}O$, wustite phase, surface elec. props. 78−76133
$Fe_{1-x}O$ wustite whiskers form. 79−77972
$Fe_{1-x}O$-ZnO at 900°C, some peculiarities *(French)* 77−70037
$Fe_{1-z}O$, wustite, struct. evolution, mean isotropic thermal agitation factor, depend. on equil. temp. and comp. *(French)* 77−68947
iron compounds continued
$Fe_{1-z}O$, wustite, struct. at high temp., neutron diffr. obs. *(French)* 79−86754
$Fe_{1-z}O$, wustite, struct. at high temp., neutron diffr. *(French)* 80−1982
Fe_2O, for UPS, rel. to 3d photoelectron spectrum of Fe_3O_4 77−1785
α-Fe_2O_3 (haematite), X-ray diffr. compression studies under hydrostatic isothermal conditions 78−85539
Fe_2O_3, absorption spectra, 0.1-6 eV, one electron energy level diagram 78−52487
γ-Fe_2O_3 acicular particles, coercivity, magnetic recording tape appls. 78−14983
γ-Fe_2O_3 acicular particles, coercivity increase by Co ferrite surface crystn. 80−44866
γ-Fe_2O_3 acicular particles, remanent coercive force 80−44872
Fe_2O_3, amorphous, magnetic props. *(French)* 80−80490
Fe_2O_3, amorphous, temp. depend. of hyperfine field, Mossbauer spectroscopy 78−84508
Fe_2O_3 amorphous film, Mossbauer spectra, mag. props. 80−15851
Fe_2O_3 amorphous layer on graphite, Mossbauer spectra, superparamag. props. 80−60474
Fe_2O_3 amorphous RF sputtered thin films, Mossbauer and mag. study 80−34711
Fe_2O_3 amorphous thin films, Mossbauer and magnetisation data 80−34712
α-Fe_2O_3, analysis of car exhaust by Mossbauer spectroscopy 78−92963
α-Fe_2O_3 and α-Fe_2O_3:Mn, linear mag. birefringence near Morin transition 77−52052
α-Fe_2O_3, antiferromag., muon spin rotation meas. 78−48106
α-Fe_2O_3, antiferromag., muon spin rotation *(German)* 80−54877
α-Fe_2O_3, antiferromag., reson. two magnon Raman scatt. obs. 77−63417
α-Fe_2O_3, antiferromag., two magnon reson. Raman scatt. 79−33703
α-Fe_2O_3, antiferromag. reson. in absence of external field, 150 and 320K *(Russian)* 79−4730
Fe_2O_3 based catalysts for NH_3 synthesis, sintering of powders 79−61551
Fe_2O_3 based γ defective spinels, elec. cond. behaviour during transform. to α rhombohedral phases *(French)* 80−49354
α-Fe_2O_3, Bragg diffr. of 14.4 keV reson. γ-quanta in inclined mag. field *(Russian)* 78−2784
α-Fe_2O_3 ceramics, semiconducting, gas sensor for city gas appl. *(Japanese)* 80−61498
γ-Fe_2O_3, clean and SiO_2 coated, reduction temp. influence on coercivities, coercivity factors and rheological props. 79−69698
α−Fe_2O_3 colloids, absorpt. index and colour 79−92009
Fe_2O_3, core and valence level XPS spectra meas. 78−15290
Fe_2O_3, cryst. growth using $K_2S_2O_7$ as flux material 80−71582
α-Fe_2O_3, crystalline grain growth during heat treatment 78−11252
Fe_2O_3 crystallite formation in B_2O_3 and $Na_2O.B_2O_3$ glasses, Mossbauer obs. 78−68429
Fe_2O_3, data base development for phase diagram calc., quasibinary and quasiternary oxide systems 79−96006
γ-Fe_2O_3, densified, rheological and mag. props. 80−44873
Fe_2O_3 deposition on Zircaloy heated surfaces in pressurised boiling water 79−93714
Fe_2O_3, diffusion in gas phase during firing of MgO-Cr_2O_3 bricks *(French)* 78−80495
Fe_2O_3, direct reduction by H_2 reaction kinetics 80−40689
Fe_2O_3, EM and acoustic energy attenuation in domain magnets 80−7140
Fe_2O_3, effect on nitridation of Si powder *(Japanese)* 77−60123
Fe_2O_3, effect on UV absorption of sodium borate glass 77−16340
γ-Fe_2O_3, effects on comp., lattice imperfections and sintering of Ni-Zn ferrites 78−3080
α-Fe_2O_3, elec. resist. and phase transition under shock compression 80−72496
α-Fe_2O_3, electrical conductivity 77−69365
Fe_2O_3, electrochem. doping 77−76430
α-Fe_2O_3 electrode, carrier density determ. by optical absorpt. and photoelectrolysis spectra 80−71462
n-Fe_2O_3 electrodes, characterisation and behaviour in acetonitrile solns. 80−25004
n-Fe_2O_3 electrodes, enhanced photoeffects by electrocatalysis and peroxide effects 80−16815
γ-Fe_2O_3, elongated particles, mag. struct. 78−88096
Fe_2O_3 exam. of mechanism and kinetics of reaction with NiO-ZnO, ferrite formation 80−3309
α-Fe_2O_3, exchange parameters including temp. effects 79−24153
Fe_2O_3, exsolution from iron bearing, TiO_2 79−61597
Fe_2O_3, Fe_3O_4, α-FeOOH, γ-FeOOH, X-ray photoelectron spectra 77−73483
β-Fe_2O_3 film, CVD and characterisation 77−44172
β-Fe_2O_3 film, hyperfine interactions below and above mag. ordering temp., Mossbauer obs. 77−69745
α-Fe_2O_3 film, prep. by reactive condensation and mag. props. 78−64241
Fe_2O_3 film deposition, by reactive sputtering, increased capacity deposition system *(Bulgarian)* 78−60572
Fe_2O_3 films, DC reactively sputtered, for selectively semitransparent photomasks, struct., mech. and chem. props. 80−59835
Fe_2O_3 films, DC reactively sputtered, for selectively semitransparent photomasks, deposition conditions and optical props. 80−60782
γ-Fe_2O_3, fine particles, surface effects on saturation magnetisation 77−69630
Fe_2O_3, flocculated suspension in ethylene glycol, intrinsic viscosity rel. to shear rate 80−1502
α-Fe_2O_3 formation during oxidation of $ZnFe_2O_4$-Fe_3O_4 solid solns. 80−25889
α-Fe_2O_3, H-T phase diagram 79−87258
Fe_2O_3, haematite, anal. of refl. spectrum by Kramers-Kronig relations 80−16058
Fe_2O_3, haematite, annealing of nonequil. defects 79−43283
α-Fe_2O_3, haematite, birefr. under uniaxial stress in mag. field *(Russian)* 78−88285
Fe_2O_3, haematite, dendrite formation from high temp. soln. *(Japanese)* 80−107684
Fe_2O_3, haematite, effect of boiling on the mass transfer of corrosion products in high temperature, high pressure water circuits 80−71766
α-Fe_2O_3, haematite, etch figure shapes on most stable faces *(French)* 77−16707
α-Fe_2O_3, haematite, linear mag. birefr., Morin transition 77−8309
Fe_2O_3, haematite, mag. domain distrib., appl. of mag. Laue neutron diffr. method 78−95455
Fe_2O_3, haematite, mag. field induced phase transition meas. by magneto-optic methods 78−10686

iron compounds continued
α-Fe_2O_3, haematite, mag. susceptibility meas. near Morin temp. 77−59404
α-Fe_2O_3, haematite, mag. susceptibility, near high temp. mag. phase transition 79−56510
α-Fe_2O_3, haematite, magnetic field induced phase transition 78−41337
Fe_2O_3, haematite, Morin transition, Mossbauer expt. using selective excitation method 78−25375
Fe_2O_3, haematite, natural and synthetic samples, thermomag. anal. 77−56622
Fe_2O_3, haematite, needle-like crystal growth during porous metallised Fe pellet re-oxidation 80−35431
Fe_2O_3, haematite, optical indicatrix deform. and rot. during field induced phase transition 78−68482
α-Fe_2O_3, haematite, reduction by H_2, mag. field effect 77−12827
Fe_2O_3, haematite, SHG, acoustic detect. of modulated sound wave *(Russian)* 78−43623
Fe_2O_3, haematite, single domain, defect moment origin and props. 79−16438
α-Fe_2O_3, haematite, substituted, Morin transition, neutron diffr. study 80−54897
α-Fe_2O_3, haematite, temp. mag. hysteresis near Morin temp. 79−56566
Fe_2O_3, haematite, weak ferromag., Hall effect mag. field depend. *(Russian)* 77−11937
Fe_2O_3, haematite, X-ray diffr. of high temp. anomalous behaviour of cryst. lattice 77−58991
Fe_2O_3, haematite nodules with fayalite and Ca ferrite additives, stressed state parameters *(Russian)* 80−45352
Fe_2O_3 haematite platelets, growth and cross-connection in consolidation of haematite pellet *(Chinese)* 80−104186
Fe_2O_3, heat of adsorpt. of pyridine and ethyl pyridine, flow microcalorimetry 78−85193
Fe_2O_3 heat treatment, effect on pulse parameters of $Li_{0.5}Mn_{0.15}Fe_{2.35}O_4$ ferrite cores with rectangular hysteresis loops 80−60370
γ-Fe_2O_3, heats of transition by quantitative thermography 77−9110
α-Fe_2O_3, hematite, field-induced domain struct., neutron diffr. meas. *(German)* 77−16101
α-Fe_2O_3, hematite, high temp. anomalous behaviour of cryst. lattice 77−69087
α-Fe_2O_3, hematite, interdomain phase transition 79−65675
α-Fe_2O_3, hematite, Morin transition, Mossbauer mag. diffr. spectra 80−20562
Fe_2O_3, hematite, reduction, exam. of role of convective mass transfer 78−52724
α-Fe_2O_3, hematite, surface magnetism, magneto-optical meas. 77−20831
α-Fe_2O_3, hematite, weakly ferromag. domain struct., X-ray topography obs. 79−28551
Fe_2O_3, hematite, weakly ferromag., transverse galvanomag. parity effects anisotropy *(Russian)* 80−49770
Fe_2O_3, hematite crystal, press. depend. of elec. resistivity and contacts 79−65476
α-Fe_2O_3, hydrostatic compression, X-ray diffr. meas. 79−99269
Fe_2O_3, hydrothermal crystallisation for mag. appl., review, book contrib. 79−69974
γ-Fe_2O_3, hyperfine mag. field at ^{119}Sn, Mossbauer expt. 80−50232
α-Fe_2O_3, IR lattice vibr. and dielectric dispersion 78−6679
Fe_2O_3, impurity in sintered TiO_2 ceramics, effect on props. 78−35329
α-Fe_2O_3, inclusions in α-Al_2O_3, superparamag. props. 78−48405
α-Fe_2O_3, interpretation of microcrysts. observed on faces (01.2) *(French)* 79−51038
Fe_2O_3, isothermal sintering, surface area reduction 77−8779
Fe_2O_3, $K_{\beta 1}$ X-ray emission line, optical effects 79−91534
Fe_2O_3, L_l and L_η X-ray emission spectra 78−39631
γ-Fe_2O_3, magnetisation distribution in isolated transitions 80−29580
α-Fe_2O_3, magneto-optical meas. of orientation of antiferromag. vector accompanying phase transition *(Russian)* 78−14961
α-Fe_2O_3, magneto-optical near UV reflection-spectra, meridional and polar intensity effects *(Russian)* 78−39572
α-Fe_2O_3, magneto-optical refl. spectra by equatorial Kerr effect *(Russian)* 77−32400
α-Fe_2O_3, magnetoelastic coupling in nonlinear acoustic phenomena, exchange interaction effects *(Russian)* 77−90010
α-Fe_2O_3 microcrystals, surface phonon modes, IR study 80−55089
γ-Fe_2O_3, microstruct. and magnetisation 80−44875
Fe_2O_3, mol. aerosol cluster, sticking probability to solid surface 77−12833
α-Fe_2O_3, Morin transition, Mossbauer spectra meas. 78−31071
α-Fe_2O_3, Mossbauer spectra near Neel temp., critical indices, magnetisation *(Russian)* 80−66094
α-Fe_2O_3, muon spin rotation above and below Morin transition 78−43762
α-Fe_2O_3, muon spin rotation expts. 80−71282
α-Fe_2O_3, muon states, local mag. fields 80−75911
α- Fe_2O_3, mutual orientations and morphology obs. *(French)* 79−37647
α-Fe_2O_3, μSR meas. 79−56666
Fe_2O_3, natural haematite, weakly ferromag., magnetoresist. *(Russian)* 78−23110
α-Fe_2O_3, neutron Laue diffr. investig. of domain distrib. 77−24712
Fe_2O_3, nuclear quadrupole interactions, role of antishielding effects 78−47748
Fe_2O_3, PMMA-metal oxide composite powder, prep. and props. *(Japanese)* 78−95708
Fe_2O_3, paint type coating layer with spherical pigment, radiative transfer theory 80−61405
γ-Fe_2O_3, particle interactions, in inhomogeneous anisotropic magnetic materials, average field effect 77−32217
γ-Fe_2O_3 particles, growing Fe-Co ferrite, coercivity increase 79−56571
γ-Fe_2O_3 particles, mag. props. rel. to mag. tape appl. 80−15762
Fe_2O_3, pelletised, internal stresses, X-ray investigation *(Russian)* 78−19684
α-Fe_2O_3, photochem. props. of sintered and doped samples for solar photoelectrochem. cell appls. 80−89651
Fe_2O_3, plasma sputtered coatings, oxide dissociation, coating props., struct. and composition *(Russian)* 80−54577
Fe_2O_3, plasmochemical synthesis, oxidised from metals, exam. of props. 80−2984
α-Fe_2O_3, polycryst., pure and TiO_2 doped, flatband potentials, donor densities, photocurrent meas. 78−76089
Fe_2O_3, porous deposit, effect on impurity transfer in steam-generating pipe 78−38398

iron compounds continued
Fe_2O_3, powder, compression in moulds, meas. apparatus *(Dutch)* 77−44205
Fe_2O_3 powder, heat of adsorpt. of stearic acid, surface area meas., flow microcalorimetry 78−81974
α-Fe_2O_3 powder, hematite, AES study, ion and electron bombard. effects 80−76114
Fe_2O_3, powder, preparation conditions rel. to morphology 77−8777
γ-Fe_2O_3 powder filled polymer films, packing and particle orientation *(Japanese)* 80−104115
γ-Fe_2O_3 powders, influence of densification on mag. props. 78−95481
γ-Fe_2O_3 powders, mag. props., effect of Co plating 79−69699
α-Fe_2O_3, precipitation in $Ni_{2/3}Fe_{7/3}O_4$ *(French)* 80−11650
α-Fe_2O_3, prep. by evaporative decomposition of $Fe(NO_3)_3.6H_2O$ soln. 79−20011
γ-Fe_2O_3, prep. from thermal decomp. of $[Fe_3(HCOO)_6(OH)_2]HCOO.4H_2O$ and characterisation 78−80741
α-Fe_2O_3, prod. by α-FeOOH dehydration, mosaic struct. and twin form. 79−86802
α-Fe_2O_3, pure and Mn doped, charact. of Morin phase transition, linear mag. birefringence meas. 77−69560
α-Fe_2O_3, pure and TiO_2 doped, electrode, photooxidation of H_2O appl. 78−76886
Fe_2O_3 reaction with NiO, ZnO, and (Ni,Zn)O solid soln., microstruct. 79−87834
γ-Fe_2O_3 recording tapes, orientation, Mossbauer, X-ray and electron microscope meas. 77−16219
Fe_2O_3, reduction, double reaction, reaction kinetics exam., expt. verification *(French)* 78−31705
Fe_2O_3, reduction by H_2, kinetics and mechanism 77−48619
Fe_2O_3, reduction rate by C 77−73468
α-Fe_2O_3, reduction to active magnetite and direct air oxidation to α-Fe_3O_4 *(German)* 78−7060
γ-Fe_2O_3, sat. moment *(French)* 77−85431
Fe_2O_3, semicond. anode in aq. electrolyte, electrolum. and electrochem. 80−76080
Fe_2O_3 semiconductor electrodes, photoassisted electrolysis of water 77−77771
Fe_2O_3, semisintered, shear strength at high press. 80−76308
Fe_2O_3, shocked hematite, Mossbauer exam. 78−64304
α-Fe_2O_3, single cryst., hematite, X-ray topographic obs. of domain struct. changes in external mag. field 80−88785
γ-Fe_2O_3, single mag. particle, remanent coercive force and remanent loop meas. 78−95480
α-Fe_2O_3, single particle material for tape and disc manufacture, prep., props., and appls. 78−52308
n-Fe_2O_3, sintered and flame-oxidised, photoelectrochemical props. 79−70355
Fe_2O_3, sintered semicond. electrode, photoeffects 79−51669
γ-Fe_2O_3, small particle composite, preparation methods, superparamagnetism, optical transparency 78−60315
γ-Fe_2O_3 small particles, hyperfine field below superparamag. blocking temp., Mossbauer obs. 78−19392
γ-Fe_2O_3 small particles, noncollinearity as crystallite-size effect, Mossbauer study 80−39939
γ-Fe_2O_3, small particles, vacancy sintering 77−65975
α-Fe_2O_3, solubility in BeO, Al_2O_3 and synthetic chrysoberyl Mossbauer studies 77−7867
Fe_2O_3 sputtered films, optical transmission and reflection spectra depend. on substrate temp. 79−91517
γ-Fe_2O_3, struct. vacancy distrib., effect on $\gamma \rightarrow \alpha$ transform. heat 78−6051
α-Fe_2O_3, superparamagnetism, magnetisation vector diffusion coeff., anisotropy energy, vol. distrib. of particles by Mossbauer effect 78−48099
α-Fe_2O_3, surface struct., adsorptive interactions rel. to rusting process, IR spectra 79−34363
Fe_2O_3 thin films, reactively sputtered, mechanical stresses rel. to deposition conditions 80−80146
γFe_2O_3, transform. to α-phase, effect of preliminary pressing or vibromilling 78−84798
Fe_2O_3, transformation to Fe_3O_4 in oxide scales on steel, conversion kinetics 80−7561
Fe_2O_3, twinning dislocations, electron microscopy obs. 79−99218
Fe_2O_3 ultrafine particles in PTFE matrix, EPR and Mossbauer study 80−100625
Fe_2O_3, ultrafine powders, prod. by cryochemical, freeze drying, spray drying or soln. techniques 80−55336
γ-Fe_2O_3, vibro-milled, energy storage and liberation 78−83941
Fe_2O_3 X-ray absorpt., heat treatment effects, chem. and struct. interpretation 80−84806
Fe_2O_3, X-ray absorpt. spectra, effective co-ordination charges 80−84805
α-Fe_2O_3, X-ray diffr. exam. at phase transition from weakly ferromag. to pure antiferromag. state 77−51904
Fe_2O_3, X-ray diffr. studies, crystallite size, phase transformation 77−21138
Fe_2O_3, XPS and UPS 79−91565
α-Fe_2O_3:Al, hematite, spin reorientation, Mossbauer spectra obs. 78−72356
α-Fe_2O_3:Al^{3+}(Ga^{3+})(Cr^{3+})(In^{3+}), substitution effect on Morin transition, neutron diffr. study 80−44827
γ-Fe_2O_3:Co, impact-induced demagnetisation, magnetostriction and coercive force, appl. in mag. recording 77−16111
γ-Fe_2O_3:Co acicular powder epitaxially doped, coercivity increase, surface anisotropy *(Chinese)* 80−7130
γ- Fe_2O_3:Co powder, increased coercivity by epitaxial doping 79−82833
γ-Fe_2O_3:Cr, pure and doped, acicular particle suspensions, mag. props., optical meas. 80−44874
γ-Fe_2O_3:Fe_3O_4, magnetite impurity determ. by C_p calorimetry 78−2152
Fe_2O_3:Mn, surface props. 79−65302
α-Fe_2O_3:Sn, Mossbauer investig. of mag. hyperfine interactions 77−32306
α-Fe_2O_3:Sn^{4+}, antiferromag. reson. *(Russian)* 80−7175
α-Fe_2O_3:TiO_2 electrode, water photooxidation appl. 78−15684
Fe_2O_3/Fe_3O_4 transformation matrices, higher-order orientation relationships 80−100846
xFe_2O_3-(1−x)PbO-3B_2O_3 glass, Mossbauer study of Fe cations 79−91325
Fe_2O_3-Al_2O_3, solid solns., effect on Fe on point of zero charge 78−61021
Fe_2O_3-Al_2O_3 mixed oxide, X-ray diffr. and elec. cond. 80−79954
Fe_2O_3-B_2O_3-PbO glass, semicond., elec. resist. meas. 78−95300

iron compounds continued
- Fe_2O_3-$B2O_3$-PbO glasses, visible and UV optical props. *(Rumanian)* 78−48196
- Fe_2O_3-BaO-B_2O_3, magnetic props. of Fe-rich amorphous oxide *(French)* 80−80511
- Fe_2O_3-BaO-B_2O_3 glass, Mossbauer spectra, ^{57}Fe hyperfine interactions 80−39969
- Fe_2O_3-Bi_2O_3 sintered material, elec. switching effects for temp. range 700-850°C *(Korean)* 80−70775
- Fe_2O_3-Bi_2O_3 system, mag. props., hyperfine parameters, Mossbauer spectrum 77−69746
- α-Fe_2O_3-Cr_2O_3 solid solution, Mossbauer effect studies 80−71249
- Fe_2O_3-Dy_2O_3-Na_2O-B_2O_3 glass, AC mag. susceptibility, antiferromag. interactions 77−32179
- Fe_2O_3-Fe composite mixture, preferential sputtering, XPS expts. 79−87544
- γ- Fe_2O_3-Fe_3O_4, lodestone, microstructure and mag. props., source of mag. hardening 79−82828
- Fe_2O_3-Fe_3O_4 equilibrium in BaO-B_2O_3 melt, ferrite prep. 77−36428
- Fe_2O_3-FeO, sinter, heating and reduction effect of phase transform. and fracture *(Russian)* 78−15375
- Fe_2O_3-FeO, sintered and pellets, reduction in H_2 *(Russian)* 78−15705
- Fe_2O_3-H_2, interaction with surface, quantum chemical study 80−45549
- Fe_2O_3-martensitic steel, mag. and dielec. emulsion, prep. by abrasion of steel surface 78−27826
- Fe_2O_3-MgO-NiO, tie-lines between solid solns. of oxide and spinel at 1273K *(French)* 79−100124
- Fe_2O_3-MoO_3, on SiO_2 and Al_2O_3, Mossbauer effect 79−47365
- Fe_2O_3-Na_2O-BaO glass, mag. props. 4.2-295K, mictomagnetism *(French)* 80−39782
- Fe_2O_3-NiO-Na_2O-Li_2O-B_2O_3-SiO_2 glass, EPR meas. of exchange interactions 77−32243
- γ-Fe_2O_3-organic interfaces, mag. struct., Mossbauer effect, IR absorpt., and magnetisation meas. 80−44869
- Fe_2O_3-P_2O_5 system, vitreous, struct. obs. using neutron scatt. 78−22667
- Fe_2O_3-PbO-B_2O_3 glass, X-ray and electron microscope studies, mag. and Mossbauer effect meas. 80−28919
- Fe_2O_3-PbO-V_2O_5 fluxed melt system, solubility and relative supersaturation meas. 80−64934
- Fe_2O_3-TeO_2 system, mag. props. 78−27020
- Fe_2O_3-TiO_2 system, high temp. intergrowth struct., metal-atom ordering in intergrowth boundaries 78−79573
- Fe_2O_3-V_2O_5 system, elec. transport 79−51576
- Fe_2O_3-WO_3, phase relations 78−92249
- α-Fe_2O_3+CaO, additive in ZrO_2 sintering 78−76617
- Fe_2O_3+MoO_3 coreduction kinetics, thermodynamic equilib. in Mo-Fe-O-H system 78−60657
- α-Fe_2O_{3-x}, nonstoichiometry effect 77−47583
- $(Fe_2O_3)_x$-$(3B_2O_3.PbO)_{1-x}$ glass, thermal cond. and diffusivity obs. 79−60561
- Fe_2O_4, suspension in oil, motion in rotating mag. field *(German)* 77−75983
- Fe_2O_y, powder sintering, surface area reduction, exam. 78−44039
- $Fe_{3-\Delta}O_4$, mag. aftereffects near Verwey temp. 79−87294
- $Fe_{3-x}O_4$, vacancy diffusion from relax. of deviations from stoichiometry 79−23769
- Fe_3O_4, 3d-photoelectron spectrum, final state effects, compared with Fe_xO 77−69964
- Fe_3O_4 (magnetite), mag. susceptibility under hydrostatic press. and implications for tectonomagnetism 80−26504
- Fe_3O_4 (magnetite), multidomain particles magnetisation 79−66686
- Fe_3O_4 (magnetite), piezomag. response depth depend. rel. to tectonomagnetism as earthquake precursor 80−26465
- Fe_3O_4, absorption spectra, 0.1-6 eV, one electron energy level diagram 78−52487
- Fe_3O_4, adsorption of Cs, meas. of contamination using washing test 78−62597
- Fe_3O_4 and $Fe_{3-x}Ti_xO_4$, IR transmission spectra changes at Verwey temp. 77−85714
- Fe_3O_4, anomalous sp. ht. obs. at 10K 77−85454
- Fe_3O_4 aqueous mag. fluids, dilution-stable, prep. by extended peptization techniques 80−60373
- Fe_3O_4 briquettes, porous, struct. changes during reduction 77−21064
- Fe_3O_4, Co modified, synthesis with autoclave in H_2 atm. 80−35117
- Fe_3O_4, core and valence level XPS spectra meas. 78−15290
- Fe_3O_4, Coulomb gap and hopping cond., effects on thermopower and Verwey ordering 80−44583
- Fe_3O_4, crit. exponents meas. by polarized neutron scatt. 80−44828
- Fe_3O_4, dielec. function and polar Kerr rotation, 0.5-3.6 eV 80−66221
- Fe_3O_4, dielec. props. of low temp. phase, at microwave freq. 78−64309
- Fe_3O_4, doped, electron correls. above and below Verwey transition, Green function theory 77−51687
- Fe_3O_4, effect of Al ion on formation and structure *(Japanese)* 77−59727
- Fe_3O_4, electron energy band theory, thermodynamic functions *(Korean)* 79−7785
- Fe_3O_4, electronic struct. and charge density oscills. near Verwey transition, Mossbauer expt. 78−27150
- Fe_3O_4, FeO, effect of mag. field on reduction rates 77−44461
- Fe_3O_4 ferrofluid, mag. birefringence, estimation of particle size 79−33511
- Fe_3O_4 ferrofluid suspension, mag. props., stability 79−87293
- Fe_3O_4 ferrofluids, spin glass behaviour 80−71120
- Fe_3O_4, ferromag. ferroelectrics *(Japanese)* 79−65804
- Fe_3O_4 film, prep. by reactive condensation and mag. props. 78−64241
- Fe_3O_4 film, quantitative sputter rates, AES, ellipsometry determ. 78−72661
- Fe_3O_4, film formed in caustic electrolyte, deform. 77−25181
- Fe_3O_4 film prep. and form. by Fe naphthenate thermal decomposition *(Japanese)* 77−32519
- Fe_3O_4, finely dispersed, electronic phase transition, cond. and DTA meas. 78−91736
- Fe_3O_4, finely dispersed powder, volt-ampere characts. *(Russian)* 77−62967
- Fe_3O_4, hopping conduction and the Coulomb gap 80−44605
- Fe_3O_4, hydrothermal growth in Au capsule in presence of H_2 77−1793
- Fe_3O_4, hyperfine field temp. depend., Mossbauer meas. near Verwey transition 77−69749
- Fe_3O_4, hyperfine fields and spin densities below 20K 78−52405
- Fe_3O_4, hyperfine mag. field at ^{119}Sn, Mossbauer expt. 80−50232
- Fe_3O_4, IR refl., ATR, Voigt and Faraday expts. 80−66180

iron compounds continued
- Fe_3O_4, identification by ion microprobe analysis *(French)* 77−86408
- Fe_3O_4 in kerosene, thermal and electrical cond. in mag. field *(Russian)* 78−6188
- Fe_3O_4 in suspension, ferromagnetic colloid, optical meas. 78−10906
- Fe_3O_4 interstellar grains, stellar light circular polarisation, two-cloud model 77−78838
- Fe_3O_4, inverse spinel ferrite, spontaneous magnetisation, mag. field theory 80−25104
- Fe_3O_4, lattice parameters, NMR freqs., and magnetoelec. pots. near 12K 80−71146
- Fe_3O_4, low temp. phase, Mossbauer spectra *(Japanese)* 77−43917
- Fe_3O_4, low temp. phase, sp. ht. and elec. cond. 77−59308
- Fe_3O_4, low temp. phase 77−69751
- Fe_3O_4, low temp. phase ionic ordering, NMR *(Russian)* 78−23354
- Fe_3O_4, low temp. sintering 78−92221
- Fe_3O_4, mag. crit. scatt., neutron spectroscopy 77−20614
- Fe_3O_4 mag. fluid particles, comp., struct., and mag. props. 80−60374
- Fe_3O_4, mag. ink, prep. 77−9128
- Fe_3O_4, mag. relax., permeability and loss tangent determ. at 4.2 to 300K 77−32263
- Fe_3O_4, magnetic after-effect by valency fluctuations assoc. with cond. transition 77−8365
- Fe_3O_4, magnetically biased, linear and bilinear magnetoelec. susceptibility, 4.2K 77−40106
- Fe_3O_4, magnetite, ARM, TRM and magnetic interactions: concentration dependence 79−44177
- Fe_3O_4, magnetite, and related Jente spinels, mag. crit. point behaviour 80−60342
- Fe_3O_4, magnetite, anomalous electrical conductivity, press. effects 79−56222
- Fe_3O_4, magnetite, cation diffusion, correlation and isotope effects 80−96686
- Fe_3O_4, magnetite, change in state due to applied mag. fields obs. in magnetoresistance meas. 77−43623
- Fe_3O_4, magnetite, charge order-disorder and metal-insulator transition 77−20241
- Fe_3O_4, magnetite, charge carriers, optical props. 80−34874
- Fe_3O_4, magnetite, comparison of anhysteretic remanence and thermoremanence 77−5191
- Fe_3O_4, magnetite, Compton profile, 100 and 300K 78−35219
- Fe_3O_4, magnetite, defect content, gas-phase comp. effects 77−43336
- Fe_3O_4, magnetite, diffusion of Cr, as function of O partial press. 78−43183
- Fe_3O_4, magnetite, electronic cond. mechanisms, review 77−20314
- Fe_3O_4, magnetite, electronic struct. at low temps., NMR anal. 78−67686
- Fe_3O_4, magnetite, ferrimag. reson. at 9.3 GHz near Verwey temp., g-factors *(French)* 78−91959
- Fe_3O_4, magnetite, final-state effects in 3d photoelectron spectra 77−1785
- Fe_3O_4, magnetite, grain size limits for pseudosingle domain behaviour, rel. to palaeomagnetism 80−11215
- Fe_3O_4, magnetite, hydrothermal crystal growth 80−66411
- Fe_3O_4, magnetite, identification in freshwater magnetotactic bacteria, Mossbauer obs. 80−3657
- Fe_3O_4, magnetite, isothermal compression up to 70 kbar under hydrostatic conditions 78−30698
- Fe_3O_4, magnetite, linear electric field effects in mag. anisotropy and ferromag. reson. 80−65854
- Fe_3O_4, magnetite, low temp. phase, magnetocryst. anisotropy 77−20584
- Fe_3O_4, magnetite, low temp. phase transition, magneto-optical exam. 78−27193
- Fe_3O_4 magnetite, low temp. phase transition, diffuse electron scattering *(Japanese)* 80−24591
- Fe_3O_4, magnetite, mag. aftereffect meas. 79−82834
- Fe_3O_4, magnetite, mag. aftereffects, 4.35K 80−80571
- Fe_3O_4, magnetite, magnetoelec. effect at 77K and cryst. symm. 80−29593
- Fe_3O_4, magnetite, magnetoelec. effect at 77K, elec. field depend. of mag. anisotropy 80−29594
- Fe_3O_4, magnetite, magnetoelec. effect temp. depend. obs. by mag. field rot. in a-c plane at 10K 80−71145
- Fe_3O_4, magnetite, magnetoresist., applied mag. field effects 80−80301
- Fe_3O_4, magnetite, Mossbauer spectra of Fe^{2+} 79−91319
- Fe_3O_4, magnetite, Mossbauer spectra of low temp. phase 80−20541
- Fe_3O_4, magnetite, nonstoichiometry, depend. on prep. conditions *(German)* 78−3081
- Fe_3O_4, magnetite, optical props. in IR 80−97271
- Fe_3O_4, magnetite, oxidation kinetics, influence of cryst. size 78−79778
- Fe_3O_4, magnetite, oxidation rate anomaly at Curie temp. 79−96298
- Fe_3O_4, magnetite, oxidation mechanism during roasting of nodules *(Russian)* 80−40567
- Fe_3O_4, magnetite, phase transition, X-ray diffr. meas. 80−15238
- Fe_3O_4, magnetite, polarisation screening effect on charge ordering, pure ionic model 78−6272
- Fe_3O_4, magnetite, polycryst., X-ray struct. anal. *(German)* 77−72598
- Fe_3O_4, magnetite, precip. with urea, prep. and props. 80−20854
- Fe_3O_4, magnetite, reduced A-site moments, polarised neutron study 79−47253
- Fe_3O_4, magnetite, suspension analysis using magnetovibr. analyser 78−4668
- Fe_3O_4, magnetite, valence instabilities, Mossbauer effect 80−20543
- Fe_3O_4, magnetite, vaporisation, mass spectrometric analysis of gaseous phase 78−48652
- Fe_3O_4, magnetite, Verweg transition temp., isotope effect, elec. resist. and DTA meas. 80−24976
- Fe_3O_4, magnetite, X-ray diffr. investig. of low temp. phase symm. 77−15364
- Fe_3O_4, magnetite crysts., skull melter growth 79−24430
- Fe_3O_4, magnetite film, coercive force and lattice const. 78−2707
- Fe_3O_4, magnetite Mossbauer spectra, mag. dipolar and elec. quadrupole effects 80−20544
- Fe_3O_4, magnetite nodules with fayalite additives, stressed state parameters *(Russian)* 80−45352
- Fe_3O_4, magnetite particles, interaction fields effect on hysteretic props. 80−54921
- Fe_3O_4, magneto-electric effect temp. depend. at 10K 79−78498
- Fe_3O_4, magneto-optical refl. spectra by equatorial Kerr effect *(Russian)* 77−32400
- Fe_3O_4, magnetocrystalline anisotropy, anomolies in magnetostriction and elastic constants 80−60244

iron compounds continued
Fe_3O_4, magnetoelastic coupling effect on anisotropy below transition temp. 77−69657
Fe_3O_4, magnetoelastic props. *(Japanese)* 78−23316
Fe_3O_4, magnetoelectric effects from electric field depend. macroscopic mag. anisotropy energy 77−69656
Fe_3O_4, metallic phase, photocond. and mag. permeab., photoinduced changes 80−15566
Fe_3O_4, molten, rate of dissolution of zircon, porosity effects *(Japanese)* 77−11699
Fe_3O_4, monoclinic phase, saturation magnetisation near Verwey temp. 77−77038
Fe_3O_4, Mossbauer linewidth of octahedral Fe 77−66446
Fe_3O_4, Mossbauer spectra at 80K, Fe electronic states and hyperfine interactions *(Russian)* 78−43696
Fe_3O_4, Mossbauer spectra above Verwey transition 78−68415
Fe_3O_4, multistage phonon softening in Verwey transition region, Mossbauer spectra 77−72670
Fe_3O_4, muon states, local mag. fields 80−75911
Fe_3O_4, NMR exam. of low temp. phase 78−56401
Fe_3O_4, NMR of low temp. phase, electron ordering anal. 78−56402
Fe_3O_4, neutron diffuse scatt. due to mol. polarons 80−15460
Fe_3O_4, neutron diffuse scatt. due to molecular polarons 80−88488
Fe_3O_4, nuclear gamma reson. investig. of high temp. electronic struct. 77−20751
Fe_3O_4, optical cond. anisotropy calcs. below Verwey transition 80−50289
Fe_3O_4, optical props. in spectral range 0.03 to 12 eV 79−51977
Fe_3O_4, orientation on α-Fe_2O_3 after low-temp. reduction, X-ray texture analysis *(French)* 77−39738
Fe_3O_4, partial thermal dissociation in air, using solar concentrator *(French)* 79−20015
Fe_3O_4 particle suspensions in non-conducting and metallic liqs., review 80−60372
Fe_3O_4 particles, entrapped in drug carrying microsphere, intravascular mag. guidance method 78−73188
Fe_3O_4 particles, nonstoichiometric, morphology and enhanced coercivity, Mossbauer meas. 80−7132
Fe_3O_4, photocond. 70-130K, temp. range including metal-semicond. transition *(Russian)* 78−56178
Fe_3O_4, polar Kerr effect invisible and near IR spectral regions 80−108187
Fe_3O_4, porous deposit, effect on impurity transfer in steam-generating pipe 78−38398
Fe_3O_4 powder, magnetite, AES study, ion and electron bombard. effects 80−76114
Fe_3O_4 powder, oxidation to γ-Fe_2O_3, coercivity changes 80−44864
Fe_3O_4 powder, used for prod. of Fe, Fe alloy sintered compacts *(Slovak)* 79−15626
Fe_3O_4, precipitation in YIG 78−84815
Fe_3O_4, reduction, double reaction, reaction kinetics exam., expt. verification *(French)* 78−31705
Fe_3O_4, relax effects, Mossbauer expt. using selective excitation method 78−25375
Fe_3O_4, SCF X_α calcs. of one-electron energy levels 78−47727
Fe_3O_4, selective excitation double Mossbauer exam. of electron hopping 77−69750
Fe_3O_4 single cryst., Mossbauer γ-ray diffr. 77−84600
Fe_3O_4, single cryst., surface magnetism, spin polarized photoemission 78−52622
Fe_3O_4, single cryst. growth by melt transport in DC arc 77−8745
Fe_3O_4 solar absorber surface spectral selectivity rel. to temp. and UV ageing 79−62027
Fe_3O_4, solubility in H_2 saturated LiOH soln., meas. 150 to 300°C 77−60179
Fe_3O_4, spherulitic film growth, elec. and mag. props. 78−68627
Fe_3O_4, spin polarised photoemission, surface magnetism 79−52083
Fe_3O_4, standard free energy of formation, by EMF method with solid oxide electrolyte at low temps. *(Japanese)* 80−88338
Fe_3O_4, substituted magnetite, oxidation kinetics 77−1889
Fe_3O_4, substituted magnetite, correl. between IR spectra, X-ray diffr., and struct. vacancy distrib. 80−84753
Fe_3O_4, superexchange interactions, three-sublattice anal. 79−61095
Fe_3O_4, suspensions, ferrofluid motion, rot. mag. field effects 77−950
Fe_3O_4, tetrahedral-site Fe^{3+} ion, spin-transfer due to covalency 79−15285
Fe_3O_4, typical spontaneous symmetry breakdown in solid state 80−34737
Fe_3O_4, ultrafine particles in ferrofluid, superparamag. and ferromag. reson. 78−15026
Fe_3O_4, ultrafine powders, prod. by cryochemical, freeze drying, spray drying or soln. techniques 80−55336
Fe_3O_4, Verwey transition, electron-phonon versus Coulomb interaction effects 80−39280
Fe_3O_4, Verwey transition, charge density-phonon condensation 80−65217
Fe_3O_4, Verwey transition, cond. processes 80−96787
Fe_3O_4, Verwey transition as potentially incommensurate but eventually commensurate phase transition 79−95120
Fe_3O_4, X-ray absorpt. spectra, effective co-ordination charges 80−84805
Fe_3O_4, XPS and UPS 79−91565
Fe_3O_4:^{119}Sn, hyperfine field exam., Mossbauer meas. 77−69753
Fe_3O_4:^{119}Sn, magnetic interactions, Mossbauer spectra 79−15301
Fe_3O_4:Cd^{2+} (Zn^{2+}), Verwey transition 80−6513
Fe_3O_4:Co, impact-induced demagnetisation, magnetostriction and coercive force, appl. in mag. recording 77−16111
Fe_3O_4:Sn, hyperfine field temp. depend., Mossbauer meas. near Verwey transition 77−69749
Fe_3O_4:Zn, and pure, influence of mag. order on charge delocalisation, Mossbauer spectra 78−68423
$Fe_3O_4/\gamma Fe_2O_3$ surface layers formed on small Fe particles, Mossbauer expts. 79−8081
Fe_3O_4-Co_3O_4 spinels, phase diagram anal., thermodynamic props. 80−3009
Fe_3O_4-Cr_2O_3-Ni_2O mixture, reduction by gases heated by electric arc discharge *(Russian)* 78−15704
Fe_3O_4-$Fe_{2.8}Ti_{0.2}O_4$, interdiffusion expts. 78−55991
Fe_3O_4-Fe_2O_3, two phase film form. during Fe anodisation 77−16737
Fe_3O_4-Fe_2O_3 thin film on passivated Fe, electron diffr. study *(German, English)* 80−89418
Fe_3O_4-$FeAl_2O_4$ spinels, Fe^{59} diffusion 80−59721
Fe_3O_4-$FeAl_2O_4$-$FeTiO_3$ titaniferous magnetite, chlorination, 1273 to 2273K 80−55752

iron compounds continued
Fe_3O_4-$FeTiO_4$ solid soln. spinels, domain wall formation inhibition, effect on bulk mag. props. 80−11220
Fe_3O_4-$NiFe_2O_4$, solid soln., activities determ. from EMF of galvanic cell 80−16290
Fe_3O_4-$ZnFe_2O_4$, spinel type solid soln., thermodynamic study by EMF meas. 78−15379
Fe_3O_6, O_2 annealed, optical absorpt., spin struct., polaronic absorpt., cryst. field transitions 78−68493
Fe_xO, antiferromag., surface magnetism probe by photoelec. currents 77−73214
Fe_xO, core and valence level XPS spectra meas. 78−15290
Fe_xO, standard free energy of formation, by EMF method with solid oxide electrolyte at low temps. *(Japanese)* 80−88338
Fe_xO, wustite, subphases in range of stoichiometry, comments and reply 77−47585
Fe_xO, wustite, width of d-level final-state struct. obs. in XPS 78−19633
Fe_xO, X-ray absorpt. spectra, effective co-ordination charges 80−84805
Fe_xO_x, passivation, semicond. model for oxide film 80−2493
Fe_xO_y, adsorption of H_2O, oxidation and reduction effects on adsorption 78−43237
Fe_xO_y, and $Fe_x(OH)_y$ surfaces, chem. changes induced by Ar^+ bombardment, XPS obs. 79−83084
Fe_xO_y, colloid prep., thermal decomposition of metal chelates 80−71953
Fe_xO_y crystal dissolution, electrical potential effect, review 79−46809
Fe_xO_y electrodes, photoassisted electrolysis of water 78−15683
Fe_xO_y epitaxial film, ferromag. reson. 77−51964
Fe_xO_y film, thermally evaporated, contamination effects obs. 80−49545
Fe_xO_y films, electron microscopy and energy-loss spectroscopy 80−80137
Fe_xO_y, passivity, electrochem. exam. *(Japanese)* 78−39946
Fe_xO_y phase comp. on equilib. heating to 3300K *(Russian)* 80−16285
Fe_xO_y powder coated with $NaPO_3$, anomalous coercivity increase 77−89980
Fe_xO_y, prep. by reactive sputtering, struct. and props. *(Japanese)* 78−92190
Fe_xO_y, sintered metallised compacts, pore struct. by Hg porosimetry 80−40280
Fe_xO_y thermal oxide film on Fe, capacitance, temp. and freq. depend., in aq. electrolyte soln. 80−54776
Fe_xO_y-coated n-Si heterostruct. photoanode for photoelectrolysis of water 80−61384
Fe_zO, non-stoichiometric, mag. struct., neutron diffr. exam. 79−42737
FeOCl, cathodic reduction in organic electrolytes, intercalation complex production 79−1833
FeOCl intercalation cpds. with Li and amines, cryst. struct. 78−51512
FeOCl, Mossbauer spectra, lattice dynamics, hyperfine interactions 80−44985
FeOCl/ferrocene (cobaltocene) intercalation cpds., X-ray diffr. obs. 79−65066
FeOCl-pyridine intercalate, mechanism, nucleation and diffusion 80−49420
$Fe_3O_{4-x}F_x$ ($0 \leq x \leq 0.25$), Mossbauer spectra 78−15075
$Fe_3O_{4-x}F_x$, low temp. Mossbauer spectra, electron transfer and spin density distribution 78−52404
$Fe_3O_{4-x}F_x$, specific heat in neighbourhood of Verwey temp. 79−33500
$Fe_3O_{4-x}F_x$ substituted magnetite, low temp. resistivity, Seebeck coeff., thermopower 80−20234
FeOH, gas, thermochem. props., mass spectrosc. meas. 80−101034
$Fe(OH)_2$, gel, coprecipitation of divalent metal ions in soln. *(Japanese)* 78−31714
$Fe(OH)_3$, adsorpt. of CO_2 rel. to prep. method 79−39192
$Fe(OH)_3$, adsorption of CO_2 79−66344
$Fe(OH)_3$, coprecipitation with Cu, Ag, Au; Ge, Sn, Pb; Mn and Ca 79−70415
$Fe(OH)_3$ thin films, elec. cond. var. with temp., amorphous struct. 80−75566
$Fe(OH)_3$ thin films, Mossbauer spectra obs., chemical and thermal anal., X-ray diffr., saturation magnetisation 80−88896
$Fe(OH)_3$-Cr_2O_3 catalysts, for water-gas shift react., porous struct. 79−29407
$Fe(OH)_3$-$Fe(OH)_2$ suspension system, potential-pH diagram 80−55728
α-FeO_2H, asymmetric line shapes of Mossbauer spectra *(Chinese)* 80−103902
FeO_2H, growth in alkaline solution, phase composition *(Chinese)* 80−108334
$FeOHSO_4$, mag. props., Mossbauer spectra meas. 79−19824
$FeOHSO_4$, mag. structure, modulation of moments, neutron diffr. meas. 77−69499
$Fe(OH_2)_6(SiF_6)$, phase transitions, spectrometric exam. *(French)* 78−88291
β-FeOOH, akaganeite, struct. changes due to radiation damage 79−28014
δ-FeO(OH) and its solid solns. synthesis, X-ray diffr. and TEM studies 80−29891
β-FeOOH, colloidal suspension, ionic spin relax. theory for Mossbauer spectra 78−19384
FeOOH, core and valence level XPS spectra meas. 78−15290
αFeOOH, core line X-ray photoelectron spectra 78−7263
FeOOH, crystal growth in $FeSO_4$ solution with NaOH or NH_4OH as precipitant, phase diagrams *(Chinese)* 80−44158
δ-FeO(OH) crystallites, TEM imaging investigation 80−39096
FeOOH crysts., prep. by hydrolysis, struct. and reactions with silica 78−35678
β-FeOOH, dehydration 80−79767
FeOOH, ferric hydroxide gel, struct. determ. 79−11832
FeOOH gels, Mossbauer spectra, mag. props. 80−11303
FeOOH, goethite, hydrothermal crystallisation, review, book contrib. 79−69974
FeO(OH), goethite, Mossbauer effect exam. of annealing effect on struct. 78−19396
α- FeOOH, goethite, surface OH groups, D_2O isotopic exchange, IR investig. 80−2254
α-FeOOH, goethite small particles, mag. hyperfine field, bulk and surface contribs. 77−69758
FeOOH, H-bonding, strong, stochastic model and IR spectra temp. effects 78−62805
α-, γ-FeOOH, heats of form. of Fe_2O_3 by quantitative thermography 77−9110
FeOOH, high-pressure phase, neutron diffraction study 78−52212
β-FeOOH, lattice imaging and pore struct., high resolution electron microscopy obs. 80−103310

iron compounds continued
β-FeOOH, Mossbauer investigation of the quadrupole splitting 78−76370
α-FeOOH, sol, mixtures with CuO and TiO_2 sols, differential surface coagulation 79−79303
FeOOH stability on lunar surface 77−33371
δ-FeOOH, structure and phase transform., Mossbauer, X-ray, DTA study *(Chinese)* 80−54368
δ-FeO(OH), study of thermal decomp. by X-ray diffr., electron diffr. and TEM 80−66790
α-FeOOH, surface struct., adsorptive interactions rel. to rusting process, IR spectra 79−34363
ε-FeOOH, synthesis, mag. struct. 78−34961
β-FeOOH, ultrafine particles, mag. struct., Mossbauer spectroscopy 78−72372
α-FeOOH ultrafine particle NGR spectra, size distrib. and surface effects 80−11299
FeOOH:Cl(F), quadrupole interaction, Mossbauer spectra 80−15895
γ-FeOOH-Cr_2O_3 catalysts, for water-gas shift react., porous struct. 79−29407
$Fe_2O(OH)_4$, Mossbauer spectra obs., chemical and thermal anal., X-ray diffr., saturation magnetisation 80−88896
α-FeOOH.nH_2O, hydrogoethite, Mossbauer spectra, Neel point, Fe^{3+} config. 77−32310
α-FeOOH.nH_2O, hydrogoethites, weak ferromag. props. 77−53042
α-FeOOh, goethite, superstructure form. on dehydration, electron microscopy obs. 80−3327
$xFe_2O_3(1-x)[PbO.3B_2O_3]$ glasses, mag. props. 77−73012
$(Fe_2O_3)_x(3B_2O_3.PbO)_{1-x}$ glass, X-ray diffr. struct. obs. 79−32915
$FeO.Fe_2O_3.MgO.P_2O_5$ glass, conversion electron Mossbauer anal. of surfac struct. and chem. state 77−63333
$2FeO.SiO_2.2MnO.SiO_2$ melt, free energy of mixing 79−61572
$2.33FeO.TiO_2.2.33MnO-TiO_2$ melt, free energy of mixing 79−61572
$xFe_2O_3.(1-x)[3B_2O_3.PbO]$ glasses, diffuse refl. spectra 79−51982
$2Fe_2O_3.3H_2O$, bog Fe ore, Mossbauer effect exam. of annealing effect on struct. 78−19396
$20Fe_2O_3.80[3B_2O_3.(1-x)PbO.xGeO_2]$ glass, phys. props. 80−49119
FeP, mag. suscept., resistivity and thermal expansion meas. 78−2661
FeP, valence electron energy spectrum, deduced from X-ray spectra and XPS 79−99984
α-FeP_4, diamag., semicond., Mossbauer study 80−50243
FeP_4, prep. and props., struct. anal. 79−14775
FeP_4, twinned cryst., synthesis and cryst. struct. 79−4278
Fe_2P, grown in liq. Cu medium, composition and mag. props. 79−11313
Fe_2P, mag. moments and form factors, polarised neutron diffr. study 79−65650
Fe_2P, mag. struct., neutron diffr. study 78−23246
Fe_2P, magnetisation, susceptibility, thermal expansion and elec. resist. meas. 77−77037
Fe_2P, Mossbauer spectra and mag. props., Curie temp. dispersion 77−36162
Fe_2P:Cu, Mossbauer spectra, mag. transition 80−50240
$Fe_{2-x}P$, first order ferro- to paramag. transition, 216K, susceptibility obs. 78−39322
Fe_3P-type structures, atomic coord. and bonding 79−60330
$Fe_2P_{1-y}As$, mag. props., Mossbauer effect 77−40156
$Fe_2P_{1-y}As_y$, band model of mag. props. 77−40029
$Fe_{80}P_{13}C_7$, amorphous and crystalline, electrochemical and semicond. behaviour *(Russian)* 80−101021
$FePO_4$ coating on Armco Fe, Fourier transform IR absorpt.-reflection spectra 80−71500
$FePO_4$, XPS of cryst., inner shell binding energies of elements 79−43092
$Fe_2(PO_4)Cl$, Mossbauer study of mag. ordering and local co-ordination 80−39972
$Fe_2(PO_4)Cl$, temp. depend. of mag. susceptibility 80−70962
$Fe_3(PO_4)_2(OH)_2$ synthetic barbosalite, temp. depend. quadrupolar and mag. hyperfine interactions 80−25255
$FePS_3$ and $FePSe_3$, antiferromag., mag. props., NMR meas. 79−24223
$FePS_3$, Goldanskii-Karyagin effect, Mossbauer spectra 79−99798
$FePS_3$, layered semiconductors, optical and electronic props. 80−70761
$FePb_4Sb_6S_{14}$, photosensitive semiconductor, with high permittivity, elec. props. 79−65518
$Fe_xPd_{82-x}Si_{18}$ metallic glass, mag. phase diagram, weak ferromagnet-spin glass transition 80−54893
$FeRO_3$, enhanced nuclear resonance scattering in dynamical diffraction of gamma-rays 80−44982
$FeRb_2(SO_4)_2.6H_2O:Mn^{2+}$, EPR, 298K, spin-Hamiltonian parameters, cryst. fields 78−27086
$FeRh_2S_4$, mag. semicond., mag. and elec. props. 80−93121
$Fe_xRh_{3-x}S_4$, thermal stability and thermochem. props. 79−86904
FeS crystal centering, and diffractometer alignment errors calcs., appl. to high pressure crystallography 80−22494
FeS, hollow particle growth by sulphuration of Fe 77−68934
FeS, inclusion in steel, effect of high temp. heating on size, number and distrib. 78−44145
FeS polymorph formation, Fe corrosion in aq. H_2S 80−81231
FeS, pressure effect on elec. resist. and thermoelec. power 80−70308
FeS quadrupole splitting and ground state, Mossbauer spectra 80−29657
FeS, S and S^{2-} states, identification from Auger line shapes 79−92034
FeS, structural chem., influence of itinerant 3d electrons and valence-band holes 79−23563
FeS, thermal switching, resist.-temp. charact. 78−64071
FeS, X-ray and visible spectra, SCF-Xα scatt. wave anal. 78−5138
FeS, zinc blende type, crystallographic and Mossbauer obs. 78−87650
FeS, zinc blende type, mag. struct. *(French)* 78−91846
FeS-Cu_2S, FeS-CoS, FeS-Ni_3S_2, melt viscosity 77−51536
FeS-Ga_2S_3 system, intermediate phases crystallographic study *(French)* 79−51061
FeS-MnS phase relationships in presence of excess Fe 77−4768
FeS-MnS(MnO), melt, exam. of viscosity and self-diffusion 79−95198
FeS-Ni_3S_2-Cu_2 S melt, enthalpy *(Russian)* 78−95730
FeS_2 (marcasite), temp. depend. mag. susceptibility 80−20391
FeS_2, (pyrite), angle-independent Mossbauer effect 80−20570
FeS_2 (pyrite), glide elements study by electron microscopy and electron diffr. 78−83817
FeS_2 (pyrite) formation in sulphide-rich sediments, Fe diagenesis studies by Mossbauer spectroscopy 79−74917
FeS_2, acid bacterial leaching, lixiviant alteration by fungal absorpt. of Fe 80−108617

iron compounds continued
FeS_2, adsorption mechanism in selective etching 77−7727
FeS_2, band gap temp. depend., optical absorpt. studies up to 425K 79−95758
FeS_2, coincidence-site lattice interfaces 80−15381
FeS_2, core-level and valence-band XPS 80−93450
FeS_2, cryst. growth, literature review 78−31318
FeS_2, cubic, d-orbital occupancies refinement, from X-ray diffr. data 79−68971
FeS_2, diatomic crysts. electron induced X-ray emission, channelling effects 79−56888
FeS_2, dielec. constant meas. 79−15395
FeS_2, dislocations and stacking faults, TEM obs. *(French)* 79−99204
FeS_2, EXAFS at high press., bond compressibility, at. spacings 78−39628
FeS_2, electric field gradient and mean-square displacement of Fe sites 79−95690
FeS_2, etching of dislocations 77−7726
FeS_2, ionisation loss spectra, density of unoccupied states 80−55241
FeS_2, mag. props. rel. to Hubbard model 79−78373
FeS_2, mag. susceptibility press. depend., bandstruct. calcs. 78−19212
FeS_2, marcasite, Mossbauer elec. field gradient meas. 78−56407
FeS_2, marcasite and pyrite phases sp. ht., thermodynamics of transform. 77−28016
FeS_2, Mossbauer effect in mag. field, absence of mag. moment 77−12288
FeS_2, Mossbauer elec. field gradient and mean square displacement 80−39991
FeS_2, natural pyrite, photocond. spectra 80−70758
FeS_2, natural single cryst., mag. susceptibility, 4.2-620K 77−40031
FeS_2, optical absorpt. 79−43002
FeS_2, oxidation, Mossbauer spectroscopic and magnetokinetic studies, 400-500°C 80−44880
FeS_2, pyrite, elec. field gradient, Mossbauer spectrum 80−15493
FeS_2, pyrite, eqn. of state, rel. to constraints on Earth S content 79−70789
FeS_2, pyrite, heat capacity meas. by differential scanning calorimetry 80−8987
FeS_2, pyrite, high-resolution electron micrograph of twin boundary 77−65983
FeS_2, pyrite, magnetokinetics of oxidation, appl. to mag. separation from coal 77−12161
FeS_2, pyrite, semiconducting props., energy gap press. and lattice parameter depend., Mossbauer obs. 80−44494
FeS_2, pyrite, single cryst. growth by chem. vapour transport, surface struct. and morphology 79−23550
FeS_2, pyrite, stacking faults, TEM obs. *(French)* 79−28004
FeS_2, pyrite, stacking fault model *(French)* 80−39117
FeS_2, pyrite, Van Vleck susceptibility, temp. depend. 80−34589
FeS_2, superficial degradation in air and water, XPS obs. *(French)* 80−89110
FeS_2, X-ray and visible spectra, SCF-Xα scatt. wave anal. 78−5138
FeS_2-$CaCO_3$-C, reaction on heating, dissociation, reduction to Fe *(Russian)* 78−44041
FeS_6^{10-}, electronic struct., SCF-Xα scatt. wave calcs., rel. to spectra of FeS, FeS_2 78−5138
$Fe_{0.9}S$, ferrimag. transition, mag., thermodynamic props., kinetics 79−47280
$Fe_{0.9}S$, pyrrhotite, eqn. of state, rel. to constraints on Earth S content 79−70789
$Fe_{0.996}S$, antiferromag., energy dispersion of spin waves, inelastic neutron scatt. meas. 77−69522
$Fe_{0.996}S$, $Fe_{0.93}S$, determination of quadrupole splitting sign, ground state appl. 78−76363
$Fe_{1-\delta}S$ chemical diffusivity and nonstoichiometric props. 78−10217
$Fe_{1-x}S$, NC-type, wave distrib. of vacancies 79−99178
$Fe_{1-x}S$, pyrrhotite, modulated struct., struct. refinement 79−94966
$Fe_{1-x}S$, pyrrhotite, S activity at 1073K 77−72700
$Fe_{1-x}S$, soft X-ray emission and AES study 79−91535
Fe_2S_3, existence and thermal stability, Mossbauer study 78−83733
Fe_3S_4, galvanomagnetic props., resist. and Hall effect meas., 4.2-300K 80−54673
Fe_7S_8, 3C pyrrhotite, cryst. struct. refinement 79−42017
Fe_7S_8, pyrrhotite, thermocond. and thermoelec. power 80−96926
Fe_9S_{10}, antiferro- to ferrimag. transition, Mossbauer and mag. exam., diffusion of Fe during transition 79−73716
Fe_9S_{10}, polytypism, Fe diffusion near antiferromag. to ferrimag. transition 80−44830
FeS_2(-CoS_2)(-NiS_2), ^{57}Fe isomer shift, quadrupole splitting, Mossbauer study 80−15832
FeS−Li_2S−Cu_2S system, Mossbauer spectra and lattice parameters 79−78584
$FeSO_3$, anhydrous, X-ray cryst. struct. determ. *(French)* 80−92486
$FeSO_4$, anhydrous, γ, β and γ-phases, Mossbauer spectra, polymorphism 77−12287
$FeSO_4$ aq. soln., oxidation by high-energy electrons 79−52700
$FeSO_4$, α- and β-forms, magnetic interactions, neutron inelastic scatt. study 80−107980
$FeSO_4$ dosimeter compared with ionisation chamber meas. at 6 radiotherapy centres *(French)* 77−37057
$FeSO_4$ dosimetry by NH_4CNS method 79−2136
$FeSO_4$ dosimetry for electrons, a re-evaluation 80−68963
α-$FeSO_4$, electronic and mag. struct., semiempirical MO cluster calcs. 78−62733
$FeSO_4$ Fricke dosemeter solns., G-value determ. for 20 MeV protons 77−52884
$FeSO_4$, G-values, C_λ and C_E reevaluation using extended cavity ionisation theory 78−92706
β-$FeSO_4$, high-temp. polymorph, stability, mag. struct., mag. props. 77−43815
$FeSO_4$ oxidation by SO_2-O_2-H_2SO_4 soln. 80−61083
$FeSO_4$, X-ray absorpt., heat treatment effects, chem. and struct. interpretation 80−84806
$FeSO_4$-$CuSO_4$ dosimeter, intense γ-radiation field effects *(Spanish)* 77−48876
$Fe_2(SO_4)_3$, aq. soln., solute struct. by X-ray scatt., Fe(III) sulphate complexes 79−32875
$Fe_2(SO_4)_3$, Mossbauer isomer shift in rhombohedral and monoclinic forms 78−6609
$Fe_2(SO_4)_3$ soln., precipitation of Fe as Jarosite *(Korean)* 79−87842

iron compounds continued
$Fe(SO_3F)_2$, Mossbauer and electronic spectra, cryst. field splittings, mag. hyperfine interactions 77−48096
$FeSO_3.2^1/_2H_2O$, X-ray cryst. struct. determ. 80−88107
α-$FeSO_3.3H_2O$, X-ray cryst. struct. determ. 79−60310
β-$FeSO_3.3H_2O$, X-ray cryst. struct. determ. 80−15063
$FeSO_4.4H_2O$, Fe sites asymmetry parameter, mean square displacement, Mossbauer spectra 78−6608
$FeSO_4.7H_2O$ and $FeSO_4.7D_2O$, frozen solns., isotope effect of Mossbauer parameters 80−34835
$FeSO_4.7H_2O$, γ-ray irradiated, Fe^{3+} formation, Mossbauer study *(Russian)* 78−84509
$FeSO_4.7H_2O$, single cryst., elec. and dielec. props., temp. depend. 79−19826
$FeSO_4.n\ H_2O$ (n=1,4,5,7), Fe^{2+} ion mag. interaction with crystallisation water protons, proton NMR obs. 80−60447
$Fe_4S_4(SH)_4^{0,2-,3-}$, HFS-LCAO calcs., 4-Fe active site model in high pot. Fe protein and ferredoxin 80−42929
$Fe_7S_8(Se_8)$, magnetocrystalline nature 78−41337
FeSb alloy films, vapour-deposited, formation of metastable phase 80−44437
FeSb solid solution, supersaturated, mag. hyperfine field, Mossbauer study 80−44961
$FeSb_2$, heat capacity and thermodynamic props. from 5 to 1021.2K, heat of decomposition 77−90636
$FeSb_2$, quasi-magnetic semicond., mag. susceptibility 80−39757
$Fe_{0.545}Sb$, temperature effect on lattice consts., Mossbauer spectra and density 80−88124
$Fe_{1+\delta}Sb$, nonstoichiometry influence on mag. props. *(Russian)* 80−65813
$Fe_{1+x}Sb$, hyperfine interactions of ^{57}Fe, room temp. Mossbauer meas. 79−47374
$Fe_{1+x}Sb$-CoSb solid soln., mag. props., Mossbauer spectra, solubility limits, and lattice consts. *(Russian)* 77−59394
$Fe_{1+x}Sb$-NiSb solid soln., mag. props., Mossbauer spectra, solubility limits, and lattice consts. *(Russian)* 77−59394
$FeSb_2O_4$, Mossbauer spectra, molecular field effects 78−91997
$FeSb_xO_{4-y}$, defect struct. and mag. transition, elec. transport and Mossbauer expts. 78−59803
$FeSb_2S_4$, berthierite cryst., anomalies in elec. and dielec. props. 77−47821
$Fe(Sb_{1-x}Te_x)_3$ system cpds., prep., cryst. struct., elec. and mag. characteris. 80−108349
$FeSc_2S_4$, prep. and X-ray cryst. struct. determ. *(French)* 79−60335
$Fe_{0.85}Sc_{2.10}S_4$, prep. and X-ray cryst. struct. determ. *(French)* 79−60335
$FeSe_2$, mag. props. rel. to Hubbard model 79−78373
$^{57}FeSe_2$ and $^{57}FeTe_2$, isomer shift, quadrupole splitting, Mossbauer study 80−15832
$Fe_{0.96}Se$, Mossbauer diffusional line-broadening 77−55734
$Fe_{1-x}Se$, phase relation 79−14926
Fe_3Se_4, Fe_7Se_8, phase gap, Mossbauer spectra 80−20552
Fe_3Se_4, mag. props., 4.2-600K 78−43570
Fe_3Se_4, Mossbauer diffusional line broadening 77−43370
Fe_3Se_4, thermal expansion, compressibility, magnetisation, susceptibility and magnetostriction 77−66318
Fe_7Se_8, 3c struct., spin axis transition 78−14967
Fe_7Se_8, Fe_3Se_4 and $NiFe_2Se_4$, thermal cond., temp. depend., 100 to 400K 77−35764
Fe_7Se_8, test of Okazaki's 3c and 4c superstruct. model, Mossbauer expt. 77−66445
3C-Fe_7Se_8, X-ray cryst. struct. study 79−55708
$FeSeO_4$, electron capture and γ-radiolysis, radn. damage 80−16705
FeSi and $FeSi_2$, inner level ESCA spectra, many particle effects, hole lifetime *(Russian)* 79−91560
FeSi, $FeSi_2$, valence shell XPES 79−43105
η-Fe_5Si_3, thermal and mag. props. 77−36080
$FeSiF_6$, isotropy of Lamb-Mossbauer factor, Debye model 80−60465
$FeSiF_6$, phase transform. and relax., EFG and quadrupole spectra 77−51995
$FeSiF_6.6D_2O$, ^2H NMR spectrum, correl. effects 78−76324
$FeSiF_6.6H_2O$, dielec. props., 100-270K, rel. to $NiSiF_6.6H_2O$ 78−35088
$FeSiF_6.6H_2O$, Lamb-Mossbauer factor isotropy in the Debye model *(French)* 80−44962
$FeSiF_6.6H_2O$, paramag., nucl. and electron spin lattice relax. 78−84494
$FeSiF_6.6H_2O$, phase transform. exam. by X-ray and DSC methods 78−83948
$FeSiF_6.6H_2O$, powder, far IR mag. reson., zero field splitting 77−81000
$FeSiF_6.6H_2O$, submillimetre EPR and zero field spectra, spin Hamiltonian 80−29604
$FeSiF_6.6H_2O$:Mn^{2+}, EPR line positions and intensities, spin Hamiltonian 79−65714
$FeSiF_6.6H_2O(.6D_2O)$, near IR spectrum, 80K, assignments 78−48164
$FeSiO_3$, high pressure and temp. phases rel. to Earth's mantle 77−9403
$FeSiO_3$, UV and soft X-ray spectra, band gap determ. 79−61468
$FeSiO_4$, hydrothermal growth, effect of NaOH soln. conc. and O_2 fugacity on morphology 79−65996
Fe_2SiO_4 (fayalite), shear strength and press. distrib. in diamond anvil press 78−12710
Fe_2SiO_4, determ. of electronic polarisabilities of ions 79−7570
Fe_2SiO_4, elec. cond. under defined thermodynamic activities, up to 20 kbar, 340-1100°C 80−6832
γ-Fe_2SiO_4, electron density distrib. 77−35514
Fe_2SiO_4, fayalite, Czochralski growth under controlled O_2 fugacity conditions 80−84843
Fe_2SiO_4, fayalite, elec. cond. obs. under shock compression 80−81873
Fe_2SiO_4, fayalite, single crystal growth by floating zone method, exam. 78−60570
Fe_2SiO_4 in equilib. with buffers, electrical conductivity *(German)* 79−93162
Fe_2SiO_4, nonstoichiometry influence on plasticity *(German)* 79−24592
Fe_2SiO_4, spinel, isothermal compression up to 75 kbar hydrostatic press. 77−43280
Fe_2SiO_4, UV and soft X-ray spectra, band gap determ. 79−61468
Fe_2SiO_4-$KAlSi_2O_6$-SiO_2, phase relations at 1 atm., and low temp. liq. immiscibility 79−47664
$Fe_{2-x}SiO_4$, fayalite, oxidation kinetics and growth of Fe_2O_3 whiskers 78−84113
$Fe_4Si_4O_{12}$-$Fe_3Al_2Si_3O_{12}$ system, pyroxene-garnet solid-soln. equilibria at high press. and temps. 77−81895

iron compounds continued
$Fe_6Si_4O_{10}(OH)_8$, greenalite, metamag. clay mineral, mag. props. *(French)* 78−88817
Fe_2SiS_4, Mossbauer effect and magnetisation meas. of mag. struct. *(French)* 77−12282
Fe_3Sn_2, mag. props., neutron diffr. and magnetisation meas. 79−11294
$FeSnO_3$, Mossbauer spectral anal. *(German)* 79−19819
$FeSnO_3$ particles in EBBA liq. cryst., Mossbauer study of Brownian motion 79−95691
$Fe_2(SnO_3)_2$, Mossbauer spectral anal. *(German)* 79−19819
$Fe_{3-x}Sn_xO_4$, mag. hyperfine fields, ^{57}Fe and ^{119}Sn Mossbauer spectra 80−39944
$FeSn(OH)_6$, mag. props. 78−43574
$FeSnO(OH)_5$, mag. props. and cryst. struct. 78−43574
Fe_2SnS_4, cryst. struct. *(French)* 78−18595
$(Fe_{0.5}Ta_{0.5})O_2$, rutile, cation distrib. and mag. ordering *(German)* 80−107116
1T-$Fe_{0.1}Ta_{0.9}S_2$, mag. modulation of lattice electric field gradient 77−85628
$Fe_{1/3}TaS_2$, Hall coefficient and resistivity 80−39610
$Fe_{1/3}TaS_2$, magnetic susceptibility, function of temp. 80−39756
Fe_xTaS_2, metallic, mag. susceptibility at low temp. 80−70972
Fe_xTaS_2, vacancy ordering, transition state cluster model, electron diffr. 77−47547
$Fe_xTa_{1-x}S_2$ (1T), low-spin high-spin equilib., susceptibility and Mossbauer expts. 77−48109
1T-$Fe_xTa_{1-x}S_2$, Anderson localisation, elec. resist. and magnetoresist. meas. 80−44596
$Fe_xTa_xV_{2-2x}O_4$ complex solid solns., synthesis and phase diagram, semicond.-metal transition temp. 79−43214
FeTe film, on amorphous substrates, Mossbauer obs. of struct. 78−27142
$FeTe_x$, Mossbauer spectra, 80 to 750K, quadrupole splitting and isomer shift 77−4590
$Fe_{1-x}Te$, fluctuating localised mag. moments, d band motion, Mossbauer study 80−65768
$Fe_{1+x}Te$, ^{129}I transferred hyperfine field, Mossbauer spectroscopy study 80−44972
$FeTe_2Fe_2Te_3$, defect struct. compounds, room temp. ^{57}Fe Mossbauer spectra 79−47371
Fe_2TeO_5 and $Fe_2Te_3O_9$, evolution of coord. of Te IV and Fe III *(French)* 77−35537
Fe_2TeO_5, mag. struct. 78−27020
Fe_2TeO_6, CC ^{57}Fe Mossbauer spectrum, hyperfine field, Neel temp. 79−56636
$FeTh_2S_5$, mag. struct. and props., neutron diffr. and mag. meas. 80−60201
$FeTh_2S(Se)_5$, synthesis, cryst. characts. *(French)* 78−51517
$FeThSe_3$, synthesis, cryst. characts. *(French)* 78−51517
$Fe_{2.6-x}Ti_{0.4}Al_xO_4$, $Fe_{2.4-x}Ti_{0.6}Al_xO_4$, titanomagnetite, monodomain, mag. props. 78−56346
β-FeTiD, neutron diffr. exam. of struct. 78−47282
$FeTiD_x$ ($0\leq x\leq 1.9$), structural phase transitions, absorpt. and desorpt. isotherms 80−19948
$FeTiD_x$, γ-phase struct., neutron diffr. study 79−51085
$FeTiH_x$, (x=0.65 to 1.03) diffusion of H, neutron scatt. exam. 79−65243
$FeTiNdO_5$, isomer shift, hyperfine field and distrib. of Fe^{3+} ions, Mossbauer spectrum 77−69747
$FeTiO_3$, electronic struct., Mossbauer expt. 78−27150
$FeTiO_3$, Fe_2TiO_4, Fe_2TiO_5, prep. and Czochralski cryst. growth 77−21017
$FeTiO_3$, Fe_2TiO_4, and Fe_2TiO_5 anodes, appl. to photoelectrolysis of water 77−63920
$FeTiO_3$, Fe_2TiO_4, influence of cryst. struct. on photoresponse of electrodes 78−43471
$FeTiO_3$, HP phase transform. 80−19941
$FeTiO_3$, ilmenite, prep. at focus of solar furnace *(French)* 80−29908
$FeTiO_3$, photoacoustic spectra, spectrometer sample cell design investig. 77−74520
$FeTiO_3$, single cryst. growth by floating-zone method 79−19991
Fe_2TiO_4, cooperative Jahn-Teller effect, neutron scatt. study 80−49678
Fe_2TiO_4, cooperative Jahn-Teller phase transition, crit. diffuse scatt. 80−59930
Fe_2TiO_4 magnetisation, Mossbauer spectra 79−87244
Fe_2TiO_4, ulvospinel, containing magnetized inclusions, mag. behaviour, cooling through Curie point 78−56314
Fe_2TiO_4, ulvospinel, mag. props. weak ferromag. in 4-200K temp. range 78−56351
Fe_2TiO_4-Fe_3O_4, titanomagnetite, prepared at different oxidation conditions, hysteresis props. 78−56352
Fe_2TiO_5, anisotropic spin glass behaviour 79−99707
Fe_2TiO_5, anisotropic spin glass type behaviour 80−60296
Fe_2TiO_5, grain size pseudobrookite oxide, microcracking relations 79−29194
Fe_2TiO_5, pseudobrookite, single cryst. growth by chem. transport 78−80464
Fe_2TiO_5, spin glass system, cation distrib. Mossbaeur spectra 80−71248
$Fe_{2.4}Ti_{0.6}O_4$, TRM acquired by multi-domain single cryst. 80−36293
$Fe_{2.4}Ti_{0.6}O_4$, titanomagnetite, single-crystal, mag. props. of multidomain TRM 78−56345
$Fe_{3-x}Ti_xO_4$, $0.5\leq x\leq 1$, mag. props. of antiferromag. phase 80−70960
$Fe_{3-x}Ti_xO_4$, elec. transport near Verwey transition, thermoelec. power and cond. meas. 79−95455
$Fe_{3-x}Ti_xO_4$, Mossbauer study at low temp. 78−27133
$Fe_{3-x}Ti_xO_4$, Mossbauer spectra in paramag. phase 80−39943
$Fe_{3-x}Ti_xO_4$, spin glass behaviour, susceptibility and hysteresis meas. 80−65917
$FeTiRO_5$, R=Pr,Nd,Sm,Eu,Gd,covalency contribs. to Mossbauer spectra 78−10808
$Fe_{(1+x)}Ti_{2(1+x)}S_4$ non-stoichiometric cpds., vacancy-cation distrib., Mossbauer spectra 80−15900
Fe_xTiS_2, lattice dynamics and hyperfine interactions, Mossbauer spectra study 80−108135
FeU_2S_5, mag. struct., exchange energy, magnetisation and neutron diffr. expts. 78−68170
$FeVO_4$, Neel temp., mag. susceptibility meas. 80−29550
$FeVO_4$, temp. depend. of heat capacity, 60-1080K, Debye temp. 77−7869
FeV_2O_4, free energies of form., 1400-1750K, electrochem. method determ. 79−43613

iron compounds continued
θ-$Fe_{0.35}V_2O_5$, NMR of ^{51}V 80−71232
$Fe_{0.35}V_2O_5$, spin glass phase, low temp. mag. susceptibility meas. 80−29565
$Fe_{1+x}V_{2-x}O_4$ spinels, prep. and negative resist. charact. *(Korean)* 78−39119
Fe_xVO_2, reduced, microstruct., crystallographic shear planes, electron microscope obs. 79−1443
$Fe_xV_{\frac{1}{2}-x}O_2$, mag. props. and Mossbauer spectra meas., exchange-coupled Fe^{3+} clusters at lower temp. 78−31136
$Fe_xV_{1-x}O_2$, X-ray diffr. obs. 77−27858
$Fe_xV_{1-x}O_2$, $x \simeq 0.25$, synthesis and cryst. struct. *(French)* 79−55713
$(Fe_xV_{1-x})_2O_3$, impurity doping effects, elec. props. obs. 80−75609
$Fe_xV_{2-x}O_4$ solid solutions, specific heat near semiconductor-metal transition 80−24612
θ-$Fe_xV_2O_5$, spin glass and paramag. props., susceptibility, EPR and Mossbauer studies 80−75782
$Fe_xV_2O_5$, spin glass transition range, cluster blocking distrib. function 80−80548
$FeV_2O_6H_{0.5}$, synthesis and cryst. struct. *(French)* 79−55720
Fe_xVS_2 ($0.20<x<1.00$), phase diagram and order-disorder transition of vacancies 80−81039
$(Fe_xV_{1-x})V_2S_4$, and $(Fe_xV_{1-x})V_4S_8$, mag. props. 78−27034
Fe_2WO_6, neutron diffr. patterns and mag. struct. 77−66250
FeX_4^-, (X=F, Cl and Br), electronic struct. and isomer shift 80−63545
$FeYb_2S_4$, cryst. struct. determ. 79−77572
$FeYb_2S_4$, structural study, X-ray diffr., Mossbauer spectroscopy 80−107159
$Fe_{0.76}Yb_{2.16}S_4$, cryst. struct. determ. 78−26533
$Fe_{1+x}Yb_{2-x}S_4$, X-ray and Mossbauer obs. 77−77132
$Fe_{1-x}Zn_xF_2$, dil. antiferromag., Raman scatt. expts. 79−78666
$Fe_{1-x}Zn_xF_2$, dil. antiferromag., electronic and mag. props., Raman scatt. and optical absorpt. study 80−108207
$Fe_{1-x}Zn_xF_2$, electronic Raman scatt., mag. anisotropy 80−66184
$Fe_xZn_{1-x}F_2$, Neel point and short range order, dilution effects, mag. birefr. obs. 80−71019
$Fe_xZn_{1-x}F_2$, Neel temp., CPA calc. 78−68233
$Fe_xZn_{1-x}F_2$, Neel temp. mag. cone depend., CPA calcs. 78−88122
$FeZnF_5.7H_2O$, Mossbauer spectra, thermal decomp. products 78−80258
$FeZnMo_6S_8$, mixed Chevrel phases, crystallography 80−39038
$Fe_{1-y}Zn_{3y/2}O_3$, solid soln. prep., struct. and mag. moment 78−52228
$Fe_{3-x}Zn_xO_4$ low temp. Mossbauer spectra, electron transfer and spin density distribution 78−52404
$FeZrF_6$, phase transition at 212.3K, Mossbauer, EPR study, quadrupole splitting, Jahn-Teller effect *(German)* 78−68430
Fe_xZrS_2, ($0<x\leq 0.50$), intercalation compounds, ordered phases obs. 80−33962
Fe_xZrSe_2, intercalation compound, IR spectra 78−88300
γ-Fe_2O_3 and glass mixtures, calibration standard for magnetic susceptibility meas. 79−88989
α-FeO0H, chemisorption of pyridine, acetic acid, CO_2, NO or trimethylchlorosilane, IR spectra 80−7855
^{57}Fe interstitial cpds. and solid solns., Mossbauer spectra 80−20557
^{57}Fe Mossbauer isomer shift from electron capture rate of ^{57}Fe 80−7203
$Fe_2[As^{III}(As^VO_4)_3]$, cryst. struct., partial disorder of As^{III} atoms with linear order *(French)* 79−90600
$Fe_3[Co(CN)_6]_2.12H_2O$ struct. dehydration fluorescence and IR studies 80−28976
$Fe_2[Fe(CN)_6]$, and $Fe_3[Fe(CN)_6]$, mag. susceptibility, reflectivity spectra and cryst. field 79−56808
$Fe_2[PO_4]F$, synthetic, cryst. struct. determ. 79−14780
$FrCr_2S_4$, second-order phase transition, Mossbauer spectra 80−20569
Ga_2O_3-Fe_2O_3 system, anomalous Mossbauer lineshapes, incomplete annealing 77−51998
Ga_2Se_3-FeSe, phase diagram, elec. cond., mag. susceptibility 80−88301
Gd_2O_3-Fe_2O_3-PbO-B_2O_3, primary crystallisation regions 77−12604
Ge-Se-Fe films, metallic and semicond., amorphous, mag. and elec. props. 78−52319
Ge-Se-Fe phase system, amorphous films, mag. and elec. props. 79−51695
$H_2Fe(CO)_4$, mol. struct., gas phase electron diffr. expt. 78−13623
$HFeN_2$ complexes, electronic configuration calc. using SCCC-LCAO-MO method *(Chinese)* 80−1082
$Hg_{1-x}Fe_xTe$ mixed crystals, zero gap, magneto-optical evidence of exchange interactions 80−45045
$Hg_{1-x}Fe_xTe$, struct. invest. using X-ray diffr. and electron microscopy 80−75365
$Ho_{12}Fe_{32}O_2$, struct. and ferrimag. props., neutron diffr. obs. 79−78319
InAs-FeAs, eutectic, growth from melt, electrical props. 77−11911
$KCl:Fe(CN)_6^{4-}$, electron irrad., Mossbauer and ESR study 80−7238
KCl-NaCl-$FeCl_3$ system, shape eutectics line calc. *(Russian)* 79−96016
$K_3Fe(CN)_6$, electronic struct., electron density, elec. field gradient, mag. susceptibility and g-tensor 79−91006
$K_3Fe(CN)_6$, pressure induced reduction, Raman spectra 80−66776
$K_3Fe(CN)_6$-KCl, press. induced reduction, IR spectra after pressurization 80−66776
$K_4Fe(CN)_6.3H_2O$, dynamic disorder and ferroelec. transition, Raman spectra obs. 77−81069
$K_4Fe(CN)_6.3H_2O$, effect of ordering on OH Raman bands 79−51959
$K_4Fe(CN)_6.3H_2O$, ferroelec., sp.ht. and spontaneous polarisation, −65 to 0 degrees C, mol. field model 78−64333
$KFe(CrO_4)_2$, cryst. struct., structural filiation with $KFe(CrO_4)_2.nH_2O$ series *(French)* 77−27855
$KFeF_4$, amorphous, Mossbauer study 80−39970
K_2FeF_4, antiferromagnet, two-dimensional, mag. excitations 80−80492
$K_{1+x}Fe_xGa_{11-y}O_{17}$, electron hopping and excitation at room temp., ^{51}Fe Mossbauer spectra 80−25257
$K(Fe_{1.5}Mg_{0.5}Si_4O_{10})(OH)_2$, cryst. struct. refinement 78−26545
$KFe(MoO_4)_2$, ferroelastic domain struct. *(Russian)* 79−90719
K_2FeO_4, XPS of hexavalent iron binding energies calcs. 80−43013
$K_{10}(Fe_3O(SO_4)_6(H_2O)_3)_2.12H_2O$, mag. exchange interaction of trinucl. Fe^{3+} complex *(German)* 78−14947
β-$K_5Fe_3O(SO_4)_6.10H_2O$, monoclinic struct. *(German)* 78−34473
$K_xFe_xTi_{8-x}O_{16}$, ionic cond. meas. 78−67856
$K_2Mn_{1-x}Fe_xF_4$, layered antiferromag., anisotropy effects on mag. ordering, neutron diffr. study 79−47254
$K_2Mn_{1-x}Fe_xF_4$, mag. and neutron scatt. exam. 79−33466
$K_2Mn_{1-x}Fe_xF_4$, tetracrit. line in x-H-T phase diagram, neutron scatt. exam. 78−47977
K_2O-Al_2O_3-B_2O_3:Fe_2O_3, glasses, liq.-liq. phase separation, Fe^{3+} ions rel. to mag., optical props. 77−15322
iron compounds continued
K_2O-B_2O_3-Fe_2O_3, γ-irrad., Mossbauer spectroscopic study 80−108132
K_2O-B_2O_3-Fe_2O_3 glass, Mossbauer expts., 85-500K 78−80260
K_2O-Fe_2O_3-SiO_2, subsolidus sector of phase diagram, X-ray obs. 80−40335
$K_2O_{5-x}Ga_2O_3.xFe_2O_3$, K ion cond. 78−83998
KPO_3-Fe_2O_3 glasses, γ-irrad., ESR 80−50182
$K[Fe_4S_3(NO_7)]$, valence levels, X-ray photoelectron and X-ray spectra 77−88500
$LaFe_{1-x}Co_xO_3$, UPS, XPS, X-ray absorpt. spectra, band struct. study 79−56885
$LaFe_4P_{12}$, single crystals grown from Sn flux, struct. 78−14314
$La_2Fe_{1.76}S_5$, cryst. struct. *(French)* 78−51499
$LaKFe(CN)_6.4H_2O$, cryst. struct. determ. 78−55844
Li nonaqueous battery iron sulphides preparation, charact. and appls. 80−97778
Li-Al-FeS, high temp. battery, ceramic powder, as electrode separators 79−61966
Li-FeS_x molten salt battery, anodic corrosion rate of candidate current collector metals 79−100512
Li-FeS_x molten salt battery, anodic corrosion rate of candidate current collector metals 79−100513
LiAl/FeS, battery system research developments at ANL 80−61323
LiAl/FeS experimental cells with molten salt electrolyte, self-discharge behaviour 80−104501
LiAl/FeS_x cell with negative electrode prep. by powder metallurgy, performance 80−26130
LiAl(Si)/$FeS(S_2)$ battery developments for electric vehicle propulsion and load levelling appls. 80−61325
$Li_{0.5}Fe_{1.32}Ga_{1.18}O_4$, temp. depend. on mag. moments, neutron diffr. data *(Russian)* 77−28371
$Li_3Fe(MoO_4)_3$, paramag. props., 90-800K *(French)* 80−39734
$Li_{0.5}Fe_{2.5}O_4$, superexchange interactions, three-sublattice anal. 79−61095
$Li_{0.5}Fe_{2.5}O_4$, temp. depend. of mag. moments, neutron diffr. data *(Russian)* 77−28371
$Li_{0.5}Fe_{2.5}O_4$-$CuFe_2O_4$-$MnFe_2O_4$, structural characteristics and mag. props. of solid solutions 77−35696
$Li_xFe_yV_{1-y}S_2$, physical props., effect of metal substitution of Li intercalation 79−100395
$LiNbO_3$-SiO_2:Fe_2O_3 glasses, Li^+ ion cond. 80−107471
Li_2O-B_2O_3-Fe_2O_3 glass, Mossbauer expts., 85-500K 78−80260
Li_2O-Fe_2O_3-siO_2 glass, struct. and crystallisation behaviour 78−83738
$(Li_2O$-Al_2O_3-$SiO_2)$:Fe_2O_3, glass, pyroceramic form., colour centres, magnetochem. investig. 77−16537
$Li_xV_{1-y}Fe_yS_2$, intercalated battery cathode material, Mossbauer studies 80−44984
$Ls_6Fe_4S_{14}$, antiferromag., neutron diffr. study 80−70954
(Mg, Fe)SiO_3, orthopyroxenes, cation distrib., electronic and Mossbauer spectra 80−7370
$(Mg,Fe)_2SiO_4$, dislocation recovery rate affected by high-press. 80−94515
β-$(Mg, Fe)_2SiO_4$, high-press. spinel phase identification in Tenham chondritic meteorite 79−80284
$(Mg,Fe)_2SiO_4$, olivine, fayalite rich, single cryst., UV absorpt. spectra at high press. 78−85545
$MgAl_2O_4$-$MgFe_2O_4$-$FeAl_2O_4$-$FeFe_2O_4$-$FeCr_2O_4$ solid soln., thermodynamic model for natural spinel *(French)* 78−32065
$MgFeGe_2O_6$-$Ca(Mg_{0.5}Fe_{0.5})Ge_2O_6$, solid solns., phase equilibria, cryst. optical, X-ray struct. charact. 79−11577
$MgFe_2O_4$, epilayer, perpendicular anisotropy 80−39769
$MgFe_2O_4$, vaporization 79−99308
$Mg_cFe_{1-c}O_{1+\delta}$ cluster component method calc. of lattice params., composition, imperfection 77−25031
$Mg_xFe_{1-x}O$, diffusion of ^{59}Fe and elec. cond. 80−59700
$Mg_xFe_{3-x}O_{4-y}$ precipitates, g-factor, ferrimag. reson. meas. 78−60337
$(Mg_xFe_{1-x})_2SiO_4$, olivine, Fe-rich superparamagnetic clusters, Mossbauer study 79−82831
MgO-Al_2O_3-Fe_2O_3-SiO_2, cordierite, in ceramic, effect of heat treatment on cordierite content 79−20039
MgO-CaO-Fe_2O_3-Al_2O_3-SiO_2, clinker production from dolomite and magnesite 80−55339
MgO-CaO-FeO-Fe_2O_3-SiO_2-Cr_2O_3-Al_2O_3 spinel refractories, physicochem. prod. conditions 80−89185
MgO-CaO-SiO_2-Al_2O_3-$Na_2O.P_2O_5$, effect of $NaPO_3$ on phase composition rel. to basic refractories 78−80528
MgO-Fe_2O_3, composition obs. by thermogravimetry 79−16081
MgO-Fe_3O_4-Cr_2O_3, isothermal sections, development of calculation data base 79−96006
MgO-Fe_xO_y-CuO, phase relations and microstruct. 79−74140
MgO-$FeCr_2O_4$, fused, thermoplastic and thermophys. props. for steel vacuuming installations 80−35281
MgO-FeO-P_2O_5 system, glass, ESR spectra, heat treatment conditions effect 79−65722
MgO-ZnO-Fe_2O_3 ternary system, phase equilibria 77−21116
Mg_2SiO_4-Fe_2SiO_4-$CaAl_2Si_2O_8$-SiO_2 system phase relations rel. to lunar basalts origin 78−65512
$(MgV_2O_4)_c(FeFe_2O_4)_{1-c}$, struct. parameters, IR spectra, cluster-component analysis 77−47425
MnFe ferrite, mechanically induced anisotropy, effect on mag. permeability 78−47970
MnFe ferrites, reson., effect of EM propagation 78−64277
$Mn_{1-x}Fe_xCr_2S_4$, Fe II electronic struct., Mossbauer spectra 80−15876
$Mn_{1-x}Fe_xP$, magnetisation, susceptibility and mag. transitions 79−47256
$(Mn_{1-x}Fe_x)_5Si_3$, solid soln., mag. transitions sp. ht., magnetisation and thermal expansion meas. 77−16075
$(Mn_{1-x}Fe_x)_5SiC$, magnitude of quadrupole splittings, Mossbauer study 78−43747
$(Mn_xSn_{1-x})Fe_2O_4$ thin film LPE on Bridgman grown Zn_2TiO_4 substrate 79−100065
$Mn_{1.18}Zn_{0.06}Co_{0.01}Fe_{1.75}O_4$, transport props. near Curie points 78−88100
N-Fe solid soln. in equilibrium with N_2 gas, partial molar enthalpy and excess entropy 80−60838
$(NH_4)_4Fe(CN)_6.1.5H_2O$, cryst. struct., and possible ionic transport mechanism 79−14758
α-$NH_4Fe(CrO_4)_2$, cryst. struct. *(French)* 77−47398
NH_4FeF_4, mag. and Mossbauer obs. *(French)* 78−19389
NH_4FeF_4, two-dimens. antiferromagnetism 77−66444
$N_2H_6FeF_5$, one-dimens. magnetism, mag. suscept. and Mossbauer reson. exam. 77−51893
$N_2H_6FeF_5$, one-dimens. antiferromagnetism 77−66444

iron compounds continued
$N_2H_6FeF_5$, one-dimensional antiferromagnetism, Mossbauer study 80−65872
Na-Fe fluorophosphate glass, EPR and Mossbauer resonance study 80−15838
Na-Fe fluorophosphate glass, Mossbauer study, mag. and optical props. 80−16065
$Na_4Fe(CN)_6.10H_2O$, single cryst., X-irradiated product ESR, 4.2K 77−48659
$Na_2Fe(CN)_5NO.2H_2O$, absolute Mossbauer fraction of ^{57}Fe nuclei 80−80648
$Na_2(Fe(CN)_5.NO).2H_2O$, powder, Mossbauer absorption in mag. field 78−68418
$NaFeF_4$, amorphous, Mossbauer study 80−39970
$NaFeF_4$, two-dimens. antiferromagnetism 77−66444
$NaFe(MoO_4)_2$, domain struct., phase transition, and dielec. props. 79−56748
$Na_2Fe_3(PO_4)_3$, synthetic alluaudite, cryst. struct. 78−83802
$Na_3Fe_2(PO_4)_3$, crystallographic data, ionic conductivity *(French)* 80−88077
α-$Na_3Fe_2(PO_4)_3$ orthophosphate, cryst. and vitreous, Mossbauer spectroscopy and mag. susceptibility *(French)* 80−80657
$Na_3Fe_2(PO_4)_3$, synthesis and cryst. struct. *(French)* 79−32964
$Na_{0.56}Fe_{0.28}Ti_{1.72}O_4$, non stoichiometric, X-ray cryst. diffr. determ., heavy atom method 79−4293
$Na_2Fe_2Ti_6O_{16}$ bronze, synthesis in $NaBO_2$, growth conditions *(French)* 78−43998
$Na_2Fe_2Ti_6O_{16}$, characterisation and mag. props., 90-800K, $Na_xTi_4O_8$ bronze isotypes *(French)* 80−39735
$Na_2Fe_2Ti_6O_{16}$, freudenbergite, cryst. struct. determ. 78−26519
Na_2O-B_2O_3-Fe_2O_3, and Na_2O-Al_2O_3-B_2O_3-Fe_2O_3 glass, Mossbauer expts., 85-500K 78−80260
Na_2O-B_2O_3-SiO_2:Fe_2O_3, effect of liquid phase separated structure on transparency in near UV and visible regions 79−4823
Na_2O-CaO-B_2O_3-Fe_2O_3 glass, Mossbauer expts., 85-500K 78−80260
Na_2O-CaO-SiO_2-Fe_2O_3 molten glass, optical props., temp. depend. *(French)* 80−100667
Na_2O-Fe_2O_3-SiO_2, Mossbauer spectra, crystallisation study *(Russian)* 79−19816
Na_2O-Fe_2O_3-SiO_2 glass, partially crystallised, mag. props. 78−23302
Na_2O-Fe_2O_3-SiO_2 glass and crystals, leucite type, Mossbauer ESR study of Fe^{3+} distrib. 79−65774
Na_2O-Fe_2O_3-TiO_2 ternary systems, X-ray investigation 79−51067
Na_2O-FeO-Fe_2O_3-SiO_2, chemical durability at different pH values 78−72902
Na_2O-FeO-P_2O_5 metaphosphate glass, internal friction *(Polish)* 79−96078
Na_2O-Li_2O-B_2O_3:Fe_2O_3, Mossbauer spectra, isomer shift and quadrupole splitting *(Korean)* 79−51889
Na_2O-SiO_2-CaO:Fe_2O_3, Mossbauer spectra, isomer shift and quadrupole splitting *(Korean)* 79−51889
Na_2O-SiO_2-Fe_2O_3, glass, X-ray absorpt. spectra, effective co-ordination charges 80−84805
Na_2O-SiO_2-H_2O-FeO system, 'heavy phase', recrystallisation and struct. 78−2089
NaOH:$Fe(Cn)_6^{3-}$, electron tunnelling, pulse radiolysis 80−108722
$5Na_2O.Fe_2O_3.8SiO_2$, glass crystallisation study by Fe^{3+} EPR and Mossbauer spectra 80−64904
$Na_20.3B_2O_3.xFe_2O_3$, borate glass, Fe^{3+} spin state and distrib. meas. 80−39966
$Na[Fe(CN)_5NO].2H_2O$, X-ray spectroscopy of single crysts., use of polarised radiation 78−8481
$Na_2[Fe(NO)_2(S_2O_3)]_2$, valence levels, X-ray photoelectron and X-ray spectra 77−88500
Ni-Fe_3O_4 system, interdiffusion 79−69301
$Ni_{1-3x}^{2+}Fe_{2+2x}^{3+}Vac_xO_4^{2-}$ (Vac=cation vacancy), solid solns., cryst. lattice imperfections 80−39069
$Ni_{0.6}Fe_{2.4}B_7O_{13}I$, boracite, orthorhombic-trigonal transition region, Mossbauer investig. 79−87342
$Ni_{0.6}Fe_{2.4}B_7O_{13}I$, boracite, mag. hyperfine interactions, Mossbauer study 80−39935
$NiFe_2O_4$-Fe_2O_3, effects of excess Fe_2O_3 on mag. props. 77−85495
$(Ni_{1-x}Fe_x)S$, solid solns., electronic props., X-ray, thermal and Mossbauer study 79−78376
$(Ni_{1-x}Fe_x)_{1-\delta}S$, anisotropic spin glass, mag. props. 80−39793
$(Ni_{1-x}Fe_x)_{1-y}S$, anomalous thermal hysteresis in metal-semicond. transition 80−39640
$Ni_{1-x}Fe_xS_2$ (x=0 to 0.075), weak ferromag. exam. 79−51755
NiO-CdO-Fe_2O_3 system, phase equilibria 79−11582
NiO-Fe_2O_3, isoelectric point meas. 80−88609
Os complex, 2,2′-bipyridine, visible spectra of cryst. 79−47424
PLZT, Fe doped, photochromic effect 77−16347
Pb_2FeReO_6, new seignettomagnets and ferroelectrics 78−19425
$PbFeTi(PO_4)_3$, cryst. struct. and prep., rhombohedral lattice *(French)* 77−27856
PbO-$2B_2O_3$-Fe_2O_3 glass, Mossbauer study, struct., crystallite formation, broadened quadrupole doublet 78−59761
PbO-Fe_2O_3 melt, used for growth of LPE garnet films, struct. and cond. 80−10808
PbO-SiO_2-Fe_2O_3(0,2,10 wt.%), conduction process 77−8096
$(PbO.2B_2O_3)_{1-x}(Fe_2O_3)_x$ glass, mag. resonance studies 79−78509
PbO.$3B_2O_3$:Fe_2O_3, EPR of Fe^{3+} ions 78−72400
xPb0.(1−x)B_2O_3:Fe_2O_3, Mossbauer spectra 79−87338
(1,10-phenanthroline-2-carbaldehyde phenylhydrazone) iron perchlorate, high spin to low spin transition, X-ray diffr. and Mossbauer obs. 79−38418
$RbFeCl_3$, linear chain cryst., quadrupole and mag. reson., rel. to $CsFeCl_3$ 79−38403
$RbFeCl_3.2H_2O$, pseudo-one-dimens. canted Ising antiferromag., spin cluster reson. 79−61235
Rb_2FeF_4, antiferromagnet, two-dimensional, mag. excitations 80−80492
α-Rb_xFeF_3, mixed valence compound, Mossbauer effect appl. to charact. 79−51883
Ru complex, 2,2′-bipyridine, visible spectra of cryst. 79−47424
S-Ni-Fe system containing monosulphide solid soln., elec. and struct. relations 80−90038
$SbNbO_4$:Fe_2O_3, growth, pyroelectric and ferroelectric props. 79−73886
$ScFe_{0.25}Si_{1.75}$, X-ray determ. of struct., new representative of struct. type $ZrSi_2$ 78−79595
$Sc_2Fe_3Si_5$, cryst. struct. determ. 78−18620
Se-Fe amorphous films, mag. and elec. props. 79−51695

iron compounds continued
SiO_2-Al_2O_3-CaO-MgO-FeO-Fe_2O_3 glasses, struct. transforms during heating 80−15014
SiO_2-Al_2O_3-Fe_2O_3-K_2O, form. of Al-Fe leucite, inversion temp. *(Japanese)* 77−62481
SiO_2-Al_2O_3-Fe_2O_3-CaO-MgO-Na_2O-SO_3 glass, thermophysical props. 78−18849
SiO_2-Al_2O_3-Fe_2O_3-CaO-MgO-Na_2O-B_2O_3-SO_3, exam. of white flaky inclusions, causes and formation time 79−29237
SiO_2-Al_2O_3-Fe_2O_3-CaO, basalt glass ceramics, crystallite form. due to heat treatment 80−38917
SiO_2-Al_2O_3-Fe_2O_3-Na_2O-K_2O-CaO-MgO glasses, Mossbauer spectra study 80−39967
SiO_2-Al_2O_3-FeO-CaO-MgO pyroxene glasses, phase changes 80−15013
SiO_2-Al_2O_3-Li_2O:TiO_2(ZrO_2),Fe_2O_3, pyroceramic glass, coloration, absorpt. spectra obs. 77−8615
SiO_2-Al_2O_3-MgO-CaO-Fe_2O_3, glass ceramic, crystn., microstructures rel. to conditions 80−11638
SiO_2-CaO-Na_2O-Fe_2O_3 system, water, alkali, acid resist., chem. durability 79−34162
SiO_2-Na_2O-CaO-MgO-Fe_2O_3-Al_2O_3-SO_3-Sn thermally polished, exam. of strength of surfaces 80−25887
$((SiO_2)_{45}(CaO)_{55})_{65}(Fe_2O_3)_{35}$ glass, effect of melt atmosphere on mag. props. 78−68299
$SnFe(CN)_6$, Mossbauer spectral anal. *(German)* 79−19819
$Sn_2Fe(CN)_6$, Mossbauer spectral anal. *(German)* 79−19819
$Sn_{0.225}Fe^{3+}_{0.575}Fe^{2+}_{1.465}Mg_{0.735}BO_3O_2$, hulsite, cation distrib., X-ray determ. 79−19225
Sr_2FeEuO_5, ^{57}Fe Mossbauer study 80−39976
$SrFe_6Ga_6O_{19}$ ferrite, mag. struct., Mossbauer study 80−93087
$Sr_6Fe_{10}O_{22}$-Fe_2O_3-$ZnFe_2O_4$ system, phase relations at 1100°C 78−68676
Sr_2FeReO_6, new seignettomagnets and ferroelectrics 78−19425
SrO-Fe_2O_3, EMF meas. with solid state cell, Mossbauer effect and magnetic props. *(Korean)* 77−28493
SrO-Fe_2O_3, splat quenching struct. and crystn. mechanism *(French)* 78−51426
$Sr[Fe(CN)_5NO].2H_2O$, cryst. and mol. struct. 78−91311
$Sr[Fe(CN)_5NO].4H_2O$, cryst. and mol. struct. 77−58982
$Tb(NO_3)_3$-$Fe(NO_3)_3$-$(NH_4)_2CO_3$-H_2O system, cpd. form., comp. and props. 80−100832
TeO_2-Fe_2O_3 system, glass structure 79−90562
TeO_2-V_2O_5-Fe_2O_3 system, phase equilib. and analysis, primary crystn. fields 77−66628
$Th_7Fe_3H_{14.2}$, Mossbauer spectra, mag. props. 80−15852
β-$TiFeH_{1.03}$, H diffusion, NMR meas. 80−10707
Ti(IV)-Fe(II) oxide, U adsorption, U extraction from seawater 80−24730
TiN-FeO, solid-phase reactions 79−11774
TiO_2-Fe_2O_3, comp. waves, Young's modulus minima rel. to crystallographic shear orientations 78−43034
$UFe_3B_2(B_4)$, Mossbauer effect of ^{57}Fe nuclei, mag. props. 80−103907
$V_{1-x-z}Fe_xMo_2O_2$, Mossbauer effect exam., Fe conc. and precise struct. characteristics 78−31141
$V_{0.986}Fe_{0.014}O_2$, metal-insulator phase transition, effect of hydrostatic press. 80−6725
$V_{1-x}Fe_xO_{2-y}$, Mossbauer effect exam., Fe conc. and precise struct. characteristics 78−31141
$V_{1-x}Fe_xO_{2-x}F_x$, $0<x<0.2$, phase diagrams, ^{57}Fe-Mossbauer spectra, X-ray diffr. studies *(German)* 80−29663
$V_{1-x}Fe_xO_{2-x}F_x$, $0<x<0.20$, magnetic susceptibility and electron cond. *(German)* 80−39754
V_2O_5-Fe_2O_3 solid solution, Mossbauer investig. of cryst. props. *(French)* 77−4592
V_2O_5-Fe_2O_3-Li_2O ternary system, charge compensation of Fe ions, Mossbauer obs. 78−52410
WO_3-$NiCO_3$-Fe_2O_3, reduction alloy form. 80−60801
$(Y,Sm,Lu,Cu)_3(Fe,Ge)_5O_{12}$, ion implanted, hard bubble suppression 80−11238
Y-Fe-O, phase equilib. and thermodynamics, solid state high temp. electrochem. obs. 79−56967
$Y_{3-x}Bi_xFe_{5-y}Ga_yO_{12}$-PbO-$B_2O_3$-$Bi_2O_3$ system, crystn. fields 78−43996
$(YEuYbCa)_3(FeGe)_5O_{12}$, garnet film, isolated straight stripe domain, dynamic behaviour 80−39809
YFe_2O_4, parasitic ferrimagnetism 79−4703
$Y_3Fe_5O_{12}$, amorphous, mag. moments, susceptibility, Mossbauer studies 79−78345
$(YGdYbBi)_3(FeAl)_5O_{12}$, epitaxial film, 360° domain walls with periodically distrib. Bloch lines 80−7127
YIG, crit. behaviour, Mossbauer and magnetisation meas. *(Russian)* 79−61106
YIG, double layer struct., LPE growth from molybdate and Pb borate fluxes 80−39827
YIG film, with periodic mag. struct., dispersion characts. anal. *(Japanese)* 79−42809
YIG, relax. after spin wave excitation in ferrite *(Russian)* 79−19783
YIG, substituted, magnetite nucleation in transitional zone, ionic process, lattice imaging 80−107424
YIG:Be^{2+}, LPE film, microwave relaxation props. 79−65741
Y_2O_3-Fe_2O_3-Ga_2O_3-PbO-P_2O_5, primary crystallisation regions 77−44222
Y_2O_3-Lu_2O_3-Eu_2O_3-CaO-GeO_2-Fe_2O_3-PbO-B_2O_3 system, garnet crystn. fields 78−43995
$Y(OH)_3$-α-FeOOH, physicochem. props. rel. to growth of $Y_3Fe_5O_{12}$ 77−40418
$(YSmLuCa)_3(FeGe)_5O_{12}$, bubble material, dynamic characterisation, comparison between transport and FMR methods 80−39833
(Zn,Fe)S (sphalerite), FeS content as geobarometer, experimental extension to 10 kbar 78−85703
Zn-Ti-Fe-O, spinel solid solns. 77−48409
$ZnFe_2O_4$-Fe_3O_4 solid solns., form. of α-Fe_2O_3 during oxidation 80−25889
$Zn_{0.005}Fe_{2.995}O_4$, phase transitions, neutron elastic scatt. and resist. meas. 77−28000
$Zn_xFe_{0.85-x}O$, prep. and struct., mag. and semicond. props. *(French)* 78−51506
$Zn_xFe_{3-x}O_4$, cond. mechanism, collective electron description 77−4588
$Zn_xFe_{3-x}O_4$ ferrite, mag. struct., Mossbauer spectra and magnetisation study, 4.2K 80−103818
$Zn_2Fe(PO_4)_2.4H_2O$, phosphophyllite, chem., optical and X-ray data 77−15366
(ZnFe)S, marmatite, optical properties 78−39555
$(Zn_{0.877}Hg_{0.116}Fe_{0.002})_{0.995}S$, unit cell dimensions *(Chinese)* 79−90616

iron compounds continued
ZnO-Fe_2O_3, isoelectric point meas. 80−88609
ZnO-Fe_2O_3:Fe, ceramics, impurity at. states, elec. cond. 79−11130
$((ZrO_2)_{0.92}(Y_2O_3)_{0.08})_{1-x}(Fe_2O_3)_x$, Fe solubility and elec. cond. 79−99354
$ZrSiO_4$-Fe_2O_3, pink colour form. kinetics 79−60360
$ZrSiO_4$-Fe_2O_3, solid soln. formation, zircon stability 77−48377
iron phosphate semiconductor glasses *see amorphous semiconductors*
irradiation effects *see radiation effects*
irradiation induced creep
alloy, order strengthening as method of reducing irradiation creep 77−48485
alloys, austenitic, neutron irradiation effect on tensile, creep-rupture, deform., fracture props. 79−65120
alpha irrad., 60 MeV 80−92597
anisotropic dislocation struct. effect on irradiation creep due to stress induced preferred point defect absorption 79−42140
bias factors, estimated from self-consistent model 80−88249
C, pyrolytic, electron induced irradiation creep, dislocation process obs. 77−47483
CANDU, stress anal. of fuel channel interaction with end shields 79−59161
carbide fuels, vibro-compacted, initial stages of sintering and hot-pressing 80−16254
ceramic fuel, irradiation device for creep and swelling study 77−42063
ceramic fuels, vibro-compacted, initial stages of sintering and hot-pressing 80−16254
ceramic nuclear fuel, irradiation induced creep 77−42056
ceramic nuclear fuel, model based on nonstationary creep in out-pile tests, neutron flux and stress depend. 78−17316
ceramic reactor fuel, nonsteady radiational creep, theoretical-experimental model 80−35282
climb-enabled glide of dislocations resulting from preferred absorpt. of point defects 79−82280
conference on fusion reactor materials [Miami Beach, Florida, Jan. 1979] 80−31407
correlation of theory with expt. evidence 80−88255
creep and growth, radiation induced, fundamental mechanisms 80−92596
cubic crystal, irradiation creep mechanisms, theoretical assessment 79−55817
defect precip. rate, solute effects 80−88252
deformation due to stress induced perferred adsorption induced dislocation anisotropy 80−75265
dislocation climb and glide 77−69009
dislocation glide enabled by preferred absorption of point defects 80−88250
Dounreay fast reactor creep-measuring machine 77−42015
Earth mantle, creep rate, influence of natural radioactivity 79−92520
EBR-II, duct dilation expts. 79−93702
EBR-II, multiaxial in-reactor creep in presence of significant void swelling 79−55818
EBR-II reactor components, creep and swelling 79−54499
elastomer, radiation mechanical props., creep *(Russian)* 77−16641
fast reactor steels and alloys, neutron damage development, irradiation conditions, chemical composition 80−34082
fast reactors Na cooled, core component material irradiation induced void swelling and creep, technological consequences summary 79−36327
FBR components, in-reactor creep measurements 79−57082
FBR structural materials, design appl. of irrad. creep and swelling data 79−59167
FCC materials, climb induced glide model 80−89292
fission reactor core system, bowed, NUBOW-3D program for static anal. including irrad. creep and swelling 80−5215
fission reactor materials, radiational growth due to diffusional anisotropy 79−71897
fisson reactor materials, irradiation induced creep, fundamental mechanisms *(Italian)* 80−55457
Frenkel pairs, unstable, mechanism for radiation stimulated processes in solids 80−34050
fuel element modelling, interpreting and predicting irradiation creep 77−42058
fusion reactor, stainless steel first wall, swelling and irradiation creep, FWLTB computer code 80−32446
fusion reactor materials, ion bombarded, swelling induced stresses, crystalline orientation effects 80−34093
fusion reactor materials, irradiation creep by the climb-controlled glide mechanism in Tokamaks 80−102304
fusion reactor materials, material requirements exam., review 78−50257
fusion reactor metals, He embrittlement, grain boundary cavity model 80−34075
graphite, creep irradiation expt., design, operation, initial results 77−42067
graphite, creep rig, high temp. 77−44423
graphite, irradiation induced creep, UKAEA reactor group studies 77−42065
graphite, reactor grade, irrad. creep, 850 to 1100°C 78−44167
graphite, reloadable creep facility for tensile or compressive expts. 77−42070
graphite, uniaxial tensile creep capsules with continuous strain registration 77−42071
graphite 77−42064
graphite 77−42066
HTR annular compacts, creep strain limit expt. 77−42069
HTR compact and matrix material, uniaxial creep meas. under tensile load at 900°C 77−42068
HTR reactor graphite, meas. 77−46279
in-reactor tests, meas. of creep information 79−83427
Incoloy-800, annealed, mech. behaviour anal. for elevated-temp. LMFBR appl. 80−18428
irreversible thermodynamics, appl. of internal forces concept 77−9971
light ion irradiation creep apparatus 79−70264
LMFBR, in-reactor irrad. creep expt., thermal anal. 79−67854
LMFBR core design, irradiation creep data 77−46211
LMFBR core materials, effect of swelling and creep on performance 78−13261
LMFBR fuel channels, measurement of irradiation creep in bending 80−104406
LMFBR performance, effects of irradiation creep and swelling 78−78482
irradiation induced creep continued
LMFBR permanent reactor structures, design, irradiation effects 78−21623
LMFBR reactor materials, simulation of void swelling and radiation-induced creep 78−8907
mechanisms, conference, Chalk River, Ontario, Canada (May 1979) 80−86031
metal, creep, point defects 78−48462
metal, irradiation creep and swelling, cascade damage effect 77−19991
metal, microstructural evidence supporting SIPA creep mechanism 79−61679
metal, radiation damage effects, neutrons and heavy ions, rel. to reactor technology, review 77−43255
metal, radiation stimulated diffusional flow, neutron irrad. *(Russian)* 79−29132
metallic materials, irradiation behaviour, review *(Italian)* 80−55457
metals, irradiation creep strain, produced by vacancy loops, calc. of magnitude 78−72815
metals, irradiation-induced creep, transient stage, vacancy loop contrib. *(Russian)* 80−29115
metals, radiation creep speed and swelling, self diffusion mechanisms *(Russian)* 80−92595
metals, radiation-induced creep and swelling, radiation dose depend. *(Russian)* 80−29050
metals and alloys, radiation damage prediction and measurement 78−75693
metals and alloys, stress relaxation, in-reactor study at low temps. 80−93588
metals under stress, thermally and radiation induced creep, constitutive relns. 77−90413
Nabarro-Herring creep, stress and irradiation induced mass transport, anal. soln. 79−60401
neutron, high-energy, apparatus for in situ creep testing during irradiation 79−79200
Nimonic PE16, irradiation creep data obtained in fast and thermal neutron spectra correlation with displacement cross-sections 80−84993
nonfissile metals and alloys 77−42072
nuclear fuel cladding, slightly oval cylindrical shells, creep anal. 78−78468
nuclear fuel compacts for HTR, irrad.-induced creep 78−44168
nuclear fuels, radiation enhanced kinetics in the fuel lattice 80−59522
nuclear fuels, transient state, kinetic eqn. treatment 80−88251
nuclear materials, conf., Petten, Netherlands (May, 1976) 77−42055
ordered alloy, point defect annihilation kinetics and correlation creep, analysis 78−75659
oxide fuel in reactor creep, LMFBR design aspects 77−42057
point defect absorption at dislocations 78−19842
point defect trapping, effect on irradiation induced creep and swelling 78−71756
point defect-dislocation interaction, radiation-induced creep, rate expression 78−87706
polyethylene, radiation heating effect 80−35285
polymer fibre, lifetime under load, in presence of UV radiation stress depend. 78−48534
polymer fibre, lifetime under load, in presence of UV radiation, stress depend. 78−48535
radiation creep rate as function of point defect formation rate and temp. 79−69187
rate equations, irrad. induced voids, swelling, creep 80−49274
reactor core bowing history computer program 79−9688
reactor fuel rods, cladded, thermo-irradiation induced creep, stress analysis 80−35275
reactor materials, radiation creep due to stress-induced preferential absorpt., theoretical model 79−89379
rubber, radiation heating effect 80−35285
SGHWR fuel pins, fuel cladding ratchetting study 78−54855
SIPA irradiation creep, material with preferred direction for dislocation Burgers vector, cold worked 79−20118
stainless steel, type 316, deuteron and proton bombarded, irrad. creep under stress 80−39209
steel, austenitic, types M316, FV548, 304, irradiation creep data obtained in fast and thermal neutron spectra correlation with displacement cross-sections 80−84993
steel, austenitic AISI 310, creep damage and rupture 79−20127
steel, austenitic cladding stability of fuel element for gas-cooled fast reactors *(Russian)* 77−83042
steel, austenitic stainless, creep, effect of temp. and dose rate variations, Dounreay fast reactor 80−93603
steel, austenitic stainless, creep dependence on electron irrad., in type SS316 steel, dislocation motion *(Russian)* 80−108495
steel, austenitic stainless, fast neutron irrad., effect on mech. props. 78−92309
steel, austenitic stainless, irrad. creep of type 316 in HVEM 80−97523
steel, austenitic stainless, irradiation induced creep, AISI 316, 20% cold worked effect of temp. change 78−72816
steel, austenitic stainless, irradiation induced creep by alpha particles, in type 316 steels *(French)* 78−72791
steel, austenitic stainless, multiaxial creep equations for nonlinear and volume-nonconservative in-reactor creep 79−59164
steel, austenitic stainless, type 316, deuteron bombarded 80−93606
steel, Cr-Mo (2.25, 1.0 wt.%), thermally aged and Na decarburised, stress-rupture props. 80−21102
steel, microstructure of 0Kh16N15M3B after creep tests in BR-10 reactor, electron, microscope invest. *(Russian)* 80−92531
steel, stabilised, pressurised capsules in-pile creep meas. 77−42077
steel, stainless, 20% coldworked 316, irradiation creep, depend. on temp. and atom displacements 77−42075
steel, stainless, 304L, irrad. induced creep and swelling 79−93723
steel, stainless, AISI 316, irrad. creep in bending at low fluence, LMFBR fuel duct deform. 79−61680
steel, stainless, cladding, irradiation enhanced creep 77−42074
steel, stainless, cold worked, 316, prior stress history effect on irradiation creep 79−87648
steel, stainless, dilation and bowing in EBR II ducts and cladding 80−625
steel, stainless, EBR-II fuel pin cladding, obs. of in-reactor creep and swelling 80−13600
steel, stainless, EBR-II reflector assembly irrad. induced bowing, implications for core restraint design 80−104234
steel, stainless, electron induced irradiation creep, dislocation process obs. 77−47483

irradiation induced creep continued
steel, stainless, fast neutron irradiated, solution annealed tubing, residual stress behaviour 80−65054
steel, stainless, FBR cladding stress distrib., effect of irradiation-induced swelling 80−19850
steel, stainless, in-pile creep measuring rig 77−42083
steel, stainless, irradiation creep and swelling, microstructural modelling 77−52407
steel, stainless, irradiation creep during 4 MeV proton bombardment 77−43256
steel, stainless, irradiation creep in bending 77−42078
steel, stainless, irradiation induced creep in BR2 reactor using resonant cavity method 77−42080
steel, stainless, neutron induced swelling, neutron flux and irrad. temp. depend. 78−79636
steel, stainless, proton simulation of fusion reactor first wall environment 79−24707
steel, stainless, solution annealed 304L, in-reactor deform. 77−42076
steel, stainless, type 304, previously irrad. in fast neutron flux 78−80600
steel, stainless, type 316, cold worked, effect of prior neutron irradiation on burst strength 78−62599
steel, stainless, Type 316 and 321, irradiation-induced creep following 4 MeV H^+ bombardment 78−14390
steel, stainless 304, previously irradiated, irradiation induced stress relaxation in fast flux environment 77−25104
steel, stainless 316, carbide precipitation rel. to in-reactor deform. 79−8302
steel, stainless creep behavior of ribbed cladding in prototypic GCFR coolant environment 80−16480
steel, tubular, type 0Kh16N15M3B, reactor irradiated, creep resist. *(Russian)* 80−25762
steel stainless capsules, soln. annealed He pressurised, type 304L, neutron irradiation-induced creep 79−42111
steels, austenitic and type 316, neutron irradiation effect on tensile, creep-rupture, deform., fracture props. 79−65120
strain measurement, design and construction of apparatus 78−15634
stress induced preferential attraction of interstitials to dislocations, contrib. to radiation creep 80−2064
stress-induced interaction between point defects and dislocations and irrad. creep 79−19313
stressed crystal, point defect interaction with dislocation 77−80537
temperature dependence 77−43252
transient irradiation environments 80−92598
vacancy dislocation loop contribution to irrad. induced creep rate 79−42141
void swelling and irradiation induced creep 77−44297
void swelling and radiation creep, bias factors in reaction-rate-theory anal. 79−46700
zircaloy, in-pile creep measuring rig 77−42083
Zircaloy, in-reactor creep meas. appl. in design of PWR fuel 77−42073
Zircaloy, irradiation growth in annealed and cold worked samples 77−88225
Zircaloy, PWR fuel induced cladding deformation, creep correl., in-pile meas. 80−97547
Zircaloy, textured, interactive creep and growth, upper-bound evaluation 80−89293
Zircaloy 2 irradiation creep strain meas. technique 77−42084
Zircaloy cladding tubes, under internal and external overpressure in FRG-2 in-pile creep 77−42082
Zircaloy fuel sheathing, NIRVANA high temp. creep model 79−87704
Zircaloy pressure tubes, effect of microstruct. on irradiation creep 79−74208
Zircaloy-2, anisotropic irradiation creep 79−8333
Zircaloy-2, irradiation creep under H^+ bombardment at 5.5 MeV 78−14392
Zircaloy-2, irradiation induced creep in reactor claddings under biaxial stress conditions 79−30912
Zircaloy-2, irradiation-induced creep following 4 MeV H^+ bombardment 78−14390
Zircaloy-2, pressure tubes, irrad. creep and growth, anisotropy factors 80−97536
Zircaloy-2, yielding creep theory, time depend. of irrad. growth 77−26845
Zircaloy-2 pressure tube, elongation in Douglas Point CANDU reactor 80−78398
Zircaloy-2 pressure tube elongation, neutron induced creep and growth, meas. and anal. 80−93628
Zircaloy-4, in-pile PWR creep meas., comparative eval. of 10 creep correl. 80−652
Ag-Zn (30 at.%), electron irrad. exam. of defect supersaturation by elasticity, and creep meas. 78−47366
Al, creep and dislocation struct., electron irrad. effects 80−49268
C materials, testing method 77−12769
Fe-Cr-Ni, solid soln. strengthened and precipitation hardened, in-reactor creep 79−43327
NaCl whiskers, X-irrad., stress oriented dislocation loop nucleation 79−33213
Nb, creep induced by neutron irrad. 79−74221
Nb, dislocation struct. after tensile creep test under reactor radiation conditions *(Russian)* 80−45348
Ni, creep, irrad. induced with 17 MeV deuterons 80−93607
Ni, creep, volumetric, irradiation induced, stress effect on swelling 77−43253
Ni, D bombardment, 22 MeV at 224°C 78−80597
Ni, deuteron irrad. induced creep mechanisms 80−39171
Ni, irradiation-induced creep following 4 MeV H^+ bombardment 78−14390
Ni, irradiation-induced creep, mechanism for large transient strains 78−14391
Ni, pure, irradiation creep during 4 MeV proton bombardment 77−43256
Ti-Al-Mo, type Ti-6242S, irrad. induced creep 80−39163
Ti-Al-Sn, type Ti-5621S, irrad. induced creep 80−39163
Ti-Al-V, irrad. induced creep 80−39163
Ti-V-Cr, type Ti-15-333, irrad. induced creep 80−39163
(U, Pu) C, nuclear fuel, irradiation induced creep meas. 80−93605
(U, Pu)C, ceramic fuel, plastic deform. behaviour at stress changes 80−35261
$(U,Pu)O_2$, in pile creep 77−42060
U-alloys, thermal creep and swelling, characterisation 79−74226
UN ceramic fuel, fission enhanced creep, in-pile meas. 77−67807
irradiation induced creep continued
UN, fission enhanced creep and swelling, in-pile meas. 77−42061
UO_2 and UC, creep props. under irradiation 77−42059
UO_2-PuO_2, ceramic fuel, plastic deform. behaviour at stress changes 80−35261
Zr alloys, creep and growth, irradiation induced, rate theory approach 80−89294
Zr alloys, creep and growth, irradiation induced, microstruct. depend. 80−93602
Zr alloys, factors affecting anisotropy of irradiation creep and growth, calcs. from crystallographic texture 79−83255
Zr, and its alloys, TEM obs. of irradiation damage, critical review 79−10879
Zr, electron induced irradiation creep, dislocation process obs. 77−47483
Zr, single crystal, irradiation creep 77−42081
Zr, yielding creep theory, time depend. of irrad. growth 77−26845
Zr-Nb (2.5 wt.%), channel tubes, in-reactor creep and irrad. growth 80−93604
Zr-Nb (2.5 wt.%), fuel cladding, anisotropy after creep and irradiaton 78−7001
Zr-Nb (2.5 wt.%), pressure tubes, irrad. creep and growth, anisotropy factors 80−97536
$ZrSiO_4$, heavy ion irrad., metamict zircon form. 80−2088

Ising lattices
see also Ising model
1-D with random transverse field at T=0, real space renormalisation group method 80−4656
Abelian and non-Abelian models, dual transforms., phase transition points *(Russian)* 79−2735
anisotropic 3-D Ising lattice 79−156
antiferromagnetic Ising model on triangular lattice, phase diagram, free energy 78−23283
approximate renormalisation group transformation, Kadanoff (1975) 77−33954
Ashkin-Teller-Potts model, in two dimensions, renormalisation group study 77−53837
Ashkin-Teller-Potts model, renormalisation group anal. 79−154
asymmetrical Ising model, phase transitions 80−17891
block spins, defined by random field, convergence 80−101759
boundary free energy, natural iteration and cluster variation methods, critical points 77−17913
cluster size and shape, Whitney polynomial 79−33080
cluster size and shape in random and correlated percolation 79−35633
cluster size distribution, percolation problems, asymptotic behaviour, essential singularity 79−2731
cluster statistics for random and Ising percolation 78−32766
coexistence curves for fourth-neighbour Ising models on FCC lattice 79−80543
collective excitations in 1-D systems with extended interactions 77−65006
confinement criteria for gauge invariant, lattice, and Abelian models 79−22023
connected diagram expansion for lattice Hamiltonian models 79−21916
correlation functions of general Ising Hamiltonians, renormalisation group calc. 77−9963
correlation length, renormalisation group calc. *(Russian)* 78−77811
correlation-function identities for general planar Ising systems 78−93616
critical behaviour, stochastic model simulation method 77−45804
critical behaviour of 3-D Ising model 80−4672
crystal growth, stochastic models, anal. treatment, comparison of two interface dynamics 77−89397
crystal growth, stochastic models, diffusion and relax. kinetics 79−37642
cubic lattices, fully frustrated, overblocking effect 79−69678
cubic lattices, fully frustrated, phase transitions, Gaussian and spherical model, free energy calcs. 80−60281
decimation transformation for 2-D and 3-D systems 78−12649
decimation transformations in lattice systems of continuous spins 79−25997
dilute frustrated lattice, spin-glass ordering, triangle and FCC lattices, Monte Carlo simulation 80−15746
dimer and Ising models on the Lobacheveskii plane 79−21677
double well model, Ising limit 80−62587
duality between blocked Ising models 79−12735
field theory, Ising model and scaling 77−5991
finite, series expansion anal. of crit. temp. shifts 79−61134
fixed points, determ. by lower bound renormalisation transformation 80−62586
fluid, classical, elementary molecular theory 77−19859
fractal lattices, crit. phenomena 80−105587
free energy, direct high-temp. star graph expansion 80−46985
free energy, derivatives, bounds, upper and lower, renormalisation group methods 80−68162
gas, Mayer cluster sums 79−153
generalised Glauber-Ising chain, dynamics in a mag. field, biopolymer appl. 79−155
Ginibre inequality, positivity and monotonicity 80−68141
Griffiths singularities of random harmonic chain 77−72665
ground state struct. in 3-D model with three steel interaction 79−21676
heteropolymer in random mag. field, Ising chains, statistical mechanics, free energy, numerical calcs. 78−77803
heteropolymers, melting theory, correlated chains 79−25996
heteropolymers, melting theory, random chains 79−25995
high temperature series renormalization group method 80−4660
high temperature-low field expansion, derived from low temp.-high field expansion 78−2636
high-temperature low field expansions extension 79−93045
impurity, soft, static and dynamic behaviour 77−72669
isoperimetric problems, convex-set theory and lattice symmetry 80−46988
kinetic, finite size effects in critical dynamics 80−46990
lattice gas, Ising-like, thermodynamic props., Monte Carlo calcs. 79−6054
lattice gases with linear clusters, phase transitions 80−90787
layered two dimensional Ising lattice, phase transitions, spin glasses *(Russian)* 80−65945
linear chain, kinetics, u.s. absorpt. in polypeptide solns. 77−4980
linear chain molecules, cooperative ligand binding, teaching approach 77−87610
lipid phase transition, cluster model, appl. to bilayer mol. passive permeation and struct. relax. 78−53346

Ising lattices continued
liquid-vapour transition, lattice gas model, nonsingular diameter without particle-hole symmetry 80−88311
low-temp. approach to renormalisation-group eqn. for lattice of discrete spins 77−61030
magnet coupled to isotropic elastic medium, first order transition, renormalisation method 80−68151
magnetisation probabilities and metastability 80−29516
Markov property, global, for + and − states 80−82725
microscopic free energy zero fluctuation 77−5740
monolayers of coadsorbed atoms, phase transitions 80−19909
Monte Carlo renormalisation group analysis, Ising model and three state Potts model calcs. 79−44880
Monte Carlo simulation of Ising chain showing several phase transitions 79−12732
Monte-Carlo method appl. to evaluation of Niemeijer-van Leeuwen cumulant expansion 78−16751
non-perturbative quantum field theory, lattice renormalisation construction 80−9098
one dimensional Ising system with random long-ranged interaction, density of eigenvalues of random matrix PV 79−12733
one-dimens. Ising model in external field 77−57284
one-dimensional compressible Ising chain with general spin 80−90791
one-dimensional system, thermodynamic limit, finite-range random interactions 77−45806
parametric eqn. of state 77−30102
polymer melt, eqn. of state analysis w.r.t. Ising fluid model 80−79907
polymer model equivalent 80−37914
position-space renormalisation-group transformations, problems and proofs 78−93619
protein folding, incorporation of 1-dimens. Ising model into 3-dimens. model 77−90723
random Ising model, press., variational principle 78−8352
random Ising model on cacti lattices 78−49773
real-space renormalisation giving differential renormalisation-group eqns., two-dimens. triangular Ising lattice 78−65881
real-space renormalisation group, dimensionality effect 80−77716
rectangular ferromagnet, pair correlation function using spinor technique 78−70063
recursive method in one-dimensional Ising model 80−90790
relaxation, 1-D Glauber model, effect of disorder 80−65761
renormalisation group recursion relations 79−97310
renormalisation group study of 2-D model with directional bonding 80−28894
renormalisation group theory, critical props. of generalised 2D Ising model 80−4665
renormalisation group theory, numerical method for calc. of free energy and correl. length of generalised Ising model 80−4664
renormalisation group transform., cell size effect on 1st order cumulant expansion 77−5772
renormalisation theory, variational principles 78−73951
renormalisation transformations, two- and three-dimens. models, cumulant expansion 77−49691
rotators, multicomponent, Gaussian inequality 78−29058
roughening transition, crit. slowing down of solid on solid cryst. surface model 77−5773
semi-infinite system, order-disorder transition, Landau-Ginzburg theory 78−47500
single-particle properties of systems undergoing struct. phase transitions 78−26654
spacial cluster or mixing props. in classical lattice systems 77−37818
spin systems on union jack lattice, non-universal behaviour of pair or three-spin interactions 80−57206
spin transformation, universality classes 79−17358
spin-1 Ising chain, sp. ht., presence of impurities and magnetic field 80−93128
square lattice, correlation functions of 2D fully frustrated Ising system 80−103805
stochastic eight-vertex model, universality in critical dynamics, Ising model appl. 78−41246
structural phase transformations in Ising universality class, real-space renormalisation calc. 80−39255
thermal relaxation, nonideal behaviour, stochastic theory 80−22312
thermodynamics of S=1 system, one-dimens., uniaxial anisotropy 79−49173
time dependent real-space renormalisation group for Ising system on triangular lattice, critical dynamics 78−60289
time-dependent Ising model, hydrodynamic soln. 79−54066
time-dependent Ising model and Cayley trees 79−75472
transverse 1-D model, dynamics 80−29515
triangular, with next nearest neighbour interactions, Monte Carlo calc. of order 77−53836
triangular and honeycomb lattices, triplet order parameters 77−87700
triangular Ising lattice, anal. of Kadanoff lower-bound renormalisation-group, approx. 80−8930
triangular Ising model coupled to honeycomb model via four spin interactions 79−30386
triangular renormalisation group transformation, var. approximation 78−49776
two dimensional spin s Ising system with lattice anisotropy, crit. props. 78−73932
two-dimensional, interstitial impurity effect on sp. ht. 77−89957
two-dimensional, Monte Carlo renormalisation-group method 80−4673
two-dimensional finite square, sp. ht. anomaly 80−27230
two-dimensional Ising system, phase coexistence, translation invariance and instability 79−80541
Union Jack lattices, non-universal Ising spin systems 80−68145
Fe-Al, spin glass transition, Monte Carlo study 80−39801
Fe-Al (0.27 to 0.50 at.%), spin glass behaviour, microscopic model, Ising lattice, exchange and superexchange 80−39800
$K_2Pt(CN)_4Br_{0.3}.3H_2O$, spin-lattice model for elastic anomalies 80−15179
ND_4Cl, order-disorder transformation, elasticity and heat capacity temp. depend., US obs. 78−71851
NH_4Cl, molar heat capacity near order-disorder transform. under high press. 78−51697
$SnCl_2.2H_2O$, layered, dielectric anomaly calc. using Ising model, possibility of antiferroelectricity 77−12341

Ising model
see also Ising lattices
1-D with random transverse field at T=0, real space renormalisation group method 80−4656
(2+1) dimensional Ising model, O(2), O(3) model in (1+1) dimens., finite lattice approach 80−86227
ϕ^4 fields, critical exponents and elementary particles 77−26243
ϕ^4 model, correlation length exponent, universality and twisted fans 77−2623
adamantane, Ising, diffuse scatt., hard-core correl., weak-graph method 80−49137
adiabatic susceptibility and specific heat at const. magnetisation 80−7114
adsorbate layer, phase transition theory, review 80−44433
adsorbed monolayer, classification of continuous order-disorder transitions 80−19910
adsorbed monolayer, phase transitions *(Russian)* 79−95269
adsorbed overlayer, order-disorder transition, Ising model, LEED superlattice beam intensity distrib. 80−65371
alcohols, H-bond system, liq., high-press. effect 80−49080
alkali halides, anomalous sp. ht. Ising model and Monte Carlo calcs. 78−47989
alloy, binary, quenched, computer simulation of cluster dynamics of two dimensional model systems 78−31434
alloy, binary, quenching, cluster growth, first order phase transition, computer simulation anal. 79−34039
alloy, FCC, binary, on Ising system, sublattice magnetisation, tricrit. point, simulation 79−33491
alloy, surface disorder, source of magnetism 79−56487
alloy between ferromag. and antiferromag. species, competing order parameters, Bethe-Peierls approx. 77−48003
alloys, AB stoichiometry, mean field theory of ordering 78−2233
alloys, binary, BCC, order-disorder transform., three-body interaction effects 80−39257
alloys, binary, ferromagnetism and spatial long-range order 80−60159
alloys and compounds, ordering, atomistic approach 79−94947
alternating spins of 1/2, and general S, appl. of transfer matrix method 80−80529
ammonium halides, phase transitions by Monte Carlo method using cubic Ising model 80−70408
amorphous antiferromagnetic finite chain, thermodynamic behaviour 79−61028
amorphous chain, thermodynamics 80−108022
amorphous Ising antiferromagnetic model, frustration effects 80−103838
amorphous semiconductor, cooperative charge disproportionations 80−54649
amorphous system, computer simulation 80−60299
amplitudes and extended lattice-lattice scaling 78−6495
anisotropic antiferromagnet, phase transition, with external mag. field 79−11316
anisotropic linear spin chain, two-magnon problem with arbitrary interaction radius 78−72320
anisotropic model high-field expansions, metamagnetic tricritical point 77−63198
anisotropic paramagnets, temp. depend. single ion excitation 79−33445
anisotropy, cubic, three-dimens., scaling-field study 79−73731
annealed magnetic mixture with continuous distrib. of random bonds 77−16023
antiferroelectric, Ising model with dipole interaction, crit. behaviour 78−48133
antiferromagnet, 3-dimens., with finite entropy at zero temp. 77−40021
antiferromagnet, anisotropic, correction to scaling in specific heat 78−80168
antiferromagnet, BCC, crit. behaviour in mag. field, Monte Carlo calc. 78−31088
antiferromagnet, BCC, in mag. field, Monte Carlo calcs. 78−31032
antiferromagnet, cluster approximation, Neel temp. and specific heat calc. 80−54901
antiferromagnet, crit. props., calc. 80−65946
antiferromagnet, disorded spin-flop, random-field effects 80−11208
antiferromagnet, FCC, mag. phase diagram, ordering, Monte Carlo calc. 80−103833
antiferromagnet, FCC, nearest neighbour interactions, Monte Carlo method 80−80544
antiferromagnet, finite field, second-order phase boundary, series investigation 79−42777
antiferromagnet, in mag. field, new perturbation approach 78−56336
antiferromagnet, induced staggered mag. fields, g-factor mechanism 77−55676
antiferromagnet, modified Kadanoff variational renormalisation method 80−88710
antiferromagnet, nonlinear response to high freq. mag. field, quantum theory *(Russian)* 80−93066
antiferromagnet, one-dimens., nonlinear dynamics 80−80521
antiferromagnet, phase boundary, crit. temp. field depend., Monte Carlo anal. 78−34995
antiferromagnet, phase boundary determ. by real space renormalisation group methods 78−88134
antiferromagnet, triangular, improved mol. field approach 79−73745
antiferromagnet, two-dimens., mag. susceptibility calc. 80−60225
antiferromagnet, two-dimensional, approx. to susceptibilities 78−47928
antiferromagnet, two-dimensional, expansion for susceptibilities 80−70963
antiferromagnet, with next nearest neighbour ferromag. interaction, tricrit. behaviour 77−40062
antiferromagnet, with zero field splitting, multicritical behaviour 77−12136
antiferromagnet chain, renormalisation group nearest neighbour interactions 80−60357
antiferromagnet with next-nearest-neighbour interactions, tricritical exponents and crossover behaviour 77−16089
antiferromagnetic, triangular, with transverse field, zero temp., ground-state props. 80−7115
antiferromagnetic 2- and 3-dimensional lattices, appl. of Kadanoff's variational approx. 80−2583
antiferromagnetic dilute-bond Ising model, spin-glass phase transition 77−69569
antiferromagnetic Ising lattice, degeneracy at crit. mag. field and zero temp. 79−8007
antiferromagnetic Ising model on triangular lattice, phase diagram, free energy 78−23283

Ising model continued
antiferromagnetic next nearest neighbour coupling, mean-field model and disorder points 77−69470
antiferromagnetic phase boundaries, hard-core lattice gas calcs. 80−80542
antiferromagnetic triangular cactus tree, bond-diluted, ordered phase 80−71037
antiferromagnetic triangular Ising model with anisotropic interactions, phase diagram 79−51798
antiferromagnets, disordered spin flop, bicritical behaviour, critical experiments 80−65899
antiferromagnets, magnetic susceptibilities in Heisenberg and Ising models 79−24185
antiferromagnets, n=4 type II, phase transitions, Landau Ginzburg Wilson Hamiltonian 80−15735
antiferromagnets in mag. field 80−11203
aqueous mixtures, lower crit. soln. pt. theory 79−4415
asymmetrical Ising model, phase transitions 80−17891
atomic order, interaction with localised ferromagnetism 77−72965
austenite, activity of C, computer simulation 79−37852
band-diluted random Ising model, criticality and crossover 78−56320
Baxter model and scale invariant field theory 78−32764
BCC and square lattices, crit. exponents, series-expansion approach 79−61138
BCC Ising model with competing interactions, fluction-induced first-order transition 80−20424
behaviour on closed Cayley tree 80−17886
Bethe lattice, bootstrap percolation 79−30376
Bethe lattice, Ising model with competing antiferromag. and ferromag. interactions, phase diagram 78−64177
Bethe-ansatz excitations, observability in Heisenberg-Ising spin systems 79−82738
bicritical points, eqns. of state, Ising-like ordered phases 77−55678
bilinear and biquadratic interactions, mag. transitions 78−23275
binary alloy, annealed Ising ferromagnet 78−47927
block spins, defined by random field, convergence 80−101759
block spins in the edge of an Ising ferromagnetic half-plane 79−47220
Bloom-Chapel model, phase transition 79−78418
Blume-Capel model for plane-triangular and FCC lattices 78−80114
Blume-Emery-Griffiths model, renormalisation group centred, tricriticality 80−42165
Blume-Emery-Griffiths-Potts model, 2-dimens., phase diagram and crit. props. 77−20620
bond dilute, bond-dil. two-dimens., phase transition 80−60320
bond-dilute two-dimensional, crit. behaviour 79−8009
bond-diluted, percolation-thermal crossover index calc. 80−11145
bond-diluted ferromagnet with first and second neighbour interactions 78−91870
bosonisation of Heisenberg-Ising chain, spin wave vel. calc. 80−54905
boundary free energy for phase interface, scalar-prod. expression, Ising model and cluster approx. 78−34591
Bravais lattice, ferromagnetic ground state conditions in Ising and Heisenberg models 80−50129
cactus tree, ferromagnetic and antiferromagnetic interactions 77−9964
Callan-Symanzik equation, perturbation analysis, crit. indices 78−52294
on Cayley tree, equilib. props. in external mag. field 77−59421
Cayley tree, phase transition of continuous order 79−40488
cell membrane nuclear hydrodynamic shear, non-equil. Ising model, master eqn. 78−61146
central peak with transverse field 80−7306
cerium ethylsulphate, elec. susceptibility evidence for electronically driven lattice dilation 77−76781
chain, in transverse field, correlation function from 1D $S=^1/_2$ X-Y model 77−77018
chain in 3-dimensional phonon field, rel. to spin-glass models 79−56540
chains, spin 1/2 Ising and classical Heisenberg models with alternating exhange, static props. 79−82737
classical, crit. dynamics simulation in transverse field 78−59930
classical, in transverse field, Monte Carlo simulation, statical props. 78−56326
classical, molecular dynamics exam. in transverse field 78−80115
classical, quantum renormalisation group approach 79−61126
cluster approximation for dilute Ising and Heisenberg ferromagnets, Curie temp. 77−89916
cluster expansion of partition function of Ising model 78−49759
cluster mean size in Ising model, series expansion 77−28350
cluster of two spins, time-depend. perturbation theory 77−45799
cluster shape and size in two-dimens. model 77−61024
cluster size and boundary distrib. near percolation limit threshold 77−20624
cluster size and percolation 79−65630
cluster size distribution 80−54855
clusters and Ising critical droplets, global phase diagram 80−100575
coexistence of phases, equiv. of different order parameter 78−49772
collective variables representation *(Russian)* 77−28353
collinear metamagnets, two-sub-lattice Ising model 78−95410
comb-like ramified linear structures, Ising model in transverse field 79−71374
commensurate phases, spatially modulated, in simple Ising model 80−79909
competing interaction systems, R-S model, series expansion and rigorous results 78−19201
compressible, critical behaviour at marginal dimensionalities 79−69677
compressible, elastic anomalies inducing first order transitions 79−47288
compressible, position space renormalisation group approach 79−56552
compressible, transform. into continuous spin Hamiltonian, renormalisation group treatment 77−66347
compressible crit. behaviour, applic. of renormalisation group methods 77−82464
compressible dilute Ising systems, critical behaviour 80−108017
compressible Ising double chain, mag. susceptibility and thermodynamic props. 79−15320
compressible Ising magnet, critical temperature shift due to spin-phonon interaction 79−99712
compressible random Ising model, crit. behaviour 78−80160
computer simulations of mag. model systems 80−65924
confluent singularities and hyperscaling in spin 1/2 model 79−73655
constant-coupling approx., successive phase transitions 80−97108
continuous Ising model, first and second order phase transitions 77−9965

Ising model continued
continuous spin Ising model, strong coupling expansion on ν-dimensional lattice 80−17888
continuous spin Ising model and $\lambda\phi^4_d$ field theory, high temp. anal. 79−63161
continuous spin systems, thermodynamic limit of free energy and correl. functions 77−9962
continuous symmetry breaking in Ising, XY- and Heisenberg model 79−82787
continuous-spin Ising ferromagnets phase transitions 78−60260
copolymer model with alternating spins, kinetics 80−9768
corner transfer matrices of eight vertex model, Ising model case 77−89915
correlated disorder in 1-D system at 0K 77−16022
correlation function identities for models with general interactions 78−95409
correlation function near free surface of Ising ferromagnet 78−21076
correlation functions of nondynamic interacting systems 78−57814
correlation index of Ising model with transverse field 77−63196
correlation inequalities for continuous-spin Ising ferromagnets 77−16020
correlation inequalities for ferromag. lattice models and Euclidean $P(\phi)$ theories 77−51865
correlation inequalities for Ising ferromagnets with symm. 78−21073
correlation quadratic identities, discrete-time Toda eqn. 80−105582
correlation-function identities and inequalities for Ising models with pair interactions 78−84375
correlations decay in SO(n)-symmetric ferromagnets 77−47956
coupled Ising chains, Monte Carlo anal. 79−42721
coupled Ising systems, variational renormalization group approach 77−2616
coupled one-dimens. system, first-order phase transition 79−42720
critical amplitudes, universal relations 77−66341
critical behaviour, non-universality in the Ising model with nearest and next-nearest neighbour interactions 79−44870
critical behaviour, scaling functions for quantum crossover 78−68249
critical behaviour in transverse field 77−66330
critical behaviour of Ising pair correlation function, density fluctuations *(Russian)* 77−33969
critical dynamics, real-space renormalisation group approach, Migdal approx. 79−63088
critical dynamics, real-space renormalisation group approach, Migdal approx., review 80−27257
critical dynamics, real-space renormalisation group approach 80−31699
critical dynamics, time-dependent real-space renormalisation group 80−60282
critical exponent γ estimates for 3-D model 79−12727
critical exponent γ for the three-dimensional Ising model 79−93051
critical exponents, determ. using Kadanoff lower-bound renormalization transform. 77−40074
critical exponents for high temperature series expansion 79−99701
critical exponents universality using entangled scale transform. on lattice 77−66346
critical indices, of 3-dimens. Ising model, high temp. series anal. 80−22295
critical isotherm of the four-dimensional Ising model 79−44871
critical phenomena, renormalisation group theory, numerical method for calc. of free energy and correl. length of generalised Ising model 80−4664
critical phenomena, use of renormalisation group, review 77−20625
critical properties, real-space renormalisation techniques 79−78420
critical properties and exact results 80−93129
critical props. of random mixtures, 3-D Ising model with Monte Carlo simulation 77−69573
critical systems, wall effects, scaling theory 80−80539
critical temp. for 2-D Ising ferromagnet with quenched bond disorder 78−56328
critical temperature, modulated Pade approximant 80−84605
critical temperature and sp. ht. in Ising model with regularly spaced blocks of impurities 77−69576
critical temperature for Ising systems with regularly arranged impurities 80−44785
critical temperatures of small clusters, Monte Carlo calc. 77−63209
critical wall perturbations and a local free energy functional for spin $^1/_2$ Ising model strip 80−80533
crystal growth disorder, 3D model, rel. between Ising models 79−51025
crystal growth-disorder models and Ising models 79−46585
cubic, site impure, crit. behaviour 77−66357
cubic Ising ferromagnet, three spin interaction effect on mag. props. 80−54910
cubic lattices, high temp. expansion at magnetisation of ninth order in Ising model *(Russian)* 80−54858
cumulant approximation is crit. region 78−76255
cumulant expansion in renormalisation group transforms, convergence 77−17915
Curie point in quenched bond model 78−56318
Curie-Weiss model, with bilinear and biquadratic interactions 78−41238
(d+1) dimensional, reln. with d-dimens. quantal spin systems 77−16031
decimation method for two-dimens. quantum model 77−47958
Devil's staircase and harmless staircase, oscillating interactions through elastic stairs or other harmonic fields 80−88296
diffusion in the one-dimensional Ising model 80−77719
dilute, macroscopically large system, observability of Griffiths singularity 77−63055
dilute ferromagnet, Ising model, crit. props. in percolation limit 79−1677
dilute ferromagnet, linear spin-wave theory, effective medium approach 80−20393
dilute ferromagnet, spin wave excitations, multicomponent CPA theory 78−68135
dilute ferromagnets, with site and bond disorders, Curie temp. 77−59407
dilute film, surface enrichment as possible source of surface magnetism 80−15731
dilute magnetic alloy, sp. ht. evaluation role of fluctuations 77−69580
dilute magnetic alloys, local mag. fields and fluctuations 77−40061
dilute magnetic systems, with nearest-neighbor and next-nearest neighbour interactions, crit. temp. 79−61121
diluted antiferromagnet, linear spin-wave theory, effective medium approach 80−20393
diluted ferromagnetic systems, cluster theory, second-neighbour interaction 77−89965
diluted Ising and Heisenberg magnets with competing interactions, phase diagrams and mag. props. 80−34672

Ising model continued
diluted systems with competing interactions, mag. ordering, appl. to $Eu_xSr_{1-x}S$ 80−65914
(2+1/N)-dimensional, XY model in 1+1/N dimensions 79−93071
dimerised Ising chain, free energy, mag. moment, static susceptibility 77−55651
dipolar antiferromag., phase transition at negative absolute temp., Monte Carlo procedure *(Russian)* 78−43594
dipolar ferromagnet, renormalisation group appls. to critical phenomena 77−57296
disorder points, correspondence to cryst. growth model model 77−47366
disorder variable, quantum field operators of D=2 Ising model 78−32773
disordered, dynamics in transverse field 77−59367
disordered, two-dimens. Ising models, real space renormalisation group 79−42788
disordered chain, linear renormalisation transformations, appl. to dil. soln. model 78−34941
disordered chains, ferromag., long-time relax. 80−34652
disordered Ising chain, equivalent formulations for thermodynamics 77−28346
disordered Ising model at low temperatures, thermodynamic pot., ferro- and antiferromagnetic bonds, mag. moment and entropy *(Russian)* 79−19714
disordered Ising model on Cayley tree, mag. transition above percolation threshold 79−73757
disordered Ising spin chains in mag. field 78−57869
disordered Ising spin system on Cayley tree 79−51783
disordered magnet, effective field approx. 77−8261
disordered magnet, spatial correl. of spins 78−23276
disordered one-dimensional system, Hubbard model 78−10642
disordered spin systems, crit. dynamics 77−43844
disordered spin systems, dynamic crit. behaviour 77−66343
displacive phase transitions in discrete cubic model 77−32198
DNA, soln., phase transitions, light absorption oscills. obs. 80−26197
DNA solution, thermodynamic props., phase transition, one-dimens. Ising model study 79−16125
domain wall parameters, temp. dependences 79−69797
domain wall type soln., transverse field model 78−14917
double Ising chain, model in external field *(Russian)* 79−82735
double Ising chain, model in zero external field *(Russian)* 78−84430
double Ising chain, transverse susceptibility *(Russian)* 80−88727
double spin $^1/_2$ lattice gas model, phase diagrams 77−20521
duality relations and replica method 80−77222
duality transformations, interfacial energies and correlation functions, 2D Ising model 78−24741
dynamic critical phenomena, real-space renormalisation group methods, appl. two-dimens. kinetic Ising model 78−77810
Dyson's hierarchical model, essential singularities of borderline Ising case 78−31077
Dyson's hierarchical model, one-dimens., crit. props. 77−79038
dysprosium ethylsulphate, pure dipolar Ising ferromag., critical thermodynamics 77−16095
education, linear chain Ising model, energy states 77−33779
Edwards-Anderson spin glass model in two dimensions, numerical results 80−97100
effective field theory 79−4684
effective field theory 80−7116
eight-vertex and q-state Potts model, relation between temp. exponents 79−93055
elastically coupled, effects of dipolar forces on crit. sound attenuation in uniaxial systems 80−50158
equilibrium characteristics in the condensed state with the nearest-neighbours interaction *(Russian)* 79−12726
equivalence of (d+1)-dimensional Ising systems of arbitrary spin to a d-dimensional spin-$^1/_2$ quantum system 79−73657
equivalent neighbour model, high-temp. series expansions 79−44877
exact differential renormalisation at criticality 79−73755
exact renormalisation group equations 79−73749
exactly soluble with new boundary conditions 77−85472
exchange-type kinetic, early stage evolution of quenched binary mixture 77−69468
extremal Λ-inequalities for Ising models with pair interactions 79−56485
FCC Blume-Capel model, Monte Carlo study 80−103453
FCC continuous spin model, universality and confluent corrections to scaling 77−24663
FCC Ising ferromagnet., cluster variation approx. 78−68278
FCC lattice, phase transitions of fully frustrated models 80−29517
ferrimagnets, one-magnon light scatt., temp. dependence, two-sublattice systems 78−31061
ferro and antiferromagnet random bond mixture, on s.c. lattice, phase transition 77−12131
ferrodistortive spin-phonon systems, crit. props. 80−88315
ferroelectric, anomalous sp. ht. Ising model and Monte Carlo calcs. 78−47989
ferroelectric, H-bonded, central peak, thermal cond. 80−93250
ferroelectric, relaxation processes, cluster approx., complex dielectric const. *(Russian)* 80−11352
ferroelectric, transverse Ising model, mean-field approach 77−28528
ferroelectric, uniaxial, crit. behaviour, electrostrictive coupling role 80−71329
ferroelectric, uniaxial, dipolar crossover effects from Ising crit. behaviour 77−89961
ferroelectrics, central peak in Ising model in transverse field, mode-coupling theory 80−75987
ferroelectrics, order-disorder, pseudo-one-dimens. kinetic Ising model 80−71333
ferromagnet, 3-D, critical behaviour in random mag. field 78−68250
ferromagnet, 4-D, correction to leading singularity of order parameter 80−25061
ferromagnet, amorphous, Ising model, Curie temp., exchange integral fluctuation effects 80−50121
ferromagnet, anisotropic, in external mag. field, continuous phase transition existence 80−108011
ferromagnet, annealed Ising, of binary alloys 77−59368
ferromagnet, correl. functions, boundary conditions 78−27009
ferromagnet, crit. correlation-function approxs. 78−56324
ferromagnet, crit. exponents in integral representation 78−56325
ferromagnet, crit. props. of site and bond diluted Ising model 79−42766
ferromagnet, critical behaviour at field-induced transition at mag. displacive limit 77−66335
Ising model continued
ferromagnet, diamond lattice, phase transition, crit. props. 80−93127
ferromagnet, diluted, theory generalisation 79−78283
ferromagnet, disordered, approximate treatment 78−52262
ferromagnet, disordered, short-range mag. order 80−50119
ferromagnet, equivalence of different order parameters 77−36082
ferromagnet, exponent inequalities at roughening transition 77−32204
ferromagnet, FCC, cluster variation approx. 78−27049
ferromagnet, four-dimensional, logarithmic correction to mean-field order parameter 79−73754
ferromagnet, gaussian fluctuations of mol. field, magnetisation and free energy 80−70918
ferromagnet, general Ising, Lee-Yang theorem GHS inequality, spin-$^1/_2$ approx. 77−20524
ferromagnet, in mag. field, new perturbation approach 78−56336
ferromagnet, Ising, with transverse single-ion anisotropy, phase transitions 78−19259
ferromagnet, Ising amorphous, crit. temp. 80−11207
ferromagnet, Ising-Heisenberg-XY crossover, bicritical-point, partial differential approximants for susceptibility series 77−85466
ferromagnet, linear Ising-Heisenberg, spin waves vs. bound states, exact soln. 78−68202
ferromagnet, linearisation assumption, crit. correlation function 80−60158
ferromagnet, one-dimens., symm. crossover from Heisenberg to Ising behaviour 79−87269
ferromagnet, one-dimens., with mag. impurity, one-magnon states 77−36042
ferromagnet, one-dimens., with phase transition, thermodynamic props. calc. 80−80536
ferromagnet, percolation threshold, real-space rescaling approx. 77−40073
ferromagnet, phase boundary rigidity, Onsager Temperley model 77−28394
ferromagnet, phase coexistence, translation invariance and stability 80−80513
ferromagnet, phonon thermal cond., crit. anomalies *(Russian)* 78−80159
ferromagnet, randomly dilute, conc. expansion study 80−60315
ferromagnet, randomly dilute, determ. of transition temp. by Monte Carlo simulations 77−12130
ferromagnet, randomly dilute, essential singularities 77−20615
ferromagnet, randomly dilute, with second neighbour interaction, concentration expansion study 77−85452
ferromagnet, rectangular, n-point functions 77−63054
ferromagnet, rectangular, n-point functions 78−76250
ferromagnet, rectangular, susceptibility, determ. of critical indices 79−28537
ferromagnet, rel. to plane rotor 80−60348
ferromagnet, renormalised crit. behaviour 78−52272
ferromagnet, rigorous inequality for sp. ht. 79−78413
ferromagnet, S=1, single-ion type uniaxial anisotropy, cluster-variation method appl. in pair approx. 78−68281
ferromagnet, site diluted, crit. props. 78−72351
ferromagnet, spin 1/2, integral representation 78−2639
ferromagnet, spin 1/2 three-dimensional model, transition temp. in integral representation 77−77059
ferromagnet, spin S, integral representation 78−43543
ferromagnet, spin-1, with random anisotropy, Curie temperature 77−28399
ferromagnet, spin-one, uni- and biaxial anisotropy, phase transitions 78−34989
ferromagnet, spin-operator reduction relations, representation 78−95443
ferromagnet, spin-s Ising model, crit. curve 79−4679
ferromagnet, surface tension using real-space renormalisation group methods 79−73760
ferromagnet, three-dimens., transition temp. with two- and four-spin interactions 79−42769
ferromagnet, transition point calc. 80−20408
ferromagnet, two-dimens., order parameter and induced susceptibility 80−71036
ferromagnet, two-dimens., surface tension of diagonal interface 77−59369
ferromagnet, two-dimensional, with second-neighbour interaction, computer simulation, series-expansion method 77−63052
ferromagnet, uniaxial, dipolar crossover effects from Ising crit. behaviour 77−89961
ferromagnet, uniaxial dipolar, crossover behaviour, theory 80−29559
ferromagnet, upper bounds for correlation functions 79−42718
ferromagnet, with antiferromag. next-nearest-neighbour coupling, relative mag. scattering intensity and anomalous scatt. 77−69469
ferromagnet and antiferromagnet, two-dimens. square, ground state, apparent 3-spin interactions 80−88709
ferromagnet and spin glass systems, random, crit. dynamics 80−34666
ferromagnet of spin 1/2, Lee-Yang theorem 78−45572
ferromagnet ordering conditions 79−42719
ferromagnet with two- and four-spin interaction, improved product average decomposition method 80−20406
ferromagnet-spin glass transition, Monte Carlo calc. 80−60287
ferromagnetic, anisotropic, Green-function theory 77−16025
ferromagnetic, band-mixed square-lattice, approx. crit. surface 80−70921
ferromagnetic, Diophantine moment problem and analytic struct. in activity 79−61026
ferromagnetic and antiferromagnetic susceptibilities, with transverse field 80−60160
ferromagnetic binary alloy, atomic and mag. ordering, critical slowing down 78−14915
ferromagnetic fluid, 1D Ising and 3D Heisenberg solns. 77−85478
ferromagnetic ground state, threshold inequalities 80−7064
ferromagnetic half-plane, surface, pinned domain wall, free energy and magnetisation profile 80−60361
ferromagnetic Ising chains, metamagnet, absence of first-order transitions 79−51794
ferromagnetic Ising model, spin-one three dimensional, single-ion anisotropy, crit. behaviour 80−80540
ferromagnetic mixed Ising model, renormalisation group calc. 79−56547
ferromagnetic planar Ising model, spinor algebra and odd operators 78−45570
ferromagnetic state, random field instability 77−40072
ferromagnetic systems, relation between quenched and annealed random systems 79−82794

Ising model continued
ferromagnetic-antiferromag. mixture, triangular cactus tree, statistical theory of bond-random Ising model 80−75702
ferromagnetic-paramagnetic transitions, critical surface calc. 79−4692
ferromagnetically coupled semi-infinite, with free surface, renormalisation group approach 78−14975
ferromagnetism, basic models, classification of theories *(Rumanian)* 78−91840
ferromagnetism, microcanonical high-temp. expansion 78−2638
ferromagnetism, nonuniform mag. field method, crit. correlation function approximations, calc. 80−20407
ferromagnetism, percolation theory 77−61022
ferromagnets, 2-D, boundary conditions and cluster property, translation-invariant correlation functions 80−54856
ferromagnets, coexistence of phases, new inequalities 77−80946
ferromagnets, correlation decay, zero-field susceptibility, mass gap 80−50116
ferromagnets, high-freq. props. quantum theory, susceptibility tensor calcs. *(Russian)* 80−11143
ferromagnets and pyroelectrics, internal energy relationship to moment 77−16028
ferromagnets with biquadratic exchange, uniaxial anisotropy, susceptibility calc. 79−99670
field theory, 2-D, $T<T_c$, three point function string structure 79−270
field theory 2-D, $T<T_c$, Green's function strings in n-point functions 79−271
field theory in mag. field, cut breakup in two point function 79−272
film, diluted, surface and bulk magnetic phases 79−82797
finite, statistical mechanics 77−36081
finite amorphous Ising system, exact ground state calcs. 79−12725
finite arrays of coupled chains, exact soln. 77−4485
finite one-dimens. Ising systems, renormalisation group transform. 79−40485
first order phase transitions, droplet models, renormalisation, singularities 80−95050
first-order phase transition, nonlinear relaxation, Ginzburg-Landau theory including fluctuations 79−35658
Fisher renormalised Ising exponents in compressible spherical model 77−30113
five states discrete vector model, transition point 80−157
fluctuations and FKG inequalities 80−77712
four-dimensional Ising-like model, excitation spectrum, mol. dynamics 78−95411
fractal lattices, crit. phenomena 80−105587
Fredholm determinant representation, Ising model two-point function 78−54314
free energy, recursion method calcs. 78−52186
free energy, variational calc. for 3 dimens. system 80−42167
free energy analytic continuation and eigenvalue analytic continuation 77−26236
free energy and susceptibility inequalities for Ising models, phase transition 78−43541
free energy upper bound by renormalisation group methods 77−61026
frustration network, phase transitions 80−2596
frustration pots., phase transition 80−52142
functional integral method appl. to classical and quantum spin models 80−15676
gauge field models, universality 80−18068
gauge invariant Ising model, statistical mechanics, phase struct. 79−71373
gauge theories, large space-time dimension, strong coupling phase 80−27397
gauge theory phases 79−97486
generalised compressible, one-dimens., exact thermodynamics, renormalisation group method 77−20525
generalised Glauber-Ising chain, dynamics in a mag. field, biopolymer appl. 79−155
Gibbs states, non-translation invariant with coexisting phases, analyticity 80−8923
Ginibre inequality, positivity and monotonicity 80−68141
GKS and correlation inequalities for model with random interactions 78−34940
Glauber-Ising model, 2-dimens., crit. dynamics, real-space renormalisation group theory 78−70070
Glauber-Ising model, crit. showing-down of energylike perturbation, renormalisation group anal. 79−61133
Glauber-Ising model, real space-time depend. renormalisation group 78−49774
Green's function theory of systems with dipolar and quadrupolar pair interactions 77−63222
Green's two time functions in model with transverse field 80−2543
Green functions, commutator and anticommutator, in Ising model with transverse field 78−76211
Griffiths inequalities, generalisation 77−32141
Griffiths singularity, and upper bounds on cluster distrib. functions 79−7958
Griffiths singularity in a non-dilute Ising chain 79−78285
ground state spin orderings, several neighbour interactions, appl. to HCP lattice 77−4483
hard-core square lattice gas, 3-parameter isotropic atom distrib. 78−24740
harmonic analysis and generalised GKS inequalities 77−30112
Heisenberg-Ising bonds, randomly mixed three dimens. system, critical props. 78−76249
Heisenberg-Ising chain, correlation functions at T=0 79−24123
Heisenberg-Ising magnets, random, critical temps., binary mixture, amorphous magnet and spin glasses 80−54911
Heisenberg-Ising spin chain quantum inverse scatt. method, Jordan-Wigner transformation 80−93068
Helmholtz free energy, approx. expressions 77−16024
hierarchical model, critical and tricritical behaviour 78−10712
high temperature expansions of arbitrary magnetisation 77−43800
high temperature series expansions, hyperscaling 77−37823
high temperature-low field expansion, derived from low temp.-high field expansion 78−2636
high-field expansion constraints for Ising and crystal growth models 77−58964
high-temperature expansion methods for Ising system with quenched impurities 79−78422
high-temperature low field expansions extension 79−93045

Ising model continued
honeycomb lattice, real space renormalisation, ferromag. (antiferromag.) appls. 80−11200
hydrogen-bonded ferroelectric, Ising model in transverse tunnelling field and proton-lattice interaction 80−7307
hyperfinite spin system, Markov semigroup, phase transition, nonstandard anal. 79−97302
hyperscaling, renormalisation group theory examination 77−66337
hyperscaling in 3-D spin-1/2 model, limitations of high-temp. series terms 79−93052
impure Ising paramagnet, influence of spatial short range order 78−43542
impurities, local crit. behaviour 77−48001
impurities and probe independence of hyperfine crit. exponents 79−87267
impurity effects on at. ordering-spontaneous magnetisation reln. in BCC magnetically ordered alloys *(Russian)* 78−19261
impurity uniaxial ferromagnet, thermodynamics below Curie point *(Russian)* 77−43801
incommensurate phase transition, Bethe-Peierls and mol. field approx. 80−20599
independent chains in transverse field, equivalence with spin 1/2 dimerized XY chain 79−19713
induced moment paramagnet, singlet ground state, mag. fluctuations 77−4482
inequalities in classical lattice and continuum systems 77−90
infinite, metastable states 80−34577
inhomogeneous mixture of Ising and Heisenberg substances, quenched system, critical temp. 80−88770
insulating systems, magnetic, review of expts. 78−68240
interacting linear Ising spin chain, phase transitions *(Russian)* 80−70920
interface entropy, phase transitions in frustrated Ising systems 79−19711
interface free energy 78−60261
interface free energy and crit. line, nearest and next nearest neighbour interactions 78−39352
interface free energy and transition temp. 77−73041
interface roughening transition, Monte Carlo study 77−67384
Ising chain in transverse magnetic field, SLAC renormalisation group approach 79−67476
Ising metamagnet, dilute tricritical point calcs. 80−50099
Ising model, convergence of Feynman diag. expansions 78−16750
Ising model, renormalisation of the interaction amplitude 79−30384
Ising spin gass, glass, Edwards-Anderson order parameter instability 80−71043
Ising spin system, coupled to acoustic and optic lattice modes, critical behaviour 80−71044
Ising system, two-state, crit. behaviour, Bragg-Williams approx. calcs. 78−86223
Ising-system, two-state, crit. behaviour, Monte Carlo calcs. 78−86222
isobutyric acid-water system, liq.-liq. critical pts., Ising exponents, extended scaling 77−20072
isotropic Lifshitz point in $2<d<4$ dimens. 78−29062
Kadanoff's variational approximation applied to the 2-D antiferromagnetic Ising lattice 79−73659
Kadanoff block transformation by Monte Carlo technique 77−69574
kinetic, crit. dynamics, real-space renormalisation group study 78−49785
kinetic, exact susceptibilities and spin flip rates 80−7063
kinetic, Migdal type renormalisation group calcs. 79−93069
kinetic, nonlinear crit. relax. 77−32140
kinetic, nonlinear critical relaxation 78−34988
kinetic, pseudospin formulation 78−10634
kinetic, quenched relaxing impurities, crit. dynamics 78−10167
kinetic, reliability of real space renormalisation approach 80−90793
kinetic, with triplet interactions, Monte Carlo study 80−7061
kinetic chain relaxation, randomly signed exchange 80−70919
kinetic Ising chain, renormalisation group transform. for master eqn. 80−11214
kinetic Ising model, physical content, Glauber methods 77−12074
kinetic Ising model, quenched relaxing impurities, critical dynamics 79−40484
kinetic Ising model in Bethe approx., nonlinear cooperative system 77−13709
kinetic model, nonlinear crit. slowing down, first moment relax. time 77−51910
kinetic model of ferromagnetism, simulation of equilib. critical props. 78−89410
kinetic one-spin-flip model, metastable state lifetime, size depend. 77−69472
kinetic processes, 1-D chain, magnetic relaxation, quantum stat. mechs. 80−80471
kinetic processes, reduction of statistical description of system during evolution 80−80470
kinetic Weiss-Ising model, birth and death process, relaxation mode anal. 77−49681
Kramers-Wannier transform. for systems with Z(n) symmetry *(Russian)* 78−77812
Landau's second-order phase transition theory, appl. to two order parameters systems, Ising model 78−43599
lattice gauge theory and spin systems review 80−22528
lattice spin systems, matching conditions for crit. props., group struct. of block transforms 80−22305
lattice-lattice scaling, reln. to scaled eqn. of state, appl. to Ising model 78−70067
layered Ising model, spontaneous magnetisation, spatial variations 77−16029
layered two dimensional Ising lattice, phase transitions, spin glasses *(Russian)* 80−65945
Lee-Yang branch point and crit. behaviour 78−68253
Lee-Yang theorem on generalised models with degeneracy 78−65879
Lifshitz point, ferromag., renormalisation-group anal. of crit. modes in cryst. systems 79−82806
Lifshitz points, phase diagram transition temp. determ. interface free energy vanishing 79−99716
linear, in 3D phonon field 77−73036
linear chain, disordered, q-depend. mag. susceptibility 78−27010
linear Ising chain, differential real space renormalisation 79−85092
linear Ising chain in mol. field 79−61027
linear Ising mixture, frozen system, thermodynamic props. 77−40064
linear Ising-Heisenberg ferromagnet, excitation spectrum and thermodynamic props. 80−50118

Ising model continued
linear Ising-Heisenberg ferromagnet, spectrum of elementary excitations 79−61091
linear spin chains interacting with asymmetric pot. *(Russian)* 79−93074
liquid crystals, generalised Suzuki formula application *(Chinese)* 80−107045
liquid-gas transitions in the spin-1 asymmetrical Ising model 79−42212
local magnetisation, semi-infinite 2-D Ising model 80−71074
long-range interaction in Ising model, dynamical props. 80−100593
looped tree-like lattice, phase transition 80−7113
low temp. expansions for 4-D simple hypercubic lattice 79−61025
low temperature expansion data for cubic and quadratic lattices 80−42155
macromolecular systems, phase transitions, temp. and press. depend. theory, Ising model appls. 78−43105
magnet coupled to isotropic elastic medium first order transition, renormalisation method 80−68151
magnetic alloy, binary, spinodal decomp. modelling at interface 80−84913
magnetic binary alloy, computer simulation, time evolution 79−56488
magnetic binary alloys, phase separation, double Ising system 78−91835
magnetic field and lattice gas 78−10703
magnetic gap, soliton bound states in Ising model, quantum double sine Gordon eqn. solns. 79−78288
magnetic mixture of triangle-bond elements 77−69467
magnetic resonance, in 2-D Ising model, appl. to $FeCl_2$ 79−47323
magnetic specific heat, effect of spin-lattice coupling 78−80157
magnetically dilute ferromagnets, Curie temp. 79−11312
magnetization reversal of the two-dimensional Heisenberg ferromagnet with weak Ising anisotropy 80−107977
many point correlation functions, two dimens. model 78−16744
Markov chains in 2-d Ising lattice gas model 79−88885
master eqn., dynamical renormalisation group transform., Ginzburg-Landau model, kinetic Ising model 80−42170
Mattis model, modified, mag. relax. 80−65947
maximum susceptibility locus crit. behaviour 80−71040
mean cluster size near T_c, exponent interpretation 77−37820
metal-insulator transition, Ising model, for transition temp., Green's function calc. 79−15084
metamagnet, compressible, renormalisation group theory of pseudocritical point 80−60337
metamagnet with dilution, variation of tricrit. point 79−87266
metamagnetic Ising model, phase diagram and crit. points, const. coupling approx. 78−34991
metastability in 2-D model 79−58648
metastability in two dimensional Ising model, dynamic Monte Carlo method, transfer matrix 78−72354
metastable, in negative field, near criticality 80−84608
MFA transition temp. for transverse Ising model, ferroelectric with dipolar interaction 78−31161
microscopic theory of formation of macroscopic order 80−42164
mixed, spin-$^1/_2$ Ising ferromagnet, crit. props. 80−34655
mixed ferromagnetic Heisenberg and Ising bonds, appl. of effective Hamiltonian method 80−50023
mixed ferromagnetic-antiferromagnetic systems with arbitrary spin, critical temp. 79−78407
mixed Ising and Heisenberg coupling, crit. props. 78−19256
mixture, binary, off-critical, quenched, struct. functions and mobilities renormalisation 79−82343
mixture, one-dimens., random, of Ising S=1 and $^1/_2$ spins, mag. props., spin distrib. 78−95407
modified F model, rel. to nearest-neighbour Ising model, crit. polarisation 79−93058
modular group and dimer problem, Ising model 77−5763
modulated phase with solitons, phasons and devil's staircase 80−95044
molecular crystal spin model for orientational phase transition 78−30735
molecular field theory with corrections, Callen identity 80−54857
Monte Carlo renormalisation group for n≥2 models 79−75470
Monte Carlo simulation of model with logarithmic exchange interaction 79−19712
Monte Carlo studies, review, book contrib. 79−82809
multispin correlation functions, two-dimens. model 77−47957
n-replica model transformation to Ising model 80−4669
n-spin correlation functions for 2-dimens. model in quantum field theory 77−37821
nearest-neighbour Ising model on tetrahedron lattice, four spin interactions 77−28349
neural network theory, analytic soln. based on Ising spin system analogy 80−12074
non-universality, polarisation and magnetisation exponents 79−40480
non-universality for Ising-like spin systems 77−24704
nonequilibrium, intensive parameters and detailed balance, computer simulation calcs. 78−76208
nonequilibrium, intensive parameters and detailed balance, theoretical estimate 78−76209
nonlinear excitation and coherent states, Ising model in transverse field 80−68143
nonrandom Ising system, random-field singularities in position-space renormalization-group transformations 80−13000
nuclear two-dimens. Ising struct., shell-cluster model 77−26601
nucleation and crystal growth, two-dimensional, simulation using kinetic Ising model 80−54156
nucleation processes, computer simulation, single spin flip kinetic Ising model 77−62613
O(2), O(3) and O(4) spin systems, Hamiltonian string-coupling expansions 80−20426
O(N) Heisenberg spin systems, N=2,3,4, and Ising model, strong coupling expansions and phase diagrams 79−71378
one dimensional anisotropic Heisenberg model, spin 1/2, Ising like antiferromag., dynamic correlation function 80−75704
one dimensional in skew mag. field, zero-temp. dynamical props. 78−80153
one dimensional Ising system with random long-ranged interaction, density of eigenvalues of random matrix PV 79−12733
one dimensional random Ising model, exact result in transverse field 79−75469
one dimensional randomly dilute Ising ferromagnet, dynamics 80−70922
one dimensional spin-1/2 XY model, finite temp. transverse autocorrelation function 80−50024
one-dimensional, in transverse field, variational treatment, static props. at zero temp. 79−4642
one-dimensional, infinite radius of interaction in transverse magnetic field 80−2587
one-dimensional, long range, metastability 80−42166
one-dimensional, time-dependent correl. functions in high-temp. limit 79−73727
one-dimensional, wavevector depend. of fluctuations in cluster approx. 80−12999
one-dimensional, with finite range interaction, exact renormalisation transformation 77−72963
one-dimensional, with long-range interaction 77−41548
one-dimensional, with mag. field, renormalisation group soln. 77−24664
one-dimensional alloy, end effects 79−35634
one-dimensional classical and quantum chains, spin-Peierls transition theory 77−66375
one-dimensional disordered spin system with isotropic antiferromag. interaction, susceptibility and Knight shift *(Russian)* 78−88202
one-dimensional disordered systems, magnetism 80−25152
one-dimensional energy conserving relax. 80−20420
one-dimensional ferromagnet with long range interaction, correlation weakening 79−95561
one-dimensional Ising chain with generalized molecular field 79−91242
one-dimensional kinetic Ising model, real-space renormalization group 79−15317
one-dimensional kinetic Ising model in a field 79−42722
one-dimensional magnetic models, fluctuations in energy-energy correlation function 79−73726
one-dimensional magnetic system, spin anisotropy and exchange alternation 80−34644
one-dimensional semi-infinite chain, enhanced surface exchange interaction, mag. relax. 80−29558
one-dimensional spin system, with next-nearest neighbour interactions, mag. responses to spin-Peierls transition 80−71054
one-dimensional transverse, time-depend. longit. correl. function 77−66332
one-dimensional transverse-field, in complex longitudinal field, real-space renormalization group method, T=0 80−103806
orbital degeneracy, one dimensional two spin models *(Russian)* 80−54899
orbitally degenerate interacting impurity thermodynamics, stress field depend. due to point defects, dislocations 79−69477
order, disorder and generalized statistics 80−99055
order parameter dimensionality n≥2 components 78−10633
order-disorder transitions in gauge and spin systems 78−70072
order/disorder quantum field operators associated with 2−D Ising model in continuum limit 79−9276
ordering and phase transitions in Ising systems with competing short range and dipolar interactions 79−91200
pair-quartet interactions, PAD approx. 80−11202
paramagnet, in transverse field 77−8260
paramagnet, transverse, spectral density approach 77−80897
paramagnet, transverse field model 78−68138
paramagnet, transverse Ising, dyson eqn. 79−82736
paramagnets, at very low temps., formalism 79−4647
particle struct. at low temps. 78−57865
partition function for three dimens. Ising model, closed form approx. *(Chinese)* 78−52185
partition function of the three-dimensional Ising model 79−71381
partition functions in terms of infinite determinants 80−62593
percolation and phase transitions 77−13704
percolation as the zero-temperature limit of the dilute Ising model 79−93053
percolation points and critical point 77−20608
Percus-Yevick type approx. 78−148
periodically layered system, cooperative effects in crit. phenomena in sp. ht. 78−23284
phase boundary, line of analytic singularities 80−60283
phase struct. of replica magnets 80−39777
phase transformations Ising and other models, review, book contrib. 77−37825
phase transition, basis distrib. 78−16748
phase transition, Monte Carlo method in Ising system with biquadratic interactions 80−60352
phase transition in 2-dimens. Coulomb gas, interfacial roughening transition 77−20394
phase transition in X-Y and Heisenberg models, Ising free energy and susceptibility 78−43595
phase transition near percolation threshold 77−33956
phase transition of spin-one Ising system with biquadratic interaction 79−4683
phase transition probability, system size depend., consequences for stochastic eqns. 78−41258
phase transition theorems, Ising model with nearest neighbour ferromagnetic interactions 77−22501
phase transitions, critical points of Ising Hamiltonian, many-spin interactions 78−6532
phase transitions, in 3D model with long range pot. 77−66379
phase transitions, in systems with competing interactions 78−14963
phonon relaxation for transverse field model, soft mode and central peak roles 80−59615
planar, higher order correl. functions calcs. 78−95408
planar, scaling analytic corrections universality 80−105586
planar Ising ferromagnet solvable model with roughening transitions 80−71069
planar spin system with annealed bond disorder 80−57212
planar three-body, duality theorem, vertex model equivalences 77−20609
plane Ising lattice, local magnetisation depend. on linear defects *(Russian)* 80−2595
polyethylene, pressure phase transition, function of pressure and temp., Ising model anal. 79−77745
polymer liquid, Ising fluid equation of state 77−51469
polypeptides, mean field Ising-type model for helix-coil transition 77−70416
position-space renormalization group transformations, mathematical props. 79−75466
positivity constraints for ferromag. Ising model 77−28348
Potts model, 1st and 2nd order transitions, renormalisation group soln. 79−99706
Potts model, dil. random bond 80−29556
Potts model, first-order phase transform., three-state model, Monte Carlo renormalisation group method 79−99709

Ising model continued
Potts model, spin anisotropy and crossover 78−56339
Potts model, three-state, phase transition continuity 80−22302
Potts model on square lattice, conjectured singularity loci 79−93049
pseudo one-dimensional kinetic Ising model, dynamic susceptibility 80−50025
quadrupolar systems of restricted dimensionality, absence of ordering 78−89411
quantal and finite-sized, dimensional crossover 78−95444
quantum classical crossover critical behaviour in transverse field 77−66331
quantum compressible Ising model, critical behaviour 80−108016
quantum field theory and two dimens. model 77−69471
quantum Ising chain, in real or complex field, real space renormalisation group method 80−71050
quantum lattice spin theory, Jastrow wave functions 79−25999
quantum spin systems, S=1/2, manifestation of frustration effect 80−65767
quantum systems, two-dimens. Ising model, zero temp. renormalisation group method 79−82801
quantum-classical crossover crit. behaviour in transverse field 77−5766
quasi-one-dimensional electron gas with strong on-site interaction 78−67966
quenched bond disorder, effective medium approx. 80−42163
quenched bond mixtures, statistical theory of random ordered phase 77−12075
quenched bond-diluted, new approach 77−32138
quenched dilute random-bond system, CPA difference eqn. and crit. curves 80−2584
quenched mixture, spinodal decomposition theory, self-consistent method, structure function 78−68671
quenched models with random ferromag. interactions magnetisation upper bound 77−66233
quenched random Ising ferro- and antiferromagnet, Bethe approx. for phase transition 77−16082
quenched random magnets, thermodynamic behaviour from position-space renormalisation group 78−68244
quenched random mixtures on Cactus tree, phase transition 77−16081
quenched two-dimensional single spin-flip kinetic Ising model, Monte Carlo simulation 78−34943
quenched-bond disorder, cluster extension of effective-interaction approximation 80−93130
random, in transverse field, CPA approach 77−36040
random anisotropy model in Ising model, Monte Carlo simulation 80−80546
random annealed one-dimensional Ising spin system, site model, specific heat, susceptibility 77−32139
random band, cumulant expansion to glass-like phase 77−8319
random band square lattice, frustrated plaquettes distrib. 80−108015
random binary Ising system with transverse field, Curie temp., paramagnetic susceptibility 80−65938
random binary magnetic systems, quenched, Neel temp. calc. 77−89963
random binary system, mag. transition temp. and sp. ht. 77−77065
random bond chain in mag. field, magnetisation 78−39281
random bond Ising chain, low temp. behaviour 80−57211
random bond Ising chains, thermodynamics and correl. functions 79−15270
random bond Ising model, susceptibility and specific heat in glass like phase, cumulant expansion 78−6533
random bond mixtures, triangular cactus tree, statistical theory 80−39790
random bond model, two-dimens., evidence against spin-glass order 80−15747
random chain, low temp. sp. ht. calc. 79−56562
random exchange bonds, phase diagram 78−43604
random field method, generalisation of var. principle 77−77020
random field method, magnetisation and critical indices 77−77064
random Glauber chain, relax. of magnetisation, numerical studies 80−60313
random Ising bond interactions, paramag. phase, thermodynamic props. 77−20523
random Ising chain, Bethe approx. for free energy 79−78287
random Ising ferromagnet, upper bounds 80−34663
random Ising magnet, phase diagrams 80−7065
random Ising model, susceptibility and magnetisation 77−80899
random Ising model, thermodynamic limit 80−17885
random Ising model Cayley tree, thermodynamic limit 77−87702
random Ising model on Cayley tree, phase transition 80−42150
random Ising model with transverse field term 79−56545
random Ising system, critical index and temp. 79−56543
random Ising system, mag. critical index 79−56544
random local magnetic fields, effects on Ising model 78−23226
random magnet, ROP type, dynamics 79−15269
random magnet with frustration, zero-temp. props. from series expansions 79−61129
random magnetic alloys, mean field effective medium theory, Ising model appl., phases 78−84438
random magnetic bonds, phys. props. near crit. point 78−84440
random magnetic system, correlation function, upper and lower bounds 80−25063
random magnetic systems, gauge symmetries, Ising and X-Y models anal. 79−38295
random mixture of classical spins on infinite Cayley tree, susceptibility 77−89917
random mixture of Heisenberg and Ising bonds, singularity 77−59411
random mixture of Ising systems of different spin values 80−11144
random mixtures of three-dimens. Ising site model Monte Carlo simulation 78−73935
random mixtures of three-dimens. Ising site model Monte Carlo simulation 78−73936
random model, restricted annealing 78−80154
random model, variational principle for distrib. function in the Bethe approx. 80−15674
random ordered phase, effective field approx. 79−1676
random ordered phase, of Ising model, random quenched effective field approx. 78−84432
random quenched broken bond disorder, bounds on crit. temp. 78−2688
random site Ising model near percolation threshold 78−23282
random spin systems, gauge symm., phase transitions *(Russian)* 80−77929

Ising model continued
random spin systems, non-analyticity of entropy and Nernst's law 78−2692
random system, $\varepsilon^{1/2}$ expansion of crit. behaviour, higher order corrections 78−27050
random-bond, upper bond to sp. ht. on Nishimori's line 80−71068
random-bond Ising chain, entropy, depend. on temp. and mag. field 79−1679
random-bond Ising chain, ground-state energy, magnetostriction and zero-point entropy calcs. 79−7957
random-bond Ising systems, thermodynamic props. at low temp. 79−28532
randomly dilute, crit. and thermodynamic props. 79−8005
randomly diluted lattice, phase transitions, near percolation threshold, scaling theory 77−40066
randomly distributed interaction centres, mol. field distrib. function *(Russian)* 80−44834
randomly located spins with oscillatory exchange interactions 79−42778
rare earth iron garnets, level intersection and instability of mag. struct. *(Russian)* 77−43816
real fluids, static and dynamic crit. phenomena, theory, summer school lecture series 80−6344
real liquids, quenched to glassy state, struct., one dimens. Ising model appl. 80−54134
real space renormalisation group for arbitrary dimension 80−4666
real-space renormalisation group method, continuous-variable Ising model 80−100589
recurrence technique for confluent singularity analysis of power series 80−73277
relativistic quantum field theory of D=2 Ising model 78−21081
relax. behaviour, Ising model with degeneracies 78−65880
relaxation dynamics in cluster approx. *(Russian)* 78−10635
relaxation phenomena, Monte Carlo studies, review, book contrib. 79−80531
remanence and non-exponential relax. in Ising chain with random bonds 79−73751
renormalisation, zero-temp. method, Ising model in transverse field in one-dimens. 79−38347
renormalisation group, scaling factor, 2-D model 78−41237
renormalisation group calc. for cells with inequivalent spins 79−73658
renormalisation group calcs. on critical phenomena 80−42171
renormalisation group calculation of crit. props. of free mag. surface 77−40068
renormalisation group theory, critical props. of generalised 2D Ising model 80−4665
renormalisation group transform. of three-dimens. Ising models 78−62163
renormalisation group transformation for quantum spins 78−47984
renormalisation group transformations, cumulant expansion 78−70064
renormalisation group transformations, Kadanoff's variational approx. 77−37822
renormalisation group treatment, stochastic weight function 79−51734
renormalisation transformations in position space, parameters determ. criterion 79−17357
renormalisation-group transformation of three dimens. Ising model 77−87704
renormalised mean-field approach to crit. behaviour, two- and three dimens. Ising models 79−38339
renormalization-group transformation, real-space, for finite thickness Ising systems 80−15749
renormalization-group transformation for quantum lattice systems at zero temperature 79−71379
replica method and solvable spin glass model 79−38327
rotational phase transition in ferroelectrics and other crysts., Ising model 77−4605
roughening transition of crystal surface, exactly solvable model 77−47368
S=1 generalised Ising model, stability conditions 80−20427
S=1 Ising model and third law of thermodynamics 79−17372
scaling, amplitude universality and confluent corrections 77−80898
scaling and multiplicative renormalising in solid state physics, review *(Hungarian)* 79−11289
scaling limit of Ising model 78−45573
self-consistent cellular methods 77−16026
sequential term prediction 78−57866
series anal. of model with free surface 80−25062
shape and size of two-dimensional percolation clusters with and without correlations 79−93054
short-range ordered mag. cluster pinning by localised optical excitation 78−68279
site-disordered spin systems, generalised CPA 77−20513
solid solutions, binary, growth-disorder model, three-dimensional, rel. to pair-interaction Ising model 78−26462
solid-on-solid model, roughening transition, Temkin approx. 77−39739
soliton field theory, construction of Green's functions from an exact S matrix 79−71629
solitons and phasons in Ising model with competing interactions 80−34653
soluble model for crit. behaviour of imperfect mag. cryst. 77−66355
solution by star-triangle relations 79−9191
space renormalisation group calc. 78−27046
spacial cluster or mixing props. in classical lattice systems 77−37818
spatially modulated phase, Monte Carlo study 79−95598
spatially modulated phase, with competing interactions 80−60334
spatially nonhomogeneous, correl. functions 80−60314
spherical ferromagnetic models, Yang-Lee edge singularity density in thermodynamic limit 79−30378
spherical Ising model with regularly spaced defects 79−56486
spherical random field model, low dimensionality for transition 80−68150
spin 1/2, susceptibility and fourth field derivative for $T>T_c$ and d=4 79−61024
spin 1/2 model on FCC lattice, exponent γ 79−73656
spin $^1/_2$ dilute magnet, crit. props. 80−15733
spin $^1/_2$ Ising model in four-dimens., hyperscaling test 80−46986
spin $^1/_2$ system, renormalisation group approach 80−2582
spin anisotropic Ising-Heisenberg chain, appl. of zero temp. quantum renormalisation group 80−80526
spin correlation functions, class of inequalities, identities 79−44878
spin dynamics of one-dimens. system 77−4486
spin fluctuation waves in critical point region *(Russian)* 77−33970

Ising model continued
spin glass, calc. of wavevector depend. susceptibility 77−63223
spin glass, computer simulation 77−66370
spin glass, crit. behaviour, appl. of n-replica method to Ising system 79−42767
spin glass, d-dimensional, frustration effect 80−108019
spin glass, d-dimensional, frustration effect and dilution problems 80−108018
spin glass, dil., at zero temp., (1/2)-state Potts model 79−42768
spin glass, dil., conc. expansions at zero temp., Ising model 80−60303
spin glass, dil., low temp. phase diagram and crit. props. 78−60291
spin glass, dipolar, anomalous sp. ht. Ising model and Monte Carlo calcs. 78−47989
spin glass, dynamical theory of quenched site model 79−19742
spin glass, Edwards-Anderson model, appl. of Migdal's recursion relations 77−40070
spin glass, effective field distrib., time dependent order parameters 77−43843
spin glass, existence of phase transition 78−56327
spin glass, five-dimensional, Edwards-Anderson ordering possibility 80−60295
spin glass, frustration and ground-state degeneracy 78−31090
spin glass, frustration model, ground states 80−60294
spin glass, generalised mean field theory with spin correls. 78−2691
spin glass, infinite ranged models 78−80166
spin glass, internal field distribution 79−73740
spin glass, Ising, cryst. field effects 77−85460
spin glass, Ising, two-dimensional, Monte Carlo evidence for absence of phase transition 78−19260
spin glass, mean field theory 79−4680
spin glass, mean field theory and ϵ-expansion 78−10705
spin glass, nature of ordering 78−80172
spin glass, nearest-neighbour Ising model, search for spin glass transition 77−89960
spin glass, nearest-neighbour random exchange bonds, short-range mag. order 79−51791
spin glass, one dimens. ideal, dynamical susceptibility and relax. behaviour 80−65950
spin glass, phase diagrams and order parameters, Oguchi-Kaneyoshi method 80−15727
spin glass, phase transitions 77−8327
spin glass, phenomenological theory 78−19263
spin glass, principle of minimum free energy 80−88773
spin glass, random-bond Ising model with continuous distrib. of exchange interactions 77−43837
spin glass, remanent magnetisation, Monte Carlo exam. 79−61166
spin glass, remanent magnetisation using Monte Carlo methods 79−78421
spin glass, replica symm. and massless modes 79−33486
spin glass, RKKY, low temp. susceptibility, spin-depend. curvature, Ising model MRF approx. 77−66366
spin glass, Sherrington Kirkpatrick model, entropy calc. 80−20411
spin glass, Sherrington-Kirkpatrick, white and weighted averages over solns. of Thouless-Anderson-Palmer eqns. 80−108012
spin glass, Sherrington-Kirkpatrick model, finite system, low temp., susceptibility, entropy 78−34993
spin glass, Sherrington-Kirkpatrick model generalisation m-component spins 79−11320
spin glass, spherical approx. 77−28392
spin glass, spherical model 77−66364
spin glass, three-dimensional mag. correlations 80−103849
spin glass, vanishing of Edwards-Anderson parameter 78−43597
spin glass, with RKKY interaction, props. 79−24177
spin glass behaviour, 3-dimens., using real space scaling transform. 77−69570
spin glass binary mixture at T=0, energy and variational props. 80−39794
spin glass freezing temp., conc., Fermi-momentum depend. 78−14970
spin glass in Bethe-Peierls-Weiss and other mean-field approximations 79−65682
spin glass in d dimensions, Ashkin Teller model 79−65691
spin glass Monte Carlo calc. of mag. susceptibilities 78−31079
spin glass near percolation threshold 78−72352
spin glass phase, of Ising model, random quenched effective field approx. 78−84432
spin glass phase in site Ising model 79−95592
spin glass phase of random model, spins distrib. and thermodynamic props. 79−51786
spin glass phase transitions, instability 78−23285
spin glass state, magnetisation of dil. mag. impurities, molecular field approx. 77−20623
spin glass state, mixed nearest-neighbour exchange interaction 78−39341
spin glass transition, lower crit. dimensionality 80−60291
spin glass transition, rel. to roughening transition in crystal growth theory 78−27045
spin glass transition, renormalisation group approach, Ising model of bond mixtures 78−43601
spin glass transition in random bond Ising model in 2-D, and 3-D, renormalisation group approach 78−68275
spin glass with non-random interactions 77−55673
spin glasses, anisotropic, crossover effects 79−65692
spin glasses, dilute, at zero temperature, low concentration series expansion 80−93131
spin glasses, dual transformation into ferromagnetic models, critical temp. in frustrated models 79−73763
spin glasses, Edwards-Anderson model autocorrelation function logarithmic decay account 79−78406
spin glasses, extended field theory description 77−63205
spin glasses, fluctuation theory, mag. susceptibility and sp. ht. 79−24176
spin glasses, frustration model, lifetime of excited states 80−15750
spin glasses, in effective interaction approx. 80−60288
spin glasses, Ising long and short ranged bond models in cluster approx. 80−20419
spin glasses, Ising type random bond, scaling, eqn. of state and instability 79−73753
spin glasses, long-range Gaussian-random Ising model 79−15319
spin glasses, mean field theory, broken replica symmetry 80−34659
spin glasses, mean field theory, replica method 80−34658
spin glasses, Monte Carlo simulation 79−78428
spin glasses, phase transition, fluctuations of local spins, mean-field theory 80−34661
Ising model continued
spin glasses, phase transition, mag. susceptibility, specific heat, Ising model calcs. *(Russian)* 80−34671
spin glasses, quartic operators in Ising, X-Y, and Heisenberg systems 79−33498
spin glasses, random mixture of Ising systems, phase boundaries 80−60285
spin glasses, recent progress in numerical simulation 79−69689
spin glasses, relax. of magnetisation and order parameter 78−27043
spin glasses, self-consistent internal field distrib. 77−16084
spin glasses, thermodynamic props., cluster mean-field theory using Ising Hamiltonian 79−33499
spin glasses, two-, three- and four-dimensional, defect energies 78−39330
spin glasses, vector and Ising, lower critical dimensionality 78−43603
spin glasses and dil. magnets, real-space renormalisation group calcs. 77−12134
spin glasses and other glasses, symmetry and topology concepts 79−28541
spin lattice models, continuous-integral method 78−93615
spin operators, general commutator eqn. 79−4638
spin phase boundaries, in BCC Ising model, struct., excess free energy 77−59097
spin system, random thermodynamic props. using Bethe-Peierls-Weiss approx. 79−78387
spin system, variational approx. for renormalization group transforms. 79−61139
spin systems, model, Monte Carlo simulation appl. 80−20421
spin systems on Cayley tree-like lattices, spontaneous magnetisation, correlation function far from boundary 78−68137
spin-1 Ising mean field model dynamics 79−67232
spin-1/2 models on square lattice, sublattice renormalisation transform. 78−23225
spin-1/2 system, mol. field theory with correlations 79−82804
spin-flop multicritical points in systems with random fields and in spin glasses 79−33495
spin-glass, renormalisation group calc. for two dimens. models 78−14968
spin-glass, two-dimensional Ising model, low temp. dynamic props. 80−20425
spin-glass model, high temp. series expansion 78−16741
spin-glass models, long-range, Ising spins and classical m-vector spins 80−15739
spin-one, bilinear and biquadratic interactions, phase diagram 80−75772
spin-one, high temp. series expansion, arbitrary biquadratic exchange, field and anisotropy 77−20526
spin-one Ising model with bilinear and biquadratic interactions 79−65677
spin-one Ising system, phase diagram 78−95441
spin-one Ising system with bilinear and biquadratic interaction 77−87703
spin-one system, correlation functions with bilinear and biquadratic interactions 78−91876
spin-oscillator coupled system, stochastic model for dynamics 77−22500
spin-s, corrections to scaling for spin-pair correls., series anal. 77−16027
spin-s Ising model, renormalisation group transformation 78−14916
spin-spin correlation, high temp. expansion and equipartition theorem 78−31089
spin-spin correlation function, series expansions 78−2637
spin-systems, double-time Green functions method, thermodynamics 79−15313
spontaneous magnetisation in d-dimensional models for $d \geq 2$ 78−72319
square frustration model, numerical study of ground state correl. 80−34638
square lattice, phase transitions, next nearest neighbour interactions 80−50128
square lattice, theory of frustration effect 77−89959
square lattice, two-spin correlation functions of an Ising model with continuous exponents 80−57216
square lattice bond dilute, renormalisation group attempts to obtain transition line 80−44836
square lattice Ising model, series expansions from corner transfer matrices 80−154
square lattice Ising model with a free surface 80−42153
square lattice Ising system, crit. relax. of temp. 79−82793
square lattice Ising type models statistical mechanics, variational approx. 79−44873
square lattice variational approximations applied to the Ising model 79−56555
square-lattice, four-spin correl. function 78−39345
square-lattice Ising antiferromagnet, interface props. and transition temp. 79−42787
statistical mechanics, one-dimens. Ising and Potts models with exponential interaction, comparison 78−21079
statistically layered system, finite, crit. phenomena 78−95446
steam, crit. region, universality, revisions and corrections to scaling 78−38810
stochastic, conc. binary magnetic systems, spin glass behaviour, Monte Carlo study 78−2694
stochastic dynamics 77−49690
stochastic Ising model, stationary measure as Gibbs state 77−71274
structural stability theory, phase transition models, mean field theories, Ising model appls. *(German)* 78−77822
SU(2)-flavour Schwinger model on the lattice, Hamiltonian lattice perturbation exam. 78−16747
subdominant critical indices for the ferromagnetic susceptibility of the spin-1/2 Ising model 80−100574
supersymmetric Ising field theory, 'doubled' model, and supersymmetric sine-Gordon kink struct. 79−71614
surface crit. behaviour, layer and local susceptibility 80−71058
surface critical behaviour, renormalisation group theory 78−47988
surface magnetic order, Cayley tree approx. 77−72964
surface of magnetic systems, multicritical phenomena 77−32208
surface susceptibility exponent for the polymer problem 80−42151
surface tension, using real-space renormalisation group methods 78−47985
susceptibility, crit. behaviour, with transverse field 77−12127
susceptibility, Ising model, appl. of integral approx. methods 79−71392
symmetric models of crystal growth disorder graphical solns. for correlations 79−1401
Takada model, central peak 79−4641
TCNQ alkali salt, spin-Peierls transition 80−29395

Ising model continued
temperature Green's function for tunnelling model, new contraction method 79−35635
thermodynamic limit asymptotic equivalence of three 1D disordered models 77−77019
thermodynamic limit in stochastic systems 78−73938
thermodynamic properties, of interacting particle ensemble, by simulation of stochastic disordering 77−87697
thermodynamic properties, variational calc. 77−85405
thermodynamics, randomly diluted Ising model on honeycomb lattice 80−54902
thermostatistical props. in model with second neighbour and four body interactions 80−31682
thin film alloys, surface magnetism props., Curie temp., Ising model 80−108039
three dimensional, crit. exponents, scaled eqn. of state 77−8262
three dimensional, crit. index. for correl. length 78−84444
three dimensional, free energy, lower bound approx. 78−10707
three dimensional, partition function integration, collective variables method *(Russian)* 77−37824
three dimensional, partition function integration by collective variables method *(Russian)* 77−33957
three dimensional cubic structures, Ising model with mag. field 77−28391
three-component model, global phase diagram 77−37835
three-dimensional, confluent singularities 77−40022
three-dimensional, recurrence relations *(Russian)* 77−74330
three-dimensional, statistical sum 77−82465
three-dimensional, two-spin correlation function, method for phase diagram 78−56323
three-dimensional, two-spin correlation function 79−28533
three-dimensional, with four-spin interaction, exact soln. 80−88711
three-dimensional spin 1/2, real space renormalisation group calcs. 77−66345
three-spin triangular Ising model, nature of critical point 77−2617
three-state Potts model, antiferromag. ordering 78−23279
TMMC, one-dimens. antiferromagnet, XY-Ising transition under mag. field 79−91244
TMMC, XY-Ising crossover transition, quasi-elastic neutron scatt. obs. 80−44826
Toulouse frustration effect 79−24167
transformation methods in anal. of crit. prop. 78−49771
3d-transition metal complexes, low spin-high spin paramag. transition, Ising model calc. 80−93073
transition point of random Ising model with bond dilution 79−93060
transition probabilities in Monte Carlo simulation 80−27234
transition temperature for square cactus tree with random bonds 78−41240
transition temperature in new mean-field theory 79−51785
transverse, dipolar interaction and crit. behaviour 77−81071
transverse, quantum crossover 78−43596
transverse, three-peak struct. for crit. relax. function 77−63204
transverse 1-D model, dynamics 80−29515
transverse bond-diluted model, appl. of CPA 79−56551
transverse field, dynamic struct. factor calc. 78−22814
transverse field, spin dynamics, mode coupling 78−56332
transverse field critical props., two-dimens. Ising system renormalisation and scaling 78−21080
transverse field model, for positive and negative exchange interactions 77−77016
transverse Ising model, dipolar interaction, crit. relax. function 79−40487
transverse Ising model, temp. depend. of transverse spin 77−32137
transverse mag. field, phase transition accuracy of variational method calc. lattice Hamiltonian 78−16746
triangular, antiferromag. to ferrimag. transition 77−20522
triangular, phase diagram, renormalisation appl. to adsorbed layers 78−10631
triangular Ising lattice with anisotropic interactions 78−47926
triangular Ising lattice with small second neighbour interaction crit. temps. 78−56331
triangular Ising model, anisotropic ferromag., corner transfer matrices, spontaneous magnetisation 78−10629
triangular Ising model in mag. field, Markov process anal. 77−13708
triangular Ising model percolation props., renormalisation group anal. 78−93620
triangular lattice, antiferromag., mag. field depend. transition temp. 77−8323
triangular lattice, pair and triplet interactions, mean-field eqn. of state 77−16021
tricritical phenomena, nearest neighbour and next nearest neighbour interactions 77−69566
tricritical relaxation in Ising-Glauber model with competing interactions 77−8326
tricritical two dimensional behaviour, ϵ expansion universal quantities 79−35642
tricritical two-dimensional behaviour, finite size effects, model depend. 79−35641
trimethyl ammonium cobalt chloride, magnetisation temp. depend. 80−7128
trimethylammonium cobalt chloride, low-dimensional Ising-like system, nucl. spin-lattice relax. of protons meas. 77−85609
trimethylammonium cobalt trichloride dihydrate, Ising-like system, nucl. spin-lattice relax. of ^{1}H and ^{35}Cl 80−29638
triplet Ising model on triangulated dice lattice, phase transitions 77−17918
triplet model, numerical evidence for two critical points 77−37819
two dimensional, nonlinear partial difference eqns., two point function 80−101762
two dimensional, surface critical exponent $\eta_{\perp}$ 79−44879
two dimensional second neighbour interaction, Pade approximant, critical behaviour 79−4682
two point correlation, renormalisation group methods 78−8353
two-component random chain in zero field, free energy and derivatives 77−59371
two-dimens., real-space calc. of spin-spin correl. 79−42724
two-dimensional, frustration in periodic systems 79−61023
two-dimensional, in transverse mag. field, renormalisation group studies 80−71042
two-dimensional, infinite cluster method for non-translation invariant equilibrium states 79−73654
Ising model continued
two-dimensional, physical realisation, surface reconstruction 80−15351
two-dimensional, renormalisation group approach 78−52261
two-dimensional, soln., connection with Korteweg de Vries eqn. 77−65004
two-dimensional, three-spin correlation functions 80−84583
two-dimensional, variable bond strength, partition function calc. 79−25998
two-dimensional, with transverse field, phase diagram and crit. props., from real space renormalisation group 78−52295
two-dimensional exponents, one-dimensional three-spin cell calc. 78−68280
two-dimensional ferromagnet with three spin interactions 80−2542
two-dimensional in external field, variational approach 79−80538
two-dimensional Ising antiferromagnet, neutron scatt., review 80−50103
two-dimensional Ising frustration model, ground-state correl. 80−15732
two-dimensional Ising model, real space renormalisation transform. 78−2687
two-dimensional Ising system, crossing over to two-dimensional Heisenberg system 80−93123
two-dimensional kinetic, dynamic correlation functions, real space renormalisation group approach 80−62589
two-dimensional kinetic, randomly diluted, determ. of spin diffusion and thermal cond. by computer simulation 77−36039
two-dimensional lattice, cluster expansion method 78−34942
two-dimensional model, small mag. field approx. near T_c 79−42773
two-dimensional n-spin correl. functions 78−52296
two-dimensional regular model, frustration effects 80−39784
two-dimensional spin glass, crit. temp. 80−11206
two-dimensional spin system on square lattice, exact duality-decimation transform. 80−17890
two-dimensional spin systems, decimation transforms. 77−77017
two-dimensional square Ising model in transverse magnetic field, renormalisation-group method 80−20428
two-dimensional with periodically distributed frustration, rigorous props. 80−46987
two-point correl function near coexistence surface 80−44847
two-spin correl. function of two-dimens. model, quantum field theory calc. 77−32205
uniaxial dipole system, order-disorder transition, computer expt. and high temp. expansion 79−38494
uniaxial Lifshitz point, Monte Carlo calcs. 78−39353
uniaxial spin systems, quasiclassical method appls. 80−8931
Union Jack lattices, non-universal Ising spin systems 80−68145
Ursell function inequality 79−4640
valency transition 78−60297
variational renormalisation group method, Ising model on square and triangular lattice 78−16740
water, Ising model and config. heat capacity 79−33096
water, lattice fluid model on 2D quadratic lattice 79−93056
weakly disordered uniaxial ferromagnet, phase transition *(Russian)* 78−23291
Weiss Ising model, stability anal. C*-algebra formalism 78−57868
Yang-Lee edge singularities at high temps. 80−20422
Yang-Lee edge singularity, field theoretic formulation 79−17354
Yang-Lee edge singularity, real-space renormalisation group method 80−34643
Yang-Lee edge singularity and ϕ^3 field theory 78−65882
Yang-Lee edge singularity from a real-space renormalization-group method, Ising model 79−97317
Z_2 duality algebra in D=2 quantum field theory 79−75685
Z(2)(3) Ising spin systems, Hamiltonian formulation in 1+1 dimens. 80−57491
zero field susceptibilities and correlations 78−34454
$AgNa(NO_2)_2$, order-disorder ferroelec., influence of hydrostatic press. on polarisation dynamics 80−103913
Au-Fe, dil. alloys, spin glasses, modified bond model calcs. 79−33489
Ba_2NiF_6, specific heat capacity, critical amplitude, cross-over from 2-D Ising to Heisenberg behaviour 80−39791
$(CH_3)_3NHCoCl_3.2H_2O$, chain ferromag. two magnon bound state, nuclear spin-lattice relax. 78−88206
$Ca_2La_8(SiO_4)_6O_2$, cation ordering, X-ray diffr. meas. 79−23577
$CoBr_2.6[(D_2O)_{0.48}(H_2O)_{0.52}]$, antiferromag. ordering, quasi-elastic neutron scatt. study 79−61068
$CoCl_2.2H_2O$, Ising antiferromag., high field transverse magnetisation meas. 80−93143
$CoCl_2.2H_2O$, magnetisation temp. depend. 80−7128
$CoCl_2.2NC_5H_5$, magnetisation temp. depend. 80−7128
$CoCl_2.2NC_5H_5$, quasione dimens. Ising system, thermodynamic props. 78−27042
$Co(urea)_2Cl_2.2H_2O$, two-dimens. mag. props., cryst. struct., specific heat 80−75777
$CrBr_3$, crit. anomaly in transverse spin-spin relaxation rate 79−15310
$CsCoBr_3$, quasi ID Ising antiferromag., polarised Raman scatt. from mag. excitations 80−66182
$CsCoCl_3.2H_2O$, pseudo one-dimens. Ising-like system, mag. heat capacity and metamag. transitions 77−66351
$CsCoCl_3$, 1-D Ising antiferromag., mag. phase transitions 79−51779
$CsCoCl_3$, Ising antiferromagnet, electronic Raman scatt. on Co^{2+} 78−10878
$CsCoCl_3$, Ising like antiferromag., mag. phase transition, ^{133}Cs NMR 80−7184
$CsCoCl_3$, Ising-like antiferromag., spin dynamics 79−42747
$CsCoCl_3$, Ising-like antiferromag., instantaneous spin correlations 79−42746
$CsCoCl_3$, mag. struct., neutron diffr. meas. 78−43563
$CsCoCl_3.2H_2O$ interchain exchange low temp. susceptibility 78−19240
$CsFeCl_3.2H_2O$, rectangular Ising cpd., Mossbauer meas. 80−71252
$CsMnF_3$, isotropic antiferromag., crossover behaviour of mag. phase boundaries 79−78370
$CsMnF_3$, mag. phase boundaries, XY to Ising crossover, virtual bicritical point 80−50095
Cu-Mn, molecular field distribution function in disordered Ising model *(Russian)* 80−54859
Cu-Mn, spin glass, meas. of order parameter 80−34642
Cu_3Au type antiferromagnet Ising lattice, finite entropy at T=0, phase transition 77−89958
$Dy_3Al_5O_{12}$, antiferromag., optical birefringence in fields along [111] meas. 77−28540
$DyPO_4$, mag. transitions under hydrostatic press., neutron diffr. study 80−71030

Ising model continued
Fe complex, $Fe(Br)[S_2CN(C_2H_5)_2]_2$, 3-D Ising ferromag., cryst. susceptibility, 1.5-20K 80−20390
Fe complex, $Fe(Cl)[S_2Cn(C_2H_5)_2]_2$, 3-D Ising ferromag., cryst. susceptibility, 1.5-20K 80−20390
Fe complex, $Fe(1,2,4\text{-triazole})_2(NCS)_2$, quasi-2-dimens. $S=^1/_2$ antiferromag., mag. props., hidden canting 80−107986
Fe complex, hexa(pyridine-N-oxide)$(ClO_4)_2$, sp. ht., comparison with simple cubic S=1/2 Ising magnet 78−23290
Fe-Al-Fe, phase diagram, microscopic model 80−34630
$FeCO_3:Mn^{2+}$, far IR host and impurity excitations, antiferromag. and paramag. temp. ranges 77−52140
$Fe_xMg_{1-x}Cl_2$, metamag. percolation, Ising model calc. 79−28542
^3He-^4He mixtures, superfluid transition temp., Green's function calc. method 77−72735
Ho-YIG, magnetic props. in strong fields at low temp., Ising approx. calcs. *(Russian)* 80−54920
K_2CoF_4, pseudo Ising antiferromag., inelastic light scatt. by mag. excitons 80−11377
K_2CoF_4, specific heat capacity, critical amplitude, cross-over from 2-D Ising to Heisenberg behaviour 80−39791
K_2CoF_4, two-dimens. Ising antiferromag., nearest neighbour correl. function, birefr. expts. 80−71386
KH_2PO_4, ferroelec. transition temp., transverse Ising model 77−90110
KH_2PO_4 type ferroelectrics above T_c, soft mode and central-peak dynamics 78−87763
KH_2PO_4, variational treatment of proton-photon system 78−88261
K_2MnF_4, specific heat capacity, critical amplitude, cross-over from 2-D Ising to Heisenberg behaviour 80−39791
K_2NiF_4, specific heat capacity, critical amplitude, cross-over from 2-D Ising to Heisenberg behaviour 80−39791
$KNi_xMn_{1-x}F_3$, two-magnon Raman scatt. 77−66509
$MnBr_2.4H_2O$, high-resolution sp. ht. meas. near Neel temp. 77−28393
MnF_2, specific heat, Heisenberg to Ising crossover near Neel temp. 78−47980
$Mn_xZn_{1-x}F_2$, three dimens. Heisenberg-Ising antiferromag., fluctuations near percolation threshold 79−78390
$ND_4D_2PO_4$, cryst., transverse and longit. elec. susceptibilities, modified Ising model calcs. 80−97203
$NH_4H_2PO_4$, cryst., transverse and longit. elec. susceptibilities, modified Ising model calcs. 80−97203
αNH_4HgCl_3 quasione dimensional type cryst., phase transition statistics, molecular field approx. calcs. 80−34190
$(NH_4)_2SO_4$, phase transition theory 79−24275
$NaNO_3$, order-disorder transition point, hyper-Rayleigh scatt. due to rotation of NO_3^- 78−52520
Ni, Ising-type system, impurities, local crit. behaviour 77−48001
$Ni(OH)_2$, quasi-two-dimensional antiferromagnet, specific heat 79−11317
Pd-Fe, molecular field distribution function in disordered Ising model *(Russian)* 80−54859
$RbAg_4I_5$, struct. transition at 209K, Ising like behaviour 78−14460
Rb_2CoF_4, pseudo Ising antiferromag., inelastic light scatt. by mag. excitons 80−11377
Rb_2CoF_4, two dimens. Ising like antiferromag., spin wave excitations 78−72342
$Rb_2Co_cMg_{1-c}F_4$, magnetic specific heat, dilution on a two-dimensional Ising-like antiferromagnet 78−91871
$Rb_2Co_pMg_{1-p}F_4$, dilute antiferromag. two dimens. Ising system, phase boundary effective medium theory 80−50130
$Rb_2Co_xMg_{1-x}F_4$, two-dimens. Ising antiferromag., fluctuations near percolation threshold 79−78390
$RbFeCl_3$, $2H_2O$, pseudo one-dimens. Ising-like system, mag. heat capacity and metamag. transitions 77−66351
$RbFeCl_3.2H_2O$, 2D Ising system, crit. fluctuations, Mossbauer spectra study 80−44842
$RbFeCl_3.2H_2O$, pseudo one-dimens. Ising cpd., multiple magnon bound states 79−42723
$RbFeCl_3.2H_2O$, pseudo-one-dimens. canted Ising antiferromag., spin-cluster reson. 79−61233
$RbFeCl_3.2H_2O$, pseudo-one-dimens. canted Ising antiferromag., spin cluster reson. 79−61235
$RbFeCl_3.2H_2O$, pseudo-one-dimensional canted Ising antiferromag., spin-cluster excitations 80−70989
$RbFeCl_3.2H_2O$, rectangular Ising cpd., Mossbauer meas. 80−71252
$Rb_2Mn_xMg_{1-x}F_4$, two dimens. Heisenberg-Ising antiferromag., fluctuations near percolation threshold 79−78390
Rb_2NiF_4, specific heat capacity, critical amplitude, cross-over from 2-D Ising to Heisenberg behaviour 80−39791
Si, spin-depend. recomb. at exchange-coupled dislocation centres 77−89725
$SrTiO_3$, stressed, trigonal-to-tetragonal transition, EPR data, realisation of 3-state Potts model 77−28525
UPTe, and UAsTe, crit. behaviour 78−43605

island-like metallic thin films *see discontinuous metallic thin films*

islet-like metallic thin films *see discontinuous metallic thin films*

isobaric analogue resonances
see also nuclear collective states and giant resonances
analog-antianalog gamma transition strength 80−13429
analogue states and resonances in semimicroscopic shell model *(Russian)* 80−86872
compound nucleus, giant resonances, force functions for partial E1-transitions 78−12985
configurations in few nucleon systems, review 78−37294
continuum shell model description of resonant structures in nuclear reactions 79−13345
Coulomb displacement energies, isobaric analogue resonances, TDHF calcs. 80−42518
dipole radiative decay of analogue states 78−17135
finite Fermi systems, polarisation effects *(Russian)* 78−46041
fission, isobaric widths, frozen quantal fluctuations, charge equilibration 80−37365
fission isomeric states population via isobaric analogue resonances 77−34231
giant isobaric resonances, A* resonances, appl. to pion-induced reactions 79−67776
giant isobaric resonances, isobar doorway model 79−85428
giant multipole resonances, isotopic splitting 79−6378
heavy nuclei, photoproton reaction, isospin effect 79−80926
nuclear forces and isobar configs. in nuclei, review 78−50093

isobaric analogue resonances continued
particle-hole calc. of isobaric analogue and isovector monopole reson. 78−21537
reduced normalisation of isobaric analogue resonances from (p,p) reactions 78−86522
strength functions for isobaric analogue resonances 78−50143
total neutron widths, isobaric analogue reson. 79−6540
NN hard (soft) core pots., FPT and ACCBA anal. 77−18404
(p,p), microscopic and phenomenological parameters, S-matrix eval. methods 78−13045
(p,p), statistical significance of spreading widths for doorway states, reply to comments 80−63147
(π,π), intermediate energies, collective isobaric resonance 80−63208
^{A}Ag, A=104, 106, levels, J^π, and isobaric analogue resonances from Pd(p,n) 80−32180
^{25}Al, T=3/2 isospin-forbidden reson. via ^{24}Mg(p,p), 5.65-6.25 MeV 77−18507
^{26}Al compound nucleus, isospin impurity from fluctuations in mirror reactions $^{12}C(^{14}N,t)^{23}Mg$, $^{12}C(^{14}N,^3He)^{23}Na$ 78−33157
^{27}Al isobaric analogue resonances, spectroscopic factors and γ-rays from (p,p), (p,γ) 80−86873
^{28}Al analogue dipole state excitation in ^{28}Si(n,p) 77−30571
^{40}Ar(d, p)^{41}Ar, 1.354 MeV, spectroscopic factor comparison with isobaric analogue reson. 79−30787
^{71}As, intermediate struct., props. 78−93948
^{71}As, isobaric analogue reson. through ^{70}Ge(p,p) 3.5 to 5.3 MeV study 79−75951
^{139}Ba, obs. of IAR in ^{138}Ba(p,p′) with 10-11.7 MeV polarised protons 77−2991
^{207}Bi $3p_{1/2}$ isobaric analogue resonance from ^{206}Pb(p,p_0), polarised p, analysing power 78−78346
^{208}Bi $3p_{1/2}$ isobaric analogue resonance from ^{207}Pb(p,p_0) analysing power, polarised p 78−78346
^{208}Bi isobaric analogue resonances, spin assignments, decay amplitudes from ^{207}Pb(p,p) 79−75946
^{208}Bi M1 isobaric analogue resonances and giant spinflip resonances from ^{208}Pb(p,n) 80−106030
^{80}Br isobaric analogue resonances and spectroscopic factors from ^{80}Se(p,n) 79−36212
^{12}C, anologue states from reson. proton scatt. 77−38260
$^{12}C(\pi,\pi')$, collective resonances 78−78415
^{13}C, resonances analogue to states ^{13}N level reached in ^{12}C(p,p) 78−13046
^{13}C-^{13}N mirror nuclei, 15.1 MeV resonance width, isospin forbidden transitions 79−13265
^{110}Cd, n spectra of isobaric analogue resonance decay from ^{115}In(p,n)^{115}Sn *(Russian)* 78−89841
^{33}Cl, T=3/2 isospin-forbidden reson. via ^{32}S(p,p) 3-3.8 MeV 77−18507
^{35}Cl, resonances determ. from ^{34}S(p,p) meas. 77−65222
^{55}Co, 1 $g_{9/2}$ analogue state fragmentation using analogue resonances from ^{54}Fe (p,γ), 3450 keV 78−70506
^{55}Co excited levels and IAS meas. with ^{54}Fe(p,γ) 77−18509
^{55}Co isobaric analogue resonances, J^π, partial widths and spectroscopic factors from ^{54}Fe(p,γ), (p,p′) 79−85431
^{55}Co, resonance decays, branching ratios and analogue resonances from ^{54}Fe(p,γ) 80−52643
^{57}Co, $g_{9/2}$ IAR in ^{56}Fe(p,γ) 78−70504
^{57}Co, gamma decay of $g_{9/2}$ isobaric analog resonance 79−63674
^{57}Co obs. of $g_{9/2}$ IAR in ^{56}Fe(p,γ) 78−82332
^{52}Cr, γ-decay of analogue states obs. in ^{51}V(p,γ) 78−70503
^{137}Cs, anal. of ^{136}Xe(p,p_1), 11.82 MeV 78−66282
^{A}Cu, A=59, 61, 63, 65, f and p shell analogue resonances, γ-decay *(Russian)* 79−30800
^{59}Cu, excited in ^{58}Ni(p,γ), γ-decay 78−13005
^{63}Cu, decay of analogues, γ-ray ang. distribs. and spins of resons. 78−13002
^{65}Cu analogue $P_{1/2}$ resonance, γ-decay and energy levels from ^{64}Ni (p, γ) 79−80907
^{65}Cu analogue resonance direct n decay, stat. anal. from ^{64}Ni(p,nγ) *(Russian)* 80−5104
^{65}Cu, isobaric analogue reson. anal., from ^{64}Ni(p,p), (p,p′) 78−78351
D, double isobar intermediate state probability 78−25066
^{145}Eu, IAS, J^π via polarised proton scatt. 77−74825
^{56}Fe isobaric analogue resonances corresponding to ^{56}Mn 335.5 and 340.9 keV states from ^{55}Mn(p,γ) 78−78342
^{56}Fe isobaric analogue resonance levels, branching ratios, from ^{55}Mn(p,γ) 80−68617
^{56}Fe(p,p), 6 MeV, elastic and inelastic, quadrupole deformation, IAR excitation, optical pots. *(Russian)* 80−63149
^{67}Ga, isobaric analogue reson., statistical reaction model anal. 79−13267
^{69}Ga, IAR corresponding to $1/2^-$ and $9/2^+$ ^{69}Zn states from ^{68}Zn(p,γ), 3.8 MeV 78−66257
^{75}Ge, via ^{74}G(p,p′) 3.3-5.4 MeV J^π, spectroscopic factors 77−34278
^{2}H(n, γ), slow neutrons, mesic interaction current, isobaric resonance *(Italian)* 78−25179
^{4}He+π^+, 120-165 MeV, non-elastic interaction 79−76041
$^4He(\pi^+,\pi^+p)$, 120-165 MeV, isobaric resonance excitation, total inelastic cross section 79−85427
$^4He(\pi^+,\pi^+n)$, 120-165 MeV, isobaric resonance excitation, total inelastic cross section 79−85427
$^4He(\pi^+,\pi^+p)$, 120-165 MeV, isobaric resonance excitation, total inelastic cross section 79−85427
^{139}La, IAS, J^π via polarised proton scatt. 77−74825
^{139}La(e,e′p), $f_{7/2}$ ground isobaric analogue resonance, proton decay mode 78−29450
^{24}Mg(e,e′), 6^-, T=1 reson. discovery at 15 MeV 77−41940
^{53}Mn fragmented $g_{9/2}$ isobaric analogue resonance, transitions, J^π assignments from ^{52}Cr(p,γ) 79−45240
^{53}Mn fragmented $g_{9/2}$ isobaric analogue resonances, γ-transitions from ^{52}Cr(p,γ) 79−85430
^{53}Mn fragmented $g_{9/2}$ isobaric analogue resonance, γ-spectra and excitation functions from ^{52}Cr(p,γ) 80−68627
^{55}Mn(p,n)^{55}Fe, 1.35-5.42 MeV, total cross section and isobaric analogue resonances, shape anal. 79−6604
^{55}Mn(p,n)^{55}Fe, neutron polarisation at isobaric analogue resonances 78−54759
^{92}Mo(p,p′), time development function at isobaric analogue resonances, compound nuclear level decays 79−3124
^{94}Mo, analogue resonances, direct neutron decay, anal. of ^{93}Nb(p,n)^{93}Mo data *(Russian)* 79−3128
^{94}Mo, direct neutron decay of analogue resonances 80−22824

isobaric analogue resonances continued
^{99}Mo, activation analysis, excitation functions of ^{98}Mo+d reactions 80−22842
Mo(p,p′γ), odd isotopes, excited d-states from analogue resonances and p-γ correlations 80−68546
^{22}Na, analogue resons., γ-ray ang. distrib. and mixing ratios in ^{21}Ne(p,γ)^{22}Na 78−62504
^{90}Nb giant particle hole resonances, Gamow-Teller strength from ^{90}Zr(p,n) 80−86877
^{90}Nb isovector resonance analogues, Gamow-Teller transition from ^{90}Zr(^{3}He,t) 79−9539
^{97}Nb high spin analogue resonance near N=50 neutron shell, DWBA anal. of ^{96}Zr(^{3}He,d) 80−42613
^{145}Nd(p,p), (p,p′), 8.7-10.3 MeV, isobaric analogue reson. and seniority model 77−57642
^{59}Ni, and N=29 nuclei f-p shell nuclei, unified model description 78−78343
^{29}P, T=3/2 isospin-forbidden reson. via ^{32}S(p,p) 5.6-5.9 MeV 77−18507
^{141}PR(e,e′p), $f_{7/2}$ ground isobaric analogue resonance, proton decay mode 78−29450
^{208}Pb(^{3}He,t)^{208}Bi, 80 MeV, Gamow-Teller M1 state excitation 78−50184
^{208}Pb(p,γ), γ-ray ang. distribs. asymmetry effects through IAR, direct-semidirect model 80−42581
^{143}Pm, IAS, J^π via polarised proton scatt. 77−74825
^{140}Pr isobaric analogue resonances, de-excitation cascade, K-shell ionisation, spin depend. from ^{140}Ce(p,n) 80−78202
^{141}Pr, IAS, J^π via polarised proton scatt. 77−74825
^{45}Sc, fragmented analogue state, ^{44}Ca(p,p′γ) amplitudes 79−17882
^{49}Sc isobaric analogue states and resonances, J^π from ^{48}Ca(p,p) 80−13426
^{28}Si+n, isobaric analogue resonances from total and differential elastic cross sections 78−41715
^{30}Si(p,p), 1.1-3.0 MeV, analogue reson. obs., Coulomb energies, spectroscopic factors determ. 77−2988
^{147}Sm(p,p), (p,p′), 7.5-10.8 MeV, isobaric analogue reson. and seniority model 77−57642
^{119}Sn(p,n′)^{119}Sb, 17-19 MeV, analogue state excitation and decay 79−6542
Sn(p,n)Sb reson. reaction, direct neutron decay of isobaric anal. reson. *(Russian)* 77−88145
^{88}Sr(p,p′)^{88}Sr(2_1^+), 7-7.5 MeV polarised protons, scatt. at IAR 77−318
^{93}Tc high spin analogue resonance near N=50 neutron shell, DWBA anal. of ^{92}Mo(^{3}He,d) 80−42613
^{95}Tc, energy levels from ^{95}Mo(p, nγ)^{95}Tc 80−37372
^{49}Ti(p,γ), 0.74-3.25 MeV, cross section and thermonuclear reaction rates, nucleosynthesis, IAR effects 80−102187
^{235}U(p,f), 13.7-14.2 MeV, isobaric analogue resonances, fission width 78−21616
^{238}U(p,p′), isobaric analogue reson., modified KASTOR code calc. 77−14132
^{51}V(p,n), 1.56-5.53 MeV, total cross section, excitation functions, isobaric analogue resonance 78−4943
^{51}V(p,n)^{51}C neutron polarisation at isobaric analogue resonances 78−54759
^{51}V(p,n)^{51}Cr, 2.34 MeV, shell model anal. of analogue resonance 77−14122
^{87}Y, IAS spectroscopy and compound nuclear enhancement 77−61396
^{A}Zn(p,γ), A=64, 66, $g_{9/2}$ isobaric analogue resonances 79−63663
^{90}Zr(^{3}He,t)^{90}Nb, 80 MeV, Gamow-Teller M1 state excitation 78−50184
Zr(p,p′γ), odd isotopes, excited d-states from analogue resonances and p-γ correlations 80−68546

isobaric analogue states
see also isobaric analogue resonances
analogue states and resonances in semimicroscopic shell model *(Russian)* 80−86872
asymmetric nuclear matter, isospin waves, IAS and giant Gamow-Teller resonance 80−91142
compound nucleus reactions, consequences of isospin mixing 78−25168
Conference on meson-nuclear physics, Houston, USA (Mar. 1979) 79−85489
Coulomb displacement energies of analogue states in mirror nuclei, review 78−78242
Coulomb energies and nuclear radii in energy density formalism 77−82810
Coulomb isospin mixing, self consistent theory, isobaric states in RPA, isovector forces *(Russian)* 79−22181
doorway states, fragmented, micro-resonances, strength functions, K-matrix width 80−57754
doorway states spreading width, statistical significance, isobaric analogue states 79−93588
fine structure of fragmented analogue states produced in proton-nucleus reactions 77−6391
fission isobaric yield distribs., pairing effects 77−50107
high energy nuclear collisions, isobaric-gas model, shock waves, temp., density, pionisation 78−94022
hypernuclei, strangeness analogue states 77−14054
inelastic collisions, charge equilibration, collective model and independent particle model 80−18270
isobaric quartets in nuclei, T=3/2 states, isobaric multiplet mass eqn. 79−93519
level density isospin depend. 77−61349
light nuclei, schematic model for isospin mixing 78−66198
light nuclides, proton rich, mass excesses 78−37259
N=27 nuclei levels and analogue states, DWBA anal., from (^{3}He,α) reaction 79−17808
narrow resonances in the continuum 79−85435
neutronrich nuclei, analogue energy splitting, isoinvariant linearisation 77−65205
pion-nucleus single charge exchange and inelastic scatt. cross sections relationship 80−102204
separation of alkali and alkaline earth elements using surface ion source 80−37688
superallowed Fermi β-decay, analogue symmetry breaking 77−65215
two-step direct reactions through doorways, fluctuation effects 80−13445
Wigner scheme, Γ-decay of analogue states, β-decay 77−41930
(d,^{3}He) on ^{12}C, ^{16}O, ^{24}Mg, ^{40}Ca, 29 MeV, polarised d, low lying analogue states, DWBA anal. 78−82285
(d,t) on ^{12}C, ^{16}O, ^{24}Mg, ^{40}C, 29 MeV, polarised d, low lying analogue states, DWBA anal. 78−82285

isobaric analogue states continued
Δ(1236), virtual isobar admixtures in complex nuclei, OBE approx. 78−17107
(p,γ), isobaric analogue doorway states, excitation functions 80−47388
(p,n) reactions, alignment and decay of IAS, depend. on higher multipole contrib. 77−3003
(p,n) scattering, charge exchange, isobaric analogue state, giant resonance effect, semimicroscopic model 78−89868
(π^+,π^0), isobaric analogue state obs. in CH_2, ^{7}Li, ^{13}C, ^{27}Al, ^{58}Ni, ^{90}Zr, ^{120}Sn, ^{208}Pb 80−106078
^{51}Mn levels studied via high resolution proton scatt. from ^{50}Cr 77−54151
^{26}Al 1^+T=0 states, isobaric analogue state, spin-isospin effective interaction from ^{26}Mg(p,n) 80−68553
^{26}Al excited states, isobaric analogues, spins, DWBA anal. of ^{27}Al(^{3}He,α) 80−105981
^{27}Al, analogue-antianalogue M1 transitions, nucl. shape change influence 78−13006
^{32}Ar, isobaric analogue states via β-delayed protons 78−558
^{A}As, A=73,75,77, probabilities for analogue-antianalogue transitions 79−6496
^{73}As bound and isobaric analogue states, spectroscopic factors, DWBA anal. of ^{72}Ge(^{3}He,d) 79−54391
^{11}B analogue of ^{11}C 6478 keV state, lifetime from ^{7}Li(α,γ) 80−5092
^{9}Be(p,pn)^{8}Be$_{gs}$, ^{9}Be-^{9}B isobaric doublet asymmetric excitation 77−26678
^{10}Be analogue states from ^{10}B(e,e′) anal. 79−75898
^{10}Be ang. distribs. to isobaric analogue states cross section ratio from ^{9}Be(p,π^+) 79−89274
^{208}Bi, 0^+ IAS, spreading width and isospin impurity, isovector monopole state influence 80−78155
^{A}C(p,$\pi^\pm$), A=12,13, 200 MeV, analogue and nonanalogue state cross sections 80−99130
^{10}C ang. distribs. to isobaric analogue states cross section ratio from ^{9}Be(p,π^-) 79−89274
^{12}C(^{3}He,^{3}H), (^{3}He,^{3}He′), 44 MeV, study of ^{12}N(2.43 MeV) and ^{12}C(17.77 MeV) analogue states 77−6235
^{12}C(p,n), 62, 120 MeV, isobaric analogue states, differential cross sections 80−18202
^{12}C(p,p′), 62, 120 MeV, isobaric analogue states, differential cross sections 80−18202
^{13}C(π^+,π^0)^{13}N, comparison with isobar doorway calcs. 77−41999
^{14}C(πγ), collective resonances, A=14 isobaric states, shell model predictions 79−85386
^{36}Ca mass via ^{40}Ca(^{4}He,^{8}He), isobaric multiplet mass eqn. deviations 77−74754
^{40}Ca+p, fine struct. levels sign meas., off-diagonal strength function, analogue state broadening theory test 78−78381
^{48}Ca, isospin purity violation, dominant role of noncollective monopole states 78−12964
Cd, A=110, 112, isobaric analogue resonances, QRPA anal. of (p,p) reactions 78−576
^{32}Cl, isobaric analogue states via ^{32}Ar β-delayed protons 78−558
^{35}Cl, fine struct. of $7/2^-$ isobaric analogue states 79−9466
^{55}Co f-wave resonances, inelastic p amplitudes, analogue state spectroscopic factors from ^{54}Fe(p,p′γ) 80−47451
^{55}Co, γ decay and splitting of analogue states from ^{54}Fe(^{3}He,dγ) at 18 MeV 78−70505
^{55}Co, IAR, J^π via ^{54}Fe(p,p) 3.28-4.53 MeV 78−574
^{55}Co, spectroscopic study via ^{54}Fe(^{3}He,d)^{55}Co and ^{54}Fe(τ,dp)^{54}Fe reactions 77−88029
^{57}Co levels and analogue states, J^π from DWBA anal. of ^{58}Ni(^{3}He, α) 79−63592
^{58}Co, fine struct. of ground hole-state analogues 78−50065
^{58}Co, fragmentation of hole-state analogues 78−54731
^{59}Co(p,d), 50 MeV, fine struct. of ground hole-state analogues 78−50065
^{49}Cr ground analogue state fine struct., l=3 states differential cross section from ^{50}Cr(p,d) 80−63152
^{50}Cr, $1f_{7/2}$ shell isobaric analogue states, displacement energies 79−13207
^{51}Cr levels, spectroscopic function and analogue states, PWBA anal. of ^{52}Cr(^{3}He,α) 80−68547
^{52}Cr, shell model study and gamma decay of isobaric analogue states 78−86492
Cu, A=61,63, analogue state decay modes from Ni (^{3}He,dp) 79−67702
^{59}Cu, γ decay and splitting of analogue states, from ^{58}Ni(^{3}He,dγ) at 18 MeV 78−70505
^{59}Cu, time struct. of the $2d_{5/2}$ analogue state 79−6591
^{61}Cu analogue states, γ-ray ang. distribs. obs. 77−82848
^{63}Cu $g_{9/2}$ analogue state fragmentation from γ-transitions in ^{62}Ni(p,γ) 79−22202
^{63}Cu, $g_{9/2}$ isobaric analogue state, using ^{62}Ni(p,γ) 79−22258
^{A}Eu, A=144,148,150,152, ground and excited state analogues, two-phonon coupling effects from Sm(p,n) 79−89277
^{52}Fe, $1f_{7/2}$ shell isobaric analogue states, displacement energies 79−13207
^{A}Ge, A=70, 72, 74, appl. of crystal blocking technique to study highly excited nuclear continuum using (p,p′) 79−45261
^{2}H(d,n)^{3}He and ^{2}H(d,p)^{3}H, comparison of analysing powers 2.5 to 11.5 MeV 79−6628
^{3}H isobaric analogue state excitation, cross section from ^{3}He(π^-, π^0) 80−42544
^{3}He(π^-,π^0)^{3}H, isobaric analogue state ang. distrib. 79−85508
^{3}He(t,d)^{4}He, charge asymmetry effects 79−3159
^{3}He(t,d)^{4}He asymmetry, cluster model anal., isobaric analogue states 78−78389
^{41}K nucleus 11.36 MeV analog state total angular momentum from ^{40}Ar(p,p) reaction *(Russian)* 80−102169
^{20}Mg, β-delayed proton obs., mass excess of T=2 state in ^{20}Na 79−22234
^{27}Mg excited analogue states high resolution study in ^{26}Mg(p,p) 78−78377
Mg(n,γ), A=24, 25, 26, E=0.1-1800 keV, determ. of isobaric analogue impurities 77−6386
^{52}Mn, $1f_{7/2}$ shell isobaric analogue states, displacement energies 79−13207
^{53}Mn, γ decay and splitting of analogue states from ^{52}Cr(^{3}He,dγ) at 18 MeV 78−70505
^{53}Mn, isobaric analogue states via ^{52}Cr(^{3}He,d) and ^{52}Cr(^{3}He,dp) 77−6237
^{91}Mo, fine struct. of ground hole-state analogues 78−50065

isobaric analogue states continued
^{92}Mo(p,d), 50 MeV, fine struct. of ground hole-state analogues 78−50065
^{12}N, ^{12}C*, comparison of ^{12}C(p,n) and ^{12}C(p,p′) cross section meas., scintillation counter efficiency 80−37713
^{13}N isobaric analogue state excitation, cross sections from ^{13}C(π^+,π^0) 80−42544
^{15}N-^{15}O, study of excited states, spin and parity *(French)* 78−33158
^{22}Na bound and analogue state lifetimes, branching ratios, DSA method from ^{21}Ne(p,γ) 0.5-6.0 MeV 78−93967
^{91}Nb analogue state decay modes from ^{90}Zr (^{3}He,dp) 79−67702
^{18}Ne analogue and nonanalogue states, π double charge exchange form factors from ^{18}O(π^+,π^-) 80−13405
^{18}Ne cross section, excitation function and double isobaric analogue state from ^{18}O(π^+,π^-) 80−27596
^{21}Ne-^{21}Na, study of excited states, spin and parity *(French)* 78−33158
Ni, A=57, 59, 61 and 63, fine struct. of ground hole-state analogues 78−50065
^{A}Ni, A=57, 59, 61, 63, fine structure of hole-state analogues, isospin mixing from (p, d) 80−13401
^{57}Ni levels and analogue states, J$^\pi$ from DWBA anal. of ^{58}Ni(^{3}He, α) 79−63592
^{58}Ni(p,d), 50 MeV, fine struct. of ground hole-state analogues 78−50065
^{59}Ni, fragmentation of hole-state analogues 78−54731
^{64}Ni, isospin purity violation, dominant role of noncollective monopole states 78−12964
Ni(p,d), A=60, 62 and 64, 50 MeV, fine struct. of ground hole-state analogues 78−50065
^{15}O, level scheme determ. from ^{14}N(p,γ) 77−38243
^{15}O, reson. widths and branching ratios meas. from ^{14}N(p,γ)^{15}O 77−38244
^{15}O-^{15}N, Coulomb energy anomaly and charge-dependent nuclear forces 79−58997
^{16}O T-mixed analogue states, (^{3}He,p)/(t,p) cross section ratio from ^{14}N(t,p), ^{14}N(^{3}He,p) 79−9478
^{18}O-^{18}F, study of excited states, spin and parity *(French)* 78−33158
^{18}O(e,e′), isovector mag. dipole and quadrupole transitions, analogues, ($\pi^-\gamma$) relation 80−106010
^{18}O(π^+,π^-)^{18}Ne double-charge-exchange, isobaric analogue transition 77−38300
^{28}P, T=1 positive parity analogue states 77−34249
^{31}P, analogue-antianalogue M1 transitions, nucl. shape change influence 78−13006
^{207}Pb isobar-like isospin forbidden state excitation from ^{206}Pb(n,p) *(Russian)* 79−75855
^{207}Pb, T=45/2 isobaric analogue state obs. in ^{208}Pb(^{3}He,α)^{207}Pb 78−93928
^{207}Pb(n,p) reaction, isobar analogue state excitation *(Russian)* 80−102124
^{208}Pb, isobaric analogue states, effects of Coulomb isospin coupling, random-phase method *(Russian)* 80−86808
^{208}Pb, isospin purity violation, dominant role of noncollective monopole states 78−12964
Pb(p,n), A=207,8, proton decay of isobaric analogues of ground states 77−26692
^{32}S(d,t) and (d,^{3}He), ^{31}S, ^{31}P analogue spectroscopic factors, charge asymm., DWBA anal., optimum Q-value 77−54229
^{119}Sb, p decay, isobaric analogue states from ^{119}Sn(p,n′) 79−6542
^{A}Sc, A=44,46,48, 1f$_{7/2}$ shell isobaric analogue states, displacement energies 79−13207
^{45}Sc, e.m. decay of fragmental analogue states 77−2987
^{82}Se(p,p) elastic, inelastic 4.5-77 MeV scatt., IAS, ^{83}Se low-lying states 78−573
^{83}Se, IAS, J$^\pi$ via ^{82}Se(p,pγ) 4.5-7.7 MeV 78−573
^{24}Si, isobaric multiplet mass eqn., test from decay 79−40890
^{28}Si, γ-spectra, isobaric analogue resonances via ^{27}Al(p,γ)^{28}Si 2.4-2.74 MeV 77−57646
^{28}Si, T=1 positive parity analogue states, lifetimes and branching ratios 77−34249
^{28}Si(d,t) and (d,^{3}He), ^{27}Si, ^{27}Al analogue spectroscopic factors, charge asymm., DWBA anal., optimum Q-value 77−54229
^{28}Si(n,p)^{28}Al*, obs. of analogue dipole state 77−30596
^{143}Sm, T$_>$ hole analogue states, p decay, deduced states and p branching ratio 78−70451
Sn deeply bound hole states and isobaric analogue states populated in ^{116,118,120,124}Sn neutron pick-up reactions 77−30570
Sn odd-mass isotopes, hole-state analogues, line broadening and Coulomb displacement energies 80−52560
Sn(^{3}He,t), 45.9 MeV, IAS, Coulomb displacement energies 77−6337
^{A}Sn, A=111,115,119, neutron hole distribs., IAS and spectroscopic factors from Sn(^{3}He,γ) 80−42519
^{114}Sn, isospin purity violation, dominant role of noncollective monopole states 78−12964
^{119}Sn(p,n)^{119}Sb, 16-20 MeV, isobaric analogue state, ang. distrib. meas. 78−29468
^{124}Sn, isospin purity violation, dominant role of noncollective monopole states 78−12964
Sn(d,t)Sn, even A=112 to 124, deeply bound hole states of odd A Sn 78−8725
Sn(p,n) (A=112,116,124), 22.8 MeV, ang. distribs. to isobaric analogue states, nuclear matter distrib. 77−10405
Sn(p,n)Sb, A=115-120, between analogue states via (p,p) and (p,np) anal. 77−88132
Te(^{3}He,t), 45.9 MeV, IAS, Coulomb displacement energies 77−6337
^{A}Ti, A=44-46, 48,49, 1f$_{7/2}$ shell isobaric analogue states, displacement energies 79−13207
^{47}V 3/2$^-$ analogue state decay amplitudes, common doorway state phase relation from ^{46}Ti(p,p′γ) 79−89276
^{49}V proton hole, analogue and high spin states, distorted wave anal. from ^{52}Cr(p,α) 79−9482
^{50}V, 1f$_{7/2}$ shell isobaric analogue states, displacement energies 79−13207
^{50}V, isobaric analogue states anal. from ^{51}V(p,d)^{50}V 78−33182
Zr, A=90-95, levels, J$^\pi$, neutron-hole struct., ^{95}Zr IAS 78−508
^{89}Zr, fine struct. of ground hole-state analogues 78−50065
^{89}Zr, IAS and bound hole states via ^{90}Zr(^{3}He, ^{4}He)^{89}Zr 39 MeV 78−492
^{90}Zr, isospin purity violation, dominant role of noncollective monopole states 78−12964
^{90}Zr(p,d), 50 MeV, fine struct. of ground hole-state analogues 78−50065
^{90}Zr(p,n), IAS transition, 18.5 to 45 MeV, microscopic model anal. 77−82927
isobaric analogue states continued
^{90}Zr(p,p′), polarised protons, compound nuclear contribs. to IAR inelastic decay 78−8813
^{97}Zr, T$_>$ hole analogue states, p decay, deduced states and p branching ratio 78−70451

isobars *see atmospheric pressure and density*

isoelectronic series
3d photoabsorpt. spectra, continuum and discrete states 79−81176
acetylene, HCN, N_2, vibr. fine struct. accompanying core ionis., STO calcs. 78−62844
alkali anions, autodetaching sub $^2P_{1/2}$ threshold states 79−22611
alkali isoelectronic series, transition probabilities, oscill. strengths, lifetimes, branching ratios 78−33470
alkali metal, excited state lifetime var. along isoelectronic series *(French)* 77−46538
atomic systems, elastic X-ray scatt. intensity, rel. to average electron density, isoelectronic changes 80−91424
atoms, Politzer's energy rel. determ. using HF data 80−91425
beam-foil spectra oscillator strengths, neutral and ionised atoms, nonclosed shell many electron theory 77−38612
Cu isoelectronic sequence, fine structure separations for ^{2}D terms 79−89804
diatomic mols., electronic transition probabilities, isoelectronic, isovalent correls. for transition strength and vibr. consts. 80−87182
electron density relation between adjacent members 79−72222
electron impact, intermediate-coupling strengths for fine struct. transitions 80−32837
14-electron isoelectronic series, ab initio calcs., equilib. geometry and electronic struct. 77−83489
energy level ordering 78−21863
energy-density relationship, for 2 to 36 electron sequences 80−9486
excited state ions energy level ordering 78−21863
f-value distribs., regularities 77−38642
Group IV tetrabromides, intramol. force fields and mean vibr. amplitudes 80−106316
H-like atoms, nuclear size and hyperfine struct., theory 80−924
Hartree-Fock expectation values, systematic behaviour 79−3365
hexafluoride ions of group IIIA elements, molecular consts., normal coord. anal. 77−1187
hexafluoride radicals, prep. and EPR spectra comparison, hyperfine splitting 78−68381
hexahalo ions, octahedral, mol. consts. calcs. 80−106317
hydrogen atoms, threshold behaviour of multiphoton ionisation 80−954
hydrogen-like ions, beam-foil excitation, relative initial populations, lifetime curves 80−14210
hydrogenic atoms, Compton profile and X-ray scatt. factors, elec. field and elec. field gradient effects 79−31458
hydrogenic Green's functions, reduced, power moments, and 2nd-kind Green's functions 79−85891
hydrogenic ion + H^+, electron capture in highly excited s-state 79−45839
hydrogenic ions, break-up processes, eikonal approach 80−91676
hydrogenic ions, electron impact excitation, modified Coulomb-Glauber approximation 79−81285
hydrogenlike ions, electron impact excitation, Coulomb-Born-Oppenheimer calcs. 79−10211
inert gas isoelectronic sequences, positive ion p-subhsell photoionisation cross-sections calcs. 77−50374
inert gas series, polarisabilities and shielding factors 79−98008
ions, H-, He-like, Z=4 to 34, wavelengths, radiative transition probabilities, autoionisation rates 79−25776
ions with partly filled L-shells, relativistic Hartree-Fock energy calcs. 78−82656
isoelectronic sequence, X-ray spectra 80−87071
methane, core ionis., single orbital relax., LCAO MO SCF calcs. 78−29739
molecular, Compton profile, empirical correlation with energy 78−78758
neutral atom, nonrelativistic binding energy, rel. to isoelectronic ions 80−18782
neutral atom and isoelectronic ions, non-relativistic binding energies 79−59334
non-closed shell many-electron-theory at. charge wavefunctions, Be through Ne and Si 77−57849
one-electron ion+He(N)(Ar), sum-rule Born cross sections, excitation and ionis. contribs. 79−22812
optical dipole transitions, first order model pot., appl. to Li isoelectronic sequence 78−25474
oxygen-type atoms, subdivision of 2p-shell 78−82609
plasma, photon escape probabilities for Stark-broadened Lyman series lines 80−24143
plasma diagnostics using spectral line intensity ratios 78−14203
relativistic effects in central field approximation, RELAC method and use 80−9520
relativistic effects in oscillator strength calculations, ab initio methods 80−9519
s^2x^2, Koopmans atomic valence electron ionisation energy, 1/Z expansion method, reorganisation corrections 78−78623
s^2xy, Koopmans atomic valence electron ionisation energy, 1/Z expansion method, reorganisation corrections 78−78623
semiconductor, atomic displacements and enthalpy of vacancy formation 78−38690
semiconductors, isoelectronic series and trends in band struct. 77−89696
sxyz, Koopmans atomic valence electron ionisation energy, 1/Z expansion method, reorganisation corrections 78−78623
ten-electron positive ions, ionic size rel. to Koopmans' ionisation pot. 79−85892
total electronic energy, atoms and mols., SCF binding energy, Z^{-1} perturbation theory 80−83268
total HF SCF energy, of ats. and ions, approximation methods comparison 79−31366
transition integral, Z-representation 77−27029
two electron, Hartree-Fock energies, scaled 1/Z expansion, integral eqns. 80−47886
two-electron atom, exchange and correlation pots., density functional theory 80−52848
two-electron atom, long-range electron density, function reliability test 79−26875
two-electron atom, Schrodinger local energies 79−41090
two-electron atom in spherical box, CI calcs., appl. to He, Li^+, and Be^{2+} 79−97984

isoelectronic series continued
two-electron atomic systems, correl. energy calcs. 79−36543
two-electron atoms, doubly excited resonances assoc. with N=4 hydrogenic threshold 80−106283
two-electron atoms, S autoionising states, at. reson. theory appl. 80−23329
two-electron ions, ground state, quadratic Stark effect 80−37775
two-valence electron systems, valence Rydberg and continuum orbitals 77−3259
vector perturbation series based upon a representation in a finite Banach space 79−63893
X-ray absorption edge-shifts, empirical relations, effective ionic charge for isoelectronic series 78−55136
Ag, excitation energies and oscillator strengths 79−54918
Ag I isoelectronic sequence identification of W radiation generation in Tokamak 80−83981
Ag isoelectronic sequence, UV spectra (60-600 Å), resonance line identifications 78−33455
AgBr:I, isoelectronic trap 79−43016
AgI, oscill. strengths, relativistic HF calcs. 79−98034
Al I isoelectronic sequence, forbidden transition probabilities for ground terms 77−2376
Al sequence, $4s^2S$-$4p^2P$ transition, f-values 78−78651
Al(^{2}P) series, Sternheimer valence shielding and antishielding factors 80−18807
Ar, and isoelectronic sequence, E1 transitions, relativistic oscill. strengths 78−949
Ar, isoelectronic sequence, many-body photoionization calcs. 78−17631
Ar isoelectronic series, orbital binding energies within statistical exchange approx. 79−85895
Ar, Koopmans' ionis. pot., virial scaling corrections 79−45655
Ar XVI, lithiumlike ions, excitation by electron impact 78−13606
Ar-like atoms, gradient expansion of atomic kinetic energy functional 80−95530
AuI, oscill. strengths, relativistic HF calcs. 79−98034
B I, weighted oscillator strengths for elec. dipole and forbidden transitions, data tables 80−37779
B I isoelectronic sequence, forbidden transition probabilities for ground terms 77−2376
B, ionization equilib. balance, solar and stellar atms. appl. 79−36587
B isoelectronic series, dipole oscill. strengths, multiconfigurational Hartree-Fock calcs. 77−83540
B series, Rydberg electron-ionic core nonadiabatic long-range forces 80−23328
B^{2+}, multipole polarizabilities and shielding factors, calcs. on open shell ions 78−46263
B^{3+}, few-parameter two-electron wavefunction of ground state 77−75051
B-like ions, autoionisation states calcs. 80−43006
B-like ions, EUV emission density sensitivity 79−16910
BF, isoelectronic sequence, Rydberg transitions, term value-ionisation pot. correl. 80−58276
BF_3, BO_3^{3-}, CO_3^{2-}, NO_3^-, 78−86887
B(^{2}P) series, Sternheimer valence shielding and antishielding factors 80−18807
Be, and isoelectronic sequence, oscillator strengths, relativistic RPA calcs. 77−57929
Be, and isoelectronic sequence, correlated and HF electron density differences 78−46275
Be, beam-foil obs. of oscillator strengths for E1 transitions 80−14112
Be, dynamic multipole polarisability, coupled Hartree-Fock 78−82858
Be, electric field variant orbitals, STO field gradient depend., atomic quadrupole polarisability 80−23295
Be, excitation energies, oscillator strengths, using relativistic RPA 80−47925
Be, excited states, oscill. strengths calcs., influence of wave function determ. method 80−99478
Be, excited states, transaction oscill. states and wavefunctions 79−59367
Be I, radiative props. determ. by model-pot. method 78−70788
Be I, weighted oscillator strengths for elec. dipole and forbidden transitions, data tables 80−37779
Be I isoelectronic series, $2p^2$-2s2p and 2s2p-$2s^2$ transitions, oscill. strengths, transition probabilities 77−46532
Be I like ions, resonant-scatt. contributions to excitation rates 80−58393
Be I-like spectra, low configs., isoelectronic consistency 79−93940
Be, inner-shell photoionis. cross sections 78−74623
Be, ionization equilib. balance, solar and stellar atms. appl. 79−36587
Be ions, isoelectronic series, correlation energy and size, empirical relationship 77−79546
Be, isoelectronic sequence, transition probabilities, relativistic effects calcs. 77−27028
Be, isoelectronic sequence, relativistic transition probability calcs. 77−54533
Be isoelectronic sequence, mag. quadrupole transition probabilities calcs. 78−21865
Be isoelectronic sequence, mag. quadrupole transitions, multiconfig. HF calcs. 78−33420
Be isoelectronic sequence, mag. quadrupole transitions probabilities 78−37592
Be isoelectronic sequence, electron impact excitation 79−81286
Be isoelectronic sequence, electron impact excitation of reson. transitions 80−63825
Be, isoelectronic series, Coulomb holes and correl. coeffs. 77−88398
Be isoelectronic series, transitions involving $2s3l^3L$ states, oscill. strengths 77−3308
Be isoelectronic series, Z=22-34, spectral lines from laser prod. plasma 77−50388
Be, mag. dipole transition contrib. isoelectronic sequence, mag. dipole transition contrib. 79−81153
Be, pot. energy relationships 79−22584
Be sequence, $2s3p\ ^3P_1$-$2s^2\ ^1S_0$ intercombination line transition probabilities 80−18823
Be sequence, (Z=4 to 10, 14), $^3P_1 \rightarrow {}^1S_0$ intercombination line, CI calc., Breit interaction 78−78641
Be series, oscill. strengths calcs. 79−72275
Be series, Rydberg electron-ionic core nonadiabatic long-range forces 80−23328
Be^+, multipole polarizabilities and shielding factors, calcs. on open shell ions 78−46263
Be^{2+}, few-parameter two-electron wavefunction of ground state 77−75051
isoelectronic series continued
Be-like ions, $2s2p(^3P_1^0) \rightarrow 2s^2(^1S_0^e)$ transition probabilities, CI calcs. 79−36544
Be-like ions, oscill. strengths and transition probabilities, Breit-Pauli approx. calcs. 79−36570
Be-like ions, photoionisation, 2-channel relativistic random phase approx. calcs. 79−59407
Be-like system, numerical many-body perturbation calcs. using multiconfig. model space 80−47907
$Be+H^+$, low-lying ^3P term excitation, cross-sections and rate consts. 79−94069
Br I, isoelectronic sequence, multiconfiguration HF calc. of sp^6-s^2p^4d interaction 78−9072
BrVI(VII), reson. line oscill. strengths, beam-foil spectra 77−38630
C, correlated and HF electron density difference 78−46275
C I, weighted oscillator strengths for elec. dipole and forbidden transitions, data tables 80−37779
C I series, ^3P_J fine structure transitions, proton impact excitation 80−37864
C I to Ni XXIII, forbidden transitions calc. 79−31444
C III, electron collisional excitation, R-matrix calc. 77−58169
C III, solar emission line ratios interpretation 78−28598
C IV, lithiumlike ions, excitation by electron impact 78−13606
C^{4+}, few-parameter two-electron wavefunction of ground state 77−75051
C-like ions, solar emission lines, density depend. 80−21963
CO, isoelectronic sequence, Rydberg transitions, term value-ionisation pot. correl. 80−58276
C(^{3}P) series, Sternheimer valence shielding and antishielding factors 80−18807
^{13}C V, high energy hyperfine struct. meas. 77−57915
Cl I, isoelectronic sequence, multiconfiguration HF calc. of sp^6-s^2p^4d interaction 78−9072
Cl I isoelectronic sequence, forbidden transition probabilities for ground terms 77−2376
Cl(^{2}P) series, Sternheimer valence shielding and antishielding factors 80−18807
Co (VII), semiempirical investigation of spectra 78−33434
Cs I, oscill. strengths, relativistic HF calcs. 79−98035
Cu, collision strengths and Gaunt factors 79−98227
Cu, dipole polarisability, numerical Coulomb approx. 80−43199
Cu I, $3d^{10}$nl, CC Mo XIV, spectrum and energy levels, ionisation energy 79−49954
Cu I isoelectric sequence, fine struct. separations for reson. transitions 78−17588
Cu I series, oscill. strengths, formula for cancellation disappearances 78−90124
Cu, ionisation energy, multiplet strengths, diagrammatic MBPT theory calcs. 80−9500
Cu isoelectronic sequence, 4s-4p reson. transition in highly charged ions 77−75087
Cu isoelectronic series, Hartree-Fock line strengths 78−9122
Cu isoelectronic series, hard-core pseudopotentials and struct. maps 80−44168
Cu, isoelectronic series, semi-empirical oscillator strengths, lifetime, transition probability 80−32672
Cu, oscillator strengths of reson. transitions 79−22666
Cu-like atoms, core polarisation influence on oscillator strengths 79−45672
Cu-like ions, 4s-4p reson. lines and transitions obs. by means of laser prod. plasma, appl. to Tokamaks 80−99468
Cu-like ions, E1 transitions, wavelengths, oscillator strengths and transition probabilities, data tables 80−37780
F I, Fe XVIII, Zn XXII, Ge XXIV, Se XXVI, spectral line identification 79−72230
F I isoelectronic sequence, forbidden transition probabilities for ground terms 77−2376
F, isoelectronic sequence, X-ray spectra 80−87071
F isoelectronic series, transitions between $1s^22s^22p^5$-$1s^22s^22p^43d$ and $1s^22s^22p^5$-$1s^22s^22p^43s$ configs. 79−26925
F series, Ni XX, Cu XXI, Fe XVIII, Zn XXII, Ge XXIV and Se XXVI spectra 79−93948
F(^{2}P) series, Sternheimer valence shielding and antishielding factors 80−18807
Fe group ions, spectra, calcs., allowance for d^n shell pair excitations 77−42261
Fe I, abnormal intensities in multiplets 79−22635
Fe IX radiative and collisional data rel. to solar coronal emission spectrum 77−49350
Fe^{3+} isoelectronic series, radial charge distrib. calc. 80−9507
Ge XXIV, $2p^5$-$2p^43s(2p^43d)$ transitions in laser produced X-ray spectra 78−13460
H, C VI, cylindrical plasma, XUV gain calc. 79−72995
H isoelectronic sequence, electron impact ionisation cross section 80−91688
H, isoelectronic series, X-ray line excitation 79−44453
H like, metastable 2S state in weak elec. field, radiative decay, bound state QED 80−42959
H^-, and isoelectronic sequence, correlated and HF electron density differences 78−46275
H^+, isoelectronic sequence, quenching radiation anisotropy calcs. 77−27021
H-like, average spectral lifetime, asymptotic expression 79−45671
H-like atom, spin-orbit interaction and single electron excitations rel. to mag. dielectrics 79−54780
H-like atom, Stark effect on fine struct. 79−26929
H-like atom+bare ion, electron capture to continuum, cross-section cusp 78−90289
H-like atom+bare ion, inner-shell electron capture, 2nd Born effects 80−48085
H-like atoms, bound states, so(2,1) algebra 79−10016
H-like atoms, dipole polarisability of arbitrary hybrid bound states 80−87237
H-like atoms, dipole transitions, asymptotic expansion of radial-dipole integral 78−82667
H-like atoms, electron exchange scatt., high impact vels. 79−22846
H-like atoms, multipole polarisability, dynamic, for S state, closed-form expression 78−82857
H-like atoms, spectra, interaction with external quantised EM field, H-like atom 79−68332

isoelectronic series continued
H-like atoms, Stark broadening, ion dynamics correction to unified classical path theory 79−76382
H-like atoms, Stark shift, classical adiabatic theory of Stark ionis. threshold 78−82687
H-like ion channelling, reson. coherent excitation 79−51178
H-like ion plasma, population inversion, soft X-ray transitions in cooling plasma 78−87437
H-like ion+H, two-body dispersion interaction, freq. depend. multipole polarisability, variational calc. 80−37758
H-like ion+H^+, 1s-2s excitation probabilities, low energy, Coulomb-Born approx. 80−37870
H-like ion+H^+, electron capture, Coulomb-Born approx. 79−45838
H-like ions, departure coeffs. from thermodynamic equilib., rel. to radio-sources recomb. lines 79−76369
H-like ions, elastic electron (positron) scatt., relativistic Glauber amplitudes 79−31681
H-like ions, electron impact ionis. from 3s sub-level 78−90297
H-like ions, electron impact excitation, Coulomb modified Glauber approx. calcs. 78−94324
H-like ions, emission spectrum, depend. on electron density in laser plasma 79−27248
H-like ions, excitation regimes, nucl. orientation due to hyperfine interaction 78−70928
H-like ions, fluoresc. polarisation of Stark quenched spin-polarised beam 78−66501
H-like ions, Glauber exchange amplitudes for electron scatt. 78−74772
H-like ions, ground-state, elastic electron (positron) scatt., relativistic Glauber amplitudes 80−23550
H-like ions, n=2→1 transitions, collision strength Z-dependence 80−91675
H-like ions, spectral broadening in plasma 79−46431
H-like ions, spectral line intensity, density depend., plasma diagnostic appls. 78−83617
H-like ions in steady-state plasma, excited level population probabilities 80−19552
H-like ions+H^+, charge transfer cross sections 79−18286
H-like systems in arbitrary mag. field, excited states, variational approach 79−77973
H^--like ions, electron correlation and Coulomb hole in momentum space 78−86793
HF, core ionis., single orbital relax., LCAO MO SCF calcs. 78−29739
H_2O, core ionis., single orbital relax., LCAO MO SCF calcs. 78−29739
HOCl, chloramine, isoelectronic mols., vapour phase UV photoelectron spectra, struct. 78−66600
He 2^1S state isoelectronic series, Fermi and Coulomb correlations 78−921
He, (H^- to C^{4+}), correl. energy calcs. 79−36543
He, and isoelectronic sequence, correlated and HF electron density differences 78−46275
He, $\delta(r_1)$ matrix elements using spatially distrib. operators 80−102445
He, electric field variant orbitals, STO field gradient depend., atomic quadrupole polarisability 80−23295
He, excitation energies, oscillator strengths, using relativistic RPA 80−47925
He, ground state, Coulomb holes and correl. pots. 79−89594
He ion isoelectronic series, X-ray line excitation 79−44453
He isoelectronic sequence, electron correlation effects on one-electron distribs. 77−10598
He isoelectronic sequence, few-parameter wavefunctions of ground state 77−75051
He, isoelectronic sequence, Schrodinger eqn. finite difference soln. 79−31373
He, isoelectronic sequence, 2^1S states, analytic wave function 80−9525
He, isoelectronic sequence, E1 and E2 oscillator strengths, MCHF calcs. 80−106292
He isoelectronic sequence to Z=10, D and F states fine struct. 77−544
He, isoelectronic series, dipole matrix elements derivation 77−83519
He isoelectronic series, dipole oscillator strength distrib. moments, systematics 78−86821
He isoelectronic series, electron correlation and Coulomb hole in momentum space 78−86793
He, isoelectronic series, ground state specific mass shift, HF variation perturbation calc. 80−47889
He, isoelectronic series, transition moments, exchange and core polarisation effects 77−54531
He isoelectronic series, time depend. Hartree Fock theory, reduced Green's function anal., multipole polarisability 79−3358
He isoelectronic series, Z=2-10, hyperfine struct. calcs. 77−31018
He isoelectronic series 79−85894
He, isoelectronic spectra autoionisation states n=3 hydrogenic threshold, complex rot. method 79−31477
He, Koopmans' ionis. pot., virial scaling corrections 79−45655
He like atoms, dipole transitions, transition integral cancellation 80−69052
He like ions Z=12-19, $1s^2\ {}^1S_0$-$1s3p\ {}^1P_1$ lines satellites obs. in laser 79−22640
He, pot. energy relationships 79−22584
He, screening constants, ground and excited states 78−62701
He series, energy level and classifications of doubly-excited states 78−62736
He^-, isoelectronic sequence, triply excited bound state, variational calc. 80−9526
He-like atoms, oscillator strength calc., allowed np-n'd and nd-n'f transitions 79−31467
He-like atoms and ions, gradient expansion of atomic kinetic energy functional 80−95530
He-like ions, ^1P and ^3P energy levels, relativistic RPA calcs. 80−47913
He-like ions, $2^3P_1{}^0$-1^1S_0 and $2^1P_1{}^0$-1^1S_0 freqs. and transition rates, relativistic calc. 79−68210
He-like ions, electron impact excitation, cross-sections, modified Oppenheimer approx. 78−82843
He-like ions, excitation regimes, nucl. orientation due to hyperfine interaction 78−70928
He-like ions, Fe XXV, dielectronic satellite line spectra as measure of nonthermal electron energy distribs. 80−21911
He-like ions, ground-state electron impact excitation strengths, close-coupling calcs. 80−23561
He-like ions, multiple charged, reson. photoionis. 79−54818
He-like ions, n=2→1 transitions, collision strength Z-dependence 80−91675
isoelectronic series continued
He-like ions, $P_1{}^0$-1^1S_0 and $^3P_1{}^0$-1^1S_0 intercombination-line transitions 78−70771
He-like ions, photoionisation, 2-channel relativistic random phase approx. calcs. 79−59407
He-like ions, radiative 2^3S_1-1^1S_0 transition, correlation effects 79−97989
He-like ions, spectral broadening in plasma, theory, high-Z 80−6223
He-like ions, spectral line intensity, density depend., plasma diagnostic appls. 78−83617
He-like ions, spectroscopy, review 79−10060
He-like ions, triplet-state, electron impact excitation cross sections obtained by Coulomb Ochkur Rudge approx. 80−102576
He-like ions, X-ray form factors and total scatt. X-ray intensities 79−10063
He-like ions of third sequence elements, blue satellite to resonance lines 80−70013
He-like positive ions, electron impact excitation, electron exchange, CBO approx. calcs. 79−36771
He-like three-electron atoms and ions, inelastic-reson. quasiprojection operators 79−3581
He-like two electron atoms, three-body problem 79−3372
$^4He^+$+H, electron transfer calc., electron ionization calc., Monte Carlo method, 79−72387
I I, isoelectronic sequence, multiconfiguration HF calc. of sp^6-s^2p^4d interaction 78−9072
^{191}Ir, magnetic hyperfine struct. 78−934
K I isolectronic sequence, transition probabilities, cancellations 80−91503
K II, isoelectronic series, photoionisation, multichannel CI calcs. 79−93931
K isoelectronic series, hard-core pseudopotentials and struct. maps 80−44168
Kr VII(VIII), reson. line oscill. strengths, beam-foil spectra 77−38630
LaIr(g), thermodynamic stability, high-temp. mass spectra obs., W_2 dissoc. energy estimation 80−7781
Li, and isoelectronic sequence, correlated and HF electron density differences 78−46275
Li, and isoelectronic series, photoionisation resons. characts., Z depend. 77−50412
Li, Be^+, B^{2+}, C^{3+}, ^2S, $^2P^0$ and ^2D autoionising states, positions and widths 79−26944
Li, dipole polarisability, numerical Coulomb approx. 80−43199
Li, electron impact, inner shell excitation cross-sections 79−59580
Li I to F I, and isoelectronic series, Z=10-100, L-shell energy struct. and level classification 78−55129
Li I to Ne VIII isoelectronic sequence, quartet spectra, Hylleraas method calcs. 80−9524
Li I to Ne VIII isoelectronic sequence, term level diagrams of doubly excited states 80−14093
Li I-like spectra, energy struct., accurate semiempirical formulae 79−49970
Li, ionization equilib. balance, solar and stellar atms. appl. 79−36587
Li isoelectronic sequence, oscill. strengths 77−3309
Li, isoelectronic sequence, transition probabilities, relativistic effects calcs. 77−27028
Li isoelectronic sequence, Hartree-Fock wavefunctions *(French)* 77−34586
Li, isoelectronic sequence, photoionisation cross section, core polarisability effects 77−57944
Li, isoelectronic sequence, radiative transition probabilities calcs. 77−83544
Li isoelectronic sequence, quartet states hyperfine consts., Hartree-Fock and CI calcs. 78−919
Li isoelectronic sequence, Hartree-Fock eqns., perturbation calcs. 79−5846
Li isoelectronic sequence, doubly-excited states, relative ordering 79−31424
Li isoelectronic sequence, self-consistent relativistic density-functional theory 80−91441
Li isoelectronic sequence, electron impact ionisation cross section 80−91688
Li isoelectronic sequence of three electron atoms, pair correlation study 80−74096
Li, isoelectronic series, Hartree-Fock line strengths 78−9122
Li isoelectronic series, hard-core pseudopotentials and struct. maps 80−44168
Li isoelectronic series, ionisation pot. relativistic corrections calcs. 77−46484
Li isoelectronic series, quartet states, HF and CI calcs. 78−17582
Li isoelectronic series, relativistic pseudopot. appl. in HF calcs. 80−27960
Li isoelectronic series, semiempirical prediction of energy levels 79−72243
Li, isoelectronic series, transition moments, exchange and core polarisation effects 77−54531
Li, isoelectronic series (Be,B,C) best optimised one-electron wave functions 77−38598
Li, model potential field, pseudopotential calcs. 79−59339
Li, pot. energy relationships 79−22584
Li, screening constants, ground and excited states 78−62701
Li, wave functions, effective pots. and energy values 79−68182
Li^-, and isoelectronic sequence, correlated and HF electron density differences 78−46275
Li^+, few parameter two-electron wavefunction of ground state 77−75051
Li^+, isoelectronic series, electron correlation and Coulomb hole in momentum space 78−86793
Li-like atoms, $^4S^e$ doubly excited states, orbital config. assignment 79−41118
Li-like ions, cross sections for electron impact ionisation 79−45850
Li-like ions, electron impact excitation, config. and parentage mixing effects 77−58176
Li-like ions, electron impact, ionisation cross section including excitation-autoionisation contributions 80−28105
Li-like ions, fine struct. in $1s2p^2\ {}^4P$ and $1s2s2p\ {}^4P^0$ states 78−66471
Li-like ions, highly charged, innner shell excitation, intermediate coupling collision strengths 80−1074
Li-like ions, in plasma, ion electron collisional radiative recomb. coeffs., bottleneck calc. 80−53942
Li-like ions, partial photoionization cross sections and radiative recomb. rate coeffs. 79−49994

isoelectronic series continued
Li-like ions, partial photoionis. cross-sections and radiative recomb. rate coeffs. 80−52951
Li-like multiply charged ions, spectra, radiative corrections 79−98015
Mg, and isoelectronic sequence, relativistic effects on transition probabilities 77−54532
Mg, excitation energies, oscillator strengths, using relativistic RPA 80−47925
Mg I isoelectronic sequence, intercombination line oscillator strengths 80−23360
Mg I sequences for elements Cr to Zn, $n=3\rightarrow n'=4$ transitions 79−26922
Mg, isoelectronic sequence, excitation energies and line strengths, MC Hartree-Fock calcs. 77−83658
Mg isoelectronic sequence, mag. quadrupole transitions probabilities 78−37592
Mg isoelectronic sequence, electron impact excitation of reson. transitions 80−63825
Mg isoelectronic sequence, static dipole quadrupole polarisabilities and shielding factors calc. using HF scheme 80−99450
Mg, isoelectronic series, D-F transitions, Mg sequence, D-F transitions oscillator strengths 79−54809
Mg, isoelectronic series, oscill. strengths and excitation energy, RRPA calcs. 78−13471
Mg XI-S XV ions, 2l3l-1s3l and 2l2l-1s2l radiative transitions and non-radiative decay probabilities 78−70781
Mg-like V XII, Cr XIII, Mn XIV and Co XVI, level struct. and predicted intercombination lines 80−14098
$Mg+H^+$, low-lying ^3P term excitation, cross-sections and rate consts. 79−94069
MnO_4^-, CrO_4^{2-}, VO_4^{3-}, electronic struct. determ. from X-ray spectra 78−86885
N I, weighted oscillator strengths for elec. dipole and forbidden transitions, data tables 80−37779
N IV, intercombination lines, transition probabilities determ. 79−89645
N isoelectronic sequence ions, atomic struct. and electron scatt. data 80−51649
N_2 oscillator strength calc. for $^4S^0$ to ^4P sequences 78−25485
N^{4+}, 2s-2p excitation absolute cross sections by electron impact, rate coeffs. temp. depend. 79−94087
N^{5+}, few-parameter two-electron wavefunction of ground state 77−75051
N_2, isoelectronic sequence, Rydberg transitions, term value-ionisation pot. correl. 80−58276
NH_3, core ionis., single orbital relax., LCAO MO SCF calcs. 78−29739
Na, Cu XIX-Br XXV, laser-produced at. spectra 79−49974
Na, dipole polarisability, numerical Coulomb approx. 80−43199
Na I isoelectronic sequence, K IX to Mn XV, wavelengths and energy levels, spectral obs. 77−428
Na isoelectronic sequence, electron impact excitation, transition probabilities, oscill. and collision strengths 78−25718
Na isoelectronic sequence, theoretical f-values 78−37593
Na isoelectronic sequence, Bethe excitation cross-sections 78−82657
Na isoelectronic sequence, hypervirial theorem, screening parameters and oscill. strengths 79−6882
Na isoelectronic sequence, dielectronic recombination rate coeffs., $2\text{-}10^3$ eV 80−10357
Na isoelectronic series, Hartree-Fock line strengths 78−9122
Na isoelectronic series, hard-core pseudopotentials and struct. maps 80−44168
Na isoelectronic series, oscill. strengths, effective orbital quantum no. method 80−9521
Na isoelectronic series, wave functions and effective pots. of valence electron 80−47873
Na like ions, dielectronic recombination rate, scaling props. 80−32668
Na-like ions, Kr-Mo, 2-3 transitions, plasma X-ray spectra classification 79−37544
Na-like ions, transition probabilities for reson. transitions 78−66494
NaI isoelectronic sequence, 3s-3p and 3p-3d transitions, ionisation energy 78−70773
NaI, isoelectronic sequence, X-ray spectra 80−87071
NaI-SVI isoelectronic series, radiative lifetimes calc. 79−72276
Ne, core ionis., single orbital relax., LCAO MO SCF calcs. 78−29739
Ne, excitation energies, oscillator strengths, using relativistic RPA 80−47925
Ne I, reson. lines in Cl VIII and A IX beam foil spectra 78−94210
Ne I isoelectronic sequence, X-ray spectra, K X to Fe XVII 79−22641
Ne I isoelectronic series, radiative lifetimes calc. 79−98037
Ne, ionisation pot. values 78−5363
Ne ions, isoelectronic series, correlation energy and size, empirical relationship 77−79546
Ne, isoelectronic sequence, many-body photoionization calcs. 78−17631
Ne isoelectronic sequence, level energies and lifetimes 79−89644
Ne, isoelectronic sequence, excitation energy and oscillator strength, level crossing anomaly, relativistic RPA calc. 80−14077
Ne isoelectronic series, $2s^22p^53l$ and $2s^22p^63l$ configs., excited state energy levels 79−54781
Ne, isoelectronic series, dipole matrix elements derivation 77−83519
Ne, isoelectronic series, ionisation pots., Ritz law and Edlen formula 80−32854
Ne isoelectronic series, orbital binding energies within statistical exchange approx. 79−85895
Ne isoelectronic series, second order correl. energy, Z depend. of irreducible-pair energies 80−91417
Ne, Koopmans' ionis. pot., virial scaling corrections 79−45655
Ne, one-electron and two-electron one-photon transitions 78−58775
Ne-like atoms and ions, gradient expansion of atomic kinetic energy functional 80−95530
Ne-like ions, E1 and M2 transitions, HF calcs. 79−59401
Ne-like ions, Kr-Mo, 2-3 transitions, plasma X-ray spectra classification 79−37544
Ni (VIII), semiempirical investigation of spectra 78−33434
Ni-like isoelectronic sequence (Hf, Ta, W, Re) X-ray spectra from laser produced plasmas 80−42981
O I, isoelectronic sequence, X-ray spectra 80−87071
O I, weighted oscillator strengths for elec. dipole and forbidden transitions, data tables 80−37779
O I isoelectronic sequence, excited level populations, line intensity ratios, solar corona appl. 80−32637
O I-like ions, solar emission lines density depend. 79−40165

isoelectronic series continued
O II, III, IV, beam-foil spectra, mean lives, 270-490 angstrom 78−55223
O isoelectronic sequence, optical oscillator strengths 80−63589
O, isoelectronic sequences, energy spectra inc. relativistic corrections 78−924
O, two photon transition probabilities 79−22680
O V, electron collisional excitation, R-matrix calc. 77−58169
O V, solar emission line ratios interpretation 78−28598
O-like ions, spectral line intensity, density depend., plasma diagnostic appls. 78−83617
$O(^1D, ^3P)$ series, Sternheimer valence shielding and antishielding factors 80−18807
OH_n, LCAO-MO-SCF with Gaussian polarisation functions, energetic effect of p-, d-, and f-functions 78−41944
RbI_3 oscill. strengths, relativistic HF calcs. 79−98035
Ru^{3+} isoelectronic series, radial charge distrib. calc. 80−9507
$S(^1D, ^3P)$ series, Sternheimer valence shielding and antishielding factors 80−18807
SH_n, LCAO-MO-SCF with Gaussian polarisation functions, energetic effect of p-, d-, and f-functions 78−41944
SO_2 photo-oxidation products, smallest particle size detectable by condensation nucleus counters 78−24364
Se XXVI, $2p^5\text{-}2p^43s(2p^43d)$ transitions in laser produced X-ray spectra 78−13460
Si I sequences for elements Cr to-Zn, $n=3\rightarrow n'=4$ transitions 79−26922
Si isoelectronic sequence, CI calcs. of oscillator strengths, L-S framework 80−14089
^{181}Ta, magnetic hyperfine struct. 78−934
^{183}W, magnetic hyperfine struct., 78−934
Xe like ions (I^-, Cs^+, Ba^{2+}, La^{3+}) $3d^94f$ config., collapse of 4f electron, X-ray spectral obs. *(Russian)* 80−58204
$^{129}Xe^+$, hyperfine struct., ion-beam mag reson., laser induced fluoresc. for signal detect and state selection 78−41986
$^{131}Xe^*$, hyperfine struct., ion-beam mag reson., laser induced fluoresc. for signal detect and state selection 78−41986
Y III to Mo VI, $4p^64d\text{-}4p^54d5s$ transitions, level assignments 79−22631
Yb II, III to Bi XV, XVI isoelectronic sequences, wavelengths and ionisation energies 77−429
Yb II $4f^{14}nl$, ionisation energies, 5g, 6g term identification 79−49953
Zn, excitation energies, oscillator strengths, using relativistic RPA 80−47925
Zn I, $4s4d\,^1D\text{-}4p^2\,^1D$ interaction, multiconfig. Hartree-Fock calcs. 79−76351
Zn I, theoretical oscillator strengths for resonance transitions 78−74616
Zn I series, $4s4p\,^1P$ lifetimes meas. 80−42998
Zn isoelectronic sequence, 4s-4p reson. transition in highly charged ions 77−75087
Zn isoelectronic sequence, RRPA calcs. of resonance transitions from $4s^2\,^1S_0$ 78−17612
Zn isoelectronic sequence, resonance oscill. strengths 79−3413
Zn isoelectronic sequence, electron impact excitation of reson. transitions 80−63825
Zn, isoelectronic sequence, oscill. strength and MCHF wavefunctions, outer correl. 80−91505
Zn, oscillator strengths of reson. transitions 79−22666
Zn XXII, $2p^5\text{-}2p^43s(2p^43d)$ transitions in laser produced X-ray spectra 78−13460
Zn-like ions, 4s-4p reson. lines and transitions obs. by means of laser prod. plasma, appl. to Tokamaks 80−99468
Zr IV, energy levels, spectrum obs. 440 to 2670 Å 80−99470
^{91}Zr, magnetic hyperfine struct. 78−934

isolators, microwave *see microwave isolators*

isomer shift
actinide ions, electronic props., Dirac-Fock studies 78−60094
actinides, Mossbauer isomer shifts, book contrib. 79−87362
alkali borate glass, Mossbauer expts., 85-500K 78−80260
alkali metal nitroprussides, Mossbauer spectra, dehydration effects 79−24237
allophane, synthetic, amorphous mineral struct. obs. using ^{57}Fe Mossbauer effect 80−34836
2-aryl-3-benzylidenamino-4-thiazolidones, IR and NMR spectra, solvent effects and isomer conform. *(Italian)* 79−3596
BBOA:Sn-BBA, liquid crystal glass, unresolved Mossbauer quadrupole doublet, orientation depend. 77−84645
camphor separated optical isomers, inverted IR Lamb dips, IR-RF double reson. obs. 78−21951
2-chloropropane, conformation, vibr. spectrum, from simple harmonic force field 78−33494
core electron contribution to Mossbauer isomer shift, variation with ionic size 79−73866
^{57}Fe, isomer-shift calibration by lifetime variations in electron capture decays of ^{57}Fe 80−75902
ferromagnet, amorphous and crystalline, evaluation of complex Mossbauer spectra 78−43755
ferromagnet, amorphous and crystalline, evaluation of complex Mossbauer spectra 78−60370
glass: ^{57}Fe, 2-parameter distrib. analysis using general inversion method 80−66079
group IV elements, ^{57}Fe isomer shift, quadrupole coupling and interat. distance correl. 78−52408
inorganic compounds, chemical bonds using $K\alpha_1$ line chem. shifts, Mossbauer isomer shifts 77−27089
ionic charge relaxation effects on Mossbauer line shape 77−28495
iron (III) salicylates, Mossbauer and IR spectra, mag. susceptibility 80−50242
magnetic metals, hyperfine mag. fields at ^{119}Sn nuclei 80−60248
matrix isolation of atoms and ions, Mossbauer isomer shift calibration scheme for ^{59}Fe and ^{119}Sn, book contrib. 79−85924
metal, Mossbauer isomer shift, pseudopot.-Born-Oppenheimer theory development 78−2775
metal, noncubic, possibility of isotopic mass effect on quadrupole coupling consts. 78−43725
metal-H systems 79−82906
mixed valence cpds. $M_2^{I}Sb_{0.5}M_{0.5}^{IV}Cl_6$, ($M^I=NH_4$, Rb or Cs, M^{IV}=Se, Te or Sn), ^{121}Sb Mossbauer effect 78−84506
Mossbauer, energy equivalents of one mm/sec, tabulation, book contrib. 79−87365
Mossbauer, for calc. of charge and spin densities in solids, book contrib. 79−87350

isomer shift continued
Mossbauer, introduction, book contrib. 79−87347
Mossbauer, measurement, book contrib. 79−87349
Mossbauer, press. effects, book contrib. 79−87353
Mossbauer, theory book contrib. 79−87348
Mossbauer ^{57}Fe spectra, ferrous charact., cryst. field interactions 80−108133
Mossbauer effect, isomer shift, rel. to orbital occupation numbers 80−39983
Mossbauer Effect Data Centre, isomer shift reference scales 80−37147
Mossbauer Effect Data Centre 80−37148
Mossbauer isomer shift expressions tabulation of consts., book contrib. 79−87367
Mossbauer isomer shift reference scales, book contrib. 79−87368
Mossbauer isomer shifts, book 79−87346
Mossbauer isomer shifts, book contrib. 79−87363
Mossbauer isomer shifts and nuclear models, book contrib. 79−85385
Mossbauer isotope shifts, electron density at nuclear determ., book contrib. 79−87351
Mossbauer source preparation, tabulation, book contrib. 79−87366
Mossbauer spectroscopy, isomer shift cancellation with resonant detectors 80−80664
Mossbauer transition characts. tabulation book contrib. 79−87364
muonic, book contrib. 79−86093
neopentane:tetramethyltin, Mossbauer exam. of plastic phase transition 77−69759
niobates, mixed metal, Eu oxidation state, mag. props., Mossbauer study 80−66080
phase transitions, Mossbauer isomer shift, book contrib. 79−87352
Prussian blue analogues, Mossbauer spectra 80−15898
pyrite type dichalcogenides, ^{57}Fe isomer shift, quadrupole splitting, Mossbauer study 80−15832
quadrupole splitting-isomer shift linear rel., elec. field gradient sign 77−1624
rare earth, heavy calibration of isomer shifts by conversion electron spectroscopy 80−39918
rare earth intermetallics, RFe_2 and $R(Co_{0.98}\ Fe_{0.02})_2$, magnetostrictive material, changes in vibr. modes near mag. phase transition 79−90736
rare earth ions, Dirac-Fock exam. of electronic props. 79−56106
rare earth metals, Mossbauer isomer shifts, book contrib. 79−87361
rare earth-Fe-Al alloys, RFe_4Al_8, mag. props. 78−52250
rare earth-transition metal intermetallics, H absorpt., Mossbauer studies 80−39987
rare-earth impurities in s-p metals, isomer shifts 80−15839
ratio of $\Delta\langle r^2\rangle$ for pairs of elements with analogous electronic structure, tabulation, book contrib. 79−85410
ratios of $\Delta\langle r^2\rangle$ for two transitions in the same element or nuclide, tabulation, book contrib. 79−85409
semiconductors and metals, Mossbauer spectra of implanted ^{83}Kr, line widths, isomer shifts 80−39899
small metal clusters, isomer shift of ^{57}Fe, nearest neighbour effect 80−44988
sodium nitroprusside, isomeric molecular states generated by polarised light, Mossbauer resonance obs. 77−20781
spectrometer, high resolution, for meas. of isotope, isomer shifts and hyperfine struct. 77−61141
spherical nuclei, isomer and isotope shifts, theory of finite Fermi systems 80−39929
steel, Hadfield, Mossbauer spectra meas., 25-250°C *(Russian)* 77−51994
steel, hydrogenated austenitic stainless ^{57}Mossbauer obs. 77−7758
steel, stainless, type 310, antiferromag. ordering, press. depend., Mossbauer meas. 79−73861
tantalates, mixed metal, Eu oxidation state, mag. props., Mossbauer study 80−66080
tin containing organic compounds, $[R^IR^{II}R^{III}PO]_2SnR_nCl_{4-n}$, $[R^IR^{II}R^{III}PO]SnR_3Cl$, Mossbauer spectra, isomer shift and quadrupolar splitting *(Russian)* 79−61285
total conversion coefficients, nuclear electron and gamma transitions importance 79−85411
transition metal, change of charge radius for 2^+-0 transitions of ^{178}Hf, ^{182}W and ^{186}Os 78−25109
transition metal dichalcogenides:^{57}Fe, Mossbauer spectra, isomer shift 80−15885
transition metal diiodides, (V, Cr, Mn, Fe, Co, Ni, Cd), Mossbauer spectrum, electronic and mag. props. 77−32302
transition metal hydrides, Mossbauer studies, book contrib. 79−82906
transition metal impurities, volume corrected isomer shift, orbital electronegativity scale 77−73103
transition metal impurities, volume-corrected Mossbauer isomer shifts 78−68434
transition metal intermetallic cpds., H absorption and mag. props. 80−60224
transition metal nitroprussides, Mossbauer spectra, dehydration effects 79−24237
transition metals, 4d and 5d, Mossbauer isomer shifts, book contrib. 79−87355
transition metals, vol. corrected isomer shifts, effects in alloys 78−39470
vermiculite, firing temp. depend. of Mossbauer parameters 80−15837
Ag, contact charge density, press. depend., trends for Ag-Te 78−39077
$AgFeTe_2$, Mossbauer parameters in phase-transition region 80−11308
Al, hyperfine interactions of implanted Fe, conversion electron Mossbauer spectroscopy 78−52391
Al-Co alloy, dil., fast neutron radiation damage, interstitial trapping, Mossbauer spectra and elec. resist. meas. 77−27914
Al-Fe alloy, dil., quenched secondary defects, Mossbauer spectroscopy 77−28491
$^{240}Am^m$, spontaneously fissioning isomer optical shift in pumped $^8S_{7/2}\rightarrow{}^{10}P_{7/2}$ transition, nuclear deformation 80−27971
Au (I) compounds, electronic config. and nucl. quadrupole interaction, atomic SCF Hartree-Fock calcs. 79−60777
Au alloy, charge density perturbations, ^{197}Au isomer shift obs. 77−20771
Au alloys, ^{197}Au Mossbauer isomer shifts, theory, book contrib. 79−87357
Au compounds, ^{197}Au Mossbauer isomer shifts, book contrib. 79−87356
Au-Cs(Mg)(Rb)(Zn), charge transfer, Mossbauer effect ^{197}Au isomer shifts, XPS valence-band spectra 80−2676
Au-M (M=Cd, In, Sn, Sb, Te), Mossbauer isomer shifts 79−60695
Au-Te, elec. field gradients and charge transfer, Mossbauer spectra 80−25268

isomer shift continued
Au-transition metal alloys, ^{197}Au Mossbauer isomer shift cellular atomic model 80−84673
$AuAl_2(Ga_2)(In_2)(Sn_2)(Sb_2)(Te_2)$, core-level binding energy shifts and charge transfer 80−25268
$Ba_x(Ba_{1-x}Al_x)Fe_2S_6[S_{1-y}(S_2)_y]$, cryst. struct., Mossbauer and mag. behaviour 77−55273
BaF_2, Eu^{2+} isomer shift Mossbauer spectroscopic anal. 79−56649
$Ba_3Ru_2MO_9$, (M=Mg, Ca, Sr, Co, Ni, Cu, Zn, Ca), Mossbauer spectra 80−108136
$BaSr_xCa_{1-x}Fe_4O_8$, substituted hexagonal ferrites, mag. split Mossbauer spectra obs. and X-ray struct. data 80−71250
$BaTiO_3$, Mossbauer spectrum, interal elec. field effects, quadrupolar splitting 79−56648
Ba_2XRuO_6(X=La,Eu), ^{99}Ru Mossbauer spectra and other techniques 80−29659
$CaBaFe_4O_8$, overlap contribution to $^{57}Fe^{3+}$ isomer shifts, nuclear size change 80−39903
CaF_2, Eu^{2+} isomer shift, Mossbauer spectroscopic anal. 79−56649
$CaFe_2O_4$, overlap contribution to $^{57}Fe^{3+}$ isomer shifts, nuclear size change 80−39903
Ca_2XRuO_6 (X=Y,La,Eu), ^{99}Ru Mossbauer spectra and other techniques 80−29659
Cd, contact charge density, press. depend., trends for Ag-Te 78−39077
Cd nitroprussides, Mossbauer spectra, dehydration effects 79−24237
$Cd_xFe_{3-x}O_4$, collective electron states, ^{57}Fe Mossbauer meas. 77−69748
$CdGeAs_2$, amorphous and cryst., short-range order, Mossbauer expts. 78−22648
CdTe, diamond-like semicond., Mossbauer isomer shift meas. 77−16233
Co complex, bis-(β-diketonato) Co(II) dihydrate, Fe chem. states, Mossbauer emission 80−15917
Co complex, diimine complexes with ^{57}Co II, ^{57}Fe II anomalous spin states, Mossbauer spectroscopy 77−12261
Co complex, diimine complexes with ^{57}Co (II), Mossbauer spectra, temp. depend. 77−12262
Co complex, Werner complexes, ^{57}Fe partial quadrupole splitting, emission Mossbauer spectra 80−15919
Co-Fe, dil., hyperfine mag. fields, press. effect, Mossbauer meas. 80−71277
$CoAl_{2-x}Fe_xO_4$ system obs., using Mossbauer spectroscopy *(Rumanian)* 79−78575
$(Co_xFe_{1-x})_5Ge_3$, Mossbauer investig. of hyperfine field at Fe nuclei 77−20776
$Co_2Mn_xFe_{1-x}M$, (M=Ga,Ge,Si,Sn), hyperfine fields of Fe impurities, Mossbauer effect meas. 78−31130
$CoSO_4.7H_2O$, time differential Mossbauer coincidence technique, time depend. of electron capture aftereffects 80−39927
$Co^{2+}[Fe^{III}(CN)_6]^{3-}$, time depend. linewidth of Mossbauer spectrum 80−15911
$CrTiRO_5$, R=Pr,Nd,Sm,Eu,Gd,covalency contribs. to Mossbauer spectra 78−10808
Cs-graphite intercalated compounds, anisotropy of Debye-Waller factor, Mossbauer meas. 77−55738
$Cs_2Au_2Cl_6$, electronic state of Au at high press., Mossbauer spectra 80−60467
Cs_2SbCl_6, mixed valence compound, ^{121}Sb Mossbauer spectroscopy 79−51890
^{133}Cs, Mossbauer isomer shifts, book contrib. 79−87363
Cu-Te system, cryst. chem., Mossbauer investig. 77−16220
Cu-Zn(Ga)(Ge)(As), Mossbauer effect of Fe impurities 78−31131
$CuCr_{2-x}Fe_xO_4$, charge transfer, Mossbauer spectroscopy 80−15836
$CuFe_2O_4$, Jahn-Teller type crystal distortions 80−103904
$Cu_2MnAl_{1-x}Sn_x$, Mossbauer effect study 80−60473
$(Cu_2SnS_3)_x(3CdS)_{1-x}$, second co-ordination sphere atoms effect on ^{119}Sm Mossbauer spectra *(Russian)* 77−63348
$(Cu_2SnS_3)_x(3ZnS)_{1-x}$, second co-ordination sphere atoms effect on ^{119}Sn Mossbauer spectra *(Russian)* 77−63348
Cu_xZn_{1-x}, positron annihilation and Mossbauer effect exam. 79−65775
Dy, and $DyMn_2(Fe_2)(Co_2)(Ni_2)$, H_2 absorpt., Mossbauer study 80−44987
$Dy_2(Fe_{1-x}Co_x)_{17}$, hyperfine interactions, Mossbauer spectra 78−2780
$DyFe_2H_2$, mag. props., ^{57}Fe and ^{161}Dy Mossbauer spectra and magnetisation meas. 79−78579
DyMg, Mossbauer spectroscopy and mag. props. 77−85624
ErMg, Mossbauer spectroscopy and mag. props. 77−85624
Eu intermetallic compounds, Mossbauer effect isomer shift, charge density at nucleus, trends 77−48112
Eu, Mossbauer isomer shift and magnetic hyperfine field, press. effect 78−52386
Eu^{3+} compounds, chloride, sulphate, nitrate, carbonate, oxalate and acetate, Mossbauer study 79−99801
Eu-Cd compounds, Mossbauer effect, mag. props. and lattice consts. 77−36164
Eu-salt solutions, frozen, Mossbauer parameters depend. on pH and halide conc., Eu(III) complexes form. 78−3330
$EuMg_5$, Mossbauer effect, effective moments, mag. ordering temp. and isomer shifts 80−34833
Eu_2Mg_{17}, Mossbauer effect, effective moments, mag. ordering temp. and isomer shifts 80−34833
$EuMg_2H_x$, Mossbauer effect exam. 78−48094
$Eu(Ni_{1-x}Cu_x)_5$, mixed valency, isomer shift temp. depend. 78−84511
$EuNi_xCu_{5-x}$, comp. depend., Mossbauer obs. of mixed valency of Eu 78−52407
$EuNi_5H_x$, Mossbauer effect exam. 78−48094
$EuNi_xZn_{5-x}$, comp. depend., Mossbauer obs. of mixed valency of Eu 78−52407
EuO, electronic struct. and props., mol. cluster approx. 77−11852
$EuPt_x$ compounds, partial valence change, ^{151}Eu Mossbauer and magnetisation obs. 80−70167
EuS, electronic struct. and props., mol. cluster approx. 77−11852
EuTe, Neel temp. and hyperfine interactions, press. depend. up to 60 kbar, ^{151}Eu Mossbauer obs. 77−63181
EuX_5, X=Cu, Zn, Ag, Au, cond. electron spin polarisation effects 77−63136
Fe complex, $[Fe(CN)_6]^{3-}$, electronic struct., optical transitions, XPS, Mossbauer isomer shift, valence ionisation pot., SCF-MSX calc. 79−6864
Fe complex, dithiocyanato bis(4-methyl-1, 10-phenanthroline) iron, Mossbauer effect and magnetism down to 0.98K 77−28490
Fe complex, $FeCl_3L_3$ type, L=ligand, Mossbauer study 78−2783

isomer shift continued
Fe complex, tris(monothio-β-diketonato) Fe (III), spin equilib., Mossbauer spectra 80−15910
Fe complex (2, 9-dimethylphenanthroline) sulphate, mag. props., Mossbauer spectra 80−66081
Fe complexes, 2- or 3-pyridyl imine complexes of $FeCl_2$, Mossbauer and mag. props. 80−15896
Fe complexes, high spin ionic with halogen ligands, Mossbauer isomer shift calibration 77−16210
Fe complexes, Mossbauer isomer shift and core electron binding energies of Fe 78−82620
Fe dilute alloys, with s-p elements of third or fourth periods, Mossbauer spectra meas. 77−63344
Fe epitaxial film, Mossbauer effect, depth profiling of mag. hyperfine field 80−11295
Fe halides, electronic charge and spin distrib. from interpretation of hyperfine interactions 79−60776
Fe hexacyanoferrates, $M_4Fe(CN)_6.nH_2O$, Mossbauer and IR spectra 80−2739
Fe, Mossbauer energy shift near Curie temp. 78−52388
Fe powder, Mossbauer spectra parameter calc. with aid of computer *(Russian)* 78−76361
γ-Fe precipitates, antiferromag. ordering, press. depend., Mossbauer meas. 79−73861
α-Fe, uniaxial stress effect on Mossbauer spectrum 80−71244
Fe^{3+} compounds, Mossbauer spectra, temp. depend. of isomer shift *(Russian)* 78−39479
Fe^{3+} ion compounds, effect on Mossbauer spectra of thermal vibrs. rel. to covalently populated 4S shell nucleus 78−72444
Fe:N, ion implanted foil, Mossbauer effect study, nitride form. 78−27149
Fe-Al, electron density distrib. vs. at. order 79−60309
Fe-As system, mag. props., Mossbauer study 80−88897
Fe-B amorphous alloys, Mossbauer spectra, mag. moment conc. depend. 80−15847
Fe-B(Si) amorphous alloys, Mossbauer spectra, struct. 80−15840
Fe-Co, equiatomic, atomic order, Mossbauer study *(French)* 78−27135
Fe-Cr, influence of annealing on hyperfine interaction parameters, Mossbauer effect 80−71263
Fe-Cr (1.20, 3.63, 7.98 wt.%), Mossbauer spectra shape depend. on deformations 79−61272
Fe-Cr-Co, mag. alloys, Mossbauer spectra 78−19386
Fe-Cu clusters, mag. interaction, Mossbauer study 79−82895
Fe-Cu metastable dil. alloy film, hyperfine interactions 78−52398
Fe-Ni, hydrogenated, Mossbauer effect meas. 78−92002
γ-Fe-Ni, local magnetisation of Fe atoms, Mossbauer effect meas. 80−75891
Fe-O compounds, MO cluster calc. of charge densities and elec. field gradients 77−76783
Fe-P-B, amorphous alloy, Mossbauer effect and short-range order 80−2675
Fe-P-C, amorphous alloy, Mossbauer effect and short-range order 80−2675
Fe-P-C amorphous alloys, Mossbauer spectra, struct. 80−15840
Fe-Pt-Ir, Mossbauer effect of ^{193}Ir and ^{57}Fe, hyperfine field, isomer shift 78−15072
Fe-Se, low conc. binary system, Mossbauer spectroscopy meas. 79−24239
Fe-Si, electron density distrib. vs. at. order 79−60309
Fe-Y(Th)(Zr), amorphous, charge transfer and mag. props., ^{57}Fe Mossbauer spectra 79−19719
FeAl, isomer shift, electronic charge density 78−80264
FeB and Fe_2B, ESCA and mag. spin data, electronic struct., isomer shifts, valence bands and chemical bonding 80−75489
$Fe_{1-x}B_x$, amorphous, hyperfine fields and local mag. moments, Mossbauer study 80−75895
Fe_3B, mag. props., ^{57}Fe Mossbauer spectra meas. 79−95693
Fe_xB_{100-x}, amorphous, mag. props., ^{57}Fe Mossbauer spectra and magnetisation meas. 79−95693
$Fe_{78}B_{12}Si_{10}$, amorphous, Mossbauer study of hyperfine interaction and mag. anisotropy 80−40027
$Fe(CN)_6$, Mossbauer isomer shift const., ab initio SCF calcs. 78−43751
$(Fe_{0.5}Co_{0.5})_{1-x}B_x$, amorphous, hyperfine fields and local mag. moments, Mossbauer study 80−75895
$Fe_{3-x}Co_xO_4$, charge transfer, ion distribs., Mossbauer effect 77−20767
$(Fe_{0.2}Co_{0.8})_{80}P_{17}Al_3$, Mossbauer spectra, isomer shift, mag. hyperfine field 80−11301
$Fe_{0.5}Co_{0.5}TiH_x$, transmission Mossbauer spectra 80−44964
FeF_3 isomer shift, using LCAO form of molecular orbital method 78−62856
FeF_3, overlap contribution to $^{57}Fe^{3+}$ isomer shifts, nuclear size change 80−39903
FeF_6, Mossbauer isomer shift const., ab initio SCF calcs. 78−43751
FeGe, hyperfine interactions of ^{119}Sn atoms, Mossbauer spectra *(Russian)* 80−29665
$FeLu_2S_4$, structural study, X-ray diffr., Mossbauer spectroscopy 80−107159
$Fe_2(MoO_4)_3$, ^{57}Fe Mossbauer effect obs. 77−48108
$FeNb_2O_6$, low temp. Mossbauer exam. 79−28659
$Fe_{0.33}NbS_2$, lattice dynamics and hyperfine interactions, Mossbauer spectra study 80−108135
$Fe_{40}Ni_{40}B_{20}$, amorphous, hyperfine field distrib., Mossbauer effect meas. 79−4755
$(Fe_{1-y}Ni_y)_{0.8}B_{0.2-x}P_x$, amorphous, hyperfine fields and local mag. moments, Mossbauer study 80−75895
$Fe_{40}Ni_{40}P_yB_{20-y}$, amorphous, mag. props. effect of metalloid elements 79−28658
$Fe_{0.5}Ni_{0.5}S_2$, hyperfine field at ^{57}Fe, Mossbauer effect *(Japanese)* 77−43916
FeO_4^{2-} ion, electronic struct., hyperfine interactions, SCF Xα calcs. 79−37951
α-Fe_2O_3, Morin transition, Mossbauer spectra meas. 78−31071
Fe_3O_4, Mossbauer spectra at 80K, Fe electronic states and hyperfine interactions *(Russian)* 78−43696
Fe_3O_4, nuclear gamma reson. investig. of high temp. electronic struct. 77−20751
Fe_3O_4:Zn, and pure, influence of mag. order on charge delocalisation, Mossbauer spectra 78−68423
α-FeP_4, diamag., semicond., Mossbauer study 80−50243
$Fe_{80}P_{20}$, binary amorphous ferromagnet, Mossbauer study 80−34829

isomer shift continued
$Fe_{48}Rh_{52}$, hyperfine mag. field at ^{57}Fe and ^{119}Sn nuclei, press. depend. *(Russian)* 78−80266
$Fe_2(SO_4)_3$, Mossbauer isomer shift in rhombohedral and monoclinic forms 78−6609
$Fe(Sb_{1-x}Te_x)_3$ system cpds., prep., cryst. struct., elec. and mag. characteris. 80−108349
Fe_xSn_{1-x}, amorphous alloy, Mossbauer spectra, charge transfer and atomic vol. effects 80−39959
$Fe_xTa_{1-x}S_2$ (1T), low-spin high-spin equilib., susceptibility and Mossbauer expts. 77−48109
$FeTe_x$, Mossbauer spectra, 80 to 750K, quadrupole splitting and isomer shift 77−4590
$FeTiNdO_5$, isomer shift, hyperfine field and distrib. of Fe^{3+} ions, Mossbauer spectrum 77−69747
$FeTiRO_5$, R=Pr,Nd,Sm,Eu,Gd,covalency contribs. to Mossbauer spectra 78−10808
Fe_xTiS_2, lattice dynamics and hyperfine interactions, Mossbauer spectra study 80−108135
FeX_4^-, (X=F, Cl and Br), electronic struct. and isomer shift 80−63545
$FeYb_2S_4$, structural study, X-ray diffr., Mossbauer spectroscopy 80−107159
^{57}Fe, hyperfine interactions in implanted metals, Mossbauer spectra 80−108141
^{57}Fe, implanted in 3d, 4d and 5d metals, conversion electron Mossbauer spectra 77−12286
^{57}Fe, isomer shift calibration const. rel. to biological cpds. 80−7227
^{57}Fe, Mossbauer, isomer shift, book contrib. 79−87354
^{57}Fe Mossbauer isomer shift from electron capture rate of ^{52}Fe 80−7203
Ga-Fe dilute alloy, Mossbauer spectrum 77−90080
GaP:Fe_x electron exchange via val. band between Fe acceptor centres, Mossbauer spectra 77−55741
GaP(As)(Sb), site selective doping by ion implantation of radioactive nuclei 80−34023
Gd impurities in s-p metals, isomer shifts 80−15839
$Gd_2(Fe_{1-x}Co_x)_{17}$, hyperfine interactions, Mossbauer spectra 78−2780
$GdRh_2H_x$, $GdRu_2H_x$, struct. and mag. props., Mossbauer and magnetisation meas. 80−71271
Ge:^{125}I(^{125}Te), implanted atom sites and quadrupole interaction, Mossbauer spectra 77−20758
Ge:Fe, amorphous film or ion-implanted, comparison of ^{57}Fe Mossbauer data 77−40159
H_2Te, solid, and photodissociated H_2Te in solid Ar, Mossbauer expts. 77−20769
Hf_2Fe, moment form. on H_2 absorpt. 79−87343
HgTe, diamond-like semicond., Mossbauer isomer shift meas. 77−16233
I, atoms, Mossbauer isotopes, isomer shift 80−78573
^AI, A=127, 129, Mossbauer isomer shifts, book contrib. 79−87360
^{127}I, isomer shift calibration, using lifetime variations in electron capture decay of ^{123}I 80−39925
^{127}I, Mossbauer isomer shift 80−39922
^{129}I impurities implanted in semiconductors, isomer shift 80−20522
^{129}I in transition metals, calibration of Mossbauer isomer shift 80−20520
^{129}I, internal conversion electron and Mossbauer spectra, calibration of isomer shift 80−39921
^{129}I, isomer shift calibration, using lifetime variations in electron capture decay of ^{123}I 80−39925
^{129}I, Mossbauer isomer shift 80−39922
In, contact charge density, press. depend., trends for Ag-Te 78−39077
InP(Sb)(As), site selective doping by ion implantation of radioactive nuclei 80−34023
$(In_2SnTe)_x$-$(2InSb)_{1-x}$ system, semicond., Mossbauer absorption line of ^{119}Sn 78−27146
In_2Te_3, nuclear gamma resonance of ^{57}Fe, isomer shift scale construction *(Russian)* 78−35070
$KAl[Fe(CN)_6]$, isomer shift of Mossbauer spectra 80−29662
$KFeO_2$, overlap contribution to $^{57}Fe^{3+}$ isomer shifts, nuclear size change 80−39903
K_2O-B_2O_3-Fe_2O_3 glasses, nonbridging O formation, Mossbauer spectroscopy 80−55001
$KTl[Fe(CN)_6]$, isomer shift of Mossbauer spectra 80−29662
^{40}K Mossbauer isomer shifts, book contrib. 79−87363
Kr isotopes, spectrometer for meas. of isotopic, isomeric shifts and hyperfine structure 79−6191
KrF_2, Mossbauer spectra, quadrupole coupling strengths, isomer shift and bonding 77−50458
$KrF_2.AsF_5(SbF_5)$, Mossbauer spectra, quadrupole coupling strengths, isomer shift and bonding 77−50458
$La_xCa_{1-x}RuO_3$, metallic, mag., electronic and structural props., ^{99}Ru Mossbauer spectroscopy 77−48107
La_2Co_7, mag. props. changes upon H_2 absorpt. 80−71270
$LaNi_{1-x}Fe_xO_4$, Mossbauer spectra, mag. hyperfine field 80−20537
$La_xSr_{1-x}RuO_3$, metallic, mag., electronic and structural props., ^{99}Ru Mossbauer spectroscopy 77−48107
$Li^{129}I$, Ar matrix isolated and cryst., Mossbauer verification of distortion overlap 77−63325
$LiTaO_3$, electric field gradients and isomer shift ^{181}Ta 78−39453
$Li_xV_{1-y}Fe_yS_2$, intercalated battery cathode material, Mossbauer studies 80−44984
$LuFe_2$, mag. props. changes upon H_2 absorpt. 80−71270
$MgIn_xFe_{2-x}O_4$ and $MgSc_xFe_{2-x}O_4$, Mossbauer spectra, elec. and mag. props. *(Russian)* 77−69737
$Mg(OH)_2$:Fe, crystal field properties, Mossbauer spectra, isomer shift and quadrupole splitting 79−61278
Mn TiRO$_5$, R=Pr,Nd,Sm,Eu,Gd,covalency contribs. to Mossbauer spectra 78−10808
β-Mn-Fe-Sn alloys, weak itinerant electron antiferromagnetism, Mossbauer spectra meas. 77−36158
MnO, ^{19}F isomer shift, time differential PAD 77−12280
N_2 solid matrix, ^{57}Fe Mossbauer spectra, Fe_xN mol. form., IR spectra confirmation 77−59496
NH_3-^{57}Fe, solid, Mossbauer study of iron bonding to solid ammonia and its photofragments 80−15833
$(NH_4)_2Sn_{1-x}Sb_xCl_6$ (x=0.13, 0.21, 0.28, 0.33), mixed valence compound, ^{121}Sb Mossbauer spectroscopy 79−51890
$Na_2(Fe,Mg)_5Si_8O_{22}(OH)_2$, riebeckite, low temp. Mossbauer obs. of oriented single cryst. behaviour and mag. props. 80−84674
NaI, temp. varying Mossbauer spectra, isomer shift 80−4726
Na_2O-Li_2O-B_2O_3:Fe_2O_3, Mossbauer spectra, isomer shift and quadrupole splitting *(Korean)* 79−51889

isomer shift continued
Na_2O-SiO_2-CaO:Fe_2O_3, Mossbauer spectra, isomer shift and quadrupole splitting *(Korean)* 79−51889
$Na_2O.2Al_2O_3.5SiO_2$:Fe^{3+}, Mossbauer effect and magnetometric exam. 78−6613
$NaTaO_3$, electric field gradients and isomer shift ^{181}Ta 78−39453
Ni-Al system, Mossbauer spectroscopy investigation *(Russian)* 80−20523
Ni-Fe, dil., hyperfine mag. fields, press. effect, Mossbauer meas. 80−71277
$Ni_{1-x}Au_x$-Co, dil., hyperfine field and isomer shift, precip. process, Mossbauer expts. 80−25267
Ni_3Fe, Mossbauer spectra, long range order 78−10810
$NiFe_2O_4$ precipitation from silicate glass, Mossbauer study 80−54998
NiSn, thermally prepared Mossbauer spectroscopy 79−61269
Ni_3Sn_2, thermally prepared Mossbauer spectroscopy 79−61269
Ni_3Sn_4, thermally prepared Mossbauer spectroscopy 79−61269
^{61}Ni, Mossbauer, isomer shift, book contrib. 79−87354
Np, ternary oxides, electronic and structural props., ^{237}Np Mossbauer spectroscopy 79−33570
$NpAs_2$, magnetic props., 4.2 to 77K, Mossbauer study 80−39937
$NpBa_6Zr_{12}F_x$ glass, Mossbauer spectrum 80−11304
$NpCo_2Si_2$, mag. props., high press. studies with ^{237}Np(60)-resonance 80−39924
$NpFe_{2-x}Co_xSi_2$, mag. and hyperfine props. 79−51887
$NpFe_{2-x}Co_xSi_2$, mag. and hyperfine props. 80−7247
$Pb(FeTa)_{1/2}O_3$, Mossbauer spectra, 78-480K 79−51885
^{208}Pb, muonic, isomer shift of 2.61 MeV gamma transition 77−38753
$xPb0.(1-x)B_2O_3$:Fe_2O_3, Mossbauer spectra 79−87338
Pd-Fe-H alloy, Mossbauer line shift with H conc. *(Russian)* 77−40165
$Pd_{1-x}Ag_{1-x}$-Au, dil., electron density at Au, Mossbauer reson. 78−39473
PdH_x-Au, dil., electron density at Au, Mossbauer reson. 78−39473
$Pd_2MnIn_{1-x}Sb_x(Sn_x)$, Heusler alloy, Mossbauer effect exam., hyperfine interactions in ferromag. phase 79−69756
Pd_2MnSb, mag. hyperfine field of ^{129}I, Mossbauer spectra 78−43706
$Pd_2MnSn_{1-x}Sb_x$, Heusler alloy, Mossbauer effect exam., hyperfine interactions in ferromag. phase 79−69756
$Pd_{100-x-y}Si_xFe_y$, amorphous, ^{57}Fe Mossbauer spectra, X-ray diffr., ageing behaviour 79−28651
$Pt_{0.72}Fe_{0.28}$, isomer shift and effective mag. field at ^{57}Fe, press. depend. 77−16232
$RbNiFeF_6$, pyrochlore, Mossbauer spectra in paramag. and mag. ordered states 77−52003
Ru complex, HF calc., electron densities and Mossbauer isomer shift, chemical binding 78−50470
Sb compounds, Mossbauer effect, isomer shifts, quadrupole splitting, CNDO/II calcs. 77−24766
Sb, contact charge density, press. depend., trends for Ag-Te 78−39077
Sb-containing glasses, ^{121}Sb Mossbauer spectra 77−20764
^{121}Sb, Mossbauer isomer shifts, book contrib. 79−87360
$ScAl_2$-Eu, intermediate valence on Eu ions, Mossbauer isomer shift 80−84587
$ScFe_2$, Mossbauer effect of ^{57}Fe 80−75903
$ScFe_2H_2$, Mossbauer effect of ^{57}Fe 80−75903
$Sc_xY_{0.95-x}Sm_{0.05}$, ^{153}Eu isomer shift, at. vol. depend. 77−43915
Si:^{57}Co/^{57}Fe, Mossbauer spectra, deep level Co impurity study 80−29666
Si:Co, substitutional Co and Co precipitates, identification by Mossbauer spectroscopy 79−11631
Si:Sb, Mossbauer spectra of ^{119}Sn defect struct. 80−97174
Si:Te, Mossbauer spectra of ^{119}Sn defect struct. 80−97175
Si:Te implanted, laser annealing, Mossbauer obs. 80−39127
SiC, α- and β-phases, isomer shift in Mossbauer spectra of implanted ^{129}I 78−15067
SmS, divalent and trivalent ion doped, electronic struct., Mossbauer spectroscopy 78−39022
SmS, electronic config., Mossbauer spectra meas. 77−16228
$Sm_{1-x}Y_xS$, electronic config., Mossbauer spectra meas. 77−16228
Sn, α- and β-phases, isomer shift in Mossbauer spectra of implanted ^{129}I 78−15067
Sn compounds, Mossbauer effect, isomer shifts, quadrupole splitting, CNDO/II calcs. 77−24766
Sn compounds, Sn(II) valency config., Mossbauer and X-ray electron determ. *(Russian)* 77−8483
Sn, contact charge density, press. depend., trends for Ag-Te 78−39077
α-Sn, ion implanted, defect struct., Mossbauer spectra 80−80214
Sn Mossbauer isomer shifts, book contrib. 79−87359
Sn organometallic cpds., chem. shifts in ESCA and Mossbauer spectra *(French)* 77−28685
Sn-Ni alloys, electrodeposited Mossbauer spectroscopy 79−61269
Sn-O system, amorphous, characterisation by appl. of Mossbauer effect 79−61283
$^{119m}SnCl_2$ adducts with O and N containing cpds., Mossbauer emission 80−15918
$Sn_{0.5}Eu_{0.5}Mo_6S_8$, supercond., spin polarisation, NMR, Mossbauer effect and bulk magnetisation meas. 77−43782
$Sn_{1-x}Eu_xMo_6S_8$, supercond., Mossbauer effect, struct. phase transition 77−12290
Sn(IV)-, Sn(II) halide mols., rare gas matrix-isolated ^{119} Sn spectra 77−48097
SnO_x films, phase composition, Mossbauer spectra 80−20051
SnO_x films reactive DC sputtering prep., phase comp., X-ray diffr. and Mossbauer meas. 79−90914
SnPb eutectic alloy, Mossbauer spectra, isomer shifts 79−82903
$Sn_{1-x}Pb_xSe(Te)$ films, Mossbauer effect of ^{119}Sn, spectral characts., conc. depend. 80−103903
SnS-SnTe, solid solns., synthesis, Mossbauer spectra 77−24768
$SnS_{2-x}Se_x$, ($0 \le x \le 2$), ^{119}Sn Mossbauer spectrum, lattice dynamics 78−71809
SnSe-SnTe, solid solns., synthesis, Mossbauer spectra 77−24768
SnTe, mechanochem. and thermal oxidation comparison, Mossbauer obs. 80−104310
SnTe, temp.-depend. ^{119}Sn isomer shift, calcs. 77−8457
^{119}Sn isomer shift calibration const. 77−28496
^{119}Sn resonance from inert gas matrix, Mossbauer isomer shift calibration 77−46530
^{119}Sn temp. depend. isomer shift, pseudopot. approach 80−84675
^{119m}Sn in FCC metals, isotope separator implanted, Mossbauer spectroscopy 79−24240
SrF_2, Eu^{2+} isomer shift, Mossbauer spectroscopic anal. 79−56649
isomer shift continued
Sr_2FeEuO_5, ^{57}Fe Mossbauer study 80−39976
SrO-Fe_2O_3, EMF meas. with solid state cell, Mossbauer effect and magnetic props. *(Korean)* 77−28493
Sr_2YRuO_6, ^{99}Ru Mossbauer spectra and other techniques 80−29659
Ta, surface layers, Mossbauer conversion electron studies 78−15068
$TaSe_2$ (1T), CDW obs. by Mossbauer reson. of ^{57}Fe impurity 77−73104
^{181}Ta, isomer shifts of 6.2 keV γ-rays, book contrib. 79−87358
Tc:^{57}Fe, dilute, quadrupole splitting and isomer shift, Mossbauer spectrum 78−48096
Tc-Fe alloy, Mossbauer spectra, hyperfine field 80−20526
Te complexes of thiourea, Mossbauer spectra 80−15914
Te compounds, X-ray photoemission, core level binding energy shifts rel. to Mossbauer isomer shifts 78−2984
Te, contact charge density, press. depend., trends for Ag-Te 78−39077
Te, Mossbauer spectra under press. up to 8000 MPa 80−80647
^{125}Te, Mossbauer isomer shifts, book contrib. 79−87360
$Th_7Fe_3H_{14.2}$, Mossbauer spectra, mag. props. 80−15852
Ti-Al alloys, comp. depend. *(Russian)* 78−6611
Ti-Fe, diffusion of stored H, Mossbauer study 80−34838
$TiFeH_x$, metallurgical and electronic struct., Mossbauer effect meas. 77−16223
Tl_2Se-As_2Se_3-SnSe system alloys, covalent component of chem. bond effect in vitrification processes, Mossbauer obs. 77−36156
Tl_2SnSe_3, preparation, Mossbauer spectra 77−28489
Tl_4SnSe_4, preparation, Mossbauer spectra 77−28489
^{203}Tl, ^{205}Tl, core excitations to low-lying states, e.m. props., hyperfine splittings, isomer shifts 78−89794
$UFe_3B_2(B_4)$, Mossbauer effect of ^{57}Fe nuclei, mag. props. 80−103907
$V_{1-x}Fe_xO_{2-x}F_x$, $0<x<0.2$, phase diagrams, ^{57}Fe-Mossbauer spectra, X-ray diffr. studies *(German)* 80−29663
V_2O_5-Fe_2O_3 solid solution, Mossbauer investig. of cryst. props. *(French)* 77−4592
Xe compounds, Xe chemical and isomer shifts, electron valence struct. *(Russian)* 80−53056
^{A}Xe, A=129, 131, Mossbauer isomer shifts, book contrib. 79−87360
^{133}Xe/^{133}Cs, implanted in various hosts, isomer shift values, Mossbauer spectra 80−7240
$Y_2(Fe_{1-x}Co_x)_{17}$, hyperfine interactions, Mossbauer spectra 78−2780
YIG, Al substituted, transferred hyperfine fields, Mossbauer effect meas. 79−1726
^{170}Yb in some metal and metal-like compounds, Mossbauer study, isomer shift and intermediate valence state 79−33569
Zn nitroprussides, Mossbauer spectra, dehydration effects 79−24237
Zn, quadrupole interaction, ^{67}Zn Mossbauer expt. 78−27120
$Zn_xCu_{1-x}Fe_2O_4$, mag. props., Mossbauer spectra 79−87344
ZnF_2, 93.3 keV Mossbauer transition in ^{67}Zn, isomer shifts 80−39978
$Zn_xFe_{3-x}O_4$, collective electron states, ^{57}Fe Mossbauer meas. 77−69748
$ZnMn_{1-x}Cr_xFeO_4$, Mossbauer effect, quadrupole splitting 80−29664
$Zn_xMn_{1-x}Fe_2O_4$, Mossbauer spectra exam. 77−40155
ZnO absorbers, ^{67}Zn isomer shift 80−39920
^{67}ZnO absorber, Mossbauer effect of ^{67}Zn 77−55737
ZnO(S)(Se)(Te), 93.3 keV Mossbauer transition in ^{67}Zn, isomer shifts 80−39978
ZnTe, diamond-like semicond., Mossbauer isomer shift meas. 77−16233
^{67}Zn Mossbauer spectroscopy with 93 keV reson. 80−66095
^{67}Zn spectrometer, double freq. interferometer for absolute velocity calibration of piezoelectric transducer 80−37146
Zr-Fe alloy, Mossbauer spectra parameters of Zr_2Fe particles *(Russian)* 80−29654
Zr-Fe-Cu-W alloy, Mossbauer spectra parameters of Zr_2Fe particles *(Russian)* 80−29654

isomerisation
E,E-1,4-diphenylbutadiene-(1,3), photoisomerisation, reaction quantum yields, exciting light bandwidth influence study *(German)* 80−21310
acetone, adsorbed on ZnO, decomp., IR and kinetic obs. 80−59780
acrolein, s-trans and s-cis, trapping from thermal mol. beams and UV-induced isomerisation in Ar matrices, enthalpy determ. 80−97688
alkenes, π bond dissoc. energies, derivation from isomerisation kinetics, for teaching 79−58498
allyl isocyanide, state-selected, visible absorption spectra and photoisomerisation kinetics 80−11879
amino acid radioracemisation, geochem. and cosmochem. implications 80−45975
anthracenophanes, fluoresc. and photoisomerisation 79−33781
bis(9-anthryloxy)polyoxaalkanes,, intramolecular excimer form. and photodimerisation, kinetic anal., rate constants determ. 80−66800
7-azaindole dimers, photoautomerisation by double proton transfer, fluoresc. kinetics 80−11880
azastilbenes, trans-cis photoisomerisation, theory 77−50466
azo dyes, cis-trans photochem. isomerisation 78−27785
azo dyes, tautomerisation, structs., laser Raman spectra 77−38672
azoethane, in hydrocarbon glass, 77K, photoisomerisation, matrix memory effect, quantum yield 78−7213
azomethane, trans-cis isomerisation, INDO-SCF and CI calc. 78−25440
bacteriorhodopsin chromophore, light-induced isomerisation 80−108956
bacteriorhodopsin chromophore photoisomerisation rel. to purple membrane proton pump 78−35804
bacteriorhodopsin isomers, dark equilib. and photochem. 78−15771
benzene, fluoresc., triplet state and isomerisation yields, photochem. 77−1942
benzene, fluoresc. triplet state and isomerisation yields, low vibr. levels 79−64035
benzene, ionised, H atom scrambling, SCF calcs. 77−9062
benzene, monosubstituted, dipole moments, isomerisation and H bonding, INDO calcs. 77−54515
benzene-Dewar benzene, lower excited states pot. energy surfaces for isomerisation 80−104429
benzenoid-o-quinoidal systems, valence isomerisation, EHT calcs. 77−77757
bimolecular isomerisation in liq., kinetic theory, spatial nonequilib. effects 79−5138
binaphthyl anion radicals, photoisomerisation, local heating effects 78−85179
bipyridines, torsional isomerisation of biologically active bicyclic molecules 80−27996
1-butene, adsorbed on δ-Al_2O_3, isomerisation, IR study 80−76554
trans-2-butene, Ar matrix, TEA CO_2 laser irrad. photoisomerisation study 80−21303

isomerisation continued
cis-2-butene, cis-2-butenenitrile, isomerisation, SCF perturbation theory 79−91918
butene, isomers, ion-mol. reactions, photoionisation mass spectra 80−81298
1-butene adsorption on delta alumina, microgravimetric-IR study 80−75432
n-butoxy radicals, intramol. isomerisation, following n-butyl nitrite pyrolysis 79−20355
carbocyanine dye solns., photoisomerisation and internal conversion rates, time-resolved spectra 77−75201
carbocyanine dyes, sterically hindered short-lived isomers, laser photolysis study 78−40063
catalytic activity of solid acids *(Chinese)* 78−31635
catalytic isomerisation apparent failure of Box-Hill procedure for model discrimination 77−63951
chiral molecules, prochiral centres, electronic and structural chirality 80−30220
chlorin in n-alkane host, photoautomerisation and hole-burning 79−47954
N-5′-chlorosalicylideneaniline, photochromism and thermochromism, NQR spectra, temp. and UV irrad. depend. 80−54968
cholesteryl cimmanate, photoreaction in solid, mesomorphic, and isotropic phases 79−87863
competitive decomposition and stabilisation models for collisional efficiency in external activation systems 80−25989
cyanine dyes, trans-cis isomerisation, ps kinetics 79−87853
1-cyano-2-methyl-3-(cis-propenyl) cyclopropanes, rotational propensities and bond rupture identity 80−104437
cycloheptatriene, and substituted forms, vibr. highly excited, steady-state photoisomerisation 80−16704
cycloheptatrienes, highly vibr.-excited thermal isomerisation in shock waves 79−79236
cycloheptatrienes, substituted, photoisomerisation, rate consts. 78−35708
cyclohexane, isomerisation, proton spin-echo NMR 77−9053
cyclopentadienyl radical, vibronic valence isomerisation, Jahn-Teller effect, D_{5h} symmetry 79−97986
cyclopropane, multiphoton IR laser-induced reactions 79−66312
cyclopropane, surface isomerisation to propylene, role of vibr. energy 79−74376
cyclopropane, thermal unimol. isomerisation, vibr. energy transfer, diffusion cloud method 80−26001
1,1-cyclopropane($-d_2$), isomerisation in He bath, vibr. transfer, temp. depend. 79−24723
1,1-cyclopropane-d_2, isomerisation transient vibr. energy distrib., collisional relax., variable encounters method 80−50836
1,1-cyclopropane-d_2, rearrangement, collisional vibr. energy transfer, temp. depend. 78−15668
1,1-cyclopropane-d_2, struct. isomerisation, vibr. distrib. collisional relax. dynamics, surface collisions 79−91926
cyclopropene fragment ions, from photoionisation, efficiency curves, isomerisation 80−53062
11-cis-13-demethylretinal, photoisomerisation, high quantum yield 79−57253
1,2-di(1-naphthyl)-ethylene, cis-trans photoisomerization in condensed phase, polycryst. phase transition 79−10139
dialkyl carbonates, liq., US, microwave dielect. relaxation 79−56717
dicarbocyanine solns., photoisomerisation, fluoresc. and absorpt. spectra of photoisomer 78−85181
1,5-dichloroanthracene, photodimerisation, orientational defects, lattice energy 78−80724
trans-1,2-dichloroethylene, Ar matrix, TEA CO_2 laser irrad. photoisomerisation study 80−21303
trans-dichloroethylene, isomerisation by laser multiphoton vibr. and electron excitation radiation *(Russian)* 78−73041
1,2-dichloroethylene, photodissoc., photoisomerisation, sensitised laser-induced reactions 78−7179
1,2-dicyanocyclopropane, stereomutations, isomerizations, reaction rate consts., extended Huckel calcs. *(Italian)* 79−20348
6,6′-diethoxy-thioindigo, cis⇌trans isomerisation, nanosecond flash photolysis and steady state methods, triplet state 78−35648
3,3′-diethyl-2,2′-thiatricarbocyanine iodide, solns., photoisomerisation and internal conversion rates, time-resolved spectra 77−75201
3,3′-diethyloxadicarbocyanine iodide, lasing and photoisomerisation, conc. and temp. effects 77−7081
difluorodiazine, cis-trans isomerisation, mechanism and kinetics, CNDO/2 study 77−90589
dihydroporphin free base, in n-octane cryst., zero-field optically detected mag. reson., triplet state kinetics 78−42103
1,2-diiodoethylene, form. from I_2+acetylene, isomerisation 80−85157
p-dimethylaminoacetophenone, ps reversible isomerisation kinetics, O_2 quenching obs. 79−5133
dioxane, isomerisation, proton spin-echo NMR 77−9053
2,3-dioxogulonic acid, reversible transformation to enol, kinetics, pH effects 79−5152
DNA, torsionally stressed, transitions between B- and Z-conformations, theoretical anal. 80−94166
dynamics, in liquid solutions, statistical mechanics, transition state approx. 78−60999
dynamics in condensed phases, kinetic theory, trajectory anal. 79−66273
electrocyclic isomerisation of ground state induced by IR laser multiphoton absorpt. 77−32811
ethyl isocyanide, N isotope enrichment, IR laser isomerisation 79−27096
ethyl isocyanide, thermal isomerisation in presence of at. gases, vibr.-translational energy transfer 78−23924
ethylene isomerisation, SCF perturbation theory anal. 79−91918
ethylene oxide-d_0, -d_4, ion chemistry, photoionisation and ion cyclotron reson. obs. 77−21373
ethynol, struct., isomerisation, ab initio SCF MO calcs. 78−41941
2-fluoro ethanol, Ar matrix, induced conformational isomerisation by IR irrad. 80−101010
fluoroformaldehyde, pot. energy surface characts., substitution effect 80−89505
formaldehyde, rearrangement to hydroxycarbene, pot. energy surface 79−79271
fumaronitrile exciplexes, photoisomeris. and photoionis, dissolved O_2 effect 78−27789
generalised isomerisation modes 77−68135
guanine-cytosine system rearrangement, reaction tree algorithm, using pot. surfaces 77−70286

isomerisation continued
1,5-hexadiene, D-labelled, IR laser induced isomerization via electronic ground state 77−25289
1,5-hexadiyne, time-depend. mass spectra, ionisation efficiency and breakdown curves 80−95747
hexafluorobutadiene, electronic ground state photochem., isotope separation by IR multiphoton isomerisation 79−79264
hexafluorocyclobutene, electronic ground state photochem., isotope separation by IR multiphoton isomerisation 79−79264
hexafluorocyclobutene, ground state, electrocyclic isomerisation of ground state induced by IR laser multiphoton absorpt. 77−32811
hexamethyl-2,2′-indotricarbocyanine iodide, solns., photoisomerisation and internal conversion rate, time-resolved spectra 77−75201
n-hexane, isomerisation over Mo-containing catalyst 77−86361
highly excited molecular systems, high energy photochem. 80−66831
hydrocarbon chain, gauche-trans isomerisation, ^{13}C relax. times and nucl. Overhauser enhancement model 78−33520
hydroxymethyl radical $+O_2$, rate coefficient meas. by laser magnetic resonance flow tube method 80−66767
interconversion pot. energy surfaces, geometries, electronic structs. 78−35660
isopropyl alcohol, adsorbed on ZnO, decomp., IR and kinetic obs. 80−59780
isovaline radioracemization, cosmochemical implications 80−62087
ketocarbene-ketene rearrangement, reaction path, ab initio calc. 78−20008
lactam-lactim tautomeric equilibria, quantum chem. calcs. 80−50833
laser specific and thermal reactions classifications 80−11919
d-limonene-1,2-epoxide, isomerisation *(Japanese)* 79−8435
maleic anhydride-styrene copolymer, photochromic, recording material for holograph 79−72537
methyl cyanides and isocyanides, isomerisation, ab initio (STO-3G) geometry optimised calc. 78−46265
methyl isocyanate, isomerisation RRKM theory using effective strong collision freq. 78−44365
methyl isocyanide, CO_2 laser induced isomerisation 78−35644
methyl isocyanide, intracavity CW dye laser state-selective activation of isomerisation 78−11533
methyl isocyanide, laser induced thermal isomerisation, obs. by new time resolved IR photographic technique 80−57400
methyl isocyanide, laser initiated thermal isomerisation, thermal explosion 78−80725
methyl isocyanide, laser initiated thermal isomerisation, time behaviour of CN radicals 80−11887
methyl isocyanide, N isotope enrichment, IR laser isomerisation 79−27096
methyl isocyanide, thermal isomerisation in presence of at. gases, vibr.-translational energy transfer 78−23924
methyl isocyanide, unimol. isomerisation to methyl cyanide 79−24725
methyl isocyanide photoisomerisation, laser isotope separation, C-isotope enrichment by one-photon vibr. photochemistry 80−81336
cis-3-methyl-1,3-pentadiene-1,2-d_2, nonrandom isomerisation, internal energy relax. 79−70313
m-methyl-p-cyanodimethylaniline, ps reversible isomerisation kinetics, O_2 quenching obs. 79−5133
methylenimine, lowest excited state, singly excited config. interaction calcs. 79−59361
11-cis-14-methylretinal, photoisomerisation, high quantum yield 79−57253
methylsilylene, closed shell states, isomerisation, config. calcs. 78−35652
methylsilylene, isomerisation, lowest triplet state reaction surface studies 79−15963
1,4-Bis(2-methylstyryl)benzene, laser dye, picosec. laser obs. 79−36891
model reaction, SCF-SI theory calcs. 80−23399
norbornadiene-quadricyclene photoisomeric interconversion for solar energy chemical conversion and storage 80−89664
organic dyes, stimulated fluorescence, energy level scheme, photoisomerisation effect 77−70310
organic solids, one- and two-photon laser photochem., hole burning appls. 80−21304
organic unimol. rearrangement, principle of least motion technique 77−36737
oxiranylidene, struct., isomerisation, ab initio SCF MO calcs. 78−41941
s-trans-1,3-pentadiene, photoisomerisation, excited state pot. energy curves, CIPSI calc. CNDO/2 parametrisation 78−11505
phenoxyacetic acid, photoinduced selective isomerisation in comparison with X-ray induced decomp., aq. soln., 25°C *(German)* 77−63931
phenylcarbene, singlet and triplet ground states, rearrangement to cycloheptatrienacarbene, MINDO/3 calc. 78−13430
photochemical reactions, isomerisation, complexing, proton transfer, initiation of internal conversion processes 80−40713
photochemical smog, rate parameters and computer simulation 78−48677
photoisomerisation, SCF MO pot. surfaces 79−11772
PMMA-spirobenzopyran mixed monolayers, photoresponsive effects 79−66316
PMMA-spiropyran Langmuir monolayers, reversible photochemical strain 80−50867
polyacetylene, soliton formation and cis trans isomerization 80−76505
polyacetylene, thin film, ESR study, effects of O_2, NO and halogens 80−25186
polyacetylene, trans- and cis-isomer, electronic struct. calcs. 80−24788
cis-polyacetylene film, unpaired electrons, isomerisation, EPR obs. 80−60405
polybutadiene networks, cis-trans isomerisation, γ-ray induced 79−74374
polyenes, photoisomerisation, triplet pot. energy surfaces and normal mode anal. 80−108700
polyethylene film, gauche-trans transition, activation energy meas. by IR spectra 79−57220
polyethylene terephthalate film, gauche-trans transition, activation energy meas. by IR spectra 79−57220
polymethine, IR-140 laser dye, photoisomerisation processes 78−27800
polymethine dye behaviour in lasers, efficiency and photoisomer generation 80−14335
polymethine dye unstable photoisomers, superluminesc. and stimulated emission 79−31896
polymethine dyes, excited mols., photoisomeric transformations 79−87854
polypeptide copolymer, trans-cis photoisomerisation 78−3331
polyphenylacetylene cis-trans isomers, rel. mol. wt. distrib., heating effect 80−106409

isomerisation continued
porphin in n-alkane host, photoautomerisation and hole-burning 79−47954
porphyrin free base in n-octane crystal at 4.2K, laser-induced photochem. isomerisation 77−12815
potential surfaces, electron correl. theories 79−39125
propene+^{38}Cl→$CH_3CHCH_2{}^{38}Cl(CH_3CH{}^{38}ClCH_2)$, thermal, terminal and central addition 77−86341
proteins, gel permeation chromatography of interacting multicomponent systems 78−68950
proteins, kinetic consts. determ. by gel permeation chromatography of interacting multicomponent systems 78−68951
racemization, relative and absolute rate consts., kinetic isotope effects 79−43558
rate processes in condensed media, anharmonicity effects 79−19349
11-cis-retinal, donor energy effects on triplet-sensitized isomerization 78−3353
retinal, proton donor-acceptor isomerisation coupling, bacteriorhodopsin as light driven proton pump 79−79473
retinal isomers, dark equilib. and photochem. 78−15771
retinal photoisomerisation mechanism for light-driven proton pump in H. halobium 78−35820
retinals, catalysed cis-trans isomerisation by crude tissue extracts 78−64925
reversible reaction, rate consts., rate kernels 78−40020
rhodopsin, bovine, photochem. cis-trans isomerisation at liq. He temps. 78−64939
rhodopsin, cis-trans isomerisation on psec time scale 77−86498
rhodopsin, primary photophys. and photochem. processes in visual excitation 78−15773
rhodopsin, thermal isomerisation rel. to visual transduction mechanism in retinal obs. 79−74651
rhodopsin, transient light-induced conform. changes 78−15774
salicylamide, excited state proton transfer, kinetics, picosec. fluoresc. 79−59502
salicylidene-2-chloroaniline, photochromism and thermochromism, NQR spectra, temp. and UV irrad. depend. 80−54968
silaethylene, closed shell states, isomerisation, config. calcs. 78−35652
silaethylene, isomerisation, lowest triplet state reaction surface studies 79−15963
silylcarbene, closed shell states, isomerisation, config. calcs. 78−35652
silylcarbene, isomerisation, lowest triplet state reaction surface studies 79−15963
solar energy chemical storage, photosensitization mechanisms for energy storing isomerizations 80−89679
solar energy chemical storage using novel photocyclization reactions of 1-alkenyl-2-pyridones 80−89680
stereoselective rearrangement reaction, electron impact induced, temp. depend. 77−25288
stilbene, cis→trans photoisomerisation rate const., direct meas. 80−30250
stilbene, cis and trans, transient spectra, radiative lifetimes and quantum yields 80−78640
stilbene, cis- and trans-, picosecond flash photolysis, intramol. charge-reson. transition obs. 80−7810
stilbene, diphenylpolyenes, photoisomerisation, 'phantom' photochem. singlet state, PPP SCF CI calcs. 78−73058
stilbene, direct photoisomerisation theory, from fluoresc. and absorption spectra 79−79262
trans-stilbene, fluoresc. decay, picosecond anal. 79−31569
stilbene, ps photoisomerisation, time-resolved spectra obs. 79−57252
stilbene anion radicals, photoinduced isomerisation, 77K 80−66818
trans-stilbene photoisomerisation, ps dynamics under collision-free conditions 79−91975
succinonitrile, plastic phase, mol. motions correlation times, incoherent neutron scatt. 80−49138
succinonitrile, plastic phase, mol. reorientation and rotational isomerization, anal. of elastic incoherent struct. factor 78−22674
symmetry of nonrigid molecules 79−22859
p-terphenyl anion radicals, photoisomerisation, local heating effects 78−85179
thermal electrocyclic reactions, anal. using topological model 80−78512
thermal isomerisation rate theory 79−34291
thioindigo, cis⇌trans isomerisation, nanosecond flash photolysis and steady state methods, triplet state 78−35648
thioindigo, in nonpolar solvent, photoisomerisation mechanism, fluoresc. obs. 77−63933
thioindigo adsorbed on Al_2O_3, photoisomerisation 80−89503
transition state determination and characterisation ab initio calcs. 77−28975
tricarbocyanine solns., photoisomerisation, fluoresc. and absorpt. spectra of photoisomer 78−85181
trifluoromethyl cyanides and isocyanides, isomerisation, ab initio (STO-3G) geometry optimised calc. 78−46265
2,4,6-trimethoxy-s-triazine, thermal isomerisation, nematic solvent effects 79−91944
visual pigment retinal chromophore, role of protein in photochem. 78−15772
water, heat capacity and structure, isomerisation reaction role 79−33097
AlOH→HAlO system, intramol. rearrangement, ab initio calc. of pot. surfaces and min. energy paths, geom. parameters 80−32623
BNC⇌BCN, isomerisation energy/barrier correlation, rel. to HNC(LiNC) 80−50840
BOH→HBO system, heterovalent isomerism, ab initio calc. of pot. surfaces and min. energy paths, geom. parameters 80−32622
CH_3PF_4, nonrigid mol., tunnelling mechanisms, spectrosc. theory 80−78605
$ClO+NO_2+M$, reaction rate constants 79−100350
ClONO, form., reaction kinetics, IR spectra 78−35641
$ClPF_4$, nonrigid mol., tunnelling mechanisms, spectrosc. theory 80−78605
$Fe(CO)_4$, IR laser induced isomerisation, non-Berry pseudorotation 78−31658
H_2, ortho⇌para conversion, on CoO, MnO mag. surfaces 79−47969
HNC→HCN, transition state determination and characterisation ab initio calcs. 77−28975
HNC⇌HCN, intrinsic reaction coord., ab initio SCF calc. method 77−48626
HNC⇌HCN, isomerisation energy/barrier correlation, rel. to LiNC(BNC) 80−50840
HNO^+, ab initio pot. surface, and isomerisation barrier of lowest states 79−22622
HPN-HNP, isomerisation energies, ab initio MRD-CI calcs. 80−106271
HSO-HOS, isomerisation energies, ab initio MRD-CI calcs. 80−106271
HSiC-HCSi, isomerisation energies, ab initio MRD-CI calcs. 80−106271
LiNC⇌LiCN, isomerisation energy/barrier correlation, rel. to HNC(BNC) 80−50840
N_2H_2, model rearrangement system, electron correlation and basis set effects 80−3317
NO^++metal atom reaction, obs. using magnetically confined afterglow 77−34750
NO_2+Cl+M, reaction rate constants 79−100350
NOH^+, ab initio pot. surface, and isomerisation barrier of lowest states 79−22622
$(NbCl_nBr_{6-n})^-$ complexes in acetonitrile soln., ^{93}Nb spin relax. and mag. shielding 80−44944
OClNO, form. in matrix reaction, IR absorpt. obs., photoisomerisation 78−15667
$SSCl_2$, IR spectra, prod. in S_2Cl_2 photolysis 78−61033
o-semiquinone, radicals, intra- and intermolecular H^+ transfer, ESR 77−16840

isomerism
see also isomerisation; nuclear isomerism; rotational isomerism
acetamide, IR spectra, amino group inversion transitions and pot. functions 80−43041
acetic acid and isomeric methyl formate, Compton profiles 77−30928
2-acetylfuran, IR spectra, cis/trans equilib. 77−469
acrolein, mol., conformational anal., inapplicability of MINDO/3 79−94105
adenine, hydroxy and methoxy derivatives, absorption UV spectroscopy and electronic struct. of ionic and tautomeric forms 80−74177
adenine, tautomers, polarisation, barriers and tunneling times calcs. 79−41114
adenylyl 3'-5' adenosine, conform. equilib., Raman temp. jump obs. 78−8450
4-alkyl-3-phenyl-3 4-dihydrocoumarins cis- and trans-, ^{13}C NMR spectra 80−43067
allylamine, N-cis lone electron pair trans isomer, total dipole moment, rel. orientation 80−69259
amino acids, positron annihilation in D and L isomers 77−12887
aminopyrazine, far IR spectra, barrier to planarity, pot. function and energy levels 80−69137
aniline, amino group inversion and torsion, far IR spectra 77−10670
anthracenes, bridged, photochemistry and spectra 77−77793
bacteriorhodopsin, 13-cis and trans isomers, photochem. and dark equilib. 77−90798
bacteriorhodopsin, dark-adapted, photocycle and light adaptation 77−73508
bacteriorhodopsin isomers, dark equilib. and photochem. 78−15771
benzene cation, internal energy selected, dissoc. dynamics 79−66274
bicyclo(3.2.0)hept-6-ene, LF vib. spectra, conformations 78−58685
bicyclo(4,2,0)octane, cis and trans isomers, struct. mol. mechanics and electron diffr. 77−54608
bicyclo [4.4.0] dicane, cis and trans forms, mol. struct., electron diffr., mol. mechanics 78−50658
bromoacetic acid, microwave spectrum, rot. consts., nucl. quadrupole coupling, conform. 79−13702
bromochlorofluoromethane, narrow saturated reson. absorpt., weak current detection 77−14433
butadiene, mol., conformational anal., inapplicability of MINDO/3 79−94105
n-butane, trans or gauche, solute mol., solvent mol. distrib. 80−96433
2,3-butanedione, mol., conformational anal., inapplicability of MINDO/3 79−94105
1-butanol, IR and Raman spectra, vibr., conformers 78−25532
t-butyl alcohol, and deuterates, gaseous and matrix IR spectra, liq. Raman spectra, vibr. assignment 79−10113
n-butyl bromide conformers, IR and Raman spectra, vibr. anal. *(German)* 77−88451
camphor, optical isomers, separated, IR Lamb dip obs. 78−90197
carbocations, degenerate $(CH)_N^+$ type, permutation description *(German)* 79−45658
carborane, ortho- and para-, phase transition and mol. reorientation, isomer effects, PMR obs. 80−80628
3-carboxy-2,2,5,5-tetramethylpyrrolidinyl 1-oxyl system, enantiomer solid soln., cryst. struct. and phase diagram 79−86778
chain mols., conformational transition kinetics 80−83339
chemical compounds, complete set, chiral subset, algebraic props. 77−70282
chiral molecules, averaged discriminatory interactions, chem. effects 78−13562
chiral molecules, positron interactions, selectivity between optical isomers 77−83751
chiral molecules, theory 79−41121
2-chloro-3-fluoro-1-propene, struct. and conformers, force field and vibr. amplitudes 78−25747
2-chloroanisole and sulphur analogue, benzene dipole moment anal. 78−25748
chlorobenzaldehyde, a^3A''→X^1A' phosphoresc., conformations and ground state fundamentals 80−78642
chloromethyl oxirane, microwave spectra and conformations of cis and gauche-2 forms 80−5534
2-chlorophenol and sulphur analogue, benzene dipole moment anal. 78−25748
N-5-chlorosalicylideneaniline, H^+-^{14}N double reson. NQR spectra temp. depend. thermochromism and tautomeric mech. 78−70849
conformers, dynamic interaction between ground states, effect on IR spectra 78−58767
2-cyanoaziridine, microwave rot. spectrum, assignments 80−91546
cyanomethyl (isocyanomethyl) radicals, electronic struct. and props. 79−49938
cyanopyridine, isomeric forms, adsorbed of Ag electrodes, Raman scatt., orientational specificity 79−69822
cyclic mol. struct., topological characterisation 80−74254
cyclic monocarboxylic acid radicals, ring inversion barriers, EPR 80−53025
cycloheptanone, vibr. spectra, pot. functions and conformers 77−83569
cyclohexanecarbonitrile, rot. consts., conformers, struct., microwave spectrum 77−42314

isomerism continued
cyclohexyl halide-thiourea clathrate, conform., Raman spectra 77−77200
cyclophanes, double and triple-layered, triplet state zero field splitting parameters, HMO calc. 77−50366
cyclopropyl ketones, photoelectron spectra, MO calcs. 77−27115
cytosine, adenine, tautomeric equilibria, in aq. solns, electrostatic model of solvation, SCF MO calc. 79−96305
cytosine, hydroxy and methoxy, derivatives, absorption UV spectroscopy and electronic struct. of ionic and tautomeric forms 80−74177
decanoic acid, mol. config. change in cryst., IR spectra, normal coord. anal. 78−33506
2,4-diamino-6-hydroxy-pyrimidine, IR absorption spectrum, vibr. anal., tautomerism 80−58253
diazomethane, isomers, electronic and isomerization energies calc. 79−50161
1,2-dibromoethane, gauche and trans conformers, photoelectron spectra 78−50574
2,4-dichloroanisole and sulphur analogue, benzene dipole moment anal. 78−25748
2,4-dichlorophenol and sulphur analogue, benzene dipole moment anal. 78−25748
dicyanobenzene, deuterated isomers, vibr. spectra 79−31521
dicyanoketene, and isomeric forms, heat of form., ab initio STO-3G calcs. 80−58190
1,2-difluoroethane, matrix isolation, trapping from thermal mol. beam, IR spectra 78−46330
1,2-difluoroethylenes, ab initio HF comparison of cis and trans energies 77−18786
dihaleothanes, CNDO/2-type calc., FORCE method, relative stability, intramolecular atomic interaction energies 78−41957
dihaloethylene, CNDO/2-type calc., FORCE method, relative stability, intramolecular atomic interaction energies 78−41957
2-5-dihydrofuran, liq. phase far IR spectra, ring puckering *(French)* 78−92068
2,5-dihydroxy-p-benzoquinone, proton tautomerism dynamics, ^{13}C NMR obs., CNDO calc. 79−52632
diimide, trans-cis conversion in lowest excited states, SCF calcs. 78−46284
dimethyl tartrate, chirality detection with chem. ionis. mass spectroscopy, meso ion obs. 77−68139
cis-3,4-dimethylcyclopentanone, conformational analysis, vib. spectra 77−75325
N,N′-diphenyl-m-phenylenediamine, crystal and mol. struct., X-ray diffr. 78−47312
diphenylethylene, UV spectra, quantum-mechanical investigation of isomerisation pathways 80−43065
directional effects of σ conjugation 78−37769
dithiocarbamate complexes of Cr, Mn, Sn and Pb IR, electronic and mass spectra, mag. susceptibility, cond. meas. 80−97270
DNA, proton transfers between base pairs, LCAO SCF all-electron PRDO method 78−80829
DODCI, absorption relax. lifetime, isomers, pulse excitations 77−9098
DODCI, rot. diffusion time, time depend. fluoresc. depolarisation meas., photoisomer effects 77−71825
dynamic isomers and spontaneous generation of optical activity, phase rule prediction 79−34421
enantiomers, discrimination using liq. crystalline solns., IR rot. dispersion meas. 79−16064
energy component hypersurfaces, local behaviour regularities 77−42256
ethane derivatives, diastereoselective form. and symm. props., semirigid mol. model 80−48099
ethyl cation, rearrangement pseudorotation modes, reaction mechanisms, permutation theoretic anal. 78−44369
ethylamines, torsional Raman spectra 77−77195
ethylene deuterates, deuteration and isomeric effects on triple point temp. 77−43337
ethylene glycol, IR spectra, ab initio calcs., vibr. anal., conformations of isotopic modifications 78−5210
ethylene oxide cation, existence of open isomer, ab initio calcs. 79−22593
ethynol, ab initio calc., energy levels and geom. struct. of C_2H_2O isomers 78−62716
1-fluoro-2-propanol, conformational energies and rot. barrier, ab initio calc. 79−31390
4-fluoroaniline, amino group inversion and torsion, far IR spectra 77−10670
fluoroanilines, isomers, thermodynamic functions and fundamental vibr. freqs. 80−9581
2-fluoroethanol-d_0-d_1, IR spectra in Ar, N_2 and Ar-N_2 matrices, normal coordinate anal. 78−25538
formaldazine, mol., conformational anal., inapplicability of MINDO/3 79−94105
formamide, IR spectra, amino group inversion transitions and pot. functions 80−43041
free energy of conformational changes, microwave spectroscopic intensities 77−75227
furan-2-aldehyde, mol. struct., electron diffr. and IR spectroscopic examination 79−10106
gauche-trans isomers, 2-iodo-2,3-dimethylbutane 79−54846
generalised isomerisation modes 77−68135
glyoxal, mol., conformational anal., inapplicability of MINDO/3 79−94105
graph theoretical basis for mol. struct. ordering 79−59326
guanine, ^{15}N and D substituted, in acid and base solutions, vibr. anal. 79−26994
1-halo-1-n-propylcyclohexanes, conform. equilib., and pot. barriers, IR spectra *(Russian)* 78−21928
1-haloalkanes, microwave spectra, conformation 78−21913
2-haloethanols, gauche conformer stability, exchange interaction 79−18311
2-haloethyl ethers, relative conformational energies, Raman obs. 79−27002
2-halopropionates, liq., dielec. relax. and permittivity 80−15948
heptanol isomers, static permittivity and density, press. and temp. depend. 78−35078
hexanes, isomeric, unimol. decomp. processes following field ionisation, temp. depend. 80−95733
HOAB, nematic liq. cryst., thermotropic mesophase, DMR chain segments assignment 80−24356
homotetrahedryl cation, rearrangement pseudorotation modes, reaction mechanisms, permutation theoretic anal. 78−44369

isomerism continued
hydrides, first row, bending pot. calc. using MINDO approx., force const., equilib. geometry 80−95544
hydrocarbons, liq., Compton profiles, bond additivity 80−93423
3-hydroxymethyl-2,2,5,5-tetramethylpyrrolidinyl 1-oxyl system, enantiomer solid soln., cryst. struct. and phase diagram 79−86778
hydroxymethylene radical cation stability, $CH_2O^{+\cdot}$ isomers, ab initio MO study 80−42965
hydroxypyrimidines, ^{14}N NQR, tautomerism 77−83620
2-iodoacetamide, mol. struct., electron diffr. obs. 80−63819
isocyanates, nonbonding and π-orbital interactions, photoelectron spectra 80−32774
isopropylphosphine, gauche form, microwave spectrum, identification 78−58674
isotactic polystyrene gel, anomalous X-ray diffraction effects, rel. to chain conformation and isomeric homogeneity 77−50576
isothiothiocyanates, nonbonding and π-orbital interactions, photoelectron spectra 80−32774
isotope and isomer separation in an inhomogeneous magnetic field 80−9752
isotopic isomers, spectroscopic obs. 80−53009
ketene, ab initio calc., energy levels and geom. struct. of C_2H_2O isomers 78−62716
Kruszewski's rule, for stability of isomeric polycyclic conjugated cpds., proof 80−106249
L-amino acids, weak neutral currents and biological stereoselection 80−26196
lactam-lactim tautomeric equilibria, quantum chem. calcs. 80−50833
lactams, N-methylated, cis-trans isomerism, ^1H and ^{13}C NMR obs. 80−106335
metastable isomers as new class of interstellar molecules 79−48872
methanol, enantiomers, racemic mixture nucleation 78−26677
methyl ethyl ether, charact. vibrs., isomer and isotope effects, rel. to reverse spectral problem 80−63613
methyl formate and isomeric acetic acid, Compton profiles 77−30928
methylphosphinosilane, IR and Raman spectra, vibr. assignment and asymmetric potential function 79−85962
3-methylthiomethylpropionate, liq., dielec. relax. and permittivity 80−15948
mirror image molecules, parity non-conserving energy difference 79−76366
molecular topology, branching, distance matrix, information theoretic calcs. 78−25405
multi-molecular clusters, isomeric structures, weights and effective characts. 79−31759
nitronaphthylamines, ESCA and UV photoelectron spectra, assignments 78−50588
nonracemic mixtures, theory of chirality functions, concept of qualitative completeness 80−69255
optical isomer crystal, energy difference due to parity nonconservation *(Russian)* 80−106405
optical isomers, separated, IR Lamb dip obs. 78−90197
optically active chiral molecules, photodissoc. fragments, ang. distrib. theory 77−10713
oxirene, ab initio calc., energy levels and geom. struct. of C_2H_2O isomers 78−62716
2-oxybicyclo(3.2.0)hept-6-ene, LF vib. spectra, conformations 78−58685
palladium bis-β-diketonates, IR and Raman spectra 78−46327
pentane, isomers, gas and liq. phases, electron transport, density and temp. depend. 79−91114
pentofuranosyl nucleosides, isomeric, ^1H NMR coupling consts., SCF FPT INDO approx. calc. 80−14156
perchloro-[4]-radialene, IR and Raman spectra 77−77198
perfluoro-1-heptene, electron attachment, $\lesssim$3 eV, rel. to perfluoromethylcyclohexane 79−36755
perhalonitrosomethanes, gas phase IR spectra, assignments, isomerism 80−28017
permutational isomers, enumeration by combinatorics, Polya's theorem 78−93501
phenacyl halides, IR spectra, $\delta(CH_2)$ vibrs. correlation with structs. *(French)* 80−23417
phenanthrene, and dideuteroisomers, vapour phase fluoresc. lifetimes, position dependent D effects 77−30901
phenylnaphthalenes isomers, fluoresc. lifetime difference and mol. geometry 80−69176
poly(m-methylene terephthalate) polymers, IR and Raman spectra 77−52088
poly-p-chlorophenyl glycidyl ether, struct., tacticity and addition isomerism, ^{13}C NMR 80−58427
polyacetylene, dynamic nuclear polarisation of protons *(French)* 80−43217
polyacetylene, pristine and acceptor doped isomers, EPR, DC cond., evidence against solitons 80−15782
polybutadiene networks, cis-trans, thermoelastic obs. 79−74220
polydiacetylene, urethane substituted, conjugated polymer soln. spectral shift on planar-nonplanar conformational transition 79−64129
polyenes, twisting force consts., CNDO theory potential energy surface 78−50474
polyethylene film, gauche-trans transition, activation energy meas. by IR spectra 79−57220
polyethylene terephthalate film, gauche-trans transition, activation energy meas. by IR spectra 79−57220
polymer single chain, coil-globule transition obs. 80−1098
polymers, symmetric, combinatorial enumeration of chemical isomers 80−28114
polymethine dyes, laser action and photoisomeric transforms. 79−89905
polymethyl acrylate, head-to-head, high-resolution PMR spectra 79−73834
polymethyl cinnamate, head-to-head, high-resolution PMR spectra 79−73834
polymethyl crotonate, head-to-head, high-resolution PMR spectra 79−73834
polystyrene, atactic, stereoregularity study using Fourier transform IR spectroscopy 79−59612
polysubstituted peri-condensed compounds, combinatorial enumeration of chemical isomers 80−28114
polyvinyl carbazole, and ring chlorinated derivatives, dielectric and NMR relaxation 79−73883
porphin, hypersurface of adiabatic pot. calc. by CNDO/2 method, vibr. freqs., absorpt. spectra calc. 80−95543

isomerism continued
porphin in host n-alkane crystals, phototautomerism, IR spectral obs. 80−34963
porphyrin free lasers, radiationless decay of triplet state, position dependent D effect 77−30902
porphyrins, isomers, enumeration by combinatorics, Polya's theorem 78−93501
n-propanol, centrifugal distortion constants, OH-trans-trans and OH-trans-gauche conformers *(Russian)* 79−10089
propene, (cyclopropane), triplet states, electron impact and photosensitised dissoc., chem. effects 77−14592
propenoyl chloride, IR bands, torsional struct. 80−28018
purple membrane protein retinal chromophore, role of protein in photochem. 78−15772
pyrimidines, substituted analogues, absorption UV spectroscopy and electronic struct. of ionic and tautomeric forms 80−74177
racemic liq. soln., mirror isomeric mol. separation by RF rot. polarisation elec. field 78−80317
retinal, isomeric triplets, low temp. spectrosc. and kinetic flash photolysis obs. 79−85972
retinal, isomers, intersystem crossing quantum efficiencies, solvent effects 79−22751
9-cis retinal, visual pigment chromophore, twisting mechanism 80−58333
retinal isomers, dark equilib. and photochem. 78−15771
11-cis retinal visual pigment chromophore, twisting mechanism 80−58333
rhodamine Zh, isomer separation, identification and emission efficiencies *(Russian)* 77−83871
rhodanines, tautomeric, electronic struct. and spectra, MO calcs. 79−13629
silaethylene, triplet carbenoid isomers, thermodynamic stability 78−90076
Sodium ammonium tartrate, L- and D-mol. energy difference, parity violation 78−25744
stereoisomer generation, algorithm and implementation 80−1080
stereoisomer generation, specification and enumeration, config. symmetry group appl. 80−1079
stilbene, radiolysis, electron transfer and protonation, vis. spectra, isomer effects 77−60085
structural formulae, graphs generation by computer *(Russian)* 79−49967
symmetry of nonrigid molecules 79−22859
tautomeric transform., quantum-statistical model 77−38739
tautomerism and alternating bonds, representation, Chemical Abstracts Systems 80−63851
TCNE-stilbene complexes, and analogs, charge transfer energy calc. isomer prediction 78−21854
terphenyl, ortho-, para-, meta-, total neutron cross sections for subthermal energies 78−74779
s-tetrazine, pot. surface of low-freq. out-of-plane modes 78−62741
1,2,4-thiadiazolidine derivatives, isomers, negative ion mass spectrometry *(Japanese)* 78−5367
thiazolidine, valence force field transferability *(French)* 79−10091
thioacetamide, IR spectra, amino group inversion transitions and pot. functions 80−43041
thioureas, alkyl and phenyl groups trisubstituted, conformation, steric and stacking interaction 80−95587
thirene, ab initio SCF calc., thermodynamic stability 78−25420
thymine, tautomers, polarisation, barriers and tunneling times calcs. 79−41114
thymine monoanions in soln., tautomer identification by laser Raman spectroscopy 80−14148
trans-propargyl amine, microwave spectra, dipole moments and struct., isotopic species 78−974
trialkylthioureas, N-H stretching vibrs. and conformation 80−95586
triazastilbenes, photoelectron spectrosc. 80−106353
2,4,5-trimethylbenzaldehyde, in durene, cryst., photochem. and photophys. processes 77−60092
uracil monoanions in soln., tautomer identification by laser Raman spectroscopy 80−14148
ureas, alkyl and phenyl groups trisubstituted, conformation, steric and stacking interaction 80−95587
vibration spectra analysis, applic. to identification between similar structures *(Russian)* 77−83577
vibrational spectroscopy, structure identification 79−10092
vinyl isocyanate, and vinylcyano ether, geometry and conform., ab initio minimal STO-3G MO calcs. 80−23337
vinyl isocyanate, conformers, geometrical and electronic structures, microwave spectra 78−9142
vinyl isocyanate, microwave and photoelectron study of cis- and trans-forms 78−70819
vinylcyano ether, and vinyl isocyanate, geometry and conform., ab initio minimal STO-3G MO calcs. 80−23337
weak electron-nucleus interaction, parity violation, mol. evidence *(Russian)* 77−30793
C_n aggregates in equilib. C vapour, MINDO/2 calc., isomerism 78−29873
C_3Li_4, structure calculations 78−5364
o-D_2, solid, up to 150 kbar, 5K, Raman spectrum 80−50332
F compounds, ground states, mol. parameters, MINDO calcs. 78−41955
FCN, CNF, isomer pairs, mol. orbitals calcs., using PLA and LEDO integral approx. methods 78−13418
F_2S_2, electronic struct. and stability of isomers, gaussian SCF MO calc. 79−93921
$Fe(CO)_5$, microwave dielec. relax., fluxional mechanism 78−94235
$Fe_2(CO)_6(HC_2R)_2$, R=H, Bu^t, Ph, binuclear complexes, isomer identification and stability *(Italian)* 77−54620
GeH_3^-, electronic struct., electron affinity, inversion barrier, ab initio SCF Gaussian basis calc. 80−63552
H_2, cryst. ortho-para mixtures, vibr. coherence decay 80−78903
p-H_2+^{4}He, vibr. relax., analytical approx. 80−63761
HCN, CNH, isomer pairs, mol. orbitals calcs., using PLA and LEDO integral approx. methods 78−13418
H_2CN^+ isomers, role in interstellar HCN and HNC form. 78−81672
HCNO, isomers, geometry, spectra, rot. and force consts., ab initio calcs. 77−34574
$H_2(D_2)(T_2)$, ortho-para transition, catalytic-, radiation-, and self-induced conversion, review 77−90633
HNCO, barrier to linearity, ab initio SCF and CI calcs. 79−3363
HNO, isomerism, low lying electronic states, ab initio MRD-CI calcs. 80−83291
HNO_2, isomers, protonation mechanism, electrostatic pot. prediction limits 78−11506
HNSi, and HSiN, electronically excited states, MRD CI calc. 79−49947
H_2S_2, electronic struct. and stability of isomers, gaussian SCF MO calc. 79−93921
HSiN-HNSi isomers, MRD-CI calcs. of struct. and stability 78−82635
Hg complex, trihalogenomercurate II ions in amide solvents, config. equilib. 79−26997
$H_2(j=0)+F(^2P_{1/2})$ quenching, quantum mech. study, ortho-para mixing role 79−76485
$^{129}I_2$, frozen soln. in o- or p-xylene, Mossbauer effect obs. 80−78637
ND_3, relax. rates determining the inversion spectra 77−454
NH_3, inversion barrier, pot. energy surface by MS Xα method 79−13656
N_2H_2, isomers, photoelectron spectra, vibr. struct., ionisation pots., Green's function calcs. 77−75213
N_2H_2, $N_2H_2^+$, ab initio calcs., electronic struct., geometries relative energies 77−46487
NO dimerisation, equilib. const. anal., trans-/cis-$(NO)_2$ zero pt. correlation energy difference 78−11509
NO_2, peroxy isomer, stability, ab initio SCF calcs., bond strength 77−14605
NO_2^-, $NO_2^-.H_2O$, and peroxy isomers, photodissoc. and photodetachment 3500-8250 Å, rel. to ionosphere 80−35554
$(NO_2)_2$, struct. and force fields of isomers, ab initio calcs. 77−18783
NO_3^-, $NO_3^-.H_2O$, and peroxy isomers, photodissoc. and photodetachment 3500-8250 Å, rel. to ionosphere 80−35554
NOH, groundstate electronic struct., MRD CI calc., dissoc. energy, isomerisation energy 80−14088
NOH isomerism, low lying electronic states, ab initio MRD-CI calcs. 80−83291
Na_2, conversion rate determ. using laser induced molecular fluorescence 79−43568
$Na_2Fe(CN)_5NO.2H_2O$, new isomeric mol. state, Mossbauer data 77−23513
O_3, analytical potentials from spectroscopic data, vibr., bond length, dissoc. 77−10613
O_3, open and closed forms, energy separation 77−83511
O_3, wave function calc. rel. to energy separation, cyclic and open isomers 79−93929
$O_3^-+X\rightarrow O^-+O_2+X$, X=He, Ar, CO_2, long-lived excited (or isomeric) state of O_3^- 78−5318
O_3H^+, isomeric structs. ab initio MO calcs. 80−83270
$(PF_2)_2O$, IR and Raman spectra, vibr. assignment 78−50544
S_3, open and ring isomers, electronic struct., ab initio SCF calcs. 77−57862
SSF_2, FSSF, and ^{34}S isotropic forms, matrix IR and Raman spectra *(German)* 79−89674
SbH_3, inversion barrier, ab initio SCF calcs. 78−78615
Sr Nb_2O_6, crystallography, polymorphism and isomerism, X-ray diffr. and DTA study 80−100216
T_2, solid, radiation-catalyses ortho-para transition 79−73832
XeF_5^+, pseudopot. SCF MO studies, steric aspects of struct. and force fields, Jahn-Teller effect 80−99444
XeF_6, pseudopot. SCF MO studies, steric aspects of struct. and force fields, Jahn-Teller effect 80−99444
Yb, isomers and hyperfine struct., selective detection through Rydberg states 80−52903

isomorphism
alkali halides, ^{14}N impurities, molecular point defects, EPR isotropic hyperfine triplets 80−2636
compound spaces of tolerance of chemical elements, mutual relationship of compounds 79−19177
groupoids, inductive, of finite cyclic rings *(German)* 80−6375
hysteresis processes, characterisation by isomorphic transform method *(Russian)* 80−80562
iron-transition metal oxinates, Mossbauer spectra 77−90082
lithium potassium tartrate monohydrate: Mn^{2+}, isomorphism with lithium ammonium tartrate monohydrate, EPR obs. 80−29607
molecular crystal, polymorphism and isomorphism, cryst. forces and mol. conform. relation 79−46592
organic compounds, crystallographic pedigree 78−91287
perfect isomorphism, predictiveness of tolerance spaces for atoms in binary and complex systems 80−107094
rare earth trihydroxides, cryst. structs., trends 77−35529
semiconductor morphotropic and isomorphic series, cryst. struct. stability 77−51353
ternary systems, triangulation parameters correl. with isomorphic intermediate phases *(Russian)* 79−52203
tetrathiofulvalene-based salts, isomorphous series systematic investig. of solid-state props. 77−55517
$(Ca_xCd_{1-x})CO_3$, cryst. struct. and cation isomorphous miscibility 80−33972
$CaFe_3O_5$, cryst. struct., isotypism with $Ca_3Y_2Fe_{19}O_{30}$ *(French)* 77−43203
$CaO-SiO_2/GeO_2-H_2O$ system, phase relations, influence of Si/Ge isomorphous substitution 79−52180
$CaS_2O_6.4H_2O$, isomorphic substitution effect on optical activity 77−32347
$CdLn(TiNb)O_7$, Ln=La-Lu, synthesis physicochem. props. 77−43186
$Cs_8Nb_{22}O_{59}$, melt growth and isomorphism with $Rb_8Nb_{22}O_{59}$ 78−35294
$Gd_xSm_{1-x}S$ K X-rays chem. shifts, electronic phase transition, semicond.-metal transition 77−28116
$GeSe_2$, struct. rel. with GeS_2 high temp. phase *(French)* 77−51359
$K_2C_2O_4.H_2O:Cu^{2+}$, ESR and isomorphism of Cu^{2+} 77−32252
$K_8Hf(MoO_4)_6$, and $K_8Zr(MoO_4)_6$, X-ray structural investigation 78−79597
Li_4GeO_4, Mg_2GeO_4, Li_3PO_4, structural relns. *(French)* 77−47433
$Li_2MgSiO_4-Li_2ZnSiO_4$, solid soln. formation, phase relns. *(Japanese)* 77−25037
Li_3PO_4, Li_4GeO_4, Mg_2GeO_4, structural relns. *(French)* 77−47433
$MgGeO_3-Ca_{0.5}Fe_{0.5}GeO_3$, solid solns., physicochem. props. 77−44223
Mg_2GeO_4, Li_4GeO_4, Li_3PO_4, structural relns. *(French)* 77−47433
$NaAlSiO_4$ (nepheline), high-press. to transform. to first silicate Ca ferrite isotype 77−64270
$Na_2MoO_4-Na_2SO_4$, phase diag. and isomorphism 78−27486
$Na_2(MoO_4)_3-Nd_2(SO_4)_3$ system, sulphatomolybdates and isomorphous substitution 80−19763

isomorphism continued
β-Na_2O-Al_2O_3, isomorphous replacement of Al^{3+}, solubility of Cr^{3+}, Ti^{3+}, Fe^{3+} 77−85926
$Nd_xSm_{1-x}S(Se)$, K X-rays chem. shifts, electronic phase transition, semicond.-metal transition 77−28116
$Ni_7I_2B_{16}O_{30}$, isomorphous phase transition ~120K 78−79764
$PbS_2O_6.4H_2O$, isomorphic substitution effect on optical activity 77−32347
$Pr_2(MoO_4)_3$-$Pr_2(SO_4)_3$ system, sulphatomolybdates and ismorphous substitution 80−19763
$PrNH_4P_4O_{12}$, cryst. struct., and isotypism with $NdNH_4P_4O_{12}$ *(French)* 77−24301
$Rb_8Nb_{22}O_{59}$, melt growth and isomorphism with $Cs_8Nb_{22}O_{59}$ 78−35294
$Sm_{1-x}Gd_xS$ system, semicond. to metallic isomorphous phase transition mechanism 80−2338
$SrAl(Ga)_2Si(Ge)_2O_8$, isomorphous replacements of Al by Ga and Si by Ge 77−84713
$Sr_2Nb_2O_7$, crystal struct. and phase transitions, rel. to isomorphous crystals *(Japanese)* 80−49208
$SrS_2O_6.4H_2O$, isomorphic substitution effect on optical activity 77−32347
Tl-Se-$TlInSe_2$, struct. and growth peculiarities, epitaxial heterojunctions *(Russian)* 79−11038
$TlGaS_2$, $TlGaSe_2$, and β-$TlInS_2$ confirmed by Raman scatt. expts. 78−43876
Tl_5SbO_6, isomorphism with Tl_2SnO_3 *(French)* 78−10012
YTa_7O_{19}, crystal struct., isomorphism with rare earth tantalates 77−7698
$ZrSiO_4$, isomorphous replacement of Zr^{4+} by Tb^{3+}, charge compensation 77−47424

isothermal transformations
binary alloy, diffusion limited transform., planar phase interface stability 78−67809
binary alloy, effect of phase boundaries *(Russian)* 79−1857
binary alloys, isothermal phase transformations, impingement and impoverishment effect 79−51234
binary alloys, simple model to describe isothermic phase transform. 78−75832
binary system, isobaric and isothermal phase transform., exchange processes, entropy meas. *(German)* 80−90798
ethane, solid, thermodynamic props. between double solid-to-solid transition and triple point temp. 78−75828
steel, alloy, transform. kinetics of supercooled austenite in 12Kh1MF, structural method 78−52801
steel, and alloy, austenitic transformation, temp.-conc. range of product formation 79−100135
steel, austenitic, decomposition, exam. of phase transformation kinetics, using new method 79−52509
steel, austenitic decomposition kinetics, crack sensitivity, H_2 effect *(Russian)* 80−20885
steel, C, structural strength, increase by high temp. mech. treatment with austenite isothermal decomp. 79−24555
steel, Cr, and Cr-Mo-Ni, austenite decomposition, deform. effects, ferrite reaction 79−1842
steel, Cr (10 wt.%), precip. free ferrite form., STEM 80−84941
steel, Cr (3 wt.%), $\gamma \rightarrow \alpha$ transformation singularities in intermediate transformation temp. interval *(Russian)* 79−91644
steel, Cr-Mo-V, creep fracture, microstruct. effects 78−64668
steel, Cr-Ni, bainitic habit plane determ. 79−1927
steel, Cr-Ni, microstruct. effect on temper brittleness *(Korean)* 79−70092
steel, eutectoid, Si partitioning during pearlite transform., analytical electron microscopy applic. 80−108458
steel, high Cr, V additions effect on brittleness near 475°C *(Russian)* 78−19890
steel, Ni-B, B effect on temperability and microstructure 79−15710
steel, plain C eutectoid, schematic isothermal transform. diagram 78−48393
steel, Si, lower bainite morphology *(Czech)* 79−78959
steel, Si, upper bainite morphology *(Czech)* 78−64537
steel, stainless, δ-ferrite, isothermal decomposition and transform. of heating at 550 to 950°C *(Chinese)* 79−43239
Au-Pt (60 at.%), solid soln. neutron small-angle scatt. study of phase decomp. 79−15646
BN, wurtzite type, phase and struct. changes at high temps. 77−12618
Cu-Ti (4 wt.%), electron and optical microscopy obs. of microstruct. 80−16307
CuCr alloys, supersaturated solid soln. dissociation *(Russian)* 79−52201
Fe, cast, grey Al-Si, eutectoid decomp. of austenite 80−29951
Fe, cast, high-strength bainitic with spheroidal graphite, mech. props., isothermal transform. 79−96023
Fe cast, Mg, austenite isothermal transform., Sn addition effect 79−87611
Fe, cast, Mg, high strength bainitic transform. in C-shape diagram *(Russian)* 79−1860
Fe, cast, Mg, isothermal dissociation of supercooled austenite, exam. of kinetics *(Russian)* 79−29013
Fe, cast, thermal treatment influence on mechanical props. *(German)* 80−29980
Fe, cast white Cr 78−44124
Fe-C (0.25 wt.%), austenitising temp. effect on proeutectoid ferrite reaction kinetics, scanning Auger microprobe exam. 78−44144
Fe-C-Si-Mn, cast, high C, K_1 phase formation due to peritectoid transitions *(Russian)* 79−11548
Fe-Cr-C (10,0.2 wt.%), isothermally transformed, precipitate orientations 80−50640
Fe-Cu-Ni (2,2 wt.%), isothermally transformed, precipitate orientations 80−50640
Fe-Mn-Ni-V-C (0.5, 3.0, 1.0, 0.2 wt.%), austenite decomp., isothermal transform. characts. 80−97477
Fe-Mn-V-C (0.5, 1.0, 0.2 wt.%), austenite decomp., isothermal transform. characts. 80−97477
γFe_2O_3, transform. to α-phase, effect of preliminary pressing or vibromilling 78−84798
$FeTiD_x$ ($0 \leq x \leq 1.9$), structural phase transitions, absorpt. and desorpt. isotherms 80−19948
Ni-S incongruently subliming system, SEM and TEM obs. of high temp. transitions, temp.-comp. diagrams 80−104136
Ni-W-Co-Cr, superalloy MAR 200, with Hf, cellular composite prod. by isothermal dendrite ripening 78−44150

isothermal transformations continued
Pt-Cu (49.37 at.%), coexistent phases in homogeneous ordering 79−29052
Pu, $\beta \rightarrow \alpha$ and $\gamma \rightarrow \alpha$ transforms., microstructures and kinetics 77−25048
Pu, $\beta \rightarrow \alpha$ transform. after full and partial β phase form., kinetics 77−21139
Pu, $\beta \rightarrow \alpha$ transform. after partial β phase form., kinetics 77−28809
Pu-Ga alloys, $\delta \rightarrow \alpha$ transform. kinetics 77−25047
RbI, single crysts., mosaic struct. changes, press. induced 77−51507
Ti β III alloy, elastic and anelastic phenomena associated with α and ω phase isothermal precipitation *(French)* 79−52288

isotope detection
see also mass spectra
automatic evaluation of isotope anal. of nuclear fuels, isotope dilution, mass and α spectrometry 78−55120
ethylene, ^{13}C substituted, isotope analysis by CO_2 laser absorpt. spectroscopy 77−44529
mass spectrometric isotope composition determ. using RMO-4S omegatron mass spectrometer 78−5368
mass spectrometry, thermal-ionis. type, controllable isotope fractionation *(German)* 80−42299
mass spectroscopy, δ values calc. method 79−10234
nuclear power plant vent-air monitoring by nuclide-specific detection system 79−3249
radioactive spots on thin layer chromatograms, autoionographic detect. 78−86960
radioisotope identification by coincidence methods *(German)* 78−90038
transuranium nuclides, production in reactor, yields, nuclide fractional concs, determ. 77−63986
CO_2, $^{12,13}C$, $^{16,17,18}O$ isotope analysis by PbS diode laser absorpt. spectroscopy 77−44529
CO_2 lasers, transition strength of 00°2 9.4 μm sequence band, appl. to IR isotope anal. 79−18395
$^{13}C/^{12}C$ variations, mass spectrometric analysis using double inlet system with viscous flow 77−18131
^{14}C dating of small samples via proportional counting 80−82102
^{14}C, detect. via small van de Graaff accelerator 79−11844
^{131}I in milk, extreme low level determ. 78−92703
^{40}K, isotope relative abundance, radioactivity expt. for schools 79−21511
Li isotope composition determ., α prod. by d bombardment 79−7029
LiCl, Li isotopic comp. determ. by mass spectrometry 80−66899
^{15}N, anal. by proton scatt. 79−61926
^{15}N, use in determ. denitrification rate seasonal var. in sediment 79−100883
$^{18}O/^{16}O$ variations, mass spectrometric analysis using double inlet system with viscous flow 77−18131
^{187}Os isotopic anomalies from different ore deposits, LAMMA determ. 80−61800
Pu isotope ratios, γ-ray spectrometric determ. 77−6518
S isotopic composition in CS, spectroscopic meas. *(Russian)* 80−91696
$^{235}U/^{238}U$ isotopic ratio determination, by γ-ray spectroscopy 79−5240

isotope effects
see also isotope shifts
acetaldehyde, carbonyl addition, model transition states, vibr. anal. 80−71898
acetic acid-$^{13}C_1$, in nematic phase soln., dipole-dipole couplings, selective spin population transfer investig. 80−60427
acetic acid-d_0(-d_1,-d_3,-d_4), cryst., H bonds, stretching, temp., isotope effects 79−51938
acetic acid-d_1(-d_2), equilib. config. from microwave spectrum 79−59442
acetone, vibr. dephasing theories, test using selective coherent ps. Stokes scatt. 80−59609
acetonitride-d_1, ^2H NMR spectra, vibr. and asymmetry corrections to quadrupole coupling consts. 80−74184
acetonitrile, soln., vibr. relax., isotropic Raman spectrosc. obs. 79−50025
acetylene(-d_1,d_2), integrated IR intensities 80−23457
acetylene (-d_2), fluoresc., in matrix-isolated acetylene and ethylene photolysis 79−59505
acetylene-d_0(-d_1)(-d_2) metastable state, mol. beam elec. deflection obs. 80−74137
acetylene-d_2, IR spectra of ν_5 bending fundamental, and $^{12}C^{13}CD_2$ isotope 79−50020
adipic acid crystals, H bonds, harmonic couplings, IR vibr. modes, isotope effect origin 80−34902
agarose-water gels, stability, conc. and isotope effects, photometric obs. 79−66362
alcohols, electrochem. oxidation, kinetic isotope effect *(German)* 78−15681
alkali halide:O_2^-, frozen soln., impurity luminesc., zero-phonon lines interpretation 79−87488
alkali halide solutions, ionic hydration, review 78−92501
alkali halides, solubility press. coeffs. and solvent isotope effect 80−96649
alkali metal chlorides, thermal diffusion in H_2O, D_2O, potentiometric calcs. 78−18807
alkane glass, γ-irradiated, charge trapping, isotope and mol. struct. effects 79−5164
alkanes, glassy, radiation chem., D isotope effects 77−36767
alkanes, polycryst., radiation chem., D isotope effects 77−36767
n-alkanes, single cryst., γ-irrad., ESR, energy deposition rel. to alkyl radical form. 77−16844
allene(-d_4), IR absorption intensities 80−1026
allylamine, N-cis lone electron pair trans isomer, total dipole moment, rel. orientation 80−69259
amino acids, isotopic enrichment determ. by chem. ionis. mass spectra 79−79694
2-aminopyrimidine(-d_1), amino inversion vibr., planarity, far IR obs. 79−31515
anthracene:rhodamine, triplet exciton density, isotope substitution effect, in weak mag. field 77−90184
anthracene, and deuterate, electron drift mobility temp. depend., transient photocond. obs. 77−66164
anthracene, pure and d_n, PMMA soln., triplet lifetimes, 77-300K 78−25594
anthracene-aliphatic amine, photochemically induced H isotope exchange 79−11771
anthracene-tetracyanobenzene, charge transfer complex, phase transitions, deuteration effect, mag. reson., spectral and thermal meas. 79−4412
anthracene-tetracyanobenzene crysts., deuteration effect on phase transition, triplet state EPR study 80−50163

isotope effects continued
L-ascorbic acid, cryst. isolated OH iscillators, IR absorption, temp. and H-bond effects 80−7351
atom+diatom potential, asymmetric, isotope substitution effect, Legendre expansion coord. transformation 78−70894
atom+heavy ion, inner at. shell ionisation, binary collision model, low vel. 80−5612
azoalkanes, fluoresc., solvent isotope effect 78−25591
azulene(-d_8), ultrafast $S_2 \rightarrow S_0$ internal conversion 79−3474
bacteriorhodopsin, kinetic isotope effects in photochem. cycle 77−44592
BCC metal, diffusion of H isotopes, self-capture effect and activation energy *(Russian)* 78−75879
$^3\pi\pi^*$benzaldehyde, zero field splitting and sublevel decay rates, deuteration and host effect 80−37750
benzaldehyde gas, nonradiative electronic transition 80−83413
benzene, $-d_0-d_8$ vapour at low press., intersytem crossing and internal conversion, press. depend. of triplet form. 77−30918
benzene, benzene-d_6, vibrational anharmonicity, condensation effect, vap. press. isotope effect 78−58657
benzene, isotope-mass effects in self-diffusion 80−92695
benzene, mixed deuterated crysts., triplet energy transfer mechanism 77−16365
benzene, mol. transilicon consignment, two-photon gas-phase spectra 77−54582
benzene, vapour press., 5-80°C, isotope effects 78−59939
benzene(-d_1,d_2,d_4), two-photon $^1B_{2u} \leftarrow {}^1A_{1g}$ spectrum, deuterium effect 80−32788
benzene in 3-methylpentane glass, phosphoresc. polarisation and intensity, 77K 77−46588
benzene-cyclohexane system, vap. press., excess free energies, isotope effects 78−59939
benzene-cyclohexane system, vap. press., isotope effects, theory 78−59940
benzene-d_0, -d_6, electronic relax., absorpt. spectra 77−75129
benzene-d_0, -d_6, in glass matrix, phosphoresc. lifetime and polarisation, rot. relax. time meas. 77−79648
benzene-d_0, -d_6, intramol. vibr. energy relax. calcs. 78−33574
benzene-d_0,-d_6, phosphoresc., Boltzmann population and spin-lattice relax., decay processes 78−31230
benzene-d_0(-d_3)(-d_6), vibronic coupling, hot band absorpt. spectra 78−58708
benzene-d_0(-d_6), radiationless triplet decay, non-Condon effects 80−83405
benzene-d_1, ^{2}H NMR spectra, vibr. and asymmetry corrections to quadrupole coupling consts. 80−74184
benzene-d_1, (-d_2)(-d_3), oriented, order, D nucl. quadrupole coupling, mag. reson. spectra 78−74683
benzophenone, and d_{10}, ODMR and phosphorescence spectra in organic matrix 79−36671
benzophenone, triplet, optically detected EPR, ENDOR and ODMR, HFS, isotope and spin-orbit effects 78−86898
benzophenones, triplet state fine struct. parameters and phosphoresc. spectra 79−50065
p-benzoquinone, second order Stark shift of zero-field transitions, isotope effects 77−24860
p-benzoquinones, chlorinated, transferable force field for in-plane vibrs. 80−964
benzoyl peroxide, photodecomp. low temp., isotope effects 77−42365
betamethylnaphthalene in $C_{10}D_8$, exciton percolation and coherence 77−59258
9,9′-bianthryl, excited, proton-induced radiationless processes 77−88486
bilayer membranes, permeation of water mols. meas. using fluoresc. quantum yield solvent-isotope effect 79−34710
bromobenzene -d_0(-d_5) radical cation, electron impact dissoc., secondary isotope effect 80−63836
bromochlorofluoromethane-d_0, -d_1, Urey-Bradley force field calcs. 77−57968
bromomethanes, ^{13}C-Br spin-spin coupling consts., isotope effects 78−13522
1,3-butadiene, matrix isolation, trapping from thermal mol. beam, IR spectra 78−46330
t-butanol and -d_1, deuteration effect on self-assoc., dielectric polaris meas. 79−28672
t-butyl formate, deuteration effects, IR and Raman spectra 79−50016
calcium copper acetate hexahydrate, and deuterated cpd., tunnelling reson. effects in nonreson. spin-lattice relax. 79−86726
calcium copper acetate hexahydrate, $CaCu(CH_3COO)_4.6H_2O$ and $CaCu(CD_3COO)_4.6H_2O$, antiferromag. props. 78−2680
carbazole, excited state, dissociation rate, normal isotope effect 77−32767
carboxylic acid systems, H(D) complexes and dimers, ν_{CO} IR band intensities 80−63715
chemical reaction dynamics, Franck-Condon factors rel. to information theory for vib.-rot. distribs. and isotopic branching ratios 77−60041
chemical reactions, Brownian dynamics simulation in soln. 80−104422
chemical reactions with electronic isotopic substitution in flow and stopped flow NMR 77−25265
chlorobenzene-d_0, -d_1, mol. reorientation and D nucl. relax. time, temp. depend. 78−39424
chloroethane-d_1, laser multiphoton dissoc., intramolecular isotope effect 78−17733
chloroform, and d, polar soln., Raman line shape of ν, band 78−74705
chloroform-d_0(-d_1), Raman and IR intensity anal. 80−18857
chloroform-d_1, and isotopic forms, liq., neutron diffr. obs. 79−32878
chloromethyl formate(-d_1,d_2,d_3), gas, solid. and liq., IR spectra assignments and struct. 80−32715
chloromethylethyl ether, GT isomer, microwave spectra and geom. config. 79−59444
chlorophyll-a radical cations, in disordered systems, electron spin echo envelope modulation, isotope effects 78−61141
copper porphin, IR spectra and vibr. anal., and deutero-derivatives 79−22705
crystal, vibr., isotopically disordered, quantum transport eqn., electron-phonon coupling 78−39081
cyanomethane-d_0, -d_3, vacuum UV photodissociation spectroscopy 79−834
cyanotrifluoromethane, vacuum UV photodissociation spectroscopy 79−834
cyclobutanol-d_0,-d_1, conformation, microwave spectrum 78−86852
cyclododecane, force field, PMR of deuterated isotopomers 79−45695
cyclohexane, isotope-mass effects in self-diffusion 80−92695
isotope effects continued
cyclohexane, vapour press., 5-80°C, isotope effects 78−59939
cyclohexane-d_0, -d_{11} ^{13}C-^{1}H coupling constant 78−13519
1,1-cyclopropane(-d_2), isomerisation in He bath, vibr. transfer, temp. depend. 79−24723
n-decane-n-decane-d_{22}, γ-irrad., H_2/D_2 product ratio mass spectra, mechanism 77−40558
di thioformic acid, cis and trans isomers, rot. microwave spectra and config. 79−63989
diacetylene derivatives, solid-state polymerisation, isotope effects 80−66799
diacetylene radical cation, and deuterated forms, electronic spectrum in solid inert gases 79−94026
diaminoazobenzene, photodecomp., low temp., isotope effects 77−42365
diatomic dissociation equilibrium, isotopic mass depend. theory 79−74372
diatomic gas, vibr. excited, large V-T relax. and isotope effect 79−3548
diatomic molecules, Franck-Condon factors, isotope effects calcs. 78−1031
diatomic mols., doublet states, spin-orbit and spin-rot. coupling cals., isotope depend. 77−57902
p-diazines, polycyclic, $T_1(\pi\pi^*) \rightarrow S_0$ intersystem crossing, isotope effects, ODMR and phosphoresc. obs. 80−91586
dibenzoylperoxide, triplet sensitized photolysis, mag. isotope effect 77−60081
1,4- dibromonaphthalene, highly disordered quasi-one-dimens., excitation transport 80−34961
dichloroacetic acid-d_0, -d_1, ^{35}Cl, ^{37}Cl NQR, isotope effects 77−46578
p-dichlorobenzene(−d_4), mixed cryst. phases, mol. reorientations and intermol. interactions, Raman obs. 79−28751
dichlorodifluoromethane, IR photolysis, isotopic selectivity factors 79−47946
1,1′-dicyanoethene(-d_2), microwave spectrum, Coriolis interaction, rot. assignments 78−82721
O-, p-, m-diethynylbenzene, vibrational spectra, deuterated isomers 78−58705
diffusion of small light solutes in solvent of larger heavier mols., search for mass effects 78−34639
1,3- difluorobenzene radical cation, and deuterated forms, laser-induced fluoresc. matrix. study 79−98138
dihalomethanes, mol. vibr. spectra internal coord. model, and d_2 substitution 79−63974
dilute alloys, solubility of H, isotope effect 78−14470
N,N-dimethyl acrylamide (−d_3,d_6,d_9), force field, IR and Raman spectra obs. 80−47979
dimethylbenzaldehydes, in durene single cryst., zero-field splitting, guest and host isotope effects 80−107752
dimethylether, and d_6, microwave spectra of torsionally excited states 79−26974
dimethylsulphite(-d_6), cryst., liq., and oriented film, vibr. spectra, force fields 79−91443
dioxan-$H_2{}^{16}O(H_2{}^{18}O)(D_2{}^{16}O)$, solns., FP determ., equilib. method 77−20048
diphenylmethylene-d_0,-d_{10}, in benzophenone, ground triplet state, electron spin echo expts. 77−16144
dithiosuccinimide-d_0,-d_1, normal coord. anal. calcs. 77−30844
DMBCA, nematogen, incoherent neutron quasielastic scatt. 79−32887
dodecylamine (−NH_2)/H_2O_2 and deuterated cpd., liquid crystal, phase relationships, isotope effects 79−19358
electron impact desorption of CO, isotope effect 77−55460
elimination reaction, D kinetic isotope effects, tunnelling, zero-point energy effects 78−56889
ethane, force consts., vibr. stress and isotope effects 78−21897
ethane(-d_6,d_3,d_1), electro-optical parameters from IR intensities, least-squares calc. 80−9584
ethane-d_0,-d_6, normal coord. and IR intensity anal. 79−36604
ethanol-d_0, -d_1, -d_5, γ-irrad., trapped electron spin-lattice relax. 77−60089
ethanol-d_0,-d_1, solvated electrons reacting with scavengers, inverse isotope effects 78−31751
ethanol-d_1(d_2)(d_3), glassy state, solvated electron geometry, electron spin echo modulation obs. 80−66009
ethylchloride, d_0-d_5, microwave spectra, elec. field gradient tensor at Cl nucleus *(German)* 78−46325
ethyldifluoroborane, microwave, Raman, IR spectra, conform., dipole moments, vibr. assignment 78−90155
ethylene, -$d_{0\text{-}4}$, UPS using 584Å line, adiabatic ionis. pot. of excited states 79−76467
ethylene, condensation, zero point energy shift, isotope effects 78−95147
ethylene, deuteration effect on thermal conductivity 77−11301
ethylene, isotopically mixed, crystal, dilute guest probe orientational energy, IR, Raman spectra 78−68496
ethylene+HBr, low temp. chain hydrobromination, kinetics and mechanism 80−93735
ethylene(−d_4), Rydberg states assignments, electron energy loss specta 80−53153
ethylene deuterates, VP isotope effect in liq. and solid, chromatographic purification 77−43337
ethylene oxide-d_0, -d_4, ion chemistry, photoionisation and ion cyclotron reson. obs. 77−21373
ethylene-d_0, -d_4, electron impact, vibr. excitation cross-sections, 1 MeV 79−22850
ethylene-d_0, -d_4, hindered internal rotation, vibronic luminesc. and absorption spectra 79−54883
ethylene-d_0,-d_4, IR band intensity and Coriolis interactions 79−54851
ethylene-deuteroethylene copolymer, polymeric unit heterogeneity *(Russian)* 79−55017
ethyleneoxide, elec. dipole moment, g-values, mag. susceptibility, moments and charge distrib. 77−58077
FCC metals, props. of vacancies and divacancies 80−10545
ferroelectrics, displacive and order-disorder type, thermal cond. at low temps. 80−75391
pfluorobenzaldehyde(-d_1), in smectic mesophase, mol. struct. and reorientation, NMR 77−27093
fluoroform., ^{13}C vap. press. isotope effect 78−59938
fluoromethane, $^{13}CH_3F$ and $^{12}CH_3F$, vibr. energy transfer between ortho- and para-mols. *(Russian)* 78−29845
fluoromethane-^{12}C+fluoromethane-^{13}C, vibr. energy transfer, IR double resonance monitor 77−61833
fluoromethane-d_0, -d_1, vibr. relax. in matrix, rot. effects, double reson. obs. 78−46375

isotope effects continued
fluoromethanes, condensation, zero point energy shift, isotope effects 78−95147
fluoromethyl methyl mercury-d_0, -d_3, vibr. spectra, normal coord. anal. 79−50017
formadelhyde(-d_2), S_1 rot. levels, collisionless nonradiative decay rates 79−72346
formaldehyde, 4_0^1 band anal., isotope effects 78−86878
formaldehyde(-d_1, d_2), and isotopic forms, microwave spectrum, ν_4-ν_6 vibr. states Coriolis reson. 78−82719
formaldehyde-d_0, -d_2, $^1(n\pi^*)$ radiationless transition, ab initio CI calc. 79−767
formaldehyde-d_0, -d_2, $^1(n\pi^*)$ transition, vibr. struct., ab initio CI calc. 79−766
formaldehyde-d_0, -d_2, fluoresc. quantum yields, rot. depend., single rovibronic level values 79−22748
formaldehyde-d_0(−d_2), S_1 single rot. level lifetimes, isotope, elec. field and vibr. state depend. 80−78655
formaldehyde-d_1 (-d_2), single vibronic levels, fluoresc. emission, radiative lefetimes and vibr. relax 80−23521
formaldehyde-d_2, inert gas and N_2 matrix fluoresc. spectra, radiationless transitions and lifetimes 79−3469
formaldehydes, (deuterated), A^1A_2 state, photoluminesc. in low temp. matrices, vibr. relaxation 79−50070
formamide, near-IR spectra, anharmonic pot. 77−14430
formamide(-d_2), vibr. spectra NH_2 stretching modes assignment 79−89675
formic acid, ^{16}C, ^{18}O, microwave spectra and centrifugal distortion consts. 80−83352
formic acid, adsorpt. and decomp. over Ni surface, obs. using combined SIMS-FDS-AES system 78−40076
formic acid anhydrides, valence force consts., IR spectra, isotope effects 79−93997
formic acid crystals, low temp. IR spectra 77−48153
formic acid crystals $\nu_{O\text{-}H...O}$ and $\nu_{O\text{-}D....O}$ vib. anharmonicities 77−48154
formic acid monomer, vib. spectra and normal coordinate analysis 77−58003
formyl fluoride, and isotopic forms, mol. struct., from electron diffr. and microwave data 80−23570
formyl radical, -d_0, (-d_1), first ionis. pot., photoelectron spectrosc. determ. 80−48039
formyl radical-d_0,-d_1, microwave spectroscopy, high field Zeeman effect 78−37631
fragmentation processes in mass spectroscopy, rate constant *(Rumanian)* 77−26429
fulminic acid-d_0, -d_1, rot. Zeeman effect and nucl. quadrupole coupling 78−78683
glycerol(-d_3), single cryst., glassy, and supercooled, polarised Raman spectra, anharmonic multiphonon interactions 79−91419
glycerol-d_3(-d_4), compressed viscous liq., reorientational motion, NMR obs. 80−7183
glyoxal, ^1A_u state energy transfer, D effects 77−58066
glyoxal-d_0, -d_2, triplet kinetics, microwave-saturation recovery and MIDP obs. 77−71823
graphite (0001), scattering and selective adsorption of H_2 (D_2) 80−71553
guanine nucleotides, purinic 8-CH exchange kinetic isotope effect, Raman spectral study 80−83381
guest/host mixed crystal systems, thermally activated intermolecular effect of deuteration on guest phosphoresc. 79−43010
gypsum, struct., vibr. spectroscopic obs. *(Russian)* 78−15175
halogen hydride lasers, vibr. energy transfer, from metastable diatomic molecules 79−31882
heavy water, VUV reflectance, refr. index, absorpt. coeff., isotope effects 78−6695
heterocyclic N compounds, radiationless transitions, isotope effects 80−48033
N-heterocyclics, radiationless transitions, vibronic coupling effect 78−33543
hexamethylbenzene, exciton band struct. for first singlet state 77−55483
1-hexene-water(-D_2O), field-induced surface reactions, field ionis. mass spectra obs. 78−95949
hydrazonium tartrate enantiomers, and deuterates, struct. and opt. props. 77−68954
hydrocarbons, deuterated, mol. polarisability and intermol. dispersion energy, 1-D delta pot. function 78−29862
p-hydroxyazobenzene, acidic soln., reson. Raman spectra, ring deuterated derivatives 79−26987
ice, cryst. Ic and Ih phases, diffr. patterns and far IR spectra, isotope effects 78−6662
ice, $H_2{}^{16}O$ and $H_2{}^{18}O$ samples, vap. press. isotope effects, −50 to 0°C 78−18757
ice, Ih, polycryst., vibr. spectrum anal., OH stretching region 79−11412
ice, polycryst., natural abundance PMR, chem. shift meas. 79−67365
ice Ih, polycryst., Raman spectra, OH stretching region 79−11410
intramolecular H-bonds, H, D and T NMR, isotope effects and pot. energy surfaces 79−76447
iodomethane cation, photodissoc., mass spectrometric obs., isotope effects 77−75241
iodomethane-d_1, ^{13}C enriched, NMR, oriented, symmetry related isotope effects 77−61772
iodomethane-d_1, in nematic soln., D NQR coupling const., isotope effect 79−27009
ion-molecule equilibria in solvolysis, secondary β ^2H isotope effects, hyperconjugation 80−50874
IR absorption intensities, electro-optical parameters transferability to isotopic species 77−6850
IR spin flip laser, matrix isolated photochemistry, isotopic, stereochemical and lattice site selectivity 78−92492
isobutene-d_0, -d_6, torsional pot. functions, spectra anal. 78−25528
isocyanic acid, molecular structure and centrifugal distortion constants 80−47974
ketene-d_0, -d_2, Coriolis coupling, centrifugal distortion and force consts., mean vibr. amplitudes calcs. 79−36607
ketene-d_0,-d_2, mol. ion reactivity, vibr. energy effects, mass spectrometric obs. 77−44470
ketene-d_1(d_2), microwave and millimetre spectra, rot. transition, centrifugal distortion anal. 77−57991
light nuclei, investigation using NMR frequency-ratio spectrometer 79−21793
linear chain, isotope effect on lattice const. 80−103306

isotope effects continued
$LiNO_3.3H_2O(3D_2O)$, density, thermal apansion coeff., isotope effect 78−87733
liquid binary mixtures, proton mag. relax. and mol. motion 77−28471
liquid crystals, dipole coupled ^{13}C NMR technique 79−99073
liquid metals, diffusion, isotope effect determ. using radioisotopes 79−95191
liquids, medium cluster model, vapour press. isotope effects, mol. orientation effect 77−72542
liquids, medium cluster model, vapour press. isotope effects 77−65943
lysine, aq. solns., $H^+(D^+)$ exchange rates, ^{17}O NMR linewidths, pH depend. 80−91661
matrix isolated molecules, IR isotope frequency and intensity patterns 78−46338
meson capture, chemical, hydrogen and H isotope effects 80−69277
metal, C content determ., isotope-spectral method *(Russian)* 80−55766
metal, diffusion of H(D), slow neutron scatt. obs., review 80−34248
metals, BCC and FCC, H-diffusion and trapping 80−70447
metals, dissolution of interstitial H_2 and D_2, diffusion coeffs., reverse isotope effect *(Russian)* 80−88368
metals, FCC, diffusion of H_2, anomalous isotope effect 77−24444
metals, FCC, H_2 diffusion, isotope depend. 80−59727
methane, ^{13}C and ^{12}C, line strength ratios of $2\nu_3$ singlet 80−78616
methane, and -d_4, electron impact K-shell excitation spectra, isotope effects 77−71879
methane, and isotopic forms, anharmonic force field, equilib. struct. 79−76365
methane, condensation, zero point energy shift, isotope effects 78−95147
methane, deuteration effect on thermal conductivity 77−11301
methane, diffusion in Kr, isotope effects at various densities 77−68732
methane, liq., medium cluster model, vapour press. isotope effects 77−65943
methane, liq., medium cluster model, vapour press. isotope effects, mol. orientation effect 77−72542
methane, rotational partition function, isotope effects 80−14130
methane, torsional ground state splitting in cryst. field 80−15019
methane+tritium reaction, reaction ergodography 77−21371
methane(-d_1,d_2,d_3), electro-optical parameters from IR intensities, least-squares calc. 80−9584
methane(-d_4), vibrationally-hot, bond lengths, simple treatment 79−68202
methane (methane-^{13}C) band strength, spectral line breadth in ν_3 bands 79−98069
methane and methane-d_4, low energy electron impact dissoc. autoionisation 80−9744
methane-d_4, isotope effect on rot. and vibr. consts. 79−22688
methane-d_4, solid, rot. tunnelling, neutron scatt. obs., isotope effect 80−92468
methanol, and deuterates, dissoc. ionisation mechanisms, photoionisation mass spectra, ionic struct., interstellar formation 79−3503
methanol, free O-H overtone absorpt. in vis. region, thermal lensing spectra 77−34644
methanol, multiphoton decomposition with laser, isotope separation 79−66306
methanol, vibr. dephasing theories, test using selective coherent ps. Stokes scatt. 80−59609
methanol and deuterated methanols, vibr. energy transfer probabilities, breathing-space theory 79−86039
methanol and deuterates, H^+, H_2^+, and H_3^+ kinetic energy distribs., electron impact dissoc. ionisation, time of flight mass spectra 80−32843
methanol-d_1, CH_2DOH optically pumped CW far IR laser lines and frequencies 80−102707
methanol-d_1(-d_4), far-IR internal rotation spectrum 80−47989
methoxytrimethylsilane-d_0,(−d_3) 78−86853
methyl(-d) radical recombination rate const. calcs. in low press. limit 77−4891
methyl bromide, ν_6 band, CO_2 and N_2O laser Stark spectroscopy 78−78698
methyl bromide, far IR laser lines, rot. anal. of ν_6 perpendicular band 77−3359
methyl bromide, NQR and A_1-A_2 splitting, RF spectrosc. inside laser cavity 80−91579
methyl cyanide (-d_3), vib. dephasing, Raman obs. 77−59566
methyl ethyl ether, charact. vibrs., isomer and isotope effects, rel. to reverse spectral problem 80−63613
methyl fluoride, solid, IR and Raman spectra, cryst. struct., and deutero deriv. 77−36218
methyl group, ^2H quadrupole coupling const. by high-resolution NMR spectroscopy 78−25563
methyl hypochlorite-d_0, -d_3, microwave Zeeman spectra, dipole moment, nuclear quadrupole tensor 77−459
methyl iodide, and -d_1, dissolved in nematic phase, C-H bond orientation, ^{13}C NMR 78−46371
methyl isocyanide, vacuum UV photodissociation spectroscopy 79−834
methyl oxirane, centrifugal distortion consts. and struct. parameters calcs. 77−34616
N-methyl thiopropionamides, normal coord. calcs. 79−36598
methyl transfer reactions, Marcus theory 80−21279
4-methyl-2,6-di-tert-butylphenol, γ-irrad. cryst., ENDOR transitions, ELDOR detect. 78−95531
4-methyl-2,6-di-tert-butylphenol, methyl group rot. mechanisms, Raman effect 78−71691
methylammonium chloride, torsional motion, harmonic oscillator and free rotor bases calcs. 79−72232
methylene fluoride, anharmonic pot. function and equilib. struct. 78−78774
methylene radicals, rotational transitions, laser mag. resonance spectra 80−5538
molecular force constant evaluation using isotopic freq. 77−38650
molecular force field iterative consistency calcs. using geometric interpretation 77−6746
molecular force field representations, vibr. stress, isotope effects and struct. of ethane 78−21897
molecular ions, spontaneous IR rot.-vibr. emission probability 78−50535
molecular IR integrated intensities, rel. to mol. consts., isotopic sum rule 77−27118
molecular solid, isotopically-mixed, electronic excitation localisation, off-diagonal disorder effects 79−99503
molecular spectra, isotopic isomers, spectroscopic obs. 80−53009
molecular spectral line shape, vibr. overtone lineshape 79−27040

isotope effects continued
molecular structure, isotopic relations for rot. and Coriolis consts. 79−3377
molecule, intensities dipolaris. ratios, polarisability, matrix rotation, isotopic rules 78−5288
molybdenum ternary sulphides, Chevrel phase, synthesis and superconductivity *(German)* 80−25038
multiphoton absorption induced reactions, appl. of effective photon concept 78−88651
multiple reactions, Cl isotope effects, mass spectrometric monitoring 79−39135
muon spin rotation method, review *(Polish)* 80−88901
muonic radicals, μSR spectra obs. 80−69279
muonium, bimol. rate consts., Larmor precession relax., kinetic isotope effect rel. to H 77−38752
muonium chemistry, isotope effects and collision theory 79−57273
muonium-substituted transient radicals observed by muon spin rotation 78−74678
MXY type molecules, vibr. isotope effect 78−25506
naphthalene, and deutero derivatives, fluoresc., absorpt. spectra under Shpolskii conditions 80−2825
naphthalene $^1B_{2u}$ resonance pairs, energy denominator depend. of excitons absorpt. 77−39783
naphthalene ($-d_8$), gamma irradiated soln., fluoresc. mag. field depend., spin correls. 77−44492
naphthalene charge transfer complexes, cryst., vibr., factor group splittings 79−7658
naphthalene in $C_{10}D_8$, exciton percolation and coherence 77−59258
naphthalene-d_0, ($-d_4$), ($-d_8$), inequivalent local C-H modes, subpicosec. dephasing, high energy overtones 79−86850
naphthalene-d_0($-d_8$), fluoresc. spectra, vibronic intensities 77−50464
naphthalene-d_0($-d_8$), radiationless triplet decay, non-Condon effects 80−83405
naphthalene-tetracyanobenzene, charge transfer complex, phase transitions, deuteration effect, mag. reson., spectral and thermal meas. 79−4412
naphthalene-tetracyanobenzene, Raman spectra, phase transition and isotopic substitution 78−80364
nonafluorobutane($-d_1$), and halo-substituted forms, gas and liq., IR and Raman spectra, normal coord. anal. *(German)* 79−72318
nonlinear symmetric XY_2 type molecules, isotopic invariants, Coriolis coupling constants, centrifugal distortion constants 80−923
nuclear, review of Soviet research 79−36168
nuclear spin isotope effects 80−69167
octaethylporphin, radiationless transitions, fluoresc. and phosphoresc., isotope effects 77−65502
organic solid, isotopically mixed, electronic energy transfer, Anderson transition 80−44545
oxazole($-d_1$), dipole moment, quadrupole coupling tensor, from microwave spectrum 78−55166
PAA, quasielastic neutron scatt., isotope effects 78−83719
PAA-d_6, $-d_8$, H and D spin-lattice relax. 77−59475
PAA-di, nematic liquid crystal, NMR data, appl. of Landau-de Gennes theory 80−64893
palladium porphin, IR spectra and vibr. anal., and deutero-derivatives 79−22705
palygorskite, uncoupled H_2O, isotopic dilution IR obs. 77−8568
paraelectric tunnelling systems, broadening mech. 79−28701
partition function ratio, reduced, of isotopic mols., generalised finite polynomial approx. 78−66529
pentacene in naphthalene (p-terphenyl), mol. mixed crysts., optical dephasing and vibronic relax. 80−95957
pentacene-d_0, $-d_{14}$, in p-terphenyl-d_0, mixed cryst., photon-echo relax. 77−72034
4-n-pentyl-4′-cyanobiphenyl, nematogen, incoherent neutron quasielastic scatt. 79−32887
perdeuterio-N-1-oxyl-2,2,6,6-tetramethyl-4-piperidinyl maleimide, spin label, biological EPR 80−32746
phenanthrene, and dideuteroisomers, vapour phase fluoresc. lifetimes, position dependent D effects 77−30901
phenol($-d_1$)-dioxan(-acetonitrile), in carbon tetrachloride ($CDCl_3$) solns., H-bonds vibr. relax. bands anal. 78−84560
phenol ($-d_1$, d_5, d_6), excited A state, normal vibr. freqs, force consts., compliance coeffs. 78−50534
bis-(phenylethinyl)-mercury, spin-orbit coupling, heavy atom and D isotope effects 79−59372
1-phosphapropyne, microwave spectrum, vibration-rotation analysis, dipole moment, structural parameters 79−93989
photosynthetic carboxylation reactions, ^{13}C kinetic isotope effect 79−57566
photosynthetic pigment, intersystem crossing 77−58057
plasma magnetic confinement system, surface problems caused by dissolved H_2 80−57946
poly-4-vinylpyridene, protonated and deuterated vibr. spectra *(Russian)* 77−19120
polyatomic molecule, laser photochem. dissoc., isotope effect rel. to dissoc. probability 80−23472
polyatomic molecules, isotopic reduced partition function ratio approx., by polynomial perturbation method 78−66530
polyatomic molecules, mol. parameters isotopic depend. 80−9522
polyatomic mols., ground rot.-vibr. energy, internal coord. Morse oscill. 77−79596
polyatomic mols., isotopic depend. of mol. parameters, contact transformations 77−79550
polyethylene, C muonic X-ray spectra, H(D) isotope effects 77−75344
polyethylene, protonated and deuterated, neutron scatt. at intermediate Q-values 79−10807
polyisoprenes, partly deuterated, ^1H-NMR spectra, struct. 80−50202
polymer film, glassy and rubbery, isotope effect in H_2 and D_2 diffusion, T_g region behaviour 80−84327
porphin ($-d_2$,d_4,d_6,d_8,d_{10},d_{12},d_{14}), nonradiative transition probabilities, deuteration effects 79−3485
porphin-d_n, (n=2-14) electronic-vibr. interaction, quasi-line absorption (fluoresc.), mirror symmetry 78−55197
porphyrin free base, spin-dependent D isotope effect in triplet state decay, N-H vibrs. 77−30909
porphyrin free base in n-octane crystal at 4.2K, laser-induced photochem. isomerisation 77−12815
porphyrin free lasers, radiationless decay of triplet state, position dependent D effect 77−30902
prelumirhodopsin, psec. kinetics, primary photochem. event in vision, proton translocation 78−44508

isotope effects continued
propane and deuteropropane, fragmentation, threshold photoelectron photoion coincidence mass spectra 77−14505
propane-d_0($-d_6$)+thermal energy reaction, mass spectra 77−9067
propyne-d_0($-d_3$), absolute and integrated IR intensities of fundamental modes 80−87179
proton transfer reactions, kinetic isotope effects, quantum theory 80−3301
PTFE, $H_2(D_2)$ solubility and diffusion, activation enthalpy 78−79775
pyrazine ($-d_4$), single vibronic level fluoresc. spectra, rel. to vibronic coupling 80−28043
pyrene+N,N-dimethylaniline (deuterate)(3,5 dimethoxy-N,N-dimethylaniline), geminate recomb., solvent, isotope, mag. field effects 78−56888
pyrene-tetracyanobenzene, charge transfer complex, phase transitions, deuteration effect, mag. reson., spectral and thermal meas. 79−4412
pyridine, elec. dipole moment, g-values, mag. susceptibility, moments and charge distrib. 77−58077
quantum crystals, discontinuous orientational phase transitions, thermodynamics, isotope effects 80−6590
racemization, relative and absolute rate consts., kinetic isotope effects 79−43558
radiationless transition rate constants, effect of geometry change in molecular vibrational promoting modes 80−5569
radical pair recombination reactions, spin multiplicity 77−81393
Raman spectra, isotropic, of liq. (isotope) mixture, intermol. vibr. mode coupling 79−31535
ring gas laser interaction of elliptically polarised opposing waves 80−38044
slow atomic collision, electron detachment, energy spectrum and isotope effects *(Russian)* 77−30984
sputter deposits, isotope enrichment 77−59656
squaric acid-d_0,-d_2, 2-dimens. antiferroelec., dielec. props. and phase transitions, press. effects 79−95700
styrene ($-d_3$, d_5, d_8), fluoresc. quantum yields and lifetimes, 298 and 77K 79−59500
superconducting transition temperature, isotope effect, theory 78−91806
superconductors with energy depend. electronic density of states, gap and crit. temp. 80−84538
p-terphenyl solns., deuteration effect on scintillation in mag. field, solute ion hyperfine interac. 77−16835
1,2,4,5-tetrachlorobenzene, excited triplet state dimer, intermol. exchange integral, isotope effect 80−15826
s-tetracyanobenzene+p-xylene, photoassoc., exciplex form., excitation energy and isotope depend., vibr. effects 80−55634
tetracyanoethylene(d), charge-transfer complex, fluoresc. quantum field and decay time 78−42107
tetracyanoethylene charge transfer complex, nonradiative decay of excited states, D isotope effect 79−31580
tetracyanoethylene-benzene(-toluene), and isotopic forms, excited charge-transfer state nonrad. decay, vibrs. role 78−82765
tetrafluoromethane, pot. consts., IR spectra 78−82808
tetramethylammonium hexachloroplatinate, order-disorder transitions due to weak CH-Cl hydrogen bonding 78−92060
tetramethylammonium hexachlorotellurate, order-disorder transitions due to weak CH-Cl hydrogen bonding 78−92060
tetraphenylchlorin-d_0, $-d_1$, lowest triplet state, intersystem crossing rates, temp. and isotope effects 80−48026
tetrathiofulvalene, Raman spectra 77−24832
s-tetrazine, cooled supersonic jet, Van der Waals complex, isotope effects, fluoresc. obs. 78−55194
s-tetrazine($-d_1$), and $^{15}N_2$-substituted, rot. consts., ground and $^1B_{3u}$ excited states geometries 78−82862
TGFB, deuterated, single cryst. growth and props. 79−24422
thioformaldehyde-d_0, $-d_2$, A^1A_2-X^1A_1 vis. absorpt. system, rot. anal. 80−5559
2-thiohydantoin-d_0, ($-d_2$), mol. vibr. and force field calcs. 78−62779
thioketen, microwave spectrum, substitution structure and dipole moment 80−975
thiomethoxyl anion, and deuterate, electron photodetachment, affinities, vibr. freq. and spin-orbit splitting 80−53063
thiosuccinimide-d_0,-d_1, normal coord. anal. calcs. 77−30844
toluene in ethanol-d_0-d_1, dry electron scavenging efficiency, isotope effect on electron localisation 78−27784
toluene-d_0, $-d_1$, mol. reorientation and D nucl. relax. time, temp. depend. 78−39424
toluene-d_8, soln., fluoresc. quantum yields, temp. and deuteration effects 77−3396
transition metal hydrides, isotope effects on supercond. props. 79−65580
transition metal hydrides, supercond., isotope effects, depend. on cryst. field energies 79−56353
transition metal hydrides and deuterides, conc.-temp. depend. of mag. susceptibility 80−29523
tri-i-propygermylamine, and isotopomers, IR and Raman spectra, normal coord. anal. *(German)* 80−32716
tri-t-butylstannylamine, and isotopomers, IR and Raman spectra, normal coord. anal., Mossbauer spectrum *(German)* 80−32716
triatomic negative ion fragmentation, energy partitioning isotope effects, Monte-Carlo calcs. 77−27126
1,2,3-triazole, nucl. quad. coupling in microwave spectrum 77−57987
2,2,2-trichloroethanol($-d_2$), vibr. spectra and normal coord. anal. 79−72319
triethylsilylamine, and isotopomers, IR and Raman spectra, normal coord. anal. *(German)* 80−32716
1,3,5-trifluorobenzene-d_0($-d_3$), cation, emission spectrum, Jahn-Teller effects 79−89680
trifluoroethane($-d_3$), IR and Raman spectra, normal coord. anal. *(German)* 80−32726
2,2,2-trifluoroethanol($-d_2$), vibr. spectra and normal coord. anal. 79−72319
trifluoroethene-d_0,d_1, mol. struct., microwave and electron diffr. obs. 80−58384
trifluoromethane-d_1, IR photolysis, kinetics of multiphoton dissoc., ^3H isotope separation 79−79276
trifluoromethyl bromide, microwave spectra, mol. rot., isotopic variation in bond lengths, Stark meas., dipole moments determ. 80−74165
trifluoromethyl iodide, microwave spectra, mol. rot., isotopic variation in bond lengths, Stark meas., dipole moments determ. 80−74165
triglycine sulphate: Cu^{2+}, cryst., struct., hyperfine coupling consts., ^1H ENDOR, isotope effects 77−71822

isotope effects continued
trimethylammonium chloride and deuterated forms, cryst., inelastic neutron scatt. H bond vibr. obs. 77−7796
triphenylene($-d_{12}$), lowest $T_1[^3A_2'(\pi\pi^*)]$ state vibronic coupling 80−47955
TTF-TCNQ, deuterated, isotope effect on mag. susceptibility 80−25080
TTF-TCNQ, isotope effect on Peierls transition temp. 78−43367
uranyl hexafluoroacetylacetonate tetrahydrofuran, IR laser photodissoc., O and U isotope selective 80−50868
vapour pressure isotope effects, bibliography 80−77558
vibrational anharmonicity, condensation effect, vap. press. isotope effect 78−58657
vinyl bromide-d_3, ^{13}CBr bond, coupling consts., correl. with C hybridisation s-character 80−34806
vinyl mercaptan -d_0, -d_1, anti rotamer, conform., microwave spectrum 80−9592
vinyl mercaptan -d_0, -d_1, synrotamer, conform., microwave spectrum 80−5535
water, and isotropic forms, IR band intensities estimation 78−86916
water, $H_2{}^{16}O$ and $H_2{}^{18}O$ samples, vap. press. isotope effects, 0-170°C 78−18757
water, low-density amorphous solid, IR spectrum, OH stretching region 79−11411
water, low-density amorphous solid, OH stretching spectrum 79−11413
water, nine isotopes, harmonic vibr. of unsymmetrical forms calc. 77−452
water, VUV reflectance, refr. index, absorpt. coeff., isotope effects 78−6695
water molecules, isotopic, vibr. intensities, ab initio and empirical calcs., band strengths 80−78593
water molecules, isotopic 80−78592
water-methanol mixtures, viscosity at 25°C, isotope substitution effects 80−92700
WINIMAX weighting factor, for isotope chem. and mol. struct. calcs. 80−27940
X_2Y linear molecule, isotope effect on spectroscopic parameters *(Russian)* 77−54577
X_2Y nonlinear molecule, isotope effect in harmonic vibrs. 77−452
X_2Y nonlinear mols., isotopic relations, anharmonicity, reson. interaction, vibr.-rot. consts., rot. energy levels 77−10663
(X=H,D; n=1,2,3), thermodynamic function in ideal gas state 80−14871
$X^+ + HD \rightarrow X + HD^+$, kinetic (orientation) isotope effect, reaction model 78−23931
XY_2 nonlinear symmetrical molecules, isotopic invariants 79−36599
XY_3 planar symmetrical molecules, isotopic invariants 79−36599
XY_4 molecules, centrifugal consts., isotope relations 79−59427
XY_4 molecules, isotope effect on rot. and vibr. consts. 79−22688
p-xylene, isotopically mixed cryst., phosphoresc. triplet state, ESR and MIDP obs. 77−58071
p-xylene-d_{10}, soln., fluoresc. quantum yields, temp. and deuteration effects 77−3396
Yang's biradical, EPR, g- and D-tensors, electronic struct., deuteration and conformation effects 77−42343
zinc octaethylporphin, radiationless transitions, fluoresc. and phosphoresc., isotope effects 77−65502
Zircaloy-2, radiation and isotope effects on corrosion in H_2O/D_2O mixture 77−21314
acetone-d_0, d_6, Raman spectral study of aq. soln. struct., H-bond effects 77−88454
Ag-Cd dilute alloy, isotope effect and correlation factor for Cd diffusion 78−14501
AgO, electronic spectra in rare gas matrix 78−996
Al, film, superconducting transition temp. and lattice dynamics 80−93028
Al, muonic atoms formed by muon transfer free μp and μd systems, isotope effect on Lyman series 79−86090
AlCl, A-X system, vibr. anal. 80−23394
Ar, thermal diffusion factors, isotopic 78−22450
Ar+H(D), differential collision cross sections, diffraction oscills., data anal. 79−22783
ArHBr, ArHCl, and isotopic forms, rot. spectra, mol. struct., mol. consts. 80−58246
Au, temp. depend. of isotope effect for self-diffusion and Co impurity diffusion 78−47563
AuO, electronic spectra in rare gas matrix 78−996
BCl_3-H_2, photochem. with Ti, Pb catalysts, isotopic excitation by laser 78−64882
BHX_2, X=F, Cl, Br, and isotopic forms, mol. pot. consts., amplitudes, Coriolis coupling, centrifugal distortion 78−50662
$BX_2{}^{14}NCS$ (X=Cl, Br, I), soln., force fields and normal modes, vibr. spectra, IR and Raman obs. *(French)* 80−58266
^{135}Ba,^{137}Ba Fourier transform NMR, NQR studies 78−94261
BeH, BeD, linewidth, indirect predissoc., anomalous isotope effect, ab initio calc. 77−58101
Br+HCl(ν'), Br+DCl(ν'), reaction and relax., classical trajectory calcs. 77−48625
$Br + HI \rightarrow HBr + I$, thermal rate const., 220-400K, H/D isotope effect 79−47906
Br_2, condensed phases, spontaneous and stimulated Raman scatt., weak and strong radiation fields 79−3450
BrF, $B^3\Pi(0^+)$ states, collision-free lifetimes laser fluoresc. obs. 78−94278
^{79}BrF, (^{81}BrF), hyperfine struct., elec. dipole moment, rot. transitions, microwave spectral obs. 80−32695
$Br(4^2P_{1/2}) + {}^{12}CO_2({}^{13}CO_2)$, electronic-vibr. energy transfer, temp. depend. meas. 79−10136
$Br(4^2P_{1/2}) + H_2(HD)(D_2)$, electronic-vibr. energy transfer, fluoresc. meas. 79−72347
CF_2Cl^+, and parent cations, IR spectra assignments, ^{13}C-forms verification 78−80767
CH_3^+, CD_3^+, reactions with acetic acid methyl acetate, dimethyl ether and ethylene oxide 77−63901
$CH_2(CD_2)$, pionic X-ray intensities in polyethylene($-d_n$) 80−32858
CNC radical vibr. and electronic spectra, in VUV photolysis of matrix-isolated cyanomethane 78−85180
$C(NH_2)_3Al(SO_4)_26H_2O{:}Cr^{3+}$, isotope effect, zero field splitting, vibr. coupling temp. depend. 78−6570
CO, (CO^+), Franck-Condon factors, isotope effects calcs. 78−1031
CO, and isotopic forms, fundamental bands, absolute wavenumbers, mol. consts. 79−59458
isotope effects continued
CO, Dunham vibration-rotation coefficients, isotope dependence 80−83518
CO, electron impact desorption from W (110), isotope effects 77−76658
CO laser output power, active species and buffer He isotope effects *(Russian)* 80−63986
CO, multiphoton UV photolysis, isotope effects obs. 80−55679
CO, two-photon spectroscopy with tunable ArF laser 80−37843
CO-myoglobin, mol. tunnelling, isotope effect, time resolved IR Fourier transform obs. 80−72126
$CO + {}^{14}N_2$ ($^{14}N^{15}N$),($^{15}N_2$), vibr. energy transfer, laser fluoresc. obs. 80−28050
$CO + {}^3He({}^4He)$, vibr. relax., deactivation rates, pulsed fluoresc. meas. 79−89698
$CO + Kr(^3P_1)(^1P_1)$ $A^1\Pi$-$X^1\Sigma^+$ and $b^3\Sigma^+$-$a^3\Pi$ sensitised fluorescence, isotope effects 78−82761
CO_2 enriched in ^{17,18}O, diode laser spectroscopy of Q branches 80−78621
CO_2, isotope effect on spectroscopic parameters *(Russian)* 77−54577
CO_2, photodissoc., isotope effects 77−75238
CO_2^+, fluoresc. quantum yields, isotope effects, photon-photoion coincidence meas. 78−90200
CO_2+deuteromethane, time resolved fluoresc. for vibr. relax 79−31659
$CO_2 + H_2(D_2)$, ab initio LCAO-MO-SCF intermolecular pot. energy surface, V→T transfer 77−50489
$CO_2 + H^+(D^+)$, vibr. excitation, 10-30 meV 80−58358
$CO_2 + H^+(D^+)$, vibr. excitation, isotope and time effects 80−63773
CO_2+HF(DF), vibr. relax. rate, chemiluminescence depletion method meas. 79−72399
CO_3, and isotopic forms, struct., normal coord. anal. 78−965
$COCl_2$, photodissociation, C isotope effects, photocatalysed isotope exchange with CO 77−36764
CS, UV vibronic spectra, isotope analysis method *(Russian)* 79−50041
CS_2, liq., vap. press., isotope effects, mass spectrometric determ. 77−24412
CS_2, vapour pressure, ^{13}C and ^{33,34}S isotope effects 78−18756
CS_2, vibr.-rot. bands at .46 μm, isotope effects 78−94245
$^{12}C^{34}S_2$, $^{13}C^{34}S_2$, high resolution IR spectra *(French)* 80−58249
CX_n radical, (X=H,D; n=1,2,3), thermodynamic function in ideal gas state 80−14871
Ca+HF(DF), beam reaction, vibr. excitation 78−68877
CaD, absorption spectra, extension of F-X system 79−18205
CaF_2, cation jump freq., isotope effect, lattice dynamical calc. 80−88357
CaH, absorption spectra, extension of F-X system 79−18205
Ca^+NO^-, $Ca^+NO_2^-$ in solid Ar, IR spectra at 15K 77−57996
CaO, formation of surface O_2^- ion by O_2 adsorpt., EPR 80−61155
$Ca(OH)_2$, V-centres, EPR obs. 77−48051
CdFCl, CdFBr, existence and vibr. characterisation, IR and Raman matrix isolation obs. 78−78706
CdF_2(FCl)(FBr), matrix isolated IR and Raman spectra, assignments, force consts., isotope effects and thermodynamic props. 80−63631
CdH, lifetime, Λ-doubling, hyperfine struct., in $A^2\Pi$ excited states 77−58083
$Cd(^3P_J)(^1P_1) + H_2(HD)(D_2)$ reacts., CdH(CdD) yields, quenching cross sections 79−1948
CdX_2, (X=Br, Cl), spectroscopic parameters of mols. from vibr. isotopic effects 78−74798
CdXY, (X, Y=Cl, Br, I), spectroscopic parameters of mols. from vibr. isotopic effects 78−74798
Ce, gettering of H, mass spectrometry and microgravimetry study, rel. to HTGR gas purification 80−73374
$Cl + D_2 \rightarrow DCl + Cl$, LEPS pot. energy surface, rate consts., isotope effect, quasiclassical trajectory calc. 78−56887
$Cl + DI \rightarrow DCl + I$, thermal rate const., 220-400K, H/D isotope effect 79−47906
Cl_2, Ar ion laser excited, normal and reson. Raman spectra 79−26993
Cl_2+H(D), uni- and bimodal product energy distribs. 79−57207
ClCN, Cl and N quadrupole coupling, spectroscopic meas. 79−72337
$^{38}Cl + H_2(D_2)$ reactions, characterisation, effect of ethylene-I_2 scavenger 78−73071
Co, FCC, self-diffusion and isotope effect, influence of mag. order-disorder transition 80−29205
Co, magnetic aftereffects of H isotopes, book contrib. 79−82835
CoIII salen complexes, O binding, reson. Raman obs. 80−58267
CoO, isotope effects in CoO diffusion rel. to vacancies 80−84319
Co_5R-H(D) system, R=rare earth, mag. orientation aftereffect 80−50148
β-CrOOH(D), crystal struct., isotope effects on bond lengths 77−15371
α-CrOOH(D), isotope effects in bond lengths 77−80488
Cs-NH_3, Cs-ND_3, solns., US absorption, metal-nonmetal transition 79−69194
$Cs(D_xH_{1-x})_2PO_4$, D distrib. during crystallisation from aq. soln. 77−11496
CsI, isotope diffusion 78−75875
Cu, diffusion in Al 78−84006
Cu, diffusion of stable Ge isotopes, isotope effect 79−60552
Cu, H_2 diffusion, isotope depend. 80−59727
Cu, impurity diffusion, mass depend. of energy factor of isotope effect 78−30795
Cu, isotope effect for diffusion of Ge 78−2285
Cu-Ge solid soln., isotope effect for Ge diffusion 78−2285
Cu-Sb melt, eutectic struct. by neutron diffr., isotopic substitution 78−47233
CuO, electronic spectra in rare gas matrix 78−996
^{63}Cu,^{65}Cu, Fourier transform NMR studies 78−94262
D isotope effect, corrosion stability in high temp. aqu. soln. 78−9091
$D + D_2$, collinear reaction, transmission coeff. isotope depend., statistical theory, invariance 77−36748
$D + H_2$ reaction, transition state theory calculations, kinetic isotope effect explanation 80−66784
D_2+Y, high temp. equilib. meas. 80−66780
DBr, IR absorpt. in 5-0 band, high-resolution spectra 77−14431
DBr, vibr. energy transfer, laser selective isotope excitation 78−82790
DBr+DBr, vibr. energy transfer, dissimilar isotopic species 79−27067
DCN, photofragmentation, vibr. distribs. 77−18992
DCl, vibr. energy transfer, laser selective isotope excitation 78−82790
DCl+DCl, vibr. energy transfer, dissimilar isotopic species 79−27067
DF, vibr. relax., isotope effect, quantum model 80−91460
$DF(\nu=1) + F \rightarrow DF(\nu=0) + F$, isotope effect 77−30959
D_2O, $H^+(D^+)$ exchange rates, ^{17}O NMR linewidths, pH depend. 80−91661

isotope effects continued
D_2O ice, thermal cond., H and D order effects 78−67871
D_2O-H_2O ice, thermal cond., H and D order effects 78−67871
D_2O+Ar, energy transfer isotope effect, rate consts. 79−8422
$D_5O_2^+$, isotope effects, easily polarisable H and D bonds 78−94231
$D_2{}^{16}O(HD^{16}O)$, isotopic depend. of mol. parameters, contact transformations 77−79550
$Dy(NO_3)_3$ in nonaqueous solvents, anharmonic vibrs. in electronic energy degradation 77−23541
F+H_2 dynamics, Franck-Condon factors rel. to information theory for vib.-rot distribs. and isotopic branching ratios 77−60041
F+$H_2(D_2)$, absolute reaction rate coeffs., time resolved IR emission meas. 79−68258
F+$H_2(D_2)$, rate consts., temp. depend. 80−81302
F+HCl(DCl)→HF(DF)+Cl, dynamical props., pot. energy hypersurface computer anal. 77−77735
F+HX or DX, (X=I, Br, Cl), H abstraction, absolute reaction rate, H/D isotope effect 78−80721
F_2+X→XF+F (X=Mu,H,D,T), isotope effects, quantum mech. and information theoretic calcs. 78−44360
FCP, microwave spectrum, struct., dipole moment and vibr.-rot. props. obs. 80−91549
$^{18}F+H_2$, hot-atom reaction, nonequilib. vel. distrib. and reaction rate calcs. 77−63942
Fe, magnetic aftereffects of H isotopes, book contrib. 79−82835
Fe meteorites, radial distrib. of spallogenic K, Ca, Cr, Ti, V and Mn isotopes 80−67488
Fe:Xe, isotope ion implantation control *(Flemish)* 78−79623
Fe-C melts, short-range order, neutron scatt. obs. *(German)* 78−71669
Fe-Pt alloy, diffusion of ^{197}Pt and ^{59}Fe *(Czech)* 79−77804
Fe-Ti, magnetic aftereffects of H isotopes, book contrib. 79−82835
Fe-Ti:H(D), isotope effects of diatomic TiH and TiD complexes 79−47259
$Fe(BF_4)_2.6H_2O(6D_2O)$, phase transition, mag. susceptibility and anisotropy and permittivity meas. 79−23718
$Fe(CO)_2(NO)_2$, vib. assignment using ^{15}N isotopic substitution, solid, liq. and soln. spectra 77−48152
$FeCl_2.4H_2O$, frozen solns., isotope effect of Mossbauer parameters 80−34835
Fe_3O_4, magnetite, cation diffusion, correlation and isotope effects 80−96686
$FeSO_4.7H_2O$ and $FeSO_4.7D_2O$, frozen solns., isotope effect of Mossbauer parameters 80−34835
$FeTiD_x$ ($0\leq x\leq 1.9$), structural phase transitions, absorpt. and desorpt. isotherms 80−19948
Ga, isotope shift and HFS, isotope effects, UV spectra obs. 80−42973
GaP:Ni, optical and EPR study of two-electron-trap state 79−73806
GeH_4, ν_2 fundamental, isotope effect 80−43024
$GeH_3.NCS$, mol., IR, Raman and microwave spectra, $^{70,72,74}Ge$ and $^{1,2}H$ isotopes 79−89663
GeO, UV spectra of mol., rot. anal. 79−81210
GeS, band system vibr. anal. 80−48009
H and D atom, recombination model 78−20001
H bond length and vibr. freq., deuteration effect 79−26911
H bonded systems, IR spectra, theoretical interpretation 79−31519
H bonds, linear triatomic model, adiabatic approx., freqs. and isotope effects 77−65448
H diffusion in Nb 78−6182
H isotope diffusion coeffs. calc. for FCC metals *(Russian)* 78−91483
H^+/D^+, 15-keV ion bombard. of sapphire, chem. implantation, isotopic trapping effects and induced hygroscopicity 77−59030
H-bonded crystal, IR absorpt. spectra band shape, X-H stretching vibr. temp. depend., isotope effect 78−76445
H+Cl_2 dynamics, Franck-Condon factors rel. to information theory for vib.-rot. distribs. and isotopic branching ratios 77−60041
H+$Cl_2(H_2)$, activation energy and trajectory calcs., temp. and isotope effects 78−76835
H+D_2 reaction, transition state theory calculations, kinetic isotope effect explanation 80−66784
H+H_2, collinear reaction, isotope depend. transmission coeff., transition state theory 77−36747
H+H_2, collinear reaction, transmission coeff. isotope depend., statistical theory, invariance 77−36748
H+H_2 dynamics, Franck-Condon factors rel. to information theory for vib.-rot. distribs. and isotopic branching ratios 77−60041
H+$H_2(D_2)(T_2)$ reactions, accurate pot. energy surface, isotope effects, quasiclassical trajectory study 80−97698
H+He, D+He, low energy elastic scatt., pot. well depth determ. 77−6884
H+Ne(Ar)(Kr)(Xe), free electron production, integral cross-sections determ. 79−89754
H_2, cluster beam formed from nozzle flow, isotope effect 80−6127
H_2, D_2, electron impact, Balmer-α, β, γ radn. emission cross sections 78−1091
H_2, D_2, photoionisation, body-frame Hund's case b description 78−94295
H_2, liq., vibr. energy transfer, isotopic impurities, relax. 79−6993
H_2, two-photon spectroscopy with tunable ArF laser 80−37843
H_2^+, HD^+ electron reduced mass use in electronic Schrodinger eqn. 77−10576
H_2^+, spontaneous emission lifetimes in ground electronic states 80−32810
H_2/D_2 solubility ratios in Pd alloys, meas. 79−99325
H_2+H(D)(T) reactions, accurate pot. energy surface, isotope effects, quasiclassical trajectory study 80−97698
H_2+H(I), activation energy and trajectory calcs., temp. and isotope effects 78−76835
H_2+He(2^3S_1), isotope effects, 77 to 300K 79−36752
H_2+Y, high temp. equilib. meas. 80−66780
$H_2^+ + H_2 \rightarrow H_3^+ + H$, reaction dynamics, isotopic variations 78−27745
$(H_2)_2$, $(D_2)_2$, $(HD)_2$ and H_2-D_2, Van der Waals complexes, mol. symmetry 80−42963
H_3BPF_3 and D_3BPF_3, laser augmented decomposition 79−52713
HBS, and isotopic forms, force consts., coriolis consts., vibr. amplitudes, shrinkage effects 80−43021
HBS, force consts., Coriolis const., vibr. amplitude, shrinkage and isotope effect 79−22863
HBr, and DBr, in monatomic matrices, near IR spectra and aggregate structs. 79−89667
HBr, isotopic struct. and spectral characts. of vibr. band, using liq. N_2 Raman laser source 78−50859
HBr, vibr. energy transfer, laser selective isotope excitation 78−82790
HBr+HBr, vibr. energy transfer, dissimilar isotopic species 79−27067
HCC^+, equilib. struct., rot. const. 79−98003
HCN, Franck-Condon transition amplitudes for mol. dissoc., semiclassical evaluations 78−62860
HCN, photodissoc., isotope effects 77−75238
HCN, photofragmentation, vibr. distribs. 77−18992
$HC^{14,15}N$ dimer, and $(DCN)_2$, microwave rot. spectrum identification and struct. 77−50427
$(HCN)_2$, and isotopic forms, microwave spectroscopic investigations of hydrogen-bonded complexes 78−62794
HCN(DCN), photodissoc. dynamics, rot. (vibr.) energy disposal 78−48672
HCl, and DCl, in monatomic matrices, near IR spectra and aggregate structs. 79−89667
HCl, intermol. partial struct. factors, isotopic substitution and neutron diffr. obs. 80−53157
HCl, vibr. energy transfer, laser selective isotope excitation 78−82790
HCl+HCl, vibr. energy transfer, dissimilar isotopic species 79−27067
$H^{35}Cl+H^{37}Cl$, reson. isotopic vibr. energy transfer, temp. depend. 79−72395
$HCl^+(DCl^+)$, spin-rot. consts., Van Vleck approx., ab initio calcs. 77−34610
HD, isotopic effects in predissociations 78−86924
H(D), penetration, into Ni-Cu alloy, reversed kinetic isotope effects 77−43387
H(D), spin-aligned, stability at low temp. and high mag. field 77−10723
HD^+, HT^+, DT^+, accurate rot.-vibr. energy and transition moment calcs. 77−14412
HD^+, spontaneous emission lifetimes in ground electronic states 80−32810
$H^+(D^+)$ discharge activation energies in the $H_2O(D_2O)$ at the Hg cathode 80−40707
$H^-(D^-)$+He, collisionally induced electron detachment, 0.5 MeV, target effect 80−37858
$H_2(D_2)$, dissociative electron attachment and vibr. excitation, low-energy 80−23565
$H_2(D_2)$, electron dissociative attachment rates, rot. (vibr.) excitation depend., in plasma 80−43848
$H_2(D_2)$, electron impact dissoc., cross sections, isotope ratios and polarisation, B H_α and H_β emission 78−25729
$H_2(D_2)$ permeation in Pd *(Russian)* 78−75881
$H_2(D_2)$ pumping by Ti film, pumping speed comparison 78−51819
$H_2(D_2)$, Rydberg states, nonadiabatic effects, elec. field ionis. 80−9528
$H_2(D_2)$+Ag(111), energy transfer, quantum mech. theory 77−8699
$H_2(D_2)$+Ar*, de-excitation processes, pulse radiolysis, isotope effect 77−65529
$H_2(D_2)$+Cd($5^3P_{0,1}$), absolute quenching cross sections 80−5604
$H_\alpha(D_\alpha)$ Stark broadening in Ar arc plasma 79−36582
$H_2(D_2)$(HD) chemisorbed on Ni (100), vibr. excitation and struct., electron energy loss spectra 78−47660
$H_{2-n}D_nSe$(n=0, 1 and 2), ^{77}Se NMR on XL-100 spectrometer, isotope effects and spin-lattice relaxation 80−71211
HF-ClF complex, and isotopic forms., mol. beam elec. reson. spectra, config., bonding, spectroscopic consts. 77−30860
HF-HCl, H bonding , struct., mol. beam-elec. reson. spectra 78−29777
HF+H(D), kinetic isotope effect and temp. depend. 78−53202
$HF^+(DF^+)$, spin-rot. consts., Van Vleck approx., ab initio calcs. 77−34610
$H_2^+(HD^+)$, $1s\sigma_g$ state, pot. energy curves, relativistic corrections 77−57892
HNO_3, centrifugal perturbation in microwave spectrum 77−57981
H_2O (D_2O), O muonic X-ray spectra, H(D) isotope effects 77−75344
H_2O, and D_2O, Feshbach-reson. and dissoc. electron attachment 79−41246
H_2O, D_2O, electron impact dissoc. excitation, Balmer-α emission obs., Doppler profile meas. 79−31706
H_2O, D_2O, fragment ion formation on photoionisation, energetics and mechanism 77−501
H_2O dimer, partially deuterated, microwave spectra and struct. 80−74212
H_2O, $H^+(D^+)$ exchange rates, ^{17}O NMR linewidths, pH depend. 80−91661
H_2O, isotope derivatives, mech. anharmonic problems, spectroscopic consts. 79−63983
H_2O isotopes, spectrophone meas. at selected CO, CO_2 laser wavelengths 78−57310
H_2O, line strengths and intensities, ab initio calcs. 79−72300
H_2O, vibr. anal., normal coord. calcs., nucl. corrections to mol. props. 77−88441
$H_2{}^{16}O$, $HD^{16}O$, $H_2{}^{18}O$, mol. diffusivities in N_2, isotope effects 79−1282
H_2O-HF heterodimer, H bonding, microwave rot. spectrum, mol. geometry and moment 80−99501
H_3O^+ (D_3O^+), plasma dissociative ion electron recomb., rate coeffs. 80−63747
HOCl, ν_1 band IR spectrum, rot. anal. 79−98095
$H_2O(D_2O)$, positronium formation, isotope effects 80−93432
$H_2O_2(D_2O_2)$, vibr. consts rot. struct. doubling, Raman spectra assignment 77−54563
H_2SO_4, frozen soln., EPR of trapped H-atoms produced by UV and X-irrad. 80−3369
HTO, atmospheric condensation-evaporation model 77−29326
HX, chemical laser performance isotope effects, computer simulation 78−29944
He, accurate empirical intermol. pot. 79−68291
He^+, incident on Zn, In, Sn and Pb, isotope effects in ion-scatt. double spectroscopy curves 77−59658
He^+, isotope effects in elastic surface scatt. on sol. and liq. Ga 80−71536
He-Xe 3.51 μ laser mode competition in axial mag. field 80−63974
He+HCl(HF)(DCl)(DF), slow collisions, rot. excitation cross-sections, quantum mech. calcs. 77−12795
He^++acetylene-d_0(-d_2), $CH^+(CD^+)$, A-X luminesc., in near-thermal charge exchange 78−50632
HeH^+, (HeD^+), rot. predissoc., nucl. motion effects on rovibr. energies and widths 78−70885
^{3}He-^{4}He isotope mixtures, mag. resonance line widths of 2^3S_1 states, metastability exchange cross sections *(Russian)* 77−10614
He(2^3S)+H(D), Penning and assoc. ionis. cross sections, vel. depend. 79−22815

isotope effects continued
He(2^3S_1), isotopic g_J-factor ratio 77−10608
He(2^3S and 2^1S)+$H_2(D_2)$, Penning, rearrangement and total ionis. cross sections, vel. depend. 79−22816
$HfV_2H_x(D_x)$, superconducting transition temp. var., isotope effect 77−12047
$Hf_{0.5}Zr_{0.5}V_2H_x(D_x)$, enhanced supercond. transition temp. on H(D) additions 78−80083
Hg complex, methylethynylmercury(II)(-d_1,-d_3,-d_4), vibr. spectra and normal coord. calcs. 80−58259
HgFCl, HgFBr, HgFI, existence and vibr. characterisation, IR and Raman matrix isolation obs. 78−78706
HgF_2(FCl)(FBr), matrix isolated IR and Raman spectra, assignments, force consts., isotope effects and thermodynamic props. 80−63631
HgX_2, (X=Cl, Br), spectroscopic parameters of mols. from vibr. isotopic effects 78−74798
HgXY, (X, Y=Cl, Br, I), spectroscopic parameters of mols. from vibr. isotopic effects 78−74798
I+methane $^-d_0(^-d_3)$,$(^-d_4)$, excited atoms, quenching, isotope effects, time resolved reson. fluoresc. 80−32656
$^{129}I_2$, $^{129}I^{127}I$, $^{127}I_2$ high resolution saturated absorption spectra at 633 nm using He-Ne laser 80−95637
$I^*+H_2O(D_2O)$(HDO), $5^2P_{1/2}$ electronic to vibr. energy transfer, quenching and time resolved IR fluoresc. 79−3537
$I(5^2P_{1/2})$+benzene-d_0(-d_6), fluoresc. quenching, spin-orbit interaction, isotope effect obs. 78−62763
$I(5^2P_{1/2})+H_2O(D_2O)$(HX)(DX), collisional quenching, isotope effects 77−34583
$I(5^2P_{1/2})+H_2$(HD)(D_2), electronic to vibrational energy transfer 79−68259
In, isotope shift and HFS, isotope effects, UV spectra obs. 80−42973
$KAlCl_4$, cryst., Raman spectra, orthorhombic space group, Cl splitting of $AlCl_4^-$ 77−85700
KCNS, single cryst., IR and Raman multiphonon bands, factor group anal. 77−4644
KCl:H, dynamical superhyperfine interaction 80−2663
KCl:H, ENDOR and ESR study of anion sites 80−108118
KCl:Li^+, defect induced tunnelling states, depend. on strain, pot. model calcs. 79−69865
KD_2AsO_4, ferroelec., phase transition and Raman scattering 78−84540
$K(D_xH_{1-x})_2PO_4$, D distrib. during crystallisation from aq. soln. 77−11496
KDP-type cryst., Raman scattering and phase transitions, deuteration effects 78−76400
KD_2PO_4, KH_2PO_4, proton, deuteron tunnelling, barrier height and energy level calc. 80−6482
$KD_3(SeO_3)_2$, central peak, soft acoustic shear mode, light scatt. study, isotope effects 78−52518
$KDy(MoO_4)_2$, polarised IR and Raman struct., $^{92}Mo/^{100}Mo$ isotope effect 80−108198
$K(H,D)_2PO_4$ crystals, effect of isotopic replacement on growth kinetics 78−95006
KH-H_2 crystal-gas system, with D impurity, thermodynamic equilib. 78−59954
KH_2AsO_4, ferroelec., phase transition and Raman scattering 78−84540
KH_2AsO_4, Raman linewidth, isotope effect 77−8565
KH_2PO_4,(KD_2PO_4), photoelectric phenomena, nonlinear optical rectification *(Russian)* 79−19628
KH_2PO_4, paraelectric, dynamic central peak depend. on deuterium content 79−65752
KH_2PO_4 type ferroelectrics, Raman spectra, coupled tunnel-phonon modes 79−69205
KH_2PO_4:AsO_4^{4-}(SeO_4^{3-}), ferroelec., low freq. fluctuations, isotope effects, EPR, ENDOR, ESCA 77−73118
$K_3H(SO_4)_2$, and $K_3D(SO_4)_2$, dielec. props. and phase transitions 80−60482
$K_2HgCl_4.H_2O$, cryst., IR spectra, water mol. struct., H-bonding 77−81089
KNO_3-$RbNO_3$, liq., electromigration cation and mobility and isotope effect 80−10691
K_2TeO_3, D_2O soln., ^{123,125}Te Fourier transform NMR 78−15046
Kr, thermal diffusion factors, isotopic 78−22450
Kr^++HD, kinetic isotope effect, cross sections, rot. transfer 77−9041
Kr^++HD, reactive collision dynamics, isotope effects 78−23930
KrF, laser spectrum, discharge-pumped, absorption bands and lines, assignment 78−79004
KrHBr, KrCHl, and isotopic forms, rot. spectra, mol. struct., mol. consts. 80−58246
KrHCl, van der Waals complexes, struct., RF and microwave spectra, isotope effects 80−37806
Kr^+.+$H_2(D_2)$(HD) reactions, temp. depend., isotope effect 78−31630
La, nucl. mag. moments and ratios of quadrupole moments, NMR spectroscopy in aqueous soln. 77−73088
$La_2(SO_4)_3.9H_2O$, and isotopic forms, water librations, Raman obs. *(French)* 79−28754
$La_2(SO_4)_3.9H_2O(D_2O)$, cryst., polarised Raman spectra, phase transition *(French)* 77−66497
$La_2(SO_4)_3.9H_2O(D_2O)$, dynamic disorder of water mols., isotope effect obs. 80−55015
LiF, RF spectra, spin interactions and moments, mol. beam elec. reson. meas. 77−18912
LiH, cryst., specific heat at const. vol., isotopic modifications effects 80−103490
LiH, $X^1\Sigma^+$ ground state, spectroscopic and pot. functions, method for combining spectroscopic data 79−45782
LiH+HCl(DCl), rot. inelastic collisions, sudden theories 79−98201
LiH+HCl(DCl), state-to-state rot. inelastic cross sections, new laser fluoresc. technique 79−98200
LiH(D), isotope effect on Wannier-Mott exciton levels 80−103633
$LiH_2(LiD_2)(LiT_2)$, pot. surfaces, fundamental freqs. and thermodynamic functions 80−69205
$Li_2H(Li_2D)(Li_2T)$, pot. surfaces, fundamental freqs. and thermodynamic functions 80−69205
$^{6,7}LiNO_3$, cryst. vibr., Raman and IR spectra 79−15445
$LiNO_3.3H_2O(D_2O)$, crysts. and melts, density, mol. vol., thermal coeff. of expansion, rel. to struct. 80−15270
Li_2O-B_2O_3 glass, conductivity, permittivity, and dielectric loss obs., mixed isotope effect 78−95182
^{6,7}LiOH, LiOD, polycryst., Raman active modes and isotopic effects 79−87424

isotope effects continued
LiOH(D)(T), thermal decomposition rates 530-690K, activation energy and enthalpy meas. 80−3321
LiX-alcohol mixtures, (X=Cl, Br, ClO_4), OH(OD) vibr. bands in sat. solns. and crysts. 77−8564
MnH(MnD), $^7\Sigma$-state, mol. parameters, ESR and optical spectrosc. 78−94264
$MnH_2(MnD_2)$, $^6A_1$ state, mol. parameters, ESR and optical spectrosc. 78−94264
$(Mn_xRe_{1-x})_2(CO)_{10}$, Raman spectra, intramol. vibr. coupling, ^{13}C substitution 79−47431
Mo complexes, oxo-bridged dimers, ^{16}O and ^{18}O-substituted synthesis, IR spectra 77−77188
Mo, superconducitng, isotopic vol. effect confirmation by energy-dispersive X-ray diffr. 77−36019
MoS_4^{2-}, S isotope effect on ^{95}Mo nucl. mag. shielding 77−63301
Mo_6Se_8, Chevrel phase, isotope effect on supercond. T_c 78−52141
Mo_6Se_8, Chevrel phase, isotope effect on supercond. transition temp., phonon modes 79−51713
Mo_6Se_8, Chevrel phase, supercond. isotope effect meas. *(German)* 80−25038
Mo_6Se_8, isotope effect, theory 78−91806
Mo_6Se_8, isotope effect on transition temp. 79−73615
N^++H_2(DH), >6 eV reaction dynamics 77−32779
N^++methane, charge transfer reaction, dissoc., isotope effects, mass spectra 77−21382
N_2, (N_2^+), Franck-Condon factors, isotope effects calcs. 78−1031
N_2 adsorbed on W, effect of SIMS sputtering induced recomb. anal. 80−55243
ND_3, Hg-photosensitised luminesc. at low press. 78−13542
$(ND_4)_3D(SO_4)_2$, ferroelectricity and isotope effect on ferroelec. activity 77−85660
$(ND_4)_3D(SeO_4)_2$, phase transitions, isotope effect, dielectric and dilatometric meas. 79−38500
$ND_2(NH_2)$, ν_2 band, laser mag. reson., 9-10 micron 80−9601
$(NH_4,Cs)Cl$, negative isotope effect on II-III phase transition *(German)* 78−95155
$(NH_4,Rb)Cl$, negative isotope effect on II-III phase transition *(German)* 78−95155
NH, ND, ($b^1\Sigma^+$) states quenching by deuterated cpds., kinetic isotope effects 77−63891
NH, ND, $d^1\Sigma^+$ state lifetimes, rot. struct., electron excited emission spectra 77−79654
NH, ND, vib. relax. in amorphous solid inert gas systems 77−7817
NH, ND, $X^3\sigma^-$ state vibr. relax. Ar matrix, energy gap law breakdown 77−30963
NH+CO, vibrational energy transfer in solids, rot. mode participation 78−63815
NH_2, free radical, isotope effect on spectroscopic parameters *(Russian)* 77−54577
NH_3, and ND_3, new electronic state, multiphoton ionis. obs. 78−74717
NH_3, Hg-photosensitised luminesc. at low press., isotope effects 78−13542
NH_3, inversion spectra, ν_4 state 80−47965
NH_3, inversion-vibration interactions, pot. energy function calcs., isotope effects 78−33567
NH_3, liq., vapour press., isotope effect, relevance to isotope exchange reaction calcs. 80−39272
NH_3, photodissociation in A←X absorption region, D isotope effects 77−77790
$^{14}NH_3$, $^{15}NH_3$ and $^{14}NH_2D$, IR laser Stark spectroscopy 80−47978
$NH_3+HD\rightleftharpoons NH_2D+H_2$, deuterium separation factors, calc. 80−3310
$NH_3+NH_3(ND_3)(HCl)(H_2O)$, inversion relax., isotope effects, beam-maser ang. resolution effects 77−30964
N_2H_2, vibr. assignment and pot. function, cis- and trans. mols., d_0-d_2 species 79−85952
NH_4ClO_4, with 0.015% and 0.1% D, proton Zeeman relaxation 78−6592
$NH_4H_2PO_4$:AsO_4^{4-}(SeO_4^{3-}), antiferroelec., low freq. fluctuations, isotope effects, EPR, ENDOR, ESCA 77−73118
$(NH_4)_{1-x}M_xX$, and $(ND_4)_{1-x}M_xX$ M=Tl, Rb, Cs, X=Cl, Br, phase diagrams birefringence obs. *(German)* 79−83185
NH(ND), $b^1\Sigma^+$ state, collisional quenching, isotope effects, rate coeffs. 77−19018
NH(ND) $X^3\Sigma^-$, in inert gas solid, vibr. relax., matrix and isotope effects 80−95713
$NH_3(ND_3)$, chemisorbed on W, decomposition mechanism, isotope effect 79−29409
$NH_3(ND_3)$ in solid Ar, UV absorption spectra, temp. depend. of matrix spectra 80−63652
NO ($a^4\Pi$), condensed phase vibr. relax., isotope effect, time resolved obs. 78−94233
NO, and isotopic forms, $X^2\Pi$ state, IR obs., mol. consts. 78−42045
NO, and isotopic forms, ν=0 electronic states, spin-rot. doubling 80−5540
NO, Fourier transform spectra, intensity and self-broadening coeff. meas. 80−102503
NO isotopes, spectrophone meas. at selected CO, CO_2 laser wavelengths 78−57310
NO_2, reson. fluoresc. excited by visible laser, force consts. of ^{15}N mol. 79−72343
$^{15,14}NO_2$, predissoc. rot. struct. in 2490 Å band 80−87192
N_2O, photoionisation and ion dissoc., isotope effects, mass spectra 78−9203
N_2O+deuteromethane, time resolved fluoresc. for vibr. relax 79−31659
$(^{14}NO)_2$ and $(^{15}NO)_2$ solids, Raman spectra at 20K 77−73139
NOCN, struct., dipole moment, quadrupole coupling, microwave spectra 78−94238
NSF_3, microwave spectra in vibr. excited states, mol. consts. 79−50009
$NaClO_3$-$NaBrO_3$, Raman spectra, mode coupling and ^{79}Br-^{81}Br isotope effects 79−19873
$NaClO_4$, frozen soln., EPR of trapped H-atoms produced by UV and X-irrad. 80−3369
$Na(D_xH_{1-x})_3(SeO_3)_2$, Raman spectra and nature of phase transitions 78−80341
$Na^{15}N_x{}^{14}N_{1-x}O_3$, reflection spectra, Kramers-Kronig anal. with preliminary dispersion anal. 78−49915
Na_2O-TeO_2:Ho^{3+}(Er^{3+})(Yb^{3+}), luminesc. quenching by OH and OD *(Russian)* 79−28839
NaOH, frozen soln., EPR of trapped H-atoms produced by UV and X-irrad. 80−3369
Na_2TeO_3, D_2O soln., ^{123,125}Te Fourier transform NMR 78−15046

isotope effects continued
Nb, diffusion of ^{95}Zr, diffusion coeff., effect on Nb self diffusion isotope effect 78−47602
Nb, diffusion of H, book contrib. 79−82390
Nb, diffusion of H_2, crystal field stabilisation 80−59728
Nb, elec. resist. due to interstitial H (D) 80−96848
Nb, Fe diffusion mechanism, self diffusion enhancement 77−84992
Nb-D-H, equilib. H/D separation factors 80−59668
Nb-H(D) system, anelastic behaviour, 0.5-15K 80−49300
Nb-H(D) system, solubility, entropy and enthalpy, isotope effects 77−20069
Nb-H(D)(T) system, BCC, US vel. changes caused by H isotope dissolution 80−65117
Ne^+, isotope effects in elastic surface scatt. on sol. and liq. Ga 80−71536
Ne^*+Ne, metastability exchange by optical pumping *(French)* 77−61845
Ni, diffusion of D, isotope effect, elec. resistivity meas. 79−86928
Ni, diffusion of H, book contrib. 79−82390
Ni, magnetic aftereffects of H isotopes, book contrib. 79−82835
Ni:C, H(D), isotope effects of C-H and C-D complexes 77−20129
Ni-C, magnetic aftereffects of H isotopes, book contrib. 79−82835
Ni-Fe, magnetic aftereffects of H isotopes, book contrib. 79−82835
$Ni^+ + H_2(HD)(D_2)$, endothermic reactions, investig. 80−97692
$Ni_{98}M_2$, M=impurity metal, formation of MH(D)-complexes 80−65236
$NiSiF_6.6H_2O$, and hexadeuterate, optical absorption spectrum, 300 and 80K 79−73966
O ion, A=16, 18, +atom collisions, K-X-ray production 77−23554
O_2, electron impact desorption from W (110), isotope effects 77−76658
O_2, predissoc. of $B^3\Sigma_u^-$ state, Rydberg-valence crossing model 80−1032
$^{18}O_2$, Raman spectrum and mol. parameter 77−46565
$(O_2)_2$, struct., vibr. relax., local modes, isotope effects 78−25669
O_3, anharmonic force field and isotopic relation 77−58198
O_3, isotope effects, complete quartic force field calc., algorithm 80−37736
OH, isotope effects, Zeeman effect, far IR laser mag-reson. spectra obs. 80−63674
OH(OD) radical, photoelectron spectra 77−27113
OH(OD), spin-rot. consts., Van Vleck approx., ab initio calcs. 77−34610
$OH^+(OD^+)$, $A^3\Pi_i \rightarrow X^3\Sigma^-$ emission branching ratios, r-centroid depend. 77−6830
$O(^3P)+H_2S(D_2S)$, reaction rate, flash photolysis-reson. fluoresc. obs. 77−4918
$^{13}O^{16}O$ and $^{12}C^{18}O$, emission bands of $E^1\Pi$-$A^1\Pi$ tfansition 78−90177
$O_2(b^4\Sigma_g^-, v'=4, N', F')$ predissociation fragments, ang. distribs., separation energies 80−5588
$O_2(b^1\Sigma_g^+)$, temp. dependent quenching, photochemical study by H_2-VUV laser 80−63702
OsO_3F_2, OsO_4 matrix-isolated IR and Raman spectra 77−75166
PH_3, and d_3, ^{31}P NMR of liq. and gas, isotope effect on coupling consts. 79−76451
PO_4^{3-}, O isotope effect in ^{31}P NMR spectra 78−42100
Pb and Pb alloys, interstitial substitutional model for anomalous diffusion 80−84330
Pb stable isotopes, 2-photon spectroscopy, isotope shift of $6s^2\ ^3P_0$-$7p\ ^3P_0$ transition 80−87070
Pd, diffusion of H, book contrib. 79−82390
Pd, elec. resist. due to interstitial H (D) 80−96848
Pd, H(D) interstitial interactions rel. to diffusion and ordering transition 80−34249
Pd, soln. of $H_2(D_2)$, isotope effect model 77−66026
Pd-D-H, equilib. H/D separation factors 80−59668
Pd-H(D), isotope effect, theory 78−91806
Pd-H(D), isotope effects in supercond. properties 78−6471
Pd-H(D), superconductivity and electron-phonon interaction 80−49975
Pd-H(D) system, normal state phonon resist. and supercond. tunnelling density of states 79−56402
Pd-Si-H(D) alloys, superconductivity in solid solution and amorphous phase regions 79−56347
$Pd_{1-y}Ag_yH_x$, electronic struct. and supercond., APW calc. 79−95318
PdD, isotope effect on transition temp. 79−73615
PdH, isotope effect in supercond. *(Russian)* 77−89892
PdH, supercond., simple scaling theory of isotope effect 78−14878
PdH_x, PdD_x, ordering, resistivity, annealing and neutron diffr. obs. 79−34030
PdH_x, superconducting transition temp., inverse isotope effect, Einstein model 80−65734
PdH(D), stoichiometric, ^1H and ^2D NMR, rel. to supercond. T_c 78−72430
PdH(D), supercond., isotopic vol. effect 77−1511
PdH(D), superconducting, electronic spin density, isotope effects 78−39262
$PdH_x(D_x)$ films, electron-phonon coupling, elec. cond. obs. 80−50011
$PdH_x(D_x)$, optical mode phonons, nonadiabaticity 78−55916
$PdH_x(D_x)$, supercond. transition temps. *(Russian)* 80−88665
$Pd_{1-y}Rh_yH_x$, electronic struct. and supercond., APW calc. 79−95318
Pd(100) surface, of O, obs. of O^- and O^+ during electron bombardment 79−95883
Pt (111) and Pt (S)-12(111)X(111)surfaces, adsorption of 0, thermal desorption, AES, XPS, and LEED study 80−70534
Pt, catalysts, supported, characterisation, hydrogenation and H_2-D_1 equilib. 78−76910
^{85}Rb, $5^2P_{3/2}$ state, Hanle effect *(French)* 78−42018
Rb+methane (and deuterates), $5^2P_{1/2} \rightleftarrows 5^2P_{3/2}$ excitation transfer, isotope effects, temp. depend. 80−91630
RbBr, hyperfine struct., qudrupole coupling consts., vibr. depend. *(German)* 77−34565
RbCNS, single cryst. factor group anal. of IR and Raman multiphonon bands 77−4644
RbCl:H, dynamical superhyperfine interaction 80−2663
$Rb_2CuX_4.2H_2O$, (X=Cl, Br), fine struct. due to indirect coupling of nuclear spins 79−78541
$RbHSO_4$, isotope effect, dielec. const. and spin polarisation investigation 80−20574
$Rb_3H(SO_4)_2$, and $Rb_3D(SO_4)_2$, dielec. props. and phase transitions 80−60482
$^{85}Rb^+(^{87}Rb^+)$, hyperfine struct., in-flight saturated absorption laser spectrosc. 78−78650
$^{85,87}Rb$, first excited D-level, hyperfine struct. meas. by cascade, fluoresc. spectrosc. 80−69101

isotope effects continued
Re, atomic masses and mass differences, mass spectrometric obs. 77−42433
Ru complexes, $Ru(bipy)_3Cl_2.6H_2O$ and $Ru(bipy\text{-}d_8)_3\ Cl_2.6H_2O$, soln. electronic excitation energy, deactivation determ. 80−55173
$^{99,101}RuO_2$, NQR spectroscopy 80−63664
SF_6, isotopically selective photodissociation under CO_2 laser pulses, geometrical effects 77−16852
SH, $X^2\Pi_{3/2}$-state, far IR LMR spectra 79−6954
SO, $a^1\Delta$ state, laser mag. reson. spectrosc. 78−94265
SO, and isotopic forms, $X^3\Sigma^-$ state, CO_2 laser mag. reson. spectroscopy 80−9602
SO_4, and isotopic forms, struct., normal coord. anal. 78−965
SbN, 3300-4000 Å, rot. and vibr. perturbations and rot. anal. *(French)* 78−37651
SeH, isotope effects, Rydberg levels-ground state transitions, rot. const., VUV spectra obs. 80−58279
$SeH(X^2\pi_{3/2})$, far IR LMR spectrum 78−66564
SeO, mol., mm wave spectra, $X^3\Sigma^-$ state 79−85959
Si:Sb, dopant implantation, activation analysis errors due to isotope comp. *(German)* 80−34037
$SiH_4(SiD_4)+F_2$, chemilum., at. absorption, and laser-induced fluoresc. obs. 80−3315
SiO, nearly degenerate $G^1\Pi$-$I^1\Pi$ energy spectra, predissoc., extended virial theorem 79−22771
SiS, chemiluminescent flame spectra, electronic states and rot. struct. obs., vibr. assignments, Franck-Condon factors determ. 80−85179
SiX_n radical, (X=H,D; n=1,2,3), thermodynamic function in ideal gas state 80−14871
Sm, and isotopes, hfs, laser-RF double reson. spectroscopy 80−58170
Sn diffusion in liq. Sn and Pb, $^{113,117m,125}Sn$ diffusion coeff. meas. *(Ukrainian)* 80−10690
$SnMo_6S_8$, isotope effect props. *(Russian)* 80−37751
^{119}Sn-^{117}Sn primary isotope effect on mag. shielding, NMR of Sn cpds. 79−72338
Sr+HF(DF), beam reaction, vibr. excitation 78−68877
T_2+Y, high temp. equilib. meas. 80−66780
TBr, mol. consts., calcs., rel. to HBr, DBr *(French)* 77−57855
Ta, diffusion of H, book contrib. 79−82390
Ta, diffusion of H_2, crystal field stabilisation 80−59728
Ta, elec. resist. due to interstitial H (D) 80−96848
Ta-H(D), lattice expansion due to interstitially dissolved impurity, isotope effect 77−39600
Te_2, laser excited fluoresc. Fourier transform spectrosc. obs., isotope effects 79−59504
$Th_4H_{15}(D_{15})$, normal and supercond., low-temp. sp. ht., Debye temp. and supercond. props. 77−4466
Ti, electromigration of H(D) 80−34247
Ti, gettering of H, mass spectrometry and microgravimetry study, rel. to HTGR gas purification 80−73374
$TiH_x(D_x)$ positron annihilation *(Russian)* 78−6807
TlH_2PO_4 and TlD_2PO_4, dielec. props. under hydrostatic press. up to 7 kbar 80−29696
U isotope separation using ion exchange chromatography, U(IV)-U(VI) exchange isotope effects 79−36376
UH_3, UD_3, dissoc., isotope effect 80−26174
UO_2F_2, in soln., UV-visible spectra, ^{18}O isotope effects 77−52116
$UO_2(NO_3)_2$, aq. soln., pulsed NMR relax. time, ^{235}U enrichment depend. 80−2658
V, diffusion of H, book contrib. 79−82390
V, diffusion of H_2, crystal field stabilisation 80−59728
V, elec. resist. due to interstitial H (D) 80−96848
V-D, exam. of phase diagram, using DTA and calorimetry, isotope effect 78−80527
V-H(D), anelasticity due to long-range diffusion 80−60904
V-H(D), metallographic and thermal differential anal., potential for H energy storage appls. 80−45281
V-H(D)(T) system, BCC, US vel. changes caused by H isotope dissolution 80−65117
VO_2, semiconductor-metal transition, effect of ^{18}O substitution 78−84268
VO_2, V_2O_3, V_3O_5, isotope effect on metal-dielectric phase transitions temp. *(Russian)* 78−34771
VO_2, V_3O_5, V_2O_3, metal-insulator transitions, effect of isotopic substitution 80−2337
V_2O_3, semiconductor-metal transition, effect of ^{18}O substitution 78−84268
V_3O_5, semiconductor-metal transition, effect of ^{18}O substitution 78−84268
W, atomic masses and mass differences, mass spectrometric obs. 77−42433
Xe, thermal diffusion factors, isotopic 78−22450
YD, electronic spectra *(French)* 77−14442
YH, electronic spectra *(French)* 77−14442
YH, YD, 3800-9000 Å negative glow spectra, triplet and singlet systems 77−79608
Yb, $4f^{14}6s6p\ ^3P_1$ and $^1P_1$ levels, Stark effect, tensor polarisabilities 80−87080
Zn, diffusion in Al 78−84006
Zn-porphin($-d_4,d_8,d_{12}$), nonradiative transition probabilities, deuteration effects 79−3485
ZnFCl, existence and vibr. characterisation, IR and Raman matrix isolation obs. 78−78706
$ZnF_2(FCl)(FBr)$, matrix isolated IR and Raman spectra, assignments, force consts., isotope effects and thermodynamic props. 80−63631
ZnH, lifetime, Λ-doubling and hyperfine struct. of $A^2\Pi$ excited states 77−58083
ZnX_2, (X=Cl, Br, I), spectroscopic parameters of mols. from vibr. isotopic effects 78−74798
ZnX_2, ZnXY, X and Y=halogen, matrix isolation IR and Raman spectra 78−55171
ZnXY, (X, Y=Cl, Br, I), spectroscopic parameters of mols. from vibr. isotopic effects 78−74798
Zr, gettering of H, mass spectrometry and microgravimetry study, rel. to HTGR gas purification 80−73374
Zr, H(D) implanted, superconductivity enhancement obs. 80−70884
β-Zr, temp. depend. of isotope effect 79−86918

isotope exchanges
acetaldehyde-d_1($-d_3$), fragmentation processes, H scrambling, photoionis. mass spectra 78−42139

isotope exchanges continued
acetylene+acetylene-d_2(D_2O), H-D exchange, equilib. consts. 77−86299
chloro-1-propanol, ^{38}Cl for Cl substitution, optical enantiomers use 78−73031
cluster ions, formation and reactions, SIFT study, review 80−58435
coupled isotope effects in exchange reactions, vibr. freq. and atomic masses 80−18843
cyanoacetylene, and isotopic forms, $^{13}C/^{12}C$ effects on partition function 79−29352
determination in organic cpds. and biological samples by combustion method with isotope exchange 79−57333
2,2-dichloro-1,1,1-trifluoroethane, redeuteration H-D exchange with water 79−64112
ethane hydrogenolysis mechanism and kinetics on evap. Ir film 79−100436
feldspar/water O isotope exchange, effect of fluid press. 78−57204
geothermal steam samples from Lanzarote (Canary Islands), high-temp. isotope exchanges 77−49048
glycine-d_2 crystal, X-irrad., H-D exchange reactions 77−16837
lithium formate, isotope exchange during crystallisation from aqueous solns. 78−18569
methyl(-d_3) ions, association reactions, isotopic exchanges, SIFT study, review 80−58435
polypeptide chain, helix-coil transition and isotope exchange reaction 79−3602
propylene, chemisorbed on η-Al_2O_3, desorption and D exchange obs. 78−51827
pyridine-3,4,5-d_3, vibr. spectra, IR and Raman, H exchange rates meas. 80−102518
pyridine-3,5-d_2, vibr. spectra, IR and Raman, H exchange rates meas. 80−102518
radiation induced exchange reaction kinetics of H_2, D_2 and T_2, review 78−61005
reactions, equilib. consts., adiabatic correction, electron correl. effects 78−88626
RMO-4S omegatron for isotopic comp. determ. 78−5368
semiconductor, prereduced surfaces, room temp. activity for oxygen isotopic exchange 79−91998
tetrahedral molecules, thermodynamic isotope effect 78−20000
trigonal planar molecules, thermodynamic isotope effect 78−20000
tropomyosin, isotopic H exchange as function of state of ionisation of side groups 78−68979
tryptophan, fluoresc. intensity increase due to deuteration 78−78739
water vapour, H-D isotope exchange, mass spectroscopic sensitivities and equilib. const. 77−42434
AgI-I_2 system, 115 to 195°C, exchange rate 77−77756
B compound isotope exchange reactions, equilib. consts. 78−19999
BF_3-$BF_3.SO_2$, gas-liq., multistage ^{10}B isotope exchange, low temp. *(Japanese)* 78−33636
^{10}B enrichment by low-temp. exchange in $BF_3.SO_2$ system *(Japanese)* 78−55251
Br_2 in environmental water samples, determ. by neutron activation, isotope exchange 77−44550
C in interstellar molecules 77−87533
C isotopes, lack of exchange, methane and C oxides, high temperature 79−84263
C^+, association reactions, isotopic exchange, SIFT study, review 80−58435
$CD_n^+ + H_2(HD)(D_2)$, isotopic exchange, interstellar implications 80−61087
$CH_n^+ + H_2(HD)(D_2)$, isotopic exchange, interstellar implications 80−61087
CO, chemisorbed on supported Rh surface, activated surface processes, IR spectra 80−16724
CO, dissociative chemisorption of Ru, isotope exchange 79−34354
$CO + {}^{13}C^+(HCO^+)$, isotopic exchange, interstellar implications 80−61087
$C^{18}O_2$, isotope exchange with $CeMoO_4$, $LaMoO_4$, $PrMO_4$, $NdMoO_4$, 300-500°C 77−63884
$COCl_2$, photodissociation, C isotope effects, photocatalysed isotope exchange with CO 77−36764
$^{12}C^{16}O + {}^{13}C^{16}O$, vibr. distrib., electron impact excitation, isotopic composition, interaction depend. 79−29332
^{13}C, ^{14}C, substitution during catalytic oxidation of CO over NiO 78−80786
$^{13}C^+ + {}^{12}CO$ exchange in dust cloud Lynds 134, rel. to CO isotope fractionation 80−26924
$Cd(OH)_2$, highly dispersed precipitate, microstruct. and exchange props. 77−36793
$Cs(D_xH_{1-x})_2AsO_4$, isotope exchange during crystallisation from aqueous solns. 78−18569
$Cs(D_xH_{1-x})_2PO_4$, isotope exchange during crystallisation from aqueous solns. 78−18569
D enrichment by CW vibr. photochem. of methane, economic aspects 80−11920
$D+D_2$, collinear reaction, transmission coeff. isotope depend., statistical theory, invariance 77−36748
$D+HCl \rightarrow HD+Cl$ or $DCl+H$, branching ratios determ. 78−40046
$D+HI \rightarrow H+DI$, Franck-Condon theory 78−60984
D_2+H_2O, isotope exchange on Pt over hydrophobic support 79−11823
D_2+H_2O, isotope exchange on Pt, CO poisoning effects 79−11824
D_2O adsorbed on Pt surface, ^{18}O, H exchange reacts. 77−80695
D_2O+methanol-d_0(-d_2)(-d_4), D exchange reaction, thermodynamics 78−94328
$D_3O^+(D_2O)_n + H_2O$, binary reactions, rate coeffs. and product ion distributions determ. 80−81305
$D_3O^+(H_2O)_{0,1,2} + H_2O$ reactions, SIFT studies, review 80−58435
$^{152,154}Eu$ fixation in solid/liquid systems 79−13530
α-FeOOH+D_2O isotopic exchange surface OH groups, IR investig. 80−2254
^{59}Fe fixation in solid/liquid systems 79−13530
H isotope exchange between clay minerals and seawater 78−69329
H isotopes, separation in H-Pd system 77−50551
H/D isotope separation factors, and exchange efficiency at Pd electrodes 79−50149
H-D exchange, catalysis by α-$Cr_xAl_{2-x}O_3$ solid solutions 77−52631
$H+DCl \rightarrow HD+Cl$ or $HCl+D$, branching ratios determ. 78−40046
$H+H_2$, collinear reaction, isotope depend. transmission coeff., transition state theory 77−36747
$H+H_2$, collinear reaction, transmission coeff. isotope depend., statistical theory, invariance 77−36748
isotope exchanges continued
$H^+ + D_2 \rightarrow D^+ + HD$, low energies 78−62911
H_2-D_2, exchange on stepped Pt surface 77−1945
H_2+D_2, exchange on Pt stepped surface mol. beam incidence angle depend. 78−31686
H_2+D_2, exchange reaction, at. vs. mol. mechanism, at. absorpt. spectrometry 78−7190
H_2+D_2O, isotope exchange and separation with Pt hydrophobic catalyst *(Japanese)* 80−37901
$H_2+D_2 \rightarrow 2HD$, transition state, study of Jahn-Teller instability of H_4 78−60995
$H_2+D_2 \rightarrow 2HD$ on stepped Pt surface, selective adsorption effect 78−20066
$H_2+D \rightarrow HD+H$, three dimens. ab initio pot. energy surface 80−55646
H_2+O_2, on Pd (111), mol. beam relax. and isotopic exchange meas. 80−35575
$H_2O+D_2O \rightleftharpoons 2HDO$, vibr. anharmonicity effect on equilib. 79−74410
H_2O+HDO, isotope exchange in liq.-vapour system, r.i. and thermal cond. obs. *(German)* 77−4902
H_2O+methanol-d_0(-d_1)(-d_4), D exchange reaction, thermodynamics 78−94328
$H_3O^+(H_2O)+D_2O$ reactions, SIFT studies, review 80−58435
$H_3O^+(H_2O)_n+D_2O(NH_3)$, binary reactions, rate coeffs. and product ion distributions determ. 80−81305
H_2S+D_2 homogeneous exchange reacts., kinetics 77−48633
I_2 in environmental water samples, determ. by neutron activation, isotope exchange 77−44550
^{131}I fixation in solid/liquid systems 79−13530
$KB_5O_8(D_xH_{1-x})_2O$, isotope exchange during crystallisation from aqueous solns. 78−18569
$K(D_xH_{1-x})_2PO_4$, isotope exchange during crystallisation from aqueous solns. 78−18569
$KDy(MoO_4)_2$, polarised IR and Raman struct., $^{92}Mo/^{100}Mo$ isotope effect 80−108198
Li_2O-SiO_2 glasses, Li self-diffusion, mass spectrometric method 80−79982
MnO_4, aqueous soln., ^{55}Mn nuclear mag. shielding, NMR obs., O isotope exchange 77−10691
^{99}Mo fission product, sequential cation-exchange separation from neutron irrad., U_3O_8 77−90898
N isotope exchange in HNO_3-HNO_2 aq. soln. in presence of NO 80−16662
N_2, radiation chem., primary neutral dissoc. excitation, isotopic exchange mechanism 78−48670
N_2+N^+, collision, isotope exchange, ion cyclotron reson. obs. 77−52618
NH_3, adsorbed on partially-deuterated amorphous silica, Raman scatt. obs. 80−11948
NH_3, liq., vapour press., isotope effect, relevance to isotope exchange reaction calcs. 80−39272
$^{14}N^{14}N+{}^{14}N^{15}N$, vibr. distrib., electron impact excitation, isotopic composition, interaction depend. 79−29332
Nb_2O_5, diffusion of O_2, solid-gas isotope exchange method *(French)* 78−34650
Ni, reaction with CO_2 interfacial kinetics, $^{14}CO_2$-CO exchange reaction, S effect 79−47978
^{18}O and ^{16}O in natural feldspars heated in ^{18}O-enriched water *(French)* 77−55400
$^{17}O+{}^{16}O$, fractionation by chemical equilib. 80−89513
$^{18}O+{}^{16}O$, fractionation by chemical equilib. 80−89513
$^{18}OH+CO_2(CO)$, evidence for at. exchange 79−47910
^{18}O in quartz silt, resistance to isotopic exchange when buried and weathered 79−39709
Pd (111), scattering, adsorption, and absorpt. of H_2 and D_2, mol. beam study 80−29277
^{238}Pu fuel form facility at Savannah River Plant 79−9846
$Rb(D_xH_{1-x})_2PO_4$, isotope exchange during crystallisation from aqueous solns. 78−18569
Re, O_2 and CO isotope exchange reactions 77−70338
Rh (111), chemisorbed CO, dissociation probability, isotopic exchange and AES meas. 80−40743
S isotope exchange between sulphate and sulphide in acid solns., expt. determ. at 300°C and 1000 bars 78−62937
Si_3N_4, ^{15}N self-diffusion, isotope exchange meas. 77−11724
SiO_2, D-impregnated, vitreous, radiation induced isotope exchange 79−99240
$SrSO_4$, mass transfer in precip. from mixed solvents *(German)* 78−67674
$SrSO_4$, surface crystn., on $BaSO_4$, isotope exchange and electron microscopy study 80−34332
$SrTiO_3$ surface oxidation and reduction by D_2O, D_2, $H_2{}^{18}O$, isotope exchange study 80−104461
T+chloroethane(cyclobutane), recoil reaction, 5×10^{-2} torr 78−44389
$T+HT \rightarrow TH+T$, collinear reactivity bands 78−85143
^{132}Te, fission product, sequential cation-exchange separation from neutron irrad. U_3O_8 77−90898
ThO_2, ^{18}O self-diffusion, isotope exchange meas. 77−11725
$UO_2(DMSO)_5^{2+}$ in DMSO soln. kinetics of DMSO exchange by NMR method 79−81214
UO_2(acac)DMSO, in DMSO soln. kinetics of DMSO exchange by NMR method 79−81214

isotope relative abundance
see also element relative abundance
$^{13}C^{16}O/^{12}C^{16}O$ double ratio, isotopic fractionation evidence in interstellar dark clouds 80−73017
$^{143}Nd/^{144}Nd$ initial ratio in Moon, lunar crust and mantle differential evolution 79−35156
^{14}C evidence in tree rings 78−7962
$^{29}I/^{127}I$ early solar system chronometer 80−62043
$\delta^{18}O$, variations in snow on Devon Island ice cap, NWT, Canada 80−4050
S.African kimberlites, $^{40}Ar/^{39}Ar$ anals. of phlogopite nodules and phlogopite-bearing peridotites 79−34769
Allende C3 chondrite, search for Xe fission fragment recoil 80−62083
Allende meteorite, $^{33}S/^{32}S$ ratio anomaly 78−49402
Allende meteorite, evidence for isotopically and chemically distinct form. reservoir for inclusion HAL 80−109399
Allende meteorite, isotopic anomalies rel. to cosmochronology 80−4462
Allende meteorite, Mg isotope anomalies 77−78725
Allende meteorite, Mg isotopic anomalies rel. to ^{26}Al stellar nucleosynthesis 79−5809

isotope relative abundance continued
Allende meteorite, O isotope anomalies 77−78724
Allende meteorite FUN inclusion Cl, search for ^{26}Al effects 79−16896
Allende meteorite inclusions, genetic implications of isotopic anomalies in mineral separates 78−49400
Allende meteorite isotopic anomalies, rel. to He-driven r-process in supernovae 78−57567
amino acids, ^{15}N-labelled, nanomole isotopic assay by collision induced dissoc. MS 78−20095
anomalies from neutron reactions during stellar explosive C burning 80−12651
Antarctic meteorite Yamato 74123, new ureilite 79−35206
Archaean migmatites in Lofoten-Vesteralen, Norway, Nd, Sr and Pb isotope data interpretation 79−34773
Archaean precious-metal hydrothermal systems, Ontario, rare earth element and 0 isotope relations 80−12383
atmosphere precipitation, D-^{18}O relationship global climatic interpretation 80−17331
atmospheric pollutants, $^{14}C/^{12}C$ ratios rel. to origins and residence times 78−69445
basalt magma sources during opening of N.Atlantic, Nd and Sr isotopic comp. 79−100821
basalt-seawater interaction, trace element and Sr isotopic vars. in glassy basalt 80−8286
big bang nucleosynthesis, cosmology and neutrino physics constraints 79−30154
bromotrifluoromethane, multiphoton decomp., ^{13}C enrichment 79−830
Bruderheim L6 chondrite, Pb isotopic abundances rel. to U-Pb age and 500 Ma shock event 80−98616
C3 carbonaceous chrondrite (Ornans), noble gas component of minerals 80−51698
calcrete deposits from Europe, Africa and India, isotopic comp. 78−73368
Caledonian granites of Scotland, Nd and Sr isotope study rel. to provenance 80−109146
carbonaceous chondrite Kr and Xe isotopes, studies of ^{248}Cm and ^{250}Cf spontaneous fission products 80−63215
carbonaceous chondrites, H/D ratio study 80−46497
cave waters, stable isotope geochemistry rel. to climatic change, 230000 to 100000 BP 79−2234
Central American andesites, Sr isotope evidence for mantle petrogenesis 79−20833
chemically peculiar (CP) stars, isotope abundance vars. rel. to planetesimal impact hypothesis 78−20834
cherts, deep sea, stable isotope geochem. 77−5182
chondrite Kirin H, inert gas content interpretation *(German)* 80−46505
chondrite Yamato-74191, inert gas composition and neutron capture effects 80−46504
chondritic meteorites, isotopic anomalies rel. to supernovae-prod. presolar grains 78−24520
CO isotope mapping of L 134 N 79−30108
coastal muds, interstitial water isotopic behaviour during evaporation *(French)* 79−79811
coral C isotope composition, rel. to environmental factors 80−46202
coral reef O isotope abundance, ice age origin in Antarctic ice surge 80−51525
coral reef water, O isotope composition rel. to evaporation and precipitation 80−46202
cosmic ray Be isotopes meas., 200-1500 MeV/nucleon 79−12366
cosmic ray Fe and other Z=20-25 nuclei, isotopic composition 77−82091
cosmic ray He, isotopic comp. meas. and anal. from 123 to 279 MeV per nucleon 78−49251
cosmic ray isotope abundance meas. for C to Ni 77−60555
cosmic rays, isotopic comp. rel. to origin and containment time 78−53781
cosmic rays from supernovae, cosmogenic isotope obs. 80−101503
cosmogenic concs. in lunar samples rel. to past solar activity 78−61828
cosmogenic isotopes, vertical turbulent diffusion in ocean 80−12428
cosmogenic radioisotopes, in Dhajala chondrite, rel. to interplanetary cosmic ray vars. 79−35207
cosmoradiogenic ghosts in meteorites, rel. to origin of Ca-Al rich inclusions 78−12162
Deccan Traps volcanic rocks, India, $^{40}Ar/^{39}Ar$ date and volcanic history 80−46178
deep sea sediment core from E.Mediterranean, stable isotopes abundances and palaeoclimatic record 78−57294
diabase intrusions, Newark trend, basins, Ar isotope geochronology 80−51350
diabase pebbles of val d'Illiez conglomerates (Haute-Savoie), ages and initial $^{40}Ar/^{36}Ar$ ratios *(French)* 78−92810
diamonds, rare gas isotopic compositions, rel. to atm. comp. 78−24270
dibenzylketone, photolysis in micellar soln., quantum yield and ^{13}C enrichment 80−97711
digital isotope ratio meas. system, using programmable calculator with double collector mass spectrometer 80−63845
digital measurements using double collecting mass spectrometer with inexpensive device 80−31932
diopsides from kimberlite nodules mantle Nd and Sr composition 80−51363
distribution among the elements 78−74781
DNC/HNC, interstellar ratio, difficulties of chemical equilib. hypothesis for D enrichment 77−82298
Donegal granite, Ireland, emplacement age by isotope chronology 80−67356
DSDP Leg 37 basalts, O, Sr and Pb isotopes rel. to petrogenesis 77−91076
Duxbury massif (2.5 Ga), Quebec, initial $^{87}Sr/^{86}Sr$ rel. to remobilised pre 3.0 Ga sialic basement hypothesis 80−76970
early solar system, isotopic anomalies and proton irradiation 77−49317
Earth, isotopic comp. and trace elements concs. rel. to mantle and crustal reservoirs mean age 80−51359
Earth, Sr, Pb isotope geochemistry rel. to catastrophic or continuous core form. 78−57178
Earth crust, isotopic ratios rel. to rel. to mantle chemical evolution 80−90043
Earth mantle, Nd-Sr isotope correl. and constraints on continental crust comp. and nature of lower crust 80−94498
Earth mantle differentiation and crustal growth, geochem. model 80−21684

isotope relative abundance continued
Earth mantle materials, Nd-Sr isotopic correl. and geodynamic consequences 79−92512
Earth mantle melting, past and present, isotope and trace element evidence 78−65238
El Tatio geothermal field waters, N.Chile, isotopic comp. rel. to sources 79−16525
elemental evolution and isotopic composition, teaching 78−41128
enrichment coefficient under focused IR laser pulse, kinetic treatment *(Chinese)* 79−50093
environmental isotope study of Kalamos springs, Greece, recharge area determ. 79−53393
eruptive gases, thermodynamic and isotopic studies 78−69316
ethylene, laser-induced IR photolysis mechanism 78−56909
explosive r process cooling process 78−69791
feldspar/water O isotope exchange, effect of fluid press. 78−57204
fission reactor fissile materials safeguards, quantity and isotopic comp. meas. *(Russian)* 80−63287
fission reactor fuel, analytical capabilities for accurate prediction 79−85620
fission Xe isotope dating technique 79−21043
formation waters from deep drillings in S.Israel, isotropic comp. 77−86945
fumarole B isotope composition, Satsuma Iwo-Jima, Japan 80−67358
galactic abundances of stable isotopes of common elements 79−44615
galactic cosmic rays, isotopic composition of Fe-group elements 78−89024
galactic cosmic rays, Ne, Mg and Si isotopes high resolution meas. 80−51631
galactic cosmic rays, secondary tracer approach 79−96864
Galaxy, distrib. from interstellar mol. obs. 80−109550
gas source stable isotope mass spectrometry, press. effect, peak broadening 77−88600
GC/MS system for isotope ratio monitoring 79−22855
geochemical $\delta^{18}O$ scales, proportional vars., interlaboratory comparison 78−69326
geological samples, f/α particle track anal. for U, Th and isotropic disequilibria 78−7799
geothermal steam samples from Lanzarote (Canary Islands) isotopic comp. 77−49048
geothermal vapour dominated field, Larderello, Italy, gases and H_2O isotopes content of steam 79−74920
geothermal vapour dominated field, Larderello, Italy, noble gas concs. 79−74919
geothermometry, chemical and isotopic techniques 78−69501
giant planet atmospheres, IR radiation, review 80−8568
granitoid rocks, Nd-Sr isotopic relationship and continental crust development, chemical approach to orgogenesis 80−94522
Greenland ice, O isotope ratios rel. to late-Wisconsin glaciation in NW.Greenland in N.Ellesmere Island 78−57232
Grenville series of Ontario, palaeomag. rel. to Ar isotope dating 80−98232
groundwater of Milk River aquifer, Alberta, isotope and ion geochemistry 80−8351
gypsum hydration water, isotopic comp. 79−20829
Hawaiian glaciation chronology, K/Ar and ^{14}C ages 77−33113
heavy isotope labelled mols., isotopic distrib. calcs. 77−56265
heavy water concentration meas. by neutron thermalisation method *(Japanese)* 79−93746
hexamethylethane, ^{13}C-^{13}C dipolar interaction, NMR longit. cross relax. 80−93196
HR 6766, weak G-band star, light-element abundances and $^{12}C/^{13}C$ ratio 78−57548
E.Iceland lava, $^{40}Ar/^{39}Ar$ dates and ocean ridge growth 80−36273
inert gases in Murchison meteorite, possible relics of s-process nucleosynthesis 79−21243
interstellar CH^+ 3957 A line towards ζ Ophiuchi rel. to $^{12}C/^{13}C$ ratio 77−87529
interstellar dust, grains growth in supernova and nova ejecta rel. to isotopic anomalies 80−26941
interstellar formamide, ^{13}C isotope detect. and column densities 79−25680
interstellar K and Ar, isotopic anomalies in dust grains 78−28761
interstellar molecular clouds 78−16513
interstellar molecules, microwave astronomy, modern aspects, book contrib. 80−56921
interstellar molecules (DCO^+, N_2D^+, DCN, DNC), obs. and interstellar chemistry implications 79−5891
interstellar N_2D^+/N_2H^+ ratio, meas. 78−16492
interstellar southern molecular clouds, $^{12}C/^{13}C$ abundance ratio derived from H_2CO obs. 79−84838
IRC+10216, isotope abundance anomalies in C star 79−5814
irradiated nuclear fuel, determ. of one group cross-section ratio from meas. isotopic comp. 80−612
island arc lavas, sources as indicated by Nd and Sr isotopic studies 78−32044
Kakangari meteorite, unique chondrite, noble gases abundances and isotopic comps. 78−65570
Kapoeta howardite, $^{40}Ar/^{39}Ar$ chronology of lithic clasts 80−46501
Kerguelen igneous rocks, petrology and isotopic geochemistry rel. to continental or oceanic character 79−57924
kimberlites and garnet lherzolite inclusion minerals, Sm-Nd systematics 80−51397
kimberlites and mantle-derived xenoliths from Southern Africa, Pb and Sr isotopes 77−60372
Kirin meteorite shower, $^{18}0$ abundance *(Chinese)* 79−16900
Lake Lisan-Dead Sea aragonite, element and isotropic comp. rel. to pleistocene geochemical evolution 78−49047
lake studies, isotope techniques appl., advisory group meeting, Vienna (1977 August 29 to September 2) 80−41950
Late Cretaceous granodiorites, Jamaica and Haiti, Greater Antilles, Sr isotope geochemistry 79−57927
late Precambrian mafic dykes, Montana, initial $^{87}Sr/^{86}Sr$ ratios and Rb-Sr geochronology 78−77196
Lewisian gneisses, $^{143}Nd/^{144}Nd$ and Sm/Nd ratios rel. to granulites origin 79−20777
light elements formation, thermal cycle, isotopic abundances problem *(French)* 78−96574
limestone cave deposits, O isotopes for palaeotemp. of mid-Wisconsin 80−82069
LL-chondrite, noble gas isotope anomalies 80−51697

isotope relative abundance continued
Luna 24 soil samples, Ne isotopic comps. rel. to depositional history 79−88608
lunar regolith, light element chemistry of Apollo 12 site 78−65515
lunar soil samples from Luna 24, inert gas element and isotope composition 80−67593
lunar soil samples from Luna 24 and Apollo 16, natural radioactivity meas. 80−67595
lunar surface mass fractionation by solar wind sputtering 78−49350
magnetosphere noble gas precipitation, gas of solar and terrestrial origin, Skylab foil obs. 80−41653
Manicouagan melt sheet, Rb-Sr isochron age and initial $^{87}Sr/^{86}Sr$ ratio 78−81168
mantle Nd and Sr isotopes, differentiation occurring in episodes 80−67352
marine plankton, C isotope ratio rel. to surface water masses 79−29783
Mars atmosphere, comp. of surface layer 78−20706
Mars atmosphere, isotopic ratios rel. to supernova and solar wind 77−87307
Mars near surface atmosphere isotope ratios and noble gas upper limits 77−17408
Mars upper atmosphere isotopic composition, Viking 1 obs. 77−17405
mass spectra, elemental compositions, computer assignment from isotopic abundance 78−20085
mass spectroscopy, δ values calc. method 79−10234
maximum abundances rel. to nucleosynthesis of elements 78−45219
measurement using RMO-4S omegatron mass spectrometer 78−5368
metagabbro at bottom of Michigan Basin deep drill hole, Rb-Sr geochronologic anal. 79−39680
meteorite, role of supernovae in solar system formation 79−44380
meteorite, Unter-Massing iron, cosmic-ray exposure age and preatmospheric size *(German)* 80−46507
meteorite inert gas isotope and element anomalies, He and Xe 80−56779
meteorite Springfield specimens, mass spectroscopic element and isotope anal. 77−60731
meteorites, abundance anomalies, astrophysical implications 80−46511
meteorites, abundance anomalies, cosmological implications 80−46510
meteorites, abundance anomalies, rel. to explosive neutron processing of stellar He burning shells 79−58302
meteorites, Antarctic, stone, inert gas content, isotopic composition 80−46506
meteorites, isotopic anomalies rel. to explosive nucleosynthesis 79−62795
meteorites, isotopic anomalies rel. to supernovae and solar system origin 80−17509
meteorites, noble gases isotopic anomalies in separated minerals from Allende chondrite 77−33430
meteorites, polymict brecciated, O isotopic comp. rel. to multiple parent bodies 78−57513
meteorites, rel. to supernova trigger for solar system formation 78−77499
meteorites isotopic anomalies, role of grains as carriers in early solar nebula 80−26757
methane isotopic mixtures, enrichment of D using vibrationally sensitized reaction 80−76532
mid-ocean ridge basaltic glasses, U-Pb, Sm-Nd and Rb-Sr systematics 80−36277
mineral processing isotope on-stream anal. 78−35777
minerals spatial isotope distributions, recovery from stepwise degassing data 79−34967
molecular isotope partition function ratios, perturbation calcs., convergence 80−87239
natural waters, pollution tracing via ^{18}O and ^{34}S contents *(Italian)* 77−53078
natural waters of Mt. Everest, mass spectrometric chem. anal. of D, ^{17}O and ^{18}O *(Chinese)* 80−77016
noble gas anomalies in josephinite and assoc. rocks 79−79761
noble gases in meteorites, isotopic anomalies origin, comment 80−26818
noble gases isotopic anaomalies in Murchison meteorite, evidence for stellar condensates 80−41772
non-destructive assay techniques for irradiated fissile material in extended configurations 80−71872
nondestructive measurement of U and Th conc. and quantities using XFA and gamma spectrometry 80−71877
nuclear fuels, elemental and isotopic conc. anal. using nondestructive assay 79−49691
nuclear materials analysis using plasma desorption mass spectrometry, isotope ratio determ. using TOF mass spectrometry 80−78375
nuclear materials safeguarding; 80−68835
nuclear materials safeguarding, determ. of U and Pu content of fuels using isotope correl. tech. 80−68834
nuclear materials safeguarding, isotopic correl. tech., R and D by ESRADA 80−68836
nuclear materials safeguarding, isotopic correlations in irradiated fuel from VVER power reactors *(Russian)* 80−68838
nuclear materials safeguarding, isotopic inventory prediction employing a Monte Carlo Dancoff factor 80−73924
nucleocosmochronology, model, r-process elements discrete addition to presolar cloud 78−4121
nucleosynthesis equilibrium processes and neutron-rich Si burning 79−62816
oceanic basalts, differential Sm/Nd evolution 78−61391
oceanic basalts, variations in $^{143}Nd/^{144}Nd$ and $^{87}Sr/^{86}Sr$ ratios 77−29295
Oklo natural fission reactor, dating from U-Pb isotopic data 80−21763
Oklo natural reactor, rare earth elements behaviour 78−49019
Oklo phenomenon, isotopic abundances, long-term radioactive waste storage information 80−52769
ophiolite petrogenesis in oceanic crust, Nd and Sr isotope study 80−61782
ophiolite rocks of Samail, Oman, study of petrogenesis and hydrothermal alteration 80−46177
orogenic lherzolite petrogenesis in oceanic crust, Nd and Sr isotope study 80−61782
p-nuclei, abundances produced by low-temp. photonuclear nucleosynthesis in degenerate H burning zones 78−57540
p-process isotopes nucleosynthetic origin in supernova explosions 78−57541
N.Pacific Ocean sediments, 150000 yr ^{18}O-pollen record for palaeoclimate marine-continental correl. 79−80008
isotope relative abundance continued
Pacific Pliocene benthonic foraminifera, O isotopes for deep ocean temp. 80−56492
pelitic sediments, Sr and Ar isotopic homogenisation during low grade regional metamorphism 79−62511
planetary atmospheres 79−58284
primary cosmic ray N and O, isotopic comp. with consequences for source models 79−84609
primary cosmic rays, isotope abundances, Cr to Ni 79−70937
PWR, Pu isotope calcs. for steady-state core anal. 79−59126
quantitative ion-microprobe analysis, geochem. appls. 79−34976
r-process nuclei, isotopic anomalies 79−5740
radioactive particulates in gaseous effluents at nuclear fuel reprocessing facility 79−9848
radionuclide ratios in clam from Galapagos Rise hot spring field, rel. to growth rate determ. 79−84300
rare earth metals, isotopic analysis at Oklo natural fission reactor *(French)* 80−21761
rare gas elemental and isotopic ratios in Luna 24 drill core soil samples 80−26760
rare gas isotopic anomalies in Nigorikawa geothermal area, Japan 79−88314
rare gases in volcanic rocks, isotopes mass fractionation as indicator of gas transport to or from magma 80−98292
rare-earths, isotopic analysis, Oklo natural fission reactor fluence distrib. meas. *(French)* 80−21759
Red Sea brines, $^{18}O/^{16}O$ and D/H ratios rel. to origin 78−96236
resonance ionization source for mass spectroscopy appl. isotope anal. and time of flight spectrometer 80−81380
rinneite, Rb-Sr dating of potash salt deposits 80−67429
rock chem. weathering rate, meas. new with U isotope method 80−77142
Ryu, isotopic composition of Oklo reactor and other samples *(French)* 80−21765
San Juan Capistrano meteorite, rare gas isotopic abundances rel. to cosmic ray record 78−57512
NW Scotland Tertiary continental volcanics, Nd and Sr isotope evidence for crustal contamination 79−66693
sea-surface microlayer, ^{210}Pb and ^{210}Po enrichment obs. 80−56496
in seawater, Ra and Th isotopes in Pacific surface waters 78−96234
sedimentary organic matter, ^{13}C enrichment prod. by subaerial weathering 78−57206
Shaw meteorite, L-group chondrite, missing metal 77−5511
Shergotty achondrite, $^{40}Ar/^{39}Ar$ age and post-shock thermal history 80−46502
slates, $^{40}Ar/^{39}Ar$ ratios and ages by stepwise outgassing model 79−29721
slow novae, CNO isotopic ratios in Z=0.3 envelope model 78−32468
solar cosmic rays, interpretations of isotopic comp. of H and He 77−45266
solar particles, isotope composition, form., effect of ion-sonic turbulence 80−101574
solar system, early isotopic anomalies 79−22161
solar system, early isotropic anomalies 79−25522
solar system, isotopic anomalies injection into early solar nebula 79−101094
solar system, local proton irradiation model for ^{16}O and ^{26}Al isotopic anomalies 78−93128
solar system abundance anomalies rel. to grans ejected from supernovae 77−87285
solar system isotopic anomalies rel. to supernova neighbour or presolar carriers model 78−12110
solar system s-process elements, isotopic ratios rel. to ^{22}Ne neutron source model 80−72926
solid microvolume mass spectrometric isotopic analysis 78−58088
speleothems, stable isotope geochemistry rel. to climatic change, 230000 to 100000 BP 79−2234
speleothems in N.America, stable isotope studies rel. to late Pleistocene palaeoclimates 78−57297
spent fuel burnup determ., U, Pu, Nd, isotopic comp. and conc. determ. by mass-spectrometric isotope dilution 79−89373
spent reactor fuel burnup determ. using anal. chem. [conf. Piestany, Czechoslovakia (Sept. 1978)] 79−89371
stable isotope abundances in natural compounds, meas. standards 78−32246
stainless steel, neutron dose determ., from isotope abundance ratio, mass spectra obs. 80−61220
stalagmite, New Zealand, $^{18}O/^{16}O$ ratios rel. to temps. and climate change during last millennium 79−62574
stellar collapsed core, neutrino prod. of bypassed isotopes, neutrinos role in nucleosynthesis 79−40182
stony meteorites, cosmogenic ^{26}Al and ^{22}Na *(Russian)* 77−9719
sulphide minerals, K-bearing, age meas. by $^{40}Ar/^{39}Ar$ technique 79−29720
superheavy elements, possibility of occurrence in nature 78−20407
Tertiary sediments from North Sea area, ^{18}O abundances and palaeotemps. 78−88903
thermal fluids of Abano region, N.Italy, O isotopes rel. to sources and circulation paths 79−20883
transuranic trace analysis using resonance ionisation spectroscopy of inert gases 80−93833
trifluoromethane, D ultrahigh single-step enrichment by CO_2 laser photolysis 80−45527
Tuscany hot springs, O isotopic comp. rel. to geothermal areas location 77−49049
volcanic rocks, Sr isotopic comp., role of ancient lithosphere in young continental volcanism 77−2133
volcanic rocks from Aleutian Islands and Pribilof Islands, Alaska, Pb and Sr isotopes 78−57185
water, density, effects of isotopic comp., temp., press., and dissolved gases, review 78−26616
water vapour in air-water interfacial layer, isotopic distrib. rel. to bulk evaporation coeffs. 78−85576
waters from high altitude region north of Jolma Longma mountain, geochem. characts. of isotopic distrib. *(Chinese)* 79−2304
Yellowstone thermal waters, subsurface boiling and dilution effects on isotopic comp. 78−49048
Yugoslav biotites, search for giant halos assoc. with superheavy elements 78−16008
^{107}Ag excesses in Santa Clara and Pinon Fe meteorites, meas. 80−85902

isotope relative abundance continued
Al isotopes, yield from C and Ne zones of massive star supernova 80−90406
Al^{26}/Al^{27}, prod. or collapse of stellar core *(Russian)* 80−77285
Al_2O_3, single cryst., self-diffusion of O, isotope exchange investig. 80−100348
^{26}Al activity in ureilitic meteorite Kenna 77−41368
^{26}Al content of Dalgety Downs meteorite 79−75167
^{26}Al content of stony meteorites with gas losses 78−32418
^{26}Al from meteorites, possible 'record' of solar wind action and luminosity variations 78−61830
^{26}Al in early solar system, fossil or fuel 77−17387
^{26}Al in Fe meteorites and past cosmic ray intensity 79−44422
^{26}Al in N.Pacific deep sea sediments, rel. to prod. by cosmic rays in atm. 77−5181
^{26}Al, meteorite capturing solar flare cosmic ray particles 80−36461
$^{26}Al/^{10}Be$, meas. in oceanic sediments using $^{26}Al/^{26}Mg$ separation via negative ion mass spectroscopy 80−31146
$^{26}Al/^{27}Al$, prod. ratio from stellar evolutionary sequence 79−5809
$^{26}Al/^{27}Al$, ratio from ^{26}Al synthesis in explosive H burning 80−85929
$^{26}Al/^{27}Al$ and ^{26}Al nucleosynthesis in novae and supernovae outbursts 80−62143
$^{26}Al/^{27}Al$ in unstable He shell in red giant stars 80−67712
$^{26}Al^{g,m}$ relative yields from $^{25}Mg(p,\gamma)$ reaction 79−101058
Am, vertical distribution in Mediterranean Sea 79−84301
Ar in ancient atmos., degassing from shungite 80−85749
Ar in Fe meteorites 78−12165
Ar in Venus lower atmosphere, isotopic abundance results from Pioneer Venus 79−48720
Ar isotope abundances in Venus thermosphere, upper limits 80−4281
Ar-K isotopic dilution method for absolute age determ. *(Rumanian)* 78−20562
^{36}Ar excess in Venus atmosphere, implications for Venus accretion 80−12700
$^{36}Ar/^{40}Ar$ in Alpine biotites, rel. to excess Ar evolution 80−94521
$^{36}Ar/^{40}Ar$ in Mars atmosphere, composition at surface, Viking 1 lander preliminary analysis 77−13268
^{39}Ar in meteorites, evidence for Maunder minimum in solar activity 78−57529
^{40}Ar concentrations in sialic crust and atmosphere, rel. to form. from upper mantle 79−44153
^{40}Ar, mobility in metamorphic terrain, excess in biotite 80−17260
$^{40}Ar/^{36}AV$ in Devonian atmosphere, isotopic ratio from Rhynie chert 77−66917
$^{40}Ar/^{36}Ar$, atmospheric abundance ratio for use in geochronology and cosmochronology 78−28189
$^{40}Ar/^{36}Ar$ ratio, North Mountain Basalt, Nova Scotia, K-Ar isochron age 80−3960
$^{40}Ar/^{36}Ar$ trapped in Cretaceous deep-sea basalts 79−16423
$^{40}Ar/^{38}Ar/^{36}Ar$ in Type I diamond from Arkansas 80−94493
$^{40}Ar/^{39}Ar$, IIE iron meteorites, Weekeroo Station and Netschaevo 80−77360
$^{40}Ar/^{39}Ar$, in Mesozoic tholeiites from Antarctica, interpretation of discordant age spectra 77−49047
$^{40}Ar/^{39}Ar$ age and thermal history of Kirin H5 chondrite meteorite 80−101567
$^{40}Ar/^{39}Ar$ ages and ophiolite obduction in W.Newfoundland 77−33034
$^{40}Ar/^{39}Ar$ dating, felsic and mafic mineral separates from an Abitibi dike 80−17237
$^{40}Ar/^{39}Ar$ dating of Frontenac Axis dikes, Ontario, implications for Grenville palaeomagnetism 79−62466
$^{40}Ar/^{39}Ar$ radioactive dating, appl. to K-bearing sulphide minerals age determ. 79−29720
$^{40}Ar/^{39}Ar$ studies of deep-sea igneous rocks 79−53325
^{40}Ar-^{39}Ar dating of magnetizations in Archaean Shelley Lake granite 80−30982
^{40}Ar-^{39}Ar stepheating analyses of clay concentrates in Irish orebodies 79−66684
^{40}Ar-^{39}Ar systematics, temp. and pressure effects 79−44178
B, isotopic analysis, by AAS, using Ne-filled discharge lamp source 78−20097
B, meteoritic isotopic anomalies rel. to protosolar cosmic ray fluxes 80−4462
B, primary cosmic ray nuclei, isotopic composition using nuclear emulsions 79−80155
$BCl_3+N(CH_3)_3 \rightarrow BCl_3N(CH_3)_3$, complex formation, reaction product isotopic composition change *(Russian)* 80−81316
Ba isotopic anomalies in Allende meteorite 78−32409
^{7}Be as a tracer for helio-geophysical phenomena 80−98525
^{7}Be, cosmic ray accel. probe 78−81512
$^{7}Be/^{9}Be$ data rel. to cosmic ray acceleration mechanisms 80−31183
^{10}Be abundance in cosmic rays rel. to age, balloon meas. technique 77−29602
^{10}Be, abundance in galactic cosmic rays rel. to age 78−12060
^{10}Be, abundance rel. to cosmic ray age 77−60554
^{10}Be, concs. in environment rel. to cyclospectrometry dating techniques *(French)* 80−21859
^{10}Be in 1000 and 5000 yr old Antarctic ice, meas. 79−2305
^{10}Be in Mn nodules, meas. using tandem Van de Graaff accelerators 79−74967
^{10}Be in ocean surface layer, conc. and residence time 79−66714
^{10}Be, mass spectrometric meas. with cyclotron, geochronological appl. 79−57338
^{10}Be, meteorite capturing solar flare cosmic ray particles 80−36461
^{10}Be var. in deep sea sediments, critical evaluation 78−7615
$^{10}Be/^{9}Be$ and ^{10}Be deposition rates at Earth surface, seasonal vars. 80−26707
$^{10}Be/^{9}Be$ in North Pacific during Pliocene 80−101356
$^{10}Be/^{9}Be$ ratio meas. using electrostatic tandem accelerator 80−76579
$^{214}Bi/^{214}Pb$ in S.California coastal air 78−49087
C at DSDP sites rel. to palaeoenvironment of NE.Atlantic during Cainozoic 78−96239
C isotope geochemistry of small groundwater system, NE. Ontario 79−84324
C isotope ratio, in comets, stars, and interstellar matter 79−5766
C isotope stratigraphy, appl. to late Miocene shallow marine sediments, New Zealand 80−26479
C isotopes in brines and sediments, in Orca Basin 79−88369
C isotopic comp. of groundwater correction for CO_2 outgassing effects during pH meas. 79−66718

isotope relative abundance continued
C, isotopically light, in diamonds from Lesotho kimberlite pipes 79−48487
C, mass spectrometric anal. double inlet system with viscous gas flow 77−18131
C, mass transfer and isotope evolution in natural water systems 79−20882
C, mud volcanoes, Copper River Basin, Alaska, composition of emitted gases 79−84308
C, organic, dissolves and particulate, in marine environment, stable isotope comp. 79−20862
C, primary cosmic ray nuclei, isotopic composition using nuclear emulsions 79−80155
C stars, C and N isotope ratios from spectral analysis 79−30057
$^{13}C/^{12}C$, terrestrial, appl. to planetary nebulae CNO abundances and central stars masses 78−85992
CNO isotope abundances in interstellar clouds 77−87527
CNO isotopes, origin and evolution 78−93201
CNO isotopes abundances in giant stars, role of mag. mixing rel. to α Bootis (Arcturus) problem 80−105229
CNO isotopes as probes of chem. evolution of Galaxy and spiral galaxies 77−91636
CNO isotopes in Galaxy, interpretation of obs. 78−4356
CNO rare isotopes, prod. in novae by explosive hot CNO-Ne cycle H burning 79−44489
CO, interstellar, isotope fractionation in Lynds 134 dust cloud 80−26924
CO_2, isotope ratios, optical anal. method 78−85228
$^{A}C(p,\gamma)$, A=12, 13, isotopic anal., estimation of $^{13}C/^{12}C$ conc. ratio 79−48014
$^{12}C/^{13}C$, evidence for telluric ratio in atmospheres of Jupiter and Saturn 78−20723
$^{12}C/^{13}C$, in cool giant stars, from obs. and anal. of CO at 5 μm 78−36569
$^{12}C/^{13}C$, ratio and chemical fractionation in cyanoacetylene in Sagittarius B2 mol. cloud 77−29900
$^{12}C/^{13}C$, ratio in atmospheric of cool C star V460 Cygni 78−93223
$^{12}C/^{13}C$ and CNO abundances in red giant envelopes 77−29825
$^{12}C/^{13}C$ determ. in C stars 78−73710
$^{12}C/^{13}C$ in α Orionis expanding shell, determ. from CO circumstellar absorpt. obs. 80−26858
$^{12}C/^{13}C$ in G and K-type giant stars, correl. with Li abundance 80−41819
$^{12}C/^{13}C$ in IR C star CIT 6 (IRC+30219), lower limit from CO obs. 80−12761
$^{12}C/^{13}C$ in Jupiter, ratio determ. using new spectroscopic method 79−84734
$^{12}C/^{13}C$ in NQ Vulpeculae (Nova 1976) upper limit from CO emission obs. 79−25609
$^{12}C/^{13}C$ in Population I giant stars, theoretical surface abundances 80−94796
$^{12}C/^{13}C$ in solar atmosphere from CH photospheric lines 77−5518
$^{12}C/^{13}C$ interstellar ratio, rel. to ^{13}C enriched matter ejection from red giants 77−9788
$^{12}C/^{13}C$ interstellar ratios from radioastronomical obs. 77−87530
$^{12}C/^{13}C$ ratio and stellar turbulent diffusion 80−21993
$^{12}C/^{13}C$ ratio correl. with Fe/H ratio in K-type giant stars atms. 79−48798
$^{12}C/^{13}C$ ratio determination in atmospheres of C stars, peculiar red giants 80−17580
$^{12}C/^{13}C$ ratio in atmosphere of HD 122563 metal-deficient giant star 78−4201
$^{12}C/^{13}C$ ratio in atms. of luminous cool stars 77−13336
$^{12}C/^{13}C$ ratio in atms. of giant and supergiant stars 77−13337
$^{12}C/^{13}C$ ratio in C stars 79−35257
$^{12}C/^{13}C$ ratio in cool C stars 77−91533
$^{12}C/^{13}C$ ratio in cool C stars 78−4205
$^{12}C/^{13}C$ ratio in G-K giant stars, explanation constraints 79−5817
$^{12}C/^{13}C$ ratio in giant interstellar molecular clouds, formaldehyde obs. 80−51837
$^{12}C/^{13}C$ ratios in G-K giants and C stars, origin of freq. distrib. 77−78780
$^{12}C/^{13}C$ ratios in Population I K-type giant stars, rel. to CN strengths 78−93229
$^{12}C/^{13}C$ ratios in red giant stars, effect of meridional circulation 79−48786
$^{12}C/^{13}C$ ratios in Sagittarius B2 and Orion A 79−21374
$^{12}C/^{13}C$ ratio in red giants after main-sequence mixing 77−33475
$^{12}CH^{+}/^{13}CH^{+}$, interstellar abundance ratio, meas. 80−67809
^{13}C and ^{18}O fractionation in calcite-depositing spring, chemical vars. and calcite precipitation 79−44202
^{13}C distribution in cyanoacetylene at thermodynamic equilib. 79−59590
^{13}C, enrichment in multiphoton dissoc. products of trifluoromethyl halides 79−18302
^{13}C, Isua sediments, W.Greenland, isotope averages and Archaean C and O cycles 79−84262
^{13}C record in tree rings, vars. in N.hemisphere trees during last 150 years 80−17363
$^{13}C/^{12}C$, ratio analysis in organic materials by mass spectrometry *(Portuguese)* 80−7875
$^{13}C/^{12}C$, ratios in N.American ancient wood cellulose (9500-22000 BP) 77−60462
$^{13}C/^{12}C$ dating of New Zealand kauri cellulose for last millennium 80−21819
$^{13}C/^{12}C$ for rocks in Tertiary igneous complex of Skye 77−33012
$^{13}C/^{12}C$ fractionation and isotope geothermometry in the Larderello geothermal field 78−69312
$^{13}C/^{12}C$ from tree ring ^{13}C records, interpretation problems 79−62573
$^{13}C/^{12}C$ in atmosphere CO_2, vars. in last 22 yrs. 80−104530
$^{13}C/^{12}C$ isotope fractionation of organic matter assoc. with U ores induced by alpha irradiation 79−57932
$^{13}C/^{12}C$ ratio analysis in carbonates by mass spectrometry *(Portuguese)* 80−7875
$^{13}C/^{12}C$ ratio in magmatic gases of Afar ridge volcanism 80−21732
$^{13}C/^{12}C$ ratio of atm. CO_2, recent trends rel. to tree ring studies 79−25311
$^{13}C/^{12}C$ ratio variations in Pinus longaeva (bristlecone pine) cellulose during the last millennium 79−44217
$^{13}CO/^{12}CO$, intensity ratios in external galaxies 80−4416
$^{13}CO/^{12}CO$ ratio in interstellar clouds, theory 77−29912
$^{13}CO/C^{18}O$ fractionation in interstellar dark clouds 80−46638

isotope relative abundance continued
^{14}C, abundance rel. to cosmic rays and solar activity cyclic vars. 79−16776
^{14}C anomaly in groundwater from regional carbonate aquifer, Great Basin, Nevada 77−45042
^{14}C, concs. in Florida annual coral rings 79−16513
^{14}C content in tree rings correl. with solar cycle, 1744-1892 period *(Russian)* 78−16390
^{14}C dating rel. to magnetic and other dating methods 78−57359
^{14}C dating using electrostatic accelerators and negative ions 78−32917
^{14}C direct detection at natural concs. by mass spectrometry, for dating 78−32916
^{14}C, dissolved in groundwater initial activity determ., new model and review 80−8458
^{14}C, distrib. in submersible-taken deep sea cores from Project FAMOUS 77−37179
^{14}C distribution, Ross Ice Shelf Project ice hole 79−88371
^{14}C in atmosphere, variability due to variable Sun 80−85730
^{14}C in atmosphere content variation, past geomagnetic and cosmic ray intensity variations 78−61691
^{14}C in groundwater, possible subsurface prod. rel. to dating 80−85690
^{14}C, in red giant stars, nucleosynthesis and possible detectability 77−26005
^{14}C in tree rings, radial flow and chemical pretreatment for meas. 78−28346
^{14}C in wines, abundance vars. with 11-year solar cycle, (1909 to 1952) 80−109249
^{14}C measurement in known age specimens, cosmic ray intensity determ. 80−101516
^{14}C pollution of Atlantic from nucl. weapons tests 80−89683
^{14}C variations in terrestrial atmosphere rel. to 11-year solar cycle 78−92885
^{14}C/^{12}C, in tree rings, rel. to solar activity long-period vars. *(French)* 78−73695
^{14}C/^{12}C and Suess effect determ. accuracy rel. to natural ^{14}C var. 79−96801
^{14}C/^{13}C/^{12}C vars., Bermuda coral 200 yr. record 79−16570
Ca and Mg isotopic anomalies and lack of ^{26}Al in Allende meteorite unsual inclusion 79−40142
Ca isotope anomalies in Ca-Al-rich inclusions in Allende meteorite 78−32410
Ca, isotope fractionation on Earth and other solar system materials 79−20835
Ca, isotopic anal. using double vaporizer 80−106398
Ca isotopic comps. of magnetic spherules in marine sediments 79−44423
Ca, Mg, isotopic comp. of Allende meteorite individual crystals 78−32417
^{40}Ca, cosmic ray source abundance meas. 80−8502
^{41}Ca/^{40}Ca, ratio rel. to ^{41}Ca radioactive dating 79−21063
Cd abundances in 28 meteorites and three terrestrial rocks 78−53891
^{116}Cd/^{106}Cd, isotope fractionation in fractions of H3 chondrites Tieschitz and Brownfield 80−94764
^{36}Cl in environmental water samples, anal. using electrostatic accelerator 79−20895
^{36}Cl in meteorites from Antarctic, cosmic irrad. histories 80−21950
^{38}Cl and ^{39}Cl in lower stratosphere, chemical form 78−44913
^{242}Cm and ^{244}Cm in global fallout, lichen sample results 78−57263
^{247}Cm in early Solar System, Allende ^{238}U/^{235}U ratio evidence 80−90347
^{56}Co, synthesis in Type II supernovae, determ. from light curves analytic solns. 80−77427
^{134}Cs and ^{137}Cs in Clyde Sea Area 80−3541
^{137}Cs distrib. in upper layer of equatorial Indian ocean *(Russian)* 77−60426
^{137}Cs/^{134}Cs radioisotopes in seawater, Cs-selective resin determ. 80−94137
D, abundance rel. to pair prod. in intense mag. fields 77−13505
D anomaly in Chainpur meteorite *(French)* 79−88628
D areal distribution in California and Nevada precipitation, 1968-1969 period 79−100918
D, form and abundances in inhomogeneous cosmologies 79−21471
D, galactic distrib., radial gradient, from DCN/H^{13}CN and DCO^+/$HC^{18}O^+$ ratios 79−40232
D in pectolite (hydrous silicate), lowest δD value 79−62513
D, Indian radioactive thermal spring water D content, mass spectrometric anal. 79−39765
D, T and ^{18}O composition of Sahelian rain, 1975-6 period *(French)* 80−21809
D universal abundance 80−62356
D/H, in Jupiter, determ. from methane-d_1 phase 78−28572
D/H climate indicator rel. to solar luminosity and sunspot cycle 79−75176
D/H for rocks in Tertiary igneous complex of Skye 77−33012
D/H in Jupiter, ratio determ. using new spectroscopic method 79−84734
D/H of river runoff on US east coast 79−100879
D/H ratio, in Jupiter atmosphere 78−45265
D/H ratio, interstellar, evidence for nearby intersteller cloud 78−93352
D/H ratio an interstellar medium, meas. from obs. of methylamine-d_1 77−33610
D/H ratio and cosmic ray ionization in interstellar clouds 79−17063
D/H ratio for Jupiter from 8-9 μm IR spectrum 80−67638
D/H ratio in early Solar Systems, H and O isotope study in chondritic meteorites 80−36518
D/H ratio in galactic centre direction, 327 MHz obs. upper limit 80−26949
D/H ratio in pre-main-sequence stars, effect on early evolution with D burning 80−51736
D/H ratio in Saturn and Uranus atms. 78−57495
D/H ratio in speleothem fluid inclusions rel. to meteoric precipitation 79−44201
D/H ratio in Uranus atm. from visible spectra obs. 80−82296
D/H ratio in Uranus atmosphere, meas. 78−57497
D/H ratio towards δ, ε and ι Orionis 79−53865
D/H ratio upper limits for Jupiter and Saturn 78−85892
D/H ratios in meteoric water over N.America (9500-22000 BP), climatic implications 77−60462
D/H ratios of natural serpentines, rel. D/H fractionation factors between serpentine and water at 100-500°C 79−34803
DC_3N/HC_3N, ratio in IRC+10216 rel. to DC_3N detect. possibility 78−69901
Fe nuclei in galactic cosmic rays, isotopic comp. 80−72729

isotope relative abundance continued
^{55}Fe and stable Fe forms and availability in oceanic aerosols 79−12241
Ga, atomic weight from solid-source mass spectra 77−541
^{156}Gd/^{155}Gd isotopic ratio, eval. of neutron temp. in Oklo natural reactors *(French)* 80−21766
$^{74}GeH_4$, transition moment for ν_3, rel. to Jovian atmosphere 79−72363
H, isotope ratio, determ. in microwave induced plasma 79−41868
H, O, isotopic comp. in plutonic granitic rocks 78−65221
H, O, Si isotope systematics in lunar samples 77−60676
H/D, mass spectrometric method 78−8462
H_2-He mixtures, isotopic anal. using high resolution mass spectrometer 77−77844
HCN, interstellar, isotopic abundance vars. 77−53657
$H_2{}^{13}CO$/$H_2C^{18}O$ mol. isotopic abundance ratio, interstellar determ. from 6.8 cm obs. 79−35347
$H^{15}NC$, interstellar, J=1→0 emission obs. rel. to ^{15}N enrichment 77−82299
^{3}H/^{1}H, ratio in solar wind 77−5407
^{3}H/^{3}He dating as meas. of O_2 utilisation rates, appl. to Sargasso Sea 77−56654
He in Earth interior, incorporated from immature Sun *(Russian)* 80−81856
He, isotope ratios in Yellowstone and Lassen Park volcanic gases 79−16425
He nuclei isotopic comp. in primary cosmic rays 79−80145
He^3/He^4 high isotope ratio in technical-grade metals and semiconductors 79−86080
He-Ne ring laser, Ne isotopic composition changes during prolonged discharge *(Russian)* 78−22110
^{3}He excess in Mid-Atlantic Ridge bottom waters, hydrothermal activity 80−101383
^{3}He/^{4}He, high ratios in Hawaii lavas olivine phenocrysts and xenolithic dunites 79−34814
^{3}He/^{4}He, ratio in mantle volatiles injected into Gulf of California, meas. in Guaymas Basin 80−85640
^{3}He/^{4}He from He I 6678 Å obs. of Feige 86, He deficient blue horizontal-branch star 79−92774
^{3}He/^{4}He in heavy-ion-rich solar energetic particle events, energy depend. and temporal evolution 80−90299
^{3}He/^{4}He in Red Sea brines, evidence for mantle He 77−25693
^{3}He/^{4}He in solar cosmic rays, ^{3}He rich events during 1976 November to December 80−61972
^{3}He/^{4}He ratio in atm. He, mass spectrometric meas. 77−9447
^{3}He/^{4}He ratio in atmosphere of primary component of 60=μ Herculis 77−57045
^{3}He/^{4}He ratio in deep ocean water, rel. to mantle He in oceanic basalts 77−64259
^{3}He/^{4}He ratio in josephinite 78−65313
^{3}He/^{4}He ratio in Jupiter atmosphere, determ. from albedo neutron fluxes 78−45271
^{3}He/^{4}He solar cosmic ray isotopic composition from Venera 9 obs. 80−72725
^{3}He/^{4}He ratio in interstellar cloud assoc. with open cluster (NGC 6530) 77−45504
^{4}He content of fracture zone water of N.Kirgizia 77−33108
^{4}He excess in Teggau Lake, NW.Ontario, rel. to U ore body 78−65353
^{4}He production, nonzero neutrino rest mass effects 80−105413
Hg isotopic anomalies in meteorites, possible prod. by extinct radioactive nucleus ^{202}Pb 77−49343
^{202}Hg/^{196}Hg anomalous ratios in meteorites, interrelations, cosmological inferences 77−2375
^{123}I product radionuclidic purity using ^{124}Te(p,2n), reply 79−29622
^{123}I product radionuclidic purity and quality, comments from ^{124}Te(p,2n) 79−29621
^{129}I, in iodyrite and marshite, determ. by radiogenic ^{129}Xe meas. 77−63983
K, abundance ratios for use in geochronology and cosmochronology 78−28189
K isotopic comps. of magnetic spherules in marine sediments 79−44423
^{40}K, isotope relative abundance, radioactivity expt. for schools 79−21511
^{39}K/^{40}K ratio for inclusions in Allende meteorite, normality confirmed 80−26820
^{40}K anomaly in Allende meteorite inclusions, evidence from pre-4550 Myr ^{40}Ar-^{39}Ar ages 79−35212
^{40}K/^{41}K in deep-sea sediments magnetic spherules, poss. meteorite origin 78−11874
^{41}K in Allende meteorite, search for anomaly prod. by proton-associated alpha-irradiation 78−49398
Kr in Fe meteorites 78−12165
Kr, s-process contributions 79−5739
^{82}Kr/^{86}Kr in Murchison C2 chondrite, presolar gas component evidence 80−85904
^{86}Kr/^{84}Kr in Murchison meteorite, rel. to s-process neutron capture time scale 80−73080
Li, Be, B, isotopic ratios rel. to cosmic-ray nucleosynthesis and extragalactic matter infall 79−17084
Li, Be, B production in ^{12}C(p, spallation) reactions, 45-100 MeV 77−23053
Li, isotope abundance, spectrographic determ. *(Chinese)* 79−68325
Li isotope composition determ., α prod. by d bombardment 79−7029
Li isotopic comp. determ., using coincident meas. of complementary particles in ^{6}Li(p,α) and ^{7}Li(p,α) 79−5201
Li, natural isotope ratio, spectroscopic determ. *(Russian)* 78−23996
^{6}Li, determination using nuclear track techniques 80−95504
^{6}Li/^{7}Li abundance ratio, meas. using isotope ratio mass spectrometer 77−88601
^{6}Li/^{7}Li ratio in C stars, low-energy spallation model 78−40927
^{6}Li/^{7}Li ratio of interstellar matter towards ζ Persei and ε Aurigae 78−49494
^{176}Lu/^{175}Lu isotopic ratio, eval. of neutron temp. in Oklo natural reactors *(French)* 80−21766
Mg isotopes, yield from C and Ne zones of massive star supernova 80−90406
Mg isotopes in Ba star HR 774, Reticon spectra 79−25594
Mg isotopes in red giants and planetary nebulae, ^{22}Ne neutron source effects 78−49430
Mg isotopic anomalies in meteorites, role of ^{26}Al synthesis in explosive H burning 80−85929
Mg isotopic vars. in hibonite from Murchison meteorite, ion microprobe study 79−58305
Mg, isotropic abundances in five G and K dwarf stars 80−51757

isotope relative abundance continued
$^{24}Mg/^{25}Mg/^{26}Mg$ of interplanetary dust particles 80−72879
^{26}Mg excess in Allende meteorite anorthite crystal, ion microprobe obs. 78−40882
^{26}Mg negative anomalies and ^{26}Al, effects of proton irradiation on gas phase with condensation 79−13289
Mn nodules, from sea-bed, isotopic and elemental composition, U, Pa, Th, radiochem. anal. 78−77215
N abundance and isotopic comp. in stony meteorites 78−65558
N in Mars atmosphere, Viking obs. 77−17406
N isotope comp. in NH_4^+ and NO_3^- in rain water collected at Julich, Germany 78−57284
N_2, isotopic composition, spectrosc. determ. in systems below natural ^{15}N levels *(Russian)* 77−68130
$^{14}NH_3$, $^{15}NH_3$, CW and pulsed $Pb_{1-x}Sn_xSe$ diode laser spectroscopy 79−26980
$^{14}N/^{15}N$ in water, for trace anal. of total N by isotopic dilution 77−5253
$^{14}N(p,\gamma)^{15}O$, isotopic anal., estimation of $^{15}N/^{14}N$ conc. ratio 79−48014
^{15}N, enrichment in Mars atm. due to cosmic ray interactions in early solar system 78−73669
^{15}N rel. to atmospheric nitrogenous trace gases 78−73470
$^{15}N/^{14}N$ in carbonaceous chrondrites, N isotope fractionations in Fischer-Tropsch and Miller-Urey reactions 80−46496
$^{15}N/^{14}N$ ratio and solar nebula differentiation 80−36519
$^{15}N/^{14}N$ ratio from $^{15}NH_3$ interstellar detection at 23 GHz 79−44590
$^{15}N/^{14}N$ ratio in Jupiter atmosphere, results from 10 to 13 μ spectrum 79−8876
$^{15}N/^{14}N$ ratio in lunar microbreccias indicating ancient solar wind composition 80−62046
$^{15}N/^{14}N$ ratio in solar wind from lunar samples 77−87354
$^{15}N/^{14}N$ ratios in gaseous NH_3, NO_2 and NO_3^- in aerosols and precip. 78−44896
$^{15}N(p,\alpha\gamma)^{12}C$, isotopic anal., estimation of $^{15}N/^{12}C$ conc. ratio 79−48014
$^{16}N/^{17}N$ levels in reactor, primary coolant flow rate determ. 77−65254
^{22}Na, meteorite capturing solar flare cosmic ray particles 80−36461
^{92}Nb, half life determ. by gamma spectroscopy, comparison of ^{92}Nb, ^{94}Nb activities and abundances 78−29423
Nd and Sr geochemistry of volcanic rocks, Grenada, Lesser Antilles 80−21724
Nd and Sr isotope ratios, Icelandic basalt, Reykjanes Peninsula 80−21725
Nd composition of ocean bed sediments 80−21704
Nd, in flood basalts, Earth struct. models 80−72475
Nd in spent reactor fuel, isotopic comp. and conc. determ. by mass-spectrometric isotope dilution 79−89373
Nd isotopes conc. in ocean floor basalts and ferromanganese deposits 78−61395
Nd isotopic anomalies in Allende meteorite 78−32409
Nd, Sr isotope geochemistry of hydrous mantle nodules and host alkali basalts, rel. to mantle heterogeneities 80−56420
Nd-Sr isotopic patterns rel. to petrogenetic mixing models 80−3965
Nd-Sr isotopic var. implications for crustal and mantle chemical evolution 79−66655
$^{143}Nd/^{144}Nd$, ratios in Cretaceous mid-ocean ridge basalt (MORB) from DSDP Holes 417D and 418A 80−94520
$^{143}Nd/^{144}Nd$ in Bay of Islands ophiolite complex, rel. to midocean ridge basalts source evolution 80−85651
$^{143}Nd/^{144}Nd$ in calc-alkaline andesites and plateau lavas from S.America 79−29726
$^{143}Nd/^{144}Nd$ in flood basalts from Siberian Platform 80−56435
$^{143}Nd/^{144}Nd$ in Isua supracrustals, implications for mantle evolution 78−36129
$^{143}Nd/^{144}Nd$ in Kerguelen Islands igneous rocks, inferences on enriched oceanic mantle sources 80−98319
$^{143}Nd/^{144}Nd$ in mantle xenoliths, equilibrated isotopic comp. meas. with unequilibrated Sr isotopes 80−98321
$^{143}Nd/^{144}Nd$ in Norwegian eclogites, rel. to crustal origin 80−76978
$^{143}Nd/^{144}Nd$ ratio in basalts from Sao Miguel 79−74873
$^{143}Nd/^{144}Nd$ ratio in Recent continental volcanic rocks 78−53635
$^{143}Nd/^{144}Nd$ vars. in continental and oceanic basalts, rel. to magma sources and mantle struct. 77−21708
Ne, Ar isotopes meas. in Allende meteorite 77−87344
Ne I, isotopic components of spectral line, separation by numerical method 78−21227
Ne in meteorites, isotopic comp. rel to $Mg(n,\alpha)Ne$ cross sections 79−96874
Ne-E, anomalous meteoritic Ne component, thermonuclear origin, supernova models 78−45292
^{20}Ne in Venus lower atmosphere, abundance from Pioneer Venus 79−48720
$^{20}Ne/^{21}Ne/^{22}Ne$ in Murchison C2 chondrite, presolar gas component evidence 80−85904
$^{20}Ne/^{21}Ne/^{22}Ne$ of energetic flare particles 79−92741
$^{20}Ne/^{22}Ne$ and ^{22}Ne nucleosynthesis in novae and supernovae outbursts 80−62143
$^{20}Ne/^{22}Ne$ of solar flare-accelerated Ne nuclei 79−92740
$^{20}Ne/^{36}Ar$ ratio in chondrites, abundance pattern established in solar nebula 78−32424
^{22}Ne anomalous abundance in Orgueil meteorite, evidence for presolar grains 80−41773
$^{22}Ne/^{20}Ne$, ratio in galactic cosmic rays 79−101036
$^{22}Ne/^{21}Ne$, ratio in Djermaia (H) chondritic breccia rel. to preirradiation history 80−36579
^{237}Np in invertebrate tissues, uptake from water 79−74765
O, anomalously heavy isotope, mass spectrometric search 79−81290
O at DSDP sites rel. to palaeoenvironment of NE.Atlantic during Cainozoic 78−96239
O in solar photosphere from O I 7774.177 Å line asymmetry 77−17530
O isotope abundance in Luna 16 and 20 soil 77−22120
O isotope anomalies in meteorites 77−87354
O isotope comp. and origin of high $^{87}Sr/^{86}Sr$ andesites 79−34817
O isotope comp. of water in Sea of Azov 77−49083
O isotope composition of Matanuska Glacier, Alaska, rel. to basal zone origin 79−79884
O isotope fractionation in decarbonation metamorphism, Mottled Zone Event 78−65307
O isotope profiles of glacial ice, Greenland and Devon Island during last 10^5 years 80−41470
isotope relative abundance continued
O isotope records rel. to global freshening of upper ocean layer during deglaciation 78−53658
O isotope stratigraphy and Late Pleistocene coral terraces in Barbados 77−78182
O isotope study of lower crust xenoliths 80−89992
O isotope thermometry for sulphate-water reaction in geothermal systems 78−69383
O isotopes in dissolved sulphate and water from hot springs and drill holes, reservoir temp. indicators 78−69382
O isotopes rel. to diagenetic silica minerals in Monterey Shale 77−64267
O isotopic composition of fallen snow in Antarctica, controlling factors 78−36237
O isotopic composition of Canadian Shield surface crystalline rocks 79−62496
O, marine isotope record in Pleistocene coral, Barbados, West Indies 79−66675
O, mass spectrometric anal. double inlet system with viscous gas flow 77−18131
$^{17}O+^{16}O$, fractionation by chemical equilib. 80−89513
$^{18}O+^{16}O$, fractionation by chemical equilib. 80−89513
^{16}O, enrichments in carbonaceous chondrite minerals, rel. to distrib. of pre-solar component 77−37582
$^{16}O/^{17}O$, $^{16}O/^{18}O$, in cool giant stars, from obs. and anal. of CO at 5 μm 78−36569
$^{16}OH/^{18}OH$, interstellar abundance ratio obs. 78−54024
^{17}O, in red giant stars, nucleosynthesis 77−26005
$^{17}O/^{16}O$, $^{18}O/^{16}O$ in Chainpur meteorite, meas., rel. to D conc. in early Solar system 80−36518
$^{17}O/^{18}O$, ratio in red giants after main-sequence mixing 77−33475
$^{17}O/^{18}O$ abundances in interstellar clouds 77−87528
$^{17}O/^{18}O$ ratio in Allende meteorite inclusion HAL, possible member of FUN family 80−105211
^{18}O analysis, parallel changes in species diversity and palaeotemp., Lower Miocene 79−39866
^{18}O and palaeomagnetic evidence for early Northern Hemisphere glaciation 78−7752
^{18}O composition of metamorphosed chert and Fe formation from W.Greenland 78−81155
^{18}O concentration in Amazon Basin water, evidence for recycling 80−81955
^{18}O concs. and rel. discharges in Negro and Solimoes rivers in Amazon 77−5268
^{18}O distrib. among mineral triplets in igneous and metamorphic rocks 78−32071
^{18}O enrichment during ocean-floor hydrothermal metamorphism of ophiolitic metabasic rocks in Italy 78−7613
^{18}O, in belemnite rostra, effects of post-depositional alteration on palaeotemps. determ. 77−29455
^{18}O, in E.African carbonates, vars. rel. to Pleistocene climatic changes 77−56723
^{18}O in equatorial Pacific core, glacial time scales and climate 80−21817
^{18}O in formaldehyde, interstellar 4389 MHz absorption line 79−44591
^{18}O in Indian Ocean, Subtropical Convergence fluctuations and Quaternary climates 77−13087
^{18}O in quartz silt, resistance to isotopic exchange when buried and weathered 79−39709
^{18}O, Isua sediments, W.Greenland, isotope averages and Archaean C and O cycles 79−84262
^{18}O, T and D composition of Sahelian rain, 1975-6 period *(French)* 80−21809
$^{18}O/^{16}O$, for rocks in Tertiary igneous complex of Skye 77−33012
$^{18}O/^{16}O$, groundwater seepage, control Kentucky karst 80−8370
$^{18}O/^{16}O$, in SiO_2 from diatoms, 20000 yr record in deep-sea sediments 78−32247
$^{18}O/^{16}O$ fractionation and isotope geothermometry in the Larderello geothermal field 78−69312
$^{18}O/^{16}O$ geochemistry, of potassic igneous rocks from Roccamonfina volcano, Roman comagmatic region, Italy, 80−41420
$^{18}O/^{16}O$ in Antarctic ice core, 30000 yr isotope climatic record 79−92586
$^{18}O/^{16}O$ in Archaen clastic metasediments, rel. to use as petrogenetic indicator for Archaean gneisses 78−20410
$^{18}O/^{16}O$ in cellulose, lignin and whole wood from tree rings, climatic appls. 78−24355
$^{18}O/^{16}O$ in DSDP Leg 37 rocks, ratios and geochemistry 77−91072
$^{18}O/^{16}O$ in deep sea cores, rel. to rapid ice-sheet growth and last glaciation initiation 80−51530
$^{18}O/^{16}O$ in estuaries 80−26532
$^{18}O/^{16}O$ of river runoff on US east coast 79−100879
$^{18}O/^{16}O$ ratio analysis in carbonates by mass spectrometry *(Portuguese)* 80−7875
$^{18}O/^{16}O$ ratio in precipitation over KFA Julich, (1974-1978) *(German)* 79−12227
$^{18}O/^{16}O$ ratio in precipitation, correl. with temp. and altitude 80−77067
$^{18}O/^{16}O$ ratio of dissolved O during FLEX 76 in North Sea 78−73404
$^{18}O/^{16}O$ ratios in granites from British Late Caledonian 80−36276
$^{18}O/^{16}O$ ratios in tropical Quelccaya Ice Cap, rel. to climatic ice core records 80−8345
$^{18}O/^{16}O$ ratios of rocks from Canadian Precambrian Shield, N.W.Ontario 77−78130
$^{18}O/^{16}O$ rel. to coral growth rate (1944-74) 79−62524
$^{18}O/^{16}O$ stratigraphy of deep sea sediments rel. to Eemian interglacial 79−29770
$^{18}O/^{16}O$ trends, Middle Pliocene climate change in W.Mediterranean 80−26605
$^{18}O/^{16}O$ variations in deep sea carbonate shells from East Pacific Rise hydrothermal field 80−109173
$^{18}O/^{17}O$, abundance, ratio in hot CNO nucleosynthesis 77−78767
$^{17,18}O$ of minerals in ureilitic meteorite Kenna 77−41367
^{187}Os isotopic anomalies from different ore deposits, LAMMA determ. 80−61800
$^{187}Os/^{186}Os$ in meteorites, rel. to solar system early chronology and Galaxy age 80−41778
$^{187}Os/^{186}Os$ in terrestrial samples, rel. to use of Os isotopes as petrogenetic and geological tracers 80−89989
^{231}Pa, determ. in coastal sediments and seawater, activity ratios, disequilib. 78−27851
Pb and Sr isotopic compositions of elemental concs. and Pb and Sr isotopes 79−34775
Pb, concs. and comp. in DSDP Leg 37 cores 77−91074

isotope relative abundance continued
Pb in Richardton and Farmington chondrites, excess radiogenic Pb and inhomogeneous initial isotopic comp. 80−56778
Pb, isotope comp. in oceanic basalts, rel. to mantle evolution 78−65217
Pb, isotope comp. of Archaean plutonic rocks 78−65223
Pb isotope inhomogeneity in Precambrian igneous K-feldspars 78−32095
Pb, isotope measurements and ages of oldest recognised Lewisian gneisses of NW.Scotland 77−70625
Pb isotope studies of ore deposits of circum-Kisseynew volcanic belt, Canada, ages 79−5479
Pb isotopes, terrestrial evolution during core formation time 78−7601
Pb isotopes conc. in ocean floor basalts and ferromanganese deposits 78−61395
Pb isotopes struct. of basic-ultrabasic layered complex 80−81847
Pb, least radiogenic ore occurrence in Isua supracrustal rocks, W.Greenland 78−44816
Pb of Amitsoq gneiss, W.Greenland, initial isotopic comp. and implications for Earth age 78−20371
Pb, Sr, Nd isotopic correl. and chemistry of N.Atlantic mantle 80−90023
Pb sulphides, isotopic composition, mineralisation time determ. 78−73372
$^{206}Pb/^{207}Pb/^{204}Pb$ ratios rel. to Earth age and chemical evolution 79−88315
^{202}Pb, extinct radioactive nucleus, meteoritic abundance rel. to Hg isotopic anomalies 77−49343
$^{206}Pb/^{204}Pb$ evolution during Earth crust development, rel. to U, Th and Pb fractionation 79−57879
$^{206}Pb/^{207}Pb$ ratio and Pb conc. in subalpine pond sediments, anthropogenic source var. 80−85315
$^{207}Pb/^{204}Pb$, $^{206}Pb/^{204}Pb$ ratios in basalts from DSDP Leg 37 cores 77−91123
^{210}Pb chronology of Long Island Sound sediment core, biological mixing effects 79−66672
^{210}Pb conc. or climatic changes at South Pole 78−7748
^{210}Pb, distrib. in submersible-taken deep sea cores from Project FAMOUS 77−37179
Pd, isotopic comp. and at. wt., using solid source mass spectrometry 79−864
^{107}Pd existence in early solar system, evidence from meteorites 79−40096
$^{210}Po/^{210}Pb$ atmospheric ratio, modification by volcanic emissions 80−41507
Pu accountability, computerised gamma spectrometer system for meas. isotopic and total Pu conc. in solns. 80−63363
Pu, alpha-energy and mass analyses, using single sample mount 78−15744
Pu, assay and accountability using neutron correlation meas. tech. 80−69015
Pu, assay of large samples using portable neutron coincidence counter 80−69041
Pu, calorimetric nondestructive assay for in-field meas. 80−71874
Pu content in nuclear fuels, appl. of isotopic safeguards tech. 80−99210
Pu in spent reactor fuel, isotopic comp. and conc. determ. by mass-spectrometric isotope dilution 79−89373
Pu, isotope compositon, determ. using gamma spectrometry 80−66915
Pu isotopes in Antarctic snow layers, deposition and accumulation 79−70820
Pu, isotopic analysis by resin-bead mass spectrometry for materials safeguards 80−78392
Pu, isotopic composition, determ. using thermal ionisation spectrometry with automatic data eval. 80−66913
Pu, isotopic composition, determ. using precise absolute gamma spectroscopic meas. 80−66916
Pu, isotopic composition, nondestructive anal. using gamma spectrometry 80−63392
Pu, isotopic conc. in soln., on-line gamma spectrometric meas. 79−11872
Pu, nondestructive assay of large samples 80−71871
Pu, nondestructive element and isotope assay in nuclear materials 80−71870
Pu passive assay using Euratom variable dead-time neutron counter 80−69042
Pu, remote contamination and total inventory from Rocky Flats, mass spectroscopic anal. 77−73739
Pu safeguards, product soln. gamma-ray NDA using K-absorption edge densitometer 80−83162
Pu safeguards accountability, gamma-ray meas. of Pu and Am in molten salt residues 80−83165
Pu safeguards assay, isotopic meas. by gamma ray spectrometry using two-detector method 80−83161
Pu, vertical distribution in Mediterranean Sea 79−84301
^{239}Pu, $(U,Pu)O_2$ fuels 80−71873
$^{226}Ra/^{222}Rn/^{238}U$ ratios in fracture zone water of N.Kirgizia 77−33108
$^{226}Ra/^{238}U$ dating of quaternary corals by γ-spectrometry 79−88221
^{226}Ra-^{222}Rn disequilib. and pumice radioactivity, Sakurajima volcano 77−33033
$^{228}Ra/^{226}Ra$ activity ratio in Gulf of Mexico 79−66713
Rb-Sr isotopic study of Precambrian metavolcanics in Orange River region, S.Africa 79−44147
Rb-Sr isotopic systems, geologically meaningless total rock isochron prod. by secondary alteration 80−31014
$^{81}Rb/^{81m}Kr$ ratio as radioactive tracer study of organic bleeding *(Dutch)* 80−3807
$^{85}Rb/^{87}Rb$, abundance ratio for use in geochronology and cosmochronology 78−28189
$^{87}Rb/^{86}Sr$ in L chondrites 80−51705
$^{87}Rb/^{87}Sr$ studies of waters in geothermal area, Cantal, France 78−61443
^{87}Rb-^{87}Sr chronology of H chondrites, parent body evolution 79−44421
^{222}Rn conc. over intertropical convergence zone of Atlantic 80−26648
^{222}Rn continuous meas. for air-sea gas exchange field determ. 78−73534
^{222}Rn daughters emission and enrichments from Etna volcanic magma 77−21736
^{222}Rn enhancements and gas upflow possibility in Earth 79−74893
^{222}Rn evasion rates in Atlantic and Pacific, Geosecs determ. 79−79875
^{222}Rn, excess bottom distrib. in deep ocean passages 79−16514
^{222}Rn exhalation meas., soil and meteorological effects *(Spanish)* 80−31082
^{222}Rn meas. during marine fog off Nova Scotia 78−40624
$^{222}Rn/^{226}Ra$ ratio in fracture zone water of N.Kirgizia 77−33108
S in gypsum from Mackenzie, Canada rel. to Devonian-Cambrian stratigraphy 78−61413

isotope relative abundance continued
S isotope variations as pollution index in lakes near Sudbury, Ontario 78−57228
S isotopic comp. in atm. precip. around Sudbury, Ontario 78−81361
S, isotopic comp. in sulphide and sulphate minerals from DSDP Leg 37 77−91101
S isotopic composition in precipitation within Great Lakes Basin 79−16625
SO, S isotope composition, vibronic spectroscopic determ. *(Russian)* 79−10124
$^{33}S/^{32}S$ ratio in ocean water SO_4^{2-} 78−65340
^{34}S, in CS mol., UV vibronic spectral anal. method *(Russian)* 79−50041
^{34}S in troilite, enrichment rel. to lunar soil 80−77303
$^{34}S/^{32}S$, interstellar abundance ratio from SO emission obs. 78−24535
$^{34}S/^{32}S$ in marine sediments 79−92523
$^{34}S/^{32}S$ ratio in magmatic gases of Afar ridge volcanism 80−21732
$^{34}S/^{32}S$ ratio meas. using SO_2 and SF_6 methods, discrepancies 78−65405
$^{34}S/^{32}S$ ratios in California stratus rel. to aerosol and cloud drop origin 77−29407
Si whisker field desorption ion source, Cu, Sn, Ag, Te, Cd and Sb isotope abundance ratios 80−11975
$^{28}Si/^{29}Si/^{30}Si$ isotopic abundance ratio determ. from SiO isotopic lines in sunspots 79−30044
Sm in solar system rel. to Allende inclusion EK1-04 isotopic anomalies 79−35208
Sm isotope anomalies in Allende meteorite 78−89134
Sr, abundance ratios for use in geochronology and cosmochronology 78−28189
Sr and O isotope abundances of Loch Uisg granophyre, Isle of Mull, origin hypotheses 78−65303
Sr anomalies and p-process odd-A abundances 78−93101
Sr in batholith between Princeton and Okanagan Lake 77−17096
Sr, in flood basalts, Earth struct. models 80−72475
Sr isotope anomalies in Allende meteorite 78−89133
Sr isotope comp. of Alpine tectonite lherzolites, evidence for mantle origin 78−65302
Sr isotope evidence for petrogenesis in Mexican andesites 78−28203
Sr isotopes and trace element geochem. of impact melt at Mistastin Lake crater, Labrador 78−32105
Sr isotopes conc. in ocean floor basalts and ferromanganese deposits 78−61395
Sr isotopes of rholitic ignimbrites, Batopilas area, Mexico 80−94501
Sr isotopes rel. to petrogenesis of N.Chilean ignimbrites 79−44146
Sr, isotopic comp. of Pacific Ocean Basin basalts, rel. to mantle comp. 78−65218
Sr isotopic composition, comment 77−29323
Sr, isotopic homogenisation in multiply deformed Precambrian terrain rel. to discrete events chronology 79−57895
Sr, Pb, O isotopic analyses of rocks from Skaergard intrusion, E Greenland 79−29763
$^{84}Sr/^{86}Sr$, chondrites, CI and CM, discordant, leaching experiments, Rb-Sr studies 79−84754
^{87}Sr, enrichment in Cyprus ophiolitic sulphides confirms ore form. by circulating seawater 77−81887
$^{87}Sr/^{86}Sr$, in rocks of Cantal continental volcanic system, constraints on genesis and evolution 79−88327
$^{87}Sr/^{86}Sr$, initial ratio in Norton County enstatite achondrite 77−5508
$^{87}Sr/^{86}Sr$, initial ratios in Archaean rocks of English River subprvince, NW.Ontario rel. to crust form. 80−94486
$^{87}Sr/^{86}Sr$, ratios in Cretaceous mid-ocean ridge basalt (MORB) from DSDP Holes 417D and 418A 80−94520
$^{87}Sr/^{86}Sr$, ratios in oilfield brines from Kansas and Colorado 78−57225
$^{87}Sr/^{86}Sr$, ratios in Recent andesites in Ecuador and N.Chile 78−32042
$^{87}Sr/^{86}Sr$ ancient seawater composition, Jurassic to Pleistocene, Israel groundwater obs. 80−61804
$^{87}Sr/^{86}Sr$ and crustal contamination model for calc-alkaline igneous rocks 79−79762
$^{87}Sr/^{86}Sr$ for plutonic rocks from Whitehorse map area, Yukon 80−31005
$^{87}Sr/^{86}Sr$ in Bay of Islands ophiolite complex, rel. to midocean ridge basalts source evolution 80−85651
$^{87}Sr/^{86}Sr$ in calc-alkaline andesites and plateau lavas from S.America 79−29726
$^{87}Sr/^{86}Sr$ in Kerguelen Islands igneous rocks, inferences on enriched oceanic mantle sources 80−98319
$^{87}Sr/^{86}Sr$ in L chondrites 80−51705
$^{87}Sr/^{86}Sr$ in mantle xenoliths, unequilibrated isotopic comp. meas. with equilibrated Nd isotopes 80−98321
$^{87}Sr/^{86}Sr$ in Murrumbidgee Batholith, isotopic equilibration 77−41026
$^{87}Sr/^{86}Sr$ in Norwegian eclogites, rel. to crustal origin 80−76978
$^{87}Sr/^{86}Sr$ initial ratios in Gondwanaland Mesozoic tholeiites, rel. to lithosphere chemistry vars. 78−28201
$^{87}Sr/^{86}Sr$ initial ratios and Rb-Sr ages, from Oxford Lake-Knee Lake greenstone belt, N.Manitoba 80−94485
$^{87}Sr/^{86}Sr$ ratio for fracture-filling calcite in granitic basement 77−29267
$^{87}Sr/^{86}Sr$ ratio in basalts from Sao Miguel 79−74873
$^{87}Sr/^{86}Sr$ ratio in Central North Atlantic basalts, evidence for Azores mantle plume 77−5179
$^{87}Sr/^{86}Sr$ ratio in Recent continental volcanic rocks 78−53635
$^{87}Sr/^{86}Sr$ ratio in Susquehanna River basin 77−29349
$^{87}Sr/^{86}Sr$ ratio in volcanic rocks from W.Pacific island arcs 77−33031
$^{87}Sr/^{86}Sr$ ratio reduction during hydrothermal alteration of basalts 79−16446
$^{87}Sr/^{86}Sr$ ratios, Indian kimberlites 79−92536
$^{87}Sr/^{86}Sr$ ratios in calc-alkaline volcanic rocks from Cerro Galan, NW.Argentina, evidence for crustal contamination 80−98318
$^{87}Sr/^{86}Sr$ ratios in granites from British Late Caledonian 80−36276
$^{87}Sr/^{86}Sr$ ratios in magma genesis, mineral phases and parental rocks 77−25671
$^{87}Sr/^{86}Sr$ ratios of calc-alkaline volcanism rel. to Peru-Chile Trench granulitic basement 78−28204
$^{87}Sr/^{86}Sr$ ratios of interstitital waters from DSPD sites rel. to sediment geochem. 79−34794
$^{87}Sr/^{86}Sr$ ratios of Upper Cretaceous ophiolitic rocks of Troodos Massif 78−7614
$^{87}Sr/^{86}Sr$ systematics of geothermal water-rock association in Massif Central, France 77−60373
^{90}Sr and T in N.Pacific surface water during 1974, conc. meas. 80−26181

isotope relative abundance continued
T, concentrations in Caspian Sea 79−34858
T, D and ^{18}O composition of Sahelian rain, 1975-6 period *(French)* 80−21809
T distribution, Ross Ice Shelf Project ice hole 79−88371
T distribution in Weddell Sea water masses 79−39728
T fallout at South Pole in 1954-1978 snow samples 80−16867
T, in Pacific Ocean, source function for transport models 78−32122
Te isotopic composition in meteoritic and terrestrial materials 78−82856
Te, Xe and Kr isotopes in Allende meteorite, record of nucleosynthesis 79−40147
^{132}Te in lower troposphere, airborne levels and lifetime 79−12242
Ti, in α Tauri (Aldebaran), isotopic ratios 77−22212
Ti, isotopic abundance ratios in cool stars 80−26840
Ti isotopic anomaly from meteoritic materials study 79−53716
U at Oklo natural fission reactors, radiometric meas. and isotopic anal. *(French)* 80−21754
U, determ. from EPR hyperfine struct. of $NaF:U^{5+}$ 79−91296
U, determ. in environmental samples, neutron activation, neutron assay and fluorometric methods 78−61087
U exchange during low-temp. alteration of oceanic basalt, isotopic evidence 79−29744
U fuel, correlation of U and Pu isotope compositions with burn-up 79−63746
U, hollow cathode discharge, opto-galvanic spectroscopy-electron temp., isotope ratio analysis 79−77437
U in phosphorite nodules on sea floor off Peru and Chile 78−7612
U in rocks isotope disequilibrium, due to α-recoil and soln. effects 80−98314
U in spent reactor fuel, isotopic comp. and conc. determ. by mass-spectrometric isotope dilution 79−89373
U, isotopic analysis by resin-bead mass spectrometry for materials safeguards 80−78392
U, isotopic comp. in chondritic meteorites 78−4157
U, isotopic composition, determ. using thermal ionisation spectrometry with automatic data eval. 80−66913
U, isotopic compostion, determ. using thermal ionisation mass spectrometry 80−66914
U, nondestructive element and isotope assay in nuclear materials 80−71870
U ore dating from meas. of ^{238}U and Ru conc. 80−21863
U-bearing minerals, isotopic composition due to terrestrial neutron flux *(Spanish)* 77−5195
U-bearing rocks, radioactive disequilib. determ., isotopes relative abundance meas. 78−57330
U-Pb geochronology in Lac Seul region, English River Gneiss Belt 77−5148
U-Th-Pb isotopic study of Precambrian metavolcanics in Orange River region, S.Africa 79−44147
UO_2-P-uO_2 rods, isotopic anal., gamma-ray spectrometric meas. calibration appl. 77−81440
^{233}U safeguards, expt. nondestructive assay using a random driver 80−83164
^{234}U excess, ageing effect in confined waters, comment 77−9449
^{234}U excess in groundwater, ageing effect in confined waters, comment 77−5252
$^{234}U/^{235}U/^{238}U$ ratios in sediment from W. coast of India 77−41020
$^{234}U/^{238}U$, ratio in Edwards carbonate aquifer, Texas, rel. to aquifer oxidation/reduction state 80−98362
$^{234}U/^{238}U$ ratio disequilibrium in natural samples, mechanisms involving recoiling alpha-emitting nuclei 79−16466
$^{234}U/^{238}U/^{226}Ra$ ratios in fracture zone water of N.Kirgizia 77−33108
^{235}U burn-up determ. by mass spectrochemical anal. 80−71989
^{235}U, determ. in coastal sediments and seawater, activity ratios, disequilib. 78−27851
^{235}U in Uf_6, mass spectrometric determ. 80−68961
^{235}U isotopic content determ. of nuclear materials using gamma spectrometry 79−85756
^{235}U, nondestructive active assay in $(U,Pu)O_2$ fuels 80−71873
^{235}U var. and natural abundance in ore bodies 77−41014
$^{235}U/^{238}U$ isotope ratio determ. in UF_6 samples using gas quadrupole mass spectroscopy 80−78376
$^{235}U/^{238}U$ ratio, non-destructive field meas. for geophysical prospecting 80−21862
$^{238}U/^{235}U$, abundance ratio for use in geochronology and cosmochronology 78−28189
$^{238}U/^{235}U$ in Allende meteorite rel. to early Solar System ^{247}Cm 80−90347
$^{238}U/^{235}U$ in chondritic meteorites, search for isotopic anomalies 80−85903
Xe, fissiogenic isotopes in CO_2 well gas 78−73374
Xe, from ^{248}Cm spontaneous fission, rel. to origin of carbonaceous chondrite fission Xe 77−37581
Xe in Fe meteorites 78−12165
Xe, in meteorites, anomalies rel. to extinct radioactivites and presolar grains 77−45367
Xe in Murray carbonaceous chondrite meteorite, evidence for multiple trapped Xe components 80−98618
Xe isotopes in Te ores, geochem. test of nucleon stability 78−8667
Xe, isotopic composition anomaly in Murchison meteorite 79−44424
Xe, isotopic composition anomaly in Murchison meteorite, reply 79−44425
Xe, s-process contributions 79−5739
^{129}Xe, excesses in Hawaii lavas olivine phenocrysts and xenolithic dunites 79−34814
^{129}Xe in meteorites, rel. to extinct radioactivities and presolar grains 77−49342
$^{130}Xe/^{132}Xe/^{136}Xe$ in Murchison C2 chondrite, presolar gas component evidence 80−85904
Yb, in meteorites and terrestrial samples 78−32419
Zr in S-type stars R Cygi and V Cancri 78−53957
Zr, isotopic composition, at. wt., rock standards, chondrite composition 79−3591

isotope separation
see also isotope exchanges; laser isotope separation; radiochemistry
12.16 μm radiation, two-photon pumping of $^{14}NH_3$ 78−90414
^{237}U isotope generator based on ^{241}Pu 79−71980
actinide partitioning from high-level radioactive wastes, arguments against 77−61570
isotope separation continued
actinide partitioning in LWR fuel reprocessing, conceptual methods 79−85810
actinide separation from high activity liquid waste, OXAL process *(French)* 79−85813
actinide separation from high-level waste, nuclear transmutation 77−61569
actinide separation in highly active nuclear waste solns. *(French)* 79−85812
actinide separation in nuclear fuel and wastes, hazard assessment 79−85806
actinide transmutation, nuclear fuel cycle impact studies 79−85752
actinide transmutation, research activity status, Japan 79−85807
actinide transmutation and chemical separation from radioactive waste 79−85808
actinides, chemical separation from PUREX raffinates using organic solvents 78−66676
actinides, recycling and recovery in fission reactor wastes 79−85699
actinides, separation from high level radioactive fuel reprocessing waste 79−85809
aerodynamic separation technique based on vel. slip in freejet expansions 80−19441
alcohol-water solutions, containing radioisotopes, radiochemical purification *(Russian)* 77−86432
alpha-radioactive nuclides separation from waste solution *(Japanese)* 77−54318
anion-exchange refinement of Pu and Np separated during extraction refinement of spent fuel elements 78−70624
asymmetric process, separative power, resoln. of inconsistencies 78−29622
asymmetric separation process, value function, separative power 77−75001
asymmetric separation processes, two types of ideal cascade 79−36377
atomic beam separation by light press. in isotope-separation setup 80−52943
atomic diffusion pulling in and pushing out by light field *(Russian)* 79−98047
binary gas mixtures, separation and isotope separation in curved shock wave 79−94753
binary isotopic gas mixture, convection-diffusion eqn. soln. for centrifuge axisymm. vel. field 78−17434
calutron, EM isotope separator, instability limit 79−22477
carbon tetrachloride, isotropically selective dissoc. by NH_3 laser radiation 78−17815
cascade, random walk model 77−58190
cascade separation of two component mixtures, limits of applicability of weak enrichment approx. 77−71696
centrifuge, crossed-field, ion wind effect on separation 80−79591
centrifuge method, rotating plasmas analysis, ^6Li enrichment *(Japanese)* 79−41248
centrifuges, gas, liquid, appls., review 79−53289
chemical vapour deposition, from gaseous or liquid source, as isotope separation methods 79−50148
chlorotrifluoromethane, multiphoton dissoc., ^{13}C enrichment *(French)* 80−91615
chromatographic, derivation of comprhensive expression for conc. profile 78−29856
collisional plasma rotating inside cylindrical annulus, anal. rel. to isotope separation 78−22466
combined laser gas centrifuge technique 77−74946
computerized mass spectrometer for isotopic analyses of solids 78−78026
conference, actinide nuclear transmutation, Ispra, Italy (April 1977) 79−85698
conference on nuclear spectroscopy of fission products, Grenoble, France (May 1979) 80−77546
cosmic ray telescope, solid state, detection system for heavy ions, element and isotope separation 80−67563
crossed-field plasma centrifuge, effect of ion wind on separation 79−31722
CVD system appl. to isotope enrichment 77−23301
cyclone separator, 3D flows and turbulence intensity *(Chinese)* 79−36418
DC discharge, isotope enrichment by reson. trapping and cataphoresist. 77−27752
denatured Th fuel cycle safeguards against proliferation 79−13422
deuterium distillation at desalination plants 77−67894
dichlorodifluoromethane, laser photolysis for Cl isotope enrichment 78−58859
discharge, cylindrical, rotation by elec. and mag. fields, isotope separation appl. 77−39486
displacement chromatography, isotope separation appl., mathematical model 79−10219
electron microscope isotope separation and electron spectroscopy 80−32850
element 114, search in galena using EM isotope separator and fission track detectors 77−27203
EM isotope separation and in-beam electron spectroscopy, Pt target preparation 80−52812
EM isotope separators, appl. to extended Pt target preparation 78−70676
EM sector separators, variable geom. multipocket collector 77−14611
EM separation, appl. to heavy-ion implantation, He ion backscatt. meas. 77−14322
EM separation, reln. to electron and positron spectroscopy 77−23329
EM separators and related ion accelerators 77−14276
EMIS separator, secondary effects of parking, design of HV power supply 77−14268
enhanced resonant atomic and mol. scattering 77−61825
enriched gaseous isotopes, recovery systems 78−58525
enriched isotope target preparation, design of quasi-hyperbolic electrostatic fields 80−23597
enrichment by isotope separation, HAGA radial-separating-nozzle centrifuge process 79−67954
enrichment by plasma centrifuge, rotational velocity meas. 78−74502
enrichment factor meas. in reln. to flow distrib. 77−71697
enrichment requirements of expanding nuclear economy with advanced reactors 77−61624
fast chemical separation procedures for short-lived nuclei 77−25351
FEBIAD ion source for fission fragment isotope separation 80−78483
fission product separation using Lohengrin mass separator, high flux reactor in Grenoble 78−17436

isotope separation continued
fission reactor fuel, preparation technology modifications *(Czech)* 80−9388
fluoromethane, deuterium separation at high press. by ns CO_2 laser multiple-photon dissoc. 80−91616
formaldehyde, selective laser photolysis for ^{14}C enrichment 80−108720
formaldehyde, UV photolytic separation of D from H in cryogenic solns. 78−95937
formic acid decomposition by IR laser radn., photochem. isotope enrichment 79−52712
Freon, photochemical ^{13}C and ^{37}Cl isotope enrichment using CO_2 laser pulses 79−36787
Freon 123, deuterium separation at high press. by ns CO_2 laser multiple-photon dissoc. 80−91616
fuel reprocessing waste ^{137}Cs, ^{90}Sr and rare earth radioisotope separation by cation exchange 78−78486
gas centrifuge, fluid flow anal., computer calcs., appl. to UF_6 77−75924
gas centrifuge, numerical anal. of weakly compressible rotating flows 80−47726
gas centrifuge, pressure recovery of supersonic flow in diffuser 78−29104
gas centrifuge rotating differentially, non-rotating side wall 77−67895
gas centrifuge with differential rot., U enrichment 77−54363
gas centrifuges, pressure recovery in diffuser at high Mach number rotation 79−22480
gas centriguge, effect of compressible flow on max. separating power 78−70644
gas discharge with travelling mag. field, isotope separation by mass diffusion 80−44050
gas in rot. cylinder, velocity profile meas. 79−50737
gas jet recoil transport system, continuous separation of Se and Te from fission products 78−70674
gas jet recoil transport system for fission products, appl. to chemical separation in gas phase 78−17459
gas membrane separation cascades, efficiency comparisons 79−13529
gas mixture-isotope inertial gas-kinetic separation 80−69927
gas separation performance of tapered cascade with membrane 79−22478
gaseous diffusion, aerodynamic effects 78−59469
gaseous mixtures, diffusion, laser separation 79−77331
He-jet fed online mass separator for recoil atom mass spectroscopic anal. 80−98998
heavy isotope separation using nozzles, jets and channels, investig. 79−94097
heavy water production, laser photodesorption 77−54365
heavy-ion separator SIS, at GSI, velocity filter 77−26425
heterogeneous chromatography, meaning of chromatographic diffusion coefficient in isotope separation 79−50147
hexafluoride molecule selective excitation via Doppler free multiphoton process 78−55178
hexafluoroacetone, IR multiphoton dissociation, isotopic selectivity and yield, temp. effect 80−53069
hexafluoroacetone, natural isotopic abundance, selective multiphoton decomposition at threshold 79−89723
hexafluorobutadiene, electronic ground state photochem., isotope separation by IR multiphoton isomerisation 79−79264
hexafluorocyclobutene, electronic ground state photochem., isotope separation by IR multiphoton isomerisation 79−79264
HF stationary discharge, travelling mag. field, barodiffusion separation 80−44049
high-level waste, hot cell facility and equipment for tests of radionuclide removal process 80−18675
highly excited atoms, review of recent expts. 80−23325
ideal cascade with variable separation factors, separative power 79−22479
ideal cascades, 2-up 1-down, separative power and interstage flow anal. 78−58499
impulse plasma centrifuge with circulation, theory *(Russian)* 80−38553
in-resonator spectroscopy using dye laser *(Russian)* 77−54752
inert gas isotope separation in RF discharge in travelling magnetic field 80−78719
interstellar clouds, isotope fractionation expts. under simulated space conditions 78−73623
ion beam instrumentation systems, CAD 77−13819
ion beams, mass separation in EM field, model mass separator 78−9855
ion implantation, isotope separator, prep. of p-n junction particle detectors 80−34034
ion source fission product separators 80−78479
ion sources, high temperature, for on-line isotope separation appl. 80−74063
ion space charge neutralisation, influence on mass separator transmission 78−82073
IR laser induced isomerization of labelled compounds 77−25289
isobar nuclear reaction products separation in on-line separators *(German)* 78−33291
ISOCELE high-current on line separator development 77−26922
ISOL novel ion source, Nielsen-type geom. 77−14286
ISOLDE as a source of neutron-rich nuclei 80−78480
ISOLDE-2 on-line isotope separator at CERN 600 MeV synchrocyclotrons 77−23330
isotope and isomer separation in an inhomogeneous magnetic field 80−9752
isotope centrifuge, effect of thermal convection on separative power, numerical anal. 78−58500
isotope production at LAMPF, hot cell chemistry 80−18674
isotope separation, microwave reson., triplet state photochem. technique 77−32818
JEN experimental reactor design, development and construction in Spain *(Spanish)* 77−38384
Kyoto University reactor, He-type on-line isotope separator 80−23152
laser-excited atoms deflection by elec. field, isotope separation appl. 78−955
laser-induced selective multistep processes: impact on nuclear physics, chemistry and biology 80−61122
Leuven isotope separator on-line at CYCLONE cyclotron 78−70682
light induced diffusion of gases, isomer, isotope separation *(Russian)* 80−79430
liquid-liquid extraction column online control by modal control techniques 78−54865
magnet design for high-current implanters or small isotope separators 80−68222
isotope separation continued
mass diffusion cascade, effectiveness increase using asymmetric schemes for combining stages 79−45392
mass diffusive separative unit, math. model 77−50300
mass separation by weakly ionised plasma centrifuge 80−106985
mass separator facility on-line to UNILAC heavy ion accelerator 77−14299
mass separator operating on heavy-ion beam, surface ionis. ion source 78−5083
mass spectrograph type separators, throughput limit 78−65995
mass-diffusion element, anal. of separative power 79−41039
MEIRA, deflection radius and operational characteristics 77−19161
MEIRA separator, MV power supply and automatic ion source control system 77−13778
metal, isotope enrichment by combined elec. migration and zone melting 78−76600
metal, isotope enrichment during zone refinement *(Russian)* 77−59686
meteorites, isotope fractionation expts. under simulated space conditions 78−73623
methane isotopic mixtures, enrichment of D using vibrationally sensitized reaction 80−76532
methyl isocyanide photoisomerisation, laser isotope separation, C-isotope enrichment by one-photon vibr. photochemistry 80−81336
molecular selective photodissociation of differing isotopic comps. 77−75244
molecule, IR radiation induced vibr. excitation and dissoc. 77−27135
molecules, polyatomic, isotopically selective photodissoc. 77−6868
molecules beam selection by quadratic Stark effect *(Russian)* 78−78823
molten salts, transport processes by ionic dynamics, mass depend. 78−22616
multicomponent isotope separating cascade composed of elements with large separation factors 79−26753
multicomponent isotope separation, synthesis of value function 79−67955
multistage cascades, nonlinear processes, computer calc. 78−5370
neutral atoms, spatial mass separation, in rot. weakly ionised plasma *(Russian)* 79−3590
neutron rich nuclei, beta decay half lives, expt. techniques 80−78224
neutron-rich fission products, gas-filled on-line separator *(German)* 77−18708
nitromethane, multiquantum absorption in intense IR field, isotope shift 77−19000
nondeliverable fabrication plant fuel material with various enrichment, determ. of optimal comp. 78−13312
nondisplacement chromatography for chromatographic isotope separation 79−50146
nuclear fuel, U and Pu decontamination, sorption and distillation methods, review *(Czech)* 78−82496
nuclear fuel cycle, extraction, concentration, UF_6 conversion, isotope separation *(French)* 80−63354
nuclear fuel production, continuous gas flow control simulation *(German)* 80−78416
nuclear isomers, photochem. separation 79−50153
nuclear power station, liquid discharge, radionuclide isotopic anal. *(Spanish)* 78−13250
nuclear reaction products, approaches, facilities 77−23358
on-line, hollow cathode ion source and He-jet system 77−14304
on-line, preparation of radioactive targets for nuclear bombardment 77−23328
on-line, progress in targets and ion sources 77−14300
on-line gas phase separations of ^{252}Cf fission products 77−14615
on-line isotope separation facility HELIOS at the Mainz reactor 80−102350
on-line mass separator for fission-produced alkali isotopes 80−98997
on-line separators, fast tape transport system 77−14328
on-line separators, progress, ion sources, ultra-high-temp. targets 77−23337
on-line system employing cooled and NaCl loaded He-jet methods 77−14288
online, ISOLDE-0 facility 77−22364
online isotope separator, SOLIS, communication channel between data acquisition system and computer 80−74030
organic non-volatile compounds ionisation by fast heavy ions, separation by TOF mass spectrom. 77−27170
ORNL, isotope separations programme 77−19109
ORNL EM isotope separation program 80−18673
OSIRIS, target/ion source system for isotope separation in on-line mass separator, mol. ion prod. 80−99366
OSIRIS on-line mass separator, study of short lived fission products 77−23352
plasma, recombining, possible isotope enrichment due to reson. trapping 77−58203
plasma centrifuge, enhanced isotope separation in crossed E×B fields 79−18305
plasma centrifuge, isotope and element separation mechanism 80−6291
plasma column, rot., in hollow cathode discharge 78−75454
plasma ion cyclotron reson. 77−10787
plasma ponderomotive force effect near ion-cyclotron reson. 80−43998
polyatomic molecules, multistage IR dissoc., collisionless energy-gathering process 80−99526
polymer membrane, laser stimulated active diffusion, appl. to isotope separation *(Russian)* 78−2302
porous barrier fabrication for U isotope separation, powder metallurgy problems *(Italian)* 78−88439
Princeton Cyclotron data acquisition system 80−102415
probe in supersonic flow, Monte Carlo simulation 79−94098
radioactive ion beams, for nucl. expts., review 79−97922
radioactive rare gas separation, using cell with two membranse of differing permeability 78−29590
radioactive rare gas separation by membrane permeation, improvement in separation factor 80−18559
radioactive rare gas separation performance of a two-unit series-type separation cell 79−41008
radioactive target production for use in charged particle reaction spectroscopy 78−70670
radioactive waste, chem. treatment prior to evaporation 77−54327
rapid automated nuclear chemistry, short lived fission products, reactor safety 80−81353
rapid automated nuclear chemistry facility for the study of short lived fission products 79−71978
rare earth fission products, isotopic separation after recoil in Ta foil 77−14614

isotope separation continued
rare gas separations using SIDONIE and PARIS separators 77−14269
rare gases in volcanic rocks, isotopes mass fractionation as indicator of gas transport to or from magma 80−98292
rare-earth fission product isotopes, separation in thin-films chromatography *(German)* 80−37635
reactor fuel gaseous mixtures separation by supersonic acceleration 79−22482
recoil separator, Lohengrin, ion optics, nuclear fission product spectroscopy 77−22607
refractory matrices, fast release of reaction products from 600 MeV irradiation 78−29652
retardation collector system for special target preparation with isotope separator 77−14284
review of new isotope separation methods 78−1111
RF separators, review 77−13821
rotating plasma technique, skewed mag. and elec. fields *(Russian)* 78−70969
rotating plasmas, balance and separation processes 78−1911
Scandinavian low output isotope separator, upgrading to 300 kV 78−66008
selective photoionisation of atoms by laser radiation, appls. 78−5189
semipermeable membrane, secondary-stage processes, photoexcitation effects *(Russian)* 77−6962
separation cascades, several outlets, theory 78−17437
separation cell with two kinds of membrane, characteristics *(Japanese)* 79−36419
separative power functions for enriched and depleted streams 80−47678
SIRIUS facility for neutron rich fission fragment studies 80−78484
SISAK 2, chemical separation method for short lived fission products in spectroscopic studies 80−74068
SOLIS, surface ionisation integrated target-ion source 77−14303
spiral ion exchanger for rapid radiochem. separations 77−25296
sputter deposition, isotope enrichment 77−27198
sputter-induced isotopic fractionation at solid surfaces 80−55244
steady-state rotating plasma, for mass separation of elements *(Russian)* 78−25732
steam, supercritical, isotopic separation of metals 77−63922
sulphonic ion exchangers Ar selective separation of U and Th from lanthanides 78−58860
superheavy element prod. in ^{48}Ca ion+^{248}Cm, spontaneous fission 78−74390
supersonic molecular beam technique using RF spectroscopy, mag. reson. 80−47725
Taylor diffusion device 78−25752
temperature-controlled multireflection absorption cell design and performance 77−18108
s-tetrazines, mol. crysts., laser-induced photochem., isotope separation and hole burning 78−85185
Tokamak plasma exhaust, packed distillation column for isotopic enrichment 80−838
transuranic element separation from radioactive waste and fuel reprocessing *(French)* 79−85811
trifluoroiodomethane, highly excited, intermol. vibr. energy transfer, transient UV absorpt. spectra 80−106381
trifluoromethyl chloride, IR multiphoton dissociation, isotopic selectivity and yield, temp. effect 80−53069
TRISTAN facility, target developments 77−23353
TRISTAN II mass separator, ion source, beam optics, computer system 80−78481
TRISTAN II mass separator at Brookhaven HFBR, research programme for fission products 80−78482
TRISTAN II on-line separator, study of non-gaseous fission product activities 79−67956
ultracentrifuge, flow, isotope conc. field, numerical model 79−1199
ultracentrifuge, thermally-controlled, for isotopic separation, gasdynamic features 77−54362
UNISOR integrated target-ion source 77−14302
UNISOR ISOL data aquisition system 77−14324
unslowed fission product separators, gas filled JOSEF, parabola LOHENGRIN 80−78478
velocity separation of isotopic mixtures in supersonic beams 77−54626
velocity slip separation process, effect of collisions with background gas 77−23578
Warsaw University isotope separator, machine parameters *(Polish)* 80−86987
wedge type ion beam divergence profile calc. 78−82555
Z=114, existence in S.American hypogene lead ores, exptl. evidence *(German)* 79−55019
Am isotopes (241, 243) separation, chemical treatment of irrad. targets *(French)* 77−26883
Am, production of transuranium elements by neutron irrad. of ^{241}Am *(Japanese)* 80−52731
Ar binary mixtures, separation performance of Kr and Xe by thermal diffusion column 77−42192
Ar, isotope separation by axial mol. flow turbomachine 78−17816
Ar isotope separation by axial flow turbomachine model 78−78500
Ar isotopes, double-spiking procedure for K-Ar dating 77−60473
Ar-Kr mixtures, liq.-vap. isotope fractionation factors 78−33626
Ar-N_2 and Xe-Kr, evaporation equilibrium data method *(German)* 77−67846
^{36}Ar, separation, calc. of thermal diffusion cascade *(Rumanian)* 78−58862
^{36}Ar-^{40}Ar, thermal diffusion column transport coefficients *(Rumanian)* 78−51274
^{75}As(α,2n)^{77}Br 79−85468
B, using anion exchange resin *(Japanese)* 78−33625
BCl_3, frozen, selective evaporation of $^{10}BCl_3$ and $^{11}BCl_3$ by CO_2 laser irrad. *(Russian)* 77−3422
B_2O_3 laser-produced plasmas, isotopic enhancement 80−92349
^{10}B separation using anion exchange resin, isotopic plateau holding displacement chromatography *(Japanese)* 78−56886
^{138}Ba separation from $BaCO_3$ by method of internal reduction 77−14613
^{210}Bi, separation from ^{210}Pb, radiochem. determ. 77−56266
^{210}Bi, separation from ^{210}Pb, using silica gel ion exchanger 78−86961
Br isotope enrichment in BrI after isotopically selective excitation 77−90581
^{A}Br A=84-88, fission products, rapid electrophoretic separation technique 79−54982
^{79}Br(p,3n)^{77}Kr→^{77}Br production excitation curves 79−85468
isotope separation continued
^{79}Br(p,3n)^{77}Kr→^{77}Br^{-} production, separation and radiopharmaceutical labelling 79−79649
^{87}Br, prod. by radiochem. separation, for neutron decay obs. 78−70951
CO, ^{13}C isotope enrichment by 123.58 nm Kr reson. radiation photolysis 78−33624
CO, ^{13}C/^{12}C and ^{18}O/^{16}O liq.-vapour isotopic fractionation factors 79−90770
^{13}C, enrichment in multiphoton dissoc. products of trifluoromethyl halides 79−18302
^{13}C in interstellar cyanoacetylene, evidence for chemical fractionation 77−87532
^{13}C/^{12}C isotope fractionation of organic matter assoc. with U ores induced by alpha irradiation 79−57932
^{13}CO/C^{18}O fractionation in interstellar dark clouds 80−46638
^{14}C dating, thermal diffusion enrichment, N. American glacial history extended to 75000 yrs ago 78−77284
^{14}C dating, time scale extension by thermal diffusion enrichment, appl. to NW. Europe climatology 78−77314
^{13,14}C, thermal diffusion separation column, effective vol. calc. *(German)* 78−42235
Ca, isotopic anal. using double vaporizer 80−106398
CaF_2, appl. of theory of sputter-induced isotopic fractionation at solid surfaces 80−55244
Cd isotope enrichment, by refining and pulsed currents 78−3032
Cd vapour, RF discharge, isotope separation 80−79619
^{144}Ce, anodic deposition on Pt anode, electrochem. separation 79−91958
Cl, isotope enrichment using laser photolysis of dichlorodifluoromethane 78−58859
Cl isotope separation by liquid-phase thermal diffusion 79−89502
Cl isotopes, thermodiffusion in carbon tetrachloride 79−90810
^{37}Cl, enrichment by ICl+acetylene selective photoaddition 77−60084
Cm isotopes (242, 244, 248) separation, chemical treatment of irrad. targets *(French)* 77−26883
Cm, production of transuranium elements by neutron irrad. of ^{241}Am *(Japanese)* 80−52731
^{137}Cs, separation from nucl. waste using sodium zirconate 80−27760
Cu(II), selective separation from rare earth elements on chelate ion exchangers 78−58861
D exchange reaction between H_2 and water á hydrophobic catalyst supporting Pt 80−30208
D, isotope enrichment by CW CO_2 laser-induced vibr. photochem. 79−36790
D isotope enrichment in methane-H_2 mixture, by glow discharge exposure 78−13343
Dy, hyperfine structure of odd isotopes, two step photoionisation, mass filtration *(Russian)* 77−46550
EM separation of rare earth isotopes, ^{135}Ba and Mo isotopes using SIDONEI II 77−14612
^{166}Er target preparation by retardation and direct deposition technique in mass separator 77−14285
^{253}Es, separation and α-spectra identification following neutron irradiation of Cf 78−17435
^{151}Eu (^{153}Eu) excitation transfer, effect on selective photoionisation 80−99538
^{18}F recovery during transport from reactor 78−78821
Fe, proton bombardment, stable nuclide form. and separation 78−20045
Fe(III), selective separation from rare earth elements on chelate ion exchangers 78−58861
H containing mixture extraction from D compounds, ionis. radiation effects *(Russian)* 77−6961
H cryogenic isotope distillation for fusion power reactors 79−93833
H isotope removal from flowing Ar, U and Ce as hydriding materials 78−17438
H isotope separation in DC-arc plasma, mass spectrometric anal. 79−90457
H-^{2}H, rotating plasmas, balance and separation processes 78−1911
H-D mixture, selective chemisorption by KC_8 intercalation cpd. *(French)* 77−32830
H-isotope enrichment using low-temp. glow discharge technique 78−66675
H_2, isotope separation in Ti-fluidised bed 80−18676
H_2-D_2 isotope separation by permeation through Pd membrane 80−68959
H_2-Pd system, effect of isotopic conc. on separation coeff. of H-T, H-D and D-T mixtures 79−71979
H_2+D_2O, isotope exchange and separation with Pt hydrophobic catalyst *(Japanese)* 80−37901
$H_2{}^{16}O$, $H_2{}^{18}O$, isotope fractionation, H-bonds, force consts., liq. water struct. 77−76288
H_2−D_2, separation by Taylor diffusion 79−18303
^{3}H, by water distillation 79−63812
He-jet online mass separator, improvements in total yield 80−98999
He-jet system, appl. for isotope separation 77−14287
^{4}He, liq., isotopic purification 77−35769
^{4}He, superfluid, purification technique from ^{3}He, for neutron source bottle 78−17823
^{203}Hg separation from chlormerodrin-203, electrophoretic method 77−56283
^{123}I, production in LASL radiochemistry hot cells 80−72326
^{127}I(p,5n)^{123}Xe→^{123}I^{-} production, separation and radiopharmaceutical labelling 79−79649
^{129}I and organic compound determ. in LWR irradiated fuel solns. *(French)* 79−3230
^{131}I-4-iodoantipyrine preparation from ^{131}I-iodide 80−12256
^{115m,113m}In, separation from ^{113}Sn and ^{115}Cd by chem. extraction 78−74783
K isotope separation in solution by thermal diffusion 80−87236
K, using cylindrical RF mass analyser 79−80718
KOH gas-crystal system, isotopic equilibrium near phase transition points *(Russian)* 80−91697
^{43}K, prod. by V target bombard. with medium energy protons, separation medical appls. 77−81572
Kr, separation in fission fuel reprocessing plants *(German)* 79−85719
Kr, transient separation of thermal diffusion column, non-active end vol. influence 77−35300
Kr-Xe, isotopic mixtures, separation in high-freq. discharge in mag. field *(Russian)* 77−75317
^{78}Kr/^{86}Kr, by thermal diffusion *(Rumanian)* 80−86988
^{85}Kr, atmos. separation technique, preliminary results *(German)* 78−16222

isotope separation continued
^{85}Kr monitoring system with permselective membranes 79−3260
^{85}Kr/Xe separation from nucl. engineering off-gases, low temp. distillation *(German, English)* 77−18671
Li, isotope separation by plasma centrifuge, static characts. anal. *(Japanese)* 80−5326
$^{6}Li^{+}$ enrichment, countercurrent electromigration cell containing molten NH_4NO_3 78−47547
Li_2, isotope separation, by two-photon ionisation, ionisation pot. determ. 78−70950
Li_2, isotopes fractionation in two step photoionization, due to Ar laser beam 78−25631
Mg, sputtering by He^{+}, isotope fractionation 79−87542
^{28}Mg carrier-free production by 50-180 MeV protons on Si, P, S, Cl, Ar and K 79−83934
^{99}Mo separation from ^{131}I and ^{103}Ru uranium fission products 77−25297
^{99}Mo separation from neutron irradiated ^{235}U, HNO_3 soln., S collector 77−42161
^{99}Mo, separation regeneration of breeder reactor fuel *(Czech)* 78−82496
^{99}Mo, sublimation separation from neutron irrad. UO_2 77−9257
N, isotope fractionations in Fischer-Tropsch and Miller-Urey reactions, appl. to carbonaceous chondrites 80−46496
N_2-Kr-Xe, liquefaction, retention of ^{85}Kr from fission exhaust gases, separation technique *(German)* 80−27753
N_2+N_2, isotopic variants, V-T and V-V exchanges 78−90270
^{15}N, isotopic anal., collector sensitivity error source 77−42441
NaOH gas-crystal system, isotopic equilibrium near phase transition points *(Russian)* 80−91697
^{24}Na carrier-free production by 50-180 MeV protons on Si, P, S, Cl, Ar and K 79−83934
Nb, separation from fission products, fast chem. methods 77−16856
Nd isotopes, determ. in nuclear fuels as burnup indicator, separation, mass spectrometric method 77−44553
^{147}Nd, anodic deposition on Pt anode, electrochem. separation 79−91958
Ne, isotope separation by cataphoresis in DC gas discharge 80−103213
Ne isotope separation by gaseous diffusion transport in regular geometries 79−94099
Ne, separation by jet-background interaction 79−54983
^{A}Ne, A=20, 22, isotope separation by mass-diffusion cascade 79−31218
Ni(II), selective separation from rare earth elements on chelate ion exchangers 78−58861
Np, production of transuranium elements by neutron irrad. of ^{241}Am *(Japanese)* 80−52731
O isotope fractionation in alkali halide H_2O and D_2O solns. 78−22629
O_2, supersonic molecular beam technique using RF spectroscopy, mag. reson. 80−47725
O_2-^{85}Kr-Xe, liquefaction, retention of ^{85}Kr from fission exhaust gases, separation technique *(German)* 80−27753
P, separation from fission product solns. by inorganic ion exchange review 79−85625
^{203}Pb production by proton reactions on natural Tl 79−88184
^{143}Pr, anodic deposition on Pt anode, electrochem. separation 79−91958
Pu accumulation in Purex process, first extraction, computer simulation, SEPHIS code 80−68907
Pu isolation, neutron irrad. of natural U in Japan Material Testing Reactor *(Japanese)* 80−52730
Pu, production of transuranium elements by neutron irrad. of ^{241}Am *(Japanese)* 80−52731
Pu separation-free nuclear power economy using LWHR, feasibility study 78−13313
Pu-U partial separation in fuel coprocessing 79−89419
^{238}Pu, chemical treatment of irrad. targets *(French)* 77−26883
^{242}Pu preparation by EM isotope separation, for use as α-spectrometry and mass spectrometry tracer 78−9011
^{223}Ra, ^{228}Ra, activity ratio and separation from Indian spring water 78−86962
^{228}Ra, separation from thorium oxalate 80−45600
Rb, isotopically selective ionisation through Rydberg states 78−5186
^{84}Rb targets for nuclear bombardment, on-line separation 77−23328
Rh, A=108-111, prod. by fission of ^{235}U, ^{238}U, ^{239}Pu, ^{249}Cf, separation, identification 78−89924
^{103m}Rh, separation from ^{103}Ru by solvent extraction 78−58857
Rn, A=220, 222, barrier technique, U prospecting appl. 78−21770
Ru isotopes, A=107-113, prod. by fission of ^{235}U, ^{238}U, ^{239}Pu, ^{249}Cf, separation, identification 78−89924
Ru, neutron deficient isotopes, gas thermochromotographic separation from AgCl 79−865
Ru, selective on-line gas phase separation from fission products 79−97907
Ru short lived isotopes, gas phase fast separation 77−23582
^{97}Ru, preparation, separation from TC isotopes 77−37054
S isotope exchange between sulphate and sulphide in acid solns., expt. determ. at 300°C and 1000 bars 78−62937
SF_6, inhibition of homogeneous condensation by vibr. excitation, isotope separation appl. 78−37688
SF_6, isotopically selective collisionless laser induced dissoc. 78−1037
SF_6, laser excitation in low temp. matrices, possible isotope selectivity 79−36788
SF_6, TEA CO_2 laser irradiation *(Japanese)* 80−11885
Sb separation from fission products, fast chem. methods 77−16856
Se+p→ ^{77}Br production excitation curves 79−85468
Sm, two step photoionisation method 77−58205
Sn, A=131, 132 prod. by ^{232}Th reactor induced fission, yield, radiochem. separation, anal. 78−89923
Sn, by radical reaction of dissoc. of $(CH_3)_3SnH$ *(Russian)* 79−59604
^{119}Sn, isotope, fractionation during zone recrystn. 80−2946
^{89}Sr and ^{90}Sr, radiochem. determ., error anal., comparison of methods 77−16873
T enrichment in water by electrolysis for low-level T activity meas. 78−17536
Tc, selective on-line gas phase separation from fission products 79−97907
Tc, separation from fission products, fast chem. methods 77−16856
^{99}Tc separation regeneration of breeder reactor fuel *(Czech)* 78−82496
Th(IV), selective separation from rare earth elements on chelate ion exchangers 78−58861
^{234}Th, isotope separation by extraction column chromatography using TnOA and filter paper 79−43659
^{234}Th, separation from natural U by extraction column chromatography using TnOA and filter paper 79−43659

isotope separation continued
^{201}Tl production by proton reactions on natural Tl 79−88184
U binding, by brown coal from seawater, IR spectroscopic obs. 78−82855
U, cascade, chemical and ion exchange unit 77−34474
U, countercurrent vortex tube method, energy consumption *(German)* 79−27099
U, diffusion enrichment plant by Eurodif and Coredif, France 77−358
U enriching gas centrifuge cascade, reflux effect, enrichment enhancement control 77−54346
U enriching gas centrifuge cascade, computer program for performance anal. 79−85805
U enrichment, centrifuge, URENCO facilities at UK and Netherlands *(German)* 78−86666
U enrichment, HAGA radial separating nozzle centrifuge process, cost 78−46155
U enrichment, jet membrane process 79−26683
U enrichment, layout of gas centrifuge cascades 79−26587
U enrichment, project using gas centrifuge at Centar, USA 77−357
U enrichment, random-walk model of holdup time of gas mols. in separation process 79−22481
U, enrichment, separation nozzle process 79−31124
U enrichment, using advanced gas centrifuge technology, for commercial use 77−356
U enrichment by electrostatic filtration *(French)* 77−18707
U enrichment by gaseous diffusion process *(French)* 78−70622
U enrichment by plasma centrifuge, partial pressure distrib. obs. 78−74501
U enrichment facility, based on separation nozzle process, materials management w.r.t. safety 79−85747
U, enrichment methods, efficiencies and costs *(Dutch)* 80−37634
U, enrichment plants, 1979 status *(French)* 80−807
U, enrichment plants, general world situation, survey 77−355
U enrichment processes development *(French)* 78−66361
U, enrichment processes in France *(French)* 79−31127
U, gas centrifuge 79−3227
U, influence of flow field struct. in the separation nozzle 78−82498
U isolation, neutron irrad. of natural U in Japan Material Testing Reactor *(Japanese)* 80−52730
U, isotope separation, new processes 79−31128
U isotope separation using ion exchange chromatography, U(IV)-U(VI) exchange isotope effects 79−36376
U, isotope separation with rot. plasma 79−13842
U isotopes (234, 237) separation, chemical treatment of irrad. targets *(French)* 77−26883
U, selected enrichments for minimisation of blending losses, optimal set 78−17402
U, separation from fission product solns. by inorganic ion exchange, review 79−85625
U, separation in Fe^{3+}(III) water-glycerine solution-U(IV) cationic resin 79−41025
U, throughput limit in mass spectrographs 79−21850
U, using gas centrifuge 79−49815
U, various processes comparison w.r.t. economics, reliability and safety *(French)* 80−806
U-Pu, isotope separation in HNO_3 by exchange resins 78−74782
U-Th, in natural waters, anal., separation and purification *(German)* 78−70952
UF_6 centrifuge cascade, power supply loss accidents anal. 79−13502
UF_6, isotope enrichment, ^{19}F NMR in gas, liq. and solid 78−23364
UF_6, isotope separation by NH_3 laser far IR radiation 77−38867
UF_6, isotope separation cascade, random walk model 77−58190
UF_6, U isotope separation by velocity slip process, calcs. 79−94100
UH_3, UD_3, dissoc., isotope effect 80−26174
UO_2(II), selective separation from rare earth elements on chelate ion exchangers 78−58861
UX_1, separation from U, using silica gel ion exchanger 78−86961
^{230}U, production, tracer appls., α-spectra 77−61644
^{235}U enrichment, separation nozzle process 79−31106
^{235}U enrichment, using double deflection separation nozzle *(German)* 77−46383
^{235}U enrichment by pulse gas diffusion 79−36380
^{235}U enrichment by separation nozzle systems with dynamic flow deflection 79−49825
^{235}U isotope separation, efficiency improvement by nuclear excitation by electron transition 78−55039
^{235}U, large scale enrichment using separation nozzle 79−94654
^{235}U, separation nozzle process for enrichment 78−21739
^{235}U, separative performance transients in a gas centrifuge 79−67957
^{235}U to ^{238}U enrichment, ultracentrifuge, gas diffusion and nozzle separation techniques comparison, w.r.t economics 77−18680
$^{235}UF_6$ enrichment equipment, running-belt and rotary-disc concentrators, transient Knudsen diffusion 80−32421
^{236}U in LWR spent fuel, recycling in enriching plant 77−18684
^{236}U separation in PBR OTTO fuel cycle, numerical anal. *(German)* 77−83030
^{178}W, productions in ^{181}Ta(p,4n), purification procedure 80−12252
Xe, centrifuge in RF discharge, rot. mag. field 79−10737
Xe discharge, HF, with propag. EM wave, isotope distrib. *(Russian)* 77−76235
Xe isotope separation in HF discharge, thermodiffusion *(Russian)* 77−46649
Xe, isotope separation in RF discharge light inert gas admixture effects 79−41250
Xe-He(Ne), gas mixture, element and isotope separation in impulse plasma centrifuge *(Russian)* 80−38725
^{133}Xe, atmos. separation technique, preliminary results *(German)* 78−16222
Zn, zone melting by electron beam, isotope fractionation enhancement 80−45229
^{64}Zn isotope, fractionation during zone recrystn. 80−2946
Zr, separation from fission products, fast chem. methods 77−16856
^{88}Zr, spallogenic, radiochem. separation for photoneutron source 77−14296

isotope shifts
see also atomic spectra
^{176}Lu, hyperfine struct, and isotope shift of 605.5 nm line by laser spectroscopy 79−41137
acetic acid-d_0, -d_1, -d_4, cryst., IR spectra, H bonding 77−40217

isotope shifts continued
acetic acid-d_0, -d_1, -d_4, H bonding in solid, IR spectra, vibr. and librational modes 78−43843
acetylene, and -d_1, 1.1 μm band, rot. struct. 77−27069
acetylene, vibr.-rot. IR spectra, mol. force field determ. ^{14}C effects 77−61748
actinide configurations, isotope shifts rel. to $|\psi(0)|^2$ 78−17580
alene, -d_2, -d_4, harmonic force field, ground state average struct. 77−61732
alkali bisulphites, and disulphites, and isotopic forms, solid and soln., Raman spectra assignments 79−42968
alkali hydrogen selenites, and deuterated analog, vibr. spectra 79−24311
alkali metal radioisotopes, hyperfine spectroscopy, nucl. props. 80−57677
aniline-ND_2(-NHD), far-IR vap. phase spectra, assignments pot. function calcs. 77−75144
anisole and -d_3, Raman spectra, low freq. vibrs., torsional barrier 78−25543
anthracene-TCNB, charge transfer cryst., Raman spectra, assignment of modes on basis of isotopic shifts 79−19885
aromatic aldehydes, and deuterated forms, $n\pi^*$ and $\pi\pi^*$ assignments in 0-0 band, pot. surface method 78−9197
atomic beam high-resolution laser spectroscopy *(Dutch)* 79−50166
atomic energy level isotopic shifts and nuclear polarisation *(Russian)* 78−13444
atomic field isotope shift off-diagonal parameter in $(5d+6s)^N$, ab initio evaluation 80−47912
atomic metastable states, Doppler-free linear single-photon spectroscopy 78−50487
atoms, highly selective multistep ionisation by laser radiation 79−59408
atoms, nucl. vol. isotope shift theory, many electron effects 80−47851
benzaldehyde, and deuterated forms, in p-xylene, 4.2K, $n\pi^*$ phosphoresc. assignments 78−9197
benzene, and deuterated forms local mode oscill. strengths 79−27039
benzene(−d_6), prereson. Raman effects, intensity enhancement mechanism 78−42069
benzene and deuterates, highly vibr. excited intramolecular V-V transfer, visible and photoacoustic spectra 80−32729
benzene-^{13}C, liq., vibr. spectra, band assignments 78−13500
benzene-d_0, -d_6, vapour absorpt. spectrum, band intensities meas. 79−81212
benzene-d_0,-d_6, $^1B_{2u}$ excited states, high resolution two-photon spectra 77−506
p-benzoquinone(-d_4), n-π^* excited states, distant intramol. interaction between identical chromophores 78−90203
bibliography at. energy levels and spectra, (July 1971-June 1975) 77−71764
bibliography on experimental optical isotope shifts, (1918 to October 1976) 77−57932
bromoacetonitrile, ground state microwave spectrum assignments, mol. struct., rot. consts., quadrupole coupling 77−6763
bromobenzene-d_0, -d_1, -d_4, vibr. spectra and force fields 77−65463
bromomethane, and isotopic forms, self-broadening and self-shifting of rot. spectra 78−13551
bromomethane, microwave spectra, isotope substitution, Br quadrupole coupling, J=0←1 transitions 79−45709
bromomethane(-d_1,d_2,d_3), F and G sum rules as vibr. intensity data error indicators 79−3494
bromomethane-d_3, IR spectra of ν_3 band, $^{79/81}Br$ substitution 79−64000
3-bromopropene, $^{79,81}Br$, microwave spectrum, mol. struct., nucl. quadrupole coupling consts., rot. consts. 77−6767
bromotrifluoromethane ^{79}Br (^{81}Br), vibrational spectra and force constants of symmetric tops, rotational analysis 79−98090
bromotrifluoromethane-^{12}C, -^{13}C, matrix IR spectra and harmonic force fields *(German)* 79−76431
bulge effect, in rot. inelastic scatt., isotope shift 79−86047
t-butyl alcohol, and deuterates, gaseous and matrix IR spectra, liq. Raman spectra, vibr. assignment 79−10113
butylsilane-d_0,(−d_n), vibr. spectra, normal vibrs. and rot. isomerism 79−31523
α-chloroacetic acid, ^{35}Cl and ^{37}Cl pure NQR, H bonding, isotope effects 78−27111
p-chlorobenzaldehyde in methylcyclohexane, matrix perdeuteration effects on $^3\pi\pi^*\rightarrow S_0$ phosphoresc. 77−20903
p-chlorobenzene, and deuterated forms, in p-dibromobenzene and p-dimethoxybenzene, 4.2K, $\pi\pi^*$ phosphoresc. assignments 78−9197
chlorobenzene-d_5, and isotopic forms, microwave spectrum, rot. consts. 78−58667
chloromethane, and isotopes, $\nu_2+\nu_3$ band, Coriolis reson. with $\nu_3+\nu_5$ band *(French)* 78−5229
Coulomb displacement energies, charge and mass number depend. in isotope shifts 78−8729
coupled isotope effects in exchange reactions, vibr. freq. and atomic masses 80−18843
cyanoacetylene, ^{13}C and ^{15}N isotopic species, rot. transitions, 8-220 GHz 77−61740
cyanoacetylene, and deuterate, microwave spectrum, ground and excited vibr. states 78−90157
cyanobutadiyne-d_0,d_1, microwave spectrum, substitution struct., dipole moment 77−3348
cyanomethane, heavy nucleus isotope shift calcs. 78−86917
3-cyanothiophene-^{34}S(-^{15}N), partial r_0-struct., microwave spectra 80−91552
cyclopropane-d_0, -d_6, force fields, Raman spectra 77−71806
cyclopropane-d_0, d_6, absolute IR intensities, dipole moment derivatives and polar tensors 78−90165
diatomic molecule, Born-Oppenheimer approximation, breakdown 79−3497
diatomic molecules, NMR isotope shifts, theory 77−75186
dichlorodifluoromethane, IR spectrum and mol. force field 79−72309
dichloromethane, (-d_2), liq. and vap., IR spectra, intensity anal. 79−64003
diethylsilane-d_0(−d_n), vibr. spectra, normal vibrs. and rot. isomerism 79−31524
1,2-difluorobenzene-d_0, -d_4, IR spectra, vibr. anal., force field 77−27063
cis-1,2-difluoroethylene oxide, substituent and isotope effects, microwave assignments 78−78682
difluoromethylborane, microwave spectra and struct. obs. 80−43036
1,5-dihydroxyanthraquinone-d_0,-d_2, mol. vibr., IR spectra 77−467
dimethyl ether -d_0, -d_3, -d_6, internal rot., far IR and Raman spectra 77−79612
dimethyl ether-d_0,d_3,-d_6, microwave spectra, torsional splittings 77−3347
dimethyl selenide-d_6, microwave spectrum in ground and excited torsional states *(German)* 77−57992
dimethyl sulphoxide-d_6, intensities in inelastic electron tunnelling, IR, and Raman spectroscopy *(French)* 79−822
2-dimethylaminoethanol(-d_1), microwave spectrum, hydrogen bonding, rot. consts., struct., dipole moment 77−6764
1,1-dimethylcyclopropane-d_0,-d_6, internal rot., Raman spectra 78−985
trans-dimethyldiazene-1, 1, 1-d_3, IR and Raman spectra, vibr. assignments and pot. functions 78−33507
trans-dimethyldiazene-d_0,d_6, IR and Raman spectra, vibr. assignments and pot. functions 78−33507
dimethylether-HCl(I)(Br) mixture in N_2 matrix, IR induced proton transfer isotope effects, bond strengths 79−29335
durene:quinoline-d_0,(-d_n), phosphorescent triplet spins, phase coherence, spectral diffusion effects 79−87334
ethane, $^{13}CH_3{}^{12}CD_3$, $^{12}CH_3{}^{13}CD_3$, microwave spectra, Stark effect, C-C bond length and mol. consts. 77−50428
ethene, general valence force field, ab initio calcs., IR and Raman intensities 77−71746
ethyl cyanide, isotopic species, rot.-torsion-vibr. interaction in rot. spectra 77−458
ethylene, and ^2H, ^{13}C, ^{15}N, ^{18}O isotopic derivatives, vibr. freqs. using MINDO/3 force consts. 77−71793
ethylene(-d_1,d_2), high-resolution UPS, mol. ion vibr. assignments, symmetry 79−27032
ethylene carbonate, Fermi reson., isotopic substitution meas. 78−86870
ethylene glycol, IR spectra, ab initio calcs., vibr. anal., conformations of isotopic modifications 78−5210
ethylene oxide, ^{13}C and D variants, T_2-relax., 2_{20}-2_{11} rot. transition by microwave pulse spectrometer 80−47976
ethylene ozonide-d_4, isotopic species, microwave rot. spectrum assignments, struct. 77−57982
ethylgermane, microwave, IR and Raman spectra, struct., internal rot., dipole moments 77−79605
ethylmethylether(-d_3), low freq. vibr. spectra, methyl torsional pot. functions, internal rot. 79−26978
ethylmethylsilane-d_0(−d_n), vibr. spectra, normal vibrs. and rot. isomerism 79−31524
fluoroacetylene, and -d_1, vibr. Zeeman effect, g-factors 78−46391
fluoroacetylene-d_0,-d_1, microwave spectrum, laser enhancement effects 79−41161
fluorobenzene, 2644 Å band system, rovibronic anal., isotope effects 79−6949
fluorobenzene radical cations, in gas phase, laser-induced fluoresc. 79−27022
fluoromethane ν_2, ν_5 rot.-vibr. Raman bands, anisotropic components, ^{13}C shifts 78−74667
formaldehyde, unique force field, parametric representation method 77−18897
formaldehyde (−d_1,d_2), isotopic forms. vac. UV Rydberg spectra, vibr. assignments origin isotope effect 77−61763
formaldehyde-d_0,-d_2, higher Rydberg states, vac. UV transitions assignments 77−42334
formamide, force consts. and dipole moment derivatives, ab initio MO calcs. 80−95521
formic acid, cryst., H bonded, IR spectrum computer simulation 80−97253
formic acid(−d_1), dilute deuterated mixture, high-sensitivity NQR, double quadrupole reson. 78−68412
cis-formic acid (-d_2,d_2), and isotopic forms, bond lengths and angs., microwave spectrum obs. 78−55169
formic acid and isotopic species, microwave spectra, Coriolis reson. between vibr. excited states 79−13700
formic acid-d_0, -d_2, OH(OD) stretching, vibr. band struct. 77−6751
formic acid-d_0(-d_1)(-d_1)(-d_2), vibr. spectra, CNDO/2 interpretation *(French)* 80−58155
glycylglycines, isotope substituted, IR and Raman vibr. spectra 78−42051
group IV tetrahalides, isotope shifts, Coriolis coupling and force consts., isotope substitution and matrix isolation 77−42322
guanine, ^{15}N and D substituted, in acid and base solutions, vibr. anal. 79−26994
halomethanes, -d_0 and -d_3, IR intensity anal. 77−58082
heavy atom substitution, vibr. freqs. and anharmonicity consts., general isotopic rules 77−75122
hexafluoropropane(-d_2), IR and Raman spectra, gas and liq., normal coord. anal. 79−68235
hydrogen-bonded ion-pair complex, anomalous isotropic freq. ratio of stretching $\nu_{N(+)H}$ vibrs. 77−3366
ice, II and IX, deuterated forms, 10K, OD stretching bands interpretation 78−2836
ice, isotopic, I_H, single crystal Raman intensities, OH bond polarisability, librational modes 78−27208
iodomethane, and isotopic forms, self-broadening and self-shifting of rot. spectra 78−13551
IR ν_s absorption band profile of isotopically diluted OH group in crysts. 79−69821
isopropylamine-d_0,-d_1,-d_2, microwave spectra, struct., dipole moments and quadrupole coupling consts. 77−34613
laser spectroscopy of unstable isotopes, nucl. props. determ. from atomic spectra using fast beams 80−9720
linear triatomic molecules, NMR isotope shifts, theory 77−75186
linear triatomic mols., isotopic relations, harmonic freq. calc. 77−23486
maleic anhydride, struct., DRM microwave spectra, isotope shifts 78−21918
metallooctaethylporphyrin, ^{15}N-enriched, reson. Raman spectra, haemoprotein oxidation state marker bands 77−58008
metalloporphins, deuterated, resonance Raman spectra, vibr. and vibronic levels 78−62812
methane, ^{12}C and ^{14}C, line parameters for ν_2 and ν_4 bands, isotope shifts, appln. to planetary atmospheres 80−95622
methane, ^{13}C enriched, IR spectrum, ν_3-band forbidden lines, ground state consts. 77−18922
methane, $^{13}CH_4$ line hyperfine splitting at 3.39 μm, laser saturated absorpt. obs. 79−76470
^{13}C-methane, ν_1 fund., quasi-CW inverse Raman spectra 80−48004
methane, and d_1-d_4, absolute Raman intensities of fundamental, overtone and combination bands 77−65468
methane, and deuterates, absolute Raman intensities, depolaris. ratios, bond polaris. theory 77−10705

isotope shifts continued
methane, heavy nucleus isotope shift calcs. 78−86917
methane, isotopic variants, IR intensity anal. 77−58081
methane, microwave Q branch distortion moment Stark spectrum, rot. transitions, C isotope shifts 77−455
methane(-^{13}C), absorpt. spectra. optoacoustic laser meas. 78−37635
methane in condensed inert gas matrices, optical excitation of rotational transition, far IR absorption spectra 80−37808
methane-d_4, Stark effect, rot. transitions in vibr. ground state, isotope shift 79−27029
methoxy radical and deuterate, vibronic level fluoresc. spectrum 80−58305
methyl bromide, rot. absorption spectrum of ν_3 and $2\nu_3$ excited vibr. states, mol. consts. determ. 78−82732
methyl bromide, rot. spectrum, microwave region *(Russian)* 78−70823
methyl chloride, ^{13}C shifted force consts., anharmonic vibr. 78−21899
methyl chloride, cryst., Raman band anomalous splitting, isotope effects 77−8562
methyl chloride, far IR laser lines, vibr. isotopic shift value 78−42055
methyl chloroformate, struct., microwave, Raman, far IR and NMR spectra 77−34614
methyl cyanide, isotopically substituted species, IR spectra, vibr. freq. displacements, harmonic pot. function 78−42057
methyl fluoride, ^{13}C shifted force consts., anharmonic vibr. 78−21899
methyl formate(-d_1,d_3,d_4), mol. vibr. spectrum, struct., beginning with PCILO calc. *(French)* 80−23401
methyl halides, harmonic force fields, high-low freq. separation calcs. 78−90067
methyl isocyanide, microwave spectrum, anal., N isotope effects 77−50430
methyl isocyanide photoisomerisation, laser isotope separation, C-isotope enrichment by one-photon vibr. photochemistry 80−81336
methyl orange, aq. soln., reson. Raman spectra of D and ^{14}N isotopes 80−91566
methyl selenocyanate, and isotopic forms, microwave spectrum 79−13705
N-methylacetamide, and isotopic forms, low-freq. Raman spectra, internal torsional mode 79−26992
N-methylacetamide, vibr. spectra and normal coord. calcs. 79−36632
methylamine, and ^{2}H, ^{13}C, ^{15}N, ^{18}O isotopic derivatives, vibr. freqs. using MINDO/3 force consts. 77−71793
methylamine, multiphoton discoc., N isotope separation 80−35553
methylborodichloride-d_0(-d_3), vibr. spectra and force constants *(German)* 79−26982
methylene bromide-d_0-d_2, liq., nucl. spin-lattice relax., rot. correl. times 77−59476
methylene-d_0, -d_2, in Xe matrix, EPR, temp. depend. 78−5255
methylenimine, mol. struct., microwave spectra, isotope effects 77−61738
methylpropylsilane, vibr. spectra, normal vibrs. and rot. isomerism 79−31524
N-methylthioacetamide(-d_1), reson. Raman spectra obs. and mechanism 78−17672
molecular energy levels, isotopic rules for heavy atom substitution perturbation theory 77−83660
molecular force field eval. from isotopic freqs. 78−33493
molecular geometry, minimum necessary no. of isotopic substitutions 77−3484
molecular isotope spectra, from unseparated natural mixture, spectrosc. technique 79−31736
molecular vibration analysis, isotopic frequency ratios, using high- and low-freq. separation method 79−26971
molecules, isotopically tagged, normal vibr. freq. calc., eigenvalue behaviour, perturbation theory obs. 80−52973
monothioformic acid, cis-, trans-rotamers, rot. spectrum, force consts. and isotopically substituted struct. 78−9145
Mossbauer isotope shifts, electron density at nuclear determ., book contrib. 79−87351
mucochloric acid-d_0, -d_1, vibr. spectra, struct. 78−46326
MXY type molecules, vibr. isotope effect 78−25506
N-methylhydroxylamine, microwave spectra, struct., moments, internal rot., HFS and rot. consts. 79−45708
naphthalene, $C_{10}H_8$ and $C_{10}D_8$, optical absorpt. spectra of hydronaphthyl radicals, isotope effects 78−60487
naphthalene crystal, vibronic spectra at 1.6K, two-photon fluoresc. excitation 77−59604
napthalene-$d_{0\text{-}8}$, fluoresc. and absorpt. Shpolskii spectra *(Russian)* 78−90208
nearly closed shell atoms, binding energy and isotope shift correl. 80−27980
nitrobenzene-d_0(p-d)(d_5), vibr. spectra 79−26966
nitromethane, multiquantum absorption in intense IR field, isotope shift 77−19000
nitromethane-d_0,-d_3, polycryst., methyl torsion, Raman spectra 79−82970
N-nitroso-dimethylamine-d_0, -d_3, -d_6, struct., microwave spectra 79−59446
Peierls-Frohlich state on many-phonon-coupling model, dynamical props. 78−47773
peroxyacetic acid, and isotopic forms, matrix IR spectra, force spectrum, force const., thermodynamic props. calc. 77−14427
phenols, ^{13}C and D substituted, microwave spectra, substitution struct. and absolute dipole moment 79−31511
PMMA, atactic, FT IR spectrum, ^{18}O substitution effects 80−23581
PMMA, C-H stretching and bending vibs., IR spectra, selective deuteration 80−23582
polyatomic molecules, fundamental stretching freq. 78−50530
polyatomic molecules, NMR isotope shifts, theory 77−75186
polyethylene(-d_4), vibr. freqs., MNDO semiempirical SCF calcs. 78−1114
polythylene, and perdeuteropolyethylene, crysts., IR and Raman intensities, factor group splittings 79−65851
propargyl mercaptan (−d_1), microwave spectra, struct., rot. anal. 77−18916
propylsilane-d_0(−d_n), vibr. spectra, normal vibrs. and rot. isomerism 79−31523
pyridine and salts, deuterium NQR, double reson. method, ring charge distrib. 80−53015
pyridine-d_0, -d_5, vap. fluoresc. spectra 78−82771
pyridine-d_0-d_5, $n\pi^*$ excited state vibronic coupling, vis. and Raman spectra 77−14438
resonance scattering methods in atomic spectroscopy 80−53167
isotope shifts continued
ring laser, nonlinear polarisability of two-isotope active medium 80−14369
rubidium tetramethylborate, vibr. spectra and force constants *(German)* 79−26981
selenoacetaldehyde, microwave spectrum, struct. internal rot. barrier 78−74645
semicarbazide hydrochloride, vibr. spectra, normal coord. anal. 80−58255
semicarbazide-d_0, -d_6, vibr. spectra, normal coord. anal. 80−58255
semiconductors, shallow impurity centre spectra, isotopic shift of zero-phonon lines 80−66249
separated product rules for high and low vibr. freqs. in isotopic mols. 77−34611
spectrometer, high resolution, for meas. of isotope, isomer shifts and hyperfine struct. 77−61141
spherical nuclei, isomer and isotope shifts, theory of finite Fermi systems 80−39929
styrene, and isotopic forms, IR and Raman spectra, normal vibr. assignments 77−18930
superconductors, effects of local and quasi-local impurity modes on crit. characts. *(Russian)* 79−19692
tellurophene(-d_4), cryst., struct., phonon spectrum, exciton splittings, assignments 77−81088
1, 2, 4, 5-tetracyanobenzene and -d_2, IR and Raman spectra, vibr. anal. 79−36629
1,4,5,8-tetrahydroxyanthraquinone-d_0,-d_4, mol. vibr., IR spectra 77−467
tetramethylurea-d_0,-d_{12}, IR spectra, normal coord. anal. 78−978
sym-tetrazine, isotope selective mol. spectroscopy and isotopically pure mols. prod. with dye laser 80−11926
sym-tetrazine, mol., isotope spectra, from unseparated natural mixture, spectrosc. technique 79−31736
s-tetrazine, visible absorpt. band assignment, vibr. anal. 78−994
1,2,4-thiadiazole, struct., double reson. modulation microwave spectra 77−14424
thioacetaldehyde (-d_1), microwave spectrum, substitution struct. internal rot. barrier, dipole moment 77−6762
thiocarbonyl bromide, IR spectra, gas, liq. and matrix isolated, mol. force consts. *(German)* 79−36640
thioformaldehyde, and -d_2, $\tilde{A}^1A_2$-$\tilde{X}^1A_1$ visible electronic absorpt. spectra, vibr. anal. 79−45733
thiophosgene, IR spectra, gas, liq. and matrix isolated, mol. force consts. *(German)* 79−36640
thiophosgene, laser Raman spectra, vibr. anal., Cl isotope splitting 77−65486
toluene-d_0,-d_8, polycryst., methyl torsion, Raman spectra 79−82970
transition metal complexes, isothiocyanates with pyridine, far IR spectra, vibr. bands 78−25535
triatomic molecules, microwave spectra, mol. parameters 79−31513
s-triazine(-d_3), gas phase IR band contours obs., computer simulation 77−6774
trichloromethane, matrix isolation IR spectra, $^{35/37}$Cl and $^{12/13}$C isotope shifts 78−977
1,2,3-trifluorobenzene, ^{13}C, ^{19}F, and ^{1}H NMR spectral anal. 78−37659
trifluorochloromethane, Raman and IR spectra, $^{35/37}$Cl isotope splitting and mol. constants *(German)* 77−83595
trimethylborane, vibr. spectra and force constants *(German)* 79−26981
triphenylene, triplet state, MIDP and T-S excitation spectrosc. 79−81233
tryptophan, Raman line characterisation 79−26996
TTF-d_0, -d_4, IR and Raman spectra, vibr. assignments 78−23436
TTF-TCNQ, ^{15}N, ^{2}H isotope labelled, IR, Raman spectra, mol. vibrs., electron-phonon interactions 77−69835
tunable dye laser, isotope shift meas. at Isolde mass separator CERN *(German)* 78−41863
two-photon spectroscopy, Doppler-free *(Dutch)* 79−50167
vibrational frequencies, band intensities and Coriolis coupling const., isotopic sum rule derivation 80−83343
vinyl bromide, mol. struct., from gas-phase electron diffr. and microwave data 80−23571
vinylfluoride, gas phase electron diffr. and microwave spectra, rot. consts., struct., isotope shifts 79−31686
vinylsilanetriol-d_0,(-d_3), soln., vibr., IR and Raman spectra 78−86854
water, solvated electrons, photon-induced electron transfer transitions 79−8154
X_3Y_3 molecules, isotopically substituted, IR freq. and intensity patterns 78−21926
AlBr, UV emission spectrum, vibr. consts., isotope displacement and dissoc. energies 77−3381
Al_2Cl_6, matrix isolated, vibr. spectra, isotopic fine struct. and valence force field calcs. 80−58258
AlH_4^-, AlD_4^-, intramol. force fields, F_2 vibrs., isotope shifts 77−3336
α-Al_2O_3, IR absorpt. spectra of OH^-, OD^-, and OT^- 80−55145
2-aminoethanol(-d_2)(-d_3), microwave spectra, hydrogen bonding, rot. const. 77−6765
Ar, metastable ion beam, collinear laser spectroscopy, isotope shift, fluoresc. detect. 80−37771
Ar-acetylene van der Waals molecule, radiofreq. spectroscopy and Stark effect meas., equilib. struct. and props. 80−91543
^{38}Ar, low abundant, isotrope shift meas., time averaging using dye laser spectrometer 80−101850
$AsH_3(AsD_3)(AsT_3)$, harmonic force fields, equal coord. method calcs. 77−30845
BCl_3, frozen, selective evaporation of $^{10}BCl_3$ and $^{11}BCl_3$ by CO_2 laser irrad. *(Russian)* 77−3422
BCl_3, in solid Ar, Kr, high resolution IR absorpt. spectra, isotopic splitting 80−87109
BCl_2F, in solid Ar, Kr, high resolution IR absorpt. spectra, isotopic splitting 80−87109
BH_4^-, BD_4^-, intramol. force fields, F_2 vibrs., isotope shifts 77−3336
$^{10,11}B_5H_9$ gas (liq.) phase, vibr. dephasing and Raman spectra 80−48101
BH_3CO, struct., quadrupole coupling consts., dipole moment, microwave spectra 77−54557
$B_3N_3H_6$, isotopic variants, pure rot. Raman spectra 77−71803
BS, and isotopic forms, two new emission bands, mol. consts. 77−18960
Ba, atomic beam, optical isotope shifts and hyperfine struct. 79−50154
Ba, atomic beam and resonance spectroscopy 80−58180
Ba, hyperfine splitting and isotope shift of high lying levels, Doppler-free 2-photon laser spectroscopy 80−58215
Ba I, isotope shifts, hyperfine struct., neutron deficient nuclei, laser resonance fluorescence study 79−72436

isotope shifts continued
Ba II, $5d^2D_{3/2,5/2}$, isotope shifts, hyperfine struct., collinear fast beam laser spectroscopy 80−83310
Ba II, ab initio calc. of isotope shifts 78−37555
Ba II, even isotopes, optical isotope shifts, Lamb-dip spectrosc. obs. 78−78666
Ba isotopes, isotope shifts and hyperfine struct. from laser spectroscopy 79−9460
Ba, radioisotopes, at. beam laser spectroscopy, hyperfine struct., nucl. moments and radii 80−57678
Ba, two-photon spectra, isotope shift and hyperfine splitting 78−33491
Ba^+, hyperfine struct. of $5d^2D_{3/2}$ to $6p^2P_{3/2}^0$, laser absorpt. expt. 78−21870
$Ba(ClO_3)_2.H_2O(HDO)(D_2O)$, hydrate group vibr., IR spectra, isotope effects 77−8557
$BaCl_2.2H_2O(D_2O)$, lattice vibr., IR and Raman spectra 79−15443
BaI resonance transitions, hyperfine struct. and isotope shifts, atomic beam laser spectroscopy 80−102141
^{128}Ba, charge radius determ. using Doppler free laser spectroscopy 77−71558
^{131}Ba, magnetic mom. and charge determ. using Doppler free laser spectroscopy 77−71558
BeCl, $^2\Sigma^+$ predissoc. state, vibr. and rot. calcs. 77−42363
Br_2, absorpt. spectrum, laser isotope separation *(Japanese)* 77−34649
Br_2, and isotopic forms, new rot.-vibr. lines, laser reson. fluoresc. obs. 78−991
Br_2, resonant fluoresc. at 5145 Å, isotope mols., rot.-vibr. states 77−61782
BrCN, ICN, and isotopic forms, force field calc., freqs., rot. consts. 79−22693
$BrCN+N_2$*, vibr. energy transfer, α_3 vibr.-rot. const., microwave meas. 77−83578
$BrCl(H_2O)_n$, mean vibr. amplitudes, Raman spectra, isotope effects 77−58014
BrF, laser excitation spectrum, 4850 to 5200 Å, rot. anal. 77−6840
$Br_2(H_2O)_n$, mean vibr. amplitudes, Raman spectra, isotope shifts 77−58014
C, ^5S-$^3P_2$ and $^5S_2$-$^3P_1$ transitions, ^{13}C isotope shift 80−58201
CD^+, $A^1\Pi$-$X^1\Sigma$ band system, spectroscopic consts. and isotope shifts 79−59485
CO_2 and isotopic forms, laser freqs., Dunham coeffs. 79−64207
CO^+ ^{14}C and ^{18}O isotope shifts, vibr. anal. of first negative, comet-tail and Baldet Johnson systems 80−28029
$^{12}C^{16}O$, ^{13}C ^{16}O, Heizberg system, rot. anal. 79−59423
$^{12}C^{16}O$:CO isotopes, IR and Raman spectra, vibron band, vibron-phonon combination bands 78−68495
CO_2, and isotopic forms, bending fund. region, IR spectra, rot. consts. 80−47988
CO_2 and isotopic species, high-resolution Fourier spectra near 4.3 micron 80−47982
CO_2, isotopic relations, harmonic freq. calc. 77−23486
CO_2 laser stability and heterodyne frequency calibration 78−59031
CO_2, matrix isolated Raman and IR spectra, fundamental freqs., isotope effects 77−88457
CO_2, Σ-diads, Raman spectra, O isotope effects 77−83610
CS, isotopic variants, IR absorpt. spectra, $v=2\leftarrow1$ hot band 79−45721
CS, isotopic variants, IR absorpt. spectra, vibr.-rot. transitions 79−45720
CS_2, condensation vibr. shift, intermol. interaction, vap. press. isotope effect 77−61742
CS_2, isotopic variants, $2\nu_1+\nu_3$ band IR spectra, rot. and rovibr. consts. 79−41166
CS_2, matrix isolated Raman and IR spectra, fundamental freqs., isotope effects 77−88457
CS_2, ν_3 band, dipole moment correl. function, isotope splitting and band contour 78−74650
$^{12}CS_2$, $^{13}CS_2$, vibration-rotation bands 2700-2900 cm^{-1} *(French)* 78−25521
$^{13}C^{16}O$, IR emission, vibr.-rot. lines 77−3355
Ca, A=40,42,43,44,46,48, laser spectroscopy 77−14392
Ca, A=40-48, meas. using enriched isotopes in atomic beam 78−17610
Ca, muonic isotope shifts 78−33640
Ca, stable and radioisotopes, hfs, isotope shifts, dye laser saturation spectroscopy, beam expt. 80−58169
Ca stable isotopes, nucl. charge distrib. from isotope shift in Ca I resonance line 79−9461
Ca- intercombination line, nuclear charge radius, spin, moments of ^{45}Ca, by laserspectroscopy 80−18187
Ca_2, van der Waals mol., in Kr matrix, absorpt. and emission spectra 77−83611
^{A}Ca, A=40, 42-44, 48, pionic X-rays, strong interaction and isotope shifts, π-nuclear optical pot. 80−53169
^{A}Ca, A=40 to 46,48, nuclear charge distrib., from isotope shift of 6573 angstrom line 80−57674
^{43}Ca, atomic beam and resonance spectroscopy 80−58180
^{43}Ca, isotope shift and hyperfine struct. by laser spectroscopy 79−41139
^{43}Ca, nucl. quadrupole moment, HFS in at. beam mag. reson. 79−63940
Cd, A=110, 116, difference in nuclear charge radius, X-ray isotopic shift meas. 77−18382
Cd, optical isotope shifts and hyperfine struct. 77−3316
$Cd(^{15}NH_3)_4^{2+}$, IR spectrum, force consts. *(German)* 77−6781
CdX_2, CdXY, (X,Y=Cl,Br,I), matrix isolated vibr. spectra, isotopic effects, force consts. 77−3358
Ce II, isotope shift and screening, pseudo-relativistic HF calc. 78−90096
Ce, isotope shift in IR spectrum *(French)* 77−54523
Cl, $3p^5$, $^2P_{1/2}\leftarrow{}^2P_{3/2}$ fine struct., tunable IR diode laser detection 80−23348
Cl metastable ion beam, collinear laser spectroscopy, isotope shift, fluoresc. detect. 80−37771
Cl_2, isotope shift and absorption spectrum for laser isotope separation 77−34701
Cl_2, resonance Raman spectrum, Q-branches of $^{35}Cl_2$ and $^{35}Cl^{37}Cl$ 78−25542
ClCN, and isotopic species, force field calc., freqs., rot. consts. 79−22692
$ClCN+N_2$*, vibr. energy transfer, α_3 vibr.-rot. const., microwave meas. 77−83578
ClH-dimethyl ether, H bonded complex, IR and Raman spectra, mech. and elec. anharmonicity 79−89672
$Cl_2(H_2O)_n$, mean vibr. amplitudes, Raman spectra, isotope effects 77−58014

isotope shifts continued
$^{35}Cl^{35}Cl$, $B^3\Pi(0^+)\rightarrow X^1\Sigma^+$, 6300 to 9900 Å, rot. anal., mol. consts., equilib. internuclear separation 78−42082
$^{35}Cl^{37}Cl$, $B^3\Pi(0^+)\rightarrow X^1\Sigma^+$, 6300 to 9900 Å, rot. anal., mol. consts., equilib. internuclear separation 78−42082
^{244}Cm, emission spectrum, 2400-11200 Å, wavelengths, rel. intensities, Zeeman effect 77−46514
Cs, HFS, isotope shift related to nucl. charge rad. 78−78826
$Cs_2LiCo(CN)_6$, mol. vibr. in cryst., normal mode anal., Raman and IR obs. 77−76494
$CsUO_2(NO_3)_3$, ^{15}N isotope shifts in electronic spectrum, internal mode identification 80−55098
^{A}Cs, A=133, 135, 137, isotope shifts and hyperfine struct. of 5s-7p transitions 79−13677
^{A}Cs, A=133, 137-139, hyperfine struct., isotope shifts, nuclear moments and radii, laser spectroscopy 79−10071
^{A}Cs, A=138 to 142, nucl. moments and charge radii changes from hyperfine struct. and isotope shifts 79−17804
Cu complex, glycylglycine, isotope substituted, IR and Raman vibr. spectra 78−42051
Cu, Doppler-free laser spectroscopy in hollow cathode discharge 80−9537
Cu, electron configs., isotope shifts, visible and UV spectra 80−32641
CuBr, new bands in emission spectrum 77−68052
Cu_2O, exciton spectrum, effect of isotopic substitution 78−67955
$CuSO_4.5H_2O$, IR spectra, internal modes and pot. environment, isotope effects 77−8563
D, 1S Lamb shift and 1S-2S isotope shift 80−91464
D_2^+,(DT^+), IR transition freqs. calcs. 77−88452
DBr, (1,0) fundamental IR band meas., isotope shifts 78−42052
$D^{35}Cl$, $D^{37}Cl$, IR absorpt. $3\leftarrow0$ band, dipole moment series expsn. 77−61747
D_2O, $(D_2O)_2$, isotopic forms, Ar matrix isolated IR spectra, assignments, config. 77−6779
D_2O, isotopic species, far IR spectra, assignments, moments 77−6761
$(D_2O)_2$, isotopic forms, Ar matrix isolated IR spectra, assignments, config. 77−6780
Dy I, hyperfine struct. and isotope shift, fluoresc. meas. on at. beam 78−9109
Dy II spark spectrum, isotope shift, config. mixing 78−58628
Dy, isotope shift meas. using laser atomic beam technique specific mass shift determ. 80−91497
Dy, isotope shifts and hyperfine structs. 78−37600
DyO, UV emission spectrum, high resolution, band systems and isotopic shifts 80−87146
^{161}Dy, ^{163}Dy, HFS, isotope shifts and hyperfine splittings 78−37595
Eu I, high resolution study of $4f^7 6s^2\rightarrow4f^7 6s6p$ 79−54790
Eu I, isotope shift meas., level classification in $4f^6 5d6s^2$ and $4f^7 5d6p$ configs. 77−30831
FCN, and isotopic forms, force field calc., freqs., rot. consts. 79−22691
$Fe(CN)_6$, adsorbed on Al_2O_3, tunnelling spectra, isotope shifts 80−29262
FeH, FeD, matrix isolated IR spectra, mol. vibr. 79−93992
FeO_2, matrix isolated IR spectra, cyclic complex struct. 77−88449
Fe_3O_4, magnetite, Verweg transition temp., isotope effect, elec. resist. and DTA meas. 80−24976
Ga, isotope shift and HFS, isotope effects, UV spectra obs. 80−42973
GaBr, rot. spectrum hyperfine struct. 79−13838
GaH_4^-, GaD_4^-, intramol. force fields, F_2 vibrs., isotope shifts 77−3336
GaI, $A0^+$-$X0^+$ and B1-$X0^+$ transitions, isotope shifts, UV and visible spectra obs. 80−53005
Gd I and II spectra, 3930 to 4140 Å, isotope shift meas. 77−61713
Gd, isotope shifts and deform. obs. 77−65433
GdO, high resolution visible emission spectrum 77−18932
Ge shallow hydrogenic centres, ground states, isotope shifts, photoelectric spectrosc. 78−39055
GeF_4, $\nu_3(F_2)$ IR band contour, isotopically pure cpds., mol. consts. 77−61746
GeH_4, IR laser sideband obs., ro-vibr. struct., isotope shifts, line widths 79−72306
GeH_4, Stark effect, rot. transitions in vibr. ground state, isotope shift 79−27029
GeO_4^{4-} compounds, vibr. pot. function, force consts., isotopic shifts, mean vibr. amplitudes 80−23395
Ge_3O_3, isotopically substituted, IR freq. and intensity patterns 78−21926
H, 1S Lamb shift and 1S-2S isotope shift 80−91464
H_2, HD and D_2, nonadiabatic coupling of EF and GK $^1\Sigma_g^+$ states 79−59431
HBr, isotope chem. shift of μ^+ 79−55005
HBr(DBr), isotopic forms, Stark hyperfine struct., polarisability anisotropy 77−83645
HCN, and isotopic forms, l-type doublet transitions 79−13704
HCN, and stable isotopic species, mol. struct., ground vibr. rot. transitions and consts. 77−10666
HCN, isotopic relations, harmonic freq. calc. 77−23486
H(D), ground state Lamb shift, isotope shift and relativistic nuclear recoil correction 78−82696
$H_2(D_2)$, dissolved in vitreous SiO_2, Raman spectra, Q-band freq. shift 79−33707
$H_2^+(HD^+)(HT^+)$, IR transition freqs. calcs. 77−88452
HN_3, and DN_3 pure rot. Raman spectra, rot. consts., K-depend. parameters 78−29791
HNC, and stable isotopic species, mol. struct., ground vibr. rot. transitions and consts. 77−10666
HNCSe, struct., microwave spectrum 79−18178
H_2O,$(H_2O)_2$, isotopic forms, Ar matrix isolated IR spectra, assignments config. 77−6779
H_2O, (D_2O), vac. UV absorption spectra, Rydberg series vibr. anal. 78−42093
H_2O, and ^2H, ^{18}O isotopic derivations, vibr. freqs. using MINDO/3 force consts. 77−71793
H_2O, and D_2O, local model vibrs. 79−76414
H_2O, dimers, IR spectra in N_2 matrix, assignments and force consts., isotope effects 77−61744
H_2O dimers, IR spectra in N_2 matrix, temp. and IR irrad. effects 77−61745
H_2O, $H_2{}^{18}O$, D_2O, low freq. Raman spectra, isotope shifts, ice-like struct. 79−28732
H_2O, heavy nucleus isotope shift calcs. 78−86917
H_2O, isotopic species, far IR spectra, assignments, moments 77−6761
H_2O, liq., intermol. coupling, isotope and salt effects, Raman spectra 78−90169

isotope shifts continued
H_2O, vibr. freqs. from anharmonic ab initio/empirical PE functions 79−76406
$H_2{}^{16}O$, $H_2{}^{18}O$, determ. of line intensities from Fourier absorpt. spectra *(French)* 79−18186
$H_2{}^{18}O$, $H_2{}^{17}O$, IR spectra, 5030-5640 cm^{-1}, line centre positions 78−5220
$H_2{}^{18}O$, $H_2{}^{17}O$, IR spectra, 6974-7387 cm^{-1}, line centre positions 78−5221
$H_2{}^{18}O$, $H_2{}^{17}O$, rot. spectra, 650-50 cm^{-1} 77−65458
$(H_2O)_2$, isotopic forms, Ar matrix isolated IR spectra, assignments config. 77−6780
$H_2O(D_2O)$, solvated electrons, optical absorpt. spectra. temp., isotope effects 80−55124
HOI, $O_3(O)+HI$ matrix reaction, IR spectra, isotope shifts and band assignments 78−80737
H_2S, D_2S, separated product rules for high and low vibr. freqs. 77−34611
H_2SeO_3, and deuterated analog, vibr. spectra 79−24311
$H\alpha(D\alpha)$ plasma red shift meas. in Ar arc, ion dynamic depend. 80−10364
He, 1s2s $^1S_0$ isotopic shift meas. using tunable vacuum UV anti-Stokes light source 79−18149
He, Doppler-free two-photon high resolution spectroscopy 80−58197
^{3}He and ^{4}He superimposed spectra, isotope shift, mass and vol. effect, Fe arc spectrum calibration, teaching 80−46763
^{3}He atom forbidden singlet-triplet anticrossings, D levels 80−99491
^{A}He, A=3,4, pionic 1s state energy shift and line broadening *(German)* 80−48107
Hg, 188, 186, 184, shape staggering laser spectroscopy isotope shifts 77−74755
Hg II, hyperfine struct. of 194.2 line, $^2S_{1/2}$-$^2P_{1/2}$ transition *(French)* 77−27009
Hg, IR arc spectrum, fine struct., HFS and isotope shifts 77−79559
Hg, IR arc spectrum, fine struct., HFS and isotope shifts 77−79560
Hg isotopes, nuclear ground state props. via atomic spectra 77−22874
Hg, short-lived isotopes, HFS and isotope shift 78−37594
^{A}Hg, A=198-202 and 204, nuclear charge radii variations from K X-ray isotope shifts 78−70441
^{190}Hg ($T_{1/2}$=20 m) isotope, IS in 2537 Å line, on-line laser spectroscopy 77−61712
^{190}Hg, isotope shift by on-line laser spectroscopy 77−34589
I_2, two-photon excitation of rovibronic levels and gerade states 77−14508
ICl, ^{35}Cl and ^{37}Cl, $B^3\Pi_{0+}$ state IR spectra, mol. consts. 80−28016
ICl, two photon UV absorpt. spectrosc. 79−89687
^{129}I, hyperfine struct. and isotope shift of 1.3 μm transition 80−102486
In, 451.1 nm transition, HFS and ^{113}In-^{115}In isotope shift 78−82674
In, isotope shift and HFS, isotope effects, UV spectra obs. 80−42973
$InCl_3$ in Kr lattice, Raman and IR spectra, vibr. assignments, force consts., isotope shift and config. 79−89671
K, isotope shifts of individual nS and nD levels 80−102489
K+CO, bulge effect, in rot. inelastic scatt., isotope shift 79−86047
KBr:Li, paraelectric reson. meas. 77−36190
$K_2(Cd(CN)_4)$, vibr. spectra, isotope substitutions, force consts. determ. *(German)* 77−61750
$KD_{2x}H_{2(1-x)}PO_4$ crystals, $0<x<0.98$, light scatt. by polaritons 80−96802
$K_3N(SO_3)_3.2H_2O$ and ^{15}N derivative, Raman and IR spectra, $N(SO_3)_3{}^{3-}$ normal coord. anal. 79−91433
KOH, KOD, mm wave spectra, rot. transitions in excited vibr. states 77−3351
$K_2Pt(CN)_4Br_{0.3}.3.2H_2O$, deuterated, coupling of charge density wave and water mode 77−4646
$K_2(Zn(CN)_4)$, vibr. spectra, isotope substitutions, force consts. determ. *(German)* 77−61750
Kr arc spectrum, shifts in near IR lines 79−72257
Kr, even isotopes, isotope shifts of 557 nm transition 77−61710
Kr I, (A=78 to 86), saturated absorpt. technique 77−75102
Kr I, laser spectroscopy, isotope shifts, hyperfine struct. *(French)* 78−33457
Kr, isotope shifts using IR laser lines 77−27026
Kr isotopes, changes in nuclear charge radii 79−93504
KrHCl, weak complex, rot. spectra 80−52980
^{138,139}La, Fourier transform NMR 80−57354
$La_2(SO_4)_3.9H_2O$, and isotopic forms, water librations, Raman obs. *(French)* 79−28754
Li, A=6,7 two-photon intracavity dye laser spectroscopy 78−82706
Li, hyperfine splitting and isotopic shift, Doppler-free two-photon spectroscopy 79−36592
Li, isotope shift in 2^2P states and spatially resolved laser-induced fluoresc. 80−14103
Li_2, and isotopic variants, low-lying X-B transition freq. calc. 78−90180
$^7Li_2CO_3$, and $^6Li_2CO_3$, polycryst., low freq. IR and Raman bands assignments 79−42970
$^7Li_2CO_3$, and $^6Li_2CO_3$, polycryst., Li-O Raman bands 79−42969
Li_3F_3, isotopically substituted, IR freq. and intensity patterns 78−21926
LiH, isotopic species, $A^1\Sigma^+ \rightarrow X^1\Sigma^+$ bands 78−42091
LiH_2PO_3, Raman and IR spectra of transverse and longitudinal modes *(French)* 80−60573
Li_3N, superionic conductor, far IR absorption, temp. and isotope effects 79−51969
$Li_2SO_4.H_2O$, $^6Li/^7Li$ and H/D substituted, IR and Raman spectra, vibr. and librational modes 77−85716
$^ALi^+$, A=6,7, 2^3_1-2^3P, dye laser saturation spectroscopy, hyperfine struct. 80−18821
^{A}Lu, A=175,176, 5d6s$^{22}D_{3/2}$-5d6s6p$^4F_{3/2}$ transition, isotope shift and hyperfine struct. 80−83309
Mg I, isotope shift, hyperfine struct. 78−42011
Mg I, isotope shifts, extended meas. 79−72279
Mg I atomic transitions 77−71771
Mg^+ laser cooled ions bound in Penning trap, high-resolution optical spectra 80−102487
Mg_2, Ar matrix isolated laser photoluminescence spectra, electronic absorpt., emission, vibronic and vibr. relax. 78−82744
Mg_2, mol. consts. calcs., inverted perturbation approach 77−57969
MgH, and MgD, $B^2\Sigma^+$-$X^2\Sigma^+$ band system, ab initio CI calcs. 79−93970
$MgO(O_2)$, from $Mg+O_3$ matrix reaction, IR spectra, isotope shifts and blue matrix shift 78−80736
isotope shifts continued
$Mn_3(Co(CN)_6)_2.xH_2O$, mol. vibr. in cryst., normal mode anal., Raman and IR obs. 77−76494
MnO_4^- ion, ^{18}O enriched, matrix isolated IR spectra, force consts. 80−52985
Mo complex, ^{97}Mo and ^{95}Mo nuclear elec. quadrupole moment, nuclear quadrupole double reson. spectra 78−10802
Mo, isotope shift meas. 78−42010
MoO_3, $^{16}O^{18}O$ substitution, isotope shift, vibr. amplitudes and consts., normal coord. anal. 79−36610
N_2, isotopic forms, visible spectra, rovibronic and rot. anal., $C'\ ^3\Pi_u$ and $C\ ^3\Pi_u$ interaction 77−18933
$^{14}ND_3$, $^{15}ND_3$, ν_2 fundamentals and isotope shift 79−59456
ND_4ReO_4, ^{185}Re NQR temp. and press. depend., deuteration shift 79−65756
NH_3, heavy nucleus isotope shift calcs. 78−86917
$^{14}NH_3$, $^{15}NH_3$, submm-wave rot.-inversion transition, ν_2 state 77−75138
NH(D) radical, and isotopic species, laser mag. reson., hyperfine parameters 77−10694
NH_4HS, and ND_4DS, polycryst., vibr. spectrum and lattice dynamics 77−90138
$N_2H_2(N_2D_2)$, ground and first excited state small vibr. coupling, ab initio CI calc. 78−62791
$NH_3(ND_3)(NT_3)$, harmonic force fields, equal coord. method calcs. 77−30845
NHO(DNO), fundamental vibr. bands, laser Stark spectra 77−38692
$NH_2(X^2B_1)$ radical, and ND_2, ionisation pot., vibr. anal., ab initio calcs. and vacuum UPS obs. 80−53047
NO dimer, asymmetric, characterisation, Raman, IR spectroscopy 79−41176
NO, Rydberg absorpt. bands 800-850 Å, isotope shift 79−13734
NO_2, Ne matrix isolated, 6K, B←X band system 78−993
N_2O, submm wave spectra, 375-565 GHz, isotopic species, mol. consts. 77−3346
NO_2Br, ^{15}N-isotopic shifts, IR spectrum 79−98097
NO_2I, ^{15}N-isotopic shifts, IR spectrum 79−98097
$^{14}N^{16}O$, $^{15}N^{16}O$ isotopic species determ. using Zeeman scanning of atomic line, vibr.-rot. line profiles 79−49983
$^{14}NH^+(^{15}NH^+)(^{14}ND^+)$, ab initio CI calc. Λ type doubling in $X^2\Pi$ states 78−82714
$NaPF_6.H_2O$, IR and Raman spectra 77−61749
^{A}Na, A=21-31, hyperfine struct., mag. moments and isotope shifts, laser spectroscopy 79−10072
^{20}Na, D-line absorption, isotope shift determ. *(French)* 78−42008
^{22}Na and ^{23}Na, isotope shift, HFS, saturation spectroscopy 77−50409
^{22}Na, spectrometer for meas. of isotopic, isomeric shifts and hyperfine structure 79−6191
Nd, A=148, 150, pionic X-rays in 4f→3d transition, neutron isotope shift 77−75347
Nd I, isotope shifts in energy levels of neutral Nd atom 80−69095
Nd I and II, isotope shifts in spectrum, 3900 to 4760 Å, config. mixing 77−30812
Nd, new lines, 3930-6450 Å, isotope shifts 80−47929
^{143}Nd, ^{145}Nd, visible spectra, relative isotope shift, odd-even staggering parameters 77−10615
Ne, atom, isotopic shift and fine struct. for $2p^54d$ and $2p^55s$ config., Doppler-free two-photon spectroscopy 80−23387
Ne, ground level isotope shift between ^{20}Ne and ^{22}Ne, obs. 79−31451
Ne, metastable state, Doppler-free linear single-photon spectroscopy 78−50487
Ne+Ne(He), 7d′ states, isotope shift, press. shift, press. broadening, two-photon spectra obs. 78−55155
^{20}Ne, ^{22}Ne, 1.15 μm line isotopic shift, phase-polarisation nonlinear high-resolution spectroscopy in longit. mag. field 79−41423
Ni complexes, $Ni(glycinate)_2(pyrazine)$ and $Ni(glycinate)_2(pyridine)_2$, and isotopic forms, IR band assignments 79−22710
Ni I isotope shift for stable isotopes, nuclear charge radii 80−99484
O_2, $^3\Sigma_u^-$-$^3\Sigma_u^+$ spin-orbit mixing in Schumann-Runge predissoc. 77−6875
O_2, $A^3\Sigma_u^+$, $C^3\Delta_u$ and $C^1\Sigma_u^-$ states in van der Waals solids, electronic spectra, dynamics 78−1000
O_2 isotopes, $^{17}O_2$, $^{16}O^{17}O$, $^{17}O^{18}O$, pure rot. Raman spectra, bond lengths 78−42071
O_3, UV absorption bands, new vib. quantum no. assignments, based on isotope effect 79−94008
O_3 vibr. and rot. variational calc., isotope shifts 77−57967
OAlCl and OAlF, IR matrix spectra, vibr. freqs. *(German)* 79−11785
$OCBr_2$, IR spectra in Ar matrix, force consts. *(German)* 79−36641
OCS, millimeter wave rot. spectra, isotope shifts, freqs. and mol. consts. 80−78611
OCS, T_2 relax. meas. using budge-type superhet. microwave spectrometer 80−91551
$^{16}O^{12}C^{34}S$ and $^{16}O^{13}C^{34}S$, IR spectra, ν_3 band anal. 80−95620
OCSe, isotopic species, microwave and IR spectra 77−38658
OGaF, matrix IR spectrum, vibrs. and force consts. 79−11787
ONCN, IR spectra isotope shifts and ab initio calc. for harmonic force field 79−13715
^{A}O, A=16,18, pionic 1s state energy shift and line broadening *(German)* 80−48107
$^{12}O^{16}O$, $^{12}C^{18}O$, IR emission, vibr.-rot. lines 77−3355
^{16}O, $^{18}O_2$, vac. UV absorpt. spectra, band intensities and designations 78−5245
$^{16}O_3$ and ^{18}O isotopic species, rot. spectra 18 to 382 GHz, force and Coriolis coupling consts. 77−75137
^{18}O isotope shift in ^{13}C NMR, struct. depend. 80−69165
$O_2(c^1\Sigma_u^-, C^3\Delta_u, A^3\Sigma_u^+)$ generation from at. recomb. in O_2-He afterglow, fluoresc. obs. 79−31576
OsO_4, and isotopic forms, stretching fundamental, 961 cm^{-1}, high resolution spectroscopy 78−90162
OsO_4, IR laser dissociation isotope separation appl. 77−18993
OsO_4, tunable diode laser spectrosc. obs. 78−82061
PCl, visible and near IR emission, $A^3\Pi \rightarrow X^3\Sigma^-$ and $b^1\Sigma^+ \rightarrow X^3\Sigma^-$ systems vibr. anal. 78−21938
$PH_3(D_3)$, ^{31}P NMR, chemical shielding, centrifugal distortion, anharmonic vibr., cubic force consts. 78−82752
$PH_3(PD_3)(PT_3)$, harmonic force fields, equal coord. method calcs. 77−30845
$P^{18}O$, UV absorpt. spectra, valence and Rydberg states, rot., vibr., anal., predissoc. 79−41184
PbBr, $b^1\Sigma^+$-$X^3\Sigma^-$ band system, microwave discharge obs., mol. consts. 79−81203

isotope shifts continued
Pt complexes, cyano and cyanohalide hydrates, IR absorpt. spectra 77−6771
Pt, ground state configs., isotope shifts and fine struct. anal., visible and UV spectra 80−42987
PuF_6, near IR spectrum, isotope shifts, vibronically induced transitions 77−6773
PuN, in Ar matrix, IR spectra, stretching freq. and isotope shifts 78−78690
PuN_2, in Ar matrix, IR spectra, stretching freq. and isotope shifts 78−78690
PuO, in Ar and Kr matrices, IR absorption spectra, normal coord. anal., assignments, force consts. 78−78681
PuO_2, in Ar and Kr matrices, IR absorption spectra, normal coord. anal., assignments, force consts. 78−78681
Rb, Doppler-free two-photon absorpt. spectrum 80−42975
Rb, high lying Rydberg states, atomic beam laser spectra 79−94101
Rb, high resolution laser fluoresc. spectroscopy in deep blue spectral region 77−82622
Rb I, D_2 resonance line ^{85}Rb-^{87}Rb shift, mean square charge distrib. values inversion *(French)* 77−57931
$^{85,87}Rb$, high Rydberg levels, press. broadening and shifts 80−52902
^{A}Rb, A=90-93, nucl. moment and charge radius using fast-beam laser spectroscopy 79−40839
^{89}Rb, nucl. moment and charge radius using fast-beam laser spectroscopy 79−40839
Re I, isotope shift meas. by HFS, methods, $5d^46s^26p$ level classification 79−49988
Rh, adsorption of $C^{16}O$ and $C^{18}O$, inelastic electron tunnelling spectra obs. 79−65331
RuO_4, $\nu_3(F_2)$ IR band contour, isotopically pure cpds., mol. consts. 77−61746
SCF_2, IR, Raman and matrix isolation spectra, isotopic shifts, anharmonicity consts. *(German)* 77−83600
SF_6, ν_3 Q-branch, CO_2 laser pumped 78−21924
SF_6, tunable diode laser spectrosc. obs. 78−82061
SF_5Cl, pure rot. spectra, 300 GHz, isotope effects 80−5533
$S_{8-x}(NH)_x$, (x=1,2,3,4), and deuterates, IR and Raman spectra, isotope shifts, mol. vibr. assignment 79−10110
$S^{16}O_2$,$S^{18}O_2$, (0,0) band rot. anal., a^3B_1 state electron spin fine struct. consts. 77−10687
SO_2, T_2 relax. meas. using budge-type superhet. microwave spectrometer 80−91551
$SO_2+H_2O(N_2)(SO_2)$, linewidths, intensities, isotope shifts, 91.5-95.5 GHz 78−42044
SPF_3, IR spectra, $^{32}S/^{34}S$ shift 78−62802
SPF_3, isotopic forms, microwave spectra, centrifugal distortion consts., vibr. and rot. states, IR matrix spectra 77−10665
SPF_3 vibr. spectrum, assignment using matrix isolation and isotope substitution *(German)* 78−13498
^{A}Sb, A=121, 123, elec. and mag. hfs. 79−10224
$SeCF_2$, IR, Raman and matrix isolation spectra, isotopic shifts, anharmonicity consts. *(German)* 77−83600
SeF_6, IR vibr. band contours, isotope substitution, force consts. 78−17670
SeO, IR bands of 10296 and 10491 Å, rot. struct. 78−5224
Si:S, existence of isotope shift for S deep level, isothermal transient capacitance meas. 78−63999
SiF_4, mol. cryst., giant anomaly of intensity of vibrs. of isotopic impurity, Raman spectrum 79−73276
SiF_4, $\nu_3(F_2)$ IR band contour, isotopically pure cpds., mol. consts. 77−61746
SiH_4, Stark effect, rot. transitions in vibr. ground state, isotope shift 79−27029
Si_6H_{12}, and Si_6D_{12}, Raman and IR spectra, vibr. force consts., config. *(German)* 79−22715
SiH_2DF, $SiHD_2F$, microwave spectra, harmonic force field, mol. struct. 77−18913
SiH_3NCS, microwave spectrum, mol. consts., isotope effects 77−46559
SiH_3NCS, microwave spectrum, rot. Zeeman effects 79−54847
SiH_3X^-, X=Cl, Br, I, and isotopic forms, EPR spectra, mol. struct. 79−94023
SiO, interaction between $G^1\Pi$ and $I^1\Pi$ states 79−50040
SiO_2, low-lying electronic states, vib. assigned perturbations 77−27082
SiO^+, rot. spectrum, isotope shift, mol. consts. 79−59483
SiO_4^{4-} compounds, vibr. pot. function, force consts., isotopic shifts, mean vibr. amplitudes 80−23395
Si_3O_3, isotopically substituted, IR freq. and intensity patterns 78−21926
SiS, and isotopes, microwave spectra and consts., review 77−23493
Sm, (A=147,149), hyperfine struct. second order effects on isotope shifts 78−25476
Sm, excited states hyperfine struct., isotope shifts, laser-RF double reson. obs. 79−41140
Sm I $^{144}Sm^{152}Sm$ isotope shift J depend., in ground term. 77−75101
Sm I spectrum from laser-atomic-beam spectroscopy 78−37578
Sm II isotope shifts for $4f^66s$ and $4f^65d$ 79−67647
Sm, optical isotope shifts, optical heterodyne method 79−22630
SmI, laser atomic beam spectroscopy, isotope shifts, hyperfine struct., transitions 80−102468
Sn tetrahedral molecular solids, ^{119}Sn Mossbauer and Raman spectra 78−15070
Sn_2, matrix isolation Raman spectrum, overtone bands breadth 78−33515
$SnBr_4$, matrix-isolation and $^{79/81}Br$ and $^{116/124}Sn$ isotope shifts in IR spectra 77−46561
$Sr^{16}O$, ($Sr^{18}O$), $A^{\prime1}\pi$ state, vibr. anal., isotope shifts, vibr. consts. 77−18903
Te II, odd-even staggering *(French)* 79−85936
Te II, vis. spectral lines, relative isotope shifts 78−37579
$Te^{VI}O_6$ ion in $A_2B^{II}B^{VI}O_6$ perovskites vibr. anal. using isotope shifts and perturbation theory 77−59073
TiO_2:H(D)(T), IR spectra, 300, 77 and 8K 78−35175
^{A}Ti, A=46, 48, 50, pionic X-rays, strong interaction and isotope shifts, π-nuclear optical pot. 80−53169
^{205}Tl, solvated and adsorbed, NMR studies *(Rumanian)* 79−82888
Tl(7^2P) states, isotopic forms, HFS, press. self-broadening, two-photon spectra 77−18879
U I, 5027 Å line, ^{235}U odd-even staggering coeff. 77−30828
U I, isotope and relative isotope shifts for ^{234}U, ^{236}U and ^{238}U 77−30823
U I, relative isotope shifts, specific mass shifts 78−90122

isotope shifts continued
U I, visible spectrum, ^{238}U-^{233}U isotope shift 79−788
U, isotope shift and configuration interaction 79−31468
UF_6, room temp., IR absorpt. obs., isotope shift of fund. band and combination bands, freq. depend. 80−23421
UI, precision isotope shifts meas. in visible, near IR 80−63587
UO_2F_2, ^{18}O isotope effects on electronic spectrum, temperature effect 79−31541
^{235}U, hyperfine struct. and isotope shift meas., laser separation by two-step photoionisation 78−78822
^{236}U, isotope shifts and inherent quadrupole moments *(French)* 79−7032
W, atomic spectra, isotope shifts in visible region and HFS 78−82694
WCl_6, force fields, IR spectra, isotope shifts 77−14432
Xe, $5d_{7/2}\rightarrow6p_{5/2}$ transition struct., laser spectrosc. and double reson. obs. 78−1210
Xe II, $5d^4D_{7/2}$-$6p^4P_{5/2}{}^0$ transition, isotope shift, h.f.s., laser-ion beam expt. 79−93945
Xe isotope shifts of 1s electron in K-X-rays following electron capture 77−23454
Xe, three level systems, obs. of isotope shifts 78−82670
Xe^+, $5p^45d^4D_{7/2}$ and $5p^46p^4P^0_{5/2}$ levels, HFS, ion-beam laser fluoresc. 77−75319
XeF, supersonic expansion jet, B←X system rot. and vibr. anal., isotope intervals, fluoresc. spectra 80−14174
Xe(II, IV, VI and VIII) compounds, Mossbauer study 79−65772
XeO, excited state spectra, subpicosec. predissoc., solvation, in solid rare gas hosts 77−68050
^{131}Xe, nuclear moments and optical isotope shift 78−33118
^{89}Y in $Y(NO_3)_3$, YCl_3 and $Y(ClO_4)_3$ aqueous solns., NMR study 77−24754
Yb, high resolution laser fluoresc. spectroscopy in deep blue spectral region 77−82622
Yb I isotope shift studies in 3900 to 6500 Å region 80−74144
Yb, optical isotope shifts and hyperfine splittings 79−93943
YbH(YbD), and isotopic forms, optical and EPR matrix isolated spectra, HFS, bonding 77−83613
^{A}YbI, A=170,171,173, $6s6p\ ^1P_1$-$6s^2\ ^1S_0$ transition, spectrosc. 80−23368
ZnXY, (X,Y=Cl,Br or I), matrix isolation, vibr. spectra, isotope effects, force consts. and geometry 78−46337
ZrO, band identifications in $^1\pi$-$X^1\Sigma^+$ system 77−18931
ZrO, γ system anal., isotopic band shifts in stellar spectra calc. 79−50029

isotopes
see also radioisotopes
natural reactor in Oklo, isotopic composition 77−56628
pivalic acid($-d_1$, d_9), liq. and soln., Raman assignments, CH_3 rot. barrier, dimerisation 79−26991
Pu radioactive waste, oxidation by radiation, effect on migration rate 80−13714
transuranium, accumulation losses in isotope producing reactor 77−61595
Ga, atomic weight from solid-source mass spectra 77−541
H anomalous isotopes, including quarks of unit charge, search using cyclotron 77−61879
Ne, separation by jet-background interaction 79−54983
O, lung perfusion determination by dilution principle with expiration detection of indicator *(German)* 78−85326
O, lung perfusion determination using O isotopes and dilution principle *(German)* 78−85327
^{238}U, natural spontaneous fission, Xe prod., determ., extraction from granite 78−96216

isotopic generators *see radioactive sources*

isotopic spin (elementary particles)
see also baryon spin and parity; lepton spin and parity
$\Delta I=1/2$ rule violation and Melosh transform. 79−93377
baryonium, importance of isospin *(French)* 79−85260
broken isospin symmetry in chiral SU(4)⊗SU(4) and D^+-D^0 mass difference 78−89691
Cabibbo angle physical interpretation, weak interactions nonleptonic $\Delta I=1/2$ rule, four-quark scheme 77−22679
charmed baryons, nonleptonic decays 78−66118
charmed particle decays, semileptonic, nonleptonic, isospin restriction on charge distibs., branching ratios 77−54099
classical particle in external Yang-Mills field and SU(2) coherent states 78−74150
coherent states and isotopic spin 80−4843
conformal relativity, particle species classification, symms., space time origin of isospin 78−93815
exotic baryon resonance with isospins $\geq5/2$, existence, sum rule in Regge-on field theory *(Russian)* 78−93824
extended conformal symmetry origin, Yukawa interaction 79−40684
finite isospin groups for hadron classification, expt. consequences 79−360
four flavour $SU(2)_L\times U(1)$ gauge model with unconfined colour, and heavy leptons, $\Delta I=1/2$ rule 77−82708
four-quark scheme, $\delta I=1/2$ rule, existence of $K_L{}^0$, $K_S{}^0$ 77−22688
hadron isospin classification, same finite group for mesons and baryons *(Chinese)* 80−62887
hadrons, relation between spin, isospin, strangeness and charm 80−37183
hadrons interacting, isospin-spin polarisations, dynamical characts. 80−32035
heavy quark weak isospin, constraints from nonleptonic transitions 79−85257
hierarchy in asymptotic reconstruction of spontaneously broken isotopic symmetry *(Russian)* 79−2968
hyperon nonleptonic decays, $\Delta I=1/2$ rule violation 79−45087
induced second-class currents from isospin and chiral-symmetry breaking 79−97538
isospin violating effects from nonvanishing quark mass difference 79−63385
isospin violating mass differences and mixing angles, quark mass and QCD 80−52505
isospin-violating mixing in meson nonets, $d\bar{d}$-$u\bar{u}$($s\bar{s}$) mass differences 80−32096
isotopic symmetry group in strong interactions, possible geom. origin 79−17628
kinematics of relativistic particles with isotopic spin, geometric quantisation 80−62871
motion of singularities and co-ordinate covariance, gauge theories 80−12977

isotopic spin continued
multiparticle production, quasi-classical description of isospin conservation 78−58134
neutrino experiments on neutral currents, expt. verification of theoretical predictions, review 79−89097
(non)conservation of isospin, parity, charge conjugation, and time reversal invariance in intermediate energy phys. 79−80772
nonleptonic hyperon decays, CP violation, deviations from $\Delta I = {}^1/_2$ rule 78−70367
nonleptonic processes, quark sea and $\Delta I = 1/2$ rule 77−79255
quark mass effects as isospin and SU(3) violations in radiative decays of vector mesons 79−22091
S-matrix, relativistic, factorised, in two-dimens. space-time with isotopic symmetry *(Russian)* 78−8547
standard model neutral current predictions, uniqueness 79−80789
SU(2), unification of isospin and hypercharge, electroweak interactions of leptons 80−27439
SU(2)⊗U(1) gauge models, neutral current couplings 79−40715
SU(2) gauge invariance, spontaneously broken, $\Delta I = 1/2$ rule, nonleptonic weak interactions model 77−41786
SU(5) grand unification, spin from isospin, half integer spin charge monopoles 80−68406
supersymmetry, superfield notation for supermultiplets spontaneous breaking, Lagrangians and internal symmetry incorporation *(German)* 78−74167
weak charge of electron, $SU_2 \times U_1$ theories, $\bar{\nu}_\mu e$ scatt., isospin 78−16974
weak neutral current isospin props. in ν-p and $\bar{\nu}$-p scatt. 77−2812
weak neutral currents, light-cone algebra anal. 79−6311
Weinberg model, universality and weak isospin leptons, nucleons, quarks 78−70273
Yang-Mills theory, conversion of isospin degree of freedom into spin degree of freedom 78−89617
b quark weak isospin and possible non-existence of t-quark 79−36010
$D \rightarrow K^- \pi\pi$, branching ratios, isospin anal. 78−70363
D^+-D^0 mass difference, form factors, SU(4) coupling, vector meson dominance model 79−391
D^+-D^0 mass differences, chiral SU(4)×SU(4) model, broken isospin symm. 77−87917
$D^\pm$ nonleptonic and semileptonic decays, isospin selection rule tests 80−73700
ed, polarized scatt., parity violation Weinberg-Salam model without parton model 79−40787
$\gamma n \rightarrow \rho^0(p\pi^-)$, 7.5 GeV, cross channel isospin amplitude meas. and anal. 77−18299
$K \rightarrow 2\pi$ and 3π, transition amplitude determ. using least-squares anal. 79−58956
$K^{*0} \rightarrow K^0\gamma$, SU(3) and isospin symmetry breaking effects 80−95272
$\bar{K}K$ S-wave enhancement, 1300 MeV in πN interactions, characteristics 77−6158
$\bar{K}N \rightarrow \pi\Sigma^*$ or $K\xi$, isospin restrictions on spin density matrices *(Russian)* 77−30446
$K^-n \rightarrow K^-n$, I=1 reaction, from 1.2 to 2.2 GeV K^-d scatt. 78−29353
K^-p, 4.2 GeV/c, backward axial vector meson prod., isospin and SU(3) struct. 79−93458
$K^-p \rightarrow \pi^+\Sigma^\pm$, cross-sections, 1470-1550 MeV 79−13154
NN I=1 amplitudes struct. at 6 GeV/c 78−70395
$NN \rightarrow NN\pi$, isovector exchange, comparison with πN elastic scatt. 78−37189
$\bar{N}N \rightarrow N\pi N$, 9 GeV/c, isospin cross sections, differential anal. 80−431
NN scatt., impact parameter representation, taking into account spin, isospin and Pauli principle 78−58198
NN T=1 phase shifts, imaginary components, effect on spin depend. cross sections 79−36092
$np \rightarrow d\pi^0$, 795 MeV, test of isospin invariance 79−75786
$\nu(\bar{\nu})$ N interactions, π charge distrib., isospin and V,A struct. of weak neutral currents 77−38157
$\nu n \rightarrow \mu^- n\pi^+$, weak current isospin struct. study 79−49507
$\nu n \rightarrow \mu^- p\pi^0$, weak current isospin struct. study 79−49507
$\nu p \rightarrow \mu\ p\pi^+$, weak current isospin struct. study 79−49507
$\omega'(1675)$, prod. in $\pi^+p \rightarrow \Delta^{++}\pi^+\pi^-\pi^0$ 78−37241
$pN \rightarrow NN\pi$, 6 to 1480 GeV, cross channel isospin amplitudes 78−45964
$\bar{p}N \rightarrow \bar{N}(N\pi)_{I=1/2}$, 5.7 GeV.c ρ exchange contrib., cross channel isospin amplitude anal. 78−45938
$\bar{p}p$, isospin anal. of energy shifts 78−62961
$pp \rightarrow n\Delta^{++}$, unconventional behaviour of isospin-one exchanges 78−21445
π, photoproduction in E<450 MeV region, dispersion relations, CT invariance, review, book contrib. 80−47311
π condensation and tensor binding, parity and isospin 78−33139
$\pi \rightarrow e\nu_e\gamma$, isospin-breaking, chiral limit, conserved-vector-current violation, σ model 80−62988
$\pi \rightarrow e\nu\gamma$, vector form factor, quark masses and isospin breaking 79−13111
$\pi^-{}^3He$, isospin anal. of energy shifts 78−62961
πN scatt., isospin violation from π^0-η mixing, partial wave anal., N*(1540) struct. 80−27426
π^-p, isospin anal. of energy shifts 78−62961
π^-p backward elastic scatt., 3.5 GeV/c, polarisation parameter, isospin anal. 77−13974
$\pi^+\pi^-$, isospin anal. of energy shifts 78−62961
ψ', ψ decay branching ratios, isospin and flavour symmetry breaking 80−95264
$\psi'(3.7) \rightarrow \psi\pi^0$, isospin violating decays 78−37205
ρ-meson production and charged-neutral correlations in high energy pp interactions 79−17760
$\pi N \rightarrow K\Sigma^*$ isospin restriction on spin density matrices *(Russian)* 77−30446

iteration methods *see iterative methods*

iterative methods
see also predictor-corrector methods
ρ-filter reconstruction from incomplete projections 77−25582
acceleration of, linear systems 79−63722
acceleration technique for iterative methods in diffusion equation *(Japanese)* 79−80971
acoustics, low freq. field calc. 78−29876
adaptive-wall wind tunnel, iterative anal. of subsonic flow 78−22364
adsorption isotherms, Adamson and Ling's analysis 77−31906
adsorption isotherms, Adamson and Ling's analysis 77−31907
AGA two-sweep iterative methods, appl. to critical reactor calc. 79−36298

iterative methods continued
Aitken's δ^2 transformation generalisation, summing perturbation series 78−24652
Aitken method, integration of highly oscillatory functions 77−13593
algorithm for continuous stress and displacement solns. 79−1109
anisotropic source flux iteration techniques, interpolation schemes 80−99200
astrometry, photography against stellar background, iterative trajectory search algorithm *(Russian)* 77−17376
astronomical images iterative reconstruction, non-negativity constraint 79−101081
asymptotic method using projection iteration, linear and nonlinear differential eqn. systems, errors, convergence *(Russian)* 77−57169
atmosphere, iterative method for barotropic flow crossing mountain barrier 77−21855
atom-solid elastic scatt., iterative integration scheme using Green function 77−48294
atomic emission spectrometry, blackening transformation parameters and computers use *(German)* 80−30300
atomic struct., numerical HF radial function during SCF iteration, convergence 78−58574
atoms, variation-iteration procedure, by numerical integration scheme 78−17551
averaging methods, n-th order asymptotic convergence for autonomous systems 79−97188
axisymmetric stationary mag. field calc. on nonlinear ferromag. media by iterative method *(Ukrainian)* 79−94127
Ball-Zachariasen model of diffractive scattering, numerical soln. near singularity of Frechet derivative 80−9158
Bayesian deconvolution, convergent props. 78−57861
beam, rotating slender, bending vibrs., Galekin method anal. 80−1465
beam vibration frequencies by Schelkunoff iteration with HP-65 calculator 78−1592
beams, tapered hinged, large-amplitude free vibrs. 78−38226
beams and plates, lateral deflection, determination by iterative method 80−19241
biharmonic eqn. finite element approx. 77−2524
block iterative finite element preprocessed scheme, large nonlinear problem simulation 79−53
Block-Stodola eigensoln. technique for large algebraic systems with nonsymmetrical matrices 77−26163
body of revolution, flow interaction near tail, iterative procedure 77−35128
body of revolution, iterative soln. for flow within and exterior to boundary layer and wake 77−35129
Boltzmann eqn. for dilute simple gas, transport coeff. determ. 78−38439
Boltzmann eqns., soln. for electron-LO phonon scatt. 79−19586
Bouleyev-Marchuk eqn. soln. methods *(Russian)* 79−100967
bound polaron, non-perturbative approach 79−69439
boundary value problems, second order 78−32660
bounded metalworking process, iterative numerical anal. technique 79−83212
Boussinesq problem for material with different moduli in tension and compression 78−55564
broadband modulation of resonance conditions, general solution of Bloch equations 79−65706
bubble and dew points calc. 79−19359
buckling, tall vertical column, optical load, optimal shape, nonlinear differential-integral equation 80−53663
BWR transient anal., iterative procedure for predicting critical power ratio 80−42816
CAD of solar heating and air conditioning system, w.r.t. maximum solar heat gain 79−57466
cell kinetic parameters estimation from flow microfluorometry 78−73143
CG method generalisation, linear and nonlinear problem appl. 79−30243
Chandrasekhar nonlinear H-eqn., iteration 79−58652
Chandresekhar's H-equations in multigroup neutron transport, iterative solns. 78−37389
Chebyshev polynomial method, 2-D fast reactor models 79−97752
chemical kinetics meas. computational processing iterative optimisation techniques 77−32765
chemical laser, steady state operating characts. calc. 77−19241
chemically reactive flow characts., simultaneous heat-mass transfer *(Japanese)* 78−22431
chemistry, method of successive approx., teaching 78−89281
Cholesky factorisation method for mixed boundary conditions and discontinuous material prop. problems 79−81715
Cholesky-conjugate gradient method, incomplete, for iterative soln. of systems of linear eqns. 78−28932
circular elastic-plastic plates, numerical anal. under press. and temp. cycles 78−30199
CLEAN method, iterative beam removal, mathematical-statistical description 78−57464
close binary systems, convergence of Kopal's iteration method for light curve soln. *(Chinese)* 79−62872
coastal trapped ocean waves, anal. and numerical calc. by inverse iteration 78−69360
coaxial cylinders, contact problem, iterative soln. technique *(Russian)* 80−23963
coherent optical iterative extrapolation of 2-D band-limited signals 80−78780
cold rolling, non-circular arc roll force model 78−48423
columns, shear deformation effect on post buckling behaviour, iterative analysis 80−38299
compact storage for iterative soln. of large sparse linear systems of eqns. 78−57713
complex alpha-spectra evaluation using program ALFUN 78−74552
composite signal anal., by cepstral inverse filtering, biomedical appl. 78−69243
compressible flow study, gas dynamics method based on iterative techniques *(Hungarian)* 78−94757
compressible laminar boundary layer analysis, on yawed cone 77−23973
computational methods, book 78−81820
computer-generated hologram spectrum shaping and image reconstruction 80−106475
computerised tomographic image boundary finding and complex object localisation 80−109016
computerised tomography, iterative three dimensional reconstruct. from twin cone beam projections, simulation study 78−80949
conference, computational methods in nonlinear problems in mechanics and engineering, Austin, Texas, USA (March 1979) 80−51945

iterative methods continued
configuration interaction, iterative variational method calcs. 78−55127
conjugate gradient method, 2-D fast reactor models 79−97752
conjugate gradient solution to discrete ordinates equation 78−21622
conjugate gradients, appl. to nonlinear inverse thermal cond. 80−23865
contact stress problems, counterformal, improved numerical method and program 79−41632
continuation method, adaptive step size selection 78−45476
contribution transport, deterministic approaches 80−555
convergence assisting method for inclusive iterative processes *(German)* 77−9876
convergence in finite element anal. of reinforced concrete 78−38186
convergence of standard and damped least squares methods, Newton Raphson algorithm 77−9878
convergence rate, comparative study, appl. to hypersonic flow problem 79−40374
convergence speed of a posteriori variance estimation *(German)* 79−100984
convergent and asymptotic iteration methods in general relativity 79−93002
convex nonlinear boundary value problems, iterative bounds for stable solns. 78−54167
corona discharge computing, electrons and ions distribution determ. 79−4204
corrective gradient projection method applied to seismic array processing 77−17222
counter current extraction column, efficiency, using nonlinear PD model *(Russian)* 79−64808
coupled eqns. for heavy ion scatt., iterative method of soln. 77−46148
coupled large linear damped structures, eigenvalue anal. 78−1561
coupled problems in transient fluid and structural dynamics, appl. to nucl. engineering 77−71646
cross section adjustment in anal. of benchmark expts. 79−63718
cross-section data adjustment iteration procedure 79−9696
CTR, model blanket expt., neutron spectra sensitivity analysis 78−29648
cylindrical fibre with symmetric index distrib., matrix analysis 77−84001
decomposition method applied to transonic flow problems 77−58725
depth determ. from seismic refraction data, iterative method 78−96302
detector distorted data analysis, appl. to beta ray spectroscopy 79−13583
DH stripe geometry lasers, three-dimensional anal. of mode props. 80−64020
diatomic molecule, wave function computation, iterative method compared with Langer's method 78−86762
diatomic molecule electron scatt., iterative static exchange method 80−53155
difference equation system of radiative heat transfer *(Russian)* 77−58540
differential equations solution, parabolic, with M-matrices, w.r.t. rate of convergence *(German)* 80−1405
diffraction theory, iterative method based on spectral domain approach for corner diffr. coeff. 80−87304
diffusion equation, sols. by Picard's method 79−7273
diffusion flames, appl. of quasi-linearisation techniques 79−20368
diffusion nonlinear equation, perturbation, iterative and optimal techniques for arbitrary diffusivity 77−66943
diffusion problems, approximate solutions using Galerkin method 80−166
diffusion-type problems, mixed explicit implicit iterative finite element scheme, theory 77−22399
diffusion-type problems, mixed explicit-implicit iterative finite element scheme, soln. and examples 77−26155
Dirichlet problem for semilinear eqn. $\Delta^k u = f$ on a disc, approx. techniques 79−40377
Dirichlet problem for semilinear eqn. $\Delta^k u = f$ on a disc, series soln. 79−40376
disc calc. by iterative method *(Polish)* 79−14252
discrete time series spectral estimation novel aspects 77−91336
dislocation surface source, calc. of critical shapes and stresses 79−46659
dual-beam tissue absorptiometry, iterative method for K_β filter elimination 77−70533
dusty gas, two fluid model field eqn., time interval for soln., iteration method *(German)* 78−63489
dynamical local field corrections in dielectric function 80−88500
dynamical systems equations 77−57167
eigensystem derivatives, convergence of iterative method 78−28926
elastic contact problems with friction, nodal parameter soln. *(French)* 79−10475
elastic deformation of continuous flexible member, shooting method with Newton-type iteration 80−48575
elastic design problems, optimality, iterative solutions, finite element analysis and variational method 80−23887
elastic shells, stable solutions, finite element and Newton-Raphson methods 80−14593
elastic unitarity integral, angle-dependent lower bound on soln. and new uniqueness condition 79−40414
elastic-plastic finite element analysis, interpolation vs. iterative soln. for Tresca yield condition 78−59312
elastic-plastic initial value problem, iterative numerical integration 77−62170
elastoplastic structures under cyclic loads, small displacement finite element analysis 77−62171
electrochemical system, multiply connected region, iteration process for calc. of elec. fields 77−81412
electrodynamics, low freq. field calc. 78−29876
electromagnetic wave scattering by inhomogeneous sphere, iterative soln. to p-tuple series eqns. 78−62976
electron density, bulk and surface atoms, from ab initio model calcs. 79−4590
electron microscope autoradiographs, iterative anal., sample sizes and confidence limits 79−35896
electron microscope autoradiographs, iterative anal. method 79−35895
electron-hole transitions, nonstationary processes, numerical anal. *(Ukrainian)* 78−84229
electronic structure, Hartree problem, iterative diagonalisation soln. 79−6829
electronic structure calcs., self-consistent, accelerating convergence of iterative process 80−87037
electronic wave functions, iterative scheme for simultaneous calc. of m 1st eigenstates of real symmetry matrix 79−85888
electronic wavefunction, correlated, graphical unitary group approach, abelian point group symmetry utilisation 79−68193

iterative methods continued
electrostatic Vlasov turbulence, iterative soln. 80−10375
EM field calculation by successive overrelaxation (SOR) method 79−92964
EM induction pumps, fluids, laminar flow, characts. anal. 79−32699
EM prospecting, inverse problem 79−53583
fast reactor finite difference diffusion theory codes, optimised iteration strategies and data management 77−83005
Fermi normal coords., expansions of the affinity, metric and geodesic eqns. 80−104
ferromagnetic bodies calc., rectangular, magnetic surface charge distribution *(Slovak)* 79−4656
ferromagnetic plates eddy current phenomena numerical computation method *(German)* 80−65952
film, surface density of states calc. within tight-binding scheme 77−55594
filter, interference type, transmission band splitting elimination, oblique incidence 77−765
finite difference Newton Raphson algorithm, multiconfiguration Hartree Fock calc., He $1s2s\,^1S$ appl. 77−6663
finite element discretisation, two-dimens. stationary heat cond. using successive overrelaxation and conjugate gradients 78−83206
finite element method using Kantorovich meth., appl. to MHD duct flow 77−74205
finite elements method, iterative algorithm for continuous stress field anal. 77−72179
finite single- and two-phase systems, atomic diffusion, iterative solns. 77−4224
finite-difference method, for crossed (doubly-periodic) gratings 79−1002
finite-element magnetic field calc. allowing for saturation and hysteresis 79−41278
finitely conducting cross grating theory 80−106635
fission reactor, criticality calculations by source-collision iteration technique for cylindrical system 77−65268
fission reactor reactivity perturbation calc. by difference iterations in the Monte Carlo method 80−5210
fission research reactor computing, three-dimensional SNAP diffusion theory, including up-scattering 80−5208
flagellar propulsion, hydrodynamic anal. 79−53072
flat plate module design evolution, influence of module requirements 80−94065
flow, confined, numerical simulation, anal. of higher order methods 80−19316
flow, plane parallel, finite amplitude stability, perturbative and iterative methods 78−38293
flow, supersonic, parabolic Navier-Stokes equations, implicit finite-difference method using fractional steps technique 80−69866
flow, transonic wedge, parabolic series method, drag coeff., press. distrib. 77−89142
flow, two-dimens. boundary layer, viscous-inviscid flow matching, transonic and supersonic flow *(French)* 78−79334
flow modelling, boundary layer, vortex, atmospheric, two-eqn. turbulence model soln. 77−91237
fluid dynamics, free boundary flow, surface tension effects, finite element fluid flow simulators 80−82647
fluid dynamics, groundwater flow, finite element eqns., Newton iteration and modified conjugate gradient method 80−77622
fluid dynamics, stationary Navier-Stokes eqn., discretisation, splitting of linear operators, iterative methods 80−69755
foil bearing, deflection due to finite width bump 78−77691
four step finite difference method for hyperbolic systems *(Japanese)* 79−77185
Fourier anal. of light curves of eclipsing variable stars 79−25632
free electron band theory wave function detn. 78−22996
Galerkin finite element-finite difference soln. of laminar boundary layer flows 78−42586
Galerkin methods, quadrature rules using B-spline basis functs. 80−30
gamma-ray detection, scintillator response, pulse height spectra unscrambling, computer program 78−55092
gas mixture, binary, condensation in boundary layer flow, numerical method 79−1236
gas transport coeff. data inversion iterative procedure, pot. energy function determ. 78−91051
Gauss-Seidel convergence criterion for elastic structural stability 77−53781
Gauss-Seidel technique for Mississippi Pascagoula Estuary water quality planning 78−73402
generalized rebalance, common framework for transport acceleration methods 79−22356
generalized WKB method, sufficient conditions for rapid convergence of iterations 80−53195
geodesy, Molodensky's problem in gravity space, existence and uniqueness of soln. by Newton's method 79−12061
geodesy, soln. of downward continuation problem by initial value method *(German)* 77−86750
Gibbs-Duhem eqn. for binary system, direct soln. 77−79041
gradient restoration algorithms, sequential ordinary and sequential conjugate, optimal control initial states conversion appl. 78−4474
gradient-type methods convergence, singular parameter optimisation problems 77−82375
gravity anomalies interpretation, computer modelling 79−34971
groundwater flow 2-dimens. eqns. soln., iterative methods 77−64351
Hall effect coeffs., linearised Boltzman eqn. solved 79−1595
hard corrugated surface, wave scatt., iterative series 78−89355
Hartree iterative solution of general SCF eqns., convergence criteria 77−61675
Hartree-Fock and linear response, coordinate space representation and gradient iteration 80−18216
Hartree-Fock calcs., fast iterative procedure 80−47414
heat conduction, inverse nonlinear problems, simulation methods 78−94513
heat conduction in solids, nonlinear, direct and inverse problems, approx. soln. method 78−94510
heat conduction problems solution, quasilinear *(German)* 80−33418
heat transfer, nonlinear, iterative-variational method 78−94511
heat transfer coefficient prediction, in drag reducing turbulent pipe flow 77−51052
heavy-ion scatt., inelastic, with Coulomb interaction, soln. of coupled eqns. 77−65232
Heisenberg chain, one-dimens. spin 1/2 dimerised, spectral excitations, renormalised group calc. 79−78295

iterative methods continued
Hermitian matrix, low lying eigenvectors, pseudo-convergence in iterative method 79−92970
Hermitian operator low lying eigenvalue calcs., iterative method 77−60965
heterogeneous multiaquifer systems, iterative quasi-three-dimens. finite element model 79−79905
HF, adiabatic time-depend. description of nucl. collective motion 77−74786
high precision voltage meas. automatic error correction algorithm *(Russian)* 78−70089
hologram construction from X-ray views or acoustic views 80−69339
holographic spatial filter, CAD, optimisation method *(Russian)* 80−28171
holography, rel. to phase problem in electron microscopy 80−99681
homogeneous doped semiconductor, influence of internal elec. field on diffusion of ionised impurity 79−55940
hot wire anemometry method for the flow patterns in an array of heat exchanger tubes 79−90357
Hubbard model, functional derivative study, perturbation method and first-order approx. 77−43465
Hubbard model, functional derivative study, self-energy correction, self-consistent eqn. 77−43466
hydrodynamic forces and moments, acting on body emerging from infinite plane 77−3802
hydrodynamics codes, Eulerian and Lagrangian, pressure iteration, multigrid method 80−53738
hydrometeorological data, Weibull distrib. appl. 78−65415
hyperbolic differential eqn., charact. initial value problems, interval-analytic soln., iterative procedure *(German)* 78−8234
hypervirial scaling iterative method 80−73196
hysteresis modelling and digital simulation, using cubic spline functions, real dipole element appl. *(German)* 79−4706
image reconstruction principles, in X-ray computer tomography 78−88745
image restoration, compare to singular value decomposition method 78−58930
images with linear spatially-varying degradations, singular value decomputation and projection iterative restorations 77−58274
implicit fast iterative numerical method for solving multidimensional partial differential eqns. 78−93519
implicit nonstationary iteration, appl. to 3D neutron diffusion 79−63712
impurity predeposition diffusion profiles, errors in iterative numerical calcs. 78−26591
incompressible Newtonian fluid flow through sinusoidal tube 80−14816
inelastic electron scattering in crystals, extension of Yoshioka theory 80−103219
inhomogeneous medium, effective cond., iteration series and variational estimates, Herring method 80−70663
instrument operation speed increase, additive-iterative correction method *(Russian)* 78−89423
integral eqn. soln. *(Russian)* 77−53765
interferometry, high fringe density technique, appl. to heat transfer *(German)* 78−21212
interplanetary trajectories determ. procedure *(Italian)* 79−44341
inverse heat conduction problems, iterative approach to soln. 80−10111
inverse iteration method convergence, for nonlinear elliptic eigenvalue problems 79−40353
inverse problems with nonnegative solns., descent approach 77−67244
inverse scatt. problem for scalar wave eqn., nonlinear approach 79−44778
inverse vibr. problem, Lowdin orthogonalisation, Kashiwagi-Sasaki generalisation 79−6928
ion beam source, optical props., convergent iterative numerical procedure 79−3620
ion optics, high current beam extracted from plasma, iteration scheme 78−50693
Ising model, boundary free energy, natural iteration and cluster variation methods, critical points 77−17913
iterative solutions, method of moments 80−18251
jet symmetrical flow around curvilinear obstacle *(Russian)* 79−81933
Kepler's equation for elliptic orbits, soln. using general algorithm 80−21898
Lambert's problem, recursive formulation for enhanced computation time 77−89016
laminar flow, entry region and numerical soln. for square channel 77−84325
laminar non-Newtonian flow in porous annulus 77−72333
laminate, time and temp. effects, mech. response, computer simulation 78−35466
large algebraic eqn. systems, direct and iterative solns. 79−41274
large scale general eigenvalue problem iterative method for soln. 78−89318
large-aperture Pockels cell design 77−19438
left ventricular ejection and valvular regurgitant fraction determ., noninvasive radiocardiographic data parameter estimation 78−48886
lens design, automatic, algorithm for accelerating convergence 80−38085
linear differential equation with two strong singularities, second order, iterative numerical soln. method *(German)* 77−30000
linear elastic arbitrary deformable bodies *(Polish)* 79−10476
linear multiplane coherent optical processors, iterative Fourier transform description 79−94164
linear systems, 3-part splittings 79−9088
linear systems, multicoordinate problem *(Russian)* 79−9102
liquid, mol. assembly, iterational soln. to integrodifferential eqn. 79−77473
liquid radial distribution functions, method of reducing termination errors 80−24332
lunar motion, literal soln., formal convergence *(French)* 80−36482
LWR core power distrib. calc., convergence of reiterating process *(French)* 80−5200
Lyapunov functions construction by iterative process, almost diagonal systems of differential eqn. *(Russian)* 77−57168
magnetic anomalies interpretation, computer modelling 79−34971
magnetic fields, slot permeance ratio evaluation *(Italian)* 78−86987
magnetotelluric anisotropic data, inversion technique 77−60475
magnetotelluric sounding, natural source obs. one-dimensional inversion 79−92479
matrix formulation of large deformation analysis 79−98608
matrix games, monotonic iterative algorithm 79−12563
matrix Riccati eqn., quasi-linearisation, iterative approx. 78−57871

iterative methods continued
Maxwell's time depend. eqns., solns. by successive overrelaxation (SOR) method 79−92963
MC-SCF equations, restricted, open- and closed-shell, soln. algorithm 79−63891
MCSCF method improvement 80−52857
membrane, rectangular under uniform pressure, large deflections 78−55560
metal, kinetic equation, iteration soln. 77−43564
metal clusters, distortions induced by finite size in regular clusters 77−35507
MHD equilibrium equations, convergence of iterative schemes 80−59115
micropolar fluids, stability of laminar flows between parallel walls 79−1160
molecular force field iterative consistency calcs. using geometric interpretation 77−6746
Monte Carlo iterative scheme for adaptive multidimensional integration 78−57762
Moser twist mapping theorem, new proof 77−25919
moving interfacial cracks, dynamic stresses, finite difference approx., iterative process 77−46966
multifluid Tokamak transport code, two dimens., time evolution 77−58880
multigrid iteration strategy appl. to neutron diffusion eqn. 79−85577
multiple input/output data, system identification 77−37750
multiple pot. scatt., soln. by finite iteration 78−28993
multiple quadratic regressions, programmable desk calculators in the laboratory 80−42048
multispectral radiance method for temp. distribution meas. *(Japanese)* 78−77912
multistep damped Picard iteration method for soln. of two-dimens. premixed laminar flame eqns. 79−94738
mutlicompartment analysis, direct estimation of parameters, appl. to drug conc. 77−44580
natural factor iterative approach to accurate stress calc. 79−94490
Navier equations of elasticity, iterative solns., depend. on Poisson's ratio 79−1107
Navier Stokes eqns., block iterative finite element algorithms 78−20971
Navier Stokes eqns., pseudo-spectral soln. method for incompressible flow *(French)* 80−52032
Navier-Stokes eqn. boundary problem, soln. via successive approximations 80−36865
Navier-Stokes eqns., soln. by efficient numerical method 78−9619
Navier-Stokes equations, laminar flow through cylinder array, finite difference method 78−42585
Navier-Stokes equations soln. method for steady flow past cylinder 77−54956
Navier-Stokes solutions using Stetter's method 79−32551
Navier-Stokes solvers, efficiency, vorticity-stream function form 77−58632
nematic liquid crystal mixtures, extended range, iterative method for eutectic range 78−83728
neutron, p-cell homogenization, transient flux effects, incorporation into 2-D iteration scheme 78−17301
neutron diffusion, linear eqns., soln. by method of implicit non-stationary iteration 78−70581
neutron spectra evaluation, computer-aided, by multisphere response meas. *(Slovak)* 77−83444
neutron spectrum unfolding, optimised smoothing, FERDOR method 80−27860
neutron transport, 2-D, diffusion synthetic acceleration method 79−22357
neutron transport, finite element diffusion and P_1 eqns. soln. by iteration 77−50188
neutron transport acceleration method, generalised rebalance 78−29525
neutron transport eqn., iterative soln. by diffusion techniques 78−29534
neutron transport eqn., optimal choice of initial flux for iterative solns. 77−26819
neutron transport integral eqn., iterative and direct approaches to critical dominant eigenfunction 77−38313
neutron transport theory, Chandrasekhar H-eqns., comparison of iterative methods 80−47521
Newton's method, appl. to renal network flows 77−16945
Newton's method soln. of steady transonic Euler eqns., nozzle appl. 80−38437
Newton method, two-point, soln. of nonlinear eqns. *(French)* 77−9871
Newton Raphson matching of Schrodinger eqn. trial solns., asymptotically Coulomb pot. eigenvalues 77−57214
Newton-Raphson, appl. to nonlinear heat transfer 79−23189
Newton-Raphson, for structural optimisation in aeroelastic conditions *(Italian)* 79−41600
Newton-Raphson and incremental methods in finite element anal. of thin structures 79−27514
Newton-Raphson method, stability anal. of nonlinear dynamical systems 77−72150
Newton-Raphson method cf. method of Scoring 79−17201
NMR, high resolution, automated anal., principles and computational strategy 80−58287
NMR analysis system, LAOCOON3-type, reliability efficiency and error estimates 78−258
NMR bandshape, complex exchange-broadened, iterative computer anal. 79−35805
nodal equations, numerical approach to numerical anal. 80−13554
non-LTE radiative transfer, rapidly convergent iterative method for Wiener-Hopf integral eqns. 78−12089
non-Newtonian fluid in cylindrical annulus, axial flow iterative calc. *(German)* 77−11225
nonlinear chaotic iterations, local convergence *(French)* 77−67241
nonlinear differential equations for gas nonisothermal stationary motion in pipe anal. 77−89086
nonlinear diffusion eqns., finite difference methods *(French)* 77−5654
nonlinear elastic half-space, dynamic contact stresses due to axisymmetrical projectile impact 78−42573
nonlinear elliptic problems for doubly connected domains, heuristic method *(Russian)* 78−86159
nonlinear evolution equations, exact solns. 79−25873
nonlinear field eqns., time discretisation and mixed finite element methods 79−40384
nonlinear image restoration with signal-dependent noise, decomposed local algorithm 78−78951

iterative methods continued
nonlinear Kalman filter for soln. of inverse heat cond. problem 80−19212
nonlinear shell theory, numerical method *(Russian)* 78−34006
nonlinear structure stability problems, incremental displacement algorithms 79−81717
nonmetrical method for paired comparisons *(Japanese)* 78−77833
nonseparable system semiclassical quantisation, invariant tori and energy levels calc. scheme 79−97225
nonstationary radiation diffusion system, iterative soln. method 79−31796
nozzle, convective heat transfer, turbulent boundary layer regime 78−9670
nuclear potential energy surfaces, folded Yukawa-plus-exponential model 80−86816
nuclear reactor kinetics, quasistatic solutions, nonlinear system, iterative procedure 80−52711
nuclear reactor neutron-physical calc., FBR, multi-group diffusion equation solution *(Czech)* 78−66332
nuclear reactor transient thermal hydraulic analysis, RELAP4 transform. into fully implicit iterative code 77−65257
one-dimensional oscillator, matrix elements of position coord., upper and lower bounds 79−35578
optical image quality enhancement, adaptive methods *(Russian)* 80−28163
optical imager, linearly degraded, iterative restoration 80−95807
optical images, linearly degraded, iterative restoration, reblurring procedure 80−99640
optimal iteration strategies, geometric interpretation 79−22358
optimal restoration filter for Poisson noise impaired and linearly blurred images 80−106481
organ flue pipes, self-sustained oscillations, integral eqn. soln. 78−51015
orientation distribution function analysis from incomplete pole figures normalised by iterative method 80−59344
p-i-n structure, forward biased, with band to band Auger recombination, numerical simulation 79−7879
pair distrib. functions on non-crystalline materials determ. from diffraction data 77−72522
parabolic procedure for three-dimens. compressible viscous flow prediction in ducts of arbitrary cross section 79−94716
partial differentiations of vis-viva and Lambert equations, Keplerian orbit calc. 78−7864
partially eclipsing binary stars, soln. of light curve by Kopal's iterative process 79−35310
particle tracks momentum determ. 78−70723
particle velocity distrib. functions in nonuniform background, iterative calc. 78−71438
penalty function solns. of algebraic systems 78−57770
Percus-Yevick equation, numerical calc. of crit. exponents 78−91212
periodic secondary motions in plane channel, num. soln. method 77−55092
peristaltic flow, Navier-Stokes eqns., implicit finite difference method using orthogonal curvilinear coords. 77−39346
permanent magnet, iterative calc. method for magnetisation 77−83777
perturbed energies, 2nd order, coupled HF iterative procedure, geometric approx. 79−9991
phonon scattering at multilevel impurities, dispersion, damping, Green's function calc. 79−14892
phonons, self consistent iterative method, economic method 77−84859
photoelastic characteristic parameters, fast iterative determ. procedure 79−27530
photographic process, reaction tensor analytical treatment *(German)* 79−83481
physiological compartment tracer flow modelling and digital imaging 80−101257
piezoelectric thin plate, electroelastic equilib. anal. *(Russian)* 78−19417
planetary disturbing function expansion, convergence of Newton's iteration 77−64629
plano-plano interferometer modes, FFT computation, Fresnel numbers 80−86392
plasma, Langmuir turbulence, large-scale, renormalisation group method 80−38650
plasma, neutral transport, one-group treatment 77−39408
plasma probe, spherical, slightly ionised continuum, current-pot. curves 77−72494
plasticity, large deflections and creep problems, soln. strategy 77−42750
plasticity, operator equations solution by iterative methods using 'near' operators 79−58547
Poisson's type eqn., reliability of iterative solns. 79−96837
polar semiconductor, HF mobility in longitudinal quantising mag. field 79−51619
polymer solution, semidilute, hydrodynamic interaction of two permeable spheres, method of reflections 78−71394
polytropes, uniformly rotating, equilib. struct. investig. using iterative method 78−32441
positron image reconstruction in nuclear medicine, three-dimens., fast iterative method 78−7443
potential energy with iterative correction or deterioration 78−89315
potential scattering, inverse problem, radial Schrodinger eqn. solns., analytic investigation *(Russian)* 79−87
potential scattering, refined Born approx. 80−77
projection-iterative methods, appl. to first kind equations *(Russian)* 79−9087
pseudo nonlinear regression 77−64933
PWR manoeuvring strategy optimisation 79−629
PWR thermodynamic design calcs., using iteration system based on secondary circuit system model *(German)* 80−13571
quadratically convergent SCF procedure based on Newton-Raphson iteration procedure 79−59335
radar attenuation in rain, iterative correction 78−92923
radiant heat transfer in absorptive and scattering medium, calc. by iterative zonal method 77−72138
radiative transfer eqn. soln. methods for model atmosphere light scattering 77−66986
radiative transfer in finite media, new technique for exact and unique soln. 78−77479
radionuclide tomographic section synthesis and enhancement 79−25103
radiosources cosmological evolution, free-form analysis, self-consistent luminosity function 80−46716
radiotelescope with minimum noise, maximum gain by iterative relaxation 78−65498
iterative methods continued
radiowaves, multiple scattering, iterative treatment method 79−8709
random digital scene generation with specified statistics 80−99666
random heat eqn. soln. 79−9195
rapid interpretation method for gravity anomalies caused by sedimentary basins 77−87110
Rayleigh-Kohn and Newton Raphson methods and their appl. to vibration analysis of single-junction branched systems 80−52035
Rayleigh-Schrodinger perturbation theory, formal treatment 79−18103
reactor neutrons, high level field stability, iterative calc. method 79−63714
rectangular matrix pseudoinverse using column approx., inconsistence systems of linear eqns. solns. 78−62061
refinement method for finite element eqns. 77−2521
regenerative Markov decision models 77−53756
relaxation methods for time depend. conservation eqns. in fluid dynamics 77−80137
relaxation time spectrum determ. from components on complex shear modulus 77−50965
reload core design optimisation 79−604
remanence direction from converging remag. circles 77−45182
remote sensing of stratified media, pulse-spectrum technique, permittivity determ. 79−8722
restrained acceleration 78−29530
restricted withdrawal of vertical cylinders from quiescent liquids, numerical treatment 77−72756
Reynolds eqn., one-dimensional, with slip boundary conds., perturbation soln. 79−14372
Riccati equation, matrix differential, steady-state soln. calc., iterative algorithm *(Russian)* 77−49585
Ritz approach to lattice columns with stochastic imperfections, buckling 79−18757
Ritz procedure, appl. to non-conservative elastic stability 77−22422
Ritz-Galerkin method, lateral beam buckling anal. 80−48607
rod, thin elastic, with causally mixed inputs, iterative numerical soln. 80−79161
rotating fluids, computation of velocity fields 78−59401
rotationally inelastic scatt., coupled eqns. for single initial state, variation-iteration method 79−68301
scattering amplitude phase construction by iteration of bounds from unitary integral 80−57142
scattering amplitudes, unitarity condition homogeneous linear inequalities, calc. program 79−85013
scattering length 80−86100
scattering theory, nonsingular potential, scatt. length by iterative-perturbation method 80−27160
SCF iterative sequences, convergence accel. 80−91435
SCF open shell orbitals, iterative process 78−90066
seismic inversion for boundary shape between two layer stacks 79−16684
seismic reflection data inversion 78−96307
seismic reflection recordings, control theory appl. to inverse problem *(French)* 77−87081
seismic stratum velocities determination, iterative method convergence *(Russian)* 79−74982
seismic velocities inversion for rock pore aspect ratio determ., linearised iterative method 80−51387
seismograms, iterative identification of noninvertible autoregressive moving average systems 77−81816
seismology, higher-order refl. moveout spectra computation procedure 79−92501
self-conjugate and positive definite operator, simultaneous calc. of eigenvalues *(Ukrainian)* 78−54154
semiconductor, one-dimensional phenomenological transport equation set 78−39102
semiconductor, polar, mobility in mag. field, extreme quantum limit, iterative technique 78−2498
semiconductor concentration calc. in weakly doped sample, iterative method, GaAs appl. *(French)* 77−72634
separating boundary-layer flow calculations 79−68678
shell calc., parabolic, shallow, thin, elastic behaviour calc. 79−57
shells, cylindrical, large elastic deflections, numerical anal. 79−98613
shock propagation, nonlinear hydrodynamic field equations, finite element anal. and method of weighted residuals 80−53813
short rectangular prism, field-depend. local surface magnetisation, numerical calc. 77−36110
shunt heated by current pulse, iterative method for overcoming errors 79−21766
siesmic reflection coefficient calc. from digital data *(German)* 77−70853
single-mode obs. distributions, invalid data rejection algorithm *(Russian)* 79−21690
soft shells, geometrically nonlinear strain *(Ukrainian)* 79−50589
soil diffusion eqn. soln. with exponential diffusivity comparison of iterative and perturbation techniques 77−41097
soil infiltration eqn. soln., comparison of perturbation and iterative techniques 77−41096
spectral estimation techniques for discrete time series 78−53734
spectroscopic measurement, convergence of iterative deconvolution technique, effect of errors 77−53849
stable operational processes appl. to inverse geophys. problems 78−85718
static electric field determ., numerical methods, monodielec./multidielec. regions, iterative solns. *(Spanish)* 80−106419
static fields in inhomogeneous anisotropic medium *(Ukrainian)* 78−81837
stationary discrete and adjoint continuous iteration processes, hybrid computation appl. 78−45472
stationary magnetic field calc. in nonlinear ferromag. medium *(Russian)* 79−13861
stationary magnetic field modelling with hybrid analyser 77−42463
stationary magnetic fields calc., in nonlinear ferromagnetic medium *(Russian)* 79−59613
steady state Navier-Stokes equation, numerical method and appl. *(Japanese)* 77−68564
steady-state response of difference eqns., digital computation schemes 78−57718
steepest descent approach, determ. of nuclear density matrix 78−17125
stellar model linear stability anal. by inverse iteration method 77−33469
stochastic approx. processes, law of iterated logarithm *(Russian)* 77−37746
stochastic constraints on iterative maximisation of system of differential eqns. 78−57757

iterative methods continued
stream-well-aquifer system groundwater flow anal., linear system models 78−77289
strength of axisymmetric body, optimum shape calc., finite element technique 78−51060
structural analysis, dynamic, soln. of quadratic eigenproblems 77−89017
structural optimisation problems, iterative methods 79−18690
structural vibration anal. using subspace iteration 78−38233
structurally disordered systems, with diagonal and off-diagonal disorder in non-orthogonal basis set, numerical study 79−69387
subsonic and slightly supercritical aerodynamic flow, rapid finite-difference computation 77−23979
subsonic flowfield, three dimensional geometrics, correction for viscous effects 79−98744
subsurface hydrology, finite element method using mixed explicit-implicit scheme 79−79900
successive over-relaxation procedure, optimum accelerating factors 79−92928
successive overretardation processes, estimation of optimum accelerator when applied to finite element anal. 78−16629
successive point upper relaxation method, 2-D fast reactor models 79−97752
successive reduction method for shell optimisation model *(Russian)* 79−76966
superconducting magnetic field problem, model, iterative soln. 79−65605
superharmonic approximation for quantum crystal 80−92615
swarm transport coefficients, iterative method calcs. 80−96336
tensile conc. optimisation using iterative method *(German)* 78−87271
terrestrial electricity, DC resist. meas. interpretation 79−5449
thermal diffusivity of solid, iterative estimation method 80−43603
thermal expansion, characterisation in minerals 79−70795
thermal properties of plane-shaped solids, simultaneous meas. method using iterative calcs. 77−42713
thin films, unbacked, optical constants by transmission interferometry 79−78778
Thomas-Fermi eqn., iterative soln., nonlinear eigenvalue problem technique 78−909
Thomas-Fermi eqn. solns. 79−9185
tissue pulse-echo US absorption estimation model 79−48304
Tokamak equilibrium, inverse problem, iterative metric method 80−106883
torsional vibration analysis, change of stiffness method 80−74589
transient field initial-boundary value problems, hybrid simulation 77−41469
transient vibration problems, solution bounds 77−67226
transonic aerodynamics, finite element method, book contrib. 79−32556
transonic flow, far-field boundary conditions solution 77−55024
transonic flow, relaxation solutions, convergence acceleration using cyclic iterative method 77−62272
transonic flow numerical calculation methods and problems, review 77−58723
transonic flow solution method using acceleration technique based on Wynn's ε-algorithm 77−58724
transonic nacelle flow fields, accelerated iterative calc. 78−26145
transonic shock free profile flow at zero incidence, iterative computation 79−50750
transonic small-disturbance eqns., shock-fitting appl. to relax. solns. 77−84275
turbulent boundary layer downstream of step change in surface temp. 79−81862
two-dimensional pattern distortion analysis, biproportional matrix projection method 79−88229
two-dimensional supersonic viscous in reactions near walls, prediction method 77−58726
two-electron integral transformations for 2nd order multiconfig. Hartree-Fock method 80−87045
two-media Milne problem in two-group neutron transport theory 78−17275
two-phase flow through porous media, simulation by finite elements 79−41752
unbounded Hermitian operators, low-lying eigenstates, method 80−98812
valvular regurgitant fraction meas. by radionuclide angiocardiography, iterative estimation 79−34668
variable direction method, 2-D fast reactor models 79−97752
variable direction method, choice of optimal variant for 2-D reactor models 79−97751
variable-thickness elastic orthotropic annular plate nonlinear oscillations 79−68630
variation-iteraction soln. of Hartree Fock eqns., Green's integral operator, SCF formalism 79−6842
vibrating beams, calc. of higher freqs. by simultaneous iteration technique 79−23258
vibrating beams, optimal design, iterative procedure 80−1457
vibration analysis, of singly curved rectangular sandwich plates with clamped boundaries, using Kantorovich method *(Japanese)* 80−5970
vibrational anal., iterative methods, accelerated automatic root search algorithm 78−59321
viscoelastic fluid, stability of laminar boundary layers *(German)* 77−72335
viscoelastic half-space, dynamic indentation and impact by axisymmetric rigid body, iterative method anal. 80−14626
viscous flow, past thin obstacle, boundary layer *(Japanese)* 79−94599
viscous laminar jet flow in slipstream calculation *(Russian)* 79−77209
water network anal. using sparse matrix and successive linearisation methods 78−85614
water table response to sequence of recharges 78−11937
wave equation, reduced, fixed incident field, inverse problem 80−62484
waveguides propagation constants calc. *(Japanese)* 78−42423
weakly coupled linear systems, block iterative LU solution technique 77−60941
weather forecasting, balance eqn. soln. with min. correction of mass field 78−36246
Wilkinson method, anal. of hydromagnetic thermal instability of rotating fluid layer, Hall current effects 79−27699
wind tunnel, convergence to interference-free conditions 78−38419
wings, low aspect ratio, computation of nonlinear characts. 79−41690
X-ray fluoresc. element anal. in pulps, conc. calcs., iterative method 78−61109
X-ray image reconstruction, iterative scheme 78−66014
X-ray structure determination, information theory aspects 77−51258
X-ray tomography, iterative reconstruction algorithms 77−12988

iterative methods continued
XPS, achromatic X-ray source, spectrum iterative deconvolution 78−72689
C materials, fine structure characteristics by integral method 77−43153
$Cu(NO_3)_2$, electronic struct., relative energies, iterative EHT calculations 77−38615
Fe, nonlinear magnetostatic problem soln. *(Russian)* 79−64138
GaAs, photoluminescence, electron-acceptor, from non-Maxwellian distrib. of photo-excited electrons 80−45138
H_2, electron scatt., iterative approach to Schwinger variational principle 80−99580
HgTe-type crystals, inverted band structure, influence of interband scattering on cond. *(Russian)* 79−51563
n-InSb, mobility in mag. field, extreme quantum limit, iterative technique 78−2498
InSb, polar semicond. longit. magneto-Seebeck coeff., effect of polar-optical-phonon scatt., iterative soln. of Boltzmann eqn. 79−56250
Li^++He, interaction pot., direct determ. from gaseous ion mobility 77−10720
LiH, direct optimisation of orbitals for multiconfiguration self-consistent field theory by unitary transformations 80−63544
$LiNO_3$, electronic struct., relative energies, iterative EH calcs. 77−38615
SF_6, arc, temp. determ. accounting for demixing 80−70057
Si, divacancy, positive, EHT calcs. 79−99184
Si, inversion layers, first order intervalley scatt. 80−29484
SiO_2, amorphous electron transport and breakdown at high elec. fields 79−78108
SiO_2, transport of electrons at high electric fields 80−20208
$TlNO_3$, electronic struct., relative energies, iterative EH calcs. 77−38615
$ZrH_{1.66}$, thermal neutron inelastic scatt., phonon spectra determ. *(Chinese)* 79−10906

itinerant model of magnetism *see band model of magnetism*

IV-VI semiconductors
amorphous, thermoelectric power and transport models 78−10482
atomic displacements and enthalpy of vacancy formation 78−38690
crystal binding, transverse effective charges 79−37651
crystal binding energy 79−37650
crystal growth of mixed cpds., morphology and transport rates, in microgravity 77−77353
crystal structure and symmetry of electron spectra, doping effects *(Russian)* 79−7696
diatomic molecules, He(I) photoelectron spectra, calcs. 80−1023
dielectric constant from band struct. calc. 80−15463
dielectric properties, elec. meas. 78−15119
electroless film deposition with variable comp. and polymorphic structs. 79−95952
ferroelectric, vibronic model of lattice instability 80−80723
film photodiodes, quantum efficiency 79−75596
film technology, review 78−3034
high temp. Fermi level position 79−90948
impurity levels, intergap interaction effects, T-matrix approx. *(Russian)* 77−31973
IR focal planes in intrinsic semiconductors 78−37994
layered materials, prep. and growth, book contrib. 78−19651
magnetic field induced displacive transition 80−50278
magnetic susceptibility near ferroelec. transition pt. *(Russian)* 79−95568
mean square atomic displacements, in single crysts., X-ray determ. *(German)* 78−30726
metal-GeS-metal system, current-voltage characts., band struct. effects in field emission region 79−42667
mixed, structural phase transition 80−15242
monochalcogenides, interaction of outer s states 79−10825
monochalcogenides interaction of internal s states 79−10826
multicomponent solid solutions for improved lasing 78−1232
narrow gap, fabrication, IR laser and detector appls. 77−77415
optoelectronic devices, MBE techniques 79−95942
orthorhombic, atomic pseudopots. 79−42453
p-n junction formation in doped semiconductors by laser radiation *(Russian)* 77−15947
n-PbTe, dynamical cond. in freq. range of LO-phonon-plasmon excitations 79−19592
phase transitions induced by electron-phonon interaction 80−10656
photodiode, lateral-collection, for 3-5 μm region 78−32871
production and physical props. for microelectronics *(Russian)* 78−11108
properties and use for making devices, review 78−60131
small gap semiconductor alloys, band edge parameters 80−49594
SnTe film, polycrystalline, anomalous resist. at struct. phase transition 80−29488
structural instabilities and transverse effective charges 77−27999
structural phase transitions, anomalous resist., electron-soft phonon interactions 80−108167
structural transitions, rel. to many-band model of electronic struct. 77−51497
transverse effective charge from one dimens. band struct. calc. 80−15038
transverse effective charge from three dimens. band struct. calc. 80−15039
two photon spectra, quantitative investigation 80−50373
vapour growth and transport in microgravity 77−77400
XPS, bond ionicity, struct. stability and charge transfer 77−44127
Au-Pb_xSn_{1-x}Te-Au structure, third harmonic variations at 77K and 300K 78−84313
CdS(Se)(Te):Co^{2+}, IR luminesc. quenching, Co^{2+} level position, ionisation energy 80−16079
GaTe, transport anisotropy 79−23975
Gd_2Se_3/PbTe, N type selenide segmented element fabrication, thermoelectric props. 80−107835
Ge-Bi-Te system, thermal cond. change during phase transitions 80−100368
Ge-$Pb_{1-x}Sn_x$Te, amorphous/crystalline heterojunction, rectification props., IR detector appl. *(Japanese)* 78−60197
Ge-S, Ge-S-Ag, amorphous prop. and origin of paramagnetic defects 79−10801
GeO amorphous semicond. films, photostructural changes by photomodulation ellipsometry 79−71510
GeS (001), density of empty states, core-level EELS and photoemission spectra meas. 79−78145
GeS (001) surface, electronic struct., Auger and electron energy loss spectra meas. 77−59314

IV-VI semiconductors continued
GeS, (001) surface struct., LEED expt. 78−84034
GeS, absorpt. spectra, electron-phonon interactions 80−80810
GeS, amorphous, UPS and XPS, valence band struct. 77−90247
GeS, angular resolved UV photoemission and band structs. 77−85144
GeS, anisotropic EXAFS, cryst. struct. determ. 80−66323
GeS, conc. depend. of rate of formation on Ge surface 79−43152
p-GeS, crystalline, photoelectric props. 80−70769
GeS, density of valence states, tight binding calc. 79−77976
GeS, dielec. function, optical and electron energy loss spectroscopy 78−15189
GeS, electron-hole interaction in d-electron excitations, photoelectron and optical spectra 78−34776
GeS, exciton luminescence 78−52555
GeS, far IR reflectivity spectra, lattice vibr. and dielec. const. 77−52068
GeS, film, effective electron mass determ. 77−1506
GeS film, effective electron mass determ. from current-voltage characts. in thermionic region 77−85135
GeS film, photocond. kinetics 77−39897
GeS, gas-phase single-cryst. growth, photoelec. props. 77−36381
GeS, growth parameter meas. during cryst. growth from vapour in closed ampules 79−19168
GeS, IR reflectivity meas. 77−8570
GeS, in metal-semicond.-metal struct., thermionic electron emission model 77−28260
GeS, interband transitions, intrinsic photocond., anisotropy 80−20244
GeS, layer cpds., Raman spectra, press. coeffs. and mode Gruneisen parameters 78−10891
GeS, low temp. photoluminesc. 77−77287
GeS orthorhombic layer crystals, photolum. spectra 80−2851
GeS, orthorhombic single cryst., fine struct. in reflectivity 79−19903
GeS, phonon dispersion relations, neutron scatt. study 79−42182
GeS, physical basis for Urbach's rule 80−93366
GeS, rot. spectra, Born-Oppenheimer approx., adiabatic corrections *(German)* 77−57994
GeS, Si doped and undoped, elec. cond. and thermally stimulated currents 80−20194
GeS, thin layer cryst., far IR transmission spectra 79−56870
GeS, Urbach's rule, absorption edges 80−97224
GeS_2-$GeSe_2$ cross section, $GeSe_2$ single cryst. growth 77−52305
GeS(Se), screw dislocations in layer crystal growth from vapour *(Russian)* 80−1953
GeS_xSe_{1-x}, form. of solid soln. and phys. props. *(Russian)* 77−1232
GeS_xSe_{1-x}, IR spectra, differential calorimetry, phase diagram *(Russian)* 78−52513
GeS(Se)(Te), XPS investig. of valence band struct. 77−48311
GeS(Se)(Te)(O_2), K X-ray spectra, Ge atoms effective charge, energy-gap widths 77−28657
GeSe (001), density of empty states, core-level EELS and photoemission spectra meas. 79−78145
GeSe, amorphous, UPS and XPS, valence band struct. 77−90247
GeSe, amorphous film, photocond. meas. 77−43647
GeSe amorphous films, blocking metal contacts characteris. and photo/EMF obs. 77−76924
GeSe amorphous films in Al-GeSe-Al structs., AC cond. and capacity, thickness depend. 79−65566
GeSe amorphouse sputtered film, DC and AC behaviour, effect of contact material 79−95513
GeSe, antiferromagnetic behaviour, res. to negative magnetoresistance effect 79−73719
GeSe, density of valence states, tight binding calc. 79−77976
GeSe, dielec. function, optical and electron energy loss spectroscopy 78−15189
GeSe, galvanomag. meas., anisotropy, metal to semiconductor transition 80−6847
GeSe, layer cpds., Raman spectra, press. coeffs. and mode Gruneisen parameters 78−10891
GeSe, low temp. photoluminescence 77−77287
GeSe, optical absorption edge meas. 77−63430
GeSe, photoelectron spectra, rel. to ionicities and phase transitions 77−69960
GeSe, rot. spectra, Born-Oppenheimer approx., adiabatic corrections *(German)* 77−57994
GeSe, single crystal, optical absorption 80−25383
$GeSe_2$ amorphous film, laser induced oscillatory phenomena 80−84711
$GeSe_2$ powdered crystalline, photoluminescence intensity under continuous excitation 80−71480
Ge_xSe_{1-x}, bonds and band struct. determ., tight-binding model 78−18959
Ge_xSe_{1-x}, thin film Schottky diode, photovoltaic effect 77−15895
$GeSe_xS_{1-x}$ solid solutions, long-wavelength optical phonons, Raman spectra 80−25378
$Ge_xSn_{1-x}S(Se)$, lattice parameters, optical energy gap and IR refl. 78−23021
$Ge_{0.5}Sn_{0.5}Te$ film, elec. and optical props. 77−12028
GeTE, density of valence states, tight binding calc. 79−77976
GeTe, amorphous, UPS and XPS, valence band struct. 77−90247
γ-GeTe, anisotropy of elec. props. 79−73515
GeTe, antistructural disordering 77−15402
GeTe based thermoelec. materials, creep mechanisms 77−16643
GeTe, bond orbital model of band struct. 80−59853
GeTe, concentration of carriers, rel. to stoichiometry 80−6847
GeTe, crystal binding energy 79−37650
GeTe, crystallisation in constant electric field, thermoelectric parameters 77−44146
GeTe, degenerate semiconductor, EPR experiments on Mn^{2+} 79−11339
GeTe, effect of phase transition on mech. and elec. props. 77−51746
GeTe, effective masses for cond., density of states 80−88472
GeTe, electron-phonon interactin induced phase transition 79−82338
GeTe, enthalpy and specific heat, 0 to 860°C, polymorphic transitions obs. 77−43350
GeTe, ferroelec. with strong cubic anisotropy, phase transition 77−52026
GeTe film, elec. props. 77−51831
GeTe, film, local order, electron diffraction study 79−77485
GeTe, film, semicond., supercond. energy gap and crit. field, tunelling meas. 77−24644
GeTe film 79−43055
GeTe films, elec. props. and struct., influence of annealing and condensation conditions 80−15388
GeTe, Hall coeff., temp. depend. rel. to order parameter 80−96921

IV-VI semiconductors continued
GeTe, heterophase state, plasma refl. spectra, twinning domain distrib. study 79−69845
GeTe, heterophase state with nonuniform distribution of free carriers *(Russian)* 78−2849
GeTe, heterophase state with nonuniform free carrier distrib. 79−56798
GeTe, high pressure effects on hole conc. and thermoelec. props. 78−26894
GeTe, high temp. mass spectrometric obs. of vaporis. 77−76542
GeTe, interpretation of polymorphic transformations 80−15032
γ-GeTe, investigation by elec. resist., latent heat of phase transform. and plasma refl. of light 79−99317
GeTe, liq., neutron diffraction study 79−77485
GeTe, machining effects on electrophys. props. 77−86199
GeTe, nonstoichiometric, homogenisation 78−44004
GeTe, oxidation kinetics 77−44380
GeTe, quenched, phase transitions and electrophysical props. 79−51250
p-GeTe, reflectance, and thermorefl. spectra 80−80814
GeTe, single cryst., hole mobility 78−6379
GeTe, stoichiometry deviations influence on mech. props., 25-500°C 80−103410
GeTe, structural transitions 77−51497
GeTe, supercond., metal-insulator transition, electron pairing, effect on optical props. 80−60139
GeTe, X-ray emission spectra, amorphous and cryst. struct. *(Russian)* 78−88385
GeTe:I, ferroelectric transition exam. 78−88264
GeTe:Mn, thermoelec. power, 2.5-25K, magnon drag effect 78−56169
GeTe-In, solubility, thermo-EMF coeff. meas. 78−43124
GeTe-Sb_2Te_3, solid solutions, cond., density of states 80−88472
$(GeTe)_x$-$(AgSbTe_2)_{1-x}$, thermoelectric props. of monolithic and pressed samples at 300K 78−80009
$Ge_{0.5}Te_{0.5}$, strucutral anal. by neutron diffr., radial distribution functions 80−15010
α-$Ge_{1-x}Te_x$, anisotropy of elec. props. rel. to cubic phase transition and band struct. 77−76820
HgSe, Dingle temp. exam. 79−65358
HgTe, gapless semicond., effect of nonlocal pot. on hole energy spectrum in mag. field 78−39017
HgTe, temp. depend. of energy gap, oscillatory magnetotransmission meas. 79−15441
(Pb,Sn)Se IR detector diode, junction resist. comparison with (Pb,Sn)Te 78−24858
(Pb,Sn)Te diode laser, grating coupled emission 77−79860
(Pb,Sn)Te IR detector diode, junction resist. comparison with (Pb,Sn)Se 78−24858
(Pb, Sn)Te-type semiconductors, displacive ferroelec. phase transitions, vibronic theory 80−11354
Pb chalcogenide, solid solution, thermoelectric efficiency 79−95429
Pb chalcogenide films, epitaxial, orientation on fluorite struct. substrate 77−35824
Pb chalcogenide mixed crystals, intraband absorption due to chemical disorder 79−56789
Pb chalcogenides, Auger recomb., theory 80−65586
Pb chalcogenides, elec. cond. anisotropy in strong electric fields *(Russian)* 79−38082
Pb chalcogenides, interband absorpt., optical absorpt. coeff., two- and six-band models 79−33728
Pb chalcogenides, interband transitions, absorpt. coeff., multiband calc. 80−29738
Pb chalcogenides, warm electron cond. 79−91066
Pb salt tunable diode laser-integrating sphere system, output intensity characts. 80−78881
Pb-S melt, absolute thermo-emf obs. 77−85251
Pb-Sn-Te, microhardness meas. as function of applied load, elec. props. exam. 78−48493
Pb-Sn-Te, solid solution, scattering mechanism of carriers 80−49710
Pb-Sn-Te system, investigation of liquidus surface by simplex lattice method 79−46784
Pb-SnTe semiconductor, spectral response calcs. 77−87826
Pb-Te, molten mag. susceptibility, conc. and temp. depend. 78−80121
p-$Pb_{1-x}Sn_xTe$, carrier mobility, acoustical phonon and impurity scatt., deform. impurity const., conc. depend. 80−39570
$Pb_{1-x}Be_xTe$, anomalous resist. near ferroelec. phase transition 80−20196
$Pb_{1-x}Cd_xS$, epitaxial, resist. and Hall coeff., substrate temp., thickness and comp. depend. 78−72290
$Pb_{1-x}Cd_xTe$, IR absorpt. study of Cd impurity levels, energy gaps 80−45081
$Pb_{1-x}Ge_xTe$, band struct., tunnelling obs. in MIS struct. 80−54795
$Pb_{1-x}Ge_xTe$, degenerate semiconducting ferroelectric, structural phase transition temp., mag. field effects 80−45017
$Pb_{1-x}Ge_xTe$, dielec. const. determ. near ferroelec. transition 78−88269
$Pb_{1-x}Ge_xTe$, electron-phonon interaction effect on ferroelec. transition 78−76416
$Pb_{1-x}Ge_xTe$ epitaxial layers, phase transition obs. by far IR reflectivity spectroscopy 79−33691
$Pb_{1-x}Ge_xTe$, ferroelec. phase transition, IR refl. and resist. meas. 80−11353
$Pb_{1-x}Ge_xTe$, ferroelec. constants, C-V and C-T characts. of abrupt p-n junctions 80−25323
$Pb_{1-x}Ge_xTe$, ferroelectric phase transition effect on forbidden band width 80−24794
p-$Pb_{1-x}Ge_xTe$ film, cyclotron reson. above and below struct. phase transition 80−88879
$Pb_{1-x}Ge_xTe$, mag.-field-induced displacive phase transition 80−50278
$Pb_{1-x}Ge_xTe$ magnetoplasma reflectivity and transmission spectra 80−71428
$Pb_{1-x}Ge_xTe$, n- and p-type, effective masses 80−44481
$Pb_{1-x}Ge_xTe$, p-n junctions, elec. characts., effect of ferroelec. phase transition 79−33338
$Pb_{1-x}Ge_xTe$, phase transitions 78−60408
$Pb_{1-x}Ge_xTe$ solid solns., phase transition influence on elec. props., 77 to 450K 80−103689
$Pb_{1-x}Ge_xTe$, solubilities, elec. and optical props. 77−35940
$Pb_{1-x}Ge_xTe$, TO phonon interaction with acoustic phonons near phase transition temp. 79−90776
$Pb_{1-x}Ge_xTe$:Ga, Fermi level stabilization, transport props. meas., 77-400K 78−56065
$Pb_{1-x}Ge_xTe$:Ga, influence of hydrostatic compression on elec. props. 79−73516

IV-VI semiconductors continued
$Pb_{1-x}Hg_xS$ epitaxial films, electroless deposition and struct. props. 79−90915
$Pb_{1-x}Hg_xS$, soln. growth, variable gap film for i.r. detector 77−1796
$Pb_{1-x}Hg_xS$-Si heterojunctions, elect. props. 80−100513
$Pb_{0.97}Hg_{0.03}Te$ photovoltaic detector produced by Sb^+ ion implantation 80−82821
PbO, reactively evaporated photoconductive film, phase transform. induced by water vapour 79−78233
PbO single crystals, current-voltage charact., electrolum. *(Russian)* 80−2863
PbO:Ag film, X-ray stimulated diffusion, current-voltage charact. 77−80653
PbO_2, compressed powder, electric conductivity obs. 77−32013
PbS, (100), angular resolved UV photoemission 78−2989
PbS (100) surface, electronic struct., O_2 adsorption effects, UPS study 80−54756
PbS, anisotropy of vol. plasmon dispersion, electron energy loss meas. 77−35878
PbS, anomalous magnetoresist. 80−107813
PbS, chem. deposited thin film, effect of morphological struct. on photosensitivity 80−70760
PbS, chemically deposited film, photosensitivity, effect of morphological struct. 79−82647
PbS, clean surface, AES and LEED exam. 80−10762
PbS, conduction band nonparabolicity and carrier scattering mechanism 79−11065
PbS, crystallisation and stability in high-temp. alkaline solns. 77−52240
PbS current tunable p-n junction laser *(Polish)* 80−32985
p-PbS, dispersion law investigation, valence band density of state effective mass 79−95314
PbS, electrodeposition, using nonaqueous solvents 80−76200
PbS, energy gap and dielec. props., 77 to 373K 80−66100
PbS, energy gap anomaly, relativistic band struct. calc. 79−4510
PbS, energy gap temp. depend., electron-lattice interaction, dilatation effect 79−65377
PbS epitaxial film, struct., optical and elec. props. 78−19583
PbS, epitaxial film, struct. perfection, two cryst. X-ray spectrometry 78−26792
PbS, epitaxial layer, structural nonuniformities and dislocation struct. 79−23852
PbS, epitaxial layer on rock salt substrate, stresses, hydrostatic press. effects 78−51831
PbS epitaxial layers, ion bombardment effects on struct., and annealing 79−10882
PbS film, appearance of EPR centres in initial form. stage *(Russian)* 77−63283
PbS film, form. by chem. spraying, elec. and optical props. 78−2588
PbS film, moisture drift origin 77−20187
PbS film, photosensitivity, role of surface oxide and ion bombardment 77−24631
PbS film, polycryst., chem. deposition from soln. and characterisation 78−72743
PbS, film, total current spectrum and energy struct. 80−100719
PbS film, used as absorbing surface in solar collector 78−5580
PbS, film condensation on amorphous substrate, struct. and growth 78−38981
PbS, film prep. from aqueous soln. of thiourea 77−8767
PbS film surface with oxysulphate layer, photoelec. memory effect 77−55584
PbS films, polycryst. and epitaxial, small-angle X-ray scatt. and electron density inhomogeneities 80−96758
PbS, first-principles calc. of eqn. of states 80−49649
PbS heterojunctions nonideal, photoelec. props. and elec. charact. 79−15215
PbS islands, vacuum deposited, electron microscope obs. 80−103601
PbS, liquid encapsulation zone-refining, source material for sublimation growth 78−27399
PbS, low carrier conc., prep. and props. 77−39846
PbS, microwave incremental conductivity, high-field, 77K 80−11026
PbS, nonstoichiometric, increase of rest pot. with p-type semicond. character 78−56170
n-PbS, $PbS_{1-x}Se_x$ layers prepared by hot-wall epitaxy 77−16481
PbS photocells, multicolour detectors in combination with Si photodiodes *(Czech)* 79−26126
PbS, photosensitive film, electron bombard. effect on elec. cond. 80−93019
PbS, plastic deform. on compression along ⟨100⟩ direction 79−28036
PbS, relativistic electronic mol. struct., calcs. 79−761
PbS single crystals, plastic deform. thermal activation anal., dislocation behaviour, point defect influences 79−65095
p-PbS, struct. of valence band, transport processes study 80−20081
PbS, surface optical phonons, anal. of LEED results 79−69339
PbS, temp. effects on valence bands, UPS study 80−11537
PbS, thermomech. props., SCF $X\alpha$ scatt. wave theory 78−71704
PbS, thin film, photoconductivity expts. 79−78130
PbS, thin film comp. and struct. rel. to precip. by allyl thiourea 77−48356
PbS, vacuum deposited film, orientation axis tilt rel. to vapour angle of incidence 80−88456
PbS, valence band struct., angle-resolved photoemission spectra obs. 77−48310
PbS, valence band struct. determ. by optical absorpt., size quantization effects 80−59871
PbS, vap. deposited film, island growth obs. by optical diffr. from electron micrograph 78−10291
PbS, wave-vector depend. of electron energy losses 78−11041
PbS:Tl, Hall and Seebeck coeffs., Hall mobility, impurity states 80−15545
PbS:Tl, self-compensation of acceptors by vacancies, Hall coeff. meas. 80−92913
PbS-$(PbSO_4)_x(PbO.PbSO_4)_y$ heterosystem, cathodoluminescence spectra 79−24370
PbS-Al coatings, absorptivity, emissivity, as function of PbS thickness 78−46731
PbS-base photodetectors, struct. invest. by proton irrad. 80−104388
PbS-$Cd_{1-x}Zn_xS$ heterojunctions prepared by spray pyrolysis 79−60917
PbS-Ge heterojunction, influence of conduction band discontinuity on lux-ampere charact. 78−39200
PbS-In_2S_3, phase investigation 80−66488
PbS-Ni, phase diag., cpd. formation and electrophys. props. 77−85997

IV-VI semiconductors continued
PbS-PbO vacuum evaporated films, elec. cond. and photocond. 80−75656
PbS-$PbS_{1-x}Se_x$-PbS DH diode laser props., comparison of theory with expt. 78−22128
PbS-PbSe epitaxial bicrystals, direct scatt. of channelled He ions at dislocations 80−65110
PbS-PbSe-PbS DH laser, Peltier cooled, IR gas spectroscopy appl. 77−23690
PbS-PbSe-PbS DH laser, fabrication, CW operation up to 120K 77−23692
PbS-PbSe(Te), thermoconductivity and thermoresistance 79−23992
PbS-Si, photosensitive p-n heterojunction, energy band diagram 79−95489
PbS-Si heterojunction, struct. and comp. 80−54530
PbS-Si heterojunction, chem. struct., AES anal. 80−76115
PbS-Si heterojunction, related optical and IR detector props. 80−77866
PbS-Si heterojunction, space charge capacitance, PbSn film thickness depend. 80−88630
PbS-Si heterojunction, PbS film growth and struct. 80−96762
PbS-Si heterojunction detector, direct injection readout 80−4765
PbS-Si p-n heterojunction, charact. and operation, IR detector appls. 78−52075
PbS-Si p-n heterojunctions, AC admittance meas. 80−96979
PbS_xS_{1-x} epitaxial film, Hall mobility meas., surface charge transport 77−20473
PbS(Se), photoionisation cross section of atomic and final state effects on 5d core levels 78−84699
$PbS_{0.1}Se_{0.9}$ 4.6 μm LED, room temp., band gap and electrolum. 80−66302
$PbS_{1-x}Se_x$, material props. and use in diode lasers, review 80−5732
$PbS_{1-x}Se_x$ (X=0.18) homojunction injection lasers, near-field emission 80−95896
$PbS_{1-x}Se_x$ diffused homojunction diode lasers, 140K operation 79−18415
$PbS_{1-x}Se_x$ diode laser, contact degradation due to diffusion 80−102734
$PbS_{1-x}Se_x$, single heterostructure tunable diode lasers formed by compositional interdiffusion 77−38896
$PbS_{1-x}Se_x$, single heterostruct. laser, wide tunability 77−79846
$PbS_{1-x}Se_x$ thin film, stimulated emission, temp. depend. 80−66232
PbS_xSe_{1-x}, chalcogen interdiffusion, electron microprobe obs. 79−28145
PbS_xSe_{1-x} film, prep. by co-evaporation method *(Japanese)* 78−64477
PbS_xSe_{1-x}, film prep. by co-evap., elec. props. *(Japanese)* 78−80470
PbS_xSe_{1-x}, multispectral photovoltaic IR detectors 80−105710
PbS_XSe_{1-x}, Schottky-barrier IR detector, comp. tuning 78−12752
PbS(Se)(Te), angle resolved UPS and electronic band struct. 79−37981
PbS(Se)(Te), bond orbital model of band struct. 80−59853
PbS(Se)(Te), chemisorption of O_2, room temp., UPS and XPS obs. 78−91529
PbS(Se)(Te), crystal binding energy 79−37650
PbS(Se)(Te), photoemission interpretation 80−25531
PbS(Se)(Te), strongly anisotropic polar semicond., electron-hole liq. in mag. field 80−59890
PbS(Se)(Te), XPS investig. of valence band struct. 77−48311
$Pb_{1-x}Sb_xTe$ DFB laser, CW operation 77−58338
PbSe, carrier density depend. of cyclotron mass, Shubnikov-de Haas effect 79−73533
PbSe, complex-composition film production method from vapour *(Russian)* 78−95702
PbSe, electron gas magnetisation, energy band parameters determ., use of Faraday effect 80−45047
PbSe, energy gap and dielec. props., 77 to 373K 80−66100
PbSe, energy gap anomaly, relativistic band struct. calc. 79−4510
PbSe, energy gap temp. depend., electron-lattice interaction, dilatation effect 79−65377
PbSe epitaxial film on NaCl, far IR reflectivity obs. 77−40251
PbSe, Faraday effect and electron gas magnetisation, Kane two band model calcs. *(Russian)* 80−34899
PbSe film, 50 μ, prep. in double quasiclosed volume 79−38745
PbSe film, influence of pot. barrier on thermoelec. props. 78−39239
PbSe film, moisture drift origin 77−20187
PbSe film, partly oriented, electron diffr. dynamic effects 77−7996
PbSe, film, photoconductivity, temp. depend. 79−38200
PbSe film, stimulated photoluminesc. charact. meas., room temp. 77−90193
PbSe, film with pot. barrier, magnetoresistance anisotropy 79−91172
PbSe films, current carrier conc. and type control, elec. cond., synthesis process *(Russian)* 80−100412
PbSe films, synthesis charact. 80−35094
PbSe, Hall effect and elec. cond. under strong anisotropic pressure 77−55549
n-PbSe, heterodiffusion of Sn 80−34245
PbSe, lattice dynamics, slow neutron inelast. scatt. 77−31740
PbSe, monocrystalline film prod. by laser pulse *(Russian)* 78−3059
PbSe on NaCl, epitaxial-substrate system, far IR transmission and refl. 78−6802
PbSe, photoluminesc. spectra and stimulated emission, effect of temp. 77−8638
n-PbSe, polar semicond., mag. field influence on high-freq. relaxation time 79−95438
PbSe, polycryst. film, low temp. illumination, residual cond. 77−43756
n-PbSe, pressure induced transition to gapless state 78−2533
PbSe, pressure tunable CW injection laser, emission spectra 79−18419
PbSe, relativistic electronic mol. struct., calcs. 79−761
PbSe, spin-orbit splitting in valence bands, angle-resolved UV photoemission 78−2991
PbSe surface, clean and O_2-exposed, XPS (UPS) obs., electronic struct. 78−52637
PbSe, temp. effects on valence bands, UPS study 80−11537
PbSe vacuum deposited thin films, struct. and growth 79−19482
PbSe, vacuum evaporation, composition of condensates 78−44012
p-PbSe, valence band structure, IR refl. and absorpt. meas. 77−55791
PbSe, valence band structure from angular resolved photoemission spectra 78−84143
PbSe, valence band struct., Hall and transverse Nernst-Ettingshausen effects, optical absorption 79−11064
PbSe, valence band struct. determ. by optical absorpt., size quantization effects 80−59871
PbSe, wave-vector depend. of electron energy losses 78−11041
PbSe, X-ray diffr. exam. of struct., and luminescence props. 80−55209
PbSe:Tl, elec. props. and IR reflection 78−6686

IV-VI semiconductors continued
PbSe:Tl, impurity states, optical absorption and Hall effect meas. 78−18995
PbSe:Tl, scatt. of holes and phonons by impurities 78−19068
PbSe:Tl, self-compensation of acceptors by vacancies, Hall coeff. meas. 80−92913
PbSe-CdSe heterojunction, elec. props. 77−1478
PbSe-flux, interfacial tension at boundary of fused systems 77−35797
PbSe-PbS(Te) and PbS-PbTe epitaxial layers, electron microscope contrast of misfit dislocations 77−85113
$PbSe_{0.5}S_{0.5}$, valence band struct., absorpt. spectra, elec. props. 80−44505
$PbSe_xS_{1-x}$, comp. depend. of density, effect of defects 77−11538
p-$(PbSe)_{1-x}(SnTe)_x$, absorpt. edge temp. depend. *(Russian)* 78−34765
$(PbSe)_{1-x}(SnTe)_x$, lattice dynamic props., Gruneisen parameters *(Russian)* 78−83984
$(PbSe)_{1-x}(SnTe)_x$ solid solution, band struct. and some optical props. *(Russian)* 77−76752
PbSe(Te), NMR, chemical shift and linewidth determ. 79−19792
PbSe(Te), single cryst. growth, reaction kinetics in binary melts of KCl, NaCl and $PbCl_2$ 77−16486
$PbSe_{1-x}Te_x$, for-IR reststrahlen spectra, mode behaviour 80−7345
$PbSe_{1-x}Te_x$, p-n junction, inversion of conduction level 78−47856
$PbSe_{1-x}Te_x$, symmetry change in cond. levels, photovoltaic effect and reflectivity obs. 78−34766
$PbSe_xTe_{1-x}$ epitaxial layers, growth, struct., elastic strain and Hall mobility 77−15717
$Pb_{1-x}Sn_xGe$:In, press.-induced transition to gapless state, galvanomag. effects 78−19108
$Pb_{0.2}Sn_{0.8}S$, Mossbauer spectra, effect of optical emission *(Russian)* 78−60367
$Pb_{0.59}Sn_{0.41}Se$, struct. phase transition, temp and hydrostatic press. influence, Hall effect, resistivity *(Russian)* 78−51675
$Pb_{0.65}Sn_{0.35}Se$, solid soln., elec. props. 78−39112
n-$Pb_{0.83}Sn_{0.17}Se$, carrier mobility, 77-300K, scattering mechanism *(Russian)* 78−2486
$Pb_{0.93}Sn_{0.07}Se$ crysts., sublimation growth, controlled carrier concs. for IR lasers and detectors 77−52237
n-$Pb_{0.94}Sn_{0.06}Se$ solid solns., Burstein-Moss effect and energy band struct. 80−40118
$Pb_{0.975}Sn_{0.025}Se$, film, acoustic wave modulation of electron current 78−64067
$Pb_{0.995}Sn_{0.045}Se$ pulsed laser for high-resolution NH_3 spectroscopy 79−64252
$Pb_{1-x}Sn_xSe$, (x=0.125), pressure induced band inversion, effect on energy spectrum *(Russian)* 78−39007
n-$Pb_{1-x}Sn_xSe$, absorption spectra investigation 80−2768
$Pb_{1-x}Sn_xSe$, band inversion effect on phonon spectra 78−79699
$Pb_{1-x}Sn_xSe$, band struct. parameters, thermoelectric power meas. in strong mag. fields 79−51474
$Pb_{1-x}Sn_xSe$, band struct. and transport props., hydrostatic press. effects 80−15452
$Pb_{1-x}Sn_xSe$, carrier density depend. of cyclotron mass, Shubnikov-de Haas effect 79−73533
$Pb_{1-x}Sn_xSe$, carrier effective mass, thermomag. effect meas. 77−24572
$Pb_{1-x}Sn_xSe$, determ. of anisotropy coeff. of Fermi surface, magnetoresist. meas. 78−51878
$Pb_{1-x}Sn_xSe$, displacive transition, temp. and press. depend., elec. meas. 80−10672
$Pb_{1-x}Sn_xSe$, energy band parameter determ. from Shubnikov-de Haas effect 77−69227
$Pb_{1-x}Sn_xSe$ epitaxial film, Hall mobility meas., surface charge transport 77−20473
$Pb_{1-x}Sn_xSe$ epitaxial layers, radiative and nonradiative recomb. processes 80−60670
$Pb_{1-x}Sn_xSe$ epitaxial layers obtained by LPE, growth conditions correl. with morphology 80−104079
$Pb_{1-x}Sn_xSe$, film struct. and elec. props. 77−80708
$Pb_{1-x}Sn_xSe$, gapless state and phonon spectrum *(Russian)* 78−30715
$Pb_{1-x}Sn_xSe$, material props. and use in diode lasers, review 80−5732
$Pb_{1-x}Sn_xSe$, n- and p-type, with band inversion, study of transport phenomena 80−49741
$Pb_{1-x}Sn_xSe$, plasma reflection spectra, carrier effective masses and relax. times determ. 78−2858
$Pb_{1-x}Sn_xSe$, single crystal and film, X-ray spectral investigation of solid solution 77−16477
n-$Pb_{1-x}Sn_xSe$, single crysts. and diodes, elec. props. under high press. 77−47809
$Pb_{1-x}Sn_xSe$, single heterostructure tunable diode lasers formed by compositional interdiffusion 77−38896
$Pb_{1-x}Sn_xSe$, single heterostruct. laser, wide tunability 77−79846
$Pb_{1-x}Sn_xSe$ solid solns., photoluminesc. spectra, energy band parameter determ. 80−71484
$Pb_{1-x}Sn_xSe$, thin film, opt. props. *(Japanese)* 77−1750
$Pb_{1-x}Sn_xSe$, transport phenomena in solid solutions with band inversion 80−107792
$Pb_{1-x}Sn_xSe$, valence zone struct. effect on mobility/inherent conc. ratio *(Russian)* 79−73437
$Pb_{1-x}Sn_xSe$, X=0.03-0.07, monocrystal film, edge of intrinsic absorpt. *(Russian)* 80−71368
$Pb_{1-y}Sn_ySe$, characts. of IR absorption 77−1681
$Pb_{1-y}Sn_ySe$, electron-irradiated, elec. and recomb. props. 79−56227
$Pb_{1-y}Sn_ySe$, spontaneous emission, temp. and carrier conc. depend. 78−10990
$Pb_{1-y}Sn_ySe$-PbSe heterojunction laser, tunable 10.6-15 nm 77−58346
$Pb_{1-y}Sn_ySe$-PbSe pulse laser diode, temp. tuning of modes 78−50777
$Pb_xSn_{1-x}Se$ laser, electron-beam-pumped 77−50689
$Pb_ySn_{1-y}Se$, multispectral photovoltaic IR detectors 80−105710
$Pb_{1-x}Sn_xSe$(Te) epitaxial layers, growth, phase diagram, p-n junctions, optical, elec. props. 78−44029
$Pb_{1-x}Sn_xSe$(Te) single crystals, Bridgeman grown, X-ray exam. 79−56926
$Pb_{1-x}Sn_xSe$(Te):I epitaxial layers, photoelectric props., doping donor impurity behaviour 77−80810
$Pb_{1-x}Sn_xSe_{1-y}Te_y$ optically pumped heterojunction laser with matched gratings, photolum. obs. 79−89909
$Pb_xSn_{1-x}Se$(Te) film, Bi and Tl impurity dopant incorporation and diffusion during MBE growth 79−66012
$Pb_{0.76}Sn_{0.24}Tc$, background radiation, influence on elec. props. 80−20226
PbSnTe and PbSnTe, epitaxial-substrate system, far IR transmission and refl. 78−6802
PbSnTe, anomalous avalanche breakdown 80−80284

IV-VI semiconductors continued
PbSnTe DH laser, anodic oxide film to avoid degradation by thermal cycling 78−50809
PbSnTe detector and preamplifier modules for heterodyne detection of CO_2 laser radiation 78−32875
PbSnTe, electron irradiated, high temp. defects 79−78122
PbSnTe IR detectors, spectral response depend. on surface carrier concentration *(Japanese)* 79−44929
PbSnTe IR photovoltaic detectors for 8-14 μm range, review *(Italian)* 78−54451
PbSnTe laser diode, tunable emission, 5-15 μm 77−50686
PbSnTe long-wavelength IR photovoltaic detectors, radiation testing 80−37084
PbSnTe, Magneto transport anomalies at low carrier densities, Wigner crystallisation 80−20222
PbSnTe, optical dielectric const. variation with carrier conc. 80−84709
PbSnTe/PbTe inverted heterostructure mosaics, long wavelength, energy gap-Fermi level temp. depend. 79−85182
PbSnTe-like semicond., Auger recomb., nonparabolic approx. 79−15161
PbSnTe-PbTe heterostructs., effect of electrical grounding on electron irrad. 78−60194
$Pb_{0.41}Sn_{0.59}Te$, Hall coeff., elec. cond. meas. 80−44615
$Pb_{0.56}Sn_{0.44}Te$, press. induced ferroelec. phase transition 79−65809
p-$Pb_{0.65}Sn_{0.35}Te$, transport coeffs. and dispersion law 80−44629
$Pb_{0.72}Sn_{0.28}Te$, Hall effect and elec. cond., 77 to 480K, energy band struct. 77−76817
$Pb_{0.72}Sn_{0.28}Te$, Hall mobility, temp. and carrier conc. depends. *(Russian)* 77−39877
$Pb_{0.76}Sn_{0.24}Te$ single crystals, current-voltage charcts. at He temps. 80−20197
$Pb_{0.78}Sn_{0.22}Te$, $Pb_{0.91}Sn_{0.09}Se$, radiative and nonradiative recombination 80−80849
$Pb_{0.78}Sn_{0.22}Te$:In, low current carrier conc., Hall effect, lattice constant 79−82603
$Pb_{0.78}Sn_{0.22}Te$:In, transport phenomena, below 20K *(Russian)* 79−38074
$Pb_{0.78}Sn_{0.22}Te$:In epitaxial layers, dislocation density, Hall effect, conductivity, photoeffects 80−25024
$Pb_{0.79}Sn_{0.21}Te$ epitaxial film on $Pb_{0.79}Sn_{0.21}Te$, far IR reflectivity obs. 77−40251
$Pb_{0.8}Sn_{0.2}Te$ film, growth in quasi-closed space, single and polycryst. 79−33930
n-$Pb_{0.8}Sn_{0.2}Te$ film, magnetophonon reson., 55-90K 79−7913
$Pb_{0.8}Sn_{0.2}Te$, film photodiodes, quantum efficiency 79−75596
$Pb_{0.8}Sn_{0.2}Te$, hole conc. at 77K from room temp. thermoelec. meas. 78−56155
$Pb_{0.8}Sn_{0.2}Te$, implantation of S^+ and In^+ ions 77−19973
$Pb_{0.8}Sn_{0.2}Te$, LPE layers, carrier conc. variation with annealing and growth temp. 77−39878
$Pb_{0.8}Sn_{0.2}Te$, magnetophonon effect obs. 78−23115
$Pb_{0.8}Sn_{0.2}Te$, p-n homojunction breakdown voltage for onesided abrupt junctions *(German)* 78−56210
$Pb_{0.8}Sn_{0.2}Te$, single cryst. and epitaxial film, far IR refl. spectra, carrier density, Hall const., and plasma freq. 80−20629
$Pb_{0.8}Sn_{0.2}Te$ surfaces, oxidation in air and thermal desorption, XPS and LEED meas. 79−47830
$Pb_{0.8}Sn_{0.2}Te$, susceptibility effective mass, carrier conc. depend. 80−20069
$Pb_{0.8}Sn_{0.2}Te$:Cd, defect struct., Hall effect and solubility meas. 77−11571
$Pb_{0.8}Sn_{0.2}Te$:Cd, influence of Cd doping on high field magnetoresist. and Hall effect 80−75590
$Pb_{0.8}Sn_{0.2}Te$:In, absorption spectra meas., 475-725K 77−4664
$Pb_{0.8}Sn_{0.2}Te$:In, implanted thin epitaxial films, laser annealing 79−65104
$Pb_{0.8}Sn_{0.2}Te$:La, evaporated thin films, low carrier conc. 80−65414
$Pb_{0.8}Sn_{0.2}Te$-Pb, Schottky barrier form., Auger depth profiling and I-V meas. 80−49903
$Pb_{0.8}Sn_{0.2}Te$-PbTe p-n heterojunction, prep., elec. and photoelec. props. 79−51664
n-$Pb_{0.82}Sn_{0.18}Te$, conduction band struct., determ. by Shubnikov-de Haas meas. 78−2504
$Pb_{0.82}Sn_{0.18}Te$ epitaxial films, surface transport of carriers at 77K 79−28419
$Pb_{0.82}Sn_{0.18}Te$, film, effect of hydrostatic pressure on props. 80−70862
$Pb_{0.82}Sn_{0.18}Te$ films, piezoresist. effect 79−38197
$Pb_{0.82}Sn_{0.18}Te$ films, VPE, hot wall technique, struct., elec. props. 79−37926
$Pb_{0.82}Sn_{0.18}Te$, Hall mobility, scatt. mechanisms, temp. and carrier conc. depend. 77−55548
$Pb_{0.82}Sn_{0.18}Te$, layers on mica substrate, Hall constant peculiarities 80−75588
p-$Pb_{0.82}Sn_{0.18}Te$, mag. susceptibility, inversion layers effect *(Russian)* 77−72996
$Pb_{0.82}Sn_{0.18}Te$, narrow band gap, relax. time for Shubnikov-de Haas effect 78−80006
$Pb_{0.82}Sn_{0.18}Te$, narrow-gap, Hall effect quantum oscillations *(Russian)* 77−4377
$Pb_{0.82}Sn_{0.18}Te$ solid solution, energy band spectrum charcts., Hall effect meas. 77−76737
$Pb_{0.82}Sn_{0.18}Te$, thermomagnetic, thermoelectric props., valence band struct. *(Russian)* 80−54724
$Pb_{0.82}Sn_{0.18}Te$:Cd, effective distrib. coeff. of Cd *(Russian)* 79−73203
p-$Pb_{0.82}Sn_{1.8}Te$, Hall coeff. sign-inversion temp. 78−52010
$Pb_{0.83}Sn_{0.17}Te$, carrier tunnelling through potential barrier in p-n junctions *(Russian)* 78−52074
$Pb_{0.83}Sn_{0.17}Te$, recomb. at high levels of optical excitation 78−10503
$Pb_{0.84}Sn_{0.16}Te$ single cryst., anelastic relax., helicon wave dispersion *(Russian)* 77−51437
$Pb_{0.86}Sn_{0.14}Te$/PbTe, interface recomb. velocity in DH laser diodes 79−64222
n-$Pb_{0.88}Sn_{0.12}Te$, stimulated spin-flip Raman scatt. 79−72621
$Pb_{0.92}Sn_{0.08}Te$, photoelec. props. 78−6415
$Pb_{0.9}Sn_{0.1}Te$, situated in quantizing magnetic field, photolum. spectra 79−71461
$Pb_{1-x}Sn_xTe$ film, epitaxial, patterns of diffuse bands on electron diffr. patterns 79−11021
$Pb_{1-x}Sn_xTe$ (x=0.15 to 0.20), SEM study, dislocation density, and carrier density and mobility 79−69107
$Pb_{1-x}Sn_xTe$, absorption edge shift, energy gap determ. 78−88308
$Pb_{1-x}Sn_xTe$, anomalous resist. near ferroelec. phase transition 80−20196
$Pb_{1-x}Sn_xTe$, band struct. and phonon energies, tunnelling spectroscopy 78−72070

IV-VI semiconductors continued
$Pb_{1-x}Sn_xTe$, band struct. changes due to displacive phase transition, Hall coeff. meas. 80−10671
$Pb_{1-x}Sn_xTe$, basic electrons energy spectrum near mag. phase transition *(Russian)* 79−90955
$Pb_{1-x}Sn_xTe$, Cd-In diffusion, changes in elec. props. 78−91348
$Pb_{1-x}Sn_xTe$, charact. of photocond., 12-130K 78−26914
$Pb_{1-x}Sn_xTe$, characts. of IR absorption 77−1681
$Pb_{1-x}Sn_xTe$, continuously tunable electron beam pumped laser 78−50802
$Pb_{1-x}Sn_xTe$, correlation between elec. props. and crystalline environment 77−80773
$Pb_{1-x}Sn_xTe$, cryst. growth rel. to IR detector fabrication 77−85911
$Pb_{1-x}Sn_xTe$, DH laser, gain-freq.-current relation, k.p band model 77−61951
$Pb_{1-x}Sn_xTe$ DH laser, minority carrier lifetimes and lasing thresholds 80−19031
$Pb_{1-x}Sn_xTe$, diamag. reson. *(Russian)* 78−23347
$Pb_{1-x}Sn_xTe$, diffusion of Cd, Hall effect, cond. and solubility meas. 79−69292
$Pb_{1-x}Sn_xTe$ diode laser, contact degradation due to diffusion 80−102734
$Pb_{1-x}Sn_xTe$, displacive phase transition, effect of interband hybridisation 79−33233
$Pb_{1-x}Sn_xTe$, distributed feedback DH lasers, design fabrication and charcts. 77−10944
$Pb_{1-x}Sn_xTe$, effect of mag. field on thermal cond. 79−65263
$Pb_{1-x}Sn_xTe$, effective mass of holes, thermoelec. power, Hall coeff., carrier conc. 79−65371
$Pb_{1-x}Sn_xTe$, electron-irradiated, elec. and recomb. props. 79−56227
$Pb_{1-x}Sn_xTe$, electron-phonon interaction 78−71819
$Pb_{1-x}Sn_xTe$, electroreflectance, Faraday rot., elec. band struct. parameters 77−66113
$Pb_{1-x}Sn_xTe$, energy band parameters from IR Faraday rotation 78−48154
$Pb_{1-x}Sn_xTe$, energy band parameter determ. from photoluminescence. spectra in mag. field 79−11066
$Pb_{1-x}Sn_xTe$, energy spectrum under hydrostatic pressure 79−65381
$Pb_{1-x}Sn_xTe$ epitaxial films, adsorption-induced accumulation layer form. on surface 80−60117
$Pb_{1-x}Sn_xTe$, epitaxial growth on $LiNbO_3$, electron diffr. and microscopy exam. 77−1331
$Pb_{1-x}Sn_xTe$, epitaxial layers, cond. *(Russian)* 77−24629
$Pb_{1-x}Sn_xTe$, epitaxial layers, In doping, donor impurity singularities, distrib. coeff. 77−80526
$Pb_{1-x}Sn_xTe$, epitaxial layers, carrier lifetime meas. 79−42559
$Pb_{1-x}Sn_xTe$, epitaxial layers, photolum. in mag. field 79−83033
$Pb_{1-x}Sn_xTe$, Faraday effect and electron gas magnetisation, Kane two band model calcs. *(Russian)* 80−34899
$Pb_{1-x}Sn_xTe$, ferroelec. phase transition, hybridization effect *(Russian)* 79−61319
$Pb_{1-x}Sn_xTe$ film, Burstein-Moss effect, absorpt. and photocond. spectra 78−18961
$Pb_{1-x}Sn_xTe$ film, deposition, elec. and piezoresist. props. 78−6465
$Pb_{1-x}Sn_xTe$ film, sputtered, for IR detector appl. elec. and optical props. 80−35084
$Pb_{1-x}Sn_xTe$ films, pure and Bi doped, polycryst., struct., elec., optical props. 79−42542
$Pb_{1-x}Sn_xTe$ films, size quantisation, optical orientation of free carriers 80−20725
n-$Pb_{1-x}Sn_xTe$, galvanomag. effects, alloy scatt., 4.2K 77−39880
$Pb_{1-x}Sn_xTe$, grown by LPE, solid-liquid tie line determ. 78−64526
$(Pb_{1-x}Sn_x)Te$, growth by sublimation technique *(German)* 77−73224
$Pb_{1-x}Sn_xTe$, growth of epitaxial layers, activation by UV and IR radiation 80−71598
$Pb_{1-x}Sn_xTe$, heteroepitaxial film, fundamental absorpt. edge and Shubnikov-de Haas effect 79−24381
$Pb_{1-x}Sn_xTe$ heterojunction lasers, instantaneous vacuum evaporation grown, threshold current density 80−5759
$Pb_{1-x}Sn_xTe$ heterostructure laser, fabrication and props. 79−10306
$Pb_{1-x}Sn_xTe$, hole effective mass near zero bandgap, IR refl. study 80−108205
$Pb_{1-x}Sn_xTe$ homojunction laser, increased freq. tuning range 77−75546
$Pb_{1-x}Sn_xTe$ IR detector, ESCA meas., surface leakage currents 77−20402
$Pb_{1-x}Sn_xTe$, impurity defused IR detector, spectral response depend. on impurity conc. *(Japanese)* 78−58036
$Pb_{1-x}Sn_xTe$, in MIS struct., tunnelling investig. of band gap and phonon energies 77−43733
$Pb_{1-x}Sn_xTe$, in MOS junction, phonon-assisted tunnelling 77−76928
$Pb_{1-x}Sn_xTe$, injection laser, use in high-resolution spectroscopy 79−76714
$Pb_{1-x}Sn_xTe$, inter- and intraband magneto-optical transitions 80−25346
$Pb_{1-x}Sn_xTe$, interband absorpt. edge for single cryst. epitaxial films 78−43948
$Pb_{1-x}Sn_xTe$, LPE grown heterostructures, improved nucleation and planar interface 79−95949
$Pb_{1-x}Sn_xTe$ LPE grown heterostructures, dislocation etch pitch, interfaces 80−2023
p-$Pb_{1-x}Sn_xTe$, LPE layer, carrier conc. and mobility 79−99639
$Pb_{1-x}Sn_xTe$, large non-seeded single cryst. growth by sublimation method, and characterisation 79−78860
$Pb_{1-x}Sn_xTe$, large single crystal growth, on quartz surface, non-seeded 78−48293
$Pb_{1-x}Sn_xTe$, lattice and electronic props. and g-value 80−80161
$Pb_{1-x}Sn_xTe$, lattice instability and phonon lifetimes, neutron scatt. 78−55932
$Pb_{1-x}Sn_xTe$ layers, LPE, phase diagram rel. to lattice const., distrib. coeffs. 79−37925
$Pb_{1-x}Sn_xTe$ layers, LPE growth on metal-etched substates 80−55313
$Pb_{1-x}Sn_xTe$, MBE, O_2 uptake, AES, XPS and UPS expts. 78−95227
$Pb_{1-x}Sn_xTe$, MBE, state-of-the-art 79−24450
$Pb_{1-x}Sn_xTe$, mag. and kinetic props. near ferroelec. transition 80−11160
$Pb_{1-x}Sn_xTe$, material props. and use in diode lasers, review 80−5732
p-$Pb_{1-x}Sn_xTe$, mobility meas., impurity and phonon scatt. mechanisms 78−23091
$Pb_{1-x}Sn_xTe$ monocrystal and sinter thermoelec. inhomogeneity 78−91713
$Pb_{1-x}Sn_xTe$, Mossbauer investig. of phonon softening at semicond.-semimetal transition 77−43908
$Pb_{1-x}Sn_xTe$, narrow gap, many-body interaction effects, Bloch electron scatt. lifetimes, energy renormalisation 80−49637

IV-VI semiconductors continued
$Pb_{1-x}Sn_xTe$ narrow gap solid alloys, hole Fermi surface, galvanomag. and oscill. effect obs. *(Russian)* 77−69345
$Pb_{1-x}Sn_xTe$, narrow gap solid solns., mag. susceptibility and energy band spectrum 79−28276
$Pb_{1-x}Sn_xTe$, narrow gap semicond., theory of mag. susceptibility 80−93070
$Pb_{1-x}Sn_xTe$ optically pumped lasers, power output and wavelength, 4 to 30K 78−79035
$Pb_{1-x}Sn_xTe$ p-n heterostructure, VPE, struct. and electrophysical characts. 78−10547
$Pb_{1-x}Sn_xTe$, photoconduct., photoelectromag. effect, laser intensity depend., carrier lifetimes 77−15896
$Pb_{1-x}Sn_xTe$, photoelec. props. 30 to 4.2K, temp. depend. of electron density 80−20246
$Pb_{1-x}Sn_xTe$, photomagnetic effect at low temps. 77−62960
p-$Pb_{1-x}Sn_xTe$ piezoresistance, temp. and conc. depend. *(Russian)* 79−1601
$Pb_{1-x}Sn_xTe$, polycryst. powder, low temp. prep. in PbI_2 flux 79−61524
p-$Pb_{1-x}Sn_xTe$, pressure-induced transition to zero-gap state, changes in energy band parameters 79−69413
$Pb_{1-x}Sn_xTe$, reststrahlen band, reflection spectra 79−8162
$Pb_{1-x}Sn_xTe$, segregation during solidification by Bridgman technique 79−38735
p-$Pb_{1-x}Sn_xTe$, single crysts. and diodes, elec. props. under high press. 77−47809
$Pb_{1-x}Sn_xTe$ single crysts, energy gap determ. from density and lattice const. *(German)* 78−26812
$Pb_{1-x}Sn_xTe$, single cryst. grown from vapour, photocond. meas. 79−24016
$Pb_{1-x}Sn_xTe$ single crystals, selection using travelling solvent method *(German)* 80−2936
$Pb_{1-x}Sn_xTe$, small-gap, recomb. mech. 79−38099
$Pb_{1-x}Sn_xTe$, soft mode, ferroelec. phase transition crit. temp. and dielec. const. calcs. 77−8530
$Pb_{1-x}Sn_xTe$, soft-phonon-induced Raman scatt. 77−77209
$Pb_{1-x}Sn_xTe$ solid solution, electron scatt. by charged Te vacancies 77−69328
$Pb_{1-x}Sn_xTe$ solid solution, radiative recombination 79−52016
$Pb_{1-x}Sn_xTe$, solid-liq. phase equilib. above 750°C 79−82316
$Pb_{1-x}Sn_xTe$, soliton modulation widths for TO-phonons 77−80588
$Pb_{1-x}Sn_xTe$, spontaneous emission, temp. and carrier conc. depend. 78−10990
$Pb_{1-x}Sn_xTe$, surface photo-EMF under laser excitation conditions 80−6897
$Pb_{1-x}Sn_xTe$, Te-rich growth by ingot nucleation method, laser fabrication 77−77362
$Pb_{1-x}Sn_xTe$, temperature gradient LPE, PbTe substrate 78−3066
p-$Pb_{1-x}Sn_xTe$, thermoelec. power, carrier conc. and temp. depend., interband scatt. 80−24957
$Pb_{1-x}Sn_xTe$, thermoelectric effects, characteristics at low temps. 80−107831
$Pb_{1-x}Sn_xTe$, VPE crystals, X-ray diffr. data interpretation 77−15712
$Pb_{1-x}Sn_xTe$, valence band struct., Hall effect meas. 78−39016
$Pb_{1-x}Sn_xTe$, x=0.2, monocrystal, photoelectric props. of p-n structures *(Russian)* 80−70808
$Pb_{1-x}Sn_xTe$, X=0.2, monocrystal, edge of intrinsic absorpt. *(Russian)* 80−71368
$Pb_{1-x}Sn_xTe$:^{119}Sn, symm. breaking of Sn local environment, Mossbauer splitting obs. *(Russian)* 77−40166
$Pb_{1-x}Sn_xTe$:Cd, Cd diffusion obs. using Hall mobility and Cd solubility expts. 78−26584
$Pb_{1-x}Sn_xTe$:Cd, deep energy level, temp. depend. of elec. cond. 78−18994
$Pb_{1-x}Sn_xTe$:Cd, impurity photocond. spectra 80−6902
$Pb_{1-x}Sn_xTe$:Cd, long-wavelength photosensitivity shift on annealing, Cd influence 78−26912
$Pb_{1-x}Sn_xTe$:Cd, photocond., photomag. effect, carrier lifetimes 80−44658
$Pb_{1-x}Sn_xTe$:Cd, photoelec. props., surface recomb. effect 80−44659
$Pb_{1-x}Sn_xTe$:Cd(In), solid solutions, impurity states in photoluminescence spectra *(Russian)* 80−97333
$Pb_{1-x}Sn_xTe$:Ge, anomalous behaviour of impurity centres under press. *(Russian)* 80−65491
$Pb_{1-x}Sn_xTe$:In, carrier spectroscopic g-factors, magnetoresistance, temp. depend. 80−6705
$Pb_{1-x}Sn_xTe$:In, energy spectrum under combined effect of mag. field and hydrostatic press. 79−65382
$Pb_{1-x}Sn_xTe$:In, energy spectra modifications due to comp. changes and press. appl. 80−10915
$Pb_{1-x}Sn_xTe$:In, Hall const. depend. on temp., autocompensation, band gap temp. depend. explanation 79−69527
$Pb_{1-x}Sn_xTe$:In, Hall effect and photoconductivity *(Russian)* 80−103720
$Pb_{1-x}Sn_xTe$:In, high temp. Fermi level position 79−90948
$Pb_{1-x}Sn_xTe$:In, impurity influence on photoluminescence at large excitation levels *(Russian)* 80−93384
$Pb_{1-x}Sn_xTe$:In, nonequilib. metallic state *(Russian)* 79−33300
$Pb_{1-x}Sn_xTe$:In, semiconductor-metal-semiconductor transitions under press. 80−34491
$Pb_{1-x}Sn_xTe$:In, tunnelling impurity self-localisation, anomalous props. nature *(Russian)* 80−59915
$Pb_{1-x}Sn_xTe$:In, with low carrier conc., transport phenomena 80−49783
$Pb_{1-x}Sn_xTe$:In epitaxial layers, growth, elec. props., and luminesc. 80−54542
$Pb_{1-x}Sn_xTe$:In film, anomalous elec. props. 78−10477
$Pb_{1-x}Sn_xTe$:In(Cd), photoconductivity 78−23129
$Pb_{1-x}Sn_xTe$:In(Ga)(Al), elec. props., dopant influence 79−51599
$Pb_{1-x}Sn_xTe/PbTe_{1-y}Se_y$ lattice-matched buried heterostructure lasers with CW single mode output 80−74386
$Pb_{1-x}Sn_xTe$-$Pb_{1-y}Sn_yTe$, p-n heterojunction, prep. and props. 79−51662
$Pb_{1-x}Sn_xTe$-PbTe, amorphous/crystalline heterojunction, rectification props., IR detector appl. *(Japanese)* 78−60197
$Pb_{1-x}Sn_xTe$-PbTe heterojunction, Sn diffusion and elec. effects of dislocations, elec. and metallurgical expts. 77−89839
$Pb_{1-x}Sn_xTe$-PbTe heterojunction, Sn diffusion profile, X-ray diffr. data interpretation 78−51832
$Pb_{1-x}Sn_xTe$-PbTe heterojunctions, interface recombination velocity reduction with decreasing lattice parameter mismatch 79−98370
$Pb_{1-x}Sn_xTe$-PbTe heterostructures, MBE produced on mica and $LiNbO_3$, elec. props. study 80−88629
$Pb_{1-x}Sn_xTe$-PbTe pulse laser diode, temp. tuning of modes 78−50777

IV-VI semiconductors continued
$(Pb_{1-x}Sn_x)_{1+y}Te_{1-y}$ system, VPE parameters influence on epitaxial film props. 79−28229
$Pb_{.87}Sn_{.13}Te$, phonon dispersion, mode softening 79−42175
$Pb_xSn_{1-x}Te$, for appl. in IR detector arrays, comp. control 80−31872
$Pb_xSn_{1-x}Te$, grown by vap. transport in closed system, quality improvement 77−40341
$Pb_xSn_{1-x}Te$, RF sputtered films, struct., lattice parameter, stoichiometric comp., RHEED 78−38975
$Pb_xSn_{1-x}Te$, RF sputtered film IR detector, photocond. response speed improvement by annealing 79−58790
$Pb_xSn_{1-x}Te$, RF-sputtered epitaxial single-cryst. films, thermorefl. spectra 77−63476
$Pb_xSn_{1-x}Te$, thin film, oxidation, appl. of Mossbauer method 80−45410
$Pb_xSn_{1-x}Te$-PbTe p-n junction, epitaxial, elec. props. and photoresponse 78−56225
PbSnTe(Se) Schottky barrier diode and n-p diffused junction IR detectors, comparison 80−9039
$Pb_{1-x}Sn_xTe_{1-y}Se_y$, narrow-gap solid soln., lattice parameter, energy gap and Hall mobility of carriers 79−73154
$Pb_{1-x}Sn_xTe_{1-y}Se_y$, quarternary solid solns. with const. lattice parameter, cryst. growth and characts. 80−108332
$Pb_{1-x}Sn_xTe_{1-y}Se_y$ solid solutions with constant lattice parameter, phase comp. 80−108417
$Pb_{1-x}Sn_xY$, Y=Te, Se, S, photocond. anisotropy rel. to lifetimes 78−52032
PbTe (111), adsorption of O_2, UPS and XPS exam. 78−71962
PbTe (111), lattice vibr. amplitude anisotropy, RHEED study 80−39408
PbTe (111) epitaxial films, localised electron irrad. effects on elec. props. and O_2 sorption 80−49472
p-PbTe, absorpt. coeffs. meas. 77−24850
n-PbTe, accumulation layer, quantised surface states 80−20279
PbTe, and $Pb_{1-x}Sn_xTe$, VPE growth control by EM irrad. *(Russian)* 80−34338
PbTe and solid solns., optimal synthesis conditions for single cryst. growth 80−100776
PbTe, asymm. strip line wall, EM wave propag. in mag. field 77−76854
PbTe, Auger recomb., photocond. decay time expts. 77−72879
p-PbTe based composite material thermoelec. props. degraded by strengthening additive 79−47114
PbTe based thermoelec. materials, creep mechanisms 77−16643
PbTe, CDW in strong mag. fields, Peierls-type transition 80−34362
PbTe, carrier conc. inhomogeneity 78−52019
n-PbTe, cold hydroextrusion, plastic deform. rel. to thermoelec. props., struct. 77−11945
PbTe, complex-composition film production method from vapour *(Russian)* 78−95702
PbTe, continuous epitaxial film, grain size, growth cond. depend. 78−26786
PbTe, crystallisation in constant electric field, thermoelectric parameters 77−44146
PbTe, crystallite size in epitaxial layers by X-ray diffraction rocking curves 80−20052
PbTe, diffusion of Ag, effect of gamma irradiation 80−59515
PbTe, diffusion of Cd, Hall effect, cond. and solubility meas. 79−69292
PbTe, electrochemical surface reactions 80−76389
PbTe, electron scattering interaction with coupled plasmon-polar-phonon modes 79−42536
PbTe, electron-phonon interactin induced phase transition 79−82338
PbTe, electronic struct. near band gap 77−69226
p-PbTe, energy band struct. and scattering of holes 80−10874
PbTe, energy gap and dielec. props., 77 to 373K 80−66100
PbTe, energy gap anomaly, relativistic band struct. calc. 79−4510
PbTe, energy gap temp. depend., electron-lattice interaction, dilatation effect 79−65377
n-PbTe, epitaxial, time dependent negative weak field magnetoresist. 78−64151
n-PbTe epitaxial film, magnetophonon and Shubnikov-de Haas oscills. 78−60234
PbTe epitaxial film, many valley semicond., band population effects, intraband magneto-optical props. 79−78007
PbTe epitaxial film, stimulated emission, absorption spectra and recombination 78−80409
PbTe, epitaxial film on fluorphlogopite, effects of annealing in Te vapour 77−80709
PbTe epitaxial films, carrier recomb. and deep levels, photocond., Hall effect, and luminesc. meas. 79−38024
PbTe epitaxial films, quantum size effect, optical meas. 80−11121
n-PbTe, epitaxial layers, elec. characts. rel. to explosive evap. in closed vol. 77−89885
PbTe epitaxial layers, orientation on different faces of $LiNbO_3$ 78−79907
PbTe, epitaxial layers, carrier lifetime meas. 79−42559
PbTe epitaxial layers, submillimetre spectroscopy 79−83048
PbTe, far IR magnetorefl., band struct. 80−76010
n-PbTe, far IR magnetotransmission and refl., dielec. function 77−52091
p-PbTe, far IR obs. of shallow bound states in high mag. fields 78−23444
PbTe, far IR spin flip reson. 79−82979
PbTe film, 50 μ, prep. in double quasiclosed volume 79−38745
PbTe film, (001), two-photon transition rate calc. 79−95869
PbTe film, Bi and Tl impurity dopant incorporation and diffusion during MBE growth 79−66012
PbTe film, characts. of photocond. spectra and reflectivity 77−55624
PbTe film, elec. transport props. 79−42679
PbTe film, electronic thermal cond. and thermoelec. power 80−93018
n-PbTe film, epitaxial, hot electron transport effects 77−12035
p-PbTe film, for IR magneto-optics, 8-30K 78−23543
PbTe film, ion-implantation-induced lattice defects 77−68985
PbTe film, light absorpt. 79−83043
p-PbTe film, magnetophonon effect obs. 78−23115
PbTe film, of uniformly varying thickness, photovoltaic effects 77−51774
PbTe film, on NaCl and TGS substrates, photo-EMF investig. of induced elec. inhomogeneity 77−15909
PbTe film, optical consts., support roughness effect 80−2882
PbTe film, residual conductivity 78−2595
PbTe film, struct. anal. and sensitisation 78−22982
n-PbTe film, transverse magnetoresistance oscillations, depend. on film thickness 79−65567
PbTe, film photodiodes, quantum efficiency 79−75596

IV-VI semiconductors continued
PbTe films grown from vapour, optimum conditions and elec. characts. 79−52117
n-PbTe, free carrier absorpt. and electron mobility 78−43392
PbTe, growth of epitaxial layers, activation by UV and IR radiation 80−71598
n-PbTe, Hall effect of hot electrons 77−55547
PbTe, high field drift vel. and Hall coeff. 78−26875
PbTe, high mobility polycrystalline layer, mol. beam deposition 79−83138
PbTe homogeneity region investig. in Pb-Te system, equil. consts. of quasichem. reactions 80−108405
PbTe IR diode, epitaxially grown and ion implanted, minority carrier lifetimes, efficiency 77−20411
p-PbTe, IR reflection and Faraday rotation angle meas. 77−1680
PbTe, index matching far i.r. method for static dielectric const. meas. 77−1678
PbTe injection laser, freq. tuning using press. and temp. combination 78−17978
PbTe, ion implantation induced damage and reson. levels 80−49255
PbTe, ion implanted, magneto-optical expts. *(German)* 79−28848
PbTe, ion-implanted, doping profile evaluation by Hall effect and sheet resist. meas. 78−59831
PbTe, LPE, solvent choice, equilib. in Pg-Sn-Te system 79−87589
n-PbTe, LPE layer, carrier conc. and mobility 79−99639
p-PbTe, lattice dielectric const. in far IR region, magnetotransmission meas. 79−78605
PbTe, lattice permittivity determ. by magnetoplasma waves method 78−19075
PbTe layers, quality control of carrier conc. using Hall effect graphical representation 77−1500
n-PbTe, low temp. elec. cond. 80−20227
n-PbTe, low temperature electrical transport, Hall effect 80−84478
PbTe, MBE homostructure diode lasers with CW operation up to 100K 78−22129
p-PbTe MIS capacitors 5 μm IR detector appl. 78−52101
p-PbTe, MIS struct. inversion layer sub-bands, IR magnetoreflectance obs. 80−44731
PbTe, Magneto transport anomalies at low carrier densities, Wigner crystallisation 80−20222
PbTe, magneto-optical pinning phenomena 79−82962
PbTe, magneto-optical transitions and band parameters 79−82961
p-PbTe, magneto-optics of free and bound carriers 79−82985
PbTe, magnetoreflectance of surface space charge layers 78−52475
PbTe, microhardness meas. as function of applied load, elec. props. exam. 78−48493
PbTe, microwave magnetoplasma exam. of lattice and electronic props. 77−69364
PbTe N-type, TE figure of merit, integral form 77−24577
n-PbTe, noncubic (111) oriented epitaxial films, weak field magnetoresistance 80−75584
PbTe, nonstoichiometric, evap. and growth of epitaxial layers 80−104072
PbTe p-n junction, minority carrier lifetime, step pulse recovery 77−11995
PbTe, phase convection for effective g-factors and role of g-factors in Knight shifts 79−51473
PbTe photovoltaic detector, detectivity limits 80−105709
PbTe, polycryst. film, RF sputtered, time stability 77−43758
p-PbTe, quantum oscillations in inversion layer 77−85245
PbTe, radioelectric effect in far IR 80−24967
PbTe, recombination radiation polarisation direction, two-photon selective energy valley occupation *(Russian)* 77−20924
p-PbTe, relax.-time anisotropy 77−35954
PbTe, resonant scattering, photocond. 80−6910
PbTe, semiconductor polycrystalline thin films, low-frequency 1/f noise meas. 80−15629
PbTe single crystals, growth from vapour phase under micro-gravity conditions 80−80957
PbTe, solidus line anal., carrier conc. 78−75806
PbTe, spin orientation under two-photon pumping 79−74000
PbTe, struct. of second valence band 77−89697
PbTe, structural transition 77−51497
PbTe substrate for MIS capacitor, C-V and G-V characts. 78−26962
PbTe surface space charge layers, far IR magnetoreflectance meas. 78−64349
PbTe surfaces, oxidation in air and thermal desorption, XPS and LEED meas. 79−47830
PbTe surfaces, Te coating, struct. and junction characts. 80−50743
PbTe surfaces, tunnelling spectroscopy in MOS and Schottky barrier junctions 80−49945
PbTe, TO phonon mode softening, sub mm spectra 78−6665
PbTe, TO phonon softening, free carriers and defects effects 78−79720
PbTe, TO-phonon mode softening, far IR Fourier transform spectroscopy 77−40248
PbTe, thermodynamic props. 77−28023
PbTe thermoelectric alloys, phase diagrams, and imperfection chemistry 80−108422
PbTe thermoelectric materials, microstructure anal. using SEM X-ray microanalysis 80−107211
p-PbTe, thermorefl., 1.0-4-6 eV 78−76492
PbTe, thick epitaxial film, laser deposition technique 78−68629
PbTe, two photon magnetoabsorption *(Russian)* 80−60553
PbTe, uncontaminated films on mica sustrates, elec. props. obs. 77−76967
PbTe, uncontaminated films prepared by mol. beam deposition, elec. props. meas. 78−15316
PbTe, VPE, on $LiNbO_3$, struct. and morphology obs. 80−54561
PbTe, VPE film growth under near equilib. conditions 77−32526
PbTe vacuum deposited thin films, struct. and growth 79−19482
PbTe very thin epitaxial films, transmission and refl. spectra, 1 to 5 eV 80−7430
PbTe, wave-vector depend. of electron energy losses 78−11041
PbTe, wedge shaped film, photovoltaic effect 77−1454
PbTe:As, hole conc. control, in LPE layers, plasma reflectivity and thermoelec. probe meas. 79−99640
PbTe:Bi-PbSmTe-PbTe, epitaxial laser struct., growth, p-n junction position and lasing region 79−89908
PbTe:Bi(Sb)(Cr)(Ag), thermoelec. props., thermal and elec. cond. 79−82616

IV-VI semiconductors continued
PbTe:Cd, Cd diffusion obs. using Hall mobility and Cd solubility expts. 78−26584
PbTe:Cd, defect struct., Hall effect and solubility meas. 77−11570
PbTe:Fe, single crystals, state and behaviour of Fe, mag. props. 80−93080
PbTe:Ga, location, behaviour of Ga, electrophysical props. meas. 79−38016
PbTe:In, absorption spectra meas., 475-725K 77−4664
PbTe:In, electron mobility, temp.-independent part, Hall effect and elec. cond. meas. 80−92914
PbTe:In, mag. susceptibility, temp. depend., 4.2 to 200K 80−65773
PbTe:In, Shubnikov-de Haas oscillatory effects, quasilocal impurity level 80−92912
PbTe:In based solid solutions, impurity states, elec. props. 79−87054
n-PbTe:Pb(Bi)(In), thermoelectric props., 300-750K 78−34851
PbTe:Ti, effect of impurities on transport props. 79−11158
PbTe:Tl, influence of Tl impurity states 80−20121
PbTe:Tl, thermoelectric power, elec. cond., Hall coeff. and optical absorpt. coeff. 80−39584
PbTe:Zn, defect struct., Hall effect and solubility meas. 77−11572
PbTe-(Pb,Sn)Te DH laser, CW operation over 1500 h at 77K 78−17950
PbTe-$AgBiTe_2$, solid solution, prep. and thermoelec. props. 77−47839
PbTe-based solid solns., 79−23990
PbTe-based structures, zero anomaly of tunnel cond. 79−24107
PbTe-CdTe heterojunctions, fabrication and characterisation *(German)* 80−89151
PbTe-CdTe(InSb) superlattices, laser deposition of multilayer heteroepitaxial structs. 80−44450
PbTe-flux, interfacial tension at boundary of fused systems 77−35797
PbTe-Ga_2Te_3, phase interaction, DTA, XPA and microstructural anal. 80−96625
PbTe-In contacts, fabrication and props. 80−60078
PbTe-In_2Te_3 system, phase diagram, elec. props. 78−35361
PbTe-InTe, solid solns., anomalies in electron mobility 77−80772
PbTe-metal barrier device, I-V and C-V characts., barrier energies, and depletion widths 77−85316
PbTe-MnTe solid solns., elec. and thermal props. 79−1599
n-PbTe-p-$Pb_{1-x}Sn_xTe$, heterojunctions, heavily doped, current-flow mechanisms 80−96974
PbTe-$Pb_{0.82}Sn_{0.18}Te$, p-n heterojunctions, electrical and photoelectrical properties 78−39193
PbTe-$Pb_{1-x}Sn_xTe$ n-p^+ heterojunction photodetector, hot wall evaporation technique 80−65673
PbTe-$Pb_{1-x}Sn_xTe$-PbTe DH, LPE and VPE, stimulated emission 77−75526
PbTe-PbS, solid-phase solubility, use of diffusion couple 77−12602
PbTe-PbSnTe heterjunction, misfit dislocations, etch pit and electron probe study 79−77926
PbTe-SnTe, solid soln. single crysts., TSM growth and elec. characts. 78−68625
PbTe-SnTe compound semiconductors, lattice instability by mm-wave magnetoplasma refl. 80−54336
PbTe-SnTe solid solns., directional solidification 77−44149
$Pb_{1-y}Te$-$Pb_{1-x}Sn_xTe$ (x,y≲0.3), double heterostruct., LPE growth, heterointerface morphology 80−70550
Pb_xTe_{1-x} film, highly absorbant, complex index of refr. determ. method 78−54445
$PbTe_{1-x}Se_x$, epitaxial layers synthesis, cryst. struct. perfection and elec. characts. 79−87587
$PbTe_{1-y}Se_y$:In, high temp. Fermi level position 79−90948
$PbySn_{1-x}Se$ epitaxial film narrow band photovoltaic detectors, detection at long wavelengths 78−8443
PdS-CdS heterojunctions, photoresistive props. 80−6970
Si-Te system, phase diagrams 80−89209
SiTe:Ge(Sn), substitution of Si, thermoelectric props. *(Russian)* 80−11023
SiTe-ATe, A=Ga, In, Tl, solid solns., mag. suscept. meas., defects 78−43552
SiTe-GaTe, thermo-EMF, elec. cond. and solubility 77−20346
Si_2Te_3, growth by Bridgman technique and sublimation, cryst. struct. 77−1106
Sn-S melt, absolute thermo-emf obs. 77−85251
$Sn_xGe_{1-x}Se$, ^{119}Sn Mossbauer and elec. conductivity study 79−19595
$Sn_{0.9}Ge_{0.1}Te$, Mossbauer spectra, soft modes 80−20550
$Sn_{1-x}Ge_xTe$, evaporated thin films, characts. 79−60944
$Sn_{1-x}Ge_xTe$, solid soln. series, Mossbauer study 80−39985
$Sn_xGe_{1-x}Te$ ($0.62<x<0.91$), specific heat anomaly at struct. phase transform. 77−69095
$Sn_xGe_{1-x}Te$, ferroelec. semicond. structural phase transition, X-ray study 79−37836
$Sn_xGe_{1-x}Te$, structural transitions 77−51497
SnO_2, gas sensor, CO, H_2O vapour, surface temp. effect on cond. 78−76067
SnO_2, heat treated film, electrical conductivity 77−8211
SnO_2:ThO_2, exposed to H_2, temp. depend. of resistivity 79−56219
$Sn_{1-x}Pb_xSe(Te)$ films, Mossbauer effect of ^{119}Sn, spectral characts., conc. depend. 80−103903
$Sn_{1-x}Pb_xSe(Te)$ films, oxidation rel. to annealing temp. and time, Mossbauer spectra, X-ray and microstruct. obs. 80−104311
$Sn_{1-x}Pb_xSe(Te)$ thin films, resistance to oxidation, Mossbauer study 80−39986
$Sn_{1-x}Pb_xTe$, elec. and struct. props. of epitaxial layers *(Russian)* 78−64147
$Sn_{1-x}Pb_xTe$, epitaxial layers synthesis, cryst. struct. perfection and elec. characts. 79−87587
$Sn_{1-x}Pb_xTe$, film, production under quasi-equilibrium conditions 80−45241
$Sn_xPb_{1-x}Te$ mixed crysts, cryst. growth and assessment 78−80463
SnS, coupling of plasma waves with optical phonons 78−31204
SnS, dielec. function, optical and electron energy loss spectroscopy 78−15189
SnS, electron-hole interaction in d-electron excitations, photoelectron and optical spectra 78−34776
SnS, far IR optical props. 77−12375
p-SnS, IR photocond., direct and indirect gaps 78−2514
SnS, photoconductivity 77−72888
SnS photoelectron spectra, rel. to ionicities and phase transitions 77−69960
SnS, single cryst. growth and struct. props. 79−52109
SnS, splitting and coupling of lattice modes 77−76503

IV-VI semiconductors continued
SnS, tight-binding calc. of density of valence states 78−34760
SnS, X-ray photoemission intensity, nearest-neighbour backscatter 79−65977
SnS-PbS, phase diag. 77−36476
SnS(Se), electron diffr. struct. anal. 80−44449
SnSSe, electron mobility, elec. cond. and Hall effect meas. 78−80004
SnS(Se), IR reflectivity and Raman spectra, phonon frequencies and dielec. const. 77−48166
SnS(Se), layer crystals, optical phonons, Is and Raman spectra 77−73148
$Sn(S_xSe_{1-x})_2$, valence band states, composition depend., photoemission spectra study 80−100434
SnS_xSe_{2-x}, thermal changes in optical props. 78−19504
SnS(Se)(Te), reaction with II-VI compounds, thermodynamic anal. 80−40728
SnS(Se)(Te) XPS investig. of valence band struct. 77−48311
SnS(Te):O, impurity assoc. with Fe microtraces, Mossbauer effect meas. 77−20763
SnSe, dielec. function, optical and electron energy loss spectroscopy 78−15189
SnSe, electron states anal. by pseudopotential method 77−66115
SnSe, electronic band struct. determ. 78−51890
SnSe, electronic props., region of existence *(French)* 77−35885
SnSe, far IR reflectivity spectra, lattice vibr. and dielec. const. 77−52068
SnSe, IR-active optical phonons, vibr. spectra 79−69848
SnSe, lattice refl. spectra in long-wavelength IR range 78−27236
SnSe, mag. susceptibility components 78−43551
SnSe, Mossbauer spectra, effect of optical emission *(Russian)* 78−60367
SnSe, photoelectron spectra, rel. to ionicities and phase transitions 77−69960
SnSe, Raman scatt., zone centre optical phonons, layer-like struct. 78−48158
SnSe, single crysts., growth by Bridgeman technique, electron diffr. anal., lattice consts., carrier conc. 79−47616
SnSe, sublimation growth, deviation from stoichiometry, elec. props. 78−76594
SnSe, tight-binding calc. of density of valence states 78−34760
$SnSe_2$-$GeSe_2$, phase diag., electrophys. props. of solid solns. 77−52306
$SnSe_yTe_{1-y}$, semicond. chalcogen interdiffusion coeffs., antifrenkel defects, interstitials *(German)* 77−43375
SnTe, ^{117}Sn diffusion coeff. meas., stoichiometric deviation, SIMS 80−34236
SnTe, annealed, iodide method of prep., props. meas. 80−71591
SnTe, bond gap, phase transform., optical dielec. const. meas. 80−10630
SnTe, bond orbital model of band struct. 80−59853
SnTe, carrier density depend. of soft TO-phonon, Raman scatt. meas. 78−6684
p-SnTe, cathodoluminescence and Fermi level hole effective mass 80−25467
SnTe, complex-composition film production method from vapour *(Russian)* 78−95702
SnTe, crystal binding energy 79−37650
SnTe, crystallisation in constant electric field, thermoelectric parameters 77−44146
SnTe, diffusion of ^{125}Te 80−84325
SnTe, displacive phase transition at 22K, Mossbauer spectra and elec. resist. meas. 80−6514
SnTe, displacive transform., interband electron-phonon interactions, phase diagram 80−93252
p-SnTe, elec. resist. anomaly in vicinity of struct. phase transform. 79−19597
SnTe, electron-phonon interaction effect on ferroelec. transition 78−76416
SnTe, electron-phonon interactin induced phase transition 79−82338
SnTe, expitaxial film, early stages of growth, replication and TEM obs. 79−65348
SnTe, ferroelec. transition, quantising mag. field effect 79−87403
SnTe film, 50 μ, prep. in double quasiclosed volume 79−38745
SnTe film, electroreflectance effects 79−43055
SnTe, film, heat treatment in air, effect on struct., props. 79−11037
p-SnTe, film and bulk, weak-field magnetoresistance 78−84236
SnTe, Hall coeff., temp. depend., interpretation 78−87988
SnTe, isothermal meas. of galvanomag. and thermomag. effects *(Russian)* 78−56160
SnTe, LO phonons affected by dielec. screening 79−77697
SnTe, LPE, solvent choice, equilib. in Pb-Sn-Te system 79−87589
SnTe, light scatt. from soft modes, theory above and below displacive transform. temp. 79−95791
SnTe, low-temp. sp. ht., thermal expansion and Gruneisen parameter 77−15601
SnTe, mag-props., effect of structure transition 78−6158
SnTe, NMR of ^{119}Sn and ^{125}Te, low hole conc., 64-440K *(Russian)* 79−15365
SnTe, obs. of soft TO-phonon by Raman scatt. 77−69838
SnTe, phase transition at high hydrostatic pressure, Mossbauer study 79−95762
SnTe, phase transition obs. by Mossbauer spectroscopy 77−55740
SnTe, polymorphism, high press. and temp., X-ray diffr. study 80−54375
SnTe, press.-temp. phase diagram 77−51497
SnTe, Raman scatt. from soft TO-phonon modes 79−95773
SnTe, self-consistent relativistic energy bands 80−10870
SnTe, softening of TO phonon mode *(Japanese)* 78−2225
SnTe, solidus line anal., carrier conc. 78−75806
SnTe, sp. ht. mean field behaviour at phase transition 77−66023
SnTe, standard free energy of form. 79−57287
SnTe, strongly anisotropic polar semicond., electron-hole liq. in mag. field 80−59890
SnTe, structural phase transition threshold instability in strong EM field 80−103477
SnTe, supercond., metal-insulator transition, electron pairing, effect on optical props. 80−60139
SnTe surfaces, oxidation in air and thermal desorption, XPS and LEED meas. 79−47830
SnTe, temp.-depend. ^{119}Sn isomer shift, calcs. 77−8457
SnTe, tight-binding calc. of density of valence states 78−34760
SnTe:Mn, ferromag.-ordering, transverse magnetoresist. and Hall effect meas. 77−85240

IV-VI semiconductors continued
SnTe-Al_2O_3-Al junction, tunnelling, Fermi level depend. on carrier conc., influence of surface states 80−25016
SnTe-Al_2O_3-Al structure, tunnelling characts., model anal. 80−29480
SnTe-In, solubility, thermo-EMF coeff. meas. 78−43124
SnTe-InTe, SnTe-In_2Te_3, solid soln. region, lattice constant variation 77−35697
SnTe-PbSe, semicond. film, growth, phase composition, condensation temp. rel. to cond. type 77−28266
SnTe-PbSe mixed system layers, struct. and props. *(Russian)* 77−28082
SnTe-PbTe solid solns., defects from susceptibility meas. 77−84737
SnTe-PbTe-GeTe, alloy semiconductor, phase transition *(Japanese)* 78−91443
SnTe-Sn epitaxial system, electron microscope contrast of misfit dislocations 77−85113
$Tb_{1-x}Sn_xTe$, ferroelectric transition calc., effect on carrier density 77−85673
TiO_2 electrode, photoelectrolysis of H_2O, solar energy conversion 79−52959
TiO_2, photoelectrochemical systems, solar energy utilisation *(German)* 80−45713
TiO_2 semicond. films for water photoelectrolysis 80−26146
ZnS(Se)(Te):Co^{2+}, IR luminesc. quenching, Co^{2+} level position, ionisation energy 80−16079
$ZnSe_xS_{1-x}$, melt grown, 10K, band edge photoluminesc. 78−84628

J particles *see psi mesons*

Jahn-Teller effect
A15 compounds, high-temp. superconductors, martensitic transform., microscopic theory based on 3-dimens. band struct. 78−19752
A15 compounds as Jahn-Teller systems, multiple band electron-phonon transport theory 80−24902
A-15 type compounds, relation between martensitic and supercond. phase transition 80−29497
activated crystals, Jahn-Teller effect in optical bands of impurity centres 78−6706
alkali halide:In, high press. studies of luminesc. phenomena 79−43017
alkali halide, polarization dichroism in the optical spectra of Jahn-Teller excitons 79−69435
alkali halide, Tl^+-type centres, struct. of Jahn-Teller induced B absorption band 77−12410
alkali halides:Ga^+, Jahn-Teller effect, EPR study 78−43690
alkali halides:Ga^+, optically detected EPR in relaxed excited states of Ga^+ 78−72437
alkali metal halide crystals, g-tensor anal. of S− and Se^- centres, ESR 80−84650
alkali metal hexacupronitrates, incommensurate Jahn Teller phase transitions 79−95156
allene, non-degenerate vibr. mode induced Jahn-Teller effect, photoelectron spectra calc. 79−817
benzene, and derivatives, Jahn-Teller instability 79−47062
benzene, first-ionisation Rydberg spectrum assignment via John-Teller splitting 80−69155
benzene, Jahn-Teller active states, vibronic struct., vibr. perturbation, spectral obs. 78−13440
benzene-d_6, splitting of vibrationless level in Jahn-Teller active state of D_{2h} symmetry 77−58080
C_{3v}-type mols., double degenerate electronic states, Jahn-Teller and spin-orbit coupling 78−50537
C_{3v}-type mols., doubly degenerate electronic states, Jahn-Teller interaction 78−50536
chabazite, Cu^{2+}-exchanged, cation and water mol. positions 78−15709
chromium tetraphenylporphyrin, reson. Raman spectra, excitation profiles, nucl. distortion and Jahn-Teller effects 77−58018
closely coupled electronic states, vibronic level calcs. using derived anharmonic pots. 77−23423
cluster expansions in cooperative Jahn-Teller T-systems 80−4661
commensurate and incommensurate structural phase transitions in Jahn-Teller system 80−70403
complex, (E+A)*e systems, Jahn-Teller, pseudo Jahn-Teller coupling and circular dichroism 79−68247
configurational co-ordinate model, predictive use 79−19918
cooperative Jahn-Teller effect and paramagnetic susceptibility of S=1 systems 78−68134
cooperative Jahn-Teller effect and related problems 77−62878
cooperative Jahn-Teller ordering of elec. dipoles in non-Kramers doublets 78−15115
cooperative Jahn-Teller phase transition, crit. behaviour 80−108016
cooperative Jahn-Teller system, US attenuation, appl. to TmZn 79−78053
cooperative Jahn-Teller systems, low-freq. dynamics 79−82565
cooperative Jahn-Teller systems of T nature, electron-phonon excitation branches 78−63823
cooperative Jahn-Teller T-systems dynamics vibronic excitation branches 80−10934
cooperative phase transition, helical ordering 79−46778
cooperative phase transitions, crit. diffuse scatt. 80−59930
cooperative T−(e+t) systems, heat current operator 80−34405
cooperative T−(e+t) systems, pseudo spin thermal cond. 80−34406
cooperative T-(e+t) Jahn-Teller system, thermal cond. 80−70479
cooperative T-systems, dynamics, elastic props. 80−65511
copper porphin, Zeeman expt. on phosphoresc. triplet and quartet states 79−33786
corundum, Jahn-Teller effect of $3d^n$ ions in trigonal symm. 77−35894
croconate ion, Jahn-Teller coupled vibrs., reson. Raman profiles 77−83602
crystal t(A_{1g}+E_g+T_{2g}) system, dynamic Jahn-Teller effect 79−28327
crystals with Jahn-Teller centres, sound absorpt. 79−37765
cubic crystal, Jahn-Teller effect, soft mode influence 80−59937
cubic crystal, multimode Jahn-Teller coupling, orbital triplet 78−23062
cubic crystal E state ion in tetragonal cryst. field, static Jahn-Teller effect 77−24539
cubic crystal with antiferrodistortive interactions, Jahn-Teller induced structural phase transitions 77−11657
cubic crystals, electrooptic absorption of anisotropic Jahn-Teller centres 78−27188
cubic lattice, multi-mode Jahn-Teller effect for T⊗e 77−76782
cubic linear pseudo-Jahn-Teller effect, rotational invariance 80−15482
cyclopentadienyl ion, electron affinity and Jahn-Teller effect, laser photoelectron spectra 77−88499

Jahn-Teller effect continued
cyclopentadienyl radical, vibronic valence isomerisation, Jahn-Teller effect, D_{5h} symmetry 79−97986
cyclopropenyl radical and anion, planar, E state pot. surfaces, CI and SCF calcs. 78−5155
degenerate Jahn-Teller active mode, depolaris. dispersion in resonance Raman scatt. 77−58012
deoxy ferrous haemoglobin, Fe atom distortion, pseudo-Jahn-Teller effect 80−55984
diamond:N, electronic struct. of deep levels, LCAO, SCF method 79−82555
diamond:N, spin-lattice relax. of Jahn-Teller N centre 77−66412
diamond:N(B)(Si)(O), substitutional impurities 79−87056
diamond, dynamic Jahn-Teller distortions at trigonal optical centres 79−87069
diamond, ESR studies, review 78−95521
diamond, GR1 and UV band, fine struct. 80−20678
diamond, GR1 band, anal. of satellite lines by quadratic Jahn-Teller computing 80−97295
diamond, GR1 band, E to T state transitions coupled to e vibrs. 77−12430
diamond, Jahn-Teller coupling at neutral vacancy 80−71453
diamond, low lying levels of GR 1 centre, satellite line struct. 77−20269
diamond, magnetic field and stress splitting of GR1 line 78−60095
diamond, optical transitions between E and T electronic states each coupled to e-modes, GR1 band 80−20677
diamond, pseudo-Jahn-Teller effects in H3 vibronic spectrum 77−90182
diamond, relaxation about the vacancy 78−71722
dielectric crystal, APR and phonon spectroscopy to study paramagnetic ions 80−84634
dilute Jahn-Teller system, simple model 80−44547
displacive phase transition, second-order, discontinuous freezing-out of local order 79−42204
ditetraethylammonium manganese bromide $^4T_1$ excited state, absorpt., MCD, Jahn-Teller model 78−43907
doubly degenerate mode systems, excitation profiles, depolarisation ratios, reson, Raman scatt. 79−98108
dynamic Jahn-Teller effect in ESR spectra, Green's functions calcs. 80−84643
dynamic Jahn-Teller systems, calc. of absorption band shapes, use of Lanczos algorithm 80−45023
dynamic weak and intermediate strength effects, ion-lattice and spin-orbit coupling 77−66143
E-e problem, diagonalisation by means of transformed basis 79−82566
E-e system, low lying vibronic energy levels, variational calcs. 77−76780
electron transfer between degenerate states 77−38727
electron transport between degenerate states, rel. to Jahn-Teller effect 77−31987
electron-phonon interactions, structural phase transitions *(Japanese)* 79−4384
electronic doublet coupled with two vibr. modes, reduction factors 77−15803
EPR spectra, Jahn-Teller effect, multistate theory for ^2E orbital states 78−56369
EPR spectra of orbital triplet, intermediate Jahn-Teller effect 80−34756
equal coupling to ε and τ_2 vibrs., Γ_8 quartet 78−2454
ethylene, C atom pyramidalisation rel. to bonding, ab initio SCF calcs. 79−93936
exact solutions to a class of Jahn-Teller systems 79−60774
F-centre optical absorption bandshape calc. for transition to state with Jahn-Teller and spin orbit couplings 80−55135
ferrimagnetic spinel, magnetostriction effects from Mn^{3+}, Co^{2+} and Fe^{2+} ions 79−91277
ferroelectrics and antiferroelectrics, elastic and dielec. anomalies, microscopic model 80−71332
ferrohaemoglobin, R-T conformational change due to pseudo Jahn-Teller effect 79−70521
ferrohaemoglobin excited state wave functions *(Japanese)* 79−8475
fluorobenzene cations, emission spectra, Jahn-Teller effects and vibronic coupling 79−10120
fluorobenzene radical cations, in gas phase, laser-induced fluoresc. 79−27022
fluorobenzene radical cations, matrix laser fluoresc. spectra 80−1009
formaldehyde$^+$, excited state dissoc., nonadiabatic interactions, conical and Jahn-Teller intersections, classical trajectory method 80−25997
fourfold symmetric systems, Jahn-Teller effects 78−58599
garnet, magnetostriction effects from Mn^{3+}, Co^{2+} and Fe^{2+} ions 79−91277
ground state calculation for T-t Jahn-Teller system by exponential transform. approach 79−4540
haemoglobin, Jahn-Teller pseudo effect rel. to Fe release and conformational changes 80−76701
halobenzene cations, in solid Ne matrix, slow vibr. relax., fluoresc. obs. 80−74194
halomethanes, vibronic struct. in electron spectra, Jahn-Teller and spin-orbit coupling 78−50537
Ham factors in multi-mode system 80−100446
Hams reduction factors, exponential transform. method, comment 78−47746
hexafluorobenzene, cation, visible emission spectra of gas, Jahn-Teller effect 79−50034
Hubbard model, degenerate in mag. field, appl. to Jahn Teller systems 77−28358
hydrides, first row, bending pot. calc. using MINDO approx., force const., equilib. geometry 80−95544
icosahedral molecules and complexes, Jahn-Teller effect, pot. surface 78−78642
II-VI compounds, Jahn-Teller effect, average phonon energy 79−15122
impurity centre, electroabsorption moments 77−48205
impurity centres, piezo-optics and magneto-optics 78−39579
impurity centres in crystals, quadratic Stark effect, Jahn-Teller effect 78−68536
induced electron tracks and structural phase changes in MCr_2O_4 type cryst. *(Dutch)* 79−1585
interacting systems, predominant states and matrix elements 80−89033
ionic crystals, recent developments 78−64015
iron poprhin, A_{2u} out of plane vibration, pseudo-Jahn-Teller effect 78−82712
IV-VI semiconductor, Cr^{2+} doped, Jahn-Teller interaction energy calc. 78−2455

Jahn-Teller effect continued
Kramers doublets strong spin-lattice coupling, due to Jahn-Teller effect 77−85181
lattice relax., photo-absorpt.-luminesc. polarisation correl. in Jahn-Teller system 77−51708
ligand trajectories, octahedral T_1 system 78−76028
linear Jahn-Teller E-e effect, canonical transformation 78−67993
linear Jahn-Teller system E⊗ε, analytical treatment 80−34404
linear Jahn-Teller systems, continuous group invariances, icosahedral systems 80−49677
linear Jahn-Teller systems, continuous group invariances 78−60092
linear pseudo-Jahn-Teller effect, in strong coupling, anal. formulae for props. 80−92863
magnesium porphin soln., mag. circular dichroism spectra, Jahn-Teller coupling 77−3391
magnetic insulators with Jahn-Teller ions, temp. depend. of exchange integrals 80−103827
magnetic materials, elastic props., review 80−7142
martensite formation, and lattice props. rel. to elastic constants 80−50630
metal porphyrins, Jahn-Teller instability 79−47062
metalloporphyrins, Jahn-Teller effects 78−58599
metalloporphyrins, reson. Raman specta, intra- and inter-manifold couplings interference 80−28020
metalloporphyrins, Soret excited, reson. Raman excitation profiles, Jahn-Teller distortion and vibronic anal. 78−58698
methane, mol. cations, struct., Jahn-Teller effect, MINDO/3 calcs. 80−74135
methoxy, Jahn-Teller induced rovibronic effect, nuclear spin-electron spin hyperfine Hamiltonian 80−83298
microclusters, morphology, Hund and Jahn-Teller tendencies 79−46996
molecular dissociation, nonadiabatic interactions, conical and Jahn-Teller intersections, classical trajectory method 80−25997
molecular forbidden rot. transitions, expt. and theory, review 77−34612
molecular shape, second-order Jahn-Teller effect, highest occupied mol. orbital postulate 78−86780
molecular system, quasiclassical dynamics 79−6880
molecule, fast electron scatt. theory 79−89784
molecule, pre-reson. Raman scatt. by t-type mode near A⟶T electronic transition 80−58261
molecule, reson. Raman scatt., by doubly degenerate vibr. 79−59460
molecule with fourfold symmetry axis, coexistence of two kinds of stable Jahn Teller distortions 78−84176
molecules, ang. overlap model for different symmetries 79−10043
molecules with double minimum pots., resonance Raman scatt. 77−58011
monopyrazine zinc sulphate trihydrate:Cu^{2+}, ESR meas. 78−84478
Mossbauer ^{57}Fe spectra, ferrous charact., cryst. field interactions 80−108133
multimode coupling of impurities in solids, at finite temps., quasi-mol. description 77−7832
multimode effect for E-term with strong vibronic coupling, IR and Raman spectra band shapes 80−20139
multimode Jahn-Teller effect for E-term with strong vibronic coupling, local and resonant states 80−24858
nickel etioporphyrin, reson. Raman spectra, excitation profiles, nucl. distortion and Jahn-Teller effects 77−58018
niobates, ferroelectric, anomalous bulk photovoltage effect, Jahn-Teller mechanism 77−28218
nitrocomplexes, planar dynamic Jahn-Teller effects 77−15804
noncentrosymmetryic crystal with cooperative Jahn-Teller effect, ferroelectric transition 77−8532
occupation dynamics of E-e type Jahn-Teller system 77−35900
octahedral clusters, quadratic Jahn-Teller effect and tunnelling splitting 77−72840
optical band polarisation dichroism, forbidden transitions 80−55062
optical response of E-e Jahn-Teller system 77−35898
orbit degenerate electron state localised at point defect, T-term multimode Jahn-Teller effect *(Russian)* 80−15490
orbital doublet with weak Jahn-Teller interaction, ESR spectra 77−28427
orbital ordering in crystals with direct Coulomb interaction 78−26833
orbitally degenerate interacting impurity thermodynamics, stress field depend. due to point defects, dislocations 79−69477
orbitally degenerated electronic level instability *(French)* 79−31421
orthovanadates, centrosymmetric exhibiting cooperative Jahn-Teller effect, dielec. props. 79−28694
oxocarbon ions, reson. Raman scatt., Jahn-Teller effect 79−18190
oxyhaemoglobin, deoxygenation, Jahn-Teller effect 77−21474
palladium porphin, triplet state, optically detected EPR and Zeeman meas. 79−19809
palladium porphin, Zeeman expt. on phosphoresc. triplet and quartet states 79−33786
palladiumporphin in n-octane cryst., lowest triplet state, ESR-optical detect. 77−58050
para-Bose operator, explicit representations 79−85064
paraelectric resonance of orbital doublet in presence of Jahn-Teller interaction 78−15137
paramagnetic impurity ions in crystals, Jahn-Teller effects, review 78−34809
pentatetraene, non-degenerate vibr. mode induced Jahn-Teller effect, photoelectron spectra calc. 79−817
perovskite structure crystals, Jahn-Teller effect for surface impurities 78−47744
phonon spectroscopy, HF, using supercond. tunnel junctions 80−65178
photoferroelectric phenomena, physical models derivation for pseudo- and Jahn-Teller optical centres 79−15407
polar crystal, vibronic levels for Jahn-Teller impurities 78−68520
polar crystals, vibrational Raman scatt. induced by Jahn-Teller systems 79−69830
polarization dichroism effects in many-phonon optical bands of multiplet-multiplet transitions 79−15125
polyatomic molecule, Jahn-Teller theorem, adiabatic approx. calcs. 77−10575
praseodymium ethyl sulphate, cooperative Jahn-Teller antiferroelec. ordering 77−66144
praseodymium ethyl sulphate, specific heat, electric suscept. and thermal cone., one-dimens. electric dipolar XY system 77−32148
pyrazine, vibr. struct. and nonlinear vibronic coupling, pseudo Jahn-Teller effect 78−94234

Jahn-Teller effect continued
quasi-Jahn-Teller optical absorption line shape due to transition from A_{1g} to $(A_{1g}+T_{1u})\times t_{1u}$ system 80−92862
quenching factors (Ham factors) for linear E-e problem, dynamical treatment 77−59271
rare earth compounds, cooperative Jahn-Teller phase transition, theory of optical side-bands 77−1398
rare earth intermetallics, quadrupole interactions, magnetoelasticity 80−15489
rare earth intermetallics, structural instabilities 80−24587
rare earth orthovanadites, phase transitions and Jahn-Teller distortions 79−28548
rare earth orthovanadites, RVO_3, magnetic and cryst. struct., Jahn-Teller effect 77−32169
rare earth oxysulphides:Eu^{3+} concentration enhanced phonon sidebands, model 78−15214
rare earth zircons, Jahn-Teller cooperative phase transition, crossover effects 80−88316
reduction factor calculations, diagram approach 78−19003
reduction factors for dynamic Jahn-Teller systems in strong coupling 79−42498
resonant phonon scatt. at trigonal Jahn-Teller centres 77−66010
resonant Raman scatt. in (E×e) system 79−28736
Rochelle salt, optical characteristics in UV region *(Russian)* 78−84550
ruby, resonant cross-relaxation to Jahn-Teller Cr^{4+} ion 79−65723
sandwich compounds, orbitally degenerate, EPR 78−86893
SO(4)-invariant pseudo-Jahn-Teller system with equal coupling 80−15029
soft mode in Jahn-Teller effect 79−69221
spin Hamiltonian for Jahn-Teller ions, temp. depend. 78−30891
spin-orbit allowed tunnelling splitting in T×ε_g Jahn-Teller problem, zero-phonon line splitting 78−19006
strongly coupled Jahn-Teller system, cluster model for optical absorption spectrum 80−89034
strongly coupled T×t Jahn-Teller system, many body theory 77−28147
symmetric molecule, quasiclassical energy and momentum range *(Russian)* 77−3342
tetra-ammine cadmium acetate:Cu, EPR dynamical effects 79−61204
di-(tetraethylammonium)tetrahalomanganate, mag. circular and linear dichroism obs. 80−29725
tetragonal complexes, meas. of covalency 77−47781
tetragonal symmetry, dynamic Jahn-Teller vibronic coupling 78−60091
thermodynamic properties, internal stress effects in Jahn-Teller system 80−59679
Thorson-Moffitt Jahn-Teller degeneracies 77−88402
transition metal compounds, Jahn-Teller effect in solid state chem. 79−47061
transition metal compounds, Jahn-Teller induced high spin-low spin transitions 79−69676
transition metal hexafluorides, quadratic Jahn-Teller vibronic coupling calcs. 79−6881
transition metal ion, Jahn-Teller coupling consts., parametrisation method based on ang. overlap model 79−78052
3d transition metal ions in crystals, Jahn-Teller coupling constants calcs. 80−49679
triatomic potential surfaces, global topology 77−50381
1,3,5-trichloro,2,4,6-trifluorobenzene radical cation, $B^2A_2'\rightarrow X^2E''$ laser-induced fluoresc. spectra 80−14172
sym-1,3,5-trichlorobenzene, cation, emission spectrum, Jahn-Teller effect 79−89681
trichlorobenzene cations, Jahn-Teller distortions, quadratic and mode mixing effects., distortion geometry determ. 80−91462
trichlorobenzene radical cation, gas and matrix isolated vibr. resolved electronic spectrum 79−68252
trifluorobenzene, cation, visible emission spectra of gas, Jahn-Teller effect 79−50034
symtrifluorobenzene cation, Jahn-Teller effects, intermode interactions and intensity anomalies 80−78553
sym-trifluorobenzene cation, Jahn-Teller effects, quadrupole coupling 80−78554
trifluorobenzene cations, Jahn-Teller distortions, quadratic and mode mixing effects., distortion geometry determ. 80−91462
1,3,5-trifluorobenzene radical cation, laser induced fluoresc. spectra, vibronic anal., Jahn-Teller distortion 79−3470
1,3,5-trifluorobenzene-d_0(-d_3), cation, emission spectrum, Jahn-Teller effects 79−89680
trifluoroiodomethane, X⟶B Rydberg transition, Jahn-Teller coupling parameter, vibronic level calc. 78−50536
trigonal symmetry 79−82563
trigonal symmetry case, with strong vibronic interaction 77−35894
triphenylene(-d_{12}), lowest $T_1[^3A_2'(\pi\pi^*)]$ state vibronic coupling 80−47955
triplet state on trigonally distorted site 77−89739
triply degenerate singlet electronic states, reson. Raman scatt. 78−78714
tris(trimethylstannyl)amine, gas phase electron diffraction 80−106401
tunnelling splitting existence in dynamic effect 77−69275
tunnelling splitting in T×($\varepsilon_g+\tau_{2g}$) problem 77−8059
uranocene, reson. Raman spectra, anomalously polarised electronic band, energy level assignment 79−59451
variational approach to linear Jahn-Teller effect 77−71759
vibronic coupling for orbital triplet, T×τ_2 and T×($\tau_2+\varepsilon$) 78−47745
vibronic coupling model, for mol. spectra, rel. to pseudo Jahn-Teller effect 78−94234
vibronic theory of ferroelectricity 79−19854
vibronically coupled systems, cluster model 79−19540
zeolite-S layers, high-temp. activated dipole moments in S clusters *(Russian)* 80−20575
zinc porphin, in n-alkane crystals. at 4.2K, Zeeman spectra for Jahn-Teller instability 78−27256
zinc porphin soln., mag. circular dichroism spectra, Jahn-Teller coupling 77−3391
$AgBr_{1-x}Cl_x$, ESR of self-trapped holes, Jahn-Teller and reorientation effects 78−27092
$AgBr_{1-x}Cl_x$, Jahn-Teller type self-trapping of holes 79−65709
$AgBr_{1-x}Cl_x$, self-trapped holes, Jahn-Teller and reorientation effects in ESR 78−64273
$AgBr_{1-x}Cl_x:Cu^{2+}$, EPR of $(AgBr_6)^{4-}$, Jahn-Teller effect 79−91294
AgCl:Pd^+, ESR spectrum, quasistatic Jahn-Teller effect 80−71170
$Al_2O_3:Co^{3+}$, corundum, Jahn-Teller effect in trigonal symmetry 79−82563
$Al_2O_3:Cr^{2+}$, Jahn-Teller study, EPR data anal. 78−84172

Jahn-Teller effect continued
$Al_2O_3:Cr^{3+}$, Jahn-Teller system, zero-phonon line broadening due to non-radiative transitions 80−108258
α-$Al_2O_3:Cr^{3+}$, stress-induced linear dichroism in $^3A_2(^3T_1)\rightarrow{}^3T_2$ transition, Jahn-Teller effect 80−34884
α-$Al_2O_3:Cr^{4+}(V^{3+})$, ground state spin Hamiltonian parameters and electric field effect 77−15801
$Al_2O_3:Mn^{3+}$, Jahn-Teller Mn^{3+} ions, phonon spectroscopy and thermal cond. meas. 80−88282
$Al_2O_3:Mn^{3+}$ under uniaxial stress, Jahn-Teller model 80−88521
$Al_2O_3:Ni^{3+}$, effect of uniaxial stress on EPR spectra 79−82862
$Al_2O_3:Ni^{3+}$, Jahn-Teller effect for Ni^{3+}, EPR 79−82564
$Al_2O_3:Ni^{3+}$, phonon-spin interaction study by thermal cond. meas. 79−82395
$Al_2O_3:Ti^{3+}$, dynamic Jahn Teller effect, role of nonadiabatic operators 77−59270
$Al_2O_3:V^{2+}$, Jahn-Teller effects, ground state 80−75528
$Al_2O_3:V^{3+}$, phonon scattering, comparison between theory and experiment 78−95116
α-$Al_2O_3:V^{3+}$, stress-induced linear dichroism in $^3A_2(^3T_1)\rightarrow{}^3T_2$ transition, Jahn-Teller effect 80−34884
α-$Al_2O_3:V^{4+}$, emission spectrum, Jahn-Teller effect in $^2T_{2g}$ and ^2E_g states 79−83007
$BaF_2:Pb^{2+}$, band struct., Jahn-Teller effect, UV luminesc. and optical absorpt. spectra 80−66243
$Ba_2NaNb_5O_{15}$, ferroelastic transition sequence, cooperative pseudo-Jahn-Teller model 77−35689
$BaTiO_3$:Cu, photoferroelec. props., Jahn-Teller effect, laser irrad. effect on pyroelec. props. 78−60400
$BaTiO_3:Fe^{3+}$ bulk photovoltaic effect and photoinduced Rayleigh scatt. 77−77226
CH_4^+, Jahn-Teller distortion, energy and angular distrib. of collisional dissociation fragment 80−66356
$C_6H_6^+$, gas, laser-induced-fluoresc., rel. to photodissoc. and Jahn-Teller X and A states distortion 79−72345
$CaF_2:Co^{2+}$, designation of optical transitions near 5.40 nm, temp. evolution of absorption spectra meas. 77−55806
$CaF_2:Co^{2+}$, MCD spectra 77−28603
$CaF_2:O^-$, Jahn-Teller distortion, electronic struct., MS Xα calc. 78−23057
$CaF_2:Pb^{2+}$, band struct., Jahn-Teller effect, UV luminesc. and optical absorpt. spectra 80−66243
$CaF_2:Sm^{2+}$, pseudo-Jahn-Teller effect 79−69476
CaF_2:Tb, EPR in new photoexcited centre 78−19319
$CaF_2:Yb^{2+}$, spectra, kinetics and polarisation of luminesc. 77−69892
$Ca_3Mn_2Ge_3O_{12}$, crystal struct. distortion due to cooperative Jahn-Teller effect *(Russian)* 77−1119
CaO, $^3T_{1u}$ of F-centre, EPR, unaxial stress effects 78−48040
CaO, F^+ centre, dynamic Jahn-Teller effect 79−28327
CaO, F^+ centre in octahedral Jahn-Teller system 79−42499
CaO F^+-centre, Lie group theory aspects of Jahn-Teller effect 77−20279
CaO, F-centres, $^3T_{1u}$ relaxed excited state, uniaxial stress effect and spin-lattice coupling 78−72405
CaO, phosphoresc. F-centre, phonon assisted conversion of Jahn-Teller states, ODMR under uniaxial stress 78−48084
CaO, random intrinsic strain effect on ODMR, PMDR, of F-centre in Jahn Teller states 78−84499
CaO, relax. in $^3T_{1u}$ state of F centres 80−24443
$CaO:Ag^{2+}$, EPR spectrum, static, quasistatic and quasidynamic Jahn-Teller effect 77−85561
$CaO:Cr^{2+}$, APR spectra 79−87313
$CaO:Cr^{2+}$ Jahn-Teller system, APR spectrum, zero strain site energy level diagram 79−99756
$CaO:Fe^{2+}$, octahedral symm., vibronic effects from Zeeman field induced Mossbauer spectra 77−8477
CaO:Ir, quadrupole interactions and static Jahn-Teller effect in EPR spectra 77−72842
$CaO:V^{3+}$ orbital triplet, intermediate Jahn-Teller effect, APR 80−34758
$Ca(OD)_2:Cu^{2+}$, ESR, secondary spectra 78−88174
Cd complex, dichlorobis (pyrazole) cadmium:Cu(II), ESR, compressed tetragonal symmetry 78−6568
$CdBr_2:Ag^{2+}$, strong Jahn-Teller coupling, EPR 79−28605
$Cd(Ca)F_2:Co^{2+}$, Jahn-Teller split $^4A_{2g}\rightarrow{}^4T_{1g}(P)$ absorption band, elec. field effect 78−15202
$CdCl_2:Ag^{2+}$, strong Jahn-Teller coupling, EPR 79−28605
$CdF_2:Co^{2+}$, MCD spectra 77−28603
$CdF_2:Cr^{2+}$, orthorhombic Jahn-Teller distortion 78−19007
$Cd(NH_3)_4Cl_2$:Cu, EPR dynamical effects 79−61204
CdTe:Cr^{2+}, absorpt. and luminesc. of $Cr^{2+}(d^4)$, cryst. field theory interpretation 79−83000
CdTe:Ti^{2+}, effect on $^3T_1(^3F)$ state, resonance on $^3T_1(^3P)$ state 78−27271
$CeAg_xIn_{1-x}$, cubic to tetragonal phase transform., conc. dependence by resist. meas. 78−2252
$CeAl_2$, dynamic Jahn-Teller effect, neutron energy loss obs. 79−78060
$Cl_2O_3:Ni^{3+}$, EPR spectra anal. using dynamic Jahn-Teller model 79−82863
Co complex, $Co(NO_2)_6^{4-}$, bond. props. and Jahn-Teller distortion, INDO-LCAO-MO calcs. 80−75532
CoV_2O_4:Fe, spinel, prep. and Mossbauer spectra 79−28660
$CrEr_2S_4$, cryst. struct. *(French)* 77−15356
Cs-halide, optical response function from Jahn-Teller systems, F-band absorpt. band shape 79−43005
$CsAsF_6$, γ-irrad., EPR spectra, hyperfine interactions and g-value determ. 77−81416
$CsCrCl_3$, co-operative Jahn-Teller distorted struct. determ. 78−63713
$CsCrCl_3$, Jahn-Teller induced phase transitions 80−70391
$CsCrI_3$, neutron diffr. expts. at 300, 77 and 1.2K 80−107163
$CsCuCl_3$, cooperative Jahn-Teller transition with trebling of period *(Russian)* 77−76557
$CsCuCl_3$, Jahn-Teller induced phase transition, helical at. displacements 77−43301
$CsCuCl_3$, Jahn-Teller effect induced phase transitions 79−47439
$CsCuCl_3$, Jahn-Teller induced phase transitions 80−70391
$CsCuCl_3$, piezoelectricity, Jahn-Teller type phase transform. 80−40065
CsF, F-centre optical absorption bandshape calc. for transition to state with Jahn-Teller and spin orbit couplings 80−55135
CsI:Tl^+, Jahn-Teller split luminesc., high press. study 78−52565
$Cs_2LiFe(CN)_6$, struct., phase transformations, temp. depend. Raman spectra 79−11416

Jahn-Teller effect continued
Cs_2MX_6(M=Se, Te, X=Cl, Br), $\Gamma_4^-(^3T_{1u})$ state, Jahn-Teller effect, luminesc. obs. 80−60650
$CsMnF_4$, planar ferromag., cryst. and mag. struct., Jahn-Teller effect 80−75715
$Cs_2PbCu(NO_2)_6$, α-modification, Jahn-Teller induced α to β transition, neutron diffr. obs. 79−1498
$Cs_2PbCu(NO_2)_6$, incommensurate Jahn-Teller transition, Huang scatt. 80−70401
$Cs_2PbCu(NO_2)_6$, low-temp. γ-modification, struct., powder neutron diffr. study, 160K 80−84151
$Cs_2PbCu(NO_2)_6$, one-dimensional stacking order 80−28941
$Cs_2PbCu(NO_2)_6$, successive Jahn-Teller phase transitions, neutron and X-ray diffr. 78−95154
$CsSbF_6$, γ-irrad., EPR spectra, hyperfine interactions and g-value determ. 77−81416
$Cs_2SiF_6:Mn^{4+}$, Jahn-Teller effect in $^4T_{2g}$ state, Zeeman meas. 80−29367
$Cs_2TeCl_6:Re^{4+}$, vibronic transitions progressions, intensity distrib. 79−78735
$Cs_2TiF_6:Mn^{4+}$, spin-orbit and field splitting, Jahn-Teller effect, Zeeman meas. 80−80234
Cu complex, bis(N-methylsalicylaldimine) copper (II), Jahn-Teller effect in EPR 77−80994
Cu complex, $Cu(NO_2)_6^{4-}$, bond. props. and Jahn-Teller distortion, INDO-LCAO-MO calcs. 80−75532
Cu complex, $Cu(ONC_5H_5)_6X_2$, X=ClO_4, BF_4, cooperative Jahn-Teller ordering and mag. struct., EPR meas. 79−60505
Cu complex, $Cu(en)_3Cl_2.0.75$ en, X-ray and ESR data, Jahn-Teller distortions 78−80206
Cu complex, hexakis pyridine-N-oxide cuprate ion, pure and Zn doped, EPR, Jahn-Teller effect 78−10754
$CuCr_{2-x}Fe_xO_4$, charge transfer, Mossbauer spectroscopy 80−15836
$CuCr_2O_4$-$MgCr_2O_4$, X-ray investig. 77−44224
$Cu_{2-x}Se$, nonstoichiometric, diamag. and paramag. props., susceptibility meas. 80−70936
$Cu_xZn_{1-x}SiF_6.6H_2O$, heat capacities and thermodynamic props., 14 to 300K, cooperative Jahn-Teller transition 80−21314
$Cu_xZn_{1-x}ZrF_6.6H_2O$, distortions of nearest Jahn-Teller $[Cu(H_2O)_6]^{2+}$ centres 78−68000
$DyAsO_4$, cooperative Jahn-Teller phase transitions, dielec. anomalies 78−64312
$DyAsO_4$, cooperative Jahn-Teller transition, optical study 80−15240
$DyAsO_4$, cryst. struct. by X-ray diffr. co-operative Jahn-Teller transition 77−89411
$DyAsO_4$, first order Jahn-Teller phase transition, sp. ht. and refr. index meas. 80−59645
$DyAsO_4$, first-order cooperative Jahn-Teller phase transition, dielec. suscept. studies 80−19940
$DyAsO_4$, phase transitions obs. 80−70412
$DyVO_4$, antiferromag.-ferromag. structural phase transition induced by elec. field *(Russian)* 79−46802
$DyVO_4$, basal plane magnetisation anisotropy under Jahn-Teller distortion 78−68222
$DyVO_4$, cooperative Jahn-Teller distortion, mag. field depend. 77−47777
$DyVO_4$, cooperative Jahn-Teller phase transitions, dielec. anomalies 78−64312
$DyVO_4$, cooperative Jahn-Teller transition, optical study 80−15240
$DyVO_4$, cooperative Jahn-Teller phase transition, linear birefr. meas. 80−88960
$DyVO_4$, dielec. anomaly and improper antiferroelectricity at Jahn-Teller transition 77−24802
$DyVO_4$, electric field influence on elastic props., electron state initial splitting 80−34123
$DyVO_4$ Jahn-Teller crystal, deform. induced transitions, elastic and dielectric characts. *(Russian)* 80−80726
$DyVO_4$, Jahn-Teller domains obs. by cryogenic X-ray topography 77−39507
$DyVO_4$, Jahn-Teller phase transition and improper antiferroelectricity *(Japanese)* 78−80294
$DyVO_4$, mag. field depend. of cooperative distortion 78−79733
$DyVO_4$, phase transitions obs. 80−70412
$EuAsO_4$:Gd, dynamical interactions, EPR meas. 80−7162
$EuVO_4$:Gd, dynamical interactions, EPR meas. 80−7162
Fe group, mol. Jahn-Teller reson. states as possible antecedents to magnetism 80−75701
Fe^{2+}, in octahedral symm., vibronic effects from Zeeman field induced Mossbauer spectra 77−8476
$FeBO_3$, mag. linear dichroism and absorpt. spectra, Jahn-Teller effect 80−54662
$FeBO_3$, mag. linear dichroism and absorpt. spectra, exciton-magnon absorpt. mechanism 80−66160
$FeBr_2$, dynamic Jahn-Teller system, Raman scatt. from electronic excitations and phonons 78−56474
$FeBr_4^-$, in various solvents, $^4A_1$ ^4E d-d band reson. Raman spectra, solvent depend., ν_3 mode Jahn-Teller effect 80−55085
$FeCl_2$, dynamic Jahn-Teller system, Raman scatt. from electronic excitations and phonons 78−56474
$Fe(ClO_4)_2.6H_2O$, single cryst. polarised opt. spectra 77−48188
$FeCr_2S_4$, normal ferrimag. spinel, NMR studies 2-77K, Jahn-Teller symm. distortions *(Russian)* 79−19785
$Fe^{2+}{}_{1+x}Cr_{2-2x}Ti_xO_4$ spinel, low temp. crystallographic transitions 77−15589
$Fe^{2+}Fe_{0.2}{}^{3+}Cr_{1.8}{}^{3+}O_4$, acoustic props. rel. to cooperative Jahn Teller effect and structural phase transform 80−24538
FeS, zinc blende type, crystallographic and Mossbauer obs. 78−87650
$Fe(SO_3F)_2$, Mossbauer and electronic spectra, cryst. field splittings, mag. hyperfine interactions 77−48096
Fe_2TiO_4, cooperative Jahn-Teller effect, neutron scatt. study 80−49678
Fe_2TiO_4, cooperative Jahn-Teller phase transition, crit. diffuse scatt. 80−59930
$FeZrF_6$, phase transition at 212.3K, Mossbauer, EPR study, quadrupole splitting, Jahn-Teller effect *(German)* 78−68430
GaAs:Co^{2+}, piezoabsorption meas. tunnel splitting and Jahn Teller effect in $^4T_1(P)$ state 79−15494
GaAs:Cr, O, effect of O in photoluminesc. meas. 80−29799
GaAs:Cr, semi-insulating, Zeeman studies of 0.839 eV emission 80−103987
GaAs:Cr^{2+}, dynamic Jahn-Teller effect, relaxation time for reorientation 80−6798
GaAs:Cr^{2+}, effect of uniaxial stress and temp. variation on Cr^{2+} centre, EPR expts. 79−95636

Jahn-Teller effect continued
GaAs:Cr^{2+}, Jahn-Teller effect for ion impurities 80−107753
GaAs:Cr^{2+}, US attenuation meas. of Jahn-Teller distorted Cr^{2+} centres 79−28048
GaAs:Cr^{2+}($3d^4$), Jahn-Teller distortion, photoinduced charge conversion, EPR 78−10758
GaAs:Cr^{3+} ($3d^3$), EPR, 5K, evidence for strong Jahn-Teller effects 77−43875
GaP:Ni, optical and EPR study of two-electron-trap state 79−73806
$Gd(OH)_3$, dynamical effects of interaction between 4f electrons and optical phonons 80−108196
Ge, entropy and enthalpy of vacancy form., comparison of theory with quenching expts. 77−11872
H_3, electronically excited state obs., vibr. level struct. determ., predissoc. 79−41204
H_3, Rydberg states, Jahn-Teller calcs. 80−9494
InAs:Mn^{3+}, Jahn-Teller effect for ion impurities 80−107753
InP:Cr^{2+}, Jahn-Teller effect for ion impurities 80−107753
InP:Fe_3 resonance photocond. 80−44651
InP:Fe^{3+} (Cr^{2+}), EPR, symm., spin Hamiltonian parameters 78−10759
$(IrCl_6)^{2-}$, electronic Raman spectra, spin-orbit components of ground state, vibr. 78−5231
IrF 6, $\Gamma_{8g}(^2T_{1g})$ state, electronic Raman scatt. and absorption spectra at 1.6 μ, resolution of Jahn-Teller problem 79−36648
IrF_6, in mixed crysts., Jahn-Teller effect, $\Gamma_{8g}(t_{2g})^3$ state, 6800 Å 78−76032
IrF_6, ligand field theory analysis of spectra 79−72248
IrF_6, neat and mixed cryst., Raman scatt., Jahn-Teller interaction in ground state 79−38540
KBr:Ga^+, Jahn-Teller effect in orbital triplet, optically detected EPR meas. 77−66441
KBr:S^-, Jahn-Teller model of S^- ion centre 79−82567
KBr:Tl, Jahn-Teller system, negative mag. circular polarisation in emission spectrum 80−20694
KBr:Tl^+, Jahn-Telier split luminesc., high press. study 78−52565
KBr:Tl^+, quadratic Jahn-Teller effect, totally symm. vibr. mode effect, ang. overlap model 80−49680
KCl, MCD of R_1 band 77−8551
KCl:Au^-, fluorescence, stress and mag. field depend., Jahn-Teller effect and relax. processes 77−48220
KCl:Pb, photolum. in A band region, spectral and time decay anal. 79−33823
KCl:S^-, Jahn-Teller model of S^- ion centre 79−82567
KCl:Tl^+, quadratic Jahn-Teller effect, totally symm. vibr. mode effect, ang. overlap model 80−49680
KCl-KI:Tl, spectral, polarisational and kinetic characts. 78−80385
KCl-Tl, Jahn-Teller system, negative mag. circular polarisation in emission spectrum 80−20694
KCl(Br)(I):Ga^+, polarisation of Ga^+ centre A_T emission, temp. depend. 80−80842
KCl(Br)(I):In^+, Jahn-Teller split luminescence, high press. study 78−52565
$K_3Co(CN)_6$, Raman scatt. and electronically-induced phase transition at 130K 77−90142
$KCrF_3$, mag. struct. and cooperative ordering or orbitals 79−99687
$KCuF_3$ crystals, with Jahn-Teller distortion, electron density distrib. X-ray diffractometry 79−69061
$KCuF_3$, mag. struct. and cooperative ordering or orbitals 79−99687
K_2CuF_4, 2-D ferromagnet, optical and magneto-optical props. 77−52062
K_2CuF_4, two-dimens. ferromag., magneto-optical props., absorpt., MCD and MLD 79−87419
$K_2Cu_{1-x}Mn_xF_4$, Cu-Mn exchange interaction, optical determ. 78−72551
$KDy(WO_4)_2$, Jahn-Teller transition, permittivity behaviour 80−55012
$KDy(WO_4)_2$, low temp. phase transitions *(Russian)* 78−87787
$KDy(WO_4)_2$, phase transition mechanism, absorpt. spectra, symmetry props. *(Russian)* 80−55130
$K_3Fe(CN)_6$, Raman scatt. and electronically-induced phase transition at 130K 77−90142
KH_2PO_4:Tl, 5.76 eV absorpt. band, temp. effects on doublet struct. 79−78713
KI, perturbed by Jahn-Teller centres, lattice dynamics 80−107394
KI:Tl, Jahn-Teller system, negative mag. circular polarisation in emission spectrum 80−20694
KI:Tl^+ type phosphor, press. effects on triplet relaxed excited states, quadratic Jahn-Teller interaction 78−23510
KI:Tl(In) and KBr:In, A-luminescence spectra and polarisation, Jahn-Teller minima 77−20914
$KMgF_3:Fe^{2+}$, US relax. absorpt., acoustic wave-impurity coupling, spin-orbit splitting 79−4375
$KMgF_3:Co^{2+}$, $^4T_1$-$^4T_2$ transition, zero-phonon lines intensities 80−75529
$KMgF_3:Cr^{2+}$, APR and US relax. 77−66416
$KMgF_3:Fe^{2+}$, Jahn-Teller quenched spin-orbit, splitting of $^5T_{2g}$ state 77−63442
$KMgF_3:Fe^{2+}$, octahedral symm., vibronic effects from Zeeman field induced Mossbauer spectra 77−8477
$KMgF_3:Fe^{2+}$, super hyperfine struct., Zeeman splitting and dynamic Jahn-Teller effect 77−85555
$KMgF_3:Fe^{2+}$, transferred hyperfine interactions, EPR exam. 78−31105
$KMgF_3:V^{2+}$, combined spin-orbit and Jahn-Teller coupling, method of soln. 79−60773
$KMgF_3:V^{2+}$, dynamical Jahn-Teller effect on spin orbit multiplets, intensity quenching 79−95374
$KMgF_3:V^{2+}$, first and second order Jahn-Teller coupling const. calc. 79−65906
$K_2Mn_{1-x}Cu_xF_4$, dynamic Jahn-Teller effect, NMR *(Japanese)* 78−19347
$KMnF_3$, exciton and exciton-magnon emission 79−33779
$K_2NaGaF_6:Cr^{3+}$, magneto-optical study of $^2T_{1g}$, $^4T_{2g}$, ^2E_g-$^4A_{2g}$ transitions 80−71384
K_2O-B_2O_3 glass, PbO-activated, rel. to negative polarisation of luminesc. *(Russian)* 78−10979
$K_2PbCu(NO_2)_6$, effect of hydrostatic press. on successive Jahn-Teller phase transitions 78−43120
$K_2PbCu(NO_2)_6$, incommensurate Jahn-Teller transition, neutron scatt. meas. 77−69065
$K_2PbCu(NO_2)_6$, incommensurate Jahn-Teller phase transition 78−79730
$K_2PbCu(NO_2)_6$, incommensurate Jahn-Teller transition, Huang scatt. 80−70401
$K_2PbCu(NO_2)_6$, Jahn-Teller phase transitions, order-disorder model 78−79762
Jahn-Teller effect continued
$K_2PbCu(NO_2)_6$ Jahn-Teller phase transitions, X-ray and neutron measurements 78−91438
$K_2PbCu(NO_2)_6$, phase transitions induced by Jahn-Teller effect, uniaxial stress effects 80−6512
$K_2PbCu(NO_2)_6$, US vel. near cooperative Jahn-Teller phase transitions 79−23680
$KZnF_3$, exchange interactions of transition metal ions in orbitally degenerated excited states 80−65512
$K_2Zn(ZrF_6)_2.6H_2O$, EPR of Cu^{2+}, temp. depend. 78−80201
$LaAlO_3$, exchange interactions of transition metal ions in orbitally degenerated excited states 80−65512
$La_{2-x}Sr_xNiO_4$, ($0 \leq x \leq 1$), rel. to cryst. struct. and elec. props. 78−2088
Li_3, BO hypersurface and vibronic states, coupled electron pair approx. 78−94203
$LiTmF_4$, Van Vleck paramag., mag. reson. on uniaxial and uniform compression *(Russian)* 79−61243
methane cation, Jahn-Teller distortion 80−48098
Mg complex, $Mg(H_2O)_6H_2(EDTA)$, Cu^2 doped EPR and ground state wavefunction of Cu^{2+} 79−56605
MgO, transition metal ion doped, phonon spectroscopy using freq. crossing techniques 79−42193
MgO:Ag^{2+}, EPR spectrum, static, quasistatic and quasidynamic Jahn-Teller effect 77−85561
MgO:Co^{2+}, weak dynamic Jahn-Teller coupling, neutron inelastic scatt. obs. 80−59934
MgO:Cr^{2+}, APR spectra 79−87313
MgO:Cr^{2+}, critically coupled spin-phonon mode 78−67779
MgO:Cr^{2+}, dynamic Jahn-Teller effect, APR obs. 77−20693
MgO:Cr^{2+}, Jahn-Teller parameters determ. using heat pulses 77−62876
MgO:Cr^{2+}(Mn^{2+}), phonon spectroscopy using supercond. tunnel junctions 79−65157
MgO:Cr^{3+}(V^{2+}), $^4A_{2g}$→$^4T_{2g}$ spectra, new expt. results 80−11441
MgO:Fe^{2+}, Jahn-Teller effect in ^5E_g state, tunnelling splitting obs. 78−19517
MgO:Ir^{2+}, quadrupole interactions and static Jahn-Teller effect in EPR spectra 77−72842
MgO:Ir^{2+}, superhyperfine struct. of ^{25}Mg in EPR spectra of Ir^{2+} 77−69683
MgO:Mn^{3+}, ground state exam., thermal conductivity meas. 79−42497
MgO:Pt^{3+}, Jahn-Teller effect in EPR spectrum 80−7160
MgO:Rh^{2+}, EPR of Jahn-Teller ions, ^{17}O superhyperfine structure 77−32253
MgO:V^{2+}, first and second order Jahn-Teller coupling const. calc. 79−65906
MgO:V^{2+}, Jahn-Teller system, zero-phonon line broadening due to non-radiative transitions 80−108258
MgO-Ti^{3+}, orthorhombic distortion, Jahn-Teller effect 77−66140
$MgSO_4.7H_2O$:$(Cu[H_2O]_6)^{2+}$, EPR and optical spectra anal. 79−38377
Mg_2TiO_4:Cu(Ni), ESR of Cu^{2+} and Ni^{3+} 80−97131
Mn^{2+}, in nearly tetrahedral clusters, ^4E levels, orbit-lattice interaction and Jahn-Teller effect, spectra obs. 80−24860
τ-MnAl, estimated theoretical limit of mag. moment 80−97072
$Mn_xCr_{3-x}O_4$, cubic and tetragonal structs., neutron diffr. obs. 79−19369
MnF_6^{2-}, $A_2^IM^{IV}F_6$ hosts, luminesc., IR and Raman spectra, 5K, assignments 77−20904
MnO, Jahn-Teller effect on optical absorption spectra 78−52484
$Mn(PO_3)_3$, cryst. struct. determ. *(French)* 78−55843
ND_4Br:Cu^{2+}, pseudo-Jahn-Teller effect manifestation in ESR spectrum 80−71168
NH_3^+, ionisation pot. of ^2E state, Jahn-Teller effect 78−62948
NH_3^+, two-mode Jahn-Teller effect calcs. 80−83297
NO-Fe(II)haemoproteins, orbit-orbit interaction, low temp. mag. circular dichroism obs. 80−30645
Na, in Xe matrix, 3s excitation, UV and vis. spectra 78−46291
Na_3, electronic struct., pot. energy surface, ab initio CI study 78−70996
$NaCa_2Cu_2V_3O_{12}$, crystal struct. distortion due to cooperative Jahn-Teller effect *(Russian)* 77−1119
NaCl:Ga^+, polarisation of Ga^+ centre A_T emission, temp. depend. 80−80842
Na_xVS_2, intercalation cpd., mag. phase transitions 77−69558
Na_xVS_2, Na_xVSe_2, charge density waves, electron localisation 79−47038
$Na_xVS_2(Se_2)$, mag. and elec. props. rel. to struct. transitions 78−91848
Na_xVSe_2, intercalation cpd., mag. and structural phase transitions 77−69558
Nb-H, BCC, quasimolecular Jahn-Teller reson. states 80−44550
Nb_3Sn, elastic instability in cubic to tetragonal phase transitions 78−39767
$Nd(OH)_3$, dynamical effects of interaction between 4f electrons and optical phonons 80−108196
$NiCr_2O_4$, acoustic props. rel. to cooperative Jahn Teller effect and structural phase transform 80−24538
$NiCr_2O_4$, cooperative Jahn-Teller phase transition, channelling obs. 78−38839
$NiCr_2O_4$ single crystal, appl. of particle channelling to the study of a cooperative Jahn-Teller phase transition 79−4413
$Ni^{2+}Fe_{0.75}^{3+}V_{1.25}^{3+}O_4$, acoustic props. rel. to cooperative Jahn Teller effect and structural phase transform 80−24538
NiZn ferrite, dielec. props., Jahn-Teller ion effects 80−97181
O_2 monolayers, on graphite, mag. α-phase and α-β-phase transition 80−70530
Pd-Er, dynamic Jahn-Teller effect of Er^{3+} 79−73478
Pd-Er, fine struct. of Er^{3+}, dynamic Jahn-Teller effect of electronic Γ_8 quartet 77−35895
$PrAlO_3$, ^{27}Al NMR, electronic spin dynamics at Jahn-Teller phase transition 78−68403
$PrBr_3(Cl_3)$, cooperative Jahn-Teller antiferroelec. ordering, struct. phase transition 77−66144
$PrCl_3$, cooperative Jahn-Teller ordering of elec. dipoles in non-Kramers doublets 78−15115
$PrCl_3$, one-dimensional X-Y system, far IR absorpt. spectra, cooperative spin excitations 78−95584
$PrCu_2$, cryst. field transitions near cooperative Jahn-Teller transition 78−84178
$PrCu_2$, Jahn-Teller transition, susceptibility, elec. resist., thermal expansion and acoustic meas. 77−20276
$PrCu_2$, mag. excitations and cooperative Jahn-Teller transition 79−65196
$Pr(OH)_3$, Jahn-Teller antiferroelectric ordering 78−10859
$PrVO_3$, neutron diffr. exam. of first order mag. transition 78−2685
$RbAg_4I_5$, 208K phase transition, Jahn-Teller-like model 77−35694
$RbAg_4I_5$, US attenuation near 208K phase transition 79−33085

Jahn-Teller effect continued
β-$RbCrCl_3$, co-operative Jahn-Teller distorted struct. determ. 78−63713
γ-$RbCrCl_3$, cooperative Jahn-Teller distorted structure 79−90604
$RbCrCl_3$, Jahn-Teller induced phase transitions 80−70391
$RbDy(MoO_4)_2$, low temp. phase transitions *(Russian)* 78−87787
$RbI:Pb^{2+}$, optical and elec. props. 79−15493
$RbMnF_3$, exciton and exciton-magnon emission 79−33779
$RbMnF_3$, Jahn-Teller coupling consts., LCAO calc. 80−59940
$Rb_2PbCu(NO_2)_6$, incommensurate Jahn-Teller phase transitions 79−65185
$Rb_2PbCu(NO_2)_6$, incommensurate Jahn-Teller transition, Huang scatt. 80−70401
$Rb_2TeCl_6:Re^{4+}$, vibronic transitions progressions, intensity distrib. 79−78735
ReF_6, cryst., Raman and absorpt. spectra, Jahn-Teller effect 78−6675
ReO_3Cl, near UV absorpt. spectra, dynamical Jahn-Teller effect 78−86881
$SO_3(SO_3^+)$, Jahn-Teller interaction, Franck-Condon factors and vibronic energy level calc. 78−50536
Si, entropy and enthalpy of vacancy form., comparison of theory with quenching expts. 77−11872
Si, extended Huckel theory calc. of hyperfine interactions of positive divacancy 77−89742
Si, extended Huckel theory calculations for positive divacancy 78−87938
Si, Jahn-Teller distorted vacancy, electronic struct. 80−10869
Si, Jahn-Teller Mn^0 centre ESR spectrum, depend. on axial press. 80−44911
p-Si, vacancy, charge states, Jahn-Teller stabilisation energy 80−80209
Si:Cr, spin-lattice relax. of Jahn-Teller Cr^0 centre *(Russian)* 78−72402
$Si:Cr^0(Mn^)$, spin-lattice relax. of Jahn-Teller centres, coexistence of minima with different symmetries 80−80602
Si:N, laser-annealed, Jahn-Teller distorted donor, EPR meas. 80−84642
Si:P, optically induced divacancy reorientation, EPR spectra 78−80216
$SrF_2:Pb^{2+}$, band struct., Jahn-Teller effect, UV luminesc. and optical absorpt. spectra 80−66243
$SrF_2:Sm^{2+}$, pseudo-Jahn-Teller effect 79−69476
SrO, electronic struct. of F-centre 78−30887
$SrO:Ag^{2+}$, EPR spectrum, static, quasistatic and quasidynamic Jahn-Teller effect 77−85561
$SrO:Ni^+$, noncentral Jahn-Teller ion, energy minimum localisation, ESR study 80−25198
$SrO:Ni^+(Cu^{2+})$ noncentral Jahn-Teller ion, coupled polar-tetragonal strains 80−44555
$SrO:Ni^{2+}$, EPR line splitting rel. to Jahn-Teller coupling and soft localised mode 80−66022
$SrTiO_3:Cr^{5+}$, nonlinear Jahn-Teller coupling, local dynamics, near struct. transition 80−2625
$SrTiO_3:Cr^{3+}$ Jahn-Teller system, EPR, electric field effects 79−28599
Ta-H, BCC, quasimolecular Jahn-Teller reson. states 80−44550
Tb compounds, anisotropic magnetoelastic props., Jahn-Teller transitions 77−69660
$TbAsO_4$, cryst. struct. by X-ray diffr. co-operative Jahn-Teller transition 77−89411
$TbFeO_3$, mag. phase transitions, Van Vleck interaction and R-Fe exchange *(Russian)* 79−61105
$TbFeO_3$, metamag. phase transitions, mag. struct. instability *(Russian)* 79−61107
$Tb_cGd_{1-c}VO_4$, cooperative Jahn-Teller effect, linear birefringence 77−76550
$Tb(OH)_3$, dynamical effects of interaction between 4f electrons and optical phonons 80−108196
$TbVO_4$, co-operative Jahn-Teller transition, low freq. dynamics, light scatt. study 80−88317
$TbVO_4$, cooperative Jahn-Teller effect, linear birefringence 77−76550
$TbVO_4$, dielec. meas. at Jahn-Teller transitions 77−24802
$TbVO_4$, Jahn-Teller phase transition, γ-ray diffractometry 78−91205
$TbVO_4$, mag. field depend. of cooperative distortion 78−79733
TcO_3Cl, near UV absorpt. spectra, dynamical Jahn-Teller effect 78−86881
Ti-Nb-H, proton spin-lattice relax. time, conc. depend., diffusion effects 77−4576
$TiBr_4$, reson. Raman spectrum, vibr. analysis, Jahn-Teller coupling 79−85965
TiH_2, electronic density of states and tetragonal distortion, APW calc. 79−37986
$TiSe_2$, structural distortion, band Jahn-Teller type mechanism 77−62875
$Tl_2PbCu(NO_2)_6$, incommensurate Jahn-Teller phase transitions 79−65185
$Tl_2PbCu(NO_2)_6$, incommensurate Jahn Teller phase transitions 79−95156
$Tl_2PbCu(NO_2)_6$, incommensurate Jahn-Teller transition, Huang scatt. 80−70401
$TmAsO_4$, optical side bands, absorpt. spectra in mag. fields 77−52123
$TmAsO_4$:Gd, cooperative Jahn-Teller system, dipolar and random strain effects 77−40124
$Tm_{0.82}Lu_{0.18}VO_4$, elastic consts. at 9 GHz 77−62576
$TmPO_4$, Jahn-Teller induced elastic constant changes, 4.2 to 300K 78−79657
$TmPO_4:Gd^{3+}$, EPR spectrum and Jahn-Teller induced nonuniform dynamic strains 77−85565
$TmVO_4$, dielec. meas. at Jahn-Teller transitions 77−24802
$TmVO_4$, elastic consts. at 9 GHz 77−62576
$TmVO_4$, Jahn-Teller distortion, RF susceptibility and NMR meas. 80−44930
$TmVO_4$, Jahn-Teller system, critical dynamics and acoustic phonon coupling, Z-branch 77−84887
$TmVO_4$, type crystals with cooperative Jahn-Teller effect, acoustic NMR *(Russian)* 77−28460
$TmVO_4:Gd^{3+}$, EPR linewidth temp. var., random strains due to Jahn-Teller effect 77−12200
$TmVO_4$-type crystals, dipole nuclear spin-phonon coupling and US absorpt., theory 77−24753
TmZn, cooperative Jahn-Teller effect 78−67998
UF_6, matrix isolated, laser fluoresc. spectrosc. at 12K 79−68253
UF_6, matrix isolated, vibronic fine struct. in fluoresc. spectrum 80−83406
UF_6, neat and mixed cryst. emission spectra, lowest charge transfer state, Jahn-Teller effect 78−67992
$U(OH)_2SO_4$, cooperative Jahn-Teller effect, mag. susceptibility meas. 78−72121
Jahn-Teller effect continued
$U(OH)_2SO_4$, mag. susceptibility, heat capacity anomalies at 21K 80−11151
V^{4+} on tetragonally distorted tetrahedral sites, Jahn-Teller effect and hyperfine parameters 77−69276
V-H, BCC, quasimolecular Jahn-Teller reson. states 80−44550
VBr_4, mol. struct., vibronic interactions, dynamic Jahn Teller effect, gas phase electron diffr. 79−31711
$V(CO)_6$, cryst. and mol. struct., Jahn-Teller distortion, mol. vib. and librational correction 79−32949
VCl_4, Raman spectra and selection rules, Jahn-Teller splitting 78−988
V_3Si, intra-atomic Coulomb interaction effect on band type of Jahn-Teller effect 79−78057
XeF_5^+, pseudopot. SCF MO studies, steric aspects of struct. and force fields, Jahn-Teller effect 80−99444
XeF_6 molecules with Jahn-Teller pseudo-effect, ang. depend. of inelastic scatt. of electrons 80−69246
XeF_6, pseudopot. SCF MO studies, steric aspects of struct. and force fields, Jahn-Teller effect 80−99444
$YAG:Nd^{3+}$, nonradiative multiphonon relaxation of isolated impurity level, transition probability calcs. 79−56853
$Y(OH)_3$, dynamical effects of interaction between 4f electrons and optical phonons 80−108196
$Zn(BrO_3)_2.6H_2O:Cu^{2+}$, Jahn-Teller system, EPR and spin-lattice relax. 78−10760
$Zn_xCu_{0.1}Fe_{2.9-x}O_4$, ferromag. reson., g-factors, Jahn-Teller ion effects 80−66043
$Zn_{1-x}Cu_xGeF_6.6H_2O$, depression of dynamic Jahn-Teller effect 77−16164
$Zn_xFe_{3-x}O_4$, ferromag. reson., g-factors, Jahn-Teller ion effects 80−66043
$ZnMn_{1-x}Cr_xFeO_4$, Mossbauer effect, quadrupole splitting 80−29664
ZnS:Co, Jahn-Teller interaction energy determ., piezospectroscopic expt. *(Russian)* 77−4623
ZnS:Co Mossbauer source, Fe^{2+} abnormal populations and vibronic props. 80−15912
ZnS:Cr, anomalous temp. depend. of near IR absorption 79−28794
ZnS:Cr^{2+}, Cr^{2+} $^5T_2$ and ^5E states, Jahn-Teller effect calcs. 80−39539
ZnS:Cr^{2+}, Jahn-Teller interaction energy calc. 78−2455
ZnS:Cu^{2+}, Jahn-Teller effect, stacking faults and formation of polytypes, absorption and emission spectra 77−4660
ZnS:Fe^{2+}, low temp. Mossbauer spectra, in source and absorber expts. 77−28500
ZnS:Mn^{2+}, $^4T_1$ excited state, absorpt., MCD, Jahn-Teller model 78−43907
ZnS:Mn^{2+}, $^4T_1$ state, magneto-optical meas. 77−20833
ZnS:Mn^{2+}, $^4T_2$ level, Zeeman splittings, Jahn-Teller effect 80−40141
ZnS:Mn^{2+}, Jahn-Teller effect in fluorescent level 78−52566
ZnS(Se)(Te):$Ag^{2+}(Cu^{2+})$, absence of EPR spectra due to strong spin-lattice coupling of Kramers doublets 77−85181
ZnS(Se)(Te):Cr^{2+}, absorpt. and luminesc. of $Cr^{2+}(d^4)$, cryst. field theory interpretation 79−83000
ZnS(Se)(Te):Cr^{2+}, Jahn-Teller coupling 78−67997
ZnSe:Co^{2+}, depression of vibronic levels, transition of Jahn-Teller states from dynamic to static 78−43337
ZnSe:Cr, piezodichroism due to reorientation of Jahn-Teller centres 80−11363
ZnSe:Cr^{2+}, Cr^{2+} $^5T_2$ and ^5E states, Jahn-Teller effect calcs. 80−39539
ZnSe:Cr^{2+}, stress-induced alignment of Jahn-Teller centres 79−78651
ZnSe:Mn^{3+}, Jahn-Teller effect in fluorescent level 78−52566
ZnTe:Cr^{2+}, Cr^{2+} $^5T_2$ and ^5E states, Jahn-Teller effect calcs. 80−39539

jamming
see also clutter
digital frequency meter impulse noise effect on accuracy *(Russian)* 77−41575
nonlinear coded waveforms, optical signal processing 79−72517

jellies *see gels*

jellium
adsorbed atom on metal surface, Hellmann-Feynman theorem 79−95262
adsorbed CO, surface plasmon relax. energies 80−70537
adsorption of He on metal surface, HF calc. of repulsive pot. contrib. 77−43434
alkali chemisorption on metallic surface, calc. for jellium substrate 77−7975
atom near metallic surface, resonant state, Schrodinger eqn. soln., jellium model 78−80033
atomic chemisorption, chemical trends, core-hole relax. effects, jellium model 78−76909
atomic chemisorption on simple metals, chem. trends, core-hole relax. 78−14586
bimetallic adhesive force at small separation 77−35823
bimetallic interface energies 78−2545
bounded, linear response function in RPA 79−69444
CDW in two- and three-dimens. jellium, appl. to liq. He surface and semiconductors 80−65476
CDW system, attenuation of collective excitations 78−84157
chemisorbed atom on metal, core electron binding energy 78−10280
chemisorption, effective-medium theory of chem. binding 80−65367
chemisorption of H_2, contraction of mol. band 79−28202
chemisorption of H_2, interpreted by one-parameter analytic model 77−39735
chemisorption of H_2, simple model 77−69171
chemisorption of H on metal surface, relax. energies in UPS 78−91544
chemisorption of H on metal surfaces, linear response theory 78−91543
chemisorption of Li(H), simple model 79−60625
chemisorption on metals, self consistent jellium+adatom calc. 77−66093
coupling of molecules to surface plasmons in resonant elastic scattering 80−20102
DC electrical conductivity, microscopic fields and currents 78−56121
deformable jellium model, long-range order HF-type orbitals 80−2349
deformable-jellium model, self-consistent long-range order in terms of non-plane-wave HF states 79−19533
degenerate electron liquid, compression modulus, perturbative calc. 80−36942
diamond Schottky barrier, electronic struct., pseudopot. calc. 78−95364
diamond Schottky barrier, electronic struct., pseudopotential method, jellium model 79−38162
disordered alloy with strong impurity scatt., adiabatic approx. 77−66161
dynamic correlations, first-order perturbation theory 80−44527
electromigration, driving force, strong-coupling theory 80−65300

jellium continued
electromigration, driving force, weak charge solutions 79−55917
electron density profiles, pots. and charge overlap forces 77−32061
electron gas, ang. correl. in positron annihilation 80−24821
electron gas, two-dimensional, variational approach to ground state, CDW instability 80−39517
electron gas with surface, Green function theory, exchange and correlation effects 77−8164
electron liquid, local field factor, freq. depend., dynamical exchange effects 80−29342
electron solid in superstrong mag. field, bifurcation theory approach 80−4640
electron transport, local electric field, appl. to electromigration 78−30896
finite step potential model, response function 77−1466
graphite intercalation cpds., dispersion relations of intercalate modes 80−34379
image charge pot. at interface of two semi-infinite media, Thomas-Fermi soln. 79−87155
impurities and photoexcited ions in metal, jellium model 80−39523
impurity interactions in pseudo-molecule form. 78−47735
inhomogeneous electron gas at jellium surface, exchange energy 80−10901
inhomogeneous strain effects on surface props., rel. to fracture model development 77−72907
liquid metal, surface ion density, nonmonotone, perturbative discrete ion introduction into jellium 78−72222
metal, H and He impurities, electronic struct. 78−10402
metal, secondary electron emission, Monte Carlo calc. 79−69932
metal, surface energies and work function, simple analytic model 80−49862
metal, surface props. in linear pot. approx. 77−43689
metal, surface region, absorption of EM radiation 78−43456
metal, work function changes on single crystal planes 79−99604
metal adhesion to ionic surface 78−18914
metal superconductivity with an account for ion core repulsion *(Russian)* 79−11260
metal surface, effect on ground state of approaching H atom 77−35979
metal surface, hydrodynamic model of linear response, nonretarded limit 80−44526
metal surface, indirect long-range oscillatory interaction between adsorbed atoms 78−71997
metal surface, integro-differeneial eqn. for electron density and formula for surface tension of jellium 80−44689
metal surface, nonlocal density based self consistent surface calc. 77−72898
metal surface, step potential model, static semiclassical response of bounded electron gas 78−72221
metal surface, virial theorem for jellium model 79−60892
metal surface densities, electronic density, variational calc. 79−15205
metal surface energies, variational calc. 77−24603
metal surface energies in infinite and step-pot. approx. 77−47876
metal surface exposed to external radiation, solns. of Maxwell's eqns. 78−52054
metal surface interaction with external mol. complex 79−47140
metal surface props., Rayleigh-Ritz variational calcs. 79−69570
metal surface props. in square barrier and linear one electron potential model 79−19645
metal surfaces props., statistical calc. 80−24987
metal work function temp. depend. 79−78154
metal-metal junction, effect of non-local exchange correlation pot. on charge density profile and electrostatic pot. 77−28239
metallic film, electron density and potential, variational calc. 79−78218
metallic films, interacting, surface pot. 78−30968
metallic sphere, very small, surface plasmon dispersion, RPA 77−47886
metallic surface, corrections to local density approx., gradient expansion vs. wave-vector analysis 77−51796
metallic surface, exchange-correlation energy, wave-vector analysis 77−47877
metallic surface, self-consistent electron theory, review 80−88616
metals, adhesion theory for two surfaces 80−20270
metals, density of states and spin susceptibility, normal and giant surface effects 78−10322
metals, free-electron-like, electron struct. of single and interacting H impurities 79−95365
metals separated by dielectric, electronic component of metal-metal interaction force, calc. 78−52056
nontransition metals, jellium approach to vacancy energetics 78−47347
one component plasma, mag. props. 79−86558
one-dimensional, wall effects 79−46468
oscillating dipole-metal surface interaction, jellium model and random phase approx. 80−92955
phenomenological theory of first- and second-order metal-insulator transitions at absolute zero 79−69420
proton in jellium, self-consistent screening 78−2441
pycnonuclear reactions, and pair correl. function in dense plasma 78−32445
rare earth atoms at surface, photoionisation of 4f electrons 78−11077
residual resistivity of vacancies 78−6348
Schottky barrier theory at jellium-semicond. interface, role of ionicity, pseudopot. method 77−47888
screening of light impurities 77−85177
screening of proton, Anderson model calc. 80−59895
simple metals, atomic chemisorption, atom-jellium model 78−84066
static dielectric function exam., Wigner distrib. function 77−66132
surface, adsorbed H, charge density oscills. and adatom-adatom interaction 79−42389
surface, H_2 chemisorption, self-consistent calc. 79−95260
surface, interaction with H_2 80−29259
surface, review of electronic struct. calcs. 77−28226
surface, spin susceptibility, density-functional approach 77−90011
surface energy of metals 78−91528
surface phase shift rule, and density of states 78−2538
surface photoelec. effect, surface photoemission spectroscopy on jellium, appl. to Al 79−4900
surface props., statistical calc. 79−60897
surface-atom polarisability derivation from field-ion energy deficits 80−76155
vacancy formation energies and volumes, exam. of models 78−47349
vacancy formation volume, self consistent electron theory 77−89426
vacuum interface, charge distrib., nuclear density profile 78−30962

jellium continued
work function calc. 79−65536
Ag film, chemisorption effects on optical reflectance and elec. resistance, jellium model surface 79−33361
Ag film, evaporated, chemisorption effects on reflectance and elec. resist. 80−11495
Al (001), enhanced photoexcitation 80−80937
Al, alkali metal adion-surface interaction energy, density formalism calcs. 78−68069
Al, chemisorption of H_2, calc. of bond lengths vibr. freq. and activation energy 79−46953
Al, one-electron calcs. of X-ray absorpt. and emission, jellium model 78−56543
Al:H, impurity energies and geometrics, self-consistent jellium calc. 79−99507
Cs, soft X-ray outer-shell absorption and emission, one-electron calc. 79−69904
Ge, Schottky barrier, electronic struct., pseudopot. calc. 78−95364
Ge Schottky barrier, electronic struct., pseudopotential method, jellium model 79−38162
K, soft X-ray outer-shell absorption and emission, one-electron calc. 79−69904
$K:F^-$(Ne), ground states and core hole states, self-consistent soln. using density functional formalism 79−69467
LaB_6, work function, thermionic emission charact., jellium model 77−8710
Li, one-electron calcs. of X-ray absorpt. and emission, jellium model 78−56543
Mg, one-electron calcs. of X-ray absorpt. and emission, jellium model 78−56543
Mg:H, impurity energies and geometrics, self-consistent jellium calc. 79−99507
Na, adsorbed on Ni, substrate, hybridisation between s and p resons., jellium model 80−6932
Na, impurities and photoexcited ions 80−39523
Na, one-electron calcs. of X-ray absorpt. and emission, jellium model 78−56543
$Na:F^-$, ground states and core hole states, self-consistent soln. using density functional formalism 79−69467
Pd-H sytem, electronic struct. of H, mol. cluster and pseudojellium models 80−24832
Rb, soft X-ray outer-shell absorption and emission, one-electron calc. 79−69904
W, alkali metal adion-surface interaction energy, density formalism calcs. 78−68069

jet stream *see atmospheric movements*

jets
see also plasma jets; sprays
abrasive, parameters affecting particle velocity 77−65788
acetylene-air flame, eddy entrainment and combustion in depth process, three-region model 79−100384
acoustic flow noise with fluid dilatation as source fluctuation, causality correlation analysis 79−72742
acoustic gas-jet generator, HF high-intensity 79−64376
acoustic noise, directivity, peak spectra freq., and Strouhal no. *(Japanese)* 78−9489
acoustic noise, large-scale struct. importance 78−94792
acoustic noise, shear layer instability effect 78−94791
acoustic noise, shear term role 77−72114
acoustic noise, two-point correlations, comments and reply 79−32492
acoustic noise diagnostics, spurious sound generated by hot-wire turbulence interaction 80−33304
acoustic oscillations, effect on laminar to turbulent flow transition 80−14656
acoustic pipe entrance, experimental study of vel. field *(French)* 80−33395
acoustic power distribution in a turbulent jet 78−67238
acoustically active turbulent structs. in cold subsonic jet, conditional sampling anal. *(French)* 79−18881
acoustically excited jet, discrete noise spectrum, vortex pairing 80−74847
adiabatic, spatial form 79−46284
adiabatic jets with inclined barriers, interaction 79−94694
aerodynamic noise, acoustic interference effects and role of Helmholtz number 79−94392
aerodynamic noise, generation by jets and boundary layers *(French)* 79−81867
aerodynamically generated noise *(French)* 77−75951
aerodynamics and mass transfer for jet entering fluidised bed 80−14809
aerofoil with jet flap, incompressible flow past 78−59414
aerosol coagulation and diffusion in turbulent jet 79−23355
aerosol fractionator for large-scale sampling, impacting jet system 77−9140
aerosol jet, turbulent, normalised radial conc. profiles meas. using laser-Doppler anemometer 77−84311
aerosol particle-size classification by opposing jets, secondary effects 79−70383
Agulhas Current, topographically induced changes in struct. of inertial coastal jet 80−72545
air, axially symmetric, velocity field in tube entrance region 80−38471
air, effect on high-voltage spark spectroscopic light source 80−3441
air, injected horizontally into liquid metal, Hg, physical behaviour 77−3857
air, interacting two-plane parallel jets, turbulence props., hot wire meas. 80−14767
air, subsonic, fully pulsed, near field vel. meas. 80−19540
air entrainment in water jet impinging vertically on water surface 80−14772
air flow, turbulent, in infinite medium spatial speed distrib. *(Rumanian)* 80−53826
air in supersonic nozzle, shock activation with overexpansion, jet form. 78−18330
air jet, heat transfer coeff. for quenching of hot plate 77−47053
air jet, heated, turbulent, discharged downward, temp. profiles 79−27677
air jet, vertical axisymmetric buoyant, profile meas. 78−90906
air jet/piston dynamical interaction pressure transducer errors 77−80245
air jets, free and constrained, acoustic emission, gas leak detection conditions 80−5895
air jets with suspended polystyrene spheres, effect of particle proximity on drag force 80−96306

jets continued
air wall-jet immersed in uniform flow, aerodynamic forces on circular cylinder 77−62287
air-bubble two dimens. plume, anal. 78−1715
airblast atomizer, drop size 78−3375
aircraft jet noise reduction test facility 77−845
aircraft jet noise reduction test facility 77−11096
airfoil noise measurement for high Reynolds numbers, investigation using adjacent plane jets 80−28372
alkyl benzenes, jet-cooled, intramol. vibr. relax., reson. fluoresc. and excitation obs. 80−14152
amorphous metal ribbon form. by cylindrical jet on flat moving substrate, uniformity 78−52718
AMTE/OUEL underwater jet noise rig, working report for 1977/78 80−79286
AMTE/OUEL underwater jet noise rig, working report for 1978/79 80−79287
annular, conditions for self-excitation of oscills. 78−94782
annular, discrete freq. noise generation props. and flow pattern 77−51092
annular, initial region, with or without central bullets 78−34173
annular, small inner diameter, investigation of vortices by schlieren photography 80−74935
annular jet, outer mixing region coherent structs. 79−32613
annular jet inner regions, jet and wake vortices 79−86479
aortic coarctation distal flow profiles 78−44528
arc, plasma, of free jet laminar core, axial flow, strong localised disturbance effect 78−91178
arc column in free turbulent jet, electric field strength 80−49021
array, propag. in bounded drift flow 77−84288
array of jets, thermal diffusion downstream meas. 78−94785
array of jets impinging surface, convective heat transfer 78−90953
asymmetric two dimensional jet efflux, from channel, two-jet three end plate problem 77−39319
atmosphere, hydrodynamical model of inner struct. of planetary jet stream *(Russian)* 77−64371
atmosphere asymmetric jets, instability 80−56537
atomic beam, produced from He nozzle flow, high speed ratio 80−5636
atomic beam production, He skimmed from freejet zone of silence 80−5635
atomisation of liquid by impinging jets, expt. and theory 78−87373
atomizing jets, ultra-high speed filming 79−68777
attached, turbulence and random switching anal. *(Japanese)* 79−68779
attached jet characteristics, aspect ratio effect *(Japanese)* 80−87791
axially symmetric, impingement on plate, heat transfer characts. inner peak in heat flux 80−28540
axially symmetrical turbulent free jets, in wind tunnel, higher order moments measurement *(German)* 80−33648
axisymmetric, counterflow problem, num. soln. procedure 77−58757
axisymmetric, turbulent mixing of gases with different densities 77−58749
axisymmetric, vel. distrib. and swirl effects, low speed results 79−46351
axisymmetric and flat jets, heat transfer in vicinity of stagnation point, turbulence effect 80−48697
axisymmetric free shear flow with Reynolds stress closure 80−19469
axisymmetric impinging jet, transfer characteristics at conical surfaces 77−3889
axisymmetric isothermal jet, flow at low Reynolds number *(Russian)* 78−47007
axisymmetric jet, interaction with plane obstacle, Navier-Stokes eqn. solns. *(Russian)* 80−1659
axisymmetric jet array from perforated plate, axial vel. semiempirical calc. 80−48757
axisymmetric jet flows, appl. of Meksyn's method 79−64729
axisymmetric jet of magnetisable fluid, stability 80−14835
axisymmetric jets, coherent structs. using optical technique, convection vel. 80−69888
axisymmetric jets and wakes, calc. with turbulence model 78−67239
axisymmetric laminar jet diffusion flame, split operator finite difference solns. 78−51252
axisymmetric subsonic and supersonic, in parallel stream, turbulence meas. 77−31349
axisymmetric swirling jets, stationary flows in surrounding inviscid medium *(Russian)* 80−69892
axisymmetric turbulent, impingement region, model 77−42886
axisymmetric turbulent impinging, mass transfer 77−42887
axisymmetric turbulent jet initial region, annular free shear layer 80−106826
axisymmetrical jet of viscous incompressible fluid, absorption effect *(Russian)* 78−1711
axisymmetrical two-phase jet, integral method for calculation *(Russian)* 78−47023
axisymmetry jet, inblow parameter effect on separation, boundary layers and heat transfer *(Russian)* 80−24064
base flow at supersonic vel., rockets and re-entry vehicles appl. 78−67243
benzene, $^1B_{2u}(\pi\pi^*)$-$^1A_{1g}(6_0^1)$ band, in supersonic jet, rot. anal. 79−31578
Bickley's jet, nonparallel effects on stability 79−46356
binary gas mixture, vel. slip and temp. difference in free-jet expansion 80−14774
bluff buoyant jets, laterial temp. distrib. profile 79−1224
blunt body problem in nonuniform flow fields 78−5748
blunted solid of revolution in gradient flow, shock wave form *(Russian)* 79−64697
boiling, forced-convection, burnout 78−38378
boiling burnout, for heaters cooled by liquid jets 79−59979
Bose-Einstein statistics, wave packet formulation of multiparticle production at high energies 80−13338
bottom flow control of liquid around sphere with peripheral annular jet *(Russian)* 79−77204
boundary layer in stratified medium, shear flow 79−64736
boundary layer separation from wall, nature of reversed flow 77−75956
bounded coaxial jets, convective heat transfer in turbulent mixing, swirling 80−64541
break-up effect of nonlinear concentration profiles on jets undergoing mass transfer 80−79371
bubble collapse and jet formation in vicinity of wall, effect of polymer additives 79−81956
bubble condensation, in subcooled liquid, high-speed photographic study 78−42654
jets continued
buoyant, turbulent in cross flow, finite difference method 78−90907
buoyant jet entrainment from single and multiple sources, rel. to draft cooling tower 79−32617
buoyant surface jet, 2-D flow props. *(Japanese)* 80−48762
buoyant surface jet, entrainment intermittancy props. at stratified interface *(Japanese)* 79−81940
buoyant surface jets analysis for heated plume characts. prediction 77−15087
buoyant surface jets of incompressible fluid, turbulent energy balance appl. 80−38469
bursts in turbulent shear flow 77−11178
n-butane, freejet flow, vibr. relax. time 79−98760
n-butane-CO_2, freejet flow, vibr. relax. time 79−98760
cantilever pipes, internal flow induced instabilities 78−63496
capillary instability, determ. of dynamic surface tension of inks 78−84031
capillary jets, flow and instability of jets interacting with surrounding medium 80−6110
capillary oscillations, meas. 80−96291
catchment areas, large, jet flow similitude *(French)* 79−66423
cavitating flow past jet-flapped second-order theory on wall effect 77−42879
centrifugal injectors, submerged flow characts. 77−58701
chemical reaction in turbulent jet, light probe meas. 77−62310
chordal jet mixing in transverse flow 78−5779
circular air jet, zero entrainment, vel. field 78−51213
circular impinging jet, heat transfer characts., stagnation point, boundary layers 80−79303
circular jet, turbulent shear layer, shear fluctuations 79−81936
circular jet asymmetry in flowfield and surrounding acoustic field, turbulence characts. 79−77197
circular jet coupled with whistler nozzle, formula for acoustic resonance freqs. 79−72741
circular jet staggered array with crossflow, heat transfer characteristics 80−6057
circular jet turbulence under suction conditions *(Bulgarian)* 78−59437
circular jets with crossflow, inline and staggered arrays, heat transfer coeff. variations 80−74873
circular semi-infinite liquid jet, harmonically forced at nozzle, instability and wave propagation 79−32618
circular turbulent jet in transverse flow, inlet section 79−94690
closed-circuit water jet pump construction 79−67272
cluster beam, nozzle flow formation and detection, high energy beam 80−5638
Coanda effect, potential model 79−77198
Coanda effect in water jet, cavitation effect on wall-attachment element *(Japanese)* 77−39321
Coanda effects, simulation of discontinuous diffusing flow 78−9622
coaxial, analysis for method of superimposition momentum fields 77−58805
coaxial, correl. covariance meas. in initial region 77−84289
coaxial, initial swirl of inner and outer flows effect on aerodynamics 77−68652
coaxial air stream, self-oscillatory liquid film flow regime 79−86498
coaxial annular jet, in circular tube 78−9667
coaxial jet, aeroacoustic characts., sound power spectral density 77−62285
coaxial jet, Raman scattering diagnostics of turbulent flow field 78−18328
coaxial jet noise and isothermal jets 79−86423
coaxial jets with and without swirl 80−48759
coaxial round, turbulent mixing, eddy Reynolds number var. 78−75179
coaxial round jet turbulence characts., obs. 78−87372
coaxial suction jet, pneumatic gauging system 80−9001
cocurrent flow, jet initial zone, boundary mixing layer turbulisation, fluctuations 80−1657
coherent structure 80−10282
coherent structures in coflowing jets and wakes, strobing laser beam visualisation 79−32610
cold subsonic coaxial jets, emitted noise *(French)* 79−37308
colliding gas-slurry jets, dispersed material motion, numerical anal. *(Russian)* 79−32653
colliding supersonic coaxial underexpanded, investigation of flow 78−67237
combustion in laminar diffusion gas jets, computation of diffusion flare 80−10276
combustion of opposed gas-air jets, convective heat transfer 79−72960
compressible and incompressible flows, recent theoretical and expt. developments, book 80−1620
compressible hodograph eqn., numerical soln. 79−60042
compressible laminar wall jet 80−28542
conduit with lateral outlet, two-dimens. flow past barrier 80−64642
cones, axisymmetric impingement of supersonic air jets, shock pattern 80−48741
confined, flow pattern and turbulence quantities prediction *(Japanese)* 79−18923
confined burning jet, droplet vaporisation, expt. and theory 78−94855
confined coaxial jet, mixing region, simultaneous laser measurements of instantaneous vel. and conc. 77−35287
confined coaxial jets with and without swirl, vel. characts., recirculation regions 80−103055
confined jet, instability modes, visualisation using laser-induced fluoresc. 77−35283
confined turbulent coaxial jet, vel. characts. 80−64601
continuum source particle beam properties, comput. modelling 80−26062
contraction ratio of horiz. jets, vel. profile effect 77−31353
contrary wall jet, interaction with supersonic flow on plate with turbulent boundary layer *(Russian)* 78−22398
control jets, gasdynamic features, 3-D subsonic and supersonic flows 80−6112
controlled break-up, droplet prod. by imposed flow perturbation 77−68667
controlled disintegration in melts, for equal-sized spherical particles prod. 80−7515
controlled perturbation of circular jets, smoke visualisation 78−90956
convective heat transfer from a confined jet in a centrifugal force field 79−98720
convergent supersonic jet, wave struct. in interaction with infinite 2-dimens. obstruction 77−55064

jets continued
converging bi-conical pipe, 3-dimensional internal blocking *(French)* 79−50751
convex wall jet, characterisation of external boundary, indentation lengths and velocities at interface *(French)* 78−1705
cooling of metal plates, heat transfer coeff. 80−10107
core noise and jet noise separation, mean square pressures 80−69779
core noise from gas turbine exhausts 78−13850
corona discharge, force exerted on electrode 77−19803
correlation techniques to detect azimuthally coherent structures 80−53765
cross stream injection boundary layer, flow and temp. field 79−1225
cross stream-jet mixing, near field influence on mass, momentum and vorticity fluxes 77−39320
cumulative jet form. on cavitation of deformed bubble near wall 77−934
curvature in bounded crossflow with stagnant zone 79−46355
curved jets, deflection due to impact of other jets *(German)* 78−26180
curved surface impingement 78−14051
curved wall power fluidics characts. 80−103053
cyclic liquid jet production in pulsating bubbles 80−33640
cylindrical channel, sudden expansion of supersonic jet 80−48800
density distribution for free supersonic jet emerging against pressure difference *(German)* 80−1666
diatomic gas, transient flow, temp. and conc. profiles, by rot. Raman scatt. 77−75995
die swell problem, free surface separation 79−90295
dielectric jet with plane laminar flow, waveguide effect stability, anal. *(Russian)* 77−7546
dielectric liquids, electrical convection and jet flow 80−1692
diffuser, stream struct. meas. by laser Doppler anemometer 79−86477
diffuser efficiency, fine turbulent jet injection at outlet sections 78−1707
diffusion flames, blowout and attachment mechanisms 79−72957
diffusion of jets in cross flow 79−27674
diffusion pump jet assembly and vaporiser design optimisation 78−81999
discharge into flaming ambient fluid, model of plume rise 80−7973
discharging into quiescent ambient, finite difference anal., turbulence modelling 78−30332
discrete-hole cooling, near-field character of jet discharged normal to main stream 77−15088
discrete-hole cooling, three-dimens. num. prediction for laminar flow case 77−15089
dispersive compressible fluid, steady two-dimens. jet flow 80−64598
dissipation rate for turbulent plane and circular jets 80−69889
driven mixing layer of circular jet, turbulent static pressure fluctuations spectra 79−77195
drop formation, continuous phase mass transfer, perforated plate extractor column design 79−90299
drop formation in a circular liquid jet, book contrib., review 80−19467
droplets, atomized, polydisperse system, nonisothermal vaporisation, algorithm for calc. vaporisation parameters 80−48782
droplets from bursting bubbles at air/water interface, electrification and size 77−48700
dual jet discharged into rectangular duct, flow and heat transfer 80−43751
duct noise radiation, aircraft turbojet and turbofan engines 80−23834
dust laden jet, particle turbulent diffusion 78−83455
dye laser jet stream, thickness meas. in real time, by optical technique 78−82975
dynamic liquid surface tension determ. from drop oscillation frequency and capillary jet instability 78−56026
dynamic surface tension, meas. by excited capillary jet axisymmetric disturbance growth rate 78−95205
dynamics and wave propagation 80−19464
eddies, large, in axisymmetric jet, harmonic forcing, modelling 78−90957
eddies, large, numerical model for axisymmetric jet 80−79375
edgetone oscillation analysis *(Japanese)* 79−10599
edgetone sound, prediction of amplitude 80−74568
EHD, numerical anal. of two unipolar jet interaction *(Russian)* 77−39352
EHD flow, return currents 79−86521
EHD transducers, jet turbulization by EHD action *(Russian)* 77−24031
EHD vortex convertor, power jet distrib. stage anal. calcs. *(Russian)* 77−7470
elasticoviscous capillary jet stability 79−90303
electrically conducting plane and annular, in axial mag. field, instability 77−35247
electrically driven jet, charge distrib. and forces 79−77268
electrogasdynamic jet, approx. calc. *(Russian)* 77−19641
electrohydrodynamic convertor or nozzle for jet printer, output parameter exact solns. *(Russian)* 78−75230
electrohydrodynamic flow of plane jet, conducting dielec. liq. in nonuniform field 79−77275
electrolyser, rotating, flow field 79−52682
electrostatic ink jet drop formation characteristics *(Japanese)* 78−25766
elliptical cross-sections, steady motion 77−72340
elliptical water jets, stability and noise 78−38377
engine exhaust noise, orderly struct. as a source 78−94786
engine exhaust noise, source coherence 78−94787
entrainment at density interface in thermally stratified vessel 80−6119
entrainment in turbulent jets and plumes 78−94781
entrainment mechanism 78−1649
entrainment mechanism 79−41721
Erlangen windowless high density gas target for nuclear scattering experiments 79−54735
erosion with plain jets and jets with cavitation inducers 79−15805
evaporation by air jets, hydrocarbons on surface 79−72919
excess noise from supersonic underexpanded jets in flight 80−69815
excited jets, aerodynamic characterisation of broadband noise amplification 79−32491
exhaust jet, swirling, noise and flow characts. obs. 77−75950
exhaust noise, role of shear-layer instability waves 77−47054
expansion into uniform counterflow, conf., Haifa, Israel, (July 1977) 79−15683
expansion into uniform counterflow boundary layer approx. 79−14445
extruded polymer soln. through capillary, flow instability and electrostatic effects 79−60035
fan jets with swirling, self-similar soln. 78−90950
fibre suspension in water, turbulent jet, analogous behaviour to polymer solns. 78−1732
film cooling effectiveness 78−14052

jets continued
flame, diffusion type, oppositely directed jets, elec. props. 78−56896
flame, free-jet diffusion type, ionis. meas. and combustion progress 80−30238
flame, laminar jet diffusion flame size prediction, Burke-Schumann theory extension 78−14096
flame, laminar jet diffusion flame size prediction from diffusion coeff. 78−14097
flame, round jet type, mass exchange between recirculation zone and outer flows, stabilisation 80−14842
flame jet, premixed, impinging on plane surface, turbulent heat transfer 79−4054
flame quenching, by narrow cylindrical passage 78−15674
flame stabilisation in subsonic and supersonic flows 78−34206
flame stabilisation mechanism in two-phase fuel-air mixture flow 79−81996
flames, multi-diffusion configurations 77−51134
flat and axisymmetric, submerged in incompressible fluid, calc. using turbulent energy balance eqn. 77−47051
flat surface, jet impingement, rotational flow model calcs. 80−64596
flow, slotted test sections, inviscid theory of wall interference 78−9665
flow around cylinder 79−64725
flow around thermally insulated porous surface, optimal suction from boundary layer 77−35123
flow characteristics for jets normal to the crossflow 80−64597
flow field during screech 77−15086
flow field meas., near nozzle outlet using laser Doppler anemometer 80−28582
flow hydrodynamic model, three-dimensional 80−79369
flow in porous layer 77−39341
flow noise anal. 78−1654
flow past airfoils with oscill. jet flaps, quasisteady theory 78−63467
flow patterns within confined jets, turbulence models 79−64720
flow visualization of cavitation in water jets and nuclei distribution measurement by holography 80−106862
flowfield behind laser-supported detonation wave 78−26171
fluidised bed, gas blowing from orifice to fluidised bed 80−1678
fluidised bed, heat transfer enhanced by turbulent jet 79−72940
fluidised bed, jet and bubble formation 77−84318
fluidised bed, plasma jet cooling mechanism 78−79371
fluidised bed, quasisteady axisymmetric jet 78−83470
fluidised bed, steady vertical jet discharge 77−65789
fluidised bed discharge, bubble form. and growth 77−47084
forced convection in two-phase flow from jets, mass transfer near interface *(German)* 80−53782
free, aeroacoustic characterisation *(French)* 79−41727
free, coefficients of eddy diffusion, rel. to mean scalar quantity 77−84287
free, heated, turbulent, high temp., eddy diffusion, methane combustion obs. 78−30329
free, streamlines and local velocities in rarefied atm. 77−42884
free annular jet with finite radial dimens. under entrainment conditions, initial part 79−98772
free boundary capillary MHD flows 80−43794
free boundary layer turbulence, calc. of mean and fluctuating characteristics 79−72885
free gas jets, acoustic field emission *(French)* 78−42595
free jet, homogeneous nucleation of clusters, noncryst. struct. *(French)* 78−79760
free jet, into rarefied chamber *(French)* 79−7395
free jet development, turbulence effects *(German)* 77−84291
free jet dynamic response investigation 77−37842
free jet expansion from laser vaporised surface 78−1703
free jet flow after slit orifice determ. by quasi-stationary rheoelectric field analogy 79−27675
free jet silencing, operational engineering principle *(French)* 79−32494
free jets, concentration probability distrib. function by laser-scatter technique *(German)* 79−64732
free round cold subsonic jet, noise from axisymmetric shear flow, numerical results 79−77206
free round cold subsonic jet, noise from axisymmetric shear flow, analytical results 79−77207
free shear flow, appl. of multiscale transport model *(French)* 79−50763
free shear layer transition of circular jet, wave development 78−94643
free turbulent flow of incompressible liquid, self-consistency of expt. data 80−6031
free turbulent jet directed against a flat surface, phenomena accompanying the impact, diversion, and distribution *(German)* 80−106827
free-jet expansion of N_2, expt. tests of energy balance eqn. 79−98777
Freon electrohydrodynamic flow, jet dynamic pressure obs. *(Russian)* 80−59117
freshwater, jet in salt water laboratory exptl. results on mixing *(Russian)* 77−68654
galaxies, accretion wake model of radio jets *(Japanese)* 79−84857
gas, absorbing and radiating, soln. of one-dimensional transfer eqn. by discrete ang. subdivision method 77−35256
gas, acoustic wave generation, Hartmann whistle 80−87695
gas, nonstationary, wave structure and density distrib. 77−62286
gas, terminal speed ratio in spherical source expansion 77−84285
gas, transient section and position of turbulent zone *(Russian)* 78−47010
gas, visualisation by laser induced I_2 molecular fluorescence 77−80257
gas bubble dynamics in turbulent jet 79−41741
gas bubbles, on liq. surface, bursting, jet and droplet form., math. model *(German)* 77−24012
gas conc. profile determ. by laser Raman optical multichannel analyser 78−73098
gas diffusion in supersonic jet 79−32604
gas distribution in a deep granular bed injected by flat jets 80−19501
gas ejector, energy separation 79−68774
gas ejector, energy separation mechanism *(Russian)* 78−34178
gas flow in duct, self-excited oscillations 78−55670
gas flow to liquid jet mass transfer 80−53827
gas injection into liquid stream, heat transfer rates 78−14075
gas injection technique, rapid response, design 78−94865
gas jet, heat transfer to porous baffle 79−98776
gas jet blowing into supersonic flow without 3-dimens. boundary layer separation, nozzle shape 80−100009
gas jet discharge into stationary bed of granular material 77−42905
gas jet expsn. into vacuum, rot. relax. 79−32625
gas jet injection into liq. in tank, math. model 78−63473

jets continued
gas jet source, emission spectrographic analysis appl. *(French)* 79−34390
gas jet system for meas. of fission product decay props. 77−88364
gas jet-liquid bath interaction for different degrees of assimilation during blowing 80−43754
gas jets, laminar homogeneous, combustion process *(Russian)* 78−94850
gas layer impact against obstacle at very high vel., plasma heating and radiation 80−19602
gas leakage effect on jet characts. *(Russian)* 79−68780
gas mixture-isotope inertial gas-kinetic separation 80−69927
gas mixtures, background gas penetration into underexpanded jets, densitometric obs. 79−94655
gas mixtures, velocity slip in free jet expansions 79−94656
gas mxitures, velocity slip in free jet expansions 78−90951
gas stream distrib. near plane jet in granular layer 79−14471
gas-jet generators, operation at elevated pressures 79−32616
gas-jet sound generator, Hartmann type, influence of jet temp. on characts. 78−51025
gas-liquid system discharging from nozzle, phase slip *(Russian)* 77−55067
Gaussian circular jet with normal impingement, velocity field 77−47057
granular layer, bubble coalescence for jet injection under constrained flow conditions 77−89197
Guderley's transonic small disturbance equation, exact solns. 80−19315
gun tunnel flow, Mach 7 jet, anal. of hot wire anemometer signals 78−14054
hadronic reactions, trajectory slopes in gauge-dual-topological approach, jet multiplicity 80−18142
Hartmann-Sprenger tube, air jet from convergent nozzle, air column oscillations generative mech. 80−14828
Hartmann-Sprenger tube, thermal effects, finite difference method for analysis 80−14771
heat exchange between jet and obstacle, turbulence effect *(Russian)* 80−1579
heat exchange of concave surface, with single jet in crossflow 80−1661
heat transfer and hydrodynamics of an array of round impinging jets with one-sided exhaust of the spent air 80−79374
heat transfer during impingement on sphere or cylinder rel. to turbulence *(Russian)* 78−38327
heat transfer in wall jet with vectored surface mass transfer 78−26174
heat transfer of impinging jet on rotating disc 78−30394
heated, temp. fluctuations in turbulent flow, ramp model 77−3819
heated circular jet, outer part, temp. and vel., simultaneous meas. errors 80−87830
heated disc with impinging jet, saturated forced convection boiling, CHF upper limit 79−81891
heated planar jet, turbulent diffusion, second-order closure anal. 77−39364
heated round turbulent jet, in coflowing stream, vel. and temp. profiles 77−27569
heated turbulent jet, local isotropy and large structs. 80−6116
heated turbulent round jet, intermittency in free turbulent shear flows 80−19348
heated water jet impingement melting, cavity formation, expt. and simulation 78−95133
heavy isotope separation using nozzles, jets and channels, investig. 79−94097
heavy laminar jet flowing into nonmixing medium 78−51212
heavy species velocity, in low density supersonic free jet 79−94754
helical disturbances amplification in round jet 77−68655
helical instabilities of slowly divergent jets 79−68776
high-temperature supersonic jet, noise spectrum 79−94691
high-velocity gas jets, interaction, photographic study 78−42695
hole with sharp edged inlet, gas discharge jet, contraction ratio 80−48758
hollow drop production by injection of gas bubbles into liquid jet and US excitation 78−1710
horizontal cylinder with different end temps., natural convection, jets 80−99996
horizontal five-layer jet instability 78−79348
horizontal jet penetration in stratified fluid, unsteady laminar flow 77−7430
hot jet, crossed beam technique for characterisation of noise sources *(French)* 77−35284
hot jet mixing, heat diffusion as source of aerodynamic sound 77−7382
hot surface quenching rate, countercurrent single- and two-phase flow effects 78−59451
hydrocarbon vapour, spontaneous condensation in submerged turbulent jet 79−64721
hydrodynamic cumulation regimes during lining collapse, cumulative jet 80−69891
hydrodynamic sound generation mechanism 79−32172
hydrodynamic stability of liquid films and jets, effect of soluble surface-active substances 80−6027
hydrodynamics conditions for jet heat transfer, impact model 78−83447
hydromagnetic capillary instability of a liquid jet with an axial flow 80−74990
hydromagnetic free jet boundary layer equations, similar soln. 79−50811
hypermixing nozzle in thrust augmentor, three dimens. turbulent mixing 78−51214
hypersonic, high temp., noise rel. to gas parameters *(Russian)* 79−32132
hypersonic liq., moving into gas, shock layer anal. 78−26177
ideal fluid jet theory for free plane and axisymmetric jets 80−6117
ideal gas flow, choked and supercritical, through orifices and convergent conical nozzles, numerical soln. 80−38474
ideal radial free jet, nozzle length effects 80−14768
immersed nozzle, liq. gas discharge processes 78−83451
immiscible liquid-liquid system, laminar jet, vel. profiles and form 79−64752
impact jets system, with unilateral flow outlet, local heat exchange *(Russian)* 79−64730
impact on flow around rectangular projection *(Russian)* 77−65777
impact system with unilateral outlet, air flow, heat exchange *(Russian)* 78−83449
impingement calculations by finite element methods 80−28541
impinging, eddy struct. effect on heat transfer 79−1227
impinging free shear layers, self sustained oscillations, book contrib., review 80−19466
impinging jet cooling on heated plate, surrounding fluid effect 78−79350
jets continued
impinging jet flames, stabilizing limit 77−89177
impinging jet flow, efficiency of Navier-Stokes solvers 77−58632
impinging jets, heat transfer, appl. to compact heat exchangers 79−1071
impinging on concave semi-cylinder surface, heat transfer, theory and expt. 78−94794
impinging slot jet on surface, mass transfer coeff. 79−32606
impinging wall, heat and momentum transfer, approx. solns. 79−60041
impringement flow, skin friction and heat transfer meas., hot and cold-film sensors 77−27629
impulse drive jet used in character printing, model for fluid ejection and refill 77−68656
inclined turbulent jet exhausting from flat plate into turbulent subsonic crosswind 77−42885
incoherent jet noise line source, for scale modelling *(Japanese)* 80−33337
incompressible power law fluid, laminar flat radial jet 79−64731
inert gas supersonic jets as vacuum UV source 77−75639
inertial confinement targets, hollow H_2 droplet prod. by acoustic excitation of superheated liq. H_2 jet 79−85766
injected into lifting wing-shed vortex, modification effect 78−63434
injector mixing chamber, flow field 78−34175
injector with distrib. multijet liquid supply, efficiency and performance 80−74939
ink jet drop formation, scale model 77−75952
ink jet droplet charging, math. model 79−50184
ink jet nozzle flow, 100:1 scaled-up model 77−75957
instabilities in planar and cylindrical jet streaming rel. to glassy alloy casting 80−35129
instability induction, by corona discharge, use in automatic systems *(Russian)* 77−11269
integral relns. for jet in wake flow *(Russian)* 79−77202
interaction in deflecting stream of incompressible liq. 79−81932
interaction of liq. jet with confined wet entraining vap.-liq. flow 79−32635
intermittency determ. from probability density function of passive scalar 77−3827
intersecting plane turbulent air jets, temp. distrib. study using Mach Zehnder interferometer 79−86476
irrotational strain dissipation eqn. sensitisation 80−106794
isobaric turbulent reacting jet issuing into costream 78−63509
isolated porous tube with nonuniform wall thickness, generated flow, jets 80−24087
isothermal annular jets, vel. characts. 79−34309
isothermal incompressible gas jets, mass transfer eqns., nonlinear thermodynamic anal. *(Russian)* 79−18925
isotope separation techniques based on vel. slip in freejet expansions 80−19441
jet, large scale struct. and vortices, linear stability theory 78−26179
jet flow noise mechanisms and principal notions 78−1653
jet noise, cross-spectral densities, extension of Ribner's theory 80−69804
jet nozzle, meas. of plane-wave noise radiation 77−58758
jet-flap flows, near wake region, mean and fluctuating vels. 79−4051
jet-generating nozzle system, hydraulic characts. 77−84295
Jupiter surface, equatorial jet stream form. due to cylindrical shear layer 78−16340
laminar, axisymmetrical, with and without buoyancy *(German)* 78−83450
laminar, dynamic and heat problems 78−67241
laminar, linear stability 78−38379
laminar, mass transfer due to impinging on flat surface 77−68651
laminar, uniform exit vel. profiles, developing region 78−79354
laminar axisymmetric impinging, heat transfer 77−42888
laminar circular jets, friction heat effect on temp. distrib., anal., forced convection 80−10279
laminar coaxial annular jets in a circular cylinder and influence of temperature on them 80−14770
laminar gas jets, heat exchange *(Russian)* 80−53829
laminar impinging jets, heat and mass transfer 78−94777
laminar jet at wall, heat transfer 79−41725
laminar jet impingement heat transfer to melting ice surface 78−22394
laminar jet in liq.-liq. system, vel. profile, numerical method 80−28545
laminar jets interaction, turbulent cone formation 77−84290
laminar non-Newtonian fluid jet, swirling, impinging on normal plane 77−42889
laminar plane jet in gas medium 79−32622
laminar plane wall jet, temp. distrib. due to variably heated wall 80−19463
laminar semi-infinite jet on porous surface, initial part calc. *(Russian)* 79−77203
laminar slot type, flow field and impingement heat transfer, num. prediction 77−42891
laminar swirling impinging jet, heat transfer, numerical calc. 79−1228
laminar vertical round jets, weak buoyancy effects due to temp. differences *(German)* 80−64595
large water jet trajectories, aerodynamic drag, max. throw distance 80−19459
laser beam degradation by two-dimens. turbulent jet 80−14375
leak detector pickups, halide, optimal flow rate determ. 80−48825
liquid, axisymmetric laminar viscous flow through pipe *(Japanese)* 77−42892
liquid, behaviour in electric and mag. fields 80−43783
liquid, breakup, 3rd perturbation Cosserat soln. 79−32615
liquid, capillary breakup, random initial perturbation, drop size distrib. 78−38380
liquid, cylindrical, flowing into pulsating stream of immiscible liq., stability 78−83444
liquid, falling in gaseous atmosphere, laminar and turbulent flow boundary layers *(German)* 77−7427
liquid, turbulent, gas absorpt. *(Japanese)* 80−38473
liquid, two-dimensional laminar, high Reynolds number flow 80−38467
liquid axisymmetric jet on baffle, heat and mass transfer 79−98775
liquid dynamic surface tension meas. instrument 80−42313
liquid flow through closely woven screens 79−14446
liquid fuel flames in open air, noise from jet and flames *(French)* 77−19476
liquid He jet pump, for circulating refrigeration systems 79−205
liquid jet, axisymmetric, impingement onto horizontal plane, hydrodynamics and mass transfer 78−94780
liquid jet, burnout in nucleate boiling 78−90991
liquid jet, capillary instability, effect of harmonics 78−71378

jets continued
liquid jet, instability, one-dimens. Cosserat theory 78−42638
liquid jet, interaction with hypersonic gas flow, shape and breakup 80−10277
liquid jet air wake boundary layer eqns. 77−75954
liquid jet breakup, second perturbation soln. for one-dimensional Cosserat theory 79−86478
liquid jet hydrodynamic development, surface active materials effect 79−46883
liquid jet impingement, on disks, in zero gravity, free surface shape determ. 78−94783
liquid jet launched into transverse liquid flow, calc. velocity and width *(Russian)* 77−68653
liquid jet penetration, rel. to drop breakup 78−94798
liquid jet penetration and breakup in subsonic airstream 78−26170
liquid jet satellite droplet formation 77−75953
liquid jet vacuum seal, inflow, rel. to electron beam emergence into atmosphere 80−78469
liquid jets, high speed, mechs. of emergence and flight 77−80193
liquid metal, jets, breakup in mag. field *(Russian)* 78−47062
liquid metal jet, borehole casing perforation feasibility, nozzle design, theory *(Russian)* 78−51216
liquid metal jets, 3D fluid flow model induced in ladles or holding vessels 80−10278
liquid vertical jet on horizontal plate, supercritical and subcritical flow, hydraulic jump *(French)* 78−59441
liquid-liquid mass transfer in systems agitated by submerged jets 78−22393
liquid-liquid ternary mass transfer in ejectors with cocurrent flow 79−46368
LMFBR LOF accident, surface ablation in impingement region of liquid jet 79−54549
LMFBR piping tee, multiple jet thermal mixing 78−8879
LMFBR vented assembly hydraulic modeling and testing, vent flow discharge coeff. determ. 79−59148
local heat exchange during axisymmetric air jet interaction with cylinder lateral surface *(Russian)* 79−60043
locally elliptic calculation procedure 80−103054
longitudinal instabilities in exit flow from a slit, surface tension origin 79−98684
low frequency sound radiation due to the interaction of unsteady flows with a jet pipe 80−69787
low Reynolds number supersonic air jets, noise generation by instabilities 80−23831
Mach wave radiation of hot supersonic jets 80−69894
Mach waves, kinematics inside and outside supersonic jets, book contrib. 80−1640
magnetisable liquid, stability 80−83831
mass dependent molecular beam focusing by cross-jet deflection 79−93257
mass transfer on cylinder in developed region of two-dimens. jet 77−31352
measurement of 1st normal stress difference, water rel. to polymer solns. 79−98829
Meksyn's method applied to jet flows 80−96292
melt reacting with gas jet, heat and mass transfer, mathematical modeling 80−87819
metal, liquid, jet disintegration by electric pulse, powder and granule prod. 79−33968
metal specimen preparation for TEM, two-stage, jet-stagnant electrolytic thinning, Ti, Mo appls. 77−71405
metallic coating, hot dip, on strip, analytical description of jet finishing 77−28935
methane, concentration along line in jet, spatially resolved coherent anti-Stokes Raman spectra 79−74476
methane, jet, free turbulent flow, diffusion coeff. variation, mixing processs velocity 77−7480
methane jet, turbulent conc. field meas. by Raman spectrum, data interpretation 79−32609
methane jet flow, average conc. meas. by Raman scatt. 79−98827
methane tracers, single-jet mixing in turbulent tube flow, similarity and scaling law 80−14765
methylene radical, vibronic bands obs. in pulsed supersonic jet 80−28024
MHD expanding free jet with incident EM wave, mag. press. 80−33698
MHD instability of quasi-parallel jets 78−83495
MHD jets, laminar and turbulent, elec. cond. fluid with transverse mag. field 79−77261
MHD laminar plane-wall jet flow 79−55424
MHD Landau-Squire jet, radially diverging elec. current, exact soln. *(Russian)* 78−5816
MHD shear flow, struct. turbulence, anomalous impulse transfer *(Russian)* 77−27610
microjet noise and micropore diffuser-muffler design 78−30335
micropolar fluid jet normal impingement on curved surface, flow near stagnation point 78−90949
micropolar fluid jets 80−28536
mixing in side flow, secondary zone characts. *(Russian)* 77−84292
mixing in transverse subsonic crossflow, vortex strength 79−14447
mixing layer, axisymmetric, influence of initial and boundary conditions 79−94689
mixing layer, free, axisymmetric, turbulent spot, data processing 80−79280
mixing layer, free, axisymmetric, turbulent spot, vorticity and Reynolds stress 80−79281
mixing layer of round jet, large-scale turbulence and vorticity 79−32611
mixing nozzle reattachment of two-dimensional turbulent jet 79−23347
mixing process induced by the vorticity associated with the penetration of a jet into a cross flow 79−7396
molecular beam experiments, high temp. and press. supersonic nozzle beam 80−37907
motor oils, polymer-thickened, rapid extensional flow through small orifice 78−1709
multiphase mixture, two-dimens. nozzle and jet supersonic flows 80−48780
multiple, in crossflow, characts. obs. 79−14444
multiple-jet thermal mixing in a piping tee 79−81938
near wake of disc, annular jet, vel. characts. 78−38336
near-field jet entrainment, overlaid viscous/inviscid model, BOAT computational model 80−19457
near-wake phenomena, with and without external compression, axial and radial air injection effects 80−10273

jets continued
neutral waves in a barotropic zonal jet 79−46333
Newtonian die swell eval. for axisymm. tube exits using finite element anal. 78−1741
Newtonian jet, axisymmetric, die-swell, Galerkin finite element method 80−83830
noise, characts. of shock assoc. noise 77−54831
noise, characts. of turbulent mixing noise 77−54830
noise, current research 79−32602
noise, effect of spatial source coherence 78−38138
noise, external boundary-layer flow effect in flight 77−75901
noise, geometric acoustics model, computer prediction program 78−34118
noise, hot and cold mixing, scaling laws based on geometric acoustics model 79−37306
noise, two-point correlation model 78−42493
noise amplification by higher mode acoustical excitation 78−9664
noise from large scale structure 78−34174
noise generation by jet mixing, eval. of Lighthill analogy using LV turbulence, source location and spectral noise data 80−69803
noise geometric acoustics model inside the cone of silence 78−34117
noise in flight, prediction, importance of jet temp. 80−69814
noise meas., source location, appl. of acoustic mirror, telescope and polar correl. techniques 78−83169
noise modelling by geometrical acoustics, outside silence cone 78−34177
noise prediction, nonlinear Lilley equation 80−69805
noise production, as example of flow-acoustics 77−75903
noise radiated from convecting quadrupoles, flight effects 79−32601
noise source characterisation, conditional sampling 79−41722
noise source distrib., from far-field cross-correlations 77−84039
noise source identification using direct measurements of correlation between axial in-jet vel. fluctuations and far-field noise 79−81629
noise source modification due to forward flight 78−63466
noise sources, meas. using shallow surface-wave simulator 77−80146
noise spectrum, turbulent jet, approx. calc. 78−67236
noise suppressors, lab. comparison 78−59193
non-Newtonian fluid, stretching jet profiles, simple rheological models 77−75955
non-Newtonian fluids, Prandtl-Eyring law appl., jetstream pump parameters *(German)* 78−30331
non-Newtonian laminar jet flow 80−1662
non-Newtonian liquid with power-law behaviour, flat submerged jet theory 80−59078
non-Newtonian plane jet, stability to infinitely small perturbations 78−51211
non-self-similar turbulent jets, flow restructuring and relaminarisation 79−98770
nonequilibrium free jet expansion, rotational temp. meas for N_2 80−69890
nonequilibrium free jet expansion, translational temp. meas. in N_2 80−64600
nonisothermal, acoustic energy 77−7431
nonisothermal, turbulence fluctuation meas. by hot-wire anemometer 77−35189
nonisothermal axisymmetric turbulent transfer, vel. and temp. fluctuations, correl. coeffs. 78−83445
nonisothermal laminar and turbulent plane free jets with buoyancy effect, boundary layer theory *(German)* 80−53830
nonisothermal turbulent heterogeneous jet entering air filled half space 80−64599
nonisothermal turbulent jet, physiochemical processes, temp. and conc. effects 80−14849
nonlinear capillary instability, satellite drop formation and control 80−33646
nonlinear capillary instability, theory 80−33644
nonlinear capilllary instability, behaviour effects before droplet formation 80−33645
nonlinear flow, boundary value problems, solvability for analytic functions 79−98677
nonstationary two-stage axisymmetric escape of gas into a submerged space, numerical modeling 79−77200
nonuniform flow through propulsion nozzle 78−94796
nozzle expansion in turbulent flow, downstream heat and mass transfer 80−1669
nozzle in different jet regimes, internal and external flows, separation and wakes 80−100023
numerical modelling of boundary layer 78−22397
oblique high-drag heat exchangers, turbulent flow and pressure losses 79−94710
ocean, nonlinear coastal and equatorial jets theory 80−51427
ocean, stable jet modes, eddy and mean flow interaction 79−16490
ocean coastal jet and warm front propagation, theory with appl. to Sagami Bay Kyucho phenomenon 80−94538
open channel flow with side discharge, recirculation zone, depth-averaged model 78−63499
open wind tunnel jet flow, convection and refraction of acoustic waves *(French)* 77−24007
organ flue pipes, sound prod. 77−7265
organ pipes and edge tones, jet drive mechanisms 77−831
Orr-Sommerfeld eqn., continuous spectrum and eigenfunctions 78−67176
oscillating jet in moving air stream, vel. meas. 78−22396
over-wing-blowing configurations, aerodynamic characts. determ. 78−5774
oxalyl fluoride, $^1A_u(n\pi)$-^1A_g fluoresc. excitation spectrum in pulsed supersonic jet 79−31577
parallel flows of unmixed reactants, temp. and conc. distrib. in reaction region 80−92236
parallel jets exhausting from ducts, acoustic wave propag. 80−64257
parallel jets systems, aerodynamics calc. *(Bulgarian)* 80−28543
particle meas. concentration in turbulent jet, laser scatt. technique 77−39372
particle separation property of impactor stage with nonstationary flow *(German)* 78−18335
particle size distribution in breakup of jets prod. by shaped explosive charges 80−23957
penetration depth of multiple vertical grid jets in fluidised bed 80−38486
penetration in deflecting stream, estimation method 79−37373
perforated plate, axisymmetric jet array, transverse vel. profiles 80−92195

jets continued
permeable contour in flow with jet separation, impulses and impact effects 80−92196
phase turbulent impinging jet, struct., vortex stretching 79−32476
phthalocyanine, free base, fluoresc. excitation spectrum, cooling in supersonic free jet 80−95670
pipe-exit flow visualisation using high-speed photography 80−106863
pipe-jet system in crossflow, turbulent vortex shedding modes 80−10274
pipes and bends, structure-borne sound behind a jet nozzle *(German)* 80−87804
pipes carrying fluid flow, oscillation stability *(German)* 78−87298
planar sonic nozzle, three dimens. wave struct. of nonstationary gas outflow 77−55068
plane and cylindrical jet streams, e.m. reflectivity and scatt., anal. 77−579
plane horizontal turbulent buoyant jet, parameter calcs. *(Russian)* 80−79373
plane isothermal jet propagation in bounded secondary stream 77−24008
plane jet, heated, ventilated, heat transfer to plane wall 80−59025
plane jet, stability and autooscillations from channel anal. 80−100018
plane jet in laminar cocurrent flow, eddy viscosity decay, phenomenological theory 79−98700
plane jet normal impingement on flat surface 78−14056
plane jet propagation in incompressible liquids, numerical solution *(Russian)* 80−43753
plane laminar gas jet in infinite space, thermal characts. *(Russian)* 79−18926
plane laminar relaxing gas jets, mixing with radiation accounted for, boundary layer eqns. 79−90349
plane Newtonian jet with surface tension, computer solns. by finite element anal. 79−64722
plane turbulent jet, interface crossing freq. as self-preserving flow variable 80−38472
plane turbulent jet, outer intermittent turbulent motion structural characts. 79−77208
plane turbulent jet flow in incompressible liquid *(Russian)* 77−55060
plane turbulent jet spreading rate, external disturbances 77−55062
plane wall jet, nonlinear stability *(Russian)* 80−24066
plasma jet on baffle, flow behaviour and heat exchange 79−98774
plate with impinging hot gas jet with low Re, convective heat transfer 80−96256
plume, buoyant, turbulent, issuing vertically into stratified or uniform ambients 77−58756
plume, low altitude, matched press. props. 78−26176
plumes, vertical, round, diffusion, flow props. 80−43755
plunging turbulent gas jets, submerged biphasic region 77−31350
polymer solns., unstable flow, reservoir to capillary, jet instability onset and flow patterns, obs. 78−87364
polymer solution, elastic, load bearing capaicty of squeeze film flow 80−103051
polymer solution, flow in exit region of tube, jet swell problem 80−38452
polymer solution, jet thrust technique for normal stresses 78−9669
polymer solution, turbulent jet behaviour 78−1732
polymer thickened motor oil, flow in convergent jet thrust nozzles 77−75959
polymer-thickened oil, flow in convergent jet-thrust nozzles at 84°C 79−23348
porous plate skin friction, injection or removal from boundary layer due to turbulent wall jet 78−47029
power law liquid, comparison of 2-D and axisymmetric jet flows 78−79351
power-law fluid laminar jet flow 79−32619
Prandtl supersonic jet problem, linear aerodynamic theory formulae, validity, book contrib. 80−6090
pressure-head thermal jet devices, cycle plotting, basic thermodynamic and gasdynamic conditions 79−18924
profile with jet flap, discrete vortex method *(Russian)* 79−77201
propagation in deflecting airstream, trajectories, density influence 79−86480
propane, freejet flow, vibr. relax. time 79−98760
propane-air flame, eddy entrainment and combustion in depth process, three-region model 79−100384
propane-CO_2, freejet flow, vibr. relax. time 79−98760
pseudoplastic incompressible fluid, weak jet 78−30330
pseudoturbulent mixing efficiency in fluidised bed 77−39342
pulsating, thermal convection in step wake *(French)* 80−10240
pulsations at discrete freq., Navier-Stokes eqns. for fluid behind plate in channel *(Russian)* 80−74979
pulse-jet fabric filter, high vel., dust retention effect on pressure drop 80−103072
pulsed, flowing out of supersonic nozzles, wave struct. in nonstationary flow stage 80−59094
pulsed nozzle jet struct., direct shadow method and streak photography 80−10323
pulsed supersonic He jet, space time characts. 77−51093
pulverised coal reactors, cold flow mixing rates with recirculation 79−50762
pump, finite-difference performance anal. 77−31348
radial turbulent, flow, attachment to disc plate, flow patterns, nozzle dimension effects 78−83443
radial wall jet, circular jump characts., boundary layer form. 77−24005
radial wall jet, linear stability anal. 80−19458
radiation properties of a turbulent jet excited by a sinusoidal acoustic disturbance 80−69789
radio sources, compact, relativistic jets model 80−4448
radio sources, extragalactic, jets configuration and propag. 80−31374
Raman scattering and laser Doppler velocimetry techniques for turbulent flow field investigs. 78−34224
rapidly rot. gas, free jet expansion, Newtonian thin shock layer approx. 80−74888
rarefied free jet, N_2^+ UV spectra for rot. temp. 80−6184
rarefied gas, free expsn. and interference 79−46353
rarefied gas expanding in vacuum, asymptotic props., jet for flow field *(Russian)* 77−55041
rarefied supersonic CO_2 flow, fluctuations in intensity of radiation excited by electron beam in jet core 77−55104
reacting gas, steady axisymmetric supersonic free jet, approx. analytical soln. 77−55099
reaction, turbojet engine internal noise 80−87644
reactive gas mass spectrometric analysis with free-jet expansion sampling 80−89566
reattachment flow issuing from finite width nozzle, bubble press. parameter 80−10275
reciprocal blow of two jets, stagnation region formation *(Russian)* 79−32620
rectangular, heated high vel., noise characts. 79−94604
rectangular cavities, end effects, vortex flow and wall jet 80−10309
rectangular jet distrib. in cross flow, expt. 80−19465
resonance tube, jet flow and heating, unsteady complex shock struct. 80−6115
resonance tube, oscillation excitation from supersonic jet *(Japanese)* 80−24116
resonance tube, thermodynamic characts. 77−89174
resonance tube driven by subsonic jets, aerothermodynamic characts. vortex shedding 78−51208
resonant oscills. in tube with jet inlet 78−59440
respirator based on jet-flow vortex-type components *(Russian)* 79−79683
reversed flow characteristics due to jet issuing from dead end channel *(Japanese)* 80−100021
ring vortices under water, vel. and momentum rel. to form. parameters 77−62257
rocket exhaust anemometry, Doppler difference and two focus methods, correlator and photon counting 79−60084
rotating annular jets, velocity distrib. and profile meas. 79−50829
rotating disc heat transfer with liq. jet impingement 79−4055
rotating hollow gas jets, nozzle exit flow angle and pressure forces effects *(German)* 80−69887
round, instabilities, cocurrent flow effects 79−60045
round buoyant jets in stratified flows, integral eqns. 79−27680
round free jet, aerodynamic noise, propagation of wavelike disturbances 80−69806
round heated jet, heat and momentum transport, intermittency, entrainment 79−32608
round jet in cross flow, injection angle effect on vortex props. 78−94779
round jet of inviscid liquid from nozzle of slowly varying profile 78−14055
round laminar jet, flow field development 77−55061
round laminar jet in spherical envelope, nonlinear soln. 79−94693
row, influence of geom. asymmetry on downstream flow of discharge into free stream 79−81941
row of jets, mixing with confined crossflow 77−58748
second-order fluid, stick-slip and die swell 78−30325
self excited oscillations, impact of liquid jet against plane barrier 79−32545
self-oscillations of underexpanded jet flowing into barrier 79−68773
self-preserving turbulent flow over convex surface 77−58754
shaped charge jet formation, Pugh-Eichelberger-Rostoker solution representation 79−94692
shaped charge jet stability 78−13919
shear flow, stratified, free-turbulent, buoyancy effects on large scale struct. 78−90849
shear layer acoustic refraction theories, comparison, parameters for open jet wind tunnel shear layer correction 78−90556
shear layer instability noise produced by various jet nozzle configurations 80−69791
shear layer scatt. of acoustic wave, linearised theory with causality 77−42643
shear turbulence, acoustic field, convective amplification, jet noise appl. 77−23943
shear turbulence, temp. fluctuations, struct. functions 78−30274
shield-hot turbulent jet interaction, nonstationary heat transfer 80−92136
shock wave, quasilinear hyperbolic system of gas dynamics *(Russian)* 80−33629
single and multiple, buoyant and nonbuoyant jets, trajectories in arbitrary crossflow 80−43756
single point jet injection on boundary layer over flat plate, direct calc. method 79−68772
slender streams for incompressible inviscid heavy liquids, jets, wall and channel flows 79−77205
slender streams with gravity, outer asymptotic expansions 78−13986
slender streams with gravity, outer asymptotic expansions 78−13987
slightly heated small perturbation jets and wakes in press. grad., self-preservation 80−96290
slow EM wave theory in conducting jets 80−91731
slowly spreading jets, MHD instability 80−87818
sluice gate problems with gravity 77−39349
small air jet and quiet valve noise obs. 78−83165
solid particle concentration profiles in turbulent jet, laser Doppler anemometer meas. and theoret. calcs. 79−27686
solid-gas jet issuing into transverse stream 79−32649
sonic boundary layer counterjet interaction with supersonic flow 79−64728
sound and aircraft noise spectral broadening by turbulent shear layer 79−37076
sound diffraction of high speed jet at subsonic flight 77−50806
sound emitted by axisymmetric steady-state free gas jet, review *(French)* 78−67244
sound generation by flow-acoustic coupling 80−69793
sound generation in flows, conf. Gottingen, Germany (Aug. 1979) 80−67937
sound generator, vortex, separation of acoustic energy and spent-air jets 80−102953
sound power output, turbulent jet into gas with different sp. ht. 78−94789
sound production in moving stream, Lighthill's acoustic analogy, jet noise 78−79313
sound radiation by instability waves of a compressible axisymmetric jet 80−69792
sound radiation field near cylindrical jet in motion 77−31169
sound radiation from a simulated jet flow, calc. of vortex configuration and sound field 80−69786
sound radiation from convecting monopole and dipole sources in jet flow, forward vel. effects 79−94603
sound radiation from turbulent jet, directivity and Mach number depend. 79−72921
sound scatt. by aircraft fuselage, coordinate stretching 79−23123
sound sinks in flows, low freq. sound absorpt. of jets 80−69788

jets continued
sound spectra radiated by gas jets, influence of closely located solid surfaces 80−69800
sound transmission through turbulent shear layer 79−37075
sounding rocket attitude stabilisation H_2O_2 jet system *(Japanese)* 78−28482
sounding rocket three-axis attitude control system *(Japanese)* 78−24422
source flow expsn., distrib. function model 79−27667
spatial viscous instability of axisymmetric jets 77−11228
splitter plate acoustics, zones of silence in sound wave-jet flow interaction 79−3819
spouted bed, theory for predicting maximum spoutable height 78−14077
spouted beds of spherical particles, spout termination, parameters 80−64621
spray, droplet vel. meas. using laser Doppler velocimeter *(German)* 79−50818
stability criteria for time-dependent flows 78−79305
stagnation point heat transfer on plate, turbulance effects, liquid crystal meas. 78−18327
standing surface waves, double boundary layers and jet-like motions 77−25694
steam jet condensation, dynamical pressure pulse effects 78−94549
steam jet condensation in turbulent liquid flow, heat transfer 80−33599
steam turbine turbulent flat jet condenser, nozzle hydraulic and heat transfer characts. 78−94793
stenotic flow models, fluid dynamic wall interactions 77−56414
straight elliptical jet motion, influence of twist using nonlinear differential equations 79−46354
stratified liquid, free convective flow struct. over point heat source 80−79323
stretching jet, convected Maxwell model 78−71379
Strouhal number influence on flight effects on jet noise radiated from convecting quadrupoles 80−69781
structure functions of temp. fluctuations, turbulent shear flows 78−71380
submerged gas injection into liquids, flow regimes 80−59101
submerged jet closed vessel recirculation flow, temp. distrib. and buoyancy 78−90958
submerged jet cone angle from bubble theory 80−79372
submerged jets impinging on baffle, flow and mass transfer, polymer additive effects 80−92194
submerged jets in water with slit nozzles, interaction between two opposed jets 80−6113
submerged jets issuing from conical radially slit nozzles 77−35195
submerged multiple-jet buoyant discharges, expt. 78−30333
submerged steam jet into unbounded space, temp. field 79−72920
submerged turbulent isothermal jet development and min. entropy prod. principle 79−77199
submerged water jet, interaction of US waves with turbulence 80−87619
subsonic, flow and heat transfer near blunt body stagnation point 77−65774
subsonic, injected into subsonic cross flow, laser-Doppler meas. 77−42893
subsonic, jet-mainstream interaction 80−79271
subsonic, noise study by method of causality *(French)* 77−7428
subsonic, of gas, vortices, flow visualisation patterns 78−63471
subsonic, sound propagation due to a source near the duct exit 78−83446
subsonic coaxial, initial region, vortices 77−80191
subsonic coaxial jets large scale coherent structures 77−7429
subsonic free-jet, directional characts. of noise radiation 80−23820
subsonic hot free, coherent structures in mixing zone, acoustic effects 79−4052
subsonic jet, acoustic far field, azimuthal struct. *(French)* 79−14150
subsonic jet in simulated motion, sound radiation 80−74846
subsonic jet issuing from semi-infinite cylindrical pipe, sound interaction 78−22395
subsonic jet noise, peak Strouhal freq. as function of Reynolds number 79−77196
subsonic jet noise, prediction method for flight effects 78−1502
subsonic turbulent jet, entry zone flow wave struct., eddies 80−14773
superheated liquid discharge from nozzle, pressure calc. 80−92199
supersonic, acoustic perturbations *(Russian)* 77−58751
supersonic, acoustic radiation using double-pulse holographic interferometry 80−14678
supersonic, acoustic reflections effect on discrete component of noise spectrum 79−68775
supersonic, cold, coaxial jet, acoustic, flow characts. 80−1656
supersonic, flowing onto infinite perpendicular barrier, limiting expansion ratio 78−59439
supersonic, from nozzle with inclined rim 79−64724
supersonic, imperfectly expanded, model describing sound generation 79−4053
supersonic, jet flow from nozzle, coords. of acoustic cross-section 78−5778
supersonic, Mach wave emission 78−26172
supersonic, noise, Reynolds number depend. 78−14053
supersonic, nonsteady interaction with barrier, math. model of oscillatory cycle 80−19462
supersonic, shock layer ahead of barrier 79−64723
supersonic, stream model 77−89180
supersonic, two-dimens., impingement on flat plate, shock-interference heating 79−94688
supersonic, two-dimensional, impingement on normal ground surface 77−24003
supersonic air ejector, constant-area-mixing type, design theory 79−86482
supersonic and sonic annular jets, 80−100019
supersonic axisymmetric gas jet, interaction with plane barrier *(Russian)* 77−27571
supersonic beam skimmers, transition regime behaviour 77−3491
supersonic conical nozzle, flowfield induced by secondary gas injection 77−62290
supersonic flow, jet injection, separation zone, boundary layer thickness and transverse curvature effects 80−48745
supersonic flow, self-induced oscills. 78−67215
supersonic flow, sonic injection, auxiliary blowing effect on conc. profiles downstream *(French)* 77−65778
supersonic gas jet, penetration into the ground *(Russian)* 80−28544
supersonic inflow into cavity, press. fluctuations and heating 79−64726
jets continued
supersonic jet, thermogasdynamic interaction with inclined permeable baffle 79−98773
supersonic jet, turbulent wake, laser velocimeter meas. 78−26173
supersonic jet flow over obstacle, discrete tones generation 78−1708
supersonic jet noise spectrum, discrete component 78−9493
supersonic jet noise suppression by coaxial cold/heated jet flows 78−63468
supersonic jet spectroscopy, appls., teaching approach 80−41996
supersonic jet structure produced by slit orifices *(German)* 79−77210
supersonic jet-barrier interaction, shock layer flow near axis 79−90282
supersonic round jet, flow characts. of large scale wave-like struct. 77−89178
supersonic underexpanded jet, press. pulsations on flat plate 78−94778
supersonic underexpanded jets, discharging into opposing supersonic stream, wave structure anal. 80−19461
surface ages of water jets 78−83442
surface buoyant jet, horizontal discharge into denser media, theory 78−90954
surface buoyant jet entrainment, meas. of velocity and concentration fluctuations *(Japanese)* 79−14450
surface discharging heated turbulent jet, 3D finite difference model, turbulent diffusivities 80−74845
surface friction dependence on compressible fluid injection and removal by suction from wall jet 77−47052
surface jets, heated, three-dimens., modelling 80−24065
surface noise from turbulent hot jet, temperature effects 80−69782
swirled jet, stream parameters at exit cross section of annular nozzle 77−15090
swirled jet propag. in channel 77−58755
swirling, radial, in free space, velocity components 78−55669
swirling aerosol jet streams, impingement zone, particle motion soln. and expt. 77−65773
swirling air jet, heat transfer of conical tube, with internal cooling by swirling air jet 77−55063
swirling annular capillary jet flow *(Russian)* 78−75180
swirling jet from vortex filament, Navier-Stokes eqn. soln. 80−38470
swirling jets, confined, axisymmetric viscous incompressible flow, numerical prediction 77−84286
swirling jets and plumes, turbulent, integral method model 79−60040
swirling recirculating reacting turbulent jets passing through diffusers 79−50764
symmetric gas jet, flow computation *(Russian)* 79−37374
symmetrical flow around curvilinear obstacle, iterative soln. *(Russian)* 79−81933
tall-form spray chamber, residence-time distribution of air 78−9679
Taylor-Helmholtz instability, jet diameter, appl. to mineral wool fibre prod. 77−35191
temperature, concentration, and velocity in jets, flames, and shock tubes 79−68778
temperature gradient meter for gas flow study 79−86539
thermal plume modelling, review 79−4056
thermal turbulence, laser beam propagation *(French)* 77−7007
thin jet in infinite viscous fluid, flow of centrally-located drop 79−32614
three dimensional turbulent rectangular jets 80−14769
transformer oil electrohydrodynamic flow, jet dynamic pressure obs. *(Russian)* 80−59117
transient jet of propelling gas during diaphragm rupture in shock tube, holographic images 79−77181
transition to turbulence in jets 78−18326
transonic free jet, overexpanded two-dimens., eqns. formulation and soln. method 80−6109
transverse, turbulent mixing with high Mach number stream 79−32603
trench flow, square section, viscous liquid, laminar and turbulent conditions obs. 77−75981
triple correlation of the pressure in subsonic circular jets and nonlinear interaction of instability waves 80−69893
turbojet engine noise interaction of entropy fluctuations with turbine blade rows 77−80149
turbojet noise suppression investigations using hydrodynamic press. meas. and cross-correlation techniques 78−79157
turbulence, large scale struct., vortex rings, similarity region 78−90847
turbulence, laser velocimeter correlation meas. 80−106785
turbulence, noise, coherent struct. 77−89176
turbulence energy dissipation, preferential spectral transport by irrotational straining 80−1551
turbulence generated noise at edges 80−103020
turbulence generated noise on both sides of double layer jet 77−47056
turbulence models, integral-relation model appl. 80−43691
turbulence of free coaxial jets with independent air supply to nozzles *(Bulgarian)* 78−59436
turbulence of hot free jet, mixing zone coherent struct. 78−94788
turbulent, acoustic emission from coherent structures *(French)* 77−65775
turbulent, axial momentum conservation 78−67240
turbulent, axisymmetric, spatial correlations 80−19539
turbulent, behaviour in presence of body forces and non-self-similarity 78−1706
turbulent, chem. reaction at metal surface, modelling 78−64885
turbulent, circular, three-dimensional, in crossflow 79−98769
turbulent, convective heat transfer to flat plate 79−1226
turbulent, drop motion 78−5789
turbulent, dye dilution laser induced fluoresc. meas. 78−30397
turbulent, free, round, initial region flow struct. 79−50765
turbulent, free, three-dimens., k-ε model calc. using finite difference procedure 80−19468
turbulent, heated, joint probability densities and quadrant contribs. 79−32597
turbulent, injected into crossflowing stream, trajectory predictions 77−51094
turbulent, mixing layers, exptl. investig. of large scale structs. *(French)* 79−41728
turbulent, plane, impinging on plane surface, RMS boundary press. pulsations 78−59438
turbulent, power spectrum of scattered acoustic signal 79−94695
turbulent, quasi-periodic structure 79−81935
turbulent, quasi-two-dimensional description of rapid-type nucleation 77−35190
turbulent, radial, flow at and after attaching point 79−37369
turbulent, radiative transfer 78−94578
turbulent, round jet/plane jet spreading rate anomaly 78−63469

jets continued
turbulent, slowly diverging, linear instability modes 77−3856
turbulent, sound transmission expts. 79−32600
turbulent, spreading rate, virtual origin 77−3855
turbulent, temperature fluctuations, local isotropy 79−1191
turbulent, trailing edge noise mechanism 79−41720
turbulent, velocity and concentration profiles in core and transition regions *(German)* 78−34172
turbulent, wavelike eddies 77−89175
turbulent Ar-Ti powder two-phase jets, with Ti combustion, high temp. study 79−81934
turbulent axisymmetric, spatial waves 77−19630
turbulent behaviour caused by nozzle wall laminar boundary layer 77−55065
turbulent boundary layer separation suppression by sequential wall jets 77−31354
turbulent bulge structure in axisymmetric jet 78−90955
turbulent buoyant, integral props. 77−58752
turbulent buoyant, turbulence struct. 77−58753
turbulent buoyant jet, in uniform environment, near field 79−32607
turbulent circular jet, in presence of co-flowing free stream 78−1704
turbulent coaxial flow analysis, mixing length calc., two-equation model solution, using finite element method 78−38295
turbulent curved, investigation along curved streamline 77−51095
turbulent deflected jet, 3-dimens. vel. field, finite-difference soln. 78−47009
turbulent diffusion flame, combustion model and calc. 78−35684
turbulent diffusion flame jet, anal., pulsations of conc. and Archimedian forces *(Russian)* 77−51130
turbulent diffusion flames, statistical props. *(Japanese)* 79−81939
turbulent energy and length scale eqn., mean vel., similar solns. 77−89102
turbulent flames and isothermal free jets, mathematical model *(German)* 79−74387
turbulent flow, film cooling performance 80−79272
turbulent flow, jet type, concentration-pulsation eqn. use 79−90300
turbulent flow in free jet, large scale struct., discrete values meas. 78−90840
turbulent flow struct. at moderate Reynolds no. 78−18329
turbulent free jets, acoustic effect, dual nature 78−18325
turbulent free jets, subsonic and supersonic, laser velocimeter meas. 79−77307
turbulent free-jet, experimental investigation of acoustic radiation 79−46102
turbulent gas jet, evaporation of semidispersive drop system 77−55077
turbulent heated jet, temp. and vel. meas. 78−94784
turbulent impingment, curved plate, surface press. fluctuations 78−9666
turbulent incident on plate, convective diffusion 78−67242
turbulent incompressible jas jets, thermodynamic transfer theory *(Russian)* 79−32621
turbulent jet, interaction with pure tone sound 78−94790
turbulent jet, large scale flow struct. 79−72923
turbulent jet, sound radiation due to nonlinear interaction of instability waves 79−50720
turbulent jet, upstream influence on near field 77−89181
turbulent jet entering air, jet with dissimilar density 79−72922
turbulent jet flame, stabilisation using thick burner rim *(Japanese)* 77−68706
turbulent jet flow, aeroacoustic interaction, review 80−87765
turbulent jet flow, simulation by discrete eddy system, statistical characts. 79−98771
turbulent jet flow modification of uniform flow along a plane wall *(German)* 80−6120
turbulent jet flow past ellipsoid of revolution 79−81937
turbulent jet impinging on cylinder wall, heat transfer and fluid mechanism study *(Japanese)* 80−83800
turbulent jet in concurrent stream at permeable surface 77−7444
turbulent jet mixing, effect of nozzle wall boundary-layer state 77−27568
turbulent jet mixing rates with self-excited acoustic oscills. 78−47008
turbulent jet noise, press. depend. for choked and subsonic jets *(Chinese)* 78−67235
turbulent jet noise and diffusors *(Chinese)* 79−55367
turbulent jet structure, turbulence and coherent eddies, review 80−48760
turbulent jet temperature fluctuations, laser beam deflection *(French)* 77−24038
turbulent jet vel. in conical annulus 77−55069
turbulent jet with negative bouyancy, penetration into LMFBR upper plenum, safety evaluation 77−23221
turbulent jets, heat, mass and momentum transport, into ambient air 78−51210
turbulent jets, influence of drag reducing polymers on cavitation inception 80−106823
turbulent jets, two-dimens., vel. and press. distribs. at confluence 77−24004
turbulent jets, vortex-street structure 80−10280
turbulent large-scale struct., noise prod. 79−7394
turbulent liq. jets, breakup length 77−84293
turbulent liquid streams vel. profiles using laser Doppler velocimeter 79−64807
turbulent mixing coefficient correlations for compressible coaxial submerged and coflowing jets 77−42883
turbulent mixing layer, conditional meas. 79−32598
turbulent mixing layer, wave dispersion on vortex pairing 79−32612
turbulent mixing noise, aircraft, in-flight simulation expt. 78−1501
turbulent mixing of coaxial jets, conc. fluctuations 77−39318
turbulent near-wake behind step with supersonic jet 79−14448
turbulent plane jet, development and struct. 79−37371
turbulent plane jet, impinging on solid wall, spectral characts. of pulsations 78−9668
turbulent plane jet, signal transit velocities 77−35192
turbulent plumes in laminar cross flow, entrainment 77−24006
turbulent power law, rel. to marginal instability principle 79−32458
turbulent pressure fluctuations on jets, long range effects, book contrib. 80−1663
turbulent recirculating jet flow, initial mixing region meas. 77−27570
turbulent round buoyant jet, flow, algebraic stress modelling technique appl. 79−55403
turbulent round jet, incompressible flow, numerical prediction 79−1171
turbulent shear flow, free, of plane jet, initial condition effect 78−90850
jets continued
turbulent shear flow without solid boundaries, effect of polymeric additives 79−77084
turbulent source coherence effect on noise 79−32599
turbulent two-dimens., parallel, mixing 78−51209
turbulent two-phase isobaric jet, anal. *(Russian)* 77−27586
turbulent vertical buoyant jet decay in uniform environment, unified scaling law 78−90905
turbulent wall, with cylindrical streamwise surface curvature 77−35193
turbulent wall jet, algebraic Reynolds stress model calc. 80−1668
turbulent wall jets, self-preserving flow 78−79352
turbulent-jet-diffusion flame, effect of mol. gas radn. 77−80232
two parallel flow, noise reduction, exptl. investig. 79−41723
two plane parallel jets interaction 78−26175
two-dimensional, charact. when produced by series of coplanar 3-dimens. jets 77−80192
two-dimensional, effect of density and cond. discontinuities on MHD stability 77−31396
two-dimensional, finite disturbances and growing vortices 77−47055
two-dimensional jet flow in ideal compressible gas, calc. method 78−83448
two-dimensional supersonic flows of mixture, vapour and drops in nozzle and submerged jet, determ. 79−23357
two-dimensional transverse sonic jet interaction with supersonic stream, application factor 80−24047
two-dimensional turbulent, in moving stream, preferential entrainment 80−1660
two-dimensional underexpanded jets, analysis *(Japanese)* 78−90952
two-dimensional wall jets under stationary and pulse conditions 78−18324
two-dimensional water, sensitive to sound, behaviour *(Japanese)* 80−79376
two-phase, discrete phase penetration into constant cross flow *(Russian)* 78−47024
two-phase, turbulence struct. modification model energy dissipation 77−58769
two-phase, turbulent, particle or droplet size effect on diffusion 80−1658
two-phase flow, energy dividing props. in discharge from supersonic jet *(Russian)* 77−39332
two-phase flow, mixing and condensation in high-speed flow, review 78−47014
two-phase supersonic jet flow around a sphere 80−6114
two-phase turbulent jet model 79−60044
two-phase turbulent jets 79−32636
two-phase turbulent round jet, turbulence dissipation 77−35208
underexpanded, first roll geometrical struct., cone angle and degree of contraction effects 77−11229
underexpanded flow between two bodies *(Russian)* 80−43752
underexpanded gas jet issuance into supersonic flow 80−38468
underexpanded jet development, transient expt. using multiple-pulse laser light source 78−14114
underexpanded jet interaction with flat plate 79−94674
underexpanded jets, nonstationary processes 79−41724
underexpanded plane free jets *(French)* 79−37372
underexpanded supersonic jet, impinging on barrier, sound field 78−9495
underwater turbulent jets, velocity field calcs. for expansion region *(Russian)* 77−31351
unexpanded jet flow interaction with spherical obstacles, anal. 80−19460
unflanged duct exit, high temp. effects on acoustic radiation impedance 77−84069
unsteady subsonic jets, entrainment charact. 78−63470
unsteady subsonic turbulent jets, book contrib. 80−1664
upstream acoustic disturbances, effects of upstream tones on the large scale instability waves and noise of jets 80−69790
US gas jet evacuation system in vacuum UV source chamber 77−13763
US scatt. by submerged turbulent jet in liquid 78−50992
variational methods, book contrib. 79−32456
velocity of jets from perforated plate *(Russian)* 77−80194
velocity sensor, calibration equipment and technique, oceanographic appls. 80−8447
vertical buoyant jets, decay, unified correlation and prediction in turbulence model 80−6118
vertical gas jet in fluidized bed, temp. field and dynamics 77−11258
vertical jet, 2-D, under gravity integral equation method of soln. 80−59093
vertical jet under gravity, Riemann-Hilbert problem, numerical soln. 80−36858
vertical laminar jets, weak buoyancy, book contrib. 80−1665
vertical plane turbulent buoyant jet in confined depth channel, stability and mixing 79−90302
viscoelastic capillary jets, stability 79−46352
viscoelastic fluid flow, die swell problems with free surface, collocation and Galerkin finite element 80−14751
viscoelastic fluid flow in fixed geometry, collocation and Galerkin finite element methods 80−14750
viscoelastic fluids, die-swell theory, anlaytical results 77−58624
viscous and inviscid, circular and elliptical, breakup and instability 80−48763
viscous capillary jet, oscills., investigation of axisymmetric perturbation 79−37370
viscous compressible liquid, bubble behaviour analysis by finite method 77−55072
viscous gas flow, similarity of flows in strongly underexpanded jets 80−6111
viscous incompressible opposing jets, collision, numerical calc. 77−7432
viscous jet with surface tension, jet shape, finite element soln. 78−79349
viscous laminar flow, tangential twist eddy flow form., numerical soln. 77−89179
viscous laminar jet flow in slipstream calculation *(Russian)* 79−77209
viscous two-dimens. incomp. flow with separation at cascade inlet edge, num. calc 79−90232
vortex collapse, periodic oscills. *(Russian)* 77−58697
vortex pairing in jet noise generation 80−69807
vortex stretching, due to shear layer instability 77−65776
vortex structure rearrangement in wake and jet, ideal fluid calc. *(Russian)* 78−5780
vortex with top-hat jet core, stability 77−19612
vortex zone from turbulent jet impinging on external stream plane surface 79−90301
wall boundary layer, induced turbulence influence from jet and vortex generator *(Russian)* 79−59970

jets continued
wall impact gas jet model, subsonic 78−34176
wall jet, 3-dimens., surface layer props., computation 80−1667
wall jet, 3-dimens., two-point statistical props. 79−1223
wall jet, axisymmetric radialwise, flow pattern on impinged wall 80−79370
wall jet, radial, linear stability 78−22392
wall jet, radial, temp. field and heat transfer meas. 77−72341
wall jet, three dimens., expt. 78−1702
wall jet, three-dimens., press. and vel. meas. 80−19456
wall jet, two-dimens., linear stability 78−22391
wall jet flow, compliant walls, influences of flow convection and refraction on sound radiation 80−74595
wall jet negotiating a trailing edge 79−41726
wall jet on flat smooth plate, mean vel., turbulence and press. distribs. 77−62288
wall jet over convex surface, turbulent flow characts., Reynolds shear stress 77−42890
wall jet turbulence, cylindrical streamwise surface curvature 77−55066
wall reattachment device, loading effects on switching *(Japanese)* 79−10548
water, destruction of rock, theory based on drag force on grains in permeable medium 78−55691
water, impinging on ice block, heat transfer in melting process 77−935
water, sub-surface, interaction with artificially-created wind *(Russian)* 79−4025
water, surface ablation of melting solids in impingement region of jet 80−14766
water, turbulent surface, steam condensation 79−64748
water, two-dimensional, effects of applied sound *(Japanese)* 78−79353
water, under gravity, cross-section shape 77−3854
water jet, penetration through water surface, high-speed photography 78−42693
water jet, round, impinging, heat transfer in interference zone of film flow along wall 77−58750
water jet, turbulence fine struct., polymer addition effects, high speed photography 78−26178
water jet appearance, nozzle shape and polymer additive effects, boundary layers 80−53828
water jet impinging on horizontal heated surface, single-phase convection and nucleate boiling regions *(Japanese)* 80−48761
water jet impinging on hot surface, boiling heat transfer 78−90993
water jets, waves 78−5775
water jets sensitive to sound, two-dimensional, velocity fluctuations behaviour *(Japanese)* 80−100020
water-jet ejector, performance improvement measures *(Japanese)* 79−14449
wave propag. on acoustically perturbed jet 79−81592
wave structure of weakly or under-expanded stationary rotationally symmetric supersonic jet *(German)* 79−86483
weakly conducting dielectric liquid, plane jet in strong nonuniform mag. field *(Russian)* 78−94838
wind simulation, air jets perpendicular to wind-tunnel stream 77−56691
xylene liq. jets induced by electrostatic field, disintegration and convergence 79−81986
zonal ocean, narrow jets model 79−2264
pN, charm-pair production 80−22643
$p\bar{p}$, hadronic jets, possible intermediate bosons 80−18149
$pp \rightarrow \pi^0$, large transverse momentum jets investig. at 52.4, 62.7 GeV 80−18151
AgBrI photographic emulsion prep., double-jet nucleation turbidimetry 79−100446
Ar, clusters in supersonic beam, electron diffr. study 80−5655
Ar jet, supersonic, electron beam-excited, continuous VUV emission spectrum origins 79−6964
Ar, nonequilibrium condensation and surface tension in supersonic jet flow *(Russian)* 80−65210
Ar, supersonic, ultrasoft X-ray emission following electron excitation 77−27015
Ar supersonic jet, spark line emission, 300-1000 Å 77−19793
Ar-He rarefied mixture in supersonic nozzle and jet, longit. translational nonequilib. 79−27678
CO, rot. distrib. in supersonic beam, IR bolometry using tunable diode laser 80−63869
CO_2, free expsn. of jet, nonequilib. effect 79−27676
CO_2 free jet, rarefied flow, homogeneous condensation scaling law 80−6121
CO_2, nonequilib. expansion, retardation temps. ≤1200K, vibr. relax. and condensation influences 78−5777
CO_2, rarefied jet beam, Raman scatt., for rot. temp. and density 80−6185
CO_2 single and multiple free jet conc. meas., CW laser Raman spectroscopy 79−97447
CO_2, single and multiple free jets, CW laser Raman spectroscopy 80−32727
Cu, meas. of density of hollow-charge jet, appl. of light radiography *(French)* 78−44344
Cu_2, in supersonic free jet expansion, laser induced excitation spectrum obs. 80−14151
$D+O_3+CO_2$ mixture supersonic jet, gain meas. for CO_2 laser 79−89902
H-air, laminar diffusion flames, chem. nonequilib. effects model 78−48654
H_2, liquid, acoustical break-up for uniform solid spheres prod. 77−74409
H_2, supersonic combustion in vitiated airstream, using transverse injection 78−14095
H_2-N_2-Na jet, ignition and extinguishment in simulated LMFBR accident conditions 78−8932
He, calibration of acoustic emission transducers and systems 77−835
He gas jet noise source, absolute calibr. 78−59228
He-benzene, van der Waals, complexes, $^1B_{2u}(\pi\pi^*)$-$^1A_{1g}(6_0^1)$ band, in supersonic jet, rot. anal. 79−31578
He-I_2, SS jet, collisional relax. of vibr. excited I_2 79−64081
He-N_2-CO_2 mixture in supersonic nozzle, shock activation with overexpansion, jet form. 78−18330
^{4}He, superfluid, turbulence in counterflow jet 77−72732
I_2 pure supersonic jet, hyperfine struct. in B-X transition, laser spectroscopy 79−81234
I_2 seeded in supersonic free jet, collision-induced rotational relax. 80−102556
I_2+H_2, vib. relax. in supersonic jet 77−58134
jets continued
Kr supersonic jet, electron beam excited, vac. UV spectrum 77−88414
N_2 (-CO_2 mixture), jet, molecular rot. level population during condensation 79−86481
N_2 free jet expansion, rot. level population kinetics, electron-beam diagnostics 78−5776
N_2, freely expanding, quantum effects in rot. relax. 80−58355
N_2 gas jet injection into Hg, interaction at submerged orifice 80−59102
N_2 in supersonic nozzle, shock activation with overexpansion, jet form. 78−18330
N_2, interaction with liq. Pb and Sn streams in metal powder prod. 79−43170
N_2 jet, mixing zone in continuous to free mol. transition 79−32605
N_2 molecular beam generation, parameters rel. to stream perturbation before skimmer 79−86468
N_2 single and multiple free jet conc. meas., CW laser Raman spectroscopy 79−97447
N_2, single and multiple free jets, CW laser Raman spectroscopy 80−32727
$N_2+^{20}Ne(^{22}Ne)$, isotope separation by jet-background interaction 79−54983
Na vapour jet target, gating and pumping action 80−10281
Pb, filament production, ejection of molten metal through nozzle, jet stability *(Japanese)* 78−52719
SF_6, supersonic jet, condensation and gasdynamic cooling 80−6089
SO_2 collection from low-vel. jets, efficiency 79−16683
U enrichment, jet membrane process 79−26683
UO_2-Na interaction, thermophysical behaviour of type 304 stainless steel impacted by jet of molten core debris 77−46319
^{235}U, large scale enrichment using separation nozzle 79−94654
XeF, supersonic expansion jet, B←X system rot. and vibr. anal., isotope intervals, fluoresc. spectra 80−14174
j.f.e.t. *see junction gate field effect transistors*
Johnsen-Rahbek effect *see adhesion; electrostatics*
Johnson noise *see thermal noise*
joining processes
see also brazing; cable jointing; soldering; welding
acrylic pieces of small surface area, cementing technique, appl. to light guides 78−13404
arc fusion splicing of low-loss single-mode fibres 80−53489
bimetallic electrodes for plasma torches, Cu to W joining methods 80−24266
bonded joints, adhesive nonlinearities, optimal length, performance 79−1103
diffusion bonding, in Ar atmosphere, investigation *(Japanese)* 78−11491
fibres joining, for transmission appl., losses causes and reduction *(Norwegian)* 77−14801
glue joints, axisymmetric with optimal shearing stress distrib. within glue layer *(Polish)* 79−66256
hot pressing ferrite and ceramic, bulk interaction *(Russian)* 80−40277
lined interference filter cementing technique 79−72729
metals, surface pretreatment effect on joint bond strength by cyanoacrylate adhesive Kanokonlit-E *(German)* 79−57202
Mirror Fusion Test Facility supercond. coil development 79−31202
optical fibre butt-joining to Ti-diffused $LiNbO_3$ waveguide 79−76812
optical fibres, multimode, splicing method using elec. arc 77−27391
optical fibres, multimode, using semi-automatic splice machine *(Japanese)* 79−59854
optical fibres, single-mode, low-loss detachable connector *(Japanese)* 80−33163
powder layer on steel backing plate, joint form. kinetics for hot pressing 80−100961
screw-fastened joints for thermal contact at low temperatures 79−35760
thermoelectric module fabrication, with Bi-Te thermoelements and Pd electrode, biomedical implantable sources appl. 79−52952
Si, joining and recrystallisation using thermomigration process 80−65298
SiC, dense, joining by hot pressing, and bond strength 80−66458
Ti, low-pressure diffusion bonding 80−11873
jointing, cable *see cable jointing*
jointing (electric connectors) *see electric connectors*
Jordan-Thiry field *see cosmology; general relativity*
Josephson effect
absorption effect current steps, inflexion point structure anal. 77−20496
AC, appl. to parametric convertor type pulse amplifiers 78−19184
AC Josephson-Fiske effect, coherence 78−88082
air-bath enclosure for standard cell group monitoring by AC Josephson effect 77−82556
alternating field tunnelling current 77−16003
applications, recent developments *(Japanese)* 78−91819
applications, review 77−20503
applications in magnetometry and meas. standards, review 77−8243
automatic thermal cycling apparatus, for superconductive thin film devices 78−37014
barrier inhomogeneities, effect on junction behaviour *(German)* 78−91818
barrier nonuniformities influence on resonance amplitudes of high-Q Josephson tunnel junctions 79−56430
BIPM voltage standard, France 77−82484
bistability model, coherently driven Josephson junction 80−15661
breatherlike and other exact solutions to Josephson's eqn. in 2+1 dimensions 80−34560
bridges, electric field penetration and collective oscillations, review 80−88678
capacitively shunted microbridge, I-V characts., subgap struct. 77−15998
cavity-coupled Josephson device, parametric dependences, I-V characts. 80−20356
Clarke solder-blob junctions, hysteresis studies 79−28478
coherent microbridges coupled by external shunts, props. 79−28460
coherent transient effects 79−33406
coherent transient effects in Josephson junctions 77−63032
coherent tunable Josephson radiation generation, 2-18 GHz, with narrowed linewidth 78−88078
coherent-state formalism in supercond. and Josephson-junction calcs. 79−51723
contact microwave detector sensitivity and cutoff frequency rel. to capacitance 78−49902
contacts will semicond. layer, critical current *(Russian)* 79−99661

Josephson effect continued
coupled Josephson weak links, phase locking 78−72309
critical current and order parameter in Josephson arrays 79−33410
cryogenic current standard based on AC Josephson effect 77−82557
current biased resistively shunted Josephson junction model, frequency analysis of voltage oscill. 77−8239
current in superconductors with nonmagnetic impurities 78−39269
current thresholds in long Josephson junctions, resonant fluxon propagation, loss, bias and open-circuit boundary conditions 80−50003
current tunnelling fluctuation, exchange mechanism 79−24106
current-carrying junction in strong mag. field *(Russian)* 79−33411
Current-monitored superconducting bridge junctions *(Russian)* 78−23205
current-phase relation, Josephson contacts 78−76195
current-switched Josephson gate 79−82713
current-versus voltage source model 78−6484
cylindrical Josephson tunnelling, proposed expts. 79−65608
Dayem bridges, two interacting, coherent behaviour 78−14891
DC, spin-glass phase transition exam. 80−100594
DC Josephson current meas., automatic recorder 79−17444
DC voltage monitor for standard cell using AC Josephson effect 77−82552
detection of microwave and far IR radiation, Josephson junction response 77−61119
differential heterodyne freq. conversion at 0.4 mm wavelength, Josephson-effect receiver 79−26125
diffraction and interference phenomena 77−69457
digital Josephson technology−present and future 79−28472
double Dayem bridge structures, Josephson-like behaviour 77−8238
double Josephson junction interferometer, dynamics 78−68118
doubly-connected loops containing two Josephson junctions, flux penetration 77−85391
dynamics of Josephson-junction ccts. 79−73635
edge-grown low-capacitance supercond. tunnel junctions props. 80−54837
electrically controlled Josephson elements *(Russian)* 79−91189
EM radiation due to moving Josephson vertex in inhomogeneous junction 79−73642
exotic spinors in supercond., charge depend. of quantised flux and Josephson current 79−33400
far IR Josephson junction voltage-tunable differential heterodyne spectroscopy 79−30578
film structure with degenerate semiconductor bridge, physical model 80−20359
films with periodic thickness modulation, pinning effects 80−88702
FIR detectors, Josephson-junction direct devices and transition edge bolometers, review 80−77865
flux flow characteristics, large Josephson junction 78−84351
fluxon-breather-plasma oscill. decay in long Josephson junctions 79−56428
fluxons on a Josephson line with loss and bias 80−103794
Fokker-Planck solution for thermal noise 77−89906
frequency conversion of Josephson junctions in self-pumping mode of operation, anomalies 80−54839
frequency modulation appl., review 79−82724
functions, with linear-periodic current-phase relation, radiation-induced steps 77−59358
Ginzburg-Landau theory 77−89905
granular films as weak link in Josephson devices 80−88685
granular metal, supercond. transition, increased resistance rel. to quasiparticle tunnelling 80−88689
granular metal film, supercond. quenching when charging energy exceeds Josephson coupling energy 77−47943
granular supercond. contact, Josephson-coupled, behaviour in microwave field *(Russian)* 78−52158
granular superconductor, quantum interference, coherence and percolation *(French)* 79−56434
granular superconductors, coherence transition, structural disorder effects 80−88657
granular superconductors, effect of charging energy on transition temp. 79−91181
granular superconductors with Josephson coupling, transition to coherent behaviour *(German)* 78−84362
granulated superconductors, phase transitions, Josephson energy *(Russian)* 80−84540
half-harmonic parametric oscills. 80−50001
heterodyne receivers 78−12754
HF losses in tunnel junctions 78−88083
HF theory, electronic analogue prototype 80−100560
higher harmonics, flux tunnelling, thermodynamic free energy 80−60147
hybrid Josephson FET, feasibility 80−80451
impurity mode effects on crit. characts. of superconductors, Josephson current amplitude *(Russian)* 79−19692
inelastic electron tunnelling spectroscopy, advantages of supercond. electrodes 79−4625
inelastic tunnelling, pair-quasiparticle interference current 80−84566
inhomogeneous distributed Josephson struct., mag. flux dynamics 78−34932
inhomogeneous superconductivity, Ginzburg-Landau theory 80−88672
interaction between two Josephson junctions separated by small superconducting granule 79−33399
interference current component, Riedel peak width in supercond. tunnel junction *(Russian)* 80−11137
interferometer, observability of decay of off-diagonal long-range order in supercond. films 77−59352
interferometer flux detrapping by ground plane thickness modulation 80−2923
interferometer logic circuits, nonlinear current injection switching 79−11269
interferometers, large arrays, device parameter meas. 80−75682
interferometers, symmetric two-junction, self-induced reson., theory 80−107962
inverse AC Josephson effect voltage standard 78−16808
Josephson AC effect applications in precision metrology and novel voltage source *(German)* 80−70902
Josephson array, relation between critical current and order parameter 79−87197
Josephson coupled layered supercond., upper critical field *(Russian)* 80−100551
Josephson element principles, applications to precision meas. of electric potential and magnetic flux at high freq. *(Norwegian)* 80−80447
Josephson effect continued
Josephson interferometer resonance amplitude theory, SFQ memory cells 80−27317
Josephson junction interferometer, loop inductance 80−97034
Josephson junctions, applications in plasma physics 80−103194
Josephson oscillators, synchronisation props., single point junctions and chains 79−19703
Josephson tunnel junction, nonresonant vortex motion 80−97037
Josephson-junction arrays, radiation props. *(German)* 78−88077
Josephson-junction capacitor, QED theory 80−93049
junction, coherent radiation induced bistability 80−80453
junction, computer simulation of vortex motion, induced by phonon injection 79−73636
junction, current biased, eigenstates and eigenvalues 80−60148
junction, discriminating props., use in microwave spectral anal. 77−49748
junction, extended, I-V charact. perturbation calc. 79−69632
junction, externally pumped, singly and doubly degenerate microwave parametric amplifiers 79−26122
junction, fabricated by RF plasma oxidation, IV charcts. *(Japanese)* 80−84564
junction, finite size, current distribution *(Russian)* 78−80103
junction, frequency-agile, biasing for precise freq., analogue computer study 79−28455
junction, in inhomogeneous field *(Russian)* 78−84350
junction, millimetre-wave, far-infrared and infrared detectors *(Japanese)* 78−32872
junction, quantum interference, determ. of characteristics *(Russian)* 78−88081
junction, space appl. 80−85836
junction, with linear periodic current-phase relations, phase locking and microwave impedance 80−93043
junction array, granular supercond., phase transitions 80−88684
junction dynamics, sine Gordon eqn. solns. 79−28481
junction fabrication, sputtering system *(Japanese)* 80−55293
junction fabrication by ion implantation, electron beam lithography and dry etching 80−88693
junction of finite width, vortex penetration *(Russian)* 77−12065
junction phase-depend. cond. and nonequilib. props. probed by flux entry into weakly closed loops 77−66228
junction position measurement method 77−69458
junction threshold viewed as crit. point 78−56264
junction transients, effect of order parameter relax. 79−56423
junction with linear periodic current phase relation, AC Josephson like effect 77−32124
junction with matched RF source, analogue simulation 80−75683
junctions, collective excitations in superconductors below T_c, tunnel current fluctuations 79−33403
junctions, coupled, I-V charact., model calc. 80−84559
junctions, mixing in the FIR 79−26121
junctions, types, props., and limitations 79−28456
junctions fabrication, tunnelling through edge-grown barriers 80−100567
junctions with Sn-Ge barriers, adjustable tunnelling transmission 79−65613
large tunnel junctions, current steps in current-voltage characts. 79−65612
laser frequency measurement using supercond. point contacts 80−90824
layered composite, Josephson current, effect of lattice defects and localised mag. moments *(Russian)* 77−80879
layered superconductor, Josephson coupling between layers 77−77009
layered superconductors, Josephson coupling effects, review 80−84554
layered superconductors, surface supercond. *(Russian)* 78−31018
layers, mixed state struct. rel. to Josephson effects 79−4628
light induced weak link 78−34926
light sensitive tunnel junctions, self-reson. modes 77−63033
light-sensitive Josephson junctions, post developments, future appl. 79−28462
light-sensitive junctions, locally lowered tunelling barriers 80−100558
long Josephson contact, parametric reson. 77−8245
long Josephson function, driving of single vortex 77−63034
long Josephson junction, switching behaviour 77−77007
long Josephson tunnel junction, current steps induced by vortex motion 79−47199
long junction, boundary between static and dynamic states *(Russian)* 77−40002
long junction, oscills., exact solns. of sine-Gordon eqn. 78−68115
long junctions, microwave induced vortex motion 80−39715
long superconducting bridges with variable thickness, Josephson effects 78−14897
longitudinal electric field in superconductors and oscillations 80−15664
low-capacitance Josephson junctions, calc. of current-voltage characts. *(Russian)* 77−51848
macroscopic quantum phenomena in superfluid He and supercond., appl. *(Chinese)* 79−38263
magnetic field penetration into Josephson junction, solns. of static mag. field distrib. *(Russian)* 78−39270
magnetic field penetration into layered supercond. 77−80872
magnetic flux annihilation in a large Josephson junction 80−11139
magnetic flux propagation, appl. of elliptic sine equations in two space dimens. 77−55640
metal, granular superconductivity, instability 80−103796
metal inhomogeneous granular, superconductivity 80−103795
metals, granular, supercond. stability 79−82722
microbridge, high-resistance, with Bi crosspiece 80−93050
microbridge, Josephson radn., subharmonic energy gap struct. 79−91186
microbridge, thin film, nonreson. detection of Josephson radiation 78−43523
microbridge, thin-film, millimeter-wave conversion 79−73644
microbridge, variable thickness, DC and UHF props. *(Russian)* 78−10620
microbridge Josephson junction, current-phase relation, size dependence 80−44767
microbridge Josephson junction, fabrication using electron beam lithography 79−28457
microbridge SUPARAMPs, phase instability noise in Josephson junctions 79−26124
microbridges, Josephson submicron; fabrication using optical projection lithography and liftoff techniques 79−28458
microbridges, short, dynamic props. 79−47202
microbridges, ultrasmall, step-edge fabrication 80−49997

Josephson effect continued
microbridges, with paramag. impurities, Josephson steady-state effect *(Russian)* 80−93042
microbridges and arrays, I-V characts. temp. depend., Josephson radiation 79−28459
microbridges in resonant cavity, enhanced Josephson radiation and linewidth-narrowing 79−56433
microscopic theory of Josephson effect in supercond. constrictions 79−60989
microscopic theory of Josephson effect on supercond. bridges *(Chinese)* 78−14887
microwave induced resistive state in long tunnel junction 78−47914
microwave oscill. regenerative effects *(Russian)* 78−2630
microwave source, short term emission fluctuations 79−15263
military appl. for Josephson junction technology 80−50004
mixers, mm wave, using Nb point contacts 79−26123
mixers for heterodyne reception at submillimetre wavelengths present expt. status, future developments 79−26120
mm wave superconducting devices, Josephson-effect mixers and parametric amplifiers, present status 79−26119
mm waves video detection by capsule type point-contact Josephson junctions 80−13141
motor, rotational solns. in BCS theory 78−72310
moving junctions, theory 80−7041
multiple flux quantum transitions, comparison with I-U characts. using Nb-point contacts 80−60149
multiple junctions, higher voltage standard 79−26069
multipolar superconductive tunnelling device, theory and technical feasibility *(Chinese)* 79−38253
near-ideal Josephson junction, fabrication and behaviour, expt. 77−20502
nematic liquid crystals, AC Josephson effect, phase slippage 79−46565
noise down-conversion in pumped Josephson junction 79−56432
noise thermometer, comparison with nuclear orientation thermometer, 0.011-0.05K 79−63218
nondestructive readout RAM cells, design criteria 80−50000
nonequilibrium state influence 77−51855
nonequilibrium superconductivity, theory in coherent longitudinal phonon field 79−47205
nonlinear behaviour, qualitative theory 78−52159
nonlinear effect of Josephson junctions *(Russian)* 79−65603
nonstationary Josephson effect in short supercond. junctions *(Russian)* 79−78273
nonstationary nonlinear eqn., auto-oscills. *(Russian)* 78−60255
NPL standard voltage monitoring system based on AC Josephson effect 77−82554
optical modulator with weak-link diffraction grating 79−98486
optical waveguide controlled Josephson junction 78−66955
oscillator, current-drive, quantum modelling 80−75687
oxide formation process, for Josephson junctions, ellipsometic meas. *(Japanese)* 80−11561
pair quasiparticle interference, in meas. of flux entry into supercond. interferometer 78−14895
pair transfer, quantum-mechanical description, commutator and anticommutator of collective operators 80−60146
pair transfer in absence of phase coherence, theory 78−23207
parametric amplification at 35 GHz 79−95547
parametric amplifiers, gain-dependent noise temp. 80−84552
parametric inductance fluctuations in up-convertor 80−25052
parametrically coupled Josephson bridges, resistive state, promixity effect *(Russian)* 80−100550
partially phase-correlated junction states 79−65606
pendulum type mechanical analogue of Josephson junction *(Japanese)* 77−72948
periodic pair-current modulation in Josephson junction 80−25049
phase slip centre, charge imbalance waves and nonequilib. dynamics 80−54830
phase-locked loop analogue to study effects of thermal noise 77−47939
physical principles, appls. to electrical and magnetic meas. *(Croatian)* 79−11271
plasmon states in ultrasmall Josephson junction, dynamic Stark splitting 80−103790
point contact junctions, HF props. 79−28461
point contacts, phase-depend. cond. at microwave freq. 77−16001
point contacts, three-dimens. assembly, crit. currents and penetration depth 80−84560
point junction, nonlinear effects 77−40003
point junction chain, solitary wave soln. 79−87212
point junction under high voltage, nonstationary Josephson effect *(Russian)* 79−60987
point-contact resonance responses 79−99658
power spectrum of radiation from junction 78−43522
preset Josephson point contact for use at sub mm. wavelengths 77−22600
proximity effect bridge, thermal effects 77−63030
proximity junction, DC Josephson current temp. depend. 79−78271
proximity Kondo alloys, DC Josephson effect 80−88690
proximity systems, DC Josephson effect 79−56425
proximity systems with magnetic impurities, DC Josephson effect 80−100554
pulsars emission mechanism, AC Josephson effect hypothesis 80−82404
QED, compact, in 3-dimens., Josephson effect comparison 77−79238
quantum mechanics of nonconservative systems appl. to thermal decay of AC Josephson current near T_c 79−81
quasi-autonomous contacts, props. 78−88084
quasi-two-dimensional dirty superconductor, nonstationary Josephson effect *(Russian)* 80−100556
radiation interaction, of system of two Josephson junctions *(Russian)* 79−82715
radiation line width, eddy fluctuation influence *(Russian)* 78−19186
ratio/detection system, flexible, for comparing DC voltage developed by AC Josephson effect 79−21774
resistive junction, I-V characteristics 78−91820
resistively shunted Josephson junctions, AC, DC components of source current *(Chinese)* 79−11270
response times and low-voltage behaviour of SNS microbridges 79−65602
restored symmetries, quark system, Pomeron as Josephson current 77−61211
retarded Josephson eqn., critical limit cycles 79−1644
retarded Josephson equation, adiabatic and pendulum approx. 78−68119
retarded Josephson equation 79−19697
Riedel anomaly and nonlinear effects in Josephson point contacts 78−60253
ring system with weak coupling, mag. impurity tunnelling, current in ground state *(Russian)* 77−47944
ring with low capacitance Josephson point contact junction, flux transition mechanisms 80−44770
S-C-S(N) pure short microjunctions, nonstationary Josephson effect theory *(Russian)* 80−50010
sandwich system, near transition temp., proximity effect and Josephson current 80−7039
scattering model 80−93046
scattering model for DC Josephson effect, penetration depth 80−54838
self-oscillating Josephson mixer as submillimetric and far IR detector 77−38004
self-resonant modes analysis using mechanical analogue model *(Chinese)* 80−34563
self-resonant modes in junction exhibiting nonuniform max. current distrib. 78−56263
semiconductor-barrier, cavity resonances 78−84352
series array of proximity coupled bridges, mode locking 77−51852
series-connected Josephson junctions, noise characts. 77−66229
shunted Josephson junction model, autonomous case 78−34929
shunted Josephson junction model, nonautonomous case 78−39267
shunted superconducting bridges, transition from relaxational to Josephson oscillations 78−72312
sine-Gordon eqn. two dimens. solns. 79−82725
sine-Gordon solitons, boundary effects 80−62481
SINIS junction proximity system, crit. Josephson current calcs. *(German)* 78−88079
SNS junction with impurities, Josephson current theory 79−42705
solitary phenomena in dissipative driven Josephson junctions 79−56429
soliton solutions of Josephson transmission line oscillators 79−87211
solitons, theory and applications 78−36811
spin-pairing state investig. via Josephson current between weakly-coupled superconductors 77−47942
spontaneous magnetic-flux in junction with mag. impurities 78−47915
SQUID, A/D conversion, conditions for countable pulse train 79−91191
SQUID, oxidised Nb granules as three-dimens. Josephson junction array 79−67362
SQUID, thermodynamic equilibrium fluctuations generation by Josephson junction, Werthamer theory 80−100564
SQUID, with two Josephson junctions, limiting magnetic field sensitivity *(Russian)* 77−77010
SQUID magnetometers, AC-biased, macroscopically quantised, higher harmonics in Josephson effect 80−98952
SQUID signal strength versus frequency 79−28453
SQUIDs, multiple mag. flux entry, cosϕ conductance exam. 79−4623
strip line coupled Josephson junctions, microwave response *(Japanese)* 77−69454
submillimetre wave mixers, review 78−45712
submillimetric Josephson mixer receivers, potentials and limitations 77−38003
subMM and MM detection by Josephson junctions mounted in a waveguide 80−4767
superconducting alloy, transition metal impurities, described by Anderson model, Josephson tunnel effect 77−16000
superconducting bridge, DC Josephson effect, microscopic theory *(Russian)* 78−56258
superconducting bridges, Josephson effect and collective modes 79−56435
superconducting film, memory device storage of Abrikosov vortices 79−28487
superconducting interferometers, threshold curve anal. 80−49999
superconducting Josephson point contacts with low capacitance *(Russian)* 79−4624
superconducting loop, transition between quantum states, erratic behaviour 77−55641
superconducting loop broken by damped Josephson junction, anomalous flux penetration 80−97033
superconducting loop of N Josephson junctions, kinetic momentum quantum effect 79−87199
superconducting magnetic field problem, model, iterative soln. 79−65605
superconducting magnetometers for very weak fields 79−30510
superconducting microbbridges and point contacts, nonstationary Josephson effect 79−38256
superconducting order parameter, rel. to macrowave function, near T_c 79−47191
superconducting point contacts, DC Josephson effect investig. *(German)* 80−39713
superconducting weak links, current steps *(Chinese)* 79−91187
superconducting weak links, review of physical processes 79−60983
superconductive bolometers for submillimetre waves 78−37063
superconductive film, microwave irradiation stimulated superconductivity 79−47201
superconductivity, basic principles *(German)* 77−89896
superconductivity characterisation, non-equilibrium 80−100557
superconductor-degenerate semiconductor-superconductor structures, critical Josephson current calc. 78−52162
superconductor-insulator-superconductor contacts, critical Josephson current near T_c *(German)* 78−84361
superconductor-insulator-superconductor contacts, Josephson tunnelling *(German)* 78−84359
superconductor-metal-insulator-metal-superconductor system, Josephson current, weak supercond. *(Russian)* 80−54842
superconductor-semicond. device research, future prospects 79−28467
superconductor-semiconductor-superconductor system, semiconductor barriers *(German)* 78−84360
superconductors, type I, mixed state, Josephson condition, phase jumps *(Russian)* 80−107967
surface acoustic waves, nonlinear interaction with Josephson junction 77−85392
surface phenomena and topological singularities, Josephson phenomena, EM surface waves, transient phenomena 79−99653
thermometer, absolute noise, resolution of unmodelled errors 78−62196
thin film superconducting bridges, Josephson effect and collective oscillations *(Russian)* 78−31022
thin film technology, appls. in energy, optics, and electronics, review 80−78932

Josephson effect continued
transmission line, appl. of perturbation anal. of fluxon dynamics 79−11280
transmission line, quantum flux propag., soliton dynamics 77−76714
tunnel characteristics, effect of paramagnetic impurity 77−69455
tunnel current, Bogolyubov, quasi-particle calc. 79−1647
tunnel current, paramag. impurities, singularities of second derivatives in Abrikosov-Gor'kov model 77−69456
tunnel current in Josephson junctions, natural fluctuations *(Russian)* 77−47937
tunnel junction, finite length, steady oscillatory states 80−44773
tunnel junction, flicker (1/f) noise 77−1520
tunnel junction, paramag. impurities effect on Josephson current *(Russian)* 80−70903
tunnel junction, Q-factor and reson. amplitude calc. 78−10617
tunnel junction, quasi-particle heterodyne mixing 79−56395
tunnel junction, thin-film, stability testing standard cell EMF appl. 77−67468
tunnel junction, two gap state induced by singular IV charact. 79−1645
tunnel junction, vortex motion induced by phonon injection 79−4622
tunnel junction array parameter amplifier 79−65611
tunnel junction in arbitrary cct., response 78−39265
tunnel junction parameters, microwave freq., temp. depend. 80−34561
tunnel junction parameters near transition temp. 79−65610
tunnel junctions, current density distrib. Fiske mode field depend. 79−78264
tunnel junctions, fabrication and four terminal resistance study *(Chinese)* 78−68116
tunnel junctions, large, current-voltage charact. 78−6483
tunnel junctions, resistively shunted 78−47916
tunnel junctions, with single flux vortices, current-voltage charact. 77−59360
tunnel junctions containing vortices, excess DC current, mag. field depend. 79−38259
tunnel junctions of nonuniform width, max DC Josephson current vs. external mag. field charact. calc. 80−65747
tunnel junctions of superconds. with paramag. impurities *(Russian)* 77−80878
tunnel microwave coupling, influence resistance effects *(Chinese)* 78−80099
tunnelling current, theory of cos ϕ term. 78−14890
tunnelling junctions, self resonant modes with zero external magnetic field, theory 79−24105
tunnelling junctions, self-resonant modes with zero external mag. field 80−15660
tunnelling junctions, supercond. fluctuations, below trasntiion temp. 78−84354
two- and three-dimensional superconducting constrictions, static props. 79−28479
two-dimensional junction, stationary current flow, approximate linear analysis 77−8240
two-junction Josephson interferometer, reson. phenomena, anal. 78−47910
type I superconductors, spectroscopy using mag. impurity relax. of Josephson junction-Fiske modes 77−80880
ultrahigh resolution sampling system 80−90828
ultrashort current pulse generation and meas. with Josephson devices 80−90827
ultrasonic effects 79−42706
undergraduate experiment, 3rd yr, Nb-Pb-Sn junction 78−54126
unit voltage standard, precision comparison with working standards 77−53941
variable thickness Josephson microbridge, I-V charact. microwave irradiation depend. 80−25051
video-detector, optimisation for mm wavelengths 80−4768
voltage, standard cell group enclosure monitored by AC Josephson effect 79−26076
voltage cell using Josephson junction, computer simulation 79−93089
voltage divider influence on Josephson voltage standard system 78−74027
voltage measurement standard *(German)* 78−93722
voltage reference system, description of system and principles *(French)* 77−67470
voltage response of Josephson junctions, functional relation, extrapolation technique for accelerating computation 80−107963
voltage standard, Josephson effect, at zero current bias 80−57245
voltage standard, resistive divider *(Japanese)* 79−63266
voltage standard and Josephson devices *(Japanese)* 77−51851
voltage standard based on Josephson junction, commercial prototype 79−26068
voltage standard realization *(German)* 79−71401
voltage standards, BIPM- and NLP-standard comparison 79−21778
voltage standards, future of superconducting instruments in metrology 79−26020
voltage transfer standard based on AC Josephson effect, standard cell calibration appl. 77−82553
voltage-standard instrument, features 78−93729
vortex motion in Josephson junction line *(Japanese)* 78−91824
vortex pinning in Josephson contact *(Russian)* 78−68117
vortex width broadening in long Josephson tunnel junction 79−82718
weak link, model *(Russian)* 78−88080
in weak link, phenomenological model 77−8241
weak link, solns. of nonlinear eqn. of resistively shunted model 78−2628
weak links, applicability of Josephson effect theory in tunnel junctions 79−56431
weak links, nonequilib. effects, Ginzburg-Landau model *(Chinese)* 78−95396
weak links, quasiparticle-injected, simple-heating-induced Josephson effects 80−70904
weak links and films, scatt. model for Josephson behaviour 78−56261
weak-link, simplification of resistively shunted junction model 77−72946
weakly coupled supercond.-insulator multilayer stack, crit. field calc. 78−52161
weakly coupled superconductors in singlet and triplet spin-pairing states 78−14896
Werthamer equation, soln. at finite temp. 79−42703
Werthamer equation for tunnel junction at finite temps. and capacitance, resulting charact. 79−56427
zero field steps in Josephson junctions 79−47206
Al film with magnetically weakened section 77−28302

Josephson effect continued
Al granular films, inhomogeneous supercond. transitions, microwave meas. 80−103789
Al microbridges, non-equilibrium phenomena 79−56410
Al, point contact Josephson junction, microwave-enhanced critical currents 77−8242
Al, small particles, Josephson-coupled, local fluctuation effects 78−72308
Al-Al_2O_3-Pb Josephson junction, nonuniform, paracond., fluctuation effects 77−59359
Al-formvar-Sn junction, supercond. order parameter fluctuations below T_c 77−66227
Al-In_xO_y-Pb tunnelling junctions, fabrication 77−36027
Al-Pb proximity sandwiches, Josephson and quasi-particle tunnelling expts. 79−65616
Au/In proximity effect bridges, square arrays, transition temps. 80−84557
Au/Pb/In-oxide-PbBi tunnel junctions, supercurrent interference patterns and excess currents 80−100563
Cu-Cr, Kondo alloy, Josephson tunnelling effect 80−60145
$(Er_{1-x}Ho_x)Rh_4B_4$, superconducting ferromag., Josephson effect, point contact junction meas. 80−7043
Ge-Sn barrier Josephson tunnel junctions 78−68114
Ge-Sn barriers, Josephson tunnelling 79−28468
^{4}He, liquid, second sound, quantised vortex creation at constrictions, excitation model 80−44383
In film, Josephson arrays, proximity effect junctions 80−84553
In microbridges, non-equilibrium phenomena 79−56410
In, superconducting bridge, Josephson effect, flux tube nucleation 77−36028
In whiskers from Sn-In alloys, current carrying, superconductivity breakdown 80−60133
In-CdS-In, tunnel junction light-induced DC Josephson current 79−47204
In-CdS-In Josephson junction, exhibiting nonuniform max. current distrib. self-resonant modes 78−56263
In-In_2O_3-Pb, tunnel junction fabrication for MM-wave detector 80−100427
In-In_xO_y-Pb tunnel-junction barriers, evidence for chemical annealing effects 79−42701
In_2Bi-In(Bi) laminar eutectic alloy, SNS struct., Josephson behaviour *(French)* 78−26996
Mo_5PbS_8 embedded in resin, composite supercond., high transition temp. 80−88660
Nb bridges, variable thickness, microwave mixing 77−85390
Nb, bulk granular supercond., thermal fluctuations compared to Josephson weak link array 78−43520
Nb Josephson junctions, excess current anal. 79−28465
Nb Josephson junctions, submicron, fabrication by evaporation 79−28920
Nb Josephson point-contact far IR detector props. 79−30543
Nb, nanobridges Josephson effect, quasiparticle diffusion time, inelastic scatt. time 80−34556
Nb on thin Si membranes, super-Schottky and Josephson-effect devices 79−28469
Nb point contact, far IR freq. depend., of AC Josephson effect 79−33407
Nb, point contact Josephson junctions, thermally recyclable, as low-noise mixers 78−62224
Nb point contacts, AC Josephson effect meas. at 604 GHz 77−80876
Nb point contacts, Josephson effects in far IR, high freq. behaviour 79−1643
Nb, superconducting bridges by electron beam lithography and ion implantation Josephson effect 80−20355
Nb superconducting point contacts, DC and HF behaviour 78−31021
Nb superconducting point contact, singularities of I-V curve and voltage fluctuations 80−93044
Nb thin film microbridge, video detection of far IR radiation *(Japanese)* 80−97038
Nb thin film microbridges, fabrication and charact. 79−19705
Nb thin-film Josephson tunnel junctions, fabrication and props., in situ ellipsometric meas. 80−65749
Nb tunnel junction, temp. dependent props., 2-9L 77−24642
Nb, variable thickness bridges on GaAs substrates, props. 79−28464
Nb, variable thickness bridges, mm wave response 79−28463
Nb-Al film, Josephson junction, tunnelling exam. 79−38257
Nb-Cu-Nb junctions, Josephson effect meas., critical current, temp. depend. 80−93041
Nb-Nb Josephson junctions, submicron, thermally recyclable, fabrication and charact. 80−100566
Nb-Nb point contact junction, supercond. weak couplings, high-freq. props. 78−68122
Nb-Nb superconducting point junctions, I-V charact. *(Russian)* 79−51727
Nb-Nb_2O_5-Pb Josephson junction formed on Nb film edge 80−107960
Nb-Nb_2O_5-Pb(In) Josephson junctions, props. of Nb_2O_5 thermally grown tunnel barriers 80−100568
Nb-Nb_xO_y-Pb, two-dimens. Josephson junction, supercurrent vs. mag. field charact. 80−34562
Nb-Nb_xO_y-Pb Josephson tunnel junction form. and ageing, adsorbed gas effect *(Russian)* 78−14899
Nb-Nb_xO_y-Pb Josephson junction current-biased on Fiske steps, mag. field depend. 80−84567
Nb-Nb_xO_y-Pb junction, thin Al layer effect on tunnelling charact. 77−85393
Nb-Nb_xO_y-Pb(In) Josephson junctions, preparation and props. *(Russian)* 79−91188
Nb-Nb_xOy-Cu/Pb supercond. proximity junction, max. DC Josephson current, thickness depend. 79−82719
Nb-NbO_x-Pb, miniature tunnel junction, gap voltage determ. 79−7939
Nb-NbO_x-Pb Josephson junction, self-reson. modes 78−64169
Nb-NbO_x-Pb Josephson junctions with high current densities, critical current 80−100552
Nb-NbO_x-Pb Josephson tunnel junctions, fabrication using FR glow discharge oxidation 80−34559
Nb-NbO_x-Pb junction, static charact. of tunnelling cryotrons 79−28480
Nb-NbO_x-Pb tunnel junction, crit. Josephson currents, temp. depend. 78−2629
Nb-NbO_x-Pb tunnel junctions with high normal resists.,, crit. currents 79−56399

Josephson effect continued
Nb-NbO_x-Pb tunnel junction, temp. depend. of effective Nb energy gap 80−80454
Nb-NbO_x-PbIn Josephson junctions, penetration depth of supercond. films 79−42691
Nb-NbO_x-PbIn window type junctions, critical Josephson current depend. on magnetic field 79−65607
Nb-NbO_x-Sn long Josephson junctions, flux-flow voltage, dynamic vortex motion 79−4620
Nb-NbO_xPb tunnel junctions, current density distrib. 80−39717
Nb-Nb(Nb_3Sn) supercond. point contacts, crit. currents, effect of laser radiation *(Russian)* 79−28484
Nb-oxide-Pb tunnel junction, capacitance and ellipsometrically determined oxide thickness 77−4469
Nb-oxide-Pb tunnel junction, anomalous microwave-induced voltages 78−39266
Nb-Pb, long, magnetic field behaviour of zero field steps 80−100561
Nb-Pb tunnel junction, crit. Josephson current, proximity effect model 80−93047
Nb-Te-Pb Josephson junctions, prep. and props. 80−65754
Nb_3Al, quantum interference and Josephson effect *(Russian)* 78−56259
Nb_3Ga Josephson junctions, excess current anal. 79−28465
Nb_3Ge, bridge contact, Josephson effect 80−70906
Nb_3Ge, superconducting thin films, energy gaps from tunnelling meas. 80−25050
NbN embedded in resin, composite supercond., high transition temp. 80−88660
NbN film, ultrathin granular, zero dimensionality and Josephson coupling 78−10612
NbN granular microbridges, Josephson effects 80−84556
NbN weak links, granular, Josephson behaviour 80−75681
NbN-NbN point-contact Josephson junction, fabrication and charact. 78−19189
NbN-V_3Ga point-contact Josephson junction, fabrication and charact. 78−19189
NbO_x-Pb junction, with high tunnel current density, fabrication and appl. to high speed switching 77−24645
Nb_3Sn, nonstationary Josephson effect, 13-18.3K, 9-10 GHz, 20 MW *(Russian)* 78−2631
Nb_3Sn, superconducting thin films, energy gaps from tunnelling meas 80−25050
Nb_3Sn thin film bridges, AC Josephson effect 79−42702
Nb_3Sn-Nb_3Sn supercond. point contacts, crit. currents, effect of laser radiation *(Russian)* 79−28484
Nb_3Sn-Pb tunnel junction, Josephson props. 79−7937
NbV-VO_x-Pb Josephson tunnel junction, VO_x effect on props. 79−87203
Pb alloy Josephson tunnelling gate, thermal cycling 78−19188
Pb granular film, Josephson coupled, resistive transition 80−88683
Pb, granular film, superconducting, Josephson-coupled, role of clusters in localisation 80−39716
Pb, narrow film strip, weak link induced by optical guided waves 78−14886
Pb, small junction, temp. and mag. field variations in resist. cos ϕ conductance and effective capacitance 78−84357
Pb superconducting variable thickness microbridge, microwave response 79−82717
Pb thin strips, supercond., optical wave illum., critical current behaviour 80−50012
Pb, tunnel junction, basis Josephson parameters, depend. on temp. below T_c 79−56442
Pb-alloy Josephson tunnel junctions, effect of process variables on elec. props., cryogenic memory appls. 80−65748
Pb-Bi counterelectrode Pb alloy Josephson junctions 80−65743
Pb-CdS-In Josephson junction, light-sensitive, structural fluctuations *(Russian)* 78−56265
Pb-In, series-connected Josephson tunnel junctions, fabrication procedure diagnostics 78−47909
Pb-In film, RF sputter anodisation, Josephson junction form., ellipsometry anal. 79−29258
Pb-In_xO_y-Pb tunnelling junctions, fabrication 77−36027
Pb-In-Au, series-connected Josephson tunnel junctions, fabrication procedure diagnostics 78−47909
Pb-In-Au alloy, Josephson junction electrode materials, strain relax. 79−38255
Pb-In-Au tunnel junctions, strain relax. effects 79−65617
Pb-In(-Au) base electrode film Josephson junctions, tunnel barrier oxide struct. 80−65750
Pb-Pb bridge, variable thickness, DC and AC Josephson effect 78−31016
Pb-Pb bridge, variable thickness, static mag. field effects, Josephson effects 78−31017
Pb-Pb_xO_y-Pb Josephson junction, long-term stability at liq. N_2 temp., voltage standard 77−72945
Pb-Pb_xO_y-Pb thin film Josephson junctions, prep. *(Slovak)* 79−42699
Pb-PbO_x-Pb, long Josephson tunnel junction, current steps induced by vortex motion 79−47199
Pb-PbO_x-Pb small supercond. tunnel junctions, effect of capacitance in I-V charact., high-freq. obs. 80−80448
Pb-PbO-Pb, tunnel junction fabrication for MM-wave detector 80−100427
Pb-Sn junctions, small area high current density normal resistance, RC times 80−34555
Pb-Te-Pb Josephson junction, cavity resonances 78−84352
Pb-Te-Te oxide-Pb Josephson junctions, prep. and props. 80−65754
PbIn-oxide-Pb junction, two-particle tunnelling and microwave effects 78−43527
Pd-CdS-In, tunnel junction, light induced DC Josephson current 79−47204
Si strongly-doped monocrystal Josephson junctions 79−56400
Sn, cross-like film structures, microwave irrad. stimulated superconductivity and Josephson effect 79−60988
Sn film, vac. deposition rate effect on supercond. Josephson tunnel junctions 80−2954
Sn microbridges, non-equilibrium phenomena 79−56410
Sn microbridges, nonequilibrium enhanced supercurrents 78−43526
Sn, small particles, Josephson-coupled, local fluctuation effects 78−72308
Sn, superconducting variable thickness microbridge, microwave response 79−82717
Sn thin-film superconducting bridge microwave impedance anomalies 79−7942
Josephson effect continued
Sn tunnelling-coupled fine particles, fluctuations of Josephson current 77−63031
Sn, variable thickness bridges on GaAs substrates, props. 79−28464
Sn-O-Sn, tunnel junction, parametric amplification on RF-induced steps 79−78266
Sn-oxide-Sn tunnel junctions meas. temp. depend. of cos 0 conductance 78−10611
Sn-Sn bridge, variable thickness, static mag. field effects, Josephson effects 78−31017
Sn-Sn_xO_y-Sn long Josephson tunnel junction, flux flow, crit. conditions 80−80452
Sn-SnO_x-Sn long Josephson junctions, flux-flow voltage, dynamic vortex motion 79−4620
Sn-SnO-Sn Josephson junction current-voltage charact., resonance detection cct. 78−54406
Sn-SnO-Sn tunnel junction, temp. depend. of cosϕ conductance, plasma reson. expt. 79−33405
TaS_2 intercalated with methylamine, supercond. layer cpd., crit. field enhancement and reduced dimensionality 80−60152
TaS_2 intercalation complexes, superconductivity 78−91803
TaS_2(2H), supercond. transition temp., upper crit. field, and interlayer coupling strength 79−56406
$TaS_2(pyridine)_{1/2}$ intercalation complex, supercond. transition temp., upper crit. field, and interlayer coupling strength 79−56406
V/Al-Al_xO_y-Pb tunnel junction, superconducting transition, critical currents, Josephson effect *(Russian)* 80−29507
V-CdS-In Josephson structures, light-sensitive 79−99660
V-CdS-In preparation and behaviour obs. Josephson junctions 80−100559
V-V_xO_y-Pb tunnel junctions, Josephson characteristics *(Russian)* 77−47938
V-VO_x-Pb tunnel junction, crit. currents exam. 78−23209
VNb-NbO_x-Pb Josephson tunnel junction, compared with VNb-VO_x-Pb 79−87203
V_3Si embedded in resin, composite supercond., high transition temp. 80−88660
V_3Si, superconducting thin films, energy gaps from tunnelling meas. 80−25050
V_3Si-SiO_x-Mo_3Re_2, supercond. tunnel junctions 80−107961
Joshi effect *see glow discharges*
Joule-Thomson effect
acetone, isothermal Joule-Thomson coeff. 80−43828
benzene vapour, flow calorimeter 79−58688
chloroform, isothermal Joule-Thomson coeff. 80−43828
cyclohexane vapour, flow calorimeter 79−58688
ethane, use of high press. recycle-flow calorimeter 80−42228
ethanol vapour, isothermal Joule-Thomson coefficient, equation of state 80−24119
forced convection heat transfer in porous medium with Joule-Thomson effect 77−89198
gas mixtures, thermodynamic props. prediction 78−83512
gas pipe flow, turbulent Graetz problem, Joule-Thomson effect 78−75204
methanol vapour, isothermal Joule-Thomson coefficient, equation of state 80−24119
pipeline compressible flow and heat transfer simulation program 77−19638
CO_2, Joule-Thomson coeff. at 20-583°C 77−42956
Cs, 768-1234K 78−71420
Cs vapour, thermodynamic props. calc. from Joule-Thomson data 78−94886
junction gate field effect transistors
flicker noise absence comparison with highly doped semicond. number-fluctuation model 79−60882
generation-recombination noise at 77K 79−60883
neutron-prod. defects, investigation by transcond. meas. 77−15455
photodetector low-noise amplifiers using J-FETs for optical fibre receivers 78−37997
radiation dose measurement using radiation induced changes *(Japanese)* 78−78504
semiconductor depth profiling by electron beam induced junction current meas. 80−96977
sensors for high direct voltages meas. 79−44916
Si, junction FET, annealing of neutron induced defects, transductance meas. 78−43052
Si-sapphire, interface radiation induced charge trapping, rapid anneal phenomena 79−19666
junction lasers *see semiconductor junction lasers*
junctions, waveguide *see waveguide couplers*
Jupiter
1.4 GHz radio emission, circular polarisation 77−64692
1979 J 1 discovery by Voyager 2 camera 80−77334
1979 J 1-3, satellite periods from Voyager 1 and 2 data 80−105196
1980 LB, 2:1 resonance with Jupiter 80−82259
β Scorpii occultation, turbulent scatt. 77−37562
absolute reflectivities and limb darkening, 4100-8300 Å Si vidicon imaging 78−7916
acetylene formation, by photolysis or thunderstorms 79−66957
Amalthea, effect of proximity to Roche limit on dynamical behaviour of ejecta 80−98592
Amalthea (J V), UBV photoelectric photometry near greatest W. elongation 78−36493
Amalthea and Galilean satellites, 1976-8 absolute and relative posns. 79−62789
angular momentum effects on early evolution 77−71055
asteroid, mean motion resonant with Jupiter, short-periodic perturbations 78−53803
asteroid 1125 China, long period motion near 2:1 commensurability 77−13276
astrolabe obs., 1976-77 winter period *(French)* 78−32387
astrometric position determ. *(French)* 80−77326
astrometric position determ. 80−77327
astrometry, positions determ. with Odessa meridian circle, (1974 to 1975) *(Russian)* 79−44394
astrometry, positions of Jupiter and Galilean satellites obtained in 1978 at ESO-La Silla *(French)* 80−21943
astrometry using image photometric anal. technique *(French)* 80−85880
atmosphere, $^{12}CH_4(^{13}CH_4)$ ν_4 band, line parameters, 7.7 micron transmission 78−85894

Jupiter continued
atmosphere, $^{74}GeH_4$ transition moment for ν_3 79−72363
atmosphere, acetylene abundance 78−16337
atmosphere, circulation and weather 77−22134
atmosphere, cloud microphysics anal. 79−16853
atmosphere, CO obs. at 5 μm, airborne spectroscopic obs. 78−36491
atmosphere, convective instability of fluid layers 80−56754
atmosphere, D abundance 78−45265
atmosphere, density model and total reflection of light *(Italian)* 79−21221
atmosphere, dynamical activity in 1975, photographic and photoelec. obs. 79−21224
atmosphere, effective transport coeffs. of plasma in LTE approx. 78−1801
atmosphere, equatorial belt, spectrophotometry in 0.6-1.1 μm range 79−96960
atmosphere, future spacecraft missions 77−37564
atmosphere, GeH_4, ν_3 fundamental, theoretical absolute J-manifold intensities 78−74707
atmosphere, GeH_4 abundance from IR spectrum anal. 78−61791
atmosphere, GeH_4 IR laser sideband obs., ro-vibr. struct., isotope shifts, line widths 79−72306
atmosphere, greenhouse effect 80−101544
atmosphere, H_2 2-O quadrupole spectrum obs. 77−45351
atmosphere, H_2 content from spectral line equivalent width *(Russian)* 78−12143
atmosphere, ionisational nonequilib. shock layer effects on entry heating 77−25979
atmosphere, IR laser heterodyne spectroscopy for trace gases remote detect. 78−61606
atmosphere, IR obs. by Fourier transform spectroscopy 78−61747
atmosphere, IR radiation, review 80−8568
atmosphere, IR radiation absorpt. induced by press., mol. collision between CO_2, N_2, O_2 *(Russian)* 80−56600
atmosphere, light polarization and scattering 79−96814
atmosphere, low order effect of cosmic ray albedo neutron decay (CRAND) input 78−45271
atmosphere, mean temp. struct. from far IR spectral obs. 80−17540
atmosphere, methane absorpt. interpretation 77−29707
atmosphere, methylamine prod. and distrib. 77−64693
atmosphere, microwave spectrum 78−85889
atmosphere, NH_3 photochemistry 77−45354
atmosphere, NH_4OH aerosols existence, IR reflectivity spectra, Kramers-Kronig anal. 78−68500
atmosphere, particles, environments and possible ecologies 77−33394
atmosphere, PH_3 photochemistry rel. to Great Red Spot 77−16807
atmosphere, PH_3 photolysis and abstraction reactions 79−66327
atmosphere, probe flight characts., scale model expts. 78−7854
atmosphere, probe heat shield C vaporisation 79−1264
atmosphere, production and interaction of solitary waves 78−36496
atmosphere, radiation-induced cooling 78−85885
atmosphere, Raman scatt. 78−28571
atmosphere, response to heat sources and perturbations *(Chinese)* 80−85748
atmosphere, review 77−5470
atmosphere, scavenging reactions of acetylene and ethylene for P containing radicals 78−81582
atmosphere, spacecraft entry, modelling by H_2-He mixture 78−71413
atmosphere, spectroscopic results *(French)* 77−33403
atmosphere, struct. and comp. models, aerosols occurrence *(Russian)* 77−53465
atmosphere, subliming boundary layer flow, simulation 78−65545
atmosphere, temp. struct. from inversion of IR spectral meas. 79−75141
atmosphere, temporal characts., IR obs., north-south temp. asymm. 80−41760
atmosphere, thermal struct. 79−84735
atmosphere, thermodynamics of trace elements 79−66956
atmosphere, trace constituents upper limits from 5 μm spectrum anal. 78−61790
atmosphere, transport props. 78−57490
atmosphere, turbulent mixing coeff. and homopause height 78−49354
atmosphere, UV emission from excited atoms and molecules 78−40865
atmosphere, wind vector, eddy mmtm. and energy conversion obs. 80−72851
atmosphere abundance ratios determ., new spectroscopic method appl. 79−84734
atmosphere circulation and thermal regime, survey 80−8584
atmosphere coloration due to Si compounds 80−51689
atmosphere composition, IR spectral obs., 800-1000 cm^{-1} 78−16336
atmosphere constituents, comparison with Saturn, visible spectra obs. *(French)* 80−101550
atmosphere differential rotation, origin 80−46467
atmosphere disturbances and dislocations, triggering factors 80−72867
atmosphere IR absorpt. profiles of GeH_4, computer simulation 78−81584
atmosphere map at 2400 Å from Voyager 2 obs. 80−77336
atmosphere probe, mass and shape var. due to aerodynamic heating 79−84630
atmosphere simulation, synthesis of UV photoprod. organic solids, mol. anal. 78−69740
atmosphere zonal flow, baroclinic instabilities 80−31245
atmospheric, review 78−32377
atmospheric absorption in blue and UV 79−40125
atmospheric banding, hydrodynamic mechanism 79−44386
atmospheric circulation, quasi-geostrophic model 80−41761
atmospheric composition and cloud struct., deduced from absorpt. bands in refl. sunlight 80−56758
atmospheric constitution, struct. and dynamics 80−105186
atmospheric differential rotation, convective instability and geostrophic mode of motion 77−17426
atmospheric differential rotation, eqns. of momentum variation in convective shell 77−25978
atmospheric methane and ammonia abundance photoelectric obs. 77−33397
atmospheric probe, mass loss, shape change, real-gas aerodynamic effects 78−4055
atmospheric probe vehicles, SiO boundary layer surface opacity 79−45641
atmospheric structure and 5 μ limb-darkening 79−25539
atmospheric temp. struct. recovery from inversion of thermal radiance data 77−82154

Jupiter continued
atmospheric upper layer struct. model *(Russian)* 77−25976
atmospheric VHF refraction 80−98608
aurora due to protons, nightside 80−85890
auroral hot spots, Io- and Europa-related, longit. asymm. 79−75138
auroral hot spots, Lyman alpha obs. 78−16333
beaming model of Io-independent decametric radiation 79−53755
bounce averaged synchrotron loss in dipole field 77−87316
bow shock, Voyager 1 plasma wave turbulence 79−96954
brightness coefficient of disc features, phase effect 80−98602
brightness distrib., 1.3 cm wavelength, interferometric obs. 79−12424
brightness temperature at sub-mm wavelengths 79−53743
Callisto, brightness temp. at 1.3 cm wavelength 77−67062
Callisto, evolution and surface age 80−56755
Callisto, evolution from derived crustal description 80−82265
Callisto, icy satellite, mass-radius relationship 80−31222
Callisto, identification of water frost 78−4141
Callisto, IR emission spectra 80−82264
Callisto, surface affected by internal processes 80−21944
centre location in Voyager image transformation 80−101534
chemical structure of deep atmosphere 78−45270
circular polarisation of 1.4 GHz emission from radiation belts 77−37556
circulations in atmosphere rel. to terrestrial turbulence and baroclinic instability 79−40132
Clairaut eqn., connection to satellite geodesy and Jupiter 78−11795
close encounter with planet crossing objects, orbit changes 80−77329
close encounters with minor bodies, importance of nearly tangent orbits 80−82248
close encounters with minor bodies 79−35184
cloud, vertical struct. models, based on methane band photometry 80−56757
cloud configurations, Pioneer and Voyager obs. interpretation in time-depend. framework 80−26787
cloud distrib. between Voyager 1 and 2 missions, 5 micron obs. 80−77345
cloud features, Voyager velocity data 79−92710
cloud structure and vel. fields 79−92712
cloud zones, IR obs. 77−29712
clouds, vertical struct. from 5 μm meas. 77−29710
clouds spectropolarimetry, lines equivalent widths information content 80−31215
colour filter obs. in 1975-76 period 77−91470
colour photographs from space probe *(German)* 77−53445
colour pictures from Voyager space probes, 800 line scan TV system, land based receiver systems *(German)* 80−101549
cometary orbits evolution in sphere of action of Jupiter 78−7938
convective interior, turbulent viscosity and tidal Q 77−29713
cooling rate, rel. to surface condition 77−29714
corotating magnetosphere, self-consistent model 78−89109
cosmic ray electrons originating from Jupiter 80−72726
cosmic ray ionization of atmosphere 80−17538
current disc of magnetosphere, modeled using Pioneer 10 data 80−101551
dawn magnetodisc, energetic electrons 79−70987
dayside magnetosphere, departure from rigid co-rotation 79−96957
decametre radio emission, dynamic spectrum modulation lines origin 80−67643
decametre radiotelescope facility at Mt. Zao Observatory, Japan 80−51656
decametric and hectometer radio emission obs. 80−67644
decametric emission assoc. with corotating interplanetary mag. sector struct. 80−26710
decametric emission features and vars. *(Russian)* 78−65546
decametric emissions, obs. by spaced receiver network 79−48730
decametric harmonic radiation generation 77−45353
decametric noise and solar activity effects *(Russian)* 77−64694
decametric radiation, bandlike emissions 77−37558
decametric radiation, burst morphology and drift rates 77−37557
decametric radiation, Io-independent emission mechanism, theory 79−62788
decametric radiation, non-Io associated, obs. at freqs. above 30 MHz 80−85886
decametric radiation, origin of modulation lanes in dynamic spectra 79−53765
decametric radiation beaming, first direct meas. 78−89114
decametric radiation induced emission by Io accelerated electrons 77−45349
decametric radiation modulation by Io, charged particles acceleration 78−89110
decametric radiation source, synchrotron process 77−71056
decametric radiation sources, locations 79−75148
decametric radio bursts, modulation lanes in dynamic spectra 80−17535
decametric radio bursts, polarisation patterns in dynamic spectra 77−5490
decametric radio bursts hyperfine polarisation struct. 77−33400
decametric radio emission, correl. with solar activity 79−21222
decametric radio emission, dynamic spectra *(Japanese)* 79−8877
decametric radio emission, extraordinary mode, nonlinear phase bunching effects 77−2366
decametric radio emission, freq. and time depend. 78−89113
decametric radio emission, S-bursts dynamic spectra 78−20722
decametric radio emission, similarity with pulsar emission *(Russian)* 80−77333
decametric radio emissions, observational study of origins of L-bursts *(Japanese)* 79−70988
decametric radio S-bursts, Io-modulated theory *(Russian)* 80−8582
decametric source locations and Io phase motion 78−40866
decimetric radio spectrum, 1975 December 77−60718
dense ionised plasma, thermodynamic props., electron screening corrections 77−972
differentially rotating models, gravit. field and figure 78−7893
diffuse aurora, influence of plasma injection from Io 80−4289
dynamics and He distribution, in He-He fluid planet 78−28555
dynamo theory for mag. field generation *(German)* 78−40852
eclipses of Galilean moons, obs. program 77−9703
Elara radius and albedo 77−33399
electrically conducting fluid core 79−75147
electron bursts, low energy, Jovian origin 77−2367
electron density profiles, Voyager 1 radio occultation meas. 79−96953
electron flux propagation to Earth orbit 80−90357

Jupiter continued
electron intensity modulation in interplanetary space by corotating interaction regions 77−13283
electron modulation, Pioneer 10 and 11 obs. 78−61690
electron propag. out of solar equatorial plane, Pioneer 11 obs. 79−40123
electrons, interplanetary modulation and transport 78−45175
electrons influence on terrestrial outer radiation belt 79−88548
electrons obs. at 1 AU 78−4150
electrons pitch angle distribution in radiation belt 77−33402
electrons propagation close to Sun (≲0.5 AU) 79−101034
EM noise and radiowave propag. below 100 kHz in atm., equatorial region 80−26782
energetic heavy ions from Jupiter, possible detect. at Skylab orbit 80−26684
equatorial atmosphere, Voyager obs. of small-scale waves 79−92713
equatorial jet stream form. on surface due to cylindrical shear layer 78−16340
equatorial light and dark spots, comments on analysis 79−84739
equatorial regions, light and dark spots lifetimes and motions 78−57493
Europa, icy satellite, mass-radius relationship 80−31222
Europa, liquid water layer beneath ice crust, model 80−26780
Europa, UV emissions and possibility of O and H clouds 79−5775
EUV observations, from Voyager 1 encounter 80−26792
faint satellites, astrometric obs. during 1976 to 1977 opposition 80−26778
faint satellites (VI-XII), astrometric obs., (1974 to 1977) 78−89107
far IR spectra, airborne interferometry 77−25942
far IR spectrum, 45-115 μm obs. 77−29681
far IR spectrum, depend. on atm. vertical thermal struct. 77−60713
far UV (1200-1900 Å) spectrum, rocket-borne multichannel spectrometer obs. 77−25974
fictitious satellites motion, long-period effects at 1/1 reson. 78−85830
figure, hydrostatic equilib. eqn. numerical soln. 79−62773
figure parameters and gravit. moments, fifth approximation calc. 78−65547
first order theory, pertubed by Saturn, critical term elimination 79−35183
formation by accretion from rotating gas cloud 78−20630
formation of planet and satellites *(Chinese)* 78−69712
Galilean means, results from Voyager spacecraft 80−56759
Galilean satellites, 12.6 cm radar obs. 77−71057
Galilean satellites, 1975-6 astrometric obs. 80−4288
Galilean satellites, astrometric obs. in (1977) 79−48728
Galilean satellites, contrib. of water products to Jupiter magnetosphere 78−45268
Galilean satellites, diameters from Pioneer data 78−85893
Galilean satellites, dynamical coupling of periodic systems, resonance *(French)* 77−73938
Galilean satellites, dynamo mag. fields possible strengths 79−16873
Galilean satellites, eclipse spectrophotometry 79−96949
Galilean satellites, eclipses rel. to light hesitation determ. by Romer *(Danish)* 77−57140
Galilean satellites, ephemeris using Samson's theory *(French)* 78−16334
Galilean satellites, icy crater model to explain radar scatt. results 78−61789
Galilean satellites, improved ephemerides for Voyager mission 80−62066
Galilean satellites, interior structure from possible flyby meas. 78−36495
Galilean satellites, long period behaviour of orbits 78−40864
Galilean satellites, max. permissible exospheric temps. calc. 79−70989
Galilean satellites, mutual phenomena during 1979, obs. 79−80266
Galilean satellites, mutual phenomena in 1979 *(French)* 79−12427
Galilean satellites, near IR spectra rel. to surface composition 79−35180
Galilean satellites, orbit-orbit reson. of I_0, Europa and Ganymede 78−4093
Galilean satellites, orbits from numerical integration *(French)* 80−26779
Galilean satellites, photometric eclipses anal. rel. to theory of motion 78−53864
Galilean satellites, photometry of Io, Europa and Callisto, 1976 to 1979, possible solar variability detect. 80−98623
Galilean satellites, Pioneer 10 and 11 photographs 77−9699
Galilean satellites, pole positions 79−66954
Galilean satellites, positioned within dipole-like Jovian mag. field, rel. to form. 79−2516
Galilean satellites, radar obs. during 1976, results 78−61788
Galilean satellites, review 79−5777
Galilean satellites, spectral reflectivities in 0.32-0.86 μ range 79−35181
Galilean satellites, water ice existence, IR spectral reflectance obs. 80−82263
Galilean satellites as CO source in upper atmosphere 79−40128
Galilean satellites atmospheres, existences and gas concs. upper limits 78−96415
Galilean satellites magnetospheres, plasma and mag. field perturbations 80−46465
Galilean satellites motion theory 77−45352
Galileo Jupiter Orbiter Mission CCD camera 80−85859
Ganymede, atmosphere erosion by radiation belt energetic atomic particles 80−72736
Ganymede, brightness temp. at 1.3 cm wavelength 77−67062
Ganymede, evolution and surface age 80−56755
Ganymede, icy satellite, mass-radius relationship 80−31222
Ganymede, O atmosphere stability 77−29708
Ganymede, phase curve and surface microstructure from Voyager 1 photopolarimetry 79−96958
Ganymede, surface affected by internal processes 80−21944
Ganymede, surface model and characts. from radar obs. 80−90359
Ganymede disturbing Jovian magnetosphere 80−72856
Ganymede image restoration by maximum entropy method 77−60624
gravity field, results from Pioneer 10 and Pioneer 11 tracking data 77−37554
Great Red Spot, as plane vortex with elliptical nucleus, theory 77−53466
Great Red Spot, atmosphere baroclinic model, solitary waves on unsymmetric shear flow 80−82266
Great Red Spot, depend. on solar activity 79−101110
Great Red Spot, ionospheric plasma MHD effect *(Russian)* 79−37466
Great Red Spot, super hurricane model *(German)* 77−9704
Great Red Spot and South Temperate Belt white spots motion and struct. 77−67065
H_2 quadrupole lines in spectrum 79−70990
haze layers, Voyager 1 obs. from UV to IR 79−92714

Jupiter continued
hectometric radiation, Voyager spacecraft radio obs. 79−84732
HF observations, using interference-excising correlator 79−75110
Himalia, radius and albedo 77−33399
inflated magnetosphere, similarity model of rot. effects 78−57492
inhomogeneous atmospheric model anal., H_2 4-0 S(1) line 77−71054
inner magnetosphere, whistler mode noise 78−89112
inner plasmasphere, possible source by photoionisation of Io's H I ring 77−60715
inner satellites mutual phenomena in 1979, ephemerides 78−53866
insolation, latitudinal, seasonal and atmospheric effects 77−60704
interior, dense fluid mixture of nuclei, phase separation calcs. 77−56849
interior, rel. to phase separation of metallic H-He alloys 77−43333
interior models, water and rock abundances 77−33398
interior Vashchenko Zubarev formula for Gruneisen parameter 80−90030
internal magnetic field geometry rel. to particle trapping 78−28575
internal structure, model, central temp. calc. 78−28576
Io, 5 micron variability 80−46463
Io, 'volcanic' outbursts, elec. current origin explanation 80−82276
Io, absorpt. bands in near IR spectrum 79−5776
Io, active volcanic eruptions and hot spots, Voyager 1 discoveries 79−40131
Io, albedo distrib. on surface 79−53761
Io, albedo stability and colour markings, historical meas. 79−96951
Io, atmosphere, review 77−5479
Io, atmospheric models with NH_3, N_2 and Na 77−37559
Io, bright dawn terminator due to thermoluminesc. 78−96425
Io, brightness increase after eclipse, colour TV obs. 77−87318
Io, charged particle absorpt. in Jupiter's magnetosphere 77−25971
Io, cometary ionosphere model 78−69738
Io, correlation of posteclipse brightening with major solar flares 78−28573
Io, currently active volcanism discovery 80−26789
Io, erosional scarps 79−92699
Io, evidence of SO_2 from UV obs. 80−36561
Io, flux tube wobbling and surface cond. effects on Jupiter's decametric emission and magnetosphere 80−26783
Io, form. of Na clouds and regolith by micrometeoroid impact 80−77330
Io, gaseous SO_2 identified and upper limits for other gases 79−92704
Io, global SO_2 abundance upper limit 80−77332
Io, H_2O loss and anhydrous surface form. 79−53756
Io, implications of Na and K salts spectral refl. changes and luminesc. during proton bombardment 79−96950
Io, intense transient brightening obs. near 5 micrometres 79−101113
Io, interaction with plasma torus 80−98604
Io, IR refl. spectra, 2.8-5.2 μm 80−56756
IO, IR reflectance spectrum, absorption features 79−92706
Io, local gas emission mechanism *(Russian)* 80−82275
Io, long term light vars. *(Italian)* 78−93147
Io, mag. moment prediction from scaling law test 80−21934
Io, melting by tidal dissipation 80−4292
Io, morphology of Na emission region 77−49329
Io, Na cloud, comparison of models and two-dimens. images 79−12426
Io, Na cloud direct images 78−61792
Io, Na cloud distrib. and intensity 78−36494
Io, Na I D_2 emission line profiles, var. with orbital phase angle and mag. latit. 78−4139
Io, Na I D-line emission synoptic obs. 77−13281
Io, non-linear standing Alfven wave current system 80−72869
Io, periodic variations obs. in Na and K clouds 78−4138
Io, pictures of Na cloud 79−12425
Io, Pioneer 10 probe and Earth based obs. *(French)* 77−74006
Io, plasma torus, ion density spatial distrib. 80−72861
Io, post eclipse brightening, BV photometry 77−37560
Io, reflectance spectrum, evidence for sublimates and adsorbates 79−92707
Io, role of SO_2 in volcanism 79−92700
Io, search for colour changes and brightening upon eclipse reappearance 77−91469
Io, SHF radioemission and radiation belts *(Russian)* 80−36565
IO, SO_2 atmosphere stability 79−92705
Io, SO_2 frost IR spectra and deposition processes 80−77331
Io, SO_2 frost or adsorbate on surface, IR spectrum 79−92708
Io, SO_2 model atmos. and ionosphere 80−72853
Io, sulphur chemical cycles, involving S, sulphite, sulphide and sulphate 80−50837
Io, surface albedo rel. to laboratory samples 78−53865
Io, surface and environs, magmatic-volatile model 80−17537
Io, surface composition, comparison of observed and lab. reflectance spectra 77−60716
Io, surface composition 77−87314
Io, surface flows of quenched molten S 79−92703
Io, terrain units, map from Voyager 1 data 79−92696
Io, thermal and EM phenomena *(French)* 77−60714
Io, visible spectrum, search for new features 79−35185
Io, volcanic activity model based on plasma obs. 80−72870
Io, volcanic eruption plumes 79−92698
Io, volcanic features 79−92697
Io, volcanic plume dynamics 79−92701
Io, volcanic resurfacing rates rel. to volatiles 79−92702
Io, volcanism, sulphur as volatile material 80−51688
Io's torus, charged particle radial diffusion 80−72859
Io interacting with jovian magnetosphere, model 80−36563
Io interaction with environment, Jupiter Voyager imagery analysis 80−105197
Io Na cloud, distrib. implications 80−46464
Io Na cloud, monochromatic imaging using filters, slitless (multislit) spectrograph, and interferometers 79−8840
Io Na cloud, solar radiation press. as cause of east-west asymmetries 80−36560
Io Na D-line emission, comparison of observed and theoretical line profiles 78−93145
Io plasma disc, model of plasma injection 80−72860
Io plasma torus, auroral hiss obs. (by Voyager 1) 79−92709
Io plasma torus, radiative cooling and spectra 80−72850
Io plasma torus props. from Voyager EUV data 80−82262
Io surface composition, implications of Na and K doped NH_3 frosts reflectance spectra 78−84561
Io tidal heating rel. to Galilean satellites orbital reson. locks 79−75145
Io torus, latitudinal plasma oscills. 80−85892

Jupiter continued
Io-Jupiter electrodynamic interaction, theory 78−81583
Io-related decametric radiation, geometrical beaming model 79−101112
Io-related radio emission, Jovian longitudinal control 79−30004
ion fluxes, Voyager 1 and 2 obs. out to 1200 Jupiter radii 80−94667
ionosphere, daytime electron temp. calc. 77−25972
ionosphere, effect of electron precipitation, Pioneer 10 and 11 S band occultation obs. 77−56871
ionosphere, electron collision processes with hydrogenic ions 79−72424
ionosphere, energetic electrons precip. fluxes upper limit 79−75143
ionosphere, hydrocarbons, semiempirical electron impact ionis. cross-sections 78−1089
ionosphere, Pioneer 10 and 11 obs. of magnetic field orientation 79−25540
ionosphere, spectral broadening meas. by Pioneers 10 and (11) 80−109391
ionosphere, Voyager 2 occultation, radio obs. 80−77337
ionospheric Na, deposition and sputtering on Io 79−44405
ionsophere, secondary electrons 79−75140
IR, high-resolution spectra in 10.2-13.4 μm range 79−96947
IR and visible spectrum, C/H ratio 79−48729
IR images at 5 microns wavelength during Voyager 1 encounter 80−26799
IR imaging in 8-14 μ spectral region 77−41350
IR multiple freq. sounding of anomalous clouds 79−2515
IR observations of Jupiter and satellites, from (Voyager 1) 80−26790
IR spatial scans 80−82268
IR spectrum, 5-8 μm obs. 77−29711
IR spectrum, high resolution obs. around 80 μm 78−45267
IR spectrum, high resolution obs. between 30 and 50 μm 80−46462
IR spectrum 17-25 μ, comparison with thermal struct. models 77−45348
isotope abundances in atmosphere 79−58284
Jupiter/Ganymede, Jupiter/Callisto systems, satellite aided capture of external body 79−75087
kilometric radiation, 10-56 kHz, Voyager obs. 80−26781
kilometric radiation, ray tracing 80−72866
kilometric radiation, spatial and temporal studies 80−77328
L-bursts in decametric radio spectra 78−96424
Leda (Jupiter XIII), continuation ephemeris (1978 Sept.-1979 May) 78−69739
Leda (Jupiter XIII), ephemeris for 1977/78, Aug.-Apr. 77−82156
Leda (Jupiter XIII), orbit and ephemeris for 1974-2000 period 79−8875
Leda (Jupiter XIII), precise positions for 1976 Nov. 2 and Dec. 13 77−22135
lightning flashes, first results, geometric reduction 79−96952
line profile obs., effect of atmospheric point spread seeing function 78−3952
linear polarisation, obs. at 6, 11 and 21 cm wavelengths 77−87313
longitude measurements for surface details, phase exaggeration effect *(French)* 78−36497
longitudes, System III(1965), new system 77−33395
Love numbers 78−16338
low energy charged particle flux, Voyager LECP results 80−98605
Lyman α albedo rel. to solar activity 80−98601
Lyman α emission var. with solar cycle 80−41759
Lyman alpha albedo, calc. from hydrocarbon and H I photochemistry 80−105194
magnetic field, influence on Galilean satellites volcanism and rot. 80−31247
magnetic field, spacecraft meas. 79−2503
magnetic field apparent source depth, rel. to planet interior struct. 78−57478
magnetic field dipole and multipole models 77−33401
magnetic field origin 80−36564
magnetic field studies by Voyager 1, preliminary results 80−26793
magnetic tail, solar wind interaction with planetary field 79−96956
magnetic tail, traversal by Voyager 2 and Saturn, 1981 prospects 80−12706
magnetodisc, props. from mag. field meas. 79−58297
magnetopause motion, longitudinal control 78−49375
magnetoplasmadisc, struct. and props. 80−12704
magnetosheath sunward flow, depend. on solar wind press. 80−72857
magnetosphere, 1.79-2.15 MeV protons residence lifetimes in equatorial region 80−26785
magnetosphere, centrifugal distortion by equatorially confined current sheet 79−40134
magnetosphere, comparison of Earth-based and Pioneer results 78−12076
magnetosphere, compression by solar wind 79−12429
magnetosphere, current sheet plasma 79−84731
magnetosphere, diffusion coefficients determ. from Io observed effects 78−32388
magnetosphere, electron pitch-angle diffusion by whistler mode waves near Io plasma torus 80−4290
magnetosphere, electrostatic waves obs. 80−72865
magnetosphere, energetic electrons ten-hour modulation phase 80−26784
magnetosphere, energetic ions and electron, Voyager 2 obs. 80−77342
magnetosphere, energetic particle flux modulation rel. to current disc penetrations 79−44404
magnetosphere, energetic particles recirculation 78−89108
magnetosphere, energetic protons 79−101111
magnetosphere, equatorial confinement and vel. space distrib. of satellite ions 77−53464
middle magnetosphere, equatorial protons instability 80−67642
magnetosphere, field-aligned currents, Pioneer 10 and 11 obs. 77−25975
magnetosphere, high β plasma in dynamic current sheet 79−16872
magnetosphere, impulsive penetration of solar wind filamentary plasma elements 77−78581
magnetosphere, inner, L dependence of protons radial diffusion coeff. 78−16339
magnetosphere, longit. asymm. and energetic particles periodic escape 77−25973
magnetosphere, lossy radial diffusion model 79−53764
magnetosphere, low energy electron obs. comments 77−71053
magnetosphere, low-energy charged particle environment, Voyager 1 first look 80−26797
magnetosphere, mode coupling of Z-mode waves, decametric radiation source 77−29537
magnetosphere, outer, protons accel. at 32 Jovian radii 78−57489
magnetosphere, particle accel. 79−12428
magnetosphere, particle flux ang. distrib. in rot. system 77−9700
Jupiter continued
magnetosphere, planetary spin period accel. of particles 77−9701
magnetosphere, plasma cloud injection from Io, S and O ions discontinuities 80−90358
magnetosphere, plasma corotation lag from Voyager 1 obs. 80−90361
magnetosphere, plasma sheet theory 77−64697
magnetosphere, plasma wave propag., CMA diagrams 77−87317
magnetosphere, plasma waves from Voyager 2, radio obs. 80−77343
magnetosphere, props. from Pioneer 10 and 11 meas. 78−12145
magnetosphere, proton flux along magnetic field lines 79−53763
magnetosphere, radial diffusion eqn. for collision-affected plasma 78−49310
magnetosphere, radial diffusion of energetic particles 77−9702
magnetosphere, radial diffusion of Io-injected plasma 79−75144
magnetosphere, revised Pioneer 10 absolute electron intensities 77−37563
magnetosphere, S nebula 77−87315
magnetosphere, S plasma discontinuities 80−4291
magnetosphere, stability of electron shell distrib. to parallel propag. plasma waves 78−4032
magnetosphere, tailward directed ion beam 80−72854
magnetosphere, thermal electron density 79−40133
magnetosphere, time dependent model of current sheet 79−16875
magnetosphere, Voyager 1 meas of various ionic species 79−96955
magnetosphere, Voyager 1 obs. of energetic ions and electrons 80−26798
magnetosphere, Voyager 1 planetary radio astronomy obs. 80−26796
magnetosphere, Voyager 1 plasma wave obs. 80−26795
magnetosphere, Voyager 2 obs. of hot plasma environment 80−77341
magnetosphere, Voyagers to test magnetic anomaly model 79−44403
magnetosphere 80−72858
magnetosphere and bow shock, plasma densities from Voyager 2 obs. 80−77340
magnetosphere and bow shock, Voyager 2 magnetometer obs. 80−77339
magnetosphere and nonthermal radio emission, exploration methods *(Czech)* 78−32374
magnetosphere and radio emissions, conf. Snowmass, Colorado, USA (Aug. 1978) 80−41939
magnetosphere Birkeland currents and Io plasma torus, model 80−105198
magnetosphere corotation lag, inertial limit, theory 80−41660
magnetosphere dust derived from Io volcanoes 80−85889
magnetosphere energetics, comparison with terrestrial magnetosphere 79−58201
magnetosphere HF and LF events from Voyager 2 obs. 80−77344
magnetosphere low energy plasma, Voyager obs. 80−72855
magnetosphere plasma observations, Voyager 1 initial results 80−26794
magnetosphere shape and field, model 80−72868
magnetosphere trapped energetic particle spectrum 80−72711
magnetosphere-satellite interactions, aspects of energetic charged particle loss 80−36566
magnetotail structure inferred from plasma obs. 80−72864
Mariner Jupiter/Saturn 1977 mission 77−73932
Mariner-Jupiter-Saturn low energy charged particle expt. 77−70971
measures of photographs of 1974/75 apparition 77−60717
meteorology, large-scale moist convection 77−37555
methane and NH_3 bands, longitudinal variability, visible obs. 80−82270
methane and NH_3 bands spectropolarimetry, 6800-8200 Å 79−66955
methane band photometry, absolute reflectivity, centre-to-limb vars. 79−53759
methane band photometry, SEB and STrZ reflectivity, atm. models 79−53760
methane emission at 76 GHz correl. with decameter activity 78−4140
methane line profiles near 1.1 μ, as probe of cloud struct. and C/H ratio 80−62067
MF radio emissions latitudinal beaming 80−31246
millimetre radiation, short wave, obs. with wide-band radiometer based on superconducting point contact 79−96916
mm wavelength spectral lines detectability 79−5769
mutual phenomena of Jupiter's satellites (1973 Sept.-1974 Jan.) 79−40129
natural vibration spectrum, rot. effects, calc. 80−8583
near IR mapping spectrometer design and testing for Galileo Jupiter Orbiter 80−90336
near IR polarisation, obs. 78−85899
near IR spectral albedo, obs 80−31242
Neptune occultation, 1613 January 4, prediction rel. to obs. by Galileo 80−105485
North Temperate Current C, fast moving bright spot obs. 80−67640
nuclear energy sources, D-burning star hypothesis 77−13282
oblateness, correction using de Sitter theory for Io 77−29715
occultations by eclipsed Moon, 100 BC to 3000 AD period 77−49319
orbit, stability of Jupiter-Saturn-Sun system 77−9679
orbit second-order perturbations, semi-major axis secular vars. *(French)* 79−2474
orbital and solar resonance of inner three Galilean satellites 80−56753
orbiter mission, periodic orbits in restricted six-body problem 77−13216
orbiter probe mission, 1981, planning 78−4056
orbiting spacecraft motion and risk of collision with Galilean satellite 77−2322
organic compounds in atmosphere, hot-atom synthesis 79−101109
origin, implications for transneptunian planets and nature of long-period comets 79−8856
origin and evolution, arguments against Kumar's theory 78−45266
original evolution, evidence for accretion hypothesis 77−87311
outer magnetosphere, charged particles energisation 78−89111
outer magnetosphere, solar wind dynamic press. variations 77−71051
outer magnetosphere, solar wind magnetic field variations 77−71052
outer magnetosphere, temporal var. in heavy ion plasma 78−61787
outer magnetosphere neutral sheet, relativistic electron accel. 77−17424
outer satellites, origin rel. to libration-point capture theory 77−29636
particle accel. near Jupiter, effect of solar activity on MHD oscills. 78−57526
perturbations on cometary orbits, missing periodic objects 77−67072
perturbations on orbital elements of short-period comets 78−40871
perturbations on Periodic Comet Ashbrook-Jackson (1978 XIV) *(French)* 80−41767
Pioneer 10 and 11 photographs and Earth-based obs. 77−67064
Pioneer 10 imaging data for prominent belt and zone, haze particles 78−45269
Pioneer 11 post-Jupiter trajectory midcourse manoeuvre sequence for Saturn targeting options 78−7857

Jupiter continued
planetary model using fourth order theory and molecular eqn. of state 77−82155
plasma sheet, self-consistent model 78−57494
plasmapause theory rel. to Io as ion source 77−22133
plasmasphere, stop zones for decametric radiation 77−2368
plasmasphere, thermal struct. 78−93148
plasmasphere models 78−77517
polar moment of inertia determ. 80−94694
polar systems, limb darkening obs. and atmospheric props. 79−62790
position determ. in 1978 using Double Zeiss Astrograph, Belgian obs. *(French)* 80−72809
probe entry, Rankine-Hugoniot eqns., soln. using reduction-of-ionisation-pot. 77−9651
probe-to-relay communication MFSK frequency acquisition and tracking 77−64613
proton flux anisotropies, Pioneer 10 obs. 79−53762
radiation belt, nucl. meas. techniques 78−85895
radiation belts, 21 cm maps from all rot. aspects 80−105195
radiation belts, review 79−58296
radiation belts and atmosphere, Pioneer 10 ratio obs. 79−35179
radio brightness distrib. across disc 77−87319
radio bursts, obs. with student-designed radiotelescope, multidisciplinary teaching exercise 80−17759
radio emission, mag. field, energisation, comparison with pulsars 80−46466
radio emission, non-Io-related, solar wind effect 78−57491
radio emission, Stokes parameters obs. at 11 and 18 cm wavelength 80−67637
radio emission, study at 2.7 GHz with Cambridge 5 km telescope 80−82272
radio emission in decimetre range, Pioneer 10 data 77−45355
radio emission in H_2O 1.35 cm line 78−20664
radio emission modulation below 8 MHz 78−81581
radio emission obs. at 327 and 1410 MHz during Pioneer 11 fly-by 77−13280
radio emissions, investigation of mechanisms using VLBI *(Japanese)* 80−21927
radio S-bursts, source of 2.5-35 MHz radiation 80−36562
radiobursts of short duration, model 77−13279
radioemission, short-duration bursts, magnetospheric EM cyclotron instability mechanism 78−7919
radioemission at 100 kHz, from magnetosphere 80−85891
rapidly rotating magnetosphere, interchange stability 77−17423
Red Spot 90 day oscillation, coincidence with position of Mercury 77−82158
reflectivities during 1976 opposition 79−40124
regular satellite system, form. model rel. to masses 78−69714
relativistic electron distrib. in interplanetary space, 1 to 11 Au, continuously emitting point source 78−4149
resonance in the restricted problem of three bodies with short period perturbations in elliptic case 79−25455
resonance with Periodic Comet Boethin (1975 I), libration 80−72883
ring, dust EM scatt. lifetimes 80−82273
ring, Pioneer 11 obs. 79−88620
ring, Voyager 1 detection 79−40131
ring and Galilean satellites, origin 79−84736
ring and regular satellite system formation 80−41746
ring detect. at 2.2 μm 79−66958
ring system, origin and location of narrow rings 80−56764
ring system, radii rel. to break-up and accretion limits and origin 79−84737
ring system, summary of recent research 80−72875
ring system, Voyager 2 obs. 80−12707
ring system dust, derived from Io volcanoes 80−85889
rings, Voyager I obs. *(French)* 80−82281
rotation period, decametric radio meas. 80−17541
S-burst drift rates 79−75146
S-bursts, drift rates 78−36492
S-bursts, drift rates from 26-33 MHz obs. 80−12705
S-bursts, freq. drift meas. at different freqs. throughout several storms 80−85888
S-bursts, obs., assoc. with Io, and origin 78−36499
S-bursts, obs. at 32 MHz 78−36498
S-bursts radio emission, occurrence with L-bursts and freq. upper limit 80−85887
satellite, orbits near Jupiter and Saturn, post-Newtonian effects 79−101054
satellite, XIII, precise positions during 1975-76 opposition 77−64691
satellite orbits, three dimens. periodic orbit determ. 80−67526
satellite predictions of Galileo 79−88784
satellite speckle patterns, image retrieval 77−22100
satellite XIII, rel. to satellite system struct. 77−67066
satellites, astrometric obs. of faint objects during 1975-6 opposition 79−75139
satellites, atmosphereless, micrometeorite impact, ion emission 80−77362
satellites, diameters from lunar occultation meas. 78−45272
satellites, light curve, surface meteoroid bombardment effects 80−26786
satellites, mutual eclipses and occultations, diameter calcs. *(Swedish)* 79−92695
satellites, precise positions during 1973 77−17421
satellites 1979 J 1 and 2, Voyager 1 imagery analysis 80−67639
satellites icy interiors and surfaces evolution 78−61771
satellites position meas. 78−81573
solar heating and internal heat flow 78−85888
South Equatorial Belt disturbances discovery 79−58295
south temperate belt white spot annual oscills. obs. 79−70991
spacecraft braking problem in Jupiter atmosphere, ballistic and navigation aspects 80−61981
spectra of upper atmosphere, lab. determ. of ethane $^RQ_0$ branch intensity in ν_9 fundamental 77−6856
spectrophotometric and polarimetric obs. *(Russian)* 77−71050
spectrophotometry at 0.6 and 1.1 μm, brightness distrib. and atmosphere optical parameters is tropical and temperature belts 79−92715
spectrophotometry in 0.6 to 1.1 μ region, Jovian atmosphere optical parameters latit. vars. 80−46468
spectrophotometry in far IR 78−85890
spectrum, obs. from 1500 to 2000 Å with IUE 80−56752
spectrum between 10 and 13 μ, Jovian $^{15}N/^{14}N$ ratio estimate 79−8876
spectrum in far IR showing NH_3 rotational bands 78−85891
Stokes parameters of 11 cm radiation, meas. 78−12141

Jupiter continued
stratosphere, acetylene photopolymers aerosol 80−31244
stratosphere, NH_3 mixing ratio 79−16874
structure and evolution, effect of dense cores 80−98603
Sun-Jupiter-asteroid circular and elliptic problem comparison at commensurabilities 77−56819
surface temperature excess, attributed to EM phenomena *(French)* 77−60714
temperature depend. of possible S_8 IR bands 77−29709
thermal profiles and NH_3 distribs. from IR spectral meas. 79−40126
thermal radiation spectrum between 12 and 24 μ 77−17425
thermal structure from IR spectral meas., filtered iterative inversion method 78−7918
thermosphere, heating by soft electrons precip. 77−82157
three-body problem, restricted, families of three-dimens, double-symm. periodic orbits, Sun-Jupiter case 80−26722
triple shadow phenomena caused by Galilean satellites (AD 1900-2100) ephemerides 80−67641
Trojan asteroids, long-period effects in motion and problems of 1/1 resonance 80−41755
two phase NH_3 stratiform clouds 77−25977
upper atmosphere, heating by solar wind energy 77−37471
upper atmosphere, photochemical models 80−36567
upper atmosphere, spectral emission, Galatry profile 77−78642
upper atmosphere aerosol content from Ganymede eclipse obs. 77−41349
upper atmosphere temperature, Voyager 1 meas. 80−17536
Voyager, telecommunications system and broadcast from Jupiter 80−26715
Voyager 1, encounter with Jovian system 80−26716
Voyager 1, photographic obs. of Jupiter atmosphere ring and major satellites 80−26788
Voyager 1, preliminary radio profiles of atmosphere and ionosphere 80−26791
Voyager 1 data summary *(Russian)* 80−82274
Voyager 1 mission 79−96948
Voyager 1 mission photographs 79−84698
Voyager 1 results 80−4293
Voyager 2, data from Jovian system 79−84740
Voyager 2 encounter, trajectory and sequence modifications 80−77265
Voyager 2 imaging science results of planet and Galilean satallites 80−72871
Voyager 2 IR obs. 80−77335
Voyager electrostatic discharge protection 78−89042
Voyager I encounter, general description of planet and satellites environment 80−12642
Voyager I flyby, discoveries *(German)* 79−96961
Voyager I results, diverse features 79−84738
Voyager imaging experiment 78−24427
Voyager IR spectroscopy and radiometry experiments 78−24428
Voyager low energy charged particle experiment 78−20618
Voyager magnetic field experiment 78−24431
Voyager mission objectives 78−24426
Voyager photopolarimeter experiment 78−20616
Voyager planetary radioastronomy experiment 78−24433
Voyager plasma experiment 78−20617
Voyager plasma wave system 78−24432
Voyager project, colour photographs of Jupiter, Amalthea and four Galilean satellites *(German)* 79−96959
Voyager project, purpose and experiments *(Norwegian)* 79−92646
Voyager radio science experiment 78−24430
Voyager reconnaissance missions *(German)* 78−20619
Voyager spacecraft, receiver for measuring LF planetary radio emissions 78−4075
Voyager UV spectrometer experiment 78−24429
Voyagers 1 and 2, general results, satellites 80−17542
whistler mode chorus obs. and Io torus implications 80−72862
whistler obs. by Voyager 1, lightning detect. 79−84733
whistler propagation in magnetosphere, theory 80−72863
wind, correl. with Earth surface winds questioned 79−25290
X-ray flux upper limits 77−5491
atmosphere, zonal vel. and texture from Voyager 1 images 79−92711
C/H, $^{12}CH_4/^{13}CH_4$ ratios, from 0.1 cm^{-1} resolution near-IR spectra 77−9698
C/H and D/H ratios from 8-9 μm IR spectrum 80−67638
CO, detect. and abundance 78−49374
CO in Jupiter upper atmosphere, extraplanetary source 78−93144
CO thermochemistry, implications for atm. convection 78−36500
$^{12}C/^{13}C$, evidence for telluric ratio in atmospheres of Jupiter and Saturn 78−20723
D/H, C/H ratios, determ. from methane-d_1 phase 78−28572
GeH_4, ν_3 and 2 ν_3 bands, high resolution IR spectra, rel. to Jovian atm. 78−37636
H I Lyman α albedo, Copernicus UV obs. 80−94747
H I Lyman α emission and Io torus, Voyager 2 EUV obs. 80−77338
H Lyman-α brightness, longit. asymm. 80−72852
H quadrupole absorption, spatial and temporal variations 77−37561
H-He immiscibility, chemical differentiation rel. to excess luminosity 78−69798
H_2, metallic, solubility of He, Gibbs energy, fluid state model, He conc. in giant planets 79−60602
H_2 rotational quadrupole lines, theoretical brightness temps. 78−7917
HD search at 6045 Å, D/H ratio upper limits 78−85892
Hα auroral activity, obs. 77−45350
Io, Na and H clouds 77−64695
Io, Na I, Ca I, Fe I, and Mg I emission lines in spectrum 79−21223
NH_3 1.56 μ band study 77−17422
NH_3 6450 A absorption band obs. 77−33396
NH_3 abundance determ. from 2 μ spectrum 79−35182
NH_3 abundance from visible obs. 80−82269
NH_3 and PH_3 photochemistry in stratosphere 77−53463
NH_3 atmospheric abundance 78−12142
NH_3 distrib. and photochemical products 77−67063
NH_3, spatial distrib. from optical band strengths and curves of growth 80−46386
NH_3, spectral line meas. using 10μm superheterodyne receiver 78−16335
NH_3 vertical density profiles from IR and radioelectric emissivity data 80−82267
Na cloud moving with Io, first photographs 78−32389
Na D-emission photography using Mach-Zehnder interferometer 77−60617

Jupiter continued
Na I emission from Region C, attributed to terrestrial airglow 77−64696
Na I emission from region C_2, Na transport from Io 79−53758
O^+, forbidden emission detect. in inner magnetosphere 80−51687
P in upper atmosphere 79−40130
PH_3 obs. at 5 μ 77−33393
S II forbidden line emission from thermal plasma 78−93146
S II forbidden line emission nebula studies 80−67636
S II forbidden line emission round planet, distrib. and intensity 80−85885
S II ring, var. in characts., link with Io, visible obs. 80−90360
S II torus, longitudinal asymmetry visible spectra 80−82271
S nebula, temp. anisotropy 80−17539

K-capture *see nuclear electron capture*

K mesons *see kaons*

K-N interactions *see kaon-nucleon interactions*

Kalman filters
adaptive beam forming processor formulation 80−91967
adaptive filter structures, for seismic signals deconvolution 80−98451
adaptive model for flood warning system, on-line, desk-top computer appl. 79−34977
air pollution episodes in Venetian region, real-time forecasting via Kalman predictor 80−82046
air pollution level prediction by nonphysical models 77−29428
air pollution levels, stat. prediction by Kalman filtering method 79−57535
beta gauge, optimal filter design 77−1904
blood flow-velocity meas. by US techniques, Kalman filter appls. 79−100686
blood-flow velocity estimation 79−62325
cardiovascular system, identification and parameter estimation 80−35947
cell kinetics stochastic model using DNA microfluorometric data 79−83723
chemical analysis, multicomponent analysis computations based on Kalman filtering 80−40772
computed tomography, limited data, image reconstruction using polar pixel Kalman filter 80−98095
cyclone forecasting applications to typhoons 77−25801
deconvolution smoother, for reflection seismograms simultaneous spherical divergence correction and optimal deconvolution 80−98258
digital, phasemeter appl., synthesis with a priori uncertainty of data 80−98934
digital speech processing, linear prediction parameter estimation using Kalman filtering *(German)* 80−96134
eclipsing binaries orbits, appl. of Kalman filter to light curves 77−5546
EEG signals with changing spectra, anal. using Kalman estimator 78−24167
EEG sleep pattern feature extraction and recognition by real-time anal. *(Japanese)* 78−73271
gamma-ray flaw detect. appl. 79−5121
Givens transformation techniques, numerical stability and accuracy 78−4473
gyrocompass levelling and setting for gyrostabilised platforms *(Russian)* 80−52190
heat flux meas. by battery heat flowmeter using Kalman filter 79−37143
holographic image reconstruction, unconditionally stable algorithms *(Russian)* 79−22909
HTGR fuel rod fabrication, estimation and control 80−83215
human motion and force sensory mechanism model 80−8094
hurricane and typhoon forecasting appl. 77−64409
hydrological prediction models, adaptive algorithm 79−53381
hydrological system, state space modelling and identification 79−79908
hydrology, river quality modelling by sequential extended Kalman filters 78−81248
irradiance meas. appl., dynamic 77−5914
Kalman-Bucy filters, extended, for passive microwave sounding of atmospheric temp. 79−21053
laser adaptive optical control with closed-loop estimation and predictive filtering 77−19298
laser pointing and tracking, adaptive optimal filtering appl. 77−88959
laser system, focused apertured Gaussian beam, focal length and target range estimation 77−19299
meteorology inverse problems, estimation theory appls. 79−35018
nonlinear, iterative filter for soln. of inverse heat cond. problem 80−19212
nuclear reactor noise analysis, time series modelling methods, comparative eval. *(Japanese)* 80−13552
nuclear reactor reactivity insertion, unexpected, rapid detection 78−58370
oil exploration seismic data processing, white noise estimators 78−3973
optimum filtration, rel. to inverse thermal conductivity problem 78−5628
prediction error filter, quantitative evaluation 78−40496
prosthesis, multifunctional upper extremity, control signal generation using EMG signal processing 80−8219
pulmonary blood flow estimation, Ljung's algorithm sensitivity 80−56107
rainfall, Delhi, recursive prediction model 79−79998
respirometer process appl. *(French)* 79−5408
road traffic noise abatement, noise propag. characts. identification under different conditions, appl. *(German)* 80−99896
seismic data, single-channel white-noise estimators for deconvolution 78−77345
seismic data deconvolution, overview 77−91060
sonobuoy position meas., sound speed adaptive estimation 79−72773
sounding rocket attitude estimation using star sensor data 79−25435
star pattern sensors for real time spacecraft attitude determination 78−96380
thermokinetics of coupled radiative and conductive transfer, Kalman filtering identification *(French)* 79−41558
visual evoked cortical potential meas., signal optimisation using Kalman filter *(Japanese)* 80−72348
voltammetry, linear sweep anodic stripping time, real time anal., recursive estimation 80−26067
water quality modelling, Kalman filter theory and practice 78−45058
white noise estimators for deconvolution 77−29472

kaon-baryon interactions
see also kaon-baryon scattering; kaon-hyperon interactions; kaon-nucleon interactions
quark mass differences in high energy collisions 78−45868
$K^{\pm}$ induced interactions, integrated cross sections, compilation 80−439
$K^-p \rightarrow \Lambda X$, 8.25 GeV/c, off shell KK and p$\bar{p}$ interactions, KNO scaling 80−52534

kaon-baryon scattering
see also kaon-baryon interactions; kaon-hyperon scattering; kaon-nucleon scattering
No entries

kaon decay
see also kaon hadronic decay; kaon leptonic decay
30 T pulsed solenoid construction and life tests 79−31297
Cabbibo fit, generalised, appl. to quark mixing angs. in sequential Weinberg-Salam model 79−17655
current algebra approach, symmetry-breaking Hamiltonian, chiral SU(3)×SU(3) or SU(4)×SU(4) 80−68450
experimental problems, review, book contrib. 79−21890
exponential decay law, corrections 77−67639
form factors, semi-leptonic weak interactions, book contrib. 78−78162
form factors and (8,8) model of chiral breaking, unitarisation 77−18286
Higgs boson couplings, charged, K_L-K_S mass differences 80−62917
mesonic octet decays, chiral QFT description using one loop approx. *(Russian)* 79−63471
nondegenerate decay system, anal. 78−447
pseudoscalar mesons, muonic double β-decay, tree and box diagram approx., K^- and F^- 79−17717
six-quark model, predictions *(Russian)* 79−93379
SU(2)×U(1) theory with very heavy quarks, comparison with superweak predictions 77−38123
SU(3) rules for non- and semi-leptonic weak decays 78−45916
$K \rightarrow \pi^+\pi^-e^+\nu$ decay form factors, relativistic quark model 77−38160
$K \rightarrow \pi^+\pi^-\mu\nu$ decay rate 77−6113
$K \rightarrow \pi e(\mu)\gamma$, quark mass ratios 80−105884
$K \rightarrow \pi e(\mu)\nu$, form factors, SU(3) σ-model one loop calc., chiral symmetry breaking 80−52506
$K \rightarrow \pi e\nu$, radiative correction amplitudes from Ke_4 decay anal. 78−86451
$K \rightarrow \pi l\nu$ strangeness changing suppression factor, $SU(3)_E$-invariant form factor 77−61288
$K \rightarrow \pi l\nu_l$, form factor, parameter-free hard-meson prediction via current algebra sum rules 77−49954
$K \rightarrow \pi\pi e\nu$, Ke_4 decay, radiative correction amplitudes 78−86451
$K^- \rightarrow \pi\mu\nu$, μ polarisation and T-odd correlations, Weinberg model of CP violation *(Russian)* 80−62969
K^0 decay, T-violation without assumed CPT 79−26249
$K^0 \rightarrow \mu e$, flavour changing neutral current search 80−105836
$K^+ \rightarrow \pi^0\mu^+\nu$, $K^+_{\mu 3}$ decay spectrum and form factors 80−57587
$K^+ \rightarrow \pi^+e^+e^-$, decay amplitude using simple model with PCAC 80−9162
$K^+ \rightarrow \pi^+e^+e^-$, neutral-current process, strong interaction corrections 80−62968
$K^+ \rightarrow \pi^+e^+e^-$, pole contribs., test of theory by comparison with expt. 78−70360
$K^+ \rightarrow \pi^+e^+e^-$, quantum chromodynamics *(Russian)* 77−2822
$K^+ \rightarrow \pi^+e^+e^-$, short distance analysis of weak interactions, asymptotically free theory 77−54068
$K^+ \rightarrow \pi^+\mu^+\mu^-$, radiative corrections in Weinberg model *(Russian)* 77−38163
$K^+ \rightarrow \pi^+\mu e$, decay mode calc. in model with heavy neutral leptons 78−45898
$K^+ \rightarrow \pi^+\nu\bar{\nu}$, calc. of number N_ν neutrino types 79−26321
$K^+ \rightarrow \pi^+\pi^-e^+\nu$, $\pi\pi$ energy, phase shift difference, hadronic current form factors, scatt. length 77−41840
$K^{\pm} \rightarrow \pi^0 l^{\pm}\nu_l(\bar{\nu}_l)$, decay form factors in relativistic symmetry SO(4,2)⊗SU(3)⊗SU(3) 79−36068
K_1^0-K_2^0 system, semi-leptonic decays, time depend., book contrib. 78−78173
K_{e3}^0 decays, vector form factor slope parameter *(Russian)* 79−67547
K_{e4} decay, scattering lengths, data compared to prediction *(Russian)* 79−93459
$K_L \rightarrow 2\gamma$, limit on mass of charm quark 77−57491
$K_L \rightarrow 2\gamma$, Weinberg-Salam model, weak radiative decays, large dist. contribs. *(Russian)* 77−82740
$K_L \rightarrow 2\gamma$, Weinberg-Salam model, weak radiative decays 78−41541
$K_L \rightarrow 2\gamma$ decay, contribution of Hamiltonian derived for weak two-photonic decays *(Russian)* 78−66119
$K_L \rightarrow e\mu^-$, muon number nonconservation 78−8542
$K_L \rightarrow \gamma\nu\bar{\nu}$, calc. of number N_ν neutrino types 79−26321
$K_L^0 \rightarrow (\pi\mu)\bar{\nu}$, energies and intensities of π-μ atoms *(Russian)* 78−54629
$K_L^0 \rightarrow (\pi\mu)\nu$, prod. and detect. calcs. 79−81306
$K_L^0 \rightarrow \gamma\gamma$, $(\pi^+\pi^-\gamma)$, chiral quark model anal. *(Russian)* 80−105900
$K_L \rightarrow \pi^-\mu^+\nu_\mu$, transverse polarisation of μ, violation of time-reversal invariance 80−68448
$K_L^0 \rightarrow \pi^{\pm}e^{\mp}\nu$, vector form factor meas. in large H bubble chamber 78−93875
$K_L^0 \rightarrow \pi^{\pm}\mu^{\mp}\nu$, form factors 4-momentum depend., μe universality *(Russian)* 80−68449
$K_L^0 \rightarrow \pi e\nu_e$, Dalitz plot anal., form factors 78−37204
$K_L^0 \rightarrow \pi\mu^+\nu_\mu$, form factor from μ polarisation meas. 77−38161
$K_L^0 \rightarrow \pi\mu\nu$, Dalitz plot anal., vector and scalar form factors 79−71744
$K_L \rightarrow \pi\mu\nu_\mu$, anomalous short-range $\pi\mu$ interaction anal. 78−8660
K_{l3} decay, form factor and propagator bounds *(German)* 80−37265
K_{l3} scalar form factor, chiral symmetry breaking model 77−71506
K_{l4} decay in relativistic quark model, axial vector form factors and decay rate 78−66109
K_{l4} decay vector form factor *(Russian)* 80−105900
$K_{l4} \rightarrow \pi\pi\gamma$, form factors in chiral quantum field theory *(Russian)* 79−67550
$K_S^0 \rightarrow 3\pi$, CP violation, book contrib. 78−78173
K_S^0 decays and Lorentz invariance 79−26250
K° decay, extended relativity, T-violation and new particle 80−37182
K_L^0−K_S^0 transmissions regeneration on H in 14-50 GeV range 77−22732
$K^* \rightarrow K\gamma$, quark loop model, SU(3) splitting of quark masses 80−62990
K^{*0}−$K^0\gamma$, SU(3) and isospin symmetry breaking effects 80−95272
$\lambda n\gamma(Z)$ vertex in vector-like model of weak and EM processes, appl. to K decay 77−6071
$K \rightarrow \pi e^+e^-$, six-quark model, CP violation 80−78055
$K_s \rightarrow \gamma\gamma$, decay rate, vector-meson exchange contribs. 79−49523

kaon hadronic decay
see also kaon regeneration
$1/N_c$ expansion in colour model 78−25042
$\Delta I=1/2$ dominated weak decays of strange hadrons, Weinberg-Salam scheme 80−27499
$\Delta S=1$ nonleptonic weak decays, $\Delta I=1/2$ rule, quark models and current algebra 80−47282
asymptotically nearly-free theories, hadronic weak decays anal. 77−65154
branching ratio $(K^+\rightarrow\pi^0\mu^+\nu)/(K^+\rightarrow\pi^0e^+\nu)$ meas. 78−8661
CP violation, statistical theory, K^0 decay 77−41784
extended PCAC hypothesis, soft-meson chiral symm. breaking, K decays 78−21353
$K_L^0\rightarrow\pi^+\pi^-\gamma$, branching ratios and γ-energy spectrum 80−47280
K_L^0-K_S^0 transmission regeneration in H, comparison of expt. data and theoretical prediction *(Russian)* 77−49955
Kobayashi Maskawa model, QCD effects and CP violation 80−42427
mixing of p-wave axial vector resonances 77−30374
non-leptonic weak interactions, book contrib. 78−78163
nonleptonic interactions, enhancement and suppression factors for left handed current, K decay 79−385
parity violating vector meson-pseudoscalar meson interaction, relativistic quark model 77−54102
quark sea and $\Delta I=1/2$ rule 77−79255
renormalisable gauge scheme of weak interactions, asymptotically free theory of strong interactions *(Russian)* 77−46048
SU(2)⊗U(1) theory of weak interactions, with spiral chromatic currents *(Russian)* 77−221
SU(3) rules for weak decay 78−45916
without dynamics enhancement *(Russian)* 79−30733
$(K^\pm,X)$ symmetry violating kaon decay as nuclear probe 80−42704
$K\rightarrow2\pi$, comment of appl. of current algebra and bag model 79−97622
$K\rightarrow2\pi$, decay amplitudes in SU(2)×U(1)×U(1) model with new neutral current 80−4986
$K\rightarrow2\pi$ and 3π, transition amplitude determ. using least-squares anal., review 79−58956
$K\rightarrow3\pi$, CP violation, current algebra anal., six quark Weinberg-Salam model 80−47281
$K\rightarrow3\pi$, radiative correction amplitudes from Ke_4 decay anal. 78−86451
$K\rightarrow3\pi$, relativistic quark model anal. 80−99096
$K\rightarrow\pi^0\pi^0$, contrib. of 2nd. class currents to nonleptonic decay 79−13117
$k\rightarrow\pi^+$+axion, bounds 78−33064
$K\rightarrow\pi\pi$, $\Delta I=1/2$ rule using PCAC 80−4990
$K\rightarrow\pi\pi$, $\pi\pi\pi$, struct. of weak interaction symmetry *(Russian)* 79−22016
$K\rightarrow\pi\pi\gamma\gamma$, scalar meson model for radiative decays involving $\delta(980)$ 78−82204
$K\rightarrow\pi\pi\pi$, S_3 permutation group approach 79−17723
$K\rightarrow\pi\pi\pi$ in relativistic quark model 77−10248
$K\rightarrow\pi\pi\pi\gamma$, scalar meson model for radiative decays involving $\delta(980)$ 78−82204
K^0 CP violating decays, review 77−57532
$K^0\rightarrow\pi^0\pi^0$, phase and magnitude of CP nonconservation parameter η_{00} 80−4988
$K^0\rightarrow\pi^+\pi^-$, CP nonconservation parameter η_{+-} phase and magnitude 80−4989
$K^0\rightarrow\pi\pi$, six-quark model, $\Delta I=1/2$ rule and CP violation 79−54323
$K^0\rightarrow\pi\pi\pi$, CP test, book contrib. 79−21890
$K^+\rightarrow\pi^+$+axion, upper bound determ. 78−50031
$K^+\rightarrow\pi^++\pi^0+\pi^0$, π^+ meson energy spectrum below 30 MeV 78−12906
$K^+\rightarrow\pi^+\pi^-\pi^+$, τ^+ decay anal. 77−82739
$K^+\rightarrow\pi^+\pi^0\pi^0$, decay matrix element parameters expt. determ. 77−13956
$K^+\rightarrow\pi^+\pi^0\pi^0$, meas. of π^+ spectrum below 30 MeV 77−6115
$K^+\rightarrow\pi\pi$, branching ratio meas. by mag. spectrometer with streamer chambers 77−18275
$K^\pm\rightarrow\pi^\pm\gamma\gamma$, expt. upper limit determ. 77−30375
$K^\pm\rightarrow\pi^\pm\gamma\gamma$, scalar meson model for radiative decays involving $\delta(980)$ 78−82204
$K_2^0\rightarrow k\pi$, k=2 or 3, Racah time reversal, a C,P,T scheme 80−78056
$K_S^0\rightarrow\pi^0\pi^0$, MIT bag model 78−33066
$K_b^0\rightarrow D^+\pi^-$, mass splitting of beautiful mesons 80−47288
$K_L\rightarrow2\pi$, eight quark model, CP violation, heavy quark degeneracy 77−26490
$K_L\rightarrow\pi^0\gamma\gamma,\pi^0e^+e^-$, decay rates calc. in baryon-loop model 78−70365
$K_L\rightarrow\pi^+\pi^-$, branching fraction meas., CP violation parameter determ. 78−8663
$K_L\rightarrow\pi^+\pi^-(\pi^0\pi^0)$, CP violation parameters in six quark model *(Russian)* 80−62974
$K_L\rightarrow\pi^+\pi^-\gamma$, Weinberg-Salam model, weak radiative decays, large dist. contribs. *(Russian)* 77−82740
$K_L\rightarrow\pi^+\pi^-\gamma$, Weinberg-Salam model, weak radiative decays 78−41541
$K_L^0\rightarrow\pi^0\gamma\gamma$, scalar meson model for radiative decays involving $\delta(980)$ 78−82204
$K_L^0\rightarrow\pi^++\pi^-\pi^0$, matrix element for data fit, branching ratio 77−38165
$K_L^0\rightarrow\pi^+\pi^-\pi^0$, Dalitz plot 78−4859
$K_L\rightarrow\pi^+\pi^-\pi^0$, matrix element expt. study *(Russian)* 78−78174
K_L^0-K_S^0 regeneration on hydrogen in 14-50 GeV range *(Russian)* 77−6121
K_L^0-K_2^0 transmission regeneration on deuterons and neutrons, 10 to 50 GeV/c 80−4985
K_{l3} decay, scalar form factor, quark mass ratio determ. 79−93409
K_s coherent regeneration on C and Regge pole exchange theory 77−49957
$K_S^0\rightarrow\pi^+\pi^-\gamma$, branching ratio and photon spectrum meas. 77−2828
$K_s\rightarrow\pi\pi$ in terms of spectral function integrals, short distance approach 77−61242
K_S^0 regeneration amplitude from K_L^0 in C 77−34150
$K^*(1420)\rightarrow K^*(890)\pi\pi$, possible evidence 77−2823
$K^*(1760)$, prod. in 9 GeV/c K^+d, spin, parity masses, widths, and branching ratios 78−8693
$K^*(2100)$, prod. in 9 GeV/c K^+d, spin, parity, masses, widths, and branching ratios 78−8693
$K^*(892)\rightarrow K\pi\pi$, decay width upper limit 78−78177
$K^*(982)\rightarrow K\pi\pi$, finite energy sum rules and finite dispersion relns. 77−22731
$K^*\rightarrow K+\gamma$, radiative decay in the MIT bag model 78−66110
$K^*\rightarrow K\pi\pi$, decay width for $V\rightarrow3=$ in Bethe Salpeter model 79−58955
$K^*\rightarrow K\pi\pi$ rate, vector meson pole dominance in coupling-constant models 77−30373
$K^{*-}(1420)\rightarrow K^{*-}(892)\pi^+\pi^-$, partial width for decay mode 78−78177
$K^{*0}\rightarrow K^0\gamma$, quark anomalous mag. moments 79−17693
$K^{0*}\rightarrow K^0\gamma$, SU_3 symm. breaking schemes, radiative width 77−6114

kaon hadronic decay continued
$K_S^{0*}\rightarrow K_S^0\gamma$ and Primakoff conversion of K_L^0 to K_S^* 80−73695
$K_b^*\rightarrow K_b\gamma$, mass splitting of beautiful mesons 80−47288
$K^{**}(1420)\rightarrow K^*(890)\pi\pi$, decay width anal. 77−46047
$K_L^0C\rightarrow K_S^0C$ coherent regeneration in range 10-30 GeV/c 77−13955
$KL_L^0\rightarrow\pi^+\pi^-\gamma$, branching ratio meas. 77−18280

kaon-hyperon interactions
see also kaon-hyperon scattering
No entries

kaon-hyperon scattering
see also kaon-hyperon interactions
No entries

kaon interactions *see kaon-baryon interactions; kaon-nucleus reactions; lepton-hadron interactions; meson-meson interactions; photon-hadron interactions*

kaon leptonic decay
Higgs bosons, effects on experimental observables, and fermion mass scale 80−32061
$K_L\rightarrow\bar\mu\mu$, strangeness changing neutral currents, avoidance in gauge theories of weak and EM interactions 79−22005
SU(6) exotic gauge model, lepton-quark symm., CP-violation and k^0 decay 78−12875
SU(6) unified gauge model, mechanism of electron number nonconserving decay 78−12847
$K\rightarrow l\nu$, strangeness changing suppression factor, $SU(3)_E$-invariant form factor 77−61288
$K\rightarrow l\nu_e\gamma(l\nu_e l'^+l'^-)$ in review of weak-EM decays *(Russian)* 77−2818
$K\rightarrow\mu\mu$, mesonic wave functions at zero point *(Chinese)* 77−10242
K^0_{e3} and $K^0_{\mu3}$ decays, form factor parameters anal., SU(3) symm. violation *(Russian)* 78−450
$K_L^0\rightarrow\mu^+\mu^-$, meas. of decay rate 79−63474
$K^+\rightarrow e^+\nu\gamma$, experimental investigation, branching ratio and γ-helicity 79−36066
$K^+\rightarrow eee$, branching ratio meas. by mag. spectrometer with streamer chambers 77−18275
$K^+\rightarrow\mu\mu(\mu)$, branching ratio meas. by mag. spectrometer with streamer chambers 77−18275
K_L, weak radiative decays in chiral theory using virtual π^0 and η pole diagrams *(Russian)* 78−78172
$K_L\rightarrow2\mu$, K_L-K_S mass difference, strong interaction effects from short-dist. gluons 77−82737
$K_L\rightarrow e\bar\mu$, symmetry violation natural suppression, muon and electron lepton number nonconservation 78−8574
$K_L\rightarrow\mu^+\mu^-$, and $n\lambda Z$ vertex in Weinberg-Salam model *(Russian)* 77−2821
$K_L\rightarrow\mu e$, decay mode calc. in model with heavy neutral leptons 78−45898
$K_L\rightarrow\mu\bar e$, V-A gauge model, muon and electron number nonconservation 77−74667
$K_L\rightarrow\mu\mu$, heavy particle decoupling effects in broken symmetry theory 78−82140
$K_L\rightarrow\mu\bar\mu$, quark mixing angle upper bounds in standard 6 quark model 80−18131
$K_L\rightarrow\mu\bar\mu$ short distance analysis of weak interactions, asymptotically free theory 77−54068
$K_L\tilde\rightarrow\mu^+\mu^-$, SU(3)×U(1) symmetry, gauge theory 78−58153
$K_L^0\rightarrow e^+e^-(\mu^+\mu^-)\gamma$, Dalitz decay modes, branching ratios 80−47276
$K_L^0\rightarrow\mu^+\mu^-$, decay probabilities in strong electromagnetic field *(Russian)* 79−80825
$K_L^0\rightarrow\mu^+\mu^-$, VDM calc. of decay probabilities *(Russian)* 78−41539
$K_L^0\rightarrow\mu^+\mu^-/K_L^0\rightarrow$all branching ratio 77−67647
$K_L^0\rightarrow\mu^+\mu^-\gamma$, VDM calc. of decay probabilities *(Russian)* 78−41539
$K_L^0\rightarrow\mu e$, unified theory with right handed currents, lepto-quark masses 77−49890
$K_{L\ \mu3}^0$ decays, CP invariance violation limits 79−89146

kaon-nucleon interactions
see also kaon-nucleon scattering; kaon-proton interactions
100 GeV/c, multiplicities and pseudorapidity distrib. 78−82241
Adler-Weisberger sum rule and the σ-commutator for the kaon-neutron system 80−101957
cross-sections related by sum rules, pomeron hypothesis, heavy-quark channels and threshold predictions 78−89755
elementary properties, general review 79−85340
finite energy rules, Regge pole models, exchange amplitudes 78−470
hadronic reaction total cross sections, correl. between maxima positions, and hadronic spectroscopy *(Russian)* 79−54356
inclusive hadroproduction of μ pairs, 39.5 GeV/c $\pi^\pm$, $K^\pm$, p, $\bar p$ beams on Cu target 78−62470
K^-n interactions, 680-840 MeV/c, cross sections, resonance prod., polarisations 77−18320
low-energy interaction in I=0 state, model 77−13979
multiperipheral n-particle prod., KNO scaling deviation at high energies *(Russian)* 77−34141
nuclear interactions of strange particles and resonances, conf. Warsaw, Poland (Ict.,1976) 78−70406
quark parton model, total cross sections 78−45859
resonance region below 3 GeV/cd review 77−6163
transversely polarised deuteron target 80−37669
K_S^0 regeneration amplitude from K_L^0 in C 77−34150
K^0_L+Cu, 4-20 GeV/c, $\mu^+\mu^-$ prod. from vector meson decay 78−45951
K^-+light emulsion nuclei, 1.5 GeV/c, K^-p and K^-n channels, probability distrib. 78−13161
$K^*(890)$ prod. at 13 GeV/c, Regge models 78−45961
Kd interactions, 9 GeV/c, prod. of $K^*(1760)$ and $K^*(2100)$ 78−8693
K^-d, information on coupling consts. for $\bar KN\Lambda(1405)$, $\bar KN\Sigma(1385)$ and $\bar KN\Sigma(1197)$ 78−8689
$K^-d\rightarrow K^-\pi^+\pi^-d$ or $K^0\pi^-\pi^0d$, 12 GeV/c coherent interactions, cross sections, resonance signals 77−50016
$K^-d\rightarrow\Lambda p\pi^-$, Λp invariant mass distrib., ΣN bound state 77−30428
$K^-d\rightarrow\Lambda p\pi^+\pi^-\pi^-$, 1.45, 1.65 GeV/c, Λp mass enhancement 79−416
$K^-d\rightarrow\pi^-\Lambda p$, anal. of Λp enhancement at 2.129 GeV in cross section meas. 79−22141
$K^-d\rightarrow\pi^-\Lambda p$, low energy Faddeev calc. 79−85341
$K^-d\rightarrow\pi^-\Lambda p$, three body Faddeev formalism, unstable dibaryon bound state search 80−32130
$K^-d\rightarrow\pi^-\Lambda p$ breakup process, appl. of Faddeev eqns. 79−75797
$K^-d\rightarrow\pi\Lambda p$, ΣN bound state and Λp enhancement 80−47326
K^-d scatt., effect of hyperon channels, <120 MeV/c 79−9406
$K^-d\rightarrow\Sigma^-p\gamma(\Lambda n\gamma)$, energy spectra, hyperon-nucleon scatt. anal. *(Russian)* 78−29347

kaon-nucleon interactions continued
K^+d inclusive reactions, 4.6 GeV/c, topological cross sections, π^-, K^0, Λ prod. 77−50004
$K^\pm d$, total cross section determ., 200 to 370 GeV/c 79−26352
$K^-{}^4He \rightarrow \pi^- \Lambda^3 He$, final state interaction model, Muskhelishvili Omnes eqn. soln., πmomentum distrib. 77−30285
$\bar{K}N$, 360-1320 MeV/c, partial-wave anal. 78−82235
KN, 50-200 GeV/c, multiparticle production, multiplicities, cross sections and ang. distribs. 80−86768
$\bar{K}N$, below 1 GeV/c, Y^* states, SU(6)⊗O(3) quark model classification 80−27523
$\bar{K}N$, kaonic H atom and $\Lambda(1405)$ 80−68479
$\bar{K}N$, reson. region, <2 GeV, energy-depend. multichannel K-matrix formalism 77−82771
KN, Z_0^* and composite resonances 77−22795
KN CEX interactions, construction of tensor exchange amplitudes 79−58974
$\bar{K}N$ CEX interactions construction of tensor exchange amplitudes 79−58974
$\bar{K}N$ interactions, low energy, K matrix and dispersion relns., $\Gamma(1405)$ resonance 78−70408
$\bar{K}N \rightarrow \bar{K}N$, $\pi\Sigma$, $\pi\Lambda$, <2 GeV, multichannel anal. 77−82772
$KN \rightarrow K^*\Delta$, positivity conditions in joint vector-meson Δ prod. 77−13975
$KN \rightarrow K^*\Delta$, $\rho\Sigma$, or ϕ^*, polarisation, selection rule on ang. momentum transfer 77−34180
$\bar{K}N \rightarrow \bar{K}^*N$ energy depend. partial wave anal. 1830 to 2170 MeV 79−3046
$\bar{K}N \rightarrow \bar{K}^*N$ energy depend. partial wave anal. 1830 to 2170 MeV 79−22138
$KN \rightarrow K\pi N$, isobar model, unitarity, two-body discontinuities 78−418
$\bar{K}N$ low energy scatt., dispersion relation constraints 77−13981
$\bar{K}N \rightarrow \Lambda\pi$, 1480 to 2170 MeV, partial wave anal. 77−22782
$\bar{K}N$ partial wave analyses and Y^* resonances 77−22790
$\bar{K}N \rightarrow \pi\Sigma^*$ or $K\xi$, isospin restrictions on spin density matrices *(Russian)* 77−30446
$\bar{K}N \rightarrow \pi$+hyperon, hypercharge exchange reactions in quasieikonal model *(Russian)* 79−3041
$\bar{K}N$ reaction below 1.9 GeV, dispersion theoretic discrepancy anal., SU(3), hadron coupling 78−21457
KN σ-term, uncertainties in determ., K-matrix formalism 80−27522
$\bar{K}N \rightarrow \Sigma\pi$, 1480 to 2170 MeV, partial wave anal. 77−22782
$\bar{K}N \rightarrow \Sigma\pi$, 1520-1745 MeV, partial wave anal. 77−18324
$\bar{K}N \rightarrow \Sigma\pi$ around 1660 MeV, partial wave anal. 77−22788
$\bar{K}N$ T-matrix, off-shell 77−13978
Kn total cross sections from Kp and kaon-nucleus scatt. data 80−102069
$\bar{K}N$ two body data, energy-depend. multichannel K-matrix anal., amplitudes, resonance parameters 77−22785
$\bar{K}N$ two channel system, Y_0^* (1405) couplings, K-matrix parametrizations 78−21452
$\bar{K}N$ two-body data multichannel anal. in resonance region 77−88006
$\bar{K}N$ two-body reactions, 1480 to 2170 MeV, partial wave anals. 77−34177
K^-n, 1800 to 2200 MeV 77−22787
$K^-n \rightarrow (\Sigma\pi)^-$, 680-840 MeV/c differential cross-sections 77−18324
K^-n cross sections, 1750-2200 MeV, from K^- deuterium bubble chamber expts. 78−8690
$K^-N \rightarrow K^-\Delta K$, diffractive excitation at 14.3 GeV/c and 500-1500 GeV/c 77−6175
$K^-N \rightarrow K^-N\pi$, diffractive excitation at 14.3 GeV/c and 500-1500 GeV/c 77−6175
$K^-N \rightarrow K^-N\pi\pi$, diffractive excitation at 14.3 GeV/c and 500-1500 GeV/c 77−6175
$K^-n \rightarrow K^-\pi^+\pi^-n$, 12 GeV/c, kinematic fit, cross section 78−41592
$K^-n \rightarrow K^0\Xi^-$, formation of cascade hypernucleus in nuclear emulsion 80−52603
$K^-n \rightarrow K^{*-}(890)n$, energy-dpend. partial-wave anal. 77−50003
$K^-N \rightarrow \bar{K}^{*0}X$, inclusive cross sections and spin density matrices, 3-Reggeon model anal. *(Russian)* 79−80858
$K^-N \rightarrow \bar{K}^*\Delta$, energy depend. 79−63524
$K^-n \rightarrow \Lambda^0\pi^-$, 1.55-1.65 GeV, energy-depend. partial wave anal. 78−41584
$K^-N \rightarrow \Lambda\pi(\Sigma\pi)$, review 79−85339
$K^-N \rightarrow \mu^+\mu^-X$, K^-/π^- structure function ratio using Drell-Yan process 80−86718
$K^-n \rightarrow \pi^-\Sigma^0$, 1750-2200 MeV, partial wave anal. 77−79280
$K^-n \rightarrow \pi^0\Sigma^-$, 1750-2200 MeV, partial wave anal. 77−79280
K^-n reactions, quasi two-body final states at 8.25 GeV/c 79−22139
$K^-n \rightarrow \sigma^{-(0)}\pi^{0(-)}$, CM 1850-2160 MeV, cross-section, $\Sigma(2030)$ reson. 77−67673
$K^-n \rightarrow \Sigma^-\pi^0(\Sigma^0\pi^-)$, 1.85-2.15 GeV, $\Sigma(2030)$ prod. and decay 78−41583
$K^-n \rightarrow \Sigma^-\pi^+\pi^-(\pi^0)$, 2.87 GeV/c, search for exotic I=2 hyperons 78−82234
K^0n interaction, 10 to 50 GeV/c, transmission regeneration *(Russian)* 78−41590
K^+N experiments below 2 GeV/c and status of Z^* resonances 77−22794
$K^+n \rightarrow K^0p$, 6,12 GeV/c polarised n, polarisation measurements 79−63521
$K^+n \rightarrow K^0p$ charge exchange at 6 and 12 GeV/c, polarisation meas. 79−22140
$K^+n \rightarrow K^+\pi^-p$, 4.6, 8.25, 12 GeV/c, spin-parity anal. of $K^+\pi^-$ system 77−82766
$K^+n \rightarrow K^+\pi^-p(K^{*0}(890))$, comparative study of ρ^0, ω, $K^{*0}(890)$ and $\bar{K}^{*0}(890)$ production 78−58200
$K^+N \rightarrow K^*\Delta$, energy depend. 79−63524
$K^+N \rightarrow \mu^+\mu^-X$, 225 GeV/c, muon pair prod., 2 to 11 GeV/c^2, differential cross section 79−67612
$K^+N \rightarrow \mu^+\mu^-X$, Higgs boson effects 80−32061
$K^\pm n$, high-energy, react. differences and annihilations 78−74279
$K^\pm n$, inelastic charge exchange scatt., diffraction approach, convergent polynomial expansion, scaling 80−78095
$K^\pm N$, ψ hadronic production, gluon contrib. in QCD framework 78−78139
$K^\pm N$ charge exchange reaction, tensor exchange amplitudes 79−63522
$K^\pm N$ charge exchange reacts. at 8.5 and 13.5 GeV/c 78−29351
$K^\pm N \rightarrow K^+ + X$, double hypercharge kaon exchange *(Russian)* 78−29368
K^+n^0p, 0.7. 0.8 and 0.9 GeV/c, differential cross-section meas. 77−50007
$n \rightarrow p\pi^-\pi^0$, diffractive dissociation induced by 12 GeV K^- 79−40805
$NK \rightarrow NK^*$, diffractive process, Pomeron current model 77−87958

kaon-nucleon interactions continued
$^4He + K^- \rightarrow \Lambda + \pi^- + p + d$, 180 MeV, final state study, double impulse model 79−30855
$K^-n \rightarrow \pi^-\Lambda$, 1750 to 2000 MeV, ang. distrib. and polarisation, comparison with PWA 79−75796
$K^+n \rightarrow K^{*0}p$, $\bar{K}^{*0}$ 890 decay density matrix elements 77−22779

kaon-nucleon scattering
see also kaon-nucleon interactions; kaon-proton scattering
Blankenbecler-Sugar multichannel eqn., $J = {}^1/_2$ particle wave soln. 78−37230
charge exchange, Regge-pole model anal. 77−74719
compilation of coupling constants and low-energy parameters 79−22159
forward amplitudes, information from $K_L^0 \rightarrow K_S^0$ coherent regeneration on C, optical model calcs. 77−30427
pseudoresonance Argand loops *(Russian)* 79−9354
resonance region, t-channel couplings, hyperbolic dispersion relations 80−57643
S-wave I=0 KN scatt. length and forward cross-sections 78−37231
two component Pomeron, πN, kN, NN forward scatt. amplitudes 80−37245
(K,X) optical pot. from KN scatt. and kaonic atom pot. models 79−97731
$K(\bar{K})N \rightarrow K(\bar{K})N$, 1.5-280 GeV/c, Regge pole residues and trajectories, review 78−45886
$K_L^0\,{}^{12}C \rightarrow K_S^0\,{}^{12}C$, elastic regeneration, 10 to 50 GeV/c, differential cross section slope 78−646
$K_L^0\,n \rightarrow K_s^0 n$, 10-50 GeV/c, regeneration, coherent production model 78−33220
K_L^0-K_2^0 transmission regeneration on deuterons and neutrons, 10 to 50 GeV/c 80−4985
$K^\pm$+light nuclei, high energy cross section calc., complex ang. momentum theory *(Russian)* 78−46067
$K^-d \rightarrow K^-n(p_s)$, 4.5 GeV/c, Glauber formalism, amplitudes, cross section 77−88004
K^-d scatt., effect of hyperon channels, <120 MeV/c 79−9406
K^+d low momentum scatt., 250-600 MeV/c, cross sections, phase shift anal. 77−50006
$\bar{K}N$, energy-depend. multichannel K-matrix anal., amplitudes, resonance parameters 77−22785
KN, null plane current anticommutators, sum rules and appls. 80−52436
$\bar{K}N$ elastic and charge exchange phase shift anal., 0.44 to 2.0 GeV/c, resonance parameters 77−22784
$\bar{K}N \rightarrow \bar{K}N$, 1480 to 2170 MeV, partial wave anal. 77−22782
$\bar{K}N$ systems, energy depend. PWA in 365 to 1320 MeV/c range 77−46078
$\bar{K}N$ two-body reactions, 1480 to 2170 MeV, partial wave anals. 77−34177
K^-n, cross section 1.2 to 2.2 GeV in K^-d collision 78−29353
K^-n elastic differential cross section, 1.2 to 2.2 GeV/c 77−22789
K^-n scatt., 610-840 MeV/c, differential cross section meas. 78−8691
K^+n, 0.851 to 1.351 GeV, polarisation parameter meas. 80−42498
K^+n, QCD, one-gluon-exchange, resonating group method, soft-core approx. 80−63025
K^+n charge exchange at 6 GeV/c, polarisation meas. 77−30426
K^+n elastic scatt., 0.851-1.351 GeV/c, polarisation parameter 80−68478
$K^+n \rightarrow K^0p$, ρ and A_2 exchange amplitudes, 2.5-200 GeV/c 77−34174
K^+N scatt., quantum-number-exchange reactions, phenomenological quark model 77−87950
$K^\pm n$ elastic scattering, 10 GeV/c, real part of forward amplitude, dispersion relation, Kd study 78−45950
n-hadron amplitudes from p-hadron and d-hadron amplitudes in Glauber-model 77−22803

kaon-nucleus reactions
for inelastic kaon-nucleus scattering, see "kaon-nucleus scattering"
see also kaon-nucleon interactions
$^AZ(K^-,\pi^-)_\Lambda{}^AZ$, strangeness exchange reaction ang. distribs., Glauber theory 79−75892
Conference on meson-nuclear physics, Houston, USA (Mar. 1979) 79−85489
deep nuclear levels, practicability of kaon probe 78−25237
distorted waves, 100 to 200 MeV, difference between Schrodinger and Klein-Gordon wave functions 78−94033
emulsion, K^- capture, neutron to proton ratio on surface 79−76024
fast particle production on nuclei in quark model *(Russian)* 79−6612
(k^-,π^-) meson-nuclear phys. in 1979, current status and new development 79−85490
light nuclei, low energy scatt. and reaction, review 79−85563
low energy, nuclear density shape optical pot. kaonic atom level shifts 80−63213
meson-nuclear physics, International Topical Conf. 77−6436
nuclear emulsions, $_\Lambda{}^9B$, decay mode obs. 79−36186
photoemulsion, kaon$^-$ capture, doubly charged particle yield 79−40959
strangeness exchange reactions and hypernuclear spectroscopy 79−67699
(K^-,π), Σ hypernuclei production 79−85392
(K^-,π^-), 390 MeV/c, formation of hypernuclear excited states in ^{12}C, ^{16}O, ^{27}Al 78−74402
(K^-,π^-), elementary properties, general review 79−85340
(K^-,π^-), excitation of unitary analogue states in hypernuclei 78−17131
(K^-,π^-), hypernuclei generation, γ-spectroscopy and lifetimes 79−75890
(K^-,π^-), kaons at rest, $^AZ_\Lambda$, hypernuclear γ-emitters prod. rates 78−46108
(K^-,π^-), strange giant resonance, DWIA calc. 77−14187
(K^-,π^-), strangeness exchange reaction, DWIA anal. 77−14186
(K^-,π^-), strangeness exchange reactions producing hypernuclei, shell model calcs. 78−17130
(K^-,π^-), strangeness exchange reactions, CERN 79−85561
(K^-,π^-), sum rules for recoilless lambda prod. 77−3053
(K^-,π^-) light hypernuclear quasifree formation and supersymmetry 77−14057
(K^-,π^-) on light nuclei, hypernuclear spectroscopy 78−50116
(K^-,π^-) reaction on ^9Be, ^{12}C, ^{16}O, ^{32}S, and ^{40}Ca 77−14183
(K^-,π^-) reactions, 900 MeV/c, sum rule for hypernuclear formation, distorted wave impulse approx. 78−70572
(K^-,X), 20, 37 GeV/c, ang. distribs., multiplicity distribs. and particle correlations 79−93664
(K^-,X), emulsion, 1.8 GeV/c, $_{\Lambda\Lambda}{}^ALi$, A=10, 11, double hypernuclei, prod. and decay 80−57718
$(K^\pm,X)$ symmetry violating kaon decay as nuclear probe 80−42704
K^-, in nuclear emulsions, 1.8 GeV/c, ^8Li emission 77−30637
K^-, stopping in emulsion nuclei, ^8Li fragments prod. 78−17244

kaon-nucleus reactions continued
K^- absorption at rest in C nuclei, study of final states containing Λ-hyperon 77−41997
K^- capture by emulsion nuclei, double charged particle yield *(Russian)* 78−78420
K^- capture on emulsion nuclei, investig. of Σ^- to Σ^+ prod. ratio below K^-p threshold 78−70407
K^- meson interaction in emulsion nuclei, mesonic hypernuclei form. 78−13158
K^- tracks, 1.5 GeV/c, fast stable particles from light emulsion nuclei, emission probabilities 78−17245
K^--nucleus reaction, in emulsion, ^{8}Li fragment energy, evaporation theory 78−62577
K^0 inclusive prod. from 10 GeV/c K^+ on nuclei and hydrogen 78−4882
K^0 regeneration in nuclei, effect of inelastic intermediate states, Glauber-Regge model anal. 79−54458
K^+ interaction with nuclei 78−13165
$K^\pm$ absorption cross section on nuclei, 60-280 GeV/c 79−22293
K^-+emulsion nuclei, star with hammerlike prong, ^{8}He, ^{8,9}Li or ^{8}B fragment 80−52695
K^-+light emulsion nuclei, 1.5 GeV/c, K^-p and K^-n channels, probability distrib. 78−13161
K^-+photonuclear emulsion nuclei, hypernuclei in hammer-like events 78−13162
$K_L{}^0C \rightarrow K_S{}^0C$ coherent regeneration in range 10-30 GeV/c 77−13955
$K^-{}^4He \rightarrow \pi^- {}^4_\Lambda He$, final state interaction model, Muskhelishvili Omnes eqn. soln., πmomentum distrib. 77−30285
Ag(K^-,K^0), cascade hypernucleus identification in nuclear emulsion 80−52603
Ag(K^-,f), 1.8 GeV, ternary, quaternary and cascade fission 79−63708
Al+K_L, 30 to 150 GeV, total cross sections, inelastic screening evidence 79−17936
Al+K_S, 20 to 140 GeV, precise coherent K_S regeneration amplitudes 79−17937
Al+K^-, stopped kaon capture, Doppler shifted nuclear gamma rays 78−62578
^{27}Al(K^-,π^-), relative ang. distribs. 77−14185
Au+K^-, 380 MeV, binary decay 79−93671
Be, 200 GeV/c, forward inclusive prod. spectra of K_s, Λ^0, $\bar{\Lambda}^0$, n, 200 GeV/c 78−82393
^{9}Be(K^-, Π$^-$), 720 MeV/c, Sigma hypernuclei prod., missing mass spectrum 80−57721
^{9}Be(K^-, π^-)$^9_\Lambda$Be*, ang. distribs. of strangeness exchange reactions, PWIA anal. *(Chinese)* 79−80956
^{9}Be(K^-,π^-p), stopped K^-, ^{8}Li$_\Lambda$ possible γ-transition 80−106002
^{9}Be(K^-,π), narrow Σ-hypernuclear states, estimated widths, quantum number assignments 80−42576
Br(K^-,K^0), cascade, hypernucleus identification in nuclear emulsion 80−52603
Br(K^-,f), 1.8 GeV, ternary, quaternary and cascade fission 79−63708
C+K_L, 30 to 150 GeV, total cross sections, inelastic screening evidence 79−17936
C+K_S, 20 to 140 GeV, precise coherent K_S regeneration amplitudes 79−17937
^{12}C(K^-,π^-), 800 MeV/c, $^{12}_\Lambda$C low lying excited states, ang. distribs. 80−32226
^{12}C(K^-,π^-), 900 MeV/c, sum rule for hypernuclear formation, distorted wave impulse approx. 78−70572
^{12}C(K^-,π^-), relative ang. distribs. 77−14185
^{12}C(K^-,π^-)$^{12}_\Lambda$C*, 800 MeV/c, ang. distribs. from DWIA calcs. 80−32225
^{12}C(K^-,π), narrow Σ-hypernuclear states, estimated widths, quantum number assignments 80−42576
^{12}C(k^-, π^-)$^{12}_\Lambda$C, strangeness exchange reaction, ground state ang. distrib., 11 MeV excitation 79−85560
^{12}C(k^-,π^-)$^{12}_\Lambda$C, Λ-nuclear spin-orbit coupling, ΛN effective interaction 79−85562
^{13}C(K^-, Π$^-$) ^{13}C$_\Lambda$, ang. distribs. of strangeness exchange reactions, PWIA anal. *(Chinese)* 79−80956
^{40}Ca(K^-,π^-), 900 MeV/c, sum rule for hypernuclear formation, distorted wave impulse approx. 78−70572
^{40}Ca(K^-,π^-), Λ particle full set of nuclear shell orbitals 79−63623
^{40}Ca(K^+,Kp$^+$), DWIA calc. of proton knockout as probe of deep hole states 78−13163
$^{40}_\Lambda$Ca(k^-,π^-), energy excitation spectra, nuclear shell orbitals for Λ 79−85565
Cu+K_L, 30 to 150 GeV, total cross sections, inelastic screening evidence 79−17936
Cu+K_S, 20 to 140 GeV, precise coherent K_S regeneration amplitudes 79−17937
Cu(K^-, φX), *(Russian)* 79−9637
^{4}He+K^- → Λ+π^-+p+d, 180 MeV, final state study, double impulse model 79−30855
^{8}He obs., in hammer tracks from K^-+emulsion, 1.8 GeV/c 79−6711
^{6}Li, γ-ray spectra of stopped K^-, transitions in $^4_\Lambda$H and $^4_\Lambda$He 79−63621
^{6}Li$_\Lambda$, supermultiplet struct. and decay props. of hypernuclear 1^+ resonances from (K^-,π^-) 80−78186
^{6}Li(k^-,π^-)$^6_\Lambda$Li, strangeness analogue reson. 79−85566
^{7}Li, γ-ray spectra of stopped K^-, transitions in $^4_\Lambda$H and $^4_\Lambda$He 79−63621
^{7}Li(K^-, π^0)$^7_\Lambda$He, prod. cross sections from shell model theory 78−62501
^{7}Li(K^-,π^-)$^7_\Lambda$Li, prod. cross sections from shell model theory 78−62501
^{7}Li(K^-,π^-γ), hypernuclear γ-ray line 78−37377
^{7}Li(K^-,π), narrow Σ-hypernuclear states, estimated widths, quantum number assignments 80−42576
^{16}O+K^-, total cross section calc., complex momentum theory anal. with $\alpha_P{}^0 > 1$ *(Russian)* 79−9638
^{16}O(K^-,π^-), spin orbit interactions of Λ hyperons 79−9628
^{16}O(k^-,π^-)$^{16}_\Lambda$O, Λ-nuclear spin-orbit coupling, ΛN effective interaction 79−85562
Pb+K_L, 30 to 150 GeV, total cross sections, inelastic screening evidence 79−17936
Pb+K_S, 20 to 140 GeV, precise coherent K_S regeneration amplitudes 79−17937
Pb+K^-, 380 MeV, binary decay 79−93671
Pt+K^- interactions, 12 GeV/c, Λ^0 prod., search for di-hyperon resonance 77−82970
^{32}S(K^-,π^-), Λ particle full set of nuclear shell orbitals 79−63623
$^{32}_\Lambda$S(k^-,π^-), energy excitation spectra, nuclear shell orbitals for Λ 79−85565
^{30}Si(K^-,$\bar{K}^0$), 300 MeV, microscopic particle-hole shell model calcs., DWIA anal. 79−59091

kaon-nucleus reactions continued
Sn+K_L, 30 to 150 GeV, total cross sections, inelastic screening evidence 79−17936
Sn+K_S, 20 to 140 GeV, precise coherent K_S regeneration amplitudes 79−17937
^{122}Sn(K^-, X), 0 MeV, E2 nuclear resonance effects, γ and X-ray meas. 78−41774
Ta+K^-, 12.6 GeV/c, backward particle emission, energy depend. 78−25236
Th, K^- meson induced fission at 700 MeV/c, fragment mass distrib. 78−13168
Th+K^-, 380 MeV, binary decay 79−93671
U, K^- meson induced fission at 700 MeV/c, fragment mass distrib. 78−13168
U+K^-, 380 MeV, binary decay 79−93671

kaon-nucleus scattering
see also kaon-nucleon scattering
elementary properties, general review 79−85340
kaonic ^{12}C, coupled channel formalism, role of Λ(1405), binding effect, Pauli blocking 78−55261
light nuclei, low energy scatt. and reaction, review 79−85563
multiple Coulomb scattering angle meas. 50 to 200 GeV/c 80−9315
universality of the ω intercept and Inelastic rescattering of kaons in nuclei 80−102212
(K,K), excitation of unitary analogue states 78−17131
(K,$\bar{K}$), isobar doorway model, optical pot., Λ-nuclear matter binding energy 80−106079
($K^\pm$,$K^\pm$) from Be, C, Al, Cu, Sn, Pb, 70, 125, 175 GeV/c 80−83128
(K,X) optical pot. from KN scatt. and kaonic atom pot. models 79−97731
$\bar{K}$-nucleus optical pot. at low energy 78−94032
K^- nucleus scattering, optical pots. 77−2962
K^0 regeneration on C, Regge behaviour and nuclear effects, ω-pomeron cut 79−13347
K^+ interaction with nuclei 78−13165
K^1-nucleus optical pot. for kaonic atoms 79−98255
KN coupling const. from kaon-nucleus forward scatt. amplitudes 79−85418
C, $K_L{}^0 \rightarrow K_S{}^0$ coherent regeneration, optical model calcs. 77−30427
C($K^\pm$,$K^\pm$) intermediate energy, forward scatt. amplitudes, Glauber model calcs. 79−30856
C($K_L{}^0$, $K_S{}^0$), 10-50 GeV/c, regeneration, coherent production model 78−33220
^{2}C(K^+,$K^{\pm\prime}$), 300-800 MeV, microscopic particle-hole shell model calcs., DWIA anal. 79−59091
^{12}C (K^+,$K^{+\prime}$)^{12}C*, DWIA, Fermi motion effect 77−54258
^{12}C+$K^\pm$, application of forward dispersion relns. to scatt. amplitude and length 77−18626
^{12}C(K,K), appl. of forward dispersion reln. 77−14188
^{12}C($K_L{}^0$, $K_S{}^0$)^{12}C, elastic regeneration, 10-50 GeV/c, differential cross section slope 78−646
^{12}C(K^+,K^{+1}), 300 MeV inclusive scatt., plane wave impulse approx. 78−50214
^{12}C(K^+,$K^{+\prime}$), form factors, cross sections, interior probing capability 80−73866
^{12}C(K^+,K^+), 0.4-1.2 GeV/c, optical potl., cross-sections determ. 77−14184
^{12}C(K^+,$K^\pm$), 100-1000 MeV, differential and total cross sections, nucleon motion 80−102206
^{12}C($K^\pm$,$K^\pm$), Glauber model anal. 80−42697
^{12}C(K^+,$K^\pm$), kaon-nucleus coupling const. from scatt. amplitudes 80−32304
^{12}C(k^-,k^-), 800 MeV, differential cross sections 79−85564
^{40}Ca(K^+,K^+), 0.4-1.2 GeV/c, optical potl., cross-sections determ. 77−14184
^{40}Ca($K^\pm$,$K^\pm$), Glauber model anal. 80−42697
^{2}H+$K^\pm$, high energy cross section calc., complex ang. momentum theory *(Russian)* 78−46067
^{2}H(K^+,K^+)^{2}H, low energy, diagram formalism anal. *(Russian)* 77−26543
^{4}He+$K^\pm$, high energy cross section calc. complex ang. momentum theory *(Russian)* 78−46067
^{16}O(K,K′), low lying collective state selective excitation, ang. distribs. and cross sections 79−6368
^{16}O(K^+,$K^{+\prime}$), plane and distorted wave impulse approx. anal., plane waves 79−9630
^{16}O(K^+,K^+), 0.4-1.2 GeV/c, optical potl., cross-sections determ. 77−14184

kaon production
electroproduction, inclusive particle ratios on H and D targets 77−18291
hadronic large p_T reactions, K^+ and K^- prod. as model test, hard quark scatt. 79−40735
inclusive interactions, double Reggeon representation of energy depend. of cross sections *(Russian)* 77−74737
inclusive particle production in C+p and W+p reactions, nuclear size depend. 77−46168
inclusive prod. in $\bar{p}p$ interactions in 9.1 GeV/c 79−6355
$K^-p \rightarrow K^-\pi^+n$, 6 GeV/c, $K^*(1780)$ 78−33087
multiple prod. in ν interactions, possible semileptonic decay of charmed meson 77−2819
nuclear multi-particle rescatt. effects, cumulative π, p, K prod. *(Russian)* 80−52638
$\bar{p}p$ annihilation, 3.0 GeV/c, differential cross sections and polarisation of $\bar{\Lambda}^0$ and $K_s{}^0$ 78−58197
proton-nucleus inclusive single particle prod. of $\pi^\pm$, $K^\pm$ and $p^\pm$ at 28.5 GeV 77−18346
quark jet fragmentation, large momentum transfer reactions, implication of large vector meson prod. 79−345
relativistic nuclear collisions, K prod. in multiple collision model 80−99157
review, hadron-nucleus interactions at high energies, phenomenological models 78−8859
strange axial vector meson non-diffracture prod. in Kp and πp interactions 80−32122
Veneziano model anal., $K\bar{K}\pi$ Dalitz-plot density calc. 79−26331
$D \rightarrow K\pi l\nu$, charm-changing weak hadronic current, models 80−57585
$D^0 \rightarrow K^-\pi^+$, quark total number conservation, D^+ lifetime longer than D^0 80−57590
$D^0 \rightarrow K^-\pi^+\pi^-$, obs. in 3.77 GeV e^+e^- annihilation 78−37206
$D^0 \rightarrow \bar{K}^0\pi^0$, ΔT=1 constraints and final state interactions 80−95267

kaon production continued
$D^0 \to \bar{K}^0\pi^0$, quark total number conservation, D^+ lifetime longer than D^0 80−57590
$D^0 \to K^+K^-$, $\pi^+\pi^-$, branching ratio, $\Delta I = {}^1/_2$ rule violation, colour radius interactions calc. 79−93412
$D^+ \to \bar{K}^0\pi^+$, quark total number conservation, D^+ lifetime longer than D^0 80−57590
ed, $K^\pm/\pi^\pm$ ratio and symmetry props. of quark- parton model, fragmentation functions 78−93888
e^+e^-, hadron production, inclusive study, momentum distrib., energy and multiplicity 80−57613
e^+e^- annihilation, 3.6-5.2 GeV, charged π, K, N inclusive prod. 79−30743
e^+e^- annihilation, 3.6-5.8 GeV, inclusive D and K meson prod. cross sections 79−93439
$e^+e^- \to$hadrons, 12, 30 GeV, π,k,p,$\bar{p}$ production 80−105916
$e^+e^- \to$hadrons, 53 GeV^2, $\pi^\pm$ and $K^\pm$ cross sections, scaling 78−78201
e^+e^- inclusive hadron prod., polarisation and p nonconservation asymmetries, π, $K^\pm$, $D^\pm$ prod. 80−78084
$e^+e^- \to K_S^0K_L^0$, ϕ meson mass meas., $\omega\phi$ interference obs. *(Russian)* 78−45935
$e^+e^- \to K_S^0X$, 3.6-5 GeV, prod. cross section 77−49991
$e^+e^- \to K^+K^-$, 1.6 GeV, total cross-section meas., kaon form factor 77−46064
$e^+e^- \to K^+K^-$, asymmetry, one- and two-photon terms interference 77−10270
$e^+e^- \to K^\pm X$, 13 and 25 GeV^2, cross sections, scaling 77−49989
$e^+e^- \to K^\pm X$, 3.6 to 5 GeV, total cross section 77−49990
$e^+e^- \to K^\pm X$, at CERN ISR with x=0 77−18303
$e^+e^- \to K$+anything, statistical model anal., two-parameter fit 77−6138
$e^+e^- \to \pi^+\pi^-(K^+K^-)$, $\sqrt{s}$=1.5 GeV, EM timelike form factors for π and K 80−91089
ep, K inclusive electroproduction, K/π and K^+/K^- prod. ratios 78−37217
ep, $K^\pm/\pi^\pm$ ratio and symmetry props. of quark- parton model, fragmentation functions 78−93888
ep deep inelastic inclusive K_s^0 and Λ electroproduction, quark fragmentation 78−66123
$ep \to eK^+\Lambda^0$, scalar transverse separation 77−71520
$ep \to eK^+\Sigma^0$, scalar transverse separation 77−71520
$ep \to eK^+$+anything, invariant cross section, DESY studies 78−41553
$\gamma \to K\bar{K}$, EM radius, low-energy approx., comparison with pion 78−50033
$\gamma d \to K^+\Delta n$, differential cross section, influence of Δn interaction *(Russian)* 79−394
$\gamma\gamma \to K\bar{K}$ amplitude, coupled channel calc. of final state interactions 77−2809
$\gamma N \to K^+\Sigma$, meas. of asymmetries and cross sections using 16 GeV linearly polarised photons 80−13318
$\gamma N \to K^\pm$+anything, 9-18 GeV, forward hemisphere 77−6134
γn to 5.3 GeV, multipion and strange particle prod., reson. 77−10261
$\gamma p \to K^+K^-p$, 20-36 GeV, Φ(1019) prod., cross sections 80−105907
$\gamma p \to K^+K^-p$, 7 GeV, S-P wave interference near K^+K^- threshold, $S^* \to K^+K^-$ cross section 79−6343
$\gamma p \to K^+K^-\pi^+\pi^-$, photoprod. at CERN SPS and search for charmed mesons 79−26336
$\gamma p \to K^+K^-\pi^+\pi^-p$, 20-70 GeV, $K^+K\pi$ threshold enhancment 80−78076
$\gamma p \to K^+\Lambda$, meas. of asymmetries and cross sections using 16 GeV linearly polarised photons 80−13318
$\gamma p \to K^+\Lambda^0$ 1.1 to 1.3 GeV, polarised proton target 78−66125
$\gamma_v p \to K^+X^b$, $K^+\Lambda$, or $K^+\Sigma^0$, K^+ electroprod. along virtual photon direction, cross sections 77−41848
$J/\psi \to K_sK^-\pi^+$, low lying resonance saturation 79−54338
K^0 inclusive prod. from 10 GeV/c K^+ on nuclei and hydrogen 78−4882
K^0 meson production cross section *(Russian)* 78−82394
K^0 prod. in e^+e^- annihilations, 3.4-7.6 GeV 77−87987
K^0 production in pp interactions, inclusive and exclusive, 6 GeV/c, polarised beam 77−65171
K_L^0 n$\to K_s^0$n, 10-50 GeV/c, regeneration, coherent production model 78−33220
K_s regeneration in K_Le scatt. 30 to 100 GeV, K^0 charge radius meas. 79−400
K_s^0 inclusive prod. in π^-p 6 GeV/c interactions 79−93454
K_S^0, neutral strange-particle prod. by 300 GeV protons in Be, Cu, Pb 79−17905
K_S^0 prod. cross-section, scaling in pp, K^+p, π^+p 80−52539
K*(890) and K*(1420) prod. in 405 GeV/c pp interactions 79−30757
K*(890) prod. at 13 GeV/c, Regge models 78−45961
$\bar{K}$*(890)(1420), in K^-p at 32 GeV/c, vector and tensor meson prod., with quark model anal. 79−80854
K*(892) prod. in e^+e^- multihadron annihilation 78−66132
K^{*0},$\bar{K}^{*0}$, production by charge exchange reactions, production cross section 78−58200
$K^{*\pm}$(890) production in 205 GeV/c pp interactions 78−54659
$K^{*\pm}$(892), inclusive prod. in π^-p 6 GeV/c interactions 79−93454
Kd interactions, 9 GeV/c, prod. of K*(1760) and K*(2100) 78−8693
K^0d interaction, 10 to 50 GeV/c, transmission regeneration *(Russian)* 78−41590
K^+d inclusive reactions, 4.6 GeV/c, topological cross sections, π^-, K^0, Λ prod. 77−50004
K_s^0e prod. in e^+e^-, charmed particle weak decay 77−2853
$K\bar{K} \to K\bar{K}$, dispersion model, matrix N/D method *(Russian)* 78−45954
$\bar{K}$K S-wave enhancement, 1300 MeV in πN interactions, characteristics 77−6158
$K^0\bar{K}^0$ pair detection, interference correlations, struct. function behaviour, statistical model *(Russian)* 79−93421
$K\bar{K}^*$ mass enhancement in $\pi^+p \to (K^+K^-\pi^+)p$ 77−26547
$K^-n \to \bar{\Sigma}(\Sigma\pi)^-$, 680-840 MeV/c differential cross-sections 77−18324
K^0n interaction, 10 to 50 GeV/c, transmission regeneration *(Russian)* 78−41590
$\bar{K}$p, 70 GeV/c, total and differential cross-sections for π and K production 80−63050
$Kp \to \pi(K)(p)X$, 4-250 GeV/c, Pomeron factorisation 77−14005
K^-p, 32 GeV/c, exclusive reactions, diffractive dissociation processes, $\pi^+\pi^-$ and K^+K^- prod. 80−86760
$K^-p \to K_s\pi^+\pi^-n$, 6 GeV/c, K* and Q_2 signals, partial wave anal. 80−86754
$K^-p \to K^0X$, 32 GeV/c, struct. functions *(Russian)* 77−264
$K^-p \to \bar{K}^0\pi^-p$, 4.2 GeV/c, non-charge exchange $\bar{K}^0\pi^-$ prod., spin-parity struct., mass 78−45949
$K^-p \to K^*(890)\Delta(1236)$, 10 GeV/c, multidimens. anal., reaction subchannel separation 80−32127
kaon production continued
$K^-p \to \Lambda(\Sigma)K^0$, $K^\pm\pi^\pm$, 4.2 GeV/c, 1550 MeV, I=1 enhancement in $(\Lambda\pi)$ and $(\Sigma\pi)$ systems 78−89735
$K^+p \to K^0X$, 32 GeV/c, associated average charged particle multiplicities 77−2882
$K^+p \to K^0X$, 32 GeV/c, inclusive cross sections, single particle distribs. 78−41598
$K^+p \to K^0X$, 5-32 GeV/c, transverse momentum distribs. *(Russian)* 77−30467
$K^+p \to K^0(\pi^-)$+anything, 32 GeV/c, associated multiplicities *(Russian)* 77−34197
$K^+p \to K^0p\pi^+$, 3 to 16 GeV/c, resonance production, cross sections and density matrix elements 78−17048
$K^+p \to K^0p\pi^+$, resonance production at 5, 8.25, and 16 GeV/c 78−12931
$K^+p \to pK^0X$, 32 GeV/c, total cross section and structure functions 79−40809
$K^+p \to (K\pi)^+p$, 10 GeV/c, amplitude and natural parity exchange anal. 78−50053
$K^+p \to K_S^0\pi^+p$, 10 GeV/c, Kπ prod., two arm spectrometer studies 78−50052
$K^+p \to K^{*+}p$, 10 GeV/c, amplitudes and exchange mechanisms 78−8692
$K_L^0p \to K_S^0p$, 4 to 14 GeV, in range $0.1 \leq |t| \leq 2$ GeV^2 79−3045
Kπ, KK, and K$\bar{K}$, correlations in multiperipheral resonance prod. model, broken SU_3 symmetry 78−45891
$K_s^0\pi^+\pi^+\pi^-$ narrow peak at 2.6 GeV in 12 GeV/c $\bar{p}$p interactions 77−30452
$\Lambda_c^+ \to p\bar{K}^0\pi^+\pi^-$, kaonic decay observation, prod. rates 79−26332
$\mu p \to K_s^0X$, 225 GeV, deep inelastic scatt., strange neutral particle prod. 80−105902
n+C$\to$(n*$\to\Lambda$kπ)X, 45 GeV, production cross section 77−82795
n+N$\to$(n*$\to\Lambda$kπ)X, 45 GeV, decay prob. 77−82795
$\nu,\bar{\nu}$ experiments at Gargamelle, strange particle production by neutral currents 78−37200
ν and $\bar{\nu}$ inclusive processes for neutral currents, sea quark effects, meson prod. 79−22088
$\bar{\nu}$ interactions, Λ, Σ^0, K^0 prod. 78−8647
$\bar{\nu}$N, K^0 and π^- prod. rates, SU(3) symmetry violation in quark jet 80−82966
$\bar{\nu}_\mu$N, K^0 and Λ inclusive prod., fragmentation function and transverse momentum squared 80−32093
$\nu_\mu N \to \mu^-e^+X$, associated K_s^0 production 77−57528
$(\bar{\nu})\nu N \to e^-e^-e^+\mu^+K^0$+7$\gamma$, exptl. obs. 79−9361
$\bar{\nu}$p, strange particle prod. at CERN PS 78−82195
$\nu p \to \mu^-K^+p$, E>5 GeV, cross-section meas. 78−93872
(p,X), 400 GeV, A=6-180, $\bar{p},\pi^\pm$ and $K^\pm$ backward prod., invariant cross sections 80−102188
(p,X), 70 GeV/c *(Russian)* 80−52681
$\bar{p}$ annihilation in nucl. emulsion, statistical theory of multiple prod. *(Spanish)* 77−67669
p-nucleus collisions, subthreshold prod., struct. function 78−21564
p+Be(Cu), 70 GeV, π^+, K^+, p large p_T yields *(Russian)* 77−82778
$p+Z \to \pi^\pm(K,p,\bar{p})X$, 28.5 Gev/c, invariant cross-sections, for P_T 0.75-2.25 GeV/c 77−30456
pd, 70 GeV, $\pi^\pm$, $K^\pm$, p, $\bar{p}$ prod. with 0.5-2.2 GeV/c transverse momenta, yield ratio, QCD *(Russian)* 80−83012
$pd \to \pi^\pm(K^\pm)pX$, 11.75 GeV/c, meas. of left-right asymmetry far inclusive $\pi^\pm$, $K^\pm$, p prod., polarised p-beam 79−22155
$pd \to V^0X$, 18 GeV/c, K^0s, γ, Λ, $\bar{\Lambda}$ prod. 77−87993
pN, 67 GeV/c, in Be, Al, Cu, inclusive $\pi^\pm$, $K^\pm$, p, $\bar{p}$ prod. cross sections *(Russian)* 80−86769
pN, 67 GeV/c, nuclear targets, $\pi^\pm$, $K^\pm$, p,$\bar{p}$ yields *(Russian)* 80−68501
pn$\to$n$K\Lambda$, field current relations *(Chinese)* 79−22126
$\bar{p}$p, 14.75 GeV/c, inclusive and semi-inclusive $K^{*\pm}$(890) and $\Sigma^\pm$(1385) prod. 80−5027
$\bar{p}$p, 22.4 GeV/c, γ, K_s^0 and Λ inclusive prod., structure functions *(Russian)* 79−58985
$\bar{p}$p, 22.4 GeV/c, inclusive γ, K_S^0, Λ $\bar{\Lambda}$ production, KNO scaling test *(Russian)* 79−30759
pp, 300 GeV/c, inclusive prod. of K^0, Λ^0 $K^{*\pm}$(890) and $\Sigma^*\pm$(1385) 80−95290
pp, 400 GeV/c, inclusive and semiinclusive prod. of π^0, K_s^0, Λ^0, $\bar{\Lambda}^0$, Σ^0, $\bar{\Sigma}^0$, η^0, ω^0 79−93472
pp, 70 GeV, $\pi^\pm$, $K^\pm$, p, $\bar{p}$ prod. cross sections, QCD-parton model anal. *(Russian)* 80−63044
pp, D, B, K prod., QCD model for heavy flavour prod., two gluon annihilation 80−86744
pp, total inclusive cross sections for δ^0, g^0, K^{*0} and $\bar{K}^{*0}$ at 53 GeV 79−17771
$\bar{p}$p 14.75 GeV/c, search for $K_s^0\pi^\pm\pi^+\pi^-$ resonance near 2.6 GeV/c 78−74289
pp$\to$(K_s^0, Λ, or $\bar{\Lambda}$)$\pi^\pm$+X, 405 GeV/c cross section determ., vector meson dominance 79−89207
pp$\to(\pi^\pm,K^\pm,p,d)$X, 6 and 11.8 GeV/c, polarised proton, L-R asymmetry meas. 77−30455
$\bar{p}$p annihilation, asymptotic props., parton model, kaon prod. *(Russian)* 78−466
$\bar{p}$p annihilations, 0.76 GeV/c, inclusive $K^{*\pm}$(892) and K_S^0 prod. 78−62465
$\bar{p}$p annihilations, 0.76 GeV/c, K$\bar{K}$ correls., effect of resonance prod. 78−78205
pp collisions, high momentum $\pi^\pm$ and $K^\pm$ prod., 45 GeV, cross sections 78−93910
pp collisions, multiplicities of pion, kaon or proton prod. at ISR 77−259
pp inclusive K and Λ prod. at 19 GeV/c 77−13998
pp inclusive reacts., charged particle associated multiplicities at ISR energies 78−21473
$\bar{p}$p interactions, 100 GeV/c, inclusive distribs. for γ, K_s, Λ^0, $\bar{\Lambda}^0$ prod. 77−38213
$\bar{p}p \to K_{S^0}^{0\pm}\pi^\pm$, K* (890), EM mass difference determ. 79−390
$pp \to K_{S^0}X$, 69 GeV/c, cross-section 77−22812
$\bar{p}p \to K_S^0X(\Lambda X)$ ($\bar{\Lambda}X$), 3.6 GeV/c, cross section anal. and Λ polarisation 79−45095
$\bar{p}p \to K_S^0$+X, 4.6, 9.1 GeV/c, inclusive total, topological and invariant differential cross sections 79−408
$pp \to K_S^0K_S^0X^{++}$ 19 GeV, strong dynamic correlations 79−93468
$pp \to K_s^0\pi^-$ +anything, 28.4 GeV/c, cross-sections and mass distribs. meas. 77−38212
$\bar{p}p \to K^-K^+$, 1.0 to 2.2 GeV/c, polarisation parameter meas. 77−74711
$\bar{p}p \to K^-K^+$, 1.0 to 2.2 GeV/c, polarisation parameter 77−87995

kaon production continued
$\bar{p}p \rightarrow K^0_S K^0_S$+pions, 700-760 MeV/c, $K^0_S K^0_S$ threshold enhancement in final states 78−82228
$pp \rightarrow K^0(\Lambda)(\Delta^{++})X$, 6 GeV/c, polarised proton 77−30400
$\bar{p}p \rightarrow K^+K^-$ 6.2 GeV/c, ang. distrib. 77−18330
$pp \rightarrow K^+K^+X$, search for narrow six quark resonance 78−89757
$pp \rightarrow K^{\pm}$+anything, 100-400 GeV expt. techniques and data analysis 78−58216
$pp \rightarrow K^{\pm}$+anything, large p_T, 200 to 400 GeV 77−22816
$pp \rightarrow KK$, 12 and 24 GeV/c, strangeness transfer distribs. 79−22142
$pp \rightarrow K^{*\pm}(892)X$, 12 and 24 GeV/c 80−86765
$\bar{p}p \rightarrow K^*(890)X$, 12 GeV/c, prod. cross sections 78−93911
$\bar{p}p \rightarrow K^*(892)X$, 3.6 GeV, factorisation hypothesis test 80−102055
$pp \rightarrow \Lambda K^0_3 X^{++}$, 19 GeV, strong dynamic correlations 79−93468
$pp \rightarrow \Lambda K^0_s X$, 19 GeV/c, single particle props. 80−32139
$pp \rightarrow \Lambda(\bar{K}^0)X$, 12 GeV/c, beam polarisation induced asymmetries 80−42507
$pp \rightarrow p\Lambda K^+$, 12, 24 GeV/c, diffr. dissoc. 77−82779
$pp \rightarrow \pi^+\pi^-(K^+K^-)$, 1.0-2.2 GeV/c, polarisation parameter 77−30401
$\bar{p}p \rightarrow \pi^{\pm}K_s{}^0X^{\mp}$, low energy, thermodynamical anal. of charged pion momentum spectra 77−65169
$pp \rightarrow \pi^{\pm}(K^{\pm})pX$, 11.75 GeV/c, meas. of left-right asymmetry far inclusive $\pi^{\pm}$, $K^{\pm}$, p prod., polarised p-beam 79−22155
$pp \rightarrow \pi(K)X$, 50-175 GeV, Regge parametrisation 77−14002
$pp \rightarrow \pi(K)(p)X$, 4-250 GeV/c, Pomeron factorisation 77−14005
$p\pi^-$ interaction, K+hyperon prod., mass quantisation anal. *(French)* 78−70401
$\pi^-{}^{12}C$, 40 GeV/c, Λ and $K_1{}^0$ inclusive distribs. *(Russian)* 77−34196
$\pi\mp U$ interaction at 55 GeV/c, search for long lived heavy mesons *(Russian)* 80−5029
πd quasielastic and inelastic rescattering as cumulative particle prod. source *(Russian)* 79−22340
π^+d, 6 to 100 GeV/c, $P_\perp$ distribs. of K^0, π^-, ρ^0, f, equilibrium temp. 79−49540
π^+d interactions, strange-particle cross-sections at 4 GeV/c 78−89734
$\pi^+d \rightarrow K^+Yp$, E>1 GeV, Glauber correction and final state interaction *(Russian)* 77−6161
π^-n, 40 GeV/c, cross sections of Λ and K prod. *(Russian)* 77−6184
$\pi^+n \rightarrow K^-K^+p$, 6 GeV/c, f, f' and $A_2{}^0$ interference 77−253
$\pi^+n \rightarrow K^-K^+p$, f,f' mesons, high statistics study at 6 GeV/c 77−79279
πp, 16 GeV/c, diffr. dissoc. into $\bar{K}K^*$, $\bar{K}^*K$ 78−41594
$\pi p \rightarrow K(p)X$, 50-175 GeV, Regge parametrisation 77−14002
$\pi p \rightarrow \Lambda K$, associated prod. of strange particles at resonance energies 77−22775
$\pi p \rightarrow \pi(K)(p)X$, 4-25 GeV/c, Pomeron factorisation 77−14005
$\pi p \rightarrow \Sigma K$, associated prod. of strange particles at resonance energies 77−22775
π^-p, 100, 200, 360 GeV/c, inclusive prod. of π^0, $K_S{}^0$, Λ^0, $\bar{\Lambda}^0$, cross sections 80−73745
π^-p, 147 GeV/c, neutral particle prod., K_S, Λ, $\bar{\Lambda}$, γ, multiplicity scaling form 80−22645
π^-p, 16 GeV/c, inclusive $\bar{K}^{*0}$ (890) inclusive prod. 78−8710
π^-p, 200, 300 GeV, relative π^+, K^+, p, $\bar{p}$ prod., charge ratios, high p_T 80−47335
π^-p 5 GeV/c interactions, inclusive distrib. of Γ^0 and $K^0{}_1$ *(Russian)* 78−54652
π^-p interactions, 15 GeV/c, K^0_s, Λ, $\bar{\Lambda}$ prod., Regge anal. 78−45981
π^-p interactions, 5 and 40 GeV, inclusive struct. functions of γ, $\pi^{\pm}$, K^0, and Λ *(Russian)* 79−80856
$\pi^-p \rightarrow K_{S^0}, \Lambda, \bar{\Lambda}$, prod. in 16 GeV/c interactions 80−37308
$\pi^-p \rightarrow K_1{}^0K_1{}^0n$, 40 GeV/c *(Russian)* 77−261
$\pi^-p \rightarrow K_1{}^0K_1{}^0n$, 50 GeV/c, cross section, ang. distrib., mass spectrum *(Russian)* 77−34186
$\pi^-p \rightarrow K_s{}^0K^{\pm}\pi^{\mp}n$, 3.95 GeV/c, E(1420) quantum numbers and branching ratio 80−95286
$\pi^-p \rightarrow K_s{}^0X$, 205 GeV/c cross-sections 77−71544
$\pi^-p \rightarrow K^-K_S{}^0p$, 9.8 and 18.8 GeV, decay ang. distribs. and differential cross sections 79−17754
$\pi^-p \rightarrow K^-K^+n$, 6 GeV/c, f, f' and $A_2{}^0$ interference 77−253
$\pi^-p \rightarrow K^-K^+n$, f,f' mesons, high statistics study at 6 GeV/c 77−79279
$\pi^-p \rightarrow K^-K^+\pi^0n$, D, E, and δ mesons, obs. at 12 and 15 GeV/c 79−9410
$\pi^-p \rightarrow K^-K^+\pi^0n$, D, E, and δ mesons obs. at 12 and 15 GeV/c 79−3052
$\pi^-p \rightarrow K^0\Lambda$, 3.5 GeV/c, Λ polarisation, high statistics meas. 80−57637
$\pi^-p \rightarrow K^0\Lambda$, threshold to 2350 MeV, partial wave analysis 78−29349
$\pi^-p \rightarrow K^0\Lambda^0$, 1375 to 2375 MeV, new results and anal. 80−438
$\pi^-p \rightarrow K^0\Lambda^0$, 1400 to 2380 MeV/c, differential cross sections and polarisations, partial wave anal. 78−70405
$\pi^-p \rightarrow K^0\Lambda^0$, up to 1334 MeV/c, cross sections and polarisation, energy depend. phase shift anal. 78−70404
$\pi^-p \rightarrow K^0\Lambda^0$, up to 1334 MeV/c, differential cross sections and polarisation, phase shift anal. 79−412
$\pi^-p \rightarrow K^0\Lambda^0$ up to 2.375 GeV/c, resonance parameters, partial wave anal. 80−32133
$\pi^-p \rightarrow K^0\Sigma^0$, 1395 to 2375 MeV/c, differential cross-section and polarisation meas. 80−9183
$\pi^-p \rightarrow K^0\Sigma^0$, 1395 to 2375 MeV/c, differential cross-section and polarisation 80−57635
$\pi^-p \rightarrow K^0\Sigma^0$, threshold to 1334 MeV/c, differential cross-section and polarisation 78−89733
$\pi^-p \rightarrow K^0\Sigma^0$, threshold to 1334 MeV/c, differential cross section and polarisation data 79−17755
$\pi^-p \rightarrow K^0+X$, 4.9-40 GeV/c inclusive and semi-inclusive distribs. *(Russian)* 78−41610
$\pi^-p \rightarrow K^+K^-K^+K^-n$, 22.6 GeV/c, ϕ prod., Okubo-Zweig-Iizuka rule test 78−89743
$\pi^-p \rightarrow K^+K^-n$, 10 GeV/c, obs. of new structure in K^+K^- system at 2.20 GeV, width approx. 200 MeV 79−80843
$\pi^-p \rightarrow K^+K^-n$, 62 GeV, spin-5 boson resonance at 2300 MeV 80−102078
$\pi^-p \rightarrow K^+\Sigma^-$, 5 and 8 GeV, differential cross section 78−21456
$\pi^-p \rightarrow \bar{K}KN$, S-wave anal., scalar mesons and branching ratios 80−13328
$\pi^-p \rightarrow K^{*0}(890)\ \Lambda^0/\Sigma^0$, 10 GeV/c, K^{*0} polarisation meas. in hypercharge exchange reaction 80−63017
$\pi^-p \rightarrow \Lambda K$, low energy, amplitude anal., Lagrangian model 80−82995
$\pi^-p \rightarrow \Lambda K^0+X^0$, 4.35, 4.85 GeV/c, mass spectra of N* resonances *(Russian)* 77−6159
$\pi^-p \rightarrow \Lambda K^+ + X^-$, 4.35, 4.85 GeV/c, mass spectra of N* resonances *(Russian)* 77−6159

kaon production continued
$\pi^-p \rightarrow nk_s{}^0K_s{}^0$, 6, 7 GeV/c, cross section, decay ang. distribs. and S-wave amplitude 79−49539
π^+p, 32 GeV/c, inclusive strange particle prod., Σ^+, $K_S{}^0$, Λ and $\bar{\Lambda}$ cross sections 80−52541
π^+p, 6 to 100 GeV/c, $P_\perp$ distribs. of k^0, π^-, ρ^0, f, equilibrium temp. 79−49540
π^+p, strange-particle cross-sections at 10.3 GeV/c 77−87999
$\pi^+p \rightarrow$four prong final states, 10.3 GeV/c, resonance prod. cross-sections 78−74276
$\pi^+p \rightarrow K^+K_S{}^0p$, forward $A_2{}^+$ prod. at 12.7 GeV/c 79−22149
$\pi^+p \rightarrow K^+\Sigma^+$, 4, 7, 11.5, 70 GeV/c, weak exchange degeneracy, Navelet-Stevens model generalisation 79−93462
$\pi^+p \rightarrow K^+\Sigma^+$, exchange degeneracy in hypercharge exchange reacts. 78−41581
$\pi^+p \rightarrow K^+\Sigma^+$, exchange degeneracy in hypercharge exchange reacts. 78−82239
$\pi^+p \rightarrow K^+\Sigma^+$ and $K^-p \rightarrow \pi^-\Sigma^+$, exchange degeneracy 80−57634
$\pi^+p \rightarrow K^+Y^+$, $Y^+=\Sigma^+$ or $Y^{*+}(1385)$, 7 GeV/c, hypercharge exchange in line-reversed π^+p and K^-p 80−82998
$\pi^+p \rightarrow K^+Y^*(1385)$, 11.5 GeV/c confirmation of exchange degeneracy predictions in line reversed reacts. 78−82247
$\pi^+p \rightarrow K^{*+}(890)Y^+$, $Y^+=\Sigma^+$ or $Y^{*+}(1385)$, 7 and 11.5 GeV/c, hyperon polarisation, vector meson decay angular distribs. 80−82997
$\pi^+p \rightarrow K^{*\pm}(892)X$, 16 GeV/c 80−86765
$\pi^+p \rightarrow \Lambda K^+\pi^-$, 10.3 GeV/c, p diffractive dissociation into ΛK^+ and $(\Sigma K)^+$ 78−45966
$\pi^+p \rightarrow \Sigma^+(1385)K^+(K^{*+}(890))$ 10.3 GeV.c, Y*K and Y*K* prod. 79−49544
$\pi\pi \rightarrow K\bar{K}$, I=0 state scatt. amplitude 77−18325
$\pi\pi \rightarrow K\bar{K}$ amplitude in the unphysical region, hyperbolic dispersion curves 79−9407
$\pi\pi \rightarrow K\bar{K}$ study via $\pi^-p \rightarrow K_S{}^nK_S{}^0n$ at 8.9 GeV/c 77−22796
Al+p, 200 GeV/c, relative yields of $\pi^{\pm}$, $K^{\pm}$, p, $\bar{p}$ 78−93995
Al+p, relative yields of K-mesons, $\bar{p}$ and $\bar{d}$ with 25 GeV/c momenta *(Russian)* 77−38277
Be+p, 200 GeV/c, relative yields of $\pi^{\pm}$, $K^{\pm}$, p, $\bar{p}$ 78−93995
Be+p, relative yields of K-mesons, $\bar{p}$ and $\bar{d}$ with 25 Gev/c momenta *(Russian)* 77−38277
Be+p($\bar{p}$)(K^-)(π^-), 200 GeV/c, forward inclusive prod. spectra, of K_s, Λ^0, $\bar{\Lambda}^0$, n 78−82393
$^{12}C+\pi^-$, 40 GeV/c, cross sections of Λ and K prod. *(Russian)* 77−6184
Cu+p, relative yields of K-mesons, $\bar{p}$ and $\bar{d}$ with 25 GeV/c momenta *(Russian)* 77−38277
e^+e^- annihilation, 30 GeV, inclusive K^0 prod. $K^0K^+/\mu^+\mu^-$ prod. ratio 80−91103
$\gamma p \rightarrow K^+\lambda(\Sigma^0)$, π^+n, π^-p, $K^+\Lambda$, $K^+\Sigma^0$ final state comparisons above resonance region 80−105906
$pN \rightarrow K_s{}^0$, 300 GeV, inclusive prod., triple-Regge behaviour 77−61328
W+p, relative yields of K-mesons, $\bar{p}$ and $\bar{d}$ with 25 GeV/c momenta *(Russian)* 77−38277

kaon-proton interactions
see also kaon-proton scattering
Adler-Weisberger sum rule and the σ-commutator for the kaon-proton system 80−101956
DC K^+p, 32 GeV/c, resonance inclusive prod. cross sections, quark model comparison 78−93913
exchange degeneracy evidence, Kp and πp total cross sections anal. 77−82796
hadronic multiple prod. and average charged multiplicity, strato-gluon mechanism in pp, Kp, πp *(Chinese)* 80−22586
inclusive, estimate of ω, ϕ and baryonium mixing at $t\approx 0$ 79−40814
inclusive, thermodynamic model calcs. of single particle distribs. 77−30453
inclusive vector and tensor meson prod. in beam fragmentation region, Mueller-Regge formalism 78−17057
$K^-p \rightarrow K^-\pi^-n$, 6 GeV/c, K*(1780) 78−33087
meson diffraction dissociation and helicity conservation, Deck model description 77−38153
meson fragmentation region, meson spectra, quark cascade model 77−67689
pion inclusive production at 32 GeV/c 78−482
quark fragmentation function universality, inclusive hadron interactions 78−66082
quark parton model, total cross sections 78−45859
quasi two body processes extraction from three body final states: program EXTRA 78−82238
Regge exchange building by strange quarks, K^-p data anal. 79−2995
strange axial vector meson non-diffracture prod. in Kp and πp interactions 80−32122
strong exchange degeneracy analysed in Kp and πp reactions, pomeron behaviour 78−41515
two-body hypercharge exchange reactions, planar and nonplanar, cross section energy depend. 79−75790
$ap \rightarrow cX$, a, c=$\pi^{\pm}$, $K^{\pm}$, p, $\bar{p}$, low P_t hadron fragmentation at 100, 175 GeV/c 79−85346
η and ω prod. at 10 and 16 GeV/c 77−34191
η/π^0 prod. ratio at high transverse momenta 78−41602
$K^-p \rightarrow \Upsilon\pi$, narrow hyperon state of mass 3.17 GeV 80−37298
K^++, 32 GeV/c, 4 and 6 body final states, principal-axis variables anal. 78−58206
$K^+d \rightarrow K^+\pi^-p(p)$, 5.44 GeV/c, absorbed pion exchange 77−82768
$K^+n \rightarrow K^0p$, 10 to 1000 GeV.c^{-1}, $d\sigma/dt$ calc. from ρ-A_2 exchange degeneracy breaking in π^-p 79−13162
$K^{\pm}N$ charge exchange reacts. at 8.5 and 13.5 GeV/c 78−29351
$\bar{K}p$, 70 GeV/c, total and differential cross-sections for π and K production 80−63050
kp, large P_T pion^0 prod., meson structure functions, quark distrib. functions 80−86714
$Kp \rightarrow K^*p(K^{**}p)$, diffractive prod. and Reggeon-photon coupling analogy 78−45890
$\bar{K}p \rightarrow \bar{K}\pi^+n(\bar{K}^{*0}(890))$, comparative study of ρ^0, ω, $K^{*0}(890)$ and $\bar{K}^{*0}(890)$ production 78−58200
$Kp \rightarrow \pi^-\Sigma^+$, exchange degeneracy in hypercharge exchange reacts. 78−41581
$Kp \rightarrow \pi X$, central region, Regge Mueller approach, inclusive cross sections *(Russian)* 78−58218
$Kp \rightarrow \pi(K)(p)X$, 4-250 GeV/c, Pomeron factorisation 77−14005

kaon-proton interactions continued
Kp→Qp, diffractive production, unitary analytic coupled channel model 79−36051
Kp→$\Sigma^+\pi^-$, 500 MeV/c, meas. of polarised Σ^+ magnetic moment 80−22614
Kp/πp total cross section ratios in SU(3) 77−46089
K^-p, 10, 16 GeV/c, Σ^+, Σ^- inclusive prod. Λ prod. comparison 80−86766
K^-p, 10 and 16 GeV/c, diffractive dissociation, multiplicity structure 79−89197
K^-p, 10 GeV.c, prod. of φ and f' 78−4874
K^-p, 10 to 16 GeV/c, hypercharge-exchange reactions 80−13335
K^-p, 110 GeV/c, charged multiplicity distrib. 80−78101
K^-p, 110 GeV/c, prod. of large $p_\perp$ single and multiparticle systems (jets) 79−85345
K^-p, 14.3 GeV/c, $0^-1/2^+$ and $0^-3/2^+$ final states, cross sections, polarisations 77−13989
K^-p, 14.3 GeV/c, momentum transfer distribs. of some diffractive enhancements 77−65179
K^-p, 14.3 GeV/c, three body final states, mass spectrum 78−37240
K^-p, 200 GeV/c, high p_T charged particle prod. and correlations 79−89199
K^-p, 2.87 GeV/c, Ξ prod. and decay anal. 78−41582
K^-p, 32 GeV/c, exclusive reaction anal. in terms of multiparticle variables *(Russian)* 80−86757
K^-p, 32 GeV/c, exclusive reactions, diffractive dissociation processes, $\pi^+\pi^-$ and K^+K^- prod. 80−86760
K^-p, 32 GeV/c, inclusive cross sections and average multiplicities 77−67687
K^-p, 32 GeV/c, vector and tensor meson prod., with quark model anal. 79−80854
K^-p, 4.2 GeV/c, backward axial vector meson prod., isospin and SU(3) struct. 79−93458
K^-p, 4.2 GeV/c, Ω^- prod., lifetime, mass, decay asymm. parameter 79−3044
K^-p, 4.2 GeV/c, $\Sigma^\pm$ inclusive prod. 77−82773
k^-p, 4.2 GeV.c^{-1}, enhancement in ΣK̄ mass spectrum at threshold (1680) MeV 79−17756
K^-p, 8.25 GeV/c, study of inclusive Λ, Σ^0 and Σ(1385) prod. 79−30749
K^-p, 8.25 GeV/c, Ξ*(2370) prod., mass and width determ. 80−47327
K^-p, <1.0 GeV^2, backward ω prod., ω(1670)→Bπ, decay mode cross section 80−37257
K^-p, χ_J P-wave charmonium states, hadronic prod. cross section 80−37292
K^-p, inclusive prod. of Ξ^- and Ξ*(1530), 10 and 16 GeV/c 80−13341
K^-p, inclusive Ξ^- production at 4.2 GeV/c, triple Regge formalism 78−4875
K^-p, neutral channel cross section meas., 1470 to 1560 MeV CM energy 78−82237
K^-p, production of Y*, Ξ*, Ω^-, data relevant to spectroscopy 77−22791
K^-p→$1^-3/2^\pm$, 4.2 GeV/c, hypercharge exchange, cross sections, momentum transfer depend. 77−71531
K^-p 14.3 GeV/c, inclusive and exclusive cross sections 77−82787
K^-p→$(\bar{K}\pi\pi)^-$p, 4.2 GeV/c, partial wave anal. in Q region 80−13330
K^-p→$(\Sigma\bar{K})^-K^-$, 4.2 GeV/c, Ξ^{*-}(2030) identification 77−61320
K^-p→$(\pi^+\pi^-)_{s\text{-wave}}\Sigma^0$(1385) amplitude anal., additive quark model and duality diagram predictions 77−30430
K^-p→$A\pi^+\Sigma^\pm$, 4.2 GeV/c, differential cross sections 77−30431
K^-p→B^-Y^{*+}(1385), 8,25 GeV/c, quasi-two-body channel data 80−63023
K^-p collisions, charged particle multiplicity, Bose distrib. 77−50022
K^-p→Δ^{++}X, 32 GeV, inclusive and total cross sections 80−105936
K^-p→Δ^{-*}(1232)+X, 16 GeV/c, cross sections 78−66169
K^-p→ηΛ, 4.2 GeV/c, total and differential cross sections, forward production peaks 79−40801
K^-p→η'Λ, 4.2 GeV/c, total and differential cross sections, forward production peaks 79−40801
K^-p→η'Λ, 4.2 GeV/c spin parity assignment of η'(958) 77−82769
K^-p→f'(1514)Λ, 4.15 GeV/c, cross sections, Λ polarisation, tensor meson density matrix elements 77−46077
K^-p inclusive interactions, 10, 16 GeV/c, polarisation of forward produced Λ 78−62466
k^-p interaction in hydrogen bubble chamber, <300 MeV/c track sensitive target 80−13333
K^-p interactions, 14.3 GeV/c, two body diffraction dissociations, cross sections, mass spectra 78−62464
K^-p interactions, 8.25 GeV/c, flow of strangeness and baryon number 78−74277
K^-p interactions at 8.25 GeV/c, charge distribs. 77−82785
K^-p→$K_s^0\pi^+\pi^-$n, 6 GeV/c, K* and Q_2 signals, partial wave anal. 80−86754
K^-p→$K^-(\pi^+\pi^-$p), 4.2 GeV/c, partial wave anal. of low mass $\pi^+\pi^-$p system 77−61318
K^-p→K^-X, 32 GeV, single and double diffractive dissociation 79−58982
K^-p→$K^-p\pi^0$, amplitude calc. for soft pion emission, using PCAC 79−13153
K^-p→$K^-p\pi^+\pi^-$, 14 GeV/c, peripherally prod. π, possible preequilibrium π evaporation 79−80850
K^-p→$K^-\pi^-\pi^+$p, 10, 14.3 and 16 GeV/c, partial wave anal. of $p\pi^+\pi^-$ system 78−82251
K^-p→$K^-\pi^0$p, c.m. energy 1775 to 1957 MeV 79−22138
K^-p→$K^-\pi^0$p, cm. energy 1775 to 1957 MeV 79−3046
K^-p→$K^-\pi^+$n, 10 and 16 GeV/c, (Kπ) mass enhancement 77−74726
K^-p→$K^-\pi^+$n, c.m. energy 1775 to 1957 MeV 79−22138
K^-p→$K^-\pi^+$n, cm. energy 1775 to 1957 MeV 79−3046
K^-p→$K^-\pi^+\pi^-$p, 10, 14.3, 16 GeV/c, partial wave anal. of $(K\pi\pi)^-$ system in the L-region 79−17764
K^-p→$\bar{K}^0\Delta^0$(1232), 5 GeV/c, differential cross section 77−18322
K^-p→K^0X, 32 GeV/c, struct. functions *(Russian)* 77−264
K^-p→$\bar{K}^0$X, inclusive multi-Pomeron corrections in the Regge-eikonal model 79−63557
K^-p→$\bar{K}^0$X, pseudoscalar meson prod. in triple Regge region, absorpt. corrections 78−78228
K^-p→$\bar{K}^0(\Lambda^0)$+X, 6.5 GeV/c total inclusive cross sections, multiparticle prod. characts. 79−89188
K^-p→$\bar{K}^0$n, 10 to 1000 GeV/c^{-1}, dσ/dt calc. from ρ-A_2 exchange degeneracy breaking in π^-p 79−13162
K^-p→$\bar{K}^0$n, 1.934-2.516 GeV/c, partial wave anal., SU_3 classification of Y* states 78−25077
kaon-proton interactions continued
K^-p→$\bar{K}^0$n, 25 and 40 GeV, differential cross section meas. *(Russian)* 78−25083
Kp^-→$\bar{K}^0$n, 25 and 40 GeV/c, differential cross sections 78−8699
K^-p→$\bar{K}^0$n, 4.15 GeV/c, differential cross-section and K^-p→K^-p 77−61321
K^-p→$\bar{K}^0$n, 5 and 8 GeV/c, differential cross section 77−18322
K^-p→$\bar{K}^0$n, 515 to 956 MeV/c, differential cross section 78−66153
K^-p→$\bar{K}^0$n, 515-1065 MeV/c, total cross section meas. 77−50005
K^-p→$\bar{K}^0$n, 515-1065 MeV/c, total cross section meas. 78−66152
K^-p→$\bar{K}^0$n, partial wave anal. below 1.2 GeV/c, Y* resonances 77−22783
K^-p→$\bar{K}^0$n or $\bar{K}^0\Delta^0$, 13 GeV/c, differential cross sections, Regge exchange, SU_3 sum rule 77−41862
K^-p→$\bar{K}^0\pi^-$p, 4.2 GeV/c, multichannel anal. 80−73736
K^-p→$\bar{K}^0\pi^-$p, 4.2 GeV/c, non-charge exchange $\bar{K}^0\pi^-$ prod., spin-parity struct., mass 78−45949
K^-p→$\bar{K}^0\pi^-$p, c.m. energy 1775 to 1957 MeV 79−22138
K^-p→$\bar{K}^0\pi^-$p, cm. energy 1775 to 1957 MeV 79−3046
K^-p→$\bar{K}^0\pi^-$p, determ. of $(K_s^0\to\pi^+\pi^-/K_s^0\to A11)$ branching ratio 79−3046
K^-p→$\bar{K}^0\pi^-$p, determ. of $(K_S^0\to\pi^+\pi^-/K_S^0\to$all) branching ratio 79−22138
K^-p→$\bar{K}^0\pi^+\pi^-$n, 10 GeV/c, partial wave anal. of $(\bar{K}^0\pi^+\pi^-)$ system 78−45969
K^-p→$K^+K^-\Lambda$, at 10 and 16 GeV/c 77−88013
K^-p→$\bar{K}$N around 2 GeV/c, resonance parameters 77−22786
K^-p→$\bar{K}N\pi$, discussion of new data 77−22782
K^-p→K* (890) Δ (1236), 10 GeV/c, multidimens. anal., reaction sub-channel separation 80−32127
K^-p→$\bar{K}^{*-}$(1420)p, channel cross sections and two-body reactions investig. at 32 GeV/c 80−18148
K^-p→$\bar{K}^{*-}$(890)N^0(1688), channel cross sections and two-body reactions investig. at 32 GeV/c 80−18148
K^-p→$\bar{K}^{*-}$(890)p, channel cross sections and two-body reactions investig. at 32 GeV/c 80−18148
K^-p→K^{*-}(890)p, determ. of mass and width of K^{*-}(890) 79−3046
K^-p→K^{*-}(890)p, determ. of mass and width of K^{*-}(890) 79−22138
K^-p→$K^{*-}\pi^+$n, doubly peripheral exchange model 77−13980
K^-p→$\bar{K}^{*0}$X, 7.3 GeV/c, comparison with π^+n→ρ^0X 77−30459
K^-p→$\bar{K}^{*0}$n, $\bar{K}^{*0}$ (890) decay density matrix elements 77−22779
K^-p→$\bar{K}$*(1420)X, at 10 and 16 GeV/c 77−18338
K^-p→$\bar{K}$*(890)X, at 10 and 16 GeV/c 77−18338
K^-p→$\bar{K}\pi$N, 14.3 GeV/c, low-mass Kπ system and $\bar{K}$* prod. mechanisms 77−74725
K^-p→Λ^0+pions, 8.25 GeV/c, resonance prod., fluctuations cluster emission model 78−93904
K^-p→$\Lambda^0(\Sigma^0)$+vector mesons, 3.1-3.6 GeV/c, exchange model anal. 77−74718
K^-p→$\Lambda^0\pi^0$, strong reaction asymmetry and mass quantisation, particle struct. *(French)* 79−3043
K^-p→ΛD, 4.2 GeV/c, D(1285) prod. and decay props. 79−49517
K^-p→ΛK^+K^-, 10 and 16 GeV/c, proton dissociation in 3-body final states 79−85338
K^-p→ΛX, 4.2 GeV/c, polarisation and triple Regge framework 78−45948
K^-p→ΛX, 8.25 GeV/c, off shell KK̄ and pp̄ interactions, KNO scaling 80−52534
K^-p→ΛX or Λ(Pions) or Λp_{slow}X, multiperipheral model with heavy clusters *(Russian)* 78−485
K^-p→$\bar{\Lambda}$+X, 32 GeV/c, total and differential cross sections, energy dependence 80−63048
K^-p→Λ+anything, 4.2 GeV/c, dual anal. of target fragmentation 77−57561
K^-p→λ+pions, 4.2 GeV/c, multiplicities, hadronic temps. and ang. distribs. in KK, pp̄ annihilations 79−45101
K^-p→$\Lambda(\Sigma)K^0$, $K^\pm\pi^\pm$, 4.2 GeV/c, 1550 MeV, I=1 enhancement in (Λπ) and (Σπ) systems 78−89735
K^-p→Λη, 6 GeV/c, baryon exchange reactions, ηNN coupling constant, Λ polarisation, nucleon-Regge exchange 80−78098
K^-p→Λη, cross section meas. near reaction threshold 77−82765
K^-p→Λγ at rest, photon search using NaI(Tl) detector 80−13332
K^-p→Λω_0 around 2 GeV/c, resonance parameters 77−22786
K^-p→Λπ^0, 5 GeV/c, differential cross section, polarisation 77−18322
K^-p→Λπ^0, 6 GeV/c, baryon exchange reactions, ηNN coupling constant, Λ polarisation, nucleon-Regge exchange 80−78098
K^-p→Λπ^0, baryon Regge exchange, FESR anal. 80−63022
K^-p→Λπ^0, Λη, Λη' at 4.2 GeV/c differential cross sections, polarisations meas. 77−65176
K^-p→Λπ^0, polarisation and differential cross-section calc. in Regge-pole model 77−54122
K^-p→Λ$\pi^+\pi^-$, 4.2 GeV/c, ρ-ω interference 77−30429
K^-p→Λ$\pi^+\pi^-$, CM energies 1.65 to 1.72 GeV 77−41861
k^-p→Λ$\pi^+\pi^-$, partial wave anal. in Λ(1520) region, Λ partial decay widths *(Russian)* 80−32131
K^-p→Λππ, discussion of new data 77−22782
K^-p→Λρ(760), transversity amplitude analysis 79−80847
K^-p→M^0+Λ(Σ^0)(Σ^0-1385), 4.2 GeV/c, quark model relations 78−82233
K^-p→N$\bar{K}3\pi$, 10 and 16 GeV/c, diffractive dissociation of K^-→$\bar{K}3\pi$, p→N3π 77−46085
K^-p→Ω^-+X, Ω^- lifetime and spin 78−93877
K^-p→ωΛ, 1.934-2.516 GeV/c expt. data, threshold to 2.436 GeV partial wave anal. 77−82767
K^-p→p$K^{0-}\pi^-\pi^{+0}$, 10 GeV/c, dynamical mechanism from cluster anal. *(Russian)* 80−42499
K^-p→φΛ, ωΛ, ρΛ, φΣ^0, or ρΣ^0, 4.2 GeV/c, cross sections, density matrix elements, hyperon polarisation 78−41580
K^-p→$\pi^-\Sigma^+$ 79−93462
K^-p→$\pi^-\Sigma^+$ and line reversed reaction π^-p→$K^-\Sigma^+$, simple Regge pole model 80−78093
K^-p→$\pi^-\Sigma^+$ and π^+p→$K^+\Sigma^+$, exchange degeneracy 80−57634
K^-p→$\pi^-\Sigma^\pm$(1385), 1775-2170 MeV, partial wave anal. 78−54653
K^-p→π^-Y^+, Y^+=Σ^+ or Y^{*+}(1385), 7 GeV/c, hypercharge exchange in line-reversed π^+p and K^-p 80−82998
K^-p→π^-Y^* 4.25 GeV/c, universality and broken SU(3) 77−30425
K^-p→π^-Y^{*+}, 4.25 GeV/c, amplitude anal. 77−18321
K^-p→π^-Y^*(1385), 11.5 GeV/c, confirmation of exchange degeneracy predictions in line reversed reacts. 78−82247
K^-p→π^-Y^*(1385), 11.5 GeV/c, line reversed reaction, Y*(1385) diff. cross section and decay ang. distribs. 79−89193

kaon-proton interactions continued
$K^-p \to \pi^0\Lambda$, 4.2 GeV/c, total and differential cross sections, forward production peaks 79−40801
$k^-p \to \pi^0\Lambda$ (1520), 1.71 to 2.17 GeV, partial wave analysis 78−29352
$K^-p \to \pi^0\Lambda(1520)$, 1710 to 2170 MeV CM energy, partial wave anal. 78−33085
$K^-p \to \pi^0X$, 100, 200 GeV/c high transverse momentum π^0 prod., quark scatt. 78−45976
$K^-p \to \pi^+\Sigma^-$, box diagram calcs. unitarity corrections in strong interactions 80−91110
$K^-p \to \pi^+\Sigma^+$ 78−82239
$K^-p \to \pi^+\Sigma^\pm$, cross-sections, 1470-1550 MeV 79−13154
$K^-p \to \pi^+\pi^-\pi^0\Lambda$, 4.2 GeV/c, partial-wave anal. of 3π system 77−82770
$K^-p \to \pi^+\pi^-\pi^0\Lambda$, Dalitz arrays for ω,ϕ,A_2 resonances 80−105924
$K^-p \to \pi^+\pi^+\pi^-\Sigma^-$, Dalitz array for A_1 resonance 80−105924
$K^-p \to \pi^+\Sigma^\pm(1385)$, 1775-2170 MeV, partial wave anal. 79−6348
$K^-p \to \pi\Sigma(1385)$, 4.2 GeV/c, total and differential cross sections 77−41860
$K^-p \to \pi X$, 32 GeV/c, struct. functions *(Russian)* 77−264
K^-p reactions, 1.934 to 2.516 GeV/c, channel cross-sections 78−469
K^-p reactions of 8.25 GeV/c, planarity study 78−21454
$K^-p \to \rho^-Y^+$, $Y^+ = \Sigma^+$ or $Y^{*+}(1385)$, 7 and 11.5 GeV/c, hyperon polarisation, vector meson decay angular distribs. 80−82997
$K^-p \to \rho^-(760)+\Sigma^+(1385)$, amplitude anal. 79−97635
$K^-p \to \rho^0$+anything, or f+anything, 10, 16 GeV/c, central and fragmentation contribs., quark model predictions 78−62467
$K^-p \to \Sigma^-\pi^+$, 430-493 MeV/c, Σ prod. and decay props. 78−29350
$K^-p \to \Sigma^-\pi^+$, backward differential cross section 80−63024
$K^-p \to \Sigma^-\pi^+$ or $\Sigma^+\pi^-$ at rest, interaction ratio for charged Σ prod. 78−78213
$K^-p \to \Sigma^-\pi^+(\Sigma^+\pi^-)(\Lambda\pi^+\pi^-)$, study in K^-d bubble chamber, in the c.m. energy range, 1.6-1.74 GeV 80−13331
$K^-p \to \Sigma^-\pi^+\omega$, 4.2 GeV/c, B (1235) backward prod., $\pi^+\omega$ mass enhancement 78−89736
$K^-p \to \Sigma^-\pi^+\pi^-\pi^+$, 4.15 GeV/c, nondiffractive A_1 production, double-Regge model 80−78097
$K^-p \to \Sigma^-\pi^+\pi^+\pi^-$, spin-parity $1^+\rho\pi$ enhancement at 1.04 GeV 77−71532
$K^-p \to \Sigma^0\gamma$ at rest, photon search using NaI(Tl) detector 80−13332
$K^-p \to \Sigma^0\pi^+\pi^-$, 4.2 GeV/c, ρ-ω interference 77−30429
$K^-p \to \Sigma^+$+anything, 4.2 GeV/c, dual anal. of target fragmentation 77−57561
$K^-p \to \Sigma^+(1385)+X$, 16 GeV/c, spin density matrix of $\Sigma^+(1385)$ by statistical tensor method 78−37235
$K^-p \to \Sigma^+\pi^-$, 460 MeV/c, Σ^+ decay and polarisation props. determ. 77−30432
$K^-p \to \Sigma^+\pi^-$, 460 MeV/c, Σ^+ mag. moment meas. in HYBUC 77−54119
$K^-p \to \sigma^\pm$ (1385)X, 32 GeV, inclusive and total cross sections 80−105936
$K^-p \to \Sigma^\pm(1385)+X$, 10, 16 GeV/c, inclusive prod. 77−26552
$K^-p \to \Sigma^\pm\pi^\mp$, 1.934-2.516 GeV/c, reson. states identification 77−38200
$K^-p \to \Sigma^\pm\pi^\mp$, around 2 GeV/c, resonance parameters 77−22786
$K^-p \to \Sigma^+\pi^-$, threshold and below, ratio of $\Sigma^-\pi^+$ to $\Sigma^+\pi^-$ production 78−70407
$Kp^- \to X^0\Lambda$ anal. and $X^0(958)$ spin determ. 77−14010
$K^-p \to \Xi^-K^0\pi^+\pi^0$, $K\rho$ resonances, spin-parity 1^+ backward prod. at 1.28 GeV 78−70409
$K^-p \to Y^*\pi$, using Massachusetts Univ. polarised proton target, expected rates and performance in strange particle phys. 79−63833
$\bar{K}^0p \to K^+n$, 0.6-1.5 GeV/c, charge exchange, differential cross sections meas. 77−61319
$\bar{K}^0p \to \Lambda^0\pi^+\pi^+\pi^-$, 1.5 to 2.5 GeV, effective mass distrib. 77−22792
$\bar{K}^0p \to \Sigma^0\pi^+\pi^+\pi^-$, 1.5 to 2.5 GeV, effective mass distrib. 77−22792
$\bar{K}^0p \to \Sigma^\pm\pi^+\pi^+$, 1.5 to 2.5 GeV, effective mass distrib. 77−22792
K^+p, 100 GeV, topological cross-sections and multiplicity distribs. meas. 77−30464
K^+p, 147 GeV/c, inclusive Δ^{++} prod., cross section energy depend. 80−57651
K^+p, 32 GeV/c, inclusive and semi-inclusive, Bose-Einstein interference effect 79−22152
K^+p, 32 GeV/c, use of Hough-Powell digitizer for processing film from bubble chamber Mirabelle 80−69040
K^+p, 32 GeV/c, vector meson inclusive spectra 79−30703
K^+p, 4.3 GeV/c, hyperon and multikaon prod. 78−4876
K^+p, 70 GeV/c, cross sections and charged multiplicity distribs. 80−63053
k^+p, multiple production processes regularities, Monte Carlo model 80−102082
K^+p, phase shift anal., exotic reson. Z_1^* 78−62456
K^+p, π multiplicity and asymmetric fireballs 79−93474
K^+p, two-particle inclusive and semi-inclusive correls. at 32 GeV/c *(Russian)* 77−88020
$K^+p \to \Delta^{++}(1232)+X^0$, 32 GeV/c 80−52540
K^+p exclusive reactions, 32 GeV/c, transverse momentum correlations and impact-parameter bounds 79−49543
$K^+p \to \gamma X$, 32 GeV/c, inclusive and semi-inclusive distributions of γ 80−27525
K^+p inclusive and semi-inclusive 32 GeV/c interactions, Λ and $\bar{\Lambda}$ prod. 78−21475
$K^+p \to K_S^0X$, 147 GeV/c, cross-section, scaling 80−52539
$K^+p \to K^0\Delta^{++}$, 13 GeV/c, differential cross sections, Regge exchange, SU_3 sum rule 77−41862
$K^+p \to K^0\Delta^{++}$, cross-sections below 2 GeV/c, data compilation 77−22780
$K^+p \to K^0X$, 32 GeV/c, associated average charged particle multiplicities 77−2882
$K^+p \to K^0X$, 32 GeV/c, inclusive cross sections, single particle distribs. 78−41598
$K^+p \to K^0X$, 5-32 GeV/c, transverse momentum distribs. *(Russian)* 77−30467
$K^+p \to K^0X$, inclusive multi-Pomeron corrections in the Regge-eikonal model 79−63557
$K^+p \to \bar{K}^0X$, pseudoscalar meson prod. in triple Regge region, absorpt. corrections 78−78228
$K^+p \to K^0(\pi^-)$+anything, 32 GeV/c, associated multiplicities *(Russian)* 77−34197
$K^+p \to K^0p\pi^+$, 3 to 16 GeV/c, resonance production, cross sections and density matrix elements 78−17048
$K^+p \to K^0p\pi^+$, resonance production at 5, 8.25, and 16 GeV/c 78−12931
kaon-proton interactions continued
$K^+p \to K^0\pi^+p$, 32 GeV/c, non-diffractive two body channel contributions 79−75801
$K^+p \to K^+(1420)p$, 3 to 16 GeV/c, resonance production, cross sections and density matrix elements 78−17048
$K^+p \to K^+(890)p$, 3 to 16 GeV/c, resonance production, cross sections and density matrix elements 78−17048
$K^+p \to K^+p$, 6,12 GeV/c, polarised p, poalrisation measurements 79−63521
$K^+p \to K^+p2\pi^+2\pi^-$, 16 GeV/c, azimuthal correls., Bose Einstein symmetrization effects 78−37239
$K^+p \to K^+\bar{p}pp$, 12 GeV/c, $\bar{\Lambda}(1520)$ ang. distribs. and correlations 80−441
$K^+p \to K^+p\pi^+\pi^-$, 2.7 to 32 GeV/c, impact parameter bounds, energy and effective mass dependence 80−57640
$K^+p \to K^+\pi^-\pi^+p$, 32 GeV/c, non-diffractive two body channel contributions 79−75801
$K^+p \to \Lambda X$, 147 GeV/c, cross-section, scaling 80−52539
$K^+p \to \bar{\Lambda}X$, 32 GeV/c, $\bar{\Sigma}^{*-}$ and $\bar{\Xi}^{*-}$ antibaryon resonance prod., mass enhancements 80−13340
$K^+p \to \Lambda$+anything, 4.3 GeV 78−4876
$K^+p \to \bar{\Lambda}pn\pi^+$, 12 GeV/c, narrow resonant state in $\bar{\Lambda}\Delta^{++}(1232)$ and $\bar{\Sigma}^+(1385)p$ combinations 78−89744
$K^+p \to pK^0X$, 32 GeV/c, total cross section and structure functions 79−40809
$K^+p \to pX$, 32 GeV/c, total cross section and structure functions 79−40809
$K^+p \to p$+anything, 16 GeV/c, study of slow inclusive protons 77−65184
$K^+p \to \pi^-\Sigma^+$, 7 and 11.6 GeV/c, Σ^+ polarisation meas. 78−41573
$K^+p \to \pi^-X$, 32 GeV/c, associated average charged particle multiplicities 77−2882
$K^+p \to \pi^-X$, 8.2-32 GeV/c, transverse momentum distribs. *(Russian)* 77−30467
$K^+p \to \pi^-X^{+++}$ inclusive double-charge-exchange π^- prod., 100 GeV/c 78−37250
$K^+p \to \pi^-\pi^-X$, 32 GeV/c, two-pion correlations, Monte Carlo model 80−83008
$K^+p \to \pi^-\pi^-X$, inclusive distribs. in statistical model, correl. function 77−18354
$K^+p \to \pi^0X$, 32 GeV/c, inclusive and semi-inclusive distributions of π^0 80−27525
$K^+p \to \Sigma^+\pi^+$, strong reaction asymmetry and mass quantisation, particle struct. *(French)* 79−3043
$K^+p \to X\Delta^{++}$, absorption corrections to three Reggeon formulas *(Russian)* 79−9423
$K^\pm p$, 130, 200 GeV, jet prod. cross sections, QCD anal. and scale breaking 80−99111
$K^\pm p$, 200 GeV/c, high p_T jet prod., QCD expt. test 79−89200
$K^\pm p$, 32 GeV/c, ρ, K^*, ϕ inclusive prod., quark fusion model 80−32135
$K^\pm p$, effective radius and total cross sections Pomeranchuk theorem confirmation *(Russian)* 78−89737
$K^\pm p$, fireball model, universal scaling function 80−57646
$K^\pm p$, high energy, impact parameter props. from σ_{tot}, σ_{el} data 77−6183
$K^\pm p$, high energy, mean charged hadron multiplicity, modified Heisenberg approach 78−45988
$K^\pm p$, high-energy, react. differences and annihilations 78−74279
$K^\pm p$, inelastic charge exchange scatt., diffraction approach, convergent polynomial expansion, scaling 80−78095
$K^\pm p$, π^+/π^- inclusive ratio in quark recombination model 80−102022
$K^\pm p$, total cross section determ., 200 to 370 GeV/c 79−26352
$K^\pm p \to (K\pi)^\pm p$, 10 GeV/c, amplitude and natural parity exchange anal. 78−50053
$K^\pm p \to$ hyperon+X, 4-16 GeV/c, unified descript. of $\Lambda,\bar{\Lambda}$, Σ^+, Ξ^- prod., urbaryon model 78−66173
$K^\pm p \to K_S^0\pi^\pm p$, 10 GeV/c, $K\pi$ prod., two arm spectrometer studies 78−50052
$K^\pm p \to K^0\pi^\pm p$, double Regge exchange phenomenology 79−3008
$K^\pm p \to K^\pm X$, triple Pomeron coupling, Reggeon treatment 80−68488
$K^\pm p \to K^\pm+X$, 140-175 GeV, differential cross-section meas. 77−18345
$K^\pm p \to K^\pm$+anything, 50 to 175 GeV/c, cross sections, factorisation 77−50027
$K^\pm p \to K^\pm(\Delta^{++}\pi^-)$, 8.25 GeV/c, proton diffraction region 79−9405
$K^\pm p \to K^\pm p\pi^+\pi^-$, study of low-mass $p\pi\pi$ system 77−22781
$K^\pm p \to K^\pm\pi^+n$ or $K^\pm\pi^-\Delta^{++}$, 13 GeV/c, elastic $K\pi$ partial wave anal. 78−41593
$K^\pm p \to K^\pm\pi^+\pi^-p$, 13 GeV/c, mass depend. of $1^+K^*\pi$ and ρK partial waves 78−8705
$K^\pm p \to K^{*\pm}p$, 10 GeV/c, amplitudes and exchange mechanisms 78−8692
$K^\pm p \to \Lambda(\bar{\Lambda})X$, 32 GeV/c, Λ and $\bar{\Lambda}$ polarisation 79−45122
$K^\pm p \to p\Lambda p(\Lambda\bar{p})$, 50 GeV/c, strange bosons decaying into baryon-antibaryon pairs 80−37306
$K_L p \to K_S p$, 5 to 10 GeV, differential cross-section, ω Regge trajectory 80−22637
$K_L p \to K_S p$ 30 to 130 GeV/c, coherent K_S regeneration amplitude, ω exchange 79−30754
K_L^0p experiments, probe for S=+1 and S=−1 baryon resonances 77−22793
$K_L^0p \to K_S^0p$, 1.54 to 1.71 GeV, search for narrow states 78−29354
$K_L^0p \to K_S^0p$, 4 to 14 GeV, in range $0.1 \le |t| \le 2$ GeV^2 79−3045
$K_L^0p \to K_S^0p(\pi^+\Lambda)(\pi^+\Sigma^0)(\pi^+\pi^0\Lambda)$, differential and polarisation cross sections near 550 MeV/c 79−17757
$K_L^0p \to K_S^0p\pi^+\pi^-$, 1.5 to 2.5 GeV, effective mass distrib. 77−22792
$K_L^0p \to K_S^0\pi+\pi^-p$, up to 17 GeV/c, Q^0-$\bar{Q}^0$ prod., cross sections 80−32129
$K_L^0p \to K_s^0p$, $\Lambda\pi^+$, $\Sigma^0\pi^+$, $\Lambda\pi^+\pi^0$, 1.54-1.71 GeV 78−33086
$K_L^0p \to \Lambda\pi^+$, 1.54 to 1.71 GeV, search for narrow states 78−29354
$K_L^0p \to \Lambda\pi^+\pi^0$, 1.54 to 1.71 GeV, search for narrow states 78−29354
$K_L^0p \to Q^0(\bar{Q}^0)p$, differential cross section slope, further Deck model anal. 80−73737
meson diffr. dissociation, Deck model and helicity conservation 77−30344
$pK^- \to \Sigma^+$+anything, beam and target fragmentation processes, triple Regge anal. 77−82786
$K^-p \to p\bar{p}\Lambda$, at 10 and 16 GeV/c 77−88013
$K^+p \to \pi^\pm X$, 32 GeV, topological cross sections 80−102085

kaon-proton scattering
see also kaon-proton interactions
elastic, Regge-pole model anal. 77−74719
elastic scattering, relativistically invariant scaling law 77−13986

kaon-proton scattering continued
hadron-nucleon total cross-section, regularities and systematics 77−38205
high energy diffraction scatt., model with shielded pomeron, pp, πp, Kp investigation 78−17004
impact param. anal. in range 50-175 GeV/c 77−22799
impact parameter representation *(Russian)* 80−5019
string model, string geometrical shape and overlapping functions 79−13073
total cross-sections, new tabulation suitable for dispersion relations 79−417
Kp→kp, polarisation phenomena in hadron collisions at small momentum transfer *(Russian)* 78−58196
K^-p, backward elastic scattering, backward differential cross section 80−63024
K^-p, cross section, 1.2 to 2.2 GeV, in K^-d collisions 78−29353
K^-p, cross-sections, 1470-1550 MeV 79−13154
K^-p, elastic differential cross-sections at 8 and 16 GeV/c 77−71536
K^-p, partial wave anal. below 1.2 GeV/c, Y* resonances 77−22783
K^-p, slope of forward diffraction peaks 79−36103
K^-p elastic scatt., 0.955, 1.272 GeV/c, polarisation parameter meas. 80−37299
K^-p elastic scatt., 0.955-1.272 GeV/c, polarisation parameter 80−86753
$K^-p \rightarrow K^-p$, 1.934-2.516 GeV/c, partial wave anal., SU_3 classification of Y* states 78−25077
$K^-p \rightarrow K^-p$, 4.15 GeV/c, differential cross-section and $K^-p \rightarrow \bar{K}^0n$ 77−61321
$K^-p \rightarrow K^-p$, elastic scatt. at low energies, polarisation parameter 78−12932
$K^-p \rightarrow K^-p\pi^+\pi^-$, partial wave anal. of low-mass $p\pi^+\pi^-$ system 78−25070
$K^-p \rightarrow \bar{K}^0\Delta^0$, 13 GeV.c^{-1}, sum rule in kaon-nucleon cross section meas. 78−82236
$K^-p \rightarrow \bar{K}^0n$, 13 GeV.c^{-1}, sum rule in kaon-nucleon cross section meas. 78−82236
$K^-p \rightarrow \bar{K}^0n$, ρ and A_2 exchange amplitudes, 2.5-200 GeV/c 77−34174
K^-p, 0.7 to 1.9 GeV/c, differential cross-section meas. 78−21455
K^+p, elastic scatt., 6 and 12 GeV/c, polarisation meas. using CERN polarised d target 79−49542
K^+p, geometrical scaling as low energy phenomena 77−22797
K^+p, geometrical scaling at inelastic threshold 77−18323
K^+p, QCD, one-gluon-exchange, resonating group method, soft-core approx. 80−63025
K^+p at 45 GeV/c, polarisation parameter *(Russian)* 77−34179
K^+p elastic scatt. in Coulomb-nuclear interf. region at 42.5 and 52.2 GeV/c 77−18332
$K^+p \rightarrow K^+p\pi^+\pi^-\pi^0$, 8.2 and 16 GeV/c cross section determ. 77−22808
$K^+p \rightarrow K^+\pi^+\pi^+\pi^-n$, 8.2 and 16 GeV/c cross section determ. 77−22808
K^+p phase shifts, 0.87 to 1.89 GeV/c, tests 77−6164
K^+p scatt., Z_1*(1800) resonance from elastic spin-rotation angle 79−63523
K^+p scatt. anal. to 2 GeV/c, coupled-channel K-matrix parametrization, resonance poles 79−17758
$K^\pm p$, 32.1 GeV, elastic scatt. cross section 80−102076
$K^\pm p$, 39, 44.5 GeV/c, differential cross section meas. 77−74720
$K^\pm p$, 50, 100, 200 GeV/c, differential cross sections meas. 77−18329
$K^\pm p$, elastic differential and total cross-sections, 50 to 175 GeV/c 77−74721
$K^\pm p$, elastic scatt. and diffractive dissociation, Regge model with $\alpha_P(0)>1$ *(Russian)* 80−57630
$K^\pm p$, peripheral reaction model, large angle behaviour 78−442
$K^\pm p$ elastic scatt., dominant exchanges using Reggeon-photon coupling analogy 78−78204
$K^\pm p$ elastic scattering, 39, 44.5 GeV/c, polarisation, spin rot. meas., Regge phenomenology 77−30438
$K^\pm p$ forward scatt. amplitudes, dispersion anal., effective KNY coupling constant 80−22636
$K^\pm p$ forward scattering amplitude, positivity of real part 77−88005
$K^\pm p$ scatt., KNΛ and KNΣ coupling constant constraints 80−32128
$K_L^0p \rightarrow K_L^0p$, 3-13 GeV/c, elastic cross section, effective linear trajectory 80−9184
$K^\pm p$, 100 and 175 GeV/c, inclusive scatt. results from Fermilab single arm spectrometer 78−89746
$K^\pm p$, 40-45 GeV, Regge anal. differential cross sections *(Russian)* 78−25081
$K^\pm p$, geometrical Schrempp model 77−74659

kaon regeneration
SU(2)×U(1), $K^0 \leftrightarrows \bar{K}^0$ transition amplitude in MIT bag model 79−63450
universality of the ω intercept and Inelastic rescattering of kaons in nuclei 80−102212
K^0 on C regeneration, Regge behaviour and nuclear effects, ω-pomeron cut 79−13347
K^0 regeneration in nuclei, effect of inelastic intermediate states, Glauber-Regge model anal. 79−54458
$K_L^0{}^{12}C \rightarrow K_S^0{}^{12}C$, elastic regeneration, 10 to 50 GeV/c, differential cross section slope 78−646
$K_L^0\,n \rightarrow K_S^0n$, 10-50 GeV/c, regeneration, coherent production model 78−33220
K_L^0-K_2^0 transmission regeneration on deuterons and neutrons, 10 to 50 GeV/c 80−4985
K_S regeneration in K_Le scatt. 30 to 100 GeV, K^0 charge radius meas. 79−400
$K_Lp \rightarrow K_Sp$, 5 to 10 GeV, differential cross-section, ω Regge trajectory 80−22637
$K_Lp \rightarrow K_Sp$ 30 to 130 GeV/c, coherent K_S regeneration amplitude, ω exchange 79−30754
$K_L^0p \rightarrow K_S^0p$, 1605 to 1910 MeV, differential and channel cross section meas. 79−75768
$K_L^0p \rightarrow K_S^0p$, 1.54 to 1.71 GeV, search for narrow states 78−29354
$K_L^0p \rightarrow K_S^0p$, 4 to 14 GeV, in range $0.1 \leq |t| \leq 2$ GeV^2 79−3045
$K_L^0p \rightarrow K_S^0p(\pi^+\Lambda)(\pi^+\Sigma^0)(\pi^+\pi^0\Lambda)$, differential and polarisation cross sections near 550 MeV/c 79−17757
$K_L^0p \rightarrow K_S^0\pi+\pi^-p$, up to 17 GeV/c, Q^0-$\bar{Q}^0$ prod., cross sections 80−32129
$K_L^0p \rightarrow K_S^0p$, $\Lambda\pi^+$, $\Sigma^0\pi^+$, $\Lambda^+\pi^0$, 1.54-1.71 GeV 78−33086
$K_L^0p \rightarrow \Lambda^+\pi^-$, 1605 to 1910 MeV, differential and channel cross section meas. 79−75768
$K_L^0p \rightarrow \Lambda\pi^+$, 1.54 to 1.71 GeV, search for narrow states 78−29354
$K_L^0p \rightarrow \Lambda\pi^+\pi^0$, 1.54 to 1.71 GeV, search for narrow states 78−29354

kaon regeneration continued
Al+K_S, 20 to 140 GeV, precise coherent K_S regeneration amplitudes 79−17937
C+K_S, 20 to 140 GeV, precise coherent K_S regeneration amplitudes 79−17937
Cu+K_S, 20 to 140 GeV, precise coherent K_S regeneration amplitudes 79−17937
Pb+K_S, 20 to 140 GeV, precise coherent K_S regeneration amplitudes 79−17937
Sn+K_S, 20 to 140 GeV, precise coherent K_S regeneration amplitudes 79−17937

kaon resonances *see meson resonances*

kaon scattering *see kaon-baryon scattering; kaon-nucleus scattering; lepton hadron scattering; meson-meson scattering; photon-hadron scattering*

kaons
see also kaon regeneration
4.2 GeV cyclotron kaon facility, parameters 77−54380
beam, intense low-momentum at Argonne ZGS, design and operation 77−10515
bound state relativistic effective range approx., EM form factors and charge radii 80−95270
Cabibbo angle universality and association with K, π and D meson mass 79−12974
charge radius, coloured quark field theory 80−62945
coloured, possible M(1.86) particle, Han-Nambu weak interaction theory 77−2799
deep inelastic structure functions in massive quark model 80−86717
dimensions, mass, elec. and mag. moments *(French)* 80−13305
EM mass difference, up quark mass effect on Dashen's formula 79−63461
EM mass differences, quark behaviour 79−58941
EM radius, low-energy approx., $\gamma \rightarrow K\bar{K}$, $\pi\pi \rightarrow K\bar{K}$ comparison with pion radius 78−50033
form factor, quark-antiquark systems combined by Coulomb type attractive force 78−89677
form factor and charge radii, isovector part using dispersion relations 79−22096
form factor and structure function, extended vector meson dominance model 78−25046
form factor extraction from high energy scatt., Chou-Yang model 77−6127
K_L^0-K_S^0 transmission regeneration in H, comparison of expt. data and theoretical prediction *(Russian)* 77−49955
$K^0 \rightarrow \bar{K}^0$ transition in the standard SU(3)⊗SU(2)⊗U(1) scheme *(Russian)* 80−82951
K^0-$\bar{K}^0$ system, constraints on weak current angles of six quark model 79−71685
KEK synchrotron low energy kaon beam line charact. 79−72053
Klein Gordon equations superposition, meson model, φ, f', F, K spectrum 78−58121
mass shifts 78−45920
mass-sum rule, Veneziano-type amplitudes π and K mesons 78−74180
polarisabilities of hadrons, quark models 77−82703
QCD exclusive processes, π, K, ρ form factors, hadronic wavefunction evolution eqns. 80−18135
quark effective-bare mass distinction 78−12866
quark model relation for K charge radii 78−4835
quark model relation for K charge radii 78−16990
quark model with 4 quarks pseudoscalar meson masses 77−46021
radii determination using geometrical model of hadron hadron collisions 79−89137
structure function, comparison between results from ep→epX and Kuti-Weisskopf model *(Russian)* 80−13291
structure functions, prediction in quark cascade model 79−36033
structure functions from inclusive prod. data, nonstrange quark distribs. 80−86715
SU_3 couplings of scalar mesons to two pseudoscalars, S* to ππ and ε to $K\bar{K}$ 80−22580
$SU(2)_L \times U(1)$, strong CP-violating phase, one-loop corrections, Higgs particles 80−62910
SU(2)×U(1), $K^0 \leftrightarrows \bar{K}^0$ transition amplitude in MIT bag model 79−63450
SU(4)×SU(4) chiral symmetry breaking, axial vector current divergences, kaon PCAC 79−45032
valance quark distribs. in π, K, D, Regge trajectories, SU(3), SU(4) breaking 79−30703
Veneziano-type K electromag. form factor *(Japanese)* 78−17019
$e^+e^- \rightarrow \pi^+\pi^-(K^+K^-)$, $\sqrt{s}$=1.5 GeV, EM timelike form factors for π and K 80−91089
K^- EM form factor direct meas. from elastic scatt. cross section 80−86716
K^- mass, influence on limit of ν_μ mass 77−14619
K^0, charge radius, quark models 78−45854
K^0-$\bar{K}^0$ mixing, strong interaction corrections in six quark model, QCD calcs. 80−82957
K^0-$\bar{K}^0$ type systems, CP invariance under particle phase choices 80−52433
K^+-K^0, Coulomb and tadpole contributions to EM mass differences 78−89713
K_L and K_S mass difference in asymptotically free gradient theory *(Russian)* 77−30333
K_L-K_S mass difference, quantum field theory with chiral Lagrangian 77−65110
K_L-K_S mass difference, restrictions on quark masses 77−57491
$K_L^0 \rightarrow K_S^0$ coherent regeneration on C, optical model calcs. 77−30427
K_s^0, differential cross section from $p\bar{p}$ annihilation 78−58197
$K_L - K_S$ mass difference, Kobayashi-Maskawa six quark model, mixing angles, mass matrix and CP violation 80−13284
K*, EM mass splitting determ. 79−3046
K*, EM mass splitting determ. 79−22138
$K^* \rightarrow K\pi\pi$, decay width for $V \rightarrow 3=$ in Bethe Salpeter model 79−58955
K0*, Klein paradox and the mass spectra of the neutral vector mesons 79−26299
$K_S^0{}^* \rightarrow K_S^0\gamma$ and Primakoff conversion of K_L^0 to K_S* 80−73695
$K^*\pi \rightarrow K^*\pi$, analytic quasi-unitary isobar model anal. 79−36099
$K^0 \rightleftharpoons \bar{K}^0$, weak neutral current diagonality, mixing amplitude, multi-quark gauge model *(Russian)* 80−68414

kaons continued
$K_S^0K_S^0$ pair rapidity correlations, quark level strangeness compensation in multiparticle production 79−36024
πK phase shifts, perturbation expansion about SU(3)×SU(3) symm. limit 79−58975

Kapitza-Dirac effect
see also Schwarz-Hora effect
atom scattering effectiveness, standing light wave field, quasiclassical approx. 80−83334
electron beam scattering by laser standing wave, classical theory 79−94143
quantum modulation in field of opposite EM waves 78−74188

Kapitza resistance
axiomatic acoustic mismatch theory, with loss 79−33132
direct electronic contribution to Kapitza cond. 78−95221
Evanohm-superfluid He, meas. of Kapitza conductance using supercond. current comparator 77−41645
freshly cleaved surface, absence of anomalous Kapitza conductance 79−73390
freshly cleaved surface, zero phonon transmission for transverse phonons, absence of anomalous Kapitza conductance 79−73391
hexa-antipyrene iodide of Ce or CIP, heat transfer with dil. ^{3}He below 50 mK 79−51413
interface three-phonon processes, Kapitza conductance and pulse expt. applications 80−2261
Kapitza conductance, dislocation depend. near acoustic mismatch 79−33172
liquid He-solid interface, tunnelling as mechanism of anomalous Kapitza resist. 79−55982
metal-He interface, theory of thermal boundary resist., heat tranport and Boltzmann eqn. 77−62730
metal-liquid He interface, electron-phonon interaction, thermal boundary resistance 78−67899
phonon mismatch theory comparison to computer expts., analogue of Khalatnikov theory 78−79834
phonon reflectivity and Kapitza resist. between solids and liq. He 79−86941
quartz-liquid ^{4}He interface, saturation effects in phonon refl. 80−92736
sapphire-^{4}He interface, transmission of ballistic longitudinal and transverse phonon pulses at 0.25K 79−51416
solid-liquid ^{4}He interface, macroscopic calc. of Kapitza resistance 77−11754
solid-liquid He, interface, Kapitza resist. and phonon scatt. 79−55983
solids-^{3}He liquid boundary, size effect description of thermal boundary resistance 77−62698
superconductor-dielectric boundary, Kapitza discontinuity *(Russian)* 79−51732
surface roughness effects on heat exchange 78−75923
thermal boundary resistance, determ. in transport approach 78−51815
thermal resistance calc., acoustic-mismatch theory 77−89631
tunnelling states of atoms, contrib. to heat transfer between solid and quantum medium 77−85046
Ag-^{4}He interface, Kapitza conductance, proof of surface superfluidity in enhanced power anomaly 80−15359
Ag-^{4}He interface, Kapitza cond. and enhanced power anomaly, 1-2K 80−88378
Ag-liquid ^{3}He interface, thermal boundary resist. from 0.4 to 10 mK 79−56000
Al, heat transport through subcooled He II 79−23794
Al, interfaces with liq. ^{3}He and ^{4}He, 0.3-1.4K 77−24475
Au-dilute ^{3}He-^{4}He mixture interface, Kapitza resist., dynamic meas. 79−28188
CMN-^{3}He, superfluid thermal boundary resistance, preliminary meas. 77−66060
CaF_2:Ce^{3+}, Kapitza limited spin-bath relax., paramag. Faraday effect meas. at liq. He temp. 79−95642
$Ce_2Mg_3(NO_3)_{12}.24H_2O$, pure and dil., heat transfer with dil. ^{3}He below 50 mK 79−51413
$Ce_2Mg_3(NO_3)_{12}.24H_2O$/He, appraisal of expt. results 79−51414
$Ce_2Mg_3(NO_3)_{12}.24H_2O$-^{3}He interface, Kapitza resist. around the mK, effect of ^{4}He impurity 79−55999
$Ce_2Mg_3(NO_3)_{12}.24H_2O$-solid ^{3}He boundary, thermal contact below 35 mK 79−60598
Cu, anomalous power depend. of Kapitza resist. 77−28072
Cu, interfaces with liq. ^{3}He and ^{4}He, 0.3-1.4K 77−24475
Cu, sintered, in contact with ^{3}He, thermal conductance, rel. to elec. resist., heat flow model calc. 80−10728
Cu superfluid ^{4}He interface, Kaptiza conductance, depend. on dislocation density near interface 79−33170
Cu-He(solid), heavy thermal load 0.45-1.5K *(Russian)* 77−11767
Cu-liquid ^{4}He interface, macroscopic calc. of Kapitza resistance 77−11754
Cu-liquid ^{4}He interface, time depend. of anomalous Kapitza conductance 79−56066
Cu-superfluid ^{4}He interface, static and transient anomalous Kapitza conductance 79−19444
$CuK_2(SO_4)_2.6H_2O$-liquid ^{3}He interface, thermal boundary resist. from 8.5 to 110 mK 79−56001
D_2, solid, interface with Cu, thermal boundary resist., 1-3K 77−20178
D_2, solid, thermal boundary resist. meas. at interface with Cu plate 77−72769
H_2, solid, interface with Cu, thermal boundary resist., 1-3K 77−20178
H_2, solid, thermal boundary resist. meas. at interface with Cu plate 77−72769
He, bulk, Kapitza conductance, acoustical mismatch 77−76637
He, liq.-solid interface, heat transfer rel. to adsorbed monolayer *(Russian)* 78−51758
^{3}He, liq., interface with $Cu(NH_3)_4SO_4.H_2O$, anomaly near Neel temp. of solid 77−69139
^{3}He, liq., interface with nonmag. solid, Kapitza resist., quantum perturbation treatment 80−88385
^{3}He, liq., thermal contact with Pd sinter down to 0.4 mK, anomalous Kapitza boundary conductance 79−69312
^{3}He, liquid, interface with antiferromagnet, anomalous thermal behaviour and nucl. spin relax. 79−56002
^{3}He liquid in contact with magnetic substrate nuclear spin relaxation 78−43200
^{3}He, liquid-ordered ferromagnet interface magnetic Kapitza conductance, surface spin wave effects 79−99406

Kapitza resistance continued
^{3}He, spin relaxation to paramagnetic centres, in surfaces at very low temps. 79−33552
^{3}He, superfluid, mag. Kapitza conductance betweeen paramag. substances 77−4235
^{3}He/ordered Heisenberg ferromagnet system, mag. Kapitza cond. calc. 79−51415
^{3}He-magnetic salt boundary *(Japanese)* 78−51780
^{4}He, liq., Kapitza heat-transfer model for boundary with solid 80−107591
^{4}He, liq., phonon energy spectrum due to thin-film heater 77−76633
^{4}He, liquid, meas. using transient temp. response 77−59164
^{4}He, liquid-solid boundary, capillary sound motion, Kapitza resistance *(Russian)* 80−92737
^{4}He liquid-solid interface, phonon transmission and Kapitza resist. 79−65271
^{4}He, solid, Kapitza resist. below 1K 78−34673
^{4}He, solid, thermal boundary resist. meas. at interface with Cu plate 77−72769
^{4}He, superfluid, Kapitza resist. meas. using second sound *(Russian)* 80−88375
^{4}He-Cu interface, thermal boundary resist., 1-3K 77−20178
LiF-He interface, absence of anomalous Kapitza resistance 78−63923
NaF-^{4}He liquid interface, phonon propagation 78−14526
NaF-He interface, absence of anomalous Kapitza resistance 78−63923
NaF-liquid He interface, phonon transmission in both directions 79−28164
Nb-epoxy, interface, Kapitza resist. in supercond. and normal states 77−66085
Ne, solid, interface with Cu, thermal boundary resist, 1-3K 77−20178
Ne, solid, thermal boundary resist. meas. at interface with Cu plate 77−72769
Ni, interfaces with liq. ^{3}He and ^{4}He, 0.3-1.4K 77−24475
Pb, interfaces with liq. ^{3}He and ^{4}He, 0.3-1.4K 77−24475
Pb, supercond., quasi-particle recomb. time, Kapitza resistance 78−68123
Sb, effect of surface layer current, on transport coeffs., and meas. of Kapitza resist. 77−69348

KDP *see potassium compounds*

Kelvin-Helmholtz instability *see flow instability*

Kennelly-Heaviside layer *see E-region; ionosphere*

keratin *see proteins*

Kerr electro-optical effect
3--phenylpropanol-n-hexane, Kerr effect near crit. pt. 79−61336
AC Kerr effect meas. in conducting liquids 78−23431
alkali halide:CN^-, Kerr effect and birefringence from paraelectric CN^- defects 78−43838
alkali halide:NH_2^-, paraelectric alignment, UV electroabsorpt. and Kerr effect 77−12413
alkanes, mol. electro-optical props. 79−50162
p,p′-n-alkoxyazoxybenzene homologous compounds, nematic, DC Kerr constants 78−27185
alkoxyazoxybenzenes, isotropic-nematic transitions, RI, orientational relax. times 77−24390
N-alkyl amides in H_2O, dioxan solns., Kerr consts. 80−2727
alkyl chlorides, mol. electro-optical props. 79−50162
α-amino acids, naturally occurring, in aq. soln., Kerr constants 80−85353
benzene, Kerr const., elec. field distrib. *(Russian)* 77−63395
benzene, substituted benzenes, liq., Kerr effect in UV region, mol. optical anisotropy dispersion 78−72488
binary mixture, Kerr effect near crit. pt. 79−61336
camphor, d- and dl-solns. in carbon tetrachloride, electro-optical Kerr effect 79−91406
carbon tetrachloride, non-polar liq., microwave induced Kerr effect meas. 78−76435
carbon tetrachloride dil. solns., ellipsoidal cavity model, electro-optical quantities *(French)* 78−35114
chlorinated naphthalene, h.v., device appls. 77−4625
chloromethanes, vapour phase, Kerr effect temp. depend., polarisability and hyperpolarisability 79−31568
coaxial Kerr cell built on coaxial 50 Ω transmission line, He-Ne laser 79−72606
conductive liquid Kerr constant meas. 78−88279
CPHB, nematogenic liq. cryst., above T_c, Kerr effect response time, temp. depend. 78−34434
cubic crystal, electrobirefringence from paraelectric defects 78−39529
cyanobiphenyl nematic homologous series, Kerr consts., relax. times, refr. index, dielectric const. 79−19863
cyanobiphenyls, isotropic phase, pretransitional behaviour, optical and elec. Kerr effects 79−10928
cyanobiphenyls, physical props., appl. to Kerr cells 79−19142
4-cyanophenyl 4-n-pentyloxybenzoate, electrical Kerr effect studies 80−25339
cyclohexane, non-polar liq., microwave induced Kerr effect meas. 78−76435
dense fluid of nonpolar mols., static Kerr effect 78−19442
depolarised Rayleigh scatt. and Kerr effect, dipole-induced dipole model 79−72321
di-(4-n-alkyloxy) benzoic esters, of hydroquinone series, effect of polar substituents on electro optical props. 79−46569
2,2-dimethylpropane, gas, Kerr effect, virial coeffs. 79−50843
distributed Bragg reflector for saturable resonator, bistability using Kerr effect 77−46737
dye laser amplifer, DC elec. field effects 80−64006
fluid, rarefied, symmetries of static elec. field induced opt. effects 78−55713
Freon-11, liq., elec. birefringence *(French)* 78−88278
gas, intermol. interactions of spherical tops affecting Kerr virial coeffs. 79−50842
gases, weakly ionised, in presence of mag. field, dielectric tensor, birefringence 77−35313
glycerol, highly viscous state, static and dynamic Kerr effect obs. 80−60545
helical wormlike chain, dipole moment, elec. birefringence, elec. dichroism, statistical mech. calcs. 80−14262
4′-n-heptyl-4-cyanobiphenyl, nematogenic liq. cryst., above T_c, Kerr effect response time, temp. depend. 78−34434
n-hexane, non-polar liq., microwave induced Kerr effect meas. 78−76435

Kerr electro-optical effect continued
high-speed Kerr cell, high power switching with picosecond precision 78−1327
HV nanosecond transient meas. from pulsed low inductance gas discharge, Kerr cell appl. 78−51380
HV pulse controller and temp. monitor microcomputer-based, Kerr effect study appl. 79−6103
insulator surface flashover in vacuum, electro-optical meas. 80−38823
Kerr effect of charged dipolar macromolecules without condensed counterions in conducting solution 80−53171
liquid, optically induced birefringence in elec. field 79−78648
liquid crystal, nematic, electrode reactions control using dopants, Kerr meas. *(French)* 80−11898
liquid crystal, positive, dielec., Kerr effect and orientational relax. 77−77171
liquid crystal and solns. laser and pulsed electric field Kerr effect 77−40210
liquid crystals close to nematic-isotropic transition, Kerr effect meas. 79−99302
liquid laser and pulsed electric field Kerr effect 77−40210
liquid motion induced by unipolar injection, solid spacer influence 78−87406
low-temperature measurements using Kerr cell 80−52199
macromolecular solution rigid ellipsoidal macromols. in cond. soln. at low ionic strength, specific Kerr consts. 80−84718
macromolecular solutions, electric field-induced optical rectification, rel. to electro-optic kerr effect 80−84726
materials, and device applications *(Italian)* 77−42626
methane, gas, Kerr effect, virial coeffs. 79−50843
methanes, substituted, Kerr consts., depolarisation ratios and hyperpolarisabilities meas. 78−25624
p-methoxybenzoate-p′-n-pentyl benzene, slow non-critical mol. reorientation in isotropic phase 80−84062
methyl acetylene, Kerr consts., depolarisation ratios and hyperpolarisabilities meas. 78−25624
molecular anisotropy from molar Cotton-Mouton and Kerr constants 77−46652
molecular reorientational motions rel. to dielec., Kerr effect relaxations 77−4599
nematic homologous series, even-odd effect in Kerr effect 77−43970
nematic liquid crysts. of mols. containing nitrile groups, dipole moments determ. 77−19872
nitrobenzene, temp. depend. of electro-optic Kerr coeff. 80−2725
4-nitrophenyl 4-n-octyloxybenzoate, electrical Kerr effect studies 80−25339
4-nitrophenyl 4-n-pentyloxybenzoate, electrical Kerr effect studies 80−25339
nondipolar liquids, axially-symm., diamag. mols., Kerr effect and Cotton-Mouton effect meas. 78−39524
nonpolar fluid, permittivity, Kerr const., in terms of at.-at. correlation functions 77−36200
nonpolar molecule solutions, birefr. kinetics 80−100648
octyl-cyanobiphenyl nematic cryst., optical and DC Kerr effects 79−7183
organic electrooptical materials for light modulators and deflectors, charcts. *(Japanese)* 77−73128
organic liquid systems, dielectric and dynamic Kerr-effect studies 80−60496
organic molecule solns., stimulated Raman scatt., self-focusing, rel. to Kerr const. *(German)* 79−61355
pentyl cyanobiphenyl, laser and electric field induced Kerr effect 80−84061
4-n-pentyl-4′-cyanobiphenyl, isotropic, optical and electrical Kerr effect 79−32886
pentyloxy-cyanobiphenyl, liq. cryst., laser and electrical Kerr effect 78−68477
piezoceramic articles, nonuniform polaris. investig. using microwave Kerr effect 78−72969
plane-parallel absorbing layer, nonlinear optical props. 80−58631
PMMA, birefringence in elec. field 80−88962
PMMA, relative phase retardation meas. in elec. stressed samples between crossed polarisers using He-Ne laser 80−84716
polychlorinated biphenyls, h.v., device appls. 77−4625
polydisperse rod suspension, elec. birefringence relax. 78−23430
polyethylene, relative phase retardation meas. in elec. stressed samples between crossed polarisers using He-Ne laser 80−84716
polyethylene oxide, elec. polarisation in suspension, Kerr effect 77−63359
polypeptide, conformational change induced by strong elec. field 80−85336
polypropylene glycol, low freq., multiple relaxation behaviour, dielectric and dynamic Kerr-effect techniques 80−29682
polypropylene glycol melt, mol. motion, dielectric and Kerr effect relax. obs. 80−60498
polystyrene-polyethylene oxide copolymer, elec. polarisation in suspension, Kerr effect 77−63359
polystyrenes, p-halogenated, optical anisotropies, Kerr consts. 78−27246
propionitrile-hydrocarbon systems, critical solns., Kerr electrooptical Kerr effect meas. 80−100645
random copolymer solution, electrooptics of crystal-like mols. *(Russian)* 77−63396
rod-like macromolecules in conc. soln., basic kinetic eqn. and appl. 78−67637
succinonitrile, plastic crystal, HF electro-optical Kerr effect, orientation depend. 77−24822
tetrafluoromethane, gas, Kerr effect, virial coeffs. 79−50843
time-dependent birefringence, linear dichroism, and optical rotation resulting from rigid-body rotational diffusion 79−47411
transient Kerr effect relaxation, in strong unidirectional elec. field 79−69811
water, Kerr const., 280 to 350K temp. depend 78−35113
water, Kerr constant, meas. at 30°C and 441 and 633 nm 77−55771
water and conducting liquids, Kerr effect meas. apparatus 79−12832
water-dioxane(acetone) systems, Kerr constant meas. at 632.8 nm 79−4788
Ar, gas, Kerr effect, virial coeffs. 79−50843
CO_2, Kerr consts., depolarisation ratios and hyperpolarisabilities meas. 78−25624
CS_2, intensity dependent total refl., ps pulses 77−14781
CS_2, liq., electronic optical Kerr effect, subpicosec. optical gating 79−46548
Kerr electro-optical effect continued
CS_2, liq., Kerr effect in UV region, mol. optical anisotropy dispersion 78−72488
CS_2, measurement between 170 and 300K 80−52199
CS_2, non-polar liq., microwave induced Kerr effect meas. 78−76435
CS_2 travelling wave Kerr cell, ultrafast pulse shaping and picosecond rise time elec. pulses 80−33152
$Gd_2(MoO_4)_3$, spontaneous birefringence, pulsed field switching, compression effect, domain movement 78−27187
$KCl:Pb^{2+}(Cu^{+})$ 80−34890
KD_2PO_4, noncentrosymmetric monocrystals, quadratic electro-optic coeffs. 79−28718
KH_2PO_4, noncentrosymmetric monocrystals, quadratic electro-optic coeffs. 79−28718
Kr, gas, Kerr effect, virial coeffs. 79−50843
$LiNbO_3$, hologram, light diffr. with electro-optical rot. *(Russian)* 78−1190
$NaNbO_3$-$BaTiO_3$, unidirectionally solidified transparent ceramics 80−25677
4′-n-pentyl-4-cyanobiphenyl, nematogenic liq. cryst., above T_c, Kerr effect response time, temp. depend. 78−34434
SF_6, gas, Kerr effect, virial coeffs. 79−50843
Xe, gas, Kerr effect, virial coeffs. 79−50843

Kerr magneto-optical effect
amorphous toroidal core, switching characts. and domain structs. 78−95477
critical binary mixtures, dielec. props., droplet model 79−69762
ellipsometric measurement 79−49271
ferrite spinels, magneto-optical refl. spectra by equatorial Kerr effect *(Russian)* 77−32400
ferrites, anomalous permeability in Polder-Smit region, magneto-microwave Kerr effect 78−19278
ferrites, EM wave effects on mag. and optical props., lecture 78−27031
ferrites, magneto-microwave Kerr effect *(German)* 78−2742
ferrites, partially magnetised, magneto-microwave Kerr effect 78−48003
ferrites, permeability tensor element in Polder-Smit region, magneto-microwave Kerr effect data 77−36090
ferromagnetic metal, anomalous magnetooptic effects near Curie temp., s-f exchange model 80−2736
ferromagnetic transition metals, electron spin polarisation, review 78−76591
film, ferromagnetic, transverse Kerr magneto-optical effect, thickness depend. 77−59559
garnets, ferro- and paramag., gyromag. ratio determ. by magneto-optical method *(Russian)* 77−32356
high speed magneto-optic camera system, for obs. of mag. bubble domain devices 77−79186
historical background, and modern appls. 77−69806
imaging by magneto-optics, domain struct. obs. 77−48151
K-band interferometer for measuring the magneto-microwave Kerr effect in semiconductors and ferrites 80−52263
laser radiation frequency spectrum control, phase polarisation method 77−75583
magnetic domains, demonstration expt. for teachers 78−69949
magnetic material domain structure obs. by Kerr-magneto-optical effect, laser speckle suppression 80−85093
meas. device with accuracy up to 0.001°, using receiving microscope, reading microscope and recording unit 80−47087
measurement of magneto-optic rotation and ellipticity, spinning analyser ellipsometer *(Japanese)* 80−73419
microwave, rel. to ESR, review 77−69667
multiple-reflection-type light modulator using Kerr effect in mag. thin film 78−79110
orientational correlation parameter for liquid 79−73090
orthoferrites, magneto-optical refl. spectra by equatorial Kerr effect *(Russian)* 77−32400
perfluorobenzene, orientational correlation parameter for liquid 79−73090
Permalloy, T- and I-shaped elements with cylindrical mag. domains, magnetisation distrib. 77−77074
permalloy film, Fe-overcoated, optical and magneto-optical characts., mag. preps. 79−82956
Permalloy I bars, hysteretic props., Bitter soln. obs. and Kerr effect meas. 79−78439
Permalloy I-bars, Kerr magneto-optical effect meas., domain wall location determ., Kerr effect probe 78−68328
Permalloy thin film cores, domain wall motion and flux patterns, Kerr magneto-optic effect obs. 80−34721
rare earth-Co systems, anomalous Hall effect and Kerr rotation obs. 77−11897
rare earth-transition metal amorphous film, Kerr and Hall effect meas. 77−24722
s-triazine, molar Cotton-Mouton const., Kerr const., 298K, 633 nm 77−16286
2,4,6-trichloro-s-triazine, molar Cotton-Mouton const., Kerr const., 298K, 633 nm 77−16286
CS_2, orientational correlation parameter for liquid 79−73090
$CdCr_2S_4$, $Cd_{1-x}X_xCr_2Se_4$, (X=Zn, Hg), optical and magneto-optical surface effects 79−82953
$Cd_{1-x}Mn_xTe$ mixed cryst., giant exciton Faraday rotation 78−27260
Co catalyst, magnetooptical investigation of mag. props. 79−69858
Co, film, Kerr magneto-optical consts. 78−76541
Co, Kerr equatorial effect freq. spectra anisotropy, dielectric permeability tensor *(Russian)* 80−55072
Co-Fe amorphous alloys, worked, perminvar type mag. hysteresis loop, longit. Kerr effect obs. 80−65958
Co-P, amorphous electrodeposited films, domain wall motion, Kerr effect 78−60322
$CoAl_tFe_{2-t}O_4$, Kerr effect, magneto-optical refl. spectra 79−82954
$CoCr_xFe_{2-x}O_4$, magneto-optical refl. spectra by equatorial Kerr effect *(Russian)* 77−32400
Co_5Sm, magnetic domains, nucleation and pinning, magneto-optical Kerr effect 80−39811
CrTe, film, attenuated total refl., magneto-optical effects 77−52196
Dy-Fe, amorphous film, Kerr readout characts. 79−15439
Dy-Fe alloy film, amorphous, contact printing 77−73061
EuS film, magnetic props. using transverse Kerr and Voigt effects 77−52054
Fe film, transverse Kerr magneto-optical effect enhancement by surface magnetoplasma waves 77−52056

Kerr magneto-optical effect continued
Fe single crystal frames, use in transient field meas., surface magnetisation meas. 79−59324
Fe thin layers, vacuum coated on PMMA, mag. behaviour during mech. stress cycles *(German)* 80−80581
Fe whisker, optimisation of magnification of magneto-optic Kerr effect by interference layers 79−51808
Fe whiskers, elastically and plastically deformed, mag. domain structs. 80−15752
Fe whiskers, magnetisation in small mag. fields, investigation using Kerr magneto-optic effect 80−2603
Fe-B, sputtered amorphous film, strong stripe domains, Kerr effect obs. and theory 79−91265
Fe-P electrodeposited foil, amorphous, mag. domains 80−75821
Fe-Si, domain structure of Neel oriented samples 77−69601
Fe-Si (3 wt.%), transformer steel, grain-oriented, magneto-optical domain obs., magnetisation mechanism 77−12364
Fe-Si (3 wt.%) domain struct., tensile load effects *(Russian)* 78−47995
Fe-Si (4 wt.%), freq. depend. of Fe losses in single crysts. with (100)[001] 79−51803
Fe-Si (4%), (110)[001] and (100)[001], dynamic domain struct., AC excitation 77−16097
$Fe_{1-x}B_x$ film, optical and magneto-optical charcts., mag. preps. 79−82956
$Fe_{80}B_{20}$ amorphous alloys, domain struct. exam., magneto-optic Kerr effect 79−28550
$Fe_{80}B_{20}$, metallic glass, optical and magneto-optical props. 80−84728
$Fe_{46}Ni_{40}P_{16}B_6$, ferromagnetic amorphous alloy, even magneto-optic effects 77−55776
α-Fe_2O_3, magneto-optical refl. spectra by equatorial Kerr effect *(Russian)* 77−32400
Fe_3O_4, dielec. function and polar Kerr rotation, 0.5-3.6 eV 80−66221
Fe_3O_4, magnetite, low temp. phase transition, magneto-optical exam. 78−27193
Fe_3O_4, magneto-optical refl. spectra by equatorial Kerr effect *(Russian)* 77−32400
Fe_3O_4, polar Kerr effect invisible and near IR spectral regions 80−108187
$Fe_{1-x}Si_x$ film, optical and magneto-optical charcts., mag. preps. 79−82956
Fe_xSi_{1-x}, amorphous film, magneto-optic Kerr effect 80−66158
Gd, magneto-optical Kerr effect spectra in UV region using synchrotron radiation 77−52127
Gd-Co amorphous film, magnetisation processes near compensation point 77−69644
Gd-Co film, amorphous, Kerr and Hall loops 77−89996
Gd-Co film, amorphous, magnetisation processes near compensation point 77−40101
Gd-Co films, anomalous magneto-optical hysteresis loops obs. 77−12174
Gd-Fe, amorphous film, Kerr readout charcts. 79−15439
Gd-Fe, co-evap. amorphous film, anomalous hysteresis loop, domains obs. 77−89995
Gd-Fe alloy film, amorphous, contact printing 77−73061
Gd-Fe amorphous films with CeO_2 coatings, Kerr magneto-optical effect enhancement 79−19866
a-GdCo film 77−12458
GdFe homogeneous amorphous films, compensation point switching, magneto-optical Kerr signal anal. 80−15726
GdFeBi, amorphous ferrimag. films, magneto-optical props., optical spectra 80−76008
$(Gd_{1-x}Fe_x)_{1-y}Bi_y$ amorphous films, saturation magnetisation, Kerr and Faraday rotation 80−40093
p-Ge, magneto-microwave Kerr effect, expt., scatt. mechanisms 78−39139
$HgCr_2Se_4$, optical and magneto-optical surface effects 79−82953
$HoCo_3$, Ho_2Co_7, $HoCo_{5.5}$ and Ho_2Co_{17}, Kerr effect determ. of domain structure, Bloch wall energy 80−39806
$Ho_2Fe_3Co_{14}$, Kerr effect determ. of domain structure, Bloch wall energy 80−39806
$Li_{0.5}Fe_{2.5}O_4$, magneto-optical Kerr effect, reflectivity spectra 80−66157
$Li_{0.5}Fe_{2.5}O_4$, magnetooptical spectra, polar Kerr rotation, dielectric tensor elements spectra 80−40091
$Li_{0.5}Fe_{2.5}O_4$, polar Kerr rotation spectra, 2-5.7 eV, comparative study with YIG 79−47413
Mn-Cu-Ni-Bi, magneto-optic film for storage appl. 77−12165
MnBi, Kerr effect and TEM obs. of mag. domains 77−89974
MnCuBi film, coated with SiO layer Kerr readout charcts. 77−85509
$Mn_xFe_{3-x}O_4$, dielec. function and polar Kerr rotation, 0.5-3.6 eV 80−66221
$Mn_{1.15}Sb$, Kerr effect and TEM obs. of mag. domains 77−89974
MnZn ferrite, high cond., magneto-microwave Kerr effect 77−43888
Nd-Co film, amorphous, exam. of domain struct. 78−68336
Ni catalyst, magnetooptical investigation of mag. props. 79−69858
Ni film, crit. mag. surface phenomena 77−69811
Ni film, surface magnetoplasma waves, ATR meas. 77−69639
Ni film, transverse Kerr magneto-optical effect enhancement by surface magnetoplasma waves 77−52056
Ni, magneto-optical Kerr effect in UV region, electronic struct. 77−52127
Ni-Co-P, amorphous electrodeposited films, domain wall motion, Kerr effect 78−60322
Ni-Fe, film, obs. of domain wall motion, magnetisation reversal 77−16132
Ni-Fe film, appl. to waveguide type optical modulator, theory 77−11015
$NiAl_xFe_{2-x}O_4$, Kerr effect, magneto-optical refl. spectra 79−82954
$NiCr_xFe_{2-x}O_4$, magneto-otpical refl. spectra by equatorial Kerr effect *(Russian)* 77−32400
Ni_3Fe, domain struct. after tensile deform., dislocation effects 80−71083
Ni(100) platelet surface optical and magneto-optic consts. 78−15151
$SmCo_5$, and $SmCo_{3.5}Cu_{1.5}$, anisotropy and coercivity, Kerr effect, magnetisation and aftereffect expts. 77−8300
$SmCo_5$, sintered alloy permanent magnets, temp. depend. of domain struct. *(Russian)* 77−66380
$Sm(Co_{1-x}Cu_x)_{7.8}$ alloys, coercive fields, domain wall energies, mag. and metallographic exam. 78−91897
$SmCo_4Cu$, nonuniform comp., domain struct. and mag. reversals process *(Russian)* 79−1681
$Sm_{0.5}Pr_{0.5}Co_5$, sintered alloy permanent magnets, temp. depend. of domain struct. *(Russian)* 77−66380
Tb-Fe, amorphous film, Kerr readout charcts. 79−15439
Kerr magneto-optical effect continued
Tb-Fe, amorphous film, thermomag. writing using He-Ne laser, Kerr contrast 77−12163
Tb-Fe alloy film, amorphous, contact printing 77−73061
Tb-Fe amorphous film, thermomag. contact printing 77−89986
Tb-Fe amorphous thin films, magnetic after-effect, Kerr magneto-optic effect obs. 80−97123
$Tb_{0.27}Dy_{0.73}Fe_2$, domain configurations, obs. by Kerr effect and synchrotron radiation topographs 78−64215
$(Tb_{0.27}Dy_{0.73})Fe_2$, magnetisation, ferromag. domains 80−25162
$TbFe_2$, domain configurations, obs. by Kerr effect and synchrotron radiation topographs 78−64215
$TbFe_2$, magnetisation, ferromag. domains 80−25162
Te, Faraday-type microwave Kerr effect 79−23998
YIG, diamagnetic substituted, anal. of polar Kerr rot. spectra 78−68485
YIG, magneto-optical Kerr effect, reflectivity spectra 80−66157
YIG, magnetooptical spectra, polar Kerr rotation, dielectric tensor elements spectra 80−40091
YIG, polar Kerr rotation spectra, 2-5.7 eV, comparative study with $Li_{0.5}Fe_{2.5}O_4$ 79−47413
YIG:Ga(Sc), magneto-optical Kerr effect, reflectivity spectra 80−66157
$Y_{2.8}Pr_{0.2}Fe_5O_{12}$, magneto-optical props. 78−72489
Zr-Ni, surface layer, segregation of ferromag. Ni, magnetooptic investigation 80−2256
Zr-Ni-H_x(x=2.8 to 3), surface layer, segregation of ferromag. Ni, magnetooptic investigation 80−2256

keyboards
optical fibre connector for keyboard lens finger detection 80−19095
verbal communication aid for nonvocal patients 79−57816

kicksorters *see counting circuits*

kidney
acoustic parameters of freshly excised tissues of Sprague Dawley rats 77−86573
albumin transport kinetics in renal cortical interstitium, heterogeneity model 80−30632
allografted, normally functioning, ^{67}Ga localisation 79−100717
angiocinedensitometry, methods and appl. in kidney diagnostics *(German)* 79−2127
angiography, selective, renal and peri-renal inflammatory lesions, correl. with histopathology 79−74740
anoxic kidney cell sensitivity to 35 MeV electron single pulses 80−26292
artificial, anal. of the ultrafilter-adsorber 78−48937
artificial, automatic extrasomatic dialysis system 80−98177
artificial, design anal. for an ultrafilter adsorber 78−40410
artificial, dialysate recycling method 78−40411
artificial, effects of blood and dialysing soln. flow rates on efficiency 78−36053
artificial, electrochem. removal of urea, basis for a regenerative dialysis system 80−26417
artificial, filtration-adsorption type, filtrate treatment system 80−51293
artificial, fundamental step for development of wearable type 78−48926
artificial appl. of systems anal. techniques for evaluation 78−36074
artificial kidney, a processing system *(German)* 79−2161
artificial kidney and liver, wearable, fundamental studies 79−44051
artificial kidney-patient system simulation, lumped-parameter haemodialyser model 80−56281
artificial organ, problem of removing urea from ultrafiltrate *(German)* 80−21574
automatic measurement of renal, thyroid and hepatic clearance 79−34644
autregulation, mathematical model of transient adjustments 77−90842
blood detoxification methods *(German)* 79−5405
blood flow in a renal artery with a deformed vascular wall 78−65063
brushorder membrane vesicles, proline and glycine uptake 77−44614
calculus extraction under fluoroscopic control 79−92342
calyceal structures, echopyelographic visualisation of pacemaker-induced contractility 78−48850
cattle, concs. of ^{210}Pb and ^{210}Po 80−30904
cells, inactivation by high-energy monoenergetic heavy-ion beams 80−72256
computerised tomographic image boundary finding and complex object localisation 80−109016
cortical imaging and renal mass lesion detect. 80−46016
counter-current mass transport, spatially discrete models for kidney appl. 79−39442
countercurrent equations solving, comparison of numerical methods 77−40698
countercurrent mechanism, transient and steady state simulation 77−36967
countercurrent transport theory 79−5307
counterflow system modelling, numerical soln. by multiple shooting 80−104609
counterflow systems, numerical soln. of differential eqns. 77−21545
counterflow systems, transient solns. computing 77−40699
counterflow systems efficient numerical method for solving the differential eqn. 78−24082
counterflow systems numerical soln. of differential eqns. 78−92662
cryogenically preserved canine kidneys, simultaneous microwave and HF thawing 77−5059
damage following perinatal γ-radiation in the beagle, characterisation 78−31866
deconvolution analysis of the scintillation camera renogram 77−21599
dialysing system, portable, development 79−44055
dialysis, clinical appl. of single compartment model to urea and creatinine kinetics 78−48931
dialysis, electrolyte, urea and osmolarity comparisons *(German)* 79−2165
dialysis, improved patient management by computer simulation 79−70703
dialysis and simultaneous diafiltration for blood purification *(German)* 78−31967
dialysis without circulating dialysate, portable artificial kidney appl. 77−48949
differential renal function in dogs using ^{99m}Tc-dimercaptosuccinic acid 79−79639
diseases, value of computerised tomography *(German)* 80−76832
EEGs recorded from renal patients, anal. 77−40882
EEGs recorded from renal patients, discriminant anal. 78−28115
efflux calculation of urea, sodium or inulin following injection into the distal or proximal tubules 77−40700

kidney continued
electrical properties of living tissues at VHF through microwave freqs., determ. technique 77−78071
electron microscopic diagnosis using clinical pathology liver and kidney samples, computer assisted 80−85485
enzyme activities, early effects after irrad., rat expts. 80−51162
enzyme activities of the kidney after irrad. 77−12976
extracorporeal blood correcting unit 78−7535
extracorporeal processing devices, review, book contrib. 80−12308
extraction fraction, determ. by a double-tracer method 77−37045
filtration fraction determ. by dual-tracer technique 77−86596
flow absorption system, reaction vel. parameters rel. to absorbed solutes conc. profile *(Japanese)* 79−74710
function studies, comprehensive, technical aspects 77−90884
functional study, rat, γ-camera obs. 77−56454
glomerular filtration rate biotelemetry in man 78−44591
glomerular filtration rate determ., limitations of the single sample tracer method 79−16271
glomerular filtration rate meas., comparison of 4 commercial preps. of ^{99M}Tc(Sn)DTPA 80−81704
graft evaluation with pertechnetate and ^{131}I Hippuran 80−46017
haemodialysis, use of reinforced expanded PTFE grafts 80−8211
haemodialysis and haemoperfusion, joint, evaluation of novel sorbent systems 78−7542
haemodialysis rel. to EEG 78−31968
haemodynamics, simulation of unsteady flow at renal branches 78−27983
haemofiltration, clinical, appl. and limits *(German)* 79−5402
haemofiltration, technical possibilities *(German)* 79−5403
haemofiltration treatment, chronically intermittent, technical foundations and clinical results *(German)* 79−5404
Henle's loop, descending limbs, osmotic equilibration, simulation study 77−40701
Henle's short loop, microperfused, of rates, computer simulation of flow-depend. absorpt. 79−83820
hippuran transit times in the kidney 78−40317
histopathological information obtained from US tissue signatures and microscopy of biopsy samples 80−51195
histopathological section image dissection and analysis 79−79679
hollow fibre dialyser, mass transfer 80−66873
human, PIXE and neutron activation anal. appl. to cancer tissues 80−56199
hypertension occurring in end-stage renal failure, mathematical model study 78−31829
imaging with radionuclides, US and computerised tomography 80−17095
insufficiency, assessment method by EEG quantification 77−73609
inverted microscope, differential interference contrast, appl. to study of in vitro perfused nephron 80−51303
irradiation of the spleen in lymphoma, renal consequences patients 79−20615
ischemia, a computer study 78−73142
magnification renal arteriography 79−53209
mathematical modelling of renal functions 79−83841
medulla, human, theoretical model 78−24081
medulla solute cycling model, transient soln. using laplace transforms 77−40694
medulla transient behaviour of the single loop solute cycling model 78−73167
medullary Na depletion during diuresis, digital computer simulation 77−60226
microorganisms use in renal support 77−48950
microwave imagery of isolated canine kidney, use of orthogonal polarisations 80−81783
microwave scattering parameter imagery of isolated canine kidney 80−3755
microwave time delay spectroscopic imagery of isolated canine kidney 80−46109
models, anal. of transient behaviour 78−65065
models, introductory remarks on solution 77−40692
multinephron kidney equations, numerical soln. 79−83822
multinephron models of the renal medulla, danonical mass balance eqn. 77−12941
neonatal whole body, γ-irrad. in growing dog, renal morphological and functional adaptations 80−41131
neonatal whole body γ-irrad. in growing dog, plasma renin activity and arterial press. 80−41132
nephro-urography by rapid intravenous injection 77−86694
nephron, operating model 79−48283
nephron, rat, functional model 79−62282
nephron functioning, diffusion and selective osmosis *(French)* 80−45864
nephron functioning model *(French)* 80−36218
network flows, a priori bounds 77−40693
network flows, eqns. anal. 79−11961
nuclear medicine, role of midi-maxi computer interaction 78−7176
nuclear medicine conference, Karlovy Vary, Czechoslovakia (May, 1979) 80−12840
nuclear medicine studies, automated interpretation 80−8164
numerical continuation method for a system of parallel flow tubes 79−43944
pattern recognition approach to US trssue characterisation 78−73186
pelvic size changes in childten after fluid intake, US demonstration 77−77951
perfusion, meas. by heated thermocouple probes' temp. transients anal. 79−96598
perfusion dynamics during preservation 79−25006
photodynamic induction of an oncogenic virus in vitro, hamster 79−25029
physiological compartment tracer flow modelling and digital imaging 80−101257
physiopathology, new concepts acquired from a quantitative kidney function exam. *(French)* 77−70518
preservation, analogue model of perfusion dynamic changes 79−83724
proximal tubule brush border and the intestinal mucosa 78−15815
radiation biophysical studies with mammalian cells and a modulated C ion beam 79−11978
radiation injury in the mouse kidney, sequential light microscopic study 78−35891
radiation nephropathy, glomerular and juxta-glomerular lesions 77−9233
radioelementry of renal and iliac blood flow from exercising heart autotransplant recipients 77−90822
radiology, conf., Brussels, Belgium (Oct. 1978) 80−31409
kidney continued
radionuclide imaging, evaluation of ^{99M}Tc-dimercaptosuccinic acid 78−77102
radionuclide imaging techniques, book contrib. 80−36113
recirculation dialysis systems, assessment mathematical theory and appl. *(German)* 79−39601
relative renal blood flow, simple meas. technique 77−2036
renal arteries model, human, qualitative and quantitative flow studies *(German)* 80−21483
renal function, identification techniques 79−96658
renal osteodystrophy, bone scintigraphy obs. 79−70611
renal tubulus, digital picture anal. 79−70712
renography, comparative study in hydration and dehydration *(Japanese)* 80−81726
renography, new technique with electronically assisted kidney localisation 78−11716
renovascular hypertension, computer-assisted static/dynamic imaging evaluation as screening test 79−79635
scintigraphic images, improved means of correcting motion blurring 79−39493
scintigraphy, bilateral, quantitative anal., importance of correctly identifying kidney struct. 79−34662
scintigraphy, value of additional lateral scans 80−36074
scintillation-camera renography, new method for estimation of single-kidney function 77−40736
shear properties of mammalian tissues at low MHz freqs. 77−29174
simulation of biological system, the kidney 78−44524
single needle haemodialysis 78−48936
six-tube vasa recta model as test problem 80−104610
solute concentration in the kidney, central core model, input-output studies 77−56405
solute concentration in. the kidney, renal medulla model 77−52821
sorbent perfusion systems, characterisation of solute removal 78−44689
stagnant filtration of human plasma 77−48948
stenosis of renal artery, effect on renovascular hypertension 80−108934
stereology conference, Salzburg, Austria (Sep. 1979) 80−22134
stones, human, X-ray anal. 80−36081
stones, touchless destruction, expts. with focusing devices 79−48300
stones method for no-contact destruct. by means of shock waves *(German)* 78−7517
sugar reabsorption rel. to Na transport in isolated rabbit kidney perfused in vitro 78−20155
T1 cell cultures, fast neutron effects on reproductive capacity 79−62307
telemetered renal responses in dogs during detect. of explosives 77−32927
telemetric detection of radionuclide tracers in the study of renal function rhythms 77−86586
thermocouple probe, spherical heated, for perfusion meas. 79−92456
tissue water freezing study, ^{1}H NMR obs. 80−8027
tomography with short exposure times in paediatric urigraphy 79−48336
transplant, dynamic ^{99M}Tc imaging supplemented by perfusion index 79−34653
transplanted, effect of local irrad. on the acute rejection process 78−24117
tubular cells, ultrastruct. of unfixed plasma membranes 78−65161
tubular haemodialyser-effect of untrafiltration and dialysate conc. anal. 78−7544
tubular mass transport simulation using perfectly mixed compartments 77−40696
tubule fluid reabsorpt., online meas. 79−92442
ultrasonography of the kidney in 1979 *(French)* 80−56149
uptake measurements using $^{197}HgCl_2$, single tracer method for background subtraction 80−67217
urography, kidney distension obs., rat 79−62334
urological illnesses, US exam. *(Hungarian)* 78−35900
US determination of renal size and position 78−31874
US echoes from the kidney, computer anal. 78−35901
US in renal diagnosis 78−18027
US local lesions in rabbit kidney, liver, and testicle, thresholds 77−81527
US measurement of renal inclination, its importance in renal length meas. 78−77092
US renal volumetry in children, accuracy and simplicity of the method 80−98044
US shockwave focusing for touchless destruction of kidney stones 77−32946
UV damage in mammalian cells, excision repair 78−53332
vascular resistance and I washout during angiography 77−77927
visually evoked cortical potentials in renal failure, transient pots. 79−16200
volume determination by US scanning 80−17034
volume measurements obtained with diagnostic US, in vivo, anal. 77−2033
X-irradiated, degenerative and age related changes, rat 79−57723
X-irradiation, unilateral, late effects in the mouse 80−21505
X-irradiation and induced autoallergic glomerulonephritis effects, rat obs. 80−76793
X-ray diagnostics, intra-operative, detection and localization of residual concretions 80−41202
Cd conc. in kidney and liver, neutron activation anal., organ depth determ. 80−72321
Cd measurement by neutron capture prompt γ-ray anal. 78−15885
^{131}I-ortho-iodohippurate absorbed kidney dose calc., literature review 80−76841
$(Na^+ + K^+)$ATPase, subunit comp. 79−83704
T radiation dose absorbed in rat organs, after feeding with organically bound T 80−51262
^{99M}Tc compounds, localisation in the rat, autoradiographical obs. 77−56463
^{99m}Tc methylene diphosphonate, immediate renal imaging and renography, clinical evaluation 80−98126
^{99M}Tc penicillamine, relative accumulation as an index of differential function 78−65115
^{99m}Tc-EDTA complex production method and renal retention obs. 80−12254

Kikuchi lines *see electron diffraction crystallography*

kinematic viscosity *see viscosity*

kinematics
see also acceleration; ballistics
artificial heart valve closing element, kinematics photoelectric recorder 79−48370
autonomous system instability, sufficient criteria, Lyapunov instability *(Russian)* 79−17210
axisymmetric rigid body in air, stability of unperturbed motion *(Russian)* 78−86146
bodies with binary material and kinematic-kinetic structure 78−73848
CA 0340−538 (3U 0328−523), southern cluster of galaxies, vel. dispersion and global parameters 78−36705
cable dynamics, nonlinear finite segment approach 77−2532
Cassiopeia A, supernova remnant, anal. of motion of details in thin shell model *(Russian)* 80−56920
cell cycle, biochemical approach 78−24039
Centaurus I cluster of galaxies, resolution into two velocity systems 80−77499
Cepheus OB3 association, star form. and kinematics rel. to supernova explosion 78−12306
clusters of galaxies, optical vel. dispersions rel. to X-ray temps. 77−91668
co-ordinatization of the kinematical vectors 79−35543
cyclic pursuit in a plane 80−12896
disclination, mathematical theory 78−63764
Earth mantle subduction zone, kinematics and thermal structs. evolution 80−56440
education, braking distance versus mass for automobiles 77−45644
education, kinematic strategy of self-preservation for the jogger 79−97157
education, momentum flow as force, alternative conceptualisation for teaching mechanics 80−67993
education, speed, Galilean and Einsteinian concepts, vel., rapidity and celerity 80−73130
elliptical galaxies, vel. dispersion radius depend. 80−51876
finite rigid-body rotations, kinematics 78−12482
galaxies and clusters, large-scale distrib. and random motion 78−54056
galaxies nuclei, vel. dispersions meas. 77−57083
Galaxy, stellar kinematics rel. to local struct. determ. *(Russian)* 78−77608
Galaxy, three-dimensional motion, of dwarf stars and RR Lyrae variables 80−12754
Galaxy central region, barlike model of inner Galaxy gas based on improved H I data 80−67845
galaxy cluster halos, vel. distribs. as probe for expanding Universe primordial inhomogeneities 80−22122
galaxy clusters, ratio of escape rel. to mean vel. *(German)* 78−53995
galaxy clusters, vel. dispersion in relativistic spherically-symmetric inhomogeneities model 77−71147
granular materials, rolling, granule kinematics 80−84875
gravitational fields whose brachistochrones and isochrones are identical curves, for teaching 79−25807
group theoretical foundations of classical and quantum physics, kinematical symmetry groups and state spaces 80−52008
He 2-111, planetary nebulae, giant halo with very high vels. discovery 79−25691
icebergs, drift in Grand Banks 78−81200
Iceland, continuum model of crustal generation, kinematic aspects 80−90059
inertial systems constructed on double-gyroscope frame base, generalised models *(Russian)* 78−28937
interstellar H I, 21 cm obs. of small vel. bridge 78−28755
interstellar molecular clouds, radiation transport and kinematics 78−93347
jaw, growth anal. in human using kinematic fundamentals 79−16243
joint instantaneous centre of rotation, least square analysis 79−29555
kinematic equivalence of system of forces *(Polish)* 79−12590
Lagrangian gyroscope, hodographs of ang. velocity *(Russian)* 78−86133
Lagrangian gyroscopes, moving ang. velocity hodograph *(Russian)* 78−86134
linear systems, stability of motion rel. to part of variables *(Russian)* 78−86144
linked rigid body systems, nonlinear eqns. of motion *(German)* 78−87254
LMC, kinematics and dynamics compared to galaxies of Magellanic type *(German)* 80−105348
Local Group, motions of Sun, Galaxy and Andromeda nebula (M31) 77−91518
Lorentz invariant multiparticle amplitudes, massive particle relativistic kinematics, spinor amplitudes 78−41156
M31, major axis rel. plots from high-resolution H I obs. 78−41057
machine tools for optical glass grinding and polishing semiautomatic *(Czech)* 78−63208
Magellanic Stream, kinematics rel. to Hypergalaxy mass 77−5573
manipulator and man's hand purposeful motion, modelling 77−78969
matrix differential equation, rotations as solns., for teachers 78−62021
multilink spatial mechanism structure and analysis *(German)* 79−21544
NGC 1313, barred spiral galaxy, rot. and kinematics, interferometric study 77−49474
NGC 3256, peculiar galaxy, kinematics 78−96537
NGC 4945, late-type spiral galaxy, excited gas kinematics, obs. 80−109547
NGC 5128 (Centaurus A), morphology and kinematics rel. to tubelike model of dust band 80−56945
NGC 5474, peculiar Scd galaxy, H I distrib. and kinematics 80−8683
NGC 650/1, planetary nebula, internal kinematics from emission line profiles 80−17639
NGC 7822 (W1) optical studies of kinematics rel. to supernova remnant struct. 78−54028
non-Euclidean geometry and physical basis, Galilean geometry and relativity, book 79−62989
OB stars Local complex, kinematics 78−16396
ocean surface gravity waves during Tropical Storm Delia, directional spectra and kinematics 79−48506
oceans, kinetic energy dissipation field struct. *(Russian)* 77−13082
open flow cross sections, local velocity variations *(Bulgarian)* 78−18268
ρ Ophiuchi dark cloud, atomic and mol. obs. rel. to contraction 78−41013
optoelectronic apparatus for classroom demonstrations 80−46773

kinematics continued
photon, stochastic phase space kinematics 79−2649
plane mechanism, dynamic balancing *(Russian)* 79−35538
planetary nebulae, spatial and vel. distrib. statistics 80−109518
planetary nebulae in M31 (Andromeda galaxy) and companions, rel. to vel. dispersions and virial masses 80−109520
planetary nebulae kinematics, radial vel. meas. 80−46633
plastic shells, kinematics at large strains and displacements 78−79221
plates undergoing oscillatory bending, particle trajectories *(Russian)* 79−37209
point mass systems, dynamically and kinematically controlled, motion *(Russian)* 77−33858
precession of rigid body, geometric and kinematic props. *(Italian)* 79−63009
radio sources, extragalactic, with speeds exceeding speed of light, kinematic models *(Danish)* 78−36715
radio sources, superluminal, kinematic quantities from mag. dipole model 80−56959
relativistic scalar particle, positive mass, conformal group in classical phase space 77−57151
relativistic transformations, Newtonian force and EM field, for teaching 78−49601
rolling object, frictional force, student lab. expt. 80−17764
rotating and turning platforms 79−30220
rotation kinetics anal. with air cushion apparatus *(Hungarian)* 79−25811
Sa spiral galaxies, internal vel. dispersions from H I study 80−98714
southern high-velocity stars, kinematical and orbital props. 79−25600
space vehicle, disordered rotation damping by elastically suspended ballast *(Russian)* 77−45287
spacecraft, flexible, in gravitational field, stability 77−25906
spherical analogue of elliptic motion *(German)* 77−53777
star clusters, ratio of escape rel. to mean vel. *(German)* 78−53995
stellar kinematics, appl. to galactic spiral structure parameters derviation 80−17665
straight-line kinematics demonstration 77−57124
subduction zone, kinematic model for inter-arc basins 78−81127
sunspot groups, kinematic parameters rel. to convective zone cophasal regions 78−96469
thrown string problem 78−89331
uterine deformation during labour, thin shell model and kinematic analysis 79−2090
Venus atmosphere, vertical extent of zonal winds 78−85875
W33, H II region, recomb. lines as evidence for mass flow 78−49501
wrist, human, kinematic and kinetic analysis by stereoscopic instrumentation 79−92274
H I clouds in solar vicinity, kinematics from Nancay 21 cm absorpt. survey 79−8971
H I in region $348° \leq l \leq 12°$, $+3° \leq b \leq +17°$, 21 cm obs. and vels. 78−45377

kinematography *see cinematography*

kinerecording *see telerecording*

kinescope *see television picture tubes*

kinetic theory
see also Boltzmann equation; collision processes; intermolecular mechanics; kinetic theory of gases
BBGKY hierarchy, classical statistics 78−16721
BBGKY hierarchy, scaling method of kinetic eqn. derivation 78−54286
binary liquid mixture, diffusivity from simple kinetic model 79−23752
binary mixtures, diffusion processes master eqns., kinetic eqns. 79−75446
Bogolyubov chain equations, solution 77−74311
Boltzmann kinetic eqn., influence of stochastic sources 77−2627
Bose condensation, kinetics 79−63139
boson system, multicomponent, transport coeffs., crit. behaviour, kinetic theory 77−2611
Brownian motion, kinetic fluctuations 79−25984
Brownian motion, kinetic theory, fluctuation effects 80−150
Brownian motion in Bogolyubov's method of abbreviated description 79−21669
Brownian motion in fluid, repeated-ring kinetic theory 78−59729
Cauchy problem, global soln. in discrete kinetic theory *(French)* 79−12710
ceramic, sintering kinetic laws with involvement of a liq. phase 80−55335
changes of variables 78−133
classical liq., kinetic theory, dynamical struct. factor calc. 78−21050
classical liquids, kinetic model, dynamic struct. factor 79−10768
classical liquids, kinetic theory for coherent scatt. function 78−42875
classical particles in box, continuous system, phase transform. 77−82444
cloud drops stochastic coagulation, kinetic eqn. 78−92944
coagulation, stability ratio of primary and secondary minimum coagulation, kinetic theory model 80−3415
collisionless evolution of particle system with elliptic interaction potential 77−61004
condensation, kinetic theory, stochastic approach *(Russian)* 77−72676
continuum theory, nonlocal, using kinetic theory, stress, energy density *(Japanese)* 78−32677
convective diffusion to a particle in a fluid with linear kinetics 80−69943
convex body aerodynamics in rarefied mol. flow, kinetic theory 78−59424
correlation functions, asymptotic time behaviour, kinetic and pot. terms. 77−5737
correlation functions, asymptotic time behaviour, local equil. and mode coupling theory 77−5738
cosmic ray propagation, applicability limits of quasilinear approximation to kinetic eqn. 77−91383
Coulomb systems and coupled harmonic oscills., generalised Stratonovich method *(German)* 77−87686
Crookes radiometer, physics anal., for teaching 79−35504
crystal growth, multi-component, master equations in lattice model 80−75194
crystal growth from melt, multi-component, kinetic equation theory 80−79721
Curie-Weiss model, with bilinear and biquadratic interactions 78−41238
dense fluids, derivation, transport coeffs., soln. of kinetic eqn. by moment method 79−54032
dense fluids, generalised Chapman-Enskog soln. 79−54033
dense fluids, HF kinetic sum rule 77−27803

kinetic theory continued
dense fluids, kinetic theory, entropy abalance eqn. and irreversible thermodynamics 79−94758
dense plasmas transport coefficients, kinetic theory 80−77280
desorption rates, stochastic description 77−20184
dissipative dynamical systems of macroscopic phys., common formal struct. of kinetic theory, fluid mechs., nonequilibrium thermodynamics 79−140
dynamical fluctuations in simple fluids, kinetic theory 77−7652
dynamical systems, kinetic theory, ergodic props. 77−82
electron diffusion in gas, Maier-Leibnitz expt. reexamined 78−83516
electron liquids, two-dimensional, self-diffusion constant, molecular dynamics 80−34372
electron stimulated desorption 78−14613
equation derivation in nonequilib. statistical mechanics, approx. results 79−2712
evaporation, disequilibrium conditions 78−79755
evaporation and condensation, BGK eqn., kinetic anal. 77−11683
explosive fracture, time criteria, kinetic theory appl. 79−14347
Fermi liquids 78−87841
fluid, of rough spheres, translational and rot. motion, particle roughness depend. 78−26403
fluid, rough sphere, kinetic theory, density fluctuations 78−131
fluidised beds, soln. to kinetic eqns. *(Russian)* 79−10610
fluids, classical, linear irreversible thermodynamics, derivation 79−2740
fluids, memory functions for kinetic theory models of density fluctuations 80−38886
fluids, one and two dimensional, hydrodynamics, viscosity, heat conductivity, kinetics *(Russian)* 80−79972
formal struct. of kinetic theory 77−13683
galaxies, kinetic theory of differentially rotating interstellar medium *(Russian)* 77−91617
gas-liquid droplet system, phase transition kinetics and kinetic eqns. 78−83933
gas-surface interaction theory 79−87002
generalised kinetic theory with memory 79−35625
glass-forming materials, ion activation, energy parameters determ. 80−24634
gravitational systems 77−5748
H-theorem for the (modified) nonlinear Enskog equation 79−60242
hard disc system, 4-point vel. correls., long time behaviour 78−93598
hard dumbbell fluid, RAM perturbation theory 79−72980
hard quadrupolar diatomics, free energy, perturbation theory and Monte Carlo calc. 79−90361
hard rods, in finite 1-D mixture, time displaced correlation functions 78−54287
hard sphere gas, H-theorem for Enskog kinetic eqn. 77−68905
hard sphere model of chemical reaction in condensed media 79−29349
hard sphere system, kinetic eqns., Boltzmann and modified Enskog eqns. 80−130
hard-sphere fluid, kinetic theory of self-diffusion 79−4225
hard-sphere fluid, translational correl. functions, stochastic theory 77−84608
heat and mass transfer in capillary-porous body, kinetic eqns. 78−5796
high-energy low-mass particles interaction with crystal *(Russian)* 79−23660
hydrocarbons, heavy liq., vapour press. and enthalpies of vaporisation by group-contrib. method 80−40726
infinite diffusion velocity and causality in special relativity 79−63027
interstellar dust condensation in clouds, importance of reaction kinetics 80−26939
ionosphere plasma conductivity, kinetic theory 79−53609
irreversibility, Liouville eqn. in Gell-Mann-Goldberger limit 77−61005
irreversibility postulates 78−24750
Klein-Gordon charged particles, perturbation theory for non-equilibrium stat. Green's functions 80−31994
Klein-Gordon charged particles, quantum distrib. function 80−31993
Klein-Gordon particles, charged, quantum kinetic theory, Feynman rules and thermal eqn. 80−57177
Klein-Gordon particles, charged, quantum kinetic theory, linear kinetic eqn. 80−57178
Landau-Fokker-Planck eqn., for arbitrary statistics, relativistic and nonrelativistic case 80−36935
linear and nonlinear kinetic equations, quantum mech. theory 77−9969
linear dynamic system with Poisson parameter fluctuations 80−31675
linear Onsager relation, mol. kinetics basis 79−67242
linearised hydrodynamics, derivation from kinetic theory 79−21679
liquid surface tension, kinetic tunnel model 78−56022
liquid surface tension, mol. theory, teaching 77−57123
liquid viscosity, simple kinetic model 78−55793
liquid-gas bubbles system, phase transition kinetics and kinetic eqns. 78−83933
liquid-vap. transform., nonequilib. conds., phys.-math. model 77−62631
liquid-vapour interface, kinetic eqn. at mean field level 79−37905
liquid-vapour transformations, statistical kinetic theory 77−20044
liquids, associated, mechanism of structural dielectric relaxation 80−107034
liquids, equilib. and non-equilib. props., book contrib. 79−60246
liquids, relaxation, binary collision theory 78−6000
liquids, transverse correlations in simple liqs., effective field approach 79−82135
Lorentz gas, calc. of velocity correlation function in ring approx. 79−44849
Lorentz gas, Fourier's law of heat cond. 79−58620
macromolecular crystallisation, kinetic statistical theories *(Chinese)* 77−84683
macromolecular solution, flexible mols., mol. models for mech. props. 79−59957
macromolecular solutions, kinetic theory and rheology 77−7424
many-body distrib. function, dilute system generalised Boltzmann equation 79−30351
many-body kinetic eqn., mol. chaos, generalised hypothesis 77−30088
Markovian equations, derivation, generating functional technique 77−9946
master kinetic equation for a particle in the field of randomly varying scatterers 79−58634
memory functions for transport fluxes 80−42172
memory operator identity, using ordinary time-correlation functions 77−57271
molecular dynamics, angular velocity autocorrelation function of fluid of rough spheres, long time behaviour 77−6879
kinetic theory continued
molecular dynamics, fluctuation driven reson., hydrodynamic and kinetic theory simulation 77−55124
molecular theory teaching, expt.-oriented approach 80−12868
molten metal binary mixtures with wide immiscibility range, gravitational layering of components *(Russian)* 80−104092
molten salts, compressibility hard sphere calcs. 77−51295
monatomic fluid, collision induced light scatt., correlation function, relative radial motion contrib. 80−20647
monatomic liquids, kinetic theory of self motion, memory function of vel. autocorrel. function 80−14986
multi-component crystal growth, binary system crystallisation 80−88071
neutrino+antineutrino system, relativistic kinetic theory, Wigner functions 77−26239
neutrino component of $e\bar{\nu}_e\bar{\nu}_e$ mixture, transport eqn. 77−33941
neutrino system, relativistic transport eqn. 77−33940
neutrino systems, relativistic kinetic theory of transport processes 80−73283
nondegenerate optical transitions of excited atom in buffer gas, line shape kinetic theory 80−42997
nonequilibrium states, by Kubo and Callen-Welton formulae *(Russian)* 79−17351
nonequilibrium statistical mechanics, kinetic eqns. derived 77−57269
nonequilibrium statistical mechanics, space-time coarse graining scaling, kinetic eqns. 79−75445
nonlinear oscillator interaction with discrete system of oscillators 78−70050
nonlinear viscous flow, in two and three dimens., 78−71372
normal quantum fluid, kinetic theory, transport props. 78−77799
one dimensional infinite particle systems with hard core interaction, nonequilibrium dynamics 77−82443
pair configuration space diffusion eqn., thermal fluctuations, kinetic theory 79−17362
paramagnetic nonresonance absorpt., kinetic eqns. 80−7151
phase transitions, master equations *(Russian)* 78−47498
planetary atmospheres, non-Maxwellian effects assoc. with minor constituent thermal escape 79−80264
plasma, EM wave reflection, kinetic theory 77−27682
plasma, kinetic expressions for transport coeffs. 77−27652
plasma, magnetic field operation, in resonant absorption of light 79−73013
plasma, one-component, dilute, kinetic eqns. and fluctuations in μ space 77−89230
plasma, one-component, nonlocal shear viscosity, long-time behaviour 77−35321
plasma, self-consistent kinetic theory of stochasticity 80−59179
plasma, strongly coupled one-component, shear viscosity, microscopic theory 77−51157
polarisation dynamics, fully relativistic kinetic model 78−62134
polyethylene glycol solns., US vels. rel. to mol. kinetic theory 77−72655
polymer, glass transition kinetic nature, sp. ht. 79−10929
polymeric liquids, rheology and kinetic theory, review 78−38611
projection and variational methods 80−6189
quantum fluid relaxation, renormalised perturbation expansion in kinetic theory 78−21061
quantum kinetic equations, derivation, nonlocal Uehling Uhlenbeck eqn. 78−70054
quantum kinetic equations, derivation by collision expansions, three particle term 78−70053
quantum kinetic theory, three-particle collision term 77−64994
quantum mechanical eqn. of Kadanoff and Baym, time reversal noninvariance 79−17332
quasi-particle transport eqns., statistical T-matrix approx. 77−65011
Rayleigh model, one-dimens., initial conditions and time reversal 79−9176
relativistic, continuity of summational invariants for massless particles 79−25968
relativistic, statistical expressions for relativistic thermodynamics 77−82423
relativistic, statistical expressions for relativistic thermodynamics 77−82424
relativistic Boltzmann eqn., series convergence 78−36949
relativistic Boltzmann kinetic eqn. derivation 80−68161
relativistic kinetic eqns. 77−67376
relativistic kinetic theory, continuity of summational invariants for nonzero rest mass 79−25967
relativistic kinetic theory, scalar proper time and vectorial relativistic entropy 77−22461
relativistic kinetic theory, thermodynamics, symmetry props. role 80−27117
relativistic kinetic theory of $e\nu_e$ and $e\nu_\mu$ systems, transport coeffs. 79−21680
relativistic quantum theory, $e\nu_e$ and $e\bar{\nu}_e\bar{\nu}_e$ mixture 79−63140
renormalised theory of time-depend. pair distrib. function 77−2601
renormalized kinetic theory of nonequilibrium many-particle classical systems 79−82038
Robertson-Walker and Petrov G_4 VIII cosmologies, general relativistic kinetic theory 78−24586
rough sphere fluid, dynamical correlations, renormalised kinetic theory 77−19858
rough sphere fluid, kinetic theory, matrix elements 77−71262
rough sphere fluid, linear and ang. vel. correl. functions 77−42951
scaling method for obtaining kinetic eqns. from BBGKY hierarchy 77−45785
simple classical liquids, kinetic theory, formal justification for memory function approx. 78−87598
simulator, for student lab. expt. 79−35461
sine-Gordon chain, displacement fluctuations, long-time behaviour and dynamic scaling props. 80−101764
single-particle density matrix kinetic eqns., linked cluster expansions in eqns. of motion method 77−33933
single-particle motion in a fluid, kinetic theory 79−41922
solids, large thermal fluctuations, kinetic eqns. for many-body treatment 79−54037
solute transport in porous media, statistical theory 80−28899
spherical condensed phase, motion in uniform vapour gas flow, kinetic theory 78−1725
spin systems, far-from-equilib. states, metastability and anomalous fluctuations 79−80561
square well fluid, self-diffusion coeff. density depend., repeated ring approx. 79−77326

kinetic theory continued
stochastic dynamical systems, kinetic eqn. derivation based on cumulant function props. 80−12995
Stokes-Einstein law for Brownian particle, kinetic theory derivation 77−49686
sulphate aerosol, stratospheric, kinetics of growth by condensation in homogeneous medium *(Russian)* 80−94566
symmetry breaking, kinetic model 80−129
system acted upon by non-delta-correlated random forces *(Russian)* 77−74323
systems in random fields 79−21652
teaching method for secondary schools 78−81767
tearing instability kinetic theory, collisional to collisionless regimes 77−84425
three-particle scatt. operator, correl. pattern representation 77−13684
time-evolution of the scattering kernels for half-space gas-solid systems 79−25849
Tolubinskij's stochastic theory of nonequil. processes and rel. to kinetic eqns. *(Russian)* 78−21053
transient relativistic thermodynamics and kinetic theory 79−17330
transport coefficients near critical point, dynamical spherical model 77−49695
transport collision frequencies, integration of empirical data 79−25969
transport collision frequencies, temp. depend. by approx. method 79−25970
turbulence, kinetic model *(French)* 79−14382
turbulence kinetic theory, fundamental soln. 80−27137
turbulent flow 77−75891
two-level system, kinetics at diffusion modulated local interactions *(Russian)* 79−2716
two-phase flows, particle interaction, obs. and calc. 79−72875
vacuum system, rate of molecular impact on surface or orifice, possible conflict with second law of thermodynamics 80−46954
vaporisation and condensation, physical-mathematical problems *(Italian)* 79−40505
vapour pressure, temp. depend. two-parameter eqn. based on kinetic theory of fluids 77−89520
virial inequalities, quantum and relativistic 80−62609
weakly coupled non equilibrium systems, time asymptotics and reversibility 79−54049
weakly interacting system, kinetic eqns. *(Russian)* 77−64992
weakly relativistic system with gravitational interaction, kinetic eqn. 77−49671
weakly-coupled classical fluid, kinetic eqn. for test particle 77−74310
weakly-coupled test particle 79−54039
Ar, liq., numerical anal. of density fluctuations 78−21051
Ar, liq., numerical anal. of transverse current correl. 78−21052
Ar, liq., transverse correlations in simple liqs., effective field approach 79−82135
Ar plasma, thermal equilibrium properties, estimation 78−1793
H plasma, kinetic eqn. for departures of electron energy distrib. from Maxwellian 77−80266
^{3}He-He II solns., magnetokinetic effects 79−19419
^{4}He, liquid, atomic kinetic energy 77−69126
Rb, liq., transverse correlations in simple liqs., effective field approach 79−82135

kinetic theory of gases
see also Brownian motion; collision processes; equations of state; intermolecular mechanics; Joule-Thomson effect
A+BC→AB+C, reactive collision model for use in kinetic theory 78−35665
alkali ion+inert gas, interaction pots., gaseous ion mobilities 77−54584
alternant Takahashi nearest neighbour type, exactly soluble case rel. to soft rods 80−33718
Ar, light scattering, collision induced, low density limit, mol. dynamics and memory function approach 80−43841
asymptotic equation for classical scattering angle 77−42950
atom interaction in reson. light field *(Russian)* 79−54936
atom scattering, from solid surfaces, undergraduate course 77−60863
atomic gases, cooling by reson. EM radiation, kinetic theory 79−77327
Barnett approximation for distrib. function, super-Barnett terms 80−28587
barometric distribution, elementary kinetic derivation 77−62323
BBGKY system, irreversibility, velocity correlations and non-Hamiltonian dynamics 80−77686
BGK model, time-depend. linearised, half-space anal. 77−47127
bi-particle correlations in gas, relax. time 80−83875
biatomic molecular gas, quantum kinetic theory *(Rumanian)* 78−91053
binary gas mixture, drop thermophoresis 80−93806
binary gas mixture, isothermal creep along flat surface, half-space moments method 77−42873
binary gas mixture thermal fluctuations in renormalised kinetic theory 77−22492
binary gas mixtures epochal relax. 79−41783
binary gas phase collisions, rates, translational energy depend., statistical mech. theory 79−44844
binary inert gas systems, determ. of (m,6,8) pot. parameters 79−46414
binary mixture, moderate density diffusive creep along flat surface 80−43822
binary mixtures, use of diffusion and second virial coeffs. to predict viscosities 79−14506
binary mixtures of monatomic gases, Chapman-Enskog theory, thermal cond. calc. 80−24118
Boltzmann collision operator with cut-off for intermolecular potentials 78−42697
Boltzmann eqn., linearised, uniqueness theorem 78−32774
Boltzmann eqn., separation of inhomoogeneous kinetic operator 77−74333
Boltzmann eqn. exact solns. for N-component systems 77−47131
Boltzmann equation, initial value problem 79−44885
Boltzmann equation asymptotic solution, kinetic theory of gases problem 80−33720
Boltzmann equation generalisations, relatively dense systems 79−98851
Boltzmann equation with average force field caused by anisotropic momentum changes 77−13714
Boltzmann gas, heat transfer between parallel plates 77−87688
Boltzmann kinetic eqn. for weakly ionised gas 77−57288
Boltzmann kinetic equations, soln. methods 78−83511
Boltzmann linearised eqn. with long range pots., numerical anal. 77−35168

kinetic theory of gases continued
Boltzmann-Lorentz kinetic equation, exptl. test 78−94875
Bose gas, spatially inhomogeneous, kinetics in presence of condensate 78−16730
boundary value problem, non-equilibrium thermodynamics 80−19544
boundary value problems, mixed type, arising in kinetic theory of gases 79−55440
canonical ensemble partition function, incorporation of long range electrostatic effects 78−21065
Cauchy problem, global soln., discrete kinetic theory, two dimensional model *(French)* 77−68727
Chapman-Enskog method for a multivelocity, multitemperature mixture of reacting gases *(Russian)* 79−15995
Chapman-Enskog method for reacting mixture of gases 78−15656
chemically reactive gas, wave structures, kinetic theory of gases calcs. 79−94678
classical Boltzmann kinetic theory justification using Liouville theory 80−87838
classical nonrelativistic two-dimens. gas, initial pair correlations effect on kinetic eqn. 78−34249
classical systems, minimal specific energy 79−90364
cold gas, noninteracting particles, nonlinear periodic motion *(Russian)* 80−14868
collision processes, kinetic theory, density effects expts. 78−12468
compressible turbulent flow, kinetic theory, comparison with classical theory 77−3814
conductive heat transfer between two concentric spheres with internal degrees of freedom 78−30399
cooling to broad band reson. light press. 80−48835
correction of errors which cast doubt on principle of material frame indifference 78−30400
coupled system, time depend. projection operator anal., classical gas and quantum systems 78−16720
dense gas, quasiparticle kinetic eqn. construction 80−53905
dense gases, density dependence of transport coeffs., viscosity 79−94757
dense gases, vel. autocorrelation function, memory function 80−59154
dense gases, viscosity and thermal cond. 79−46415
diatomic gas, flow around a sphere, using kinetic eqns. 77−906
diatomic gases, harmonic oscill. system, vibr. energy relax. 78−66632
diatomic molecular gas, atomic versus mol. description 77−7495
diffusion eqn., recoil/sticking probabilities at wall 77−51149
dilute gas, Boltzmann-Langevin eqn., light scatt. and density correlation function 77−11307
dilute gas, kinetic perturbation theory 80−100051
dilute gas, kinetic-hydrodynamic transition obs., Brillouin scatt. 77−7508
dilute hard sphere gas, vel. autocorrelation function, diffusion coefficient 77−62324
dilute monatomic gas flow round macroscopic object 77−965
dilute polyatomic gases, nonequilib. alignment phenomena in elec. and mag. fields 78−71414
discrete kinetic theory, maths. and numerical aspects, Couette flow appls. 80−19413
discrete velocity gas, boundary conditions and Couette flow 78−30254
disparate mass gas mixtures, near-normal behaviour 79−94762
dissociation equilibrium, phase space allocation 79−27746
distance force consts., pseudocritical volumes 78−58765
droplet model for gas above T_c and the metastable phase 78−34608
education, irreversible processes, linear coeff. calc., kinetic and Onsager reciprocity theorems, gas flow appl. 79−9053
education, kinetic theory, mean time between collisions paradox 77−33771
elastic cross-section analytical approximation *(Russian)* 78−75248
electron motion in weakly ionised gases, stochastic theory of homogeneous systems, review 80−77735
electron swarms in gases with large inelastic cross sections, accuracy of numerical solns. of Boltzmann's eqn. 79−94756
Enskog eqn., possible generalisation *(Russian)* 77−39392
equilibrium constant and parameters of interaction pot. of at. particles 78−1045
equilibrium correlation functions, turbulent flow kinetic theory *(German)* 78−90886
ethane gas, electron-mol. collision freqs. from breakdown data in crossed mag. field 80−43835
evaporation and condensation in nonlinear half-space 79−27500
extended principle of corresponding states, rel. to pair interaction potential 78−51269
fast atom slowing down, by nonlinear Boltzmann eqn. 79−98196
Fermi acceleration and RF heating 80−33790
flow in plane-parallel channel, integral entropy derivation *(Russian)* 77−84382
Frey-Salmon closure hypothesis *(French)* 77−68728
friction const. of Brownian particle density expansion 77−87694
gas, Boltzmann eqn. for transport coeff. 78−38439
gas, in contact with condensed phase, hydrodynamic eqn. and slip boundary condition 80−14791
gas breakdown by large amplitude EM fields, kinematic theory 80−24295
gas flow over cylinder at low speeds under constant force, kinetic theory description 80−79354
gas flows, entropy prod. determ. using Boltzmann's H-theorem, Knudsen effusion 80−106867
gas suspension, closed dynamic eqn. system using kinetic theory 80−6190
gas-solid suspension, kinetic eqn. for gas phase from Boltzmann eqn. *(Russian)* 79−85059
gaseous transport coefficients, rot. inelastic collisions effects 79−82020
Gaussian model of imperfect gas, possible transition 77−80260
general physics and heat, book 79−25814
generalised kinetic eqn. of Boltzmann type, eikonal approx. *(Russian)* 77−35297
global existence theorem for Cauchy problem in discrete kinetic theory *(French)* 77−68729
H-theorem for hard sphere gas 77−7498
hard rod gas, one-dimens., exact nonlinear driven response 78−22447
hard sphere gas interacting with hard wall, density profile, virial expansion 78−63928
hard sphere gas mixture, vel. autocorrelation function calc. 80−75019
hard sphere gas with step repulsive barrier, generaralised Enskog eqn. 80−87836
hard sphere gases, two and three dimens., free flight times and densities 79−98846

kinetic theory of gases continued
heat propagation, finite vel. problem, kinetic theory anal. 77−46881
heavy ions in light gases in electric field, limits of Kihara distrib. 80−87837
history, Bernoulli and other contributors 80−17782
hole-burning in at. vel. distrib. by EM radiation 80−64674
hydrocarbon, internal degrees of freedom, Eucken factor, effect on transfer props. 78−22445
ideal gas, law of iterated logarithm for dynamic system *(Russian)* 77−51153
ideal gases, solns., basic props. kinetic derivation from elastic collision processes 78−91048
ideal monatomic gas, thermal cond. coeff., appl. of simple variational principle 77−968
inert gas, transport and equilib. props., using LJ (12-7) pot. 79−98849
inhomogeneous, structure of three particle kinetic operator 77−35294
inhomogeneous Boltzmann gas, lumped phase space, non-linear diffusion approx., stochastic hydrodynamic theory 80−64666
inhomogeneous systems, stochastic version of Boltzmann eqn. 79−55442
intensive evaporation processes, mechanism 78−30746
interionic force pot. in ideal dipolar gas 80−96330
ion mobility and diffusion in elec. fields of arbitrary strength 78−30398
ion transport, three temperature theory 79−46412
ion transport, three-temp. theory generalisation, appl. to $Cs^+ + Ar$ 80−6202
ion transport theory, perturbation treatment of thermal motions 79−64820
ionosphere E-region, effective electron collision frequency determ. rel. to gas kinetic theory 79−58153
ionosphere plasma, cond. via mean free path and kinetic theory formulae 77−60512
Landau equation for weakly coupled gases soln. for homogeneous plasma relaxation 79−41798
light induced kinetic effects in gases *(Russian)* 80−92244
light scattering, nonequilibrium gas 79−46421
linear heat equation from kinetic theory of gases 78−94877
linearised Boltzmann eqn., constructive soln., scalar BGK model eqn. 79−161
Lorentz Fokker-Planck equation eigenvalues 79−46413
Lorentz model, hydrodynamic kinetic stages asymptotic equivalence 79−55438
mass transfer in highly rarefied gas 77−11222
matrix representation of the kinetic theory differential operator 80−14867
Maxwell's gas velocity law functional eqn. derivation 77−13
Maxwell-Boltzmann eqn., exact soln. generation 79−94760
Maxwellian molecule gas, heat transfer between parallel plates, Navier-Stokes eqns. 80−87839
mean free flight time of molecules, soln. of apparent concept inconsistency 78−63525
methane, gas, electron transport, kinetic theory 77−84391
methane, liq. and gas, mol. dynamics simulation, thermodynamic props., struct. factors, etc. 79−50976
microwave radiation, kinetic theory of interaction with diatomic gas, j=0, j=1 transitions 78−9750
microwave radiation, kinetic theory of interaction with polyatomic gas 78−9749
mixture, binary, Wassiljewa coeffs., thermal conds., 50 and 100°C appls. 79−37437
mixture, Boltzmann collision operator matrix elements 79−86545
mixture, multicomponent, transport equations near catalytic surfaces 80−43821
mixture, multivel. multitemp., gasdynamic eqns. 79−77052
mixtures, eigenfunctions positivity in time depend. kinetics theory 77−19660
mixtures of heavy and light gases, kinetics and thermodynamics *(Russian)* 77−76015
mixtures of reacting gases, extension of Chapman Enskog method *(Russian)* 78−57878
moderately dense gas, Bhatnagar, Gross and Krook model from Chapman-Enskog equations 80−106864
mole, introduction in teaching of ideal and real gases 77−87611
molecular flow in vacuum, kinetic method analysis, flux in elementary structs. 78−55663
molecular flow in vacuum, kinetic method for analysis basic formulation 78−51201
molecular fluid, hard-core triatomic, Monte Carlo simulations 80−38880
molecular fluids, coupling of rotation and translation 80−38892
molecular fluids, diatomic, struct. and dynamics 80−38889
molecular gas, diffusion coeff. and mean free path, higher order approx. calcs. 79−27734
molecular velocity redistribution by optical processes 78−38448
monatomic fluid, collision induced light scatt., correlation function, relative radial motion contrib. 80−20647
monatomic gas, between parallel plates, higher kinetic moments, differential eqns., boundary conditions 77−75921
monatomic gases, quantum corrections to transport coeffs. 77−15148
multicomponent system, with internal energy states, kinetic eqns. 77−15145
multidroplet system, condensation-evaporation by kinetic theory 80−7873
multitemperature gas-mixture, linearised Boltzmann operator, matrix elements 78−47085
mutlicomponent dilute gases under EM and gravity fields 79−77328
neutral radiant gas, kinetic eqns. with allowance for radiation polarisation 79−23399
NMR, single relax. time approx. 77−14451
non-equilibrium gas, Doppler broadened spectral and time correl. functions 78−14122
non-ideal gas, internal degrees of freedom, kinetic equation *(Russian)* 79−23390
non-Maxwell molecular interaction model, integrable representation 80−100050
non-Maxwellian distribution integral representation and approach to equilib. 80−10343
nonequilibrium gas, small fluctuations, theory *(Russian)* 80−69962
nonequilibrium processes, integro-differential eqn. approx. by Fokker-Planck type 78−91049
nonequilibrium states, by Kubo and Callen-Welton formulae *(Russian)* 79−17351
nonideality effect, student experiment with surprise value 77−82351
kinetic theory of gases continued
nonisothermal gas motion in plane channel, S-model kinetic eqn. 80−83816
nonlinear effects in polarised gases, complex dielectric constant evaluation 78−1787
nonlinear kinetic eqns. soln. by Monte Carlo method *(Russian)* 77−5735
nonlinear viscous flow in 2-D and 3-D, kinetic theory 79−50694
nonpolar gases, eqn. for prediction of third virial coefficients 80−33717
nuclear mag. relax., DWBA cross sections from S-matrix formalism 77−27151
one-component gas, relativistic Burnett eqns. and sound propag. 77−15150
one-dimensional hard sphere gas, initial value problem, exact soln. 80−92243
optical breakdown, quantum kinetic eqn. for electrons *(Russian)* 79−60092
optically excited gas, kinetic effects 80−1721
orientational correlation functions, for mol. reorientation 79−36798
Penning collision processes, review *(Japanese)* 79−64092
percolation theory 78−5839
photodissociation, kinetic theory analysis 78−82795
planetary gravitational field, kinetic eqn. soln. for gas 78−16322
plasma, nonequilib., kinetic theory of spectral line broadening 80−59187
plate infinite, oscill. in strong rarefied gas under constant force 79−10623
polyatomic chemically reacting gases, hydrodynamic eqns. 79−32711
polyatomic gas, in non-hydrodynamic domain, Rayleigh-Brillouin scatt. *(French)* 78−86872
polyatomic gas, thermomagnetic phenomena at intermediate press. *(Russian)* 79−77329
polyatomic rarefied gases, vibrational modes, energy exchange *(Russian)* 80−32811
pressure, 'stress' calculation and virial theorem 79−37433
quantum momentum distribution, asymptotic form 79−98850
quantum state diffusion, in nonequilib. polyatomic gas, kinetic theory 77−62325
rarefied flow, closure relations 79−98757
rarefied gas dynamics projection and variational methods 80−6189
rarefied gas flow through finite length slots 77−72331
reacting spheres, Enskog theory of transport processes 78−35668
real gas thermodynamics, Van der Waals model approach 80−38515
reciprocity and conservation theorems, for fields with general time dependence 79−80452
reduced pressure in centrifugal field 79−58491
relativistic, hard sphere gas, binary mixture diffusion coeffs. 77−3908
relativistic, hard sphere gas transport coeffs., temp. depend. 77−3907
relativistic, propagation eigenmodes, Marle's 14-moment description 77−27626
relativistic electron beam relaxation in dense gas, radiative energy transfer 80−69968
relativistic gas, one-component, transport eqns. 77−966
relativistic kinetic gas theory, electron-neutrino system 77−5756
relativistic Lorentz gas of hard spheres, diffusion coeff. 77−5743
relativistic transformation of energy and momentum, for teaching 78−24618
rigid spherical mols., relax. of translational energy in perpendicular directions 77−72398
scaling method for obtaining kinetic eqns. from BBGKY hierarchy 77−45785
second virial viscosity coefficient, temp. depend. 80−19543
self-diffusion of hard sphere gas, scaled Boltzmann theory of correl. functions 79−68894
self-structure factor, kinetic modelling 79−41791
self-trapped electron effective mass, appl. to He 79−60090
shear viscosity, nonlinear in steady Couette flow 80−28588
shock tube boundary-value problem global soln. *(French)* 78−63449
slip flow in porous medium, effective diffusion coeff., variational method 79−90325
slit and crack type leaks, calc. model and results of its use 80−35490
sphere slow rotation in confined vol. of dilute gas 79−77187
spherical waves focusing and reflection, numerical soln. *(Russian)* 77−7501
stochastic approach 78−9744
stochastic approach and functional models 79−60091
structureless polyatomic molecules, phenomenological energy exchange, kinetic models 78−42168
student experiment, computer modelling of mol. vel. distribs. 79−30169
surface integrals for triple collision integrals 77−84381
symmetric-top molecules, dilute gas, non-reson. microwave absorpt., kinetic theory 79−68901
temperature-jump problem with arbitrary accommodation 78−67221
test particle diffusion, in conservative field, integral Boltzmann eqn. solns. 79−97324
thermal stresses effect on motion of simple gas 78−22444
Thorne equation test, from He-Ar$(N_2)(O_2)(CO_2)$ binary diffusion coeffs. press. depend., 300 and 323K 80−1724
three-particle collision processes, kinetic eqns. 78−1044
time-dependent boundary-value problem soln., half-range, orthogonality relations 79−14508
time-local gaussian processes, path integrals and nonequilib. nonlinear diffusion 77−13726
transient relativistic thermodynamics, kinetic theory, dilute gas 77−76014
transpiration, thermal, effect of gas-surface interaction, dusty gas theory 77−19634
transport coeff. data inversion iterative procedure, pot. energy function determ. 78−91051
transport coeff. for real gases *(Russian)* 79−10624
transport coefficients density expansion, 1st logarithmic term, moderately dense gas 78−94878
transport collision frequencies, integration of empirical data 79−25969
transport collision frequencies, temp. depend. by approx. method 79−25970
transport processes, alternative approach for teachers 78−28890
transport processes, kinetic cross sections, temp. depend. 77−80259
Tsuge kinetic theory, applic. to turbulent gas flow reaction rates 79−7418
two component Boltzmann gas, fluctuating kinetic eqn. 80−171
two particle distribution function, Bogoliubov eqn. soln. 80−96332

kinetic theory of gases continued
unbounded linear transformation arising in kinetic theory of gases, spectral representation 79−55441
unsteady heat transfer from suddenly heated infinite plate in rarefied gas 78−34166
vacuum science and technology, undergraduate and post-experience courses 79−62954
vane radiometers, elementary model 77−64901
velocity correlation functions, transport props. predictions, medium density 77−7500
very low pressure pyrolysis, gas-gas and gas-wall average energy transfer 80−93739
virial coeffs., quantum mech. second, square-well plus hard core pot. 78−1778
viscomagnetic effect, collision cross sections, linear mol. gas 80−10353
viscomagnetic heat flux, in a Burnett regime, gas kinetic theory 78−71400
viscosity, coeff. for mol. gas 79−41784
viscosity, in transition regime, density depend., appl. to He 79−1280
viscous gases, simplified transport coeffs. for vibr.-rotational relaxation *(Russian)* 78−51270
weak second law of thermodynamics, classical gas in rectangular box 77−82442
weakly ionised gas, kinetic theory of electron component 77−47132
weakly ionised gases, in electrostatic field, Maxwell model, ion vel. distrib. and moments 78−94879
C, monatomic, transport properties, rel. to spacecraft entry into planetary atms. 78−87424
CO_2, kinetic cooling by laser radiation 79−31621
CO_2, viscosity, density expansion near critical temp. 80−53909
Cs, dense plasma near saturation line elec. cond. 80−38559
H_2, electron swarm transport coeffs. determ. by Boltzmann and Monte Carlo methods 79−90359
H_2-He mixture, collision integrals, modelling of spacecraft entry into Jupiter atmosphere 78−71413
H_2-N_2(Ar), correl. between kinetic theory of thermal cond. and expt., 90 to 300K, 1 bar 79−81707
He, dense gas, transport eqns., shear viscosity and acoustic vel., quasi-particle kinetic eqn. calcs. 80−53906
He, elec. breakdown by pulsed high freq. field, electron distrib. function *(Russian)* 80−14876
He-Ar, gas mixtures, thermal cond. meas. in the range 0.5-15 MPa 80−14874
He-N_2, correl. between kinetic theory of thermal cond. and expt., 90 to 300K, 1 bar 79−81707
He+CO(HCl), effective pot. and coupled states approx., differential and gas kinetic cross sections 77−61827
Mg atoms, cooling to broad band reson. light press. 80−48835
N_2(-CO_2 mixture) jet, molecular rot. level population during condensation 79−86481
NH_2D, heat cond. gas, nonequilib. vel. distrib. function, laser absorption obs. 78−22448
Ne-Ar, gas mixtures, thermal cond. meas. in the range 0.5-15 MPa 80−14874
Ne-Ar-Kr, gas mixtures, thermal cond. meas. in the range 0.5-15 MPa 80−14874
O_2, thermal conductivity, calcs. 79−37434
SF_6, equilib. composition and transport props., 300 to 15000K 77−24051
SF_6+H_2 mixture, equilib. composition and transport props., 300 to 15000K 77−24051
Xe, gas, two-body time correls., Van Hove scatt. function meas. 80−100053
Xe, thermal cond., 500 to 2400K, interatomic pots. 77−39393

kinetic theory of liquids *see kinetic theory; liquid theory*

kinetics of chemical reactions *see reaction kinetics*

kink bands
camphor, rhombohedral, polycryst., compressive deform. and dynamic recrystn. 80−71698
creep and dislocation velocities 78−95783
dislocation damping during electron irradiation, new model for peaking effect 78−87683
dislocation kink stationary propag. 80−2016
dislocation structure and orientation gradient development 79−90667
Frenkel-Kontorova system, discreteness effects, perturbation formalism, Peierls pot. and kink vel. reduction 80−34001
ice, dislocation vel. theory, glide plane influence 80−79805
jog-kink interaction, nonlocal continuum theory 77−59043
kyanite, deformed, defect struct. 77−31668
metals, Snoek-Koster relaxation, theory 80−16369
polyethylene, oriented chain-extended, Young's modulus, fracture and compression behavior 80−11747
polyethylene, ultradrawn linear, kink bands by compression, interfibrillar motion 79−24581
rocks, ultimate locking angles for conjugate and monoclinal kink bands 78−88821
semiconductors, covalent, quantum mechanics of dislocation kinks 77−19951
steel, mild, Luders band front 78−3168
Ag, FCC crystal, stress-strain curve, stage I to stage II transition *(Japanese)* 78−19834
$BaTiO_3$, deform. and stress relax. of single crysts. 77−59542
CsI, exam. of kinking process, using cholesteric liquid crystals 80−7629
Cu alloys, jog formation and glide on dissociated dislocations, direct obs. 77−68977
Cu FCC crystal, stress-strain curve, stage I to stage II transition *(Japanese)* 78−19834
Cu-Ge (1 at.%), FCC crystal, stress-strain curve, stage I to stage II transition *(Japanese)* 78−19834
MgO, Peierls mechanism for dislocation motion, formation of double kinks 77−68973
Nb, deformed polycryst., γ-peak obs. and interpret. in internal friction, 300-500K 80−81098
$(SN)_x$, deform. and defects, lattice strain, fibrillation 80−3139
$(SN)_x$, kink bands, deform. and defects 79−52308
Si, heavily doped, electronic effects on dislocation velocities 77−62531

kinoforms *see computer-generated holography*

Kirchhoff adders *see summing circuits*

Kirkendall effect *see diffusion in solids*

kitchen appliances *see domestic appliances*

KKR calculations
A15 compounds, band theory, semiself-consistent band calcs. 78−2406
adsorbates, photoexcitation theory rel. to angle-resolved UPS and surface EXAFS 80−39426
atomic sphere approximation, one electron energy states 77−72811
crystal surface, band structure calc., multi-scattering method 80−2439
crystals, matching Green function method 77−85129
Cu_cNi_{1-c}, soft X-ray emission spectra 78−95620
deformation potentials calc. by Green's function method 79−1568
disordered solid, l-depend. pseudopot. in theory of band struct. 78−84124
disordered system electron energy system, calc. methods 80−75485
free electron Green function singularities 78−10320
fundamental Korringa-Kohn-Rostoker eqn. version of coherent potential approx. 80−59847
HEED, band theory, zone axis crit. voltage effect 78−83659
HEED atomic string approximation use in obtaining dispersion surfaces 80−100143
KKR-CPA equations, numerical solution 80−44474
metal, chemisorption, theoretical models, chemical and solid state approaches 78−18911
momentum matrix element calc. using Green's function method 77−1351
relativistic KKRZ theory of energy bands of heavy solids 79−82512
relativistic multiple scattering method 77−20214
structure constants, electronic struct., KKR calc. 80−80152
transition metal, model potential, generalised APW formulation 78−91579
transition metal, one-electron theory, atomic sphere approx. to KKR and LMTO methods 78−91584
transition metal carbonitrides, carboxides and oxynitrides, electronic struct., theoretical approach 80−54584
transition metals, 3d, ferromag., itinerant electron magnetism, magnetic excitation props., theory 80−34581
transition metals, chemisorption on, theoretical model, formalism 80−6651
transition metals, liq., electronic struct. and transport props. 80−29314
Ag, deformation potentials for isotropic strains 79−42506
Ag, electronic and mag. structure calcs. of mag. impurities 80−80213
Ag-transition metal, dil., mag. impurities, electronic struct., KKR-Green's function calc. 80−65783
AgI, FCC and γ phase, electronic struct., relativistic KKR calc. 77−85140
Al (111), ordered O overlayer, angle-resolved photoemission, band struct. 80−40229
Al, energy bands, densities of states and X-ray spectra, superposed self-consistent pots. 78−39010
β-Ce, electronic energy band calcs. by KKR method 79−95317
Co-Al, band struct. and density of states, KKR method and X-ray meas. 80−10863
Cr, band structure and Fermi suface of paramag. solid *(Russian)* 79−65375
Cr-Al, band struct. and density of states, KKR method and X-ray meas. 80−10863
CsAu, photoelectron spectroscopy and energy bands calc. 78−76581
Cu, crystalline FCC, theoretical tensile strength, three separate first-principles calcs. 80−50683
Cu, deformation potentials for isotropic strains 79−42506
Cu, electronic and mag. structure calcs. of mag. impurities 80−80213
Cu-Ni, alloys, electronic states, KKR-CPA calc. 78−84125
Cu-Ni, soft X-ray emission and local densities of states 79−83059
Cu-Ni(Zn)(Ga)(Ge), dil. impurity electron struct., self-consistent Korringa-Kohn-Rostoker Green's function calc. 79−78040
Cu-transition metal, dil., mag. impurities, electronic struct., KKR-Green's function calc. 80−65783
CuBr(Cl)(I), energy bands, relativistic KKR method, UV absorpt. spectra 80−39501
Cu_cNi_{1-c}, solutions of KKR-CPA equations for paramagnetic alloys 78−95256
Cu_xNi_{1-x}, paramag., electronic struct., atomic sphere approx. to KKR-CPA 79−19502
Eu, band struct. and Fermi surface 77−62814
Fe, electronic band struct., generalised k.p. interpolation method 80−6709
Fe, ferromag., effect of pressure on electron struct. *(Russian)* 79−77987
Fe-Al, band struct. and density of states, KKR method and X-ray meas. 80−10863
FeAl B2 struct., band struct. and density of states, KKR calc. 78−63969
$Fe_{76}P_{24}$, amorphous alloy, electronic struct., KKR calc. 80−96775
Gd, band structure and Fermi surface using KKR formalism 79−77993
Gd, HCP, ferromag. band struct. and Fermi surface, KKR band calcs. 77−62815
HfC, quasi-self-consistent energy band structures using relativistic KKR calcs. chemical bonding 79−51484
HfC_xN_{1-x}, X-ray valence photoelectron spectrum, 4f signal calc. 80−66391
Hg, expanded fluid, opt. gap, KKR band calcs. 77−1354
Hg, expanded liq., electronic props. 77−55477
In, Fermi surface dimensions, ab initio KKRZ calc. 77−89686
In, Fermi surface dimensions, RF size effect meas., KKRZ calc. 77−89687
In, relativistic energy bands, density of states, and optical spectra, KKRZ calc. 79−51478
Mg, bandstruct. using potentials with exchange and correlation 79−11060
Mo ternary chalcogenides, supercond., band struct., muffin-tin orbitals and atomic-sphere approx. 78−51871
MoS_2, KKR calc. of energy bands 80−34355
α-$MoTe_2$, KKR calc. of energy bands 80−34355
Nb, de Haas-van Alphen study of Fermi surface, cyclotron effective masses, mag. breakdown effects, KKR calcs. 78−43288
Nb, deformation potentials calc. by Green's function method 79−1568
Nb, Fermi surface, Fermi velocity, electron-phonon interaction parameter 79−7778
Nb, high field de Haas van Alphen spectroscopy compared with KKR calcs. 79−73425
$NbSe_2$, KKR calc. of energy bands 80−34355

KKR calculations continued
Ni, ferromag., effect of pressure on electron struct. *(Russian)* 79−77987
Ni, liquid, electronic struct. and transport props. 80−29314
Ni-Al, band struct. and density of states, KKR method and X-ray meas. 80−10863
NiH_x, electronic band struct. and interatomic bond 78−43295
Pd, dil. alloy, electronic struct. calc. using KKR method 80−15438
Pd, electronic structre, Compton scatt., soft X-ray emission and X-ray photoelectron spectra 79−77999
Pd, high field de Haas van Alphen spectroscopy compared with KKR calcs. 79−73425
Pd, phonon linewidths and electronic mass enhancement, electron-phonon contrib. 79−95099
Pd-Cu compound, KKR electronic struct. 80−59864
Pd_cAg_{1-c}, possibility of superconductivity 80−10862
Pt, Fermi surface 78−47693
Pt, high field de Haas van Alphen spectroscopy compared with KKR calcs. 79−73425
PtTe, electronic struct., self-consistent and non-self-consistent band calcs. 80−44499
RbAu, photoelectron spectroscopy and energy bands calc. 78−76581
Sc, band structure, density of states, absorpt. spectra, KKRZ calc. 80−70593
ScCl, electronic struct., self-consistent and non-self-consistent band calcs. 80−44499
ScH_2, electronic struct., band theory 79−78006
ScH_2, self-consistent bond struct., charge transfer 80−49590
ScH_2, self-consistent energy bands, KKR method with Hedin-Lundqvist approx. 80−49593
TaC, quasi-self-consistent energy band structures using relativistic KKR calcs. chemical bonding 79−51484
TaS_2 (1T), generalised electronic suscept. and CDW 77−43471
$TaSe_2$ (1T), generalised electronic suscept. and CDW 77−43471
Tc, band structure calc., effect of correlation 79−60699
Tc, Fermi surface, constant-energy-search KKR band theory calc. 77−89689
TiC_xN_{1-x}, (O_{1-x}), electronic struct., KKR-ATA method 80−65447
TiN_xO_{1-x}, electronic struct., KKR-ATA method 80−65447
UC, quasi-self-consistent energy band structures using relativistic KKR calcs. chemical bonding 79−51484
$U_xTh_{1-x}As$ (Sb), electronic struct., relativistic KKR-averaged T-matrix approx. method 80−107702
V-Al, band struct. and density of states, KKR method and X-ray meas. 80−10863
YH_2, electronic struct., band theory 79−78006
YH_2, self-consistent energy bands, KKR method with Hedin-Lundqvist approx. 80−49593
ZrB_2, self-consistent band struct., XPS, reflectance, NQR, Hall effect and density of states meas. 80−107689
ZrBr(Cl), electronic struct., self-consistent and non-self-consistent band calcs. 80−44499

klystrons
see also reflex klystrons
Darmstadt linear accelerator high resolution scatt. facility 78−70653
electron synchrotron storage ring RF power supply *(German)* 78−17453
EPR spectrometer, 2 mm band, with re-entrant resonator 78−86311
ETL linear electron accelerator, energy increased up to 40 MeV by improvement of klystron efficiency *(Japanese)* 78−78515
far IR laser line frequency meas. by klystron harmonic comparison 77−7113
frequency-agile phase lock system for mm wave klystrklystron 77−5446
gyrotrons and gyrokylstrons, small signal theory, fusion reactor appl. 78−70633
harmonic generation of subMM radiation, monochromatic, simple tunable source 80−5788
heavy ion beam buncher control system 79−72148
high-power low-freq. klystron as drive for LAMPF Alvarez sections 77−83174
laser frequency measurement using supercond. point contacts 80−90824
MM-wave, for radiospectroscopy, phase stabilisation 77−5456
particle accelerator, power supply system transient behaviour theory *(German)* 78−5077
power capabilities for plasma heating *(French)* 78−9801
power transmission system design, for solar satellite power system 79−52893
pulsar magnetosphere, vibrations generation by klystron mechanism 78−53971
quasioptical superheterodyne radiometer for upper atmosphere 77−41241
self excited oscillator with short time delay microwave pulse 77−6578
stabilizing resonator of high-power klystron self-oscillator for microwave supply system of linear accelerator 80−42878
UHF, 600 kW, for particle acceleration and plasma heating *(German)* 80−106211
UHF klystron, high efficiency, high power, performance at SLAC PEP storage ring 77−83296
UHF TV klystron, pulsed operation for lower hybrid heating in ATC machine 78−66404

Knight shift
see also nuclear magnetic resonance
alkali metals, magnetic property volume depend., Knight shifts, electron spin response 80−88729
alkali metals, muon Knight shift 79−56656
alkali metals, positive muon spin rotation frequency, Knight shift meas. 79−38421
alkaline earth metals, muon Knight shift 79−56656
alkaline earths, positive muon spin rotation frequency, Knight shift meas. 79−38421
alloys, d-metal, magnetic susceptibility and Knight shift meas. 80−66055
chalcogenide, charge transfer, influence of cryst. field 79−99516
diastereomeric compounds, nonrigid mols., in soln., conform. determ., NMR, lanthanide shift reagents 77−30887
dilute alloy with impurity ion of Z>83 77−12275
Fermi surface points with changing topology, Knight shift theory *(Russian)* 80−34794
ferromagnetic alloys, conc., spin fluctuations, SCR theory and CPA calcs. 78−64290
graphite intercalation compound, LiC_6, ^{7}Li NMR *(French)* 78−35050
graphite lamellar cpds., ^{13}C NMR studies 80−44936
linear conductor, dynamical aspects of fluctuations 79−33715

Knight shift continued
liquid metal, electron states, esp. opt. and mag. props., review 78−2882
liquid metals, nonlocal pseudopot. calc. of Knight shifts 78−91965
liquid metals, review of research, phys. aspects, Knight shift, elec. resist. *(Dutch)* 77−7657
liquid metals and alloys, review 78−2755
metal, muon screening spherical solid model 79−56654
metal, spherical solid model for muon and H in metals 79−78601
metal enhancement factor for strong electron correl., Gutzwiller theory at finite temp. 77−43527
metal-H system, NMR depend. on struct., H diffusion and electronic struct., book contrib. 79−82887
metals, hyperfine fields at positive muons 78−43758
metals and alloys, pseudopotential investigation of phys. props. 77−43526
Ni-Pt-P, metallic glass, electronic structure, pulsed NMR study 80−75869
nuclear isomeric states, time gated stroboscopic method 78−43660
nuclear orientation and NMR of oriented nuclei, appl. to solid state magnetism, review 80−44928
one-dimensional disordered spin system with isotropic antiferromag. interaction, susceptibility and Knight shift *(Russian)* 78−88202
paramagnet, free electron, muonic and hydrogenic Knight shifts 78−43759
pnictides, charge transfer, influence of cryst. field 79−99516
positive muon spin rotation frequency, Knight shift meas. 79−38421
rare earth chalcogenides, cryst. field splitting, press. depend. 80−24852
rare earth Cu_2Si_2, interconfiguration fluctuation system, NMR meas. 80−15817
rare earth monopnictides, Knight shift systematics 78−43661
rare earth pnictides, cryst. field splitting, press. depend. 80−24852
(rare-earth)Al_2Ga_2, synthesis, NMR and X-ray absorpt. studies 80−108083
simple metal, Knight shift, single-ion approach 80−44935
solid, hydrostatic pressure shifts, appl. of parametrisation 78−72120
superconductors, surface relax. time of conduction electron spins 78−91814
TCNQ salt, Qn(TCNQ)$_2$, one-dimens. spin glass with antiferromag. exchange, Knight shift meas. 80−25231
transition metal group VIII aluminide, NMR near equiatomic composition *(Russian)* 80−20479
triplet exciton contrib. 77−59472
Ag_2F, NMR of ^{109}Ag and ^{19}F, modified Korringa relation in two-dimens. metal 80−93199
Al particles, supercond., Zeeman crit. field, NMR spin echo meas. 79−56453
Al small particle, NMR study, Knight shift, spin-lattice relax. time, supercond. effects 80−39710
Al-Li, dilute substitutional alloy, impurity Knight shift and electric field gradient 80−44940
Al-Mn, dil., ^{54}Mn Knight shift meas. using nucl. orientation 78−68396
Al-Ni (10 to 70 at.%). NMR of ^{27}Al *(French)* 77−51974
Al-Ni system, Knight shift, NMR line widths determ. *(French)* 77−77113
Al_2O_3 void formation by fast neutron irradiation, TEM exam., and Knight shift expts. 78−51591
As, muonic Knight shift, temp. and mag. field depend. 79−91331
Au-Co, dil. alloy, crystalline electric field and spin-orbit splitting, NMR results 77−32274
Au-Co, liquid alloys, ^{59}Co NMR studies 79−95660
Au-V Kondo alloys, mag. susceptibility and NMR Knight shift in conc. independent region 77−77027
$AuGa_2$ film, supercond., mag. susceptibility and Knight shift press. depend. 77−43777
Be, electronic struct., NMR study 80−108085
Be, Knight shift of μ^+ 79−56657
$Be_{1-x}Mn_x$, Be-rich, NMR and paramag. susceptibility 80−71206
BeNi, dil., electronic struct., NMR study 80−108085
Bi, muonic Knight shift, temp. and mag. field depend. 79−91331
Bi-BiI_3 mixture, molten, NMR meas. 77−51976
Cd, temp. depend. Knight shift 80−2655
n-CdSe, ^{113}Cd and ^{77}Se Knight shifts, impurity carrier wavefunction 78−35049
Ce intermetallics, CeX_2Si_2 (X=Cu, Ag, Au), ^{29}Si NMR and mag. susceptibility 79−61246
CeAs, evidence for valence fluctuations, ^{75}As Knight shift data 78−91966
$CeCu_4$ Knight shifts and mag. susceptibility 79−95656
$CeCu_5$, Knight shift and mag. susceptibilities 79−95656
$CePt_3$, ^{195}Pt NMR and susceptibility meas. 77−63299
$CeSn_3$, valence instabilities 79−78546
Co, NMR in paramagnetic and ferromagnetic states, crit. nucl. relax. 79−56622
Co-based Heusler alloys, Co_2TAl, (T=Ti, Zr, Hf), paramag. state NMR and susceptibility meas. 79−65643
Co_xGa_{1-x}, NMR expts. interpretation 80−75870
$Co_{1-x}Ni_xAl$, Knight shift and mag. susceptibility study, electron struct. peculiarities *(Russian)* 80−15814
CoS_2, microscopic mag. props., NMR meas. 79−91306
$CoSe_2$, bulk mag. susceptibility, anomalous temp. depend., NMR and X-ray diffr. meas 79−87229
$CoSe_2$, temp. induced local mag. moments, ^{59}Co NMR 79−65747
Co_2TiAl, paramag., ^{59}Co NMR 78−2760
$Cr_{1-x}V_xCo$, mag. state of Co impurity, NMR exam. 78−27100
CsAu, semicond. and metallic, NMR line shape, Knight shift, X-ray diffr. study 78−68402
Cu:Cr(Mn)(Fe), NMR satellite data rel. to impurity struct. 78−35052
Cu-Cr, dil., spin-density magnetisation near Cr atoms, NMR study 80−80626
Cu-Cr, dil. alloy, Knight shift temp. depend., electronic struct. 78−84488
Cu-Cr(Mn)(Fe), dil., NMR satellite data, rel. to electronic struct. 78−68398
Cu-Cr(Mn)(Fe), dil., NMR data, ionic model and Kondo temp. 78−68399
Cu-Fe alloys, Kondo system, static and dynamic susceptibilities, NMR and Mossbauer spectra 77−63090
Cu-Fe group, dil., NMR satellite data calc., struct. of mag. impurities 80−103894
Cu-V, dilute, Knight shift of ^{51}V reson., and host satellite resonances 77−85594

Knight shift continued
CuV_2S_4, preparation, cryst. struct. and physical props. *(French)* 79−55714
Fe, BCC, high field Knight shift and hyperfine anisotropy of ^{57}Fe 80−71205
Fe, nuclear orientation and NMR/ON on implanted ^{114m}In 79−47345
$Fe_{1-x}Co_xAl$, Knight shift and mag. susceptibility study, electron struct. peculiarities *(Russian)* 80−15814
$Fe_{1-x}Ni_xAl$, Knight shift and mag. susceptibility study, electron struct. peculiarities *(Russian)* 80−15814
Ga, liq., Knight shift of ^{69}Ge 77−12271
Ga, liq., nucl. acoustic reson. Knight shift, rel. to spin-lattice relax. 78−19351
Ga, NQR, press. depend. of elec. field gradient and Knight shift tensors 78−19366
$Gd_2Co_6Al_{11}$, ^{27}Al Knight shift, mag. susceptibility 79−15367
$Gd_2Cu_6Al_{11}$, ^{27}Al Knight shift, mag. susceptibility 79−15367
$GdRh_4B_4$, magnetic and electrostatic props., NMR study 80−93195
Ge:As, NMR, conduction electrons in impurity band, metal-nonmetal transition 79−78544
$H_{1.6}MoO_3$ bronze, proton shift tensors PMR meas. 80−71202
$HfV_2H_{2.1}$, proton NMR relax. time and Knight shifts, diffusional activation energies meas., sorption props. 80−75871
Hg, expanded liq., band model for electronic struct., Knight shift and electronic transport 77−89690
Hg, liquid, expanded, Knight shift interpretation in terms of electronic struct. and transport 77−43895
Hg:^{212}Rn, Knight shift and absolute mag. moment meas. in ^{212}Rn 78−37278
$Hg_{2.86}AsF_6$, linear chain compound NMR exam. 78−19359
$Hg_{3-x}AsF_6$, incommensurate chain compound, anisotropic Knight shift, spin-spin interactions 78−80233
In-Hg, liq., Knight shift of ^{115}In, temp. and conc. depend. 79−47343
InBi, Knight shift and quadrupole interaction of ^{115}In 77−55717
InBi single crysts., Knight shifts and quadrupole interaction 80−84662
$In_{1-x}I_x$, molten mixture, NMR, reson. shifts, relax. rates, quadrupole relax. 80−2654
InP:Te, mag. props. of conduction electrons 78−6510
K, conduction electron contrib., band struct. calcs. 77−1359
K, Pauli susceptibility and Knight shift meas., electron wave functions 80−44937
$K_2Pt(CN)_4Br_{0.3}3.2H_2O$, linear conductor, dynamical aspects of fluctuations 79−33715
La, FCC, NMR 4.2 to 296K, mag. susceptibility and sp. ht. 80−15813
LaAg, electronic struct., susceptibility, sp. ht. and Knight shift meas. 77−43485
$LaH_{2.69}$ ^{139}La NMR, Knight shift 79−91307
La_3In, mag. susceptibility and normal state NMR meas. 78−31118
$LaNi_5H_x$, μ^+ spin relax. and Knight shift 79−56699
$LaPt_3$, ^{195}Pt NMR and susceptibility meas. 77−63299
La_3Tl, mag. susceptibility and normal state NMR meas. 78−31118
Li, Knight shift volume depend. 80−84663
Li-Cd alloy, liq., elec. resist. and Knight shift 80−75537
Li-In, liquid alloy, elec. resist., Knight shift of ^{115}In and ^{7}Li nuclei 79−11352
Li-methylamine solution, NMR investig. of metal-nonmetal transition 77−40142
Li-NH_3 concentrated solution, NMR relaxation of ^{7}Li 80−108084
$LiCd_{1-x}Tl_x$, intermetallic, X-ray and Knight shift meas. of ^{205}Tl and ^{113}Cd 79−42851
$LuRh_4B_4$, magnetic and electrostatic props., NMR study 80−93195
Mg, electric field gradient and Knight shift, temp. depend., OPW calcs. 78−56387
α-Mn, localised spin fluctuations, Knight shift obs. 80−60181
α-Mn, NMR and susceptibility max., paramag. phase 78−56386
MnSi, μ^+ Knight shift, temp. depend. 78−80270
MnSi, μ^+ probe, itinerant electrons spin fluctuations 79−56671
MnSi, NMR and susceptibility above T_c 78−43665
Mo, Knight shift and mag. susceptibility, temp. depend. *(German)* 78−10791
Mo, Knight shift and mag. suscept. temp. depend. 78−15043
Mo-Co Kondo alloy, Co impurity susceptibilities, Knight shift 80−88721
$Mo_{1-x}Re_xCo$, mag. state of Co impurity, NMR exam. 78−27100
$(Mo_{0.5}Ru_{0.5})_{80}P_{20}$, amorphous normal and mixed supercond. state, ^{31}P NMR 79−87193
Mo_6S_8Sn, triple chalcogenide, NMR spectra in supercond. state *(Russian)* 80−93194
Mo_6Se_8Sn, triple chalcogenide, NMR spectra in supercond. state *(Russian)* 80−93194
$Mo_{1-x}V_x$, supercond., NMR and mag. susceptibility meas. 79−56388
Na-Li, liq., Knight shift calc. by multiple scatt. Xα method 80−54961
Na_xWO_3, $(0.22 \leq x \leq 0.84)$, ^{183}W NMR, electronic struct. near metal-semicond. transition, Knight shift 78−48063
Na_xWO_3, Knight shift, spin-lattice and spin-spin relax., high press. NMR obs. 80−50211
Nb, NMR study up to 1700K, Knight shift and spin-lattice relax. time 80−2653
Nb-Al, A15 and σ-phases, supercond. and normal state electronic props. 77−43765
Nb-Al alloy, σ-and A15-phases, Knight shift and supercond. 77−15984
Nb-Pt, A15- and δ-phases, Knight shift of ^{195}Pt meas. 78−19350
NbD, orthorhombic β phase, ^{93}Nb Knight shift and quadrupole coupling parameters 78−19352
NbH, orthorhombic β phase, ^{93}Nb Knight shift and quadrupole coupling parameters 78−19352
$NbH_{0.026}$, nucl. acoustic reson. of interstitial H 79−51867
NbH_x, proton Knight shift and mag-suscept., high resolution meas. 77−55716
$NbSe_2$, 2H phase, layered type II supercond., NMR meas. 77−36024
$NbSe_2$ (2H), CDW amplitudes determ. by ^{77}Se NMR 77−77116
$NbSe_2$ (2H), charge density waves state, NMR meas. 78−39421
$NbSe_2$, charge density wave state, NMR meas. 77−8430
$Nb_{1-xy}V_xyH_x$, interaction between interstitial H and V, NMR meas. 77−59471
Ni, band structure, μSR Knight shift meas. 79−56663
Ni, critical NMR obs. near mag. transition 77−81026
Ni, ferromag., Knight shift of hyperfine field at positive muon 77−43925
Ni:^{192}Ir, NMR/ON, resonant freq. shift with applied field 77−28462
Ni-P alloy, amorphous, NMR expts. and interpretation 79−8060
Knight shift continued
Ni-Pd-P, metallic glass, electronic structure, pulsed NMR study 80−75869
Ni-Pd-P, Ni-Pt-P, amorphous and electronic structs., NMR Knight shifts and linewidths meas. 78−68400
NiPB amorphous alloys, ^{31}P and ^{11}B NMR near paramag.-ferromag. transition 79−33558
$NiSe_2$, paramag. props., NMR, mag. susceptibility 80−60175
^{61}Ni, paramag. solid and liq. phases, nucl. spin relax. and Knight shift 78−76327
P+Nb, dil. alloy, NMR obs. of ^{93}Nb 80−71203
Pb:^{215}Ra, abs. mag. moment of $(h_{9/2})^n$ proton states from Knight shift obs. 77−82821
$Pb_{1.125}Mo_6Se_{7.5}$, Chevrel phase supercond., NMR study 80−49989
PbTe, phase convection for effective g-factors and role of g-factors in Knight shifts 79−51473
Pd, Knight shift calcs. 79−56620
Pd, metallic, positive muon Knight shift 80−71280
Pd-Fe alloy, NMR of ^{27}Al meas. 77−12215
Pd-Fe and Pd, muon$^+$ Knight shift, cond. electron polarisation, RKKY oscill. 77−66450
Pd-Mn alloy, NMR of ^{27}Al meas. 77−12215
Pd-Ni alloy, NMR of ^{27}Al meas. 77−12215
Pd-Rh, dil., hyperfine anomaly between bound negative muon and Rh nucleus 79−56707
PdNb, dilute, NMR obs. of ^{93}Nb 80−71203
$PrCu_4$ and $PrCu_5$, Knight shift, mag. susceptibilities 79−95570
PrN, compressibility, mag. susceptibility and NMR freq. shift meas. 77−85595
$PrPt_3$, ^{195}Pt NMR and susceptibility meas. 77−63299
PrSb, compressibility and NMR freq. shift 77−85595
Pt, Knight shift and spin-lattice relax., up to 1358K 78−72425
PtV, dil. alloys, NMR obs. of ^{51}V 80−71203
RbAu, NMR line shape, Knight shift, X-ray diffr. study, struct. props. 78−68402
Sb, muonic Knight shift, temp. and mag. field depend. 79−56659
Sb, muonic Knight shift, temp. and mag. field depend. 79−91331
Sc-Ag(Cu)(Pd)(Rh)(Ir)(Ru), electronic struct., susceptibility, sp. ht. and Knight shift meas. 77−43485
Sc_3In, itinerant electron ferromag., NMR and relax. 78−6586
SmB_6, intermediate valence, ^{11}B NMR study 80−93193
$SmSn_3$, NMR Knight shift, extension to low temp. 77−20735
Sn small particles, electron level quantisation effects, Knight shift meas. of electron spin susceptibility 78−2624
Sn, white, nuclear acoustic reson., Knight shift 80−71204
$Sn_{0.5}Eu_{0.5}Mo_6S_8$, supercond., spin polarisation, NMR, Mossbauer effect and bulk magnetisation meas. 77−43782
SnTe:Mn, NMR shift meas. 80−97154
TTF-TCNQ, ^{13}C Knight shift and spin-lattice relax. meas., local susceptibility determ. 77−4571
Ta, nucl. acoustic reson. determ. 79−51868
TaH_x, proton Knight shift and mag. suscept., high resolution meas. 77−55716
Ta_6SH_x, H locations and motions, PMR linewidth meas. 77−77115
$TaSe_2$ (2H), CDW amplitudes determ. by ^{77}Se NMR 77−77116
Te, diffusion and cond. props., NMR investigation 79−78547
Te, enriched with ^{125}Te, spin-lattice relaxation and Knight shift, high temp. behaviour 77−1614
Te, NMR spectrum, electron paramagnetism and atomic self-diffusion mechanism 78−72426
ThC_xN_y, NMR, Knight shift and spin-lattice relax. 80−100621
$Ti_{1-x}Nb_xH_{1.94}$, electronic struct. MNR meas. 80−15439
$TiSe_2$, electronic instability, ^{77}Se NMR 78−10790
$(Ti_{1-x}V_x)_2O_3$, susceptibility and ^{51}V NMR expts., spin glass behaviour 77−66369
Tl:^{212}Fr, abs. mag. moment of $(h_{9/2})^n$ proton states from Knight shift obs. 77−82821
$UC_{1-x}N_x$, NMR of ^{13}C and ^{15}N, 5f electrons nature, mag. susceptibility, spin fluctuations 77−20736
UCu_5, mag. props. and NMR 77−20734
$UNi_{5-5x}Cu_{5x}$, NMR and press. effects 80−25230
U_3P_4, Knight shift, paramag. susceptibility 77−66430
VB, nuclear quadrupole parameters 80−103896
$V_{1-x}Ga_x$, nuclear spin-lattice relax. and supercond. 79−56387
V_3Ga, NMR and mag. suscept. *(Russian)* 78−39420
VH_x, Knight shift and spin-lattice relax. of proton NMR, local electronic environment of protons 77−16194
VH_x, proton Knight shift and mag-suscept., high resolution meas. 77−55716
V_2(Hf,Zr), NMR and mag. susceptibility, density of states determ. *(Russian)* 80−66053
V_2Hf, NMR meas., mag. susceptibility, Knight shift and elec. field gradient determ. *(Russian)* 78−23359
$V_{0.62}Ir_{0.38}$, supercond., Knight shift contrib. to reson. line shift meas. 77−4467
$V_{2-x}Nb_3Hf$, NMR of ^{51}V and mag. susceptibility, 20-300K *(Russian)* 80−93192
$V_{0.76}Pt_{0.24}$, supercond., Knight shift contrib. to reson. line shift meas. 77−4467
$V_{1-x}Pt_x$, A-15 struct., Knight shift in normal state, upper crit. field curves *(French)* 78−43519
V_3Pt, supercond., Knight shift contrib. to reson. line shift meas. 77−4467
V_3S_4, and V_5S_8, itinerant antiferromag. spin fluctuations, NMR studies 80−93198
V_3S_4, antiferromag. order, ^{51}V NMR spectrum 79−56625
VSe_2, CDW states, correl. mag. and transport props. 79−73494
VSe_2, CDW states, intrinsic mag. props., mag. susceptibility and NMR obs. 78−68397
V_3Se_4, antiferromag. order, ^{51}V NMR spectrum 79−56625
V_3Si, exam. of superconductivity and props. 79−1649
V_3Si, NMR meas. near struct. transform. *(Russian)* 80−44942
V_3Si, NMR of ^{51}V above and below 21K struct. transition *(Russian)* 80−34796
V_2Ta, NMR meas., mag. susceptibility, Knight shift and elec. field gradient determ. *(Russian)* 78−23359
V_2Zr, NMR meas. mag. susceptibility, Knight shift and elec. field gradient determ. *(Russian)* 78−23359
W, Knight shifts obs. with 6.2 keV ^{181}Ta Mossbauer resonance 79−11369

Knight shift continued
W, with H adatoms, PMR meas. of adsorption state, surface migration 78−10275
Y, low temp. Knight shift meas. 77−28466
$(Y_{1-x}Gd_x)Co_2$, spin echo NMR of mag. states 80−7190
YRh, electronic struct., susceptibility, sp. ht. and Knight shift meas. 77−43485
$YbAl_3$, valence instabilities 79−78546
Zn, HCP metal, pulsed ^{67}Zn NMR studies at 4.2K 79−91315
Zn, liq., NMR and relax. 79−8061
Zn, liq. Knight shift, temp. depend. 78−80232
$Zr_{0.9}Fe_{0.1}V_2$, NMR and mag. susceptibility 78−95527
$ZrMn_2H_x$, proton NMR relax. time and Knight shifts, diffusional activation energies meas., sorption props. 80−75871
$Zr_{1-x}Nb_xZn_2$, microscopic mag. props., NMR investigation 80−15807
$Zr_{0.99}Pt_{0.99}V_2$, NMR and mag. susceptibility 78−95527
ZrV_2, Knight shift vs. susceptibility plot 80−75712
ZrV_2, NMR and mag. susceptibility 78−95527

Knudsen flow
aerosol, high Knudsen number, coagulation rate measurement 80−71954
aerosol particles, large, diffusional phoresis theory 79−55408
aerosol photophoresis, low Knudsen number spherical particles 77−63965
angular number distribution function, Knudsen flow through single and double-slit orifices 80−53816
binary gas mixture, vel. slip and temp. difference in free-jet expansion 80−14774
Boltzmann equation, soln., for small Knudsen nos. *(Russian)* 77−61033
Boltzmann equation, solution for small Knudsen numbers 79−81924
Boltzmann equation, solution for small Knudsen numbers 79−81925
Boltzmann equation, solution for small Knudsen numbers 79−81926
boundary conditions for gasdynamic eqns. in presence of evap., condensation and chem. reactions 77−47042
diffusion through noncircular pores 78−14076
dilute gas transport processes over whole range of Knudsen numbers, general theory 79−86467
drop growth in atmosphere by condensation, cloud physics appl. 79−44216
effusion cell, high temp. mass spectroscopy, thermodynamic and physicochemical behaviour, review 80−52354
effusion chamber with low axial temp. gradient for high temp. thermodynamic tests 77−71329
effusive beam source, heterogeneous reaction type, chem. equilib. 80−52362
equilibrium pressure of gaseous components, metallic refractory compounds, determ. by Knudsen method 79−52529
evaporation from capillary pore, mass transfer kinetics 78−51233
external potential field, Boltzmann eqn. 77−3848
gas, in contact with condensed phase, hydrodynamic eqn. and slip boundary condition 80−14791
gas creep along solid surface, half-space moments method calcs. 78−67222
gas dynamics eqn. boundary conditions in Chapman-Enskog Boltzmann eqn. soln. 80−96284
gas flow over cylinder at low speeds under constant force, kinetic theory description 80−79354
gas flows, entropy prod. determ. using Boltzmann's H-theorem, Knudsen effusion 80−106867
gas kinetic boundary value problem, non-equilibrium thermodynamics 80−19544
gas mixture in Knudsen layer, transport eqns. 77−47045
gas with rotational degrees of freedom, macroscopic description of motion *(Russian)* 78−46999
glass, porous, free molecule flow and interdiffusion 79−32658
heat transfer between two plates at unequal temp. in Knudsen gas 79−86469
high temperature gas and vapour characterisation, conf., Gaithersburg, USA (Sept. 1978) 80−53910
Knudsen layers, by linearised Boltzmann eqn. 79−98759
molecular flow, in long tubes, effect of cross-sectional shape 79−14437
molecular gas in mag. field, transport phenomena 80−33684
monatomic gas, rarefied flows in two-dimens. expansion nozzle 80−28547
multiphase mixture, two-dimens. nozzle and jet supersonic flows 80−48780
multiple barriers 78−63451
nonequilibrium free jet expansion, rotational temp. meas for N_2 80−69890
nonisothermal gas motion in plane channel, S-model kinetic eqn. 80−83816
novel Monte Carlo binning technique 79−160
nuclear reactor fuel element gap conductance, heat transfer over range of Knudsen number 78−13213
outgassing from surface, Monte Carlo method in one-dimens. 78−47001
oxide system, complex, mass-loss Knudsen effusion method for phase equilib. determ. 77−11668
packed beds, pressure drop in low Knudsen number regime 79−50792
parallel plates, isothermal heat flux, and Knudsen layer 78−5638
particle slip, temp. depend. in gaseous medium, free mol. regime 77−11249
pipes with const. annular cross section, mol. cond. calc. method 80−79353
polyatomic gas, plane Couette flow in Knudsen regime, wall induced polarisation 80−19443
polymer membrane gas permeation, pore size distrib. *(Japanese)* 78−79372
pores, periodically constricted, anal. of flow *(Japanese)* 79−72911
porous material, effect of cross sectional pore shape on Knudsen diffusion 77−24021
porous media, Knudsen to Poiseuille flow transition, capillary model 78−55689
porous media, random networks, gaseous Knudsen flow, capillary model 77−80212
porous solids, diffusion of gases, Monte Carlo simulation 80−65299
powder, Knudsen diffusion, gas diffusion relationship of Knudsen flow permeametry 77−55087
powder, Knudsen diffusion, pore size distrib. effect on surface areas obtained by diffusion meas. and Hg porosimetry 77−55088
powders, surface area measurement using Knudsen diffusional flow of gas 79−40536

Knudsen flow continued
random capillary networks, interdiffusion of gases, struct. factor calc. 78−14080
reactive gas flow through porous barrier, exit flux, composition depend. 77−31383
rectangular channels, long, Poiseuille and thermal creep flow, mol. and transition flow 77−7418
Scott effect Knudsen mol gas., thermo-mag. force on heated cylindrical body *(Russian)* 78−26235
slightly rarefied flow over specularly reflecting body, sphere and thermophoresis 77−55040
sphere, drag in low velocity rarefied gas flow 80−48752
spontaneously condensing and wet steam discontinuous flows in steam turbines, subsonic, transonic and supersonic, numerical investigation *(Russian)* 80−87800
steam, thermal cond. in large Knudsen range, theory and expt. 78−94888
structure of Knudsen layer, collision freq., Prandtl no. effect, book contrib. 80−1648
thermal accommodation coefficients from heat transfer data for low-density gases 77−35167
thermal creep for gas flow in flat channel, accommodation coeff. 77−11264
thermal creep of gas at interface, arbitrary accommodation coeff. 78−5766
thermal gas slip coeff., using Onsager symm. principle 77−58737
thermodynamic activity meas., new appl. of the Knudsen method 78−79783
torsion-effusion method, vapour press. meas., automatic data acquisition 80−52188
transition flow, macroscopic theory *(Japanese)* 80−1647
transition Knudsen regime, nonstationary heat and mass transfer, book contrib. 80−1649
two parallel plates, heat conduction, gaseous molecules bimodal two stream relaxing distrib. *(Chinese)* 80−6097
vacuum valve, Monte Carlo method for conductance 78−71398
vapour pressure measurement, effusion method, review 80−51995
viscous flow theory, exact soln. of integral eqn. 77−65764
Fe-Zn, homogeneous phases, Gibbs free energies of form., Knudsen effusion method 80−66481
^4He, superfluid, phonon heat transport and Knudsen's minimum below 0.6K 79−33136
Ni-S system, Knudsen effusion and thermodynamics 78−79759
RbI, vaporisation thermodynamics, mass-loss Knudsen effusion, mass spectrometry 79−28093

Knudsen number *see Knudsen flow*

Kohn effect *see lattice dynamics*

Kondo effect
3d element, low temp. props. 80−2569
actinide metallic systems, magnetism 80−7076
alloy, amorphous, magnetic, transport props. 79−73485
alloy, dil., thermoelec. power in asymmetric single-orbital Anderson model, perturbation calc. 79−99534
alloy, highly concentrated, Kondo effect in terms of quasi-spins 79−24134
alloy, mag. interactions 77−59385
alloy,dil., electrical resistivity, Kondo effect vs. spin glass behaviour 78−68269
alloy systems, conc., Kondo type effects, phenomenological dilution model 77−72858
alloys, dil., Kondo coupling, hyperfine and exchange interactions 79−65647
alloys, dilute, mag., press. effects 79−99676
alloys, low temp. props. book 80−3
alloys, magnetic localisation and charge oscillations 80−75781
amorphous alloys, mag. and nonmag., thermoelec. power, 15 to 580K 80−80255
amorphous ferromagnet, effective-field distrib. and resistivity minima 79−73501
Anderson model, dynamical susceptibility of impurity electrons 77−12090
Anderson model, perturbation expansion in infinite conduction bandwidth limit, Kondo temp. 79−28506
Anderson model coupled to boson field, HF approx. and RPA 77−40033
Anderson model for dilute magnetic alloys, static suscept., functional integral approach 80−50050
binary magnetic alloys, Monte Carlo calc. beyond homogeneous mol. field approx., anomalous Kondo effect 77−8308
concentrated magnetic alloys, density of states, Kondo effect, theory 80−65780
DC Josephson effect for superconducting proximity Kondo alloys 80−88690
degenerate Anderson model, Fermi liq. theory 79−19715
dilute alloy, perturbation expansion for the asymmetric Anderson Hamiltonian 80−80202
dilute alloys, Kondo temperature, lattice vibr. effect 78−19025
dilute and concentrated alloys, magnetism *(Rumanian)* 78−91843
dilute Kondo alloys, calc. of host nucl. spin-lattice relax. 78−88215
dilute local moment local magnetisation, Kondo-like deviations from free spin behaviour 80−44800
dilute magnetic alloy, configuration fluctuations 79−33449
dilute magnetic alloy, magneto-transport theory 80−15509
dilute nearly magnetic alloys, magnetoresist. calc., LSF approx. of Anderson model 77−62901
dispersion theory, in low mag. field, Hilbert problem, numerical investigation 78−84387
dispersion theory for low mag. field 78−27015
doped electrode junction, tunnelling, Kondo scatt., coherence distance 78−31001
electron dynamics, additional sp. ht. 80−15688
generating functional method appl. to dil. mag. alloy kinetics *(Russian)* 77−43579
Hamiltonians, rotationally invariant, universality and renormalisability 79−95573
Hamiltonians diagonalisation, zero-temp. mag. susceptibility 80−93078
Hamiltonians with non-zero ground-state spin 79−51746
impurity interactions, ground state calc., impurity conc. effect 80−65782
impurity interactions in system with spin glass temp. below Kondo temp. 77−66360
impurity-impurity interaction effects on Kondo resist. 78−51981

Kondo effect continued
intermediate valence, phase diagram and Kondo behaviour 80−29366
irradiated dilute alloy, containing self-interstitials and vacancies 78−60105
Kondo Hamiltonians, s-d exchange, ground states, renormalisation group calcs. 80−50046
Kondo lattice and Kondo effect 79−78312
lattice Hamiltonian, ground state props., real-space renormalisation study 80−34590
localised magnetic impurity problem, functional-integral approach, sp. ht. calc. 77−77026
low temperature nuclear orientation investigation 80−15825
low-temperature, Nozieres-Wilson relation, renormalisable quantum field theory 79−95572
magnetic alloys, dil., in finite mag. field, Suhl's dispersion eqns. 77−24673
magnetic alloys, dil., transition metal hosts, props. review 78−84417
magnetic alloys, dilute, thermopower 79−65455
magnetic impurities and Kondo effect, theoretical model 79−33455
magnetoresistance of dilute magnetic alloys, calc. 77−62918
metal, magnetic impurity, model of resonance level in Kondo problem *(Russian)* 78−80129
metal, quasimagnetic impurity, exact solution of Wolff's model 78−56105
metal with paramagnetic centres, sound absorption temp. and freq. depend. *(Russian)* 78−34827
metallic glasses, tunnelling two-level system, Kondo-like state 80−88547
metals, Kondo effect, Anderson hamiltonian 80−60187
MIM structure, zero-bias anomalies due to Kondo scatt., hopping model, mag. field effect 77−59334
mixed valence compounds, electronic levels, impurity model 79−99513
nuclear orientation and magnetisation expt. comparison 77−63297
one dimensional system, Kondo lattice and weak antiferromagnetism 77−73038
order parameter spatial variation near Kondo impurity 80−103813
phase diagram of Kondo lattice 80−7077
polarized neutron diffractoin in high magnetic fields, for Kondo systems 79−73684
potential scattering, Wilson's numerical technique 78−79972
quantal spin systems, classical representation and scaling props. of spin Hamiltonians 78−14919
rare earth alloys, Kondo effect, review 79−69506
rare earth alloys and cpds., intermediate valence, models for anomalous systems 80−96827
rare earth compounds, Kondo effect, review 79−69506
rare earth compounds, valence mixed state, Kondo lattice, Anderson localisation models *(Japanese)* 78−51945
rare earth impurities in s-band metals, Kondo anomaly 78−52208
rare earth systems, Kondo singularity, Anderson-Smith model 80−80479
rare earth systems, metallic, with unstable valence, model for thermodynamic props. 77−69487
rare earth-Al_2, cubic Laves phases, prep. and phys. props. *(German)* 78−23075
rare earth-transition metal alloys, amorphous, electronic and mag. props. 80−93093
renormalisation group approach 77−63086
renormalisation group method, zero-temp. real-space, for Kondo-lattice model Hamiltonian 78−34960
resonant level model, for soln. of Kondo problem 80−60190
scaling and multiplicative renormalising in solid state physics, review *(Hungarian)* 79−11289
single-impurity Kondo system, fluctuation conductivity 78−76064
spin 1/2 Kondo impurity, minimal effort scaling approach 79−1657
spin 1/2 Kondo system, static susceptibility and relax. rate 79−65646
spin 1/2 Kondo system, thermodynamical props. 78−52209
spin glass, resist. max. rel. to Kondo temp. and RKKY interaction 77−20307
spin glass Kondo transition resist. max. 79−19584
spin glass to Kondo transition 78−68266
spin glasses, anomalous Hall effect including Kondo effect in molecular field approx. *(Russian)* 80−34424
spin glasses under high press., resist. meas. 78−52277
steel, stainless, low-temp. electroresistance anomalies *(Ukrainian)* 77−32006
superconducting alloys, specific heat jump at transition temp. 78−6479
superconducting order parameter, spatial variations in presence of impurity near transition temp., Anderson model calcs. 79−38245
superconducting proximity effect and Kondo alloys 78−19190
superconductive tunnelling study of localised bands 78−10613
superconductivity, magnetic impurity effects, Anderson model 78−52148
superconductor, effect of mag. impurities with high Kondo temp., in Anderson model 77−63023
superconductor, Kondo, nucl. spin-lattice relax. 78−52156
superconductor, Kondo, transport props. 79−65600
superconductor type II, upper critical field and Ginzburg-Landau parameter 78−14874
superconductor with impurities, Green's function calcs. 77−89894
superconductor with low conc. of mag. impurities thermoelec. effect 77−69448
superconductors, Kondo impurities, self-consistent theory of pairbreaking 78−26989
superconductors, transition temp. and upper crit. field 77−55634
transition metal impurities, Kondo problem exptl. advances and trends 78−84384
transition metal magnetic alloys, dilute, props., review of theory 79−15282
two or three electrons, interacting with localised mag. moment, wave function determ. *(French)* 79−12636
two-impurity spin correl., self-consistent treatment 77−24672
valence fluctuation system, ground state and elementary excitations, Anderson lattice model Hamiltonian, dense Kondo problem 80−54656
Zn-Mn(Cr), dil., mag. anisotropy below 1K, low field magnetisation meas. 80−20382
Ag, transport props. meas., 20 mK-4.2K 77−20292
Ag-Cr dilute alloys, elec. cond. meas., 1.5 to 30K 77−62914
Ag-Fe, dil., estimate of Kondo temp. from static mag. susceptibility meas. 78−19214
Ag-Fe, Kondo system, magnetisation, Mossbauer expts. 77−77028
Ag-Mn alloys, dilute, low temp. elec. resist. *(Russian)* 78−68024
Ag-Mn dilute, magnetoresist. and Hall effect, field-depend. electron scatt. 77−43581

Kondo effect continued
$Ag_{1-x}Au_xYb_y$, thermopower and resistivity 79−65457
AgCr, dil., specific heat, impurity contrib. Kondo temp. 80−65903
Al-3d transition metal, dil. alloy, preasymptotic charge oscillations around 3d impurities 77−36055
Al-Al_2O-Al tunnel junction, Fe doped, Kondo-type zero-bias conductance 78−56237
Al-Cr, Kondo alloys, spin and phonon resistivity independ. 78−47777
Al-insulator-Au tunnel junction, conductance peaks produced by Kondo scatt. from O_2 78−95387
Al-Mn, dil., magnetoresist. meas. 77−28160
Al-Mn, Kondo alloys, spin and phonon resistivity independ. 78−47777
Al-Mn (0.55-5 at.%), magnetoresist. depend. on mag. field and impurity conc. 77−62896
Al-Mn alloys, dil., magnetoresist. meas. 77−62900
Al-Mn(Cr), dil. alloys, single impurity and interaction effects in susceptibility 77−8269
Al_3Ce and $Al_{11}Ce_3$, Kondo cpds., mag. behaviour obs. by neutron diffr. 80−50049
Al_3Ce, thermal expsn. below 1K, single ion Kondo effect model 79−90803
Au-^{171}Yb, nuclear induced resistivity drop 78−10431
Au-^{174}Yb, nuclear induced resistivity drop 78−10431
Au-Co, dil. alloy, crystalline electric field and spin-orbit splitting, NMR results 77−32274
Au-Cr, dil., elec. resist., generalised phase shift anal. of Kondo effect 80−75556
Au-Cr, dil. spin glass elec. resist., press. and conc. depend. 80−24864
Au-Cr Kondo alloy, effect of press. on resistivity 78−79978
Au-Fe; anomalous Hall effect, asymm. scatt. of itinerant electrons 77−43569
Au-Fe, dil., approach to saturation of magnetisation 78−56293
Au-Fe, Kondo system, magnetisation, Mossbauer expt. 77−77028
Au-Fe, spin glass, spin relaxation rates, neutron scatt. study 79−47235
Au-Fe, spin-glass, characteristic temps. 79−38348
Au-Fe, very dil. alloy, Kondo temp. 78−91688
Au-Fe(Mn) dil. spin glass alloy, impurity-impurity interaction press. depend., resistivity meas. 77−20308
Au-Mn, dil., ^{52}Mn γ-ray anisotropy down to 3 mK, Kondo and relax. effects 77−81034
Au-Mn(Cr)(Fe), dil., spin glass state and Kondo effect, nucl. orientation of ^{54}Mn 78−6514
Au-Pd(Pt), elect. resistivity, temp. depend. between 1.6 and 4.2K *(German)* 79−28337
Au-V, dil., ^{51}V CW NMR line width anal., RKKY broadening 78−15033
Au-V, dil., Kondo alloy, spin dynamics, nuclear spin relax obs. 78−68155
Au-V Kondo alloys, mag. susceptibility and NMR Knight shift in conc. independent region 77−77027
Au-Yb thin films, ESR spectra, strain effects 80−71172
$Au_{1-x}Cu_x$-Fe, dil., resistance maximum 79−61056
Be, resistivity minimum temp. depend., 4.2 to 40K *(Russian)* 79−87077
Bi-Mn, dil. liq. alloy, static and dynamic props. of localised Mn moments 79−82755
Cd-Cr, dil., estimates of s-d interaction from supercond. transition temp. and mag. susceptibility 78−43561
Cd-Mn, dil., lattice state effects on pair breaking 77−8219
(Ce, La)In_3, heat capacity and elec. resist. 80−71049
Ce alloys, Kondo effect, mag. suscept. exam., appl. to $CeIn_3$ 77−8270
Ce alloys, Kondo system, mag. susceptibility calc. in Anderson model 77−55661
Ce compounds, Anderson model, exchange parameter, Kondo temp., mag. susceptibility 79−1656
Ce compounds, Kondo coupling, hyperfine and exchange interactions 79−65647
Ce dilute alloys, cryst. field and Kondo effect 77−43809
β-Ce, elec. resist., 2-300K, quenched Kondo scatt. 77−4320
Ce impurity Kondo system, crystal field effects on thermopower and Kondo effect 77−66163
γ-Ce, Kondo-like anomaly 80−96857
Ce-alloys, abnormal ordered Kondo lattice 78−47947
Ce-La alloys, DHCP, low temp. mag. and elec. props. 77−62911
$CeAl_2$, Anderson lattice system, volume collapsed strongly mixed valent state 79−38033
$CeAl_2$, antiferromag. ordering between 4f shells, Kondo effect 80−20417
$CeAl_2$, antiferromag. ordering and Kondo behaviour, ^{27}Al NQR study 80−71231
$CeAl_2$, $CeAl_3$, Kondo lattice theory 80−20380
$CeAl_2$, conf. Kondo system, sp. ht. meas. 78−52210
$CeAl_2$, low temp. mag. props., Kondo effect 80−20381
$CeAl_2$, mag. behaviour 2.5 to 300K, neutron scatt. meas. 77−63110
$CeAl_2$, mag. ordering and anomalous ground state, neutron diffr. obs. 79−78331
$CeAl_2$, magnetisation under high mag. field and hydrostatic press., Kondo temp. 77−63233
$CeAl_2$, neutron diffr. at low temp., magnetism 80−20383
$CeAl_2$, pure and $LaAl_2(YAl_2)$ diluted, collective phenomena 80−65933
$CeAl_2$, sp. ht. in high mag. fields, Kondo effect 78−52284
$CeAl_2$, specific heat between 0.02 and 1K 79−1680
$CeAl_3$, magnetic susceptibility, dense Kondo system 77−63087
$CeAl_3$, singlet ground state at T=0, mag. ordering 2.5-6K 78−84388
$CeAl_3$, sp. ht., Kondo effect and ferromag. order coexistence 80−65927
Ce_3Al_{11}, Kondo system, competition between ferro- and antiferromag. interactions 80−60258
Ce_3Al_{11}, sp. ht., Kondo effect and ferromag. order coexistence 80−65927
CeB_6, mag. and electronic props. 80−71048
CeB_6, magnetostriction, US absorpt. and thermal expansion 80−66004
Ce(In, Sn)$_3$, heat capacity and elec. resist. 80−71049
$CeIn_3$, Kondo effect, mag. suscept. exam. 77−8270
$CeIn_{3-y}Sn_y$, electrical resist. and thermal expansion meas., 1.5-300K 80−34400
$Ce_xLa_{1-x}Al_3$, mag. susceptibility, 1.5 to 20K 79−78310
$CePd_{3-x}Rh_x$, resistance behaviour and intermediate valence effects 79−78068
Co-Al system, nucl. spin relaxation exam. 79−19798
$Co_2Ti(Y)(Zr)(Nb)$, Laves phase, elec. resist. rel. to mag. props. 77−59282
Cr-Co, dil., antiferromag., elec. resist. min., press. and impurity effects 80−59970

Kondo effect continued
Cr-Co (up to 8 at.%), antiferromagnetic, resist. minimum, Kondo effect by pairs of Co atoms 80−39566
Cr-Co-V alloys, dil., elec. resist. min. 80−54680
Cr-Fe, dil., antiferromag., elec. resist. min., press. and impurity effects 80−59970
Cr-Fe (0.6 at.%), antiferromag., anomalous press. effect on resist. minimum 79−15138
Cr-Fe alloys, antiferromag., elec. resistivity, Kondo effect 79−60812
Cr-Fe_x (x=0.5, 1.5 and 3.5 at.%), antiferromag., Kondo anomaly 80−11163
$Cr_xPd_{82-x}Ge_{18}$, amorphous, RF sputtered, elec. resist. and magnetoresist., Kondo type behaviour 78−76066
Cu-Al-Mn liq. alloys, susceptibility behaviour 80−93077
α-Cu-Al(Fe) dil. alloys, Al ion charge screening, elec. resist. obs. 77−4500
Cu-Co, Kondo system, NMR, spin-lattice relax., impurity spin dynamics 77−69724
Cu-Co-Fe, dil. alloy, low temp. resistivity maxima *(Russian)* 79−87091
Cu-Cr, dil., spin-density magnetisation near Cr atoms, NMR study 80−80626
Cu-Cr, dil. alloy, Kondo resist. at 35 GHz 79−60814
Cu-Cr, dil. alloys, Frenkel defects, effects on anomalous resistivity and thermopower 77−8084
Cu-Cr, Kondo alloy, Josephson tunnelling effect 80−60145
Cu-Cr, Kondo alloy, NMR of Cu satellites, 1 to 4K 79−73837
Cu-Cr, vapour deposited, electron irrad., resistance behaviour *(German)* 78−47779
Cu-Cr alloys, dil., mag. susceptibility 77−63092
Cu-Cr dilute alloys, elec. cond. meas., 1.5 to 30K 77−62914
Cu-Cr(Mn)(Fe), dil., NMR satellite data, rel. to electronic struct. 78−68398
Cu-Cr(Mn)(Fe), dil., NMR data, ionic model and Kondo temp. 78−68399
Cu-Fe, classical Kondo system, impurity spin dynamics, NMR relax. of impurity neighbour nuclei 77−36056
Cu-Fe, dil., powder, transferred orbital hyperfine field on near neighbours, NMR meas. 78−27098
Cu-Fe, dil., transmission ESR meas. 2 to 40K 78−68364
Cu-Fe, dil. alloy, spin relaxation rates, neutron scatt. study 79−47235
Cu-Fe, highly dil., mag. impurity scatt., and deviations from Matthiessen's rule 78−43371
Cu-Fe, Kondo system, magnetisation, Mossbauer expts. 77−77028
Cu-Fe, static and dynamic susceptibilities, hyperfine studies 77−63090
Cu-Fe, vapour deposited, electron irrad., resistance behaviour *(German)* 78−47779
Cu-Fe (0.04 to 0.9 at.%), film, resistivity temp. depend., 1.5 to 17K, impurity interactions 77−63007
Cu-Fe (1.2 at.%), Fe moment and lattice distortion, neutron scatt. meas. 79−24133
Cu-Fe alloy, dil. dynamic susceptibility around T_k, satellite nucl. spin-lattice relax. time meas. 77−4573
Cu-Fe clusters, electronic states and mag. props., MO calc., appl. to Kondo problem 77−20219
Cu-Mn, dil., Kondo deviations of Mn electron spin relax. and g-factor, NMR meas. 79−51747
Cu-Mn, dil., spin density magnetisation near magnetic atoms 79−33545
Cu-Mn, dilute, magnetoresist. and Hall effect, field-depend. electron scatt. 77−43581
Cu-Mn dil. spin glass alloy, impurity-impurity interaction press. depend., resistivity meas. 77−20308
Cu-Mn Kondo system, ^{54}Mn nucl. orientation 78−68421
Cu-Mn(Fe)(Co), Kondo system, host NMR exam. 78−80246
Cu-Ni(Fe)(Mn)(V), dil., local mag. moments and Kondo effect, theoretical model 79−69651
Cu-transition metal, alloys, satellite NMR study, lineshifts and splitting 80−34786
CuCr, dil., specific heat, impurity contrib. Kondo temp. 80−65903
$Cu(Rh_{1-x}Cr_x)S_4$, spinel system, susceptibility and metallic resistivity, anomalies due to s-d interaction 80−70958
Eu^{2+}, in metallic hosts 80−39739
$Eu_xLa_{1-x}Al_2$, cryst. fields and exchange parameters, ESR meas. 80−71175
Fe_xNbSe_2, transport props. and mag. ordering 80−65527
$Fe_{65}Ni_{28}Mn_7$, disordered, mag. struct. near ferro-antiferromagnetic transition 80−60211
GaAs:Te, heavily doped degenerate semicond., Kondo effect 79−61053
$Gd_xLa_{1-x}Al_2$, cryst. fields and exchange parameters, ESR meas. 80−71175
Ge, degenerate, doped with nonmag. impurities, Kondo effect 78−14746
In-Mn, dil., film, ion implanted, supercond, and mag. props. 77−15987
InMn, ion implanted, influence of O and lattice disorder on Kondo resist. 79−38061
n-InSb, low temp. resonance excitation of Kondo effect *(Russian)* 78−56159
InSb:Te, heavily doped degenerate semicond., Kondo effect 79−61053
$(La,Ce)Al_2$, conf. Kondo system, sp. ht. meas. 78−52210
$(La,Ce)B_6$ dil. alloy, Kondo effect, impurity-impurity interaction, mag. susceptibility, mag. to non mag. transition 78−47948
$(La,Gd)Al_2$, reverse Kondo alloy, transport props. at finite mag. field 80−6812
$(La,Gd)Al_2$, very dil., resist. 79−23958
$(La,Nd)Sn_3$, reverse Kondo effect in presence of crystalline elec. field splitting 80−103684
(La,Y)Ce, dil., Kondo supercond., transition temp., susceptibility and resist. 80−65733
La-Ce, Kondo system, intermediate temp. supercond. under hydrostatic press. 79−24097
La-Ce alloy, press. induced spin glass to Kondo phase transition, resist. meas. 79−24174
La-Sm-Sn, dil. alloy, Kondo effect obs., supercond. transition temp. meas. 77−51837
$La_{1-x}Pr_xSn_3$, Kondo effect from excited cryst. field levels, elec. resist. 78−14723
LaB_6:Ce, Kondo system, magnetoresist. down to 0.04K, anisotropy 77−11904
$La_{1-c}Ce_cAl_2$, Kondo superconductor, self-consistent theory of pairbreaking 78−26989
$(La_{1-x}Ce_x)Al_2$, Kondo supercond., tunnelling density of states 78−14900
$(La_{1-x}Ce_x)Al_2$, Kondo supercond., tunnel junction fabrication with wax barriers, tunnelling meas. 78−19191

Kondo effect continued
$La_{1-x}Ce_xAl_2$, Kondo system, low temp. thermal expansion behaviour 79−19382
$(La_{1-x}Ce_x)Al_2$, Kondo system, antiferromag., specific heat 79−24179
$La_{1-x}Ce_xB_6$, Kondo system, low-field impurity susceptibility, 0.03 to 8K 77−63095
$La_{1-x}Ce_xPd_3$, resistance behaviour and intermediate valence effects 79−78068
$La_{1-x}Ce_xSn_3$, electrical resist. and thermal expansion meas., 1.5-300K 80−34400
$(La_{1-x}Gd_x)Al_2$, dil., reverse resistance anomaly 78−76054
$La_{1-x}Pr_xSn_3$, singlet ground-state system, mag. susceptibility 78−19215
$La_{1-x}Sm_xSn_3$, Kondo scatt. from Sm ions 77−51734
$LaSn_3$, dilute alloy containing light rare earth impurities, press. depend. of supercond. transition temp. 79−47184
$La_{1-x}Y_x$ alloys, PAC obs. of hyperfine field fluctuation at ^{140}Ce, Kondo effect interpret. 77−20761
$(La_{1-x}Y_x)_{1-y}Ce_yAl_2$, resistivity meas., Kondo temp. enhancement 77−62917
Lu-Gd, dil., positive exchange Kondo system, magnetisation and resist. 78−68158
Lu-Gd, positive exchange const. Kondo system, resistivity meas. 78−47775
Mg-Fe, dil. alloy, single impurity Kondo behaviour in elec. resist. *(French)* 79−60815
Mg-Fe alloy film, quench-condensed, resistance meas. 79−15235
Mg-Mn, dil. alloy, de Haas-van Alphen effect, exchange interaction, Kondo effect 78−88093
Mg-Mn, dil. alloy, single impurity Kondo behaviour in elec. resist. *(French)* 79−60815
Mg-Yb, dil., Kondo scatt. from Yb, low temp. elec. resist. meas. 80−44578
Mo-Co Kondo alloy, Co impurity susceptibilities, Knight shift 80−88721
Mo-Fe, dil., Kondo effect of RKKY interaction 78−31052
Mo-Fe, Kondo system, magnetisation, Mossbauer expts. 77−77028
Mo-Fe, local magnetisation from Mossbauer meas. 77−20549
MoFe, occurrence of spin glass and mictomagnetic regimes, props. meas. 77−16085
NbI_4, metallic state, resistivity anomaly 79−15136
$NbSe_2$:Mn, Kondo effect, mag. ordering and superconductivity 77−62915
$NbSe_2$-Fe, dil. alloy, magnetotransport and superconductivity 77−55516
$NbSe_2$-Fe, layered supercond. quenching of Kondo anomaly by cryst. anisotropy field 79−60972
Ni-Al-Fe(Co), electrical and mag. anomalies due to substitutional atoms 77−15839
Ni-Cu, hydrogenated, Curie point, cluster magnetism 78−14960
Ni-P-B alloy, amorphous, giant moments and short-range orders 77−4499
$(NiAl)_{1-x}M_x$, M=3d transition metal, elec. resist. and magnetoresist. 77−43580
Pd, hydride and alloys, electronic band struct., comparative study of electric and mag. props. 78−95259
Pd-Co, nuclear orientation expt., Co impurity in singlet Kondo state 77−63296
Pd-Co alloy, dil., giant moment and Kondo-like coupling, nuclear orientation meas. 77−32160
Pd-Cr, dil., temp. dependent scatt. 80−59973
Pd-Pt, elect. resistivity, temp. depend. between 1.6 and 4.2K *(German)* 79−28337
$Pd_{1-y}Cr_yH_x$, resistive Kondo behaviour as function of Cr and H conc. 80−59971
$PdH_{0.97}$:Fe(Cr), supercond. transition temp. depression, coexistent mag. behaviour 80−49976
PdH_x (α')$Fe_{0.003}$ 79−61054
PdH_x-Fe, dil., Kondo system, local moment hyperfine studies, Mossbauer expt. 80−39908
$PdH_xFe_{0.003}$, Kondo system, local moments, hyperfine fields, Mossbauer study 80−80478
$Pd_{0.98}Pr_{0.02}$, dil. alloy, mag. susceptibility 79−19583
Pr, DHPC single cryst., Kondo-like resist. between 15 mK and 5K 79−60816
Pr-Ce(Tm), mag. order onset, elec. resistivity 80−20416
Pt-Co, dil., skew scatt. Hall effect, magnetoresist. and mag. anisotropy, orbital magnetism of impurity 80−70678
Pt-Cr(Nb)(Re)(Rh)(V), dil. alloy, 0.5 at.%, ^{195}Pt NMR for local mag. susceptibility 78−84484
Pt-Mn alloy, dil., low temp. susceptibility, spin glass and Kondo behaviour 77−66372
Pt-Mn dilute alloys, spin glass, low temp. resist. meas., cluster model explanation 78−26851
$(SN)_x$, thermoelec. power, 0.1 to 4.2K, phonon drag contrib. and supercond. transition 79−56356
$(SN)_x$, thermopower from 0.15 to 4.2K 80−34427
Sc, sp. ht. data rel. to electronic props. 78−83971
Sc-Gd, dil., reverse resist. anomaly and negative magnetoresist. 80−84459
$TaSe_2$-Fe, dil. alloy, magnetotransport and superconductivity 77−55516
$Tb_cY_{1-c}P(As)$, singlet ground state systems, resistivities 77−62912
Th-Cr, supercond., press. meas. to 20 kbar 80−88667
Th-U, Kondo alloys, spin and phonon resistivity independ. 78−47777
ThH_2:Er^{3+}, EPR of Er localised electron mag. states, Kondo effect 80−25202
Th_4H_{15}:Er^{3+}, EPR of Er localised electron mag. states, Kondo effect 80−25202
$Tm_y(La,Y)_{1-y}S$, microwave resistivity 77−11949
$Tm_y(La,Y)_{1-y}Te$, microwave resistivity 77−11949
TmS, far IR refl. and DC resist., 1-300K, interconfig. fluctuation effects 78−35136
TmSe, Kondo lattice model 80−97063
TmSe, Kondo lattice theory 80−20380
Tm_xSe, valence instabilities, antiferromag. order 80−20128
$Tm_xY_{1-x}Se$, Kondo effect, Van Vleck behaviour 80−25085
UCo_2, Kondo like resist. minimum, non-stoichiometry influence 77−63088
W-Co, dil., excess resistivity, temp. depend., Kondo effect 78−68011
Y-Ce, Kondo system, spatial extent of Ce moment, neutron diffr. meas. 78−68159
Y-Gd, dil., reverse resist. anomaly and negative magnetoresist. 80−84459

Kondo effect continued
Yb, FCC, nucl. orientation of 3d impurities and magnetisation meas. 78−64280
Yb impurity Kondo system, crystal field effects on thermopower and Kondo effect 77−66163
$YbMo_6S_8$, supercond., low temp. thermal and mag. props. 78−14904
Zn based Kondo alloys, with magnetic breakdown, anal. of de Haas-van Alphen effect 78−34751
Zn-Al dilute alloy, Kondo effect anisotropy 77−43578
Zn-Cr, Kondo alloys, spin and phonon resistivity independ. 78−47777
Zn-Mn, dil., Kondo effect and impurity interactions in resist., 0.05-14K 78−14721
Zn-Mn, Kondo alloys, spin and phonon resistivity independ. 78−47777
Zn-Mn, Kondo-system, ion implantation as method for study 80−70241
Zn-Mn dilute alloy, Kondo effect anisotropy 77−43578
Zr-Mn (up to 0.3%), high-magnetic field magnetisation and magnetoresistance 78−10652

Korringa-Kohn-Rostoker calculations *see KKR calculations*

Koster effect *see dislocation damping*

k.p calculations
A15 compounds, elec. struct., 3-D k.p model 78−2405
A-15 compounds, appl. of three-dimens. model to V_3Si 78−23015
III-V semiconductors, k.p perturbation theory 77−43484
Kane model, three-band, Auger recombination overlap integrals, kp approx. *(Russian)* 78−87897
Lifshitz's criterion for symmetry changes in second-order phase transitions 79−4392
semiconductor, direct gap, one-photon Keldysh absorption coeff. derived using k.p method 77−8599
semiconductor with relativistic electron spectrum, bound and reson. states 77−51701
semiconductors, electronic band shape, k.p perturbation theory *(Korean)* 78−23020
two band model with electron-phonon interactions for narrow-gap electron spectra 79−90961
zero-gap semiconductors, anisotropy of IR absorpt. coeff., k.p. calc. 80−97285
Bi, energy dispersion of electron Fermi surface, deform. model and k.p. calcs. 79−51469
BiSb, alloys, semimetallic, camera, dispersion relations 80−59854
Fe, electronic band struct., generalised k.p. interpolation method 80−6709
GaAs, k-linear coupling, E_1' transitions 78−91583
GaP, overlap integrals and Auger recomb. coeff. direct calc. 79−69524
$InAs_{1-x}P_x$, electron effective mass cyclotron reson. and magnetophonon effect 80−24786
n-InSb, anomalous Hall effect at high mag. field 77−15876
n-InSb, effective mass and Lande factor, stress depend. calcs. *(German)* 79−95313
InSb, semiconductor, Brillouin zone spin dependent wave functions calcs. 79−56126
Nb_3Sn, electronic struct. from three-dimens. k.p model 78−84139
Pb chalcogenides, interband transitions, absorpt. coeff., multiband calc. 80−29738
$Pb_{1-x}Sn_xTe$, DH laser, gain-freq.-current relation, k.p band model 77−61951
$Pb_{1-x}Sn_xTe$, narrow gap, many-body interaction effects, Bloch electron scatt. lifetimes, energy renormalisation 80−49637
PbTe epitaxial film, many valley semicond., band population effects, intraband magneto-optical props. 79−78007
n-Si (001) on sapphire, galvanomag. effect for holes, valence band 79−91166
Si, phonon-assisted Auger recomb., direct calc. of overlap integrals 80−107808
Te, hole cyclotron reson. with B⊥c 78−10777
Te, uniaxially stressed, submm. cyclotron reson., deform. pots. and k.p coeffs. 80−54606
V_3Si electronic struct. from three-dimens. k.p model 78−84139

Kramers-Kronig relations
alcohols, opt. consts. in IR, stretch band obs. 79−91421
alkali halides, refractive index calculation 80−88949
anisotropic crystal, refl. spectra, phase difference determ., Fresnel formula validity 77−43956
anthracene, O-O exciton absorption bands, thermomodulation study 78−39563
anthracene-pyrometallitic dianhydride cryst., refl. and absorpt. spectra of singlet charge transfer excitons 80−71442
complex reflection amplitudes of photons, sum rules 78−63006
9-cyanoanthracene, cryst., polarised refl. spectra at 2K, 360-460 nm, dielec. function 79−91461
deoxyhaemoglobin high spin ferrous ion, low lying electronic states, far IR mag. reson. 80−48110
deoxymyoglobin high spin ferrous ion, low lying electronic states, far IR mag. reson. 80−48110
dielectric permittivity, allowed sign, validity of relations 77−32346
electroreflection exam., short range order in surface layers 78−6703
ellipsometric function, Kramers-Kronig relations and sum rules, Lorentz oscillator model 80−102617
film, optical const. determ. from meas. of normal incidence reflectance and transmittance 77−85825
films, optical constants, reflection spectra by Kramers Kronig method 80−76099
Fourier method numerical soln. by computer 78−2825
Fourier series algorithm 77−85679
gas, virial expansions for dielec. and refr. indices, rel. to collision-induced absorption bands 79−86547
glass, refractive index freq. depend., dispersion enq. calc. 80−40083
graphite, pyrolytic, dielectric function from IR reflectance meas. 77−55781
graphite-$FeCl_3$ intercalation cpd., electronic excitation spectrum, high resolution EELS meas. 80−45182
inelastic electron scatt. data anal., appl. to Cu 77−73199
ionic conductive crystal, statistical theory of relaxation current and low-freq. dielectric dispersion 78−60391
IR reflection spectrum, dispersion formula fitting, Kramers-Kronig anal. 80−50311
modulation spectroscopy, anal. of Kramers-Kronig relations 78−23423
n-order nonlinear phenomena, dispersion rels. 79−41410
normal reflectance of conductors and insulators, dispersion relations and sum rules 80−29706
optical constants calculation *(Russian)* 80−80740
organic charge transfer complexes, refl. spectra, excitons 79−47477
petrols, optical consts. in 0.25 to 25 micron region, sea pollution detection appl. *(Russian)* 78−76976
phenanthrene, cryst., refl. spectra of first singlet transition 78−88323
plasmon dispersion, correlation correction 80−43917
polyacetylene, pure and heavily doped, optical and IR studies, electronic struct. calcs. 80−7347
polydiacetylene, cryst., refl. spectra, Kramers-Kronig transforms 78−43889
prep. by electron beam evaporation, and optical and elec. props. 80−20793
quadrupole distorted NMR powder patterns, simulation, Fortran program 77−77105
quartz, cryst. and fused, far UV optical consts. 77−81078
reflection spectra, Kramers-Kronig anal. with preliminary dispersion anal. 78−49915
reflection spectra, phase correction in Kramers-Kronig anal. 79−56815
reflection spectroscopy, validity of K-K transform. 77−66468
reflectivity extrapolations in Kramers-Kronig anal. 78−19438
resonance Raman spectrum, rel. to Kramers-Kronig relations 80−97267
sapphire substrate surface evaluation for SOS 77−76653
spatially dispersive media, generalised Kramers-Kronig formula, vac. polarisation tensor 77−17798
TCNQ, salt, $(NMe_3H)(I)(TCNQ)$, semicond. 'metal-like' complex, optical props. 79−95761
TCNQ salt, K^+TCNQ^- particles, light scatt., absorpt. spectra 79−24332
TCNQ salt, K-TCNQ, single crystal, charge transfer band interpretation, refl. spectrum obs. 80−25353
TCNQ salt, MTPA $(TCNQ)_2$, IR refl., dielec. function and cond. 80−34924
transition metal dichalcogenides, layer type, reflectivity meas., 6-40 eV 77−55801
transition metal oxides, energy loss spectra, ion polarisability 78−68585
US attenuation and dispersion, appl. to haemoglobin 78−83135
water, IR spectrum, influence of Cu^{2+} ions 78−72501
water, optical consts., 400-5000 cm^{-1}, 1, 16, 27, 39 and 50°C, rel. to intermol. struct. 77−66469
water, Van der Waals interaction, Kramers-Kronig eqn. with full spectral data vs. oscillator model approx. 78−5998
Ag, single cryst. electrodes, electroreflectance obs. in aqueous solns. 80−25342
β-AgI thin film, exciton spectrum 80−55216
Al_2O_3-SiO_2, mullite 2:1 cryst., dielectric tensor components 77−48142
As, rhombohedral, electronic struct. and optical props. var. with internal displacement parameter 79−60702
As-S, glass, IR vibr. spectra, optical characts. calc. 80−40119
Au, dielectric const. by multiangle reflection meas., optical props. 79−95723
Au, optical consts., dispersion, temp. depend., Kramers-Kronig calcs. *(Russian)* 77−69796
Au, single cryst. electrodes, electroreflectance obs. in aqueous solns. 80−25342
Au-Cu, dielectric const. by multiangle reflection meas., optical props. 79−95723
$BaTiO_3$, UV refl. spectra, optical consts. 0 to 32 eV Kramer-Kronig anal., band struct. calcs. 78−43903
BeO film, amorphous or polycryst., dielec. function, refl., from electron energy loss meas. 78−43947
$Bi_{12}GeO_{20}$, reflectivity spectrum and band struct. 79−47474
BiI_3, layered single crystal, band-edge excitons, optical constant meas. *(Russian)* 77−90171
CC GaAs, n- and p-types, optical consts., 2.5-3.5 eV, normal incidence reflectance meas. 79−15428
$CaCl_2(Br_2)$, aq. solns., IR spectral reflectance meas., Kramers-Kronig anal. 77−4633
$CdCr_2S_4$, ferromag. semicond., IR refl. spectra, phonon props. and dielec. function 80−66191
$CdCr_2Se_4$, magnetic red shift origin, specular reflectivity, band struct. 80−40127
$CdCr_2Se_4$, optical reflectivity, dielectric const. by expt. data Kramers-Kronig anal., spinel struct. 79−99903
$CdGa_2S_4$, IR refl. spectra 80−60604
$CdGa_2Se_4$, IR refl. spectra, optical phonon dispersion 80−29746
$CdIn_2S_4$, fundamental optical constants 78−84549
CdSe, undoped and Cr doped, far IR transmission and reflectance spectra 80−71429
$CdSnAs_2(P_2)$ single crysts., refl. spectra, band struct., dielec. consts. 77−44022
CeN, optical props. and valence mixture 78−56450
Co, X-ray refl. near $L_{2,3}$ absorpt. edge 80−71513
$Co_{1-x}Fe_xSi$, solid solution, optical props. 78−72556
$Co_{1-x}Ni_xSi$, solid solution optical props. 78−72556
CoSi, absorpt spectrum, phase correction in Kramers-Kronig anal. 79−56815
CoSi solid solution, optical props. 78−72556
CrSb, optical props., 0.05 to 5 eV 77−48194
$Cs_3CoCl_5(Br_5)$, single cryst. polarised vibr. spectra 78−39535
Cu, dielectric const. by multiangle reflection meas., optical props. 79−95723
Cu, inelastic electron scatt. data anal. 77−73199
Cu, single cryst. electrodes, electroreflectance obs. in aqueous solns. 80−25342
CuBr, exciton absorpt. band shape, dielectric const. real part derivatives *(Russian)* 80−25413
$CuCl_2$, aq. solns., IR spectral reflectance meas., Kramers-Kronig anal. 77−4633
$CuGaTe_2$, mode energies from Kramers-Kronig anal. of IR lattice vibr. spectra 79−28765
$CuInSe_2$, mode energies from Kramers-Kronig anal. of IR lattice vibr. spectra 79−28765
$CuSO_4$, single cryst., IR optical consts., comparison with soln. 77−66470
Dy_2S_3, optical props. and electronic struct. in fund. absorpt. region 80−80817
FeF_2, dielectric properties, IR spectra, lattice dynamics *(French)* 80−76026
FeF_2, IR reflectivity spectrum 79−51952
$FeGe_2$, Fe_2Ge, optical consts., electron energy loss spectra meas. 77−90121

Kramers-Kronig relations continued
Fe_2O_3, haematite, anal. of refl. spectrum by Kramers-Kronig relations 80−16058
Fe_3O_4, optical props. in spectral range 0.03 to 12 eV 79−51977
Ga film, optical props., 2-15 eV 77−77308
$Ga_{1-x}Al_xAs$, IR refl. spectra and Raman spectra 80−20623
GaAs, exciton parameters near absorption edge 79−73448
GaAs, reflection spectra, optical consts. *(Russian)* 79−38571
ε-GaAse, optical consts. for ⊥ and ∥ light polarisation, reflectivity, interf. meas. 77−52077
$Ga_{1-x}In_xAs$, IR reflectivity, cluster effect on optical phonons 80−97259
$Ga_{1-x}In_xSe$ solid solution, IR spectra of static reflectivity 79−69849
GaS, reflectivity from 4 to 32 eV, Kramers-Kronig anal. 80−34943
GaS(Se), polar optical phonon ang. behaviour, IR refl. meas. 80−20633
$GaS_{1-x}Se_x$, mixed crystals, IR reflectivity spectra 80−66204
GaSe, long wavelength IR refl. spectra 80−11401
GaSe, reflectivity from 4 to 32 eV, Kramers-Kronig anal. 80−34943
GaSe, refr. index 0.45 to 330 μm, interf. and refl. meas. methods 77−63387
GaTe, vibr. spectrum 77−89513
GeS, far IR reflectivity spectra, lattice vibr. and dielec. const. 77−52068
GeS_2, energy gap and optical props. in IR region 79−51948
GeS_2, single cryst., IR polarised reflectivity spectra, 79−56775
$GeSe_2$, far IR reflectivity meas. 77−28565
$GeSe_2$, single cryst., IR polarised reflectivity spectra, 79−56775
p-GeTe, reflectance, and thermorefl. spectra 80−80814
$Hg_{0.75}Cd_{0.25}Te$, single crystal, reflection spectra 80−40140
$Hg_{0.75}Cd_{0.25}Te$ thermorefl. spectra, spectral dependence of thermally-induced permittivity changes, calc. 80−16057
InP, Kramers-Kronig electroreflection spectra 77−4655
InSe, optical const. and interband transitions 77−20816
InSe, polar optical phonon ang. behaviour, IR refl. meas. 80−20633
InSe, reflectivity from 4 to 32 eV, Kramers-Kronig anal. 80−34943
α-In_2Se_3, far infrared optical study of ordered and disordered forms 78−84572
K double fluorides, IR refl. spectra, vibr. modes, optical vibr. freq., Kramers Kronig anal. 80−66190
K-intercalated graphite (stage-1), electron energy loss expts. and band struct. theory 79−100001
$KMgF_3$, extreme UV spectra, 9-30 eV 78−23486
K_2MnF_4, perovskite type layer struct., far IR reflectivity and Raman spectra 77−15511
Kr, solid, reflectivity, Kromers-Kronig anal. 77−73122
LaB_6 film, prep. by electron beam evaporation, and optical and elec. props. 80−20793
LaOF, features of formation of band structure 79−33232
La_2S_3, optical props. and electronic struct. in fund. absorpt. region 80−80817
Li deposits, optical consts., Kramers-Kronig anal., 0.5-10.7 eV 77−40201
α-$LiIO_3$, statistical theory of relaxation current and low-freq. dielectric dispersion 78−60391
$LiNbO_3$, ferroelec. phase, soft vibr. modes, far IR refl. meas. 79−87407
$LiNbO_3$, IR reflectivity temp. depend. 78−27202
$LiNbO_3$, Raman spectra and dielec. props. near Curie point 79−38530
$LiTaO_3$ high-temp. ferroelec. transition, soft mode IR reflectivity spectroscopy 79−33692
$LiTaO_3$, paraelectric phase, soft vibr. modes, far IR refl. meas. 79−87407
$LiTaO_3$, Raman spectra and dielec. props. near Curie point 79−38530
$MgCl_2$, aq. solns., IR spectral reflectance meas., Kramers-Kronig anal. 77−4633
5 wt.% MgO-Si_3N_4, hot-pressed, dielec. props. 78−10822
MnAs, optical props., 0.3-14 eV 77−52122
$MnAs_{0.85}P_{0.15}$, optical props., 0.3-14 eV 77−52122
$Mn_xFe_{3-x}O_4$, optical props. 80−20606
MnSb, optical props., 0.05 to 5 eV 77−48194
$MnSe_2$, IR lattice vibrs., dielectric dispersion 79−28735
Mo film, polycryst., energy loss function, Kramers-Kronig anal., reflectivity, optical props., EELS 80−40194
$MoS_2(Se_2)(Te_2)$(2H) polytypes, Kramers-Kronig anal. of reflectivity spectra, 0-30 eV, band model 79−51976
NH_4Br, thermorefl. spectra, band energy anal. 77−12402
NH_4Cl, thermorefl. spectra, band energy anal. 77−12402
NH_4I, thermorefl. spectra, band energy anal. 77−12402
NH_4X, X=OH, Cl, Br, aq. soln., IR reflectivity spectra, Kramers-Kronig anal. 78−68500
NaCN, aq. solns., IR spectral reflectance meas., Kramers-Kronig anal. 77−4633
$NaMgF_3$, extreme UV spectra, 9-30 eV 78−23486
Nd_2S_3, optical props. and electronic struct. in fund. absorpt. region 80−80817
NiAs, optical props., 0.05-5 eV 77−48194
NiI_2, far IR study of lattice dynamics 78−80359
NiSb, optical props., 0.05 to 5 eV 77−48194
PbF_2 optical props. 77−32394
$PbHAsO_4$, ferroelec., far IR and microwave dielec. props. 80−55108
$PbHPO_4$, microwave permitt. and far IR refl. spectra in paraelec. and ferroelec. phases 80−40033
PbI_2, exciton absorpt. band shape, dielectric const. real part derivatives *(Russian)* 80−25413
PbI_2, optical props. 77−32394
$(PbO)_x(SiO_2)_y$ glass, vibrational spectroscpic exam. 79−11417
$Pb_{1-x}Sn_xTe$, reststrahlen band, reflection spectra Kramers-Kronig anal. 79−8162
$Pb_xSn_{1-x}Te$, RF-sputtered epitaxial single-cryst. films, thermorefl. spectra 77−63476
PdO, optical props., 0.5-5.4 eV 79−56813
$Pd_{81}S_{19}$ and $Pd_{84}Si_{16}$, metallic glasses, optical refl. spectra and optical consts. 79−87464
PtO film, electrochemically formed, anisotropy of optical constants, reflection spectroscopy and Kramers-Kronig analysis 77−32456
Rb_2MnCl_4, perovskite type layer struct., far IR reflectivity and Raman spectra 77−15511
$(SN)_x$, reflectivity spectra meas. by synchrotron radn. 79−91513
SbSBr glass, IR reflectivity spectra 80−71403
Sb_2Te_3, semiconductor, appl. to optical props. determ. 77−8537
Sc, HCP, optical examination of electronic struct. 77−89694
ScH_2, optical interband struct. and low energy plasmons 78−31200
Si, effective mass from Kramers-Kronig analysis for various doped crysts. 77−31942
Kramers-Kronig relations continued
Si, optical constants, heavily doped crystals, Kramers-Kronig analysis 77−85676
Si, optical properties of monocrystal by electron energy loss meas. *(German)* 79−24283
$Si_{(6-z)}Al_zO_zN_{(8-z)}$, sialons, hot-pressed, dielec. props. 78−10822
SiC, semiconductor, appl. to optical props. determ. 77−8537
Si_3N_4, hot-pressed, dielec. props. 78−10822
SiO evaporated film, dielec. function 8 to 33 μm, spectrophotometric and refl. meas. 80−80883
SiO_2, amorphous, and layers on Si substrate, IR optical props. 79−56780
SiO_2 deposited on Ge, optical constants, reflection spectra by Kramers Kronig method 80−76099
SmB_6 film, prep. by electron beam evaporation, and optical and elec. props. 80−20793
SmS, optical props. and electronic struct., Kramers-Kronig model anal. 79−69859
Sn film, white, optical props. between 2-15 eV 78−19584
SnS, far IR optical props. 77−12375
SnS_2, refl. using Kramers-Kronig anal., optical functions 79−95798
SnS_2, single cryst., far IR reflectivity 79−56774
SnSe, far IR reflectivity spectra, lattice vibr. and dielec. const. 77−52068
SnSe, lattice refl. spectra in long-wavelength IR range 78−27236
$SnSe_2$, refl. using Kramers-Kronig anal., optical functions 79−95798
$SrTiO_3$, surface EM wave propag., IR refl. expts. 78−39553
$SrTiO_3$, UV refl. spectra, optical consts. 0 to 32 eV Kramer-Kronig anal., band struct. calcs. 78−43903
Ti, clean and oxidised surfaces, refl., 2-25 eV 80−55123
Ti, X-ray refl. near $L_{2,3}$ absorpt. edge 80−71513
TiN, optical props. at 300K 78−19466
TiO, electronic excitations, electron energy loss spectra in 3 to 60 eV range *(French)* 78−80440
TiO_2, electronic excitations, electron energy loss spectra in 3 to 60 eV range *(French)* 78−80440
TiO_2 single cryst., refl. and electrorefl. spectra 78−2870
Ti_2O_3, optical consts., polarisation dependent reflectivity 78−52531
TiS_2, electron energy loss spectra, dielectric function, reflectivity and absorption coefficient 79−69937
$Ti_{1+x}Se_2$, superlattice form. and phase transition, IR reflectivity meas. 79−24322
Tl_3AsS_4, optical phonons, Raman and refl. spectra 80−11400
$TlGaS_2$, IR refl. spectrum, Kramer-Kronig analysis, transverse optical phonons 78−19489
$TlGaS_{2x}Se_{2(1-x)}$ layer solid soln., long wave lattice vibrs., IR reflection spectra 80−11388
$TlInS_{2x}Se_{2(1-x)}$ layer solid soln., long wave lattice vibrs., IR reflection spectra 80−11388
TlS_2, amorphous semiconductor, optical consts. 79−11400
TlSe, vibrational spectrum, IR spectra meas. 78−35146
UO_2 and U_4O_9 single crysts., optical props. rel. to chem. bonding 77−28598
V_6O_{13}, semicond., IR vibration spectra 80−88997
W, chemisorbed H, surface cond. and intrinsic surface states, surface refl. spectra 80−15378
W, optical consts., dispersion, temp. depend., Kramers-Kronig calcs. *(Russian)* 77−69796
W-Fe spin glass, optical props. and electronic states 80−20412
Y, reflectivity spectrum, 3.5 to 30 eV dielectric function and plasmons 77−44014
$YAlO_3$, reflection spectra, Kramers-Kronig anal. of optical characts. 79−8161
(ZnFe)S, marmatite, optical properties 78−39555
$ZnIn_2S_4$, fund. optical consts., Kramers-Kronig analysis, reflectivity spectra 78−39573
$ZnIn_2S_4$ layered semiconductor, fundamental optical constants, experimental result analysis 79−56757
ZnS(Se)(Te), thermoreflectance spectra, at energies from absorption edges to 9 eV *(Japanese)* 79−11436
$ZnSnAs_2(P_2)$ single crysts., refl. spectra, band struct., dielec. consts. 77−44022
ZnTe, excitonic effects on E_0 and E_1 gaps, anal. of measured spectrum, derivation of dielectric const. 79−61400
ZnTe, wavelength modulated reflectivity spectra *(Japanese)* 79−11435
ZrN, optical props. at 300K 78−19466

Kramers systems *see determinants*

Kromayer lamps *see mercury vapour lamps*

Kronig-Penney model
channeling in Kronig-Penney pot., band struct. and Bloch wavefunctions 80−65112
crystal in static elec. field, true width of electron levels 77−66145
cubic lattice, soluble dispersion reln. for 3-D band struct. 77−8007
education, deep one-dimens. periodic pot., zero energy gaps, Kronig-Penney model 80−62426
electron eigenstates in ordered and disordered ensembles of scatterers 79−99466
energy band structure, nearly-free and tightly-bound electron approxs. 78−73792
energy bands, low-lying, Mathieu and Kronig-Penney potentials comparisons 80−70583
EXAFS, one-dimensional model calc. 77−20957
insulator, in inhomogeneous elec. field, localized states in forbidden band 77−8060
Koster-Slater method, convergence and interleaving theorem 78−23051
liquid-like random Kronig-Penney model, electronic density of states, CPA calc. 79−1567
localised energy levels, lower bounds, intermediate Hamiltonian approach 80−54643
metallic state, one dimens. model, stability *(Russian)* 77−85171
nonseparable band problems, in higher dimensions 79−46995
one-dimensional lattice, impurity levels, transfer matrix approach 79−42489
one-dimensional semi-infinite crystal with arbitrary potential at boundary, surface states 77−43681
polytypes, one-dimens. Kronig-Penney model and calcs. 80−75494
quantum particle in one-dimensional potentials with incommensurate periods 80−34345
semiconductor, possible role of surface states in FIM 77−47883
semiconductor-vacuum interface, phase rule 78−52049

Kronig-Penney model continued
semiinfinite, existence conditions for surface states 77−89826
Shockley states in a semi-infinite Kronig-Penney model 79−73562
simple solution for teachers 79−22
Stark ladder levels, width and spacing 78−72124
surface states, semiinfinite cryst., generalised existence conditions 77−51794
surface states, transfer matrix approach 78−95321
surface states in one-dimens. model of cryst. in external field 77−72896
theta function-modulated plane wave appl. to band theory models 77−39763
GaAs-AlAs superlattice, folded acoustic phonons obs., Raman scatt. 80−88996
$GaAs-Ga_{1-x}Al_xAl$ superlattice, reson. Raman scatt., 2-D quantum states 77−8577
SiC crystal, energy band struct. and optical spectra 78−18962

krypton
see also nuclei with .....
absorption on graphite, monolayer regime phase diagram 80−49507
accommodation coeff. meas., on O_2 covered Pt wire, 400-1400K 77−63948
adatom-graphite surface interaction, polarisation energy from opt. data 77−72792
adsorbed dense monolayer on graphite cleavage face, phase transition 78−56034
adsorbed layer on graphite, heat capacity 79−60621
adsorbed layer on W, effect on field emission energy distrib. 77−8730
adsorbed layers on graphite, neutron diffr. obs. 77−72789
adsorbed mono- and bilayers on graphite, two-dimens. struct., neutron diffr. study 79−42393
adsorbed monolayer, Lennard-Jones fluid eqns. of state predictions vs. expt. 79−69223
adsorbed monolayer, on graphite basal face, fluid-registered solid transition 80−49491
adsorbed monolayer on graphite, gas to condensed phase transition 77−7968
adsorbed on graphite, commensurate-incommensurate transitions, low temp. theory 80−103582
adsorbed on graphite, nonregistered-registered phase transition 80−39414
adsorbed on graphite, overlayer-substrate spacing, LEED determ. 80−103579
adsorbed on graphite, Potts lattice gas, renormalisation-group treatment 78−67908
adsorbed on graphite, X-ray diffr. from 2-D solid 78−75498
adsorption, on porous C, Henry's constant, pre-exponential factor *(German)* 78−22961
adsorption on activated C, equil. adsorption coeffs. at low partial press. 77−52673
adsorption on BN_3 and graphite 79−73397
adsorption on Ge (111) plane, adsorpt. pot. 78−26768
adsorption on graphite, finite size effect and temp. depend., multicritical phase diagrams 79−42372
adsorption on graphite, substrate deform. meas. 80−54520
adsorption on graphitized carbon black, virial coeff. theory anal. 78−34697
adsorption on hexagonal BN_3 79−73395
adsorption on NaCl, energy distrib. using numerical algorithm HILDA 77−55443
adsorption on SiC coated UO_2, small surface area determ. 80−44429
adsorption potential energies on NaBr and KBr, calc. 78−71993
afterglow, stationary, singly charged atomic ion obs. 80−38757
afterglow plasma, electron energy distrib. function 80−38748
afterglow spectra of pulsed discharge, levels populated by dissociative recombination 78−83640
anomalous isotope composition at Oklo natural reactor deposit 77−56630
arc lamp, acoustical resonances and instabilities 77−58907
arc spectrum, isotope shifts in near IR lines 79−72257
atmospheric activity meas. using ^{85}Kr 77−78454
atom, $3d_{3/2}$ subshell impact ionis., coincidence exptl. method, theory 80−1066
atom, 3d-shell electron impact ionis., Auger electrons ang. distrib. 77−27183
atom, 3p core hole spectrum, many electron description 78−50517
atom, 3p X-ray photoelectron spectrum, many-electron effects 78−50513
atom, $4p^55p$ and $4p^56p$ configs., level radiative lifetimes meas. 78−58625
atom, $4p^55s$ state, electron excitation fine struct. neg. ion reson. 77−14585
atom, 4p asymmetry parameter and cross section photoelectron energy depend. pseudopot. method 78−9130
atom, 6p levels, two-photon excitation, time resolved fluoresc., quenching, lifetimes and photoionisation cross section 80−78587
atom, $^3P_1$ state, reson. fluoresc., Zeeman beats, time-resolved VUV spectra using synchrotron radiation 78−33454
atom, absolute photoionis. cross sections for VUV region 77−46547
atom, absorpt. spectrum, using vacuum UV storage ring source 77−7165
atom, approximate relativistic Hartree-Fock eqns., soln. using Slater-type functions 80−58168
atom, Compton profile, local density approx., Kohn-Sham self consistent scheme 78−94193
atom, Compton profiles using Gaussian expansion of at. orbitals 80−945
atom, double ionisation by electron impact, soft X-ray emission *(Russian)* 77−34766
atom, elastic positron scatt., phaseshifts and elastic, diffusion and annihilation cross section 80−53134
atom, electric dipole lines, absolute transition probabilities 80−9560
atom, electron energy loss spectra, energy-depend. multichannel quantum defect theory anal. 77−61860
atom, electron impact, near threshold UV-emitting level excitation 78−25711
atom, electron impact, struct. near $M_{4,5}$ edges 77−75083
atom, electron impact autoionisation, cross-section parametrisation 77−6932
atom, electron impact excitation, rel. differential cross-section meas., 15 to 100 eV *(French)* 78−13602
atom, electron impact excitation of autoionis. states 78−90302
atom, electron impact ionis. of inner shells, coincidence expt. theory 78−58837
atom, electron impact ionisation, cross section ratios 78−94326
atom, electron ionis. cross section, Born approx. 77−83745

krypton continued
atom, electron pulse radiolysis, 2p levels formation and decay kinetics 78−31665
atom, electron scatt., threshold excitation spectra 78−70936
atom, electron scattering, elastic, low-energy, polarised-orbital calcs. 80−37882
atom, ESCA, lifetime broadening, CI resonances 77−18853
atom, Feshbach reson. classification, relation to ionis. pots., appl. Ne, Kr, Ar, Xe 77−54519
atom, first excited config., intermediate coupling coeff. 80−83450
atom, fluoresc. lifetimes, time resolved VUV spectra 78−17601
atom, g-factors meas. by optical pumping and mag. reson. 80−14246
atom, heavy ion induced MNN Auger electron spectra 77−6907
atom, impulse Compton profiles, atomic optimised pot. model 78−74618
atom, incoherent scatt. factors calc. by direct integration over impulse approx. Compton profiles 80−102475
atom, independent particle pots. comparison 80−52846
atom, inner shell alignment calc. in electron impact ionisation 77−14586
atom, kinetic energy functional, gradient expsn. 77−6665
atom, Koopmans' ionis. pot., relax. correction 79−18308
atom, large angle elastic and inelastic electron scatt. differential cross section, exchange corrections 80−28111
atom, line strength calcs. for 7s-6p and 4d-5p transitions 77−14384
atom, metastable, electron impact excitation cross-sections calcs. 78−94323
atom, metastable, photoionisation rel. to laser development 78−13476
atom, ns→εp photoelectrons, spin polarisation 80−37792
atom, nucl. mag. relax. meas. in gas 80−43072
atom, optical and Auger spectra, discrepancies anal. 79−93944
atom, outer $p_{1/2}$ subshell photoionisation, polarised electrons, relativistic RPA calcs. 80−83331
atom, outer shell photoionisation, relativistic RPA calcs. 80−9571
atom, photoelectron asymmetry parameters 80−95684
atom, photoelectron emission, polarisation depend. on incident unpolarised VUV radiation wavelength 80−52952
atom, photoionisation, absolute cross-sections, exptl. meas. techniques 80−63598
atom, photoionisation, appl. of valence electron spectroscopy using polarized He I radiation 77−492
atom, photoionisation cross sections for excited states 77−75110
atom, photoionisation cross-sections, ground state inversion pot. method 78−33481
atom, polarisation transfer collision with Rb atom, NMR of Kr 78−33453
atom, population inversion, intershell transitions, photoionisation, from UV irradiation *(Russian)* 78−70803
atom, primary ionisation by ~2 MeV relativistic electrons *(Russian)* 77−75309
atom, props., calculation from optimised potential model 79−6895
atom, radioactive, spectrometer for meas. of isotopic, isomeric shifts and hyperfine structure 79−6191
atom, reson. levels relax. consts. determ. by alignment method in discharge 79−26936
atom, rotation of plane of polarisation close to reson. 79−41129
atom, self-broadening of first reson. line 79−26933
atom, shake-up energies, Slater transition-state calcs. 79−89651
atom, spin-polarised photoelectrons by circularly polarised synchrotron radiation 80−91516
atom, twelve-photon ionis. at 10^{13} W cm^{-2} laser field 80−32687
atom, ultrasoft X-ray emission near $M_{4,5}→N_{2,3}$ transition 79−76377
atom, VUV fluoresc. under monochromatic excitation 78−9237
atom, X-ray scattering, anomalous, Kramers-Heisenberg dispersion calc. 79−89628
atom+H(D), ion pair formation, curve crossing model 80−87216
atom+Li(Na)(K)(Rb), quenching cross sections of alkali n^2P states, 5-100 eV 79−76505
atom-atom collision with Rb, disorientation cross-section temp. depend. 77−23546
atomic, XPS calc. 78−958
atomic beam, partially metastable, composition, charge exchange 79−85914
atomic electron pot. scatt., 100 and 500 eV, extended Glauber approx. calcs. 77−54610
atomic electron scattering, 20-300 eV, total cross sections 79−36778
atomic isotope shifts using IR laser lines 77−27026
atomic structure, Hartree-Fock electron density, kinetic energy functional 79−26879
atomic structure, Thomas-Fermi model with Fermi-Amaldi correction 79−81156
atomic three-body collision-induced light scatt. spectrum moments 78−9226
atoms, absorpt. spectra, field induced autoionisation near ionisation threshold 80−106301
atoms, electron ionisation and excitation coeffs. in low E/N region 80−48090
atoms, free, electron bombard., subsequent X-radiation ang. distrib. 80−53144
atoms, inner-shell level energies, absorpt. spectroscopy with synchrotron radiation 80−99583
atoms, metastable, in afterglow, spectra, collisions 77−427
atoms in Ne matrix, radiative and nonradiative lifetimes in excited states 80−69106
breakthrough characts. of Kr in charcoal bed, effect of carrier gases, temp. and intraparticle diffusivity *(Japanese)* 79−73392
broad beam ion source used for sputtering and etching 80−69002
carbonaceous chondrites, fission Kr and Xe origin 79−35199
Clausius-Mossotti function, exam. of variation with gas density 78−52418
clustering, in W (100) He desorption spectrometry 80−77908
convective instabilities in closed vertical cylinder heated from below 79−77072
critical region, thermodynamic properties, correlation experimental data 78−6139
cryogenic distillation from gaseous effluents in nucl. fuel reprocessing 80−5309
cryogenic distillation process for noble gas removal from gas streams at Japanese power stations 77−61538
crystal, exciton exam. 78−51898
crystal, pure and benzene-doped, photoelectron emission, exciton states 77−44116

krypton continued
crystallite on Be substrate, crystallite dimensions determ. using synchrotron radiation X-ray diffr. photographs 80−24313
crystals, internal energy, Monte Carlo calcs. 77−72577
DC glow discharge excited atoms, radial conc. distrib. obs. 78−67494
dense, depolarised Rayleigh scatt. 79−69851
diffusion, of methane, isotope effects at various densities 77−68732
diffusion coefficients and mobilities of F^- ions in Kr and Xe 80−100048
diffusion in tetrafluoromethane, 243.15K, density depend., size effect 78−75859
diffusion in Xe, diffusion coeff. density expansion, search for log. term 79−82024
diffusion of ^{85}Kr in fluid Kr, apparatus and expt. results 78−54520
dilute gas, transport props., simple pair pot. model 80−87835
discharge, non-self-maintained, ionis. instability of excited ats. and excimers *(Russian)* 77−84557
discharge, secondary ionisation processes 78−59711
EBR-II cover-gas cleanup system 79−97874
energy loss straggling for H^+ and He^{x+}, ion energies of 50-500 keV per nucleon 77−46620
entrapment in pulse biased sputter deposited metals 79−28255
epitaxial monolayer on graphite, second order phase transform. obs. by LEED 77−76687
EPMA of Kr in sputtered layers of GaAs 80−3443
equation of state, perturbed-hard-sphere, applicable to sub- and supercritical temps. 79−19350
excimer lasers, stimulated emission kinetics in nonself-sustained elec. discharge 78−50753
excimers and excimer lasers 80−48217
excited atom+molecules reactions, electronically excited atoms and alkali metal atoms analogy 80−76490
excited levels, lifetimes, measurement by photon-photon delayed coincidence technique 79−89640
field ion appearance potential spectroscopy, temp. effects 79−19978
filament lamps, Kr-Ag-N gas mixture, thermal conduction coefficient calculational methods *(Russian)* 80−96335
film, absorpt. in exciton region 78−52529
fission gas release from UO_2-Zr high burnup nuclear fuel rods 80−57846
fission products formation and behaviour, Kr and Xe separation and processing *(Czech)* 79−49707
fluoroform($-d_1$)-trimethylamine-Ar(Kr), cryospectroscopic IR study of association 77−468
fluoromethane, in Kr matrix, vibr. relax. IR double reson. 77−79635
gas, compressed, 3371 to 1124 Å conversion by nonresonant freq. tripling of N_2 laser 79−64279
gas, ion mobility and longit. diffusion coeff. of Na^+ 80−106866
gas, Kerr effect virial coeffs. 79−50843
gas, laser-induced breakdown wavelength depend. meas. of threshold 79−41895
gas, liquid, solid, refractive index, density and dielectric const. 80−66138
gas, nonlinear susceptibility meas. via third harmonic generation, Lyman-α 1216 Å source 80−95947
gas, proportional scintillation mechanism 79−81131
gas, thermal cond., 90-270K, 1 atm. press. 78−42700
gas, thermal conductivity, reduced temp., atmospheric press. 77−84385
gas, thermal conductivity meas. at elevated temps. by hot wire method 80−6199
gas, thermal conductivity meas. at elevated temps. by hot wire method 80−6200
gas, third harmonic generation, bandwidth limitations in Lyman-α vicinity 79−81482
gas, tunable narrow-band coherent VUV source for Lyman-α region 80−38070
gas atoms, electron thermalization time and position distribution meas. 80−93771
gas discharge plasma, electron impact depolarization 80−43847
gas structure, by neutron diffr., three-body pot. contrib. 79−90358
gas structure, three-body-contrib., neutron diffr. obs 80−43820
gaseous adsorption in fission reactor fuel reprocessing 79−31094
gaseous effluents from LWR and reprocessing plants, treatment and control 77−61589
gaseous fission product, continuous determ. of content in reactor loop 79−30905
gaseous mixtures, binary and ternary, viscosity meas. 78−18367
gaseous reactor waste treatment in PWR and BWR 79−54570
Gaussian basis sets, Ga, Ge, As, Se, Br, and Kr, HF calcs. 77−38611
glow discharge, electron energy distrib. function, electrical characts. investig. 80−24279
glow discharge, Kr_2^+ dissoc. recombination coeff., electron temp. depend. 78−30501
harmonic generation for H conc. reson. fluoresc. plasma diagnostics *(Russian)* 77−79895
high-frequency discharges, at sub. atm. press. 78−67460
hollow-cathode glow discharge with gas flow 78−67532
HTR individual coated fuel particles, gas anal., optimum heating and crushing 77−56294
HTR individual coated fuel particles, mass spectrum. determ. of Xe, Co and Kr gases 77−56293
immobilisation by incorporation into metallic matrix by ion implantation and sputtering 80−27794
implantation in GaAs, influence of damage on diffusion 78−6082
impurities in alkali metal films, optical excitation spectra obs. 77−24876
impurities in magnetic GdCo and GdCoMo films prepared by RF bias sputtering 77−44163
inner electron energy characteristics, validity of Hartree-Fock-Pauli approx. 80−42957
interatomic potential and transport props. 77−14519
interatomic potential functions 79−68293
intermolecular potential energy function determ. from thermal diffusion data 77−54590
ion+Kr target collisions, quasimol. KX-ray spectra, Doppler shift 77−19044
ion+target collisions, K-X-ray yields, 1sσ excitation 77−19051
ion+target collisions, K-X-ray yields, 2pσ excitation 77−23549
ion+target collisions, K-X-ray yields, K-vacancy sharing 77−23548
ion+target collisions, X-ray yields, K-L level matching 77−19052
ion bombardment of polycryst., kinetic energy reflection 77−85869
ion collisions, 200-330 MeV, K-vacancy production, multiple and single collisions in mol. orbital excitation 77−83717
ion impact on C foil, energy loss 78−55902
krypton continued
ion implanted in Si, migration during anneal 78−18834
ion laser, mode-locked, near UV, 50 ps pulse width 78−79030
ion source, HF, proton yield increase, influence of various admixtures to H_2 obs. 80−57422
ion-atom collision, K-vacancy prod., mol.-orbital method 77−68095
ionisation relaxation, stepwise, multilevel models 78−13592
ionising shock wave refl., interferometric meas. 79−55553
ions, high energy stripping by solid foil, charge state distribs. 77−6912
IR lasers pumped by U fission fragments 80−28198
isotope separation, HF stationary discharge, travelling mag. field, barodiffusion separation 80−44049
isotope separation, non-active end vol. effect on transient separation of thermal diffusion column 77−35300
isotope separation using SIDONIE and PARIS separators 77−14269
isotopes, even, isotope shifts of 557 nm transition 77−61710
isotopic abundances, s-process contributions 79−5739
Kerr effect in gas, statistical theory 79−50842
L-shell fluorescence yield 80−47937
laser, CW UV emission, power enhancement 78−17906
laser, He-Kr mixture, hollow cathode, internal anode system, CW 78−9396
laser, high output power in visible and near UV 78−1249
laser, new IR laser transitions, 3.725 to 17.233 μm 80−87374
laser, nuclear pumped, energy pathways by proton excitation 78−5459
laser, recombination, in expanding CO_2 laser prod. plasma 77−88698
laser, tunable, Lyman alpha radiation, nonlinear generation 78−87038
laser oscillation obs. in transversely initiated laser-produced plasma 77−88696
laser wavelength measurement using digital interferometer 80−37079
lattice heat capacity, thermal vibrations, Lindeman parameter, lattice dynamic model *(Russian)* 80−29141
Lennard Jones (12,6) pot. distance parameter, transport props. calc. 80−79423
liquid, comparison on interaction induced light scatt. and IR absorption 80−60561
liquid, compressibility, long wavelength limit of liquid struct. factor 78−67633
liquid, electron drift vel., mol. solute effects 77−4338
liquid, electron mobility, role of shallow traps 80−34440
liquid, excess electron mobility, Cohen-Lekner theory failure 78−19112
liquid, high-field electronic conduction obs. 79−4587
liquid, ionisation and scintillation, application to radiation detectors, review *(Japanese)* 78−35206
liquid, perturbation theory for sound prop. vel. *(Russian)* 77−15500
liquid, principle of corresponding states for viscosity 77−84959
liquid, Ramsauer-Townsend minimum in electron scatt. cross section 77−89821
liquid, recomb. and self-trapped exciton luminesc., free electron dynamics, excited states 80−25463
liquid, T_c, P_c, V_c, from eqn. of state 78−2228
liquid, triplet state of self-trapped exciton states, evidence of existence, luminescence meas. 78−72608
liquid, US attenuation and bulk viscosity 80−49304
liquid and solid, absorpt. and luminesc. spectra of self-trapped excitons 79−65893
liquid independent structure model, critical point, liquid-vapour equilib., second virial coeff. *(Spanish)* 77−4031
liquid ionisation chamber media, review of physical props. 79−41071
low-press. glow discharge, elec. characts. of positive column 80−100112
Mars, atmospheric Kr and Xe, Viking obs. 77−56856
mass spectroscopic chemical anal. using quadrupole mass spectrometer for fissile material accounting 80−63300
matrix isolated NO 3sσ($A^2\Sigma^+$) Rydberg state 'bubbles', reson. fluoresc. obs. 77−83636
methane-Kr mixtures, rot. self-diffusion and spin-lattice relax. *(Russian)* 79−69745
methanol+Kr, methoxy radical prod., UV emission spectra 80−91572
molecular dynamics simulations, three effective interactions 79−69224
monolayer, adsorbed on Cu surface, many-body interactions 78−84068
monolayer, density profile, adsorption isotherm, in superposition approx. 79−33182
monolayer, on graphite, misfit dislocations and lattice parameters, model 78−34708
monolayer, on graphite (0001), liq. state model appl. 77−69185
monolayer, on graphite commensurate-incommensurate transition, X-ray scatt. 79−73382
monolayer on graphite, disregistry transition 78−30825
monolayer on graphite, phase transition from localised to nonlocalised solid 77−11787
monolayers adsorbed on (0001) graphite, continuous phase transitions 78−34698
photoionisation, 3d subshell absorption spectra 77−10648
physisorbed monolayer on graphite, neutron scatt. studies 80−107655
physisorbed on metal, polarisation due to short range interaction with substrate 80−39428
physisorbing on Ni, stay time meas. 78−56044
plasma, dense, shock-heating, calc. of equilibrium props. *(Japanese)* 80−79513
plasma, electron beam excited plasma UV absorpt. by diatoms 79−68907
plasma, energetic binary collisions 79−77337
plasma, high-press. arc discharge, elec. cond. 80−59181
plasma, of positive column, at. alignment, radiative lifetimes, collision cross sections 79−4203
plasma, shock-heated, continuum radiation emission coefficient meas. 79−64835
plasma, shock-heated, dense, continuum radiation and optical transmittance diagnostics 80−24202
plasma, thermodynamic functions, composition, and elec. cond., calc. method 79−32738
plasma Tokamak discharge, impurity emission spectra for diagnostics 77−11403
plasma trap for magnetic flux, loop probe meas. 79−14621
potential, predictive ability for dilute gas, bulk and microscopic data 79−81250
radioactive, adsorbed on charcoal, release in spill accident 77−50262
radioactive effluent gases from nuclear power industry, ambient contamination *(Spanish)* 78−61540
radioactive ion implantation using Lublin separator 79−82251
refractive index meas. using low temp. refractometer 77−57382

krypton continued
removal from irradiated UO_2 in fuel reprocessing 77−67850
resonance lamp in vac. UV, new developments 79−32017
s-process Kr in meteorite, $^{86}Kr/^{84}Kr$ ratio rel. to s-process neutron capture time scale 80−73080
scintillation detectors appl. *(Czech)* 78−86727
second virial coefficients from compressibility meas., mol. pot. parameters calc. *(Spanish)* 77−47133
self-diffusion coeff. behaviour at low density, 293K 78−67302
self-diffusion coefficient, radioactive tracer meas. 77−13534
separation in fission fuel reprocessing plants *(German)* 79−85719
separation performance from Ar binary mixture, in thermal diffusion column 77−42192
shear viscosity determination under high pressure, using capillary viscometer 78−55708
single crystal, Pockel coeffs. and short-range-interaction parameters 79−73962
solid, absorption spectra of self-trapped excitons 78−43879
solid, anharmonic contributions of $O(\lambda^4)$ to mean-square atom displacement 79−42155
solid, core excitons, integral eqn. formalism, isolated atoms and cryst. 78−47704
solid, dead layer effects in UV reflectance of excitons 78−72553
solid, density at melting and isochoric equations of state 78−83915
solid, electronic struct. of self-trapped excitons 79−19525
solid, enthalpy of sublimation, internal energy, determ. from vapour pressure 78−91435
solid, H_2 and D_2 CoM freq. matrix shifts calc. 79−6969
solid, HCP, vap. phase grown thin films 78−18917
solid, high-temp. thermal expansion characts. 80−59680
solid, improved unsymmetrised SCF approx. for strongly anharmonic crysts. 78−75791
solid, lattice dynamics calc. using Kihara hard core pot. 77−1193
solid, liquidus lines in liq. air component mixtures *(German)* 77−84915
solid, n=1 surface excitons and LO-TO splittings of bulk excitons 79−73445
solid, NMR study of dilute o-H_2 impurity 80−25228
solid, particle track obs. in condensed matter by emission method *(Russian)* 77−57824
solid, phonon dispersion, many body pot. assuming variable at. polarisability, mech. props. 79−55840
solid, phonon freqs., lattice heat capacities, and Debye charact. temps. 79−10905
solid, reflectivity, Kramers-Kronig anal. 77−73122
solid, self-trapped exciton, pseudopotential method 79−82529
solid, surface excitons 77−76892
solid, thermodynamic props., behaviour near m.p. *(French)* 77−1212
solid, vacancy conc., X-ray study at const. vol. 80−64991
solid, vibr. and thermal props., effect of polarisability 78−71807
solid film, electron MFP, vacuum UV photoemission data 77−28690
solid monolayer on graphite, commensurate to incommensurate transition 80−80079
solubility in liq. scintillator solvents, meas. using radioactive tracers 77−57808
submonolayer, adsorbed on graphite, melting, X-ray scatt. obs. 78−95234
submonolayer films on graphite, mol. dynamics simulation 80−88425
substrate uniformity, Kr vapour press. isotherms at 77K as standardized meas. 80−107657
superheated liquid, nucleation rates 79−23741
supersonic jet, electron beam excited, vac. UV spectrum 77−88414
surface, desorption of He, appl. of simplified continuum model 78−87860
tetracene-Kr(Xe), intramol. intersystem crossing in supersonic beam, external heavy atom effect 80−14167
thermal conductivity, 100-1200K 77−35305
thermal conductivity, at high press. 80−103099
thermal conductivity, law of corresponding states *(Russian)* 78−87426
thermal conductivity, near 300K, density depend., 1.1-16 MPa 78−67304
thermal conductivity coeff. meas. 1100-2200K range, differential technique 77−33989
thermal conductivity Lennard-Jones (12-6) pot. parameters calcs. 80−28591
thermal release from amorphous $Gd_{0.27}Co_{0.64}Kr_{0.09}$ UHV mass spectrometric technique 80−3439
total electron impact excitation cross section, first Townsend coeffs. 77−536
triple point realisation, reference temperature appl. 78−73997
UV light source for plasma diagnostics, 121.5-121.6 nm *(Russian)* 78−25942
vapour press., entropy and enthalpy, thermodynamic consistency, two-parameter eqn. 77−80613
viscosity, 130-1300K, up to 10^9 dyne cm^{-2} 79−60536
viscosity, near solidification, 50°C, up to 6500 bar, meas. and simulation using Lennard-Jones pot. *(French)* 78−67301
viscosity, vibr. disc method meas. 80−75020
viscosity coeff., density expsn. 78−91054
VUV radiation, narrowband tunable, at Lyman-α wavelength 80−78907
VVER fuel elements, T and ^{85}Kr content obs. 77−54349
water-cooled arc lamp, anode, temp. distrib. along length, anode geometry effects 80−106994
Al:Kr foil, ion implantation, low-temp. on-line Mossbauer meas. of ^{83m}Kr 78−35071
^{40}Ar:^{41}K, matrix isolation model system 78−45722
Ar-Kr, internal pot. function calcs. 79−68292
Ar-Kr, liq. mixture, excess thermodynamic props. 78−75836
Ar-Kr, mol. force const. from viscosity data, thermal cond. 78−33565
Ar-Kr, pair pot. energy functions, gas phase bulk property reproduction 77−27642
Ar-Kr, pair pot. function calcs. 78−74726
Ar-Kr, thermal cond., 90-270K, 1 atm. press. 78−42700
Ar-Kr jet, electron excited, VUV emission spectra 80−933
Ar-Kr liq. and gas. solns., collision-induced dipole moment, far IR band obs., self-diffusion coeff. 77−38627
Ar-Kr liquid mixtures, volume and shear viscosities *(Russian)* 77−84961
Ar-Kr mixture, thermal cond., 120-273K 78−83514
Ar-Kr mixtures, liq.-vap. isotope fractionation factors 78−33626
Ar-Kr white light lasers *(Russian)* 77−27303

krypton continued
Ar-Kr-F_2 discharge, inelastic electron collisions, energy distrib. and rate consts. 80−87980
Ar-Kr-F_2 excimer laser, kinetics of excimer formation 80−14328
Ar-Kr-F_2 mixture, electron beam pumped, spectroscopy and kinetics of 248, 414 nm bands 78−63081
Ar-Kr-F_2 mixture, nucl. induced excimer fluoresc. for I laser excitation 80−78846
Ar-Kr-F_2 nuclear pumped laser, high energy beam deposition 80−63999
Ar-Ne(Kr) systems, pot. parameters from binary diffusion coeffs. 78−37700
Ar^+-Kr^+ ion lasers, I_2 stabilized, beat frequency 80−95916
$Ar+H_3^+$, collision-induced dissoc. 77−42383
Ar+Kr, $(4p^5p)$ and $(4p^5p')$ states, radiative lifetimes and two-body collisional deactivation rate consts. 80−95572
Ar+Kr, binary diffusion coeff. pressure depend. meas. 80−43826
$Ar+Kr(^3P_2)$, flowing afterglow metastable decay rates, diffusion, two- and three-body rate consts. 78−73027
$Ar^{2+}+Ne(Ar)(Kr)$ single electron capture cross-section 77−88550
$Ar^{x+}+Kr(N_2)$, (x=2-7), electron capture cross sections, 10-110 keV 77−6923
$Ar^{*+}+Kr$, flowing afterglow, energy transfer reaction and quenching rates 80−23529
$Ar^*(4s^3_{2,0})+Kr(Xe)$, elastic and reactive scatt., ang. distribs. 77−6919
B+Xe(Kr), reson. radn. quenching 77−30820
Ba+Kr, collision induced dipole transition, elec. quadrupole transition, oscillator strengths 79−41128
$Ba^{+}+Kr$, quasimolecular states interference, degree of polaris. oscill. *(Russian)* 77−6917
Cl^--Ne(Ar)(Kr)(Xe), longitudinal diffusion coeff., generalised Einstein relation 79−86552
$Cs_2+He(Ne)(Ar)(Kr)(N_2)(CH_4)$, collision-induced dissoc., atom-mol.-exchange optical pumping 78−22008
$CsCl(Cs_2Cl_2)+Ar(Kr)(Xe)$, collision-induced ion-pair form., absolute cross sections 78−73029
Cu:^{85}Kr 80−15145
F ions+Ne(Ar)(Kr) and C foil and slab, K shell X-ray spectra 78−17599
F+Ne(Ar)(Kr), thermal energy interaction pots., crossed beam study 79−68288
F_6S-Kr, compressibility 0 to 50°C, second virial coeffs. calcs. 77−15147
Fe:K, mag. hyperfine interaction, temp. depend. 78−68420
$H+H^+(Arq^+)(Kr^{q+})(B^{q+})(C^{q+})(N^{q+})(O^{q+})$ charge transfer and impact ionis. cross sections calcs. 77−88555
H+inert gas atom, interaction pot. from electron gas model 79−31637
$H^++He(Ar)(Kr)(O_2)(H_2)(N_2)$, 2.2-8.2 keV, H(n=3) form., absolute cross sections 77−34755
H^++Kr, mol. orbit approach, spin-orbit interaction, adiabatic pot. and projected valence band treatments 77−533
$H^++Kr(Ar)$ charge exchange, oscillating cross sections 77−58158
$H^++Kr(Xe)$, electron capture into 3s state, cross-section meas. 78−42209
H_2-Ar(Kr)(Xe) mixtures, intermol. forces 78−62867
H_2-Kr, bound complex form., anisotropic intermol. pot., IR spectra anal. 78−37634
H_2+Kr, differential cross-sections, diffraction undulations, anisotropic pot. calcs. 78−9223
H_2+Kr, elastic total cross section, orbiting effects, Regge theory 78−82814
$H_2^++He(Kr)(Xe)$, collisional dissociation, ion-pair prod., negative ion prod., cross sections 77−14529
HCl-Kr, rot. for IR spectra, anisotropic density fluctuations 79−54848
HCl+Kr(Ar), pot. energy surface determ. from rot. line broadening data 79−13784
HD-Kr, $R_1(1)$ absorpt. spectra, positive intercollisional interference 79−54843
$H(2S)+Kr(Ne)(Xe)(H_2)$, metastable atom total quenching 77−46628
He-Ar(Kr)(Xe), 208 and 707K, intermol. forces, virial, diffusion, and viscosity coeffs. 77−75256
He-Kr, ion laser transitions, hollow cathode excitation 80−1184
He-Kr, Kr I TEA lasers, energy characteristics 80−63977
He-Kr HV hollow cathode laser, gain meas. of Kr II 4694 Å, 4318 Å CW transitions 79−45928
He-Kr high voltage hollow cathode discharge, new Kr II CW laser lines 79−13947
He-Kr hollow cathode CW laser, Kr II 4584 Å generation 80−58510
He-Kr hollow-cathode dischage, CW and pulsed lasing at Kr ion lines 79−3679
He-Kr hollow-cathode discharge, CW laser oscills. on Kr II 4694 Å, 4318 Å lines 79−3680
He-Kr ion lasers, hollow cathode, CW operation and excitation mechanism 80−69363
He-Kr mixture, diffusion coeff. meas. by diffusion in flowing gas 80−83876
He-Kr mixture, diffusion coeff. meas. by diffusion in flowing gas 80−83877
$He-Kr^+$ ion laser, He metastable atom concentration and time variation 79−55111
$He-Kr^+$ ion laser, microwave-pulse-excited, spectroscopic expts. 77−71973
He-Kr(Xe), scaling parameters for thermal diffusion factors, viscosity, mutual diffusion coeff. calcs. 77−35292
He+Ar(Kr), translation band spectral moments, induced dipole moments 78−55218
$He+Ar(Kr)(Xe)$, $He^*(2^1S)$ scatt., low energy repulsion systematic struct. 78−22000
He+Ne(Ar)(Kr)(Xe), energy transfer, time-resolved VUV spectra 77−19028
^3He-Hg (−Kr)+$^3He(n,p)T$, high press. plasma excitation, luminesc. spectra 80−38719
^3He-Kr, direct nuclear pumped lasers using $^3He(n,p)^3H$ reaction 79−31863
^3He-Kr, nucl. lasing, population inversion mechanism 80−63980
^3He-Kr laser, nucl. pumping by volumetric $^3He(n,p)^3H$ reaction 77−10886
^3He-Kr volume pumped nuclear laser survey of lasing 80−63979
^4He stopping cross sections, 1-8.5 MeV 78−58558
$He^*+Ar(Kr)(Xe)$, elastic scatt., repulsive rainbows and optical pots. 79−840
$He^*+D_2(Ar)(Kr)$ interaction pots. 77−83674
Hg, 2537 Å line satellites, Kr broadening 77−83523

krypton continued
Hg-Kr, mixtures, prebreakdown discharges, discharge current depend. on electron mobility 79−77433
Hg-Xe(Kr)(Ar), fluoresc. emission, high press., electron beam excitation, laser appl. 77−34676
K-He(Ne)(Ar)(Kr)(Xe), oscill. strengths, for induced dipole transitions, pot. energy curves 77−75100
K+H(H_2), orbiting resons., van der Waals pots., beam scatt. obs. 79−89739
K^++Kr, differential elastic cross-section meas. *(German)* 77−58130
Ke^++CO_2, CO_2^+ electronically excited states prod. 77−3454
Kr 4s, photoelectron ang. distrib., relativistic Dirac-Fock calc. 79−59411
Kr arc discharge, radiative characts. computational model requirements 80−64812
Kr I, 5871 Å line, transition probability meas. 77−3291
Kr I, (A=78 to 86), isotope shift, saturated absorpt. technique 77−75102
Kr I, high resolution polarisation spectroscopy of 557 nm transition 78−74602
Kr I, laser spectroscopy, isotope shifts, hyperfine struct. *(French)* 78−33457
Kr I, saturated absorpt. profile of 557 nm line, collision effects 78−9121
Kr I, Stark broadening in visible spectra 78−37590
Kr I, transition probabilities in transition arrays 80−32667
Kr I 6058 Å line, asymmetry rel. to cause of anomalous astron. redshifts 77−13458
Kr I atom, $4p^5$ nd (n=4,5,6,7) configurations, experimental lifetimes 80−27981
Kr I lines from wall-stabilised arc measurements, transition probabilities 78−22569
Kr I spectra, theoretical transition probabilities and lifetimes, data tables 79−54793
Kr I-III, hollow cathode discharge, excitation and ionis. mechanisms, spectra obs. 77−15261
Kr I-VIII, beam foil mean life meas., f-values 77−30974
Kr II, absorption spectrum in vac. UV region, ionisation energies 79−49972
Kr II, CI calcs. on $4s^24p^44d+4s^24p^45s+4s4p^6$ configs. 77−3277
Kr II, calcs. of radiative lifetimes, absolute transition probabilities and oscillator strengths 77−50405
Kr II, excited states lifetime meas., photon-photon delayed coincidence technique 77−68011
Kr III, CW laser, short wavelength multiline performance 79−926
Kr IV, very strong laser emission at 195.827, 175.641 nm 78−63060
Kr IV emission spectral lines, classification 80−95563
Kr, Kr-Xe, detection gas suitability for proportional scintillation counter *(German)* 78−41901
Kr, thermal diffusion factors, isotopic 78−22450
Kr V, emission spectral lines, classification 80−95563
Kr VII, beam-foil excitation, 4s4p $^1P_1^0$ level decay simulation 80−78578
Kr VIII, beam-foil decay curves for reson. transitions simulation 80−9721
Kr VIII, beam-foil lifetime meas. using ANDC anal. for reson. doublet 79−93964
Kr VIII, excited state energies and lifetimes, beam foil spectra 80−63591
Kr VIII, ionisation energy, multiplet strengths, diagrammatic MBPT theory calcs. 80−9500
Kr VIII beam-foil decay curves for resonance transitions 78−74755
Kr VII(VIII), reson. line oscill. strengths, beam-foil spectra 77−38630
Kr XI-XIV, X-ray and UV spectra, 30-300 Å range 80−95566
Kr XXVI, electron impact excitation, transition probabilities, oscill. and collision strengths 78−25718
Kr XXVII, ionisation pot. in Ne isoelectric sequence 78−5363
Kr XXXIII, energy levels and transition 79−59383
Kr XXXIII and Kr XXXIV, beam-foil obs. of transition wavelengths and oscillator strengths 80−14115
Kr^-, electron capture expts. to search for long lived states 79−72410
Kr^+, and isotopes, trajectory in const. mag. field plus orthogonal sinusoidal elec. field 78−50687
Kr^+, beam metastable fraction determ., by W surface impact, secondary electron obs. 79−28873
Kr^+, beam-tilted C foil interactions, charge-state distrib., photon emission, 100-400 keV 79−22814
Kr^+, equilib. charge state distribs. and multiple scatt. angles in C foil 80−59532
Kr^+ ion laser, mode-locked near UV output, chem. and appls. 79−45966
Kr^+, Kr_2^+, $^2P_{1/2}$ and $^2P_{3/2}$ states, mobilities in Kr, spin state depend. 77−3913
Kr^+ laser plasma lines for Raman spectrometer calibration 80−57394
Kr^+ mode-locked ion laser, pulse width and linewidth meas. 80−102696
Kr^{2+}, beam metastable fraction determ., by W surface impact, secondary electron obs. 79−28873
Kr^{2+}, mobility in He gas, drift-tube meas. 78−66657
Kr^{2+}, mobility in parent gas 79−7439
^{86}Kr, discharge, metastability-exchange cross section 80−99464
Kr:^{86}Sr, 8^+ state, nucl. g-factor and nucl. spin relax. in gas phase 77−22884
Kr:methane, impurity rotational states, inelastic neutron scatt. study 79−51020
Kr:Mg_n, matrix isolated Raman spectra 78−90170
Kr:N_2O, cryodeposited film, exciton-enhanced KrO excimer luminescence 77−36288
Kr:N_2O, photoluminesc. from KrO (^1S) excimers 78−68544
Kr:O, laser, electron beam excitation 77−711
Kr:OCS, O(^1S) and S(^1S) photodissociative prod., photoluminesc. excitation spectra, exciton energy transfer 80−89508
Kr:S_2, absorpt. spectra, matrix-isolated in van der Waal solid 77−52139
Kr-Ar, mol. interactions, thermodynamic props., mol. dynamics calcs. 77−61044
Kr-Ar, phase matched, generation of Lyman-α radiation 80−91845
Kr-Ar, solubility in Ar, and related functions, three-body forces 79−10776
Kr-Ar binary mixture, expt. determ. of temp. depend. of thermal diffusion factors *(Russian)* 79−60095
Kr-Ar mixture, shock-heated, ionisation relax. processes 77−84277
Kr-Ar(N_2) gas mixture, vapour-liq. equilib. data *(German)* 77−84915
Kr-Ar(Xe)-F_2 mixtures, excimer emission bands *(Russian)* 77−71885
Kr-Cl_2, UV transient absorption following flash photolysis 79−61879
Kr-Cl_2 mixture, glow discharge positive column, electron energy distrib. and rates of inelastic processes, negative Cl ions form. 80−19632

krypton continued
Kr-Cs^+, ion mobility and interaction pot., drift tube meas. at 300K 78−59537
Kr-F_2 mixture, preionised electric discharge stability 79−64865
Kr-Freon, saturation curve 1 to 8 atm., for ionography ionisation chambers 77−12997
Kr-H_2**, ionising collisions, KrH^+ form. 79−100338
Kr-HCl, intermol. pot. energy surfaces calcs. 80−91625
Kr-He(Ne)(Ar)(Xe), gas, diffusion coeffs. meas., 350-1200K 80−14869
Kr-K, afterglow of laser plasma, fluoresc. spectra 79−19085
Kr-Kr(Ar)(Xe), glory structure in total cross section, crossed supersonic atomic beam, n(x)-6 potential 80−48060
Kr-methane, liq., Soret coeff. at low temp. 77−89565
Kr-methane mixture, self-diffusion of Kr, density depend. 77−76587
Kr-N_2, liq., N_2 Raman scatt. parameters, high resolution coherent active spectroscopy 80−66207
Kr-N_2 plasma, afterglow ion prod. and loss processes 77−11401
Kr-N_2O, thermal diffusion factors meas. 80−10344
Kr-N_2O gas mixture, thermal diffusion const. 78−67300
Kr-N_2(He) gas mixtures, separation using silicone rubber, cellulose acetate membranes, separation factor 77−36791
Kr-NO, thermodynamics, monomer-dimer assoc. of NO, vap. press. meas. 79−90798
Kr-O_2, high press. mixtures, gain profile near 5577 Å 77−68204
Kr-plated graphite, possible Ising transition in ^{4}He adsorbed monolayer 80−34298
Kr-SF_6, cryogenic liq., SF_6 mol. motions, IR and Raman spectra 79−69823
Kr-Xe, absorpt. spectra line-narrowing, with reson. excitation transfer 79−89973
Kr-Xe, glow discharges, AC cataphoresis meas. using light spectrometry 79−60096
Kr-Xe, isotopic mixtures, separation in high-freq. discharge in mag. field *(Russian)* 77−75317
Kr-Xe, phase matched, generation of Lyman-α radiation 80−91845
Kr-Xe-F_2 excimer laser, kinetics of excimer formation 80−14328
Kr-Xe(Ar), UV absorption spectra, induced lines and line-shift meas. *(French)* 77−61697
Kr^+-He laser, microwave-pulse-excited, internal plasma parameter, time variation 77−38858
^{86}Kr-^{78}Kr, discharge, metastability-exchange cross section 80−99464
Kr^+-$^{35}ClF(^{37}ClF)$ potential, asymmetric, isotope substitution effect, Legendre expansion coord. transformation 78−70894
Kr^+-^{75}As, slowing down of atoms/ions with KE≤5 eV by inert gases 79−31650
Kr^+-$^{75}As^{n+}$, slowing down of atoms/ions with KE≤5 eV by inert gases 79−31650
Kr+acetylene, vibr. relax. study using laser-induced fluoresc. 80−74219
Kr+Ar, elastic collision total cross-section, low energy 80−5603
Kr+Ar,(Ne), elastic scatt., Monte Carlo averaging of differential cross-section data 78−21997
Kr+Ar^+(Ar_2^+)(Ne^+)(Ne^{2+}), thermal energy charge transfer reaction rates, mass spectrometric obs. 78−61000
Kr+Ar^{2+}, electron transfer cross-section, <100 eV 78−66654
Kr+Ar^{2+}(Ne^{2+}), single electron capture excitation, photon emission, VUV spectroscopy 80−58379
Kr+Ar^{6+}, collisional excitation, excitation cross sections 79−98209
Kr+Ar*, 123.6 nm emission excitation of Kr by metastable Ar, press. depend. 78−5331
Kr+Ar(He)(Ne), thermal diffusion, conc. depend. determ. 77−11300
Kr+Ar(Kr)(Xe), total scatt. cross-sections, glory undulations 77−10732
Kr+C_2H_4 liquid mixtures, intermol. forces effect on phase diagram and excess props., perturbation theory 80−39287
Kr+C^+(H^+)(N^+)(O^+)(S^+), charge exchange cross-sections *(German)* 77−10753
Kr+CHF_3, vibr. relax. times at 298K 77−525
Kr+CO, intermol. pot. energy surfaces from electron gas model, ang., distance, and vibr. depend. 79−3520
Kr+CO_2, collinear atom-triatom transition probabilities for anharmonic triatom pots., quantum mech. calcs. 80−83455
Kr+CO_2, collision dynamics, generalised Langevin eqn. approach 78−70900
Kr+CO_2, collisional energy transfer, anharmonicity effects 80−28097
Kr+CO_2, vibr. energy transfer rate, anharmonicity, quasi-classical calc. 78−46431
Kr+CO_2 (methane), ^{13}C-mag. shielding density depend. 78−9173
Kr+CO_2(001), deactivation pathways, quantal close-coupling calcs. 78−58787
Kr+carbon tetrachloride, differential elastic scatt. cross-section 79−45784
Kr+Cl_2, $KrCl^+$ form., mass spectrosc. obs. 79−29346
Kr+Cl^-(Br^-), total electron detachment cross sections, near threshold energies 79−3555
Kr+CsF_3, sudden, body-fixed and semiclassical approx. calcs. 78−42164
Kr+Cu^{q+}, (16≤q≤23), 1.4 MeV/amu, X-ray emission, charge state dependence 78−37713
Kr+Cu^{q+}, K-vacancy production, impact parameter depend. 79−72390
Kr+ethene, liquid mixture thermodynamic excess functions 78−48690
Kr+F_2, KrF form., relax. and quenching 80−81314
Kr+F^-, inner-shell ionisation, X-ray cross sections 80−58369
Kr+Fe^{4+}, 20 MeV, gaseous targets, electron loss, charge state yields 79−54957
Kr+H, 20-500 eV, ion pair and free electron production, integral cross sections 78−46437
Kr+H, low energy elastic scatt. cross section MCSCF calc., van der Waals forces 78−70897
Kr+H_2^+(H_3^+), collisional dissoc., 6 to 60 keV *(German)* 77−10733
Kr+H_2O(D_2O), ($^3P_{0,2}$) state quenching cross sections 78−70912
Kr+H_2S^+(CS_2^+)(CH_3I^+)(CF_3I^+), collision induced molecular ion dissociation, mass spectra *(Russian)* 77−88549
Kr+H^+, electron capture, 4-20 keV, production of highly excited H atom 79−54963
Kr+H^+, electron capture, charge-state distrib. 80−32814
Kr+H^+, electron capture cross sections 79−86061
Kr+H(D), free electron production, integral cross-sections determ. 79−89754
Kr+H(2s), 5-25 keV, H(n=3) excitation, Balmer α emission obs. 80−53113
Kr+H(2s), collisional de-excitation, 5-26 keV 79−59546
Kr+He, 2^1S and 2^3S assoc. and Penning ionisation cross sections vel. depend. 79−3551

krypton continued
$Kr+He^+(2s)$, metastable ion electron capture, loss and de-excitation 77−6904
Kr+He*, Penning and assoc. ionisation, correl. diagrams calcs. 77−50521
$Kr+He(2^1S,2^3S)$, Van der Waals forces, one-electron model pot. calcs. 80−14094
Kr+K, differential cross-section meas. by multi-crossed-beam method 79−45797
Kr+K, photon emission polarisation anal., coincidence studies 80−5614
Kr+Kr, isotropic intermolecular forces evaluation using semi-empirical approach 79−36726
Kr+Kr, low-energy collision induced UV radiation 79−50125
Kr+Kr, Thomas-Fermi-Dirac interaction pots. 77−75253
$Kr+Kr^+(Kr^+)$ collisions, quasimol. Auger transitions 77−19070
Kr+Kr(Xe), X-ray prod. cross sections for Kr L-shell vacancies 79−10190
$Kr+Li(2^2P_J)$, collision induced fine struct. transition rate coefficients determ. 80−74220
$Kr+NH_3$, pure rot. line, press. broadening calcs. 80−78656
Kr+NO, angle depend. intermolecular pot., crossed beams study 80−9682
Kr+Na, excimer bands, multiperturber interactions 78−66497
Kr+Na, non-Lorentzian spectral line shape 80−106297
Kr+Na, reson. line broadening, press. depend. 78−66596
$Kr+Na(3P_{1/2})$, vel.-changing collisions, effect on 2 photon and stepwise absorpt. line shape 80−87221
Kr+Ne, elastic scatt. absolute total cross section, long range interaction 78−58768
Kr+Ne, K-L vacancy sharing process, Nikitin two-state model 80−9684
Kr+Ne (Ar)(Xe), collision induced microwave absorpt. spectra 80−74216
Kr+Ne slow collisions, four-state treatment of K-L vacancy sharing 79−45793
$Kr+Ne_2$, total integral cross sections for excitation, exchange and dissoc. 80−1044
$Kr+Ne^{n+}$, (n=1, 2, 3, 4), energy spectra of electrons produced 79−45822
Kr+Ne*, quenching rate const. for metastable $Ne(^3P_2)$, flowing afterglow 78−46295
Kr+O, magnetically selected $O(^3P)$ state scatt. 80−99543
$Kr+O^-$, 0.2-1 keV, elastic and inelastic reduced differential cross-sections 80−32829
Kr+OCS, gas, EPR of rot. transitions, T_1 press. depend. 80−9621
$Kr+O(^1D)$, deactivation rate consts., 110-330K 78−88628
$Kr+O(^1D)$, inelastic collisions, spin-orbit coupling 80−5605
Kr+Rb(Cs), metal atom spectral line breadth and shift, Van der Waals pot. calc. 78−90126
Kr+S, collision-induced emission of $S(^1S)$, 232 and 425K 79−81264
Kr+target atom, 200-330 MeV, K-vacancy cross sections, target depend. 77−19026
Kr+Ti, 200 MeV, collision, quasimol. bremsstrahlung, semiclassical calcs. 77−88530
$Kr+TlF(Tl_2F_2)$, collision-induced ion-pair formation 78−17749
$Kr+U_3$ momentum transfer cross-section, 0.1 eV 79−45783
$Kr+U^{36+}$, radiative charge exchange, 16, 64, 256 MeV/amu 78−55234
Kr+Xe, excitation transferred populations, absorpt. profile analysis 78−74748
Kr+Xe, nonresonant excitation transfer, Doppler profiles, donor levels *(French)* 77−30824
$Kr+Xe^{10+}$ depend. of charge transfer on ionisation pot. of atoms 79−64096
Kr^++2Ar, three body reaction, rate coeffs., temp. depend., 100 to 300K 80−108703
$Kr^++2Kr\rightarrow Kr_2^++Kr$, gas phase reaction rate const. calc. 78−92457
$Kr^++2Kr\rightarrow Kr_2^++Kr$, reaction rate const. in afterglow period 77−9044
Kr^++Cs, total charge-transfer cross-sections meas. 77−50527
Kr^++ethylene (haloethylenes), 2-stage ion beam mass spectrometric obs. 77−9061
Kr^++F^-, in Ar, high press. ion-ion recomb. rate calcs. 78−31621
Kr^++F^- and $Kr_2^++F^-$, ionic recomb. rates in buffer rare gases 79−8425
Kr^++F^-+Ar, three body ion-ion recombination probability, Monte Carlo simulation 80−85160
Kr^++HD, kinetic isotope effect, cross sections, rot. transfer 77−9041
Kr^++HD, reactive collision dynamics, isotope effects 78−23930
Kr^++Kr, diabatic correl. diagrams for quasi-mol. description 79−3525
Kr^++Kr, diatom. quasimolecule form., shielded-orbital model 79−10165
Kr^++Kr, quasi-resonant charge transfer at thermal energies 80−48082
Kr^++Kr, symmetric charge exchange, below 1 keV, cross sections calcs. 77−532
Kr^++Kr collisions, quasimol. Auger transitions 77−19070
Kr^++molecules, $^2P_{3/2}(^2P_{1/2})$ doublet ground state reactions at 300K 80−108702
Kr^++O_2, charge transfer mech., implication of inner-shell level mixing 77−61852
Kr^++SO_3, in mass spectroscopy of SO_3 mixtures 78−3415
Kr^++fluoromethanes, thermal energy charge transfer reactions mechanism 77−63889
$Kr^{18+}+N$, highly charged very slow Ne recoil ions, K X-ray transition 80−91649
$Kr^{2+}+H_2(N_2)(O_2)$ (inert gas), charge transfer reaction rate consts. 80−7779
$Kr^{2+}+H_2(N_2)(O_2)(CO)(CO_2)$(methane), charge transfer reactions, rate coeffs. and product-ion distributions meas. 80−104431
Kr^{2+}+inert gas, low energy reactions, SIFT and drift tube obs. 80−97705
$Kr^{2+}+Kr$, radiative charge transfer coeffs. 79−7010
$Kr^{2+}+Kr$, symm. reson. double charge transfer, 0.04-20 eV 78−66657
$Kr^{24+}+Ge$, K X-ray prod., impact parameter depend. 78−58800
$Kr^{n+}+H_2$, charge transfer, collision defects and dynamics, cross section meas. 80−53099
$Kr^{n+}+Ta(W)(Pt)(Au)(Pb)(Bi)(Th)(U)$, K-L level matching, X-ray obs. 79−63948
$Kr^{Z+}+H_2$, Z=4-7, electron capture 80−37875
Kr_2, collision-induced Raman spectra, absolute cross sections 78−46351
Kr_2, electron impact ionisation, relative cross-sections, mass spectrometric meas. 79−86078
Kr_2, electron-beam pumped, visible absorpt. rel. to laser development 79−59671
Kr_2, excimer laser action in coaxial field emission diode, comparison with Ar_2, Xe_2 80−28201
Kr_2, kinetics of optically excited electronic states 78−63059
Kr_2, mean force constants and rectilinear law of mean force calcs. 78−33414
Kr_2, near IR absorpt. spectra 78−66547
Kr_2, photoelectron spectra 78−78748
Kr_2, photoionisation 77−54578
Kr_2, prod. and decay of 0_u^+ and 1_u states, synchrotron excited 80−43109
Kr_2, vibr. level spacings calc. from Lennard-Jones pot. 77−42369
Kr_2^+, $A^2\Sigma_{1/2u}^+\rightarrow D^2\Sigma_{1/2g}^+$ system, theoretical absorption spectrum 80−32734
Kr_2^+, dimer ions, electronic struct., chem. binding 79−31376
Kr_2^+ dissoc. recomb., rate coeff. and excited state prod., electron temp. depend. 78−22040
Kr_2^+, electronic states, pot. curves, with/without spin-orbit interaction 78−33443
Kr_2^+, electronic struct., pot. energy curves, spectroscopic consts. 79−18114
Kr_2^+, formed in 50 keV Kr^++Kr collisions, Auger transitions obs. by electron-scattered-ion coincidence method 80−74243
Kr_2^+, mobility and clustering reaction in Kr 79−10628
Kr_2^+, near UV absorption spectra, config. interaction methods 78−17680
Kr_2^+, photodissoc. cross sections at 3.0 and 3.5 eV 78−62861
Kr_2^+, photodissoc. cross-section, 6200-8600 Å 78−78761
Kr_2^+, photodissociation cross sections, 3500-5400 Å 79−81243
Kr_2^+, photofragment energy spectra, pot. energy curves 78−55207
Kr_2^+, weakly bound excited states, dissoc. energies 78−78748
$Kr_2^++F^-$, in Ar, high press. ion-ion recomb. rate calcs. 78−31621
Kr(-He) arc, wall-stabilised, atm. press. 79−46503
$KrF^*+Kr+Kr\rightarrow Kr_2F^*+Kr$, recombination rate consts. calc. 77−75488
KrI, p-s lines, transition probabilities meas. 80−23366
$Kr(^3P_1)+H_2O$, decomposition, $OH(A^2\Sigma^+)$ internal energy distrib. 79−10183
$Kr(^3P_2)$, quenching mechanisms and rate consts. 79−13801
$Kr(^3P_2)$+F donor reagent, quenching, excimer form. 79−63953
$Kr(^3P_2)+F_2(NF_3)(CF_3OF)$, KrF* bound-free oscill. emission spectra calc. 80−7799
$Kr(^3P_2)$+fluorine containing molecules, quenching rate consts., KrF* formation branching ratios 77−9072
$Kr(^3P_2)+XeF_2\rightarrow XeF^*$ KrF* mechanisms 77−30897
$Kr(^3P_1)(^1P_1)+CO$, $A^1\Pi$-$X^1\Sigma^+$ and $b^3\Sigma^+$-$a^3\Pi$ sensitised fluorescence, isotope effects 78−82761
^AKr, A=78, 82, appl. for PWR gas tagging 79−59222
^{76}Kr, ^{77}Kr production, excitation function meas. 79−88191
$^{78}Kr/^{86}Kr$, isotope separation by thermal diffusion *(Rumanian)* 80−86988
^{79}Kr, kinetics after inhalation in man, rel. to internal dosimetry calcs. 78−28073
$^{81}Kr^m$, new type generator using cellulose chromatography paper, for hospital use 79−8541
$^{81}Kr^m$ generator for lung ventilation studies, test for free Br in carrier gas 79−79642
^{83}Kr, $^3P_1$ and $^1P_1$ levels, quadrupole coupling consts. 80−23434
^{83}Kr, $4p^55p$ config., HFS meas. using level crossing technique 80−18827
^{83}Kr I, hyperfine structure in arc spectrum 78−41988
^{83}Kr, NMR gaseous study *(German)* 80−52917
^{83}Kr spin dephasing 80−38524
^{83}Kr, weak hyperfine component detect., time averaging using dye laser spectrometer 80−101850
^{85}Kr absorption in liquid CO_2 (KALC process), mass transfer efficiencies of packed columns 79−36354
^{85}Kr aerosol discharge devices, fabrication and use 79−1969
^{85}Kr, atmos. separation technique, preliminary results *(German)* 78−16222
^{85}Kr atmospheric concentration in North and South Hemisphere 80−93756
^{85}Kr conc. in midwest USA air 77−73834
^{85}Kr concentration in atmosphere over USSR (1971-1975) 78−37453
^{85}Kr, diffusion in Al *(Russian)* 79−65258
^{85}Kr entrapment in continuous-biased sputter-deposited glassy metals 80−24603
^{85}Kr extraction, occupational doses in gas liquefaction industry 78−15905
^{85}Kr, fission product, separation from Xe for storage by distillation *(German, English)* 77−61516
^{85}Kr immobilization, evaluation of methods 79−26578
^{85}Kr, nuclear reactor radioactive gaseous effluents, abatement techniques 79−3221
^{85}Kr, pressurised cylinder storage tests 80−5269
^{85}Kr, radioactive pollution in atmos., Warsaw 1975 to 1977, meas. methods 79−34458
^{85}Kr radioisotope, estimation of radiation safety 80−5346
^{85}Kr reactor radwaste, gas processing with low temp. rectification for quasi-null release 79−67877
^{85}Kr removal from HTGR reprocessing plant off-gas streams 79−30972
^{85}Kr waste encapsulation, in amorphous alloy 80−47589
^{85}Kr waste management, strategy anal. 80−37531
^{81M}Kr, blood flow and tracer uptake in normal and abnormal canine bone 80−17072
^{81M}Kr, continuous intravenous infusion, pulmonary regional perfusion assess., compared to ^{99M}Tc macroaggregates 79−39477
^{81m}Kr dosimetry, internal conversion electrons, error in previous work 79−12005
^{81m}Kr, lung, regional distrib. of (dV/dt)A/(dQ/dt) in man, at rest and with exercise 79−16232
^{81m}Kr ventilation rel. to ^{99m}Tc labelled aerosol particles imaging for lung function assess. 79−100716
Kr*+Ar*, metastables, chemi-ionis,, merging beams. 0.01-10 eV 80−14198
Kr*+He, $^3P_2$ metastable state, disorientation cross-sections 77−71853
Kr*+He, persistence of velocity following elastic collisions 78−78779
Kr*+He(Ar), vel. changing collisions studied by saturated absorpt. 78−62892
Kr*+Kr, $^3P_2$ state, metastability-exchange and depolarisation, press. broadening of mag. reson. curves 77−71853
Kr_2*, form. and UV fluoresc. under monochromatic excitation and collision processes 78−9237

krypton continued
Kr_2*, radiative lifetime and quenching rate consts. 78−63056
Kr_2*, VUV time resolved spectra, formation and decay kinetics 79−31544
Kr*(Kr^+)+NF_3, rate consts., electron attachment coeffs., flowing afterglow 78−13578
Kr**+HCl rot. effect on collisional ionis. 77−83702
Kr^+.+$H_2(D_2)$(HD) reactions, temp. depend., isotope effect 78−31630
Li-Kr, oscill. strengths, for induced dipole transitions, pot. energy curves 77−75100
LiF+Kr, anisotropic system intermol. pot. determ. 77−58121
N^++Kr, single electron detachment cross-sections, 35 to 140 keV 77−6909
N_2-Kr, liquid, high resolution CW CARS spectra 80−63635
N_2-Kr-Xe, liquefaction, retention of ^{85}Kr from fission exhaust gases, separation technique *(German)* 80−27753
NH_3-$N_2(H_2)$(Ne)(Ar)(Kr)(Xe), as R(1,1) vibr-rot. line parameters, ν_2 band, using CO_2 laser light 79−3444
NO+Kr^+, charge-transfer reaction rel. to vibr. state of NO^+ 77−1916
Na-(Ne)(He)(Ar)(Kr)(Xe), oscill. strengths, for induced dipole transitions, pot. energy curves 77−75100
Na+Kr collisions in laser beam, transition probability 79−50120
Na^++He (Kr) thermal, two trajectory model from meas. cross-sections 77−75257
NaKr, red wing radiation and pot. 80−87180
Ne:Kr, luminesc. in vacuum UV 79−15519
Ne-Kr, mol. force const. from viscosity data, thermal cond. 78−33565
Ne-Kr, partially miscible mixture, high press. mol. dynamics using Lennard-Jones pot. 79−41929
Ne-Kr mixture, collision-induced microwave absorpt. 77−88411
Ne-Kr Penning mixtures, Townsend ionisation coeffs. and breakdown pot. meas. 80−19641
Ne+Ar(Kr), translation band spectral moments, induced dipole moments 78−55218
Ne+Kr and Ne+Kr+Xe glow discharge, Kr^+ and Xe^+ excitation in negative luminesc. *(Russian)* 77−68883
Ne^++Kr, low vel. collision, enhanced K-L vacancy sharing ratios, X-ray prod. cross section 78−78790
Ne^{2+}+He(Ne)(Ar)(Xe)(Kr), cross sections for electron capture, 60 to 200 keV 78−46442
Ne*+Kr, Penning and associative ionisation 77−6910
Ni:Kr, ferromagnetic, hyperfine field and relax. time obs. of impurity heavy nuclei 80−75533
Ni:Kr gas trapping and release, thermal evolution mass spectrometric study 80−34026
O+NO+M→NO_2+M, (M=He, Ne, Ar, Kr), 217-500K, absolute rate consts. 77−16787
$O^{4,5,6,7+}$+Ne(Ar)(Kr)(Xe), 10-30 MeV, charge exchange 77−34757
O_2-^{85}Kr-Xe, liquefaction, retention of ^{85}Kr from fission exhaust gases, separation technique *(German)* 80−27753
O_2+Ar, binary diffusion coeff. pressure depend. meas. 80−43826
OCS photodissociation by Kr_2* excimer in OCS-N_2-SF_6 laser, electric dipole forbidden transition 79−68389
O(^{1}S)+Ne(Ar)(Kr)(Xe), total cross sections 78−42188
Rb^+, ionic mobility in Ar, Kr and Xe, interaction pot. determ. 79−18991
Rb:Kr film, metal-insulator transition, cond. and optical absorption meas. 77−24598
Rb+Kr, STS components shift and broadening 77−68014
^{81}Rb/^{81m}Kr ratio as radioactive tracer study of organic bleeding *(Dutch)* 80−3807
^{87}Rb+Kr, D_1 line broadening and shift 77−38640
Si:^{85}Kr, ion-implanted, impurity distrib. 80−15145
Si:Kr, amorphous, implanted and sputtered, epitaxial regrowth, influence of noble gas atoms 80−2289
Si:Kr, ion implantation damage, annealing, comparison with Si:Ne and Si:Ar 79−10867
Si:Kr, ion implanted, amorphous, epitaxial regrowth 79−10869
SiO_2:^{85}Kr, ion-implanted, impurity distrib. 80−15145
W:Kr, He trapping at substitutional Kr, vacancy creation 77−43258
Xe-Kr binary mixture, expt. determ. of temp. depend. of thermal diffusion factors *(Russian)* 79−60095
Xe-Kr gas mixture, vapour-liq. equilib. data *(German)* 77−84915
Xe-Kr mixtures for gas proportional scintillation counters 77−83464
Xe-Kr-Ar mixtures, VUV continuous spectrum prod. in low volt. lamp *(Russian)* 78−75451
Xe+Ar(He)(Ne)(Kr), thermal cond., 800 to 2000K from Wassiljewa's expression 79−27736
Xe^++$H_2(N_2)(O_2)$(CO), near-resonant charge transfer, 4-45 keV 77−27176
XeCl*+Kr, substitution efficiency during excitation in transverse AC electric discharge 80−50850
Xe_2(−Kr,He), time-resolved excitation spectra, 1500 Å region, fluoresc. lifetime 77−75195

krypton compounds
ArKr, mol. interactions, differential scatt. cross-sections meas. 79−89732
K(5S)Xe, K(5S)Kr, excimer, visible emission band, exptl. results relative to theory 78−82779
KrAr, photoionisation spectra of ground and excited states 78−5297
$KrAr^+$, quasimolecule Auger spectra 79−68269
KrB, excimer, collisional quenching rates, photolysis meas. 78−63066
KrBr, B(1/2)-A(1/2) system, emission spectra 79−6934
KrCl, B and C states, energy ordering from temp. depend. of emission spectra 80−78837
KrCl, intense lasing with HCl halogen donor 78−90411
KrCl laser, lifetime extension by H addition 80−91773
KrCl, laser expts. on $^2\Sigma$-$^2\Sigma$ transitions 78−63080
KrCl, stimulated emission obs. from electron beam excited Ar-Kr-Cl_2 mixture 77−672
$Kr_2Cl(F)$, ab initio diatomics in mols. pot. surface, spin-orbit coupling 79−3519
KrCl*, excimer formation rate consts., B state radiative lifetimes, quenching, VUV excitation 80−55631
KrCl*+Xe, substitution efficiency during excitation in transverse AC electric discharge 80−50850
KrF, 0.8 J multi-atm. laser, glow discharge characts. 78−58992
KrF, 1/4J discharge pumped laser 78−74927
KrF 1J avalanche discharge laser unstable resonator expts., beam divergence 80−74404
KrF, 25 J unstable resonator oscillator, injection locking 80−28218

krypton compounds continued
KrF, covalent and ionic states, ab initio CI calcs. 78−78634
KrF, diffraction-limited laser, with negative branch unstable resonator 77−38937
KrF, discharge excited laser operation at elevated temps., transitions, output power 80−43359
KrF, discharge laser, operating characts. 79−22937
KrF discharge laser, steady state amplification 80−5726
KrF, discharge pumped laser, efficient amplification 78−78997
KrF discharge pumped laser, circuit and UV preioniser parameters effect 79−55143
KrF discharge pumped laser, stable-unstable resonator for beam control 80−23722
KrF discharge pumped laser, energy extraction, collisional coupling between B, C and D-states 80−28213
KrF, double discharge laser amplifier, small signal gain meas. 77−79807
KrF, double discharge laser, operating parameters, discharge characts. 77−88704
KrF, double discharge laser, prism tuning 78−37892
KrF, efficient 1/4 J laser with corona preionisation 79−59713
KrF efficient discharge-pumped laser, amplification characts. 79−59679
KrF, efficient short pulse lasing 80−28217
KrF, elec. discharge laser, pulsed, high-power UV emission *(Russian)* 77−79808
KrF, electric discharge pumped laser, model for UV preionisation 77−23658
KrF, electrically excited laser, theoretical model 78−42321
KrF electroionisation laser, energetic, threshold and spectral characts. 80−99705
KrF, electron beam controlled discharge laser, plasma elec. characts. 79−59680
KrF, electron beam pumped laser system at 2 to 7 MW/cm^3 excitation rates 80−32968
KrF, electron beam pumped laser medium, time depend. fluoresc. spectrum in high current density range 80−78842
KrF, electron beam sustained discharge excitation, threshold power density meas. 78−63078
KrF, electron impact deexcitation cross sections and rate consts. calcs. 80−32848
KrF, electron quenching rate consts. meas. by fluoresc. anal., laser implications 80−32969
KrF electron-beam pumped laser, performance model 80−53273
KrF electron-beam-excited amplifier, master-oscillator power-amplifier expt. for gain coeff. and saturation intensity determ. 80−48222
KrF, electronic states, ab initio CI calcs., spin-orbit coupling, pot. curves, dissoc. energy, dipole moments 77−38619
KrF, electronic states, ab initio POL CI calcs. 78−66474
KrF excimer, collisional quenching rates, photolysis meas., rel. to laser performance 78−63066
KrF, excimer laser, development of dielectric mirror *(Japanese)* 79−72588
KrF excimer laser, high brightness performance using high magnification unstable resonator 79−59716
KrF excimer laser, operating and beam characts. 79−59715
KrF excimer laser, passive mode-locking using saturable absorber dyes 80−1244
KrF excimer laser, water dielec. Blumlein-driven fast elec. discharge pulser 79−10318
KrF, excimer laser power and efficiency, review 79−937
KrF, excimer laser pumped dye laser *(Chinese)* 80−1234
KrF excimer laser using corona preioniser 80−33016
KrF, excimer laser with improved beam quality 77−72007
KrF excimer lasers, lasing action *(Chinese)* 79−59682
KrF excimer lasers, review *(Japanese)* 78−33723
KrF, excimer lasers, state of art 80−95879
KrF, excimer UV discharge laser, emission spectra 77−79809
KrF, excimers, power superluminesc. in elec. discharge *(Russian)* 77−7621
KrF, excimers and excimer lasers 80−48217
KrF, fast discharge laser in NF_3, N_2F_4 or SF_6 mixtures 77−31097
KrF, fluoresc. spectrum, theoretical modelling using electronic potential curves 78−63086
KrF, form., relax. and quenching 80−81314
KrF, formation and quenching of electronic excited states 77−673
KrF, high efficiency laser with short pulse electron excitation 80−33032
KrF high power lasers, const. E/N pumping 77−88711
KrF, high pulse rate, 10 W excimer laser 78−42348
KrF, high-power, dye laser pumping characterisation at 248 nm 80−1199
KrF high-power electron-beam pumped lasers, optical performance 78−46640
KrF high-power laser, efficiency and energy scaling 79−36887
KrF high-power laser, X-ray preionisation 80−33031
KrF, inert gas halide lasers, 60-ns electron beam excitation 80−74340
KrF injection locked unstable resonator discharge laser, narrow linewidth and high spatial quality 80−53323
KrF, injection-locked narrow-band discharge laser, using unstable resonator cavity 78−25893
KrF, kinetics simulation of high-power gas lasers 79−59676
KrF, Kr_2F, in electron beam pumped Ar-Kr-F_2 mixture, spectroscopy and kinetics of 248, 414 nm bands 78−63081
KrF, Kr_2F, time depend. emission meas., Ar-Kr-F_2 laser mixture kinetics 80−32768
KrF laser, closed cycle characts. 80−33030
KrF laser, closed cycle flow type, operating characts. 80−43349
KrF laser, collisional coupling between B, C, D states from fluoresc. meas., influence on energy extraction 80−1189
KrF, laser, e-beam pumped Kr-F_2 mixtures, form. and quenching processes 78−42322
KrF laser, e-beam sustained, glow discharge stability 79−55117
KrF laser, electron beam stabilised, electron kinetics 77−83888
KrF laser, electron beam pumped, high press. UV emission 78−25866
KrF laser, electron beam pumped, with Ne-Ar diluent 79−22936
KrF laser, electron-beam sustained discharge excitation, threshold power density meas. 77−88699
KrF laser, kinetic model, limiting behaviour and scaling 80−78838
KrF laser action in return-current discharge-excited F_2/Kr/He mixtures 78−94920
KrF laser beam, Raman pulse compression, for fusion expts. 78−59086
KrF laser compatible materials, gas purification techniques 80−38037

krypton compounds continued
KrF laser driven methane backward Raman amplifier, high-efficiency energy extraction 80−106533
KrF laser efficiency optimisation, photoionisation cross sections for excited states of Kr and Ar 77−75110
KrF, laser emission, ab initio config. interaction calcs. on electronic states 78−63083
KrF laser excitation of tunable UV Ce:$LiYF_4$ laser 80−38022
KrF laser induced preionization of XeCl discharge 80−84020
KrF, laser spectra, absorpt. lines 80−9604
KrF, laser spectrum, discharge-pumped, absorption bands and lines, assignment 78−79004
KrF lasers, discharge and electron beam pumped, review 78−71083
KrF linac-excited gas mixture, UV fluoresc. meas. 80−28216
KrF, matrix isolated, absorpt. and emission spectra 77−14446
KrF, matrix isolated, mag. circ. dichroism, UV and vis. absorpt. and saturation 78−46379
KrF mini-laser operation at high repetition rate 80−74396
KrF oscillator at excitation rates of 2-7 MW/cm^3 80−5727
KrF, photoionisation excimer laser charact. 80−102712
KrF pump laser, scaled Raman pulse compression experiments at 248 nm 80−38071
KrF, radiative lifetime and quenching 78−63063
KrF, Raman shifting of laser wavelengths 77−75539
KrF, simple high-power TEA laser operating in UV 79−94251
KrF, small signal gain meas. and kinetic modelling 78−63077
KrF, spark-preionised large-vol. discharge laser 78−1218
KrF, stability enhancement of electron beam sustained laser discharge 79−98381
KrF superradiance laser excited by electric discharge 77−19236
KrF, UV bound-free emission after electron excitation 77−27279
KrF, UV excimer laser, fast helical pin discharge, 50 μJ 77−23660
KrF, UV preionised transverse discharge laser, theoretical model 79−22938
KrF, UV preionized discharge pumped laser 77−10889
KrF X-ray-preionized high-pressure laser 79−18403
KrF^+, selected valence-electron split-shell MO calc., ground state props. 79−22585
KrF^* radiative lifetime, pulsed photolysis obs. 78−29819
^{84}KrF in polycrystalline KrF_2 ESR spectra, struct. and dynamic parameters of radical sites determ. 80−84652
KrF+He(Ne)(Xe)(NF_3), quenching rate consts. meas. 79−24718
KrF_2, Mossbauer spectra, quadrupole coupling strengths, isomer shift and bonding 77−50458
KrF_2, photoionisation mass spectrometric study 79−45772
Kr_2F, absorpt. in near UV wing of 410 nm band, fluoresc. efficiency 80−14323
Kr_2F, semi-empirical VB calcs. of hyperfine interactions and struct. 79−85902
$^{83}Kr_2F$ radical, in UV-irrad. Kr/CF_3OF, 10K, ^{83}Kr hyperfine EPR spectrum, struct. 78−42101
KrF(Cl), discharge pumped multiwavelength lasers *(Chinese)* 80−102703
KrF*, bound-free emission spectra, simulation 78−29806
KrF* constant E/N pumped high-power laser, parametric study 78−42346
KrF*, elec. discharge excimer lasers, stimulated emission 79−31884
KrF*, electron beam controlled laser, plasma processes 79−930
KrF*, excimer electronic struct., config. interaction, electrostatic model 78−927
KrF* excimer laser, discharge pumped, influence of electron-F_2 collisions 78−42326
KrF*, excimer laser, electron beam controlled discharge pumping 77−10893
KrF*, Kr_2F*, kinetics of proton-excited KrF_2 mixtures, time-resolved and time-integrated spectra 79−36883
KrF* laser, electron beam pumped, dominant formation and quenching processes 79−938
KrF* laser, gain and absorption meas. 77−79802
KrF* laser, generation of high-spectral-brightness tunable XUV radiation at 83 nm 80−91846
KrF* laser, influence of F_2 dissociation and degree of ionisation 78−50756
KrF* laser discharges, electron beam sustained, instability onset 78−63065
KrF* laser system, trimer form. rates 80−50831
KrF* nuclear pumped lasers, excited state prod. rate and fission power pulse shape matching 80−63998
KrF*, oscillatory bound-free emission spectra, semiclassical anal. method 80−7799
KrF*, pressure depend. of C to B state ratios 79−24731
KrF*, three-body quenching by Ar and broad-band emission at 415 nm 77−75486
KrF* tunable ultrahigh spectral brightness excimer laser source 80−64046
KrF*, waveguide laser excited by capacitively coupled discharge 78−94391
KrF*+Ar(Kr)+Ar(Kr), recomb. rate consts., 300 to 800K, appl. to KrF* laser efficiency 79−45930
KrF*+Ar(Kr)+Ar(Kr)→Ar(Kr)KrF*+Ar(Kr) recombination rate consts. calc. 77−75488
Kr_2F*, gain meas. at 4416 Å 78−50758
Kr_2F*, radiative lifetime and quenching rate consts. 78−63056
$KrF_2.AsF_5(SbF_5)$, Mossbauer spectra, quadrupole coupling strengths, isomer shift and bonding 77−50458
KrH_2 van der Waals mols., rot. predissoc. 80−63721
KrHBr, KrCHl, and isotopic forms, rot. spectra, mol. struct., mol. consts. 80−58246
KrHCl, van der Waals complex, prod. and rot. spectra assignments 80−5532
KrHCl, van der Waals complexes, struct., RF and microwave spectra, isotope effects 80−37806
KrHCl, weak complex, rot. spectra 80−52980
KrHF, ^{83}Kr nucl. quadrupole coupling, charge transfer 80−53012
KrO, high press., optical gain profile near 5577 Å 77−68204
KrO, in doped inert gas matrix, photoluminesc. 79−31579
KrO, lasing, low-lying electronic states, ab initio config. interaction calcs. 78−63084
KrO, low lying state characterisation 80−99543
KrO^+, $X^4\Sigma^-$ state, pot. energy curves and correl. effects, elastic scatt. cross sections 80−23502
krypton compounds continued
KrS, photoluminesc. in rare gas matrices 80−5568
KrXe, electron impact ionisation, relative cross-sections, mass spectrometric meas. 79−86078
^{83}Kr Mossbauer isomer shifts, book contrib. 79−87363
$Kr.2SiO_2$, props. of vitreous deposits 78−22664
Na(4S)Xe, Na(4S)Kr, excimer, visible emission band, exptl. results relative to theory 78−82779
Kuhn-Thomas sum rule *see molecular energy levels*
Kurie plots *see beta-decay theory*
Kyropoulous method *see crystal growth from melt*
labelled atoms *see radioactive tracers*
labelled compounds *see radioactive tracers*
labelled molecules *see radioactive tracers*
laboratories
see also acoustical laboratories
ACCMOR collaboration spectrometer and expts. *(Dutch)* 77−46454
ACS Tenth Biennial Education Conference on Safety and Health in Academic Lab., recommendations 79−80387
activation analysis laboratory in Noril'sk mining-metallurgical complex 77−23185
air-conditioned laboratories, automatic temp. control and meas. *(Japanese)* 78−86245
ambient air analysis, area survey and sampling mobile laboratory 80−104528
Australian National Measurement Laboratory and cryogenics 79−35753
Austrian Dosimetry Laboratory, calibration and meas. standards 80−5362
BESSY, a 800 MeV storage ring dedicated to synchrotron radiation, review 79−68021
BNL 79−45411
British Calibration Service 80−22319
CAMAC instrumentation in European labs. 77−54482
cell cultures, equipment used in a modern labroatory 78−85457
CERN, international scientific cooperation *(Dutch)* 77−45669
CERN 400 GeV super proton synchrotron, review *(Dutch)* 77−46432
CERN experiments in 1979 80−408
CERN super proton synchrotron, experimental programme *(Dutch)* 77−46431
CERN super proton synchrotron, experiments with light particles *(Dutch)* 77−46433
chemical laboratory, airborne contaminants monitoring, USA regulations 80−12869
dosimetry, secondary standard laboratory organisation in India 80−5366
dosimetry, secondary standards laboratory, role in a nuclear power utility 80−5365
dosimetry standards labs., international network 77−67898
electric equipment testing laboratory, movable, type ETL-35, design *(Russian)* 80−95088
electrical standardising laboratory for developing countries 80−101774
energy resource development role of Sandia Laboratories' photometrics division 78−58077
engineering metrology laboratory, design and equipping 77−82479
environmental climatic, features of McKinley laboratory 79−16798
Fermi National Accelerator Laboratory, description 77−57782
Fermilab, microprocessor based timed reading and time plot CAMAC modules 77−54484
Fermilab, multi-user control and data acquisition systems 77−54480
forensic laboratory applications of combined chromatography/mass spectrometry techniques 78−92556
free neutrinos investigations, research installations 77−50336
French CGE laboratory work on lasers and applications *(Spanish)* 78−30004
frontiers in education, conference, Urbana-Champaign (1977) 78−81779
gamma irradiation of Bulgarian Academy of Sciences *(Russian)* 77−38592
heavy ion research facilities, Darmstadt *(German)* 77−67916
high-pressure, for chem. engng. development 79−21507
hospital test instruments, scientific and medical instrumentation capability 78−69242
hot laboratories, post irrad. work, trends and prospects 78−41844
hot laboratory design and construction *(Japanese)* 78−29623
HV laboratory ion density due to repetitive impulse generation 78−65913
ICPE spectroscopy laboratory, electrical engineering materials research *(Rumanian)* 80−4774
Indian Secondary Standards Dosimetry Laboratory, development and functions 80−41244
integrated optics laboratory for teaching and research in optical waveguides 77−39034
integrated surface physics and chemistry laboratory planning for automation 79−67269
Japanese National Research Institute for Metals, cryogenic appls. 80−4693
Laboratoire d'Optique de Besancon, recent work 77−68177
LAMPF, neutron physics programme 77−26951
laser fusion Optical Evaluation Laboratory, Antares CO_2 laser system 80−14346
LLL, microprocessors appl. 77−54481
low temperature research activities and facilities in Italy 79−93146
Mexican Solar Energy Experimental Center optimum site determ. 79−57380
MIT, recent developments in elec. scatt. expts. 77−82916
mobile, radiation calibration appl., design 77−38582
National Radiological Protection Board low-background laboratory, research summary 77−48880
Naval Research Laboratory, USA, inertial confinement fusion programme 78−59042
Netherlands National Institute for Nuclear and High Energy Physics, exptl. programme *(Dutch)* 77−46475
neurofunction, clinical trials appl. 79−96541
neutron installations and facilities 77−23317
nuclear engineering, process instrumentation meas. 78−17447
Nuclear Reactions Lab., Dubna, USSR, review of 30 years work 79−36204
nuclear science, undergraduate teaching, courses, facilities 80−27086
occupational physiology and psychology laboratory 77−48885
Omega laser system for fusion studies, Rochester Univ. 78−59041
optics laboratory, undergraduate, in American universities, status 80−62411

laboratories continued
permit-to-work certification scheme, for use in health building laboratories 80−22338
photometric, facilities at National Measurement Laboratory, Australia 78−82019
radiopharmacy optimisation by redesign 77−90899
Regional Calibration Laboratory at the M.D. Anderson Hospital, Texas, USA 80−8189
safety standards, realisation 78−77879
Scripps Institution of Oceanography, research projects and education review 78−69464
Secondary Standards Dosimetry Laboratory, review of role 80−5361
SERI, Solar Energy Research Institute, CO, USA, R and D program, organisation 80−89599
space environment simulation laboratory 79−48644
Spacelab and space platform solar array programmes 79−96884
Spacelab atmospheric trace contaminant meas. and identification 79−70387
Spacelab launch conditions for absorption spectroscopy *(French)* 79−8791
Spacelab of European Space Agency 80−85837
SPEAR, charmed meson, review of three years e^+e^- research 79−63490
standards room, in factory air-raid bunker, general description 78−93646
Stanford Synchrotron Radiation Laboratory, operation and development, review 79−68020
Stanford Synchrotron Radiation Laboratory, status report 80−91327
Suttle pallet satellite power module for Spacelab power augmentation 79−96882
test results, international acceptance *(Danish)* 80−8952
transuranic element meas. in vivo at CRNL 77−77993
University of Liege beam-foil facility 79−45866
vision research laboratory, clinically oriented, tasks and goals 80−12083
Pu fuel research facility for advanced LMFBR fuel *(Japanese)* 78−29624

laboratory apparatus and techniques
see also specific instruments and techniques, e.g. balances, plasma probes, vacuum techniques
see also instrumentation; instruments; measurement; student laboratory apparatus; test equipment; test facilities; testing
200 W power supply, series-regulated, programmable, 0-50 V range 77−82543
β source laboratory apparatus for radiation chemistry research 79−34340
accidents involving instrumentation, causes and prevention 79−80594
air blowers, noise emission 78−61975
amino acid analyser, LKB 400 automatic ninhydrin, new sampler loader 80−101916
annealing of electron field emitters and multiple multichannel analyser, precision temp. regulator 78−86384
articulated support system, appl. to Ganzfeld ophthalmological stimulator 79−83970
automated systems and digital techniques 78−57922
automatic curve slope meter for physical or chemical quantities 78−49812
automatic purge and trap concentrator, gas chromatography, determ. volatile organic compounds in water 80−97739
automatic speech recognition, equipment used for experimental purposes *(German)* 79−46129
automatic titrator, microcomputer controlled, for chem. anal. 78−27841
automation in laboratories *(Japanese)* 78−93664
balance, microprocessor based, capabilities 80−13067
biomedical instrument to computer coupler 80−41271
broadband time relay for automatic activation 79−88940
cable-driven large-angle rotator used in superconducting solenoid 77−2640
calorimeter, dynamic differential types comparison, in linear macromol. heat capacity meas. 78−89482
cantilevered bench, vibration isolation for balances 80−68183
capacitance-based micropositioning system for X-ray rocking curve measurements 80−205
cardiac catheterization laboratory sensitometric system application and clinical evaluation 78−20263
ceramic, deform. test apparatus and method *(Russian)* 78−35613
chemical monitoring, complete laboratory, installation 78−61123
chemical reaction apparatus, automatic, for low temp. inert atmosphere system 78−93695
chromatographic Micronova computer interfacing scheme 80−93813
chromatography, high performance radial 78−80802
cine film colour duplication, Laboratory Aim Density control method 77−5953
clean air cabinets, standards 79−67273
clinical ECG laboratory methods and difficulties 78−7482
clinical electrophysiolgy laboratory automatic control system 78−57110
closed-circuit water jet pump construction 79−67272
co-ordinate machines for mark-out of workpieces 80−62643
co-ordinate measuring machines, development 80−62644
cold-bath, precision, low-cost, design and construction 79−26048
collection device for capturing a spray sample 78−57920
complex material atomic structure study, laboratory extended X-ray absorpt. fine structure technique 79−17589
computer system architecture for laboratory automation 79−12777
computer systems, minicomputers, microprocessors, uses 77−79072
computer-controlled experimentation and laboratory automation, interfacing system 79−49213
concrete optical table 79−50449
container for volatile inorganic hydrides of specially high purity 80−47043
continuous temperature gradient incubator, fungal growth 80−47044
conversational data processing system for instrumental analysis *(Japanese)* 77−82496
corrosive atm. pressure or vacuum meas. isolation chamber 77−30174
creep testing of refractories, high-temperature at different loadings *(Russian)* 78−19970
cryo-ultramicrotomy and myofibrillar fine struct., review 78−53592
current balance, modified, for elementary physics laboratory 77−67163
cuvette for studying optical nonuniformities in aggressive liquids 79−2810
dilatometer, meas. thermal dilatation of metallic amorphous ribbons 80−86258

laboratory apparatus and techniques continued
distribution function parameters determ. in real time, instrument description 80−202
dual resistance wire wavestaff system for laboratory and coastline 80−46324
Earth resources, remote sensing by Skylab microwave radiometer 78−16273
electric field probe, miniature 60 Hz 78−77930
electric furnace, 2300K, oxidising atmosphere *(French)* 80−27311
electrical contacting method, Au wire-semiconductor, spark welding, for elec. meas. *(German)* 79−49215
electrical instruments in photometric laboratory, selection, care, and use 80−86283
electrodialysis and its applications 80−55702
electrolyte-gas interface motion control by electric field 77−35248
electromagnets, design criteria *(Czech)* 79−88985
electromedical devices of the angiohaemodynamical catheterisation laboratory 80−85515
electron microscope laboratory floor vibration detection by record-player cartridge 79−54233
electronic industry, Spain measuring equipment choice, criteria *(Spanish)* 78−36963
electronics, undergraduate laboratory course 80−105478
electronics influence on laboratory technology and instrumentation over last 25 years 77−67422
electrothinning, laser-monitored, for preparing ultrathin metal foils 78−53074
equipment for the measurement of ions in solution, review 80−71983
ergometer for small-animal research 80−101295
experimental data interpretation, chemical analysis appl. 78−77827
fatigue crack growth testing equipment 80−81247
ferrite materials and components, laboratory meas. automation *(Polish)* 80−101789
fibre microtome 78−16780
flash point measurement, liquid wastes 80−47051
flexible fused silica columns for gas chromatography 80−45590
flow and volume meas. devices, repair and checking *(German)* 78−32803
fluid heating mantle using heat-exchanger principles 78−93665
foil mounting technique, wrinkle-free 80−77767
fume hood performance evaluation by face velocity meas. 80−37011
gas adsorption installation, static characts. of porous and nonporous materials 80−81361
gas chromatograph, N504 type charact. 78−11599
gas chromatograph glass open ended tubular columns, electric heating device for straightening ends 79−6106
gas gun, short-barrelled, for impact studies 80−64501
gas supply generator for gas discharge units 79−88927
gas-supply line which permits high voltage across its ends without breakdown 77−9998
glass breakage, minimisation methods 80−77580
glass capacity measures testing, measurement standards, appl. 79−6085
glass tube cutter, hot wire technique 78−20925
graphite furnace, between-sample cleaning 79−87889
grinding device for radioactive tracer diffusion studies in hard ceramics 78−41291
helical marking of cylindrical specimens, device for holding and scratching 79−58679
high performance liquid chromatography, sample introduction, syringe injection 80−66906
high performance liquid chromatography, SLIC-1400 universal interactive controller 80−55731
high-pressure cell, low temp. gas mixture expts. 80−86334
holography table effective size increase 79−35694
honeycomb optical tables development 78−18073
humidity test chamber, convectively mixed, calibration appl. 78−54379
hydraulic microdrive for recording single nerve cell activity 79−70727
ignitrons, high current, for plasma physics expt. equipment *(German)* 78−75435
incubator, choice 80−68187
instrumentation system, computerised, real-time 79−12786
integrated optics laboratory for teaching and research in optical waveguides 77−39034
jet impinger, SO_2 collection efficiency low velocity studies 79−16683
laboratory test instruments 79−30444
linear regression, least-squares eqns. derivation, appl. to g determ., for teaching 78−45450
liquid chromatograph for homogeneous mixture analysis 80−16757
liquid chromatography, automatic fraction-separating system 80−45589
liquid chromatography, high performance low pressure equipment 78−80801
liquid level detection, audible alarm system, thermistor appl. 79−12764
liquid-friction bearing tester, description and improvements over existing designs 80−64503
low temp. sample holder using thermal cycling to reduce stress 79−49238
LV short-circuit testing station, equipment and measurement methods *(Polish)* 80−77773
magnetic domain dry colloid observation apparatus, 90K to 290K 80−73394
magnetic stirrer with no external moving parts, digital cct. 78−93666
manipulation system, mech. props. 79−85132
manipulator for rotating spheres 78−73975
materials science experiments, use of closed circuit TV as teaching aid 79−71209
measurement accuracy, evaluation 79−17380
Measurement Standards Laboratory, capability improvement 78−54332
mechanical isolation device, super spring 80−47042
mechanical testing of materials automation, using 500 kN and 2.5 MN ATE *(Czech)* 80−66710
medical laboratory techniques, materials chemical resistance 79−88926
metrology standards and measurements laboratory, used by Matsushita Communication Industrial Co. Ltd. *(Japanese)* 80−82738
micro-sample handling device, various appl. 80−62642
microcomputer and A/D convertor interfacing 80−22337
micromanipulator for use in closed system 80−37013
micromanipulator using microscope focus, appl. to yeast asci single spare isolation 78−61292
micropipet, digital high precision device 78−24774
microprocessor controlled vector scan pattern generator, scanning electron microscopes 80−13188

laboratory apparatus and techniques continued
microprocessor-based, programmable laboratory equipment controller and data acquisition system 79−6104
microtome, automatic for cutting 400 μ fibre snippets 77−9999
microtome based on MBR-1 microscope for polymer sections of min. thickness 5 μ 77−71306
minicomputer appls. in analytical laboratory 79−75508
minicomputer data system for polymer characterisation, gel permeation chromatography 80−45591
mixer for powders 79−61828
mobile test laboratory for analyzing gases 79−71435
mobile testing laboratory PPLII-3 for ionizing radiation 79−74761
modified window air conditioner, laboratory temperature control 80−68192
molecular spectroscopic laboratory strategies, queueing theory and digital simulation use 80−30299
molecular weight determination in microgram quantities, lab. system 78−33634
monitoring instrument for continuous tissue pressure meas. 79−100762
Mossbauer spectra recording apparatus, effect of gate setting on spectral parameters 80−90938
multimeter with microprocessor, precision *(French)* 79−6139
multiwire chambers, setup for washing and drying 80−105624
muzzle flange alignment technique for gas gun 79−67271
neutron detector, expt. control and data acquisition system 79−45589
NMR of tritiated samples, use of plastic tube insert 79−40546
ohmmeter and capacitance meter sensitivity measurement, new checking method for instruments having both uniform and non-uniform scales 80−62654
optical bench fixtures 78−13822
optical fibre alignment tool 80−23814
optical instrument evaluation definition and test criteria 77−39119
optomechanical element system, Hungarian development *(Hungarian)* 79−81574
organic carbon analysis, automation 80−45592
oscilloscope, 25 MHz, LBO 515, performance and serviceability *(German)* 78−41294
pH meters, revised British Standard BS3145 77−70371
pharmaceutical dissolution testing, microprocessor controlled sampling system 80−86273
photographic film-slitting in printing laboratory problems *(German)* 79−6199
photometric, light sources props. meas. *(Slovak)* 80−17990
physiological response measurement, multiplexing system 80−56292
piezoelectric displacement generator, annular, mathematical theory 78−62185
pipettes, automatic precision instruments 79−21734
plasmon surface polariton dispersion curve, optical obs. 80−101690
plasterboard sound reduction indices and meas. 78−87196
positioning equipment, hardware tradeoffs 78−62187
powder handling in the laboratory 80−45475
practical physics course for undergraduates 77−9836
precision axial translator with high stability 79−88930
pressure transducer testing apparatus, freq. charact. meas. 80−62650
programmable desk calculators, multiple quadratic regressions, simple laboratory data processing approach 80−42048
programmable pipette, microprocessor controlled stepping motor, repetitive dispenser appl. 80−42205
psychophysical laboratory unit organisation and meas. system for persons with impaired locomotor system *(Croatian)* 78−44667
pulverised char feeder, laboratory scale 77−61058
quartz spectrograph, Littrow, spectrochemical anal. appl. 77−86396
radioimmunoassay, fitting of general form of fundamental physical model 80−94150
radioimmunoassay, plasma renin activity estimation, microprocessor controlled 80−46023
radioimmunoassays in clinical chemistry laboratory, statistical quality control, computerised approach 77−90878
real time data acquisition system for controlling and collecting data from laboratory instruments 78−54348
resonance meas. in solids *(Spanish)* 80−86285
rider for optical bench, construction and specifications 80−28369
rotating sample holder without mechanical linkages 79−35697
Rutherford, pulsed neutron facility 78−29208
safety, in-house design and construction 79−80595
safety, survey of sources of information 79−80596
sample chamber for ultrasonic vels. and elastic consts. meas. in Mo, 4.2 to 300K *(German)* 78−46868
sample heater, high vacuum, using Zener diode 78−12690
sample orienting device with 2 degrees of freedom for galvanomagnetic meas. 78−81958
sample rotation, biaxial, in supercond. solenoid *(Czech)* 80−37010
semi-automatic grain size separation apparatus 78−54351
short tube drawing from thin metal sheets 78−86248
SIINC laboratory instrumentation information system, proposed structure 80−98908
silicone rubber mould for solid models, appl. to Pb Fermi surface modelling *(Japanese)* 77−26277
solid-particle ejector, pneumatically operated 80−73339
Space lab integrated UV and X-ray astronomical payload proposal *(Italian)* 77−82112
Spacelab optical techniques for liquid flow and temp. meas. 79−82007
Spacelab passive atm. sounders, attitude control and stabilisation 78−65483
Spacelab passive atmospheric sounders 77−82113
specimen clamps for X-ray angle-tensile meas. of cotton fibres 78−4603
specimen containers, thin-walled silica glass, technique of construction 80−31724
spectrophotometric standards, glass filter SRM 930 by NBS, clinical laboratory appl. 78−54331
spherical nuclear fuel particle porosity, testing equipment for fuel production consistency 80−27795
stable frequency standards comparison by TV carrier beat note transmission 78−57909
stand, expts. on kinetic reactions during phase transitions in $PbTiO_3$ *(Polish)* 80−77766
standard cell calibration against Josephson voltage reference 77−5874
strip chart recorder future in laboratory 80−57279
stripping cells, comparison of time-of-flight and stripping cell low-energy ion scattering methods 80−73522
laboratory apparatus and techniques continued
student computer aided laboratory instruction Karlsruhe Univ. 79−12556
superconducting solenoid, control of field-changing tasks by microcomputer 79−216
surface emittance, determ. total hemispherical calorimetric emissometer 80−86309
temperature regulation cct. 77−45836
temperature wave generator for diurnal temp. wave propag. simulation 78−85735
thermal neutron high press. sample container for diffr. and spectroscopy on fluids 79−46513
thermo-optical measurements at six European laboratories compared *(French)* 78−29107
thermomechanical devices for motions in small inaccessible volumes 77−33979
thermometers test equipment, thermoelectric and resistance, using zero-setting and steam thermostats 77−74400
thermometry below 1.5K 77−57332
thermostats, electronic device for precision temp. regulation 79−88931
timekeeping clock synchronisation and comparison problems and equipment 77−71302
timer based on electronic clock module 79−67282
timers, electronic progammable, Xanadu up-timer, industrial lab. appl. 79−9207
Toepler pump, all-metal automated 80−52180
transportable 1000 pF capacitance standard 77−5870
tritiation system for tritium introduction for phase composition and struct. determ. 79−39068
tuning forks, electrically driven, Melde's experiment apparatus 80−42022
turbulent gas flow in annular channels, heat transfer apparatus and technique *(Russian)* 78−34199
two plate capacitor with aerostatic electrode regulation for precise determination of capacitor loss factor *(German)* 78−74021
ultrathin metal film mounting method on cylinders 79−35696
undergraduate course, in advanced physical instruments 79−21486
US crystal cleaner, use of US 79−49216
V block, low cost precision block for heavy loads 80−57273
vacuum gap breakdown initiation by microparticle impact 80−96413
Varian Model 63 C rod atomiser, device for positioning and dispensing samples into C rods 80−42206
vibratory polisher for semicond. single crystal, construction 78−80659
vortex flowmeter for student laboratory use 79−7424
water level short-term meas., systems 78−93654
wire spark erosion machine for hard metals, control cct. 79−35695
Ar purifier, portable, 0.3 m^3/h, design and appl. *(Polish)* 79−12781
CaF_2 vapour deposition apparatus, Na-resistant glass cell 80−90874
Cs atomic time standard data combination 77−5814
He-Ne laser, rejuvenation methods 77−37687
^{125}I, procedures for safe working in labs. 79−35698
Ir, recovery from laboratory residues 78−81957
$(La_{0.8}Ca_{0.2})MnO_{3+y}$, sample preparation using O_2 partial pressure controller *(Japanese)* 78−73977
N_2 purifier, 2.5 m^3/h *(Polish)* 79−12782
organohalogen analyser system, drinking water total organic halogen anal. 80−93830
Pu laboratory stack monitoring, computerised system 79−3256
Rb, portable clock for transcontinental and intercontinental time comparison 78−57908
Rn, diffusion coefficient and exhalation rate from building materials, meas. technique 80−4694
S meter, model XA-300, for laboratory use 80−26085
SO_2 transfer resistance of European soils, laboratory meas. 77−37384
Si solar cells, undergraduate teaching expts. 77−74177
^{133}Xe storage and dispensing device for nuclear medicine *(Czech)* 79−43986

labryrinth speakers *see loudspeakers*

Lacertids *see BL Lacertae-type objects*

ladder filters *see filters; ladder networks*

ladder networks
see also filters
electrochemical impedance simulation, by AC ladder networks 77−12806
wire spark chamber 77−65396

lakes
see also rivers
acid rain, neutralization in Hubbard Brook ecosystem 79−74922
acidification of Canadian lakes, effects on fish populations 77−37259
Agassiz, northern extent in E Saskatchewan 77−91161
ambient air/water interface, frictional coefficient at low wind strength, obs. *(French)* 78−16020
American Southwest, Pleistocene palaeolakes rel. to cold, dry full-glacial climate 78−57296
Antarctic dry areas geochemical problems 79−79844
Antarctic saline lakes−stable isotopic ratios, chemical compositions and evolution 79−74911
aqueous heavy metals, adsorption on inorganic minerals 78−49006
Arabian Desert, ^{14}C chronology of late Quaternary lakes 77−5161
Aral Sea, anthropogenic effects on level and salinity, 1951-75 period 79−44211
Aral Sea, water balance model, thirty year projection 80−41471
artificial, time evolution of stress, rel. to induced seismicity 79−25272
Assal (FTAI), geothermal zone, geochemical and expt. studies 78−69314
atmosphere light refraction, rel. to image distortion and lake monsters 80−46259
Baikal, ice covered, statistical props. of velocity and temp. profiles *(Russian)* 77−78269
Baikal lake and rift zone, windows into Earth interior, geophysical exploration *(Russian)* 80−12364
Balkhash, wind driven water level vars. 78−81237
Baltic Ice Lake levels, dating rel. to S.Finland Salpausselka moraines 79−20872
Barrett Reservoir, chronological strategies and metal fluxes in semi-arid lake sediments 79−34860
biochemical and physical model interfacing for large lakes 77−21822
Biwa, central Japan palaeoclimate from sediment compositions 79−12230
Biwa (Japan), sedimentary sequence rel. to late glacial age chronology 79−34872

lakes continued
Biwa basin, hydrological cycle, system theoretic study *(Japanese)* 77−81951
Biwa basin, hydrological cycle 79−53400
boat wake effects on shoreline of Lake Manapouri 79−25278
Bogoria, Kenya Rift Valley, radiocarbon date 79−44207
Bonneville, SW.Utah, shoreline features rel. to probable Holocene ground deform. 79−79803
Bonneville sediments, EM depth sounding 77−45173
Boone Lake ^{14}C dates rel. to ice-free corridor in Late Pleistocene Alberta 80−26552
Bosumtwi, Ghana, Holocene lake level variations, palaeoclimatological evidence 77−78249
Bosumtwi, Ghana, water-level, Late Pleistocene-Holocene 80−81931
bottom sediments, in situ neutron activation anal., pollution, mapping and prospecting appl. 77−87115
Canyon Lake, Texas, ^{90}Sr in molluscs 77−81590
Carl Blackwell, Oklahoma, atmospheric contrib. of P to aquatic system 79−100545
Caspian Sea, biogenous elements balance during period of regulated streamflow runoff 80−31073
Caspian Sea, diagnostic calcs. of currents *(Russian)* 77−13091
Caspian Sea, evaporation processes, evaluation of temporal spectral density *(Russian)* 77−5337
Caspian Sea, short internal waves in near-surface thermocline *(Russian)* 78−81231
Caspian Sea, spatial struct. of storm waves *(Russian)* 79−29790
Caspian Sea, stationary hydrodynamic model 79−39774
N.Caspian Sea, storm surge simulation using bottom friction *(Russian)* 77−21810
Caspian Sea, T content 79−34858
Caspian Sea, thermocline depth determ. using sonar *(Russian)* 77−13132
Caspian Sea, Turkmenian sector, magnetotelluric sounding results 77−40980
Caspian Sea, water balance and level vars. statistical forecasting 77−78263
Caspian Sea, water density and composition obs. 80−101388
Caspian Sea ice formation, aircraft radiometry 77−70712
Caspian Sea shallow areas, wind waves freq. spectra *(Russian)* 79−16477
chemistry, geology and physics, book 79−44215
circular basin, variable depth, time dependent response to wind stress 78−24320
circulation, seiches, tides and storm surges, finite element methods, book contrib. 79−34876
circulation driven by wind, 3-D transient response 80−77021
Clear Lake, California, absence of Mono Lake geomagnetic excursion in sediment palaeomagnetic record 78−11801
closed basins, three-dimens. rigid-lid model 78−32131
Clutha Lakes, inflow rel. to atm. circulation indices and rainfall 78−11926
coastal boundary layer with friction, wind stress forcing, time depend. model 79−34861
cold-air advective conditions, lake moderating effects on surface temps. 79−25299
Constance, eutrophication effects on sedimentation 79−79889
Constance, heavy storms and wind strength and direction *(German)* 77−56695
cooling pond, heat transfer processes evaluation 78−61458
cooling pond with waves, heat transfer through thermal skin 79−100878
cooling ponds, atm. effects of heat transfer, numerical model study 80−8380
cyclonic mean circulation of large lakes, surface-wind and solar-heating effects 78−16071
Daisetsu Dam, artificial reservoir, Hokkaido, Japan, winter ice cover study *(Japanese)* 77−81945
Dead Sea, KCl and H_2O activities in brine 78−31673
Dead Sea, mixolimnion deepening and water column overturn 80−61822
Derwent Reservoir, N.England, Zn, Cd and Pb in water, sediments and submerged plants 79−25286
discrete model 79−96767
drift, wind-induced, in contained water bodies 79−48512
Duluth-Superior Harbour, ice growth meas. 79−2299
dynamics, isotopic techniques appl., advisory group meeting, Vienna (1977 August 29 to September 2) 80−41950
ecological models, time and length scales for one-dimens. assumption 80−12455
ecosystem management at Lake George, model development 78−36217
ecosystem modelling, real-time estimation methods appl. 79−5541
effluent P standards impact on eutrophication control 79−88015
Erie, elutriate-primary productivity bioassays of dredge spoil disposal 79−88016
Erie, geomorphology and origin of Point Pelee, SW.Ontario 78−92857
Erie, heat storage and advection 77−41078
Erie, sedimentary record of heavy metal pollution 79−83644
Erie, three-dimens. circulation, free-surface and rigid-lid models 79−20894
Erie terrestrial radiation in 1952-1968 period 77−29343
estuaries, nontidal, hydrographic network changes under influence of natural factors and water management measures 79−29792
eutrophication modelling and control 77−21820
evaporation, climatological estimates 80−12449
evaporation from shallow lakes and ponds, simple determ. method 77−5352
evaporation from water surface, scaling theory 80−109179
evaporation from water surfaces in Armenian SSR 78−7673
evaporation of large lakes, aerodynamic evaporation technique 80−61833
evaporation variation with salinity and temp. 77−53083
Eyre North, S.Australia, bottom profile 78−69376
fjord lake, short period internal waves near river induced shear zone 77−81939
fjord-type lake, river-induced currents 78−49051
Flevo, Netherlands, Priestley-Taylor evaporation model of shallow lake 80−51443
flood and tidal flows, network hydraulic model 79−12162
flood event real-time predictors, stochastic model 80−67383
flood wave propagation in Lake Maggiore, recursive parameter estimation and outflow forecast 79−8650
flooding after breakthrough of Lake 2 at Tuyuksuy moraine *(Russian)* 77−53091
lakes continued
flow, unsteady, numerical model validation 80−72559
flow-through reservoir, vel. and temp. fields, num. simulation 77−17152
Fox Chain of Lakes, Illinois, wind-generated circulation patterns 79−53391
freshwater thermocline, migrating thermal struct. 79−79880
frozen Arctic lakes, L-band imaging radar obs. 77−21816
George, New South Wales, water levels, balance and chemistry 79−84332
Georgian Bay, chlorophyll conc. from airborne spectral refl. meas. 78−16202
Georgian Bay, water balance estimate during 1974, Lake Huron water exchange 80−12450
Gippsland, Victoria, Pliocene eustasy and sand barrier form. onset 79−74886
Glacial Lake Whittlesey, ice frontal position in eastern Erie basin 80−12436
glacier-fed lake with low sediment input, sedimentation processes and patterns 78−88849
Gordon, geomagnetic variation caused by ground loading during lake filling 80−8346
Gow Lake, N.Saskatchewan, terrestrial meteorite impact crater 78−7640
Great Lakes water quality, remote sensing data interpretation 80−98364
Great Lakes, flow var. through Straits of Mackinac 77−64352
Great Lakes, ice formation, freeze-up, breakup predictions 77−45038
Great Lakes, LANDSAT obs. of whitings and chlorophyll distribs. 78−77283
Great Lakes, sediment chemical composition, anthropogenic loadings 77−37256
Great Lakes, toxic substances 80−55949
Great Lakes coastal waters, thermal plume meas. systems 78−44891
Great Lakes shoreline erosion, meas. of W. Lake Michigan 79−5542
Great Slave Lake fallout estimation from Cosmos 954 satellite 79−85830
Greatlakean Substage replacing Lake Michigan basin Valderan Substage 77−17104
groundwater flow near lakes, numerical simulation 79−2322
Hamilton Harbour on Lake Ontario, O_2 depletion 79−16554
Harp Lake, Ontario, Canada, atm. N and P loading 79−53383
heat flow meas. in small lakes in N.W. Ontario, discussion and reply 77−53016
heat fluxes, latent and sensible, prediction from surface water temps. 80−72562
heavy metal concs. in small Norwegian lakes 79−16551
heavy metals, distrib. and speciation in aquatic systems, analytical techniques 78−69390
heavy metals and organic C conc. in surface microlayer, physical processes effects 79−57978
high-resolution ocean subbottom survey data analysis model 80−46211
Holocene lake sediments, N.Poland, palaeomag. 80−21616
Huron, east coast, mag., physical and lithological props. and age of till, discussion 78−20404
Huron, north shore, resedimented conglomerates of Huronian age, deposition from sediment gravity flow 78−36164
Huron, Saginaw Bay, Georgian Bay and North Channel, gravit. oscills. 77−60435
Huron, sediment composition, anthropogenic inputs 79−79419
Huron, sediment radioactivity, mixing by benthic organisms 78−16060
Huron, shore contamination from radioactive fallout 77−86897
Huron, wet and dry deposition of P 79−57991
Huron, winter circulation meas. 79−84309
hydrographic surveys optimization 79−53378
hydrologic settings classification, north central USA 78−11939
ice, microwave radar and radiometric remote sensing meas. 80−85691
ice cover, dissipation, effect of surface meltwater accumulation, heat flow 80−8364
ice-cover thickness, pulsed radar meas. method 78−92862
ice-covered lakes (North Slope, Alaska), radar return differences 79−2298
interactive lake survey programme for water resource surveillance 78−81257
internal long nonlinear waves, obs. in Babine Lake, Canada 78−69377
internal surges, nonlinear internal wave model 78−63442
internal wave of two-layer lake, due to wind stress, theory 80−98365
Iowa lakes, water transparency survey 79−2308
Isar River, Bavaria, trace elements distrib. in sediment, suspension and water samples by neutron activation analysis 78−3834
Jocassee, S.Carolina, seismicity rel. to Rn content of groundwater 80−94466
Jocassee reservoir, South Carolina, stress distrib. 77−91047
Kainji, W.Africa, water columns movement, LANDSAT data 79−25284
Kainji Lake particulate distrib. patterns, LANDSAT-1 spectral data 77−5255
Kalahari, evidence for widespread late Pleistocene humid period 79−58083
Kama Reservoir, USSR, forecasting spring inflow 80−105008
Kamloops, fjord lake, internal Kelvin waves obs. 78−73411
Kamloops Lake, B.C., Thompson River effects 78−49051
Kariba, crustal deformation following filling 77−9391
Keowee, S.Carolina, USA, 1978 earthquake swarm following filling 80−36255
Kinneret, limnological modelling 77−21821
Kinneret (Sea of Galilee), mean flow in rotating basin 80−81937
Kivu, multiple components transport through thermohaline diffusive interfaces 80−12396
La Cygne Lake, Kansas, wind generated waves, statistical props. 77−41093
Lagoa dos Patos, Brazil, shallow water circulation modelling 78−77286
lagoon sediments, Mahalanobis' D^2 distance appl. *(Portuguese)* 78−61388
Lahontan Basin, Nevada, pluvial lake level fluctuations 79−2310
Lake Chad, brines and evaporites 80−41463
Lake George, New South Wales, Australia, water level fluctuations 80−51440
Lake Jocassee area, S.Carolina, seismicity, earthquake prediction algorithms 80−51345
Lake Lisan-Dead Sea system, Pleistocene geochemical evolution 78−49047
Lake Michigan and Chicago area lake breeze, numerical study 78−7682
Lake Shlavantas, deep autumnal cooling and freezing *(Russian)* 78−36213

lakes continued
Lake St George, Ontario, Fe diagenesis in sulphide rich sediments from Mossbauer spectroscopy 79−74917
Lake Toya, Japan, acid mine drainage, pH effect 79−34449
Lake Van tectonic activity and sedimentation study *(German)* 78−3843
land-lake precip. relationships, using Lake Michigan data 78−44942
landslide wave generation digital simulation by Galerkin finite element method 78−92879
Langmuir circulations, controlled laboratory expts. 79−23330
Langmuir circulations, generation by instability mechanism 77−64304
Late Pleistocene and Holocene dry lake deposits, Mexico, palaeomag. record 80−21618
Late Quaternary lake levels in S.Afar and Ethiopian Rift 77−64337
Lebsko and Sarbsko, Poland, water level changes due to storm tides in Port of Leba *(Polish)* 78−40568
Lebsko water level analysis and wind effects *(Polish)* 77−70708
level and velocity meas., surface wave random signal anal. 77−45205
level oscillations and influence on river runoff in Lithuania *(Russian)* 78−16068
limnological theses and dissertations concerning Texas waters, 1897 to 1976 period 78−7680
N.Lithuania, karst lake replenishment *(Russian)* 79−8643
Lithuania, lake vegetation influence on river runoff *(Russian)* 79−12154
N.Lithuania, surface karst craters and lakes *(Russian)* 78−49053
Lithuanian lake catchment area soil N and P distrib. *(Russian)* 79−96780
Lithuanian lake overflow influence on river runoff *(Russian)* 78−16070
Lithuanian lake water temperature rise (spring 1974) *(Russian)* 79−8644
Llyn Goddionduon, sediment influx, magnetic susceptibility meas. 79−74915
Loch Lomond, Scotland, palynology, palaeomag. and ^{14}C dating of Flandrian marine and freshwater sediments 78−81234
Loch Lomond sediments, geomagnetic secular var. record 79−44088
Loch Ness, bubble clouds in freshwater lake, detect. by acoustic refl. 79−66722
Loch Ness, Kelvin-Helmholtz billows, rel. to thermocline fine struct. 77−66935
Loch Ness, near surface mixing layer microstruct. in stable heating conditions 78−85568
Loch Ness, Scotland, turbulence and mixing meas. 77−70702
Lugano, bathymetric map 78−96252
Magadi basin (Kenya), hydrochemistry 77−49098
magnetic remanence acquisition in Finnish lake sediments 79−66682
Maneri Bhali Hydel hydroelec. scheme, stage I, model; India 77−9452
McIlwaine, Rhodesia, distrib. of P, N and organic C in sediments 77−33114
Mets and nearby peat bogs, thickness meas. by radar 80−21860
Michigan, aerosol mass conc. and scattering coeff. in midlake region 80−61839
Michigan, atmos. boundary layer modified by cold lake 80−72571
Michigan, Chicago Area Program, mesoscale meteorology 78−77294
Michigan, circulation during annual temp. cycle 80−36341
Michigan, diurnal wind var., lake breeze and general lake effects 79−39809
Michigan, model and obs. currents 78−24321
Michigan, natural oscill. of Green Bay, theory 80−61806
Michigan, O_3 formation rel. to power plant emissions 79−74575
Michigan, pot. benefits from wave forecasting service for Port of Milwaukee 78−77357
Michigan, sulphate deposition in stable atmos. conditions 80−81494
Michigan, surface microlayer and subsurface element concs. 80−77022
Michigan, surface normal modes calc. compared with water level obs. 77−2185
Michigan, trace element input by aerosol deposition, pollution study 80−76672
Michigan, W. shore, breeze circulation cell 79−88445
Michigan dry deposition loading by airborne particulate matter 77−29410
Michigan sediment cores, palaeomag. records of geomag. secular var. 77−60347
Michigan surface waters, N_2O concs. 78−57223
microcystis removal ship, Seimei, Japan *(Japanese)* 77−56753
microseisms in lakes, longitudinal waves, origin from atm. press. variations *(Italian)* 77−81798
midlake region, aerosol mass conc. and scattering coeff. 80−61839
NW.Minnesota, Recent palaeolimnology 77−2186
mixed layer growth, penetrative convection in stratified fluid 78−44908
mixing in upper layer during heating cycle 77−29335
modelling, temperate ecosystem, literature review 80−81949
moderating effect on downwind temp. and humidity, model simulation 79−88400
Monona Lake, Wisconsin, Cu environmental chemistry 79−44214
Morskie Oko in high Tatra, Poland, specific resistivity of ground and water *(Polish)* 79−96735
multi-inflow reservoirs, flow dynamics 78−20452
Musos Tyrelis (N.Lithuania) bog stratigraphy and palaeogeography *(Russian)* 78−49054
Naini Tal, India, metal pollution in water and sediment 80−97828
Naivashi, Kenya, level changes rel. to equatorial westerlies over E.Africa 80−61819
neutron activation analysis of Cr after preconc. on activated C 78−3993
New Guinea Highlands lake sediments, evidence for recent palaeomag. secular var. 79−12069
Nipissing Great Lakes, radiocarbon dating of organic material, alluvial sediments 79−84251
nonlinear waves in closed basin, random behaviour 80−26557
numerical modelling appls., conf., Southampton, England (July 1977) 78−77285
Ontario, airflow in boundary layer, aircraft obs. 77−37295
Ontario, circulation from mirex patterns in sediments, simulation 80−26556
Ontario, coastal boundary layer forced wave model 78−7669
Ontario, coastal zone, mean summer circulation 80−90106
Ontario, current fluctuations during IFYGL (winter 1972-3) 79−57981
Ontario, downwelling fronts generation and propag. 79−20893
Ontario, evaporation during IFYGL 79−2318
Ontario, Hamilton Harbour, numerical model of unsteady flow 80−72559
Ontario, inertial currents, 1972-73 winter 79−79882

lakes continued
Ontario, intermittent full upwelling 77−33110
Ontario, internal oscillation characts. 77−53084
s. central Ontario, lake P budget, snow and ice effects 79−62540
Ontario, Late Wisconsin sediments, aspartic acid racemisation and ^{14}C dating 78−73415
Ontario, north shore coastal boundary layer response to storm 78−24322
Ontario, objective forecast method for lake induced snowfall systems 80−51484
Ontario, sediment and nutrient loading 77−81922
Ontario, sediment and nutrient loadings, methodological arguments 78−77278
Ontario, sedimentation rates determ., ^{210}Pb dating method 78−73408
Ontario, summer circulation, three-dimens. model, diagnostic study 79−79881
Ontario, summer circulation three dimens. model, comparison with obs. 78−7668
Ontario, tributary waters, N and P conc. determ. 79−79418
Ontario, water quality model limitations 80−98373
Ontario, water quality near Port Granby radioactive waste storage site 80−97829
Ontario, winter circulation 77−60436
Ontario and Erie, comparative ^{210}Pb, ^{137}Cs and -pollen geochronologies of sediments 79−66728
Ontario and Erie, comparison of bluffs and sediments composition 77−5248
Ontario atmosphere turbulence, vel. and scalar statistics 77−33128
Ontario coastal waters, optical props. determ. 80−36337
Ontario drainage basin, evapotranspiration climatonomy model 77−5266
Ontario water masses, nonzero subsurface irrad. refl. at 670 nm 80−101387
Oroville, 1975 August earthquake and nearby surface faulting 77−9345
Oroville, California, possible rel. to 1975 earthquakes 77−9344
Oroville, California, weight-induced crustal stresses rel. to seismicity 77−9347
Oroville, reservoir-induced pore pressure and seismic activity 79−2190
oxbow lakes, Yukon River basin, Alaska, morphometric definitions and classifications 77−66941
palaeoclimatology and vegetation changes during 2000 years BP, from anal. of varved lake sediments 79−25279
palaeohydrologic phenomena recorded by lake sediments 77−66936
Par Pond, reactor cooling reservoir, seasonal cycling between water and sediment 79−100881
particulate cores., remote sensing 80−105056
Perch Lake Basin, Ontario, hydrological and geochemical studies conference, Chalk River, 1978 April 25 to 26 80−51955
Pitt Lake, BC, sedimentation rates from ^{137}Cs measurements 80−4048
N.Poland, Holocene lake sediments palaeomag. records anal. rel. to short period secular geomag. vars. 80−98221
polar desert pond, dynamic chemical equilib., as sensitive index of meteorological cycles 80−12441
pollution, crude oil spill spreading 78−16079
ponds, solar radiation absorption 79−16530
Poplar Bay, Lac du Bonnet, Manitoba, possible meteorite impact crater 77−17150
Powell, Utah-Arizona USA, 1972-5 circulation and stratification 80−61829
pure water PVT properties, use and misuse for lake waters 77−49095
radioisotope applications in agriculture, hydrology, medicine industry etc., booklet 78−35947
Ramganga reservoir, Kalagarh, India, filling rel. to seismic activity 77−25657
reserviors, suspended load sedimentation, analysis and prediction method 78−53664
reservoir, stratified layer config. *(Japanese)* 78−20454
reservoir, stratified layer turbidity *(Japanese)* 78−20455
reservoir, surface layer turbulence and water masses dynamic stability *(Russian)* 77−33107
reservoir, well-mixed shallow water, evaporation estimation model 78−20453
reservoir, wind driven currents, turbulent viscosity and bottom friction *(Russian)* 77−70700
reservoir management, dynamic programming and release rules 77−73776
reservoir on River Elta, rock slide stability, geological survey *(German)* 78−7636
reservoir operation, multigoal anal. 79−96768
reservoir operation under conflicting objectives 77−73777
reservoir storage, distrib. of max. deficit of partial sums of variables 80−4651
reservoir surface area from LANDSAT imagery 79−66834
reservoir surface water, T balance inc. molecular exchange 80−72565
reservoir with inclined bottom, gas motion under press. penetration *(Russian)* 77−81952
reservoir with silty bottom, sound refl. coeff. freq. and ang. response 77−11078
reservoirs, asymptotic distrib. of functions of partial sums of stationary processes 77−41091
reservoirs, bars, longitudinal axis when formed at a shore inlet within a contour *(Russian)* 79−92522
reservoirs, thermal stratification during winter season 79−5532
reservoirs at Kiev and Kremenchug, wind-induced currents in shallows *(Russian)* 77−29329
reservoirs of Uttar Pradesh, sedimentation 80−31076
reservoirs with Markovian inflows, modelling 78−16080
riffle-pool sequences morphology 77−45024
riverine lakes, spring circulation, lake temps. and inflow effects 80−26555
Rostherne Mere, Cheshire, ^{137}Cs dating confirmation by algal stratigraphy 79−12156
runoff management, ecosystem model WINGRA III 78−36216
Salton Sea, California, tectonic tilt rates from lake level obs. 80−90065
Salton Sea geothermal field, test of shallow-hole temp. meas. 78−11849
sand transported by wave motion near lake bottom 80−98306
Saroma (Hokkaido), wind stress meas. over ice *(Japanese)* 78−88842
Sava River and Lake, possible interconnection with Ranney wells determ. by environmental T meas. 78−20447
Sava water pollution influence on ranney wells in Belgrade 78−40602
Schlegeis reservoir, water level var. and seismic microactivity 77−81807
Searles Lake, California, ^{14}C and ^{230}Th ages 79−2311
seasonal reservoir, optimal releases, deterministic case 80−8362

lakes continued
sediment leachates, trace element anal., multielement-direct reading method 78−69514
sediment mixing and accumulation, near-shore, fallout radionuclide tracer obs. 80−81864
sediment pollution records in New York State 80−85311
sediment regulation in reservoirs in silt-laden Chinese streams *(Chinese)* 77−70711
sediment sequences, pre-Pinedale, Yellowstone National Park, geology, palynology, climatology 79−66727
sediment vertical mixing by tubificid oligochaetes 80−101390
sediment-water interface sampling with gravity corer 79−88512
sedimentation process, entrainment of cohesive sediments 80−90107
sediments, ^{210}Pb dating, results from Lake Ipea and Lough Erne 78−28202
sediments, E_h meas. reliability conditions 79−48528
sediments, microbial degradation of organic molecules 79−84331
sediments, PO_4^{3-} adsorption equilibria 79−66354
sediments, polymodal, of river-lake system, interpretation 79−25273
sediments, radionuclide geochronology and pollution history 78−61451
sediments, Recent unconsolidated lacustrine, organic geochemical analysis 78−49016
sediments, selective chem. extraction of CO_3^{2-} associated metals 78−65406
sediments as indicators of heavy-metal pollution 77−25710
sediments denitrification rate seasonal var. determ. by use of ^{15}N 79−100883
sediments from Lake Zurich, magnetisation of detrital and chemical samples 79−70787
sediments transport and resuspension in shallow lake 79−70816
seiches, tidal energy amplitude in lakes *(Italian)* 77−49092
shallow lake evaporation, simple model 79−39767
shallow lake heat balance, simple model, Lake Chad appl. 79−66716
shallow water basin, wind-driven current, eddy viscosity, bottom friction 78−65319
shallow water eqns., ADIF, FORTRAN IV soln. program 79−84493
E.Sivash waters, ^{90}Sr content *(Russian)* 78−77282
Skeleton Lake, Ontario, Canada, evidence for Palaeozoic impact crater 79−92553
Slate Islands structure, partially submerged meteorite impact crater in Lake Superior 77−78183
Solar Lake, Gulf of Elat, recent hot brine dolomitization 77−70634
sonar mapping of lake bottom sapropel and sea shelf sediments *(Russian)* 77−9562
Soufriere Crater Lake, use as calorimeter, erupted lava heat loss rate calc. 78−28207
Spain, induced seismicity of dams and reservoirs 80−61776
spatially averaged flow over a wavy surface 77−53085
stagnant, thermal stratification 80−36340
stratified flow, finite element analysis, book contrib. 79−34875
stratified fluid density interface, wind-wave interaction 77−62291
stratified lakes, temp. distrib. seasonal var., two-dimens. model, wind-induced currents effects 77−29327
stratified turbulent flow digital simulation using finite element method 78−90964
streamflow calc. from discharge vols. for winter periods 79−25285
subglacial lake, Antarctica, radar sounding 79−29798
subsurface bubble clouds caused by breaking waves 80−46185
subsurface water chemistry study, coring and squeezing technique 78−57332
Superior, coastal upwelling/downwelling cycles 78−44889
Superior, Huron, St. Clair, Erie and Ontario, N distrib. and C/N ratio in sediments 78−28250
Superior, Keweenaw Current, surface temp. structure 78−40597
Superior, LANDSAT-1 obs. of internal standing wave pattern 78−96244
Superior, organic C as nonspecific water quality indicator 79−25287
Superior, particulate concs., remote sensing 80−105056
Superior, primary production model including circulation influences in Lake Superior 78−49041
Superior, remote determ. of chem. loading due to spring runoff 78−96243
Superior, sediment composition, anthropogenic inputs 79−79419
Superior, shore surface water temp., spatial var. during upwelling 80−36322
Superior, shoreline inheritance in coastal histories 77−33112
Superior, silica mass balance and dynamic response to eutrophication 79−74912
Superior, transports using depth integrated model 77−37252
surface cooling, under free and forced convection regimes *(Russian)* 78−36179
surface films and foams, source and metal transport 79−16549
surface mixed layer of lakes, scaling of vel. fluctuations 77−45009
surface reverberation, statistical props. 79−1020
surface to bottom fronts, wind effects 79−2261
surface winds, small-scale, vars. over water surface, computation model 78−61480
suspended sediment rating curves, accuracy assessment for small basin 77−91170
suspended sediments in surface waters of Mississippi reservoirs 77−45041
suspended solids, anal. using Landsat multispectral data 79−16523
Sutlej catchment annual rainfall and Bhakra dam site annual runoff statistics 77−53082
Suwa, wind driven currents, obs., numerical calcs. *(Japanese)* 77−37254
synthetic aperture radar L-band imagery computer processing 78−36311
Tahoe, California-Nevada, effects of coastal front on chlorophyll distrib. 79−2301
Tahoe, California-Nevada, LF turbulence spectra in mixed layer 77−21804
Tahoe, California-Nevada, sediments, palaeomag. and sedimentological studies 80−41371
Tahoe, neutrally buoyant capsules dynamics from experimental drop 80−12438
Tanganyika, acoustic absorpt. $MgCO_3^0$ ion-pair relaxation 79−74914
Tanganyika, acoustic attenuation explanation 79−34851
Tarbela reservoir, Pakistan Himalayas, seismicity during initial filling 80−56388
Tarmanskii Marsh, influence of human activity on hydrological and thermal regimes 78−92864
Teggau, NW.Ontario, excess ^4He rel. to U ore body 78−65353
Teletsk lake valley, limnoclimate *(Russian)* 77−21881
temperate lakes, finite element analysis of one dimensional thermocline problem 78−49042
temperature and current meas., vertical automatic profiling system 78−36327
temperature distribution in deep and shallow lakes *(German)* 78−85618
terminal lakes water levels, statistical predictability of long-term processes *(Russian)* 77−49105
Texas impoundments, critical levels of P and N_2 78−11929
thermal boundary layer near air-water interface, fine struct. *(Russian)* 78−22332
thermal structure, modified wind speed influence 78−11943
thermosolutal convection in saline lakes, Antarctica *(Japanese)* 78−20448
Thunder Bay, Lake Superior, element conc. in post-glacial sediments 77−78237
Toba (Sumatra), ignimbrite ages rel. to Sumatra late Cenozoic rot. 77−60363
Tofutsu, Hokkaido, ice crystallography *(Japanese)* 80−36347
trace elements determination using routine neutron activation analysis 78−3992
trophic state index for inland lakes using remote sensing data 77−5256
Tsengwen reservoir, Taiwan, seismicity due to fault and lake filling 80−81930
Uchinskii reservoir, ice covered, statistical props. of velocity and temp. profiles *(Russian)* 77−78269
NE.United States, effects of soil Al leaching response to acid precip. 80−12442
unsteady energy transfer in surface layers of stratified water 77−41092
USA, benzo(a)pyrene conc. of sediment 80−61476
Val Tresa glacial lake, glaciolacustrine sediments dislocations due to Wurm glacier melting *(Italian)* 79−8647
Vanern, Sweden, wind, fetch and water depth rel. to sediment distrib. 77−66934
vertical temp. profile determ. by one-dimensional heat transfer eqn. soln. 78−77290
Victoria, incident global solar radiation, 1970-1974 obs. 80−81940
Volcan Poas, Costa Rica, subaqueous S lake 78−28206
Volta Lake, hydrological models, data bases and computerised control 80−4057
Vuokonjarvi, Finland, palaeomagnetic secular variation 78−32004
Waiau, Mauna Kea, sediment thermal diffusivity 77−2253
water, Gran's plot, acid-base titration 79−79432
water, level fluctuations since 30000 yr BP, global maps 80−51447
water flow low velocities meas. with submerged floats 78−7813
water levels and environmental conditions at 18000 yr BP, continental record initial evaluation 80−51529
water natural temp. and man-made variations *(Dutch)* 79−83642
water pollution control mathematical modelling, book 78−73418
water quality from colour imagery reflectances 79−53376
water quality from Landsat imagery of Wisconsin 80−41469
water quality monitoring, multidate Landsat data extraction progrm 80−17299
water surface, free, roughness determ., from air flow struct. anal. 78−63441
wave sensor array, high resolution, for wave directional spectra meas. in nearshore zone 78−36329
wilderness lake, Canada, hydrocarbons, detect. in water and sediment 79−12155
wind effect eqns., finite difference schemes 79−12163
wind stress coefficient over water surfaces, new evaluation 80−72603
wind-driven circulation, numerical models 77−37243
wind-driven lake circulation models, boundary conditions 80−85688
wind-induced circulation and water level changes, two-dimensional finite difference model 78−77287
wind-induced heat and mass transfer over large bodies of water 77−11186
Windermere, catchment area, dissolved Hg conc. meas. 79−24924
Winnipeg, lake surface fluctuations and mass flow through Narrows 79−57982
winter season energy balance *(Polish)* 78−24315
Wyoming, bathymetry and temp. of glacial lakes 80−94550
Yellowstone, heat flow meas., Yellowstone caldera thermal struct. 78−48997
Yellowstone, seismic refl. and refr. surveys and palaeomag. study 78−49049
Yellowstone, submerged hydrothermal explosion crater in Mary Bay, bathymetry, seismic and mag. surveys 78−49050
Yellowstone and Jackson, mag. props. and secular var. in sediment cores 78−48968
Yuzhny Bug river, wind-induced currents in shallows of brackish lagoon *(Russian)* 77−29329
B abundance determ. 78−85559
Ca, determ. in lake sediments, by atomic absorption spectroscopy 78−95970
Cd, determ. in sea and fresh waters, interlaboratory comparison 78−81209
^{137}Cs movement and loss in small lake 78−24317
Cu, rate of loss and speciation in lakewater 80−7967
Fe, determ. in waters, colorimetric-acid digestion method 78−61088
Hg determ. in sea and fresh waters, interlaboratory comparison 78−81209
Hg, determ. in sea and inland waters, differential pulse anodic stripping voltametry method 77−70361
Hg determination, error anal. 78−69519
Mn nodules in Oneida Lake, New York, growth rate 80−46208
P input, uncertainty analysis 78−81262
PO_4^{3-}, removal kinetics in small alkaline lakes, natural and artificial processes 79−79417
Pb conc., rel. to boating activities and sediment interactions 80−104523
^{210}Pb dating of annually laminated Finnish lake sediments 79−74916
^{210}Pb determination in lake and marine sediments 79−48582
Pu ecological export from reprocessing waste pond 78−53533
Pu from fallout in alkaline, saline lakes 80−97826
S isotope variations as pollution index in lakes near Sudbury, Ontario 78−57228
^{90}Sr concentration in freshwaters of USSR 79−39770
U in natural waters, field meas. technique 78−85705

Lamb shift
1S Lamb shift and 1S-2S isotope shift 80−91464
atom, two-level chirping in emitted light 78−37598
atom between two perfectly conducting plates, effect on Lamb shift 78−78122
atom interaction with pair of conducting plates 79−97990
atomic ground state energy, relativistic and radiative corrections *(Russian)* 77−67991
camphor separated optical isomers, inverted IR Lamb dips, IR-RF double reson. obs. 78−21951
decaying atomic states, behaviour in applied fields, Lamb shift expt. 79−63963
Dicke state N two level atom assembly, radiation emission theory 80−69350
electron internal dynamics, rel. to Lamb-Rutherford shift and microwave generation 80−13239
EM vacuum fluctuation effects on atom between conducting plates 79−72278
formaldehyde, width of inverted Lamb dip, meas. using low-noise He-Xe lasers 79−54915
glass:Cr^{3+}, absorpt. spectra, Fano antireson. and vibronic Lamb shift 80−71458
harmonic oscillator in random EM field radiative corrections stochastic electrodynamic treatment 77−45736
heavy ion, one and two electron systems, Lamb shift and radiative decays 77−38643
high-Z electronic and muonic atoms, QED, strong and supercritical fields, book contrib. 78−74193
hydrogenic ions, radiative decay of $2S_{1/2}$ metastable state 77−67992
hydrogenic ions of high-Z, expt. and calc. of Lamb shift, review 77−54534
intracavity inverted Lamb dip, of laser with nonlinear absorpt. cell 77−14765
iodomethane, dressed mol., ν_6 band, saturated absorption spectrosc. 79−54844
Lamb-Mossbauer factor for crystalline lattice 79−78592
light muonic atoms, nuclear size effects, energy levels, Lamb shift 80−14254
methane, ground state, dipole oscill. strength distrib., rel. to molar refractivity and dispersion energy 77−71835
molecular lasers, IR-FIR transferred Lamb-dip, standing wave saturation effects 80−58520
muonic atom, heavy, $1s_{1/2}$ levels, self-energy corrections 78−55262
muonic atom, self-energy corrections, Lamb shift 77−75343
muonic atom energy levels, $\alpha^2(Z\alpha)^2$-vacuum polarisation contrib. 79−22867
muonic atoms, Dirac-Fock method 78−74805
non-relativistic limit, physical interpretations of electron radiative corrections 78−37567
one-electron atoms, corrected for fine struct., lamb shift and QED shift, tables 77−79529
polarised H^- and $^2H^-$ source at Giessen polarisation facility 77−65372
propynal, IR-microwave double reson. and two-photon expts. 80−83396
radiative corrections to electron form factors, book contrib. 78−82213
radiative transitions, classical theory appl. 78−74597
resonant scattering of laser pulses by a system of N atoms 78−74617
slow proton beam spin polarisation meas. 78−78031
superfluorescence quantum beats, chirping role, Lamb shift sign change 79−31474
temperature dependence, theory 79−97991
temperature dependent term, classical calc. 79−59371
two atom system near metallic surface, cooperative Lamb shift 77−3317
two-level atom, EM radiation interaction, elec.- and mag.-dipole contribs., reaction field 78−94215
two-photon light shift and two-photon Lamb dips 79−36591
$\pi\mu$ atom, energy levels, fine struct. and Lamb shift calc. *(Russian)* 79−31744
Al XIII, $1s2p^3P_2$ and $1s2p^3P_0$ levels, radiative lifetimes and hyperfine induced decay 80−74149
Ar, hydrogenlike, Lamb shift meas. by motional elec. field quenching time-of-flight expt. 80−9550
Ar^{17+}, Lamb shift, elec. field quenching time of flight method 79−13674
Ba II, even isotopes, optical isotope shifts, Lamb-dip spectrosc. obs. 78−78666
Ba, saturation spectroscopy with laser optical pumping 80−83324
CaF, $A^2\Pi$-$X^2\Sigma^+$ transition, HFS and fine struct., intermodulated fluoresc. spectra obs. 80−63695
Cl, XVI, 1s2s ^{3}S-1s2p ^{3}P transitions, Lamb shift, VUV beam foil spectra obs. 80−52919
Cl^{16+}, Lamb shift meas. using beam-foil excitation, QED test 80−9551
^{35}Cl XVI, beam-foil excitation, Lamb shift and fine struct., QED test 80−9549
^{35}Cl XVI, n=2, Lamb shift, fine struct. 79−13675
D, 1S Lamb shift and 1S-2S isotope shift 80−91464
D, Lamb shift, from elec. field quenching radiation anisotropy 78−66502
Fe, highly ionised, 1s to 3p Kβ-like X-ray spectrum 77−50394
Fe $SiF_6.6H_2O$, phase transform., temp. depend. of Mossbauer parameters 77−73102
Fe XXI, relativistic energy levels, Dirac-Fock multiconfig. calc., triplet state fine struct. and Lamb shift 80−23315
Fe XXV resonance line wavelength, influence of 1s-electron Lamb shift 80−18819
H, $3P_{3/2}$-$3D_{3/2}$ Lamb shift, double quantum saturation spectrosc. obs. 78−94223
H, $(2^2S_{1/2}, F=0)$-$(2^2P_{1/2}, F=1)$ interval RF at. beam meas. 77−6728
H, (n=2) Lamb shift meas. 77−75336
H, double-quantum saturation spectroscopy, laser and RF 80−77880
H, excited states calc., use of Coulomb Green's function 77−57907
H interacting with EM vacuum fluctuations, ground state energy in multiply connected universes 80−87050
H, Lamb shift, anomalous mag. moment relativistic Dirac eqn. 80−42954
H like, metastable 2S state in weak elec. field, radiative decay, bound state QED 80−42959
H, microwave determ. 79−45676
H, n=2 levels, Lamb shift and fine struct. reson. meas. 80−23321
H, n=2 state, lamb shift determ., atomic interferometer method 80−23324
H polarised ion source, Lamb-shift type, charge exchange processes *(Rumanian)* 77−46445

Lamb shift continued
H, self-interaction of excited at. with radiation field 78−86794
H, Stark-induced anticrossings, Lamb shift meas. 78−33467
H, Stark-induced anticrossings, $^2P_{3/2}$-$^2D_{3/2}$ Lamb shift meas. 78−33468
H, subnatural linewidth resolution $2^2S_{1/2}$, $2^2P_{1/2}$ level crossing, Lambshift, pulse technique 79−22669
H, temperature-dependent Lamb shift 79−787
H^- polarised ion source, pulse operated, Lamb shift type, for acceleration of polarised protons *(Japanese)* 77−67929
H^+, isoelectronic sequence, quenching radiation anisotropy calcs. 77−27021
H-like atoms, E1-M1 interference in radiative decay, $2S_{1/2}$ metastable state, effect on Lamb shift expts. 78−41994
H-like atoms in intense long wave EM field 79−89652
H-like ion, ground state, Lamb shift, classical theory 79−97992
H_2CO stabilised He-Xe laser, freq. stabilisation using inverted Lamb dip 79−22991
H(D), ground state Lamb shift, isotope shift and relativistic nuclear recoil correction 78−82696
^{1}H Lamb shift measurement, estimate of proton RMS charge radius 77−50047
H*, radiative magnetic energy shift, H in 2p state 78−58601
He^+, isoelectronic series, variational approach, Z=2-10 78−9092
He^+ Lamb-shift measurement by the quenching-radiation anisotropy method 80−18824
^{4}He, muonic, Lamb shift calcs. 78−94199
O, He-like, $1s3s^3S$-$1s3p^3P$ transition 79−89637
Pb, muonic high-lying states transitions, electron screening effects 77−34786
S XV, 1s2s ^{3}S-1s2p ^{3}P transitions, Lamb shift, VUV beam foil spectra obs. 80−52919
Si XIII, 1s2s ^{3}S-1s2p ^{3}P transitions, Lamb shift, VUV beam foil spectra obs. 80−52919
Si^{12+}, $1s2s^2S$-$1s2p$-^3P transitions 79−22632
SiH_4, second-order stark effects, RF-IR double reson. 78−58739
SnO_2, finely dispersed, Lamb-Mossbauer factor 80−39930

lambda point *see liquid helium-4; superfluidity*

laminar flow
see also laminar to turbulent transitions
ablating Jovian probe heat shield, C vaporisation into nonequilib. stagnation point boundary layer 79−1264
ablation front, laminar, stability model 78−42680
acetone, electrification during laminar flow in metal pipe 80−6954
acoustic field effect on compressible liquid flow in laminar boundary layer *(Russian)* 77−68617
aerodynamic laminar boundary layer on curvilinear thermally conducting surface, optimum suction *(Russian)* 77−54968
aerodynamically heated body, stable shape during ablation *(Russian)* 78−75162
aerofoil, dynamic forces acting, subsonic instabilities *(French)* 78−67213
aerosol, in cylindrical tube, conc. distrib. of free and attached Rn and Tn decay products 79−29412
aerosol, through inclined circ. tubes, gravitational deposition of particles 77−89192
aerosol particle gravitational deposition from developing flow in horizontal circular tube 79−50776
aerosol particle thermophoretic deposition, from laminar-flow gas streams 77−58766
aerosols, particle deposition from laminar flow 79−47988
agitated vessel, flow behaviour and transport phenomena, correlation eqns. *(Japanese)* 78−38300
air, heat transfer in laminar natural convection in cubical cavity 80−24022
air flow over water surface instability 79−46290
air scoops at supersonic and hypersonic vels., throttling, separation and central body cooling 80−14739
air-vapour flow in channel, laminar, with wall vapour-ice transition 79−94617
amonium alginate, aq. solns., laminar flow heat transfer in helical coils 80−59030
annular ducts, eccentric approx. solns. for wall tangential stress profiles, viscous friction coeffs. 77−35238
annular flow, heat transfer at entrance, finite-difference method 79−4013
annular flow, linear stability 78−63497
annular gap turbulent flow calcs., laminar boundary layer thickness 79−55417
annular pipe heat exchanger, laminar flow heat transfer coeffs. 79−72779
annuli, laminar flow, pressure drop and heat transfer with dissipation allowance 80−74858
annulus laminar flow of Newtonian fluids, kinetic energy correction factor 77−31271
annulus with negligible diffusion, laminar non-Newtonian flow, residence time distrib. 80−79357
arc, electrical characts., effects of laminar and turbulent flows 80−1870
arc, laminar flow, equilib. composition deviation 80−24274
arc, plasma, of free jet laminar core, axial flow, strong localised disturbance effect 78−91178
artificial heart blood pump ventricle, mech. driven, visual study of flow field 77−56539
asymptotic laminar thermal convection, unified treatment *(Italian)* 79−18883
autocorrelation, photon correl. laser Doppler anemometer appl. 79−50826
axial, flow study by shear stress meas. 79−77126
axial air flows, heat transfer from wire 80−48700
axial turbine blades, spatial streamline flow calcs. using pot. flux of incompressible liq. 80−59000
axially symmetric laminar boundary layer, on finite disc, vel. profile *(Russian)* 77−84219
axisymmetric boundary layer flow between wall and paraboloid *(Russian)* 78−75121
axisymmetric channel, laminar boundary layer in presence of external stream swirls 80−64631
axisymmetric free shear layer, effects of initial momentum thickness 78−71325
axisymmetric laminar boundary layer, swirling flow through conical hydrocyclone, heat transfer 79−98733

laminar flow continued
axisymmetric laminar jet diffusion flame, split operator finite difference solns. 78−51252
axisymmetric rotating round nosed bodies, flow and heat transfer, buoyancy effects 80−79306
axisymmetric stagnation flow on circ. cyl. 78−79298
axisymmetric streaming flow past torus, Stokes eqn. soln. method 78−14026
benzene, electrification during laminar flow in metal pipe 80−6954
biharmonic equation, analogue technique, cylinders falling between parallel walls 78−55628
binary boundary layer with press. pulsations, friction and heat and mass transfer 80−14653
binary mixture flow in vertical channel, film condensation 78−75139
bistable wall attachment fluid amplifier, flow field anal. *(Japanese)* 80−53743
Blasius flow, Orr-Sommerfeld eqn., spectral props. 77−89097
blood, atherogenesis at branching sites, steady laminar flow field 77−21553
blood flow, gas and heat transport, platelet and protein diffusion 78−92669
blood plasma, human, hydrodynamic props. 77−73538
bluff bodies in confined flow, free-streamline model 78−46931
bluff body, laminar incompressible flow, separation, reattachment, eddies, drag 79−59964
blunt biconic at incidence, laminar viscous shock layer, supersonic/hypersonic flow 78−30313
blunt body, boundary and wake, supersonic viscous gas flow, numerical soln. 80−38441
blunt circ. cylinder, separated, reattached, redeveloped air flow, heat transfer characts. 77−58692
body of revolution, slender, nonlinear normal forces, Reynolds no. influence *(German)* 78−51191
body of revolution with heating and cooling, boundary layer transition and separation 80−64518
boundary alyer flow, heat transfer, rel. to vel. fluctuations 78−94710
boundary flow, periodic wavy surface, nonlinear anal. 78−90826
boundary flow on circular cylinder, axisymmetric flow 78−9623
boundary flow over spinning blunt body of revolution, Magnus forces 78−94745
boundary laminar flow on a flat plate 79−68677
boundary layer, 3-dimens., surface heat transfer and curvature effects, numerical soln. 79−1173
boundary layer, acceleration on partially moving surface *(Russian)* 77−51032
boundary layer, along a heated horizontal hollow cylinder, buoyancy and variable viscosity 78−46964
boundary layer, approx. soln. of Von Mises eqn. 77−27503
boundary layer, characteristics 77−35114
boundary layer, convective diffusion due to incident turbulent jet 78−67242
boundary layer, direct finite difference calc. of through separated regions 77−35115
boundary layer, finite amplitude high frequency oscillations 80−6024
boundary layer, flow stagnation with suction 79−68676
boundary layer, fourth-order numerical method 79−1174
boundary layer, heat transfer, mass transfer and friction coeffs. *(German)* 80−74881
boundary layer, heated, stability 78−9626
boundary layer, hydrodynamic stability over flexible surface with constant suction 79−77070
boundary layer, in elevated-free stream turbulence 77−80139
boundary layer, laminar, skin friction, determ. with small Pitot probe 78−18269
boundary layer, laminar, subsonic, strong slot injection, triple deck theory 80−74831
boundary layer, laminar, with separated bubble 77−23935
boundary layer, laminar separation, from upstream-moving wall 78−13989
boundary layer, local self-similarity method 79−32453
boundary layer, local wall deform. effect on evol. of natural instabilities *(French)* 78−30263
boundary layer, longit. surface curvature effects calc. 80−19337
boundary layer, low free stream perturbations influence, hydrodynamic waves 79−98738
boundary layer, nonstationary, with self-induced press. 78−34164
boundary layer, optimal control, group theoretic approach 79−32452
boundary layer, optimal control by wall suction or blowing 79−1242
boundary layer, second-order unsteady stagnation pt. solns. 77−89092
boundary layer, semiempirical calc. using arbitrary free stream press. gradient 78−94640
boundary layer, separating incompressible flow over smooth step of small height 80−19325
boundary layer, separation, control, heating and suction effects 78−9625
boundary layer, separation, transverse surface curvature effect 79−64644
boundary layer, separation in water, heating and suction, comments 79−14378
boundary layer, sharp press. gradient, calc. method 78−1628
boundary layer, similarity method with universal eqn. 79−90215
boundary layer, small amplitude oscillation development, stability characts. 80−48674
boundary layer, small temp. factor, high Mach no. 78−34156
boundary layer, solution of the Falkner-Skan equation by quasilinearization 79−1156
boundary layer, transient convective heat transfer 78−30286
boundary layer, turbulent 'spot' 77−19587
boundary layer, two dimens., encountering three dimens. hump 78−5725
boundary layer, two-point finite difference method 77−19617
boundary layer, universal eqn. in differential form 78−46925
boundary layer, unsteady, past wavelike bulge on flat plate, num. soln. of Navier-Stokes eqns. 77−58644
boundary layer, vorticity genesis 78−1630
boundary layer, with press. fluctuations heat transfer, friction *(Russian)* 77−89114
boundary layer, with suction or injection, parametric calc. method 78−22323
boundary layer along concave wall, vortex instability analysis 77−55000
boundary layer anal. of convection on horizontal heated plates 77−7396
boundary layer behaviour on continuous accelerating surfaces 78−22320
boundary layer calc., experimental wing profile surface pressure, spine function, single-parameter method 80−33556

laminar flow continued
boundary layer development under continuous incipient separation conditions 78−63415
boundary layer eqns. for liquid with temp. dependent thermophysical props. *(Russian)* 77−84220
boundary layer eqns. soln. by inverse series method 79−41662
boundary layer extraction through a system of slots of finite width *(Russian)* 79−27692
boundary layer flow, Gortler functions, uniqueness *(German)* 80−52034
boundary layer flow, laminar, thermal response behaviour 78−75136
boundary layer flow, three-dimens., soln. using method of integral relations 77−58645
boundary layer flow, three-dimensional, in orthogonal curvilinear coordinates 77−23940
boundary layer flow, unsteady, compressible, 3-D, near axisymmetric stagnation point 80−103011
boundary layer flow along vaporising liq. layer *(German)* 78−83403
boundary layer flow convection anal. by integral and characts. methods 78−34137
boundary layer flow over porous flexible surface, oscillatory flow 80−92107
boundary layer flow past two dimens. slot 78−5724
boundary layer flow with suction (blowing) and pressure gradient, finite element anal. 79−18866
boundary layer heat transfer along static and moving cylinders 80−79316
boundary layer heat transfer over rot. bodies 79−32517
boundary layer induced wake behind cylinder attached to plate 80−43712
boundary layer instabilities, Mach number 7 77−65760
boundary layer mass transfer with thermal diffusion 80−19323
boundary layer of dilute suspension during application of elec. field *(Russian)* 78−63503
boundary layer of incompressible liquid, electro-hydrodynamic analogy, design 77−27627
boundary layer on body in simple harmonic motion, three dimens. unsteady flow 77−27507
boundary layer on circular cylinder started impulsively from rest 79−64627
boundary layer on conical body with gas injection *(Japanese)* 78−59417
boundary layer on heated plate, numerical results 79−10545
boundary layer on moving surface under combined action of free and forced convection *(Ukrainian)* 79−50695
boundary layer on porous plate, wall shear stress with mass transfer 78−47032
boundary layer on rot. cylinder 77−89130
boundary layer on rot. disc in counter-rot. fluid 77−35113
boundary layer on rot. sphere 79−27648
boundary layer on rotating sphere in still fluid *(Japanese)* 77−35112
boundary layer reattachment in supersonic flow, num. soln 80−53809
boundary layer separation, on moving walls, use of integral theory 77−58640
boundary layer separation, review, book contrib. 77−51033
boundary layer separation at angular inflection on solid surface 78−67169
boundary layer solns. on moving surfaces, series method 79−32455
boundary layer stability rel. to transverse curvature for laminar flow with disturbances *(Russian)* 77−62233
boundary layer swirling flow with heat and mass transfer in conical nozzles and diffusers 79−81842
boundary layer velocity measurement by single-beam laser time-of-flight method 79−77298
boundary layer with hard suction 78−26097
boundary layer with press. fluctuations, friction and heat transfer 79−64652
boundary layers, compressible, Prandtl=0.72, sharp pressure rise effect 80−83782
boundary layers, hot wire readings, wall proximity effects heat transfer 80−48822
boundary layers, integral eqn. finite element soln. 80−10127
boundary layers, nonsimilar incompressible heat transfer analysis using method of strained coords. 77−42811
boundary layers, regular separation free from Goldstein singularity *(Italian)* 79−41657
boundary layers in incompressible micropolar fluids 77−80140
boundary layers in three dimens., integral relation method 77−31277
boundary layers on concave curved walls, heating effect on stability 77−65745
boundary-layer flow over parabola, second approx. 78−63414
boundary-layer flows with swirl and large suction 80−1519
boundary-layer reattachment in supersonic flow 79−46342
buoyancy cross-flow effects on longitudinal boundary layer flow 77−58687
buoyancy driven flows originating from heated cylinders submerged in a finite water layer 80−59024
Burgers' turbulence model, uniqueness and stability 79−27693
capillary fluid, in rectangular channel, free surface shape *(Russian)* 77−51117
capillary penetration problem, refined mathematical anal. 80−24713
carboxymethyl cellulose, aqueous soln., diffusion and mass transfer from rotating disc 80−83827
catalytic reactive flow, normal velocity in laminar boundary layer *(French)* 77−75988
cavities, advanced numerical anal. of 2-D time depend. free convection 80−43704
cavity, horizontal, laminar natural convection heat transfer 79−55383
cavity flow at high Reynolds numbers 77−31276
channel, curved (straight), entry flow, slender channel approx. 78−47042
channel, cylindrical, horizontal, mass transfer across interface of two concurrent laminal flowing liquids 80−79397
channel, heat-insulated, laminar flow with nonuniform vel. and heat input distribs. *(Russian)* 79−64662
channel, laminar boundary layer, Gortler vortices 80−64572
channel, rectangular, laminar forced convective heat transfer for 3rd kind temp. boundary conditions 78−87341
channel bounded by two hyperbolas, steady laminar flow, vel. distrib. 77−68565
channel flow, entry region and numerical soln. for square channel 77−84325
channel flow, heat transfer 78−79317
channel flow, heat transfer in entrance region 79−32518

laminar flow continued
channel flow, heat transfer internal conjugate problem 79−90254
channel flow, symmetrical, with wall suction 77−31389
channel flow, upstream flow processes effect on hydrodynamic development 78−47041
channel flow, upstream interactions 77−35240
channel flows of high temp. gases, heat transfer 78−94722
channel height effect on nearcritical flow past circular cylinder 80−14818
channel laminar flow, thermal entrance zone, heat transfer, optically thin gas layer effects 80−74861
channel thermal inlet zone, heat transfer in laminar boundary layer 79−1178
channel with blocked branch, laminar flow, nonregular domain transformation into rectangular domain 80−64635
channel with mass transfer across porous walls 79−41759
channels, buoyancy induced flow, general correl. eqn. 77−58790
channels, lune-shaped, analytical soln. 77−19585
chemical laser nozzle, effect of geometry and boundary layers on flowfield 77−27622
chemical reactors, annular, cylindrical, mass transfer in laminar flow 78−22429
chemically nonequilibrium mixture flow, characts. of combined heat and mass transfer *(Russian)* 79−59965
chemically reacting gas, chemically reacting noncondensable components 78−51258
circular channel, convective heat transfer *(French)* 78−63424
circular channel with rod clusters, heat transfer characts. 78−75140
circular cone, axisymmetric laminar boundary layer, exact similar soln. 80−14650
circular cylinder, local heat transfer by turbulence of free-stream flow of viscous liquid, theoretical determ. of influence *(Russian)* 80−96252
circular cylinder in laminar incompressible viscous flow, finite element anal. 77−84216
circular cylinder moving in stationary fluid, skin friction and heat transfer 79−50701
circular jets, friction heat effect on temp. distrib., anal., forced convection 80−10279
circular slot, flow conditions and testing *(Hungarian)* 78−67267
circular tube laminar flow, heat transfer with temp. depend. heat generation 77−68582
circular tube thermal entrance region, laminar droplet flow convective heat transfer 80−6049
circular tube under centrifugal accel. field, condensation heat transfer 80−74713
circulation flows near wall, ideal liq., two-dimens. anal. in Cartesian coords. 78−51173
classical fluid near critical point, nonequilib. steady state fluctuations with laminar shear flow 79−81844
classical fluids, critical phenomena in mean field approx. 80−59001
Coanda effects, simulation of discontinuous diffusing flow 78−9622
coiled tubes, laminar flow and heat transfer, efficient numerical procedure 80−64633
colloidal dispersions, stability in flow fields, trajectory anal. 78−5782
combined convection flow along vertical surface, fluctuating boundary layers 80−96254
combined convection heat transfer in rod arrays, numerical anal. 78−90898
combined convective laminar boundary flow, vertical cylinder in horizontal flow, finite difference approx. 78−90893
combined forced and free convection in horizontal tubes with temp. depend. viscosity 77−15023
combined free and forced convection across horizontal cylinder, flow and heat transfer characts. 77−84245
combustion in laminar diffusion gas jets, computation of diffusion flare 80−10276
complex heat exchange in scatt. laminar flow in cylindrical channel 78−83490
compressible 3D stagnation pt. boundary layer, large injection rate 77−89139
compressible boundary layer, at large Prandtl numbers, pressure gradient effects 80−19321
compressible boundary layer, with adverse press. gradient, separation and development 78−26144
compressible boundary layer, with vectored mass transfer 77−23974
compressible boundary layer flow at stagnation pt., vectored mass transfer 79−27661
compressible boundary layer flow at stagnation pt. 79−10583
compressible boundary layer on rot. sphere with heat transfer, buoyancy and viscous dissipation effects 77−15053
compressible boundary layer swirling flow in nozzle, flow and heat transfer 78−94795
compressible boundary layers, stagnation point flow with continuous moving surfaces 77−15054
compressible boundary layers, Taylor-Gortler instability 78−26140
compressible flow through duct, numerical method 79−4030
compressible laminar boundary layer analysis, on yawed cone 77−23973
compressible laminar boundary layer with large acceleration and cooling 77−11213
compressible laminar boundary-layer, 2D eqn., near separation, numerical soln. 77−46989
compressible laminar wall jet 80−28542
compressible Navier-Stokes equations, mixed explicit-implicit splitting method 77−58715
compressible Newtonian fluid, flow between rotating discs 77−31320
compressible nonadiabatic gas flow in tube, eqns. system numerical integration *(Russian)* 78−83427
compressible stagnation pt. boundary layers for laser heated flows 77−89141
computational fluid mechanics, book 80−1517
condensate film flow on finned surfaces, heat transfer, heat exchanger design 78−75038
condensation on falling laminar liq. sheet 77−42815
condensed film, flow down vertical surface, effect cooling conditions on heat exchange *(Russian)* 78−46934
conducting fluid, laminar rot. in cylindrical vessel, elec. and mag. field effects *(Russian)* 78−75222
conducting fluid in annulus, MHD laminar flow 77−42922
conducting fluid in cylindrical MHD induction pump, laminar flow 80−43788

laminar flow continued
conduits, two-dimens., suddenly expanding, laminar flow patterns, temp. influence 80−19505
cone, rotating, flow and heat transfer obs., disc theories applicability 77−58673
conical body laminar boundary layer with heat transfer *(Japanese)* 78−30257
conical diffuser, with suction, compressible boundary layer swirling flow 78−38360
conical nozzle and diffuser, laminar compressible boundary layer swirling flow 80−48768
conical surface, boundary layer due to swirling flow with throughflow 77−47024
convection, combined free and forced, in internally finned square ducts 77−51060
convection, conjugate, steady, incompressible fluid in flat channel 77−75919
convection, following injection of a hot-fluid against plate 79−32502
convection, forced, over rot. bodies with non-uniform surface temp. 79−23315
convection, free, laminar, three-dimens., about surface, numerical anal., visualisation *(French)* 78−87343
convection, free flat plate problems, new formulation *(Italian)* 79−46302
convection, free laminar flow, between two parallel vertical walls 77−47010
convection, heated vertical surface, boundary-layer thickness and Prandtl number 78−51161
convection, in vertical cylinder, const. heat flux 79−46307
convection, laminar assisting forced and free, comprehensive correlating equation 77−51051
convection, laminar mixed forced/free, about sphere, buoyancy effects 77−75907
convection, natural, laminar, enclosure with heat source and sink on horiz. boundary 78−90882
convection, natural, laminar, in open vertical channel, numerical soln. method 78−5799
convection, unsteady laminar, in uniformly heated vertical pipes 78−38323
convection flow through co-axial circular pipes 79−86431
convection from upward-facing inclined flat plate 77−7395
convection in flow between coaxial cylinders *(French)* 78−38314
convection in forced upflow, with radiative transfer 78−47064
convective coupled heat transfer, Nusselt no. computation 78−59398
convective diffusion to surfaces of poorly streamlined bodies 80−6041
convective flow over horizontal plate, laminar, wave instability 79−32499
convective heat and moisture transfers with const. heat flux *(French)* 80−33582
convective heat transfer augocentation thermal entrance regions using thermal instability 79−81887
convective heat transfer from perforated surfaces 78−94727
convective heat transfer in flow over plate 77−39290
convective heat transfer in internally finned tubes 78−94724
cooled pipe, droplets from vapour condensation, size distrib., laminar flow 80−79111
corner boundary layer, press. gradient and leading edge effects 80−14652
Couette flow, permeable wall layer, heat transfer and temp. distrib. 78−51165
Couette flow, plane, past permeable bed, buoyancy effect 80−92215
Couette flow between parallel plates, heat transfer 77−31299
Couette flow in rot. fluid between coaxial cylinders, Taylor instability 77−51066
Couette-type channel flow, laminar equalising flow *(German)* 78−51239
countercurrently flowing fluids separated by thin wall, heat transfer 77−23949
creeping Newtonian flow through sinusoidal tubes, collocation solns. 80−14817
cross-flow effects in unsteady flow past yawed infinite cylinder 78−30258
crossflow developing in boundary layer during longit. flow around right dihedral angle 80−59049
cryogenic systems, circulating cooling time for laminar and turbulent flow coolant 77−5849
curly-viscous fluids, free convection under boundary conditions of second kind 77−75942
curly-viscous fluids, three-dimens. free convection about slender bodies of revolution 77−75943
curved annulus, heat transfer effects 77−42820
curved circular pipe, steady laminar flow, laser anemometer obs. 78−47037
curved duct laminar flow and heat transfer 78−75144
curved semicircular duct laminar flow, secondary vortex flow 80−106847
curved tubes, fully developed laminar flow and heat transfer 80−79308
cylinder, circ., inclined, laminar 3-dimens. free convection, stability *(French)* 79−18884
cylinder, circ., separated wake stagnation pt., 2nd order boundary-layer soln. 78−63432
cylinder array, 2-dimens. viscous laminar flow field, finite difference method 78−42585
cylinder drag, low Reynolds number flow transverse to axis, wall effects 79−64624
cylinder in conducting fluid, radial mag. field effects *(Russian)* 77−3874
cylinder moving in fluid, flow pattern and heat transfer 80−28487
cylinders, vertical and coaxial, theory of convection, velocity profile and heat transfer 80−59036
cylindrical annuli, concentric, eccentric horizontal, natural convection heat transfer 79−55382
decaying vortex core, boundary layer dynamics, atmospheric appl. 79−55394
density stratified reservoir, selective withdrawal from line sink 77−14980
developed flow in curved channels, vortex formation *(German)* 80−1689
developed flows in rotating channels having rectangular cross section *(German)* 79−86516
DHAB, nematic, ordering change due to external DC elec. field, permittivity obs. 78−94990
dibutylphthalate, supersaturated vapour, aerosol form. by mixing of flows 79−39212
dielectric fluid, flow and heat transfer in annular channel, electric field effect 80−103077

laminar flow continued
dielectric jet with plane laminar flow, waveguide effect stability, anal. *(Russian)* 77−7546
dielectric organic liquid, concentric annuli, heat and momentum transfer, electric field effects 80−96315
diffuser, self-similar MHD flows with induced mag. fields 78−34205
diffuser entrance region, suspension laminar flow and particle deposition 80−53845
diffusion boundary layers, with surface reactions, laminar or turbulent regimes, thermal simulation method 77−75912
diffusion direct optical meas. of vel. gradients 80−59132
diffusion flow on interacting surfaces, laminar and turbulent, in Newtonian or nonNewtonian fluids *(French)* 77−27516
dilatant liquid, plane laminar boundary layer 79−64712
dimensionless equations for heat transfer in laminar flow with variable physical properties 78−83384
directional dispersion coefficients in anisotropic porous media 77−89195
disc, rotating, convective mass transfer 80−43707
disc in electrically conducting fluid, hydromagnetic flow due to torsional oscillations about non-zero mean 80−74992
discrete-hole cooling, three-dimens. num. prediction for laminar flow case 77−15089
disperse systems, plastic, laminar flow in circular tubes 80−87798
dispersion in porous media, pore distrib. and flow segregation effects 80−10302
dispersion in rectangular conduits, side wall effects, convection 78−94636
dispersion of contaminant mol. in laminar flow 77−39347
dissociated high enthalpy hypersonic laminar air flow, heat transfer to flat plate 80−69828
dissociating air, non-equilibrium laminar boundary-layer 77−952
downstream development of velocity-profiles behind flat plates 79−18870
downward-facing flat plate, stable film boiling heat transfer 77−23954
drag, on circular cylinder low Reynolds number 77−84218
drag minimised bodies, given length and base, Newtonian theory calcs. 77−84267
drag reduction polymer additive in helicoidal flow, screw pump press. head 78−26166
driven, in square cavity, finite element study 80−23983
driven polar cross section cavity, laminar incompressible recirc. flow 78−46988
drop in ternary mixture, laminar condensation heat and mass transfer at stagnation point 79−14227
droplets, vaporising, in gas stream in channel, laminar entry region 78−30347
duct, circ., laminar convective MHD heat transfer for 3rd kind temp. boundary conditions 78−87342
duct, curved, laminar incompressible viscous flow 78−46932
duct, dispersion with variable viscosity and diffusion coeff. 80−87808
duct, narrow, plane, temp. distrib., heat flow to dense blown layer *(Russian)* 78−83402
duct, nonconducting walls, MHD volumetric flow rate under uniform mag. field 80−1691
duct, plane, with sudden expansion, aerodynamics 79−94722
duct, rectangular, laminar non-Newtonian flow, vel. profiles 80−92217
duct, rectangular, MHD flow under uniform transverse mag. field at high Hartmann no. 77−55094
duct, streamwise-periodic variations of cross-sectional area, flow, heat transfer 77−80156
duct, thermal entrance region, laminar forced convection, finite-element soln. 80−10118
duct, various complex geometries, press. drop and vel. distrib. calcs. 77−51031
duct, vertical, laminar steady flow, combined forced-free convection, finite element anal. 79−27637
duct confined turbulent flames, laminar burning vel. effect on struct. and propagation 79−90351
duct entrance flow, 2nd order numerical method 78−38407
duct entrance region, laminar heat transfer, finite element method 80−69836
duct flow, compressible laminar flow, superimposed sound field effect 77−75933
duct flow, laminar, finite element methods compared to Doppler meas. 79−1253
duct flow, numerical solns. to Navier-Stokes equations 78−22424
duct flow, stationary viscous, 3D, generalised Prandtl eqns., analytic and numerical solns. 78−5726
duct flow development, step-by-step anal. for laminar flow 80−64634
duct flow with oscill. plate, numerical soln. 79−50794
duct of strong curvature 78−13988
duct wall cavities, heated bottom surface, forced convection heat transfer 80−6048
ducts, determ. of friction factors in hydrodynamic entry length region 78−94825
ducts, entrance region, finite element anal., marching technique 80−69761
ducts, spanwise-periodic and corrrugated, heat transfer and laminar flow 80−64547
ducts and pipes intricately shaped cross section, heat transfer, Laplace and structural method 78−83477
dust erosion by shock wave in air 78−42648
dust-liquid channel flow, with varying inlet temp., transient forced convection soln. 78−87375
dusty fluid, laminar boundary layer flow, 2-D stagnation point near oscillating plate 80−64606
dusty fluid flow past plate, small amplitude oscillations 80−14792
dusty fluid unsteady flow through long pipe with time depend. press. gradient 79−18863
dusty fluid unsteady laminar flow through circular pipe 77−11236
dusty viscous flow through a cylinder of elliptic section under time-dependent pressure gradient 79−77248
dusty viscous fluid, unsteady flow through tube 78−59449
dusty viscous fluid, unsteady flow through uniform pipe 78−59450
dusty viscous liquid, laminar flow through tube 79−37399
dynamic characteristics, in rot. mag. field, symm. effects *(Russian)* 78−47063
eddy motion in horizontal fluid layers, resulting from thermal lift *(German)* 77−11171
Ekman boundary layer, suspended particles effect 78−24349
elastic liquids, stability of plane Poiseuille flow 78−9662
elasticoviscous flow along plane wall with periodic suction 79−10594
laminar flow continued
elasticoviscous flow between rotating disc and stationary porous disc 77−54964
elbow primary flow field, 2-dimens. laminar flow 80−43779
electrically conducting fluid, laminar flow mass transfer at high Peclet numbers 80−43784
electrodes, sheet, mass transfer to continuous moving surface 80−69821
electrodynamically coupled streams, MHD flow in tubes *(Russian)* 77−27609
electrohydrodynamic stability in rigid cylinder, dielectric viscous fluids, eigen wavenumbers 78−59497
electrolyte, diffusion interactions between electrodes spaced on oscillating cylinder *(French)* 78−64849
electrostatic image force charged particle deposition in rectangular and cylindrical channels with laminar flow 78−83491
EM induction pumps, fluids, laminar flow, characts. anal. 79−32699
entrance flow, ducts of arbitrary cross-section finite element anal. 77−72351
entrance region heat transfer in tube 78−26119
entrance region heat transfer in tube 78−26120
entrance region of straight channel with uniform heat flux, heat transfer 77−58688
entry laminar flow in curved parallel plate channel 77−31386
equilibrium dispersed-ring water vapour flows, liq. distrib., film paramters and hydraulic resist. 80−24079
ethyl alcohol, electrification during laminar flow in metal pipe 80−6954
evaporation with natural convection, simultaneous heat and mass transfer in laminar boundary layer, numerical anal. *(French)* 80−53778
exit region central source flow, between finite close parallel rot. discs 77−42849
extended Graetz problem, approx. soln. by orthogonal collocation 77−89118
Eyring model fluid, dispersion in laminar falling film 77−89167
falling film, finite amplitude equilib. surface waves 77−19614
falling film, linear stability theory, applicability 77−23938
falling film flow, equivalence of spatial and temporal formulations for linear stability 77−19589
falling liquid film, laminar and turbulent, local mass transfer *(German)* 79−77080
falling liquid films, mass transfer with heat transfer and interfacial shear 80−80033
ferrofluid devices, magnetostatic and centrifugal, nonmagnetic body motion 80−33700
ferrofluid flow in circular pipe, uniform mag. field effects 80−43782
film, condensation of moving vapour on horizontal cylinder, exptl. dependences 80−58892
film, mass transfer with dissolution 78−26098
film, wavy, of fluid, instantaneous vel. profile meas. 78−79299
film boiling heat transfer, thermal conductivity and convection effects 80−74864
film boiling of binary liquid mixture, heat transfer rates *(German)* 77−7398
film condensation from moving vapour, with suction 78−59459
film condensation inside tubes, conf., Haifa, Israel, (July 1977) 79−15683
film condensation inside tubes, with noncondensable gas 79−14234
film cooling, expts. in hypersonic flow 79−94648
film flow down vertical cylinder, linear hydrodynamic stability 77−19588
film heating in axisymmetric flow around cylinder, bulk flow twist effect on efficiency 77−23952
film on rough surface, calc. of mean thickness *(Russian)* 79−77061
film rupture in laminar and turbulent lubrication, inertia forces effect 80−74813
filtration through porous metal gauzes, hydraulic resist. 80−100034
fin array, shrouded, with, without tip clearance, laminar heat transfer 79−55376
fine particles aggregation, mechanism and rate at uniform shear field 80−101046
finite amplitude wave propagation in nearly parallel flow 80−74899
finite element algorithm *(Chinese)* 79−72874
finite length plate in supersonic low density flow, surface pressures and corrections 80−14741
finite shrouded disc, laminar boundary layer in rot. compressible isothermal flow 80−43727
first-order reaction, algebraic expression 79−94585
fission reactor 61-tube bundle with wire wrap 80−32329
flame, laminar jet diffusion flame size prediction, Burke-Schumann theory extension 78−14096
flame, laminar jet diffusion flame size prediction from diffusion coeff. 78−14097
flame, laminar long wave stability, EHD problem anal. 80−53866
flame, laminar mixed-mode forced-free diffusion type, on vert. burning fuel slab 78−91033
flame, premixed, two-dimens. elliptic partial differential eqns. soln. 79−94738
flame, premixed laminar, multiplicity and stability, bifurcation theory applic. 80−16681
flame front, laminar, diffusion-thermal stability *(Russian)* 77−7477
flame in tube, diffusion-thermal instability 79−86320
flame jet, premixed, impinging on plane surface, turbulent heat transfer 79−4054
flame spread over PMMA sheets in laminar forced oxidising gas flow 80−35535
flames, laminar and turbulent, normal vels. of propag. calc. 77−84342
flames, laminar diffusion flames, struct. and extinction by suppressive agents 79−32705
flames, premixed, laminar, time-depend. soln. determ. 78−67282
flat insulated plate, supersonic laminar boundary layer stability 79−98749
flat plate, adiabatically densified fluid film, turbulent two-substance boundary layer *(German)* 78−90845
flat plate streaming potential investigations: hydroynamics and electrokinetic equivalency 80−106777
flat-plate solar collectors, laminar mixed convection in fully developed flow *(French)* 80−61411
floating heat layer interaction with solid wall, computation, book contrib. 80−1642
flow between circ. tube and cylindrical eccentric capsule 78−79377
flow measurements employing white light fringe image velocimeter 79−64816

laminar flow continued
flow round circular cylinder at low Reynolds number *(German)* 78−94641
flowmeter, 360 degree bend, discharge coeffs. 79−27717
fluctuating flow past a cylinder at high frequencies 80−1518
fluid containing particles, laminar throughflow between corotating disks 79−77136
fluid film, heat transfer, variable viscosity influence 80−64561
fluid with free surface, in triangular-shaped open channel *(Russian)* 77−51028
fluidised bed, effect of particle proximity on drag force 80−96306
fluidised gas-solid flow in standpipes 77−75970
forced and free convection in laminar flow over plate 80−24005
forced and free convective flow past a semi-infinite vertical plate 79−37286
forced convection, multiple finite spheroidal transform and its application 80−12910
forced convection, over horizontal plate, buoyancy-induced streamwise press. gradient effects 77−58681
forced convection between concentric spheres, num. soln. 77−42831
forced convection film boiling on plate with varying heat flux 78−5737
forced convection with rheological systems, review 79−1222
forced convective laminar heat transfer in annulus 80−48688
forced flow in convectively cooled parallel plate channel, asymmetric solidification anal. 78−38404
forced flow laminar filmwise condensation of vapour in vertical tube 80−43762
forced laminar convection flow on inclined surfaces, buoyancy force effects 80−6046
forced- and free convection joint flow past flat plate 77−47002
free and surface-mounted obstacles, topology, flow visualization 78−51157
free convection, boundary layers, similar solns. 77−27524
free convection, in horizontal eccentric annular channel 78−38310
free convection along nonisothermal vertical flat plate, soln. technique 77−58682
free convection boundary layer in three-dimens. system 80−33587
free convection boundary layers on cylinders of elliptic cross section 78−90877
free convection duct connecting fluid reservoirs 79−55421
free convection due to point source of buoyancy 77−15029
free convection effects in vertical tubes 78−5722
free convection flow past vertical porous plate set in impulsive motion 80−69818
free convection heat transfer from vertical thin wire to air, laminar-turbulent transitions *(Japanese)* 80−92152
free convection in laminar boundary layer along rot. plate, nonsimilarity solns. 77−31307
free convection laminar flow, viscous dissipation and pressure stress effects importance 78−63428
free convection loops, dissipation effects in laminar and turbulent flow 80−19372
free convection past heated vertical plate, leading and trailing edge and discontinuous temp. effects 77−15028
free convection with uniform heat flux on vertical plate *(French)* 77−39292
free convective flow, three-dimens., num. soln. 77−42826
free convective laminar flow, non-uniform gravity effects, finite difference soln. 80−33604
free surface gravity flow, finite element anal. with variable domain 78−79294
free surface in uniform laminar stream 79−98678
freely interacting laminar boundary layers in channels 79−81981
freon-114 boundary layer, stability, press. gradient and heating effects 79−18891
frustum of cone, laminar natural convection flow 80−53768
fully developed laminar flow with internal heat generation between horizontal parallel plates, thermal instability 78−90899
Galerkin finite element-finite difference soln. of laminar boundary layer flows 78−42586
gas, liquid flows in catalyst static granular bed, transfer processes 80−45554
gas, perfect, vortex sheet, separation from smooth body at large Reynolds number *(French)* 80−74908
gas flow, heat exchange to selectively emitting liq. in radn. field 77−84343
gas flow, high-temp., heating of graphite body, numerical soln. 79−37318
gas flow, transverse migration of individual particles 80−96240
gas flow in ducts, global solns. for quasilinear hyperbolic system 79−86511
gas flow through cracks 79−98693
gas jets, heat exchange *(Russian)* 80−53829
gas mixture, binary, condensation in boundary layer flow, numerical method 79−1236
gas mixture, flowing, separation by thermal diffusion 79−68755
gas mixtures, removal of condensing component by suction through porous walls 79−98787
gas particulate flow on flat plate, laminar boundary layer, finite difference method 80−43688
gas-liquid compressible flow, numerical investigation *(German)* 77−15111
gas-liquid flow, mass transfer in laminar streams with circulation in wet-walled columns 79−94698
gas-liquid moving interface diffusion 78−22404
gas-particulate laminar boundary layer on a flat plate 79−77068
gaseous microbubble growth in laminar separation bubbles 80−106821
glass sintered powder porous bodies, liq. penetration mechanism *(Japanese)* 80−53853
Gortler vortices in the nonlinear region, book contrib. 80−1607
groundwater nonlinear laminar flow into eccentrically placed well 77−66929
H-shaped section cylinder in laminar flows, aerodynamic charact. 80−106813
Hartmann flow in heated channel, thermal instability 77−7461
heat and momentum transfer, viscous incompressible laminar flow, constricted duct 77−80155
heat convection, liq. flowing in annular channel with const. heat flux, numerical soln. 78−83392
heat exchange in complex domains, new soln. techniques 78−94509

laminar flow continued
heat exchange in thermally initial portion of tube with variable wall temp., asymptotic soln. 77−58675
heat transfer, downstream of sudden duct enlargement 78−67196
heat transfer, flow in planar (quasiplanar) channel of variable cross section 78−1661
heat transfer, laminar periodic flow regime in channel, appl. heat exchanger 77−58678
heat transfer and flow instability of natural convection over upward-facing horizontal surfaces 78−94698
heat transfer and friction factors for laminar flow through finned tube 78−94730
heat transfer and press. drop for laminar flow through heat exchanges 80−19379
heat transfer at supercritical pressure 79−81872
heat transfer between two moving fluids separated by wall containing heat sources 77−23948
heat transfer characteristics for laminar flow between parallel plates with suction 80−79301
heat transfer flow enhancement low porosity surfaces of heat exchanger cores 78−38402
heat transfer for boundary layers with mass injection and chemical reactions *(Chinese)* 80−59020
heat transfer in circular tube during laminar flow *(Russian)* 78−38175
heat transfer in circular tubes and annular passages 77−72133
heat transfer in duct with one moving wall 77−7456
heat transfer in flow between porous plates 79−68708
heat transfer in internally finned tubes 78−94725
heat transfer in laminar cyclone 78−55548
heat transfer in laminar freely convecting boundary layer, series soln. predictive capability 78−71335
heat transfer in laminar longitudinal flow over cylinder, numerical investig. 80−19389
heat transfer in noncircular ducts, Schwarz-Neumann technique 77−80161
heat transfer in rarefied MHD laminar channel flow 80−48687
heat transfer in tube, liq. solidification in thermal entrance region 78−18346
heat transfer to laminar flow with internal heat source in channel 80−64532
heated curved pipe laminar flow anal. 79−32674
heated water laminar boundary layer props., approx. methods 79−64628
helical channel flow, heat transfer 80−6150
helical coil, effect of Schmidt number on laminar dispersion 77−80145
helical coil, residence time distrib. of flow 79−68806
helical coiled tubes, laminar convective heat transfer 78−94678
helically coiled tubes, residence time distrib. 77−54963
n-heptane, electrification during laminar flow in metal pipe 80−6954
high Reynolds no. flow past rough walled circ. cylinder 78−46952
holonomic formulation of boundary layer eqns., use of tensors 79−1153
horizontal concentric annuli, free and forced convection heat transfer for fully developed laminar flow *(Japanese)* 78−30150
horizontal cylinder, laminar free convective heat transfer 78−75130
horizontal cylindrical surface, free convection, local nonsimilarity anal. 78−75120
horizontal flat plate, heat transfer in natural convection flow *(Japanese)* 79−64658
horizontal jet penetration in stratified fluid, unsteady laminar flow 77−7430
horizontal parallel plates, unsteady laminar flow of viscous fluid, Navier-Stokes eqn. solns. 80−1683
horizontal pipe subjected to external convection and radiation, laminar forced convection 80−79307
horizontal tube, fully developed laminar flow, combined free and forced convection, expt. 78−87391
horizontal tube, heat transfer with filmwise condensation, vapour vel. influence 80−33598
hydrocarbons flowing through circular pipe, streaming currents developed in laminar and turbulent flows 78−87413
hydrodynamic control of increase of diffusional boundary layer upon plate immersed in Ostwald fluid *(French)* 78−87329
hydrofoil cavitation noise and inception, boundary layer development 77−55057
hydromagnetic flow, suction effect near accelerated plate 80−92232
hydromagnetic viscous fluid between rotating surfaces of revolution *(Polish)* 77−55096
hypersonic axisymmetric flow with const. momentum, shock wave, ideal and laminar regions *(Russian)* 77−55033
hypersonic boundary layer, nonequil. ionis. problem 80−59129
hypersonic boundary layer, shock wave interactions 77−89151
hypersonic boundary layer at stagnation pt., slip, mass transfer 77−19625
hypersonic flow about yawed blunted cone, similar boundary layer anal. for lee-surface heating 77−27553
hypersonic flow over insulated accelerating slender wedge 78−1685
hypersonic flow past blunt axisymmetric body, shock layer 78−9654
hypersonic laminar boundary-layer flow over expansion corner 77−65758
hypersonic laminar heat transfer to cones at angle of attack 79−1211
hypersonic laminar near wake of blunted cone, convective heat and mass transfer 79−98752
hypersonic unsteady airfoil aerodynamics, viscous and elastic perturbation effects 78−26150
hypersonic viscous shock layer, leeward vortex-induced heat transfer 77−80179
hypersonic viscous shock layer, three-dimens., numerical calc. on sharp cone at incidence 77−47041
hypersonic viscous state stability of sharp cone at incidence 77−23987
ice growth in laminar flow through a channel with two parallel flat walls 79−3908
ice layer profile on const. temp. plate in forced laminar convection flow 80−24006
ideal liquid flow around spherical segment *(Russian)* 78−63411
ideal plastic material, film flow along oscillating wall 79−81927
immiscible liquid-liquid system, laminar jet, vel. profiles and form 79−64752
inclined flat plate, laminar film condensation on underside 79−50700
inclined surfaces, wave instability of laminar mixed convection flow 80−69837
incompressible boundary layer eqns. finite element soln. 78−79304
incompressible flow past rot. elliptic cylinders 77−27538

laminar flow continued
incompressible fluid laminar boundary layer, Gortler function existence problem *(German)* 80−64516
incompressible laminar boundary layer, three-dimensional, hyperbolicity of integral equations of momentum 77−27505
incompressible laminar planar flow between parallel plates, ang. vorticity formulation 80−64643
incompressible laminar transient forced convection heat transfer in circular pipe 79−50798
incompressible liquids, laminar heat transport anal. using nonlinear temp. transform. *(Spanish)* 79−68693
incompressible power law fluid, laminar flat radial jet 79−64731
incompressible pseudoplastic fluid, laminar two-dimens. wake 77−51089
induction melting, fluid velocity, large scale meas. and predictions 77−46985
inhomogeneous medium, two-dimens., light propag. problems rel. to thermogasdynamic waveguide development 80−32914
injection flow in straight duct, vel. distrib. and press. drop 77−11263
inlet flow with slip, laminar in incompressible Newtonian fluid 79−94659
instabilities in gaseous heated channel, temperature-viscosity induced, nuclear rocket reactor appl. 77−18689
instability, ideal fluid flow with free surface, reson. surface wave buildup 78−34106
instabiliy in multiple channels 79−90217
insulated plate thermometer, incompressible boundary layer flow 78−55626
interacting boundary layers in high Reynolds number laminar separated flow 77−42865
ion wind enhancement of evaporation into a laminar air stream 80−53773
ionising Ar flows, shock wave and laminar boundary layer coupled interaction 80−59071
irrigating films, laminar, entry zone length for vertical plate wetting 80−53742
isothermal continuous cylinder, thermal laminar boundary layer 78−22321
isothermal horizontal circular cylinder, laminar free convection, thick boundary layer 80−64566
jet, dynamic and heat problems 78−67241
jet, heavy, flowing into nonmixing medium 78−51212
jet, laminar, in liq.-liq. system, vel. profile, numerical analysis 80−28545
jet, laminar axisymmetric impinging, heat transfer 77−42888
jet, laminar rectangular, mass transfer due to impinging on flat surface 77−68651
jet, liquid, falling in gaseous atmosphere, laminar and turbulent flow boundary layers *(German)* 77−7427
jet, slot type, flow field and impingement heat transfer, num. prediction 77−42891
jet, surface age meas. 78−83442
jet, uniform exit vel. profiles, developing region 78−79354
jet flow, appl. of Meksyn's method 80−96292
jet impingement heat transfer to melting ice surface 78−22394
jet on porous surface, initial part calc. *(Russian)* 79−77203
jet-wall boundary layer, heat transfer 79−41725
jets, axisymmetrical, with and without buoyancy *(German)* 78−83450
jets, impinging, heat and mass transfer 78−94777
jets, interaction, turbulent cone formation 77−84290
jets, laminar, vertical, round, weak buoyancy effects due to temp. differences *(German)* 80−64595
jets, linear stability 78−38379
jets in circular cylinder, influence of temp. 80−14770
journal bearing in rotating MHD flow, system characts. *(French)* 79−1263
Kelvin-Helmholtz-like instability of a shear layer subject to free boundary conditions 79−68726
Knudsen flow, through periodically constricted pores *(Japanese)* 79−72911
laminar bubble separation, stalling, lecture 78−22325
laminar compressible MHD boundary layer flow, effect on heat transfer 79−14489
laminar convection in vertical tube, thermophysical prop. temp. depend., effects 78−90895
laminar dispersion, effect of tube curvature and pulsations 77−3858
laminar dispersion in circular tubes, approx. anal. 77−46986
laminar flow, coupled heat and mass transfer, around flat plate with uniform heat flux 78−1631
laminar free convection in 1-D solar induced flows, theory 80−3495
laminar liquid films, dependence of temp. variation of film substance viscosity 79−41686
laminar natural convection over a slender vertical frustum of a cone *(German)* 79−77116
laminar plume above a line heat source in a transverse magnetic field 78−67269
laminar steady free surface flow past a permeable bed, buoyancy effects *(German)* 79−41665
large Reynolds number, 2-D hydrodynamic lubricating theory *(Russian)* 78−59368
laser heated nozzle flow with swirl, axisymmetric comp. boundary layer 80−14775
laser-Doppler technique, local size and vel. probability distrib., two-phase suspension flow 78−59517
latex suspension liquid film flow, local thickness meas. 79−4070
Laval nozzle, two-dimensionality of flow 79−90305
laws of motion of solid particles in laminar flow 80−83779
lifting surface, varying thickness shear layer, soln. using kernel function 77−89137
limiting relative law of heat and mass transfer and friction, permeability parameter effect 80−23999
linear pressure losses *(Rumanian)* 79−23298
liquid film, absorption with chem. reaction 77−42929
liquid film, boiling, laminar, with chem. react. on catalyst surface, model 80−45553
liquid film, falling, evaporation model 79−46305
liquid film, falling, laminar, transport augmentation by surface waves 78−71343
liquid film, falling, O_2 adsorpt. with zero order react. in entrance region 80−64652
liquid film, flow down vertical or inclined surface, surface tension effects 80−106778
liquid film, flow over horiz. smooth tubes 78−38273

laminar flow continued
liquid film, subcooled, heat transfer and film breakdown 78−34121
liquid film, with nucleate boiling, heat transfer and film breakdown 78−34122
liquid film breakdown, numerical anal. 79−46285
liquid film condensation on vertical wall, linearised stability anal. 79−55381
liquid film flow affected by streaming turbulent gas *(Russian)* 79−14386
liquid film flow on vertical wall 77−62237
liquid film in vertical flow down solid surface, coherence *(German)* 78−22322
liquid film moving along sloping surface, hydrodynamics 77−7365
liquid film stability adjacent to supersonic boundary layer 77−930
liquid flow around a self-propelled body 79−86399
liquid flow around plate, boundary-value problem soln. for generalised diffusion eqn. 77−7366
liquid flow in tube with frozen layer, crust profile method 78−30359
liquid in centrifugal atomizer, air vortex radius 77−80201
liquid in ribbed slot, free laminar convection 80−96261
liquid in rotating channel 79−68717
liquid jet, axisymmetric laminar viscous flow through pipe *(Japanese)* 77−42892
liquid jet, capillary breakup, random initial perturbation, drop size distrib. 78−38380
liquid jet, two-dimensional laminar, high Reynolds number flow 80−38467
liquid metal, laminar convective heat transfer along cylinder 77−914
liquid metal flow in curved channels, transversely applied mag. field 80−14829
liquid metal jets, 3D fluid flow model induced in ladles or holding vessels 80−10278
liquid metal transient flow at electrode in linear cond. motor 80−43792
liquid metal vapour, laminar film condensation under effect of electromotive force 79−1258
liquid metals laminar flow in curved channels, transversely applied mag. field, flow anal. 80−59116
liquid metals with variable thermal cond. and capacity, forced convection 79−37310
liquid motion in channels with permeable walls, hydraulic resistance 78−5797
liquid-gas mixer, perforated disc stirring cascade type, power dissipation, mechanism and correlation 79−1238
LMFBR wire wrap spaced rod bundles, laminar, transition, and turbulent parallel flow press. drop 79−26478
localised optical heating, principle of meas. on flows *(French)* 77−31406
longitudinal dispersion in saturated porous media 79−4080
longitudinal gas flow in cylindrical channel, heat transfer with elec. arc 77−11189
longitudinal internally finned tubes, analysis of fully developed laminar flow 78−13991
Lorenz model, Feigenbaum sequence of bifurcations 80−83783
low Mach number duct flows, combustion noise generation by chemical inhomogeneities 80−92237
low Reynolds-number flow in the vicinity of axisymmetric constrictions 80−6147
low speed flow up a step 78−79303
macromolecular solutions, laminar filtration under low polarization conditions 80−24056
magnetic field as a tool for investigating transition and turbulence 80−1696
magnetic fluid (cable coolant), natural convection heat transfer 78−94846
magnetic fluid boundary layer, flow stability 79−64782
magnetic liquid film flow in mag. field, laminar regime 78−34203
magnetically suspended cones, laminar near wake meas. probe interference 77−84257
magnetoelectrolysis in steady Hartmann flow cells, hydrodynamics, mass transport 77−36759
mass exchange in flat channel during electrochemical reaction 79−74394
mass transfer, electrochem. meas. 77−58794
mass transfer, linear wall resist. entrance region solns. 78−67168
mass transfer between a flowing fluid and a solid wavy surface 80−14681
mass transfer by forced convection, at rough surfaces in annuli, rate meas. 77−27532
mass transfer from rotating cylinders 78−42613
mass transfer in laminar flow between two plane parallel plates 79−37321
mass transfer in semi-cylindrical hollows, electrochemical measurements 79−23365
mass transfer with axial diffusion and chem. reaction 79−23376
MBBA, nematic mesophase, struct. of flow in cylindrical capillary 77−7671
melting heat transfer in steady laminar flow over flat plate 77−15027
metal, liquid, fluid flow during blast furnace tapping, mathematical model 78−85117
metal, thermal boundary layers, variable thermal cond. 79−59962
MHD, gas boundary layer swirling nozzle and diffuser flows with mag. field 80−1693
MHD, in entrance region of flat duct 78−30367
MHD, nonsimilar incompressible laminar boundary layers, finite-difference scheme 78−79386
MHD, sink flow with transverse mag. field, boundary layer thickness 80−69940
MHD, slow flow in channel, porous walls, periodic mag. field effects 77−27599
MHD axial flow in triangular pipe with transverse mag. field 78−59498
MHD boundary layers, laminar, control problem *(German)* 78−91024
MHD coaxial induction machine travelling mag. field, laminar flow *(Russian)* 78−5815
MHD convection in boundary layer, overplane and axisymm. bodies, theory 79−77270
MHD flow, impulsively started plate, Hall effect 78−1747
MHD flow in rot. mag. field *(French)* 78−51248
MHD flow of electrically conducting fluid in axial mag. field *(French)* 78−42667
MHD flow past moving plate with const. suction 77−11268
MHD flow past vertical plate, similarity solutions 77−65803
MHD flow with chem. reactions, solute dispersion 79−23378

laminar flow continued
MHD generator, compressible laminar boundary layer separation from segmented electrode wall 77−27598
MHD induction pump channel press. loss, laminar liq. metal flow friction losses *(Russian)* 78−75224
MHD jets, laminar and turbulent, elec. cond. fluid with transverse mag. field 79−77261
MHD laminar boundary layer with variable elec. cond., nonstationary flow *(French)* 77−39356
MHD laminar flow, longitudinal dynamic effects determination for Na, Al, Sn and Hg *(Rumanian)* 80−64792
MHD laminar flow, suspended particle motion stabiity *(Russian)* 78−5808
MHD laminar flow down vertical wall 77−11270
MHD laminar flow in liquid metal slip contacts 80−43795
MHD laminar flow in parallel-plate channel with unequal wall temperature, thermal entry heat transfer 77−42927
MHD laminar plane-wall jet flow 79−55424
MHD pipe flow with heat transfer 79−14482
MHD pulsating viscous flow superposed on steady laminar motion 80−92228
MHD stability of laminar boundary layer flow along flat plate with transverse mag. field 79−27709
MHD viscoelastic free convection boundary layer flow past porous plate 80−10317
MHD viscous laminar unsteady flow over infinite flat plate 79−37406
micropolar fluid, laminar boundary layer, longitudinal surface curvature effects 80−48669
micropolar fluid, laminar flow through slot 80−10313
micropolar fluid, nonsimilar incompressible laminar boundary-layer flow 77−35184
micropolar fluid flow, circular cylinder asymptotic boundary layer 79−18916
micropolar fluids, stability of laminar flows between parallel walls 79−1160
micropolar laminar radial channel flow, heat transfer 78−30328
micropolar liquids, laminar plane channel flow, stability *(German)* 78−94773
mixed convection on a horizontal plate with uniform surface heat flux 78−90903
mixed convection on vertical plate with unheated starting length, num. soln. 77−42827
mixed-convection heat transfer around an isothermal flat surface of finite length 78−90891
mixing layer growth from turbulent and nonturbulent boundary layer 79−68686
molecular gas radiation in the thermal entrance region of a duct 80−6051
molecular lasers with gas pumping, temp. field calc. 79−76673
moving horizontal flat plate, laminar boundary layer, buoyancy effects 80−74877
moving surface, free liquid layer, laminar and turbulent flow, Navier-Stokes anal. 79−94589
multidimensional two phase flow eqn. derivation, general constitutive principle appl., laminar stresses 80−10297
multidimensional unsteady laminar flames, scaling transformations for numerical computations 80−19522
multigranular suspensions, aqueous, sedimentation in oblique plate separator under laminar flow conditions *(German)* 77−44513
multiphase, with heat conduction, numerical soln., implicit difference method *(German)* 77−15110
narrow ducts and circular tubes, laminar flow-heat transfer, series solutions 79−72946
natural convection, heat transfer in enclosed cavity 77−51056
natural convection air flows, vel. meas. using laser velocimeter 79−82016
natural convection along cylinder, stability 78−1663
natural convection boundary layers on horizontal circular discs 79−77067
natural convection flow adjacent to vertical surface, leading edge effect 79−55389
natural convection from inclined cylinder 80−33586
natural convection from line thermal source, buoyancy-induced flow 77−19603
natural convection in horizontal cylinders, asymmetric boundary conditions, numerical anal. 77−39282
natural convection mass transfer along porous vertical plate 78−90876
natural convection on horizontal surface 77−80159
natural convective flow through duct with restricted entry 79−14393
natural laminar and turbulent convection, from isothermal spheres, correlation eqn. *(German)* 80−33607
natural laminar convection, side wall effects on heat transfer through vertical air layer 80−19377
natural laminar convection about isothermal cylinder, Navier-Stokes eqn. soln. 80−92143
natural laminar convection flows, variable viscosity effect 80−33589
natural laminar convection over cone with const. wall heat flux *(German)* 80−38414
natural laminar convective heat transfer in triangular enclosures 80−38404
Navier-Stokes eqns., spatial decay estimates, appl. to entry flow 79−14370
Navier-Stokes equation, incompressible, soln. using primitive variables 80−6017
Neumann-Kelvin problem, steady flow over finite obstacle on horizontal bottom *(French)* 77−72267
Newtonian and non-Newtonian fluid, laminar heat transfer, in tubes 78−9624
Newtonian calibrating oil, stress transient data obtained from cone and plate flow 77−31407
Newtonian fluid, recirculating flow in rectangular cavity, free convective flow in enclosed container 80−74852
Newtonian fluids, momentum transfer in curved pipes 79−68813
Newtonian liquids in straight horizontal elliptical tubes, heat transfer 79−94584
Newtonian vapour, with liquid droplets, throughflow between corotating disks, numerical anal. 78−94802
NMR spin-echo difference meas. method, plug and laminar flow, appl. to plant stem 78−14110
noise generation by laminar flames in tubes 79−86422
non-Newtonian boundary layer flow, mass transfer 77−27562
non-Newtonian duct entrance region flow, loss coeffs. calcs. 77−89166

laminar flow continued
Non-Newtonian falling film, hydrodynamic entrance length 77−58743
non-Newtonian falling film, Taylor diffusion of solute 77−39317
non-Newtonian falling liquid films, dynamics 79−7393
non-Newtonian flow along thin needle, vel. profile, skin friction 78−67229
non-Newtonian flow in noncircular pipes 78−18315
non-Newtonian flow in porous annulus 77−72333
non-Newtonian fluid, effective diffusion of impurity in laminar flow of liquid 78−67228
non-Newtonian fluid, laminar boundary layer, surface heat transfer rate 80−24055
non-Newtonian fluid, laminar flow in thin layer, two-dimensional problem 79−86474
non-Newtonian fluid, laminar forced convection heat transfer in square duct, numerical solns. 78−18318
non-Newtonian fluid, laminar pipe flow, nonisothermal, heat transfer, with internal heat sources 79−68763
non-Newtonian fluid, laminar source flow betweens parallel disks 79−37363
non-Newtonian fluid, unsteady laminar incompressible boundary layer eqns., flow, heat and mass transfer, similarity solns. 79−32590
non-Newtonian fluid duct flow, heat transfer 79−1219
non-Newtonian fluid film flow along vertical oscillating plate *(German)* 78−59431
non-Newtonian fluid flow through helical coils, studies 78−51204
non-Newtonian fluid jet, swirling, impinging on normal plane 77−42889
non-Newtonian fluid solution, film flow over soluble wall, solvent layer form 78−42634
non-Newtonian incompressible fluid flow through curved pipe, asymptotic theory *(German)* 77−24000
non-Newtonian laminar falling liq. films with smooth wave free gas-liq. interface, heat transfer 79−7389
non-Newtonian laminar flow through parallel plates, kinetic energy correction factor 77−31271
non-Newtonian laminar jet flow 80−1662
non-Newtonian liquid, isothermal Couette flow in slowly converging channel with complex shear 77−15069
non-Newtonian liquids and gases, annular two-phase flow, press. drop and gas vol. fraction 80−10286
non-Newtonian non-similar laminar boundary layers, rapid calc. procedure 78−90943
non-Newtonian power law fluid, laminar far wake flow 80−53824
non-Newtonian pulsatile laminar flow in tube 78−79346
non-Newtonian pulsatile laminar pipe flows, multiviscous approx. 77−3871
nonaxisymmetric flow between rot. and stationary disks with eccentric source 77−84215
noncircular pipes, laminar and turbulent flow 78−18315
noninertial particle transfer to rotating in laminar flow under external force field 80−10250
nonisothermal boundary layer, laminar flow of dilute particle suspension, self similar soln. 77−65785
nonisothermal flow of viscous or non-Newtonian fluids over rotors of centrifugal heat exchangers 79−77097
nonisothermal laminar and turbulent plane free jets with buoyancy effect, boundary layer theory *(German)* 80−53830
nonisothermal laminar flow in pipes 77−58741
nonisothermal steady flow in flat gap *(German)* 80−38376
nonlinear effects in laminar stability theory *(French)* 80−103012
nonlinear laminar flow of fluid into fully penetrating cylindrical well 78−75198
nonlinear perturbations, secondary flow existence *(Russian)* 78−22326
nonlinear stability, subcrit. Re, small disturbance asymptotic theory 77−84223
nonlinear viscoplastic media, dispersion in circular tubes for laminar motion case 77−58626
nonNewtonian duct flow, wall heat transfer in entrance region 79−4049
nonsimilar axisymmetric stagnation flow on a moving cylinder 78−79297
nonsimilar laminar free convection flow along a nonisothermal vertical plate, finite difference method 78−75119
nonsteady MHD thermal boundary layer, in incompressible laminar flow with variable elec. cond., approx. soln. 78−91022
nose separation for laminar boundary layers on body of revolution 80−59091
nozzle, heat transfer of transonic air flow 79−1230
nozzle and diffuser flow, laser heated, laminar compressible boundary layers 80−53831
nozzle boundary layer, hypersonic, static press. variation and Reynolds stress 77−84294
nozzle boundary layer equations for laser heated flow, similarity soln. 77−31355
nozzle wall laminar boundary layer, effect on jet turbulence 77−55065
nuclear reactor, buoyancy effects on pressure loss in rod arrays under laminar flow 80−27735
numerical methods, conf., Swansea, Wales, July 1978 79−1155
oil, channels formed under electron beam action *(Russian)* 77−72353
oil and polyisobutylene-oil, laminar plane stagnation flow kinematics, laser Doppler anemometry 78−38374
open channel with submerged rectangular orifices, laminar flow profiles *(Japanese)* 80−14827
optimal coords. for 3-D incompressible laminar boundary layers 77−72273
organ pipes and edge tones, jet drive mechanisms 77−831
Orr-Sommerfeld eqn., continuous spectrum and eigenfunctions 78−67176
Orr-Sommerfeld eqn. for laminar flow stability, accurate soln., Blasius profile neutral curve 80−33559
oscillating airfoil drag in fluctuating free stream, laminar and turbulent boundary layer anal. 80−53746
oscillating flow past flat plate, heat transfer, viscous dissipation effect 77−80151
oscillating source flow of ducting fluid between parallel discs 80−99986
oscillations in flows over shallow cavities 77−89091
oscillatory hydromagnetic free convection flow past an infinite vertical flat plate with suction 79−32687
parallel channels with short flow constriction, laminar transport phenomena 79−81886
parallel fixed planes, incompressible viscous flow *(French)* 77−72269
parallel flow between concentric cylinders, stability, heat transfer 77−11190
parallel flows, stability anal. by finite element anal. 79−81843

laminar flow continued
parallel plate channel, combined forced and free convective laminar flow, solute disperison 79−98801
parallel plates, longitudinal dispersion in laminar flows homogeneous in streamwise direction 79−98811
parallel plates, reactant injection effects 78−34208
parallel porous discs of different permeability, laminar flow heat transfer 80−14810
parallel porous discs with equal suction and injection, in mag. field, laminar source flow 77−84331
parallel streams with interfacial mass transfer, laminar boundary-layer anal. 77−31272
parallel viscous compressible flows, linearised disturbances, asymptotic anal. 79−27618
parallel-plate channel, convectively-cooled, liq. solidification 77−68666
parallel-plate channel wall solution in electrolyte laminar flow *(Russian)* 78−64848
partially filled container rot. about horiz. axis, stable laminar secondary flow 77−51026
particle capture from laminar flows, review, book contrib. 77−47078
particle deposition, in laminar flow in tube, thermal effects 77−58764
particle shape, in laminar flow, by optical mixing *(Russian)* 79−10619
particle transport in laminar stream *(Russian)* 77−58768
particles in laminar tube flow, thermophoretic deposition 79−46371
passage, arbitrary cross-section, fully developed flow prediction method 79−1254
periodic boundary layer, with large Strouhal number, parametric method 77−51030
periodic surge flow in circular tube, wall shear stress vel. distrib. *(German)* 79−10613
periodic wavy surface, laminar boundary layer, nonlinear anal. for long waves, separation 80−87759
pipe, corrugated, steady flow analysis 80−38492
pipe, laminar friction factor and heat transfer, finite-element technique 80−10247
pipe, laminar pulsating flow, heat transfer 79−94621
pipe, smooth, entrance regions, laminar flow 79−50696
pipe, toroidal, extended Stokes series 78−51242
pipe entrance, unsteady effects of fluctuating main flow on laminar boundary layer thickness 77−39274
pipe flow, curved pipes, fully developed oscillatory flow 80−83846
pipe flow, curved pipes, oscillatory flow development 80−79400
pipe flow, developing, arbitrary curvature, Navier-Stokes eqn. 78−79378
pipe flow, entrance region, anal. 77−80214
pipe flow, finite amplitude stability theory 78−63498
pipe flow, laminar with nonlinear wall heat fluxes, axial cond. 79−27636
pipe flow, low Reynolds number, in vicinity of three dimensional obstacles 80−74981
pipe flow, numerical calc. 78−79376
pipe flow, solute diffusion 77−39345
pipe flow heat transfer, simultaneous wall and fluid axial conduction 80−74870
pipe flow of anomalously viscous liqs., heat transfer 78−59485
pipe gas flow, fluid-wall mass transfer, sonic oscills. enhancement 77−910
pipe rotating perpendicular to axis, liq. fully developed heat transfer 77−58689
pipe subjected to circumferentially varying external heat transfer coeff., laminar heat transfer 80−10242
pipe with chem. reaction, laminar flow mass transfer with axial diffusion 77−55101
pipe with laminar flow in boundary layer and const. wall temp., initial section heat exchange 79−86432
pipes, laminar heat transfer data with step-varying wall heat flux 77−50210
pipes with regular artificial wall roughness, laminar flow stability, turbulence 79−98803
plane jet in gas medium 79−32622
plane jet in laminar cocurrent flow, eddy viscosity decay, phenomenological theory 79−98700
plane laminar gas jet in infinite space, thermal characts. *(Russian)* 79−18926
plane laminar relaxing gas jets, mixing with radiation accounted for, boundary layer eqns. 79−90349
plane non-Newtonian Couette flow, heat transfer 79−86471
plane stagnation flow, vel. and temp. profile determ. by variational method 77−72293
plane thermal boundary layer, temp. distrib. determ. by var. formulation 77−23947
plane wall jet, temp. distrib. due to variably heated wall 80−19463
plastic non-Newtonian fluids in circular pipes, laminar flow stability loss 78−79342
plate, flat, optically thin boundary layer, of grey medium near leading edge, radiative-convective heat transfer 78−91027
plate, flat, with uniformly distributed vectored surface mass transfer, flow and heat transfer analysis 77−42838
plate, heat transfer from high enthalpy hypersonic air boundary layer 78−34210
plate, heated, semiinfinite, vertical, with heat sources and sinks natural convection 80−59035
plate, thin, in gradient current flow, coupled heat exchange *(Russian)* 78−83398
plate, vertical, free convection boundary layers and heat transfer 80−59002
plate, vertical, heat transfer coeff., interpolating eqns. between two limiting cases 79−37309
plate, with temp. and vel. profile nonuniformities, laminar flow and heat transfer 77−75913
plate and laminar slug flow with periodically changing temp., transient heat transfer 80−74872
plate temp. oscillations, response of horizontal free convection boundary layer 78−59391
plate with nonsteady temp. on lower surface, laminar flow, conjugate heat transfer 80−74879
plume generated from heat source in liquid, temp. field 79−59984
point source of heat, laminar flow pattern, press., enthalpy, vel. 78−79316
Poiseuille flow, horizontal plane, heated from below, axial heat cond. effects on thermal instability 77−42825
Poiseuille flow, subcrit. Re, nonlinear stability, finite axisymmetric disturbances 77−84224
laminar flow continued
Poiseuille flow in channel of variable cross section and porous walls *(Polish)* 79−64768
polybutadiene soln., rheological behaviour of flow patterns around agitators 77−31269
polyethylene oxide, dilute aq. soln., laminar viscous tube flow, scale-depend. effect 79−7367
polyethylene oxide, dilute solution, flow round circular cylinder 80−69882
polyethylene soln., conc., laminar steady flow, expt. *(German)* 79−14443
polyethylene solns., conc., viscosity, shear speed depend. *(German)* 79−27671
polyethylene solutions, conc., flow behavior in laminar steady flow field, mol. wt. numerical freq. distrib. *(German)* 79−68673
polymer flow on inclined plane, edge effects 80−19451
polymer melt, composite flow anal. in sandwich sheeting die 78−94637
polymer melts, laminar and melt fracture flow through successive capillaries 80−59085
polymer solns., anomalous defect pressure in laminar orifice flows 80−48664
polymer solution, boundary layer having laminar, transitional and turbulent flow zones *(Russian)* 77−80185
polymer solution, effect of anisotropy on stress and strain-rate tensors *(Russian)* 78−22387
polymer solution, flow visualization near rot. disc 79−72914
polymer solution, laminar capillary tube, critical shear rate 78−34170
polymer solution flow through porous media *(French)* 79−46376
polymer solution laminar capillary flow, excess press. drop 79−60038
polymer solutions, aqueous, diffusion and mass transfer from rotating disc 80−83827
polymer solutions, laminar flow, effect of capillary entrance *(French)* 78−87330
polymer solutions, rigid-chain, flow birefr., hydrodynamic and dynamic-optical props. 79−24286
polymer solutions, viscoelastic, tubular entry flow, vortex characts. in stable flow 79−32428
polymer solutions, wake, behind cylindrical body 79−37355
polymeric liquids in pipes, non-steady two-phase stratified laminar flow 79−81832
polymethylphenylsiloxane liquid, pumped, improved heat transfer near crit. press. 77−7421
polyoxyethylene, dil. solns., laminar flow in tubes, scale effect 79−86472
polystyrene, 7% in tricresyl phosphate and Arochlor, stress transient data obtained by cone and plate flow 77−31407
polystyrene monomer, high purity, soln., rheological behaviour of flow patterns around agitators 77−31269
polystyrene soln., rheological behaviour of flow patterns around agitators 77−31269
polystyrene suspension, laminar flow, augmentation of heat and mass transfer, correl. of data 80−53840
porous ducts, fully developed laminar flow 78−47038
porous media, electrokinetic effects, analysis *(Russian)* 78−1748
porous media, laminar flow, velocity and longitudinal dispersion, deterministic model 80−83842
porous medium, laminar isothermal flow of two immiscible compressible fluid phases 80−69919
porous pipe in a pipe heat exchanger, laminar flow, vel. changes 80−64512
porous surface, heat exchange optimal control 79−32661
porous tube or channel, nonunique solns. 78−94816
porous tubes and flat plates, with wall resistance, laminar mass transfer 79−60053
porous vertical wall, boundary layer and film thickness 78−90825
porous vertical wall, laminar flow integral approach to flow 79−77059
power law fluid, approx. soln. of two-dimens. laminar boundary layer flow *(Japanese)* 77−72337
power law fluid, laminar flow heat transfer in helical coils 80−59030
power law fluid in pipes and channels, extended Leveque solns. 80−24095
power law fluids, laminar flow through granular beds 80−38488
power law fluids laminar pipe flow, heat transfer 78−59425
power law liquid, flow between eccentric rotating cylinders 77−65766
power law non-Newtonian liquid, stability of laminar boundary layer 77−55048
power law pseudoplastic laminar tube flow, heat transfer 77−80184
power-law fluid, nonsteady heat exchange during steady flow in initial thermal section of tube 77−47046
power-law fluid, two-stream mixing along flat plate, variational solns. 80−53817
power-law fluid laminar jet flow 79−32619
power-law fluid laminar tube flow, dispersion 77−27561
power-law fluids flowing between two rot. coaxial circular cylinders, heat transfer rates 77−58742
power-law non-Newtonian conducting fluid, laminar boundary layer in transverse mag. field 80−33694
power-law non-Newtonian fluids, laminar flow in concentric annuli, vol. flow, press loss. calcs. 79−94681
Prandtl-Batchelor closed streamline theory, 3-dimens. analogue, helical streamline flow 79−81895
pseudoplastic fluid, flowing upward in vert. heated tube, variable physical props. 78−90945
pseudoplastic fluids, heating in laminar flow 78−34128
pseudoplastic liquid flow in planar laminar boundary layer 79−86470
pseudoplastic non-Newtonian liquid, laminar natural convection heat transfer 79−64713
pulsatile flow in tubes, heat tranfer 78−30289
pulsating channel flow, heat transfer 77−31297
pulsating laminar compressible flow in cylindrical pipe with through flow 77−80216
pulsating laminar-boundary layer, heat transfer and skin friction 78−94711
pulsation effects on laminar heat transfer between two parallel plates *(German)* 80−33681
quasiviscous fluid, thin film flow over surface of rotating nozzle 77−54965
radial in fixed bed reactor, two-dimensional calc. by Runge-Kutta method 79−10546
radial vane grids, numerical calcs. *(German)* 78−90824
radially rotating pipe, heat transfer coeffs. in various flow regimes 78−1668

laminar flow continued
radiating laminar boundary flow over flat plate at large free stream Mach no. 79−1270
radiative heat transfer between isothermal parallel plates, flow models, numerical analysis 80−14547
radical species, tube electrode generation, laminar flow through EPR cavity, decomp., convection 77−24746
radiotracer methods for laminar flow in small channels, liq. tracer method 77−58816
radiotracer methods for laminar flow in small channels, response model 77−58814
radiotracer methods for laminar flow in small channels, tracer-sphere method 77−58815
rarefied gas, laminar boundary layers with swirl in slip regime 77−31336
re-entry vehicle heat transfer meas. in separated laminar base flow 78−61708
reactive liquid in tube, props. varying with total conversion 78−42678
real gas laminar boundary-layer separation prediction methodology 80−19322
reattaching laminar and turbulent separated flow, three-dimens. heat and mass transfer 77−65759
recirculating flow, numerical prediction 79−1152
recirculating laminar flow between shrouded rotating disks, num. soln. 79−64667
rectangular body, laminar flow, separation bubble and stagnation line 80−64514
rectangular ducts, fully developed laminar forced convection, general inequality theorem 80−43780
rectangular prisms, galloping in smooth and in turbulent flow 77−75840
renal branch unsteady blood flow simulation 78−27983
reversal in circular pipe, water reactor LOCA anal. 78−50271
roll wave formation in thin laminar flow down inclined plane wall 80−48673
roll-cell instability, rot. laminar and turbulent channel flows 77−946
roll-wave stability on thin laminar flow down inclined plane wall 80−28488
rotating annulus, stable stratification effect 78−94797
rotating bodies in axial flows, laminar and turbulent boundary layers *(Japanese)* 79−77127
rotating body, axisymmetric, arbitrary surface temp. distrib., thermal boundary layer, exact solns. 78−75133
rotating cone-cylinder body, boundary-layer flow in uniform stream 77−23965
rotating disc, local heat transfer, Prandtl's mixing length hypothesis 77−27540
rotating disc with axisymmetric surface heat source distrib., in laminar flow, heat transfer 79−46314
rotating discs, drag reduction in polymer soln., laminar to turbulent transition 78−75173
rotating porous annuli, Navier-Stokes eqns. 77−68687
rotating short radial blade, laminar and turbulent flow, heat transfer 78−18294
rotating sphere, small yaw ang., laminar boundary layer *(Japanese)* 78−38272
rotating square cavity, laminar flow, flow problems with body forces soln. 79−68715
rough subliming surface, laminar boundary layer, anal. 78−51148
rough wall with blowing and heat transfer, boundary layer struct. 79−81863
round laminar jet, flow field development 77−55061
round laminar jet in spherical envelope, nonlinear soln. 79−94693
round tube flow, laminar dispersion 80−64638
rubber toughened plastics, ABS- and AAS-resin, flow props., effect of heating and shearing hysteresis *(Japanese)* 79−94685
sand, fluidised, determ. of flow parameters by simple model and new distributor design 78−83493
saturated vapour, on horizontal melting surface, laminar film condensation 77−15661
Separan, 1.5% in 50/50 glycerine water, stress transient data obtained by cone and plate flow 77−31407
separated flow between periodically varied walls, num. simulation using perturbed primitive variables method 77−54971
separated flow with laminar mixing region, heat and mass transfer, math. simulation 78−59397
separated flows, upwind and central difference schemes 80−28539
separated high Reynolds number flow past a corner, numerical solns. 79−81855
separating boundary-layer flow calculations 79−68678
separating laminar boundary layer, horseshoe vortex 80−19405
separation, incipient, viscous interaction, laminar and turbulent boundary layers, similitude props. 77−72325
separation bubbles, airfoil performance effects, turbulent shear layer reattachment 80−48774
separation due to curvilinear obstacle, successive approx. algorithm, convergence *(Russian)* 78−75117
separator intertray space, development of liq. laminar flow 79−81893
sharp cone, symmetry plane viscous layer 77−58639
shear layer on oscill. plate 79−32454
shear stress determination, in laminar and Taylor vortex flows, using flush-mounted hot film probe 80−28486
shear-thinned fluid, laminar heat transfer and drag 79−68764
short cylindrical channel, laminar axisymmetric nonstationary viscous gas flow, oscillations 80−38495
silicone, electrification during laminar flow in metal pipe 80−6954
simple law of wall formulation for Newtonian fluid, unified time mean velocity profile model 80−103017
singularities in unsteady boundary layers 80−14651
sintered composite-liq. metal interaction, mass transfer eqn. approx. soln. 78−67262
sinusoidally curved pipe, pulsating laminar flow, anal. 78−87390
skewed boundary layers in duct with streamwise press. grad. variation 78−79302
skin friction in supersonic laminar and turbulent flows 79−98751
slag and metal flow in ESR process, mathematic model 77−73249
slender channel laminar flows, numerical soln. 77−78985
slip flow, developing, vel. distrib. and press. drop, Navier-Stokes analysis 77−55039
slow viscous flows over flat plate with mixed boundary conditions 78−1632

laminar flow continued
small sphere in slow viscous flow, shear and rot. flow, forces calc. 79−37282
smoke 78−90863
solid particles lateral migration in laminar flow near plane 77−35207
solid reacting particles, ordered system at high Peclet numbers, mass transfer, convection 80−69830
solid spheres, reacting, in periodic array, convective mass transfer in liq. laminar flow 80−96176
solid-liquid two-phase mixtures in open channels *(German)* 77−15123
soluble fluids in laminar, turbulent flows, stretch model appls. to mixing, diffusion, react. 79−94736
sphere, external laminar boundary layer vel. profile, photographic-tracer film anal. 79−50698
sphere, transient flow, unsteady matched Stokes-Oseen soln. 79−32448
spherical particle in circular tube flows, lateral migration 80−92221
spherically blunted cone with massive surface blowing, laminar and turbulent flows, shocks 80−38445
spheroid at incidence, flow separation, laminar separation lines, turbulent separation 79−72878
spinning disc causing laminar and turbulent flow, mass transfer 79−41691
square cavities, laminar and turbulent incompressible flows 80−10307
square cylinders, smooth/turbulent lift, drag, vortex shedding 77−89109
square duct entrance region, Laminar flow and heat transfer to non-Newtonian fluid 80−10243
stagnation flow, nonlinear stability 78−90831
stagnation point, surface curvature effect on heat transfer 78−38316
stagnation point boundary layer on subliming surface with roughness elements 78−94635
stagnation point boundary layers, unsteady, three dimensional, compressible, numerical soln. 79−37335
stagnation point steady and non-steady laminar viscous flow, variational solns. 77−27510
static pressure probe, laminar limiting boundary layer *(French)* 77−31402
stationary disc in rotating cylinder, laminar compressible flow 80−43728
steady and pulsatile, velocity meas. for flow in 90° branch, appl. to atherogenesis 78−38277
steady flow in tubes of slowly varying cross section 79−32680
steady flow prod. by rot. disc, series soln. anal. 78−71308
steady flow through curved cross section 80−14649
steady heat transfer, between parallel plates, with conduction in wall 77−47003
steady laminar flow through channel with symmetrical constriction in step form 80−100036
steady laminar interacting boundary layers *(German)* 80−14655
steady low Reynolds number flow, past circular cylinder, soln. and drag calc. 79−37287
steady state Navier-Stokes equation, numerical method and appl. *(Japanese)* 77−68564
steady viscous flow past circular cylinder, numerical study, vortices and separation 80−92108
steady-state in turbulence amplifier, numerical integration *(Bulgarian)* 80−106779
steady-state recirculating flows, finite difference schemes, practical evaluation 80−106776
steam-water mixture, with high vap. content, annular flow, heat transfer, press. loss 78−75193
steel pipe corrosion, mass transfer coeffs. under isothermal flow conditions 80−97628
stellar atmospheres, free convection effects on unsteady laminar boundary-layer flow 79−35237
Stokes flow past circ. arc, separation 79−90214
Stokes flow past slender body of revolution 77−14986
Stokes flow through channel and tubes with sinusoidal boundaries as model for porous media 78−18337
Stokes problem of motion of Cassinian cylinder in viscous fluid 78−71312
straight tube, hyperbolic cross section, steady flow of incompressible viscous fluid 79−32457
stream flow over right circular cone, method of singular perturbations 80−69763
stream swirling, effect on laminar flow struct., heat exchange in round tube 77−11265
streaming, of vel. and temp., in oscill. boundary layers 78−83358
streaming, past axisymmetric bluff bodies, approx. theory 77−84217
streaming, uniform, past fixed semicirc. infinite strip 79−23299
styrene-butadiene copolymer, soln., rheological behaviour of flow patterns around agitators 77−31269
subsonic laminar viscous gas flow in flat channels and in shadow regions *(Russian)* 79−50749
suction controlled boundary layer flow, perturbation caused stability loss 77−75886
suction effects on shock wave-boundary layer interaction, numerical Navier-Stokes soln. 79−1243
suction or blowing flows through openings in the wall of a boundary layer *(French)* 79−18947
suction-induced asymptotic boundary layers, exptl. and predicted props. 80−1553
supercavitation flow, cylinder between parallel walls, Efros' model 78−42637
supersonic boundary layer, prediction by hybrid marching integration procedure 77−65761
supersonic boundary layer, separated bubble induced by wall depression 78−9651
supersonic boundary layer on plate with leading edge blunting, stability 79−64688
supersonic boundary layer response to oblique slot blowing 77−11220
supersonic cone flow at high angle of attack, numerical simulation, laminar and turbulent flow 79−77178
supersonic corner flow, boundary region 79−32559
supersonic corner flow, viscous-inviscid interaction 79−32563
supersonic flow, viscous, past corner, energy eqn., asymptotic solns., heat transfer 79−32564
supersonic flow over compression ramp, laminar separation, second order asymptotic soln. 80−83828
supersonic flow past slender cone at high incidence 78−90932
supersonic laminar boundary layer separations, quasi-3-dimens. 78−46995

laminar flow continued
supersonic laminar boundary layer with conjugated heat transfer 79−64687
supersonic laminar boundary layers, strong slot injection, flow separation 80−48738
supersonic laminar boundary-layer separation by slot injection 79−98747
supersonic laminar flow over backward facing step, numerical soln. at high Reynolds number 77−47040
supersonic separated flow changes, caused by throttling in round duct 78−63446
supersonic stream, laminar separation, Reynolds no. effect 80−19432
supersonic trailing edge flow, numerical soln. of 2D laminar and turbulent flows 79−77172
supersonic viscous, numerical anal., separation 80−24062
surface diffusion flux in Newtonian or nonNewtonian fluid, laminar flow, double pulse meas. *(French)* 78−40055
surface friction dependence on compressible fluid injection and removal by suction from wall jet 77−47052
surface with sharp boundary condition change, laminar flow, concentration distrib., convective diffusion *(Russian)* 79−94590
surgery cell with laminar air flow *(German)* 79−16335
suspension, laminar Poiseuille flow, particle lateral migration, tubular pinch effect 79−98783
suspension, parallel flows with boundary layer characts. 77−15093
suspension deposition in entrance of a diffuser, electrostatic and gravitational effects, numerical investigation 80−14785
suspension in inclined channel, two dimensional model 80−106834
suspensions, deposition in channel entrance, combined influence of diffusion, electricity and gravity 80−1674
suspensions, flow in cylindrical pipe, using ultrasonic debitmetry Doppler spectra *(French)* 80−96303
suspensions, with diffusive gravit. deposition at entrance of converging and diverging channels 80−14825
suspensions of charged particles, laminar tube flow, entrance deposition 80−59100
swirl dynamics 79−50732
swirled flow in annular channel 79−90260
swirling flow, integral method of anal. *(Japanese)* 80−28512
swirling impinging jet, heat transfer, numerical calc. 79−1228
symmetric sink flow between parallel plates 80−1524
symmetrical wake calc., two-dimens. laminar and turbulent flows 80−14707
T-junction laminar flow, partially elliptic flow numerical calcs., recirculation 80−64632
Taylor vortex flow with imposed laminar axial flow and isothermal surface heat transfer, velocity profiles 80−103031
Taylor-Gortler instability of boundary layer with suction and blowing 77−27512
temperature boundary layer on rotating curved surface, constant wall temp. case 79−81903
thermal markers for liq. vel. field meas., error reduction 78−91036
thermal-ignition analysis in boundary-layer flows 79−64800
thermally developed duct flow, boundary conditions rel. to Nusselt numbers 78−91016
thermoacoustic vibration generation, in heated channel laminar flow 78−14029
thermoviscous fluid, steady flow through straight tubes 80−33636
thin flat plate parallel to supersonic stream, laminar near wake, centreline velocity 79−55392
thin sheet fluid, example of kinematic waves *(German)* 77−72310
three dimensional laminar flow in curved pipes, Navier-Stokes eqn. numerical soln. technique 79−10611
three-dimensional laminar incompressible internal flow, general computation method 77−42803
three-dimensional laminar stream tube network, convective mixing 80−14815
three-dimensional stagnation point with large injection rates 77−23934
three-phase pipe type cables, friction factor prediction 77−75880
throughflow between closely spaced rot. discs 78−51170
throughflow between rotating and stationary disk calc., finite difference method appl. *(Japanese)* 80−6064
tracer gas axial dispersion through tube constrictions 80−64625
trailing edge stall, triple-deck eqns. num. soln. 77−55020
transient boundary layer on porous plate, coolant injection, laminar flow stability and heat transfer 78−83389
transient boundary layers between porous plates 77−46990
transient coaxial entry tube flows, numerical program 77−15117
transient forced convection eqn. soln., circular pipe flow 78−30282
transient free convection from an isothermal horizontal circular cylinder *(German)* 79−77115
transonic boundary layers, freely interacting, compressive and expansive flow 77−89145
transonic flow, viscous effects, Navier-Stokes eqns. soln. method 77−55023
transonic flow around lifting round-nosed airfoil, extended integral eqn. method 77−62271
transonic laminar boundary layer flow near convex corners 79−64686
transonic nonseparating normal shock-laminar boundary layer interaction, approx. anal. theory 77−23992
trench flow, square section, viscous liquid, laminar and turbulent conditions obs. 77−75981
triple deck problem for supersonic and subsonic flow, numerical technique for separation 80−14757
Trombe wall channel, convective heat transfer 79−86397
tube, elliptical, laminar liq. flow, nonsteady heat transfer 78−42598
tube, horizontal, laminar combined convection, circumferentially nonuniform heating effect 78−71331
tube, severely-contricted, symmetric, separating flow 79−50697
tube, vertical, laminar and turbulent heat transfer, air and Ar 78−71332
tube, with heated inner eccentric rod, steady convective laminar heat transfer 78−38311
tube banks, heat transfer, viscous flow, numerical anal. 79−55375
tube drag in different rows of banks in transverse streamline air flow *(Russian)* 79−94583
tube entrance laminar flow, influence of film condensation *(German)* 79−77260
tube flow, bifurcating, blocked or constricted, entry flow effects 77−19636
tube flow, drag reducing additives and sudden enlargement of diam. 79−37397
tube flow, gel-walled 79−90334
laminar flow continued
tube flow, gravitational deposition of growing aerosol particles 80−59099
tube flow during periodic pressure drops and transverse oscills. 77−7452
tube flow with varying wall temp., heat transfer anal. 78−38318
tube with two hyperbola bounded cross section, steady laminar flow 79−94723
tubes, circular, forced and combined convection, finite difference anal. 80−48711
tubes, entry length heat transfer by combined laminar convection, computation methods 78−38312
tubes, liquid filled Al and PMMA longitudinal wave experiments, laminar flow 79−64604
tubeside laminar flow heat transfer augmentation 78−94726
tubular reactor with non-Newtonian laminar flow, diffusion and raction analysis 77−68703
turbulence models for heat transfer, review 79−4017
turbulent flow relaminarisation, flow visualisation 78−75244
turbulent plumes in laminar cross flow, entrainment 77−24006
through twisted pipes, loss of flow rate 77−14979
two dimensional Laval micronozzles, laminar boundary layer approx. calcs. 80−24070
two dimensional recirculating flow, finite difference grid for non-rectangular flow fields 79−14374
two immiscible liquids, mass transfer into laminar fluid stream from moving interface 78−1717
two parallel corotating discs, laminar flow and heat transfer, shear pump appl. *(German)* 80−69840
two-dimensional boundary layer, Coriolis force stabilising and destabilising effects 79−81841
two-dimensional laminar boundary layers, perturbation development, secondary flows 80−1521
two-dimensional laminar flow between porous walls 79−14477
two-phase boundary layer, successive approx. method 79−32647
two-phase flow between parallel corotating discs, laminar or turbulent throughflow, bulk-parameter anal. 77−39336
two-phase flow particle interaction, coagulation and rebound calc. 79−98789
two-phase flows, particle interaction, obs. and calc. 79−72875
two-phase laminar boundary layer, forced convection condensation *(Japanese)* 78−34191
two-phase laminar channel flow, forced convection energy eqns. 77−55090
two-phase laminar channel flow, vel. profile 78−9675
two-phase laminar flow, in circular pipe, heat transfer, inlet temp. effects 78−67265
two-phase medium,, laminar boundary layer eqns. 80−38476
two-phase pressure driven stratified laminar pipe flow 80−64609
two-phase stratified flow through fractures in porous media 78−5792
two-phase zero net flow in inclined pipe 78−83457
underground cable system, convectively cooled, temp. distribs., heat transfer correlations 78−71262
underground cable system, convectively cooled, vel. distribs., press. drop correlations 78−71330
uniform fluid flow, general nondimensional relationship *(Bulgarian)* 78−12571
unstable laminar boundary layer, response to acoustic excitation 79−98681
unstable laminar boundary layers, nonlinear evolution and breakdown 80−92109
unsteady airfoil stall in laminar boundary layer, water tunnel visualisations 80−53745
unsteady boundary layer on infinite yawed wedge 77−42800
unsteady boundary layers, separated and attached, review 78−71313
unsteady boundary layers with reversal and separation 78−75163
unsteady comp. laminar boundary layer flow, num. anal. 79−94586
unsteady flow of an electrically conducting dusty viscous liquid through a channel 79−14484
unsteady flow of viscous fluid through elastic tube with outward suction 77−68690
unsteady flow past flat plate finite difference method 79−18864
unsteady free convection flow past vertical flat plate, effect of suction 78−18296
unsteady heat transfer effect on boundary layer growth at forward stagnation point 79−10555
unsteady imcompressible laminar boundary layers around impulsively started cylinders *(French)* 79−72876
unsteady incompressible laminar boundary layer, eqn. soln. for 2-dimens. flow 80−48672
unsteady laminar boundary layer, approx. solns. 77−23936
unsteady laminar boundary layer flows induced by impulsive accelerating motion *(Japanese)* 80−69765
unsteady laminar boundary layer with separation, reattachment 79−59963
unsteady laminar boundary layers, collision at equator of rotating sphere 79−72896
unsteady laminar boundary layers behind blast waves, num. soln. 80−69776
unsteady laminar boundary layers in an incompressible three-dimensional stagnation flow 79−81848
unsteady laminar boundary layers in an incompressible three-dimensional stagnation flow, book contrib. 80−1525
unsteady laminar flow of elastic viscous fluid through porous channel, applied mag. field effects 80−38499
unsteady laminar flow through porous media in presence of transverse mag. field 79−37394
unsteady laminar forced convections in elliptic pipe 77−11184
unsteady laminar heat transfer in circular duct flow in receiver tubes in solar collectors *(Japanese)* 79−77058
unsteady laminar separation and stall from aerodynamic surfaces 80−59090
unsteady laminar viscous incompressible fluid flow through channels 77−68566
unsteady magnetohydrodynamic flow through a channel 79−37413
unsteady mass transfer, laminar flow past sphere, heterogeneous chemical reaction 77−55102
unsteady thermal boundary layer, parametric method appl. 77−11170
unsteady three dimens. laminar boundary layer separation, anal. 79−32451
unsteady two-dimens. boundary layers, fluctuations in external vel. 77−51043

laminar flow continued
unsteady two-dimensional and axisymmetric compressible boundary layers 79−27616
unsteady viscous flow near axisymmetric stagnation point on circular cylinder 79−23302
unsteady viscous plane stagnation flows, incompressible boundary layer, heat transfer 80−1584
unsteady viscous separated laminar flow, numerical modelling 78−46933
vapor flow calculations in a flat-plate heat pipe 80−23869
vaporising liquid layer at nonadiabatic evaporation, binary laminar boundary layer flow *(German)* 80−1588
vapour condensation on vertical surface, laminar flow in film condensate 78−75057
vapour flow between parallel disks with asymmetric sublimation 79−18865
vapour flow in film boiling, stability limits 78−90832
vapour-air mixture flow, around circ. cyl. with vapour desublimation, numerical anal. *(Russian)* 79−60051
velocity distrib., wall friction in rotational turbulent laminar boundary flow *(German)* 80−1526
velocity field measurements of a laminar thermal 79−68674
velocity measurement, repetitive pulse NMR technique 80−31829
velocity profile for boundary layer flow along a rectangular corner *(Japanese)* 80−74832
vertical annular laminar flow, of immiscible liqs., heat transfer 78−14082
vertical cones in laminar free convection, integral method 79−81881
vertical flat plate, wave instability of liminar mixed convection flow 80−10245
vertical free convective cavities, laminar flow struct. 78−34125
vertical internally heated annulus entry region, mixed convection in water 80−24015
vertical laminar jets, weak buoyancy, book contrib. 80−1665
vertical natural flow, adjacent to surface transition limits 79−50726
vertical natural laminar convection flows in cold water, buoyancy force reversals 80−59034
vertical plate, laminar natural convection heat transfer, supercritical CO_2 and He 80−64544
vertical plate with uniform blowing, laminar combined forced and free convection 80−74876
vertical tube with laminar combined convection, water, finite difference anal. 78−90894
visco-plastic steady-state flow finite element solns. 77−5670
viscoelastic boundary layers, role of fluid relaxation time 79−81829
viscoelastic flow at stagnation point over moving wall 78−18319
viscoelastic fluid, axial laminar flow, force exerted on wall *(German)* 77−68643
viscoelastic fluid, natural convection heat tranfser 78−83436
viscoelastic fluids, unstable tubular entry flow 79−90218
viscoelastic fluids in concentric annuli with axially moving boundaries 78−79295
viscoelastic laminar flow, combined generalised measure approach, pseudo-plasticity 80−64586
viscoelastic laminar flow round spherical obstacle, finite boundaries effect 77−15076
viscoelastic linear fluid, viscous dissipation of flow between eccentric rotating discs 77−58745
viscoelastic liquid, heat transfer in rot. flow, suction and injection effects 80−33596
viscoelastoplastic laminar tube flow, heat transfer 80−10269
viscous conducting fluid, laminar flow, boundary effect in helical induction machine *(Russian)* 77−47105
viscous dissipation effect on heat transfer, circ. cylinder axisymmetric stagnation flow 78−51164
viscous drag reduction by polymer injection at high Reynolds number *(Chinese)* 79−32582
viscous dusty fluid flow through rotating circular cylinder 77−68675
viscous electrically cond. fluid, laminar free shear flow, transverse mag. field effect 80−48811
viscous flow, 3D, finite difference method 79−32447
viscous flow, time-dependent two-dimensional, moving boundary walls 78−14059
viscous flow down an open inclined channel with naturally permeable bed 80−69764
viscous flow equations num. soln. using integral represents. 77−54966
viscous flow field inside locally constricted cylindrical duct *(French)* 77−51115
viscous flow fields in moving curved channels 77−72352
viscous flow in constricted or widened tube, analytic solns. 79−18959
viscous flow over flat plate, comput. method developments 77−54970
viscous flow past circular cylinder, two coord. systems description 77−58643
viscous flow past two-dimensional bluff body, new approx. theory 77−918
viscous flow through pipe orifice 79−98807
viscous flow through rough wall cracks, friction factor formula *(Rumanian)* 80−69925
viscous fluid, laminar flow, Navier-Stokes eqns., central difference scheme 80−69762
viscous fluid, steady laminar flow through tube with bi-circular cross section 79−90331
viscous fluid, variable thermal conductivity, variational calc. of vel. profile and temp. in laminar boundary layer *(French)* 78−55625
viscous fluid, vortex dipoles 80−48718
viscous fluid flow through slot between fixed and rotating surfaces of revolution *(Polish)* 78−79300
viscous fluid in channel, laminar steady forced convection flow 79−32505
viscous fluid in toroidal tube, oscillations 80−79253
viscous fluid magnetic throughflow in slot, inertia effect 79−37418
viscous impressible fluid bounded by cylindrical boundaries, slow motion of small sphere 77−14978
viscous incompressible flow problems, two-dimens., Navier-Stokes eqns. soln. and contaminant effects 77−58638
viscous incompressible fluid, laminar divergent flow through porous cone *(French)* 80−83838
viscous incompressible fluid, perturbation theory of stationary flow 77−3803
viscous incompressible fluid flow through partially filled cylinder 80−74973
laminar flow continued
viscous incompressible heat generating flow past porous plate with free stream oscillations, laminar free convection 79−37312
viscous incompressible heat generating flow past porous plate with free stream oscillations, laminar free convection 79−37311
viscous incompressible laminar flow entry problem in porous ducts, anal. 77−62302
viscous incompressible liquid, vibrational displacement, wave mechanism 80−43777
viscous incompressible liquid flow in plane channel 80−23985
viscous laminar jet flow in slipstream calculation *(Russian)* 79−77209
viscous liquid, linear radial flow between parallel infinite discs 77−904
viscous liquid, unsteady laminar flow between parallel plates 80−10310
viscous liquid film instability under the influence of an adjacent gas flow 80−92110
viscous liquid laminar flow in gap, nonstationary Reynolds differential eqn. *(German)* 77−58641
viscous mixing at trailing edge 78−1635
viscous sheet flow over sloping dry bed 77−72270
viscous-inviscid flow interaction method, using blowing and suction flows 79−1154
von Mises' eqn., finite element solution to eqns. of laminar boundary layer *(French)* 77−72268
vortices, laminar and turbulent, decay mechanism 79−50732
wake, of flat plate, vel. distrib. 78−34140
wake formation in shock wave prod. from plate edge 79−77120
wake of thin flat plate set parallel to stream, centre line vel. variation 78−14042
wall plumes in transverse mag. field 79−86398
water, electrification during laminar flow in metal pipe 80−6954
water, forced laminar convection in horizontal pipe, density inversion effects, numerical anal. 78−90900
water, hot, film, wavy laminar flow down vertical plate at high surface tension numbers 79−94587
water, Tollmien-Schlichting waves and transition 79−81845
water adjacent to vertical uniform flux surface, buoyancy driven flow, transition and transport 79−27631
water boundary layer along heated cylinder, buoyancy and variable viscosity effects 80−79256
water boundary layers on heated cones, variable viscosity effect, heat transfer, shear stress 79−32520
water jets sensitive to sound, two-dimensional, velocity fluctuations behaviour *(Japanese)* 80−100020
water vapour, 2-D laminar boundary layer 80−19492
water vapour, wet, boundary layer in compressible flow 80−10295
water viscosity changes close to quartz surface, fine capillary calcs. 80−54422
water viscosity changes effect on electrokinetic phenomena in capillaries 80−53867
wedge, with separation, forced convection calc., using perturbation method 80−1523
wetting of a vertical plate by a liquid, model 78−22319
wind tunnel contraction section, smoothly varying nozzle construction method 78−47081
wing, 3-dimens. boundary layer calc. method 80−1622
wing, permeable, moving through a stationary liquid, flow calcs. *(Russian)* 80−38377
wing flow, tip vortex stability 77−19611
wing-body configurations, boundary layer induced secondary flows 80−48671
wire, in longitudinal laminar air stream, heat exchange *(Russian)* 78−83401
wire-wrapped 61-rod bundle edge subchannel flow distrib. 79−9676
Ar bubbles injected into Sn, Pb and Cu melts, under laminar flow, characts. 78−38394
Ar ionised gas flow, quasi-steady laminar boundary layers 79−10544
Ar, ionising boundary layer in shock-tube side-wall flow 79−60144
Ar, stabilised electric arc, laminar plasma flow section, length and characts. 78−91177
CO_2, laminar free convection at supercrit. press. under cooling conditions, heat transfer analysis 79−86428
CO_2-N_2 downstream mixing gasdynamic laser, Navier Stokes eqns., laminar mixing flows 80−23662
H_2-O_2 gas mixture in chem. equilib., elemental diffusional separation in nonisothermal flow 79−55429
He, supercritical, laminar free convection heat transfer, analytical study 79−23311
^{4}He superfluid, laminar flow through capillary tubes 79−55949
Hg, liq., flow in transverse mag. field, laminar and transition, channel wall effects 78−63500
N_2, cryogenic, shock wave-boundary layer interaction *(German)* 78−71370
N_2O_4, dissoc. flow in tube, heat transfer and drag 78−71402
N_2O_4, dissoc. laminar gas flow, heat exchange with triangular bundle of rods 77−42930
$(NO_2)_2 \rightleftarrows 2NO + O_2$, chemically unstable mixture laminar flow in channel, heat and mass transfer *(Russian)* 77−68707
$(NO_2)_2 \rightleftarrows 2NO_2 + O_2$, nonequilibrium mixture laminar flow in channel, zone method anal. of heat and mass transfer *(Russian)* 77−72370
Na vapour in heat pipe *(Russian)* 77−80166
TiO_2 suspension in glycerine, Bingham plastic flow through annuli 80−64521

laminar to turbulent transitions
accelerated flow past rough surface, unsteady, turbulent boundary layer generation 78−90828
acoustic oscillations, effect on laminar to turbulent flow transition 80−14656
aerodynamic drag on heated spheres and cylinders, effective Reynolds no. 77−89090
aerosol precipitation from laminar gas stream, free convection effect 78−83459
air wall-jet immersed in uniform flow, aerodynamic forces on circular cylinder 77−62287
airflow in pipe at low Reynolds numbers, effect of flow laminarisation on heat transfer 77−23942
airfoil, leading-edge separation bubbles, shear layer and transitional reattaching flow 77−27580
annulus, laminar-turbulent flow 79−32681
atmosphere, turbulent shearing layers, dominant eddy scale, growth, limiting thickness 77−87022

laminar to turbulent transitions continued
axial flow between cylinders, stability to asymmetric disturbances 78−38294
axisymmetric flow stability 79−23300
axisymmetric starting plume cap, transition from laminar flow 79−18872
Blasius flow, horizontal, heated from below, longitudinal vortices onset 78−71342
bluff body, turbulent near wake, vel. correlation struct. 78−30298
blunt-body boundary layers, three dimensional, surface curvature effects 80−1520
body of revolution with heating and cooling, boundary layer transition and separation 80−64518
boundary layer, elongational viscosity and secondary instability 77−23997
boundary layer, heated, stability 78−38332
boundary layer, heated, with nonuniform surface temp. distrib., stability 78−67175
boundary layer, in supersonic wind tunnel 78−38437
boundary layer, intermittent laminar/turbulent transition, local skin friction 78−30260
boundary layer, laminar to turbulent transition, Tollmien Schlichting wave development *(French)* 78−38285
boundary layer, nonlinear wave development during laminar to turbulent transition *(Russian)* 77−80173
boundary layer, numerical method *(French)* 78−38289
boundary layer, oscillating *(French)* 78−38288
boundary layer, second-order closure model 78−38276
boundary layer, semiempirical calc. using arbitrary free stream press. gradient 78−94640
boundary layer, temp. factor effect 78−63417
boundary layer, transitional, natural convection instabilities effect *(French)* 78−38333
boundary layer, transitional, oscills., stability waves, vortices 78−38287
boundary layer, transport eqns. *(French)* 77−62234
boundary layer, two-dimens., nonlinear wave interaction, numerical calc. 78−38281
boundary layer, vorticity genesis 78−1630
boundary layer, wall heating effect 78−38334
boundary layer, with press. grad. and suction, nonparallel stability 78−38282
boundary layer along concave wall, vortex instability analysis 77−55000
boundary layer flow, unsteady past wavelike bulge on flat plate, num. soln. of Navier-Stokes eqns. 77−58644
boundary layer flows, outer-stream turbulence effect 77−75881
boundary layer in shock tube 77−23995
boundary layer instabilities, Mach number 7 77−65760
boundary layer on cone at Mach 5 78−38368
boundary layer on cone at Mach 5 78−38369
boundary layer shear flow, three-dimens., stability eqns. 78−38284
boundary layer stability, nonlinear effects 78−1636
boundary layer transition, detection using holography 78−14101
boundary layer transition, results of photographic expt. *(Russian)* 77−62243
boundary layer transition, two-equation model, mean velocity profiles *(French)* 77−65736
boundary layer transition region, IR emission meas. 78−38438
boundary layer transition region extension, initial turbulence effects *(Russian)* 79−90233
boundary layer transition research at AEDC, review 78−38290
boundary layer transitions, conference, Lyngby, Denmark (May 1977) 78−38278
boundary layer with suction, stability theory 78−38274
boundary layers, engineering predictions 78−38275
channel, corrugated wall 77−80157
channel flow, laminar to turbulent alternating transition, crit. Reynolds no. 78−46935
channel flow, nonerodible porous lining thickness effects 77−58788
chemical shock tube flow, laminar to turbulent boundary layer transitions 77−48642
circular cylinders and spheres, fluid flow and convective heat transfer *(German)* 79−94624
circular straight pipe with protrusions, turbulence onset in low Reynolds no. flow 77−84222
combined laminar and turbulent flow, over a rotating disc 77−3809
cone in transition Reynolds no. domain, tangential injection effect on heat transfer 79−64654
convection, natural, from vert. DC current-heated plate, linear stability anal. 78−90873
Couette flow, laminar to turbulent transition spectrum evolution 80−103034
Couette flow, turbulence transition, Landau picture, stochastic attractor representation *(Russian)* 79−98692
Couette-Taylor flow, laser Doppler velocimetry obs. of transition to turbulence 80−92163
critical Reynolds numbers for Newtonian flow in concentric annuli 80−64517
crossflow developing in boundary layer during longit. flow around right dihedral angle 80−59049
cylinder, circ., inclined, laminar 3-dimens. free convection, stability *(French)* 79−18884
determination of transition in hypersonic flow using boundary layer acoustic monitor 78−34237
diatomic gas, transient flow, temp. and conc. profiles, by rot. Raman scatt. 77−75995
dielectric polar liq., electroviscosity rel. to cond. process, EHD model 78−1750
disc, rotating, convective mass transfer 80−43707
disc rotating in jacket in presence of transitional boundary layer, local heat transfer 79−94608
dissociating gas in pipe flow, heat transfer crisis, flow laminarisation 79−1265
dissociating gas in pipes, heat and mass transfer 80−24105
disturbance growth mechanisms in buoyancy induced flow 77−39275
doubly periodic flows, transition to turbulence 80−83790
duct of arbitrary cross section, parabolic procedure for three-dimens. compressible viscous flow prediction 79−94716
dusty gas, Stokes layer stability 80−19493
dynamic heat transfer meas. at Mach 8, digital Fourier anal., boundary layer transition 80−14682
laminar to turbulent transitions continued
dynamical systems, dissipative, intermittent transition to turbulence 80−79132
early nonperiodic transitions in Couette flow 80−59056
eccentric rotating cylinders, flow where clearance is relatively large 78−1667
Ekman boundary layer, incompressible, nonlinear stability, numerical soln. 80−38378
elementary model for transition to turbulence *(Russian)* 79−86402
external noise effect on transition to turbulent convection 80−96263
fibre suspension flow in pipes, transition regime analysis, drag reduction 77−89186
finite amplitude stability, perturbative and iterative methods 78−38293
finite amplitude wave propagation in nearly parallel flow 80−74899
flame front, laminar, hydrodynamic instability, nonlinear integro-differential eqn. 78−51253
flame front, laminar, hydrodynamic instability, numerical solns. 78−51254
flat insulated plate, supersonic laminar boundary layer stability 79−98749
flow, unsteady, transitional and turbulent boundary layers, expt. and calc. methods *(French)* 78−75125
flow structure, light scatt. and hot-wire anemometer expts. 78−18271
fluctuation correlations *(Japanese)* 77−14988
fluid flow in pipes, boundary between laminar and turbulent conditions *(Bulgarian)* 79−60066
free convection flow, spectral energy distrib. in transition region *(French)* 79−64651
free convection heat transfer from vertical thin wire to air, laminar-turbulent transitions *(Japanese)* 80−92152
freestream turbulence effects on boundary layer development 80−48684
fully turbulent environment with transitional boundary layer spot 78−26110
gas discharge, perturbation by longitudinal turbulence 80−24271
gas liquid flows in catalyst static granular bed, transfer processes 80−45554
gas-liquid film interface stability behind slipping shock wave front *(Russian)* 78−55630
gas-liquid flow with small gas contents, liq. phase vel. profiles distrib. 77−35216
Gortler vortices, high value eigenstates, stability diagrams, book contrib. 80−1606
Hagen-Poiseuille flow, natural transition freq. 79−32459
Hartmann flow, evolution of resonance disturbances 79−90220
heat transfer behaviour, turbulent boundary layer on rough surface with blowing 78−71334
heat transfer flow enhancement low porosity surfaces of heat exchanger cores 78−38402
heat transfer from cylinder to air cross flow, surface roughness effect 77−39287
heat transfer from single sphere, turbulent air stream 78−22342
heated flat plate in water, critical Reynolds number, heat transfer 80−69766
high Reynolds no. flow past rough walled circ. cylinder 78−46952
highly accelerating flow near smooth wall, prediction method 80−1550
hot wire signal conditional sampling techniques for transition intermittency studies *(French)* 79−77066
hydrodynamic calculations for container pipeline systems with non-Newtonian liquids 80−106817
hydrodynamic instabilities, transition to turbulence, Couette flow, vertex streets, Rayleigh-Benard instability 78−83362
hydrodynamic instabilities, transition to turbulence 80−28491
hydrofoil profile for accelerating cascade, surface press. distribs. 78−18321
hypersonic transitional/turbulent boundary layer, wall cooling effect 78−26149
ice layer profile on const. temp. plate in forced convection, laminar to turbulence transition regime 80−24007
inclined surface, natural convection flow, transition, vortex system, meas. method 79−27632
incompressible fluid streaming past smooth surface, laminar separation 77−75897
incompressible separated boundary layers including viscous-inviscid interaction, transition bubble 80−64515
instability, transition to turbulence and predictability 78−87332
intermittancy in transition zone of boundary layer *(French)* 77−72274
intermittency coefficient measurement circuit 78−9733
intermittent transitions to turbulence, intermittency in dissipative dynamical systems 80−106781
internal currents, struct., kineticity effects 77−68570
jet, axisymmetric, vel. distrib. and swirl effects, low speed results 79−46351
jet, circ., free shear layer transition wave development 78−94643
jet, mixing layer, axisymmetric, influence of initial and boundary conditions 79−94689
jet, subsonic, of gas, vortices, flow visualisation patterns 78−63471
jet, viscous laminar flow, tangential twist eddy flow form., numerical soln. 77−89179
jets, transition to turbulence 78−18326
jets, wakes, and shear layers, turbulent, power laws, rel. to marginal instability principle 79−32458
laminar boundary layer, characteristics during increased turbulence in bulk stream *(Russian)* 77−23937
laminar boundary layer, heated, stability 78−9626
laminar forced convection to turbulent free convection transition over heated plate 79−32516
laminar vapour flow in film boiling, stability limits 78−90832
laminarisation in turbulent duct flow 78−30358
Larunar boundary layer, low free stream perturbations influence, hydrodynamic waves 79−98738
laser Doppler velocimetry expt. 79−77073
leading edge bubble formation, peaky airfoil *(French)* 80−64524
leading edge transition on swept wings 78−38361
linear stability theory, transition prediction 78−38279
liquid flow in conduits, turbulence development 79−68809
liquid flows in channels with porous walls, turbulence development *(Russian)* 77−27590
liquid-gas mixer, perforated disc stirring cascade type, power dissipation, mechanism and correlation 79−1238
LMFBR wire wrap spaced rod bundles, laminar, transition, and turbulent parallel flow press. drop 79−26478

laminar to turbulent transitions continued
local heat transfer from inline tube bank to air crossflow *(Russian)* 78−5746
Lorenz model, Feigenbaum sequence of bifurcations 80−83783
lubrication, turbulent, eqn. derivation using friction law 79−98694
magnetic field as a tool for investigating transition and turbulence 80−1696
MBBA, electrohydrodynamic instabilities, power spectra and autocorrel. in flow transitions 77−68914
MBBA, nematic, EHD transitions, white noise effects 80−6159
mixing layer at high R_e, large struct. dynamics and entrainment 77−15001
mixing layer growth from turbulent and nonturbulent boundary layer 79−68686
natural convection boundary layer, laminar to turbulent transition, critical values for air *(Japanese)* 80−14657
Navier-Stokes equations for turbulent and transition flows, num. soln. methods 77−54979
near-wake for slender cone, Mach number depend. of laminar transition 77−62277
non-steady boundary layer, turbulence development 78−90829
nonlinear interaction of two waves in boundary-layer flows 80−59016
nonlinear theory, perturbation amplitude threshold 78−63416
nonNewtonian flow between rotating porous cylinders, stability wide gap case 79−68761
nozzle, critical air flow, heat transfer, numerical study 79−98778
nozzle, heat transfer of transonic air flow 79−1230
oil, US flow measurement in laminar-turbulent transition region 79−68850
one-dimensional turbulent flow at rough wall, heat transfer and hydraulic resist., effect of viscosity variation 77−42816
Orr-Sommerfeld eqn. eigenvalues, boundary layer, series representation 78−38280
parallel flow, role of negative energy waves in some instabilities 79−59967
permeable surface, injection, laminar to turbulent transition, heat and mass transfer 78−83361
pipe flow, transitional Reynolds no. *(Russian)* 78−38406
pipe flow, triggered laminar to turbulent transition, random coiling macromolecular soln. 78−26195
pipe flow, wall region mass transfer 78−1638
plane Couette flow, bifurcation from infinity, nonlinear differential eqn. 79−98806
plane Couette flow, transition to turbulence and finite amplitude disturbances 80−33558
plane Poiseuille flow, transition to turbulence and finite amplitude disturbances 80−33558
plate, flat, with suction, boundary layer turbulence and momentum props. 80−1679
Poiseuille flow in pipe, bifurcation from infinity, nonlinear differential eqn. 79−98806
Poisseuille pipe flow transitional behaviour, effect of inlet flow disturbances 79−90216
polymer solns., laminar-turbulent transition 78−9663
polymer solution, boundary layer having laminar, transitional and turbulent flow zones *(Russian)* 77−80185
pulsatile flow, laminar-turbulent transition, appl. to blood flow *(French)* 77−5022
radially rotating pipe, heat transfer coeffs. in various flow regimes 78−1668
Rayleigh-Benard instability, vel. field, transition to turbulence 80−6029
rigid circular cylinder in confined flow, fluctuating lift and drag forces 77−15118
roll-wave stability on thin laminar flow down inclined plane wall 80−28488
rotating disc, local heat transfer, Prandtl's mixing length hypothesis 77−27540
rotating disc boundary layer, stability 78−38283
rotating disc boundary layer transition regime, spiral vortices 80−59040
rotating discs, drag reduction in polymer soln., laminar to turbulent transition 78−75173
rotating radial convergent duct, air flow heat transfer boundary conditions, turbulent and transition flow 78−83476
rough cylinder in critical Re water crossflow, heat transfer 80−1571
rough pipe, gas-liq. flow pattern transition model 78−14084
round tubes, non-Newtonian fluid transition and turbulent flow regions *(Russian)* 80−59077
separated incompressible boundary layer prediction, including viscous-inviscid interaction 80−1548
shock tube, unsteady boundary layer obs., behind moving shock wave 78−46998
shock tube wall boundary layer instability, transition evolution 79−64642
shock wave, laminar to turbulent boundary layer transition, effect on current flow 79−41709
simulation of two-dimens. boundary layer transitions 78−38286
slender body, axisymmetric wake, transition and instability 79−32524
statically stressed fluid, transition to turbulence, inverted bifurcation 77−7370
stratified gas-liq. film flow, eqns. of motion 79−37376
stratified shear flow, wave breakdown 77−31358
structures and mechanisms of turbulence, conference, Berlin, Germany (Aug. 1977) 78−94647
subsonic streamwise corner, laminar-turbulent transition 77−62269
suction-induced asymptotic boundary layers, exptl. and predicted props. 80−1553
supersonic compressed boundary layer on two-dimens. plate, unstable localised disturbance characts. 77−55031
Taylor-Gortler instability in turbulent shear flows and boundary layer transitions 78−90836
three dimensional parallel shear flows, stability and transition for rot. disc 80−74887
three-dimensional disturbances, instability, turbulence generation *(Russian)* 77−27511
three-wave resonance interaction of disturbances in a boundary layer 79−90264
Tollmien Schlichting wave, two-dimens., flat plate downstream flow field 78−38357
Tollmien-Schlichting waves, sound field 78−18090
Tolman-Schlichting waves in boundary layer effected by external perturbation 79−90265
transition in the infinite swept attachment line boundary layer 80−19326
transitional flow conditions on rot. disc 78−46980
transitional turbulent pulsatile flow in channel 77−46993
tube, oscillating and pulsating flow, critical Reynolds numbers *(German)* 80−1687
tube bank heat transfer in air crossflow at high Reynolds nos. *(Russian)* 78−14010
tubes, viscous liquid turbulent unsteady flow, pressure drop in transition region 80−74978
turbulence separation, subsonic and supersonic, ultra-short duration visualisation *(French)* 78−75128
turbulent boundary layer, compressible, extended mixing length appls. 78−94655
underground cable system, convectively cooled, temp. distribs., heat transfer correlations 78−71262
uniform fluid flow, general nondimensional relationship *(Bulgarian)* 78−12571
unstable laminar boundary layers, nonlinear evolution and breakdown 80−92109
velocity distribution in cylindrical pipes 79−37299
velocity gradient factor, use as pressure gradient parameter 77−27506
vertical layers, struct. of laminar-turbulence transition and turbulent convection conditions 80−6040
vertical natural flow, adjacent to surface transition limits 79−50726
viscous fluid flow down inclined plane, development of roll waves 78−75160
vortex shedding from smooth and roughened cylinders in crossflow near plane surface 79−81911
wake, axisymmetric, instability and laminar to turbulent transition 78−38337
wake, supersonic, of transverse circ. cylinder, laminar to turbulent transition, external noise effect 78−38367
wake, transition artificial control by external sound 78−34139
wakes, transition to turbulence 78−94739
water adjacent to vertical uniform flux surface, buoyancy driven flow, transition and transport 79−27631
water film flow over cylinder, laminar to turbulent transition, heat transfer rates 77−58691
water jet, turbulence fine struct., polymer addition effects, high speed photography 78−26178
water jet appearance, nozzle shape and polymer additive effects, boundary layers 80−53828
water pulsating flow in heat exchanger effect of pulsations on heat transfer 79−94614
He, liq., Rayleigh-Benard expt., freq. locking and turbulence onset 79−90255
Hg, liq., flow in transverse mag. field, laminar and transition, channel wall effects 78−63500
Hg, transition and turbulent flow in curved channels under transverse mag. field 80−79396

laminates
Γ-shaped crack elastic energy evolution rate in laminate determ. by pliability vibr. meas. 78−83348
adhesively bonded metallic panels, 2-ply, finite element and integral eqns. anal. of fatigue crack growth 78−92347
adhesively bonded sheets, fracture anal. 77−50996
Al alloy 2024-T81, adhesive bonded multi-ply laminate, effective remote stresses and stress intensity factors 77−73328
analysis, desktop calculator library module appl. 80−77764
angle ply composite, impact props. 77−56054
angle ply laminate, fibre reinforced, interlaminar strength test for delamination 78−88523
angle ply laminates, 3D finite difference soln. of free edge effect 80−79152
angle-ply laminate, edge effects 78−19803
anisotropic cylindrical shell, optimal problems of vibrations 78−1602
anisotropic elliptical layered plates, deflection, interlayer shear effects 79−98622
anisotropic layers, fibre reinforced, effective moduli of elasticity 77−4802
anisotropic plates, transverse shear deformation effect 80−19237
anisotropic reinforced resin laminate, cyclically reversing load, strain behaviour determ., approx. method *(German)* 79−5096
anisotropic shells, nonlinear eqns. of Timoshenko-type theory 80−69669
anisotropic shells, thermal stresses *(Ukrainian)* 77−68399
anisotropic shells, transverse shear stiffness calc. 78−42526
balsa wood laminates, thermal and mech. characts. 80−25819
beam, steady-state response to moving load 78−26030
beams interlaminar thermoelastic stresses 80−1432
bi-layer struct., radiation attenuation technique for simultaneous layer thickness determ. 77−12758
biaxially fibre reinforced composites, two dimens. mixture theory, dynamic crack appl. 78−87301
bimaterial interface, wave propagation in non-uniform motion of displacement discontinuities 80−19264
bonded Al-CFRP single lap joint strength 79−29328
bonded dissimilar materials, crack along bond, stress intensity factors 78−55607
bonding inspection, by acoustic amplitude method 78−48591
calculation of stress distrib. and X-ray elastic consts. *(German)* 78−52883
carbon fibre reinforced plastic, fracture energy improvement by delamination promoters 77−8909
cast iron with lamellar graphite, tensile strength, reactor appl. 77−57718
ceramic multilayer capacitors, fracture mechanics approach to structural reliability assessment 80−89328
cermet coating on Cu, thermal shock performance 78−7081
circular sandwich plates, free asymmetric vibr. 80−1459
club sandwich, elasto-plasticity anal., comparison to shells 80−43625
cold rolling of laminated composite sheet, finite element anal. 78−39797
composite, laminate, crack normal to interface, impact response 80−14628
composite beam, multilayered, anisotropic, exam. of shear stress distrib. under transverse loading 79−18731
composite laminate in combined stress state, fracture models 80−10211
composite laminates, proof test and fatigue study 80−93643
composite plates, stress/strain relation, finite element anal. 79−17219
composite shells, mixed isoparametric finite element models 77−78979
composites, effective length of reinforcing component 80−25797

laminates continued
composites, multicomponent layered, time depend. of flexibilities 80−39205
computer simulation of time and temp. effects, mech. response 78−35466
cord reinforced rubber laminate, interlaminar-shear-strain meas. 79−57043
cord-rubber laminates, two-ply balanced, interlaminar-shear strain study 80−97526
creep behaviour, natural weathering, of glass fibre-reinforced polyester laminates 79−66107
cross-plied factors controlling transverse cracking 77−77566
cross-ply, symmetric composites, edge effects, traction-free-edge condition satisfaction 80−79151
curved sandwich beam, finite elements for linear static elastic anal. 77−62153
cylinder, imperfect, buckling under combined loading 80−7620
cylinder, thin-walled, laminated, non-uniform, elastic equilib. with surface loads and displacements 80−69671
cylindrical and plane parallel layered materials, thermographic determination of heat transfer coeff. 80−19221
cylindrical ceramics-metal laminated components, X-radiography 79−5123
cylindrical non-axisymmetric wave propagation in laminated medium, continuum theories 79−14293
cylindrical shell, coupling effect under internal press. *(Japanese)* 80−55449
cylindrical shell, reinforced laminer, intrinsic oscill. 80−99957
cylindrical shell containing elastic filler subject to axial compression and external press., weight minimization 79−86352
cylindrical shells, prepared by continuous filament winding calc. of strength and reliability 80−10194
damage zone failure analysis 80−85059
deformation charact., pliability and rigidity 78−23798
delamination failure mode of composite bars in compression 80−11772
delaminations in thin sheets, elongated, interaction with Lamb waves, book contrib. 79−98574
discontinuity type defect revealability, comparison of thermal inspection methods, computer simulation 79−79207
dynamic behaviour, simulation of effect of bonding materials 79−46216
dynamic response under large deformation, nonlinear mixture theory 78−56717
edge effects, new results in symmetric laminates 77−46971
edge stresses in multilayer laminates, calc. by substructuring 78−34022
elastic dissimilar semiinfinite strips, different widths, plane symmetric contact problem 78−55615
elastic nonlinear beam of thin-walled open cross-section, sectorial coord. 77−35036
elastic reinforced shells, stability 80−58948
elastic static problems *(Russian)* 78−30187
elastic wave propag., complex transfer matrix approach 77−42768
elastic-ideally-plastic beams, sectorial coord. 77−68406
elasticity of multilayered slab, boundary value problems 77−35047
elastomeric bearings, high-capacity, laminated, finite-element anal. 80−96197
EM wave propag., bonding material influence 80−91726
EM wave propagation in laminated waveguides, continuum modelling 79−55031
epoxy laminate, fatigue residual strength degradation model and theory of periodic proof tests 77−70158
epoxy laminate, glass-fibre reinforced, with circular holes, tensile fracture 80−25789
epoxy laminate, surface prep. to promote electroless Cu bonding 77−21300
epoxy resin, E-glass fibre reinforced, flexural fatigue properties 79−66138
epoxy-graphite composite creep behaviour humidity effects 77−66682
ethylene-vinyl alcohol laminated copolymer film, O_2 permeability *(Japanese)* 79−24824
fabric reinforced laminates, stress-strain relationship *(Polish)* 79−91750
failure mechanics, damage development 79−43427
fatigue damage anal. 80−104253
fatigue failure of angle ply laminates 77−4833
fibre cross-reinforced, moment effects in plane problem 80−64393
fibre reinforced, elastic law for materials with different tensile and compressional moduli 80−11713
fibre reinforced, nonlinear response 77−70107
fibre reinforced composite, fatigue damage, early detection by NDT 77−28951
fibre reinforced composite, moisture diffusion, 3-D Fick's law 78−10218
fibre reinforced composite laminate, fracture mode determ. by AE 79−57187
fibre reinforced epoxy, interlaminar failure 80−81207
fibre reinforced epoxy, static and impact props. 77−63725
fibre reinforced laminated composite, reliability anal. approach to fatigue life dispersion *(Japanese)* 79−61704
fibre reinforced laminated hybrid, tensile first cracking strain and strength 80−81175
fibre reinforced plastic laminate with circular holes, stress conc. and breaking strength *(Japanese)* 78−23816
fibre reinforced plastic/Al/adhesive laminate, interlaminar behaviour under thermal loading 77−81309
fibre reinforced plastics, spread of strength rel. to stress conc. *(Japanese)* 79−24610
fibre-reinforced, optimum design under natural frequency restraints, nonlinear mathematical programming 80−53688
fibreglass/epoxy composites, laminates, rings, tubes, thermal contraction at low temps., report 80−19968
fibreglass/epoxy laminate curing by microwave heating 77−77457
fibrous laminated composite, tensile failure, quantitative fault tree anal. 77−59891
filament wound laminated composites, thermal residual stresses 80−49290
filament wound material, lamination theory for failure envelope prediction under biaxial loading 79−38931
filler containing beam reinforced three layer plates *(Russian)* 80−43613
fracture, effect of adhesive layers 78−90791
fracture, multiple, anal. 80−10206
fracture and delamination combined, simple idealised example 77−68529
free edge stress fields, in composite laminates 78−67039

laminates continued
fusion reactor anisotropic B_T-coil two-dimens. finite element anal. of laminate sliding 78−50382
fusion reactor coil, multilayer structs., laminated beam theory anal. 78−55011
fusion targets, laminated coatings, strength optimisation 78−60883
GFRP cross-ply laminate, constrained cracking 78−19870
GFRP laminate, damage assessment by stress wave emission and dynamic mech. meas. 78−11461
glass, narrow sandwich seals, shape factor, finite element anal. 78−75111
glass applications, review 78−3306
glass fabric laminate, nontransparent dielectric, laser emission reflection and destructive action *(Russian)* 79−74031
glass fabric reinforced organic-matrix, interlaminar fracture studies 80−55495
glass fabric reinforced phenol resin effect of thermal loading on physicomech. props. 79−24622
glass fabric reinforced plastic laminate, fatigue strength rel. to test frequency 79−8362
glass fibre epoxy cross-ply laminates, multiple transverse cracking 78−95800
glass fibre reinforced bakelite, laminate, internal stresses occurring during production 79−66034
glass fibre reinforced diallyl polymer, thermally stable, prep. *(Japanese)* 78−92232
glass fibre reinforced epoxy, epoxy matrix, strength in twisting, stretching and transverse bending 80−11622
glass fibre reinforced epoxy, exam. of interlaminar shear stress distribution 79−43308
glass fibre reinforced epoxy, fracture mechanics 80−35294
glass fibre reinforced epoxy, multilayer circuit board, holographic interferometry appl. to real-time studies of heat effects 79−91873
glass fibre reinforced epoxy cross ply laminates, transverse cracking and long. splitting, strain effects 79−61723
glass fibre reinforced epoxy laminate, failure, fractographic study 79−96111
glass fibre reinforced epoxy laminate, internal moisture condition effect on strength 79−15736
glass fibre reinforced epoxy laminate, mech. strength meas., comparison with theory, tensor polynomial failure criterion 78−39886
glass fibre reinforced epoxy laminate, metallization by Cu and chem. treatment by H_2CrO_4 *(German)* 80−93670
glass fibre reinforced epoxy laminate, tensile testing, monitoring cond. effect on stress wave emission data 79−87814
glass fibre reinforced epoxy laminates, exp. determ. of nonlinear shear behaviour 80−66575
glass fibre reinforced epoxy resin laminate, sliding behaviour against Cu or Al speres at cryogenic temps. 80−66671
glass fibre reinforced epoxy-aniline, laminate, work required to rupture along interfaces 79−43413
glass fibre reinforced laminate, failure process 78−31529
glass fibre reinforced non woven epoxy laminates comparison with paper phenolic and woven glass epoxy 78−35635
glass fibre reinforced plastic, cemented joint of cylindrical shell with cover, stressed state 80−69668
glass fibre reinforced plastic, comparison of single and multi-hole bolted joint strength 79−91739
glass fibre reinforced plastic, failure in compression 80−11755
glass fibre reinforced plastic, fatigue strength under normal and interlaminar shear stresses 80−11758
glass fibre reinforced plastic, laminate, stress anal. finite element modelling 79−59924
glass fibre reinforced plastic, pin-bearing strength, stacking sequence effect 77−70105
glass fibre reinforced plastic, strain disintegration under repeated static load 80−11756
glass fibre reinforced plastic, strength and deformability, artificial ageing effect 80−60893
glass fibre reinforced plastic laminate, crack resistance under prolonged loading 77−21276
glass fibre reinforced plastic laminate, mixture law of tensile and fracture strength and variation *(Japanese)* 79−43337
glass fibre reinforced plastic laminate in plane-stress state, strength depend. on reinforcement struct. 78−23796
glass fibre reinforced plastic laminates, failure models, reinforcement struct. effect 80−66641
glass fibre reinforced plastic/polyurethane foam/Al sandwich, flexural props. *(Japanese)* 78−56707
glass fibre reinforced plastics, laminated ring with extra steel pin radial reinforcement, mech. props. 80−11714
glass fibre reinforced plastics, load carrying capacity, interlaminar imperfections influence *(German)* 79−100218
glass fibre reinforced polyester, 90° cross-ply laminates, multiple transverse fracture 77−8913
glass fibre reinforced polymer matrix laminates, compressive strength 78−64609
glass fibre-reinforced polyester cross-ply laminates, effect of resin failure strain on tensile props. 78−3212
glass laminate 27-63S, shear fracture toughness charact., strain rate effects 77−8950
glass narrow sandwich seal, correction factor for thermal expansion mismatch 78−75110
glass reinforced epoxy resin laminator, strength tests *(Polish)* 77−12772
glass reinforced laminates, damage accumulation during tensile loading 79−83262
glass reinforced plastic laminates, stress, strain anisotropy, tensor calculus *(Polish)* 77−12678
glass strip reinforced epoxy resin, temp. relationship of fracture toughness 80−3196
glass textolite, failure charact., effect of test conditions 78−27635
glass textolite cylindrical shells, parallel wound, feasibility of diagnosing strength 78−67157
glass textolites, three layer construction diagnostics of physicomech. props. 77−73254
glass wool reinforced polymer, relationship between Young's modulus and dissipation of energy *(German)* 79−96064
glass-epoxy laminate, superconducting magnet insulators, gamma-ray radiation effects 80−24495
glass-epoxy laminate post failure behaviour, stress concentration 77−48521

laminates continued
glass-fibre reinforced plastic specimens, prep. of three-layer cylindrical with syntactic foam base 80−3267
glass/C fibre reinforced plastic, hybrid effects between interlaminar and translaminar config., mech. props. 79−52351
glass/C hybrid reinforced plastics, fatigue props. and flexural rigidity *(Japanese)* 80−55510
graphite, reinforced epoxy angle-ply laminate wave propag. during transverse impaction 79−83295
graphite epoxy laminate, mixed mode fracture, fracture strength 77−70156
graphite fabric reinforced organic-matrix, interlaminar fracture studies 80−55495
graphite fibre epoxy laminates, low thermal expansivity, design considerations 80−81031
graphite fibre filled phthalocyanine composites, cure cycle investigation 80−81030
graphite fibre filled polyimide composite laminates, space environment, phys. and mech. response 80−81140
graphite fibre filled polyimide composite prepreg laminates, room-temp. ageing effect 80−81093
graphite fibre reinforced epoxy, fracture mechanics 80−35294
graphite fibre reinforced epoxy, laminated plate under tension, stacking sequence and lay up angle effect on free edge stresses round hole 78−88524
graphite fibre reinforced epoxy laminate, containing interlaminar paper inclusions, AE monitoring 79−34229
graphite fibre reinforced epoxy laminate, fracture, comparison of anal. and expt. 79−61713
graphite fibre reinforced epoxy laminate tension-compression fatigue loading, fatigue residual strength degradation model, comparison with expt. results for 78−35491
graphite fibre reinforced epoxy laminates, expt. investigation of tensile moduli and strength 78−52870
graphite fibre reinforced epoxy matrix laminates, microscopical anal. 78−3288
graphite fibre reinforced panels, low energy impact testing 78−72845
graphite fibre/epoxy laminates, free edge induced failure 80−11775
graphite reinforced epoxy, accelerated characterisation procedure 79−34263
graphite reinforced epoxy angle ply laminates, statistical fatigue in shear 79−11690
graphite reinforced epoxy laminate, cantilever shells and late, natural modes 79−91737
graphite reinforced epoxy laminate, edge effects 78−19803
graphite reinforced epoxy laminate, fracture behaviour 79−83294
graphite reinforced epoxy laminate, fracture by three point bend 79−83297
graphite reinforced epoxy laminate, mech. strength meas., comparison with theory, tensor polynomial failure criterion 78−39886
graphite reinforced epoxy laminate plates with cracks, strain and failure anal. 79−29170
graphite reinforced epoxy laminate with arbitrarily symmetrical struct., stability 79−61649
graphite reinforced epoxy laminates, cracked, deformation and failure in biaxial stress fields 79−47763
graphite reinforced epoxy laminates, imminent fracture detection using acoustic emission 79−20302
graphite reinforced epoxy/Al laminate, cantilever shells and late, natural modes 79−91737
graphite-epoxy composites, Thornel 300/Fiberite 1034, effects of thermal spiking on moisture absorpt. characts., tensile strength and buckling modulus 79−43330
graphite-epoxy hybrid laminates, low level Charpy impact response 78−11333
graphite-epoxy laminates, AS/3501-5, compressive fracture strength 79−43396
graphite/epoxy 5208/300, proof test and fatigue study 80−93643
graphite/epoxy composite laminates, splitting process charact. 80−25843
graphite/epoxy laminate, T300/5208, proof testing under cyclic tension-tension fatigue 80−81249
graphite/epoxy laminate containing holes, high temp. tensile strength 77−25105
graphite/epoxy laminate with third phase reinforcement, static and impact behaviour 77−40447
graphite/epoxy laminates, statistical fatigue, high load effect 80−93642
graphite/epoxy laminates, stress wave damage 80−93611
graphite/epoxy laminates, T300/5208, effect of curing stresses on first ply failure 79−43329
graphite/epoxy laminates fatigue characts. under compression loading 78−84971
graphite/polyimide laminates, effect of ply stacking sequence and orientation on residual stresses 77−52378
Griffith cracks, partial immobile equilib. in two media plates 80−33529
heat conduction, anisotropic to orthotropic transform. 80−38217
heat conduction, laminated stack of metal 79−41556
heat conduction eqns. *(Russian)* 77−75767
heat propagation, longitudinal, in 3-phase laminate, at high exciting freqs. 78−90684
homogeneous continuum model 77−58546
impact testing, machining 78−3272
insulating element, laminated, vac. drying in inert heat-transfer vap. 78−56875
interlaminar stresses 79−10472
isotropic plane sandwich plates, constant shear theory 80−99943
Kapton, substrate, electron beam evaporation of uniform Al film 78−11373
laminate, stress anal. finite element modelling 79−59924
laminated plate, moderately-thick, biaxial buckling 77−58573
laminated plates flutter and buckling anal. 77−65698
layer interface, SH type disturbance due to shearing stress discontinuity 78−34011
layered cylinder, axisymmetric delaminations 78−79269
layered cylindrical shell, with transversely isotropic core stability in axial compression 77−3722
layered material with through cracks, transverse conductivity 77−84122
layered orthogonally reinforced plastics, strength and stiffness prediction in interlaminar shear 77−9025
layered reinforced plastic, light propagation for NDT 77−9024
layered rod on sagging elastic supports, aeroelastic stability, vibr. modes 78−51115

laminates continued
layered system, thermal stresses and displacements 80−23891
layered thin composites, optimum design and strength 80−10210
linear elastic three layered rings, transient response 77−80075
local heating in layer with absorption *(Russian)* 77−42716
Love wave diffraction, by stress-free crack in plane interface 80−33501
magnetoelastic surface Love wave propagation 80−38322
mechanics of composite mats., homogenisation and random evolutions 80−28423
metal clad fibre reinforced composites, debonding risk 80−3132
metal panels, adhesively bonded, cracked, fracture anal., crack tip stress intensity factors 78−90792
metal-composite rods, compressed, delamination 80−64396
metal-polymer, ply-separation resist. polymer polarity effect *(Russian)* 80−61064
metallic, laws governing development and retardation of fast cracks 78−15527
metallic laminated composite, crack growth retardation *(Russian)* 77−70144
microplastic strain development *(Russian)* 79−34102
multidirectional, general fatigue failure criterion and test program 80−7658
multilayer, stress-strain state 78−18177
multilayer built-up plate with crack, rigidity determ. 79−90190
multilayer cylinder, exam. of stresses, considering layer contact characts. 78−63399
multilayer cylindrical shell, theory in inhomogeneous temp. field 80−1434
multilayer fibre reinforced composite, alternate hybrid stress elements for anal. 77−50926
multilayer hybrid-stress finite element analysis of through-thickness edge crack 77−54928
multilayer materials, vacuum rolling at high temp. *(Russian)* 79−15708
multilayer object, layer separation detection by thermal method using thermal visualizer 78−53127
multilayer parts, thermal quality inspection two dimensional problem soln. 79−70283
multilayer plates, viscoelastic, equations of forced vibrs. 78−67084
multilayer product, theory of laid-on shielded transducers for inspection 78−88610
multilayered basements, harmonic oscills. anal. *(Ukrainian)* 77−68474
multilayered composite soft interlayer, limiting stressed state and carrying capacity 78−30201
multilayered shells, nonlinear anal. 78−18168
Mylar film/adhesive/Al foil laminate, mech. interactions 80−81112
Nimonic alloy reinforced Al, Cu and brass, creep singularities at low temps., struct. defect changes *(Russian)* 80−11696
nonlinear elastic laminated composite, wave propag., geometrical acoustics anal. 77−42774
nonlinear stress-strain response 79−91738
nonlinear transient pulse propag., interface reflection effect 78−63222
notch strength 79−57095
orthotropic laminate composite, broken layer 78−38254
orthotropic laminate composite containing layer with crack, stress intensity factors 78−5694
orthotropic laminates, torsion strength and shear modulus determ. 80−92587
paper, decorative, deform. and internal stresses 79−61671
periodically layered composites in plane strain, dispersion eqn. for waves 80−79212
piecewise continuous eigenfunction solns. 78−18178
piecewise-homogeneous elastic medium with plane parallel boundaries of separation, vibrations 77−84188
pipe, layered, support layer thickness effect on stress-strain state *(Russian)* 80−43614
plane strain state with transverse crack 80−38338
plastic, glass, C, Kevlar fibre reinforced, US evaluation of hygrothermal effects 80−7730
plastic, glass- and fibre-reinforced, strength anisotropy comparative anal. 80−19872
plastic laminate removal from metal using laser beam 78−7061
plate, laminated, high-order deformation theory 78−63309
plate, laminated composite, under tension, interlaminar stresses around circ. cutout 78−34010
plate, three layer, thermoelasticity problem, soln. method *(Ukrainian)* 80−48574
plate under tension, stacking sequence and lay up angle effect on free edge stresses round hole 78−88524
plates, laminated, cylindrical bending, random loading, dynamic response 80−58902
plates, laminated anisotropic composite, penalty plate bending element 80−96200
plates, optimum design under shear 80−23925
plates, rectangular cross-ply laminated, with nonlinear stress-strain behaviour, buckling 80−64415
plates, symmetric, specially orthotropic, thermoelastic anal. 80−92058
plywood shallow shells, orthotropic, mech. charact., effect of restraint of sliding or expansion *(Japanese)* 77−77522
polyester laminates, glass fibre reinforced, enhanced elasticity, chem. resist. tests *(Polish)* 80−60901
polyester resin, Polimal 109, open pore density and content *(Polish)* 80−59665
polymer blends, selective staining method for TEM obs. of morphology 80−84103
polymer laminate thin films, adhesive strength determ. 79−57178
polymer matrix, residual stresses 77−25007
polymer multilayer composites, wire-reinforced, dynamically loaded, crack propagation and arrest 80−97567
polymer soft lossy, viscoelastic props. determ. from torsional vibr. of laminated bar 77−62218
polymer-metal laminate, bone fixation plate fabrication 79−79685
polymeric adhesive layer, interlaminar stresses, direct determ. 77−86237
polypropylene-polyurethane laminates, meas. of dielectric losses at cryogenic temps. 80−25301
polyurethane foam/glass reinforced plastic/Al, sandwich construction, non-symmetric, flexural fracture 79−74233
poroelastic layered media, waves and apparent additional mass effect 80−53675
post-failure behaviour, no stress conc. 77−28895
randomly imperfect periodic laminated composites, wave propagation, diffusion approx. 79−98659

laminates continued
rectangular antisymmetric angle ply plates, shear deform. effects on vibr. 78−63356
rectangular laminated plate, free vibrs., freq. and shape determ., complex boundary conditions 80−79203
rectangular plate on elastic foundation, uniform loading, computer anal. 77−46915
reinforced epoxy angle-ply laminate wave propag. during transverse impaction 79−83295
reinforced in two directions, cracking 79−96139
reinforced UP resin laminate under dynamic stress, anisotropic, mech. behaviour determ. *(German)* 79−83268
residual stress form. during hardening 78−1575
residual thermoelastic stresses 80−106721
resonance splitting in ultrasonic spectroscopy 78−87214
rosette cylinder, elastic response under axisymmetric loading 77−58549
rubberized cloth, service life determ. under cyclic load 78−31535
sandwich composite beam, four point bending stress, multilayer built-up theory anal. *(Japanese)* 79−8322
sandwich composite beam, impact bending behaviour *(Japanese)* 80−55468
sandwich disc, axisymmetric deformation 80−10148
sandwich panels, discrete field mechanics 77−62151
sandwich plate, modified Berger method, large thermal bending anal. 78−63297
sandwich short beams, departure from classical beam theory 78−26034
sandwich strips, plane deform., Saint Venant end effects 78−46893
sheet moulding compound, laminate, charge pattern influence on tensile strength *(Japanese)* 80−55513
sheet-metal laminate effect of interstage annealing on stretch formability 77−55917
shell, cylindrical, effect of material orthotropy on stress state around circular hole 78−34023
shell, cylindrical, three-layered, stress-strain state *(Russian)* 80−90677
shell, multilayer, cylindrical, viscoelastic strain equations under axisymmetric load 77−80079
shells, laminated composite circular cylindrical, prebuckling deformation effects on buckling 80−48609
shells, with viscoelastic binder, stability 80−10165
shock wave propag., stress history recording 78−38242
simple shear charact., comparison of test methods 78−44283
single ply, thickness effect on percolation and conductivity 80−92953
sital, structural glass component, strength in complex stress state 79−91763
solute diffusion, conc. depend., with/without chem. reactions 80−54427
spherical shell, stability 77−65700
square laminated panels, forced transverse vibr. expt. *(Japanese)* 78−22298
steel, laminar, high hardness, ballistically damaged, fracture mech. approach to residual strength 77−56050
steel, laminar composite, crack extension, rising tensile load effect 77−36642
steel, laminated, tensile props. 77−52441
steel, middle and low C, clad plate, inhomogeneity and residual stresses, heat treatment effects *(Japanese)* 78−6955
steel, sheets bonded with low density polyethylene, static fatigue *(French)* 80−108522
steel, stainless, clad Al, sandwich sheet material, forming limits 80−3131
steel, stainless/Al laminate, sandwich sheet material, plane strain compression and rolling 79−57062
steel, stainless/Al laminate, sandwich sheet materials, deform. in uniaxial tension 79−57061
steel Co-Ni three layer composite, high strength with increased damping capacity 77−1850
steel laminate, acoustic emission rel. to fracture at 77K *(Russian)* 80−93633
steel plates, plastic coated, RF welded, quality and strength *(German)* 79−34185
steel pressure vessel, multilayer, without longitudinal seam, model investigation *(German)* 79−34276
steel-Al-steel plate, fatigue damage analysis and life predictor 77−25120
steel-aluminium plates, exam. of adhesion strength by impulse loading 78−84943
steel/polypropylene bar, torsional vibr., polymer viscoelastic props. determ. 77−62218
strength anal. and distribution, failure prediction 78−88522
strength optimisation, anisotropic laminated plates, within supercritical range 79−59934
strength properties of a 3 component beam *(German)* 80−35269
stress field in composite laminates, theory based on Reissner's variational principle 78−67038
stress free and problem, plane elastostatic problem, crack across interfaces 78−34076
structural elements, stress intensity factors determ. 80−99973
surface EM waves, wave phase velocity *(Russian)* 79−45889
tensor polynomial failure criterion 78−39886
Textolite, mech. props. in elastic symmetry planes 77−21211
Textolite, shear strength behind the front of a plane shock wave 79−15752
thermal diffusivity for multimaterial composite laminate 78−90643
thermal monitoring by near surface thermoelectric receivers 78−53107
thermal NDT using liquid crystals, fibreglass laminates 80−93709
thermally induced stresses, edge effect 77−84142
thermoelastic laminated media, aggregate response modelling 77−50897
thermopiezoelectric laminae, coated with electrodes, two dimens. vibr. theory 78−35092
thermoviscoelastic laminate beam, stress anal. *(German)* 80−106727
thick multilayer laminates, hybrid-stress finite element formulation 80−92043
thin, optimal struct. and strength in two-dimens. stress state 80−64395
Thornel 300/Fiberite 1034 graphite epoxy laminates, tensile strength, 200 to 422K, moisture effects 77−48486
Thornel reinforced epoxy laminates, strength and biaxial stress-strain response, analytical expt. correlation 79−29131
three layer cylindrical shell having low stiffness filler, resistance to axial compression 79−86353
three phase laminated composite, longitudinal heat propag. at low exciting freqs. 80−58889
three-layer plates, circular, stability 80−79188
transient moisture sorption induced stress field 78−34021
transverse dynamic loading, transient response 77−31245
laminates continued
transverse elastic wave propag. theories, comparative study 79−14324
unidirectionally reinforced composites, large deflection, plastic constitutive relations 80−43624
vapour deposited coatings, mech. props. 78−6247
vibroacoustic quality control 79−70274
viscoelastic composite, wave propag., dispersion relations, mode shapes, variational methods 78−18215
viscoelasticity measurement using mech. drive viscoelastic tester *(Japanese)* 79−34232
water/Al/adhesive/Al/water five layer struct., time domain anal. of US propag. 79−20319
wave propagation in imperfectly periodic structures, random evolution approach 79−14339
wave propagation in laminated initially strained medium 80−38321
wood-epoxy bond system, cleavage fracture toughness *(Japanese)* 77−77574
Young's modulus determination, dynamic high-speed method *(German)* 80−85123
Al alloy, adhesive-bonded-laminated, fatigue props. 80−50695
Al alloy, laminates, fracture of bonded 2024-T3/7075-T6 78−56722
Al alloy adhesively bonded laminates, axial fatigue 80−40491
Al alloy bimaterial laminates, crack growth 80−16424
Al alloys, epoxy bonded sheet, fatigue crack initiation, propagation 79−15776
Al/Al_xO_y vacuum deposited laminates, struct. and mech. props. 79−28219
Al/Cu laminates, vapour deposited, strength enhancement 79−24576
Al/polyethylene/Al sandwich construction, flexural fatigue props. *(Japanese)* 78−56751
Al-304 stainless steel laminate composite, fatigue crack nucleation and propagation 79−100244
Al-Ag, thin-layered laminates, yield strength rel. to dislocation generation and motion 79−20137
Al-Cu, thin-layered laminates, yield strength rel. to dislocation generation and motion 79−20137
Al-Cu-Mg-Mn (4.5, 1.5, 0.6 wt.%), alloy 2024-T3, exam. of residual strength of plate containing crack, fracture anal. 78−90792
Al-Cu-Mg-Mn (4.5, 1.5, 0.6, wt.%), alloy 2024-T81, plates, adhesively bonded, exam. of fatigue crack growth 78−92349
Al-Mn-Mg laminated composite, fatigue fracture, fatigue strength enhancement 79−87725
Al-PMMA laminated composites, shock wave propag., flash radiographi obs. 79−4370
Al-Zn-Mg-Cu alloy, laminated, adhesively bonded alloy 7075-T6, exam. of fracture resistance 78−76754
Al-Zn-Mg-Cu-Cr, (5.6, 2.5, 1.6, 0.3 wt.%), laminates, 8 and 22 layers, adhesively bonded exam. of fatigue crack propag. 78−92345
Al-Zn-Mg-Cu-Cr, (5.6, 2.5, 1.6, 0.3 wt.%), alloy 7075, plates, adhesively bonded, exam. of fatigue crack growths 78−92348
Al_2O_3/Nb laminates, metal to ceramic joints, adherence props. 80−45386
Au-Mo-Si multiple layer structure, bombarded with P ions, calc. of P ion profile in substrate *(Russian)* 79−55771
B epoxy laminate, notched, fatigue damage 78−3215
B fibre reinforced Al alloy 6061, cross plied laminate, tension-compression fatigue 79−38940
B fibre reinforced Al laminate with discontinuities, fracture 78−19877
B fibre reinforced Al laminate, unidirectional, interlaminar shear strength exam. 78−35434
B fibre reinforced Al laminate, effect of ply by-up sequence on fracture toughness 78−35492
B fibre reinforced epoxy, fracture mechanics 80−35294
B fibre reinforced epoxy laminate, energy release approach for stable crack growth in free edge delamination problem 78−19878
B fibre reinforced epoxy resin, anisotropic laminate, effective modulus of elasticity 77−4802
B fibre reinforced epoxy resin laminate, fatigue damage, stiffness/strength comparison 77−90451
B fibre/Al laminates, use in neutron collimators 79−45506
B reinforced Al laminates, applic. of linear elastic fracture mechanics 77−28893
B-epoxy-Al sandwich laminate. influence of residual stresses on tensile strength 78−60703
C fabric reinforced plastic laminates, tensile and compressive strength determ., 20-1500°C 80−100880
C fibre reinforced epoxy, fatigue strength 78−15495
C fibre reinforced epoxy, wound, strength in twisting, stretching and transverse bending 80−11622
C fibre reinforced epoxy cross ply laminates, transverse cracking and long. splitting, strain effects 79−61723
C fibre reinforced laminate, elastically orthotropic or isotropic, stress around pin loaded holes 77−84143
C fibre reinforced plastic laminates, axial and short beam shear fatigue 78−15492
C fibre reinforced plastic, laminate, non Hookean behaviour in fibre direction, effect of fibre waviness on tensile props. 78−19804
C fibre reinforced plastics, ply multidirectional effects 78−95165
C fibre reinforced plastic, laminate, free-free plates, predicted and expt. natural modes 79−10520
C fibre reinforced plastics, angle ply specimen, calc. of strength and elastic response 79−20108
C fibre reinforced plastics, fatigue behaviour visualised by moire fringe method 80−21110
C fibre reinforced plastic multilayer laminate, strength and deform. *(Russian)* 80−30019
C fibre-Kevlar 49 fibre epoxy laminate, impact props. 78−44164
C/epoxy, moisture distribution determination low cost method 79−65252
C-fibre reinforced epoxy resin, laminated structs. mech. props. 80−50672
C-fibre reinforced resin laminate for IR mirror, design and fabrication *(French)* 77−54770
Cr/Cu/Cr layer composite, influence of phase boundary on flow stress 78−60717
Cu-P (8.4 wt.%) metallic laminate, laws governing development and retardation of fast cracks 78−15527
Cu-polymer composite foils, fracture surface exam. by XPS *(German)* 78−84992
Fe laminates, superplastic bonding 80−25981
Fe-B alloy reinforced polysulphone exam. of tensile and flexure props. 78−72823

laminates continued
Fe-Si (3 wt.%), loss dependence on lamination, orientation and stacking *(Slovak)* 79−4696
Mn-Cr-Ti layers on low C steel, composite, residual stresses rel. to arc-spraying parameters *(German)* 80−104077
Mo-TiC lamellar eutectic composite, deformation and strength, room temp. to 2073K *(Japanese)* 80−71702
PLZT/TFPD thermal/flash protective lens assembly, polarised delamination investigation 80−78929
Si_3N_4/Zr laminates, metal to ceramic joints, adherence props. 80−45386
SiO_2 reinforced decorative laminates, abrasion resistance, abrasive paper deterioration 77−16696
TiN-VN refractory powder composite, resistors, produced in low temp. 78−11182
TiO_2-polycarbonate laminate, impulse surface flashover in vacuum, effect of normal elec. stress 79−4199

laminations
ethylene-vinyle acetate lamination, solar cell encapsulation, double vac. technique 80−93510
minor loop hysteresis loss in thin laminations calc. 78−90342
Permalloy thick film coercivity control 80−15764
steady-state eddy-current dominated magnetic domain wall motion with severe bowing and necking 79−91248
transient skin effect in laminated cores with sectionally different material props. *(German)* 79−41280
Fe-Si, grain-oriented, surface coating effect on transverse magnetostriction 77−66402
Fe-Si, influence of stress on rotational loss, lamination appl. 78−35384
Fe-Si, mag. props., stress and reannealing effects 80−88844
Fe-Si (3 wt.%), grain orientated, negative magnetostriction, theory 78−91917
Fe-Si (3 wt.%), grain-oriented, stacking effect on power loss, mag. props. 80−88795
Fe-Si (3 wt.%), grain-oriented, power loss and domain wall variation with lamination thickness 80−88814
Fe-Si (3 wt.%) laminations, isotropic and cube-on-face, magnetostriction behaviour 80−39843
Fe-Si (3 wt.%) laminations, magnetostriction behaviour associated with closure domain spikes 80−75834
Fe-Si (3 wt.%) laminations, grain oriented, plastically deformed, anomalous losses 80−88853
Ni-Fe multilayered films, mag. domain structures 79−82847

lamp accessories
see also lamps
Fresnel zone plate support UV window as lens and monochromator 80−1326
halogen projection lamps and light fittings *(German)* 77−58408
photographic flashlamp trigger circuit 80−62750
reflector, rotationally symmetrical, physical modelling *(Slovak)* 80−38088
sound-controlled flashlamp trigger circuit *(Spanish)* 80−13175
Na vapour lamp reflector design *(Spanish)* 79−23042

lamps
see also discharge lamps; filament lamps; light sources
blue light phototherapy of neonatal icterus, comparison of lamps 78−44582
camera slit lamp, fluorescence angiography of vascularised camera 78−48855
camera slit lamp, ophthalmic appl. of stereophotography 78−48904
centring projector 10, installation of halogen projection lamp 79−76782
electric lamps, historical review of development 80−9977
gonioscopy, foot-operated camera trip for Nikon photo slit lamp 78−80986
illuminants which give prescribed tristimulus values to given object colours, design technique *(Japanese)* 78−94420
illumination system, optical design 80−64135
illuminators light distribution indication method for computerised illumination projecting *(Hungarian)* 80−27333
luminaire photometry, new concepts using automatic photometer 80−4752
photolamps, thermal interference reduction using Therm-O-lux 85 film 78−41302
pulsed, destruction in liq. coolants 79−94312
slit lamp photodocumentation of ocular structure 80−67181
solar simulator lamp, for photovoltaic cell expt. 80−42004
spectral, plasma appl., using surface wave microwave excitation structures 79−19059
UV emitting lamps, method for estimation of O_3 concs. in vicinity 80−81765
UV high energy photoionisation detector in gas chromatography appl. 78−92561
UV radiation from lamps, medical appls. 79−66504
UV radiation from lamps, properties and harmful effects *(Swedish)* 80−35996
UV sources for curing 78−88443
He, low press. discharge lamps, reson. line broadening O I and N I 78−9123

Landau levels
analytic function theory, energy eigenvalues and eigenfunctions determ. 77−69259
Anderson localisation, transport props. of 2D disordered electron systems in strong mag. fields 78−95318
beat effect of sp. ht. due to impurities, in external mag. field 78−10401
Bloch electrons in mag. field, energy spectrum, struct. of Landau levels 80−54623
CDW instability of electron gas in a strong magnetic field 78−79950
CDW state of two dimensional electrons in mag. field 79−90978
CDW system, nonlinear de Haas-van Alphen effect 77−43523
charged particle scatt. in quantising mag. field 80−46853
charged particle scattering in homogeneous mag. field, transition amplitude 79−10218
cyclotron frequencies near mag. subband 80−39512
cyclotron reson. at model interface in transverse mag. field 79−4726
degenerate semiconductor, conduction electron acoustic spin resonance, oscillations of absorbed power 80−108075
density operator P-representation for Landau electrons 77−20215
diamagnetic band structure, second order calc. using Landau functions 80−24784
electron gas, thermodynamic properties, weak field expansions, in uniform mag. field at T=0K 79−85066

Landau levels continued
electron-impurity system in two dimensions, theory of cyclotron reson. lineshape 78−19332
electron-phonon system, two-dimensional cyclotron resonance lineshape, quantum theory 79−47336
excitonic insulator in mag. field, two-band model 80−80192
excitonic phase, collective excitation modes under strong mag. field *(Japanese)* 77−43502
ferrimagnetic semiconductor, electron transitions between Landau levels under action of alternating EM field 79−69725
ferrimagnetic semiconductors, magnetomagnon reson. 79−69663
ferroelectric semiconductor, magnetic field influence, ferroelectric transitions 80−55049
ferroelectric semiconductors, vibronic, mag. field effect on phase transition 77−40193
film, electron states in longitudinal mag. field 78−91784
Friedel sum rule in static mag. field, impurity-induced mixing between Landau levels 77−31976
gapless semiconductor valence band in mag. field 80−49600
graphite, far IR magnetospectroscopy of Landau level structure 79−73906
graphite, giant quantum attenuation of sound waves 80−54741
graphite, magnetoreflection under press., Landau level transitions 80−50303
graphite intercalation compounds, interband Landau level transitions, magnetorefl. 77−52095
hexagonal lattice, mag. subband struct. of electrons 79−95307
holes, in degenerate bands, variational principle for Landau levels, const. mag. field 79−33219
hot electron distribution functions, expts., review 78−27231
n-InSb, intraband processes exam. by stimulated spin-flip Raman scatt. 77−19362
inversion layer in quantising mag. field, Einstein relation 78−19156
inversion layers, mag. field depend. of reson. line width 78−56380
itinerant electron ferromagnet, effective Lorentz force and Landau level 78−80120
layered crystal, mag. quantisation investig. *(Russian)* 78−23054
light absorption due to electron-electron interaction of electrons occupying Landau levels 78−27195
longitudinal thermo-EMF in quantising mag. field *(Russian)* 77−28204
magnetoelectronic density of states for model cryst. 79−77978
magnetoresistance, longitudinal, in weak mag. fields, Landau level depend. *(Russian)* 78−87965
Matthiessen's rule and its variation for cyclotron reson. width in two and three dimensions 78−6578
metal, electron scatt., effect of surface on lattice defects, surface Landau level reson. 79−65534
MIS, magnetooptic absorption by electron gas, optical phonon effects 80−97248
MOS inversion layer, hot electron effects in Landau levels 80−6998
MOS inversion layer, hot electron effects in Landau levels 80−20315
MOSFET, two-dimens. electron gas, determ. of fine struct. const. based on quantised Hall resist. 80−96997
narrow-gap semiconductor, heavy holes, energy spectrum in mag. field, effect of nonlocal pot. 79−90959
nondegenerate semiconductor electrons in strong elec. and quantizing mag. fields 78−10457
nonequilibrium electrons, thermalisation and linear response 80−65422
piezoelectric semiconductor, photocurrent in quantising magnetic field in presence of nonequilibrium photoelectrons, spectral oscill. and energy relax. by interaction with acoustic phonons 79−91100
polar semiconductors, anharmonicity influence on cond. in quantising mag. field 80−2406
polar semiconductors, secondary cyclotron emission giant oscillations of intensity and line shape 80−66192
quasi-local level, line shape induced by impurity 80−100441
quasi-two-dimensional superconductivity in quantising mag. field *(Russian)* 77−40001
semicond. alloy, spin splitting and effective g-factor of T-holes *(Russian)* 77−51643
semiconductor, antiferromagnetic, spin-magnetomagnon resonance 80−2566
semiconductor, diamagnetic excitons, odd states, oscillator strengths and optical absorption line positions 79−11072
semiconductor, diamagnetic excitons in strong elec. field 79−38002
semiconductor, excitation spectrum and optical props. in field of standing EM wave and homogeneous field 78−91625
semiconductor, influence of impurities on Raman scatt. by Landau levels 77−1668
semiconductor, interband absorpt. in strong parallel mag. and elec. fields 80−6799
semiconductor, magnetophonon resonance oscills., peak shape, theory 80−107824
semiconductor, nondegenerate nonpolar, quantum theory of magnetophonon reson. 77−28200
semiconductor, optical absorption of diamagnetic excitons in crossed mag. and elec. fields 78−10874
semiconductor, piezoelec. and nonpiezoelec. cyclotron-phonon resonance due to polarisation scatt. from phonons 79−95649
semiconductor, saturated state, interaction with weak EM wave in quantising mag. field 77−16288
semiconductor, uniaxially stressed, zincblende struct., band edge Landau levels 79−60706
semiconductor film, electron-phonon interactions in quantizing mag. field 79−69610
semiconductor in quantising mag. field, Stark effect *(Russian)* 77−73126
semiconductor in quantized mag. field, multiphoton Stark effect *(Russian)* 78−72541
semiconductor in quantizing mag. field, plasma surface states of electrons 79−11195
semiconductor with nonparabolic bands, diamag. excitons, optical absorpt. in mag. field 77−55487
semiconductor with nonspherical bands, diamag. excitons and Franz-Keldysh effect 78−72554
semiconductors, hot electron maximum mobility in longitudinal quantising mag. fields 79−69519
semiconductors, hot electrons in longitudinal quantising mag. fields 80−39593
semiconductors, light induced electron drift, two-photon transitions *(Russian)* 80−107853

Landau levels continued
semiconductors, mixed, containing paramag. atoms, Landau levels and interband Faraday rot., appl. to $Cd_{1-x}Mn_xTe$ 79−61348
semiconductors, nondegenerate, free carrier absorpt. in quantising mag. fields 80−45044
semiconductors, two-dimensional, Mott exciton formation in high mag. fields *(Russian)* 80−65467
semiconductors, weakly polar, intraband magnetoabsorption theory 79−42949
semiconductors with neutral impurity, transverse cond. in quantising mag. fields, finite radius scatterers *(Russian)* 80−29400
semimetal, degenerate, conduction electron acoustic spin resonance, oscillations of absorbed power 80−108075
semimetal, longit. cond. in extremely strong mag. field 77−89779
semimetals, two-dimensional, electron-hole rearrangements in high mag. fields 79−87028
spin-splitting factor for Landau levels from de Haas-van Alphen effect first 3 harmonics 77−20226
superlattice, electronic band struct. in mag. fields 79−65355
two photon transitions to Landau levels, selection rules 77−69240
two-dimensional, Hartree-Fock soln. of CDW in mag. field 79−28302
two-dimensional electron impurity system, quantum theory of cyclotron reson. lineshape 78−64083
two-dimensional electron system in strong mag. field, Anderson localisation 77−15929
two-dimensional electron-impurity system, theories of cyclotron resonance lineshape 77−85573
two-dimensional quantum plasma in mag. field, exchange energy 77−72904
two-phonon transitions, phonon assisted, in mag. field, four-band model 77−36260
wave function for crystalline electrons in mag. field 78−51918
Wigner crystal, two-dimens., in strong mag. field, classical and quantum theory 78−79948
zinc-blende semiconductors, quantum resonances in valence bands under uniaxial stress 79−99480
Ag, surface Landau level resonances, effect of k_H-broadening 79−65533
Al, anisotropic Fermi vel., surface Landau level reson. 78−10333
Al, Fermi surface, scattering anisotropy of conduction electrons on dislocations *(Russian)* 78−60051
Au, conduction electron g-factor meas. 77−35859
Bi electron properties, carrier spectrum 78−84137
Bi, gas-liquid type transform. and sound attenuation in strong mag. fields, electron-hole correl. effects 80−88598
Bi, giant quantum attenuation anomalies of sound waves at high mag. field, temp. and freq. depend. 80−70587
Bi, giant quantum attenuation anomalies of sound waves at high mag. field, extra attenuation peaks 80−70588
Bi, Landau level spin splitting factor, US exam. 77−20281
Bi, magnetoacoustic attenuation peak at low temp. 79−91105
Bi, magnetoreflection spectra, reson. Landau level transitions 77−52096
Bi, quantum-EM excitations 80−88471
Bi, US attenuation in strong mag. fields, electron-hole correlation effects 80−11049
$Bi_{1-x}Sb_x$, reson. Landau level transitions, magnetorefl. 77−52096
$Bi_{1-x}Sb_x$, semicond. alloy, EM wave propag. in direction perpendicular to mag. field 79−60687
C, glassy and fibrous, density of states, magnetoresistance theory appl. 80−44620
$Cd_{1-x}Mn_xTe$, semimagnetic, exchange interactions between localised and delocalised electrons 80−97245
CdS(Se), magnetoreflectance spectra of anisotropic II-VI semiconds. by mag. field modulation 77−66519
$CdS(Se)_3$ excitons and Landau levels meas. by magneto-optical spectroscopy apparatus 77−34032
n-GaAs, heavily doped, test of cond. band edge random fluctuations by MCD 77−63438
n-GaAs, hot electron magnetophonon resonance, Fourier anal. 80−54718
n-GaAs, Landau level lifetimes for electrons 79−87112
n-GaAs, mechanism of cyclotron reson. induced cond. 78−43396
n-GaAs tunable far IR Landau emission with subnanosecond rise time 79−32015
$GaAs-Al_xGa_{1-x}As$, heterojunction and superlattice, magnetophonon reson., polaron mass 80−44715
$GaAs-Al_xGa_{1-x}As$ superlattice, mag. field induced dimensionality change 78−64381
GaSb, E_1 and $E_1+\Delta_1$ edges using electroreflectance, Franz-Keldysh oscills., high mag. fields 77−66518
GaSb, oscillatory magnetoabsorption and excitons 77−55777
Ge, electron-hole droplets, reson. scatt. of free carriers 78−2500
Ge, luminescence circular polarisation in mag. field, Landau levels paramag. splitting 77−32435
Ge, mag. field luminesc. lifetime, quantum oscills., phonon wind effects 80−93385
Ge, photocurrent oscillations in mag. field, intense excitation *(Russian)* 78−26915
He, liq., effect of short-wave surface excitations on damping in two-dimens. electron gas *(Russian)* 79−10995
He liq. surface, cyclotron reson. of two-dimens. electrons *(Russian)* 80−88374
^{4}He superfluid, phonon-roton excitation 80−107586
$Hg_{1-x}Cd_xSe$, (x=0 to 0.15), Shubnikov-de Haas oscillations, influence of level broadening 79−11155
HgCdTe, interband magnetoabsorption and band struct. 79−82959
$Hg_{0.77}Cd_{0.23}Te$, spin-flip, Raman laser,, quantum oscills. from n=0, 1, 2 Landau levels 77−79832
$Hg_{1-x}Cd_xTe$, semimetallic state, magneto-optical investig. of Landau levels and band parameters 77−63410
HgMnTe, interband magnetoabsorption and band struct. 79−82959
$Hg_{1-x}Mn_xTe$, energy levels at Γ-point in intense mag. fields, Shubnikov-de Haas effect meas. 80−24951
$Hg_{1-x}Mn_xTe$ mixed crystals, zero gap, effect of exchange on interband magneto-absorption 78−23443
$Hg_{1-x}Mn_xTe$, semimagnetic, exchange interactions between localised and delocalised electrons 80−97245
$Hg_{1-x}Mn_xTe$, semimetallic, giant spin splitting induced by exchange interactions 77−28150
HgSe, thermoelec. power, spin split quantum oscills. 77−11948
n-HgTe, far IR magnetoabsorption involving resonant acceptor states 79−69813
Landau levels continued
HgTe, gapless, nonlinear effects in transverse quantising mag. fields 77−69353
HgTe, gapless semicond., magnetophonon conc. oscills. *(Russian)* 77−11943
HgTe, mag. sub-band struct. under uniaxial stress 77−11883
HgTe, magnetooptical study of Γ_8 bands anisotropy 79−82984
HgTe, uniaxial stress effect on magneto-optical props. 77−59558
HgTe, uniaxially compressed, anomalous magnetoresist. and band crossing 79−65501
InAs surface accumulation layers, magneto-transconductance meas. 78−64137
InAs-GaSb superlattices, mag. field induced semimetal-semicond. transition 80−65656
p-InSb, deformed, photocurrent spectra obs. 78−19097
n-InSb, deformed, spectral oscills. of absorption in quantising mag. field 80−34486
InSb, doping depend. of high-field donor spectra 77−90175
n-InSb, electron recombination between Landau-levels 79−38096
n-InSb, electronic lifetime in N=1 Landau level, far IR cyclotron emission 79−61226
InSb film, threshold singularity on quantising mag. fields 78−87904
n-InSb, helicon wave propag., quantum mechanical features 79−42571
n- InSb, hot electron energy relax. in quantizing mag. fields 78−31259
p-InSb inversion layer, magnetotransport 78−64138
n-InSb, Landau emission spectra, influence of bakcground radiation 78−43935
InSb, Landau level struct., magneto-electroreflectance 80−25349
n-InSb, Landau-level-electron lifetimes, saturation meas. of magnetoabsorption 78−48150
n-InSb, magnetophonon effect in non parabolic band 79−37962
InSb, phonon assisted cyclotron resonance exact sol. of integral eqn. for Green's function 79−61227
InSb, pinning struct. of cyclotron-phonon reson., effect of nonequidistant Landau levels 77−11881
InSb, polar semicond., magnetophonon struct. for several occupied Landau levels 79−56250
n-InSb, spin polarisation, anisotropic size effect, effect on CESR signal 80−70743
n-InSb tunable far IR Landau emission with subnanosecond rise time 79−32015
InSb-Au Schottky barrier, photovoltaic spectra and magneto-optical transitions, Landau levels and excitons 77−47858
Li, first Landau spin parameter, transmission ESR obs. 77−20703
Pb, de Haas-van Alphen effect, spin-splitting factor for Landau levels 77−20226
$Pb_{0.82}Sn_{0.18}Te$, narrow band gap, relax. time for Shubnikov-de Haas effect 78−80006
$Pb_{1-x}Sn_xTe$, epitaxial layers, photolum. in mag. field 79−83033
PbTe epitaxial film, many valley semicond., band population effects, intraband magneto-optical props. 79−78007
p-PbTe, MIS struct. inversion layer sub-bands, IR magnetoreflectance obs. 80−44731
PbTe-Au Schottky barrier junctions, Landau level oscills. in tunnelling data 80−49945
Pd-Ni, dil., Zeeman splitting of cond. electrons 77−11884
Si, (100) surface space-charge layer, intersubband cyclotron combined resonances 79−69571
n-Si channel ⟨100⟩ inversion layer MOSFET, valley splitting, conductivity 80−70840
Si inversion layer, cyclotron resonance in extreme quantum limit, collective ground state 80−50191
p-Si, inversion layer, screening effect and quantum transport in strong mag. fields 78−19155
Si, inversion layer, voltage tunable far IR emission 80−25018
Si inversion layers, cyclotron and subband emission 78−64128
n-Si inversion layers, electronic g-factor, spin-split Landau levels 80−80346
Si inversion layers, magnetocond. in ground Landau level, defect diffusion in Wigner cryst. 77−39914
Si, inversion layers, magnetic localisation of electrons 78−43481
n-Si MOS inversion layers, Hall cond. meas. 80−39676
Si n-channel ⟨100⟩ MOSFETS, Shubnikov-de Haas oscills. on mag. fields up to 35 T 79−91154
Si, surface space charge layer, electron subbands, mag. field effect 77−20393
TlBr, resonant polaron coupling and excitons under mag. field 80−71383
V_3Si, CDW instability and anharmonicity 78−79734
ZnS, two-photon absorpt. in crossed elec. and mag. fields 77−85693
p-ZnTe 79−43028

Lande g-factor *see g-factor*

Lande splitting factor *see g-factor*

landing fields *see airports*

Langmuir films
acetate, aq. soln. current-potential curve, influence of NO_3^-, SO_4^{2-}, PO_4^{3-} and Cl^-, obs. *(Japanese)* 78−85172
anisotropic optical waveguides based on Langmuir organic films 80−64177
anthracene, lightly substituted, AC and DC cond. 80−80425
anthracene derivative, Langmuir-Blodgett multilayer film, semiconducting props., optical and elec. meas. 80−11122
anthracene derivatives, Langmuir-Blodgett built-up multilayer, prep. and characterisation 79−95293
anthracene Langmuir film, lightly substituted, electrolum., photolum. and electroabsorption 80−20726
barium stearate single-layer Langmuir films, elastic and inelastic tunnelling 80−80403
built-up, static dielectric const. thickness depend. 77−12297
cadmium arachidate mixed with cyanine dyes, mol. layers, photoelec. props. 80−80401
cadmium arachidate monolayer, Ag(Au) substrate, reson. surface plasmon reflection 78−56536
cadmium arachidate monolayer on Au, surface plasma reson., optical consts. 77−90210
cadmium arachidate monolayer transfer from air-water interface to solid, contact angles 77−55424
cadmium behenate in Langmuir multilayer assembly system, single layer conductance 79−51701
cadmium stearate, multilayer Langmuir films, DC cond., $T^{-1/2}$ law 77−12022

Langmuir films continued
cadmium stearate based, deposition on p-CdTe, charcts. and MIS struct. 80−92998
cadmium stearate monolayer in CC CdTe/Langmuir film photovoltaic structures for solar cells 80−49918
carboxylate, aq. soln. current-potential curve, influence of NO_3^- and SO_4^{2-}, obs. *(Japanese)* 78−85173
chlorophyll a, Langmuir-Blodgett films, deposition onto SnO_2 optically transparent electrode 80−80093
chromophore phospholipid Langmuir films, photoeffects 80−80409
deposition, dipping and raising device, new design 77−24954
diacetylene monocarboxylic acids, multilayers, struct. phase transitions and polymerisability 80−80129
dielectric relaxation, dark and photo-stimulated relaxation similarity 78−92021
dye monolayer coating Ag film, anomalous dispersion of surface plasma oscills. 79−8203
dye-sensitized, anisotropic photocond. 80−80327
electrical and photoelec. transport props. of Langmuir-Blodgett films, device appl. 80−80431
esters, long-chain, X- and Y-type multilayers, form. conditions and struct. characterisation 80−80127
fatty acid, AC and DC cond. 78−56239
graded refractive index optical fibre process 79−76836
integrated optics applications 77−75711
lead stearate, Langmuir-Blodgett multilayers, comp. and transfer mechanism 80−80125
lightguiding in Langmuir-Blodgett films 80−79006
manganese stearate: cadmium stearate, dil. quasi two-dimensional, ESR line width 80−71155
manganese stearate, Langmuir-Blodgett layers, high resolution X-ray diffr. 80−80126
manganese stearate, literally two-dimensional magnet, mag. ordering, EPR 79−28597
manganese stearate, two-dimensional mag. struct. 80−108040
manganese stearate Langmuir-Blodgett layers on Ag, IR surface EM wave prism spectroscopy 78−52587
manganese stearate Langmuir-Blodgett type multilayers, periodic and near-periodic, small-angle interferences of reflected X-rays 79−94846
metal-barium stearate-metal structs., internal voltage work function meas. 79−82684
MIS structure, InP surface state distrib. obs. 77−89859
monolayer, phase separation without gravity effects *(French)* 80−54534
monolayer to multilayer, Langmuir-Blodgett 80−80031
monomolecular and multimolecular built-up film, present status and future potential 78−71906
monomolecular layers, Langmuir-Blodgett, mol. orientation determ. by IR absorpt. 79−11423
multilayer, structure-dependent carrier transport obs. *(Japanese)* 80−20339
multilayer assembly Langmuir film structure, X-ray diffr. results 77−39740
multilayer films with and without dye-sensitisers, elec. props. 80−97006
optical anisotropic waveguide for integrated optics, monomolecular layered film 78−66954
optical waveguide mode selection using organic Langmuir films 79−98495
PMMA-spiropyran Langmuir monolayers, reversible photochemical strain 80−50867
Raman spectra of very thin Langmuir-Blodgett films 80−31911
refractive indices and mol. lengths meas. by optical waveguide probe 77−40294
sodium stearate, Langmuir-Blodgett multilayers, comp. and transfer mechanism 80−80125
stearic acid layers, charge transport processes 78−84316
stearic acid multilayer films, dark and photo-generated dielec. response 77−72882
stearic acid multilayer films, lattice and carrier contribs. to dielec. polarisation 77−69775
stearic acid-based, layer periodic structure, prep. and optical props. 77−69199
stearic acid-calcium stearate monomolecular films, multilayer deposition 80−54550
surface balance, monolayer parameters meas. in radiation field 78−82092
tetramethylsiloxane dicarbonxylic acid Langmuir films on Cu surface, surface EM wave absorpt. study 80−97359
thickness step gauge, Ba stearate multilayer films on EDF glass, interference colours 77−5900
vinyl stearate multilayers, struct. determ. by electron diffraction 79−4469
Cd salts of pure and mixed fatty acids mixed assemblies, prep. and structure *(Japanese)* 78−6232
CdTe-Langmuir film MIS structures 79−65551
Cu surfaces, with Langmuir films, surface EM wave absorpt. using CO_2 laser excitation 80−97365
In, oxidised surface, bonding of Cd arachidate monolayers, XPS 79−15011
InP substrate for Langmuir film growth, surface chemistry, ESCA study 80−103552
p-type InP/Langmuir film MIS diodes, charcts. 80−80384
Rh, oxidised surface, bonding of Cd arachidate monolayers, XPS 79−15011
Si, oxidised surface, bonding of cadmium arachidate monolayers XPS 79−15011
Sn, oxidised surface, bonding of cadmium arachidate monolayers, XPS 79−15011

Langmuir probes
see also plasma diagnostics
absolute wave amplitude determ., Langmuir probe RF coupling 78−75425
afterglow, electron energy distrib. meas., Langmuir probe characteristics 77−80350
antenna characteristics, in low-freq. ion-acoustic wave expts. 78−42819
arc, ion density, voltage drop, heat conduction by neutrals 77−4012
automatic recording system of probe meas. for plasma parameters *(Japanese)* 79−41870
characteristics at low plasma densities, numerical analysis 78−63592
control system for maintaining probe at plasma potential 78−5943

Langmuir probes continued
cylindrical, orbital-limited conditions, collisional plasma charge density diagnostics 79−50888
double modulation probe, current ratio optimisation 79−48576
electron distrib., Langmuir probe effect on meas. 78−83609
electron energy determ. using analogue computer and Langmuir probe 78−14212
electron temp. meas., continuous, automatic, using double Langmuir probe 80−43977
finite-β collisional plasma, temp. fluctuations and wave induced losses with draft-Alfven instability 77−3934
floating double probe, electronic circuit for pulsed plasma diagnostics 77−62403
flow velocity measurement, in flame or collision dominated plasma 79−46475
fluctuations, LF, diagnostics by probes and optical line radiation 79−64905
flush probe studies of plasma flow over flat plate 80−24147
frequency depend. in Hg vapour plasma under HF voltage *(Russian)* 77−11407
HF discharge, plasma density and electron temp. meas. using Langmuir probe *(Russian)* 79−37559
high pressure plasmas, use of Langmuir probes, review 77−3982
hollow cathode arc, Langmuir probe meas. for discharge model 78−87533
hollow cathode arc with reduced gas flow, operation mode 80−38783
hollow current profile form. in Tokamak LT-3 77−72500
inflection-point method of interpreting emissive probe characteristics 79−37550
ion acoustic waves method of plasma potential meas. 80−59289
ion beam diagnostics by means of electron saturated plane Langmuir probe 79−94144
ion temperature of low density plasmas by two-probe method 78−55749
ion-acoustic wave excitation with probes 77−68780
ionosphere, electron densities and temps. from Intercosmos-10 Langmuir probe expts. *(German)* 79−2469
ionospheric D-region, electron density and energy distrib., meas., modulation technique 77−82078
ionospheric electron temperature, cylindrical Langmuir probe technique 79−2379
ionospheric rocket expt. high-power electron gun *(Japanese)* 78−61566
ionospheric structure studies by space vehicle obs. 79−53540
laser plasma, Langmuir probe meas. of parameters and expsn. 78−18456
leakage velocity through low-β line cusp meas. 77−35380
magnetic field affecting characteristics, for teachers 79−21502
magnetosheath effects on cylindrical Langmuir probes 80−28820
magnetosphere, lower, electron densities and temps. from Intercosmos-10 Langmuir probe expts. *(German)* 79−2469
microwave discharge, electron energy distrib. 77−47293
multidipole plasma, probable errors assoc. with minicomputer anal. of Langmuir probe charcts. 77−24193
plasma perturbation, by probe stem 77−35388
pulsed DC discharge afterglow, electron conc. and temp., double-probe technique 78−63632
reaction energy anal. using pulsed plasma diagnostics with Langmuir probes 77−89308
RF sputtering system, Langmuir probe study of glow discharge at various freqs. 80−55294
spherical and cylindrical drift probes, in collisionless plasma, comparative study 80−6286
sputtering, plasma charcts. by Langmuir probe technique 80−80929
student experiments on elec. cond. and similarity laws 78−24605
temperature measurement in flame plasma 77−24181
Tokamak, large magnetic field ripples, electric probe meas. 80−83976
Tokamak, TM-3, near wall region, Langmuir probe obs. *(Russian)* 77−47261
torus plasma, fluctuation induced particle transport, strong DC elec. and mag. fields 77−89322
transitional charcts., effect of ion distrib. and electron relaxation *(Russian)* 79−7486
Ar plasma boundary layer, ion number density and electron temp. meas. *(Japanese)* 78−5933
Ar plasma density meas. by Langmuir probe and microwave interferometer 80−28819
H^- surface ion source, plasma parameters, diagnostics 78−9849
N_2, electron beam produced, plasma, energy distribution of electrons 77−3959

language translation
measurement technical term translation problems *(German)* 80−36965

languages, formal *see formal languages*

lanthanides *see rare earth metals*

lanthanons *see rare earth metals*

lanthanum
see also nuclei with .....
abundance in HD 18474 giant star *(Spanish)* 79−25605
addition to Cr-Mo and Ni-Cr-Mo-V low-alloy steels, remedy for temper brittleness 80−66659
addition to Ni-Cr austenitic stainless steel, effect on heat resist. and comp. of non-metallic inclusions 80−76315
adsorbed atoms on W (112), strongly anisotropic interaction *(Russian)* 77−11798
adsorbed monolayer on W (112) face, LEED and contact pot. difference meas. *(Russian)* 77−1316
adsorbed on 4d or 5d metal, work function, O_2 coadsorpt. effects, thermionic emission obs. 78−11064
adsorption on W, specific charcts. *(Russian)* 79−1543
adsorption on W, with B, field emission meas. 78−47662
adsorption on W (100), depend. of work function, heat of adsorpt. on surface coverage, contact potential study 78−67912
adsorption on W (112) face, coating growth and struct. obs. *(Russian)* 78−14618
adsorption on W and Mo (011) face, influence of substrate electronic struct. on props. 78−60032
adsorption with O on W, work function changes *(Russian)* 77−35816
atom, 4d subshell spectra, strong interaction regime 79−18165
atom, arc spectrography, applic. of equidensitometry *(German)* 77−1962
atom, coexistence of 'collapse' and 'blow' states 80−32587
atom, intense 4d-f resons., cross-sections, spectra, calcs. 79−31426

lanthanum continued
atom, ionisation cross sections for L_1 and L_2 subshells by 250-500 keV protons *(Russian)* 77−6918
atom, Kβ/Kα rel. intensity obs. 80−32665
atom, La I, lifetimes of $z^2F_{5/2}$, $z^2D_{3/2}$, $z^4G_{5/2}$ and $y^2D_{3/2}$ states 78−66489
atom, laser at. beam spectrum, HFS resolution at 5930.6 Å 78−9110
atom, photon-bound-electron scatt. meas. 77−14394
atom, term dependence of position of 4f electron in $4d^94f$ configuration 77−26973
atom on transition metal, surface, intermediate valence state 79−69367
bremsstrahlung resonances and APS near 3d threshold 77−69937
buffer action, in at. absorpt. spectrosc. of alkaline earths, mechanism *(Russian)* 79−29441
coadsorption with B on W, field emission and field ion microscopy 80−104049
crystal structure rel. to d-band occupancy 77−35510
density functional theory 80−15442
determination, in Ta-Re-Y-La alloy, spectrochem. method 79−16076
determination by X-ray fluorescence 78−61127
electrical resistivity, 5-300K, α and β phases 78−10417
electron and positron multiple scatt. 80−15171
electron impact excited soft X-ray spectra, resonances and many body effects 80−50468
electronic structure, 4f band *(German)* 77−55479
electronic structure vol. depend., rigorous cellular method 77−20233
electrotransport of C, N_2 and O_2 80−24674
FCC, band struct., linear APW method 79−51467
FCC, ground-state props. 78−75989
film, superconducting, tunnelling investig., multiple band effects 77−8244
ground state properties of f band metals 78−91607
heat capacity and supercond. props. 80−65247
horizontally dipped LPE film, inhomogeneities, spin wave reson. meas. 79−91298
Hubbard model, two band, almost mixed valence system, new ground state 78−84171
liquid, resist. and thermoelec. power, t-matrix calc. 78−26840
liquid, solubility of Am, heat of mixing, 1200-1600K 80−15232
liquid, struct., neutron diffr. meas. 77−51305
liquid, trivalent, electrical resist. 79−42514
liquid, viscosity from 940 to 1220°C *(German)* 79−28123
liquids, optimised cluster expansion, struct. function evaluation 80−49085
low temperature P-T diagram 77−47550
lunar drill sample, neutron activation and radiochemical anal. *(German)* 80−51673
mode softening and lattice instability under press. 77−51833
NMR 4.2 to 296K, mag. susceptibility and sp. ht. 80−15813
normal spectral emittance above 1000K 77−28028
particles, supercond. props. *(Russian)* 80−7018
phonon density of states, in DHCP and FCC phases 78−67791
preparation on chelate ion exchangers 79−61538
quasimol. KX-ray spectra, Doppler shift 77−19044
soft phonons, f-band induced instability 78−83907
submonolayer film, on W (011) or Mo (011), disordering, LEED obs. *(Russian)* 77−89655
superconducting, electron-phonon coupling, hydrostatic press. depend. 78−80087
superconducting film, A1-type quench-condensed, prep. and crit. temp. 77−69443
superconducting transition temp., press. depend., mode softening 78−14847
surface and volume props., flow props., surface layer thickness *(Russian)* 80−59760
SXAPS from 0 to 1400 eV 77−4703
thin layer chromatography 78−20105
X-ray emission spectra *(Russian)* 77−77322
X-ray L emission spectrum, diagram lines obs. 77−6715
X-ray reson. emission, appearance pot. and charact. electron energy loss spectra 80−16126
XPS valence band spectra meas. 77−48306
α-induced X-ray anal. of Y, La, Ce, Nd content of apatite minerals 79−16084
$BaF_2:La^{3+}$, nuclear spin relax. orientation depend., point defect self-diffusion mechanism 77−48078
$BaF_2:La^{3+}$, phonon reson. and IR absorpt. 80−84752
$BaF_2:La^{3+}$, relaxation processes, studies by ionic-thermocurrent techniques 79−69769
$BaF_2:La^{3+}$, thermal depolarisation of La^{3+}-F_i^- defect dipoles 80−75926
$BaF_2:La^{3+}$ ionic conductivity meas., computer analysis, point defect parameters 80−54429
$Ba_{0.54}Sr_{0.46}Nb_2O_6$:La, dielectric and electrooptic props. 78−68466
$BaTiO_3$:La and undoped, defect chemistry elec. cond. at high temp. meas. 77−39858
$^{140}Ba/^{140}La$ radio-nuclide generator, separation methods *(German)* 77−25298
$CaF_2:La$, dielec. relax. spectrum, ion size trends 78−72460
$CaF_2:La^{3+}$, thermal depolarisation of La^{3+}-F_i^- defect dipoles 80−75926
$(Ce_xLa_{1-x})_2Mg_3(NO_3)_{12}.24H_2O$, adiabatic demagnetisation temp., mag. entropy *(Russian)* 80−65892
EuO:La, metallic, photothreshold, correl. and exchange energy of electron gas 77−62852
EuO:La, photoelectron spin polarisation, temp. depend. 77−69966
EuO:La, photothreshold reduction by mag. induced space charge layer 78−72692
EuO:La, photothreshold changes below mag. ordering temp. 80−97406
$GdAlO_3$:La, antiferromag., random-field crit. and multicritical behaviour 80−65939
$GdAlO_3$:La, random antiferromagnets, crit. and multicritical props. 80−60332
H, and He, stopping powers meas. 80−42904
La I, extension of even energy level system 77−3285
La II, $y^3F_{4,3,2}^0$ levels, lifetime meas. using beam-laser method 77−30827
La IV, spectrum and energy levels 79−72261
La XI, UV spectra, 60-600 Å reson. lines 78−33455
La^+, cascade free lifetime meas., beam-laser method 78−17618
La^{2+}, XPS in oxide and chromite, multicomponent struct. of 4d orbital 78−74620
La^{3+}, 3d photoabsorpt. spectra, continuum and discrete states 79−81176

lanthanum continued
La^{3+} $3d^94f$ config., collapse of 4f electron, X-ray spectra obs. *(Russian)* 80−58204
$La:Eu^{2+}$, liquid, γ-ray spectra observation of exchange interaction 80−84672
$^{138}La/^{139}La$ nuclear electric quadrupole moment ratio, laser RF double reson. obs. 80−23447
$La\text{-}F_2(ClF)(Cl_2)(SF_6)$, visible chem. laser development from reactions yielding visible chemilum. 78−63111
$La+H_2O(D_2O)$(alcohols), O atom abstraction, product internal state distrib., fluoresc. study 78−48643
$La_{1-x}Ce_xAl_2$, supercond., nucl. relax. and impurity magnetism 77−20495
$LaNi_{5-y}Al_y$ alloys and related hydrides, thermodynamic and struct. props. for H_2 storage appl. 80−16847
$LaNi_{1-x}Co_yO_3$, UPS, XPS, X-ray absorpt. spectra, band struct. study 79−56885
^{139}La, hyperfine struct. of excited odd-parity levels, laser at. beam fluoresc. obs. 79−13663
^{139}La II $5d^2\ ^3F_4 \rightarrow 5d4f\ ^3F_4^0$, hyperfine structure, $\Delta F = \pm 2$ transitions, three-quantum process 80−63848
$O_2+La(Y)(Sc)$, crossed beam chemiluminescence reaction, spectral simulation, hyperthermal energy meas. 78−80732
$Pb_{0.8}Sn_{0.2}Te$:La, evaporated thin films, low carrier conc. 80−65414
Pb(Zr,Ti)O_3:La, electro-optical ferroelec. ceramic, secondary electron emission yield 79−91546
$Sr_{0.5}Ba_{0.5}Nb_2O_6$:La, ceramic, additive effect on ferroelec. and pyroelec. props. 77−16256
SrF_2:La, type-I dipole reorientation, activation vol. determ. from dielec. const. 80−88916
$SrF_2:La^{3+}$, thermal depolarisation of La^{3+}-F_i^- defect dipoles 80−75926
W:La, B coadsorption and work function, FEM and FIM obs. 79−52087
YIG, epitaxial, temp. stabilisation of ferrimag. reson. field by Ga, La substitution 77−77104
YIG:La,Ga, film, LPE-grown, Ga incorporation, depend. of magnetisation on growth rate 80−84627
YIG:La,Ga film, uniaxial anisotropy, variation along growth direction 77−28416
YIG:La film, for microwave applics., growth and ferromag. reson. meas. 78−3008
ZnO:La, electrolum. brightness, field strength and freq. depend. 80−100696
ZnO:La phosphor, electrolum. brightness waves, −168 to +85°C 78−52580

lanthanum alloys
see also lanthanum compounds
binary alloys, use as tritium extractors from breeder blankets 79−67946
$La_{1-x}Gd_xRu_2$, mag. ordered superconductor, re-entrant superconductivity 78−88059
LaAg, exchange coulombic contrib. of cond. electrons to cryst. elec. field 79−95376
Magnico alloy, with Si, Nb, Ti and La, low-temp. thermomag. treatment 77−63812
Mischmetal-Mg alloy, hydrogen storage materials *(French)* 79−66419
Mischmetal-Ni alloy, H_2 adsorption and desorption *(Japanese)* 77−47668
pnictides, superconducting props. 77−85366
steel, austenitic, Cr-Ni-La(Na,Pr,Ce), nonmetallic inclusions modification using rare earth metals *(Russian)* 80−40369
steel, low alloy, Mn-P, temper brittleness, rare earth mischmetal effect *(Chinese)* 80−104249
thermoelectric materials, B_4C_x and $(B,Si)_4C_x$ P-type LaS_x N-type alloys, fabrication and thermoelectric props. 80−107771
transition metal intermetallics, LaM_5H_4 and LaM_5H_6, H_2 storage appl., desorption isotherms dependence on d-bandfilling 78−18912
transition metal intermetallics ESR of Nd^{3+} and Gd^{3+} 79−87315
Al-La, thermodynamic interaction in liquid phase *(Russian)* 78−44080
$Al_2La_xCe_{1-x}$, low temp. mag. props. 80−20564
(Ce,La)Al_2, collective phenomena 80−65933
(Ce, La)Al_3, near stabilisation of Ce moment upon dilution 79−91209
(Ce, La)In_3, heat capacity and elec. resist. 80−71049
Ce-La, DHCP, low temp. mag. and elec. props. 77−62911
Ce-La, mag. ordering, sp. ht., susceptibility and resist. 78−68238
Ce-Le H_2 charging effect on nodularizing efficiency of Ce-La additions to cast Fe 78−27544
$Ce_{1-x}La_x$ alloy, thermoelectric power 79−78080
$Ce_{1-x}La_x$, dil., γ−α transition temp. and press., elec. resist. meas. up to 10 kbar 80−59643
$Ce_{1-x}La_x$, electrical resist. T^2-depend. under high press. 80−29383
$Ce_{1-x}La_x$, thermoelectric power, mag. transition temps. 80−20154
$Ce_{0.99}La_{0.01}Al_3$, effect of disorder on cond. transition into ground state 77−89755
$Ce_{1-x}La_xAl_2$, extraordinary Hall effects, 4.2-300K, cryst. field interaction 78−79980
$(Ce_xLa_{1-x})Al_2$, inelastic neutron scatt. cross-section, effect of cryst. field 79−65642
$Ce_xLa_{1-x}Al_3$, Kondo system, mag. susceptibility, 1.5 to 20K 79−78310
$(Ce_xLa_{1-x})Be_{13}$, mag. intermediate valence behaviour 79−24131
$Ce_{1-x}La_xSn_3$ (x=0 to 1), mag. susceptibility and magnetisation, lattice parameters, X-ray and neutron diffr. meas. 80−49675
$Ce_{0.9-x}La_xTh_{0.1}$, mixed valence state, static and dynamic mag. response 80−103816
$Ce_x(La_yY_{1-y})_{1-x}Al_2$, local mag. moments, neutron scatt. study 79−61058
$Ce_x(La_{0.76}Y_{0.24})_{1-x}Bi$, mag. phase diagrams 79−56535
$Ce_x(La_{0.76}Y_{0.24})_{1-x}Sb$, mag. phase diagrams, exchange interaction variation-thermodynamic model 79−65673
Co-mischmetall system, phase relations, microstruct., mag. props. 80−104118
Cr-La, cast, B additions effect on struct. and props. *(Russian)* 78−19891
Cr-La-V-Nb-Ta, La, V, Nb Ta effect on hardness and strength *(Russian)* 79−34050
Cr-M, optimum alloying with rare earth metals, Ti, Zr, Hf, Nb, Ta 78−68651
Cu-Ge-La, Cu+Misch metal, eutectic alloy, internally oxidised, mech props. *(Japanese)* 77−52411
Cu_xLa_{1-x}, splat-cooled, phase diagram and supercond. props. 80−70881
$Dy_{0.9}La_{0.1}Al_2$, hyperfine field, NMR spectra 80−15811
Er-La, HCP, mag. phase diagram, neutron diffr. meas. 80−70950
$Er_xLa_{1-x}Be_{13}$, ESR studies 80−108064

lanthanum alloys continued
$Er_xLa_{1-x}Be_{13}$, mag. sp. ht. and ESR, cryst. field interactions 80−60290
$Er_xLa_{1-x}Cu$, antiferromagnetic, mag. and resist. behaviour 80−34412
$Eu_xLa_{1-x}Al_2$, binding energy and workfunction charges using XPES 80−33928
$Eu_xLa_{1-x}Al_2$, cryst. fields and exchange parameters, ESR meas. 80−71175
$Eu_xLa_{1-x}Al_2$, dil. EPR, cryst. fields and effective exchange interaction 80−66029
$Eu_{0.25}La_{0.75}Rh_2$, high press. Mossbauer spectra, interconfig. charge fluctuations 77−63341
$Eu_{1-x}La_xS$, electron struct., lattice consts., X-ray spectral study *(Russian)* 80−100432
Fe, cast, La effect on graphite nodularisation *(Japanese)* 77−55999
Fe-Cr (20 wt.%) high temp. oxidation behaviour with small La additions (0 to 1.3 wt.%) *(Japanese)* 78−85039
Fe-Cr-La-Al, La or Y with Al addition effect on high-temp. oxidation 79−100302
Fe-La, Fe-rich alloys, mag. props. for bulk amorphous deposits *(Japanese)* 79−95971
Fe-La amorphous films, mag. props., Mossbauer effect and magnetisation meas. 79−69701
Ga-La, energy band struct. and atomic radius 79−73434
Gd-La, Curie temp. and saturated mag. moment, nonmag. solute effects 78−39301
Gd-La, magneto-optic reson. *(Russian)* 79−47426
Gd-La alloy, optical freq. cond. in 0.5-3.1 eV range, paramag.-ferromag. transition 80−29761
$Gd_xCe_yLa_{1-x-y}Be_{13}$, high electron lattice relax., Gd EPR meas. 78−2736
$Gd_{0.9}La_{0.1}Al_2$, ferromag., NMR of ^{139}La 78−52377
$Gd_xLa_{1-x}Al_2$ ($x<0.05$), Hall effect measurements 80−44569
$Gd_xLa_{1-x}Al_2$, cryst. fields and exchange parameters, ESR meas. 80−71175
$Gd_xLa_{1-x}Be_{13}$, $0.001\leq x\leq 1$, EPR, indirect exchange, bottleneck effect 77−16171
$Gd_{0.9}La_{0.1}Ni_2$, Ni contrib. to ordering, ^{139}La NMR spin echo 77−63317
$Gd_{0.1}La_{0.9}Ni_5H_x$, $Gd_{0.1}La_{0.9}Co_5H_x$, ^{155}Gd Mossbauer spectra 77−63340
$Gd_xLa_{1-x}Pd_3$, EPR of Gd, g-factor and thermal broadening, temp. and comp. depend. 77−48048
$Gd_{1-x}La_xPt_2$, Laves phase alloy, NMR, nonstoichiometry 77−63298
$Gd_{1-x}La_xRh_2$, NMR, contribution of Gd neighbours to Gd hyperfine field 77−8423
$Gd_xLa_{1-x}Zn$, magnetisation and paramag. suscept. 78−88101
Ho-La, HCP, mag. phase diagram, neutron diffr. meas. 80−70950
$(La,Ce)Al_2$, conf. Kondo system, sp. ht. meas. 78−52210
$(La,Ce)Al_2$, magnetic impurity effect on thermal cond., normal and supercond. states 77−63027
$(La,Ce)B_6$ dil. alloy, Kondo effect, impurity-impurity interaction, mag. susceptibility, mag. to non mag. transition 78−47948
$(La,Ce)Ru_2$, supercond. transition temp., its press. depend., and structural phase transform. 78−6473
$(La,Ce)Sn_3$, dil. alloys, supercond. and normal state props. 78−76184
$(La,Er)Al_2$, cryst. field parameters, inelastic neutron scatt. study 79−23937
$(La,Gd)Al_2$, dil. alloy, magnetoresistivity determ. 79−73495
$(La,Gd)Al_2$, mag. props. 78−52299
$(La,Gd)Al_2$, magnetic impurity effect on thermal cond., normal and supercond. states 77−63027
$(La,Gd)Al_2$, normal and supercond. state, US attenuation, freq. depend. and mechanisms 80−49992
$(La,Gd)Al_2$, reverse Kondo alloy, transport props. at finite mag. field 80−6812
$(La,Gd)Al_2$, spin glass, cluster glass and magnetisation characts. for different comps. 77−69585
$(La,Gd)Al_2$ spin glass, suscept. and sp. ht., mag. field depend. 79−61173
$(La,Gd)Al_2$, spin glass materials, mag. field dependence of susceptibility peak 80−103840
$(La,Gd)Al_2$ spin glasses, reversible and irreversible mag. susceptibility 80−15738
$(La,Gd)Al_2$ spin glasses, time depend. mag. props. 80−65909
$(La,Gd)Al_2$, very dil., resist. 79−23958
$(La,Gd)B_6$, dil. alloy, spin glass behaviour, 4.2 to 200K AC mag. susceptibility, RKKY calcs. 78−47994
(La,Na)Sn alloys, supercond. transition temp. 79−78254
$(La,Nd)Sn_3$, cryst. field effects, normal and supercond. props. 79−60973
$(La,Nd)Sn_3$, reverse Kondo effect in presence of crystalline elec. field splitting 80−103684
$(La,Nd)Sn_3$, superconducting props. 79−60958
(La,Th)-Ce, dilute alloys, mag.-nonmag. transition of impurity moments, environment effects 77−40034
(La,Y)Ce, dil., Kondo supercond., transition temp., susceptibility and resist. 80−65733
La-Ag alloys, amorphous, elec. resist. and supercond. 80−70885
La-Al, XPS valence band spectra meas. 77−48306
La-Al amorphous alloys, internal friction, relaxation process 80−92607
La-Al(Ge)(Au), amorphous, alloying effect on supercond. props. 79−60951
La-Au, splat-quenched, Mossbauer effect and elec. resist., amorphous struct. 80−84676
La-Au liq.-quenched alloys, Mossbauer spectra, struct. 80−15841
La-B, amorphous, B-rich, low freq. modes, Raman scatt. obs. 80−108202
La-B, phase and thermodynamic props., vaporisation 78−51660
La-Bi, phase diagram, struct. of intermetallic compounds 77−44214
La-Ce, dil., cryst. fields and Kondo effect 77−43809
La-Ce, Kondo system, intermediate temp. supercond. under hydrostatic press. 79−24097
La-Ce alloy, press. induced spin glass to Kondo phase transition, resist. meas. 79−24174
La-Ce-Al_2, dilute alloy, cryst. fields and Kondo effect 77−43809
La-Co-H, catalytic props. in hydrogenation of propylene, dehydrogenation of propane 80−30277
La-Cu alloys, cryst. struct. exam. 77−58978
La-Dy, elec. resist. temp. depend. 78−2462
La-Er, superconducting, EPR for localised Er mag. moments *(Russian)* 77−47931
La-Eu, dil., DHCP, impurity effects on supercond. T_c, electron pair breaking 77−36013
lanthanum alloys continued
La-Eu, EPR investig. of local moment, correl. with supercond. props. 77−63282
La-Fe, amorphous alloy film, spin reson. meas. 78−68389
La-Fe, FCC, Mossbauer spectra, Fe atom position 80−20549
La-Fe, liquid quenched, X-ray diffr. and Mossbaeur effect exam. of structure 78−76678
La-Fe alloy, amorphous, sputtered at high rate, mag. props. 80−75753
La-Fe amorphous alloy film, mag. props. 77−16121
La-Fe bulk amorphous alloys, mag. props. *(Japanese)* 79−95588
La-Gd, dil., DHCP, impurity effects on supercond. T_c, electron pair breaking 77−36013
La-Gd, EPR investig. of local moment, correl. with supercond. props. 77−63282
La-Gd, exchange-coupled localised moments, Korringa relaxation rate 80−75851
La-Gd (8 at.%), FCC, under hydrostatic pressure, resistivity meas., comparison with positive-J spin glasses 80−59958
La-Gd-An, amorphous, high Gd content, bulk mag. props. 77−59426
La-Gd-Au, amorphous, mag. field depend. of resist. minima 77−59275
La-Gd-Au, amorphous spin glasses, mag.-cluster description 79−42776
La-Gd(Tb,Dy,Ho,Er,Tm) alloys, FCC, supercond. transition temp. 79−4614
La-In, heat of formation meas. using differential direct isoperibol calorimeter 77−21101
La-In alloys, cohesive and superconducting props. from electronic struct. calcs. 79−99113
La-Ni, D_2 absorption, 500-700°C 79−23736
La-Ni, hydriding characts., applicability for H_2 storage material 78−83955
La-Ni-H, catalytic props. in hydrogenation of propylene, dehydrogenation of propane 80−30277
La-P-Ce, dilute, NMR investig. of anisotropic cond. electron exchange 77−63309
La-Pr, superconductive tunnelling, cryst. field effects 78−88085
La-rare earth metal/AlO_x/Al tunnel junctions, cond. meas., cryst. field effects 80−88694
La-Re-B, annealed and quenched, X-ray structural and phase anal. 78−11207
La-Sb, heat of formation for various phases, 300K 79−91988
La-Sm-Au, amorphous, surface effects on Sm valence, XPS and X-ray absorption meas. 80−108325
La-Sm-Sn, dil. alloy, Kondo effect obs., supercond. transition temp. meas. 77−51837
$La_{1-x}Ca_xNi_5$, H_2 sorption props. 78−91533
$La_{1-x}Pr_xSn_3$, Kondo effect from excited cryst. field levels, elec. resist. 78−14723
LaAg, band calcs., rel. to mag. and electronic props. and martensitic transform. 77−8014
LaAg, direct Coulomb contrib. of cond. electrons to crystalline elec. field 77−76784
LaAg, direct coulombic contrib. of cond. electrons to cryst. elec. field 79−91005
LaAg, electronic struct., susceptibility, sp. ht. and Knight shift meas. 77−43485
LaAg, electronic struct., NMR relax. times meas. 79−51871
LaAg, press. depend. of martensitic and supercond. transition temp. 79−19681
LaAg, Tb and Pr substituted, superconductors, cryst. field transitions linewidths 80−24854
LaAg, under hydrostatic press., supercond. and phase transform, elec. resist., 1-300K 78−10595
$LaAg_xIn_{1-x}$, crystal struct., neutron diffr. obs. 80−49187
$LaAg_xIn_{1-x}$, phonon dispersion, elastic consts. and struct. instability, soft mode behaviour 80−103436
$LaAg_xIn_{1-x}$, structural instability 78−79562
$LaAg_2Si_2$, ^{29}Si NMR and mag. susceptibility 79−61246
$LaAl_2$, calc. of energy band-structure and Fermi surface by APW method 80−70590
$LaAl_2$, cryst. field splitting and spin-spin interaction of Eu^{2+} and Gd^{3+}, ESR meas. 78−68370
$LaAl_2$, de Haas-van Alphen effect, Fermi surface 80−15436
$LaAl_2$, doped with Tb, Nd, or Pr, crystal field effects, tunnelling within mK range 80−70907
$LaAl_2$, electronic struct., APW method and local-spin-density approx. 80−65434
$LaAl_2$, inelastic neutron scatt. 80−11165
$LaAl_2$, magnetoresist. and de Haas-van Alphen effect, Fermi surface model 79−15069
$LaAl_2$, rare earth ion impurities, mag. moments 78−6515
$LaAl_2$, supercond. and normal states, anomalous US attenuation and velocity-change 80−80446
$LaAl_2$, Tb and Pr substituted, superconductors, cryst. field transitions linewidths 80−24854
$LaAl_2$:Gd^{3+}(Eu^{2+}), cryst. field parameters, relax. rates 78−84482
$LaAl_2$:Gd(Ce), supercond., electronic thermal cond. 77−12063
$LaAl_2$-Er(Dy)(Nd), dil., EPR and mag. susceptibility 80−15797
$LaAl_3$-Ce, dil., linewidth of cryst. field excitations 78−67988
$LaAl_2Ga_2$, synthesis, NMR and X-ray absorpt. studies 80−108083
$La_{1-x}Au_x$, supercond. splat cooled amorphous alloy, sp. ht. 78−19182
$La_{100-x}Au_x$, amorphous film, stability, supercond. temp. and residual resistivity 79−4636
$La_{18}Au_{22}$, amorphous, evidence for short wavelength cutoff in fluctuation spectrum 78−68113
$La_{76}Au_{24}$, disordered ribbons, production of quenched samples using arc furnace 80−71612
$La_{78}Au_{22}$, amorphous supercond., T_c and fluctuation cond. under high press. 79−7935
$LaAu_2Si_2$, ^{29}Si NMR and mag. susceptibility 79−61246
LaB_6 cathode gun from transmission electron microscope appls. 80−18048
LaB_6, de Haas-van Alphen effect and Fermi surface 77−15743
LaB_6-Cu, form. by wetting of LaB_6 with Cu 80−100813
LaB_6-Ni-WC(TiC)(NbC)(TiB_2), thermionic emission 77−28678
$LaBe_{13}$, lattice spacings and susceptibilities 80−65778
$LaBe_{13}$:Er, ESR spectra, Er spin-spin exchange broadening 78−23338
$LaBe_{13}$-Er(Dy), dil., ESR, crystalline elec. field splitting, exchange parameters 78−52348
$La_{1-n}Ce_n$, supercond. mag. alloy, effect of interconfigurational fluctuations 78−19175

lanthanum alloys continued
$(LaCe)Al_2$, unstable valence system, model for thermodynamic props. 77−69487
$La_{1-c}Ce_cAl_2$, Kondo superconductor, self-consistent theory of pairbreaking 78−26989
$(La_{1-n}Ce_n)_3Al$, mag. impurity effects in normal and supercond. state, NMR 78−2622
$(La_{1-x}Ce_x)Al_2$, Kondo supercond., tunnelling density of states 78−14900
$(La_{1-x}Ce_x)Al_2$, Kondo supercond., tunnel junction fabrication with wax barriers, tunnelling meas. 78−19191
$La_{1-x}Ce_xAl_2$, Kondo system, mag. susceptibility calc. in Anderson model 77−55661
$La_{1-x}Ce_xAl_2$, Kondo system, low temp. thermal expansion behaviour 79−19382
$(La_{1-x}Ce_x)Al_2$, Kondo system, antiferromag., specific heat 79−24179
$La_{1-x}Ce_xPd_3$, resistance behaviour and intermediate valence effects 79−78068
$La_{1-x}Ce_xSn_3$, electrical resist. and thermal expansion meas., 1.5-300K 80−34400
$La(Ce)Sn_{3-x}Pb_x$ system, mag. impurities in supercond., supercond. transition temp. and sp. ht. 78−39244
LaCeY, three normal supercond. transitions 78−26989
$LaCo_5$, N_2 absorpt. at low temps. 80−24599
$LaCo_x$, sorption at press. up to 1500 atm. 80−97819
$La_{1-x}Co_x$, amorphous, conc. depend. of Co moment 78−56300
$La_{1-x}Co_x$, amorphous alloys, thermal stability, elec. cond. enthalpy 80−100172
La_2Co_7, mag. props. changes upon H_2 absorpt. 80−71270
La_2Co_7, mag. saturation and anisotropy, density, lattice parameters 77−85426
$LaCoAl_4$, X-ray anal. of crystal structure *(Russian)* 77−55263
$La(Co_{1-x}Ni_x)_5$, distrib. of Co and Ni atoms, neutron diffr. obs. *(Russian)* 80−64954
$La(Co_{1-x}Ni_x)_5$, mag. props. and mag. reversal phenomena *(Russian)* 77−51924
$La_3Co_2Sn_7$, prep. and crystal structure *(German)* 80−84138
$La_{70}Cu_{30}$, disordered ribbons, production of quenched samples using arc furnace 80−71612
$LaCu_2Si_2$, ^{29}Si NMR and mag. susceptibility 79−61246
$LaCu_2Si_2$, resistivity, thermal conductivity and thermopower between 1.5 and 300K 78−87963
LaEu, mag. supercond., phase diagram, bulk susceptibility meas. 77−59353
$La_{0.9}Eu_{0.1}Ni_{4.6}Mn_{0.4}$, absorption-desorption props. of H_2, degradation mechanism, Mossbauer study 80−88431
$LaFe_4Al_8$, mag. props. 78−52250
$La_{0.8}Ga_{0.2}$, amorphous, Hall effect at 4.2, 78K and room temps. 79−60797
$La_{1-x}Ga_x$, amorphous foil, Hall coeff. meas. 80−20153
$La_{1-x}Ga_x$ foils, amorphous, splat cooled, calorimetric and resistive meas. 79−33417
$La_{75}Ga_{25}$, amorphous, local symmetry around glass-former sites, elec. quadrupole effects, NMR 80−80618
$La_{1-x}Gd_xAg$, antiferromagnet, spin echo NMR anal. 80−15821
$La_{1-x}Gd_xAg$, NMR ^{139}La 78−15038
$(La_{1-n}Gd_n)_3Al$, mag. impurity effects in normal and supercond. state, NMR 78−2622
$(La_{1-x}Gd_x)Al_2$, dil., reverse resistance anomaly 78−76054
$(La_{1-x}Gd_x)Al_2$, spin glass, susceptibility maximum freq. depend. 79−61172
$La_{1-x}Gd_xAl_2$, spin glass, thermoremanent and isothermal remanent magnetisation 79−87276
$La_{1-x}Gd_xAl_2$, supercond., nucl. relax. and impurity magnetism 77−20495
$La_{80-x}Gd_xAu_{20}$, amorphous dil. alloy, RKKY interaction, magnetisation meas. 77−32207
$La_{80-x}Gd_xAu_{20}$, amorphous, supercond. and spin-glass regime, magnetisation and resist. meas. 77−36011
$La_{3-x}Gd_xIn$, mag. impurity ordering and superconductivity, EPR exam. *(Russian)* 77−8400
$La_{1-x}Gd_xZn$, NMR ^{139}La 78−15038
$LaGe_2$ film, supercond. obs. 77−72939
$LaGe_x$, specific heat in range $0.07 \leq T \leq 10K$, comp. depend. 78−43517
$La_{11}Hg_{45}$, cryst. struct. determ. 79−77555
La_3In, mag. susceptibility and normal state NMR meas. 78−31118
La_3In, supercond. T_c, alloying effects 79−38227
$LaIr_2(Rh_2)$, ESR of Nd^{3+} and Gd^{3+} 77−85564
LaIr(g), thermodynamic stability, high-temp. mass spectra obs. 80−7781
$(La_{.993}Lu_{.007})_{1-x}Gd_xRu_2$, exchange enhanced supercond., compensation effect on H_{c2} 77−4474
LaM_2, (M=Rh, Ru, Pt, Ir, Al), H_2 sorption props. 79−86980
LaM_2:Nd^{3+}, M=Ru, Rh, Ir, Pt, ESR investigation 79−78514
LaM_2-Gd, M=transition metal, correl. between g-shift and stability, EPR study 80−88874
LaMg, Pauli paramagnet, mag. susceptibility, nonlinear band behaviour 80−75706
La_2Mg_{17}, sorption of H_2 77−84933
La_2Mg_{27}, reversible alloys, hydrogenation for H_2 storage *(French)* 79−74549
La_xMg_y, hydrogen storage materials *(French)* 79−66419
$(LaNd)Sn_3$, containing Nd impurities, supercond. and normal state props. 80−49967
$LaNi_4$, absorption and desorption of H_2 77−81400
$LaNi_5$, absorption of H_2, kinetics, diffusion consts. 78−14508
$LaNi_5$, absorption of H_2, 77-300K 79−23737
$LaNi_5$, activated, slow step for H_2 absorpt. (desorpt.) 78−18894
$LaNi_5$, adsorption and desorption charact. of H_2 *(Japanese)* 77−47667
$LaNi_5$, aspects of electrochem. storage of H 79−24917
$LaNi_5$, crystal field investigation from inelastic slow neutron scatt. expts. 80−39538
$LaNi_5$ effect of Ni, Ce, Co alloying additions on H_2 absorption for storage appls. 80−45790
$LaNi_5$, H storage using metal hydrides, self restoring of active surface 80−45815
$LaNi_5$, H_2 absorpt. kinetics *(Chinese)* 80−103561
$LaNi_5$, H_2 absorption in thin film hydriding alloys 80−65238
$LaNi_5$, H_2 sorption kinetic studies using high-accuracy volumetric device 79−56071
$LaNi_5$, H_2 storage appl. 78−18785
$LaNi_5$, Haucke compounds, low temp. heat capacity, Debye temp. 80−96663
lanthanum alloys continued
$LaNi_5$ hydrides, 4.2K paramag. susceptibility 80−70934
$LaNi_5$ hydrides (Al, Ga, In, Si, Ge and Sn substituted) appl. in chemical heat pumps for solar energy conversion 80−89667
$LaNi_5$ hydrogen storage capacity, intermetallic compounds research results 77−7843
$LaNi_5$, magnetism and H_2 storage 80−70941
$LaNi_5$ metal hydrides, numerical physical property data for H storage 80−40929
$LaNi_5$, Pauli paramagnet, adsorption of H, proton and ^{139}La NMR 79−78535
$LaNi_5$, self restoring of active surface, photoemission, mag. susceptibility study 78−48280
$LaNi_5$, surface segregation induced by O_2, LEED and AES exam. 79−11009
$LaNi_5$ surface segregation, influence of O_2, H_2, H_2O, SO_2 *(German)* 80−51008
$LaNi_5$ type ternary alloys, H_2 sorption/desorption reaction kinetics 80−45813
$LaNi_5$:Gd, ESR, exchange induced g-shift, H_2 uptake effect 77−4556
$LaNi_5$/H system, thermodynamics of H trapping 80−107444
$LaNi_5$/Ti-Zr-Cr-Mn hydriding alloy mixtures for H energy storage 80−45788
$LaNi_5$-Gd, dil., ESR spectra, fine struct. and random stresses 80−25203
$LaNi_5$-H, thermodynamics of solution of H at small content 77−21104
$LaNi_5$-H, with small Cr additions, NMR parameters *(Russian)* 80−29637
$LaNi_5$-H system, rel. partial absorption (desorption) enthalpies 80−50881
$LaNi_5$-type ternary alloys, H_2 absorption and desorption kinetics 80−55932
$LaNi_5 + 3H_2 \rightleftarrows LaNi_5H_6$ reaction, absorpt. capacity and reaction kinetics 79−43626
$LaNi_x$, sorption at press. up to 1500 atm. 80−97819
$LaNi_4Al$, solubility and sorption props. of H_2, effect of Al 80−103482
$LaNi_{5-x}Al_x$, Al addition effects on structural and H_2 absorpt. props. 79−52761
$LaNi_{5-x}Al_x$, HYCSOS chemical heat pump, low grade heat enhancement using 80−61467
$LaNi_{5-x}Al_x$, use in hydride conversion and storage system chemical heat pump 80−72077
$LaNi_{5-x}Al_x$, versatile alloy system for metal hydride appls. 77−86308
$LaNi_{5-y}Al_y$ alloys and their hydrides, for H storage appls. 80−45816
β-$LaNi_{5-y}Al_y$ hydrides, H diffusion, NMR studies 80−15298
$LaNi_{4.4}B_{0.6}$, H_2 absorpt. props. 80−88432
$La(Ni_{1-x}Cu_x)_5$, H_2 sorption props. 78−91533
$LaNi_4Cu$, H_2 absorption, cell volumes and desorption pressures correlation 78−22860
$La_7Ni_3D_2$ storage material, neutron, X-ray diffr. study 78−83954
$LaNi_4Fe$, H_2 absorpt. cracking, acoustic emission charact. *(Japanese)* 80−66631
$LaNi_{5-x}Fe_x(Cr_x)$, Fe and Cr electron hydride formation, X-ray and SEM obs. *(Japanese)* 79−43202
$LaNi_2H_{4.6}$, effect of synthesis, heat treatment, on comp. stability, chemical props. 80−29985
$LaNi_3H_x$ (x=4.7, 4.9), NMR line width, spin-lattice relaxation time temp. depend., H self-diffusion *(Russian)* 79−61248
$LaNi_5H_6$, H storage material, H diffusion, neutron diffr. obs. 80−51013
$LaNi_5H_{6.6}$, $LaNi_5H_{6.2}$, H diffusion NMR spectra *(Russian)* 78−2287
$LaNi_5H_{\geq 3.0}$, H diffusion coeff., neutron scatt. obs. 80−24643
β-$LaNi_5H_x$, H_2 diffusion, NMR meas. 79−82378
$LaNi_5H_x$ hydrogen storage system, $(0 \leq x \leq 6)$, neutron scatt. obs. of static and dynamic props. 78−14323
$LaNi_5H_x$, μ^+ spin relax. and Knight shift 79−56699
$LaNi_6H_6$, solar energy storage by metal hydride 80−61455
$La_2Ni_7H_x$ (x=9.9, 11.4), NMR line width, spin-lattice relaxation time temp. depend., H self-diffusion *(Russian)* 79−61248
$La_xNi_yH_z$, thermokinetics of H evolution 80−30593
$LaNi_5H_6(D_6)$, low energy excitations of H and D 79−77699
$LaNi_{4.6}In_{0.4}$, H_2 absorption props., desorpt. pressure calc., and decomp. pressures 79−24827
$LaNi_4M$ (M=Pd,Ni,Ag,Cu,Co,Fe,Cr), H_2 storage appl., desorption isotherms dependence on d-bandfilling 78−18912
$LaNi_{4.6}Sn_{0.4}$, H_2 absorption props., desorpt. pressure calc., and decomp. pressures 79−24827
La_3Os, cryst. struct. 80−96474
$LaPb_3$, doped with Tb, Nd, or Pr, crystal field effects, tunnelling within mK range 80−70907
$LaPb_3$, Tb and Pr substituted, superconductors, cryst. field transitions linewidths 80−24854
$LaPd_3$, heat capacity at low temps. 79−28547
$La_{80-x}Pr_xAu_{20}$, amorphous, mag. and supercond. props. 80−75713
$(LaPr)Sn_3$, supercond., free energy and thermodynamical crit. field 77−32127
$La_{1-x}Pr_xSn_3$, singlet ground-state system, mag. susceptibility 78−19215
$La_{1-x}Pr_xSn_3$, supercond., 0.6 meV cryst. field transitions, neutron spectroscopy 78−67991
$La_{1-y}Pr_ySn_3$, neutron spectroscopy of 0.6 meV cryst. field transitions 78−30894
$(La_{1-x}Pr_x)_3Tl$, mag. props., simple phenomenological model 77−16041
$LaPt_3$, ^{195}Pt NMR and susceptibility meas. 77−63299
$LaPt_5$, cryst. field effects on transport props. 78−72133
La_3Pt_2, structure determ., rhombohedral Er_3Ni_2 type 77−80443
$LaRh_2$, ESR of Yb^{3+} 79−87315
$LaRh_2$:Nd^{3+} cubic metallic host, spin-lattice relaxation, ESR obs. 79−1710
$LaRu_2$, H absorption induced Ce valence change, mag. and supercond. props. 80−50042
$LaRu_2$, supercond. disappearance on H absorption 79−47185
$LaRu_2$, type II supercond., ESR of Nd^{3+} meas. 79−28444
LaSb, lattice dynamics 79−37783
$La_{1-x}Sm_xSn_3$, Kondo scatt. from Sm ions 77−51734
$LaSn_3$, dilute alloy containing light rare earth impurities, press. depend. of supercond. transition temp. 79−47184
$LaSn_3$, doped with Tb, Nd, or Pr, crystal field effects, tunnelling within mK range 80−70907
$LaSn_3$, inelastic neutron scatt. 80−11165
$LaSn_3$, mag. susceptibility and magnetisation, lattice parameters, X-ray and neutron diffr. obs. 80−49675
$LaSn_3$, Tb and Pr substituted, superconductors, cryst. field transitions linewidths 80−24854

lanthanum alloys continued
La_3Sn, cubic phase, high press. and high temp. synthesis, and characterisation 78−19687
La_5Sn_3, low temp. modification with tetrogonal struct. 80−1963
$La_{1-x}Tb_xAg$, supercond., 0.6 meV cryst. field transitions, neutron spectroscopy 78−67991
$La_{1-y}Tb_yAg$, crystal field effects, normal and superconducting states 78−2621
$La_{1-y}Tb_yAg$, neutron spectroscopy of 0.6 meV cryst. field transitions 78−30894
$La_{1-x}Tb_xAg(Sn_3)(Al_2)$, paramag. anisotropy of Tb^{3+} in cubic cryst. field 80−15687
$La_{1-x}Tb_xAl_2$, competing paramag. anisotropy from cryst. field and indirect quadrupolar coupling 80−60180
$La_{1-x}Tb_xAl_2$, supercond., 0.6 meV cryst. field transitions, neutron spectroscopy 78−67991
$La_{1-y}Tb_yAl_2$, neutron spectroscopy of 0.6 meV cryst. field transitions 78−30894
$La_{1-x}Tb_xSn_3$, supercond., 0.6 meV cryst. field transitions, neutron spectroscopy 78−67991
$La_{1-y}Tb_ySn_3$, neutron spectroscopy of 0.6 meV cryst. field transitions 78−30894
$La_{0.80}Th_{0.20}Ce$, re-entrant supercond. matrix-impurity system additive pair breaking 77−69460
$(La_{1-x}Th_x)_{1-n}Ce_n$, supercond. mag. alloy, effect of interconfigurational fluctuations 78−19175
La_3Tl, mag. susceptibility and normal state NMR meas. 78−31118
$La_{1-x}Y_x$ alloys, PAC obs. of hyperfine field fluctuation at ^{140}Ce, Kondo effect interpret. 77−20761
$(La_{0.80}Y_{0.20})Ce$, three superconducting crit. point behaviour 78−10625
$La_{1-y}Y_y(Ce)$ system, mag. impurities in supercond., supercond. transition temp. and sp. ht. 78−39244
$(La_{1-x}Y_x)_{1-y}Ce_yAl_2$, resistivity meas., Kondo temp. enhancement 77−62917
Mg-La, appl. to H_2 storage 80−72093
Mg-La, workability, aging characts. and tensile strength 80−55416
Mo-Ti-La-C, influence of high pressure on mech. preps. after nitriding *(Russian)* 79−57137
Nd-La, mag. ordering, sp. ht., susceptibility and resist. 78−68238
$Nd_{1-x}La_x$ alloy, thermoelectric power 79−78080
$Nd_{1-x}La_x$, thermoelectric power, mag. transition temps. 80−20154
$Nd_{0.25}La_{0.75}Mg$, cryst. field, neutron diffr. meas. 78−34810
$Nd_{0.2}La_{0.8}Zn$, cryst. field, neutron diffr. meas. 78−34810
Ni-Cr-Si (10, 1.8 wt.%), Zr, Hf, La or Sm alloying additions effect on oxidation resist. 77−63831
Ni-La ion implanted surface alloys, solid solubility and radiation-induced disorder, backscatt. obs. 79−46692
Pb-La, vacuum deposited supercond. films, T_c chem. comp. depend. *(Russian)* 78−19174
$Pr_{1-c}La_cAl_2$, mag. props. 79−65658
$Pr_xLa_{1-x}Al_3$, cryst. elec. field 80−24856
$Pr_xLa_{80-x}Au_{20}$, amorphous, low temp. excitations, specific heat 80−100337
$(Pr_xLa_{1-x})_2In$, mag. props. 80−108009
$Pr_{0.25}La_{0.75}Mg$, cryst. field, neutron diffr. meas. 78−34810
$Pr_xLa_{1-x}Sn_3$, anomalous resistivity maxima in metallic magnetic system 78−79977
$Pr_{0.25}La_{0.75}Zn$, cryst. field, neutron diffr. meas. 78−34810
$R_{0.2}La_{0.8}Ni_5$ (R=Er,Y,Gd,Nd,La,Th,Zr), H_2 storage appl., desorption isotherms dependence on d-bandfilling 78−18912
$Sm_{1-x}La_xCo_5$, mag. props., domain boundary pinning on statistical conc. heterogeneities *(Russian)* 79−99728
$Sm_{1-x}La_xS$, electron struct., lattice consts., X-ray spectral study *(Russian)* 80−100432
Sn-La system, heats of form. 80−89517
Ta-Re-Y-La alloy, Y, La determ., spectrochem. method 79−16076
Tb-La, mag. ordering temps., susceptibility meas. 80−25136
$(Tb_cLa_{1-c})Be_{13}$, mag. struct., cryst. field effects, neutron diffr. study 80−65789
Th-La-H, hydride form. and supercond. 77−36007
$(Tm,La)Al_2$ disordered alloys, cryst. field transitions, inelastic neutron scatt. obs. 80−50055
Zr-Mo-Al-La, metastable deform. induced transform. 78−52805

lanthanum compounds
see also lanthanum alloys
adsorption on LaB_6 (100) surface, UPS and LEED study 80−49519
C La_2O, La_2O_2, atomisation energies and stand. ht. of formation 77−54622
dihydirdes, structs. and stabilities 80−107146
disc LaB_6 cathode for plasma production in magnetic field 80−106951
ethyl sulphate.$9D_2O$:$^{166}Gd^{3+}$, EPR transition energies at low mag. fields 77−12198
ethyl sulphate:Gd^{3+}, EPR lineshape distortion in weak fields with zero-field splitting 77−48034
ethyl sulphate:Gd^{3+}, spin Hamiltonian, higher-order spin terms 77−48044
ethyl sulphate=Gd^{3+}, proton position determ. by ENDOR 77−51992
ethyl sulphate nonahydrate: Tb^{3+}, ESR spectrum, spin lattice relax., effect of hydrostatic compression 78−88185
ethyl sulphate nonahydrate:Pr^{3+}, absorpt. spectrum, 400-700 nm, 78K, 22 kbar press. effects 77−81133
ethylsulphate:Gd^{3+}, zero-field splitting, contributory mechanism 80−80231
ferrite, hexagonal, with M, W and Y structures containing Fe^{2+} and Fe^{3+} mag. ions, saturation moment and anisotropy 80−71009
field emission patterns and emission characts. *(Japanese)* 77−85900
formate, IR spectra and phase transitions, under pressure 78−31179
high current discharge from cold LaB_6 cathode 80−107011
IR and Raman spectra 79−78671
LaF_3:Tm^{3+}(Nd^{3+})(Er^{3+}), vacuum-UV excitation spectra 78−80381
lanthanum bicarbamide acetate, cryst. struct. 79−19240
lanthanum ethyl sulphate:Gd^{3+}, X-band EPR, near room temp., spin Hamiltonian parameters 77−63275
lanthanum ethyl sulphate:Pr, phase transition under pressure, absorpt. spectra *(Russian)* 80−92667
lanthanum nicotinate dihydrate:Nd^{3+} cryst., H coords., EPR and ENDOR determ. 77−59005
lanthanum nicotinate dihydrate, cryst., nucl. quadrupole interactions, D atom coords., ENDOR obs. 80−97161

lanthanum compounds continued
oxalates, separation from high level radioactive waste by precipitation 79−49720
oxychromates (La_2CrO_6, $La_7Cr_2O_{16}$, $La_{16}Cr_7O_{44}$), form. from O_2 reactions with La_2O_3-Cr_2O_3 and $LaCrO_3$ *(French)* 77−52524
phase form. and relations, phys. props. 79−43218
piston engine using $LaNi_5H_x$ as energy conversion medium, prototype 79−70458
PLZT, diffuse phase transitions 79−33628
PLZT ceramics, ferroelec., special props. 79−42916
PLZT ceramics as electro-optic shutter material for IR appls. 79−72679
PLZT coarse-grained solid solutions, electro-optical processes induced by longitudinal electric field *(Russian)* 80−80750
PLZT ferroelectric ceramic, anomalous bulk photovoltaic effect and cond. *(Russian)* 80−54733
silicides, valence band struct. *(Russian)* 79−15076
thermodynamic study of form. 78−48685
Al_2O_3-La_2O_3:Eu^{3+} system, optical and struct. exam. 77−4674
Al_2O_3-Ln_2O_3, Ln=La,Ce,Pr,Nd,Sm,Gd,Tb, struct. and thermal characts. of amorphous phases *(French)* 77−72558
Al_2O_3-Y_2O_3-SiO_2 containing TiO_2, La_2O_3, exam. of elastic moduli and refractive indices 78−80502
(Ba,La)TiO_3, defect chemistry and elec. cond., thermogravimetric meas. 77−39580
$Ba_xLa_{1-x}CoO_3$, x=0 to 0.5, structural, elec. and mag. props., Zener double exchange and Goodenough's model 79−65663
$Ba_{1-x}La_xF_{2+x}$, enhanced ionic motion in solid solutions 80−107491
$BaLa_2Fe_2O_7$, Mossbauer exam. of mag. struct. 77−40157
$BaLaMnO_4$, and $Ba_{1+x}La_{1-x}MnO_4$, cryst. struct. determ. *(French)* 78−6042
BaO-$La_{0.6}$O-VO_2-SiO_2, glass, elec. cond. rel. to ion polarisability, polarons 80−49729
BaO-La_2O_3-B_2O_3, glass, refraction, refractive index from 0.365 to 2.50 μm 80−88953
BaO-La_2O_3-GeO_2, exam. of glass forming region, properties and crystallisation 78−88454
$Ba_{0.50}Sr_{0.50}Nb_2O_6$:$La_2O_3$, Raman spectra 79−78678
$BaTiO_3$:La_2O_3 and $BaTiO_3$:La_2O_3.$3TiO_2$ capacitor, permittivity ageing obs. *(Korean)* 80−25325
$BaZrO_3$-$LaAlO_3$ systems, sintering conditions, elec. props. 79−43184
$BiFeO_3$-$LaFeO_3$, solid solns., antiferroelec.-antiferromag., magnetoelectric effect at antiferroelec. transition 80−100637
CC LaB_6, adsorption on Ta, work function 80−20039
CaF_2-LaF_3, solid soln. with fluorite struct., phase diagram 79−100119
$CaLaBO_4$, crystallographic and Pb^{2+} luminesc. data 79−32971
$CaLaFeO_4$, two-dimens. mag. props. rel. to cryst. struct. 80−75776
$Ca_2LaFe_3O_8$, Fe replacement by diamag. cation, Neel temp. *(French)* 79−73712
$Ca_2LaFe_3O_8$, physico-chemical characterisation, Mossbauer exam. and mag. props. *(French)* 77−28494
$Ca_{1-x}La_xMgAl_xSi_{2-x}O_6$, crystalline and vitreous phase comp. and props. 77−44221
$Ca_8La_2(PO_4)_5(VO_4)O_2$, IR and Raman spectra 79−78671
$CaLa_4(SiO_4)_3O$:Nd, laser damage initiating inclusions 77−68246
$CaLa_4(SiO_4)_3O$:Nd^{3+}, spectra, stimulated emission 77−85755
$Ca_2La_8(SiO_4)_6O_2$, cation ordering, X-ray diffr. meas. 79−23577
$Ca_4La_6Si_4P_2O_{26}$, and derivatives, synthesis, physicochemical props. 77−21066
$Ca_8La_2(VO_4)_6O_2$, IR and Raman spectra 79−78671
$CaTiO_3$-$LaAlO_3$ solid soln., phase redistrib. during roasting in H_2 78−52735
Ca_2TiO_3-La_3AlO_3, synthesis of solid solution by coprecipitation 79−1836
$Ce_x(La,Y)_{1-x}Sb$, and $Ce_x(La,Y)_{1-x}Bi$, antiferromag. spin arrangement, neutron diffr. obs. 77−63106
$Ce_xLa_{1-x}B_6$ solid solutions, Weiss const. antiferromagnetic ordering calcs., mag. props. *(Russian)* 79−91212
$Ce_xLa_{1-x}F_3$, paramag. mixed crystal, scattering of optical phonons by rare earth ions 78−68518
$Ce_xLa_{1-x}F_3$, phonon self-energy and electron-phonon interaction 79−65159
$(Ce_xLa_{1-x})_2Mg_3(NO_3)_{12}.24H_2O$, mag. susceptibility meas., AC method meas., appl. as thermometer in mK region 77−17999
$Ce_xLa_{2-x}Mg_3(NO_3)_{12}.24H_2O$, magnetically diluted thermometer 79−17420
CeO_2-La_2O_3 system, surface microphases investigation by X-ray electron spectral anal. 79−51269
$CeO_2La_2O_3$, ceramic, thermal stability, sintering, deform., effect of La_2O_3 79−11532
CsCl-$LaCl_3$ molten binary mixtures, thermal cond. 79−86931
$Dy_{0.7}La_{0.3}FeO_3$, reorientational phase transitions, influence of La^{3+} ions 80−7108
$(Eu,La,Ca)_3(Fe,Ga,Al)_5O_{12}$ film, LPE growth and induced orthorhombic anisotropy 77−20652
$Eu_xLa_{1-x}Ta_7O_{10}$, polycryst., luminesc. and excitation spectra 80−60659
Eu_2O_3-R_2O_3-Ta_2O_5, R=La, Gd, Y, quasibinary cross sections 77−90333
Ga_2S_3-La_2S_3-Nd_2S_3:Nd^{3+} chalcogenide glass, Nd^{3+} emission and absorption spectra, nonradiative relax. 77−40268
$Gd_xLa_{1-x}B_6$, solid solns., mag. susceptibility, 80 to 1000K *(Russian)* 80−88713
$Gd_{0.67}La_{0.33}P_5O_{14}$, photoemission spectra, 4f, 5p and 5s giant reson. enhancement 78−95660
$Gd_xLa_{1-x}Pd_3$, ESR linewidths, g-shifts, effective electron interaction, spin-lattice relax., spin-flip scatt. 78−68372
β-Gd_2S_3:Nd^{3+}, spectroscopic props. from absorpt., photoluminesc. and excitation spectra 80−34968
HfF_4-BaF_2-LaF_3 glass system, IR transmitting, synthesis and props. 80−71623
HfO_2-La_2O_3 system, phase form. and relations, phys. props. 79−43218
K-La-NH_3 system, cpd. formation, phase analytical and X-ray expts. *(German)* 79−66043
K_2CrO_4+$La_2(NoO_4)_3$, X-ray phase analysis, IR absorption spectra, and thermogravimetric anal. 79−1944
$(K_{0.5}La_{0.5})_xBa_{1-x}TiO_3$, cryst. struct., dielec. and IR spectral meas. 79−46614
$KLa(MoO_4)_2$, solubility in aq. K_2MoO_4 solns., hydrothermal conditions 80−96651
$K_5La(WO_4)_4$, formation possibility 77−36392
L_n-F_3-CaF_2 membrane electrode development, ion selective *(Japanese)* 80−61203
$(La,Ca)_nTi_nO_{3n+2}$, (n=4.5,5 or 6), cryst. struct. determ. *(French)* 79−65039

lanthanum compounds continued
(La,Ce)B_6, low temp. mag. props. 79−61043
(La,Gd)B_6, mag. susceptibility, zero field, 0.04 to 10K 78−10696
(La,Nd)P_5O_{14}, optical props., ferroelastic phase transition induced 79−95731
(La,Nd)$_3PO_7$, IR and Raman spectra, vibr. assignments, cryst. struct. characts. 80−97258
(La, Pb)MnO_3, flux growth 79−83113
(La, Y, Sc)B_6 solid solns. electron work function, thermal emission technique 80−20755
La, $(SO_4)_3.9D_2O$, soln. growth, struct., props. 77−77363
La ferrite, composition and mag. props., anisotropy field, magnetisation 80−71109
La-Co-O system, stability of ternary phases, nonstoichiometry 80−24434
La-D, phase transition, NMR meas. 80−66508
La-Ge-B, X-ray investigation of phase equilibrium 79−99294
La-H, ordered struct. near $LaH_{2.65}$ at 250K, NMR 80−66508
La-H, phase equilibria 80−66492
La-H(D), inelastic neutron scattering exam. of lattice dynamics 80−29128
La-H(D), lattice parameters 80−64982
La-N-C system, metallographic investigation *(German, English)* 77−52600
La-Ni-H compounds, prep. by gas absorpt. in La-Ni system, struct. 77−9078
La-S system, phase diagram above 1600°C 79−78938
La-Si-As ternary cpd., synthesis, stoichiometry 80−104083
La-Si-O-N, comments on new apatite phase 80−15255
La-Si-O-N system, new compound form. with fluorapatite struct. 79−4941
La-Sm-Lu iron garnet film grown as NdGaG substrates, mag. props. 80−44888
$La_{1-x}Eu_xB_6$ solid solutions, cryst. lattice defectiveness, mag. susceptibility and elec. conductivity 80−15083
$La_{2-x}A_{1+x}Cu_2O_{6-x/2}$ (A=Ca, Sr), synthesis and characterisation *(French)* 80−104085
$LaAMTeO_6$, A=Ba, Pb, Sr, M=Li, Na, antiferroelectric, synthesis and charact. 77−55758
La_2ASe_5, A=Ge, Sn, diffuse refl. spectra and band gaps 79−51963
$LaAl_{0.85}Mg_{0.15}O_{2.925}\square_{0.075}$, $LaAl_{0.8}Mg_{0.2}O_{2.9}\square_{0.1}$, $LaNb_{2.6}Zr_{0.4}O_{8.8}\square_{0.2}$, ionic conductivity 77−20119
$LaAlO_3$, exchange interactions of transition metal ions in orbitally degenerated excited states 80−65512
$LaAlO_3$ perovskite electrolytes for high-temp. fuel cells 79−29467
$LaAlO_3$, Pm3m to R3c or R$\bar{3}$c phase transitions, TEM method for domain identification 80−14980
$LaAlO_3:Bi^{3+}$, and related Bi^{3+}-activated hosts, cryst. struct. effs. on luminesc. 77−16376
$LaAlO_3:Cr^{3+}$ enriched in ^{17}O isotope, flux growth 79−87573
$LaAlO_3:Tb^{3+}$, cathodo- and photoluminesc. 77−12448
La_4As_3, superconductivity 77−20481
LaB_6 (001), surface state exam. by angular resolved UPS 78−19114
LaB_5 gun, optimum brightness problem 78−21298
LaB_6, ^{11}B nucl. quadrupole interaction, NMR meas. 80−2660
LaB_6, (La,Eu)$_6$, (La,Y)B_6, (La,Ba)B_6, (La,Cs)B_6, single crystal growth for thermionic emission 78−92183
LaB_6 (001) surface, struct., initial oxidation, XPS, UPS, LEED, AES, work function meas. 79−99403
LaB_6, (001) surface struct., XPS, LEED meas. 78−63909
LaB_6 (100), (110), and (111), surface structs. and work functions 80−70512
LaB_6 (210) surface, work function, struct. and chemisorpt. stability, XPS, UPS and LEED 80−65344
LaB_6, adsorpt., surface migration and thermal desorpt. on W 79−56075
LaB_6, and related cpds., thermionic props. *(French)* 78−60541
LaB_6, arc floating zone prep. technique 77−12521
LaB_6 cathode, beam current stability in high vacuum 77−40321
LaB_6, cathode, brightness, cryst. orientation and purity effects 77−12483
LaB_6 cathode, directly heated, for electron beam instruments, design and optimisation 78−93783
LaB_6 cathode, thermal, illumination systems for round beam electron probe systems 80−57436
LaB_6 cathode electron gun, current beam intensity and brightness meas. *(French)* 77−590
LaB_6 cathode poisoning, by residual gases, organic solvents, oils and greases 77−66568
LaB_6 cathodes, mounting methods and operating characts. 80−57437
LaB_6 cathodes, residual gas poisoning in vac. system, thermionic emission decay 78−27364
LaB_6 cathodes, single crystal, of <100> and <110> orientations, brightness meas. from 1500 to 1950K 80−62808
LaB_6 cathodes for Kohler illum. and brightness meas. 80−68296
LaB_6, chemical vapour growth of whiskers, and single crystals 78−72710
LaB_6, clean and oxidised (100) surface, LEED, AES, work function, evaporation meas. 78−71989
LaB_6, collector for low temp. thermionic convertor 79−27842
LaB_6 crystals, zone refined, chem. characterisation 80−93821
LaB_6, de Haas-van Alphen effect, low-field 80−75497
LaB_6, direct recomb. and Auger deexcitation channels of La 4d to 4f reson. excitations, photoemission spectra 80−66395
LaB_6, elastic consts. at room temp., US vel. meas. 77−43268
LaB_6, elec. cond. under hydrostatic press. 79−7832
LaB_6 electrodeposition, cathodic behaviour 79−20378
LaB_6 electron gun source, grid aperture contamination, emission instability 79−12907
LaB_6, electronic struct., APW method and local-spin-density approx. 80−65434
LaB_6 electronic structure calc. and obs., by APW method and X-ray photoelectron spectroscopy *(Japanese)* 79−15074
LaB_6, emissivity at 650 nm, 1600 to 2100K 79−90806
LaB_6 emitters, thermionic emission *(Japanese)* 77−44114
LaB_6, FIM study 80−71578
LaB_6, field emission and FIM expts. 77−90255
LaB_6 film, prep. by electron beam evaporation, and optical and elec. props. 80−20793
LaB_6 film, structure, stoichiometry, elec. properties 78−60043
LaB_6, growth by soln. method, struct. mech. and elec. props. 80−16168
LaB_6, gun, 100 kV, combined CTEM and STEM 80−86516
LaB_6 gun, Broers type, design, for SEM 78−21283
LaB_6, high temp. interaction with 0_2, AES and mass desorption expts. 80−7698

lanthanum compounds continued
LaB_6 highly stable single cryst. cathode for conventional electron microprobe instruments 78−78043
LaB_6 hollow cathode for dense plasma production 78−55729
LaB_6, hollow cathode mag. multipole ion source 80−102369
LaB_6, measurements of O adsorption using retarding potential method in axial magnetic field 79−80719
LaB_6, metallic, energy bands and bonding 77−43486
LaB_6, metallic, energy band structure and Fermi surface, self-consistent APW method 77−69221
LaB_6, negative surface ionisation 77−77335
LaB_6, negative surface ionisation, intense halogen ion source 79−93850
LaB_6, plasma light reflection by free charge carriers 80−11403
LaB_6, polycrystalline, negative surface ionisation of I atoms, negative ion desorption heat 79−78848
LaB_6, porous, field emitter cathode sputtering and surface damage 79−11492
LaB_6 rods, chem. and electrolytic reaction in HNO_3 aq. soln. 79−87850
LaB_6, Shockley surface states, angle-resolved photoemission 79−56278
LaB_6 single cryst. tips with [100], [110], [111] and [210] orientations, thermionic emission patterns 80−66379
LaB_6, single cryst. work function, thermionic emission, evaporation 77−24922
LaB_6 single crystal cathode, thermionic emission, surface struct. 80−97395
LaB_6 single crystal needles, thermal field emitted electron total energy distribution spread 80−45218
LaB_6, single crystals, thermionic work function meas. 78−11067
LaB_6, single crysts., growth by laser heated floating zone method 77−81213
LaB_6, single-crystal thermionic electron emission anisotropy 77−24920
LaB_6, sintered, work function and Richardson const., Mo poisoning effects 79−52070
LaB_6, surface (100), atomic struct., angle-resolved XPS, LEED and ISS investigation 80−10765
LaB_6, surface ionisation of halogens, using ion source 78−60538
LaB_6 surface stoichiometry, thermionic emission B conc. effects 79−87556
LaB_6 surfaces, (100), (110) and (111), electron states, UPS study 80−100752
LaB_6, synthesis and props., review *(Japanese)* 80−40255
LaB_6 synthesis by heating BN with lanthanum citrate hydrate 80−100819
LaB_6 tablets, electron injector cathode appl. *(Russian)* 77−38535
LaB_6 thermal and electrical conductivities, 1000-2100°C 77−69293
LaB_6, thermal expansion, X-ray method, room temp. to 1300 C 80−96670
LaB_6, thermal field emitted electrons, total energy distrib. spread 77−52227
LaB_6, thermionic emission props. *(Japanese)* 77−63523
LaB_6, thermionic emission rel. to surface state 78−39654
LaB_6 three-electrode 250 A pulsed electron gun 78−82553
LaB_6, time of flight atom-probe FIM study 80−6652
LaB_6, transverse magnetoresistance meas. 80−107764
LaB_6, UPS and XPS of valence band 78−84703
LaB_6, US comminution of refractory compound powders 78−23656
LaB_6, valence band dispersions, angle-resolved photoemission 80−11536
LaB_6, work function, thermionic emission characts., jellium model 77−8710
LaB_6, work function, thermionic and field emission retarding pot. meas. 77−90233
LaB_6, work functions from thermionic and field emission retarding pot. methods 79−65537
LaB_6:C, AES, LEED and energy-loss spectra study of C layer on (100) surface 77−62715
LaB_6:Ce, Kondo system, magnetoresist. down to 0.04K, anisotropy 77−11904
LaB_6:Y, Sc effects of impurities thermionic emission 78−60542
LaB_6-SmB_6(YbB_6), exam. of secondary ion-ion emission, due to bombardment with 8 keV Ar ions 79−33882
LaB_6-YB_6-ScB_6, thermionic emission 78−11068
LaB_x, phase relationships, chemical activity and work function obs., thermionic appls. 77−90234
LaB_x x=4.24 to 29.2, thermoelectric electron emission, work function, 1400-2100K 78−60539
LaB_2C_2, ordering of B and C atoms in struct. 80−96481
$La(BH_4)_3$, synthesis from chloride salts and $NaBH_4$ in tetrahydrofuran 80−30222
$LaBO_3$ (B=V, Cr, Mn, Fe, Co, Ni), chem. stability X-ray and thermal anal. 79−79242
$LaBO_3$, flux growth 79−38732
$LaBO_3$, single cryst., not cut parallel to principal axes, Raman spectra birefringence effect 79−69837
LaB_6(001) surface, struct. and initial oxidation, UPS, XPS and work functions meas. 77−86195
$La_4Ba_6(BO_3)_9$, flux growth and chem. characts. 78−23595
$La_{1-x}Ba_xCoO_3$, electronic and mag. props., itinerant ferromagnetism obs. 78−10660
$La_{0.003}Ba_{0.66}Sr_{0.34}TiO_3$ ceramic, positive TCR near Curie temp. rel. to charge dispersion *(Russian)* 80−16511
$LaBe_{13}$:Er, ESR, appl. of exchange induced broadening in low lying crystalline field system 80−108062
$LaBe_{13}$:Er(Dy)(Gd), ESR, crystalline field single ion effects 78−84481
$La_2Be_2O_5$:Nd^{3+}, laser cryst. props. 77−19260
$La_2Be_2O_5$:Nd^{3+}, optical absorpt. and fluoresc. intensities 80−29793
$La_2Be_2O_5$:Nd^{3+} (Pr^{3+}), cryst. growth, spectral and laser properties in $^4F_{3/2}\rightarrow{}^4I_{11/2}$ and $^4F_{3/2}\rightarrow{}^4I_{13/2}$ transitions 80−80853
LaBi, thermal expansion, 20-800°C 79−14942
LaBi:Er, ESR of non S-state ions 77−43881
La_4Bi_3, La_4Bi_2Pb and La_4BiPb_2, superconductivity 77−20481
$LaBr_3$, ionisation energies, satellite struct., photoelectron spectra, MS Xα calcs. 78−13425
$LaBr_3$:Np^{3+}, energy level anal., polarised absorpt. and fluoresc. spectra 80−76056
$LaBr_3$:Pr, continuous wave and pulsed laser pumped Pr IR quantum counters 79−93219
$LaBr_3$:Pr^{3+}, IR absorption, energy values for Stark manifolds 80−34955
$LaBr_3$:Pr^{3+}, laser-induced fluoresc. line-narrowing, hyperfine struct. and Zeeman effect 77−85789
$LaBr_3$:U^{3+}, luminesc., fluoresc. lifetimes 79−33768
$La(BrO_3)_3.9H_2O$, IR and Raman spectra, vibr. asignments 78−84569

lanthanum compounds continued
LaC_2, high-temperature carbide targets for fast on-line mass separation of alkali and noble gas elements 79−22515
La_2C_3, solid solution, lattice const. and superconducting transition temp. *(Russian)* 80−92496
$LaCO_{1-x}M_xO_3$, M=Mg, Ti, cryst. struct., elec. and mag. props. 79−86748
$La_{1-x}Ca_xCoO_3$, electronic and mag. props., itinerant ferromagnetism obs. 78−10660
$La_{0.9}Ca_{0.7}CrO_3$ polar semiconductor, elec. props., slight reduction effect 80−20183
$(La_{0.8}Ca_{0.2})MnO_{3+y}$, mag. sp. ht. and Debye temp. 79−61124
$(La_{0.8}Ca_{0.2})MnO_{3+y}$, mag. props., Faraday method meas. 80−103832
$(La_{0.8}Ca_{0.2})MnO_{3+y}$, non-stoichiometry and lattice consts. 80−100212
$(La_{0.8}Ca_{0.2})MnO_{3+y}$, sample preparation using O_2 partial pressure controller *(Japanese)* 78−73977
$La_xCa_{1-x}RuO_3$, metallic, mag., electronic and structural props., ^{99}Ru Mossbauer spectroscopy 77−48107
$La_{1-x}Ca_xVO_3$, struct., elec. and mag. props., temp. and conc. depend. *(French)* 77−4293
$La_{1-x}Ce_xB_6$, Kondo system, low-field impurity susceptibility, 0.03 to 8K 77−63095
LaCl-Pr(Dy)(Sm), mech. for X-ray luminesc. and thermolum. 79−8170
$LaCl_2:U^{3+}(5f^3)$, polarised absorption spectra and energy levels 80−16063
$LaCl_3$, aq. soln., H_2O coordination of metal ion, X-ray diffr. 79−69000
$LaCl_3$, Raman intensity anal. 79−33710
$LaCl_3$, Schottky anomalies, ht. capacity meas., 5-350K 77−31784
$LaCl_3:Gd^{3+}$, ^{139}La ENDOR, hyperfine and elec. quadrupole interactions 77−20749
$LaCl_3:Gd^{3+}$, EPR spectra, linear-electric-field effect 79−73808
$LaCl_3:Ho^{3+}$ parametric energy level anal. 78−18991
$LaCl_3:Nd^{3+}$, coherent interactions of Kramers doublet system with microwaves in zero static mag. field 77−73078
$LaCl_3:Nd^{3+}$, cryst., appl. to phosphoroscope IR detector 79−49293
$LaCl_3:Nd^{3+}$ radiation upconversion, 1.06 to 0.873 μm 78−19530
$LaCl_3:Np^{3+}$, energy level anal., polarised absorpt. and fluoresc. spectra 80−76056
$LaCl_3:Np^{3+}$, phonon-induced relax. in excited optical states, linewidth temp. depend. meas. 80−100688
$LaCl_3$:Pr, continuous wave and pulsed laser pumped Pr IR quantum counters 79−93219
$LaCl_3:Pr_1$ optical absorpt. and Zeeman spectra, zero mag. field splitting 79−91482
$LaCl_3:Pr^{3+}$, coherent transients by optical phase switching 80−95962
$LaCl_3:Pr^{3+}$, crystal field parameters using multiple-scatt.-X_α method 78−95271
$LaCl_3:Pr^{3+}$, dipole transition probabilities between states, electron correl. effects 80−23364
$LaCl_3:Pr^{3+}$, hyperfine Zeeman effects, fluorescence line-narrowing technique 77−62881
$LaCl_3:Pr^{3+}$, hyperfine struct. of 6011 Å line, laser-induced absorpt. line narrowing 78−15196
$LaCl_3:Pr^{3+}$, IR absorption, energy values for Stark manifolds 80−34955
$LaCl_3:Pr^{3+}$, Nd^{3+}, single cryst., optical double reson. excitation, energy transfer and transform. 77−69891
$LaCl_3:Pr^{3+}$, satellite lines in optical absorpt. spectra, Zeeman effect 79−65911
$LaCl_3:Pr^{3+}$, second order Zeeman hyperfine effect *(French)* 77−52162
$LaCl_3:Pr^{3+}$, Zeeman second-order effects, fluoresc. line narrowing technique 80−16103
$LaCl_3:R^{3+}$, cryst. field parameters, angular overlap model calcs. 78−26830
$LaCl_3:U^{3+}$, cryst., spectrum anal., cryst. field parameters 80−76057
$La(ClO_4)_3$, osmotic coeffs. 80−45556
$LaCo_5N_n$, formation by N_2 absorpt. by $LaCo_5$ 80−24599
$LaCoO_3$, ^{59}Co NMR, quadrupolar and hyperfine interactions 79−15366
$LaCoO_3$, conducting oxide powder prod. by freeze drying 79−95984
$LaCoO_3$, conducting oxide prod. by amorphous citrate process 79−95985
$LaCoO_3$, Mott isolator, paramag. props., calc. 80−93071
$LaCoO_3$, reduction, direct obs. using high voltage TEM 77−63817
$LaCoO_3$, spin states, XPS meas. 78−68599
$LaCoO_3$, structural phase transition involving changes in spin and valency 78−79765
$LaCoO_3$, synthesis and characterisation by powder X-ray diffr. 78−79580
$LaCoO_3$:Ca(Sr), anomalous $^{57}Fe^m$ charge states, Mossbauer study 80−40017
La_2CoO_4, mag. behaviour obs. 80−70971
La_2CoO_4, synthesis and characterisation by powder X-ray diffr. 78−79580
$La_4Co_3O_{10}$, cryst. struct., stability 80−24434
$La_4Co_3O_{10}$, synthesis and characterisation by powder X-ray diffr. 78−79580
$LaCr_3$ alloy development for thermoelec. appls. 80−35705
$LaCr(Co)O_3$, conducting oxide prod. by amorphous citrate process 79−95985
$LaCrO_3$, reactions with O_2 *(French)* 77−52524
$LaCrO_3$, sp. ht., enthalpy, entropy, 298-900K, polymorphic transition 77−69094
$LaCrO_3$, spin states, XPS meas. 78−68599
$LaCrO_3$, vaporization in oxidizing atmos. 80−24579
$LaCrO_3$-CeO_2, quadrupole interactions and moments, ^{137}La Mossbauer obs. 78−27121
$LaCrO_3$-Cr ceramic, prep., phase comp. and elec. cond. *(Polish)* 80−71621
$LaCrO_3$-Cr cermet, effect of explosive compacting on props. 77−12557
$LaCrO_3$-MgO, LC20M electrode material in open cycle MHD systems, thermionic emission characts. 80−97394
$LaCrO_3$-TiO_2 photoactive anode, for photoelectrolytic production of H_2 and electricity 80−12024
$LaCrO_3$-W(Mo)(Cr) eutectics, eutectics, prep. and microstruct. 80−108380
$LaCrOS_2$, single cryst. X-ray diffr. struct. determ. *(French)* 79−23581
$LaCrOS_2$, X-ray cryst. struct. anal. *(French)* 80−92484
$LaCrS_3$, crystal atomic struct., X-ray diffr. analysis *(German)* 78−10003
$LaCrSe_3$ alloy development for thermoelec. appls. 80−35705
$LaCuO_2$, enthalpy of formation and high temp. stability from EMF of galvanic cell 80−11942
lanthanum compounds continued
$LaCuO_3$, struct. rel. to phys. props., high-pressure series of perovskite-like oxides 78−51493
La_2CuO_4, catalytic props., mag. and elec. props. 79−66350
La_2CuO_4, enthalpy of formation and high temp. stability from EMF of galvanic cell 80−11942
La_2CuO_4, high pressure phase transformation, small polaron cond. to semicond. transition 78−6156
La_2CuO_4, magnetic properties obs. 80−70937
$LaCu_3Ru_4O_{12}$, synthesis, cryst. struct., mag. and elec. props. *(French)* 80−107151
LaD_3, stoichiometric, structural phase transform., neutron diffraction evidence 80−88319
$La_{0.9}Er_{0.1}Al_2$, crystal field study rel. to $ErAl_2$ 78−76036
$La_xEu_{1-x}B_6$, EPR linewidth conc. depend., $Sr_xEu_{1-x}B_6$ comparison, exchange interaction in EuB_6 80−20457
$La_xEu_{1-x}B_6$ solid solns., thermal cond., 300 to 2000K 80−59741
LaF, Franck-Condon factors and R-centroids, rot.-vibr. effects 78−50596
LaF^+, electronic spectra, rot. anal. and orbital configurations 80−83240
$LaF_2:Pr^{3+}$, ultraslow optical dephasing for $^3H_2$-$^1D_2$ transition 79−64290
LaF_3, ^{19}F NMR study, relaxation times meas. 80−108093
LaF_3, bomb calorimetric determ. of enthalpy of formation 80−50879
LaF_3, coating materials for IR laser components 80−33105
LaF_3 films, electron beam evaporated, dielec. props. 79−91375
LaF_3, force consts., Coriolis coupling consts., vibr. amplitudes 78−17650
LaF_3, gamma-irrad. induced coloration and role of impurities 77−35586
LaF_3, heat capacity of 350K, enthalpy to 1477K, calorimetric determ. 78−79781
LaF_3, high-frequency phonon lifetimes 80−70338
LaF_3 insulators for MIS structs. 79−78182
LaF_3, ionic transport, NMR and cond. studies 80−107555
LaF_3, ionisation energies, satellite struct., photoelectron spectra, MS $X\alpha$ calcs. 78−13425
LaF_3 laser coating, UV damage obs. 80−33056
LaF_3, MS $X\alpha$ electronic struct. calc., inner shell photoelectron spectra 77−10594
LaF_3, mol. consts., kinetic consts. and L-approx. methods 80−18839
LaF_3, mol. force, compliance and Coriolis consts. 79−31726
LaF_3, monocrystal, thermal cond., temp. dependence 77−55402
LaF_3, new coating materials for IR laser optical components 79−65821
LaF_3, pre and Nd^{3+}-doped, thermal cond., 300-1450K 80−24686
LaF_3, quantum yield, photoelectron spectra, density of states struct. 78−68601
LaF_3, self diffusion studied with ^{19}F relaxation 78−6180
LaF_3 single cryst., electron diffr., superlattice struct. 78−42993
LaF_3 superionic conductor insulating layer, used for photocapacitive detectors 80−92976
LaF_3, UV visible absorpt. by laser calorimetry, wavelength modulation spectroscopy 78−66876
LaF_3, VUV luminescence, conference, Moscow, USSR (Apr. 1978) 80−62378
LaF_3, zone centre optical phonon stress dependence, point group symm., Raman spectra meas. 79−78686
LaF_3:Ce, cryst. field parameters, optical transitions and g-factor determ. 78−2456
$LaF_3:Ce_3$ optically pumped laser at 286 nm 80−99738
$LaF_3:Ce^{3+}$, UV fluoresc. potential tunable laser 2760 to 3220 Å 78−15206
$LaF_3:Dy^{3+}$, $^4F_{9/2}$ and $^4I_{15/2}$ levels, radiative decay rates 79−61415
$LaF_3:Dy^{3+}$, high temp. fluoresc., Dy^{3+} G-level emission 78−27295
$LaF_3:Dy^{3+}$, laser excited fluoresc., lifetimes meas. 79−24353
$LaF_3:Dy^{3+}$, magnetospectroscopy with optically pumped far IR laser 79−33737
$LaF_3:Er^{3+}$, impurity centre interaction with external. elec. field 77−89727
$LaF_3:Er^{3+}$, optically excited, direct-process spin-lattice relaxation 80−93378
$LaF_3:Er^{3+}$, spin-lattice relax. meas. in excited $^4S_{3/2}$ state by purely optical method 79−19923
$LaF_3:Eu^{3+}$, absorpt and laser fluoresc. spectra 77−52159
$LaF_3:Ho^{3+}$, laser excited fluorescence absorption spectra, symmetry groups 78−60514
$LaF_3:Ho^{3+}$ single crysts., multiphonon relax., fluoresc. obs. 79−47495
$LaF_3:Ho^{3+}(Dy^{3+})$, laser excited fluoresc. rise and decay meas., expt. 80−22448
$LaF_3:Nd^{3+}$, cryst., $4f^3$ config., ground level energy state var. rel. to press. *(Russian)* 77−16358
$LaF_3:Nd^{3+}$, laser-excited fluoresc., self-adsorpt. 78−15210
$LaF_3:Nd^{3+}$, luminesc. decay times 80−2811
$LaF_3:Nd^{3+}$, radiative transition rates of Nd^{3+}, Judd-Ofelt theory 79−33753
$LaF_3:Nd^{3+}$, spin echo envelope modulation exam. 79−61212
$LaF_3:Nd^{3+}$, vacuum UV luminesc. *(Russian)* 78−64414
$LaF_3:Nd^{3+}(Er^{3+})(Tm^{3+})$, VUV fluorescence and tunable coherent sources from 1650 to 2600 Å 77−688
$LaF_3:Pr^{3+}$, $^1D_2$ metastable state, hyperfine splittings, enhanced and saturated absorpt. spectra 78−43694
$LaF_3:Pr^{3+}$, 2K, optically detected coherent transients in nuclear hyperfine levels 79−19806
$LaF_3:Pr^{3+}$, anomalous luminesc. decay, phonon reson. trapping and bottlenecking 79−43023
$LaF_3:Pr^{3+}$, fluoresc., time resolved excitation technique 79−95820
$LaF_3:Pr^{3+}$, hyperfine splitting of $^1D_2$ metastable state, RF optical double reson. 78−35067
$LaF_3:Pr^{3+}$, laser-induced fluoresc. line narrowing 77−40280
$LaF_3:Pr^{3+}$, Nd^{3+}, fluorescence linewidth and energy transfer 77−8635
$LaF_3:Pr^{3+}$, nuclear hyperfine interactions, photon echo relax. obs. 79−59771
$LaF_3:Pr^{3+}$, nuclear quadrupole interaction, optical-RF double reson. meas. of ground electronic state 77−48092
$LaF_3:Pr^{3+}$, optical coherence storage in spin states, echo lifetime 80−58649
$LaF_3:Pr^{3+}$, optical free induction decay exam. of dephasing time 77−3637
$LaF_3:Pr^{3+}$, optical free induction decay meas. of low temp. dephasing 79−46009
$LaF_3:Pr^{3+}$, optical line narrowing by nuclear spin decoupling, photon echo meas. 80−48353
$LaF_3:Pr^{3+}$, optical meas. of spin-lattice relaxation of dilute nuclei 80−93212

lanthanum compounds continued
$LaF_3:Pr^{3+}$, optical transition, spin decoupling and magic angle line narrowing 80−28286
$LaF_3:Pr^{3+}$, photon echo lifetimes, conc. independ. 78−74951
$LaF_3:Pr^{3+}$, photon echo decay as modulation process 78−79078
$LaF_3:Pr^{3+}$, photon-echo quantum beats in $^3P_0$-$^3H_4$ transition 79−86219
$LaF_3:Pr^{3+}$, pseudo-Stark effect meas. using population hole burning and optical free-induction decay 79−24292
$LaF_3:Pr^{3+}$, spectroscopic and relaxation character of $^3P_0$-$^3H_4$ transition, photon echo 80−39897
$LaF_3:Pr^{3+}$, ultrahigh resolution photon echo spectroscopy 80−28285
$LaF_3:Pr^{3+}$, ultraslow optical dephasing 80−58648
$LaF_3:Pr^{3+}$, ultraslow opt. dephasing at 2K 80−91864
LaF_3:Pr(Nd)(Sm)(Eu)(Gd)(Dy)(Ho)(Er)(Tm), cryst. field anal. of triply ionised ion spectra 80−2796
$LaF_3:R^{3+}$, R=rare earths, crystal field anal., intensity calcs. 80−100670
LaF_3-alkali fluoride binary liquid mixtures, thermochemistry 80−45538
LaF_3-BaF_2-ZrF_4(-MF), M=Na, Li, glassy transition, refr. index, density and molar refr. 80−1937
LaF_3-$La(OH)_3$, high pressure phases, X-ray diffr. and IR spectroscopic anal. 79−47679
$LaFe_4As_{12}$, synthesis and cryst. struct. 80−84154
$LaFe_{1-x}Co_xO_3$, UPS, XPS, X-ray absorpt. spectra, band struct. study 79−56885
$LaFe_{1-x}D_xO_3$:Sn, D=Al, Ga or Sc, Mossbauer effect, hyperfine mag. fields at Sn 77−24772
$LaFeO_3$, doped, effect of doping on hyperfine fields, supertransfer model 79−47057
$LaFeO_3$, electronic struct., super transfer effects, Mossbauer expt. 78−27150
$LaFe_{12}O_{19}$, high field Mossbauer effect on ^{57}Fe at room temp. and 4.2K 79−24238
$LaFe_4P_{12}$, single crystals grown from Sn flux, struct. 78−14314
$La_2Fe_{1.76}S_5$, cryst. struct. *(French)* 78−51499
$La_2Fe_2S_5$, $La_2Fe_{1.87}S_5$, struct. *(French)* 77−55277
$LaFe_4Sb_{12}$, prep. and cryst. struct. 80−100211
$La_2Ga_2BeO_7$, melilite struct., synthesis 77−81236
$La_{10}Ga_3Co_7$, X-ray cryst. struct. determ. 80−33977
$LaGaOS_2$, cryst. struct. determ. *(French)* 78−79575
$LaGaS_3:Ce^{3+}$, phosphor, luminesc. props. 80−103979
$(La_{1-x}Gd_x)_{1.0}Mo_6Se_8$, Gd-rich, supercond. state, phase transition, lambda-type sp. ht. anomaly obs. 78−6480
$La_{1-x}Gd_xMo_6Se_8$, supercond. transition temp., upper critical field, local spin fluctuations 79−38250
La_2GeSe_5, elec. props., 300 to 1100K 79−51585
LaH, $^1\Sigma$ state, Dirac-Fock one-centre calcs. 80−23301
LaH_2, lattice thermal expansion and point defect form. energy 77−51524
$LaH_{2.08}$, proton mag. relax. by pulse NMR 78−88217
$LaH_{2.69}$ ^{139}La NMR, Knight shift 79−91307
$LaH_{2.69}$, low temp. phase transition, specific heat meas. 78−14665
$LaH_{2.69}$, low-temp. sp. ht., mag., elec., and cryst. field splitting effects 80−49379
$LaH_{2.69}$ two-phase behaviour, ^{1}H-NMR evidence 80−93189
$LaH_{2.96}$, elastic props. at high press. 77−84825
$LaH_{2.98}$, electrical resistance anomalies at high pressures 80−29381
$LaH_{2.98}$, proton mag. relax. by pulse NMR 78−88217
LaH_x, x=2.3 to 2.98, EPR investigation 79−78513
$3La(IO_3)_3.HIO_3.7H_2O$, pyroelec., cryst. struct. 79−1410
$3La(IO_3)_3.HIO_3.7H_2O$, pyroelec. p_3 and piezoelec. d_{33} coeffs. 79−19840
La_3InS_6, cryst. struct., four-circle diffractometer data and Fourier synthesis determ. *(French)* 79−14739
$LaIr_3B_2$, supercond. and mag. props. 80−97028
$La_3Ir_3O_{11}$, prep. and cryst. struct. *(French)* 79−51084
$LaKFe(CN)_6.4H_2O$, cryst. struct. determ. 78−55844
$La_2Li_{0.5}Co_{0.5}O_4$ phase, intermediate electronic configuration 80−80226
$LaLi_{0.5}Ir_{0.5}O_3$, perovskite, prep. and mag. study 80−80486
$(LaLuSm)_3(GaFe)_5O_{12}$ bubble garnet film, coercivity 79−78459
$La_xM_3(BO_3)_4$, M=Ba,Ca, thin-film capacitor mat. synthesis and props. 77−48128
$La_{1-x}M_xCrO_3$, M=Mg, Sr, electronic struct. study by XPS 80−25518
La_2MRuO_6, (M=Mg, Co, Ni, Zn), cubic ordered perovskites Mossbauer obs. and absence of mag. order 80−75889
$LaMg(NO_3)$:Ni^{2+}, pressure depend. of zero-field splitting of two mag. centres *(Russian)* 77−32249
$LaMg(NO_3)_2$:Cu^{2+}, spin-lattice recovery rate 78−10760
$La_2Mg_3(NO_2)_{12}.24H_2O$: Ce^{3+}, electron spin-lattice relax. under uniform compression 77−90028
$La_2Mg_3(NO_3)_{12}.24D_2O$, use of neutron time-of-flight technique for cryst. structs. investigation 79−19126
$La_2Mg_3(NO_3)_{12}.24D_2O$:$Mn^{2+}$, ESR spectra and non-diagonal cryst. field paremters 77−55705
$La_2Mg_3(NO_3)_{12}.24D_2O$:Nd, dynamic polarisation of deuterons in individual sites 77−59484
$La_2Mg_3(NO_3)_{12}.24H_2O$, appl. in cryogenic neutron polarisation filter 77−23341
$La_2Mg_3(NO_3)_{12}.24H_2O$, neutron diffr. obs. 78−18598
$La_2Mg_3(NO_3)_{12}.24H_2O$:$Mn^{2+}$, ESR spectra and non-diagonal cryst. field parameters 77−55705
$La_2Mg_3(NO_3)_{12}.24H_2O$:$Ce^{3+}$, mag. circular dichroism of Ce^{3+} 77−69869
$La_2Mg_3(NO_3)_{12}.24H_2O$:$Mn^{2+}$, linear electric field effect on ground state splitting, EPR 78−80198
$La_2Mg_3(NO_3)_{12}.24H_2O$:$Co^{2+}$, Ce^{3+}, relax. and ESR in magnetically cooled systems 78−88225
$La_2Mg_3(NO_3)_{12}.24H_2O$:Ce, bottlenecked Orbach relax. process, phonon lifetime 79−65151
$La_2Mg_3(NO_3)_{12}.24H_2O$:$Nd^{3+}$, polarised neutron diffr. from dynamically and statically polarised protons 80−44078
$La_2Mg_3(NO_3)_{12}.24H_2O$:$Nd^{3+}$, proton raser, self-radiating nuclear spin system *(German)* 80−53298
$La_2MgSn_{1-x}Ti_xO_6$, luminescence and energy transfer 77−28619
$LaMn_{1-x}Cu_xO_{3-y}$, prep., struct., selected catalytic props. 77−36433
$LaMn_{1-x}Cu_xO_{3+y}$, O_2 stoichiometry by thermogravimetry 77−36434
La_2MnFeS_5, antiferromag., mag. props. and mag. struct., neutron diffr. and magnetisation meas. 80−65801
$LaMnO_3$, ferromag.-paramag. phase transition, neutron diffr., calorimetric investigs. 78−31072
$LaMnO_3$, monoclinic and cubic perovskite struct., mag. props., neutron diffr. meas. 78−27022

lanthanum compounds continued
$LaMnO_3$, O_2 environment, phase stability and nonstoichiometric behaviour, 1200°C 78−43134
$LaMnO_3$, orthorhombic lattice distortions, mag. props. rel. to prep. conditions 77−20592
$LaMnO_3$, phase diagram, mag. moments, neutron diffr. study 80−108414
$LaMnO_3$, solid phase synthesis mechanism 80−21268
$LaMnO_3$, stoichiometric manganite form. reaction, thermodynamic charcts. 80−108727
$La_2(MnO_3)_3$, hydrostatic press. effect on mag. struct., neutron diffr. 77−51886
La_2MnZnS_5, antiferromag., neutron diffr. study 80−25099
$La_2(MoO_4)_3$, crystn. from Na_2MoO_4 based melt 80−20920
La_2MoO_5, cryst. struct., IR spectra, elec. and mag. props. 80−33954
La_2MoO_6, paramag. resonance and struct. 80−84162
$LaMo_6S_8$ thin films, crit. currents and pinning forces 80−34575
$La_{1.0}Mo_6S_8$, Chevrel phase supercond., compressibility and vol. depend. of Tc 78−31008
$La_xMo_6S_8$, Chevrel phase, lattice instabilities, X-ray diffr. meas. 78−34491
$La_{1.0}Mo_6Se_8$, Chevrel phase supercond., compressibility and vol. depend. of Tc 78−31008
$La_xMo_6Se_8$, supercond., mag. props., 0.7 to 295K 77−32113
$LaMo_6X_8$ (X=S, Se), supercond., sp. ht., 1 to 14K 79−51720
LaN, form. conditions 80−101019
LaN, m.p. N_2 press. depend., Pirani-Alterthum meas. 78−43103
LaN, miscibility with UC *(German)* 80−96654
LaN-RN systems, (R=Ce,Nd,Gd), mutual solubilities *(German)* 79−19374
$La(NO_3)_3.6H_2O$ single cryst. polarised Raman spectra *(French)* 77−1670
$La_{1-x}Na_xFeO_{3-x}$, defect perovskite system, Mossbauer effect 77−36159
$(La_{0.5}Na_{0.5})RuO_3$, mag. props. 78−27027
$LaNbO_4$ crystals, ferroelastic, w′ walls, temp. depend. 80−10560
$LaNbO_4$, doped, modulated struct., characterisation in ABO_{4+x} phase 79−99148
$LaNbO_4$, ferroelastic, cryst. struct. and twinning struct. 79−27965
$LaNbO_4$, ferroelastic phase transition exam. 77−27934
$LaNbO_4$, Raman scatt. and fluoresc. spectra 80−20625
$LaNbO_4$, room temp. form., symmetry determ. by convergent beam electron diffr. 80−79723
$LaNbO_4$, room temp. phase exam. 78−26536
$LaNbO_4$, single cryst., grown by Czochralski method, props. 77−52247
$LaNbO_4$:Eu^{3+}, single cryst., photoluminesc. obs., vibronic transition dichroism 77−69890
$LaNbO_4$:Ho^{3+} crystal, 3 μm stimulated emission by Ho^{3+} ions 79−99910
$LaNbO_4$:Tb^{3+}(Ho^{3+}), EPR and spin-lattice relax., Stark levels *(Russian)* 77−85563
La_3NbO_7, synthesis and cryst. growth 80−71590
La_3NbO_7, weberite-type, elec., mag. and opt. props. 77−85212
$La_{1-x}Nd_xP_5O_{14}$, Nd^{3+} luminesc. anomalously weak quenching 77−75533
$La_{2-x}Nd_xTi_2O_7$, luminesc. and absorpt. props. 79−65928
$LaNi_{1-x}Fe_xO_3$, UPS, XPS, X-ray absorpt. spectra, band struct. study 79−56885
$LaNi_5$, appl. as H storage system for heat engines *(Ukrainian)* 78−67022
$LaNiC_2$, struct. determ. using X-ray diffraction *(Ukrainian)* 80−33949
$LaNi_{1-x}Co_xO_3$, mag. props. 77−85411
$LaNi_5D_6$, cryst. struct., neutron diffr. obs. 79−19221
$LaNi_{1-x}Fe_xO_3$, mag. props., 7 to 300K 79−4648
$LaNi_{1-x}Fe_xO_3$, magnetisation meas. and ^{57}Fe Mossbauer studies 80−93217
$LaNi_{1-x}Fe_xO_3$, Mossbauer spectra, mag. hyperfine field 80−20537
$LaNi_{1-x}Fe_xO_3$, semicond. and metallic phases, elec. and mag. props. 79−78102
$LaNi_3H_x$ (x=9.7, 4.9), NMR line width, spin-lattice relaxation time temp. depend., H self-diffusion *(Russian)* 79−61248
$LaNi_5H_6$, diffusion const. in presence of large background gradients, modified pulsed gradient technique 80−31831
$LaNi_5H_6$ sponges, Al or Mn substitution, neutron diffr. 80−24427
$La_2Ni_7H_x$ (x=9.9, 11.4), NMR line width, spin-lattice relaxation time temp. depend., H self-diffusion *(Russian)* 79−61248
$LaNi_{1/2}Mn_{1/2}O_3$, Curie point rel. to Neel points of $Sr_{1-x}Ca_xMnO_3$, superexchange interactions 77−77055
$LaNi_{1-x}Mn_xO_3$, ^{55}Mn NMR study, magnetisation meas., ferromag. and Pauli paramag. components 80−7191
$LaNiO_3$, form. conditions and props. 80−21270
La_2NiO_4, free energy of formation 77−1240
La_2NiO_4, magnetic properties obs. 80−70937
$La_6Ni_6P_{17}$, synthesis and cryst. struct. 78−75634
LaO, absorption spectra, in flame, optogalvanic spectrosc. obs. 79−18202
LaO, chemiluminescence due to bimolecular oxidation of La metal 77−29011
LaO, fluoresc. spectra, atom+ROH O atom abstraction reactions, fluoresc. study 78−48643
LaO, Franck-Condon factors rot. depend. 80−58319
LaO molecule, potential energy curves, Rapid method by Morse function 77−26998
LaO, spectral intensity of $B^2\Sigma$-$X^2\Sigma$ bands, Rydberg-Klein-Rees pot. 79−31611
LaO_4^{5-}, ionisation energies, satellite struct., photoelectron spectra, MS Xα calcs. 78−13425
La_2O_3, 4f states of La, diagram lines in L-spectrum obs. 77−20959
La_2O_3, activator in Na_2O-B_2O_3-SiO_2 glass, exam. of distribution by absorption study 79−4832
La_2O_3, aerosol, controlled production technique 78−76929
La_2O_3, atomic interaction effects in X-ray emission spectra *(Russian)* 79−69905
La_2O_3, cryst. struct., X-ray powder diffr. and electron diffr. study 80−107161
La_2O_3, effect of elec. cond. of fused CaF_2 78−43157
La_2O_3, elec. cond. and dielec. const., 400-1180K, phase transition 79−56224
La_2O_3, electronic struct. study by XPS 80−25518
La_2O_3, fast ionic O_2 diffusion, neutron scatt. evidence 79−99357
La_2O_3, from reactive evaporation, struct. and polymorphic transform. 79−51441

lanthanum compounds continued
La_2O_3, high refractive index core glass for high NA optical fibres *(Japanese)* 79−59853
La_2O_3, microhardness anisotropy of single cryst. *(French)* 77−52489
La_2O_3, neutron diffraction study of high temp. struct. *(French)* 79−65050
La_2O_3, Raman spectra, lattice vibrs. 79−87440
La_2O_3, reaction with liq. Li and liq. Li-N 79−66276
La_2O_3, reduction by Si in solar furnace *(French)* 80−16784
La_2O_3, thermal expansion, 100 to 300K, X-ray method 79−99335
La_2O_3:Eu(Tb)(Tm), powder layer, electrolum., comparison with Y_2O_3 and Y_2O_2S 77−20927
La_2O_3:Mn^{2+}, position and intensity of forbidden hyperfine lines, ESR spectra 79−19775
La_2O_3-Al_2O_3 system, alumina rich phase, X-ray obs. 79−29030
La_2O_3-B_2O_3-P_2O_5, glasses, struct. changes during heat treatment, NMR obs. 77−7672
La_2O_3-CeO_2, microstruct. of La_2O_3 rich crystallites, electron microscopy and diffr. *(French)* 78−35374
La_2O_3-CeO_2, quadrupole interactions and moments, ^{137}La Mossbauer obs. 78−27121
La_2O_3-Cr_2O_3 mixtures, reactions with O_2 *(French)* 77−52524
La_2O_3-Cr_2O_3-Y_2O_3 ceramics, fireproof, direct energy conversion appl. *(Czech)* 79−70455
La_2O_3-GeO_2 system cpds., physicochem. characts. 80−97469
La_2O_3-GeO_2-$Ta_2O_3(HfO_2)(ZrO_2)$, vitrification, crystn. 77−15559
La_2O_3-Mn_2O_3-Cr_2O_3, synthesis and properties of solid solutions 78−44038
La_2O_3-P_2O_5-H_2O, solubility, regions of crystallisation, 100-500°C 77−16483
La_2O_3-SiO_2, gels, microstruct. and crystallisation, prep. method and thermal treatment effect 79−61913
La_2O_3-SiO_2, glass synthesis by hot pressing of gels 79−15637
La_2O_3-WO_3, melt, glass formation on rapid quenching 77−20055
La_2O_3-Y_2O_3, phase diagram at high temps. *(Japanese)* 77−70038
La_2O_3-Y_2O_3 phase, diagram at high temps. *(Japanese)* 77−1218
La_2O_3-Y_2O_3-Al_2O_3-SiO_2, coloration by transition metal oxides, absorpt. bands *(Japanese)* 80−55148
$La_2O_3+NH_4H_2PO_4 \rightarrow La(PO_3)_3$, solid phase reaction 79−79235
$(La_2O_3)_{1-x}$-$(CeO_2)_x$:Mn, valence state of Mn, effect of annealing in H_2 atm., ESR obs. *(French)* 80−71164
La_2O_5-$Na_2Si_2O_5$ molten glasses, surface tension and density, 900-1500°C 80−15334
LaOBr:Tb phosphor X-ray mottle reduction by multilayer screen construction 78−4756
LaOBr:Tm X-ray emission spectra and screen-film system design 78−11024
$(La_2O_3)_{0.95}(CeO_2)_{0.05}$:$Mn^{2+}$, X-band EPR study 80−60409
LaOCl, tetragonal, lattice coupling with cubic and hexagonal ZnS and ZnSe, heterojunctions 79−60919
LaOCl:Eu^{3+}(Sm^{3+}), rel. band intensities in luminesc. spectra *(Russian)* 77−48238
LaOCl:Sm^{3+}, conc. quenching of X-ray and UV-excited luminescence *(Russian)* 77−55829
LaOF, features of formation of band structure 79−33232
LaOF-LaF_3, high pressure phase transitions 80−55368
$La_2O_3GeO_2$-$Ga_2O_3(B_2O_3)$, vitrification and crystallisation 77−15558
$La(OH)_3$, heat capacity from near 5 to 350K, lattice and Schottky contribs. 80−49374
$La(OH)_3$, mol., XPES, satellite phenomena 79−27035
$La(OH)_3$, thermal decomposition, TGA, DTA, X-ray diffr. study *(Japanese)* 77−36436
$La(OH)_2Br$, hydrothermal phase equilib., cryst. struct. 78−35372
$La_7(OH)_{18}Br_3(I_3)$, hydrothermal phase equilib., cryst. struct. 78−35372
$LaOHCO_3$, $La_3Cl(CO_3)_4$, synthesis of rare earth carbonates under hydrothermal conditions 78−72714
$La_7(OH)_{18}I_3$, cryst. struct. 78−42968
$(LaO)_2S$-$(LnO)_2S$ system (Ln=Y or Lu), TEM, X-ray diffr. and fluorescence spectroscopy 79−64957
La_2O_2S, compact specimen prep. 77−85951
La_2O_2S penetration phosphor, penetration and cathodoluminescent props. 80−20718
La_2O_2S:Eu, high press. effect on luminesc. efficiency and lifetime, charge transfer absorpt. 80−66266
La_2O_2S:Eu, slow phosphoresc., high press. study 80−80839
La_2O_2S:Eu^{3+}, luminesc. props., charge transfer effects 78−15214
La_2O_2S:Eu^{3+}, luminesc., excitation spectra, cooperative phonon sidebands 79−33771
La_2O_2S:Tb, cathodoluminesc., nonlinear depend. on activator concs. 79−8190
La_2O_2S:Tb, cathodoluminesc. efficiency changes due to processing, XPS meas. of surface changes 79−99951
La_2O_2S:Tb, recomb. processes and emission spectra *(Russian)* 78−6797
La_2O_2S:Tb based barrier layer phosphors, prep. and cathodum. props. in penetration phosphors 77−1738
La_2O_2S:Yb^{3+}, charge transfer type luminesc. 79−33797
La_2O_2S:Yb^{3+},Er^{3+}, IR excited visible luminesc. of Er^{3+} 78−2910
La_2O_2S:Yb^{3+},Ho^{3+}, anti-Stokes emission band assignments, energy transfer mechanism 77−40277
La_2O_2S-AgS-Ga_2S_3, ionic conducting glasses *(French)* 78−79804
La_2O_2S-Ga_2S_3, exam. of preparation and props. *(French)* 78−80504
La_2O_2S-Ga_2S_3 system, phase diagram determ. by DTA and X-ray diffr. *(French)* 77−43309
La_2O_2S-R_2O_2S (R=rare earth), solid solubility, differences in ionic radii 77−15593
$La_2O_2S_2$, cryst. struct. determ. 79−51087
$3La_2O_3.2WO_3$, X-ray charact. and thermal props. 77−43194
$LaOs_4As_{12}$, synthesis and cryst. struct. 80−84154
$La_3Os_2O_{10}$, cryst. struct., Os_2O_{10} clusters with metal-metal bonds 79−86753
$La_4Os_6O_{19}$, prep. and struct., metal-metal interaction exam. *(French)* 77−27865
$LaOs_4Sb_{12}$, prep. and cryst. struct. 80−100211
LaP(As)(Sb)(Bi), coupling between Gd 4f electrons and conduction electrons, EPR linewidth 78−52347
$La(PO_3)_2$, vitreous, microhardness 80−25864
$La(PO_3)_3$, form. reaction form $La_2O_3+NH_4H_2PO_4$ 79−79235
$La(PO_3)_3$, X-ray struct. characts. 80−54202
$LaPO_4$ catalyst crysts., high resolution electron microscopy, morphological characts. rel. to catalytic activity 80−107193

lanthanum compounds continued
$LaPO_4$, cryst. struct., pattern-fitting struct. refinement method for X-ray powder diffractometer patterns 77−76251
$LaPO_4$:Bi, fluoresc. props., blue emission mechanism 79−52002
$LaPO_4$:Eu^{3+}, vac. UV luminesc.-excitation spectra 77−85774
$LaPO_4$:Yb^{3+}, charge transfer type luminesc. 79−33797
LaP_3O_9, X-ray powder data 79−51079
LaP_5O_{14}, continuous ferroelastic transition elastic and mechanical props. 80−92668
LaP_5O_{14}, coupling effects between soft optic and acoustic modes at ferroelastic transition 80−70358
LaP_5O_{14}, ferroelastic transition, soft acoustic mode 77−11656
LaP_5O_{14}, ferroelastic phase transition, thermal expansion and elastic consts. tensors 79−42236
LaP_5O_{14}, ferroelastic transition, polarised Raman study 80−16035
$La_{1-x}Pb_xMn_{1-y}Fe_yO_3$, magnetically ordered, NMR, spin echoes and relax. 77−48087
$La_{0.65}Pb_{0.35}MnO_3$, transport props. near Curie points 78−88100
$La_{0.71}Pb_{0.29}MnO_3$, metal-semicond. transition at Curie point, transport props. obs. 79−73554
$La_{1-x}Pb_xMnO_3$, spin polarised XPS and UPS, elec. struct. 77−8717
$La_xPb_{1\pm x}Mo_{6+y}S_8$, sputtered, supercond. props. 80−50019
$La_xPb_{1-x}Zr_yTa_{1-y}O_3$, ferroelec. with diffuse phase transition, electrostriction-optical props. 78−68457
$(La_{1-x-y}Pr_xA_y)Cl_3$ (A=Ce, Gd, Y), satellite lines in optical absorpt. spectra, Zeeman effect 79−63912
$La_{1-x}Pr_xP_5O_{14}$:Pr^{3+}, fluorescence spectrum 79−83014
$La_{1-x}Pr_3(Sn_3)$, superconducting, cryst. field excitations, inelastic neutron scatt. obs. 80−15653
La_3ReO_8, cryst. struct. *(French)* 79−90614
$La_6Re_4O_{18}$, X-ray cryst. struct. determ. Patterson and Fourier methods *(French)* 79−14745
$LaRe_2Si_2$, cryst. struct. 78−26551
$LaRu_4As_{12}$, synthesis and cryst. struct. 80−84154
$LaRu_4B_4$, X-ray cryst. struct. determ. 79−32959
$LaRu_xFe_{1-x}O_3$ perovskites, cryst. struct., elec., mag. and Mossbauer behaviour 77−55274
La_3RuO_{11}, prep. and struct. study, metal-metal bonding *(French)* 78−91325
$La_3Ru_3O_{11}$, crystal struct., X-ray diffr. study 78−67688
$La_{3.5}Ru_4O_{13}$, perovskite-type cryst. struct., X-ray determ. *(French)* 80−75206
$La_4Ru_6O_{19}$, prep. and struct., metal-metal interaction exam. *(French)* 77−27865
$La_8Ru_4O_{21}$, mixed valence oxide of new hexagonal struct. type 78−51503
$LaRu_4Sb_{12}$, prep. and cryst. struct. 80−100211
LaS, chemiluminesc. vibr. analysis of $C^2\Pi \rightarrow X^2\Sigma^+$, D_0^0 determ. 77−48645
LaS elec. cond. and diff. thermo-EMF in 77-300K range 77−24573
LaS, heat carrier scatt., thermal and elec. cond. from 5-400K 79−14974
LaS, plasma light reflection by free charge carriers 80−11403
$LaS_{1.33}$-$LaS_{1.40}$, low temp. sp. ht. 80−15259
$LaS_{1.47}$ elec. cond. and diff. thermo-EMF in 77-300K range 77−24573
$LaS_{1.500}$-$LaS_{1.333}$, solid soln. region, density meas. 80−95075
LaS_2, cryst. struct. *(French)* 78−34476
La_2S, unsaturated and saturated vapour press., 673-1173K, thermal dissoc. pattern 80−104457
La_2S_3 glass *(French)* 80−71369
γ-La_2S_3, indirect electron transitions, diffuse refl. and vibr. spectra 78−84576
La_2S_3, optical props. and electronic struct. in fund. absorpt. region 80−80817
La_2S_3 single crystals, optical props. 79−87458
La_2S_3, vibr. spectra, factor-group anal. 80−80793
La_2S_3-Ag_2S-Ga_2S_3 glass system, prep., thermal and elec. props. *(French)* 80−89192
La_2S_3-Ga_2S_3 system, phase diag. *(French)* 78−3108
La_2S_3-LaS_2, p-T-x phase diagram of La-S system 77−21112
$La_{3-x}S_4$, mag. ordering and elec. cond. 78−10681
La_3S_4, high crit. mag. field supercond., elec. resist., sp. ht. and magnetisation 80−2532
La_3S_4, structural transitions, symm. anal. 80−92671
La_3S_4-La_2S_3, low temp. sp. ht. 80−15259
La_xS_y, stoichiometry and opt. props. during hot pressing 78−23653
$La_2(SO_4)_2.9H_2O$, Raman spectra meas. *(French)* 77−20855
$La_2(SO_4)_3.9H_2O$, and isotopic forms, water librations, Raman obs. *(French)* 79−28754
$La_2(SO_4)_3.9H_2O$, crystal struct. refinement 77−15369
$La_2(SO_4)_3.9H_2O$:Gd^{3+}, single cryst., EPR study, spin Hamiltonians 80−80606
$La_2(SO_4)_3.9H_2O(D_2O)$, cryst., polarised Raman spectra, phase transition *(French)* 77−66497
$La_2(SO_4)_3.9H_2O(D_2O)$, dynamic disorder of water mols., isotope effect obs. 80−55015
La_2S_3=1.8Ga_2S_3 glass, vibr. spectra electronic transitions, short range order 77−69820
$La_2S_3.3Ga_2S_3$:Er^{3+} glass, fluoresc., and possibility of lasing 78−23514
LaSb, cryst. field effects on transport props. 78−72133
LaSb, plasma light reflection by free charge carriers 80−11403
La_2Sb, X-ray cryst. struct. determ. 80−33943
La_4Sb_3 and $La_4(Sb_{0.5}Bi_{0.5})_3$, superconductivity 77−20481
La_4Sb_3, X-ray cryst. struct. anal. 80−39013
$LaSbO_3$, single crysts., hydrothermal synthesis and crystallographic characteristics 79−95916
LaSe, plasma light reflection by free charge carriers 80−11403
La_2Se_3, La_2Te_3, mutual solubility 77−21113
La_2Se_3-Ga_2Se_3-$GeSe_2$ ternary system, phase diags., glass formation *(French)* 78−3109
La_3Se_4, structural transitions, symm. anal. 80−92671
$LaSi_2$, thin film, exam. of phase transitions during vacuum annealing 79−95281
La_5Si_3 thin film, exam. of phase transitions during vacuum annealing 79−95281
$LaSiO_3F(Cl)(Br)$, phosphor host, luminesc. and struct. props. 78−48212
$LaSiO_2N$, cryst. struct. 78−10017
$LaSiO_2N$, cryst. struct. 78−10019
$La_4Si_2O_7N_2$ single cryst. growth by floating zone method with SiO_2-Si_3N_4 additions 80−93481
$La_{0.58}Sm_{0.42}B_6$, FIM study 80−71578
$La_xSm_{1-x}B_6$ solid solns., mag. susceptibility meas. *(Russian)* 79−28501

lanthanum compounds continued

$La_ySn_xMo_6S_8$, supercond. props. 80−97023
$La_{0.98}Sn_{0.02}Mo_6Se_8$, Chevrel phase supercond., hyperfine interaction, microscopic study 79−56650
$La_{0.98}Sn_{0.02}Mo_6Se_8$, Mossbauer spectra 80−15926
$La_{0.5}Sr_{0.5}CoO_3$, conducting oxide powder prod. by freeze drying 79−95984
$La_{0.5}Sr_{0.5}CoO_3$, conducting oxide prod. by amorphous citrate process 79−95985
$La_{0.5}Sr_{0.5}CoO_3$, semicond. oxide O_2 electrode characts. 79−24073
$La_{1-x}Sr_xCoO_3$ ($0.5 \leq x \leq 1.0$), mag. props. 79−24154
$La_{1-x}Sr_xCoO_3$, ($0.5 \leq x \leq 0.9$), ferromag., elec. props., itinerant electron model 80−107785
$La_{1-x}Sr_xCoO_3$, electronic and mag. props., itinerant ferromagnetism obs. 78−10660
$La_{1-x}Sr_xCoO_3$, specific heat meas., using laser-flash method, phase transitions obs. *(Japanese)* 80−54898
$La_{1-x}Sr_xCoO_{3-y}$, Seebeck coeff. meas., small polaron hole conduction model 80−20233
$La_{2-x}Sr_xCoO_4$, mag. behaviour obs. 80−70971
$La_{0.75}Sr_{0.25}CrO_3$, struct. refinement by X-ray powder diffr. profile analysis 77−84721
$La_{0.84}Sr_{0.16}CrO_3$, sintering 77−77440
$La_{1-x}Sr_xCrO_3$ ($0 \leq x \leq 0.4$), localised level hopping transport 80−10974
$La_{1-x}Sr_xCrO_3$, densification 77−8780
$La_{1-x}Sr_xCrO_3$ system, phase relationships, cryst. struct. 77−69073
$La_{1-x}Sr_xCrO_3$, x=0-0.2, AC and DC cond., 77-1300K, hopping of polarons 78−2477
$La_{2-x}Sr_xNiO_4$, ($0 \leq x \leq 1$), cryst. struct. and elec. props. 78−2088
$La_xSr_{1-x}RuO_3$, metallic, mag., electronic and structural props., ^{99}Ru Mossbauer spectroscopy 77−48107
$La_{1-x}Sr_xVO_3$, Anderson transition, elec. resist. and thermopower meas. 80−100488
$La_{1-x}Sr_xVO_3$, high-temp. transport meas. 77−11917
$La_{1-x}Sr_xVO_3$, semiconductor-metal transition, Anderson localisation, Hall mobility and 1/f noise meas. 79−78142
$La_{1-x}Sr_xVO_{3-0.1x}$, elec. cond. and mag. susceptibility, temp. depend., 77-300K 77−47816
LaT_2, ^3He detrapping and release after ^3H decay, strain model 77−60101
$LaTaO_4$, doped, modulated struct., characterisation in ABO_{4+x} phase 79−99148
$La_{1-x}Tb_xOBr$ phosphor, concentration quenching of Tb^{3+} luminesc. 80−29785
LaTe, metallic, phonon density of states, Raman scatt. expt. 78−23451
La_3Te_4, thermal cond., thermoelec. power abd elec. cond. meas., 80 to 750K 78−18853
La_3Te_4, thermoelectric material, thermal cond. meas., 1100-2000K 78−24798
$LaTiO_3$, spin states, XPS meas. 78−68599
$La_2Ti_2O_7$, crystal struct. and phase transitions, rel. to isomorphous crystals *(Japanese)* 80−49208
$La_2Ti_2O_7$, ferroelec., layer type struct., cryst. growth 80−108348
$La_2Ti_2O_7$, ferroelecs., nonlinear optical props. 80−33086
$La_2Ti_2O_7$, layered ferroelectric anomalous photovoltaic effect, photovoltaic current 80−75603
$La_2Ti_2O_7$-$CaTiO_3$ system, mode of formation and stability of $A_nB_nO_{3n+2}$ phases *(French)* 78−3110
$La_4(TiO_4)_3$, electrical props., effect of initially used La_2O_3 *(Polish)* 77−59508
$(LaTmCa)_3(FeGe)_5O_{12}$, mag. loss and domain wall mobility 80−65980
$(LaTmCa)_3(Fe_{5-x}Ge_x)O_{12}$ film, high g, for mag. bubble applics. 77−85529
$La_{0.9}Tm_{0.1}Se$, sp. ht. meas., 1.6 to 20K, mag. contrib. 80−65934
$LaV_{1-x}M_xO_3$ (where M=Cr or Fe), solid solns., elec. and mag. props 79−23967
$LaVO_3$, successive phase transitions, X-ray anal. 80−108437
$LaVO_4$, dimorphic, NMR of ^{51}V and ^{139}La 77−63310
$LaVO_4$, electron energy loss spectra, primary excitation processes in cathodolum. 79−11490
$LaVO_4$, monazite struct., IR and NMR spectra 79−78534
$La_2V_{10}O_{28}.20H_2O$, cryst. struct., monoclinic unit cell parameters, X-ray anal. 79−86772
$La_2V_{10}O_{28}.20H_2O$, X-ray cryst. struct. anal. 80−39060
$La_{3-x}V_xS_4:Gd^{3+}$, EPR study of interaction between localised mag. moment and conduction electrons *(Dutch)* 77−63277
$La_{3-x}V_xS_4:Gd^{3+}$ localised moment-conduction electron interact., ESR obs. 78−88183
$La_{10}W_2O_{21}$, enthalpy and heat capacity at high temp. 80−70424
α-La_2WO_6, enthalpy and heat capacity at high temp. 80−70424
La_2WO_6, growth from soln. in melt 77−1806
$La_6W_2O_{15}$, enthalpy and heat capacity at high temp. 80−70424
$La_xY_{3-x}Ga_yFe_{5-y}O_{12}$, solubility model in PbO/B_2O soln. 79−46807
LaYSb, superconductivity 77−20481
$La_2Zn_3(NO_3)_{12}.24H_2O:Mn^{2+}$, pair spectra and mag. props. of Mn^{2+} 77−8396
$La_2Zn_3(NO_3)_{12}.24H_2O:CO^{2+}$, Mn^{2+}, Ni^{2+}, mag. exchange interactions, EPR 77−36118
$La_2Zr_2O_7$-$La_2Hf_2O_7$ system, cryst. struct., phase diagram 78−83806
$La_{3-x}\square_xS_4:Gd^{3+}$, localised moment-cond. electron interactions, EPR data interpretation 77−63280
Li-La phosphate glass, Nd, Cr activated, Nd luminesc. quantum efficiency meas., Nd-Cr nonradiative transfer 80−66296
Li-$La_{1-x}Nd_x$ phosphate glasses, stimulated emission spectroscopy of $^4F_{3/2}$ to $^4I_{11/2}$ and $^4F_{3/2}$ to $^4I_{13/2}$ transitions 79−38573
Li-Nd-La phosphate glass, nonradiative losses, pulse periodic stimulated emission and luminesc. 77−83878
Li-Nd-La phosphate glass active elements, laser characts., comparison with Nd:YAG 80−33002
$(Li_{0.5}La_{0.5})_xBa_{1-x}TiO_3$, cryst. struct., dielec. and IR spectral meas. 79−46614
$LiNd_{0.5}La_{0.5}P_4O_{12}$ laser, stabilised dual-polarisation oscill. 77−54723
$Ls_6Fe_4S_{14}$, antiferromag., neutron diffr. study 80−70954
$(Lu, La, Y, Ca)_3(Ge, Fe)_5O_{12}$, temperature compensated high mobility bubble garnet, LPE and props. 77−20656
Mo-Mo_2C-La_2O_3-Pt cathode, Pt effect on work function *(German)* 79−74048
$Na_3La(AsO_4)_2$, allotropes, prep. and cryst. struct. *(French)* 78−63724
$Na_xLa_{1-x}B_6$, electrodeposition 79−47643
$(Na_{0.5}La_{0.5})_xBa_{1-x}TiO_3$, dielec. and IR spectra exam., ferroelec. transition 78−23418

lanthanum compounds continued

$Na_3La_{1-x-y}Ce_xTb_y(PO_4)_2$, optical props. *(French)* 80−103991
$Na_3La_{0.98}Eu_{0.02}(VO_4)_2$, luminesc. spectrum 77−4673
$Na_2LaGeO_4(OH)$, cryst. struct. and refinement 77−65970
$NaLa(MoO_4)_2$, luminesc. centres, EPR meas. *(Russian)* 77−28442
$Na_3La(PO_4)_{1.9}(VO_4)_{0.1}$, luminesc. spectrum 77−4673
$Na_3La(VO_4)_2$, luminesc. spectrum 77−4673
$Nd^{3+}:LaCl_3$, laser-induced fluoresc., hyperfine structs. 80−100677
$Nd^{3+}:LaCl_3$, laser-induced fluoresc. energy transfer effects 80−100678
$NdLaP_5O_{14}$, large crystal growth technique *(Chinese)* 79−24418
$Nd_{0.5}La_{0.5}P_5O_{14}$ laser, FM mode-locked 79−86184
$Nd_{0.75}La_{0.25}P_5O_{14}$, miniature laser system bonded mirrors, side pumped by LEDs 78−87058
$Nd_xLa_{1-x}P_5O_{14}$, crystal growth, laser generation characts. 80−38020
$Nd_xLa_{1-x}P_5O_{14}$, large single crystal growth from hot conc. H_3PO_4 and oxide, props. *(French)* 77−4723
$Nd_xLa_{1-x}P_5O_{14}$ laser, pumped by nanosecond pulses, performance 77−38897
$Nd_xLa_{1-x}P_5O_{14}$, laser properties 79−22957
$Nd_xLa_{1-x}P_5O_{14}$, Nd^{3+} stoichiometric materials, luminesc., conc. quenching 78−27315
$Nd_xLa_{1-x}TaO_4$, polycryst. optical centres, thermodynamic equilib., 1600-1700K *(Russian)* 77−68970
$NiLa_2O_4$ electrochemical electrodes, kinetics of O_2 evolution, appl. to electrolytic H energy prod. 80−30430
PLZT ceramic, ageing, dielec. props. 80−88940
PLZT ceramic, bonded lens assembly manufacture 80−79018
PLZT ceramic, dielectric anisotropy, role of 90° domain processes 77−63384
PLZT ceramic, ferroelec., cathodlum. spectral and temp. depend. 78−84665
PLZT ceramic, optical gate, dielec., optical props., electro-optical effect meas. 78−42418
PLZT ceramic, possible construction of matrix-addressable controlled transparency 78−71222
PLZT ceramic, proton implanted, photoferroelectric effect for image storage and display devices 80−80315
PLZT ceramic, thin waver electrode slotting process 80−79017
PLZT ceramic, thin wafer production polishing process 80−81214
PLZT ceramic, transverse electro-optical effect, matrix-addressable transparency 79−27431
PLZT ceramic birefringence props., transverse electro-optical meas. 78−72487
PLZT ceramic with memory, domain reorientation, alternating elec. field effect 79−47405
PLZT ceramic;, visible light scatt. depend. on photoferroelectric space charge fields 80−80806
PLZT ceramics, electro-optic characts., w.r.t. future instrument applics. *(German)* 78−33792
PLZT ceramics, electro-optical props. *(Korean)* 79−11406
PLZT ceramics, electro-optic; defect struct. and prop. 79−42910
PLZT ceramics, modified by $Ca^{2+}(Sr^{2+})(Nd^{3+})(Y^{3+})$, dielec. behaviour 80−60519
PLZT ceramics, optical information storage and spatial light modulation 78−83097
PLZT ceramics, photoferroelectric image storage in antiferroelectric phase 79−47404
PLZT ceramics, photoferroelectric effects, image storage device appl. 79−42924
PLZT ceramics, photoinduced charge transfer process 79−50362
PLZT ceramics, SHG, anomalous phase transition 79−45996
PLZT ceramics, sp. ht., 2-25K, field depend., phonon modes 77−47586
PLZT ceramics, stress-induced ferrelec. transition, pseudoelasticity and shape memory, bending meas. 79−24274
PLZT ceramics, transparent ferroelec., photorefraction and photocond. study 79−42581
PLZT, coaxial magnetron sputtering techniques 79−83123
PLZT colour cell for real time two colour incoherent to coherent image convertor 78−38039
PLZT composition, effect on its switching characts. 79−42917
PLZT, controlled light scatt. 78−10909
PLZT, diffuse phase transitions, Curie temp., dielectric props. 80−75979
PLZT, effect of ageing on temp. depend. of permittivity, for ferroelectric and antiferroelectric compositions 78−48121
PLZT, electrically polarised, size and conc. of light scatt. centres 77−28549
PLZT, electro-optical, physical elec. and optical props. and fabrication *(Polish)* 78−56458
PLZT electro-optic shutter stereoscopic display applications 80−90826
PLZT electrooptic shutters as thermal/flash protective devices 77−46808
PLZT, exam. of grain growth in hot pressing, and liquid phase sintering 79−33981
PLZT, Fe doped, photochromic effect 77−16347
PLZT ferroelec. ceramics, piezoelec. props. 79−42897
PLZT, ferroelectric domain struct. obs. by SEM and optical microscopy *(Japanese)* 78−15136
PLZT ferroelectric display electro-optical props. *(Russian)* 79−9211
PLZT ferroelectric ceramic, photovoltaic effect 79−99585
PLZT film, electro-optic effects 78−6799
PLZT film, epitaxial growth by RF sputtering, and characterisation 77−85937
PLZT, fine grained 90° electric domain wall movement, interpretation of dielectric losses *(German)* 79−33646
PLZT, light scatt., time depend., switching, memory modes 77−12362
PLZT, light scatt. under switching conditions, time characts. 77−52045
PLZT, light scattering, IR laser radiation recording 78−4695
PLZT, mech. and elec. losses, correl., theory and expt. 80−66133
PLZT modified high voltage dielectric, permittivity, Curie temp., loss meas. 80−80720
PLZT, phase transitions, permittivity, birefr. and light scatt. meas. 77−81074
PLZT porosity and transparency affected by vacuum hot pressing 77−12556
PLZT powder preparation, hyrolysis ball mixing 80−81006
PLZT, prep. by liquid phase sintering of oxides 79−38778
PLZT pyroelectric detectors, fast response to MW CO_2 laser pulses 79−54187
PLZT pyroelectric detectors, piezoelectric oscillations, in response to CO_2 laser pulses 79−61305
PLZT, RF sputtered thin film, ferroelectric props. 79−69780

lanthanum compounds continued
PLZT real time 2 colour incoherent to coherent image convertor 79−3805
PLZT, reduced, exam. of ageing phenomena, using dielectric hysteresis *(German)* 79−33647
PLZT, refr. index, 405-764 nm, surface layer 78−35110
PLZT slim-loop and linear ceramics, longit. electrooptic effects, display appl. 80−80751
PLZT slugs, powder hot pressing technique 80−81007
PLZT, Sn substituted, antiferroelectric ceramics research and their applications *(Chinese)* 79−33617
PLZT spatial light modulator for a 1-D hologram memory 80−37963
PLZT thermal, flash, ferroelectric protective goggles 80−81746
PLZT, thin film epitaxial growth and characteris. 79−28918
PLZT, thin film prep. by RF sputtering, struct. and ferroelec. props. *(Japanese)* 77−69992
PLZT, transparent, optical exam. of small signal behaviour, of 90° electric domain walls *(German)* 79−33645
PLZT transparent ceramics, electro-optical anisotropy due to hot pressing 77−12720
PLZT, transparent ferroelec., RF sputtering and film characterisation 78−72727
PLZT, transparent ferroelectric, ceramics obtained by hot pressing, optimum conditions *(German)* 79−43176
PLZT type ceramics, calorimetric meas. of energy of electrical polarisation 79−2770
PLZT/TFPD thermal/flash protective lens assembly, polarised delamination investigation 80−78929
(PLZT)(PLZN) system, ferroelec. transparent, prep. and study 79−42911
$(Pb,La)TiO_3$ ceramic, ferroelec. Curie temp. comp. depend. 77−16258
$(Pb,La)TiO_3$, paraelec. phase, anomalous dielec. behaviour 78−23387
$(Pb,La)TiO_3$, soft E(TO) phonons, and phase transitions, Raman spectra, −200 to 400°C 78−15109
$(Pb_{1-y}Ba_y)_{1-x}La_xNb_{2-x/5}O_6$, transparent ferroelec. ceramic, optical transmittance, electrooptic props. and Curie temp. 77−32395
$Pb(Fe_{1/2}Nb_{1/2})O_3$-$La_2O_3(CeO_2)$ ferroelec. ceramics, electrophysical props. 78−35099
$Pb_{1-\alpha x}La_xTiO_{3+x(1.5-\alpha)}$, permittivity as function of temp. 79−33586
$Pb_{0.97}La_{0.02}(Zr_{0.92}Ti_{0.08})O_3$, ferroelec. ceramic, stress effects 80−2119
$PbTiO_3$-$La_2O_3.3TiO_2$, struct. and dielec. props. 80−54200
$Pr_{0.2}La_{0.8}F_3$, fluorescent line narrowing, time depend. effects 78−31244
Si_3N_4-SiC-La_2O_3, reactively sintered, microstruct. and strength 80−25631
SiO_2-Al_2O_3-Y_2O_3-La_2O_3-TiO_2 glasses with high elastic moduli, alkaline durability 80−85071
SiO_2-CaO-Na_2O-La_2O_3 system, water, alkali, acid resist., chem. durability 79−34162
$Sm_{0.8}La_{0.2}AlO_3$, high temp. Raman spectra, phase transition 79−61367
$Sm_{1-x}La_xB_6$, valence transition, lattice parameter and mag. susceptibility meas. 80−59929
$Sm_xLa_{1-x}B_6$, solid solns., exam. of structure, elec. props. 80−39290
$Sm_{1-x}La_xS$, mag. suscept., moment, impurity effects, indirect exchange interaction 78−68147
$Sm_{1-x}La_xS$, magnetoresist. in semicond. and metallic phases 80−96914
$Sm_{1-x}La_xS$, press.-induced semicond.-metal transition, refl. and lattice compression meas. 77−62826
$Sm_{1-x}La_xS$, valence transitions, theoretical model 79−69474
$(SrCaLa)_2(Cr,Ga_{1-x})O_4$, mag. 2-D oxide, phys. props. 78−47974
SrF_2-LaF_3, tentative phase diagram 80−71633
$SrLaBO_4$, crystallographic and Pb^{2+} luminesc. data 79−32971
$SrLaCoO_4$, struct. and mag. props., electronic struct. of trivalent Co *(French)* 79−86760
$SrLaCrO_4$, mag. struct. determ. by neutron diffr. *(French)* 79−28507
$SrLaFeO_4$, mag. and cryst. struct. determ. *(French)* 80−54866
$SrLaFeO_4$, Mossbauer spectra 80−15880
$SrLaFeO_4$, two-dimens. mag. props. rel. to cryst. struct. 80−75776
$Sr_{1-x}La_xFeO_3$, Mossbauer spectra, charge disproportionation 80−20542
$Sr_{0.5}La_{1.5}Li_{0.5}Fe_{0.5}O_4$, high spin configuration stabilisation for Fe^{4+} *(French)* 80−88519
$Sr_{1+x}La_{1-x}MnO_4$, cryst. struct. determ. *(French)* 78−6042
$Tb_xLa(Y,Gd)_{1-x}$.DAM.Sal_3, DAM=diantipyrylmethane, luminesc. *(Russian)* 77−55830
TiO_2-$LaCrO_3$-GaP photoelectrochem. reactor for materials synthesis using solar energy 80−45712
$Tm_y(La,Y)_{1-y}S$, microwave resistivity 77−11949
$Tm_y(La,Y)_{1-y}Te$, microwave resistivity 77−11949
(U,La)C, U self-diffusion 80−92711
$(Y,La)B_6$, superconducting transition temps., impurity effects 80−20341
Y-W(Mo)-B, phase equilibria, struct. of crysts. 77−21122
YIG, La- and Ga-substituted, inhomogeneous epitaxial films, spin wave reson. 79−99773
YIG:La, films, ferromagnetic resonance, ion implantation effect 80−97145
$Y_{1-x}La_xAl(Sc)O_3:Ho^{3+}$, stimulated emission of Ho^{3+} ions 77−81126
$(YLaBi)_3(FeGa)_5O_{12}$, pure and In^{3+} doped, near IR absorpt. and Faraday rot. 78−95580
$Y_{1-x-y}La_xEr_yAlO_3$, $Y_{1-x-y}La_xEr_yScO_3$, stimulated emission of Er^{3+} ions 78−6705
$Y_{2.85}La_{0.15}Fe_{3.75}Ga_{1.25}O_{12}$ epitaxial film, spin wave reson. spectrum 77−69703
$Y_{2.85}La_{0.15}Fe_{3.75}Ga_{1.25}O_{12}$ LPE films, ion implantation effect on spin waves 80−71124
$Y_{2.85}La_{0.15}Fe_{3.85}Ga_{1.15}O_{12}$ garnet, mag. props., ion implantation effect, Mossbauer study 80−97166
$Y_{3-x}La_xFe_{5-y}Ga_yO_{12}$ film, horizontally dipped LPE grown, FMR, anisotropy field obs. 79−78449
$Y_{3-y}La_yFe_{5-x}Ga_xO_{12}$, garnet film, radial oscillation of bubble lattice 79−73787
$Y_{3-x}La_xFe_5O_{12}$, mag. props. rel. to ionic struct. 80−75756
ZnO-La_2O_3-B_2O_3, glass, refraction, refractive index from 0.365 to 2.50 μm 80−88953
ZnO-La_2O_3-GeO_2, exam. of glass forming region, properties and crystallisation 78−88454
ZrF_4-BaF_2-LaF_3 F^- ion cond. glasses, cond. process 80−107477
α-$ZrH_{0.74}La_{0.42}(PO_4)_2.4.6H_2O$ cryst., self-diffusion of La^{3+} ions 78−34648

Laplace transforms
acoustic response, transient, of two fluid-coupled spherical elastic shells to incident pressure pulse 79−68454
aerosols, asymmetric deposition motion in circ. tube, anal. by Laplace transform methods *(Chinese)* 79−37379
airfoil, thin, pulsating, HF subsonic flow 79−59998
arterial bifurcation, steady convective diffusion model 77−21546
beam, homogeneous, initial boundary value problem of transverse vibr. 79−41601
beam transient response prediction by Laplace transform techniques 78−1596
biological model mathematically exact soln. *(German)* 79−1991
Birman-Schwinger bounds for the Laplacian with point interactions 80−137
cascade flow problem reduction of part-channel of varying width 80−83843
Cauchy problem, linear eqns. with const. coeffs., absolute instability, 3-dimens. 79−12622
colloid size distrib., photon correl. spectroscopy, methods of cumulants, histogram and Laplace transform 79−58801
compound unbounded cones, temp. fields *(Ukrainian)* 78−54317
concrete creep under nonuniform temp. distrib., linear viscoelastic analysis 77−62172
convergence acceleration method for lattice sums from electronic struct. of crystalline solids 78−30577
coordinate transformation of Laplace operator in 2-D, for teachers 78−61999
cracks, penny-shaped, ductile, dynamic effects in propagation, Hankel and Laplace transform methods 80−87741
cylinder, composite circular, transient thermal stresses 78−79217
diffuse reflection problem for combination of Rayleigh and isotropic scatt., Laplace transform 79−84661
diffusion of particles, time-depend. problem, spectral anal. 78−45582
double transform technique, appl. to semiconductor charge carrier transport 77−39836
ducts and pipes intricately shaped cross section, heat transfer, Laplace and structural method 78−83477
Earth EM sounding, interpretation of transients in Laplace space representation *(Russian)* 78−40483
education, nabla^2 derivation in cylindrical and spherical polar coords. 77−78927
elastic wave propagation in heterogeneous bars with varying cross-section 77−65707
electric field between conical electrode with hyperboloid end and earthed plate, mathematical formulation *(Czech)* 79−27125
electrocoating, cell design, Fourier transform soln. of Laplace eqn. 78−76609
EM quasistationary time-varying field, diffusion into spherical shell 79−13870
EM wave diffr. by unidirectionally cond. strip, transform and Wiener-Hopf techniques 78−58883
emergent intensity from semi-infinite atmosphere, Laplace transform and Wiener-Hopf technique, exact soln. 79−75095
ferroelectric ceramics, 1-D linear dynamic electromechanical responses 79−47397
finite decomposition of tr e^{-A} as function of diagonal of A determ. from Laplace transform *(French)* 79−25824
finite element Laplace transform soln. 78−4488
fluidised glass ballotini-packed fixed bed, at low/intermediate Reynolds nos. 79−1244
forced oscillations in rotating stratified liquid 78−63478
generalised transform props. 77−67212
geodesy, soln. of downward continuation problem by initial value method *(German)* 77−86750
heat conduction, elliptic cylinder, interior value problem 79−37123
heat transfer, in thick slabs, inversion problem 77−27460
impurities dispersion in river, model *(Dutch)* 79−88011
inert gas mixtures, interatomic pots. and interaction dipole moments, IR spectra calcs. 77−75082
integral eqn. method for potential problems with source function not located on boundary 78−24643
invariant phase space integral evaluation via Laplace transforms 80−31573
inversion, non-unitary representations of MH(2) and group ax+b 80−4866
inversion methods for integral transforms of class L_2 functions *(Russian)* 78−20940
kidney model transient behaviour 78−65065
LANDSAT geoexploration, digital mosaicking and lineament enhancement *(Japanese)* 80−82169
Lie theory and wave eqn. in space-time, SO(4,C) group 79−12968
light intensity probability density determ., from photoelectron statistical distrib. 78−24840
linear differential equations with variable algebraic coeffs. *(Czech)* 78−86115
linear time dependent partial differential eqns., solns. by Laplace transform and FFT 78−57763
liquid metal flow, in open channel, MHD regulation, armature reaction calc. *(Russian)* 77−47107
Maxwell fluid, unsteady flow past flat plate, transform technique 78−59428
MHD unsteady free convection flow, past hot vertical plate, calcs. 77−75986
modal anal., formulations for numerical calcs. 78−57767
neutron slowing down and transport in medium of const. cross-section 78−33235
nonlinear oscillators, Brownian motion, projection operator method, double well potential oscillator appl. 79−2723
nonlinear relaxation processes governed by rotational Smoluchowski eqn. 79−71365
nonlinear transient heat transfer, through multilayer wall *(Russian)* 77−23857
nonlinear unsteady heat conduction, Laplace transform, small parameter, R-function and variational methods joint appl. 79−94451
numerical inversion, Mellin transform expressed as two sided Laplace transform 78−77694
numerical inversion method and relax. distrib. function approx. 80−84720
numerical inversion of Laplace transform and Fredholm integral eqns., eigenvalues and eigenfunctions 78−81800
particulate suspensions, weak wave propagation 77−80207
penny-shaped crack, sudden twisting in a finite elastic cylinder, stress calcs. 78−67110

Laplace transforms continued
photodielectric layer, Laplace transform of small-charge current, trapping level parameters 77−69337
photon statistics, unsaturated k-photon absorption, exact soln. of master eqn. 80−37984
piezoelectric transducers, calculation of inverse Laplace transform for functions describing pulsed operation 79−64480
pipes, hydraulic, with nonlinear boundaries, transient waves 80−43722
plane two-dimensional motion in acoustic medium caused by kinematic excitation, Laplace transform study *(Russian)* 80−43503
planetary finite atmospheres, radiative transfer key eqn. exact soln. 80−67536
plasmatron gas average enthalpy, forced heat exchange calcs. *(Russian)* 80−38724
porous elastic half space, Lamb's line load problem 79−30248
potential problems, numerical solution, integral equations without Green's function 78−20950
quantum mechanics, Feynman path integrals with Gaussian measure, Laplace transform method 80−62522
radiative transfer, exact soln. of diffuse refl. and transmission problem in Rayleigh scatt. 79−35116
radiative transfer, exact soln. of problem by Laplace transform and Wiener-Hopf technique 79−53711
radiative transfer, time-dependent, exact soln. of integro-differential eqn. via Laplace transform 80−94703
radiative transfer eqn. exact soln. for semiinfinite plane-parallel isotropic scatt. atm. 79−12396
radiative transfer H-function, expression using Laplace transform and Wiener-Hopf technique 79−35111
radiative transfer in finite atmosphere, exact soln. of basic eqn. via Laplace transform 80−94702
radiative transfer in semi-infinite Rayleigh scattering atmosphere, exact soln. 79−35112
radiative transfer in stellar atmosphere, soln. using Laplace transform and Wiener Hopf technique 79−84784
Rayleigh scattering transport eqn. exact soln. by Laplace transform and Wiener-Hopf technique 79−8827
reactor fuel pin heat transfer, digital transfer matrix 78−29548
real variable inversion, plasma physics application, for teachers 79−21496
renal medulla single loop solute cycling model, transient behaviour 78−73167
renal medulla solute cycling model soln. by Laplace transforms 77−40694
resistance thermometer transmission function approximation *(Russian)* 78−62197
reversible reactions, first order, time depend. behaviour 80−97699
Riemann function derivation for Klein-Gordon eqn. with nonconstant coeff. 77−57153
river pollution, dynamic behaviour of distributed systems *(Dutch)* 80−3542
scattering experiments, deconvolution of thermal averaging using integral transform methods 78−92442
Schrodinger eqn., hyperspherical coords., discrete spectrum of charged particles 77−49627
Schrodinger equation, scatt. theory 78−57806
second order fluid, unsteady motion between parallel plates 78−30321
shock wave diffraction on plane with semicircular cylindrical roughness, numerical integration *(Ukrainian)* 80−22201
skin impedance, Laplace plane anal. 79−39458
soil consolidation under distributed shear loads, complex Fourier and Laplace transform. technique 79−57936
solar UV continuum, absolute intensities, centre to limb vars. and Laplace inversion between 1400 and 2100 Å 79−62803
sound pulse diffraction by circular cylinder 78−30107
specific equilib. recombination rate coeffs., Laplace transform calcs. of temp. depend. 78−60989
spray drying, of highly viscous conc. solns., heat and mass transport *(Russian)* 78−83230
stellar finite atmosphere, radiative transfer key eqn. exact soln. 80−72762
stochastic temperature fields in a solid spheric cone *(Ukrainian)* 79−50566
stress anal. in 3-D, numerical-experimental hybrid technique 78−22265
stress analysis of beam, Timoshenko, non-stationary loaded 80−14564
stress waves in heterogeneous media, Laplace transform inversion 77−80103
tall-form spray chamber, residence-time distribution of air 78−9679
tensor spherical harmonics on S^2 and S^3 as eigenvalue problems 79−17324
thermal desorption model analysis *(German)* 78−63940
thermoelasticity, one-dimensional direct approach anal. 80−8797
third-order nonlinear systems with aperiodic excitations 78−81830
Timoshenko beams, effect of rotary inertia and shear deform. on freq. eqns. 78−83296
transient elasto-dynamic response of circular crack in thick plate under torsion 80−5993
transient EM wave transverse propagation in non-homogeneous half-space 77−75374
transient forced convection eqn. soln., circular pipe flow 78−30282
transient heat conduction, Laplace transform and boundary integral eqn. 77−72129
transient piezoelectric wave scatt. from crack 79−52615
triangular aperture, EM field scattering 79−50192
tube with variable boundary conditions, heat transfer, Laplace transform appl. 80−74859
two-photon spectroscopy, Laplace transform method 79−10084
unsteady aerodynamic modelling for arbitrary motions 80−19433
unsteady subsonic and supersonic pot. aerodynamics for complex config. aircraft 77−72320
viscoelastic 78−1576
viscoelastic bar, transient wave propag. 80−106745
viscoelastic beam, continuous, dynamic response 78−9569
viscoelastic liquid, pulsatile flow in elliptic cross-section channel 79−7392
viscoelastic materials, stress waves generated by internal heating in Voigt and Maxwell materials *(Japanese)* 80−69693
viscoelastic wave propagation, integration contour deform. for Laplace transform inversion 80−74801
viscoelasticity equations, stability of numerical soln. 78−16647
viscoelasticity problems, direct soln. method 79−17228

Laplace transforms continued
weighted residual classification of approximate methods 79−10540
X-ray small angle scattering, slit-height correction, exact soln., general method 78−42852
CO_2 supercritical boilers, forced flow, frictional pressure drop 80−14689
Zn single cryst., dislocation velocity and plastic deform. 80−64998

large scale integration
contactless measurement of sheet conductivity and mobility of semiconductor wafer by using eddy current 80−62693
counter design, 1 GHz, use of custom LSI 80−8973
counters, digitisers of time and pulse height, monolithic flash A/D convertor 80−63475
counting cct., frequency measurement appl. *(Japanese)* 77−18003
digital automatic blood pressure recorder *(Japanese)* 78−24168
digital frequency counter for microwave band 80−213
digital Josephson technology−present and future 79−28472
digital multimeter appl., cost effective design 77−45858
digital panel meters appl. 77−37867
digital thermometer, using LSI ADC 79−44907
DVM constructed using Intersil ICL 7106 evaluation kit 79−80599
electron beam lithography, triple slit scheme for high current variable-shaped beam forming 80−68290
epitaxial films, model for autodoping lateral variation 80−103595
failure analysis, wafer defect classification using modified scanning electron microscope 79−21876
frequency counter, 100 MHz, microcomputer controlled, Hewlett Packard (5315A) *(French)* 79−88938
frequency counter, high quality using wideband preamp and LSI pair 77−87782
function testing with stroboscopic microcomputer-controlled SEM 80−68294
high energy physics and microcircuits 79−89572
lithographic manufacturing techniques *(German)* 79−71547
MOS LSI passivation using reactive plasma deposited Si-N films 78−56584
MOS-LSI organ circuits *(German)* 77−19493
movement-activated recording monitor for motor activity 77−25565
multimeter, digital, Philips (PM 2517) 79−80640
multimeter design, digital, portable 79−71427
NMOS VLSI circuits manufacture process and problems *(Norwegian)* 80−60090
portable instruments, battery powered employ LSI ccts. for versatility and economy 77−33999
radiation damage in oxide layers due to ion processing techniques 79−24088
SOS for LSI/VLSI technology *(German)* 79−95918
surface analytical techniques applied to electronic components [Si LSI chip inspection] 80−81392
swept-frequency heterodyne receiver with CRT display for spectral analysis *(Spanish)* 77−37875
VLSI, low temp. differential oxidation for double poly Si devices 80−16521
VLSI multilayer metallisation interlayer dielectrics, CVD films 80−45235
VLSI processing by low-pressure CVD, review 79−87581
X-ray lithography laboratory apparatus *(Polish)* 79−89050
Al and Al alloy metallisation sputter deposition for VLSI 80−66429
SiO_2 film growth technology *(Japanese)* 77−40381
SiO_2 layers in LSI cct. device, cathodoluminesc. obs. 80−80867

large-scale systems
see also hierarchical systems
combined sewer system detention storage, real-time control algorithm 77−37281
commercial large-scale laser displays using path-controlled galvanometers 77−17963
environmental pollution control system methodological approach problems 77−21899
interconnected dynamical systems on Banach spaces, well posedness, instability, Lagrange stability 78−69976
large-scale hydrodynamic system simulation programs 77−21799
nuclear power station safety consideration 78−8961
H_2 generation by water solar photolysis, large-scale impracticability 80−26172

laser accessories
2 Gbit/s electro-optic modulator for visible lasers 79−86262
α-crystal quartz as IR dichroic laser mirror 79−36908
ablative flashlamps for high peak power dye lasers 77−79836
absorption of laser materials, static profile calorimetry meas. 78−25908
acoustic suppression, acoustic attenuator development for pulsed chemical lasers 79−76680
acousto-optic isolator for stabilisation of optically pumped submm. lasers 79−31918
acousto-optic mode locking device, for Nd garnet ring laser with return mirror 80−99764
acousto-optic modulator, pumping laser modulation for CW dye laser mode-locking 79−18456
acousto-optic modulator and driver for CW dye laser 77−61984
acousto-optic modulator for CO_2 laser beams and detect. using W-Ni point contact diode 79−3730
acousto-optic Q-switches for Nd:YAG lasers 79−7166
acousto-optical deflector, design and appls. *(Czech)* 78−5573
acousto-optical frequency and intensity control system for CW lasers 77−88804
acousto-optical high resolution deflector demonstrated in laser scanner 78−46827
acousto-optical modulator, for intracavity laser intensity modulation, 0.01 Hz to 12. GHz 79−41400
acousto-optical modulator, metrological certification of photodetection devices 80−23727
acousto-optical modulator, standing wave, thermal detuning effects 78−71197
acousto-optical modulator for gas laser radiation, using acoustic surface waves 78−25901
acousto-optical modulator laser beam transverse mode and polarisation effects on perform 77−58469
acousto-optical modulators, for laser freq. changes 78−74932
acousto-optical modulators for laser beams 77−19355
acousto-optical tunable filter, for optical coherent detect. 77−88932
acousto-optical variable-ratio laser beam splitter 79−81538

laser accessories continued
acoustooptic modulator intensity servo, optical isolation and amplitude noise reduction 79−98472
actinometer, photooxygenation type for beam intensity meas. 77−30193
adaptive optical control with closed-loop estimation and predictive filtering 77−19298
adiabatic laser calorimeter design for window and mirror evaluation 79−13971
aerosol deflector operation at high radiation intensities 80−9922
AFC system, zero beat, two laser injection locking system 77−88737
alignment accuracy of Helios CO_2 laser 80−33071
alignment fixtures for laser beams 80−74414
alignment system for Antares CO_2 fusion laser beams 80−74422
alignment system for CO_2 fusion laser 78−46706
alignment system for Helios CO_2 fusion laser 80−33070
alignment system for Helios CO_2 fusion laser 80−74420
alignment system for large high-power pulsed CO_2 laser fusion system 78−59075
alkali halides, behaviour as materials for optical components *(Rumanian)* 79−18462
alkali halides, finished optical components, forging 77−46824
alkali metal vapour arc lamp, source for Nd^{3+}:YAG laser pumping 80−78924
alkaline earth fluorides, UV window and coating materials, two-photon absorpt. coeffs. 79−59734
amplifier, free electron laser, storage ring appl. 80−871
amplifier gain computing, program for programmable calculator 79−18442
annular lens soft aperture for high power laser systems 77−72014
annular lens soft aperture for high power laser systems 77−72015
antireflection coating, two-layer, error considerations in design 80−74477
antireflection coating evaluation by attenuated total refl. 77−50783
antireflection coatings, three layer 77−50775
antireflection coatings on window materials for DF chemical lasers 79−64262
antireflective window coatings using rare earth fluorides, 10.6 μm 77−61963
aplanatic waxicon insensitive to tilt errors, for high power laser beam transport 80−74460
apodised apertures, Faraday rotators, and spatial filters 77−19290
apodized aperture used in the laser oscillator *(Chinese)* 79−68408
ATR prism for IR laser absorpt. spectroscopy 79−98480
attenuator of CO_2 laser radiation, using multilayer Dacron filters 80−58616
autocorrelator, rapid-scan, for monitoring CW mode-locked dye laser pulses 80−87421
automated gain measurement system for high-energy chemical lasers 79−36914
automatic alignment system, for OMEGA-10 multibeam laser system 78−50847
automatic bias control cct. for injection lasers 78−71110
automatic frequency control system design 77−3619
avalanche transistor switchout, high performance, for external pulse selection at 1.06 μm 79−7158
axial mode selector for laser with active Q-switching 79−13996
axicon and related optical component diagnostic techniques 80−14417
beam deflector development, holography appl. *(Russian)* 80−1158
beam deflector using computer-generated holograms 77−38979
beam expander, Galilean or Keplerian form telescope 78−50839
beam expander design corrected for Petzval curvature 80−74461
beam expander for short cavity dye laser 80−87532
beam expanind telescope, on-axis reflective, for pulsed dye laser cavities 79−41398
beam intensity control circuit 78−9394
beam pointing control system, visible to IR wavelengths 79−98426
beam sampling mirror gratings, optimal design 77−14791
beam scanner, background signals anal. 77−19425
beam scanner status 79−89921
beam scanning by acousto-optic deflector array 80−10017
beam simultaneity system for CO_2 Helios fusion laser 80−74419
beam splitters, use in rel. to fluctuating polarisation 77−79884
beam splitters, variable ratio, for high energy glass laser systems 79−45952
beam steering device, magneto-optic stripe domain approach 78−13816
beam transport optics for laser fusion 78−83017
benzene derivatives, monohalogenated, saturable absorpt. of CO_2 laser 80−69465
birefringent, tuning filters without secondary peaks 78−29994
birefringent filters for tuning flashlamp-pumped dye lasers 78−74914
bisanthenes, phototropic Q-modulators for ruby lasers *(Russian)* 77−83910
bolometers, laser beam energy distribution reconstruction using data from grid of bolometers 80−53350
bolometric laser emission convertors, thin wire, EM energy absorption, thermal processes *(Russian)* 77−18094
bolometric laser power meter, sensitive meas. IR to vacuum UV spectral range 78−82031
Bragg mirror reflectance, dielectric waveguide inhomogeneity effect 80−28356
brightening filter for solid laser, ultrashort light pulse optimum generation 79−36903
calorimeter, absolute reference, for high power laser pulse meas. 77−19268
calorimeter, large aperture, for fusion laser meas., design 80−43382
calorimeter, variable aperture for unstable laser resonator 77−7136
calorimeter development for laser power meas. 78−22161
calorimeter for pulse energy meas., 0.1 to 30 J *(Polish)* 78−29998
calorimeter types and techniques 80−69441
calorimetric data, automated anal. 80−4714
calorimetric energy meters, KDM and BKDM, for pulsed laser radiation 79−17494
calorimetric energy meters, KDS and BKD, for high-power laser pulses 79−17496
capacitive mesh output couplers for optically pumped far IR mol. lasers 78−74916
capacitor modification for N_2 laser 77−14735
capacitor modification for Schenck-Metcalf N_2 laser 79−18439
cathode, aerodynamically stabilised, for CO longit. discharge lasers 77−10955
cathodes for He-Ne lasers, Al, cold, vapour deposited, performance improvement by Cu addition 80−5748

laser accessories continued
cell, molecular I, impurity gas detection, He-Ne laser stability *(French)* 77−73496
cell for high temp. transverse discharge 77−38914
cell for laser stabilised by saturation absorption in $^{127}I_2$ 78−17971
ceramic capacitor for N_2 laser, failure elimination 78−33740
chalcogenide cubic compounds, melt grown, physical properties, application as lens or laser window materials 79−98450
chalcogenide glass two-layer low-absorpt. antirefl. coating, for KCl laser window 78−37927
chalcogenide glass Z 79−14063
chalcogenide spinels, Faraday effect optical isolators for CO_2 laser system 78−50816
chemical laser nozzle, temperature profiles meas. by thermal imaging system 80−14376
chemical laser window materials evaluation 77−46769
chopper, simple submicrosecond optical, for rectangular-shaped pulse prod. 80−14373
chopper-wheel gas pulsar for foilless anode electron-beam laser 78−63122
circuit for prod. and recording pulse flashes 15 to 400 μsec of He-Ne laser *(Russian)* 80−1235
coated optical component, damage resist. for pulsed CO_2 laser 79−45989
coating damage thresholds in CO_2 laser systems 79−14006
coatings, for IR optical components 79−65821
coaxial Kerr cell built on coaxial 50 Ω transmission line, He-Ne laser 79−72606
coaxial relay current pulse generator for laser pumping 78−59014
coherent optical adaptive Modal Wavefront Control System 77−19295
coincidence detection fo optical pulse streams, high resolution heterodyne system 77−690
cold cathode electron gun, in compact high-press. laser system 78−5496
combined pulse transformer for electronic pumping of CdS laser 78−1255
communication system components characts. and appl. *(Flemish)* 80−5836
compact 5×10^{12} A/s rail-gun pulser for laser plasma shutter 80−70017
compact cold cathode electron beam gun, appl. CO_2 laser *(German)* 80−86501
computer generated hologram for CO_2 laser beam shaping 77−14726
cone absorption calorimeter for pulsed laser meas. 80−98980
conical optics for radiation conversion from laser with unstable resonator 80−91831
continuous deformable mirror multidither coherent optical adaptive system operation 77−19296
continuous deformable mirror multidither coherent optical adaptive system characteristics 77−19297
control element, external, for CW laser radiation power stabilisation 80−91832
control system for fusion gas laser using distributed microcomputer 77−61975
controlled flashlamp illuminated phototropic switch 77−88735
controlled photomultiplier tube with subnanosecond input gate 77−87830
convex beam integrator for laser beam shaping, heat treating appl. 80−53346
cooling, use of mechanical refrigerators, heat pump and thermoelectric coolers 78−22136
cooling system, low temp. ruby laser with optical delay line inside resonator 79−36922
coupling arrangement, for tunable diode lasers far-IR spectroscopic light sources appl. 80−73481
coupling reflector, involute-related, for flash lamp pumped laser systems 78−90425
cratings, SiO_2-TiO_2, for Shiva laser optics 79−7135
crystal evaluation, testing and meas. instrument 77−7226
current pulse formation from pulse gas-discharge lamp using thyristor keys *(Bulgarian)* 78−33795
cutoff filter for CO_2 lasers 77−88938
cuvette for Cu laser with excitation by transverse discharge 80−106532
CW CO_2 laser power meter, 0 to 500 W range *(Russian)* 77−37992
CW X-ray preioniser for high-repetition-rate gas lasers, appl. to HF pulsed laser 80−64037
damage in optical materials, conference, Boulder, USA (Oct. 1977) 79−14048
damage limits for optical components exposed to nanosecond pulses 77−38976
damage of laser components, threshold meas. 78−13740
damage thresholds at 1064 nm, 125 psec, three-beam expt. 77−61990
damage-resistant components for 2-5 μm laser systems 77−19282
damaged laser mirror reuse using simple mirror holder 79−36910
deflecting system, electro-optic, using Kerr cell and birefringent calcite prism 77−7103
deflector, electromechanical, for data transmission through free atmosphere *(German)* 80−38053
deflectors, tilted surface acoustic wave, and tilted electrodes n electro-optical beam deflector *(German)* 77−19417
deformable mirror design for wavefront correction in CO_2 laser fusion system 80−74427
deformable mirror for wavefront error correction in Gemini CO_2 laser fusion system 80−74426
deformable mirror high-reflectance dielectric coatings 79−14085
delay line for investigation of fast processes 77−764
diametral blower in flow-through laser with closed gas-circulation system 80−23701
dichroic beam splitters, high-performance, for DF chem. lasers 80−95932
dichroic mirror, shared aperture, for high energy DF laser 77−88885
dielectric mirror, for KrF excimer laser *(Japanese)* 79−72588
dielectric thin film multilayer systems, polarisation effects and use in laser physics *(German)* 78−33912
differential ball screw actuator driven deformable mirror design and performance 80−33137
diffraction grating, refl. type elec. controllable, for intracavity laser modulation 77−58357
diffraction grating as beam expander in dye laser cavity 78−66858
diffraction grating tuners for CW lasers 79−86183
diffraction structure as laser mode selector 79−89951
digital beam switch for 10.6 μm laser radar 80−102836
digital beam switch for agile beam laser radar 80−58620
digital frequency-offset lock system designed for use with stabilised lasers 78−29960

laser accessories continued
diode laser output stabilization by bevelled-end fibre coupling 80−91806
diode modulator using current switching bipolar transistors 78−1288
diodes life testing, with constant light output current 80−1215
diphenyl butadiene, absorption recovery lifetime, use in UV mode-locked lasers 80−19075
discharge chamber for N_2 laser, metal-ceramic, with transverse excitation 80−48285
discharge circuitry for Cu vapour laser 78−5479
discharge gap characts., laser-radiation-triggered, influence of discharge medium, electrooptic switch control appls. 80−64818
discharge power source for CO_2 laser, pulse forming network 78−74928
discharge tubes, He-Ne, Czechoslovak design and construction *(Czech)* 79−76702
dispersive delay line, optical pulse squaring effects 77−88808
dispersive modulator for CO_2 and N_2O laser light 77−54793
driving circuit for laser cavity dumper 78−13717
dual Bragg cell local oscillator, for laser heterodyne radar 77−19279
dye, bleachable no.3955, relax. time meas., laser passive shutter appl. 80−23759
dye accessory invertor for LG-21 serial N_2 laser 77−68224
dye bleaching, no. 3955 in soln., relaxation and correlation times meas. 80−28281
dye cell, contacted mode-locking, for use with Nd^{3+}:glass laser 79−18454
dye compositions bleachable by I laser, for passive Q-switching 80−91826
dye passive switch for Nd laser pulses, transmission coeff. depend. on power density 77−23686
dye ultrafast saturable absorbers for Nd lasers 80−53386
dynamic power supplies for TEA lasers 79−7136
electro-optic microwave modulator, broadband electronically tunable, for CO_2 lasers 79−64256
electro-optic modulator, servo controlled, for CW laser power stabilisation and control 80−19060
electro-optic phase modulator for single-mode laser freq. modulation 78−13737
electro-optical deflector streak camera system, for picosecond laser pulse diagnostics 78−33909
electro-optical gate for nonpolarised emission *(Russian)* 78−59132
electro-optical modulation with MBBA liq. crystal 77−20826
electro-optical modulator use in or outside cavity for laser freq. shifting or stabilisation 78−5512
electro-optical phase modulator, for dye laser freq. stabilisation 77−88802
electro-optical Q-switch for pulse-periodic Nd^{3+}:YAG laser 79−45975
electro-optical shutter, for CO_2 laser pulse prod. 78−37926
electro-optical shutter, piezo-opt. effect on dynamics and spectral characts. *(Russian)* 77−83912
electron accelerator, high current, with rectangular cold cathode, for laser excitation 78−25358
electron accelerator, high-current, for optical pumping of gases 80−32544
electron accelerator, high-current pulsed, for compressed gas laser pumping 79−692
electron accelerator for gas laser pumping 78−5483
electron beam accelerator for gas laser, design 78−13720
electron beam coaxial excitation system for high power excimer lasers 80−53310
electron beam diode, radially converging, for gas laser excitation 79−94239
electron beam sources for pulsed lasers 79−36913
electron beam system for laser excitation, coaxial diode 80−86509
electron gun, glow discharge cold-cathode, for pulsed ionisation of high-pressure CO_2 laser 79−27269
electron gun, grid-controlled, for electron beam controlled CO_2 laser 78−46635
electron gun, long pulse high current, for e-beam sustained excimer laser 77−88733
electron gun, long-pulse, high-current, for e-beam sustained excimer lasers 78−29967
electron gun coupled to pulsed blowdown apparatus, for supersonic flow electronic transition lasers 79−59723
electron gun using HV glow discharge, for electron beam pumping 77−62428
electron gun with photocathode for electron beam controlled laser 77−50678
electronic stabilisation system for radiated power of semicond. laser 80−23702
electrooptic gate, ns pulse train generation with ruby laser *(Russian)* 77−79871
electrooptic shutter, passive switching to produce ruby laser picosecond pulse generation 79−36942
electrostatic droplet source suitable for laser targets 77−34074
EM transducer for laser fine-tuning 77−79862
emission power fluctuation statistical meas. system 77−79881
energy coupling arrangement for parallel concentric lasers *(German)* 78−33757
excitation generator for GaAlAs semicond. injection lasers 78−33748
Fabry Perot wide-band electrooptic type modulator, modulation sensitivity 79−3724
Fabry-Perot cavity acoustooptic modulator for internal laser modulator *(Japanese)* 77−88814
Fabry-Perot interferometer for CO_2 laser pulse generation 78−29996
Fabry-Perot interferometer for sub ns pulse stretching and spectroscopy 77−42555
Fabry-Perot non-linear optic media devices, instability and regenerative pulsation phenomena 78−46685
Fabry-Perot variable output coupler for optically pumped FIR laser 77−68220
far IR laser hybrid output couplers, metal mesh dielectric mirror design and fabrication 80−58554
far IR laser output detection by MOM point-contact diodes *(Japanese)* 79−21811
far IR laser stabilisation servo electronics 77−38928
Faraday effect for laser output power external stabilisation, control unit design *(German)* 79−18455
Faraday element fabrication for intracavity laser appls. 78−66852
Faraday filter, freq. locking of CW dye laser to Na D-lines 78−5487
Faraday filter, freq. locking of CW dye laser to Ne absorpt. lines 79−22989

laser accessories continued
Faraday rotator isolator, with solid state switching 77−88734
Faraday rotator using low Verdet constant material 80−69520
fast Pockel cell and GaAs switch for active pulse shaping in ps domain 80−28257
fibre optic components, radiation strength for ruby laser transmission 77−7108
fibre waveguide photosensitivity, appl. to refr. filter fabrication 78−63171
field meas. Fourier transform spectrometer 80−86470
film photopot detector characteristics for adaptive optical systems 79−59741
film polariser, design, prep. and optical characterisation 79−76866
filter, bleachable 78−50937
filter for altering spectrum of multiple-frequency lasers 80−58553
flash lamp, 1 kJ per pulse, for tunable organic-dye laser 79−36907
flash lamp, ballast volume effect on pumping efficiency 77−707
flash lamp, for dye laser pumping 77−19334
flash lamp, Hg capillary, high efficiency, for pumping pulsed dye laser 77−14710
flash lamp, high-energy, short-pulse, operating characts. in ablation regime 77−23724
flash lamp drive circuit discharge currents, Fourier anal. 80−23695
flash lamp high-power radiation for laser pumping, interaction with cooling fluid 78−13718
flash lamp pumping of lasers, optimal lamp filling, review *(Russian)* 78−63123
flash lamp pumping of rectangular cross section active elements, efficiency 77−695
flash lamp pumping source for lasers 77−50679
flash lamps, discharge development effects on pumping efficiency 78−71114
flash tube, discharge brightness radial profile, laser illuminator effects 77−692
flash tube, enhancement of luminous efficiency using high power preionisation 78−37958
flash tube radiation, interaction with cooling liq., nonlinear hydrodynamics 77−11121
flashlamp array supplied from storage inductor, current and voltage distribution 77−83940
flashlamp drive circuit optimisation for lasers 77−75534
flashlamp pumped thyratron switched reliable dye laser 79−31930
flashlamp pumping and triggering cct., for Nd^{3+}:$YAlO_3$ laser 78−55378
flashlamp reflectors for I photodissoc. laser 77−79848
flashlamp technology for pulsed lasers, design requirements 79−36912
flashlamps, coaxial and preionised linear, comparison as pumping sources for high power dye lasers 80−102730
flat top beam profile production for high energy lasers 80−58618
flexible IR waveguides, high power laser output steering appl. 80−48409
fluorophosphate and fluoroberyllate glass laser damage thresholds and solid inclusions 80−33054
focus alignment sensor, for collimated light beam 78−59065
focusing device for laser radiation 78−13742
focusing lens design for hot spot elimination 79−72658
FP and FPU electron-trap photocells, for laser flux intensity meas. 78−286
frequency and spectral parameter check system 77−79880
frequency doubler crystals for solid lasers 78−46725
frequency selector, ZnS thin film, for laser pumped dye laser *(Russian)* 77−54736
frequency stabiliser using electronic servocontrol system 78−1240
frequency stabilizer using single-photon detection, D/A lock-in circuit 79−50334
frequency trimming circuit, automatic *(Russian)* 80−1217
frequency-locking system for wide-band tunable laser 79−18432
fused quartz flashlamps, correlation between static stress distrib. and explosion energy 77−10931
fusion research lasers, advanced components and systems for beam lines 79−18466
gas isolator mixes for CO_2 laser system 78−46663
gas laser and developmental laser, apparatus and applications *(Japanese)* 77−61961
gas laser cavity unit for radiation lead-out *(Russian)* 78−90433
gas mixture, absorbing, for isolation between amplifiers in TEA CO_2 laser 80−95911
gas pumping arrangement, for relativistic electron-beam pumped lasers 77−701
gas saturable absorber, formic acid and SF_6 cells, as isolator for 9 μm band CO_2 laser amplifier 79−76709
gasdynamic windows of gas lasers *(Russian)* 77−58335
generator, high voltage, for 1 kJ electro-ionising CO_2 laser *(Russian)* 77−19316
generators for power pulse meas., using semiconductor radiators 80−23710
glass, TI-20, laser window material, IR thermooptic coeff. meas. 77−36208
glass window, polished, 1.064 μm laser damage threshold rel. to pulse duration and surface roughness 80−33055
graphite electrode open channel config. for N_2 laser 78−55379
grating mirror, loss of periodic mode in IR laser resonator 80−28254
grating reflector for thin film Fabry-Perot laser 78−55471
grazing incidence grating efficiencies, rel. to dye laser tuning 79−36990
Gunn device, planar, high-bit-rate pulse regeneration and modulation of injection lasers 79−59731
halides, melt grown, physical properties, application as lens or laser window materials 79−98450
heat exchanger, high capacity, inexpensive construction 78−49826
heterodyne receivers of CO_2 laser emitters, antenna characts. meas. 77−67498
high current plasmadynamic discharges light source 77−38923
high pressure chamber for diode laser tuning 77−46742
high reflectivity surfaces for high energy laser appl., sputter deposition of Cu and AG 79−47181
high speed rot. mech. shutter design for pre-pulse protection 80−96032
high voltage microsec. pulse-forming network for CO_2 laser 78−5494
high-energy, IR laser component optical characterisation techniques 80−14347
high-energy laser diffraction grating evaluation approach 80−14474
high-energy laser mirror thermal distortion test facility 80−14348
high-power glass laser users' facility with computer control 77−19341
high-power laser luminance contrast meas. 78−87055

laser accessories continued
high-pressure laser cell with a transverse excitation scheme 80−78859
high-speed shaping device, for address control of laser beam deviation 78−5554
hole grating attenuator, for beam steering investig. 78−59071
hollow cathode, sputtering problem, temp. control 77−88769
hollow dielectric waveguides, 10 micron propagation losses 77−50756
holograms, computer-generated, prod. of two-dimens. laser beam deflections 78−58956
holographic beam scanner using auxiliary reflector 77−83951
holographic grating, for spectral narrowing and tuning of CW dye laser 78−71109
holographic laser beam deflector performance characteristics 77−19287
holographic total internal reflection selector for tunable lasers 77−79840
HV pulser development for CS_2 laser cavity 80−23707
HV pulser for discharge into CS_2 laser cavity, with triggered spark gap 79−13973
II-VI semiconductor Franz-Keldysh effect modulators for laser radiation *(Russian)* 77−88813
image phase conjugate laser adaptive control, isoplanatic effect simulation 77−19294
improved free-vortex, subsonic aerodynamic window 80−23663
impulse shape regulation, electro-optic deflectors *(Russian)* 77−19354
in-cavity hot cell with sequence CO_2 lasers 78−5495
inductive storage bank for rhodamine 6G dye-laser pumping 80−5742
inductive storage unit for laser pumping, design and construction 79−89916
inductive storage unit used to pump SF_6-H_2 laser 79−98409
inhomogeneous interface laser mirror coatings, durability improvement 80−1252
injection diode modulated laser pulse generator and digital control cct. *(Russian)* 80−14372
injection laser output regulation by NTC resistor cct. 80−14353
injection laser/optical waveguide connection module 78−59023
integrated electro-optical modulator, 12GHz continuous tuning of CO_2 laser lines 77−83907
integrated interferometric reflector 77−58490
intense ion beam lens system for X-ray laser 77−34053
intensity stabiliser, using variable transmission element 79−36905
interference coatings perpared by electron beam evaporation, UV optical strength 79−59779
interference filters, nonlinear, spectral characts. in strong fields *(Russian)* 77−54718
interference polarisers for lasers, development 78−83108
interferometer, angle-scanned, as coherent energy modulator in coherence discriminating laser receiver 79−58777
interferometer with increased resolution to analyse FM laser output 78−4688
interferometric digital wavemeter for CW lasers 77−162
intermetallic coatings, possible use in power optics elements 79−14084
intracavity Brewster-angle birefr. filter, line narrowing and tuning of Nd:glass 77−38916
intracavity versus extracavity absorpt. cells, fractional absorpt. with single-mode laser 77−23700
IR coating for high energy laser reflector and window 79−45951
IR coating nonuniformity effect on precision optical systems, compensation by auxiliary laser 80−78926
IR electrooptic waveguide for CO_2 laser modulation 77−27349
IR laser power transmission waveguides 77−19430
IR laser radiation visualiser 77−38974
IR laser window material extrinsic absorption 79−14049
IR laser window material refractive props., temp. depend. 79−14052
IR materials, high transparency, state of the art 77−27326
IR materials, laser residual absorpt. 2 to 10 μm, review 78−25906
IR materials, optical phenomena, conf., Annapolis, MD, USA (Dec. 1976) 78−25933
IR optical components and aspherics, 10.6 μm interferometric testing 80−74523
IR optical elements, adsorbed water effect on optical strength 77−79886
IR optical train handling high pulse powers, thermal distortion thresholds 77−46745
IR Smartt interferometer, alignment tool for CO_2 laser fusion systems 80−74425
IR transmissive material guide, laser window appl. 77−39004
IR window coatings, new materials 77−50736
IR window heating, interferometric meas. 77−46748
IR window materials, optical phenomena, book contrib. 78−9420
IR windows, optical properties measurement 77−54788
isolator, based on Faraday rotator, for diode laser, struct. simplification 80−1209
Kerr shutters, for Q-switching and radiation pulse shaping in Nd-glass lasers 79−3729
KS glasses for passive shutters of ruby laser for genrating subnanosec. pulses 80−102728
large optical components for high-power lasers, refl. and transmission meas. 79−44927
large-aperture Pockels cell design 77−19438
laser and electro-optical systems, conf., San Diego, USA (May 1976) 77−19278
laser mirrors cooled by open pore structures, radiation damage 79−72603
lens, aspheric, stigmatic, for ruby or He-Ne laser, CAD *(Czech)* 78−55427
lens, high aperture, for laser plasma compression expt. 79−14076
lens array for extended coherent light source *(Russian)* 78−30040
lens design and ghost focus problem in fusion lasers 79−86247
lens design and testing for laser systems, assets and liabilities 78−46753
lens design for laser beam shaping 78−13781
lenses, laser compression expts., design principles, geometrical optics theorem appl. 79−55203
light guide for laser beam diffusion and homogenisation 79−68436
light pulse parameter meas., integral method 77−72018
light-controlled light modulator, fast resonantly enhanced, for laser beam modulation 78−5509
lightwave pulse regenerator for triggerable semiconductor lasers 80−69408
liquid absorption cell, for pulse energy meas., digital readout *(Russian)* 78−18000
liquid calorimeter, for laser pulse energy meas. *(Russian)* 78−22163
liquid Kerr cell, pulse compression inside actively AM mode-locked Nd-YAG laser 79−22990
liquids for cooling and index matching of Nd:glass laser systems 80−33015
low-absorption grating beam sampler design, fabrication and testing 80−14475
low-inductance spark gap switch for Blumlein-driven N_2 laser 80−33010
low-level pulse meas. system at 1.064 μm, transfer standards 80−86253
luminescence filters, efficiency for Nd:glass lasers 80−1213
Luneberg lens for laser diode coupling to graded-index fibre *(German)* 78−33875
magnetic mirrors in gas lasers with non-self-sustaining discharge *(Russian)* 80−106530
magnetic tuning system for dye laser 77−75541
magnetooptic bounce-cavity modulator, direct AM 80−5769
magnetooptical switch for synchronization of CO_2 and red laser beams 80−58615
mass production and radiated power meas. improvements 78−37064
metal and alloy surfaces, highly reflecting, pulsed laser stress phenomena 79−14015
metal film mirror prep. by ultraclean DC sputtering, optical props. 77−50748
metal film reflection filter for CO_2 laser line selection 78−55368
metal foils for pulsed laser appls. 78−5480
metal IR window materials, diamond machinability 78−5586
metal mesh dielectric mirrors for far IR lasers 77−54727
metal mirrors, diamond turned, evaporated and sputtered, surface and optical studies 78−79098
metal mirrors, diamond turned, surface, optical and laser damage characts. 77−50705
metal mirrors, dielec. enhanced, absorptance at 5.3 μm 77−50709
metal mirrors, for high-power appls., multithreshold damage analysis 77−88884
metal mirrors for CO_2 laser fusion systems, material constraints and fabrication 78−5476
metal mirrors for high power appls., multithreshold damage analysis 79−980
metal optics, diamond turned, book contrib. 79−32104
metal oxide/fluoride mirror coatings, light scatt. and optical strength in UV range 80−106595
metal surfaces for laser mirrors, ion polishing and vac. annealing 78−5588
metal-ceramic discharge tube for high power Ar laser 78−29962
metallic mirrors for laser fusion reactors, neutron and gamma irrad. response calc. 80−23121
metallic wired grids as far IR semitransparent mirrors, use in HCN laser cavity 78−71188
methane absorber for He-Ne laser, reson. obs. in output freq. stabilisation 77−83854
methane absorption cell for He-Ne laser, hyperfine struct. influence on freq. reproducibility 78−50864
methanol waveguide laser radiation modulation by Stark cell 77−38962
Michelson coupler with variable output for far IR methyl fluoride CW laser 78−55372
Michelson output coupler with one-dimensional grid, for optically pumped near MM laser 80−58555
mid IR laser window materials, absorption props. 77−46770
MIM point-contact diode harmonic generators and mixers 80−60105
minicomputer-controlled diagnostic and display system for high-energy lasers 79−36915
mirror, 6320 Å, refl. anisotropy 79−98413
mirror, depth concentration profile determ. by ion microprobe mass anal. 77−31126
mirror, diffusive component meas. using heterodyne method 77−68217
mirror, multi-segmented, for laser thermal blooming reduction vice phase correction, experimental demonstration 79−98449
mirror, off-axis parabolic, for laser fusion expt., fabrication process 79−23103
mirror, SEM obs. of laser induced damage *(German)* 78−37929
mirror aligner, providing translational and ang. motions 77−7142
mirror and window absorption, reflection and transmission obs. at 10.6 μm 79−14014
mirror for beam focusing, dielec. coatings on metal 77−62034
mirror for Fabry-Perot interferometer, coeff. of reflection meas. *(Russian)* 78−1237
mirror for laser resonator to minimize output beam divergence 78−13735
mirror for semiconductor laser output stabilisation 79−45954
mirror grating mount, compact stepping motor design 80−87402
mirror machining of nonconventional shapes 78−5589
mirror manufacture, ion beam/plasma chemical etching mixed batch process *(French, English)* 77−83880
mirror mount, of high-resolution, appls. 77−3618
mirror positioner, tip/tilt, high performance 79−59795
mirror quality specifications for CO_2 Antares laser system 80−74423
mirror reflectance meas. using multiple wave interferometer *(French)* 77−42585
mirror reflectivity meas. technique, precision 78−17947
mirror surfaces degradation on 10000 hr. lifetime tests on CW heterolasers 80−106542
mirrors, damage threshold at 10.6 μm, up to 10^{10} W/cm^2 77−50707
mirrors, high precision reflectivity meas. technique 77−23698
mirrors, optical fabrication techniques 77−65600
mirrors, sputtered films production and props. *(Hungarian)* 80−53483
mode-locking saturable absorber for rhodamine laser using pinacyanol 77−42554
modulation circuit, with 1 ns pseudo-random impulses 78−50836
modulator, 1 Gb/s 77−79965
modulator, acousto-optical for microwave frequencies 78−1282
modulator using acoustic Fabry-Perot resonator, for gas laser mode locked operation 79−45976
modulator using rotary diffraction grating 78−87080
modulator/repetitively pulsed field emission electron beam gun interface for CO_2 laser 78−5482
modulators, electro-optical and acousto-optical devices comparison 80−43380
monitor for divergence and intensity distribution of pulsed laser oscillator output 78−5515
monolithic deformable mirror/heat exchanger unit evaluation 80−33139
multi-gigahertz modulation concepts, for CO_2 laser communications 77−3681
multi-lens focusing systems for energy Nd:glass lasers 78−50848

laser accessories continued
multiactuator mirrors, wavefront error compensation capabilities 79−59797
multichannel surface spark gaps 79−18436
multichannel system, MIK-48, for laser pulse energy meas. 79−17497
multichannel system, MIS-20, for laser pulse energy recording 79−17495
multicomponent gaseous saturable absorber for CO_2 laser Helios system, optimisation 80−74393
multielement objectives synthesis, for focusing monochromatic laser beam *(German)* 77−68231
multielement resonant reflector design, temp. and wavelength depend. props. 78−17945
multifrequency Bragg acousto-optic deflector, laser beam AM suppression 80−53426
multilaser beam combination system 79−68402
multilayer, dielectric reflectors, simplified description 79−89984
multilayer dielectric enhanced mirrors for 2 to 6 μm 79−14086
multilayer dielectric mirrors, exam. of reflectance, optical thickness and refractive index 78−59106
multilayer mirrors, high refl. at fundamental, second and third harmonic laser wavelengths 78−90490
multiple spatial filters, imaging props. to reduce self-focusing in fusion lasers 77−58360
multistage interference-polarization filter for wavelength selection in dye lasers 80−64091
nanosecond source for semiconductor laser pumping 77−14746
nonlinear absorber for gas laser, reson. obs. in output freq. stabilisation 77−83854
nonlinear absorbing filter, for CO_2 laser self-modulation 78−37925
nonlinear holographic gratings for high energy laser beam sampling 80−14476
nonlinear interferometers for laser pulse shaping 78−59097
nonlinear interferometers for laser pulse shaping 78−79051
optical attenuator, for TEM_{00} mode laser beam, using collimators and iris diaphragm *(Japanese)* 79−98378
optical attenuators, review *(Japanese)* 79−98475
optical coating abrasion resistance characterisation test 79−14129
optical coating adhesion characterisation pull-off tests 79−14128
optical coatings, conf., Washington, USA (March 1978) 79−46028
optical component laser damage mechanisms 78−83016
optical component manufacture and evaluation, seminar, Los Angeles, USA (Jan. 1979) 80−12850
optical component props. depend. on material flow props. *(Russian)* 80−38047
optical component replication 79−55253
optical delay lines to control solid state laser output characts. 80−99758
optical fibre interconnection *(Danish)* 77−88911
optical filters, nonlinear distortion of laser beams 79−7170
optical isolators, elimination of polarisation depend., fibre communication appl. 80−5844
optical isolators for semiconductor laser, in laser-to-fibre coupling module 80−48267
optical Kerr effect modulator, for laser passive mode-locking and Q-switching 78−9403
optical materials, laser induced damage, symposium, Boulder, USA (Sep. 1978) 80−31417
optical multichannel analyser for picosecond spectroscopy, mode locked laser synchronisation 77−38022
optical noise filter with two aperture stops, numerical analysis *(Japanese)* 77−14812
optical path electronic simulator in GaAlAs laser power control loop *(German)* 78−82987
optical power meters for laser photometry 78−65953
optical radiation power photometry, USSR system of standards 77−30194
optical shutter for fusion laser, Faraday cell highly uniform mag. field production 78−13719
optical shutters, fast acting, for Nova laser fusion reactor 78−66854
optical surface, target containing alkali metals and alkaline earths, chemical sensitisation after ion bombardment 80−3227
optical system for laser induced plasma compression 80−14382
optical system for laser light transformation, parameter calc. *(Russian)* 77−65614
optoacoustic power monitors for laser radiation 79−41404
optoelectronic ps switch using pulsed lasers and photoresistive semiconductor *(German)* 77−72066
optomechanical element system, for laboratory meas., Hungarian development *(Hungarian)* 79−81574
organic dye attachment for wavelength conversion of pulsed solid state and gas lasers 79−7147
oscillatory circuit with current breaker for discharge excitation 77−14759
p-ν-n diode modulator, for CO_2 laser 77−79873
p-ν-n Si diode, for CO_2 laser modulation, temp. and switching characts. 79−81467
paper, yellow and white bond, as inexpensive detector for CO_2 laser 80−78880
paraffin oil coatings for high power laser system components 77−88730
parallel plate technology, polarisation problems obs. and solution 80−1225
passive contrast enhancer for ultrashort pulses in high gain system 77−88873
passive nonresonant technique for pulse contrast enhancement and gain isolation 78−63142
passive pulse shapers, etalons and multiple beam splitters, interpulse interf. 77−19265
passive Q-switch, relax. time effect on Nd:YAG laser pulse length 77−38960
passive switch of KS-19 glass for controlling time of appearance of laser giant pulses 77−38959
permalloy film, Fe-overcoated, magneto-optical characts., appl. to Kerr effect mirrors for ring laser gyros 79−82956
phase autotrimming system, beat frequency setting up to 400 MHz *(Russian)* 78−1238
phase diffraction grating as laser beam coupler, radiation parameters monitoring 80−10033
phase interferometer control of mode locking in gas laser 77−72009
phase-rotating plate, smooth transverse intensity distrib. form. in light beam 79−59837
phased array of optical fibres for laser beam scanning 79−81514

laser accessories continued
photoacoustic detector, for laser beam energy monitoring, construction and calib. *(Czech)* 78−29156
photocell, FEK-37, for HV pulse shaping and electrooptic switch control in lasers 79−64340
photodiode circuit, for small power-radiation instability levels meas. of gas lasers 80−23704
photoelectric digital energy meter for laser pulse meas. 77−71375
photographic amplitude filter for laser radiation uniform intensity distrib. *(Russian)* 77−54748
photographic semiconducting device, for high-speed CO_2 laser output meas. 79−14008
photopreionization-stabilized discharge scheme for inert gas halogen excimer lasers 80−33009
photoresist microlens production for semiconductor lasers 78−9398
picosecond pulse generation scheme for injection lasers 80−87418
piezo mirror translator for freq. control of dye laser 79−72582
piezoceramic transducer for laser freq. stabilisation, freq. response *(Russian)* 79−10315
piezoelectric beam deflector, basic characts., multielement 77−54808
piezoelectric beam deflector, bimorph, theory and expt. 77−54807
piezoelectric micrometer for precision movement in optical alignment applics. 77−65017
piezoelectric mirror translator, stabilisation of narrow-bandwidth CW dye laser 80−33036
piezoelectric mirror-driving transducer for gas lasers, distortion measurement 77−10006
piezoelectric stack for beam control 77−72012
piezoelectric transducer as monitor for optically pumped far IR laser 80−102729
pinhole closure due to intense laser radiation 77−79877
pinhole plasma shutter for optical isolation in high-power glass lasers 80−23733
PIR-1 instrument for laser radiation divergence meas. 79−23001
plasma, intracavity laser breakdown, for laser short pulse generation 78−37924
plasma diode, prevention of laser damage by back-reflected light 78−87057
plasma isolator for retropulse in CO_2 laser amplifier chain 79−22959
plasma mirror in electron beam controlled CO_2 laser 78−17976
plasma mirror refl. characts., in electron beam controlled CO_2 laser 78−59064
plasma polymerised ethane for laser window coatings 77−50737
plasma pulse clipper and optical isolator for IR lasers 77−65601
plasma shutter, expanding supersonic plasma 79−68412
plasma shutter, self-triggered, for laser beam switching 77−58367
plasma shutter for CO_2 laser, transmission cut-off time depend. on breakdown intensity 80−6259
plasma shutter for multichannel Nd:glass laser 80−64088
plasma spatial filter for high power laser system 77−72056
plasma spatial filter for high-power lasers, mechanism 77−19269
plasma tube impedance changes for CO_2 laser power variation detection 80−69437
Pockels cell, variable length subnanosecond laser pulse prod. 78−94405
Pockels cell, variable pulse width generation for CO_2 lasers 78−46691
Pockels cell drive pulser in multiarm laser 79−14001
Pockels cell for subns. pulse prod. 77−83904
Pockels cells, optically timed, electrooptic prepulse suppression for fusion laser systems 80−102743
Pockels switching system producing single and double variable length pulses 77−724
point contact IR detector tunnelling and rectification characteristics, geometrical and multiple image interactions 80−57376
polarisation beam splitters for F II-centre laser pumping 79−45960
polarisation flipper, for i.r. beams, using five mirrors 77−699
polarisation flipper for IR laser beams mirror and prism systems 77−75586
polarisation rotator, broad band, for high power appls. in IR 79−981
polarisation rotator, tunable damage-resistant, for UV and visible laser radiation 77−83964
polariser, thin film, design and fabrication 79−37010
polarising optical components for high power glass laser systems 77−46727
polarizer, matching type to applic. 78−18051
polarizing beam splitter coating, theory 77−596
Polaroid film, developed, use as recording medium for pulsed laser radiation 79−94270
porous structures for cooling laser reflectors, theoretical study 80−91809
power and energy meters, calorimeter system for calibration 80−38024
power meas., scale comparison for calorimeter and radiometer systems 79−76729
power meter, absolute CW laser, based on momentum transfer *(French)* 78−37932
power meter, Al slab, for output meas. from high power CW CO_2 laser 79−59739
power monitor, nearly transparent for optically pumped FIR lasers 80−5773
power supply, high efficiency and high stability *(Rumanian)* 79−64248
power supply circuit, N_2 laser discharge dynamic characts. 79−18446
power supply for Ar laser, discharge current and output power control 77−38912
power supply for He-Ne laser 79−36906
power supply inductive pulse shaping for periodically pulsed CO_2 laser 80−53311
power supply type selection for capacitor charging in pulsed laser 77−79838
power-per-line analyser for real-time display of laser spectra on oscilloscope 80−58552
preset Josephson point contact for use at sub mm. wavelengths 77−22600
primary regulated dual power supply 79−98396
prism anamorphic system, for Gaussian beam expander 79−3716
prism beam expander for dye laser, dispersion 78−17968
prism raster focusing device 77−19272
prism used as beam expander in N_2 laser pumped dye laser, dispersion 78−74924
prismatic polygon mirror, laser beam deflection for scanning system 77−19267
prisms for producing slit beams 77−72020
production planning problems, system of indices 77−31145
pulse detector, using SAW generation 77−57392

laser accessories continued
pulse electron accelerator for CO_2 laser preionization 77−88780
pulse energy digital indicator *(Russian)* 79−22995
pulse energy monitor 78−66839
pulse forming network design interface with electron beam sustained gas discharge 78−5481
pulse forming network for CO_2 TEA laser 78−9389
pulse generation and modulation devices 78−25899
pulse generator, 100 ps risetime, for GaAs laser drive 77−7149
pulse generator, multiple-cct., for high repetition rate rare gas halide lasers 78−94399
pulse generator for heterojunction laser *(Polish)* 79−3701
pulse generator for pumping injection semiconductor laser oscillators 77−27299
pulse generator for semiconductor laser pumping, cct. parameters 78−74919
pulse monitor, 50 psec detector 77−3600
pulse power requirements for laser isotope separation 79−13972
pulse shaping and display, electro-optic technique 77−19270
pulse shaping for laser fusion 77−88806
pulse shaping system, using grating pair and filters 79−89940
pulse stackers, comparative flexibility and efficiency 77−19291
pulse synchronisation system for fusion laser 77−88807
pulsed acousto-optical modulator RF driver for laser mode locking 78−90438
pulsed lamp for pumping *(Russian)* 78−22138
pulsed lamps for laser systems, bulb transmittance changes 80−5740
pulsed laser energy measurement system and calibration facility 79−27301
pulsed power systems for high energy gas laser 78−9390
pulser, high average power, for Cu halide laser systems 78−5497
pulsers, low-impedance, high-voltage, for travelling wave excitation of UV gas lasers 77−3608
pump, active medium and interference coating effect, temp. profile, electro-optical characts. 77−19275
pump system, analytical theory 80−106540
pumping lamp ignition pulse semiconductor shaper 79−72585
pumping oscillator for transverse excitation lasers 78−5488
pyroelectric detector for subnanosecond CO_2 laser pulse meas. 80−78884
pyroelectric detector of transmitted power, coordinate-sensitive, for laser beam displacement determ. 79−75599
Q-switch, ultrasonic, for Nd:glass laser 80−64034
Q-switched laser pumping lamp trigger circuit 79−68403
Q-switched pulse stretching by intracavity nonlinear ellipse rot. 78−17991
quadraxial high repetition rate adapter for coaxial flashlamp pumping of laser dyes 79−45949
quarter-wave dielectric reflector, spectral absorptance approximation 80−33131
quartz:Ti tube for I photodissoc. laser, C deposit elimination 77−10945
radially converging electron beam accelerator for gas laser excitation 78−9391
rare earth fluorides, CeF_3, PrF_3, LaF_3, coating materials for IR laser components 80−33105
reflector, uniaxial cryst., optic axis orientation determ. by polarisation meas. 77−3598
reflector with non-quarter-wave design, enhanced damage resist. 77−88819
resonant chopper performance characteristics and limitations 80−64084
resonator mirrors, optimal reflection coeff. selection, for intraresonator Q-switching 80−48302
restricted laser beam polar diagrams *(Russian)* 80−14381
retropulse isolator for CO_2 laser light 78−9388
retroreflective array as resonator mirror 80−95973
rhodamine 6G soln. in ethanol, luminesc. liq., pump radiation conversions to enhance laser efficiency 80−48293
rotating mirror in Ar^+-Kr^+ laser for time multiplexing of multicolour laser light 78−17999
rotator, low loss, and appl. for isolator design 77−58447
ruby, one-freq. tunable one-pulse, selector parameter optimisation 78−74935
rutile prism, high dispersion, for tuning dye lasers 77−7107
sapphire, fabrication of optics 79−23099
saturable absorber gases, for CO_2 laser gain isolation 78−59095
saturable absorbers, large scale flowing gas, for CO_2 lasers 78−59096
saturable absorbers, laser multipass power amplifier stabilisation in CO_2 system 78−46664
saturable absorbers, stabilisation of CO_2 laser triple-pass power amplifier system 78−46619
saturable absorbers for CO_2 10.6 μm band, Ge:Ga and SF_6 77−88868
saturating absorber efficiency increase apparatus for ruby laser generation of ultrashort light pulses 80−23700
SAW acousto-optical total internal reflection modulator 77−19435
scanner, using acoustic travelling wave technology 77−58470
scanning electro-optical deflectors 78−79060
scanning system, telecentric, wide-aperture, for PWB holes counting 80−1264
seals high-temp. metal foil, formed by seam welding 79−80597
Seebeck effect position sensor for CO_2 laser beam alignment 80−5772
self-adjusting laser-target system for laser fusion 79−14024
self-focusing suppression through low-pass spatial filtering and relay imaging 78−74938
self-modulating system, external for producing variably separated pulse pairs 77−83902
semiconductor, IR radiation ultra-fast switching by laser-produced carriers 79−98417
semiconductor convertor in pump system of Nd:YAG laser 77−7129
semiconductor films with anomalous photovoltages for radiation recording 77−37989
semiconductor laser pumping thyristor current pulse generator 78−79024
semiconductor laser pumping thyristor nanosecond current pulse generator 78−79025
semiconductor reflection switch for CO_2 laser 77−3609
semiconductor thin-film nonlinear Fabry-Perot interferometer for optical pulse shaping 79−89945
semiconductors, laser window materials, residual lattice absorpt., freq. and temp. depend. 78−25910
servo system for phase control of HF chemical lasers 80−33063
Shiva, laser-target and laser isolation 78−59035
Shiva fusion laser, development of components and subsystems 78−5491
Shiva laser, 25 MJ energy storage and delivery system 78−59038
laser accessories continued
Shiva mechanical systems 78−63135
Shiva optical system 78−59039
shock isolator for closed-cycle refrigerator of diode laser 78−50796
shutter, controllable phototropic, synchronization of single pulse ruby laser 80−23699
shutter, differential electro-optic with ns pulse operation 78−74994
shutter for laser pulse shaping, Pockels cell with programmable transmission control 80−64162
side cathode for high-power Ar laser 80−99742
silica reflectors, ageing under flash lamp light pulses *(Russian)* 77−54737
skimming discharges for pulsed gas-discharge laser preionisation, spectral characts. 80−99740
sliding reference interferometer for two-dimensional phase meas. 77−19280
sliding-spark arrays for laser pre-ionization 77−46726
Smartt interferometer as alignment tool for IR laser systems 80−33072
smooth pulse oscillator for single mode operation in I laser 78−59057
soft aperture, radial intensity distrib. form. 77−7110
soft diaphragms, prepared by induced absorption method at 1.06 micron in CaF_2 78−5477
solid-state laser miniature power pack 78−59015
solid-state measurement lasers, single-pulse with uniform distribution of energy density, correction equipment 80−23703
space-time light modulator for laser radiation control 80−48310
spatial filter imaging relays in high power lasers 77−88760
spatial profile meas. by pyroelectric vidicon camera 80−87425
spectral shared aperture beam splitter for high-energy laser systems 80−14477
spectrophone, use in controlling and stabilising pump freq. of far IR laser 77−31105
spectrum analyser for optical laser oscillator radiation 77−26403
spring-loaded partial kinematic mount 80−74518
stabilisation of output power using acousto-optical method *(Polish)* 79−13994
Stark cell noise reduction for CO_2 laser beam 78−59059
Stark external cell containing 1-1 difluoroethane, CO_2 laser possible freq. stabilisation 79−94266
steel, stainless, mirror acted on by laser radiation, reflectivity meas. 79−10342
steerer-expander device, two-mirror afocal telescope design 78−46700
stimulated Brillouin scatt. complex conjugate mirror for ruby laser 80−87438
stimulated Brillouin scattering mirror, wave-front inversion of laser output 79−14038
sub-mm-wave laser interferometer, use of low-inertia semiconductor structs. to modulate radiation 80−31848
submillimetric and IR laser absolute frequency meas. 77−79882
subnanosecond blast shutter, isolator for high-power laser system 77−79842
surface cleaning, liquid spraying technique, appl. to laser glass, metal surfaces 78−72921
surface generated by diamond turning machine, physical and optical props. 80−33263
surface irregularity statistics for laser component materials 79−14057
surface spark discharges high current, light emission props. and appls., book contrib. 79−77449
target positioning system for Helios CO_2 fusion laser beams 80−74421
temperature-compensating drive circuit using Si bipolar transistor, for injection lasers used in optical communications 79−45971
thermal blooming cell design for adaptive optics evaluation 80−33096
thermal compensator for diode laser closed-cycle refrigerator stabilisation 78−50797
thermal length control, for lasers and etalons 78−87056
thermal neutron traps description 80−64041
thermionic gun with beam extraction through Al foil 77−13817
thermo-gasdynamic control in laser beam guidance, review of developments 78−74942
thermoelectric detector, for CO_2 laser power meas. *(French)* 77−58365
three mirror HF laser modulator 79−3728
thyratron ignition of gas lasers *(German)* 79−64245
thyratron pulser, high-power, HF, for photo-impulse ionised lasers 79−18444
thyratrons for short pulse laser circuits 79−18437
thyristor convertor for Ar laser discharge current control 77−14747
thyristor oscillator for injection laser pumping 79−13982
tilted birefringent Fabry-Perot etalon, for dye laser tuning *(Japanese)* 77−54735
tracking system testing by 1 m unobscured IR collimator 80−78991
transmissive optics for high power CO_2 lasers 78−79057
transparent solids, absorpt. coeffs. by laser calorimetry, wavelength modulation spectroscopy 78−66876
travelling wave lens, optically excited soft X-ray laser technique development 78−59016
travelling-wave electro-optic element, CW laser freq. shifting for subnanosecond FID 80−38075
trichromatic acousto-optical laser-beam deflector for TV scanning *(Czech)* 79−98502
tunable laser linear scan control by Fabry-Perot interferometer 79−76693
two-laser frequency difference stabilisation electronic system 79−68401
two-mirror laser beam steerer-expander design 79−18460
two-scatter-plate low-speckle-noise integrator for atmospheric laser beam transmission meas. 80−90252
two-wave laser coatings for 0.63 and 3.39 μ line prod. *(Russian)* 77−83895
UV damage resistance of laser coatings 80−33056
UV high power μs light source for photodissoc. laser pumping 77−27295
UV high-power laser material, refractive props. and optical constants 80−106555
UV laser window material absorption obs. 79−14012
UV lasers, Blumein circuit transient anal. for effective operation 77−68230
UV light source, surface spark discharge type, for H_2/F_2 laser initiation 80−78923
UV source using surface discharge plasma 77−58917
vacuum UV coating technology 79−46030
vacuum UV special application coatings, reflectance, transmission, technology 79−59788
variable attenuator for Gaussian laser beams 79−22987

laser accessories continued
vidicon, Si target, and minicomputer system, for laser intensity profiles meas. 79−27267
visualizer for infrared laser emission field 80−23732
wall ablation lamps for high energy dye laser pumping 78−29961
water continuously variable filter for I laser 78−55397
wavefront analyser for diagnosing high-energy lasers 79−59740
wavefront analyzer for diagnosing high-energy lasers 79−59738
wavefront visualizer for coherent IR beams 78−25986
wavelength meter, compact static, based on Fizeau interferometer, for pulsed and CW lasers 79−36947
wavelength meter, He-Ne laser/monochromator/interferometric system 77−18086
wavelength scanning with microcomputer control 79−94248
wavelength tuning gratings, damage resist. 77−19283
wavemeter for CW lasers 79−26112
waxicon, nonlinear, for laser beam transform., design and fabrication 78−5543
waxicons for high-power chemical lasers, interferogram analysis 80−14418
window, elec. fields and power dissipation at oblique incidence 77−46746
window, thermal lens form. due to giant laser pulse 77−3602
window and rod critical orientations for stress-induced depolarisation elimination 79−14054
window coating materials with low index, laser damage at 10.6 μm 77−61991
window construction, for type 300.1 TEM_{00} He-Ne laser *(Rumanian)* 80−9898
window degradation interactions and impurity clustering effects 79−14050
window materials, pulsed HF-DF laser damage 79−14011
window materials, refr. index, temp. and stress effects 77−46771
window materials for CO_2 lasers, optical suitability 77−58361
window materials for HF-DF laser, surface and bulk absorpt., photoacoustic meas. 78−25912
window materials for high-power lasers, stress birefr. elimination 77−58362
windows, damage threshold at 10.6 μm, up to 10^{10} W/cm^2 77−50707
windows, single cryst., stress-induced birefr. elimination 77−88818
wire diffraction grating, potential use in meas. of IR laser beam parameter 77−730
X-ray phototube detector, with Al and Fe interchangeable cathodes *(German)* 77−10107
AlAs-GaAs three-layer heterostruct. spectrum convertor, in Nd:YAG laser pumping system 79−27272
$Al_xGa_{1-x}As$-$Al_yGa_{1-y}As$ DH superluminesc. diode, for Nd:YAG laser pumping, room temp. CW operation 77−7122
Al_2O_3 coated Al mirrors, highly efficient refl. type polarisers for 10.6 μm laser radiation 78−71177
Al_2O_3-Si, alternating layers, dielec. facet reflector for semiconductor lasers 78−66841
Au film, laser absorpt. vs. temp., calorimetric meas. 79−98423
BCl_3 gaseous phototropic shutter control of CO_2 laser PRF 78−50833
BaF_2, piezo-optical coeffs. meas. at 0.6328, 1.15 and 3.39 μm 80−34888
BaF_2, polycryst., laser window material, IR thermooptic coeff. meas. 77−36208
BaF_2 purification for laser components, selective ion filter design and construction 79−14051
BaF_2, single cryst. windows for high power lasers, stress-induced birefr. elimination 77−88818
BiF_3 coating materials for IR laser components 80−33105
BiI_3, coating materials for IR laser components 80−33105
CO_2, 100 kJ laser, optical design and components 78−82990
CO_2 high power laser beam monitor 78−74943
CO_2 laser amplifier isolation from target reflection 77−19288
CO_2 laser Antares fusion system power amplifier optics 80−74394
CO_2 saturable absorber, heated, for passive Q-switching of CO_2 laser 78−25900
CS_2 travelling wave Kerr cell, ultrafast pulse shaping and picosecond rise time elec. pulses 80−33152
$CaCO_3$ calcite linear polarizer, role in laser technology 80−64165
CaF_2 ⟨111⟩ oriented windows, optical distortion coeffs. at chem. laser wavelengths 79−94269
CaF_2 antireflection coated, 3.8 μm CW laser damage threshold obs. 80−33053
CaF_2, fine-grained, forging and bulk optical props. 80−33103
CaF_2, hot forged, laser window material, fabrication, props. 77−46773
CaF_2, laser window material, absorpt. at CO wavelengths, calorimetric meas. 78−25911
CaF_2 laser window surface O_2 detection by X-ray photoelectron spectroscopy 79−14056
CaF_2, laser windows, intermediate temp. forging 77−46775
CaF_2 low-loss laser window material, surface absorpt. meas. at 2.8 and 3.8 μm 79−94267
CaF_2, piezo-optical coeffs. meas. at 0.6328, 1.15 and 3.39 μm 80−34888
CaF_2, polycryst., laser window material, IR thermooptic coeff. meas. 77−36208
CaF_2, press-forged laser window, polishing, cleaning and grinding 79−59849
CaF_2 trapezoid, ThF_4 and ZnSe coated, IR characterisation by internal-refl. spectra 78−71161
CaF_2 window, hot forged, refr. index, temp. coeff. 77−46772
$CdCr_2S_4$ Faraday effect isolator, laser damage tests 77−46750
$CdCr_2S_4$, hot-pressed, optical isolation appl. at 10.6 μm, intrinsic absorpt. props. 78−42368
CdHgTe detectors for CO_2 laser appls. 79−40615
CdS, fast modulator for CO_2 laser, using two-photon magnetoabsorpt. 77−88805
CdS, fast optically controlled modulator using two-photon magnetoabsorpt., for CO_2 laser 78−13736
CdS nonlinear lens, with variable focal length 79−81511
CdTe crystal Pockels modulator, PCM of CO_2 TEA laser pulse 80−102742
CdTe, electron-beam-controlled transmission of 10 μm radiation 79−81466
CdTe intracavity electrooptic modulator, for high pulse repetition freq. CO_2 oscillator 77−88801
CdTe, laser window material, absorbing Te inclusions, damage threshold 77−46749
CdTe, laser window material, vap. deposition, mech. props. 77−46776
CdTe, laser window material, vap. deposition 78−27391
CdTe linear electro-optic translation of IR laser wavelengths 80−78878
CdTe optical applications, review 77−42580
CdTe, polycryst., laser window material, IR thermooptic coeff. meas. 77−36208
CdTe, single cryst. IR laser window, low absorption at 10.6 μm 78−79081
CdTe single crystal IR window for CO_2 laser 77−75566
CdTe, window material, catastrophic laser damage threshold estimate 78−25913
CdTe, window material with absorbing inclusions, damage thresholds 77−38971
CeO_2 coating of laser optical components, electron microscope obs. 80−43342
$CoCr_2S_4$, Faraday effect, appl. to CO_2 laser systems, radiation damage resist. 78−95579
$CsCuCl_3$, optical props. rel. to IR electro-optical modulator appl. 78−42393
^{133}Cs vapour external selective mirror for semiconductor laser 79−45961
Cu film self-generation on Cu doped glass ceramics, for low-expansion IR laser mirrors 79−14127
Cu halide laser driving ccts., parametric study 80−83610
Cu mirror, microstruct. effect on Ag overlayer deposition, 10.6 μm reflectivity 77−42543
Cu mirror, single-point diamond-turned, evaluation for 8-beam CO_2 laser, Helios 79−23044
Cu plated substrates for Antares CO_2 laser mirrors 80−14349
Cu, polished mirror, optical props. ageing 77−79912
Cu vapour deposited mirror on SiC substrate, pulsed laser damage charcts. 80−48314
Cu-Sn(Al)(Ga) reflecting surface absorpt. coeffs. at 10.6 μm 80−95984
$Fe_{1-x}B_x$ film, magneto-optical charcts., appl. to Kerr effect mirrors for ring laser gyros 79−82956
$Fe_{1-x}Si_x$ film, magneto-optical charcts., appl. to Kerr effect mirrors for ring laser gyros 79−82956
GaAs 400 MHz TW laser modulator 80−87541
GaAs, absorption coefficients, method of meas. 78−83048
GaAs laser reliability, protective facet coatings 79−81452
n-GaAs, microwave biased, fast rise-time modulation of 337 μm radiation 77−54794
GaP acoustooptic pulse modulator 78−46814
n-GaP low absorption monitors for HF laser 79−31964
p-Ge, broadband modulation of 3 μm light by 10 μm light 78−42389
p-Ge broadband passive isolator for CO_2 laser system, pulse shaping 78−46662
Ge, electron-beam-controlled transmission of 10 μm radiation 79−81466
Ge optical switch, picosecond pulse generation at 10.6 μm 79−7159
Ge reflection switch, N_2 laser controlled, mode-locking of CO_2 laser oscillator 80−1247
p-Ge saturable absorber, passive mode locking of TE CO_2 lasers 78−71127
p-Ge saturable absorber for CO_2 laser 77−88869
p-Ge, saturable absorption isolator for CO_2 laser systems 77−19284
Ge window, thermal lensing 77−72021
$Ge_{0.45}Se_{0.55}$-As_2S_3, antirefl. coating, performance at 3.8, 5.3 and 10.6 μm 77−61964
HFO_2, vacuum deposited film, use in multilayer reflector for near UV 77−34924
He, hollow-cathode type discharge, spectroscopic obs., laser light source appl. 80−59335
He recovery and recycling system, for CO_2 lasers 78−82974
He-Ne lasers parallel plate development 80−1224
Hg, optically pumped, saturable absorber overlap of ^{127}I 77−83932
$Hg_{1-x}Cd_xTe$, Faraday effect at CO_2 laser freq. 78−64348
I hot wall cell, freq. stabilisation of He-Ne laser 77−65598
I passive switch for 1.315 μm radiation 77−23685
I saturable absorpt. cell for I 1.315 μm laser wavelength 77−10985
I switch, active modulation of transmission based on Zeeman effect 79−22994
I_2 absorption cell for He-Ne laser 77−79867
I_2 vapour passive Q-switch for ruby laser 77−79872
I_2 hot wall cell for He-Ne laser freq. stabilisation 77−83914
$^{127}I_2$, weakly saturable absorber for He-Ne laser, high contrast power reson. 78−29976
InSb, 100 W average power 10.6 μm isolator based on interband Faraday effect 79−59706
K-Rb arc lamp development for space laser communications 78−46646
KBr, IR laser window appl., crystal growth, polishing and optical absorpt. 77−7102
KBr, plate, distortions due to 10.6 μm laser irrad., interferometric obs. 78−46697
KBr purification for laser components, selective ion filter design and construction 79−14051
KCl, bulk and surface absorpt., 2 to 10 μm, calorimetric meas. 78−71160
KCl crystals with NaF surface absorpt. regions, photoacoustic detect. 79−87466
KCl diamond turned window surfaces, 10.6 μm pulsed laser damage 77−50704
KCl, doped, saturable absorber for CO_2 laser 79−10363
KCl IR window material, polish layer effect, ellipsometric meas. 78−55419
KCl laser window, thermal lensing, effective optical distortion parameter 77−83916
KCl, laser window material, absorpt. at CO wavelengths, calorimetric meas. 78−25911
KCl laser windows at 10.6 μm, optical distortion parameter 78−79036
KCl low-loss laser window material, surface absorpt. meas. at 2.8 and 3.8 μm 79−94267
KCl plate, distortions due to 10.6 μm laser irrad., interferometric obs. 78−46697
KCl, single cryst., laser window material, IR thermooptic coeff. meas. 77−36208
KCl surface texture and optical props. after forging between polished dies 80−33102
KCl window, thermal lensing 77−72021
KCl, window material, photoelastic consts. meas. at 10.6 μm 78−25934
KCl window with antirefl. coating, laser damage at 10.6 μm 77−61992
KCl, zone refined single crystal growth for high power CO_2 laser optics 78−22181
KCl:Eu IR laser window lattice equilibrium obs. 79−14055

laser accessories continued
KCl:RbCl, $SrCl_2$, laser window material, prep., grain boundary stability 77−46774
KCl:ReO_4^- nonlinear absorption for CO_2 laser pulse compression and mode locking 80−74443
KD_2PO_4, cryst. high-freq. modulation in Pockels cell, acoustic phenomena 78−1336
KD_2PO_4 crystal, electro-optical extraction of Nd:YAG laser pulses *(German)* 80−87416
KD_2PO_4 r_{63} modulator *(Chinese)* 80−28260
KD_2PO_4, ultrafast electro-optical modulator design and application 77−19432
KD_2PO4 transmission line Pockels cells, optical rise time meas. 78−46778
$KGaF_4$ coating materials for IR laser components 80−33105
KH_2PO_4, cryst. high-freq. modulation in Pockels cell, acoustic phenomena 78−1336
KN_bO_3, single domain crystal growth, SHG with Nd:YAG laser 78−74954
LaF_3-MgF_2 multilayer mirrors, optical strength in Xe laser 77−27294
LiF mech. and optical props. rel. to forging conditions 80−33101
$LiNbO_3$ crystal in laser resonator, thermo-optical effect *(Chinese)* 80−106546
$LiNbO_3$ electro-optic phase modulator for unpolarised laser beam 79−50403
$LiNbO_3$ electrooptic phase modulator, axial mode locking of CW Nd^{3+}:YAG ring laser 78−50835
$LiNbO_3$ electrooptic phase modulator, freq. shift device for optical range 78−59147
$LiNbO_3$ electrooptic switches used in Nd^{3+}:YAG lasers, contrast and configs. 80−33012
$LiNbO_3$ fast-response broad-band electrooptic elements for laser beam control systems 79−89944
$LiNbO_3$ volume holographic grating as spatial-freq. selector for tunable dye laser 80−53240
$LiNbO_3$:Cu, holographic grating, for electro-optical laser beam modulation 77−3672
$LiNbO_3$-Ge, acoustooptic modulator for CO_2 lasers 78−42365
$LiNbO_3$-Ge acousto-optic modulator for 10.6 μm CO_2 laser 80−99776
$LiTaO_3$ fast electro-optic deflector, arbitrarily shaped optical pulsed generation 80−53421
$LiYF_4$, UV window and coating materials, two-photon absorpt. coeffs. 79−59734
Mo laser mirror, optical and metallurgical characterisation 80−33129
Mo sputtering for laser mirror refurbishment 80−14498
NH_3 incavity cell, technique for obtaining CW CO_2 sequence laser lines 79−18438
NH_2D Stark active mol., cavity dumping for CO_2 laser pulse generation 77−88800
$NH_4H_2PO_4$, total internal refl. diffr.-type modulator as laser cavity switch 78−5511
NaCl 46 cm window optical evaluation facility 80−74526
NaCl, bulk and surface absorpt., 2 to 10 μm, calorimetric meas. 78−71160
NaCl Czochralski crystal growth for large CO_2 laser windows 80−74525
NaCl large window continuous polishing 80−74527
NaCl, plate, distortions due to 10.6 μm laser irrad., interferometric obs. 78−46697
NaCl Polytran laser windows, for CO_2 lasers, fusion appls. 78−59067
NaCl window production for Antares CO_2 laser system 80−74524
Nd:YAG, operational characts. of $LiNbO_3$ Q-switch for generating single laser pulse *(Korean)* 77−704
Nd:YAG K vapour arc lamp as optical pump source 79−86261
Nd:YAG mode-locked laser picosecond pulse profile and power meas. 77−7112
Ne discharge Faraday filter, dye laser freq. locking to absorpt. lines 77−79870
Ni complex soln., BDN II, saturable absorber for 1.315 I laser 79−27297
Ni_xP_{1-x}surface, laser produced ripple patterns, appl. to cavity mirror 77−79878
OsO_4 absorber for freq. stabilised CO_2 laser, output freq. reproducibility 78−50800
PLZT transparent ceramic laser modulator *(German)* 78−5553
PbF_2, antireflection coating deposition technique, 2.87 μm laser damage threshold 80−33264
PbF_2-TlI graded coatings on KCl laser windows, photoacoustic spectroscopy 80−33052
$PbMoO_4$ acousto-optical modulator for wideband laser recording system 79−89942
$PbMoO_4$, polychromatic acousto-optical deflector *(Russian)* 77−58429
PbO-SiO_2 glass, optical coating for GaAs-$Al_{1-x}Ga_xAS$ laser 78−71113
PbS exploding film, Q-switching of Nd^{3+}:glass laser 78−42361
Pt-Pd discontinuous film MIM point-contact diode detector 77−5917
SF_6 based broadband gas isolator, for high power CO_2 lasers, design and evaluation 78−42339
Si Fabry-Perot couplers for optically pumped far IR lasers 80−69404
Si position-sensitive detector for CW and pulsed laser beams 80−78883
SiC nonlinear lens, with variable focal length 79−81511
SiO_2 facet coating film effect on self-sustained pulsation suppression in GaAlAs DH lasers 80−95894
SrF_2 antireflection coated, 3.8 μm CW laser damage threshold obs. 80−33053
SrF_2 fusion-cast prism refractive index obs., 0.2138 to 11.475 μm 80−34882
SrF_2, laser window material, absorpt. at CO wavelengths, calorimetric meas. 78−25911
SrF_2 piezo-optical coeffs. meas. at 0.6328, 1.15 and 3.39 μm 80−34888
SrF_2, press-forged laser window, polishing, cleaning and grinding 79−59849
SrF_2 purification for laser components, selective ion filter design and construction 79−14051
Te acousto-optic modulator, props., for IR laser beam control *(Russian)* 77−72073
TeO_2 acousto-optic laser deflector scanning 80−14486
TeO_2 acousto-optic laser beam deflector using shear wave propag. slightly off (110) crystal axis *(Japanese)* 80−102818
TiO_2, reactively sputtered optical coating for inertial confinement fusion laser components 80−23705
TiO_2-SiO_2, multilayer dielec. mirrors, laser-induced damage resist. 79−10335
laser accessories continued
TlI coatings on KCl laser windows, photoacoustic spectroscopy 80−33052
TlI films, polymorphic, double epitaxy and growth on KCl, X-ray and optical obs. 79−77944
TlI laser window films, stoichiometry, Rutherford backscatt. study 80−59831
TlI window coating, epitaxial growth habit rel. to light scatt. 77−50738
TlI-PbF_2 graded-index film coating technique and results 80−33265
W-Ni(Co) point-contact diodes as harmonic generators and mixers, DC bias dependence 80−75653
Xe flashlamp efficiency for photoinitiation of HF pulsed laser 80−69403
Xe flashlamps with interf. coatings, laser pumping efficiency improvement 79−10316
YIG Faraday rotation optical isolator, intensity fluctuation suppression in $LiNdP_4O_{12}$ laser 79−81437
$ZnGeP_2$, synthesis, characts., applic. to laser windows *(French)* 78−80467
ZnS CVD window, IR lattice absorption, phonon assigments and image spoiling 80−33104
ZnS(Se), polycryst. laser window material, IR thermooptic coeff. meas. 77−36208
ZnSe, CVD, laser window material, impurity absorpt. meas. 78−25909
ZnSe coatings on CaF_2 laser windows, photoacoustic spectroscopy 80−33052
ZnSe, electron-beam-controlled transmission of 10 μm radiation 79−81466
ZnSe, Faraday effect visible optical isolator 77−75657
ZnSe, IR laser window coating absorption rel. to deposition conditions 79−14061
ZnSe, laser window material, multiphonon absorpt. temp. depend., calorimetric meas. 78−25907
ZnSe, laser window material, absorpt. at CO wavelengths, calorimetric meas. 78−25911
ZnSe laser window photoacoustic spectroscopy 80−33052
ZnSe laser windows, AR coated, photoacoustic chopping freq. studies using CO_2 laser 80−83629
ZnSe laser windows, photoacoustic signal var. with chopping freq. 80−75309
ZnSe, RF bias-sputtered CVD films on CaF_2 79−14060
ZnSe sputtered laser window coatings, prep. and evaluation 77−50739
ZnSe window, laser induced thermal stresses 77−46747

laser beam applications
see also holography; integrated optics; laser beam machining; laser beam welding; laser isotope separation; matrix isolation spectroscopy; measurement by laser beam; modulation spectroscopy; optical communication; optical radar; patient treatment; plasma production and heating by laser beam; Raman spectra; Raman spectroscopy; remote sensing by laser beam; spectroscopy; surgery; two-photon spectroscopy
1 Gb/s laser space communication system 77−7213
absolute mass detection limits using laser microprobe anal. with cross excitation 78−7297
acceleration of macroscopic particles by laser radiation 80−6290
accelerator diagnostics using laser beam 80−95497
acoustic fields in quartz, $LiIO_3$ and quartz piezoelectric transducers 80−97231
acoustic microscope, using scanning laser beam 79−7263
acoustic microscopy using scanning laser beam as remote sensing microphone 77−81382
acoustic transducer-receiver activation, flexible configuration 80−83724
adaptive phased arrays driven by independent laser oscillators 80−33005
adhesion determination, thin films 80−71833
advancements and development trends *(Japanese)* 78−13745
aeronautical technique utilising laser and microwave beams *(Russian)* 77−3838
aerosol size distribution by means of laser-induced fluoresc. 77−40576
aerosols, monodisperse, mass concentration, laser monitoring 80−98878
agricultural *(Chinese)* 77−68216
air pollution, ambient sulphate aerosols laser-Raman monitoring 78−69532
air pollution, laser-Raman microprobe anal. of suspended particulates 80−76687
air pollution above urban site, monitoring by Lidar meas. *(French)* 77−25780
air pollution detection, reviews 77−9569
air pollution studies, laser absorpt. techniques 77−9570
aircraft velocity and altitude measurements using a tunable diode laser 80−13042
alignment of crystal face perpendicular to axis of rot. 77−15283
alloy, laser surface melting 77−90492
alloy surface composition modification by high-power CW lasers 80−93699
alphanumeric character generator for line printer and COM 80−33067
ametropia determination with laser refractor 78−35907
annealing, ion implanted Si, pulsed electron and laser beam annealing, comparison 79−52256
annealing, pulsed ruby laser annealing of ion implanted Si 79−52255
annealing Au diffusion barrier, at metal-semiconductor on metal-metal interface 80−80373
anthology, lasers and their applications in physical research 80−17724
arrangements and appls., including mining *(Croatian)* 77−697
atmospheric analysis, from orbiting satellite 77−9571
atmospheric communication line, error probability 77−14731
atmospheric constituents, detection by laser beam, review *(French)* 79−34952
atmospheric pollutants, selective quantitative meas. using CO and CO_2 lasers 78−69526
atmospheric properties meas. using Spacelab lidar 77−21943
atmospheric research using Spacelab lidar 77−21948
atmospheric scatter channel for ELOS optical communications system 79−29862
atmospheric science, conf., San Diego, USA (Aug. 77) 78−85748
atmospheric spectroscopy and pollution monitoring by tunable dual CO_2 laser 78−3977
atmospheric studies, review 79−66789
atmospheric topside sounding using Spacelab lidar 77−21942
atmospheric transmission meas. using IR lasers and Fourier spectroscopy 77−70885
atmospheric transparency meas., laser radar meas. *(Italian)* 77−91333

laser beam applications continued
atmospheric UV propagation and optical communications range 77−79770
atom detection technique 79−26950
atom in laser field, reson. light press. forces, cooling and trapping appls. 79−98045
atomic beam, focused with laser beam, Na beam and dipole forces 79−7066
atomic beam, produced by laser-metal surface impact 80−5637
atomic beam velocity spectrum, determ. via tunable CW laser 77−3210
atomic motion control, vel. selection, cooling, trapping, spectroscopy appl. 77−30833
atoms in resonant laser fields, cooling, trapping and storage 79−59421
automatic inspection of materials 80−66734
back pointer for ^{60}Co radiotherapy unit 77−86583
ballistic missile destructor and weapons technology 77−50710
bar code reader, using optically generated holograms 77−14673
basic principles and future aspects *(French)* 77−3601
bathymetry using Nd;YAG Q-switched laser 80−8461
beacons, increase of range of visibility in fog using coaxial beams technique 80−101434
beam-addressable optical display using supersaturated vapour photonucleation 80−4691
benchless laser structural model, control system 79−81464
benchless laser with autoalignment for airborne electro-optical systems 79−76723
binary optical communication system, atm. scintillation effects 77−71943
biological microsample preparation and manipulation *(German)* 80−56307
biological tissue, coagulation by irradiation with laser light 80−41113
biology and medicine *(Japanese)* 80−3752
biomedical developments review 77−13017
biomedical laser absorption spectroscopy with ATR plates *(German)* 78−36084
biomedical research, diagnostic probe 77−9298
biomedical research, influence of lasers, review 80−26318
biomedical research in USSR 78−48858
blood vessel photocoagulation 79−39467
body dither laser gyro, scale factor nonlinearity 78−79062
boring and sampling, conc. determ. of ^{137}Cs fission product in coated-particle fuel 80−18416
Bragg diffraction imaging for medical use 78−53462
Bragg imaging in the reflection mode and designs for improved optics 80−17040
Brillouin ring laser, fibre-optic, use for inertial sensing 80−87411
bubbly flows, simultaneous meas. of local liquid vel. and void fraction by gas laser, accuracy *(Japanese)* 78−67295
buried-heterostructure laser packaging for wideband optical transmission systems 78−74920
calorimetry, absorption meas. 79−55308
camera, with scanning head and photosensitive detector, nuclear reactor surveys appl. 80−52748
[cc] He-Ne laser scanning system, for video record player, information identification *(German)* 80−106557
cell microsurgery using UV laser beam *(German)* 77−60235
cellular microsurgery, microscope vertical illuminator adaptation by laser microbeam 79−20727
ceramic powder synthesis from laser-heated gas phase reactants 80−93525
chalcogenide glass, prep. by laser evaporation, and characterisation 77−12533
charged particle beams, energy spread reduction, laser pulse technique 80−87279
chemical analysis, industrial appl. of lasers 80−87427
chemical analysis, tunable-diode-laser IR spectroscopy applics. 80−40798
chemical reaction control using chemical lasers 77−70312
chemical spectroscopy and dynamics, higher-order susceptibility effects 79−40625
chemistry, laser spectroscopy applications, conf., Anaheim, USA (Mar. 1978) 80−36781
chemistry, review 80−45535
chemistry, review of laser systems *(German)* 78−13744
clinical medicine *(Japanese)* 80−12211
clinical otorhinolaryngology, Ar^+ laser application 77−90870
clinical rhinology, Ar^+ laser instrument *(German)* 78−69177
clinical surgery appls., advantages 79−34704
cloud clearance, atmosphere liq. water content and temp. fluctuations in clearance zone *(Russian)* 78−44999
cloud hole-boring by high-intensity laser beams, theory 78−28319
coherence implications 77−75599
coherent THz acoustic wave launching by far IR photon-phonon conversion 77−39135
coherent-radiation spectral power density unit reproduction, USSR standard 78−37957
cold atoms, trapping and storage in laser field 78−86826
colliding beam arrangement using laser linac, feasibility study, laser accelerator problems 78−78521
colour image scanner, using one-colour laser and modified γ-Ruticon image buffer 79−27373
colour TV digital signal holographic recording on photographic film *(German)* 78−22101
COM system recording module 77−18120
communication, gigabit link development 78−66860
communication system, using US light modulator, for teachers 79−40321
communication systems, transmission of information in the optical waveband, book 79−3645
computer controlled optical system for quantitative diagnosis of early pulmonary oedema 77−77981
computer output to microfilm, using laser imaging dry process development film *(German)* 79−9253
computer printer using laser *(Japanese)* 78−90446
conference, appls. of low power lasers, San Diego, Calif., USA (Aug. 1976) 77−75536
conference, Dresden, Germany (Mar.-Apr. 1977) 77−83881
conference, laser and electro-optical systems, San Diego, CA, USA (Feb. 1980) 80−62392
conference, laser and electrooptical systems, San Diego, CA, USA (Feb. 1978) 78−42340
conference, laser engineering and appls., Washington, USA (May-June 1979) 80−1216

laser beam applications continued
conference, lasers and applications, Erice, Italy (May-Jun. 1970) 77−38906
conference, lasers and their appls., Dresden, East Germany (Mar.-Apr. 1977) 79−7137
conference, Masnuy-St-Jean, Mons, Belgium, Oct. 1979 80−82570
conference, Washington, DC., USA (Jun. 1977) 78−46610
conference, Washington, DC, USA (June 1977) 77−88732
conference on laser and fibre-optics communications, San Diego, CA, USA, Aug. (1978) 79−86203
conference on laser optoelectronics, Munich, Germany (June 1977) 78−33739
continuous radiation relative power-density distribution unit reproduction, USSR 78−37956
cooled ion storage frequency standard possibilities 79−54102
cooling tower plumes, lidar meas. *(German)* 77−25781
CVD, using CO_2 laser for substrate heating 78−39698
CVD using focused laser beam 80−93493
CW laser appls. 80−58550
dark photography, laser as flash-lamp+image intensifier *(Russian)* 77−79177
data recording on disc using diode laser 80−19001
deflection system, X-Y beam, accuracy and repeatability improvement 77−58480
deflector quality factor N/τ, comparison of holographic and acousto-optical deflectors *(French)* 78−55318
dental sealant application by laser 78−48868
dentistry, laser interactions 77−52840
dentistry, preventive, laser processes 78−7530
dermatological high-intensity laser therapy *(German)* 79−2117
dermatology, photobiologic phenomena 78−35909
dermatology investigation and therapy with dye lasers 78−35910
designation system spot motion model identification 79−94277
deuteron source for pulsed neutron generator 80−27844
diabetic retinopathy therapy, laser photocoagulation efficiency factors 79−79622
diagnostic irradiation of fluid-suspended cell flow 77−21594
diameter meas. by laser scanned gauge *(Chinese)* 80−77756
dichromated PVA specific wavelength sensitisation for laser beam recording 78−5531
dielectric crystal, phase transitions, laser spectrometry, use of diamond anvil devices *(Japanese)* 80−49362
dielectric films, low temp. epitaxy in laser sputtering 80−34335
dielectric thin film deposition by CW CO_2 laser, optical and struct. props. 80−7506
diffraction gratings, laser produced, review *(Rumanian)* 80−87542
diffraction pattern approximation by laser simulation 78−55287
digital communication systems, acousto-optical multiplexing and demultiplexing techniques for multigigabits/sec transmission 79−86132
diode laser communications for remote utility meter reading 79−86195
direct conversion of CO_2 laser energy to HV electrical energy using laser-produced plasma 78−18427
direct energy conversion, CO_2 laser to HV elec. energy 77−88834
direct picture printers on photographic paper, appl. in life sciences *(French)* 80−72119
discharge channel migration control by laser beam *(Russian)* 77−55198
discharge gap characts., laser-radiation-triggered, influence of discharge medium, electrooptic switch control appls. 80−64818
discharger, fast response, sealed triggered by laser radiation 78−51391
discotheque light effects, safety considerations with respect to output power and exposure time, regulations and recommendations *(German)* 80−101224
dissociation of SF_6, focused beam approach 78−42369
dolorimetry, cerebral response to noxious CO_2 laser stimulation 78−31882
doppler anemometer feasibility assessment method *(Russian)* 79−98832
Doppler anemometry, instrumentation, appls., explanation using Moire patterns 77−7490
Doppler velocimeters, blood flow meas. in fish *(Japanese)* 79−84052
drop size time variation meas., in aerosol continuum and non-continuum evap. 79−43639
dye laser, pulsed, high energy, moderate energy, tunable coherent light 77−23681
dye laser for holographic contours generation 77−14671
dye laser induced photochemistry 79−39182
dye-polymer system, diffusion based direct marking process, laser induced, spectral thermal characteristics 79−76779
dynamic data display on large screen by brightness enhancing system 77−58462
dynamic range measurements on streak cameras 80−73490
dynamic wind-tunnel balance, two-component, for mounted flying insects 80−22350
electric welding, interferometric study using laser source *(Russian)* 78−37049
electro-optic laser scanner, background signals anal. 77−19425
electro-optics, conference, Utrecht, Netherlands (Oct. 1978) 80−31420
electrocyclic isomerisation of ground state induced by IR laser multiphoton absorpt. 77−32811
electromechanical mirror scanning devices 77−58477
electron accel. in laser-beam focus 77−10574
electron accelerator 79−93847
electron accelerator powered by laser beam, parameter estimates 77−83167
electron beam focusing by laser beam fields 78−74833
electron beam laser technology and applications 77−19262
electron collective acceleration 79−76166
electron gun cathode heating using focused laser beam *(German)* 78−89591
electron ring accelerator, particle focusing with rectified laser light 80−42879
electron-beam exposure system, distortion correction and deflection calibration by laser interferometry 80−69310
electrophoresis, laser Doppler, high current-density electrodes 80−89500
electroradiographic image laser readout 80−41225
electrothinning, laser-monitored, for preparing ultrathin metal foils 78−53074
emission spectroscopy, laser microprobe, matrix effects, appls. 77−16870
end preparation and fusion splicing of fibre array with CO_2 laser 80−10051
endoscope treatment of urinary tract strictures *(German)* 78−35914

laser beam applications continued
endoscopic Ar ion laser photocoagulator for bleeding digestive lesions 78−40287
endoscopic laser coagulator with recirculating gas-jet assist 78−48867
endoscopic laser photocoagulation, use of gas jet appositional pressurisation 78−53468
endoscopic photocoagulation in human digestive tract using Ar ion laser *(German)* 78−35915
endoscopic photocoagulation of bleeding lesions, using Ar laser *(French)* 79−34627
endoscopy, comparison of optical waveguides *(German)* 77−78037
energy flux channel close-up time *(Russian)* 77−55994
engineering advances, conf., San Diego, CA, USA (Aug. 1977) 78−59017
engraving unit, direct dry preparation of offset printing plates 79−18434
environmental diagnostics using laser beams 80−35802
EPR spectrometer, high temp., CO_2 laser-heated 80−68233
etching, of Si monocryst., by Br, Ar laser beam initiation *(Russian)* 77−73358
ether wind first-order expt. with stabilised lasers 77−5665
excimer laser systems appls., book contrib. 79−81441
excimer lasers, review *(Japanese)* 78−33723
excitation of stationary molecular states 77−68084
eye tissue coagulation, OK-2 laser ophthalmocoagulator 79−11991
Fabry-Perot laser spectrometer, for nonlinear superhigh-resolution spectroscopy 78−49912
facsimile printing comprising real-time diffr.-limited reading, transmission and printing of large images 77−42559
far IR technology and applications, conf., Reston, USA, (Apr. 1977) 78−45711
fast-response photocell time characteristics meas. 77−5913
fatigue damage measurement by laser scanning, exoelectron display 77−73391
ferrous metallurgy, surface purification using laser and N_2 jet 78−92392
fibre drawing, CO_2 laser system limitations 78−1447
fibre drawing, tension rel. to drawing vel. and ultimate strength 78−74986
fibre optic break detection, time-domain reflectometer with gated photomultiplier receiver 77−65620
fibre optic laser gyro signal detection and processing technique 79−37037
fibre optics in medicine, diagnostic and therapeutic appls. 79−39466
fibre splicing with low-power CO_2 laser 77−72098
film deposition, Al, using pulsed ruby laser *(Czech)* 79−52126
film deposition, evaporation of chem. element films with Nd:glass laser 79−47633
film deposition using pulsed plasma generators *(Russian)* 77−21037
film deposition with periodically pulsed CO_2 laser, film characts. 79−28926
fission fuel coated particles, laser boring for material sampling 78−55399
fission products, release and distrib. in coated particles *(German)* 78−82403
fixed-frequency laser beam scanning device 78−59135
flame, OH concentration measurement, local and instantaneous, by laser induced fluoresc. obs. *(French)* 79−15999
flame temperature meas. using laser induced fluoresc. spectrosc. of OH 80−90839
flexible holographic disc for laser scanner 79−94188
flow measurement, axisymmetric jet coherent struct. obs. 80−10282
fluorescence bronchoscope for occult lung tumor localisation 80−30832
fluorescence correlation spectroscopy, profile of focused collimated laser beam near focal minimum 80−43386
fluorescence life time decay curve meas. and anal. 78−54465
fog clearing, thermal self-defocusing effect 77−64432
fog hole boring with pulsed high-energy lasers 79−16662
Fourier transform spectrosc., new developments−passive heterodyne spectrosc. and diode laser absorpt. spectrosc. 80−95148
French CGE laboratory work on lasers and applications *(Spanish)* 78−30004
Freon, photochemical ^{13}C and ^{37}Cl isotope enrichment using CO_2 laser pulses 79−36787
frequency division, laser-to-microwave, using synchrotron radiation 79−76562
frequency-domain nonvolatile optical storage scheme 80−43282
fundamental techniques *(Japanese)* 77−72022
fundamental techniques *(Japanese)* 77−75535
fusion, high-energy gas-laser facility, distrib. microcomputer control system 77−61975
fusion expts., focusing X-ray spectrograph 80−31962
fusion reactor, high power laser appl., review *(German)* 77−54361
fusion reactor ignition *(French)* 79−41037
fusion reactors, laser-induced acceleration of macroparticles 80−27813
fusion system for radiolytic H_2 production 77−25294
fusion target irrad., laser specification 77−18696
n-GaAs-Ge laser alloying to from ohmic contacts 80−58546
galvanometer scanning system, CAD 77−58475
gas cooling method, laser pumping followed by reradiation at higher freq. transitions 79−827
gas etching technique 77−63815
gas ionisation path formation by laser beam with retractable focus 79−18992
gas laser and developmental laser *(Japanese)* 77−61961
gas laser and its appls. *(French)* 80−83590
gas laser applications, book contrib. 77−50680
gastric lesion bleeding control using lasers, comparison of Ar and Nd laser damage 78−48831
geodesy, accuracy with transportable lunar laser ranging station 77−48988
geodesy, artificial satellite laser ranging, high precision, earthquake anal. 80−98215
geodesy, base line estimation using single passes of laser data 80−3910
Geos 3 tracking systems, intercomparison 80−4227
glass, laser decoration technology 80−84810
glass fibre waveguide drawing using CO_2 lasers 79−59857
glint tracking by adaptive optical techniques 77−19458
Glissada laser landing system 79−31920
graphic arts imaging material and laser source cost tradeoffs 80−14383
ground-to-satellite power transfer 79−62724
gyroscopes, possible appl. of diffraction biased unstable ring resonators, 80−1238

laser beam applications continued
gynaecological cancer care, Ne-He laser appl. *(German)* 78−24176
gyro, integrated 3 axis design 80−1268
gyro, low-scatter low-loss mirror prod. 80−1272
gyro, ring laser, dispersion and gas flow effects 80−1267
gyro, ring laser, for military appl. 78−42370
gyro, ring laser, Rockwell programme 80−1271
gyro, ring laser, two-mode, four-mode soln. to locking problem 80−1270
gyro, ring laser *(German)* 80−53337
gyro, tutorial review 80−1266
gyro, two-mode ring laser, multioscillator approach to locking problem 79−59742
gyro, Zeeman laser, beat-note sensitivity 80−53340
gyro evaluation plan and test results 80−9934
gyro performance analysis using fast Fourier transforms 80−9933
gyro progress 78−46704
gyro technology 77−75598
gyrooptical compass, signal measurement time *(Russian)* 80−33007
gyroscope, accuracy limit *(Russian)* 79−10343
gyroscope, concepts and status 77−88827
gyroscope, Litton LC-2717, for missile appls. 79−72598
gyroscope, nuclear radiation vulnerability 80−9935
gyroscope, operation principle 79−23007
gyroscope, ring laser, Raytheon four freq., mag. mirror, Faraday and Zeeman biassing 80−1269
gyroscope, structure and basic characts. 79−23006
gyroscope, using passive ring resonator 77−88828
gyroscope, vibratory laser, steepness characts. and S/N ratio anal. *(Russian)* 78−59070
gyroscope applications 79−23008
gyroscope with induced mode locking, limiting sensitivity 79−59744
hard copy imagery from remote sensing systems, laser beam recorder appl. 79−80715
hardening temperature determ. using pulsed laser 78−72942
head surgery, possible Ar laser appl. 79−8529
heating system, for meas. of high-temp. props. of materials over wide press. range 77−77699
heavy water production, by photodesorption 77−54365
heterodyne radar, dual Bragg cell local oscillator 77−19279
high power lasers, conf., San Diego, Calif., USA (Aug 1976) 77−46730
high power lasers and their applications 78−87092
high power lasers for practical appls., conference, Reston, Va., USA (Mar. 1976) 77−34895
high resolution laser spectrometer, 10^{13} resolving efficiency *(Russian)* 77−38027
high resolution spectroscopy, comparison with level crossing method 77−30835
high resolution two-photon FM laser spectroscopy of gas atoms, free of Doppler broadening 80−95748
high speed framing photography *(Japanese)* 79−2847
high speed optical techniques, conf., San Diego, USA (Aug. 1976) 77−79182
high-speed cinematography *(Russian)* 80−279
high-speed photography of fast processes, ruby laser based apparatus 77−68236
high-temperature laser microscope, design details 80−90891
hitting high speed targets by laser beams, CO_2 laser capabilities 77−68235
hole melting in metal films, for real-time, high density digital data storage 78−71135
hologram scanner for supermarket point-of-sale bar-code symbol reader 80−48182
holographic grating production by laser irradiation of photoresist *(German)* 80−33254
holographic storage system, laser apparatus for recording transparencies of ROM 80−28177
holography, laser coherence length meas. 77−7100
hydrophone, optical interferometric, with homodyne detection, signal stabilization by light source tuning 80−87477
ice, surface, interaction of laser burst, possible appl. 80−7444
image convertor, pulsed, exposure time meas. using N_2 laser 77−30205
image storage mass memory 80−102752
imaged intracavity laser absorpt. spectroscopy 77−41703
imagery transmission, appl. of 3M and Kodak dry silver recording materials 78−70209
immunocompetent human cell irradiation, abscess removal example *(German)* 77−77960
impulse transformer for pulser-sustained laser appls., high voltage 80−1263
industrial, multikilowatt CO_2 lasers, survey 77−46731
industrial applications and historical development *(French)* 77−38904
industrial CO_2 high-power laser system, for welding, cutting, heat treating and irrad. 78−55380
inert gas halides, laser mechanism, excitation methods and appls. 80−95871
inertial rotation sensors, conf., San Diego USA (Aug. 1978) 80−1265
interferometer, acoustic vibration meas. 78−71253
interferometer, He-Ne laser, microtremor meas. *(Japanese)* 80−9025
interferometer, prism optics testing, interf. meas. 80−105698
interferometer for angular measurement, autocollimating telescope calibration *(German)* 78−77853
interferometer for sensing of respiratory sounds 77−90872
interferometric manometer, using He-Ne laser 77−110
interstellar ramjet powered by space-based laser 77−70975
interstellar rocket, laser powered, mass ratio and instantaneous efficiency 79−21134
intracavity laser spectroscopy, with continuous and quasicontinuous operation lasers *(Russian)* 78−37080
introduction to lasers, fundamental physical processes and appls. 77−75466
ion+atom, projectile charge dependence *(Dutch)* 79−50121
ion photofragment spectroscopy, via laser-ion coaxial beams spectrometer 78−12775
ion prod. in GeV range from laser irradiated targets, limitations 78−55068
ion source, appl. in mass spectrometry, review 80−89564
ionisation chamber calibration and testing using N_2 laser beam 80−27890
ionisation source for ICR spectroscopy, metal at. ion chem. appl. 80−45597
IR laser and defectograph, semicond. flow detection 78−3299

laser beam applications continued
IR laser applications in chemistry 80−16710
IR laser Stark spectroscopy, absorption of laser radiation in Stark tunable mol. gases *(Rumanian)* 79−86157
isotope separation, at. and mol. beams in nonuniform mag. and laser fields *(Russian)* 77−6960
isotope separation, by mol. dissociation in strong IR field, appl. of CO_2 laser 77−83755
isotope separation, counterstreaming laser beam-at. beam, in crossed DC elec. field 78−955
isotope separation, high power lasers for nuclear fuel reprocessing 77−38378
isotope separation, isotope shift and absorption spectrum of Cl_2 77−34701
isotope separation, laser photochemical method using relativistic electron beam microwave source 77−38750
isotope separation, laser stimulation-filtering diffusion method *(Russian)* 77−555
isotope separation, new methods review 78−1111
isotope separation, system requirements, dye and rare gas halogen lasers 77−46405
isotope separation, U enrichment, laser R&D 77−54364
isotope separation 77−38743
isotope separation and selective photochem. reactions 77−77800
isotope separation of mol. gas by mol. laser *(German)* 77−6954
isotope separation using tunable lasers, U enrichment appl. 77−6953
isotopic filtration of radiation of dye laser, in-resonator spectroscopy *(Russian)* 77−54752
jet engine, air-breathing 79−7172
jet engine reactive thrust using lasers 77−38905
large angle laser interferometer for 'curved' crystal spectrometer, precision 78−77973
laser and electro-optical systems, conf., San Diego, USA (May 1976) 77−19278
laser chemistry, conf., Pasadena, USA, (March 1978) 79−39181
laser fusion in power engineering, future prospects 77−38401
laser interference microphone for US and nonlinear acoustics 77−46874
laser iridectomy, energy required, hazards and techniques 78−11713
laser location for cosmic space appl. *(Polish)* 79−27311
laser Raman spectrometer, Chinese WFL model design *(Chinese)* 79−30573
laser range-differencing, Earth pole posn. and rotation determ. 80−101312
laser spectroscopy conf., Jackson Lake Lodge, WY, USA, 1977 July 78−82666
laser-compatible materials for graphic arts 80−13180
laser-induced optical activity, QED theory of multiphoton processes 79−31794
laser-plasma source, for pulsed X-ray lithography 79−30636
LASSO experiment on Spiro-2 spacecraft laser synchronisation from stationary orbit 80−82211
lens, optical axis designation method 80−102798
lidar antenna aerosol vol. optical field scatt., laser atmospheric sounding 77−88641
light-coupled logic with triggerable semicond. laser 80−74360
line art optical processor, optimal enhancement filter 79−59648
linear laser spectroscopy, review of absorption, opto-acoustic and fluorescence techniques 78−29170
liquid film, micron thick, optoacoustic spectroscopy using pulsed dye laser 80−42265
liquid mixture, shallow, laser separation, thermal mechanism 80−5925
liquid mixtures, thin layer separation by laser heating 79−29404
liquids, impurity separation, laser thermal method *(Russian)* 77−7859
lithographic focused laser system, integrated optical device fabrication appl. 78−55477
logic elements, transients during switching *(Russian)* 80−23697
low jitter spark gap triggering through fibre optics 80−107000
low vel. airflow facility for calibration of wind-speed measuring instrums. 80−1718
low-inertia scanner selection 77−58476
lunar laser ranging, orbital dynamics and selenodetic results 77−29672
Mach-Zehnder four-framing laser interferometer system, using TEA N_2 lasers 80−4761
magnetic material domain structure obs. by Kerr-magneto-optical effect, laser speckle suppression 80−85093
marksmanship training, moving target screen system with laser beam firing 78−54488
mass spectrometric analysis of laser induced microplasmas from organic samples 79−57315
mass spectroscopic analysis of gaseous impurity microconcentrations in nonconducting materials 80−73518
material processing, high power lasers, comparison of available systems 78−30003
material processing, IR holographic elements appl. 80−37964
material processing, overview 78−56826
material processing, welding, cutting, drilling and surface hardening 78−80663
material processing for welding, drilling and heat treatment, basic physical processes 77−23682
material treatment, projection diaphragm diam. determ. *(Russian)* 77−59792
materials processing, seminar, San Diego, CA, USA (Aug. 79) 80−90609
materials processing, thermophys. and hydrodynamic effects 78−19957
materials processing appls. of CO_2 and Nd:YAG lasers *(German)* 78−1294
materials processing with CO_2 laser holographic scanner systems 79−18367
materials testing, generation of stress waves for determination of elastic consts. 79−20309
measurement and testing, state of art in Poland 77−5790
medical, 1980 development trends 80−85464
medical, light penetration depth in tissue, spectral depend., 0.35 to 1 μ 78−11714
medical and biological fields, status of laser use 77−77961
medical laser beam operation, safety 78−35903
medical laser video recorder 80−36065
medical research, laser applications, biophysical aspects 80−51201
medical science, laser therapy and endoscope for holographic diagnosis *(German)* 79−96645
medicine, appls. and equipment development 78−48862
laser beam applications continued
medicine, development trends 80−51198
medicine, developments in diagnosis and surgery *(German)* 77−9235
medicine, diagnosis and treatment *(German)* 78−73192
medicine, possibilities, limits and prospects *(Italian)* 80−56156
medicine, review of appls. in USSR 77−73555
medicine *(French)* 80−41165
medicine and biology, bibliography, 1963-74 77−25539
medicine and biology, book 78−48857
medicine and surgery, review *(French)* 79−34626
medicine to newsprint, brief review 79−72577
memory disc, large capacity (ten billion bits), using diode laser, Philips development 79−81369
metal, evaporation under laser irradiation *(German)* 78−52599
metal, thin film, heating by light pulse of linear intensity time dependence *(Russian)* 77−59827
metal film, laser photodeposition 79−100061
metal layers, thin, atomic absorption analysis with laser atomisation 80−30308
metal machined surface, defect detection by laser scanning 78−40018
metal thin film, preheating as aid to laser recording 80−102753
metal working, surface hardening and alloying using high power CW CO_2 lasers 78−79026
metal working by CW CO_2 lasers 77−90493
metal working with high power lasers 78−80682
metalcutting element rectilinearity testing appl. *(German)* 77−44419
metallic film, scanner laser marking 80−43385
metals heating kinetics in oxidising medium, exam. using CO_2 continuous laser emission *(Russian)* 79−57135
metrology and testing by lasers, review 77−5817
MHD propulsion, by laser radiation absorption 77−3998
Michelson interferometer, active stabilization by electrooptically tuned laser 80−86386
micro-Raman spectrometer, for individual aerosol microparticles identification 78−68970
microanalysers, possible applications in electronics and elsewhere *(Polish)* 80−33008
microemission spectroscopy for local determ. of impurities in graphite reactor material *(German)* 78−7161
microfilm, laser transfer printing 78−65994
microfilm laser transfer printing 77−18121
microirradiation for biological tissue exam. 80−26422
microlocal analysis using laser mass spectrometer *(Russian)* 77−12862
microprobe analysis, crater formation, gas medium effects *(Russian)* 79−18428
microprobe analysis, impulse synchronous discharge effects, water formation *(Russian)* 79−18429
microprobe mass analyser, development for biological specimens 79−17554
microprobe mass analyser achievements and appls. 80−73536
Microprobe Mole/plasma chromatograph system, for anal. of compounds on micron scale 80−101049
microprobe system for spectrochemical anal. *(Italian)* 77−25323
microscope, Doppler, capillary blood flow of frog web study 77−36964
microscope, neuronal cell culture appl. *(German)* 78−3694
microscope, scanning, high resolution and depth of field 79−26118
microscopic equipment, methods, appls. and related topics, bibliography 80−73124
microscopic image projection system with quantum amplifier 80−33116
microspectral analysis, forensic appl. 80−81385
microsurgery, CO_2 laser use and laryngology applics. 78−35905
mirror aligner for laser cavity using He-Ne beam 77−7142
molecular beam, laser-induced alignment 77−31025
molecular beam detector, state-resolved, using laser and optical fibres 79−54999
molecular gas, laser-stimulated cooling 80−5594
molecular gas orientation by reson. radiation, optical detect., laser spectroscopy appl. 79−27742
molecule, laser-induced processes, conf., Edinburgh, Scotland (Sept. 1978) 80−9577
MOSFETs, short channel, fabrication by ion implantation and laser annealing 80−20312
Mossbauer spectrometer, absolute vel. control via laser interferometer 77−71715
movie camera, laser based, operation and applications 80−57405
multiphoton ionisation spectroscopy, sequential, appl. to I_2 79−50163
Multiple Mirror Telescope guide alignment system 79−75107
nautical, near-shore charting 80−8463
nematic liquid crystal, viscoelastic properties, spectral noise intensity of scattered laser light obs. 79−23522
neurosurgery, CO_2 laser uses *(German)* 78−35912
neurosurgery, review 80−26317
noncontact material testing using laser energy deposition and interferometry 80−71846
nondestructive testing of steel, using laser speckle photography 78−76797
nonlinear high resolution laser spectroscopy, review of techniques 78−29171
nonlinear optics, 1978 state of art and appl. *(Czech)* 79−18468
nozzle fluid concentrations, probability density functions in free-diffusion flames, laser-light technique 80−10235
nuclear fusion, photolytic atomic I and rare gas oxide lasers 77−46403
nuclear fusion using H-B reaction, research in Australia 79−3234
nuclear orientation, laser-induced ^{24m}Na appl. 80−57680
nuclear orientation effects 77−30740
nuclear physics applications, review, book contrib. 80−68504
nuclear reactors, laser-fission-fusion systems coupled nuclear-thermohydrodynamic anal. 79−13520
ocean optics, blue-green laser technology 77−78458
oceanology, lidar techniques *(Russian)* 79−39975
ophthalmological instrument manufacture, development trends 78−48903
ophthalmological treatment with photocoagulation systems *(Croatian)* 78−44581
ophthalmology, applic. of lasers 77−90869
optical communication, Montreal area laser propag. statistics 80−4099
optical communication line using laser at 0.63 micron wavelength, expt. 78−38022
optical communications system, OCULT, for naval appls. 79−86133
optical components testing for thermal imaging systems 78−33911
optical data processing 77−88832

laser beam applications continued
optical data transmitter, laser and LED comparison *(German)* 80−14432
optical fibre, end preparation using CO_2 laser 78−55478
optical fibre drawing, split beam CO_2 laser heat source 77−19465
optical fibre splicing using CO_2 laser, thermal conditions 78−13820
optical frequency standard, highly stable, utilising an atomic beam 79−35685
optical frequency standards, use of lasers *(Chinese)* 79−173
optical illuminator light source, geometrical optical anal. *(Russian)* 78−79094
optical information processing *(Japanese)* 78−1170
optical levitation of dielec. or metallic spheres, by TEM_{01}^* mode laser beam 79−983
optical levitation of spheres by laser beam *(French)* 79−98428
optical links, integrated optics, review *(German)* 77−54810
optical mechanical scanning system, phase relations, grating screen quality *(Russian)* 78−94451
optical memory disc development and capacity *(German)* 79−68364
optical motion control applied to Atmospheric Cloud Physics Laboratory on Shuttle/Spacelab 80−12634
optical particle counter, portable, using He-Ne laser, for particles with 0.06 to 10 μm diameter 79−75674
optical PCM with envelope modulation, pulse detection characteristics 77−11010
optical reading and recording instruments using lasers, review *(Japanese)* 77−72023
Optical Society of America meeting, Rochester, USA (Oct. 1979) 80−12841
optical surface figuring by laser controlled chem. reactions 78−63209
optical tracking system for space laser communication 80−33068
optical transmission *(Japanese)* 77−68269
optical transmission devices, including laser optical modulators and solid-state techniques *(Spanish)* 79−23079
optical video disc, acoustooptic travelling wave transcription signal recording 79−36986
optical video discs, laser read-out system diffraction theory, focus error alteration influences 79−50338
optically pumped cell for visible display of inhomogeneous mag. field or RF freq. spectrum 77−65027
optics experiments using He-Ne laser beams, book 77−27246
opto-acoustic pulse generation in atmospheric pressure flame 80−43345
optoacoustic imaging and image processing 80−95143
optoacoustic material probing and imaging, far IR 80−83559
optoacoustic sound focusing device using YAG laser 80−87692
optoacoustic sound-focusing device based on laser beam absorption in thin liquid film 79−90107
optoelectronic ps switch using pulsed lasers and photoresistive semiconductor *(German)* 77−72066
optoelectronic vibration transducer based on coordinate photodetector 79−75495
optoelectronics, conference, Munich, Germany (June 1975) 77−7111
organic film, scanner laser marking 80−43385
organic surface contaminants, anal. by plasma chromatography-mass spectroscopy, and Raman microprobe technique 80−108773
osteotomy, new results *(German)* 78−24114
otology, microsurgery, ablative and anal. appls., review 78−48860
overview of laser applications to chemistry 79−58800
overview of laser technology, past, present and future 77−75537
particle acceleration along cryst. channel axis by laser beams 77−30677
particle accelerator, laser focusing, phase-adjusted 80−63434
particle levitation in air or vac., feedback stabilisation 77−27290
patient-positioning laser alignment instrument 78−53471
pellet refuelling for JET and reactor uses 80−9408
phase-nulling fibre optical laser gyro 79−36949
phasometric method of measuring the thicknesses of transparent recording carriers and substrates *(Russian)* 80−73514
Philips video long play system, bi-aspherical objective lens 79−46026
photochemical hole-burning memory magnetic and electric field addressing 79−81371
photochemical separation of metals in aq. soln. 77−60082
photochemistry, and nuclear wastes processing appl. 79−31719
photochemistry, appl. of chirping laser 77−38902
photocoagulating scalpel for laser surgery 78−48866
photoelectrochemistry, laser sources use for solar energy conversion 80−40873
photoexcitation effects during laser trimming on thin film resistors on Si 80−64093
photographic materials, automatic inspection by IR laser beam 79−30593
photographic paper quality improvement, colour spots detection *(German)* 80−57412
photolysis installation for investigation of phototransformations of substances in nanosecond time interval 80−33006
photon source for bubble chamber expts. 77−38521
photon-photon scattering obs. in vac., possible laser expt. 77−74741
physical sciences, review of recent appls. 79−81440
picosecond fluorescence spectroscopy using CW laser and radio 77−27200
picosecond resonant spectroscopy, using nonlinear cryst. parametric excitation, stroboscopic method *(Russian)* 77−83930
picture colour component detection in SAW scanning 78−59149
piezoelectric surface excitation by far IR laser beam 79−46906
pistonphone with Michelson interferometer for microphone calibration 77−58519
plasma density measurements, via quadrature interferometer 78−1900
plasma sprayed coating consolidation by laser remelting 80−93697
plasma-ion analyser for H conc. in metals using pulsed laser and thin film scintillation detector 78−15746
plastic laminate removal from metal 78−7061
pnp switching transistors, anomalous breakdown regions, laser scanning obs. 80−34854
point transfer machine, TRANSMARK, performance testing 78−81438
pointing and tracking, adaptive optimal filtering appl. 77−88959
polarised nuclear beam production by reson. at. ionis. 79−13576
pollution detection, atmospheric, comparison with other optical methods *(Czech)* 79−21001
polymer membrane, laser stimulated active diffusion, appl. to isotope separation *(Russian)* 78−2302
portable LIDAR for antipollution problems *(German)* 79−74583
laser beam applications continued
pressure vessel, defect detection, strain evaluation laser holographic and speckle photography methods 77−81365
printer scanning system with f-θ lens 80−78942
printers and scanners, fractional picture element registration clock generation 77−58486
printing, dry Ag material technology 80−13179
printing, seminar, Los Angeles, USA (Jan. 1979) 80−12852
PROBE, profile resolution obtained by excitation 78−76938
progress survey (1979) *(Japanese)* 80−1262
projection microscope, transmitted light, Cu vapour laser as image amplifier 80−73446
projection microscope, with brightness amplifier for biology and medicine 80−76875
projection microscope with image-brightness amplifier using Pb and Mn vapour 80−106541
projection system with brightness amplifier, laser appl., for medicine and biology 80−36060
proportion counter pulse height fluctuations, resonant ionisation studies 78−90025
propulsion system, pulsed laser, fluid mech. model, real gas effects 79−60089
proton beam, relativistic, energy monochromation using laser 78−90010
proton beam characts. control by laser-induced selective multistep processes 80−61122
pulse laser appls., figure of merit 78−59069
pulse tracking position-sensitive photodetector characteristics 77−18098
pulsed and Doppler CO_2 laser radar, for simultaneous velocity and range determ. 77−19320
pulsed coherent radiation intensity unit reproduction, USSR standard 78−37955
pulsed laser stereophotography, of electrically exploded bridges 77−79190
pulsed US field display by laser *(Chinese)* 79−32158
PWB holes counting, wide-aperture telecentric laser scanning system design 80−1264
quantum communication theory, appl. of generalised quantum meas. theory 78−13668
quantum electronics, conf., New York, USA (Jun. 1980) 80−90614
radiation press cooling of ions in Penning EM trap 78−66527
radioisotope dating, sensitive laser techniques 79−59707
radiometry, laser based characterisation facility 78−29140
radiotherapy sidelight using laser cross-hair image 78−35939
Raman spectroscopy of powders, optimum conditions *(Russian)* 77−28580
Raman tunable IR lasers, isotope separation and photochem. appls. 77−54709
raster-scanned laser display using TeO_2 acousto-optical deflector 77−10930
Raytheon laser gyroscope using MnBi magnetic mirror 78−79064
Raytheon multioscillator ring laser gyroscope 78−79063
reaction kinetics measurement and control using laser technology, free electron laser appl. 80−81349
reaction motor, using laser breakdown of air, expt. model *(Russian)* 77−7106
real time laser recording, plastic versus metal coatings 77−74536
recorder of video signals, on dry-developed photosensitive paper *(French)* 78−92998
recording and information handling, seminar, San Diego, CA, USA (Aug. 1979) 80−101663
recording systems development *(Russian)* 77−54751
recording with truncated Gaussian beams and focusing lens 79−81474
rectilinear laser scanning of wide formats application of additional mirrors 78−33803
refractometer, digital, automatic measurement appl. 77−67492
resonance fluorescence diagnostics, of high temp. H_2 plasma 80−48971
retinal function, laser interference fringes meas. *(German)* 77−12910
retinoscope using He-Ne light source 80−41159
review in brief 80−91807
ribbon growth using scanned focused CO_2 laser beams 80−66417
ring laser gyro, anomalous dispersion and gas flow effects 79−98430
ring laser gyroscope for missile guidance using magneto-optic bias mirror 78−79061
ring laser gyroscopes, multioscillator approach to locking problem 78−79042
rocket engine, laser evaporated target, nozzle for impulse augmentation 79−23439
rotating mirror deflector design cost/performance tradeoffs 77−58485
rotation rate sensors, Air Force appls. 80−9932
rotor vibration control and meas. appl. *(Russian)* 78−70115
safe operation control measures 80−9928
Sagnac fibre-ring interferometer gyro with electronic phase sensing 79−17472
sand detectors to discriminate between bubbles and sand, oceanography appl. 79−58109
satellite laser ranging system, 2cm accuracy, for geodetic research 77−21932
satellite photograph production using laser beam recorder *(German)* 80−5777
satellite ranging, picosec. pulse freq. doubled Nd:YAG laser system 77−21933
saturation spectroscopy, beam profile effect, appl. to species conc. determ. in flame 79−29425
SAW device, amplitude response meas. 79−94435
SAW generation using CW laser, NDT appl. 80−87683
SAW study, optical heterodyne method *(Russian)* 80−64271
scale-measuring laser interferometer 77−5804
scalpel and micromanipulator for neurosurgery, CO_2 laser system *(German)* 80−3753
scanner, augmented resolution eqns. 78−55398
scanner, replication process 77−58496
scanners, compensated moving-coil mirror galvanometer 77−58479
scanning, electro-optical deflectors 78−79060
scanning, flat-field telecentric lens design 77−58424
scanning, multidimensional scan generation by single rotating component 77−58482
scanning, rotating mirror deflector motor and control system selection 77−58484
scanning, two-dimens. using computer-generated holographic grating 78−58956

laser beam applications continued
scanning and recording system, resolution, intensity, and power distribution 77−58425
scanning components and techniques, San Diego (1976) 77−58474
scanning detector for gyroscope rotor vibration meas. *(Russian)* 80−22351
scanning device, distortion correction using parabolic mirror 79−7171
scanning dye laser, microprocessor controlled, for spectrometric anal. systems 78−20081
scanning optical microscope 79−9242
scanning optical microscope for semicond. materials and devices 80−95136
scanning optical microscope operation and appls. 80−47098
scanning optical microscope using semiconductor laser with longitudinal electron pumping 80−18012
scanning optical microscopy examination of grain boundaries of polycryst. solar cells 78−79618
scanning system, laser beam deflection by prismatic polygon mirror 77−19267
scanning system design, stable fixed freq. 77−58478
scanning system with multifaceted mirror, tracking sweep 80−33123
schlieren probe method for measurement of refractive index profile of shock wave in fluid 80−23785
seawater transmission props. for underwater laser communication 80−33069
selective laser excitation of atoms and mols., photophys., photochem. processes, appls. 77−54630
selective photoionisation of atoms by laser radiation, appls. 78−5189
semiconductor, annealing of ion-implanted defects and other processing 80−55431
semiconductor amorphous film, laser crystallisation, for production of large grained sheets for solar cells 80−93570
semiconductor background heating for laser annealing 79−96047
semiconductor devices, resistivity and lifetime inhomogeneities, laser scanning method detect. 79−30489
semiconductor laser annealing to round edges of Si structures 80−25742
semiconductor laser developments *(German)* 77−61962
semiconductor laser screens, scanning optical microscopy appl. 80−86398
semiconductor wafer 80−25741
semiconductor-metal system, light sensitivity for high exposure densities *(Russian)* 79−6212
semiconductors, ion implanted, laser annealing 80−65023
SHG, computer controlled intracavity, in CW ring dye laser 80−91841
Shiva project, control and alignment systems development trends 79−85764
shock wave physics, interferometric laser technique for accurate vel. meas. 77−50972
shocked specimens, laser-illuminated of diffuse surface vel. meas. by Michelson interferometer 77−61050
silicate glass surface, photodichroic for laser recording 80−102785
skin, treatment of chromatic maculae, ruby laser appl. *(German)* 78−24177
skin melanoma therapy by laser irradiation *(German)* 80−12208
solar cell defects detection, optical scanning technique 80−81460
solar cell fabrication, laser-induced p-n junction formation 80−93880
solar cells, fabrication using continuous or pulsed lasers *(French)* 80−61350
solar reflector paraboloid surface inspection using LG-75 gas laser system 77−75643
solenoid, for fusion power appl. 77−47250
solid state and semiconductor, apparatus and applications *(Japanese)* 77−68215
sonar echo acoustic imaging 77−58501
sound detection, fibre-optic technique 78−13871
sound generation by long laser pulses incident on liquid surface 80−5900
sound track recording, laser light modulating device *(Russian)* 80−1399
space communications, K vapour arc lamp as optical pump source 79−86261
space communications appl. of Nd:YAG laser 78−28483
space communications system, evaluation of optical coatings required for components 79−86248
space isotropy test, special relativity, laser version of Michelson-Morley expt. 80−52021
spallation, meas. of film-substrate bond strength 80−50821
speckle photography, for nondestructive testing 77−67515
speckle photography for fluid flow vel. meas. 78−14112
spectrochemical analysis, plasma obtained without supplementary elec. discharges *(Russian)* 77−29081
spectrochemical analysis, rate consts. determ. with diode laser 79−70310
spectrometer, appl. to hyperfine struct. of $F_2^{(2)}$ line of methane 77−58201
spectrometer, diode laser dual-beam, long-term temporal and scanning characts. 80−90902
spectrometer, for submicronic aerosols, conc. and dispersity determ. 79−54244
spectrometer, high resolution, with separate optical laser heterodyne, appl. to Mandel'stam-Brillouin scatt. *(Russian)* 78−29180
spectroscopy, absorpt. coeff. determ. of threshold generation characts. *(Russian)* 79−49302
spectroscopy, appls., conf., Graz, Austria, (Jun. 1978) 79−26137
spectroscopy, high-resolution, by at. beam-laser beam interaction *(Dutch)* 79−50166
spectroscopy, high-resolution, with tunable dye laser, appl. to SO_2 77−22601
spectroscopy, two-photon, Doppler-free *(Dutch)* 79−50167
spectroscopy conf., Rottach-Egern, Germany (Jun. 1979) 80−51957
spectroscopy methods based on laser light's props. 80−62739
spectroscopy of Na neutron rich isotopes, nuclear ground state props. 77−22875
spectroscopy uses, multiphoton transitions and Doppler effect elimination 77−57398
spectroscopy uses and applics. 77−57397
spherical laser fusion target, uniform illumination 78−13317
spiralling resistors with laser beam *(Polish)* 80−28242
sputtering, structuring of GaAs and Permalloy-type alloy coatings *(Russian)* 77−59689
stainless steel, laser surface melting for corrosion protection 80−93698
standing wave and pellicle, proposed design for very large space telescopes 79−92672
steel, Cr-plated, H_2 distrib., laser-mass spectrometer investig. 78−61113
steel, En8, surface hardening by 2 kW CW CO_2 laser 79−83396
laser beam applications continued
steel, laser beam melting kinetics *(Russian)* 77−56121
steel, laser-irradiation surface treatment *(Russian)* 77−59978
steel, microhole working by laser irrad., accuracy increase *(Russian)* 80−55434
steel hardening, surface, using linear-contour laser beam *(Russian)* 77−12731
steel hardening, uniform surface heating by focused laser beam *(Russian)* 78−27670
stethoscope for respiratory sounds meas., comparison with acoustical method *(German)* 80−98058
storage, recording and retrieval systems 78−33688
storage rings, free electron laser amplifier operation 79−68399
strain measurement, photoresist grating and diffraction pattern method *(German)* 80−68195
stratosphere, O_3 vertical profile determ. by lidar sounding from ground 78−11972
stratosphere, trace constituents, laser heterodyne spectroscopy 80−109257
stratosphere aerosol, laser radar meas. *(Japanese)* 80−21810
stratosphere aerosol microstructure, sounding by multifrequency lidar *(Russian)* 77−64374
striascopic imaging of profiles with laser light, surface tension measurement 79−2845
structural material hardening by laser irradation *(Russian)* 79−15851
submicrosecond pulses, use in laser gas dynamics *(Russian)* 78−29940
submillimeter wave heterodyne detection, with a laser LO 78−70183
submillimeter wave polarimeter, for plasma diagnostics 78−91158
submillimetre waves and applications, conf., San Juan, Puerto Rico (Dec. 1976) 78−4712
submillimetre waves and applications, conference, San Juan (1976) 77−38785
submillimetric heterodyne receiver with laser local oscillator 77−38042
subMM laser spectroscopy of solids 80−31895
superalloy, laser melted, epitaxial resolidification 77−90491
superlattice synthesis from erosion laserplasma, InSb, CdTe, PbTe 80−44450
supermarket checkout system, laser/photomultiplier optical and scanning system 78−83021
supersonic optoacoustic antenna, acoustic field 78−1540
surface, alloying, glazing and cladding using laser beams 79−69912
surface finish automatic inspection by laser scanning *(German)* 78−170
surface hardening of steel and cast Fe 77−90490
surface inspection with defined flaw analysis using microcomputer-controlled scanning laser beam *(German)* 80−3278
surface roughness measurement, highly-polished metal *(German)* 80−52155
surface transformation hardening, heat flow model for cylinder 80−93700
surface velocity meas. using laser beams 78−49806
surgery, acute and long term laser beam effects on fibroblasts and smooth muscle cells in culture 78−40268
surgery, Ar ion laser treatment of haemangiomas, teleangectasia, radiodermatitis and tattoos 78−35906
surgery, effects on blood vessels 79−66505
surgery, flexible fibre-optic beam-guiding system, oto-rhino-laryngology appls. *(German)* 79−83886
surgery, healing of tissue wounds following CO_2 laser action *(German)* 78−35913
surgery, laser medicine in Japan, current status *(German)* 80−98059
surgery, partial hepatecomy using high power CW and Q-switching Nd:YAG laser *(German)* 77−44734
surgery, Sharplan 791 CO_2 laser 78−35904
surgery, state of the art 77−40729
surgery, using CO_2 laser 77−9297
surgical lasers, effect on lining tissue and applics. 77−90871
synchronous spot-scanned underwater viewing system 77−21934
target designator, 10.6 μm 77−88927
target position checking by light beam using automatic two-coord. system 78−5564
teeth, human, thermal stress effects and surface cracking assoc. with laser use 78−80915
television, appl. of distrib. feedback epitaxial waveguide laser *(Russian)* 78−29973
text information micro-recording *(Russian)* 77−54750
therapeutic applications of lasers *(French)* 80−108996
therapy in lower female genital tract disease medical and engineering problems 78−48865
therapy of skin defect using Ar ion laser *(German)* 78−35916
therapy using CO_2 laser 80−56155
thermal diffusivity meas. by laser-pulse technique, instrumental recording and data processing 77−45846
thermal imaging system design for graphic arts, laser scanning unit 80−14487
thermonuclear power plant, conceptual design study 80−78441
thermonuclear power station 'Argus' system *(Czech)* 79−67943
thermoplastic recording, IR laser heating 78−71065
thin film magnetic recorders of optical images, sensitometry using glass Nd laser *(Russian)* 77−79178
thin film optical circuit fabrication using CO_2 laser 80−99881
thin film processing, review 77−23684
thin metal layers testing *(German)* 80−35436
thin-film distributed optically excited laser, signal suppression by superluminescence radiation *(Russian)* 78−87091
thin-film laser logic elements, characts. and limiting capability optimisation *(Russian)* 79−18431
time-of-flight spectrometry, vel. selection using pulsed tunable laser fluoresc. detect. 77−49804
time-resolved absorption spectra, with picosecond laser *(Japanese)* 80−22451
tissue sampling in biochemistry, laser microbeam *(German)* 78−69175
tool steel transformation hardening by CO_2 laser 80−16483
trabeculotomy in glaucoma treatment 78−53470
trace analysis in gases by laser-induced schlieren technique 80−3436
tracker, target induced pointing noise 78−5519
tracking system testing by 1 m unobscured IR collimator 80−78991
transfer printing of volatile dyes 77−53998
transient jet experiment, multiple-laser light source 78−14114
transmission of communications, laser light and fibre optics techniques *(German)* 80−5827

laser beam applications continued
transmitter-receiver system, nearly coaxial, limiting detect. range through water 77−78461
transverse displacement of distant body, interferometric meas. 77−82488
triggered vacuum gap for high energy appl. 80−78888
triggering lightning by pulsed laser 80−72626
troposphere, O_3 distribs. meas. with airborne laser absorpt. spectrometer 79−2344
tropospheric aerosol monitoring using Spacelab lidar system 77−21876
tunable, principles, characts. and appl. review *(Japanese)* 80−74330
tunable CO_2 laser calorimetry for bulk and surface absorption in NaCl and KCl in 9.2-10.8 μm region 79−95808
tunable diode lasers and applications 78−25886
tunable dye laser, isotope shift meas. at Isolde mass separator CERN *(German)* 78−41863
tunable lasers and applications, conference, Loen (1976) 77−54720
TV image formation using laser projection electron-beam tubes 79−59743
TV picture, acousto-optically modulated laser beam 79−55237
TV scanner, rotating mirror, development programme *(Japanese)* 80−74369
TV systems, trichromatic acousto-optical laser-beam deflector for TV scanning *(Czech)* 79−98502
two-phase bubbly flow, void fraction meas. by laser beam attenuation technique, theory *(Japanese)* 79−50779
two-phase bubbly flow, void fraction meas. by laser beam attenuation technique, expt. *(Japanese)* 79−50780
two-phase bubbly flow, void fraction meas. by laser beam attenuation technique, meas. accuracy determ. *(Japanese)* 79−50781
two-photon molecular spectroscopy using two synchronised tunable dye lasers 77−34783
Udimet 700, microstruct. of resolidified zones formed by laser melting single crysts. 79−78953
underwater surveying with laser, description of portable laser device *(German)* 78−37890
urinary calculi in vitro destruction by laser-induced stress waves 78−77100
US power meas. via acousto-optic method 77−832
US tomography using laser-generated acoustic fan beam 79−83862
vacuum evaporation, isotope target deposition 80−18735
vapour deposition of complex films, laser heating *(Russian)* 77−48353
vapour pressure meas. up to 5000K, pyrometric-laser heating technique 77−1239
vapour pressure measurement, torsion-effusion method, automatic data acquisition 80−52188
vibration control and meas. appl. *(Russian)* 78−71299
vibratory processes investigation, laser interferometry appls. 77−118
vibrometer for gyrosystem *(Russian)* 80−8983
video recording NTSC colour signals on to 16 mm colour print film 77−74537
Viking Ground Reconstruction Equipment for facsimile picture recording 77−38051
virology and immunology using laser correlation spectrometer 80−56158
visible and UV lasers for diverse appls., new families 79−59705
water, interaction of laser bursts, possible appl. 80−7444
water drop in heated plate, interferometric study using laser source *(Russian)* 78−37049
waveguide fabrication, laser heating technique for glass multimode channel guides 77−7220
waveguide fabrication by CW Ar laser irrad. of $Al_xGa_{1-x}As$ 80−5849
wideband archival optical storage technology assessment 80−43283
wideband optical disc data recorder systems 80−102751
workpiece focal point window tolerances in laser material processing 80−5776
wound healing with laser irrad. *(German)* 78−35918
wound healing with laser radiation, immunological aspects *(German)* 78−35917
wound-healing stimulation, clinical and expt. results of action mechanism 77−9299
X-ray laser holography, pumping by synchrotron radiation from storage rings 78−55322
X-ray picture digital transmission over voice-grade telephone channels, laser scanning system 78−80953
X-ray picture transmission over voice grade telephone channels 78−44607
X-ray spectra spatial resolution recording by spherical crystal analyser 78−74114
zone plate production by laser irradiation of photoresist. *(German)* 80−23782
Al aircraft alloy, fatigue resistance improvement by laser shock 80−93654
Al, alloy, laser surface melting 78−48557
Al-As_2Se_3-Al, photographic process based on electrochem. reactions *(Russian)* 79−6213
As-Se chalcogenide glass, semicond. film, laser stimulated refr. index change, writing/erase cycle 77−50677
As_2S_3 thin film, diffr. grating production, using laser photolithographic process, image evaluation 78−42479
Ba^+ ion cloud containment in RF trap, <50 ions, optical sideband cooling 78−75407
n-$BaTiO_3$, ohmic contact form. 80−92969
CO_2 Doppler-tuned CW IR radiation for highly excited atomic beam source 77−27204
CO_2 freq.-tunable laser for photoreceiver characts. meas. 77−14728
CO_2 high power laser, design and fabrication 77−46732
CO_2 laser, electroionisation, testing X-ray mirror objectives with soft X-rays from plasma mirror 78−85850
CO_2 laser, NASA high power system 78−5493
CO_2 laser heterodyne meas. of $01^11\text{-}11^10$ hot band transition frequencies 77−7063
CO_2 waveguide laser and appls. 77−75568
CoO deposition on glass 79−83364
Cr $^7P_0^0$ state, radiative lifetime in matrices, meas. using laser ablation and selective excitation 80−71959
Cr film, pattern generation by laser-induced oxidation 80−61009
Cr-Ni-Mo-Cr_xC_y wear resistant coating prep. by laser beam melting, and props. 80−40607
Cs clock, laser synchronisation between observatories of Paris and San Fernando *(French)* 78−89461
Cs film vaporisation by laser impact for production of atomic beam pulses 80−37123

laser beam applications continued
Cu-As-Se glasses, recording and erasure by laser beam *(Russian)* 78−71170
GaAs DH laser, alloying of ohmic contacts, Nd:YAG laser irrad. 80−43357
GaAs diode laser in communication system using PPM methods *(Rumanian)* 77−68260
GaAs injection laser, appl. to meas. of photomultiplier linearity in pulsed mode 77−37961
GaAs, ion implanted, laser pulse annealing 80−19825
GaAs, laser alloying of Au-Ge ohmic contacts 79−73583
GaAs, laser reordering of implanted amorphous layers 78−43042
GaAs laser-annealing behaviour, Si_3N_4 encapsulation effect forming n-type layers 79−79131
GaAs, laser-induced microscopic etching 80−76379
GaAs:Zn, implanted, laser annealing, elect., Rutherford backscattering and SEM meas. 80−100273
GaAs:Zn, pulsed laser annealing, expt. 78−34828
GaInPAs, narrow-band tunable injection laser, 1.06 μm, description and appls. 79−76713
Ge, amorphous film, large aligned grain solid-phase growth during scanned laser crystallisation 80−49100
H, atomic spectrum 79−72267
H laser-fusion prod. by radiolytic-thermochem. cycles 80−45811
H^+ beam, control using laser radiation 79−27112
H_2, laser-heated, analysis of nozzle flow 80−10283
He-Ne, monochromatic directed radiation source, long-life 80−33021
He-Ne laser demonstration of continuously varying refractive index *(German)* 80−8
He-Ne laser for original equipment manufacturer, aligning, recording and meas. appls. 77−75597
He-Ne laser interferometry for vibration control and meas. *(Russian)* 78−70117
He-Ne lasers, Original Equipment Manufacturer applics. 78−33765
I_2, $X^1\Sigma_g^+$ ground state, Le Roy's theory, continuous wave oscillation 79−94006
InP, laser-induced microscopic etching 80−76379
InP:Cd, doping by UV laser photodeposition 80−84191
p-InP-Cd(Zn), ohmic contact formation on InP by laser photochemical doping 80−80369
$LiNbO_3$ acoustophotorefractive memory correlator enhancement 79−55080
MgO, atomic C anal. by laserflash induced mass spectrometry 80−108767
Mo film, constrained, 20 MHz thermoelastic wave generation 79−47880
Mo, microhole working by laser irrad., accuracy increase *(Russian)* 80−55434
N_2, liq., impurity separation, laser thermal method *(Russian)* 77−7859
NH_3, laser-induced excitation at 1076 cm^{-1} in megawatt region 80−10354
NO_2, g-factors of electronic transitions determ., use of resonance optical rot. 79−54876
$^{14}NH_3$, four level system, two-photon jumping to obtain 12.16 μm radiation for isotope separation 78−90414
Na, laser orientated vapour, rotary power determ. 79−32737
Nd:YAG laser integration into optical systems 80−78887
Nd-YAG laser driven 3 kA X-ray source 78−41389
Ni films, laser CVD 79−78897
PbSe, monocrystalline film prod. by laser pulse *(Russian)* 78−3059
PbSe(Te), low-temp. epitaxial film form., on KCl(Br), laser spraying *(Russian)* 77−73238
$Pb_{1-x}Sn_xTe$ diode laser, appl. to high resolution IR spectroscopy *(Japanese)* 79−49306
PbTe, thick epitaxial film, laser deposition technique 78−68629
Pd-Cu-Si, laser melting and splat quenching to form foils for TEM obs. 80−29986
Re film, prep. by laser melting 80−84859
SF_6, laser isotope separation model 77−31016
SF_6, multiwavelength phase conjugation using multiline CO_2 TEA laser 80−91847
SF_6, spark gap, KrF laser triggered, low jitter timing 80−106999
SO_2, absorption spectrum, meas. using frequency doubled pulsed dye laser 80−87144
SO_2, absorption spectrum, meas. using frequency doubled CW dye laser 80−87145
Si, amorphous film, epitaxial laser crystallisation 78−84078
Si amorphous layer recrystallisation 80−93566
Si, CVD using CO_2 laser 78−56589
Si, cast polycryst., annealing for solar cell appl. 80−93918
Si film, polycryst., laser-induced CVD growth from $SiCl_4$ 80−84852
Si film deposition by CO_2 laser irrad. of SiH_4 80−16190
Si, heavily doped implantation layers, laser beam annealing 78−88481
Si, laser assisted doping, ohmic contacts and p-n junction form. 78−79621
Si planar diode, Al coated, binary memory device, laser writing 79−69593
Si powders, laser synthesis using SiH_4 79−74119
Si ribbon growth by laser zone melting 80−93482
Si ribbon solar cells, defect anal. using laser scanner 80−94089
Si, ribbon to ribbon crystal growth, solar cell appl. 78−35299
Si semiconductor switch using laser-excited solid-state plasma for pulse shaping, expt. 77−19397
Si solar cell processing, pulsed laser techniques for annealing ion-implantation damage 80−81453
Si solar cells, laser annealing, conversion efficiency improvement *(French)* 80−66976
Si solar cells, preparation using laser processing 80−81454
Si solar cells, realisation by laser induced diffusion of deposited Sb 80−93998
Si, surface cleaning by pulsed laser irrad. 80−45173
Si:As, dual wavelength, laser ion implantation damage annealing 79−69117
Si:As^+, annealing by scanning Ar ion laser, dislocation loop density comparison 78−47438
Si:B, lattice location of implanted ions after laser annealing 78−30660
Si:B, P, high temp. diffusion, effects of laser irrad. on diffused layer 79−14834
Si:P diffused solar cells, laser treatment to dissolve diffused P precipitates 80−45667
Si:P solar cells, improved P diffusion using laser treatment 80−55850
Si:Pb, implanted, laser annealing 78−75685

laser beam applications continued
Si-B, diffusion-free annealing, use of scanning CW Kr laser 78−91345
SiC, fibre growth kinetics in laser-heated system 77−81203
Si_3N_4, hot-pressed, thermal cond. by laser flash method 79−69302
Si_3N_4 powders, laser synthesis using NH_3-SiH_4 gas mixtures 79−74119
Si_3N_4, pyrolytic, crystn. and amorphous, thermal diffusivity, thermal cond., specific heat, by laser flash method 79−69303
SiO_2-Ta_2O_5 film channel optical waveguide, fabrication using CO_2 laser 79−27386
Sn foil irradiated by Nd laser, psec optical shutter 78−1350
Ti-Ni, laser melting and splat quenching to form foils for TEM obs. 80−29986
TiC, laser CVD, coating characterisation 80−93494
TiO_2 film, laser CVD 79−78897
$(U,Pu)O_2$ fuels, eqn. of state up to 5000K, high-temp. laser technique 77−27971
U enrichment, implications for nucl. weapons proliferation 77−67849
UF_6 laser isotope separation for fuel enrichment 77−54618
UF_6+H_2, laser induced dielectric breakdown obs. 77−28992
^{235}U enrichment, using laser based two-phase photoionisation and photodissociation methods *(Czech)* 77−61583
^{235}U enrichment by laser isotope separation process, cost anal. 77−42160
Y_2O_3 sintered bodies, thermal cond. and diffusivity *(Japanese)* 79−55944
$Zn/ZnSO_4/Zn$ system, laser interferometric study of corrosion of coated and uncoated metals, technique standardisation 79−35815
ZnS, film, vac. sputtering deposition by CW CO_2 laser beam *(Russian)* 77−21024

laser beam effects
see also plasma-beam interactions; plasma production and heating by laser beam
ablative acceleration of laser-irradiated thin-foil targets 79−71952
absorbing film, damage by high-power optical pulses, two-phase model 80−93438
absorbing inhomogeneity molten zone, laser beam nonlinear scatt. 79−89969
absorption of laser materials, static profile calorimetry meas. 78−25908
acoustic wave generation from thermal sources in fluid scanned by laser beam 80−38161
acoustic wave generation in liquid half-space bounded by solid layer 80−38158
acoustic waves in nonviscous liqs., laser-induced 78−63808
adatom laser stimulated migration and multiphoton excitation, relax. and reaction enhancement 79−39200
adenine, nucleic acid component, selective action by ps light pulses 80−72213
aerosol, H_2O-droplet, CO_2 laser beam clearing process, transmission function ratios 78−88919
aerosol, moving droplet, bleaching kinetics by CO_2 laser radiation 78−13743
aerosol, plasma production by CO_2 laser beam, brightening channel 80−6272
air, breakdown threshold meas. using pulsed HF(DF) laser 77−11423
air, elec. discharge, effect of long laser spark ionis. channel 78−67468
air, laser breakdown, very long spark prod. *(Russian)* 77−1031
air, low threshold breakdown, near target, by pulsed laser radiation *(Russian)* 78−22594
air, optical breakdown threshold reduction near dielectric surface 77−51211
air, plasma, slow burning gasdynamics, due to Nd laser beam *(Russian)* 80−108715
air breakdown initiated on aerosol *(French)* 79−73021
air breakdown near solid, thermal stress cracking effects reducing threshold 79−69924
air near solid dielectric surface, reduction of laser breakdown threshold 79−77446
alkali bromides and iodides, self-trapped exciton and F-centre form. by picosecond laser pulses 80−10546
alkali halide, avalanche impact ionisation, in optical breakdown 79−42895
alkali halide and other crystals, damage induced by $CaF_2:Er^{3+}$ laser radiation at 2.76 μm 79−91539
alkali halide crystal, laser induced breakdown, avalanche ionisation theory *(Russian)* 77−44095
alkali halide crystal, vol. damage anisotropy under laser irrad. 77−89469
alkali halide surface light emission, 10.6 μm laser pulse irradiation *(Russian)* 78−27352
alkali halides, behaviour as materials for optical components, for high power lasers *(Rumanian)* 79−18462
alkali halides, cryst., optical emission following pulsed 10.6 μ irrad. 79−28847
alkali halides, laser induced breakdown, 10.6 μm, reproducibility 77−62023
alkali halides, laser induced damage *(Russian)* 79−43070
alkali halides, optical breakdown, damage threshold calcs. 79−95708
alkali halides, optical breakdown 1.06 to 0.172 μm 78−35089
alkali halides, photon induced sputtering 80−35013
alkali halides, pulsed-laser-induced damage, role of avalanche multiplication and multiphoton absorpt. 80−48316
alkali metal halide, laser damage morphology simulation 80−35015
alkali metal halide optical breakdown, multiphoton carrier generation theory 79−19953
alloy, laser surface melted, heat transfer props. and microstructs. 79−70085
amber, natural, optical strength and laser induced rupturing 78−7039
amorphous materials, laser irrad., electronic struct., one-electron approx. 80−70576
amorphous semiconductor film, laser induced nucleation, long wavelength instability 80−84126
annealing mechanisms, continuous and pulsed laser impact, melting 80−84964
anthracene, single crystals, TSC excited by Q-switched ruby laser 80−29417
aqueous aerosol, optical thickness change due to CO_2 laser pulses 77−75591
aqueous polydisperse aerosol, bleaching by high intensity beam 77−58394
atomic beam deceleration and monochromatisation laser radiation press. 80−102491

laser beam effects continued
atomic beam focusing and defocusing using reson. radiation press. 80−47143
atomic electron scatt. in laser field without optical pumping, theory 78−17804
atomic electron scattering, reson. laser induced negative ion production 79−64104
atomic momentum distrib. modification by travelling wave reson. light field 79−72280
atomic motion in resonant EM wave, two-level atom 79−18155
atomic spectrum nonresonance perturbation in strong light field, review 77−46543
atoms, interaction of laser radiation, review 78−13473
avalanche ionisation in optically transparent medium, recomb. effect 80−7295
benzene, liq., laser pulsation kinetics, optical damage effects 80−58614
benzyl anion, IR multiphoton electron detachment, by CO_2 laser 79−94043
biological, laser medicine in Japan, current status *(German)* 80−98059
biological damage due to fast pulse laser 78−48827
biological material, generation of acoustic transients by laser pulses 78−48830
biological systems, nonthermal laser effects, phys. model 78−35885
biological tissue, laser-irradiated, moving phase transitions, tissue heating 79−83848
biological tissue, temp. distrib. with laser irrad., thermodynamic analysis 79−29562
biomedical research in USSR 78−48858
biomolecules, selective photochemical mechanics 79−66450
breakdown, obs. by two-wave interferometry *(French)* 77−3597
brightening of disperse media, role of laser fluctuations 79−41405
bubble formation by action of focused laser radiation *(German)* 77−42882
bubble formation in liquid, dynamics of growth and pulsations 78−51226
calorimetric absorption coefficient measurements using pulsed CO_2 lasers 80−9918
carbon tetrachloride, supersaturated vapour, photonucleation 79−7682
cavitation bubbles, appl. of HF holography with ruby laser *(German)* 77−75437
cavitation bubbles in water, behavioural study by holo-cinematography *(German)* 78−87371
cavitation in liq., bubble collapse 77−89171
cavitation in liquid crysts. 80−87633
cell flagella, laser damage, high speed cinematography 80−81785
cell functional activity regulation, human 79−43957
cell ultrastructure *(Chinese)* 79−53187
cellulose hydrate, pulsed laser irrad., struct. changes *(Russian)* 77−66560
cellulose triacetate, pulsed laser irrad., struct. changes *(Russian)* 77−66560
ceramics, fracture by single pulse 10.6 μm irrad. 79−99988
chalcogenide glass film, optical waveguide form. by laser and electron beam irrad. 77−79978
chalcogenide glass two-layer low-absorpt. antirefl. coating, for KCl laser window 78−37927
charged particle potential scattering, in presence of mag. and laser field 79−81248
charged particle potential scattering in laser field, eikonal theory 79−81249
chemical decomposition, unimolecular of octafluorocyclobutane 77−32775
chemical laser window materials evaluation 77−46769
Chlorella microalgae cells, laser damage mechanism 78−3550
chlorotrifluoroethane, IR photoreaction *(Japanese)* 80−11885
cloud clearance, atmosphere liq. water content and temp. fluctuations in clearance zone *(Russian)* 78−44999
cloud medium evaporation by CO_2 laser radiation, self-focusing possibility 79−27306
coal, laser pyrolysis in He or H_2, products exam. 79−20356
coated optical component, damage resist. for pulsed CO_2 laser 79−45989
coating damage thresholds in CO_2 laser systems 79−14006
coating materials, 100 ns pulsed laser damage at 2.7 and 3.8 μm 80−33057
coating materials for high power laser elements, selection 77−50735
collisional ionisation in intense laser field, quasimol. state reson., quantum mechanical anal. 78−33589
complex solid, laser induced explosion 77−40308
Compton scatt., bound and free electron Compton scatt. in coherent EM field 78−94225
conference, Masnuy-St-Jean, Mons, Belgium, Oct. 1979 80−82570
conference on laser-solid interactions and laser processing, Boston, MA, USA (Nov. 1978) 79−69911
conical lens, to produce large diameter openings using laser beam *(Russian)* 80−19061
cooled laser mirror construction, possible use of open pore structures 79−31952
corneal damage induced by near-UV laser, cumulative effects 80−85448
corneal epithelium, predictive equation for IR laser damage 79−25031
corneal temperature range, implications in prediction of laser thermal damage 80−108848
corneal temperatures, normal and laser injured rabbits 79−11919
Coulomb electron atom scatt. in laser field, asymptotic dynamics 79−94084
crack development and light absorption 78−2193
crater evolution, quasisteady, in laser-evaporated material, heat cond. anal. 77−48283
crystal electronic spectrum, EM wave influence 79−33218
Cu vapour deposited mirror on SiC substrate, pulsed laser damage charcts. 80−48314
damage history of Argus 4 TW Nd laser system 79−18463
damage in optical materials, conference, Boulder, USA (Oct. 1977) 79−14048
damage limits for optical components exposed to nanosecond pulses 77−38976
damage of laser components, threshold meas. 78−13740
damage protective coating, electric field interference 80−33062
damage threshold, optical performance meas. 78−59066
damage threshold meas., statistical methods 79−18464
damage thresholds at 1064 nm, 125 psec, three-beam expt. 77−61990
damage thresholds for mirror and window materials, 10.6 μm 77−50708
damage-resistant components for 2-5 μm laser systems 77−19282

laser beam effects continued
desorption, laser induced, appl. to adsorbed CO and H_2 layers on Ni surface 79−1548
desorption, laser stimulated, quantum theory 78−79876
diamond, dielec. breakdown, two-photon absorpt. and other optical damage mechanisms 78−84684
diamond, homogeneous formation in gas phase, laser beam effects *(Russian)* 80−104052
diamond drilling, process mech., thermal stresses elec. surface forces *(Dutch)* 77−7759
diamond processing, quality improvement and monitoring *(Russian)* 78−31595
diamond-like solids, laser irrad. effect on cohesion 80−50470
dielectric, criterion for breakdown by single light pulse *(Russian)* 77−12311
dielectric, thermal mechanism of plastic deformation and fracture by laser beam 77−11553
dielectric, transparent, laser-induced damage, role of absorbing microinclusions, passive methods 79−31969
dielectric breakdown by picosecond laser pulses, many-photon and impact ionisation 78−18002
dielectric breakdown with picosecond laser pulses, SHG sharp increase 80−102769
dielectric coated mirrors, large-spot DF laser damage obs. 79−14022
dielectric liquids, laser induced breakdown 79−91363
dielectric materials, laser induced microwave damage, space simulation 77−81050
dielectric mirror, temp. field during laser radiation absorpt. 80−19063
dielectric multilayers, laser damage, elec. field strength role 77−61993
dielectric protective coatings for diode laser facets, optimisation 78−63144
dielectric solid, absorpt. of laser radiation by defects in surface layer *(Russian)* 80−25497
dielectric solids, laser damage, conduction-band electron interaction theory 80−35017
dielectric surface, nonlinearly-absorbing, laser-induced evap. 78−80438
dielectrics, surface heating by laser, optical temp. meas. 79−55911
dimethyl silicone oil, laser-induced breakdown mechanism *(Japanese)* 77−43935
dipalmitoyl phosphatidyl choline vesicle damage by picosecond laser pulses 79−79599
discharge channel migration control by laser beam *(Russian)* 77−55198
DNA light induced diffusion in solutions due to laser cutting *(Russian)* 80−81646
dosimeter glass, radiophotoluminescence intensity change by intense laser light 80−89050
dosimetry, standardisation of practice 77−16998
drop fragmentation 79−7169
droplet aerosol optical bleaching, influence of free convection 80−9924
dye proflavine bound to synthetic polynucleotides, selective laser photodamage 80−99525
ebonite, nontransparent dielectric, laser emission reflection and destructive action *(Russian)* 79−74031
elastic wave excitation by laser beam, through thermoelastic effect 80−103503
electrolyte aqueous soln. drops, ion emission due to laser heating 78−59063
electron+atom potential scatt. in low freq. laser field, perturbation theory 80−43191
electron+atom resonance scattering in laser field 79−859
electron beam, quantum modulation in field of opposite EM waves 78−74188
electron beam polarisation in storage ring by laser beam interaction 79−93860
electron beam-produced plasma, visible and UV high intensity spectral lines 79−73012
electron scatt. in laser field, photon correl. effects 80−83481
electron scattering in LF laser field, sum rule and classical limit 80−18978
electronic structure of solids under laser irradiation 78−91614
electroplating, enhanced, and maskless pattern generation 80−20803
energy flux channel close-up time *(Russian)* 77−55994
Escherichia coli, exogeneously photosensitized, effect of tunable laser radiation 77−90849
ethylene, laser-induced IR photolysis mechanism 78−56909
evaporated thin film filter, durability and stability 77−75686
evaporation of drop, explosive evap. criteria 77−953
explosive mechanism for press. on solid due to CO_2 laser pulse 77−16434
eye, aqueous temperature stabilisation, laser induced temp. changes and model 77−40713
eye, human, max. permissible exposure to 1.54 μm laser radiation 79−11966
eye lens fibre damage, rat 79−39374
eye maximum permissible exposure to 1.06 μm picosecond laser pulses 79−25033
eye retina laser radiation dosimetry 80−12268
fast electron energy spectra and preheating of laser irrad. target 79−55528
fast ion beam, laser beam interaction, high-resolution obs. 77−6959
Fe, cast, compact graphite inclusions, surface hardening by continuous action laser emission *(Russian)* 78−15567
ferroelectric, tetragonal, irradiated by laser pulses, spatial temp. and bound-charge distrib. 80−103927
ferroelectric oxide crystals for electrooptics and nonlinear optics, optical inhomogeneities, review *(Japanese)* 77−65613
ferroelectric phase transition, laser induced, centrosymmetric and noncentrosymmetric media 80−7312
fibre optic components, radiation strength for ruby laser transmission 77−7108
fibre optic elements, laser radiation damage 80−102747
fibroblasts and smooth muscle cells in culture, acute and long term laser beam effects 78−40268
film, defect-caused laser damage, statistical analysis 77−75587
film, laser-damage thresholds, meas. and identification 79−45988
film, single-layer, 2.8 μm and 3.8 μm absorpt. meas. 78−90463
film absorptive laser damage analysis by Weibull distrib. 80−33061
film coating, IR absorpt. meas. by laser calorimetry 78−25905
film deposition, evaporation of chem. element films with Nd:glass laser 79−47633
film on absorbent support, laser heating *(Russian)* 80−7441
laser beam effects continued
film pulsed laser damage determ., optical techniques 80−33060
flame, ruby laser-induced gas breakdown thresholds 79−1951
flare image danger reduction in laser focusing objectives 79−22997
floating optoacoustic antenna, statistical characteristics 79−27485
fluorescence redistribution after photobleaching rel. to cell membrane translational dynamics 80−21491
fluorophosphate and fluoroberyllate glass laser damage thresholds and solid inclusions 80−33054
fog, droplets evaporation rel. to laser beacons visibility range extension 80−101434
fog clearance, by laser-beam induced heat and mass transfer 78−93635
free convection in photoabsorption in liqs., gases and plasmas 77−11191
free-free transitions, mutiphoton, energy absorption laser pulse shape-independ. 80−43184
fundus oculi tissue, thermal effects on exposure to laser radiation 80−26261
fused and cryst. laser pulse breakdown freq. depend., self-focusing elimination 77−55855
garnet, epitaxial film, mag. bubble props., permanent local modification by laser annealing 80−2612
garnet film, mag. bubble domain, annealing by laser pulse 80−15769
gas, laser absorpt. wave propag., shock waves 80−28597
gas breakdown, book contrib. 77−51256
gas breakdown, effective photon theory, critical analysis 77−68735
gas breakdown, laser and microwave field induced, press. depend. 79−55446
gas breakdown, laser-supported, finite absorpt. length model 80−107005
gas breakdown at high intensity *(Russian)* 79−98853
gas breakdown by pulses from a CO_2 laser, air, Ar and He 80−6206
gas breakdown intensity threshold at 1.06 micron, of air $(N_2)(Xe)(Ar)$ 80−28594
gas cooling to broad band reson. light press. 80−48835
gas mixture, laser irradiated, anisotropy of inelastic scatt. and selective diffusion 80−53907
gas stream, chem. reacting, thermal crisis suppression by laser radiation reson. interaction 80−75000
gas-dielectric interfaces, initiation of low threshold breakdown 79−68900
gas-liquid phase transition, resonant field influence on critical parameters 77−84914
gas-surface scattering, energy transfer in laser field 79−69941
gases, optical breakdown, mol. ion reactions influence 80−96341
glass:Nd, surface struct., laser beam effects, IR spectra appl. 79−95250
glass, GLS, surface radiation strength, grinding and polishing press. effect 77−72104
glass, irrad. with laser beam, damage accumulation kinetics 79−99991
glass, K-8, radiation coloured, msec laser pulse effects 77−16435
glass, laser induced damage 80−66335
glass, laser irrad. effects, SEM meas. *(German)* 80−24492
glass, optical anisotropy due to laser-induced electrostriction *(Russian)* 79−99846
glass, optical K8, advanced evaporation mechanism under laser irrad. 77−79887
glass, polished, 1.064 μm laser damage threshold rel. to pulse duration and surface roughness 80−33055
glass, surface damage, free electron density meas. 77−40309
glass, ZhS-12 type, optical discharge, dynamics and props. 79−61471
glass cutting technology using CO_2 laser, damage effects 79−7173
glass destruction, by laser radiation, Brillouin-Mandelshtam scatt. influence *(Russian)* 77−72039
glass fabric laminate, nontransparent dielectric, laser emission reflection and destructive action *(Russian)* 79−74031
glass shell, laser compression, two-dimens. effects *(Russian)* 77−4124
glass spheres levitated by two horizontal laser beams, stable equilib. positions 77−46743
glass surface catastrophic optical breakdown development dynamics *(Russian)* 78−2951
glass surface roughness effect on 1064 nm 150 ps laser pulse damage 79−14013
graded-index antireflection coatings, high laser damage threshold 80−83628
graphite, laser pyrolysis in He or H_2, products exam. 79−20356
graphite artificial single crystals, failure under action of laser emission, exam. *(Russian)* 80−10573
graphite surface, laser-induced impulse 79−43071
graphite target in air, refl. of CO_2 laser radiation, plasma layer form. 80−25500
graphite vapour cloud, laser-prod., temp. conditions investig. 80−59290
grating phenomena, laser-induced review 77−46752
gratings, amplitude and phase, laser-induced 79−94302
gratings, holographic and ruled, laser damage resistances compared 77−19283
gratings, laser-induced, method for study of optically excited solids, forced light scatt. 79−41408
hazards and protection standards 80−46069
health hazards calc., for various viewing conditions 79−39447
heated surface colour temp. meas. pyrometer 78−57956
heating of disc of laser flash technique, error analysis 77−6552
heavy hydrocarbons, surface transient deformation by laser-induced thermocapillarity 79−33157
heterogeneous medium, laser irrad., prebreakdown stage evaporation *(Russian)* 79−24393
heterogeneous photocondensation process initiation by laser radiation 80−67410
high impact strength materials, laser beam effects, review 80−21073
highly absorbing media melting by laser radiation, liq.-phase surface shape 79−28082
hole drilling, ring focal pattern of lens-axicon doublet 78−55421
human eye exposed to single IR pulse, max. permissible exposure for safety 77−37009
hydrocarbon layer, influence on laser-induced surface damage 78−60533
hydrocarbons, heavy, self-holograms of laser-induced surface depressions 78−82927
hydrodynamic effects in laser radiation action on condensed medium 80−93439
hygroscopic aerosol interaction 77−79888
hypervelocity particle-surface impact simulation, using high-power pulsed laser 77−44094
ice, surface, interaction of laser burst, possible appl. 80−7444
II-VI semiconductor, spontaneous action of laser beams *(Russian)* 77−88820

laser beam effects continued
image recording on cinefilm, acousto-optical light modulator *(Russian)* 79−89027
impure solids, laser pulsed, mechanism for point defect generation 78−47368
impure solids, pulsed irrad., point defect generation 77−1150
infrared multiphoton dissociation of molecules, review *(Japanese)* 80−11885
infrared multiphoton processes, reaction rate, scale factors, pulse structure 80−32791
inhomogeneous interface laser mirror coatings, durability improvement 80−1252
insulator, transparent, laser breakdown, acoustic characts. 80−50269
insulator, transparent absorpt. wave struct. associated with optical breakdown 78−68581
insulator, wide-gap, damage by UV laser radiation 80−76110
interface of two phases or liquids, selective processes induced by resonance laser radiation 78−64867
interference coatings perpared by electron beam evaporation, UV optical strength 79−59779
ion, electromagnetically confined, laser cooled, double resonance and optical pumping 80−87155
ion emission from laser-driven implosions, routine monitoring using multichannel digitizer 80−57268
ion implantation by laser annealing, characterisation, solar cell applications 80−70247
ionic desorption, Ge, Ni, KI substrates, mechanism 77−15686
ionising particle beam interactions with liquids, acoustic effect, laser beam simulations 80−23262
IR detector materials, irreversible laser damage 78−25914
IR materials, laser residual absorpt. 2 to 10 μm, review 78−25906
IR materials, optical phenomena, conf., Annapolis, MD, USA (Dec. 1976) 78−25933
IR optical elements, adsorbed water effect on optical strength 77−79886
IR optical train handling high pulse powers, thermal distortion thresholds 77−46745
IR optics elements, breakdown dynamics near surface in gaseous media 79−45986
IR window heating, interferometric meas. 77−46748
IR-optical material surface breakdown, adsorbed water evaporation model 80−35020
isotopically selective heterogeneous reactions, stimulation with laser light 77−25309
Josephson junction, coherent radiation induced bistability 80−80453
large-spot laser damage meas., multibeam apparatus 77−19286
laser radiation, interaction with free atoms, review 78−13473
laser radiation-matter interactions, dissertation 79−86555
laser stimulated desorption, multicomponent systems, absorbent surfaces, Langmuir kinetic theory, laser rate equation 79−99407
laser-fusion reactor, surface heating of 1st wall by pulsed photon and ion irrad. 78−89979
levitation of solid transparent spheres by two horizontal beams 77−7104
liquid, absorbing intense IR radiation, behaviour of pressure 80−102749
liquid, laser breakdown, photoacoustic and photohydrodynamic parameters 78−52597
liquid, laser excited acoustic field, effect of surface perturbation 77−15499
liquid, laser induced breakdown, high speed holography 78−18360
liquid, laser induced shock wave 77−7413
liquid, steady-state crater form. due to high-power DW CO_2 laser irrad. 78−48260
liquid, superheated, under intense EM irrad., effect of spinodal singularities on evaporation *(Russian)* 77−89533
liquid drop cloud medium dissipation by CO_2 laser radiation 79−39858
liquid drops, optically dense, motion in laser radiation field 78−50842
liquid half-space, sound generation by FM modulated laser beam 78−38781
liquid interaction, air shock-wave generation at surface 78−19608
liquid layer floating on liquid half-space, acoustic field generated by laser beam 78−51615
liquid mixtures, decomposition into components by thermal action of continuous laser irradiation 79−19362
liquid surface deform. due to laser radiation thermal action, lens effect 80−33048
liquid surface response to intense laser pulse, hydrodynamic anal. 77−24468
liquid with absorbing particles, laser beam illum., refr. index change, bubbles form. 80−25334
liquids, highly voltatile light beam interaction, photohydraulic effect *(Russian)* 80−69440
liquids, laser pulsation kinetics, optical damage effects 80−58614
low-level prolonged exposure effects on visual function 80−3714
macromolecular solutions, orient. in laser beam elec. field, anisotropic light scatt. 79−1768
macromolecules, nonlinear laser photomodification, radiation damage 80−61120
macroparticle impact with meteoritic vels., physical modelling principles, quasi-full laser modelling 79−52049
mammalian cell, thermal sensitivity to pulsed CO_2 laser irrad. and hyperthermia 78−15802
mammalian cell exposure using evanescent fields created in optical waveguides 78−73298
mammalian cells, laser radiation effects obs. using optical waveguide evanescent fields 80−12183
mass spectrometer ion-field source emitter, influence of laser irradiation on ion current 80−101874
material interactions and effects due to absorpt. 78−35229
materials processing, seminar, San Diego, CA, USA (Aug. 79) 80−90609
matter interaction, picosecond exposure scanning camera, and associated recording system *(French)* 78−42429
mechanical response to giant laser pulse, recoil impulse meas. 80−80910
medical laser beam operation, safety 78−35903
metal, action of intense optical radiation, behaviour of surface temp. and refl. coeff. 78−15260
metal, chemiluminescent oxidation using laser vaporisation, kinetics 79−100385
metal, crater deepening, expt. testing of models *(Russian)* 77−20962
metal, EMF appearance due to mag. field and laser pulse irrad. 77−76797
metal, evaporation under laser irradiation *(German)* 78−52599
laser beam effects continued
metal, foil, surface temp. meas. during laser irradiation heating *(Russian)* 79−74030
metal, heating by laser emission, spatial nonlinear problems *(Russian)* 80−7440
metal, irrad. with 10.6 μm pulses, time-resolved specular reflectivity 79−69819
metal, laser heating kinetics, influence of oxide film interf. effects 80−11841
metal, laser-photoinduced etching, photodissociation of dissolved complexed halogens in soln. 80−100929
metal, negative ion emission during microsecond laser pulse irrad. 78−2981
metal, oxidizable, laser heating in air by obliquely incident radiation 80−71815
metal, pulsed laser irrad. effects on struct. and props. *(Russian)* 78−30665
metal, steady-state crater form. due to high-power DW CO_2 laser irrad. 78−48260
metal absorptivity under laser radiation action, time and temp. depend. 79−95724
metal and alloy, characts. and effects of laser generated stress waves 79−69192
metal and alloy surfaces, highly reflecting, pulsed laser stress phenomena 79−14015
metal combustion, laser-initiated, time-resolved spectroscopy 77−77765
metal evaporation, Nd laser and Cu example, numerical analysis *(Russian)* 77−40312
metal film, grating etching process, transient signals 77−19263
metal film, laser damage determ. using quartz resonator 78−31286
metal film, surface effect on laser-induced damage 77−16436
metal film, vaporisation kinetics on absorbing laser radiation *(Russian)* 77−43423
metal film vaporisation by laser, vaporisation front relativistic velocities *(Russian)* 80−66337
metal foil with thin film coating, failure by laser pulse *(Russian)* 78−23561
metal heating by laser radiation, calc. allowing for thermal props. temp. depend. 78−30770
metal melting by laser emission, laws governing fluid phase spattering *(Russian)* 77−20963
metal mirrors, diamond turned, evaporated and sputtered, surface and optical studies 78−79098
metal mirrors, diamond turned, surface, optical and laser damage characts. 77−50705
metal mirrors, dielec. enhanced, absorptance at 5.3 μm 77−50709
metal mirrors, for high-power appls., multithreshold damage analysis 77−88884
metal mirrors for high power appls., multithreshold damage analysis 79−980
metal oxide/fluoride mirror coatings, light scatt. and optical strength in UV range 80−106595
metal particle, ultra-fine, form., pulsed laser breakdown of carbonyl vapours 80−84881
metal plate, penetration by combined CW and pulsed laser radiation 79−89955
metal pulse evaporation, metal-insulator transition 77−81181
metal reflectance changes during laser irrad. 80−93261
metal surface, charged-particle emission caused by beam scanning 80−11518
metal surface, flash mechanism caused by monochromatic laser radiation 79−95878
metal surface, high-intensity laser beam interaction 80−19600
metal surface, reflectivity, single laser pulses, plasma burst effect 78−19609
metal surface crater form., by laser pulse, frontal method, approx. soln. 77−77327
metal surface laser beam irrad., effective absorpt. coeff., temp. field determ. *(Russian)* 80−76108
metal surface-ultrashort coherent IR pulse interaction, inertialess radiation *(Russian)* 79−95879
metal surfaces, laser heat treatment, wear resist., corrosion protection, hardening, review 78−72939
metal systems, mech. prop. improvement by pulsed laser generated shock wave 77−48443
metal target, gas breakdown near surface, pulsed CO_2 laser focusing effect 79−52051
metal target, irradiated by pulse-periodic CO_2 laser, absorpt. coeff., air breakdown effect 79−52052
metal target, recoil impulse on microsecond CO_2 laser irrad. 77−36322
metal target heating by CO_2 laser pulses, breakdown initiation in vapour 79−91540
metal targets, laser radiation absorption in craters 80−97386
metal vaporisation by laser irrad., effect of plasma 79−1800
metallic film, failure processes due to powerful light pulses *(Russian)* 80−7443
metallic film machining by laser-induced explosion 78−15258
metallic layers, heating, impulsive and continuous 77−40311
metallic mirrors, laser damage, temp. depend. of absorptance, melting 79−81470
metallic mirrors, laser damage, temp. depend. of absorptance, vaporisation and vap. heating 79−81471
metallic plate, subject to laser heating, nature of thermoelastic stresses *(Russian)* 77−21199
metallic surface, heat treating and melting with scanning laser or electron beam 78−11406
metallic surface rippling induced by surface tension during laser melting 78−11405
metallic target, laser produced shocks rel. to material damage 78−31285
metallised coating on polyethylene terephthalate film, fracture under laser irrad. *(Russian)* 80−76333
metals, erosion accompanying simultaneous action of laser emission and ultrasound *(Russian)* 80−7442
metals, fracture due to laser irrad. and shock compressed plasma *(Russian)* 80−55500
metals, fracture during laser working, depend. on physico-chem. props., heat cond. *(Russian)* 80−55432
metals, laser and nuclear radiation induced emission anomalies, current sources *(Russian)* 80−25536
metals, optical erosion, interpretation of screening effects 77−66559

laser beam effects continued
metals, optimal heating, in oxidised medium, by CW CO_2 laser radiation 80−69445
metals, specular refl. anomalous behaviour after 10.6 μ pulsed laser irrad. 80−93260
metals and alloys, laser erosion, influence of metallic target temp. *(Russian)* 79−39028
metals erosion, of IV-VI and VIII groups *(Russian)* 77−12702
metals in water , light beam interaction, photohydraulic effect *(Russian)* 80−69440
metals vaporisation by laser beams, effect of delivery pressure time dependent behaviour *(Russian)* 79−55877
microcline, continuous laser emission effects on surface, spectroscopic obs. 79−94271
microcline, laser torch effects, spectroscopic investig. *(Russian)* 78−76560
microdiscs, energy transport to rear surface under high laser irrad. 80−33797
microprobe analysis, crater formation, gas medium effects *(Russian)* 79−18428
microprobe analysis, impulse synchronous discharge effects, water formation *(Russian)* 79−18429
microscopic particles, heating by laser beams 78−50838
mid IR laser window materials, absorption props. 77−46770
mirror, SEM obs. of laser induced damage *(German)* 78−37929
mirror surface, high power optical damage threshold elevation by hypervapotron cooling 79−23002
mirror-damage thresholds for laser-fusion pulse shapes 78−74467
mirrors with temperature-dependent absorptance, laser-induced thermal runaway 80−91882
molecular collisions, laser radiation field effects, quantum mechanical close coupled expansion 77−50485
molecular gas, thermalisation under reson. excitation by laser radiation *(Russian)* 78−26231
molecular ion formation on molecular cryst. surface UV laser irrad. *(Russian)* 80−71521
molecular nonsteady-state luminesc. behaviour under narrowband laser excitation 80−87159
molecular system dissociating in laser radiation mass action law 77−70298
molecular vibrations, coherent interaction with strong monochromatic laser light, classical calc. 80−28079
molecules in degenerate electronic state, IR laser radiation effects 80−81351
moving target for coherent radiation test of k-factor of Bondi's calculus 79−75435
multilayer, electric field distrib. and laser damage reduction 80−87420
multilayer 532/1064 nm laser reflector damage resistance improvement by non-λ/4 design 79−14019
multilayer coating design with reduced elec. field intensity 77−72046
multilayer film, intrinsic and thermal stress modelling and interferometry 79−14059
multiphoton ionisation by lasers, localised and dispersive states 77−27041
muonic atom muon capture probability and laser effect on hyperfine level population *(Russian)* 77−75348
nematic liquid crystal, laser breakdown, plasma-acoustic cavitation phenomena *(Russian)* 77−65947
nepheline, continuous laser emission effects on surface, spectroscopic obs. 79−94271
nepheline, laser torch effects, spectroscopic investig. *(Russian)* 78−76560
new materials properties achievable by ion implantation doping and laser processing 79−69127
nonabsorbing materials, laser radiation scatt., destructive effects *(Russian)* 78−30001
nonequilibrium phase transformation theory homogeneous fluctuation effect 80−84277
nonlinear crystals, water soluble, characts. of laser pulse damage 79−45987
nonlinear diffusion equation, general class of similar solns., laser interactions, thermal cond. 77−37827
nonmetallic infinite plate, temp. field calc. *(Russian)* 78−59061
nonspherical particle, optical levitation for light scattering obs. 80−58455
normal metal-superconductor structure, laser irrad. theory of current voltage characts. *(Russian)* 77−80877
nuclear energy level transitions, laser radiation effects on lifetime 80−22760
nuclear orientation, induced by laser, at. and nucl. applications, review 78−37310
octafluorocyclobutane, laser induced unimolecular decomposition 77−32775
octyl-cyano-biphenyl, influence of laser light wave field on nematic phase *(Russian)* 80−92456
ocular hazard of short pulse Ar laser irradiation, primates 79−25030
opaque solid, laser heating and burnthrough 77−69940
opaque solid slab, laser heating and burnthrough, anal. 77−48284
opaque targets in air, pulsed laser heating 77−52204
optic cavitation and laser-produced bubbles 80−38463
optical cavitation in liquids, ruby laser pulse effect *(German)* 77−75949
optical coatings, conf., Washington, USA (March 1978) 79−46028
optical coatings on glass in liquids, damage threshold 77−61994
optical component laser damage mechanisms 78−83016
optical component thermal failures in long and short laser pulse regimes 77−19281
optical fibre, parabolic index, selective excitation by Gaussian beams 80−95992
optical fibre coupling efficiency and surface damage threshold for giant and free-running laser pulses 80−33212
optical glass, coloured, laser damage threshold, optical absorpt. influence 80−91830
optical glass, damage threshold for 10 ms pulses, temp. depend. 77−75595
optical glass, K-8, laser pulse heating, softening and hardening points obs. 78−33794
optical glass, K-8 type, laser irradiated, transient thermal self-focusing and melting 77−50733
optical glass, laser bulk damage, stimulated Brillouin scatt. influence 79−59762
optical glass, laser induced pre-threshold changes 78−29999
laser beam effects continued
optical glass, surface damage by wide beam 77−79885
optical glass exposed to laser radiation, absorpt. coeff. temp. depend. 79−89979
optical glass irrad. with quasi-CW laser pulse, obs. of absorpt. waves 79−89952
optical glasses, laser induced destruction threshold, types *(German)* 77−75631
optical material, phototransport laser damage mechanism 77−63498
optical material radiation resistivity *(German)* 77−58363
optical material radiation strength, dissipative characteristic 79−27344
optical materials, damage threshold at 10.6 μm, up to 10^{10} W/cm^2 77−50707
optical materials, laser beam damage thresholds of CO_2 fusion laser optics 80−38050
optical materials, laser induced breakdown, breakdown thresholds and multiphoton absorpt. coeffs. 79−3735
optical materials, laser induced damage, symposium, Boulder, USA (Sep. 1978) 80−31417
optical materials at 1.06 μm 80−28263
optical materials for high power lasers, conf., Boulder, Colo., USA (July 1976) 77−46729
optical surface roughness dependence of laser induced damage threshold 79−81469
optical system surface damage from fusion experimental lasers, high fluence and contamination effects 80−38049
optical waveguide, diffused, light-induced damage 80−9925
optogalvanic effect, theory based on multiplication of electron within plasma 80−38741
organic liquid, laser induced breakdown 77−81056
oxidising metal heating by periodically pulsed CO_2 laser 80−7445
p-n junction formation in doped semiconductors by laser radiation *(Russian)* 77−15947
particle properties, particle heating by radiation absorption, effect of radiation press. *(German)* 80−106556
particle properties, radiation pressure effect on particle motion *(German)* 80−102755
phage T7, inactivation by visible laser light *(German)* 80−98010
phosphate glasses, optical breakdown rel. to nicroscopic inhomogeneous struct. 80−102784
photoabsorption convection in horizontal tube, unsteady-state convection, num. investig. 80−33594
photoabsorptive convection, steady states in field of continuous laser radiation 79−14212
photoacoustic pulse phenomena in liquids 78−1486
photoexcitation effects during laser trimming on thin film resistors on Si 80−64093
photographic emulsions used in optical correlators, laser damage 79−27303
photographic films, Kalvar and Polaroid, damage threshold variation with spot size at 10.6 μm 79−36945
photosynthetic membranes, anal. of laser-induced fluorescence with Pauli master eqn. 79−39350
piezoceramic cell, fluid-filled, response to pressure generated by axial laser pulse 79−72746
pinhole closure due to intense laser radiation 77−79877
pinholes irradiated by Nd:glass laser pulses, plasma closure phenomena 79−89946
planar laser explosion near a target in air 80−19601
plane evaporation boundary instability in laser radiation-matter interactions *(Russian)* 80−76111
plane target, laser-matter interactions, wavelength, intensity and target type depend. 77−43002
plasma mirror refl. characts., in electron beam controlled CO_2 laser 78−59064
plastic flow influence on laser optical component props. *(Russian)* 80−38047
PMMA:butlacrylate, breakdown threshold to ns IR laser pulses *(Russian)* 77−81179
PMMA, absorbing defect role in laser damage 80−108308
PMMA, damage mechanism due to multiple laser pulse exposure 77−731
PMMA, laser damage mechanism rel. to viscoelastic props. 80−55233
PMMA, laser damage threshold, freq. and size depend. 80−104018
PMMA, laser damage threshold, microstructural defects effect 77−52205
PMMA, light absorption, laser crack development 78−68780
PMMA, optical strength rel. to surface defectiveness 77−28665
PMMA, thermochem. instability at Pt sphere inclusions caused by CW laser beam 80−29689
PMMA film, Plexiglas, penetration depth of 10.6 μm laser radiation, transmission, refl. and absorpt. meas. 79−74010
polyatomic mol. gas, laser-induced rate processes, collision-free dynamics 77−30934
polydiacetylenes, reversible creation of defects by laser pulses 78−23480
polyethylene, laser irrad., mol. emission from unionised gas 78−42777
polyethylene, laser irrad. chem. and struct. modifications *(Russian)* 79−27931
polyethylene, X-ray emission spectra of CO_2 laser-irrad. targets, nonlinear processes 80−33793
polymer, transparent, damage mechanism due to multiple laser pulse exposure 77−731
polymer, transparent, form. of linearly extended destruction zone by pulsed laser radiation 77−69942
polymer, transparent, high-temp. zone form. in laser induced mech. breakdown 77−56086
polymers, orientation of plane of large cracks prod. by laser pulses 80−11753
polymers, transparent, absorbing defect role in laser damage 80−108308
polymers with various atomic composition and viscoelastic props., laser damage 80−104017
polymethine dye solution, optoacoustic response 80−6465
polymethine dye solutions, brightening depend. on laser pulse length 79−41425
polystyrene, laser irrad. chem. and struct. modifications *(Russian)* 79−27931
polyvinyl alcohol, laser irrad. chem. and struct. modifications *(Russian)* 79−27931
polyvinylidene fluoride films, 200 ps laser pulse heating, pyroelectricity meas. 79−4768

laser beam effects continued
propane, and propane-N_2 gas mixture, CO_2 laser radiation absorpt. coeff. 77−58366
propellant solid, pyrolysis craters due to laser pulse heating 78−23921
pulse heating, high speed pyrometry and spectroscopy, review of techniques 80−52225
pulsed heating profile width and total coupling changes with pulse length and press. 80−71520
pulsed laser atom-probe FIM, development and appls. 80−66402
pulsed laser damage to optical surfaces, multithreshold analysis 79−18465
pulsed laser induced damage at DF laser wavelengths 77−46751
pulsed laser light stimulated desorption and local vaporization 77−16432
pulsed laser-induced shattering of water drops 80−50471
pulsed pressure on targets, measurement using optical pressure-sensing element based on interferometer 79−35771
Pyroceram, enhanced failure by combined pulse and CW laser 79−29182
pyrolysis of organic liqs., *(Russian)* 77−56226
quarter-wave dielectric reflector, spectral absorptance approximation 80−33131
quartz, fused, continuous laser emission effects on surface, spectroscopic obs. 79−94271
quartz, fused, laser torch effects, spectroscopic investig. *(Russian)* 78−76560
quartz, fused, picosecond-pulse optical breakdown, direct obs. of dynamics 78−6629
quartz, laser-induced spherical defects 77−44093
quartz, stimulated Brillouin scatt. correlation with laser induced damage 77−38984
quartz glass, laser breakdown and absorption, 1800-2400K 79−64296
quartz glass, optical breakdown by sharply focused laser beam 79−69776
α-quartz twinning and tailored domain patterns 77−40197
radiation pressure on a moving resistive sheet 80−18989
rare earth fluorides, antirefl. laser window coatings at 10.6 μm 77−61963
rare earth oxide (R_2O_3)-M_xO_y glassy systems (M=Ti,Nb,Ta), rapid quenching by laser beam, exam. of composition and crystallization 78−52856
rate calorimetry analysis with coating absorption 80−33050
reflector with non-quarter-wave design, enhanced damage resist. 77−88819
refractory oxide optical coatings, laser damage resist., spectral depend. 77−62022
resonant defect enhancement of laser elec. field 77−63499
resonant electron scatt. by atoms in laser field, negative ion formation, polarisability 77−19089
retina, primate, temp. rise and tissue damage due to Ar laser irrad. 78−44559
retina thermal injury following laser irrad., asymptotic rate process calcs. 78−80916
retinal damage by 325 nm He-Cd laser radiation 78−69136
retinal damage from a white-light laser, thresholds and mechanisms, rhesus monkey obs. 80−108955
retinal damage from suprathreshold Q-switch laser exposure 79−5274
retinal injury mechanics, laser exposure limits 79−66485
retinal morphological and functional changes and safe energy levels 80−3712
retinal photocoagulation by laser beam, temp. and bleaching dynamic meas. *(German)* 79−2098
retinal tissue damage, by single ultrashort laser light pulses 78−96065
ruby:Cr, lifetimes of laser-induced population density gratings, comparison with fluoresc. lifetimes 79−64276
ruby, optical strength rel. to surface defectiveness 77−28665
ruby, structural defects due to laser irrad. *(Russian)* 80−100303
ruby laser rod, exoemission parameter rel. to optical strength 77−732
ruby single crystal, laser induced damage, influence of pores 77−83918
safety, basic classification concepts 79−39524
safety considerations 77−77940
safety eyewear, filter glasses 79−39525
sapphire, absorbing microdefects effect on anisotropy of optical strength 78−2952
sapphire constant diameter cryst., laser heated float zone growth, meniscus angle meas. 80−108347
satellite retroreflector arrays, method of calculating transfer functions 80−5778
SAW velocity dispersion induced by laser radiation absorpt. 77−51585
scanned visual displays, pulsed light data extrapolation 80−3713
segregation, nonequilibrium, during pulsed laser annealing, model 80−108451
semi-infinite solid, laser surface melting and subsequent solidification, computer heat flow models 79−69916
semiconducting plate, optical thermal breakdown, laser hysteresis 79−56889
semiconducting plate, with temp. depend. absorption coeff., heating kinetics *(Russian)* 77−54867
semiconductor, damage by 10.6 μm CW CO_2 laser beam 77−63497
semiconductor, dynamics of surface melting and resolidification during laser annealing 79−69918
semiconductor, ion implanted, epitaxial regrowth, laser annealing dynamics 80−92548
semiconductor, ion implanted, laser annealing 79−69124
semiconductor, ion implanted, laser annealing *(Japanese)* 80−19821
semiconductor, ion implanted, pulsed laser and electron beam annealing comparison 80−92547
semiconductor, ion implanted, ruby laser pulse effects 79−69125
semiconductor, ion-implanted, laser annealing dynamics 79−69121
semiconductor, laser induced superconducting props. 77−72960
semiconductor, laser-induced damage 77−20961
semiconductor, laser-photoinduced etching, photodissociation of dissolved complexed halogens in soln. 80−100929
semiconductor, optical heating, coupled diffusion eqns. for heat and excess carrier density 80−60718
semiconductor, optical props. under intense laser field 79−43040
semiconductor, optical thermal breakdown, fluctuations and wave processes 80−20587
semiconductor, or insulator, laser stimulation of light interstitial diffusion, theory 77−15630
semiconductor, pulsed laser irrad. effects on struct. and props. *(Russian)* 78−30665
laser beam effects continued
semiconductor, surface melting during laser annealing 79−74023
semiconductor epitaxial regrowth, ion implantation induced defects, annealing 80−24479
semiconductor film, laser-induced transmittance oscills. and struct. phase transitions 79−87516
semiconductor films, structure, influence of laser beam 79−7761
semiconductor laser damage, role of carrier diffusion 79−19954
semiconductor layer, implanted, effectiveness of annealing by millisecond laser pulses 78−55885
semiconductor physics, conf., Edinburgh, Scotland (Sept. 1978) 79−95303
semiconductor plate, light irradiation, heating and thermoelastic stress 80−25499
semiconductor with impurities, laser beam induced synergetic phenomena 79−74021
semiconductors, ion-implanted, laser pulse annealing, TEM and channelling study 80−100264
semiconductors, laser annealing after ion implantation, temp. distrib. 80−54265
semiconductors, laser beam annealing of ion implanted layers 80−24469
semiconductors, laser processing, bibliography 79−74028
semiconductors, laser window materials, residual lattice absorpt., freq. and temp. depend. 78−25910
semiconductors and insulators, nonequilib. electron Coulomb collisions during optical pulse interband interaction 80−76049
shells, creation of finite perturbations by use of laser beam 79−18849
shells, cylindrical, subjected to localised perturbations, equilib., states 79−18850
shock production rel. to material damage 77−90221
shock wave, implosive spherical, produced by laser pulses, shadowgraphic detection 80−87529
shock wave optical diagnostic system 80−79421
silicate glass darkening due to UV radiation from laser produced plasma jet 78−52598
slab, with temp. depend. surface absorbance, laser heating 80−48545
sodium nitroprusside, isomeric molecular states generated by polarised light, Mossbauer resonance obs. 77−20781
soft X-ray photography, extra-fast shutter *(French)* 78−41397
solid, avalanche ionisation, multiphoton ionis., in laser induced breakdown *(Russian)* 79−51906
solid, temp. rise induced by laser beam 78−11025
solid in gas, mech. effect of CO_2 laser pulses 77−77329
solid phase reactions induced by scanning CW laser, reaction rates, analytical model 80−66334
solid Raman laser damage avoidance, methods for increasing efficiency 77−79853
solid surface, laser irrad., temp. rise calc. *(German)* 78−68580
solid surface, mol. dynamic processes interaction with laser radiation 80−71943
solid surfaces under laser irrad., electronic struct. and chemisorption 80−84812
solid target, abrasion and evaporation by focused CO_2 TEA laser radiation *(German)* 77−40305
solid targets in Ar atom., laser radiation effects, plasma cloud form. 79−11488
solid transparent dielectric, surface damage caused by laser radiation 79−31968
solid-state amplifying medium interaction with laser radiation *(Rumanian)* 78−59011
solids, optical absorption under laser irrad. 80−34940
soot conglomerate destruction dynamics in pulsed laser radiation field 80−58617
sound generation by absorpt. of modulated laser radiation in liq. waveguide, theory 78−1539
sound generation by intensity-modulated laser beam in liquid half-space 79−91403
sound generation by moving pulsed optoacoustic sources 80−87634
sound generation in liquid, effect of harmonic variation of modulation freq. 79−19321
sound generation in liquids and solids by laser heating 78−1485
sound generation in moving inhomogeneous fluid 78−34568
sound wave generation in liquids 78−83882
sound wave generation in water 77−50812
sound with finite tracks, generation by laser beam 79−90731
spark, laser-produced, light pulse narrowing and power density increase 80−28862
spark in focused laser beam, and continuous optical discharge, numerical study 79−14632
spatial distribution of temperature rise induced by Gaussian laser beam 79−69917
speckle dynamic statistical props. due to diffuse object longit. motion under Gaussian beam illum. 80−99628
sphere, force exerted by laser beam, stable optical levitation conditions 79−76733
spherically symmetric molecules, many-photon excitation in IR laser field 80−95596
spinach chloroplasts, laser photoinduced changes in high freq. dielectric constant 80−85449
spot thermal history, surface heating with laser-coaxial gas jet 77−63494
SQUID, laser irrad. effects 79−56419
stainless steel, optical breakdown threshold, illuminated spot dimension effects 78−68582
steel, AISI 1045, laser transform. hardening, fatigue and wear rates 79−70198
steel, alloy, Cr, austenitic boundary layers, form. by short laser pulse reaction 78−88555
steel, alloy, interaction with Nd^{3+}-glass laser light 78−92147
steel, C, structural transform. and surface hardening by laser treatment 77−70233
steel, Cr plated, laser treatment 80−21191
steel, hardness, effect of laser irrad. in inert gas atm. *(Russian)* 79−38935
steel, high speed tool, laser surface melting 79−24654
steel, laser beam melting kinetics *(Russian)* 77−56121
steel, laser-irradiation surface treatment *(Russian)* 77−59978
steel, low C, rapidly solidified laser surface alloyed, electron microprobe obs. 79−70201
steel, medium C, type 35 laser treatment effect on struct. and mech. props. 79−39041

laser beam effects continued
steel, microhardness changes under high-press. and laser irrad. *(Russian)* 77−59903
steel, multiple crater refl., effect on refl. props. 78−52596
steel, Ni and W, recrystallisation mech. during laser treatment 80−50658
steel, reflectivity at 10.6 μm, calorimeter meas. 78−55393
steel, stainless, CW CO_2 laser radiation coupling coeffs. 80−84811
steel, stainless, laser induced damage 80−66335
steel, stainless, O_2 desorpt. during laser irrad., etching, AES study 80−66338
steel, stainless, sensitised surface normalisation by laser melting 78−60869
steel, stainless, type 304, laser surface melted, topographical charact. 79−70200
steel, tool, M2, laser surface melted, heat treatment effects on struct. 79−70086
steel, tool type M2, surface hardening and microstruct. refinement by laser melting, electron beam melting, heat treatment *(Korean)* 79−70093
steel, W-Mo-Cr-V tool, laser surface melted, struct., heat treatment effect 80−76424
steel 1018, laser surface melted, topographical charact. 79−70200
steel melting, effects of laser light focusing conditions *(Russian)* 77−59823
stomach tissue, canine, temp. increase comparison for Ar and Nd:YAG laser irrad. 79−92290
stomach tissues, canine, Ar and Nd laser damage 78−48831
stress waves, high amplitude, laser generated in materials 79−78797
structural phase transitions in crystals, effect of high-power visible and IR laser radiation 78−71825
superconductor, optically induced non-equilibrium, heating effects *(Russian)* 78−95398
surface evaporation, vapour free jet expsn. 78−1703
surface evaporation spectral-line absorption 79−19951
surface generated by diamond turning machine, physical and optical props. 80−33263
surface impact, transient momentum transfer, pulsed and CW modes 77−89013
surface impact on transparent dielectric, shock wave dissipation from imperfections 79−69925
surface irradiation shielding time with CO_2 laser beam, appl. to Al and graphite 79−55530
surface thermal working by laser, laser annealing parameters *(Russian)* 80−100848
surfaces, laser-annealed, characterisation by ellipsometry 80−103544
target exposed to intense pulsed beam, kinetic temp. meas. method 77−82524
teeth, human, optical interaction, thermal field and micro-crack form. 77−52840
teeth, human, thermal stress effects and surface cracking assoc. with laser use 78−80915
teeth, rel. to laser appl. of durable dental sealants 78−48868
Teflon, nontransparent dielectric, laser emission reflection and destructive action *(Russian)* 79−74031
tendon, rat-tail, coherent optical SHG 80−89796
tetramethyldioxetane, gas phase unimol. decomp. and chemiluminesc. initiated by TEA CO_2 laser 77−60068
thermal acoustooptical effect, laser beam incident on plane interface 77−11639
thermal coupling of 2.8-μm laser radiation to metal targets 80−76107
thermal halo effect, nonlinear scatt. by moving particles, symm. distortions 78−66875
thermooptical excitation of acoustic fields in liquid by periodic train of laser pulses 80−103945
thermooptical sound source in liquid, anal. of wave zone 80−87631
thermooptical US generation due to moving laser source in liquid 80−102903
thin absorbing films, laser-induced removal, two-phase mechanism 80−97384
thin absorbing films, laser-induced removal, two-phase mechanism 80−97385
thin film, laser damage, photoacoustic study 80−80098
thin film waveguides, optical damage thresholds 79−46033
thin-film reactions, solid phase, laser annealing 79−51438
tissue, significance of blood flow in temp. calcs. 80−104563
tissue, temp. distrib. during laser irradiation 79−39449
tissue heating temp. profile and scatt. determ. *(German)* 79−2099
tissue temperature calcs. in laser irrad., significance of blood flow 80−55993
transition metal nitrides of group IV-V, laser irrad. action, erosion strength *(Russian)* 77−56112
transparent dielectric, enhanced localised intensities in surface scratches rel. to laser damage 79−22999
transparent dielectric, laser damage, appl. of gas breakdown model 77−63496
transparent dielectric, laser damage probability and avalanche breakdown 77−12471
transparent dielectric, laser destruction, impact mechanism diverting energy from absorb. inclusions 78−43962
transparent dielectric, laser induced fracture *(Russian)* 77−51406
transparent dielectric, laser induced plasma at surface 80−79531
transparent dielectric, laser pulse energy absorption, refr. wave form. *(Russian)* 79−55167
transparent dielectric, laser-induced damage by thermal explosion of absorbing inhomogeneities 79−10340
transparent dielectric, nondirectional glow under laser irrad. 78−52575
transparent dielectric, optical stimulation of compression pulses, absorbing layer effects *(Russian)* 77−1174
transparent dielectric, spot size and pulse duration depend. 77−61995
transparent dielectric destruction by laser radiation, review 77−50702
transparent dielectric optical breakdown, thermal instability *(Russian)* 77−55854
transparent dielectric with inclusions, thermal stresses 77−729
transparent dielectric with metallic inclusions, light pulse shape effect on optical breakdown threshold 80−20588
transparent dielectric with radioimpurities, intense radiation absorption *(Russian)* 78−74939
transparent dielectrics, breakdown of air near surface 78−34381
transparent dielectrics, cumulative ionisation by strong light pulse, numerical soln. *(Russian)* 77−28667
laser beam effects continued
transparent dielectrics, laser damage, electron avalanche and multiphoton ionisation roles 80−35016
transparent dielectrics, with inclusions, laser-induced stresses 79−28012
transparent materials, absorpt. coeffs. meas., interf. effects 78−46699
transparent materials, defective surface layer formation during abrasion, laser-induced breakdown *(Russian)* 78−53007
transparent materials, laser irradiated, in-depth and surface temp. meas. by Moire-Schlieren technique 80−53392
transparent media with random inhomogeneities, optical breakdown 77−59647
transparent medium with random absorbing inclusions, laser heating statistics *(Russian)* 77−28666
transparent optical material surfaces and films, pulsed laser induced damage 79−89948
transparent optical materials, laser induced damage and lattice strain due to lattice defects 80−48315
transparent polymers, laser-induced optical breakdown, chem. reactions effects *(Russian)* 78−35676
transparent solid, laser damage by electron avalanche ionisation 79−19952
transparent solid dielectric, laser evaporation, analytic eqns. 80−35014
transparent solid optical materials, laser damage statistics rel. to structural defect statistics 80−91829
trapped ion, laser cooling, theory 80−58414
treatment of material, influence of oxidising atmosphere *(Russian)* 78−23840
tumour irradiation, immunological processes *(German)* 78−40242
two film struct., laser heating *(Russian)* 78−15259
two-layer chemical coating, laser radiation damage thresholds 79−76739
two-level atom, radiation by intense laser beam, resonance fluorescence, photon antibunching, Doppler shift 80−74146
Udimet 700, superalloy, melted by laser beam, microstructure and topography exam. 79−69919
uracil, nucleic acid component, selective action by ps light pulses 80−72213
US field, 2 MHz, in water, expts. on intensity modulation of traversing laser beam 79−76906
UV coating, damage resistance 80−33047
UV damage resistance of laser coatings 80−33056
vanadyl phthalocyamine dye solns., laser destruction, highly excited states participation 78−53231
vaporisation, hydrodynamic effects, in thermal model of condensed media under action of intense EM radiation *(Russian)* 79−69922
water, interaction of laser bursts, possible appl. 80−7444
water, laser-induced acoustic waves 78−25996
water aerosol clearing by CO_2 laser beam, transmittance change at 0.63, 1.06 μm 78−37933
water aerosols, pulsed laser radiation action 80−14378
water drop evaporation by 10.6 μm laser radiation 77−75589
water drop thermal explosion by high-power laser radiation 77−75590
water droplet, explosive vaporisation on 10.6 μm radiation exposure, inhomogeneous internal heat evolution 80−29162
water droplet, laser induced evaporation, diffusion coeff. temp. depend. 77−20062
water droplets, small, weakly absorbing, motion in bounded laser beam 79−12269
water surface subjected to laser radiation, repulsion of bodies, optically generated vapour cushion 79−10339
water vapour, i.r. CO laser beam absorpt., optoacoustic meas. 77−2241
weakly absorbing solid medium, opacity fluctuations, heating by intense radiation and thermoelastic stresses problem 80−38048
weakly ionised gas, low threshold optical breakdown 79−27860
window, elec. fields and power dissipation at oblique incidence 77−46746
window, thermal lens form. due to giant laser pulse 77−3602
window coating materials with low index, laser damage at 10.6 μm 77−61991
window materials, pulsed HF-DF laser damage 79−14011
window materials, refr. index, temp. and stress effects 77−46771
window materials for CO_2 lasers, optical suitability 77−58361
window materials for HF-DF laser, surface and bulk absorpt., photoacoustic meas. 78−25912
wound-healing, clinical and expt. results of action mechanism 77−9299
Ag film, inertialess glow induced by picosecond laser pulses *(Russian)* 80−100714
Ag-Cu (6.6% at.wt.), melted by laser beam, microstructure and topography exam. 79−69919
Ag-Cu surface alloyed films, laser melt quenched, microstruct. 80−76423
AgBr, Herschel effect, latent image centre struct. changes under laser irrad. 80−77900
$AgGaS_2(Se_2)$, IR nonlinear material, laser induced surface damage 77−19266
Al alloy, 2024 T-351, laser surface melted, topographical charact. 79−70200
Al alloy rod, wave profiles generated by laser shock pulse 78−6125
Al alloys, laser surface melted, porosity form. 78−44279
Al, and Al-Cu(Pb) dil. alloys, pulsed ruby laser irrad., noncryst. phase form 80−35012
Al, anomalous resistive state due to light pulse 78−52157
Al, film, bleaching possibility by laser pulse, liq. metal-insulator transition 77−43498
Al foil, laser irrad., fracture props. *(Russian)* 80−108523
Al foil, transparency, UV laser irrad. effects *(Russian)* 77−1768
Al foil, with Au overlay, impedance-match expts. using laser-driven shock waves 80−29119
Al, laser irrad., charged particle emission from back side of target 78−2949
Al, laser irradiated, conditions for appearance of bleaching 78−35228
Al, laser pulse damage at 10.6 μm, single cryst. target in vac. 77−50706
Al, laser radiation absorptance at 1.064μm 79−87528
Al, laser strengthening, struct., hardness and dislocation density *(Russian)* 80−76399
Al mirror acted on by laser radiation, reflectivity meas. 79−10342
Al, multiple crater refl., effect on refl. props. 78−52596
Al, polished, target in air, refl. of CO_2 laser radiation, plasma layer form. 80−25500
Al, polycrystalline, high dose implanted with Cu and Pb, doping profile after laser pulse irradiation 80−88194
Al, reflectivity at high temps. pulsed laser heating 77−63388
Al, rhodamine 6G laser radiation interaction 80−97387

laser beam effects continued
Al, shock-waves, ultrahigh-press., laser-driven 79−55823
Al surface, CO_2 laser energy coupling into ionised blowoff material 78−72641
Al surface, laser impact, 30-350 MW cm^{-2}, surface press. meas., atm. depend. *(Russian)* 77−77328
Al surface, thermal and impulse coupling by pulsed KrF laser 80−45171
Al target interaction with pulsed CO_2 laser beam, pulse shape importance 80−108307
Al, X-ray emission spectra of CO_2 laser-irrad. targets, nonlinear processes 80−33793
Al-alloys, laser-induced, Rayleigh waves 79−51407
Al-Cu, implanted metal system, Cu redistrib. after laser irrad. 79−69163
Al-Cu (2.12 at.%), irradiated by 8J CO_2 laser pulses, metastable precipitate and amorphous phase *(French)* 78−80552
Al-Mg-Cu-Si-Cr (1,2.7,0.6,0.2wt.%), laser shock hardening of weld zones 78−39800
Al-Mg-Mn-Cr (4, 0.45, 0.15 wt.%), laser shock hardening of weld zones, exam. 78−39800
Al-Sb, laser induced surface alloy formation and Sb diffusion 80−54439
$Al_xGa_{1-x}As$ DH laser material, Ar laser induced catastrophic damage 79−86178
Al_2O_3-B_2O_3-P_2O_5 system, glass formation by laser melting 78−44074
AlSb film, laser-induced metal-semicond. transition in Al-Sb mixed film 80−6661
AlSb, laser pulse annealing, induced nucleation, crystal growth 80−84966
Ar, breakdown threshold meas. using pulsed HF(DF) laser 77−11423
Ar crystal, laser breakdown as model of fast high-energy processes, shock waves motion 79−91541
Ar gas, supersonic radiation waves generated by CO_2 laser radiation 79−10593
As-S system glasses, photostruct. transforms. under laser radiation, use in holographic recording 77−76316
As-S-Se glasses, solubility, photostimulated changes 80−24602
As-S(Se) glasses, solubility, photostimulated changes 80−24602
As-Se glassy film, photostimulated changes in microhardness 77−15723
As-Se-Cu system glass films, elec. and photoelec. props. variation with photostruct. transforms. 77−76980
As-Se-Te thin films, laser induced crystn. kinetics 77−76317
As-Se(Te) films, laser-beam recordings by thermal creation of holes 80−35010
As_2S_3, As_2Se_3, antireflection coatings, multithreshold damage meas. at HF and DF laser wavelengths 80−33058
As_2S_3 coating defects and impurities affecting damage threshold and absorptance 79−14065
As_2S_3 glass, at. struct. changes due to irrad., comp. variations and annealing 77−76323
$As_2S_3(Se_3)$ containing coatings, 10.6 μ laser damage obs. 79−14021
As_2Se_3, amorphous, laser radiation induced struct. changes, electron microdiffr. obs. 79−10874
As_2Se_3 amorphous film, comp. ratio variation by annealing and laser irrad., ESCA meas. 79−99447
As_2Se_3, AsSe and As_3Se_2 films, photostimulated changes in opt. and elec. props. 77−76979
As_2Se_3 coating defects and impurities affecting damage threshold and absorptance 79−14065
As_2Se_3, IR window coating, prep. and optical props. 77−50736
As_2Se_3, photodarkening and photostructural effects, Raman, IR and NQR studies 80−16036
Au film, inertialess glow induced by picosecond laser pulses *(Russian)* 80−100714
Au film, laser absorpt. vs. temp., calorimetric meas. 79−98423
Au film, on glass or quartz, laser-induced damage, determ. of surface fluctuation of slide 77−1279
Au, laser radiation absorptance at 1.064μm 79−87528
Au, metallised coating on polyethylene terephthalate film, fracture under laser irrad. *(Russian)* 80−76333
Au/Si films, laser-irrad., phase transform. study 80−49536
Ba atom, laser excited, ionisation studies 80−83330
BaF_2, illuminated over large area, optical strength 77−75593
BaF_2, optical breakdown threshold, illuminated spot dimension effects 78−68582
Bi surface, laser irrad., press. pulse 79−24392
C particles in flame, laser heating and sublimation 78−61012
C phenolic surface, laser-induced impulse 79−43071
CO-haemoprotein photolysis, transient Raman study, quantum yield origin 80−67155
CO_2 laser irradiation at 10.6 micron, irreversible damage threshold meas. 80−83627
CO_2 laser pulse induced vaporisation and thermoelastic press. in water 80−84227
CO_2-N_2, kinetic cooling effect by CO_2 laser radiation, temp. dependence 80−10347
CO_2-N_2 gas mixture, kinetic cooling by CO_2 laser radiation *(Russian)* 77−89229
Ca atom, laser excited, ionisation studies 80−83330
Ca+Sr, laser-induced collisions, large cross sections meas. 79−64075
Ca+Sr, laser-induced dipole-quadrupole collision 79−98207
$CaCO_3$, calcite Raman laser, methods for increasing efficiency, optical damage avoidance 77−79853
CaF_2 ⟨111⟩ oriented windows, optical distortion coeffs. at chem. laser wavelengths 79−94269
CaF_2 antireflection coated, 3.8 μm CW laser damage threshold obs. 80−33053
CaF_2, illuminated over large area, optical strength 77−75593
CaF_2, laser window material, absorpt. at CO wavelengths, calorimetric meas. 78−25911
CaF_2 low-loss laser window material, surface absorpt. meas. at 2.8 and 3.8 μm 79−94267
CaF_2, picosecond laser-induced breakdown at 5321 and 3547 Å, freq. depend. 77−63495
$CaLa_4(SiO_4)_3O$:Nd, laser damage initiating inclusions 77−68246
$Ca^+(4s\ ^2S_{1/2})+Sr(5s^2\ ^1S_0)$, laser induced charge transfer to excited electronic state 79−81274
$CdCr_2S_4$, hot pressed, Faraday effect isolation 10.6 μm, damage tests 77−46750
$CdCr_2S_4$, hot-pressed, optical isolation appl. at 10.6 μm, intrinsic absorpt. props. 78−42368
laser beam effects continued
$CdGeAs_2$, IR nonlinear material, laser induced surface damage 77−19266
n-$Cd_xHg_{1-x}Te$, conductivity inversion under laser radiation *(Russian)* 79−15198
CdP_2, surface destruction by ruby laser irrad. *(Russian)* 77−20964
CdS, defects formed by laser radiation of subthreshold intensity, bulk photo-EMF investigation 79−91098
CdS laser irrad. native defect formation, influence on photoelectric props., IR luminescence *(Russian)* 80−11039
CdS type semiconductors, bulk laser damage mechanism, photocond. meas. 80−15567
CdS_xSe_{1-x}, laser damage, self-focusing influence 78−50844
CdS_xTe_{1-x}, surface layer conductivity type inversion by ruby laser radiation *(Russian)* 77−15948
CdSb heterojunction, formation by laser irradiation, photoelec. meas. *(Russian)* 77−76915
CdSb single crystals, surface layer melting and recrystallisation due to laser irradiation *(Ukrainian)* 79−46699
CdSb:Al, p-n junction formation by laser emission, photoelectric effects *(Russian)* 80−70815
CdSb:Al(In)(Ga)(Te), p-n junction formation by laser radiation 80−96983
CdSe, diffusion of Cu, effect of laser radiation on diffusion 79−10983
CdSe film, laser annealing effects on surface struct. and elec. characts. 79−73605
CdSe film, vac. deposited, elec. resist. and surface changes by laser annealing 80−2491
n-CdSe, laser excited stimulated emission, optical gain spectrum 80−76050
CdSe, O_2 desorption by laser irradiation *(Russian)* 77−55462
CdTe, absorbing precipitates, catastrophic laser damage threshold estimate 78−25913
CdTe, laser annealing, surface layer temp. distrib. 79−74029
CdTe, laser annealing of ion bombardment damage 80−25502
CdTe, laser window material, absorbing Te inclusions, damage threshold 77−46749
CdTe, window material with absorbing inclusions, damage thresholds 77−38971
Co, ferromagnetic, EMF generation by pulsed laser irrad. 78−68021
Co film, on Si substrate, laser irrad., cellular struct. and silicide form. 80−10710
$CoCr_2S_4$, Faraday effect, appl. to CO_2 laser systems, radiation damage resist. 78−95579
Cr foil, laser irradiated, low-angle X-ray scatt., angular block misalignment and hardness *(Russian)* 80−103413
Cr-SiO, thin film, laser beam-treated, emission mode of SEM 79−28226
Cs cell, laser beam excitation, multipass, optical pumping and weak neutral current parity violation 80−58207
CsH, crystallisation in Cs+H_2 gas mixture, laser snow effect 80−40712
Cu, drilling with CO_2 laser pulses, influence of laser-supported detonation waves 79−28866
Cu film, inertialess glow induced by picosecond laser pulses *(Russian)* 80−100714
Cu foil, laser irradiated, low-angle X-ray scatt., angular block misalignment and hardness *(Russian)* 80−103413
Cu, foils and powder compacts, pulsed action of laser radiation, dimens. effect *(Russian)* 77−16437
Cu, metallised coating on polyethylene terephthalate film, fracture under laser irrad. *(Russian)* 80−76333
Cu, multiple crater refl., effect on refl. props. 78−52596
Cu, reflectivity at high temps. pulsed laser heating 77−63388
Cu, shock compressed, release isentropes, eqn. of state at high energy density *(Russian)* 80−54340
Cu target absorptivity under laser radiation action, time and temp. depend. 79−95724
Cu-Cr alloy, laser irrad., structural changes *(Russian)* 80−100247
CuO, desorpt. of ions by low power laser beam 80−80092
D_2O laser induced breakdown, comparison with H_2O 78−68453
F+Xe, enhanced quenching in intense KrF laser light, computer modelling 78−55232
Fe alloys, ferromagnetic, EMF generation by pulsed laser irrad. 78−68021
Fe, Armco, discontinuous laser beam effect on mass transfer *(Russian)* 79−33109
Fe, Armco, Nd^{3+}-glass laser light interaction in high press. N_2 medium 79−99990
Fe, atom mobility, laser irrad. effects *(Russian)* 77−59139
Fe, cast, grey, surface hardening by continuous laser emission *(Russian)* 77−70212
Fe, erosion by laser beam, in self-consistent mode *(Russian)* 77−69945
Fe, ferromagnetic, EMF generation by pulsed laser irrad. 78−68021
α-Fe, laser irrad., Mossbauer effect and positron annihilation *(Russian)* 78−19390
Fe, laser radiation absorptance at 1.064μm 79−87528
Fe surface, laser doping with V *(Russian)* 78−95065
Fe-Al (40 wt.%), defect elimination by laser irradiation *(French)* 79−65960
Fe-Mo doping surfaces of Fe with Mo under laer emission *(Russian)* 77−70211
Fe-Ni, alloy 20N24, martensitic, exam. of structure after laser treatment, and recrystallisation *(Russian)* 79−11608
Fe-Si (3 wt.%), pulsed laser induced deform. 77−36605
Fe-W(Ni), recrystallisation under laser irradiation *(Russian)* 78−35396
$Fe_{50}Co_{50}$, disordering by laser irradiation, Mossbauer transmission spectroscopy and electron microscopy study *(French)* 79−23639
GaAlAs laser, CW operation, self coupling phenomena caused by optical fibre, exam. 78−55355
GaAs, damage by 1.06 μm laser radn. 79−56890
GaAs, destruction mechanisms by intense IR laser radiation *(Russian)* 78−39633
GaAs epitaxial layer, AuGe ohmic contact production by laser alloying 78−88026
GaAs, implanted p-n junction form. using laser pulse annealing 77−15946
GaAs, ion damage, TEM study of laser annealing 80−88215
GaAs, ion implanted, laser annealing 79−69124
GaAs, ion implanted, laser induced damage and recrystallisation by freq.-doubled Nd:YAG laser 79−73197
GaAs, ion implanted, laser induced recrystn. and damage, ion backscatt. and Raman scatt. obs. 80−49248

laser beam effects continued
GaAs, ion implanted, laser annealing 80−107296
GaAs, ion implanted, mode-locked Nd:YAG laser annealing, recrystn. 80−19817
GaAs, ion implanted and laser-annealed, photoacoustic meas. 80−47117
GaAs, ion-implantation induced damage profile, ellipsometric study, annealing 80−103400
GaAs, ion-implanted, laser pulse annealing of amorphous surface layer, TEM 80−55436
GaAs, ion-implanted semiconductor, annealing, crystallisation, laser pulse energy depend. 78−34528
GaAs, laser annealed, Ga precipitation, Rutherford backscattering and TEM study 79−79127
GaAs, laser annealing, optical refl. meas. of melted layer 79−78796
GaAs, laser annealing of ion bombardment damage 80−25502
GaAs, laser heating of lightly damaged material, carrier diffusion effect 80−84809
GaAs, laser irradiated, origin of periodic surface struct. 78−91513
GaAs, laser irradiation effects, capacitance spectra 79−99987
GaAs, laser-annealed ohmic contacts for microwave devices 79−73584
GaAs, laser-induced bulk breakdown and free carrier generation, photocond. meas. 80−35018
GaAs, laser-induced recrystallisation and damage of ion-implanted amorphous samples 79−47557
GaAs p-n junction formation, laser assisted, TEM and elec. props. 79−69138
GaAs, photoabsorption and magnetoabsorption effects 77−16332
GaAs, point defects, laser annealing 80−107224
GaAs, radiative yield improvement by laser annealing 80−45128
GaAs single crystals, laser damage statistics rel. to structural defect statistics 80−91829
GaAs structures produced by laser doping, recombination radiation, anomalous temp. depend. 80−2847
GaAs, trapping levels obs. using deep level transient spectroscopy, laser irrad. effects 79−99499
GaAs vaporisation during laser annealing 80−25495
GaAs:Cr, redistrib. of Cr during laser annealing 80−88192
GaAs:Cr,Zn, implanted, doping profiles after laser annealing, elec. props. 80−2058
GaAs:Cr erosion *(Russian)* 78−2950
GaAs:Cr plane-parallel photocond. plate, oscills. in current and light intensity in laser irradiation 80−49819
GaAs:Mg(C)(Te)(Ge), ion implanted, laser annealing, ellipsometric and Hall meas. 79−73193
GaAs:Se, implantation and laser annealing 80−24476
GaAs:Se, ion implanted, laser annealing 80−24482
GaAs:Se ion implanted samples, Q-switched ruby laser annealing, improvement in elec. props. 80−100460
GaAs:Se^+, implanted semi-insulating, pulsed electron and laser beam annealing effects on elec. characts. 79−73196
GaAs:Si, ion-implanted, annealing with Nd:glass laser 79−73194
GaAs:Si, pulsed laser annealing of implanted layers, defect structure and Hall effect meas. 79−69118
GaAs:Si(Se), ion implanted, laser annealing, microwave device appl. 79−69139
GaAs:Si(Sn), ion implanted, laser annealed, high doping levels 80−88181
GaAs:Te, implanted and laser annealed, surface crystallinity, refl. and channelling meas. 79−95036
GaAs:Te, ion implanted, laser annealing 79−73192
GaAs:Te, ion implanted, surface crystallinity and stoichiometry of laser annealed samples 79−73198
GaAs:Te, ion implanted, ohmic contacts produced by laser-annealing 79−73585
GaAs:$Te^+(Se^+)(Sn^+)(Ge^+)$, ion implanted, laser annealing effect on elec. characts. 79−73195
GaAs:Te-implanted by laser-annealing, ohmic contacts 79−19658
GaAs:Zn, ion implanted, TEM study after laser and furnace annealing 80−70234
GaAs:Zn, laser annealing of implanted layers 77−55296
GaAs/AlGaAs, DH laser, degradation under Ar laser irrad. 79−98375
GaAsP photocathode, negative electron affinity process obs. by laser beam scanning *(Japanese)* 80−55262
$GaAs_{0.6}P_{0.4}$:N, isoelectronic tape by ion implantation and CO_2 laser annealing 80−24464
n-GaP, CO_2 laser induced photon drag effect 79−42589
GaP films on Si, epitaxial crystallisation by nanosecond laser pulses 80−107674
GaP, ion implanted, mode-locked Nd:YAG laser annealing, recrystn. 80−19817
$Gd_2(MoO_4)_3$, ferroelastic, laser-induced twinning 77−76422
Ge, amorphous, laser reordering of implanted amorphous layer 79−19270
Ge amorphous film, crystn. front velocity during scanned laser crystn. 80−107662
Ge, amorphous film, large aligned grain solid-phase growth during scanned laser crystallisation 80−49100
Ge, amorphous film, laser pulse annealing 80−15006
Ge, amorphous film, persistent photoconductivity, dangling bonds 80−84487
Ge, amorphous layer, comparison of laser and electron beam pulsed annealing 79−69374
Ge, amorphous layer, on single cryst. Si, heteroepitaxy by laser annealing 79−77952
Ge, amorphous thin films, fast crystn. and void precipitation in laser pulse annealing, TEM exam. 79−56086
Ge, deform. of laser induced electron-hole drops under high magnetic fields *(German)* 78−23027
Ge, elec. damage, carrier removal, mobility degradation 77−80791
Ge film, electrical cond. during laser-induced crystallisation 79−47175
Ge, IR nonlinear material, laser induced surface damage 77−19266
Ge, ion-implanted amorphous layers, melting model for pulsing-laser annealing 79−56080
Ge, laser annealing, optical refl. meas. of melted layer 79−78796
n-Ge, laser irrad., accumulation of defects, effect on elec. props. 80−107317
Ge, laser irradiation, photoacoustic detection 80−2901
Ge, laser pulse annealing, induced nucleation, crystal growth 80−84966
Ge, laser-induced bulk breakdown and free carrier generation, photocond. meas. 80−35018

laser beam effects continued
Ge, multiple refls. contrib. to thermal runaway, heat cond. eqn. 80−33044
Ge, plastic deform. under laser irrad. rel. to diamond-type structure *(Russian)* 77−56023
Ge, regrowth under laser irrad. 80−24481
Ge, surface recomb. before and after laser annealing, 10-μm transmission meas. 80−1247
Ge, thermal relaxation time, laser heating effect at 1.3K , book contrib. 80−11519
Ge:Au under laser illumination, non-equilibrium conduction 80−6896
Ge:B(P), ion implanted, laser-induced regrowth 79−69130
Ge:Ga surface, antireflection coated, laser pulse damage resistance obs. 79−14020
Ge:Hg photoconductive detector, laser damage thresholds calc. 78−90443
Ge:Pb, ion implanted damaged layer, laser induced reorder 80−84201
Ge-Fe, laser annealing of implanted ^{57}Co sources, Mossbauer obs. 80−39139
Ge-S(As)-Se glasses, solubility, photostimulated changes 80−24602
Ge-Se(Te) films, laser-beam recordings by thermal creation of holes 80−35010
$GeSe_2$ amorphous film, laser induced light absorpt. oscillation, exciton model 80−50446
$GeSe_2$ amorphous film, laser induced oscillatory phenomena 80−84711
$GeSe_2$ chalcogenide film, struct. changes due to laser induced transmittance oscill., SEM obs. 78−6240
$GeSe_2$ film, light induced transmittance oscillations 77−81171
$Ge_{0.45}Se_{0.55}$-As_2S_3, antirefl. coating, performance at 3.8, 5.3 and 10.6 μm 77−61964
H_2 ortho-para transition as means of observing weak interaction parity nonconservation *(Russian)* 80−900
H_2O, laser induced breakdown, comparison with D_2O 78−68453
He, laser-induced breakdown 80−96339
$He^*(^3S)+Ar+\hbar\omega \rightarrow He+Ar^+(^2P)+e^-$, intense laser radiation assisted collisional ionis. 79−76497
HgBr(B→X) radiative lifetime, laser induced fluorescence 77−30900
$Hg_{1-x}Cd_xTe$, avalanche formation, high intensity IR transmission limit 79−78684
$Hg_{1-x}Cd_xTe$, Faraday effect at CO_2 laser freq. 78−64348
n-InAs, avalanche formation, high intensity IR transmission limit 79−78684
InP:$S^+(Se^+)$, ion-implanted VPE layers, laser annealing, elec. and struct. anal. 79−73199
InP:Se, implantation and laser annealing 80−24476
$InP/In_{1-x}Ga_xAs_yP_{1-y}$ heterostruct., optically induced degradation 79−86791
InSb, Auger-governed decay of laser-induced plasma, optical probing 80−76105
InSb, avalanche formation, high intensity IR transmission limit 79−78684
p-InSb, low-resistivity n-type layer form. by laser pulse irrad. 77−69944
n-InSb, Shubnikov-de Haas effect expts. on optically heated electrons 79−73529
InSe luminescent film, production and characterisation *(Russian)* 78−39581
InSe, photoconductivity anisotropy at high optical excitation levels *(Russian)* 80−103721
In_2Se with p-n junctions produced by laser radiation, photoelec. characts. *(Russian)* 78−56226
$In_{1.9}Sn_{0.1}O_3$ laser-damage-resistant transparent conductive coatings, appl. in Pockels cells 79−50333
K vapour, mag. props. changes under laser irrad., induced EMF obs. 80−100059
$KAlSi_3O_8$, feldspar microwedge, melting by CO_2 laser, deform. of IR absorpt. spectra 77−19984
KBr, colour centre form. under polarised UV irrad., dichroism in absorption spectra 80−107232
KBr, optical damage threshold anisotropy, polarised laser radiation 77−16433
KBr, plate, distortions due to 10.6 μm laser irrad., interferometric obs. 78−46697
KBr, transparent, plasma form. at surface due to CO_2 laser irrad. 78−60534
KCl, bulk and surface absorpt. of CO_2 laser radiation, calorimetric data analysis 78−25904
KCl, bulk and surface absorpt., 2 to 10 μm, calorimetric meas. 78−71160
KCl, cryst., optical breakdown plasma effects 77−66558
KCl, cryst. laser irrad. effects, electron microscopic obs. 77−73192
KCl crystal, F-H centre formation by opt. conversion of self-trapped excitons 78−91335
KCl diamond turned window surfaces, 10.6 μm pulsed laser damage 77−50704
KCl, internal damage threshold for CO_2 laser pulses rel. to absorption 77−75594
KCl, laser produced shocks rel. to material damage 78−31285
KCl, laser window material, absorpt. at CO wavelengths, calorimetric meas. 78−25911
KCl laser-induced breakdown fields rel. to wavelength and focal spot radius 80−35019
KCl low-loss laser window material, surface absorpt. meas. at 2.8 and 3.8 μm 79−94267
KCl, optical breakdown, γ-irrad. effects, rel. to appl. in high power lasers 77−8507
KCl, optical breakdown from 0.53-10.6 μm 80−7292
KCl, optical breakdown threshold, illuminated spot dimension effects 78−68582
KCl plate, distortions due to 10.6 μm laser irrad., interferometric obs. 78−46697
KCl, surface radiative absorption meas., acoustic technique 77−3596
KCl, TEA-CO_2 laser irradiated, damage struct. optical microscopy obs. 77−19983
KCl window with antirefl. coating, laser damage at 10.6 μm 77−61992
KCl:Na, F_A reorientation and $F_A \leftrightarrows F'_A$ conversions, laser induced, kinetic studies 80−10547
KD_2PO_4, transparent dielec., thermal analysis of laser-induced damage 80−66336
KH_2PO_4, cryst. laser irrad. damage threshold, surface finish and defects effects *(German)* 78−59058

laser beam effects continued
KH_2PO_4 crystal, laser freq. conversion to produce UV coherent pulse, 45 GW, for laser fusion 80−69450
KH_2PO_4, picosecond laser induced breakdown at 5321 and 3547 Å, freq. depend. 77−63495
KH_2PO_4, real structure influence on optical strength 79−7187
KNO_3, aq. solns., laser induced breakdown 79−87530
K_2O-B_2O_3 glass, laser decolorisation of colour centres 79−43008
KOH, aq. solns., laser induced breakdown 79−87530
Kr-Ar, phase matched, generation of Lyman-α radiation 80−91845
Kr-Xe, phase matched, generation of Lyman-α radiation 80−91845
LaF_3-MgF_2 multilayer mirrors, optical strength in Xe laser 77−27294
Li vapour, photoionisation, cross-section obs. by absorpt. spectroscopy 77−71782
LiF, laser irrad., Li^+ emission, time and energy characts. 80−100710
LiF, laser-irrad., emitted electrons and positive ions delay 80−29830
LiF, optical damage threshold anisotropy, polarised laser radiation 77−16433
LiF, picosecond laser-induced breakdown at 5321 and 3547 Å, freq. depend. 77−63495
LiF single cryst. with vac. deposited Bi film, surface failure induced by laser impulse *(Russian)* 77−35585
$LiNbO_3$, chemical control of optical damage, due to laser beams 78−38056
$LiNbO_3$, laser induced optical damage, pyroelec. contrib., electrostatic obs. 78−37935
$LiNbO_3$, laser-induced optical damage, electrostatic obs. 78−18030
$LiNbO_3$, light induced ultrasonic wave velocity change, refractive index 80−97236
$LiNbO_3$, optical stability to laser pulse, 1.54 μm 79−3734
$LiNbO_3$, optical strength, surface layer influence 78−50843
$LiNbO_3$, optical strength anisotropy, excitation of second harmonic 79−69923
$LiNbO_3$, photoinduced grating contrib. to acoustic wave vel. 77−77154
$LiNbO_3$, pyroelectric induced optical damage 78−52446
$LiNbO_3$:Fe, local photodeform. and photorefraction 80−16003
$LiNbO_3$:Fe, refractive index change induced by light irrad. *(Japanese)* 79−65824
$LiNbO_3$:Ti, in-diffused waveguides, optical damage thresholds 79−46033
$LiNbO_3$, Li_2O diffusion for chemical control of laser induced optical damage 78−46693
Mg atoms, cooling to broad band reson. light press. 80−48835
Mg^+, Penning trap, laser cooling, optical spectrum from laser freq. sweeping 80−52916
MgF_2 film, 1064 nm 150 ps laser pulse damage rel. to OH content and refr. index 79−14016
$MgSi_2$, laser irrad. induced form., cryst. microstruct. 80−35011
Mo film, on Si substrates, laser irrad., cellular struct. and silicide form. 80−10710
Mo, laser irradiation, shock wave formation relationships, surface propagation, elastoplastic wave effects 79−55825
Mo single cryst., laser induced dislocation struct. 80−70210
Mo single crystal surface, shock wave form. due to laser radiation interaction 77−81180
Mo wire, laser shock induced microstructural changes, rel. to explosive shock induced phenomena 78−67768
N_2, breakdown threshold meas. using pulsed HF(DF) laser 77−11423
N_2 cryogenic liq., laser sonoluminesc., at elevated hydrostatic press. 80−71498
N_2, low threshold breakdown, near target, by pulsed laser radiation *(Russian)* 78−22594
Na atom, cyclic interaction with circularly polarised laser radiation 80−78581
Na atoms cooling by resonant laser radiation *(Russian)* 80−74155
Na free atom cooling in resonant laser field at scanning freq. *(Russian)* 79−72272
Na neutral atom beam, focusing and defocusing forces, radiation press. from CW dye laser 80−52944
Na, neutral atom production by pulsed laser heating 77−85848
Na vapour, assoc. ionis. by CW dye laser and applics. *(Japanese)* 80−5515
Na vapour, laser induced diffusion *(Russian)* 80−6195
Na vapour, photoionisation, cross-section obs. by absorpt. spectroscopy 77−71782
Na+Na, crossed-beam collision, laser-induced Penning and assoc. ionisation, struct. obs. 80−83476
NaCl, bulk and surface absorpt., 2 to 10 μm, calorimetric meas. 78−71160
NaCl, CO_2 laser pulse transmission, breakdown dynamics near surface in gaseous media 79−45986
NaCl cryst., laser pulse breakdown freq. depend., self-focusing elimination 77−55855
NaCl, cryst., optical breakdown plasma effects 77−66558
NaCl, damage caused by CO_2 laser radiation 77−90222
NaCl, damage induced by CaF_2:Er^{3+} laser radiation at 2.76 μm 79−91539
NaCl, dislocation density, laser beam effect, electron microscopy of etch pits 77−11553
NaCl, F-centers, laser irrad. optical bleaching kinetics 80−66244
NaCl, illuminated over large area, optical strength 77−75593
NaCl, internal damage threshold for CO_2 laser pulses rel. to absorption 77−75594
NaCl, laser damage, phenomenological theory 80−19836
NaCl, laser damage simulation, optical breakdown probability at 6943 Å 77−12470
NaCl, laser irradiated, electron emission, surface layer electric discharge effects 79−74032
NaCl laser-induced breakdown fields rel. to wavelength and focal spot radius 80−35019
NaCl, laser-induced damage threshold variations 80−14380
NaCl, optical breakdown threshold, illuminated spot dimension effects 78−68582
NaCl, optical breakdown from 0.53-10.6 μm 80−7292
NaCl, optical strength, effect of irrad. in mechanically stressed state 80−80695
NaCl particles, laser irradiated, white light flash obs. 79−15565
NaCl, picosecond laser-induced breakdown at 5321 and 3547 Å, freq. depend. 77−63495
NaCl, plate, distortions due to 10.6 μm laser irrad., interferometric obs. 78−46697

laser beam effects continued
NaCl, transparent, plasma form. at surface due to CO_2 laser irrad. 78−60534
NaCl(I), aq. solns., laser induced breakdown 79−87530
NaF, antireflection coating, multithreshold damage meas. at HF and DF laser wavelengths 80−33058
NaF coating defects and impurities affecting damage threshold and absorptance 79−14065
NaF, IR window coating, prep. and optical props. 77−50736
NaF_2, picosecond laser-induced breakdown at 5321 and 3547 Å, freq. depend. 77−63495
Na_2O-CaO, enhanced failure by combined pulse and CW laser 79−29182
Na_2O-CaO-SiO_2, glass, formation of colour centres, linear absorption of UV radiation 80−103328
Nb films, ion beam sputtered, supercond., laser annealing effects 80−97024
Nb-Fe, formed on laser irradiation of Nb-Fe interface, Mossbauer spectra *(Russian)* 79−60560
Nb-Nb(Nb_3Sn) supercond. point contacts, crit. currents, effect of laser radiation *(Russian)* 79−28484
Nb_3Sn-Nb_3Sn supercond. point contacts, crit. currents, effect of laser radiation *(Russian)* 79−28484
Nd laser, excited stimulated Mendelstam-Brillouin scatt. phase fluctuations *(Russian)* 80−89014
Nd:glass, laser bulk damage rel. to temp. and conc. 79−14023
Ne, at. spectra, Doppler broadening compensated by light shifts 79−41136
Ne, hollow cathode discharge, role of Penning ionisation of minor species 79−86633
Ne spectral line broadening as diagnostic for compressed laser fusion targets 79−98979
Ni, ferromagnetic, EMF generation by pulsed laser irrad. 78−68021
Ni, ion-implanted and virgin, laser irrad. effect, epitaxial lattice regrowth 80−108306
Ni, laser irrad., elec. cond. recovery *(Russian)* 77−55512
Ni, mass transfer parameters, lattice defect effects under laser pulse action *(Ukrainian)* 80−6537
Ni, metallised coating on polyethylene terephthalate film, fracture under laser irrad. *(Russian)* 80−76333
Ni_xP_{1-x} surface, laser produced ripple patterns 77−79878
$NiSi_2$, amorphous, crystallisation by energy beam annealing 79−69012
P-Se glasses, solubility, photostimulated changes 80−24602
PLZT pyroelectric detectors, piezoelectric oscillations, in response to CO_2 laser pulses 79−61305
Pb, erosion by laser beam, in self-consistent mode *(Russian)* 77−69945
Pb, evaporation under action of laser beam, recoil press. behaviour 80−25501
Pb, laser irradiated tunnel junction, nonequilibrium quasi-particle distrib. function, thermal regime *(Russian)* 79−42700
Pb, shock compressed, release isentropes, eqn. of state at high energy density *(Russian)* 80−54340
Pb, surface, Q-switched ruby laser irrad., recoil momentum 79−65961
Pb, X-ray emission spectra of CO_2 laser-irrad. targets, nonlinear processes 80−33793
PbF_2, antireflection coating deposition technique, 2.87 μm laser damage threshold 80−33264
PbF_2, laser damage resistant antirefl. coatings for 16 μm region 79−31963
PbI_2-Ag light sensitive system, photochem. conversion process under continuous laser radiation, nonreciprocity *(Russian)* 77−79179
$PbMoO_4$, elastic wave excitation and amplification by laser radiation 80−103419
$Pb_{0.8}Sn_{0.2}Te$:In, implanted thin epitaxial films, laser annealing 79−65104
$Pb_{1-x}Sn_xTe$, surface photo-EMF under laser excitation conditions 80−6897
Pd coated Si wafers, interference effects on irrad. with laser beam 80−66333
Pd film, on Si substrate, laser irrad., cellular struct. and silicide form. 80−10710
Pd, silicide formation due to laser and electron beam annealing 80−84849
Pd-Si, amorphous thin films, laser irrad., metastable phases 80−96622
Pd-Si layers, form. by laser irrad. of Pd film on Si substrate 79−99438
Pd_2Si, form. by laser irrad. of Pd film on Si substrate, Rutherford backscatt. obs. 79−42317
Pd_4Si and Pd_2Si, amorphous, crystallisation by energy beam annealing 79−69012
Pt films, optical props. and radiation stability 80−34999
Pt, silicide formation due to laser and electron beam annealing 80−84849
Pt-Si, amorphous thin films, laser irrad., metastable phases 80−96622
Pt-Si layers, form. by laser irrad. of Pt film on Si substrate 79−99438
Pt-Si Schottky barriers on Si, laser formation and characts. 80−60079
Pt-Si:As, silicide form. during laser irrad., p-n junctions and ohmic contacts 80−84397
Rb vapour, mag. props. changes under laser irrad., induced EMF obs. 80−100059
Re, thin film preparation, by laser melting *(Japanese)* 79−78909
S_2 mol. $B^3\Sigma_u^- \rightarrow X^3\Sigma_g^-$ fluorescence induced by N_2 laser *(Japanese)* 80−14175
SF_6, film, IR laser induced processes at low temp. and under ultrahigh vac. 79−69914
SF_6, gas, heating effect on optical props., transmittance meas., CO_2 laser IR irradiation 79−27737
SF_6, isotope separation, TEA CO_2 laser irradiation *(Japanese)* 80−11885
SF_6, laser excitation in low temp. matrices, possible isotope selectivity 79−36788
SF_6, multiple-photon dissoc. rate determ. 77−60079
SF_6, surface ionisation on W cathode, laser irrad. effects 80−93440
Sb-S films, laser-beam recordings by thermal creation of holes 80−35010
$Se_{1-x}Te_x$, amorphous film, photo-crystallisation 80−59839
Si, ^{75}As implantation, scanned CW electron beam annealing 79−99225
Si, ^{75}As implanted, comparison of effects of pulsed ruby laser and pulsed electron beam annealing 79−69135
Si (100), self-ion implanted, laser annealing, channelling and TEM meas. 80−24466
Si, amorphous, implanted, struct. transition under laser irrad. 79−50992

laser beam effects continued
Si, amorphous, ion implanted, laser annealing, reflectivity meas. 80−29039
Si, amorphous, Raman spectra, vibrational properties 79−99881
Si, amorphous, small dia. laser beam annealed, temp. distrib. and microstructure 79−73098
Si, amorphous, substrate orientation effect on regrowth by laser pulses, channeling, backscatter 80−84409
Si, amorphous and crystalline, heating by Q-switched laser radiation 80−84963
Si, amorphous deposited, laser induced epitaxy 79−69372
Si, amorphous film, selective laser recrystn. over heavily doped lines 80−84947
Si amorphous films, laser beam annealing, optical information storage possibilities 79−87515
Si, amorphous laser effects 79−69921
Si, amorphous layer, comparison of laser and electron beam pulsed annealing 79−69374
Si, amorphous layer, epitaxial growth by laser annealing 78−79899
Si amorphous layers, glow-discharge, laser-annealed, elec. props. 80−75661
Si, amorphous layers, laser induced As profile broadening 79−95045
Si amorphous layers, on Si substrates, deposited and ion-implanted, laser-annealing behaviour 79−69373
Si, amorphous layers, RF-sputtered on sapphire, crystallisation by CW ion laser annealing 80−80109
Si, amorphous layers, recrystallisation, pulsed laser annealing 80−65404
Si, amorphous-implanted, laser induced struct. changes related to pulse shape 79−69123
Si, annealing, using laser pulses, impurity incorporation at melt-cryst. interface 80−59504
Si, CW laser annealed, defect luminesc. 80−50388
Si, crucible grown, virgin and implanted laser irradiation effects on surface struct. 80−92768
Si, cryst. and amorphous surface layers, ruby laser pulse effects 79−69920
Si, crystalline, repeatable order-disorder transformation 80−39150
Si, deep amorphous layer implantation, laser effects, channelling diffr. study 80−25494
Si, defect annihilation depth by pulse laser annealing 80−16128
Si, dense plasma dynamics during pulsed laser annealing, carrier density, recombination 80−84479
Si, destruction mechanisms by intense IR laser radiation *(Russian)* 78−39633
Si, dopant segregation by pulsed-laser annealing, test case for thermal melting concept 80−24489
Si, elec. damage, carrier removal, mobility degradation 77−80791
Si, electronic defect levels in self-implanted CW laser annealed samples 79−87053
Si epitaxial layer regrowth due to laser annealing mechanism, liquid and solid phase regimes 80−100712
Si, epitaxial regrowth of thin amorphised layers by laser annealing, absorpt. coeff. influence 79−46968
Si film, crystallographic orientation using surface relief grating and laser crystn. 79−95277
Si, furnace preannealed (111) ion implanted, laser irrad. 80−65015
Si, graphoepitaxy on fused SiO_2 using surface micropatterns and laser crystn. 80−70554
Si high efficiency solar cells, laser annealing, reviews 80−93976
Si, hydrogenated amorphous, laser annealing 80−100713
Si, implanted amorphous, comparison of laser and thermal annealing 79−70084
Si, implanted crystal, laser induced annealing and diffusion behaviour 80−88202
Si, implanted semiconductors, laser annealing, review 80−107301
Si, implanted with low solubility dopants, laser annealing, TEM study 80−70233
Si, impurity solubility limit after laser induced melting 80−107426
Si, ion damage TEM study of laser annealing 80−88215
Si, ion implantation and pulsed laser annealing of group III and group V dopants, supersat. alloy form. 80−54267
Si ion implanted, amorphous to crystalline transition due to laser irrad. 80−103451
Si, ion implanted, CW laser annealing 80−92550
Si, ion implanted, difference between ruby and Nd:YAG laser annealing 79−37723
Si, ion implanted, dynamic behaviour of pulsed-laser annealing, time depend. optical reflectance meas. 79−60393
Si, ion implanted, extent of annealed or melted regions as function of pulsed laser irrad. energy 79−74025
Si, ion implanted, laser annealing, periodic regrowth phenomena 78−67724
Si, ion implanted, laser annealing 79−69124
Si, ion implanted, laser annealing 79−69126
Si, ion implanted, laser annealed, elec. characterization 79−69137
Si, ion implanted, laser annealed, deep levels study 79−69457
Si, ion implanted, laser annealed, elec. props. and annealing kinetics 79−69508
Si, ion implanted, laser annealed microstructure 79−74027
Si, ion implanted, laser-annealed, theoretical anal. of thermal and mass transport 78−91364
Si, ion implanted, mode-locked Nd:YAG laser annealing, recrystn. 80−19817
Si, ion implanted, pulsed-laser annealed, Raman obs. 79−73189
Si, ion implanted, scanning CW and pulsed laser annealing 80−92549
Si, ion implanted, SiO_2 antireflection coating effect on CW laser annealing 80−49242
Si, ion implanted, transient optical reflectivity study of laser annealing, thresholds and kinetics 79−60390
Si, ion implanted and laser annealed, characterisation 80−29043
Si, ion implanted layers, laser annealing 78−67732
Si, ion-implanted, annealing using scanning CW laser system 80−100265
Si, ion-implanted, effect of free-carrier absorpt. on annealing by pulsed laser 79−55757
n-Si, ion-implanted, elec. characts. after laser annealing 80−88562
Si, ion-implanted, laser annealing at 1.06 μm, computer simulation 79−47556
Si, ion-implanted, laser annealing, appls. 79−73202
Si, ion-implanted, laser irrad., characterisation by X-ray topography 79−74026
laser beam effects continued
Si, ion-implanted, period surface struct. in laser annealing, new expt. evidence 80−29836
Si, ion-implanted, pulsed-laser annealing, dynamic behaviour by optical reflectance meas. 79−69122
Si, ion-implanted amorphous layers, melting model for pulsing-laser annealing 79−56080
Si, ion-implanted amorphous, laser epitaxial recrystallisation threshold energy 80−70571
Si ion-implanted dopant redistribution under laser annealing 80−70242
Si ion-implanted laser-annealed solar cells 80−93881
Si, ion-implanted layers, crystn. by ns laser pulses, TEM and RHEED 80−100421
Si, ion-implanted layers, epitaxial regrowth by laser beam and flash annealing 80−100420
Si, ion-implanted semiconductor, annealing, crystallisation, laser pulse energy depend. 78−34528
Si, laser annealed, charge collection microscopy, carrier lifetime determ. 79−69136
Si, laser annealed, EPR and cyclotron resonance 80−34773
Si, laser annealed, elec. props. 79−69609
Si, laser annealed, solubility of impurities 79−69247
Si, laser annealed ion implanted, elec. props., melting threshold 80−10969
Si, laser annealing, nonlinear dynamic transport processes 80−93437
Si, laser annealing, optical refl. meas. of melted layer 79−78796
Si, laser annealing, surface layer temp. distrib. 79−74029
Si, laser annealing after ion implantation, temp. distrib. 80−54265
Si, laser annealing at 1.06 μm, free carrier absorpt. role 80−24964
Si, laser annealing for improved stacked-struct. oxide quality 80−65386
Si, laser annealing mechanisms, disordered overlayers, crystalln. 80−84967
Si, laser annealing of ion bombardment damage 80−25502
Si, laser annealing of point defects 80−107224
Si, laser heating of lightly damaged material, carrier diffusion effect 80−84809
Si, laser induced cryst. regrowth 79−69913
a-Si, laser induced crystallisation mechanism, epitaxial regrowth 80−84962
Si, laser induced damage, effect of applied electric field 77−40310
Si, laser induced dense plasma, dynamics 80−65612
Si, laser induced formation of metal silicides 79−70366
Si, laser induced reactions with metal films, silicide formation 79−70365
Si, laser induced surface deforms. 79−82262
p-Si, laser irrad., accumulation of defects, effect on elec. props. 80−107317
Si, laser irrad., anisotropic melting and epitaxial regrowth, surface struct. 79−33163
Si, laser irradiated, positron annihilation crystal struct. imperfection monitoring 80−11506
Si, laser pulse induced amorphous to cryst. transition, thickness depend. 78−47678
Si, laser pulse train shaping for polycrystal recovery in self-ion implanted samples 79−47555
Si, laser pulsed annealing, carrier diffusion role in lattice heating 80−45172
Si, laser pulsed heating, lattice temp., Raman meas. 80−80780
Si, laser-induced bulk breakdown and free carrier generation, photocond. meas. 80−35018
Si layers amorphized by molecular ions, laser annealing 80−103379
Si, melting and resolidification, laser-induced, surface morphology 79−87529
Si, minority carrier lifetime improvement through laser damage gettering 80−65589
Si, misfit dislocations removal by laser irrad. 79−83063
Si n-p planar diode, Al layer covered, laser beam produced alloy areas, characterisation 79−69594
Si, new materials properties achievable by ion implantation doping and laser processing 79−69127
Si, non thermal laser induced ordering, plasma life time, phonon interactions 80−84481
Si on sapphire, laser annealing dynamics epitaxial regrowth, optical reflectivity 80−29285
Si on sapphire, stress-relieved regrowth by laser annealing 80−65389
Si on sapphire film, laser annealing non-thermal theory expt. test 80−89273
Si, order-disorder transformation, pulsed UV laser induced 79−60400
Si p-n homoepitaxial junctions, elec. and struct. characts. 80−6662
Si p-n junction formation, laser assisted, TEM and elec. props. 79−69138
Si, photoacoustic signal changes assoc. with crystallinity, recrystallisation after laser annealing 80−16127
Si photocathode, negative electron affinity process obs. by laser beam scanning *(Japanese)* 80−55262
Si, plasma effects during pulsed laser annealing 80−84480
Si, point defects, H passivation 80−75515
Si, polycryst., recrystallisation, charges at laser recrystallised poly Si/insulator interface 80−54789
Si polycryst. film, ion-implanted, pulsed laser annealing 79−77612
Si polycrystalline film resistivity reduction by Nd:YAG laser annealing 80−100539
Si, polycrystalline layer, laser-induced single cryst. transition, RHEED and backscatt. obs 78−87704
Si processing technology, appls. of scanning CW lasers and electron beams 80−100932
Si, pulsed laser annealing, nonthermal, plasma annealing 80−25498
Si, pulsed laser annealing, mechanism 80−25739
Si, reflectivity time dependence during pulsed laser annealing 80−66214
Si, regrowth under laser irrad. 80−24481
Si, self implanted, and additional impurity implanted laser induced recrystn., threshold power density 79−69131
Si, self-implanted, ⟨100⟩ and ⟨111⟩, crystallised layers by laser annealing, struct. 78−47644
Si, self-implanted layer, grain size, laser irrad. energy density depend. 78−72012
Si, self-ion implanted, amorphous to polycrystalline transition induced by laser beam 77−84771
Si single crystals, laser damage statistics rel. to structural defect statistics 80−91829
Si, slip dislocation nucleation during laser annealing 80−84179

laser beam effects continued
Si, solar cell, open-circuit voltage at ultrahigh light intensities, plasma reflection effects 80−96928
Si surface formation during etching of thin thermally grown oxide layers, ellipsometric control *(Russian)* 80−104315
Si, surface structure changes by laser pulses 78−14548
Si, surface structures after pulsed laser annealing, LEED obs. 80−54494
Si, surface topography changes due to pulsed laser annealing 80−84348
Si, temp. rise induced by laser beam, nonlinear heat cond. 79−11487
Si, temperature during CW laser heating, Raman scatt. meas. 80−76109
Si temperature field determ. under laser irradiation *(German)* 80−25496
Si wafer processing, CO_2 laser heating dynamics 80−76106
Si:Ar, As, ion implanted, laser annealing, doping profiles, channelling 80−97506
Si:Ar, ion-implanted, epitaxial regrowth by laser annealing, microstruct. 80−84404
Si:As, CW CO_2-laser annealing, comparison with thermal annealing 80−84193
Si:As, CW laser annealing mechanism, annealed spot size, solid phase epitaxial regrowth 79−78798
Si:As, diffused, laser irrad., stability study 80−65547
Si:As, diffusion of implanted As induced by laser annealing 77−89590
Si:As, dual wavelength, laser ion implantation damage annealing 79−69117
Si:As, high-dose implanted, irrad. time and subsequent heat treatment effects on laser annealing 80−29041
Si:As, implanted, laser annealing reduction in defect conc. 77−62559
Si:As, ion implanted, amorphous-cryst. transition induced by multiple-pulsed ruby laser 79−90555
Si:As, ion implanted, laser scanning apparatus for annealing 78−34526
Si:As, ion implanted, laser annealed, lattice defects, epitaxial regrowth 80−103334
Si:As, ion implanted, pulsed laser annealing, partial solid-state regrowth 80−103591
Si:As, ion implanted, recrystallisation by free running ruby laser 79−73185
Si:As, ion implanted layers in device structures, boundary effects in laser annealing 79−73188
Si:As, ion-implanted, CW IR laser annealing 80−34022
Si:As, ion-implanted, channelling anal. of CW Ar laser annealing 79−73186
Si:As, ion-implanted, laser annealing, channelling obs. of As cluster form. 79−69128
Si:As, ion-implanted, laser recrystallisation by freq.-doubled Nd:YAG laser 79−77613
Si:As, ion-implanted layers, ellipsometric anal. of laser annealing 79−73190
Si:As, laser annealing, channelling, optical obs., and resist. meas. 79−1444
Si:As, laser annealing of implanted layers 77−55296
Si:As, laser induced diffusion and annealing processes 77−69943
Si:As, melting by high power ns laser pulsing, As diffusion 78−79789
Si:As, p-n junction form. by laser annealing, space charge region, effects on reverse current 80−54772
Si:As, solid solubility of As determ. by ion implantation, CW laser annealing 80−6517
Si:As ion implanted, laser induced diffusion modelling 80−24672
Si:As ion implanted layers, annealing by CO_2 laser, doping profile shift 80−84965
Si:As laser annealing, heat and mass transport model 80−92546
Si:As wafers, laser annealing, Rutherford backscatt., optical, and TEM obs. 79−1445
Si:As^+, implanted, CW laser annealing, electron-beam induced current 80−100709
Si:As^+ layers, laser annealing, optical constants, ellipsometry observation 80−34024
Si:As^+(P^+) ion implanted, laser annealed, correlation of struct. and elec. props 80−70855
Si:As^+(P^+)(Sb^+), implantation damage removal by laser irrad. and its thermal stability, TEM study 79−74024
Si:As(B), implanted CW laser annealing, elec. props., cryst. struct. and limitations 80−39131
Si:As(B), ion implanted, pulsed laser annealing appl. to device fabrication 79−73180
Si:As(B), ion-implanted, scanned laser and electron beam annealing 79−73182
Si:As(B)(P), ion-implanted polycrystalline films, laser annealing 79−73181
Si:As(P), ion implanted, TEM study after laser and furnace annealing 80−70234
Si:As(P) film, polycryst. laser annealed, resistivity changes during thermal annealing 79−91163
Si:As(Pb), ion-implanted, impurity redistrib. during laser irrad. 80−100280
Si:As(Sb), implanted, pulsed ruby-laser annealing, Rutherford backscatt., TEM and ion channelling study 79−86805
Si:As(Sb), ion implant lattice location after pulsed ruby laser annealing 79−73204
Si:As(Sb), ion implanted, lattice location of impurities after pulsed laser annealing 80−88196
Si:As(Sb), ion-implanted, CO_2 laser annealing 79−73183
Si:B, implanted laser annealed, lattice strain, X-ray study 80−96554
Si:B, implemented laser annealed samples, unidirectional contraction 78−71747
Si:B, ion implanted, laser annealing 78−34525
Si:B, ion implanted, laser annealed, thermal annealing effect 79−73191
Si:B, ion implanted, laser annealed, IR and Raman spectra 79−73914
Si:B, ion implanted, laser annealed, Raman scatt., Fano interactions, lattice damage 79−78711
Si:B, ion-implanted, annealing by incoherent light source 79−19267
Si:B, laser damage obs. by DLTS 78−76023
Si:B, p-n junction form. by B deposition and laser-induced diffusion 78−87690
Si:B,P, double implanted layer, n-p-n struct., single pulse laser annealing 80−49247
Si:B MOS structures, implanted laser beam irrad. effects on interface electrophys. props. 79−1627
Si:B(P), ion implanted crystalline and amorphous laser annealing 80−97509
Si:B(P)(As)(Cu)(Fe), dopant profile changes induced by laser irrad. using SIM and backscatt. meas. 79−69148
Si:B(P)(As)(Sb), ion implanted, redistrib. of dopants by pulsed laser annealing 79−7620
Si:B(P)(As)(Sb)(Cu)(Fe), ion implanted, doping profile, pulsed laser annealing effects 80−88197
Si:Bi, ion implanted, channelling obs. of pulsed Q-switched ruby laser annealing 80−59542
Si:Cu, segregation effects after laser pulse melting 79−1843
Si:Fe, ion implanted, laser annealing studies using Mossbauer spectroscopy 80−79827
Si:Fe, laser annealing of implanted ^{57}Co sources, Mossbauer obs. 80−39139
Si:Fe, laser implantation, Mossbauer obs. 80−39125
Si:Fe(Cu), impurity segregation and microstructural changes by pulsed laser irrad. 79−82254
Si:Fe(Cu)(Pt), implant redistrib. and enhanced solubility following laser irrad. 79−69129
n-Si:Ga laser doped, segregation, Rutherford backscattering 80−103483
Si:Ga(As), laser-doped, impurity distrib., Rutherford backscatt. and channelling anal. 80−59507
Si:Ga(As) 80−19824
Si:H, amorphous, glow discharge deposited, laser annealing 80−49104
Si:In, implanted, laser annealing 79−52050
Si:N, laser-annealed, Jahn-Teller distorted donor, EPR meas. 80−84642
Si:O, incorporation of O during pulsed-laser irrad. 80−96557
Si:O(C), implant redistribution, annealing effects, SIMS meas. 80−96561
Si:P, depth of melting produced by pulsed-laser irrad. 79−55756
Si:P, diffusion-doped laser irradiation effects, electrical reactivation of P 80−39124
Si:P, distrib. of implanted impurity after laser annealing, e.s.r. and neutron activation analysis 77−4122
Si:P, implanted, SiO_2-film-covered, laser annealing behaviour 79−86808
Si:P, implanted, two-stage laser annealing of lattice disorder 79−1452
Si:P, ion implanted, irrad. by laser of different wavelengths, annealing behaviour 79−69132
Si:P, ion implanted, laser and thermal annealing, elec. cond. and Hall effect meas. 79−69145
Si:P, ion implanted, regrowth of damage structs. by laser annealing 80−107289
Si:P, ion implanted, selective annealing of amorphous layers by Nd^{3+}:YAG laser irrad. 79−14823
Si:P, ion implanted with small doses, defect annealing by nanosecond laser pulses 80−107297
Si:P, ion-implanted, laser annealing 80−10564
Si:P, ion-implanted and unimplanted, laser annealing, photoluminesc. study 80−2049
Si:P, polycrystalline laser recrystallised film on Si substrate, cryst. struct., thermal oxidation 80−65391
Si:P, thermally annealed, high dose, ion-implanted, dislocation array prevention by prior laser annealing 79−73187
Si:P(As)(B), nonequilibrium solid solutions obtained by heavy ion implantation and laser annealing 80−92544
Si:Pb, low-solid solubility ion-implanted, pulsed and continuous laser annealing and furnace annealing comparison 79−73184
Si:Pt, implanted and laser annealed, segregation and increased dopant solubility 80−65016
Si:Sb, laser doping, evaporation loss and diffusion of Sb, under pulsed laser irrad. 80−59508
Si:Sb, redistribution of thin impurity layers after laser annealing, theoretical model and expt. results 79−69147
Si:Sb wafers, laser annealing, Rutherford backscatt., optical, and TEM obs. 79−1445
Si:Sb(Ga)(Bi)(In), dopant solubility limit, laser irrad. effects 80−84295
Si:Te, laser melting, surface Te atom accumulation, profiles 80−100258
Si:Te implanted, laser annealing, Mossbauer obs. 80−39127
Si:Zn, implanted atom diffusion during laser annealing 79−37725
Si-H (up to 15 at.%), amorphous, ion implanted, laser annealing obs. 79−69133
Si-metal thin film reactions, laser annealing 79−70364
Si-Pt(Ni)(Pd), laser-induced reactions of metal films with Si, surface struct. obs. 79−19471
Si-saphhire, Si ion implanted wafer, laser annealing 79−99989
Si-Te, laser and thermal annealing, Mossbauer resonance lines 79−99810
SiC ion implanted, laser induced ordering and defects 80−84754
SiC(6H), ion-implanted, laser-induced recrystallization and defects 80−44221
Si_3N_4, surface etching by laser-generated free radicals 80−71772
SiO_2, cryst. and amorphous, laser-induced breakdown, electron avalanche damage mechanism 80−100711
SiO_2 film, 1064 nm 150 ps laser pulse damage rel. to OH^- content and refr. index 79−14016
SiO_2, fused, laser damage threshold rel. to surface roughness 77−40306
SiO_2, fused, laser damage threshold rel. to subsurface struct. 77−40307
SiO_2, fused, surface damage threshold rel. to prep. and OH^- conc. 77−62026
SiO_2, fused, surface roughness rel. to prep. and treatment history 79−14058
SiO_2, fused, US cleaning effect on laser damage threshold 77−62024
SiO_2, fused silica optical surface, ion polishing rel. to laser damage thresholds 77−75717
SiO_2, picosecond laser induced breakdown at 5321 and 3547 Å, freq. depend. 77−63495
SiO_2, surface etching by laser-generated free radicals 80−71772
SiO_2-TiO_2 antireflection coatings, 1064 nm 150 ps laser pulse damage rel. to barrier layering and smoothness 79−14018
SiO_2-TiO_2 antireflection coating, 1.064 μm laser damage, barrier 80−33059
SiO_2-TiO_2 stack reflector and antireflection coating, 1064 nm 180 ps laser pulse damage 79−14017
SiO_x film, damage mechanisms 77−75592
SmS, energy of metal-semicond. phase transition and threshold recording energy density 79−28386
SmS, film, laser generation of US using metal-insulator transition 79−90734
Sn microstrip, optically illuminated, resistive transition and supercond. props. 80−54821
Sn-Pb supercond. loop, laser irrad. effects 79−56419

laser beam effects continued
SrF_2 antireflection coated, 3.8 μm CW laser damage threshold obs. 80−33053
SrF_2, IR window coating, prep. and optical props. 77−50736
SrF_2, laser window material, absorpt. at CO wavelengths, calorimetric meas. 78−25911
ThF_4 film, 1064 nm 150 ps laser pulse damage rel. to OH^- content and refr. index 79−14016
Ti-Al-V (6,4 wt.%), laser surface melted, topographical charact. 79−70200
Ti-Pt link on Si_3N_4-SiO_2-Si substrate, laser vaporisation, interference effects 77−69941
TiO_2, reactively sputtered optical coating for inertial confinement fusion laser components 80−23705
TiO_2-SiO_2, multilayer dielec. mirrors, laser-induced damage resist. 79−10335
TiO_x film and crystal, damage mechanisms 77−75592
Tl, neutral atom production by pulsed laser heating 77−85848
Tl_3AsSe_3, IR nonlinear material, laser induced surface damage 77−19266
TlCl-TlBr, internal damage threshold for CO_2 laser pulses rel. to absorption 77−75594
TlCl-TlBr, KRS-5, KRS-6 crystals, optical strength pulsed CO_2 laser radiation 79−27307
U extraction by transfer between liq. phases, laser radiation effect 80−66795
UC, transient capillary wave generation on laser irradiated surface 78−21653
UF_6, laser chemistry 80−69198
V, oxidised in air during laser irradiation, switching effect *(Russian)* 80−24977
VO_2, film, semiconductor-metal phase transition, fast laser kinetic studies 79−69419
VO_2, laser induced metal-insulator transition, thermal switching dynamics 77−76885
V_2O_5, laser induced damage *(Russian)* 79−43069
W (100), laser induced desorption, mirror electron microscopy 78−84067
W, desorption of D_2, meas. of fast desorption kinetics by laser heating technique 79−23837
W, erosion by laser beam, in self-consistent mode *(Russian)* 77−69945
W foil, integral heating by msec laser pulses *(Russian)* 77−59824
W, hot electron emission using ruby laser pulses 79−28883
W, laser heating in air by obliquely incident radiation 80−71815
W, laser irrad., charged particle emission from back side of target 78−2949
W, laser irrad., negatively charged particle emission 77−8690
W, point target, temp. depend. of electron emission caused by laser illumination 79−43107
W wire, laser shock induced microstructural changes, rel. to explosive shock induced phenomena 78−67768
WSi_2, amorphous, crystallisation by energy beam annealing 79−69012
XeCl discharge, KrF laser induced preionization 80−84020
Zn, erosion by laser beam, in self-consistent mode *(Russian)* 77−69945
Zn, stacking faults, plastic deformation, due to laser beam irrad. *(Russian)* 80−15121
Zn, surface, Q-switched ruby laser irrad., recoil momentum 79−65961
$Zn_xCd_{1-x}S$, laser damage, self-focusing influence 78−50844
ZnP_2, surface destruction by ruby laser irrad. *(Russian)* 77−20964
ZnS, film, laser evaporation synthesis, surface struct. 79−28954
ZnS-MgF_2 dielectric film, laser irrad. and microscopic inhomogeneities 78−2157
ZnS-MgF_2(SrF_2), dielec. films, transparent, microscopic inhomogeneities and optical breakdown 78−10844
ZnS-SrF_2 dielectric film, laser irrad. and microscopic inhomogeneities 78−2157
ZnSe, CVD, laser window material, impurity absorpt. meas. 78−25909
ZnSe, laser window material, multiphonon absorpt. temp. depend., calorimetric meas. 78−25907
ZnSe, laser window material, absorpt. at CO wavelengths, calorimetric meas. 78−25911
ZnSe sputtered laser window coatings, prep. and evaluation 77−50739
ZnSe window, laser induced thermal stresses 77−46747
ZnSe/water, interface, laser-induced damage in ZnSe 80−102746
ZnTe, secondary emission, transient behaviour under band-to-band excitation 80−108266
ZnTe:Bi, laser annealing, channelling, reflectivity spectra 80−66215
Zr, pure, laser microprobe damage, metallographic exam. of craters formed 78−39988
ZrC, destruction delay time under laser impact 79−38976
ZrC, fracture by laser beams, macrocrack propag. 79−15789
ZrH_x, laser irrad. effect on interstitial phases, metallographic obs. 79−37734
ZrO_2, film, 1064 nm 150 ps laser pulse damage rel. to OH^- content and refr. index 79−14016

laser beam machining
composite film structures, micromachining, interference effects 77−88825
contour-projection method for laser processing of materials 79−91825
cutting laser beam appl. in material-cutting, processing optimisation *(German)* 80−43384
dimensional processing of materials by ruby laser emission in free generation and single-pulse modes *(Russian)* 77−70274
drilling of diamond, process mech., thermal stresses, elec. surface forces *(Dutch)* 77−7759
drilling using TEA CO_2 and Nd lasers, absorption mechanisms 77−88826
electro-optics, conference, Utrecht, Netherlands (Oct. 1978) 80−31420
electrospark coating improvement by laser action *(Russian)* 79−15850
ferrites, laser drilling and cutting, anal. of results using computer model 79−70180
focusing, linear, annular and radial, with axicons, laser machining appl. 78−66856
glass cutting technology using CO_2 laser, damage effects 79−7173
holographic appl., single versus multiple exposure investigation 77−77645
industrial CO_2 high-power laser system, for welding, cutting, heat treating and irrad. 78−55380
instrumentation engineering, laser beam appls. in drilling, welding, cutting, definite abrasion and surface treatment *(German)* 80−108608
laser-assisted hot spot machining, advantages and potential 79−70199
laser beam machining continued
lasers as modern machine tools for hardening, glazing, boring welding and cutting *(Dutch)* 80−91808
material interactions and effects due to absorpt. 78−35229
material processing, IR holographic elements appl. 80−37964
material processing, overview 78−56826
material processing, welding, cutting, drilling and surface hardening 78−80663
materials classification, according to behaviour under CO_2 laser processing 77−5820
materials processing, alloy fabrication, laser systems, theory, appls. 77−2639
materials processing with CO_2 laser holographic scanner systems 79−18367
metal drilling velocity and efficiency 77−24913
metal drilling with Nd lasers, absorption phenomena 78−30002
metal plate, penetration by combined CW and pulsed laser radiation 79−89955
metallic film machining by laser-induced explosion 78−15258
metals and alloys, laser erosion, influence of metallic target temp. *(Russian)* 79−39028
microscopically rough substrate local smoothing for optical storage 80−14288
nonmetallic material cutting by CO_2 laser beam 79−45992
nuclear reactor irradiated fuel, anal. of α-emitting isotopes through laser micro-boring 80−37444
opaque solid slab, laser heating and burnthrough, anal. 77−48284
operational principles *(German)* 78−5522
optical communication fibre endface preparation by AC discharge heating and stretching 80−64232
optical disc data recorder, laser machining for recording 78−71136
optoelectronic pattern tracer for laser plate cutting 79−55170
pyroceramic plate scribing by pulsed CO_2 laser 79−52410
quartz SAW resonator tuning by shorted reflector opening 78−59246
refractories, erosion resistance during action of highly concentrated energy fluxes 80−55562
review *(Japanese)* 78−4674
steel, laser erosion value depend. on metallic props. anisotropy during plastic deform. *(Russian)* 78−31452
thin film processing, review 77−23684
thin films, projection method 77−26276
transition metals and their compounds, erosion resistance increase obs. *(Russian)* 77−53871
workpiece focal point window tolerances in laser material processing 80−5776
Al_2O_3, laser drilling and cutting, anal. of results using computer model 79−70180
Bi film, granular, enhancement of laser machining and ageing charact., using $Mg_{0.25}In_{0.75}$ sensitising layer 77−62020
Bs film, hole machining 80−30207
CO_2 for macnine tools 77−40517
CO_2 laser, construction, industrial appls. *(German)* 77−88731
CO_2 laser, feasibility study *(Czech)* 77−19274
CO_2 laser, pulsed, design improvements 77−46733
CO_2 laser processing of materials, interfacing with modern prod. engng. technology 78−33767
Cu, drilling with CO_2 laser pulses, influence of laser-supported detonation waves 79−28866
Mo powder, struct. changes under action of high-powder pulses 79−70018
Se film, hole machining 80−30207
YAG laser trimmer for wafer level products 80−87428

laser beam welding
basic physical processes 77−23682
creep capsules, multiaxially stressed, remote pressurization and laser closure welding 79−54514
electro-optics, conference, Utrecht, Netherlands (Oct. 1978) 80−31420
glass sphere targets, small, for laser fusion, technique for full surface exam. in SEM 79−21874
heat transfer model for CW laser material processing 80−64336
Incoloy, oxide-dispersion-strengthened, pulsed YAG laser welding 79−70075
industrial CO_2 high-power laser system, for welding, cutting, heat treating and irrad. 78−55380
instrumentation engineering, laser beam appls. in drilling, welding, cutting, definite abrasion and surface treatment *(German)* 80−108608
lasers as modern machine tools for hardening, glazing, boring welding and cutting *(Dutch)* 80−91808
material processing, overview 78−56826
material processing, welding, cutting, drilling and surface hardening 78−80663
metal working with high power lasers 78−80682
penetration hydrodynamic limit 77−40313
steel, cold crack formation following laser welding *(Russian)* 79−38938
stress wave emission techniques for monitoring laser welds 79−100329
weld material penetration hydrodynamic limit 77−40313
CO_2 and Nd:YAG systems *(German)* 78−1294
CO_2 lasers appl., CW, 5 kW 79−15879

laser beams
see also holography; laser frequency stability; Schwarz-Hora effect
aberrating Gaussian beam, free-space propagation, wave eqn. solns. 78−87008
aberration sensor for high-energy laser system, interference problems 79−98422
absolute calibration of grating spectrograph for laser wavelength meas. 78−90528
active medium, EM field self-focusing, laser transverse struct. form. 80−87442
active optical systems, real-time control over optical wave fronts 78−71187
adaptive control of laser beams 77−88833
adaptive control process, optimal estimation techniques 77−88660
adaptive optics, atmospheric compensation, book contrib. 79−31972
adaptive optics, book 79−31921
adaptive optics in high energy laser systems, book contrib. 79−31971
adaptive optics technology overview, book contrib. 79−32030
adaptive optics technology status and prospects 80−33132
adaptive phased array expt. with independent laser sources, compensation for atm. effects 78−42367
aerodynamic effects of supersonic flow past laser beam 78−38366

laser beams continued
aerosol, thermal clearing by laser radiation *(Russian)* 78−28312
aerosol deflector operation at high radiation intensities 80−9922
algebraic model for CW thermal-blooming effects 79−94303
alignment, reticle method, for teachers 78−12495
alignment accuracy of CO_2 laser on target, Hartmann test, direct meas. 79−23004
alignment accuracy of Helios CO_2 laser 80−33071
alignment fixtures 80−74414
alignment of pulsed or CW beam by Si position-sensitive detector 80−78883
alignment system for CO_2 fusion laser 78−46706
alignment system for Helios CO_2 fusion laser 80−33070
alignment system for large high-power pulsed CO_2 laser fusion system 78−59075
amplifier system, small-scale self-focusing 80−106580
amplifier with spatial filters, graphoanalytic determ. of energy parameters 80−48322
amplifier with spatial filters, optimal length and operating conditions 80−48323
amplitude fluctuation statistics in turbulent atmosphere 80−106458
amplitude modulated laser beam prog. in random inhomogeneous medium, phase fluctuation anal. 78−87017
angular divergence from electron-beam-controlled laser, refr. and diffr. contribs. 79−59668
angular divergence minimisation with optimal resonator output mirror 78−13735
annular beam profile changing by aperturing diffr. pattern 80−18991
apodizing of intense laser beams with saturable dyes 79−31965
arbitrary profile beam, diffr. by periodically modulated layer 80−43252
artificial mist, laser radiation propag., intensity fluctuations *(Russian)* 78−37806
Asterix III and German laser fusion programme 78−63136
astigmatic, active laser cavity resonator systems *(German)* 78−1269
asymmetry detection of short pules by three-photon fluoresc. meas. 78−1289
atmosphere, freq. spectrum of random displacements meas. *(Russian)* 79−96813
atmosphere propagation, IR radiation attenuation by ice platelets 80−66141
atmosphere propagation, light focusing and defocusing in exploded aerosol 80−8426
atmosphere radiative t0ansfer, nonlinear propag. effects, conference, San Diego, California (1979 August 29 to 30) 80−62376
atmospheric absorption by dust, spectrophone meas. 77−9513
atmospheric aerosol, laser beam propag., UV, visible and IR regions *(Russian)* 78−28313
atmospheric aerosol extinction measurements, multiple scatt. corrections 80−98445
atmospheric attenuation, H_2O continuum, meteorological factors 77−2242
atmospheric attenuation, reson. absorption by water vap., ruby laser pulse *(Russian)* 78−49138
atmospheric attenuation at 6328 Å statistical meas. 77−45144
atmospheric cloud clearance, liq. water content and temp. fluctuations in clearance zone *(Russian)* 78−44999
atmospheric extinction at 10.6 μm CO_2 laser wavelength, from meteorological records 79−39848
atmospheric optical communication line operating under photon counting conditions, adaptation to turbulence 80−9930
atmospheric optical communication link, laser beam size 80−33064
atmospheric propagation, book 79−34955
atmospheric propagation, conf., San Diego, USA (Aug. 77) 78−85748
atmospheric propagation, detector nonlinearity effects on statistics of fluctuating signal 78−55301
atmospheric propagation, high-energy, simplified aberrated lens model 78−69454
atmospheric propagation, integrals evaln. 77−79879
atmospheric propagation, interferometric evaluation of imaging characts. 77−88643
atmospheric propagation, Kolmogoroff's theory of turbulence and intermittency 79−7368
atmospheric propagation, problems and trends review 79−100947
atmospheric propagation, thermal blooming, mirror deform. for phase compensation 80−8423
atmospheric propagation, thermal self-action on heterogeneous paths *(Russian)* 78−28311
atmospheric propagation, turbulence effects, wave parameter fluctuations 77−38805
atmospheric propagation, turbulence effects 77−38975
atmospheric propagation of high energy beam, thermal blooming in stagnation zone 77−75588
atmospheric propagation of modulated laser beam, acoustic pulse generation, thermal defocusing 79−92597
atmospheric propagation of repetitively pulsed beam, target intensity enhancement, thermal blooming 77−65604
atmospheric propagation through turbulence, K distribs. 79−80023
atmospheric scattering coeff. as function of visibility and wavelength, empirical formula 79−34944
atmospheric surface layer turbulence effects, optical parameter determ. model *(Russian)* 80−12481
atmospheric transmission, anomalous effects during August, 1976 at Farnborough, England 79−39862
atmospheric transmission, scintillation and multiwavelength coherence in absorpt. spectrometer 78−40653
atmospheric transmission at 10.6 μm, analytic model of bleaching 78−85688
atmospheric transmission meas., losses 3.5 to 4.0 μm 77−91266
atmospheric transmission meas., using IR lasers, Fourier transform spectroscopy, gas-filter correl. techniques 77−70873
atmospheric transmission meas. at 10.6 μm 78−92977
atmospheric transmission of far IR laser lines 77−19237
atmospheric turbulence, corner-cube reflector and plane mirror comparison in folded-path and direct transmission 78−85697
atmospheric turbulence degradation compensation by nonlinear optical mixing 77−42558
atmospheric turbulence distortions of spatial coherence 77−79756
atmospheric turbulence effects on target irrad. by laser beam 77−58254
atmospheric turbulence induced laser beam spread, isoline approach 77−72016
laser beams continued
atmospheric water vapour, narrowing of collision shape of mol. absorpt. line in powerful laser field 79−29860
atmospherically degraded, detection effects on statistics of intensity fluctuations 79−16672
atmospherically degraded, higher-order propag. statistics, recording process effect 79−14004
atmospherically degraded, log-normally distributed intensity fluctuations 79−50228
atomic system, hydrogenlike, polarised monochromatic laser radiation absorption in electronic transitions, DC mag. field effects 80−9563
attenuation by snowfall, characts. 80−26611
attenuation for spatial profiling of small focal spots 80−99780
autocorrelation by optical processing of Fabry-Perot spectrograms 80−58465
automatic alignment system, for OMEGA-10 multibeam laser system 78−50847
automatic target alignment of Helios CO_2 laser system 80−74416
backscattering from dense water-droplet clouds 79−53513
beam divergence, mode competition effect 80−48303
beam expander for short cavity dye laser 80−87532
beam splitting device for use with smoke chamber ray optics demonstrations 80−67990
beamed signal propagation through diffractive inhomogeneous media 77−71920
blue-green pulsed propagation through fog 79−39846
bolometric laser power meter, sensitive meas. IR to vacuum UV spectral range 78−82031
bulk absorption homogeneity, Doppler interferometric meas. 79−14010
calibration of wavelength and bandwidth using optogalvanic effect 78−5514
calorimeter response, spatial var. 77−65603
calorimetric energy meters, KDM and BKDM, for pulsed laser radiation 79−17494
calorimetric energy meters, KDS and BKD, for high-power laser pulses 79−17496
calorimetry for incident laser energy in laser fusion expts. 78−51361
chemical CW laser, optical diagnostics 79−36916
chirp-free picosecond pulse generation 77−79869
chirped steady π-pulses of arbitrary duration in lossy, exactly resonant inverted medium 79−89947
chopper, simple submicrosecond optical, for rectangular-shaped pulse prod. 80−14373
circularly polarised, intense, multiphoton ionis. pots. for H(He) 80−43010
coaxial digital pulse compression for high power Nd:glass lasers 77−7101
coherence, review 80−48140
coherence and divergence *(Spanish)* 80−87424
coherence discrimination laser detect., angle-scanned interferometer as coherent energy modulator 79−58777
coherence length meas., for holographic appl. 77−7100
coherence length measurement problems *(German)* 78−79052
coherence meas. and fibre modal noise simulation by Michelson interferometer 80−48324
coherence of light beam through optically dense turbid layer 78−55300
coherence oscillations in nonlinear media, coherent state lifetime 78−66862
coherence props. 77−75408
coherent, two component system producing by static phase modulation a directional light beam *(Russian)* 78−50940
coherent fast IR wavefront aberration sensor interference problems 80−74499
coherent Gaussian beam in laser Doppler velocimeter, interference 80−69444
coherent light beam, azimuth of plane of polarisation determ. *(Russian)* 78−29143
coherent optical pulse synthesis using phase-locked lasers and nonlinear optical processes 79−76724
coherently combined, phase lock control considerations 80−5743
collimated laser beam interactions with SAW-induced bulk particle motion 79−76742
collimated laser radiation, directivity pattern axis spatial location 80−102748
collimation and focusing at given distance *(Russian)* 78−29959
compensation using phase plates 77−42556
composite waveguide laser with end-fire excitation, output characts. 80−23738
concentration using inversion of wave front technique *(Russian)* 78−63154
cone-type light beam structure in nonlinear medium 79−98437
confined beam small-scale self-focusing 79−89977
confocal unstable resonator beam props., astigmatism due to Brewster angle windows 78−46670
conical optics for radiation conversion from laser with unstable resonator 80−91831
conical scattering of laser beams in active dye solutions 79−94294
contraction dynamics due to thermal transient self-focusing 79−10368
contrast magnification of spectral distrib. by freq. spatial filter *(Russian)* 77−747
convex beam integrator for laser beam shaping, heat treating appl. 80−53346
correlation method for meas. beam parameters *(Russian)* 78−50705
coumarine dye laser, N_2 laser-pumped, pulse time behaviour 79−31894
coupling efficiency of semicond. laser beam into fibre, matching element misalignment influence 80−48432
curvature radius mem. using Talbot effect *(Polish)* 79−86200
CW, radiated power meas. *(German)* 78−79053
CW digital wavemeter, moving cube-corner interferometer system 78−50840
CW laser radiation power stabilisation by external control element 80−91832
dark laser wavelength monitoring using fibre interferometer 80−74413
deflection, complementary control of scanner 77−83982
deflection, optically controlled, based on CdS_xSe_{1-x} thin-film waveguide 80−33206
deflection angle determ. from holographic shear interference patterns 80−95848
defocusing in weakly absorbent medium, reduction by circ. scanning *(Russian)* 77−83917
degradation by two-dimens. turbulent jet 80−14375

laser beams continued
detection using tunable acoustooptic filters 78−29159
detector, using transverse voltage generated in refractory metal film 78−41350
DFB laser, limiting spectral characts. 79−64197
diagnostics, use of subpicosecond proximity-focused visible streak camera 78−59155
diameter fluctuations meas. 78−87086
diameter measurement 79−7168
diameter measurement of laser beams using a grating 80−102745
dielectric layer transmission, phase and intensity distribs. *(Russian)* 77−88821
difference frequency generation, Gaussian intensity profile effect 80−78906
diffracted rays in turbulent medium 80−48153
diffraction, teaching approach 79−71177
diffraction by absorbing inclusions in solid, thin lens approx. 77−79757
diffraction focusing by sequence of irises 79−50332
diffraction of high intensity light by ultrasound in nonlinear liquids 80−64270
diffraction of laser beams in near and far zones, calc. 79−94274
diffraction theory of interactions with single skeletal muscle fibres 80−56110
diffraction-limited CW optically-pumped far IR lasers, beam characts. 77−38953
diffractive ray tracing 77−27291
digital beam switch for agile beam laser radar 80−58620
digital wavemeter for CW lasers 78−89447
diode laser, mear and far field characterization 80−48242
directional beam generation from globally incoherent source 80−53211
directionality of light beams and spatial coherence 79−36834
distortionless propagation of 5 psec-wide pulses in fibres, use of mode-locked colour-centre laser 79−94358
distributed aperture effect in laser rods with negative lenses 78−66857
disturbed wavefront in nonlinear medium, dynamic holographic correction *(Russian)* 78−55326
divergence, for inhomogeneous active medium with gain saturation 77−50703
divergence angle definition 77−54747
divergence influence on axicon axial intensity distrib., Kirchkoff-Fresnel integral soln. 80−95934
divergence meas. using lateral shearing interferometry 78−13739
divergence measurement, focus errors 78−46692
divergence measurement of Guassian beam 77−72013
divergence measurement using PIR-1 instrument 79−23001
divergence reduction using phase masks *(Russian)* 79−27308
divergent laser beam, influence on signal of optical system misalignment in space filtering scheme *(Russian)* 78−37815
diverging beam conversion into plane wave by dynamic vol. hologram 79−18376
Doppler broadened laser amplification line frequency characteristics meas. 78−59060
Doppler scattering by ocean ripples due to acoustic and capillary waves 78−3807
dosimeter, health physics evaluation of operating conditions at laser installations 80−76835
double scattering contribution to lidar returns from clouds 79−5615
dual-beam laser Doppler anemometer, beam waist location and meas. 78−37931
dye CW laser, spectral narrowing and continuous tuning by grating beam-expansion 79−59720
dye CW laser, spectral narrowing by intracavity Na atomic beam 79−55159
dye laser, continuously pumped, pulse compression with slow saturable absorber 79−31959
dye laser, CW, double mode locking, parametric study 79−45978
dye laser, divergence of emitted radiation, excited transverse modes determ. 79−94228
dye laser, flashlamp pumped, freq. tunable ns duration pulses by pulsed Q-modulation 79−41403
dye laser, flashlamp-pumped, linear, thermal effects on spatial mode struct. 79−36943
dye laser, highly synchronous CW double mode-locked, picosecond pulse shape meas. 79−64257
dye laser, N_2 laser pumped, spectral narrowing 78−25903
dye laser, passively mode-locked, parameters affecting subps pulse duration 79−45979
dye laser, pulsed, beam divergence *(Russian)* 78−25902
dye laser, second harmonic pulse structure and cavity length determ. 80−95935
dye laser, short constructional length with folded mirror beam expansion system 80−53328
dye laser, unstable ring resonator, good beam quality and low divergence 80−53326
dye laser cavity, pulsed, concave grating for beam expansion and spectral dispersion 79−59721
dye laser fast light deflection, ultrahigh resolution 78−63178
dye laser multimode beam, spectral distrib. meas. using speckle patterns 77−14730
dye laser picosecond pulse generation, excitation by passively mode locked Ar laser 80−95930
dye laser pulse output, accurate numerical simulation 79−41380
dye laser radiation directivity improvement 77−72003
dye laser reference wavelengths, two-photon transitions to Rydberg levels 78−94221
dye lasers, beam divergence, transverse mode saturation, kinetics *(Russian)* 78−74931
dye lasers, mode-locked, exponential SHG autocorrelation function rel. to pulse to pulse var. 80−9920
dye pulsed laser, light polarisation with thin wedge plate in cavity 78−55394
dye TEM_{00} tunable laser system high-power, with frequency-doubling crystal 79−50306
dynamic three-dimens. phase holograms for light beam parameter correction 77−10876
dynamic-focusing mirror system, umbrella-type 79−36971
education, laser beam UHF and audio freq. difference heats 80−73139
effective photon hypothesis, expt. test 77−46709
electron beam scattering, intensity differential cross-section 77−71914
electrooptic prepulse suppression for fusion laser systems, using optically timed Pockels cells 80−102743
laser beams continued
elliptical Gaussian beam, propagation and focusing anal. 79−50873
elliptically polarized Gaussian beams, nonlinear precession 80−28269
emission from circular inphase Gauss excited antenna aperture, Fresnel area 77−46741
emission power fluctuation statistical meas. system 77−79881
energy distribution analysis, film calibration method 77−79875
energy distribution reconstruction using data from grid of bolometers 80−53350
energy exchange between free electrons and EM waves in vacuum, anal. 80−18975
energy meter *(French)* 80−102790
energy meters for calibrations at most principal laser wavelengths 80−99741
energy monitoring, medium power, photoacoustic detector, construction and calib. *(Czech)* 78−29156
energy parameters of IR beam, aerosol deflector meas. 78−25916
energy photometry, meas. of parameters of pulsed and steady-state radiation 79−14007
energy pulse measurement, liquid absorption cell technique, digital readers *(Russian)* 78−18000
energy standards, inequivalence, simplification 77−79876
errors in mode parameters determ. of spatial distribution of radiation 80−95055
evanescent wave holography using Gaussian beam, recording geometry and colour sensitivity 80−58473
excimer laser, double discharge, improved beam quality using unstable cavity 77−72007
excimer laser Raman pulse compression for appl. to laser fusion 79−59756
excimer laser Raman pulse compressor systems for laser fusion 79−59757
expanded beam use in optical correlation expts. 77−23629
expander, Galilean or Keplerian form telescope 78−50839
expander design corrected for Petzval curvature 80−74461
expansion in dye laser cavity, use of diffr. grating 78−66858
externally self-modulated laser producing two pulses 77−83902
extraterrestrial laser signals detect. likelihood, instrumentation 80−4276
Fabry-Perot resonator filled with transversely inhomogeneous active medium, radiation field struct. 79−55157
far field of Gaussian beam 79−76583
far IR CW optically pumped lasers, simple accurate method for wavelength meas. 80−106554
far IR laser intracavity polarisation modulation by CdTe AC Faraday rotation 80−58613
far-field profile, focal plane technique 78−87087
fast beam-laser interactions, review 79−30607
fibre laser high-power stimulated emission pulses, substruct. 80−9890
field properties of multiple coherently combined lasers 79−36944
fine structure of He-Ne laser radiation, Fabry-Perot scanning interferometer meas. 77−54749
Fizeau wavelength meter, laser and other monochromatic sources, digital display 78−89450
flat top beam profile production for high energy lasers 80−58618
flexible IR waveguides, high power laser output steering appl. 80−48409
fluctuating polarisation rel. to use of beam splitters 77−79884
fluctuations of laser beam diameter of single-mode laser, lens effect 80−64090
fluoromethane TEM_{00} far IR laser with integrated pump laser 80−43348
FM laser output analysis by interferometer with increased resolution 78−4688
focus and alignment sensing of a collimated light beam 78−59065
focus path of beam deflected by prismatic polygon mirror 77−19267
focused, scattering by moving particles 80−48149
focused beam ray tracing for laser fusion 80−83218
focused gaussian beam optical parameters, SR-52 calculator programme for calc. 78−79056
focused light beams, phase anomaly, intuitive explanation 80−99622
focusing, linear, annular and radial, with axicons, laser machining appl. 78−66856
focusing by random phase screen 77−79755
focusing by vertical temp. gradient in aerated water 78−33661
focusing device for laser radiation 78−13742
focusing device using prism raster 77−19272
focusing lens design for hot spot elimination 79−72658
focusing of CO_2 laser beam by reflection kinoform 77−79780
focusing of single mode laser, geometrical optics model, focusing system design 77−7109
focusing optics for fusion appl., lens and mirror design 77−3641
focusing properties of high power laser beam, influence of nonlinear refractive index medium *(French)* 78−46696
fogs, radiational and advective, laser beam multiple scatt. 79−100950
formic acid laser 311 μm line, freq. meas. by mixing with HCN laser 79−76728
four-channel laser system with four-ellipsoidal-mirror set-up for focusing laser beams 79−94276
four-point coherence function measurement, turbulent atmosphere 80−23623
four-point field coherence function meas. in laser random focusing region *(Russian)* 78−58910
Fourier optics described by operator algebra 80−48163
free electron laser, intense-beam, beam quality expts. 80−58619
free-electron laser amplification on relativistic electron beam in spatially periodic transverse mag. field 80−19014
frequency and spectral parameter check system 77−79880
frequency chirped pulse compression using phonon-polariton propag. modes 78−46689
frequency doubling in isotropic-dielectric waveguide *(Russian)* 79−94285
frequency measurement, interferometric method based on Doppler shift 77−165
frequency shifting by refl. from moving blazed grating 77−88822
frequency shifting via rotating half-wave retardation plate 80−9800
frequency spectrum control, phase polarisaton method 77−75583
fresnel diffraction images of periodic objects under gaussian beam illumination 79−94148
fusion laser energy meas. using large aperture calorimeter 80−43382
fusion research lasers, advanced components and systems for beam lines 79−18466

laser beams continued
fusion system beam quality, Laser Optical Train Simulation code 80−78886
gas, resonance four-photon shift, optimal focusing of high-power pumping 80−95574
gas flow through optical train, thermal blooming control, optical degradation 80−33045
gas laser, intensity fluctuations, spatial distrib. 79−18458
gas laser, interferometric correction of output charact. *(Russian)* 77−79855
gas laser, modulation method, for relative excitation level, cavity bandwidth and at. temp 80−5771
gas laser cavity, universal unit for beam extraction, design 80−1230
Gaussian, construction of nomographs 79−98421
Gaussian, focused, apertured, focal length and target range estimation 77−19299
Gaussian, Fraunhofer diffr. by single slits 80−87298
Gaussian, geometric props. 77−19276
Gaussian, nonlinear self-focusing in plasma, variational approach 79−27786
Gaussian, transverse self-focusing and self-trapping investig., moment method 80−58652
Gaussian beam, equal phase, self-focusing effect calcs. 77−23722
Gaussian beam, focused truncated, spot size evaluation 79−59737
Gaussian beam, generalized spot size for higher-order beam mode 79−72612
Gaussian beam, plane-wave-type expansion, errors incurred 80−48312
Gaussian beam, tilted, modal expansion *(Japanese)* 78−30000
Gaussian beam at oblique incidence on plane interface of dielectrics, refl. and transmission *(Japanese)* 80−5687
Gaussian beam diameter measurement, Ronchi ruling method 79−55169
Gaussian beam far-field 79−81357
Gaussian beam propagation, Fresnel-Kirchhoff integral anal. 79−45984
Gaussian beam propagation beyond the paraxial approximation 79−72476
Gaussian beams, increase of axial brightness during wave front smoothing *(Russian)* 80−5774
Gaussian beams, off-axis, aberrated Fraunhofer diffr. patterns 78−66753
Gaussian beams of pulsed IR radn., parameters determ. 80−1260
Gaussian instability growth 80−69469
Gaussian laser beam, transmitted field at total internal reflection 78−13654
Gaussian laser beam focus, intensity distrib. determ. 79−14002
Gaussian laser beams, spatial modulation 79−7162
Gaussian light beam, diffr. by plane acoustic waves at oblique incidence 80−69326
generalized Collett-Wolf sources 79−31793
geometric parameters determ. of quasi-Gaussian beams, interf. methods 79−64265
geometrical optics, spatial structure 78−83014
heat flux and power profiling, using swept null point calorimetry 80−69439
helical wave surface light beams, interf. props. 80−1121
heptafluoroiodopropane light amplifier, wave-front distortion due to photolysis-gas dynamic effects 79−18412
Hermite Gaussian beam, spot size and divergence 80−69436
heterodyne optical radar S/N ratio in atmospheric turbulence 80−106558
heterojunction lasers, for fibre optic data systems 79−55149
HF laser nanosecond pulse generation using Ar gas breakdown 79−81465
high energy laser system, optical distortion, active control 78−83019
high energy laser system, optical distortion sources 78−83018
high energy laser system, thermally induced optical distortion 80−38051
high power, optimal focusing conditions for freq. doubling 79−14036
high power, pulsed radiation recording using developed Polaroid film 79−94270
high power laser propag., thermal blooming review 78−30035
high power laser radiation, transmission through silica fibre, role of stimulated Raman scatt. 79−37011
high power sharpened pulse form. in amplifying system 77−75584
high precision laser freq. meas., sigmameter, motionless two-channel Michelson interferometer 78−89449
high-power annular lasers, uniform beam transformation, mirror system 78−94403
high-speed shaping device, for address control of laser beam deviation 78−5554
higher order beam modes in complex lenslike media and resonators 77−27308
holographic elements, moving, laser beam deflection appl. *(Russian)* 80−63956
holographic method for laser radiation divergence reduction *(Russian)* 78−63147
image convertor camera, for laser and laser-plasma diagnostics 78−38550
image phase conjugate laser adaptive control, isoplanatic effect simulation 77−19294
image quality of diffuse objects, laser coherence influence 79−31820
image resolution through atm. turbulence over ocean, optical transfer function 78−85695
image-bearing, nonuniformly polarized, generation of time-reversed replica 80−69459
impulses, 10^{-12} sec, anal. using Kerr cell and streak camera *(Italian)* 78−54477
indicator/visualiser made from new thermochromic material 80−9976
inert gas halide excimer laser, operating and beam characts. 79−59715
inert gas halide laser, stable-unstable resonator for beam control 80−23722
information transmission capacity, review 77−38821
injection laser, high-power coupled-multiple-stripe phase-locked, beam characts. 79−50307
intense laser beam diffraction by long US wave in liquid column 78−60421
intensity control circuit 78−9394
intensity distrib., far field laser and partially coherent sources, comparison 78−66751
intensity distrib. meas. by thermal deform. method 79−64267
intensity distrib. uniformity, use of photographic amplitude filters *(Russian)* 77−54748
intensity distribution meas., Bragg diffraction of light 80−64092
laser beams continued
intensity fluctuations, averaging effect saturation with distance, expt. *(Russian)* 78−46512
intensity fluctuations, influence of transmitting aperture diffr. size and turbulence 79−45906
intensity fluctuations, statistical props. of sum of partially correlated complex variables 77−79754
intensity fluctuations due to beam wandering 77−88824
intensity fluctuations in medium with Kolmogorov turbulence, distrib. function *(Russian)* 78−71034
intensity fluctuations in rainfall, statistical characts. 80−101433
intensity fluctuations in turbulent atm. over water surface *(Russian)* 78−69449
intensity fluctuations of thin laser beam in waveguide channel with large-scale random inhomogeneities 80−33194
intensity fluctuations produced by multimode lasers in combination with dielectric beam splitters 78−22160
intensity mapping aberrations 78−66855
intensity meas. by photooxygenation actinometer 77−30193
intensity profile analysis using video equipment 78−59068
intensity profile distortions in turbulent media, theory 78−22162
intensity profiles meas., using Si vidicon and minicomputer system 79−27267
intensity ratio increase by possible use of stimulated Brillouin and Raman scatt. 80−5796
interaction with inclusion defects in isotropic solids 79−76741
interference pattern fluctuation statistics in turbulent atmospheric layer 78−53727
interferometric wavelength measurements through post-detection signal processing 80−42254
interferomic wavelength meas. with post-detection signal processing 80−105699
internal modulation of laser radn., freq. limitation 79−72607
intracavity phase perturbations effect on beam quality 77−38968
intraresonator formation of laser fields, transverse mode influence *(Russian)* 79−50327
IR, measurements of 3-dim. energy characts. and imaging methods 79−76842
IR, thermal imaging screens for visual display 78−66903
IR beam parameters meas., potential use of wire diffraction grating 77−730
IR Gaussian laser beam truncated by annular aperture, diffraction study 79−18344
IR laser pulse recording using ZnS:Ag, Ni and CdS:Ag, Ni luminesc. screens 79−64342
IR laser system alignment using Smartt interferometer 80−33072
IR laser window material extrinsic absorption 79−14049
IR phase conjugation adaptive array 77−46790
IR pulse laser intensity profiles meas. *(Japanese)* 80−22413
IR pulse recording, semicond. ionisation-type photographic system 78−49903
IR pulsed laser spectral characts. determ., interferogram display on luminesc. screen 79−10341
IR wavelength meas. by radiation conversion method, error anal. 79−7175
irradiance enhanced variance from target glint 80−5691
irradiance profile, short-term average, in turbulent medium 77−7098
irradiation symmetry calcs. for spherical laser targets 80−23140
kinetic cooling of CO_2 laser beam 77−62018
large system beam transport optics for laser fusion 78−83017
large time-bandwidth acousto-optic signal processors 79−46118
laser, double-current-confinement channelled-substrate struct., near-field and beam-waist position 80−106553
laser beam broadening and depolarization in dense water-droplet fogs 78−92981
laser nonstationary generation induced interference pattern phase distortion, holographic meas. 78−58945
laser radiation distrib. characteristic determ. in vicinity of focus 79−50871
lateral displacement meas. using position-sensitive photodetector, selection of parameters 79−17490
lensless method of measuring gaussian beam divergence 79−18459
Lidar return from fogs, effect of non-uniform extinction coeff. on double scatt. contrib. 79−100952
light fluid transformation by stochastic coherent optical filters *(Russian)* 79−982
light scattering, appl. to simulated microbes, suspension, size determ. 79−71178
line radiation transfer, Grad moment method 79−98877
line spread instrumentation for propag. meas. 78−83013
line spread instrumentation for propag. meas. 78−83015
lineshape, non-Lorentzian, reversed peak asymmetry in double optical reson. 80−69443
linewidth effect on mol. collisions in laser field 79−6980
liquid crystal laser self-focusing, effect of spatially dispersed nonlinearity 80−38908
liquid-drop aerosol, laser beam distortion in illumination channels *(Russian)* 77−14727
low energy output from CO_2 laser, absolute calorimeter meas. 78−55396
low level pulse simulation and calibration, tracking system evaluation 78−59074
low-absorption grating beam sampler design, fabrication and testing 80−14475
low-level laser pulse meas. at 1.064 μm, transfer standards 80−86253
magnetooptical switch for synchronization of CO_2 and red laser beams 80−58615
magnetoplasma, laser beam self-focusing 80−102778
matrix pyroelectric detector for laser oscills. investigation 77−74502
Maxwell equations, exact soln., with Gaussian beam as limiting case *(German)* 77−71907
MBBA liquid crystal wedge as a polarizing element and its use in shearing interferometry 80−53444
measurement laser, single-pulse, radiation stabilisation and control 80−23734
methyl fluoride, 496 μm line, freq. meas. 77−42557
microsecond pulse production, with quadratic loss in laser cavity 77−7147
mirror and window absorption, reflection and transmission obs. at 10.6 μm 79−14014
mode coupling by circular apertures 77−6995

laser beams continued
modulated signal, electron-optical recording with sub-picosecond resolution *(Russian)* 77−7105
modulated wave propag. in turbulent atm., correlation functions and freq. spectrum 79−34954
modulation by Fresnel acousto-optic conversion 77−27371
modulator using rotary diffraction grating 78−87080
monochromatic, atmospheric propag. problems 78−92988
monopulse energy meas., time-resolved spectroscopic method *(Russian)* 79−94272
multi-lens focusing systems for energy Nd:glass lasers 78−50848
multichannel system, MIK-48, for laser pulse energy meas. 79−17497
multichannel system, MIS-20, for laser pulse energy recording 79−17495
multicolour laser light time multiplexing using rotating mirror 78−17999
multicomponent laser systems with two-photon absorbents 79−94240
multidither hillclimbing adaptive optical system, secondary intensity maxima correction 80−106593
multifrequency laser radiation, nonlinear power type interaction with matter 80−53356
multimode, optical coherent spectrum analyser energy estimate smoothing 78−55311
multimode laser field, effect of intensity time variation on mol. collision processes 79−31620
multimode structure effects in many-photon resonant absorpt. 77−23708
multiphoton detectors of laser radiation, statistical characts. 80−86408
multiple pulse detection in atmospheric turbulence 78−92974
multiple pulse thermal blooming, phase compensation 77−50732
multiple-beam pellet irradiance, diffraction analysis 78−50845
multiplication, interferometric method *(Ukrainian)* 78−90442
multiwavelength laser illuminators, colour distortion compensation in plastic fibres 77−58435
nanosecond laser pulse stretch meas. in underwater propagation 80−87426
narrow band high power laser radiation transmission through fibres, nonlinear optical processes 80−53443
near IR laser beam profile recording using phosphor convertor camera 79−81468
noise immunity of optical signal reception with unstable modulator characts. 78−46690
nonlinear absorption and pulse shaping in InSb 78−79077
nonlinear distortion of laser beam transverse struct. by light filters 79−7170
nonlinear interferometers for laser pulse shaping 78−59097
nonlinear optical phase conjugation for laser systems 78−79072
nonlinear optical phase conjugation for pulsed laser systems 78−59092
nonlinear optical technique for laser focus movement 80−74446
nonlinear propagation in corundum particle aerosol 79−23033
nonlinear propagation of elliptically shaped Gaussian laser beams 80−43409
nonlinear propagation through fog, thermal blooming 77−91268
nonlinear scattering by molten zone near absorbing inhomogeneity 79−89969
nonlinear transmission of fog 80−1256
ns pulse length continuous control, appl. to Nd laser 78−1280
off-axis gaussian beam, third order spherical aberration, diffr. pattern 77−14665
off-axis gaussian beam focusing props. optical system primary spherical aberration depend. 79−76735
off-axis propag. in low visibility weather conditions, non-small-angle scatt. 80−102621
offset two-dimensional Gaussian beam wave, scatt. by cylinder 79−50207
on-axis reflective beam expanding telescope, for pulsed dye laser cavities 79−41398
optical antennas combined with laser beam, parameters optimisation 79−81475
optical distortions in large-aperture disc amplifier, holographic interferometry meas. 79−10338
optical heterodyne simulation expts., first order correlation meas., fluctuating laser beam 78−83008
optical noise filter with two aperture stops, numerical analysis *(Japanese)* 77−14812
optical propag. through turbulent atmosphere, He-Ne laser transmitter/receiver 80−98450
optical rectification effect, meas. of power, polarisation and profile of laser pulses 80−91835
optical systems with spherical and nonspherical diopters, in three-dimens. space, calc. method *(Rumanian)* 79−13898
optical waveguide, parabolic index with random dielectric constant gradient, Gaussian beam propag. 80−58698
optics in adverse environments, conf., San Diego, USA (Aug. 1977) 78−82976
optoacoustic detection using Stark modulation 79−94325
optoacoustic power monitors for laser radiation 79−41404
optoacoustic radiation detector, IR, spatial resolution 79−17493
optooptic modulated based on gain saturation in laser amplifier 79−22988
Osterberg problem and wave propag. in inhomogeneous plasma, numerical study 80−63925
paraxial beams, in vacuum, theory 79−55035
partially coherent source, highly directional, superposition of independ. laser beams 79−14070
particulate media propagation, radiative transfer eqn. soln. 79−50222
passive mode locking, transient evolution 77−34900
passive picosecond pulse shapers, throughput efficiency limitations 78−90436
passive pulse shapers, etalons and multiple beam splitters, interpulse interf. 77−19265
passive pulse shaping by delayed superposition using grating 77−75580
passively mode locked pulse stability in fast absorber limit 78−59052
path design for reduced thermal blooming in axial pipe flow 79−94268
PCM of injection laser radiation, optimal conditions 79−59733
phase aberration correction via stimulated Brillouin scatt. 78−37944
phase adaptation by nonlinear techniques, optical propag. distortion compensation, book contrib. 79−31973
phase compensated laser beam propag. through atm. turbulence 78−83012
phase compensation, optimization techniques 78−1291
phase compensation of laser beam modes 77−3599
phase compensation of thermal defocusing of light beams 80−64121
laser beams continued
phase conjugate adaptive optical systems, convergence 77−46688
phase conjugate adaptive optics using perimeter phase meas. 77−46791
phase conjugation, stimulated Mandelstam-Brillouin scatt. 80−5786
phase control of HF chemical lasers by servo system 80−33063
phase diffraction grating as laser beam coupler, radiation parameters monitoring 80−10033
phase distrib. measurement using interference from two openings 79−18461
phase front profile, optical inhomogeneity meas. of laser medium 77−79841
phase front radius of curvature meas., polarising interferometer ultimate resolution 79−88997
phase measuring sliding reference interferometer, for high power beam 77−19280
phase variation determ. using optical heterodyne interferometer 77−5896
phase-conjugate backscatt., large-signal theory 79−86211
photocount distribution for laser radiation scatt. by atm. 80−9921
photocounting distribution obs., dead-time-modified, for modulated laser radiation 79−12846
photoelectric laser radiation energy meter, digital output 78−58040
photomultipliers appl., sensitivity to incidence angle obs. 80−31843
photon behaviour 80−28185
picosecond and subpicosecond pulse display, by real-time intensity autocorrelation interferometer 79−17468
picosecond beam, spatial struct. in a non-linear medium 79−94287
picosecond chronoscopy of repetitive weak light sources 78−38033
picosecond laser impulse, characterisation by sweeping slit cameras *(French)* 78−42366
picosecond laser pulse length meas. using fast optical shutter and echelette grating 79−64266
picosecond laser pulse stabilisation, attenuation and shaping by dye two-photon absorpt. 79−55165
picosecond light pulse shape and duration determ. by bleaching of dyes 79−86220
picosecond light pulses, spectral meas. using microcomputer-controlled multichannel analyser 79−93890
picosecond photochronoscopy, generation and meas. of pulses from mode-locked lasers 79−76734
picosecond pulse diagnostics, using electro-optical deflector streak camera system 78−33909
picosecond pulse generation at 10.6 μm, using Ge optical switch 79−7159
picosecond pulse generation with a CW GaAlAs laser diode 79−50329
picosecond pulse meas. using streak camera 78−33902
picosecond pulse parameter meas. 77−19271
picosecond pulse time behaviour, background free meas. using SHG in $LiIO_3$ 79−59758
picosecond pulses generation and meas. 79−41401
piezoelectric positioner three-axis coordinate convertor for optical scanners 79−63199
piezoelectric stack for beam control 77−72012
planar sources generating same radiant intensity distribs., equivalence theorems 79−89843
plasma shutter, expanding supersonic plasma 79−68412
pointing and tracking through air-sea interface 77−79776
pointing control system, visible to IR wavelengths 79−98426
polarisation flipper, for i.r. beams, using five mirrors 77−699
polarisation flipper for IR laser beams mirror and prism systems 77−75586
polarisation of laser light, review *(Japanese)* 78−5516
polarisation of output radiation, gas laser with resonator weak phase anisotropy 79−64264
polarisation rotator, broad band, for high power appls. in IR 79−981
polarization of intense beam propag. in liquid, DC elec. field influence 80−91828
position determ. using ordinary paper 80−33046
power, measurement using miniature calorimetric convertor 79−22998
power and coherence requirements for holography 79−50260
power meas., radiometric and calorimetric scales' equivalence 77−7115
power meas., scale comparison for calorimeter and radiometer systems 79−76729
power measurement, calorimetry development at NBS and Calorimetrics Inc. 78−22161
power measurement at 633 nm, international intercomparison 78−37930
power measurement by new thermoelec. detector *(French)* 77−58365
power measurement by thermoelec. meter 78−63124
power meter, absolute CW laser, based on momentum transfer *(French)* 78−37932
power meter, Al slab, for output meas. from high power CW CO_2 laser 79−59739
power meter calibration for the range 5-1000 W using electrically calibrated calorimeters and beam splitters 78−1241
power monitor, nearly transparent for optically pumped FIR lasers 80−5773
prism beam expander in N_2 laser pumped dye laser, prism material dispersion 79−27285
prism used as beam expander in N_2 laser pumped dye laser, dispersion 78−74924
processing and appl., 1979 progress survey *(Japanese)* 80−1262
profile measurement, wide-range monitor system using photodiode or pyroelec. array 77−58364
profile measurement using spatial sampling, Fourier optics and holography 79−86201
propagation eqn., finite difference approx. *(French)* 77−72017
propagation experiment in low visibility atm. 77−88829
propagation experiment in low visibility atmosphere 78−46703
propagation in evap. liq. drop medium, wind refr. 77−5322
propagation in thermal turbulence *(French)* 77−7007
propagation in turbulent atm., phase fluctuations spectrum 78−78914
propagation in turbulent medium, light intensity two-freq. fluctuations correl. 79−98280
propagation in water, multiple scattering effects *(Japanese)* 78−78915
propagation through atmosphere, wind, thermal turbulence effect 77−83814
propagation through atmospheric turbulence, long- and short-term Strehl ratios 79−62577
propagation through atmospheric turbulence 80−41550
propagation through inhomogeneous media, appl. to spin-flip Raman laser 77−79883
propagation through snowfall, characts. 79−74958

laser beams continued
ps light pulse length determ. by parametric amplification in nonlinear crysts. 78−1306
pulse amplification through energy exchange with electron beam via nonlinear radiation press. effects 80−95776
pulse broadening in multiple-scatt. media, closed form expression 78−42277
pulse duration by second harmonic beam anal. 80−1275
pulse duration measurement, 0.1 to 100 psec., nonlinear autocorrelation methods 78−46702
pulse energy, picoseconds order meas. *(French)* 80−74412
pulse energy measurement, by liquid calorimeter *(Russian)* 78−22163
pulse energy monitor 78−66839
pulse generation, double, gradual cutting-off resonator losses 80−69433
pulse generation, temporally shaped, for inertial confinement 78−50831
pulse generation and meas., 0.2 psec., from passively mode locked dye laser 78−50830
pulse generation using up to five independent CO_2 waveguide lasers 77−38907
pulse intensity depend. of two-photon fluoresc. contrast ratio 80−1255
pulse profiling in high power lasers for fusion, methods 79−50870
pulse profiling in high power lasers for fusion, pulse evolution in amplifiers 79−50872
pulse propagation, high intensity, in absorbing medium *(Russian)* 79−59752
pulse recording with picosecond, femtosecond resolution, using image convertor tubes 78−33903
pulse shape in cavity filled with Kerr dielectric, bistable behaviour 80−99787
pulse shaping by nonlinear interferometers 78−79051
pulse shaping by passive optical Fourier techniques 77−10934
pulse shaping for laser fusion 77−88806
pulse shaping in Nd:glass amplifier, variable spectrum input 77−14758
pulse shaping with grating pair and filters 79−89940
pulse shortening by intensity dependent total refl. in CS_2 77−14781
pulse squaring effects in dispersive delay line 77−72035
pulse synchronisation system for fusion laser 77−88807
pulse synchronization in Q-switched and mode-locking regime 78−5510
pulse tailoring and termination, by Fabry-Perot cavity self-sweeping 80−23760
pulse width, meas. by two-photon absorpt. fluoresc., contrast ratio variation 79−76737
pulse width from solid-state measurement lasers, meas. using Fabry-Perot interferometer 80−23736
pulse width meas., integral method with direct reading 77−72019
pulse width meas., picosecond, tunable laser resources development and appl. 80−48262
pulsed, output spatial characts. using FTIROS material 79−68414
pulsed chemical laser amplifier, beam deflection 79−50331
pulsed gas laser with unstable resonator, beam shaping 78−17987
pulsed imitators of laser radiation 80−23765
pulsed laser energy measurement system and calibration facility 79−27301
pulsed laser intensity evaluation using saturation, organic mol. photophysical parameters 79−59735
pulsed laser power meas. 79−86202
pulsed laser radiation beams, energy flux density meas. based on thin-film thermometry 79−81472
pulsed laser radiation intensity fluctuations, thermal selfinteraction in turbulent medium 80−102781
pulsed laser radiation pattern divergence meas., focal spot method 77−23683
pulsed lasers beams shape measuring technique 80−1214
pulsed output, from mode-locked laser, quantised field representation 78−79054
pulsed radiation energy measurement using multichannel instrum. 79−76731
pulsed solid laser radiation reproducibility *(German)* 77−58331
pyroelectric detector of transmitted power, coordinate-sensitive, for laser beam displacement determ. 79−75599
Q-switched pulse stretching by intracavity nonlinear ellipse rot. 78−17991
quasi-homogeneous Gaussian source, spatial coherence 80−48145
radial intensity distrib. form. by soft apertures 77−7110
radial intensity distrib. formation by use of Faraday effect 77−54746
radiance produced by beam transversing particulate multiple scatt. medium 78−9325
radiant flux density, thin film thermometry 77−38967
radiation asymmetry, in laser with inhomogeneous active layer *(Russian)* 79−23003
radiation density of CO_2 lasers, quantitative estimation using PVA-I_2 film 77−58368
radiation fluctuation-spectrum recording for USSR state standard 78−45696
radiation intensity distrib. meas., high-speed unit 77−38969
radiation kinetics, photoelectric transducer conversion factor measurement 79−2820
radiation monitoring for pulsed oscillators 78−5515
radiation pulse length meas., discussion 80−1259
radiation pulse-length monitor testing, precision test system 78−45697
random medium, finite beam propagation 80−91748
randomly diffusing surface, laser beam scatt., simplified statistical model *(Chinese)* 79−50217
Rayleigh-Debye scattering with focused laser beams 78−71030
reciprocity theorem, for polarised laser beams 78−79055
reflection from sea surface, effect of water surface wavenumber spectrum 80−31121
refraction at spherical surface, distortion, geometrical optics calc. 80−95929
refraction into a nonlinear medium: wave profiles and hysteresis 80−43395
regerative compression of mode-locked laser pulses using saturable dye 80−95925
resonant propagation of two concomitant optical pulses interacting with three-level atomic system, num. modelling 80−9942
resonant-pulse propagation method for line-shape parameters analysis 79−55168
resonator, unstable telescopic, precision of some methods of adjustment *(Russian)* 80−38040
resonator-focusing system, power density improvements, anal. 79−50335
laser beams continued
retroreflecting mirror for dynamic compensation of optical inhomogeneities 79−31970
rhodamine 6G, halo laser device 79−72597
rhodamine 6G dye laser, degree of polaris., solvent effect 79−41375
rhodamine 6G dye laser, N_2 laser-pumped, pulse time behaviour 79−31894
rhodamine 6G laser amplifier pumped by N_2 laser, sub nsec pulse generation 80−1232
rhodamine B dye laser, N_2 laser-pumped, pulse time behaviour 79−31894
rhomb laser beam sampler, two-grating, inherent aberration correction, inverse filter description 80−37954
rotating, generation by ruby laser with nonorthogonal resonator *(Russian)* 79−10330
rotating beam generation in ruby laser 80−1258
ruby, beam characts. using DC induced SHG in gas 77−7093
ruby, spatial coherence meas. with holographic coherence meter 80−9837
ruby laser, wavefront restoration *(Russian)* 77−38989
ruby laser beam spatial coherence interferometry 79−14003
ruby laser with small active volume, mode-locked ultrashort pulse generation 79−89932
ruby lasers, freq. synchronisation and locking by passive modulator 80−1249
ruby passively mode-locked laser, subnanosecond pulse generation using saturable absorber 79−86197
ruby Q-switched laser, photographic film calibration for energy meas. 78−5517
safety, beam diameter meas. methods survey 80−53348
safety aspects of LED- and laser-fed cables 78−74968
safety aspects of LED- and laser-fed cables 78−74969
safety standards, calc. of max. permissible exposure levels 79−96666
saturation parameter from gain meas. 78−66797
SAW propagation study based on coherent light diffraction *(Russian)* 79−14172
scaling props. of laser light, photoelectron and photon statistics 77−14729
scanner status 79−89921
scanning, nonlinear distortions 80−14407
scanning by acousto-optic deflector array 80−10017
scanning using phased array of optical fibres 79−81514
scanning using rotating mirrors, specifications and tolerances 80−9979
scattering by diffusing surfaces *(Chinese)* 80−1128
scattering from rough-surface materials, anal. and prediction 79−72493
scattering of ultrashort laser pulse by large spherical particle 79−906
scintillation, in turbulent atmosphere 79−80018
scintillation beyond turbulent atm., numerical calc. 77−7005
second order coherence function, phase determ. 78−9406
self diffraction of laser beam by liquid crystal struct. 80−5803
self-adjusting laser-target system for laser fusion 79−14024
self-channeling, Schrodinger nonlinear eqn., exact soln. *(Ukrainian)* 79−94278
self-focusing in nonlinear media 80−48360
self-focusing stability in isotropic phase of liquid crystal 80−99812
semiconductor, high-power radiation propagation, rel. to interband absorption or amplification 79−76727
semiconductor DFB lasers, operating in higher Bragg interaction orders, radiation spatial characts. 79−89933
semiconductor junction laser, radiation coherence, interferometric analysis methods *(Polish)* 80−19065
semiconductor laser, HF AM, near-zone radiation field delay fluctuations 77−61987
semiconductor laser pulse radiation, coherence rel. to Fourier hologram recording 78−50738
semiconductor laser with electron-beam-induced stripe waveguide, radiation directionality 80−28237
shadow cast by half-screen when illuminated by Gaussian beam, props. 80−28156
shaping by lens system, design 78−13781
Shiva laser beam diagnostics 78−59037
Shiva laser performance, nominal interstage beam energy, power 78−59032
Shiva optical system 78−59039
side band spatial elimination associated with acoustooptical pulse-picking 79−59732
signal distortion due to beam pointing error 78−37937
signal measurement with nonlinear conversion of multimode laser radiation 77−23715
simulator for 1.06 μm laser radiation 77−38903
single axial mode laser, degenerated by mag. field, light props. *(Japanese)* 79−64254
single mode fibre cable, 4.15-km, interf. and polarisation characts. using AlGaAs laser 79−81535
single mode laser, photon statistics, intracavity two-photon absorption effect *(German)* 77−10933
single particle scattering with focused laser beams 77−58248
single picosecond pulse, freq. sweeping and self focusing, direct streak meas. 78−25915
single pulse extraction from mode locked train using dye amplifier 77−19314
single pulse spectral distrib. meas., using Fabry-Perot interferometer and CCTV system 79−3732
single transverse mode radiation, spatial coherence 77−14733
single-mode, modal noise suppression by dithering laser's operating point 79−94357
single-mode formation anal. by nonconfocal optical system *(Russian)* 78−71132
smooth transverse intensity distrib. form. by phase-rotating plate 79−59837
in snowfall, intensity fluctuations *(Russian)* 80−94602
soft apertures, method of controlling inversion profile in amplifier 79−98427
solid laser, measurement, radiation pulses formation and stabilisation 80−23735
solid laser, passively mode-locked, statistical props. of ultra-short pulses 79−36941
solid laser wavelength identification using reference absorber 78−5513
solid state directly coated laser rods, beam divergence and refractive power 79−59736
solid state laser, refraction effects and gain meas. 79−31905

laser beams continued
solid state laser satellite rings, energy losses caused by diffusion, refl. in cavity 79−89911
space-time characteristics, pyromag. detector meas. *(Russian)* 79−93220
spatial and temporal fluctuations of nanosecond radiation pulses in CO_2 amplifiers 79−14009
spatial characteristics control of single-pulse laser 78−79058
spatial characteristics meas. by modulation method 79−31967
spatial coherence control by progressive US wave 80−78885
spatial coherence degree correlation with wave vector variance 79−45985
spatial coherence in a randomly inhomogeneous medium, effect of thermal nonlinearity 80−9926
spatial coherence of radiation transmitted by MBBA near isotropic transition 78−18003
spatial distribution of laser radiation control 80−64086
spatial filtering function for collimated laser beam amplitude fluctuations in turbulent atm. 80−9810
spatial scanning by nonlinear freq. conversion *(Russian)* 79−50336
spatial structure, inaccuracy of reproduction in amplifying medium with reversing mirror 80−14379
spatial-temporal intensity distrib., Charlier curve 77−14732
spatially coherent laser beam form., phase transitions 78−17898
spatially inhomogeneous, induced scatt. 80−28274
speckle, non-Gaussian, contrast variation 80−83554
speckle motion in laser refraction, expt. obs., vision appls. 80−45879
speckle reduction in image plane by US modulation of spatial coherence 80−106459
spectral analysis, photomixing method 78−46698
spectral characteristics measurement, high resolution spectroscopy appl. 78−89555
spectral purity of high intensity beam, spectroscopic, interferometric and filtering anal. 77−88823
spectrum analyser for laser oscillator radiation 77−26403
spot size, simple accurate measurement technique 78−63146
spot size meas. by scanning with opaque ribbon 77−38972
square law medium excitation by optical wave beam *(Japanese)* 80−38052
stability theory of coherent laser pulses in inverted medium 77−10936
statistical characteristics of laser field, influence on two photon absorpt. *(Russian)* 80−37842
steerer-expander device, two-mirror afocal telescope design 78−46700
steering, using hole grating attenuator 78−59071
stimulated Brillouin scatt., three dimensional, for focused Gaussian beam 80−69456
stimulated Raman scattering with spatially inhomogeneous pump, enhanced gain 80−28279
stochastically fluctuating, saturation and Stark splitting of resonant transitions 80−53245
streak camera for subpicosecond chronoscopy 78−38030
strong intensity fluctuations in turbulent atm., similarity relations and expt. verification, book contrib. 79−34958
structural conversion of coherent beam, using volume phase hologram in $LiNbO_3$ 79−59656
sub-picosecond optical pulses, generation and meas. 80−23731
submillimeter radiation field, transverse distribution, scanning device for visualisation 78−4693
submillimetric laser wave propagation, range and resolution 77−41242
subMM wave mixing in metal-metal and metal semiconductor point contact diodes 80−4769
subnanosecond optical free-induction decay with novel laser freq. shifting 80−38075
subnanosecond pulse production, of variable length 78−94405
subnanosecond pulses, stretching and spectroscopy using Fabry-Perot interferometer 77−42555
subnanosecond pulses from longer pulses using Pockels cells 77−83904
subpicosecond spectroscopy, high intensity, broad wavelength tunability 79−44950
superradiant dye laser, coherence and beam geometry 78−37876
tachyon, EM analogue, production by reflected ultrashort laser pulse *(Russian)* 77−46680
TEA-CO_2 laser, transverse profile pulse evolution 79−98425
TEM_{10} laser mode for IR holography at 10.6 μm 79−27199
temporal characteristics analysis of short laser pulses, SHG soln. 78−22171
temporal compression of dye laser 5890 Å CW output, using Na vapour delay line 78−46688
temporal pulse shape of Ar ion laser system, streak camera meas. 77−79799
thermal blooming: round beam vs square beam, computer study 80−38076
thermal blooming, continuum-lens model 80−78918
thermal blooming, enhanced focal plane irradiance 77−7096
thermal blooming, theoretical aspects of compensation 78−32226
thermal blooming cell design for adaptive optics evaluation 80−33096
thermal blooming cell design for use in evaluating adaptive optics 80−102780
thermal blooming compensation, equivalent thin lens model 78−87108
thermal blooming compensation with multidither COAT system 78−33789
thermal blooming effect on laser beam propag. with on-axis null 77−27323
thermal blooming in a diagonal wind 80−95965
thermal blooming in atmosphere, book contrib. 79−34961
thermal blooming in axial pipe flow: comment [and reply] 80−95966
thermal blooming in laboratory expts., index of refr. turbulence effects 79−50357
thermal blooming of slewed laser beam, stagnation and transonic effects 77−34903
thermal blooming of slewed laser beam with stagnant absorber region 77−38966
thermal blooming reduction vice phase correction, experimental demonstration 79−98449
thermal lensing in SiO_2 plate, aberration effects 78−63148
thermal lensing in window materials 77−72021
thermal self-action over path in medium moving at variable vel., expt. and numerical simulation 79−32003
thermal self-focusing of laser beams in moving media 80−64122
thermal self-interaction of annular laser beams in moving medium 78−71159
laser beams continued
thermal-blooming compensation, using closed-loop adaptive single parameter system 78−94407
thermally induced self-focusing, laser beam with spatial and temporal inhomogeneity 79−32002
thermo-gasdynamic control in laser beam guidance, review of developments 78−74942
thermoelectronic laser energy convertor, Cs plasma device 78−90421
threshold recording energy density meas. method 78−5520
tracking turbulence induced tilt errors with shared and adjacent apertures 77−46792
transformation for improved angular charact., transverse mode struct. depend. 79−89950
transformation of Gaussian beam by laser anemometer elements 79−45991
transformation of space-angular characteristics of the Gaussian beams by means of phase masks *(Ukrainian)* 80−69438
transient self-diffraction in absorbing liquid 80−9927
transmission through fibre light guide, spatial coherence 78−71133
transmitted Gaussian laser beam, critical angle phenomena 77−27298
transparent materials, laser light refl. and transmission, high power densities 79−27305
transverse mode struct., laser field transformation *(Russian)* 78−37934
traveling Michelson interferometer with phase-locked fringe interpolation 78−89451
truncated Gaussian beam variation effects in laser saturation spectroscopy 77−31119
turbulent absorbing liq. medium, laser radiation thermal self-interaction 80−91868
turbulent atmosphere, beam props. of partially coherent curved beam waves 80−95798
turbulent atmosphere, laser beam propag. Huygens-Kirchhoff method 78−32228
turbulent atmosphere propagation, spectral expansion soln. method 79−18350
turbulent atmosphere reflection, laser radiation intensity fluctuations 77−50621
turning of beam through const. ang. by prism, for teaching 79−25805
TV analyser of laser radiation 79−3702
two-beam mirror interferometer, accuracy, emission beam divergence effects 79−26115
two-mirror laser beam steerer-expander design 79−18460
two-photon absorbents, laser pulse propagation 78−50862
two-photon laser beam, breathing mode of EM field 78−46558
ultrashort laser pulse onset, first or second order phase transition 78−78986
ultrashort light pulse formation optimisation 80−64085
ultrashort light pulses, duration and reproducibility improvements *(Russian)* 78−22159
ultrashort pulse operations using flat lenses 78−66883
undersea transmission charact. of laser beam in Tago Bay, Japan 77−21782
underwater laser beam transmission charact. in Tago Bay *(Japanese)* 77−21797
unstable resonator containing small-scale phase inhomogeneities, laser props. 80−19057
UV laser window material absorption obs. 79−14012
variable attenuator for Gaussian laser beams 79−22987
variable ratio beam splitters, for high energy glass laser systems 79−45952
vertical propagation through troposphere 79−39851
very high-intensity laser beam, autofocusing propag. effects *(Italian)* 79−68420
vibrating laser speckle in diffr. field, dynamic statistical props. 79−22895
volume attenuation coeff., invalidity 80−95791
wandering in turbulent atm., error probability in binary signal reception 79−10337
wandering in turbulent atm., fluctuation power probability density distrib. 79−10336
water aerosol, propagation of intense radiation at 10.6 μm 80−5692
water vapour absorption of CO_2 laser beam, optoacoustic detector meas. 77−9512
wave beam distortion by thermal self-interaction in droplet medium 80−19082
wave conjugation by three photon mixing, effect of strong wave front distrib. 80−5783
wavefront analyser for diagnosing high-energy lasers 79−59740
wavefront analyzer for diagnosing high-energy lasers 79−59738
wavefront conjugate complex prod., scatt. and diffr. in non-uniform phase film *(Russian)* 77−38973
wavefront correlation transformations *(Russian)* 80−99778
wavefront curvature meas. of small diam. laser beams using Fourier imaging 79−94273
wavefront rotation for light beam nonlinear deformation compensation *(Russian)* 80−64094
wavefront visualizer for coherent IR beams 78−25986
waveguide propag. in frozen gaseous layers at 4.2K 80−64168
wavelength, automatic reading by wavelength-modulation technique *(Japanese)* 78−1286
wavelength, comparison of 2 beams, two-wave interference, book contrib. 78−9408
wavelength and linewidth measurement using high-resolution monochromotor-interferometer 80−33153
wavelength calibration using optogalvanic effect, atlas 80−62727
wavelength comparison by two-beam interferometer, I_2 stabilised He-Ne laser 78−86326
wavelength comparison with standard, using interferometric digital wavemeter 77−162
wavelength determ., random/systematic errors statistical estimation 78−17996
wavelength intercomparison between methane and I_2 stabilised He-Ne lasers 78−87089
wavelength meas., review 78−89446
wavelength meas. using material spectral transmission curves 79−76738
wavelength meas. with Michelson and servocontrolled Fabry-Perot interferometers 78−89452
wavelength measurement, review 78−50841
wavelength meter, compact static, based on Fizeau interferometer, for pulsed and CW lasers 79−36947

laser beams continued
wavelength meter for pulsed or CW lasers, Fizeau interferometer system 78−46701
wavemeter, inexpensive broadband optics and minicomputer interface 78−89448
wavemeter for CW lasers 79−26112
wavenumber calibration of Pb salt tunable diode lasers, using etalons 78−45738
weak optical laser radiation in random-pulse sequence, recording 77−37988
(AlGa)As, CW, accelerated ageing effect on optical props. 77−38898
Ar ion laser radiation, Faraday effect, polarisation plane negative rot. 79−98424
Ar laser emission under passive mode-locking conditions, temporal structure 80−9923
CO, CW output spectral content meas. with scanning Fabry-Perot interferometer 77−27292
CO_2 10 kJ laser for fusion research, automated alignment 79−76703
CO_2 10.6 μm laser pulse spatial distrib. recording, nanosecond photography with Ag halide film 79−89016
CO_2, 30 ps laser pulse generation by free induction decay 77−14738
CO_2 9.4μm band R(14) line, absolute wavelength meas. for light speed determ. 77−82485
CO_2 amplifier, method for radiation pulse shape control 80−43367
CO_2 atmospheric propag. enhancement due to offline centre tuning, thermal blooming reduction 79−84472
CO_2, beam shaping with computer generated hologram 77−14726
CO_2 CW electric discharge laser, output beam props. 79−36877
CO_2 CW laser, energy distrib. meas. using heat resistant camera shutter 77−58369
CO_2, continuously tunable multiatom. laser, real time linewidth meas. 78−9405
CO_2 electric discharge CW laser beam properties 79−76736
CO_2 gas transport laser with cylindrical geometry 79−7108
CO_2 high power laser beam monitor 78−74943
CO_2, high press., pulse temporal struct. using up-conversion 77−3603
CO_2 highly multimode pulsed electron beam laser, beam divergence 79−3731
CO_2 laser, active medium obs. using heat camera system 80−1257
CO_2 laser, Gaussian beams energy profile 79−64247
CO_2 laser, intense sub ns pulse attenuation and reshaping 77−88870
CO_2 laser, pulse flow stretching *(Chinese)* 78−90435
CO_2 laser, radiation detection by PbSnTe detector and preamplifier modules 78−32875
CO_2 laser, Stark cell noise reduction 78−59059
CO_2 laser, with anisotropic resonator, radiation polarisation *(Russian)* 79−27309
CO_2 laser amplifier, short pulse propagation calcs. 79−76730
CO_2 laser Antares fusion system beam alignment 80−74422
CO_2 laser Antares fusion system optical diffraction computation 80−74424
CO_2 laser beam Al target interaction, pulse shape importance 80−108307
CO_2 laser beam alignment, accuracy, Snout test 78−59073
CO_2 laser beam attenuation by air discharge plasma column 80−19062
CO_2 laser beam focal zone rel. to luminesc. duration of NaCl particle 80−34983
CO_2 laser beam meas. using pyroelectric vidicons 78−49907
CO_2 laser beam-diagnostics techniques, laser beam parameter monitoring 80−64089
CO_2 laser fusion system phase conjugation 80−74429
CO_2 laser Helios fusion system, beam simultaneity system 80−74419
CO_2 laser Helios fusion system alignment 80−74420
CO_2 laser Helios fusion target positioning with orthogonal telescopes 80−74421
CO_2 laser Helios fusion system beam diagnostics 80−78882
CO_2 laser noise, fluctuations and output power stabilisation, 1 Hz to 150 kHz *(Polish)* 78−5447
CO_2 laser pulse, nonlinear propagation, computer simulation *(Japanese)* 80−95963
CO_2 laser pulse meas., single sweep 5 GHz oscilloscope detector system 77−88817
CO_2 laser pulse meas., pyroelectric detector development 80−78884
CO_2 laser pulse temporal shaping by controlled plasma switching 79−3725
CO_2 laser radiation, intracavity modulation of polarization direction 80−102744
CO_2 laser radiation, single pulse, thermal blooming 80−19080
CO_2 laser radiation reson. absorpt., atm. NH_3 conc. determ. on long path 79−29904
CO_2 mode-locked hybrid TEA laser, variable width stable pulse prod. 79−76726
CO_2 multiatmosphere laser, mode-locked pulses 80−1248
CO_2, pulse evolution 77−10884
CO_2 pulse generation by free induction decay in KCl:$KReO_4$ 80−53388
CO_2 pulsed laser beam, thermal coupling 78−63145
CO_2 pulsed laser output, spatial distrib. meas. by photographic device 79−14008
CO_2 pulsed laser radiation field, energy density distrib. recording 78−1292
CO_2, single ultrashort pulse generation in Fabry-Perot interferometer 78−29996
CO_2 single-pulse laser, emission spectrum photographic recording by parametric conversion 79−10357
CO_2, TEA, pulse stretching by CO addition 77−14754
CO_2 TEA laser, shortening of pulses *(Rumanian)* 79−86199
CO_2 TEA laser mode locked by positive Ge, pulse shape meas. 78−46694
CO_2 TEA Laser pulse, PCM with CdTe crystal Pockels modulator 80−102742
CO_2 TEA laser pulses, interaction with aerosol particles 77−7097
CO_2 ultrashort pulse generation by free-induction decay in KCl:$KReO_4$ 80−74444
CO_2 waveguide laser, parameters meas. 79−31859
CO_2 waveguide laser pulse shaping on multiple rot. lines 80−78879
CO_2, weak laser lines around 10.6 μm, wavenumber meas. 78−17998
CO_2-He-N_2, absorpt. coeff. for 10.6 μm CO_2 laser radiation, 295 to 650 K 80−92252
CO_2-N_2-He self-sustained TEA discharge laser, config. for high beam qualtiy 77−14753

laser beams continued
CO_2 laser short pulse diagnostics, using upconversion linearity in Ag_3AsS_3 79−27304
CdTe linear electro-optic translation of IR laser wavelengths 80−78878
Cu vapour laser, coherent props., dynamic holography in VO_2 films 79−13929
D_2O far IR laser pulses, real-time spectral anal. using SAW dispersive delay line 79−45983
GaAlAs DH laser-diode-to-diffused-waveguide coupling calcs., Gaussian beam model 79−94372
GaAlAs, diode laser, CW radiation, intensity noise spectra of axial mode groups 77−34890
GaAlAs laser diode, CW, ps pulse generation 79−50329
(GaAl)As low-beam-divergence CW DH laser, grown by low press. metal-lorganic CVD 80−74376
$Ga_{1-x}Al_xAs$ visible diode lasers, transverse-mode stabilised, nonstigmatic laser beams 79−76694
GaAs single-channel injection laser, polarisation characts. 80−48256
GaAs single-frequency injection laser, coherence of emitted radiation 79−31904
GaAs:Zn optically pumped ribbon-whisker laser, picosecond pulses 80−99771
GaAs-AlGaAs DH injection laser with stripe contacts, radiation pulse stepped shape 80−91799
GaAs-GaAlAs injection laser, radiation divergence reduction by non-waveguide mode excitation 80−91797
GaInAsP/InP DH lasers, direct modulation charact. meas. by sharp pulse method 80−1245
GaInAsP-InP DH lasers with low threshold; narrow-beam divergence 79−36892
HCN, CW 337 μm laser, spatial coherence meas. 77−3595
HF, beam spectral anal. using near field holography 77−23680
HF CW chemical laser with unstable telescopic resonator, diffr. effects 79−94265
HF chemical laser beam, phase fluctuation meas. 80−48317
HF, high-energy laser, energy extraction, beam quality, for fusion ignition 78−63102
HF laser, Phoenix oscillator-amplifier system, laser-beam characts., rel. to plasma heating 79−76701
He-Ne, 0.63 μm emission intensity fluctuations, spectral correl. 78−1212
He-Ne, internal mirror laser, polarisation props. of output beam 77−46744
He-Ne beams, detection by surface barrier position sensitive detectors 79−36485
He-Ne laser, atmospheric extinction meas. 78−40654
He-Ne laser, field distrib. and spatial coherence of superluminescence at 3.39 μ transition *(Russian)* 78−13682
He-Ne laser, radiation field spatial distrib. distortions due to multilayer dielectric mirrors 77−38970
He-Ne laser freq. determ., interferometric comparison with upconverted CO_2 laser radiation 78−55395
He-Ne laser near threshold, intrinsic third-order intensity correlation 77−10887
He-Ne laser radiation, frequency shifting via rotating half-wave retardation plate 80−9800
He-Ne laser radiation, spatial and temporal correlation of intensity fluctuations 79−81473
He-Ne lasers, wavefront curvature and diffraction effects in high precision wavelength comparisons with a Michelson interferometer 80−99781
I, energy profile meas. using hypersensitised photographic plates 78−5518
I laser, 100 ps pulse generation and amplification 77−19301
I laser, Asterix III, light-plasma interaction expt. and light pulse props. 80−53349
I laser, high-power, beam quality, gain saturation effect, for fusion ignition 78−63149
I photodissociation laser, diffr. limited output beam 79−27286
InGaAsP buried stripe laser, modulation characts. 79−98418
KrF 1J avalanche discharge laser unstable resonator expts., beam divergence 80−74404
KrF discharge pumped laser, stable-unstable resonator for beam control 80−23722
KrF excimer laser, passive mode-locking using saturable absorber dyes 80−1244
KrF injection locked unstable resonator discharge laser, narrow linewidth and high spatial quality 80−53323
KrF laser beam, Raman pulse compression, for fusion expts. 78−59086
KrF* tunable ultrahigh spectral brightness excimer laser source 80−64046
$LiNbO_3$ laser beam/SAW mode conversion 79−46056
$LiNdP_4O_{12}$ laser, fluctuations in bath of strong Gaussian noise 79−55166
N_2 helical TE laser with circular beam cross section 80−33023
N_2 laser, 3371 Å, fringe visibility curve 78−46695
N_2 liquid Raman laser with slowly relaxing active medium, radiation divergence 79−98352
N_2 multichannel Blumlein type laser, elec. and optical characts. 79−59719
N_2^+ high-pressure laser, superradiance spatial structure 79−64215
Nd, multifreq. laser, coherence time meas. using bleaching dyes 80−23739
Nd:glass, mode locked, picosec. pulse form., expt. technique 77−38957
Nd:glass, Q-switched laser, radiation polarisation 77−27293
Nd:glass, subnanosecond pulse oscillator, investigation by high-speed oscillography 80−74411
Nd:glass laser, stable ultrashort light pulses generation *(German)* 80−91823
Nd:glass laser amplifiers, self-focusing and suppression by spatial filtering 80−14406
Nd:glass laser array, mode locking, spatially coherent beam form. 77−88811
Nd:glass laser array, spatially coherent beam form., mode locking 78−29989
Nd:glass laser beam distrib. in focal region, transmission monitoring through pinhole 78−90441
Nd:glass laser in Tl vapour, output conversion from 1.06 micron to 388.1 nm 80−91850
Nd:glass laser picosecond pulses, background energy content meas. with saturable absorbers 78−59062
Nd:glass laser radiation, spatial coherence of fundamental and second harmonic 80−69442

laser beams continued
Nd:glass laser six beam system, output characts. *(Chinese)* 80−83612
Nd:glass laser system, beam spatial profile optimization in amplifier channel 80−74407
Nd:glass laser with continuously tunable ps output, polaris. filter 79−22985
Nd:glass laser with unstable resonator and additional feedback, angular divergence 80−48307
Nd:glass ring laser, single synchronizable ps pulse generation 77−14739
Nd:glass ultrashort pulse length, passive switch relax. time effect 77−38960
Nd:phosphate glass, single ps pulse props. 77−19273
Nd:YAG, actively mode locked laser, short pulse generation for fusion 77−88809
Nd:YAG, CW mode-locked, diagnostics of radiation using nearly online picosecond streak camera 79−49314
Nd:YAG, electro-optical extraction of ps laser pulse *(German)* 80−87416
Nd:YAG, injection locked oscillator, pulse duration var. 77−88772
Nd:YAG, passive mode-locked, picosecond pulse duration, determ. from luminesc. intensity 78−71134
Nd:YAG high performance laser system efficiency and beam uniformity 77−19327
Nd:YAG laser, high repetition rate stimulated Raman scatt., thermal blooming in liquid N_2 80−91865
Nd:YAG long-pulsed laser, resonator config. for relax. oscills. suppression 79−72599
Nd:YAG mode-locked laser pulse, quadratic phase evolution direct meas., time resolved interferometry 80−48318
Nd:YAG passively locked laser, pulse width meas. by SHG method *(Chinese)* 80−87432
Nd:YAG Q-switched laser beam and waist, knife-edge profiling 79−45982
Nd^{3+}:phosphate glass laser, brightness enhancement by spatial filtering in amplifying channel 80−48321
Nd^{3+}:YAG Q-switched picosecond laser radiation, pulse duration and energy fluctuations 79−89949
Nd+YAG, beam divergence in short interferometers 77−27310
Pb salt tunable diode laser-integrating sphere system, output intensity characts. 80−78881
Pb-salt tunable diode lasers, beamshaping and polarisation control props. of flexible hollow metallic rectangular pipes in mid-IR 79−76856
Xe 3.5 μm self-mode-locked laser pulse, waveform analysis 78−1290
Xe_2 excimer laser pulse temporal evolution, cavity mirror depend. 79−76732
XeCl 80−53323
XeCl, high-energy subnanosecond pulse amplification 80−99770
XeCl laser pulse backward Raman compression in Pb vapour 80−19068
YAG stable resonator, yielding high output energy and very low divergence beam 80−23721

laser cavity resonators
active control techniques 78−71122
adaptive, intracavity phase variations 77−88793
adaptive laser resonator techniques for CO_2 laser, phase error correction 79−59729
adaptive optical components, seminar, Washington (1978) 79−59792
adaptive optical system, intracavity deformable mirror 78−87078
adaptive optics technology overview, book contrib. 79−32030
adaptive resonator expt. config. 78−55386
adaptive resonator techniques, multidither COAT system 78−42360
adiabatic invariant of oscillatory systems, laser mode sweeping interpretation 79−31950
anisotropic inhomogeneous medium with axial symm., mode struct. 78−18069
annular, adaptive mirror effects on performance 80−58596
annular converging wave resonator 78−29981
annular gain volume lasers, unstable resonators 78−46672
annular HSURIA resonators, testing with CO_2 laser, polarisation effects 80−58599
annular mode volume lasers, unstable resonator concepts 77−88791
antiresonant ring laser and electrooptic phase modulator, for cavity dumping 77−88792
with aperture in mirror, natural type vibr. excitation *(Russian)* 77−46739
apodized aperture used in the laser oscillator *(Chinese)* 79−68408
astigmatic laser beam generation *(German)* 78−1269
asymmetric waveguide structure semicond. laser, anomalous stimulated emission, theory 79−64228
asymmetric waveguide structure semicond. laser using external resonator, anomalous stimulated emission 79−64227
atomic beam tube with laser pump, interaction eqns. *(Russian)* 78−74801
automatic adjustment system for lasers with unstable cavities 77−50693
axicon and related optical component diagnostic techniques 80−14417
BBOT dye, vapour phase, optical props. *(Japanese)* 80−9879
BBOT dye vapour single-pass gain obs. 79−55136
beam divergence in short interferometers 77−27310
beam expander for short cavity dye laser 80−87532
beam expanind telescope, on-axis reflective, for pulsed dye laser cavities 79−41398
beam expansion with diffr. grating in dye laser cavity 78−66858
benchless laser structural model, control system 79−81464
benchless laser with autoalignment for airborne electro-optical systems 79−76723
birefringent filters for tuning flashlamp-pumped dye lasers 78−74914
bistability, optical, dispersive, beyond mean-field theory 80−43408
bistability of saturable-absorber containing laser, semiclassical and quantum theories 78−82943
Bragg mirror emission and absorpt. losses in waveguide mode *(Russian)* 78−1272
cavity with optical delay line 77−720
chemical CW laser, unstable resonators effect on performance 79−41397
chemical laser, CW, small-signal gain meas., cavity scans by chem. probe laser 78−22119
chemical laser, power spectral performance, coupled fluid dynamic, kinetic and physical optics model 78−79040
chemical laser, resonator design rel. to output beam quality, book contrib. 77−10964
chemical laser nozzle, effect of geometry and boundary layers on flow-field 77−27622

laser cavity resonators continued
chemical laser resonator modelling, LAMP and BLAZER code calcs. comparison with CL XV meas. 79−36890
cholesteric liquid crystal resonator for distrib. feedback dye laser, theory 79−31956
colour centre laser with superfluid He cooling 80−48282
colour centre pulsed broadly tunable IR laser 79−76706
complex resonator with internal diaphragm, diffr. losses and field distribs., integral eqns. 80−95921
computer generated hologram for CO_2 laser beam shaping 77−14726
concave grating mirror stable resonator, approx. anal. *(Chinese)* 79−50324
confocal spherical cavity, spatial-temporal intensity distrib. 77−14732
confocal strip resonator, diffr. performance, mirror defects effect 77−19349
confocal unstable resonator beam props., astigmatism due to Brewster angle windows 78−46670
confocal unstable resonators, high Fresnel no., optical extraction efficiency 80−14363
confocal unstable resonators, near- and far-field laser modes, free space and saturable gain media 78−46674
conical elements in resonator, mode structure, polarisation effects 79−98411
conical laser plasma tube, electron density distrib. 78−58981
conical resonator, high-order circular mode selection 77−75569
cooled laser mirror construction, possible use of open pore structures 79−31952
coupled generator and amplifier system, stationary modes 79−64196
coupled laser oscillators, injection modulation 80−99773
coupled transitions with arbitrary polarization of radiation 80−78827
coupled waveguide laser as optical oscillator 78−9399
coupling reflector, involute-related, for flash lamp pumped laser systems 78−90425
CW optically pumped far IR waveguide lasers, high-power operation and scaling 77−38949
cylindrical resonator thermal distortion due to surface absorbed energy *(Russian)* 78−13729
cylindrical-mirror confocal resonator design with high transmissivity region *(Russian)* 80−14361
cytochrome c, fast Raman spectroscopy using dye laser intracavity reson. Raman amplification 77−66794
decay time dependence on resonator type 78−25897
DFB film laser, wavelength control by elec. field 77−3616
DFB resonators, dielectric waveguide with periodic surface inhomogeneity 77−7146
dielectric laser mirror production with variable transmissivity *(Russian)* 80−14362
3,3-diethyl thiadicarbocyanine iodide dye, stimulated fluoresc. and stimulated reson. Raman scatt. relationship 80−91853
diffraction experiment in cavity with 1-D diaphragm 80−95920
diffraction grating, refl. type elec. controllable, for intracavity laser modulation 77−58357
diffraction losses for symmetrically tilted plane reflectors in open resonators 80−58598
diffraction structure as laser mode selector 79−89951
diffraction-limited CW optically-pumped far IR lasers, beam characts. 77−38953
1,1-difluoroethylene mm laser, waveguide cavities comparison, CW props. 78−42328
difluoromethane, using variable coupling open structure resonator, CW FIR laser line 79−94219
difluoromethane laser, optically pumped, FIR lines, performance efficiency 79−94220
diode, modulated, with short external cavity, single mode operation 80−5756
diode DH lasers, optimal cavity design for low-threshold-current-density operation 79−94259
diode laser in external cavity, linearized theory 80−69391
diode lasers coupled to external resonators, tutorial review 79−94231
distributed aperture effect in laser rods with negative lenses 78−66857
distributed Bragg reflector, coupled wave anal. 77−27305
distributed Bragg reflector for saturable resonator, bistability using Kerr effect 77−46737
distributed Bragg reflector laser design, waveguide struct. 77−27306
distributed Bragg reflector lasers, tunability using electro-optic effect 77−38938
distributed Bragg reflector optical resonator, response to light pulses 78−63141
driving circuit for laser cavity dumper 78−13717
dye, CW, mode selection by nonlinear absorpt. 77−705
dye, simultaneous tunable two-wavelength operation, cavity config. 77−3610
dye CW laser, double-mode-locked, config. for independent tunability 79−72590
dye CW laser, freq. locking to Ne absorpt. lines by Faraday filter 79−22989
dye CW laser, spectral narrowing and continuous tuning by grating beam-expansion 79−59720
dye CW laser, spectral narrowing by intracavity Na atomic beam 79−55159
dye CW lasers sharing common amplifier medium, synchronous mode locking 77−7119
dye CW synchronously mode locked laser, cavity length detuning 80−5768
dye grazing-incidence pulsed laser, operation in single longit. cavity mode 78−94398
dye high gain mm. bore laser, transverse mode control in waveguide resonator 78−1268
dye laser, cavity dumped flashlamp pumped 79−13987
dye laser, continuously pumped, pulse compression with slow saturable absorber 79−31959
dye laser, CW, pumped, stable multifreq. picosecond pulse emission, phase-locked radiation pumping 80−91789
dye laser, CW, synchronous pumping and passive mode-locking, for picosecond pulse generation 79−3727
dye laser, CW single-mode, 'double Michelson' mode selector and press. scanning 78−46686
dye laser, double grazing-incidence single-mode type 80−95906
dye laser, double wavelength operation using gratings at grazing incidence 80−53317
dye laser, efficient cavity dumped operation 78−46684

laser cavity resonators continued
dye laser, emission locking on to wavelength of I_2 mol. fluoresc. 80−99721
dye laser, flash lamp pumped, tuning by grazing incidence grating technique 80−95914
dye laser, flashlamp-pumped high-energy, spectral narrowing by two-stage injection locking 79−81450
dye laser, freq. locking of Na flame atomic transitions 78−50795
dye laser, frequency locking by selective refl. 78−29992
dye laser, generation subpicosecond light pulses 78−42354
dye laser, intracavity absorpt. of I_2 vapour 79−22992
dye laser, long pulses using resonator with spherical mirror and thermal lens 78−22149
dye laser, longit. pumped, simultaneous two-wavelength operation using intracavity prism *(French)* 79−970
dye laser, mode-locked, synchronously pumped, pulse-width stabilization 80−83622
dye laser, N_2 laser pumped, single mode operation 78−87060
dye laser, N_2 laser pumped, two wavelength outputs with orthogonal polarisations 78−50792
dye laser, narrow band CW oscillator/pulsed amplifier system for precision nonlinear spectrosc. 80−53318
dye laser, narrow linewidth short pulse operation, using dual prism beam expander and grating 79−971
dye laser, passively mode-locked, parameters affecting subps pulse duration 79−45979
dye laser, pulsed, without intracavity beam expansion, narrowband operation 78−17957
dye laser, second harmonic pulse structure and cavity length determ. 80−95935
dye laser, self frequency locking, strong field effect on intracavity atoms 79−86198
dye laser, self-injected laser-pumped, nanosecond pulse generation by cavity flipping 79−18457
dye laser, short constructional length with folded mirror beam expansion system 80−53328
dye laser, short resonantor, tunable, pumped by travelling wave N_2 laser 80−48291
dye laser, short-cavity, tunable blue picosecond pulses 77−88740
dye laser, small linewidth, N_2 laser pumped *(German)* 78−1246
dye laser, spectral selection and tuning using thin layer Fabry-Perot interferometer *(German)* 79−94242
dye laser, spectrally narrow pulsed, without beam expander 78−79028
dye laser, synchronously mode-locked CW, intracavity SHG in thin $NH_4H_2PO_4$ cryst. 80−95945
dye laser, transverse flow, unstable resonator mode control 77−88789
dye laser, transverse flow, unstable resonator mode control 78−46671
dye laser, tunable, N_2-laser pumped, using single prism beam expander *(Chinese)* 80−74389
dye laser, tuning and active mode-locking, interferometry technique 79−22982
dye laser, two-wavelength single mode operation, using grazing incidence grating 80−53329
dye laser, unstable resonator, injection locking 79−979
dye laser amplifier system, electro-optical injection 79−22975
dye laser cavity, pulsed, concave grating for beam expansion and spectral dispersion 79−59721
dye laser characteristics with forced mode synchronisation, intraresonator absorpt. effect 80−78873
dye laser design, short-cavity picosecond 79−41390
dye laser design for nonlinear spectroscopy, cavity and ruby pumping laser 77−79852
dye laser emission freq. tuning with cholesteric liq. cryst. Bragg mirror 79−89931
dye laser emission spectral condensation near absorpt. lines of intracavity atoms 80−53286
dye laser frequency locking by intracavity stimulated Raman scatt. 78−79050
dye laser resonator, CW, astigmatism compensation using lenses 78−29978
dye laser resonator with slow saturable absorber, pulse distortion *(German)* 78−33732
dye laser short cavity design with multiple prism beam expander, high performance 78−1250
dye laser single-mode mag. tuning system 77−75541
dye laser spectral props., hole-burning effects 80−102718
dye laser synchronisation, CW laser injection, spectral purity *(French)* 78−63118
dye laser tuning by dielectric interference filter-coated prism 79−10322
dye laser with modes locked to atomic absorption lines, spectral characts. 80−9881
dye lasers, book contrib. 80−106517
dye lasers, freq. locking by injection, CW and delta pulse regime anal. 80−87389
dye millimetre cavity laser, dual freq. subnanosecond pulses 78−17956
dye oscillator-amplifier system, high power, pumped by Nd-YAG laser 79−18443
dye pulsed laser, light polarisation with thin wedge plate in cavity 78−55394
dye short-cavity laser, nearly transform-limited pulses 79−45965
dye standing wave laser, single mode operation using intracavity Michelson reflectors 79−89918
dye synchronously pumped mode-locked CW system, pulse characts., cavity detuning effect 79−3726
eigenvalue translation method for mode calculations 79−71515
electro-optical modulator use in or outside cavity for laser freq. shifting or stabilisation 78−5512
electron-beam-controlled laser, angular divergence with unstable telescopic resonator 79−59668
EM transducer for laser fine-tuning 77−79862
emission asymmetry, laser with inhomogeneous active medium 80−28191
emission field structure of active medium with thin-lens type heterogeneity *(Russian)* 77−83899
empty off-axis unstable resonators with rectangular mirrors, modes 79−76787
empty unstable resonators, effects of small misalignments 77−79857
energy coupling arrangement for parallel concentric lasers *(German)* 78−33757
esculin in ethanol, coherent pumping, intracavity absorpt. anal. method sensitivity 79−57328
exact cavity eqns. for lasers with large output coupling 80−64079

laser cavity resonators continued
excimer laser, double discharge, improved beam quality using unstable cavity 77−72007
excimer laser, with elec. discharge pumping, model 80−58516
excitation energy conversion efficiency in laser cavities 78−90432
External cavity operation with complete removal of sub-cavity effects for mode-locking injection lasers 80−58545
F_2-centre, pulsed tunable laser, IR spectral characts., 1.1-1.26 μ region 80−91805
F II centre laser, cavity design incorporating polarisation beam splitters 79−45960
Fabry-Perot, and confocal resonators, comparison of diffraction formulas 78−87077
Fabry-Perot cavity, gas filled, optical bistability described by stochastic master eqn. 79−76652
Fabry-Perot cavity, optical pulse tailoring and termination by self-sweeping 80−23760
Fabry-Perot cavity containing ruby, optical bistability and differential gain, 85 to 296K 77−39025
Fabry-Perot cavity with Faraday filter, for freq. locking, polarisation props. 77−46738
Fabry-Perot etalon effect on laser resonator modes 78−25896
Fabry-Perot resonator, laser mode sweeping dynamics, optical length effects 78−83001
Fabry-Perot resonator cavity, dielectric film effect on characts. 79−94134
Fabry-Perot resonator filled with transversely inhomogeneous active medium, radiation field struct. 79−55157
Fabry-Perot resonator of gasdynamic laser, collisional relax. effect on fundamental mode 79−31948
Fabry-Perot resonator with quadratically nonuniform active medium, radiation field *(Russian)* 78−46682
Fabry-Perot resonators, second-order perturbation theory 79−18451
Fabry-Perot with short pulse lasers, spectral selection and analysis in dye lasers 78−46669
far IR CW optically pumped lasers, resonator designs 78−46588
far IR gas lasers, common resonator with CO_2 pump laser 77−38950
far IR laser, intracavity pumped by TE CO_2 laser 80−87382
far IR laser, optically pumped, electronic tuning and phase-locking 78−59055
far IR laser intracavity polarisation modulation by CdTe AC Faraday rotation 80−58613
far IR lasers, Fabry-Perot vs. waveguide lasers 78−13733
far IR waveguide cavities, coherently pumped, geometrical design criteria 77−54739
far IR waveguide laser cavity design criteria 77−38951
fibre optic CW Raman laser, freq. spectrum and temporal behaviour 77−61965
fibre optical CW Raman oscillator, using two-mirror resonator config. 79−7152
fibre Raman lasers 80−102767
field distribution, Rensch finite difference method calcs. *(Chinese)* 80−87412
filled telescopic resonator, steady-state lasing, oscillation modes 80−95922
fine structure of laser lasing spectrum in transparency microwindows 79−3722
flowing medium, EM anal. 77−79856
fluctuations of laser beam diameter of single-mode laser, lens effect 80−64090
fluoromethane, 496 μm high-power smooth-pulse laser systems 77−19332
fluoromethane, far IR laser, electronic tuning and phase-locking 78−59055
fluoromethane, vel.-tuned multiphoton processes in laser cavity 77−27134
fluoromethane far IR laser FM and stabilisation by Stark effect 78−59056
fluoromethane for IR laser, evidence for Stark induced freq. shift 77−58358
fluoromethane laser emission from unstable resonator 79−22983
fluoromethane TEM_{00} far IR laser with integrated pump laser 80−43348
fluoromethane TEM_{00} far IR laser with integrated pump laser 80−58578
FM mode locked laser, dispersion effect 80−74406
focusing system, power density improvements, anal. 79−50335
fourth harmonic generation cascade process *(Russian)* 80−99797
free electron laser, small-signal gain, space charge effect 79−920
frequency selection, resonator losses due to oblique Fabry-Perot etalon *(Russian)* 77−38944
fundamental-mode laser intracavity optical second-harmonic generation 77−10972
gain saturation in laser resonator, interf. effects 80−37987
Gardner-Fresnel-Kirchhoff propag. algorithm 80−83621
gas laser, coupling modulated, mode coupling distortions minimisation 78−55384
gas laser, freq. modulated, threshold conditions for gain and freq. 77−88816
gas laser, long pulse electron beam accelerator 77−23321
gas laser, mode-locking operation using modulator with acoustic Fabry-Perot resonator 79−45976
gas laser, modulation method, for relative excitation level, cavity bandwidth and at. temp 80−5771
gas laser, polaris. effects 80−58605
gas laser, reference freq. and resonator length fluctuations effect 77−3619
gas laser, resonator parameters effect on mode volume *(Hungarian)* 80−58603
gas laser, theory of polarisation effects 80−23660
gas laser 78−83084
gas laser and its appls. *(French)* 80−83590
gas laser cavity, universal unit for beam extraction, design 80−1230
gas laser cavity light intensity optimisation for three-mirror system utilising Fabry-Perot resonators 80−48305
gas laser cavity unit for radiation lead-out *(Russian)* 78−90433
gas laser resonator, simple method of adjusting mirrors 80−19054
gas laser with resonator weak phase anisotropy, output radiation polarisation 79−64264
gas laser with short resonator, single freq. emission condition 77−58356

laser cavity resonators continued
gas lasers, single-mode in transverse mag. fields, polarisation props. 79−7167
gas ring laser, opposite wave freq. difference, mag. field 79−7156
gas waveguide laser, mode comp. of radiation 80−28192
gasdynamic CW laser, multipass cavity 78−63140
gasdynamic high speed lasers, optical cavity anal. using geometrical optics methods *(Chinese)* 79−31854
gasdynamic laser resonator cavity, flow fields and amplification coeffs., 2-D calc. 80−5722
gasdynamic laser with thermal excitation and mixing in ultrasonic flow, output power and resonator efficiency *(Russian)* 77−23646
gasdynamic lasers, plane flows in presence of weak supply of energy *(Russian)* 79−32498
gaussian beam resonator, optical nutation 80−99807
glass laser, dynamic tuning of polarisation of radiation *(Russian)* 77−38945
glass laser rods, silicate and phosphate, pumped in pseudoelliptic cavities, thermal effects 79−76692
HF chemical laser, CW, with unstable telescopic resonator, radiation field structure 80−91786
HF self-modulation of laser with unstable resonator *(Russian)* 77−83911
high power industrial gas laser system design, 1 kW 77−19321
high speed flow lasers, stable oscillation condition mode struct., output power characters 79−76660
high yield triggered laser *(French)* 78−37916
high-energy laser cavity diagnostics, holographic subtraction technique 77−19285
high-power submillimetric laser oscillator-amplifier system design 77−38927
higher order beam modes in complex lenslike media and resonators 77−27308
hollow rectangular dielectric waveguide laser resonator and external spherical mirrors, coupling radiation 78−37914
hologram filter telescope for use in dispersive laser cavity 80−9839
holographic selector in external resonator of semiconductor laser 79−98406
homogeneously broadened with constant loss, optimum output efficiency 80−74403
Huygens-Fresnel integral in circular coords., asymptotic soln. 78−87013
imaged intracavity laser absorpt. spectroscopy 77−41703
inert gas halide laser, stable-unstable resonator for beam control 80−23722
inert gas ion laser, wall confined, high CW power UV generation 77−19232
inert gas-halogen bearing molecule three-component mixture, self-sustained electric photoionization discharge 80−54073
inertial feedback, T-modulated giant pulses 77−19353
inhomogeneous active medium, angular correction, telescopic systems 78−1276
injection hetero laser with low generation threshold current, Bragg distributed mirrors *(Russian)* 77−38943
injection heterojunction laser with short resonator, construction and output radiation characteristics 79−98408
injection laser, external resonator, threshold temp. depend. at fixed wavelength 78−25882
injection laser, transverse mode control by strip loaded waveguide 77−75543
injection laser with composite resonator, active region internal parameters determ. 80−106548
injection laser with external dispersive resonator as narrow-line tunable emission source *(Russian)* 77−83898
injection laser with external selective resonator, mode deformation due to self-focusing 79−13966
injection laser with index-guiding structure, single longit. mode operation 79−98362
injection lasers, mode comp., control with selective cavities 80−19037
injection lasers, with external dispersive cavity, mode competition 79−31901
integrated interferometric reflector with elec. control for laser reflector 77−58490
integrated twin guide laser, coupled wave theory 77−27307
integrated twin guide lasers, axial mode selectivities 77−75519
intensity distributions in unstable resonator, geom. optics limit 77−50691
interferometer, for phase changes $<10^{-5}$Å 77−18087
internal CW parametric upconversion using Ar laser and $LiNb_3$ 78−42376
internal mirror laser, polarisation mode, freq. stability *(Japanese)* 78−46675
internal modulation of laser radn., freq. limitation 79−72607
intracavity absorpt. spectroscopy, short pumping pulses and restricted mode competition, numerical anal. 77−82607
intracavity absorption model in CW multimode dye laser 80−47119
intracavity absorption spectroscopy, using semicond. injection laser 79−7157
intracavity absorption spectroscopy at reduced pressures, using dye laser 80−47118
intracavity absorption spectroscopy theory, mode competition 78−32890
intracavity absorption spectroscopy utilizing sweep dye lasers 79−89015
intracavity acousto-optical modulation 77−19356
intracavity atomic spectroscopy, fluoresc. detection of narrow absorpt. lines 79−52830
intracavity dye laser quenching, quantitative detect. of Na absorpt. 77−36817
intracavity dye laser spectrometer, double beam, flash lamp pumped 79−75620
intracavity dye laser technique for spectroscopic and kinetic meas. of transients 78−62239
intracavity enhancement of absorpt. in nanosecond regime 78−78839
intracavity laser Raman spectrometer, appls. 78−65973
intracavity laser spectroscopy, absorpt. line profiles determ. 78−12776
intracavity laser spectroscopy sensitivity, saturation absorpt. influence 79−63312
intracavity method for optical densities meas., dynamic range extension 79−9231
intracavity method of analysis sensitivity *(Russian)* 78−46680
intracavity Nd:glass laser spectrometer for 1.35 μm 79−63316
intracavity optical SHG, $LiIO_3$ crystal in Nd^{3+}:YAG laser cavity. *(Russian)* 80−28272
intracavity phase lock control system 79−76718
laser cavity resonators continued
intracavity phase perturbations effect on beam quality 77−38968
intracavity Raman laser theory 79−27296
intracavity resonance asymmetries, nonlinear freq. depend. diffraction effect 80−99760
intracavity SHG, phase effects, harmonic feedback case 80−9945
intracavity SHG, phase effects 80−1276
intracavity spectrometer, using continuous jet dye laser *(Russian)* 78−70197
intracavity spectroscopy, laser output spectrum, lineshape 79−55155
intracavity spectroscopy, quantitative information acquisition on absorpt. line parameters 78−49911
intracavity spectroscopy, spectrometer based on continuous jet dye laser 79−52831
intracavity spectroscopy rel. to laser spectral charact. *(Russian)* 78−46561
intracavity tip/tilt adaptive control system 79−59728
intraresonator absorption spectroscopy in plasma jet, laser stimulation optimisation 80−77881
intraresonator atomic spectroscopy, element determ. by narrow line fluoresc. recording *(Russian)* 78−73124
intraresonator forced Raman radiation with polariton excitation *(Russian)* 79−94286
intraresonator formation of laser fields, transverse mode influence *(Russian)* 79−50327
intraresonator high-sensitivity meas., using Nd:YAG laser with min. amplitude noise 79−63317
intraresonator spectroscopy, competing-beams method sensitivity *(Russian)* 79−93228
introductory concepts and results, book contrib. 80−106504
inverted Lamb dip, of laser with internal absorpt. cell 77−14765
ion laser frequency using inclined Fabry-Perot etalon within cavity 79−55161
ionised-gas lasers, refr. during pump pulse due to gasdynamic motion 79−3723
IR laser cavities, rot. equilib. 80−1239
isotopic filtration of radiation of dye laser, in-resonator spectroscopy *(Russian)* 77−54752
Israel Physical Society 1980 annual meeting, Rehovot, Israel (April 1980) 80−94909
kinetics, self-coordinated problem *(Russian)* 79−27238
laser coupled output, importance on intracavity effects *(Chinese)* 79 64269
laser mirrors cooled by open pore structures, radiation damage 79−72603
laser-induced line shifts and double-quantum Lamb dips 78−86825
linear three-mirror resonator, lasing, theory 79−3720
loaded strip confocal unstable resonator, theory of modes 77−50692
loaded unstable resonators with centered or corner obscurations, far field energy 77−72006
longitudinal modes in resonators filled with inhomogeneous material 79−81463
losses, phase polarisation method in lasing regime 80−87413
marginally stable, analytical solns. of Fresnel-Kirchhoff integral equation 79−94262
marginally stable resonator, gain effect on electrodynamics 80−53339
metal mesh dielectric mirrors for far IR lasers 77−54727
metallic wired grids as far IR semitransparent mirrors, use in HCN laser cavity 78−71188
methanol, far IR laser resonator for TEM_{00} mode operation 78−66847
methanol far-IR laser, optically pumped, intracavity polarization modulation 80−23726
methanol laser, optically pumped, use of crystalline reflector in cavity 80−64080
methyl alcohol submm wave laser, optically pumped, intracavity double resonance obs. 80−58522
methyl fluoride, deuterated, optically pumped near-MM laser 80−69379
methyl fluoride, double-ended unstable resonator submillimetre laser characts. 79−81461
Michelson interferometric output coupling for NH_3 sub mm laser 77−14744
micro-resonators, high flux, for X and γ-ray lasers 79−7151
microsecond pulse production, with quadratic loss 77−7147
mirror curvature effects *(Russian)* 78−46683
mirror for laser resonator to minimize output beam divergence 78−13735
mirror misalignment sensitivity 80−53334
mirror substrates microroughness ellipsometric determ., effect on laser cavities 79−59791
mirrors optimal reflection coeff. selection, for intraresonator Q-switching 80−48302
misalignment, anal. by ray contour method 80−58602
misalignment characteristics, resonator formed by 90° cone and mirror 80−99757
mm-wave Fabry-Perot tuning and freq. modulation by electrically variable external reactance 79−68409
mode competition and frequency locking, lasers with broad homogeneous emission lines 80−23723
mode locked lasers, effects of narrow-free-spectral-range etalons 80−38041
mode locking, transverse resonator, slow saturable absorber 79−22993
mode selection, CW, laser with homogeneously broadened gain 77−61978
mode stability in resonator containing active medium 77−19346
mode structure, effects in open resonator with variable iris 80−5767
mode-locked binary laser oscillator, bistability induced by optical nutation 79−31958
molecular laser, optically pumped, development 78−13732
molecular lasers, laser pumping, dispersion 80−87375
monolithically integrated lasers and amplifiers using cleaved substrate technique 80−58590
multi-reflectivity cell, efficiency of methods of energy release *(Russian)* 77−75579
multielement resonators, canonical formulation *(Chinese)* 79−89938
multilayer resonance elements, elec. field distribution calc. *(Russian)* 78−78854
multilayered structures containing optically active medium, absorption and amplification of light *(Japanese)* 80−19052
multiline resonator, independently controllable, multifreq. injection locking 77−7141
multipass amplifier, theory and numerical anal. 80−78872

laser cavity resonators continued
multipass telescopic amplifier, energy characts. calc. 77−14763
multipath optical cavities in saturated absorpt. expts. 77−65610
multiple-pass Raman gain cell 80−48334
natural vibrations, sensitivity to transverse nonuniformity of optical resonators *(Russian)* 78−5508
near-IR fibre Raman oscillator, 1.07-1.32 μm tunable 79−72622
negative branch unstable resonator, with self imaging aperture 79−977
negative-branch confocal unstable resonator, for high radiance flashlamp pumped dye laser 78−29970
non-confocal resonator, with output-coupling aperture, eigenvalues *(Japanese)* 79−55163
nonconfocal resonator with output-coupling aperture, matrix eigenvalue analysis 79−72600
nonlinear, containing medium with quadratic susceptibility, props. 80−33074
nonlinear active medium laser, transient intracavity SHG, giant pulse generation 80−9948
nonlinear crystal in external resonator, optical rectification 78−13748
nonlinear resonators, radiation excitation, review 80−69462
nonorthogonal resonators, fund. mode props. w.r.t. rotating Gaussian beams 80−53336
nonsymmetric eigenvalue problems of optical resonators, numerical solns., Prony method 78−82992
ns pulse length continuous control, appl. to Nd laser 78−1280
off-axis focusing arrangement, compensation of coma and astigmatism 77−34898
one-dimensional, output coupling, field quantisation 77−7144
one-dimensional laser, with output coupling, linear quantum theory 77−88690
one-dimensional optical cavity with output coupling, fluctuation-dissipation theorem 79−89876
open cavity, Slater method validity 80−69428
open cavity with selector, field transverse struct. at mirrors 79−27295
open resonator with aperture in reflector, theoretical anal. 79−31955
open resonator with periodic boundary *(Russian)* 78−46679
open resonators, modes of oscillation, theory 77−38947
open resonators with aperture coupling, multimode interaction effects 80−58608
open stable cavity with axial symmetry, aberration corrections 80−43372
optical cavity with output coupling, one-dimens., quasimodes as field eigenvalue 80−9911
optical fabrication techniques 77−65600
optical feedback effects in CW injection lasers, using external reflecting surface 78−79045
optically pumped CW far IR waveguide lasers, high power, scaling 77−54731
optically pumped FIR laser with variable Fabry-Perot output coupler 77−68220
optically pumped sub mm wave regenerative amplifier 77−54728
optically pumped waveguide gas lasers 78−5490
optically pumped waveguide laser characteristics 77−38870
optically-pumped submillimetre oscillator, for plasma diagnostics 78−47184
organic molecules, polyatomic, stimulated emission, laser spectral kinetics 79−55132
organic solution laser, unstable resonator calculation 80−58600
orthogonality properties of optical resonator eigenmodes 80−38042
oscillations in open cavities, transient processes, stabilisation time 79−3721
oscillator-based powerful laser, GOS-1001 with film resonator Q-switch 79−3705
output mirror, low reflectance, reduced radiation loading 78−83000
output power calculations, laser models, sources of error 80−48207
oxazine-1-perchlorate mode-locked CW dye lasers, tunable near IR ps and subps pulse generation 79−45972
parallel-plate waveguide CO_2 laser, self-focusing 77−7139
partially open cavity, freq. shift and decay time of radiation 79−13990
partially selective resonator, for spectral line tuning in dye laser *(Russian)* 77−61980
passive resonant ring laser gyroscope design 80−99768
passively mode locked solid laser, ps pulse generation 77−717
periodic laser with unstable resonator, single-pulse emission characts., active-medium inhomogeneities effect 80−74365
periodic mode loss, use of grating mirrors in IR laser resonators 80−28254
periodic modes, diffr. props. 77−61979
periodic modes of optical resonator *(Russian)* 78−33756
periodic stratified medium, EM propag., general theory 77−65565
phase conjugate mirror component for optical cavity, Gaussian transverse modes 80−58595
phase conjugate mirror for optical resonator, longit. and transverse modes 80−14392
phase conjugate mirror forming optical cavity, Hermite-Gaussian higher-order reson. modes 80−58594
phase transitions, intracavity absorber expt. 78−13676
phase-conjugate mirrors for optical resonators, degenerate four-wave mixing 80−43393
phase-conjugate resonator using 4-wave geometry conjugate mirrors 80−58650
phosphate glass active-passive mode-locked oscillators at 1.054 μm 78−63139
photon lifetime and reflectance meas., phase-shift method 80−38039
photon statistics, optical cavity length depend. 78−94402
planar and disc-cavity lasers, volume-averaged rate eqns. 78−13734
plane mirror cavity, field structure of nonstationary oscill. modes, edge diffr. effects 79−55160
plane-parallel mirror cavity, with holes, losses calcs. 77−10962
plane-parallel resonator with wavefront reversing mirrors, mode structure 79−86196
planospherical resonator with internal lens, stability of caustic 79−31954
plasma mirror refl. characts., in electron beam controlled CO_2 laser 78−59064
plasma Q-switch in laser cavity 80−28259
polarisation capture, in 3.39 μm laser *(Russian)* 78−5456
POPOP solution dye lasers, multiplate reflectors 80−83606
porous tube array, flowfield struct., turbulence and vorticity distribs. in elec. discharge laser 77−27589
prism anamorphic system, for Gaussian beam expander 79−3716
pulse generation, double, gradual cutting-off resonator losses 80−69433
pulsed dye for laser pumped by powerful N_2 laser 79−94260
laser cavity resonators continued
pulsed laser sources using Nd 78−50784
Q-switched laser with unstable resonator, transient processes 77−75576
Q-switched Nd:YAG oscillator for stable time-tunable operation in nanosec. regime 80−99759
Q-switching, resonant vibrating mirror system 78−87082
Q-switching by acousto-optical modulation, for interferometer light source 77−7489
Q-switching mechanism by intracavity stimulated Brillouin scatt. 80−106552
quasi-optical open resonators, phase struct. of field, meas. method *(Russian)* 78−29925
radiation asymmetry, in laser with inhomogeneous active layer *(Russian)* 79−23003
radiation density, field strength superposition calcs. *(Chinese)* 80−83618
Raman amplification of optical radiation *(Russian)* 79−27333
Raman laser, CW fibre, bandwidth reduction using prisms, gratings and etalons 80−53366
Raman laser, Nd^{3+}:YAG with quartz lightguide resonator 80−99735
Raman oscillator, tunable multiple Stokes CW fibre 77−88786
Raman oscillator, two-mode fibre, group velocity matching 78−25925
rectilinear optical resonators for curved metallic waveguides 80−69425
reflector appl., 90 degrees, stability analysis, use of ray transfer matrix 80−33184
resonance phase transition in two-level lattice system, thermodynamics 80−69351
resonators folded by diffr. grating 78−33755
retroreflective array as resonator mirror 80−95973
RF spectroscopy in laser cavity, pure nucl. quadrupole spectra 78−90320
rhodamine 6G, halo laser device 79−72597
rhodamine 6G, ring struct. laser emission, resonator exit mirror effect 77−38941
rhodamine 6G, tunable UV radiation prod., intracavity freq. doubling in $NH_4H_2PO_4$ 77−3628
rhodamine 6G, ultrashort pulse generation in resonator *(Russian)* 79−50289
rhodamine 6G in polyurethane film, etched cavity 77−7140
rhodamine 6G laser amplifier pumped by N_2 laser, sub nsec pulse generation 80−1232
rhodamine 6G laser with lamp excitation, cavity thermooptical distortions effect 79−55135
rhodamine 6G synchronously mode locked CW laser, pulse width depend. on intracavity bandwidth 78−66821
rhodamine 6G water soln. laser with spatial lamp pumping, spatial coherent emission 78−82963
rhodamine 6Zh pulsed laser, simple transverse mode observation *(Russian)* 79−72565
rhodamine G in ethanol, flash-lamp pumped, intracavity absorpt. anal. method sensitivity 79−57328
rhodamine GG tunable narrowband subnanosecond dye laser, optical pumped 79−81445
rhodamine laser, induced losses in active medium during incoherent excitation *(Bulgarian)* 79−10297
ring cavity, dispersive bistability in homogeneously broadened systems 80−14306
ring dye travelling-wave CW laser, mode locking 80−43354
ring laser, freq. shift and splitting for opposite waves, spatially inhomogeneous media 79−7155
ring laser, open cavity matrix eqns. in diffraction theory 80−69429
ring laser with anisotropic resonator, polarisation and freq. splitting of opposite waves 80−33037
ring modulator, efficiency very wideband coupling modulation of CO_2 laser 77−42553
ring optical cavity, nearly confocal, with spatially inhomogeneous medium, threshold gain 80−43373
ring optical resonator with diaphragmed spherical mirror and inhomogeneous amplifying media *(Russian)* 80−28256
ring resonator with arbitrarily situated medium, axial contour and stability *(Russian)* 79−89939
ring resonators, with counter directions linked through back refl. props. *(Russian)* 77−68233
rotating anharmonic oscillators in resonator, stimulated emission power 80−99689
ruby, laser, with active phasing of spectrum, double Pockels shutter performance *(Russian)* 79−98419
ruby, lasing spectrum singularities and Q-factor, for z-dimens. beam path *(Russian)* 77−88795
ruby, negative feedback, external perturbations effect, spectral depend. 77−83908
ruby, slot method for radiation extraction 77−50694
ruby, total mode self-synchronisation 79−64259
ruby, unstable Q-switched resonator in negative branch confocal config. 79−13980
ruby and Nd:glass lasers placed parallel in cavity, for efficiency increase *(Russian)* 77−10954
ruby laser, double mode locking using dye saturable absorber 80−99763
ruby laser, modulation by US surface waves on resonator mirror 77−50699
ruby laser, negative feedback, cavity Q insertion effect on parameters of modulated pulses 80−43376
ruby laser, power enhancement by intracavity plasma 80−53330
ruby laser, radiation automodulation with passive switching of electro-optical shutter *(Russian)* 78−74936
ruby laser, weak passive Q-switching in spherical resonator 78−50834
ruby laser with electrooptical shutter, emission spectrum narrowing and single freq. giant pulse lasing 80−78877
ruby laser with nonorthogonal resonator, rotating laser beam generation *(Russian)* 79−10330
ruby laser with optical delay line inside cavity resonator 77−42552
ruby laser with special resonator Q-switching 77−38958
ruby lasers and $LiNbO_3$ cryst. in difference freq. laser, tunable MM range emission 80−5764
ruby oscillator-amplifier compact system for satellite ranging 79−966
saturable optical resonator with distributed Bragg reflectors, transient behaviour 79−23029
saturable resonator with distrib. Bragg reflectors, bistability, bleaching and loss effects 77−27309
secondary laser cavity for weak absorptions 78−92551
self-synchronising modes, saturated filter relax. time reduction *(Russian)* 77−7145

laser cavity resonators continued
semiconductor DH laser with external cavity, output power and coherence length in incoherent feedback 79−98412
semiconductor injection laser, external optical feedback effect on props. 80−58535
semiconductor injection laser, lateral mode selection 77−79861
semiconductor injection lasers, output depend. on inhomogeneous bonding 80−64015
semiconductor laser, electron beam pumped, use of periodic structs. with special profiles 80−95923
semiconductor laser, optical systems using caustic region or antiwaveguide struct. 77−61972
semiconductor laser, single mode criteria at high speed pulse modulation 79−10305
semiconductor laser, single-wavelength oscillation at high speed pulse modulation 79−7129
semiconductor laser epitaxial growth with moulded reflectors 78−42347
semiconductor laser with ^{133}Cs vapour external selective mirror, pulsed stimulated emission 79−45961
semiconductor lasers, single mode, spontaneous emission spectrum dip observation, generation saturation *(Russian)* 79−76691
semiconductor stripe geometry junction laser, waveguiding mechanism 77−75521
SHG, efficient intracavity, of unpolarised laser radiation 79−50352
single axial mode laser, degenerated by mag. field, light props. *(Japanese)* 79−64254
single frequency intra-cavity spectroscopy, anal. *(Russian)* 78−37079
single mode folded laser cavities, selection and test of parameters *(Chinese)* 79−55154
single mode laser, intracavity spectrosc., enhancement calc. 80−69426
single pulse formation kinetics with self-modulation of quality factor *(Russian)* 77−27312
single-mode emission stability rel. to active medium and resonator 78−17899
single-mode gas laser with slightly anisotropic resonator, output polarization stability 80−43370
solar pumped laser for space communications 78−46645
solid laser, multimode, with modulated resonator losses, radiation intensity fluctuations 80−74367
solid laser, passively mode locked, picosecond pulse generation, pulse compression and broadening 77−31111
solid laser, Q-switched, nanosecond and microsecond pulse generation, review 78−71130
solid laser, subnanosecond and picosecond operation 80−28262
solid laser characts. control using optical delay lines, resonator effective length increase 80−99758
solid laser Q-switching by optomechanical shutter 79−72609
solid single-mode face pumped laser, resonant-mode analysis 77−58350
solid state directly coated laser rods, beam divergence and refractive power 79−59736
solid state laser, refraction effects and gain meas. 79−31905
solid state laser cavity reson., longitudinal mode locking, free generation region *(Russian)* 77−75572
solid state laser satellite rings, energy losses caused by diffusion, refl. in cavity 79−89911
solid-state laser without external mirrors, stability conditions 80−33024
solid-state ring laser, mode locking theory 79−41399
spark control cavity dumping for ruby laser 78−59053
spatial distribution of laser radiation control 80−64086
spatial field configuration with diffuse reflector 80−53344
spatial field configuration with nonresonant feedback 79−18453
spatial field structure in resonator filled by periodically inhomogeneous active medium *(Russian)* 79−976
spatial hole burning and twisted-mode laser resonators 78−42359
spectroscopy technique, high-sensitivity, gas cell absorpt. meas. in laser resonator cavity 79−40626
spectrum analyser for laser oscillator radiation 77−26403
spherical cavities, Q-switching by rotating mirror in ruby and Nd:glass lasers 80−28261
spherical mirror folded cavities, astigmatism elimination and regulation *(Chinese)* 78−90431
spherical mirror resonator, misaligned, open, spatial struct., phase and amplitude distrib. 78−46676
spherical open resonator, approx. theory *(French)* 80−48301
spherical resonator diffraction losses, expt. meas. 78−29980
split-mode unstable resonator, phase locking 77−58351
spontaneous radiation propag. in travelling wave amplifier, spatial filtering 77−14764
stability conditions for laser cavities with two foci 78−66850
standing wave simultaneous forward and backward integration 79−94258
stationary laser oscillator with Fabry-Perot resonator, spatial coherence analysis 77−79863
statistical properties of emitted light, cavity length depend. 77−88794
stilbene tunable narrowband subnanosecond dye laser, optical pumped 79−81445
stimulated combined scattering of light, effect of generation of 'hot' vibrs. 80−58601
stimulated Mandelstam Brillouin scatt. component self-synchronisation in internal transverse resonator *(Russian)* 80−48345
stimulated Mandelstam-Brillouin scatt. component synchronisation *(Russian)* 80−48346
stimulated Raman emission component locking, in optical resonator with dispersive medium 78−50858
stimulated Raman scattering, possibility of femtosecond pulse generation 77−23717
stimulated Raman scattering of light inside a laser resonator, stationary mode *(Russian)* 80−38067
stimulated scattering, Raman and Brillouin, electrostatic and EM waves 78−34324
submillimetre laser, vibr. mirror for phase modulated pumping, amplitude stability improved 79−22967
submillimetre laser output and efficiency, rel. to pump frequency displacement 79−31866
submillimetre wave laser waveguides 78−5505
submillimetric pulsed laser with optical pumping, characts. rel. to vapour pressure *(Russian)* 79−94215
submillimetric waveguide laser for gas spectroscopy 80−33022
submillimetric-wave laser waveguides 77−38952
symmetric laser cavity with asymmetric modes 79−13989
TEM_{00} thermoinsensitive cavity *(Chinese)* 80−53335

laser cavity resonators continued
thermal distortion of active element during pumping pulse *(Russian)* 77−50696
thermal lens due to liquid in cavity, focal length 77−61977
thermal radiation, fluctuation-dissipation theorem, one-dimens. optical cavity with output coupling 79−978
thermoelastically disturbed resonator, mode calcs. 79−13992
three-mirror, for ionic Ar laser with polarised radiation 80−23712
three-mirror laser, freq. phenomena, implications for interferometry 77−3617
threshold characteristics of mirrorless lasers 77−31112
tilted mirror unstable resonator cavity 77−88790
tilted mirror unstable resonator laser cavity 78−29979
time-dispersion-tuned fibre Raman oscillator 77−42562
TOPOT vapour dye lasers with multiplate reflectors 80−83606
transverse structure of radiation from a laser with an additional mirror 80−58604
travelling wave amplifier, efficiency of methods of energy release *(Russian)* 77−75579
travelling wave generator, output beat signal freq., statistical characts. *(Russian)* 77−7148
travelling wave laser, harmonic var. in cavity freq. difference, beat signal phase 77−75571
travelling-wave, astigmatic Gaussian beams 77−723
tuning of pulse laser radiation by varying resonator length 78−29986
two-mirror resonator, efficiency of methods of energy release *(Russian)* 77−75579
two-mode laser, mutual quenching of axial modes 79−13991
two-mode optical resonator mode mutual quenching in stimulated Raman emission 79−36960
two-photon amplifier, laser pulse propag. 79−7154
two-photon laser oscill. in optical cavity, semi-classical theory 79−22928
ultrashort pulse duration control rel. to forced mode synchronisation *(Russian)* 77−46735
unfolded cavity using planoconvex lenses, for CW mode-locked dye laser 80−5765
unstable, effects of medium and gain inhomogeneities, waveguide model 77−58349
unstable, Fourier transform spline soln. to deal with sharply cut off fields at mirror edges 79−94263
unstable, optical alignment procedure 78−50826
unstable confocal resonator operating point choice 79−36938
unstable confocal resonators, operating point choice 79−59727
unstable optical resonators with tilted spherical mirrors, design eqns. 78−74930
unstable resonator, for low-gain media 79−22984
unstable resonator, gain saturation in geometric mode limit 78−1267
unstable resonator, half-symmetric, with coated rear cone, polarisation effects 80−74402
unstable resonator, power meas. using variable aperture calorimeter 77−7136
unstable resonator, thermoelastic mirror deform., influence on laser characts. 78−71124
unstable resonator analysis, ray transfer matrix approach 79−50322
unstable resonator containing small-scale phase inhomogeneities, laser props. 80−19057
unstable resonator in pulsed gas laser, beam shaping 78−17987
unstable resonator laser, conical optics for radiation conversion 80−91831
unstable resonator mirrors, diffuse scatt. effect on intensity distrib. 77−58354
unstable resonator properties, small-scale phase inhomogeneity influence 78−59050
unstable resonator with circular mirrors, asymptotic analysis 79−3718
unstable resonator with field rotation to reduce beam divergence 78−17988
unstable resonator with spatial filter, mode discrimination, phase modification 79−76719
unstable resonators, ϵ-approx. eigenvalues and eigenfunctions *(Chinese)* 80−5766
unstable resonators, quantum multimode approach 77−719
unstable resonators for high power lasers *(Italian)* 78−87076
unstable resonators with field rotation, mode structure 80−53342
unstable resonators with field rotation, props. in CO_2 laser 80−53343
unstable resonators with rounded edges, mode losses 78−79039
unstable resonators with scraper mirrors, equivalent Fresnel no. calc. 79−81460
unstable strip resonators with misaligned circular mirrors, waveguide approach 78−82991
unstable telescopic, precision of some methods of adjustment *(Russian)* 80−38040
unstable telescopic resonator laser, energy parameters calc. 77−75577
unstable telescopic resonator operation, influence of active medium inhomogeneities 77−75575
unstable-resonator laser performance at near MM wavelengths 80−58607
UV resonators for 300-700 Å 78−1279
variable band gap heterojunction laser spectral characteristics *(Russian)* 79−94236
vector resonator mode synthesis, perturbation theory 80−43374
wavefront correlation transformations *(Russian)* 80−99778
wavefront reversing mirror, oscillator modes 80−53345
waveguide, laser, pump efficiency, saturation effects 78−17981
waveguide far IR laser mode losses 77−38954
waveguide laser, construction and operation characteristics *(Rumanian)* 78−59049
waveguide lasers, operation under multimode conditions, relative efficiency of cavities, comparison 79−55158
Al coated Pyrex double ellipse cavity 78−5503
(AlGa)As CW narrow stripe injection laser with induced waveguide, expt. props. 80−32988
AlGaAs constricted DH laser with large optical cavity, CW high-power single-mode operation 80−48276
AlGaAs DH laser epilayer struct. optimization for integrated optical circuits 80−99879
(AlGa)As DH narrow stripe injection laser with rigid waveguide, expt. props. 80−32987
AlGaAs injection laser, large optical cavity, with multiple active regions 80−106538
AlGaAs laser, monolithic integration with amplifier/detector by twin-guide struct. 78−42466

laser cavity resonators continued
AlGaAs lasers, CW high-power single-mode constricted DH lasers with large optical cavity 80−64076
(AlGa)As strip buried heterostructure lasers, mode locking using external cavity 80−91791
AlGaAs-GaAs, DH semiconductor laser, influence of struct. parameters on lasing characteristics 79−45942
AlGaAs-GaAs CW injection heterolaser, single freq., tunable by external dispersive resonator 80−28236
AlGaAs-GaAs DH laser, bent-guide struct. 77−75544
AlGaAs-GaAs injection lasers, effects of single- and double-grating external cavities 79−98364
$Al_xGa_{1-x}As$, CW low threshold, high efficiency injection laser props. 78−22126
$Al_xGa_{1-x}As$-GaAs DH injection laser, active region internal parameters determ., composite resonator use 80−106548
$Al_xGa_{1-x}As$-GaAs DH laser, short cavity, performance characts. 77−83889
$Al_xGa_{1-x}As$-GaAs photopumped quantum-well heterostructure lasers grown by metalorganic CVD 79−98390
Ar high-power CW laser, resonator configs. for mode selection 79−10327
Ar laser, longit. mode locking in three mirror cavity 79−55164
Ar laser emission under passive mode-locking conditions, temporal structure 80−9923
Ar laser resonator, effect of axial mag. field on loss increase 79−76716
Ar^+ laser 582 THz stabilisation by I_2 cell, improvements 80−102741
Ar-N_2, electron-beam-excited laser lines at 337.1, 357.7, and 380.5 nm, gain conditions 79−86166
CO electric discharge laser using single vibr.-rot. transition, laser line selection 79−59687
CO electric discharge unstable resonator laser, computer model 78−58988
CO laser, water-sealed, efficiency increase by reducing resonator losses 80−64081
CO pulsed laser, stimulated emission dynamics, transition lines for isotope enrichment 80−48225
CO, simple high energy TEA laser 79−3714
CO, vibr. relax. at glass surface, glow discharge meas. 79−18409
CO-Xe-N_2-He gas laser power rel. to mixture composition *(Russian)* 79−7114
CO_2, atm. press. laser pulse duration reduction by stimulated emission quenching 79−18400
CO_2, CW, transverse mode suppression by cavity length control 77−14762
CO_2 CW continuous flow laser, unstable resonator props. using dihedral corner reflector 78−29983
CO_2 CW sequence laser lines generated using incavity NH_3 cell 79−18438
CO_2, CW waveguide laser, anodised Al waveguide construction 78−55376
CO_2 compact sealed TEA laser, single mode operation 79−968
CO_2, controlled multiline oscillator 78−1259
CO_2 electroionisation laser plasma mirror, soft X-ray emission for biological radiography 79−43983
CO_2 electron beam controlled laser, emission pulse synchronisation with plasma mirror 79−89930
CO_2, fast flow discharge laser, amplitude modulation in stable, unstable resonators 77−75478
CO_2 gas transport laser with cylindrical geometry 79−7108
CO_2 gasdynamic 16 μm laser, performance determ. using multipass cavity 79−81443
CO_2 gasdynamic laser, resonator action, output power 78−13681
CO_2 gasdynamic laser, resonator design, lasing medium model 78−29984
CO_2, gasdynamic laser, simplified model for cavity flow, population inversion calc. 78−46567
CO_2, gasdynamic laser, unstable resonator selection 77−23701
CO_2, high power pulse laser with unstable resonator 77−75564
CO_2, high-power multibeam CW laser, parallel packed tubes in common resonator 79−13984
CO_2 high-power pulsed laser, wave-optical resonator modelling, gain saturation law 80−99693
CO_2 high-power pump laser, direct narrow-line tuning 80−58579
CO_2 hybrid laser, operating regimes 79−22932
CO_2 IR laser, transients obs. by modulation of intracavity absorber 78−74933
CO_2, inverted, wavefront reversal, high efficiency 80−74436
CO_2 large aperture TEA laser, injection mode locking 77−14737
CO_2 laser, high-press. ns pulse generation *(Russian)* 77−75581
CO_2 laser, high-press. CW, output power fluctuations 80−74333
CO_2 laser, intracavity IR absorpt. of vinyl chloride, ethylene, and propylene 78−78835
CO_2 laser, mode locking obs. by intracavity plasma injection 80−83624
CO_2 laser, SF_6 intracavity hysteresis, bistability, critical behaviour onset and extinction of lasing 79−98336
CO_2 laser, single-frequency, using unstable resonator 77−38939
CO_2 laser, TEA, single longit. mode, double unstable resonator 80−106547
CO_2 laser, transverse mode-medium instability anal. 79−76662
CO_2 laser, with anisotropic resonator, radiation polarisation *(Russian)* 79−27309
CO_2 laser, with anisotropic resonator, output polarisation 80−28253
CO_2 laser bimetallic mirror coating vacuum sputtering technology 80−35086
CO_2 laser cavity and Ge phase-conjugate 10 μm reflection expts. 80−78894
CO_2 laser discharge tube, phase distortions due to heating differential 80−95865
CO_2 laser intracavity freq. modulation, transient behaviour 80−14374
CO_2, laser line selection using metal film reflection filter 78−55368
CO_2 laser modulation, plasma injection into cavity 80−83626
CO_2 laser power variation detection via plasma tube impedance changes 80−69437
CO_2 laser pulse compression and mode locking using KCl:ReO_4 nonlinear absorpt. 80−74443
CO_2, laser pulse generation, cavity dumping by NH_2D Stark active mol. 77−88800
CO_2 laser resonator, gasdynamic, optimal parameters determ. from vibr. energy exchange kinetics 80−14317
CO_2 lasers, optically pumped, use of crystalline reflector in cavity 80−64080

laser cavity resonators continued
CO_2 optogalvanic stabilised laser 79−89923
CO_2 oscillator, high power nsec. pulse selection 79−98382
CO_2 pulse-periodic laser utilising air-CO_2 mixture, emission characts. 79−89886
CO_2, pulsed TE laser, tunable single-mode operation by means of selective absorbers 79−36940
CO_2, rapid wavelength switching probe laser, J-line scan gasdynamic laser diagnostic 78−59044
CO_2 rotating-mirror Q-switched TEA laser, mode sweeping effects 80−99769
CO_2 single frequency atmospheric press. laser, with 15 cm resonator 78−13728
CO_2 TE laser, longit. mode control using intracavity gas-phase absorbers 79−72579
CO_2 TE unstable resonator laser, operation using additives 79−98403
CO_2, TEA, freq. chirp reduction, improved stability 77−10959
CO_2 TEA high-power tuned laser using three-mirror confocal unstable resonator 80−23719
CO_2, TEA injection laser, single-mode pulse prod. 77−54722
CO_2 TEA laser, compact sealed single mode operation 78−50810
CO_2, TEA laser, energy extraction improvement in multiline double band mode 78−63129
CO_2, TEA laser, mode characts. using unstable resonators 79−3719
CO_2 TEA laser, mode-locked, cavity-dumping 80−87415
CO_2 TEA laser, multiline oscill. temp. control., intercavity etalon method 79−98337
CO_2, TEA laser, pulse shape and duration, excitation method *(German)* 78−83010
CO_2 TEA laser, pulse shaping by independent excitation of coaxial discharge systems 79−7150
CO_2 TEA laser oscillator, longit. mode rejection, cavity length tuning effect 79−86189
CO_2 TEA laser oscillator, transverse mode locking by short pulse injection 80−38045
CO_2 TEA laser with long optical resonator, mode-locked operation 78−79041
CO_2 TEA single longit. mode laser with tilted intracavity etalon 78−5484
CO_2, tunable 2.75 GHz IR source 77−14786
CO_2, tunable linearly polarized TEM_{00} operation, concave diffr. grating 77−19344
CO_2, unstable resonator, gain, spatial inhomogeneity effect 77−34870
CO_2 unstable resonator laser pump for high energy density NH_3 laser 80−53327
CO_2 waveguide high press. laser, line selection and tunability 78−59026
CO_2 waveguide laser, CW, optical pumping of far-IR molecular lasers 80−83615
CO_2 waveguide laser, tunability calc. *(Rumanian)* 80−87371
CO_2, waveguide laser structures, design, construction and performance 77−88750
CO_2 waveguide laser with plane parallel mirror resonator 79−3715
CO_2 waveguide laser with pulsed high-freq. discharge 80−99755
CO_2 waveguide lasers, engineering aspects 79−31941
CO_2 whispering-gallery CW laser, design and operation 79−81447
CO_2-H_2-He 10.6 μm scan laser with programmable VO_2 mirror 80−38026
CO_2-N_2, CW mixing gasdynamic laser, saturation parameter and small signal gain 79−45923
CO_2-N_2 fast-flow laser with unstable resonator, self-oscillation instability 80−95870
CS_2 laser cavity pulser with triggered spark gap 79−13973
C_0 CW laser, unstable resonator with small-scale phase inhomogeneities, props. 80−19057
CdS crystals, one-photon pumping, active layer structure, light amplification 80−78858
CdS, laser, petal shaped cryst., high-temp. spectral characts. *(Russian)* 79−13968
CdS monocrystal petal lasers, single-photon excitation *(Russian)* 80−99736
CdS platelet laser, emission spectra, optical coupling between partial resonators 80−69400
$CdS_{1-x}Se_x$ monocrystal petal lasers, single-photon excitation *(Russian)* 80−99736
Co:MgF_2, laser, broadly tunable CW operation, output powers, optical pumping 80−32995
Co_2 injection mode-locked TEA laser, extra-cavity feedback into unstable resonators 79−72601
Cu II, laser construction and performance, novel hollow cathode discharge structs. 80−38000
Cu vapour laser, unstable resonator oscillator and oscillator-amplifier characts. 80−23720
Cu vapour laser with unstable resonator, for pumping of dye amplifier 77−88755
DCN, 250 mW continuous discharge laser at 195 μm 79−31949
DCN, CW submm. waveguide laser, high volumetric efficiency 78−42351
DF laser, CW, modelling of three-dimensional compressible mixing and reacting ducted flows 77−27621
DF laser, pulsed unstable resonator, mode control and performance studies 78−82995
DF-CO_2 CW chemical transfer laser, high pressure operating charact. 79−81449
D_2O FIR lasers, reststrahlen laser resonator for 66 μm line 78−55385
D_2O laser, 66 μm, with unstable reststrahlen resonator 80−83619
(Ga,Al)As CW diode laser, L(J) charact., external cavity induced nonlinearities 77−79824
GaAlAs CW diode laser, external cavity control, 32 MHz single axial mode 78−1271
GaAlAs, DH CW diode laser, picosecond pulse generation 78−83002
GaAlAs DH injection laser, half-ring, room temp. operation 80−58558
(GaAl)As high performance diode laser, high-reflectivity cavity mirrors 78−82994
(GaAl)As injection lasers operating with optical fibre external resonator, characts. 80−58544
(GaAl)As injection laser operating in external cavity, intensity self-pulsations 80−64013
(GaAl)As injection lasers operating with optical fibre resonators 80−91812
(GaAl)As laser, stripe struct. for horizontal transverse mode stabilisation 77−79859

laser cavity resonators continued
GaAlAs laser diode, CW, ps pulse generation 79−50329
GaAlAs mode stabilised separated multiclad layer stripe geometry DH laser, optical waveguide 80−64051
(GaAl)As oxide-stripe geometry DH laser, cavity length effect on output 79−50323
(GaAl)As-GaAs DH laser, anomalous emission intensity, cavity competition 77−79823
$Ga_xAl_{1-x}As$-GaAs heterostructure laser, suppression of internally circulating modes, effect on catastrophic degradation and efficiency 77−83896
GaAs DH laser diodes stabilised using self-apertured facet coatings 80−58609
GaAs diode lasers coupled to short external resonators, reson. amplifier model 77−31110
GaAs double cavity laser, with branching output waveguides, exam. 78−37918
GaAs double-cavity laser with branching output waveguides 78−63128
GaAs, electron beam pumped laser, far-field radiation pattern, optical confinement effects 79−86181
GaAs electrooptically tuned external-cavity CW injection laser, FM optical communication appl. 80−14351
GaAs laser, electron-beam-pumped, transient waveguide effects and lasing time delays 78−37882
GaAs, semi-insulating substrates, whispering gallery lasers 80−69405
GaAs:Zn optically pumped laser, ribbon whisker between highly refl. dielec. mirrors 80−99771
GaAs-(GaAl)As DH injection laser with pillbox resonator, characts. and fabrication 80−58581
GaAs-(GaAl)As LOC-DBR laser, high differential quantum efficiency 78−79031
$GaAs$-$Al_{0.3}Ga_{0.7}As$ laser diode, spontaneous radiation transfer 80−91796
$GaAs$-$Al_xGa_{1-x}As$ CW-diode laser, coupled to freq.-selective external cavity, self-pulsing 77−61982
GaAs-AlAs multilayer heterostructure laser, power and photoelectroluminescence characts. 80−53297
GaAs-AlGaAs CW laser coupled to external cavity, multimode operation, output intensity low freq. pulsations 79−68394
GaAs-AlGaAs short cavity laser, cleaving process for GaAs wafers 78−37915
$GaAs$-$Ga_xAl_{1-x}As$, injection laser with external resonator, mirrors of Michelson interferometer 79−81455
$GaAs$-$Ga_xAl_{1-x}As$ injection laser, external resonator, radiative characts. 77−23703
GaAs-GaAlAs CW diode laser, lateral mode stabilization using apertured facet reflectors 80−23708
GaAs-GaAlAs DH injection lasers, external cavity operated angled-stripe geometry, CW operation 80−64078
GaAs-GaAlAs embedded stripe DH laser with polycryst. GaAsP, cleaved mirrors 77−75548
GaAs-GaAlAs embedded stripe DH laser with polycryst. GaAsP, etched mirrors 77−75549
GaAs-GaAlAs grating coupled lasers, output power efficiency 77−79858
GaAs-GaAlAs injection laser, branching waveguide directional coupler, fabrication and operation 78−38047
GaAs-GaAlAs injection laser, radiation divergence reduction by non-waveguide mode excitation 80−91797
GaAs-GaAlAs nonplanar large optical cavity laser, pulsed room temp. operation 80−28244
GaInAs, electron-pumped laser, far-field radiation pattern, optical confinement effects 79−86181
GaInAsP-InP stripe laser, etched mirrors fabricated by wet chem. etch 80−99744
Ge complanar X-ray resonator circulating beam, high symm. multiple wave configurations *(Russian)* 80−78875
H_2, compressed, Raman laser, axial mode self-locking in long high-Q resonator 79−94223
HCN CW compact laser, output characts. expt. 80−38035
HCN waveguide and Fabry-Perot CW laser power scaling laws 79−76715
HF, CW chem. laser, freq. stabilisation by beat signals and anomalous dispersion 79−86187
HF CW chemical laser, design of multipass telescopic amplifiers 79−27289
HF CW chemical laser, mode competition obs. 80−33040
HF CW chemical laser, longit. and transverse mode competition in stable, unstable resonators 80−95917
HF CW chemical laser, spatial homogeneity of radiation improvement using telescopic resonator 80−106549
HF CW chemical laser amplifier with multiple pass telescope cavity, diffr. 80−19055
HF CW chemical laser with cylindrical telescopic resonator, flame front model 78−59001
HF CW chemical laser with unstable telescopic resonator, diffr. effects 79−94265
HF chemical laser, 10 kW CW arc-driven, diagnostic system for supersonic free jets 77−23667
HF chemical laser, single-line CW, with unstable resonator, temporal stability 77−50690
HF chemical laser, spherical telescopic resonator, design 78−71120
HF chemical laser with microwave excitation *(German)* 80−43326
HF chemical lasers, numerical anal. of laser generation conditions 80−9872
HF laser, pulsed unstable resonator, mode control and performance studies 78−82995
HF pulsed, chemical laser, with spherical telescopic resonator, energy characts. calcs. 80−14367
HF-DF, pulsed closed cycle laser, operation with dispersive unstable resonator cavity 77−88753
He-Ne, 0.633μm line freq. stabilisation with 3.39μm line locked to CH_4 80−28258
He-Ne, complex resonator laser, stabilisation by freq. offset-lock 77−31107
He-Ne, lasing spectrum, modulation freq. of resonator losses 77−34902
He-Ne, longit. mode locking using Fabry-Perot etalon 79−50318
He-Ne, mode locking, phase interferometer control 77−72009
He-Ne, waveguide resonator, oscill. modes 77−27311
He-Ne, weakly anisotropic resonator laser, natural polarisation fluctuations of emission 77−79801
He-Ne commercial multimode low power laser, conversion to single mode laser 80−53325
He-Ne complex resonator laser, stabilisation 78−55374

laser cavity resonators continued
He-Ne gas laser, anisotropic resonator, linear polaris. freq. depend. 77−10961
He-Ne laser, 3.39 μm, in-resonator losses, effects on power *(Russian)* 78−5455
He-Ne laser, cavity losses, phase polarisation method in lasing regime 80−87413
He-Ne laser, doubly resonant intracavity SHG of 1153 nm radiation with stabilization on HFS components of $^{127}I_2$ 80−33077
He-Ne laser, in axial mag. field, output power dependence of mode locking phenomena 78−71129
He-Ne laser, mode stabilisation by axial mag. field, long resonator case 77−7143
He-Ne laser, output power, unsaturated gain distrib. 78−50751
He-Ne laser, refl. anisotropy of 6320 Å mirrors 79−98413
He-Ne laser average output power, resonator losses, freq. modulation 77−34901
He-Ne laser cavity optimisation for thermal lens effect meas. 77−42577
He-Ne laser frequency stabilisation using mag. field tuning dip 79−55153
He-Ne laser modal configuration, interference spectrometer study *(Spanish)* 80−86458
He-Ne laser mode locking by three-level reson., Zeeman tuning of intracavity Ne absorber 79−89943
He-Ne laser model LG-10, design *(Rumanian)* 80−87407
He-Ne laser photon statistics variation with cavity length 80−53265
He-Ne laser plasma, metastable at. and electron density diagnostics 77−84499
He-Ne laser saturation resonance in static magnetic field 77−54693
He-Ne laser stabilisation, I_2 absorption cell power densities 80−99767
He-Ne laser stabilisation by I_2 612 nm saturated absorption 80−99765
He-Ne laser stabilisation by I_2 611.8 nm saturated absorption 80−99766
He-Ne laser with anisotropic cavity, fluctuations of field polaris. 79−27242
He-Ne laser with external optical resonator, SHG 79−27326
He-Ne laser with internal mirrors, mode polarisation props. 80−23672
He-Ne lasers, stabilised by saturation absorpt. in I_2 78−1270
He-Ne nuclear-pumped CW lasing 80−48216
I, radial oscills. of medium, effect on laser output 78−5507
$In_xGa_{1-x}As$-$In_yGa_{1-y}P$ DH laser, CW room temp. operation at 1.06 μm 77−19250
InGaAsP DH lasers with etched reflectors, fabrication, current density 80−64050
InGaAsP-InP DH laser with self-aligned struct., oscillation characts. 80−38017
$In_{1-x}Ga_xP_{1-z}As_z$, DH, operated in external grating cavities, inhomogeneous and homogeneous line broadening 77−10921
$In_{1-x}Ga_xP_{1-z}As_z$ near IR DH laser, constant temp. LPE, external grating cavity 77−75550
InSb pulsed spin-flip Raman laser, external cavity, low field operation at 10.6 μm 79−41394
InSb spin-flip Raman laser, external cavity CO_2-pumped, with intracavity etalon 78−42345
InSb spin-flip Raman laser external-cavity system, oscill. characts. 78−55383
$KNdP_4O_{12}$ epitaxially grown waveguide, laser operation at 1.051 μm 79−18423
KrF 1J avalanche discharge laser unstable resonator expts., beam divergence 80−74404
KrF, diffraction-limited laser, with negative branch unstable resonator 77−38937
KrF discharge pumped laser, stable-unstable resonator for beam control 80−23722
KrF, excimer laser, development of dielectric mirror *(Japanese)* 79−72588
KrF excimer laser, high brightness performance using high magnification unstable resonator 79−59716
KrF injection locked unstable resonator discharge laser, narrow linewidth and high spatial quality 80−53323
KrF, injection-locked narrow-band discharge laser, using unstable resonator cavity 78−25893
KrF mini-laser operation at high repetition rate 80−74396
KrF*, electron beam pumped laser, pulse shape and laser-energy extraction, model and expt. comparison 79−98345
Li^+:KCl, F_A (II) colour-centre laser, mode locking and tunable picosecond IR pulse generation 80−43364
LiF OH-stabilised F_2^+-centre laser, appl. to intracavity laser spectroscopy 80−32999
$LiIO_3$ Raman oscillator, high-average-power, employing shared resonator config. 78−30013
$LiNbO_3$ crystal in laser resonator, thermo-optical effect *(Chinese)* 80−106546
$LiNbO_3$ intracavity upconvertor for IR detect., limits to low noise equivalent power operation 80−74430
$LiNbO_3$, nonstationary intracavity stimulated Raman scatt. by polaritons 79−18473
$LiNd(PO_3)_4$ laser with external and Fabry-Perot resonators, 1.05, 1.32 μm CW oscill. 80−23693
$LiNdP_4O_{12}$ laser, spontaneous phase locking obs. 78−83005
$LiNdP_4O_{12}$ stable miniature laser with compact resonator, single mode operation 79−50305
N_2, coherent radiation from unstable resonator 77−71994
N_2 laser, electrode configuration for high peak powers and high repetition rates 78−55379
N_2 laser, superrad., inexpensive construction *(Korean)* 78−22147
N_2 liquid IR Raman laser with unstable resonator 79−31957
N_2 superradiant UV laser, method for brightness increase 79−36917
NH_3 high power laser, improved optical pumping geometry in Littrow cavity config. 79−22973
NH_3, waveguide cavity, efficient CW far IR output 77−72001
$NH_4H_2PO_4$ total internal reflection intercavity laser switch 77−38955
NI:MgF_2, laser, broadly tunable CW operation, output powers, optical pumping 80−32995
N_2O IR laser, transients obs. by modulation of intracavity absorber 78−74933
N_2O-N_2, CW mixing gasdynamic laser, saturation parameter and small signal gain 79−45923
Nd laser, continuously tunable, pulsed, operation and output, characts. 79−18448
Nd, with mirror plasma-optical Q-switch *(Russian)* 80−33028

laser cavity resonators continued
Nd:garnet, freq. axial mode shift, two-mirror resonator synchronisation, stabilisation *(Russian)* 78−22154
Nd:glass, dynamic mode sweep-laser, freq. tuning 78−66851
Nd:glass, laser rod amplifier of 4 cm diam., design and performance 77−19339
Nd:glass, lasing spectrum singularities and Q-factor, for z-dimens. beam path *(Russian)* 77−88795
Nd:glass, line narrowing and tuning using intracavity Brewster angle birefr. filter 77−38976
Nd:glass, oscillator, short laser pulses *(Rumanian)* 79−7165
Nd:glass, slot method for radiation extraction 77−50694
Nd:glass, spectral distrib. kinetics rel. to intracavity spectroscopy 78−1293
Nd:glass, with metallic grating in cavity, Fourier spectrum and periodic mode fields distrib. *(Russian)* 79−31915
Nd:glass intracavity laser spectrometer with dispersive resonator 77−74530
Nd:glass laser, resonant reflectors in laser cavity, freq. selection 78−55369
Nd:glass laser operation, self-focusing influence 79−13997
Nd:glass laser output, passive-mode locked, resonator length effect 78−79044
Nd:glass laser resonator deform. due to polarisability change of excited Nd ions 79−10313
Nd:glass laser with active mode locking, ultrashort pulses 80−64087
Nd:glass laser with continuously tunable ps output, polaris. filter 79−22985
Nd:glass laser with grid mirror, emission field 79−55142
Nd:glass laser with unstable resonator and additional feedback, angular divergence 80−48307
Nd:glass passively mode-locked laser, obs. of external feedback influence 80−23729
Nd:glass Q-switched laser emitting polarised radiation 79−45974
Nd:glass Q-switched with stable operation in pure transverse natural oscillation *(German)* 77−14761
Nd:YAG, cavity dumping single mode-locked pulses 77−7137
Nd:YAG, electro-optical extraction of ps laser pulse *(German)* 80−87416
Nd:YAG, intracavity modulation, sum freq. mixing, 212.8 nm pulse burst generation 78−74934
Nd:YAG, mode-volume matching of oscillating modes of laser containing several active elements *(Chinese)* 79−50325
Nd:YAG, negative feedback external perturbations effect, spectral depend. 77−83908
Nd:YAG, single freq. laser with waveguide resonator 78−1277
Nd:YAG, unstable resonator oscillator, 12 ns 200 mJ output 77−42548
Nd:YAG, unstable resonator, Q-switched laser, operating characts. 79−36928
Nd:YAG CW laser, active stabilisation, laser noise 80−48295
Nd:YAG crystal, orientation influence on thermally induced birefringence *(Chinese)* 80−88958
Nd:YAG laser, intracavity freq. doubling by $LiIO_3$ long pulse emission 80−102736
Nd:YAG laser, Q-switched, pulse stretching using Pockels cell 80−95927
Nd:YAG laser as optical pulse generator, mode locking by acoustooptic loss modulation 79−64260
Nd:YAG laser stabilisation by T-shaped four-mirror resonator *(Russian)* 78−13730
Nd:YAG laser with internal SHG in coupled resonators, CW coherent UV-source *(German)* 79−98438
Nd:YAG long laser resonator, active and passive mode-locking 78−50832
Nd:YAG long-pulsed laser, resonator config. for relax. oscills. suppression 79−72599
Nd:YAG mode-locked unstable laser, p-branch unstable resonator config. 79−31928
Nd:YAG oscillator, Q-switched, generation of high-power ns pulses 80−23730
Nd:YAG passively mode-locked unstable oscillator 79−45953
Nd:YAG pumped tunable sources, appl. to spectroscopy 80−58576
Nd:YAG unstable resonator design 79−13988
Nd:YAG unstable-resonator oscillator, stable single-axial-mode operation by injection locking 80−53331
Nd:YAG waveguide resonator laser, time characts. 77−58345
Nd:YaG laser reflection resonator with hole coupling 80−58597
Nd^{3+}:$LiYF_4$, pulsed free running laser action at 1053, 1046 nm, passive mode locking *(French)* 78−79048
Nd^{3+}:YAG, CW laser with planospherical resonator, freq. degeneracy of modes 79−31953
Nd^{3+}:YAG, Raman laser with optical-fibre resonator, expt. investigation 79−31913
Nd^{3+}:YAG, with $LiNbO_3$ or $Ba_2NaNb_5O_{15}$ crystals, AM of optical second harmonic 80−78908
Nd^{3+}:YAG CW linear laser, longit. mode self-locking 79−72611
Nd^{3+}:YAG electro-optically Q-switched pulse-periodic laser 79−45975
Nd^{3+}:YAG laser, high repetition rate electrooptic Q-switching, birefringence 80−69430
Nd^{3+}:YAG stabilised single-freq. travelling wave laser 79−18449
$Nd_{0.5}La_{0.5}P_5O_{14}$ laser, FM mode-locked 79−86184
(Pb,Sn)Te diode laser, grating coupled emission 77−79860
$Pb_{1-x}Sn_xSe$ laser, optical feedback effects on performance, external cavity modes 80−32981
n-$Pb_{0.88}Sn_{0.12}Te$ spin flip Raman laser pumped by TE CO_2 laser, characts. 80−87397
ruby Q-switched with stable operation in pure transverse natural oscillation *(German)* 77−14761
Xe_2 excimer laser pulse temporal evolution, cavity mirror depend. 79−76732
XeCl 80−53323
XeCl mini-laser operation at high repetition rate 80−74396
XeF, C-A blue-green, multipass amplification and tuning 80−43346
XeF, diffraction-limited laser, with negative branch unstable resonator 77−38937
YAG laser, resonator length effects on loss coeffs. and ouptut energy *(German)* 78−66849
YAG stable resonator, yielding high output energy and very low divergence beam 80−23721
$Zn_xCd_{1-x}S$, lasing modes and spatial distrib. under one-photon excitation, cavity model 78−74913
laser cavity resonators continued
$Zn_xCd_{1-x}S$ monocrystal petal lasers, single-photon excitation *(Russian)* 80−99736
ZnSe-ZnS semiconductor waveguide laser, electron beam excited, blue emission 79−18447

laser frequency stability
3.39 μm He-Ne laser frequency stabilisation without FM 79−55152
^3He-^{20}Ne stabilised transverse Zeeman laser, tuning characts., freq. fluctuation 80−48273
acousto-optical frequency and intensity control system for CW lasers 77−88804
atomic beam nonorthogonal to laser light, absorpt. profile, optical freq. standard appl. 78−74940
carbon tetrafluoride laser with optical pumping, freq. tuning and stabilisation 80−99706
carbon tetrafluoride optically pumped laser, stimulated emission stabilisation and tuning 80−9866
CW dye lasers, improved freq. stability using the He-Ne lasers *(French)* 79−31935
CW laser, mode selection using spatially inhomogeneous saturable absorpt. *(German)* 78−83011
1,1-difluoroethylene, optically pumped, far IR laser line assignment 79−31865
digital frequency-offset lock system designed for use with stabilised lasers 78−29960
digital-analogue lock-in circuit for freq. stabilization, using single-photon detection 79−50334
diode laser in external cavity, linearized theory 80−69391
diode laser output stabilization by bevelled-end fibre coupling 80−91806
Doppler broadened laser amplification line frequency characteristics meas. 78−59060
dual frequency laser, frequency stabilisation study *(Chinese)* 79−72578
dye CW commercial laser, freq. stabilisation for ultrahigh resolution spectroscopy 77−88802
dye DFB laser, line narrowing and wavelength stabilisation technique 77−88783
dye laser, CW freq. stabilised, spectroscopic and metrological appl. 78−9395
dye laser, double grazing-incidence single-mode type 80−95906
dye laser, freq. control by piezo mirror translator 79−72582
dye laser, freq. locking of Na flame atomic transitions 78−50795
dye laser, frequency locking by selective refl. 78−29992
dye laser, mode-locked, synchronously pumped, pulse-width stabilization 80−83622
dye laser, narrowband CW, high output power, piezoelec. mirror translator for stabilisation 80−33036
dye laser, wide bandwidth feedback loop 77−83891
dye laser frequency locking by intracavity stimulated Raman scatt. 78−79050
electro-optical modulator use in or outside cavity for laser freq. shifting or stabilisation 78−5512
extracavity absorption cell laser, inverted Bennett hole 79−64292
F_2-centre, pulsed tunable laser, IR spectral characts., 1.1-1.26 μ region 80−91805
Fabry-Perot cavity, gas filled, optical bistability described by stochastic master eqn. 79−76652
Fabry-Perot cavity with Faraday filter, for freq. locking, polarisation props. 77−46738
far IR laser, injection phase locking 80−69431
far IR lasers, optically pumped, frequency modulated noise measurements 78−55392
fibre-optic communication system performance at 1.55 μm with single-longitudinal-mode laser 80−87556
FIR laser pump lasers, variable-frequency stabilisation 79−14005
FIR lasers stabilizations, fast modulation technique 80−99777
fluoromethane far IR laser FM and stabilisation by Stark effect 78−59056
fluoromethane for IR laser, evidence for Stark induced freq. shift 77−58358
frequency and spectral parameter check system 77−79880
frequency meas. 78−12675
frequency stabilizer using single-photon detection, D/A lock-in circuit 79−50334
gas laser, radiation synchronisation, with quantum RF standard 77−68226
gas laser, reference freq. and resonator length fluctuations effect 77−3619
gas laser, single frequency, production testing techniques 78−90444
gas laser frequency stabilisation *(Japanese)* 80−9891
gas laser stabilisation using nonlinear Ramsey reson. 77−3622
gas laser with automatic freq. control, long-term instability and irreproducibility of freq. 79−45962
gas laser with nonlinear absorber, reson. obs. in output, freq. stabilisation 77−83854
gas lasers, CW, small power-radiation instability levels meas., using photodiode circuits 80−23704
gas lasers, frequency stabilised by saturated absorpt., synthesis and measurement of optical frequencies, review *(French)* 79−31966
gas lasers, vibration immunity for interference work 78−5489
gas single-mode laser with absorpt. cell, intensity and freq. fluctuations 78−17993
gasdynamic high speed lasers, freq. stability mode struct., and output power characts. *(Chinese)* 79−31854
gyroscope with induced mode locking, limiting sensitivity 79−59744
He-Ne methane saturated absorpt. stabilised lasers *(Chinese)* 79−59718
high intensity laser oscillator, output characts., stability criteria, semiclassical density matrix approach 80−63968
high-power laser emission freq. stabilization against reference laser 80−23698
hydrophone, optical interferometric, with homodyne detection, signal stabilization by light source tuning 80−87477
injection laser longitudinal mode stabilisation by temp. compensation 79−45964
instability below threshold, laser-saturable absorber system 78−94385
interference discriminator, Fabry-Perot, for laser freq. stabilisation, optimisation 79−31962
interferometry, multimode fibre optic, applications 80−86387
internal mirror laser, polarisation mode, freq. stability *(Japanese)* 78−46675

laser isotope separation continued
methanol, multiphoton decomposition with laser, isotope separation 79−66306
methyl nitrite, N-isotope separation by multiphoton dissoc. in intense IR field 77−68086
methylamine, multiphoton discoc., N isotope separation 80−35553
mixtures, two-component, two photon isotope separation, dynamics 80−102584
molecular dissociation by IR lasers 79−52710
molecular gas, by mol. laser *(German)* 77−6954
molecular ion, spontaneous IR rot.-vibr. emission probability, vibr. selective excitation 78−50535
molecular vibrational excitation, tunable IR source 77−65605
multiphoton dissociation method, using CO_2 laser 77−88598
multiphoton dissociation of mols. with high-power CO_2 laser, practical methods 79−89802
non equilibrium light gas, heavy impurity thermal diffusion under laser irrad. 80−64667
nonequilibrium condensation method, with selective laser photoexcitation, mathematical model 79−31720
nonuniform mag. field *(Russian)* 77−6960
nozzle flows with heterogeneous condensation 80−50862
overview, mol. photodissociation processes 78−55257
photochemical method using relativistic electron beam microwave source 77−38750
photochemistry in solid state, IR lasers appl. 80−11929
photochemistry two-photon, photo-fragment distrib., isotope separation appl. 80−81344
photoionisation, selective, use in laser isotope separation and spectros., review 80−83332
photomigration method *(Japanese)* 80−32849
photophysical and photochemical methods, book contrib. 79−79273
plasma science, conference, Monterey, CA, USA (May 1978) 79−37442
polyatomic molecule, laser photochem. dissoc., isotope effect rel. to dissoc. probability 80−23472
polyatomic molecule, suitability for separation by selective photodissoc. 77−68086
polyatomic molecules, collisionless dissociation by multiphoton IR absorption 77−54580
polyatomic molecules, dissociation by intense IR laser field 77−54579
polyatomic molecules, multiphoton dissoc. and isotope separation 78−62865
polyatomic mols., laser induced isotope enrichment, selective vibr. excitation mechanisms 77−18994
polyatomic mols., multiple photon IR processes, reviews 80−43125
principles and developments 79−76148
pulse power requirements 79−13972
purification of materials with overlapping absorpt. spectra 80−78452
rare earth elements, by two-step photoionisation 78−46461
rare earth isotopes laser separation 77−88597
recent advances *(Chinese)* 79−81291
recombination, in steady supersonic flow, in devices for laser isotope separation 79−31717
resonance light pressure, anal. of forces and applications, reviews 79−18156
review, basic ideas, methods and key expts. 79−36789
review, conf., USSR Acad. of Science, (June 1977) 79−18062
review *(Chinese)* 77−14610
review 77−34784
review *(German)* 78−13744
review 78−37758
review 79−18304
review 80−32851
review of 1970-77 development and future prospects *(Japanese)* 78−5048
review of principles and methods, book contrib. 78−9280
scattering of atoms by stimulated light freqs. appl. to isotope separation 78−66526
selective action of laser radiation on matter, review 80−7832
selective dissociation, ionis., and chem. reaction stimulation, by ultra-short pulses, isotope separation *(Russian)* 78−29825
selective laser excitation of atoms and mols., photophys., photochem. processes, appls. 77−54630
selective multistep processes 80−23473
selective photochem. reactions 77−77800
selective vibrational excitation effect on chem. reaction kinetics 78−33627
surface photochemistry and photodesorption, isotope separation aspects 78−64863
system requirements, dye and rare gas halogen lasers 77−46405
techniques and efficiency 79−31721
sym-tetrazine, gas phase separation of ^{13}C and ^{15}N isomers, CW dye laser 79−27097
sym-tetrazine, isotope selective mol. spectroscopy and isotopically pure mols. prod. with dye laser 80−11926
s-tetrazine in Ar matrix, laser induced isotope enrichment 77−88599
trifluoremethane-d_1, IR photolysis, kinetics of multiphoton dissoc., ^1H isotope separation 79−79276
trifluoroiodomethane, high press., selective isotope dissociation with pulsed CO_2 laser 79−72370
trifluoroiodomethane, isotope separation by multiple photon IR excitation and subsequent UV dissoc. 79−18301
trifluoroiodomethane, isotopic sensitivity of IR laser photodissociation 80−7805
trifluoroiodomethane, multiphoton dissoc., isotopically selective 80−28113
trifluoromethyl iodide, ^{13}C isotope separation by selective multiphoton dissoc. 78−25734
tunable lasers and applications, conference, Loen (1976) 77−54720
uranyl hexafluoroacetylacetonate tetrahydrofuran, IR laser photodissoc., O and U isotope selective 80−50868
B, laser photochemical isotope separation using Ti catalyst 77−61612
BCl_3, gas, isotope separation, laser stimulation-filtering diffusion method *(Russian)* 77−555
BCl_3, isotope enrichment, heterogeneous condensation in prescence of CO_2 laser irrad. 78−70953
BCl_3-N_2 mixtures, thermodiffusion props., effect of resonant excitation of mol. vibr. by laser, isotope separation 80−100047
BCl_3+methane reaction, laser-induced, vibr. excitation influence on reactivity, isotope selectivity 80−11921

laser isotope separation continued
Br isotope laser separation possibility, using Ge+Br_2 heterogeneous photochem. reaction 79−66326
Br_2, absorpt. spectrum, laser isotope separation *(Japanese)* 77−34649
Br_2, absorpt. spectrum, rel. to laser isotope separation 77−10683
C isotope separation, by multiphoton dissociation of CF_3I 79−3592
C isotopes, prospects of using hexafluoroacetone for separation 79−98172
CO pulsed laser, stimulated emission dynamics, transition lines for isotope enrichment 80−48225
CO_2 periodically pulsed laser, appl. isotope separation 79−27287
CO_2 pulse-periodic laser, multiphoton molecular dissociation 80−9931
CS_2, single-photon isotope separation using ArF laser 78−55211
^{13}C, from formaldehyde, ion laser induced photopredissociation 77−61871
^{14}C, enrichment method for radiocarbon dating 79−10220
Cl_2, isotope shift and absorption spectrum laser induced, obs. 77−34701
Cl_2, photochemical reaction using Ar ion laser, Cl isotope enrichment 78−74780
D, depletion optimisation and photon efficiency 78−46175
D enrichment, laser methods for nuclear fuel reprocessing 77−38378
D enrichment by CW CO_2 laser induced reaction of methane 79−18300
D enrichment by CW vibr. photochem. of methane, economic aspects 80−11920
D, reaction chamber for laser separation 78−55040
D_2O production, using laser isotope separation 77−83106
Dy atom isotope separation, laser excitation, charge exchange with Cs^+ ions 80−83512
Eu, laser isotope separation by two step photoionisation 77−61720
Eu+H^+, two-step laser isotope enrichment using charge transfer ionisation 79−867
^{151}Eu, ^{153}Eu, two-step laser photoionisation *(Russian)* 77−6952
Gd, laser isotope separation by two step photoionisation 77−61720
Gd, sputtered vapour, neutral ground state population, laser obs., appl. to isotope separation *(Russian)* 78−29759
ICl selective photoaddition to acetylene, isotope enrichment, influence of press., buffer and wavelength 80−11927
^{127}I, ^{129}I isotope separation possibility using photodissociation I laser 79−7030
$^{129}I_2$, selective excitation and separation in I_2+C_2H_2 laser induced chem. reaction 80−68962
Li, selective two-step photoionisation and isotope separation 77−71783
$^6Li^*$+$^7Li^*$, laser-induced Penning and associative ionis., $^7Li_2^+$ enrichment 78−58796
^7Li selective excitation, by intracavity nonlinear absorpt. in CW dye laser 79−866
MoF_6, isotope separation by laser, multiple-photon 78−58858
N, isomerisation of ethyl and methyl isocyanide 79−27096
N isotopes, selective two-step dissoc. of NH_3 by laser, book contrib. 78−9208
NH_3 laser, optically pumped 12 μm, for UF_6 isotope separation, parametric study *(Japanese)* 79−81414
NO, state selective step-wise photoionis. with mass spectroscopic ion detect. 80−43119
O, in methanolic UO_2F_2 soln., photochem. enrichment 79−36786
O, photochem. enrichment of ^{17}O and ^{18}O using ArF laser 77−16834
^{17}O enrichment by formaldehyde photopredissociation using Ne II ion laser 77−19112
$^{17,18}O$, from formaldehyde, ion laser induced photopredissociation 77−61871
Os isotopic anomalies from different ore deposits, LAMMA determ. 80−61800
OsO_4, by dissociation in two-freq. IR laser field 78−25638
OsO_4, IR laser dissociation isotope separation appl. 77−18993
OsO_4, isotope selective dissociation by IR radiation pulses, luminesc. intensity 77−83665
OsO_4, two IR pulse multiphoton absorpt. selective dissoc., obs. 78−82798
^{207}Pb, laser isotope separation using nuclear spin induced elec. dipole transitions 77−61877
S, by mol. dissociation of SF_6 in strong IR field, appl. of CO_2 laser 77−83755
S isotopes, SF_6 photodissoc. by IR laser pulse, selectively excited vibr. levels 78−9209
S, multiphoton molecular dissociation using high-power CO_2 laser radiation 80−9657
SF_6, CO_2 laser induced dissociation, energy and press. depend. 77−23523
SF_6, collisionless dissociation and isotopic enrichment, using CO_2 laser 77−18999
SF_6 cooled gas, multiphoton dissociation with CO_2 laser, enrichment with ^{33}S 80−14245
SF_6 dissociation processes using one or two TEA CO_2 lasers 78−74713
SF_6, electron capture, laser radiation influence, possible laser isotope separation appl. 79−22856
SF_6, IR laser isotope separation 79−50150
SF_6, IR laser isotopic enrichment in low temp. matrices 78−90318
SF_6, IR laser radiation induced dissoc. 77−29026
SF_6, isotope separation, laser induced multiphoton dissoc. 77−16839
SF_6, isotopic enrichment, coherent multiphoton vibr. excitation and dissociation 77−88512
SF_6, laser isotope separation model 77−31016
SF_6 laser isotope separation, rot. and vibr. relax. in mixture 78−25634
SF_6, laser-induced isotope separation, threshold intensity 77−4898
SF_6, mol. beam, selective dissoc. in intense IR laser field, wavelength and energy depends. 78−73065
SF_6, multiphoton dissoc., classical model 80−53076
SF_6, multiphoton IR dissoc., quantum or classical approach 78−82801
SF_6, multiphoton isotope selective dissoc., pulse shape, energy, press. and geometry effects 78−25733
SF_6, multiphoton reaction, laser mode-locking effect 77−46606
SF_6, photon-enhanced dissociative electron attachment, isotope selectivity 80−18939
SF_6, selective dissociation using tunable compressed H_2 Raman laser 77−34708
SF_6, selective multiphoton dissociation by CO_2 laser irradiation 77−34707
SF_6+SiH_4→S_2*+SiF_4+HF+H_2, laser augmented reaction, isotopic selectivity retention during detonation 78−48673
SF_5NF_2, multiphoton excitation, absorption and dissoc., isotope selection 79−100408

laser isotope separation continued
SeF_6, IR photolysis, $NH_3^- + CO_2^-$ laser isotope separation and dissoc. enhancement 79−29377
SeF_6, isotopically selective IR photodissociation 78−42142
Sm, laser isotope separation by two step photoionisation 77−61720
U, appl. of Ar ion laser UV lines, photoionisation expts. 78−42233
U enrichment, laser R&D 77−54364
U enrichment *(Japanese)* 80−68960
U enrichment by laser isotope separation 77−38418
U enrichment by photochemical laser, two-phase flow with condensation, mathematical model *(French)* 80−74029
U enrichment by two step photoionisation *(Japanese)* 79−49865
U enrichment plant, optimum operating conditions 79−54578
U enrichment using lasers, implications for nucl. weapons proliferation 77−67849
U isotope separation appl. to nucl. fuel cycle, teaching module 80−36805
U isotope separation by selective laser photoexcitation in reactive two-phase flow 79−94109
U, laser isotope separation, atomic spectroscopy requirements 78−33638
U, laser isotope separation by O_2 chemi-ionisation *(Japanese)* 79−13830
U, radiative lifetime, appl. to laser isotope separation 79−50152
UCl_4, UCl_6^{2-}, UCl_6^-, UCl_8^{3-}, reduced partition function ratio calc. 77−12819
UF_6, by mol. laser *(German)* 77−6954
UF_6, characts. of optically pumped 12.08 μm high power NH_3 laser 78−74923
UF_6 laser isotope separation for fuel enrichment 77−54618
UF_6 molecule dissociation in two-frequency IR laser field 80−66855
UF_6, non-equilibr. condensation calcs. for laser isotope separation 80−10132
UF_6, temp. and density profiles in freely expanding gas for laser enrichment 78−74458
UF_6, UF_4, reduced partition function ratio calc. 77−12819
$^{235}UF_6$ isotope separation by CO_2 laser beam four-photon mixing IR source 77−54760
$U(NO_3)_6^{2-}$, reduced partition function ratio calc. 77−12819
UO_2^{2+}, $UO_2F_5^{3-}$, $UO_2Cl_4^{2-}$, $UO_2Br_4^{2-}$, $UO_2(NO_3)_3^-$, reduced partition function ratio calc. 77−12819
^{235}U enrichment, laser methods for nuclear fuel reprocessing 77−38378
^{235}U enrichment, using laser based two-phase photoionisation and photodissociation methods *(Czech)* 77−61583
^{235}U enrichment by laser isotope separation 77−19113
^{235}U enrichment by laser isotope separation process, cost anal. 77−42160
^{235}U, hyperfine struct. and isotope shift meas., laser separation by two-step photoionisation 78−78822
^{235}U isotope separation enhancement with RF hyperfine transitions 79−41249
^{235}U, laser photochemistry appl., LASL developments 79−31719
^{235}U, lifetime meas. of electron excited states, rel. to laser isotope separation 77−34591
^{235}U, photoionisation, isotope separation and enrichment by Ar ion laser *(Japanese)* 79−81192
^{238}U vapour, hollow-cathode generator, energetic yield 80−47724
^{235}U, recovery from enrichment plant tailings appl. 80−83212
Yb, photoionisation cross-section of $^3P_1$ excited state *(Russian)* 78−25496

laser magnetic resonance
diatomic molecule, rel. to theory of high-precision Zeeman effect 77−14486
formyl radical, laser mag. reson. spectrum at 5.3 micron 80−47981
high magnetic field appls. in spectroscopy of simple atoms and molecules 79−72445
hydroxymethyl radical $+O_2$, rate coefficient meas. by laser magnetic resonance flow tube method 80−66767
methoxy free radical, laser mag. reson. submillimetre spectrum, linear Zeeman effect 77−46579
methoxy radical, LMR spectra anal. 80−63677
methylene radicals, rotational transitions, laser mag. resonance spectra 80−5538
spectral line narrowing of triplet state, in laser excited experiments 80−63703
spectrometers, sensitivity improvement using laser properties 80−13115
spectroscopy technique using optically pumped far IR laser 77−54725
Ba I, isotope shifts, hyperfine struct., neutron deficient nuclei, laser resonance fluorescence study 79−72436
CH, far IR laser mag. reson. spectrum 79−3466
CH_2F, far IR laser mag. reson. spectrum 78−9174
ClO radical, 2-0 vibrational overtone band, laser magnetic resonance spectroscopy study 80−48021
ClO_2 radical, ν, band, tuning by avoidance of Zeeman level crossing 78−94263
Cs, optical pumping with second resonance light 80−23376
FO free radical, detection by CO_2 laser mag. reson. 80−45594
HBr^+, laser mag. reson. pure rot. transition in far IR 79−89695
HCO, ν_2 fundamental band, laser mag. reson. spectra 78−5256
HCO, vibr.-rot. transitions, IR laser mag. resonance 77−27098
HO_2 radical, ν_3 fundamental band, laser mag. reson. 78−66566
$HO_2 + HO \rightarrow H_2O + O_2$, rate coeff. meas. by laser mag. reson., atm. chem. appl. 77−52614
$HO_2 + NO$, reaction kinetics meas. 78−31624
$HO_2 + NO_2$, reaction rate consts. by laser mag. reson. 78−27748
$HO_2 + O_3$, reaction kinetics, laser mag. reson. obs. 80−102528
$HO_2 + O \rightarrow HO + O_2$, rate coeff. meas. by laser mag. reson., atm. chem. appl. 77−52614
^4He, laser mag. reson., 7^1S-9^1P energy separation, motional Stark effect, Zeeman tuning parameters 79−6911
Hg(6^3P_0), $^3P_1$-$^3P_0$ fine struct. obs., CO_2 laser mag. res. 77−61696
^{55}Mn, metastable states, hyperfine struct., laser RF double reson. study 79−72260
NH_2, ν_2 band, laser mag. reson. 80−83523
NH_2, radical, laser mag. reson. spectra in 9 μm region, ν_2 band 79−45724
NH_2, vibr.-rot. transitions, IR laser mag. resonance 77−27098
NH(D) radical, and isotopic species, laser mag. reson., hyperfine parameters 77−10694
$NH_2(X^2B_1)$, laser mag. reson. spectra, Zeeman and hyperfine effects, rot. consts. 77−30892
NO, laser mag. reson. and IR-RF double-reson. near 5.3 μm 78−5258

laser magnetic resonance continued
Na, nonabsorption hyperfine resonances in dye laser irrad. vapour 79−93941
O, 2^3P_2-2^3P_1 fine struct. splitting by laser mag. resonance 79−98010
O, far IR laser mag. reson. 78−37576
OH, isotope effects, Zeeman effect, far IR laser mag-reson. spectra obs. 80−63674
OH, radical, far IR laser mag. reson. spectra, fine struct. transition 79−76454
OH, rot. transitions broadened by press., laser mag. reson. study 79−94020
$OH + Ar(He)(NO_2)$, collisional relax., press. broadening study of OH rot. lines 79−94020
$OH + HO_2 \rightarrow H_2O + O_2$, rate const. meas. *(German)* 79−52629
PH, far IR laser mag. reson. of $X^3\Sigma^1$ and at $^1\Delta$ states 79−54869
PH_2, 9-9,6 μm region, ν_2 band and force consts. 79−89694
PH_2, X^2B_1-state, rot. laser mag. reson. spectrosc. 80−28038
SD, $X^2\Pi_{3/2}$-state, far IR LMR spectra 79−6954
SO, $a^1\Delta$ state, laser mag. reson. spectrosc. 78−94265
SeH($X^2\pi_{3/2}$), far IR LMR spectrum 78−66564

laser modes
^3He-^{20}Ne stabilised transverse Zeeman laser, tuning characts., freq. fluctuation 80−48273
active mirror and disc amplifiers, laser glasses, physical props. 78−42337
adiabatic invariant of oscillatory systems, laser mode sweeping interpretation 79−31950
alkali halide CW single mode colour centre lasers, freq. behaviour and linewidth 77−88728
anisotropic inhomogeneous medium with axial symm., mode struct. 78−18069
anisotropic laser, oscill. props., rate eqns. 78−22135
annular HSURIA resonators, testing with CO_2 laser, polarisation effects 80−58599
atom two step reson. photoionisation, multimode and level degeneracy effects 80−78583
axial mode selector for laser with active Q-switching 79−13996
beam compensation using phase plate 77−42556
bidirectional laser amplifiers, amplified spontaneous emission intensity fluctuations 80−37988
binary laser oscillator mode-locked, bistability induced by optical nutation 79−31958
bistability of saturable-absorber containing laser, semiclassical and quantum theories 78−82943
Bragg mirror reflectance, dielectric waveguide inhomogeneity effect 80−28356
Bragg reflector laser, mode separation and selectivity 78−22153
buried heterostructure laser, DH multilayer LPE growth on etched substrate, optical read-out appls., longitudinal mode operation 80−99749
buried heterostructure laser, fund. transverse mode operation, current limitation 78−55353
CARS spectroscopy linewidth parameter from laser mode structure 80−33083
CH stripe laser, spatial coherence and modal struct. 80−87531
chemical laser, electronic phototransition, with thermal initiation by shock wave 80−53283
confocal unstable resonators, near- and far-field laser modes, free space and saturable gain media 78−46674
conical resonator, high-order circular mode selection 77−75569
coumarin dye laser, mode-locked flashlamp pumped, tunable blue ps pulses 79−13974
coumarin dye laser, passively mode-locked, saturable absorber solvent effect *(French)* 78−42335
coupled laser oscillators, injection modulation 80−99773
coupled laser-amplified system, stationary modes stability 80−1179
coupled wave analysis, DFB and DBR lasers 77−27305
CW flowing gas lasers, mode medium interaction 79−36876
CW laser, homogeneously broadened gain, longit. mode selection 78−63143
CW laser, mode selection using spatially inhomogeneous saturable absorpt. *(German)* 78−83011
CW laser with homogeneously broadened gain, mode selection 77−61978
detector frequency response meas. using laser mode beating 78−8442
DFB lasers, symmetric and antisymmetric modes, discrimination *(Russian)* 77−75573
DFB resonators, dielectric waveguide with periodic surface inhomogeneity 77−7146
DH lasers, symmetric waveguide, near and far-field analytical approx. for fundamental mode 79−50296
DH stripe geometry lasers, three-dimensional anal. of mode props. 80−64020
DH stripe lasers, field model, mode gain, mode spacing 79−7128
DH symmetric laser, beamwidth approx. for fundamental mode 79−22952
diffraction experiment in cavity with 1-D diaphragm 80−95920
diffraction structure as laser mode selector 79−89951
1,1-difluoroethylene mm laser, waveguide cavities comparison, CW props. 78−42328
diode, modulated, with short external cavity, single mode operation 80−5756
diode laser, active mode locking, effect of noise 80−19030
diode laser, longit. mode struct. depend. on injected carrier diffusion 77−54710
diode laser, mode locking to external resonator, theory 80−106550
diode laser, spatially and spectrally resolved near field patterns 78−29955
diode laser IR spectra, intermode calibration using tandem etalons 80−32982
diode laser spatial coherence, studied with reversing front interferometer 80−32993
diphenyl butadiene, absorption recovery lifetime, use in UV mode-locked lasers 80−19075
dispersive medium, incoherent, coherent stimulated Raman scatt. with multimode pump *(Russian)* 80−38063
distributed Bragg reflector lasers, tunability using electro-optic effect 77−38938
distributed feedback laser, two-mode operation, index and gain grating configurations 80−69357
dye, CW, mode selection by nonlinear absorpt. 77−705
dye CW frequency-locked mode-locked laser, for high resolution spectroscopy in freq. domain 80−43350

laser modes continued
dye CW laser, double-mode-locked, config. for independent tunability 79−72590
dye CW laser, freq. locking to Ne absorpt. lines by Faraday filter 79−22989
dye CW laser, mode locking using externally modulated pumping laser 79−18456
dye CW laser, ring resonator, mode selection 80−14371
dye CW lasers, mode-locked, prod. of picosecond and subpicosecond pulses *(French)* 79−31961
dye CW lasers sharing common amplifier medium, synchronous mode locking 77−7119
dye CW mode-locked lasers, vac. UV ps. pulse generation 80−43355
dye CW mode-locked lasers for ultra-fast spectroscopic studies 79−31960
dye CW synchronously mode locked laser, cavity length detuning 80−5768
dye grazing-incidence pulsed laser, operation in single longit. cavity mode 78−94398
dye high gain mm. bore laser, transverse mode control in waveguide resonator 78−1268
dye laser, active mode locking by saturable absorber loss modulation 77−72002
dye laser, actively mode-locked, flashlamp pumped, streak camera obs. of pulses 78−22158
dye laser, continuously pumped, actively mode locked, pulse props. 77−42546
dye laser, CW, double mode locking, parametric study 79−45978
dye laser, CW, freq. locking to absorpt. lines of Ne discharge Faraday filter 77−79870
dye laser, CW, oligo mode action, kinematic model 77−14707
dye laser, CW, synchronous pumping and passive mode-locking, for picosecond pulse generation 79−3727
dye laser, CW passively mode-locked, subpicosecond pulse generation and amplification 80−9907
dye laser, CW single-mode, 'double Michelson' mode selector and press. scanning 78−46686
dye laser, CW single-mode tunable 80−106534
dye laser, DFB, single-mode operation 80−74409
dye laser, divergence of emitted radiation, excited transverse modes determ. 79−94228
dye laser, double grazing-incidence single-mode type 80−95906
dye laser, double mode-locked CW, pulse cross-correlation studies 80−69389
dye laser, double-wavelength electro-optically tuned synchronously pumped mode-locked CW 79−89924
dye laser, flashlamp pumped, injection locking without longit. mode matching 78−33760
dye laser, flashlamp-pumped, linear, thermal effects on spatial mode struct. 79−36943
dye laser, flashlamp-pumped high-energy, spectral narrowing by two-stage injection locking 79−81450
dye laser, forced mode locked CW system 77−38880
dye laser, frequency locking by selective refl. 78−29992
dye laser, highly synchronous CW double mode-locked, picosecond pulse shape meas. 79−64257
dye laser, intense subnanosecond pulse generation, 0.58 to 0.80 μm mode locking 78−90422
dye laser, internally pumped mode-locked CW, theory 80−91787
dye laser, intracavity intensity modulated, 0.01 Hz to 1.2 GHz 79−41400
dye laser, mode-locked, synchronously pumped, pulse-width stabilization 80−83622
dye laser, mode-locked CW, subpicosecond pulse generation with slow saturable absorber 80−9915
dye laser, N_2 laser pumped, single mode operation 78−87060
dye laser, N_2 laser pumped, two wavelength outputs with orthogonal polarisations 78−50792
dye laser, N_2 laser-pumped, subns. relax. oscills. 78−82959
dye laser, passively mode-locked, parameters affecting subps pulse duration 79−45979
dye laser, passively model locked, 0.2 psec. pulse generation and meas. 78−50830
dye laser, pulsed output, mode locking with synchronous-pumping 80−5760
dye laser, single mode, flashlamp pumped, tuning by injection locking 77−19303
dye laser, single-mode CW oscills. at Na D-lines, Faraday filter freq. locking 78−5487
dye laser, subpicosecond, directly pumped by mode-locked Ar laser, pulse train autocorrelation traces 79−22969
dye laser, subpicosecond pulse production 77−83906
dye laser, synchronous mode locking, composite gain and absorber medium, sub ps pulses 78−79046
dye laser, synchronously mode-locked CW, intracavity SHG in thin $NH_4H_2PO_4$ cryst. 80−95945
dye laser, transverse flow, unstable resonator mode control 77−88789
dye laser, transverse flow, unstable resonator mode control 78−46671
dye laser, tunable CW mode-locked system, sub ps pulses 78−42362
dye laser, tuning and active mode-locking, interferometry technique 79−22982
dye laser, two-wavelength single mode operation, using grazing incidence grating 80−53329
dye laser, unstable resonator, injection locking 79−979
dye laser amplifier system, electro-optical injection 79−22975
dye laser characteristics with forced mode synchronisation, intraresonator absorpt. effect 80−78873
dye laser mode locking, absorpt. expts. to explain action of DODCI 77−9098
dye laser mode locking, picosecond pulse generation, book contrib. 77−61138
dye laser single-mode mag. tuning system 77−75541
dye laser with modes locked to atomic absorption lines, spectral characts. 80−9881
dye laser with saturable absorber, stationary pulse parameters, approximate theory 79−3690
dye lasers, beam divergence, transverse mode saturation, kinetics *(Russian)* 78−74931
dye lasers, flash lamp pumped, mode locking, picosecond, pulse generation 78−71131
dye lasers synchronously mode-locked, used for material polaris. relax. meas. 79−44952
dye mode-locked dye laser and single pulse amplification 79−27255
dye pulsed laser, mode competition with Na coloured intracavity flame 78−46594
dye ring laser, second harmonic CW, single mode operation 79−41392
dye solutions, simultaneous 2 or 3 band tunable emission, band competition 77−7082
dye standing wave laser, single mode operation using intracavity Michelson reflectors 79−89918
dye synchronously pumped mode-locked CW system, pulse characts., cavity detuning effect 79−3726
education, laser beam UHF and audio freq. difference heats 80−73139
eigenvalue translation method for mode calculations 79−71515
electro-optic laser technique for probing coherent and incoherent decay processes 77−75338
emission field structure of active medium with thin-lens type heterogeneity *(Russian)* 77−83899
errors in mode parameters determ. of spatial distribution of radiation 80−95055
etalon frequency selectivity effect on mode-locked laser, narrow free spectral range 80−38041
ethyleneglycol dye laser, conversion efficiency and tuning, solvent effect 79−55131
Fabry-Perot cavity, gas filled, optical bistability described by stochastic master eqn. 79−76652
Fabry-Perot etalon effect on laser resonator modes 78−25896
Fabry-Perot resonator, laser mode sweeping dynamics, optical length effects 78−83001
Fabry-Perot resonator of gasdynamic laser, collisional relax. effect on fundamental mode 79−31948
fibre laser-amplifier, coupled-mode theory 78−66848
fibre-optic communication system performance at 1.55 μm with single-longitudinal-mode laser 80−87556
fibre-optic transmission by laser diode analogue baseband modulation 80−58738
field properties of multiple coherently combined lasers 79−36944
filled telescopic resonator, steady-state lasing, oscillation modes 80−95922
fine structure of He-Ne laser radiation, Fabry-Perot scanning interferometer meas. 77−54749
fluorol 7GA, flashlamp pumped, passive mode-locking in green spectral region 77−38922
fluoromethane laser emission from unstable resonator 79−22983
fluoromethane optically pumped molecular laser, relax. oscills. 80−95875
fluoromethane-^{13}C optically pumped molecular laser, relax. oscills. 80−95875
FM mode locked laser, dispersion effect 80−74406
free electron laser, coherent states in single mode and multimode cases 80−102689
free-electron laser amplification on relativistic electron beam in spatially periodic transverse mag. field 80−19014
frequency locking and mode competition, lasers with broad homogeneous emission lines 80−23723
frequency modulation of single-mode laser 78−13737
frequency noninteraction of oppositely travelling waves in gas ring laser 80−38043
gain-guiding double-heterostructure laser transverse carrier diffusion effects 79−55139
gas laser, competition between high intensity modes of different polarisation 77−58311
gas laser, coupling modulated, mode coupling distortions minimisation 78−55384
gas laser, high intensity, multimode standing-wave operation, matrix formalism 77−19229
gas laser, mode interaction, transition level degeneration effects *(Russian)* 77−61940
gas laser, mode-locking operation using modulator with acoustic Fabry-Perot resonator 79−45976
gas laser, polaris. effects 80−58605
gas laser, resonator parameters effect on mode volume *(Hungarian)* 80−58603
gas laser, single mode, mode polarisation in transverse mag. fields 78−22107
gas laser, synchronous mode-locked pumping, mode-locked far IR pulse generation 79−27271
gas laser, theory of polarisation effects 80−23660
gas laser, two-mode emission in strong field, limits of stability 77−14685
gas laser beam, intensity fluctuations, spatial distrib. 79−18458
gas laser with internal mirrors, polarisation states 77−50701
gas lasers, mode interactions in longit. mag. field, active medium dispersion effects 80−63967
gas lasers, single-mode in transverse mag. fields, polarisation props. 79−7167
gas multimode laser with excitation modulation, polaris. of active medium 78−82942
gas ring laser, multimode, high-Q power resonances 78−82997
gas ring laser, opposite wave freq. difference, mag. field 79−7156
gas single-mode laser with absorpt. cell, intensity and freq. fluctuations 78−17993
gas waveguide laser, mode comp. of radiation 80−28192
gasdynamic high speed lasers, freq. stability mode struct., and output power characts. *(Chinese)* 79−31854
gasdynamic laser with partial population inversion 79−55125
gasdynamic lasers, improved perform. by selective thermal pumping 79−31858
Gaussian beam, generalized spot size for higher-order beam mode 79−72612
Gaussian beam, tilted, modal expansion *(Japanese)* 78−30000
Gaussian beams, increase of axial brightness during wave front smoothing *(Russian)* 80−5774
Gaussian laser beams, spatial modulation 79−7162
Gaussian TEM_{00} mode laser beam scatt. from surface defect, normlaization 80−48313
giant pulse lasers, passive mode-locking 79−72608
giant pulse lasers, passively mode locked, optimisation 78−83006
Goldstone mode in stationary state of non-equilibrium dissipative system *(Chinese)* 80−87365
gyroscope with induced mode locking, limiting sensitivity 79−59744
He-Ne, mode coupling, nonlinear effects *(German)* 77−19233

laser modes continued
high speed flow lasers, stable oscillation condition mode struct., output power characters 79−76660
high-power annular lasers, uniform beam transformation, mirror system 78−94403
higher order beam modes in complex lenslike media and resonators 77−27308
homogeneously broadened laser, injection locking, dynamic rate eqns. 78−37920
homogeneously broadened laser, two mode operation, analytical string signal analysis 78−55331
injection laser, bias quenching of relaxation oscillations 79−72570
injection laser, mode deformation due to self-focusing, rel. to output characts. nonlinearity 79−13966
injection laser, planar stripe SWAN, single transverse and longit. mode control 80−48281
injection laser, transverse mode control by strip loaded waveguide 77−75543
injection laser diode, single freq., for integrated optics and fibre optic appls. 80−1237
injection laser diode mode structure enhancement by backface plating 80−64056
injection laser harmonic distortion analysis 80−58537
injection laser longitudinal mode stabilisation by temp. compensation 79−45964
injection laser quantum noise in optical fibre communication systems 80−48259
injection laser with index-guiding structure, single longit. mode operation 79−98362
injection lasers, homojunction and single-heterojunction, mode competition 79−31901
injection lasers, mode comp., control with selective cavities 80−19037
injection lasers, optical ringing effects, internal loss modulation and direct modulation 78−87081
injection lasers, stripe geometry, horizontal mode deform. and anomalous lasing props. 77−19252
injection mode-locking principle and applications 80−9916
integrated twin guide lasers, axial mode selectivities 77−75519
internal, beat freq. method for speed of light meas. 80−41992
intracavity absorpt. spectroscopy, short pumping pulses and restricted mode competition, numerical anal. 77−82607
intracavity absorption spectroscopy theory, mode competition 78−32890
intracavity phase perturbations effect on beam quality 77−38968
intraresonator formation of laser fields, transverse mode influence *(Russian)* 79−50327
introductory concepts and results, Q-switching and mode-locking, book contrib. 80−106504
ion laser, intracavity intensity modulated, 0.01 Hz to 1.2 GHz 79−41400
jet stream dye laser, mode locked synchronous pumping, near IR ps pulses 78−17948
kinetic processes in lasers 80−28190
kiton red S, mol. fluoresc. decay time, self-absorption 79−68255
laser, double heterostruct. junction type, US wave freq. modulation anal. 78−83009
laser, internal mirror, polarisation mode, freq. stability *(Japanese)* 78−46675
loaded strip confocal unstable resonator, theory of modes 77−50692
locking phenomena in lasers with inhomogeneous spectral line *(Japanese)* 77−58307
many-mode laser, statistical props., generalised Volterra-Wiener method calcs. 77−38851
master equations steady state soln., chem. react., two-photon laser appls. 77−9945
memory effects and mode coupling near the laser threshold 79−55107
methanol, far IR laser resonator for TEM_{00} mode operation 78−66847
N-methylphthalimides, laser, lamp-pumped, solvent and temp. depend. 79−3692
mode locked ring-laser with two isotope medium, two-mode emission 78−1278
mode-locked frequency-doubled laser efficiency 77−19264
modelocking, soln. of 2nd order integro-differential eqns. 78−66796
multi-mode diodes, dynamic mode interaction 78−55354
multi-mode laser, coexistence and noncoexistence of modes 78−29991
multi-mode laser, competition between selected and nonselected modes 78−29990
multimode laser, Gaussian statistics, influence on reson. ionis. multiphoton process 78−29927
multimode laser, mode interaction and radiation fluctuations 80−43338
multimode laser, semiclassical theory of stability, generalised entropy 79−3699
multimode laser containing saturable absorbers, bistable operation 80−91862
multimode laser field, effect of intensity time variation on mol. collision processes 79−31620
multimode laser radiation field, multiphoton ionisation probabilities *(Russian)* 77−42560
multimode laser steady-state stimulated Raman scatt. 80−99796
multimode laser theory, quantum generalisation of Lamb's semiclassical theory 77−58309
multimode radiation, spatial coherence, mode degeneration and deformation effects 77−726
N-mode laser, emitted light correlations 78−63051
narrow double-current-confinement channelled-substrate-planar laser fabrication by double etching 80−64073
non-confocal resonator, with output-coupling aperture, eigenvalues *(Japanese)* 79−55163
open cavity, Slater method validity 80−69428
open resonator with aperture in reflector, theoretical anal. 79−31955
open resonators, modes of oscillation, theory 77−38947
open resonators with aperture coupling, multimode interaction effects 80−58608
open stable cavity with axial symmetry, aberration corrections 80−43372
operation physical principles *(German)* 79−59664
optical bistability, Dicke model of phase transitions 79−81402
optical cavity, one-dimens., with output coupling, thermal radiation, fluctuation-dissipation theorem 79−978
optical Kerr effect modulator, for laser passive mode-locking and Q-switching 78−9403
optical picosecond spectroscopy using mode-locked lasers 78−58065
optically pumped waveguide gas lasers 78−5490
laser modes continued
orthogonality properties of optical resonator eigenmodes 80−38042
oxazine-1-perchlorate mode-locked CW dye lasers, tunable near IR ps and subps pulse generation 79−45972
oxide stripe heterojunction lasers, asymm. modes 78−59006
parasitic oscillations in the static centered two-aperture limit 80−95861
partially open cavity, freq. shift and decay time of radiation 79−13990
passive mode locking, fast absorber model 78−59054
passive mode locking, transient evolution 77−34900
passive mode locking, two laser amplifiers with slow saturable absorber 80−33041
passive mode locking with fixed moment of stimulated emission 77−61973
passive mode-locking and Q-switching, theory 77−38948
passively mode locked pulse stability in fast absorber limit 78−59052
periodic mode loss, use of grating mirrors in IR laser resonators 80−28254
periodic modes, diffr. props. 77−61979
periodic modes of optical resonator *(Russian)* 78−33756
phase compensation, optimization techniques 78−1291
phase compensation of laser beam modes 77−3599
phase conjugate mirror component for optical cavity, Gaussian transverse modes 80−58595
phase conjugate mirror for optical resonator, longit. and transverse modes 80−14392
phase-locked multi-mode laser, onset of self-pulsing, Lorenz model 77−7054
phosphate glass active-passive mode-locked oscillators at 1.054 μm 78−63139
phosphate glass oscillator, passively mode-locked, stabilised with acousto-optic modulator *(Japanese)* 79−13999
picosecond photochronoscopy, generation and meas. of pulses from mode-locked lasers 79−76734
picosecond spectroscopy, methods and appls., laser mode-locking 80−42263
picosecond spectroscopy using mode-locked lasers 80−9046
planar stripe laser with deep Zn diffusion, stable transverse mode oscill. 80−14338
plane mirror cavity, field structure of nonstationary oscill. modes, edge diffr. effects 79−55160
plane-parallel resonator with wavefront reversing mirrors, mode structure 79−86196
planospherical resonator with internal lens, stability of caustic 79−31954
plasma, collisional, mixed mode operation, cross-focusing 80−83945
polymethine dye lasers, mode-self-synchronisation, broadband, picosecond pulses *(Russian)* 78−29946
POPOP solution dye lasers, multiplate reflectors 80−83606
PT asymmetry and four-fold EM degeneracy lifting, appl. to ring laser mode splitting 80−23606
pulse synchronization in Q-switched and mode-locking regime 78−5510
pulse timing by combined passive and active mode-locking, anal. 78−55391
pulsed acousto-optical modulator RF driver for laser mode locking 78−90438
pulsed output, from mode-locked laser, quantised field representation 78−79054
Raman spin-flip laser, higher modes and saturation effects, theory 78−71106
Raman-Nath standing-wave mode-locking switch, modulation index 80−78980
regerative compression of mode-locked laser pulses using saturable dye 80−95925
resonator, marginally stable, gain effect on electrodynamics 80−53339
resonator, open with variable iris, moding effects 80−5767
resonator, stimulated combined scattering of light, effect of generation of 'hot' vibrs. 80−58601
resonator containing active medium, mode stability 77−19346
resonator filled with flowing medium, EM anal. 77−79856
resonator with conical elements, mode structure, polarisation effects 79−98411
resonator with wavefront reversing mirror, oscillator modes 80−53345
resonators filled with inhomogeneous material, longit. modes 79−81463
rhodamine 590 picosecond transverse-flow flashlamp-pumped dye laser 80−38025
rhodamine 6G, Cu vap. laser pumped, axial mode struct. 77−23671
rhodamine 6G, CW laser, passive-active mode locking 78−29993
rhodamine 6G, laser, lamp-pumped, solvent and temp. depend. 79−3692
rhodamine 6G, mol. fluoresc. decay time, self-absorption 79−68255
rhodamine 6G, ring struct. laser emission, resonator exit mirror effect 77−38941
rhodamine 6G dye laser, CW synchronously mode-locked, subpicosecond pulse generation 78−71128
rhodamine 6G dye laser, induced radiation spectral characts., effect of vibr. relax. 80−64008
rhodamine 6G in ethanol, injection locked ring amplifier 77−88788
rhodamine 6G jet stream CW laser, tuning range, mode competition effects 78−50791
rhodamine 6G lasers, synchronized CW psec. pulse train generation at 2 independently tunable wavelengths 78−33758
rhodamine 6G pulsed dye laser, locking by anomalous dispersion in vapour cell 79−7163
rhodamine 6G synchronously mode locked CW laser, pulse width depend. on intracavity bandwidth 78−66821
rhodamine 6Zh pulsed laser, simple transverse mode observation *(Russian)* 79−72565
rhodamine B, laser, lamp-pumped, solvent and temp. depend. 79−3692
rhodamine B, mol. fluoresc. decay time, self-absorption 79−68255
rhodamine pinacyanol as mode locking saturable absorber 77−42554
rhodamine-6G mode locked dye laser pulse width monitoring by rapid scan autocorrelator 80−87421
ring cavity, unbalanced antiresonant, perturbed Gaussian modes 77−718
ring dye travelling-wave CW laser, mode locking 80−43354
ring gas laser under gain modulation conditions 77−72011
ring gas two-mode laser with two-isotope active medium, freq. characts. 77−79864
ring laser, anisotropic cavity single isotope type, oppositely travelling waves competition 78−50825
ring laser, coherence theory, counter-rotating laser modes 78−55387
ring laser, CW oscillation in presence of passive medium, stability 78−37913
ring laser, de-adjusted medium, optical axis and stability 78−82999

laser modes continued
ring laser, freq. shift and splitting for opposite waves, spatially inhomogeneous media 79−7155
ring laser, freq. stabilisation for two and three-mode operating regimes 77−75578
ring laser, homogeneously broadened, mode competition, intensity fluctuations 80−43375
ring laser, lock-in width calc. 79−55156
ring laser, luminesc. effects on beat signal *(Russian)* 77−54742
ring laser, mode competition at line centre 78−25898
ring laser, relativistic Doppler effect, two-wave mode instability and optimum tuning 77−38940
ring laser, self-locking type II mode, freq. depend. effects 78−5506
ring laser, solid state, beat regime with nonlinear absorber, appl. to ang. vel. sensor *(Russian)* 78−1273
ring laser, travelling wave, mode self-synchronisation 80−83605
ring laser, two-mode, correl. functions 79−76720
ring laser, two-mode, intensity fluctuations 80−33038
ring laser, two-mode, intensity fluctuations meas. near threshold 78−55388
ring laser, unidirectional, modes 80−91818
ring laser, with detuning, generation of high-frequency pulsations 80−48304
ring laser beam divergence, mode competition effect 80−48303
ring laser gyro, two-mode, four-mode soln. to locking problem 80−1270
ring laser gyro, two-mode, multioscillator approach to locking problem 79−59742
ring laser gyroscopes, multioscillator approach to locking problem 78−79042
ring laser mode competition and anticorrelation calc. and expt. 80−102740
ring laser with anisotropic resonator, polarisation and freq. splitting of opposite waves 80−33037
ring laser with reversible pedestal, freq. response, single and two-mode emission 80−48308
ring lasers, dual mode, capture zone constriction, interference effect *(Russian)* 77−88796
ring resonator, longit. mode analysis 77−14766
ring resonator, with additional return mirror, mode struct. 78−46677
ring resonators, two coupled system, mode freqs. and amplitudes 79−10328
ring Zeeman laser, interaction of modes characterized by orthogonal circular polarizations 80−48306
ruby, slot method for radiation extraction 77−50694
ruby, total mode self-synchronisation 79−64259
ruby laser, double mode locking using dye saturable absorber 80−99763
ruby laser, generation, amplification of high power picosecond pulses depend. on superluminescence 80−53305
ruby laser, passively mode-locked, output charact. 79−18424
ruby laser, peak generation for active mode phasing *(Russian)* 79−14000
ruby laser, pulsed, electronic speckle pattern interferometry 78−65961
ruby laser, self-synchronisation of modes *(Russian)* 78−74937
ruby laser, spiked regime, dynamic theory 79−27260
ruby laser mode synchronisation during loss modulation on freq. difference *(Russian)* 77−61989
ruby laser with bisanthene phototropic Q-modulator *(Russian)* 77−83910
ruby laser with small active volume, mode-locked ultrashort pulse generation 79−89932
ruby lasers, freq. synchronisation and locking by passive modulator 80−1249
ruby NMR laser, ^{27}Al nucl. spin system, collective ordering phenomena, instabilities 80−11278
ruby NMR laser, spontaneous nucl. spin system self organisation 79−916
ruby passively mode-locked laser, subnanosecond pulse generation using saturable absorber 79−86197
ruby ring laser with forced mode locking 80−95915
ruby sweep generator, spectral-kinetic charact., singularities *(Russian)* 77−83894
saturable absorber mode locking of pair of laser amplifiers, periodic pulse soln. 80−83623
self-locking, appl. to solid and ring gas lasers 78−1283
self-pulsing instability of single mode laser, critical pumping parameter 77−7055
self-selection, in Zeeman-effect laser, expts. with He-Ne laser *(Russian)* 80−1251
self-synchronisation in dye laser with continuous pumping 80−83605
self-synchronising modes, saturated filter relax. time reduction *(Russian)* 77−7145
semiconductor, optically pumped, mode broadening due to transient heating 77−75517
semiconductor, spectral dynamics, carrier diffusion, higher order transversal modes 77−75522
semiconductor DH injection laser with gain-induced waveguiding, spontaneous emission factor calc. 79−81429
semiconductor DH laser, TE_0 mode radiation confinement factor, analytical approx. 78−46603
semiconductor DH lasers, charact. explanation, multimode field theory 78−37880
semiconductor heterojunction lasers, partially homogeneous broadening and saturation, non-oscillating mode suppression 80−99775
semiconductor homostructure injection laser, mode form., spatial, spectral and temporal meas. 77−79821
semiconductor injection laser, lateral mode selection 77−79861
semiconductor injection laser, optical mode spectra, photodetector scanning and IR photography 80−48257
semiconductor injection laser, spectral modulation behaviour, theory 78−50775
semiconductor injection lasers, simplified theory for mode locking 80−64021
semiconductor injection stripe lasers, homogeneous spectral broadening multimode rate eqn. 78−79018
semiconductor junction lasers, narrow stripe geometry, non-Gaussian fundamental mode patterns, waveguide model 78−94394
semiconductor laser, dynamic behaviour, lateral mode and carrier density profile effects 78−82968
semiconductor laser, lasing characteristics, transverse modes *(Japanese)* 79−81432
semiconductor laser, polarisation control, mode competition 77−75515
laser modes continued
semiconductor laser, self-sustained pulsations 80−106522
semiconductor laser, single mode *(Japanese)* 80−14339
semiconductor laser, single mode criteria at high speed pulse modulation 79−10305
semiconductor laser, single-wavelength oscillation at high speed pulse modulation 79−7129
semiconductor laser, spontaneous-emission coupling on number of excited longitudinal modes 79−18417
semiconductor laser, transverse modes, mirror reflectivity dependence 79−68404
semiconductor laser intrinsic noise in optical communication systems 80−69394
semiconductor laser radiation, frequency self-modulation interpretation 80−64028
semiconductor laser with composite waveguide, emission characteristics 79−72592
semiconductor laser with dielec. transverse mode confinement, light intensity fluctuations 80−48258
semiconductor laser with electron-beam-induced stripe waveguide, transverse mode selection 80−28237
semiconductor lasers, multimode generation *(Russian)* 78−55357
semiconductor lasers, single longitudinal mode oscill. by optical coupling 78−22157
semiconductor lasers, single mode, spontaneous emission spectrum dip observation, generation saturation *(Russian)* 79−76691
semiconductor single mode laser, mode selection and control *(Polish)* 80−19035
semiconductor stripe geometry junction laser, waveguiding mechanism 77−75521
semiconductor super-DFB single-mode laser with periodic stripe width variations 80−58574
SHG, effect of partial mode locking 80−9960
single axial mode laser, degenerated by mag. field, light props. *(Japanese)* 79−64254
single laser mode switching, probe of phase memory and radiationless relax. 77−10698
single mode, intracavity versus extracavity absorpt. cells, fractional absorpt. 77−23700
single mode, parametric resonance 79−76656
single mode folded laser cavities, selection and test of parameters *(Chinese)* 79−55154
single mode laser, photon statistics, cooperative atomic interactions 80−43318
single mode laser, photon statistics, intracavity two-photon absorption effect *(German)* 77−10933
single pulse extraction from mode locked train using dye amplifier 77−19314
single transverse mode radiation, spatial coherence 77−14733
single-mode emission stability rel. to active medium and resonator 78−17899
single-mode gas laser with slightly anisotropic resonator, output polarization stability 80−43370
single-mode laser, cooperative effects 79−13944
single-mode laser models, Scully-Lamb master eqn. 77−38852
single-mode laser theory, nonequilibrium statistical operator method 79−89881
solid laser, multimode, with modulated resonator losses, radiation intensity fluctuations 80−74367
solid laser, passively mode locked, picosecond pulse generation, pulse compression and broadening 77−31111
solid laser, passively mode-locked, statistical props. of ultra-short pulses 79−36941
solid laser, pulse train stability with periodic Q-switching 80−28239
solid laser, two-standing mode operation with stationary ats., saturation effects and stimulated scatt. 79−68398
solid laser, undamped spiking, dynamical theory 77−14724
solid laser array spatially-coherent beam formation and mode locking 78−37898
solid laser charact. control, using optical delay lines, free-generation, Q-switching and mode-locking regimes 80−99758
solid laser mode locking, picosecond pulse generation, book contrib. 77−61138
solid single-mode face pumped laser, resonant-mode analysis 77−58350
solid state directly coated laser rods, beam divergence and refractive power 79−59736
solid state laser cavity reson., longitudinal mode locking, free generation region *(Russian)* 77−75572
solid-state laser, mode locking, importance of active medium nonlinearity 79−13967
solid-state lasers, influence of inversion depletion on ultrashort pulse evolution, mode-locking behaviour 80−5736
solid-state ring laser, mode locking theory 79−41399
soliton line constructed from an equivalent cct. of undamped spiking lasers 79−3673
spatial distribution of laser radiation control 80−64086
spatial hole burning and twisted-mode laser resonators 78−42359
split-mode unstable resonator, phase locking 77−58351
stabilisation by optically induced optical activity 79−18490
stimulated scattering, wavefront reproduction 78−1305
stripe contact injection lasers, heterostructure model, lateral mode control 80−14342
stripe geometry injection laser, lateral transverse mode instability and stabilisation 79−98358
stripe geometry injection lasers, mode deformation effects on modal gain 79−81434
stripe geometry injection lasers, rigorous boundary value soln., for lateral modes 78−71100
stripe geometry laser, device geometry effect on lateral mode content 79−98363
stripe geometry laser, oxide-insulated narrow stripe, lateral mode behaviour 79−98359
stripe geometry semiconductor lasers, transverse mode stabilisation 80−99774
stripe-geometry heterojunction lasers, review 80−53288
subharmonic lasers, quantum theory, first order non-equilib. phase transition 80−83584
subpicosecond spectroscopy, high intensity, broad wavelength tunability 79−44950
supermode locking, noise effects 79−22986

laser modes continued
superradiance waveguide laser, stimulated emission spectrum, leaky modes *(Russian)* 80−87400
symmetric laser cavity with asymmetric modes 79−13989
TEM_{00} thermoinsensitive cavity *(Chinese)* 80−53335
terraced substrate DH laser, fundamental transverse mode oscillation *(Japanese)* 80−78856
thermoelastically disturbed resonator, mode calcs. 79−13992
thin-film chirped gratings, mode coupling 80−23808
third harmonic generation, spatial modes effect 80−43400
TJS laser diode, single-mode oscill. with low threshold currents, for optical communication 80−14355
TOPOT vapour dye lasers with multiplate reflectors 80−83606
transformation of laser beams for improved angular charact., transverse mode struct. depend. 79−89950
transient laser radiation, stochastic process near an instability point, numerical solution 80−23658
transverse, phase compensated far field distrib. *(Chinese)* 79−10324
transverse junction stripe lasers, dynamic props. 77−75520
transverse mode struct., laser field transformation *(Russian)* 78−37934
transverse resonator, mode locking, slow saturable absorber 79−22993
transverse structure of radiation from a laser with an additional mirror 80−58604
travelling wave cross-saturation asymmetry 80−43371
travelling-wave ring lasers with uniform spread, free generation modes *(Russian)* 77−46736
two-dimensional DFB laser with acoustic wave and Bragg reflectors 78−79043
two-level atom in multimode EM field anal., semiclassical anal. 77−10881
two-level system in resonant multifrequency field with structureless noise *(Russian)* 80−91766
two-mode gas laser, strong coupling, transients 79−55114
two-mode laser, mutual quenching of axial modes 79−13991
two-mode laser, with smooth variation of mode separation, freq. charact. 80−53264
two-mode laser with coupled transition, quantum theory 80−43319
two-mode optical resonator mode mutual quenching in stimulated Raman emission 79−36960
two-mode oscill. gas laser, saturation-induced polaris. preferences 79−22929
two-photon laser beam, breathing mode of EM field 78−46558
ultra-short light pulse generation, review *(Japanese)* 79−45973
ultrashort laser pulses, form. dynamics and self-stabilisation *(Russian)* 77−19259
ultrashort pulse duration control rel. to forced mode synchronisation *(Russian)* 77−46735
unstable resonator, gain saturation in geometric mode limit 78−1267
unstable resonator containing small-scale phase inhomogeneities, laser props. 80−19057
unstable resonator properties, small-scale phase inhomogeneity influence 78−59050
unstable resonator with spatial filter, mode discrimination, phase modification 79−76719
unstable resonators, ϵ-approx. eigenvalues and eigenfunctions *(Chinese)* 80−5766
unstable resonators, quantum multimode approach 77−719
unstable resonators with field rotation, mode structure 80−53342
unstable resonators with field rotation, props. in CO_2 laser 80−53343
unstable resonators with rounded edges, mode losses 78−79039
variable band gap heterojunction laser spectral characteristics *(Russian)* 79−94236
vector resonator mode synthesis, perturbation theory 80−43374
wave-front estimation from phase derivative meas. 79−89856
waveguide far IR laser mode losses 77−38954
waveguide lasers, operation under multimode conditions, relative efficiency of cavities, comparison 79−55158
waveguide mode propag. in nonlinear amplifying medium 77−58308
Zeeman laser, two-transitions with common upper level *(Japanese)* 79−55112
Zeeman linearly polarised laser, Izsing atom susceptibilities, first and third order approx. *(Japanese)* 78−71071
Zeeman linearly polarised laser, mag. field reson. on laser output, freq. stabilisation *(Japanese)* 78−66798
Zeeman ring laser, four-mode operation 80−19053
(Al,Ga)As, ageing-induced self-pulsation stabilisation and initial degradation elimination by facet coatings 80−43347
(Al,Ga)As, channelled substrate planar struct. injection lasers 77−71996
(Al,Ga)As DH diode laser, double-dovetail constricted, single mode CW operation 79−22949
(Al,Ga)As proton-bomard. stripe-geometry DH lasers, optical nonliniarities and optical spikes 79−55138
(Al,Ga)As-GaAs laser, transverse junction stripe, high temp. single mode CW operation 78−74918
(AlGa)As CW narrow stripe injection laser with induced waveguide, expt. props. 80−32988
AlGaAs constricted DH laser with large optical cavity, CW high-power single-mode operation 80−48276
(AlGa)As DH narrow stripe injection laser with rigid waveguide, expt. props. 80−32987
AlGaAs heterojunction laser, single transverse and longit. mode operation 78−37887
AlGaAs high-power constricted DH diode laser, for optical recording 80−43351
AlGaAs, integrated twin-guide laser, mode selectivity 77−88723
AlGaAs laser mode, fractional spontaneous emission coupling, power fraction, expt. evaluation 79−959
AlGaAs lasers, relaxation oscillation rel. to carrier diffusion length, spontaneous emission 80−32986
(AlGa)As oxide-defined strip lasers, self-sustained oscillations, ageing effects 80−32991
AlGaAs pulse modulate DH laser, oscillatory longitudinal mode competition 79−81427
AlGaAs semiconductor lasers, single-mode stabilisation by traps 80−95893
(AlGa)As strip buried heterostructure lasers, mode locking using external cavity 80−91791
AlGaAs transverse junction stripe lasers, single longit. and fund. transverse mode oscill. 78−22124
(AlGa)As, transverse junction stripe single mode oscillating laser, gain spectra 78−55356

laser modes continued
AlGaAs transverse junction stripe laser with distributed Bragg reflector 80−106535
AlGaAs-GaAs, DH semiconductor laser, influence of struct. parameters on lasing characteristics 79−45942
AlGaAs-GaAs CW injection heterolaser, single freq., tunable by external dispersive resonator 80−28236
AlGaAs-GaAs DH laser, bent-guide struct. 77−75544
AlGaAs-GaAs multimode laser, intensity fluctuations in each longit. mode 77−75512
AlGaAs-GaAs transverse mode stabilised plano-convex waveguide laser made by single step LPE 80−48274
$Al_xGa_{1-x}As$, CW low threshold, high efficiency injection laser props. 78−22126
$Al_xGa_{1-x}As$ CW multiwavelength TJS laser, MBE, single-longitudinal modes 80−64049
$Al_xGa_{1-x}As$, mode-stabilised injection laser, longitudinal-mode behaviour 79 962
$Al_xGa_{1-x}As$ pulsating DH laser, spectral broadening 80−23686
$Al_xGa_{1-x}As$, transverse mode stabilized injection lasers 78−29964
$Al_xGa_{1-x}As$:Zn DH laser, stripe geometry, horizontal transverse mode stabilisation, lasing charact. 77−19313
Ar high-power CW laser, resonator configs. for mode selection 79−10327
Ar ion laser, mode-locked pulses, second-order intensity correls., two-quantum photoeffect 79−10332
Ar ion laser, multimode, photon statistics, autocorrelation 78−9358
Ar ion mode-locked laser system, temporal pulse shape, streak camera meas. 77−79799
Ar laser, longit. mode locking in three mirror cavity 79−55164
Ar laser emission under passive mode-locking conditions, temporal structure 80−9923
Ar laser resonator, effect of axial mag. field on loss increase 79−76716
Ar laser with passively locked modes, excitation of dye laser for picosecond pulse generation 80−95930
Ar^+ ion laser, active mode locking study 80−91827
CO CW laser emitting dominant spatial mode, output power stability rel. to CO_2 laser 80−32965
CO chemical laser, flash photolysis of time-resolved spectra and gain 79−86172
CO_2 10.6 μm laser, freq. modulation and demodulation 80−43378
CO_2, 200 J TEA laser, injection mode locking 78−79049
CO_2, CW, transverse mode suppression by cavity length control 77−14762
CO_2, CW electric discharge lasers, mode medium interaction 79−36876
CO_2 CW electric discharge laser, output beam props. 79−36877
CO_2 CW laser, sealed-off design, NaCl Brewster angle mirrors 78−55370
CO_2 CW laser, vibr. temp., dissoc. and gain limitation determ., new technique 80−87369
CO_2 CW laser emitting dominant spatial mode, output power stability rel. to CO laser 80−32965
CO_2 compact sealed TEA laser, single mode operation 79−968
CO_2 electric discharge CW laser beam properties 79−76736
CO_2, excitation by NO+N reaction, transverse flow, output power, intensity distrib. 77−79796
CO_2, gain spiking and mode-beating control by signal injection 77−71999
CO_2, gasdynamic laser possibility, transitions between levels of paired modes 79−89885
CO_2 high-power pump laser, direct narrow-line tuning 80−58579
CO_2 highly multimode pulsed electron beam laser, beam divergence 79−3731
CO_2 hybrid laser, transverse mode struct., effect on laser induced acoustic waves in liq. 79−77683
CO_2 large aperture TEA laser, injection mode locking 77−14737
CO_2 laser, CW, construction and power calibration *(Korean)* 78−17961
CO_2 laser, detuning effects of FM mode-locking 80−69434
CO_2 laser, high pressure, passive mode-locking characteristics *(Japanese)* 80−14357
CO_2 laser, high repetition rate-pulsed, weak shock wave effect 78−90409
CO_2 laser, high-press. ns pulse generation *(Russian)* 77−75581
CO_2, laser, internal modulation 80−23728
CO_2 laser, mode locking obs. by intracavity plasma injection 80−83624
CO_2 laser, optical coupling modulation in travelling-wave cavities 77−42553
CO_2 laser, TEA, single longit. mode, various prod. techniques 80−106547
CO_2 laser, transverse mode-medium instability anal. 79−76662
CO_2 laser, tri-n-propylamine in working gas 79−22935
CO_2 laser, tripropylamine additive on amplification charact., CO_2+N_2+He gas *(Russian)* 78−25848
CO_2 laser gain switch, pulse charact., approx. evaluation 80−58504
CO_2 laser modulation, plasma injection into cavity 80−83626
CO_2 laser pulse compression and mode locking using KCl:ReO_4 nonlinear absorpt. 80−74443
CO_2, laser pulse mode quality, effect on multiple photon absorpt. 78−66615
CO_2 lasers, IR saturable absorpt. in benzene, chlorobenzene and bromobenzene 80−69465
CO_2 long-pulse 2 GW single longit. mode source for laser-matter expts. 80−78860
CO_2 mode-locked hybrid TEA laser, variable width stable pulse prod. 79−76726
CO_2, multi-atm. TE laser, 10.6 μm ultrashort pulse generation by injection mode-locking 77−88799
CO_2 multiatmosphere laser, mode-locked pulses 80−1248
CO_2 oscillator, high power nsec. pulse selection 79−98382
CO_2 oscillator, multiatm. injection mode-locking, high-power subnanosec. pulses 78−29988
CO_2, pulsed TE laser, tunable single-mode operation by means of selective absorbers 79−36940
CO_2 rotating-mirror Q-switched TEA laser, mode sweeping effects 80−99769
CO_2, single mode laser, internal freq. modulation up to 350 MHz 77−19308
CO_2 TE laser, injection mode locking, press. up to 8 atm. 77−10883
CO_2 TE laser, longit. mode control using intracavity gas-phase absorbers 79−72579
CO_2 TE laser, passive mode locking using p-Ge saturable absorber 78−71127

laser modes continued
CO_2, TE multiatmos. laser, 10 μm pulse generation and amplification 79−45981
CO_2, TEA, multifreq. injection locking, resonator config. 77−7141
CO_2, TEA, pulse-forming and line-broadening in AM mode locking 77−54743
CO_2 TEA far IR laser, optimum spectral matching 79−31857
CO_2 TEA helical laser, axial mode behaviour 79−55108
CO_2, TEA injection laser, single-mode pulse prod. 77−54722
CO_2 TEA laser, actively modelocked multiline, controlled by NaCl etalon 80−23713
CO_2 TEA laser, compact sealed single mode operation 78−50810
CO_2 TEA laser, injection mode locking on P and R transitions in 9, 10 μm bands 79−89883
CO_2 TEA laser, injection tuning and mode locking on low gain rot. lines 80−95928
CO_2, TEA laser, mode characts. using unstable resonators 79−3719
CO_2 TEA laser, mode-locked, cavity-dumping 80−87415
CO_2, TEA laser, pulse shape and duration, excitation method *(German)* 78−83010
CO_2 TEA laser injection locked, tunable single longitudinal mode operation, O_3 absorpt. spectra 80−33018
CO_2 TEA laser mode locked by positive Ge, pulse shape meas. 78−46694
CO_2 TEA laser oscillator, longit. mode rejection, cavity length tuning effect 79−86189
CO_2 TEA laser oscillator, transverse mode locking by short pulse injection 80−38045
CO_2, TEA laser pumping efficiency increased by longitudinal mode control 77−38924
CO_2 TEA laser system, 20-J nanosecond pulse, based on injection-mode-locked oscillator 80−99752
CO_2 TEA laser with long optical resonator, mode-locked operation 78−79041
CO_2, TEA oscillator, injection locking, mode selection 77−653
CO_2 TEA oscillator, injection mode-locking using N_2 laser-controlled semicond. switching of 10-μm radiation 80−1247
CO_2 TEA oscillator, simultaneous freq. stabilisation and injection 78−55362
CO_2 TEA single longit. mode laser with tilted intracavity etalon 78−5484
CO_2, thermally pumped gas-dynamic laser based on deformation and symmetric modes 79−36874
CO_2 vibrational temperature determ. in gasdynamic laser with $CO_2+N_2+H_2$ mixture 80−9849
CO_2, waveguide TE laser, modes of operation 79−81451
CO_2 whispering-gallery CW laser, design and operation 79−81447
CO_2-N_2-H_2O gasdynamic laser, small signal gain and vibr. wall accomm. 79−98340
CO_2-N_2-He electroionisation laser, freq. mode, lasing conditions 80−63970
CO_2-N_2-He self-sustained TEA discharge laser, config. for high beam qualtiy 77−14753
CdS crystals, one-photon pumping, active layer structure, light amplification 80−78858
CdS, doped laser mechanism and output study 80−43340
CdS, laser, petal shaped cryst., high-temp. spectral characts. *(Russian)* 79−13968
Cu vapour, mode-locked, high pulse rate operation 77−61967
DF laser, pulsed unstable resonator, mode control and performance studies 78−82995
D_2O far IR laser pulses, real-time spectral anal. using SAW dispersive delay line 79−45983
GaAlAs actively mode-locked laser, bandwidth limited picosecond pulses 80−95905
(GaAl)As buried-heterostructure laser with buried optical guide, highly efficient operation 80−1219
GaAlAs CW diode laser, external cavity control, 32 MHz single axial mode 78−1271
GaAlAs DH injection laser, half-ring, room temp. operation 80−58558
GaAlAs, diode laser, CW radiation, intensity noise spectra of axial mode groups 77−34890
(GaAl)As heterojunction laser with distributed Bragg refl., mode switching 80−43336
GaAlAs heterostructure lasers, fine-structure in spectra 80−19033
(GaAl)As injection lasers, self-pulsations, Q-switching and mode-locking effects 78−66827
GaAlAs laser, coherent pulse generation by active modelocking 79−89941
(GaAl)As laser, stripe struct. for horizontal transverse mode stabilisation 77−79859
GaAlAs laser diode, CW, ps pulse generation 79−50329
GaAlAs lateral injection laser, low threshold, single mode operation 77−75545
GaAlAs mode stabilised separated multiclad layer stripe geometry DH laser, optical waveguide 80−64051
(GaAl)As oxide-stripe geometry DH laser, cavity length effect on output 79−50323
GaAlAs stripe laser, longit. and transverse mode dynamics on junction plane 77−38890
GaAlAs terraced substrate laser, visible-light-emitting, characts. 80−106523
(GaAl)As-GaAs DH laser, anomalous emission intensity, cavity competition 77−79823
GaAlAs-GaAs heterostruture, optical waveguide characteristics, mode spectrum, universal dispersion curves 79−72706
$Ga_{1-x}Al_xAs$ buried heterostruct. laser, rel. to stable operation during accelerated ageing at 70°C 79−7125
$Ga_{1-x}Al_xAs$, channelled substrate, planar struct. and DFB lasers 78−79032
$Ga_{1-x}Al_xAs$ junction-up TJS laser electron injection efficiency improvement 80−48300
$Ga_{1-x}Al_xAs$ stripe laser with stable transverse mode structure 80−48298
$Ga_{1-x}Al_xAs$ transverse mode DH laser with inbuilt plano-convex waveguide 80−48296
$Ga_{1-x}Al_xAs$ visible diode lasers, transverse-mode stabilised, nonstigmatic laser beams 79−76694
$Ga_xAl_{1-x}As$-GaAs heterostructure laser, suppression of internally circulating modes, effect on catastrophic degradation and efficiency 77−83896
GaAs, broadening mechanism, limitations to single mode power emission 79−961
laser modes continued
GaAs DH laser, self-induced modulation, noise, instability 80−48250
GaAs DH laser diodes stabilised using self-apertured facet coatings 80−58609
GaAs DH stripe geometry laser, horizontal mode deform. and anomalous lasing props. 77−19253
GaAs freq. retuning using electron beam *(Russian)* 77−716
GaAs injection laser, single heterostruct., mode competition effects, tuning characts. 80−48255
GaAs injection lasers, longitudinal mode spectrum, effect of carrier diffusion 78−71099
GaAs injection lasers, direct modulation enhancement effect of HF noise 80−83608
GaAs laser, refractive-index profile and resonant modes 79−86179
GaAs laser convex micromirror mode control 79−36920
GaAs laser diode, spontaneous emission reduction 80−95904
GaAs laser diodes, junction temp. meas. method 79−36895
GaAs, optically pumped DFB laser, oscills. of two- and one-dimens. modes 78−1252
GaAs, permittivity at laser transitions freq., excess carriers effect 77−14719
GaAs single-channel injection laser, radiative characts., single longit. mode 79−10309
GaAs, stripe-geometry, interaction and spectral distrib. of lateral modes *(Russian)* 78−22134
GaAs/GaInP DH, MBE grown, optically pumped laser action at 77K 80−95890
GaAs-(GaAl)As terraced-substrate injection lasers, fabrication and output characts. 79−50310
GaAs-(GaAl)As terraced substrate laser, fundamental transverse and longit. mode oscill. 79−98357
GaAs-$Al_xGa_{1-x}As$ buried-heterostructure laser, wideband optical sources *(German)* 78−37904
GaAs-$Al_xGa_{1-x}As$ channelled-substrate-planar-struct. laser with lateral-evanescent-field distributed feedback 79−98398
GaAs-$Al_xGa_{1-x}As$ current injection multi-quantum-well heterostructure lasers, MBE grown 80−19042
GaAs-$Al_xGa_{1-x}As$ strip buried heterostructure laser with passive DBR 80−14352
GaAs-$Al_xGa_{1-x}As$ transverse junction stripe laser, single-mode oscillation *(German)* 78−37885
GaAs-AlGaAs CW laser coupled to external cavity, multimode operation, output intensity low freq. pulsations 79−68394
GaAs-AlGaAs distributed Bragg reflector integrated twin-guide laser, temp. characts. 78−87064
GaAs-AlGaAs transverse junction stripe laser, single mode behaviour after 12000 hr ageing test 78−66831
GaAs-$Ga_{1-x}Al_xAs$ DH injection laser, curved junction stabilized filament, struct. and characts. 78−33744
GaAs-$Ga_{1-x}Al_xAs$ laser, optically pumped, longit. mode broadening due to transient heating 77−61953
GaAs-GaAlAs CW diode laser, lateral mode stabilization using apertured facet reflectors 80−23708
GaAs-GaAlAs CW injection laser, stripe geometry DH, temporal coherence 80−38016
GaAs-GaAlAs DH lasers, single longit. mode operation 78−22125
GaAs-GaAlAs DH laser diode, lateral modes 78−59009
GaAs-GaAlAs injection laser, radiation divergence reduction by non-waveguide mode excitation 80−91797
GaAs-GaAlAs TJS lasers, high power density single mode operation, Si_3N_4 facet coating 79−86186
GaInAsP DH laser diode CW modelocking 79−7126
GaInAsP/InP 1.5-1.6 micron integrated twin-guide lasers with distributed Bragg reflectors 80−74380
GaInAsP/InP integrated twin-guide lasers with distributed Bragg reflector, spectral behaviour 80−74381
GaInAsP/InP narrow planar stripe lasers, lasing characts. 80−95897
GaInAsP/InP terraced substrate DH lasers, fabrication and single transverse mode operation 80−58580
GaInAsP-InP DH lasers, LPE growth and operational characts. 80−53313
GaInAsP-InP planar stripe lasers, sputtered SiO_2 film as Zn-diffusion mask 80−48249
H_2, compressed, Raman laser, axial mode self-locking 79−94223
HF, CW chem. laser, freq. stabilisation by beat signals and anomalous dispersion 79−86187
HF CW chemical laser, mode competition obs. 80−33040
HF CW chemical laser, longit. and transverse mode competition in stable, unstable resonators 80−95917
HF laser, c.w., longitudinal mode beat intensities, tuning freq. depend. 77−671
HF laser, pulsed unstable resonator, mode control and performance studies 78−82995
He-^{20}Ne-^{22}Ne, orthogonally polarised laser mode interactions *(Russian)* 77−19235
He-Cd, hollow cathode laser, output characts. 77−42525
He-Cd laser, 442 nm, high order mode crossing signals from Cd II $4d^95s^2\ ^2D_{5/2}$ state 79−796
He-Cd^+, laser, cataphoretic, power noise meas. 79−36885
He-Ne, 3.39 μm laser, actively mode-locked oscill., modulation freq. depend. 77−61983
He-Ne, 6328 Å, single-mode collapse 78−94404
He-Ne, anisotropic ring laser cavity, polarisation characts. 79−59726
He-Ne, laser single frequency generation model and expt. *(Russian)* 77−58314
He-Ne, longit. mode locking using Fabry-Perot etalon 79−50318
He-Ne, mag. polarised, performance 77−14750
He-Ne, mode locking, phase interferometer control 77−72009
He-Ne, short pulses, self mode-locking *(Rumanian)* 79−13995
He-Ne, single mode laser, mode polarisation in transverse mag. fields 78−22107
He-Ne, single mode laser, emission zone nonlinear active lens effect 80−32960
He-Ne, three mode stimulated emission 77−75485
He-Ne, three-mode laser, total intensity under mode locked conditions, freq. stabilisation 77−83853
He-Ne, two-mode ring laser, stimulated emission regimes 77−657
He-Ne, waveguide resonator, oscill. modes 77−27311
He-Ne 3.39 μm laser mode-locking for ultrashort pulse generation 77−83909

laser modes continued
He-Ne commercial multimode low power laser, conversion to single mode laser 80−53325
He-Ne double mode laser in axial mag. field. *(Russian)* 79−86160
He-Ne gas ring laser, unidirectional two-mode lasing, stability region width 79−76721
He-Ne internal mirror laser, degeneration of longitudinal modes and freq. stabilisation *(Japanese)* 78−90426
He-Ne laser, 6328 Å, output power, using intracavity rot. reflector 79−7113
He-Ne laser, beat freq., high displacement sensitivity meas. 80−95926
He-Ne laser, competitive oscillation mode frequency stabilisation *(Russian)* 79−22962
He-Ne laser, freq. characts. under two-mode generation 80−53264
He-Ne laser, in axial mag. field, output power dependence of mode locking phenomena 78−71129
He-Ne laser, internal pulse-code modulation, 0.6328 μm at 150 Mbits s^{-1} 79−76725
He-Ne laser, mode interaction, transition level degeneration effects *(Russian)* 77−61940
He-Ne laser, mode selection and mode locking, effect on two-photon absorpt. efficiency 78−83023
He-Ne laser, mode stabilisation by axial mag. field, long resonator case 77−7143
He-Ne laser, optical heterodyning of spontaneous emission 78−29995
He-Ne laser, refl. anisotropy of 6320 Å mirrors 79−98413
He-Ne laser, self-locked, pulse velocity, power and mode phase 77−61939
He-Ne laser, two-mode ring laser power resons. 78−1211
He-Ne laser modal configuration, interference spectrometer study *(Spanish)* 80−86458
He-Ne laser mode locking by three-level reson., Zeeman tuning of intracavity Ne absorber 79−89943
He-Ne laser wavelength drift 80−67978
He-Ne laser with internal mirrors, mode polarisation props. 80−23672
He-Ne lasers, I_2 stabilised development, laser freq. locking 79−68380
He-Ne mode locked laser for very wide band communication system 78−17994
He-Ne multimode and single-mode lasers, phase locking to very high coherence degree 79−76710
He-Ne ring laser, opposite waves competition dynamics 77−72008
He-Ne ring laser, unidirectional, modes 80−91818
He-Ne ring laser with nonlinear absorber, competition of orthogonally polarised modes 78−17984
He-Ne single mode lasers, meas. of intensity of sources of inherent fluctuations 80−32958
He-Ne standing wave laser, two-mode locking *(Russian)* 77−79874
He-Ne two-mode gas laser, strong, coupling, transient 79−55114
He-Ne two-mode laser with methane absorbing cell, freq. stability and reproducibility 79−89934
He-Ne two-mode travelling-wave laser, Zeeman beats 78−50827
He-Ne-methane stabilised ring laser, freq. stability calcs. *(Russian)* 78−9401
He-Xe 3.51 μ laser mode competition in axial mag. field 80−63974
He-Xe laser, 3.51 μm, mode competition in axial mag. field 78−25850
^{3}He-^{22}Ne laser, interaction of orthogonally polarised modes with various transverse distribs. *(Russian)* 77−27276
Ho:$LiYF_4$ laser, TEM_{00} mode and Q-switched operation 80−74395
I laser, smooth pulse oscillator for single mode operation 78−59057
I laser radiation, 2nd, 3rd and 4th harmonic generation 80−91844
I_2 1.315 μ laser, passive mode locking *(French)* 77−68203
IBr:CO_2 photolysis, electron-vibr. pumping, 2.7 μm Br and 4.3, 10.6 μm CO_2 laser transitions 80−28196
InGaAsP low-threshold 1.25-μm vapour grown CW lasers, emission characts. 79−50308
InGaAsP single-mode CW ridge-waveguide laser emitting at 1.55 micron 80−58584
InGaAsP-InP, Zn diffused DH structures, oxide defined transverse junction stripe lasers 79−98389
InGaAsP-InP DH laser with self-aligned struct., oscillation characts. 80−38017
InGaAsP-InP DH lasers, spatial hole burning, spontaneous emission saturation, direct obs. 80−95892
$In_{1-x}Ga_xP_{1-z}As_z$ thin well in InP p-n junction, confined carrier luminesc. and laser modes 78−13703
InP-$In_{1-x}Ga_xP_{1-z}As_z$ quantum-well LPE heterostructure lasers, band filling and gain, mode groups 79−22955
InSb spin-flip Raman laser external-cavity system, oscill. characts. 78−55383
KF F_2^+-centre laser, picosecond pulse generation 1.24 to 1.45 μm, mode locking 79−89925
Kr ion laser, mode-locked, near UV, 50 ps pulse width 78−79030
Kr^+ ion laser, mode-locked near UV output, chem. and appls. 79−45966
Kr^+ mode-locked ion laser, pulse width and linewidth meas. 80−102696
KrF excimer laser, passive mode-locking using saturable absorber dyes 80−1244
Li^+:KCl, F_A (II) colour-centre laser, mode locking and tunable picosecond IR pulse generation 80−43364
LiF, picosecond generation on F_2^+ colour centres, induced mode synchronisation *(Russian)* 80−64033
$LiNbO_3$ crystal in laser resonator, thermo-optical effect *(Chinese)* 80−106546
$LiNd_{0.5}La_{0.5}P_4O_{12}$, stabilised dual-polarised oscill. 77−54723
$LiNd(PO_3)_4$ laser with external and Fabry-Perot resonators, 1.05, 1.32 μm CW oscill. 80−23693
$LiNdP_4O_{12}$ glass-clad rectangular waveguide, laser performance 80−32996
$LiNdP_4O_{12}$ laser, relaxation oscillations and mode spectra, high density pumping effect 80−69396
$LiNdP_4O_{12}$ laser, spontaneous phase locking obs. 78−83005
$LiNdP_4O_{12}$, single-transverse-mode slab waveguide laser, characts. 79−55141
$LiNdP_4O_{12}$ stable miniature laser with compact resonator, single mode operation 79−50305
N_2 laser, time shape of laser pulse 79−7120
NH_3 high power laser, improved optical pumping goemetry, mode locked operation 79−22973
NH_3 inverse level doubling mol., space and combined parity nonconservation *(Russian)* 80−52879
NH_3 laser transitions, CW, two-photon pumped 80−99702
Na_2, continuous laser oscill., optical pumping 77−88706

laser modes continued
Nd garnet ring laser, with return mirror, mode locking 80−99764
Nd, reproducible active-passive mode locked oscillators 77−88810
Nd, with mirror plasma-optical Q-switch *(Russian)* 80−33028
Nd:AlG, laser, mode locked, output stabilisation 77−61986
Nd:garnet, freq. axial mode shift, two-mirror resonator synchronisation, stabilisation *(Russian)* 78−22154
Nd:glass, CW SELFOC, actively initiated quasi-passive mode-locking 77−19306
Nd:glass, dynamic mode sweep-laser, freq. tuning 78−66851
Nd:glass, mode locked, picosec. pulse form., expt. technique 77−38957
Nd:glass, Q-switched with stable operation in pure transverse natural oscillation *(German)* 77−14761
Nd:glass, slot method for radiation extraction 77−50694
Nd:glass, TEM_{00} mode operation *(Rumanian)* 78−50798
Nd:glass, with metallic grating in cavity, Fourier spectrum and periodic mode fields distrib. *(Russian)* 79−31915
Nd:glass laser, blue tunable picosecond pulse generation by synchronous mixing with sideband radiation in $NH_4H_2PO_4$ 80−87431
Nd:glass laser, mode locking characts. using polymethine dye No. 3955 in solid host 78−17989
Nd:glass laser, mode-locked, ultrashort pulse duration meas., two-photon fluoresc. 79−27302
Nd:glass laser, tunable-wavelength mode-locked, with instant recording of temporal and spectral characts. 77−54732
Nd:glass laser array, mode locking, spatially coherent beam form. 77−88811
Nd:glass laser array, spatially coherent beam form., mode locking 78−29989
Nd:glass laser output, passive-mode locked, resonator length effect 78−79044
Nd:glass laser with active mode locking, ultrashort pulses 80−64087
Nd:glass laser with grid mirror, emission field 79−55142
Nd:glass mode locked ring laser, unidirectional travelling wave operation 77−88812
Nd:glass passively mode-locked laser, obs. of external feedback influence 80−23729
Nd:glass ring laser, actively mode-locked and Q-controlled, props. 79−18445
Nd:glass ring laser, mode-locking, unidirectional travelling wave operation 77−61976
Nd:$La_2Be_2O_5$, passive mode locking, ps pulse generation 77−7118
Nd:phosphate glass laser, CW oscillation 79−50311
Nd:phosphate glass mode-locked oscillator and amplifier system 79−81446
Nd:YAG, actively AM mode-locked Q-switched laser, pulse compression by liq. Kerr cell 79−22990
Nd:YAG, actively mode locked laser, short pulse generation for fusion 77−88809
Nd:YAG, cavity dumping single mode-locked pulses 77−7137
Nd:YAG, frequency-doubled operation, effects of absorpt. loss in $Ba_2NaNb_5O_{15}$ 79−36957
Nd:YAG, hole burning elimination in active medium 77−79851
Nd:YAG, injection locked oscillator, pulse duration var. 77−88772
Nd:YAG, laser fusion system, short pulse generation, active mode-locking and Q-switching 77−79868
Nd:YAG, mode locked oscillator, operation at 1.052 μm 80−33017
Nd:YAG, mode self locking with combined Q-switching 78−1284
Nd:YAG, mode-volume matching of oscillating modes of laser containing several active elements *(Chinese)* 79−50325
Nd:YAG, passive mode-locked, picosecond pulse duration, determ. from luminesc. intensity 78−71134
Nd:YAG, single mode Q-switched oscillator with short build up time 77−7091
Nd:YAG acousto-optically mode-locked CW laser performance and stability criteria 77−38934
Nd:YAG acousto-optically mode-locked CW laser, optical spectra obs. by interferometer 79−7134
Nd:YAG CW laser, longit. mode number reduction 79−72576
Nd:YAG CW laser, mode locking, 30 W average power 80−87419
Nd:YAG CW mode-locked laser, negative feedback power stabilization 80−69435
Nd:YAG laser, actively modelocked and Q-switched, fusion reactor appl. 79−45980
Nd:YAG laser, CW, with high output coupling modulation 80−9917
Nd:YAG laser, CW mode-locked and intracavity freq. doubled, anal. 80−58548
Nd:YAG laser, kinematic mode synchronisation *(Russian)* 77−34892
Nd:YAG laser, subnanosecond pulse generation at 100K 80−74397
Nd:YAG laser as optical pulse generator, mode locking by acoustooptic loss modulation 79−64260
Nd:YAG laser oscillator, mode-locked, pulse splitting 79−7160
Nd:YAG laser pulse tailoring/synchronization system for laser-plasma interaction expt. 79−98404
Nd:YAG long laser resonator, active and passive mode-locking 78−50832
Nd:YAG mode-locked laser pulse, quadratic phase evolution direct meas., time resolved interferometry 80−48318
Nd:YAG mode-locked unstable laser, p-branch unstable resonator config. 79−31928
Nd:YAG passively locked laser, pulse width meas. by SHG method *(Chinese)* 80−87432
Nd:YAG passively mode-locked unstable oscillator 79−45953
Nd:YAG pumped $LiNbO_3$, parametric oscillator, picosecond IR pulse generation 78−71151
Nd:YAG regenerative amplifier, expt. studies 80−95909
Nd:YAG unstable-resonator oscillator, stable single-axial-mode operation by injection locking 80−53331
Nd^{3+}:glass laser, stabilised, single-mode, Q-switched, continuous frequency scanning 79−31922
Nd^{3+}:glass laser, with contacted mode-locking-dye cell 79−18454
Nd^{3+}:$LiYF_4$, pulsed free running laser action at 1053, 1046 nm, passive mode locking *(French)* 78−79048
Nd^{3+}:YAG, CW laser with planospherical resonator, freq. degeneracy of modes 79−31953
Nd^{3+}:YAG, stabilised laser with longitudinal mode synchronisation *(Russian)* 77−19315
Nd^{3+}:YAG, with nonstationary resonator, axial mode synchronisation *(Russian)* 77−75582
Nd^{3+}:YAG CW laser, intensity fluctuations in single-freq. mode 80−91802

laser modes continued
Nd^{3+}:YAG CW linear laser, longit. mode self-locking 79−72611
Nd^{3+}:YAG CW ring laser, axial mode locking by electrooptic $LiNbO_3$ phase modulator 78−50835
Nd^{3+}:YAG laser, running pulse mode of operation, exptl. obs. 77−7089
Nd^{3+}:YAG laser, spontaneous mode locking necessary conditions, quadratic nonlinearity influence 79−64261
Nd^{3+}:YAG multimode laser radiation noise 80−74366
Nd^{3+}:YAG stabilised single-freq. travelling wave laser 79−18449
$Nd_{0.5}La_{0.5}P_5O_{14}$ laser, FM mode-locked 79−86184
Ne ring laser, two-mode, oppositely travelling waves, beat freq. obs. 77−10963
PbSe, pressure tunable CW injection laser, emission spectra 79−18419
$Pb_{0.995}Sn_{0.045}Se$ pulsed laser for high-resolution NH_3 spectroscopy 79−64252
$Pb_{1-x}Sn_xSe$ laser, optical feedback effects on performance, external cavity modes 80−32981
$Pb_{1-y}Sn_ySe$-PbSe pulse laser diode, temp. tuning of modes 78−50777
$Pb_{1-x}Sn_xTe/PbTe_{1-y}Se_y$ lattice-matched buried heterostructure lasers with CW single mode output 80−74386
$Pb_{1-x}Sn_xTe$-PbTe pulse laser diode, temp. tuning of modes 78−50777
ruby Q-switched with stable operation in pure transverse natural oscillation *(German)* 77−14761
Xe 3.5 μm self-mode-locked laser pulse, waveform analysis 78−1290
Xe IV laser excited by long current pulse discharge, double-pulsed output 80−37993
Xe laser, electron beam excited, form. of multiply-charged ions *(Russian)* 78−25853
Xe laser, high gain, ang. multiplexing for short pulse amplification 79−36924
XeF, injection locking, cross relax. rates 78−17909
XeF laser, electron beam stabilised discharge *(Russian)* 78−25894
XeF laser, transverse discharge in Xe+He+NF_3, time and energy charcts. *(Russian)* 78−25861
XeF, transverse discharge-excited laser, active mode locking 77−23656
$Zn_xCd_{1-x}S$, lasing modes and spatial distrib. under one-photon excitation, cavity model 78−74913
$Zn_xCd_{1-x}S$, platelet single cryst. one-photon optical excitation, spatial distrib. and mode struct. of laser emission 79−31912

laser radar *see optical radar*

laser theory
see also laser transitions; population inversion; stimulated emission
20 years of development 80−58501
active media, possibilities of efficient freq. conversion 79−59764
active medium, EM field self-focusing, laser transverse struct. form. 80−87442
active medium, surface transition layer effects *(Russian)* 78−71072
amplification of incoherent radiation 78−55334
amplified spontaneous emission in spherical and disk-shaped laser media 80−1177
amplifying medium with infinite energy store, quasistable state 77−75470
amplifying medium with polarisation relax. and nonresonant linear losses, 2π pulse propag. 77−75469
anharmonic oscillator in strong EM field, induced radiation model *(Russian)* 78−78988
'approximate eigenvalue' concept for integral eqn. 77−67217
asymmetrical inhomogeneously broadened line, lasing stability 79−923
atom-coupled-to-field system, coherent radiation, phenomenological theory 77−14683
atom-strong field interactions, generalised dressed atom approach, laser theory and Bloch-Siegert shift 77−71964
atomic collisional gas-discharge laser feasibility 80−91779
atomic collisions, vel. changing, saturation spectroscopy, internal coherences 78−42245
benzoxazole, aromatic derivatives, spectral luminesc. and lasing props. rel. to electronic struct. 80−99519
bidirectional laser amplifiers, amplified spontaneous emission intensity fluctuations 80−37988
bistability, in lasers containing saturable absorbers, semiclassical and quantum theory 79−3674
bistability of saturable-absorber containing laser, semiclassical and quantum theories 78−82943
bistable absorber system, in ring cavity, photon statistics 79−31847
bistable absorption in Fabry Perot ring cavity 78−50821
book, quantum electronics 80−105442
bound-free excimer lasers, radiative and kinetic mechanisms 77−88697
Bragg interactions in active medium, first and second order 78−50747
chemical CW lasers, inhomogeneous broadening effects, two-level vibrational model 79−76679
chemical laser, CW diffusion type, simplified model extension 77−3573
chemical laser, mol. constraints implied by kinetic coupling schemes, maximal work 80−38010
chemical lasers oscillating on rot., vibr. and electronic transitions, review 80−102716
Cherenkov radiation, stimulated, cooperative effects 77−19228
Cherenkov radiation at resonance frequency of amplifying medium 79−22926
classical multimode theory of the free electron laser 79−27228
CO_2, TEA, field uniformity requirements 79−3675
coherence oscillations in nonlinear media, coherent state lifetime 78−66862
coherent laser waves, stability domain 79−50280
coherent radiation generation near cyclotron resonance 80−18979
collisional laser with energy exchange between excited levels of two systems 80−28188
complex molecules, triplet state, photoinstability and quenching effects on lasing kinetics *(Russian)* 79−13778
composite waveguide laser with end-fire excitation, output charcts. 80−23738
computer model for CW optically-pumped submm laser performance prediction 78−87041
correlation function of single-mode radiation in a quasi-classical approximation 80−95815
correlation functions, lasing systems exhibiting first order like phase transition threshold behaviour 77−71969
correlation functions for laser with saturable absorber, renormalised Fokker-Planck eqn. 80−48208
counterrunning light waves interaction in mirrorless device 79−98333
coupled generator and amplifier system, stationary modes 79−64196

laser theory continued
coupled laser oscillators, injection modulation 80−99773
coupled laser-amplified system, stationary modes stability 80−1179
coupled laser-amplifier system, computation technique 79−3720
coupled system, time depend. projection operator anal., classical gas and quantum systems 78−16720
coupled transitions with arbitrary polarization of radiation 80−78827
crystal lasers, theoretical problems, current status *(Chinese)* 79−45948
CW lasers, homogeneously broadened, with uniform distribution loss, exam. of output power 78−55332
cylindrical active element with sheath, radiation intensity distrib. calc. 80−58531
degenerate system, two-photon lasing process 79−86156
DF-CO_2 CW chemical transfer laser, comprehensive kinetics model 79−81422
DFB laser, limiting spectral charcts. 79−64197
DH Injection lasers, single and dual-filament, self-sustained oscillations, theoretical model 80−64023
DH laser, model for static props. 79−98360
DH laser, threshold current rel. to interface recombinations vels. 79−98369
DH lasers, phase and group indices 80−64016
DH stripe geometry lasers, three-dimensional anal. of mode props. 80−64020
DH stripe-geometry lasers, thermal props., interpretation of thermal resistance measurements 80−64017
dispersion of opt. charcts. in amplification range, freq. spectrum of stimulated emission, calcs. *(Russian)* 77−54757
distributed feedback laser, two-mode operation, index and gain grating configurations 80−69357
double resonance Raman amplifier, theory 80−87434
dye laser, N_2 laser-pumped, subns. relax. oscills. 78−82959
dye laser, optically pumped, threshold singularities 79−3703
dye laser, radial distrib. of pumping in coaxial cell with external irrad. 80−53308
dye laser, rate eqns. 78−82961
dye laser, subnanosecond radiation pulse formation mechanism, axial period *(Russian)* 77−50700
dye laser, triplet losses, six level model 77−14711
dye laser deterioration, effect on performance 80−83602
dye laser operation, second and first order phase transition analogy 79−953
dye laser output coupling, optimisation by consideration of spatial gain distrib. 80−83603
dye laser rate equations, nonstationary solns. 79−27250
dye laser with saturable absorber, stationary pulse parameters, approximate theory 79−3690
dye lasers, anisotropic theory, oscill. model of complex mols. *(Russian)* 79−22948
dye lasers, metastable state relaxation time determ. 80−102719
dye lasers, triplet loss influence on relaxation oscills. 80−23680
Einstein theory of stimulated emission of radiation *(Hungarian)* 79−89880
electron beam self-bunching in resonantly absorbing medium, radiation amplification feasibility 80−102605
electron pumping of C and He like ions, for lasing below 1000 Å 77−65589
electron-positron pair stimulated annihilation, coherent γ-emission 79−55104
emission asymmetry, laser with inhomogeneous active medium 80−28191
emission kinetics of solutions of complex organic compounds for pumping with linearly polarised radiation *(Russian)* 77−83872
excimer lasers, physical processes and performances 80−32962
excimer oscillatory emission, analytic quantum mech. model 79−59675
exciton laser action, quantum theory 77−54754
exciton systems, dense, recombination processes 77−75531
exponentially decaying gain medium, waveguiding 78−50774
extreme UV and X-ray lasers, basic physical concepts, review 79−31850
Fabry-Perot cavity, gas filled, optical bistability described by stochastic master eqn. 79−76652
far IR oscillator, optically pumped, parametric study 80−95862
fast flow laser, active medium parameter input fluctuations, intensity response 80−53257
field autocorrelation function, in threshold region, fine struct. 79−3683
field fluctuations of two-photon coherent states 79−13937
filled telescopic resonator, steady-state lasing, oscillation modes 80−95922
first order phase transition in laser with saturable absorber 79−18394
fluctuating intensity regimes in lasers and masers 80−19015
fluctuations, semiclassical stochastic master eqn. theory, and Scully-Lamb theory 79−27236
fluoromethane optically pumped molecular laser, relax. oscills. 80−95875
fluoromethane-^{13}C optically pumped molecular laser, relax. oscills. 80−95875
FM light pulse shape change on amplification 77−3564
Fokker-Planck equation, approx. analytic solution 77−54689
Fokker-Planck equation, continuum mode laser, stationary soln. 77−54688
Fokker-Planck equation, continuum mode laser with spatially inhomogeneous dissipation and excitation 77−54687
Fokker-Planck equation solutions, polynomial expansion method 80−91771
four-level laser power and relaxation oscillation, excited-state diffusion effect 77−79834
free electron devices, nonlinear theory, book contrib. 79−27148
free electron laser, 'beats' of two coherent electron beams 79−55106
free electron laser, classical, semiclassical and quantum field theories 77−14684
free electron laser, classical theory, in moving frame 79−76655
free electron laser, coherent dynamics, conservation law, small signal theory and gain-spread relation 80−83582
free electron laser, coherent dynamics with arbitrary magnet geometry 80−83581
free electron laser, coherent quasi-classical states 80−53251
free electron laser, coherent states in single mode and multimode cases 80−102689
free electron laser, collective and single electron interactions, book contrib. 79−27234
free electron laser, generalised gain-spread expressions 80−53249
free electron laser, multiphoton analysis 80−78826

laser theory continued
free electron laser, nonlinear formulation and efficiency enhancement 80−32948
free electron laser, nonlinear theory, efficiency enhancement 80−43317
free electron laser, one-body analysis, book contrib. 79−27233
free electron laser, orotron, using Smith-Purcell effect 80−5720
free electron laser, pulse propagation equations 80−53250
free electron laser, quantum and multimode theory, Bloch-like model 80−48203
free electron laser, quantum description 79−98330
free electron laser, quantum theory 80−23656
free electron laser, quantum theory for strong fields 80−83583
free electron laser, saturation, classical theory 80−23655
free electron laser, saturation behaviour from barrier reflection 80−9846
free electron laser, single particle classical model, stimulated Thomson scatt. 78−42317
free electron laser, small signal theory for gain in strong axial mag. field 80−78825
free electron laser, strong wave amplification by electron scatt. in spatially periodic mag. field 79−76654
free electron laser, strong-signal theory 77−19226
free electron laser, theory 78−37867
free electron laser, two-element, efficiency improvement 80−43313
free electron laser as travelling wave amplifier, book contrib. 79−27232
free electron laser dynamics, coherent picosecond pulse propag. calcs. 80−95860
free electron laser dynamics with space charge and wiggler effects 80−58500
free electron laser theory, relativistic steady-state formulation 80−43316
free electron laser with nonuniform wigglers, small signal gain 80−58499
free electron lasers, boundary deform. and Robinson-Liouville theorem 80−48202
free electron lasers, Cherenkov, Smith-Purcell, and TW amplifiers, operation regimes 79−919
free electron lasers, classical theory, saturation, perturbation calcs. 80−83580
free electron lasers, energy transfer, computer simulation 80−83578
free electron lasers, low gain, analytic soln. of quasi-Bloch eqns. 80−87363
free electron lasers, nonlinear saturation, thermal effects using EM pump 80−87364
free electron lasers, quantum mechanical and classical theories 80−83579
free-electron laser, electron dynamics 77−88688
free-electron laser, gain mechanism 78−46557
free-electron laser as laser, population inversion existence 79−59665
free-electron lasers 80−48205
free-electron lasers using Smith-Purcell effect 79−50276
free-electron lasers with quasicircular undulators 79−55102
frequency conversion, interatomic cooperative effect model *(Russian)* 79−72549
frequency noninteraction of oppositely travelling waves in gas ring laser 80−38043
Fresnel formulas and law of stimulated emission 80−58489
fundamental concepts, elementary approach *(Hungarian)* 78−71070
gain measurements using amplified spontaneous emission 80−37986
gain saturation in laser resonator, interf. effects 80−37987
gain-switched laser amplifiers, analytic modelling 77−7053
gain-switched laser oscillators, analytic modelling 77−7052
gamma lasers, kinetics, quasi-classical approach *(Russian)* 80−74332
gamma-ray laser, conditions for laser threshold, use of polarized nuclei 78−37868
gas laser, freq. modulated, threshold conditions for gain and freq. 77−88816
gas laser, theory of polarisation effects 80−23660
gas laser amplifier, quasi-Gaussian pulse propagation, effect on line-shape parameter anal. 78−55333
gas laser autodyne effect 79−81404
gas laser kinetics simulation 79−59676
gas laser three-level gain medium, semiclassical theory, population pulsations and interf. effects 80−95863
gas lasers, computer modelling, book 79−41364
gas lasers, longitudinal flow, effect of flow on output power 78−58975
gas lasers, mode interactions in longit. mag. field, active medium dispersion effects 80−63967
gas lasers, relax. parameters and performance, Lamb theory 77−75467
gas lasers, single-mode, autodyne effect *(Russian)* 79−925
gas nuclear pumped laser simulation experiments 80−64042
gas waveguide laser, mode comp. of radiation 80−28192
gasdynamic CW laser, multipass cavity 78−63140
gasdynamic laser with partial population inversion 79−55125
gasdynamic layers, thermally excited quantum oscillators and second law of thermodynamics 77−34863
gaseous dipolar media, semiclassical theory, appl. to gas laser 80−83586
giant pulse lasers, passively mode locked, optimisation 78−83006
Goldstone mode in stationary state of non-equilibrium dissipative system *(Chinese)* 80−87365
heterostructure lasers, fundamental principles, book 79−36899
HF chemical laser, CW, with unstable telescopic resonator, radiation field structure 80−91786
HF self-modulation of laser with unstable resonator *(Russian)* 77−83911
high gain amplifier, amplified spontaneous emission and gain saturation nonlinearity 77−31087
high intensity laser oscillator, output characts., stability criteria, semiclassical density matrix approach 80−63968
high intensity single-mode laser theory 77−88691
high speed flow lasers, stable oscillation condition mode struct., output power characters 79−76660
high-power lasers, review 80−32950
homogeneously broadened CW lasers with nonsaturating lasers, optical extraction characts. 80−91770
homogeneously broadened laser, injection locking, dynamic rate eqns. 78−37920
homogeneously broadened laser, two mode operation, analytical string signal analysis 78−55331
homogeneously broadened with constant loss, optimum output efficiency 80−74403
inert gas halide avalanche discharge lasers, characts. and parametric behaviour 80−37998
inert gas halide electronic transition laser, quantum chem. 80−32971
laser theory continued
inert gas nuclear pumped lasers, prod. efficiency of excited states 80−63998
inhomogeneous active medium gain 79−22930
inhomogeneously amplifying medium, light beam deflection 77−88689
injection laser, comprehensive model, current depend. of spontaneous and coherent emission 80−74361
injection laser transients, phase-plane anal., effects of absorbing sections 80−64022
injection laser with index-guiding structure, single longit. mode operation 79−98362
injection lasers, current depend. of spontaneous emission and junction resist. 79−59699
injection lasers, output depend. on inhomogeneous bonding 80−64015
injection lasers, stripe geometry, nonlinearity in power output-current characts. 77−83875
instabilities, example from synergenetics 80−9848
instabilities for coherently driven absorber in ring cavity 78−50822
instabilities in the laser with injected signal and laser-phase transition analogy 79−18393
instability, example of thermodyanmic props. of nonequilibrium states subject to Fokker-Planck eqns. 77−67396
instability below threshold, laser-saturable absorber system 78−94385
instability in lasers, behaviour of cooperative systems 77−3563
intensity fluctuation linewidth, Jakeman-Pike approx., black-body and laser models 78−58960
interaction process between radiation modes and laser atoms 77−38853
internal modulation of laser radn., freq. limitation 79−72607
intracavity Raman laser theory 79−27296
intracavity spectroscopy, laser output spectrum, lineshape 79−55155
intracavity spectroscopy rel. to laser spectral characts. *(Russian)* 78−46561
intrinsic resonant freq., near-threshold behaviour 79−98367
introductory concepts and results, book contrib. 80−106504
ion-molecule processes in lasers, excitation methods 80−28221
kinetic processes in lasers 80−28190
kinetics, self-coordinated problem *(Russian)* 79−27238
laser, optical excitation by photodissoc. wave propag. in dense gas 80−74352
laserlike systems, stochastic master equation description 80−53243
lateral wave amplification through reflection from active medium 78−78987
lecture course 78−1202
limiting characteristics in self-limiting transitions 80−14311
Lorentz equation derivation for unstable dispersive physical systems 80−83786
Lorenz attractor, origin and struct., appl. to specific model systems 78−29054
Lorenz model, onset of self-pulsing 77−7054
macroscopic system, vibrational relaxation, information-theoretic approach 77−58156
magnetic free-electron laser, output power 80−32947
magnetic resonance spectrometers, sensitivity improvement using laser properties 80−13115
many-mode laser, statistical props., generalised Volterra-Wiener method calcs. 77−38851
master equations, discrete, approx. methods for stationary solns. 77−22480
master equations steady state soln., chem. react., two-photon laser appls. 77−9945
mean field model for absorptive and dispersive optical bistability with inhomogeneous broadening 78−50823
memory effects and mode coupling near the laser threshold 79−55107
memory effects in linewidth and line shape near laser threshold 78−58976
metal halide vapour lasers, kinetic model 79−94222
metastable state, theory of decay processes 77−61935
metastable states in laser phase transitions, first passage time analysis 79−922
methanol far IR laser, optically pumped, Stark effects 79−72552
methylfluoride laser, CW, 496 microns, rate equation model, review 78−55343
modified Lame eqn. with integral term, exact soln. 78−63052
molecular laser, optical pumping in damped photodissoc. wave propag. in dense gas 80−99714
molecular lasers, laser pumped, theory 79−36868
molecular lasers, laser pumping, dispersion 80−87375
monochromatic waves in amplifying two-level system 80−74331
monochromaticity, teaching approach 79−84886
moving active medium, light production *(Russian)* 79−27237
multicomponent laser systems with two-photon absorbents 79−94240
multifrequency emission, atomic states interference effect on polaris, characts. 79−27235
multilevel gas, transient and spatially inhomogeneous excitation 77−652
multimode high-intensity laser dynamics theory 79−41363
multimode laser, Gaussian statistics, influence on reson. ionis. multiphoton process 78−29927
multimode laser, semiclassical theory of stability, generalised entropy 79−3699
multimode laser theory, quantum generalisation of Lamb's semiclassical theory 77−58309
multiple-quantum-well laser, optical analysis, three-region waveguide model 80−14337
N-mode laser, emitted light correlations 78−63051
near MM wave laser synchronous pumping, ultrashort pulse generation 80−69385
negative light absorption by medium with selective freq. modulation of quantum oscillators 80−106501
non-confocal resonator, with output-coupling aperture, eigenvalues *(Japanese)* 79−55163
non-self-maintained discharge, three-body electron attachment to O_2, plasma decay obs. 80−43844
nonequilibrium phase transition, dynamical features *(Chinese)* 78−83030
nonequilibrium quantum statistics of lasers and nonlinear optics 79−31848
nonequilibrium steady states, distrib. functions and phase transitions 77−61041
nonlinear active medium in Gaussian random optical field, stimulated emission statistics 80−58488

laser theory continued
nonlinear active medium laser, transient intracavity SHG, giant pulse generation 80−9948
nonlinear active medium laser for both stimulated emission and SHG 79−64285
nonlinear laser pulse amplification in medium with single photon stimulated emission 79−45922
nonlinear optical amplifier, coherent radiation statistical props. 80−99691
nonlinear swept gain amplifiers, energy and power fluctuations 79−55095
nuclear inversion coherent excitation by relativistic electron beam *(Russian)* 80−48206
on-resonance self-focusing, optical pulses in thick absorbers 77−14783
one-dimensional laser, with output coupling, linear quantum theory 77−88690
one-dimensional model, stable and metastable states, relax. and fluctuation theory 78−49769
open systems, statistical mechanics *(Japanese)* 79−76658
open systems, statistical mechanics *(Japanese)* 79−76659
operation physical principles *(German)* 79−59664
optical bistability, Dicke model of phase transitions 79−81402
optical cavity with output coupling, one-dimens., quasimodes as field eigenvalue 80−9911
optical feedback in lasers *(Chinese)* 79−81405
optical instabilities from the entropy production point of view 79−80560
optically pumped CW far IR lasers, quantum mechanics 77−54700
optically pumped far IR laser output power, temp. depend., four-level model 79−59674
optically pumped laser three-photon transition theory 80−102690
optically pumped lasers utilizing self-terminating transitions, CW stimulated emission possibility 80−14329
optically pumped sub mm lasers 77−54699
optically pumped submillimetric laser models and rate eqns. 77−38871
organic compound lasing ability *(French)* 79−31893
organic compounds, lasing ability, substitution effects 78−82941
organic dyes, stimulated fluorescence, energy level scheme, photoisomerisation effect 77−70310
oscillation caused by two-photon process, quantum stochastic process in thermodynamic limit 77−37814
parametric resonance, response of single mode operating laser 79−76656
parasitic oscillations in the static centered two-aperture limit 80−95861
partially homogeneously broadened gas laser amplifier, wave impedance formulation 77−75468
periodic laser with unstable resonator, single-pulse emission characts., active-medium inhomogeneities effect 80−74365
phase diffusion model, Lorentzian laser lineshape, detuning 80−944
phase transitions, intracavity absorber expt. 78−13676
photon distributions of lasers with first-order phase-transition analogies 80−23659
photon reflection at the boundary of an inverted medium 79−36869
photon statistics, optical cavity length depend. 78−94402
photorecombination laser, shock wave triggered, waveguide mode optical gain 80−5730
photorecombination laser theory thermally induced behind a shock wavefront 79−76682
planar and disc-cavity lasers, volume-averaged rate eqns. 78−13734
plane waveguide laser, with semitransparent wall, kinetics 77−54740
plasma dispersion function 78−17894
plasma laser pulse amplifier using induced Raman or Brillouin processes 80−1279
POPOP vapour lasing, buffer gases influence, theory 80−91790
population inversion, maximum achievable, in finite volumes 78−50749
power as function of level of optical signal synchronisation 80−69359
power calculations, laser models, sources of error 80−48207
power output formula *(Chinese)* 79−89879
PT asymmetry and four-fold EM degeneracy lifting, appl. to ring laser mode splitting 80−23606
pulse amplification through energy exchange with electron beam via nonlinear radiation press. effects 80−95776
pulse generation, double, gradual cutting-off resonator losses 80−69433
pulsed collinearly pumped far IR amplifier, rate analysis 79−81408
pulsed laser, rel. to optical parameters of semicond. in strong EM field 77−44050
pulsed optically-pumped submillimetre-wave amplifier theory 79−31868
pump fluctuations, influence on resonance fluoresc. radiation intensity correlation 80−37981
pumping, quasi-reson. energy and charge exchange processes, new transitions 80−58526
pumping system, thermodynamic calc. method 80−58551
Q-switched four level laser dynamics, lifetime of terminal energy level *(Chinese)* 78−66832
quantum dynamical semigroups and spin multipole relaxation in isotropic surroundings 78−86813
quantum optics, transition phenomena, review 80−32944
quantum theory of spontaneous and stimulated emission of channelled electrons and positrons *(Russian)* 78−49999
Raman fibre laser oscillators, theory 79−81439
Raman spin-flip laser, higher modes and saturation effects, theory 78−71106
relativistic channelled particle beam, induced radn., tunable laser prod. 79−18391
relativistic ion beam laser, continuously IR to X-ray tunable, in negative temp. state *(Chinese)* 80−87373
resonance phase transition in two-level lattice system, thermodynamics 80−69351
resonant media, pulse steady propag. 79−72633
resonant pumping, high-power, of molecular systems *(Russian)* 77−54690
resonant two-photon ionisation in partially coherent radiation field 78−66525
resonator, sensitivity to misalignment, anal. by ray contour method 80−58602
resonator, stimulated combined scattering of light, effect of generation of 'hot' vibrs. 80−58601
rhodamine 6G dye laser, induced radiation spectral characts., effect of vibr. relax. 80−64008
riby resonator, lasing spectrum singularities and Q-factor, for z-dimens. beam path *(Russian)* 77−88795
ring cavity, dispersive optical bistability 79−18386
ring gas laser, limiting characts. of power resonances 80−19058
laser theory continued
ring laser, diffraction theory, Gaussian approx. 80−53338
ring laser, intensity fluctuations taking spatial population-inversion grating into account 80−14364
ring laser, luminesc. effects on beat signal *(Russian)* 77−54742
ring laser, quasiclassical equation of motion, spontaneous emission in lasing channel *(Russian)* 78−90434
ring laser, solid state, with intracavity bleachable filter, conditions for CW stimulated emission 80−14368
ring laser, two-mode, correl. functions 79−76720
ring laser, two-mode, intensity fluctuations 80−33038
ring laser, with detuning, generation of high-frequency pulsations 80−48304
ring resonator, with additional return mirror, mode struct. 78−46677
rotating anharmonic oscillators in resonator, stimulated emission power 80−99689
roto-vibrational molecular laser, optically pumped, rate eqn. model 78−37874
ruby laser, nonuniform amplification effects *(Russian)* 77−14722
ruby laser, spiked regime, dynamic theory 79−27260
ruby NMR laser, ^{27}Al nucl. spin system, collective ordering phenomena, instabilities 80−11278
saturable absorber, analogy with convective instability in two-component liquid layer heated from below 80−79319
saturable absorber, phase transition analogies 77−3565
saturable absorber laser and dye laser, comparison of time depend. density matrix eqns. 79−86176
saturable absorber-laser semiclassical model, stability 80−78828
saturation parameter from gain meas. 78−66797
scaling, nonequilibrium systems near instability point, anomalous fluctuation theorems in extensive region 77−2612
scaling theory of laser radiation in the transient unstable region 78−94384
self-induced distributed feedback, stability, in system without resonator 80−87368
semiclassical, incorporating spontaneous emission 77−58310
semiclassical laser theory in the stochastic and thermodynamic frameworks 80−1178
semiconductor DH lasers, current-crowded carrier confinement 80−78854
semiconductor heterojunction lasers, partially homogeneous broadening and saturation, non-oscillating mode suppression 80−99775
semiconductor injection lasers, simplified theory for mode locking 80−64021
semiconductor injection stripe lasers, homogeneous spectral broadening multimode rate eqn. 78−79018
semiconductor laser, asymmetric waveguide structure, anomalous stimulated emission, theory 79−64228
semiconductor laser, photon spectrum and distribution function, analogy with nonideal Bose gas 80−23689
semiconductor laser nonlinear theory self-consistent calc. 77−71968
semiconductor lasers, generalised expressions for turn on delay 79−94233
semiconductor lasers, triggerable, light-coupled logic appl. 80−74360
semiconductors, low carrier density, lasing action, exciton Bose condensate charact. function 79−64233
short-wave emission, initial plasma parameters 80−99692
simultaneous CW oscillation of Cd(II) and I(II) lines in positive column He-Cd-I_2 discharge *(Japanese)* 77−71977
simultaneous oscillations of different transitions in lasers 79−22927
single mode, nonlinear stochastic eqn. of motion calcs. 77−648
single mode, quantum mechanical model, exact steady state soln. 77−649
single mode laser, photon statistics, cooperative atomic interactions 80−43318
single-mode laser, cooperative effects 79−13944
single-mode laser, nonequilibrium statistical operator method 79−89881
single-mode laser models, Scully-Lamb master eqn. 77−38852
six-level model, triplet-triplet pumping 78−25870
solid laser, fluctuations in laser theories 80−83587
solid laser, freq. spectrum, linear atom-field interaction 77−19258
solid laser, multimode, with modulated resonator losses, radiation intensity fluctuations 80−74367
solid laser, passively mode-locked, statistical props. of ultra-short pulses 79−36941
solid laser, two-standing mode operation with stationary ats., saturation effects and stimulated scatt. 79−68398
solid laser active rod, effect of surface transition layer on laser action 79−50301
solid laser with brightening filter, ultrashort light pulse optimum generation 79−36903
solid pulsed laser cylindrical element, temp. distrib. anal. *(Russian)* 77−58332
solid-state ring laser, mode locking theory 79−41399
solid-state ring laser, single-freq., spontaneous antiphase fluctuations, theory 80−91821
soliton line constructed from an equivalent cct. of undamped spiking lasers 79−3673
solitons, laser physics appls. 80−48333
spatial coherence degree correlation with wave vector variance 79−45985
spatially coherent laser beam form., phase transitions 78−17898
spectrally inhomogeneous active medium, giant external pulse 78−17897
spectroscopic techniques based on Lamb's laser theory 79−35847
spectrum kinetics of polyatomic organic molecule lasers *(Russian)* 78−46560
spiking, irregular, Lorenz eqn., horseshoe-map chaos 77−41473
spontaneous coherent pulsations in laser oscillators 79−921
spontaneous noise of spatially modulated signal *(Russian)* 77−38850
stability of quantum model of CW laser, Lyapounov function approach, using Scully-Lamb theory 78−5445
stability theory of coherent laser pulses in inverted medium 77−10936
statistical properties of emitted light, cavity length depend. 77−88794
stimulated and Cherenkov radiations, differential eqns. with respect to coupling constants, S-matrix 79−50278
stimulated Raman scatt. of broad freq. spectrum pump radiation, antiStokes wave excitation and amplification *(Russian)* 79−50346
stimulated scattering, wavefront reproduction 78−1305
stochastic destruction of bound states in atomic interaction with radiation field *(Russian)* 77−10644
stochastic model, entropy and stability 79−50279

laser theory continued
stripe geometry injection lasers, rigorous boundary value soln., for lateral modes 78−71100
stripe injection DH laser, radiation emission kinetics 79−64229
subharmonic lasers, quantum theory, first order non-equilib. phase transition 80−83584
submillimetre, optically pumped lasers 78−46587
successive oscillatory fields, molecular beam resonance method 80−91706
superluminescent laser theory for dye soln. *(Russian)* 79−951
supermode locking, noise effects 79−22986
superradiance waveguide laser, stimulated emission spectrum, leaky modes *(Russian)* 80−87400
symposium contrib., Florida, USA (March 1979) 80−51946
synchronism by small external signal, capture dynamics 78−46559
synergetics, mechs. of self organisation, lasers, chem. reactions, heat transfer in fluid 77−34867
synergetics, nonequilibrium phase transitions and laser instability hierarchy 80−1180
TEA laser discharges, inhomogeneities 77−14687
TEM_{00} thermoinsensitive cavity *(Chinese)* 80−53335
thermal gasdynamic laser, energy parameters, analytic calc. method 77−75479
thin-sheet gain approx. criteria 78−25845
three boson field modes with trilinear interaction, statistical behaviour 78−87093
three level molecular system interaction with two laser fields 77−54685
three-level laser, rate equations 80−69356
three-level lasing system, one-dimens., saturation effects 80−53253
three-level molecular laser pumping and dispersion eqns. 80−69384
threshold characteristics of mirrorless lasers 77−31112
threshold range, qualitative change determ., analogy with phase transition *(Czech)* 80−32949
transient laser radiation, stochastic process near an instability point, numerical solution 80−23658
travelling wave laser, operation with periodically varying resonator parameters 78−46678
travelling-wave Zeeman gas laser operating at high radiation intensities, theory 80−9912
tricritical phenomena in laser with saturable absorber 78−78989
two level three dimensional system, phase transitions analogy with lasers 78−58965
two-level atoms, gain without population inversion 78−17895
two-level system, in strong reson. field, saturation, temp. and spectrum characts. 80−99690
two-level system, Rabi oscillations in partially coherent field 80−102688
two-level system, spontaneous emission, non-Markovian effects 80−58487
two-level system in resonant multifrequency field with structureless noise *(Russian)* 80−91766
two-level systems, spatially extended in cavity, reson. radiation mode interaction 78−37870
two-mode laser with coupled transition, quantum theory 80−43319
two-mode oscill. gas laser, saturation-induced polaris. preferences 79−22929
two-photon amplification on cascade-transitions 80−48219
two-photon inhomogeneously-broadened laser, quantum statistical anal. 79−59666
two-photon laser, atomic transitions, semiclassical stochastic description 79−76657
two-photon laser amplifier, system with population inversion, theory 78−17896
two-photon laser beam, breathing mode of EM field 78−46558
two-photon laser for optical communications, quantum noise optimum control 78−71049
two-photon laser oscill., semi-classical theory 79−22928
two-photon single-mode laser, radiated EM field statistics 79−98334
ultrashort laser pulse onset, first or second order phase transition 78−78986
ultrashort laser pulses, onset and time evolution 77−7051
ultrashort pulse duration control rel. to forced mode synchronisation *(Russian)* 77−46735
ultrashort pulse formation mechanism rel. to peak transition process *(Russian)* 77−54745
unstable resonator calculation, laser operating on organic compound solution 80−58600
unstable state decay, trajectory time spread, laser photon statistics 80−83585
van der Pol oscillator, RPA for linewidth 80−68138
VUV and X-ray lasers, amplification by ion accel. in plasma by steady state fields 80−28187
weak quantization in a nonperturbative model 79−88825
Zeeman laser, two-transitions with common upper level *(Japanese)* 79−55112
Zeeman laser or amplifer, bistability and intensity fluctuations 80−53254
Zeeman linearly polarised laser, Izsing atom susceptibilities, first and third order approx. *(Japanese)* 78−71071
Zeeman linearly polarised laser, mag. field reson. on laser output, freq. stabilisation *(Japanese)* 78−66798
Zeeman ring laser, four-mode operation 80−19053
(Al,Ga)As DH laser degradation, facet oxide formation 79−86185
AlGaAs CW heterolaser, hysteresis of output radiation power 79−64230
AlGaAs-GaAs double heterostructure laser lifetime, point defect generation model calcs. 80−32992
Ar ion laser plasma, collision radiation model appl. *(Dutch)* 78−29934
CO, gasdynamic laser working media, energy characteristic 80−14319
CO laser, analytical theory, multilevel cascade emission *(Chinese)* 80−102702
CO laser, multiphoton amplification, HF removal of forbiddenness *(Russian)* 80−53262
CO laser, simple model for power and spectra 79−7119
CO laser, steady state, parametric relation investigation 79−76677
CO laser with selective resonator, gain saturation law, lasing transition efficiency 80−48227
CO lasers, scaling laws 80−95878
CO pulsed laser emission with line selection, analytical theory 80−53277
CO sealed laser, approximate analytic theory 78−58994
CO-N_2 and CO lasers, energy and spectral characteristics 80−14327
CO_2, CW high power TE electron initiated laser, small signal gain profile calcs. 79−72550
laser theory continued
CO_2, electric discharge convection laser, saturation characts. *(Chinese)* 78−90408
CO_2 gasdynamic laser, gain supersonic flow heating effect, condition optimisation 78−82947
CO_2 high-power pulsed laser, wave-optical resonator modelling, gain saturation law 80−99693
CO_2 laser, high power, CW, electron beam sustained, performance, theory and expt. 78−71074
CO_2 laser, long and short pulse formation, optimum conditions 78−87037
CO_2 laser, multiphoton amplification, HF removal of forbiddenness *(Russian)* 80−53262
CO_2 laser, output characts. at high pump levels 80−58509
CO_2 laser, thermodynamic approach *(Rumanian)* 79−7109
CO_2 laser discharge tube, phase distortions due to heating differential 80−95865
CO_2, laser discharges, determ. of recombination coeff. 78−90407
CO_2 laser gain switch, pulse characts., approx. evaluation 80−58504
CO_2 laser short pulse propagation and energy extraction 80−74335
CO_2 multi-rotational line TEA laser, theoretical model 80−69361
CO_2 numerical soln. to nonlinear rate eqns. of population level density *(Bulgarian)* 78−33720
CO_2, stability of parallel pin electrode laser discharges, theoretical investigation 80−83588
CO_2 transverse discharge flow type laser, theoretical model *(Chinese)* 80−53255
CO_2 transverse flow CW laser, modelling and props. meas. 80−43321
CO_2 waveguide laser, gain and saturation *(Rumanian)* 80−23667
CO_2:N_2:He plasma, lasing action, gain limiting attainment possibility 79−89884
CO_2-N_2, gasdynamic laser, gain-optimisation, theory 79−76664
CO_2-N_2 fast-flow laser with unstable resonator, self-oscillation instability 80−95870
CO_2-N_2-He-CO, electron diffusion perpendicular to elec. field, second order theory 80−43322
Cu halide vapour laser, kinetic model 79−94222
Cu vapour laser, non heated, kinetic processes 80−37999
Cu vapour laser, rate processes, computer simulation 80−69371
CuCl vapour laser, output power limiting processes 80−91776
DF-CO_2 pulsed chemical transfer laser, analysis of calc. model 79−94226
GaAlAs DH lasers, SiO_2 insulated, characts. and near field 80−64019
GaAs, broadening mechanism, limitations to single mode power emission 79−961
GaAs junction laser, long time delays and Q-switching 77−3587
GaAs laser, spontaneous emission reduction at lasing with long delays 79−64226
GaAs-GaAlAs, heterostructure laser diode, lasing threshold calc. 80−28232
GaAs-GaAlAs DH stripe lasers, incremental efficiency enhancement and RF response 77−3586
H, recombining plasma, population inversion using collisional-radiative model 79−46423
H-like plasmas for short-wavelength lasers, population inversion 78−34277
HBr chemical laser, pulsed, output performance, numerical anal. 80−1197
HCl-D_2-He mixture, gasdynamic laser theory, gain depend. on parameters 78−50761
HF chemical laser, spherical telescopic resonator, design 78−71120
HF pulsed chain reaction chem. laser, scaling laws 80−32974
HF, rotational nonequilibrium, efficient model 79−22945
HF/UF_6-H_2 nuclear pumped laser, characts. 80−78847
HF-HCl chemical laser utilising ClF+H_2 chain reaction, kinetic model 80−9874
H_2O-H_2 cooling in supersonic nozzle, submillimetre wave generation 80−48229
He-Ne methane system, narrow nonlinear resonances in three level system *(Russian)* 80−78898
^{3}He-Ar nuclear pumped laser, first order model, lasing action depend. on Ar conc. 79−76668
^{3}He-Ar volumetric nucl. pumped laser, dominating processes and reaction physics 80−63981
^{3}He-Ar(Xe)(Kr)(Cl), nucl. lasing, population inversion mechanism 80−63980
^{3}He-Xe nuclear pumped laser, small signal gain coeff. and power output, theory comparison with expt. 80−63983
^{3}He(n,p)^{3}H direct nuclear pumped laser 77−83851
Hg halide electronic transition laser, quantum chem. 80−32971
Hg-N_2, optical pumping, vibr. excitation, laser theory 78−66517
I chemical laser, optically pumped, four-level model *(Korean)* 80−28224
I, laser, short pulse amplification, multilevel paraxial Maxwell-Bloch eqn. 79−36889
I, methyl iodide photodissoc. laser, kinetic model, cross-section calcs. 80−58530
I photodissociation laser, short-pulse high-press., line broadening and saturation parameters 77−3575
InGaAsP-InP, double heterostructure laser lifetime, point defect generation model calcs. 80−32992
InGaAsP-InP DH lasers, interfacial recomb., influence on oscill. characts. 80−87393
KrF electron-beam pumped laser, performance model 80−53273
KrF laser, kinetic model, limiting behaviour and scaling 80−78838
KrF* nuclear pumped lasers, excited state prod. rate and fission power pulse shape matching 80−63998
Li_2, $^3\Sigma_g^+$-$^3\Sigma_u^+$ excimer emission, ab initio calcs. 80−91608
N_2 electron impact excitation, rate coeffs., momentum transfer cross-section 78−78819
N_2, IR laser transition, excitation mechanism *(Japanese)* 80−83594
N_2 laser UV-IR pulse time lag theory *(Japanese)* 80−14325
N_2, stimulated emission kinetics under pulse-periodic conditions, theory 79−59689
Na_2, $^3\Sigma_g^+$-$^3\Sigma_u^+$ excimer emission, ab initio calcs. 80−91608
Nd laser glasses, gain coefficient meas. and modelling 79−81436
Nd:glass resonator, lasing spectrum singularities and Q-factor, for z-dimens. beam path *(Russian)* 77−88795
Nd:YAG laser, CW mode-locked and intracavity freq. doubled, anal. 80−58548
Nd^{3+}:YAG multimode laser radiation noise 80−74366

laser theory continued
$Pb_{1-x}Sn_xTe$ DH laser, minority carrier lifetimes and lasing thresholds 80−19031
Xe_2 excimer laser, electron beam excitation, VUV fluoresc., lasing 80−87379
XeF, ground state kinetics, multilevel model of energy transfer 80−99707
XeO photochemical laser, energy characts., kinetic model of physicochem. processes 80−28228

laser transitions
see also laser theory
acetylene, CO-C_2H_2 energy transfer, e-beam controlled discharge excitation 77−27277
acetylene-d_2, 17 to 21 μm laser lines generated using CO_2 laser pump 80−69375
anthracene derivatives in soln., fluoresc. and laser parameters 79−27251
asymmetrical inhomogeneously broadened line, lasing stability 79−923
atomic-transition lasers based on two-photon dissociation of metal-triiodide vapors 80−23679
Becklin-Neugebauer source in Orion, possible H Pfund β laser emission 80−12796
bromotrifluoromethane, CW optically pumped, FIR laser action obs. at 823, 883 μm 80−14321
bromotrifluoromethane 823 laser line, simple accurate method for wavelength meas. 80−106554
carbocyanine dye CW laser emission, spectral range extension up to 1020 nm 78−74901
carbon tetrafluoride, lasing action, spectroscopy of features near 9 μm lines 79−22944
carbon tetrafluoride 16 μm laser, radiance enhancement 78−87045
carbon tetrafluoride $^{12}CF_4$ laser, Doppler-limited absorption spectroscopy 80−74347
carbon tetrafluoride laser, CF_4 molecule $\nu_3+\nu_4$ band optical pumping 80−74349
carbon tetrafluoride laser, frequencies of pump and laser transitions 79−94218
carbon tetrafluoride laser, high energy output in 16 μm region, CO_2 laser pump 79−89927
carbon tetrafluoride laser oscillator amplifier meas., small signal gain and self-absorpt. 79−59683
carbon tetrafluoride optically pumped laser, pulse-periodic operation, 16 μm emission 79−27247
carbon tetrafluoride optically pumped laser, spectroscopic characts. 79−89896
chemical gas laser, mol. diluent effect on transition levels and population inversion *(Russian)* 78−25868
chemical lasers oscillating on rot., vibr. and electronic transitions, review 80−102716
chlorodifluoromethane subMM wave laser, optically pumped 80−87376
chloromethane-d_3, and isotopic forms, optically pumped mm laser transition assignments, 792 micron line 78−42328
collective processes in slightly inverted and absorbing media 80−87367
collision-induced, theory of gain and saturation 78−13677
confined plasma column, soft X-ray lasing action conditions 80−74346
coupled transitions with arbitrary polarization of radiation 80−78827
crystals with paraelectric impurities, superradiative transitions, acoustic and EM excitation 78−66872
cumarine derivatives, stimulated emission by laser and lamp excitation 79−72563
3-cyano-4-methylumbelliferone in ethanol containing water, acid or alkali, laser emission 79−955
9,10-dichloroanthracene with iso-amyl acetate or esters as solvents, dye laser material 80−74354
dichloromethane, CD_2Cl_2, CW optically pumped, submm. laser action, 100 to 900 μm 79−929
dideuteroacetylene, optically pumped laser action, 17.4 to 20.5 μm 79−935
cis-1,2-difluoroethene, CO_2 laser pumped, CW far IR laser lines 80−69372
1,1-difluoroethylene, optically pumped, far IR laser line assignment 79−31865
1,1-difluoroethylene, optically pumped mm laser transition assignments 78−42328
1,1-difluoroethylene, submillimetre laser molecules, Stark and ODR spectroscopy 79−31864
cis-1,2-difluoroethylene laser, far IR CW optically pumped 80−69368
1,1-difluoroethylene submillimetric wave emission assignments 80−102708
difluoromethane, optically pumped, CW far IR laser line frequencies 80−102706
difluoromethane, optically pumped, efficient CW far IR laser action obs. 79−928
difluoromethane, optically pumped by CO_2 laser, new CW FIR lines 79−94219
difluoromethane far IR laser gas, CW laser pumped, gain 80−69367
difluoromethane laser, optically pumped, FIR lines, performance efficiency 79−94220
diode laser IR spectra, intermode calibration using tandem etalons 80−32982
diphenyl with pyrene cryst., self induced transparency self stimulated excitation *(Russian)* 80−14403
diphenyl-stilbene dye, sulphonated, CW laser emission, tunable down to 390.4 nm 79−41379
dye laser efficient emission characts., pumping at 248 nm with KrF* discharge laser 79−954
dye mixture, possibility of tunable multiple wavelength output 80−23684
ethyl iodide submillimeter wave laser, optically pumped 80−87376
excimer systems, electronic structure and radiative transitions, book contrib. 79−81416
expanding plasma, gain on transitions of hydrogenic ions 78−17918
far IR CW optically pumped lasers, simple accurate method for wavelength meas. 80−106554
far IR laser lines, optically pumped, atm. transmission 77−19237
first order phase transition in laser with saturable absorber 79−18394
fluoromethane, 496 μm transition, laser pumped mol. laser theory 79−36868
fluoromethane, $^{12}CH_3F$, far IR CW laser emission by optical pumping 79−3687
fluoromethane, $^{12}CH_3F$, far IR Raman laser line obs., CO_2 laser pumping 80−69381

laser transitions continued
fluoromethane, angular correlation between far IR emission and CO_2 pump radiation, Dicke superradiance theory 79−41370
fluoromethane, laser pumped molecular lasers, sub MM laser expts. 80−1192
fluoromethane, near-MM-wave laser synchronous pumping, ultrashort pulse generation at 496, 193 μm 80−102705
fluoromethane laser diagnostics using two CO_2 laser pump pulses 79−31869
fluoromethane-^{13}C, pulsed far IR emission 80−69370
fluoromethane-SF_6 496-μm optically pumped laser, energy-transfer mechanisms 80−99712
formaldehyde-d_2 vapour, far IR laser emissions 78−63072
formaldehyde-d (d_2) submillimetre lasers, optically pumped, assignment of laser lines 80−58513
formic acid, CW submm. laser assignment 79−27244
formic acid, laser transitions near 5.6 μm, HF laser optical pump 78−58995
formic acid, optically pumped by pulsed HF laser, emission obs. at 5.7μm 79−50283
formic acid, vap., laser lines identification 78−1222
formic acid laser 311 μm line, freq. meas. by mixing with HCN laser 79−76728
free-free transitions in quantum electronics 80−28183
frequency conversion, interatomic cooperative effect model *(Russian)* 79−72549
Ga stimulated emission obs. on 417.2 nm line, by GaI_3 photodissoc. 79−89897
gain and refractive index for broadened laser line, sampling series representation 78−50748
gas, resonance four-photon shift, optimal focusing of high-power pumping 80−95574
group VI elements, auroral and transauroral transitions, high energy storage 77−10897
halogen-metal vapour lasers, average lasing power 79−936
inert gas fluoride laser, using NF_3-inert gas mixture, long pulse UV emission *(French)* 78−58982
inert gas halide lasers, pumped by transverse elec. discharge devices 79−41373
inert gas halide VUV lasers, pumped by travelling-wave discharges, 170 to 250 nm range 79−41372
inert gas halides, III(1/2)-II(1/2) transition 79−94211
inert gas mixture ion lasers, hollow cathode, CW operation and excitation mechanism 80−69363
instabilities in the laser with injected signal and laser-phase transition analogy 79−18393
instability in lasers, behaviour of cooperative systems 77−3563
iodomethane-d_3($^{13}CD_3I$), 690 and 806 micron laser transitions 78−42328
ion laser, $^{127}I_2$ stabilised, beat freq. intercomparisons at 514.5 nm 80−74338
IR, for 16 μm range, review *(Rumanian)* 80−87408
isotope, opposing waves competition at lasing line centre 80−1187
kinetic processes in lasers 80−28190
limiting characteristics in self-limiting transitions 80−14311
$LiNdP_4O_{12}$, fluoresc. and oscill. characts. at 1.317 μm 78−5473
metal vapour, laser operation by dissoc. of halides, alkyls and carbonyls 77−54702
metal-vapour recombination lasers using segmented plasma excitation 80−74370
metastable states in laser phase transitions, first passage time analysis 79−922
methanol, 118 μm, diagnostic experiments and modelling 80−58515
methanol, CD_2HOH, CH_2DOH, CW optically pumped, submm. laser action, 100 to 900 μm 79−929
methanol, CH_3OH and CD_3OH, far IR laser lines, optically pumped by CO_2 laser 78−90415
methanol, far IR laser, intracavity pumped by TE CO_2 laser 80−87382
methanol, far IR laser line obs. and assignment 79−31867
methanol, high power optically pumped CW laser, line assignments 77−54701
methanol, optically pumped, assignment of weak FIR laser lines 80−14320
methanol, optically pumped, far IR gain meas. 78−22114
methanol, optically pumped, far IR laser lines meas. and assignments 79−22939
methanol, optically pumped, laser line assignment 77−54698
methanol, optically pumped CW far IR laser frequency characteristics 77−38873
methanol, optically pumped CW for IR laser lines, freq. meas. 80−58514
methanol, optically pumped CW subMM emission lines 80−95876
methanol, submillimetre laser molecules, Stark and ODR spectroscopy 79−31864
methanol 118 μm laser line, simple accurate method for wavelength meas. 80−106554
methanol 70 and 118 μm laser line diagnostic expts. 80−69387
methanol far IR laser emission spectroscopy 80−58524
methanol far IR laser gas, CW laser pumped, gain 80−69367
methanol laser, CW, optically pumped, 170-μm emission, press. shift 80−106510
methanol optically pumped 118.8 μm laser line, Stark splitting obs. 80−102710
methanol subMM laser line obs. 80−58523
methanol-d_1, CH_2DOH optically pumped CW far IR laser lines and frequencies 80−102707
methanol-d_1, CO_2 laser pumped, CW far IR laser lines 79−76672
methanol-d_3, CO_2 laser pumped, CW far IR laser lines obs., 34.5 to 287 μm 78−71082
methanol-d_3, optically pumped, CW far IR laser lines obs. 78−79005
methanol-d_4, 869 micron laser transition 78−42328
methanol-d_x, optically pumped, new FIR laser lines 79−72553
methanol-d, CO_2 laser pumped, CW laser lines obs. 80−53272
methanol-d, optically pumped CW subMM emission lines 80−95876
methyl alcohol, assignment of submillimetre transitions 79−22943
methyl alcohol, optically pumped, far IR laser line assignment 77−38869
methyl alcohol, optically pumped, new CW FIR laser lines meas. and assignments 80−48224
methyl alcohol high-power optically-pumped CW laser line assignment 77−38868
methyl alcohol IR absorption, diode laser obs. 79−31518

laser transitions continued
methyl alcohol IR transitions, saturated absorption spectroscopy 77−38874
methyl alcohol-d, optically-pumped laser line freqs. 78−55345
methyl cyanide, far IR laser line assignments 80−69380
methyl cyanide submillimetric waveguide laser amplifier design and operation 77−38926
methyl fluoride, deuterated, optically pumped near-MM laser 80−69379
methyl fluoride, optically pumped mirrorless laser at 496 μm 79−31871
methyl fluoride Raman FIR laser, high-intensity CO_2 laser pumping, new emission lines 80−23675
methyl fluoride-d_3, optically pumped sub-MM wave laser 80−23676
methyl halides, candidate transition identification for optically pumped far IR lasers 79−931
methyl mercaptan, CW subMM emission lines, optical pumping 80−87381
methyl nitrile CW for IR mol. laser, optical pumping with $^{16}CO_2$ and $^{18}CO_2$ lasers 80−74343
methylfluoride, CW for IR mol. laser, optical pumping with $^{16}CO_2$ and $^{18}CO_2$ lasers 80−74343
optically pumped laser three-photon transition theory 80−102690
optically pumped lasers utilizing self-terminating transitions, CW stimulated emission possibility 80−14329
optically pumped waveguide gas lasers 78−5490
optically pumped waveguide laser characteristics 77−38870
perylene, vapour phase excitation energy transfer from pyrene 77−12802
plasma flow, spontaneous superradiance of at. and mol. ions 77−3470
plasma laser star model of QSOs 78−96558
polymethine dyes, mol. struct., lasing props. 79−3693
POPOP, polarisation of spontaneous and stimulated radiation 79−31583
POPOP-Ar-N_2, electron beam pumped, intense laser emission at 381 nm 78−74898
propynal, CW for IR mol. laser, optical pumping with $^{16}CO_2$ and $^{18}CO_2$ lasers 80−74343
pulse duration increase in self-limiting transitions *(Russian)* 78−33719
pumping, quasi-reson. energy and charge exchange processes, new transitions 80−58526
quantum optics, transition phenomena, review 80−32944
p-quaterphenyl, polarisation of spontaneous and stimulated radiation 79−31583
p-quaterphenyl vapour laser, optically excited, laser action obs. at 350 nm 79−7123
rare earths in vapour and solid phases as high intensity lasers, laser line prediction 79−3700
recombination lasers using elemental vap., metal ion transitions 78−17923
recombination lasers using elemental vap., stimulated emission conditions 78−17922
rhodamine 6G, fluoresc. polaris. spectra in glycerol soln. 79−76458
rhodamine 6G dye laser, induced radiation spectral characts., effect of vibr. relax. 80−64008
rhodamine G, in glycerine-H_2O mixture, fluoresc. polarisation spectra, 350 and 540 nm excitation 79−98139
ring laser gyro, anomalous dispersion and gas flow effects 79−98430
ring laser gyro, dispersion and gas flow effects 80−1267
ruby, far IR lasing feasibility, pumping via ruby laser 79−81435
self-pulsing instability of single mode laser, critical pumping parameter 77−7055
semiconductor diode laser, IR, for 16 μm range, review *(Rumanian)* 80−87408
simultaneous oscillation of competing laser transitions, time multiplexing 78−37869
solid laser, freq. spectrum, linear atom-field interaction 77−19258
solid state lasers, book contrib. 80−106529
submillimetre wavelength tables for gas lasers, 34 μm to 1.965 mm 77−7095
p-terphenyl, substituted, dye laser and spectral characts., output power, conversion efficiency 80−23681
tesla discharge as spectroscopic source for excimer laser transitions study 80−274
tetrafluoromethane molecule, laser spectrosc. and optical pumping from CO_2 laser 80−74202
threshold range, qualitative change determ., analogy with phase transition *(Czech)* 80−32949
TOPOT, polarisation of spontaneous and stimulated radiation 79−31583
two-photon laser, atomic transitions, semiclassical stochastic description 79−76657
UV ion lasers, metal-inert gas charge transfer reaction 78−66809
UV molecular lasers with transverse electronic pumping, review *(French)* 79−31880
XUV lasing, gain-verification problem 78−71086
Zeeman laser, two-transitions with common upper level *(Japanese)* 79−55112
Ag, hollow cathode discharges, IR transitions, discharge conditions, excitation mechanisms 79−68383
Ag II, 1 W multiline output power from 800.4, 825.5, 840.4 nm transitions 78−82953
Ag II, discharge in hollow cathode, new IR transitions 77−661
Ag II, in He-Ag, Ne-Ag mixtures, unidentified laser transitions as Lyman, spectrometer ghosts 78−5464
Ag-He CW mW-level laser source at 224 nm 80−43352
Ag-He discharges, new ion laser transitions in near IR region, CW excitation 79−59673
Al II near IR laser transitions, large diameter hollow cathode Ne-Al discharge 80−102715
$Al_xGa_{1-x}As$-GaAs, p-n heterojunction laser, low temp. operation 80−1204
$Al_xGa_{1-x}As$-GaAs, p-n heterostruct. laser, tunnel injection and phonon-assisted recomb. 80−5733
Ar, CW oscillation of 5062 Å line, reln. to laser Raman spectroscopy 80−1186
Ar, CW UV emission, power enhancement 78−17906
Ar I, high press. tunable laser emitting at 0.91 μm 78−50755
Ar II, lower laser levels, natural lifetime determ. 77−6724
Ar III, CW laser, short wavelength multiline performance 79−926
Ar laser, new IR laser transitions, 3.725 to 17.233 μm, 5.804 μm laser line identification 80−87374
Ar, line strength calcs. for 6s-5p and 3d-4p transitions 77−14384
Ar, recomb. laser in expanding CO_2 laser prod. plasma, 1.79 μm laser oscill. 77−88698

laser transitions continued
Ar-Kr-F_2 mixture, electron beam pumped, spectroscopy and kinetics of 248, 414 nm bands 78−63081
Ar-N_2, electron-beam-excited laser lines at 337.1, 357.7, and 380.5 nm, gain conditions 79−86166
Ar-N_2, proton beam pumped, laser actqn at 3577 Å 80−9861
Ar-N_2 mixture, electron beam pumped, lasing obs. at 337, 358, 380 and 406 nm 80−102700
Ar-N_2 mixture, lasing at four lines 80−99713
Ar-Xe high press. transverse discharge laser using Xe IR transitions 80−63978
Ar-Xe high-press. neutral IR laser emission from Xe 79−86159
ArF excimer, electronic structure, pot. energy curves, radiative transition probabilities, quantum mech. calcs. 79−10284
ArF^*, laser expts. on $^2\Sigma$-$^2\Sigma$ transitions 78−63080
As^+, CW laser oscill. on transitions in He-AsH_3 gas discharges 80−38004
Au hollow cathode laser, ion laser transitions 80−69366
Au II, ion laser transitions in He-Au mixture, 253.3 to 763.5 nm 77−7071
Au vapour brightness amplifier at 627.8 nm, for projection microscope 80−83616
Au vapour laser, 627.8 nm UV emission, average output power and efficiency 79−45933
Au-He CW mW-level laser source at 280 nm 80−43352
Au-He discharges, new ion laser transitions in near IR region, CW excitation 79−59673
Ba vapour laser, energy characts. at 1.5 μm 79−13953
Ba vapour laser, pulsed lasing due to 1.13, 1.5 μm atomic transitions 80−53276
Ba-N_2O flame, candidate chem. laser reactions, intracavity dye laser absorpt. meas. 78−63108
Ba-Tl laser optically pumped by pair-absorption transitions, 1.5 μm emission obs. 80−58517
Bi atom, pulse stimulated emission of 472.2 nm line 78−17920
Bi pulsed laser, stimulated emission mechanism at 472.2 nm 80−19022
Bi_2, optically pumped continuous laser oscill. 79−933
Br electronic transition chemical laser, stimulated emission at 3685 cm^{-1} 79−27249
Br, IR laser action using pulsed microwave discharge, Br_2 source gas 80−48233
Br ion UV laser transitions, performance and spectroscopy 78−22111
Br_2, optically pumped at 532 nm, lasing obs. in visible and near IR 78−63094
Br_2, UV laser transitions, electronic designation 79−944
C, atomic. in He-CO(CO_2) mixtures, direct nuclear pumped, laser action obs. 78−5460
C, IR laser action using pulsed microwave discharge, CO_2, CO and CF_4 source gases 80−48233
C ion impurity in linear Z-pinch He plasma, outer 2s-shell electron excitation emission 78−22113
C VI, n=3 and n=2 levels population inversion, possible extreme UV laser 77−7073
C VI, XUV gain in expanding cylindrical plasma 77−15170
CF_4 laser, for 16 μm range, review *(Rumanian)* 80−87408
CO, and isotopic forms, laser freqs., Dunham coeffs. 79−64207
CO, CW laser , vibration-rotation transitions 77−27292
CO cooled electron-beam-controlled laser, two-quantum transitions 79−45935
CO discharge lasers, low transitions, theory and expt. 77−3568
CO, elec. excited overtone bands lasing at 2.7 to 3.1 μm 78−13684
CO electric discharge laser using single vibr.-rot. transition, laser line selection 79−59687
CO laser, analytical theory, multilevel cascade emission *(Chinese)* 80−102702
CO laser, CW, with RF excitation in supersonic flow 80−74375
CO laser, liq. N_2 cooled, extended spectral distrib. of lasing transitions 79−89894
CO laser, multiphoton amplification, HF removal of forbiddenness *(Russian)* 80−53262
CO laser lines, spectral coincidences with NO absorpt. lines 79−86162
CO pulsed laser, stimulated emission dynamics, transition lines for isotope enrichment 80−48225
CO room temperature nuclear pumped laser, parameter optimisation and spectral props. obs. 80−63995
CO, $X^1\Sigma^+$ state elec. dipole moment function, transitions, vibr.-rot. band calcs. 77−14410
CO_2 00^01-10^00 transition in CO-N_2O reacting gas mixture, gain 80−74337
CO_2, 10.17 μm R(32) transition, appl. to He-Ne laser freq. meas. 77−31113
CO_2, 16.5 micron band generation, HF laser pumped, threshold characts. *(Russian)* 77−83846
CO_2, absolute transition freqs. by multiplication of difference-freqs. 78−90445
CO_2 CW sequence laser lines generated using incavity NH_3 cell 79−18438
CO_2, efficiency at 14 and 16 μm 79−59670
CO_2 electric discharge laser, free oscill. stimulated emission, nanosecond pulse duration 79−31860
CO_2 gasdynamic laser, 16 μm radiation, modified Anderson's time-depend. anal. 80−106505
CO_2, gasdynamic laser possibility, transitions between levels of paired modes 79−89885
CO_2, high temp. absorpt. meas. in 10.4 μm laser band 79−36870
CO_2, high-press. laser, gain contribs. from 00°2 and 00°3 sequence bands, theory 78−46565
CO_2 isotope laser transitions, abs. freq. calibration, heterodyne technique 77−19230
CO_2 laser, for 16 μm range, review *(Rumanian)* 80−87408
CO_2 laser, intense high-press. sequence-band 78−33749
CO_2 laser, intracavity IR absorpt. of vinyl chloride, ethylene, and propylene 78−78835
CO_2 laser, multiphoton amplification, HF removal of forbiddenness *(Russian)* 80−53262
CO_2 laser, SF_6 intracavity hysteresis, bistability, critical behaviour onset and extinction of lasing 79−98336
CO_2 laser, transitions, linewidth, temp. depend. 80−69360
CO_2 laser, transverse double-discharge, spectral characts. *(Russian)* 77−656
CO_2, laser hot-band transitions, heterodyne freq. meas. 77−88695

laser transitions continued
CO_2 laser light pulse amplification calc. Fortran program PULSAMP 77−58312
CO_2 laser small-signal gain coefficient calc. 80−78831
CO_2 laser stability and heterodyne frequency calibration 78−59031
CO_2 laser transition absolute freqs. by multiplication of difference freqs. 80−37992
CO_2, laser transitions, rel. to dipole strengths calcs. 77−61937
CO_2 laser transitions, absolute freq. meas. by multiplication of CO_2 difference freq. 80−105618
CO_2 laser with partial population inversion, 16 μm steady state action 79−36873
CO_2 multi-rotational line TEA laser, theoretical model 80−69361
CO_2, optical pumping in stimulated Raman scatt., tunable laser emitting at 14,16 μm, theory 78−46568
CO_2, optically pumped laser, simultaneous lasing in bands of sequence 80−5725
CO_2 oscillating laser transition, band width meas. 79−3677
CO_2 pulsed gas discharge laser, emission on molecular transitions at 14, 16 μm 80−53261
CO_2, sequence band transitions, heterodyne freq. meas. 77−71970
CO_2, sequence bands, laser power and gain meas. 77−79795
CO_2 TE pulsed 4.3 μm laser 79−89926
CO_2, TEA, 4.3-μm radiation pulse generation 80−5724
CO_2 TEA laser, injection mode locking on P and R transitions in 9, 10 μm bands 79−89883
CO_2, TEA laser, intense pulsed lasing at lines of P and R branches of 00^02-$(10^01,02^01)_{II}$ 79−89887
CO_2 TEA laser, multiline operation with CO_2 as intracavity absorber 79−94206
CO_2 TEA laser, sequence band effect on 10.4 μm band multiline oscillation 80−74334
CO_2, transition strength of 00°2 9.4 μm sequence band, appl. to IR isotope anal. 79−18395
CO_2, vibr. distrib., effect of laser radiation 77−34868
CO_2, weak laser lines around 10.6 μm, wavenumber meas. 78−17998
CO_2, weak transitions, freq. and gain meas. using diode laser 77−88693
CO_2/$^{192}OsO_4$ laser, absolute light oscill. freq., universal const. variation meas. possibilities *(Russian)* 80−5723
CO_2-N_2-He laser mixtures, electron swarm parameters, Boltzmann eqn. anal. 79−18396
$^{13}C^{16}O(^{12}C^{18}O)$, freqs. relative to $^{12}C^{16}O$, by Stark spectroscopy of formaldehyde 77−75150
$CO_2(00^01)+Br_2$, vibr. relax. rate consts., rel. to E→V transfer lasers 77−6898
$CO(\nu=1)+Br_2$, vibr. relax. rate consts., rel. to E→V transfer lasers 77−6898
$C^3\Pi_u$ effective lifetime in N and air 80−102704
CS_2 laser, for 16 μm range, review *(Rumanian)* 80−87408
CS_2, laser transition, rel. dipole strengths calcs. 77−61937
$^{13}CS_2$, laser emission at 6.9 μm, HF laser optical pump 78−58995
$^{13}CS_2$, optically pumped by pulsed HF laser, emission obs. at 6.9 μm 79−50283
Ca laser, pumped via collision-induced absorpt. in Ca-inert gas mixture 79−7117
Ca-H_2, single freq. laser, 5.54 μm emission, mag. field tuning 78−46634
Ca-N_2O-CO flame, Ca catalyzed, gain meas., emission band assignment 78−66815
Ca-N_2O-CO flame, candidate chem. laser reactions, intracavity dye laser absorpt. meas. 78−63108
CaF_2:Na, γ-irrad. cryst., spontaneous and induced colour centre emission 79−7131
CaO, tunable optical gain at 3600 Å using F^+ centres 79−45947
Cd hollow cathode laser, ion laser transitions 80−69366
Cd I, plasma recomb. process, laser oscill. at 1.40, 1.43, 1.45 and 1.64 μm 79−94217
Cd^+ in He-CdBr, He-$CdCl_2$ and He-CdI_2 discharges, CW laser oscill. 78−50765
Cd^+, in He-halide discharge, CW oscill. 78−17913
CdHg, positive gain measurements on 470 nm continuum band 78−66805
CdS, submillimetre laser emission due to transitions between free exciton level 79−27261
Ce:LaF_3 286 nm laser, optically pumped 80−99738
Ce:$LiYF_4$, tunable UV laser at 325, 309 nm, KrF laser excitation 80−38022
Ce^{3+}:$LiYF_4$, UV laser at 325 nm, stimulated emission obs. 79−72574
Cl II in CuCl and $FeCl_2$ vapours, pulse generation at 5218 Å, 5221 Å 78−58990
Cl, IR laser action using pulsed microwave discharge, Cl_2, CH_3Cl, CH_2Cl_2 and CCl_4 source gases 80−48233
Cl ion UV laser transitions, performance and spectroscopy 78−22111
Cl VII, transitions in laser heated plasma, intensity anomalies obs. 58 to 78 Å 78−1214
Cl_2, laser oscillation on 2580 Å band system, axial electron beam excitation of He-Cl_2 79−31879
ClF, interhalogen UV laser on 285 nm band, fluoresc. and laser oscill. obs. 79−76674
ClF-H_2 chemical laser, HF rot. laser emission 79−98349
ClO_2, CW for IR mol. laser, optical pumping with $^{16}CO_2$ and $^{18}CO_2$ lasers 80−74343
Cr vapour, laser transitions in near IR 80−99704
Cr^{3+}:$BeAl_2O_4$, tunable laser performance, 701 to 794 nm, long-pulse and Q-switch operation 79−72573
Cs-Xe solar-pumped MHD excimer laser, modelling 80−95873
Cs_2, fluoresc. spectra, kinetics, laser candidate 79−64027
Cu, Doppler-free laser spectroscopy in hollow cathode discharge 80−9537
Cu hollow cathode discharges, IR transitions, discharge conditions, excitation mechanisms 79−68383
Cu hollow cathode laser, ion laser transitions 80−69366
Cu II, 1 W continuous output from 780.8 nm transition 78−82953
Cu II, in Ne-Cu hollow cathode discharge, CW laser oscill. at 2703 Å 78−13689
Cu II laser, UV, operating period extension by Ar admixture 80−74342
Cu II laser with cylindrical hollow cathodes, UV performance 80−102709
Cu, laser action on 5106, 5782 Å lines in copper acetylacetonate, $Cu(NO_3)_2$ vapours 77−88712
Cu laser line structure at 510.6, 578.2 nm 80−53274
laser transitions continued
Cu vapour, comparison of copper acetate, acetylacetonate and CuCl lasants 79−31875
Cu vapour laser, fabrication, green and yellow emission *(French)* 80−43360
Cu^+ transitions in He-Cu halide gas discharges, CW laser oscill. 79−7116
Cu-He discharges, new ion laser transitions in near IR region, CW excitation 79−59673
Cu-Ne CW mW-level laser source at 250 nm 80−43352
DCN, 250 mW continuous discharge laser at 195 μm 79−31949
DCN waveguide lasers, optimised 190/195 μm, amplifying medium characts. 80−99709
D_2O, 385 μm transition, laser pumped mol. laser theory 79−36868
D_2O, angular correlation between far IR emission and CO_2 pump radiation, Dicke superradiance theory 79−41370
D_2O, candidate transition identification for optically pumped far IR lasers 79−931
D_2O, far IR CW laser emission by optical pumping 79−3687
D_2O, far IR laser, intracavity pumped by TE CO_2 laser 80−87382
D_2O, far IR superradiant laser, 114, 66 μm emission, time-resolved pulse and wavelength meas. 77−88715
D_2O, laser, emission characteristics at 50, 66, 83, 111 and 116 μm 80−58525
D_2O laser pumped molecular lasers, sub MM laser expts. 80−1192
D_2O, optically pumped, superradiant line obs., 235, 280, 97 and 98 μm 78−1215
D_2O optically pumped mirrorless laser at 385 μm 79−31871
D_2O vapour high-power 385 μm laser oscillator 80−69422
D_20, near-MM-wave laser synchronous pumping, ultrashort pulse generation at 385, 66 μm 80−102705
Dy^{3+}:oxide glass, intensity parameters and laser transitions 79−50300
dye solution output conversion of Cu vapour laser to 5782 Å 80−48241
Er^{3+} implanted crystals, laser active media, nonradiative losses due to $^4I_{11/2}$-$^4I_{13/2}$ transition 79−31911
Er^{3+}:CaF_2 crystal laser, hologram form. at 2.76 μm, laser emission linewidth meas. 79−10270
Er^{3+}:$Gd_3Ga_5O_{12}$, stimulated emission 79−91466
Er^{3+}:YErAG, $^4I_{11/2}$ to $^4I_{13/2}$ laser transition cross section, luminesc. energy 77−79833
$Er_3Al_{5-x}Ga_xO_{12}$, LPE, spectroscopic props. 80−93419
Eu atoms and ions, self-terminating lasers, energy and time characts. 77−75493
Eu^+ metastable states in discharge plasma, anomalously high speed deexcitation, modulation of induced radiation obs. 80−44014
F, at. transition intensities, press. depend. 77−659
F atomic laser, doublet and quartet transitions, spectral press. depend. 77−58318
F ion UV laser transitions, performance and spectroscopy 78−22111
F_2 discharge pumped laser, 1578 Å emission 79−31877
F_2, valence electronic states, $^1\Pi_u$←$X^1\Sigma_g^+$ absorption spectrum 79−63920
F_2-He, high-press. mixture, neutral atomic F laser lines 79−86167
FCN, CW for IR mol. laser, optical pumping with $^{16}CO_2$ and $^{18}CO_2$ lasers 80−74343
Fe vapour laser, 4529 Å emission 79−10282
GaAlAs DH laser, stripe geometry, spatially resolved emission 79−27257
GaAs, permittivity at laser transitions freq., excess carriers effect 77−14719
GaAs-$Al_xGa_{1-x}As$ current injection multi-quantum-well heterostructure lasers, MBE grown 80−19042
GaInAsP/InP, DH laser, low threshold current density, 1.3 μm emission 79−94249
GaInAsP/InP DH lasers emitting at 1.3 μm, growth and characts. 80−64057
GaInAsP/InP DH stripe geometry lasers emitting at 1.3 μm, growth characterisation 80−69410
GaInAsP/InP DH lasers, 1.3 μm wavelength, LPE growth and characterisation 80−69411
GaInAsP-InP buried heterostructure lasers, 1.6 μm wavelength 80−64055
$Ga_xIn_{1-x}As_ySb_{1-y}$ laser, efficient room temp. stimulated emission, 1.8 to 2.4 μm spectral range 79−10307
$GdAlO_3$:Er^{3+}, $^4S_{3/2}$ to $^4I_{9/2}$ transition laser action, optical and luminescence spectra 80−16082
Ge^{3+}:YAG, excited state absorpt. loss, 5d→4f rare earth lasers 78−90417
GeF, use in chemical lasers 80−64004
H, maser hyperfine transition, affected by coherently excited Zeeman transitions 79−72544
H, population inversion obs. in FM-1 spherator 77−7048
HBr, laser emission at 4 μm based on chem. generation of Br atoms 80−9878
HCCF, CW for IR mol. laser, optical pumping with $^{16}CO_2$ and $^{18}CO_2$ lasers 80−74343
HCN far-IR laser, chem. pumping, 337 μm and 311 μm stimulated emission obs. 79−13958
HCN, $H^{15}CN$, far IR laser transition assignments 78−46579
HCl, 3.8 μm, 10.6 μm CW laser emission based upon Cl atom chem. generation 79−947
HCl pulsed chem. laser, plane and helical electrode types, expt. study and modelling 80−32973
HCl-He, discharge, possible laser action on vibr. transitions 80−14332
HD, vibr.-rot. transitions, possible laser appl. 79−55122
HF chemical TE laser, 16 μm emission 80−83600
HF, double-discharge chem. laser, transitions in SF_6-C_3H_8 mixture, temporal characteristics 80−53282
HF in absorption, anomalous dispersion meas. 80−95881
HF, modelling, Lorentz broadening 77−79813
HF premixed chain reaction CW laser, spectral output 80−95882
HF, pure rotational, from exploding-wire metal atom oxidation lasers 77−14701
HF, rot. population transfer using IR-laser double-resonance expt. 79−55128
H_2O, CW laser, characts. at 118 and 28 μm 79−81411
H_2O, electronic-vibr. energy transfer from $Br(4^2P_{1/2})$, 12 laser transitions 7 to 7.7 μm 77−31094
H_2O-H_2 cooling in supersonic nozzle, submillimetre wave generation 80−48229
Hd-Cd hollow cathode laser in mag. field, Cd II stimulated emission 78−79002

laser transitions continued
He II, shock tube generated plasma ions, 1640 Å lasing on Balmer-α line 77−58317
He-Ar high voltage hollow cathode discharge, new Kr II CW laser lines new Ar II CW laser lines 79−13947
He-Ar hollow cathode discharge, laser generation on Ar II 4765 Å line 80−23671
He-As CW laser, excitation mechanism 79−3685
He-Au, UV ion laser, dominant transition at 280 nm 79−942
He-Cd bipolar hollow-cathode laser, 441.6, 533.7 and 537.8 nm Cd ion lines 79−50319
He-Cd hollow cathode laser, axial mag. field effect on oscills. 79−59681
He-Cd II, 0.5378 μm oscill. spectra meas. using scanning interferometer *(Japanese)* 80−9864
He-Cd II hollow-cathode laser, 4416 Å pulse oscillation 79−7122
He-Cd II laser, power interaction of laser lines 80−9862
He-Cd II lasers, positive column, hollow cathode types, 4416 Å oscill. charact. *(Japanese)* 78−94392
He-Cd positive-column laser discharge, excitation mechanisms from radial profiles 77−68205
He-Cd single-mode laser, linewidth meas. and population calc. 77−14694
He-Cd^+ cataphoretic laser, freq. fluctuations of 4416, 3250 Å lines 79−72556
He-Cd^+ laser plasma, interferometric anal. of spectral lines 77−10892
He-Cu hollow cathode discharge, Cu II CW laser oscill. at 8096 Å 79−31878
He-F, doublet series laser lines near 700 μm, hyperfine splitting and broadening meas. 78−63070
He-I_2 laser, sequential separate multicolour output operation *(Japanese)* 80−28205
He-Kr HV hollow cathode laser, gain meas. of Kr II 4694 Å, 4318 Å CW transitions 79−45928
He-Kr high voltage hollow cathode discharge, new Kr II CW laser lines 79−13947
He-Kr hollow cathode CW laser, Kr II 4584 Å generation 80−58510
He-Kr hollow-cathode discharge, CW laser oscills. on Kr II 4694 Å, 4318 Å lines 79−3680
He-Kr hollow-cathode dischage, CW and pulsed lasing at Kr ion lines 79−3679
He-Kr(Ar)(Xe), ion laser transitions, hollow cathode excitation 80−1184
He-metal vapour lasers, positive column electron densities, experimental study *(Japanese)* 80−69376
He-Ne, 1.15 μm laser line, 260 THz freq. synthesis using $CdGeAs_2$, Ag_3AsS_3 crysts. 79−64263
He-Ne, laser pumping transition, mol. beam obs. 77−7064
He-Ne, Ne transitions, 1.52 μm and 633 nm, mode crossing resonance shape 79−18163
He-Ne, six new transitions near 1.49 μm 77−38856
He-Ne discharge, 3071, 5665 and 10353 nm. laser transitions 77−54692
He-Ne laser, 60 mW, perturbation spectroscopy *(Rumanian)* 78−50752
He-Ne laser, double reson., RF mag. field strength and g-value depend. *(Japanese)* 78−9359
He-Ne laser, Ne $3s_2$-$2p_4$ transition, relaxation charact. of degenerate states obs. using polarisation spectroscopy *(Russian)* 80−27348
He-Ne laser, operating on 0.63, 3.39 μm coupled transitions, intensity modulation 80−69365
He-Ne laser, simultaneous oscillation at 0.63 and 3.39 μm, output power depend. on loss in mag. fields *(Japanese)* 80−32959
He-Ne laser, spatial anisotropy induced by cascade laser transitions 78−29931
He-Ne laser, two-photon amplification on cascade-transitions, power tuning curve meas. 80−48219
He-Ne laser fluctuation spectra of freq. and amplitude 78−82950
He-Ne lasers, in hollow Cu cathode, 632.8 nm output charact. 80−63975
He-Ne nuclear-pumped CW lasing 80−48216
He-Ne ring laser, nonlinear spectroscopic technique 80−91819
He-Ne-Xe, ion laser transitions, hollow cathode excitation 80−1184
He-Ne-methane stabilised ring laser, freq. stability calcs. *(Russian)* 78−9401
He-Sr laser, possibility of nucl. pumping, 4305 Å Sr II transition 80−58518
He-Xe, high-press. neutral IR laser emission from Xe 79−86159
He-Zn, hollow cathode laser discharge, selective excitation of 5894, 7479 Å transitions by Ar 77−27280
He-Zn, hollow cathode laser, gain meas. for 7588, 4924, 7479 and 5894 Å Zn^+ transitions 77−88713
He-Zn, hollow cathode laser tube, Zn II 7588 Å laser line *(Japanese)* 79−76704
He-Zn hollow cathode laser, 7588 Å in ZnII, operating charact. and upper level operating mech. 78−63071
He-Zn hollow cathode laser discharge, radiative cascade excitation effect on upper laser levels 80−102697
He-Zn hollow-cathode discharge, excitation processes, rel. to Zn II laser 79−98342
He-Zn II, 0.4924 μm oscill. spectra meas. using scanning interferometer *(Japanese)* 80−9864
^{3}He-Ar (Xe)(Kr)(Cl), volume pumped nuclear laser, survey of lasing 80−63979
^{3}He-Ar nuclear pumped laser, first order model, lasing action depend. on Ar conc. 79−76668
Hg, lifetimes and cross sections of depolaris. collisions of laser working levels 79−76387
Hg-N_2, optically pumped pulsed 546.1 nm laser emission 79−13952
HgBr, 502 nm stimulated emission, prolonged optical pumping of $HgBr_2$ 79−18414
HgBr, ab initio CI calcs., spectroscopic parameters 79−72245
HgBr, $B^2\Sigma_{1/2}^+ \rightarrow X^2\sigma_{1/2}^+$ band at 5018 Å 77−83856
HgBr, B→X transition radiative lifetime, charge transfer model 78−17719
HgBr, laser action on B→X bands, 5018 Å 77−88709
HgBr radical, laser action by $HgBr_2$ photodissociation, 502 to 505 nm 78−13695
HgBr, visible laser transitions at 5018 Å and 4984 Å 79−939
HgBr(B→X), vibr. relax., level deactivation 80−63697
HgCl, ab initio CI calcs., spectroscopic parameters 79−72245
HgCl, B→X transition radiative lifetime, charge transfer model 78−17719
HgCl, laser action on B→X bands, 5576 Å 77−88709
HgCl, photodissociation calcs., laser efficiency 80−48047
HgCl, visible laser transition at 5576 Å 79−939
HgCl*, laser action using electron-beam-controlled discharge pumping 78−42325
HgI, B→X transition radiative lifetime, charge transfer model 78−17719
HgTl excimer laser, kinetics, optical excitation obs. 80−58527
$Hg^+(7^2P_{1/2}, 7^2P_{3/2})$, excitation processes in Hg-He afterglow, rate consts. *(Russian)* 78−29848
Ho:$LiYF_4$, 750 nm laser oscill., flashlamp and dye laser pumping 78−9386
Ho^{3+}:$Gd_3Ga_5O_{12}$, stimulated emission and Ho^{3+} cascade laser action 79−91466
Ho^{3+}:$LiYF_4$, 1.392, 1.673 and 3.914 μm stimulated emission, laser cascades 80−9886
Ho^{3+}:$LiYbF_4$. laser converter for 2.06 μm radiation, ND primary laser 79−18427
Ho^{3+}:YAG, 2.09 μm stimulated emission, resonant pumping by Nd laser 78−17944
I, $^2P_{1/2}$ state, relax. between hyperfine levels 80−18880
I, $^2P_{1/2}(F=3) \rightarrow {}^2P_{3/2}(F'=4)$ transition, stimulated emission cross section determ. 79−13961
I, 1.315 μm, oscill. freq. selection hyperfine transition 77−10952
I, dye laser pumped to dissoc. point of I_2, laser action 78−63064
I I,II, radiative lifetime meas., rel. to I and He-I^+ laser transitions 79−54810
I photodissociation laser, press. induced freq. shifts 78−37875
I, photodissociation laser, 1.315 μm transition line struct. 78−59000
I, Q-switched, emission at two frequencies 79−18413
I_2, A-X system 79−63995
I_2, CW, optically pumped, performance 78−17912
I_2, CW optically pumped, laser oscill. 0.57 to 1.35 μm 79−943
I_2, efficient laser action on 342 nm band, ArF laser pumping 80−99703
I_2 laser, three-level, pumped by CW dye laser 80−63993
I_2 molecule B-X electron transition during Cu vapour laser optical pumping *(Russian)* 80−78845
I_2 molecule pumped by Cu vapour laser, pulsed stimulated emission due to electronic transitions 80−14330
I_2, optically pumped, lasing obs. on 342 nm band 78−79008
I_2, optically pumped laser, I_2 transition moment from gain 79−54917
I_2, UV laser transitions, electronic designation 79−944
I_2+Ar(Ne)(tetrafluoromethane), D-state lifetime and UV laser action 77−14471
IBr:CO_2 photolysis, electron-vibr. pumping, 2.7 μm Br and 4.3, 10.6 μm CO_2 laser transitions 80−28196
$InAs_xSb_yP_{1-x-y}$, efficient electron-beam-pumped laser at 3.1-3.7 μm 80−5738
InGaAsP, injection heterojunction laser at 1.3-1.5 μm 79−89910
InGaAsP single-mode CW ridge-waveguide laser emitting at 1.55 micron 80−58584
InGaAsP-InP DH laser, optical gain meas., low-intensity luminesc. and absorpt. spectra 79−98356
InGaAsSb based injection heterolaser, 1.9 μm stimulated emission 79−18420
$In_{1-x}Ga_xP_{1-z}As_z$, visible spectrum laser diode, continuous operation, 6280 Å, 77K 79−960
InKr, low-lying electronic states, PE curves, transition moments, emission coeffs. 79−6894
KF, tunable CW laser, using F_2^+ centres for 1.26-1.48 and 0.82-1.07 μm bands 78−79023
$K_5Nd(MoO_4)_4$, spectral and struct. props. *(Russian)* 79−52020
$KNdP_4O_{12}$ epitaxially grown waveguide, laser operation at 1.051 μm 79−18423
Kr, CW UV emission, power enhancement 78−17906
Kr III, CW laser, short wavelength multiline performance 79−926
Kr IV, very strong laser emission at 195.027, 175.641 nm 78−63060
Kr laser, new IR laser transitions, 3.725 to 17.233 μm 80−87374
Kr, line strength calcs. for 7s-6p and 4d-5p transitions 77−14384
Kr, nucl. pumping by volumetric $^3He(n,p)^3H$ reaction in He-Kr 77−10886
Kr, recomb. laser in expanding CO_2 laser prod. plasma, 3.07 μm laser oscill. 77−88698
KrCl, laser expts. on $^2\Sigma$-$^2\Sigma$ transitions 78−63080
KrF, discharge excited laser operation at elevated temps., transitions, output power 80−43359
KrF, electron beam pumped laser medium, time depend. fluoresc. spectrum in high current density range 80−78842
KrF, Kr_2F, in electron beam pumped Ar-Kr-F_2 mixture, spectroscopy and kinetics of 248, 414 nm bands 78−63081
KrF laser, collisional coupling between B, C, D states from fluoresc. meas., influence on energy extraction 80−1189
KrF, radiative lifetime and quenching 78−63063
Li I laser, 207 Å, oscillator strengths 80−83598
Li III, shock tube generated plasma ions, 729 Å lasing on Balmer-α line 77−58317
Li-$La_{1-x}Nd_x$ phosphate glasses, stimulated emission spectroscopy of $^4F_{3/2}$ to $^4I_{11/2}$ and $^4F_{3/2}$ to $^4I_{13/2}$ transitions 79−38573
$LiBi_xNd_{1-x}P_4O_{12}$ waveguide laser layer, LPE grown, CW laser oscill. at 1.05 μm 80−23709
LiF, coherent freq. tunable radiation generation in F-centres, 0.6 to 1.26 μm range 79−36902
LiF, laser action of M-centres at 700 nm 78−82972
$LiNd(PO_3)_4$ laser with external and Fabry-Perot resonators, 1.05, 1.32 μm CW oscill. 80−23693
$LiNdP_4O_{12}$, simultaneous oscillations of different transitions in lasers 79−22927
$LuAlO_3$:Er^{3+}, $^4S_{3/2}$ to $^4I_{9/2}$ transition laser action, optical and luminescence spectra 80−16082
Mg-N_2O-CO flame, Mg catalyzed, gain meas., emission band assignment 78−66815
Mn, self-terminating vapour laser, max. pulse repetition freq. 80−23677
$MnCl_2$ vapour laser, output spectrum as function of excitation conditions 79−68387
N I, laser transition obs. at 9064 Å in He-N_2 afterglow 78−74891
N ion impurity in linear Z-pinch He plasma, outer 2s-shell electron excitation emission 78−22113
N_2, 337.1 nm emission, high specific power, high pulse repetition freq. 79−45932
N_2, energy transfer from Ar, 3371 and 3577 Å laser emission, kinetic model 78−5465
N_2, IR, excitation mechanism *(Japanese)* 80−83594
N_2, IR laser transition, excitation process 80−87383

laser transitions continued
N_2 laser, 406 nm emission on C→B band 80−64047
N_2 laser 337.1 nm transition, rotational struct. variation 80−78836
N_2 laser near-threshold IR enhancement by He additive *(Japanese)* 80−14324
N_2 laser transitions, $Ar(^3P_2)+N_2(C^3\Pi_u)$ excitation transfer cross section, radiative lifetime 79−27246
N_2 molecule ω→a, a→a′ electron transitions, strong near IR generation *(Russian)* 79−76676
N_2, photostabilised UV laser, gain, fluoresc., and energy extraction charcts. 79−7118
N_2, transverse excited $C^3\Pi_u \rightarrow B^3\Pi_g$(0-0) UV laser band, spectroscopic rot. anal. 79−7115
N_2, transverse excited $C^3\Pi_u$-$B^3\Pi_g$ (0-0) UV laser band, spectroscopic analysis 79−76671
N_2-Ar, stimulated emission obs. at 337.1, 357.7 and 380.5 nm 78−17925
N_2-F_2 mixture, fast Blumlein discharge excited, intense 3371 Å laser emission 79−41365
NH, pure rot. lasing after flash photolysis of HN_3 79−86175
NH_3 12.08 and 12.81 μm transitions using unstable resonator CO_2 laser pump 80−53327
NH_3, 12.08 μm emission, CO_2 laser pumped, temp. depend. 78−46582
NH_3 CW far IR laser lines, CO_2 laser pumping and Stark tuning 80−69382
NH_3 CW far IR laser lines, CO_2 laser pumping and Stark tuning 80−106508
NH_3, far IR emissions by IR pumping using N_2O laser 80−74345
NH_3, far IR emissions from forbidden transitions, using Stark effect with CO_2 laser pumping 79−86168
NH_3, IR and far IR laser emissions, using TE CO_2 laser pump 79−934
NH_3 inverse level doubling mol., space and combined parity nonconservation *(Russian)* 80−52879
NH_3 laser, for 16 μm range, review *(Rumanian)* 80−87408
NH_3 laser, high energy output in 13 μm region, CO_2 laser pump 79−89927
NH_3, multiline IR emissions, appl. for InSb Raman laser pumping 79−94216
NH_3, near-MM-wave laser synchronous pumping, ultrashort pulse generation at 151 μm 80−102705
NH_3, two photon excited 16 μm laser 78−58986
NH_3, two-photon-excited, 16μm emission, wavelength meas. technique 78−71085
$^{14}NH_3$, CW far IR lasing using Stark tuning 79−81407
$^{14}NH_3$, far IR CW laser emission by optical pumping 79−3687
$^{15}NH_3$ far IR laser emission at 153, 375 μm, optically pumped by $^{13}C^{16}O_2$ laser 80−58507
$^{15}NH_3$, optically pumped by CW sequence band CO_2 laser, far IR laser emission 78−46578
NO, electronic-vibr. energy transfer from $Br(4^2P_{1/2})$, 5.5 μm transition 77−31094
N_2O, electronic-vibr. energy transfer from $Br(4^2P_{1/2})$, 10.9 μm transition 77−31094
N_2O isotopes, laser transitions near 4.6 μm, HF laser optical pump 78−58995
N_2O, new lines in 10 μm region, rot.-vibr. transitions in $(00^02\text{-}10^01)$ band 77−27281
$^{15}N_2O$, $^{14}N^{15}NO$, $^{15}N^{14}NO$, optically pumped by pulsed HF laser, emission obs. at 4.6 μm 79−50283
NOCl laser, for 16 μm range, review *(Rumanian)* 80−87408
$^{14}NH_3$, high power vibr.-rot. emission, optically pumped off reson. 77−7068
$^{14}NH_3$, laser emission at 16 μm by two-quantum excitation of $2\nu^-_2(7,5)$ state 79−86165
$^{15}NH_3$, far IR laser lines, optically pumped by CO_2 laser 78−90415
Na, in shock heated salt vapour, anomalous emission from atomic lines 78−63089
Na:CaF_2, tunable room temp. laser action of M-centres, luminesc. and absorpt. spectra 79−31907
Na:SrF_2, tunable room temp. laser action of M-centres, luminesc. and absorpt. spectra 79−31907
Na_2, continuous laser oscill., optical pumping 77−88706
Na_2, laser excited broadband violet emission, 420 to 457 nm 78−79006
$Na_2NdPb_6(PO_4)_6Cl_2$, self-activated mini-laser material, quantum yield determ. 79−33773
$Na_2Nd_2Pb_6(PO_4)_6Cl_2$, high-Nd conc. laser material, oscillator strengths and laser effect 79−55140
Nd:$CaY_2Ge_3O_{12}$, energy levels and laser action, fluoresc. meas. 79−81438
Nd:$CaY_2Mg_2Ge_3O_{12}$, CW room temp. laser operation, 0.941 and 1.059μm 78−66842
Nd:$CaY_3Mg_2Ge_3O_{12}$, CAMGAR low threshold CW room temp. laser operation at 0.941 μm 78−1234
Nd:glass, gain coeff. for fusion laser amplifier 77−19261
Nd:glass Q-switched laser controlled by external signal, stimulated emission charcts. 79−10312
Nd:$La_2Be_2O_5$, laser crystal properties 77−19260
Nd:Y_2O_3 single crystal fibre laser, room temp. CW operation at 1.07 and 1.35 μm 78−63121
Nd:YAG, laser transition cross sections, modulation *(Chinese)* 78−90418
Nd:YAG, mode locked oscillator, operation at 1.052 μm 80−33017
Nd^{3+}: crystal, laser transitions intensities 79−78062
Nd^{3+}:glass, fluoresc. line narrowing, hole burning and ion-ion energy transfer 79−89912
Nd^{3+}:glass, laser props., uncorrelated inhomogeneous broadening of 1.06 μm band induced luminesc. quenching 79−31914
Nd^{3+}:$LiNd_{0.3}La_{0.7}$ phosphate glass, stimulated emission charcts. 79−18426
Nd^{3+}:$LiYF_4$, pulsed free running laser action at 1053, 1046 nm, passive mode locking *(French)* 78−79048
Nd^{3+}:$POCl_3$-$SnCl_4$ laser, relaxation oscillations with high power spikes obs. 78−42331
Nd^{3+}:YAG, 1.05 to 1.44 μm tunable high-power laser emission on 18 CW transitions 77−88727
Nd^{3+}:$YAlO_3$, $^4F_{3/2}\rightarrow{}^4I_{13/2}$ transition, stimulated emission wavelength, continuous tuning 77−58334
Nd^{3+}:YVO_4, absorption and fluoresc. spectra of laser states 77−38900
Nd^{3+}:YaG, multiplet splitting, effective ligand point-charge model calcs. 77−76779
$NdAl_3(BO_3)_4$, cw laser action at 1.3 μm 79−27258
laser transitions continued
$NdAl_3B_4O_{12}$, self-activated mini-laser material, quantum yield determ. 79−33773
$NdAl_3(BO_3)_4$ miniaturised crystals with directly applied mirrors, laser emission 79−22958
NdP_5O_{14}, cw laser action at 1.3 μm 79−27258
NdP_5O_{14} laser, flashlamp excited, emission cross section at 1.32 μm 79−59701
NdP_5O_{14}, self-activated mini-laser material, quantum yield determ. 79−33773
$Nd_{1-x}Y_xP_5O_{14}$, laser emission at 1.32 μm, Ar laser pump source 79−31909
Ne, $3s_2$-$2p_4$ and $3s_2$-$3p_4$ coupled transitions, sensitivity to discharge current fluctuations 77−75484
Ne 6328 Å laser transition, homogeneous saturation due to collisions, weak collision model 78−78995
Ne II, long pulse UV laser emission, electron beam excited Ne-NF_3 mixture 78−78996
Ne laser line, 260 THz, direct freq. meas. 80−53266
Ne like multiply charged ion transitions, stimulated emission possibility in far UV 79−10292
Ne, population inversion mechanism between 4p→3d, laser generation conditions 80−1185
Ne, radial profiles of upper and lower level emission 77−31088
Ne-Ag_2 UV ion laser, dominant transition at 318 nm 79−942
Ne-Al^+, hollow-cathode laser, five Al II transitions 358 to 747 nm 77−58316
Ne-Cu, UV ion laser, dominant transition at 260 nm 79−942
Ne-Tl hollow-cathode discharge, CW laser generation on Tl II 594.9 nm line 79−76675
Ne-TlCl hollow-cathode discharge, CW laser oscill. on 594.9, 695.1 nm Tl^+ transitions 80−23674
Ni I 1.3968 μm laser transition in hollow cathode discharge 79−81409
Ni II, laser oscill. at 796.24, 797.54 nm in hollow cathode discharge 79−86161
Ni:MgF_2, efficient CW optically pumped laser, 1.63 to 1.75 μm operation 79−18425
O atoms, two-photon absorpt., auroral transition relax. obs. *(Japanese)* 80−47954
O ion impurity in linear Z-pinch He plasma, outer 2s-shell electron excitation emission 78−22113
O_2, possible high energy laser at 1.27 μm 79−13950
OCS laser, for 16 μm range, review *(Rumanian)* 80−87408
OCS, optically pumped CW subMM emission lines 80−95876
OCS-N_2-SF_6 mixture laser, OCS photodissociation, electron dipole forbidden transition, absorpt. spectra 79−68389
PH_3, laser emission 83 to 223 μm region, laser line assignments 78−71084
Pb atomic photodissociation laser, 405.8, 368.3, 364.0 nm emission lines 80−87387
Pb pulsed 722.9 nm laser with double-section gas-discharge tube 80−9902
Pb self-terminating vapour laser, max. pulse repetition freq. 80−23677
Pb vapour, long-lived sealed-off laser design, 7229 Å emission 78−50808
Pb^+ high-gain laser populated by direct electron excitation, 1.159 μm transition 80−37997
Pb-He discharge, excitation process, Pb^+ emission lines 78−66803
Pr^{3+}:oxide glass, intensity parameters and laser transitions 79−50300
PrF_3, laser action of Pr^{3+} 80−95901
$Pr_xLa_{1-x}P_5O_{14}$, laser emissions, fluoresc. 79−72572
PrP_5O_{14}, laser emissions, fluoresc. 79−72572
$Pr_xY_{1-x}P_5O_{14}$, laser emissions, fluoresc. 79−72572
Rb, in shock heated salt vapour, anomalous emission from atomic lines 78−63089
S, IR laser action using pulsed microwave discharge, SF_6 and CS_2 source gases 80−48233
S, IR transitions in SF_6-He discharge 77−79805
S ion UV laser transitions, performance and spectroscopy 78−22111
S_2 laser, optically pumped, lasing obs. 470 to 480 nm 78−63095
S_2, tunable visible and UV laser, $B^3\Sigma_u^-$-$X^3\Sigma_g^-$ transition 77−42522
SF_6 laser, for 16 μm range, review *(Rumanian)* 80−87408
Se, laser action at 489 nm or 777 nm, OCSe photolysis 79−31889
Si, IR laser action using pulsed microwave discharge, SiH_4 source gas 80−48233
SiF, use in chemical lasers 80−64004
Sn hollow cathode laser, emission obs. from Sn II, I transitions 80−106509
SnF, use in chemical lasers 80−64004
Sr atom, laser action mechanism due to 3066.2, 3011.1 nm $4d^3D_{1,2}$-$5pP^0_2$ transitions 80−9869
Sr vapour pulsed laser, power charcts. of laser transitions in Sr I, II 79−10290
Sr^+ cyclic ion laser oscillating at 1033 and 1092 nm, single and double pulse expts. 79−22940
Sr^+, inversion and lasing on optically pumped reson. line 78−70798
Sr-N_2O-CO flame, candidate chem. laser reactions, intracavity dye laser absorpt. meas. 78−63108
Sr-N_2O-CO flame, Sr catalyzed, gain meas., emission band assignment 78−66815
SrII, near IR laser transitions in hollow cathode discharge 80−1194
$TbCl_3$-$AlCl_3$ vap. complex, kinetics and laser fusion pot. 79−98343
Te_2, optically pumped continuous laser oscill., 550 to 660 nm 79−933
Tl, $6^2P_{3/2}$-$6^2P_{1/2}$ transition, population inversion 80−950
Tl atomic laser pumped by TlI photodissociation, hyperfine struct. of laser transitions 79−18411
Tl-Hg, excimer band emission from electron beam initiated discharge in TlI-Hg 80−78841
Tl-Hg excimer, emission pressure and temp. depend., blue band gain, RF excited discharge 79−22941
Tl-Xe, excimer band emission from electron beam initiated discharge in TlI-Xe 80−78840
TlHg excimer, fluoresc. at 4590 and 6560 Å, possible laser action 77−6837
Tm^{3+}:YAG, 2.014 μm, stimulated emission, resonant pumping by Nd laser 78−17944
Xe, 3.5 μm transition, quasi-Gaussian pulse propagation, effect on line-shape parameter anal. 78−55333
Xe 3.51 μm laser amplifiers, spectral narrowing and saturation induced rebroadening optical heterodyne obs. 80−63976
Xe, 3.51 μm laser transition, phase-changing broadening, inert gas perturbers 78−82949

laser transitions continued
Xe, Autler-Townes effect, i.r. laser transitions 77−425
Xe III, $5s^2 5p^3(^4S)nl$ levels, ionis. pot., from spectral data 80−47920
Xe, ionic assignment of laser lines at 3306 Å 78−1209
Xe laser, new IR laser transitions, 3.725 to 17.233 μm 80−87374
Xe, lifetimes and cross sections of laser levels, Hanle effect 77−75480
Xe, line strength calcs. for 8s-7p and 5d-6p transitions 77−14384
Xe, nucl. pumping by volumetric $^3He(n,p)^3H$ reaction 77−10886
Xe, recomb. laser in laser prod. plasma, 2.03, 2.65, 3.43 and 3.65 μm laser oscills. 77−88698
Xe-He, 3.51 μm laser amplifiers, spectral narrowing and saturation induced rebroadening optical heterodyne obs. 80−63976
Xe-Ne-He hollow cathode discharge, laser oscill. at 5314 Å Xe II line 79−3679
Xe_2, efficient vac. UV laser, 172 nm at 6 atm 78−50793
Xe_2, fluoresc. decay of O_u^+ and 1_u states, rad. decay consts. 79−86009
XeCl, efficient laser output at 308 nm, electron-beam excitation 79−59678
XeCl high specific power long-pulse supersonic flow laser at 308 nm 80−48221
XeCl laser, B→X, form. and quenching kinetics 80−74341
XeCl, UV preionised discharge pumped laser, improved performance 78−37906
Xe_2Cl, triatomic excimer, transient gain meas. at 488.0, 497.6, 514.5 nm 80−58511
XeF 2 kHz repetition rate laser action at 351, 353 nm 79−59714
XeF, C-A blue-green band, gain meas. at 488 and 475.9 nm 79−45929
XeF, direct pumping by electron beam pulses, gain and laser oscill. obs. in blue-green 80−102699
XeF, discharge excited laser operation at elevated temps., transitions, output power 80−43359
XeF discharge pumped laser at 490 nm 79−89893
XeF electric discharge laser at 490 nm 79−89890
XeF, electron beam pumped laser, gain, fluoresc. and laser output at 351, 488 nm 80−28215
XeF electron-beam pumped laser at 486 nm 79−89892
XeF electron-beam-pumped laser, characts., 300-600K 80−78839
XeF, laser action on C→A transition, pumping mechanisms, kinetics and efficiencies 80−32967
XeF laser excited by proton beam, stimulated emission at 351, 353 nm 79−98344
XeF laser performance, ground state population effect 80−63987
XeF molecule formed by XeF_2 photodissociation, laser action due to bound-free C(3/2)-A(3/2) transition 80−14334
XeF, optically excited by incoherent Xe_2* radiation, B→X band emission 78−87044
XeF, photodissociation by Xe_2*, excimers inducing blue-green excimer lasing, laser spectra 79−68382
XeF waveguide laser operation on 351, 353 nm transitions 79−22942
XeO, optical pumping, ^1S-^1D transition, 0.54 μm emission 77−667
XeO, photochem. laser performance, 0.54 μm stimulated emission 79−45938
^{136}Xe laser amplifier, pressure shifts of 3.51 μm line 79−76669
YA-O_3:Er^{3+}, pulsed laser action, $^4S_{3/2}$ to $^4I_{9/2}$ transition laser action, optical and luminescence spectra 80−16082
Zn^+ in He-ZnB_2, He-$ZnCl_2$ and He-ZnI_2 discharges, CW laser oscill. 78−50765
Zn^+, in He-halide discharge, CW oscill. 78−17913
$Zn_xCd_{1-x}S$, platelet single cryst. one-photon optical excitation, spatial distrib. and mode struct. of laser emission 79−31912
ZnSe, optically pumped stimulated emission at 4580 Å, near band edge luminesc. 78−71105

laser tuning
^3He-^{20}Ne stabilised transverse Zeeman laser, tuning characts., freq. fluctuation 80−48273
acetylene, CO-C_2H_2 energy transfer, e-beam controlled discharge excitation 77−27277
aliphatic tertiary amines, laser action feasibility, emission spectra, two photon excitation 80−23683
alkali halide, CW lasing of F_2^+-centres, 0.9-2 μm 78−29957
alkali halide host cryst. F-centre lasers, tunable IR emission 78−59030
atomic vapours, stimulated electronic Raman scatt., saturation of tunable IR lasers 78−37941
birefringent, tuning filters without secondary peaks 78−29994
bis-styryle dyes, broad tuning ranges 78−42333
bis-styryles, sulphonated, laser dyes, CW operation in blue and violet spectral region 78−42334
butyl-PBD laser, tunable narrow-band coherent VUV source for Lyman-α region 80−38070
carbon tetrafluoride laser, optically pumped, freq. tuning 80−28208
carbon tetrafluoride laser with optical pumping, freq. tuning and stabilisation 80−99706
carbon tetrafluoride optically pumped laser, stimulated emission stabilisation and tuning 80−9866
colour centre laser pumped by flashlamp-pumped dye laser, 2.4 to 3.3 μm wavelength range 80−102737
colour centre pulsed broadly tunable IR laser 79−76706
continuous broadband dynamic freq. adjustment using selective resonator *(Russian)* 78−1239
coumarin derivatives in simple dye laser, pumping by N_2^+ ion laser, tuning ranges 78−74903
coumarin dye laser, mode-locked flashlamp pumped, tunable blue ps pulses 79−13974
coumarins (C-30, C-102, C-7), synchronous pumping and mode locking 79−45966
CW laser, mode selection using spatially inhomogeneous saturable absorpt. *(German)* 78−83011
DCM laser dye, spectral props., synthesis, broad tuning range, comparison with other dyes 79−76684
detuning phase diffusion model, Lorentzian laser lineshape 80−944
DFB film laser tuning using acoustic wave 77−58359
diffraction grating tuners for CW lasers 79−86183
diode laser, IR spectroscopy *(German)* 80−43361
diode laser, pressure-tuned, appl. to high-resolution spectroscopy 80−82835
diode laser calibration by IR spectra of OCS 80−83363
diode laser instruments, tunable, developments and appls. 78−25886
diode laser tuning using autonomous high-press. chambers 77−46742
diode lasers, construction and operating characts. 77−27304

laser tuning continued
diode lasers, tunable IR, appls. to high resolution spectroscopy 80−58562
diphenyl-stilbene dye, sulphonated, CW laser emission, tunable down to 390.4 nm 79−41379
distributed Bragg reflector lasers, tunability using electro-optic effect 77−38938
dye, operation principles and tuning methods 77−10914
dye, simultaneous tunable two-wavelength operation, cavity config. 77−3610
dye, tunable superradiant emission, planar cell 77−7116
dye, wavelength shifts, surfaces model 77−7079
dye activated CLC, distributed feedback, tunable radiation generation *(Russian)* 80−102720
dye CW frequency-locked mode-locked laser, for high resolution spectroscopy in freq. domain 80−43350
dye CW laser, double-mode-locked, config. for independent tunability 79 72590
dye CW laser, electrooptically tuned, optical switching and bistability 79−59708
dye CW laser, on-line computer control, laser isotope separation appl. 78−70948
dye CW laser, spectral narrowing and continuous tuning by grating beam-expansion 79−59720
dye CW laser, tunable by holographic grating 79−27288
dye CW laser, tuning and spectral narrowing using low-loss diffr. grating 78−71109
dye CW lasers, RF tuning 80−1243
dye CW mode-locked lasers, vac. UV ps. pulse generation 80−43355
dye CW synchronously mode locked laser, cavity length detuning 80−5768
dye DFB laser, N_2 laser pumped, tunable single ps pulse generation 79−55147
dye DFB laser, simultaneous oscill. of independently tunable spectral lines 77−23673
dye DFB laser, single-freq., 10 Å continuous pressure tuning 79−76705
dye DFB pulsed laser with high repetition rate 77−27300
dye high power DFB laser, tunable 7420 to 10500 Å 77−88782
dye IR laser, Nd:YAG laser pumped, continuously tunable 10810 to 12160 Å 78−22139
dye laser, broadband tuning using electrochem. reactions 78−9397
dye laser, continuous dynamic freq. tuning of pulse radiation 78−29986
dye laser, CW, travelling wave oscills. 77−23699
dye laser, CW single-mode tunable 80−106534
dye laser, distrib. feedback formed by diverging pump laser beams, tuning curves 77−83893
dye laser, double-wavelength electro-optically tuned synchronously pumped mode-locked CW 79−89924
dye laser, filter tuning rel. to relative-gain curve determ. 78−25878
dye laser, flash lamp pumped, tuning by grazing incidence grating technique 80−95914
dye laser, flashlamp pumped, freq. tunable ns duration pulses by pulsed Q-modulation 79−41403
dye laser, flashlamp-pumped, birefr. filter for tuning, theory and design 78−74914
dye laser, for ps spectroscopy, 400-500 nm 78−82988
dye laser, freq. shifting using stimulated Raman scatt. in H_2, tunable UV source 80−9963
dye laser, high power narrowband pulsed oscillator-amplifier system 80−58570
dye laser, laser pumped, thin film interferometer freq. selector *(Russian)* 77−54736
dye laser, N_2 laser pumped, tunable ultrashort light pulse generation *(German)* 79−27275
dye laser, production of tunable picosecond pulses 79−22976
dye laser, pulsed tunable IR, pumped by flashlamp-driven dye laser 78−94400
dye laser, pumped generation by UV N_2 laser in 420-470 nm range *(Russian)* 77−88719
dye laser, short resonantor, tunable, pumped by travelling wave N_2 laser 80−48291
dye laser, short-cavity, tunable blue picosecond pulses 77−88740
dye laser, simultaneous two wavelength operation *(French)* 78−29971
dye laser, single mode, flashlamp pumped, tuning by injection locking 77−19303
dye laser, single-mode, precise freq. tuning 78−33752
dye laser, spectral selection and tuning using thin layer Fabry-Perot interferometer *(German)* 79−94242
dye laser, tunable, 545-680 nm radiation efficient conversion to 360-415 nm UV range 80−74439
dye laser, tunable, flashlamp excited, triplet quenching effect 79−31892
dye laser, tunable, flashlamp pumped, ultra-narrow bandwidth 80−9897
dye laser, tunable, improved freq. doubling for 217-360 nm 78−33781
dye laser, tunable, N_2-laser pumped, using single prism beam expander *(Chinese)* 80−74389
dye laser, tunable CW mode-locked system, sub ps pulses 78−42362
dye laser, tunable emission by pumping with Nd:YAG laser 79−950
dye laser, tunable in 1.1 μm range, 13 MW peak power, Nd:YAG laser pump 79−86190
dye laser, tunable ps high efficiency system for 340 nm to near IR 78−50789
dye laser, tunable ultrashort pulse generation 80−58612
dye laser, tuning and active mode-locking, interferometry technique 79−22982
dye laser, tuning by multistage interference polarisation filter 80−64091
dye laser, tuning for vel. selection in time-of-flight spectrometer 77−49804
dye laser, two-wavelength single mode operation, using grazing incidence grating 80−53329
dye laser, wavelength tuning by changing dye soln. conc. 78−17967
dye laser, Xe ion laser pumped, tunable output in blue region 78−46621
dye laser double-pass planar amplifier, two-wavelength operation 77−75538
dye laser emission freq. tuning with cholesteric liq. cryst. Bragg mirror 79−89931
dye laser excited by pulsed N_2 gas laser *(Korean)* 79−13963
dye laser multiple system, flashlamp pumped, energy transfer 77−88720
dye laser SHG, automatically tunable 79−985
dye laser single-mode mag. tuning system 77−75541
dye laser systems with dynamic DFB, freq. tunable over whole gain profile 79−50317

laser tuning continued
dye laser tunable coherent radiation source, 185 to 880 nm, stimulated Raman scatt. in H_2 79−31980
dye laser tunable oscillator-amplifier system, N_2 laser pumped *(Japanese)* 79−68406
dye laser tuning by birefringent Fabry-Perot etalons *(Japanese)* 77−7125
dye laser tuning by dielectric interference filter-coated prism 79−10322
dye laser tuning range extension using electrochem. reaction products 79−31895
dye laser with stimulated electronic Raman scatt. in Cs vap. 78−1300
dye lasers, birefringent Fabry-Perot etalon, electrooptic, mechanical methods 77−75500
dye lasers, independently tunable double freq., with continuously variable power ratio 80−5755
dye lasers, picosecond tunable emission, extension of spectral range 80−5731
dye lasers, review 77−38884
dye lasers, tunable narrow bandwidth 2 MW, pumped by KrF* discharge laser 79−41378
dye lasers, tuning, via high dispersion rutile prism 77−7107
dye lasers using mixed dyes, tuning props. 79−59693
dye mixture, possibility of tunable multiple wavelength output 80−23684
dye picosecond laser, tunable in 1.1 μm region, Nd:YAG laser pump 79−86191
dye pulsed laser, electronic tuning by piezo driven grating with etalon 77−42544
dye pulsed laser, spectral narrowing by tuning elements *(French)* 78−46616
dye ring CW laser, high efficiency, tunable single-freq. radiation over visible spectrum 79−72589
dye ring laser, second harmonic CW, 292 to 302 nm tuning range 79−41392
dye synchronously pumped mode-locked CW system, pulse characts., cavity detuning effect 79−3726
dye tapered DFB laser as tunable picosecond pulse source 78−22150
dye TEM_{00} tunable laser system high-power, with frequency-doubling crystal 79−50306
dye tunable laser systems 78−59029
dye UV laser, tunable picosecond, pumped by Nd:YAG laser third harmonic 79−31927
dye UV laser system, simultaneous tunable two-wavelength oscill. 77−88784
dyes, 266 nm pumped, tuning ranges in near UV, 390 to 333 nm 80−48239
dyes, 355 nm pumped, tuning ranges from 410 to 715 nm 79−76683
EM transducer for laser fine-tuning 77−79862
ethyleneglycol dye laser, conversion efficiency and tuning, solvent effect 79−55131
excimer tunable laser systems 78−59029
F_2-centre, pulsed tunable laser, IR spectral characts., 1.1-1.26 μ region 80−91805
F-centre, laser, continuously tunable near IR *(German)* 80−1207
Fabry-Perot etalon, freq. selector in laser resonator losses *(Russian)* 77−38944
far infrared lasers, tuning for time and frequency standard appl. 78−174
far IR, high speed freq. modulation using Stark effect 77−72010
far IR laser, optically pumped, electronic tuning and phase-locking 78−59055
fibre Raman ring laser, tuned by interferometer or pump pulse rate variation 79−22981
fluorescein dye laser, solvation effects on tunability 80−53285
fluoromethane, $^{12}CH_3F$, far IR Raman laser line obs., CO_2 laser pumping 80−69381
fluoromethane, far IR laser, electronic tuning and phase-locking 78−59055
fluoromethane far IR CW laser, Stark effect, large freq. tuning and resolved structures 79−45931
fluoromethane for IR laser, evidence for Stark induced freq. shift 77−58358
fluoromethane high-power laser, tuning behaviour 80−63994
fluoromethane laser emission from unstable resonator 79−22983
fluoromethane waveguide laser, tunable, for far IR freq. synthesis in 500-70 μm region 78−90439
free electron laser, relativistic, rippled static mag. field, simulation, waves and instability 77−54686
free-electron laser amplifier, exact classical electron dynamics 79−41362
frequency shift, using two acousto-optical modulators in series 78−74932
gas laser, freq. modulated, threshold conditions for gain and freq. 77−88816
gas lasers using SAW light diffraction grating *(Russian)* 78−33759
gas ring laser, opposite wave freq. difference, mag. field 79−7156
glass laser, dynamic tuning of polarisation of radiation *(Russian)* 77−38945
gratings, damage resistance 77−19283
grazing incidence grating efficiencies, rel. to dye laser tuning 79−36990
high power tunable lasers for isotope separation 77−34904
high resolution tunable laser spectroscopy, review 77−74515
high-resolution spectroscopy using tunable lasers 80−101849
holographic total internal reflection selector for tunable lasers 77−79840
hydrophone, optical interferometric, with homodyne detection, signal stabilization by light source tuning 80−87477
hysteresis effect in SHG, depend. on detuning under CW conditions 79−59766
inert gas halide lasers, discharge excited, optical loss mechanisms and tuning performance 80−32970
injection laser with external dispersive resonator as narrow-line tunable emission source *(Russian)* 77−83898
interference technique, spectrally depleted destructive two-beam, for laser freq. control 78−74941
IR generation, tunable, from four-wave mixing in room temp. Ge 80−9940
IR lasers, review 78−13724
IR source, tunable, efficient 80−5789
IR tunable lasers, principles and operating characts., review 79−98376
jet stream dye laser, mode locked synchronous pumping, near IR ps pulses 78−17948
linear scan control of tunable lasers using scanning Fabry-Perot 79−76693
methanol CW far IR laser, tuning curve asymm. rel. to anisotropic gain 77−61944
methanol far IR CW laser, Stark effect, large freq. tuning and resolved structures 79−45931
Michelson interferometer, active stabilization by electrooptically tuned laser 80−86386
mm-wave Fabry-Perot tuning and freq. modulation by electrically variable external reactance 79−68409
mobile resonances, appl. to freq. stabilisation and tunability 77−7138
molecular FIR laser design, freq. tunable by Stark effect 80−5750
molecular laser, optically pumped, review 80−58519
multi-mode laser, coexistence and noncoexistence of modes 78−29991
multimegawatt tunable IR source up to 7.7 μm, using dye laser and H_2 78−1301
multipath optical cavities in saturated absorpt. expts., freq. calibration and optical delay line 77−65610
near-IR fibre Raman oscillator, 1.07-1.32 μm tunable 79−72622
nonlinear device descriptions, characts. and potential 79−990
nonlinear materials for tunable coherent light sources in middle infrared, review 77−38991
oxazine 1 and 9 laser dyes, absorpt. and gain with picosecond pumping 79−55134
oxazine-1-perchlorate mode-locked CW dye lasers, tunable near IR ps and subps pulse generation 79−45972
parametric frequency conversion possibility of laser beam by electron beam 79−68413
paraterphenyl, efficiency, 323-364 nm tuning 77−14752
phase autotrimming, beat frequency setting up to 400 MHz *(Russian)* 78−1238
POPOP solution dye lasers, multiplate reflectors 80−83606
progress in tunable lasers, tunable range extension, power level improvement 80−43344
pulse radiation, continuous dynamic freq. tuning by varying resonator length 78−29986
Raman oscillator, tunable 1.1 μm fibre 78−1242
Raman oscillator, tunable multiple Stokes CW fibre 77−88786
Raman spin-flip laser, higher modes and saturation effects, theory 78−71106
relativistic ion beam laser, continuously IR to X-ray tunable, in negative temp. state *(Chinese)* 80−87373
rhodamine 6G, SHG for high power tunable UV source 77−42565
rhodamine 6G, spectral line tuning using partially selective resonator *(Russian)* 77−61980
rhodamine 6G, sub ns dye laser with optical pumping, spectral width, efficiency, tuning *(Russian)* 78−29974
rhodamine 6G, tunable UV radiation prod., intracavity freq. doubling in $NH_4H_2PO_4$ 77−3628
rhodamine 6G dye in quartz glass microcomp. matrix, as tunable solid laser 80−99734
rhodamine 6G jet stream CW laser, tuning range, mode competition effects 78−50791
rhodamine 6G solution laser, pulse tube pumping *(Russian)* 77−88785
rhodamine 6G-safranin-T mixed dye laser energy transfer, 31 nm tuning range 80−58532
rhodamine 6GDN, synchronous tunable ps laser 77−75560
rhodamine B, tunable freq. doubled CW laser using RbH_2PO_4 cryst. 80−53372
rhodamine B and 6G, laser wavelength and dye conc. 78−50770
rhodamine dye laser, synchronously pumped, electronically tunable pulse prod. 79−76698
rhodamine GG tunable narrowband subnanosecond dye laser, optical pumped 79−81445
ring laser, freq. shift and splitting for opposite waves, spatially inhomogeneous media 79−7155
ring laser, relativistic Doppler effect, two-wave mode instability and optimum tuning 77−38940
ring laser, self-locking type II mode, freq. depend. effects 78−5506
ring laser, with detuning, generation of high-frequency pulsations 80−48304
ruby, one-freq. tunable one-pulse, selector parameter optimisation 78−74935
ruby laser, Q-factor passive modulator unloading, in resonator with prism *(Russian)* 77−68234
ruby lasers and $LiNbO_3$ cryst. in difference freq. laser, tunable MM range emission 80−5764
scalable tunable IR laser operating characteristics and limitations 77−54713
selective laser excitation of atoms and mols., photophys., photochem. processes, appls. 77−54630
semiconductor diode laser instruments, appl. advanced meas. and anal. 77−75600
semiconductor laser, wide band electro-optical tuning using birefringent filter 77−23689
semiconductor laser with holographic selector, influence of feedback strength on tuning range 79−98406
single-mode gas laser with slightly anisotropic resonator, output polarization stability 80−43370
single-sideband generation in IR 80−78876
spectroscopy, conf., Tsakhkadzor, USSR (Jan. 1976) 77−23706
spectroscopy, tunable laser, of semiconductors 79−93231
spectroscopy applications 79−64270
stilbene tunable narrowband subnanosecond dye laser, optical pumped 79−81445
stimulated Raman scatt., creation of laser source, near IR to submillimetric waves *(French)* 79−31993
submillimetre laser output and efficiency, rel. to pump frequency displacement 79−31866
subpicosecond spectroscopy, high intensity, broad wavelength tunability 79−44950
p-terphenyl, substituted, dye laser and spectral characts., output power, conversion efficiency 80−23681
p-terphenyl in cyclohexane, 1 MW laser, conversion efficiency and tuning curve 77−58323
tetrafluoromethane optically pumped laser, tuning and stabilisation 79−13985
thermal length control, for lasers and etalons 78−87056
thin-film laser with spatially separated multiple-frequency outputs 80−43368
three-stage birefringent filter, tuning over visible region 80−58667
time-dispersion-tuned fibre Raman oscillator 77−42562
TOPOT vapour dye lasers with multiplate reflectors 80−83606
triazinyl-stilbene compounds, lasing characts. 78−29948

laser tuning continued
triazinyl-stilbenes, sulphonated, laser dyes, CW operation in blue and violet spectral region 78−42334
tunable lasers, review *(Japanese)* 79−27270
tunable lasers and applications, conference, Loen (1976) 77−54720
two-wavelength double-pulse tunable dye laser for differential absorption lidar 77−21939
unstable resonator, for low-gain media 79−22984
UV metal ion lasers, appl. to tunable dye laser, 300-400 nm 78−66809
vacuum UV tunable coherent radiation generation by lasers 77−54705
wide-band tunable lasers, frequency-locking system 79−18432
xanthene-acridine dye mixture, flashlamp pumped, tuning props. 77−3579
AlGaAs-GaAs CW injection heterolaser, single freq., tunable by external dispersive resonator 80−28236
Ar I, high press. tunable laser emitting at 0.91 μm 78−50755
Ar_2 excimer laser, tunable vac. UV action 80−48215
ArF, double discharge laser, prism tuning 78−37892
ArF laser, excimer gas-discharge tunable, intense laser oscill. obs. 77−38862
ArF laser pump source, tunable efficient VUV generation using stimulated Raman scatt. in H_2 80−38072
CO, CO_2 lasers, perturbation spectroscopy tuning for atmospheric pollutants selective quantitative meas. 78−69526
CO_2, 1 mJ line tunable optically pumped laser 78−66840
CO_2 atmospheric pressure laser, tuning for single longit. mode operation 78−13728
CO_2 CW sequence laser lines generated using incavity NH_3 cell 79−18438
CO_2, continuously tunable high press. monochromatic laser for spectroscopy 80−5762
CO_2 dual-line laser, tuning for atmospheric spectroscopy and pollution monitoring 78−3977
CO_2 freq.-tunable laser for photoreceiver characts. meas. 77−14728
CO_2, high press. electron beam controlled, continuous tuning 77−713
CO_2 high-power pulsed laser continuously tunable over wide freq. range 79−45925
CO_2 high-power pump laser, direct narrow-line tuning 80−58579
CO_2, high-press. tunable IR lasers 78−59030
CO_2, intermode beats, use in automatic frequency control system 80−48209
CO_2, laser, 16 GHz tunable sideband generation 78−90428
CO_2 laser, absorption of laser radiation in Stark tunable mol. gases *(Rumanian)* 79−86157
CO_2 laser, broadband electronically tunable resonant microwave modulators 79−64256
CO_2 laser, detuning effects of FM mode-locking 80−69434
CO_2 laser, pulsed, high-press., high-power, electron-beam-controlled, continuously tunable 80−64065
CO_2 laser, Q-switched, single rot. line-selection *(German)* 78−46562
CO_2, laser, TEA, tunable simultaneous double wavelength operation 77−61970
CO_2 laser, tunable stabilised single-mode TEA 78−5485
CO_2, laser lines, 12 GHz continuous tuning in integrated electro-optic modulator 77−83907
CO_2 multiatmosphere laser tuning for methyl fluoride laser pumping 80−69421
CO_2, narrow band TEA laser for far IR laser pumping 77−54729
CO_2, optical pumping in stimulated Raman scatt., tunable laser emitting at 14,16 μm, theory 78−46568
CO_2, possible freq. stabilisation using external Stark cell, tuning efficiency 79−94266
CO_2 pulsed laser with continuously tunable radiation frequency 80−48292
CO_2, pulsed TE laser, tunable single-mode operation by means of selective absorbers 79−36940
CO_2, pulsed TEA laser, tuning by 9.55 μm CO_2 laser radiation injection 77−38908
CO_2, pumped by energy transfer from Br, line tunable 78−5448
CO_2, pure and CO_2-He mixture, optically pumped continuously tunable lasers 78−13678
CO_2, short-pulse oscillator, variable pulse repetition freq., pulsewidth and wavelength control 77−88801
CO_2, small high press. UV preionised laser, continuous tuning characts. 79−59722
CO_2 TEA far IR laser, optimum spectral matching 79−31857
CO_2 TEA laser, fine freq. tuning 79−98405
CO_2 TEA laser, injection tuning and mode locking on low gain rot. lines 80−95928
CO_2 TEA laser injection locked, tunable single longitudinal mode operation, O_3 absorpt. spectra 80−33018
CO_2 TEA laser oscillator, longit. mode rejection, cavity length tuning effect 79−86189
CO_2 TEA single longit. mode laser with tilted intracavity etalon 78−5484
CO_2 TEA UV preionized laser, non-dispersive tuning 79−31856
CO_2, tunable linearly polarized TEM_{00} operation, concave diffr. grating 77−19344
CO_2 tunable waveguide laser 79−64249
CO_2 waveguide high press. laser, line selection and tunability 78−59026
CO_2 waveguide laser, for space link transceiver 77−19322
CO_2 waveguide laser, tunability calc. *(Rumanian)* 80−87371
$^{12}C^{16}O_2$, double-discharge Pyrex waveguide CW laser 78−9393
CO_2-CO laser, optical transfer, saturation behaviour and tunability *(German)* 77−23650
Ca-H_2, single freq. laser, 5.54 μm emission, mag. field tuning 78−46634
CaO, tunable optical gain at 3600 Å using F^+ centres 79−45947
CdS, two-photon-excitation, tunable laser emission, luminesc. processes 80−55127
CdTe, tunable high efficiency microwave freq. shifting of IR laser 78−71126
Ce:LaF_3 286 nm laser, optically pumped, 275 to 315 nm pot. tuning range 80−99738
Ce:$LiYF_4$, tunable UV laser at 325, 309 nm, KrF laser excitation 80−38022
Co:MgF_2, laser, broadly tunable CW operation, output powers, optical pumping 80−32995
Co:MgF_2, tunable transition-metal-doped solid state lasers 80−58549
Cr^{3+}:Al_2BeO_4, Alexandrite, tunable laser sources development and appl. 80−48262
laser tuning continued
Cr^{3+}:$BeAl_2O_4$, tunable laser performance, 701 to 794 nm, long-pulse and Q-switch operation 79−72573
Cr^{3+}:$BeAl_2O_4$ alexandrite laser, wavelength-tunable CW laser action 80−53300
DCN, 250 mW continuous discharge laser at 195 μm 79−31949
D_2O far IR laser pulses, real-time spectral anal. using SAW dispersive delay line 79−45983
D_2O tunable vapour laser, optically pumped with single-mode CO_2 TEA laser 79−55145
GaAlAs CW diode laser, external cavity control, coarse and fine tuning 78−1271
(GaAl)As heterojunction laser with distributed Bragg refl., mode switching 80−43336
GaAs electrooptically tuned external-cavity CW injection laser, FM optical communication appl. 80−14351
GaAs freq. retuning using electron beam *(Russian)* 77−716
GaAs injection laser, single heterostruct., mode competition effects, tuning characts. 80−48255
GaAs, tunable stimulated Raman scatt. in far IR, laser feasibility 79−50344
GaAs-GaAlAs optically pumped DFB laser, wavelength tuning effect 78−82979
$GaAs_{1-x}P_x$, continuously tunable electron beam pumped laser 78−50802
$GaAs_{1-x}Sb_x$, DH, laser operation between 0.9 and 1.1 μm 77−10922
$GaAs_{1-x}Sb_x$-$Ga_{1-x}In_xP_{1-y}As_y$ multilayer structure, continuously tunable electron beam pumped laser 78−50802
$Ga_xIn_{1-x}As_ySb_{1-y}$ tunable electron-beam-pumped laser parameters 80−106524
GaInPAs, narrow-band tunable injection laser, 1.06 μm 79−76713
H, maser hyperfine transition, affected by coherently excited Zeeman transitions 79−72544
H_2, efficient tunable Raman laser 80−28245
H_2 high power tunable IR compressed laser, for spectroscopy 80−48277
H_2 laser, tunable IR waveguide Raman type pumped by dye laser, 0.7-7 μm range 79−45959
HCN, 337 μm tunable radiation in laser-klystron link through Schottky diode or metal-semicond. point contact 78−46714
He-Cd(Zn) hollow cathode laser, upper level decay rate, mag. field tuning dip meas. 78−87043
He-Ne, narrow linewidth frequency scannable 3.39 μm laser, appls. 77−88757
He-Ne, power characteristics obs., with CH_4 cell, at λ=3.39 μ *(Russian)* 78−1207
He-Ne, scheme for automatic fine frequency tuning along the Lamb depression 80−74385
He-Ne, wavelength switching using var. methane pressure 77−19312
He-Ne laser, mode interaction, transition level degeneration effects *(Russian)* 77−61940
He-Ne laser, two-photon amplification on cascade-transitions, power tuning curve meas. 80−48219
He-Ne lasers, stabilised by saturation absorpt. in I_2 78−1270
He-Xe laser, Zeeman tuned *(Korean)* 79−7145
$Hg_{0.77}Cd_{0.23}Te$, spin-flip, Raman laser,, tuning characts. 77−79832
Ho^{3+}:$LiEr_{0.945}Tm_{0.05}Ho_{0.005}F_4$ laser, tuning at 2.06 μm 80−83611
I, 1.315 μm, oscill. freq. selection hyperfine transition 77−10952
I, photodissociation laser, 1.315 μm transition line struct. 78−59000
I photodissociation laser, tuning using Zeeman effect 79−50316
I_2 molecule B-X electron transition during Cu vapour laser optical pumping *(Russian)* 80−78845
I_2, optical pumping, quasi-tunable IR emission, appl. to absorption meas. 77−42551
$InAs_xP_{1-x}$, continuously tunable electron beam pumped laser 78−50802
$In_{1-x}Ga_xP_{1-z}As_z$ near IR DH laser, constant temp. LPE, external grating cavity 77−75550
InSb spin-flip Raman laser external-cavity system, oscill. characts. 78−55383
K atomic Rydberg state tunable subMM laser 80−69378
KF F_2^+-centre laser, picosecond pulse generation 1.24 to 1.45 μm, mode locking 79−89925
Kr, laser, tunable, Lyman alpha radiation, nonlinear generation 78−87038
KrF, double discharge laser, prism tuning 78−37892
KrF excimer laser, operating and beam characts. 79−59715
KrF* laser, generation of high-spectral-brightness tunable XUV radiation at 83 nm 80−91846
KrF* tunable ultrahigh spectral brightness excimer laser source 80−64046
Li^+,Na^+:KCl(RbCl), F_A(II) to F_B(II) centre crystals, CW laser oscill. with extended tuning range 80−32997
LiF, coherent freq. tunable radiation generation in F-centres, 0.6 to 1.26 μm range 79−36902
LiF crystal, tunable laser via F_2^+, F_2^--centres, 0.88 to 1.25 microns 77−75529
LiF crystal with F_2^+ centres, periodic pulsed tunable laser, Nd laser second harmonic excited 80−38021
LiF tunable laser production, F_2^+ centre accumulation and generation *(Russian)* 80−28238
$LiNbO_3$, tunable parametric Raman laser utilizing polaritons 79−41418
MgF_2:Ni electronic transition laser, tunable IR emission 78−59030
N_2 high power tunable liq. Raman laser, for spectroscopy 80−48277
N_2 laser, TEA, pump for dye laser amplifier system 78−82984
N_2, liq., tunable Raman laser based on third Stokes component 78−50859
NH_3 CW far IR laser lines, CO_2 laser pumping and Stark tuning 80−69382
NH_3 CW far IR laser lines, CO_2 laser pumping and Stark tuning 80−106508
NH_3 laser, high-power efficient optically pumped, tunable over 770 to 890 cm^{-1} range 80−91780
NH_3 laser, optically pumped, freq. tuning 80−28208
NH_3 laser, optically pumped, wide range line-tunable oscill. 80−53267
$^{14}NH_3$, CW far IR lasing using Stark tuning 79−81407
NI:MgF_2, laser, broadly tunable CW operation, output powers, optical pumping 80−32995
N_2O-CO_2, optically pumped transfer lasers, continuously tunable 78−13678
Na fluorescein, laser wavelength and dye conc. 78−50770
Na^+:KCl, CW laser action of $(F_2^+)_A$-centres, tunable from 1.62 to 1.91 μm 80−32998
Na^+:KCl, F_B(II) colour centres, tunable CW laser action obs. 77−83877

laser tuning continued
Na^+:RbCl, F_B(II) colour centres, tunable CW laser action obs. 77−83877
Na_2, continuous laser oscill., optical pumping 77−88706
NaF, F_2^+-like colour centre, room temp. stable, CW laser, 0.99-1.22 μm tunable 80−69399
Nd laser, continuously tunable, pulsed, operation and output, characts. 79−18448
Nd:glass, dynamic mode sweep-laser, freq. tuning 78−66851
Nd:glass, line narrowing and tuning using intracavity Brewster angle birefr. filter 77−38916
Nd:glass composite tunable laser at 1.89, 3.39 and 16 μm 79−72596
Nd:glass laser, continuous dynamic freq. tuning of pulse radiation 78−29986
Nd:glass laser, Fabry-Perot etalons tuning, narrow linewidth 79−76707
Nd:glass laser, resonant reflectors in laser cavity, freq. selection 78−55369
Nd:glass laser, tunable-wavelength mode-locked, with instant recording of temporal and spectral characts. 77−54732
Nd:glass laser with continuously tunable ps output, polaris. filter 79−22985
Nd:glass Q-switched laser, feasibility of tuning range widening 79−59724
Nd:glass travelling-wave sweep laser, emission spectrum dynamics 78−50829
Nd:phosphate glass laser beam, single ps pulse props. 77−19273
Nd:YAG pumped $LiNbO_3$, parametric oscillator, picosecond IR pulse generation, tuning ranges 1.365-4.825 μm and 0.66-2.70 μm 78−71151
Nd:YAG pumped tunable sources, appl. to spectroscopy 80−58576
Nd^{3+}:YAG, 1.05 to 1.44 μm tunable high-power laser emission on 18 CW transitions 77−88727
Nd^{3+}:YAG, CW laser, 1.05 to 1.44 μm tunability, performance 78−22142
Nd^{3+}:$YAlO_3$, $^4F_{3/2}\rightarrow{}^4I_{13/2}$ transition, stimulated emission wavelength, continuous tuning 77−58334
Ni:MgF_2, tunable transition-metal-doped solid state lasers 80−58549
Ni^{2+}:MgO laser system, optical parameters 80−48260
Pb salt, tunable IR diode lasers 78−59030
Pb salt DH lasers for IR gas spectroscopy 77−19325
$PbS_{1-x}Se_x$, single heterostruct. laser, wide tunability 77−79846
PbSe, pressure tunable CW injection laser, emission spectra 79−18419
$Pb_{0.995}Sn_{0.045}Se$ pulsed laser for high-resolution NH_3 spectroscopy 79−64252
$Pb_{1-x}Sn_xSe$ and $PbS_{1-x}Se_x$, single heterostructure tunable diode lasers formed by compositional interdiffusion 77−38896
$Pb_{1-x}Sn_xSe$, single heterostruct. laser, wide tunability. 77−79846
$Pb_{1-y}Sn_ySe$-PbSe, prep. and emission characts., tuning 10.6-15 μm 77−58346
$Pb_{1-y}Sn_ySe$-PbSe pulse laser diode, temp. tuning of modes 78−50777
PbSnTe laser diode, tunable emission, 5-15 μm 77−50686
n-$Pb_{0.88}Sn_{0.12}Te$ spin flip Raman laser pumped by TE CO_2 laser, characts. 80−87397
$Pb_{1-x}Sn_xTe$, continuously tunable electron beam pumped laser 78−50802
$Pb_{1-x}Sn_xTe$ homojunction laser, increased freq. tuning range 77−75546
$Pb_{1-x}Sn_xTe$-PbTe pulse laser diode, temp. tuning of modes 78−50777
PbTe injection laser, freq. tuning using press. and temp. combination 78−17978
Rb vapour, dynamic Stark tuned far IR laser 78−63126
S_2 laser, optically pumped, lasing obs. 470 to 480 nm 78−63095
S_2, tunable visible and UV laser, $B^3\Sigma_u^-$-$X^3\Sigma_g^-$ transition 77−42522
SiO_2 fibre, CW tunable near IR Raman oscillator 78−1235
Te, energy gap, laser emission study of press. depend. 79−82521
Xe_2 coaxial-diode tunable vacuum UV excimer laser systems 77−54738
XeCl frequency-tuned laser, coherent tunable vacuum UV near H Ly-β transition 80−99798
XeF, C-A blue-green, multipass amplification and tuning 80−43346
XeF, photodissociation by Xe_2*, excimers inducing blue-green excimer lasing, laser spectra 79−68382
ZnO, two-photon-excitation, tunable laser emission, luminesc. processes 80−55127

laser velocimeters
3-D Doppler velocimeters for use in wind tunnels 80−10331
accuracy estimate, turbulence effects 79−55433
acoustic optic cells, appl. *(Portuguese)* 77−89217
acoustic pressure level, spectral components and noise meas., directional non-contact method 77−834
acousto-optical modulators used in laser velocimetry 80−33715
aerodynamic applications and principles *(Spanish)* 80−53902
aerosol particle sizing by laser Doppler dynamic relaxation time meas. 77−21897
aerosol single particle aerodynamic relaxation time anal. 77−80205
aerosol size spectrum determ. in turbulent medium using coherent Doppler meas. 79−96841
afocal Doppler, for flow meas. 77−19652
air, untreated, shock press. meas., Teflon seeding technique 77−84348
airflow through cascade of turbine blades, laser anemometry 80−59146
anemointerferometer, for simultaneous velocity and density meas. 79−18976
anemometer, appl. to investigation of supersonic shock-wave boundary-layer interaction 77−35275
anemometer, gas-solid suspension flow meas. 77−35268
anemometer, laser Doppler, meas. of turbulent vortex flow 80−79412
anemometer, laser fibre-optic Doppler 78−30373
anemometer, two-component, using rotating radial diffr. grating 77−3898
anemometer, with differential optical arrangement, instrum. function 77−959
anemometer elements, Gaussian beam transform. 79−45991
anemometer signals, visibility characts., particle sizing appl. 77−42482
anemometry, basic principles 77−74179
anemometry, flow statistics retrieval via photon correl. 77−3896
anemometry, fringe-type, review of high-speed wind tunnel appl. in France and Germany 77−35272
anemometry, fundamental limitation and accuracy 80−87829
anemometry, laser-Doppler, microprocessor-based signal processing system 77−89218
anemometry, principles and status, survey *(German)* 78−9738
anemometry, Reynolds stress expt. analysis appl., turbulent flow in rectangular channel *(Italian)* 79−4094

laser velocimeters continued
anemometry, velocity meas. by light scatt. techniques 78−57916
atmospheric transverse velocity single-beam meas. 78−53747
backscatter, single particle correlation for wind speed remote meas. 77−91302
Benard convection, transient, laser speckle photography obs. 79−32508
bidirectional LDV system, blood cell speed absolute meas. in retinal vessels 79−83884
blood flow meas. by laser Doppler system *(Swedish)* 80−51199
boundary layer velocity measurement by single-beam laser time-of-flight method 79−77298
Bragg cell laser Doppler velocimeter, increase in optical power by using multiwavelength lasers 78−34211
bubble-flow regime, two-phase, laser Doppler anemometry 77−39366
bubbly flows, simultaneous meas. of local liq. vel. and void fraction using gas laser *(Japanese)* 77−42947
burst-like Doppler signals, processing via digital freq. meter 77−72376
circular channel with centrifugal forces, laser Doppler meas. of vel. field 78−34225
coherent Doppler anemometer for turbulent vel. meas., potential accuracy anal. *(Russian)* 78−71406
coherent Gaussian beam in laser Doppler velocimeter, interference 80−69444
coherent structure in flow fields anal. using laser Doppler anemometry 80−10339
commercial LDA instruments *(Czech)* 79−46409
compressible aerodynamics, appl. of laser velocimetry 77−35274
conference, fluid flow research instrumentation, Saint-Louis, France, May 1976 77−35271
contactless speed meas., laser Doppler difference system *(German)* 77−17957
correlation technique for surface speed measurement, industrial paper machine test *(French)* 80−95082
cross beam Doppler, moving spherical particle scatt. rel. to signal visibility 77−42478
cross-beam Doppler, for extremely low velocity meas. 77−79071
cross-beam rate correlation, advances 80−58621
differential Doppler system, transverse vel. meas. at remote point 77−65816
differential-type laser speckle velocimeter 79−31975
digital, signal processor accuracy testing *(German)* 78−86242
digital processing of laser-Doppler velocimeter signals *(German)* 78−83510
Doppler, appl. to electron-hole drops in Ge 77−43504
Doppler, Czech instruments *(Czech)* 79−23388
Doppler, for charged dust particles vel. meas. in high elec. field 80−95083
Doppler, for turbulent flow velocity meas., redesign 78−1245
Doppler, instantaneous, using fast wavelength tracking Michelson interferometer 79−7430
Doppler, light scattering visibility, Mie theory 77−19167
Doppler, meas. system for frazil ice conc. 77−25796
Doppler, output data anal., noise rejection 77−39378
Doppler, principles of operation and applications 77−68712
Doppler, signal processing using counters, biasing elimination method 78−1773
Doppler, using radiation from C_3F_7I laser 79−23005
Doppler, using wide-band-pass stroboscopic FM demodulator *(Russian)* 78−36976
Doppler and time of flight combined anemometer 79−55434
Doppler anemometer, acousto-opticalmodulator using TeO_2 78−83082
Doppler anemometer, directionally sensitive two-component 80−75004
Doppler anemometer, dual-beam, coincidence of beam waist and crossover region 80−14377
Doppler anemometer, flow field meas. in wake of blunt body, effect of chem. reaction 77−35262
Doppler anemometer, flow meas. in fluidic amplifiers *(German)* 77−961
doppler anemometer, microprocessor-based autocorrelator 77−72396
Doppler anemometer and digital correlator system for direct measurement of velocity correlation functions 79−27728
Doppler anemometer measurements, bias correction 80−24114
Doppler anemometer system, influence of Gaussian beam props. 79−41406
Doppler anemometer use for turbulent flow investig. of polymer solns. 77−58822
Doppler anemometer with microscopic intersection volume 79−94750
Doppler anemometers, rot. diffr. gratings for use as beam splitting freq. shifters 77−68721
Doppler anemometers, sensing volume and biasing corrections for dual counter processors 79−77314
Doppler anemometry, association with photographic particle tracking 80−38512
Doppler anemometry, GaAlAs laser diode sources 79−14499
Doppler anemometry, image form., wall scatt. effect on S/N ratio 79−89953
Doppler anemometry, periodic sampling in periodic fluid flow measurement 80−64657
Doppler anemometry, S/N, detector influence *(German)* 77−19651
Doppler anemometry, velocity and photomultiplier bias effects 80−59140
Doppler anemometry for meas. in oscillatory boundary layer beneath water waves 79−27719
Doppler anemometry in internal combustion engine cylinder 79−77296
Doppler anemometry of high-temp. industrial gas flow *(German)* 79−10618
Doppler anomemeter for velocity fields meas. near prosthetic heart valves 79−57814
Doppler beat signals, freq. error, due to extended scatt. particles, theory and expt. 77−7487
Doppler correlation technique for meas. of periodic flows 77−35278
Doppler flowmeter, LADO 1, non-contact meas. of liquid and gas flow rate 79−77305
Doppler for turbine-vane passage velocity meas. 80−95086
Doppler frequency discriminator 78−81954
Doppler frequency discriminator applic. 78−26220
Doppler laser velocimeter, meas. of motion of fine particles in gas flow 77−27583
Doppler laser velocitometer, fluctuation of meas. values of a constant velocity *(Japanese)* 80−6179
Doppler linear velocity meas. by YAG laser 79−26039
Doppler microscope, vel. measuring device 80−68251
Doppler microscope for blood velocity meas. 79−62329

laser velocimeters continued
Doppler microscope for flow velocity meas. in areas <10 μ dia., signal-analysing system *(Japanese)* 78−22441
Doppler microscope period meas. signal analyser *(Japanese)* 79−88998
Doppler shifted light scatt. technique for eye movement meas. 79−92322
Doppler spectroscopy, biology appls. 79−66598
Doppler system, optics and signal processor for turbulent low speed flows *(French)* 78−59521
Doppler system, rot. radial diffraction grating as beam splitting freq. shifter 77−39382
Doppler type, appl. of electro-optical freq. modulator with rot. elec. field 77−42620
Doppler type, mathematical analysis *(Russian)* 77−27245
Doppler vel.-profile meter 77−75997
Doppler velocimeter, appl. to meas. in subsonic and supersonic flows 77−35273
Doppler velocimeter, optical system with multifrequency shifting for simultaneous meas. of several flow velocities 80−43805
Doppler velocimeter, optimisation of receiving optical system for sampling volume reduction 77−72379
Doppler velocimeter, turbulent spot entrainment behaviour 78−26102
Doppler velocimeter calibration burst generator 79−77321
Doppler velocimeter description *(Russian)* 77−65822
Doppler velocimeter direction-sensitive simultaneous multivelocity component 78−94857
Doppler velocimeter for meas. of specified velocity vector 80−47040
Doppler velocimeter signal analysis for pulsatile arterial flow meas. *(Japanese)* 79−2156
Doppler velocimeter with differential photodiode array 79−76743
Doppler velocimeter with high resolution Fabry-Perot interferometer for supersonic vel. meas. 77−39377
Doppler velocimetry application to electrophoresis detection on biological surfaces 80−41359
Doppler velocimetry for plasma vel. meas., review 80−48975
Doppler velocimetry in turbulent flow meas. *(French)* 77−35276
Doppler velocimetry of transition to turbulence in Couette-Taylor flow 80−92163
Doppler velocimetry within turbulent phase boundaries 77−11289
Doppler-difference laser anemometry, appl. to wind tunnel meas. 79−7421
droplet size and falling velocity meas. using laser Doppler velocimeter 80−68185
droplets, large, size and velocity meas. equipment 78−86238
dual-focus flow velocimeter 77−39381
dual-scatter laser velocimeter, appl. to transonic flow wind tunnel 77−39376
dynamic flow characteristic determ. of electro-hydraulic servo-valve using laser velocimeter 79−32719
electrostatic precipitator, particle velocity, laser Doppler anemometry study 80−59144
flow meas., laser Doppler anemometry, practical considerations 79−27725
flow meas., laser Doppler anemometry 78−34227
flow meas., optical design and signal processing advances 77−19655
flow over dam, appl. *(Chinese)* 79−64804
flow rate measurement, using laser Doppler anemometer-computer system 79−68881
flow velocity, meas. using reson. ionisation velocimeter 79−82002
flow velocity meas. at olfactory organ nares of fishes *(German)* 78−69262
flow velocity of water streams, in wide channels, by laser Doppler method *(Russian)* 78−30370
fluid flow and reflecting objects, laser Doppler anemometer *(Russian)* 79−82009
fluid flow discharge, laser Doppler vel. meas. in open and closed conduits 79−68882
fluid mechanics, photon correlation techniques, conf., Cambridge, England (March 1979) 80−56998
fluid section flow pattern speckle photography 80−103096
fluidic element nonstationary flow meas. by laser Doppler velocimeter with frequency tracker *(Japanese)* 78−55707
follow-up-type Doppler velocimeter, using single-mode optical fibres 80−74476
frequency tracker for laser Doppler anemometry 79−72968
fringe and two-spot backscatter laser Doppler velocimeter, with burst-correlator processor 79−50827
fringe anemometers, light scatt. aspects, particle size meas. appl. 78−83020
fringe mode fluorescence velocimetry, organic dye appl. 77−39380
gas flow, two dimensional, laser streak velocimetry of streak velocimetry of two dimens. gas flow 77−42937
hemisphere-cylinder vel. meas. anal. 77−74375
high Reynolds number flow, review, data anal. for photon correl. method, simulation 79−60082
high-speed dual-lag photon-correlation signal processor development 77−18095
holographic microvelocimeter, ocean particle dynamics meas. 80−12567
human retinal blood flow meas. by laser Doppler velocimeter 79−79623
imaging system, real time Doppler, colour TV display of particle size or density 77−62038
individual realisation laser anemometry, sampling bias evaluation 77−58810
inertial method for measurements of airborne particle distributions 80−53901
instrumentation developed by Electricite de France Optical Applications Division *(French)* 78−75233
interferential laser Doppler velocimetry in HF plasma jet *(French)* 77−89307
interferometer system, Doppler, error sources analysis meas. volume structure *(Russian)* 80−27336
internal combustion engine efficiency studies using laser anemometer 80−53307
jet turbulence, laser velocimeter correlation meas. 80−106785
LADO-1, performance and specifications *(German)* 78−4598
laser Doppler anemometer measurement, effect of finite-size probe vol. 77−24036
laser Doppler techniques for flow measurement 79−68883
laser Doppler velocimeter for high speed combustion flow meas. 77−80255
laser Doppler velocity meter, operating principles, optical configs., appls. *(Dutch)* 78−1769

laser velocimeters continued
laser interference velocimeter, gas flow meas. appl., features 77−80254
laser-Doppler anemometry and photon correlation for turbulence length scales 80−87828
liquid, vel. meas. by coherent diffusion using triggered ruby laser *(French)* 77−68711
local size and vel. probability distrib., two-phase suspension flows, laser-Doppler technique 78−59517
measurement principles *(Polish)* 79−4096
metrological charcts. of laser Doppler anemometers 78−75238
microscopes for flow vel. meas. 78−37052
microwave modulated laser velocimeter for meas. speed of diffusely refl. objects 78−4599
multicomponent frequency shifting self-aligning laser velocimeters 78−87423
non-contact, using laser produced speckle patterns *(Japanese)* 78−178
oceanographic applications 78−36325
oil and polyisobutylene-oil, laminar plane stagnation flow kinematics, laser Doppler anemometry 78−38374
on-axis velocity component measurement with laser velocimeters 80−19526
opt. freq. shifting of light and laser beams 78−79392
optical scanning system 77−58481
optimal geometrical design 79−64268
outdoor velocimetry with CO_2 lasers 77−91296
particle measuring system, for size and density simultaneous determ. 80−98880
particle measuring system, using nonsinusoidal forced vibr. and bispectral analysis 78−41285
particle size distribution measurement by laser Doppler velocimetry technique *(Japanese)* 78−24913
particle size meas., using forced vibr. synchronised detection, and power spectral anal. 78−36977
phase inhomogeneous medium, interference method, appl. to pulsed flow *(Russian)* 78−30375
photon correl. laser anemometry, information extraction method 79−60081
photon correl. laser anemometry, on-line data reduction system 79−60080
photon correl. velocimetry, turbomachinery and industrial burner velocity and turbulence profiles 79−60083
photon correlation anemometer, differential Doppler system, appl. supersonic flow 77−35277
photon correlation signal processor 77−62035
photon correlation velocimetry of blood flow in retina 77−90828
polyethylene oxide, dilute aq. soln., laminar viscous tube flow, scale-depend. effect 79−7367
portable laser Doppler velocimeter for vibrating surfaces 79−68666
powder electrodeposition particles flow meas. 78−18364
principles and aerodynamic appls. *(French)* 78−63518
projection optics, afocal 80−75011
pulsating air flow, meas. instrumentation using photon correlation 78−87420
pulsed laser Doppler velocimeter signal processing, FFT and pulse-pair estimation 79−77322
random pulse train processing by linear filter *(Russian)* 78−46518
real-time statistical system for high Reynolds number low turbulence flow 77−3895
reflected-beam laser anemometry using photon correlator 80−106861
resonance fluorescence velocimeter, appl. to atom velocity meas. and flow speed meas. 78−46467
resonant Doppler velocimeter, direct flow visualisation 77−35285
resonant hydraulic circuit pulsatile water flow meas. using laser Doppler velocimeter 80−103091
retinal blood flow, laser Doppler meas. 78−69174
ring laser gyroscope, accuracy limit, model calc. 80−1241
rocket exhaust anemometry, Doppler difference and two focus methods, correlator and photon counting 79−60084
rolling mill product speed and length meas. *(German)* 79−72614
S/N ratio and scatt. power, detection angle effect 77−42936
SAW velocity meas. by phase-sensitive laser probe 79−46911
scanning, appl. to remote Doppler meas. of intensity fluctuations 77−791
seeding method for high-temp. laser Doppler velocimetry 78−9730
ship model wake meas. in wind tunnel, laser anemometer autocorrelation *(German)* 79−60085
signal processing techniques 78−59520
simultaneous laser measurements of instantaneous vel. and conc. in turbulent mixing flow 77−35287
single particle correlated time of flight velocimeter, wind speed meas. 78−32251
single scattering particle laser Doppler measurements of turbulence, data reduction 77−39379
smoke plume speed and turbulence meas., CO_2 laser 78−28345
sonic venturi nozzle, for volume or mass flow, differential interferometric meas. 79−68872
Spacelab optical techniques for liquid flow and temp. meas. 79−82007
spark discharge particle generator for Doppler measurements in turbulent flames 80−59139
spatial resolution and accuracy 77−24043
spatially constricted flow meas. 78−71409
spectral analysis of signals from a laser Doppler anemometer operating in the burst mode 80−100041
sphere drag coeff. correlation method, continuum and rarefied flows 77−84349
spherical particle velocity and size meas., crossed-beam light scatt. interferometry 80−47011
spray, droplet vel. meas. using laser Doppler velocimeter *(German)* 79−50818
stabilized model-fitting approach to the processing of laser anemometry and other photon-correlation data 80−58622
supersonic flowmeter using laser beam and Fabry-Perot interferometer 79−7420
three dimensional Doppler, using cross-bispectral analysis 79−30426
three-component laser-Doppler-velocimeter, signal processing and storage 77−39384
time-differentiated laser speckles, vel. meas. by first order statistics 80−82750
time-of-flight laser anemometer, for velocity meas. in atm. 78−69469
time-of-flight laser anemometer 77−39383
tracking laser Doppler velocimeter with direct spectral anal. 80−99782
transit anemometer signals, semiclassical processing 80−59145

laser velocimeters continued
transit anemometer system, computerised, for measurements in supersonic flow 80−10332
transit-time lidar velocimeter, detect. of atm. aerosol flow 77−13127
transonic axial compressor rotor flow field anal. 79−4009
transonic wind tunnel laser velocimeter meas. interpretation 77−31324
turbulent flow, meas. in vicinity of cation-selective membrane using scatt. laser radiation Doppler shift 79−46301
turbulent flow field investigation techniques 78−34224
turbulent flow measurement by laser Doppler anemometry, concentration and size of tracer particles, theoretical limits 78−59514
two dimensional laser Doppler anemometer, turbulent jet flow field meas. 80−28582
two dimensional velocity distrib. measuring system, using multiple line detectors and correlation analysis 80−14851
two-colour laser Doppler velocimeter *(German)* 80−10326
two-component LDV, appl. to flame induced flow meas. 79−23380
two-dimensional LDV measurement, of flow induced by flames 78−59529
two-phase supersonic streams, gas-dust, laser velocimetry and visualisation 79−68830
ultramicroscope anemometer for three-dimens. flow meas. in models of arterial branchings 78−35876
unsteady transonic flow meas. 80−10341
vaneless diffuser of centrifugal compressor, flow velocity meas. using laser Doppler anemometer 80−59147
variable frequency shift Doppler, for combustion flow meas. *(Japanese)* 78−67294
velocity and signal quality relationship in laser Doppler anemometry 79−14501
viscoelastic converging pipe flow, vel. vectors and radial stresses, rheological model and laser anemometry 79−60028
vortex breakdown regimes, in rot. cylindrical cavity, identification 79−50731
vortices, merging, in wind tunnel, surveys 79−32718
water flow anemometry 77−58818
wide-angle scattering configuration for laser Doppler measurements of electrophoretic mobility 80−33011
wind tunnel meas. appl., principles 78−71405
wind tunnel meas. appl., principles and techniques 77−80252
wind vel. determ. from laser intensity fluctuation meas. *(Russian)* 78−36302
CO_2 Doppler velocimeter for transverse wind vel. meas. 80−4115
CO_2 IR laser velocimetry, processing techniques and applications 80−87831
CO_2 laser, long range outdoor velocimetry, air pollution meas. 78−61623
CO_2, optical design for long-range anemometry 78−36333
CO_2, performance of acousto-optic freq. shifter 80−100042
He-Ne laser, based on speckle system *(German)* 77−33977
TeO_2 volume-acoustic-wave generator acousto-optical device, appl. in laser Doppler velocimeter 79−90030

lasers
see also chemical lasers; distributed Bragg reflector lasers; distributed feedback lasers; dye lasers; excimer lasers; free electron lasers; gas lasers; laser beams; laser frequency stability; laser tuning; liquid lasers; nuclear pumped lasers; Raman lasers; ring lasers; solid lasers; X-ray lasers
adjustment technique based on laws of geom. optics 78−5475
advanced lasers for fusion, modelling and anal. 78−50819
amplifier output enhancement by self-focusing suppression 79−13986
anthology, lasers and their applications in physical research 80−17724
basic principles and appls. *(French)* 77−3601
book, optics and lasers 78−22079
chirping laser for photochemical applics. 77−38902
coherent and nonlinear optics, Conf., Leningrad, USSR (June 1978) 80−27027
conference, appls. of low power lasers, San Diego, Calif., USA (Aug. 1976) 77−75536
conference, Dresden, Germany (Mar.-Apr. 1977) 77−83881
conference, laser engineering and appls., Washington, USA (May-June 1979) 80−1216
conference, lasers and applications, Erice, Italy (May-Jun. 1970) 77−38906
conference, lasers and their appls., Dresden, East Germany (Mar.-Apr. 1977) 79−7137
conference, Washington, DC., USA (Jun. 1977) 78−46610
conference, Washington, DC, USA (June 1977) 77−88732
conference on laser optoelectronics, Munich, Germany (June 1977) 78−33739
Crab Nebula, wisps, possible cosmic laser 77−87505
development, recollection by Townes 79−21517
educational course in modern optics and lasers at San Diego State University 80−62423
electro-optics, conference, Utrecht, Netherlands (Oct. 1978) 80−31420
electro-optics/laser international conference, Brighton (1976) 77−38800
EM precision meas., conf., Ottawa, Canada 1978 78−89462
energy meas. by optical calorimetry, hollow graphite cone appl., absorption charact. determ. *(Slovak)* 79−40572
energy research and laser development *(Japanese)* 80−91813
engineering advances, conf., San Diego, CA, USA (Aug. 1977) 78−59017
French CGE laboratory work on lasers and applications *(Spanish)* 78−30004
gain measurement technique for high gain amplifiers 80−1208
high power, conf., San Diego, Calif., USA (Aug 1976) 77−46730
high power, for fusion reactor appl., review *(German)* 77−54361
historical aspects *(Japanese)* 79−81403
introduction to lasers, fundamental physical processes and appls. 77−75466
IR lasers, and laser techniques in mol. spectroscopy 78−8455
laser and electro-optical systems, conf., San Diego, USA (May 1976) 77−19278
laser spectroscopy conf., Jackson Lake Lodge, WY, USA, 1977 July 78−82666
materials, new, res. progress, fibre optics communication appl. 77−14813
modern machine tools for hardening, glazing, boring welding and cutting *(Dutch)* 80−91808
operating mechanisms, characteristics and applications 80−64039
optical inhomogeneity cancellation using parametric convertor 80−33049

lasers continued
Optical Society of America meeting, Rochester, USA (Oct. 1979) 80−12841
optics conference, Los Alamos, NM, USA (May 79) 80−73095
optics in adverse environments, conf., San Diego, USA (Aug. 1977) 78−82976
optoelectronics, conference, Munich, Germany (June 1975) 77−7111
output control by semiconductor devices 78−22137
overview of laser technology, past, present and future 77−75537
physical characteristics, agricultural appls. *(Chinese)* 77−68216
physics, working principles, and historical evolution 80−91807
picosecond phenomena, conf., Hilton Head, USA (May 1978) 79−44940
practical IR optics, conference, Los Angeles, USA (Jan. 1978) 79−23085
principles, construction and applications 80−106531
quantum electronics, conf., New York, USA (Jun. 1980) 80−90614
radiation control *(Russian)* 77−54719
radiation energy, spectral and time range meas., instruments 79−35687
refractive index change of active medium, meas. by delay method 77−58336
review of research in International Business Machines Corp., USA 80−23696
review of work at Ukrainian SSR Acad. of Sci. *(Russian)* 79−45950
safety regulations, US Bureau of Radiological Health standards ref. 77−12955
stellar atmosphere, narrow laserJine detection in inhomogeneous broadening 77−41312
stellar atmospheres, He II 4686 Å laser action 77−13354
technology developments, power gains wavelength extensions *(Danish)* 80−64038
transitions gain coeff., maximal meas. method for cascade laser 77−31104
tunable, principles, charact. and appl. review *(Japanese)* 80−74330
tunable lasers and applications, conference, Loen (1976) 77−54720

latent heat
see also heat of fusion; heat of sublimation; heat of vaporisation
boiling, nucleate, subcooled, latent heat transport contrib. 78−75046
cold work heat release kinetics meas. using adiabatic elec. heating 77−52344
heat storage, periodic, heat-carrying fluid and storage material transport kinetics 79−3901
liquid crystals, thermal parameters, transition temps. and latent heats 78−22832
4-n-pentylbenzenethio-4′-n-octyloxybenzoate, liq. cryst. phase transitions, press. and temp. depend. 79−77730
rutile structure fluorides, high temp. polymorphism and thermal props. 80−75199
solar energy collection and storage, latent heat diode walls, space heating *(French)* 80−61298
solar energy thermal storage by latent heat of fusion of mineral salts *(French)* 79−24915
storage, physical and chemical processes at low temps. 80−72091
thermal energy storage by latent heat of fusion *(French)* 79−3893
thermal energy storage materials, energy density and materials cost *(Japanese)* 80−26168
thermal storage in density stratified fluids and phase change materials 80−67003
wind energy generator system, tornado-type, latent heat from moist air, effect on vortex 80−30365
Cr-Fe, dil., latent heat exam. of magnetic transitions 79−61156
Cr-Si, dil., latent heat exam. of magnetic transitions 79−61156
DyAG, cubic antiferromagnet, multiaxis phase transitions 79−78377
Ga, liq., effective pair pot. and thermodynamical props. 77−47600
$LiNH_4SO_4$, thermal props. near high temp. phase transition 78−19428

latent heat of adsorption *see heat of adsorption*
latent heat of combustion *see heat of combustion*
latent heat of crystallisation *see heat of crystallisation*
latent heat of dissociation *see heat of dissociation*
latent heat of formation *see heat of formation*
latent heat of fusion *see heat of fusion*
latent heat of mixing *see heat of mixing*
latent heat of reaction *see heat of reaction*
latent heat of solution *see heat of solution*
latent heat of sublimation *see heat of sublimation*
latent heat of transformation *see heat of transformation*
latent heat of vaporisation *see heat of vaporisation*
latent image *see photographic process*

lattice constants
see also crystal atomic structure
A15 struct., stabilized by crystal field distortion of exotic elements at chain sites 78−79555
absolute method for lattice parameters determ. *(Czech)* 80−44070
actinide metals and compounds, low temp. X-ray diffr. study 80−316
adenine hemisulphate hydrate, single cryst. growth from soln., props., cryst. parameters, X-ray anal. 79−32929
adenine sulphate, single cryst. growth from soln., props., cryst. parameters, X-ray anal. 79−32929
adsorbed monolayer, substrate-induced strain and orientational ordering 79−82460
alkali halide, static and dynamic props., appl. to KCl 77−7798
alkali halide crystal, struct. stability and repulsion 79−65028
alkali halide solid solns., lattice parameter and heat of form. 80−79739
alkali halides, bond forces, parameterless calc. 78−47275
alkali metal halides, interionic repulsive force and ion compressibility rel. to lattice consts. 77−11500
alkali metal hydrides, bond forces, parameterless calc. 78−47275
alkali metals, non-parametric calc. of binding energy *(Russian)* 77−27844
alloy, variation in interatomic interaction and lattice parameters during ordering *(Russian)* 77−81255
anthracene, lattice parameters press. depend., elastic consts. 78−38686
benzalazine, thermal expansion, lattice consts. meas. 78−47539
binary system, A^NB^{8-N}, ground state of electron subsystem, quasimolecular model 79−69055
Bond method, of meas. lattice parameters, asymmetric Bragg reflections appl. 80−38861
carnauba wax, thermoelectret, lattice parameter changes at elevated temps. 80−29674

lattice constants continued
carnauba wax thermoelectret, charge behaviour 80−7276
cellulose II, unit cell parameters, neutron diffr. 77−1086
chaoite, a new allotropic form of carbon, produced by shock compression 80−80997
cholesteryl ethyl carbonate, unit-cell dimensions and space group 80−84165
covalent semiconductors, charge density, struct. props. electron-electron interactions 78−47725
crystal, statistical thermodynamics with collective vibrations 78−54289
crystal Hartree-Fock theory, ab initio effective potentials 80−103290
cubic crystals, response to (111) loading, internal energy, elastic moduli 80−84230
Debye-Scherrer method, lattice parameter determ., influence of specimen absorption and beam divergence 77−76249
di-o-thymotide, cryst. chem. study and morphology *(French)* 79−46576
1,6-dicarbazolyl hexadiyne, solid-state polymerisation, monomer to polymer phase transformations 80−38948
dioctadecyl hydrogen maleate crystals, X-ray spectroscopic true $2d_{cr}$ value, 'effective' 2d value concept of Bragg spectrometer crystals 80−70081
disperse systems, solubility increase, phase composition, size effect calcs. 80−70418
drift and lattice const. determ., graphic method *(Chinese)* 80−87985
elastic deformation effect on lattice-parameter determ. 77−72524
electron diffraction, high order Laue zone effects, lattice parameter determ. 77−43120
Elinvar, γ to γ' transformation and γ' phase form. kinetics, lattice consts. 80−35191
equivalent neighbour model, generalised, derivation of high temp. lattice consts 80−77721
$EuSb_4S_7$, single cryst. growth, and X-ray anal. 79−100033
extended deformation fields, X-ray diffr. meas. method sensitivity 80−28880
faceted microcrystal, surface tension and lattice parameter changes 77−47660
FCC cryst., theory of response to [110] uniaxial loading 79−19310
FCC metals, props. of vacancies and divacancies 80−10545
γ-Fe particles, obtained by reactive gas evaporation from Fe-N system, lattice consts., electron microscopy 79−56919
ferrite, hexagonal, local lattice distortions, use of Mossbauer effect 78−43745
fluctuations, influence on thermal props. of cryst. 79−77715
fluctuations, rel. to theory of eqn. of state for crystals 78−30732
2-fluoronaphthalene, disordered form, thermal expansion, neutron and X-ray diffr. study 80−24621
grain boundary segregation, computer simulation using Mie type interatomic pot. 80−54259
graphite, neutron induced changes, exam. of lattice consts., elastic modulus, elec. cond 79−95053
homogeneity and struct. vacancies 77−84937
I-III-VI_2 semiconductor epitaxial layers, lattice parameters meas. using RHEED 79−90913
II-VI quaternary semiconductor alloys, energy bandgap and lattice constant contours 80−103622
II-VI semiconductors, mag. susceptibility, effect of physical parameters 80−44793
III-V compounds, lattice constant determ. of epitaxial layers and effect of misfit dislocations 79−19479
III-V quaternary alloy, $A_xB_yC_zD$ or $AB_xC_yD_z$, energy bandgap and lattice constant 79−4296
III-V quaternary alloys, energy bandgap and lattice consts. 78−67940
III-V semiconductors, effective mass, forbidden bandwidth and lattice constant relation *(Slovak)* 78−51879
inert gas in metal in gas discharge, model, lattice const. 79−65202
infinite linear array of atoms equilib. lattice parameter, Morse pairwise pot. calcs. 77−76331
intermetallic phases with $L1_2$ and $D0_{19}$ struct., atom incompressibility, lattice parameter approach 78−91294
interplanar spacings, precision determ., by means of reflection electron diffr. 79−64961
Invar, Fe-Ni (36 wt.%), alloy 36N, effect of melting conditions on thermal expansion coeff. 80−65256
Invar, phase stability, spinodal decomposition 80−88327
ion irradiated, radiation-induced damage, microhardness and lattice consts. meas. 78−2170
ionic crystals, interplanar spacings near boundaries and repulsive forces between ions 79−99165
ionic solids, lattice and defect props., modified electron gas approx. 79−42054
Ising fourth-neighbour models on FCC lattice, coexistence curves 79−80543
isoperimetric problems, convex-set theory and lattice symmetry 80−46988
Kapton H, aromatic, polyimide, conformational investig., X-ray method, pot. energy calcs. 77−3498
ketone-paraffin solid soln., dielec. relax., temp. and lattice const. depend. *(German)* 78−76383
Kossel technique in SEM for crystallographic orientation 80−75133
least squares program 79−64958
linear chain, isotope effect on lattice const. 80−103306
LJD model, fine-grained lattices and continuum, Monte Carlo studies 79−12734
Madelung parameter, expansion in terms of multipole moments, ratio of two lattice parameters 78−75618
measurement, single cryst., with $K\alpha_1$-$K\alpha_2$ doublet in two-cryst. spectrometer 79−50938
metal, entropy and lattice parameter relation 77−36464
metal, non-cubic, electric field gradient, press. and temp. depend. 77−8057
metal, textured cubic, residual stress evaluation 80−89435
metal hexaborides, ^{11}B nucl. quadrupole interaction, NMR meas. 80−2660
metal powder, milling conditions effect on densification during pressing and sintering 78−11149
metals, electron-deformation interaction, lattice contraction, Hubbard model calcs. *(Russian)* 80−59592
metals, FCC, lattice parameters in pair potentials calc., appl. to point defect props. 80−19798
methylammonium chromium selenate, lattice consts. and ferroelec. props. 79−33641
lattice constants continued
methylammonium gallium selenate, lattice consts. and ferroelec. props. 79−33641
microcrystals, method for indexing *(German)* 78−22608
$Mn_{1-x}Cu_xSb$ films, $0 \leq X \leq 0.3$, magneto-optical props. 79−51981
muscovite of regional metamorphic rocks in Xizhang, b_0 value and geological significance *(Chinese)* 79−74890
nylons 6, 66, 610, change in cryst. struct. with temp. 77−15324
order-disorder structures, X-ray powder patterns features 80−38864
organic solid solutions, cell parameters calc. *(Russian)* 77−72687
oxamide, thermal expansion tensor, calc. from lattice constant changes with temp. 77−76582
oxides, nonstoichiometric, cluster component method calc. of lattice params., composition, imperfection 77−25031
PbO-Nb_2O_5 system, X-ray and electron microscopic phase and struct. determ. *(French)* 80−92508
period determ. by axial X-ray camera 79−68974
perovskite structure oxides, solid soln., crystal lattice parameters, conc. depend. calc. 78−95041
perovskites, $(AA')(BB')O_6$, ion valency pairs determ. from lattice consts. 77−43195
perturbation stable cell comparison technique 80−49133
poly-ε-caprolactone-PVC blends, morphology 79−69019
polycaprolactam film, subjected to 9 kV elec. discharge, X-ray obs. *(Russian)* 79−23536
polycrystalline materials, lattice parameter meas., systematic errors 79−10749
polydiacetylene-bis(toluenesulphonate), single cryst., thermal expansion and optical band splitting 77−8594
polyethylene, branched, annealing effect on lattice consts. 79−14698
polyethylene cryst., unit cell variations with temp. and high press. 78−47250
polyimides, DFOPF and DFOB, X-diffr. exam. of structure and elasticity 80−6370
polymethylpentene, isotactic, crystal struct. 78−67663
polystyrene spheres, crystallised suspension, gravitational compression 78−23975
polytetrahydrofuran, line-broadness in X-ray diffr. 77−19878
polytetramethylene terephthalate, comparison of crystn. structs. in relaxed and strained forms 77−84675
polytrimethylene terephthalate single crystals, X-ray and electron diffr. obs. of cryst. struct., packing analysis 79−94924
pyrite type dichalcogenides, ^{57}Fe isomer shift, quadrupole splitting, Mossbauer study 80−15832
α-quartz, compression to 120 kbar 77−15493
quartz, synthetic, fading rel. to lattice deformation *(German)* 78−63760
quartz, synthetic local variations meas. in spacing and orientation of lattice plane, X-ray anal. 79−52099
quartz lattice constants, impurity effects 80−39034
quartz powders, CaO soln. chemisorpt. rel. to lattice parameters, work function 79−37918
rare earth alloys with Cu_3Au lattice, cryst. chemistry and supercond. crit. temp. 79−86744
rare earth dicarbides, solid solns., phase transformation, strain energy 78−51672
rare earth garnets, garnets, Debye charact. temp. and reciprocal lattice consts. 80−29144
rare earth intermetallics, RFe_2, spontaneous magnetoelastic distortion, X-ray diffr. expts. 77−63253
rare earth metal, electron interactions rel. to lattice props. *(Russian)* 77−35901
rare earth mixed molybdates, $R_2(MoO_4)_3$, $R_{2(1-x)}R'_{2x}(MoO_4)_3$, cryst. growth and crystallographic data 79−43132
rare earth orthoferrites, Neel point, cation depend. *(Japanese)* 77−43834
rare earth oxide-ZrO_2 (HfO_2), cubic solid soln., lattice parameters 79−82186
rare earth RNb_3O_9, synthesis and physicochem. props. 77−90304
rare earth-Cd double tungstates, with scheelite structure 78−44103
rare earth-Fe_2, mag. props. changes due to H_2 absorption, unit cell vol. 77−63178
(rare-earth) $Fe_3(BO_3)_4$, cryst. growth from soln.-melt, props. 80−108337
rare-earth $CaWO_4$, phase transitions of fergusonite-scheelite *(French)* 80−19942
rare-earth trihydroxides, single cryst. X-ray lattice constants determ. 80−19766
RbBr, structural phase transition, Born-model and effects of hydrostatic and non-hydrostatic stresses 79−23721
reciprocal squares of lattice parameters, determ. by solving linear eqns. *(German)* 80−10452
reduced cell for use in cryst. materials identification 77−15271
semiconductor alloys, effect of lattice const. variation in band theory 80−49596
semiconductor thin film, lattice parameter meas. 78−59720
SiAlON X-phase, X-ray diffr. data 80−49198
sigma phase structure, ionicity modified pair pot. model anal. 78−51466
single crystal, apparatus for temp. depend. meas., Bond's method 77−24243
small particles, cause of reduction in lattice spacing *(Russian)* 80−38967
sodalites, aluminogermanate- and aluminate-, IR spectra rel. to T-O bond length and T-O-T ang. 79−91445
spatial lattice distance, accurate and precise meas. *(German)* 80−19666
sphalerite materials, complex, spray pyrolysis 79−43574
steel, austenitic, Cr-Ni-Mo, Mo effect on lattice parameters and chem. comp. of σ-phase and $M_{23}C_6$ carbides 77−70072
steel, austenitic stainless, defect structure, N content depend. *(Russian)* 77−59022
steel, Cr-Ni-(Mo) (25, 28, 2 wt.%), lattice dilation by N_2 77−16592
steel, heat-resistant, 12Kh1MF, yield point rel. to dislocation density and cryst. lattice spacing *(Russian)* 77−44291
steel, Mn, tempered, sementite crystals, carbide phase segregation, X-ray study *(Russian)* 78−35391
steel, Mo and Cr-Mo, X-ray elasticity constants at high specimen temp. *(German)* 80−35239
steel, stainless, cold plastic deform. effect on struct. and props. 80−29113
steel, stainless, wire, axial texture after electroplastic drawing, X-ray struct. investigation *(Russian)* 80−104177
steel, W-Co-Mo-Cr-V-C (8.5, 8.1, 4.5, 3.5, 2.2, 1.02 wt.%), phase composition, struct. and props. 80−104163

lattice constants continued
strain-tensor components expressed in terms of lattice parameters 78−26618
talc, lattice parameters meas. by back-reflection pseudo-Kossel technique 79−82124
TBBA liquid crystal, monoclinic cell parameters of solid, smectic and metastable phases, temp. dependence 80−70122
TCNQ salt, $(TSeF)_x(TTF)_{1-x}$-TCNQ, struct., elec. and mag. props., review 80−20158
TCNQ salts, $Qn(TCNQ)_2$ impurity effects on electronic coherence length 79−73500
temperature dependence, high angle double crystal diffractometry, pt.II 80−1891
temperature dependence, meas., high angle double cryst. diffractometry, pt.I 80−1890
ternary alloys, A-15 phase, Cr_3Si type, atomic volumes deduced 78−22690
ternary semiconductors, measurement of lattice parameters of thin heteroepitaxial layers, RHEED technique 80−15406
transition metal, cohesive energy, lattice consts. and bulk modulus, renormalised atom method 77−43170
transition metal 3d monoxides, specific vol. and mag. moment calcs. 80−65822
transition metal alloys, cohesive properties and press.-vol. relation 80−92476
transition metals, interatomic forces, phonon spectra, from band structure charge densities 79−7662
transuranic compounds, 5f electrons delocalisation *(French)* 77−27857
triptycene hydrogenation products, ACC and TCC, cryst. data 80−100224
tris (3-mercapto-1, 3-diphenyl-2-propen-1-onato) Co(III), multiple twinning 80−100250
TTF-TCNQ, elastic- and inelastic-neutron scatt. study 79−69208
urea molecule, bond-length corrections for external and internal vibrs. 80−106402
vanadium bronzes of type $M_xV_{12}O_{30}$, synthesis and thermal props. of single crysts. 77−84717
vanadocene, order-disorder phase transition, sp. ht. and crystallographic study *(French)* 80−84131
X-ray spectrometer, double-beam triple-crystal, high sensitivity, for lattice parameter and topographic meas. 80−77915
YAG powder, X-ray K_α doublet diffr. peak position rel. to lattice const. precision 77−68891
zinc blende-type hosts, Co^{2+} impurities Huang-Rhys number rel. to props. of host lattice 79−83018
Ag, vacancy formation energy, thermal expansion meas. 79−14798
Ag-Au (50 at.%), thermal expansion and lattice parameters, temp. depend. 78−91456
Ag-based alloys, α-phase, mag. susceptibility correl. with lattice parameter 78−68154
Ag-Ge, thermal expansion, X-ray determ. 78−26697
Ag-Hg amalgam, temp. depend., explained in terms of Hg evaporataion 78−26704
α-Ag-In solid solutions, lattice dynamics parameters *(Russian)* 80−96477
Ag-Ni supersaturated metastable solid solns. formed by ion beam mixing 80−107425
Ag_7AsS_6, thermal, crystallographic and elec. props. *(French)* 80−40338
Ag_7AsSe_6, thermal, crystallographic and elec. props. *(French)* 80−40338
AgCl-AgBr mixed crysts., elastic consts. and cryst. symm. 80−70290
$AgGaS_2$-$AgGaSe_2$ system, phase diagram, lattice consts., and IR spectra 80−60841
AgMg two phase bicrystal, growth by solid state diffusion couple method 80−60773
Ag_2O, thermal expansion, lattice parameter determ., 150-250K 78−2267
$AgSbS_2$, synthetic crystals, DTA and cryst. struct., phase transitions *(German)* 78−42943
Al, difference between vacuum condensates and massive specimens *(Russian)* 77−31912
Al film, He^+ irrad., overpressurised bubble obs. 79−51165
Al, Gruneisen parameters, low temp. 79−23694
Al, low temperature lattice parameters and Gruneisen parameter 78−38658
Al, vacancy formation energy, thermal expansion meas. 79−14798
Al/Cu thin film couples, TEM study of intermetallic nucleation at interface 80−65305
Al-C interstitial solid solns., atomic static displacements and deform. interaction *(Russian)* 80−64953
Al-Cu films, deposition rate, mol. beam incidence angle influence on struct., film props. *(Russian)* 79−60646
Al-Mn alloys, study of solidification by rapid cooling *(Japanese)* 78−88459
Al-Zn, low temperature lattice parameters 78−38658
Al-Zn(Ag)-Mg, metastable T′ phase 77−21151
$Al_{12-4x}Be_2C_{10-3x}$(-1≤x≤1), solid soln., comp. vs lattice constants 80−45284
$Al_4C_3.3Be_2C$, X-ray difr. and TEM study 80−14973
β-AlO_3-$(Na,Li)_2O$, NMR, Raman and IR spectra, and X-ray diffr., heat treatment induced changes 80−107508
Al_2O_3, polycrystalline, conditions for formation of anion vacancies 79−10844
Al_2O_3-Cr_2O_3, solid soln., thermal expansion anisotropy, lattice consts. 80−54411
β-Al_2O_3-K2O/K ferrite, interfaces and solid soln., thermal expansion and lattice parameter variations 78−55959
$Al_4Si_2C_5$, synthesis, X-ray diffraction pattern, lattice constants 80−50581
Ar adsorbed monolayers, on graphite, equilib. config. and lattice consts. 80−54524
Ar, monolayer, adsorbed on graphite, lattice spacing and isosteric heat below 50K, LEED obs. 80−34303
Ar, solid, lattice parameter determ. at melting, X-ray diffr. 78−10174
As, band structure and cryst. energy, pseudopot. calc. 79−90954
Au, electron irradiated, interstitials and their clusters, diffuse X-ray scatt. study 80−33997
Au, fine particles, gas evaporation technique for prep., X-ray diffr. study 80−75327
Au, fine particles, gas evaporation technique of prep., X-ray diffr. study, charact. temp. 80−75328

lattice constants continued
Au-Cu, dil., electron irradiated, interstitials and their clusters, diffuse X-ray scatt. study 80−33997
Au_4Si.m, metastable phase, substruct. unit cell *(German)* 80−88091
B-B_4C materials, hot-pressed, lattice constants 79−79018
B_4C, melting and phase homogeneity range 80−20911
$BaF_{2-x}H_x$, synthesis and struct. determ. using neutron diffr. *(French)* 80−24425
$(BaF_2)_{1-x}(YF_3)_x$, crystal growth and struct. 77−12520
$(BaF_2)_{1-x}(YbF_3)_x$ and $(BaF_2)_{1-x}(NdF_3)_x$, crystal growth and struct. 77−12520
$BaFe_{12}O_{19}$, hexagonal ferrite, local lattice distortions, use of Mossbauer effect 78−43745
$BaFe_{12}O_{19}$, powder, milled and annealed, phase composition, lattice conts. and crystallite size 80−71677
β-$Ba_9Fe_4S_{15}$, and low temp. α polymorph., cryst. struct. 78−67690
$Ba_3FeTa_2O_9$, Mossbauer and X-ray diffr. studies 80−103905
$BaGd_4X_5O_{17}$ (X=Si,Ge), cell consts., luminesc. of various rare-earth activators 80−93376
BaO thin films, on (110) face of W, struct. study by LEED 79−60659
$BaR_2(MoO_4)_4$, R=rare-earth, struct., optical, mech., spectral and physicochem. props. 80−84161
$BaSi_{2-y}Ge_y$, solid solution with type $SrSi_2$ struct., lattice parameters at high press. 80−54203
$BaSiO_3$-$BaGeO_3$, phase diag. 77−48404
$BaSnF_4$, lattice constants meas. from liquid N_2 temp. up to 400°C, phase transition 79−77781
$BaTiO_3$, polycryst., phase transition obs. in −170 to 220°C range *(Russian)* 80−103474
$BaTiO_3$, transform. of cryst. struct., at cubic-to-tetragonal phase transitions 79−37827
$BaTiO_3$:Dy ceramic, sintering, grain size, characterisation and props. 77−55923
$Ba_2Ti_9O_{20}$ single crysts., prep. and unit-cell parameters 80−103302
$Ba_{0.15}VO_2$, electrical cond., thermo-EMF, and lattice consts. 80−54685
Ba_xVO_2, oxygen vanadium bronze, phase comp., heating in air 77−40417
$BaY_4X_5O_{17}$ (X=Si,Ge), cell consts., luminesc. of various rare-earth activators 80−93376
Be intermetallics, MBe_{13}, (M=Y, La, Ce, Lu, Th), lattice spacings and susceptibilities 80−65778
$Bi_2Al(Ga)_4O_9$, fluoresc. and X-ray data 78−80403
$Bi_2W_2O_9$-$BiVO_4$, solid soln., X-ray diffr. study 80−2001
C fibres, fibril dimension estimation, using lubricostatic structural models 80−54171
$CaAl_2O_4$, high pressure modifications 80−104149
CaF_2, anion-void superlattices *(Danish)* 79−14796
CaF_2, thin insulating film, lattice parameter meas. by electron microscope 77−65940
$CaGa_2O_4$, high pressure modifications 80−104149
$Ca_xGd_{2-x}Sn_{2-x}Sb_xO_7$, pyrochlorate struct. form. 80−92504
$Ca_xNi_{1-x}Fe_2O_4$, X-ray struct. anal., determ. of lattice constant and interplanar distances *(French)* 80−96487
CaO, electronic structure 80−2332
CaO, modified electron gas theory, high press. effect 77−19899
$CaSO_4$, thermal expsn., 22-1000°C 80−6530
Ca_2SiO_4, structurally related phases, high-temp. X-ray powder diffr. 80−81050
$Ca_{0.15}VO_2$, electrical cond., thermo-EMF, and lattice consts. 80−54685
$Ca_2V_2O_7$, $Ca(VO_3)_2$, and $Ca_3(VO_4)_2$, thermal expansion, lattice constants temp. depend. 80−34211
Ca_xVO_2, oxygen vanadium bronze, phase comp., heating in air 77−40417
$CaWO_4$:Nd^{3+} $4f^3$ configuration, ground level energy state variation rel. to press. *(Russian)* 77−16358
CaX-MnX, X=S, Se, Te, lattice constants rel. to comp. 80−44320
$CdCr_2Se_4$:In, influence of Se-deficiency on props. 78−30921
$Cd_{65}Hg_{35}$ and $Cd_{55}Hg_{45}$, X-ray study of cryst. struct. and thermal expansion 80−24405
$Cd_xHg_{1-x}Te$ film, vacuum deposited, struct. and elec. props. 77−59344
$CdLn(TiNb)O_7$, Ln=La-Lu, synthesis physicochem. props. 77−43186
$Cd_2(NH_4)_2(SO_4)_3$, X-ray and optical studies of ferroelec. phase transition 79−38495
CdS, rock-salt type high-press. phase synthesis using metal sulphide additives 80−104084
CdSe-Ge (111) heterojunctions, epitaxial, azimuthal rotation 78−84085
CdTe layers, on CdS substrate, cryst. perfection and defects, X-ray diffr. obs. 79−56081
p-CdTe, nondoped, heat treatment in vacuum, dissoc. obs. effects on struct. and props. *(Japanese)* 80−60662
Ce-M intermetallic cpds., M=3d transition metal, sorption of H_2, structural charges 80−88429
$Ce_xLa_{1-x}B_6$ solid solutions, Weiss const. antiferromagnetic ordering calcs., mag. props. *(Russian)* 79−91212
$(Ce_xLa_{1-x})Be_{13}$, mag. intermediate valence behaviour, lattice parameters meas. 79−24131
$Ce_{1-x}La_xSn_3$ (x=0 to 1), mag. susceptibility and magnetisation, lattice parameters, X-ray and neutron diffr. meas. 80−49675
$Ce_2(MoO_4)_3$, crystn. from Na_2MoO_4 based melt 80−20920
CeN, interconfiguration fluctuation, temp. and press. depend. 79−38031
$CeNi_2$-$CePt_2$ system, structural and mag. studies on valence behaviour of Ce 80−103809
CeO_2-PrO_x system, mixed cryst. phase characterisation 79−14936
CeO_2-rare earth oxides, complexes of the 'two impurity ions-vacancy' type 79−95004
CeP(As)(Sb), compressibility, room temp., from neutron diffr. meas. of lattice parameter variation up to 41 kbar 77−27940
$CeRu_2$, change of valence of Ce ions, induced by H absorption, supercond. disappearance 79−47185
$CeRu_2$, H absorption induced Ce valence change, mag. and supercond. props. 80−50042
$Ce_{1-x}Sc_xPd_3$, intermediate valence of Ce, susceptibility, lattice const., ESR meas. 80−103648
$Ce_4Si_2O_7N_2$, lattice consts., X-ray diffr. anal. 80−28986
$(Ce_xY_{1-x})Fe_2$, mag. susceptibility and Mossbauer meas., lattice parameters 80−97068
CmAs(N)(P)(S)(Sb)(Se)(Te), lattice consts., X-ray diffr. study 80−33953
CmO_2, lattice parameter, neutron diffr. meas. 77−63101
Co, lattice dynamics and compression curves 78−38793

lattice constants continued
Co-C, ferromag., prep. by splat-quenching, obs. of electronic struct. of interstitial C 77−62868
Co-Fe epitaxial films, singularities of $\gamma \rightarrow \alpha$ transform., X-ray diffr. obs. *(Russian)* 79−52198
Co-Ga binary system, lattice consts., phase transform *(Chinese)* 80−88108
Co-Ni-Zn, diagram of state, crystalline lattice consts., microhardness *(Russian)* 80−66479
Co-V (10 to 23 wt.%) system, phase constitution, X-ray and elec. resist. meas. 80−3007
Co-WC hard alloys, rapidly quenched struct. 80−76233
$(Co_{1-x}Mn_x)_2B$, $0 \leq x \leq 1$, magnetisation, lattice consts., press. depend. of Curie temp. 80−7137
CoO-ZnO-MgO ternary systems, solid solns., struct. charact. 80−60629
CoSb, cryst. growth from nonstoichiometric melt, and cryst. chem 78−35286
$CoSe_2$, bulk mag. susceptibility, anomalous temp. depend., NMR and X-ray diffr. meas 79−87229
Cr condensates, lattice const., internal stresses *(Russian)* 80−107141
Cr, difference between vacuum condensates and massive specimens *(Russian)* 77−31912
Cr, electronic struct., spin-density functional calcs. 80−88476
Cr film, obtained by thermo ionic precipitation, phase composition, lattice parameters *(Russian)* 80−96756
Cr film, vacuum-evaporated, with A-15 struct., prep. and characterisation 77−62768
Cr, lattice dynamics, improved Fielek model 80−59598
$Cr_xFe_{3-x}O_4$, spin and charge density oscillations due to impurities *(Korean)* 80−20565
$Cr_{1-x}Fe_xOOH$, $0 \leq x \leq 10$, prep., Mossbauer effect, Neel temp. 80−108134
CrN-MnN, synthesis and props. 77−40405
$CrSe_2$, layered, phys. and elec. props. 80−44594
$Cr_2Se_{3-x}Te_x$, mag. props. and lattice parameters, comp. depend. 77−66263
$Cr_3Se_{4-x}Te_x$, mag. props. and lattice parameters, comp. depend. 77−66263
$CrSxTe_{1-x}$ (x=0 to 0.2), lattice constants v's CrS conc. 80−11194
$CsDy_2F_7$ and Cs_3DyF_6, cryst. symm. and cell parameters *(French)* 80−81040
CsH_2PO_4, lattice consts., temp. depend. of dielec. const. and birefringence, high temp. phase transitions 79−56746
$Cs_2NaLn(III)Br_6$, prep., cryst. genesis, and charact. by X-ray powder diffr. *(French)* 79−43135
$CsPbCl_3$, lattice thermal expansion, X-ray powder technique 80−19965
Cs_2SO_4-$(NH_4)_2SO_4$ mixed cryst., ferroelec. transition, structural and dielec. props., proton spin-lattice relax. 78−39512
$CsSbO_3$, solid state synthesis *(French)* 80−104438
Cs_2UI_6, lattice constants 80−50568
Cu alloy solid solution condensed films, influence of alloying components on phase composition and lattice spacing *(Russian)* 80−20047
Cu, difference between vacuum condensates and massive specimens *(Russian)* 77−31912
Cu extended X-ray fine struct., lattice consts. 80−89085
Cu, lattice and force consts., pairwise atomic repulsions in cluster model 79−32939
Cu, plastically deformed, lattice strain distrib. *(German)* 80−85012
Cu, wire, axial texture after electroplastic drawing, X-ray struct. investigation *(Russian)* 80−104177
Cu-Ag (3 at.%), plastically deformed, lattice strain distrib. *(German)* 80−85012
α-Cu-Al, binary substitutional, short-range ordering kinetics, vacancy behaviour 78−55867
α-Cu-Al, short range order effect, atomic potential appl. 77−27850
Cu-Al system, high temp. lattice parameters by X-ray diffr. 80−28950
Cu-Al-Ni (14.5, 3 wt.%), fatigued, polycrystn., pseudoelastic, dislocation and martensite substructs. 79−82223
Cu-based alloys, α-phase, mag. susceptibility correl. with lattice parameter 78−68154
Cu-Be-Ni (1.9, 0.32 wt.%) solution treated alloy, age induced vol. changes in structural transformations *(Russian)* 79−100179
Cu-Cd alloys obtained by electrolysis, struct. 78−91552
Cu-Ge, thermal expansion, X-ray determ. 78−26697
Cu-M, M=Al,Cd,In,Ga,Zn, magnetic susceptibility, comp. and temp. depend., melting effects 78−52202
Cu-Ni-Fe, spinodal alloy, heat treatments for improved mech. props. 79−5024
Cu-Ni-Sn, thermal decomposition after prior cold work 78−15427
Cu-Ni-Zn system, tie lines in a two phase region 80−24404
Cu-S, thin film, phase formation conditions *(Russian)* 79−56078
Cu-Ti, lattice parameter change during ageing *(Japanese)* 78−35411
$Cu_xAg_{1-x}I$ crystals, layer structs., X-ray diffr. studies 80−96457
$Cu_{1-y}Ag_yInS_{2(1-x)}Se_{2x}$, lattice consts. and band gap variations 79−78000
$CuAl_2$, constitutional defect struct., from X-ray and density meas. proposed substitutional-vacancy model 79−37696
CuCl, defect and impurity bands, lattice consts. 80−54638
CuCl, energy bands and effective mass 80−10859
$CuCl_2.2H_2O$, magnetoelastic props. under press., antiferromagnetic resonance, lattice parameters 80−29598
$CuCr_2O_4$-$MgCr_2O_4$, X-ray investig. 77−44224
$CuCr_2Se_4$, crystal growth from melt, exam. of props. 80−55283
$Cu_{1-x}Cr_2Se_4$, influence of excess Cu on physical props. 80−103836
$CuFe_2S_3$, cubanite polymorph, synthesis above 200°C and 1 GPa, lattice constants 80−108367
$CuGaS_2$, tetragonal distortion, crystal field splitting, temp. depend. 79−47060
$CuGaSe_2$, epitaxial layers, lattice parameters meas. using RHEED 79−90913
$CuGaSe_2$, thermal expansion obs. 80−70432
$CuGdTe_2$, synthesis and elec. props. 78−26529
$CuInS_2$ crystals, growth, struct., and elec. props. 79−38729
$Cu_xMo_6S_8$, constitution diagram, 11-2000K 80−108407
$Cu_xMo_6S_8$, evap. film prep., supercond. props., lattice parameters 78−23195
$Cu_xMo_6S_6I_2$, x=0 to 1.2, superconducting Chevrel-phase system, lattice parameters 79−69618
$Cu_{2-x}Te$, x=0 to 0.3, elec. cond., Hall const., carrier mobility, conc., thermoelec., density, lattice parameter 77−11915

lattice constants continued
DyF_3-KF, phase diagram, cryst. symmetry and lattice constants of phases *(French)* 79−65171
$DyFeO_3$, temp. depend. of lattice consts., spontaneous magnetostriction 79−56599
$Dy_2(MoO_4)_3$, cryst. growth and props. 79−55727
Dy_2O_3-ZrO_2 phase diagram and long range ordering 80−93542
$DyRh_{1.1}Sn_{3.6}$, new supercond./mag. cpds., X-ray powder diffr. data 80−100215
$ErCo_3B_2$, rel. to mag. props. 77−24711
$ErFe_2H_{3.9}$, mag. props. and lattice consts., effect of hydrogen absorpt. 77−20561
$ErRh_{1.1}Sn_{3.6}$, new supercond./mag. cpds., X-ray powder diffr. data 80−100215
Eu_4As_3, new synthesis, trigonal anti-Th_3P_4-type compound, X-ray characterisation 79−37687
EuB_6, growth by soln. method, struct., mech. and elec. props. 80−16168
EuB_6, resistivity press. variation, lattice consts. 80−100456
$Eu_{1-x}La_xS$, electron struct., lattice consts., X-ray spectral study *(Russian)* 80−100432
$(EuLu)_3(FeAl)_5O_{12}$, film epitaxial growth on Gd_3GaO_{12} substrate, mag. props. 80−65402
EuO, nonstoichiometric film with excess EU, effect on resist. and Curie temp. 79−8204
EuO:Gd, critical specific heat depend. on doping, microwave cond. 79−95602
$Eu_{1-x}{}^2R_x{}^+O_{1-x}$ (R=Nd, Eu, Gd), lattice parameters, mag. and elec. props. 80−100578
$EuSb_2Se_4$, single cryst. growth, and X-ray anal. 79−100033
EuX_5, X=Cu, Zn, Ag, Au, cond. electron spin polarisation effects 77−63136
(Fe, Mn)B and $(Fe, Mn)_2B$, lattice constants of solid solns. *(Italian)* 77−48402
Fe, cast, influence of Y and Sb on microhardness and lattice spacing of ferrite *(Russian)* 80−19748
Fe complex, $[Fe(2\text{-}pic)_3]Cl_2.EtOH$, struct. changes, spin phase transition mechanism 79−78380
Fe, difference between vacuum condensates and massive specimens *(Russian)* 77−31912
γ-Fe, FCC film, epitaxial growth on CuAu (111) surfaces, strong ferromagnetism 80−70557
α-Fe, lattice and force consts., pairwise atomic repulsions in cluster model 79−32939
α-Fe, lattice wave dispersion, lattice consts., elastic consts. 80−24545
Fe-Al-C, gamma irrad., crystal lattice parameter reversible changes *(Russian)* 80−10576
Fe-B, rapidly solidified, metastable phases *(German)* 79−29045
α-Fe-Be(Mo_1)(Ti)(W), lattice consts. at 293K *(Japanese)* 79−42256
α-Fe-Be(W)-Co, solid soln., lattice constant at 273K *(Japanese)* 79−42257
Fe-C-Al steels, law of variation of cryst. lattice parameters X-ray diffr. analysis *(Russian)* 77−52322
Fe-C-Si alloy, lattice parameters of cementite after quenching 78−11198
Fe-Co-Ni-Al-Nb (15-20, 14, 9, 0.1-5.5 at.%), Nb effect on magnetic props., lattice parameter *(Russian)* 77−55689
Fe-Co-W-C steel, M_6C carbide behaviour during ht. treatment *(Russian)* 77−66658
Fe-Cr alloys and Fe, lattice parameters, 293 to 1273K, α to γ phase transform., X-ray diffr. exam. *(Russian)* 80−50625
Fe-Cr-C, lattice parameters of cementite, annealing effect 80−29007
Fe-Cr-Mn alloys, Mn content effect on Cr distrib. in suboxide layers *(Russian)* 77−12732
Fe-lanthanid-O systems, thermodynamic props., composition and lattice constants 78−31390
Fe-Mn-C, anomalous changes in austenite and martensite lattice parameters 80−50636
Fe-Mn-C, lattice parameters of cementite, annealing effect 80−29007
Fe-Mn-C-Si alloy, G20 type, vol. effects during $\gamma \rightarrow \varepsilon$ transform., lattice parameters of γ-and ε-phases, Si and Mn effects *(Russian)* 78−6918
Fe-Mn-Sb, phase comp. 80−16267
Fe-Mo-C, lattice parameters of cementite, annealing effect 80−29007
Fe-Mo(V), nitrided by const. activity ageing, X-ray studies 77−32720
Fe-Ni alloys, XPS of valence electrons rel. to lattice parameters *(Russian)* 77−77340
Fe-Ni films, lattice constants rel. to mag. moments *(Russian)* 77−32218
Fe-Ni-Al-Cu (25, 14, 4 wt.%), alloy YuND4, effect of Ti addition on structure, mag. props. 80−15714
Fe-Ni-C, lattice parameters of cementite, annealing effect 80−29007
Fe-Ni-Cr, Elinvar, struct. and mag. props., singularities during tempering *(Russian)* 80−50627
Fe-Ni-Cr-Ti-Al Elinvar alloys, dispersion-hardened, structural transform. *(Russian)* 79−1872
Fe-Pd (31.2 wt.%), thermoelastic FCC-FCT martensitic transformation 80−104156
Fe-Pd Invar alloys, elec. and mag. props. and thermal expansion 80−75732
Fe-Si-N alloy, BCC, N conc. depend., rel. to martensitic transform. obs. *(Russian)* 78−48397
Fe-Ti-C, rapidly quenched by splat-cooling 80−84923
Fe-V alloys, Mossbauer study, lattice constant and magnetic moment correl. 78−27134
$Fe_3Al_xSi_{1-x}$, DO_3 structured, ferromag., lattice parameters 79−42010
$Fe_{73}Al_xSi_{27-x}$, DO_3 structured, ferromag., lattice parameters 79−42010
$Fe_{3-x}Co_xSi$, structural, mag. moment, and hyperfine field behaviour, local environment model 79−65762
$Fe_{1.4}Mg_{1.3-x}Zn_xTi_{0.3}O_4$ spinel system, X-ray diffraction, Fe Mossbauer effect 80−88900
$FeMo_6S_8$, mixed Chevrel phases, crystallography 80−39038
β-Fe_2O_3 film, CVD and characterisation 77−44172
Fe_3O_4, lattice parameters, NMR freqs., and magnetoelec. pots. near 12K 80−71146
Fe_3O_4, magnetite, isothermal compression up to 70 kbar under hydrostatic conditions 78−30698
Fe_3O_4, magnetite, phase transition, X-ray diffr. meas. 80−15238
Fe_3O_4, magnetite film, coercive force and lattice const. 78−2707
Fe_3O_4, typical spontaneous symmetry breakdown in solid state 80−34737
$Fe_{1-x}P_x$ dilute alloys, electronic struct., mag., elec. and struct. props. 79−37971
FeS−Li_2S−Cu_2S system, Mossbauer spectra and lattice parameters 79−78584

lattice constants continued
$Fe_{0.54}Sb$, temperature effect on lattice consts., Mossbauer spectra and density 80−88124
$Fe_{1+x}Sb$-CoSb solid soln., mag. props., Mossbauer spectra, solubility limits, and lattice consts. *(Russian)* 77−59394
$Fe_{1+x}Sb$-NiSb solid soln., mag. props., Mossbauer spectra, solubility limits, and lattice consts. *(Russian)* 77−59394
Fe_2SiO_4, spinel, isothermal compression up to 75 kbar hydrostatic press. 77−43280
$FeZnMo_6S_8$, mixed Chevrel phases, crystallography 80−39038
$Ga_{1-x}Al_xAs$, epitaxial layers, on GaAs substrates, X-ray double-cryst. diffractometry, state of strain 79−19480
GaAs, fast neutron irrad., effect on cryst. lattice period, X-ray diffr. meas. 79−37743
GaAs:Te, superdilation and defects, lattice parameter meas. and carrier mobility 80−10569
$GaBO_3:Fe^{3+}$, ESR spectra, lattice parameters 80−93170
$GaBo_3$, coefficients of thermal expansions 80−39322
$Ga_{1-x}In_xAs_{1-x}P_x$, VPE growth and characterisation 78−22970
$Ga_xIn_{1-x}As_yP_{1-y}$/GaAs structure, LPE growth and lattice consts. matching conditions 80−59822
$Ga_xIn_{1-x}P$ MBE layers, comp., Rutherford scatt. and X-ray diffr. meas. 80−75457
$Ga_xIn_{1-x}P$:N, Delta lattice parameter model, correl. with electronic props. 78−91560
$Ga_{1-x}In_xSb$, LPE on GaSb by stepwise grading, and characterisation 78−72745
$Ga_{1-x}In_xSe$, energy spectrum and struct., X-ray diffr. and light absorption 79−11437
$(Ga_xIn_{1-x})_2Se_3$, $1 \geq x \geq 0$, phases, lattice parameters and thermal expansion between room temp. and melting point 80−39031
GaN, high-press. VPE and elec. characts. 78−14627
GaN:Zn(Fe)(Ni)(Cr), lattice parameters, variation with stoichiometry and doping 79−73153
β-Ga_2O_3-K_2O/K ferrite, interfaces and solid soln., thermal expansion and lattice parameter variations 78−55959
GaP, 1 MeV proton bombardment, lattice deformation investigation by Kossel effect 78−22775
GaP VPE layers, precision lattice parameter meas. by Umweganregung method 79−65047
GaS_xSe_{1-x}, grown by iodine vapour transport, X-ray struct. studies 79−4411
$GaS_{1-x}Te_x$, solid soln., single cryst., crystallography and optical props. 79−55711
$GaSb_{1-y}As_y$, MBE-grown, substrate effect on lattice consts. 79−77942
Gd films, electrical props. correlation with microstructure 80−97009
$GdCo_3B_2$, rel. to mag. props. 77−24711
$GdFe_2$, Mossbauer sample, X-ray diffr. obs. 78−22737
$Gd_3Ga_5O_{12}$, high energy heavy ion irrad., lattice strain 80−49278
GdIG, empirical formula for lattice const. calc. 79−27968
GdS, low temp. phase transitions, mag. moment orientation, spin flip 79−99700
$Gd_{3-x}S_4$, ferromag., elec. props. near Curie temp. 80−107788
GdSe, low temp. phase transitions, mag. moment orientation, spin flip 79−99700
GdTe, low temp. phase transitions, mag. moment orientation, spin flip 79−99700
Ge, EXAFS at high press. 80−97376
Ge, evaporated film, lattice parameters and phase transition temp., surface influence of glass substrates 78−94996
Ge, lattice parameter determ. by X-ray multiple diffr. study *(Russian)* 80−10460
$(Ge_{1-x}Ga_x)_{1-x}Te$, rhombohedral and cubic phases, transport effects 78−2481
$(Ge_{1-x}In_x)_{1-x}Te$, rhombohedral and cubic phases, transport effects 78−2481
$GeSe_2$, single crysts., 3 polymorphic forms, DTA, photolum., IR and Raman sepctroscopy 80−33923
GeTe-MnTe, heat treatment effect on struct., elec. props. 80−54725
p-H_2, solid, neutron diffr. studies up to 5 kbar 80−59436
HfO_2, high pressure polymorphism 80−59429
HfO_2-CeO_2, solid solutions 77−16549
HfO_2-PrO_x, phase equilibria and physicochem. props. in range 1000 to 1800°C 79−100117
$Hf_{1-x}Zr_xV_2$, lattice consts. at 4K and room temp., phase division at x=0.4 78−51474
Hg_2Cl_2, high press. induced phase transitions, X-ray study 79−69242
$Hg_{1-x}Mn_xS$, phase studies and hydrothermal synthesis 77−48333
$HoFe_2H_{4.5}$, mag. props. and lattice consts., effect of hydrogen absorpt. 77−20561
$Ho_{12}Fe_{32}O_2$, struct. and ferrimag. props., neutron diffr. obs. 79−78319
In, muon quadrupolar interaction expansion of crystal lattice *(Russian)* 79−15388
InAs, intrinsic point defects, nature and influence on electrophys. props. 78−79609
$InBO_3:Fe^{3+}$, ESR spectra, lattice parameters 80−93170
$In_{0.53}Ga_{0.47}As$, phase diagram at 650°C and LPE growth of lattice-matched layer 79−96009
$In_{1-x}Ga_xAs$, MBE-grown, substrate effect on lattice consts. 79−77942
InGaAsP, LPE growth techniques influence on composition 79−52130
InGaAsP-InP layers, grown by LPE techniques, lattice const., bandgap, thickness and surface morphology meas. 80−59818
$In_{1-x}Ga_xAs_yP_{1-y}$, lattice matched to InP, band gap vs. comp., and Vegard's law demonstration 79−7782
$In_{1-y}Ga_yP$-GaAs heterojunction, VPE, energy band gap and lattice parameter, lattice mismatch effects 78−95345
InGaPAs, LPE-grown on (001)-InP, lattice mismatch study using X-ray double-cryst. diffr. 79−99440
InN film, specular reflection spectra, lattice parameters 80−7428
InO_3:Sn film, prep. by spray hydrolysis, struct., elec. and optical props. *(Japanese)* 79−42678
In_2O_3, lattice defects, optimum prep. conditions w.r.t. stoichiometry 79−27974
InP, depend. of phonon spectrum on hydrostatic press., Raman spectra 80−93315
InSe-SmSe system, microhardness and electrophys. props. 79−87093
β-In_3Sn, crystn., decomp. and superconductivity 79−91579
Ir borides, MIr_3B_2 (M=La, Th, U), supercond. and mag. props. 80−97028
K, lattice parameter determ. by neutron scatt. 79−7576
K, spin susceptibility and volume dependence 79−95569

lattice constants continued
K-rare earth double sulphates, $K_{6+3n}R_{4-n}(SO_4)_9$, (n≈0.4), cryst. struct. 80−28985
KBr, analysis using density functional formalism 79−90592
KCl crystals, Eu^{2+} concentration effect on lattice parameter and density of crystals 80−88169
KCl, thermal expansion, compressibility and melting calcs. 79−33069
KCl-NaCl solid solns., equilib. decay curve *(Russian)* 79−90760
$KCoF_3$, lattice parameter temp. depend., phase transitions and thermal expansion coeff. 80−1988
$KH_3(SeO_3)_2$, ferroelastic, lattice consts. and thermal expansion tensors, X-ray diffr. meas. 79−37856
$KH_3(SeO_3)_2$, thermal anomalies rel. to acoustic phonon instability 77−76545
$K_6LiFe_{24}S_{26}Cl$, Mossbauer spectra and lattice parameters 79−78584
$K_3Li_2Nb_5O_{15}$ films for optical waveguides epitaxial growth and characterisation 80−79016
$KLiSO_4$, phase transition, lattice parameter variation with temp. 78−79767
$KMnF_3$ lattice parameters, temp. depend., 21°C to MP 77−76583
$KMnF_3$, lattice parameter temp. depend., phase transitions and thermal expansion coeff. 80−1988
$KMn_{0.9}M_{0.1}F_3$, (M=Co,Ni), lattice parameter temp. depend., phase transitions and thermal expansion coeff. 80−1988
$KMn_{1-x}Me_xF_3$ (Me=Mg^{2+}, Fe^{2+}, Co^{2+} and Ni^{2+}) Bridgman growth, 80−60764
K_2MoO_4, hysteresis of phase transitions and modulated structures 80−29169
KNO_3, paraelec., precision lattice parameters, thermal expansion 77−11517
KNa_2, binding energy and lattice const., nonparametric calc. *(Russian)* 78−51462
$KNiF_3$, lattice parameter temp. depend., phase transitions and thermal expansion coeff. 80−1988
$K_4Sb_2O_7$, solid state synthesis *(French)* 80−104438
K_2UI_6, lattice constants 80−50568
K_xVF_3 (x=0.45 to 0.56), non-stoichiometric, struct. depend. on composition 79−99152
K_2WO_4, hysteresis of phase transitions and modulated structures 80−29169
Kr monolayer, on graphite, misfit dislocations and lattice parameters, model 78−34708
La-In alloys, cohesive and superconducting props. from electronic struct. calcs. 79−99113
LaB_6 crystals, zone refined, chem. characterisation 80−93821
LaB_6, growth by soln. method, struct. mech. and elec. props. 80−16168
La_2C_3, solid solution, lattice const. and superconducting transition temp. *(Russian)* 80−92496
$(La_{0.8}Ca_{0.2})MnO_{3+y}$, non-stoichiometry and lattice consts. 80−100212
La_2Co_7, mag. saturation and anisotropy, density, lattice parameters 77−85426
$LaF_3:Nd^{3+}$, cryst., $4f^3$ config., ground level energy state var. rel. to press. *(Russian)* 77−16358
$LaLi_{0.5}Ir_{0.5}O_3$, perovskite, prep. and mag. study 80−80486
$La_2(MoO_4)_3$, crystn. from Na_2MoO_4 based melt 80−20920
La_2O_3-Mn_2O_3-Cr_2O_3, synthesis and properties of solid solutions 78−44038
$LaRu_2$, H absorption induced Ce valence change, mag. and supercond. props. 80−50042
$LaRu_2$, supercond. disappearance on H absorption 79−47185
$LaSiAs_3$, F-type phase synthesis 80−104083
$LaVO_3$, successive phase transitions, X-ray anal. 80−108437
Li cluster, density functional calcs. 77−8031
Li, cryst. and electronic props., Hartree-Fock calcs. 79−60698
Li, electronic structure and lattice const. determ. using orthogonalised modulated plane wave method *(Ukrainian)* 79−42436
Li, martensitic phase transitions, and phase diagrams at moderate press. 78−72775
Li, spin susceptibility and volume dependence 79−95569
$LiAl_5O_8$, ordered single cryst., struct. determ. *(French)* 80−15074
$LiBO_2$-In_2O_3, phase composition, mag. props, elec. cond. 80−55365
$LiBi_xNd_{1-x}P_4O_{12}$ waveguide laser layer epitaxially grown on $LiNdP_4O_{12}$ substrate 80−23709
LiF, thin insulating film, lattice parameter meas. by electron microscope 77−65940
Li_2FeS_2, Mossbauer spectra and lattice parameters 79−78584
$LiGd_3(MoO_4)_5$, single crysts., cryst. growth, optical props. 80−60763
Li_4GeO_4-Zn_4GeO_4, solid electrolyte system, phase diagram 80−66489
LiH_2F hypothetical crystal, existence, total energy calc., pseudopot. calc. 78−2442
α-$LiIO_3$, lattice consts. variation due to electrostatic field *(Chinese)* 78−83787
$LiIO_3$ single crystal, DC field effect, neutron diffr. enhancement *(Chinese)* 80−44077
Li_2MgSiO_4-Li_2ZnSiO_4, solid soln. formation, phase relns. *(Japanese)* 77−25037
$Li_{1.8}N_{0.4}Cl_{0.6}$, fast ionic Li conduction, elec. conductivity and thermodynamic stability 79−65247
$LiNH_4SO_4$, ferroelectric phase transition, lattice parameters and thermal expansion coeffs. 80−40074
$LiNbO_3$:Fe, local photodeformation 79−42932
$Li(Nb_{1-x}Ta_x)O_3$, $0 \leq x \leq 1$, LPE thin film growth on $LiTaO_3$ substrate, lattice mismatches, meas. of temp. depend 79−56087
$LiNb_{1-y}Ta_yO_3$, Czochralski growth and basic props. 77−63556
Li_2O-MgO-Al_2O_3 system, subsolidus phase equilibria 80−81036
$Li_{1+y}Ta_{1.5y}Ti_{6y}O_3$ ($0 \leq y \leq 0.028$), non-stoichiometric phase, crystallographic and dielec. props. 80−75212
$Li_{1-y}Ti_{1+y}S_2$, intercalation chemistry and electrochemical energy storage 79−100541
^7Li, lattice dynamics, temp. depend., 110-424K 77−20033
$LuBO_3:Fe^{3+}$, ESR spectra, lattice parameters 80−93170
$(Lu_{1-x}Sc_x)_2V_2O_7$, prep., cryst. chem. and chem. anal., lattice const. determ. 79−41986
$Lu_4Si_2O_7N_2$, lattice consts., X-ray diffr. anal. 80−28986
$Lu_2V_2O_7$, prep., cryst. chem. and chem. anal., lattice const. determ. 79−41986
$(Lu_{1-x}Y_x)_2V_2O_7$, prep., cryst. chem. and chem. anal., lattice const. determ. 79−41986
$M_{1-x}Sr_xSi_2$ (M=Ca, Eu, Ba), solid solution with type $SrSi_2$ struct., lattice parameters at high press. 80−54203
Mg-Nd-Zn dilute alloy, metallography and precip. kinetics 80−71655

lattice constants continued
$MgCu_{2-x}Ni_2$, X-ray and neutron diffr. investigation of Laves phases of $MgCu_2$-type *(German)* 80−15050
$MgCu_{2-x}Zn_x$, X-ray and neutron diffr. investigation of Laves phases of $MgCu_2$-type *(German)* 80−15050
$Mg_xFe_{3-x}O_4$, cation redistrib., lattice const. 79−60338
$Mg(IO_3)_2.4H_2O$, struct. and phase transition using X-ray diffr. and thermal anal. *(Chinese)* 79−51059
$MgM^{3+}{}_xFe_{2-x}O_4$, M=In,Al,Cr,Sc, comp. effects on ferrite charact. 78−52305
$MgNi_{2-x}Zn_x$, X-ray and neutron diffr. investigation of Laves phases of $MgCu_2$-type *(German)* 80−15050
MgO, electronic struct. calc., lattice const., cohesive energy and compressibility 79−78003
MgO, modified electron gas theory, high press. effect 77−19899
$Mg_yU_{1-y}O_{2+x}$, thermodynamics from EMF meas., high Mg conc. 78−43143
MgV_2O_4-Mg_2VO_4 spinel solid soln., quenching and lattice const. 77−90307
γ-Mn-Cu, changes in cell dimensions at martensitic transform. 78−19750
Mn-Cu alloy, volume effect, paramagnetic-antiferromagnetic and structural transition, lattice consts. 80−39007
Mn-Ni, thermal expansion, mag. susceptibility, lattice consts. 80−100341
Mn_2As-Mn_2Sb, structural and magnetic props. determ. 78−76248
$MnAs_{1-x}P_x$, mag. and crystallographic anal. 79−47257
$MnAs_{1-x}Sb_x$, mag. and crystallographic anal. 79−47257
$Mn_{1-x}Cu_xCr_2S_4$, phase relationships and mag. phase diagram 79−78374
MnF_2 lattice parameters, temp. depend., 21°C to MP 77−76583
MnO-MgO-ZnO-Fe_2O_3, grade 1.3 VT ferrite formation from hydroxides 77−90302
Mn_3O_4, hausmannite, tetragonal-cubic transform., X-ray anal. 80−103288
MnSb, cryst. grown from nonstoichiometric melt 77−16488
MnSb, cryst. growth from nonstoichiometric melt, and cryst. chem 78−35286
$Mn_2Sb_{1-x}Bi_x$ ($0 \le x \le 0.175$), mag. transition, thermal expansion, thermomag. effects and lattice constant changes *(Japanese)* 79−78375
$MnSi_{\sim 1.73}$ crystal growth and characterisation 80−93474
MnTe, effect of press. on Neel temp. and lattice parameter 79−95594
MnZn ferrites, neutron diffr. exam. of influence of technology on mag. and cryst. parameters 79−42741
$(Mn_{0.7}Zn_{0.3})_xFe_yO_4$, electromag. props. rel. to Fe content 78−43613
Mo, 14 MeV neutron damage 77−15460
Mo, binding energy, lattice parameters bulk modulus, self-consistent pseudopot. calc. 79−60748
Mo, lattice dynamics, improved Fielek model 80−59598
Mo, neutron irradiated, influence on X-ray diffr. patterns *(Russian)* 78−22764
Mo, neutron irradiated single crystals, vacancy reactions in III recovery 79−73220
Mo, superconducitng, isotopic vol. effect confirmation by energy-dispersive X-ray diffr. 77−36019
Mo-Ti (up to 5.48 wt.%), internal nitriding, lattice expansion and precipitation *(Japanese)* 79−79157
$Mo_{6-x}Rh_xTe_8$, synthesis, struct., and elec. props. 80−92877
$Mo_4Ru_2Se_8(Te_8)$, synthesis, struct., and elec. props. 80−92877
MoS_2 film, non-stoichiometry and sputtering conditions 78−87891
2H-MoS_2, thermal expansion between 10 and 320K, cell dimensions meas. 79−65222
MoSCl, thermal expansion and thermal transform. 78−26696
$MoSi_2$-$CrSi_2$, phase equilib., struct. and props. 80−50608
$Mo_{0.5}W_{0.5}Se_2$ single cryst. vapour growth, characterisation 80−93466
NB-H(D), lattice expansion due to interstitially dissolved impurity 77−39600
α-NH_4HgCl_3, thermal expansion, lattice constants between 302 and 364K 80−15268
$((NH_4)_xK_{1-x})_2SnCl_6$, mixed cryst., spectroscopic study 79−33712
$(NH_4)_{1-x}M_xX$, and $(ND_4)_{1-x}M_xX$ M=Tl, Rb, Cs, X=Cl, Br, phase diagrams birefringence obs. *(German)* 79−83185
NH_4MnCl_3, X-ray single crystal analysis, phase transitions, Mossbauer effect 79−19366
Na cluster, density functional calcs. 77−8031
Na, equilibrium struct. and phys. props., pseudopot. method 80−96778
Na, martensitic phase transitions, and phase diagrams at moderate press. 78−72775
Na, spin susceptibility and volume dependence 79−95569
NaBr, analysis using density functional formalism 79−90592
NaBr, EXAFS at high press. 80−97376
$NaBrO_3$, lattice parameters, thermal expansion, defect formation energy 78−79786
NaCl, thermal expansion, compressibility and melting calcs. 79−33069
NaCl with divalent impurities, lattice relax. from density meas. 80−70226
NaF, thin insulating film, lattice parameter meas. by electron microscope 77−65940
$Na_2Ge_2O_5$, crystn., from Na_2O-GeO_2 glasses, lattice constants 79−77527
$Na_{1-x}K_xNbO_3$, solid soln., crystal lattice parameters, conc. depend. calc. 78−95041
$Na_3M_2Li_3F_{12}$, M=Al, Fe, fluoride garnets, high press. form 77−76554
$NaNH_4SO_4.2H_2O$, ferroelec. and thermal props. 78−83968
$Na_2O.y(Al_{1-x}Fe_x)_2O_{3-m}$, β″-$Al_2O_3$ phase stability, lattice constants 80−45283
$Na_3R(XO_4)_2$ (R=rare earth; X=P, As, V), pressure synthesis *(French)* 80−93509
$Na_xTa_yW_{1-y}O_3$, substitution of W with Ta, Anderson type transition *(French)* 79−60879
$NaTb(MoO_4)_2$, lattice thermal expansion, rel. to temp., X-ray method 79−77782
$NaYb(WO_4)_2$, thermal expansion, X-ray determ. 80−39323
Nb based A-15 type superconductors, universal defect behaviour, transition temp. rel. to lattice parameter 77−69440
Nb films, ion beam sputtered, supercond., laser annealing effects 80−97024
Nb-Ge, supercond. A-15 phase, supercond. transition temp. after ion implantation 80−49972
Nb-Mo(Ti)(Zr), nitriding, diffusive saturation, lattice spacing and activation coeffs. *(Russian)* 80−21168
Nb-Pt, A15 phase, comp. and order effects on supercond. props. 77−85372
lattice constants continued
Nb-Re(Ru)-N system, spectral emissivity, lattice parameter, initial rate of N_2 absorption *(German)* 77−4204
Nb_3Al based ternary solid solns., supercond. transition temp., paramag. susceptibility and lattice parameters meas. *(Russian)* 77−43766
Nb_3Al, supercond. props. and lattice parameter, comp. and neutron irrad. effects 80−70880
Nb_3Ge, DC sputtered films, annealing and mech. deform. effects on struct. and supercond. props. 79−38217
Nb_3Ge film, CVD, thermal expansivity, X-ray diffr. meas. 78−6166
Nb_3Ge film, sputtered, chemical composition versus lattice parameter a_o and supercond. transition temp. relations 77−43771
Nb_3Ge film, supercond., intercorrelations between composition, lattice parameter a_0 and T_c 77−8217
Nb_3Ge supercond. thin films, He- and Ar-irradiated, X-ray diffr. studies 80−29503
NbH_2, harmonic and anharmonic elastic props. 80−10589
Nb_2N, supercond. props. and structural phase transform. induced by C^+ and N^+ implantation 80−107942
$Nb_3Nb_{1-x}Si_x(Ge_x)$, impurity stabilised A15 supercond., transition temp., lattice consts., specific heat 80−93026
NbO, single cryst. with 25% vacancies, neutron damage 77−15459
$NbSe_2$, thermal expansion, lattice parameter meas. 78−18804
Nb_3Si A15 phase from amorphous Nb-Si alloys, high-press. synthesis 80−93516
Nb_3Si, hypothetical, electronic struct., lattice parameters and possible supercond. transition temp. 79−23891
Nb_3Si, supercond., A15 film, electron beam evaporation 80−29284
Nb_3Si, supercond. phase, formation by explosive compression 79−82701
Nd_2Co_7, mag. saturation and anisotropy, density, lattice parameters 77−85426
$Nd_xEu_{1-x}B_6$ solid solution, mag. susceptibility, lattice parameters, Weiss temp. 80−29535
$Nd(Ga,Cr)_3(BO_3)_4$, cryst. growth by LPE, Nd^{3+} fluorescence, lattice constants 80−29883
$Nd(Mn_{1-x}Cr_x)_2Si_2$, mag. and structural props. 79−78342
NdO, mag. props., lattice consts., and X-ray absorpt. spectra 80−44798
$NdRh_{1.2}Sn_{4.1}$, new supercond./mag. cpds., X-ray powder diffr. data 80−100215
Ni band structure, rel. to lattice const., spin polarised APW calc. 80−20073
Ni, cold-rolled, anomalous effects during X-ray stress meas. *(German)* 80−104184
Ni, difference between vacuum condensates and massive specimens *(Russian)* 77−31912
Ni, Gruneisen parameters, low temp. 79−23694
Ni, lattice and force consts., pairwise atomic repulsions in cluster model 79−32939
Ni, magnetostriction, lattice parameter changes, direct X-ray obs. 78−15001
Ni precipitates, isothermal annealing influence on structural state, X-ray diffr. anal. *(Russian)* 80−100849
Ni-Al, electronic, mag., and cohesive props. 80−44491
Ni-Al (51 to 55 at.%), vacancy defective, TEM exam. of structure 78−76677
Ni-Al(-Si), diffusion, lattice parameter, microhardness, and constitution, effect of Si additions *(Russian)* 80−84316
Ni-C, ferromag., prep. by splat-quenching, obs. of electronic struct. of interstitial C 77−62868
Ni-Co, lattice parameter measurement, C precipitation in Ni-Co-C solid solution, Ni_3Co ordering *(Czech)* 80−60867
Ni-Co-Al alloys, continuous precip., SEM, TEM, X-ray diffr. study 80−89220
Ni-Cr, ordering in the vicinity of Ni_2Cr 79−38819
Ni-Cr, solid soln., lattice parameter meas. rel. to conc. and temp. depend. *(Czech)* 80−28949
Ni-Cr, solubility limit determ., X-ray method 79−43199
Ni-Cr-Ta system, phase equilib. of Ni rich region at 1523 and 1273K 80−93541
Ni-Cu-X (X=Sn, Nb, Ti), spinodal decomp. alloys, linear expansion coeff. influence on morphological anisotropy *(Japanese)* 80−70431
Ni-Fe alloy, FCC, density, lattice parameters, X-ray diffr. and hydrostatic weighing 78−55904
Ni-Fe-Ti-O spinel phase, single-phase region and cryst. chem. charact. 77−52301
Ni-Nb(-Cu)-C, NbC dispersed supercond. tapes, fabrication and charact. 78−19773
Ni-Pd-Mn ternary alloys, mag. charact., use for thermoseed 80−107995
Ni-Ta-Al system, phase equilibria and diagram, electron probe, X-ray diffr. anal. 80−29927
Ni_3Al, substitutional soln. and defect hardening mechanisms 77−21155
$Ni_{0.5-x}Co_xZn_{0.5}Fe_2O_4$ ferrospinal solid solutions, cryst. lattice defects and props. 80−19796
$(Ni_xCu_{1-x})_2MnSn$, mag. props. and lattice parameter, composition depend. 77−80916
$Ni_{1-3x}{}^{2+}Fe_{2+2x}{}^{3+}Vac_xO_4{}^{2-}$ (Vac=cation vacancy), solid solns., cryst. lattice imperfections 80−39069
$Ni_xFe_yCr_{1-x-y}$ films, struct., mag. props., and corrosion resist. 80−34706
$NiFe_2O_4$, effect of sintering in air in range 1373-1773K on lattice parameter 79−19208
$(Ni_{1-x}Fe_x)S$, solid solns., electronic props., X-ray, thermal and Mossbauer study 79−78376
Ni_4Mo, order-disorder phase transform., X-ray diffr. *(Russian)* 79−1855
NiO, bulk props., initial state MO Ni_4O_4 and $Ni_{13}O_{14}$, cluster model, lattice and force consts., photoemission and CT absorpt. spectra 80−84828
NiO, lattice parameters, microstrains, non-stoichiometry, comparison between mosaic microcrysts. and quasi-perfect single microcrysts. 80−24414
NiO, temp. depend. of thermal expansion and IR lattice vibrational mode 77−84950
NiO-Al_2O_3, Verneuil-grown crysts., phase comp. 77−66586
$Ni_{1-x}Rh_xS$, nonvolume effect of Rh substitution on paramag. metal-antiferromag. nonmetal transition 79−28277
β-Ni_3S_2, defect struct. 78−63754
β-Ni_3S_2, formed during sulphidation of Ni, defect struct. and chemical diffusion 78−2115
NiSb, cryst. growth from nonstoichiometric melt, and cryst. chem 78−35286

lattice constants continued
$Ni_{1+}Sb$, temperature effect on lattice consts., Mossbauer spectra and density 80−88124
NiTiCu, shape memory alloys, electron microscope and X-ray diffr. study of struct. 79−82179
$(Ni_{1-y}Y_y)_3Al_{1-x}Sc_x(Ti)_x$, quarternary gamma prime ($L1_2$) pseudobinary props. revealed by ionicity modified pair model 78−19725
$NpCo_2Si_2$, mag. struct., neutron diffr. determ. 80−93084
$NpCu_2Si_2$, mag. struct., neutron diffr. determ. 80−93084
Os borides, MOs_3B_2 (M=Lu, U), supercond. and mag. props. 80−97028
Pb-Au, interstitial and substitutional distrib. 80−84204
Pb-Au (0-0.0918 at.%), lattice parameter changes due to Au dissolution 79−77558
$(Pb_{1-y}Ba_y)_{1-x}La_xNb_{2-x/5}O_6$, ferroelec., phase transitions 79−38487
$Pb_{1-x}Cd_xS$ metastable epitaxial films, growth and physical props. 78−27417
$PbCl_2$ crystals, acousto-optical props. and photoelasticity 80−40085
$Pb_{1-x}Hg_xS$ film, solution-grown, struct., lattice parameters and optical band gap var. 77−69201
PbI_2 intercalated with organic mols., energy band splitting *(Russian)* 78−76027
PbI_2, Raman spectra, phonon dispersion curves, vibrational props., lattice parameters 79−69211
$Pb_3MgNb_2O_9$, crystal growth procedure, meas. electro-optic and dielectric props. 78−88418
$PbMgTa_2O_9$, crystal growth procedure, meas. electro-optic and dielectric props. 78−88418
$PbMo_6S_8$ and ternary sulphides, lattice parameter rel. to supercond. T_c 78−52119
$Pb_3(PO_4)_2$, temp. depend. of lattice parameters and spontaneous strain 80−29170
PbS, first-principles calc. of eqn. of states 80−49649
PbS, thermomech. props., SCF Xα scatt. wave theory 78−71704
$PbSc_{2/3}Te_{1/3}O_3$-$PbSc_{2/3}W_{1/3}O_3$($PbFe_{2/3}Te_{1/3}O_3$) ferroelec. props. and lattice consts. 80−60520
$PbSnF_4$, lattice constants meas. from liquid N_2 temp. up to 400°C, phase transition 79−77781
$Pb_{0.78}Sn_{0.22}Te$:In, low current carrier conc., Hall effect, lattice constant 79−82603
$Pb_{1-x}Sn_xTe$ layers, LPE, phase diagram rel. to lattice const., distrib. coeffs. 79−37925
$Pb_{1-x}Sn_xTe$ single crysts, energy gap determ. from density and lattice const. *(German)* 78−26812
$Pb_{1-x}Sn_xTe$-PbTe heterojunctions, interface recombination velocity reduction with decreasing lattice parameter mismatch 79−98370
$Pb_xSn_{1-x}Te$, RF sputtered films, struct., lattice parameter, stoichiometric comp., RHEED 78−38975
$Pb_{1-x}Sn_xTe_{1-y}Se_y$, narrow-gap solid soln., lattice parameter, energy gap and Hall mobility of carriers 79−73154
$Pb_{1-x}Sn_xTe_{1-y}Se_y$ solid solutions with constant lattice parameter, phase comp. 80−108417
$Pb_{0.95}Sr_{0.05}(Zr_x, Ti_{1-x})O_3$-$Nb_2O_5$, phase coexistence range, lattice consts. 80−92680
$PbTeO_3$, interplanar spacings, X-ray powder diffr. anal. 79−70046
$Pb(Ti,Zr)O_3$ solid solutions, phase coexistence discrepancies 80−96662
$PbTiO_3$, single crysts., lattice parameters and birefringence as function of temp. 79−38517
$PbZr_xTi_{1-x}O_3$ ceramics, morphotropic phase boundary 80−81035
Pd alloy-H system, α-β phase transformations, hysteresis of press., elec. resistance, review 80−60859
Pd alloys, effect of alloying on activation energy of H_2 diffusion 80−107571
Pd-Ag-Au, lattice parameters and thermal expansion coeffs., X-ray diffr. meas. 79−99121
Pd-D, crystallite size effects, simultaneous sorption and X-ray study 80−65237
Pd-Fe, dil., anomalous lattice parameters and H_2 solubilities 79−33091
Pd-H system, α-β phase transformations, hysteresis of press., elec. resistance, review 80−60859
Pd-H system, lattice parameter increase meas. by X-ray diffr. *(German)* 77−62560
Pd-Ti, hydrogenation, lattice spacings, microhardness and mag. susceptibility meas. 79−77557
Pd-Zn, $L1_0$ type intermetallic phase, X-ray diffr. study of lattic compression 80−49182
PdD_x, model of instabilities 78−75619
PdH_x, model of instabilities 78−75619
$Pd_{1-x}M_xSe_2$ (M=Ru,Co,Ni), high pressure phase transformation studies, lattice constants and densities 79−65187
Pd_2Si and PdSi films, on Si, stress obs. 80−80145
Pr_2Co_7, mag. saturation and anisotropy, density, lattice parameters 77−85426
PrO, mag. props., lattice consts., and X-ray absorpt. spectra 80−44798
$Pr_4Si_2O_7N_2$, lattice consts., X-ray diffr. anal. 80−28986
PtSi films, on Si, stress obs. 80−80145
Pu(C,N), lattice parameter variation, 50 to 300K 78−51709
PuC(N), lattice parameter variation, 50 to 300K 78−51709
$ROsB_4$, R=Y, Gd, Tb, Dy, Ho, Er, Tm, struct. and mag. props. 78−79584
$RRuB_4$, R=Y, Cd, Tb, Dy, Ho, Er, Tm, struct. and mag. props. 78−79584
$RbCaF_3$, cubic to tetragonal phase transition, neutron diffr. obs. 79−23730
$RbCaF_3$, first order improper ferroelastic phase transition at 194K, phenomenological description 80−70397
$RbCaF_3$, lattice consts. temp. depend., X-ray examination, 194K transition *(French)* 78−10184
RbCl, structural phase transition, Born-model and effects of hydrostatic and non-hydrostatic stresses 79−23721
$RbCrI_3$, radiocrystallographic study, lattice parameters *(French)* 79−46632
$RbDy_3F_{10}$, $RbDy_2F_7$ and Rb_3DyF_6, cryst. symm. and cell parameters *(French)* 80−81040
$RbH_3(SeO_3)_2$, ferroelec. phase transition, X-ray study 79−38479
$RbNbW_2O_9$ crysts., growth and props. 80−104054
Rb_2SO_4-$(NH_4)_2SO_4$ mixed cryst., ferroelec. transition, structural and dielec. props., proton spin-lattice relax. 78−39512
$Rb_4Sb_2O_7$, solid state synthesis *(French)* 80−104438
Rb_2UI_6, lattice constants 80−50568
Rb_xVF_3, non-stoichiometric, struct. depend. on composition 79−99152
Rb_2ZnCl_4, phase transitions, thermal expansion coeff. 80−100638

lattice constants continued
Re, Anderson-Gruneisen parameter, bulk modulus and compression curves 78−30690
Re-Hg-O system, solid state synthesis of 5 crystn. compounds, thermal and X-ray anal. *(French)* 79−66281
Re-Mo (up to 4.4 wt.%), X-ray diffr. study of conc. and temp. depend. of lattice parameters 79−94965
Re-W (up to 6.1 wt.%), X-ray diffr. study of conc. and temp. depend. of lattice parameters 79−94965
ReO_3, lattice parameters, thermal expansion 291 to 464K, Bond technique meas. 78−75617
Rh borides, RRh_3B_2 (R=rare earth), supercond. and mag. props. 80−97028
Ru borides, RRu_3B_2 (R=rare earth, Y, Th, or U), supercond. and mag. props. 80−97028
Ru, lattice dynamics, thermal expansion and bulk modulus, lattice parameter press. variation 77−59079
SO_2, lattice dynamics, rigid mol. model 80−44266
Sb_2S_3 crystals, X-ray and DTA methods lattice constant change *(German)* 78−43119
Sc alloying behaviour, C and B stabilising effect, lattice parameters and at. radius 77−36454
$ScBO_3$:Fe^{3+}, ESR spectra, lattice parameters 80−93170
$ScFe_2$, Mossbauer effect of ^{57}Fe 80−75903
$ScFe_2H_2$, Mossbauer effect of ^{57}Fe 80−75903
ScM, (M=Ru,Rh,Pd,Ag,Mo), self-consistent local density functional calcs., LMTO method 79−11059
ScN_x, region of homogeneity, physicochem. props. 78−52018
Sc_2O_3-ZrO_2 (HfO_2), cubic solid soln., lattice parameters 79−82186
Si, B implanted layers, damage obs. by X-ray double refl. 77−15463
Si, bulk and surface equilib. props., self-consistent pseudopotential calcs. 79−60750
Si, charge density, struct. props. electron-electron interactions 78−47725
Si, cryst., impurities rel. to lattice parameters, dislocation density, strresses *(German)* 77−51403
Si, crystalline struct. and lattice imperfections 80−24398
Si, ground state props. in density-functional pseudopot. approach 80−92803
Si, lattice constant, press. depend., X-ray diffr. meas. effect of nonhydrostaticness of press. 77−35439
Si, lattice constants anomalous temp. depend. 79−46821
Si, lattice parameter determ. by X-ray multiple diffr. study *(Russian)* 80−10460
Si, lattice parameters and perfection *(Japanese)* 79−4300
Si, neutron irrad. effects on lattice parameter and anomalous X-ray transmission 79−86821
Si, neutron irradiated, changes in lattice period, X-ray meas. 77−7767
Si powder, X-ray K_α doublet diffr. peak position rel. to lattice const. precision 77−68891
Si, preliminary X-ray interferometry results 79−7522
Si, structural props., self-consistent calc. 80−28947
Si, total energy calcs. by r-space method, Wannier functions 80−88503
Si-Ge heteroepitaxial layers on Si substrate, lattice const. meas. 79−69382
SiC, crysts., tetrahedral bond deformation variation with hexagonality and doping degree of N 79−94977
β-SiC, sintering, B transport and lattice parameter change 80−108370
SiC, synthesis by ion implantation of diamond and silicon, struct. charcts. 77−76434
SiC-Si struct. formation on ^{12}C ion implantation in Si, optical and photoelectric props. 79−91136
$Si_{1-x}Ge_x$ system, lattice energy and consts., virtual cryst. approx., pseudopot. calc. 80−44166
Si_3N_4, rapid CVD, and struct. charcts. 77−28767
α-Si_3N_4 single crysts., growth, morphology, hardness and slip system 79−83112
Si_2N_2O, fast neutron irradiation, variation of lattice parameters 80−24504
SiO_2, crystobalite form. in evacuated silica ampoules, cryst.-amorphous transform. 77−68933
Sm, electron radiation damage, elec. resistivity change rates 80−59954
SmB_6, resistivity press. variation, lattice consts. 80−100456
$SmB_4(B_6)$, growth by soln. method, struct. and mech. props. 80−16168
$Sm_{1-x}B_xS$, valence transition induced by alloying 80−96829
$SmCo_3B_2$, rel. to mag. props. 77−24711
$Sm_{0.85}Gd_{0.15}S$, metal-semicond. transition, X-ray diffr. obs. 90-473K 79−95333
$Sm_{1-x}Gd_xS$, metal-semicond. isomorphous transition curve, low temp. crit. point, lattice parameter changes 79−95334
$Sm_{1-x}La_xB_6$, valence transition, lattice parameter and mag. susceptibility meas. 80−59929
$Sm_{1-x}La_xS$, electron struct., lattice consts., X-ray spectral study *(Russian)* 80−100432
$(SmLu)_3(FeAl)_5O_{12}$, film epitaxial growth on $Gd_3Ga_5O_{12}$ substrate, mag. props. lattice mismatch 80−65402
$Sm_{1-x}M_xS$, M=Eu,Ca,Yb, valence transition under high press. 79−73551
$Sm_{1-x}Nd_xSe$, Nd substitution effect on lattice const., resist., and colour 79−56763
SmO, mag. props., lattice consts., and X-ray absorpt. spectra 80−44798
SmS, optical props. and electronic struct., Kramers-Kronig model anal. 79−69859
SmS, physical and physicochem. props., review 80−96875
SmS, press. effect on lattice parameter, mag. susceptibility, and reflectivity 79−56272
$SmS_{1-x}As_x$ solid solns., intermediate valence phase, lattice const. and mag. susceptibility meas. 79−87245
$SmS_{1-x}P_x$, intermediate valence cpd., lattice parameter and mag. susceptibility 80−7091
$SmSb_xS_{1-x}$, intermediate valence, susceptibility and lattice parameter meas. 78−51943
$Sm_{1-x}Y_xS$, metal-semicond. isomorphous transition curve, low temp. crit. point, lattice parameter changes 79−95334
$Sm_{1-y}Yb_yB_6$, valence transition, lattice parameter and mag. susceptibility meas. 80−59929
Sn, single cryst., equilib. vacancy conc., length and lattice parameter change meas. 79−60352
Sn ternary intermetallic systems, new supercond./mag. cpds., X-ray powder diffr. data 80−100215
$SnMo_6S_8$, mixed Chevrel phases, crystallography 80−39038
SnS_xSe_{2-x}, growth by I_2 vap. transport, cryst. struct. 77−73223

lattice constants continued
SnSe, single crysts., growth by Bridgeman technique, electron diffr. anal., lattice consts., carrier conc. 79−47616
SnSe-Bi_2Se_3 system, lattice constants of phases 79−87622
SnSe-BiSe system, lattice constants of phases 79−87622
SnTe, annealed, iodide method of prep., props. meas. 80−71591
$Sn_xZr_{1-x}Se_2$, growth by I_2 vap. transport, cryst. struct. 77−73223
$SrB_{0.5}B'_{0.5}O_4$, where B=Ln, Y, Sc, Fe, In, Rh and B'=Nb, Ta, synthesis and characterisation 79−69087
$SrF_{2-x}H_x$, synthesis and struct. determ. using neutron diffr. *(French)* 80−24425
$SrFe_{12-x}Cr_xO_{19}$, effects of substitution of Fe by Cr, Mossbauer spectra 80−2674
$Sr_3FeTa_2O_9$, Mossbauer and X-ray diffr. studies 80−103905
$Sr_{0.3}La_{0.7}MnO_3$, neutron-irrad. induced phase transition 77−89952
$Sr(NO_3)_2$, 261-740K, X-ray diffr. obs. 77−35720
$SrSnF_4$, lattice constants meas. from liquid N_2 temp. up to 400°C, phase transition 79−77781
$Sr_{0.15}VO_2$, electrical cond., thermo-EMF, and lattice consts. 80−54685
Sr_xVO_2, oxygen vanadium bronze, phase comp., heating in air 77−40417
Ta, lattice parameter, X-ray meas. 77−89406
Ta, muon quadrupolar interaction expansion of crystal lattice *(Russian)* 79−15388
Ta-H(D), lattice expansion due to interstitially dissolved impurity, isotope effect 77−39600
Ta-W-Hf (8,2 wt.%), T-111, O_2 absorption, effect on lattice parameter and specimen dilation 78−83958
TaC_xN_y, supercond. and normal props. under hydrostatic press. 77−12049
Ta_2H, ordered, distortion-induced superstruct. modulation, from X-ray scatt. 80−49186
TaS_2, thermal expansion, lattice parameter meas. 78−18804
TaS_xSe_{2-x}, growth by I_2 vap. transport, cryst. struct. 77−73223
$TaSi_2$-$CrSi_2$, phase equilib., struct. and props. 80−50608
$(Tb_{1-x}Gd_x)_3Co$, intermetallic cpd. mag. props., phase transform, and mag. hystersis *(Russian)* 80−93113
$Tb(OH)_3$, powder and single crystal, mag. props. 80−2558
^{99m}Tc, supercond. effect on decay rate, lattice consts., transition temp. 78−41671
$ThCo_5$, lattice consts., magnetisation, and anisotropy fields 79−78364
$ThSiO_2$, single crysts., prep. by vapour phase reaction, lattice parameters 79−28905
$Th_{1-x}Y_xCo_{5-y}Fe_y$, lattice consts., magnetisation, and anisotropy fields 79−78364
α-Ti, diffusion of O_2, 700 to 950°C, lattice parameter and microhardness meas. *(French)* 79−86929
Ti, plastic deform. dynamics, mech. characts. and phys. props., effect of O_2 *(French)* 80−45353
Ti-Al-H, H effect on mech. props. and lattice constants 80−21036
Ti-Al-Mo-Zr (Cr-Fe), effect of heating on thermal stability of phases, lattice constants and chem. comp. 78−56672
Ti-B-N, CVD, lattice const. 79−74097
Ti-Cr-B system, self-propagating high temp. synthesis, crystallochemical and mech. props. 80−20861
Ti-Fe-Al(Mn), homogeneity and lattice parameters, Mn and Al effect on hydriding cmpd. FeTi 80−108400
Ti-Mo, lattice parameter and Debye temp., comp. depend. *(Russian)* 78−47280
Ti-Mo-V (8 wt.%, 8 wt.%), FCC phase, decay of β-solid soln., electron microdiffr. 79−15670
Ti-V-C-N, solid solns., quasibinary cross sections 78−23676
$(Ti_{1-x}V_x)_2O_3$ spin glass, mag. props., metallic antiferromagnetism 79−82791
TiC-C composites, hot pressed, thermophys. props. at high temps. 80−59675
TiC_x-TiN double-layer films, on C steel, CVD in US field, X-ray and SEM characterisation 79−65338
TiC_xN_y monolayer films, on C steel, CVD in US field, X-ray and SEM characterisation 79−65338
TiC_xN_y, powder preparation, physical, chemical props. *(Russian)* 80−76212
TiC_xO_y, cubic phase, thermal expsn., lattice consts. 78−43149
TiC_xO_y, oxidation mechanism 77−86200
$TiC_xO_yH_m$, cubic phase, thermal expsn., lattice consts. 78−43149
$TiC_xO_yN_z$, homogeneity and struct. vacancies 77−84937
TiFeD, cryst. struct., Mossbauer and neutron diffr. obs. 80−34839
TiN_z-TiO_y, thermal expansion, 23-1000°C, X-ray obs. 78−91454
TiO_2, rutile, reduction by C, thermodynamic and struct. study, 1400 to 1600K 79−52650
TiO_2-ZrO_2, submicron powders, vapour phase production from $TiCl_4$-$ZrCl_4$-O_2 system 80−40301
TiO_x, anomalous difference between theoretical and expt. densities, non-vacancy character 79−90630
TiO_y, thermal expansion of cubic phase at low temp. X-ray diffr. anal. 79−1514
TiO_yH_m, cubic phases, lattice consts. meas., thermal expansion coeffs. calc. 79−55906
TiO_yH_m, thermal expansion of cubic phase at low temp. X-ray diffr. anal. 79−1514
TiOy, annealed, lattice const. meas., thermal expansion coeffs. calc. 79−55906
$TiSi_2$, crystal atomic struct., X-ray diffr. exam., lattice parameters and integrated intensities 78−75647
$TiSi_2$-$CrSi_2$, phase equilib., struct. and props. 80−50608
$Ti_xV_{1-x}H_2$ system, reaction and press.-composition isotherms meas. 80−108391
$(Ti_{1-x}V_x)_2O_3$, semicond. to semimetal electrical transition, lattice parameter changes 79−60714
Tl, thermal and elastic props., lattice heat capacity, elastic constants and thermal expansion, model 80−39321
TlCl, ground-state props., Wannier functions, and electronic struct., ab initio self-consistent calc. 80−80178
TlCl, self-consistent electronic struct. and ground state props. 80−15451
$TlCl_xBr_{1-x}$, $TlBr_xI_{1-x}$, polymorphous mixed cryst. layers, opt. props. 78−23490
Tl_xVF_3, non-stoichiometric, struct. depend. on composition 79−99152
$Tm_{1-x}Eu_xSe$, semicond. with valence instabilities, cryst. chem. considerations 80−100213
$TmFe_2H_{4.3}$, mag. props. and lattice consts., effect of hydrogen absorpt. 77−20561

lattice constants continued
TmSe, nonstoichiometry, high temp. chem. and valence instability *(German)* 79−23743
Tm_xSe, valence instabilities, antiferromag. order 80−20128
$TmSe_{1-x}Te_x$, semicond. with valence instabilities, cryst. chem. considerations 80−100213
$TmSe_{1-x}Te_x$, phase relationships and press. induced transitions 80−19771
$Tm_4Si_2O_7N_2$, lattice consts., X-ray diffr. anal. 80−28986
$Tm_2V_2O_7$, prep., cryst. chem. and chem. anal., lattice const. determ. 79−41986
$Tm_{1-x}Y_xTe$, $(0 \leq x \leq 1)$, single cryst. growth and characts. 78−23603
U-UNi_2-UCo_2, system, phase equilibria, lattice constants *(German)* 80−50598
UAs, search for lattice distortions at low temps. 80−79759
UC, low temp. reactor irradiation 80−39168
UC, miscibility with rare earth nitrides *(German)* 80−96654
UFe_2, giant magnetoelastic deform. of cryst. struct. mag. props. *(Russian)* 80−93159
UN, lattice parameters determ. by X-ray diff. 79−19212
UN, search for lattice distortions at low temps. 80−79759
US, electronic struct. calc. 78−91615
US-UC-UC_2 system, potential nuclear fuels, phase solid soln. studies, prep. and props. exam. 79−40996
USb, search for lattice distortions at low temps. 80−79759
V-C system, ordering and phase equilibrium processes 79−99311
V-Mn, equiatomic, ordering kinetics and antiphase domain coarsening 80−7559
V-N system, ordering and phase equilibrium processes 79−99311
V-Re system, discovery of supercond. A-15 phase 78−88060
$V_{3-x}Cr_xSi$, x=0 to 3, struct., supercond. and mag. props. 80−1962
V_2D, ordered, distortion-induced superstruct. modulation, from X-ray scatt. 80−49186
V_3Ga, A15 cpd., hydrogenation effects on supercond. transition temp., lattice parameters 80−103772
V_3Ge, A15 cpd., hydrogenation effects on supercond. transition temp., lattice parameters 80−103772
V_3Ge, anisotropic thermal vibrations, lattice const. X-ray study 80−34164
V_3In, hypothetical, electronic struct., lattice parameters and possible supercond. transition temp. 79−23891
VO_2, X-ray determ. of lattice constants and thermal expansion coeffs. near transition temp. 79−86747
V_2O_3, impurity doping effects, elec. props. obs. 80−75609
V_2O_3, lattice parameters and anomalous high temp. behaviour 78−87790
V_2O_3-M_2O_3, M=Ti, Cr, struct. and mag. props. 78−27041
V_3O_5, high-temp. phase transition, resistivity, valence photoelectron spectra 80−49357
V_xSe_2 (x=1.04,1.13,1.15), crystallographic parameters correlation to heats of formation and reduced length 79−27963
$VSe_{2-x}S_x$ $(0<x<2)$ solid solutions, characterisation 80−88730
V_3Si, A15 cpd., hydrogenation effects on supercond. transition temp., lattice parameters 80−103772
V_3Si, electron spectrum characts., mag. susceptibility depend. on resistivity ratio 79−95320
V_3Si, ion irradiated, influence on struct., resist., and supercond. transition temp. 80−54823
V_3Si plastically deformed cryst., lattice transform., Kossel technique 78−95153
V_3Si, powdered, Debye-Waller factors and lattice consts., 25-1000K, X-ray diffr. obs. *(German)* 79−33060
$(V_{1-x}Ti_x)_3O_5$, unit cell dimensions 80−70970
W, binding energy, lattice parameters bulk modulus, self-consistent pseudopot. calc. 79−60748
W, lattice wave dispersion, lattice consts., elastic consts. 80−24545
W-Cr solid solution, precipitation behaviour, reaction front motion, lattice parameters *(German)* 80−55401
W-Os system films, condensation temp., conc., and phase comp. effect on struct. and props. *(Russian)* 80−24749
2H-WSe_2, thermal expansion between 10 and 320K, cell dimensions meas. 79−65222
Xe adsorbed monolayers, thermodynamic props. and lattice const., quasi-harmonic theory 79−42380
Xe, crystalline, lattice constant at insulator-metal transition 80−107706
Xe monolayer, on graphite, misfit dislocations and lattice parameters, model 78−34708
Y, electron radiation damage, elec. resistivity change rates 80−59954
Y, thermal and elastic props. 79−33027
Y-M intermetallic cpds., M=3d transition metal, sorption of H_2, structural charges 80−88429
$Y_2(CO_3)_3.nH_2O$, tengerite, single cryst. hydrothermal growth 80−97417
$Y_3Fe_{5-x}In_xO_{12}$, K absorpt. and Mossbauer spectra and other phys. props. *(Russian)* 77−32467
$YFe_{3-x}Ni_x$, electronic sp. ht., saturation magnetisation and lattice parameter meas. 78−68261
$Y_{3-x}Gd_xFe_{5-y}Al_yO_{12}$, solid solns., IR absorpt. spectra, physical props. 80−55082
$Y_{3-x}Gd_xFe_5O_{12}$, solid solns., IR absorpt. spectra, physical props. 80−55082
YIG and Ga-substituted YIG, high energy heavy ion irrad., lattice strain 80−49278
YIG, empirical formula for lattice const. calc. 79−27968
YIG:Ca, oxidising effects of high temp. annealing in reducing atmosphere 80−66696
YMn_2, lattice consts. and mag. props. before and after H_2 absorption 77−36061
Y_6Mn_{23}, lattice consts. and mag. props. before and after H_2 absorption 77−36061
$YO_{1.5}$-PrO_x, phase relns. and electrophys. props. of solid solutions 78−23686
Y_2O_3, synthesis at high-press and temp., supercond. 80−2513
Y_2O_3-ZrO_2 (HfO_2), cubic solid soln., lattice parameters 79−82186
$Y(OH)CO_3$, ancylite like phase, hydrothermal cryst. growth *(French)* 80−108340
$(YSmCa)_3(FeGe)_5O_{12}$ mag. bubble garnets, ion implantation induced stress influence on props. 79−91274
Yb, electron radiation damage, elec. resistivity change rates 80−59954
YbB_{12}, valence state and mag. props. 80−50031
YbB_6, growth by soln. method, struct. and mech. props. 80−16168
YbB_6, resistivity press. variation, lattice consts. 80−100456
$Yb_{0.99}Gd_{0.01}CuAl$, intermediate Yb valence states, mag. props. 79−51743

lattice constants continued
$Yb_2V_2O_7$, prep., cryst. chem. and chem. anal., lattice const. determ. 79−41986
$Yb_{1-x}Y_xCuAl$, intermediate Yb valence states, mag. props. 79−51743
Zn island films, effect of surface press. on lattice spacings 79−11045
Zn, vacancy conc., lattice parameters meas. 78−10040
Zn, vacancy concentration meas., lattice parameter and length changes, form. parameters 79−37697
$Zn_xCd_{1-x}S$ film, prep. by soln. spray method, and struct., optical and elec. props. 78−52666
$Zn_xCd_{1-x}S$ film, prep. and use as heterojunction optical energy converters 79−95488
$ZnGeP_2$, synthesis, characts., applic. to laser windows *(French)* 78−80467
$ZnMo_6S_8$, mixed Chevrel phases, crystallography 80−39038
$ZnO-Zn_2TiO_4$, solid soln. formation 78−27490
α-ZnP_2, lattice parameters and thermal expansion, 80-320K, X-ray obs. 80−75373
ZnS, cubic, compression 80−107358
ZnS, wurtzite, ZnO solubility, 1444-1240°C 80−15248
$ZnS-MgF_2$ alloy films, struct. and optical props. 79−90910
$ZnSiP_2$, 1 MeV proton bombardment, lattice deformation investigation by Kossel effect 78−22775
$ZnSiP_2$, chem. inhomogeneities, X-ray lattice parameter meas. *(German)* 77−72693
Zr-Cr-B system, self-propagating high temp. synthesis, crystallochemical and mech. props. 80−20861
Zr_3Al, Ar^+ ion and electron irradiation, irradiation swelling, lattice parameter changes 79−65123
ZrC deposit on C steel surface, exam. of composition *(Russian)* 79−34201
ZrC, whiskers, CVD on Ni, catalytic effect 78−51865
ZrC-C composites, hot pressed, thermophys. props. at high temps. 80−59675
ZrC_x, change in lattice const. in region of homogeneity 77−25029
ZrI_4, high-temp. enthalpy, X-ray powder diffr. data 80−107446
$Zr_{1-x}In_{2x}O_{2-x}$, ionic conductivity, lattice const. 80−96688
ZrO_2, high pressure polymorphism 80−59429
$ZrO_2-Y_2O_3$, stabilised, struct. of single crysts. 77−35527
$ZrS(Se)_2$, nonstoichiometry 78−75841

lattice defects *see crystal defects*

lattice diffusion *see diffusion in solids*

lattice dynamics
see also crystal surface and interface vibrations; displacive transformations; Gruneisen coefficient; lattice dynamics of covalent crystals; lattice dynamics of ferroelectric crystals; lattice dynamics of ionic crystals; lattice dynamics of metallic crystals; lattice dynamics of molecular crystals; lattice localised modes; lattice phonons; soft modes; vibrational states in disordered systems
A-15 compounds, limiting optical freqs., in terms of force consts. 78−26636
absorption and fluorescence spectra of localised centres in crystals, multiquantum transitions, vibr. mode heating 78−10936
acoustic and long-wave optical vibrations, quasicontinuous approx., method of expanded unit cells 78−10143
activated crystals, Jahn-Teller effect in optical bands of impurity centres 78−6706
alkali metal acid oscalates, neutron inelastic scatt. spectra in 2200-200 cm^{-1} range 80−70327
alkali metal hexachlorotellurates, $A_2(TeCl_6)$, (A=Cs, Rb, K), IR and Raman spectra, lattice and internal modes, phase transition 78−6659
alkaline earth chalcogenides, atomis. energy, electron affinity, mean amplitude of vibr. *(German)* 79−51045
alkaline earth chalcogenides, crystal parameters calcs. using repulsive interaction pot. 79−37795
alkylammonium compounds with perovskite-type layer struct., symmetry of lattice vibrs. 78−22797
alloy, collective modes, computer simulation 80−54325
alloys, effects of temp. on order-depend. elec. resist. 77−31992
alloys, substitutional, influence of many electron exchange and correlation effects on vibr. props. 79−69443
alloys with diagonal and geometrically-scaled off-diagonal disorder, coherent locator approach to lattice vibr. 79−73279
ammonium compounds, rotational tunnelling, temp. dependence 80−38970
ammonium oxalate monohydrate, Raman spectrum, internal and external vibrs. 79−73924
Anderson Gruneisen parameter, expression 77−76517
Anderson-Gruneisen parameter effect of anharmonicity 78−79714
angular force models of de Launay and Clark, Gazis and Wallis 77−47524
anharmonic Brownian oscillator, canonical correlation function based on projection operator technique 78−55926
anharmonic classical oscill., dynamical struct. factor in classical stat. mech. 77−55326
anharmonic crystal, lattice dynamics and stability, self-consistent phonon theory 79−51209
anharmonic crystal, lattice dynamics and stability 78−6129
anharmonic crystal $O(\lambda^4)$, phonon self energy, monatomic linear chain model calcs. 79−42161
anharmonic crystals, neutron scatt. cross-section, sublattice displacement effects 79−77460
anharmonic crystals, unsymmetrised SCF approx. 78−63830
anharmonic crystals with complex lattice, equations of state 80−107399
anharmonic effects investigation, uniaxial press. for inelastic neutron scatt. 77−35442
anharmonic lattices, nonlinear mechanics, computer simulation 80−24557
anharmonic oscillator, highly excited, damping, asymptotically exact solution 79−33041
anharmonicity, intensities of overtones and component freqs. 77−69052
anisotropic temperature factors, anharmonic motions 78−9902
antimonates, columbite or trirutile struct., force fields rel. to cryst. struct. *(French)* 80−107104
atomic mean-square displacements, T^γ temp. depend. 80−19883
atomic movements in solids, illustration model for univ. students 77−49531
atomic thermal vibration parameters, empirical $T^{3/2}$ law 77−39652
axial shadow pattern, atomic vibr. effect on width and shape of axial shadow pattern 77−39640

lattice dynamics continued
band tailing due to zero-point vibrs. in perfect cryst. 79−28267
Bethe lattice, vibration 78−30706
Bethe-lattice dynamics, impurity and localised mode 77−62595
bond percolation problem in semi-infinite medium, Landau-Ginzburg theory 79−93068
Born-Huang invariance conditions, completeness 78−51620
Born-Huang invariance conditions 77−84856
boson linear coupling systems, general props. 80−2124
brass, thermal cond., electronic and lattice components, separation methods 80−29380
Brillouin zone summations, convergence 78−91384
Cayley tree type system, modes, densities, lattice vibrs. 78−71813
centre with close electronic levels, temp. effects 79−37804
chalcopyrite compounds, ABS_2, Urey-Bradley force fields and ionic charges calc. at zero wave vector 77−76497
charge density, effect of phonon 78−22794
chemisorbed atoms and mols., vibrational motion dynamics, infrared absorpt. line shape 78−51814
chlorotrifluoroethane, IR photoreaction *(Japanese)* 80−11885
classical crystal optics, lattice dynamical background, review 80−97221
classical Ising model, crit. dynamics simulation in transverse field 78−59930
classical quadrupole solids, correl. effects 80−10628
classical shell model, quantum mechanical foundation 77−15506
cluster-Bethe model, anharmonic and nonharmonic vibr. props. of classical solid 77−43299
collective modes in solids, computer simulation 80−54325
collective vibrations rel. to absolute stability limit *(Russian)* 77−47373
conference, Paris, France (Sept. 1977) 78−59869
continued fraction formalism 78−47475
Coulombic interaction summation in Gaussian basis 80−70575
crystal, models, dynamic systems, symm. props. 77−19888
crystal lattice oscillations and molecular oscillation, change in bond length and angles as cooridnates 80−107385
crystals, quasicontinuum theory 77−855
crystals and dislocations, spontaneous breakdown of spatial translation invariance *(German)* 79−7653
cubic and hexagonal lattices, Brillouin delta function 79−73261
cubic crystal, acoustic waves, Christoffel elastic eqns., and elastic consts. 79−51205
cubic crystal, multimode Jahn-Teller coupling, orbital triplet 78−23062
cubic crystals, overlap shell model, bond charge model 79−42156
cubic crystals, Raman scatt. from tunnelling of substitutional molecules 80−40107
cubic system, force const. models comparison, self consistency conditions 80−44264
Debye lattice, thermal props., WINIMAX approx. appl. 80−49333
density response, direct approach 78−43078
diamond structure semicond., lattice dynamics calc. prog. using adiabatic bond charge model 80−10599
diatomic solids viewed as directed media, generalised continuum model 77−69051
dielectric absorpt. spectrum, charact. lattice vibrs. 80−2766
dielectric matrix, approximate inversion 78−71797
differential pseudocontinuum models 79−69200
dilute binary alloys, formation energy, lattice relax. and zero-point vibrations 78−83771
dilute binary alloys, formation energy, lattice relax. and zero-point vibrations 78−87646
dimers, singlet-triplet energy gap, temp. depend. 79−7809
dimethylammonium manganese chloride, perovskite type layer struct., lattice dynamics 79−33053
dislocation-phonon interaction in cryst. with anisotropic slip system 80−29137
dispersion of dielectric axes in monoclinic and triclinic crystals related to lattice dynamics 78−87920
dispersive media, Ewald dynamical diffr. theory extinction theorem 78−66749
distortive transformations, lattice-dynamical model, crit. exponents calc., statistical mech. treatment 77−84880
DNA, double helix, breathing modes and induced resonant melting 79−62180
domain wall Brownian motion and diffusion constants 79−37775
effective atomic charge rel. to electronegativity and ionicity 77−24287
Einstein's work in solid-state theory, geophysical importance *(German)* 79−86848
elastic coefficients, independent 4th-order for all cryst. classes, numerical methods anal. 79−69219
elasticity, discrete lattice model transition to continuum limit, invariance conditions 77−861
electron crystal in strong mag. field, phase diagram, normal mode anal. 80−44287
electron-ion system, effective ion interaction and force consts. 80−65185
electronic structure and solid props., rel. to chemical bonding, book 80−86044
energy transfer and two-centre optical transitions in OH^- and rare earth double-doped solid 80−7398
equations of state of crystals with strong sixth-order anharmonicity 80−92637
equations of state of solids of cubic and tetragonal symm., fourth order quasi-harmonic 77−69068
Ewald dynamical theory of diffr., lattice dynamics problem *(Czech)* 79−46757
exciton motion depend. on lattice vibr., inner potential energy, ground state, effective mass *(Chinese)* 80−54610
exciton-phonon coupled-mode excitations in cryst., relax. rates, theory 80−59881
F centre luminescence polarisation, stress induced, temp. dependence 79−56857
FCC, cryst. fine particles, freq. distrib. function 79−4376
Fermi resonance theory 77−1666
ferroelastic crystal, nonideal, domains struct. 78−2191
ferroelastic phase transitions, Brillouin scatt. spectroscopy 80−55115
Fischer-Tropsch wax, NMR investigation 80−7186
flexible structures, physical props. 79−19331
fluoride, Mn^{4+} activated, configurational co-ordinate model, predictive use 79−19918
fluorite type crystal, effects of anharmonicity and disorder on Raman scatt. at high temp. 78−80349
fluxes in crystals, field theoretic approach 79−69199

lattice dynamics continued
force const. adjuster program for least squares fit to observed frequencies of molecules and crystals 78−91395
force constants, diamond and sphalerite struct. crysts. 78−91408
fracture theory based on lattice instability 80−84244
free energy, anharmonic contrib. 77−20088
free energy of crystal, uncorrelated-pairs approx. 79−42200
Frenkel-Kontorova model, equilib. config., numerical study 79−40474
gas-solid surface sticking probabilities, internal mode depend. 78−6213
grain boundary structures, lattice dynamics studies, method and appl. to stability 80−49237
graphite, atomic thermal motion comparisons at 300K based on X-ray neutron and phonon spectrum data 79−7657
graphite, frequency distribution based on unfolding technique 80−92619
graphite, new force const. model 77−72643
graphite, obs. of anomalously sharp feature in second order Raman spectra 77−81103
graphite, thermal vib. amplitudes from integrated intensities corrected for TDS 78−67780
graphite, X-ray monochromator crystal, TDS, Mossbauer obs. *(German)* 77−16230
graphite and graphitic intercalation compounds 78−34574
graphite intercalation compounds, C_8M, (M=K, Rb, Cs), Breit-Wigner line shape anal., Raman spectra 80−50336
graphite intercalation compounds, interband Landau level transitions, magnetorefl. 77−52095
graphite intercalation compounds, props. and appls. 78−71711
graphite intercalation compounds with Br_2, ICl and IBr, Raman scatt. 77−12390
graphite intercalation cpds., dispersion relations of intercalate modes 80−34379
graphite intercalation cpds., Raman scatt. and IR refl., review 80−45066
graphite-$AlCl_3$, well-staged, Raman and IR spectra 80−50339
graphite-alkali metal intercalation cpds., IR, active lattice mode obs. 80−45072
graphite-Br_2 stage 2 intercalation cpds., Raman spectra 80−80787
graphite-$FeCl_2(FeCl_3)$ intercalation cpds., lattice dynamics, Mossbauer spectra 80−15925
graphite-$FeCl_3$ layered compound, lattice modes, Raman spectra 79−95785
Green's function calculation, surface atom freq. spectrum, mean correl. displacements *(French)* 78−2206
Green's function generating coeffs., appl. to FCC lattice 77−1185
Green's functions in quantum theory, book 79−65147
half space layered cryst., vibr. spectrum, Brillouin zone *(Russian)* 80−100313
harmonic crystal lattice with extended distortions *(Russian)* 77−66003
harmonic crystals, cell cluster method, Einstein heat capacity 78−51636
harmonic lattice with point defects, exponential transformations for Hamiltonian 77−39638
harmonic oscillator one-dimens. chain with friction, discrete-continuous transition 77−849
harmonic oscillator one-dimens. chain with friction, discrete-continuous transition 77−850
harmonic vibrations, one-dimens. incommensurate lattice 78−38788
harmonically coupled particle chain in double-minimum potential well exact soln. for soliton propag. in discrete case 80−34166
heat capacity of crystals and the vibrational spectrum, historical review 80−57071
heat pulses, soliton-like props. 78−22808
heavy-particle channelling, diffr., probe for correlated lattice dynamics 78−30687
hexagonal crystal, bulk and surface-atom mean square displacements, elastic continuum theory 77−7795
hot luminescence in F centres, nonradiative quenching 80−11467
hydrates, H_2O vibration in crystal lattice, model calc. 78−75741
ice, hexagonal, Raman spectrum of translational lattice vibrs., press. effects 79−24304
ice, IR ν_s absorption band profile of isotopically diluted OH group in crysts. 79−69821
ideal anharmonic crystal, X-ray diffuse scatt. asymm. *(Russian)* 77−47300
ideal crystal, anharmonicity contrib. to X-ray scatt. 77−58920
II-VI and III-V compounds, eight-parameter bond-bending forces model 80−70334
II-VI compounds, deformable-ion model 78−91396
II-VI compounds, transition metal ion activated, vibronic struct. in absorption and luminesc. 78−6729
impurity centres, electron-phonon coupling from structured optical spectra, review 80−89038
impurity molecules in solids, vibrational relaxation, anharmonic dynamics role *(Russian)* 80−75323
impurity relaxation in nonresonance field, phonon amplification *(Russian)* 80−100310
incommensurate lattices, conditions of existence and spectra 78−55934
incommensurate lattices, optical absorption and neutron scatt., lattice dynamics 79−33039
incommensurate lattices, statics and dynamics 79−23913
incommensurate structure, Debye-Waller factors, modulation wave thermal fluctuations 80−84274
incommunsurate crystal phases, harmonic approx. 80−29147
inelastic light scattering conference, Santa Monica, CA, USA (Jan. 1979) 79−95762
inert gas, collective modes, computer simulation 80−54325
inert gas solids, book contrib. 77−47522
inert gas solids, homology of lattice vibrations 79−77695
inert gas solids, research history, book contrib. 77−49547
inert gas solids, unpaired elastic force model in lattice dynamical study 78−63820
infinite harmonic crystal, dynamics and ergodicity 77−39653
infinite harmonic crystal, dynamics and ergodicity 78−59919
infinite harmonic crystal, dynamics and ergodicity 80−10598
infinite harmonic crystals, stationary nonequilib. states, existence, props. 77−55325
inner elastic constants, symm., depend. on symm. of interlattice tensors 79−28028
inner elastic constants, tensor notation and relation to lattice dynamics 79−28027
inorganic molecular crystals, metal complexes electronic spectra and intermolecular interactions 80−55137
interatomic force consts. from lattice vibrs. 77−20020
lattice dynamics continued
internuclear density units, temp. factors, exptl. accuracy 77−55206
internuclear density units, temp. factors, theory in harmonic approx. 77−55205
inverse spectral problem, use of parameters of intermol. spectrum of condensed media to decrease nonuniqueness 77−80586
ion-lattice interactions, modelling displacement correls. in computer simulations 78−2179
IR absorption mechanisms 78−60460
Ising spin system, coupled to acoustic and optic lattice modes, critical behaviour 80−71044
Jahn-Teller E-e problem, diagonalisation by means of transformed basis 79−82566
Jahn-Teller reduction factors, vibronic states 77−15803
king and domino polynomials for polyomino graphs, lattice dynamics appl. 77−71278
Kohn discontinuities, effect on press. depend. of superconducting transition temp. *(Russian)* 77−47914
Kohn effect, dielectric response of electron gas in strong mag. field 77−4279
lattice gas model, three phase eqns. of state 78−22818
lattice instabilities, electronically driven, theory 78−10158
lattice sums by Ewald method, dipolar and Coulomb energies in infinite lattices 77−68942
layered compound, anisotropy of lattice vibrs., polarisable ion model 77−35642
layered compounds, dynamics of two-dimens. lattices perturbed by weak interlayer interactions 77−51453
layered compounds, optical props., book contrib. 77−44023
layered crystal, low freq. vibr. spectra peculiarities, normal mode density at low temp. *(Russian)* 80−70332
LEED, high temp. limit Debye model 77−1207
light diffraction, Ewald extinction theorem and Green function method for semi-infinite dipole cryst. 79−23683
Lindemann's criterion and necessary condition for melting curve maximum 80−2145
linear atomic chain model, freq. of lattice vibrs. in $A_2^{III}B_3^{VI}$ compounds *(Russian)* 77−55327
linear chain model, symmetry-adapted, layer dynamics of high-symmetry crystals 80−34148
linear conductor, IR absorption, amplitude and phase mode dynamics 77−16313
linear mixed valence compounds, longit. modes 78−95119
linear triatomic chain, lattice vibr. anal. 78−83886
localization problem of nonlocal continuum theories 79−69201
low lying lattice vibrational modes, conf., San Juan, Puerto Rico, (Dec 75) 78−10131
low-dimensional materials, pseudolattices and correlation method 78−75768
low-lying vibrational modes and theory of local and transport props. at transitions 78−14425
Lyddane-Sachs-Teller relation, cryst. with Debye polarisation 77−20256
mag. dipole transitions $^5D_3 \rightarrow {}^7F_4$, interpretation 79−42505
magnetic order coexistence with charge density waves 80−97096
martensite formation, and lattice props. rel. to elastic constants 80−50630
matrix paradox, for teaching 78−49611
metal oxides, cation ordering effect on Raman spectra 78−43850
metals, electron-deformation interaction, lattice contraction, Hubbard model calcs. *(Russian)* 80−59592
methyl compounds, rotational tunnelling, temp. dependence 80−38970
methyl group tunnelling and coupling to internal vibrations 78−79675
α-methylammonium chloride, disordered, lattice vibrs. Raman spectra 77−85699
mica tetrahedra, cation-apical O vibrs., IR spectra 79−47420
microscopic formulation of rigid ion, deformable charge densities and effective charges 78−59876
microscopic theories, developments 78−59870
microscopic theory, derivation of electron-phonon Hamiltonian of crystal 78−87746
mixed crystal, one-dimens. dynamics 79−69217
mixed valence compounds, phase diagrams, lattice props., electron hole symmetry 79−91002
molecules, Debye-Waller factors, contrib. of internal modes 79−73263
molybdates, alkaline earth, U activated, scheelite struct. luminesc. props. . vibr. modes and quenching temp. 80−60651
molybdates, hydrated, water mol. bending vibrs. at low freqs. *(French)* 79−78670
monatomic BCC lattice under intense excitation, energy transport 78−59922
monatomic three dimensional FCC lattice, solitary wave effect on shock profile 80−79874
monoclinic crystal, refl. spectra dispersion anal. 79−99877
Mossbauer effect appl., conference, Kyoto, Japan (Aug.-Sept. 78) 80−7199
Mossbauer emission and absorption spectra, effect of anharmonic US vibrations excited in cryst. 78−72443
multimode Jahn-Teller coupling of impurities in solids, at finite temps., quasi-mol. description 77−7832
n-vector model, stochastic, dynamic critical props. 77−24362
neutron anal. techniques at Grenoble high flux reactor *(Italian)* 77−15289
neutron incoherent thermal scatt., nonlinear multi-sublattice jump diffusion model 77−28034
neutron scattering conference, Gatlinburg, TN, USA (June 1976) 79−41910
niobates, columbite or trirutile struct., force fields rel. to cryst. struct. *(French)* 80−107104
NMR second moment, lattice vibrs. effect 80−20467
nonequilibrium harmonic chain, light scatt., temp. depend. 77−69827
nonlinear 1D system, ϕ^4 chain dynamical props. 80−4655
nonlinear interaction of powerful light beam with cryst. lattice vibrs. 78−46711
nonlinear lattice, one-dimens., wave propag. with arbitrary neighbour range 77−59072
nonlinear lattice dynamics, mol. dynamics simulation 78−59921
nonlinear lattice dynamics, molecular dynamics studies 79−77713
nonlinear one-dimens. Hamiltonian dynamics for lattice distortion 80−20171
nonlinear system, kink-phonon interaction 79−73262
nonlinear vibr., synchronised periodic phenomena 77−31730

lattice dynamics continued
nonlocal elasticity, rel. with lattice dynamics 77−84824
nonmetals, microscopic and model theories 78−59871
normal mode calcs. of crystals and molecules, coordinates and force matrices generation, computer program 78−91393
normal modes of crystalline solids, HF gravitational radiation 77−2586
normal modes vibrations, use of group of neutral elements of crystalline sites 79−37774
NQR pressure sensitivity, vol. depend. of elec. field gradient and lattice vibrs. 77−12225
one dimensional defect lattice vibrations 80−31454
one dimensional mixed crystal short range order, frequency spectrum 79−95093
one-dimensional complex order parameter model, mol. dynamics 78−34787
one-dimensional diatomic chain, order-disorder transition, simple model 79−4394
one-dimensional finite chain, boundary states and vibrs., tight-binding approx. 80−2317
one-dimensional molecular lattice, soliton motion, thermal vibrations *(Russian)* 80−54321
one-particle pot. formalism, site symmetrized Fourier invariant treatment of anharmonic temperature factors 79−33040
optical activity, lattice dynamical background 80−93267
optical activity in crystals, lattice dynamical theory 80−34883
optical generation of longit. phonon modes 77−43288
orbital ordering in Jahn-Teller crystal with direct Coulomb interaction 78−26833
ordered and disordered materials, continuum model, elastic wave propag. 77−1168
organic charge transfer crystals, transport props., phase transitions, mol. dynamic *(German)* 80−39507
organic linear chain cpds., diffuse $4k_F$ refls., small intramolecular Coulomb interaction 80−34376
orthogonal fibre reinforced viscoelastic composites 78−42558
paraelastic tunnelling system dynamics, intermediate coupling regime 77−55489
n-paraffins, solid and liq., Raman spectra, longitudinal acoustic vibr. mode 78−31183
partially disordered crystal, lattice dynamic model 78−83897
Pauling electrostatic valence rule, anion-cation vibr. freq. 77−35641
Peierls one dimensional model, exact solution, electron spectra, static lattice deformation *(Russian)* 80−70609
phase transition model due to nonlinear reson. of lattice oscills. *(Russian)* 77−31746
phenol formaldehyde resin reinforced with chrysotile asbestos fibres, thermal expansion, specific heat 79−55908
phenomenological models *(Polish)* 79−37769
phenomenological non-hermitian dynamical matrices 79−69202
plasma, classical two dimensional one-component, Monte Carlo simulation, solid-liquid phase study 79−94814
point defect migration in crystals, anharmonic model description 77−65976
polar crystals, gravitational wave induced IR emission 77−45769
polar semiconductors, two-phonon resonance Raman scattering 80−108204
pseudoatom potential, rel. to screening and lattice dynamics 79−60736
pyridine-Ag_5I_6, superionic conductor, dynamical aspects 78−79695
quantum crystals of spinless fermions, collective modes, vacancy motion-lattice vibr. coupling 79−86960
quantum field theory of crystals and extended objects, review 79−42164
α-quartz, Γ-A phonon dispersion curves, rel. to $AlPO_4$ lattice dynamics 78−75750
quartz, cryst. lattice nonlinearity rel. to strain amplitude depend. of internal friction 77−27939
α-quartz, interatomic forces and lattice dynamics 77−7802
α-quartz, Raman spectral lines, radiation and temp.-induced changes in width and intensity 78−2859
quasi one-dimensional conductors, conference, Dubrovnik, Yugoslavia, (Sep. 1978) 80−12853
quasi-continuous model for a crystal with ionic and electronic polarization 79−69053
random harmonic chain model, essential singularities of sp. ht. and density of states 77−72665
random system, density of states, essential singularities, sp. ht., free energy 78−18729
rare earth iron garnets, spectra calc. using exact microscopic Hamiltonian 77−8553
rare earth mixed valent compounds, lattice dynamics 79−73268
rare earth perrhenates, Raman spectra, $(ReO_4)^-$ ion normal vibrs. rel. to static field 79−65858
rare earth phosphors, Ln_2O_2S:Eu, Raman spectra, lattice vibrs. 79−78669
rare earth trihydroxides, cryst., Raman spectra, vibr. assignments 78−76455
rare gas solids, Debye Waller factors from unpaired elastic force model 80−19896
rate processes in condensed media, anharmonicity effects 79−19349
Rayleigh's theorem generalised, infinite harmonic crystal 78−55914
relaxation structs., physical props. 79−28050
sapphire, 14.8 MeV neutron damaged, optical vibronic absorption spectra 80−50384
second sound, molecular dynamics study 79−42207
second-neighbour interactions, Green's matrix and Weyl surface 78−18713
self-trapping of powerful light pulses, role of TO and LO lattice vibr. modes 80−99809
semiconductor, atomic displacements and enthalpy of vacancy formation 78−38690
semiconductor, deep centres, nonradiative de-excitation 79−38644
semiconductor, dynamical effective charges, pseudopotential calc. 78−30881
semiconductor, electronic properties, rel. to chem. bonding and lattice dynamics 80−44169
semiconductor, vibr. IR excitons, spectra *(Russian)* 78−15173
semiconductor physics, conf., Edinburgh, Scotland (Sept. 1978) 79−95303
semiconductor single crysts, mean square atomic displacements determ. by X-ray anal. *(German)* 78−30726
semiconductors, force variation due to charged defects 80−92634
lattice dynamics continued
semitransparent solids, approx. band model for radiative transfer 79−37136
sine-Gordon kinks, nonequilib. props. using mol. dynamics techniques 79−12737
solid-liquid transitions, freq. distrib. function 77−4183
soliton in solids with chain structure *(Chinese)* 79−90931
soliton scattering from mass interface in 1D nonlinear lattice, simulation *(Japanese)* 77−43306
soliton solutions to nonlinear phenomena 78−59880
solitons in condensed matter physics, theory 80−50122
specific heat, const. press., press. variation of vacancy contrib. 79−1510
spinel compounds, AB_2C_4, Urey-Bradley force constants 80−59587
strain driven thermoelastic instability toward brittle fracture 80−103415
strongly anharmonic crystals, improved unsymmetrised SCF approx. 78−75791
structural phase transitions, Landau theory 80−92639
structural phase transitions, theory 78−75797
structural phase transitions in crystals, effect of high-power visible and IR laser radiation 78−71825
structurally incommensurate systems, fluctuation spectrum, incommensurate phases 78−91419
superconductivity and lattice instability 80−88663
superconductor, non-A15, lattice instabilities 78−10591
superharmonic approximation for quantum crystal 80−92615
superionic conductor, hydrodynamic theory for collective excitations 80−107530
superionic conductors, correlation functions theory 78−79674
superionic conductors, dynamic properties 78−79673
superionic conductors, microscopic theory 78−79809
superionic conductors, Raman scattering from mobile ions, theory 78−80352
superionics, with fluorite structure, Brillouin scattering and lattice defect energetics 78−80369
tantalates, columbite or trirutile struct., force fields rel. to cryst. struct. *(French)* 80−107104
TCNQ alkaline salts, phase transitions, vibronic intensity enhanced IR spectra 78−23441
TCNQ salts, lattice vibr. freezing, Kohn anomalies, lattice struct. 77−15401
ternary alloys, vibr. freq. distrib. spectra, small cluster statistical theory 79−24317
tetraalkylammonium bromide, solid and liq., Raman spectra, longitudinal acoustic vibr. mode, mol. dimensions of ions 78−31183
tetramethylammonium hexachlorotellurate, IR and Raman spectra, lattice and internal modes, phase transition 78−6659
thermoelastic effect, lattice dynamics and energy channelling 78−22786
three-body force shell model, asymmetric matrix elements 77−27950
tourmaline, pyroelectricity, struct. mechanisms 78−10850
transition metal, dichalcogenide layer cpds., bonding and phase transitions 80−34186
5d-transition metal antifluorite crystal, struct. props. and lattice dynamics, mag. struct. 80−44268
transition metal nitrides and carbides, surface energy for brittle fracture from phonon freqs. 79−86837
transition metal oxides, electronic polarisability of ions 77−19901
transparent optical materials, laser induced damage and lattice strain due to lattice defects 80−48315
trimethylammonium cadmium trichloride, struct. phase transitions, low-freq. Raman scatt. obs. 80−80783
α-trimethylammonium chloride, disordered, lattice vibrs. Raman spectra 77−85699
TSeF-TCNQ, Kohn anomaly of metallic state, X-ray diffuse scatt. meas. 80−19887
TTF crystals, polarised Raman spectra meas. 78−6681
tungstates, alkaline earth, U activated, scheelite struct. luminesc. props. vibr. modes and quenching temp. 80−60651
two-dimensional lattice vibrations calcs. 80−2126
two-electron level with quasidegenerate levels, local phase transitions and temp. effects in lattice dynamics 80−10666
two-parameter dynamical model, appl. to Ag and Al 80−10597
uncorrelated-pairs approximation for anharmonic free energy, tests 78−59920
undamped lattice vibrations in systems with two incommensurate periodicities 79−10904
urea, internal modes contrib. to Debye-Waller factors 79−73264
valence force field, rel. to tensor force consts. 80−79888
van der Waals crystal, cohesive energy, many-body theory calc. 77−76348
variational quasiharmonic approx., free-energy *(Russian)* 77−11642
velocity autocorrelation function, long-time correlation tails 80−24541
vibration spectra and crystal symm., book 77−24365
vibrational dephasing in liquids and solids 79−38552
vibrational dynamics of liquids and solids, Raman scatt. of picosecond light pulses 78−94414
wave motion in one dimens. nonlinear, periodic, exponential lattice 78−12646
wave scattering, fluctuating inhomogeneous media, model for teachers 79−21492
wurtzite-type crystals, force constants determ., polarisable ion model 78−75740
wurtzite-type crystals, lattice dynamics including the effect of electronic extension 80−59586
X-ray diffraction and lattice dynamics, early work by I. Waller 80−62439
X-ray diffraction by coherent sound wave 77−84860
X-ray thermal diffuse scatt. effects on atomic parameters and electron density distrib. 77−19819
X-Y model, two-dimensional, with quartic anisotropy, mol. dynamics study 78−75739
zinc blende structure, rigid ion second neighbour ionic model, dispersion calc. 77−1194
zincblende crystals, internal strain and piezoelectric coefficient 78−39505
zincblende structure compounds, lattice dynamics calc. program 79−86854
zincblende type crystals, lattice dynamics, phonon freq. rel. to mass ratio 78−95121
$AgFeTe_2$, Mossbauer parameters in phase-transition region 80−11308
α-AgI, dynamic cage effect 80−107541
α-AgI, ionic motion, low freq. Raman scatt. 78−80354

lattice dynamics continued
AgI, lattice dynamics of binary superionic conductors 80−107393
AgI, phase transition, statics and local dynamics, mean field and Mori theory 80−39347
AgI, superionic conductor, dynamical aspects 78−79695
α-AgI, superionic conductor, Raman scattering evidence for sublattice melting 78−80350
AgI, superionic conductor, Raman study 78−80353
α-AgI, superionic conductor, struct. and dynamics, two-dimens. mol. dynamics model 80−49413
$AgIO_4$, dynamics of IO_4^- vibr. in lattice 79−42157
$AgNa(NO_2)_2$, ferroelectric phase transition, theory 79−24272
$AgNa(NO_2)_2$, ferroelectric transitions, group theoretic comparison with $NaNO_2$ 80−7311
Ag_3SI, superionic conductor, dynamical aspects 78−79695
Ag_3SbS_3, IR refl. spectra, permittivity, lattice vibrs. 79−65862
$Ag_2SnS_3(Se_3)(Te_3)$, Mossbauer obs. 77−43923
α-Al_2O_3, IR intensities, valence-band dynamic and electrooptic models 80−34906
β-Al_2O_3-X_2O, (X=Na,K,Rb,Ag,Tl), infrared and Raman spectra 79−1761
$AlPO_4$, vibr. normal modes, rel. to α-quartz phonon dispersion curve 78−75750
$Al_2(WO_4)_3$:Cr(Eu), and undoped crystals, luminesc. obs. 80−89047
AmO_2, IR spectra, values of transverse vibr. frequencies 77−28585
Ar, solid, vol. depend. lattice dynamics, pseudo-harmonic approach 79−99260
Ar-graphite system, effects of dynamic coupling 80−10771
As_2O_3-SO_3, polarised Raman and IR spectra, force field calc. *(French)* 78−6674
$(As_2O_3)_n$, claudetite I, vibr. spectra, force field calc. *(French)* 78−60447
As_2S_3, network dynamics, vibr. band splittings 79−42199
As_2Se_3, monoclinic, chem. bonds rel. to electronic and vibr. states 80−64951
BN, ^{15}N zero point vibr. energy from nuclear photon scattering 80−59593
BN, cubic, prediction from trends of force consts. of first-row crysts. 79−77694
BN, hexagonal, long optical vibrs., elastic consts. from valence force consts. 78−51621
BN, superhard, X-ray characts. *(Russian)* 77−80593
BaF_2, anharmonicity vibrs. and correlation effects, neutron diffr. 78−55915
BaF_2, superionic conductor, theoretical investigation of Raman scatt. 78−80351
$Ba_2KNb_5O_{15}$, Raman scatt. experiments in tetragonal tungsten bronze compounds 80−40113
$Ba_2NaNb_5O_{15}$, Raman scatt. experiments in tetragonal tungsten bronze compounds 80−40113
$BaSO_4$, barite, crystal struct. and sulphate force consts. 78−83784
$BaSO_4$, polarised IR refl., absorpt. and laser Raman spectra 77−43997
BeO, valence force fields and lattice dynamics 77−7799
BeO, wurtzite-type crystals, lattice dynamics including the effect of electronic extension 80−59586
Bi_2O_3 and sillenite struct. derivatives, $MO_x.6Bi_2O_3$, IR and Raman spectra, vibr. anal. 78−76464
Bi_2Se_3, Raman spectra, Raman and IR-active modes 79−56776
Bi_2Te_3, Raman spectra, Raman and IR-active modes 79−56776
C materials, thermodynamic props. rel. to struct. 77−80597
C_8K(Rb), graphite intercalated, phonon dispersion relations and Raman spectra 80−44272
CaF_2, superionic conductor, theoretical investigation of Raman scatt. 78−80351
$CaHPO_4.2H_2O$ powder and crystals, vibrational spectra, factor group anal. 80−45076
$CaMgSi_2O_6$, single cryst., IR reflection spectra, vibr. spectrum calc. 77−73142
$Ca(MoO_4)_{1-x}(WO_4)_x$, Raman scatt. meas. 77−28578
$CaNb_2O_6$, columbite, polarised Raman and IR spectra, normal coord. anal. 77−76500
CaO:Bi^{3+}(Pb^{2+}), impurity centres vibronic spectra, lattice dynamics and electron-phonon interactions 80−7396
β- and γ-$Ca_2P_2O_7$, IR and Raman vibr. spectra 80−25355
CaR_2S_4, R=rare earth, ternary sulphide with Th_3P_4 struct., vib. spectra 78−2844
$CaSO_4$, anhydrite, resonance splitting of complex anion internal vibrs. 80−55081
CdF_2, ionic conducting fluoride fluorite, US velocity meas. 80−107381
$CdGa_2S_4$, vibr. spectra, 33-400 cm^{-1}, symm. transform. *(Russian)* 78−23465
$Cd_{1-x}Hg_xTe$, lattice dynamics of low conc. of Hg atoms, perturbation model impurity description 79−55853
CdI_2-$CdBr_2$ mixed layer cpds., rigid layer modes and van der Waals interactions, Raman spectra obs. 79−33700
$CdIn_2S_4$, partial inverse spinel struct., detection by Fourier transform spectroscopy 80−108197
CdP_2, oscillatory states, polarised spectra of IR absorption and emission of single crysts. *(Russian)* 77−28583
CdP_2, Raman spectra, mode symmetry 79−91441
CdR_2S_4, (R=Sc, Yb, Tm), IR and Raman spectra, force consts. 78−68503
CdS, chemically precipitated film, optical spectra, annealing effects *(Russian)* 79−11424
CdS, long wavelength lattice vibr. modes 80−49318
CdS(Se), optical spectroscopy, absorpt. coeff., lattice vibr. modes, band gap, acoustic approach 77−69822
CdSe, hexagonal, anharmonicity, X-ray intensity meas. 77−43286
CdTe, lattice dynamics and phonon parameters bond bending force model 80−59595
CdTe, temp.-depend. of root-mean-square dynamic displacements, characteristic temp., X-ray study 78−83895
Ce-H(D), inelastic neutron scattering exam. of lattice dynamics 80−29128
CeBi(Sb), enhanced lattice-displacement effects on cryst. field and anomalous mag. anisotropy 79−73477
CmO_2, IR spectra, values of transverse vibr. frequencies 77−28585
$CoCl_2$, interlayer force constants 78−14406
$CoCl_2$, static displaced shell model 78−79689
$Co(NH_3)_6(IO_4)_3.2H_2O$, dynamics of IO_4^- vibr. in lattice 79−42157

lattice dynamics continued
CoO, dielec. behaviour, Dick and Overhauser shell model calcs. 80−45001
$CrBr_4$, $CrCl_4$, Raman spectra, struct. and thermodynamic functions 78−60443
Cr_2O_3, optical generation of longit. phonon modes 77−43288
Cs halides, Gruneisen and Anderson-Gruneisen parameter determ. 80−59611
$Cs_3CoCl_5(Br_5)$, single cryst. polarised vibr. spectra 78−39535
$CsCuCl_3$, Jahn-Teller induced phase transition, helical at. displacements 77−43301
$CsIO_3$, hexagonal modification, temp. depend. of NQR freq., interpretation of long-wave spectra 80−25243
$CsIO_4$, dynamics of IO_4^- vibr. in lattice 79−42157
$Cs_2NaBiCl_6$, optical props. 78−68549
$Cs_2NaTbCl_6$, mag. circ. polarised emission, MCD, $^7F_J \rightleftarrows {}^5D_4$ transitions 77−77242
$Cs_2PbCu(NO_2)_6$, incommensurate Jahn-Teller transition, Huang scatt. 80−70401
$CsPbX_3$, (X=Cl,Br), anharmonic thermal vibrs., neutron diffr. study 80−29125
Cs_2SeO_4, single cryst., orthorhombic, Raman spectra 77−73140
Cs_2TiF_6, Raman spectra, internal and lattice vibrs. 77−8569
Cu halides, lattice dynamics of binary superionic conductors 80−107393
Cu-Al, change in force constant due to volume effects 78−75778
Cu-Be solid solutions, local oscill. conc. depend., impurity bands *(Russian)* 80−75318
Cu-Fe, force constant change with pressure, relative Mossbauer fraction 80−34163
Cu-Si, change in force constant due to volume effects 78−75778
CuBr, neutron scatt. investig. of anharmonic effects on Debye-Waller factor 77−11658
CuBr(Cl)(I), LF light scatt. spectra in superionic cond. phases, ion motion obs. 80−108217
CuI, parameter calc. from zinc blende zone boundary conditions 77−1194
CuI, superionic conductor, Raman study 78−80353
$CuInTe_2$, infrared optical properties 79−82974
Cu_6PS_5Br, cryst. struct. at 293 and 473K, thermal parameters, neutron diffr. obs. 80−59450
$CuSO_4.5H_2O$ and $CuSO_4.5D_2O$, Raman and IR spectra, mode assignments 77−66493
$CuSeO_4.5H_2O$, Raman and IR spectra, mode assignments 77−66493
$Cu_2SnS_3(Se_3)(Te_3)$, Mossbauer obs. 77−43923
D_2, solid, HCP, density depend. of elastic consts. 80−6589
Fe-Ni, Invar alloys, anomalous thermal expansion coeff. *(Japanese)* 79−65225
$FeBO_3$, antiferromag., vibr. spectra, 6000-30 cm^{-1} 78−19473
$FeCl_2$, interlayer force constants 78−14406
$FeCl_2$, vibrational excitations, polarised Raman spectra 79−19888
$FeCl_3$ intercalated with graphite, vibrational excitations, polarised Raman spectra 79−19888
FeF_2, long-wavelength lattice vibr. modes, symmetry coordinates 78−43081
$Fe_{0.33}NbS_2$, lattice dynamics and hyperfine interactions, Mossbauer spectra study 80−108135
$Fe_{1-z}O$, wustite, struct. evolution, mean isotropic thermal agitation factor, depend. on equil. temp. and comp. *(French)* 77−68947
FeOCl, Mossbauer spectra, lattice dynamics, hyperfine interactions 80−44985
$FePS_3$, Goldanskii-Karyagin effect, Mossbauer spectra 79−99798
FePt lattice, symmetry, state of order, vibration, temp. effects *(German)* 77−4067
$FeSO_4.4H_2O$, Fe sites asymmetry parameter, mean square displacement, Mossbauer spectra 78−6608
Fe_xTiS_2, lattice dynamics and hyperfine interactions, Mossbauer spectra study 80−108135
GaAs, lattice dynamics, phonon freq., bond bending force model calcs. 80−70335
GaAs, piezoelectric constant due to bond bending, electron redistribution effect 79−38457
GaAs:Cu, electron-phonon interaction in optical transitions between deep impurity level and allowed bands 79−42591
GaP, dispersion of vibrational excitations, Raman scatt. 78−84588
GaP, lattice dynamics and phonon parameters bond bending force model 80−59595
GaS, factor-group analysis of high-symmetry layer dynamics 79−42160
GaS, lattice dynamics parameters, X-ray diffr. study *(Russian)* 80−29146
Ga_2S_3, IR refl. spectra, linear chain model for lattice vibrs. 78−27235
$GaS_{1-x}Se_x$, mixed crystals, IR reflectivity spectra 80−66204
GaSb, anharmonic force consts. from third order elastic consts. at 300K 77−59074
GaSb, lattice dynamics, phonon freq., bond bending force model calcs. 80−70335
GaSb, vibr. spectra, lattice dynamics ang. force model 80−29127
GaSe, factor-group analysis of high-symmetry layer dynamics 79−42160
GaSe, lattice dynamics and elastic props., Born-von Karman model study 80−70337
GaSe, lattice dynamics parameters, X-ray diffr. study *(Russian)* 80−29146
GaSe MSM struct., inelastic tunnelling investigation of lattice dynamics, electron-phonon interaction 80−20330
Ga_2Se_3, IR refl. spectra, linear chain model for lattice vibrs. 78−27235
Ga_2Se_3-Ga_2S_3 solid solutions, IR refl. spectra, linear chain model for lattice vibrs. 78−27235
GaTe, layer cryst., polarised IR refl. spectra 80−97279
GaTe monocrystal, far IR polarised complex reflectivity obs. 80−60609
Gd-Mg, X-ray determ. of Debye temp., mean amplitude of vibr. 78−38802
Gd-Zn, X-ray determ. of Debye temp., mean amplitude of vibr. 78−38802
Ge, nearest-neighbour atom mean-square relative displacements, EXAFS spectra 79−91532
$GeBr_4$, isotopic splitting in totally symm. stretching vibrations 79−42967
GeH_4, IR spectral obs. 77−36226
GeS_2, cryst. and glass, Raman spectra, struct. *(Russian)* 79−51966
$GeSe_2$, cryst. and glass, Raman spectra, struct. *(Russian)* 79−51966
H_2, solid, HCP, density depend. of elastic consts. 80−6589
$HClO_4.H_2O$, wide line PMR spectra, oxonium ion motion *(French)* 79−56616

lattice dynamics continued
$H_3Co(CN)_6$, strong NHN hydrogen bond, vibr. lattice and mol., incoherent inelastic neutron scatt. 80−39232
α-HIO_3, vibration level Davydov splitting, adiabatic potential role, dipole-dipole approx. *(Russian)* 80−29365
$HNO_3.H_2O$, wide line PMR spectra, oxonium ion motion *(French)* 79−56616
$H_2PtCl_6.2H_2O$, wide line PMR spectra, oxonium ion motion *(French)* 79−56616
$H_2SO_4.H_2O$, wide line PMR spectra, oxonium ion motion *(French)* 79−56616
H_2SeO_3, cryst., vibr. spectra in O-H stretching region 79−51949
$H_2SeO_4.H_2O$, wide line PMR spectra, oxonium ion motion *(French)* 79−56616
$H_{0.4}WO_3$, inelastic neutron spectra 77−15287
^3He, solid mag. ordering, lattice dynamical approach 78−56020
^4He, FCC high-density cryst., lattice dynamics by inelastic neutron scatt. 79−1539
$Hg_{3-x}AsF_6$, one-dimens. lattice dynamics, X-ray scatt. study 80−75317
$Hg_2(BrO_3)_2$, Raman and IR spectra, vibr. anal. 77−66492
Hg_2Cl_2 prototype phase, soft mode, inelastic neutron scattering, Raman effect 78−91411
$HgCr_2Se_4$, ferromag. semicond., Raman spectra 78−52496
$HgCr_2Se_4$, Raman scattering, as function of temp. and incident photon energy 79−95781
HgI_2, IR lattice vibr. and dielec. dispersion 80−76018
α-HgI_2, red, normal modes vibrations, use of group of neutral elements of crystalline sites 79−37774
$Hg_3In_2Te_6$, complex ordered-vacancy cpd., struct. and lattice dynamics 78−34496
$Hg_2(NO_3)_2.2H_2O$, Raman and IR spectra, vibr. anal. 77−66492
Hg_2SO_4, Raman and IR spectra, vibr. anal. 77−66492
p-HgTe, far IR reflectivity spectra, experimental and theoretical study of the dynamic dielectric function 78−92069
InAs, lattice dynamics 79−14895
$In_{1-x}Ga_xAs_yP_{1-y}$ epitaxial layer, far IR refl. spectra, lattice vibrs. 80−97282
$In_{1-x}Ga_xAs_yP_{1-y}$, lattice vibrs., Raman study 78−91391
InP, lattice dynamics 79−14895
InP, lattice dynamics and phonon parameters bond bending force model 80−59595
InP, multiphonon absorpt. bands *(Russian)* 77−85731
InP:Fe, resonance photocond. 80−44651
InS, layer semicond., Raman scatt. meas. 78−35134
InS, layer single cryst., Raman scatt. meas. 78−76478
InS, Raman scatt. spectra and interpacket interaction 79−8146
InSb, lattic dynamics 79−14895
InSe, layer semicond., Raman scatt. meas. 78−35134
InSe, layer single cryst., Raman scatt. meas. 78−76478
InSe, layer single crystal, infrared and Raman spectra 78−92070
InSe, vibr. energy spectrum *(Russian)* 79−51483
K double fluorides, IR refl. spectra, vibr. modes, optical vibr. freq., Kramers Kronig anal. 80−66190
$KAl(SO_4)_2.12H_2O$, single cryst., Raman spectra, temp. depend., SO_4^{2-} site dynamic disorder 77−40219
$K_2Al_2(SO_4)_4.24H_2O$, temp. depend. curves of quadrupole interaction parameter for $^{27}Al^{3+}$ 77−55727
$KBrO_3$, hexagonal modification, temp. depend. of NQR freq., interpretation of long-wave spectra 80−25243
$KCl:Pb^{2+}$, low temp. sp. ht. 80−2178
$K_3Co(CN)_6$, ^{59}Co quadrupole coupling const., temp. depend. 80−44557
$KDy(MoO_4)_2$, polarised IR and Raman struct., $^{92}Mo/^{100}Mo$ isotope effect 80−108198
KH-H_2 crystal-gas system, with D impurity, thermodynamic equilib. 78−59954
KIO_4, dynamics of IO_4^- vibr. in lattice 79−42157
$KMnF_3$, lattice dynamics, rigid-ion model calc. 77−15512
K_2MnF_4, perovskite type layer struct., lattice dynamics, rigid-ion model calc. 77−15512
KND_2, neutron diffr. anal. of librations of amide ion *(German)* 77−27788
KND_2, neutron diffr. exam. 31K *(German)* 77−62506
KNO_2 polymorphs, high press. Raman spectra 77−85725
$K_2NaAlF_6:Cr^{3+}$, ^2E_g-$^4A_{2g}$ phosphoresc. spectrum, vibr. struct. 79−47494
$K_2PbCu(NO_2)_6$, incommensurate Jahn-Teller transition, Huang scatt. 80−70401
$K_2PbCu(NO_2)_6$ Jahn-Teller phase transitions, X-ray and neutron measurements 78−91438
$K_2Pt(CN)_4Br_{0.3}.3H_2O$, CDW system, nonlinear amplitude-phase interaction 80−88490
$K_2Pt(CN)_4Br_{0.3}.3.2H_2O$, deuterated, coupling of charge density wave and water mode 77−4646
$K_2Pt(CN)_4Br_{0.3}.xH_2O$, dynamical props. near Peierls instability, neutron scatt. 78−14436
K_2PtCl_4, far IR reflection spectra, assignments, effective ionic charges, force consts. 77−66488
K_2SO_4, D_{2h}^{16} and C_{2v}^9 phases, internal and external vibrs., Raman spectra obs. 79−47446
K_2SeO_4, single cryst., orthorhombic, Raman spectra 77−73140
$K_2(UO_2)_3F_8.4H_2O$ and $K_3(UO_2)_2F_7.2H_2O$, IR and Raman vibr. spectra *(French)* 79−51937
Kr, anharmonic contributions of $O(\lambda^4)$ to mean-square atom displacement 79−42155
La-H(D), inelastic neutron scattering exam. of lattice dynamics 80−29128
$La(BrO_3)_3.9H_2O$, IR and Raman spectra, vibr. asignments 78−84569
$La_2(SO_4)_2.9H_2O$, Raman spectra meas. *(French)* 77−20855
$LiAl_xFe_{5-x}O_8$, IR spectra, ionic ordering in absence of fine struct. 77−8583
LiC_6, Raman spectrum, rigid band model anal. 79−4800
$LiCr_xFe_{5-x}O_8$, IR spectra, ionic ordering in absence of fine struct. 77−8583
LiD, deformable-ion model and lattice dynamics 77−47514
LiD, lattice dynamics, effect of long-range three-body forces 77−89507
LiH, lattice dynamics, effect of long-range three-body forces 77−89507
α-$LiIO_3$, hexagonal cryst., vibrs. and force consts. 79−69220
α-$LiIO_3$, pot. energy distrib. and force const. variations with temp. 80−79894
$LiIO_3$, Raman spectra and phase transitions 77−16316
α-$LiIO_3$, Raman spectra behaviour in electrostatic field *(Chinese)* 80−7333
lattice dynamics continued
$LiIO_4$, and $LiIO_4.2/3H_2O$, dynamics of IO_4^- vibr. in lattice 79−42157
$LiKSO_4$, polarised Raman and IR reflection spectra, internal and external mode assignments 77−16293
Li_3N, interstitial sites and anharmonic thermal vibrs. in cryst. struct., ionic cond. mechanism 80−107190
Li_3N phonon spectra and lattice dynamics 77−59580
Li_3N, superionic conductor, cryst. growth and struct., phys. props., book contrib. 79−42308
Li_3N, superionic conductor, far IR absorption, temp. and isotope effects 79−51969
$LiNbO_4$, dispersion of vibrational excitations, Raman scatt. 78−84588
$LiScO_2:Bi^{3+}$, luminesc., vibr. struct. 79−33790
Li_2SiO_3, IR and Raman spectra, normal coord. anal. of unit cell vibrs. 77−81090
$LiZnVO_4$, high press. spinel modification, vibr. spectra 78−35124
$Lu_2(WO_4)_3:Cr(Eu)$, and undoped crystals, luminesc. obs. 80−89047
Mg-Cd, thermodynamic props., order-disorder transitions based on Helmholtz free energy 79−37853
$MgAl_2O_4$, lattice dynamics, rel. to space group of spinel 78−59898
MgF_2, long-wavelength lattice vibr. modes, symmetry coordinates 78−43081
$Mg(NH_4)_2(SO_4)_2.6H_2O:Cr_2O^{2-}$, optical absorption study, $Cr_2O_7^-$ and CrO_4^{3-} centres 80−55128
MgO, core struct. and energy of dislocations, breathing shell model calc. 77−39586
MgO crystal, unified approach to lattice states and dynamics 78−59878
$MgO:Cr^{3+}$ (Mn^{2+}) spin Hamiltonian parameters, lattice expansion and vibr. effects 80−24851
$MgO:Cr^{3+}(V^{2+})$, $^4A_{2g}\rightarrow{}^4T_{2g}$ spectra, new expt. results 80−11441
$Mg_2P_2O_7$, α- and β-phase, vibr. spectra, Raman and IR spectra 78−19467
MgR_2S_4, (R=Sc, Yb, Tm), IR and Raman spectra, force consts. 78−68503
Mg_2SiO_4, fosterite, lattice dynamics, IR and Raman spectra meas. 79−65153
Mg_2Sn, lattice dynamics, angular force model 77−4166
Mg_2Sn, third-order elastic constant, low temp. limit of Gruneisen parameter 79−73280
$MnBr_2$, vibr. struct. in cryst. field electronic transitions 78−59895
$MnCl_2$, lattice dynamics, density of states and sp. ht. calc. 80−92624
$MnCl_2$, vibr. struct. in cryst. field electronic transitions 78−59895
$MnCl_2.2H_2O$, Raman spectra and lattice dynamics 79−28742
MnO, dielec. behaviour, Dick and Overhauser shell model calcs. 80−45001
$(Mn_xRe_{1-x})_2(CO)_{10}$, Raman spectra, intramol. vibr. coupling, ^{13}C substitution 79−47431
$MnTa_2O_6$, columbite struct., X-ray diffr., IR and Raman spectra *(French)* 78−63727
MoO_3, Raman scatt. and struct. props. 77−55780
MoS_2, entropy, enthalpy and specific heat, temp. depend. 500 to 1700K 80−15260
MoS_2, factor-group analysis of high-symmetry layer dynamics 79−42160
ND_4DS, polycryst., vibr. spectrum, lattice dynamics 77−90138
ND_4IO_4, Raman spectra, libration lattice modes 80−60575
NH_4Cl, ^{15}N zero point vibr. energy from nuclear photon scattering 80−59593
$(NH_4)_2CuCl_4.2H_2O$, lattice dynamics, anal. of Raman scatt. measurements 80−34149
$(NH_4)_2CuCl_4.2H_2O$, Raman sepctra, dynamics, struct., phase transition 79−47434
NH_4HS, polycryst., vibr. spectrum, lattice dynamics 77−90138
NH_4IO_4, dynamics of IO_4^- vibr. in lattice 79−42157
NH_4IO_4, Raman spectra, libration lattice modes 80−60575
$((NH_4)_{1-x}K_x)_2CuCl_4.2H_2O$, Raman scatt. spectra 79−15459
$(NH_4)_2PO_3F$, H_2O, X-ray diffraction and Raman spectra struct. determ., external mode temp. depend. *(French)* 78−52507
NH_4ReO_4, ND_4ReO_4, Raman spectrum, temp. depend. 78−80335
$N_2H_6SO_4$, orthorhombic, low-temp. phase transition, Raman spectra meas. 77−24849
$(NH_4)_2SO_4.Al_2(SO_4)_3.24H_2O$, temp. depend. curves of quadrupole interaction parameter for $^{27}Al^{3+}$ 77−55727
$(NH_4)_2(TeCl_6)$, IR and Raman spectra, lattice and internal modes, phase transition 78−6659
$(NH_4)_2TiF_6$, Raman spectra, internal and lattice vibrs. 77−8569
N_2O_2, IR spectra of solid, Raman spectra of solid and liq., vibr. anal. 77−81093
$NaBrO_3$, IR and Raman spectra, vibrs., dipolar coupling effect 78−43852
$NaBrO_3$, Raman spectrum, temp. depend. *(Russian)* 78−23466
$NaCl_{1-x}Br_x$, mixed cryst., vibr. and optical props. 80−29133
$NaClO_3$, IR and Raman spectra, vibrs., dipolar coupling effect 78−43852
$NaClO_3$-$NaBrO_3$, Raman spectra, mode coupling and ^{79}Br-^{81}Br isotope effects 79−19873
$NaCrS_2$, antiferromag. semicond., Raman and far-IR spectra 79−47454
$NaIO_4$, dynamics of IO_4^- vibr. in lattice 79−42157
$NaIO_4$, normal coord. anal., internal and external modes 79−23684
$NaLnO_2:Bi^{3+}$, (Ln=La, Gd, Sc), luminesc., vibr. struct. 79−33790
$Na_3M_2Li_3F_{12}$, M=Sc, Ti, V, Cr, Mn, Fe, Ce, Ni, IR spectra 79−38544
$NaNO_2$, ferroelectric transitions, group theoretic comparison with $AgNaNO_2$ 80−7311
$NaNO_3$, disordered, temp. depend. of Raman spectra, Rayleigh wing scatt. 78−31209
$NaNO_3$, lattice vibrs., order-disorder transform., IR spectra study 80−65176
$NaNO_3$, N atom velocity, NO_3^- vib. and orientation, nucl. reson. photon scatt. 78−68433
$NaNO_3$, pure cryst., NO_3^- singlet-triplet absorption, Stark effect obs. 79−8153
$NaPF_6$, high press. phase diagram, vibr. spectra 78−60446
Na_xWO_3, struct. transitions and lattice dynamics 78−79771
$NbOPO_4$, cation ordering effect on Raman spectra 78−43850
NbS_2 (3R), Raman spectra, vibr. modes 79−87449
$NbS_2.Sn$, $NbS_2.Sn_{1/3}$ intercalation cpds., lattice dynamics, hyperfine interactions 79−61273
Nb_3Sn, lattice microstrain induced metastable phase, low temp. struct. and props. 77−8482
Nb_3Sn, proton and γ-irradiated, lattice dynamics from ^{119}Sn Mossbauer studies 78−39458
Nd-H, inelastic neutron scatt. exam. of lattice dynamics 80−29128

lattice dynamics continued
$Nd(BrO_3)_3.9H_2O$, IR and Raman spectra, vibr. asignments 78−84569
Ne, crystalline, self-localized exciton, cavity radius, wave function and energy 80−6737
Ne, lattice vibrs., heat capacities 79−42169
Ni_3Al, at. displacements, characteristic temp. and lattice spacing, temp. depend. *(Russian)* 79−90598
$Ni_3B_7O_{13}I$, cubic, Raman spectrum, 88-295K, vibr. anomalies 78−76479
$NiBr_2$, vibr. struct. in cryst. field electronic transitions 78−59895
$NiCl_2$, vibr. struct. in cryst. field electronic transitions 78−59895
$Ni_{0.89}Cr_{0.11}$, phonons with disorder caused by force consts., neutron diffr. obs. and CPA calc. 80−96602
NiI_2, far IR study of lattice dynamics 78−80359
$Ni(NH_3)_6X_2$, (X=Cl, Br, I, ClO_4, BF_4) and d, far IR, Raman spectra, 80-300K 78−31190
NiO, dielec. behaviour, Dick and Overhauser shell model calcs. 80−45001
NpO_2, IR spectra, values of transverse vibr. frequencies 77−28585
PBr_3, Raman scatt. spectra in gas, liq. and solid states, mol. dynamics *(Russian)* 77−55779
$PMo_{12}O_{40}$, vibr. anal., symmetry coords. and force field anal., IR and Raman spectra 77−15522
$PbCO_3.PbX_2$ (X=Cl,Br), vibr. props. 79−24319
PbF_2, anion disorder at high temps., neutron diffr. obs. 80−59614
PbF_2, superionic conductor, theoretical investigation of Raman scatt. 78−80351
PbI_2, 2H polytype, anisotropy of lattice vibrs. 77−7807
PbI_2, cubic, elastic consts., hydrostatic press. effect, US vel. meas. 80−49292
PbI_2, factor-group analysis of high-symmetry layer dynamics 79−42160
$Pb_2M_2^{III}Ge_2O_9$, (M^{III}=Fe,Mn,Sc,In), synthesis, X-ray diffr. and vibr. anal. 79−61360
$Pb_2M^{II}M^{IV}Si_2O_9$, (M^{II}=Mg,Ni,Co,Cu for M^{IV}=Sn; M^{II}=Co, Ni for M^{IV}=Ti), synthesis, X-ray diffr. and vibr. anal. 79−61360
$PbNb_2O_6$, IR absorpt. spectra and diffuse Raman scatt., normal coord. anal. *(French)* 80−66198
$Pb_3(PO_4)_2$, IR dispersion at room temp. 79−15460
$PbSO_4$, anglesite, crystal struct. and sulphate force consts. 78−83784
$(PbSe)_{1-x}(SnTe)_x$ solid solution, band struct. and some optical props. *(Russian)* 77−76752
$PbTa_2O_6$, IR absorpt. spectra and diffuse Raman scatt., normal coord. anal. *(French)* 80−66198
PbTe-based solid solns., 79−23990
Pd-Er, dynamic Jahn-Teller effect of Er^{3+} 79−73478
Pd-H(D), thermal expansion and lattice anharmonicity 9 to 270K 80−39241
PdH_x, superconducting transition temp., inverse isotope effect, Einstein model 80−65734
Pr-H, inelastic neutron scatt. exam. of lattice dynamics 80−29128
Pt complex, $Mg_{0.82}Pt(C_2O_4)_2.xH_2O$, X-ray diffuse scatt., 1-D Peierls-Kohn anomaly and struct. transforms. 78−14680
Pt_3Mn, cryst. dynamics at 80K 79−23688
Rb halides, role of quantum effects in lattice dynamics, Debye temp., shell model calcs. 80−70336
Rb-K, lattice vibrs. in CPA, comparison to neutron scatt. meas. 79−42165
α-$RbAg_4I_5$, dynamic cage effect 80−107541
$RbAg_4I_5$, phase transition, statics and local dynamics, mean field and Mori theory 80−39347
$RbAg_4I_5$, single particle excitations, inelastic neutron scatt. obs. 80−59599
$RbBrO_3$, hexagonal modification, temp. depend. of NQR freq., interpretation of long-wave spectra 80−25243
$RbCaCl_3$, Raman scatt. study of phase transitions 80−71411
$RbCrCl_3$ crystals, $\beta \rightarrow \gamma$ structural phase transition, lattice dynamical anal. 80−84291
$RbIO_3$, hexagonal modification, temp. depend. of NQR freq., interpretation of long-wave spectra 80−25243
$RbIO_4$, dynamics of IO_4^- vibr. in lattice 79−42157
Rb_2MnCl_4, perovskite type layer struct., lattice dynamics, rigid-ion model calc. 77−15512
$RbMnF_3$, triplet states, piezospectroscopy 79−38562
$Rb_2PbCu(NO_2)_6$, incommensurate Jahn-Teller transition, Huang scatt. 80−70401
Rb_2SeO_4, single cryst., orthorhombic, Raman spectra 77−73140
$ReCl_6^{2-}$ doped in various host lattices, luminesc. spectra and vibr. struct. 79−43024
ReO_3, cubic lattice stability, screening effect on vibrs. 80−75356
SF_6, isotope separation, TEA CO_2 laser irradiation *(Japanese)* 80−11885
$(SN)_x$, lattice dynamics, pseudolattices and correlation method 78−75768
SO_2, IR and Raman spectra, mol. and lattice vibrs. 78−19464
SO_2, lattice dynamics, rigid mol. model 80−44266
Sb_2Se_3, Raman spectra, Raman and IR-active modes 79−56776
$Sc_2(WO_4)_3$:Cr(Eu), and undoped crystals, luminesc. obs. 80−89047
Se, atom positions, effect of press. 78−34465
Se, trigonal, normal mode calcs. 80−84259
Si MBE layer resistivity and carrier mobility obs. *(Russian)* 80−49962
Si:H, new IR absorpt. bands 79−87472
$SiBr_4$, isotopic splitting in totally symm. stretching vibrations, Raman spectra 79−42967
β-SiC, lattice dynamics, phonon dispersion curves 77−89509
α-Si_3N_4, Raman active modes, spectra 78−80326
SiO_2, polymorphs (cristobalite and tridymite), vibr. normal modes, GVFF calcs. 78−51627
SmS, Debye temps., vibr. amplitudes, X-ray diffr. determ. 78−2222
SmS, electron-phonon interaction, lattice dynamical model 80−96610
SmSe, Debye temps., vibr. amplitudes, X-ray diffr. determ. 78−2222
SmTe, Debye temps., vibr. amplitudes, X-ray diffr. determ. 78−2222
Sn-Pb alloy, dil., lattice dynamics, sp. ht., resist., thermal expansion and nuclear γ reson. expts. *(Russian)* 78−87749
$SnBr_4$, isotopic splitting in totally symm. stretching vibrations 79−42967
SnS_2, Mossbauer spectra, vibr. amplitudes anisotropy 80−15904
SnS_2, Raman active mode assignments 77−12387
SnSe, lattice refl. spectra in long-wavelength IR range 78−27236
$SnSe_2$, Mossbauer spectra, vibr. amplitudes anisotropy 80−15904
$SnSe_2$, Raman active mode assignments 77−12387
SnTe, LO phonons affected by dielec. screening 79−77697
SnTe, sp. ht. mean field behaviour at phase transition 77−66023

lattice dynamics continued
SnTe, thermal lattice vibrs. rel. to temp.-depend. ^{119}Sn isomer shift 77−8457
SnX_6^{2+}, (X=Cl,Br,I), spectroscopic consts., environmental cation effects 79−56779
^{119}Sn temp. depend. isomer shift, pseudopot. approach 80−84675
$SrCl_2$, anion disorder at high temps., neutron diffr. obs. 80−59614
$SrCl_2$, anion motion at high temps., quasielastic nuetron scatt. obs. 80−59715
$SrF_2(Cl_2)$, superionic conductor, theoretical investigation of Raman scatt. 78−80351
$Sr_2KNb_5O_{15}$, Raman scatt. experiments in tetragonal tungsten bronze compounds 80−40113
$SrNO_3$, single cryst., normal Raman modes, temp. effects *(French)* 77−43998
$Sr_2NaNb_5O_{15}$, Raman scatt. experiments in tetragonal tungsten bronze compounds 80−40113
SrO:Pb^{2+}(Bi^{3+}), impurity centres vibronic spectra, lattice dynamics and electron-phonon interactions 80−7396
SrR_2S_4, R=rare earth, ternary sulphide with Th_3P_4 struct., vib. spectra 78−2844
$SrSO_4$, celestite, crystal struct. and sulphate force consts. 78−83784
1T-TaS_2, nearly commensurate phase stabilisation 77−15588
TaS_2.Sn, intercalated, Mossbauer effect, hyperfine interaction, lattice dynamics 77−8473
$TaSe_2$ (2H), lattice dynamics and phase transitions 78−79727
$TaSe_2$ (2H), microscopic model of CDWs lattice dynamics in commensurate phase 77−89719
Te, anisotropic thermal motion of atoms, X-ray exam. 78−18730
Te, atom positions, effect of press. 78−34465
α-TeO_2, anisotropy of atomic vibrations, Mossbauer absorption spectra 78−27147
TeO_2, press.-induced ferroelastic transition and internal displacement, soft effective elastic const. meas. 79−73240
TeX_6^{2-}, (X=Cl,Br,I), spectroscopic consts., environmental cation effects 79−56779
ThO_2, Gruneisen coeff., lattice vibrational frequencies in range 298-2300K 78−79712
Ti-Fe, force constant change with pressure, relative Mossbauer fraction 80−34163
TiC_xO_y, elastic characts. 77−80568
TiO_2, long-wavelength lattice vibr. modes, symmetry coordinates 78−43081
TiO_2, Raman spectra and struct. at high press. 79−87442
TiO_2, rutile, first order Raman spectrum, uniaxial stress effects 80−66196
$TiSe_2$ (1T), lattice dynamics and phase transitions 78−79727
$TiSe_2$ (1T), Raman studies of lattice dynamics 80−103962
$TiSe_2$, lattice dynamics, charge density waves transverse phonon dispersion curves, model 80−49322
$(Ti_{1-c}V_c)_4O_7$ order-disorder and metal-insulator transition theory 80−24802
TlCl-TlBr, single cryst., composition determ. by reflection spectrophotometry 77−1961
$TlGaS_{2x}Se_{2(1-x)}$ layer solid soln., long wave lattice vibrs., IR reflection spectra 80−11388
$TlGaTe_2$, IR refl. and Raman scatt. spectra, lattice vibrs. 80−40108
$TlGaTe_2$, multilayer cryst., lattice vibr. symm., IR absorpt. and Raman scatt. selection rules 80−39231
$TlInS_{2x}Se_{2(1-x)}$ layer solid soln., long wave lattice vibrs., IR reflection spectra 80−11388
$TlInSe_2$ single crystals, vibr. props. by light scatt. spectroscopy 79−56804
$TlInSe_2(Te_2)$, multilayer cryst., lattice vibr. symm., IR absorpt. and Raman scatt. selection rules 80−39231
$TlInTe_2(Se_2)$, IR refl. and Raman scatt. spectra, lattice vibrs. 80−40108
$Tl_3Na(SO_3)_2$, α-phase, IR and Raman spectra, order of cryst. struct. *(French)* 77−85718
$Tl_2PbCu(NO_2)_6$, incommensurate Jahn-Teller transition, Huang scatt. 80−70401
TlSe, vibr. props., Raman and far IR spectra meas. 78−71800
TlSe, vibrational spectrum, IR spectra meas. 78−35146
$Tl_2(TeCl_6)$, IR and Raman spectra, lattice and internal modes, phase transition 78−6659
TmSe, Debye temps., vibr. amplitudes, X-ray diffr. determ. 78−2222
UC, temp. depend. of Gruneisen parameter and lattice vibr. freq., between 298 to 2500K 80−29142
UN, temp. depend. of Gruneisen parameter and lattice vibr. freq., between 298 to 2500K 80−29142
UO_2, Gruneisen coeff., lattice vibrational frequencies in range 298-2300K 78−79712
V-Fe, force constant change with pressure, relative Mossbauer fraction 80−34163
α-$VD_{0.7}$, interstitial vibr., coherent neutron scatt. study 79−42196
V_3Ge, anisotropic thermal vibrations, lattice const. X-ray study 80−34164
V_3Ge, forbidden Bragg refls., rel. to supercond. transition temp. 79−15251
V_6O_{13}, semicond., IR vibration spectra 80−88997
V_3Si, single cryst., anharmonicity determ. from X-ray refl. intensities 79−73284
WO_3, condensed modes represented by normal modes in space group D_{4h}^7 79−90747
WO_3, electronically induced lattice distortion, screening effect on vibrs. 80−75356
Xe, lattice vibrs., heat capacities 79−42169
Xe, monolayer adsorption on Ag (111), statistical mech. 80−34306
$YAl_3B_4O_{12}$:Bi^{3+}, luminesc., vibr. struct., energy transfer 79−38584
ZnF_2, long-wavelength lattice vibr. modes, symmetry coordinates 78−43081
$ZnIn_2S_4$, vibr. spectrum, Raman study 80−97278
ZnP_2, oscillatory states, polarised spectra of IR absorption and emission of single cryst. *(Russian)* 77−28583
ZnS, cubic, thermal vibr. temp. depend., anharmonic models 80−92618
ZnS, lattice dynamics, phonon freq., bond bending force model calcs. 80−70335
ZnS(Se)(Te), thermal expansion and lattice dynamics under press. 80−100316
$ZnSc_2S_4$, IR and Raman spectra, force consts. 78−68503
ZnSe 79−38457
ZnSe, reson. Raman scatt. meas. 77−66510

lattice dynamics continued
ZnSe, single cryst. and film, long wave IR emission by lattice vibrs. 77−51528
$Zn_4Si_2O_7(OH)_2H_2O$, hemimorphite, polarised IR refl., vibr. modes *(French)* 77−85698
ZnTe, lattice dynamics and phonon parameters, bond bending force model lattice dynamics and phonon parameters bond bending force model 80−59595
$ZrH_{1.92}$, total neutron cross section of protons at 77.4K 79−60444
$ZrSiO_4$, zircon, resonance splitting of internal vibr. freq. of complex anion 80−55080

lattice dynamics of covalent crystals
caesium uranyl propionate, low temp. absorpt., luminesc. spectra, intermol. interactions 80−2830
chalcopyrites, sphaleritelike vibration mode, group theoretical anal. 79 -7661
covalent, charge density, struct. props. electron-electron interactions 78−47725
covalent solid, struct. props. and valence force fields, non-empirical calc. 77−1096
diamond, acoustic phonon geometric propag., anisotropic continuum acoustics 77−4170
diamond, adiabatic bond charge model 77−69057
diamond, and isomorphic crysts., phonon dispersion relations, Born-von Karman study 79−86855
diamond, coherent nonlinear two-phonon Raman spectra 79−19878
diamond, Cosserat continuum model, elastic props., lattice dynamics 80−59552
diamond, effective ion interaction and force consts., model of Si point defect 80−65185
diamond, electron density, neutron diffraction powder data 78−38655
diamond, GR1 band, E to T state transitions coupled to e vibrs. 77−12430
diamond, Gruneisen spectroscopic mode parameters via Raman spectra 77−7876
diamond, lattice dynamical calc. using extended Born-von Karman scheme 78−59889
diamond, lattice vibrational spectrum 79−90741
diamond, low lying levels of GR 1 centre, satellite line struct. 77−20269
diamond, phonon frequencies, model calc. using tight binding Hamiltonian 78−59894
diamond, pseudo-Jahn-Teller effects in H3 vibronic spectrum 77−90182
diamond, resonant Raman scatt., first and second order 78−60471
diamond, semicond., energy band struct., elec. and optical props., review 77−35862
diamond, superhard, X-ray characts. *(Russian)* 77−80593
diamond, two-phonon Raman peak linewidth, bond polarisability model 77−77212
diamond, two-phonon Raman spectrum, harmonic pot. and bond polarisability model 77−77213
diamond, type-II_a, electron irradiated, thermal cond. reduction at low-temps. 77−47631
diamond, vibronic bands at 2.498 eV (H4), 2.417 eV and 2.536 eV, absorpt. and luminesc. under stress 77−85758
diamond, zone-centre optical phonon, effect of uniaxial stress, elastic consts. determ. 78−91399
diamond structure, extended Born-Von Karman scheme 77−27953
diamond type crystals, internal strain parameter 78−43090
diamond-structure crystals, lattice anharmonicity 77−89549
diamond-type crystals, lattice dynamics from Keating's valence force field 78−79687
graphite, long wavelength lattice vibrations, Raman and IR reflectivity spectra 78−75746
graphite, optical probe of lattice dynamics 78−35131
graphite, two-dimens. lattice vibrs. calcs. 80−2126
phonon transmission from incoherent radiator into cryst., anisotropic continuum acoustics 77−47521
pseudopotential method, phonon dispersion curves 77−43295
rubidium uranyl propionate, low temp. absorpt., luminesc. spectra, intermol. interactions 80−2830
semiconductor, electronic and struct. energies calc. 78−59874
semiconductor, structural props. using electron-ion Hamiltonian using density-fundamental methods 79−82177
semiconductors, covalent, phonon spectra calc. using dielectric matrix approach 79−4381
semiconductors, displacement correlations, adiabatic bond charge model 80−70350
semiconductors, extrinsic covalent, Raman scatt. of light by phonons 77−73147
semiconductors, total electronic energy, force consts., and phonon dispersion curves, tight-binding calc. 79−60747
sodium uranyl acetate (deuteroacetate) 80−2830
tetrahedrally bonded crysts., lattice vibration, thermal expansion and pressure effect 80−39233
unpaired forces effects 79−95096
valence force model for lattice vibr. 77−20026
C, diamond-type crystal, lattice dynamics from Keating's valence force field 78−79687
C, harmonic and cubic Einstein force consts. calc. 77−47515
Ge, acoustic phonon geometric propag., anisotropic continuum acoustics 77−4170
Ge, acoustic phonon scattering by electron-hole drops, deform. potential 78−10360
Ge, adiabatic bond charge model 77−69057
Ge, covalent semicond., piezoresistance coeffs. of holes, temp. depend. 77−39847
Ge, diamond type crystal, lattice dynamics from Keating's valence force field 78−79687
Ge, electron-hole drops, laser Doppler velocimetry 77−43504
Ge, energy band gap dilation and vibr. contrib. determ. 79−60703
Ge, extended Born-Von Karman scheme 77−27953
Ge, γ-electron-hole drop formation, time delay 77−31952
Ge, harmonic and cubic Einstein force consts. calc. 77−47515
Ge, heat capacity and phonon dispersion, using five force schemes *(Russian)* 77−62649
p-Ge, highly deformed, hole scattering 77−20309
p-Ge, hot hole relax., IR saturated absorption, LO phonon emission 77−28569
Ge, impurity modes due to point defects, comparison with IR and Raman meas. 79−4386

lattice dynamics of covalent crystals continued
Ge, interatomic force consts. from lattice vibrs. 77−20020
Ge, lattice dynamical calc. using extended Born-von Karman scheme 78−59889
Ge, lattice dynamics of group IV elements with the local Heine-Abarenkov model potential 78−63821
Ge, lattice dynamics under press 80−92627
Ge, lattice dynamics using Born-van Karman model 79−73271
Ge, lattice thermal conductivity, effect of Debye temp. var. 78−18850
Ge, localised vibrational modes of isolated impurities, Green's function method 77−39650
Ge, microscopic inverse dielec. matrix, local field correction and acoustic sum rule 77−84863
Ge, phonon assisted Auger recomb. in indirect gap semiconductors 78−39126
Ge, phonon boundary scatt., reduction of lattice thermal cond. 78−55921
n-Ge, phonon conductivity and attenuation 77−4167
Ge, phonon density of states determ. from sp. ht. 77−7809
Ge, phonon density of states from thermodynamic functions *(Russian)* 79−35631
Ge, phonon dispersion curves, appl. of deformable-ion model 78−59887
Ge, phonon viscosity tensor 78−34570
Ge, phonon-phonon scatt. strength, thermal cond. in low- and high-temp. regions 77−43296
Ge single crysts., mean square atomic displacements determ. by X-ray anal. *(German)* 78−30726
Ge, thermal expansion coeff. and Gruneisen const. 77−59128
Ge, two-phonon difference absorption spectra 78−76452
Ge type semiconductor, interimpurity zero-phonon radiative transitions 78−15222
Ge:^{119m}Sn, impurity lattice dynamics, Mossbauer spectra, Debye temp. 80−84262
Ge-Si, dil. alloy, IR absorpt. and first-order Raman scatt. due to single and paired impurity atoms 79−82976
Ge-Si alloy, phonon boundary scatt., reduction of lattice thermal cond. 78−55921
InSb, acoustoelectric phonon attenuation of X-ray anomalous transmission 77−4160
InSb, phonon dispersion curves, appl. of deformable-ion model 78−59887
Se and Te, homology of phonons, scaling formalism for phonon freqs. 80−54326
Se, trigonal, force field calc. of phonon dispersion relations 80−54328
Se, trigonal, low temp. sp. ht. and elastic consts., piezoelec. effect influence on phonons 80−54404
Se, trigonal, state-of-the-art review of model calcs. 80−54327
Se, trigonal, surface lattice dynamics, mean square displacement spectra in long wavelength limit 80−54498
Se, trigonal, vitreous and red amorphous, phonon density of states comparison 80−54329
Se, trigonal and vitreous, sp. ht. and thermal cond., 3 to 300K 80−59676
Si (111), dynamic effective charge and surface reconstruction, soft-mode theory 79−4460
Si, acoustic phonon geometric propag., anisotropic continuum acoustics 77−4170
Si, adiabatic bond charge model 77−69057
Si, charge density, struct. props. electron-electron interactions 78−47725
Si, conductivity of holes at low temp., electric field depend. 77−28179
Si, crystn. front face effect on at displacements *(Russian)* 78−67781
Si, diamond-type crystal, lattice dynamics from Keating's valence force field 78−79687
Si, dielectric screening and zone-centre phonons 78−67785
Si, electronic properties, rel. to chem. bonding and lattice dynamics 80−44169
Si, electronic response to high symmetry lattice vibr. 80−10619
Si, electronic screening of lattice vibrs. 78−59875
Si, energy band gap dilation and vibr. contrib. determ. 79−60703
Si exciton luminescence in mag. field or under uniaxial stress 78−27322
Si, Gruneisen coeff. from stress-induced phonon energy meas., inelastic neutron scatt. 79−82298
Si, harmonic and cubic Einstein force constant calc. 77−47515
p-Si, highly deformed, hole scattering 77−20309
Si, highly transparent semicond., multiphonon IR absorpt. 78−60461
Si, lattice dynamical calc. using extended Born-von Karman scheme 78−59889
Si, lattice dynamics of group IV elements with the local Heine-Abarenkov model potential 78−63821
Si, lattice dynamics under press 80−92627
Si, lattice dynamics using Born-van Karman model 79−73271
Si, lattice thermal cond., 2-1400K, phonon scatt. calcs. 78−2311
Si, microscopic inverse dielec. matrix, local field correction and acoustic sum rule 77−84863
Si, O content determ. by spectral analysis, phonon absorpt. effects *(Russian)* 77−48177
Si, optical spectroscopy, absorpt. coeff., lattice vibrs. modes, band gap, acoustic approach 77−69822
Si, phonon assisted Auger recomb. in indirect gap semiconductors 78−39126
Si, phonon boundary scatt., reduction of lattice thermal cond. 78−55921
p-Si, phonon conductivity and attenuation 77−4167
Si, phonon viscosity tensor 78−34570
n-Si, phonon-phonon relaxation 80−96609
p-Si, photosensitivity of elastic moduli and surface tension 78−83864
Si quantised inversion layers, hot electron effects 77−28188
Si, Raman spectrum, two-dimens. tensile stress effects 78−48173
Si, stretched, lattice vibr. anharmonicity, influence of stress on elastic moduli, Raman spectra 80−80791
Si, structural props. using electron-ion Hamiltonian using density-fundamental methods 79−82177
Si, TO and TA phonons, electronic and struct. energies calc. 78−59874
Si, thermal expansion coefficient and Gruneisen const. 77−59128
Si type semiconductor, interimpurity zero-phonon radiative transitions 78−15222
n-Si, vibr. excitation conditions, vol. charge redistrib. effect *(Russian)* 80−103427
Si:^{119m}Sn, impurity lattice dynamics, Mossbauer spectra, Debye temp. 80−84262
α-Sn, lattice dynamics of group IV elements with the local Heine-Abarenkov model potential 78−63821

lattice dynamics of covalent crystals continued
$SnS_{2-x}Se_x$, ($0 \leq x \leq 2$), ^{119}Sn Mossbauer spectrum, lattice dynamics 78−71809
Te and Se, homology of phonons, scaling formalism for phonon freqs. 80−54326
Te, trigonal, state-of-the-art review of model calcs. 80−54327
Te, trigonal, surface lattice dynamics, mean square displacement spectra in long wavelength limit 80−54498
VN, lattice phonons, dispersion and density-of-states 79−99283

lattice dynamics of ferroelectric crystals
see also displacive transformations; soft modes
alkali-alkaline earth ceramic solid solutions, with tetragonal tungsten bronze struct., low freq. optical modes 78−76477
anharmonic crystal, lattice dynamics and stability 78−6129
arsenates, ferroelec. phase, E-mode splitting 78−15163
Brillouin scattering spectroscopy of phase transitions, dynamical aspects 80−55115
Debye temperature, tabulation of calorimetric values 78−51639
Debye temperature tabulation of calorimetric values 78−51639
dicalcium lead propionate, Raman scatt., order-disorder type transform. 77−12373
dicalcium strontium propionate, Raman scatt., order-disorder type transform. 77−12373
displacive and order-disorder type, thermal cond. at low temps. 80−75391
displacive ferroelectric, inelastic neutron scatt. cross. section determ. 77−31737
displacive ferroelectric transition, effect of strong cubic anisotropy of lattice anharmonicity, mol. field theory 77−52026
displacive type, Ginzburg-Lavanyuk parameter 79−8106
displacive type ferroelectrics with impurities, lattice dynamics 79−28061
displacive type low-dimens. ferroelec., thermal cond. 79−61314
doped narrow gap semiconductor, two-channel vibronic mechanism of ferroelectric phase transitions *(Russian)* 79−56745
electron subsystem, crit. vibrs., order parameter 78−43813
ferroelectric semiconductor, phase transition temp., rel. to free carrier conc. 78−10860
ferroelectric theory and dynamics, optical, acoustic electro-optical props., Brillouin zone struct. 80−11347
ferroelectric-elastic phase transition, modelling, appl. to KH_2PO_4 and $LiNH_4C_4H_4O_6.2H_2O$ *(Russian)* 80−75961
ferroelectrics, one and two dimensional displacive types, phonon relaxation 78−87761
ferroelectrics, order-disorder, displacive transformations, tunnelling, phonons 80−75975
ferroelectrics, surface sound waves on domain boundaries, low temp. sp. ht. 78−71937
ferroelectrics with hydrogen bonds, phase transition into coherent state, two-level proton calcs. *(Russian)* 80−71356
ferromagnet, ferroelectric, soft mode damping, temp. anomalies *(Russian)* 80−44284
guanidinium aluminium sulphate hexahydrate, pyroelectric coeff., 1.8-300K, dynamic method, low freq. polar optic modes *(French)* 79−19844
hydrogen-bonded, incoherent and coherent inelastic neutron scatt. cross sections 77−59524
hydrogen-bonded, parametric reson., influence of lattice vibr. by parallel electric microwave pumping 77−48140
hydrogen-bonded, soft and central modes, mag. reson., review 78−15108
hydrogen-bonded ferroelectric, Ising model in transverse tunnelling field and proton-lattice interaction 80−7307
hydrogen-bonded partially-deuterated cryst., coupled tunnelling-lattice modes 77−63372
incipient ferroelectrics, mode-mode coupling 79−38464
instability and phase transition in system with interband interaction 77−12346
Ising model in transverse field, mode-coupling theory for central peak 80−75987
isotopically disordered ferroelectric cryst., thermal cond. 77−76628
IV-VI semiconductor, vibronic model of lattice instability 80−80723
large-gap type, vibronic theory and opt. props., anomalous bulk photovoltaic effect 80−103939
lithium ammonium tartrate monohydrate, Raman spectra, anomalous low-lying response 80−2746
local structural excitations model for lattice dynamics of disordered or unstable lattices 78−75790
low-lying vibrational modes and theory of local and transport props. at transitions 78−14425
magnetic ferroelectrics, mechanism of phonon relaxation *(Russian)* 79−90742
mixed crystals, CPA calc. 78−10855
mixed order-disorder displacive transition, model 77−59540
noncentral ions in ferroelectric crystals, spontaneous polarisation, phase transitions 80−15991
order-disorder ferroelectric, longitudinal phonon relax. *(Russian)* 79−55860
order-disorder ferroelectrics, exactly solvable model 77−32337
order-disorder ferroelectrics, phonon damping and freq. shift *(Russian)* 79−60471
orthophosphates, dynamics of ferroactive cryst. 79−37801
perovskites, Rayleigh scatt., crit. dynamics at struct. transition 77−12396
phase transitions, ferroelectric and structural refractive indices and electro-optics 79−19850
phase transitions soft modes and dipole relaxations 78−91409
polaron state of electron near structural instability in ferroelectrics and antiferroelectrics, polaron state of electron near structural instability 79−33245
pseudo-ionic model for ionic crystals, appl. to $BaTiO_3$ 79−33049
relaxation effects, disorder excitations, LF dielectric const., spin lattice relaxation phonon-excitation coupled model 78−10852
Rochelle salt, ferroelec. phase transition, Raman scatt. study 80−97211
Rochelle salt, ferroelectric, Raman and IR study 80−71406
Rochelle salt, paraelectric-ferroelectric phase transition, relaxing defects effects 79−61320
Rochelle salt, phase transition mechanisms by optical spectroscopy 79−15411
saccharose, single cryst. low-temp. pyroelectricity 79−42906
self-consistent phonon theory 79−37802

lattice dynamics of ferroelectric crystals continued
semiconductor, electronic density of states, effect of soft phonon-electron interaction *(Russian)* 77−80718
squaric acid, cryst., neutron diffr., bond lengths and angles, vibr. modes 77−76384
squaric acid, two-dimens. phase transition, Raman scatt. study 80−71401
susceptibility, Raman line shape of overdamped mode 79−91426
tetragonal tungsten bronze structure ferroelec. mech. for ferroelec. transition 79−38481
TGS, ferroelec., phonon contributions to anomalous sp. ht. near phase transition temp. 77−52023
TGS, nitroaniline admixture effect on thermal parameters 80−107580
TGS, pyroelectric coeff., 1.8-300K, dynamic method, low freq. polar optic modes *(French)* 79−19844
TGS, X-irrad., thermal diffusivity, cooling const. and heat transmission coeff. 79−86935
TGS(Se), optical phonons near T_c, IR refl. and Raman spectra 77−48136
TGS(Se), optical phonons near T_c, nonlinear pseudospin-phonon interaction 77−48137
TGS type crystal, phase transition model due to nonlinear reson. of lattice oscills. *(Russian)* 77−31746
TGSe, pyroelectric coeff., 1.8-300K, dynamic method, low freq. polar optic modes *(French)* 79−19844
thiourea, Brillouin scatt., Debye relax. 79−87453
thiourea, ferroelec., soft mode and Debye relax., IR reflection spectra 77−90111
thiourea, ferroelectric, Raman and IR study 80−71406
thiourea, lattice vibrs. in incommensurate phase 79−28056
thiourea, phonon modes near order-disorder transforms., hard-core modes due to pseudospin-phonon coupling 80−44285
thiourea, phonon modes near phase transitions, IR and Raman spectra 80−45084
thiourea, pyroelectric coeff., 1.8-300K, dynamic method, low freq. polar optic modes *(French)* 79−19844
thiourea, soft mode and Debye relaxations 78−80347
transverse field ferroelec., lattice vibrs. effect on parametric ferroelec. reson. 77−59525
tungsten bronze structure ferroelectrics, tetragonal, model of ferroelec. transition 77−28526
tunnelling motion, phonon vibrs. and statistical disorder in unified theory 77−63373
tunnelling systems in polariton region, linear response function 78−43799
uniaxial ferroelectric, electrostrictive interaction, mode damping 80−34862
uniaxial ferroelectrics, microscopic theory, crit. behaviour and anomalous elastic consts. 79−38463
vibrational modes, crit. behaviour of uniaxial materials 78−84539
vibronic model, fluctuations of order parameter and anharmonic interaction 77−52022
vibronic theory of antiferroelec. and struct. modulated transitions, soft modes 78−79719
vibronic theory of ferroelectricity, developments 79−33620
vibronic theory of ferroelectricity 79−19854
zero-gap semiconductor, ferroelec. phase transitions, effect of Coulomb interaction on RPA calc. 79−28691
Ag_3AsS_3, proustite, phonons and soft modes at ferroelec. transition 80−60524
$AgNa(NO_2)_2$, ferroelec., Raman scatt. and phase transitions 80−71349
$AgNa(NO_2)_2$, ultraslow crit. dynamics of order parameter, ^{23}Na spin relax. times obs. 78−76410
$As_{0.2}Sb_{0.8}SI$ cryst., ferroelec., soft mode Raman and IR spectroscopy 80−76016
$BaMgF_4$, low temp. phonon effects on polarisation 79−42905
$BaMgF_4:Mn^{2+}$ ferroelec., EPR and ENDOR study, cryst. field tensor 80−71162
$BaMnF_4$, low temp. phonon, and exciton effects on polarisation 79−42905
$BaMnF_4$, spectroscopy, ferroelectric/ferromagnetic coupling, soft optic mode frequencies 200-1000K 79−19845
$Ba_{0.5}Sr_{0.5}Nb_2O_6$, temp. depend. of Raman spectra 78−72524
$BaTiO_3$, A_1 and E optical phonons obs. in temp. range 10 to 132°C 77−27963
$BaTiO_3$, A_1-modes reflectivity meas. 79−65875
$BaTiO_3$, cubic, optical modes meas. by neutron scatt. 79−69213
$BaTiO_3$, displacive ferroelectric, effective charge determ. 80−97212
$BaTiO_3$, elastooptic effect near ferroelec. transition, temp. depend. 80−97233
$BaTiO_3$, ferroelec., appl. of pseudo-ionic model for ionic cryst. 79−33049
$BaTiO_3$, ferroelec. temp. depend. of broad A_1 (TO) phonon Raman linewidth 78−2857
$BaTiO_3$, mean square atomic displacement temp. depend., sublattice vibration anharmonicity 80−79890
$BaTiO_3$, paraelec. phase, stabilisation of soft mode 80−75985
$BaTiO_3$, polycrystalline ferroelectric, grain-size dependent props. 80−71352
$BaTiO_3$, pseudo-ionic model applic. to dynamics 77−59077
$BaTiO_3$, Raman intensity analysis, symmetry coords., optical modes, electro-opt. consts. 79−95740
$BaTiO_3$, soft mode dielec., anomalous low temp. sp. ht. 78−14423
$BaTiO_3$, undoped and Cu doped, Γ_{15} phonon freezing, electronic instability, LCAO calc. 80−25318
$BaTiO_3$, vibronic theory and opt. props. 80−103939
$BaTiO_3:Eu(Sm)$, absorption spectra, Ti^{3+} ion and Z-centre formation 77−24871
$BaZnF_4$, low temp. phonon effects on polarisation 79−42905
BiSI(Br), optical B_u modes of paraelectric phase, simple model 78−75747
$Bi_xSb_{1-x}SI$, low freq. Raman spectroscopy 78−15162
BiSeI(Br), optical B_u modes of paraelectric phase, simple model 78−75747
$Bi_4Ti_3O_{12}$, IR refl. spectrum, 60-2000 cm^{-1} 77−69843
$Cd_2Nb_2O_7$, Raman-scattering investigation of vibrational structure 78−76441
CsH_2AsO_4, and deuterated isomorph, E-mode splitting in ferroelec. phase, Raman scatt. meas. 77−16296
CsH_2AsO_4, pres. depend., LF dielec. response, ferroelec. props. 78−15120

lattice dynamics of ferroelectric crystals continued
$CsPbCl_3$, n.q.r. spin-lattice relax. near cubic-tetragonal transition, soft modes 77−1616
DBr(DCl), solid, ferroelec. and paraelec. phases, transitions, Raman scatt. 77−43980
$Gd_2(MoO_4)_3$, ferroelec., anomalous damping of phonons, Raman spectra, stress and temp. effects 79−38503
$Gd_2(MoO_4)_3$, uniaxial stress effect on ferroelec. transition, Raman scatt. 78−80360
HBr(HCl), solid, ferroelec. and paraelec. phases, transitions, Raman scatt. 77−43980
HCl, solid, orthorhombic, temp. depend. freq. spectrum 77−15510
KD_2PO_4, deuteron tunnelling, barrier height and energy level calc. 80−6482
KD_2PO_4, microwave spectra, temp. depend. mode rel. to proton subsystem 80−24548
KD_2PO_4, neutron scattering from coupled polar-elastic waves 80−92623
KD_2PO_4, soft ferroelec. mode anisotropy 78−14430
KD_2PO_4, transverse dynamics, short-range interaction effects 78−14408
$KD_3(SeO_3)_2$, acoustic phonon softening and spontaneous strains 78−26652
$K_4Fe(CN)_6.3H_2O$, dynamic disorder and ferroelec. transition, Raman spectra obs. 77−81069
$K_4Fe(CN)_6.3H_2O$, Raman spectrum and dielec. relax. 78−19476
KH_2AsO_4, and deuterated isomorph, E-mode splitting in ferroelec. phase, Raman scatt. meas. 77−16296
KH_2AsO_4, fast and slow dynamic reorientation 78−80306
KH_2AsO_4, ferroelectric phase transition under high hydrostatic press., mol. dynamics, NQR study 80−75880
KH_2AsO_4, KD_2AsO_4, slow dynamics from Cr^{5+} EPR 78−15126
KH_2AsO_4, NQR of ^{75}As, press. and temp. depend., 77K to Curie temp. 80−71227
KH_2AsO_4, pres. depend., LF dielec. response, ferroelec. props. 78−15120
$K(H_{1-x}D_x)_3P_4$, polarised impurity cluster effects in light scatt. expts. 80−71431
$KH_{2(1-x)}D_{2x}PO_4$, Raman spectra of overdamped mode 79−91427
$K(H_{1-x}D_x)_3(SeO_3)_2$, Brillouin spectrum central peak, soft acoustic mode 80−2777
KH_2PO_4, and isomorphs, ferroelectric transition and Curie temp., soft mode effect, Green's function anal. 79−24269
KH_2PO_4, damping of transverse acoustic and ferroelec. modes 78−14413
KH_2PO_4, dynamic central peak in ferroelectric phase 78−84538
KH_2PO_4, E-mode splitting in ferroelec. phase, Raman scatt. meas. 77−16296
KH_2PO_4, far IR dispersive reflection spectra 77−36213
KH_2PO_4, ferroelectric phase transition exam. by spontaneous parametric light scatt. 78−19427
KH_2PO_4, KD_2PO_4, slow dynamics from Cr^{5+} EPR 78−15126
KH_2PO_4, KD_2PO_4, high-press. struct. rel. to dynamical models 78−80307
KH_2PO_4, neutron critical scatt. in struct. transition due to homogeneous crystal deform. 79−42922
KH_2PO_4, proton tunnelling, barrier height and energy level calc. 80−6482
KH_2PO_4, pyroelectric coeff., 1.8-300K, dynamic method, low freq. polar optic modes *(French)* 79−19844
KH_2PO_4, soft mode spectroscopy, digital control system for Raman spectrometer 78−86345
KH_2PO_4 type crystals, low lying ferroelec. modes, cluster dynamical theory 78−80305
KH_2PO_4 type crysts., evidence of non-linear behaviour of soft modes, Raman spectra 79−33639
KH_2PO_4 type ferroelectrics above T_c, soft mode and central-peak dynamics 78−87763
KH_2PO_4 type ferroelectrics, Raman spectra, coupled tunnel-phonon modes, isotope effect 79−69205
KH_2PO_4, variational treatment of proton-photon system 78−88261
KH_2PO_4-KD_2PO_4 mixed crystals, static and dynamic props., proton-lattice coupled mode model 78−64328
KH_2PO_4-type cpds., collective vibr. of protons, cluster approx. 79−51210
KH_2PO_4-type crystal, LF dynamics 80−10602
KH_2PO_4-type ferroelectrics, inelastic neutron scatt. theory 78−48122
KH_2PO_4:Tl, UV absorption bands obs. 78−27266
KNO_3, and KNO_2, fused, electrolum. 79−99945
KNO_3, far IR study of dielec. function by asymmetric Fourier spectroscopy 79−51947
α-KNO_3, lattice dynamics, inelastic neutron scatt. 79−4383
KNO_3, Raman and IR spectra and lattice vibrs. 80−60565
$KNbO_3$, cubic, temp. depend. of intensity of X-ray interference 80−59613
$KNbO_3$, displacive ferroelectric, effective charge determ. 80−97212
$KNbO_3$, ferroelec. phase, phonon dispersion relations and lattice dynamics calcs., comparison with expt. 80−49319
$KNbO_3$, orthorhombic, anharmonic effects 78−79721
$KNbO_3$, pseudo-ionic model applic. to dynamics 77−59077
K_2SeO_4, ferroelec., incommensurate struct., dynamic props. *(Russian)* 80−11373
K_2SeO_4, hexagonal-orthorhombic transition, Brillouin scatt. study 80−97208
K_2SeO_4, incommensurate and ferroelec., far IR and mm dielectric response 79−73955
K_2SeO_4, lattice dynamics, displacive phase transform. 80−39248
K_2SeO_4, Raman spectra, 77-300K *(Japanese)* 77−43988
$KTaO_3$, incipient ferroelectric, mode-mode coupling 78−79717
$LiNbO_3$ and $LiTaO_3$, IR reflectivity spectra and phonon self-energy effect 77−63413
$LiNbO_3$, asymm. phononlines, IR refl. analysis 78−27197
$LiNbO_3$, comparative frustrated total refl. and Raman scatt., fundamental mode freq. and phonon dispersion 77−28579
$LiNbO_3$, ferroelec., displacive type phase transition, far IR reflection spectra 80−71339
$LiNbO_3$, ferroelec. phase, phonon dispersion relations and lattice dynamics calcs., comparison with expt. 80−49319
$LiNbO_3$, optical phonon modes and anharmonic couplings 78−60466
$LiNbO_3$, Raman line phonon relative intensities *(German)* 77−59582
$LiNbO_3$, temp. dependence of Raman scattering 77−16297
$LiNbO_3$, X-ray diffr. study of lattice dynamics parameters *(Russian)* 79−65156
$LiNbO_3$:Fe, calc. of photorefraction *(Russian)* 78−92032
$LiTaO_3$, asymm. phonon lines, IR refl. analysis in paraelec., ferroelec. phases 78−27197
lattice dynamics of ferroelectric crystals continued
$LiTaO_3$, displacive ferroelectric, effective charge determ. 80−97212
$LiTaO_3$, ferroelec., displacive type phase transition, far IR reflection spectra 80−71339
$LiTaO_3$ high-temp. ferroelec. transition, soft mode IR reflectivity spectroscopy 79−33692
$LiTaO_3$, optical phonon modes and anharmonic couplings 78−60466
$LiTaO_3$, primary pyroelec. effect, lowest order mode contrib. 78−15103
$LiTaO_3$, uniaxial ferroelec., polariton dispersion relations 77−20249
$LiTaO_3$, X-ray diffr. study of lattice dynamics parameters *(Russian)* 79−65156
$Mn_3B_7O_{13}Cl$ improper ferroelec., orthorhombic phase, Raman spectrum, lattice vibrs. 78−43849
$(NH_4)_2BeF_4$, ferroelec., incommensurate struct., dynamic props. *(Russian)* 80−11373
$(NH_4)_2BeF_4$, powder, IR spectra, assignments, mol. libration, in paraelec. and ferroelec. phases 78−88299
$NH_4H_2AsO_4$:Cr^{5+}, fast and slow dynamic reorientation 78−80306
NH_4HSO_4, Brillouin shifts and linewidths 77−16322
$NH_4H_3(SeO_3)_2$, Raman spectra meas. 78−10899
$((NH_4)_xK_{1-x})_2SO_4$, NH_4^+ dynamics, neutron scatt. study 79−42167
$(NH_4)_{2(1-x)}Rb_{2x}SO_4$, mixed crystal, dielectric and US meas. of ferroelec. phase transition *(Japanese)* 80−7305
$(NH_4)_2SO_4$, NH_4^+ dynamics, neutron scatt. study 79−42167
$(NH_4)_2SO_4$, phase transition mechanisms by optical spectroscopy 79−15411
$Na(D_xH_{1-x})_3(SeO_3)_2$, Raman spectra and nature of phase transitions 78−80341
$NaD_3(SeO_3)_2$, polarised Raman spectra, lattice vibrs., ferroelec. transition 77−24851
$NaH_3(SeO_3)_2$, proton behaviour in H-bonding, neutron spectroscopy obs. *(German)* 78−22816
$NaNO_2$, ang. dispersion of internal phonon modes, Raman meas. 79−51211
$NaNO_2$, ferroelec., X-ray diffr. topographic study of polarisation reversal 79−38441
$NaNO_2$, ferroelectric, second-order vibr. spectra and dispersion of phonon branches 79−69847
$NaNO_2$, incommensurate-and-antiferroelectric phase transition, amplitude mode, ultrasonic study 80−39227
$NaNO_2$, lattice dynamics, two-phonon Raman scatt. and IR absorpt. 79−33684
$NaNO_2$, mechanism of ordering type ferroelec. transition, vibr. spectroscopy 78−76402
$NaNO_2$, mechanism of order-disorder transition, opt. spectra 78−76403
$NaNO_2$, Raman and IR spectra, destructive Fermi reson. 77−16309
NdP_5O_{14}, ferroelastic, spectroscopy, ferroelastic/ferroelectric coupling, soft optic mode frequencies 79−19845
$Ni_3B_7O_{13}I$, cubic, Raman spectrum, 88-295K, vibr. anomalies 78−76479
$Ni_3B_7O_{13}I$, dynamics of ferroelec. phase transition, Raman spectra obs. 79−33630
PLZT ceramics, sp. ht., 2-25K, field depend., phonon modes 77−47586
$Pb_5Ge_3O_{11}$, lattice dynamics parameters anisotropy, X-ray diffr. study 80−59612
$Pb_5Ge_3O_{11}$, Raman spectrum factor group anal., external and librational modes 77−36240
$Pb_5Ge_3O_{11}$, temp. depend. of A_{LO}-modes, Raman spectra meas. 78−2213
$PbHAsO_4$, ferroelec., far IR and microwave dielec. props. 80−55108
$PbHPO_4$, ferroelec. phase transition, Brillouin and Raman spectra obs. 79−33683
$PbHPO_4$, microwave permitt. and far IR refl. spectra in paraelec. and ferroelec. phases 80−40033
$PbMg_{1/3}Nb_{2/3}O_3$, vibr. spectrum and dispersion of optical consts., coexisting ferro- and paraelec. phases 77−63422
$Pb_2Nb_2O_7$, Raman-scattering investigation of vibrational structure 78−76441
Pb_3O_4, IR and Raman study of structural phase transitions *(French)* 78−84582
PbTe-SnTe compound semiconductors, lattice instability by mm-wave magnetoplasma refl. 80−54336
$PbTiO_3$, vibronic theory and opt. props. 80−103939
$Pb(Zr,Ti)O_3$, temp. and hydrostatic press. depend of vibr. modes, rel. to phase transforms 77−89510
$Pb(Zr_{0.52}Ti_{0.48})O_3$, polycrystalline ferroelectric, grain-size dependent props. 80−71352
$RbCdCl_3$, n.q.r. spin-lattice relax. near cubic-tetragonal transition, soft modes 77−1616
RbH_2AsO_4, and deuterated isomorph, E-mode splitting in ferroelec. phase, Raman scatt. meas. 77−16296
RbH_2AsO_4, pres. depend., LF dielec. response, ferroelec. props. 78−15120
RbH_2PO_4, acoustic longit. mode coupling to order parameter and effect on ferroelec. phase transition 79−51914
$RbH_3(SeO_3)_2$, improper ferroelectric phase transformation, neutron scattering study 78−80302
$RbH_3(SeO_3)_2$, Raman spectra meas. 78−10899
Rb_2ZnBr_4, Raman scatt., normal-incommensurate-commensurate phase transitions, soft modes 80−40071
Rb_2ZnBr_4, soft modes at phase transforms., far IR spectrum study 80−107398
Rb_2ZnCl_4, US velocity and attenuation, around normal-incommensurate phase transition 80−40072
Sb_2S_3, effect of screening by conduction electrons on phase transitions 78−84537
SbSBr, optical B_u modes of paraelectric phase, simple model 78−75747
SbSI, anharmonic at. pot. and temp. depend. of thermal vibrs. 80−39246
SbSI, ferroelec. transition, inelastic neutron scatt. 77−40189
SbSI, ferroelectric semiconductor, effect of screening by conduction electrons on phase transitions 78−84537
SbSI, neutron diffr. obs. at −185, 16 and 100°C 77−43180
SbSI-SbSBr system, ferroelec., anharmonic effects in far IR reflectivity spectra 80−76014
SbSI(Br), optical B_u modes of paraelectric phase, simple model 78−75747
$Sn_{0.9}Ge_{0.1}Te$, Mossbauer spectra, soft modes 80−20550
$Sn_2P_2S_6$, ferroelec. semicond., phase transition and lattice dynamics 80−60526
$Sn_2P_2S_6$ ferroelectric semicond., polarisation Raman scatt. spectra, X-ray struct. study 79−95778

lattice dynamics of ferroelectric crystals continued
$Sn_2P_2S_6$, soft mode, temp. depend. of Raman spectra near phase transition 78−88263
$Sn_2P_2S_6$, soft mode props., Raman scatt. study 80−60525
SnTe, softening of TO phonon mode *(Japanese)* 78−2225
$SrTiO_3$ ceramic, electrocaloric effects for refrigeration at cryogenic temp. 80−77789
$SrTiO_3$, disorder manifestation, light scatt. spectra, high temp. 80−76017
$SrTiO_3$, forced thermal Rayleigh scattering 78−80371
$SrTiO_3$, hyper-Raman scatt. spectra due to lattice vibr. 80−29732
$SrTiO_3$, incipient ferroelectric, mode-mode coupling 78−79717
$SrTiO_3$, mean square atomic displacement temp. depend., sublattice vibration anharmonicity 80−79890
$SrTiO_3$, phonon interactions and the dynamic central peak near structural phase transition 77−81114
$SrTiO_3$, structural phase transition at 110K, theory 78−80300
$SrTiO_3$, tetragonal, effect of impurities on Raman spectrum 80−2770
$SrTiO_3$, thermal motion at room temp., anharmonic or disordered 79−37805
$SrTiO_3$:Eu(Sm), absorption spectra, Ti^{3+} ion and Z-centre formation 77−24871
TGSe, Raman and far IR spectra, lattice vibrs. in para- and ferroelec. phases 77−77190

lattice dynamics of ionic crystals
alkaki metal halides, cohesive energies, effect of three body interactions 77−76516
alkali chloride: V^{2+}, phonon induced zero field splitting 78−39073
alkali cyanide crystals, lattice dynamics calc. 79−77705
alkali halide: O^{2-}, photoluminesc. spectra, phonon using struct. *(Russian)* 78−2912
alkali halide:CN^-, internal modes reson. hybridization 79−42194
alkali halide, F-centres, vibronic problem in higher excited states 78−10931
alkali halide, lattice dynamics calc., extended three body force shell model 78−47491
alkali halide, lattice props. from interorbital-distance-related-repulsion approach 78−22809
alkali halide, lattice relaxation around tetragonal and rhombic defects 79−95110
alkali halide, localised mode due to U-centre 77−20036
alkali halide, static and dynamic props., appl. to KCl 77−7798
alkali halide crystal, Gruneisen parameter, vol. depend. anal. 80−2135
alkali halide crystals, anharmonic effects, modified Gruneisen relation 79−99290
alkali halide crystals, compressibility, force const. and IR absorpt. freq. 77−27955
alkali halide crystals, long wavelength optical mode frequencies and Anderson-Gruneisen parameter 80−65182
alkali halide crystals, mixed, impurity centre local vibrs., comp. depend. of spectral parameters 80−79898
alkali halide crystals, Szigeti effective charge parameter, strain derivative 79−7571
alkali halides, absorption spectra, freq. and temp. depend. of vibr. bands 80−2787
alkali halides, cryst., force consts., IR absorpt. freq., logarithmic pot. function calcs. 78−2832
alkali halides, curvature in cond. plots as consequence of anharmonicity 77−76597
alkali halides, emission spectra of O_2^- and NO_2^- centres at high hydrostatic press. 78−10943
alkali halides, exchange charge shell model analysis of strain derivatives of static polarisability, effective charge parameter 78−91296
alkali halides, interionic potentials, completely independent specification of Born-Mayer potentials 78−55828
alkali halides, interionic potentials, cryst. independent shell parameters and fitted Born-Mayer pots. 78−55827
alkali halides, IR absorpt. in molecules, clusters and microcrystals 78−80363
alkali halides, IR absorption spectrum, lattice vibrs., freq. and temp. depend. 79−65864
alkali halides, IR spectra, freq. and temp. depend. of charact. lattice vibrs. 79−65861
alkali halides, lattice dynamics using breathing shell model 80−88285
alkali halides, Lindemann's melting law, exptl. test 77−89522
alkali halides, mixed, U-centre localised modes 80−100319
alkali halides, multiphonon absorption, quasiselection rules 77−24844
alkali halides, optic mode Gruneisen parameters 78−43088
alkali halides, phonon spectra moments 77−4163
alkali halides, Poisson ratio and Gruneisen parameter, vol. depend. anal. 80−96614
alkali halides, shift and broadening of local vibr. bands, temp. depend. 78−87755
alkali halides, temp. and press. depend. of transverse-optic modes and anharmonic self-energies 77−11649
alkali halides, transverse optic mode Gruneisen parameter 80−39244
alkali halides, V_k-centres, vibr. modes, calc. 80−84269
alkali halides, vibration modes due to single ion impurities 79−51225
alkali hydrides, lattice props. from interacton pot. energy function 80−100199
alkali hydrides, thermodynamic props. calc. using ionic pots. 78−10155
alkali metal halides, vibrational modes due to three impurity cluster 78−75773
alkali metals, lattice sp. ht. and thermal vibrs. 78−30768
alkaline earth oxides, cohesive and thermophysical props., role of three-body interactions 80−92477
Anderson-Gruneisen parameter, interaction approach 80−88291
anharmonic crystal, statistical theory, quasi-classical expansion *(Russian)* 78−38803
anharmonic parameter, $\gamma\beta T$, interpretation *(French)* 80−34160
Bogolyubov chains, temp. expansion *(Russian)* 77−27949
Brownian sublattice, microscopic theory 78−79681
centrosymmetric ionic crysts., stimulated excitation of second harmonic, microscopic theory 80−91849
collective mode, computer simulation 80−54325
complex crystals, isotopic shifts, phonon freqs. 78−67787
Coulomb coeffs. for complex ionic crystals, computer program 77−39656
diamagnetic ionic cubic lattice in homogeneous mag. field, oscillations 78−91868
disorder-induced TA Raman lines 79−73929

lattice dynamics of ionic crystals continued
dispersion calcs. of cubic nonlinear susceptibility near Raman resonance 79−94292
electron-lattice interactions, ionic and partially ionic solids 77−20274
EM field interactions with ionic crystals, equations of motion and field equations 80−54319
fluoperovskites, nonlinear elastic behaviour, US velocity, 1 bar-3 kbar 78−59851
fluorite structure solids, long wavelength behaviour, elastic consts. 79−87441
Gruneisen and Anderson-Gruneisen parameters, interatomic forces 80−79904
heavy metal halides, atomis. energy, electron affinity, mean amplitude of vibr. *(German)* 79−51045
interface with degenerate semiconductor, localised plasmon-optical phonon coupled modes 77−28071
ionic crystals, surface polaron 78−60020
LiH, cubic, vibronic struct. and anisotropy of excitons, refl. and edge luminesc. spectra 78−23523
Lundqvist three-body interaction and lattice dynamics of ionic crystals 78−67775
microcrystallites, sp. ht. calc. 77−72696
microscopic and model theories 78−59871
microscopic model, for crysts. with Brownian sublattice 78−71798
model potentials 77−27845
nonlinear third-order susceptibility near Raman, two-photon resonances 79−94282
ordered vacancy compounds 78−75770
plate, line widths in spectrum of surface vibr. 79−33174
point defects, electronic and vibr. props., book 80−51962
polar crystal, Frenkel exciton effective mass temp. depend., lattice displacement interactions *(Chinese)* 80−84429
powdered stratified layers, lattice frequency 77−40222
pyridinium pentasilver hexaiodide, solid, far IR refl. spectra, incoherent neutron scatt., low freq. optical modes 78−2291
resonance Raman scattering, electron-phonon interaction for F centres 78−68519
rocksalt type, phonon dispersion relations, using extensions of shell model 79−77702
spheroids, IR spectra, calc. using point matching method 77−32377
statistical theory of surface tension and surface energy 80−17894
superionic conductors, long-wavelength density fluctuations 78−79808
superionic conductors, phase transitions and dynamics 78−59924
surface lattice dynamics, Green function approach 77−31865
surface rumpling at finite temps, Verwey model 79−51402
surface thermodynamic functions, vibrational contributions 77−47659
surface vibrational properties, review 78−71928
surface vibrations, energy level widths 80−6617
transition metal dihalides, layer struct., lattice dynamics, calc. 80−65177
wurtzite-type crystals, appl. of polarizable-ion model 77−80584
Ag halides, quadrupolar deformability theory by tight binding method 80−10614
Ag halides, temp. and press. depend. of transverse-optic modes and anharmonic self-energies 77−11649
AgBr, 295K, three-body-force shell model 77−15517
AgBr, 4.4K, neutron scatt. expts. 77−39643
AgBr, curvature of conductivity plots, consequence of anharmonicity 78−79800
AgBr, indirect near edge emission, 1.5-50K 77−16380
AgBr-$Li^+(Na^+)$, local mode freqs., Green's function calc 80−39237
AgCl, curvature of conductivity plots, consequence of anharmonicity 78−79800
Ag_2HgI_4, ordered and disordered phases Raman spectra temp. depend., ion hopping 78−23438
Ag_2HgI_4, polycryst., Raman spectra, press. depend. 77−73137
α-AgI, cation distrib. and anharmonic thermal vib. 77−66005
β-AgI, phonon-induced X-ray scatt. from lattice dynamical model 79−37790
β-AgI, thermal expansion, 4 to 270K 80−79961
β-Al_2O_3-M_2O, M=monovalent metal, superionic cond., phonon spectra and sp. ht. calc. 77−24368
BaClF, cryst., elastic consts. 80−19863
BaClF, localised vibr. of U-centres 78−75779
BaF_2, Raman spectra, 15 to 1300K, anharmonic vibr. effects 77−43990
BaF_2:Er^{3+}, fluoresc. spectra of charge compensated cryst., multiphonon and energy transfer relax. 79−87496
BaO, modified three-body shell model, lattice dynamics 77−4165
$BaTiO_3$, pot. functions of ions 80−19885
CaBr(Cl)(I), Gruneisen γ and other thermodynamic props. at zero and elevated press. 78−43142
CaF_2, anion motion at high temps., quasielastic nuetron scatt. obs. 80−59715
CaF_2, cation jump freq., isotope effect, lattice dynamical calc. 80−88357
CaF_2, Frenkel defect, entropy of form., Green function calc. 80−19898
CaF_2, high-frequency phonon lifetimes 80−70338
CaF_2, impurity modes due to interstitials, Green function formalism 80−24554
CaF_2, lattice dynamics in ang. force model, Debye-Waller factors, sp. ht., dispersion relations 77−59081
CaF_2, phonon resonances associated with vacancy 80−19893
CaF_2, Raman spectra, 15 to 1300K, anharmonic vibr. effects 77−43990
CaF_2, slab, surface modes of vibr. 78−71935
CaF_2:Ce^{3+}, thermally modulated UV absorpt. spectra, 90K 77−28602
CaF_2:Co^{2+}, elec. field effect on spectra induced by odd vibrs. 79−73973
CaF_2:Er^{3+}, fluoresc. spectra of charge compensated cryst., multiphonon and energy transfer relax. 79−87496
CaF_2:Eu^{2+}, tunable optical detection and generation of THz phonons 79−65149
CaF_2:rare earth ion, hydrogenated, local lattice modes, spectroscopy 80−50375
$CaF_{2-x}H_x$, IR spectra 80−34920
CaO, modified three-body shell model, lattice dynamics 77−4165
$CdBr_2$ crystal, transverse and longitudinal lattice mode freq., IR reflection spectra meas. 78−27227
$CdBr_2$, lattice vibr., IR absorpt. meas. 79−4380
$CdCl_2$ crystal, transverse and longitudinal lattice mode freq., IR reflection spectra meas. 78−27227
CdI_2 crystal, transverse and longitudinal lattice mode freq., IR reflection spectra meas. 78−27227
$CoSO_4.7H_2O$, electron capture aftereffects, time differential Mossbauer coincidence technique 80−39927

lattice dynamics of ionic crystals continued
$CsAlCl_4$, solid state Raman spectra, 298-80K, vibr., struct. 79−28745
CsBr, lattice statics and dynamics, deformation shell model 77−20034
CsBr, thermodynamic props., lattice dynamical calc. 77−20090
CsBr:O_2^-, Stokes' losses on cryst. vibrs. in luminesc. spectra of mol. centres *(Russian)* 77−55827
CsBr:Tl^+, impurity induced Raman spectra, breathing shell model 78−39541
CsBr:Tl^+, perturbed lattice dynamics, breathing shell model calculation 78−75744
CsCl, lattice statics and dynamics, model calcs. 77−11647
CsCl type crystals, deformable shell model including quadrupole deformation of charge cloud 79−99276
CsCl-type, elastic consts., and press. derivatives, Cauchy discrepancy, three-body force shell model 77−20004
CsF, second-order Raman spectra and phonon spectrum 77−90148
CsI, far-IR optical props., shell-model calcs. 77−28557
CsI, hyper-Raman spectrum, optical phonons, nonlinear processes 77−4640
CsI, isotope diffusion 78−75875
CsI, lattice statics and dynamics, model calcs. 77−11647
CsI, thermodynamic props., lattice dynamical calc. 77−20090
CsN_3, polycryst., IR active lattice vibr., optical consts. 77−77185
CsNCS, long-wave lattice modes 78−59881
CsNCS, vibr. spectra, multiphonon modes 77−40230
Cu-halides, phonon anomalies, dynamical model 79−73272
CuCl, anharmonic thermal vibr. X-ray diffr. exam. 78−30728
$CuCl_xBr_{1-x}$, disorder-induced TA Raman lines 79−73929
Cu_2HgI_4, ordered and disordered phases Raman spectra temp. depend., ion hopping 78−23438
Cu_2HgI_4, polycryst., Raman spectra, press. depend. 77−73137
CuI, superionic cond., Raman spectra in all 3 phases 78−19486
GaAs-polyethylene mixture, optical transmission spectra, IR filter prep. using computer appl. 80−2763
H_2SeO_3, cryst., vibr. spectra in O-H stretching region 79−51949
$Hg_{3-\delta}AsF_6$, low-temp. sp. ht., lattice dynamics, 1- to 3-dimens. crossover 79−86864
K halides, lattice dynamics in five parameter model 80−107382
K halides, surface lattice dynamics, by Green's function method 78−71936
KBr, defect modes due to H^--D^- pair impurities 80−59602
KBr, doped with F-centres, Raman spectra meas. excitation in F and K bands 80−16027
KBr, mode Gruneisen parameters, acoustic phonon dispersion relations 79−42201
KBr, spectral distrib. of triplet to singlet luminesc. of F_2 centre 77−59601
KBr, transverse optic mode self-energy at 100 and 300K, expt. determ. 80−84265
KBr:CN^-, neutron scatt. studies of $(CN)^-$ defects 80−92620
KBr:CN^- 80−49316
KBr:Ga^+, Jahn-Teller effect in orbital triplet, optically detected EPR meas. 77−66441
KBr:$HS^-(HF_2^-)$, anharmonic interaction of impurity intramol. vibrs. with cryst. phonons 77−77217
KBr(I), oscillatory and diffusive regime, above and below melting point, IR thermal emission spectra 78−83985
KCN, crystal props., log potential model calc. 78−63829
KCN, lattice dynamics in disordered cubic phase 78−38794
KCN, order-disorder transition, light scatt., Raman obs. 77−1672
KCN, phase transition at 168K, neutron inelastic scatt. line shapes for phonons obs. 78−38840
KCN, single cryst., orientationally disordered, Brillouin scatt., elastic consts. 77−85732
KCl, defect modes due to H^--D^- pair impurities 80−59602
KCl microcrystal boundary influence on IR spectrum 77−40243
KCl, phonon dispersion curves calc. 77−39648
KCl, phonon-phonon scatt. strength, thermal cond. in low- and high-temp. regions 77−43296
KCl, pure cryst., residual OH^- impurities, thermal cond. meas., zero field tunnelling splitting determ. 77−62692
KCl, spectral distrib. of triplet to singlet luminesc. of F_2 centre 77−59601
KCl, surface and bulk absorpt. at 10 μm, temp. depend. 77−28576
KCl, TSM study of lattice statics and dynamics 79−82292
KCl, thermodynamic props., lattice-dynamical calc. 77−35715
KCl, transverse optic mode self energy, freq. and temp. depend. 77−80589
KCl:CN^-, phonon-internal mode hybridisation, neutron scatt. 78−2217
KCl:CN^-, coherent admixtures of phonons with impurity libronic excitations, neutron scatt. study 80−49316
KCl:Eu^{2+}, radiationless process, vibronic spectrum analysis 78−80391
KCl:$F^-(Br^-)(I^-)$, U-centres, local defect modes, Green's functions calcs. 80−44280
KCl:Kbr(KI), enhancement in sp. ht. due to anion impurities 79−51274
KCl:Li^+, defect induced tunnelling states, depend. on strain, pot. model calcs. 79−69865
KCl:Li^+, phonon generation by EM excitation, mechanism 80−2129
KCl:$NO_2^-(O_2^-)$, Stokes' losses on cryst. vibrs. in luminesc. spectra of mol. centres *(Russian)* 77−55827
KCl:Na^+, R-centre exam., uniaxial stress effects on zero-phonon lines 78−47371
KCl:OH^-, paraelec. system, acoustic susceptibility in strong phonon-coupling approx. 78−71801
KCl:Pb, vibr. struct. of absorption band 79−33735
KCl(Br):Li^+, localised impurity modes, static lattice distortion effect 77−47530
$KCl_{1-c}Br_c$, impurity centre local vibrs., comp. depend. of spectral parameters 80−79898
$KCl_{1-x}Br_x$, phonon densities of states, dispersion relations 78−75761
$KCl_{1-x}Br_x$:NCO^-, absorpt. band defect broadening *(Russian)* 78−72526
KCl(Br)(I), lattice dynamics, bond-bending force model 80−54322
$KCl_{1-x}I_x$:NCO^-, absorpt. band defect broadening *(Russian)* 78−72526
KF(Cl)(Br)(I), surface lattice dynamics, Green function method 78−34693
KI, containing F-centres, Raman scatt. calc. 77−16306
KI, perturbed by Jahn-Teller centres, lattice dynamics 80−107394
KI, spectral distrib. of triplet to singlet luminesc. of F_2 centre 77−59601
KI:NO_2^-, Raman spectra, high press., low temp. effects 78−52479

lattice dynamics of ionic crystals continued
KI:S_2^-, Stokes' losses on cryst. vibrs. in luminesc. spectra of mol. centres *(Russian)* 77−55827
KN_3, IR refl. spectra, fundamental lattice modes, azide ion dipole derivatives 78−48166
KN_3, mono- and polycrysts., IR active lattice vibr., optical consts. 77−77185
KNCO, polycryst., IR and Raman spectra, lattice and internal modes 77−32369
KNCS, long-wave lattice modes 78−59881
KNCSe, IR and Raman spectra, internal and external modes 77−16312
$K_{1-c}Na_cCl$ and $K_{1-c}Rb_cCl$, impurity centre local vibrs., comp. depend. of spectral parameters 80−79898
K_2PtCl_6, K_2ReCl_6, K_2SnCl_6, solid state phase transitions, lattice vibr., NMR and NQR obs. 80−34814
$K_{1-x}Rb_xBr$, lattice dynamics on pseudo-crystal model 78−75762
$K_xRb_{1-x}Cl_yBr_{1-y}$, IR reflection spectra 78−76474
$K_{0.5}Rb_{0.5}I$, mixed cryst., phonons, neutron scatt. 77−1192
$KReO_4$, vibr. spectrum, Raman and IR spectra obs. 80−55104
K(TCNQ), Raman spectra from 30 to 2300 cm^{-1} 80−11392
K_2XY_6 (X=Sn, Te, Y=Cl, Br), low temp. vibr. spectra, lattice dynamics and phase transitions 79−73917
Li halides, moments of phonon spectrum from sp. ht. data 77−35649
$LiBaPO_4$, vibrational spectra and cryst. struct. 78−39536
LiCl:Ni^{2+}, first order induced Raman scatt. from Ni^{2+} and cation vacancies 77−48169
LiD, long-range three centre potentials, influence on lattice dynamics 80−96605
LiF, (001) surface, He and Ne inelastic resonant scatt. assisted by phonons 77−73201
LiF, anharmonic cryst. of order λ^4, self-energy of phonons, approximate numerical results 79−55843
LiF, bulk and (001)-surface equal-time vibr. correlation function 78−47655
LiF film, ATR spectrum, reson. between longit. phonons and substrate surface polaritons *(Russian)* 77−32384
LiF film, boundary influence on IR spectrum 77−40243
LiF, γ-irrad. pure and Mg-doped, phonon scatt. and interstitial clusters 80−70254
LiF, rel. to viscous drag of dislocations, internal friction, 4.2-300K 77−11566
LiH crystals, temp. effects on X-ray scattering factors in LCAO calcs. 80−10454
^{6,7}LiH(D), cryst., cohesive energy, force const., lattice freq., Debye temp., Gruneisen parameters, calc. 78−91293
LiN_3, evidence for N_3^- from static and dynamic props. 78−60465
LiN_3, polycryst., IR active lattice vibr., optical consts. 77−77185
$LiPbPO_4$, vibrational spectra and cryst. struct. 78−39536
$Li_2SO_4.H_2O$, far IR spectra, H_2O flipping motion, lattice modes 80−84258
$LiSrPO_4$, vibrational spectra and cryst. struct. 78−39536
MgF_2, rutile structure, dielectric props., neutron and Raman scatt. exam. 78−79684
MgO, 15-layer unrelaxed slab, lattice dynamics using breathing-shell model 79−73389
MgO, bulk and (001)-surface equal-time vibr. correlation function 78−47655
MgO, lattice dynamics and vibr. sp. ht. 78−47482
MgO, second-order Raman scatt. 78−10894
ND_4Cl, ordered phase, Raman spectrum, dipole and polarisability derivatives 77−52072
$NH_4Br(Cl)$, dynamic crit. phenomena 79−77690
NH_4Cl, dispersion of vibrational excitations, Raman scatt. 78−84588
NH_4Cl, ordered phase, press. depend. of Raman scatt. meas. 77−12388
NH_4Cl, ordered phase Raman spectrum, dipole and polarisability derivatives 77−52072
NH_4Cl, polariton Raman spectra, bound and many particle states 77−32372
NH_4Cl, Raman scatt. of light on limiting and nonlimiting dipole vibr. 80−11402
NH_4Cl Raman spectra, pressure effects 80−97268
NH_4I, ND_4I, lattice dynamics calcs. 78−6133
Na halides, surface rumpling at finite temps, Verwey model 79−51402
Na, thermal diffuse X-ray scatt. meas. in longitudinal and transverse branches 78−19598
Na-halide, extended three-body shell-model dynamics 77−7797
NaCN, Brillouin backscatter spectra of (100) LA phonons, elastic consts. determ. 79−65886
NaCN, crystal props., log potential model calc. 78−63829
NaCN, elastic const. temp. depend., Brillouin and US exam. 77−80572
NaCN, lattice dynamics in disordered cubic phase 78−38794
NaCN, single cryst., orientationally disordered, Brillouin scatt., elastic consts. 77−85732
NaCl, activation energy for mass transfer, quantum theory calc. *(German)* 79−51031
NaCl, anharmonic cryst. of order λ^4, self-energy of phonons, approximate numerical results 79−55843
NaCl, bulk and (001)-surface equal-time vibr. correlation function 78−47655
NaCl, calc. of third- and fourth-order elastic constants 79−10891
NaCl, far IR dispersive-reflection meas. at room temp., comparison with calc. 78−35139
NaCl film, UPS linewidth, phonon broadening of core levels 77−36371
NaCl, lattice thermal and optical phonon contrib. 79−14971
NaCl, microcrystallites, sp. ht. calc. 77−72696
NaCl, phonon dispersion curves calc. 77−39648
NaCl, phonon freqs. in off-symm. directions, neutron inelastic scatt. 79−46767
NaCl, polarisation mechanism and lattice mechanics, microscopic approach 78−59888
NaCl, rel. to viscous drag of dislocations, internal friction, 4.2-300K 77−11566
NaCl, single cryst., for IR dispersive refl. meas., low temp., rel. to anharmonicity calcs. 80−11371
NaCl, spectrum of intrinsic oscills., allowance for quadrupole deform. of ions 77−7810
NaCl structure, high temp. dynamics, var. approach 80−29130
NaCl, surface and bulk absorpt. at 10 μm, temp. depend. 77−28576
NaCl, thermodynamic props., lattice-dynamical calc. 77−35715
NaCl transverse optic mode anharmonic self-energy meas. by dispersive Fourier transform spectroscopy 77−39642

lattice dynamics of ionic crystals continued
NaCl, transverse optical mode anharmonic self energy, far IR spectrum 78−6131
NaCl-type, elastic consts. and press. derivatives, Cauchy discrepancy, three-body force shell model 77−20004
NaCl(Br) (F) (I), lattice dynamics and statics, three-body-force shell model 80−49323
NaCl(Br), oscillatory and diffusive regime, above and below melting point, IR thermal emission spectra 78−83985
$NaClO_3$-$NaBrO_3$ mixed crystals, internal optic modes, Raman and IR spectra meas. 79−95746
NaF, anharmonicity of lattice vibrations, neutron scatt. study, rel. to melting 77−84862
NaF, phonon linewidths at high temps. 77−62594
NaI, long wave phonon modes, IR absorpt. 78−79686
NaI:Cl^-, anharmonic effects on low-frequency impurity phonon resonances 78−75771
NaI:Cl^-, local vibr. exam. by neutron scatt. 77−24373
NaN_3, lattice dynamics and phase transition, theory 77−76501
NaN_3, polycryst., IR active lattice vibr., optical consts. 77−77185
PbBr(Cl)-Ag^+ IR absorpt. spectrum and vibr. of substitutional impurity 77−81135
PbF_2, fast ion conductor, phonon freq. distrib., temp. variation 80−84264
PbI_2, ionic layer cpd., lattice dynamics, influence of static dipole moments 79−28057
Rb halide crysts., phonon dispersion curves, shell model calc. 77−55331
Rb halides, moments of phonon spectrum from sp. ht. data 77−35649
$RbAg_4I_5$, solid electrolyte, polarised Raman scatt. meas. 77−12376
Rb_2AgI_3, cryst. struct. and polarised Raman spectrum 77−69813
$RbAlCl_4$, solid state Raman spectra, 298-80K, vibr., struct. 79−28745
RbBr, harmonic and anharmonic props. from phonon dispersion at three temps. 80−39235
RbBr, mode anharmonic self energies, freq. depend. 78−59908
RbBr, phonon freqs. at 80, 290, 370K, neutron inelastic scatt. study, comparison to Gruneisen parameters 78−51631
RbCN, crystal props., log potential model calc. 78−63829
$RbCaF_3$, 193K phase transition, lattice dynamics 78−10160
RbCl containing K additive impurity, local modes due to U-centres 78−22805
RbCl, lattice localised modes due to U-centre pairs 79−77709
RbCl, nearest-neighbour atom displacements derived from EXAFS spectra, temp. depend. 79−87524
RbCl, thermodynamic props., lattice-dynamical calc. 77−35715
RbCl:Ag^+, first-order impurity-induced Raman scatt. 77−77216
$RbCl_xBr_{1-x}$, IR refl. spectra, temp. depend. 77−28573
RbI, elastic constants determ. by inelastic neutron scatt. 78−79659
RbI, NaCl to CsCl phase transition by elastic diffuse and inelastic neutron scatt. 80−2162
RbI, non-linear press. depend. of phonon freq. 77−35650
RbI, temp. depend. of second order Raman spectra 78−68512
RbN_3, lattice vibration Raman study, tetragonal-cubic phase transitions 79−77743
RbN_3, polycryst., IR-active lattice vibr., optical consts. 77−77185
RbNCO, polycryst., IR and Raman spectra, lattice and internal modes 77−32369
$Sr_{1-x}Cd_xF_2$, IR and Raman meas. 78−75763
SrClF, cryst., elastic consts. 80−19863
SrClF, localised vibr. of U-centres 78−75779
SrF_2, high-frequency phonon lifetimes 80−70338
SrF_2:Er^{3+}, fluoresc. spectra of charge compensated cryst., multiphonon and energy transfer relax. 79−87496
SrF_2:Eu^{++}, tunable optical detection and generation of THz phonons 79−65149
$SrF_2(Cl_2)$, Raman spectra, 15 to 1300K, anharmonic vibr. effects 77−43990
SrO, modified three-body shell model, lattice dynamics 77−4165
$SrS(F_2)(Cl_2)$, nearest-neighbour atom displacements derived from EXAFS spectra, temp. depend. 79−87524
TiO_2, anatase phase, lattice vibrs. calcs., rigid ion model 80−2125
Tl halides, temp. and press. depend. of transverse-optic modes and anharmonic self-energies 77−11649
TlBr, CsCl and NaCl phases, atomic interactions and lattice statics and dynamics 78−83889
TlBr, reson. Raman scatt., forbidden one phonon and intervalley scatt. at direct exciton 80−45073
$TlBrO_3$, polycryst., Raman and IR spectral assignments, room temp. 78−15156
TlCl, Debye Waller factors of Tl^+ and Cl^-, X-ray diffr. 77−31742
TlCl, Raman spectra in melting region 78−27224
TlCl, thermal vibr. amplitudes, 296-534K, X-ray obs. 77−35656
$TlClO_3$, polycryst., Raman and IR spectral assignments, room temp. 78−15156
$TlIO_3$, polycryst., Raman and IR spectral assignments, room temp. 78−15156
TlN_3, lattice vibration Raman study, tetragonal-cubic phase transitions 79−77743

lattice dynamics of metallic crystals
actinide, transport props. and sp. ht., role of optical and acoustic phonons 77−15821
actinides, lattice vibrs. role in transport props. determ. 77−28158
alkali metal, Ashcroft pseudopotential, unified study of props. 80−39239
alkali metal, atomic props., accuracy of description depenxence on pseudopotentials *(Russian)* 78−38997
alkali metal, lattice vibr. and Gruneisen parameter 78−59917
alkali metal, phonon frequencies, depend. on atomic mass 79−14901
alkali metals, a priori pseudopot. calc., comparison of statistical and Lindgren cond.-core exchange approxs. 77−72662
alkali metals, anharmonic effects in thermodynamics *(Russian)* 78−43145
alkali metals, atomic properties, pseudopot. calcs. 77−89512
alkali metals, axially symmetric model, phonon dispersion 80−34152
alkali metals, dispersion curves using second-order perturbation theory 80−79893
alkali metals, effective ion-ion potential, compressibility and force consts. 80−70158
alkali metals, elastic and thermal props. by pseudopotential method 80−19899
alkali metals, electron fluid model 78−75738

lattice dynamics of metallic crystals continued
alkali metals, energy-independ. model pseudopot., phonon spectra 77−62890
alkali metals, Gruneisen parameters, influence of press. on lattice anharmonicity and temp. depend. 80−79905
alkali metals, lattice anharmonicity 79−19341
alkali metals, lattice dynamics, modified Bhatia model 77−51455
alkali metals, lattice excitation dispersion relations 80−100314
alkali metals, lattice vibrations, homology 80−44267
alkali metals, phonon dispersion, phenomenological model 79−60445
alkali metals, phonon dispersion and electron gas pressure, theory 78−2208
alkali metals, phonon dispersion binding energy, compressibility, elastic consts. electron screening and Ashcroft pot. calcs. 80−65174
alkali metals, phonon freqs., optimised model pot. calcs. 78−2467
alkali metals, thermal properties and Gruneisen parameters, employing model pot. 78−71815
b.c.c., modified Cheveau model for lattice waves, phonon dispersion and Gruneisen parameter 77−1189
BCC metal, angular force model 77−15509
BCC metal, angular force model 77−31735
BCC metal, Debye-Waller factors, temp. depend. calc. 78−22807
BCC metal, Debye-Waller factors, temp. variation calc. 78−55925
BCC metals, ang. forces in lattice dynamics 77−84870
BCC metals, axially symm. and ang. force models, equivalence 78−26637
BCC metals, effective valence, from phonon data, rel. to vacancy formation energies 80−79781
BCC metals, equivalence of ang. force models for lattice dynamics 78−83891
BCC metals, lattice dynamical ang. force models 79−82289
BCC metals, modified tensor force model for lattice dynamics 77−35644
BCC metals, noncentral ionic interaction 80−65172
BCC metals, phenomenological model for lattice dynamics 77−20017
BCC metals, phonon dispersion, modified de Launay model 78−34573
BCC structures, electron-ion interactions 79−4377
BCC transition metals, seven parameter model 79−90739
BCC transition metals, tensor force model, lattice dynamics 80−103428
β-brass, cryst. struct., elastic consts., central force model 78−51637
CFC metals, frequency spectra, and correlated spectral density between bulk atoms 79−19330
charged fermion system, in random external field, dielec. instability 77−85170
collective mode, computer simulation 80−54325
cubic metal, noncentral force model for lattice dynamics 79−69209
cubic metal, Sharma-Joshi model, correl. exchange effects 80−10613
cubic metal, three-body forces and condition of equilib. in models of Krebs and Cheveau 79−19333
cubic metal, three-body forces and condition of equilib. in models of Krebs and Cheveau 79−23687
cubic metal, vol. and temp. depend. of phonon frequencies 77−15514
cubic metals, central pair pot. vs. axially symm. pot. 78−87747
cubic metals, impurity-host force-constant changes from Mossbauer data, review 78−48097
cubic metals, ionic interaction in dynamical matrices 79−77693
cubic metals, ionic overlap interaction energy, press. and bulk modulus 80−29340
cubic metals, lattice dynamics, ang. force models 77−31731
d-band metals, force fields 79−33051
dilute alloys, Kondo temperature, lattice vibr. effect 78−19025
electron fluid model, phonon dispersion in Na 77−27954
electron gas model 79−14894
electron-ion metal system, dynamics eqns. in microscopic theory *(Russian)* 80−15198
electron-phonon interaction, magnetism influence 77−73040
FCC, model for lattice dynamics 78−91387
FCC, X-ray Debye-Waller factors, CGW vs. DAF models 79−37794
FCC metal, crystal equilib., lattice dynamics 78−47479
FCC metal, Debye-Waller factors, modified ang. force model 77−66013
FCC metal, phonon dispersion relations and Debye-Waller factor calcs. 78−51630
FCC metals, (100)-split interstitials, internal modes reson. hybridization 79−42194
FCC metals, dynamics of multiple interstitials and interstitial impurity complexes 78−75775
FCC metals, equivalence of ang. forces 80−49312
FCC metals, lattice-dynamical model 79−51219
FCC metals, nonequivalence of ang. force models of de Launay and Clark, Gazis and Wallis 78−63819
FCC metals, vibr. anharmonicity and Debye-Waller factors, Willis approach 77−51467
FCC structures, electron-ion interactions 79−4377
FCC transition metal, improved Fielek model 79−19335
Fermi surface local geometry effects on phonon spectrum, acoustic props. *(Russian)* 77−55333
ferromagnetic metals, itinerant electron, theory of crit. US propag. 77−69655
fine particles, anharmonic lattice vibr. theory, Einstein model appl. 78−18714
fine particles, Mossbauer fraction, anharmonic lattice vibr. 78−47489
generalised Gruneisen tensor from solid nonlinearity parameters 80−84275
HCP lattices, angular forces in lattice dynamics 80−107383
HCP metals, anharmonicity effect on neutron diffr. struct. factor 78−59907
HCP metals, lattice dynamics, local pseudopotential approach, dielectric functions 80−34151
HCP metals, model for lattice dynamics 78−22795
HCP metals, phonon dispersion 78−59883
HCP metals, phonon dispersion relations, effect of different dielec. functions on model pseudopot. calc. 79−33055
helicon-phonon interaction for parallel wave propagation 78−64054
interatomic potential determ. from phonon spectra 77−65962
interatomic potentials, from phonon spectra 80−33927
interatomic potentials from experimental phonon spectra 78−75621
interatomic potentials of Na, K, Al, Cu, Fe from phonon spectra 80−19744
ion pair potentials, asymptotic, contrib. to lattice energy, elastic consts., phonon dispersion 77−19898
ionic interaction in axially symmetric and Bhatia models 79−37767
itinerant ferromagnet, tight-binding metal, Einstein temp. 79−24126

lattice dynamics of metallic crystals continued
lattice dynamical models, phonon dispersion curves 77−89506
Lindemann's melting law, exptl. test 77−89522
metal, cryst. equilib. and Cauchy deficiency 79−19328
metal, spin scattering and spin-orbit coupling 80−29369
metal-insulator-superconductor junction, electron interactions with phonons and mag. impurities 77−16004
metals, BCC and FCC, H-diffusion and trapping 80−70447
metals, compressibility in presence of anharmonic interaction *(Russian)* 78−23763
metals, lattice surface relaxation, electrostatic model 80−49488
migration and formation energies rel. to Debye temp. and melting point 78−22710
model, homogeneous electron liquid concept *(Hungarian)* 77−27952
monovalent metal, electron-phonon coupling const., calc. 79−99286
multiphonon contribution to struct. factor 77−1206
noble metal, phonon density of states determ. from thermodynamic functions *(Russian)* 77−7800
noble metal, van der Waals forces and their contrib. to vacancy form. energy and phonon dispersion 78−91635
noble metal lattice dynamics, pseudopotential method, Cu, Ag phonon spectra 77−89508
noble metals, angular force contribution 79−37768
noble metals, energy wave number charact., by reson. model 80−10612
noble metals, lattice dynamics, central pair pot. calcs. 77−31736
noble metals, nonlocal effects 78−75754
noble metals, pseudopot. exam. of electronic props. 78−51960
OPW construction electron states in nonlocal pseudopot. calcs. of phonon spectra, exact normalization 77−7803
phonon spectra, singularities caused by local geometry of Fermi surface 78−91401
phonon spectrum, nonadiabatic effects, in mag. field *(Russian)* 78−19106
positron-phonon interaction strength 77−15796
positron-phonon scatt. effect on positron trapping at monovacancies 78−26829
pseudoharmonic effects of phonons in heat conductivity of metals 80−70326
pseudopotential investigation of phys. props. of metals 77−43526
rare earth metal, lattice dynamics and scatt. reson. 78−59872
rare earth metals, HCP, microscopic theory 77−43292
rare-earth metals, US attenuation in applied fields 77−51933
simple metals, volume forces 80−15178
surface phonons and superstructures 77−62731
thermal vibration amplitude of atoms and fusion behaviour *(Korean)* 79−69218
three-body forces inclusion and equilibrium condition in Krebs and Cheveau models 78−47480
three-body interaction and lattice dynamics 78−10139
transition metal, Animalu model potentials, nonlocality 78−6250
transition metal, BCC, crystallographic aspects of elastic dispersion 77−20032
transition metal, BCC, phonon dispersion curves and elastic, calc. using cohesive energy 78−59885
transition metal, charge fluctuation model 77−84869
transition metal, cubic, phonon dispersion, Fielek and extended Cheveau models 78−22801
transition metal, Einstein temp. and vibr. entropy, semiquantitative calc. 78−2221
transition metal, FCC, 5-parameter model dispersion relations, appl. to Ni, Pt 78−75748
transition metal, lattice dynamics and scatt. reson. 78−59872
transition metal, phonon dispersion curves, extended de Launay model 77−4162
transition metal 4d BCC, phonon dispersion 79−95102
transition metals, BCC crysts., seven parameter model calc. 79−19329
transition metals, HCP, nonlocal effects in lattice dynamics 78−91397
transition metals, interatomic forces, phonon spectra, from band structure charge densities 79−7662
transition metals, lattice excitations, classical models 80−29132
transition metals, microscopic theory 79−7664
transition metals, phonon dispersion using non-central force model 78−91392
transition-metal slab, surface lattice dynamics and density response 78−71930
transiton metals, lattice dynamics calculations, superconductivity parameters 79−7655
two-parameter shell model of lattice vibrs. in monoatomic systems 78−59877
X-ray emission edges, effect of incomplete phonon relaxation 78−35227
X-ray spectra, temp. broadening 77−69936
Ag, Debye temp., X-ray diffr. determ., anharmonic parameters of pot. function 80−100320
Ag, Debye-Waller factor temp. parameter 78−30725
Ag, electronic contribution to thermal cond. at low temps. 79−95384
Ag, Gruneisen parameters, 10-100K, phonon wave vector depend. 78−38801
Ag, Gruneisen parameters, dynamical study using modified Bhatia model 79−37797
Ag, lattice dynamics, ion-ion and ion-electron interactions 80−49321
Ag, lattice dynamics on Kreb's model 80−59594
Ag, lattice vibrations and ideal elec. resistivity 79−46770
Ag, model pseudopotential method for phonon dispersion 79−23685
Ag, modified Bhatia model, phonon dispersion, Debye-Waller factor temp. depend. 77−31729
Ag, modified CGW model calcs., phonon dispersion, sp. ht. and equiv. Debye temp. 78−10135
Ag, phonon dispersion, binding energy, compressibility, pseudopot. calc. 77−4164
Ag, phonon dispersion relations and Debye-Waller factor calcs. 78−51630
Ag, phonon dispersion relations, screened shell model 78−83894
Ag, transverse acoustic phonon branch, temp. depend., neutron scatt. *(German)* 78−71808
Ag, two-parameter dynamical model appl 80−10597
Ag, X-ray Debye temp. and isobaric Gruneisen coeff., anharmonicity effects 77−62654
Al, anharmonic lattice dynamics, computer simulation of dynamical struct. factor 78−6130
Al, Debye temp., X-ray diffr. determ., anharmonic parameters of pot. function 80−100320

lattice dynamics of metallic crystals continued
Al, Debye-Waller factor temp. parameter 78−30725
Al, electronic Gruneisen parameter in shock Hugoniot eqn. of state 80−10635
Al, empirical pot. methods, use of Wedepohl pot., vacancy form energy 80−39230
Al, film, superconducting transition temp. and lattice dynamics 80−93028
Al, Gruneisen parameters, dynamical study using modified Bhatia model 79−37797
Al, incomplete phonon relax. in X-ray emission calc. 77−52202
Al, lattice thermal cond. at low temps., Ashcroft pseudopotential method 80−19897
Al, lattice vibrations, seven parameter non-central force model 80−44270
Al, melting, existence of before and after effects, neutron scatt. 77−84895
Al, modified Bhatia model, phonon dispersion, Debye-Waller factor temp. depend. 77−31729
Al, phonon density of states by neutron scatt., sp. ht. and Debye temp. 80−2132
Al, phonon dispersion curves, lattice dynamics unpaired forces 79−42170
Al, phonon dispersion relations and lattice heat capacity calc. 77−20023
Al, phonon dispersion relations and lattice heat capacity, modified Bhatia model 77−20024
Al, phonon dispersion relations and Debye-Waller factor calcs. 78−51630
Al, polycryst., density fluctuations, neutron scatt. anal. 80−70349
Al, tilt boundary, $\Sigma=5$, struct. and atomic vibr., computer simulation 80−70223
Al, two-parameter dynamical model appl. 80−10597
Al, unpaired ion-ion interaction, transverse phonon branch, neutron scatt. expt. *(Russian)* 78−87751
Al, X-ray absorpt. and emission edges, one-electron and many-body effects 80−25484
Au, Debye-Waller factor temp. parameter 78−30725
Au, electron-ion pseudopot., form factor, liquid elec. cond., phonon dispersion 78−34785
Au, fine particles, gas evaporation technique of prep., X-ray diffr. study, charact. temp. 80−75328
Au, Gruneisen parameters, 10-100K, phonon wave vector depend. 78−38801
Au, Gruneisen parameters, dynamical study using modified Bhatia model 79−37797
Au, lattice dynamics, ion-ion and ion-electron interactions 80−49321
Au, lattice dynamics on Kreb's model 80−59594
Au, lattice vibr., electron press., central pair pot. model calc. 78−75749
Au, lattice vibrations and ideal elec. resistivity 79−46770
Au, local pseudopotential, phonon frequencies, binding energy and liq. metal resist. calc. 77−20216
Au, model pseudopotential method for phonon dispersion 79−23685
Au, modified Bhatia model, phonon dispersion, Debye-Waller factor temp. depend. 77−31729
Au, modified CGW model calcs., phonon dispersion, sp. ht. and equiv. Debye temp. 78−10135
Au, phonon dispersion, binding energy, compressibility, pseudopot. calc. 77−4164
Au, phonon dispersion, lattice phonons three body interaction model 79−99280
Au, phonon dispersion relations and Debye-Waller factor calcs. 78−51630
Au, phonon dispersion relations, screened shell model 78−83894
Au, phonon spectra, self-consistency condition for force const. models 80−44264
Au, thermal properties and Gruneisen parameter, Toya's first principle approach 78−38806
Be, HCP, electron-phonon interaction, thermal effects 79−33057
Be, HCP metal, lattice dynamical props., unpaired forces, phonon dispersion relations 79−19336
Be, noncubic crystal, temp. depend. of elec. field gradient, effect of thermal vibr. of atoms 79−99515
Be, phonon dispersion calc. 79−51218
Be, phonon dispersion relations and Debye temp. 79−42171
Be, three-body forces in math. model for phonon dispersion branches and expt. degeneracy 77−62593
Bi, optical phonon anharmonicity and melting, light scatt. study 80−60621
Ca, lattice dynamics, phenomenological model 80−44265
Cd, anharmonic interactions, elastic X-ray scatt. 78−75755
Cd, anisotropic thermal expansion 79−23750
Cd, atomic vibr. and fermion behaviour of HCP metals 80−6474
Cd, electric field gradient press. depend., lattice vibrs. effect, PAC expts. 79−61267
Cd, electron-phonon interactions, inelastic neutron scatt. meas. 79−99285
Cd, field gradients, temp. depend., electronic and lattice contribs., ab initio study 79−42501
Cd, HCP, phonon dispersion relations, effect of different dielec. functions in model pseudopot. calc. 79−33055
Cd, noncubic crystal, temp. depend. of elec. field gradient effect of thermal vibr. of atoms 79−99515
Cd, phonon density of states calc. from neutron diffr. data 77−24369
Cd, phonon density of states determ. from heat capacity *(Russian)* 80−29131
Cd, phonon dispersion 77−15513
Cd, phonon dispersion relations, specific heat by modified Cheveau model 78−38792
Cd, phonon spectra and eqn. of state, pseudopot. method *(Russian)* 77−24367
γ-Ce, lattice and spin dynamics, inelastic neutron scatt. obs. 79−86859
$CeSn_3$, intermediate valence cpd., search for phonon anomalies, inelastic neutron scatt. 80−100317
Co, Debye-Waller factor and Lindemann parameter, temp. depend., lattice dynamical model calcs. 80−59610
Co, FCC, electron response and modified Bhatia model 79−37771
Co, FCC, modified Krebs model, phonon dispersion relations 78−79682
Co, lattice dynamics and compression curves 78−38793
Co, nearest-neighbour atom displacements derived from EXAFS spectra, temp. depend. 79−87524
Cr, cryst. equilib. lattice dynamical model 78−22811
Cr, Debye-Waller factors, temp. depend. calc. 78−22807

lattice dynamics of metallic crystals continued
Cr, freq. spectra, sp. ht., Debye temp., Clark-Gazis-Wallis ang. force model 78−22799
Cr, lattice dynamics, and sp. ht., extended de Launay model 79−46762
Cr, lattice dynamics, improved Fielek model 80−59598
Cr, lattice dynamics, phonon dispersion and atomic force constants, phenomenological model 78−26640
Cr, lattice vibrations, Debye temp., freq. wave vector dispersion relations 78−63818
Cr, phonon dispersion, Debye temp. and Debye-Waller factors, lattice dynamical model 78−55920
Cs, elec. and thermal resist. calc. using modified noncentral force model 79−91016
Cs, phonon freqs, and Gruneisen parameter, model pseudopotential calc. 77−35643
Cs, phonon spectral density, pseudopotential calcs. 80−39234
Cu, Debye-Waller factor temp. parameter 78−30725
Cu, EXAFS Debye-Waller factors 80−45168
Cu, elastic constants, up to 2500 bar, −196-25°C, US pulse echo obs. 79−87680
Cu, electronic contribution to thermal cond. at low temps. 79−95384
Cu, FCC, appl. of model for lattice dynamics 78−91387
Cu, Gruneisen parameters, 10-100K, phonon wave vector depend. 78−38801
Cu, Gruneisen parameters, dynamical study using modified Bhatia model 79−37797
Cu, interatomic force consts. from lattice vibrs. 77−20020
Cu, Krasko-Gurskii model potential, test of validity 80−39485
Cu, lattice and force consts., pairwise atomic repulsions in cluster model 79−32939
Cu, lattice dynamics, ion-ion and ion-electron interactions 80−49321
Cu, lattice specific heat, from two-parameter lattice dynamical model with dispersion 80−10678
Cu, lattice vibrations and ideal elec. resistivity 79−46770
Cu, model incorporating second neighbour shell-shell interactions 77−59082
Cu, model pseudopotential method for phonon dispersion 79−23685
Cu, modified Bhatia model, phonon dispersion, Debye-Waller factor temp. depend. 77−31729
Cu, modified CGW model calcs., phonon dispersion, sp. ht. and equiv. Debye temp. 78−10135
Cu, nearest-neighbour atom displacements derived from EXAFS spectra, temp. depend. 79−87524
Cu, one-phonon scatt. of ultracold neutrons 77−61480
Cu, phonon dispersion relations and Debye-Waller factor calcs. 78−51630
Cu, phonon spectra, self-consistency condition for force const. models 80−44264
Cu, rel. to press. depend. of Mossbauer fraction for ^{57}Fe 77−16226
Cu surface, Ar ion bombardment, fast ionized recoils, thermal lattice vibr. effects 80−100737
Cu, thermal vibr. and zero-point motion effects on low-energy collision cascades 78−87705
Cu, zero to first sound transition, inelastic-neutron scatt. data 77−31738
Cu-Al(Au) alloys, HV electron microscopy, crit. voltages depend. on comp., temp. and short-range order 80−100146
Cu-Pt system, phonon dispersion relations, force constant disorder effect 80−84263
Cu-Zn-Al martensite, phonon branches meas. 80−88286
Er, Debye-Waller factor and Lindemann parameter, temp. depend., lattice dynamical model calcs. 80−59610
Er, lattice dynamics, thermal expansion, bulk modulus calcs. 77−20022
$ErFe_2$, lattice dynamics, Mossbauer spectra 80−19888
Fe, BCC, vib. entropy of $^1/_2\langle 111\rangle\{110\}$ edge dislocations 78−63768
α-Fe, cryst. equilib. lattice dynamical model 78−22811
α-Fe crystal, phonon spectrum, slow neutron inelastic scatt. meas. 77−80592
α-Fe, Debye-Waller factors, temp. depend. calc. 78−22807
Fe, EXAFS Debye-Waller factors 80−45168
Fe fine particles in matrices, lattice vibr., Mossbauer effect 80−15924
α-Fe, freq. spectra, sp. ht., Debye temp., Clark-Gazis-Wallis ang. force model 78−22799
α-Fe, lattice and force consts., pairwise atomic repulsions in cluster model 79−32939
α-Fe, lattice defects, relax. studies, computer simulation 78−79604
Fe, lattice vibrations, temp. depend. 78−95124
α-Fe, lattice wave dispersion, lattice consts., elastic consts. 80−24545
α-Fe, phonon spectrum, cold neutron inelastic scatt. obs. 77−7811
Fe small particles, Mossbauer effect study of lattice vibr., Debye temp. of metallic core 80−44963
Fe, surface phonon spectra 78−71934
Fe_3Pt, atomic thermal vibr. anisotropy, martensitic transform. model *(French)* 80−70355
Ga, elastic moduli, temp. depend., anharmonic effects *(Russian)* 77−31708
H-He, metallic solid alloys, phase separation, electron band struct. and lattice dynamics determ. 77−43333
H_2 crystal, metallic, total energy, self consistent harmonic phonon approx. 77−31629
HF, high temperature thermophysical properties 78−91404
Hf, HCP, lattice dynamics, thermal and elastic props., model 80−34155
Hf, lattice dynamics, phonon dispersion, mode softening 80−107390
Hg, phonon dispersion curves, neutron inelastic scatt. 78−14410
Ho, phonon freqs., calc. 80−15206
Ho, sp$_\sigma$ ht., using lattice dynamical model for HCP metals 79−51273
Ho, three-body forces in math. model for phonon dispersion branches and expt. degeneracy 77−62593
Ho, unpaired forces in lattice dynamics of rare-earth HCP metals 77−7805
In, lattice dynamics, pseudopot. computation *(Russian)* 80−92617
In:Sn, phonon spectrum, electron-phonon interaction *(Russian)* 78−18722
In-Tl, BCC alloys, stability and elastic consts., US vel. 79−42133
Ir, phonon/wave vector dispersion relations, Debye temp., modified axial symmetric model 80−70339
K, anharmonic lattice dynamics 78−18720
K, BCC, Gruneisen parameter temp. var. 78−6137
K, elastic constants, cryst. equilib. and electronic contrib. 79−73243
K, Gruneisen parameter, press. depend. 80−65184
K, ideal thermal resist. calc., anisotropic continuum dispersive model 77−51724
K, incomplete phonon relax. in X-ray emission calc. 77−52202
K, phonon frequencies, normal mode Gruneisen parameters, pseudopot. calcs. 79−42184
K, phonon spectral density, pseudopotential calcs. 80−39234
K, phonon spectrum calc., microscopic theory of force constants 78−26647
K, search for anomalous phonons, coherent inelastic neutron scatt. meas. 77−47525
$KMgF_3:V^{2+}$, dynamical Jahn-Teller effect on spin orbit multiplets, intensity quenching 79−95374
K_cRb_{1-c}-alloys, lattice dynamics of substitutional alloys, force constant disorder 78−75786
La, DHCP and FCC phases, phonon density of states 78−67791
Li, anharmonic props., temp. depend. 79−19340
Li, anharmonicity and low temp. phase struct., neutron diffr. study 80−107105
Li, BCC, Gruneisen parameter temp. var. 78−6137
Li, elec. and thermal resist. calc. using modified noncentral force model 79−91016
Li, ideal thermal resist. calc., anisotropic continuum dispersive model 77−51724
Li, incomplete phonon relax. in X-ray emission calc. 77−52202
Li, microscopic theory using Bloch wavefunctions 77−35648
Li, phonon dispersion curve crossing in [ζ00] direction 77−59078
Li, phonon frequency, liquid electrical resist. and interionic pair potential 78−10140
Li, phonon spectra, variable-form pot. calcs. 78−2209
Li, phonon spectral density, pseudopotential calcs. 80−39234
Li, Sharma-Joshi model, correl. exchange effects 80−10613
Li, soft X-ray spectra, phonon broadening calc. 77−63526
Li, spectrum, calc. from bandstructure 78−6134
Li, vibration modes, phenomenological calc., non-central force model 78−38791
Li, X-ray absorpt. and emission edges, one-electron and many-body effects 80−25484
^{7}Li, temp. depend., 110-424K, force consts. 77−20033
Mg, anisotropic thermal expansion 79−23750
Mg, atomic vibr. and fermion behaviour of HCP metals 80−6474
Mg, HCP metal, lattice dynamical props., unpaired forces, phonon dispersion relations 79−19336
Mg, lattic dynamics and sp. ht. in extended de Launay model 79−51217
Mg, phonon density of states calc. from neutron diffr. data 77−24369
Mg, phonon density of states determ. from heat capacity *(Russian)* 80−29131
Mg, phonon dispersion relations and Debye temp. 79−42171
Mg, phonon spectra and eqn. of state, pseudopot. method *(Russian)* 77−24367
Mg, phonon spectrum and thermodynamic functions, inelastic coherent cold neutron scatt. *(Russian)* 78−55917
Mg, X-ray absorpt. and emission edges, one-electron and many-body effects 80−25484
Mg, X-ray Debye charact. temp., powder specimens 77−84876
Mo, and alloys, lattice dynamical models, phonon dispersion curves 77−89506
Mo, Debye-Waller exponents, modified ang. force model, and lattice vibrs. 77−76515
Mo, interatomic pot. from phonon spectrum 78−67784
Mo, lattice defects, relax. studies, computer simulation 78−79604
Mo, lattice dynamics, improved Fielek model 80−59598
Mo, phonon density of states determ. from heat capacity *(Russian)* 80−29131
Mo, phonon dispersion, anomalous struct., tight-binding calcs. 78−10137
Mo, phonon dispersion, Debye temp. and Debye-Waller factors, lattice dynamical model 78−55920
Mo, phonon dispersion, lattice phonons three body interaction model 79−99280
Mo, phonon frequencies, seventh-neighbour tensor force model 78−91402
Na, BCC, Gruneisen parameter temp. var. 78−6137
Na, Debye-Waller factors, temp. depend. calc. 78−22807
Na, electron fluid model, phonon dispersion 77−27954
Na, equilibrium struct. and phys. props., pseudopot. method 80−96778
Na, Gruneisen parameter, press. depend. 80−65184
Na, incomplete phonon relax. in X-ray emission calc. 77−52202
Na, lattice dynamics, angular force model 77−31735
Na, linear potential and phonons 79−82293
Na, martensitic transform. obs. neutron scatt. meas. 77−15581
Na, model incorporating second neighbour shell-shell interactions 77−59082
Na, phonon dispersion curve, sp. ht. and Debye temp., ang. force model 77−15509
Na, phonon spectra, self-consistency condition for force const. models 80−44264
Na, phonon spectral density, pseudopotential calcs. 80−39234
Na, soft X-ray spectra, phonon broadening calc. 77−63526
Na, X-ray absorpt. and emission edges, one-electron and many-body effects 80−25484
Na_xWO_3, metallic, light-scatt. studies 80−45071
Nb, electron-phonon contrib. to phonon linewidth determ. 78−10146
Nb, high-temperature nonlinear electrical resistivity, supposed failure of Boltzmann eqn. 78−91664
Nb, modified Sharma-Joshi model 79−51221
Nb, phonon density of state determ. from thermodynamic crystal functions *(Russian)* 79−82291
Nb, phonon dispersion, anomalous struct., tight-binding calcs. 78−10137
Nb, phonon dispersion curves, extended screened-shell model 80−96601
Nb, phonon frequencies, seventh-neighbour tensor force model 78−91402
Nb, phonon linewidths and electron-phonon interaction 79−73273
Nb, phonon spectra, self-consistency condition for force const. models 80−44264
Nb, plastically deformed, changing lattice dynamics 78−67793
Nb, pure and N doped, neutron diffuse-scatt. intensities 80−59597
Nb, X-ray and neutron diffuse scatt. intensities comparison, thermal vibrs. 77−43294
Nb-H system, local frequency spectrum, mean thermal displacement of H 80−59604
Nb_3Sn, anisotropic thermal parameters of Nb 79−99282
Nb_3Sn, martensitic transition, lattice anharmonicity 79−8300
$NdH_{2.57,2.62}$, optical vibr. spectra of H, inelastic neutron scatt. study 80−107391

lattice dynamics of metallic crystals continued
Ni angular forces and normal vibration 79−73270
Ni cryst., US wave attenuation, phonon viscosity and dislocation drag coeffs. 80 and 298K 77−76491
Ni, Debye Waller factor by mol. dynamics simulation 77−80598
Ni, Debye-Waller factor temp. parameter 78−30725
Ni, dispersion curves from deLaunay angular force model 79−33054
Ni, lattice and force consts., pairwise atomic repulsions in cluster model 79−32939
Ni, phonon dispersion curves, θ-T curves 78−26642
Ni, phonon dispersion relations and Debye-Waller factor calcs. 78−51630
Ni:He, defect props., quantum-chemical and lattice-defect hybrid approach 79−4528
Os, atomic vibr. and fermion behaviour of HCP metals 80−6474
Pa, phonon density determ. and heat capacity *(Russian)* 77−24415
Pb, Debye-Waller factor, temp. variation calcs. 80−34162
Pb, Debye-Waller factor temperature parameters, vibr. depend. 79−99288
Pb, melting, existence of before and after effects, neutron scatt. 77−84895
Pb, phonon dispersion and cryst. equilib. 78−75752
Pb, phonon dispersion curves, lattice dynamics unpaired forces 79−42170
Pb, phonon dispersion relations and lattice heat capacity, modified Bhatia model 77−20024
Pb, phonon dispersion spectra from 5-parameter lattice dynamical model 78−10136
Pb, phonon spectrum, calc. by phenomenological method 78−59890
Pb, relativistic model pseudopot., appl. to elec. resist. and phonon spectra calc. 78−51866
Pb, transverse acoustic phonons, freq. and damping, supercond. transition temp. effects 79−42687
Pb, two-parameter shell model of lattice vibrs. in monoatomic systems 78−59877
Pd, Kohn anomalies and phonon dispersion, model including exchange-correl. corrections 78−59886
Pd, non-central forces and normal modes 79−99278
Pd, phonon dispersion, simplified Frielek model 78−79683
Pd, phonon dispersion curves, freq. spectrum, specific heat calc. 77−15516
Pd, phonon dispersion curves, θ-T curves 78−26642
Pd, phonon dispersion curves in highest-symmetric directions 79−51219
Pd, phonon dispersion using non-central force model 78−91392
Pd, ultrafine particles, size effect on vibr. sp. ht. 78−10153
Pd, vibrational spectrum modification relation with 55K heat capacity anomaly of PdH_x 77−51516
Pd-H, optical phonons in supercond. 77−63021
Pd-H system, local frequency spectrum, mean thermal displacement of H 80−59604
Pd-Pt, resonant modes, rel. to CPA predictions 78−75757
$Pd_{0.96}Ag_{0.04}$, phonon dispersion curves at 296K 80−24546
$Pd_{0.9}Rh_{0.1}$, lattice dynamics, inelastic neutron scatt. meas. at 296K 80−29135
Pd_xSn_y (x=0.95, y=0.05; x=3, y=1), Mossbauer spectra, high press. effects, force consts. 80−84669
Pr $H_{2.8}$, optical vibr. spectra of H, inelastic neutron scatt. study 80−107391
Pt (111) stepped surface, localised surface phonons obs. 78−95223
Pt, Debye-Waller factor temperature parameters, vibr. depend. 79−99288
Pt, EXAFS Debye-Waller factors 80−45168
Pt, generalised susceptibilities and phonon anomalies, band struct. calcs. 79−90953
Pt, lattice dynamics, ang. forces and normal vibrs. 78−22810
Pt, phonon density of states from thermodynamic functions *(Russian)* 79−35631
Pt, phonon dispersion, simplified Frielek model 78−79683
Pt, phonon dispersion, vibr. spectrum, sp. ht., modified ang. force model 77−69054
Pt, phonon dispersion curves calc. 77−20030
Pt, phonon dispersion curves, θ-T curves 78−26642
Pt, phonon dispersion spectra from 5-parameter lattice dynamical model 78−10136
Pt, phonon spectrum, Kohn anomaly 79−46766
Rb, BCC, Gruneisen parameter temp. var. 78−6137
Rb, elastic constants, cryst. equilib. and electronic contrib. 79−73243
Rb, ideal thermal resist. calc., anisotropic continuum dispersive model 77−51724
Rb, lattice dynamical props., conduction-core exchange, Lindgren approx. 79−1481
Rb, lattice vibr., modified tensor force model 79−86853
Rb, lattice vibrations, seven parameter non-central force model 80−44270
Rb, phonon freqs. and Gruneisen parameter, model pseudopotential calc. 77−35643
Rb, phonon spectral density, pseudopotential calcs. 80−39234
Re, atomic vibr. and fermion behaviour of HCP metals 80−6474
Re, lattice dynamics, third order elastic consts. and thermal expansion 77−76505
Ru, atomic vibr. and fermion behaviour of HCP metals 80−6474
Ru, Debye-Waller factor and Lindemann parameter, temp. depend., lattice dynamical model calcs. 80−59610
Ru, lattice dynamics, sp. ht., thermal expansion 79−82363
Ru, lattice dynamics, thermal expansion and bulk modulus 77−59079
Sb, optical phonon anharmonicity and melting, light scatt. study 80−60621
Sc, Debye-Waller factor and Lindemann parameter, temp. depend., lattice dynamical model calcs. 80−59610
Sc, dielec. screening and lattice dynamics 77−35646
Sc, HCP, lattice heat capacity, third order elastic consts., thermal expansion 79−82352
Sc, Kohn anomalies and phonon dispersion, model including exchange-correl. corrections 78−59886
Sc, lattice dynamics, sp.ht. and bulk modulus 78−71814
Sc, phonon dispersion, phenomenological model 79−7660
Sn, diamond type crystal, lattice dynamics from Keating's valence force field 78−79687
Sn, Grey, lattice dynamics 77−84865
Sn, harmonic and cubic Einstein force consts. calc. 77−47515

lattice dynamics of metallic crystals continued
α-Sn, lattice dynamical calc. using extended Born-von Karman scheme 78−59889
α-Sn, lattice dynamics 80−107389
Sn, white, anharmonicity in X-ray diffraction intensities 78−71626
Sn, white, lattice vibrations anharmonicity, X-ray meas. 78−51624
Sn, X-ray diffraction study of thermal motion of atoms in β-Sn 80−39243
α-Sn:^{119m}Sn, impurity lattice dynamics, Mossbauer spectra, Debye temp. 80−84262
Sr, lattice dynamics, phenomenological model 80−44265
Ta, internal equilibrium, cryst. dynamics, lattice dynamical theory of BCC metals 78−79688
Ta, lattice vibrations, Debye temp., freq. wave vector dispersion relations 78−63818
Ta, phonon density of state determ. from thermodynamic crystal functions *(Russian)* 79−82291
Ta, phonon dispersion curves compared with Ta-H and Ta-D 77−76504
Ta-H system, local frequency spectrum, mean thermal displacement of H 80−59604
Ta-H(D), phonon freqs. and dispersion curves 77−76504
Tb, phonon freqs., calc. 80−15206
Tb, phonon spectrum, obs. of one phonon transitions by nucl. reson. fluoresc. 79−38416
Tb, sp. ht., using lattice dynamical model for HCP metals 79−51273
Tb, three-body forces in math. model for phonon dispersion branches and expt. degeneracy 77−62593
Tb, unpaired forces in lattice dynamics of rare-earth HCP metals 77−7805
Th, crystal equilib., lattice dynamics 78−47479
Th, lattice dynamics, unpaired forces 80−15201
Th, lattice dynamics in reson. model pseudopot. theory 79−19334
Th, local model pseudopotential applic. 77−39646
Th phonon dispersion curves, angular force electron gas model 77−7801
Th, phonon dispersion relations and lattice heat capacity calc. 77−20023
Th, phonon dispersion relations and lattice heat capacity, modified Bhatia model 77−20024
Th, phonon dispersion relations, non-central electron fluid model 80−100312
Th, phonon dispersion spectra from 5-parameter lattice dynamical model 78−10136
Ti, HCP, lattice dynamics exam. by inelastic neutron scatt. 79−60447
Ti, high temperature thermophysical properties 78−91404
Ti, rel. to press. depend. of Mossbauer fraction for ^{57}Fe 77−16226
α-Ti, strain driven thermoelastic instability toward brittle fracture 80−103415
α-Ti, X-ray Debye charact. temp., powder specimens 77−84876
Tl, hexagonal lattice equilibrium, electron gas model with noncentral forces, lattice dynamics 78−95123
Tm, lattice dynamics, thermal expansion, spt. ht., mag. contrib. 79−37778
α-U, lattice dynamics 79−95101
α-U, superstruct. neutron scatt. obs. near 43K 79−95116
V, Debye-Waller exponent, 4.2 to 296K, incoherent elastic neutron scatt. 79−4382
V, Kohn anomalies and phonon dispersion, model including exchange-correl. corrections 78−59886
V, lattice defects, relax. studies, computer simulation 78−79604
V, lattice dynamics, phonon dispersion and atomic force constants, phenomenological model 78−26640
V, lattice dynamics, vibr. spectrum and sp. ht., CGW model 78−22793
V, lattice dynamics and cryst. equilib. 78−75753
V, modified Sharma-Joshi model 79−51221
V, phonon dispersion using non-central force model 78−91392
V, rel. to press. depend. of Mossbauer fraction for ^{57}Fe 77−16226
V-H system, local frequency spectrum, mean thermal displacement of H 80−59604
W, Debye-Waller exponents, modified ang. force model, and lattice vibrs. 77−76515
W, freq. spectra, sp. ht., Debye temp., Clark-Gazis-Wallis ang. force model 78−22799
W, lattice wave dispersion, lattice consts., elastic consts. 80−24545
W, model incorporating second neighbour shell-shell interactions 77−59082
W, Mossbauer recoilless fractions, temp. depend., Born-von Karman model of lattice vibrs. 78−15076
W, phonon density of states determ. from heat capacity *(Russian)* 80−29131
W, phonon dispersion, Debye temp. and Debye-Waller factors, lattice dynamical model 78−55920
W, single cryst., proton integral dechannelling functions *(Russian)* 78−10111
W, surface phonon spectra 78−71934
Y, dielec. screening and lattice dynamics 77−35646
Zn, anharmonic lattice vibr., 'forbidden' X-ray reflections obs., 300K 78−34586
Zn, anharmonicity of lattice vibrs., elastic neutron scatt. 77−51454
Zn, anisotropic thermal expansion 79−23750
Zn, atomic vibr. and fermion behaviour of HCP metals 80−6474
Zn, field gradients, temp. depend., electronic and lattice contribs., ab initio study 79−42501
Zn, hexagonal lattice equilib., electron gas model with noncentral forces, lattice dynamics 78−95123
Zn, mean square displacement of atoms in cryst. lattice, rel. to sp. ht. *(German)* 80−79902
Zn, noncubic crystal, temp. depend. of elec. field gradient, effect of thermal vibr. of atoms 79−99515
Zn, optical phonon anharmonicity and melting, light scatt. study 80−60621
Zn, phonon density of states calc. from neutron diffr. data 77−24369
Zn, phonon density of states determ. from heat capacity *(Russian)* 80−29131
Zn, phonon dispersion 77−15513
Zn, Raman scatt., TO optical phonon, anharmonicity 77−15520
Zn, single cryst., mean square vibr. amplitudes X-ray diffr. 77−35640
Zn single crystals, antisymmetric atomic vibrs. from elastic neutron scattering data 79−33046
Zr, BCC, lattice dynamics, 1400K, phase transform. 79−19337
Zr, BCC, phonon dispersion relations, d-electron contrib. to Cauchy discrepancy 80−92628
Zr, BCC, phonon vibrs., pseudopot. method 80−15204

lattice dynamics of metallic crystals continued
Zr, HCP, normal vibr. modes, temp. depend. 79−19339
Zr, HCP, temp. depend. of C-axis phonon dispersion curves 78−59884
Zr, high temperature thermophysical properties 78−91404
Zr, phonon density of states, scatt. law in thermal neutron field 77−72663
β-Zr, phonon dispersion, modified Sharma-Joshi model 80−100311
$ZrFe_2$, lattice dynamics, Mossbauer spectra 80−19888

lattice dynamics of molecular crystals
1,4-dithiane-1-oxide, cryst., IR and Raman spectra 79−69839
2-chloronaphthalene, vibr. and calorimetric investigation of polymorphism 78−87641
2-fluoronaphthalene, vibr. and calorimetric investigation of polymorphism 78−87641
acetic acid-d_0(-d_1), Fermi reson., IR spectra band profiles 80−60569
adamantane, plastic cryst. lattice vibr. study of phase transition 80−7355
adamantane, plastic phase, librations, phonon branches, neutron scatt. study *(French)* 79−51222
ammonium hydrogen oxalate hemihydrate, X-ray TDS effects on at. parameters and electron density distribs. 77−19819
ammonium oxalate monohydrate, IR refl. and Raman spectra, internal and external modes *(French)* 77−36231
aniline-HBr, ferroelasticity, orthorhombic to monoclinic phase transition, X-ray scatt. 80−39276
anthracene, excitation and propagation of phonons, luminesc. meas. *(Russian)* 78−35202
anthracene, IR spectra, strong anharmonicity effects *(Russian)* 77−66511
anthracene, metastable triclinic phase 80−59452
anthracene, molecular crystal, exciton-phonon coupling, absoprt. band profile in first singlet system 78−83888
anthracene, monocryst., additional absorpt. spectrum at low temp. 78−92096
anthracene, orientationally disordered cryst., lattice relax. effect 80−107278
anthracene, polariton effects in transmission and absorpt. spectra in thin crysts. 77−20886
anthracene, temp. depend. of mol. motion in lattice 79−33045
anthracene, vibr. amplitude of mol. in condensed phase, five-parameter approx. 79−82295
anthracene crystal, dynamical matrix eigenvectors from Raman scatt. 80−100315
anthracene crystal film, nonequilibrium phonon distribution, at low temp. *(Russian)* 77−47520
anthracene mol. cryst., exciton-lattice interaction and exciton absorption line shape 78−18968
anthracene plate, ballistic propagation of phonons *(Russian)* 78−34582
anthracene-phenanthrene-tetracyanobenzene, CT-cryst., mini-excitons and lattice dynamics, ESR, optical and Raman spectra 80−60406
anthracene-pyrometallitic dianhydride cryst., refl. and absorpt. spectra of singlet charge transfer excitons 80−71442
atom-atom and multipole-multipole potentials, theory 78−43077
benzamide, single cryst., far i.r. absorpt. spectrum *(French)* 77−4637
benzene, Brillouin scatt., cryst. at 0°C, elastic consts. 78−43882
benzene, cryst., vibronic spectra using 2-photon fluoresc. excitation 79−47493
benzene, IR and Raman intensity of lattice vibrs., theory 80−11381
benzene, IR spectra, vibr. exciton cluster states, percolation and pairwise interactions 78−43844
benzene, mol. cryst., quadrupole contribs. to lattice vibr. freqs. 79−82290
benzene, mol. cryst. $S_0 \rightleftharpoons S_1$ transition, non-Born-Oppenheimer phonon coupling 77−15523
benzene, Raman and IR spectra at high press. 78−35127
benzene phenol crystal, asymmetry of phonon side bands, absorption, luminesc. and specular spectra 77−1730
benzene-d_6:benzene-d_0, phonon side bands of specular optical transitions 78−26649
benzened_0:phenol, phonon side bands of specular optical transitions 78−26649
benzoic acid, dimer, cryst., IR and Raman spectra, vibr. assignments 78−31191
1,12-benzoperylene in n-alkane, zero-phonon lines in luminesc. spectra 78−56512
2-benzoyl-1,3,4-triphenyl-1-cyclopentanol, cryst., thermal vibr. of mols., rigid body anal. 78−38787
1, 12-benzperylene, in alkane matrices, zero-phonon lines, press. shifts *(Russian)* 78−76502
bicyclo[2.2.2]octane, thermal expansion coeff., Gruneisen parameter 77−76581
biphenyl, incoherent inelastic neutron scatt. time of flight spectra, vibr. spectra model calc. 78−63816
biphenyl, incommensurable phases, obs. of excitations, inelastic neutron scatt. 80−49334
biphenyl cryst., nonbonded atom-atom interact. model, low freq. vibr. modes 77−1188
bromobenzenes, intermol. forces in cryst. 77−76349
bromocyanoacetylene, cryst., IR, far-IR and Raman spectra, vibr., struct. 77−63407
carbon tetrabromide, Brillouin scatt., plastic-liquid transition 77−32389
carbon tetrabromide, solid, Raman spectrum, temp. depend. 78−52488
carbon tetrachloride, solid, phase transition, Raman study 78−80345
chloranil, neutron superlattice reflection, soft phonon and central peak scatt., phase transition 78−18732
p- chloraniline cryst., lattice vibr., IR and Raman spectra, lattice energy 78−56481
p-chlorobromobenzene, single cryst., polarised Raman and IR spectra, assignments 78−60431
chlorocyanoacetylene, cryst., IR, far-IR and Raman spectra, vibr., struct. 77−63407
chloromethane, and −d_3, cryst., IR and Raman spectra of lattice vibrs. 79−95741
m-chloronitrobenzene, cryst., low freq. vibrs., polarised Raman and IR spectra study *(French)* 80−16029
m-chloronitrobenzene, molecular crystals, translational and orientational vibr. determ. 80−55103
collective mode, computer simulation 80−54325
complex structure, continuous and discrete models 78−51625
condensed H-containing media, cold neutron total section data interpretation 80−33857

lattice dynamics of molecular crystals continued
coronene, in alkane matrices, zero-phonon lines, press. shifts *(Russian)* 78−76502
coronene, mol. vibr. amplitude of condensed phase, five-parameter approx. 79−82295
crystal, molecular lattice vibr. IR intensities, mol. polarisability calc. 80−11372
crystallography, electron densities, thermal smearing, limited resolution effects 78−71635
crystallography, X-ray neutron, charge deformation, vibr. smearing 78−71634
cyanoacetylene, and-d_1, cryst., IR, far-IR and Raman spectra, vibr., struct. 77−63407
1,1-cyclobutane dicarboxylic acids and K salts, IR and Raman vibr. spectra *(French)* 80−2758
cyclohexane, rotational reorientation anisotropy near phase transition *(Russian)* 79−4261
cyclohexane, solid, neutron scatt. spectra using inverted geometry, white beam, t. of f. spectrometer 78−34395
cyclohexane, solid, Raman spectra near 186K phase transition 78−56480
cyclopentane, solid, neutron scatt. spectra using inverted geometry, white beam, t. of f. spectrometer 78−34395
cyclopropane, lattice vibrs., IR and Raman spectra, 4 to 78K 78−27209
cytidine, cryst. powder, absorption spectrum, unusual narrow line FIR modes, cryogenic temps. 79−69824
depolarised Rayleigh-Brillouin spectra, theory 79−69850
deuteronaphthalene:β-deuteromethylnaphthalene crystal, asymmetry of phonon side bands, absorption, luminesc. and specular spectra 77−1730
diamantane, Raman study of three solid-state phase transition 79−51946
dibenzoyl, X-ray TDS effects on at. parameters and electron density distrib. 77−19819
1,4-dibromonaphthalene, S_0 to T_1 exciton transition, optical dephasing time and lineshape function 78−15183
1,12-dicarbaclosododecaborane, plastic solid, phase transitions, 10-320K, Raman and IR obs. 79−28744
p-dichlorobenzene, lattice dynamics, thermodynamic functions and phase transitions 78−67777
4,4′-dichlorobenzophenone, phase changes, Raman spectra *(French)* 80−2756
dielectric singularity, causing Kohn anomaly and soft modes 79−60470
1,1′-diethyl-2,2′-cyanine iodide, neat and mixed crysts., visible absorption and emission spectra assignments 77−1692
diethylammonium manganese tetrachloride, IR active modes, interlayer and intralayer forces 77−59575
1,5-difluoronaphthalene, IR and Raman study of crystal dynamics 78−80346
p-dihalobenzene, mixed cryst., Raman spectra, phonons and vibr. excitons, criteria for solid solns. 78−43840
p-dihalobenzene alloys, successive perturbation of phonon bands 77−35653
p-dihalobenzene series, cryst., chem. perturbation and lattice instability, X-ray and Raman scatt. 77−39654
1,4-dihalonaphthalenes, binary solid solns. lattice stability, mol. motions 78−31182
p-diiodobenzene, far IR single cryst. transmission spectrum, temp. and polaris. depends., assignments 78−72498
dimethyl tin difluoride, solid, methyl group motion, neutron scatt. study 80−10607
dimethylammonium manganese tetrachloride, IR active modes, interlayer and intralayer forces 77−59575
dimethylammonium manganese tetrachloride, phonon density of states, expt. and calc. 80−54323
4,4′-dinitrobiphenyl complexes, intermol. interacts. and geometry of non-rigid mols., vibr. spectra 78−88294
2,2-dinitropropane-d_0(-d_6), phase polymorphism, vibrational assignments, IR and Raman study 80−16031
dioxane-$HgCl_2$ complexes, IR and Raman vibr. spectra, inter- and intramol. forces 77−66489
dipolar coupling and phonon symm. *(Chinese)* 80−103437
dipole-dipole interaction rel. to internal vibr. 78−47476
DNA pyrimidines, cryst. coherent inelastic neutron scattering 78−75766
dynamic multipole interactions, lattice energy and vibr. 77−35645
dynamics of translations and rotations 79−51215
ethylene, ab initio interaction pot. 79−33043
ethylene, solid, self-consistent phonon calcs. 78−75745
ethylene crystal, partially deuterated, Raman phonon spectra 78−56470
exciton-phonon interactions, strong and weak coupling 78−51899
exciton-phonon interactions and exciton drops 79−56131
exciton-photon coupling, Hamiltonian for displaced modes 77−15507
fluorobenzene, cryst., absorpt. spectrum, vibronic states 77−59588
fluorobenzene, lattice vibs. *(French)* 77−32366
fluorobenzene crystal, localised excitons 77−31963
formic acid, lattice dynamics model to explain neutron scatt. data 79−86856
formic acid, lattice vibr., pot.-function calcs., comp. to neutron scatt. data 79−42168
formic acid, normal and deuterated, dynamic modes, neutron inelastic scatt. study 79−51214
FTF-TCNQ, libron freqs., temp. and press. effect 79−86860
furane, crystalline, lattice vibr. 78−79694
furane, lattice dynamics calc. for low-temp. phase 77−55329
group theoretical anal. by computer 77−80590
halogens, bond charge model 78−79692
halogens, crystallised, acoustic wave velocity calc. from phonon curves *(French)* 77−1180
hexachlorobenzene, Raman intensities, polarised scatt. from lattice rot. modes. 78−43845
hexamethyl benzene, high press., variable temp. Raman spectra 78−56488
high spin/low spin transition, model including lattice dynamics 77−63202
hydrocarbon crystal structure calc. by molecular packing analysis 78−14303
hydrocarbons, Coulombic nonbonded interatomic pot. functions from vibr. freqs. 77−80587
ice, H_2O:D_2O, I_c phase cryst., IR spectra, H exchange activation energy 79−99866
intermolecular interactions, correlation with absolute Raman intensities of lattice modes 77−66502
iodocyanoacetylene, cryst., IR, far-IR and Raman spectra, vibr., struct. 77−63407

lattice dynamics of molecular crystals continued
IR inteisities of mol. crystal lattice vibrs., dynamic multipoles model 80−11372
IR intensity of lattice modes 77−47516
IR spectral line shape and polarisation temp. depend. 80−88991
laser excitation of stationary molecular states, coupling of real eigenstates to phonons and photons 77−68084
librational dynamics 77−7831
libron frequencies, temp. and press. effect 79−86860
linear diatomic rigid mol. chain, mol. dynamics, rot. phase transformation, struct. factors 78−26635
lithium formate, Fermi reson. of optical phonons with two particle state zone, interference effects *(Russian)* 77−90149
localisation in ionized and excited states, conf. 77−30750
methane, solid, far IR spectra, and lattice vibr., 4.2K, 0.4-4.5 kbar 79−19868
methane, solid phase II Raman spectrum, lattice vibr. and ν bands 78−19456
methane-d_4, solid phases I, II, acoustic phonon dispersion curve meas. by neutron inelastic scatt. 78−2212
methyl halides, Raman spectra and lattice motions 77−77197
N-methylacetamide, and isotopic forms, low-freq. Raman spectra, internal torsional mode 79−26992
molecular complex, intermol. vibrs., giant mol. and sublattice limits 77−66004
molecular crystal with impurities, nonequilib. phonon excitation by laser pumping *(Russian)* 79−38664
molecular crystals, exciton-lattice interaction and exciton absorption line shape 78−18968
molecular crystals, low freq. Raman spectra, defects and lattice vibr. 78−31194
molecular crystals, Raman scatt. from external orientation vibrations 79−95776
molecular crystals, spectroscopy, bibliography for 1976 78−72585
molecular mixed crystals, electronic transition props., Redfield theory 79−46008
molecular solid, intermolecular interactions, laser induced phonon probe 80−79891
molecular solids, intermol. forces and eqn. of state, pseudoharmonic approx. calcs. 78−30731
molecules, condensed, vibr. excitation in photoemission spectra, appl. to CO 77−28689
myoglobin, atomic vibr. mean square displacement, Rayleign scatt. of Mossbauer radiation meas. *(Russian)* 80−100665
naphthalene:$\beta\beta'$-dinaphthylethylene, stimulated emission, phonons role 77−8606
naphthalene:$\beta\beta'$-dinaphthylethylene, stimulated emission suppression in phonon wing 78−2881
naphthalene:octafluoronaphthalene, cryst., interactions, Raman spectra 77−43982
naphthalene, cryst., low freq. Raman spectra, defects and lattice vibr., 80-320K 78−31194
naphthalene, doped, role of nonequilibrium phonons in stimulated radiation emission 80−103971
naphthalene, in durene and perdeutero-naphthalene mixed crystals, photon-echo decay 78−42388
naphthalene, inelastic neutron scattering 78−79690
naphthalene, mol. cryst., quadrupole contribs. to lattice vibr. freqs. 79−82290
naphthalene, multiphonon i.r. absorption 77−1686
naphthalene, phonon eigenvectors, neutron scatt. intensities determ. 80−44271
naphthalene, Raman intensities, polarised scatt. from lattice rot. modes. 78−43845
naphthalene, surface dynamics, calc. 80−92772
naphthalene, temp. depend. of mol. motion in lattice 79−33045
naphthalene, thermal diffuse scattering, errors in X-ray diffr. intensities and atomic parameters 79−73155
naphthalene, vibr. amplitude of mol. in condensed phase, five-parameter approx. 79−82295
naphthalene crystal, dynamical matrix eigenvectors from Raman scatt. 80−100315
naphthalene crystal, external phonon modes, inelastic incoherent neutron scatt. spectra and computer calc. 78−34577
naphthalene-d_8:β-methylnaphthalene -d_{10}, phonon side bands of specular optical transitions 78−26649
naphthalene-d_8, cryst., phonon dispersion curves calcs., low temp. 80−96599
naphthalene-d_8, phonon dispersion meas. and calc. 78−2211
naphthalene-d, press. depend. of lattice freqs. at 100K 79−46768
naphthalene-octafluoronaphthalene complex, Raman spectrum, intermol. vibrs. 77−66004
naphthalene-$SbCl_3$ system, phonon bands in π-electron charge transfer complex 77−39644
naphthalene-tetracyanobenzene, doped cryst., EPR of triplet state for mol. reorientation 79−38368
α-naphthol, ν(O-H) k=0 phonon band, width and splitting 77−52066
neutron scattering obs., book contrib. 77−89505
neutron spectroscopy determination, review 79−42166
p-nitrotoluene, low-freq. vibr. spectrum, Raman and IR spectra 78−56484
nonlinear interaction with light beam 78−30034
nonpolar molecular crystal phonon sidebands, Green's function mol. model 79−37779
octafluoronaphthalene, struct. phase transition exam. 77−47572
octafluoronaphthalene crystals, phase transition, Raman spectra 77−24829
one-dimensional conductor, lattice stability, phonon dispersion, Kohn anomaly 80−96603
one-dimensional systems, electronic collective excitons, EPR response 77−31960
one-dimensional systems electronic collective excitations 77−31959
organic crystal, US absorption, rel to lattice vibrs. 77−24358
organic molecular crystals, use of atom-atom pots. in interpreting behaviour, book contrib. 80−84136
organic solids, Raman phonon spectra, mol. motions 79−73921
organic solids, vibr. relax. and dephasing Raman spectra, review 80−88987
orientationally disordered cryst., translation-rot. dynamics, soft modes 78−83906
ortho-para mixtures, vibr. coherence decay 80−78903

lattice dynamics of molecular crystals continued
oxanilide, IR and Raman spectra, cryst. struct. and vibr. 79−42954
paradichlorobenzene, NQR study of the lattice dynamics *(Russian)* 80−97160
n-paraffin, rotator phase transformation, lattice dynamics Helmholtz free energy 78−34585
pentacene, in p-terphenyl mixed cryst., low temp. optical phase relax. obs., mechanism 77−52112
pentacene doped p-terphenyl mol. cryst., laser induced photoacoustic grating effects 79−55215
pentacene in p-terphenyl, intermolecular interactions, laser induced phonon probe 80−79891
perturbation theory for strong interaction, appl. to molecular crystals *(Russian)* 77−15528
perylene, intermolecular interactions, laser induced phonon probe 80−79891
perylene in n-alkane, zero-phonon lines in luminesc. spectra 78−56512
phenanthrene, IR and Raman spectra, lattice and internal mode coupling 77−20843
phenol, cryst., mol. vibrs., factor group splittings 80−16021
phonon echo in travelling and standing wave regimes 77−8521
phonon spectrum under Fermi reson. 78−34583
poly(4-methyl pentene-1), US props., glass transition, Gruneisen parameters 80−54316
polyethylene, FIR absorpt. freqs. using proved semiempirical pot. function 77−52090
polyethylene, intermolecular force field and normal vibrs. 79−73265
polyethylene, orthorhombic and triclinic lattices, eqns. of state 79−28069
polyethylene (orthorhombic), intermol. pot. functions, force consts., vibr. assignments, thermodynamic props. 77−39639
polymers and molecular crysts., vibronic spectra exam. 78−67778
polyperdeuteroethylene, IR and Raman spectra, 77K and room temp., vibr. anal. 78−72517
potassium acid phthalate, Raman spectra and lattice vibr., 77, 300K 78−27219
potassium hydrogen oxalate, oriented single cryst., Raman spectra with very strong H-bonding 80−25359
1,3-propylenediammonium manganese tetrachloride, vibr. study of phase transitions, IR and Raman spectra 80−40103
purine, single cryst., Raman spectra and lattice vibr. 77−66498
β-quinol, low frequency mode investig. by IR absorpt. and neutron scatt. *(French)* 77−36220
Raman and IR obs., review 78−43079
Raman intensities of lattice vibrations, point-dipole rigid-mol. approx. 78−43845
Raman scattering, effect of inter- or intramol. energy exchange on vibr. dephasing times 77−66506
Raman scattering by external vibrs. 77−85711
Raman scattering on nondipole vibrations 79−95751
Raman spectra, low frequency polarised, of complex mol. cryst. 78−84574
Raman spectra line polarisations, impurity mol. orientational tunnelling effect 77−77208
reorientation barriers of molecules, determ. from data on LF spectra of lattice vibrs. 77−69824
rigid molecule approx., considering only intermol. interactions 77−55328
rigid molecule approx. 77−27951
rigid molecules, invariance and stability conditions, in lattice dynamical model calcs. 79−28051
rigid molecules, with large librations, dynamic density and struct. factors 79−7515
saccharose, far IR absorption, low temp. pyroelectricity 78−80348
salicylic acid, Raman active external modes *(French)* 78−23458
self-term force consts. 80−15199
shell model for crystal with mols. having fixed multipole moments 77−76495
sodium formate(-d_1), far IR and IR absorpt. spectra, lattice mode assignment 77−85717
sodium hydrogen oxalate monohydrate, oriented single cryst., Raman spectra with very strong H-bonding 80−25359
spin-lattice relax. of mol. crystals 79−15337
squaric acid, struct. transition, US vel. meas. 78−79770
stability constraints on potential function and rotational invariance in external mode formalism 80−24543
sym-trioxane, phase transition, polarised Raman spectra obs. 80−84742
symmetrised valence and relative motion coords., force consts. 80−84134
TBBA, phonon dispersion curves in cryst. and smectic phases 79−86863
TBBA, smectic liq. cryst., crystalline at liq.-cryst. phases phonon modes, coherent neutron inelastic scatt. study *(French)* 79−51216
TBBA, smectic liq. cryst., polarised Raman spectra, 90-300K, 0-400 cm^{-1} 77−12383
TCNE, cryst. forms, '6-exp' pot. function 79−28055
TCNQ, lattice vibrs., temp. depend., NQR obs. 79−38402
TCNQ salts, conducting, Raman spectra, estimation of degree of charge transfer from vibrational frequencies 80−50344
tellurophene(-d_4), cryst., struct., phonon spectrum, exciton splittings, assignments 77−81088
p-terphenyl:pentacene, optical coherence and resonance decay 77−24859
p-terphenyl, far IR absorption spectra, 300-1.3K, phase transition obs. *(French)* 77−90140
p-terphenyl, Raman scatt., order-disorder phase transition 78−43841
tetraalkylammonium tetrahalometalates, opt. lifetimes rel. to thermal transitions 77−28608
1,2,4,5-tetrabromobenzene, lattice vibrs., Raman and far IR spectra 78−76444
1,2,4,5-tetrabromobenzene, structural phase transition, Raman and IR spectra meas. *(French)* 77−66503
tetrabromomethane, isotopic splitting in totally symm. stretching vibrations, Raman spectra 79−42967
tetracene, in p-terpheny. mixed cryst., low temp. optical phase relax. obs., mechanism 77−52112
α1,2,4,5-tetrachlorobenzene, cryst. struct. and lattice vib. freqs. 77−19939
1,2,4,5-tetrachlorobenzene, lattice dynamics, thermodynamic functions and phase transitions 78−67777
sym-tetrachlorobenzene, LF Raman bands and space symmetries 77−66504
1,2,4,5-tetrachlorobenzene, mol. solid, heat pulses, phonon-induced delocalisation of trapped excited triplet states 80−89053
1,2,4,5-tetrachlorobenzene, structural phase transition, Raman and IR spectra *(French)* 77−66503

lattice dynamics of molecular crystals continued
tetracyanobenzene-naphthalene, Raman spectra, phase transition and isotopic substitution 78−80364
tetradecane, with tetra-4-tert-butylphthalocyanine impurity mols., luminesc. 77−18965
tetramethyl germanium, methyl reorient., lattice vibrs., neutron scatt. obs. 79−51016
tetramethyl silicon, methyl reorient., lattice vibrs., neutron scatt. obs. 79−51016
tetramethyl tin, methyl reorient., lattice vibrs., neutron scatt. obs. 79−51016
tetrohydrofuran-$HgBr_2$ complexes, IR and Raman vibr. spectra, inter- and intramol. forces 77−66489
1,3,5,7-tetroxocane, vibr. spectra and intermol. forces 77−36216
thermal vibrations in molecular solids, amplitudes 78−38789
thermoelasticity anomalies and mol. reorientation 77−84676
thieno(3,2-b)thiophene, electronic and vibr. spectra, vapour phase and cryst. 77−34654
thiourea, order-disorder transitions, soft modes 78−80361
thiourea, polycryst., mol. dynamics under hydrostatic press., NMR study 80−80619
thiourea, soft mode and Debye relaxations 78−80347
toluene sulphonate diacetylene polymer, electronic and vibr. excitations, press. and temp. depend. 78−31188
transition metal hexafluorides, density of exciton states, two-particle and mixed cryst. spectra 78−2829
s-triazine, Raman spectrum, lattice vibrs. 78−19465
tribromobenzene, Raman spectra line intensities 79−65863
1,3,5-trichlorobenzene, lattice vibr., Raman spectra line intensities calc. 77−69825
1,2,3-trichlorobenzene, low freq. vibs. 77−32365
trimethylammonium chloride and deuterated forms, cryst., inelastic neutron scatt. H bond vibr. obs. 77−7796
S-trioxane, lattice vibrs. from Raman spectra 78−6672
1,3,5-trioxane, vibr. spectra and intermol. forces 77−36216
S-trithiane, lattice vibrs. from Raman spectra 78−6672
TTF-TCNQ, Kohn anomaly, electron-mol. vibr. coupling 77−31734
TTF-TCNQ, phonon anomalies and superstructures, Peierls transition, X-ray diffuse scatt. obs. 77−27962
TTF-TCNQ, phonon dispersion and Kohn anomaly, inelastic neutron scatt. 77−1196
TTF-TCNQ, temp. depend. of phonon frequencies at constant vol. 80−10616
TTF-TCNQ, three dimensional ordering 77−59087
two particle exciton-phonon interactions, optical absorpt. line shapes theory 80−55120
two-phonon resonances, bound states absorpt. coeff. 78−47486
two-phonon resonances, bound-states, general theory 78−47485
vibronic excitons, rigid lattice calcs. 77−31958
α-N_2, computer-simulation with atomic pair pot., plastic cryst., phonon dispersion 77−7679
As_4S_4, vibrational spectra, effect of temp. and press. on phonons 79−37776
$Bi_{12}GeO_{20}$, $Bi_{12}SiO_{20}$, IR reflection spectra studies of lattice vibrations 79−99879
Br_2, lattice dynamics using simple bond charge model 78−55919
CO_2-N_2O, mixed cryst., librational motion, Raman obs. 78−6661
CS_2, crystalline, far IR spectra 77−24834
CS_2, lattice dynamics of 0K cryst., phonons and lattice energy 79−73269
CS_2, second order Raman spectrum in condensed phase 80−93299
CS_2, solid, group theoretical anal. by computer 77−80590
CS_2, solid, tailoring of potentials 78−79679
Cl_2, lattice dynamics using simple bond charge model 78−55919
$Co(NH_3)_6X_3$, (X=Cl, Br, I), internal and lattice vibr. normal coordinate anal. 79−69203
p-D_2, far IR absorpt. in ordered state 79−91430
p-D_2, order-disorder phase transition 78−79726
D_2, Raman active optical phonon, density depend. 79−87432
D_2, solid, HCP, effect of internal strains on elastic consts. 77−24343
p-D_2, solid, orientationally ordered state, anomalous far IR absorption spectrum 78−10876
D_2, solid, phonons in linear chain with hard-core pot. 77−11644
D_2O_2, lattice dynamics, neutron scatt. study 79−42176
D_2O_2, lattice phonons by neutron scatt., covalent force model 78−67782
GaSe(S), layer dynamics of high-symmetry crystals with atom-atom interactions 78−71799
GeF_4, Raman spectra at 77K, scatt. angle, polaritons and space group 78−23439
p-H_2, FCC, equation of state and lattice dynamics, temp. depend. 77−76521
O-H_2, far IR absorpt. in ordered state 79−91430
H_2, mol. solid, atomic H impurities, dynamic local field approx. 79−69316
o-H_2, order-disorder phase transition 78−79726
H_2, ortho-para mixtures, 10 to 23K, rot. Raman spectra, quantum calcs. 77−6700
H_2, Raman active optical phonon, density depend. 79−87432
H_2, solid, HCP, effects of internal strains on elastic consts. 77−24343
H_2, solid, inelastic neutron scatt., theoretical analysis 78−34569
H_2, solid, neutron scattering expts. 78−79693
H_2, solid, Raman active phonons, freq. depend. on ortho-para conc. and temp. 79−73918
H_2, solid renormalised pair interactions and three-body polarisation forces 77−31732
HCN, solid state phase transition, hydrogen bond distance, stretching freq. calc. 78−10183
HF(Cl)(Br)(I), ferroelec. and paraelec. phases, elec. multipole interactions 77−59522
$Hg(CN)_2$, phonon freq. anomalous press. depend., mol. struct. distortion 80−88981
I_2, lattice dynamics, bond charge model 77−84858
I_2, lattice dynamics, internal and external modes 78−18719
K, solid, dynamical structure factor S(Q, ω), molecular dynamics simulation 77−7806
$KBr_{1-x}(CN)_x$, mixed mol. cryst., coupled rot. and translational modes 80−84267
KCN, inelastic neutron scatt. by coupled rot. and translational modes 80−79895
KCN, lattice dynamics in disordered cubic phase 78−38794
KCN, phonon freq. distrib., cubic and monoclinic phases 78−22800

lattice dynamics of molecular crystals continued
$(KCN)_{0.5}(KBr)_{0.5}$, lattice dynamics neutron scatt. obs., glass phase formation 80−15207
$(KCN)_x(KBr)_{1-x}$, Brillouin scatt. of elastic anomaly 79−28779
K_2MnF_4, IR active modes, interlayer and intralayer forces 77−59575
MnF_6^{2-}, $A_2^{I}M^{IV}F_6$ hosts, luminesc., IR and Raman spectra, 5K, assignments 77−20904
MoF_6, cryst., overall vibr. band struct., excitons 77−90136
MoF_6 crysts., density of exciton states, two-particle and mixed cryst. spectra 78−2829
MoF_6, orthorhombic crysts., Raman spectra, int./external mode separation and factor group anal. 77−90135
MoS_2, layer dynamics of high-symmetry crystals with atom-atom interactions 78−71799
MoS_2(2H), lattice dynamics, Coulomb and quasi-harmonic effects 80−39245
MoS_2(2H), Raman spectra, phonon modes, high press. effects 80−40111
α-N_2, anharmonic lattice vibrations calcs. 78−71812
N_2, cryst., screened nucl. pot. and lattice dynamics, pseudo-atom approx. 78−34575
α-N_2, crystal dynamics at 15K 77−24366
β-N_2, dynamical struct. factor S(Q,ω), digital simulation 77−76502
α-N_2 simulation of dynamical props. of molecular solids 78−30710
N_2, solid, α- and γ-forms, Raman spectra, vibron and lattice freq. shifts, libration 80−16020
N_2, solid, gamma-phase, anharmonic lattice vibr. 79−33705
N_2, solid, group theoretical anal. by computer 77−80590
N_2, solid, lattice dynamical calcs., use of anisotropic at.-at. pot. functions, α-γ transition 78−71811
N_2, solid, Raman spectra vibron and lattice freq. shifts, librational force consts., α- and γ-phases 78−19460
N_2, solid, semimicroscopic approach 78−75765
N_2:N, dynamically induced electronic transitions of matrix isolated atom 78−63825
N_2-CO mixed cryst., librational motion, Raman obs. 78−6661
N_2-N_2 anisotropic interaction pot. model, comparison with solid state data 77−34712
ND_3, atom-atom and multipole-multipole pot. lattice dynamics calc. 79−1479
NH_3, assoc. mols., struct. and dynamics, atom-atom pots., gas, solid and liq., props. 80−23487
NH_3, atom-atom and multipole-multipole pot. lattice dynamics calc. 79−1479
NH_3, atom-atom model of intermol. forces 78−75751
NH_3, IR and Raman intensity of lattice vibrs., theory 80−11381
NH_3, phonon dispersion curves, phonon lifetimes, anharmonic effects 80−15202
NH_3, solid, group theoretical anal. by computer 77−80590
NH_3BF_3 and d_3, polycryst., for IR spectra, lattice vibrs., cryst. and mol. struct. interpret. 80−2771
NH_4Br and NH_4I, Raman scatt., 1 bar-7 kbar, 86-295 K 80−34909
NH_4Br, λ-type phase transition, Brillouin scattering 78−79725
NH_4Br, partially disordered, librational modes below disorder-order phase transition temp. 78−79680
NH_4I, $(NH_4)_{0.16}K_{0.84}I$ and $(NH_4)_{0.16}K_{0.84}Br$, reorientation motion of NH_4^+ 78−79542
NaCN, lattice dynamics in disordered cubic phase 78−38794
NbS_2.(pyridine)$_{1/2}$, intercalation complex, vibr. spectra 77−59076
γ-O_2, mol.-dynamic study of struct., dynamics 80−96467
O_2, solid, lattice dynamics 79−95095
β-O_2, thermodynamics of mol. libration motion *(Russian)* 80−70328
OCS, lattice dynamics and phonon sidebands of vibr. excitons calc. 77−20028
OCS, third order coupling coeffs. for two phonon absorpt. 80−10621
γ-$PH_{3-x}D_x$, Raman and IR spectra, phase transition, internal and external modes 77−77191
PbI_2, layer dynamics of high-symmetry crystals with atom-atom interactions 78−71799
$RbClO_3/RbBrO_3$ mixed crystals, internal optic modes obs., Raman and IR reflectance spectra 80−76024
Rb_2MnCl_4, IR active modes, interlayer and intralayer forces 77−59575
α-S, zone-centre lattice vibrs., including hydrostatic press. effects 80−49314
$(SN)_x$, IR transmission spectrum assignment 78−15160
S_4N_4, Raman scatt., press. and temp. depend., 0-10 kbar, 10-295K 78−15160
S_4N_4, vibrational spectra, effect of temp. and press. on phonons 79−37776
SiF_4, mol. cryst., coupled phonon modes and IR band shapes 78−26641
SiF_4, mol. cryst., giant anomaly of intensity of vibrs. of isotopic impurity, Raman spectrum 79−73276
SiF_4, Raman spectra at 77K, scatt. angle, polaritons and space group 78−23439
SnI_4, mol. solid, dynamics, press. and temp. depend. 78−79691
SnI_4, Raman spectra, temp. and press. meas. and lattice dynamical calcs. 78−56472
SnI_7 crysts., dynamical props. of ^{119}Sn by Mossbauer spectroscopy 77−59495
TaS_2.(pyridine)$_{1/2}$, intercalation complex, vib. spectra 77−59076
TeO_2, paratellurite, atomic motions corresponding to zone centre phonons 78−76461
Ti complex, $Ti_2Cl_8(CH_3NO_2)_2$, single cryst., struct., IR and Raman spectra, X-ray diffr. 78−43000
$(TiCl_4.POCl_3)_2$, solid, IR and Raman spectra, vibr. assignments 78−43868
UF_6, cryst., overall vibr. band struct., excitons 77−90136
UF_6 crysts., density of exciton states, two-particle and mixed cryst. spectra 78−2829
UF_6, orthorhombic crysts., Raman spectra, int./external mode separation and factor group anal. 77−90135
WF_6, cryst., overall vibr. band struct., excitons 77−90136
WF_6 crysts., density of exciton states, two-particle and mixed cryst. spectra 78−2829
WF_6, orthorhombic crysts., Raman spectra, int./external mode separation and factor group anal. 77−90135

lattice energy
see also binding energy
acetic acid, hypothetical dimer-based cryst. struct. calc. 77−19940
acetylene, Coulombic energy calcs. 79−99104
acetylene, electrostatic terms in lattice energy calcs. 79−51040

lattice energy continued
acetylene cryst., lattice energy, spheroidal multipolar expsn. for intermol. energy 79−14726
alkali feldspars, structure energies 80−6387
alkali halide, melting mechanism, vol. and enthalpy changes 79−55866
alkali halide lattice energies, empirical calcs. 77−58967
alkali halides, crystal binding, electronic delocalisation *(French)* 77−24286
alkali halides, photoelastic constants, effect of many body forces 78−47464
alkali halides, photoemission, energies and lineshapes 80−89119
alkali halides, repulsive hardness parameters, crystal-independent 80−64947
alkali halides, short range interactions, static polarisabilities 78−71702
alkali halides, softness parameter, additivity rule 80−1959
alkali hydrides, thermodynamic props. calc. using ionic pots. 78−10155
alkali metal cyanide, lattice energy calc. from hydration enthalpy 77−35506
alkali metal cyanides, lattice energies calcs. 77−47375
alkali metal halides, interionic repulsive short-range interaction pot., lattice energy calc. 80−96466
alkali metal nitrates, lattice energies and related thermodynamic props. 77−51344
alkali metal nitrates, standard heat of formation, electron affinity 78−91295
alkali metals, atomic properties, pseudopot. calcs. 77−89512
alkali metals, compressibility and binding energy, Shaw's optimised model pot. 78−26620
alkali-alkali dilute alloys, lattice relax., energy of mixing 77−84936
alkaline earth chalcogenides, interionic repulsive short-range interaction pot., lattice energy calc. 80−96466
alkaline earth chalcogenides, Madelung potential, ionic radii 78−2061
alkaline earth oxides, crystalline second-neighbours contrib. to repulsive energy 79−51044
n-alkanes, even, long-chain, layer interaction energies for different twin and polytypic positions 77−65985
alloy, AB type, equilib. props. by Markovian simulation 78−91302
alloy, nonlocality and energy of form. 79−20459
alloy, substitutional, low conc., volume change calc. using Morse pot. function 77−15342
alloy phase stability, computer calc. using modified pair potentials 78−35352
amino acid, cryst., mol. dielec. function 79−7043
ammonium Rochelle salt, thermodynamics of ferroelec. transition 80−84702
Anderson-Gruneisen function exam. 79−55855
anisotropic solids, cracks, interaction energies 77−80576
anthracene crysts., mol. orientational disorder calc. vacancies, dislocations, photodimerisation 77−4915
anthracene-acridine, order parameters and lattice energy, mean field approx. 78−22688
azide salts, univalent, lattice energy using direct minimisation eqns. 77−62501
BCC crystal, held by pair interactions, asymmetry props. 77−19970
benzene, Coulombic energy calcs. 79−99104
benzene, cryst., orthorhombic, lattice energy and cell dimensions, spheroidal approx. 79−51041
benzidine, cryst. struct. and lattice energy 79−37694
binary alloys, structural aspects of energy 77−39556
biphenyl, semi-empirical lattice energy calcs. 79−73126
β-brass, cryst. struct., elastic consts., central force model 78−51637
Bravias lattice, config. energy in many-particle approx. *(Russian)* 78−47271
carboxylic acids, crystals, empirical interatomic potential functions 79−7567
dl-carvoxim, order parameters and lattice energy, mean field approx. 78−22688
charge density functions, Bertaut series, convergence props. study 80−27104
p- chloraniline cryst., lattice vibr., IR and Raman spectra, lattice energy 78−56481
p-(N-chlorobenzylidene)-p-chloraniline, cryst., polymorphism, cryst. struct. rel. to mol. conform. 78−75611
clean surface, internal pot., interplanar spacing 77−89627
complex salts, lattice energy, repulsion component eqns., minimisation eqn. derivation 77−4065
conformational props. rel. to spatial electron density determs., computer simulations 78−70763
convergence acceleration method for lattice sums from electronic struct. of crystalline solids 78−30577
Coulomb crystal energy, analysis of tail of density series 78−91300
covalent semiconductors, charge density, struct. props. electron-electron interactions 78−47725
crystal potential and lattice sums on NaCl and CsCl structures 77−72578
crystal potential and summation of diverging series 77−76354
deformation potential of crysts. formulation *(Russian)* 77−19894
depolarization correction for Coulomb lattice sums 79−10829
diamond, lattice potential, high energy electron diffr. and refr. study 80−54165
1,5-dichloro anthracene, cryst. struct. calc., use of at.-at. pots. 79−46646
1,5-dichloroanthracene, photodimerisation, orientational defects, lattice energy 78−80724
p-dichlorobenzene, α, β and γ forms, cryst. struct. and pot. energy 78−38685
dilute binary alloys, formation energy, lattice relax. and zero-point vibrations 78−83771
dilute binary alloys, formation energy, lattice relax. and zero-point vibrations 78−87646
dipolar lattice, 2-D, Monte-Carlo calc., lattice energy 78−14308
disordered distributions of vacancies or altervalent ions, electrostatic energy 78−9995
electronic potential energy and X-ray scatt., relationship 79−28311
electrostatic energy, calc., convergence of Bertaut series 79−55693
electrostatic lattice potentials, calcs. 77−39557
element, melting, vol. change, simple model 79−55865
equilibrium form of crystal *(Japanese)* 80−24395
ethylene, dimer interaction, lattice energy, multipole expsn., at.-at. pots. 78−9218
fluorite crystals, Brillouin scatt. and high temp. disorder 78−80365

lattice energy continued
formic acid, cryst., electrostatic energy, multipole moments and point-charge lattice sums 77−76350
formic acid, lattice energy, non-empirical MO SCF calc. 79−37656
group IV semiconductors, diamond type, Madelung energies, stability of high-press. phase 77−1097
hard-sphere solid, disordered, lattice energy 79−23542
harmonic crystals, Helmholtz free energy, vacancy defects interactions calc. by cell cluster method 80−107443
HCP lattice, Ewald potential calc. 80−64948
hexahalometallate (IV) complexes, A_2MX_6, A=alkali metal or ammonium, M=lanthanide or actinide, X=F or Cl, lattice energies and thermochem. 79−60307
hydrocarbons, molecular packing anal. of alkyne structs., lattice energy minima 78−95011
ice, electron-irrad., cluster-ion prod., lattice and fragmentation energies 77−4911
ice, rel. to water struct. theory pot. energy function 79−73125
idolalkylamines, conformational varieties in cryst. 78−10030
II-VI semiconductors, electronic theory, cryst. energy and bulk modulus 78−72104
III-V semiconductor, electronic theory, cryst. energy and bulk modulus 78−72104
inert gas crystal, correlation forces *(Russian)* 78−22686
inert gas crystal, quantum mech. calc. of elastic forces *(Russian)* 77−39555
inert gas crystals, internal energy, Monte Carlo calcs. 77−72577
inert gas crystals, repulsive interaction energy, Born-Mayer parameters 78−26485
inorganic binary iono-covalent compounds, cryst., inorganic static effective charge calcs. *(French)* 80−2331
ionic crystal, from modified Kapustinskii-Yatsimirskii eqn. 78−34461
ionic crystal, modified Born-Mayer eqn. 79−65024
ionic crystal, repulsive short-range interaction pot., lattice energy calc. 80−96466
ionic crystal, simple electrostatic pot. determ. 79−65026
ionic crystal, stability of polar surface planes 77−39554
ionic crystal and liquid, trace element partitioning 78−47255
ionic crystals, calc. of electrostatic fields based upon Ewald method 77−80439
ionic crystals, electrostatic lattice energy, optimisation of convergence of Ewald series 79−7569
ionic crystals, radii of simple and complex spherical ions, repulsion energy of ionic crysts. 77−62503
ionic crystals, statistical theory density functional method, dispersion interaction energy calc. 80−15043
Ising model, randomly diluted, on honeycomb lattice, thermodynamic props. 80−54902
Laves phases C14, C15 and C36, electrostatic energy calcs. 77−1095
Madelung constants, first derivatives with respect to cell lengths, calc. 78−34459
Madelung energies of tetragonal and orthorhombic systems 77−1097
Madelung energy of one-dimens. charge array, infinite series evaluation, for teaching 79−25803
Madelung parameter, expansion in terms of multipole moments, ratio of two lattice parameters 78−75618
Madelung potentials, and sizes of ions in oxides and nitrides 79−99105
metal, asymptotic ion-pair pots., contrib. to lattice energy, elastic consts., phonon dispersion 77−19898
metal, Madelung energy, rel. to lattice dynamics model *(Hungarian)* 77−27952
metal, semistatistical calcs. 77−35879
metal, surface relaxation, lattice statics calc. 78−63925
metal, third order perturbation theory self consistency 78−76014
metal complexes, lattice energies calc. methods 80−107099
metal film, lattice sum for use in self-consistent warped muffin tin pots 77−15741
metal oxides, ESCA, Madelung pot. effects 80−104036
metallic compounds, cohesive props., augmented-spherical-wave calcs. 79−94952
metallic state, one dimens. model, stability *(Russian)* 77−85171
metals, cubic, ionic overlap interaction energy, press. and bulk modulus 80−29340
metals, electric properties calc., book 79−28274
metals, Hume-Rothery's class I, Engel-Brewer theory and related phys. props. 78−2059
methane, solid, orientational order of molecules in phase III 79−51042
mica, layer deformation and cryst. energy, struct. models for 1M and $2M_1$ polytypes 79−19184
minimisation, singularity-free, static 80−10525
minimisation procedures for calc., comparison and appl. 79−32944
molecular crystal, lattice energy, dynamic multipole interactions 77−35645
molecular crystal, spheroidal multipolar expsn. for intermol. energy 79−10824
molecular crystals, Coulombic energy calcs. 79−99104
naphthalene, Coulombic energy calcs. 79−99104
naphthalene-coumarin solid solution, struct. parameters and phase diagram 77−11532
naphthoquinone series charge transfer complexes, cryst. and electronic structs. 79−73474
noncubic structures, expansion of Madelung parameters as function of ratio of two lattice parameters 77−84693
one-dimensional system, two-body pot., min. pot. energy config. 78−30582
organic carbonyl compounds, empirical pot. model EPEN/2, development, parameter testing 79−54934
organic molecular crystals, use of atom-atom pots. in interpreting behaviour, book contrib. 80−84136
oxides of alkalis and alkaline earths, O two electron affinity from cohesive energies 78−25736
partly charged organic solids, mol. energies calcs. 79−55694
pentaphenyl group V compounds, $(C_6H_5)_5M.^1/_2C_6H_{12}$, M=P, As, Sb, cryst. packing 78−9994
pentaphenylantimony, Coulombic interactions in anomalous structure 77−24285
permanent multipole, induced dipole interaction energies and vectors, computer algorithm 79−7573
phyllosilicates, dioctahedral and trioctahedral, calc. of electrostatic energy relations 80−19743

lattice energy continued
point defect migration in crystals, anharmonic model description 77−65976
point-charge lattice, pot. field depend. on specimen shape, planewise summation method 77−47376
polar crystal with impurity atom, lattice energy change, optical vibrs. freq. shift 77−11652
polar lattice, free energy, dielectric constant, Monte Carlo results 77−4594
polyatomic ions, charge distributions, rel. with cohesive energies of ionic crystals 80−70161
polytypes, ABX_3, with close-packed AX_3 layers, electrostatic lattice energies 77−80440
potential, electronic microscopy, real and imaginary terms *(French)* 77−84697
pyrazine, dimer interaction, lattice energy, multipole expsn., at.-at. pots. 78−9218
pyrene, cryst. struct. calc., use of at.-at. pots. 79−46646
quadrupoles, axially symmetric, lattice sums, error bounds 77−30803
quantum solids, Boltzmann, energy, Kirkwood-Monroe approx. 79−33155
quasi-one-dimensional systems, charge distrib. and lattice distortion 78−6317
RbBr, structural phase transition, Born-model and effects of hydrostatic and non-hydrostatic stresses 79−23721
Rietveld neutron profile refinement, interactive computer system, POWDER 80−1900
salts, containing complex ions, lattice energy calcs., problems and solns. *(French)* 80−19746
semiconductor, diamond-like, adiabatic pot. in quasi mol. model 78−2063
solid solutions binary, order-disorder transitions, long range order parameter and chemical potential 80−6487
spinel structs., thermodynamic anal. of energy of cation octahedral sites 79−10827
spinel structure, Madelung calc. 77−89403
trans-stilbene, disorder and degree of misorientation 78−38683
stoichiometric and non-stoichiometric average crystals, Madelung consts. 78−18579
strong orthogonality, requirement in calcs. dealing with crysts. by geminal method 78−14307
TCNQ salt, HMTTF-TCNQ, Madelung energy, intermol. charge transfer, 1-dimens. disorder 79−7572
TCNQ salts, charge transfer and ionic bonding 77−39558
TCNQ salts, quasi-one-dimensional, Wigner cryst. model 78−47273
TCNQ salts, Wigner crystal model 79−42008
tetra-alkylammonium halide interionic potential models and far IR spectra 79−33689
tetra-alkylammonium halides, far IR spectra, interionic pot. energy 78−27217
tetrafluoromethane, intermolecular pot., lattice energy and heat of sublimation 80−38995
tetrahedrally coordinated solids, charge distrib., localised mol. orbitals 79−23560
thianthrene, heat of sublimation, cryst. lattice and polarisation energy 79−32941
Thomas-Fermi-Dirac method for atomic interaction energy calc. 77−66130
Thomas-Fermi-Dirac method for atomic interaction energy calc., comparison with expt. 77−66131
transition intermetallic cpds., CsCl struct., charge transfer and heat of form. 78−22689
transition metal, band theory 78−34757
transition metal chalcogenides, stability criterion between spinel- and defect NiAs-type structs. 77−84696
transition metal dihalides, crystal field stabilisation energies, lattice energies 80−38994
transition metal halides and oxides, cryst. field stabilisation and lattice energy 80−75201
transition metal hydrides, interstitial solid soln., H coordination 77−24289
transition metal oxides, cryst. electronic polarisabilities and ion sizes, Madelung pot. effects 78−63693
transition metal oxides, crystal field stabilisation energies, lattice energies 80−38994
transition metal oxides, dielec. behaviour 78−71703
transition metals, 4d, theory of energy bands, s and d contrib. to eqn. of state 78−30865
transition metals, cohesive properties, correlation effects 77−69262
transition metals, correl. effects, bulk modulus and equilib. lattice spacing 78−10115
transition metals, many-electron systems, self-interaction corrected approach, beyond local spin density approx. 80−92844
s-triazine, structural phase change, lattice energy calc. 78−55945
TTF, heat of sublimation, cryst. lattice and polarisation energy 79−32941
TTF-$Br_{0.79}$, charge transfer and ionic bonding 77−39558
TTF-TCNQ, 1:1 complex, atom-atom approx. and lattice energies 79−7568
TTF-TCNQ, Madelung energy, electronic struct. *(Russian)* 78−6253
TTF-TCNQ, segregated stack stability 78−55831
TTF-TCNQ crystal, antiferroelec. ordering of electronic polarisation, simple model anal. 78−92028
TTT_2I_3, charge transfer salt, Coulomb effects, Madelung energy calcs. 80−19747
TTT_2I_3, charge transfer salt, Coulomb effects 79−46599
Wigner crystal, electrostatic energy, Fuchs method 80−79744
Wigner crystal, two-dimensional, static and dynamic props. 77−43293
Wigner solid, electrostatic energy, Fuchs calc. 80−79743
Wigner solids and Coulomb lattices, Fuchs energy, theory 80−79745
Zachariasen's rules, Madelung constant, and network topology 79−27926
Ag, stability of FCC struct. collinear three-ion interaction 80−49173
AgCl(Br)(I), van der Waal dipole-dipole and dipole-quadrupole energies, Born and Slater-Kirkwood models 79−27947
Al, energy and elastic constants 80−59435
Al, stability and strength of FCC metal using Morse pot. 80−59430
α-Al_2O_3, charge distribution determ., SCF calc., Slater-type orbitals, Madelung type const. 80−107100
β-Al_2O_3, Madelung pot. determ. by Ewald method 80−92475
Al_2O_3-Cr_2O_3, crystalline soln., microstrain rel. to lattice energy and strain energy 77−24411
As, band structure and cryst. energy, pseudopot. calc. 79−90954
As, cryst. struct. calc., pseudopot. expansion method 77−27848
As, struct., pseudopotential method calcs., using untruncated pot. 78−18582
Au, stability of FCC struct. collinear three-ion interaction 80−49173
p-azotoluene-azulene, order parameters and lattice energy, mean field approx. 78−22688
$BaGaF_5$, X-ray cryst. struct. anal., lattice energy *(German)* 79−69094
$BaTiO_3$, reduction inhibition by impurity ions 80−101018
Bi film, evaporated, lattice distortion spectrum, elec. resistance temp. variation 80−54806
Bi-layered compounds, stability in rel. to structural mismatch 80−39040
C, crystalline, intermediate form, CI lattice energy *(Russian)* 78−22693
C_2N_2, electrostatic terms in lattice energy calcs. 79−51040
CO_2, electrostatic terms in lattice energy calcs. 79−51040
CO_2, lattice energies, non-additive three body contributions, triple-dipole term 80−54168
CO_2, solid, high press. mol. libration calc. with Kihara core pots., Gruneisen parameter and lattice 80−65173
CS_2, lattice dynamics of 0K cryst., phonons and lattice energy 79−73269
CS_2, solid, tailoring of potentials, in lattice dynamics 78−79679
$CaCO_3$, calcite (aragonite), lattice energies, four-centre CO_3^{2-} charge distrib. 78−47272
CaO, absorpt. band identification of colour centres 77−40271
CaS, absorpt. band identification of colour centres 77−40271
CoO, electronic struct. calc. 78−43297
CoO-MgO, cryst. oxide demixing in O pot. gradient 79−37849
Cr, lattice dynamics, phonon dispersion and atomic force constants, phenomenological model 78−26640
Cr-Fe-Ni-Si, ternary phase equilibria for Cr-Fe-Ni rich portion, lattice stabilities 80−71628
Cs, structural energies, pseudopotential formalism 80−39519
CsCl, lattice statics and dynamics, model calcs. 77−11647
CsCl, Madelung pot. determ. by Ewald method 80−92475
CsCl structure solids, many-body effects on elastic consts. 77−1163
CsCl-structure compounds, lattice energy and elastic consts. for 3-body Van der Waals interaction 77−72580
CsI, lattice statics and dynamics, model calcs. 77−11647
Cu, cohesion, electron statistical model 77−27846
Cu crystal, cohesion and vacancy form., electron statistical model 80−54169
Cu, plastically deformed, containing dislocation distribs., X-ray diffr. line broadening 77−43218
Cu, stability of FCC struct. collinear three-ion interaction 80−49173
CuCl(Br)(I), van der Waal dipole-dipole and dipole-quadrupole energies, Born and Slater-Kirkwood models 79−27947
$DyCl_3$, vapour press. and sublimation thermodynamics, mass loss effusion meas. 80−88313
FeO, electronic struct. calc. 78−43297
GaAs, dopant atom charge effect on lattice parameter 77−31631
$GdCl_3$, vapour press. and sublimation thermodynamics, mass loss effusion meas. 80−88313
Ge, edge dislocation struct., lattice distortion and surrounding vacancy distrib. 77−19954
H, atomic crystalline phase, ground state energy calc. *(Russian)* 79−19426
H, metallic, struct. and stability 78−14305
H_2 crystal, metallic, total energy, self consistent harmonic phonon approx. 77−31629
H_2, mol. cryst., static energy determ. taking into account three particle interactions *(Russian)* 78−9996
H_2, solid, electron-irrad., cluster-ion prod., lattice and fragmentation energies 77−4911
H_2, solid, energy in vol. range 10 to 60 a.u./atom, allowance for three-particle interactions *(Russian)* 78−38654
In, face centred tetragonal, total cryst. energy with electronic screening effect, struct. stability 77−15345
In, Madelung energy, stability of f.c.t. lattice 77−1097
K, phonon spectrum calc., microscopic theory of force constants 78−26647
K, structural energies, pseudopotential formalism 80−39519
KBr, analysis using density functional formalism 79−90592
KBr, stored energy after X-irrad. at low temp., 10-50K 77−76459
KCN, polymorphic transitions, lattice energies calc. 77−1092
KCl, calc. of third- and fourth-order elastic constants 79−10891
KCl, cluster expansion of density matrix and crystal energy 78−87952
KCl:Li^+, shape of pot. energy well of impurity 79−23692
$KClO_4$, single ion props. by lattice energy minimisation 78−83769
KF:Li^+(Na^+)(K^+), shape of pot. energy well of impurity 79−23692
LaM_2-Gd, M=transition metal, correl. between g-shift and stability, EPR study 80−88874
Li, cryst. and electronic props., Hartree-Fock calcs. 79−60698
Li, electronic structure and lattice const. determ. using orthogonalised modulated plane wave method *(Ukrainian)* 79−42436
Li, energy and elastic constants 80−59435
LiH, lattice energy calc., teaching 78−16595
Li_3N, Watson sphere model, Madelung energy calc. 79−99112
$LiNbO_3$, optical absorption of hole centres, polaron model 80−97314
Li_2O, ionic atomic binding force assumption 78−79556
$MgBr_2$-ABr (A=Cs, Rb, K, Na, Tl), thermochemical and struct. investigation *(German)* 79−1423
MgH_2, lattice energy calc. 78−83768
MgO crystal, unified approach to lattice states and dynamics 78−59878
MgO-NiO, crystalline soln., microstrain rel. to lattice energy and strain energy 77−24411
Mn film, heat treated, lattice distortion energy, resist. meas. 79−19492
Mn-MgF_2 cermet, heat treated, lattice distortion, resist. meas. 79−19492
MnAs, soft mode, energy and entropy, competition with energy and entropy of spin system 79−10908
MnO, electronic struct. calc. 78−43297
α-N_2, lattice energies, non-additive three body contributions, triple-dipole term 80−54168
NH_3, cluster-ion prod. in electron-irrad. solid, lattice, and fragmentation energies 77−4911
NH_4ClO_4, single ion props. by lattice energy minimisation 78−83769
$NaAl_2O_4$-$MgAl_2O_4$ spinel solid solns., activities rel. to cation distrib. 77−15377

lattice energy continued
NaBr, analysis using density functional formalism 79−90592
$NaBrO_3$, comparative computations using explicit minimisation procedures 79−32944
$NaBr.2H_2O$, lattice energy, electrostatic, multipole expansion method 79−99107
NaCN, polymorphic transitions, lattice energies calc. 77−1092
NaCl, Coulombic energy calcs. 79−99104
NaCl, Madelung const., rel. to electrostriction consts. calc. 77−36178
NaCl, Madelung pot. determ. by Ewald method 80−92475
NaCl, plastically deformed, containing dislocation distribs., X-ray diffr. broadening 77−43218
$NaClO_3$, comparative computations using explicit minimisation procedures 79−32944
$NaClO_4$, single ion props. by lattice energy minimisation 78−83769
Nb-H, ordering of hydride phases 77−19902
NiO, bulk props., initial state MO Ni_4O_4 and $Ni_{13}O_{14}$, cluster model, lattice and force consts., photoemission and CT absorpt. spectra 80−84828
NiO, electronic struct. calc. 78−43297
$Ni_{1-x}Te_2$, mixing energies of Ni atoms and vacancies 79−27975
$PbCl_2$, binding, ionicity, covalent contrib., Madelung const., cohesive energy 78−79558
$PbMoO_4$, optical absorption of hole centres, polaron model 80−97314
PbS, first-principles calc. of eqn. of states 80−49649
PbS, thermomech. props., SCF Xα scatt. wave theory 78−71704
PdD_x, model of instabilities 78−75619
PdH_x, model of instabilities 78−75619
Rb, structural energies, pseudopotential formalism 80−39519
RbCl, structural phase transition, Born-model and effects of hydrostatic and non-hydrostatic stresses 79−23721
SO_2, lattice dynamics, rigid mol. model 80−44266
$Sc_{0.8}S$, order-disorder transition, ionic model appl. 80−107096
Se, molecular cryst., Se-Se nonbonded pot. parameters derivation from heat of sublimation 79−27945
Si (111) clean surface, internal pot., interplanar spacing, LEED 77−89627
Si, bulk and surface equlib. props., self-consistent pseudopotential calcs. 79−60750
Si, charge density, struct. props. electron-electron interactions 78−47725
Si, edge dislocation struct., lattice distortion and surrounding vacancy distrib. 77−19954
$Si_{1-x}Ge_x$ system, lattice energy and consts., virtual cryst. approx., pseudopot. calc. 80−44166
β-Si_3N_4, Madelung energy calcs. 79−46605
TTF stacks, intermolecular energy and struct. from atom-atom potentials 80−79738
$TbCl_3$, vapour press. and sublimation thermodynamics, mass loss effusion meas. 80−88313
TiO_2, interionic repulsive short-range interaction pot., lattice energy calc. 80−96466
Ti_nO_{2n-1}, long-range strain and localised relax. energies of crystallographic shear structs. 79−94948
TlCl, self-consistent electronic struct. and ground state props. 80−15451
TlCl(Br)(I), van der Waal dipole-dipole and dipole-quadrupole energies, Born and Slater-Kirkwood models 79−27947
$Tl_2Ta_2O_6$, localisation of Tll, electrostatic energy, calc. *(French)* 80−33926
UO_2, ionisation potential, cohesive, electronic and redox props. 79−47916
V, lattice dynamics, phonon dispersion and atomic force constants, phenomenological model 78−26640
YAG, optical absorption of hole centres, polaron model 80−97314
YM_2-Gd, M=transition metal, correl. between g-shift and stability, EPR study 80−88874

lattice gas *see lattice theory and statistics*

lattice localised modes
see also phonon-defect interactions; phonon-impurity interactions
adsorbed molecule vibr. excitation due to plastic deform. accompanying fracture 77−15488
alkali alloy, dil. solid solution, atomic displacement near solute atom and in asymptotic range 79−65162
alkali halide:CN radical, impurity effects on ion-induced luminesc. 77−16402
alkali halide:$H^-(D^-)$, local modes and colour centre absorpt. bands, analogy 80−60632
alkali halide:O_2^-, frozen soln., impurity luminesc., zero-phonon lines interpretation 79−87488
alkali halide, lattice relaxation around tetragonal and rhombic defects 79−95110
alkali halide, lattice vibrs., effect of NO_2^- impurity molecule, theory 77−35654
alkali halide, localised mode due to U-centre 77−20036
alkali halide, SH^- and SD^- impurities, shift of IR absorption band centre 77−16346
alkali halide, U-centre pairs, localised modes 77−7813
alkali halide crystals, mixed, impurity centre local vibrs., comp. depend. of spectral parameters 80−79898
alkali halide solid solutions, Stokes losses for crystalline vibrs. in impurity O_2^- anions luminesc. spectra *(Ukrainian)* 79−43012
alkali halides, local and reson. modes due to hydide ions, U-centres and additive cation impurities 79−77710
alkali halides, local vibr. modes excitation by ions, moving dislocation steps *(Russian)* 77−31696
alkali halides, mixed, U-centre localised modes 80−100319
alkali halides, shift and broadening of local vibr. bands, temp. depend. 78−87755
alkali halides, spectra of O_2^-, S_2^- and NO_2^- mol. ions, electron-phonon interaction 77−52174
alkali halides, V_k-centres, vibr. modes, calc. 80−84269
alkali halides, vibration modes due to single ion impurities 79−51225
alkali metal halides, vibrational modes due to three impurity cluster 78−75773
alkaline earth fluorides, hydrogenated mixed cryst., local mode absorpt. 77−81130
amorphous alloy, vibr. props., appl. to Si_xGe_{1-x} 77−4176
anisotropic crystal, vibr. characteristics at low temp., effect of substitution impurities *(Russian)* 80−103439
anisotropic crystals, infinite rectilinear dislocation, vibrs. 80−44210

lattice localised modes continued
anisotropic crystals, long-wave vibrs. localised near dislocations 80−59603
anthracene, monocryst., additional absorpt. spectrum at low temp. 78−92096
atomic chain, anharmonic, change in nature of vibr. produced by deformation 79−7666
BCC crystal lattice containing interstitial atom in split config., reson. and localised vibrs. *(Russian)* 80−84268
benzene phenol crystal, asymmetry of phonon side bands, absorption, luminesc. and specular spectra 77−1730
p-benzoquinone, mixed crysts., PMDR and thermal modulation spectroscopy, electron-phonon interaction 77−32297
Bethe lattice, vibration 78−30706
Bethe-lattice dynamics, impurity and localised mode 77−62595
bicrystal interface vibrational props., different-interface phonons and low-temp. sp. ht. 77−76656
biopolymer, local mode resonance enhancement in Raman spectra 77−77204
Cayley tree type system, modes, densities, lattice vibrs. 78−71813
chabazite type zeolite, cation substituted, IR spectra, interion vibr. bands 78−10933
collective dislocation motion, dynamic effects 78−79632
crystal, subjected to high-energy, particle flux, excitation near point defects 79−7708
crystal with long range impurity states, vibr. spectrum *(Russian)* 80−6478
cubic crystal, absorpt. saturation and radiation polarisation rot. by local vibrs. *(Russian)* 77−69797
cubic crystal, Mossbauer line, second-order Doppler shift 79−56633
cubic crystals containing substitutional impurities, slow neutron coherent scatt., phonon mass operator 79−28065
defect vibrations, resonant and localised 77−1200
defect-clusters in linear chain, effect of second neighbour interaction on freq. 78−63826
defects, behaviour at structural phase transitions 78−83904
defects, central peak at displacive phase transitions 78−83905
degenerate three dimensional local and quasi local vibration spectral distributions 80−29138
deuteronaphthalene:β-deuteromethylnaphthalene crystal, asymmetry of phonon side bands, absorption, luminesc. and specular spectra 77−1730
diamond:N(B)(Si)(O), substitutional impurities 79−87056
diamond, irradiated, optical spectrum 78−6719
diamond, natural, cathodoluminescence of defects *(French)* 80−34988
diamond, van Hove singularities, absorpt. and luminesc. electronic-vibr. spectra 80−70639
diamond, vibronic bands at 2.498 eV (H4), 2.417 eV and 2.536 eV, absorpt. and luminesc. under stress 77−85758
diamond crystal, deep centres, changes in Van Hove singularities in vibronic spectra 77−8645
diatomics in rare gas matrices, vibr. modulation effects 77−23496
p-dihalobenzene alloys, successive perturbation of phonon bands 77−35653
dilute alloy, atomic displacements around impurity and three body interaction 78−91406
dilute alloys, force const. changes due to substitutional impurities 77−24374
dislocation, thermal vibrs., mean-square displacement, double-time Green function technique 79−19345
dislocation wall, localised cryst. vibrs. 80−70346
displacive phase transition, second-order, discontinuous freezing-out of local order 79−42204
displacive phase transitions, localised modes and central peak 77−69064
distortion effects on impurity modes 78−30722
durene:naphthalene, spin-lattice relax. in photo-excited triplet states, spin axes rot. on thermal excitation 78−76294
Einstein-Kanzaki model of static and dynamic lattice relax. 78−34676
F-centre, vibronic scheme of relaxed excited state 79−90989
FCC lattice, defect modes due to substitutional impurities, Green's function anal. 77−62600
FCC metals, ⟨100⟩-split interstitials, internal modes reson. hybridization 79−42194
FCC metals, dynamics of multiple interstitials and interstitial impurity complexes 78−75775
Fermi resonance, lattice with two-phonon spectrum 78−18723
fluorobenzene crystal, localised excitons 77−31963
Ginzburg-Landau model, localised defects, nearly ferromag. system, solids near displacive phase transition 78−71820
glissile dislocations, prod. by impurity atoms, Debye-Waller factor calcs. 78−2214
Green's function calculation, surface atom freq. spectrum, mean correl. displacements *(French)* 78−2206
guanidinium aluminium sulphate hexahydrate:Mn^{2+}, NMR 78−91939
harmonic chain with molecular defect, exponential transformations 77−84872
harmonic lattice chain with impurities, dynamics 77−4174
harmonic solids, free energy, vacancy defect effects calcs. 77−1198
harmonic systems, disordered, spectrum of dynamical matrix 78−30705
HCP lattice with substitutional impurity, defect Green's function and T matrix 79−42191
highly anisotropic crystal, phonon spectrum and local vibrs. *(Russian)* 78−59912
homopolar crystals, imperfect, lattice dynamics 80−59601
II-VI compounds, local force variations due to substitution impurities 78−51633
III-V compounds, local force variations due to substitution impurities 78−51633
III-V semiconductors, manifestation of local vibrs. of dislocations in IR spectra 78−88339
impure crystals, vibrs. in average local information transfer approx. 79−46774
impurities, conc. of C, O, Si 78−59832
impurities, zero-phonon transitions, spectral characts. 78−2884
impurity atom in solid, reson. fluoresc., transient spectrum, intensity, and intensity correl. 80−84777
impurity cluster pairs, lattice localised modes 79−33058
impurity interactions with local vibrs., effect on spectral distrib. 80−96613
impurity modes localisation 79−55850
impurity molecule in solid matrix, vibr. relax., stochastic classical trajectory approach 78−79707

lattice localised modes continued
impurity molecule reorientation at phonon excitation *(Russian)* 79−51019
impurity molecules in crystals, exclusion rules for librational-tunnelling states 78−84174
impurity molecules in Debye solids, vibr. relax., stochastic classical trajectory calcs. 79−1482
impurity pinning, phonon localization, in incommensurate modulated lattices 80−39238
inert gas:Eu(Sm), absorpt. and emission spectra, phonon sidebands 79−43021
inert gas crystal, lattice vibrs. and radiative transitions of implanted ions *(Russian)* 80−69098
interface, localised, resonant and antiresonant modes *(French)* 78−71938
intermediately coupled localised electron-phonon system, transient reson. Raman scatt. Franck-Condon-like excitation 79−8141
ionic and partially ionic solids, electron-lattice interaction 77−20274
ionic crystal/degenerate semiconductor interface, localised plasmon-optical phonon coupled modes 77−28071
ionic crystals, electronic and vibr. props. of point defects, book 80−51962
isotropic medium, elastic vibrations localised near dislocation 80−79897
Jahn-Teller E-e system, low lying vibronic energy levels, variational calcs. 77−76780
KBr(I):D, inelastic light scattering of localised vibration of interstitial H atom in alkali halides 80−88998
laminary crystal, phonon spectrum and local vibrations *(Russian)* 80−10623
rel. to laser stimulation of light interstitial diffusion in semiconds. and insulators 77−15630
light impurity in infinite nonlinear lattice 80−10624
linear defects, local phonon modes and structural instability *(Russian)* 79−73275
linear mixed valence compounds, lattice modes obs. 79−46763
local modes in disordered crysts., two-time Green's functions 80−6480
localisation in ionized and excited states, conf. 77−30750
matrix isolated molecules, IR spectral line broadening, theory 78−46332
metal: ^{119}Sn, impurity force const. changes from Mossbauer parameters 77−85630
metal, diffusion of H(D), slow neutron scatt. obs., review 80−34248
metal, FCC, vibr. behaviour of self interstitials 77−4175
metal-H system, inelastic neutron scattering meas. of optical vibr. freq. distribs. 80−59605
metals, atomic displacements near impurities and many-particle interactions *(Russian)* 80−24553
metals, BCC and FCC, H-diffusion and trapping 80−70447
metals, dynamical props. of point defects, book contrib. 80−103317
metals, interstitial atom struct. and vibr. air table simulation 79−71186
metals, point defect dynamic props. and diffusion controlled reactions, book 80−101674
MIS tunnelling spectra, interaction of holes with local modes and one and two optical phonons 77−20457
mixed crystal, one-dimens. dynamics 79−69217
mixed crystals, diatomic linear chain model 77−39649
molecular crystal, Frenkel exciton, coupled coherent and incoherent motion 77−35870
molecular crystal with isotopic impurity molecule, phonon spectrum under Fermi resonance 78−34583
molecular crystals, low freq. Raman spectra, defects and lattice vibr. 78−31194
molecular mixed crystals, electronic transition props., Redfield theory 79−46008
molecular one-dimensional systems, electronic collective excitations 77−31959
molecular one-dimensional systems, electronic collective excitons, EPR response 77−31960
molecular organic solid, vibronic excitons, rigid lattice calcs. 77−31958
molecule impurity vibr. relax., rot. and translational local modes 77−75118
molecule in solid matrix, pseudolocal modes, quantum vibr. relax. theory 79−65161
Mossbauer effect anomalies assoc. with thermal relax. of localised mode 77−12279
Mossbauer resonance, time differential, theory of phonon relax. effects 77−20777
multimode Jahn-Teller effect for E-term with strong vibronic coupling, local and resonant states 80−24858
multiphonon relax., localised electron radiationless decay, continuum and cluster modes 77−52158
naphthalene, cryst., low freq. Raman spectra, defects and lattice vibr., 80-320K 78−31194
naphthalene, in durene, photoexcited triplet state spin-lattice relax., local phonons effects 78−6605
naphthalene, solid, high-energy vibr. overtone spectra, local modes, intramol. relax. 79−28052
naphthalene in durene matrix, spin-lattice relax. of phosphoresc. triplet state, PMDR study 79−27012
naphthalene in various crystals, luminesc. and stimulated emission on laser irrad. *(Russian)* 77−48236
n-nonane:H_2-tetra-4-tert-butylphthalocyanine, thermal broadening of zero phonon lines, hole burning 78−71803
nonideal crystal, dynamics of void lattice *(Russian)* 77−80594
nonmetals, Raman scatt. from impurities, phonon effects 79−24299
nonmetals, Raman scatt. of impurities, anharmonic effects 79−24300
nonresonance field heating and cooling of local and quasilocal vibrs. 79−65148
one dimensional defect lattice vibrations 80−31454
one-dimensional crystal subjected to deform., static and dynamic equilib. 79−28037
one-dimensional system, phase fluctuations, disorder, nonlinearity 80−54331
organic solid, motion of localised excitations 77−31961
organic solids, vibr. relax. and dephasing Raman spectra, review 80−88987
point defects in crystals, book 77−47442
polar crystal, vibronic levels for Jahn-Teller impurities 78−68520
polaritons appl. of IR reflectivity and Raman scatt. expts. 77−40237
polyatomic molecules in condensed medium, vibr. relax., coherence transfer processes 79−60461
lattice localised modes continued
quantum system interacting with nonequilibrium phonons, light absorption props. 78−88340
quartz, X-ray topographical chamber for work by the Lang extinction method, appl. to quartz *(Russian)* 78−83649
rare earth ions, orbit-lattice interaction empirical parameter determ. 78 38799
resonant far IR absorption by impurities 78−6715
resonant localised impurity vibrs. at finite temps., spectral distrib. 77−7814
resonant Raman scattering, intensity of electronic and vibr. contribs. 77−77186
rigid lattice, vibr. relax., rot. mechanism, impurity interaction pots. 77−72664
sapphire, 14.8 MeV neutron damaged, optical vibronic absorption spectra 80−50384
at screw dislocation, calcs. *(Russian)* 77−35652
screw dislocation, split in BCC metal 78−22804
screw dislocations, inelastic neutron scatt. 78−75774
screw dislocations, phonon dispersion curves of localised modes, inelastic neutron scatt. 77−72661
second order optical processes, localised electron-phonon system, stationary response 78−43916
second order optical processes, localised electron-phonon system, transient response 78−43917
semiconductor, recombination enhanced defect reactions 79−38094
semiconductor, Zincblende struct., localised vibrs. due to defect complexes, Green's function study 80−79896
semiconductors, force variation due to charged defects 80−92634
semiconductors, localised transition metal impurities, lattice relaxation in optical transition *(Polish)* 80−70345
semiconductors, multiphonon capture rate 79−38022
semiconductors, shallow impurity centre spectra, isotopic shift of zero-phonon lines 80−66249
simple cubic lattice, localised vibrs., isotopic defects effects 79−86862
soft, static and dynamic behaviour 77−72669
soft displacive impurity dynamics in host lattice with displacive phase transition 80−34159
solid solutions, impurity centres, internal mol. vibrs., inhomogeneous band broadening 78−92103
soliton-impurity scatt. in Toda lattice, localised modes 78−14420
solitons, lattice, scattering theory from mass impurity in cubic nonlinear lattice 79−4385
spherical-like model, isolated impurity behaviour near displacive phase transition 78−71821
square lattice isotopic impurity effects, analytic soln. 77−15526
superconductors, effects of local and quasi-local impurity modes on crit. characts. *(Russian)* 79−19692
superionic conductor, statics and local dynamics near phase transition 80−107542
tetradecane, with tetra-4-tert-butylphthalocyanine impurity mols., luminesc. 77−18965
tetrahedral lattice sites, selection rules for multiphonon transitions 80−92632
Toda lattice, surface impurity localised mode vibr. 79−60462
Toda lattice soliton, interaction with impurity atom 78−75772
transition metal, BCC, crystallographic aspects of elastic dispersion 77−20032
two-electron level with quasidegenerate levels, local phase transitions and temp. effects in lattice dynamics 80−10666
vacancy, excess entropy, effect of localised vibr. modes 77−11542
vibration entropy and mean square atomic displacements due to defects in crysts. *(French)* 79−28064
vibrational relaxation, local phonon and roton receiving modes 79−46759
vibronic splitting, effect of including higher vibronic states in calc. 79−55851
vibronically coupled systems, cluster model 79−19540
zinc blende type crystals, mass substitution, diatomic and extended linear chain model 80−44279
AgBr, phonons at elevated temp. 78−79810
AgBr:Li^+, time-depend. infrared absorpt. due to Li-localised mode 79−8133
AgBr:Li^+(Na^+), impurity induced IR absorpt. 80−7386
AgBr-Li^+(Na^+), local mode freqs., Green's function calc. 80−39237
β-AgI, phonon-induced X-ray scatt. from lattice dynamical model 79−37790
Al alloys, inelastic electron scattering by dislocations *(Russian)* 78−79988
Al, tilt boundary, Σ=5, struct. and atomic vibr., computer simulation 80−70223
$Al_xGa_{1-x}Sb$, vibr. spectra, Raman light scatt. study 80−45080
$Al_{10.4}Ga_{0.08}V$, low temp. thermal expansion 78−95167
β-AlO_3-(Na,Li)$_2O$, NMR, Raman and IR spectra, and X-ray diffr., heat treatment induced changes 80−107508
Al_2O_3, transition metal ion doped, phonon spectroscopy using freq. crossing techniques 79−42193
β-Al_2O_3:NH_4^+(Nd_4^+), polarised Raman scatt. 80−103947
β-Al_2O_3-(Na,Li)$_2O$, β-Al_2O_3-(K,Li)$_2O$ and β-Al_2O_3-(K,Sn)$_2O$, ionic cond. and Raman spectra 80−107509
β″-Al_2O_3-Ag_2O, Raman scatt. from mobile cations 80−11394
β-Al_2O_3-Ag_2O(K_2O)(Li_2O)(Na_2O), low-energy excitation spectra, localised modes 80−59606
β″-Al_2O_3-Ag_2O(K_2O)(Li_2O)(Na_2O)(Rb_2O), single cryst. Raman scatt., cond. mechanism and cryst. struct. 80−66209
β″-Al_2O_3-K_2O 80−11394
β″-Al_2O_3-Na_2O, NMR of ^{23}Na, elec. quad. interaction, 185 to 419K, ion motion obs. 80−108110
β″-Al_2O_3-Na_2O, Raman scatt. from mobile cations 80−11394
β-Al_2O_3-Na_2O-K_2O, cation interstitial pair modes in vibr. spectra 79−37788
β-Al_2O_3-Na_2O-Rb_2O, cation interstitial pair modes in vibr. spectra 79−37788
β-Al_2O_3.Li_2O(Na_2O)(K_2O)(Rb_2O)(Ag_2O), low temp. sp. ht., tunnelling states and diffusion theory 77−43345
$Al_{10}V$, low temp. thermal expansion 78−95167
$Al_{10}V$, supercond. transition temp. determ., localised phonon modes 77−63016
$Al_{10}V$, well defined local modes 78−26648
$Al_{10}V$-Ga, dil., well defined local modes 78−26648
Ar, solid, lattice dynamics calc. using Kihara hard core pot. 77−1193
Ar:H, solid, struct., pair pot. calcs. 78−2215

lattice localised modes continued
Ar:Ne, localised mode due to Ne impurity, Green function technique 77−1201
As, amorphous, vibrational excitations of defect sites 80−49332
BaClF, localised vibr. of U-centres 78−75779
BaF_2, rare earth and transition ion doped, far IR absorption and Zeeman effect 77−40246
BaF_2: rare earth, far IR electronic transitions 77−4657
$BaF_2:Dy^{3+}$, far IR absorption 80−40143
$BaF_2:R^{3+}$, far IR Stark and Zeeman splitting 77−48190
$BaF_2:Sm^{2+}(Tm^{2+})$, vibronic spectra and dynamics of impurity-contaiing lattice 79−1787
$Ba(NO_3)_2$, Raman spectra temp. depend. anomalies in symmetric stretch region 79−61361
$Ba(NO_3)_2$, vibrations of isotopic impurities, IR reflection and Raman spectra meas. 77−51465
Be-Cu, thermal expansion, vibr. characteristics at low temp., effect of substitution impurities *(Russian)* 80−103439
$Bi_{72}SiO_{20}$:Sn(Mo), Raman scatt. spectra, impurity effect 80−80795
$Bi_2Ti_4O_{11}$:PbO, anomalous temp. depend. of phonon modes, Raman spectra 78−10893
CF_2, matrix-isolated, vibr. unrelaxed fluoresc., lattice mode coupling 77−14485
CaF_2, Frenkel defect, entropy of form., Green function calc. 80−19898
CaF_2, impurity modes due to interstitials, Green function formalism 80−24554
CaF_2, localised vibrs. due to substitutional impurities 78−22803
CaF_2, phonon resonances associated with vacancy 80−19893
CaF_2, rare earth doped, force const. changes near impurity site, calc. 77−47529
CaF_2, rare-earth and transition ion doped, far IR absorption and Zeeman effect 77−40246
$CaF_2:Eu^{2+}$, second order perturbation in vibronic system 78−30893
$CaF_2:R^{3+}$, far IR Stark and Zeeman splitting 77−48190
CaF_2:rare earth ion, hydrogenated, local lattice modes, spectroscopy 80−50375
$CaF_2:Sm^{2+}$, luminesc. spectra, vibronic wing, 2K 79−8182
$CaF_2:Sm^{2+}(Eu^{2+})$, cubic crysts., vibronic spectra, induced dichroism method 77−81131
$CaF_2:Tm^{2+}$, vibronic spectra and dynamics of impurity-contaiing lattice 79−1787
$CaF_{2-x}H_x$, IR spectra 80−34920
$CaMoO_4:Mo^{5+}$, g-factor, ground state, line broadening, EPR obs. 80−39863
$Ca(MoO_4)_{1-x}(WO_4)_x$, Raman scatt. meas. 77−28578
$Ca(NO_3)_2$, Raman spectra temp. depend. anomalies in symmetric stretch region 79−61361
CaO, interstellar, zero phonon lines rel. to origin of diffuse absorpt. bands 77−57073
$CaO:Ni^{2+}$, vibronic splitting, effect of including higher vibronic states in calc. 79−55851
CaS:Ce, Na, photon sidebands in emission and excitation spectra, pseudolocalised vibrs. 79−28800
Cd:^{67}Ge, elec. quadrupole interaction temp. depend., PAC meas. 79−42877
Cd:^{67}Zn elec. quadrupole interaction temp. depend., PAC meas. 79−42877
Cd-Mg, dil., elec. resistivity, local mode effect 78−6347
$CdCl_2:Co^{2+}$, optical absorpt. spectra, Zeeman study 78−6712
CdF_2, rare earth and transition ion doped, far IR absorption and Zeeman effect 77−40246
$CdF_2:R^{3+}$, far IR Stark and Zeeman splitting 77−48190
$Cd_{1-x}Hg_xTe$, lattice dynamics of low conc. of Hg atoms, perturbation model impurity description 79−55853
$CdS:Mn^{2+}$, temp. depend. of rate of spin-lattice relax. 79−42832
CdTe:Be, impurity modes and IR absorption 78−76506
CdTe:S, reson. interaction of local S vibr. with lattice phonons 77−11654
CdTe:Si(Cl), force variation due to charged defects 80−92634
$CdTe_{1-x}S_x$, long-wavelength optical phonons, composition depend., IR and Raman spectra 78−67788
$Cd_xZn_{1-x}S$, vibr. spectra, microscopic theory 79−73949
γ-Ce, FCC, localised vibration of interstitial H impurities 80−75322
Cl_2 in Ar matrix, vibr. relax., stochastic classical trajectory approach 78−79707
Cr^{3+}, electronic states interactions with crystal odd vibrs., R-lines vibr. recurrences 78−84639
$CsBr:MNO_4^{2-}$, optical and vibronic spectra 79−65909
$CsBr:O_2^-$ Stokes' losses on cryst. vibrs. in luminesc. spectra of mol. centres *(Russian)* 77−55827
$CsBr:Tl^+$, impurity induced Raman spectra, breathing shell model 78−39541
CsBr(I), single crysts., polarisation of luminesc. and reorientation of NO_2^- centres 79−95823
$Cs_2GeF_6:Mn^{4+}$, magnetically circularly polarised emission and MCD of vibronic lines 77−16377
$CsI:H^-$, U-centres, force consts. using Green's functions 79−46775
$CsI:MnO_4^{2-}$, multiple-order Raman scatt., and absorpt. spectra 77−40229
Cu alloys, dilute, localised phonons due to substitutional impurities 79−77711
Cu alloys, inelastic electron scattering by dislocations *(Russian)* 78−79988
Cu, vacancy, lattice vibrs., reson. and localised modes 80−39236
Cu-Al, impurity concentration effects 78−75777
Cu-Al alloy, dil., lattice expansion and localised vibr. mode 79−37789
Cu-Al alloy, vibrs., average local information transfer approx. 79−46774
Cu-Be, impurity concentration effects 78−75777
Cu-Si, impurity concentration effects 78−75777
$CuGaS_2$, lattice vibr. modes, Fourier transform spectroscopy 79−33701
D_2, solid, sp. ht. effect of Ne impurities 79−33099
Eu, in inert gas matrix, pseudolocalised vibr. modes, UV/vis. spectra 78−46289
Fe, surface phonon spectra 78−71934
α-Fe, vacancy, lattice vibrs., reson. and localised modes 80−39236
Fe, vibrational spectrum with interstitial C atoms 78−67796
Fe-Ni(28 at.%), Mossbauer scattering, martensitic transformation, evidence of soft modes 80−93223
$Fe(CO)_2(NO)_2$, vib. assignment using ^{15}N isotopic substitution, solid, liq. and soln. spectra 77−48152
$Fe_{0.49}Mn_{0.01}Ti_{0.5}H_x$, localised vibrs., sp. ht. obs., room temp. 80−65248

lattice localised modes continued
$Ga_{1-x}Al_xAs$, solid solution, synthesized by ion implantation, Raman scattering 79−42972
$Ga_{1-x}Al_xSb$, small wave vector modes 78−75785
GaAs, IR absorption of isolated impurities 77−12407
GaAs, irradiated with fast neutrons, IR vibrational absorpt. 78−75776
GaAs, isolated impurities, local mode sideband IR absorption and second harmonic intensity calc. 77−85707
GaAs:B, electron or neutron irradiated, low symmetry interstitial B centre 78−79605
n-GaAs:Si, B, IR absorpt. spectra, reson. and localised modes 80−66172
GaAs:Si, Cr, carrier concs. from Hall effect, microscopy, localised vibrational modes absorption meas. 78−56104
GaAs:Si, donor-acceptor pair defects absorpt. bands 80−16064
GaAs:Si, electron irradiated, LPE layers and Bridgman crysts., IR absorption and Hall meas. 77−16345
GaAs:Si, IR absorpt. bands, localised modes, Si-related defects 80−76054
GaAs:Si, Li, IR absorpt., microstruct., charge compensation 80−107565
GaAs:Si, neutron irrad., strain detection by local mode IR absorpt. meas. 77−69828
GaAs:Si, thick LPE layer growth and characterization 77−12511
n-GaAs:Te, vibr. props. of 1.0, 1.2 and 1.3 eV luminesc. centres 77−55823
GaAs-C, ion implanted, obs. of localised vibrational mode absorption, effects of annealing temp. ~80−16068
$GaAs_{1-x}P_x$, solid solution, synthesized by ion implantation, Raman scattering 79−42972
$Ga_xIn_{1-x}As$, far IR reflectivity spectrum, damped harmonic oscill. model 77−52070
GaP donor system, local mode, random force const. change 78−38800
GaP:M, M=substitutional impurities, lattice dynamics and local mode freqs. *(French)* 77−66011
GaP:Sb(Bi), gap vibrs. and impurity conc. determ. 79−69869
GdTe:P and CdTe:P,In(Ga)(Al), IR absorpt. investig. of localised vibr. modes of impurity centres 77−52136
Ge, doped, electron or neutron irradiated, vibrational absorption 78−6718
Ge, impurity modes due to point defects, comparison with IR and Raman meas. 79−4386
Ge, localised vibrational modes of isolated impurities, Green's function method 77−39650
Ge:Si, impurity lattice modes due to single and paired defects 78−75780
Ge:Si, impurity modes and IR absorption 78−76506
Ge-Si, dil. alloy, IR absorpt. and first-order Raman scatt. due to single and paired impurity atoms 79−82976
Ge-Si, impurity concentration effects 78−75777
Ge-Si alloys, defect modes and optical spectra 80−11413
Ge-Si alloys, imperfect homopolar crystals, lattice dynamics 80−59601
p-H_2:o-H_2, solid, cryst. field interactions, impurity effects 79−82562
$Hg_3In_2Te_6$, complex ordered-vacancy cpd., struct. and lattice dynamics 78−34496
In pnictides, mixed, impurity induced Raman scatt. spectra 80−88983
In, recoilless fraction calc. of ^{57}Fe impurity atoms from mean-square displacements 78−2216
In:^{67}Ge, elec. quadrupole interaction temp. depend., PAC meas. 79−42877
$In_{1-x}Ga_xAs_yP_{1-y}$ far IR reflection spectrum 80−60612
InP:M, M=substitutional impurities, lattice dynamics and local mode freqs. *(French)* 77−66011
InP:Si, vibr. modes of Si, IR absorpt. bands 78−55922
$InP_{1-x}As_x$, long wave and short wave phonons, Raman spectra obs. 80−50317
KBr, defect modes due to H^--D^- pair impurities 80−59602
$KBr:(CrO_4^{2-})(MoO_4^{2-})(MnO_4^-)(ReO_4^-)$, absorption spectra 78−10924
$KBr:H^-$, U-centre absorpt. band shape, piezodichroism dispersion curve and electron-phonon interaction 77−24873
$KBr:NO_2^-$, effects of Mg, Ca, Sr, Ba, Pb impurities on vibrational constants of NO_2^- ion 77−20035
KBr:Rb, U-centre modes, Green's function method calc. 77−24372
$KBr:Rb^+$, elastic interaction of H-centre with impurity, dynamic effects 77−76396
$KBr:SO_4^{2-}$, $Ba^{2+}(Ca^{2+})$, IR absorpt. band parameters, temp. depend. *(Russian)* 78−31226
$KBr:SO_4^{2-}$, IR absorpt. spectra, cation impurity influence *(Russian)* 78−10901
$KBr:SeO_4^{2-}(WO_4^{2-})$, IR absorpt. spectra, vibr. splitting *(Russian)* 79−51995
$KCN:H^-$, U-centre, local mode meas. 77−1199
KCl, defect modes due to H^--D^- pair impurities 80−59602
KCl, Raman spectra and vibrational modes of V_K centre meas. 78−80338
$KCl:(CrO_4^{2-})(MoO_4^{2-})(MnO_4^-)(ReO_4^-)$, vibronic absorption spectra 78−10924
$KCl:CN^-$, phonon-internal mode hybridisation, neutron scatt. 78−2217
KCl:Ca,H, studies of localised vibrations of substitutional atomic H 78−80248
$KCl:Ca^{2+}$, cryst., hydrolysed, IR absorpt. bands 77−32404
$KCl:Eu^{2+}$, radiationless process, vibronic spectrum analysis 78−80391
$KCl:F^-(Br^-)(I^-)$, U-centres, local defect modes, Green's functions calcs. 80−44280
KCl:H, ENDOR and ESR study of anion sites 80−108118
KCl:Kbr(KI), enhancement in sp. ht. due to anion impurities 79−51274
$KCl:Li^+$, defect induced tunnelling states, depend. on strain, pot. model calcs. 79−69865
$KCl:Li^+$, shape of pot. energy well of impurity 79−23692
$KCl:NO_2^-(O_2^-)$, Stokes' losses on cryst. vibrs. in luminesc. spectra of mol. centres *(Russian)* 77−55827
$KCl:Na^+$, R-centre exam., uniaxial stress effects on zero-phonon lines 78−47371
$KCl:Pb^{2+}$(0.005% Pb), A band fine structure, electron-phonon interaction 78−60491
$KCl:SO_4^{2-}$, $Ba^{2+}(Ca^{2+})$, IR absorpt. band parameters, temp. depend. *(Russian)* 78−31226
$KCl:SeO_2^{2-}(WO_4^{2-})$, IR absorpt. spectra, vibr. splitting *(Russian)* 79−51995
$KCl(Br):Li^+$, static lattice distortion effect 77−47530
$KCl(Br):OH^-$, electron irrad., F_2^+ centre stabilisation 80−54231
$KCl_{1-c}Br_c$, impurity centre local vibrs., comp. depend. of spectral parameters 80−79898

lattice localised modes continued
$KCl_{1-x}Br_x:NCO^-$, absorpt. band defect broadening *(Russian)* 78−72526
$KCl(Br)(I):PO_2^-$, vibr. spectra and struct. of PO_2^- impurity ions 77−16354
$KCl_{1-x}I_x:NCO^-$, absorpt. band defect broadening *(Russian)* 78−72526
$K_2CoF_4:Mn^{2+}$, impurity induced mag. excitations, magnon gap mode, far IR spectra obs. 80−44821
$K_2CrO_4:SO_4^{2-}$, IR absorpt. spectra, local symmetry of impurity ions *(Russian)* 78−2893
$K_3Cu(CN)_4$, isotopic mixed crystal with ^{12}C and ^{13}C, Raman scattering 78−76476
$KF:Li^+(Na^+)(K^+)$, shape of pot. energy well of impurity 79−23692
KI, containing F-centres, Raman scatt. calc. 77−16306
KI, gap modes due to impurity pairs 77−62602
KI, gapmode calc. using Green's function technique, effect of uncertainty in eigendata 78−79708
KI, perturbed by Jahn-Teller centres, lattice dynamics 80−107394
$KI:BH_4^-$, far IR absorption in phonon gap 77−12406
$KI:H^-$, U-centres, force consts. using Green's functions 79−46775
$KI:S_2^-$, Stokes' losses on cryst. vibrs. in luminesc. spectra of mol. centres *(Russian)* 77−55827
$KMgF_3:Fe^{2+}$, US relax. absorpt., acoustic wave-impurity coupling, spin-orbit splitting 79−4375
$K_2MnF_4:Co^{2+}$, Raman spectra meas. 77−12389
KNO_3, vibrations of isotopic impurities, IR reflection and Raman spectra meas. 77−51465
$K_{1-c}Na_cCl$ and $K_{1-c}Rb_cCl$, impurity centre local vibrs., comp. depend. of spectral parameters 80−79898
$K_xRb_{1-x}Cl:HF_2^-,SO_4^{2-}$, nonuniform broadening of IR vibr. absorpt. bands of impurities *(Russian)* 77−16357
$K_2SO_4:XO_4^{2-}$, X=Cr, Se, Mo, W, lattice-impurity interactions, IR spectra 78−19522
$LaNi_5H_6(D_6)$, low energy excitations of H and D 79−77699
$LiCl:Ni^{2+}$, first order induced Raman scatt. from Ni^{2+} and cation vacancies 77−48169
LiF, manifestation of local vibrs. of dislocations in IR spectra 78−88339
LiF, Raman spectra and vibrational modes of V_K centre meas. 78−80338
$LiF:OH^-$, electron irrad., F_2^+ centre stabilisation 80−54231
$LiGaO_2$, light scatt. *(German)* 79−28730
Li_3N, superionic conductor, far IR absorption, temp. and isotope effects 79−51969
$Li_2SO_4.H_2O$, $^6Li/^7Li$ and H/D substituted, IR and Raman spectra, vibr. and librational modes 77−85716
$Li_4WO_5:U^{6+}$, vib. fine struct. in luminesc. spectra 77−8620
Mg, lattice distortion around vacancy 79−42192
Mg_xCd_{1-x} Te:P, vibr. modes of defects, IR absorpt. expts. 77−62601
MgO, interstellar, zero plasma lines rel. to origin of diffuse absorpt. bands 77−57073
MgO, transition metal ion doped, phonon spectroscopy using freq. crossing techniques 79−42193
$MgO:Cr^{2+}$, paramag., spin-phonon coupling, inelastic neutron scatt. obs. 79−60441
$MgO:Cr^{2+}(V^{2+})$, coupling of T_{1u} and T_{2u} vibr. to $^2E_g \rightarrow {}^4A_{2g}$ transition 77−63453
$MgO:Cr^{3+}(Mn^{2+})$, spin Hamiltonian parameters, lattice expansion and vibr. effects 80−24851
$NH_4Br:Cl^-$, impurity mode, far IR transmission obs. 77−16308
NH_4Cl, acoustic absorption by soft modes of defects 80−59584
NH_4Cl, cryst., impurity overtone states, interference two-photon spectrum *(Russian)* 79−24344
NH_4Cl, vibrations of isotopic impurities, IR reflection and Raman spectra meas. 77−51465
$NH_4Cl_{1-x}Br_x$, phonon dispersion 78−75760
N_2O crystal, vibrational exciton bands, impurity modes 77−28560
NaBr(:I), exciton ionisation and decay, photoluminesc. in elec. field 77−44046
NaCl, inelastic light scattering of localised vibration of interstitial H atom in alkali halides 80−88998
$NaCl:Ca^{2+}$, cryst., hydrolysed, IR absorpt. bands 77−32404
$NaCl:H^-$, U-centre absorpt. band shape, piezodichroism dispersion curve and electron-phonon interaction 77−24873
$NaF(Cl):OH^-$, electron irrad., F_2^+ centre stabilisation 80−54231
$NaI:Cl^-$, local vibr. exam. by neutron scatt. 77−24373
$NaI:H^-$, U-centres, force consts. using Green's functions 79−46775
$NaNO_3$, isotopically mixed, vibr. spectra, IR and Raman spectra 79−28770
$NaNO_3$, vibrations of isotopic impurities, IR reflection and Raman spectra meas. 77−51465
$Na_2SO_4:XO_4^{2-}$, X=Cr, Se, Mo, W, lattice-impurity interactions, IR spectra 78−19522
Nb:H, lattice distortion and migration energy of H impurities 78−30796
Nb-H, BCC, tetrahedral interstitial site H band modes, neutron scatt. obs. 79−55852
Nb-H system, lattice dynamics, local frequency spectrum, mean thermal displacement of H 80−59604
Nb-H(D) system, solubility, entropy and enthalpy, isotope effects 77−20069
$NbD_{0.85}$, localised D vibrs., temp. depend., neutron inelastic scatt. study 80−107395
$NbH_{0.82}$, localised H vibrs., temp. depend., neutron inelastic scatt. study 80−107395
$NbH_x(D_x)$, acoustic and optic phonons, neutron diffr. obs., book contrib. 79−82296
Ne, solid, lattice relax. model of n=1 exciton emission 79−47492
Ni, lattice vibrations at (111) surfaces and stacking faults 79−86974
Ni:He, defect props., quantum-chemical and lattice-defect hybrid approach 79−4528
$Ni_{1-x}Pt_x$, disordered, phonon dispersion relations using neutron inelastic scatt. 79−69212
$Ni_{1-x}Pt_x$, disordered phonon dispersion relations, neutron inelastic scatt. 78−43085
$Ni_{1-x}Pt_x$, disordered system, phonon dispersion relations using pseudo unit cell model 79−28066
P, amorphous, vibrational excitations of defect sites 80−49332
Pb, recoilless fraction calc. of ^{57}Fe impurity atoms from mean-square displacements 78−2216
Pb-Tl-Bi-In, localised phonons studies by supercond. tunnelling 79−87210
Pb-Tl-In, localised phonons studies by supercond. tunnelling 79−87210

lattice localised modes continued
$PbBr(Cl)-Ag^+$ IR absorpt. spectrum and vibr. of substitutional impurity 77−81135
$Pb(NO_3)_2$, Raman spectra temp. depend. anomalies in symmetric stretch region 79−61361
$PbSe_{1-x}Te_x$, for-IR reststrahlen spectra, mode behaviour 80−7345
Pd mixed valence-mixed metal compounds, ionic crystals, longitudinal lattice modes, Raman spectroscopy 80−40099
Pd-Cu-H(D) dilute alloy soln., thermodynamic props. at high-temp. 79−99334
Pd-H system, lattice dynamics, local frequency spectrum, mean thermal displacement of H 80−59604
Pd-H system, thermodynamic aspects of atomic vibr. 78−59913
Pd-H_2, dilute soln., high temp. thermodynamics, partial molar props. 77−15597
α-PdH_x, H-motions, conc., temp., momentum transfer, annealing depend., neutron scatt., study 79−42197
PdH_x, inelastic neutron scattering meas. of optical vibr. freq. distribs. 80−59605
α-PdH_x, local mode intensity var. with conc., temp., direction and annealing 77−11653
$PdH_x(D_x)$, acoustic and optic phonons, neutron diffr. obs., book contrib. 79−82296
$Pd_{0.99}Sn_{0.01}$, lattice dynamics of ^{119}Sn impurities, Mossbauer meas. 77−76507
Pt, mixed valence-mixed metal compounds, ionic crystals, longitudinal lattice modes, Raman spectroscopy 80−40099
Rb-K alloys, localised phonon modes, classical mol. dynamics compuer simulation 78−10147
RbCl containing K additive impurity, local modes due to U-centres 78−22805
RbCl, Raman spectra and vibrational modes of V_K centre meas. 78−80338
RbCl, U-centre local modes calcs. 77−62603
RbCl, U-centre pairs causing localisation 79−77709
$RbCl:Ag^+$, first-order impurity-induced Raman scatt. 77−77216
RbCl:Ca,H, studies of localised vibrations of substitutional atomic H 78−80248
$RbCl_xBr_{1-x}$, IR refl. spectra, temp. depend. 77−28573
$RbI:H^-$, U-centres, force consts. using Green's functions 79−46775
Rb_xWO_3, low lying phonon dispersion curves, neutron scatt. study 80−92622
Sb, amorphous, vibrational excitations of defect sites 80−49332
Si, EPR and spin-lattice relax. of dislocation spin chains *(Russian)* 79−91291
Si, electron irrad., multivacancy-O complexes, EPR expt., correl. with IR absorpt. data 77−28443
Si, H-related interstitial defects, vibr. electronic struct., extended Huckel theory 77−62604
Si, proton irradiated, IR absorption 79−33742
Si, resonant interaction of optical phonons with acceptor continuum states 78−35178
Si, vibrational properties of the ⟨001⟩ split interstitial 78−91405
Si:B, As, first and second order Raman scatt. by pair modes 79−65869
Si:B, P, first and second order Raman scatt. by pair modes 79−65869
Si:N(P), ion implanted, IR transmission and rel. spectra study 80−108244
SiC, H^+, D^+ and He^+ ion implanted, Raman scatt. obs. of localised vibr. modes 78−6689
SiC, influence of plastic deform. on struct. of photoluminesc. spectra 77−55824
SiF_4, mol. cryst., giant anomaly of intensity of vibrs. of isotopic impurity, Raman spectrum 79−73276
Si_xGe_{1-x}, vibr. props. 77−4176
Si_3N_4, CVD, chem. bound H, NH_3/SiH_4 ratio and annealing depend. 77−76680
Sm, in inert gas matrix, pseudolocalised vibr. modes, UV/vis. spectra 78−46289
$Sn:^{67}Ge$, elec. quadrupole interaction temp. depend., PAC meas. 79−42877
Sn-Pb alloys, dil., low-freq. phonon spectrum peculiarities 79−60463
$SnS_{2-x}Se_x$, layer cryst., Raman active modes 80−80767
SrClF, localised vibr. of U-centres 78−75779
SrF_2:Pr, Nd, Tb, Dy, Ho, Er, Tm^{3+} far IR spectra 79−33736
$SrF_2:Sm^{2+}$, interconfig. luminesc. spectra, vibronic wing 79−24358
$SrF_2:Sm^{2+}(Tm^{2+})$, vibronic spectra and dynamics of impurity-contaiing lattice 79−1787
$Sr(NO_3)_2$, Raman spectra temp. depend. anomalies in symmetric stretch region 79−61361
$SrO:Ni^{2+}$, EPR line splitting rel. to Jahn-Teller coupling and soft localised mode 80−66022
$SrTiO_3$, monodomain, O-D and O-H stretching vibrs., IR spectra 80−71449
Ta:H, lattice distortion and migration energy of H impurities 78−30796
Ta-H, BCC, tetrahedral interstitial site H band modes, neutron scatt. obs. 79−55852
Ta-H system, lattice dynamics, local frequency spectrum, mean thermal displacement of H 80−59604
$TaH_x(D_x)$, acoustic and optic phonons, neutron diffr. obs., book contrib. 79−82296
TbO_x, Mossbauer spectra of localised modes 79−73874
$ThC_{0.063}$, cryst. struct. and lattice dynamics 80−88088
Th_4H_{15}, H vibr. modes, neutron scatt. study, phonon density of states 79−42195
$TiCr_{1.8}$, H and D soln., enthalpy, solubility and mol. vibr. determ., comparison with soln. in metals and binary alloys 80−79951
$TiH_{1.92}$, thermal neutron inelastic scatt. phonon spectra determ. *(Chinese)* 79−10906
$TiO_2:H(D)(T)$, IR spectra, 300, 77 and 8K 78−35175
Tl, recoilless fraction calc. of ^{57}Fe impurity atoms from mean-square displacements 78−2216
V:H, lattice distortion and migration energy of H impurities 78−30796
V-H, BCC, tetrahedral interstitial site H band modes, neutron scatt. obs. 79−55852
V-H system, lattice dynamics, local frequency spectrum, mean thermal displacement of H 80−59604
V-Pt, dilute, inelastic neutron scatt. and quasilocal vibrs. *(Russian)* 77−80595
α-$VD_{0.7}$, interstitial vibr., coherent neutron scatt. study 79−42196
α-$VD_{0.7}$, vibrations of interstitial D, coherent neutron scatt. 80−96612
$VH_{0.51}$, optic modes study by neutron spectroscopy 80−19891

lattice localised modes continued
α-$V_{0.97}O_{0.03}$ solid soln., impurity vibrs., inelastic neutron scatt. study 80−92635
$V_{0.97}U_{0.03}$, phonon spectrum, quasi-local vibrs., inelastic incoherent neutron scatt. 77−15519
V=O, lattice distortion and migration energy of O impurities 78−30796
W, surface phonon spectra 78−71934
YIG:B,Pb, IR spectrum, localised modes, rel. to impurities and O vacancies 80−50377
Zn:^{67}Ge, elec. quadrupole interaction temp. depend., PAC meas. 79−42877
$Zn_{1-x}Cd_xS$ mixed crystals, Raman spectra between frequencies LO(Γ) to TO(Γ) 78−2854
$Zn_xCd_{1-x}Te$:P, vibr. modes of defects, IR absorpt. expts. 77−62601
ZnO:Cu, H(D), IR absorpt. line spectra, OH and OD vibr., optical excitation 79−15498
ZnP_2:As, local vibrs. of impurity ions, Raman study 80−29745
ZnS with cation impurity, first order transitions in Raman spectra 78−88310
ZnS with substitutional impurity, dipole and weak-dipole vibr. 79−14904
ZnS:Al, IR studies of Al complexes 79−33741
ZnS:Al-Cu, localised vibrational modes 78−63827
ZnS:Be, far IR lattice absorpt., Green's function calc. 78−43865
ZnS:Be, impurity modes and IR absorption 78−76506
ZnS:Co, Jahn-Teller interaction energy determ., piezospectroscopic expt. *(Russian)* 77−4623
ZnS:Co(Fe)(Mn)(Ni), impurity-induced Raman scatt., central force const. reduction 77−32379
ZnS:Cr(Mn)(Fe)(CoXVi), vibr. modes of transition element impurities 78−76472
ZnS:Cu^{2+}, motional averaging in excited state 77−66137
ZnS:Fe, piezospectroscopic effect on electron-vibr. lines of Fe^{2+} 78−27269
ZnS:M, M=substitutional impurities, lattice dynamics and local mode freqs. *(French)* 77−66011
ZnSe:Mg, local vibrations of impurities, IR absorpt. spectra exam. 77−7815

lattice mechanics *see lattice dynamics*

lattice phonons
see also electron-phonon interactions; lattice dynamics of covalent crystals; lattice dynamics of ferroelectric crystals; lattice dynamics of ionic crystals; lattice dynamics of metallic crystals; lattice dynamics of molecular crystals; lattice localised modes; phonon-defect interactions; phonon dispersion relations; phonon drag; phonon-exciton interactions; phonon-impurity interactions; phonon-magnon interactions; phonon-phonon interactions; phonon-plasmon interactions; polaritons; soft modes; spin-phonon interactions; tunnelling spectra; tunnelling spectroscopy
A^4-phonon theory, free energy and phase transition 78−41257
acceptor centres, radiationless transitions probabilities *(Russian)* 79−87507
acentric crystals, optical phonons, small oscillator strength meas. from frequency-angular polariton spectra 80−92629
actinide compounds, mag. ordering and struct. transforms. 77−20596
activated crystals, influence of temp. on energy transfer 79−28323
adsorbed monolayers, acoustic phonons, obs. method using Brillouin scatt. 80−59804
alkali borates, vitreous and cryst., vibr. spectra and struct. comparison 78−23470
alkali fluoantimonates, dielectric props. and structural phase transitions *(German)* 80−25274
alkali halates, NQR freq. temp. depend., phonon spectra interpretation 77−12226
alkali halides, bound polarons, vibronic theory, appl. to F-centre excited states 78−84150
alkali halides, photoemission, energies and lineshapes 80−89119
alkali hexahalogeno compounds: $ReCl_6^{2-}$ ($ReBr_6^{2-}$), low symm. splittings in vibronic spectrum due to phase transitions 80−55161
alkali metal, thermal expansion, elastic constants, phonon freq. anisotropy *(Russian)* 79−1516
alkali metal halides, elastic consts., anomalous temp. depend., phonon-lattice interaction 80−107354
alkali metals, elastic and thermal props. by pseudopotential method 80−19899
alkali metals, Gruneisen parameters, influence of press. on lattice anharmonicity and temp. depend. 80−79905
alkali metals, optimised model pot. calcs. 78−2467
alkali metals, pressure influence on absolute zero isotherms, polymorphic transform., phonon spectra *(Russian)* 80−49363
alkali tungsten bronzes, local struct. states in supercond. Tl phase, lattice props. 78−26981
alkyl ammonium copper chloride, two-dimensional ferromag., low temp. lattice cond., phonon spectrum 77−4227
alloys, concentrated, excess vibr. entropy and local environment effects 77−76498
ammonium compounds, rotational tunnelling, temp. dependence 80−38970
ammonium salts, proton spin relax. and phonons 78−84493
anharmonic crystal, lattice dynamics and stability, self-consistent phonon theory 79−51209
anharmonic crystal, lattice dynamics and stability 78−6129
anharmonic crystal $O(\lambda^4)$, phonon self energy, monatomic linear chain model calcs. 79−42161
anharmonic crystals, Debye-Waller factor, specific heat thermal behaviour 80−54335
anharmonic crystals, phonon density 77−62597
anharmonic system, generalisation of CPA 78−75783
anisotropic multilayer solids, macroscopic fields anal. 77−89547
anomalous fluctuations, neutron scatt. 78−75743
anthracene, cryst., heat pulse propag., exciton condensation, time-resolved fluoresc. spectra 80−84771
anthracene, nonequilibrium phonon propag. with freq. down-conversion 80−84260
anthracene, reson. Raman emission and hot luminesc. *(Russian)* 79−61377
anthracene films, optical props., comparison between free and optical contact mounting 80−89079
antiferromagnet, magnon and phonon damping, effect of intermediate state lifetime 79−24151
atomic beam scattering by surface and bulk phonons 77−73209
atomic chain, loaded, phonon model of breaking 80−70301

lattice phonons continued
ballistic phonon imaging, nonequilib. phonon anisotropic propag., low-temp. 80−10605
band modification caused by impurities and magnetophonon effect 79−42562
BCC transition metals, seven parameter model 79−90739
benzene, crystal, inelastic coherent neutron scatt., phonon spectra 78−51629
benzil, cryst., excited triplet state spin-lattice relax. probabilities, temp. depend. *(Russian)* 80−88860
binary alloy, one-dimens., embedded-cluster calcs. of phonon spectra 79−77703
binary alloys, random, dielec. matrix and related props. 78−51916
binary mixed crystals, phonon frequency spectra, travelling pseudofermion approx. 79−77704
bottleneck, influence on dynamic nucl. polarisation by solid effect 80−20511
brass, nonradial diffuse streaks and complex diffuse scatt. patterns of electrons 79−7527
β-brass, phonon spectra pseudo potential calcs. rel. to long range order and composition *(Russian)* 79−99279
Brillouin scattering by acoustic phonons, lineshapes 78−31208
Brillouin scattering by oblique-incidence acoustic phonons, lineshapes 78−72534
Brillouin scattering by Stoneley waves, elasto-optic and surface ripple mechanisms 80−71435
Brillouin scattering in reflection and transmission modes, rel. to intense acoustic flux, relation linearity test 80−45098
Brillouin scattering lineshape, theory in opaque material 77−16323
$CdSiP_2$, one- and two-phonon Raman scatt. 79−78681
CDW distorted linear chain, longitudinal phonon spectrum 80−24814
central phonon peaks, droplet model 77−43302
chain conductors, CDW ordering 78−79731
chalcopyrites, sphaleritelike vibration mode, group theoretical anal. 79−7661
chemisorbed atom, electronically adiabatic vibr. state lifetime 77−72768
cluster walls and phonons in structural phase transitions 79−77720
coherent THz acoustic wave launching by far IR photon-phonon conversion 77−39135
collective modes in solids, computer simulation 80−54325
complex crystals, isotopic shifts, phonon freqs. 78−67787
compressible classical Heisenberg chain, phonon dynamics and sound velocity 80−96604
conference on lattice dynamics, Paris, France (Sept. 1977) 78−59869
coupled hydrodynamic modes near structural phase transitions 77−1203
coupled phonon-linear Heisenberg chain system, phase transition 78−64208
coupled spin $^1/_2$ phonon system, existence of sharp transition 79−69204
covalent semiconductors, optical absorption by acoustic phonons related to shallow impurity levels 77−4665
critical thermodynamics, phase transition in transverse field with deform. depend., phonon anomaly separation 80−39258
crystal with long range impurity states, phonon spectrum *(Russian)* 80−6478
crystals and dislocations, spontaneous breakdown of spatial translation invariance *(German)* 79−7653
cubic crystals, phonon magnification, evaluation method 78−83890
p-$CuInTe_2$, single cryst., IR study of lattice and free carrier effects 80−45074
cyclohexane-$d_0(d_6)$, plastic crystal phase transition, mol. reorientation, Raman scatt. phonon spectra 80−20631
defect-free crystals, dielec. losses due to phonon system perturb. in elec. field 80−80693
degenerate three dimensional local and quasi local vibration spectral distributions 80−29138
densities of states, computational algorithm 80−44466
density of states, differential areas method for cryst. symm. independ. calcs. 79−82508
density of states determ. from thermodynamic functions 77−84871
di(alkyl ammonium)copper tetrachloride, two-dimens. magnon and phonon thermal cond. in high mag. fields 77−69123
diamond, coherent nonlinear two-phonon Raman spectra 79−19878
diamond, optical absorption and luminesc. spectra, review 80−2848
diamond, role of electron-hole interaction in optical spectra, review 80−45113
diamond, semiconducting, band gap temp. depend, dilation and vibr. contribs. determ. 80−10868
diamond, type Ia, max. lattice freq., IR absorpt. spectra 80−16026
diamond, type IB, electron irradiated, 2.367 eV vibronic absorpt. system, optical study 79−73975
diamond lattice, dynamic symmetry and plastic deform. 80−24527
diamonds, natural, thermal cond., 0.5 to 20K, anisotropic heat cond. in boundary scatt. regime 79−65267
diatomic crystals, phonon spectra calc. by recursion method 80−59596
diatomic mols. in Ar matrix, vibr. level energy cascades 77−79598
p-dibromo-tetrafluorobenzene mol. cryst., in commensurate phase, quasielastic neutron scatt. 80−107386
dielectric, regulated, thermal capacity, strong US waves effects *(Russian)* 80−65240
dielectric, spatially dispersive, boundary conditions for polarisation waves 79−61296
dielectric crystal, APR and phonon spectroscopy to study paramagnetic ions 80−84634
dielectric crystals, doped, phonon spectroscopy using supercond. tunnel junctions 79−90738
dielectric crystals, externally deformed, phonon transport eqn. 77−27956
dielectric deformed crystal, phonon hydrodynamics 77−20025
dielectric material, phonon gas, nonlocal hydrodynamics, second sound attenuation, thermal cond. *(Russian)* 78−47478
dielectric medium at low temp., influence of nonequilib. phonon gas on US propagation *(Russian)* 78−71795
dielectric plate, dimensional effects in ultrasonic wave absorpt. coeff. *(Russian)* 80−70321
diffusion with freq. down-conversion 80−19886
1,4-dihalonaphthalene: octafluoronaphthalene, Raman spectra, phonon band mass coeff. tuning 79−8131
dirty superconductor limit, microjunction phonon spectroscopy *(Russian)* 79−11272
discrete ϕ^4 chain, statistical mechanics 79−75463
displacive regime, lattice phonons in presence of non-linear excitations 80−44283

lattice phonons continued
displacive transformations, one-dimensional model, interaction of solitary wave soln. with phonons 78−22813
displacive transitions, continuum ϕ^4 equation, kink-phonon and kink-kink interactions 80−70354
echo, recent trends in physical acoustics *(Japanese)* 80−79889
echoes, electroacoustic and acoustoelectric mechanisms *(French)* 77−51461
elastic phase transitions, crit. dynamics 80−2146
electroacoustic echo in crystals 77−1641
electron channelling patterns, contrast mechanisms, lattice-defect images, in SEM 79−27884
electron-hole droplet phonon wind 80−107707
electronic state of excitations and their phonon coupling 79−60719
electronically driven phonon anomalies and phase transforms. 78−63834
emission into diffusive medium 79−14896
energy mismatch in multiphonon relax. 77−24371
EPR, phonon avalanche due to nonequilib. dipole reservoir, theory 79−99751
EPR, saturation of inhomogeneous broadened line under bottleneck phonon condition *(Russian)* 79−8040
ethylene, lattice dynamics of cryst., ab initio interaction pot. 79−33043
ethylene, solid, self-consistent phonon calcs. 78−75745
excitation and detection of phonon beams in GHz range 78−43080
exciton luminescence spectra, surface polaritons and Brewster waves *(Russian)* 79−43033
F-centres, relaxed excited states, vibronic model of stress effects 78−95118
ferroelectric crystal, displacive, effect of elec. field on thermal cond. 77−85002
ferroelectric phase boundary, effect of temp. gradient 79−8107
ferroelectric with orientational transition, coupled elastic, EM and polarisation oscill. spectrum 79−8103
ferroelectricity, unified model, tunnelling of atoms, phonon vibrs. and statistical disorder 78−31160
ferroelectrics, centrally-symm. displacement type, dielec. losses, weak elec. field effect *(Russian)* 80−29683
ferroelectrics, H-bonded, phonon relax. mechanism 80−79906
ferroelectrics, inelastic neutron scatt., one-phonon differential cross section 80−28883
ferroelectrics, order-disorder, displacive transformations, tunnelling, phonons 80−75975
ferromagnetic, thick film, reson. transmission of EM energy via phonons 80−60382
ferromagnetic resonance, phonon propagation 78−88194
filament, condenson energy and mass 78−91637
focusing, phonon magnification factor determ. 77−47517
focusing and cond. in orthorhombic and tetragonal crysts., boundary scatt. regime 79−42162
focusing phenomena, catastrophe theory 80−59591
Formvar, phonon spectrum from Al-Formvar-Pb junction electron tunnelling 77−59080
frequency crossing techniques appl. to high resolution phonon spectroscopy 80−107392
Frohlich model, method of functional derivatives 78−51909
frozen solution spectra, inhomogeneous broadening and phonon effects 79−33725
gas-solid collisions, phonon energy transfer model Hamiltonian 80−34307
GG GaS, indirect exciton exam. 78−39029
graphite, E_{2g} mode splitting, two-phonon spectrum 78−92077
graphite, finite-size crysts. first- and second-order Raman scatt. 79−95759
graphite, neutron irradiated, thermoelec. and thermomag. effects 77−59296
graphite intercalated with AsF_5, HNO_3 and $SbCl_5$, Raman scatt. in low stage cpds. 80−20638
graphite intercalation compounds struct., elec. props. 78−27446
graphite-Rb intercalation compounds, Raman scatt. from in-plane lattice modes 78−15168
half space layered cryst., vibr. spectrum, Brillouin zone *(Russian)* 80−100313
high energy spectroscopy using tunable dye laser 78−83893
high frequency phonon stimulated emission by fast charged particle channelling 79−73267
high resolution phonon spectroscopy at low temps., review 79−69207
highly anisotropic crystal, phonon spectrum and local vibrs. *(Russian)* 78−59912
highly excited harmonic oscillator in crystal, damping 79−40408
hydrogen-bonded ferroelectric, Ising model in transverse tunnelling field and proton-lattice interaction 80−7307
hysteresis in nonequilibrium superconducting proximity-effect bridges 79−15258
ice, hexagonal, Raman spectra of temp. depend., 80 to 250K, translational vibr. modes 77−36221
ice, Ih-phase, oriented single cryst., proton distrib., light scatt. obs. 77−16318
II-VI semiconductor:Co^{2+}, IR luminesc., local density of phonon states 79−33778
III-V semiconductors, radiative recomb., optical evaluation review 80−60647
impure crystals, vibrs. in average local information transfer approx. 79−46774
impure metals at low temperatures, conductivity 80−103669
impurities, interaction and diffusion, near structural phase transition of matrix 79−42083
impurity molecules in solids, vibrational relaxation, anharmonic dynamics role *(Russian)* 80−75323
impurity relaxation in nonresonance field, phonon amplification *(Russian)* 80−100310
incommensurate crystals, first order Raman scatt. from unbounded phonons 80−88990
incommensurate lattice, energy gap in phonon spectrum. role of Coulomb forces 80−44269
inert gas:Eu(Sm), absorpt. and emission spectra, phonon sidebands 79−43021
inert gas crystal, two-phonon bound states in high temp. limit 77−43291
inert gas solid, two-phonon Raman light scatt. 79−56783
inert gas solids, self-consistent phonon theory, book contrib. 77−51460
inhomogeneous solid, determ. of homogeneous impurity spectra 79−73982

lattice phonons continued
insulator, strong US wave absorption due to phonon interactions 77−89503
insulators, nonlocal hydrodynamics of phonon gas *(Russian)* 79−10900
interacting systems, predominant states and matrix elements 80−89033
interaction with electron-hole drops, in heat pulses, effect of phonon wind 78−6279
Invar, ferromagnetic, lattice dynamics 79−55838
Invar, influence of magnetoelastic effects on lattice vibrs., neutron scatt. meas. 78−2722
ionic crystals, centrosymmetric, stimulated excitation of second harmonic, microscopic theory 80−91849
ionic crystals, positronic atom scatt. on optical phonons, positron thermalisation 80−50457
ionic crystals, surface polaron 78−60020
Ising chain, linear, three dimensional phonon field 77−73036
Ising chain in 3-dimensional phonon field, rel. to spin-glass models 79−56540
Ising chain of alternating spins of 1/2, and general S, appl. of transfer matrix method 80−80529
Jahn-Teller effect, intermediate, in orbital triplet, effect on EPR 80 34756
Jahn-Teller multimode system, Ham factors 80−100446
Jahn-Teller problem, $T\times e_g$, spin-orbit allowed tunnelling splitting, zero-phonon line splitting 78−19006
Jahn-Teller system, reduction factor calculations, diagram approach 78−19003
Josephson junction, computer simulation of vortex motion, induced by phonon injection 79−73636
Kikuchi patterns due to plasmon and phonon excitations 77−76264
kink dynamics in one-dimens. double-well field theory 80−39247
Kramers ions, virtual phonon exchange, field theoretic formalism 80−20137
$KZnF_3$:Er excitation of 650 GHz phonons in spin-lattice relax. 78−27089
laminary crystal, phonon spectrum and local vibrations *(Russian)* 80−10623
lattice thermal cond., variational bounds improvement by scaling and Ritz procedures 77−62689
lattice thermal conductivity, general transport theory, phonon Boltzmann eqn. 80−54446
lattice thermal conductivity determ., hypercircle approach and complementary variational principles 77−47630
layered semiconductors, high pressure effects 77−51654
layered structures, sp. ht. rel. to phonon spectrum *(Russian)* 79−90794
lecture on phonons and polaritons 78−26638
light pulse resonant interaction with matter, lattice vibr. enhancement, relax. role 79−23009
light scattering near phase transition pts. in pure and defect containing cryst., review 80−93361
linear chain with anharmonic pot., SC phonon, RPA and transfer integral methods 77−51452
linear conductor, dynamical aspects of fluctuations 79−33715
linear defects, local phonon modes and structural instability *(Russian)* 79−73275
linear spin chain in uniform mag. field, spin-phonon interactions *(Russian)* 80−2594
lithium formate, optical phonons, small oscillator strength meas. from frequency-angular polariton spectra 80−92629
lithium thallium tartrate, single cryst., thermal cond. at low temps. 79−33125
lithium thallium tartrate, sp. ht., 0.3 to 25K, second-order ferroelec. transition 80−59674
magneto-optic Raman scattering of Raman-inactive phonon polaritons 80−91843
magnetocrystalline anisotropy constants, phonon-induced temp. depend. 80−65858
magnetophonon oscillation separation techniques, advanced methods 78−2499
malignant cells, evidence for a condensed phonon state 79−62214
malononitrile, displacive phase transition, 294.7K, Raman and Brillouin-Rayleigh scatt. obs. 80−16047
martensite formation, and lattice props. rel. to elastic constants 80−50630
matrix isolated NO $3s\sigma(A^2\Sigma^+)$ Rydberg state 'bubbles', reson. fluoresc. obs. 77−83636
melting temperature, Lindemann hypothesis and size depend. 80−15222
metal, low temp. phonon resist. 77−62888
metal, phonon spectra, singularities caused by local geometry of Fermi surface 78−91401
metal, positron-phonon scatt. for non-equilibrium phonon subsystem 79−15551
metal, quasi one dimensional, Peierls instability criterion *(Russian)* 77−89516
metal, spin scattering and spin-orbit coupling 80−29369
metal surface, resonant absorpt. of sound *(Russian)* 78−95216
metal-insulator-metal-superconductor junction, phonon struct., proximity effect tunnelling 79−82721
metal-metal microbridge, electron-phonon coupling and phonon generation 77−76510
metallic point contacts, nonlinear resist. rel. to phonon emission and background effects 78−68074
metals, BCC, diffusion of H_2 and its isotopes, phonon-assisted quantum-mechanical tunnelling of interstitials 80−59730
metals, electrical and thermal resistance, influence of static atomic displacements 80−103674
metals, melting theory for small particles, Helmholtz free energy 80−59629
metals, phonon limited resistivity, anharmonicity, Debye Waller factors, ^{4}multiphonon terms 80−49691
metals, phonon point-contact spectroscopy 79−65152
metals, phonon-phonon scatt. role in lattice thermal cond., phonon drag, elec. cond. 80−70483
metals, positron-phonon interaction through cond. electrons *(Russian)* 80−29126
metals, struct. of d^2J/dV^2 charact. of point contacts 80−96975
metals, surface positronium formation, stopping distance, positron-phonon interactions 80−96582
metals, X-ray photoemission line shape, Fermi surface excitations, book contrib. 79−61499

lattice phonons continued
metals and alloys, electron momentum density, positron annihilation meas., book contrib. 79−99976
methane, solid, probing phase transition with Mossbauer effect in ^{57}Fe impurities 79−4751
methane and methane-d_4, solid, thermal cond. calc. 78−51753
methyl compounds, rotational tunnelling, temp. dependence 80−38970
minerals, silicates and oxides, phonon cond. 77−73715
mixed crystal, line profile of absorpt. and Raman spectra, calc. 78−48183
mixed crystal, theory of lattice vibr., CPA, ATA and REI models 77−1190
mixed crystals, reson. Raman scatt. of light by longitudinal optical phonons 77−28577
mixed valence systems, phonons, effect of valence changes due to f⇄d electronic transitions 79−95104
molecular crystal IR spectral line shape and polarisation temp. depend. 80−88991
molecular crystals, dipolar coupling and phonon symm. *(Chinese)* 80−103437
molecular crystals, photon echoes *(Dutch)* 78−71156
molecular crystals, polariton spectra and lattice dynamics 80−49313
molecular polaron, dynamics and thermodynamics 78−14678
molecular solid, intermolecular interactions, laser induced phonon probe 80−79891
MOS structure, interface states, evidence for multiphonon emission 78−39220
multiphonon relaxation, statistical anal. 79−79223
β-Na_2O-Al_2O_3 low temp. ultrasonic vel. meas., temp. depend. 80−79885
naphthalene:$\beta\beta'$-dinaphthylethylene, stimulated emission suppression in phonon wing 78−2881
naphthalene, doped, role of nonequilibrium phonons in stimulated radiation emission 80−103971
naphthalene, external mode one-density states, low freq. Raman scatt. spectra *(French)* 80−76012
naphthalene, melting of rotational degrees of freedom near cryst.-liq. transition 80−54352
naphthalene, phonon eigenvectors, neutron scatt. intensities determ. 80−44271
naphthalene, Raman active phonon freqs., linewidths and line shapes, temp. depend. 79−47432
naphthalene, vibr. dephasing and Raman active localised internal mode temp. depend. 80−45060
naphthalenes, phonon satellite narrowing in local exciton luminesc. *(Russian)* 79−47507
narrow gap semiconductors, recombination mechanisms, review 80−96905
narrow-gap ferroelectric, phase transition due to strong mag. field 80−103924
neutron inelastic scatt. expts., book contrib. 78−1959
neutron scattering, inelastic, optical phonon strong anharmonicity effects 77−31739
neutron scattering for dynamics of liquids and solids, book 77−89350
neutron scattering from equilibrium and non-equilibrium phonons, excitons and polaritons 80−84032
neutron scattering obs. of phonons, book contrib. 77−89504
$NH_4H_2PO_4$, phonon echos in SiO_2, ADP, KDP, and Rochelle salt *(Japanese)* 79−51213
noble metals, energy wave number charact., by reson. model 80−10612
non-equilibrium phonon distrib., in cryst., spectral line shape theory 80−60530
nondegenerate semiconductor, thermomagnetic phenomena in quantising mag. field *(Russian)* 80−60014
nonequilibrium phonon gas, spontaneous breaking of symmetry *(Russian)* 77−11645
nonequilibrium superconductivity, theory in coherent longitudinal phonon field 79−47205
nonlinear optical reson. effects, phonon generation by IR radiation 78−50865
nonradiative transitions at impurity centre with participation of short-wavelength phonons 80−16099
nonresonance field heating and cooling of local and quasilocal vibrs. 79−65148
nonresonant transfer of energy between impurities in solids 78−23520
normal metal-superconductor double-layer, photon struct. induced into normal side by proximity effects 79−99659
nuclear acoustic resonance, behaviour of incoherent phonons 80−7180
nuclear operators single $\hbar\omega_0$ and models of luminescence centres, operators 79−78749
one dimensional conductors, electron-electron interactions and Kohn anomaly 80−24895
one dimensional crystal, failure of linearised phonon approx. 77−62590
one-component plasma, crystallized, dynamics and energy, self-consistent-phonon theory 80−107384
one-component systems with quartic anharmonicity, microscopic theory of statics and dynamics 79−73260
one-dimensional conductor, IR and Raman activity 78−60441
one-dimensional conductor, phenomenological eqns. of motion for electrons, phonons and librons 80−10955
one-dimensional conductor, phonon dynamics 78−79704
one-dimensional conductors, Peierls instability, dynamics, structural energy, pseudopot. calc. 80−54676
one-dimensional lattice, props. of commensurate CDW system 78−75796
one-dimensional metallic systems, theory of structural phase transitions 78−38830
one-dimensional systems, electron trapping and transport by supersonic solitons 78−72139
opaque crystal, Brillouin scatt., photoelastic and surface corrugation contribs. 79−42980
opaque crystal, inelastic light scatt. by acoustic phonons 78−43851
opaque media, Brillouin scatt. theory 79−19895
optical absorption spectrum dynamics using sub-ps. optical pulses 80−11431
optical detection of acoustic phonons at THz freqs. 80−75320
optical fibres, single-mode, normal acoustic modes and Brillouin scatt. 79−76760
optical no-phonon impurity lines, influence of local and quasilocal vibrations on thermal broadening 78−30717
order-disorder ferroelectric, phonon damping and freq. shift *(Russian)* 79−60471
ordered vacancy compounds, lattice dynamics 78−75770

lattice phonons continued
organic charge-transfer complex, mixed-stack crystalline, phonon bands 78−75767
organic conductors, Fano anti-resonance and IR props. 79−15465
oxide crysts., Fourier transform Ir spectroscopy of vibr. states at high temp. 80−97256
PAA, cryst. phase transitions, intermolecular motion, Raman and inelastic neutron scatt. spectra 80−2164
PAP, cryst. phase transitions, intermolecular motion, Raman and inelastic neutron scatt. spectra 80−2164
paradichlorobenzene, NQR study of the lattice dynamics *(Russian)* 80−97160
paraelectric tunnelling systems, broadening mech. 79−28701
paramagnetic crystal, Mandel'shtam-Brillouin light scatt. by hot phonons 77−52110
parametric excitation in field of strong EM wave 80−2133
parametric generation of acoustic phonons by laser beam, theory 77−20021
particle size effect on acoustic phonon spectrum, rel. to Debye temp. 77−72666
pentacene, in naphthalene (p-terphenyl), picosec. coherent transients obs. 79−46013
pentacene in p-terphenyl, intermolecular interactions, laser induced phonon probe 80−79891
perylene, intermolecular interactions, laser induced phonon probe 80−79891
phase transitions, rigorous bounds, quantum anharmonic phonon model 77−15541
phase transitions soft modes and dipole relaxations 78−91409
phonon anomaly near Fermi surface topological transition 78−95120
phonon conductivity correction due to three phonon normal processes in presence of dislocations 80−15318
phonon echo, review *(Japanese)* 78−14409
phonon electroacoustic echo under acoustic reson. conditions *(Russian)* 77−48131
phonon-assisted radiative transfer 77−90192
phonon-polariton modes for freq. chirped optical pulse compression 78−46689
photoemission spectroscopy, angle resolved, importance of thermal disorder 77−90243
picosecond optical phonon lifetimes, Raman scatt. meas., book contrib. 77−65057
piezoelectric crystals, acousto-optic props. exam., light scatt. by thermal acoustic phonons 78−48144
piezoelectric powders, phonon echoes and long-time storage *(Japanese)* 80−70330
piezoelectric semiconductor, nonlinear acoustic noise amplification theory, phonon distrib. function basis 78−47837
piezoelectrics, phonon echo in travelling and standing wave regimes 77−8521
plastic crystal, dipolar autocorrelation function, phonon contrib., IR absorption 78−42928
polar, directional dispersion meas. by i.r. reflection 77−1665
polar crystal, vibronic levels for Jahn-Teller impurities 78−68520
polar crystals, vibrational Raman scatt. induced by Jahn-Teller systems 79−69830
polar mode crystals, IR dispersion 77−73141
polar phonons in crysts., Raman scatt. theory 79−47447
polar semiconductor, exciton, energies, oscillator strengths, and phonon side bands 80−44512
polar semiconductor, exciton-dispersion 80−6741
polar semiconductor, Raman spectra of coupled LO phonon-plasmon mode, de Haas-Shubnikov like quantum oscills. 78−43863
polar semiconductor, TO phonon-helicon coupling 79−73539
polar semiconductors, resonant secondary radiation 78−31242
polarisation echo, physical nature 77−1635
polarisation operation in one- and two-dimensional crystals *(Russian)* 78−79676
polarization echo and induction signals excited by pulses of various duration *(Russian)* 79−61298
polycrystal cold neutron incoherent inelastic scatt., computation of phonon spectrum 78−34572
polyethylene, crystalline, Mossbauer anisotropic elastic scatt. fraction 78−6616
polyethylene, oxidised, paraelectricity, dielec. relax. obs. 77−48123
polysulphur nitride, low temp. thermal cond. 80−24689
porous glass:In, effect of press. on transition temp. 80−97027
propagation of phonon pulses in spontaneous decay mode *(Russian)* 78−34571
proximity effect sandwiches, phonon structure in tunnelling characts. 77−28304
pseudo-one-dimensional system, Ginzburg-Landau theory of phase transitions 77−15529
quantum corrections for a system of interacting phonons and the modified Korteweg-de Vries equation 79−60454
quantum crystal, model of tunnelling point defect at finite temp. 78−38907
quantum crystals, approx. second quantisation method 79−23804
quantum field theory of crystals and extended objects, review 79−42164
quantum field theory of solids, book 77−31922
α-quartz:Al, γ-irrad., thermal cond. below 10K 79−51320
quartz:Co^{2+}, far IR absorption spectra, effect of phonons *(French)* 78−31186
quartz, α-β phase transition, lattice dynamical study 79−65168
quartz, acoustic phonon geometric propag., anisotropic continuum acoustics 77−4169
quartz, Fourier transform Ir spectroscopy of vibr. states at high temp. 80−97256
quartz, fused, longit. phonon lifetimes, thermal Brillouin scatt. obs. 77−36255
α-quartz, Gruneisen constants for optical modes, neutron irrad. and press. effects *(Russian)* 78−22815
α-quartz, high-frequency phonon lifetimes 80−70338
α- quartz, Raman spectrum, piezospectroscopic behaviour 78−35138
α-quartz, Raman spectrum of optical phonon mode, stress splitting and wave-vector depend. 77−77214
quartz, resonant powder, stimulated phonon echo, ang. and powder depend. 79−8093
quartz, stimulated Brillouin scatt. correlation with laser induced damage 77−38984
quartz, x-cut, triplepass Brillouin scatt. by induced phonons 77−28588

lattice phonons continued
quasi one-dimensional spin lattice coupled system, collective modes 80−24896
quasi-elastic scattering of phonons and thermal conductivity, structural phase transition 79−82299
quasione dimensional crystal, phonon spectrum change due to struct. transition 78−67789
radiative electronic transitions of impurities, effects of hydrostatic press. 80−11446
Raman effect in solids, interacting elementary excitations, review 78−43846
Raman scatt. cross sections in simple solids 80−93334
Raman scattering, anticorrel. effects. Heisenberg eqns. of motion, Raman scattering by phonons 79−95747
Raman scattering, stimulated, oscillations, spatial and temporal, in saturated optical phonon generation 78−87099
Raman spectra, vibr. anal. 80−93312
rare earth chlorides, doubly degenerate E-phonons, mag. field splitting 77−43297
rare earth compounds, cooperative Jahn-Teller phase transition, theory of optical side-bands 77−1398
rare earth compounds, paramagnetic, Faraday and Cotton-Mouton effects for acoustic phonons 78−52476
rare earth compounds, Raman light scatt., phonons and valence fluctuations, review 77−63415
rare earth compounds, valence fluctuations, electron-phonon coupling effect 80−20134
rare earth monobismuthides, thermal expansion, thermal cond., 300-900K 78−91453
rare earth orthoferrite, phonon slowing down of domain wall *(Russian)* 79−33503
rare earth oxsulphides:Eu^{3+}, phonon sidebands 78−15214
rare earth salts, phonon field contrib. to g-shift, symm. restrictions 77−55500
rare earth systems, crystal field effects 78−67987
rare earth systems, mag. field depend. of polaritons 79−33246
rare earth trichlorides, magnetic phonon splitting, Raman spectra 77−52099
rare gas crystals, lattice heat capacity, thermal vibrations, Lindeman parameter, lattice dynamic model *(Russian)* 80−29141
reorienting or tunnelling molecular groups in solids, symmetry of rotor part of rotor-phonon interaction 80−84114
resonance Raman scattering, appl. to ultrafast dephasing and relax. obs., phonon scatt. effects 80−7337
resonance Raman scattering, in strong elec. field 77−16305
resonance Raman scattering, influence of mass defect disorder 78−35133
resonance scattering of neutrons and γ-quanta, high recoil energies *(Russian)* 78−35075
resonant Raman scattering by LO phonons 78−39551
RF vibrating crystals, inverse problem of Mossbauer spectroscopy 79−78574
ruby, 29 cm^{-1} phonon propag. and lifetime, reson. scatt. *(Russian)* 78−34581
ruby, acoustic phonon focusing, direct obs. *(Russian)* 77−59075
ruby, anisotropic 29 cm^{-1} phonon capture *(Russian)* 80−6471
ruby, high energy phonon spectroscopy 78−83893
ruby, optical pumping, bottlenecked 29 cm^{-1} phonon spectral width 77−12425
ruby, optically excited, diffusion of bottlenecked 29 cm^{-1} phonons 80−6472
ruby, phonon bottleneck of direct decay within $\bar{E}(^2E)$ state, optical detection 80−10608
ruby, phonon spectrum, thermal pulses under diffuse phonon propagation conditions 80−103434
ruby, phonon spectrum of high energy heat pulses generated in thin metal films 77−20140
ruby, phonons, at 29 cm^{-1}, stimulated emission 80−45114
ruby, resonance radiation transfer and nonequilibrium phonons *(Russian)* 78−80418
ruby, resonance trapping of 0.87×10^{12}Hz acoustic phonons in mag. field 78−91400
ruby, resonantly trapped 29 cm^{-1} phonons, spectral diffusion 78−92113
ruby, spatial diffusion of weakly bottlenecked 29 cm^{-1} phonons, quasi-stationary techniques 79−73996
ruby, spin-strain coupling tensor meas. US modulated EPR obs. 80−50170
ruby R_1 zero phonon line, resonance fluoresc. meas. 80−89055
saccharose crystal, low temp. pyroelectricity 79−42909
sapphire, acoustic phonon geometric propag., anisotropic continuum acoustics 77−4169
sapphire, constant phonon energy contours, in bc-plane, inelastic neutron scatt. obs. 77−59083
sapphire, optical detection of acoustic phonons at THz freqs. 80−75320
sapphire, phonon cond. calc., 0.4-4K 78−18852
sapphire, second sound observation by heat pulses method, phonon scatt. processes *(Russian)* 79−99273
β-Sb_2O_3, Raman spectra, vibr. anal. 80−93312
Seebeck effect, volume component determination 80−49788
semi-infinite crystals, linear wave vector effects on optical props. 77−85721
semiconducting solid solutions, optical transitions, review 78−2908
semiconductor, deformation potential, possibility of screening by free carriers 77−72826
semiconductor, doped lattice thermal cond., role of electron-phonon interactions and peripheral phonons, appl. to Ge:P 78−79702
semiconductor, EM generation of ultrasound 79−51639
semiconductor, indirect band gap, Auger recomb. of electron-hole drops 78−39600
semiconductor, light scatt. spectra, interference effects 79−82977
semiconductor, local fields, nonuniform charge distrib. 80−24826
semiconductor, multiphoton absorption by charge carriers in mag. field 77−28553
semiconductor, narrow gap, optical phonon spectrum 79−7794
semiconductor, nonequilibrium acoustic phonons, generation by interband light absorption 80−96607
semiconductor, nonequilibrium optical phonons generated by electrons in laser radiation field 78−71802
semiconductor, optical phonon generation on intraband absorpt. of EM radiation *(Russian)* 77−48235
semiconductor, phonon conduction and relaxation times 80−107585
lattice phonons continued
semiconductor, phonon spectrum in mag. field, renormalisation 79−28060
semiconductor, phonon-assisted Auger recomb., scatt. mechanisms 77−85804
semiconductor, phonon-assisted Auger recomb. transition probability 77−44064
semiconductor, polar, longwave secondary radiation *(Russian)* 78−80343
semiconductor, polaron transport in long phonon waves approx. 79−90975
semiconductor, possible phonon generation by EM wave 80−96606
semiconductor, Raman scatt., one-phonon final states and many-body effects 80−34913
semiconductor, resonant Raman scatt., book contrib. 77−36251
semiconductor, surface Brillouin scattering from acoustic phonons 80−55113
semiconductor defects, entropy of ionisation and temp. variation of ionisation levels 77−11871
semiconductor film, cyclotron-phonon absorption singularities 77−51955
semiconductor film, phonon spectrum under one-dimens. quantisation conditions 77−66007
semiconductor film, quantised, one-phonon light absorption 78−60527
semiconductor layer structure, laser-induced photolum. and collective effects *(Russian)* 79−95830
semiconductor superlattice, phonon spectrum, effect of strong elec. field, parametric reson. 80−44273
semiconductors, covalent and ionic, surface (110) atomic struct. bulk elastic consts. and phonon freqs. 79−69331
semiconductors, degenerate, resonance Raman scatt., Green's function method 80−80781
semiconductors, electron-hole drop formation, phonon wind influence *(Russian)* 80−92825
semiconductors, electron-phonon interactions, combined phonon resonance *(Russian)* 80−75321
semiconductors, impact ionisation theory 80−49752
semiconductors, lattice thermal conductivity, high temp., role of optical phonons 79−33129
semiconductors, lattice vibration amplification in field of EM wave 77−76511
semiconductors, narrow band gap, superlattices, acoustic wave absorpt. and amplification 80−29445
semiconductors, nondegenerate, free carrier absorpt. in quantising mag. fields 80−45044
semiconductors, nonradiative multiphonon carrier-capture cross section of deep traps, low temp. depend. 78−10469
semiconductors, optical props. due to phonons, book contrib. 80−80805
semiconductors, photostimulated enhancement of optical lattice vibrs. 79−55845
semiconductors, polar, resonance electron-phonon Raman scatt., cross-section oscills. 80−60598
semiconductors, relax. and reson. struct. in magneto-optical spectra 80−29723
semiconductors, resonant Raman scatt. from exciton-polaritons *(Japanese)* 80−50349
semiconductors, van Hove critical point region, electron-phonon interactions, dispersion law 80−70344
semiconductors, weakly polar, free polaron IR absorpt. effect of DC field 77−81132
semimetal, phonon spectrum, influence of mag. field induced quasi-local levels 78−18946
shear waves, rotary activity under helicon-phonon interaction 80−2412
Shpolskii systems, sensitised phosphoresc., triplet-triplet energy transfer *(Russian)* 78−76527
silicate minerals, heat capacities rel. to simple lattice vibrational models 80−4005
silicate minerals, phonon cond. and mean sound vel., linear relationships 77−21761
silicate minerals, relationship between phonon cond. and seismic parameter Φ 79−39707
silicate minerals, thermodynamics and lattice vibr. props. 79−100830
silicate minerals, thermodynamics and lattice vibrs. 79−100831
sine-Gordon system with winding-number density, low temp. soliton gas phenomenology 80−105589
small metallic particle, theory of far-IR absorpt. 79−19881
SO(4)-invariant pseudo-Jahn-Teller system with equal coupling 80−15029
solid-state theory, introduction, book 79−33215
solids, acoustic wave emission, absorpt. and propag. in THz range 80−65164
solitons in system of coherent phonons and photons 79−64291
spatially dispersive media, optical boundary value problem 80−45024
spectroscopy, HF, using supercond. tunnel junctions 80−65178
spectroscopy, phonon pulse spatial, spectral and temporal evolution 78−34580
spectroscopy, phonon pulse spectral distrib. 78−34579
spin lattice relax. and g-shift, one-phonon processes 80−15799
spin system, optical-acoustic two-phonon relax. 80−11244
spin system, thermodynamics, contrib. of spin-phonon interaction 78−2635
spin-Peierls transition in mag. field, phonon freq., Heisenberg model calcs. 80−25151
steel, stainless, Mossbauer radiation modulation by coherent US excitation 79−61277
stimulated Raman scattering, review of appls. 77−735
strongly coupled Jahn-Teller system, cluster model for optical absorption spectrum 80−89034
structural phase transforms. and phonons, book contrib. 77−89518
structural phase transitions, crit. dynamics and quasi-elastic scatt. 80−92641
structural phase transitions, de Gennes pseudospin model, lattice phonons tunnelling effects 79−73290
structural phase transitions, tunnelling effects 79−55858
structural phase transitions and anharmonic phonons 78−14433
structural transitions, method of self consistent phonon field 79−33065
sublattice and interatomic force constants from phonon meas. 77−27958
superconducting critical temp., generalised moments of phonon spectrum *(French)* 80−39702
superconducting film, illuminated, heating model and spectral charcts. of phonon emission 79−28442
superconducting film, photoexcited, phonon spectrum 80−11132

lattice phonons continued
superconducting junction electron tunnelling, effect of dissolved O^{2-} 78−80100
superconducting transition critical temperature, BCS theory, phonon spectra, review *(Spanish)* 80−84535
superconducting transition temperature, determination, influence of effective phonon spectra 79−78252
superconducting tunnel junction, nonequilibrium phonon effect on supercond. states with 2 coexisting energy gaps 80−84561
superconductive tunnelling, appl. in inelastic electron tunnelling spectroscopy 79−4625
superconductive tunnelling, phonon generation and detection by tunnelling *(Japanese)* 77−28306
superconductivity, nonequilibrium, quasiparticles and phonons 78−52146
superconductivity and phonons, review 80−84543
superconductor, nonequilibrium distribution functions of quasiparticles and phonons calc. 77−89904
superconductor, nonequilibrium excitation of quasiparticles and phonons 77−43783
superconductor, phonon mechanism for sound-affected energy gap *(Russian)* 77−43781
superconductor, quasiparticle and phonon lifetimes, theory 77−20488
superconductor, theory of tunnel injection *(Russian)* 79−47198
superconductor film, nonequilib. states induced by thermal phonon injection 77−47925
superconductors, A15 cpds., local lattice instabilities 78−19178
superconductors, effective phonon spectrum influence on T_c *(Chinese)* 79−51707
superconductors, kinetic eqns., nature and decay rate of new mode 80−49978
superconductors, nonequilibrium, T^* model of quasiparticle and phonon distribs. 80−25039
superconductors, nonequilibrium, phase transitions induced by quasiparticle injection 78−91808
superconductors with A-15 lattice, LF maxima in phonon state density and exponential term of resist. *(Russian)* 77−80871
superionic conductors, collective motion, AC conductivity rel. to acoustic phonons 79−99368
superionic conductors, light scatt. and IR absorpt. book contrib. 80−25382
superionic conductors, prefactor anomalies, effect of low dimensionality 78−48061
superionic conductors, theoretical models, review 80−107465
supernonradiative phase transition, appl. to paramag. impurities in strong mag. field 79−14898
surface, adsorbed atoms thermal desorption, one dimens. microscopic model, weak binding case 80−96729
surface Brillouin scattering, from acoustic phonons, general theory 80−34932
surface energy of solids, universal model 80−39409
sym-trioxane, phase transition, polarised Raman spectra obs. 80−84742
TCNQ salt, decamethylferrocenium, monomeric and dimeric, optical and EELS study 80−100660
TCNQ salt, NMP-TCNQ, X-ray diffuse scatt. rel. to charge transfer 77−80496
TCNQ-HMTSeF, X-ray diffuse scatt., one-dimens. distortion in phonon spectrum and interpret. 78−10144
tetracene, cryst., solid-state transitions, Raman spectra, prompt fluoresc. in mag. field 79−99865
1,2,3,5-tetrachlorobenzene, chemical perturbation of cryst. structs., Raman phonon spectra 78−26559
tetrahedral lattice sites, selection rules for multiphonon transitions 80−92632
TGS, ferroelec. single crystal, low freq. nonlinear effects 80−84490
TGS and deuterated cpd., ferroelec. US relax. time constant 80−84257
thermal broadening, inhomogeneous, of crystal vibr. spectrum 80−55100
thermal conductivity, anomalous temp. behaviour near structural phase transition *(Russian)* 80−75394
thermal conductivity, Callaway eqn., phonon scatt. in highly disordered systems 80−20000
thermal desorption and dissociation catalyzed by a solid surface 80−108734
thermal optical rotation, temp. depend. 79−8111
thermal vibrations of solid, student description in terms of lattice waves 77−62591
thin film on substrate, normal Brillouin scatt. by acoustic phonons 80−20648
thin optical irradiated superconductors, phonon spectrum and phonon temp. definition 80−93037
thiourea, phonon modes near order-disorder transforms., hard-core modes due to pseudospin-phonon coupling 80−44285
thiourea, phonon modes near phase transitions, IR and Raman spectra 80−45084
time dependent phonon irrad. of detector area from pulsed incoherent phonon radiator 78−38790
transition and noble metal dilute alloys, Einstein's temp. and vibrational entropy, rel. to electronic struct. 78−83900
transition metal, dichalcogenide layer cpds., bonding and phase transitions 80−34186
transition metal, surface lattice dynamics 78−95224
transition metal carbide, d-band effects in lattice dynamics to acoustic phonon freqs. 78−2207
transition metal compounds, electronically driven lattice instabilities, role of p-d hybridisation 79−7669
transition metal compounds, phonon anomalies due to d-band effects, electron-phonon matrix elements 78−30720
transition metal dichalcogenides, layered, optical phonon anisotropies 77−59573
transition metal dichalcogenides, layered, surface Brillouin scatt. obs., surface ripple and elasto-optic mechanisms 80−16048
transition metal dichalcogenides, optical phonon modes and localised effective charges, reflection spectra 78−76453
transition metal dichalcogenides, phys. props. and CDWs, review *(Japanese)* 80−49635
transition metal dihalides, layer struct., lattice dynamics, calc. 80−65177
transition metal tunnelling, tunnel junctions, phonon struct., junction quality 79−11274
transition metals, paramagnetic susceptibility, phonon instability, mixed localised-collective electron states 80−103811
transmission from incoherent radiator into cryst., anisotropic continuum acoustics 77−47521

lattice phonons continued
transport problems, use of generalised Langevin eqns. 78−30708
1,3,5-trichloro-2-bromobenzene, chemical perturbation of cryst. structs., Raman phonon spectra 78−26559
1,2,3-trichloro-5-bromobenzene, chemical perturbation of cryst. structs., Raman phonon spectra 78−26559
TSeF-TCNQ, X-ray diffuse scatt., one-dimens. distortion in phonon spectrum and interpret. 78−10144
TTF-Cu bis-dithiolene, dimer, mol. displacements at 4.2K 80−10539
TTF-halides, conductors with chain struct., lattice phonons and distortions, incommensurability transitions 80−24549
TTF-TCNQ, microscopic model for three low temp. phases 79−73303
TTF-TCNQ and derivatives, 1.8 to 40K, three dimens. state, specific heats 80−44333
tungsten bronzes, hexagonal, supercond. and special phonons, neutron scatt. obs. 80−15643
tunnelling, relaxation, competing models, paramagnetic defects 79−37787
two-phonon Raman scattering, double reson. 77−40226
type I and II superconductors, influence of effective phonon spectrum on T_c *(Chinese)* 79−51705
uniaxial crystal, dispersion of bulk phonon polaritons meas. by IR refl. 78−59902
uniaxial ferroelectrics, microscopic theory, crit. behaviour and anomalous elastic consts. 79−38463
uniaxial noncentrosymmetric cryst., oblique phonon symmetry props. 77−84861
US wave amplification and phonon echoes in microwave elec. field 79−19635
Wigner lattice, three-dimensional, detect. by Brillouin scatt. 77−36254
XPS, angle-resolved, phonon-assisted processes, interpretation 78−72696
XPS line shapes, phonon broadening, and independence of hole state lifetimes 77−48313
zero-phonon impurity lines in absorption and fluorescence spectra, temp. broadening and shift 77−8643
zincblende structure compounds, lattice dynamics, calc. program 79−33048
zincblende type crystals, lattice dynamics, phonon freq. rel. to mass ratio 78−95121
Ag-Sn proximity-effect bridges, crit. current hysteresis under phonon injection 79−87206
Ag-Sn proximity-effect bridges, T* anomaly under phonon injection 80−34566
Ag_3AsS_3, and Ag_3SbS_3, Raman spectra obs. of low-temp. phases 80−93327
Ag_3AsS_3, proustite, cryst., vibr. spectra 78−48172
AgBr, cyclotron reson. of polarons at high microwave fields 79−61228
AgBr, dispersive phonon modes, reson. Raman scatt. obs. 78−10896
AgBr, exciton absorpt. at high excitation rates 80−2343
AgBr, exciton relaxation by intervalley scattering 80−20644
AgBr, phonons at elevated temp. 78−79810
AgBr, streaming cyclotron motion of hot electrons, at intense microwave fields 80−6703
AgBr:I, isoelectronic trap 79−43016
AgBr:Li^+, time-depend. infrared absorpt., Li-localised mode decay into two phonons 79−8133
$AgGaS_2$, Raman spectrum, degenerate mods, temp. depend. 78−35150
$AgGaSe_2$, optical phonons, IR reflectance meas. *(French)* 77−81095
$AgGaSe_2$, polarised IR refl. spectra, optical phonon modes 77−16304
$AgGaSe_2(Te_2)$, far IR refl. obs. 78−60459
$AgGaTe_2$, optical phonons, IR reflectance meas. *(French)* 77−81095
AgI, density of states, IR cond., and Raman scatt., lattice dynamics calc. 78−30709
$AgInSe_2(Te_2)$, far IR refl. obs. 78−60459
Ag_2O, exciton luminesc. spectra, mag. field influence 80−80860
$Ag_xV_2O_5$, metallic, Raman scatt. 78−80358
$Ag_8W_4O_{16}$, high temp. Raman spectra exam. 77−36236
Al alloys, low temp. standard resist., appl. in resistors and strain gauges 77−17997
Al, Brillouin spectra, light scatt. cross section for surface ripples 80−71434
Al, electronic Gruneisen parameter in shock Hugoniot eqn. of state 80−10635
Al, empirical pot. methods, use of Wedepohl pot., vacancy form energy 80−39230
Al, film, superconducting transition temp. and lattice dynamics 80−93028
Al, Gruneisen coeff. depend. on specific volume, phonon spectra calcs. 79−65165
Al, metallic, phonon freq., binding energy, compressibility, elastic const. and energy band gap calcs., linear pot. 80−88284
Al, phonon-anharmonic response, neutron-scatt. test of computer calcs. 80−44281
Al, phonon density of states by neutron scatt., sp. ht. and Debye temp. 80−2132
Al, phonon scatt. surfaces obs., by neutron film methods 79−46761
Al, polycryst., density fluctuations, neutron scatt. anal. 80−70349
Al strips, supercond., on Si substrates, microwave-enhanced crit. currents, phonon effects 79−56451
Al, supercond., phonon absorption and pair breaking at 35 GHz 77−32120
Al, supercond. film, intrinsic and expt. quasiparticle recomb. times 77−15999
Al thin films, dielectric coating effect on superconductivity 80−7026
Al/formvar/Al(Sn) structures, low frequency phonon spectroscopy by tunnel effect 78−23206
Al-Ag, resonance splitting of phonons 78−75759
Al-Ag(Cu), alloying effect on phonon spectrum and lattice heat cond. 77−62695
$Al_{0.5}Ga_{0.5}As$, first order phonon spectrum replicas 78−60467
$Al_xGa_{1-x}As$: Sn(Te), persistent photocond., due to donor-related centres, symmetry 80−15558
$Al_xGa_{1-x}As$:Cr, exptl. verification of Cr^{2+} models of photoluminescent transitions 78−27320
$Al_xGa_{1-x}As$-GaAs, p-n heterojunction laser, low temp. operation 80−1204
$Al_xGa_{1-x}As$-GaAs, p-n heterostruct. laser, tunnel injection and phonon-assisted recomb. 80−5733
$Al_xGa_{1-x}As$-GaAs heterostructures, MO-CVD, phonon assisted recomb. and stimulated emission 80−1205

lattice phonons continued
$Al_xGa_{1-x}As$-GaAs heterostructure, quantum-well, hot electrons and phonons 80−84505
$Al_xGa_{1-x}As$-GaAs quantum well heterostructure lasers, operation 80−53292
$Al_xGa_{1-x}As$-GaAs quantum-well heterostruct., exciton in recomb. 80−103990
$Al_{1-x}Ga_xP$, IR phonons, lattice reflection spectra 78−51626
$Al_xGa_{1-x}Sb$ mixed crystal, two-phonon absorption meas., 15-48 μm 77−1682
$Al_xGa_{1-x}Sb$, vibr. spectra, Raman light scatt. study 80−45080
AlN, luminesc. excitation spectrum and band struct. 80−84783
AlN, phonon repetitions in excitation spectra 78−10956
Al_2O_3, corundum, Fourier transform Ir spectroscopy of vibr. states at high temp. 80−97256
Al_2O_3, doped, phonon spectroscopy in supercond. tunnel junctions 79−90738
Al_2O_3, high-frequency phonon lifetimes 80−70338
Al_2O_3, phonon spectra using freq. crossing techniques 78−14415
α-Al_2O_3, polarised luminescence in neutron- and proton-irradiated single crystals 80−66271
α-Al_2O_3, single crystal transmission and reflectance IR phonon spectra, polariton dispersion 80−66170
$Al_2O_3:Cr^{2+}$, HF phonon spectroscopy using supercond. tunnel junctions 80−65178
$Al_2O_3:Cr^{2+}$, multiple-ion phonon absorpt. 79−82971
$Al_2O_3:Cr^{3+}$, ruby, reson. scatt. and trapping of 29 cm^{-1} acoustic phonons 80−93403
$Al_2O_3:Fe^{2+}$, phonon spectroscopy using superconducting tunnel junctions 78−91389
β-$Al_2O_3:NH_4^+(Nd_4^+)$, polarised Raman scatt. 80−103947
$Al_2O_3:Ni_3$ heat transfer at low temp. 78−38888
$Al_2O_3:Ni^{2+}$, corundum, phaser production of transverse phonons by impurity centres *(Russian)* 78−91390
$Al_2O_3:V$, V^{3+} pairs studied by phonon freq.-crossing spectroscopy 78−39068
$Al_2O_3:V^{3+}$, frequency crossing signals of V^{3+} ions, conc. depend. study using thermal phonons 78−95115
$Al_2O_3:V^{3+}$, $g_\perp/g_\parallel$ determ. by freq. crossing spectroscopy using thermal phonons 78−23055
$Al_2O_3:V^{3+}$, phonon spectroscopy study of V^{3+} ion pairs 79−87068
$Al_2O_3:V^{3+}(Fe^{2+})$, hyperfine splitting and magnetoelastic consts., freq. crossing spectroscopy 80−107392
$Al_2O_3:V^{4+}$, dil. solution, stimulated phonon emission 78−63817
β-Al_2O_3-Na_2O-K_2O, cation interstitial pair modes in vibr. spectra 79−37788
β-Al_2O_3-Na_2O-Rb_2O, cation interstitial pair modes in vibr. spectra 79−37788
β-Al_2O_3-$Na_2O(Ag_2O)$, Raman scatt., 12-400K, 2nd order phase transition 77−81091
γ-AlOOH, boehmite, lattice vibrs., evidence for $C_{2v}{}^1{}_2$ space group 79−28756
β-Al_2O_3.$Li_2O(Na_2O)(K_2O)(Rb_2O)(Ag_2O)$, low temp. sp. ht., tunnelling states and diffusion theory 77−43345
$AlPO_4$, α-β cristobalite phase transition, Raman meas. 79−4799
α-$AlPO_4$, IR and Raman spectra, optical phonons 80−2767
Al_2SiO_5, andalusite, phonon spectra and rigid-ion model calcs. 80−11391
Ar matrix, Ca atom emission spectra, multiphonon relax. processes 78−37583
Ar small crystallite,s self consistent phonon calc. of struct. and thermodynamic props. 77−62596
Ar, solid, lattice dynamics calc. using Kihara hard core pot. 77−1193
Ar, solid, phonon spectrum, effect of 3-body forces and anharmonicity 79−77706
Ar:S_2, absorption spectra of matrix-isolated S_2 molecules 77−52139
As, amorphous and cryst., phonon density of states calc., comp. to IR absorpt. and neutron scatt. data 78−55924
As, black phosphorous struct., Raman vibr. spectra and bonding 80−11411
As, rhombohedral, phonon states 79−60464
As, zone centre phonons and elastic consts., hydrostatic press. depend. 78−59905
AsH_3, plastic cryst., dipolar autocorrelation function, phonon contrib., IR absorption 78−42928
As_4S_4, effects of pressure and temp. on phonons, Raman scattering study 80−7360
$As_xSb_{1-x}SI$ mixed crystals, phonon coupling, ferroelectric phase transition, Raman study 80−108165
As_2Se_3, cryst., electroabsorption on indirect gap 80−80812
As_2Se_3, photodarkening and photostructural effects, Raman, IR and NQR studies 80−16036
$As_2(Se_{1-x}Te_x)_3$, thermal cond., temp. and press. depend. 79−82396
Au films, thermal phonon radiation into α-quartz substrates 79−42363
Au small particles, embedded in gelatin, phonon spectrum, Mossbauer obs. 77−43921
Au, tilt boundary, Σ=11, simulated and observed struct., vibr. of individual atoms at grain boundary 80−88167
$AuSb_2$, pyrite structure, Raman scatt., phonon frequencies 77−40235
B, IR-active phonons, reflectivity and absorption spectra 79−82294
BC_x, IR-active phonons, reflectivity and absorption spectra 79−82294
$B_{12}C_x$, phonon energies and electronic props., x depend., refl. spectra and thermoelec. power meas. 80−16052
BN, hexagonal, low freq. Raman active vibr. 78−43880
BaClF, long wavelength dynamics, shell model calc. 80−29134
BaF_2, F^- interstitial and substitutional trivalent cations, phonon reson. and IR absorpt. 80−84752
BaF_2, strain induced splitting and oscillator strength anisotropy of IR transverse optic phonon 80−92625
$BaF_2:Er^{3+}$, single-site multiphonon and energy transfer relax. 78−52547
$BaMnF_4$, incommensurate phase, Brillouin spectra 79−42981
$Ba(NO_3)_2$, dynamical props., IR reflection spectra meas., 10-300K 77−1676
$Ba(NO_3)_2$, IR reflection spectra, dynamical props. 77−16303
$BaTiO_3$, A_1-modes reflectivity meas. 79−65875
$BaTiO_3$, electron energy loss spectra, 0.02-2 eV 78−39642
$BaTiO_3$, phonon scatt. surfaces obs., by neutron film methods 79−46761
$BaTiO_3$, piezoceramic, elastic normal wave propagation, phase transitions *(Russian)* 80−40067
$BaTiO_3$, undoped and Cu doped, Γ_{15} phonon freezing, electronic instability, LCAO calc. 80−25318

lattice phonons continued
$BaWO_4:Er^{3+}$, spin-lattice and spin-spin relax. times, electron spin echo obs. 79−28609
$BaY_2F_8:Nd^{3+}(Ho^{3+})(Er^{3+})(Yb^{3+})$, ESR spectra and spin-lattice relax. 80−11263
Bi, k=0 optical phonon temp. depend., Raman scatt. meas. 77−76509
Bi, phonon density of states by neutron scatt., sp. ht. and Debye temp. 80−2132
Bi, stationary I-U curve, falling portion under phonon generation conditions 79−15195
Bi, thermal conductivity at ultralow temp. 79−1532
Bi, zone centre phonons and elastic consts., hydrostatic press. depend. 78−59905
$Bi_{12}GeO_{20}$, optical phonon freq. in vicinity of Brillouin zone, linear wave-vector depend. 79−19892
BiI_3, characts. of low-temp. photoluminesc. 77−8646
$Bi_{0.9}Sb_{0.1}$, magnetophonon effect on hot electrons *(Russian)* 80−107814
$Bi_{1-x}Sb_x$, crystalline, vibrational, spectra, second order Raman scattering 79−47455
$Bi_{0.5}Sb_{1.5}Te_3$ film, effect of struct. on thermal cond. 79−28257
$Bi_{12}SiO_{20}$, film and single cryst., optical absorpt. edge and optical transitions 79−33730
Bi_2Te_3, Bi_2Se_3, $Bi_2(Te_{1-x}Se_x)_s$, Raman and far infrared investigation of phonons 78−23453
Bi_2Te_3 film, effect of struct. on thermal cond. 79−28257
$Bi_2Te_{3-x}Se_x$ films, thermal cond. depend. on grain size, phonon-boundary scatt. 79−69304
$Bi_2Ti_4O_{11}$, anomalous temp. depend. of phonon modes, Raman spectra 78−10893
$Bi_2Ti_4O_{11}$:PbO, anomalous temp. depend. of phonon modes, Raman spectra 78−10893
α-CO, IR and Raman spectra, vibron band, vibron-phonon combination bands 78−68495
CO, in Ar matrix, vibr. line shape, vibr.-phonon interaction 79−3493
$^{12}C^{16}O$:CO isotopes, IR and Raman spectra, vibron band, vibron-phonon combination bands 78−68495
CS_2, lattice dynamics of 0K cryst., phonons and lattice energy 79−73269
CS_2, second order Raman spectrum in condensed phase 80−93299
$^{12}C^{16}O$ in Ar matrix, vibr. level energy cascades 77−79598
Ca_2, in solid Kr, discrete reson. Raman scatt. and vibr. relax. 79−18188
$CaCO_3$, calcite, coherent excitation of vibr., dephasing time meas. 78−35120
$CaCO_3$, IR reflectivity, oblique phonons 78−60440
CaF_2, high-frequency phonon lifetimes 80−70338
CaF_2, optical detection of acoustic phonons at THz freqs. 80−75320
CaF_2, strain induced splitting and oscillator strength anisotropy of IR transverse optic phonon 80−92625
$CaF_2:Eu^{2+}$, Sm^{2+}, relaxed resonance acoustic phonons in vibronic anti-Stokes luminescence *(Russian)* 80−93404
$CaF_2:Gd_2$ triply ionised, lowest energy 4f-5d transition 79−24345
$CaF_2:Sm^{2+}$, phonon spectrum of thermal pulses by fluorescence 79−95860
$CaMg_2$, phonon spectra 77−20031
$CaMg(CO_3)_2$, dolomite, Raman spectra calc. 77−24848
$CaMg_{0.95}Fe_{0.05}Si_2O_6$, pyroxene, Mossbauer line integrated intensity ang. depend. 77−90083
CaO, electron irradiated, symmetry assignment of new point defect 78−31261
CaO, relax. in $^3T_{1u}$ state of F centres 80−24443
$Ca(OH)_2$ and $Ca(OD)_2$, molecular and lattice dynamics by IR^2 and Raman spectra 77−73134
$Ca_5(PO_4)_3F$: Cr^{5+}, spin-lattice relax. time and Debye temp., EPR obs. 79−28601
$Ca_{10}(PO_4)_6(OH_2)$, polarised Raman and LF IR spectra, lattice vibr. 77−77192
$Ca_{10}(PO_4)_6(OH)_{2-2x}O_x\square_x$ polycryst. sintered bodies, prep. and thermal props. 80−25624
CaS:Ce, Na, photon sidebands in emission and excitation spectra, pseudolocalised vibrs. 79−28800
$CaSO_4$, anhydrite and gypsum, phonon spectroscopy, lattice dynamical calc. 80−19889
Cd, resistivity, existence of Einstein type phonon mode 79−42519
$Cd(ClO_3)_2$ single crystals, Raman scatt. 80−55106
$CdCr_2S_4$, ferromag. semicond., IR refl. spectra, phonon props. and dielec. function 80−66191
$CdCr_2S_4$, magnetic semicond., resonance Raman scatt., mag. circular polarisation props. 80−50341
$CdCr_2S_4$, spin dependent phonon Raman scatt., resonance effects 77−73145
$CdCr_2S_4(Se_4)$, ferromagnetic semiconductors, spinel-type, resonance Raman scattering and electronic structure *(Japanese)* 79−47421
$CdCr_2Se_4$, influence of ferromag. ordering on phonon Raman scatt. 78−2853
$CdCr_2Se_4$, spin dependent phonon Raman scat., resonance effects 77−73145
$CdGa_2S_4$, IR refl. spectra 80−60604
$CdGa_2S_4$, Raman scatt. anal., optical phonons 79−73951
$CdGaS_4(Se_4)$, absorption and refl. spectra anisotropy, two-phonon processes 77−69840
$CdGa_2Se_4$, ordered vacancy compound, Raman scatt. 79−95749
$CdGeAs_2$, optical and elec. props. 79−19590
$CdGeAs_2$, polarised IR reflectivity, optical modes, optical phonons 77−69836
n-$Cd_xHg_{1-x}Te$, magnetophonon oscills. of transverse magnetoresist. 78−72177
CdI_2, interlayer interactions estimate from Raman and Brillouin scatt. 79−99884
CdI_2, optical phonon anisotropies and intralayer bonding forces from IR refl. 77−59573
$CdI_2:Fe^{2+}$, polarised electronic Raman scatt. 80−29733
CdI_2-Ni^{2+}, absorption and mag. circular dichroism, spectra, phonon density of states of CdI_2 deduced 79−19913
$CdInGaS_4$, far IR refl. and transmission spectra, lattice vibrs. 79−91439
$CdIn_2S_4$, Raman and IR spectra 78−48181
$Cd_{1-x}Mn_xTe$ mixed crystals, Raman spectra 80−103961
$Cd(NH_3)_6X_2$, X=Br, Cl, I, orientational phase transitions, Raman spectra 80−11382
CdP_2, reson. interaction of vibr. states, polarised Raman spectra meas. 77−15521

lattice phonons continued
CdP_2, tetragonal, one and two phonon states using second order Raman spectra 78−43874
CdS, acoustic phonon intensity fluctuations after strong nonlinear amplification 78−59909
CdS, bulk acoustic phonons, light scatt. from phonon-induced surface ripples 78−75924
CdS, intensity fluctuations of nonlinearly amplified phonons, Brillouin scatt. meas. 77−90163
CdS, LO phonons, size effect reson., first order forbidden light scatt. 77−44002
CdS, mode corrected TA phonons, reson. Brillouin scatt. 78−72535
CdS, phonon-coupled photoacoustic spectroscopy 80−54317
CdS, reson. Brillouin scatt. by longitudinal acoustic phonons 79−38555
CdS, reson. forbidden Brillouin scatt. by TA phonon domains 79−56802
CdS, reson. Raman scatt., temp. depend. polarisation, A-exciton 77−12386
CdS, resonant Raman scattering by LO phonons 78−39551
CdS, stimulated Mandelstam-Brillouin scatt. on acoustic phonon amplification *(Russian)* 80−71437
CdS, thermal equilib. phonon populations, acoustic intensity meas. by Brillouin scatt. intensity obs. 80−45098
CdS:Cl, resonant Raman scatt. exam. 78−39546
CdS:Mn^{2+}, temp. depend. of rate of spin-lattice relax. 79−42832
$3CdSO_4.8H_2O$, cryst., phonon assisted indirect transitions 78−72559
$CdS_{1-x}Se_x$, zone edge phonon, IR absorpt. and Raman scatt. meas. 77−76508
$CdS_{1-x}Se_x$, zone edge phonons 78−76475
CdSe, fundamental vibrs., Raman scatt. and IR refl. obs. 78−60451
CdSe, polarisation correl. of resonant Raman scatt. or hot luminesc. 80−25384
$CdSiP_2$, polarised Raman spectra 77−24853
CdTe, far IR absorpt., two-phonon density of states 78−15155
CdTe, reson. Raman scatt. by excitonic polaritons 80−11396
CdTe, time-resolved spectra, carrier relax. time, phonon lifetime 80−11433
CdTe:Li, excitation spectrum of Li acceptor and valence band parameters 79−28795
$CdTe_{1-x}Se_x$, Raman scatt. spectra, two-mode behaviour 78−60450
Cds, reson. Brillouin scatt. by piezoelectrically inactive TA phonon domains 78−84593
CeB_6, Raman spectra of phonons 79−82972
$CeCl_3$, mag. field depend. of polaritons 79−33246
$CeCl_3$, Raman spectra circ. polaris., Faraday effect phonon state splitting 78−43855
CeH_x, phonon features in IR and Raman spectra 80−93310
$Ce_cLa_{1-c}F_3$, Raman spectra circ. polaris., Faraday effect phonon state splitting 78−43855
$Ce_xLa_{1-x}F_3$, phonon self-energy and electron-phonon interaction 79−65159
Co, martensitic HCP-FCC transition, neutron scatt. obs. 79−51252
Co-P, metallic glass, phonon propagation at low temp. 78−87756
$CoBr_2$, paramag. and antiferromag., Raman scatt. from electronic excitations and phonons 79−69826
$CoCO_3$, antiferromag., Raman spectra, 2-300K 77−32380
$CoCO_3$ light scatt. from parametric magnons and phonons *(Russian)* 80−34937
$CoCO_3$, light scatt. from magnons and phonons excited by microwave pumping 80−66213
$CoCl_2.2H_2O$, phonons and electronic transitions, Raman spectra 79−28761
$CoCs_2(SO_4)_2.6H_2O$, obs. of H^2T^7 Raman spin-lattice relax. process 77−51459
$CoFe_{2-x}Ga_xO_4$, IR reflection spectra, permittivity spectra and effective ionic charges 79−69841
$CoK_2(SO_4)_2.6H_2O$, obs. of H^2T^7 Raman spin-lattice relax. process. 77−51459
$Co(NH_4)_2(SO_4)_2.6H_2O$, obs. of H^2T^7 Raman spin-lattice relax. process 77−51459
$CrBr_3$, modulation of exchange integral, contrib. to temp. depend. of exchange interaction 77−69484
$CrBr_3(Cl_3)$, two-dimensional mag. insulator, cryst. field splitting, spectroscopic g-factors 79−47059
$CrCl_3$, electronic struct. and struct. phase transition 80−59644
Cr_2O_3, IR active phonons 78−34578
Cr_2O_3, thermal magnetoresist., 0.1 to 100K, magnon-phonon interactions 79−65266
Cs, isostructural transition and lattice vibrs., relativistic LMTO calc. 80−20074
Cs, phonon spectral density, pseudopotential calcs. 80−39234
CsBr, hyper-Raman spectra by single channel method 78−84591
CsCl, phonon dispersion, temp. induced phase transition, deformable shell model calcs. 79−77698
$CsCl(Br)(I):NO_2^-$, vibronic and reson. Raman spectra of BCC cryst. 79−87468
$CsCoBr_3$, ID Ising antiferromagnet, spin dependent Raman scattering from phonons and electronic excitations 80−103948
$CsCoBr_3$, quasi ID Ising antiferromag., polarised Raman scatt. from mag. excitations 80−66182
CsH_2AsO_4, elastic props., photoelasticity near ferroelectric phase transition 80−29107
CsI crystal, incoherent phonons, nuclear acoustic resonance 80−7180
CsI, hyper-Raman spectra by single channel method 78−84591
CsI(Br), IR active and silent modes, hyper-Raman scatt. obs. 79−61376
$CsMnF_3$, mag. field- and temp.-depend. of light absorption spectra 78−52528
$CsNiF_3$, 1D ferromag., optical absorption and spin dynamics 80−71417
$Cs_2ZrCl_6:Os^{4+}$, multiple state luminesc. 78−72584
$Cs_2[ZnCl_4]$, Raman-active phonons, $[ZnCl_4]^{2-}$ distortion, press. effects 77−52073
Cu films, thermal phonon radiation into α-quartz substrates 79−42363
Cu halides, phonon anomalies for Cu^+ at off-centre sites, dynamical model and Raman meas. 80−10618
Cu, photoemission, temp. and photon-energy induced breakdown of direct transition model 78−95681
Cu, thermal disorder, EXAFS determ. 80−45167
Cu-Al, change in force constant due to volume effects 78−75778
Cu-Al alloy, lattice thermal cond. meas., 0.06-2K 77−15822
Cu-Au, dil., enhanced lattice sp.ht. 78−51699
Cu-Be solid solutions, local oscill. conc. depend., impurity bands *(Russian)* 80−75318

lattice phonons continued
Cu-halides, phonon anomalies, dynamical model 79−73272
Cu-Si, change in force constant due to volume effects 78−75778
Cu-Zn alloy, molecular dynamic exam. of perfect and imperfect cryst. 77−39647
Cu-Zn-Al alloy, lattice dynamical study of premartensitic state, phonon meas. 79−77696
Cu-Zn-Al cubic alloy, phonon sp. ht. near martensitic transform. 79−60521
Cu_3Au, elec. resistivity, temp. depend. 79−47078
$CuBr_xI_{1-x}$, disorder-induced TA Raman lines 79−73929
CuCl, neutron scatt. of TO phonon at 5K 79−60446
CuCl, zincblende struct., high press. Raman scatt., 77K 78−60463
$CuCl_xBr_{1-x}$, disorder-induced TA Raman lines 79−73929
CuCl(Br)(I), Raman spectra, Cu ions vibr. and diffractive motions 80−11412
$CuGa_xIn_{1-x}S_2$ solid soln., IR refl. spectra, comp. depend. 78−52498
$CuGaS_2$, IR lattice reflectivity spectra obs. 78−19477
$CuGaS_2$-CuGaSe, solid solutions, IR lattice reflectivity spectra obs. 78−19477
$CuGaSe_2$, IR lattice reflectivity spectra obs. 78−19477
$CuGaTe_2$, IR lattice vibr. spectra 79−28765
β-CuI, phonon spectra, model 77−89511
CuI, superionic conductor, lattice dynamic meas. and calcs. 79−99880
$CuInSe_2$, IR lattice vibr. spectra 79−28765
$Cu_2Mo_6S_8$, phonon density of states, mode softening correl. with supercond. transition temp. 79−51714
Cu_2O, exciton luminesc. spectra, mag. field influence 80−80860
Cu_2O, yellow exciton states investig. by forbidden resonant Raman scatt. 77−48165
$Cu_xV_2O_5$, metallic, Raman scatt. 78−80358
Cu_3VS_4, Raman active modes 80−11414
Cu_3VS_4, Raman linewidth of A_1 mode under high press., reson. effects 80−108210
D-T, solid, estimated heat capacity, enthalpy, thermal cond. and diffusivity 77−4228
D_2, solid, compressed, anomalons double peaked one-phonon for IR absorption 79−56788
D_2, solid, far IR absorption by phonons and librons in ordered state 78−80331
D_2, solid, press. depend. of phonon lineshape in ordered state, far IR spectra 79−56023
o-D_2, solid, up to 150 kbar, 5K, Raman spectrum 80−50332
DCN, phonons meas. by neutron coherent inelastic scatt. 79−95097
D_2O_2, lattice phonons by neutron scatt., covalent force model 78−67782
$DyAsO_4$, cooperative Jahn-Teller phase transitions, dielec. anomalies 78−64312
Dy_2S_3, vibr. spectra, factor-group anal. 80−80793
$DyVO_4$, cooperative Jahn-Teller distortion, mag. field depend. 77−47777
$DyVO_4$, cooperative Jahn-Teller phase transitions, dielec. anomalies 78−64312
$DyVO_4$ Jahn-Teller crystal, deform. induced transitions, elastic and dielectric characts. *(Russian)* 80−80726
$DyVO_4$, Jahn-Teller distortion, mag. field depend. 78−79733
$ErCrO_3$, phonon Raman spectra rel. to mag. ordering 77−52100
Eu chalcogenides, paramag., spin-disorder-induced Raman scatt. 78−19474
EuO, mag. semicond., dielec. and optical props. 78−10824
Eu_3O_4, inelastic light scatt. 77−55788
EuO(S)(Se)(Te), cryst. and electronic struct., mag., elec., and optical props., book contrib. 80−39760
Eu_3S_4, inelastic light scatt., photoluminesc., anomalous vibr. 77−48229
Eu_3S_4, inelastic light scatt. 77−55788
EuS(Se)(Te)(O), Raman scatt. near mag. phase transitions 79−47458
EuSe, mag. semicond., dielec. and optical props. 78−10824
EuTe, mag. 'Bragg' scatt. obs. through Raman scatt. 80−66179
$Eu_2(WO_4)_3$, mag. susceptibility, elec. cond. and dielec. const. meas. 77−11916
$Eu_{1-y}X_yS$ (X=Sr,Gd), spin-disorder-induced Raman scatt. from phonons, expt. investigation 80−20635
EuX(X=O,S,Se) 80−20635
Fe, lattice vibrations, temp. depend. 78−95124
Fe, microcrystal, temp. dependent lowering of Debye-Waller factor 79−1736
Fe, surface lattice dynamics 78−95224
Fe-Ni alloy, solid solution, vibr. analogue of Bain deform. and morphology of martensite in 78−2224
$FeBr_2$, dynamic Jahn-Teller system, Raman scatt. from electronic excitations and phonons 78−56474
$FeCO_3$, Mossbauer quadrupole splitting of ^{57}Fe, vibronic effects 79−19813
$FeCl_2$, dynamic Jahn-Teller system, Raman scatt. from electronic excitations and phonons 78−56474
$FeCl_2.2H_2O$, also deuterated, electronic transitions in Raman spectra 78−80337
$FeCl_2.2H_2O(2D_2O)$, phonons and electronic transitions, Raman spectra 79−28761
FeF_2, dielectric properties, IR spectra, lattice dynamics *(French)* 80−76026
FeF_2, IR reflectivity spectrum 79−51952
$Fe_{65}Ni_{35}$, ferromagnetic Invar alloy, lattice vibrations 78−91403
$Fe_{1-x}O$, wustite, phonon and magnon props., inelastic neutron scatt. 78−52236
α-Fe_2O_3, IR lattice vibr. and dielectric dispersion 78−6679
$Fe_{72}Pt_{28}$, ferromagnetic Invar alloy, lattice vibrations 78−91403
FeS_2, optical absorpt. 79−43002
$Ga_{1-x}Al_xAs$, IR refl. spectra and Raman spectra 80−20623
$Ga_{1-x}Al_xSb$, second order Raman spectra, photon combinations *(French)* 80−34912
$Ga_{1-x}Al_xSb$, small wave vector modes 78−75785
GaAs, absorption edge broadening by piezoelec. phonon fields 77−16302
GaAs, Brillouin spectra, light scatt. cross section for surface ripples 80−71434
GaAs, bulk acoustic phonons, light scatt. from phonon-induced surface ripples 78−75924
GaAs, electron capture by multiphenon emission at B centre 80−24830
GaAs epilayers and p-n junctions, anisotropic phonon generation 79−37784
GaAs, excited, LO phonon effective temp., Raman meas. 80−20639
GaAs, fundamental absorption band, influence of phonons on long-wavelength wing 79−69857

lattice phonons continued
p-GaAs, heavily doped, self energy of phonons 80−44277
GaAs, highly excited, LO phonon Raman lineshape 79−78683
GaAs, highly transparent semicond. crysts., multiphonon IR absorpt. 78−10885
n-GaAs, hot electron distrib. function with LO phonon kink, photoluminesc. 79−19925
n-GaAs, hot electron magnetophonon resonance, Fourier anal. 80−54718
GaAs, IR spectra, multiphonon absorpt., phonon density of states interpretation 77−69833
GaAs, irradiated with fast neutrons, IR vibrational absorpt. 78−75776
GaAs, lattice vibration, thermal expansion and pressure effect 80−39233
n-GaAs, longitudinal magnetophonon reson. and Fourier anal. 79−4569
GaAs, luminescence by laser excitation, photocarrier thermalisation and polariton kinetics 77−66533
n-GaAs, magnetophonon resonance, Fourier anal. 79−91080
GaAs, n-i-n three layer struct., transmitted phonon effect in strong mag. fields 77−20341
n-GaAs, non-Maxwellian electron distribution function, from electric field-depend. photolum. spectrum 79−11450
n-GaAs, non-equilibrium acoustic phonon generation by hot electrons 80−6477
GaAs, nonradiative capture, direct obs. of phonons 78−30976
GaAs, phonon viscosity tensor 78−34570
GaAs, photoluminescence, electron-acceptor, from non-Maxwellian distrib. of photo-excited electrons 80−45138
GaAs, photoluminescence and resonant Raman spectra, press. depend. 78−31251
GaAs, Raman scattering absolute cross section band struct. model calcs. 80−7349
GaAs, Raman scattering from nonequilibrium LO phonons with picosecond resolution 80−80779
GaAs, resonant Brillouin scattering 79−78695
GaAs, thermal equilib. phonon populations, acoustic intensity meas. by Brillouin scatt. intensity obs. 80−45098
GaAs, time-resolved spectra, carrier relax. time, phonon lifetime 80−11433
GaAs, valence band fine struct. from light mod. with nonequilib. opt. phonons 78−39568
GaAs:Cr, exptl. verification of Cr^{2+} models of photoluminescent transitions 78−27320
GaAs:Cr_2 zero-phonon struct. in Cr^{2+} ($3d^4$) optical absorption 80−60640
GaAs:Cr^{2+}, dynamic Jahn-Teller effect, relaxation time for reorientation 80−6798
GaAs-AlAs alternating epitaxial monolayers, Raman scatt. and zone-folding effects 77−90208
GaAs-AlAs alternating monolayers, zone folding effects on phonons 78−72510
GaAs-AlAs layered films, MBE prep., struct., rel. to optical props. 79−77950
GaAs-AlAs superlattice, folded acoustic phonons obs., Raman scatt. 80−88996
GaAs-anodic oxide interfaces, struct. and chem. props., Raman scatt. obs. 79−47168
GaAs-based mixed cryst. form. by ion beam synthesis, vibr. anal. 80−103376
GaAs-$Ga_{1-x}Al_xAs$ superlattice, Raman scatt., polar phonon anisotropy 80−45052
GaAs-Pb junctions, electron tunnelling under high press., transition temp., energy gap, phonon energies 79−15257
GaAsP, composition dependence of phonon frequencies 78−75764
$GaAs_{1-x}P_x$, indirect-gap, evidence for exciton localization by alloy fluctuations, photolum. 80−66276
$GaAs_{1-x}P_x$, piezomodulation spectra of indirect gap, zero-phonon and phonon-assisted transitions 77−48192
$GaAs_{1-x}P_x$:N, $0.6<x<1$, photoluminesc., comp. depend. 78−52546
GaAs(Sb), two-phonon diffuse scatt. of X-rays 78−26374
$Ga_{1-x}In_xAs$, IR reflectivity, cluster effect on optical phonons 80−97259
$Ga_xIn_{1-x}As_yP_{1-y}$, conduction band and phonons, Shubnikov-de Haas effect, magnetophonon resonance, Raman scattering 80−24795
GaInP, composition dependence of phonon frequencies 78−75764
$Ga_{1-x}In_xP$, mixed cryst., IR absorption by zone edge lattice vibrs. 78−19487
$Ga_{1-x}In_xP$, zone edge phonons 78−76475
$Ga_xIn_{1-x}P$, with indirect band struct., radiative recomb. of free excitons, cathodolum. meas. 77−90202
$Ga_xIn_{1-x}P$:N layers, LPE growth, luminesc. and direct exptl. obs. of band struct. effects 77−52157
$Ga_xIn_{1-x}Sb$ LO phonon obs. using Raman scatt. 78−35152
$Ga_{1-x}In_xSe$, Raman scatt. spectra, optical phonon freq., cryst. vibr. freq. types 80−29744
$Ga_{1-x}In_xSe$ solid solution, IR spectra of static reflectivity 79−69849
GaP, lattice dynamics, phonon freq. meas., valence-force-field overlap shell model 80−15205
GaP, light scatt. by LO phonons, high-resolution study 80−80798
GaP, moments of phonon spectra from specific heats 80−15203
GaP, obs. of Γ-L indirect transition, phonon struct. 78−48194
GaP, piezobirefringence above direct gap 79−51929
GaP, Raman spectra, press. depend. optical phonon anharmonicity 77−8586
GaP second order Raman spectrum, polarisation meas. 78−64368
p-GaP, spin-flip Raman scattering, review 80−108209
GaP, thermal expansion below room temp., press. depend. of elastic stiffness consts. and phonon frequencies 80−79963
GaP:N, temp.-modulated photoluminesc., phonon assisted tunnelling process 78−23511
GaP:Ni, absorpt. and luminesc. spectra 79−42996
GaP:O^-, two-electron O^- state evidence, ODMR, IR emission, phonon replicas 80−15828
GaP_xAs_{1-x} solid solns., edge absorpt. 77−16334
$(GaP)_x(InAs)_{1-x}$ solid solution, IR reflection spectra 77−69830
GaS, anisotropic phonon dispersion 77−84864
GaS, Davydov splitting of degenerate lattice modes 79−61382
GaS, infrared optical props., polarisation depend., vibr. modes 80−100658
GaS layer semiconductor, IR derivative absorpt. spectra 78−6666
GaS, sp. ht., vibr. spectra and Debye temp. 78−87796
αGa_2S_3, single crystal, lattice phonon exam., Raman and IR spectra of polycrystalline samples *(French)* 78−27229
GaS(Se), Brillouin scatt. by pure transverse phonons 79−78696
lattice phonons continued
GaS(Se), layer compound, long-wavelength phonons and elastic consts. 80−65175
GaS(Se), layered, optical phonons, IR and Raman scatt. meas. 78−59903
GaS(Se), polar optical phonon ang. behaviour, IR refl. meas. 80−20633
GaS_xSe_{1-x} layered system, neutron diffr., IR and Raman scatt. 79−87443
GaS_xSe_{1-x} solid solutions, two-mode behaviour of optical phonons, IR reflect spectra 79−78680
GaSb based eutectics, thermal cond. and diffusivity, 300-700K, phonon mechanism 80−103526
GaSb, lattice vibration, thermal expansion and pressure effect 80−39233
GaSb, phonon density of states 79−90744
GaSb, reson. two phonon Raman scatt. near E_1 and $E_1+\Delta_1$ gaps 78−60470
GaSb, second order Raman scatt. meas., comparison with photon density of states calc. 77−8579
GaSe, absorpt. and electroabsorpt. near indirect edge 77−20827
GaSe and GaS_xSe_{1-x}, multiphonon reson. Raman scatt., excitonic transition 77−59574
GaSe, cascade resonant Raman processes 80−25385
GaSe films, optical props. at lattice vibr. freqs., IR and Raman spectra 80−60696
GaSe, fine struct. of exciton spectrum 78−39567
GaSe, group theoretical anal. of phonon assisted optical transition 78−39564
GaSe, isolated layer model, lattice dynamics and elastic props. 80−24547
GaSe, lattice dynamics and elastic props., Born-von Karman model study 80−70337
GaSe, layer compounds, lattice instability, deformation dipole model 80−39249
GaSe, layer cryst., elastic props. rel. to zone-centre phonon freqs. 79−46736
GaSe layer semiconductor, IR derivative absorpt. spectra 78−6666
ε-GaSe, long-wavelength lattice vibr. 80−92631
ε-GaSe, Raman scatt., hydrostatic press. effect 80−84745
GaSe, sp. ht., vibr. spectra and Debye temp. 78−87796
GaSe, zone-centre optical phonons, Raman scatt. meas. 78−10141
$GaSe_{1-x}S_x$, struct. transition, Raman scatt. obs. 79−99888
$GaSe_{0.9}Te_{0.1}$, undulation spectra associated with acceptor complexes 78−80392
$GaSe_{1-x}Te_x$, Raman scatt., optical phonons and phase transition 80−66202
$GaSe_{1-x}Te_x$, Raman spectra, phonon freq. 80−97286
$GaSe_{1-x}Te_x$, zone-centre optical phonons, Raman scatt. meas. 78−10141
GaTe layer semiconductor, UV-visible wavelength derivative and thermorefl. spectra 78−6666
GaTe, long wavelength phonons, Raman and far IR spectra obs. 79−69210
α-GaTe, single cryst., Raman scatt. 80−60599
α-GaTe single crystals, Raman spectra, phonon modes 79−99883
GaTe, sp. ht., vibr. spectra and Debye temp. 78−87796
GaTe, vibr. spectrum 77−89513
GaTe, zone-centre optical phonons, Raman scatt. meas. 78−10141
GaI, Brillouin spectra, light scatt. cross section for surface ripples 80−71434
$Gd_xLa_{1-x}Pd_3$, EPR of Gd, g-factor and thermal broadening, temp. and comp. depend. 77−48048
$Gd_2O_2S:Eu^{3+}$, luminesc., excitation spectra, cooperative phonon sidebands 79−33771
GdS, FCC metallic phase, Raman scatt., phonon density of states 78−19480
GdS, metallic FCC antiferromag., phonon Raman scatt. 78−60458
GdS(Se)(Te), metallic, phonon density of states, Raman scatt. expt. 78−23451
Ge, acoustic phonon propag. and interaction with electron-hole drops *(Russian)* 80−29336
Ge, ballistic phonon focusing singularities 79−99277
Ge, electron-hole drop drag, interaction with thermal pulses 80−103631
Ge, electron-hole drop recombination radiation due to heat pulse action *(Russian)* 80−16087
Ge, electron-hole drop velocities, excitation wavelength depend. 78−88358
Ge, electron-hole droplet cloud form., phonon wind, luminesc. obs. 80−45136
Ge, electron-hole droplet cloud kinetics, thermalisation phonons 80−88483
Ge, electron-hole droplets distrib., and phonon wind 80−103629
Ge, electron-hole drops, accel. by IR radiation field 78−95264
Ge, electron-hole drops, phonon lifetime and acoustic attenuation due to phonon-assisted Auger recomb. 80−34462
Ge, electron-hole-droplet cloud, photoluminesc. of laser excited surface, phonon wind 78−84146
Ge, exciton recombination with emission of single phonon, luminesc. replicas, detect. and anal. 79−60728
p-Ge, heavily doped, self energy of phonons 80−44277
Ge, mag. field luminesc. lifetime, quantum oscills., phonon wind effects 80−93385
Ge, phonon energy variation under high press. band struct. changes, tunnel spectroscopy study *(Russian)* 80−2134
Ge, phonons, directional depend. of boundary scatt. mean free path 79−73354
Ge, photomag. EMF, reson. struct., energy relax. mechanisms 78−2515
Ge, reson. Raman scatt. under uniaxial stress near E_1 gaps 79−42960
Ge, thermal conductivity of semiconductors, quantum acoustical method, thermal phonon lifetimes 80−65312
Ge, thermodynamic functions and normalised moments 79−51279
Ge:^{119m}Sn, impurity lattice dynamics, Mossbauer spectra, Debye temp. 80−84262
p-Ge:Hg(Cu)(Cd)(Zn), deep levels, optical-phonon-assisted capture of carriers 79−51597
Ge:P, charact. temp. and lattice thermal cond. 80−59743
Ge:P, lattice thermal cond., role of electron-phonon interactions and peripheral phonons 78−79702
Ge:P, peripheral phonons and phonon cond. 79−14973
Ge:Sb,In, semicond. phonon assisted absorpt. processes 79−60456
Ge-Si alloys, hot-pressed, fine-grained, boundary scatt. of phonons, lattice thermal cond. 80−107583

lattice phonons continued
Ge-Si alloys, hot-pressed, fine-grained, boundary scatt. of phonons, theory 80−107584
Ge-type semiconductor, light scatt. from zero-sound 78−43857
GeS, far IR reflectivity spectra, lattice vibr. and dielec. const. 77−52068
GeS, IR reflectivity meas. 77−8570
GeS_2, single cryst., IR polarised reflectivity spectra, 79−56775
GeS(Se), layer cpds., Raman spectra, press. coeffs. and mode Gruneisen parameters 78−10891
$GeSe_2$, far IR reflectivity meas. 77−28565
$GeSe_2$, far IR reflectivity spectrum, dielec. const. and lattice vibrs. 77−52069
$GeSe_2$ multimode layer cryst., far IR transmission and reflection spectrosc., comparative merits 80−76019
$GeSe_2$, single cryst., IR polarised reflectivity spectra, 79−56775
$GeSe_xS_{1-x}$ solid solutions, long-wavelength optical phonons, Raman spectra 80−25378
$Ge_{1-x}Si_x$, vibrational and Raman-scattering props. 78−10884
o-H, one-dimens., struct. instability 79−86885
H_2, metallic, phonon spectrum, rel. to eqn. of state *(Russian)* 77−89519
H_2, metallic, phonons, supercond. transition, nonlinear self consistent screening approach 79−95537
H_2, solid, far IR absorption by phonons and librons in ordered state 78−80331
H_2, solid, orientational level structure of o-H_2 pairs, phonon renormalisation 79−47554
H_2, solid, Raman active phonons, freq. depend. on ortho-para conc. and temp. 79−73918
H_2, solid collective excitations observed by incoherent neutron scatt. 79−23690
HCN crystals, polarition spectra and lattice dynamics 80−49313
HD, lattice thermal cond., 0.2 to 4K 78−75903
HF, high temperature thermophysical properties 78−91404
HIO_3, single crystal, ang. depend. of Raman spectra 78−72518
He, solid, theory and thermodynamic props., book contrib. 77−47646
^{4}He, FCC quantum cryst., lattice dynamics 79−77859
^{3}He, solid, low temp. thermal cond., structural crystalline defects 80−2240
^{3}He, solid, phonons in linear chain with hard-core pot. 77−11644
^{4}He, FCC cryst., self-consistent phonon theory 79−4453
^{4}He, solid, boundary limited thermal cond., Poiseuille phonon flow 80−2241
^{4}He, solid, diffusion coeff. of ^{3}He, detection and study of impuriton-phonon scatt. mech. 79−56029
^{4}He, solid, interface with liq. ^{4}He, phonon transmission using heat pulse technique 79−56035
^{4}He, solid, quantum diffusion of ^{3}He, tunnelling jumping approx. *(Russian)* 78−87844
HfS_3, one-dimensional semicond., Raman spectra meas. 80−50345
HfS_3, quasi one-dimens., optical phonon anisotropy, IR spectra study 80−40112
$HfS_3(Se_3)$, phonon study of chemical bonding 80−20645
$HfSiO_4$, Raman spectrum interpretation, lattice vibrs. 77−48160
$Hg_{2.86}AsF_6$, linear chain, anomalous low temp. sp. ht. 78−14476
$Hg_{3-\delta}AsF_6$, dynamical props., Hg chain behaviour, neutron scatt. study 79−95103
$Hg_{3-\delta}AsF_6$, one dimensional phonons and chain ordering 80−24544
$Hg(CN)_2$, phonon freq. anomalous press. depend., mol. struct. distortion 80−88981
$nHg_{1-x}Cd_xTe$, single-phonon and plasmon recomb. lifetime effect, with magnetically tuned bandgap 79−38098
HgCdTe(Se) MIS junction, phonon-assisted tunnelling 79−47170
Hg_2Cl_2, neutron and Raman scatt. studies, ferroelastic transitions 80−76015
Hg_2Cl_2 single crysts., IR refl. spectra and ferroelasticity 79−99889
HgI_2, phonon-assisted recomb. of free electron-hole pair 78−23521
α-HgS, cinnabar, reson. Raman effect and luminesc. meas. 80−50338
HgTe type semiconductors, spin-flip transitions in magneto-optics and magneto-transport 80−50306
In pnictides, mixed, impurity induced Raman scatt. spectra 80−88983
In, superconducting energy gap and phonon frequencies under press., tunnelling meas. 77−32112
In-Cd, soft mode, latent heats and entropies of fusion 79−46786
n-In-Sb, polar semicond., TO phonon-helicon coupling, Doppler shifted cyclotron reson. region 79−73539
In-Sn alloy, phonon spectra and superconductivity, single-particle electron-tunnelling expts. 77−40005
In-Tl, soft mode, latent heats and entropies of fusion 79−46786
n-InAs, heated electron gas, longitudinal optical phonon form., IR absorpt. modulation 80−45079
n-InAs, oscillations in photocond. and photomag. effects 77−4405
n-InAs phonon propagation, heat pulse obs. 79−46852
InAs, Raman scatt. by LO phonons 77−20852
$InAs_{1-x}P_x$, magnetophonon effect 79−65500
InAs(P), electron irrad. at 50 MeV, elec. and optical props. 77−47486
$In_{1-x}Ga_xP$, non-isodisplacement of P atoms in long-wavelength optical phonons 79−47444
$In_{1-x}Ga_xP$, phonon density of states, cluster Bethe lattice treatment 80−6475
$In_{1-x}Ga_xP$, quantitative characterisation of chemical disorder from wavelength-modulated no-phonon absorpt. 79−15482
$In_{1-x}Ga_xP$, two-phonon IR absorpt. 78−52493
$In_{1-x}Ga_xP_{1-z}As_z$-$In_{1-x}Ga_xP_{1-z}As_z$ visible spectrum multiple-quantum-well heterostruct. lasers 80−106537
InP, depend. of phonon spectrum on hydrostatic press., Raman spectra 80−93315
InP, model for ~1.10 eV emission band 80−66289
InP, piezobirefringence above direct gap 79−51929
InP, valence band fine struct. from light mod. with nonequilib. opt. phonons 78−39568
InP-$In_{1-x}Ga_xP_{1-z}As_z$ laser, phonon-assisted recombination 79−89906
$InP_{1-x}As_x$, long wave and short wave phonons, Raman spectra obs. 80−50317
InS, IR reflection spectra 80−11389
InSb, acoustoelectric phonon attenuation of X-ray anomalous transmission 77−4160
InSb based eutectics, thermal cond. and diffusivity, 300-700K, phonon mechanism 80−103526
InSb, cyclotron resonance lineshape 80−15801
n-InSb, far IR cyclotron emission 79−61226
lattice phonons continued
InSb, impurity polarons at two LO-phonon region, magneto-optical anomalies 79−61227
InSb, lattice vibration, thermal expansion and pressure effect 80−39233
n-InSb, magnetophonon effect in non parabolic band 79−37962
n-InSb, magnetophonon oscillations by photomag. effect *(Russian)* 77−43665
p-InSb, magnetophonon reson. of holes 79−95424
n-InSb, magnetophonon struct. obs. in transverse magnetoresist. 78−23120
p-InSb, phonon assisted cyclotron harmonic transitions 78−48046
InSb, phonon viscosity tensor 78−34570
n-InSb piezoelectric semiconductors, carrier temp. effect on transverse phonon-helicon interaction 77−15886
InSb, pinning struct. of cyclotron-phonon reson., effect of nonequidistant Landau levels 77−11881
n-InSb, quantum magnetophonon oscills. of piezoresist. 77−15880
p-InSb, quantum oscills. of photocurrent due to relax. of photoelectron energies via acoustic phonons 79−73546
InSb, reson. Raman scatt. under uniaxial stress near E_1 gaps 79−42960
p-InSb, spin-flip Raman scattering, review 80−108209
InSb, two-phonon diffuse scatt. of X-rays 78−26374
InSb type semiconductor, spin-flip transitions in magneto-optics and magneto-transport 80−50306
$InSb_{1-x}As_x$, cryst. struct. and far IR reflectivity 79−56752
$InSb_{1-x}As_xBi_y$, far IR reflectivity 79−56752
InSe, absorpt. edge fine struct. *(Russian)* 77−48176
InSe, layer compound, long-wavelength phonons and elastic consts. 80−65175
InSe, layer compounds, lattice instability, deformation dipole model 80−39249
InSe, polar optical phonon ang. behaviour, IR refl. meas. 80−20633
InSe, Raman scatt. spectra 79−69846
InSe, Raman scatt. spectra, optical phonon freq., cryst. vibr. freq. types 80−29744
InSe, second order Raman spectrum and phase transition 79−38545
InSe, vibr. spectrum, IR refl. and absorpt. 500-100 cm^{-1} 77−81102
In_4Se_3, layered cryst., sp. ht. rel. to phonon spectrum *(Russian)* 79−90794
InTe, Raman spectra, phonon modes 80−40109
IrF_6, neat and mixed cryst., Raman scatt., anomalous phonon behaviour 79−38540
K, electrical and thermal resistivity determ. from first principles 79−69493
K halides, spin-lattice relax. of O_2^- centre 80−88863
K, helicon-phonon interaction 79−4379
K, helicon-phonon interaction, numerical study 79−46758
K, phonon spectral density, pseudopotential calcs. 80−39234
KAg_4I_5, superionic phase transition, dynamical and crit. pt. props. 80−107535
$KAlCl_4$, cryst., Raman spectra, orthorhombic space group, Cl splitting of $AlCl_4^-$ 77−85700
KBr:MnO_4^-, vibronic spectra interpretation 79−37770
KBr:Tl, impurity-induced first-order Raman scatt., critical-point and critical-line anal. 79−19884
$KBr_{1-x}(CN)_x$, mixed mol. cryst., coupled rot. and translational modes 80−84267
KBr(I), inelastic light scattering of localised vibration of interstitial H atom in alkali halides 80−88998
KCN, Brillouin line width of phonons 78−80370
KCN, inelastic neutron scatt. by coupled rot. and translational modes 80−79895
KCN, librational and phonon sidebands of IR CN^- stretching mode 79−15457
KCN, phonon freq. distrib., cubic and monoclinic phases 78−22800
KCN, Raman diffusion spectra, IR absorpt. in phases II and III *(French)* 80−84741
$(KCN)_{0.5}(KBr)_{0.5}$, lattice dynamics neutron scatt. obs., glass phase formation 80−15207
KCl, entropy change associated with substitutional anion defects calc. 78−79782
KCl:Li^+, phonon generation by EM excitation, mechanism 80−2129
KCl:OH^- type paraelec. systems, phonon superradiant phase transition *(Russian)* 79−69206
KCl:Tl, impurity-induced first-order Raman scatt., critical-point and critical-line anal. 79−19884
$K_3Co(CN)_6$, NMR spin lattice relax. of ^{59}Co rel. to $Co(CN)_6$ octahedra vibr. modes 80−39885
$K_3Co(CN)_6$, Raman scatt. and electronically-induced phase transition at 130K 77−90142
K_2CuF_4, Brillouin scatt. and US meas. of phonons, elastic moduli and Debye temp. calc. 79−87454
$KD_{2x}H_{2(1-x)}PO_4$ crystals, $0<x<0.98$, light scatt. by polaritons 80−96802
KD_2PO_4, microwave spectra, temp. depend. mode rel. to proton subsystem 80−24548
$KD_3(SeO_3)_2$, phase transition, neutron scatt. study 80−75351
$K_3Fe(CN)_6$, paramag. relax., phonon bottleneck effects 78−23322
$K_3Fe(CN)_6$, Raman scatt. and electronically-induced phase transition at 130K 77−90142
KH_2PO_4, anharmonic phonons and central peaks at struct. phase transitions 79−95775
KH_2PO_4, E-symmetry Raman spectra 79−38535
KH_2PO_4, paraelec., Raman scatt. spectra of B_2-polariton and B_2(LO) modes 79−28762
KH_2PO_4, paraelectric phase, forward and backward Raman scatt. 79−33681
KH_2PO_4, phonon echos in SiO_2, ADP, KDP, and Rochelle salt *(Japanese)* 79−51213
$KH_3(SeO_3)_2$, and $KD_3(SeO_3)_2$, anharmonic phonons and central peaks at struct. phase transitions 79−95775
KI, luminesc. lines due to n=2 free exciton state of Wannier series 80−29776
KI, zero phonon and LO phonon assisted luminesc. of free excitons 79−28799
KI:OH^-, HF phonon studies under uniaxial stress 79−83002
KI:Tl^+, pre-resonant enhancement of Raman scatt. 80−7354
$KMgF_3$:Cr^{2+}, HF phonon spectroscopy using supercond. tunnel junctions 80−65178
$KMgF_3$:Er^{3+}, Orbach-Aminor paramag. relax. processes, phonon bottleneck 79−28610

lattice phonons continued
$KMgF_3:Ni^{2+}$, acoustic Faraday and Cotton-Mouton effects, theory 80−65987
$KMgF_3:V^{2+}$, dynamical Jahn-Teller effect on spin orbit multiplets, intensity quenching 79−95374
$KMgF_3:V^{2+}$, first and second order Jahn-Teller coupling const. calc. 79−65906
$KMnF_3$, critical dynamics of sound 80−103424
$KMnF_3$, IR-active phonons in tetragonal phases 80−2748
K_2MnF_4, perovskite type layer struct., far IR reflectivity and Raman spectra 77−15511
$K_2NaGaF_6:Cr^{3+}$, mag. circular dichroism and absorption spectra 77−77254
$KNbO_3$, acoustic modes near orthorhombic-tetragonal phase transition, temp. depend. 79−28058
$K_2PbCu(NO_2)_6$, incommensurate Jahn-Teller phase transition 78−79730
$K_2Pt(CN)_4$, quasi-one-dimens. Peierls system, phonon dispersion and neutron scatt., calc. 80−24550
$K_2Pt(CN)_4Br_{0.3}3.2H_2O$, linear conductor, dynamical aspects of fluctuations 79−33715
$K_2Pt(CN)_4Br_{0.3}.3H_2O$, CDW pinning, phonon gap and pinning freq. at low temp. 79−7591
$K_2Pt(CN)_4Br_{0.3}.3.2D_2O$, lattice dynamics, neutron scatt. expts. 78−14412
$K_{1.75}Pt(CN)_4.1.5H_2O$, Raman scatt. and luminesc. studies 80−25394
$K_2PtCl_6:Os^{4+}$, multiple state luminesc. 78−72584
$K_2PtCl_6:Os^{4+}$, sharp line luminesc. band at 10K, vibr. assignment 78−95600
K_2SeO_4, anharmonic phonons and central peaks at struct. phase transitions 79−95775
K_2SeO_4, improved Raman spectra at room temp. 78−56487
K_2SnCl_6, phase instabilities and mode softening X-ray and neutron diffr. 77−7830
K_2XY_6 (X=Sn, Te, Y=Cl, Br), low temp. vibr. spectra, lattice dynamics and phase transitions 79−73917
$K[Ag(CN)_2]$, Raman scatt., press.-induced phase transitions and phonons 79−33698
Kr, solid, lattice dynamics calc. using Kihara hard core pot. 77−1193
$Kr:S_2$, absorption spectra of matrix-isolated S_2 molecules 77−52139
LaF_3, high-frequency phonon lifetimes 80−70338
LaF_3, zone centre optical phonon stress dependence, point group symm., Raman spectra meas. 79−78686
$LaF_3:Pr^{3+}$, anomalous luminesc. decay, phonon reson. trapping and bottlenecking 79−43023
$LaF_3:Pr^{3+}$, optical free induction decay meas. of low temp. dephasing 79−46009
$LaMo_6X_8$ (X=S, Se), supercond., sp. ht., 1 to 14K 79−51720
$LaNbO_4:Eu^{3+}$, single cryst., photoluminesc. obs., vibronic transition dichroism 77−69890
$LaNi_5H_6(D_6)$, low energy excitations of H and D 79−77699
La_2O_3, Raman spectra, lattice vibrs. 79−87440
$La_2O_2S:Eu^{3+}$, luminesc., excitation spectra, cooperative phonon sidebands 79−33771
La_2S_3, vibr. spectra, factor-group anal. 80−80793
$La_{0.98}Sn_{0.02}Mo_6Se_8$, Chevrel phase supercond. phonon anomalies at Sn site 79−56650
$La_{0.98}Sn_{0.02}Mo_6Se_8$, Mossbauer spectra 80−15926
LaTe, metallic, phonon density of states, Raman scatt. expt. 78−23451
Li, phonon limited resistivity struct. depend., Umklapp scatt., elastic consts. 80−88532
Li, phonon spectra, variable-form pot. calcs. 78−2209
Li, phonon spectral density, pseudopotential calcs. 80−39234
Li, spectrum, calc. from bandstructure 78−6134
$LiAl_5O_8:Cr^{3+}$, fluoresc. and excitation spectra, zero phonon lines 79−33785
LiF, 63 meV He atom scatt., single Rayleigh phonon interaction 78−80447
LiF, anharmonic cryst. of order λ^4, self-energy of phonons, approximate numerical results 79−55843
LiF:Mg(Ag), electron spin-lattice relax. of V_k-centre 78−95518
$LiGaO_2$, Raman scatt., optical modes determ. 79−15463
$LiGa_5O_8:Cr^{3+}$, fluoresc. and excitation spectra, zero phonon lines 79−33785
Li_3N phonon spectra and lattice dynamics 77−59580
Li_3N, photoluminesc. props. 80−50414
β-$LiNH_4SO_4$, lattice modes and phase transition, polarised Raman meas. 77−20859
$LiNbO_3$, IR reflectivity temp. depend. 78−27202
$LiNbO_3$, long wavelength phonons, low temp. lifetime 78−18710
$LiNbO_3$, Mossbauer radiation modulation by coherent US excitation 79−61277
$LiNbO_3$, optical consts. determ. by background stimulated Raman scatt. 80−48336
$LiNbO_3$, optical phonon modes and anharmonic couplings 78−60466
$LiNbO_3$, parametric phonon echo obs. 80−59588
$LiNbO_3$, piezoceramic, elastic normal wave propagation, phase transitions *(Russian)* 80−40067
$LiNbO_3$, temp. dependence of Raman scattering 77−16297
$LiNbO_3$:Ti, in-diffused waveguide, acousto-optical meas. of optical field profiles 79−23054
Li_2SO_4, liq. and plastic crystalline phases, Brillouin scatt. 79−99897
$Li_2SO_4.H_2O$, X-ray diffr., IR and Raman spectra, internal optic modes, mol. dipole model 77−76493
$Li_2Si_2O_5$, laminated cryst., IR spectra, dispersion anal. 77−1675
$LiTaO_3$, optical phonon modes and anharmonic couplings 78−60466
$LuMo_6X_8$ (X=S, Se), supercond., sp. ht., 1 to 14K 79−51720
$Lu_2O_2S:Eu^{3+}$, luminesc., excitation spectra, cooperative phonon sidebands 79−33771
$MgAl_2O_4$ spinel, low energy phonon obs. by inelastic neutron scatt. 78−43084
$MgAl_2O_4$ spinel, optic frequencies, evidence for membership of F43m space group 78−48168
Mg_2Ge, L, electron-phonon interaction and phonon cond. at low temp. L n-type semicond. 79−14903
MgO microcrystals, IR absorpt. 79−42963
MgO, phonon spectra using freq. crossing techniques 78−14415
$MgO:Cr^{2+}$, Jahn-Teller parameters determ. using heat pulses 77−62876
$MgO:Cr^{2+}(Mn^{2+})$, phonon spectroscopy using supercond. tunnel junctions 79−65157
$MgO:Cr^{2+}(Mn^{3+})(V^{3+})$, HF phonon spectroscopy using supercond. tunnel junctions 80−65178

lattice phonons continued
$MgO:Cr^{3+}$, $^4T_{2g}$ excited level of Cr^{3+} 78−43920
$MgO:Cr^{3+}$, no-phonon lines associated with broad band emission *(French)* 77−52163
$MgO:Fe^{2+}$, phonon-induced transition interf. in EPR and IR spectra, ion-lattice coupling 77−51945
$MgO:Ni^{2+}$, near IR luminesc. from isolated and exchange-coupled Ni^{2+} ion pairs, temp. depend. 80−93382
$MgO:V^{2+}$, first and second order Jahn-Teller coupling const. calc. 79−65906
$MgO:V^{2+}$, mag. circular dichroism in split zero-phonon line 78−56460
Mg_2Si, stress effects on Raman spectra 77−20851
Mg_2SiO_4, fosterite, lattice dynamics, IR and Raman spectra meas. 79−65153
Mg_2Sn, L, electron-phonon interaction and phonon cond. at low temp. L n-type semicond. 79−14903
Mg_2Sn, stress effects on Raman spectra 77−20851
$Mg_xZn_{1-x}Te$, long wavelength optical phonon replica 78−60468
$Mn_xCd_{1-x}Te$, far IR refl. spectra, phonon spectra 78−52497
$Mn_xCd_{1-x}Te$, lattice vibrs., Raman and IR spectra meas. 80−93311
$Mn_xCd_{1-x}Te$, phonons, Raman scatt. and IR absorpt. meas. *(French)* 80−97275
$MnCl_2.2H_2O$, phonons and electronic transitions, Raman spectra 79−28761
MnF_6^{2-}, $A_2{}^IM^{IV}F_6$ hosts, luminesc., IR and Raman spectra, 5K, assignments 77−20904
$Mn_xHg_{1-x}Te$, long wavelength optical phonons, IR refl. obs., 50-300 cm^{-1}, 90 and 295K 77−36243
MnO, Jahn-Teller effect on optical absorption spectra 78−52484
MnO, two phonon density of states 77−7808
$MnSe_2$, IR lattice vibrs., dielectric dispersion 79−28735
Mo and Nb-Mo alloys, superconductivity and phonon softening, between electron bands and phonons 78−14859
Mo, phonon frequencies, seventh-neighbour tensor force model 78−91402
Mo ternary chalcogenide, MMo_6X_8 (M=metal, X=chalcogen) Chevrel phase, supercond. and normal state props. 78−56267
Mo-Re (5 at.%), enhanced lattice sp. ht. due to LF reson. modes 78−14882
$Mo_6S_8(Se_8)(Te_8)$ and halogen substituted cpds., sp. ht. capacity 80−49986
MoS_2(2H), Raman spectra, phonon modes, high press. effects 80−40111
Mo_6Se_8, Chevrel phase, isotope effect on supercond. T_c 78−52141
Mo_6Se_8, Chevrel phase, isotope effect on supercond. transition temp., phonon modes 79−51713
Mo_6Se_8, Chevrel phase supercond., phonon spectra, neutron scatt. meas. 79−42174
$MoSe_2(Te_2)$, IR and Raman spectra, lattice vibrs. interlayer bonding 80−40110
Mo_6X_8 (X=S, Se), phonon density of states, mode softening correl. with supercond. transition temp. 79−51714
α-N, low freq. absorpt. spectra, libration modes *(Russian)* 80−55078
N_2, in solid N_2, phonon-assisted v-v transfer rates 79−10901
N_2, solid, semimicroscopic approach to lattice dynamics of mol. crystals 78−75765
N_2:CO, IR and Raman spectra, vibron band, vibron-phonon combination bands 78−68495
β-ND_4Br, $ND_4{}^+$ orientational fluctuations, neutron scatt. obs. 79−7557
$NH_4Ag_4I_5$, superionic phase transition, dynamical and crit. pt. props. 80−107535
NH_4Cl, orientational disorder, Raman and far IR spectra 78−23447
NH_4Cl, Raman scatt. of light on limiting and nonlimiting dipole vibr. 80−11402
NH_4I, orientational disorder, Raman and far IR spectra 78−23447
$(NH_4)_2M(SO_4)_2.6H_2O$, M=Ni, Co, Mg, IR spectra 80−97280
NH_4NO_3, Raman scatt. in region of extended IV-V phase transition 79−99887
NH_4SbF_5, dielectric props. and structural phase transitions *(German)* 80−25274
Na, dynamical structure factor calc., High temp. 80−15047
Na, electrical and thermal resistivity determ. from first principles 79−69493
Na, equilibrium struct. and phys. props., pseudopot. method 80−96778
Na, linear potential and phonons 79−82293
Na, phonon limited resistivity struct. depend., Umklapp scatt., elastic consts. 80−88532
Na, phonon spectral density, pseudopotential calcs. 80−39234
Na vacancy formation energy value from phonon data 79−77592
Na-NaO-Na struct., inelastic tunnel effect, spectra, potential barrier parameters 79−95511
$NaBrO_3$, Raman spectra, intramolecular vibrs. and lattice vibrs. *(Russian)* 77−1683
NaCN, Brillouin backscatter spectra of (100) LA phonons, elastic consts. determ. 79−65886
NaCN, librational and phonon sidebands of IR CN^- stretching mode 79−15457
NaCN, Raman diffusion spectra, IR absorpt. in phases II and III *(French)* 80−84741
NaCN, Raman spectrum, hydrostatic press. effects 78−6663
NaCl, anharmonic cryst. of order λ^4, self-energy of phonons, approximate numerical results 79−55843
NaCl, containing Na colloids, first-order Raman spectra 79−73943
NaCl, lattice thermal and optical phonon contrib. 79−14971
NaCl, positronic atom scatt. on optical phonons, positron thermalisation 80−50457
$NaClO_3$, Raman spectroscopy exam. of high-pressure phase transform. 78−10186
$NaClO_3$-$NaBrO_3$ mixed crystals, internal optic modes, Raman and IR spectra meas. 79−95746
$NaClO_4$, Raman spectra temp. depend. near 581K phase transition 78−56477
NaF-^{4}He liquid interface, phonon propagation 78−14526
NaI_3 long wave phonon modes, IR absorpt. 78−79686
$Na^{15}N_x{}^{14}N_{1-x}O_3$ mixed crystal, Raman spectra determ. of phonon density of states *(Russian)* 80−93313
$NaNO_2$, ferroelec., lattice dynamics, two-phonon Raman scatt. and IR absorpt. 79−33684
$NaNO_2$, fine struct. in luminesc. spectra in UV region 77−59607
$NaNO_2$, hot luminescence 78−10976
$NaNO_2$, incommensurate antiferroelec. phase, Brillouin scatt. freq. shift 80−93349

lattice phonons continued
$NaNO_2$, phonon side bands of triplet absorption 78−76488
$NaNO_3$, rel. to ^{23}Na spin-lattice relax. time −75.5 to +320°C *(Japanese)* 77−43897
Na^ANO_3, (A=14,15), anomalous IR reflectivity min. due to damping factor originating in two-phonon processes 79−56796
β and β-Na_2O_3-Na_2O, selection rules for spinel-block modes 79−19332
$NaPO_3$-$NaAsO_3$ system solid solutions, four-mode type IR spectra 79−51942
Na_2S, dielectric const., transverse and longitudinal optical mode, static dielectric const., effective charge 79−73892
α-$Na_2Si_2O_5$, laminated cryst., IR spectra, dispersion anal. 77−1675
$Na_xV_2O_5$, metallic, Raman scatt. 78−80358
Na_xWO_3, local struct. states in supercond. TI phase, lattice props. 78−26981
Nb and Nb-Mo alloys, superconductivity and phonon softening, between electron bands and phonons 78−14859
Nb, phonon density of state determ. from thermodynamic crystal functions *(Russian)* 79−82291
Nb, phonon frequencies, seventh-neighbour tensor force model 78−91402
Nb, superconducting phonon struct. obs. in proximity tunnelling 77−77008
Nb-H, acoustic phonon anomaly at small wavevectors 78−59882
Nb-Zr, diffuse neutron scatt. 78−71816
NbC, phonon anomaly rel. to Fermi surface 77−11853
NbC, supercond. transition temp. and lattice dynamics 79−56361
NbC(N), critical temp. enhancement, surface effect on phonon spectrum and electronic state density *(Chinese)* 80−2507
NbD_x, acoustic phonons conc. depend. 77−15515
NbH_x, HF phonons, neutron spectral obs. 80−49317
NbH_x, thermopower, role of phonon dynamics 79−33284
NbN, Raman spectra and superconductivity of various phases 78−68506
NbN, supercond. transition temp. and lattice dynamics 79−56361
$NbS_2Cl_2(Br_2)(I_2)$, absorpt. edge spectrum, fine struct. 80−66219
$NbSe_2$, 2H polytype, effect of incipient CDW on second-order Raman spectra 78−80357
$NbSe_2$ (2H), effect of CDW fluctuations on Raman active optic phonon freq. 78−87750
$NbSe_2$ (2H), Raman scatt. by supercond. gap excitations, coupling to CDWs 80−103956
$NbSe_3$, phonon study of chemical bonding 80−20645
$NbSe_2$(2H) microscopic theory of charge density wave instability 78−79732
Nb_3Sn, electronic props. calc. 79−7780
$NdH_{2.57,2.62}$, optical vibr. spectra of H, inelastic neutron scatt. study 80−107391
Nd_2O_3, Raman spectra, lattice vibrs. 79−87440
Nd_2S_3, vibr. spectra, factor-group anal. 80−80793
Ne, solid, quasi-line emission in transitions between excited states *(Russian)* 79−91494
Ni, Brillouin spectra, light scatt. cross section for surface ripples 80−71434
Ni, phonon density of states determ. from thermodynamic functions 80−96616
Ni, phonon generation and attenuation at FMR 80−39875
$Ni_3B_7O_{13}I$, Raman spectra in paraelec. phase 78−60434
$NiBr_2(Cl_2)$ two-phonon vibronic progressions, Raman obs. 80−29742
NiH_x, magnetization, elec. resist., and non-occurrence of supercond. 79−56195
NiO, temp. depend. of thermal expansion and IR lattice vibrational mode 77−84950
NiS, spin polarons exam. and metal-insulator transition 78−10377
NiS_2, Raman scatt., optical phonon peaks obs. 77−85728
$NiS_{2-x}Se_x$, first-order Raman scattering 80−108206
P, black phosphorous struct., Raman vibr. spectra and bonding 80−11411
Pb, effect of supercond. transition on phonon energies and lifetimes 79−28432
Pb, supercond., quasiparticle and phonon propagation 79−42689
Pb, supercond. film, intrinsic and expt. quasiparticle recomb. times 77−15999
Pb, superconducting, phonon density of states determ. 77−20493
Pb superconducting film, nonequilib. gap instability and phase transition under intense tunnel injection 79−28476
Pb superconducting film, quasiparticle and phonon lifetimes, tunnel junction and meas. 77−20498
$PbCl_2$, Raman spectra, phonon modes 80−2754
$PbCl_2$, single cryst., far IR refl. spectra, effective ionic charges 79−87430
PbF_2, acoustic phonon modes up to high temps., neutron scatt. meas., time averaged defect struct. 79−33052
PbF_2, orthorhombic and cubic, heat capacity, 3 to 22K 80−19955
PbF_2, phonon temp. depend., neutron scatt. study 79−60450
PbF_2, Raman scatt. exam. at high temp. 77−32367
PbF_2, US vel. near press. induced cubic-to-orthorhombic transform. 80−103476
$Pb_5Ge_3O_{11}$, anharmonic phonons and central peaks at struct. phase transitions 79−95775
$Pb_5Ge_3O_{11}$, Raman scatt., soft modes and damping near structural phase transition 79−28739
$Pb_{1-x}Ge_xTe$ epitaxial layers, phase transition obs. by far IR reflectivity spectroscopy 79−33691
PbI_2 intercalated with aniline, NQR meas. *(Russian)* 79−91311
PbI_2, low temp. thermal props. 79−95178
PbI_2, optical phonon anisotropies and intralayer bonding forces from IR refl. 77−59573
PbI_2, single cryst., far IR refl. spectra, effective ionic charges 79−87430
PbI_2 single crysts., resonant and nonresonant Raman spectra 77−69823
PbI_2, two-photon absorpt. spectrum 77−52118
$Pb(Mn_{1/2}Ta_{1/2})O_3$, ceramic, for thermal and dielectric isolation at low temp. 80−39365
$PbMoO_4$, Raman scatt. obs. of external and internal modes 79−69842
$PbMo_6S_8$, Chevrel phase supercond., phonon spectra, neutron scatt. meas. 79−42174
$Pb_{1.2}Mo_6Se_8$, Chevrel phase supercond., phonon spectra, neutron scatt. meas. 79−42174
$PbMo_6X_8$ (X=S, Se), phonon density of states, mode softening correl. with supercond. transition temp. 79−51714
$Pb(NO_3)_2$, dynamical props., IR reflection spectra meas., 10-300K 77−1676
$Pb(NO_3)_2$, IR reflection spectra, dynamical props. 77−16303
lattice phonons continued
$Pb_3(PO_4)_2$, crit. behaviour of polar modes near ferroelastic phase transition 79−95750
$Pb_3(P_xV_{1-x}O_4)_2$, ferroelastic phase transitions, lattice dynamics, dielec. and optical props. meas. 77−55334
PbSe, lattice dynamics, slow neutron inelast. scatt. 77−31740
$PbSe_{1-x}Te_x$, for-IR reststrahlen spectra, mode behaviour 80−7345
$Pb_{0.8}Sn_{0.2}Te$, magnetophonon effect obs. 78−23115
$Pb_{1-x}Sn_xTe$, band struct. and phonon energies, tunnelling spectroscopy 78−72070
$Pb_{1-x}Sn_xTe$, in MIS struct., tunnelling investig. of band gap and phonon energies 77−43733
$Pb_{1-x}Sn_xTe$, in MOS junction, phonon-assisted tunnelling 77−76928
$Pb_{1-x}Sn_xTe$, lattice and electronic props. and g-value 80−80161
$Pb_{1-x}Sn_xTe$, lattice instability and phonon-width, comprehensive model 79−14906
$Pb_{1-x}Sn_xTe$, longit. optical phonon, freq. and damping coeff. 79−8162
$Pb_{1-x}Sn_xTe$, soliton modulation widths for TO-phonons 77−80588
n-PbTe epitaxial film, magnetophonon and Shubnikov-de Haas oscills. 78−60234
PbTe epitaxial layers, submillimetre spectroscopy 79−83048
p-PbTe film, for IR magneto-optics, 8-30K 78−23543
p-PbTe film, magnetophonon effect obs. 78−23115
n-PbTe film, magnetophonon reson., 55-90K 79−7913
PbTe, index matching far i.r. method for static dielectric const. meas. 77−1678
PbTe, microwave magnetoplasma exam. of lattice and electronic props. 77−69364
PbTe-SnTe compound semiconductors, lattice instability by mm-wave magnetoplasma refl. 80−54336
$PbWO_2$, IR and Raman multiphonon spectra, struct. 77−90143
$PbWO_4$, reflectivity, dispersion parameters and optical const. temp. depend. 77−28575
$PbZr_{0.95}Ti_{0.05}O_3$, soft mode dielec., anomalous low temp. sp. ht. 78−14423
Pd complex, linear ionic mixed valence cpd., IR and resonance Raman spectra rel. to lattice modes 80−25393
Pd, diffusion of H, model 79−73338
Pd mixed valence-mixed metal compounds, ionic crystals, longitudinal lattice modes, Raman spectroscopy 80−40099
Pd, phonon density of states determ. from thermodynamic functions 80−96616
Pd, phonon mediated interaction for triplet pouring 79−23911
Pd-H(D), vibr. modes Raman study 77−85713
Pd-Pt, and other substitutional alloys with large mass disorder, phonon modes 78−95122
Pd-Si, metallic glass, phonon propagation at low temp. 78−87756
PdD_x, optical phonon spectra, supercond. tunnelling meas. 79−19701
PdH, supercond., simple scaling theory of isotope effect 78−14878
PdH, superconducting transition critical temperature, BCS theory, phonon spectra *(Spanish)* 80−84535
PdH_x, local, soft modes, superconductivity thermal neutron inelastic scatt. *(Chinese)* 80−70331
PdH_x, optical phonon spectra, inelastic neutron scatt. study 79−42186
PdH_x, x=0.915 to 0.996, thermoelec. power, 10 to 170K, rel. to optical phonon spectra 79−56201
$PdH_x(D_x)$, nonstoichiometric, phonon spectra calc., Born-von Karman treatment 77−11650
phase transition in transverse field with deform. depend., phonon anomaly separation KH_2PO_4 80−39258
Pr $H_{2.8}$, optical vibr. spectra of H, inelastic neutron scatt. study 80−107391
Pr, magnetic excitations, exchange, crystal field and magnetoelastic interactions 80−2563
Pr_2O_3, Raman spectra, lattice vibrs. 79−87440
$PrSn_3$, inelastic neutron scatt. spectra, cryst. elec. field effects 78−43336
Pr_3Te_4-Pr_2Te_3 system, characts. of thermal cond. 77−7917
Pt complex, linear ionic mixed valence cpd., IR and resonance Raman spectra rel. to lattice modes 80−25393
Pt, mixed valence-mixed metal compounds, ionic crystals, longitudinal lattice modes, Raman spectroscopy 80−40099
Pt, phonon density of states determ. from thermodynamic functions 80−96616
Rb halides, spin lattice relaxation meas. of O_2^- centre 80−88863
Rb, phonon spectral density, pseudopotential calcs. 80−39234
$RbAg_4I_5$, solid electrolyte, neutron scattering study 78−79696
$RbAg_4I_5$, solid electrolyte, Rayleigh-Brillouin and low-frequency Raman spectra 79−33720
$RbAg_4I_5$, superionic phase transition, dynamical and crit. pt. props. 80−107535
$RbCoF_3$, antiferromag., anisotropic exchange, dispersion relations of mag. excitations 77−69532
RbH_2PO_4 powder, phase transition in paraelectric (upper) phase by measuring damping const. and amplitude of phonon echoes 79−19855
RbI, hyper-Raman spectra by single channel method 78−84591
RbI, IR active and silent modes, hyper-Raman scatt. obs. 79−61376
RbI, NaCl to CsCl phase transition by elastic diffuse and inelastic neutron scatt. 80−2162
RbI, zero phonon and LO phonon assisted luminesc. of free excitons 79−28799
$Rb_{1-c}K_c$, phonon spectra, single site CPA 78−10142
Rb_2MnCl_4, perovskite type layer struct., far IR reflectivity and Raman spectra 77−15511
Re, Raman scattering spectrum at room temp. 80−25373
ReO_3, coeff. of linear thermal expansion, 100-500K 79−10972
ReO_3 type lattice, group-theoretical symmetry anal. of vibr. *(Russian)* 80−10610
α-S, zone-centre lattice vibrs., including hydrostatic press. effects 80−49314
$(SN)_x$ film and crystal, acoustic and optical phonons, Raman, i.r. and transmission spectra 77−4642
$(SN)_x$, lattice and electronic sp. ht. contribs. density of states 77−43344
$(SN)_x$, phonon spectra, four-parameter valence force model 77−20027
S_2N_2, cryst. and partly polymerised films, Raman scatt., optical absorption 77−8673
S_4N_4, effects of pressure and temp. on phonons, Raman scattering study 80−7360
S_4N_4, Raman scatt. and opt. absorpt., press. and temp. depend. 77−36227
Sb, k=0 optical phonon temp. depend., Raman scatt. meas. 77−76509

lattice phonons continued
Sb, zone centre phonons and elastic consts., hydrostatic press. depend. 78−59905
Sb_5O_7I, polytype 2MA, ferroelectric, ferroelastic, Raman scattering and symmetry anal. 79−38550
Sb_2Te_3, $(Bi_{1-y}Sb_y)_2Te_3$, Raman and far infrared investigation of phonons 78−23453
$ScMo_6X_8$ (X=S, Se), supercond., sp. ht., 1 to 14K 79−51720
Sc_2O_3, Mandelshtam-Brillouin spectra, transverse phonon contrib., elastic and photoelastic consts. 77−81115
Se, effective charge tensor, microscopic treatment 78−59879
Si, covalent semiconductor, electronic response to high symmetry lattice vibr. 80−10619
Si, dense plasma dynamics during pulsed laser annealing, carrier density, recombination 80−84479
p-Si, galvanomagnetic effects 79−33297
Si, highly transparent semicond. crysts., multiphonon IR absorpt. 78−10885
Si, Kikuchi structures, phonon scatt. and thermal diffuse scatt., transmission electron diffraction study *(German)* 80−44082
Si, multiphonon and one phonon X-ray scattering, and temp. depend. of Debye-Waller factors, shell model calcs. 79−99022
Si, phonon induced intervalley transitions, violation of selection rules 78−30875
Si, phonon-assisted Auger recomb., direct calc. of overlap integrals 80−107808
Si, phonons, directional depend. of boundary scatt. mean free path 79−73354
Si, piezo−spectroscopic study of ratio of electron−TO phonon to hole−TO phonon interaction 79−24289
n^+nn^+Si planar device, hot electron flicker noise at 78K 80−103732
Si, polarisation of recombination radiation from multiparticle exciton-impurity complexes, induced by uniaxial deform. *(Russian)* 79−78754
Si, Raman cross section and its press. depend., theoretical study 79−91448
Si, role of electron-hole interaction in optical spectra, review 80−45113
Si, shallow p-n junction, energy loss and escape depth of hot electrons 79−78159
Si, structural props. using electron-ion Hamiltonian using density-fundamental methods 79−82177
Si, thin slabs, vibr. freq. calcs., dimens. effect 80−60585
n-Si, vibr. excitation conditions, vol. charge redistrib. effect *(Russian)* 80−103427
Si:^{119m}Sn, impurity lattice dynamics, Mossbauer spectra, Debye temp. 80−84262
Si:Al, absorpt. line broadening 78−95594
Si:B(P), uniaxially stressed, impurity-assisted intervalley scatt., photoluminesc. obs. 80−34979
Si:In, backward wave phonon spectroscopy 80−2357
p-Si:Zn^-, deep levels, optical-phonon-assisted capture of carriers 79−51597
SiC (1 OH), phonon spectrum, dispersion curves energy discontinuity and vibr. modes, IR spectra obs. 80−44274
n-SiC (6H), anisotropy of thermoelectric power *(Russian)* 78−91710
SiC polytypes, free exciton luminesc. meas., phonon energies 80−80852
p-SiC, spin-flip Raman scattering, review 80−108209
α-SiC, wurtzite type cryst., temp. depend. of one phonon Raman spectra, Gruneisen parameters 77−66500
p-SiC:B (4H), absorption spectra of bound excitons 78−88338
SiO_2, phonon echos in SiO_2, ADP, KDP, and Rochelle salt *(Japanese)* 79−51213
SiO_2, transport of electrons at high electric fields 80−20208
Si_2Te_3, cryst., IR reflection, Raman spectra 77−12393
Sm^{3+} in cubic environment, importance of T^{-5} and T^{-7} terms in spin-lattice relax. time 80−25192
SmS, f-d hybridisation, valence fluctuation and phonon spectrum, Raman scatt. expts. 78−60464
Sm_3S_4, inelastic light scatt. 77−55788
$Sm_{1-x}Y_xS$, effect of valence fluctuations on lattice dynamics 78−47493
$Sm_{1-x}Y_xS$, mixed valence, phonon softening and linewidths, calc. 80−75319
α-Sn, adiabatic bond charge model 77−69057
Sn, bulk supercond., ballistic propag. of near-gap phonons 77−85384
α-Sn, gapless semicond., sound propag., RPA calc. 77−31721
α-Sn, reson. first and second order Raman scatt. 78−35144
Sn, supercond. film, intrinsic and expt. quasiparticle recomb. times 77−15999
Sn, superconductor, bulk non-equilib. quasiparticles probed by ballistic phonons 79−56391
Sn thin film, anomalous transmittance of metal-insulator interface for thermally radiated phonons *(Russian)* 80−103664
α-Sn:^{119m}Sn, impurity lattice dynamics, Mossbauer spectra, Debye temp. 80−84262
Sn-insulator-Sn, supercond. tunnel junction, phonon emission caused by subharmonic energy gap 79−56437
$SnCl_2.2H_2O$, Brillouin scatt. and thermal expansion 80−97289
SnI_2 single crysts., Raman scatt. of light 79−73950
SnI_2, single crysts. and film, optical props. 77−32437
$SnMo_6S_8$, Chevrel phase supercond., phonon spectra, neutron scatt. meas. 79−42174
$SnMo_6S_8$, phonon density of states, mode softening correl. with supercond. transition temp. 79−51714
$SnMo_6S_8(Se_8)$, Mossbauer spectra 80−15926
$SnMo_6Se_8(Se_8)$, Chevrel phase supercond., phonon anomalies at Sn site 79−56650
SnS, far IR optical props. 77−12375
SnS, splitting and coupling of lattice modes 77−76503
SnS_2, crystal growth and optical props. in visible and IR regions 77−52114
SnS_2, single cryst., far IR reflectivity 79−56774
Sn_2S_3, mixed valence semicond., long wavelength phonons, full space group theoretical anal. 79−65873
$SnS_{2(1-x)}S_{2x}$ solid soln. system, long-wavelength optical phonons, Raman scatt. study 80−80794
SnS(Se), IR reflectivity and Raman spectra, phonon frequencies and dielec. const. 77−48166
SnS(Se), layer crystals, optical phonons, Is and Raman spectra 77−73148
$SnS_{2-x}Se_x$, layer cryst., Raman active modes 80−80767
$SnS_{2-x}Se_x$, Raman spectra 79−28763
lattice phonons continued
$SnS_2(Se_2)$, optical phonon anisotropies and intralayer bonding forces from IR refl. 77−59573
SnSe, far IR reflectivity spectra, lattice vibr. and dielec. const. 77−52068
SnSe, Raman scatt., zone centre optical phonons, layer-like struct. 78−48158
SnTe, LO phonons affected by dielec. screening 79−77697
SnTe, obs. of soft TO-phonon by Raman scatt. 77−69838
SrClF, cryst., Raman intensity anal., normal coord. anal. 78−72493
SrClF, long wavelength dynamics, shell model calc. 80−29134
SrF_2, F-centres, single-phonon Raman scatt. meas. 77−20844
SrF_2, high-frequency phonon lifetimes 80−70338
SrF_2, optical detection of acoustic phonons at THz freqs. 80−75320
SrF_2, strain induced splitting and oscillator strength anisotropy of IR transverse optic phonon 80−92625
$SrF_2:Eu^{2+}$, phonon spectroscopy, phonon pulse spatial, spectral and temporal evolution 78−34580
$SrF_2:Eu^{2+}$, spectral, spatial and temporal phonon spectroscopy, new spectrometer 78−83892
$Sr(NO_3)_2$, dynamical props., IR reflection spectra meas., 10-300K 77−1676
$Sr(NO_3)_2$, IR reflection spectra, dynamical props. and phase transition 77−16303
$SrTiO_3$, anharmonic phonons and central peaks at struct. phase transitions 79−95775
$SrTiO_3$, centrosymmetric crystal, phonon polariton hyper-Raman scatt. obs. 80−76028
$SrTiO_3$, IR active and silent modes, hyper-Raman scatt. obs. 79−61376
$SrWO_4:Er^{3+}$, spin-lattice and spin-spin relax. times, electron spin echo obs. 79−28609
TR^{3+} ion excited state population depend. on lattice on IR excitation. *(Russian)* 80−50425
Ta, phonon density of state determ. from thermodynamic crystal functions *(Russian)* 79−82291
Ta phonon frequencies calc. 79−19329
TaC, phonon anomaly rel. to Fermi surface 77−11853
TaS_2, 1T polytype, charge density waves effects on phonon modes, Raman spectra meas. 77−36245
TaS_2, $1T_2$ phase, Kohn anomaly, neutron scatt. meas. 77−69056
TaS_2 (1T), commensurate and incommensurate CDW state, far IR reflection spectra 79−95755
TaS_2 (2H), Raman scatt. 77−1679
$TaS_2(Se)_2$, 2H polytype, effect of incipient CDW on second-order Raman spectra 78−80357
$TaS_2(Se_2)$, intercalated with ethylenediamine, Raman spectra 78−48182
$TaSe_2$ (1T), commensurate and incommensurate CDW state, far IR reflection spectra 79−95755
$TaSe_2$ (2H), effect of CDW fluctuations on Raman active optic phonon freq. 78−87750
2H-$TaSe_2$, commensurate superlattice vibr., Raman spectra 77−16299
$TaSe_3$, phonon study of chemical bonding 80−20645
Tb complex, in $Cs_2NaTbCl_6$, f-f transitions, mag. dipole intensities, vibronic coupling model 80−25404
Tb-Gd, spontaneous striction and phonon contributions to thermal expansion *(Russian)* 79−90800
$TbVO_4$, Jahn-Teller distortion, mag. field depend. 78−79733
Te, galvano- and thermomagnetic effects 78−30939
TeO_2, elastic wave parametric instability kinetics in dielectrics *(Russian)* 80−45035
TeO_2, paratellurite, IR refl. and Raman scatt. expts. 77−15518
TeO_2, paratellurite, phase transition at high-press., Raman and far IR spectra 78−80328
TeO_2, zone centre optical phonons under uniaxial stress 78−79700
$ThBr_4:U^{4+}$, absorpt. spectrum, zero phonon line *(French)* 80−11443
$ThBr_4:U^{4+}$, IR luminesc., zero phonon lines 79−33769
Th_4H_{15}, ThH_2, phonon densities of states rel. to supercond. props. 77−27960
$ThSiO_4$, synthetic, Raman spectrum and lattice vibrs. 77−48160
Ti, high temperature thermophysical properties 78−91404
Ti-Ni-Co cubic B_2 alloys, phonon enhancement of electronic sp. ht. near martensitic transform. 79−60522
$TiCl_3$, electronic struct. and struct. phase transition 80−59644
$TiCl_3$, lattice instability, d-electron-lattice interaction 80−44276
$TiH_{1.92}$, thermal neutron inelastic scatt. phonon spectra determ. *(Chinese)* 79−10906
$Ti_{55}Nb_{45}$, supercond., anomalous phonon thermal resist. 77−69451
TiO-MeO (Me=Ni, Co, Mn), solid soln., lattice thermal cond. 79−23791
TiO_2, anatase, natural and synthetic crysts., Raman spectra and assignments 79−28752
TiO_2 anatase, Raman spectrum, temp. depend. 80−76027
TiO_2, electron energy loss spectra, 0.02-2 eV 78−39642
TiO_2, rutile, first-order Raman spectrum, uniaxial-stress depend. 80−60586
TiO_{2-x}, plasmon and polar optical phonons 77−39794
Ti_2O_3, IR refl. spectra, IR active phonons, Ti 3d electronic effects 78−35145
$(Ti_2O_3)_{1-x}(V_2O_3)_x$, lattice polarisability, electronic contribs. IR refl. obs. 78−59904
TiS_3, linear chain compound, lattice props., Raman spectral study 80−71421
$TiS_2(Se_2)$, modelling contrasting semimetallic characters 78−43393
$TiSe_2$, IR reflectivity, phonons and free carriers 79−61379
$TiSe_2$, semimetal, IR props. 79−24318
$TiSe_2$, superlattice formation, Raman and far IR spectra 78−35135
Tl, phonon spectrum from Krasko-Gurskii pseudopot. calc. 80−96608
Tl-Bi-Pb, phonon anomaly near Fermi surface topological transition, phonon softening at X point 78−95120
$TlAsS_2$, Tl_3AsS_3, and Tl_3AsS_4, Raman and IR spectra *(Russian)* 77−66512
Tl_3AsS_4, optical phonons, Raman and refl. spectra 80−11400
TlBr, phonon struct. of forbidden-indirect transitions 79−61393
TlBr, reson. Raman scatt., forbidden one phonon and intervalley scatt. at direct exciton 80−45073
TlBr, second order Raman scatt., reson. behaviour rel. to phonon bands 80−40101
TlBr, soft mode dielec., anomalous low temp. sp. ht. 78−14423
TlCl, phonon struct. of forbidden-indirect transitions 79−61393
TlCl, second order Raman scatt., reson. behaviour rel. to phonon bands 80−40101

lattice phonons continued
$TlGaS_2$, IR refl. spectrum., LO phonons *(Russian)* 77−40221
$TlGaS_2$, IR refl. spectrum, Kramer-Kronig analysis, transverse optical phonons 78−19489
$TlGaS_2(Se_2)$, IR reflection spectra, lattice vibrs. *(Russian)* 77−85701
$TlGaS_2(Se_2)$, optical phonons, IR and Raman scatt. meas. 78−59903
$TlGaS_2(Se_2)$, phase transforms. under hydrostatic press., Raman scatt. study 80−25366
$TlGaS_2(Se_2)$, Raman spectra 78−43876
$TlGaS_{2x}Se_{2(1-x)}$, layer solid soln., mixed one- and two-mode behaviour of optical phonons 79−47445
$TlGaSe_2$, Raman and IR spectra, zone centre optical phonons 78−76462
$TlGaTe_2$, $TlInTe_2$, and $TlInSe_2$, IR refl. spectra 80−60605
TlI, magnetoabsorption, LO phonon energy 77−28593
$Tl_6I_6M_{2/n}{}^{n+}(I_4)^{2-}$, (M=Pb, Ag, Au, $(Bi_{0.5}Tl_{0.5})$), struct., rel. to phonon spectra 80−71425
$TlInS_2$, optical phonons, IR and Raman scatt. meas. 78−59903
$TlInS_2$, optical phonons, IR and Raman spectra *(Russian)* 79−10903
β-$TlInS_2$, Raman spectra 78−43876
$TlInS_2(Se_2)$, IR reflection spectra, lattice vibrs. *(Russian)* 77−85701
$TlInS_{2x}Se_{2(1-x)}$, layer solid soln., mixed one- and two-mode behaviour of optical phonons 79−47445
$TlInSe_2$, single crystals, optical phonons, Raman and infrared spectra studies 79−55842
TlSe, optical phonons, IR and Raman scatt. meas. 78−59903
TlSe, Raman spectra, phonon modes 80−40109
TmSe, intermediate valent, Raman scatt. 80−16038
TmSe, mixed valence, X-ray absorption study 80−76102
UO_2, electronic transitions, crystal field effects and phonons, phase transition 80−97303
U_3O_{8-z}, depend. of therm. cond. on porosity, phonon mean free path calcs., Debye temps. 79−37886
USb, neutron inelastic scatt. meas., phonon spectra, mag. response, anisotropy 80−50065
V film, superconducting tunnelling, meas. of annealing characteristics 79−7944
V, photon frequencies calc. 79−19329
VCl_3, electronic struct. and struct. phase transition 80−59644
$(V_{1-x}Cr_x)_2O_3$, Raman scatt. and phase transitions 80−71420
V_3Ga, phonon densities of states and Debye temp. calcs. 79−51212
V_3Ge, phonon densities of states and Debye temp. calcs. 79−51212
$VH_{0.51}$, optic modes study by neutron spectroscopy 80−19891
VI_2, mag. 'Bragg' scatt. obs. through Raman scatt. 80−66179
VN, lattice phonons, dispersion and density-of-states 79−99283
$V_{0.97}O_{0.03}$, lattice dynamics exam., neutron scatt. 79−23689
V_2O_3, polarised Raman scatt. in metallic and semicond. phases 77−90152
V_3Si, A 15 compound, Raman scatt. and phonon density of states 79−28768
V_3Si, E_g optical phonon, Raman scatt. meas. 79−24316
V_3Si, phonon densities of states and Debye temp. calcs. 79−51212
V_3Si, phonon density of states at 300K, mode softening 77−11648
V_3Si, single crystals, supercond. tunnel characts. 80−7044
$V_{0.97}U_{0.03}$, phonon spectrum, quasi-local vibrs., inelastic incoherent neutron scatt. 77−15519
W, alternating sign Hall effect and doppleron spectrum 78−79981
WC, microcrystalline, mol. dynamics, motion of H_2O and H_2 mols. adsorbed on surface, catalytic activity 78−71941
$W_xMo_{1-x}O_3$, mixed cryst., structural phase transition, Raman and IR spectra 78−79766
WO_3, condensed phonon modes in successive phases 79−46765
WS_2 (2H), layered cpd., Raman scatt. 80−103960
WSE_2, Raman spectrum, long wavelength optical phonons 77−40218
Xe, solid, lattice dynamics calc. using Kihara hard core pot. 77−1193
Xe, solid, two-phonon difference scatt. 80−60588
YAG, phonon spectrum, incoherent inelastic neutron scatt. meas. 77−66006
YAG:Ce^{3+}, photoluminescence excitation energy, crystal field and temp. effects 80−11460
YAG:Cr, optical detection of phonons 80−92630
YAG:Nd^{3+} crystal, zero-phonon linewidths, in $^4I_{9/2} \rightleftarrows {}^4F_{3/2}$ luminesc. band calc. 79−28834
$Y_3Al_5O_{12}$:Yb^{3+}(Nd^{3+}), one-phonon satellites in luminesc. spectra, rel. to effective phonon density 78−6730
YF_3:Yb,Er, multiphonon processes in IR visible light conversion *(Russian)* 77−28628
YMo_6X_8 (X=S, Se), supercond., sp. ht., 1 to 14K 79−51720
Y_2O_3, Mandelshtam-Brillouin spectra, transverse phonon contrib., elastic and photoelastic consts. 77−81115
Y_2O_2S:Eu^{3+}, luminesc., excitation spectra, cooperative phonon sidebands 79−33771
YS, supercond. transition temp. and lattice dynamics 79−56361
YS, superconductor, resonances in generalised susceptibility and phonon anomalies 79−60443
$YbCl_3.6H_2O$, paramag. relax., Mossbauer spectra 80−20536
Zn superconducting film for energy selective phonon detection 80−92621
$ZnAs_2$, thermodynamic functions 79−10961
$ZnAs_2(P_2)$, monoclinic, lattice vibr. symm., IR and Raman active frequencies *(Russian)* 77−69055
$Zn_{1-x}Cd_xS$ mixed crystals, Raman spectra between frequencies LO(Γ) to TO(Γ) 78−2854
$Zn_{1-x}Cd_xSe$, mixed crystals, antireson. in phonon spectrum, Raman spectroscopy 80−88992
$Zn_xCd_{1-x}Te$, reson. Raman scatt. of light by longitudinal optical phonons 77−28577
$ZnGeP_2$, one- and two-phonon Raman scatt. 79−78681
$ZnIn_2S_4$, lattice dynamics, IR and Raman spectra 77−81106
$ZnIn_2S_4$ layered compound, phonon freqs., IR refl. and transmission spectra 77−77210
$ZnIn_2S_4$, Raman and IR spectra 78−48181
$ZnIn_2S_4$, Raman scatt., hydrostatic press. effect 80−84745
$Zn_{1-x}Mg_xTe$, long wavelength optical phonons, IR ref. and Raman obs. *(French)* 78−60433
ZnO, acoustic phonon intensity fluctuations after strong nonlinear amplification 78−59909
ZnO, electron-hole recombination emission, temp. depend. and phonon repetitions *(Russian)* 79−15521
ZnO, intensity fluctuations of nonlinearly amplified phonons, Brillouin scatt. meas. 77−90163
ZnO, luminescent, phonon detection by shallow electronic trap states 79−14902

lattice phonons continued
ZnO, reson. Raman scatt. 78−35137
ZnO, wurtzite type cryst., temp. depend. of one phonon Raman spectra, Gruneisen parameters 77−66500
ZnO:Cu, excited state, zero phonon lines in emission and Zeeman spectra 79−38026
ZnP_2, Brillouin scattering and optical props. meas. 80−76041
ZnP_2, reson. interaction of vibr. states, polarised Raman spectra meas. 77−15521
ZnP_2, tetragonal, one and two phonon states using second order Raman spectra 78−43874
ZnP_2 tetragonal crysts., light scatt. by optic phonons 80−55116
Zn_3P_2, multiphonon absorption in IR spectra 78−39554
ZnS, phonon spectra calc. by recursion method 80−59596
ZnS, phosphor, voltage depend. of electrolum. brightness 80−45148
ZnS, Raman scatt. by phonon polaritons 80−103959
ZnS, single crystal, effect of elec. field on cond. 78−84228
ZnS, wurtzite type cryst., temp. depend. of one phonon Raman spectra, Gruneisen parameters 77−66500
ZnS:Ag_2 phospors, nature of fluorescent centres and traps 79−91484
ZnS:Cu^{2+}, Jahn-Teller effect, stacking faults and formation of polytypes, absorption and emission spectra 77−4660
ZnS:Fe^{3+}, spin-lattice relax., expt. evidence for optical phonons 80−20451
ZnS:Mn^{2+}, $^4T_1$ state, magneto-optical meas. 77−20833
ZnS:Mn^{2+}, spin-lattice relaxation, EPR, optical phonons 80−39852
ZnS-CdS:Ag, phospors, nature of fluorescent centres and traps 79−91484
ZnS(Se), highly transparent semicond. crysts., multiphonon IR absorpt. 78−10885
ZnS(Se):Ni, optical absorpt., impurity ionisation, optical phonon coupling 80−88505
ZnS_xSe_{1-x}, phonon spectra calculations by recursion method, mixed crystals 80−103430
ZnS(Se)(Te), second order Raman scatt., lattice dynamical calc. and expt. 80−25370
ZnSe film, thermostimulated polariton emission 78−2436
ZnSe films, reson. Raman spectra 80−80888
ZnSe, Gudden-Pohl effect, release of electrons from traps 80−45149
ZnSe, lattice vibration, thermal expansion and pressure effect 80−39233
ZnSe, moments of phonon spectra from specific heats 80−15203
ZnSe, relaxation processes in Raman scattering and exciton luminescence under resonant excitation 80−25386
$ZnSiF_6.6H_2O$, spin-phonon interaction between Ni^{2+} ions, phonon bottleneck effects, splitting parameters *(Russian)* 80−15796
$ZnSiP_2$, first- and second-order Raman scatt. 78−35151
$ZnSiP_2$, one- and two-phonon Raman scatt. 79−78681
ZnTE, relaxation processes in Raman scattering and exciton luminescence under resonant excitation 80−25386
ZnTe, edge luminesc. excited by electron bombard. 80−66308
ZnTe, lattice vibration, thermal expansion and pressure effect 80−39233
ZnTe, moments of phonon spectra from specific heats 80−15203
ZnTe, relax. times of secondary radiations, circular polarisation correlation 79−28816
ZnTe, reson. secondary radiation 79−99886
ZnTe, spin-flip plus phonon scatt., line shape and shift in peak position 79−73907
p-ZnTe, spin-flip Raman scattering, review 80−108209
ZnTe:As(P)(Li), electronic Raman scatt. and IR absorpt. spectra of shallow acceptors 79−73978
$ZnTe_xSe_{1-x}$, phonon spectra calculations by recursion method, mixed crystals 80−103430
Zr, high temperature thermophysical properties 78−91404
ZrC, supercond. transition temp. and lattice dynamics 79−56361
ZrS_3, one-dimensional semicond., Raman spectra 79−87447
$ZrS_3(Se_3)$, quasi one-dimens., optical phonon anisotropy, IR spectra study 80−40112
$ZrS_3(Se_3)(Te_3)$, phonon study of chemical bonding 80−20645
$ZrSe_3$, long wavelength optical phonons, Raman scatt. and IR refl. 80−34921
$ZrSiO_4$, synthetic Raman spectrum and lattice vibrs. 77−48160

lattice structure, crystals *see crystal atomic structure*

lattice theory and statistics
see also Ising lattices; renormalisation; X-Y model
1/n expansion to order $1/n^2$, crit. exponent β for d=3 79−35636
1/n expansion to order $1/n^2$, crit. exponents γ, ν for d=3 79−35637
1/n expansion up to $1/n^2$, eqn. of state and correlation function 78−89412
1/n expansion up to order $1/n^2$, critical amplitude ratio R_x 79−58646
(2+1) dimensional Ising model, O(2), O(3) model in (1+1) dimens., finite lattice approach 80−86227
20-vertex model on triangular lattice 78−70065
$\lambda\pi^4$ field theory with internal symm., string representation 78−70266
λ-bell lattice one-dimens., nearest neighbour statistics 77−61028
$\phi_4{}^4$, constructive euclidean approach 77−65001
ϕ^3 field theory with internal Potts symmetry, exactly soluble limit 79−45004
ϕ^4 fields, critical exponents and elementary particles 77−26243
ϕ^4 kink behaviour in presence of inhomogeneous perturbation 79−75692
ϕ^4 lattice field theory, d-dimens., thermodynamic props. near Ising limit 80−82860
ϕ^4 system, metastable state, decay rate calc. 80−22301
ϕ^4-model in two and three dimensions, real-space renormalisation for arbitrary single-site pot. 80−22307
ϕ^6 operators in scalar systems near four dimensions, tricritical scaling and renormalisation 79−58863
Abelian Higgs model, two dimens., multiple vacs. in lattice formulation 78−54543
Abelian lattice gauge field theory, 2+1 dimens., phase transition 78−24963
Abelian lattice gauge theories, phase transitions 78−12812
Abelian lattice gauge theory, quark confinement 78−66040
adsorbed monolayer of orientable molecules, lattice fluid model, real-space renormalisation group method 80−17882
adsorbed monolayers, groups of sites used in statistical calculations, Bethe's method *(French)* 77−70334
adsorbed particle interactions, lattice gas quasi-chem. approx. 80−49529
alloys, binary, BCC, order-disorder transform., three-body interaction effects 80−39257

lattice theory and statistics continued
analyticity and cluster props. of unbounded spin systems, lattice model 78−45571
analyticity properties of 3-component models 79−67235
Anderson localisation, statistical fluctuations in numerical approx. methods 79−6056
anharmonic chain with nearest neighbour interaction, periodic permanent waves 79−150
anharmonic lattice, Gibbs states time evolution 79−54065
anharmonic lattice with defects 78−73937
anharmonic lattices, quasisoliton solns., influence of pair pot. shape 80−22297
anisotropic bond percolation in d-dimens. hypercubic lattice 79−75464
anisotropic critical line from anisotropic scaling 80−12997
anisotropic cubic system with long-range interactions, critical behaviour 78−36941
anisotropic lattice spin systems, phase transitions 78−73930
anisotropic percolation, square random network conductivity *(French)* 80−68142
anisotropic systems, percolation in square lattices, real space renormalisation group calcs. 79−63160
anti-ferromagnetic lattice, ground-state energy calc., Kadanoff cells renormalisation procedure 77−77015
antiferromagnetic lattice, ground state energy, renormalisation procedure 79−40486
antiferromagnets, pair interaction and arbitrary fields, correlation inequalities, Ginibre-Percus double variables method 80−68147
approximation schemes, appl. to X-Y model and Abelian gauge fields 77−41547
Ashkin Teller model, exact results 79−58651
Ashkin Teller model on planar lattice, eight-vertex model on related lattice 77−49689
Ashkin-Teller model, dual and star-triangle transforms. 79−30380
Ashkin-Teller-Potts model, dil., crit. behaviour 80−65897
Ashkin-Teller-Potts model, magnetic indices for percolation problem, renormalisation group approach 79−63163
Ashkin-Teller-Potts model, renormalisation group anal. 79−154
associated solution, characteristic sums method in stat. theory 80−10480
asymmetric random walk with exponential transition probabilities, exact analytic results 79−44875
asymptotic number of lattice animals in bond and site percolation 78−54310
asymptotically free field theory of (1+1) dimens., lattice Hamiltonian results 77−6021
athermal model chains, pair distrib. function, Metropolitan Monte Carlo calcs. 78−17827
atomic migration on disordered surfaces, theory 80−54516
axioms for nonrelativistic quantum mechanics 78−12595
Backlund transformations as canonical transformations 78−81855
Banach lattice $L^1(R^3\times R^3)$, linear multiple scatt. operator. dynamics and spectrum 79−93073
Baxter model and scale invariant field theory 78−32764
BBGKY hierarchy, first eqn. exact linearisation, Ornstein-Zernicke phase instability 79−75461
BCC lattice, probability of visiting new site in random walk 79−88891
Bell-Lavis 2-D bonded lattice model, critical behaviour 79−17356
Bethe lattice, anisotropic percolation 79−58642
Bethe lattice, bootstrap percolation 79−30376
Bethe lattice, correlated site percolation, mean cluster size 80−17881
Bethe lattice, correlated site percolation probability and dangling site conc. 79−49174
Bethe lattice, displacement correl. function, random walk 78−41247
Bethe lattice, high density percolation 79−58643
Bethe lattice, random ordered phase and glasslike phase 78−29060
Bethe lattice, spatial dimens. 79−30381
Bethe lattice, vibration 78−30706
Bethe random lattice, spectral diffusion, total conductance distribution probability 80−8928
bi-lattices, transient motions 78−8357
bifurcation of solutions with crystalline symmetry 77−7650
binary alloy, morphological stability, discrete lattice theory, appl. to interfacial zones 78−3133
binary lattice gas, crit. phenomena, cluster expansions and transcriptions 80−4670
binary lattice gas, crit. phenomena, series anal. 80−4671
binary melt-crystal phase transformation kinetics, stat. modelling of cryst. growth mechanism 80−24389
block spins in the edge of an Ising ferromagnetic half-plane 79−47220
block-cluster approach to percolation 80−161
Blume-Emery-Griffiths model in 2-D, renormalisation group studies 78−54311
Bogolyubov chain temp. expansion, third approx. *(Russian)* 77−13705
Boltzmann eqn. on lattice, convergence 79−97314
Boltzmann equation, discretised, lattice limit and non-Maxwellian gases 80−52139
Boltzmann equation on a lattice, existence, uniqueness of solns. 79−80537
Boltzmann equation on a lattice, global solns. 79−80536
bond and site percolation, renormalisation group results 79−149
bond percolation, 2D, cluster size crit. exponent, Monte Carlo calc. 80−68144
bond percolation, Hamiltonian formulation, alternative derivation of Ashkin-Teller-Potts model relationship 78−81926
bond percolation in a square lattice in presence of a 'magnetic field' 80−95041
bond percolation in anisotropic square lattice 80−46989
bond percolation in bounded geometries 79−93062
bond percolation in square, cubic, hypercubic lattice, probability renormalisation group method 80−31680
bond percolation model, site-cluster distribs. and eqn. of state 77−74329
bond percolation problem in semi-infinite medium, Landau-Ginzburg theory 79−93068
bond percolation processes in d dimensions 78−70066
bond-percolation conductivity, effective-medium approx. 78−29057
bootstrap percolation conductivity on Cayley tree 80−54743
Born-Huang invariance conditions, completeness 78−51620
boson gas, rigorous second-order cumulant expansion 79−44853
boson system, ideal, lattice sums, Poisson's summation formula and Walfisz's formula 80−8903
Brownian oscillators, non markovian diffusion and Fokker Planck eqn. 77−57285
lattice theory and statistics continued
Brownian particle in periodic potential, effective diffusion coeff. 80−4649
C*-algebra, *-automorphisms, inner dynamical one-parameter groups, trace and KMS states 77−41526
chain conformations and local motions, Brownian motion simulation 79−86098
chain dynamics simulation, lattice model *(Russian)* 79−22876
chain of coupled nonlinear oscillators, large amplitude motion, numerical study 79−25993
chain-folded crystal, statistical mechs. in lattice model 78−47247
classical and quantum lattice systems critical lengths and critical temp. estimates 79−56556
classical equilibrium statistical mechanics, mathematical struct., book 79−26017
classical lattice field theory, inequalities and symmetry breaking 79−9131
classical lattice gas, surface of separation between phases 79−44868
classical lattice spin systems, Ornstein-Zernike and analyticity props. 79−12724
classical lattice system group analysis 77−67385
classical lattice systems with constraints, partition function zeros and unicity of states 77−2620
classical n-vector model, critical temp. shifts 78−36939
classical n-vector model, eqn. of state in 1/n expansion 77−65005
classical n-vector model, spin-dimensionality dependence of critical parameters 79−40479
classical n-vector models, d-2 and 4-d expansions 79−30387
classical solid solutions, beyond-mean-field approx. 77−20039
classical systems with long range forces, equilibrium forces, one-dimens. Coulomb gas appl. 79−85087
close packed lattices of ferro- and antiferromag. exchange integrals, glass-like phase 78−10697
cluster distribution, reln. between percolation and condensation 77−17916
cluster expansion with lattice approximation 78−49759
cluster expansions in cooperative Jahn-Teller T-systems 80−4661
cluster motion on surface, stochastic evolution 79−40496
cluster operator bound states 80−8899
cluster radius, below percolation threshold, speculations 78−70073
cluster shapes at percolation threshold, cluster dimensionality, reln. to critical point exponents 78−4561
cluster shapes at percolation threshold, effective cluster dimensionality, connection with percolation critical exponents 79−63166
cluster size, pair connectedness for fluid and lattice systems, percolation and condensation 77−61019
cluster size distribution, perimeter for two-dimensional percolation 77−9967
cluster size distribution, scaling function in 2-D site percolation 78−24742
cluster statistics of lattice gas model in 2 and 3 dimens. 77−13706
cluster sums, vol. depend. for lattice gases 77−17921
coherent states and lattice sums 79−2650
colloid stabilisation by polymers, excluded volume effects 77−60129
colloidal plates, parallel, polymer adsorption, excluded volume effects, polymer-solvent interactions 80−45568
coloured lattices, rot. symmetry effect, appl. to mag. structs. 79−90587
colouring problem on randomly occupied lattice, critical conc. existence for long range order 80−80519
commensurability in one-dimensional lattices at finite temperature 80−42156
commensurate-incommensurate transition and melting in two-dimensions 80−75339
complete orthomodular lattice, role of modular pairs, m-morphism 79−49175
complex solids, energy-momentum tensor, nonequilibrium relativistic dynamic eqns. *(Russian)* 80−57236
composite material, heat conduction lattice model 79−81682
composite next nearest neighbour degeneracy, one-dimens. lattice space 77−65002
composites, fibre reinforced and particulate, mechanical model 78−51105
condensation, lattice gas, one-dimens., for teachers 79−18
condensed phase, lattice gas model 78−73931
conductance network, random, simple, triangular, site percolation, effective medium theory 79−12746
conference, general congress, Societe Francaise de Physique, Toulouse, France (June 1979) 80−77536
conference on solitons and condensed matter physics, Oxford, England (June 1978) 79−75364
configurational free energy of chains Monte Carlo approach 78−16742
connected diagram expansion for lattice Hamiltonian models 79−21916
continuous Heisenberg spin chain, semi-classical quantisation and spectrum 79−85084
continuous renormalisation transformation, variational calcs., rel. to Potts model 78−93618
continuous spin Ising model, strong coupling expansion on ν-dimensional lattice 80−17888
continuous spin systems, position-space renormalisation group study 79−38350
continuous symmetry breakdown, absence in more than 2-dimens. 79−6293
corner transfer matrices of eight vertex model, Ising model case 77−89915
correlated percolation, ε expansion, appl. to gels 80−77714
correlated site percolation problem, universality, Monte Carlo tests 80−73275
correlation inequalities, systems with compact connected real Lie group config. manifold 77−33959
correlation inequalities for lattice gauge fields 77−45940
correlations decay in lattice models at high temp. 79−80534
Coulomb gas system, correl. with sine-Gordon system 79−54068
Coulomb lattice, high-temp. expansion 78−143
Coulomb vector gas in two-dimens., melting 79−69449
coupled nonlinear oscillators, large amplitude vibr. motion, coherent state representation 77−87698
coupled oscillators, macroscopic excitation relaxation 80−52135
coupled phonon-linear Heisenberg chain system, phase transition 78−64208
coupled random walk process specified by Hamiltonian in pot. field 80−42169

lattice theory and statistics continued
coupled second-order differential equations, Weyl's theory appls. 79−30375
critical dimension for lattice animals 80−57208
critical exponent induced by impurity effect 80−36961
critical exponents, diagrammatic representation, three-state Potts model appl. 78−57867
critical exponents in three dimensions, derivation from ϕ^4 field theory with Gaussian propagator 80−4686
critical indices to $O(1/n^2)$ for 3-dimens. system with short range forces 78−49775
critical phenomena, renormalisation group, appl. to lattice dynamic model 77−2624
critical temp. shifts for finite slabs in ϵ-expansion 78−41242
cross-over phenomena in asymptotic behaviour of lattice sums 78−21075
crystal, statistical thermodynamics with collective vibrations 78−54289
crystal defect clusters coupling, in linear chain 79−51144
crystal growth, Monte Carlo simulation, review, book contrib. 79−80532
crystal growth, multi-component, master equations in lattice model 80−75194
crystal growth, two-component, analytic theory 79−82168
crystal growth disorder model in 3-dimens., with cubic symmetry 79−73118
crystal growth disorder models by symmetry imposition 77−31614
crystals, cubic-tetragonal transitions, symmetry anal. 80−10636
cubic and hexagonal lattices, Brillouin delta function 79−73261
cubic crystals, temp. series in statistical theory, Vlasov eqn. 80−17895
cubic lattice, Green's function determ. 78−62162
cubic lattice, soluble dispersion reln. for 3-D band struct. 77−8007
cubic systems, axial and diagonal anisotropy crossover exponents 77−13710
cumulant expansion in renormalisation group transforms, convergence 77−17915
cumulative distributions, symmetry- and composition-dependent of normalized structure amplitude for use in intensity statistics 79−32847
Curie-Weiss model, random magnetisation, statistics, asymptotic behaviour 79−4639
cutoff and lattice models, construction of renormalised field theories 78−4787
d-dimens., quantal spin systems, reln. with (d+1) dimens. Ising systems 77−16031
d-dimensional hypercubical system, phase transition existance 79−97332
d-dimensional lattice spin model, multicritical pt. 77−36041
Debye-Waller factor, anharmonic, classical limit, calc. 80−54334
decimation transformation for 2-D and 3-D systems 78−12649
decorated lattice gas model of critical phenomena in fluids and fluid mixtures, review 78−36944
defect states in two-dimens. planar rotator model with long range interactions 80−98861
density of states in disordered one-dimensional systems 79−58640
devil's staircase, quantum fluctuation effects 80−73281
diagonalisation of the quadratic fermion Hamiltonian with a linear part 79−40445
diagonally disordered binary alloy, mass operator 80−52140
diamond lattice, Gaussian model in three dimensions, differential real-space renormalisation 80−17896
diatomic lattice, solitary wave solns., ϕ^4 kink, struct. phase transition, phonon dispersion curves 79−80544
diatomic lattice system, soliton solns. in continuum limit 80−4668
diatomic lattice system with cubic nonlinearity, soliton solns. 79−93076
Dicke model, soft modes and counter rotating terms 78−146
diffuse wave scatt. by short range order, improved mean spherical approx. 79−9127
diffusion, chemical, highly defective solids, steady-state computer simulation method for lattice gas 80−49401
diffusion in defective solids, Haven ratio in athermal lattice gas;, Monte Carlo method 80−84313
diffusion in random networks near percolation threshold, ant in labyrinth problem 80−77732
diffusion-controlled processes among partially absorbing stationary sinks 79−54074
dilute branched polymers, statistics, field theory 80−22303
dilute simple cubic lattice, short-range quadrupolar order 79−65681
dimer and Ising models on the Lobacheveskii plane 79−21677
dimer config. enumeration, n-dimensional theory, graph paths 78−54315
dimer problem, square lattice calcs. using Kikuchi method 77−71279
dipolar lattice, 2-D, Monte-Carlo calc., lattice energy 78−14308
Dirac eqn., (2+1) dimens., continuous space-time symm. 78−4799
Dirac eqn. on lattice 78−24924
Dirichlet problem response function method solution 80−27106
discrete ϕ^4 chain, statistical mechanics 79−75463
discrete Gaussian model, position-space renormalisation transformation 78−93617
discrete Gaussian model, renormalization transformation 78−81925
discrete Gaussian roughening model, Monte Carlo simulation, appl. to Coulomb gas and Villain X-Y model 78−86225
disordered spin systems, nonrandom free energy in macroscopic limit 79−40477
disordered system without centre of inversion, direct percolation 80−77725
displacive transformations, connection to dislocations and solitons 79−82300
displacive transitions, kinks in one-dimens. model, statistical mechanical treatment 79−42203
dissipative structures, non-equilibrium systems, self organisation *(Chinese)* 80−42168
dissipative Toda lattice, soliton propag. using nonlinear transmission line 80−27228
distributive lattices, bounded, Baer semigroup coordinatisation using idempotent residuated mappings 80−73280
double-layer lattice plate yield surfaces, anisotropic continuum treatment *(Japanese)* 78−22261
dual string theory, lattice approach, tachyon problem exhibited 78−4840
dualities for extended Potts models induced from the percolation problems of block elements 80−105585
duality in field theory and statistical systems, review 80−73610
duality of interaction models 77−9849
duality transform. of equilib. states, surface tension between phases 78−144
dynamic crit. phenomena and renormalisation group, appl. to lattice dynamic model 77−22515

lattice theory and statistics continued
dynamic renormalisation group in the large-n limit 80−4842
dynamic renormalization group, phenomenological fitting 79−75471
dynamic scaling near lambda point of liq. He and at bicritical points 80−15321
Dyson's hierarchical model, critical props. 79−40481
effective medium approach to real space renormalization 79−80539
effective nonintegral space dimensionality, infinite lattice, critical behaviour 77−49688
eight-vertex and q-state Potts model, relation between temp. exponents 79−93055
eight-vertex model, corner transfer matrices, low-temp. expansions, spontaneous magnetisation 77−28352
eight-vertex model, solvable, on arbitrary planar lattice 79−2733
elastic dielectric, many-body theory, appl. to NaCl-structure 78−38805
elastically coupled systems at marginal dimensionalities, crit. dynamics and stability 80−101769
electrode, porous, capillary equil. and percolation theory 79−91971
electrolyte, strong, conc. solns., thermodynamic props. of mixed electrolytes and Harned rule basis 79−90506
electron correlation problems, lattice statistical aspects, Gutzwiller approx. 78−84160
electron solid, two-dimens., shear modulus and melting, temp. depends. 80−158
electrons in magnetic and electromagnetic fields, Bloch functions, Jacobi ϑ-function determ. 80−36941
electrostatic lattice sums for semi-infinite lattices 79−71376
elementary length and time in the strong interaction, meson reson. width data 78−82189
ellipsoid assembly, solvable model with first order phase transition 77−30101
empirical relationships for random self-avoiding walks on lattices 79−9190
energy eigenvalues lower bounds for quantum Hamiltonians in lattice field theories 78−45575
entangled scale transformation on lattice, universality of crit. exponents of Ising models 77−66346
equations of state, three phases, lattice gas model 78−22818
equilibrium states in lattice systems 77−17909
equivalent neighbour model, generalised, derivation of high temp. lattice consts 80−77721
equivalent neighbour model, high-temp. series expansions 79−44877
escape probability of random walker on lattice doped with impurities 79−17353
Euclidean fermion-boson systems on lattice, appl. to field theory 78−45559
Euclidean lattice gauge theory, selfadjoint, strictly positive transfer matrix 77−65071
exponent inequalities for the percolation problem 79−63165
exponential clustering for long-range integer-spin systems 79−80744
face centred orthorhombic lattices, matrix elements of Green's function 77−5767
face centred rectangular lattice gas model, ground state struct. 78−38936
FCC lattice, Gaussian model in three dimensions, differential real-space renormalisation 80−17896
FCC lattice, repulsive lattice gas, ordered phase existence 80−77717
FCC lattices, ordered superstruct., phase diagrams, cluster variation calc. 80−39256
Fermi and Bose quasi-particles in lattice system *(Russian)* 79−75462
Fermi gas model in 1-D, review 79−58636
Fermi gas model in 1-D 79−58635
Fermi system, 1-D, and plane xy model; behaviour of correlation functions 78−56091
Fermi-Pasta-Ulam lattice, continuum approx. using Korteweg-de Vries eqn. 79−71375
Fermi-Pasta-Ulam lattice with cubic nonlinearity, novel first integrals 77−65003
ferroelectric lattice model, 2-D, six-vertex, quantum inverse scattering transform method 80−68348
ferromagnet, total spin distrib. in spherical model with long-range pot. 79−30383
ferromagnetic classical vector model, extension of high temp. free energy series 80−7062
ferromagnetic scalar spin systems, wall and boundary free energies 78−155
field theory, Ising model and scaling 77−5991
figure eights, number weakly embeddable in square lattice, bounds 77−57281
finite lattices, with traps, random walks, Monte Carlo simulations 80−52131
finite size scaling theory, static, dynamic, based on renormalisation group approach, critical phenomena exam. 78−16745
finite system, order parameter and sp. ht. for epitaxial ordering renormalisation-group calc. 80−17862
finite Toda lattice, derivation of soln. 78−36937
first order melting transition in the incommensurate phase 79−85094
first passage percolation on the square lattice, book 79−49177
first-order phase transitions, clusters, metastablility, nucleation 78−54326
Fisher-Domb cluster model, pseudospinodals in first order transitions 80−57213
fluid, classical, elementary molecular theory 77−19859
fluid, of isotropic mols., DID Rayleigh and Raman depolarised scatt., lattice-gas model 80−10356
fluids, continuous time random walks, non-equilib. Ornstein-Zernike eqn. 77−13687
fluids with triple point, lattice and continuous one-dimens. models 77−31571
Fokker Planck eqn., system in periodic pot., 1-D, elec. field perturbed, mobility 78−32776
free energy in lattice systems with long range random Hamiltonians 79−88886
free-fermion condition for generalised vertices 78−93622
Frenkel-Kontorova model, equilib. config., numerical study 79−40474
Frisch-Lloyd random system, low-lying electronic tail spectrum by path integral method and coherent state representation variational method 80−105580
fundamental Korringa-Kohn-Rostoker eqn. version of coherent potential approx. 80−59847
gas, percolation theory 78−5839

lattice theory and statistics continued
gas model, pressure estimation, computer simulation 78−4564
gas with finite range attractive potentials, cluster and percolation inequalities 77−61029
gas-liquid-solid phase diagram, modified lattice-gas model 80−62591
gauge invariant Ising model, statistical mechanics, phase struct. 79−71373
gauge theories, effective actions 78−29239
gauge theories, large space-time dimension, strong coupling phase 80−27397
gauge theories on Euclidean lattice with fermions, cluster expansion 78−58119
gauge theory, 4-D Z_2 gauge, verification of first order phase transition 79−58876
gauge theory, phase transitions, recursion relations 78−24953
gauge theory, Z(2), renormalisation group calc. 80−22514
gauge theory and spin systems, review 80−22528
gauge theory on lattice, gauge-fixing and mass renormalisation 78−24949
Gaussian core model duality relations 79−93070
Gaussian functions distributed over lattice, analytical transform. into Wannier functions 78−32768
Gaussian model, kinetic, formulation from master eqn., diffusive and relax. behaviour 77−9966
gaussian model, two-dimensional, differential real-space renormalization 79−54067
generalisation of exactly soluble models 77−82446
generalised Mobius functions for rectangles on square lattice 78−36938
generalised random walks, transform. of recursion relations 80−101757
generalized lattice representations using generalized Bloch and Wannier functions 80−22300
Gibbs condition, positive cone, Radon-Nikodym theorem, relative Hamiltonian, appl. of Tomita Takesaki theory 77−17758
Gibbs fields, absence of continuous symmetry breaking in two-dimensional models of statistical physics 79−21650
Gibbs lattice field, clustering operator invariant subspaces 80−4658
Gibbs phase rule, heuristic theory applied to lattice spin system 77−45811
Gibbs phase rule equivalence to ensembles for classical lattice systems 79−75467
Gibbs random field in lattice spin system, local central limit theorem 80−22293
Gibbsian Distribution on the Lorenz attractor, 1-dimens. Ising model representation 79−97331
Ginzburg-Landau model, crossover and scaling at low temp. 77−61023
grain boundaries, coincident site lattices theory *(Russian)* 78−2141
grain boundary soliton-like features, molecular dynamics computer simulation study 79−77610
grand canonical partition function, zeros on unit circle in complex plane, sufficiency condition 77−22498
graph-like state of matter, electrical cond. of random networks, gelation and elasticity 78−65875
graphite, Cs-intercalated, melting and staging, X-ray scatt. obs. 79−19180
ground state symmetry under perturbation 80−42161
group structure, classical systems of arbitrary spin 77−33958
group structure for general lattice systems and surface tension 80−4675
growing lattice animals and Monte-Carlo methods 80−57207
hadron mass spectrum in lattice gauge theory 78−74139
hadrons, light and heavy constituents in lattice algebra 78−16978
Hamiltonian formulation of site percolation in a lattice gas 79−12729
hard core, lattice gas against hard wall, pair correlations 80−36952
hard core lattice gas vertex models, scaling transform critical parameters 80−98860
hard core trigonal mols. on triangular lattice, phase transition, eqns. of state 77−59089
hard disk system, solid-fluid transition 79−88900
hard hexagon model, exact soln. 80−42149
hard hexagon model, site entropy 80−42152
hard sphere problem on lattice, moment method, uniform chain 79−97311
hard sphere system in equilibirum 80−86225
hard sphere system in three dimens., thermodynamic props. 80−86226
hard-core lattice gas with tricrit. point, phase transition behaviour 80−8926
hard-core square lattice gas, 3-parameter isotropic atom distrib. 78−24740
hard-sphere lattice gas, Bethe model for phase transitions 79−88884
hard-sphere solid, correl. function model 79−23541
hard-sphere solid, disordered, lattice energy 79−23542
hard-square lattice gas 80−95043
harmonic chain system, lattice thermal cond. 79−93064
harmonic crystal, generalised equipartition theorem 80−105584
harmonic crystal properties in stationary nonequilibrium state 78−16752
harmonic lattice, impurity motion, generalised hydrodynamics and microscopic theory of long time tail *(Korean)* 77−49683
Heisenberg antiferromagnet, phase transitions in quantum spin systems 78−84434
Heisenberg ferromagnet system, temp. Green's function sum rules *(Chinese)* 80−31678
Heisenberg model, validity of Fokker-Planck equation 77−89920
Heisenberg spin 1 system assembly with tunneling, phase transitions, thermodynamic behavior 80−4667
Heisenberg spin systems, phase transitions from strong coupling expansions 79−6058
hexagonal lattice, mag. subband struct. of electrons 79−95307
hierarchical model, ε-expansion anal. 77−71284
hierarchical model, renormalisation group approach 80−34580
hierarchical model ε-expansion, numerical test of Borel summability 78−12650
high density limit for lattice spin models 79−40490
high-temperature analyticity in classical lattice systems, continuous spin systems 77−2615
higher order modified pot. for effective phase integral approx. 79−44779
Hilhorst model, generalised, statistics of trees and branched polymers 79−3604
homeopolar excitations in a one-dimensional system of spinless fermions with nonlocal interaction 79−97318
honeycomb bond lattice, renormalisation group approach 79−85089
honeycomb extended lattice VB theory, long range order spin pairing 80−52136
honeycomb lattice, real space renormalisation, ferromag. (antiferromag.) appls. 80−11200
Husimi-Temperley model under a random field 79−97313
ice, two-dimens. square, correl. function calcs., approx. methods, Bjerrum fault conc. effects 80−10513
ice lattice model, 2-D, six-vertex, quantum inverse scattering transform method 80−68348
incommensurate-commensurate transition in two-dimensional sine-Gordon system 80−90789
inequalities for classical spin vector models, X-Y and Heisenberg models 77−91
inequalities in classical lattice and continuum systems 77−90
infinite anharmonic crystals, existence of time evolution 77−79039
infinite crystal, classical statistical mechanics 80−107067
infinite harmonic crystal, bound states, spectral props. 79−85086
infinite harmonic crystals, stationary nonequilib. states, existence, props. 77−55325
infinite lattice systems, perturbation velocity 79−44874
instability of evolving systems, elastic stability and catastrophe theory approaches 78−44442
instantons in U(1) lattice gauge theory, Coulomb dipole gas 78−8351
integrable field theories, as classical gases with generalised charges *(Russian)* 80−12922
interacting dimers on the simple cubic lattice as a model for liquid crystals 80−42154
interacting molecules, expansions in activity powers *(Russian)* 79−88892
interaction function, lattice duals, duality relations for correl. functions 78−8354
interactions, point, periodic, one particle theory, polymers, monomolecular layers and crystals 80−105576
interface, statistical mechs. of short chain mols. 77−43426
interface phenomena singular densities and currents at dividing surface 80−17907
interstitial solid solutions, self-diffusion activation energy rel. to partial molar energy 80−15291
invariant Gibbs states, cluster props., surface tension 79−49172
inverse scattering problem for semi-infinite crystals 79−12651
ionic crystal theory, Poisson's summation formula for lattice sums evaluation 77−2618
ionic crystals, statistical theory calcs. of surface energy and surface tension 80−17894
ionic crystals, statistical theory density functional method, dispersion interaction energy calc. 80−15043
irregular networks, self-avoiding walks, critical parameters 77−20607
Ising model, appl. of square lattice variational approxs. 79−56555
Ising model, cubic, site impure, crit. behaviour 77−66357
Ising model, dipolar antiferromag., phase transition at negative absolute temp. *(Russian)* 78−43594
Ising model, duality relations and replica method 80−77722
Ising model, hyperscaling in 3-D spin-1/2 model, limitations of high-temp. series terms 79−93052
Ising model, shape and size of two-dimensional percolation clusters with and without correlations 79−93054
Ising model, two-dimens., in external field, variational approach 79−80538
Ising model on a closed Cayley tree 80−17886
Ising problems, partition functions in terms of infinite determinants 80−62593
isothermal transport in the lattice gas 80−8927
isotropic spin system, cubic lattice, step model of phase transitions, critical behaviour 78−60290
Jacobian theta functions, evaluation of lattice sums 77−26245
Kadanoff lowerbound renormalization transformation for the q-state Potts model 79−44876
Kadanoff renormalisation for s-state Potts model in 3-d 78−21074
Kagome lattice, 8-vertex model, equivalence to triangular lattice 32 vertex model 77−26244
kagome lattice, bond percolation threshold bounds *(French)* 79−44865
Kagome lattice, renormalisation group approach 79−85089
kinetic Ising model, real space renormalisation group for arbitrary dimension 80−4666
king and domino polynomials for polyomino graphs, lattice dynamics appl. 77−71278
KMS states and chem. pot. 77−41525
Krieger-James approx. of short range order effects, antiferro- and ferromag. 78−56276
Landau model with several order parameters 78−41244
Landau-Ginzburg-Wilson model, 2 and $2+\varepsilon$ dimensions 78−36940
large lattice animals as limits of clusters in percolation clusters 80−162
large-cell Monte Carlo renormalization group for percolation 80−46994
largest cluster at two dimensional percolation threshold, Hausdorff dimens. and fluctuations 80−46982
lattice, gas, entropy and phase transitions in partially ordered sets 78−77808
lattice animal numbers, lower bounds 78−70069
lattice animals, statistics, field theory 80−22303
lattice approx. of gauge field theories 78−29225
lattice Coulomb gas representations of two-dimensional problems 78−70068
lattice Coulomb-gas representation of two-dimensional problems 79−58650
lattice gas, model of monomers and dimers with interaction 79−71380
lattice gas, phase transition on partial orders, entropy 79−63158
lattice gas, phys. correl. factor in Nernst-Einstein relation 80−105591
lattice gas, vol. depend. cluster sums behaviour *(Japanese)* 78−147
lattice gas model, critical cond., rel. to cond. in superionic conductors 78−93614
lattice gas model, double spin 1/2, for mag. annealed binary alloy and nematic mixture 77−66342
lattice gases, strong cluster props. of connected correlations, potential analyticity 78−70062
lattice gases, volume dependent cluster sums 77−17922
lattice gases of hard core molecules having two orientations, phase transitions 78−29059
lattice gauge fields, review 78−45797
lattice Hamiltonian for arbitrary couplings, variational method calc. 78−16746
lattice models with a solvable symmetry group 79−17616
lattice random walks, occupation times 80−42162

lattice theory and statistics continued
lattice renormalisation group and thermodynamic limit 78−8359
lattice spin models, high-density limit 78−29056
lattice sums, relation to EM eigenfrequency density oscills. 77−65556
lattice sums determ. using Poissons summation formula 78−4562
lattice thermal conductivity, general transport theory, phonon Boltzmann eqn. 80−54446
lattice-lattice scaling, reln. to scaled eqn. of state, appl. to Ising model 78−70067
lattice-valued random walks with Markov chain dependent steps 79−71377
lattices of mixed single particles, exact occupation statistics 79−40473
layered spin systems, phase transitions, partition functions and binary correlation functions 80−50133
Lennard-Jones for linear crystal, infinite volume ground state 79−88888
Lennard-Jones one-dimensional chain, stochastic transitions, statistical features 79−67233
Lifshitz point, critical exponents, ε-expansion 78−65899
Lifshitz points of higher character, spherical model 77−67395
linear chain, with arbitrary masses and force consts., correl. functions 77−13685
linear chain, with arbitrary masses and force consts., ergodic props. 77−13686
linear chain doublet exciton, with exponential memory, exact dynamical soln. 78−39027
linear chain molecules, asymptotic form of partition functions, renewal theory appl. 77−53835
linear classical spin chain with nearest, next-nearest neighbour and spin-lattice interactions 77−30104
linear cluster lattice gas, phase transitions, behaviour on Bethe lattice 79−97307
linear cluster lattice gas, phase transitions, interacting dimer models 79−97306
linear fermion systems, molecular field models, and the KMS condition *(German)* 79−9178
linear hard core fluid as limit of lattice fluid 80−38882
linear harmonic oscillator on lattice, wave functions, energy eigenvalues, Pade approximant method 78−57817
linear lattice of atoms, Lennard-Jones pot. basis, for teachers 78−61997
linear lattices, integration of vector valued functions 79−63157
lipid bilayer phase transition, semiphenomenological model 77−35670
liquid crystal, nematic-isotropic transition, lattice model for hard core mols. with flexible tails 78−38818
liquid crystal, nematic-isotropic transition, lattice model for hard core mols. with semiflexible tails 78−38819
liquid crystals, correlation in statistical theory 78−75536
liquid crystals, lattice models showing liquid-liquid crystal phase transitions 79−95128
liquid metals, theory combining lattice gas model and Hubbard model 77−69220
liquid theory, classical spin system, absence of ordering 78−51402
liquid-vapour interface struct. from uniformity of chemical pot. 79−60241
liquid-vapour transition, lattice gas model, nonsingular diameter without particle-hole symmetry 80−88311
LJD model, fine-grained lattices and continuum, Monte Carlo studies 79−12734
local thermodynamic stability and KMS conditions of quantum lattice systems 77−71275
logarithmic corrections to a simple power law at d=4 in 1/n expansion 78−65895
long-range site percolation, crossover from mean-field to crit. behaviour 80−82728
low temperature expansion, lattice systems with many ground states 79−88887
low-temperature series expansions, algebraic techniques 79−17352
Luttinger-Thirring model on lattice, real space-time renormalisation 80−62590
macromolecule, simulation of Brownian motion of chains, chain dynamics 79−86099
Madelung constants, first derivatives with respect to cell lengths, calc. 78−34459
magnet symmetry, and quasiparticle spectra at low momenta 79−42726
magnon-magnon interaction in square lattice 78−2669
Maier-Saupe model on square and triangle lattices, Monte-Carlo method 78−32771
manifolds of phase coexistence 78−16749
marginal local instability of quasi-periodic motion, separation distance effects 80−82633
Markov chain sampling grown lattice walks, variance reduction 79−27121
Markov processes in quantum lattice systems 79−40476
massive Schwinger model on lattice, renormalisation group approach 77−30246
Mayer graphs, general, rigorous estimates and applics., uniform upper bands 77−82363
Mayer graphs, general, two root-points, rigorous estimates and appl., long range behaviour 78−4565
mean spherical model in 1+1 dimensions, lattice Hamiltonian formulation 80−22304
melting transition, grain-boundary, in two-dimensional lattice-gas model 80−59634
metastable states of quantum lattice systems 77−71276
metric space of interactions, grand canonical pressure, thermodynamics limit 78−12652
metric tensors, in Hilbert space, geometrical approach to solving cryst. structs. 79−32846
microemulsions, lattice gas model, surfactant effects 78−23974
Migdal transformation, renormalisation group, recursion relations 80−34647
Migdals recursion relation, harmonic rotator model in two dimens. 78−89413
minimum potential energy per particle configuration, one-dimens. system 78−70084
Minkowski space, causal logic 78−16739
model factorized S matrix and an integrable Heisenberg chain with spin 1 *(Russian)* 80−101767
model with infinite number of phase transitions, equivalent neighbour limit 77−27969
modified antiferroelectric six-vertex model 79−93050
modular group and dimer problem, Ising model 77−5763

lattice theory and statistics continued
modulus lattices, ideal neutrals role, congruence relation *(German)* 79−80533
Monte Carlo methods in statistical physics, book 79−80528
Monte Carlo renormalisation group for polymers 80−42148
moving bond approach for renormalisation group transform 78−21078
multicritical phase transitions, review 79−30385
multilayer adsorption isotherms, step formation, lattice model investig. 78−14575
multimagnon bound states, unphysical solns. to Faddeev eqns. 77−18440
multistate diffusion in perfect and defective system, stochastic theory 79−93066
multistate diffusion in perfect and defective systems, stochastic theory 79−93067
n-component spin system, anisotropic Brillouin zone, Wilson-Feynman graph technique, universality 77−5764
n-vector classical model, Yang-Lee edge singularities at high temps. 80−20422
n-vector lattice spin model near two-dimens., crit. temp. 77−8324
n-vector model, spherical limit and correlation inequalities 80−22298
near-Coulombic lattice sums, Ewald evaluation, Poisson summation formulas 80−57210
neighbour-avoiding walks, asymptotic behaviour of mean square length 77−71277
nematic solution, hard rigid/flexible mols. mixture, unathermal, lattice model *(Russian)* 80−54129
nematic-isotropic transition, chain flexibility, flexible chain in rigid rod solvent 79−4400
nematic-isotropic transition, lattice model, semiflexible chain solutes 79−10927
neutron system, localised, tensor force effects, alternating layer spin config. 77−2925
non-Abelian lattice fields, duality 79−93280
non-purely ferromagnetic systems, correlation inequalities 79−47219
nonarithmetic lattice in SU(2,1) 79−88890
nonlinear 1-D lattice, wave propagation theory 77−30105
nonlinear 1D system, ϕ^4 chain dynamical props. 80−4655
nonlinear σ-model, Hamiltonian lattice formulation 77−10183
nonlinear differential difference eqns. with N-depend. coeff. 79−71274
nonlinear discrete systems, integrability 80−98858
nonlinear dynamics of first order phase transitions 79−11322
nonlinear lattice, steady motions 79−44866
nonlinear lattice dynamics, molecular dynamics studies 79−77713
nonlinear one-dimens. lattice with Lennard-Jones potential, soliton soln. 79−54069
nonlinear one-dimensional lattice, periodic solns. 77−33955
nonlinear system, chopping phenomena induced by solitons 77−30111
nonlinear systems, dynamics, heavy damping limit 80−86199
normalisation of one-dimens. lattice statistics 78−62161
O(2) Heisenberg gauge invariant model, eigenfunctions and energy spectrum 79−58875
O(n) Heisenberg model close to n=d=2 80−98862
occupation statistics for 2-dimens. lattices of single particles 77−33951
off-lattice polymer chains, Monte Carlo calcs. 78−5382
one dimensional quantum lattice systems, Cauchy problem for BBGKY hierarchy 80−46996
one dimensional system with phase transform., exact linear renormalisation 78−32769
one-component system interface with directed intermol. forces, Monte Carlo calcs. *(Russian)* 77−61031
one-dimens. lattice, phase transitions 79−40489
one-dimensional alloy, end effects 79−35634
one-dimensional hopping, moment expansions and occupancy (site) correlation functions 78−55972
one-dimensional nonlinear lattices with exactly solvable steady motion 77−79036
one-dimensional quiescent lattices, shock profiles, end condition effects 80−34138
one-dimensional site percolation, one finite lattice 80−68152
one-dimensional system, two-body pot., min. pot. energy config. 78−30582
optic mode second sound in distortive phase transitions 79−73366
optical percolation in 3-D, renormalisation group approach 80−22299
order relations for lattice sums from order relations for theta functions 77−33952
ordered media containing defects, gauge-like variables 79−88889
ordered physical line structures, nonlinear local field theory, appl. to high polymers, supercond. flux line lattices 78−81859
oriented bond percolation, threshold probability and correlation length exponent calc. 80−68146
Ornstein-Zernike lattice system, random-walk theory and pair correl. 77−5770
orthogonal lattice, interacting hysteresis dipoles, lattice sums and switching, chain breakdown 77−51860
particle dechannelling with phonon scatt., quantum theory 78−18695
particle kinetics on one-dimensional lattice with inequivalent sites, stochastic model 77−41546
particle lattice models, physical signals speed of propagation, bounds 78−93613
particle random walk without self-intersections 80−62585
partition functions, calc. methods 80−8925
Patterson superposition technique, modified, using multiple vectors 79−32856
percolation, block cluster approach, scaling laws and renormalisation groups 80−62592
percolation, combined site and bond, with nearest- and next-nearest-neighbour bonds 80−27231
percolation, correlated, in film-deposition model 80−107679
percolation, Monte Carlo anal. of cluster size distrib. 79−75465
percolation, polychromatic, coexistence of percolating species in highly connected lattices 78−8361
percolation, prefactor exponent change with valence, 3 and 4 dimens. 80−52141
percolation, sol-gel transitions, stirred percolation, and laminar flows of passive suspensions *(French)* 80−77724
percolation, two dimensions, absence of phase transitions 78−87770
percolation, universal critical amplitude ratios 80−101765
percolation and cluster distrib., cluster multiple labelling technique and crit. conc. algorithm 77−2622
percolation as the zero-temperature limit of the dilute Ising model 79−93053

lattice theory and statistics continued
percolation at surface, appl. of real-space renormalisation group 79−93057
percolation backbone problem, large cell renormalisation group 79−69481
percolation by position-space renormalisation group with large cells 78−77805
percolation cluster distribs., mean value depend. and animals distrib. 78−81928
percolation cluster number asymptotic decay 80−101760
percolation cluster numbers by real-space renormalization 79−75474
percolation cluster sizes and perimeters, scaling form 79−2728
percolation cluster sizes and perimeters in three dimensions 77−82466
percolation clusters, one dimens., crit. exponents 78−31082
percolation clusters, scaling theory of lattice 79−80542
percolation clusters, spanning lengths, Monte Carlo calcs. 79−2730
percolation clusters, teaching film 79−58509
percolation clusters and lattice animals, similarity laws for density profile, Monte Carlo data anal. 79−44881
percolation clusters density profiles, lattice animals 79−93075
percolation conduction crit. exponent, large cell renormalisation group calc. 80−12998
percolation conduction problem, position-space renormalisation 77−61027
percolation conductivity in anisotropic systems, infinite cluster struct. 79−93063
percolation dusters, fluctuations in number 80−17880
percolation exponent for lattice dimens. ≥3 77−45801
percolation in 1-D, ghost fields, pair correctedness and scaling 78−4560
percolation in one-dimension, finite size and scaling theory 79−54064
percolation in square lattice, temp. depend., effective medium theory 80−96837
percolation model, essential singularity 79−63164
percolation model, singularity of the analogue of free energy 78−36943
percolation models, infinite cluster density fluctuations and FKG inequalities 80−77712
percolation models, low density expansion of pair connectedness 79−67234
percolation network samples, cond. near crit. point 80−105578
percolation phenomena, simple cubic lattice, Monte Carlo study, cluster shapes and sizes 77−17919
percolation problem, directed-bond, for simple acyclic hypercubic lattices 77−41544
percolation problem, directed-bond, series expansions 77−41543
percolation problem, equivalence between Reynold's one-parameter renormalisation group transform. and Kirkpatrick's transform. 79−12731
percolation problem, for semiinfinite porous media, diagram technique calcs. 78−93621
percolation problem, Hausdorff dimension of largest cluster and backbone, numerical estimates 79−97316
percolation problem, high order behaviour in 0^3 field theories 78−65883
percolation problem, real-space renormalisation group approach 79−93059
percolation problem, two-dimens., crit. indexes of cond. 77−62964
percolation problem and surface effects in semi-infinite medium repulsive wall case 80−62588
percolation problems, one-dimens., exact soln. 78−16743
percolation problems, quantal 80−31554
percolation processes in 3-dimens. 77−17914
percolation processes in d-dimens., clusters, size, number and growth 77−2619
percolation processes in three and more dimens. 77−65007
percolation related to energy migration dynamics 79−85085
percolation theory, bond problem, critical probabilities, bond clusters 78−86224
percolation theory, combined site and bond percolation with nearest- and next-nearest-neighbour bonds 80−4654
percolation theory, eqn. for cluster distrib., spheres problem *(Russian)* 79−30382
percolation theory, fluctuations of infinite network 80−73278
percolation theory, infinite cluster props. 78−32765
percolation theory, review, appl. and polychromatic percolation 79−58626
percolation theory, scaling assumption for lattice animals 78−54313
percolation theory, series expansions in continuum problem 77−79037
percolation theory at the critical dimension 79−152
percolation theory kinetic eqns., Bethe lattice in spin-glass limit 79−97309
percolation threshold, computer generated pictures of infinite clusters 78−56117
percolation threshold, ramification of large clusters 78−41245
percolation threshold, random void influence 79−44872
percolation with nearest neighbour interaction 78−73934
percolation with restricted valence 79−12728
periodic exponential lattice, soliton quantum theory 77−30110
periodic lattices, random walkers, multiple trapping 79−2732
phase diagrams and catastrophes 80−8946
phase diags. of classical systems, contour models 77−30114
phase transformations in intermediate spherical model 79−30403
phase transition and surface tension 80−77713
phase transition in 2-D sine-Gordon system 79−12736
phase transition in 2D Coulomb gas, sine-Gordon theory and XY model, renormalisation group anal. 80−36950
phase transition in BCC hard sphere lattice gas with second neighbour exclusions 80−160
phase transition near displacive limit, for classical n-component lattice model 77−45807
phase transitions, percolation clusters and lattice animals 79−6057
phase transitions and critical phenomena, recent developments 77−87713
phase transitions and reflection positivity, Peierl contour probabilities, long range lattice models 78−89398
phase transitions and reflection positivity in lattice systems with short-range and Coulomb interactions 80−82715
phase transitions and renormalised struct. of lattice gauge theories with fermions 78−82105
phase transitions for lattice gas of big interacting mols. *(Russian)* 79−157
phase transitions for models with isotropic short range interactions and continuous symmetries 80−36949
phase transitions in strongly random systems, review 79−58647
phase transitions in tree like percolation 79−75473
lattice theory and statistics continued
phenomenological renormalisation group theory 80−4663
planar model, F-model and related systems, Monte Carlo test 79−9192
planar rotator model, correl. functions 79−40495
planar-rotator model with short range interaction 79−80540
plane lattices with non-standard boundaries, exact results for dimer problem 80−82727
plane rotator ferromagnetic model, equilib. state anal. 78−29055
plane rotator model, partition function and Gaussian inequality zeros 80−42158
plane rotor model, static and dynamic crit. behaviour, Monte Carlo simulation 79−38334
Poincare cycles of the linear chain of oscillators 80−4662
point clusters, classification of symmetric coordinates, method 80−57203
point clusters, classification of symmetric coordinates, rectangular tetrahedron and cube examples 80−57204
point defect trapping by extended sinks, model of cloud random walk of lattice pts. 79−82199
polarisable fluid, effective field of dipole 79−7540
polychromatic correlated site percolation, appl. to supercooled H_2O and D_2O 80−22296
polycrystalline material, scatt., lattice representation 78−65774
polymer chain, irregular, lattice distortions, SCF perturbation calcs. 78−6018
polymer chain, lattice model, Monte Carlo simulation, Rouse coord. distrib. and dimens. 79−89814
polymer chain, long, in dilute soln., 2nd order phase transform. 79−13851
polymer chain, virial expansion 78−5383
polymer chain cyclisation, lattice embedded model, discrete scatt. series representation 80−48109
polymer chain statistics and universality 78−29869
polymer chains, Edwards' model, stochastic model 80−68140
polymer chains, with volume interaction, statistical physics problems, coils and globules, review 78−94347
polymer chains and vulcanisation, discrete Hamiltonian in Potts model 79−95991
polymer conformation, correlated walk model calc. 80−78733
polymer dilute soln., critical ratio limiting values using renormalisation group methods 78−83715
polymer linear chains, excluded vol. problem 80−5650
polymer off-lattice chains, Monte Carlo anal. of excluded vol. problem 80−5647
polymer solution, simulation of macromol. dynamics, Monte-Carlo method, conc. depend. *(Polish)* 78−51404
polymers, branched, mean end to end distance 79−86097
polymers, rectilinear on square lattice, series expansion 80−5646
polymers, simulation by self-avoiding nonintersecting random chains, conc. effect 78−12639
polytypes, Monte Carlo simulation 78−6024
position-space renormalization approach 79−30404
Potts lattice gas, crit. and tricrit. exponents using Kadanoff transform. 80−101768
Potts lattice gas, renormalisation-group treatment, Kr adsorbed on graphite 78−67908
Potts model, 1st and 2nd order transitions, renormalisation group soln. 79−99706
Potts model, 2-dimens. q-state, mag. exponents 80−86220
Potts model, analyticity properties of 3-component models 79−67235
Potts model, crit. behaviour, renormalisation group calcs. *(Russian)* 79−6059
Potts model, critical dynamics 80−101766
Potts model, discrete, three spin thermodynamic behaviour, Kikuchi cluster variational method anal. 79−35640
Potts model, exact results 79−58651
Potts model, first order phase transitions, Monte Carlo renormalisation group method 80−34645
Potts model, five state spin system, phase diagram 79−58641
Potts model, four state, series studies 79−85088
Potts model, hierarchical, three-state, high temp. susceptibilities 80−77723
Potts model, Kadanoff renormalisation 79−40483
Potts model, Monte Carlo simulation in three dimens. 80−163
Potts model, presence of instability 80−17892
Potts model, q-component, mean field theory in many component limit 80−86221
Potts model, quantum field theory 79−6055
Potts model, quenched bond disorder, single-bond effective interaction approx. 80−27229
Potts model, three state, lower bound renormalisation transformation 77−28347
Potts model, three state, series anal. 80−73274
Potts model, three-state, effects of symmetry-breaking perturbations 80−105579
Potts model, three-state, first order phase transitions 80−60333
Potts model, three-state, high field series expansions and critical props. 79−85090
Potts model, three-state, phase transition continuity 80−22302
Potts model, three-state, with three-site interactions 79−12723
Potts model, triangular, at transition temp., related models 78−8358
Potts model, triangular, with two- and three-site interactions 80−36951
Potts model, two dimensional three state, critical exponents 80−105583
Potts model, zero state, in $2+\varepsilon$ dimensions, crit. exponents 78−77809
Potts model and percolation 78−54312
Potts model in 1-D with exponential interactions, statistical mechanics 78−21079
Potts model in 2-D, exact results 79−58644
Potts model on square lattice, specific heat critical exponents 77−20606
Potts model with many body interactions, site percolation 78−21077
Potts models, percolation, and duality 79−97312
Potts models, planar, critical points for various lattices 79−93061
Potts models, q-state, two-dimens., Monte Carlo renormalisation-group studies 80−77727
Potts q-state model, variational renormalisation group approach 80−31679
Potts s-state model, exact critical surface on triangular and honeycomb lattices 79−148
pressure in lattice systems, differentiability props. 80−31677
probabilistic bond percolation in random arrays 79−2729
probability estimates for continuous spin systems 77−2614

lattice theory and statistics continued
propositional systems and meas., quasi-tensor-products of certain orthomodular lattices 78−81871
pure component liquid-vapour transition, two component decorated lattice gas model 79−35650
pure fluids, critical point change of variables 79−93065
q-state Potts model multicritical point, singularities and scaling functions 80−57215
QCD, lattice-gauge theory calc. of π and ρ-meson decay consts. 78−74154
QED on lattice, ϵ separation method 78−41453
quadratic lattice, correlated percolation, critical percolation probability 80−57205
quadratic lattice, correlated percolation 80−68149
quadrupolar systems of restricted dimensionality, absence of ordering 78−89411
quantum anisotropic antiferromag. Heisenberg model, Gibbs state limitation 80−50027
quantum corrections for a system of interacting phonons and the modified Korteweg-de Vries equation 79−60454
quantum corrections for lattice gases 77−17920
quantum coupled oscillator systems, or quantum fields on lattice, low and high temp. series expansion 78−29061
quantum crystals, appl. of method of quasiaverages 80−10737
quantum field theory of crystals and extended objects, review 79−42164
quantum Heisenberg model, Yang-Lee edge singularities at high temps. 80−20422
quantum lattice, conditional entropy in microcanonical ensemble 79−80555
quantum lattice spin theory, Jastrow wave functions 79−25999
quantum lattice system, local thermodynamic stability, KMS conditions 77−17902
quantum lattice systems, linear response and relaxation functions 80−4659
quantum particle in 1-D deformed lattice, energy depend. on quasimomentum 77−30052
quantum spin model with unstable stationary states 77−67382
quantum spin system, frustration effect 80−15677
quarks and strings on lattice, appl. of renormalisation group techniques 77−22654
quasi-one-dimensional systems, statistical mech., thermodynamic props., mag. transition 77−26246
quasifree excitons and electrons impurity trapping, finite coherence effects 80−59880
quasilattice theory of solutions, use in mol. spectroscopy, thermodynamic parameters determ. 79−96350
quenched bond disorder, effective medium approx. in Ising model 80−42163
Racah coefficients for point groups, chemical space groups and mag. group symmetry 80−57214
random chain, low-energy density of states and long-time behaviour, scaling approach 79−25994
random coil polymer chain relax., lattice model with excluded vol., head movement rules 80−5642
random conductors, position-space renormalisation and exponent theory 80−153
random energy model, disordered models family-limit 80−90794
random fields, lowering of dimensionality in phase transitions 77−17923
random Gaussian lattice, mass lower bound using random walk representation 78−89409
random harmonic chain model, essential singularities of sp. ht. and density of states 77−72665
random Ising model, thermodynamic limit 80−17885
random lattice, atom site diagonal perturbation, functional integral approach 80−57218
random lattice systems, Lifschitz singularity and density of states tailing 80−155
random lattices, bond percolation and cluster form. 77−45798
random ordered phase, effective field approx. 79−1676
random quenched site model, competing exchange energies and competing anisotropy energies 80−29552
random resistor network, scaling and critical behaviour near percolation threshold 77−41545
random resistor networks, critical behaviour near percolation threshold 78−87956
random spin systems with long-range interactions, critical behaviour 78−36942
random system, dispersion theory approach to scaling function 78−70071
random walk, self-avoiding, direct renormalisation group approach 78−73933
random walk and SU(2) Clebsch-Gordan coefficients 80−17822
random walk on lattice, correl. of successive steps, absorbing walls 79−44863
random walk process, memory effects 80−27232
random walk properties on periodic and random lattices via generating function 80−42157
random walks, average number of steps to trapping on D-dimens. finite lattice 77−17912
random walks, self-avoiding and limited order, distrib., orthogonal vector anal. 78−65874
random walks, span-constrained, on cubic lattice, internal configs. 80−68148
random-walk theory and correl. functions in classical statistical mechanics 77−5768
random-walk theory and ordered phases in lattice-gas systems 77−5769
randomly diluted Heisenberg spin system with anisotropic exchange coupling, crit. temp. 79−99702
randomly driven system, strong coupling expansion for classical statistical dynamics 80−105568
randomly occupied lattice, continuous-time random-walk eqn. 80−31683
randomly packed spheres, site percolation threshold calc. 80−27233
randomly-packed spherical particle bed, coord.-no. distrib., effective thermal cond., stat. thermodynamic theory 78−75028
rare earth pnictides, phase diagram for cubic model in Kikuchi cluster variational method 79−35639
real-space renormalisation group transformation based on cumulant expansion 79−12730
real-space renormalisation of self-avoiding walk by linear transformation 78−8360
real-space renormalization-group scheme for spin and gauge systems 80−32008

lattice theory and statistics continued
recursion eqns. for renormalisation group transforms. in lattice gauge theories including fermion variables 78−62298
recursion method for the extended impurity problem 80−96814
Reggeon field theory on a lattice, critical behaviour, Monte Carlo calc. 80−18126
renormalisation group, spurious relevant eigenvalues 77−45808
renormalisation group approach to scaling, phys. appl. 78−49634
renormalisation group calculations for Reggeon field theory on transverse lattice 77−18203
renormalisation group for site and bond percolation, real space 77−45803
renormalisation group transforms, optimal variational approx. 77−87699
restricted valence site animals on the simple cubic lattice 80−77715
restricted valence site animals on the triangular lattice 79−44867
rotational like degrees of freedom system, phase transitions, thermodynamic props. 80−77737
rotators, multicomponent, Gaussian inequality 78−29058
roughening transition dynamics, renormalisation group method 78−45574
roughening transition in one dimension, dynamics at low temps. 80−159
roughening transitions of finite order 80−38975
scalar interactions, microscopic, histogram collection by FORTRAN program 78−34958
scalar macroscopic fields in anisotropic stratified media, Green's functions 79−58544
scalar QED on lattice, correl. inequalities, infinite vol. limit 77−61233
scalar quantum electrodynamics on lattice as classical statistical mechanics 78−16956
scaling invariance and percolation in a random field *(Russian)* 77−41549
scaling relations, dynamic, linear and nonlinear, in renormalisation group theory 77−8321
Schwinger model, massive QED for fermions in 1+1 dimens. 78−78121
screw dislocation high velocity motion, lattice model effects 79−77600
self avoiding chain, scatt. function, n=0 vector model, calcs. and expt. 80−90788
self avoiding random walks, exactly soluble lattices 78−32767
self avoiding walk and supersymmetry 80−101756
self avoiding walk attached to a surface, tests of scaling theory 78−81927
self-avoiding chains, strong universality of excluded contacts 80−86224
self-avoiding lattice walks, renormalisation by non-linear transforms. 79−75468
self-avoiding lattice walks, renormalisation by nonlinear transformations 79−67230
self-avoiding lattice walks with high coordination and small excluded volume 80−77718
self-avoiding random walk, external spatial constraints, 'slithering snake' calcs. 77−89
self-avoiding random walk, real-space renormalisation group approach 79−63167
self-avoiding random walks on lattice strips 80−17875
self-avoiding walk, asymptotic behaviour in continuous space 77−13700
self-avoiding walks, mean-square lengths, asymptotic behaviour 79−21673
self-avoiding walks on the face-centred cubic lattice 79−93048
self-avoiding walks on the hyper face-centred cubic lattice in four dimensions 79−17355
self-avoiding walks with nearest- and next-nearest-neighbour steps 80−86222
self-consistent screening approximation, long range interactions and the critical exponent η 80−101761
selfavoiding random walk problem, direct renormalisation method 80−77703
semi-infinite systems, critical behaviour 78−4563
semi-quantum lattice system, equilib. states, AF algebra 78−45576
semiclassical approach to lattice theories of nonrelativistic fermion model and Gross Neveu model 78−16724
semiclassical spectrum of two dimens. nonlinear σ models 78−378
sequential term prediction, appl. to Ising, X-Y and other models 78−57866
series expansions, from finite lattice method 77−45800
simple cubic lattice, orientational ordering of quadrupoles 80−44157
sine-Gordon chain, cond., finite damping correction 80−46993
sine-Gordon chain, displacement fluctuations, long-time behaviour and dynamic scaling props. 80−101764
sine-Gordon chain, evidence for breather excitations 79−63054
sine-Gordon chain, long-term behaviour 80−68051
sine-Gordon chain, T≠0, commensurability, phase-torque eqn. of state 80−39251
sine-Gordon field theory, two dimens., second order phase transition, lattice model 78−78095
sine-Gordon kinks, nonequilib. props. using mol. dynamics techniques 79−12737
sine-Gordon system, two component, phase transition in two-dimens. 80−73279
sine-Gordon system with winding-number density, low temp. soliton gas phenomenology 80−105589
site and bond percolation distribs. 79−93046
site percolation, structure of infinite cluster 80−52137
site percolation model, series expansion exam. of pair correctedness 77−5765
site percolation on 2-D lattices, Cayley tree, boundary problem 80−52138
site percolation problem, finite lattice renormalisation-group approach 78−12648
site percolation problem, numerical simulation *(French)* 79−44864
site-bond percolation, low-density series anal. of uncorrelated limit 80−4657
site-bond percolation by position space renormalization group 79−63159
site-bond problems in percolation and cluster distributions, Monte Carlo calcs. 80−42160
site-diluted resistor networks, renormalisation group approach 79−15128
six-vertex model, partition function 79−40494
sixteen vertex model, bifurcation anal. 79−85091
small systems, Monte Carlo simulation, book contrib. 79−80530
solid lattice thermodynamics, two-temp. Debye approx. *(Russian)* 80−77728
solid on solid model rel. to XY model and Coulomb gas 77−84684

lattice theory and statistics continued
solid solutions, substitutional, with immobile cryst. lattice, chain of models *(Russian)* 79−46588
solitary wave propagation in 3-dimensional lattice 80−8929
soliton lattice melting, functional integral method 80−17883
soliton lattice stability in coupled linear chain system 80−73282
soliton lattices, dynamic and stochastic oscills. *(Russian)* 77−74324
solitons, lattice thermal conductivity theory 80−46991
solitons, scatt. from mass impurity 80−46992
solution, different-sized mols., orientation effects, surface region, lattice model 79−1540
solutions with closed loop coexistence curves, directionality depend. of lattice models 78−95158
space group representations, complex conjugation 79−90583
spacial cluster or mixing props. in classical lattice systems 77−37818
spanning trees, number on large square, triangular or honeycomb lattice 77−57282
sparsely periodic and random lattices, random walk props., lattice bond enumeration 79−21675
spatial lattice of Dirac fields and Thirring fields, spontaneous breaking of chiral symm. 78−24962
spectral props. of composition operators 79−80496
spectrum of one electron Hamiltonians with impurities 79−1578
spherical and mean spherical models, correlation phenomena 77−74327
spherical ferromagnetic models, Yang-Lee edge singularity density in thermodynamic limit 79−30378
spherical limit for n-vector correls., spin correl. functions 78−24726
spherical model, phase separation 79−44869
spherical model on hypercubic lattice modified 1/d expansion for critical temp. 77−2621
spherical models, critical behaviour 77−61025
spin and pseudospin lattice systems, Green's functions diagrammatic technique 78−8355
spin and pseudospin lattice systems, Green's functions diagrammatic technique, Pauli operators 78−8356
spin dimensionality dependence of T_c in the 1/n expansion 78−32772
spin lattice models, continuous-integral method 78−93615
spin system, cubic model, Monte Carlo simulation, phase transitions 80−34646
spin systems, Gibbs states, boundary condition equivalence 80−42159
spin-1/2 models, on square lattice, sublattice renormalisation transformations 78−65878
spin-oscillator coupled system, stochastic model for dynamics, projection operator approach 78−77813
spinels, percolative phenomena in cationic B-sublattice, Monte Carlo simulation 80−17893
square lattice, appl. of real-space renormalisation group to site percolation 79−30377
square lattice, close packing of rectilinear polymers 80−48114
square lattice, critical dynamics and potential moving approx., renormalisation group approach 80−57209
square lattice, critical probability of bond percolation equals 1/2 80−77711
square lattice, no. of configs. for nonoverlapping rods 79−21674
square lattice, percolation and cluster distrib. variable range interactions, exciton cluster model, layers 79−30379
square lattice, renormalisation of self-avoiding walks 80−73273
square lattice, series expansion technique 77−57283
square lattice finite thickness slabs, long self-avoiding walks, steric stabilisation model 78−54309
square lattice Ising model, series expansions from corner transfer matrices 80−154
square lattice Ising type models statistical mechanics, variational approx. 79−44873
square lattice Potts model, corrections to series expansions 77−17917
square lattice site problem, percolating cluster, Monte Carlo study 80−77720
square site percolating system, renormalisation group approach 78−41241
stability, equilibrium and metastability 79−54070
staggered eight-vertex model with four sublattices 77−45802
star mayer graphs, ninth order, three-space lattice symmetry coeffs. *(Russian)* 78−29064
star-triangle transformation, phase boundary for planar site-bond percolation problems 80−95042
statistical crystal model, small amplitude acoustic perturbations and Debye-Waller factors 78−55930
steam-water-ice system, two-dimens. triangular lattice model, matrix calc., props. 77−27975
step model, critical behaviour, high temp. susceptibility and internal energy series 78−34987
sticky potential, 2-D, ground state, triangular lattice 80−82726
stochastic n-vector model dynamic crit. props. 77−45805
stochastic systems, infinite dimens., ergodic props. 78−32770
strong-coupling calcs. and Pade approximants for lattice Hamiltonian 78−4762
structural phase transition, computer simulation 79−77721
structural stability, phase transitions 80−8932
SU_n Heisenberg spin chain derivation 80−37184
SU(2)-flavour Schwinger model on the lattice, Hamiltonian lattice perturbation exam. 78−16747
SU(N) gauge fields, non-convergence of 1/N expansion 77−71427
super-multiplicative functions, generalisation to fundamental theorem 79−93047
superfluidity on Bose-condensed quantum crystal 78−75905
superionic conductors, cooperative phenomena within generalized lattice gas models 79−46827
supersaturated vapour, critical clusters, theory and Monte Carlo simulation, review 80−82734
superspace groups, mathematical struct. and props. 80−17884
supersymmetric spin systems, extensions 78−21344
surface percolation processes, scaling theory and real space renormalisation group 80−86223
surface roughening transition, gravitational field effects 79−58645
surface tension and phase transition in lattice systems 80−27226
surfaces and interfaces, elastic energy of point defects and inclusions 80−73272
systems with quenched random impurities, dynamics as a substitute for replicas 79−35638
Temperley-Nagle identity for graph embeddings 79−147
lattice theory and statistics continued
tetrahedron equations and integrable systems in three-dimensions *(Russian)* 80−105590
thermodynamic limitations on interaction topologies 80−57217
thermodynamic mapping relations *(Chinese)* 80−27227
Thirring model, iterative variational anal., fermion field theory on lattice 78−41426
three state Potts-Kihara model, phase transition 79−85093
three-dimensional cubic lattice, random walk of particle, polymer chain config. approach 80−22294
three-dimensional lattices, random walks, probability of eventual return calc. by matrix method 78−6172
three-dimensional lattices with coord. number 4, random walk calcs., tracer diffusion 80−13001
three-level lattice system with quadrupole type interaction, analogue of Ising model 78−29063
three-state Potts model variant, phase behaviour 78−68259
time correlation functions of one dimens. infinite system, ergodic props. 78−65862
time evolution in equilibrium states without time automorphism 79−12722
Toda, quantum mechanical lattice 80−46983
Toda chain, integrability of two dimensional generalisation *(Russian)* 80−17889
Toda equation, difference analogue 78−20975
Toda lattice, excitation spectrum, molecular dynamics study 80−105588
Toda lattice, generalised eqn., solitons 80−95040
Toda lattice, Kac-Moerbeke's eqn., scatt. problem 78−12647
Toda lattice, nonlinear network eqns. generated from Backlund transformation 77−30107
Toda lattice, poles, soliton solns. 79−75368
Toda lattice, scatt. of solitons from mass impurity 79−12739
Toda lattice, statistical mechanics and solitons 79−49176
Toda lattice, surface impurity localised mode vibr. 79−60462
Toda lattice, transformation theories 77−30106
Toda lattice, undamping of strongly nonlinear surface impurity localised mode, computer simulation 79−97315
Toda lattice, wave behaviour in nonlinear LC equivalent circuit 80−105577
Toda lattice and generalised Wronskian technique 80−90792
Toda lattice and periodic multi-soliton soln. of Korteweg de Vries eqn. 77−30109
Toda lattice as integrable system, uniqueness of Toda's potl. 77−30108
Toda lattice Darboux transformation, differential difference evolution eqns. 80−156
Toda lattice eqns. of motion, multi-soliton soln. construction, direct method 79−75360
Toda lattice soliton, interaction with impurity atom 78−75772
Toda periodic lattice, perturbations 77−13703
topological cell model in two dimens., correl. functions 79−41924
topological excitations in Abelian Higgs model 78−70275
topological excitations in U(1)-invariant theories 77−67383
topological theory of defects in ordered media 79−93072
transfer integral method, three dimens., appl. to harmonic cryst. 78−84161
transfer integral method for two-and three-dimens. cryst., ground-state expectation value 77−76492
transfer matrix of one-sided subshift of finite type with exponential interaction 77−33953
transformation methods in anal. of crit. prop. 78−49771
transition point of random Ising model with bond dilution 79−93060
triangular and honeycomb lattice gases, order-disorder transitions to 2×2 struct. 80−4674
triangular Ising model coupled to honeycomb model via four spin interactions 79−30386
triangular lattice, ferroelectric ice model 77−82463
triangular lattice, finite series expansions 80−98859
triangular lattice, self-avoiding walks 79−40478
triangular lattice, size distrib. as function of perimeter or energy 79−44882
triangular lattice bond problem, series expansion study of percolation probability 79−2727
triangular lattice gas model, multicritical behaviour 77−74328
triangular lattice gas model with up to 3rd neighbour interactions, ground state struct. 78−41239
triangular spin lattice, renormalisation theory anal. of triplet interactions 77−5771
tricritical behavior in a two-dimensional field theory 80−77726
trimer problem, square lattice calcs. using Kikuchi method 77−71279
two dimensional system, melting and condensation theory 80−57231
two-dimens. planar model, universality class of crit. lines determ. 78−4566
two-dimens. U(1)-Goldstone model, QFT on lattice 78−74158
two-dimensional anisotropic N-vector models 79−85095
two-dimensional cluster configurations, nonlinear average size-perimeter relation 79−12738
two-dimensional lattice, solitons and nonlinear resonances *(Russian)* 80−52041
two-dimensional lattice embeddings of connected graphs of cyclomatic index two 78−41243
two-dimensional lattice gas models, improvement of quasi-chemical approx. 79−69356
two-dimensional lattices, pair-correctedness for directed band percolation by series methods 77−87701
two-dimensional model of polymer with an excluded volume *(Russian)* 78−42926
two-dimensional spin system on square lattice, exact duality-decimation transform. 80−17890
two-dimensional square Ising model in transverse magnetic field, renormalisation-group method 80−20428
two-dimensional systems, phase transitions 78−68241
two-phase seminvariants, of first rank, probabilistic theory via method of representations 79−32848
unbounded n-component spin systems on lattice, statistical mech. 77−4477
uniaxial, critical behaviour studied via renormalisation group theory 78−8367
uniform cluster estimates for lattice models 79−25992
uniqueness theorem for anticommutation relations and commutation relations of quantum spin systems 79−12713
variational approximations to renormalization groups 79−63169

lattice theory and statistics continued
variational principle for quasi-local algebras over the lattice 79−71371
vertex models on A-B square lattices 80−46984
vibrational properties of Cayley tree type system, modes, densities 78−71813
virial coefficients for hard rectangular parallelepipeds and cubes on simple cubic lattice 79−97308
von Neumann lattice, discrete coherent states 79−40475
vortex model in external elec. field, exact solution *(Russian)* 80−101763
wall and boundary free energies, general domains and complete boundaries 79−49182
water, lattice fluid model on 2D quadratic lattice 79−93056
water, lattice gas model, phase transitions 79−80535
wave motion in one dimens. nonlinear, periodic, exponential lattice 78−12646
wave scattering, fluctuating inhomogeneous media, model for teachers 79−21492
Widom-Rowlinson lattice gas, grand partition function zeros 80−31681
Widom-Rowlinson lattice models, sharp interface existence in three dimens. 79−49171
WKB approximation for quantum theory on a lattice 80−32009
X-Y model, percolation in three-dimens. model 78−80113
X-Y model, self avoiding walk approx. 77−4488
XY model, one-dimens., renormalisation group method anal. 80−17887
Yang-Lee edge singularity from a real-space renormalization-group method, Ising model 79−97317
Yang-Lee edge singularity in the hierarchical model 79−35933
Z(N) spin systems, duality and phases 80−73276
Z(N) topological excitations in Yang-Mills theories: duality and confinement 79−12938
zero field susceptibility in d=4, n=0 limit, confluent logarithmic singularities 78−54308
Fe-C interstitial solid solutions, self-diffusion activation energy rel. to partial molar energy 80−15291
H bond lattice with diamond struct., 3D statistical model of phase transition *(Chinese)* 80−8924
H_2 chain, infinite, lattice distortions, CNDO/2 calcs. 78−6018
^4He, superfluid, quantum lattice gas as microscopic model 78−59986
Rb_2NiF_4, planar antiferromagnet, cluster-Bethe-lattice method 80−22306
Ti_4O_7, semicond.-semicond. transition, lattice gas model 77−1364

lattice vibrations *see lattice dynamics*

laundering
nuclear power plant personnel protective clothing, dry cleaning versus water wash 80−13691

laundries *see laundering*

Laves phases *see alloys*

lawrencium
atom, ground state config., relativistic prediction, multiconfig. Dirac-Fock calcs. 80−106277

lawrencium compounds
LrH, $^1\Sigma$ state, Dirac-Fock one-centre calcs. 80−23301

laying, cable *see cable laying*

LCAO calculations
ab initio LCAO-HF-concentrated GO crystal-orbital program 77−55471
acetaldehyde, first triplet state geometry, fragmentation into free radicals 80−47915
acetylene, chemisorbed on metal surfaces, geometric and electronic struct., UPS obs. and HF LCAO calc. 79−86988
acrylonitrile, semiempirical CNDO calcs. of electronic struct. and absorpt. spectra 78−995
activated complexes, exp. obs., bonding MO LCAO states 80−76506
addition theorems of spatial functions, multicentre integrals of arbitrary atomic functions, symmetry and analytical struct. *(German)* 80−37729
adsorption anisotropy for molecule SCF MO LCAO calcs. 77−89643
alkali borate glass networks, π-electron distrib. SCF INDO LCAO-MO calc., O basicity 78−79924
alkali halides, heteronuclear XY^- defects, spin Hamiltonian parameter anal. 80−88509
alkanes, mag. susceptibility simple additive approx. calcs. 78−86775
alkanes, saturated, ab initio LCAO MO SCF calcs., core ionis., electronic relax. 77−71745
all-valence LCAO MO SCF INDO method, for mol. ground and excited state props. 78−37556
allyl radical, ab initio SCF solns., doublet stability 78−33423
allyl radical, restricted ab initio SCF LCAO solns., doublet stability 77−79539
allyl-radical, pi-electron system, appl. of UHF Green's function method 77−61684
anisotropy of long-range interaction 79−36734
aromatic systems, alternant, sign-alternation rule for triplet state 80−102420
atom-pair interactions in molecules, semi-empirical MO calc. 80−915
atomic anions positron complexes, ground and excited states theoretical studies 80−42934
atomic d orbitals in basis sets, symmetry criterion 79−45622
atomic sphere overlap, Xα-SW MO projection of LCAOC MO's 78−25422
azabenzenes, multipole moments, polarisabilities and long-range interaction coeffs. calcs. 79−89599
band structure calcs., optimised LCAO version, appl. to Wannier states results for Cu 79−33220
benzene, LCAO-MO-SCF calcs., MODPOT, VRDDO and MODPOT/VRDDO procedures 77−71742
benzene, mol., directional Compton profile, ab initio SCF LCAO MO calc. 78−62857
benzene, protonated, electronic struct., SCF MO LCAO calcs. 78−82638
benzene, semiempirical CNDO calcs. of electronic struct. and absorpt. spectra 78−995
benzenes chemisorpt. on α-Fe, π complex form., MO LCAO calcs., thermodynamics 77−52674
benzoic acid, spectral shift due to electron-repelling substituents 79−72362
benzonitrile, LCAO-MO-SCF calcs., MODPOT, VRDDO and MODPOT/VRDDO procedures 77−71742
beryllocene, gas phase struct., ab initio LCAO SCF calc. 78−41942
bond order, maximum principle, LCAO formalism 78−29728

LCAO calculations continued
bromomethane, ab initio SCF MO calcs., ionis. pots., dipole moment, config., electronic props. 78−1104
carbenes, core ionised states, singlet and triplet state binding energy, struct. changes, LCAO-SCF calc. 79−97982
carbonic anhydrase, active site substrate binding, environmental effects, CNDO and SCF LCAO calcs. 80−8002
carbonyl halogen substituted cpds., geometric and electronic struct., LCAO-SCF calc. 79−89603
carbonyls, core ionisaton phenomena, nonempirical LCAO MO SCF investig. 80−37906
carboranes, ab initio 6-3G and 3G/MODPOT LCAO-MO-SCF calcs. 79−10026
β-carotene, optical absorpt., theory 79−62189
charge ordered state of quasi-one dimens. and finite cyclic system, ab initio LCAO-MO method 77−1343
chemical bond, MO-LCAO scheme for binding energy, correlation correction, physical fragmentation 77−46490
chemical bond anal., semi-empirical methods 77−57880
chemisorbed atoms, theory, CI calcs. *(German)* 78−31707
chemisorption, embedding problem, SCFMO formalism 78−71977
chemisorption on model insulator 77−85072
cluster systems, program for calc. electronic struct. with double self-consistency-Bersuker's method 80−69289
conjugated system, potentials of twofold ionization and electron affinity calcs. 77−3287
conjugated systems, symmetry-depend. rules 79−89592
convergence in SCF calcs., reverse level shifting technique for accel. rate 78−70735
copper (II) complex, bis(dithiocarbamate), HF-Slater-LCAO calcs., mag. coupling parameters and optical spectrum 80−99447
core level ligand field splittings in photoelectron spectra 80−43106
correlated Π-electron systems, mol. interactions, linear response theory 80−53090
covalent elements, cohesion in condensed phases, corrections to simple Huckel approx. 78−59779
covalent elements, cohesion of σ and π bonds in condensed phases, simple Huckel approx. 78−59778
covalent semiconductor, valence band calc. using many-electron theory 80−15434
crystal, Fourier transforms of Compton profiles, LCAO calc. 79−83050
cubic crystal, perfect, non-Bloch electron states, incompletely symmetric 79−23877
cubic crystals, non-Bloch electron states determ. 77−1352
cyclopentadiene, LCAO-MO-SCF calcs., MODPOT, VRDDO and MODPOT/VRDDO procedures 77−71742
d-orbital basis functions role in electronic struct. description of systems containing Si, P, S and Cl 80−9484
defect electronic struct. determ. using LCAO method, appl. of cubic harmonic expansion 77−20268
diamond, cluster, electronic struct. of deep levels, LCAO, SCF method 79−82555
diamond, Compton profiles, X-ray struct. factors, band struct., LCAO calc. 78−51889
diamond, ground-state, electronic properties, ground-state in local-density formalism 77−69223
diamond-like structure, interatomic matrix elements between s- and p-like states, LCAO calc. 80−10857
diamond-structure semiconductor, Compton profile interpretation 80−29820
diamond-type crystals, LCAO band structure, overlap and distant neighbour effects 80−49585
diatomic mol., directional Compton profiles for mol. simulation of crysts. 77−30931
diatomic molecule, electron static interaction potl., computation 77−3255
diatomic molecule nucl. mag. shielding using LCAO MO functions and gaussian expansion 79−36548
diatomic molecules, LCAO Hartree-Fock-Slater method calcs. 79−31374
diatomic molecules of 1st row, total Xα energy, LCAO calc., rel. to local density models 80−32607
diazines, LCAO-MO-SCF calcs., MODPOT, VRDDO and MODPOT/VRDDO procedures 77−71742
diazoles, LCAO-MO-SCF calcs. MODPOT VRDDO and MODPOT/VRDDO procedures 77−71742
diformamide, torsional pot. barriers, ab initio and partition of energy methods 77−88588
dipyridylethylenes, photoelectron spectra, conformation, SCF LCAO calcs. 77−79651
discontinjous approx. mol. electronic wave functions, ab initio LCAO and VB ZDO appls. 77−50340
DNA, proton transfers between base pairs, LCAO SCF all-electron PRDO method 78−80829
double groups, relativistic symmetry orbitals for LCAO calculations 79−10018
effective convergence to complete orbital bases and at HF limit through systematic Gaussian primitive sequences 80−14065
eigenvalue independent partitioning and direct minimisation of SCF theory 77−26970
electronegativity representation based on LCAO and Schrodinger eqn., new scale *(Chinese)* 77−75034
electronic structures comparison, arbitrary electronic state, distance and similarity measures appl. 80−9487
electrostatic molecular potential from completely transferable group contribs. 77−88408
energy functional, direct minimisation in LCAO-MO density matrix formalism 78−5118
ethane, nucl. spin-spin coupling, scanning MO HF LCAO calc. 79−50045
ethylene, chemisorbed on metal surfaces, geometric and electronic struct., UPS obs. and HF LCAO calc. 79−86988
ethylene, dimer interaction, lattice energy, multipole expsn., at.-at. pots. 78−9218
ethylene, nucl. spin-spin coupling, scanning MO HF LCAO calc. 79−50045
ethylene+$Cl_2(Br_2)$ complex, intermolecular interaction and struct. SCF-MO-LCAO CNDO/2 calc. 78−58763
ethylene molecules, long range forces in multipole expsn., ab initio calcs. 78−9219
Ewald method, convergence of reciprocal lattice sums 77−11834
expansion of MO wave functions into VB work functions 78−74580
extended Huckel theory, rel. to NDO LCAO theories 80−95536

LCAO calculations continued
FCC lattice, density of dynamical observables, incompletely symm. non-Bloch states 79−23879
FCC lattice, electronic density of states, incompletely symm. non-Bloch states 79−23878
Fenske-Hall LCAO method, inner-shell binding energies and chem. shift calcs. 80−47871
ferrihaemoglobin hydroxide, nucl. hyperfine interaction, HF LCAO calc. 79−2002
finite crystal, electron density of states, rel. to infinite cryst., LCAO calcs. 77−24507
first-row transition metal ions, core ionised states, ΔSCF MO calcs. 80−78523
fluoro sulphuric acid methyl ester, rot. isomerism 78−86964
fluoropolymers, linear, valence electronic struct., LCAO cryst. orbital calcs., ESCA 78−5384
formaldehyde, adiabatic CI pot. surface LCAO calc., gradient determ., mol. dynamics 80−48056
formaldehyde, core ionisation, valence orbital relax. calcs. 78−5135
formaldehyde, orbital contribs. to relax. energies accompanying core ionis., ΔSCF HF calcs. 78−82642
formaldehyde+formaldehyde, medium distance interaction, SCF LCAO MO, supermol., perturbation and MCF calc. 79−837
formamide+formamide, medium distance interaction, SCF LCAO MO, supermol., perturbation and MCF calc. 79−837
formyl-triglycyl amide-H_2O, analytical pot., ab initio calc. 79−48206
frozen core AO approx. in Roothaan's MO LCAO SCF method 77−3264
furan, ionisation pots., transition operator calcs. 77−30771
garnets, mag. props. of V^{4+} ion, effect of covalency 78−64010
Gaussian-70 MO program, LCAO-SCF eqn. soln., population anal., appl. 78−70742
generalized alternative systems, valence and forbidden band widths, LCAO calcs. *(Russian)* 79−18111
graphite, electronic props., self consistent LCAO calc., point vacancy in 2-dimens. cryst. 78−51932
graphite, electronic props., self-consistent LCAO calc. 78−51887
graphite, electronic struct. exact exchange HF calcs. 80−65438
graphite, heteroatom doped, electronic struct., energy spectrum, HMO LCAO calcs. 77−43539
graphite intercalation cpds., Fermi surface and transport props., LCAO model 80−80159
graphite monofluoride, self-consistent semi-empirical LCAO calcs. of electronic band struct. 77−85142
halogen compounds, chem. bond, MO LCAO SCF calcs. 79−41104
halomethanes, ^{13}C chem. shifts, trigonal additivity procedure 80−1002
Hartree-Fock integral eqns., soln. 79−76325
heavy atom mols., program for calc. electronic struct. by quasirelativistic method 80−69088
HEED, Bloch waves, corresponding atomic and mol. orbitals 79−27880
helical systems, energy band calcs. using Hartree-Fock SCF-LCAO formulae 78−10329
heteroconjugated molecule, LCAO MO graph-theoretical formulation 78−890
heterocyclic conjugated compounds, electronic struct., spectra, ionisation pot., INDO-CI LACO-MO-SCF calcs. 79−54834
heterojunction band-edge discontinuities, LCAO theory 77−89840
heteronuclear molecules, alternant mol. orbitals energies, generalised formula 79−6867
hydrides, third row, electron binding energies, one-centre expansion method 77−6677
hydrocarbons, conjugated, dynamic polarisability and eigenfreqs. in one-electron approx. 79−64117
2- and 4- hydroxypyridine tautomers, ab initio SCF LCAO MO calcs. 79−81154
hyperpolarizability, freq. depend., time depend. HF eqn., second order LCAO SCF pertubation theory 79−31388
III-V semiconductors, calc. using MOLCAO approx. 79−42732
inelastic electron tunnelling spectroscopy, model for electron-molecule interaction 78−90257
inert gas compounds, chem. bond, MO LCAO SCF calcs. 79−41104
infinite crystal, electron density of states, rel. to finite cryst., LCAO calcs. 77−24507
infinite polymers, long-range Coulombic interactions, LCAO-CO calcs. 79−7042
integral expression, for $(nl|n'l')$ with n, n′=3, 4 77−30769
interconversion pot. energy surfaces, geometries, electronic structs. 78−35660
β-lactam antibiotics, ab initio SCF-MO-LCAO calcs., amidic bond breaking, methoxy substitution effect 80−78533
large complex systems, mixed electrostatic-quantum chemical approach 79−89605
LCAO Hartree-Fock-Slater method, evaluation 79−31374
lone pair localised MOs, energy contribs. and second moments in 10-electron hydrides 77−14341
magnetic dipole-dipole hyperfine integrals for Slater-type orbitals 79−11095
metal, BCC, chemisorption of monolayer of atoms, charge in density of states determ. 77−47682
metal, FCC, (100) surface, chemisorption-induced interaction between electronic levels of two-level adsorbate 80−39644
metal, HCP, LCAO description of (0001) surface electron states, appl. to Sc 78−72232
metal porphin, triplet state, spin density and zero-field splitting, PPP-SCF-CI calc. 79−68200
methane, core ionis., single orbital relax., LCAO MO SCF calcs. 78−29739
methane, freq. depend. polarizability, LCAO SCF perturbation theory 79−31387
methane, pot. energy curves, Monte Carlo and SCF LCAO MO calcs. 80−63526
methanol, polymers, structs., binding energies, LCAO SCF MO calcs. 77−83498
methyl halides, mol. force field at SCF ab initio levels, quantum-mechanical calc., LCAO-MO method 80−106319
3-methyl lumiflavin in soln., optical absorption, theory 78−74569
methylamine-t_1-NH_3, β^- decay effect on H-bond, ab initio LCAO SCF MO calc. 78−76894
microcrystallites, LCAO-MO calcs, in HMO approx., influence of lattice distortion adsorption, absorpt. of gases *(German)* 78−30584
MO, LCAO method, chem. bond order, ZDO approx. 79−41102

LCAO calculations continued
MO LCAO method, improvement by directed variation of exponential parameters 79−41101
molecular complex, g-tensor components, semi-empirical LCAO calc. 77−18794
molecular electric multipole moment integrals, STO orbitals 77−50557
molecular electrical props., chem. substitution effect, LCAO calc. 79−41103
molecular electronic struct., UHF Green's function method, appl. to allyl-radical 77−61684
molecular electronic structure, semiempirical CNDO method, calc. progam 78−86782
molecular geometry optimisation in mols. with second row atoms 77−42232
molecular nuclear spin-spin couplings between ^1H, ^{13}C, or ^{19}F, LCAO-MO-SCF-MINDO/3 approx. calcs. 79−94019
molecule, anisotropic Compton profile, LCAO calcs. 77−6863
molecule, diatomic, Zeeman effect, relativistic corrections 77−83646
molecule electron density distrib. maps, graphical construction from MO LCAO calculated wave functions 77−83480
molecule with second-row atoms, bond functions in SCF calcs. 77−14349
molecules in molecule (MIM) model, appl. to π-electron systems *(German)* 79−36506
naphthalene, anion, cation and triplet, GO LCAO MO calcs. of electronic struct. 78−25416
naphthalene, LCAO SCF MO CI calcs., integral approx. scheme using semiorthogonalised orbitals 79−6873
nitrile complexes, RCN...Cl-Cl′ and RCN...$HCCl_3$, charge transfer and distrib., NQR 77−12244
NMR spin-spin coupling consts. calcs. 77−68060
nuclei acid phosphate group, analytical atom-pair pot., SCF-LCAO calc. 79−70516
one-dimensional homonuclear molecular systems, nature of energy gap 79−11063
one-dimensional molecular crystals, electronic struct., mol. orbital theory 80−54588
one-electron wave functions, optimisation procedure 77−38597
open shell SCF MO LCAO method in unrestricted Hartree Fock formalism 79−31389
open-shell clusters, semiempirical LCAO-MO method of energy spectrum and electronic struct. calc. 80−54583
ordered adlayers, electronic struct. 79−38142
organic molecules, core ionisation and electronic redrganisations, LCAO MO SCF calcs. 79−18115
organic molecules, Raman spectra intensities, electronic polarisabilities, quantum mech. calc. 79−27041
organic molecules, relax. phenomena, following core ionis., LCAO MO SCF calc. 79−10030
organic system, nonlinear second-order optical susceptibility 80−9947
overlap matrix, Slater-Koster interpolation 79−7766
oxalic acid, theoretical deformation density, ab initio Hartree-Fock calcs. 79−32982
periodic systems electronic struct., LCAO SCF ab initio HF calcs. method 80−65419
perovskites, d-band, surface electronic props., π-bands exam. 79−38145
perovskites, matrix element effects in freq. dependent dielectric function 80−70632
phytochrome chromophore, models, absorption wavelengths and oscillator strengths calc. 77−81469
pinacyanol dye, adsorbed on CdS substrate, aggregation effect on mol. electronic states 80−37757
cis-polyacetylene, electronic struct. 79−47012
polyacetylene, pure and doped, electronic props. from one-dimens., tight-binding LCAO-SCF-MO calcs. 79−56123
polyacetylenes, fluorinated, electronic struct., tight-binding LCAO-SCF-MO calcs., prep. 80−70591
polyatomic molecule, Eckart frame orientation by symmetric orthonormalisation 79−6818
polyatomic molecules, relativistic symmetry spinors, LCAO-SCF theory 77−420
polyatomic molecules, relativistic symmetry spinors, LCAS-SCF calcs. 77−419
polyatomic system, large, ALGOL-60 program for MO LCAO calcs. in Mulliken-Rudenberg approx. 77−88388
polycytosine, ab initio energy band struct. 77−70415
polydiacetylene, model chain, band struct. calcs. 77−8016
polyene, different orbitals for different spins 79−69392
polyene, energy bands, ab initio Hartree-Fock cryst. orbital calcs. 77−89717
polyene, infinite, electronic states under local perturbation 77−57878
polyethylene, displacement of electronic spectrum during stretching, LCAO calc. 80−5481
polyethylene, valence electronic struct., LCAO cryst. orbital calcs., ESCA 78−5384
polyglycine, band struct., ab initio SCF LCAO calcs. 79−22874
polymers, long-range Coulombic interaction, Fourier transform technique calcs. 79−31748
polynuclear clusters, programs for calc. electronic struct. by Mulliken-Wolfsberg-Helmholtz method 80−69288
polypyridines, photoelectron spectra, SCF LCAO calcs. 78−33551
porphin, MCD, LCAO MO SCR π-electron calcs., PPP approx. 78−9178
porphin, spin-spin coupling const., MO LCAO CNDO/2 calc. 79−41108
porphyrin a, MCD, LCAO MO SCR π-electron calcs., PPP approx. 78−9178
position space LCAO wave function, momentum space variation approx., many centre integrals 80−27926
proton magnetic shielding, chem. substitution effect on chem. shift, LCAO perturbation method 77−68064
protoporphyrin, MCD, LCAO MO SCR π-electron calcs., PPP approx. 78−9178
pyrazine, dimer interaction, lattice energy, multipole expsn., at.-at. pots. 78−9218
quantum chemistry, simple approximation method *(Hungarian)* 79−3341
quasi-relativistic SCF-MO-LCAO methods, CNDO and MWH appls. 78−41953
radical, small, isotropic hyperfine coupling consts., MINDO/3 calcs. 80−52894

LCAO calculations continued
rare earth borides, higher types, phys. props. and electronic struct., group orbitals-LCAO calcs. 80−20077
rare earth monobismuthides, LCAO calc., electronic struct. *(Russian)* 77−39777
reciprocal lattice expansion, Hartree-Fock exchange term, LCAO calcs. 78−47691
refractory compounds, electron struct. and phys. props. 80−54585
SCF-LCAO-MO calculation, semi-empirical, correct orthogonalisation of basis set 80−32613
Schrodinger eqn. soln. for electron in several Coulomb centres' field 77−57854
semi-empirical SCF-LCAO calc. including energy minimisation, GEOMO program 77−23428
semi-infinite solid, elementary excitations in surface region 79−60618
semiconductor, electronic struct. of deep levels, LCAO, SCF method 79−82555
semiconductors, deep levels, self consistent LCAO MO calcs. 80−29353
separated electronic pair functions, direct minimisation of energy functional, LCAO-MO SCF, density matrix formalism 79−31392
Slater-Koster LCAO integrals, general expressions for reduction to two-centre approx. 79−68187
Slater-type orbital band structure calcs., computable expressions, derivation 80−24776
small molecules, HMO-CI, HMO-AO-CI methods, quantum chemistry model studies *(German)* 78−29753
solid, new Hartree-Fock energy band struct. determ. using LCAO basis, appl. to diamond 77−35848
solid, self-consistent numerical-basis-set LCAO model, local density formalism 77−76725
solid-state chemistry, determ. of electronic struct. 78−2409
sparse s and p type Gaussian basis set LCAO MO SCF calc., mol. props. 80−23306
stilbene derivatives, electronic struct., frontier electron density, chem. reactivity *(Rumanian)* 79−72242
superexchange in insulators, refined LCAO scheme 78−91861
surface dielectric response in local representation, microscopic theory 77−85289
surface lattice dynamics and density response 78−71930
surface states, three-dimens. cryst. ab initio SCF LCAO calc., impurity clustering 78−56201
surfaces states of semi-infinite s-p hybrid diatomic linear chain, Green function method 77−4419
symmetry-adapted linear combinations, algebraic formulae 77−79533
symmetry-adapted Wannier functions, variational procedure 80−2323
TCNE, semiempirical CNDO calcs. of electronic struct. and absorpt. spectra 78−995
TCNE-stilbene complexes, and analogs, charge transfer energy calc. isomer prediction 78−21854
TCNQ, semiempirical CNDO calcs. of electronic struct. and absorpt. spectra 78−995
ternary alloy semiconductor, band struct., CPA calc. based on linear combination of bond orbitals 79−87035
tetrafluoromethane, valence electron binding energies, molecular symmetry restrictions effect 80−63528
tetrahedral crystal, electron localisability by LCAO band theory, Pauling ionicity 77−47776
tetrahedrally coordinated semiconductors, electronic struct. and Fourier transformed Compton profiles 79−38689
2,2,4,4-tetramethylcyclobutane-1,3-dione, Rydberg transitions, spectra, LCRO calcs. 77−34659
thiocarbonyl halogen substituted cpds., geometric and electronic struct., LCAO-SCF calc. 79−89603
three-electron bonds, strengths, ab initio LCAO MO CI calcs. 80−87046
$(TiF_6)^{3-}$ complex, open-shell cluster calcs., semiempricial method 80−54583
total energy of molecule, local spin density functional approx., LCAO SCF calc. 79−93920
transition metal, chemisorption of ordered overlayers with C(2×2) and (2×1) structs. 79−46925
transition metal borides, higher types, phys. props. and electronic struct., group orbitals-LCAO calcs. 80−20077
transition metal complex, LCAO-HFS-STO calc., basis set effects 80−52882
transition metal complexes, LCAO Hartree-Fock-Slater method calcs. 79−31374
transition metal cpds., electronic spectrum calc. by GO-LCAO method *(Russian)* 79−73420
transition metal dichalcogenides, layered, electronic band struct. and bonding by atomic orbitals methods 79−15077
3d transition metal ions in crystals, Jahn-Teller coupling constants calcs. 80−49679
transition metal nitrides, liquid interactions, ab initio LCAO MO SCF calcs. 79−18256
transition metal surface, electronic perturbations 78−95334
transition metal-oxygen compounds, salts, X-ray Lα emission spectra, excited states calcs. 79−59488
transition metals, universal LCAO parameters 80−75503
TTF-TCNQ, band struct., Fermi surface and density of states, LCAO calc. 78−60048
use of the symmetry-adapted atomic orbitals in the large unit cell approach to solids 79−77974
vinyl alcohol, struct. from ab initio calcs. 78−29857
water+glycine(serine) zwitterions, interaction pots., ab initio SCF LCAO calcs. 78−48747
X-ray scattering factors, of crysts., temp. effects in LCAO calcs. 80−10454
Z-centre 1-electron integrals and Coulomb integrals over STOs 78−82608
Ziegler-Natta type catalysis, reaction pathway, ab initio SCF-LCAO-MO calcs. 78−56891
zincblende (110), surface relaxation 79−38143
zincblende structured ternary alloy semiconductor valence bands, LCBO coherent potential approximation *(Japanese)* 78−47699
Ag clean (111) surface, absence of filled surface states in s-p gap, LCAO calc. 78−2543
Ag, cluster and microcrystal, matrix isolated, optical absorpt. spectra, photolysis and plasmon absorpt. 79−89820
Ag halide, photographic image form., defect and impurity states, LCAO calc. 78−16876
Ag halide bonding LCAO-MO treatment 79−23561

LCAO calculations continued
AgBr surface, vibr. freq. of adsorbed Ag atom, LCAO-MO calc. *(Russian)* 79−2866
Al, single vacancy formation energy, determ. using energy bands and wave functions, from LCAO calc. 78−47348
Al, single vacancy formation energy calc., SCF-LCGO modified solid state scatt. theory 80−54637
$Al_2(Al_2^-)(Al_2^+)$ configurations, ab initio study, LCAO, STO, MO-SCF and CI calcs., binding energy *(French)* 80−91447
Al_2Cl_6, ab initio LCAO SCF minimal basis set calc., struct. 79−49943
Al_2F_6, ab initio LCAO SCF minimal basis set calc., struct. 79−49943
Ar, electron binding energies, one-centre expansion method 77−6677
$Ar+HHe^+$, ab initio pot. energy data, SCF-LCAO calcs. 80−63530
$Ar_nH(H^+)$, excited and ground state struct. energies and binding energy, vibr. modes, LCAO-SCF-MO calc. 79−3608
Au, Bloch waves, corresponding atomic and mol. orbitals, in HEED 79−27880
BH, electron density and localizability partitioning calcs. 78−21847
B(I) hydrides, ab initio calcs., proton and hydride affinities 79−10029
BN, electronic struct., exact exchange HF calcs. 80−65438
$B_xN_xH_{x+3}$, energy levels and wave functions, π-electron approx. 77−38608
$BaTiO_3$, cluster surface states, LCAO calc. 77−43686
$BaTiO_3$, undoped and Cu doped, Γ_{15} phonon freezing, electronic instability, LCAO calc. 80−25318
Be cluster, multibody expansions, convergence 80−23594
Be metal, electron distribution and momentum density, Compton scatt. 80−11502
Be_4 (Be_4^-), atomic clusters, electronic struct., LCAO-MO-SCF and HF calcs. 80−63880
BeS, electronic energy bands, APW and LCAO calc. 77−20236
BeSe, electronic energy bands, APW and LCAO calc. 77−20236
BeTe, electronic energy bands, APW and LCAO calc. 77−20236
$Br^-(H_2O)_n$, hydration energies, orientation, ab initio-LCAO SCF MO calcs. 80−27944
C, amorphous, diffraction intensities, chem. bonding effects 77−72557
C, amorphous, inelastic electron scatt., valence electron contrib. 80−55240
C-C σ bonds, mag. suscept., refined variational calc. 77−68136
C-H bonds, mag. suscept., vector pot. variational calc. 77−68137
CH_2, FSGO LCAO calc., bond angles 77−34557
$(CN^-;e^+)$ complex, ab initio LCAO SCF calc., positron affinity and excitation energy 79−49945
CO, adsorbed on jellium, surface plasmon relax. energies 80−70537
CO, core ionis., electric field depend. 78−13424
CO, core ionisation and single orbital relax. calcs. 78−5133
CO, core ionisation single orbital relax. energy, LCAO-SCF basis set depend. 79−89604
CO, HF calcs., compared with optimised LCAO results 78−5139
CO, LCAO-Xα method calcs., comparison with Hartree Fock and MS Xα methods 80−95539
CO, orbital contribs. to relax. energies accompanying core ionis., ΔSCF HF calcs. 78−82642
CO_2, ionised states, core and valence, ab initio HF calcs. 77−79597
COH^+, orbital contribs. to relax. energies accompanying core ionis., ΔSCF HF calcs. 78−82642
$CaCO_3$:Li, synthetic calcite, $(CO_3Li)^{2-}$-Li^+ defect after X-irrad., EPR study 80−75852
$CdCl_2$, deformation densities, relativistic effect 80−42928
CdI_2, UV reflectivity meas., band struct., LCAO calcs. 78−72545
CdSb, energy spectrum, influence of chem. bonds 80−34356
Cl-containing systems, core Auger and core electron binding energy shifts, ab initio LCAO SCF MO UHF calcs. 77−30777
$ClHCl^-$, deuteron quadrupole coupling const., nuclear mag. shielding, geometry depend. 78−58586
Co, Auger spectrum, ab initio MO LCAO SCF CI calc. many electron contribs. 80−87169
Co complex, $Co(NO_2)_6^{4-}$, bond. props. and Jahn-Teller distortion, INDO-LCAO-MO calcs. 80−75532
Co-porphine, ab initio LCAO SCF MO calcs. 79−6860
$Co(CN)_6^{3-}$, electronic struct., ab initio LCAO SCF MO calcs. 79−18112
$Cr(CO)_6$, LCAO-HFS-STO calc., basis set effects 80−52882
CsBr, (110) surface, electronic struct. of valence bands calc. *(Russian)* 80−75621
CsCl, (110) surface, electronic struct. of valence bands calc. *(Russian)* 80−75621
CsI, (110) surface, electronic struct. of valence bands calc. *(Russian)* 80−75621
$CsPbBr_3$, $CsPbCl_3$, ionic semiconductors, electronic and optical props. 79−38594
$CsPbBr_3$, optical props. and electronic struct. 78−48198
$CsPbCl_3$, optical props. and electronic struct. 78−48198
$CsPbCl_xBr_{3-x}$, optical meas., LCAO band scheme 80−25437
Cu (001) monolayer, electronic struct., self-consistent LCAO calc. 79−4606
Cu, band structure calcs., optimised LCAO version, appl. to Wannier states 79−33220
Cu complex, $Cu(NO_2)_6^{4-}$, bond. props. and Jahn-Teller distortion, INDO-LCAO-MO calcs. 80−75532
Cu on Ag (001), ultrathin film electronic states calc. 78−6318
Cu, orbital energies and X-ray K-absorpt. spectra 80−69060
Cu, surface energy band calc., significance for photoemission 78−95330
CuCl, electronic struct. by LCAO and LMTO methods, direct gap semiconductor 80−59868
$CuCl_4.2NH_3$, g-tensor components, LCAO calcs. 77−18794
CuO, mol. orbital energies and X-ray K-absorpt. spectra 80−69060
Cu_2O, mol. orbital energies and X-ray K-absorpt. spectra 80−69060
EuO, electronic struct. and props., mol. cluster approx. 77−11852
EuS, electronic struct. and props., mol. cluster approx. 77−11852
F^-+fluoromethane, S_N2 reaction, ab initio LCAO SCF calcs. 77−81402
F_2, LCAO-GTO *Xα* calc., rel. to other LCAO calcs. 80−52871
F_2, nucl. spin-spin coupling, scanning MO HF LCAO calc. 79−50045
FH_3^+, stability, ab initio calcs. 77−30775
$FHCl^-$, deuteron quadrupole coupling const., nuclear mag. shielding, geometry depend. 78−58586
FHF^-, deuteron quadrupole coupling const., nuclear mag. shielding, geometry depend. 78−58586
$(F^-;e^+)$ complex, ab initio LCAO SCF calc., positron affinity and excitation energy 79−49945

LCAO calculations continued
Fe, ferromag. film, surface states, surface magnetisation and electron spin polarisation 80−65648
Fe, ferromag. nonrelativistic LCAO energy band calc. 78−10343
Fe_2Al, mag. moment determ., role of local environment, self consistent calcs. 80−44815
FeF_2, electronic struct., charge density and elec. field gradient, MO cluster calc. 77−51704
FeF_3 isomer shift, using LCAO form of molecular orbital method 78−62856
FeO, valence band XPS and UPS, LCAO-MO calcs. 80−45197
$Fe_4S_4(SH)_4^{0,2-,3-}$, HFS-LCAO calcs., 4-Fe active site model in high pot. Fe protein and ferredoxin 80−42929
FeX_4^-, (X=F, Cl and Br), electronic struct. and isomer shift 80−63545
GaAs, piezoelectric constant due to bond bending, electron redistribution effect 79−38457
$GaAs_xP_{1-x}$, energy band struct., CPA based on LCBO *(Japanese)* 80−44495
Ge, LCAO band structure, overlap and distant neighbour effects 80−49585
Ge, valence band splitting in mag. field, LCAO interpolation *(German)* 77−59251
GeO_2, electronic struct. and densities of states, tight-binding calcs. 80−15447
H atom finite chains, HF solns. stability and symmetry breaking, independent particle model calcs. 80−87035
H, bond energy, chem. substitution influence 80−37718
H-bonded systems, core and valence ionis., nonempirical LCAO MO SCF calcs. 77−67973
H-bonded systems, cyclic and bifurcated, ab initio MO calcs. 79−41100
H^++Kr, mol. orbit approach, spin-orbit interaction, adiabatic pot. and projected valence band treatments 77−533
H_2, anisotropic Compton profile, LCAO calcs. 77−6863
H_2, highly compressed, combined representation method for use in band struct. calc. 77−89685
H_2, mag. field depend. orbitals for mag. screening and susceptibility of mol. 78−78611
H_2, shielding const., variable screening method 79−93932
H_2, Xα theory appls. approximations 80−9510
H_2^+, electron impact dissociation variationally adjusted LCAO mol. orbitals calcs. 77−3473
H_2^+, extended LCAO method, 1sσg orbital *(Russian)* 79−93922
H_2^+, in mag. field, LCAO calcs. 78−82628
H_2^+, mol. props. in intense mag. fields 79−81169
H_4 and H_4^+, H_4^- ions rectangular configurations, stability, SCF MO LCAO calcs. 77−42235
HBr^{n+}, highly charged, repulsion energies, nucl. internal conversion, ab initio calcs. 79−76341
HCN, HNC, electronic reorganisation, with core ionisation 78−94196
HCO^+, orbital contribs. to relax. energies accompanying core ionis., ΔSCF HF calcs. 78−82642
HF, core ionis., single orbital relax., LCAO MO SCF calcs. 78−29739
HF, HF calcs., compared with optimised LCAO results 78−5139
HF, mag. field depend. orbitals for mag. screening and susceptibility of mol. 78−78611
HF+HF, medium distance interaction, SCF LCAO MO, supermol., perturbation and MCF calc. 79−837
H_2^+He, total energy, interat. dist., geometric configurations, LCAO MO SCF calcs., stability, binding energy 77−42236
HNO, HON, electronic reorganisation, with core ionisation 78−94196
H_2O, $(H_2O)_2$, mag. shielding rel. to hydrogen bonding 77−14348
H_2O, core ionis., single orbital relax., LCAO MO SCF calcs. 78−29739
(H_2O), electron affinity, ab initio SCF calcs. 79−76343
H_2O-H_2S supersystem, ab initio LCAO MO SCF calcs. of H bonding 79−89607
H_2O-lysozyme, interaction, intermol. pot. calcs. 77−75250
$H_2O+H_O(F^-)(CH_4)$, interaction energy calc. using minimal basis sets 80−9678
H_2O+H_2O, medium distance interaction, SCF LCAO MO, supermol., perturbation and MCF calc. 79−837
$(H_2O)_2$, coherent X-ray scatt. profile calcs. 77−61765
$(H_2O)_3$, geometric config. energies, SCF LCAO MO calcs. 80−63551
H_2S, electronic struct., ab initio CI SCF calc., spectra assignments 77−10586
H_2S, KLL Auger spectra of S, ab initio LCAO SCF calcs. 77−65515
He, freq. depend. polarizability, LCAO SCF perturbation theory 79−31387
$He+ArH^+$, ab initio pot. energy data, SCF-LCAO calcs. 80−63530
$HeCl^+$, interaction potential, HF dissociation energies, LCAO SCF calcs. 77−6880
HeH^+, collisional formation, SCF calcs. 77−6893
HeH^+, spectroscopic characts. in ground and first excited triplet states, Dunham pot. approach 77−42234
HeH^{2+}, LCAO MO calcs. using reduced Bessel functions 79−31361
HeH_2, collision induced dipole IR spectra, ab initio SCF LCAO calc. 79−89737
He_2H^+, quantum-mechanical calculations 78−33424
$HgCl_2$, deformation densities, relativistic effect 80−42928
InAs-GaSb superlattice energy struct. and semiconductor-semimetal transition 79−23893
InSb, zincblende and rocksalt type struct., semiempirical LCAO band struct. calc. 77−72816
Ir (001), surface electronic props. 78−95332
Ir clean (001) surface, electronic props. 77−72901
KBr, electronic states at (100) surface, accounting for spin-orbit interaction *(Russian)* 78−91750
KCl, band struct. calc. by mixed LCAO and OPW method 77−8019
KCl, Compton profile anisotropies, charge and momentum distrib., LCAO-SCF-MO calc. 79−3500
KCl, electronic states at (100) surface, accounting for spin-orbit interaction *(Russian)* 78−91750
KCl:Br^-(I^-), interstitial atomic H centres, formation kinetics and struct. MO calc. and EPR studies 80−75854
KI, electronic states at (100) surface, accounting for spin-orbit interaction *(Russian)* 78−91750
$KZnF_3$:V^{2+}, calc. of t_{2g} antibonding mol. orbital in $[VF_6]^4$, rel. to ESR 80−50174
Li (100), O adsorption, cluster models, ab initio HF LCAO theory 78−71978
Li, cluster and microcrystal, matrix isolated, optical absorpt. spectra, photolysis and plasmon absorpt. 79−89820

LCAO calculations continued
Li^++ether(thioether)(amide), pair pots., ab initio LCAO SCF MO calcs. 80−58184
Li^++He collisions, K-shell vacancy sharing, ab initio LCAO-SCF, CI calcs. 77−19054
Li_2, nucl. spin-spin coupling, scanning MO HF LCAO calc. 79−50045
$LiAlF_4$, struct. pot. energy surface, Li^+ migration, ab initio LCAO SCF calcs. 80−23305
Li_5B_4, molecular and electronic struct. 80−20107
LiCL, band struct. calc. by mixed LCAO and OPW method 77−8019
LiCl, Compton profile anisotropies, charge and momentum distrib., LCAO-SCF-MO calc. 79−3500
LiF, Ewald method, convergence of reciprocal lattice sums 77−11834
LiF, F-centre, excited state, optical absorption 77−20267
LiF, ground and excited state props., local density formalism 78−10349
LiF, LCAO calc. of Compton profiles 79−95871
LiF-NH_2 adduct, mol. consts., ab initio SCF LCAO MO calcs. *(French)* 78−13423
LiH chains, long-range Coulombic contribution to direct space LCAO CO matrix elements 78−37774
LiH, cluster cryst., extended HMO calc. of defects 79−51521
LiH, cryst., Compton profile, position space anal. 79−47536
LiH crystals, temp. effects on X-ray scattering factors in LCAO calcs. 80−10454
LiH, $LiHe^+$ and $LiHe_2^+$ systems, ab initio SCF LCAO calcs. of stability and spectroscopic consts. 77−71748
LiH, positron affinity, ab initio LCAO MO SCF calc. 78−82870
LiH, SCF calcs., undergraduate exercise 80−82597
$Li(H_2O)^+$, coherent X-ray scatt. profile calcs. 77−61765
$LiNH_3^+$, $LiNH_2$, Li_2NH, localised orbital anal., bond props. 77−6676
$Li^+NO_3^-$ ion pairs and hydrated ion pairs, MO calcs., matrix isolation data 78−46267
$MNbO_3$, tetragonal, electronic struct., optical anisotropy 80−70599
Mg cluster, multibody expansions, convergence 80−23594
MgB_2, band struct. 79−90957
MgF_2, electronic struct. and densities of states, tight-binding calcs. 80−15447
MgF_2, ground state, nonempirical LCAO SCF calcs. 78−66469
$Mg_4(Mg_4^-)$, atomic clusters, electronic struct., LCAO-MO-SCF and HF calcs. 80−63880
MgO, chemisorption on (100) surface, surface electronic struct. 79−11016
MgO, intrinsic surface states at (100) and (110) surfaces 78−91740
Mo (100) plane, surface reson., field emission energy distrib., LCAO calc. 77−32507
Mo, Bloch waves, corresponding atomic and mol. orbitals, in HEED 79−27880
Mo, surface bands of (001) surface 77−72902
N_2, ab initio MO-LCAO-SCF and Gordon-Kim intermolecular pot. for seven different orientations 80−95522
N_2, core ionisation, single orbital relax. energy contrib. calcs. 78−82637
N_2, HF calcs., compared with optimised LCAO results 78−5139
N_2, nucl. spin-spin coupling, scanning MO HF LCAO calc. 79−50045
N_2, Xα theory appls. approximations 80−9510
N_2, Xα-SW MO projection of LCAOC MOs 78−25422
NCl_3, ab initio LCAO SCF calc. for ground state, inversion barrier 78−25426
NH_3, core ionis., single orbital relax., LCAO MO SCF calcs. 78−29739
NH_3, LCAO-MO-SCF calcs., analysis of Gaussian basis sets rel. to one-electron props. 78−55122
NH_5^+, stability, ab initio calcs. 77−23419
N_2H_2, nucl. spin-spin coupling, scanning MO HF LCAO calc. 79−50045
NH_4Cl:$[MoOCl_5]^{2-}$, single cryst., struct. investigations 77−66524
NH_2TNH_3, β^- decay effect on H-bond, ab initio LCAO SCF MO calc. 78−76894
NO_2, ground state pot. surface, ab initio LCAO MO SCF calcs. 80−102461
NO_3, mag. hyperfine interactions, MO LCAO UHF calcs. 77−14369
NO_3^{2-}, coupling consts., geometry, LCAO UHF and ENDOR data calcs. 77−14369
N_2O, X-ray fluoresc. obs., ionis. pot., fine struct., LCAO SCF calc. 77−68055
NSF, geometry and stability, LCAO-MO SCF calcs. 79−31391
Na, cluster and microcrystal, matrix isolated, optical absorpt. spectra, photolysis and plasmon absorpt. 79−89820
Na^++ether(thioether)(amide) interaction, pair pots., ab initio SCF LCAO MO calc. 79−36721
NaCl, band struct. calc. by mixed LCAO and OPW method 77−8019
NaCl, Compton profile anisotropies, charge and momentum distrib., LCAO-SCF-MO calc. 79−3500
Nb-H, BCC, quasimolecular Jahn-Teller reson. states 80−44550
NbC crystals, electron energy spectra 80−49568
Ne, core ionis., single orbital relax., LCAO MO SCF calcs. 78−29739
$Ne+H_2^+$, reaction pot. energy surface, LCAO-MO-SCF energies 77−1917
$Ne+HeH^+$, collinear reaction, pot. energy surface SCF-LCAO-MO and DIM calc. 78−92467
Ne_2, total energy MS and LCAO Xα calcs., non-muffin-tin corrections, overbinding 78−46266
Ne_nH clusters, ab initio LCAO MO SCF calc., struct. and energy 78−66704
Ne_nH^+ clusters, ab initio LCAO MO SCF calc., struct. and energy 78−66704
Ni (001) film, electronic struct. by self-consistent numerical-basis-set LCAO discrete variational method 79−60938
Ni, adsorbed CO, core level spectrum, satellite struct., ab initio HF-LCAO calc. 80−40233
Ni compound, $[Ni_3(CO)_6]_n^{2-}$, n=1,2, one-electron states in polynuclear carbonyls 79−95358
Ni, FCC, H-Ni_n self-consistent electronic screening charge density 79−33255
Ni, ferromag. film, surface states, surface magnetisation and electron spin polarisation 80−65648
Ni film, ferromagnetic (100) and (110), energy bands 79−1630
Ni, film (111), ferromag., energy bands and planar densities of states, LCAO calc. 79−4509
Ni, Xα theory appls. approximations 80−9510
Ni_2, extended basis set LCAO Xalpha treatment 80−95537
NiCO, and core ionised, binding and relax. energy ab initio LCAO MO SCF calc. 78−62712

LCAO calculations continued
NiCO, liquid interactions, ab initio LCAO MO SCF calcs. 79−18256
$(NiF_6)^{4-}$ complex, open-shell cluster calcs., semiempirical method 80−54583
NiH, extended basis set LCAO Xalpha treatment 80−95537
NiNO, ground and core hole states, config. depend. HF LCAO SCF calc., relax. and binding energy 80−29453
NiZnCo ferrite, model of photomagnetic effect 77−43853
Ni(001) surface states, surface magnetisation, electron spin polarisation 80−88612
O-containing organic molecules, LCAO-SCF calc. core binding and relax. energies, rel. to polymer surface oxidation 79−76344
O_2, Zeeman effect, relativistic corrects. to g_s using LCAO wavefns. 79−3492
O_2^+, $^4\Pi$ states, spin-spin coupling consts., ab initio calc. 79−97981
$OH^- + CO_2 \rightarrow HCO_3^-$ react., MO-LCAO-SCF calcs., energy barrier 78−76846
OH_4^+, stability, ab initio calcs. 77−30775
OH_n, ab initio LCAO SCF calcs. of ionisation pot., electron, proton, H and hydride affinities 77−88387
OH_n, LCAO-MO-SCF with Gaussian polarisation functions, energetic effect of p-, d-, and f-functions 78−41944
ONF, vertical electronic spectrum, CI and SCF calcs. 77−75123
P_2H_4, nucl. spin-spin coupling, scanning MO HF LCAO calc. 79−50045
$PH_2(PH_2^+)(PH_2^-)$, electronic structure, ab initio LCAO MO SCF calcs. 79−10027
$P_2O_4(OH)_4^{2-}$ group, electronic struct. calcs. 78−67971
PbI_2, UV reflectivity meas., band struct., LCAO calcs. 78−72545
$PbMo_6S_8$, Chevrel-phase, electronic struct., LCAO calc. for idealised Mo_6S_8 cluster 77−43494
PbO_2, electronic struct. and densities of states, tight-binding calcs. 80−15447
Pd (111) clean surface, electronic struct. using LCAO band model 79−65531
Pd on Ag (001), ultrathin film electronic states calc. 78−6318
$Pd(CO)_4$, ab initio LCAO MO SCF results invalidate pseudopot. calc. 77−6675
Pt (001), surface electronic props. 78−95332
Pt clean (001) surface, electronic props. 77−72901
Pt compound, $[Pt_3(CO)_6]_n^{2-}$, n=1,2, one-electron states in polynuclear carbonyls 79−95358
$(PtCl_6)^{2-}$, quasi-relativistic SCF-MO-LCAO methods, CNDO and MWH appls. 78−41953
RbCl:Br^- (I^-), interstitial atomic H centres, formation kinetics and struct. MO calc. and EPR studies 80−75854
$RbMnF_3$, Jahn-Teller coupling consts., LCAO calc. 80−59940
$Ru(NH_3)_6^{3+}$, isotropic chem. shift, pseudocontact contrib. 80−91577
SF_2, ab initio LCAO MO SCF calcs., elec. struct., mol. props. 77−14344
SF_6, KLL spectra of S, ab initio LCAO SCF calcs. 77−65515
SH_n, LCAO-MO-SCF with Gaussian polarisation functions, energetic effect of p-, d-, and f-functions 78−41944
SN, electronic states, ab initio, SCF, and CI calcs. 77−75053
$(SN)_x$, 1-D chain, ab initio treatment, HF LCAO calc. 77−1349
$(SN)_x$ and S_2N_2, electronic band struct. for one-dimens. chain and cryst. 77−76723
$(SN)_x$, different orbitals for different spins 79−69392
$(SN)_x$, electronic props., ab initio LCAO HF orbital calc. 77−51635
S_2N_2, $(SN)_x$, (x=2 or 3), minimal STO-3G basis HF ab initio LCAO SCF MOC, geometry 78−903
S_2N_2, electronic states, ab initio, SCF, and CI calcs. 77−75053
SNF, geometry and stability, LCAO-MO SCF calcs. 79−31391
SO, Zeeman effect, relativistic corrects. to g_s using LCAO wavefns. 79−3492
SO_2, KLL Auger spectra of S, ab initio LCAO SCF calcs. 77−65515
SO_2, SF_2, SO_2F_2, bond function parameter transferability 77−30770
^6S state ions, overlap and covalency contrib. to zero field splitting, LCAO-MO calc. 80−24850
ScP, electronic struct., self-consistent Hedin-Lundqvist and Xα APW calcs. 80−29322
Sf_6, high resolution X-ray emission, valence electron struct. and chemical bonding, LCAO comparison 79−31545
Si (110), chemisorption of Cl, LCAO calcs., Auger line shapes, localized density of states 78−56202
Si (111), adsorption of Cl, electronic energy states, cluster-type calcs. 79−47149
Si (111), chemisorbed Cl layer, SCF LCAO band struct. calcs. 78−88010
Si (111), chemisorption of H, localised model, ab initio HF-LCAO calc. 80−6930
Si (111), with chemisorbed Cl and F, electronic energy struct. calcs. 79−78144
Si amorphous, diffraction intensities, chem. bonding effects 77−72557
Si, amorphous, electronic struct. and optical dielec. function, LCAO calc. 79−42478
Si, amorphous, structural disorder rel. to electronic props. 78−34756
Si, atomic wave functions localisation and band struct., LCAO calcs. 77−51648
Si, Bloch waves, corresponding atomic and mol. orbitals, in HEED 79−27880
Si, $L_{2,3}$ VV AES, local probe of atomic charge 78−48261
Si polymorphs, optical props., orthogonalized LCAO calc. 78−10345
Si, shallow donor states, substitutional donors 79−65403
Si:F(,H), amorphous, electronic struct., orthogonalised LCAO calc. 80−44486
a-Si:H, electronic states and bonding config. 80−64900
SiH_4, ab initio Hartree-Fock SCF-LCAO-MO method 78−94195
SiH_4, SiH_3F, SiH_2F_2, CH_3SiH_3, core Auger shifts, ab initio LCAO MO SCF calcs. 78−904
Si_2H_6, nucl. spin-spin coupling, scanning MO HF LCAO calc. 79−50045
SiH_2F_2, ab initio Hartree-Fock SCF-LCAO-MO method 78−94195
SiH_3F, ab initio Hartree-Fock SCF-LCAO-MO method 78−94195
Si_3N_4, electronic struct., LCAO calc. 80−96776
SiO_2, Auger line shapes, final state correlation effects 80−89095
SiO_2, calculated and measured Auger line shapes 79−83067
$Si_2O_6(OH)_2^{6-}$ group, electronic struct. calcs. 78−67971
Si(111), chemisorption of H, formation of monohydride and trihydride phases 79−15004
SnF_2, valence bands, electronic struct., UPS 78−39656
SnI_3^-, vibr. intensities, forms and freqs. anal. SCF MO LCAO CNDO calcs. 78−9274
SnO_2, electronic struct. and densities of states, tight-binding calcs. 80−15447
SnS_2, UV reflectivity meas., band struct., LCAO calcs. 78−72545
$SrTiO_3$, cluster surface states, LCAO calc. 77−43686
$SrTiO_3$, matrix element effects in freq. dependent dielectric function 80−70632
TCNQ, ab initio SCF LCAO band struct. calc. 80−70608
TTF, ab initio SCF LCAO band struct. calc. 80−70608
Ta-H, BCC, quasimolecular Jahn-Teller reson. states 80−44550
Te, trigonal nucl. elec. field gradient ellipsoid, LCAO and extended Huckel approx. calc. 77−55736
TeO_2, electronic struct. and densities of states, tight-binding calcs. 80−15447
Ti complex, bis cyclopentadienyl Ti:N_2, liquid interactions, ab initio LCAO MO SCF calcs. 79−18256
TiC, LCAO band struct., Compton profile 77−85138
TiC_x^{n-}, nonstoichiometric, ESCA spectra, MO LCAO calcs. 79−59513
$TiCl_4$, $t_1 \rightarrow 2e(^1A_1 \rightarrow {}^1T_2)$ transition, bond props. and LCAO MO calcs. 80−18889
TiO_2, cluster surface states, LCAO calc., electron energy loss peak interpretation 77−43686
TiS_2, electronic struct. and props., self consistent numerical basis set LCAO calc. 77−89698
TiS_2, valence density of states 80−44465
$TiS_2(Se_2)$, core states, energy bands, and valence densities of states 79−95322
$TiS_2(Se_2)$, valence density of states, Gilat-Raubenheimer method 80−88465
$TiSe_2$ (IT), structurally induced semimetal-to-semicond. transition, ab initio LCAO calc. 78−51896
$TlCl_xBr_{1-x}$, $TlBr_xI_{1-x}$, polymorphous mixed cryst. layers, opt. props. 78−23490
V, energy bands, Compton profile, optical cond., SCF LCAO calcs. Gaussian orbitals 78−47698
V-H, BCC, quasimolecular Jahn-Teller reson. states 80−44550
VO, $^4\Pi$ states, spin-spin coupling consts., ab initio calc. 79−97981
VO_2, semiconductor-metal transition calc., cryst. distortions 77−4294
V_3Si, electronic struct., charge distrib. and X-ray emission spectra 79−51481
W (001), adsorbed H_2, LCAO calc. of band struct. 77−8168
Zn_2, ab initio SCF LCAO MO calcs., contracted basis set effects 77−83495
$ZnCl_2$, deformation densities, relativistic effect 80−42928
ZnSe 79−38457
ZnSe:Mn^{2+}, ligand HFS calcs., comparison with other methods and expt. 77−55501
ZnSe+Mn^{2+}, LCAO calc. of d-orbital splitting 77−28148
ZnSe(Te):Cr^{2+}, spin Hamiltonian parameters and wave function coeffs., LCAO theory 77−39804
ZrC crystals, electron energy spectra 80−49568
ZrS_2, valence density of states 80−44465
$ZrS_2(Se_2)$, core states, energy bands, and valence densities of states 79−95322
$ZrS_2(Se_2)$, valence density of states, Gilat-Raubenheimer method 80−88465

lead
see also nuclei with .....
5d subshell, photoionisation partial cross-section, energy depend. meas. 80−29850
^{222}Rn released by uranium tailings piles, potential population dose 79−85824
acoustic velocity, shock-compressed uniform solid, lateral discharge ang. semiempirical formula *(Russian)* 78−55910
activation energy and primary characts. of Bordoni relax. peak 77−69040
adsorbed on Cu, Auger electron spectroscopy 77−85851
adsorbed on W (100) surface, field emission microscopy study 79−15015
adsorption, on Au, formation of $AuPb_2$ epitaxial layer, LEED, AES study of $Au/AuPb_2$ interface 78−71988
adsorption on Au(320) and (311) surfaces, LEED and AES obs. 79−86998
adsorption on Cu stepped and low index surfaces, LEED, AES and desorption anal. 79−46942
adsorption on Cu vicinal surfaces, LEED study 80−103575
adsorption on Ni (100), effects on secondary electron spectra 80−50480
adsorption on P or C contaminated Ni, AES study 80−54521
adsorption on W, low-index planes, probe-hole field emission microscopy obs. 77−47677
adsorption on W, pairwise interaction approach to adsorpt. of oriented overgrowths 77−62759
adsorption on W(100), W(110) substrates, pairwise interaction model using Morse pot. 80−6657
air pollutant, radioisotope-induced X-ray fluorescence analysis 77−17214
air pollution, effects on children, Steinbuch's Lernmatrix appl. 77−44878
air pollution, from petrol engine exhaust, deposition on plant and soil surfaces 77−87063
air pollution, statistical models with reference to Los Angeles Catalyst Study (LACS) data 80−30620
air pollution at Quillayute, Washington, Pb concs. 77−29421
air pollution neutron activation anal. using 14 MeV neutrons 77−91257
airborne particulate concentration variation at two stations in Perth, 1974-76 period 80−94127
airborne Pb, dry deposition vel. on snow surface 77−2231
alkali halide: $Ge^{2+}(Sn^{2+})(Pb^{2+})$, T-centres, absorpt. spectra, energy level diagram 77−73157
alkali halide: Pb^{2+}, charge transfer absorpt. band 79−73977
Amitsoq gneiss, W.Greenland, initial Pb isotopic comp. and implications for Earth age 78−20371
anomalous grain growth 77−8855
aqueous corrosion film, IR and Raman spectroscopy 80−55567
in atmosphere, long-range transport to Denmark 80−94131
atmosphere vehicle generated Pb concs., correl. study 79−21012
atmospheric concs. of vehicular Pb from airborne particulate Br levels 77−91254
atom, 1.4 to 5.9 MeV/u, K-shell ionisation cross-section meas. 79−31671

lead continued
atom, 5d level open shell interactions, 304 Å photoelectron spectrum 80−87087
atom, $^3P_1{}^0$ state reson. radiation, collisional quenching cross-sections 77−435
atom, α-particle impact K-shell ionisation, 40 to 110 MeV 78−17752
atom, γ-ray absorption cross-sections, 10-160 MeV 78−90136
atom, chemiexcitation of ^3P metastable states, during combustion of acetylene and C_2H_2 78−3339
atom, Compton scatt. of 1.12 MeV γ-rays by K-shell electrons 77−54539
atom, double-vacancy states, L X-ray fluoresc., K Auger electrons 77−27016
atom, elastic scatt. of 145 keV gamma rays 79−13680
atom, electron impact, relativistic, L-shell ionis., Lβ/Lα branching ratio energy depend. 79−98228
atom, electron impact excited, spectrum in 54-126 nm range 79−63942
atom, electron impact L-shell ionis., 300-600 keV 77−50542
atom, electron impact M-shell ionisation, 60-600 keV, absolute cross sections meas. 80−83493
atom, excited states, quadrupole moments, Sternheimer shielding factors 78−82630
atom, hyperfine structure 79−3375
atom, ionisation probability, K-shell, 25- 40- 74-MeV α particles 77−528
atom, K-shell electrons, Compton scatt. of 1.12 MeV gamma-rays 77−68016
atom, K-shell electrons, Compton scatt. of 1.12 MeV gamma-rays, energy distrib. meas. 77−68017
atom, L-shell electron impact ionisation, X-ray production cross sections 77−19095
atom, L-shell X-ray photoelectric cross sections, fluorescence spectra 78−58636
atom, laser excited fluoresc., three-level scheme 78−17605
atom, LL-vacancy states produced by KLL Auger transitions, X-ray fluoresc. yield 77−18832
atom, $np^6 \rightarrow np(n+1)s$ transition array, relativistic oscill. strengths 79−31465
atom, nuclear K-X-ray satellites, Z=50-83, by α-bombard., 17.5-22.5 MeV 80−42984
atom, optical activity near suppressed M1 transition *(Russian)* 78−46292
atom, optical activity of vapour as indication of electron-nucleon weak interaction *(Russian)* 77−10618
atom, optical transitions, struct. of weak neutral currents *(Russian)* 77−88420
atom, parity nonconservation in heavy atoms, weak electron-electron interaction *(Russian)* 78−55132
atom, photoelectric cross section, derived from total absorpt. cross sections 77−10646
atom, photoelectric cross sections for 323 keV gamma rays 77−88432
atom, photon-bound-electron scatt. meas. 77−14394
atom, polarisability meas. using field electron microscope *(French)* 77−543
atom, Rayleigh scatt., expt. and form factor approx. 78−33474
atom, relativistic 1s wavefunctions test, using exptl. Compton profiles 80−32600
atom, spectral transition probabilities, 200-700 nm 79−31454
atom, total to K-shell photoelectric cross section ratios, 145 to 662 keV γ-rays 77−54545
atom, VUV photoelectron spectra, spin polarisation autoionis. reson. 78−33483
atom, X-ray L shell emission spectra *(Spanish)* 79−98016
atom, X-ray production cross sections for protons, fluoresc. obs. 80−102476
atom + buffer gas, $^3P_1{}^0 \rightarrow {}^3P_0{}^0$ transition cross section 80−1058
atom total to L-shell photoelec. cross section ratio 77−30836
atom X-ray spectra, mass absorpt. coeffs. in ultrasoft region, spectral depend. 77−10622
atomic, photoelectron spectra, electron correlations and spin-orbit interaction influence 80−102495
atomic absorption graphite furnace analysis, matrix interferences reduction with L'vov Platform 79−92020
atomic beam, interaction with low-temp. glass condensation surface 78−19626
atomic beam impinging on mica and SiO in vac. deposition, thermal accommodation 79−77960
atomic electron collision cross sections 77−42410
atomic photodissociation laser, 405.8, 368.3 and 364.0 nm emission lines obs. 80−87387
atomic polarisability, oscillator strength and radial integral, Dirac eqn. calc. 79−22620
atomic spectroscopy, search for parity-violating weak interaction of electrons with nuclei 79−36571
atoms, L-shell photoelectric photon absorpt. cross section, energy depend. 80−106279
attenuating shock waves, following meteoroidal impact *(Russian)* 77−71068
Auger emission target, contrib. of reflected electrons 78−92152
Auger $N_{6,7}O_{4,5}O_{4,5}$ spectra, X-ray excited 77−85886
automobile exhaust pollutants, neutron activation analysis, distrib. of Pb particulate 78−3943
background levels in air over S.Norway 79−12239
band structure, ab initio calcs. 80−75502
band structure, and electron-phonon interaction, supercond. transition temp. determ. 79−19512
band structure, pseudopot. calc. 79−56119
band structure, relativistic Green function 77−20214
beta-ray backscattering variation with target thickness, self-absorpt. coeff., Z depend. 79−78801
binding energy and compressibility, model pot. calc. 79−99650
blood, Pb content, PIXE determination 80−51228
bone, X-ray fluorescence technique for in vivo determ. of Pb conc. 79−25084
Bordoni relaxation peak in high purity, polycrystalline Pb, high vacuum annealing effect 78−39828
bremsstrahlung, β generated, spectral shape depend. on target thickness 78−56545
Bremsstrahlung distrib. from 22 MeV electron irradiation 78−59840
in Bruderheim meteorite, L6 chondrite, isotopic abundances rel. to U-Pb age and 500 Ma shock event 80−98616
bullion production, elec. smelting of $PbSO_4$ residues 80−11592

lead continued
catalyst, BCl_3-H_2 photochem. with Ti, Pb catalysts, isotopic excitation by laser 78−64882
cathodic deposition on Ag (111) and (100) surfaces, potentiostatic obs. *(German)* 79−15616
Cauchy relations, violation for elastic moduli 79−69179
chemical shift of X-ray L-absorption edge 79−52044
chill cast and wrought cyclic voltammetry and electrochemical meas. of anodic activity, PbO_2 form. 78−31582
clusters, 2 to 500 atoms, nucleation, mass spectra 80−102596
coadsorbed with Bi on Cu (100), LEED and AES study 79−15017
coadsorbed with Sn on Al (100) surface, prep. and props. of monolayers 79−15018
cold rolling of I-section beams 78−39845
coloured surface layer form. by diffusion into glass 77−36677
concentration determ. in atm. and rainwater in Vizcaya, Spain *(Spanish)* 78−57264
concentration in a.c. arc, during interruption, time depend. *(Russian)* 78−22597
concentration in snow of Mt. Blanc rel. to air pollution 78−81258
contact area, effect of loading time *(Japanese)* 78−6230
contact formation and cohesion, influence of multiple contacting *(Russian)* 80−40548
contaminated Ni surface, coadsorption of Sn, AES study 80−88437
contamination, of soils, air exchange in cities *(German)* 79−70470
contamination of Zn electrodeposits, influence on morphology and orientation 79−56090
convertor photon detection efficiency below 500 MeV, semi-empirical formula 80−27866
corrosion, by applied alternating currents 79−70205
cosmic-ray showers in Pb and Fe, hadron-induced 77−60561
creep, low-temp., thermal heating and quantum mechanisms, supercond. transition effects 80−79868
cyclic grain boundary migration during high temp. fatigue 80−39111
cyclotron resonance, anisotropy, line shape, relax. time and identification of orbits. 77−35853
cyclotron resonance, neutron irrad. effect *(Russian)* 77−69216
cyclotron resonance, tipping effect of mag. field 77−35852
de Haas-van Alphen γ oscill. for [011] symmetry direction 79−90944
de Haas-van Alphen effect, mag. induction oscillations 77−62806
de Haas-van Alphen effect, spin-splitting factor for Landau levels 77−20226
Debye-Waller factor, temp. variation calcs. 80−34162
Debye-Waller factor temperature parameters, vibr. depend. 79−99288
deformed by torsion, stored energy and recrystallization 79−34069
deposition on Au, quantitative Auger electron spectroscopy, substrate and instrumental effects 80−71523
deposits, layers in South Niger, geological features *(Croatian)* 79−29772
Derwent Reservoir, N.England, Zn, Cd and Pb in water, sediments and submerged plants 79−25286
determ. in water and organic materials, flameless atomic absorpt. spectrometry with wire loop atomiser 80−45586
determination, in atmosphere, flameless atomic absorpt. in particle size fractionated aerosols 78−69434
determination, in blood, haematofluorometric method 78−53554
determination, in cement, by direct atomisation AAS *(Japanese)* 79−70413
determination, in complex alloy, by at. absorpt. 77−40582
determination, in flux-grown magnetic garnets, by AAS 78−92585
determination, in powder rock samples, by at. absorpt. *(Russian)* 78−85278
determination, in steel wire, AAS determ. 78−68939
determination aqueous solutions, by Delves Cup technique and flameless atomic absorpt. spectrometry 78−68973
determination in Earth materials by at. absorpt. 79−88035
determination in NaCl:$PbCl_2$ crysts., UV spectrochem. anal. 78−40101
determination in NaCl, serum or urine, AAS, background correction 78−27834
determination in ore, by universal backscattered gamma method 79−1984
determination with Tl in $ZnSO_4$ electrolyte by anodic stripping voltammetry 77−12844
diffusion and saturation solubility of Pt, melting curve, conc. profiles 80−88365
diffusion and solubility of Zn, press. effects 77−43385
diffusion coefficient in In, RF size effect meas. *(Russian)* 78−91717
diffusion coefficient in molton Li 79−93828
diffusion in Al *(Japanese)* 79−19403
diffusion in Cu, diffusion coefficient temp. depend. *(Russian)* 77−84987
diffusion in liquid Cu *(Japanese)* 78−59962
diffusion in mica, rel. to Po haloes 79−44186
diffusion of Au, ultra-centrifuge study 78−47593
diffusion of Co impurity in Pb, ion implanted, exam. by activation analysis technique 78−91488
diffusion of Hg and Cd at high press. 77−72721
diffusion of Sn, press. effect up to 30 kbar 78−10224
diffusion thermopower, inelastic electron-phonon interaction 80−96851
dislocation electron drag coeff. temp. depend., internal friction method, superconducting state 80−29031
dislocation inertial effects, internal-friction meas. on normal and superconducting states 79−38883
dislocation internal friction changes under the action of US vibr. 79−69630
dislocations, electronic damping, US meas. 79−27997
distribution function branch imbalance, relaxation 79−33401
distribution in waters of Yarra River estuary 79−16552
dry deposition onto snow surface 77−37288
DSDP Leg 37 cores, Pb concs. and isotropic comp. 77−91074
effective cyclotron masses of central and noncentral ζ orbits, de Haas-van Alphen effect 78−63968
elastic constants, from room temp. to MP, US pulse echo meas. 77−24342
elastic properties *(Russian)* 78−56678
electrical resistivity, 300-1050K 80−24868
electrode, combined electroreflectance and double layer effects 77−85692
electrode, in situ surface phase study by laser Raman spectroscopy 80−103542
electrode, porous, oxidation in H_2SO_4 solutions obs. 79−100514

lead continued
electrode, potential effect on surface struct. in H_2SO_4 in anodic region 80−16592
electrode material, influence on electric breakdown in dielectric liquids *(Russian)* 80−50265
electrodes, surface reactions during electrolysis 77−77784
electrolytic refining, adhesion of anode slime on anode surface 78−44047
electromigration, thermomigration, and solubility, of ^{64}Cu 78−71882
electromigration of Au, 165 to 270°C 80−29221
electromigration of Au and Ag 77−69116
electromigration of Cu in Pb 78−84003
electromigration of fast diffuser 78−47594
electromigration of Ni, steady-state method 78−87820
electron beam reflection, high current *(Russian)* 78−84690
electron field emission, temp. effect 80−60756
electron impact excitation, visible and UV spectra, excitation cross sections anal. 80−32840
electron irradiation at 4.7K and below 3K, annealing expts. 77−11595
electron-phonon interaction, press. depend. rel. to normal state resist. 79−28063
electron-photon cascade curves 79−44322
electronic thermal Gruneisen parameters 80−39242
electroplastic deformation, stress relax. meas. *(Russian)* 79−38894
electroplastic effect 79−24589
Eliashberg gap equation, approx. BCS-like soln. 77−1513
EM cascades caused by electrons and photons, 10-100 GeV, longit. development 79−21120
encapsulation of radioactive waste, risk assessment 80−99249
enstatite chondrite, Bi and Pb microdistribution obs. 80−62085
environmental aspects 79−34443
epitaxial growth on Ag (111) and Cu (111), LEED, RHEED, AES study 78−84090
equation of state, isentropic expansion method 78−91414
erosion by laser beam, in self-consistent mode *(Russian)* 77−69945
evaporation under action of laser beam, recoil press. behaviour 80−25501
expansion, isentropic, vaporisation and condensation kinetics anal. 77−66623
exposure, determ. from X-ray fluorescence anal. of children's teeth in situ 77−64128
extractive metallurgy, developments, review 80−20820
Farmington chondrite, U-Pb abundances and Pb isotopic studies 80−56778
fatigue testing in normal and supercond. state 78−19959
FBR blanket facility, gamma-ray heating rate meas. 80−57912
Fermi electron vel. change under press., Tomasch tunnelling *(Russian)* 77−72950
Fermi surface, cyclotron reson. obs. *(Japanese)* 78−23009
Fermi surface, de Haas-van Alphen effect obs. *(Japanese)* 78−23010
Fermi surface, uniaxial stress depend. 79−65362
Fermi surface and non-muffin-tin energy bands, calc. 80−20072
filament production, ejection of molten metal through nozzle, jet stability *(Japanese)* 78−52719
filamentary crystals, third-order elastic consts. combinations 80−92585
film, amorphous, nucleated with Mo, supercond. and normal elec. cond. 77−24633
film, conducting coating effect on supercond. transition temp. and normal-state cond. 77−16007
film, conduction electron surface scatt. phase shift, tunnelling meas. 79−51648
film, deposited on Si substrate, residual strains 78−18915
film, deposition props. on specially prepared substrate, desorption energy and surface diffusion 79−90917
film, deposition using low-energy ion beam, Rutherford backscatt. and TEM anal. 77−59699
film, deposition using low-energy ion beam, Rutherford backscatt. and TEM anal. 77−70003
film, electrolytic deposition on semicond. substrates 77−77425
film, evaporated, interaction with BCl_3, HCl, adsorpt. 78−75945
film, friction and fear in ultrahigh vacuum, effects of speed, film thickness and substrate surface roughness 79−20202
film, hillock formation by grain boundary sliding 80−107673
film, IR optical constants, determ. by surface plasmon excitation 78−76418
film, monocryst., heteroepitaxial growth, struct. defects, and elec. props. *(Russian)* 80−84403
film, near supercond. transition temp., Hall effect 79−42698
film, O ion irradiated, damage rate decrease 78−26604
film, on Ag electrode, anisotropy of optical props. 80−60534
film, on Au (100), initial stages of condensation 78−91569
film, on Cu substrate, oxidation, AES and XPS obs. 79−47833
film, oxide form. on (111) surface, orthorhombic PbO 77−63835
film, oxidised (111) surface, electron microscope anal. of oxides 78−23878
film, polycryst. or amorphous, thermal cond., 0.5-11K 78−39260
film, polycrystalline, electron diffr. evidence by off coincidence grain boundaries 77−47469
film, polycrystalline, optical transitions from d core states 77−85827
film, quench-condensed, disorder effect on optical cond. and band struct. 77−1746
film, reactive ion beam sputtering 78−19666
film, supercond., meas. of effective quasiparticle recombination times, density of electronic states at Fermi level 79−38264
film, superconductor, interaction between crystal lattice and vortices 77−28307
film, thermal strain, depend. on cryst. orientation 78−10311
film, thermal strain, strain relax. above room temp. 80−59841
film, thermal strain, strain relax. mech. 79−42427
film, thermal strain investigation multiple cycling to 4.2K effects 79−90918
film, ultra-thin, existence of double-hexagonal close packed phase 78−63952
film, ultra-thin, hexagonal phase, struct. 78−38982
film, ultrathin, quench-condensed, two-dimensional elec. cond. 78−39233
film, ultrathin on PbTe and Te, prep. and characterisation 77−7995
film, vacuum deposited, reflectance spectra, structural rearrangement effects 77−24905
film, vacuum deposited, thermal strain depend. on thickness and grain size 79−90926
film, vacuum deposited onto SiO, C and mica, quantitative study of nucleation 79−77959
lead continued
film on Cu and Ag substrates, tunnel conductivity, proximity effect *(Russian)* 79−51726
film tunnel junction, thermal cycling stability enhancement using substrate with large thermal expansion 79−87200
films, hillock growth upon cycling to cryogenic temps. 80−88448
films, splat-cooled and vapour-deposited, metastable structs. 79−87018
films, ultrathin, deposited on Si supercond. 77−66220
films, vapour deposited FCC, normal and oblique incidences, microstructure, X-ray diffr. study 80−20048
fine particles, prep. by gas evaporation technique, crystal habit 77−52239
fluxural oscillations in longitudinal mag. field, sound attenuation, magnetoelasticity *(Russian)* 80−54844
foil, type I supercond., crit. current density, pinning force density, shadow electron microscopy obs. 80−88696
friction, He environment 4.2-80K 78−48543
friction, wear in supercond., normal states *(Russian)* 78−39914
frictional behaviour, effect of mechanical properties 80−55548
fusion reactor molten-salt blanket, effect of Pb and Bi neutron multiplication zones on the fission rates of ^{232}Th and ^{235}U 80−99272
gamma photon backscattering, energy dependence *(Rumanian)* 79−76316
gamma-ray attenuation coeff. meas., 1115, 1173, 1332 keV 77−55303
gamma-ray attenuation meas. using Ge(Li) detector 78−17539
gamma-ray buildup factors for Pb/H_2O stratified radiation shields 80−86994
gamma-ray elastic scatt. cross section at 279 keV 79−26421
gamma-ray impact, absolute pair production cross-section meas. 78−43958
gamma-ray scatt., incoherent 80−40179
gamma-ray scattering, incoherent, differential cross-section determ. 78−43952
gamma-ray scattering, incoherent, total at. cross section 79−13679
geochemistry, chemical speciation in mixed freshwater, seawater and bine solns. 78−20409
geochemistry in sediments of Gulf of St. Lawrence and estuary 78−92855
glass fibre reinforced Pb, production by infiltration, tensile strength 77−59720
grain boundary self diffusion, microtome serial sectioning anal. 80−79975
grain boundary sliding, grain size and stress effects 78−27571
grain refinement, and structural stability by S, Se and Te additions *(German)* 80−55387
granular film, Josephson coupled, resistive transition 80−88683
granular film, superconducting, Josephson-coupled, role of clusters in localisation 80−39716
Gruneisen parameter, behaviour at high press. 78−83899
Gruneisen parameter and binding energy, model pot. calcs. 77−51517
Gruneisen parameters and thermal expansion coeff. 79−33103
Heine-Abarenkov potential 78−6248
hydroextrusion, effect of longitudinal US oscills. *(Russian)* 79−34071
hydrosphere, global and regional distrib. 79−16517
implantation in Fe, effect on corrosion by H_2SO_4 soln. 80−71793
implantation in Si, channelling and RHEED anals. 78−30657
implantation of ions into Fe, effect on corrosion 79−39015
implanted ^{119m}Sn, Mossbauer spectroscopy, isomer shift and Debye-Waller factors 79−24240
impregnated porous Ni, porous, internal friction and effective elasticity modulus, temp. depend. *(Russian)* 79−29118
impurity diffusion and self-diffusion activation volumes 80−2209
impurity in Nimonic 105, influence on creep and stress rupture props. 80−66602
inclusions in free-cutting steel, X-ray, light and scanning electron microscopy 77−77685
infiltrated Ti base composite sintered bearing materials, antifriction props. 80−60981
interatomic pair potential, phonon spectra 80−33927
interface with sapphire, heat transfer coeff. meas., 2-80K 80−88419
intermediate sate, Meissner effect investigation of muon technique *(Russian)* 80−107954
intermediate state, hardening 78−47917
intermediate state, thermal resist. of normal-supercond. interphase boundary 79−56384
interstitial substitutional model for anomalous diffusion 80−84330
intoxication, effects on scotopic vision of young monkeys 77−56377
ion bombardment, sputtering, re-emitted kinetic energy ang. distrib. 80−2910
ion bombardment-induced photon emission near melting point 80−100699
ion collisions, 90-110 MeV, K-vacancy production, multiple and single collisions in mol. orbital excitation 77−83717
ion impact on C foil, energy loss 78−55902
ion implanted in Al, doping profile after laser pulse irradiation 80−88194
ion plated soft film, initial wear rate 80−11795
ion recombination laser 78−17923
ion-atom collision, K-vacancy prod., mol.-orbital method 77−68095
ions, 120 keV, range in Si, Al from backscatt. obs. 80−19855
isotope composition of Archaean plutonic rocks 78−65223
isotope dating of ore mineralisations in Erma River Area, Bulgaria 78−81115
isotope evolution during Earth core formation time 78−7601
isotope inhomogeneity in Precambrian igneous K-feldspars 78−32095
isotope studies of ore deposits of circum-Kisseynew volcanic belt, Canada, ages 79−5479
isotopes composition in oceanic basalts, rel. to mantle evolution 78−65217
isotopes conc in ocean floor basalts and ferromanganese deposits 78−61395
isotopic composition, of volcanic rocks of Aleutian and Pribilof Islands, Alaska 78−57185
isotopic composition in Cretaceous kimberlites and mantle xenoliths from S.Africa 77−60372
isotopically enriched rotating sandwich targets for high intensity heavy ion beams 80−18743
J_1J_2 transition from LS, revised assignments for $d^9s^2p^2$, $d^9s^2p^3$ 79−45630
Josephson junction, oxide formation process, ellipsomesric meas. *(Japanese)* 80−11561

lead continued
Kapitza resistance of interfaces with liq. ^{3}He and ^{4}He, 0.3-1.4K 77−24475
kinetic friction re-examination using modified pin and disc machine 80−55547
lake, Pb conc., rel. to boating activities and sediment interactions 80−104523
laser, discharge-heated, 0.723 μm, improved performance by vol. scaling 77−88778
laser, long life operation at 7229 Å 78−79037
laser, long-lived sealed-off design, 7229 Å emission 78−50808
laser, pulsed 722.9 nm, with double-section gas-discharge tube 80−9902
laser, pulsed discharge in $PbCl_2$ vap. 77−79812
lattice vibrations, appl. of two-parameter shell model for monoatomic systems 78−59877
leading in glazed ceramics, colorimetric method *(Spanish)* 80−73414
liq., elec. resist. calcs., pseudopot. depend. 80−96840
liquid, ^{113,117m,125}Sn diffusion coeff. meas. *(Ukrainian)* 80−10690
liquid, collective excitations, neutron inelastic scatt. obs. 80−75148
liquid, dynamic scatt. functions, 300 and 600°C, neutron scatt. study 79−50983
liquid, dynamic struct. factor, slow neutron scatt. obs. 80−28908
liquid, elec. resist., temp. depend., calc. 78−14701
liquid, elec. resistivity, 600-860K 79−56180
liquid, electrical resistivity with spin-orbit scatt. 78−64018
liquid, electron component of entropy *(Russian)* 79−23747
liquid, evaporation in shock compression release waves *(Russian)* 78−18761
liquid, ISSEC selection for fusion reactor 80−57950
liquid, mag. relax. of excited ^{207} 77−16217
liquid, neutron diffr. meas. of pair and direct correl. functions 77−55229
liquid, new description of random stacks *(French)* 78−79512
liquid, O_2 activity from electrochem. meas. 80−55695
liquid, paracryst. struct., coordination statistics calcs. 77−1063
liquid, short range order parameters, from information theory 78−83730
liquid, short-wavelength density fluctuations 79−46550
liquid, struct. factors, neutron diffr. 78−18538
liquid, surface tension temp. depend. 77−4248
liquid, thermal conductivity meas. in Spacelab, measuring cell design and testing *(German)* 80−57303
liquid, thermoelectric power, pseudopotential calc. 80−59959
liquid, thermophysical properties rel. to clustering 77−1065
liquid, US wave velocity *(Japanese)* 79−60438
liquid, viscosity, comp. and temp. depend., up to 500°C 79−65233
liquid, viscosity, hard sphere diameter, interionic potential 79−77797
liquid, wetting of Ge surface rel. to cryst. orientation 78−43211
liquid, wetting of Si surface in H_2+HCl 78−43210
liquid and solid, UPS, optical densities of states 80−2924
liquid film, electron diffr. 78−83721
M shell prod cross section of Au, Pb and U for 75 to 150 keV p and e excitation 79−47552
magnetic interaction, de Haas-van Alphen effect 78−79921
magnetic interaction effect and Dingle temperature of de Haas-van Alphen oscills. 79−69395
magnetoresistance, linear, semiclassical transport theory 77−35925
marine pollution conc. in coastal waters of North and South Lebanon 79−12146
marine pollution determ. in Gulf of Fos, NW Mediterranean 79−12141
mass ejection from shocked surface during fusion 78−47186
measurement of content of children's teeth in situ by X-ray fluoresc. 77−16976
melt, structural factors, tetrahedral concs., neutron diffr. study *(German)* 80−19688
melt, wetting of β-SiC 77−85016
melt density, temp. depend. *(Russian)* 79−69174
melting, changes in electron image contrast 80−100147
melting, existence of before and after effects, neutron scatt. 77−84895
melting curve, high press. effect, and Pb diffusion in Cu 80−49337
melting curve, use for press. determ. in girdle apparatus 77−65043
melting theory for small particles, Helmholtz free energy 80−59629
melts, As and Sn distrib., Si, Cr and Mn influence *(Russian)* 80−16274
melts, effect on fracture stress of Armco iron *(Russian)* 77−21246
membranes, life testing 79−70256
metal cluster generator for gas-phase electron diffr., variation of microcryst. with size 78−63645
metallic coated, produced by electrospark alloying, corrosion behaviour in Cl saturated NaCl solns. *(Russian)* 79−39026
metallic compressibilities, general pseudopotential approach 80−54631
metallographic preparation, using pH controlled silica gel and superior microetchant 80−16623
micro fall-out, furnace atomic absorption spectrometry appl. 78−49125
microbridges, supercond. breakdown under electron beam irrad. 79−56418
microclusters, mol. beam electron diffr., amorphous struct. 78−66703
microstructural investigation by etching with aqueous $HClO_4$, high purity 77−56205
MIM diode, US effect on tunnel current for normal and supercond. metals 77−16006
minerals suspended in ocean waters 79−74904
model material, specimen size effect on plastic deform. around deep notches 79−70142
molten, density, surface tension, temp. depend. 77−69147
molten, thermal expansion meas. to 1300K 80−65254
monolayer, double layer with Sn, growth on Al (111), struct. 80−70567
mosaic single cryst., neutron integrated reflectivities 79−86656
motor exhausts on motorways 79−12248
multiple interior impacts on Pb target, hard target high vel. impact simulation 77−72145
muon angular distrib., Monte Carlo calc. 79−78600
muonic atom, electron screening effects 77−34786
muonic atom, nucl. polarisation correction 79−64123
muonic atom transition energy meas., tests of high-order vac. polarisation corrections 77−71895
neutron activation anal. of short lived nucl. states in aerosols of Otto carburettor engine *(German)* 77−12860
neutron radiotherapy, 14 MeV, skin-sparing, effect of metal sheets 78−35923
neutron yield calcs., electron beam incidence 78−95622
normal-superconducting transition and plastic flow in single crystal 78−3166
nuclear target, self supporting O_2 free 78−13365
Oklo natural fission reactor, dating from U-Pb isotopic data 80−21763
Oklo natural fission reactor, radioactive dating from Pb and Th meas. *(French)* 80−21762
P-V meas., 5 to 45 kb *(Chinese)* 79−23676
particles, evaporation in arc plasma, integral eqn. method calcs. 78−1942
particulate Pb levels for Perth, W.Australia, 1971-6 var. 79−34455
partitioning between volcanic glass and sanidine/plagioclase feldspars 79−74867
parts, albedo thickness meas., neutron technique 79−29309
passivation in H_2SO_4 soln. 78−76871
patination, IR spectroscopic study 77−56140
perfect and deformed, phonon mean free path from thermal cond. meas., 0.6 to 7.5K 79−65166
perturbed γ-ray angular distrib. of ^{210}Po, temp. depend., radiation damage effects 78−43736
perturbed angular distribution of ^{208}Po, temp. depend. 78−43735
phase smearing and mag. interaction, de Haas van Alphen effect 79−37961
phonon dispersion and cryst. equilib. 78−75752
phonon dispersion curves, lattice dynamics unpaired forces 79−42170
phonon dispersion relations and lattice heat capacity, modified Bhatia model 77−20024
phonon dispersion spectra from 5-parameter lattice dynamical model 78−10136
phonon softening, neutron scatt. at high press. 78−80091
phonon spectrum, calc. by phenomenological method 78−59890
phonon thermal conductivity of deformed cryst. below 2K *(Russian)* 78−60244
photoelectric cross sections, from total absorption cross sections, 5 to 130 keV 79−26947
photoelectric cross sections of low energy photons 78−46309
photoelectric cross-section at K-edge measurements 78−2983
photoelectric interaction around the K edge 78−5183
photoionisation cross section of atomic and final state effects on 5d core levels 78−84699
photoionisation cross section of d-core level synchrotron radiation study of spin-orbit branching ratio 79−74057
photon showers produced by 150 MeV electrons 77−10563
photoneutron yields released by incident electrons, improved calc. 80−27630
plasma, dense, nondegenerate, electron transport, thermal cond. *(Russian)* 79−98865
plastic deform. rate rel. to supercond. transition, temp. depend. *(Russian)* 78−31015
plastic deformation, accumulation of cryst.-lattice defects in normal and supercond. state 77−85196
plastic deformation of polycryst. sample at 4.2K, heating effect 77−15481
plastic properties over wide range of strain rates 80−71693
plastically bent, effect of dislocations on electron relax. time, cyclotron reson. 79−24217
plastically deformed, annealed, positron trapping rate, 4-100K 78−31275
poisoning in human teeth, determ. using alpha-sensitive plastic track detector 80−94433
pollution, New Zealand, battery factory and smelter emissions compared with vehicle exhausts 78−85562
pollution conc. determ. in estuarine waters, Raritan and Lower New York Bays 79−12139
pollution in Christchurch, New Zealand 78−85561
pollution near roads in Egypt 79−12255
porous electrode oxidation in H_2SO_4, potential step expts. 79−96438
positron annihilation, Doppler broadening, 4.2 to 600K 79−47540
positron annihilation, evidence for microporosity and dislocations 79−78786
positron annihilation rates, electron-electron and electron-positron correl. effects 78−76548
positron prethermalisation trapping model 77−43541
positron trapping by vacancies, high resolution lifetime meas. 77−1759
positron-vacancy interactions, equilib. temp. depend. of positron annihilation 78−76547
powder, automatic image analysis for charact. of size and shape distrib. 78−11473
powder prod. by electrolysis of fused salts 78−19690
powder production, interaction between N_2 jet and liq. Pb stream 79−43170
powder size and shape distribution via image anal. 80−16221
powders, prep. of spherical starting particles, for suspension electrolysis 78−60689
power cables, HV, Rb coverings quality estimation using mechanical tests *(Polish)* 80−97525
primitive, in Australian Zn-Pb-Ba deposit 78−11900
pseudopotential, energy-depend., for phonon dispersion calc. 77−15737
pure, friction stress for high temp. creep 78−11289
quench-condensed films, superconducting transition temp., elastic stress and strain effects 80−70883
radiation damage and recovery processes due to charged particle irrad. 77−69002
radioactive tracer for Pu nuclear fuel input accountability in reprocessing plants 80−73919
radiogenic, migration in hydrothermal metamorphism of U minerals 77−56627
radiography, ^{208}Pb spatial distrib. on microscopic scale, ^{4}He 30 MeV ion beam 77−12859
Raman conversion of XeCl-laser radiation in metal vapours, up to 40% efficient 79−23025
range of $^{27}Al^+$ ions, meas. by (p,γ) reson. broadening 79−46729
reactor shielding material, 6 MeV γ penetration, bremsstrahlung 78−58350
recrystallisation textures, and deformation formed by dry sliding against steel 79−91698
recycling, effect on comp. 80−66455
relativistic model pseudopot., appl. to elec. resist. in liq. phase and phonon spectra 78−51866
resistivity, multiple plane wave calc., Fermi surface, vel. and band struct. 77−51723
Richardton chondrite, U-Pb abundances and Pb isotopic studies 80−56778
rings, bearing capacity under compression 78−83256

lead continued
roadside soil and plants in Alexandria district, Egypt, contamination with Cd, Ni, Pb and Zn 78−81171
sample length effect on plasticity 78−44179
second Hugoniot relationship 77−35659
secondary cells, Pb-acid, cylindrical, pure lead, design features and performance experiences in float service applications 80−55831
seeding, variations of energy of the ⟨111⟩ torsion joint as a function of the angle of torsion in metallic seeds [dendritic structure] *(French)* 80−25682
sheathed cables in plastic multiway ducts, corrosion 80−7721
shock adiabatics at ultrahigh press. *(Russian)* 77−27941
shock compressed, release isentropes, eqn. of state at high energy density *(Russian)* 80−54340
shock compressed, thermal energy relaxation 77−69043
shock compression at high press. *(Russian)* 80−92608
short range order amongst cond. electrons 80−107040
single cryst. stress relax. depend. on elec. current, electron plastic effect 79−79021
sinter, thermal contact with liq. ^{3}He down to 0.4 mK 79−69312
sintering, surface oxide layer effect 79−66024
SO type, commercial purity, local deform. meas., using Moire method 80−21219
soil, Pb adsorption, Langmuir and Freundlich isotherms 77−33078
soil, specific Pb adsorption 77−33079
soil, total Pb, comparative study of analysis methods 78−16221
soil-water system interfacial reactions and heavy metal adsorption 78−3832
solenoid, partially disintegrated superhigh field, for fusion reactor *(Russian)* 77−7584
solid solubility of Au, elec. resist. meas. 80−39298
solutions, conc. changes, proton induced X-ray emission obs. 77−25325
solvent extraction with versatic acid 10 *(Japanese)* 79−4928
spectra of diffuse reflection and photoluminesc. *(Russian)* 79−11447
sphere, dissolution in H_2SO_4 in elec. field *(Russian)* 77−4867
splat quench in vacuum 79−52268
sputtering by 10 keV inert gas ions, angular distrib. 79−52061
sputtering efficiency ang. distrib. meas. using thermal particle detector 77−28671
SQUID, granular supercond. characterisation 79−28489
stable isotopes, 2-photon spectroscopy, isotope shift of $6\text{-}^2\,^3P_0\text{-}7p\,^3P_0$ transition 80−87070
stacking fault energy estimation, using phonon dispersion curve 78−43031
stain artefacts in electron microscopy, technique for minimizing occurrence 79−84040
steel, austenitic stainless, stress corrosion cracking, exam. of inhibiting action of Pb^{2+} 79−20249
steel, wires reinforced Pb, deform. behaviour and effect of volume fraction and surface treatments *(Japanese)* 79−66118
steel fibre reinforced Pb, fabrication, mech. props. *(Korean)* 77−12579
strain hardening and recovery during primary creep 78−39799
strength loss during upsetting 77−90430
strength loss in supercond. state, size factor effect *(Russian)* 80−88677
stress-strain state of central part during rolling of tall narrow strips *(Russian)* 79−52262
structure sensitive props., temp. hysteresis after melting and crystallisation *(Russian)* 79−29036
subshell photoelectron branching ratio meas., using synchrotron radiation 80−66397
substrate for polystyrene film, electrode effect on carrier injection, TSC, I-V characts. 80−34463
supercond. crit. RF mag. field, rel. to superheating 78−2632
superconducting, absolute surface reactance and penetration depth 78−68109
superconducting, amorphous film, conductivity and transition temp., ion bombardment effects *(Russian)* 80−49969
superconducting, crit. mag. field, functional derivatives 78−91798
superconducting, internal mag. field meas. by μ^+ method *(Russian)* 79−33391
superconducting, laser irradiated tunnel junction, nonequilibrium quasiparticle distrib. function, thermal regime *(Russian)* 79−42700
superconducting, mag. hysteresis meas. *(French)* 77−4463
superconducting, nonbranching laminar intermediate state structs. 80−54846
superconducting, penetration field and magnetisation curve, lattice detect effects 77−28292
superconducting, phonon density of states determ. 77−20493
superconducting, phonon struct. meas. in ultra-thin proximity effect tunnel junctions 78−80101
superconducting, press. depend. of supercond. transition temp. 78−84340
superconducting, quasi-particle recomb. time, Kapitza resistance 78−68123
superconducting, quasiparticle and phonon propagation 79−42689
superconducting, surface bound state, microwave surface impedance 77−12059
superconducting and intermediate state, thermal cond. measurements below 1K *(German)* 80−49984
superconducting contact to p-InAs, characts. 79−38254
superconducting crit. temp., functional derivative with electronic density of states, Eliashberg eqns. 79−56368
superconducting critical temp., shell model for clad particles *(Chinese)* 79−69623
superconducting film, acoustic coupling and effective quasiparticle lifetime 77−20499
superconducting film, anomalous temp. depend. of quasiparticle injection-induced voltage onset 78−56256
superconducting film, current-induced flux motion, studied at 100 ns time resolution 79−47208
superconducting film, first order transition due to quasiparticle injection 78−23208
superconducting film, flux dynamics during current-induced breakdown, magneto-optical flux detection 77−24646
superconducting film, flux nucleation in current-induced resistive state 78−23210
superconducting film, hypersonic attenuation investig. of crit. field, intermediate state 77−8246
superconducting film, intermediate state, shadow electron microscopy 79−11276
superconducting film, intrinsic and expt. quasiparticle recomb. times 77−15999
lead continued
superconducting film, nonequilib. gap instability and phase transition under intense tunnel injection 79−28476
superconducting film, quantized resistances, RF fields effects 78−10604
superconducting film, quasiparticle and phonon lifetimes, tunnel junction meas. 77−20498
superconducting film, radiation induced critical temp. 79−87179
superconducting film, spatially inhomogeneous state appearance under laser pumping conditions 80−93053
superconducting film, T_c and residual resist., variation with coating thickness 78−47900
superconducting friction with Ge, supercond. friction layers formed on Ge *(Russian)* 78−52143
superconducting junction, neutron irradiated, tunnel spectroscopy 78−10618
superconducting microbridges, two-dimens. imaging of resist. voltage changes caused by electron irrad. 80−15659
superconducting narrow film strip, weak link induced by optical guided waves 78−14886
superconducting phase condensation in bulk sample *(German)* 79−56447
superconducting RF surface resist., 136 to 472 MHz and 1.5 to 4.2K 77−63029
superconducting shell, mag. vacuum prod. by supercond. transition 78−8427
superconducting single cryst., quasiparticle propag. and recomb. 77−32126
superconducting slabs, magnetisation and migration field, reversible stage 80−65737
superconducting state parameters, dielectric screening functions effect 77−4471
superconducting strips, resistive transition in surface sheath state 79−56443
superconducting surface sheath, Brownian motion 79−19708
superconducting thin film resonator, high-freq. characts. in mag. field *(Russian)* 78−31014
superconducting transition curves, meas. during plastic deform. 79−60956
superconducting transition temp., electron-phonon mass enhancement, pseudopot. calcs. 78−2604
superconducting transition temp., perturbative corrections, direct and indirect ladder diagrams 80−49979
superconducting transition temp., theoretical calc. 79−73614
superconducting transition temp. from Eliashberg eqns. 79−51709
superconducting transition temperature, ab initio calc. 80−25036
superconducting transition temperature, resistive transition meas. 77−80861
superconducting transitions at high pressures, determ. via X-ray diffr. 77−11442
superconducting tunnel barrier, oxidation in humidity-controlled O_2 regulated atm. 78−19187
superconducting tunnel junction, basis Josephson parameters, depend. on temp. below T_c 79−56442
superconducting tunnel junction, quasiparticle recomb. times and electronic density of states at Fermi level 79−56414
superconducting tunnel junctions, nonequilibrium occupation of quasiparticle states 79−56416
superconducting variable thickness microbridge, microwave response 79−82717
superconductive fixed points for temperatures above 0.5K 79−63221
superconductor, anomalous thermal cond., transition induced creep *(Russian)* 77−36020
superconductor, effect of changes in $\alpha^2(\Omega)F(\Omega)$ on the zero-temp. energy gap 80−97025
superconductor, elastic tunnelling spectroscopy of single-particle excitations 78−56260
superconductor, law of corresponding states, Eliashberg eqn. *(Russian)* 79−87183
superconductor, strong coupling, LF EM response function 78−10605
supercooled liquid thin films, liq. struct. factor determ. by STEM 80−10487
surface, 10 eV impact of CS_2^+, CS_2^{2+}, CS^+, S^+, S_2^+, chem. modification, ESCA obs. 77−24916
surface, (100) and (110), oxidation and sulphidation, LEED and XPS obs. 78−20070
surface, (111), vacuum deposition of Ag, Cu, substrate diffusion effects, RHEED, LEED, AES 80−65410
surface, H^-, H^+, H_2^+ and H_3^+ grazing incidence collision with surface, Balmer radiation, elliptical polarisation 78−86804
surface, H ion impact, elliptic polarisation in Balmer radiation 80−35039
surface, He^+ ion neutralisation 78−35237
surface, Hg flow kinetics in temp. grad. *(Russian)* 78−6198
surface, isotope effects in ion-scattering double spectroscopy curves for He^+ 77−59658
surface, oxidation, XPS and SIMS study 79−15873
surface, Q-switched ruby laser irrad., recoil momentum 79−65961
surface analysis, quantitative, comparison of XPS results with model 78−40091
surface density of electronic states 77−20397
surface energy, self-consistent calc. including ion pot. perturbation effect 77−8166
surface erosion by supersonic plasma stream, mech. momentum role 80−2065
surface props., Rayleigh-Ritz variational calcs. 79−69570
surface props. rel. to adsorbed O_2, H_2O vapour, work function determ. 78−60187
surface tension liquidus temp. to 550°C *(Korean)* 79−90848
teeth, human, determ. of Pb distrib. by charged particle activation anal. 80−101303
Teheran atmosphere, Pb conc. 79−21011
thermal and elec. magnetoconductivities, high-field, meas. 77−59279
thermal conductivity, in normal and supercond. states, 0.6-7.5K *(Russian)* 80−6815
thermal conductivity in supercond. and normal states, press. effects 77−43779
thermal expansivity, simple eqn. of state appl. 77−27970
thermal neutron cross sections, in single crysts. 80−19672
thermodynamic props., calc. for liq. and solid phases 77−43348
thermoelectric power, absolute scale 77−71288
thermoelectric power below 17K 79−38052

lead continued
thermoelectricity, absolute scale between 10 and 350K 77−28162
thermomagnetic effect in type I superconductor *(French)* 77−63036
thermopower, Thomson heat expt. 79−65434
thick layer, evaporation neutron propag. Monte Carlo calcs. 79−89346
thin films, single and polytextured, band struct., tunnelling spectroscopy 80−80169
thin strips, supercond., optical wave illum., critical current behaviour 80−50012
total backscatt. coeffs., MeV electrons obliquely incident on target 77−63508
trace quantity determ. by atomic absorption spectroscopy with heated graphite atomizer 78−15749
tracer diffusion, atom size effect 78−84005
traces in human blood plasma, atomic absorpt. anal., nonspecific absorpt. correction using Zeeman effect 80−76881
transverse acoustic phonons, freq. and damping, supercond. transition temp. effects 79−42687
troposphere baseline, anthropogenic sources effects 78−7757
tropospheric fallout fluxes in Antarctica and Greenland 79−58007
twin boundary energy estimation, using phonon dispersion curve 78−43031
two photon photoelectric emission, photocurrent vectorial depend. 79−95906
ultrafine particle, positron annihilation exam. 78−56542
underpotential adsorption, cathodic deposition, on Ag(111) and (100) *(German)* 80−108363
underpotential adsorption on Ag (100), mean field theory and Monte Carlo simulation 79−60630
underpotential deposition on Ag single crystal cathode 78−52692
underpotential deposition on Cu substrate, phase formation 80−54538
US oscillations and dislocation unpinning in supercond. and normal states *(Russian)* 79−11648
V-V_xO_y-Pb tunnel junctions, IV charcts. of SQUID 79−19704
vacancy and divacancy props., exam. via quenching and annealing 78−47343
vacancy energy of formation, positron annihilation obs. *(German)* 78−71721
vacuum deposited metal film, elec. field effect on residual struct. 78−51836
vapour, diffusion-limited condensation meas. rel. to vacuum processing of metallurgical melts 77−8775
vapour, pulsed laser, with <20 kHz repetition freq. 78−9374
vapour, use in laser projection microscope with image-brightness amplifier 80−106541
vapour, XeCl laser pulse backward Raman compression 80−19068
vapour laser, optimum working conditions and charcts. *(Russian)* 78−13723
vapour laser, self-terminating, max. pulse repetition freq. 80−23677
vapour press., meas. using transpiration method, thermodynamic props. determ. 78−3365
water, natural, trace metals, energy dispersive X-ray fluoresc., at absorpt. anals., comparison 77−60175
whiskers, growth from metallic vapour phase, $<10^{-14}$ torr, elec. resist. 78−47686
work function temp. depend. 79−78154
work hardening, and recovery rates during steady state deformation, temp. and stress effect 80−45319
X-ray absorption, discontinuities and limits, chem. combination effects 80−93435
X-ray absorption edge, chem. shift, electron binding energy in compounds 78−62822
X-ray attenuation, 5-40 MV, rel. sensitivities of materials for half-value-layer meas. 77−45927
X-ray Debye temp. calc. 79−19348
X-ray emission spectra of CO_2 laser-irrad. targets, nonlinear processes 80−33793
X-ray M_5 absorpt. limits 78−6812
X-ray production by 9.5 to 41.8 MeV Fl ions, total L-shell cross-sections 77−85847
XPS, inelastic mean free path in 700 to 1200 eV range, bulk method 80−20763
XPS, outer core of level linewidths 77−44118
Young's modulus and internal friction, 20°C to melting point *(Russian)* 80−89278
Z dependence of thick target β-ray backscattering 80−76118
zone refining by electron transfer *(Russian)* 78−19662
Ag film-Pb sandwich, supercond., effective renormalisation interactions 79−56397
AgBr:Pb, impurity distrib., ion scattering spectroscopy obs. 77−19979
AgBr:Pb^{2+}, cubic microcryst., ion influence on ionic cond. and space charge charcts. 79−55928
AgCl:Pb^{2+}, EPR of mobile electrons, mechanism for photoinduced decomposition 78−80219
AgCl:Pb^{2+}, ionic cond. and dielec. loss relax. vacancy-impurity complex. form. 77−1259
AgCl:Pb^{2+}, recombination processes, radioluminescence 78−2915
Al film, Pb^+ implanted, ion scatt. erosion rate, Rutherford backscatt. 79−74038
Al/Pb two-layer target, moderate energy electron interactions, direct statistical modelling *(Russian)* 77−66561
Al-Al_2O_3-Pb contacts, tunnelling spectroscopy, band struct. of Pb 80−80169
Al-Al_2O_3-Pb Josephson junction, nonuniform, paracond., fluctuation effects 77−59359
Al-Al_2O_3-Pb tunnel junction, depend. of conductance corres. on chemisorbed ion conc. in barrier 79−15233
Al-Al_xO_y-Pb tunnel junction, thermal annealing effects 80−49952
Al-AlO_x-Pb junctions, organic ring cpd. doped, asymmetries in elastic and inelastic tunelling 79−95549
Al-Formvar-Pb junction electron tunnelling, phonon spectrum 77−59080
Al-I-Pb tunnel junction, clean and doped, tunnelling conductance 79−15232
Al-insulator-Pb, clean and doped tunnel junctions, barrier profiles 79−56445
Al-insulator-Pb tunnel junction doped with m-cresol, asymm. in tunnel spectra 77−6782
Al-monolayer-Pb, supercond. junction, electron tunnelling meas. 79−28482
Al-Ox-Ag-Cu-Pb and Al-Ox-Cu-Ag-Pb trilayer junctions, tunnelling charcts. 79−87208
Al-Pb junction, intensity and line-shape measurements in inelastic electron tunneling spectroscopy 79−24104
Al-Pb proximity sandwiches, Josephson and quasi-particle tunnelling expts. 79−65616
Al-Pb:Bi, tunnel-junction relax. oscillator, appl. to thermometry 79−85138
Al-SiO_2-Si-Pb, MIS system, photocurrent, effect of supercond. to normal transition in Pb 78−72271
$Al_xGa_{1-x}Sb$:Pb, doping of solid solns. during IPE *(Russian)* 77−85087
α-Al_2O_3:Pb, implantation, lattice disorder 77−80525
Ar bubbles injected into Sn, Pb and Cu melts, under laminar flow, charcts. 78−38394
atom, L-shell X-ray emission, proton induced, impact parameter dependence 77 23553
Au/Pb thin film couple, room temp. interdiffusion study 79−28154
$BaCl_2$:Pb, absorption and emission spectra *(Russian)* 78−23527
$BaCl_2$:Pb crystal phosphor, emission spectra 80−66298
BaF_2:Pb^{2+}, band struct., Jahn-Teller effect, UV luminesc. and optical absorpt. spectra 80−66243
Bi:Pb, carrier dispersion law, Shubnikov-de Haas meas. 77−20345
Bi:Pb, microhardness anisotropy 80−21079
Bi:Pb polycrystal elastic constants for US velocity obs. 79−69180
$Bi_{1-x}Sb_x$:Pb ($0.08 \leq x \leq 0.13$) Seebeck, magneto-Seebeck coeff., longitudinal Nernst coeffs. 78−56168
Bi_2Se_3:Pb, dopant influence on elec. cond. 79−51569
$^{210}Bi \rightarrow {}^{210}Po \rightarrow {}^{206}Pb$, decay chain, L-shell ionisation investig., X-ray emission during β, α decay 77−18891
CaF_2:Pb_xO_y, UV absorption, impurity centres 78−68534
CaF_2:Pb^{2+}, band struct., Jahn-Teller effect, UV luminesc. and optical absorpt. spectra 80−66243
CaI_2:Pb, recomb. processes, luminesc. charcts. *(Russian)* 80−25450
$CaLaBO_4$:Pb^{2+}, luminesc. obs 79−32971
CaO:Pb^{2+}, impurity centres vibronic spectra, lattice dynamics and electron-phonon interactions 80−7396
CaO(S):Pb^{2+}, luminesc. 77−73166
$Ca_5(PO_4)_3OH$:Pb^{2+}, thermolum. props. 80−2877
CaS-Pb,Mn, phosphors, thermoluminesc. and fluoresc. spectra 78−64396
CaSe:Pb, luminesc. and EPR props. of Pb centres 80−55168
CaSe:Pb^{2+} phosphors, luminesc., refl., emission, and excitation spectra 79−11456
$CaZrO_3$:Pb^{2+}, UV luminescence temp. depend., three-level model 77−4683
$CaZrO_3$:Pb^{2+} (Bi^{3+}) and related Pb^{2+}(Bi^{3+})-actuated hosts, cryst. struct. effects on luminesc. 77−16376
CdI_2:Pb^{2+}, luminesc. *(Russian)* 78−2913
CdS:Cu,Pb reflectivity of Ni-salt coated powder, pre-irrad. effect on defect form. 79−27973
$CsCaCl_3$:Pb, and undoped crystals, photolum. and thermolum. meas. *(Russian)* 77−85767
Cs_2O-B_2O_3:Pb^{2+} glass, optical basicity, variation with probe ion and comp. 80−2800
$CsSrCl_3$:Pb, luminesc. spectral distrib., transitions identification *(Russian)* 77−40276
Cu-Pb proximity sandwiches, tunnelling expt., barrier transmission effects 80−50002
Cu-Pb thin film couple, interdiffusion and recrystallisation, grain size effects 77−76625
CuCr-Pb, proximity effect, tunnelling conductance 78−52160
EUIG:Pb, valence of Pb in Fe-garnets 77−47480
EuIG:Pb, bubble domain film, magnetocrystalline anisotropy coeff. reduction, by Pb addition 79−11329
EuIG+Pb, (100) LPE film, magnetocryst. anisotropy and lattice mismatch 77−20647
n-Fe_2O_3:Pb electrodes, characterisation and behaviour in acetonitrile solns. 80−25004
$Fe(OH)_3$, coprecipitation with Cu, Ag, Au; Ge, Sn, Pb; Mn and Ca 79−70415
GaAs-Pb junctions, electron tunnelling under high press., transition temp., energy gap, phonon energies 79−15257
GaP-Pd contact system, low temp. alloyed contact formation 80−100519
GaSb-Pb junction, Ar ion bombard. effect on tunnelling props. 80−54783
Ge:Pb, ion implanted, lattice reordering, channelling and sheet resist. meas. 77−35577
Ge:Pb, ion implanted damaged layer, laser induced reorder 80−84201
$Ho_3Fe_5O_{12}$:Pb film, grown from fluxed metals by LPE 77−24972
In-Pb-In thin film bridge, instability current enhancement in perpendicular mag. field 77−85396
InSb-Pb, thermodynamic props. *(German)* 78−75847
KBr:Pb, luminesc. spectra obs. 78−95604
KBr:Pb, A-luminesc., 8-80K 80−2836
KCL:Pb^{3+}, interpretation of optical absorption spectra 79−51993
KCl:Pb, 420 nm A-emission band *(Russian)* 79−56852
KCl:Pb, additive coloration 77−68967
KCl:Pb, colloid centre formation, absorpt. spectra, 300-1000 nm 79−78710
KCl:Pb, colouring, room temp., influence of conc. and aggregation state of Pb 78−14339
KCl:Pb, impurity distrib., light scatt. and microhardness study, heat treatment 80−96562
KCl:Pb, impurity valence, heat treatment influence, absorpt. spectra obs. 79−38574
KCl:Pb, ionic electret behaviour, ionic thermoconductivity technique 80−7274
KCl:Pb, lead aggregation effect on yield stress, incoherent precipitates, solubility determ. method 80−50645
KCl:Pb, light induced ionic polarisation 80−7264
KCl:Pb, luminesc. spectra obs. 78−95604
KCl:Pb, photolum. in A band region, spectral and time decay anal. 79−33823
KCl:Pb, photoluminesc. induced by Suzuki-like occlusions, ionic thermocond. 79−33808
KCl:Pb, solid solution, electron microscope exam. of decomposition, of naturally aged specimens 79−96030
KCl:Pb, structural state of impurities, hydrostatic press. effect, thermostimulated depolarisation exam. 77−39614
KCl:Pb, thermoluminesc. meas. using high impedance DC amplifier 79−99955
KCl:Pb, vibr. struct. of absorption band 79−33735

lead continued
KCl:Pb crystal surfaces, Au decoration, electron microscope study 80−15144
KCl:Pb crystals, development of mechanical stresses during growth 80−19735
KCl:Pb exam. of simultaneous effect of heat treatment, Pb concentration on state, phase diagram construction 79−96008
KCl:Pb^{2+}, decay of luminescence emission 78−39593
KCl:Pb^{2+}, electrolytically coloured, elec. cond. and optical absorpt. meas. 80−100668
KCl:Pb^{2+}, γ-irrad., rel. to props. 78−31262
KCl:Pb^{2+}, highly doped, state of dispersion of Pb^{2+} 77−1144
KCl:Pb^{2+}, inner-centre luminesc., 8 to 80K *(Russian)* 78−92112
KCl:Pb^{2+}, ion energetic parameters comparison with alkaline earth fluoride crystals 80−66243
KCl:Pb^{2+}, Kerr electro-optical effect 80−34890
KCl:Pb^{2+}, low temp. sp. ht. 80−2178
KCl:Pb^{2+}, origin of 420 nm emission band 77−40279
KCl:Pb^{2+}, X-irrad. quenching effects on thermal glow curves 78−27333
KCl:Pb^{2+}, X-ray irrad., electron-trapped centres, Pb^{+} and Pb^{0}, optical absorpt. spectra 80−71461
KCl:Pb^{2+} crystals, precipitation, density changes, nucleation mode, lattice relaxation, heat treatment 79−66066
KCl:Pb^{2+}(0.005% Pb), A band fine structure, electron-phonon interaction 78−60491
KCl:Tl,Pb, X-irradiated, EPR spectra 79−28613
KCl-KF:Pb^{2+}, point defects, ionic thermal currents and optical meas. 80−6403
KCl:Pb^{3+}, relation between bonding and g-shift 80−39492
KI:Pb, absorpt. spectra of Pb^{++} centres 80−76058
KI:Pb^{2+}, absorpt., excitation and luminesc. spectra 78−19519
KI:Pb^{2+}, UV absorpt. and mag. circular dichroism spectra 80−25418
LiI:Pb, absorpt. spectra of Pb^{++} centres 80−76058
Li_2O-B_2O_3:Pb^{2+} glass, optical basicity, variation with probe ion and comp. 80−2800
liquid, polyvalent, electrical resistivity by harmonic model potential 80−54668
$LuPO_4$:Pb^{3+}, EPR, hyperfine interactions 80−108050
Mg (Fe,In)$_2O_4$:Pb,Pt film, LPE 77−77436
N_2^+ + Group IV elements and oxides, XPS and UPS prod. determ. 78−73084
NaBr:Pb, absorpt. and emission spectra of Pb centres 79−78717
NaCl:Pb, colouring, room temp., influence of conc. and aggregation state of Pb 78−14339
NaCl:Pb, γ-irrad., centres in thermoluminescent emission 77−85816
NaCl:Pb, luminesc. spectra obs. 78−95604
NaCl:Pb, Pb determ. by optical absorpt. in aq. soln. 78−85232
NaCl:Pb, precipitation of Pb impurity 78−48415
NaCl:Pb^{2+}, activation energy for clustering of Pb^{2+} vacancy pairs 77−72610
NaCl:Pb^{2+}, decay of luminescence emission 78−39593
NaCl:Pb^{2+}, emission spectra obs., and luminesc. centre model 77−36286
NaCl:Pb^{2+}, Z_4-like centre, absorpt. spectra obs. 78−76498
NaCl:Pb^{2+} crystals, grown from aq. soln., flotation study 80−39144
NaCl:Tl,Pb, X-irradiated, EPR spectra 79−28613
NaCl-NaF:Pb^{2+}, point defects, ionic thermal current and optical meas. 80−6403
NaCl + Pb, Pb aggregation effect on yield stress, incoherent precipitates, solubility determ. method 80−50645
NaI:Pb, absorpt. spectra of Pb^{++} centres 80−76058
Na_2O-P_2O_5:Pb^{2+}, metaphosphate glass, absorpt. spectra of radiation products 78−64865
Nb-I-Pb junction, double-peak structure *(Russian)* 79−82716
Nb-I-Pb junctions, fine struct. of current-voltage curves *(Russian)* 79−19693
Nb-Nb_2O_5-Pb Josephson junctions, props. of Nb_2O_5 thermally grown tunnel barriers 80−100568
Nb-Nb_2O_5-Pb Josephson junction formed on Nb film edge 80−107960
Nb-Nb_xO_y-Pb, tunnelling junction, current-voltage characts., knee struct. 79−38261
Nb-Nb_xO_y-Pb Josephson tunnel junction form. and ageing, adsorbed gas effect *(Russian)* 78−14899
Nb-Nb_xO_y-Pb Josephson junctions, preparation and props. *(Russian)* 79−91188
Nb-Nb_xO_y-Pb junction, thin Al layer effect on tunnelling characts. 77−85393
Nb-NbO_x-Al/Pb supercond. proximity function, production by RF sputtering and photolytographic techniques 77−43787
Nb-NbO_x-Pb Josephson junction, self-reson. modes 78−64169
Nb-NbO_x-Pb Josephson junctions with high current densities, critical current 80−100552
Nb-NbO_x-Pb Josephson tunnel junctions, fabrication using FR glow discharge oxidation 80−34559
Nb-NbO_x-Pb junction, static charact. of tunnelling cryotrons 79−28480
Nb-NbO_x-Pb superconductive tunnel junctions, oxide tunnelling barriers, ESCA characterisation 80−65745
Nb-NbO_x-Pb tunnel junction, crit. Josephson currents, temp. depend. 78−2629
Nb-NbO_x-Pb tunnel junctions with high normal resists.,, crit. currents 79−56399
Nb-NbO_x-Pb tunnel junctions at 4.2K, conductance of oxide barrier 80−7046
Nb-NbO_xPb tunnel junctions, current density distrib. 80−39717
Nb-oxide-Pb Josephson junctions, anomalous microwave-induced voltages 78−39266
Nb-oxide-Pb Josephson tunnel junction, capacitance and ellipsometrically determined oxide thickness 77−4469
Nb-Pb supercond. tunnel junction proximity effect, theory 80−65752
Nb-Pb tunnel junction, crit. Josephson current, proximity effect model 80−93047
Nb-Te-Pb Josephson junctions, prep. and props. 80−65754
NbV-VO_x-Pb Josephson tunnel junction, VO_x effect on props. 79−87203
Ng-Pb Josephson junctions, magnetic field behaviour of zero field steps 80−100561
Ni + Pb, inner shell vacancy prod., impact parameter depend. 77−6906
$_{28}{}^{58}Ni^{n+}$ + $_{25}Mn(_{50}Sn)(_{82}Pb)$, 45, 94, and 138 MeV Ni inner shell vacancy production, impact parameter depend. 79−41130
Pb^{-}, photodetachment cross-section, crossed beam meas. *(German)* 77−42298
Pb, effect of supercond. transition on phonon energies and lifetimes 79−28432

lead continued
Pb I, absorption spectrum, 1350-2041 Å 78−9102
Pb I and II, transition probabilities, Stark broadening parameters 80−23367
Pb II, oscillator strength meas. and trends in group IV homologous ions 80−42991
Pb II homologous ions series, Stark broadening trends 80−105157
Pb IV, relativistic oscill. strengths 77−14388
Pb, K-shell photoionisation, cross section meas. K X-ray-photoelectron coincidence method 79−72285
Pb, liq., sticky hard sphere pot., stuct. function evaluation 80−33869
Pb, melting studies by temperature wave anal. method 80−15217
Pb ore dust, pollution analyser using Harwell 6000 series electronics 79−5649
Pb, reactivity worths of fixed neutron absorbers 78−21654
Pb^{+}, adsorbed on Ag (111) or (100) surface, struct. *(German)* 78−68636
Pb^{+}, and isoelectronic ions, excited-state energy level k-ordering, l-patterns 77−88406
Pb^{+}, electron collisional laser populated by recomb. 79−18405
Pb^{+} high-gain laser populated by direct electron excitation, 1.159 μm transition 80−37997
Pb^{2+}, in soln., luminesc., halide ion effects 78−35187
Pb^{2+}, on calcite surface, ESCA, calibration 77−81432
$^{212}Pb^{2+}$, diffusion in ion exchange membrane, autoradiographic obs. 77−90637
Pb:^{215}Ra, abs. mag. moment of $(h_{9/2})^n$ proton states from Knight shift obs. 77−82821
Pb:Au(In)(Bi), type II superconducting film, penetration depth meas. 77−28285
Pb:Fe, impurity recoilless fraction calc. from mean square displacements 78−2216
Pb:Ni, paramag. impurity effect on work hardening at superconducting transition *(Russian)* 77−47915
Pb:O, thin film, microstruct. and thermal stress, doping effects 80−88458
Pb/Ag-Pd, sequentially deposited, thin film reaction kinetics, X-ray diffr. expts. 77−89594
Pb/Cu interface, thermal conductance at low temps. in normal and supercond. states 80−49436
Pb/Cu(Ag) proximity effect semiconductor, US surface wave attenuation 79−60994
Pb/oxide/InAs structure, effective mass determ. by tunnelling spectroscopy *(Russian)* 80−44482
Pb/$PbCl_2$ electrode, in chloride media, low temp. props. 78−68899
Pb/PbF_2/BiF_3/Bi thin solid film reversible galvanic cell 79−52928
Pb/U in two-billion-year granulites in Late Precambrian metamorphic basement along S.Peruvian coast 78−28204
Pb-acid battery, effect of H_3PO_4 on positive electrode, mechanism 80−26129
Pb-acid cells, PbO_2 formation on Pb and antimonial Pb alloy 80−76628
Pb-acid negative battery plate, form., physicochem. processes 77−4907
Pb-Ag proximity effect sandwich, mag. field depend. of tunnelling characts. 77−20501
Pb-Al radiation shields, build-up factors for 6.2 MeV photons 79−81093
Pb-Al_2O_3 composites, mech. alloyed, hot hardness meas. *(Japanese)* 78−84830
Pb-Al_2O_3-Al, solid-state anodisation of Al by vapour infusion, oxide growth rate 80−11830
Pb-Al_2O_3-Al tunnel junction, Pb supercond. film behaviour in mag. field 78−14894
Pb-Al_2O_3-HgSe junction, asymmetry of tunnelling characts. 79−47169
Pb-barium stearate-Pb structs., internal voltage work function meas. 79−82684
Pb-Cd thin films, electron tunnelling study of supercond. proximity effect 80−2525
Pb-Cd-Pb, supercond.−normal-metal−supercond. junction, crit. currents 80−107965
Pb-Cd-Pb junctions, pair pot., mag. field depend., crit. currents meas. 80−84555
Pb-CdS-In Josephson junction, light-sensitive, structural fluctuations *(Russian)* 78−56265
Pb-Cu contacts, proximity effect *(Russian)* 80−34558
Pb-$Cu_{91}Ni_9$-Pb superconducting junction, crit. currents 79−69633
Pb-$Cu_{99.8}Mn_{0.2}$-Pb superconducting junction, crit. currents 79−69633
Pb-Cu-Pb superconducting microbridges, response times and low-voltage behaviour 79−65602
Pb-Cu(Ag) double layers, intermetallic boundary effects, tunnelling 80−88692
Pb-Fe multilayers, zero pair pot. verification by supercond. tunnelling 80−54841
Pb-foiled plastic scintillator, γ-ray meas. *(Japanese)* 77−57825
Pb-formvar-Al tunnel junction, excitonic superconductivity, BCS theory, generalised jellium model 80−75684
Pb-H_2SO_4 battery negative plates, impedance, theory 78−27771
Pb-H_2SO_4 cells, Sb alloying effect on solid Pb electrochemical properties 80−55668
Pb-He discharge, excitation process, Pb^{+} emission lines 78−66803
Pb-I-NiCr-Cu double tunnel junction struct., supercond. energy gap suppression and instability 79−56417
Pb-Nb_3Sn tunnel junction, Josephson props. 79−7937
Pb-Nb_xO_y-Nb, two-dimens. Josephson junction, supercurrent vs. mag. field characts. 80−34562
Pb-Nb_xO_y-Nb Josephson junction current-biased on Fiske steps, mag. field depend. 80−84567
Pb-Nb-Pb bridge, fabrication technique and film parameters meas. 80−100569
Pb-Nb-Pb bridged, variable thickness, ion implant, coherent vortex motion props. obs. 80−100562
Pb-NbO_x-Nb tunnel junction, temp. depend. of effective Nb energy gap 80−80454
Pb-O-Pb, PbTl-O-Pb, Josephson tunnel junction parameters, microwave freq., temp. depend. 80−34561
Pb-oxide-Al tunnel junction, clean and doped, cond. 77−59335
Pb-oxide-PbIn superconducting junction, two-particle tunnelling and microwave effects 78−43527
Pb-Pb bridge, variable thickness, DC and AC Josephson effect 78−31016
Pb-Pb bridge, variable thickness, static mag. field effects, Josephson effects 78−31017

lead continued
Pb-Pb quasimolecular states, inner shell ionis. spectra during form. 78−33592
Pb-Pb_xO_y-Pb Josephson junction, long-term stability at liq. N_2 temp., voltage standard 77−72945
Pb-Pb_xO_y-Pb thin film Josephson junctions, prep. *(Slovak)* 79−42699
Pb-$PbCl_2(I_2)$, finely disperse system, supercond. props. 77−85376
Pb-PbO_2, bielectrodes, anodic polarisation 77−44483
Pb-PbO_2 storage batteries, gas tight with recombination, advantages *(German)* 79−52921
Pb-PbO_x-Pb, long Josephson tunnel junction, current steps induced by vortex motion 79−47199
Pb-PbO_x-Pb small supercond. tunnel junctions, effect of capacitance in I-V characts., high-freq. obs. 80−80448
Pb-PbO-Pb, Josephson tunnel junction fabrication for Mm-wave detector 80−100427
Pb-PbO-Pb, supercond. junction, tunnel effect under laser irrad. *(Russian)* 77−43788
Pb-Si heterojunction, RHEED, Mossbauer spectroscopy and I-V characts. 80−70828
Pb-Si:Sb Schottky tunnel junction, variable range hopping assisted tunnelling 80−39670
Pb-SiO_2-Au tunnel junction, obs. of conductance anomalies 78−26968
Pb-SiO_2-$Pb_{0.8}Sn_{0.2}Te$, prop. of insulating film for tunnelling study on zero bias anomaly 79−15608
Pb-SiO_2-$Pb_{1-x}Ge_xTe$, semicond. band struct., tunnelling obs. 80−54795
Pb-Sn bimetallic loop, supercond., thermoelec. flux effects due to penetration depth changes 77−24636
Pb-Sn Josephson junctions, small area high current density normal resistance, RC times 80−34555
Pb-Sn proximity effect sandwich, mag. field depend. of tunnelling characts. 77−20501
Pb-Te-Pb Josephson junction, cavity resonances 78−84352
Pb-Te-Te oxide-Pb Josephson junctions, prep. and props. 80−65754
Pb-Zn belts and their origin 79−48427
Pb-Zn-Ag, liquid system, 450-750°C, phase boundaries *(French)* 77−69081
Pb^{2+}-Cd^{2+}, solns., differential pulse and anodic stripping voltammetry, in thin-layer cell 77−36812
Pb+Cm, 1sσ excitation probability, scaling law, breakdown at very small internuclear distances 80−58365
Pb+F_2, chemiluminesc. spectrum of PbF 79−24742
Pb+H_2(HD)(D_2), intramultiplet transitions 77−54597
Pb+H^+, K-shell ionisation, 7-15 MeV, relativistic effects 78−82830
Pb+H^+, L-shell ionis., 0.5-3.5 MeV, X-ray emission obs. 77−54528
Pb+H^+(D^+), L-subshell vacancy production, Coulomb deflection effects 80−9711
Pb+He^+, at. beam and surface interaction, scatt. ion yield oscills. 78−55221
Pb+He^+, ion backscattering, emitted radiation intensity rel. to incident energy 79−89762
Pb+Kr^{n+}, K-L level matching, X-ray obs. 79−63948
Pb+$N_2O(0)(0_2)(0_3)$→PbO, chemiluminesc. spectra 77−9087
Pb+N_2O→PbO+N_2, chemiluminesc. reaction, vel. depend. 78−27762
Pb+O_3 reactions, chemiluminesc. 79−52673
Pb+Pb K-MO spectrum, impact parameter depend. 80−5613
Pb+Pb^+, δ-electrons from K- and L-shell ionisation in adiabatic collisions 80−23541
Pb+Pb^+, inner-shell ionisation of quasimolecular system, perturbation theory 79−31667
Pb+target atom, 90-110 MeV, K-vacancy cross sections, target depend. 77−19026
Pb^++Z (42≤Z≤92), 1sσ MO excitation probability and binding energy, X-ray coincidence 78−94316
Pb^{36+}+Ne, highly charged very slow Ne recoil ions, K X-ray transition 80−91649
Pb^{n+}+gas target, 50 keV, multiple scatt., target at.+energetic ion spatial correlation influence 79−27062
Pb_2, in Ar matrix, excitation and emission spectra, vibr. freq. 78−13507
Pb_2, laser induced fluoresc. *(French)* 79−13760
Pb_2, low-lying states, energy curves, bonding 79−76367
Pb_2, three photon excitation, Pb Rydberg series 80−106280
$^{206/207/204}$Pb ratios rel. to Earth age and chemical evolution 79−88315
Pb($^3P_1^o$)+H, spin-orbit relax., fluoresc. intensity meas. 78−82681
$Pb_{0.8}Sn_{0.2}Te$-Pb, Schottky barrier form., Auger depth profiling and I-V meas. 80−49903
n-PbTe:Pb thermoelectric props., 300-750K 78−34851
p-PbTe-Pb, barrier props. 79−7898
^{82}Pb+H^+, L-subshell ionisation probabilities, impact parameter depend. 77−30981
^{202}Pb, extinct radioactive nucleus, as origin of Hg isotopic anomalies in meteorites 77−49343
^{204}Pb, muonic, first excited 2^+ state, isomer shift of E2 transition 80−99150
^{204}Pb(n,n')^{204}Pb, meas. of lead content of metal fragments 79−52850
^{205}Pb, decay, orbital electron capture ratios 77−18894
^{206}Pb/^{204}Pb evolution during Earth crust development, rel. to U, Th and Pb fractionation 79−57879
^{206}Pb/^{207}Pb ratio and Pb conc. in subalpine pond sediments, anthropogenic source var. 80−85315
^{207}Pb, laser isotope separation using nuclear spin induced elec. dipole transitions 77−61877
^{207}Pb muonic isomer shifts, neutron hole anomalous moment contribs. 80−78728
^{207}Pb/^{204}Pb, ^{206}Pb/^{204}Pb ratios in basalts from DSDP Leg 37 cores 77−91123
^{208}Pb+^{208}Pb collisions, 1 GeV, mol. orbital X-rays 79−49978
^{208}Pb+Ag(Au), 5.8 MeV/amu, Pb K-shell excitation probability 78−5338
^{210}Pb, ^{226}Ra and ^{210}Po disequilibria in western N.Pacific 77−5227
^{210}Pb and ^{210}Po concs. in liver and kidneys of cattle 80−30904
^{210}Pb, atmospheric fluxes determ. from soil profiles 79−2346
^{210}Pb, balance in Long Island Sound 79−20861
^{210}Pb chronologies of lake and marine sediments, problems 78−81122
^{210}Pb chronology of Long Island Sound sediment core, biological mixing effects 79−66672
^{210}Pb, concs., physico-chem. states and residence times in marine and estuarine waters 78−11913
^{210}Pb dating, results from Lake Ipea and Lough Erne sediment cores 78−28202
^{210}Pb dating of annually laminated Finnish lake sediments 79−74916

lead continued
^{210}Pb determ. by direct gamma-ray meas. in lake sediments and air samples 77−5156
^{210}Pb determination in sediment core from ocean floor off Californian coast 80−72101
^{210}Pb determination in U ores, dusts and mill tailings 78−15736
^{210}Pb distrib. in Pacific surface waters 77−5226
^{210}Pb distrib. in S.Pacific water profiles 77−5225
^{210}Pb, distrib. in submersible-taken deep sea cores from Project FAMOUS 77−37179
^{210}Pb, external γ-counting and bioassay meas. on retired U miners 80−26332
^{210}Pb from nucl. explosions in environment 78−21774
^{210}Pb geochemistry in Galapagos Rise hot spring field, rel. to clam growth rate determ. 79−84300
^{210}Pb, in deep sea, particulate and soluble activities 77−5223
^{210}Pb, radiochem. determ. in U ores, air dusts 77−56266
^{210}Pb, sediment age determination, plastic nuclear track detector 78−20554
^{210}Pb, time variation of low concentrations in rain water 79−43994
^{210}Pb tropospheric residence time 78−85396
^{210}Pb, use as heavy metal tracer in Susquehanna River system 78−49046
^{210}Pb/^{210}Po atmospheric ratio, modification by volcanic emissions 80−41507
^{210}Pb/^{226}Ra and ^{210}Po/^{210}Pb disequilibria in seawater and suspended particulate matter 77−5224
^{212}Pb atoms and ions, attachment coeffs. on monodisperse aerosols 79−66367
^{212}Pb inhaled body burden calibration, general phantom procedure 77−64138
^{212}Pb ion clearance from rabbit bronchial epithelium to blood 77−86641
Pd-CdS-In, tunnel junction, light induced DC Josephson current 79−47204
RbI:Pb_3, absorpt. spectra of Pb^{++} centres 80−76058
RbI:Pb^{2+}, luminescence under B-band excitation 78−35192
RbI:Pb^{2+}, optical and elec. props. 79−15493
Si:Pb, diffusion behaviour of Pb in high dose implanted Si layers during isothermal annealing 79−1525
Si:Pb, He^+ Rutherford backscatt. and TEM exam., implant species effect on recrystn. 78−47452
Si:Pb, high dose implantation profiles, determ. using low angle Rutherford He ion backscatt. 79−4327
Si:Pb, high-dose ion implanted and annealed, implant redistribution 80−107309
Si:Pb, implanted, laser annealing 78−75685
Si:Pb, implanted and annealed, impurity redistrib. 78−75689
Si:Pb, ion-implanted, impurity redistrib. during laser irrad. 80−100280
Si:Pb, ion-implanted and annealed, dose depend. of residual lattice disorder 77−43228
Si:Pb, lattice location of dopant and amorphous zones, by Rutherford backscatt. 77−68990
Si:Pb, low-solid solubility ion-implanted, pulsed and continuous laser annealing and furnace annealing comparison 79−73184
Si:Pb implanted layers, recrystn. on annealing, backscatt. and TEM obs. 77−51421
Si(111):Pb ion implanted amorphous layers, recrystallisation, impurity out-diffusion model *(Chinese)* 80−88363
Sn-Pb supercond. loop, laser irrad. effects 79−56419
$SrCl_2$:Pb^{2+}, intracentre luminesc. *(Russian)* 77−16395
SrF_2:Pb^{2+}, band struct., Jahn-Teller effect, UV luminesc. and optical absorpt. spectra 80−66243
$SrLaBO_4$:Pb^{2+}, luminesc. obs. 79−32971
SrO:Pb^{2+}, impurity centres vibronic spectra, lattice dynamics and electron-phonon interactions 80−7396
Ta-Ta_xO_y-Pb, tunnelling junction, current-voltage characts., knee struct. 79−38261
U+Pb, K-vacancy form., rot. coupling effect in quasimol. L-shell 78−25692
V, effect of O ion irradiation on supercond. 78−52131
V/Al-Al_xO_y-Pb tunnel junction, superconducting transition, critical currents, Josephson effect *(Russian)* 80−29507
V-VO_x-Pb Josephson tunnel junction, crit. currents exam. 78−23209
VNb-NbO_x-Pb Josephson tunnel junction, compared with VNb-VO_x-Pb 79−87203
Xe+Pb, 4.6 MeV/amu, 1 sσ vacancy production, impact parameter depend. 79−72393
^{136}Xe+Pb, 625 MeV, probability of forming 1sσ vacancies 78−25681
YIG:B,Pb, IR spectrum, localised modes, rel. to impurities and O vacancies 80−50377
YIG:Pb, valence of Pb in Fe-garnets 77−47480
YPO_4:Pb^{3+}, EPR, hyperfine interactions 80−108050
Zn-Pb proximity sandwiches, tunnelling characts. 79−56396
ZnS:Cu, Pb, phosphors, ruby laser stimulated time delayed emission spectra 77−69874
ZnS:Cu,Pb, thermoemission of positive ions in simple gas atmos. *(Russian)* 77−28676
ZnS:Cu,Pb film, sublimated, pulse electrolum. meas. *(Russian)* 77−85806
ZnS:Pb, blue luminesc., photoexcited EPR spectrum 80−108070
ZnS:Pb, luminescence, polaris. emission 79−38634
ZnS:Pb, melt grown cryst., impurity distrib. and ionicity 77−55298
ZnS:Pb, phosphor, photocapacitive effect and Gudden-Pohl effect 79−65520
ZnS:Pb current pulses due to elec. field liberation of electrons from trapping centres by tunnel processes 79−28378
ZnS:Pb phosphor, electrolum. brightness, temp. depend. 77−48249
ZnS:Pb phosphor, ionisation mechanism of field trapping centres 80−45156
ZnS:Pb phosphor mech. of elec. field liberation of electrons from traps 78−72616
ZnS:Pb^{2+}(Mn^{2+}), high press. luminesc., localised excitations 78−19534
ZnSe:Pb, luminescence photocond. 79−38634
$ZnSe_{1-x}S_x$, luminescence, polaris. emission 79−38634

lead alloys
see also lead compounds
alkaline earth-Pb, M_2Pb, occurrence struct. 78−38663
Babbitt grade Bk-2Sh, improvement in antifriction layer props. by impulse discharge *(Russian)* 79−1917
battery anode reverse polarisation corrosion test method *(Bulgarian)* 80−50950

lead alloys continued
α-brass, leaded and Pb-free mech. damping 77−63705
brass leaded, effect of Al, Sn, Fe on solidification, differential thermal analysis exam. *(Russian)* 79−29041
DC SQUID, ultra-low-noise tunnel junction, design, fabrication and noise props. 80−29506
dilute, diffusion thermopower, inelastic electron-phonon interaction 80−96851
dilute, dislocation inertial effects in plastic deform., internal friction meas. 77−36609
dilute, solute resist. meas., multiple point defect form. 78−10433
dilute binary alloy, residual resistivity 77−1406
FCC ternary, solid soln. hardening model, compared with expt. results 77−44262
interstitial substitutional model for anomalous diffusion 80−84330
ion-selective membrane electrodes development, Ag ion conduction ceramic systems *(Japanese)* 80−61203
Josephson tunnel junctions, effect of process variables on elec. props., cryogenic memory appls. 80−65748
leaded brass, mechanical damping in terms of Granato-Lucke theory, comparison with unleaded brass and Cu_3Au 78−95772
liquid amalgams mixing, excess entropy, vibr. contrib. *(Russian)* 79−51263
melts, effect on fracture stress of Armco iron *(Russian)* 77−21246
metallographic preparation, using pH controlled silica gel and superior microetchant 80−16623
phosphor bronzes, surface Cs^+ impact, 5.5 keV negative secondary ion emission obs., rel. to Cu *(French)* 77−66562
slip band theory, model for creep based on dislocation climb at grain boundaries, comparison with expt. data 79−37756
solders, superconducting transition temp. determ. 77−28281
steel, cavitation during superplastic flow, affecting factors 78−60728
steel, continuously cast slab, liquid-solid interface obs. by Pb additions to mould 77−21128
superconducting alloys, meas. of small changes in calorimetric props. using direct difference technique 77−33988
time and spatially resolved at. absorpt. anal. 80−40760
Wood's alloy, liq. enthalpy effects when solute is added 80−39314
Ag-Bi, melt, crystal growth of Ag, conditions for transition from round to face forms *(Russian)* 79−28906
Ag-Cu-Pb coin chem. anal. by low energy γ-rays and neutron transmission meas. 80−35591
Ag-Pb, liquid alloy, thermoelectric power and magnetic susceptibility 77−8076
Ag-Pb (30 wt.%), contact material, contamination layer thickness, resist., ESCA study *(German)* 80−55561
Ag-Pb-Hg system, DTA of phase diagram 77−12594
Al-Al-PbBi double tunnel junction structs., quasiparticle relax. times, energy and temp. depend. 79−56412
Al-Bi(Cd)(Pb)-Ti, containing low-melting pt. inclusions, mech. props. 80−93632
Al-Na alloy, supercond. flux pinning by precipitates 77−47948
Al-Pb, containing low melting point inclusions, impact props., temp. depend. 78−60792
Al-Pb, dil., pulsed ruby laser irrad., noncryst. phase form 80−35012
Al-Pb, liquid, surface tension, size effect *(French)* 80−15341
Al-Pb, monotectic system, rapid cooling from melt, effect on struct. *(Russian)* 79−70053
Al-Pb, with isolated liq. phase inclusions, recrystn. *(Russian)* 80−20970
Al-Pb solid solution, thermal expansion, 10-55K *(Russian)* 77−80635
Al-PbBi superconducting tunnel junction as phonon spectrometer 78−47477
AlCuMgPb, microstruct. and flow stress during deform. at 573K 77−81307
AlPb alloy prod. under microgravity *(German)* 79−38766
As-Pb, eutectic, temp. determ. up to 35 kbar 77−85989
Au-In-Pb, $AuIn_2$-In-Pb portion of phase diagram 77−32562
Au-Pb-In solder joints, layer growth, ageing 77−32764
AuIn-Pb pseudobinary system, DTA 78−23667
$AuPb_2$, epitaxial layer, formation during Pb absorpt. on Au, LEED, AES study of $Au/AuPb_2$ interface 78−71988
$(Au_xPb_{1-x})_{1-c}Fe_c$, ferromag. and spin glass ordering 78−56335
Ba-Pb system, intermediate phases, equilib. phase diagram, cryst. struct. 77−44213
Bi-Pb, complex-regular eutectics, structural modification 78−23695
Bi-Pb, dilute, electrical cond. and thermal EMF at press. up to 12 kbar 77−47806
Bi-Pb, dilute, oxidation kinetics 80−25914
Bi-Pb, liq., conc. and temp. depend. nucl. relax. rates meas. 78−19357
Bi-Pb, supercond. crit. temp., effects of press. up to 30 kbar. *(Russian)* 77−20484
Bi-Pb amorphous alloys, superconductivity and the very strong electron-phonon interaction *(Japanese)* 79−95552
Bi-Pb-Hg, liquid, surface tension and density *(Russian)* 77−55418
Bi-Pb-Sn, eutectic alloys, struct. instability and absence of superplasticity *(Russian)* 77−8882
Bi-Pb-Sn, molten metallic system, contribution to sign inversion of effective charge *(Czech)* 78−60656
Cd-Pb, binary metallic melt, deviation from the Kopp law, specific heat *(Russian)* 80−39305
Cd-Pb, high pressure effects, eutectic temp. 80−55361
Cd-Pb alloy, molten, EMF meas. meas. of liquid separation 78−39747
Cd-Pb-Bi melts, enthalpies of form. *(Russian)* 79−51277
Cd-Pb-Bi-Sn system, ternary liq. alloys, thermodynamic props. 78−51701
Cd-Pb-Sn melts, enthalpies of form. *(Russian)* 79−51277
Cd-Sn-Pb (0.03 to 0.10 at.% Cd), Cd activity coeffs., interaction parameters, EMF depend. on temp. 80−49383
Ce-Pb, liquid, solubility and thermodynamic props. *(Russian)* 78−19717
$CePb_3$, crystalline elec. field parameters, exchange and Coulomb contrib. 77−20278
α-Cu-Ni-Zn-Pb, fire cracking and ordering *(German)* 78−60760
α-Cu-Ni-Zn-Pb, fire cracking, effect of pores and impurities 79−29207
Cu-Pb, diffusive redistrib. during friction *(Russian)* 78−52999
Cu-Pb, evaporation of Pb in vacuum induction melting 77−28742
Cu-Pb, gas-atomised, particle profiles, morphological characterisation derived from Walsh coeffs. 80−50816
Cu-Pb, liquid, surface tension, size effect *(French)* 80−15341
Cu-Pb, preferred crystallographic orientation of unidirectionally solidified polycrystals *(Czech)* 79−43233

lead alloys continued
Cu-Pb, stirred at different speeds under press., evaporation of Pb 77−47555
Cu-Pb liquid alloys, exam. of O diffusivity at 1430K using electrochemical cell 78−51713
Cu-Pb-O, liquid, dil. alloy, O_2 activity, 1100 to 1200°C 80−25662
Cu-Pb-O system, ternary miscibility gap activity determ., thermodynamic method 77−28783
Cu-Pb-S system, at 1473K, thermodynamic anal. 78−39746
Cu-Sn-Pb-Fe-graphite, bronze-based, sintered alloy, silica additions effect 77−63807
Cu-Zn-Sn-Pb (5, 5, 5 wt.%) analysis in glow discharge lamp and in ion microprobe, sputtering processes 77−52730
Fe, cast, Mg, Pb impurity effect on struct. and mech. props. 79−96089
Fe, cast, nodular graphite form. by Bi and Pb additions *(Japanese)* 77−63693
Fe-C-Pb, sintered, antifriction props., Pb introduction effect 79−96155
Ga-Pb, liquid alloy, thermodynamic activity determ. using Knudsen method *(German)* 79−34008
Ga-Pb, liquid binary alloys, magnetic susceptibility *(Russian)* 77−24671
Ga-Pb, polythermal cross sections 77−52300
Hg-Pb, dil. liq. amalgams, expanded, cond. at high temps. and press. 77−20287
In-Pb, liq., conc. and temp. depend. nucl. relax. rates meas. 78−19357
In-Pb, liquid alloy, thermodynamic activity determ. using Knudsen method *(German)* 79−34008
In-Pb, small κ supercond., phase transitions higher than second order 80−88668
In-Pb, thermal anal. solidus determ. 79−20030
In-Pb (7 at.%), supercond. cylinder, magnetisation change induced by current near upper crit. field 80−70890
In-Pb (up to 6.7 at.%) whisker, supercond. crit. temp., stress depend. 77−39988
In-Pb alloys, elastic consts. of three phases, acoustic mode softening 80−30006
In-Pb-Sn system, thermal anal. 80−35162
InPb-covered manganin wire, level detector, depth gauge, demonstration of superconductivity 79−35751
InSb-Pb, metallic soln., quasibinary alloy, association 78−15373
$La(Ce)Sn_{3-x}Pb_x$ system, mag. impurities in supercond., supercond. transition temp. and sp. ht. 78−39244
$LaPb_3$, doped with Tb, Nd, or Pr, crystal field effects, tunnelling within mK range 80−70907
$LaPb_3$, Tb and Pr substituted, superconductors, cryst. field transitions linewidths 80−24854
Li-Pb, liq. alloy, enthalpies of mixing, calorimetric study *(German)* 80−2170
Li-Pb, liq. semicond., electronic struct., resist. and thermoelec. power meas. 77−47712
Li-Pb, quasi-ionic, thermodynamic props. using EMF meas. 78−51705
Li-Pb, thermodynamic study using Knudsen effusion mass spectrometry 80−24578
Li-Pb eutectic alloys for fusion reactor solid breeder blankets, reactions with water 80−102297
Li-Pb liquid alloys, elec. resistivity, negative temp. coeff. 80−88527
Li-Pb liquid compound forming alloy, entropy of mixing 80−88328
Li-Pb-cooled blanket for tandem mirror fusion reactor, neutronic anal. 80−99273
LiPb alloy, compound-forming, vol. of mixing, conc. depend. 80−103484
$Li_{1-x}Pb_x$, liq., metal-nonmetal transition, electronic theory 78−79930
Mg-Al-Tl system, phase diags., electrode pots. *(Russian)* 78−80516
Mg-Cu-Pb system, phase equilibria in Mg-rich corner *(French)* 78−76630
Mg-Li-Pb, phase diagram, isothermal cross section *(Russian)* 80−20900
Mo_5PbS_8 embedded in resin, composite supercond., high transition temp. 80−88660
NaPb alloy, compound-forming, vol. of mixing, conc. depend. 80−103484
Nb-NbO_x-PbIn tunnel junctions with ultra-thin Nb electrodes 79−56398
Nb-PbSn, Josephson tunnel junction, 3rd yr undergrad. expt. 78−54126
$NdPb_3$, crystalline elec. field parameters, exchange and Coulomb contrib. 77−20278
Ni-Pb, conc. profiles across solid-liq. interfaces 80−55382
Pb/Au/Pb, Josephson junction, oxide formation process, ellipsomesric meas. *(Japanese)* 80−11561
Pb/Bi-I-Al tunnel injected nonequilibrium supercond. struct., diffusive quasiparticle instability, multiple gap states 80−50005
Pb-2n, work hardening in mixed state *(Russian)* 79−42707
Pb-(Sb)(Sn)(Ag) anodes, film behaviour for Cr electroplating 80−35115
Pb-Ag, Ag precipitation kinetics 78−19758
Pb-Ag, diffusion of Au, de-enhancement by Ag impurities 80−19990
Pb-Ag, high shear technique for liquidus boundary meas. 79−61564
Pb-Ag, liquid alloy, exam. of thermodynamic props. using solid oxide galvanic cell 78−75851
Pb-Ag, solid soln. hardening due to metal interstials 77−52337
Pb-Ag (0.068 wt.%), Ag precipitation kinetics and activation energy 80−66517
Pb-Ag eutectic alloy, microstruct. coarsening under isothermal and temp. gradient conditions 79−20079
Pb-Ar,(Xe) film, struct., electron diffr. meas., rel. to metal-nonmetal transition 77−51626
Pb-As (~0.01 wt.%), enhanced precip. phenomena, invest. of mechanism by elec. resist. meas. 80−104162
Pb-Au, dil., solute resist. meas., multiple point defect form. 78−10433
Pb-Au, interstitial and substitutional distrib. 80−84204
Pb-Au, Josephson tunnelling gates, thermal cycling 78−19188
Pb-Au (0-0.0918 at.%), lattice parameter changes due to Au dissolution 79−77558
Pb-Au (2.5 wt.%) film, In diffusion, alloy form. 78−22899
Pb-Bi, annular superconductor, field replication and flux shielding 77−28286
Pb-Bi, creep, low-temp., thermal heating and quantum mechanisms, supercond. transition effects 80−79868
Pb-Bi, dirty strong-coupling supercond., Ginzburg-Landau parameters, type II behaviour deviations 77−8249
Pb-Bi, elastic moduli, internal friction from US velocity meas. 79−15717
Pb-Bi, liq. calc. of electromigration forces and resist. 79−82572
Pb-Bi, liquid alloy, chemical and intrinsic diffusion coeffs., exam. *(German)* 78−83987
Pb-Bi, peritectic reaction, microstruct. changes 78−52753

lead alloys continued
Pb-Bi, splat quenched, solubility limit, vacancy conc. and supercond. transition temp. 77−12046
Pb-Bi, strong coupling superconductor, LF EM response function 78−10605
Pb-Bi, supercond., anomalous thermal cond., transition induced creep *(Russian)* 77−36020
Pb-Bi, supercond., crit. mag. fields, influence of parameters 80−75691
Pb-Bi, supercond. alloys, microwave surface resist., mag. field depend. *(French)* 77−24647
Pb-Bi, supercond. T_c evaluation, from ab initio band struct. calcs. on Pb 80−75502
Pb-Bi, supercond. tunnelling, effect of phase composition and press. 79−15261
Pb-Bi, temp. regime of crystn. on rapid cooling *(Russian)* 80−66495
Pb-Bi, thermodynamic props. 77−59743
Pb-Bi, vacuum deposited supercond. films, T_c chem. comp. depend. *(Russian)* 78−19174
Pb-Bi, X- and γ-ray attenuation obs. 79−61457
Pb-Bi (12 at.%), Sn fibre reinforced type II superconductor, flux pinning *(German)* 77−85397
Pb-Bi (4.1 at.%) solid soln., tetragonal distortion field for substitutional Bi atoms, neutron scatt. 78−51568
Pb-Bi alloy, fine powder electrodeposition and X-ray struct. obs. 78−11163
Pb-Bi alloy, liq., thermal cond. and elec. resistance up to 900°C 77−47785
Pb-Bi alloy, vapour press., meas. using transpiration method, thermodynamic props. determ. 78−3365
Pb-Bi alloys, phonon-electron interaction, normal and supercond. state thermal cond. and elec. resist. meas. 79−60460
Pb-Bi counterelectrode Pb alloy Josephson junctions 80−65743
Pb-Bi eutectic alloy flow rate meas. apparatus 77−79412
Pb-Bi eutectic melt, in contact with Cu, mutual indentation *(Russian)* 77−59853
Pb-Bi film, amorphous and polycrystalline, specific heat meas. 77−80715
Pb-Bi liquid alloy, Pb and Bi diffusivities, temp. and conc. depend. *(German)* 80−84311
Pb-Bi molten alloys, density, surface tension, temp. depend. 77−69147
Pb-Bi-Tl, supercond., crit. mag. fields, influence of parameters 80−75691
Pb-Ca-Sn, chill cast and wrought, cyclic voltammetry and electrochemical meas. of anodic activity, PbO_2 form. 78−31582
Pb-Ca-Sn, effect of Sn additions on precipitation behaviour, of Pb-Ca alloys *(German)* 78−52821
Pb-Ca-Sn, for battery grids, proposed phase diagram, grain struct. development, corrosion phenomena 77−16546
Pb-Cd, supercond. proximity effect, electron tunnelling study 78−10616
Pb-Cd (1.5 wt.%) discontinuous precipitation, metallographic study *(Japanese)* 77−48440
Pb-Cd dilute alloys, conc. depend. of Cd diffusivity enhancement 79−73348
Pb-Cd eutectic composite, mag. flux entry in proximity effect regime 79−33418
Pb-Cd lamellar eutectic composite, pair potential meas. 79−33396
Pb-Cu, charged particle irrad., damage and recovery processes 77−69002
Pb-Cu, hypoeutectic, grain refinement, and structural stability by S, Se and Te additions *(German)* 80−55387
Pb-Fe, supercond. films, modification of props. by Fe grains *(French)* 79−60957
Pb-Fe(Cu), liq., thermodynamic props. *(Polish)* 80−89199
Pb-Ga(Ge)(Si)(Mo)(Bi) amorphous films, supercond. transition temp. and residual elec. resist. *(Russian)* 79−19680
Pb-Ge thin film alloy, critical currents near metal-insulator transition 79−65626
Pb-I(-Au) base electrode film Josephson junctions, tunnel barrier oxide struct. 80−65750
Pb-In, CPA interpretation of positron annihilation *(Russian)* 80−11507
Pb-In, containing Ag particles, flux pinning in superconducting matrix 80−2534
Pb-In, Pb-In-Au, Josephson tunnelling gates, thermal cycling 78−19188
Pb-In, series-connected Josephson tunnel junctions, fabrication procedure diagnostics 78−47909
Pb-In, strong coupling effects in temp. depend. of flux-flow resist. near H_{c2} 77−36036
Pb-In, superconductive, electron tunnelling under hydrostatic press. 77−51850
Pb-In, superconductive to normal transition due to external mag. fields, dynamic behaviour 80−39722
Pb-In, viscous drag on mobile dislocations, plastic deformation, critical temp. magnetic data 78−43514
Pb-In, vortex pinning on grain boundaries *(Russian)* 77−89910
Pb-In (1 to 20 at.%), upper critical field anisotropy 77−36033
Pb-In (21 at.%), dirty type II supercond., anisotropic thermal cond. 79−56385
Pb-In (40 wt.%), solid soln., single phase, superplastic behaviour 80−21048
Pb-In (40-60 at.%), type II superconducting Ettingshausen effect, transport entropy of vortices 78−56272
Pb-In (5%), supercond. mobile dislocation density, instantaneous flux change meas. 80−15670
Pb-In (50 wt.%), supercond., pinning effect 80−15669
Pb-In alloys, flux pinning at grain boundaries 80−34572
Pb-In alloys, supercond., AC losses of EM energy, critical current densities 79−33423
Pb-In alloys, supercond. energy gap determ. by pt. contact tunnelling 78−19185
Pb-In and Pb-In/Au, Josephson junction, oxide formation process, ellipsomesric meas. *(Japanese)* 80−11561
Pb-In cylinder, vortex-surface interaction, vortex field *(Russian)* 78−27003
Pb-In film, RF sputter anodisation, Josephson junction form., ellipsometry anal. 79−29258
Pb-In film, supercond. surface sheath, dynamic pinning model of elec. dissipation 77−28320
Pb-In film, superconducting tunnel junction, pulsed quasiparticle injection 80−84565
Pb-In films, atom redistrib., ion-ion emission obs. *(Russian)* 78−18926
Pb-In multilayered superconducting film, critical currents 79−61017

lead alloys continued
Pb-In/Pb couple, FCC, Kirkendall interdiffusion, conc. depend. 77−39702
Pb-In/Sn-In proximity sandwiches, crit. currents 79−60992
Pb-In-Ag, transport current distribution in longitudinal mag. field 80−25057
Pb-In-Au, film, supercond. penetration depth 78−72306
Pb-In-Au, series-connected Josephson tunnel junctions, fabrication procedure diagnostics 78−47909
Pb-In-Au alloy, Josephson junction electrode materials, strain relax. 79−38255
Pb-In-Au Josephson tunnel junctions, strain relax. effects 79−65617
Pb-In-Sn system, liquidus and solidus isotherms 78−44088
Pb-La, vacuum deposited supercond. films, T_c chem. comp. depend. *(Russian)* 78−19174
Pb-Li alloys, ^3H breeding blanket for fusion reactor, ^2H solubility 80−18626
Pb-Li liner for fusion reactor, with controlled implosion 79−49860
Pb-Li liq. alloy internal spectral shifter and energy converter for laser fusion reactor 79−49841
Pb-Mg, dil., resistivity, multiple plane wave calc., Fermi surface, vel. and band struct. 77−51723
Pb-Mn, dil., supercond. film, H_{c2} meas., mag. impurity effects, pair breaking theory 79−42708
Pb-Na, peak-effect supercond., flux pinning 78−95403
Pb-Na, with Pb_3Na precips., flux pinning, crit. currents obs. *(German)* 78−14907
Pb-Na (8.4 at.%), supercond., surface flux pinning, crit. state model 80−97044
Pb-Ni, creep, low-temp., thermal heating and quantum mechanisms, supercond. transition effects 80−79868
Pb-Pd, diffusion of Au, de-enhancement by Pd impurities 80−19990
Pb-Pd, liq. alloy activity by effusion method *(German)* 79−29023
Pb-Pd equilibrium diagram, Pb-rich region 77−48398
Pb-Rb, phase diagram *(Russian)* 78−19720
Pb-Sb, chill cast and wrought, cyclic voltammetry and electrochemical meas. of anodic activity, PbO_2 form. 78−31582
Pb-Sb, crystal struct., supercond. after subjection to high press. 78−88064
Pb-Sb, dynamic destruction of supercond. 80−2529
Pb-Sb, improvement in antifriction layer props. by impulse discharge, impulse discharge treatment *(Russian)* 79−1917
Pb-Sb, influence of quench deform. on precipitation *(German)* 77−86064
Pb-Sb, phase transform. at high press., DTA, eta, beta thermodynamic stable phases *(Russian)* 79−66051
Pb-Sb, thermal analysis in non-faceted/faceted eutectic systems 80−71637
Pb-Sb (1 wt.%), highly averaged, fracture behaviour 79−8366
Pb-Sb alloy, Sb distrib. profile as function of depth in corrosion films 80−21177
Pb-Sb battery grids, ageing behaviour obs., effects of casting and cooling 79−100517
Pb-Sb eutectic alloys, solidification in space environment 79−47671
Pb-Sb form of growth of Sb crysts., precip. temp. effects *(Russian)* 77−21144
Pb-Sb molten alloys, oxidation and drossing *(German)* 79−74313
Pb-Sb-As (1.1-1.8, ~0.01 wt.%), enhanced precip. phenomena, invest. of mechanism by elec. resist. meas. 80−104162
Pb-Sb-Sr alloys, corrosion props. by simplex-lattice planning method 77−56148
Pb-Sb-Te-Cu-Sn, influence of specimen and grain size on mech. props. *(Russian)* 77−81297
Pb-Si superconducting solutions, effect of hydrostatic compression on tunnelling *(Russian)* 80−65746
Pb-Si-Sb amorphous alloys, electrical resistometric detection of relaxation 79−60278
Pb-Sm, vacuum deposited supercond. films, T_c chem. comp. depend. *(Russian)* 78−19174
Pb-Sn, arc electrode processes, thermodynamic approach *(Russian)* 77−27755
Pb-Sn, binary liq. soln., surface cluster functions 78−67631
Pb-Sn, controlled solidification, monograin growth, selection and struct. *(French)* 77−16568
Pb-Sn, DC arc plasma, meas. of conc. ratio of component atoms *(Russian)* 77−27754
Pb-Sn, dil., dislocation inertial effects, internal-friction meas. on normal and superconducting states 79−38883
Pb-Sn, directionally solidified lamellar eutectic, deform. induced microstruct. instability 77−32623
Pb-Sn, dirty strong-coupling supercond., Ginzburg-Landau parameters, type II behaviour deviations 77−8249
Pb-Sn, eutectic, electron emission avalanche obs., during isothermal superplastic deform., *(Russian)* 77−48324
Pb-Sn, eutectic, superplastic behaviour, grain size effect 80−7635
Pb-Sn, eutectic alloy, plastic deform., work hardening *(German)* 78−92279
Pb-Sn, eutectic alloy, spiral growth phenomenon 77−48419
Pb-Sn, eutectic alloys, struct. instability and absence of superplasticity *(Russian)* 77−8882
Pb-Sn, ingots, solidified, formation of equiaxed eutectic grains *(Japanese)* 78−39756
Pb-Sn, lamellar eutectic alloy, proximity effect, entropies, free energies and transition temps. 77−51849
Pb-Sn, lamellar eutectic stability and growth struct., fault formation 79−96019
Pb-Sn, melt viscosity rel. to phase equilib. *(Russian)* 79−69272
Pb-Sn, off-eutectic alloy growth from stirred melt 77−8809
Pb-Sn, proximity and pinning effect up to 7K *(French)* 77−51858
Pb-Sn, solidification, predicted vol. change 77−28802
Pb-Sn, superplastic eutectic, roll load and torque necessary for rolling *(French)* 78−95761
Pb-Sn, undercooled eutectic, compositional variations at various gravity levels 77−52314
Pb-Sn, unidirectionally solidified eutectic, lamellar microstructure, influence of grain boundaries on thermal stability 78−72795
Pb-Sn, with brass insert, tensile flow and fracture 78−11290
Pb-Sn (20wt.%), eddy current study of solidification 80−104141
Pb-Sn (62 wt.%), activation energy for superplasticity 77−86112
Pb-Sn (62 wt.%), intercrystalline and interface boundary sliding, tensile tests, SEM obs. 79−38886

lead alloys continued
Pb-Sn (62 wt.%), superplastic eutectic, exceptional ductility 78−27579
Pb-Sn alloy, viscoplastic flow study, appl. of Moire fringe method *(Russian)* 77−35102
Pb-Sn binary alloy, unidirectional solidification, convective and interfacial instabilities 80−60851
Pb-Sn directionally solidified eutectic alloy, morphology and crystallography 77−90340
Pb-Sn eutectic, directionally solidified, perfection and stability of lamellar struct. *(French)* 77−77468
Pb-Sn eutectic, directionally solidified, periodic array of supercond.-normal contacts, supercurrent and dynamic resist. 78−34928
Pb-Sn eutectic, strain rate sensitivity index, expt. comparison of different methods 80−3144
Pb-Sn eutectic, superplastic deform., appl. of SEM specimen holder for cold tensile deform. expts. *(French)* 77−36704
Pb-Sn eutectic, superplastic, anelasticity effect on stress relaxation 78−31443
Pb-Sn eutectic alloy, high temp. deform. 77−16637
Pb-Sn eutectic alloy, superplastic deform. of circular sheets *(French)* 77−28871
Pb-Sn eutectic alloy, superplastic deform. at relatively high strain rates 79−57042
Pb-Sn lamellar eutectic alloy, supercond. normal-supercond. junction arrays 77−24641
Pb-Sn microduplex eutectic, cavitation during superplastic flow due to hard particles 77−36575
Pb-Sn superplastic alloy, cutting, stress distrib. *(German)* 79−24682
Pb-Sn system, soft solder, elec. and thermal cond. at low temps., superconducting transition temp. 80−20150
Pb-Sn-Bi-Cd low melting point alloy block for organ shielding in radiotherapy *(Korean)* 80−36154
Pb-Sn-Ca sheet, continuously cast, for battery grids, ageing behaviour 77−16603
Pb-Sn-Cd, eutectic and monovariant eutectic, ingot struct. 78−15388
Pb-Sn-Cd, monovariant eutectic and eutectic alloys, ingot struct. 77−63656
Pb-Sn-Hg amalgam, liq., thermodynamic props. *(Russian)* 77−66624
Pb-Sn-Te, liquidus meas. by DTA 79−95999
Pb-Sn(-Sb), surface tension liquidus temp. to 550°C *(Korean)* 79−90848
Pb-Sn(Ag), dil. alloys, dislocation motion and electron-dislocation interactions 77−7728
Pb-Sn(Bi) alloys, dil., impurity effects on softening at T_c *(Russian)* 78−23220
Pb-Sn(Bi)(Ni), strength loss in supercond. transition, nonmag. and paramag. impurities influence *(Russian)* 80−70875
Pb-Sn(Sb), dil., US oscillations and dislocation unpinning in supercond. and normal states *(Russian)* 79−11648
Pb-Sn(20 wt.%), partially remelted interdendritic fluid flow 77−4771
Pb-Tl, liq., viscosity, comp. and temp. depend., up to 500°C 79−65233
Pb-Tl, low κ type II supercond., vortex motion anisotropy, intermediate-mixed state 78−47918
Pb-Tl, reversible surface superconducting magnetisation 78−43531
Pb-Tl, sliding and its accommodation during creep and superplasticity 77−40436
Pb-Tl, small κ type II supercond., flux line lattice, triangular/square transition 78−31025
Pb-Tl, supercond., crit. mag. fields, influence of parameters 80−75691
Pb-Tl, vacancies, positron capture, function of Tl concentration *(German)* 80−49213
Pb-Tl (20 wt.%) rod, supercond., critical current densities in surface pinning region 79−47216
Pb-Tl (2.5 wt.%), grain boundary sliding, grain size and stress effects 78−27571
Pb-Tl alloys, pinning parameters 78−52173
Pb-Tl alloys, positron trapping in vacancies, varying concentration effects *(German)* 80−25477
Pb-Tl-Bi-In, localised phonons studies by supercond. tunnelling 79−87210
Pb-Tl-Cd(Sn) melt, short-range order struct. 80−49088
Pb-Tl-In, localised phonons studies by supercond. tunnelling 79−87210
Pb-Zn, liquid phase immiscibility determ., DTA 78−64523
Pb-Zn, off-eutectic alloys, controlled grain growth *(Japanese)* 77−55958
Pb-Zn, pressure effect on solubility and diffusion of Zn 77−43385
Pb-Zn, unmixing alloys, mathematical model for solidification process *(Russian)* 80−81047
Pb_{1-c}-Li_c (As)(Ag)(In)(Sn)(Sb)(Te)(Au)(Tl)(Bi), liquid alloys, local fluctuations and quadrupolar relaxation 80−66060
Pb(Ag) alloys, effect of Ag content on yield strength 80−76322
PbBI-Al superconducting tunnel junctions, optically illuminated, quasiparticle energy distribution 80−75688
PbBi-AlO_x-Al tunnel junction, quasiparticle energy distrib. in nonequilib. supercond. 77−80881
$Pb_{0.9}Bi_{0.1}$, strong-coupled superconductor, quasiparticle recombination time 79−15259
$Pb_{0.98}Bi_{0.02}$-Cd, superconductor-normal-metal boundary resist., mag. field depend. 80−44772
$Pb_{0.99}Bi_{0.01}$, superconducting-normal interface, boundary resist. 80−50006
$Pb_{55}Bi_{45}$ film, amorphous, supercond. energy gap and transition temp. 78−14866
Pb_xBi_{1-x}, quench-condensed films, superconducting transition temp., elastic stress and strain effects 80−70883
Pb_3Ce, nucl. orientation meas. 78−39415
PbCu film, amorphous supercond., phonon heat transport, thermal cond. meas. 78−19181
$Pb_{0.9}Cu_{0.1}$, film, polycryst. or amorphous, thermal cond., 0.5-11K 78−39260
PbIn films strengthening, by preventing formation of misfit dislocations 80−84858
PbIn, flux flow, longitudinal geometry 78−14902
PbIn oxidised electrodes, symm. and asymmetric supercond. tunnel junctions, subharmonic gap struct. study 79−60981
PbIn superconducting films, penetration depth measured with Nb-NbO_x-PbIn Josephson junctions 79−42691
β'PbIn, thermodynamic analysis 77−36455
PbIn-oxide-Pb superconducting junction, two-particle tunnelling and microwave effects 78−43527

lead alloys continued
PbIn-oxide-Pb(PbTl) thin film tunnel junction, subharmonic group struct., multiparticle tunnelling theory 79−56438
$Pb_{0.8}In_{0.2}$, superconducting, flux-flow noise 79−95556
$Pb_{0.84}In_{0.16}$, barriers to flux entry and exit, magnetisation meas. 79−60963
$Pb_{40}In_{60}$, mixed state supercond., Hall and Ettingshausen effects, vortex entropy transport 80−44780
$Pb_{80}In_{20}$, flux pinning and flux flow noise 79−56473
$Pb_{80}In_{20}$ foil, deformed, annealed, correlation between pinning strength and flux flow noise charges 77−43792
$Pb_{80}In_{20}$ foil, flux flow current-voltage charact., and their mag. field depend. 78−23217
$Pb_{80}In_{20}$ foil, flux-flow crit. freq. and generalised bundle size depend. on fluxoid traversal distance and length 80−7054
$Pb_{83}In_{17}$, supercond., flux creep meas. 77−20508
Pb_xIn_{1-x}-Pb_yTl_{1-y} asymmetric supercond. tunnel junctions, subharmonic gap struct. 79−15260
PbInAu film, RF plasma oxidised, surface analysis using ESCA 80−50742
Pb_4Li, eutectic, ISSEC selection for fusion reactor 80−57950
PbNa, type-II superconductor, regularly ordered precipitates, peak effect, crit. current meas. *(German)* 78−19196
PbSb foil production for TEM by electrolytic and ion beam thinning *(German, English)* 77−49812
$Pb_{0.871}Sn_{0.129}$, supercond., hysteresis in flux flow charact., normal metal precipitates 78−80107
PbTl-O-Pb, Josephson tunnel junction parameters, microwave freq., temp. depend. 80−34561
Pb−(Au) (0.1 and 0.2 wt.%), single crysts., yield strength depend. at 77K on Av conc. 80−55479
Pd-Pb-Bi supercond. alloy, X-ray, microscopic, thermographic anal. *(Russian)* 77−32106
$Pd_{0.9}Ag_{0.1}$:H(D), free energy, enthalpies of soln. 78−15692
$Pd_{1+x}MnSb$ Heusler alloys, magnetic hyperfine fields on ^{111}Cd, TDPAC and magnetisation meas. 80−93219
$PdPb_2$-Rh, dil., quadrupole interaction of ^{100}Rh 79−99520
Pd_3Pb, Ll_2 ordered alloy, positive temp. depend. on strength, phase destabilization 80−81203
Pd_3PbBi, and Pd_4PbBi_3, cryst. struct. *(German)* 79−94963
PdPb.r, crystal structure *(German)* 80−96472
$Pd_{13}Pb_9$.r, cryst. struct., X-ray study 80−103293
PnBa, supercond., flux density distrib. meas. differential magnetisation loop method 77−32129
Po-Ge film, random percolation, elec. resist. meas. 79−28418
$PrPb_3$, crystalline elec. field parameters, exchange and Coulomb contrib. 77−20278
Pt-Pb fibre, CO adsorption and oxidation, AES and ESCA obs. 79−52469
$PtPb_{0.7}Bi_{1.3}$, crystal structure *(German)* 80−84139
$PtPb_3Bi$, cryst. struct. *(German)* 78−59783
Pt_4PbBi_7, cryst. struct. *(German)* 80−107113
$RhMn_2Pb$, mag. and cryst. props. 77−20568
Rh_2MnPb, hyperfine fields, ferromag., NMR and Mossbauer effect studies 80−71259
Rh_2MnPb, hyperfine mag. field at Cd impurity, TDPAC study 80−39905
$Sc_3PbC_{1-x}(B_{1-x})$, stabilising effect of C and B on alloying behaviour 77−36454
Sn-Cd-Pb system, contacting layer struct. and phase composition *(Russian)* 80−66475
Sn-Pb, dil., lattice dynamics, sp. ht., resist., thermal expansion and nuclear γ reson. expts. *(Russian)* 78−87749
Sn-Pb, dil., undercooled alloy, solidification 78−3120
Sn-Pb, effective atomic number from β-ray produced bremsstrahlung meas. 78−22046
Sn-Pb, eutectic system, interlamellar spacing meas. 77−36492
Sn-Pb, liq. calc. of electromigration forces and resist. 79−82572
Sn-Pb, liquid alloy, thermodynamic activity determ. using Knudsen method *(German)* 79−34008
Sn-Pb, refining by fractional solidification 79−61536
Sn-Pb, supercooled, dendritic growth rates *(Russian)* 78−80533
Sn-Pb, temp. regime of crystn. on rapid cooling *(Russian)* 80−66495
Sn-Pb, thermo-EMFs meas. 77−20300
Sn-Pb (15 wt.%), forging of liquid and partially solid alloys 78−80569
Sn-Pb (15 wt.%), partially solidified slurry, exam. of structure, viscosity 78−84793
Sn-Pb (26%), liq. eutectic alloy Seebeck coeff. 80−84463
Sn-Pb (38 wt.%), graphite fibre reinforced, effect of interface on fracture charact. 78−76723
Sn-Pb (38.1 wt.%), liq., self-diffusion coeff. of Sn, 466 to 786K 77−69106
Sn-Pb (5 wt.%) ingots, quenching technique, for studying formation of macrosegregations 78−52793
Sn-Pb alloys, dil., low-freq. phonon spectrum peculiarities 79−60463
Sn-Pb alloys, electron work function determ., contact pot. difference method 77−39920
Sn-Pb alloys, inhibited electrocrystn. *(German)* 79−38753
Sn-Pb alloys, stress relaxation and activation enthalpy 79−74190
Sn-Pb alloys electroplating, comparison with Au *(French)* 80−89158
Sn-Pb composition anal. of PCBs using beta-backscatter gauge 80−16631
Sn-Pb eutectic, strain rate sensitivity of flow stresses, grain boundary sliding during superplastic, non-superplastic deform. 80−7645
Sn-Pb eutectic, struct. and plasticity, thermomech. treatment effects *(Russian)* 78−60686
Sn-Pb eutectic alloy, inelastic behaviour 77−48471
Sn-Pb investment castings, graphite fibre reinforced, tensile strength 77−48487
Sn-Pb solder, wettability on Cu and mild steel plates *(Japanese)* 80−89244
Sn-Pb solder on Cu plate, spreadability, effect of fluoride and iodide addition to $ZnCl_2$ flux *(Japanese)* 80−29251
Sn-Pb surfaces ageing, detrimental effect in PC fabrication 80−108625
Sn-Pb-Bi-(Cd) infiltrated Ti base composite sintered bearing material, antifriction props. 80−60981
Sn-Pb-(Bi) infiltrated Ti base composite sintered bearing material, antifriction props. 80−60981
Sn-Pb-(Bi)(Ag)(Sb) (Cu), microduplex eutectic, cavitation during superplastic flow 78−48457
SnPb 38, superplasticity, effect of ageing *(Czechoslovakian)* 77−32644

lead alloys continued
SnPb eutectic alloy, Mossbauer spectra, isomer shifts 79−82903
Sn_xPg_{1-x}, thermal cond. and Lorenz function 78−51966
Te-Pb, amorphous, obtained by splat cooling, crystallisation, TEM obs. 77−66638
Te-Pb (20 at.%), amorphous, obtained by rapid cooling from liq. state, crystn. behaviour 78−26445
Th-Pb, liquid alloy, thermodynamic props. *(Russian)* 77−25011
Ti-Pb, eutectoid decomposition 79−24491
Tl-Bi-Pb, phonon anomaly near Fermi surface topological transition, phonon softening at X point 78−95120
Tl-Pb, in solid and liquid state, specific electric resistance 80−103662
Tl-Pb-Bi, critical field and specific heat 79−73631
Tl-Pb-Bi, supercond., electronic density of states from heat capacity meas. 79−56383
Tl-Pb-Hg system, thermodynamic props. *(Russian)* 77−25018
UPb_3, crystal field energy levels, magnetisation and susceptibility, neutron spectra obs. 80−50064
Zn-Al-Cu-Mg-Pb-Sn, Cu, Mg, Pb, Sn effects on corrosion in wet steam 77−48585
Zn-Al-Cu-Mg-Pb-Sn (12, 1, 0.02, 0.01, 0.015, wt.%), combined effects of Pb and Sn additions on corrosion, in wet steam 78−39952
Zn-Pb, liquid, surface tension, size effect *(French)* 80−15341
Zn-Pb composite, production under conditions when gravity forces are balanced out by EM forces 78−31363
Zn-Pb melt, immiscible component distrib. in crossed EM fields *(Russian)* 77−48396
Zn-Sn-Pb, intergranular and solid-liquid interfacial tensions 77−36452

lead bonding
furnacing technique for bonding Au and Ag on sapphire 78−54352
IC prod., Ag electroplated lead frames surface struct. rel. to bonding behaviour *(German)* 79−11010
NDT wire bonds on Si chips, IR microscopy 78−95867
physiological miniature strain-gauge pressure transducers 79−100778
US bonding displacement meas. by He-Ne laser interferometer 77−37972
Al-Au bimetal thin film interdiffusion zone, intermetallic phase form kinetics, 70-160°C 78−75891
Au conductor bonding performance and failure mechanisms 79−71436
GaAs, plastic deform. prod. by thermocompression bonding, elec. props. 77−76807
Ti/Cu/(Au) thin films thermocompression bonds degradation by thermal ageing 80−66546

lead compounds
see also lead alloys
air pollution, dispersion from motor exhausts 79−70491
alkyl Pb compounds, in atmosphere, detect. via gas chromatograph-microwave plasma detector 78−68975
borosilicate glass, phase separated, components distrib. by electron probe microanal. *(Japanese)* 79−52844
chalcogenide films, epitaxial, orientation on fluorite struct. substrate 77−35824
chalcogenide mixed crystals, intraband absorption, due to chemical disorder 79−56789
chalcogenides, Auger recomb., theory 80−65586
chalcogenides, elec. cond. anisotropy in strong electric fields *(Russian)* 79−38082
chalcogenides, electron-hole liquid theory, generalised RPA 78−87914
chalcogenides, interband absorpt., optical absorpt. coeff., two- and six-band models 79−33728
chalcogenides, interband absorption under linearly polarised light excitation 78−92089
chalcogenides, multicolour photodetectors *(Czech)* 79−26126
chalcogenides, spectral depend. of internal quantum efficiency 77−4402
chalcogenides, warm electron cond. 79−91066
chrome yellow, crystal lattice deform. effect on colour *(Rumanian)* 78−23422
crystal glass, chem., electrochem. corrosion *(French)* 79−20232
DH lasers for IR gas spectroscopy 77−19325
dicalcium lead propionate, effect of particle size on dielec. behaviour 79−38429
dicalcium lead propionate, ferroelec., annealed, crit. exponents, dielec. const. temp. depend. 80−55050
dicalcium lead propionate, Raman scatt., order-disorder type transform. 77−12373
dicalcium lead strontium propionate, mixed cryst., phase diagram, dielec. and dilatometric anomalies 77−11689
displacive phase transition, S ion spin Hamiltonian parameter dependence on order parameter 80−70356
eutectics, HgTe-PbTe and Au-PbTe, prep. and thermoelectric behaviour characts. 80−107774
galena, polycryst. synthetic, stress relax. 500 to 800°C 78−87737
glasses, Cu containing, crystallisation 78−47241
halide based photodevelopable materials 79−21830
halides, adsorpt. of water, mol. studies of ice-forming capabilities 77−31872
halides, doped, secondary ion emission, at. and mol. processes 78−68588
halides, exciton spectra, temp. and press. effects 77−20881
halides, metastable exciton emission, electron excitation mechanism 77−66546
halides, molecular versus atomic secondary ion emission, rel. to quantitative analysis 79−61481
halides, UV photoelectron spectra of valence d shells, gas-phase 78−62845
halides impurity distributions, in TlBr and TlI of various cryst. orientations 79−51135
heterogeneous oxidation catalysts, effects of Pb compounds 79−24817
hydroxyapatites, elec. cond., charge carrier identification 78−67855
inorganic and organometallic cpds., photoelectron spectra, valence bands, ligand field broadening 77−63525
intermolecular shielding contributions, proton mag. shielding 80−34783
ion-selective electrodes, solid-state, for potentiometric determ. of phosphate 79−92044
lead phthalocyanine:O_2, photocond., impurity-induced 79−47120
lead phthalocyanine film, switching effects 79−28384
$M^IM^{IV}IO_6$, vibr. spectra (M^I=Na,K,Rb,Cs,NH_4; M^{IV}=Ge,Sn,Pb) 77−42325
monochalcogenides, interaction of outer s states 79−10825
monochalcogenides interaction of internal s states 79−10826
myristate, multilayer analyser for X-ray spectroscopy 78−49944
niobates, pyrochlore block structs., cryst. struct. determ. *(German)* 80−70178
nitrocomplexes, planar dynamic Jahn-Teller effects 77−15804
optical glass containing PbO, effect of Al_2O_3/Na_2O ratio on rate of ion exchange 78−44377
organolead compounds, aliphatic and aromatic, ^{13}C and ^{207}Pb NMR 79−95657
organolead compounds adsorbed on atmospheric particulates in urban air 77−73831
oxides, antiferroelec., growth and props. 79−38461
oxides, effect on thermal oxidation of Si 77−36673
oxides, X-ray absorption, discontinuities and limits, chem. combination effects 80−93435
$Pb_3M_gNb_2O_9$ crystals for optical radiation control 79−81554
$Pb_4Sb_4S_{11}$, synthetic, cryst. struct. by X-ray goniometry 80−6394
$Pb_5Ge_3O_{11}:Gd^{3+}$, ESR spectra, electric-field effect and reversible permittivity 80−29614
PbI_2, trapping levels, TSC meas. 78−23107
$PbO-Nb_2O_5$ system, X-ray and electron microscopic phase and struct. determ. *(French)* 80−92508
n-PbTe, dynamical cond. in freq. range of LO-phonon-plasmon excitations 79−19592
perovskite, Pb_2XReO_6 (X=Mg, Fe, Co, Ni), new seignettomagnets and ferroelectrics 78−19425
perovskites, ordered cubic, cationic effect on intramolecular forces, stretching force const. 80−88979
phthalocyanide, thermal stability obs., by DTA *(German)* 80−11945
PLZT, diffuse phase transitions 79−33628
PLZT, optically induced birefr. change 78−43832
PLZT ceramics, ferroelec., special props. 79−42916
PLZT ceramics as electro-optic shutter material for IR appls. 79−72679
PLZT coarse-grained solid solutions, electro-optical processes induced by longitudinal electric field *(Russian)* 80−80750
PLZT ferroelectric ceramic, anomalous bulk photovoltaic effect and cond. *(Russian)* 80−54733
polymorphic transformations possibility, mag. and elec. ordering effects 80−55389
PZT, ferroelec. ceramic, mechanical props. determ. by acoustic techniques 79−28685
PZT ceramics, ferroelec. energy conversion under shock loading 80−108163
PZT/polymer composites, simplified fabrication 80−40323
rare earth lead molybdenum sulphides, $R_xPb_{1\pm x}Mo_{6+y}S_8$, R=La, Nd, Pr, Gd, sputtered, supercond. props. 80−50019
rare earth substituted lead apatites, $Pb_{10-2x}R_xM_x(PO_4)_6Z_2$, M=Na or K and Z=F or Cl, cryst. struct. and IR spectra 80−107167
schultenites, ferroelectric, sp. ht. 79−19853
stabilisers in PVC, degradation obs. using X-ray diffr. *(German)* 79−34297
stearate, Langmuir-Blodgett multilayers, comp. and transfer mechanism 80−80125
sulphides, isotopic composition, mineralisation time determ. 78−73372
tartrate, single cryst. growth in gel, dendrite form. and self-regulation 77−77352
tellurites, acousto-optical criterion estimation 79−82945
tetra-alkyl Pb compounds in urban air 78−16149
titration, amperometric, using thioxanthate 79−57326
triphenyl isocyanate, X-ray cryst. struct. determ. and refinement 79−51097
in urban aerosols, identification, rel. to health hazards 78−44991
XPS, outer core of level linewidths 77−44118
zeolites, synthetic, effect of sintering on elec. cond., porosity and microstruct. 79−29009
zinckenite, chem. and structural study *(French)* 77−43181
SnTe-PbTe-GeTe, alloy semiconductor, phase transition *(Japanese)* 78−91443
$3PbO.GeO_2$, X-ray and electron diffr. exam. *(German)* 80−11632
Ag-Pb-Te, phase equilibrium *(German)* 79−34018
$AgBr:PbBr_2$, emulsion grains, dielec. loss, ionic cond. and surface space charge 77−28038
$AgI-PbI_2$ molten mixtures, conductivity, thermodynamic excess props. 79−86914
$AgPO_3-PbI_2$ glass, elec. cond. and Raman. spectra rel. to struct. *(French)* 79−10979
$(Ag_{x/2}Pb_{1-x}Bi_{x/2})Te$ solid solution, preparation and thermoelectric props. 77−47839
$(Ag_{x/2}Pb_{1-x}Sb_{x/2})Te$ solid solns., Hall coeff., thermoelec. power, and thermal cond., 100 to 500K 79−82614
Al-Pb liquid alloy, surface tension and surface adsorpt. determ. *(French)* 79−69325
Al-PbS selective surfaces for solar photothermal conversion, prep., emissivity, absorptivity 80−12030
As_2S_3-PbS glass, DC elec. cond. and photocond. 78−39107
As_2S_3-PbS glasses, structural props. 79−27925
$Au-Pb_xSn_{1-x}Te$-Au structure, third harmonic variations at 77K and 300K 78−84313
B_2O_3-PbO glass-ceramic-cement composites, review 79−38783
$B_2O_3-PbO-GeO_2-Fe_2O_3$ glass, Mossbauer exam. of Fe valence states 79−78597
$B_2O_3-PbO-GeO_2-Fe_2O_3$ glasses, mag. props. and Mossbauer spectra, spero-mag. order at low temps. 80−80530
$(Ba,Pb)Al_{12}O_9$, LPE growth 79−100064
$BaMoO_4$-PbO and $BaMoO_4-PbMoO_4$ systems, phase diagrams 77−25034
$BaO-PbO-GeO_2-MF_2$ (M=0.45CaF_2+0.55MgF_2), MgF_2 and CaF_2 effect on physicochem. props. 80−34876
$BaPb_{1-x}Bi_xO_3$, struct. determ., X-ray and neutron diffr. study 79−42039
$BaPb_{1-x}Bi_xO_3$, supercond. T_c and crit. fields, comp. depend. 79−73623
$BaPbF_6$, Group IV hexafluoride anion radical γ-irrad., EPR spectra 78−72411
$BaTiO_3-PbO-B_2O_3$, liquid phase sintering, effect on props. *(German)* 79−33980
BamSrmPb hexaferrites, prep. by cernet procedure, mag. props. 77−32174
$BiFeO_3-Pb(Fe_{0.5}Nb_{0.5})O_3$, ferroelec., magnetoelec. obs. temp. and conc. depend. 80−50156
Bi_2O_3-PbO, glass, cond. meas. using complex impedance anal. *(French)* 80−92707
$Bi_2S_3-CuPbBi_5S_9$, solid solution, semiconductor and dielectric props. 79−69511

lead compounds continued
$Bi_2Ti_4O_{11}$:PbO, anomalous temp. depend. of phonon modes, Raman spectra 78−10893
$BiVO_4$, ferroelastic phase transition, thermodynamic theory 79−37832
$CaO-V_2O_5-Fe_2O_3-PbO$, crystallisation field of Ca-V ferrogarnet 77−16548
$CaPb(OH)_6$, cryst. struct. determ. *(French)* 77−47419
$CdCl_2-PbCl_2$, thermodynamic quantity meas. by quantitative thermal anal. of heating process 78−19730
CdI_2-PbI_2-NaI, fusion diag. and thermodynamic calc. *(Russian)* 77−48417
$(CdI_2)_x(PbI_2)_{1-x}$, layered cryst., photoluminesc., and reflection spectra obs. 78−6726
$(CdI_2)_x(PbI_2)_{1-x}$, reflection and luminesc. spectra obs. 77−8648
$Cd_xPb_{1-x}I_2$, photoluminescence comp. and energy depend., band gap 77−44045
$Cd_{1-x}Pb_xSe$, electroless film deposition with variable comp. and polymorphic structs. 79−95952
$Cd_{1.6}Pd_{0.4}Nb_2O_7$, ferroelec., sp. ht. and Debye temp. meas., 2-25K 79−73319
CdS-PbS, film production, electrochem. method 77−44180
$Co(NH_3)_6(Pb_4Cl_{11})$, cryst. struct., and relationship with the chlorolead struct. moieties in $NH_4(Pb_2Cl_5)$ and $PbCl_2$ 79−32954
$CsNO_3-Pb(NO_3)_2$, ht. of crystn. *(Russian)* 77−48418
$CsPbBr_3$, critical thermodynamic props. around successive phase transitions 79−33627
$CsPbBr_3$, $CsPbCl_3$, ionic semiconductors, electronic and optical props. 79−38594
$CsPbBr_3$, struct., Debye-Waller factor, neutron diffr. study 79−90609
$CsPbCl_3$, critical thermodynamic props. around successive phase transitions 79−33627
$CsPbCl_3$, exciton states, magneto-optical investigation 80−29328
$CsPbCl_3$, lattice thermal expansion, X-ray powder technique 80−19965
$CsPbCl_3$, O_h^1-D_{4h}^5 transition, US and thermodynamic props. 78−67826
$CsPbCl_3$, phase transition under pressure 78−51664
$CsPbCl_3$, refr. index and birefr., struct. transition effects 77−90126
$CsPbCl_3(Br_3)$, optical and photoelectronic spectra 79−24410
$CsPbCl_xBr_{3-x}$, optical meas., LCAO band scheme 80−25437
$Cs_2PbCu(NO_2)_6$, α-modification, Jahn-Teller induced α to β transition, neutron diffr. obs. 79−1498
$Cs_2PbCu(NO_2)_6$, one-dimensional stacking order 80−28941
Cu-PbI_2, thin sprayed layer, glass substrate, hologram recording *(Russian)* 77−71956
CuBr-$PbBr_2$ system, phase diagram, DTA and X-ray diffr. analysis 77−47552
CuI-PbI_2 system, phase diagram, DTA and X-ray diffr. analysis 77−47552
$Cu_2O-PbO-SiO_2$, equilibrated with liquid Cu, Pb and Ni distrib. 77−28790
CuPbBiS, ferroelec. semicond., elec. cond., photocond. permittivity, phase transitions 77−47822
$CuPb_3Br_7$, ionic cond. meas. 77−47552
$Er_2O_3-TiO_2-WO_3-PbO$, glass form., refr. indices and density meas. 77−90312
$xFe_2O_3-(1-x)PbO-3B_2O_3$ glass, Mossbauer study of Fe cations 79−91325
$Fe_2O_3-B_2O_3-PbO$ glass, semicond., elec. resist. meas. 78−95300
$Fe_2O_3-B2O_3-PbO$ glasses, visible and UV optical props. *(Rumanian)* 78−48196
$Fe_2O_3-PbO-B_2O_3$ glass, X-ray and electron microscope studies, mag. and Mossbauer effect meas. 80−28919
$Fe_2O_3-PbO-V_2O_5$ fluxed melt system, solubility and relative supersaturation meas. 80−64934
$(Fe_2O_3)_x-(3B_2O_3.PbO)_{1-x}$ glass, thermal cond. and diffusivity obs. 79−60561
$(Fe_2O_3)_x(3B_2O_3.PbO)_{1-x}$ glass, X-ray diffr. struct. obs. 79−32915
$xFe_2O_3.(1-x)[3B_2O_3.PbO]$ glasses, diffuse refl. spectra 79−51982
$20Fe_2O_3.80[3B_2O_3.(1-x)PbO.xGeO_2]$ glass, phys. props. 80−49119
$FePb_4Sb_6S_{14}$, photosensitive semiconductor, with high permittivity, elec. props. 79−65518
Ga_2S_3-PbS system, phase diagram and crystallographic study *(French)* 80−29937
$Gd_2O_3-Fe_2O_3-PbO-B_2O_3$, primary crystallisation regions 77−12604
Gd_2Se_3/PbTe, N type selenide segmented element fabrication, thermoelectric props. 80−107835
$(Ge,Pb)_{1-x}Mn_xTe$, mag. and elec. props. meas. 80−29534
$Ge-Pb_{1-x}Sn_xTe$, amorphous/crystalline heterojunction, rectification props., IR detector appl. *(Japanese)* 78−60197
Ge-Pb-Bi-O glass, photoelasticity, glass transition limits 79−33670
Ge-Pb-S, glassy, photoconductivity dependences applied elec. field 80−107857
Ge-Pb-Se-Te, glass form., DC cond., and mole volume 79−90560
GeO_2-PbO glasses, IR transmittance and thermal expansion, effect of oxides and fluorides 77−63405
$In_{1-x}Pb_xTe$, single crystals, mag. susceptibility 79−51738
$InSb/Pb_{0.79}Sn_{0.21}Te$ photodiodes, two-colour sandwich detector 77−82602
InSb-PbSnTe sandwich two-colour IR detector 78−45692
In_2Te_3-PbTe system, phase diagram, elec. props. 78−35361
KBr:PbI_2, single crysts. grown from aq. soln., growth striations obs. 77−1089
KCl:$PbCl_2$, tablet, 272 nm absorpt. band 78−84612
$KF-PbO-SiO_2$ glass shear wave velocity and its temp. depend. *(Japanese)* 78−30702
$KNO_3-Pb(NO_3)_2$ molten mixture, elec. cond., Tobolsky parameter *(German)* 80−15282
$K_2O-B_2O_3$ glass, PbO-activated, luminesc. and excitation spectra *(Russian)* 78−10979
$K_2O-PbO-PbF_2-SiO_2$ glass shear wave velocity and its temp. depend. *(Japanese)* 78−30702
$K_2O-PbO-SiO_2$, glass, mech. and optical props. *(Russian)* 77−20860
$K_2O-PbO-SiO_2$, glass, effect of DC on corrosion of SnO_2 electrodes 80−85075
$K_2O-PbO-SiO_2$, structural units, Raman spectroscopy 77−20847
$K_2O-PbO-SiO_2$ glass powders, ion exchange during leaching in HNO_3 79−100358
$K_2O-PbO-ZnO-B_2O_3-SiO_2$, corrosion and microhardness, effect of detergents 80−16518
$KPO_3-Pb(PO_3)_2$, phase diagram of binary system 77−21114
$K_2PbCu(NO_2)_6$, effect of hydrostatic press. on successive Jahn-Teller phase transitions 78−43120
$K_2PbCu(NO_2)_6$, incommensurate Jahn-Teller phase transition 78−79730
$K_2PbCu(NO_2)_6$, Jahn-Teller phase transitions, order-disorder model 78−79762
$K_2PbCu(NO_2)_6$, phase transitions induced by Jahn-Teller effect, uniaxial stress effects 80−6512
$K_2PbCu(NO_2)_6$, US vel. near cooperative Jahn-Teller phase transitions 79−23680
$La_{1-x}Pb_xMn_{1-y}Fe_yO_3$, magnetically ordered, NMR, spin echoes and relax. 77−48087
$La_{0.65}Pb_{0.35}MnO_3$, transport props. near Curie points 78−88100
$La_{0.71}Pb_{0.29}MnO_3$, metal-semicond. transition at Curie point, transport props. obs. 79−73554
$La_{1-x}Pb_xMnO_3$, spin polarised XPS and UPS, elec. struct. 77−8717
$La_xPb_{1-x}Zr_yTa_{1-y}O_3$, ferroelec. with diffuse phase transition, electrostriction-optical props. 78−68457
LiCl-$PbCl_2$, molten, struct. anal. by X-ray diffr. 78−94961
$LiPbPO_4$, vibrational spectra and cryst. struct. 78−39536
MnO_2, β and γ conductivity meas. by new method 80−45517
$xMnO.(100-x)[19TeO_2.PbO]$, EPR studies of Mn^{2+} ion distribution 80−71167
$(NH_4)_2PbCl_6$, temp. depend. of tunnel freq. 80−1947
$Na_{0.5}Bi_{4.5}Ti_4O_{15}$, hot-forged ferroelec. ceramic with layer struct. 79−43175
NaCl:$PbCl_2$ crysts., melt grown, Pb distrib. determ., UV spectrochem. anal. 78−40101
$NaNO_3-CsNO_3-Pb(NO_3)_2$, fusion diag. *(Russian)* 77−48418
$NaNO_3-Pb(NO_3)_2$, ht. of crystn. *(Russian)* 77−48418
$NaNO_3-RbNO_3-Pb(NO_3)_2$, crystn. heat of eutectic, thermodynamic anal. *(Russian)* 77−63644
$Na_2Nd_2Pb_6(PO_4)_6Cl_2$, laser material, flux growth *(French)* 78−35288
$Na_2Nd_2Pb_6(PO_4)_6Cl_2$, high-Nd conc. laser material, oscillator strengths and laser effect 79−55140
$Na_2O-PbO-B_2O_3-SiO_2$, homogeneous melt formation rate, exam. 78−64520
$Na_2O-PbO-SiO_2$, activity of PbO, EMF meas. 77−47595
$Na_2O-PbO-SiO_2$, molten glass, reactions with conducting materials 80−85186
$Na_2O-PbO-SiO_2$, PbO activity 78−44112
$Na_2O-PbO-SiO_2$ glass-ceramic composite, directionally crystallised 80−107058
$Na_2Pb_{11}F_{18}Br_6$, cryst. struct. determ., X-ray study 79−60320
Nb-NbO_x-PbIn window type junctions, critical Josephson current depend. on magnetic field 79−65607
$PBMoO_4$, ^{207}Pb mag. shielding anisotropy, Fourier transform NMR 77−90057
PLZT ceramic, ageing, dielec. props. 80−88940
PLZT ceramic, bonded lens assembly manufacture 80−79018
PLZT ceramic, dielectric anisotropy, role of 90° domain processes 77−63384
PLZT ceramic, ferroelec., cathodlum. spectral and temp. depend. 78−84665
PLZT ceramic, modulator for optical communication 80−78964
PLZT ceramic, optical gate, dielec., optical props., electro-optical effect meas. 78−42418
PLZT ceramic, possible construction of matrix-addressable controlled transparency 78−71222
PLZT ceramic, proton implanted, photoferroelectric effect for image storage and display devices 80−80315
PLZT ceramic, thin waver electrode slotting process 80−79017
PLZT ceramic, thin wafer production polishing process 80−81214
PLZT ceramic, transverse electro-optical effect, matrix-addressable transparency 79−27431
PLZT ceramic birefringence props., transverse electro-optical meas. 78−72487
PLZT ceramic photoferroelectric image storage device, characts. 77−55756
PLZT ceramic with memory, domain reorientation, alternating elec. field effect 79−47405
PLZT ceramic;, visible light scatt. depend. on photoferroelectric space charge fields 80−80806
PLZT ceramics, diffuse phase transitions and thermodynamics 80−29694
PLZT ceramics, electro-optic characts., w.r.t. future instrument applics. *(German)* 78−33792
PLZT ceramics, electro-optical props. *(Korean)* 79−11406
PLZT ceramics, electro-optic; defect struct. and prop. 79−42910
PLZT ceramics, elastooptic effect, stress induced birefr. 80−60543
PLZT ceramics, ferroelectric and struct. transitions, crystallographic, thermal, and dielec. anal. 80−29693
PLZT ceramics, modified by $Ca^{2+}(Sr^{2+})(Nd^{3+})(Y^{3+})$, dielec. behaviour 80−60519
PLZT ceramics, optical recording *(French)* 77−31078
PLZT ceramics, optical information storage and spatial light modulation 78−83097
PLZT ceramics, photoferroelectric image storage in antiferroelectric phase 79−47404
PLZT ceramics, photoferroelectric effects, image storage device appl. 79−42924
PLZT ceramics, photoinduced charge transfer process 79−50362
PLZT ceramics, phase transitions induced by elec. fields 80−29695
PLZT ceramics, pulse charging of nenofarad capacitors from shock depoling 79−42913
PLZT ceramics, SHG, anomalous phase transition 79−45996
PLZT ceramics, short circuit photocurrent, depend. on polarization 79−38121
PLZT ceramics, sp. ht., 2-25K, field depend., phonon modes 77−47586
PLZT ceramics, stress-induced ferrelec. transition, pseudoelasticity and shape memory, bending meas. 79−24274
PLZT ceramics, transparent ferroelec., photorefraction and photocond. study 79−42581
PLZT ceramics photosensitivity enhancement by H- and He-ion implantation 80−96934
PLZT, coaxial magnetron sputtering techniques 79−83123
PLZT colour cell for real time two colour incoherent to coherent image convertor 78−38039
PLZT composition, effect on its switching characts. 79−42917
PLZT, controlled light scatt. 78−10909
PLZT, deposition of transparent electrodes, opt. storage device applic. 78−74848
PLZT, diffuse phase transitions, Curie temp., dielectric props. 80−75979

lead compounds continued

PLZT, effect of ageing on temp. depend. of permittivity, for ferroelectric and antiferroelectric compositions 78−48121
PLZT, electrically polarised, size and conc. of light scatt. centres 77−28549
PLZT, electro-optical, physical elec. and optical props. and fabrication *(Polish)* 78−56458
PLZT electro-optic shutter stereoscopic display applications 80−90826
PLZT electrooptic shutters as thermal/flash protective devices 77−46808
PLZT, electrooptic systems *(Japanese)* 79−65840
PLZT, exam. of grain growth in hot pressing, and liquid phase sintering 79−33981
PLZT, Fe doped, photochromic effect 77−16347
PLZT ferroelec. ceramics, piezoelec. props. 79−42897
PLZT, ferroelectric domain struct. obs. by SEM and optical microscopy *(Japanese)* 78−15136
PLZT ferroelectric display electro-optical props. *(Russian)* 79−9211
PLZT ferroelectric ceramic, photovoltaic effect 79−99585
PLZT, ferroelectric phase transitions, phase state identification 80−45018
PLZT ferroelectric thin films, epitaxial growth and optical props. 80−70543
PLZT film, electro-optic effects 78−6799
PLZT film, epitaxial growth by RF sputtering, and characterisation 77−85937
PLZT, fine grained 90° electric domain wall movement, interpretation of dielectric losses *(German)* 79−33646
PLZT, hologram storage, book contrib. 78−25834
PLZT, light scatt., time depend., switching, memory modes 77−12362
PLZT, light scatt. under switching conditions, time characts. 77−52045
PLZT, light scattering, IR laser radiation recording 78−4695
PLZT, mech. and elec. losses, correl., theory and expt. 80−66133
PLZT modified high voltage dielectric, permittivity, Curie temp., loss meas. 80−80720
PLZT, opt. spectra and luminesc. 78−76508
PLZT, phase transitions, permittivity, birefr. and light scatt. meas. 77−81074
PLZT, photoferroelectric image storage in antiferroelectric-phase PLZT ceramics 80−71353
PLZT, photorefractive effect and photoconductivity 78−92046
PLZT porosity and transparency affected by vacuum hot pressing 77−12556
PLZT powder preparation, hyrolysis ball mixing 80−81006
PLZT powders, chemical prep. and hot pressing 78−44059
PLZT, prep. by liquid phase sintering of oxides 79−38778
PLZT, pure and doped solid soln. powders, synthetic process prep. 79−78920
PLZT pyroelectric detectors, fast response to MW CO_2 laser pulses 79−54187
PLZT pyroelectric detectors, piezoelectric oscillations, in response to CO_2 laser pulses 79−61305
PLZT pyroelectric detectors, delayed onset of piezoelec. oscills. 80−75953
PLZT, RF sputtered thin film, ferroelectric props. 79−69780
PLZT real time 2 colour incoherent to coherent image convertor 79−3805
PLZT, reduced, exam. of ageing phenomena, using dielectric hysteresis *(German)* 79−33647
PLZT, refr. index, 405-764 nm, surface layer 78−35110
PLZT slim-loop and linear ceramics, longit. electrooptic effects, display appl. 80−80751
PLZT slugs, powder hot pressing technique 80−81007
PLZT, Sn substituted, antiferroelectric ceramics research and their applications *(Chinese)* 79−33617
PLZT spatial light modulator for a 1-D hologram memory 80−37963
PLZT thermal, flash, ferroelectric protective goggles 80−81746
PLZT, thin, elec. cond. and pyroelectric behaviour 80−75954
PLZT, thin film epitaxial growth and characteris. 79−28918
PLZT, thin film prep. by RF sputtering, struct. and ferroelec. props. *(Japanese)* 77−69992
PLZT, transparent, optical exam. of small signal behaviour, of 90° electric domain walls *(German)* 79−33645
PLZT transparent ceramics, electro-optical anisotropy due to hot pressing 77−12720
PLZT, transparent ferroelec., RF sputtering and film characterisation 78−72727
PLZT, transparent ferroelectric, ceramics obtained by hot pressing, optimum conditions *(German)* 79−43176
PLZT type ceramics, calorimetric meas. of energy of electrical polarisation 79−2770
PLZT, with broad phase transition, birefr., electro-optic and dielec. props. 77−16280
PLZT:Fe, enhancement of photochromic effect by multi-reflection scatt. 77−75632
PLZT/TFPD thermal/flash protective lens assembly, polarised delamination investigation 80−78929
PLZT-based polarised ceramic, electro-opt. props. 77−52041
(PLZT)(PLZN) system, ferroelec. transparent, prep. and study 79−42911
PZT, ferroelec. film, elec. props., composition anal., AES 78−84530
PZT paraelectric ceramic one-dimensional spatial light modulator 79−55240
PZT-polymer flexible composite transducer 78−80291
$(Pb,Ba)_5Ge_3O_{11}$ ferroelectric crystals, influence of Pb replacement by Ba on props. 79−87402
$(Pb,Ba)Nb_2O_6$, polycryst., orientational polarisation and phase comp. in strong field 78−27157
$(Pb,Ba)(Zr,Ti)O_3$, diffuse phase transitions, Curie temp., dielectric props. 80−75979
$(Pb,La)TiO_3$ ceramic, ferroelec. Curie temp. comp. depend. 77−16258
$(Pb,La)TiO_3$, paraelec. phase, anomalous dielec. behaviour 78−23387
$(Pb,La)TiO_3$, soft E(TO) phonons, and phase transitions, Raman spectra, −200 to 400°C 78−15109
(Pb,Sn)Se IR detector diode, junction resist. comparison with (Pb,Sn)Te 78−24858
(Pb,Sn)Te diode laser, grating coupled emission 77−79860
(Pb,Sn)Te IR detector diode, junction resist. comparison with (Pb,Sn)Se 78−24858
(Pb, Sn)Te-type semiconductors, displacive ferroelec. phase transitions, vibronic theory 80−11354

lead compounds continued

$(Pb, Sr)_5Ge_3O_{11}$, single crysts., growth and X-ray and dielec. investigations 80−88127
$(Pb,Sr)TiO_3$, ferroelec. solid solution, dielec. nonlinearity in nonpolar phase *(Russian)* 77−32317
$(Pb,Sr)TiO_3$, ferroelec. props., press. depend., anharmonic oscillator model 80−80716
$(Pb,Sr)(Zr,Ti)O_3$, piezoceramic, effect of glass additions on props. during hot pressing 79−24475
Pb bi-univalent cpds., soln., activity and osmotic coeffs., H_2O activity, Gibbs energy, molality depend. 80−51964
Pb ceramic glaze, Cu^{2+} doped, Pb^{2+} release 80−49101
Pb chalcogenide, solid solution, thermoelectric efficiency 79−95429
Pb chalcogenides, interband transitions, absorpt. coeff., multiband calc. 80−29738
Pb complex, $Pb(C_2O_4)_2^{2-}$, stoichiometry, form. const. determ., teaching appl. 79−84916
Pb complex formation with oxyacids, IR and PMR study *(Russian)* 77−28582
Pb crystal glass melting, elec. furnace 79−58691
Pb glass counter, automated calibration system 80−106233
Pb glazes, Cu^{2+} doped, alkaline substitution, crystal field modifications, EPR study 79−95634
Pb $Mg_{1/3}Nb_{2/3}O_3$ ferroelectric semiconductors, electro-optical and elasto-optical props., appl. to optical storage *(Russian)* 80−80749
Pb multicomponent glasses, alkali evaporation, mass spectrometry study, thermal anal. 79−74464
Pb salt, tunable IR diode lasers 78−59030
Pb salt semiconductor laser, low freq. noise characts. 79−59698
Pb salt tunable diode lasers, wavenumber calibration using etalons 78−45738
Pb salt tunable diode laser-integrating sphere system, output intensity characts. 80−78881
Pb salts, inorganic 80−77081
$Pb/PbCl_2$ electrode, in chloride media, low temp. props. 78−68899
$Pb/PbF_2/BiF_3/Bi$ thin solid film reversible galvanic cell 79−52928
Pb-Ar films, atomic arrangements, high energy electron energy diffractogram study, Ar conc. depend. 79−99444
Pb-As-S semiconductor glasses, far IR transmission and Raman scattering 77−63419
Pb-Cd-Te, microhardness meas. as function of applied load, elec. props. exam. 78−48493
Pb-Cr-O system, equil. relationships, stability limits 77−59765
Pb-Ge-S semiconducting glasses, far IR transmission and struct. 79−65855
Pb-Pb_xO_y-Pb Josephson junction, long-term stability at liq. N_2 temp., voltage standard 77−72945
Pb-Pb_xO_y-Pb thin film Josephson junctions, prep. *(Slovak)* 79−42699
Pb-$PbCl_2(I_2)$, finely disperse system, supercond. props. 77−85376
Pb-PbO_2, bielectrodes, anodic polarisation 77−44483
Pb-PbO_x-Pb, long Josephson tunnel junction, current steps induced by vortex motion 79−47199
Pb-PbO_x-Pb small supercond. tunnel junctions, effect of capacitance in I-V characts., high-freq. obs. 80−80448
Pb-PbO-Pb, Josephson tunnel junction fabrication for Mm-wave detector 80−100427
Pb-PbO-Pb, supercond. junction, tunnel effect under laser irrad. *(Russian)* 77−43788
Pb-S melt, absolute thermo-emf obs. 77−85251
Pb-S-I-X-H_2O, (X=solvent) crystallisation conditions 78−80466
Pb-S-O system, phase equilib. *(Rumanian)* 78−19727
Pb-Sb, liq. alloy, Pb thermodynamic props. *(Czech)* 80−29925
Pb-Sb-S-I, chalcogenide glass film, prep. by laser evaporation, and characterisation 77−12533
Pb-Se-As-Ge, phase separation in melt centrifugal quenching 80−25701
Pb-Sn-Te, microhardness meas. as function of applied load, elec. props. exam. 78−48493
Pb-Sn-Te, solid solution, scattering mechanism of carriers 80−49710
Pb-Sn-Te system, investigation of liquidus surface by simplex lattice method 79−46784
Pb-SnTe semiconductor, spectral response calcs. 77−87826
Pb-Te, molten mag. susceptibility, conc. and temp. depend. 78−80121
Pb-Te system, crystn. of amorphous Te-Pb (20 at.%) 78−26445
Pb-Te-O, thermal stability 78−44104
Pb-Te-O system, PbTe-$PbTeO_3$ and $PbTeO_4$-PbO cross sections 78−23679
Pb-Tl-Te, liquidus of ternary system 79−8285
Pb-Xe mixture, metal-insulator transition, resistivity meas. 77−76883
Pb-Zn-SiO melt, mathematical model of thermal C reduction *(Russian)* 78−15663
$Pb_{1-x}Sn_xTe$ film, possible applic. as mechanised stress transducers 77−58621
p-$Pb_{1-x}Sn_xTe$, carrier mobility, acoustical phonon and impurity scatt., deform. impurity const., conc. depend. 80−39570
$Pb_z-Sr_{1-z}(Zr_x-Ti_{1-x})O_3$:$Cr_2O_3$, ferroelec. ceramic, reversible characts. and dielectric losses *(Russian)* 78−84517
$Pb_2AgNb_5O_{15}$, $Pb_2AgTa_5O_{15}$, ferroelec. and ferroelastic props. *(French)* 79−24266
$Pb_{1-x}Al_xF_{2+x}$, ionic cond. of quenched and annealed specimens, interstitial cond. mechanism 80−2199
$PbAl_2Se_4$, X-ray cryst. struct. determ. *(German)* 80−107174
PbAr, metal-insulator transition, resistivity meas. 78−80028
$Pb_2As_2O_7$, cryst. data, X-ray powder diffr. meas. 78−42987
$Pb_5(AsO_4)_3Cl$, mimetite, vibr. spectra, normal coord. anal. 78−88305
$Pb_9As_4S_{15}$, gratonite, single crystal, photoelectric props. 80−49822
PbAsSb, isomertieite, fengluanite, cryst. struct. *(Chinese)* 79−1417
$(Pb_{1-x}Ba_x)_5Ge_3O_{11}$, ferroelec. phase transition, dielec. const. and quasi-elastic light scatt. 80−71289
$Pb_{5-x}Ba_xGe_3O_{11}$, Raman spectra, temp. depend. of ferroelec. soft A-mode 79−33682
$(Pb_xBa_{1-x})_5Ge_3O_{11}$, electrogyration, and dielectric props. 78−19444
$(Pb_{1-y}Ba_y)_{1-x}La_xNb_{2-x/5}O_6$, transparent ferroelec. ceramic, optical transmittance, electrooptic props. and Curie temp. 77−32395
$(Pb_{1-y}Ba_y)_{1-x}La_xNb_{2-x/5}O_6$, ferroelec., phase transitions 79−38487
$Pb_{2-x}Ba_xLi_{0.5}Nb_{1.5}O_6$, elec. resistivity, Curie temp., x=0-0.15, 50-350°C 78−2478
$Pb_{2-x}Ba_xLi_{0.5}Nb_{1.5}O_6$, dielectric const., temp. and Ba conc. 78−64308
$Pb_{1-x}Ba_xMoO_4$, refr. index. and photoelastic consts. 77−63393
$Pb_{0.6}Ba_{0.4}Nb_2O_3$, piezoelectric ceramic solid soln. *(Polish)* 77−55755
$Pb_{0.94-x/2}Ba_{0.6}Nb_xZr_{1-x}O_3$, Nb dopant morphology effect on microstructure 80−81005

lead compounds continued
$Pb_{1-x}Ba_xZrO_3$, electric quadrupole interaction meas., by PAC 77−4591
$(Pb_{0.715}Ba_{0.285})_{0.991}(Zr_{0.707}Ti_{0.293})_{0.981}Bi_{0.019}O_3$, slim loop ferroelec. ceramic, shock wave compressed, elec. response 78−80293
$(Pb_{0.8}Ba_{0.2})(Zr_{0.8}Ti_{0.2})O_3$, ferroelec. ceramic, pulse-like voltage generation using polarisation reversal 78−2809
$Pb_{1-x}Be_xTe$, anomalous resist. near ferroelec. phase transition 80−20196
$Pb_{1-x}Bi_xF_{2+x}$, new solid electrolytes, conductivities and activation energies 79−28137
$Pb_{1-x}Bi_xF_{2+x}$, solid anionic conducting electrolytes, struct., elec. props. 77−84977
$Pb_{1-x}Bi_xF_{2+x}$, solid soln., struct. and ionic cond. correl., neutron diffr. study *(French)* 80−84324
$(Pb_{1-x}Bi_x)_5Ge_3O_{11}$, spontaneous and induced electrogyration 79−42946
$PbBiMTeO_6$, M=Li, Na, antiferroelectric, synthesis and charact. 77−55758
$Pb(Bi_{1/2}Nb_{1/2})O_3$, single cryst. growth from PbF_2-PbO-B_2O_3 77−48336
$PbBi_2Nb_2O_9$, bend strength, grain orientation effects 80−40375
$PbBi_2Nb_2O_9$ ceramic, grain oriented, dielectric and piezoelectric props. 79−42896
$PbBi_2Nb_2O_9$, hot-forged ferroelec. ceramic with layer struct. 79−43175
$Pb_{46}Bi_{54}S_{127}$, carnizzarite, X-ray cryst. struct. determ. 79−23567
$PbBi_4Ti_4O_{15}$ ceramic, dielec. props., temp. depend. 78−95561
$PbBi_4Ti_4O_{15}$, hot-forged ferroelec. ceramic with layer struct. 79−43175
$PbBi_8Ti_7O_{27}$, cryst. struct. 77−47428
$Pb_2Bi_4Ti_5O_{13}$, hot-forged ferroelec. ceramic with layer struct. 79−43175
$Pb_3Bi_2[\square](GeO_4)_3]$, cryst. data 78−42985
PbBr, $b^1\Sigma^+$-$X^1\Sigma^-$ band system, microwave discharge obs., mol. consts. 79−81203
$PbBr_2$, above-edge cathodolum. from metastable excitons 78−6786
$PbBr_2$, cryst., red luminesc. at low temps. *(Russian)* 78−92125
$PbBr_2$, determ. of sign and drift mobility of majority carriers *(Russian)* 79−69512
$PbBr_2$, ionic cond. and activation volumes, high press. effects 80−100353
$PbBr_2$, light sensitive material, regularities in exciton states 77−20885
$PbBr_2$, lowest exciton states 78−72082
$PbBr_2$, photoconductivity obs. 77−43650
$PbBr_2$, red luminesc., absorpt. spectra 80−2831
$PbBr_2$, reflectance spectra, exciton peaks 77−24870
$PbBr_2$, single cryst., photolum. meas. 77−69882
$PbBr_2$, valence band electronic struct., XPS and UPS obs. 78−6826
$PbCO_3$, ^{207}Pb mag. shielding anisotropy, Fourier transform NMR 77−90057
$PbCO_3$, cryst. growth, Liesegang ring form., pH effect 80−49140
$PbCO_3$, neutron diffr. topographic study of growth defects. 78−91282
$PbCO_3$ whiskers, growth kinetics in silica gel 78−75971
$PbCO_3$-$BaCO_3(SrCO_3)(CaCO_3)$, solid soln. form., regions of existence 79−11581
$PbCO_3.PbX_2$ (X=Cl,Br), vibr. props. 79−24319
$Pb_xCa_{1-x}MoO_4$, growth and props. 80−71588
Pb_2CaTeO_6, ferroelec. behaviour microwave dielec. props. meas. 77−43948
$Pb_{1-x}Cd_xS$, epitaxial, resist. and Hall coeff., substrate temp., thickness and comp. depend. 78−72290
$Pb_{1-x}Cd_xS$ epitaxial layer, metastable, optical props. and electronic struct. 79−15543
$Pb_{1-x}Cd_xS$, metastable epitaxial films, elec. props. 78−26979
$Pb_{1-x}Cd_xS$ metastable epitaxial films, growth and physical props. 78−27417
$Pb_{0.95}Cd_{0.05}Te$, solid solns., thermoelec. power and Hall effect under hydrostatic press. 79−23990
$Pb_{1-x}Cd_xTe$, IR absorpt. study of Cd impurity levels, energy gaps 80−45081
Pb_2CdTeO_6, ferroelec. behaviour, microwave dielec. props. meas. 77−43948
PbCl, rot. analysis of A-X_1 system 80−32703
$PbCl_2$, binding, ionicity, covalent contrib., Madelung const., cohesive energy 78−79558
$PbCl_2$, blue emission 78−23518
$PbCl_2$ crystals, acousto-optical props. and photoelasticity 80−40085
$PbCl_2$, determ. of sign and drift mobility of majority carriers *(Russian)* 79−69512
$PbCl_2$ emulsion layer, effect of elec. field on microcrystal sensitivity *(Russian)* 79−58831
$PbCl_2$, evidence for diffuse transition, elec. cond. and Raman spectra meas. 79−73552
$PbCl_2$, ionic cond. and activation volumes, high press. effects 80−100353
$PbCl_2$, large needles and single crysts., gel cryst. growth 80−29869
$PbCl_2$, light sensitive material, regularities in exciton states 77−20885
$PbCl_2$, lowest exciton states 78−72082
$PbCl_2$, mol. struct. determ. from gas phase electron diffr. 78−25742
$PbCl_2$, molten, struct. anal. by X-ray diffr. 78−94961
$PbCl_2$, photoconductivity obs. 77−43650
$PbCl_2$, photoionisation cross section of atomic and final state effects on 5d core levels 78−84699
$PbCl_2$, pulsed discharge, lasing on Pb atom 77−79812
$PbCl_2$, Raman spectra, phonon modes 80−2754
$PbCl_2$, single cryst., far IR refl. spectra, effective ionic charges 79−87430
$PbCl_2$, single cryst. growth using zone melting furnace 79−52110
$PbCl_2$, struct. comparison with Co_2Si, Co_2P, and SbSI *(French)* 80−84155
$PbCl_2$:NaCl, trapped exciton states, absorption spectra 80−50383
$PbCl_2$-MCl, (M=Li, Na, K, RB, Cs), molten systems, thermoelec. power 77−62658
$PbCl_2$-$ZnCl_2$, thermodynamic quantity meas. by quantitative thermal anal. of heating process 78−19730
$PbCl_6^{4-}$, model force fields and vibr. amplitudes calcs. 78−62780
$PbCl_{2-2x}Br_{2x}$, luminesc. and reflection spectra *(Russian)* 80−84762
$PbCl_{2-2x}I_{2x}$, orthorhombic, absorpt. spectra 77−59633
$PbCo_{0.33}Nb_{0.66}O_3$, ferroelectric, exam. of permittivity and dielectric props. 79−1742
$PbCo_2(PO_4)_2$, mag. susceptibility, elec. cond. and optical refl. 79−56495
Pb_2CoReO_6, seignettomagnets with perovskite struct. 79−38459
$PbCo_{1/2}Te_{1/2}O_3$, antiferroelec., high-frequency permittivity, temp. depend. 80−71325
Pb_2CoWO_6, antiferroelectric substruct. 79−38489
$PbCrO_4$, ^{207}Pb mag. shielding anisotropy, Fourier transform NMR 77−90057
$PbCrO_4$, cathode material for Li cells evaluation 78−11525

lead compounds continued
$PbCrO_4$, cryst. growth kinetics and particle size in precipitating K_2CrO_4-$Pb(NO_3)_2$ mixed soln. 78−26472
$PbCrO_4$, diffuse reflectance spectra 78−88326
$PbCrO_4$, paste, anomalous viscous flow 79−64617
Pb_2CrO_5, flux growth and chem. charact. 78−23595
Pb_2CrO_5, thermal X-ray and dielec. investigations 79−47403
$Pb_3Cr_2(PO_4)_2$, synthesis and cryst. struct. 79−19218
$Pb_{1-p}Cr_2S_{4-p}(Se_{4-p})$, modulation of intergrowth struct. 79−94967
$Pb_{5-x}(Cs, Bi)_xGe_3O_{11}$ 80−75960
$Pb(Cu_{1/4}Nb_{3/4})O_3$-$Pb(Li_{3/4}Nb_{3/4})O_3$-$PbTiO_3$-$PbZrO_3$, piezoelec. ceramic materials for SAW devices 79−11390
$Pb(Cu_{1/4}Nb_{3/4})O_3$-$Pb(Li_{1/4}Nb_{3/4})O_3$-$PbTiO_3$-$PbZrO_3$, optimisation of composition for SAW devices 79−33609
PbF, laser-induced fluoresc. of $A^2\Sigma$ state, chem. laser eval. 79−81222
PbF, rot. anal. of B-X_2, B-X_1 and A-X_1 systems 77−58001
PbF, visible spectra, A-X_1 and B-X_1 fine struct. anal. 79−36657
PbF_2, ^{19}F NMR, free induction decay, initial behaviour 78−80227
PbF_2, acoustic phonon modes up to high temps., neutron scatt. meas. 79−33052
PbF_2, anion disorder at high temps., neutron diffr. obs. 80−59614
β-PbF_2, anion mobility from noise meas. 79−46836
PbF_2, antireflection coating deposition technique, 2.87 μm laser damage threshold 80−33264
PbF_2 based solid solns., ion transport 80−107545
PbF_2, Brillouin scatt. and high temp. disorder 78−80365
PbF_2, cathode materials for Li cells, evaluation 78−11525
PbF_2 coatings, transmission and refraction dispersion spectra *(Russian)* 77−48264
β-PbF_2, complex impedance exam. 78−47579
PbF_2, cubic, dielec. const., ionic cond., soft modes 78−14427
PbF_2, cubic and orthorhombic, press. and temp. depends. of ionic cond. 79−95207
β-PbF_2, electrolytic props., AC cond. meas. 78−71878
PbF_2, fast ion conductor, phonon freq. distrib., temp. variation 80−84264
PbF_2 film, contamination by 1 MeV proton bombardment, backscatt. obs. 77−11811
PbF_2 film, IR absorpt. coeffs. meas. by laser calorimetry 78−25905
PbF_2 film, ionic conduction, effect of hydrostatic press. *(French)* 79−28259
β-PbF_2 film, ionic migration study by Rutherford scatt., defects, secondary emission *(French)* 78−55982
PbF_2 film, refr. index and struct., deposition temp. depend. 79−4857
β-PbF_2 film between metal electrodes, vac. evaporated, AC study of elec. props. 80−2207
PbF_2, gamma-ray and neutron irrad. at low temps., EPR of Pb^{3+} ions 77−63262
β-PbF_2, γ-irrad., F-band region spectrum, impurity effects 77−44026
PbF_2, inelastic neutron scatt. study of phonon dispersion relation 78−30712
PbF_2, ionic cond., activation volumes and high press. phase transitions 80−70461
PbF_2, laser damage resistant antirefl. coatings for 16 μm region 79−31963
PbF_2, lattice dynamics 78−79697
α-PbF_2, lowest exciton states 78−72082
PbF_2, motionally narrowed system, appl. of zero time resolution NMR 78−76325
PbF_2, muon Coulomb capture ratio 78−62959
PbF_2, NMR relax. and self diffusion 78−80236
PbF_2 optical props. 77−32394
PbF_2, orthorhombic and cubic, heat capacity, 3 to 22K 80−19955
PbF_2, phonon temp. depend., neutron scatt. study 79−60450
PbF_2, polarised Raman scatt. in fluorite crysts., anharmonicity, high-temp. disorder 78−35132
PbF_2, polymorphic transition temps. under hydrostatic press., DTA study 80−2156
PbF_2, Raman scatt. exam. at high temp. 77−32367
β-PbF_2, single cryst., photolum. meas. 77−69882
PbF_2 single-layer film 2.8 μm, 3.8 μm absorpt. meas. 78−90463
β-PbF_2, solid electrolyte, mobile species mobility and conc., temp. depend. 77−20113
PbF_2, sp. ht. anomalies, phase transition 79−86901
PbF_2, sp. ht. meas., Schottky-type diffuse phase transitions, defect form. energies and entropies 80−107441
β-PbF_2, spectral diffusion, coherent effects in ESR of Gd^{3+} 79−51852
PbF_2, superionic, electrical conductivity at high temp. 78−79798
PbF_2, superionic, F^- motion and F sublattice melting, NMR obs. 77−43374
PbF_2, superionic conductor, theoretical investigation of Raman scatt. 78−80351
β-PbF_2, thin films, cond. mechanisms, struct. 77−84970
PbF_2, US vel. near press. induced cubic-to-orthorhombic transform. 80−103476
PbF_2, use in vacuum sealing LiF window to Au or Cu thin-walled cylinder 77−54820
PbF_2:Fe^{3+}, F motion, ESR study 80−66023
PbF_2:Gd^{3+}, EPR and ENDOR of Gd^{3+} at cubic sites 80−7161
PbF_2:Mn, mag. tagging of ion diffusion, ^{19}F NMR meas. 80−108106
PbF_2:Mn, NMR relaxation by paramag. impurities 79−42866
PbF_2:Mn^{2+}, NMR linewidth with mag. tagging for superionic cond. parameters determ. 77−81021
PbF_2:Mn^{2+}, superionic, cryst. field fluctuation dynamics, EPR 78−23328
PbF_2:Tb^{3+}, cubic Tb^{3+} centres, energy level and cryst. field parameters 77−52181
PbF_2:Tb^{3+}, ESR spectrum of ions in cryst. field of cubic symmetry 79−38378
PbF_2:Yb^{3+}, superhyperfine interaction, ENDOR and RF discrete saturation expts. 79−73856
PbF_2-AlF_3, ionic cond., charact., effect of trivalent cations 77−89576
PbF_2-AlF_3 glass, optical props., crystn. and thermal expansion 80−48367
PbF_2-AlF_3 glass, prep. and props. 80−49120
PbF_2-MgF_2, multidielectric stacks as interf. filters, ageing charact. *(French)* 77−34939
PbF_2-Na_3AlF_6, interference filter prod. for near UV *(French)* 78−25974
PbF_2-Na_3AlF_6, semitransparent wide band dielectric mirror synthesis using dispersive and absorbing materials 79−89986

lead compounds continued
- PbF_2-TlI graded coatings on KCl laser windows, photoacoustic spectroscopy 80−33052
- PbF_2-x$PbO.ySiO_2$, freezing point depression meas., effect of SiO_2 compound additions 77−28798
- PbF_2-ZnSe multilayer 16 μm dichroic mirror, 16 μm region, mech. stress compensation 80−74465
- $^{207}PbF_6^{3-}$, radical, prep. and EPR comparison with other hexafluoride radicals 78−68381
- PbFBr, dehydration, zone refining and Bridgman cryst. growth 77−36395
- PbFBr, reflectance spectra, exciton peaks 77−24870
- PbFBr, single cryst., photoluminesc. 77−16375
- PbFBr, undoped and doped, ionic cond. 79−60545
- PbFCl, dehydration, zone refining and Bridgman cryst. growth 77−36395
- PbFCl, ionic cond. mechanism, ^{19}F NMR meas. and struct. considerations 79−55927
- PbFCl, reflectance spectra, exciton peaks 77−24870
- PbFCl, single cryst., photoluminesc. 77−16375
- PbFCl(Br), single crystal ionic cond., deviation from molecularity, effect of O_2 impurities 79−51305
- PbFI, X-ray studies 78−14320
- Pb_2F_2O, cryst. struct., X-ray obs. 77−89412
- PbFX, X=Cl, Br, photoconductivity obs. 77−43650
- $6PbF_2.PbBr_2$, X-ray studies 78−14320
- $6PbF_2.PbCl_2$, X-ray studies 78−14320
- $Pb(Fe/Al/Ga)_{12}O_{19}$, solid soln., crystallographic charact. *(German)* 79−94972
- $PbFe_{12-x}Ga_xO_{19}$ ferrite, single cryst., ferromag. reson. 80−50193
- $Pb(Fe_{1/2}Nb_{1/2})O_3$-$La_2O_3(CeO_2)$ ferroelec. ceramics, electrophysical props. 78−35099
- $2PbFe_{1/2}Nb_{1/2}O_3$-Pb_2FeReO_6, comp., struct., dielec. and mag. props. 80−2704
- $PbFe_{12}O_{19}$, bubble and stripe lattice domain wall oscills. 80−97115
- $PbFe_{12}O_{19}$, dislocation etch pit morphology study *(Chinese)* 80−88150
- $PbFe_{12}O_{19}$, Mossbauer spectra, domain magnetisation vector rotations, domain struct. 79−69761
- $PbFe_{12}O_{19}$ platelets, ferromag. reson. absorpt. of close-packed bubble lattice 77−69709
- $PbFe_{12}O_{19}$, single crystal, Mossbauer spectra 80−84670
- $Pb_2Fe_2O_5$, IR absorpt., Mossbauer spectra, Neel temp., cryst. cell *(French)* 79−42759
- Pb_2FeReO_6, seignettomagnets with perovskite struct. 79−38459
- $Pb(FeTa)_{1/2}O_3$, Mossbauer spectra, 78-480K 79−51885
- $2PbFe_{1/2}Ta_{1/2}O_3$-Ba_2FeReO_6, comp., struct., dielec. and mag. props. 80−2704
- $2PbFe_{1/2}Ta_{1/2}O_3$-Pb_2FeReO_6, comp., struct., dielec. and mag. props. 80−2704
- $PbFeTi(PO_4)_3$ cryst. struct. and prep., rhombohedral lattice *(French)* 77−27856
- $Pb(Fe_{2/3}U_{1/3})O_3$-$PbZrO_3$ solid solns., phase transition 77−48138
- $PbFe_{2/3}W_{1/3}O_3$-$BaTiO_3$ system ferroelec., antiferromag., ESR and dielec. props. meas. 77−40172
- $PbFe_{(2/3}W_{1/3)}O_3$-$Pb(Co_{1/2}W_{1/2})O_3$ solid soln., crystallographic, dielectric, magnetic props., Mossbauer spectra 78−43807
- $Pb(Fe_{2/3}W_{1/3})O_3$-$Pb(M_{3/2}W_{1/2})O_3$, (M-Mn, Co, Ni), ferroelec. phenomenological theory 79−99831
- $Pb_3Fe_2WO_9$, perovskite ferroelec., characts. of dielec. polarisation 77−8496
- $Pb_2Ga_2S_5$, X-ray cryst. struct. determ. and refinement *(French)* 80−107130
- $PbGa_2Se_4$, X-ray cryst. struct. determ. *(German)* 80−107174
- Pb_2GaTaO_6, transition from pyrochlore to imperfect fluorite struct. 80−19939
- $Pb_5Gd_3O_{11}$, trigonal Gd^{3+} centre structure 79−69720
- $Pb_3(Ge,Si)_2O$, growth from melt, struct. and dielec. props. 77−44148
- $Pb_5(Ge,Si)_3O_{11}$, dielec. and elec. props., 20 to 250°C 80−29697
- $PbGeO_3$, cryst. struct., dielec. and optical props. 77−1118
- $PbGeO_3$, single cryst. films growth, temp. depend. of dielec. constant 79−100066
- $PbGe_3O_7$, cryst. data and cryst. growth 78−47289
- $Pb_{11}GeO_3$, X-ray powder cryst. data, struct. rel. to $PbO_{17}GeO_8$ and PbO 80−84146
- Pb_3GeO_5 antiferroelectric, cryst. struct. 79−19233
- Pb_3GeO_5, cryst. struct. dielec. and optical props. 77−1118
- Pb_3GeO_5, high temp. phase, cryst. struct. 80−1995
- Pb_3GeO_5, single crystal, props., grown by hydrothermal method 79−11504
- $Pb_3Ge_2O_7$, dielectric thin film, obtained by sedimentation, exam. of dielectric props. and structure 80−2282
- $Pb_3Ge_2O_7$, vacuum condensates on US irrad. substrates, props. 77−66466
- $Pb_3Ge_3O_{11}$, uniaxial ferroelec., thermal expansion and dielec. permittivity in vicinity of transition points 77−66459
- Pb_5GeO_{11}, elastic nonlinearity and acoustic losses 80−59554
- Pb_5GeO_7, cryst. data and cryst. growth 79−51076
- Pb_5GeO_7, X-ray cryst. struct. determ. *(German)* 79−46603
- $Pb_5Ge_2O_{11}$ acoustic relax. assoc. with phase transition at hypersonic freq. 78−88267
- $Pb_5Ge_3O_1$, anharmonic phonons and central peaks at struct. phase transitions 79−95775
- $Pb_5Ge_3O_{11}$, acoustic emission, threshold electric field 79−60874
- $Pb_5Ge_3O_{11}$ acoustic relaxation near ferroelectric transition 78−2814
- $Pb_5Ge_3O_{11}$ bonded $Pb(Zr,Ti)O_3$ composites, piezoelec. props. 79−78629
- $Pb_5Ge_3O_{11}$ crystal, ferroelec., luminesc. under pulse polarisation switching conditions 77−1735
- $Pb_5Ge_3O_{11}$, Czochralski growth, secondary phase formation 78−3027
- $Pb_5Ge_3O_{11}$, Czochralski-grown oxide crystals, fluid-flow effect on gas-bubble entrapment 80−84121
- $Pb_5Ge_3O_{11}$, dielec. behaviour, 60 Hz-100 kHz, particle size effects 79−33638
- $Pb_5Ge_3O_{11}$, dielec. functions above and below ferroelec. transition 79−33588
- $Pb_5Ge_3O_{11}$, dynamic central peaks and phonon interactions near structural phase transitions 78−83903
- $Pb_5Ge_3O_{11}$, ESR of Fe^{3+} ions 79−95639
- $Pb_5Ge_3O_{11}$, electrogyration during phase transitions 79−19859
- $Pb_5Ge_3O_{11}$, electrostrictive interaction, mode damping 80−34862
- $Pb_5Ge_3O_{11}$, ferroelec., induced and spontaneous optical activity, permittivity 79−33661

lead compounds continued
- $Pb_5Ge_3O_{11}$, ferroelec., elec. cond. meas. 79−65472
- $Pb_5Ge_3O_{11}$, ferroelec., surface capacitance effect on dielec. props., DC cond. and dielec. const. meas. 79−91333
- $Pb_5Ge_3O_{11}$, ferroelec. phase transition, for IR transmission meas. 79−38478
- $Pb_5Ge_3O_{11}$, ferroelec. transition, US and elasto-optic props. 80−60527
- $Pb_5Ge_3O_{11}$, ferroelectric transition exam. by Raman scatt. 78−56439
- $Pb_5Ge_3O_{11}$, ferroelectric soft mode exam., Raman spectra 79−42202
- $Pb_5Ge_3O_{11}$, ferroelectric, anharmonic effects in low freq. symm. modes, Raman study 80−25365
- $Pb_5Ge_3O_{11}$ film, pyroelectric effects, origin 78−88258
- $Pb_5Ge_3O_{11}$, freq. and damping of ferroelec. soft mode, permittivity meas. 77−52027
- $Pb_5Ge_3O_{11}$, growth defects and polarisation switching 78−48132
- $Pb_5Ge_3O_{11}$, lattice dynamics parameters anisotropy, X-ray diffr. study 80−59612
- $Pb_5Ge_3O_{11}$, light scatt. meas., central peak dynamics at ferroelectric transition 77−4606
- $Pb_5Ge_3O_{11}$, light scatt. obs. of unresolved central peak 77−4649
- $Pb_5Ge_3O_{11}$ monocrystal, US absorption meas. by acoustooptical method, losses in boundary layer evaluation *(Polish)* 78−30701
- $Pb_5Ge_3O_{11}$, multidomain mat., opt. anisotropy meas. at mag. crit. temps. 77 16279
- $Pb_5Ge_3O_{11}$, paraelectric and ferroelectric, Raman spectra near ferroelectric transition 80−55090
- $Pb_5Ge_3O_{11}$, photodielectric effects, Curie temp., permittivity and polarisation 80−40034
- $Pb_5Ge_3O_{11}$, pulsed polarisation switching process depend. on illumination 80−93253
- $Pb_5Ge_3O_{11}$, pyroelectric radiation detector appl. *(Czech)* 79−40611
- $Pb_5Ge_3O_{11}$, Raman scatt., soft modes and damping near structural phase transition 79−28739
- $Pb_5Ge_3O_{11}$, Raman spectrum factor group anal., external and librational modes 77−36240
- $Pb_5Ge_3O_{11}$, single crystal, ferroelec., Czochralski growth 78−3024
- $Pb_5Ge_3O_{11}$, single crysts., photoemission anamoly during ferroelectric phase transitions 79−47599
- $Pb_5Ge_3O_{11}$ single crystals, switching behaviour and hysteresis 80−40077
- $Pb_5Ge_3O_{11}$, spectral diffusion, coherent effects in ESR of Gd^{3+} 79−51852
- $Pb_5Ge_3O_{11}$, sputtered ferroelec. films, prep. struct. and dielec. props. 80−75452
- $Pb_5Ge_3O_{11}$, struct. of paraelec. phase, neutron diffr. meas. 77−84720
- $Pb_5Ge_3O_{11}$, temp. depend. of A_{1O}-modes, Raman spectra meas. 78−2213
- $Pb_5Ge_3O_{11}$, ultrafine-grained crystallized from glass, ferroelectricity 78−39508
- $Pb_5Ge_3O_{11}$, uniaxial displacive ferroelectrics, domain wall dynamics 79−73890
- $Pb_5Ge_3O_{11}$, uniaxial ferroelectric, optical activity dispersion 78−48141
- $Pb_5Ge_3O_{11}$, vitreous, crystn. via metastable phase 78−30543
- $Pb_5Ge_3O_{11}$:Ba_2O, impurities, static central peak 78−92079
- $Pb_5Ge_3O_{11}$:Gd^{3+}, discrete saturation of ESR, due to superhyperfine interaction 77−28440
- $Pb_5Ge_3O_{11}$:Gd^{3+}, EPR hyperfine struct. 79−82867
- $Pb_5Ge_3O_{11}$:Gd^{3+}, ferroelec. transition, temp. depend., EPR study 80−66127
- $Pb_5Ge_3O_{11}$:Si, switching velocity, increase over that of undoped crysts. 79−51922
- Pb_6GeO_8, X-ray powder cryst. data, struct. rel. to $Pb_{11}Ge_3O_{17}$ and PbO 80−84146
- $Pb_5(GeO_4)(PO_4)_2$, crysts., acousto-optical props. 80−100644
- x$Pb_5GeO_4(VO_4)_2$, (1-x)$Pb_5SiO_4(VO_4)_2$, solid solution of centrosymmetric crystals, electrically induced optical activity 80−108180
- $Pb_5GeO_4(VO_4)_2$, centrosymmetric crysts., induced linear electrogyration 80−45039
- $Pb_5(GeO_4)(VO_4)_2$, crysts., acousto-optical props. 80−100644
- $Pb_5(GeO_4)(VO_4)_2$, elastic and dielectric props. 77−7782
- $Pb_5(GeO_4)(VO_4)_2$, elastic nonlinearity and acoustic losses 80−59554
- $PbGeS_3$, vitreous and cryst., IR and Raman spectra *(Russian)* 78−72527
- $Pb_3(Ge_{1-x}Si_x)_2O_7$, optical SHG and pyroelectric effect 77−10982
- $Pb_5(Ge_{1-x}Si_x)_3O_{11}$, dielec. spectra, ferroelec. behaviour 78−60406
- $Pb_5(Ge_{1-x}Si_x)_3O_{11}$, electrogyration, phase transition and dielectric props. 80−93269
- $Pb_5(Ge_{1-x}Si_x)_3O_{11}$, ferroelec. soft mode, temp. and Si impurity, effects Raman scatt. 79−1762
- $Pb_5(Ge_{1-x}Si_x)_3O_{11}$ solid solutions, dielec. props., ferroelec. phase transitions 80−15988
- $Pb_5Ge_{3-x}Si_xO_{11}$, ferroelec. soft mode, temp., press. and comp. depend. 78−80304
- $Pb_5Ge_{3-x}Si_xO_{11}$, ferroelec., switching vel. and spontaneous polarisation 78−84543
- $Pb_5Ge_{3-x}Si_xO_{11}$, ferroelec. phase transition, for IR transmission meas. 79−38478
- $Pb_{1-x}Ge_xTe$, band struct., tunnelling obs. in MIS struct. 80−54795
- $Pb_{1-x}Ge_xTe$, degenerate semiconducting ferroelectric, structural phase transition temp., mag. field effects 80−45017
- $Pb_{1-x}Ge_xTe$, dielec. const. determ. near ferroelec. transition 78−88269
- $Pb_{1-x}Ge_xTe$, electron-phonon interaction effect on ferroelec. transition 78−76416
- $Pb_{1-x}Ge_xTe$ epitaxial layers, phase transition obs. by far IR reflectivity spectroscopy 79−33691
- $Pb_{1-x}Ge_xTe$, ferroelec. phase transition, IR refl. and resist. meas. 80−11353
- $Pb_{1-x}Ge_xTe$, ferroelec. constants, C-V and C-T characts. of abrupt p-n junctions 80−25323
- $Pb_{1-x}Ge_xTe$, ferroelectric phase transition effect on forbidden band width 80−24794
- p-$Pb_{1-x}Ge_xTe$ film, cyclotron reson. above and below struct. phase transition 80−88879
- $Pb_{1-x}Ge_xTe$, mag.-field-induced displacive phase transition 80−50278
- $Pb_{1-x}Ge_xTe$ magnetoplasma reflectivity and transmission spectra 80−71428
- $Pb_{1-x}Ge_xTe$, n- and p-type, effective masses 80−44481
- $Pb_{1-x}Ge_xTe$, p-n junctions, elec. characts., effect of ferroelec. phase transition 79−33338
- $Pb_{1-x}Ge_xTe$, phase transitions 78−60408
- $Pb_{1-x}Ge_xTe$, Raman scatt. from soft TO-phonon modes 79−95773
- $Pb_{1-x}Ge_xTe$ solid solns., phase transition influence on elec. props., 77 to 450K 80−103689

lead compounds continued
$Pb_{1-x}Ge_xTe$, solubilities, elec. and optical props. 77−35940
$Pb_{1-x}Ge_xTe$, TO phonon interaction with acoustic phonons near phase transition temp. 79−90776
$Pb_{1-x}Ge_xTe$:Ga, Fermi level stabilization, transport props. meas., 77-400K 78−56065
$Pb_{1-x}Ge_xTe$:Ga, influence of hydrostatic compression on elec. props. 79−73516
$PbGe[Ge_3O_9]$, X-ray cryst. and powder data 80−19768
PbH_4, relativistically parameterized extended Huckel theory 79−49924
$PbHAsO_4$, ($PbDAsO_4$), Raman spectra of ferroelec. transition proton tunnelling 78−23410
$PbHAsO_4$, ferroelec., far IR and submillimetre dielec. dispersion 79−38528
$PbHAsO_4$, ferroelec., far IR and microwave dielec. props. 80−55108
$PbHAsO_4$, hydrostatic press. effect on ferroelec. transition 78−35102
$Pb(HAsO_4)_2.H_2O$, cryst. struct. 78−26552
$Pb(HAsO_4)_2.H_2O$, thermal stability, 20-1000°C, decomposition prod. struct. 79−11775
$PbH(D)AsO_4$, ferroelectric, sp. ht. 79−19853
$PbH(D)PO_4$, ferroelectric, sp. ht. 79−19853
$PbHPO_4$ cryst. for pyroelectric detector 77−82600
$PbHPO_4$, crystals, ferroelec. phase transition, hydrostatic press. influence, dielec. meas. 80−88936
$PbHPO_4$, ferroelec., far IR and submillimetre dielec. dispersion 79−38528
$PbHPO_4$, ferroelec. phase transition, Brillouin and Raman spectra obs. 79−33683
$PbHPO_4$, hydrostatic press. effect on ferroelec. transition 78−35102
$PbHPO_4$, linear response function for tunnelling systems in polariton region 78−43799
$PbHPO_4$, microwave permitt. and far IR refl. spectra in paraelec. and ferroelec. phases 80−40033
$PbHPO_4$, neutron diffr. exam. of struct. at room temp. 79−38490
$PbHPO_4$, optical props. near ferroelec. transition 79−33663
$PbHPO_4$, phase transitions study, role of cryst. struct. determ. 80−75197
$PbHPO_4$, protonic order-disorder transition 78−26478
$PbHPO_4$, Raman spectra study of ferroelec. transition, proton tunnelling 78−23410
$PbHPO_4$, single cryst., growth, optical props., ferroelec. transition 78−35285
$PbHPO_4$, single cryst., dielec. props. 79−38426
$PbHPO_4$-type crystals, ferroelec. transition, statistical model 80−25321
$Pb(HPO_4)_2.H_2O$, cryst. struct. 78−26552
$PbHfO_3$, antiferroelectric-ferroelectric phase transition in strong elec. field 80−15990
$PbHfO_3$, elec. field gradient, crit. behaviour, DPAC meas. 78−80303
$PbHfO_3$, elec. quadrupole interaction, temp. depend., DPAC meas. 79−51884
$PbHfO_3$, X-ray cryst. struct. refinement 80−44189
$PbHf_{1-x}Ti_xO_3$, phase diagram, influence of poling treatment, ferroelec. antiferroelec. transition *(French)* 77−63374
$Pb_{1-x}Hg_xS$, electroless film deposition with variable comp. and polymorphic structs. 79−95952
$Pb_{1-x}Hg_xS$ electroless-deposited films, optical and elec. props. 80−7011
$Pb_{1-x}Hg_xS$ epitaxial films, electroless deposition and struct. props. 79−90915
$Pb_{1-x}Hg_xS$ film, IR detector material, struct. and IR props. 78−26775
$Pb_{1-x}Hg_xS$ film, solution-grown, struct., lattice parameters and optical band gap var. 77−69201
$Pb_{1-x}Hg_xS$, soln. growth, variable gap film for i.r. detector 77−1796
$Pb_{1-x}Hg_xS$-Si heterojunctions, elect. props. 80−100513
$Pb_{0.97}Hg_{0.03}Te$ photovoltaic detector produced by Sb^+ ion implantation 80−82821
PbI, $^1S_0$-$^3P_1$ to $^1S_0$-$^3P_2$ multipole line intensity ratio 79−36658
PbI polytypes, phase transforms. and electrical behaviour 78−47839
PbI_2, 2H polytype, anisotropy of lattice vibrs. 77−7807
PbI_2, 2H polytype, optical mode inversion hear M-critical point, neturon scatt. mass 80−103432
PbI_2, 24-layered hexagonal polytype, growth in U-tube by silica gel method, struct. 77−4722
PbI_2 (2H), angular depend. magnetoluminesc. 79−43029
PbI_2 (2H), electronic transport and cyclotron reson. 79−28369
PbI_2 (2H), layer cpd., band parameter determ. 79−95332
PbI_2 (2H), multi-phonon scatt. near direct absorpt. edge, resonant Raman obs. 79−87448
PbI_2 (2H), photolum. spectrum, in strong photoexciton mixing region 78−48223
PbI_2, above-edge cathodolum. from metastable excitons 78−6786
PbI_2, adsorbed ^{36}Ar and CD_4 films, on cleavage faces, layer-like charact., neutron diffr. obs. 79−86994
PbI_2, complex dielectric and optical consts., ellipsometric determ. 78−23425
PbI_2, cooperative fluoresc. by excitonic reson. pumping 79−33732
PbI_2, cryst., photochem. phenomena investig. *(Russian)* 78−35204
PbI_2, cryst., photocond., energy gap localised level obs. 78−43443
PbI_2 crystal, gel-grown AgI impurity effects on struct. transformations during growth 77−76339
PbI_2 crystals, exciton condensation, excitation and luminesc. study 80−55182
PbI_2, cubic, elastic consts., hydrostatic press. effect, US vel. meas. 80−49292
PbI_2, DC elec. cond. as function of I pot. 79−24023
PbI_2, defect levels, TSC meas., photoconductor models, trap level capture cross section 79−69463
PbI_2, detector fabrication 77−54411
PbI_2, determ. of sign and drift mobility of majority carriers *(Russian)* 79−69512
PbI_2, dielectric props., elec. cond., space charge polarisation 80−100631
PbI_2, direct and indirect two photon processes 77−40261
PbI_2 direct gap polar semicond., electron hole liquid phase diagram *(Russian)* 80−93314
PbI_2 direct gap semiconductor, exciton lifetime and condensation threshold, luminescence spectra 80−34981
PbI_2, elec. props. rel. to polytypically modulated structs. 79−94971
PbI_2, electronic struct. and exciton problem, photoelectron spectra meas. 77−63540
PbI_2, electronic struct., tight-binding calcs. 80−15446
PbI_2, emission spectra, 80K, high excitation intensity effects at different pump wave lengths 77−52170

lead compounds continued
PbI_2, exciton absorpt. band shape, dielectric const. real part derivatives *(Russian)* 80−25413
PbI_2, exciton dispersion curves, influence of optical phonons 79−15091
PbI_2, exciton magneto-optical spectra 80−25347
PbI_2, exciton spectra depend. on strong excitation, crystal transmission 79−69433
PbI_2, exciton states, high field magnetoabsorption 77−52130
PbI_2, excitonic shifts of quasiatomic optical core to cond. band transitions, UPS obs. 78−11079
PbI_2, excitons in spatially dispersive medium, absorption theory 80−54618
PbI_2, factor-group analysis of high-symmetry layer dynamics 79−42160
PbI_2, film, fundamental absorption edge, complex dielec. const. *(Russian)* 77−40266
PbI_2 film, highly excited, oscillator strength of excitons, absorpt. and emission spectra 78−76001
PbI_2 film, photolyzed, refr. index change 78−11010
PbI_2, film, reflectance meas., optical consts., humidity effects 80−34994
PbI_2, film, spectral depend. of optical consts. on fundamental absorption edge *(Russian)* 77−16415
PbI_2, film exciton spectrum, Faraday rot. 77−20944
PbI_2, film intercalated with pyridine, UV absorpt. spectrum, Frenkel excitons 77−24864
PbI_2, first-order 2H-4H polytype transition, exciton spectroscopic study 80−59647
PbI_2, hexagonal to rhombohedral phase transform., SFE 79−91643
PbI_2, high press. phase diagram to 3.5 GPa 80−104126
PbI_2, high-pressure phase transition, optical props. meas., 300K and 78K 77−51495
PbI_2, ice-nucleating props., −10 to −25°C *(French)* 77−78301
PbI_2 in piperidine solution, crystn. of intercalation cryst. 80−16170
PbI_2 intercalated with organic donor mols., cryst. struct. and phys. props. 78−26543
PbI_2 intercalated with organic mols., energy band splitting *(Russian)* 78−76027
PbI_2 intercalated with organic mols., superlattice and quantum dimens. effect *(Russian)* 79−46628
PbI_2 intercalated with aniline, NQR meas. *(Russian)* 79−91311
PbI_2, ionic cond. and activation volumes, high press. effects 80−100353
PbI_2, ionic layer cpd., lattice dynamics, influence of static dipole moments 79−28057
PbI_2, kinetic parameters of water drops crystn. *(Russian)* 77−81963
PbI_2 laminar semicond., phase transition of first kind by exciton spectroscopy *(Russian)* 79−82334
PbI_2, layer dynamics of high-symmetry crystals with atom-atom interactions 78−71799
PbI_2, layered, electronic band struct., direct evaluation by angle resolved photoemission 77−51652
PbI_2, layered, photoelectromag. effect meas. of transport parameters 77−59301
PbI_2, layered compound, exciton spectra, surface and stacking fault effects 80−40134
PbI_2, layered cryst., photoluminesc., and reflection spectra obs. 78−6726
PbI_2 layered cryst. under uniaixal compression, low temp. thermal cond. *(Russian)* 80−44374
PbI_2, layered semicond., valence bands UPS and XPS obs. 78−11078
PbI_2, longitudinal-transverse splitting of anisotropic excitons 78−2431
PbI_2, low temp. thermal props. 79−95178
PbI_2, luminescence excited by high-intensity two photon pumping 77−44038
PbI_2, multiphoton cross-section determination by means of luminescence experiments 80−93377
PbI_2, octahedrally coordinated, layer cpd., electronic struct. using synchrotron-radiation photoemission spectroscopy 79−74058
PbI_2, optical phonon anisotropies and intralayer bonding forces from IR refl. 77−59573
PbI_2, optical props. 77−32394
PbI_2, photo-EMF, effect on photolysis of PbI_2-Ag *(Russian)* 80−92939
PbI_2, photocond. induced by polaritons at band-edge 79−95450
PbI_2, photoelectromagnetic investigation, expt. 79−24010
PbI_2, photoemission, book contrib. 77−44133
PbI_2, photoexciton interaction, luminescence spectra, polariton dispersion diagram 80−93397
PbI_2 photographic layers, fogged with metals, spectral sensitivity and optical absorpt. *(Russian)* 77−30209
PbI_2, photolum. and reflectivity temp. depend., cryst. anisotropy effect on electron-phonon interaction *(Russian)* 78−15225
PbI_2, photoluminesc. spectra, generation of stimulated radiation 77−8647
PbI_2, polar, layered material, quenching of excitonic diamag. shifts 79−19526
PbI_2, polymorphic phase changes of adsorbed NO 77−31900
PbI_2 polytypes, centrosymmetric space groups 77−31618
PbI_2 polytypes, elec. cond., band gap reduction due to stacking fault levels 77−32015
PbI_2, polytypic change, 5 new polytypes, X-ray diffr. anal. 79−37648
PbI_2, press. depend. of band-gap excitons, 77K, optical absorpt. spectra 79−8157
PbI_2, quasi-two-dimens layered struct., phonon dispersion surfaces 79−42180
PbI_2, Raman spectra, phonon dispersion curves, vibrational props., lattice parameters 79−69211
PbI_2, semicond., band struct., angle resolved photoemission meas. 78−15296
PbI_2 single cryst., EPR of V^{2+}, Mn^{2+}, Co^{2+} 78−68362
PbI_2, single cryst., far IR refl. spectra, effective ionic charges 79−87430
PbI_2, single cryst., luminesc., photocond. and absorpt. after thermal treatment 79−56855
PbI_2 single crystal growth, modified gel technique improved design 80−84842
PbI_2 single crysts., photo-induced AC impedance meas., photodielec. effect 78−52034
PbI_2 single crysts., resonant and nonresonant Raman spectra 77−69823
PbI_2, sputtering processes during 6 keV Xe ion bombard. 78−68590
PbI_2, stimulated photoluminesc. excitons role 77−48201
PbI_2 suspension, chem. sensitization 80−73492
PbI_2, TSC meas., localised levels in energy gap, depend. on purity and history 77−15856
PbI_2, temp. depend. of electron-hole drop emission *(Russian)* 77−16394
PbI_2, thin cryst. barrier, reson. and inelastic tunnelling 80−44739

lead compounds continued
- PbI_2, thin films, photolysis kinetics 77−36769
- PbI_2, three-photon absorpt. coeff. determ. by nonlinear luminesc. expt. 80−14384
- PbI_2, tight binding band structure using scaled parameters 78−79927
- PbI_2, two-photon absorpt. spectrum 77−52118
- PbI_2 two-photon absorpt. cond. and luminesc. meas. 77−52166
- PbI_2, two-photon photoemission 79−28890
- PbI_2, UV reflectivity meas., band struct., LCAO calcs. 78−72545
- PbI_2, valence band electronic struct., XPS and UPS obs. 78−6826
- PbI_2, valence-band XPS meas. 77−12487
- PbI_2, visible exciton spectrum, exciton-phonon interactions, dielectric const. and oscill. strengths 80−25405
- PbI_2:KI, trapped exciton states, absorption spectra 80−50383
- PbI_2:KI alloys, fundamental abs. edge, potential as solar convertor 80−101128
- PbI_2-Ag, light sensitivity for high exposure densities *(Russian)* 79−6212
- PbI_2-Ag, photographic mat., photolysis, effect of PbI_2 photo-EMF effect *(Russian)* 80−92939
- PbI_2-Ag light sensitive system, photochem. conversion process under continuous laser radiation, nonreciprocity *(Russian)* 77−79179
- PbI_2-Ag system, effect of bound and free exciton states on light sensitivity *(Russian)* 78−71169
- PbI_2-Ag(Au)(Cu), light sensitive, internal photoelectric emission 80−107910
- PbI_2-Cu photosystems, null-refl., cermet and Fabry-Perot types 78−46738
- PbI_2-$PbBr_2$ mixed systems, cryst. growth, struct. and optical props. *(German)* 80−96499
- PbI_2-$PbBr_2$, optical spectra, solid soln. struct. 78−48247
- PbI_2-piperidine intercalations rel. to NQR, spin-lattice relax. temp. depend. *(Russian)* 78−27108
- PbI_2-piperidine(aniline)(pyridine), intercalation cpds., heat capacity of low temp., intercalation effect *(Russian)* 80−92682
- $Pb_5I_2Br_8$, form., cryst. symmetry, X-ray diffr. obs. 79−23570
- $Pb_5I_4Br_6$, form., cryst. symmetry, X-ray diffr. obs. 79−23570
- PbI_2(2H and 4H), layer cryst., elec. field effect on NQR, elec. polarisation mechanism 77−20746
- $PbIn_{0.5}Nb_{0.5}O_3$, ferroelectric, dielectric props. 80−103923
- $PbIn_2S_4$, vap. press., computer-automated meas. by simultaneous Knudsen torsion-effusion method 80−73334
- $PbIn_2S_4$, X-ray powder cryst. struct. determ. 80−66488
- $Pb_4In_9S_{17}$, $Pb_3In_{6.67}S_{13}$, cryst. struct. *(French)* 78−63707
- $Pb_6In_{10}S_{21}$, X-ray powder cryst. struct. determ. 80−66488
- $Pb_{1-x}In_xTe$, $0.01 \leq x \leq 0.2$, elec. cond., Hall coeff. liquid He temp. 78−47815
- $Pb_{1-x}In_xTe$, impurity-state conduction and temp. depend. of transport coeffs. 78−47795
- $Pb_2KNb_2O_5$, SAW props., rel. to device appl. 78−71923
- $Pb_2KNb_5O_{15}$ material for SAW devices 79−56735
- $Pb_2KNb_5O_{15}$ piezoelectric coupling for SAW applications 79−56055
- $Pb_2KNb_5O_{15}$, strong electromechanical coupling of SAW 78−63919
- $Pb_{0.27}K_{0.56}Nb_{0.91}Ta_{4.15}O_{15}$, coupled ferroelastic-ferroelectric props. 77−59543
- $Pb_2KNb_{5-x}Ta_xO_{15}$, ferroelastic-ferroelectric coupling, dielec. props. 79−38433
- $Pb_{2.07}K_{0.56}Nb_{0.91}Ta_{4.15}O_{15}$, tetragonal tungsten bronze type, ferroelastic-ferroelectric coupling *(French)* 77−28522
- $PbK_2(PO_3)_4$, cryst. struct. 77−31638
- $Pb_{0.9}K_{0.1}(Zn_{1/3}Nb_{2/3})O_{2.95}$-$PbZrO_3$-$PbTiO_3$, morphotropic tetragonal-rhombohedral phase boundary 78−48129
- PbLaMTeO$_6$, M=Li, Na, antiferroelectric, synthesis and characts. 77−55758
- $Pb_{1-\alpha x}La_xTiO_{3+x(1.5-\alpha)}$, permittivity as function of temp. 79−33586
- $PbLaZrNbO_7$, dielectric with zero temp. coeff. of dielect. consts., electrophys. props. 77−52010
- $Pb_{0.97}La_{0.02}(Zr_{0.92}Ti_{0.08})O_3$, ferroelec. ceramic, stress effects 80−2119
- PbLi, gas phase thermodynamics, Knudsen effusion mass spectrosc. 80−100057
- $Pb_2Li_{1/2}Nb_{3/2}O_6$, antiferroelec. cryst. growth and props. 77−36189
- $PbLi(PO_3)_3$, cryst. struct. determ. *(French)* 77−80463
- $Pb_{1-x}M_xF_{2+x}$ (M=Bi,Th), fast ionic conduction of F^- ions 79−99360
- $Pb_2M_2^{III}Ge_2O_9$, (M^{III}=Fe,Mn,Sc,In), synthesis, X-ray diffr. and vibr. anal. 79−61360
- $Pb_2M^{II}M^{IV}Si_2O_9$, (M^{II}=Mg,Ni,Co,Cu for M^{IV}=Sn; M^{II}=Co, Ni for M^{IV}=Ti), synthesis, X-ray diffr. and vibr. anal. 79−61360
- $PbMO_6S_7$, supercond., fast neutron irrad. effects on T_c 77−55633
- $PbMO_6S_8$, supercond., upper crit. field meas. up to 600 kG 80−93057
- $Pb(Mg_{1/3}Nb_{2/3}Nb_{2/3})O_3$-$PbTiO_3$-$PbZrO_3$ ceramics, HF filters appl. additives effect obs. *(Japanese)* 80−60507
- $PbMg_{1/3}Nb_{2/3}O_3$, and its solid solns., low temp. phase transition obs. 79−69788
- $PbMg_{1/3}Nb_{2/3}O_3$, carrier mobility and photoluminesc. near ferroelec. transition *(Russian)* 78−2813
- $Pb(Mg_{1/3}Nb_{2/3})O_3$, cation disordered perovskite, elastic consts. and thermal expansion 80−96587
- $PbMg_{1/3}Nb_{2/3}O_3$, dielec. props. under high hydrostatic pressure near phase transition point 80−44997
- $Pb(Mg_{1/3}Nb_{2/3})O_3$, electrostrictive effect 80−66113
- $PbMg_{1/3}Nb_{2/3}O_3$, ferroelec., cathodlum. spectral and temp. depend. 78−84665
- $PbMg_{1/3}Nb_{2/3}O_3$, ferroelec., crit. electron-phonon phenomena and diffuse phase transition in elec. field 79−38497
- $PbMg_{1/3}Nb_{2/3}O_3$, ferroelectric with diffused phase transition, photoelectret states 80−20583
- $PbMg_{1/3}Nb_{2/3}O_3$, PMN, electro-opt., elasto-opt., opt. and photo-induced props. 78−95560
- $PbMg_{1/3}Nb_{2/3}O_3$, photocond., 20-150°C, and photoelectret state 77−24590
- $PbMg_{1/3}Nb_{2/3}O_3$, photoinduced phenomena at diffuse phase transition 78−43814
- $PbMg_{1/3}Nb_{2/3}O_3$, photoinduced birefr., reversible optical information recording 78−50874
- $PbMg_{1/3}Nb_{2/3}O_3$, photolum. near ferroelec.-paraelec. phase transition 80−16100
- $PbMg_{1/3}Nb_{2/3}O_3$, photolum. and carrier drift mobility at ferroelec. transition 80−71469
- $PbMg_{1/3}Nb_{2/3}O_3$, short-range ordering, electron microscope and diffr. study 80−10469
- $PbMg_{1/3}Nb_{2/3}O_3$ single cryst., electro-optical hysteresis curves and phase transitions *(German)* 79−28717

lead compounds continued
- $PbMg_{1/3}Nb_{2/3}O_3$, vibr. spectrum and dispersion of optical consts., coexisting ferro- and paraelec. phases 77−63422
- $Pb(Mg_{1/3}Nb_{2/3})O_3$-$PbTiO_3$, ceramic dielectric, electrostriction, relaxation, polarisation 80−80700
- $PbMg_{1/3}Nb_{2/3}O_3$-$BiMg_{2/3}Nb_{1/3}O_3$, dielectric polarisation of solid solutions 78−43776
- $Pb(Mg_{1/3}Nb_{2/3})O_3$-$PbTiO_3$-$PbZrO_3$, piezoelec. PCM ceramic, formation process *(Japanese)* 77−85978
- $Pb(Mg_{1/3}Nb_{2/3})O_3$-$PbTiO_3$-$PbZrO_3$, piezoceramics for high frequency use 78−95555
- $Pb(Mg_{1/3}Nb_{2/3})O_3$-$Pb(W_{1/2}Mg_{1/2})O_3$, struct. and dielec. props. 80−25312
- $Pb(Mg_{1/3}Nb_{2/3})O_3$-$Pb(Mg_{1/2}W_{1/2})O_3$, solid soln., electrostriction, strain gauge obs. 80−55043
- $PbMg_xNb_{1-x}O_3$, ferroelec. with diffuse phase transition, electrostriction-optical props. 78−68457
- $Pb_3MgNb_2O_9$, birefringence, pulse response of electro-optical effect 79−87417
- $Pb_3MgNb_2O_9$, crystal growth procedure, meas. electro-optic and dielectric props. 78−88418
- $Pb_3MgNb_2O_9$ crystal electro-optic deflector design and adjustment 79−72690
- $Pb_3MgNb_2O_9$ diffuse phase transition, Brillouin scatt. and acoustic phonons 78−76401
- $Pb_3MgNb_2O_9$, photoelectretic states in real time spatial light modulators, photorefractive effect 80−80676
- $Pb_3MgNb_2O_9$-CdS, electro-optical space-time light modulation 78−18056
- $Pb_3MgNb_2O_9$-$PbTiO_3$, relaxor ferroelectrics, electrostrictive effects 80−66112
- $PbMg_{0.33}Ta_{0.66}O_3$, ferroelectric, exam. of permittivity and dielectric props. 79−1742
- $PbMg_{1/3}Ta_{2/3}O_3$ ferroelectric semiconductors, electro-optical and elasto-optical props., appl. to optical storage *(Russian)* 80−80749
- $Pb_3MgTa_2O_9$, crystal growth procedure, meas. electro-optic and dielectric props. 78−88418
- Pb_2MgTeO_6, ferroelec. behaviour, microwave dielec. props. meas. 77 43948
- $Pb(Mg_{0.5}W_{0.5})O_3$-$BiFeO_3$, dielec. props., cryst. struct. 78−84534
- $PbMnF_3$, antiferromag., acoustic nuclear resonance, self-induced transparency *(Russian)* 79−91304
- Pb_2MnF_6, antiferromag. and superionic conductor, EPR and NMR meas. 79−99366
- $PbMnFeF_7$, vitreous, insulating, evidence of spin-glass transition 80−97112
- Pb_2MnFeF_9, vitreous, insulating, evidence of spin-glass transition 80−97112
- $Pb_3Mn_7O_{15}$, X-ray cryst. struct. determ. *(French)* 79−14744
- Pb_xMnO_2, synthesis, chem. stability, use *(French)* 78−80525
- $Pb(Mn_{1/2}Ta_{1/2})O_3$, ceramic, for thermal and dielectric isolation at low temp. 80−39365
- $Pb_{1-x}Mn_xTe$ (x=0.005, 0.001, 0.05), solid solns., exam. of electrical and thermal props. 79−1599
- $Pb_{1-x}Mn_xTe$, photovoltaic effect, p-n junction, energy gap determ. 80−92931
- $Pb_{1-x}Mn_xTe$, single cryst., mag. susceptibility 79−73672
- $PbMo_4$, M=Mo,W, EPR spectrum, temp. depend. of zero field splitting 79−15346
- $PbMoO_4$, acousto-optical freq. and intensity control system for CW lasers 77−88804
- $PbMoO_4$, acousto-optic interaction at high optical intensities 79−42942
- $PbMoO_4$, Brillouin spectra, photoelastic consts. and optical purity 78−60480
- $PbMoO_4$, centrosymmetric cryst., linear electrogyration study 80−60540
- $PbMoO_4$, colour origin 77−85921
- $PbMoO_4$, colour study from absorption, fluorescence and thermoluminesc. exam. 78−31245
- $PbMoO_4$, cryst. growth from gel soln., habit modifications 78−2043
- $PbMoO_4$, defect electron centres after X-irrad. 79−55738
- $PbMoO_4$ deflectors, beam quality, of acousto-optic frequency shifters 78−79127
- $PbMoO_4$, diffr. modulator, two separate opposing US waves 77−3676
- $PbMoO_4$, doped and undoped single crysts., polarisation of luminesc. and assignments 80−76069
- $PbMoO_4$, elastic wave excitation and amplification by laser radiation 80−103419
- $PbMoO_4$, electrogyration coeff. meas. 79−19859
- $PbMoO_4$, Faraday rotation, interband optical transitions *(Russian)* 80−55071
- $PbMoO_4$, hollock growht origin in gel growth 80−49139
- $PbMoO_4$, investigation of molecular light scatt. 78−72537
- $PbMoO_4$, ionic and electronic cond. 79−91107
- $PbMoO_4$, near-edge absorpt. band, fluoresc. and photocond. 77−44017
- $PbMoO_4$, optical absorption of hole centres, polaron model 80−97314
- $PbMoO_4$, polychromatic acousto-optical deflector *(Russian)* 77−58429
- $PbMoO_4$, Raman scatt. obs. of external and internal modes 79−69842
- $PbMoO_4$, refr. index, single crystals having scheelite struct. 78−79082
- $PbMoO_4$, SAW props. 78−63920
- $PbMoO_4$, single crystal growth in Na_2SiO_3 gel 77−77351
- $PbMoO_4$, vibr. props. and struct., effect of hydrostatic press. 77−28571
- $PbMoO_4$:Fe^{3+}, ESR, effective g-factors, Fe^{3+} sites 77−51947
- $PbMoO_4$:Fe^{3+}, single crystals, structure and kinetics, EPR meas. 79−99760
- $PbMoO_4$:Mn^{2+}, zero-field splitting of Mn^{2+}, EPR 80−75531
- $PbMoO_4$:Nd^{4+}, optical absorpt. intensities, 300, 550 and 4.2K, expt. and Judd-Ofelt theory 77−20894
- $PbMoO_4$-MO, M=Ca,Ba,Sr, phase diag. cross sections and reactions 78−27487
- Pb_2MoO_5, form. conditions 80−20853
- $PbMo_{5.1}S_6$, supercond. wire prep. by powder technique 78−52705
- $PbMo_6S_6$, cold-worked core-wires, supercond. transition temp. and lattice instability 78−6469
- $PbMo_6S_8$ and ternary sulphides, lattice parameter rel. to supercond. T_c 78−52119
- $PbMo_6S_8$, Chevrel phase supercond., phonon spectra, neutron scatt. meas. 79−42174
- $PbMo_6S_8$, Chevrel-phase, electronic struct., LCAO calc. for idealised Mo_6S_8 cluster 77−43494
- $PbMo_6S_8$, Chevrel-phase superconductors, lattice dynamical calcs. 79−33056

lead compounds continued
$PbMo_6S_8$, crit. current density, effect of prep. technique and press. 78−14908
$PbMo_6S_8$, high crit. field Chevrel phase 79−61003
$PbMo_6S_8$, influence of Fe on superconduction transition temp., and mag. props. *(Russian)* 79−42686
$PbMo_6S_8$, inhomogeneous superconductor, scaling laws for pinning forces 79−47214
$PbMo_6S_8$, normal state and superconducting property measurements 78−91660
$PbMo_6S_8$, normal-state electronic props., Fermi surface and supercond. parameter derivations 79−60850
$PbMo_6S_8$, prod. by solid state reaction, supercond. crit. temp. *(Japanese)* 79−42682
$PbMo_6S_8$, projected critical current, comparison with Nb_3Ge 79−69642
$PbMo_6S_8$, relationship between electronic struct. and supercond. transition temp. 77−85368
$PbMo_6S_8$, sputtered Chevrel phase films, indirect meas. of Fermi surface parameters 79−60686
$PbMo_6S_8$, sputtered film, critical current density meas. 78−84369
$PbMo_6S_8$, supercond. Chevrel phase, electron tunnelling spectroscopy expts. *(German)* 80−107966
$PbMo_6S_8$, supercond. wires prod. and characteris. 77−69462
$PbMo_6S_8$, temp. depend. of crit. currents 80−20363
$PbMo_6S_8$, thin films, low temp. normal state, resist., temp. depend. 78−91783
$PbMo_6S_8$ wire, powder processed, crit. current density and field 80−80466
$PbMo_6S_8$:Fe, elec. cond. anomalous temp. depend., mag. moments *(Russian)* 80−92878
$PbMo_6S_8$:Gd^{3+}, EPR meas. *(French)* 80−54947
$PbMo_6S_8$:Gd^{3+}, powder EPR spectra, cryst. field, supercond. energy gap 80−34769
$Pb_{1.0}Mo_6S_8$, Chevrel phase supercond., compressibility and vol. depend. of Tc 78−31008
$Pb_xMo_6S_8$, Chevrel phase supercond. prep. and supercond. props. 79−28434
$Pb_xMo_6S_8$ Chevrel phase, synthesis, stability and characts. 80−71608
$Pb_xMo_6S_{8-y}$, phase relns., stoichiometry, T_c 78−15378
$PbMo_6S_6O_2$, O-containing Chevrel phases, synthesis and props. 80−108368
$Pb_xMo_6S_8(Se_8)$, prep., metallurgical and supercond. props. 77−32102
$Pb_xMo_3S_4(Se_4)(Te_4)$, chevrel phase, anomalous elec. resist. 79−56221
$Pb_xMo_6S_8(Se_8)(Te_8)$, Chevrel phase correlation between struct. and supercond. transition temp. 80−7023
$PbMo_6Se_8$, relationship between electronic struct. and supercond. transition temp. 77−85368
$Pb_{1.125}Mo_6Se_{7.5}$, Chevrel phase supercond., NMR study 80−49989
$Pb_{1.2}Mo_6Se_8$, Chevrel phase supercond., compressibility and vol. depend. of Tc 78−31008
$Pb_{1.2}Mo_6Se_8$, Chevrel phase supercond., phonon spectra, neutron scatt. meas. 79−42174
$PbMo_6Se_8(S_8)$, anisotropy of H_{c2} 78−39274
$PbMo_6X_8$ (X=S, Se), phonon density of states, mode softening correl. with supercond. transition temp. 79−51714
α-$Pb(N_3)_2$, crystal struct., neutron diffr. exam. 78−10006
$Pb(N_3)_2$-He system, high-velocity two-layer detonation 77−84278
PbN_6, electronic transitions and energy band struct. 79−74053
PbN_x, pressed, lag time of breakdown and dielec. strength 77−36174
$Pb(NO_3)_2$, ^{207}Pb mag. shielding anisotropy, Fourier transform NMR 77−90057
$Pb(NO_3)_2$, ^{207}Pb NMR linewidth, angular depend. due to ^{14}N-^{207}Pb direct dipole-dipole interaction 80−11280
$Pb(NO_3)_2$, crystal-solution interfacial tension, from crystn. meas. 79−69045
$Pb(NO_3)_2$, dynamical props., IR reflection spectra meas., 10-300K 77−1676
$Pb(NO_3)_2$, IR reflection spectra, dynamical props. 77−16303
$Pb(NO_3)_2$, low temp. struct. changes, elec. props. 79−87377
$Pb(NO_3)_2$, Nd laser second harmonic stimulated Raman scatt., efficiency in calcite, nitrate crysts. 80−95949
$Pb(NO_3)_2$, nucl. mag. shielding tensors of $^{207}Pb^{2+}$, NMR obs. 80−44939
$Pb(NO_3)_2$, press. derivatives of elastic-moduli, ultrasonic velocity meas. 78−95102
$Pb(NO_3)_2$, Raman spectra temp. depend. anomalies in symmetric stretch region 79−61361
$Pb(NO_3)_2$, thermal expansion study to test sensitivity of X-ray powder goniometer *(French)* 80−79631
PbN_2O_3, vibr. spectra, assignments 77−38670
$Pb_3(NO_4)_2$, press. induced ferroelastic phase transition, neutron diffr. study 79−73308
Pb_2NbFeO_6, form. reacts., thermogravimetric investig. 78−35340
$PbNbO_3$ thin film microwave complex permittivity meas. 79−73879
$PbNb_2O_3$, piezoelectric ceramic solid soln. *(Polish)* 77−55755
$PbNb_2O_6$ ceramic, piezoelectric effect due to polarisation *(Polish)* 77−77151
$PbNb_2O_6$, ferroelec., cryst. struct. *(French)* 77−72588
$PbNb_2O_6$, ferroelec., sp. ht. and Debye temp. meas., 2-25K 79−73319
$PbNb_2O_6$, ferroelectric thick crystals, domain formation and dislocation loops 78−60410
$PbNb_2O_6$ ferroelectric single crysts., domain struct., cryst. planes, twinning 78−64340
$PbNb_2O_6$, ferroelectric strain polarisation interaction, domain wall formation 79−56750
$PbNb_2O_6$, IR absorpt. spectra and diffuse Raman scatt., normal coord. anal. *(French)* 80−66198
$PbNb_2O_6$, O defects and elec. props. anomalies 79−42898
$PbNb_2O_6$, permittivity and elec. cond. meas., first order transition 79−24270
$PbNb_2O_6$, sp. ht. and Debye temp. meas., 2-25K 79−73319
$PbNb_2O_6$, surface (001), microstruct. obs. by optical, etching, and interferometric techniques 79−11399
$PbNb_2O_6$-$NaNbO_3$, DTA *(French)* 77−44234
$Pb_2Nb_2O_7$, electric cond. and dielect. props. of cathodic-sputtered films *(French)* 79−33371
$Pb_2Nb_2O_7$, Raman-scattering investigation of vibrational structure 78−76441
$Pb_2Nb_2O_7$, sp. ht. and Debye temp. meas., 2-25K 79−73319
$Pb_xNb_yO_6$ pyrochlore phases, three odd superstructures *(French)* 77−68946
PbNbS(Se), struct., X-ray powder diffr. meas 80−44175

lead compounds continued
$PbNb_{0.5}Sc_{0.5}O_3$, ceramic, dielec. props. 79−11392
Pb_2NbYbO_6, X-ray structural investigation 79−65060
$Pb_{0.98}Nb_{0.02}(Zr_{0.95}Ti_{0.05})_{0.98}O_3$, PZT 95/5, ferroelec. ceramic, resist. meas. under shock wave compression 78−19031
$Pb_{0.99}Nb_{0.02}(Zr_{0.95}Ti_{0.05})_{0.98}O_3$, ferroelec. ceramic, stress effects 80−2119
$Pb_{5-x}Nd_xGe_3O_{11}$, ferroelec. props. 80−75960
$PbNdTiNbO_7$, cryst. growth rel. to investig. of PbO-KF-B_2O_3-$PbNdTiNbO_7$ cross section 77−86004
Pb_2NiReO_6, seignettomagnets with perovskite struct. 79−38459
PbO activity in ternary and binary silicates *(Japanese)* 78−6907
PbO, anharmonicity effect, Debye temp. determ. from Mossbauer spectra 77−63335
PbO, appl. of effective pots. to relativistic HF calcs. of mol. props. 78−74559
PbO, binder layer, properties of radiographic system 78−21238
PbO, chemiluminesc. spectra, Pb atom reactions, mol. consts. 77−9087
PbO containing crystal glasses, viscosity, effects of Li_2O, BaO, ZnO, MgO and SrO 80−19973
PbO containing crystal glass, viscosity-temp. depend., glass transition, and softening point 80−24637
PbO, content estimation in PZT using analytical procedure *(German)* 78−53279
PbO, disordered photoconductor, dielec. props., temp. depend. anomalies 78−43765
PbO, doped, secondary ion emission, at. and mol. processes 78−68588
PbO film, on Na_2O-B_2O_3 glass, deep penetration of Pb^{2+} ions into glass 78−79535
PbO film, on vitreous SiO_2, interdiffusion reactions, UV spectroscopy obs. 78−51750
PbO film on Na_2O-B_2O_3 glass, interdiffusion layer 79−51318
PbO formed on (111) surface of Pb, electron microscopy 78−23878
PbO glass, mechanochemical reduction 77−52628
PbO glass, reflection spectra 78−88325
PbO glass, strength, effect of HNO_3 etching 77−56124
PbO glass, thermal focusing of elliptically shaped optical beams 79−18489
PbO, high refractive index core glass for high NA optical fibres *(Japanese)* 79−59853
PbO, ion plating, X-ray sensitive photoconductor 77−44174
PbO, laser excitation IR spectra, photoluminescence obs., rot. anal., rot. const. determ. 80−95619
PbO layer vapour deposition, structure, and props. 80−65408
PbO layers, crystal platelets orientation and thickness, X-ray diffr. obs. 78−87890
PbO layers on Pb films, optical props. 79−83042
PbO, microprobe state anal. by X-ray OK and BK emission band spectra *(Japanese)* 78−19606
PbO mixtures with various oxides, solvents for garnet growth, cryoscopic study 80−24393
PbO, molecular versus atomic secondary ion emission, rel. to quantitative analysis 79−61481
PbO orthorhombic crystals grown from melt, followed by quenching 79−100038
PbO, polycrystalline layers, influence of prep. conditions on phase comp., texture and struct. 79−4495
PbO powder layers, adsorbed rhodamine B dye, charge storage and photocond. 78−64056
PbO, prep. and growth, book contrib. 78−19651
PbO, reactively evaporated photoconductive film, phase transform. induced by water vapour 79−78233
PbO, reactively evaporated, photocond., H_2O induced phase transform. 80−60122
PbO single crystals, current-voltage characts., electrolum. *(Russian)* 80−2863
PbO, single crysts., exciton and impurity luminesc. 80−60674
PbO, sintered, pure, prep. and props. 77−48361
PbO, smoke particles prep. by burning metal in Ar-O_2 gas, electron microscope obs. 77−52238
PbO, spray coated, reaction with Si, IR investig. 79−39197
PbO, standard free energy of formation, by EMF method with solid oxide electrolyte at low temps. *(Japanese)* 80−88338
PbO, stoichiometric deviations on heating in vacuum 77−25035
PbO tetragonal crystals, top-seeded soln., growth method from 6% TiO_2-PbO soln. 79−100038
PbO, thermodynamic activity in liquid, PbO-$PbCl_2$ 78−7227
PbO thin films, elec. props. *(Korean)* 79−60943
PbO thin layers on PbO-SiO_2 glass, reaction behaviour 78−34660
PbO, trap parameters, appl. of calc. method from TSC 77−8495
PbO, vapour, photoluminescent decay, a(1) state 78−58745
PbO, visible absorpt. spectra rel. to indirect exciton transitions 80−60628
PbO, X-ray powder cryst. data, struct. rel. to Pb_6GeO_3 and $Pb_{11}Ge_3O_{17}$ 80−84146
PbO:Ag film, X-ray stimulated diffusion, current-voltage characts. 77−80653
PbO/PbF_2/B_2O_3 solvent system, density, surface tension and expansivity data, effect of B_2O_3 conc. 79−19985
PbO/TeO_2 system, central region of phase diagram, X-ray and thermal anal. 79−70046
PbO-2B_2O_3-Fe_2O_3 glass, Mossbauer study, struct., crystallite formation, broadened quadrupole doublet 78−59761
PbO-Al_2O_3-B_2O_3 vitreous system with relaxation structure, spinodal decomposition 78−75553
PbO-B_2O_3, glass exam. of Raman spectra *(Japanese)* 79−19894
PbO-B_2O_3, solder glass, thermal reduction of Cu^{2+} and Cu^+:Cu^{2+} effect on thermal props. 78−15350
PbO-B_2O_3 glass, X-ray emission spectra of Fe and Cu 77−44089
PbO-B_2O_3 glass-forming melt, specific volume and viscosity, temp. depend. 80−84073
PbO-B_2O_3 glasses, microhardness 80−66612
PbO-B_2O_3 melt, activity of PbO 77−11708
PbO-B_2O_3 phase-separated glass, fracture toughness, Vickers indentation method 80−85023
PbO-B_2O_3:Cu^{2+}, glasses, ESR and optical absorpt. 80−34760
PbO-B_2O_3-Al_2O_3 glass, spinodal decomp. during continuous cooling, theoretical anal. 80−1935
PbO-B_2O_3-Al_2O_3 system melts and glasses, viscosity, phase separation, and supercritical fluctuations effects 79−65235
PbO-B_2O_3-Bi_2O_3, glass with metallic Bi granules, elec. cond. 80−84493

lead compounds continued
PbO-B_2O_3-Fe_2O_3-CuO glass, electric cond. and struct. *(Japanese)* 78−23093
PbO-B_2O_3-$Li_2O(Na_2O)(K_2O)$ melt, activity of PbO 77−11708
PbO-B_2O_3-SiO_2, glass enamel, heat treated, exam. of microstructure and chemical durability 79−29254
PbO-B_2O_3-SiO_2, molten mixture, microprobe state anal. by X-ray OK and BK emission band spectra *(Japanese)* 78−19606
PbO-B_2O_3-SiO_2-Al_2O_3-ZnO-CuO-Bi_2O_3 solder glass, crystallisation prevention by Cu addition 80−11654
PbO-B_2O_3-SiO_2-Li_2O-ZrO_2-CdO(CoO)(CuO), glass enamel, chemical durability, microstruct., CuO, CdO and CoO addition effects 79−29256
PbO-B_2O_3-SiO_2-Li_2O-MgO(CaO)(ZnO)$(Al_2O_3)(TiO_2)(ZrO_2)$, glass enamel, heat treated, chemical durability, MgO, CaO, ZnO, Al_2O_3, TiO_2, ZrO_2 addition effects 79−29255
PbO-B_2O_3-ZnO solder glass, with admixtures, crystallisation and thermal expansion 80−24364
PbO-$B_2O_3(SiO_2)$ glasses, absorpt. spectra of Cu^{2+} ions and interpret. 78−27276
PbO-$B_2O_3(SiO_2)$ glasses, structure toughness-composition relationship 80−104257
PbO-Bi_2O_3, thermodynamic props. 77−59743
PbO-Bi_2O_3-Al_2O_3, glass formation and IR transmission *(Japanese)* 80−54146
PbO-Bi_2O_3-GeO_2, exam. of glass forming and liquid phase separation regions, and optical props. 78−88453
PbO-containing binary systems, acoustooptic props. from comp. and density 80−76000
PbO-Fe_2O_3 melt, used for growth of LPE garnet films, struct. and cond. 80−10808
PbO-Ga_2O_3, phase diag. 78−80524
PbO-GeO system, pyroelec. and TSC props. 78−43798
PbO-GeO_2, glass, exam. of Raman spectra *(Japanese)* 79−19894
PbO-GeO_2, glass, structure of anionic network, IR spectra 80−103256
PbO-GeO_2 glass, synthesis, Ge coordination state 77−24271
PbO-GeO_2 melt, thermodynamic study 77−59760
PbO-GeO_2:Fe_2O_3 glass, $Fe^{2+(3)}$ impurity ions struct.-chem. state, Mossbauer data 80−40028
PbO-In_2O_3 two-phase film, quantitative analysis, use of internal calibration technique developed by AES 77−36834
PbO-K_2O-SiO_2, O tracer diffusion above transform. temp. 79−28120
PbO-K_2O-SiO_2-(Al_2O_3) glass, corrosion in acid, leaching kinetics 78−92378
PbO-MO-SiO_2 (M=Ca,Mg,Ba,Ni,Co) system, melt, viscosity meas. in temp. range 950 to 1250°C *(Japanese)* 79−77663
PbO-MoO_3-MO and PbO-WO_3-MO systems, M=Ca, Ba, Mg, Sr, perovskite type cpds. detection 80−108404
PbO-MoO_3-P_2O_5, glass phase investigation, density determ. *(Polish)* 77−70039
PbO-P_2O_5 glass, ESR of VO^{2+} ions 80−100610
PbO-P_2O_5-SiO_2 glasses, photoelastic consts. and polarisability 79−65839
PbO-$PbCl_2$-PbS, liquid system, elec. cond. meas. 78−43162
PbO-PbF_2 melt, thermodynamic study of solid-oxide galvanic cell 79−96013
PbO-$PbSO_4$ melts, thermodynamics, determination of free energies of mixing at 1253K 78−83976
PbO-$PbSO_4$ system, discussion of thermodynamics of oxide-sulphate melts 79−82358
PbO-$PbSO_4$ system, thermodynamic study of solid and liq. phases *(French)* 77−35667
PbO-$PbSO_4$ system, thermodynamics 79−82359
PbO-Re_2O_7 system, gas phase components obs. using mass spectrometry *(Russian)* 79−96354
PbO-Si-O, general features of reaction 79−11819
PbO-SiO_2, corroded in acid, IR reflectance spectra 77−20846
PbO-SiO_2, interdiffusion layer optical waveguide, prep. and props. 80−43489
PbO-SiO_2, melt, elec. cond. and struct. 80−88020
PbO-SiO_2, melt, polymer equilibria 80−88019
PbO-SiO_2, molten, activity of PbO, effect of CaO, Al_2O_3, MgO and ZnO 78−60663
PbO-SiO_2, surface flattening kinetics by sinusoidal profile decay method *(Japanese)* 80−34284
PbO-SiO_2 and Na_2O-PbO-SiO_2 system glasses, radiative paramag. and optical absorpt. centres 77−8402
PbO-SiO_2 and PbO-SO_3-SiO_2 system glasses, struct. and IR absorpt. spectra 79−41967
PbO-SiO_2 binary glasses, Pb depth profiles after acid etching, α-particle backscatt. 79−79343
PbO-SiO_2 glass, acoustic and thermal Gruneisen parameters 80−59608
PbO-SiO_2 glass, corrosion in acid, conc. profile meas. 78−92379
PbO-SiO_2 glass, distrib. of different O ions, molar refractivity meas. 80−33897
PbO-SiO_2 glass, EPR of Cu^{2+}, V^{4+}, and Mn^{2+} 78−39392
PbO-SiO_2 glass, electronic struct. and optical props. 80−2791
PbO-SiO_2 glass, IR and Raman spectra interpreted in terms of struct. 78−27213
PbO-SiO_2 glass, IR and Raman spectra, heat treatment conditions effect 79−66088
PbO-SiO_2 glass, leaching behaviour in dil. HNO_3, ellipsometry and AES obs. 78−23846
PbO-SiO_2 glass, modifier release in acid soln. 79−43450
PbO-SiO_2 glass, optical coating for GaAs-$Al_{1-x}Ga_xAS$ laser 78−71113
PbO-SiO_2 glass, reduced channel-plate, variable range hopping conductivity 80−107466
PbO-SiO_2 glass, trimethylsilylation method for silicate ion anal. *(Japanese)* 80−71975
PbO-SiO_2 glass, use of $Na_2S_2O_3.5H_2O$ in polishing 80−33258
PbO-SiO_2 glasses, absorpt. spectra of Nd^{3+} ions and interpret. 78−27277
PbO-SiO_2 glasses, charge trapping and dielec. breakdown, radiation-induced, microphase separation 78−23399
PbO-SiO_2 glasses, constitution of silicate groupings 77−7676
PbO-SiO_2 glasses, density-of-states and structural forms, Raman spectra study 80−97255
PbO-SiO_2 glasses, elec. cond. and dielec. behaviour 80−44361
PbO-SiO_2 glasses, high temp. ESR of Fe(III) 80−60410
PbO-SiO_2 glasses and crystal, silicate anion constitution 79−48023
PbO-SiO_2 melt, behavior of MgO and NiO *(Japanese)* 79−52746
PbO-SiO_2 melts, ionic transport, tracer diffusion and chem. interdiffusion 79−77785

lead compounds continued
PbO-SiO_2 optical glass melts, resistivity rel. to viscosity 77−76589
PbO-SiO_2 reduced glass, electron backscattering 77−85855
PbO-SiO_2 wall added to SPEAR Mk. I mag. detector 78−37494
PbO-SiO_2-Fe_2O_3(0,2,10 wt.%), conduction process 77−8096
PbO-SiO_2-NiO-MgO glass melt, interaction of NiO and MgO, elec. cond. and IR spectra obs. *(Japanese)* 80−24632
PbO-SiO_2-TiO_2, molten, viscosity *(Japanese)* 78−18819
PbO-SiO_2-(Al_2O_3) glass, corrosion in acid, leaching kinetics 78−92378
PbO-SiO_2-(CaO)(MgO)(BaO)(NiO)(CoO), melt, PbO activity *(Japanese)* 78−6907
PbO-SiO_2-(CaO)(SrO)(BaO)(NiO), melts, density *(Japanese)* 78−6908
2PbO-SiO_2-xSO_3 melts, crystn. 80−59400
PbO-TeO_2 glass, struct. and props. *(Japanese)* 79−32917
PbO-TiO_2, phase equilib. determ. by mass-loss Knudsen effusion method 77−11668
PbO-TiO_2, solid phase reactions, thermodynamic anal. 77−12603
PbO-xPbF_2, solvent, solubility of $Y_3Al_5O_{12}$ and phase formation in system Y_2O_3-Fe_2O_3-PbO-PbF_2-B_2O_3 78−95247
PbO-ZnO-B_2O_3, glass ceramic cements, crystallisation kinetics and character 77−85982
PbO-ZnO-B_2O_3:TiO_2 glass, circuit corrosion protection on alumina substrates 79−29236
PbO+C→CO+Pb, chemiluminesc. from gas phase reaction 79−8426
$PbO_{1.57}$, thermal expansion tensor, phase transitions, X-ray diffr. obs. *(French)* 79−1515
PbO_2 and pyrolusite compressed powder mixtures, mixing rules concerning Hall effect and Hall mobility *(German)* 78−84234
PbO_2, Auger quantitative anal. 78−73104
PbO_2 α- and β-phases prep. by anodic oxidation, electrochem. behaviour *(French)* 79−83460
PbO_2, cathode material for Li cells, evaluation 78−11525
PbO_2, compressed powder, electric conductivity obs. 77−32013
PbO_2 compressed powder magnetoresistance and apparent carrier mobility 80−35669
PbO_2, corrosion in HBF_4, redox mediator effects 77−90480
PbO_2 electrode, cyclic voltammetry for accelerated corrosion life tests 78−31582
PbO_2, electronic struct. and densities of states, tight-binding calcs. 80−15447
PbO_2, plate of Pb-acid battery, thermopassivation 80−3507
PbO_2 potentiostatic growth on vitreous C electrodes 79−43596
β-PbO_2 powders, Hall carrier mobility mixing rule *(German)* 78−52008
PbO_2 pressed powder, Hall voltage and change of cond. in transverse mag. fields 79−4567
PbO_2, thermal decomposition, heating rate effect, kinetics, mechanism, struct. 78−92473
PbO_2-Ag electrode system for potentiometric titrations, semi-auto titrator, student experiment 79−84918
PbO_2-$KInO_2(KScO_2)$, ionic cond., lamellar struct. *(French)* 77−1257
PbO_x, aq. corrosion film, IR and Raman spectroscopy 80−55567
PbO_x layer, ellipsometry, compensator inaccuracy evaluation 79−54170
PbO_x, photoconducting, phase transitions, occurrence of ferroelectricity, pyrocurrent obs. 79−11395
Pb_3O_4, cryst. struct., 5-240K, symm. change at 170K *(French)* 78−34618
Pb_3O_4, IR and Raman study of structural phase transitions *(French)* 78−84582
Pb_3O_4, isomorphous with $ZnSb_2O_4$, cell parameters evolution with temp. *(French)* 78−75642
Pb_3O_4, phase transition, texture of tetragonal and orthorhombic phases *(French)* 79−23726
Pb_3O_4, tetragonal to orthorhombic transition, heat capacity meas. 80−20929
Pb_2OFBr, mimetic twinning, cryst. struct. determ. 79−23568
Pb_2OFCl, mimetic twinning, cryst. struct. determ. 79−23568
Pb_2OFI, mimetic twinning, cryst. struct. determ. 79−23568
Pb(OH)Cl, temp. depend. of elec. cond., solid state thermal decomp. 78−19042
PbO_2(Pb) electrode, anodic impedance during suspension-electrolysis leaching of β-ZnS in 1N H_2SO_4 soln. *(Japanese)* 79−43594
$(PbO)_x(SiO_2)_y$ glass, vibrational spectroscpic exam. 79−11417
$PbO.B_2O_3$ glass, additional IR absorpt. *(Russian)* 77−85730
4PbO.GeO_2, X-ray phase and thermal anal., new antiferroelectric 79−1744
4PbO.$PbSO_4$, oxidation to PbO_2 in positive plate of Pb-acid battery 79−70336
4PbO.$PbSO_4$, paste mixing and curing for Pb acid batteries, effect of CO_2 79−61968
PbO.SiO_2 film, formation mechanism on Si, X-ray spectral anal. 79−87008
2PbO.SiO_2, glassy, DTA obs. of crystn. kinetics 77−89381
2PbO.SiO_2 melt, coding rate influence on constitution of silicate anions, crystn. kinetics 80−103248
γ-4PbO.SiO_2, synthesis and struct. 78−71716
PbO.$2B_2O_3$, vitreous, structural aspects studied by Raman scattering 77−8575
$(PbO.2B_2O_3)_{1-x}(Fe_2O_3)_x$ glass, mag. resonance studies 79−78509
3PbO.2GeO, TSC in thermoelectret state during ceramic synthesis, pyroelec. currents and energy struct. of capture centres 80−55014
PbO.$3B_2O_3$:Fe_2O_3, EPR of Fe^{3+} ions 78−72400
15PbO.$3B_2O_3$.$2WO_3$, struct. and electrophys. characts. 77−84716
PbO.$6Bi_2O_3$, IR and Raman spectra, vibr. anal. 78−76464
12PbO.$6SiO_2$.$PbSO_4$, crystn. from 2PbO-SiO_2-xSO_3 melts, struct. and vibr. spectra 80−59400
$Pb(PO_3)_2$, vitreous, microhardness 80−25864
$Pb_2(PO_4)_2$, ferroelastic, switching processes 78−2192
$Pb_2P_2O_7$, flux for RPO_4 growth, solubility 78−95687
$Pb_3(PO_4)_2$, crit. behaviour of polar modes near ferroelastic phase transition 79−95750
$Pb_3(PO_4)_2$, EPR study of Mn^{2+} around ferroelastic transition point 78−76303
$Pb_3(PO_4)_2$, ferroelastic, bending stress effect on domain struct. *(Russian)* 77−39623
$Pb_3(PO_4)_2$, ferroelastic, deform. hysteresis loop. 77−51432
$Pb_3(PO_4)_2$ ferroelastic, dielec. consts. and birefringence meas. 78−2793
$Pb_3(PO_4)_2$, ferroelastic, switching processes in pulse mech. field 78−59853
$Pb_3(PO_4)_2$, ferroelastic, Raman scatt. by soft vibr. involved in ferroelastic phase transition 80−16040

lead compounds continued
$Pb_3(PO_4)_2$, ferroelastic, dielectric anomalies, phase transitions, permittivity, relaxation *(Russian)* 80−71293
$Pb_3(PO_4)_2$, ferroelastic transition, X-ray diffr. and scatt. *(French)* 77−31769
$Pb_3(PO_4)_2$, ferroelastic transition, soft modes, inelastic neutron scatt. obs. 77−31772
$Pb_3(PO_4)_2$, ferroelastic domain struct., twinning analysis by pseudosymmetry 77−76421
$Pb_3(PO_4)_2$, ferroelastic transformations and struct. as function of temp., neutron diffr. study 79−19188
$Pb_3(PO_4)_2$, ferroelastic phase transition, thermodynamic theory 79−37832
$Pb_3(PO_4)_2$, ferroelastic phase, structure domains, electron microscope obs. 79−42078
$Pb_3(PO_4)_2$, ferroelastic phase transition, inelastic neutron scatt. *(French)* 80−24584
$Pb_3(PO_4)_2$, ferroelastic props., domain struct., electron microscopic study *(French)* 80−44216
$Pb_3(PO_4)_2$, IR dispersion at room temp. 79−15460
$Pb_3(PO_4)_2$, nonintrinsic ferroelastic properties 78−91374
$Pb_3(PO_4)_2$, phase transition at 180°C, dielectric meas. 79−37831
$Pb_3(PO_4)_2$, temp. depend. of lattice parameters and spontaneous strain 80−29170
$Pb_3(PO_4)_2$:Gd^{3+}, EPR near ferroelastic transition point 79−15350
$Pb_3(PO_4)_2$:Gd^{3+}(Eu^{2+}), EPR spectra of α- and β-phases 80−11261
$Pb_3(PO_4)_2$-$Pb_3(VO_4)_2$, direct obs. of ferroelasticity 77−21203
$Pb_3(PO_4)_2$-$Pb_3(VO_4)_2$ mixed crystal, crit. stress and phase diagram temp. depend. 78−26623
$Pb_9(PO_4)_6$, X-ray cryst. struct. determ. and refinement 80−103300
$Pb_5(PO_4)_3Cl$, pyromorphite, vibr. spectra, normal coord. anal. 78−88305
$Pb_{10}(PO_4)_6(OH)_2$, cryst., IR spectra, band assignments 78−60442
$Pb_{10}(PO_4)_6(OH)_2$, IR spectra, stretching and librational bands of OH 78−2841
$Pb_5(PO_4)_3OH$, prep. from sulphate, X-ray diffr. and IR spectrosc. 80−29893
$Pb_3(P_3O_9)_2.3H_2O$, cryst. struct. *(French)* 77−15352
$Pb_3(P_{0.95}V_{0.05}O_4)_2$, ferroelastic transition, soft mode, inelastic neutron scatt. study 80−70357
$Pb_3(P_{1-x}V_xO_4)_2$, ferroelastic, acoustooptic props. of single crysts. and solid solns. 79−69809
$Pb_3(P_{1-x}V_xO_4)_2$, x=0.1, 0.2, Raman scatt. by low freq. vibrs. 80−55111
$Pb_3(P_xV_{1-x}O_4)_2$, ferroelastic phase transitions, lattice dynamics, dielec. and optical props. meas. 77−55334
$Pb_3(P_xV_{1-x}O_4)_2$, ferroelastic phase transition, DTA, dilatometric and Brillouin scatt. study 80−70398
$Pb_3(P_xV_{1-x}O_4)_2$, phase diagram and crystallography *(French)* 78−92252
PbPo, electronic struct., relativistic band struct. calc. 79−4510
$Pb_{1-nx}R_xTiO_{3+x(1.5-n)}$, R=rare earth, ferroelec. Curie temp. comp. depend. 77−16258
$Pb_3Rh_7O_{15}$, struct. study, X-ray diffr. *(French)* 80−88100
$Pb_3Rh_7O_{15}$ thick film, temp. coeff. of resist., cond. mech. 78−84315
PbS, (100), angular resolved UV photoemission 78−2989
PbS (100) surface, electronic struct., O_2 adsorption effects, UPS study 80−54756
PbS, ab initio SCF calcs. using relativistic effective core pot. 80−95524
PbS, adsorption mechanism in selective etching 77−7727
PbS, anisotropy of vol. plasmon dispersion, electron energy loss meas. 77−35878
PbS, anomalous magnetoresist. 80−107813
PbS, band struct., angle resolved photoemission obs. 79−33899
PbS, bond orbital model of band struct. 80−59853
PbS, chem. deposited thin film, effect of morphological struct. on photosensitivity 80−70760
PbS, chemically deposited film, photosensitivity, effect of morphological struct. 79−82647
PbS, chemisorption of O_2, room temp., UPS and XPS obs. 78−91529
PbS, clean surface, AES and LEED exam. 80−10762
PbS, colloidal, light scatt. and electron microscopy 78−3379
PbS, conduction band nonparabolicity and carrier scattering mechanism 79−11065
PbS, crystal binding energy 79−37650
PbS, crystallisation and stability in high-temp. alkaline solns. 77−52240
PbS, crystals, relation of struct. and bond type to slip geometry 80−88165
PbS current tunable p-n junction laser *(Polish)* 80−32985
p-PbS, dispersion law investigation, valence band density of state effective mass 79−95314
PbS, dispersion relation for magnetoplasma waves 79−51506
PbS, electrodeposition, using nonaqueous solvents 80−76200
PbS, electroless film deposition with variable comp. and polymorphic structs. 79−95952
PbS, energy gap and dielec. props., 77 to 373K 80−66100
PbS, energy gap anomaly, relativistic band struct. calc. 79−4510
PbS, energy gap temp. depend., electron-lattice interaction, dilatation effect 79−65377
PbS epitaxial film, struct., optical and elec. props. 78−19583
PbS, epitaxial film, struct. perfection, two cryst. X-ray spectrometry 78−26792
PbS, epitaxial layer, structural nonuniformities and dislocation struct. 79−23852
PbS, epitaxial layer on rock salt substrate, stresses, hydrostatic press. effects 78−51831
PbS epitaxial layers, ion bombardment effects on struct., and annealing 79−10882
PbS epitaxial layers, obs. of NaCl single crystal surface relief 77−51577
PbS exploding film, Q-switching of Nd^{3+}:glass laser 78−42361
PbS film, appearance of EPR centres in initial form. stage *(Russian)* 77−63283
PbS film, form. by chem. spraying, elec. and optical props. 78−2588
PbS film, moisture drift origin 77−20187
PbS film, photosensitivity, role of surface oxide and ion bombardment 77−24631
PbS film, polycryst., chem. deposition from soln. and characterisation 78−72743
PbS, film, total current spectrum and energy struct. 80−100719
PbS film, used as absorbing surface in solar collector 78−5580
PbS film, vac. deposited, optical and phys. props. 80−2315
PbS, film condensation on amorphous substrate, struct. and growth 78−38981

lead compounds continued
PbS, film prep. from aqueous soln. of thiourea 77−8767
PbS film surface with oxysulphate layer, photoelec. memory effect 77−55584
PbS films, polycryst. and epitaxial, small-angle X-ray scatt. and electron density inhomogeneities 80−96758
PbS, first-principles calc. of eqn. of states 80−49649
PbS, heat of entropy of fusion 77−72701
PbS heterojunctions nonideal, photoelec. props. and elec. characts. 79−15215
PbS, hot-pressed compact, elec. behaviour, adsorbed atmos. gas effects 77−66601
PbS islands, vacuum deposited, electron microscope obs. 80−103601
PbS, liquid encapsulation zone-refining, source material for sublimation growth 78−27399
PbS, low carrier conc., prep. and props. 77−39846
PbS, microwave incremental conductivity, high-field, 77K 80−11026
PbS, mol. diamag. susceptibility, bonding types 78−31046
PbS, molecule, Ne matrix environment effects on vibronic emission systems 77−58070
PbS, molecule, vibr. anal., in neon matrix *(Russian)* 79−10094
n-PbS, natural galenite, optical and crystallographic properties 79−42975
PbS, nonstoichiometric, increase of rest pot. with p-type semicond. character 78−56170
PbS, oxidation, $PbSO_4$ distrib. in products *(Polish)* 80−25883
PbS oxide, optical excitation meas. of trap charging surface film *(Russian)* 78−76180
n-PbS, $PbS_{1-x}Se_x$ layers prepared by hot-wall epitaxy 77−16481
PbS, phase transitions under action of high press., elec. cond. meas. 77−4196
PbS photocells, multicolour detectors in combination with Si photodiodes *(Czech)* 79−26126
PbS, photoemission interpretation 80−25531
PbS photosensitive deposit precipitation, alkali and acetate conc. effects 79−76781
PbS, photosensitive film, electron bombard. effect on elec. cond. 80−93019
PbS, plastic deform. on compression along ⟨100⟩ direction 79−28036
PbS, point defects and effect on decopperization of Pb with S 79−47918
PbS, relativistic electronic mol. struct., calcs. 79−761
PbS single crystals, plastic deform. thermal activation anal., dislocation behaviour, point defect influences 79−65095
PbS, small gap, band-edge parameters 80−49594
PbS, solubility products in LiCl-KCl and LiCl-LiF molten eutectic mixtures 80−54387
PbS sputtered film microhardness, influence of gas discharge *(Russian)* 80−49560
p-PbS, struct. of valence band, transport processes study 80−20081
PbS, superficial degradation in air and water, XPS obs. *(French)* 80−89110
PbS, surface defect annealing *(Russian)* 77−47658
PbS, surface optical phonons, anal. of LEED results 79−69339
PbS, temp. effects on valence bands, UPS study 80−11537
PbS, thermomech. props., SCF Xα scatt. wave theory 78−71704
PbS, thin film, photoconductivity expts. 79−78130
PbS, thin film comp. and struct. rel. to precip. by allyl thiourea 77−48356
PbS, vacuum deposited film, orientation axis tilt rel. to vapour angle of incidence 80−88456
PbS, valence band struct., angle-resolved photoemission spectra obs. 77−48310
PbS, valence band struct. determ. by optical absorpt., size quantization effects 80−59871
PbS, vap. deposited film, island growth obs. by optical diffr. from electron micrograph 78−10291
PbS vapour, mass spectroscopic study *(Russian)* 77−65545
PbS, wave-vector depend. of electron energy losses 78−11041
PbS, X-ray determ., Debye-Waller factors, Debye temp. and vibration amplitudes 78−55928
PbS, XPS investig. valence band struct. 77−48311
$^{208}Pb^{32}S$, $^{203}Pb^{80}Se$, rot. g_J-factor meas., $^1\Sigma$ ground state *(German)* 77−30865
PbS:Tl, Hall and Seebeck coeffs., Hall mobility, impurity states 80−15545
PbS:Tl, self-compensation of acceptors by vacancies, Hall coeff. meas. 80−92913
PbS-$(PbSO_4)_x(PbO.PbSO_4)_y$ heterosystem, cathodoluminescence spectra 79−24370
PbS-Al coatings, absorptivity, emissivity, as function of PbS thickness 78−46731
PbS-As_2S_3 glass, elastic props. temp. depend. 78−71780
PbS-base photodetectors, struct. invest. by proton irrad. 80−104388
PbS-$Cd_{1-x}Zn_xS$ heterojunctions prepared by spray pyrolysis 79−60917
PbS-CdSe, phase boundary processes 78−71857
PbS-CuS, black Zn-dust pigmented solar selective coatings for solar photothermal conversion 80−66997
PbS-$CuS_{1.8}$-ZnS, phase equilib. *(Russian)* 77−28786
PbS-Ge heterojunction, influence of conduction band discontinuity on lux-ampere characts. 78−39200
PbS-In_2S_3, phase investigation 80−66488
PbS-Ni, phase diag., cpd. formation and electrophys. props. 77−85997
PbS-PbO vacuum evaporated films, elec. cond. and photocond. 80−75656
PbS-$PbS_{1-x}Se_x$-PbS DH diode laser props., comparison of theory with expt. 78−22128
PbS-PbSe epitaxial bicrystals, direct scatt. of channelled He ions at dislocations 80−65110
PbS-PbSe-PbS DH laser, Peltier cooled, IR gas spectroscopy appl. 77−23690
PbS-PbSe-PbS DH laser, fabrication, CW operation up to 120K 77−23692
PbS-PbSe(Te), thermoconductivity and thermoresistance 79−23992
PbS-PbSe(Te) epitaxial layers, electron microscope contrast of misfit dislocations 77−85113
PbS-Sb system alloys, phase diagram, composition depend. of microhardness and thermo-EMF 77−25028
PbS-Sb_2S_3 semicond., optical and photoelec. behaviour 80−96938
PbS-Si, photosensitive p-n heterojunction, energy band diagram 79−95489
PbS-Si heterojunction, struct. and comp. 80−54530

lead compounds continued
PbS-Si heterojunction, chem. struct., AES anal. 80−76115
PbS-Si heterojunction, related optical and IR detector props. 80−77866
PbS-Si heterojunction, space charge capacitance, PbSn film thickness depend. 80−88630
PbS-Si heterojunction, PbS film growth and struct. 80−96762
PbS-Si heterojunction detector, direct injection readout 80−4765
PbS-Si p-n heterojunction, charact. and operation, IR detector appls. 78−52075
PbS-Si p-n heterojunctions, AC admittance meas. 80−96979
PbS+CuS solar selective black coatings for large area appls., prep. and props. 80−21411
$(PbS)_x(As_2S_3)_{1-x}$, high field effects 79−42553
$Pb(SCN)_2$, thermal decomposition, kinetic parameters from thermogravimetric data 79−61859
$Pb_5S_2I_6$, ferroelec., synthesis and hydrothermal growth 79−38731
$PbSO_4$, anglesite, crystal struct. and sulphate force consts. 78−83784
$PbSO_4$ flotation with sodium hexadecyl sulphate, influence of heavy metal ions obs. *(Japanese)* 80−55701
$PbSO_4$-PbO.$PbSO_4$(PbS)(SO_2), solid, EMF determ. of O_2 equilib. press., 1000-1100K 78−48683
$PbS_2O_6.4H_2O$, isomorphic substitution effect on optical activity 77−32347
PbS_xS_{1-x} epitaxial film, Hall mobility meas., surface charge transport 77−20473
PbS(Se), photoionisation cross section of atomic and final state effects on 5d core levels 78−84699
$PbS_{0.1}Se_{0.9}$ 4.6 μm LED, room temp., band gap and electrolum. 80−66302
$PbS_{1-x}Se_x$ (X=0.18) homojunction injection lasers, near-field emission 80−95896
$PbS_{1-x}Se_x$ diffused homojunction diode lasers, 140K operation 79−18415
$PbS_{1-x}Se_x$ diode laser, contact degradation due to diffusion 80−102734
$PbS_{1-x}Se_x$, material props. and use in diode lasers, review 80−5732
$PbS_{1-x}Se_x$, single heterostructure tunable diode lasers formed by compositional interdiffusion 77−38896
$PbS_{1-x}Se_x$, single heterostruct. laser, wide tunability 77−79846
$PbS_{1-x}Se_x$, small gap, band-edge parameters 80−49594
$PbS_{1-x}Se_x$ thin film, stimulated emission, temp. depend. 80−66232
PbS_xSe_{1-x}, chalcogen interdiffusion, electron microprobe obs. 79−28145
PbS_xSe_{1-x} film, prep. by co-evaporation method *(Japanese)* 78−64477
PbS_xSe_{1-x}, film prep. by co-evap., elec. props. *(Japanese)* 78−80470
PbS_xSe_{1-x}, multispectral photovoltaic IR detectors 80−105710
PbS_XSe_{1-x}, Schottky-barrier IR detector, comp. tuning 78−12752
PbS(Se)(Te), angle resolved UPS and electronic band struct. 79−37981
PbS(Se)(Te), strongly anisotropic polar semicond., electron-hole liq. in mag. field 80−59890
PbS(Se)(Te)-NiSb eutectic system, crystn. 79−52190
PbS(Te)-Sb eutectic system, crystn. 79−52190
PbSb, meas. using high mag. field installation *(Dutch)* 78−252
$Pb(Sb_{1/3}Mn_{2/3})O_3$-$PbTiO_3$-$PbZrO_3$, remanent dielec. polarisation of poled ceramic, heat treatment 79−87390
$PbSbO_2Cl$, nadorite, thermal expansion, X-ray determ. 78−18802
$Pb_4Sb_7S_{13}$, synthetic robinsonite, crystal struct., lattice constants by X-ray goniometry 79−77581
$Pb_5Sb_8S_{17}$, dielectric props. 78−72452
$Pb_6Sb_{14}S_{27}$, zinkenite, electrophysical properties 78−34834
$(Pb_{0.66}Sb_{0.34})_6SnS_9$, garnet-like struct., synthetic, cryst. struct., X-ray diffr. study 79−19217
$Pb_{1-x}Sb_xTe$ DFB laser, CW operation 77−58338
$PbSc_{0.5}Nb_{0.5}O_3$, single cryst., dielec. props. 80−66126
$Pb(Sc_{0.6}Ta_{0.5})_3$ ceramics, ordering and diffuse phase transitions 80−29699
$PbSc_{2/3}Te_{1/3}O_3$, ferroelec., high-frequency permittivity, temp. depend. 80−71325
$PbSc_{2/3}Te_{1/3}O_3$-$PbSc_{2/3}W_{1/3}0_3$($PbFe_{2/3}Te_{1/3}O_3$) ferroelec. props. and lattice consts. 80−60520
PbSe, ab initio SCF calcs. using relativistic effective core pot. 80−95524
PbSe, band struct. angle resolved photoemission obs. 79−33899
PbSe, bond orbital model of band struct. 80−59853
PbSe, carrier density depend. of cyclotron mass, Shubnikov-de Haas effect 79−73533
PbSe, chemisorption of O_2, room temp., UPS and XPS obs. 78−91529
PbSe, complex-composition film production method from vapour *(Russian)* 78−95702
PbSe, crystal binding energy 79−37650
PbSe, dispersion relation for magnetoplasma waves 79−51506
PbSe, electroless film deposition with variable comp. and polymorphic structs. 79−95952
PbSe, electron gas magnetisation, energy band parameters determ., use of Faraday effect 80−45047
PbSe, energy gap and dielec. props., 77 to 373K 80−66100
PbSe, energy gap anomaly, relativistic band struct. calc. 79−4510
PbSe, energy gap temp. depend., electron-lattice interaction, dilatation effect 79−65377
PbSe, enthalpy, heat capacity, 300 to 1480K 79−60523
PbSe epitaxial film on NaCl, far IR reflectivity obs. 77−40251
PbSe, epitaxial growth, cluster mobilities, in-situ electron microscopes obs. 80−15407
PbSe, Faraday effect and electron gas magnetisation, Kane two band model calcs. *(Russian)* 80−34899
PbSe film, 50 μ, prep. in double quasiclosed volume 79−38745
PbSe film, influence of pot. barrier on thermoelec. props. 78−39239
PbSe film, moisture drift origin 77−20187
PbSe film, partly oriented, electron diffr. dynamic effects 77−7996
PbSe, film, photoconductivity, temp. depend. 79−38200
PbSe film, soln. growth 80−66437
PbSe film, stimulated photoluminesc. charcts. meas., room temp. 77−90193
PbSe, film with pot. barrier, magnetoresistance anisotropy 79−91172
PbSe films, current carrier conc. and type control, elec. cond., synthesis process *(Russian)* 80−100412
PbSe, films, synthesis and growth 80−45236
PbSe films, synthesis charcts. 80−35094
PbSe, Hall effect and elec. cond. under strong anisotropic pressure 77−55549
n-PbSe, heterodiffusion of Sn 80−34245
PbSe IR detector, pollution detection and control appl. 78−24378
PbSe, lattice dynamics, slow neutron inelast. scatt. 77−31740
PbSe, monocrystalline film prod. by laser pulse *(Russian)* 78−3059

lead compounds continued
PbSe, NMR, chemical shift and linewidth determ. 79−19792
PbSe on NaCl, epitaxial-substrate system, far IR transmission and refl. 78−6802
PbSe photocells, multicolour detectors in combination with Si photodiodes *(Czech)* 79−26126
PbSe, photoemission interpretation 80−25531
PbSe, photoluminesc. spectra and stimulated emission, effect of temp. 77−8638
n-PbSe, polar semicond., mag. field influence on high-freq. relaxation time 79−95438
PbSe, polycryst. film, low temp. illumination, residual cond. 77−43756
n-PbSe, pressure induced transition to gapless state 78−2533
PbSe, pressure tunable CW injection laser, emission spectra 79−18419
PbSe, relativistic electronic mol. struct., calcs. 79−761
PbSe, small gap, band-edge parameters 80−49594
PbSe, spin-orbit splitting in valence bands, angle-resolved UV photoemission 78−2991
PbSe, surface, clean and O_2-exposed, XPS and UPS obs., electronic struct. 78−52637
PbSe, temp. effects on valence bands, UPS study 80−11537
PbSe vacuum deposited thin films, struct. and growth 79−19482
PbSe, vacuum evaporation, composition of condensates 78−44012
p-PbSe, valence band structure, IR refl. and absorpt. meas. 77−55791
PbSe, valence band structure from angular resolved photoemission spectra 78−84143
PbSe, valence band struct., Hall and transverse Nernst-Ettingshausen effects, optical absorption 79−11064
PbSe, valence band struct. determ. by optical absorpt., size quantization effects 80−59871
PbSe, wave-vector depend. of electron energy losses 78−11041
PbSe, X-ray diffr. exam. of struct., and luminescence props. 80−55209
PbSe, XPS investig. of valence band struct. 77−48311
PbSe:Tl, elec. props. and IR reflection 78−6686
PbSe:Tl, high temp. elec. and optical props., impurity states 79−60854
PbSe:Tl, impurity states, optical absorption and Hall effect meas. 78−18995
PbSe:Tl, scatt. of holes and phonons by impurities 78−19068
PbSe:Tl, self-compensation of acceptors by vacancies, Hall coeff. meas. 80−92913
PbSe-CdSe heterojunction, elec. props. 77−1478
PbSe-flux, interfacial tension at boundary of fused systems 77−35797
PbSe-$GeSe_2$-AsSe, glass form., struct. defects, elec. cond., assoc. *(Russian)* 80−54144
PbSe-GeSe-AsSe, glass form., elec. cond., struct. defects, assoc. *(Russian)* 80−54145
PbSe-$PbCl_2$, eutectic crystallisation, visual monitoring 77−44237
PbSe-PbS(Te) epitaxial layers, electron microscope contrast of misfit dislocations 77−85113
Pb_xSe_{2-x} melts, viscosity and radial distrib. function for stoichiometric and peritectic comp. 80−1916
$PbSe_{0.5}S_{0.5}$, valence band struct., absorpt. spectra, elec. props. 80−44505
$PbSe_xS_{1-x}$, comp. depend. of density, effect of defects 77−11538
p-$(PbSe)_{1-x}(SnTe)_x$, absorpt. edge temp. depend. *(Russian)* 78−34765
$(PbSe)_{1-x}(SnTe)_x$, lattice dynamic props., Gruneisen parameters *(Russian)* 78−83984
$(PbSe)_{1-x}(SnTe)_x$ solid solution, band struct. and some optical props. *(Russian)* 77−76752
PbSe(Te), low-temp. epitaxial film form., on KCl(Br), laser spraying *(Russian)* 77−73238
PbSe(Te), single cryst. growth, reaction kinetics in binary melts of KCl, NaCl and $PbCl_2$ 77−16486
$PbSe_{1-x}Te_x$, for-IR reststrahlen spectra, mode behaviour 80−7345
$PbSe_{1-x}Te_x$, p-n junction, inversion of conduction level 78−47856
$PbSe_{1-x}Te_x$, small gap, band-edge parameters 80−49594
$PbSe_{1-x}Te_x$, symmetry change in cond. levels, photovoltaic effect and reflectivity obs. 78−34766
$PbSe_xTe_{1-x}$ epitaxial layers, growth, struct., elastic strain and Hall mobility 77−15717
$PbSiO_3$ and Pb_2SiO_4, vitreous, free energy of form. at elevated temps. 79−43195
Pb_2SiO_4-$PbSiO_3$, Raman and IR spectra of crystalline phases 80−3013
$Pb_xSi_yO_z$ films on Si, form. kinetics and props. 80−35358
$Pb_5SiO_4(VO_4)_2$, centrosymmetric crysts., induced linear electrogyration 80−45039
$Pb_5(SiO_4)(VO_4)_2$ cryst. growth and elastic props., appl. in acousto-optical devices 78−19660
$Pb_5(SiO_4)(VO_4)_2$, crysts., acousto-optical props. 80−100644
$Pb_5(SiO_4)(VO_4)_2$, elastic nonlinearity and acoustic losses 80−59554
$Pb_{1-\alpha x}Sm_xTiO_{3+x(1.5-\alpha)}$, permittivity as function of temp. 79−33586
$PbSnF_4$; allotropic transformations 80−84926
$PbSnF_4$, anionic conductor *(French)* 79−1523
$PbSnF_4$, anionic conductor, thin films and ceramics 80−107556
$PbSnF_4$, α- and β-, new solid electrolytes, conductivities and activation energies 79−28137
$PbSnF_4$, fast ionic conduction of F^- ions 79−99360
$PbSnF_4$, fast ionic cond. of F^- ions, NMR study *(French)* 80−39345
$PbSnF_4$, high anionic cond. of new solid electrolytes 80−107546
$PbSnF_4$, thermal expansion and phase transitions 79−77781
$Pb_{0.9}Sn_{0.1}F_2$, NMR study of F atom motion *(French)* 80−100622
$Pb_{1-x}Sn_xF_2$, ionic cond. of F ion *(French)* 80−6547
$Pb_xSn_{1-x}F_2$ solid soln., struct. evolutions *(French)* 80−96488
$Pb_{1-x}Sn_xGe$:In, press.-induced transition to gapless state, galvanomag. effects 78−19108
$Pb_xSn_{1-x}I_2$, thin films, photosensitivity, ageing and annealing effects *(Russian)* 78−6804
$Pb_xSn_{1-x}O_2$ film, optical props. 78−39616
$Pb_xSn_{1-x}O_2$:Sb films, DC sputtered, elec. props. 80−80426
$Pb_{0.2}Sn_{0.8}S$, Mossbauer spectra, effect of optical emission *(Russian)* 78−60367
$Pb_{0.59}Sn_{0.41}Se$, struct. phase transition, temp and hydrostatic press. influence, Hall effect, resistivity *(Russian)* 78−51675
$Pb_{0.65}Sn_{0.35}Se$, solid soln., elec. props. 78−39112
n-$Pb_{0.83}Sn_{0.17}Se$, carrier mobility, 77-300K, scattering mechanism *(Russian)* 78−2486
$Pb_{0.91}Sn_{0.09}Se$ film, Bi and Tl impurity dopant incorporation and diffusion during MBE growth 79−66012
$Pb_{0.93}Sn_{0.07}Se$ crysts., sublimation growth, controlled carrier concs. for IR lasers and detectors 77−52237
n-$Pb_{0.94}Sn_{0.06}Se$ solid solns., Burstein-Moss effect and energy band struct. 80−40118

lead compounds continued
$Pb_{0.975}Sn_{0.025}Se$, film, acoustic wave modulation of electron current 78−64067
$Pb_{0.995}Sn_{0.045}Se$ pulsed laser for high-resolution NH_3 spectroscopy 79−64252
$Pb_{1-x}Sn_xSe$, (x=0.125), pressure induced band inversion, effect on energy spectrum *(Russian)* 78−39007
n-$Pb_{1-x}Sn_xSe$, absorption spectra investigation 80−2768
$Pb_{1-x}Sn_xSe$, band inversion effect on phonon spectra 78−79699
$Pb_{1-x}Sn_xSe$, band struct. parameters, thermoelectric power meas. in strong mag. fields 79−51474
$Pb_{1-x}Sn_xSe$, band struct. and transport props., hydrostatic press. effects 80−15452
$Pb_{1-x}Sn_xSe$, carrier density depend. of cyclotron mass, Shubnikov-de Haas effect 79−73533
$Pb_{1-x}Sn_xSe$, carrier effective mass, thermomag. effect meas. 77−24572
$Pb_{1-x}Sn_xSe$, determ. of anisotropy coeff. of Fermi surface, magnetoresist. meas. 78−51878
$Pb_{1-x}Sn_xSe$, displacive transition, temp. and press. depend., elec. meas. 80−10672
$Pb_{1-x}Sn_xSe$, energy band parameter determ. from Shubnikov-de Haas effect 77−69227
$Pb_{1-x}Sn_xSe$ epitaxial film, Hall mobility meas., surface charge transport 77−20473
$Pb_{1-x}Sn_xSe$ epitaxial layers, radiative and nonradiative recomb. processes 80−60670
$Pb_{1-x}Sn_xSe$ epitaxial layers obtained by LPE, growth conditions correl. with morphology 80−104079
$Pb_{1-x}Sn_xSe$, film struct. and elec. props. 77−80708
$Pb_{1-x}Sn_xSe$, gapless state and phonon spectrum *(Russian)* 78−30715
$Pb_{1-x}Sn_xSe$ laser, optical feedback effects on performance, external cavity modes 80−32981
$Pb_{1-x}Sn_xSe$, material props. and use in diode lasers, review 80−5732
$Pb_{1-x}Sn_xSe$, n- and p-type, with band inversion, study of transport phenomena 80−49741
$Pb_{1-x}Sn_xSe$, plasma reflection spectra, carrier effective masses and relax. times determ. 78−2858
$Pb_{1-x}Sn_xSe$, single crystal and film, X-ray spectral investigation of solid solution 77−16477
n-$Pb_{1-x}Sn_xSe$, single crysts. and diodes, elec. props. under high press. 77−47809
$Pb_{1-x}Sn_xSe$, single heterostructure tunable diode lasers formed by compositional interdiffusion 77−38896
$Pb_{1-x}Sn_xSe$, single heterostruct. laser, wide tunability 77−79846
$Pb_{1-x}Sn_xSe$, small gap, band-edge parameters 80−49594
$Pb_{1-x}Sn_xSe$ solid solns., photoluminesc. spectra, energy band parameter determ. 80−71484
$Pb_{1-x}Sn_xSe$, thin film, opt. props. *(Japanese)* 77−1750
$Pb_{1-x}Sn_xSe$, transport phenomena in solid solutions with band inversion 80−107792
$Pb_{1-x}Sn_xSe$, valence zone struct. effect on mobility/inherent conc. ratio *(Russian)* 79−73437
$Pb_{1-x}Sn_xSe$, X=0.03-0.07, monocrystal film, edge of intrinsic absorpt. *(Russian)* 80−71368
$Pb_{1-y}Sn_ySe$, charact. of IR absorption 77−1681
$Pb_{1-y}Sn_ySe$, electron-irradiated, elec. and recomb. props. 79−56227
$Pb_{1-y}Sn_ySe$-PbSe, ($0 \leq y \lesssim 0.08$), semicond. junction laser, lasing investigation 78−10990
$Pb_{1-y}Sn_ySe$-PbSe heterojunction laser, tunable 10.6-15 nm 77−58346
$Pb_{1-y}Sn_ySe$-PbSe pulse laser diode, temp. tuning of modes 78−50777
$Pb_xSn_{1-x}Se$ laser, electron-beam-pumped 77−50689
$Pb_ySn_{1-y}Se$, multispectral photovoltaic IR detectors 80−105710
$Pb_{1-x}Sn_xSe$(Te) epitaxial layers, growth, phase diagram, p-n junctions, optical, elec. props. 78−44029
$Pb_{1-x}Sn_xSe$(Te) single crystals, Bridgeman grown, X-ray exam. 79−56926
$Pb_{1-x}Sn_xSe$(Te):I epitaxial layers, photoelectric props., doping donor impurity behaviour 77−80810
$Pb_{1-x}Sn_xSe_{1-y}Te_y$ optically pumped heterojunction laser with matched gratings, photolum. obs. 79−89909
$Pb_{0.76}Sn_{0.24}Te$, background radiation, influence on elec. props. 80−20226
PbSnTe and PbSnTe, epitaxial-substrate system, far IR transmission and refl. 78−6802
PbSnTe, anomalous avalanche breakdown 80−80284
PbSnTe DH laser, anodic oxide film to avoid degradation by thermal cycling 78−50809
PbSnTe detector and preamplifier modules for heterodyne detection of CO_2 laser radiation 78−32875
PbSnTe, electron irradiated, high temp. defects 79−78122
PbSnTe film epitaxial growth on BaF_2 substrates 78−11134
PbSnTe IR detectors, spectral response depend. on surface carrier concentration *(Japanese)* 79−44929
PbSnTe IR photovoltaic detectors for 8-14 μm range, review *(Italian)* 78−54451
PbSnTe laser diode, tunable emission, 5-15 μm 77−50686
PbSnTe, Magneto transport anomalies at low carrier densities, Wigner crystallisation 80−20222
PbSnTe, optical dielectric const. variation with carrier conc. 80−84709
PbSnTe/PbTe inverted heterostructure mosaics, long wavelength, energy gap-Fermi level temp. depend. 79−85182
PbSnTe-like semicond., Auger recomb., nonparabolic approx. 79−15161
PbSnTe-PbTe heterostructs., effect of electrical grounding on electron irrad. 78−60194
$Pb_{0.41}Sn_{0.59}Te$, Hall coeff., elec. cond. meas. 80−44615
$Pb_{0.56}Sn_{0.44}Te$, press. induced ferroelec. phase transition 79−65809
p-$Pb_{0.65}Sn_{0.35}Te$, transport coeffs. and dispersion law 80−44629
$Pb_{0.72}Sn_{0.28}Te$, Hall effect and elec. cond., 77 to 480K, energy band struct. 77−76817
$Pb_{0.72}Sn_{0.28}Te$, Hall mobility, temp. and carrier conc. depends. *(Russian)* 77−39877
$Pb_{0.76}Sn_{0.24}Te$ single crystals, current-voltage charact. at He temps. 80−20197
$Pb_{0.78}Sn_{0.22}Te$ film, Bi and Tl impurity dopant incorporation and diffusion during MBE growth 79−66012
$Pb_{0.78}Sn_{0.22}Te$, $Pb_{0.91}Sn_{0.09}Se$, radiative and nonradiative recombination 80−80849
$Pb_{0.78}Sn_{0.22}Te$:In, low current carrier conc., Hall effect, lattice constant 79−82603
$Pb_{0.78}Sn_{0.22}Te$:In, transport phenomena, below 20K *(Russian)* 79−38074
$Pb_{0.78}Sn_{0.22}Te$:In epitaxial layers, dislocation density, Hall effect, conductivity, photoeffects 80−25024

lead compounds continued
$Pb_{0.79}Sn_{0.21}Te$ epitaxial film on $Pb_{0.79}Sn_{0.21}Te$, far IR reflectivity obs. 77−40251
p-$Pb_{0.79}Sn_{0.21}Te$, free-carrier optical absorption 77−52101
$Pb_{0.8}Sn_{0.2}Te$ crysts., Bridgman grown, X-ray perfection study 80−107018
$Pb_{0.8}Sn_{0.2}Te$ film, growth in quasi-closed space, single and polycryst. 79−33930
n-$Pb_{0.8}Sn_{0.2}Te$ film, magnetophonon reson., 55-90K 79−7913
$Pb_{0.8}Sn_{0.2}Te$, film photodiodes, quantum efficiency 79−75596
$Pb_{0.8}Sn_{0.2}Te$, hole conc. at 77K from room temp. thermoelec. meas. 78−56155
$Pb_{0.8}Sn_{0.2}Te$, implantation of S^+ and In^+ ions 77−19973
$Pb_{0.8}Sn_{0.2}Te$, LPE layers, carrier conc. variation with annealing and growth temp. 77−39878
$Pb_{0.8}Sn_{0.2}Te$, magnetophonon effect obs. 78−23115
$Pb_{0.8}Sn_{0.2}Te$, single cryst. and epitaxial film, far IR refl. spectra, carrier density, Hall const., and plasma freq. 80−20629
$Pb_{0.8}Sn_{0.2}Te$ surfaces, oxidation in air and thermal desorption, XPS and LEED meas. 79−47830
$Pb_{0.8}Sn_{0.2}Te$, susceptibility effective mass, carrier conc. depend. 80−20069
$Pb_{0.8}Sn_{0.2}Te$:Cd, defect struct., Hall effect and solubility meas. 77−11571
$Pb_{0.8}Sn_{0.2}Te$:Cd, influence of Cd doping on high field magnetoresist. and Hall effect 80−75590
$Pb_{0.8}Sn_{0.2}Te$:In, absorption spectra meas., 475-725K 77−4664
$Pb_{0.8}Sn_{0.2}Te$:In, implanted thin epitaxial films, laser annealing 79−65104
$Pb_{0.8}Sn_{0.2}Te$:La, evaporated thin films, low carrier conc. 80−65414
$Pb_{0.8}Sn_{0.2}Te$-Pb, Schottky barrier form., Auger depth profiling and I-V meas. 80−49903
$Pb_{0.8}Sn_{0.2}Te$-PbTe p-n heterojunction, prep., elec. and photoelec. props. 79−51664
n-$Pb_{0.82}Sn_{0.18}Te$, conduction band struct., determ. by Shubnikov-de Haas meas. 78−2504
$Pb_{0.82}Sn_{0.18}Te$ epitaxial films, surface transport of carriers at 77K 79−28419
$Pb_{0.82}Sn_{0.18}Te$, film, effect of hydrostatic pressure on props. 80−70862
$Pb_{0.82}Sn_{0.18}Te$ films, VPE, hot wall technique, struct., elec. props. 79−37926
$Pb_{0.82}Sn_{0.18}Te$ films, piezoresist. effect 79−38197
$Pb_{0.82}Sn_{0.18}Te$, Hall mobility, scatt. mechanisms, temp. and carrier conc. depend. 77−55548
$Pb_{0.82}Sn_{0.18}Te$, layers on mica substrate, Hall constant peculiarities 80−75588
p-$Pb_{0.82}Sn_{0.18}Te$, mag. susceptibility, inversion layers effect *(Russian)* 77−72996
$Pb_{0.82}Sn_{0.18}Te$, narrow band gap, relax. time for Shubnikov-de Haas effect 78−80006
$Pb_{0.82}Sn_{0.18}Te$, narrow gap semicond., mag. susceptibility meas. *(Russian)* 78−84397
$Pb_{0.82}Sn_{0.18}Te$, narrow-gap, Hall effect quantum oscillations *(Russian)* 77−4377
$Pb_{0.82}Sn_{0.18}Te$ solid solution, energy band spectrum charact., Hall effect meas. 77−76737
$Pb_{0.82}Sn_{0.18}Te$, thermomagnetic, thermoelectric props., valence band struct. *(Russian)* 80−54724
$Pb_{0.82}Sn_{0.18}Te$:Cd, effective distrib. coeff. of Cd *(Russian)* 79−73203
p-$Pb_{0.82}Sn_{1.8}Te$, Hall coeff. sign-inversion temp. 78−52010
$Pb_{0.83}Sn_{0.17}Te$, carrier tunnelling through potential barrier in p-n junctions *(Russian)* 78−52074
$Pb_{0.83}Sn_{0.17}Te$, recomb. at high levels of optical excitation 78−10503
$Pb_{0.84}Sn_{0.16}Te$ solid soln., anelastic relax. in single cryst. *(Russian)* 77−51437
$Pb_{0.85}Sn_{0.15}Te$ homostructure diode laser, LPE growth, with controlled carrier conc. 80−95903
$Pb_{0.86}Sn_{0.14}Te$/PbTe, interface recomb. velocity in DH laser diodes 79−64222
n-$Pb_{0.88}Sn_{0.12}Te$ spin flip Raman laser pumped by TE CO_2 laser, charcts. 80−87397
n-$Pb_{0.88}Sn_{0.12}Te$, stimulated spin-flip Raman scatt. 79−72621
$Pb_{0.92}Sn_{0.08}Te$, photoelec. props. 78−6415
$Pb_{0.93}Sn_{0.07}Te$ tunable diode laser for IR spectroscopy 78−33511
$Pb_{0.9}Sn_{0.1}Te$, situated in quantizing magnetic field, photolum. spectra 79−71461
$Pb_{1-x}Sn_xTe$ film, epitaxial, patterns of diffuse bands on electron diffr. patterns 79−11021
$Pb_{1-x}Sn_xTe$, ($0 \leq x \lesssim 0.2$), homogeneous, spontaneous emission, temp. and carrier conc. depend., cathodoluminescence 78−10990
$Pb_{1-x}Sn_xTe$ (x=0.15 to 0.20), SEM study, dislocation density, and carrier density and mobility 79−69107
$Pb_{1-x}Sn_xTe$, (x<0.35), permittivity and soft modes, carrier density and comp. effects 80−7256
$Pb_{1-x}Sn_xTe$, absorption edge shift, energy gap determ. 78−88308
$Pb_{1-x}Sn_xTe$ and $Hg_{1-x}Cd_xTe$ quantum detector selection for 8 to 14 μm 79−80681
$Pb_{1-x}Sn_xTe$ anodic oxide film form. conditions, IR absorpt. spectra 80−11494
$Pb_{1-x}Sn_xTe$, anomalous resist. near ferroelec. phase transition 80−20196
$Pb_{1-x}Sn_xTe$, band struct. and phonon energies, tunnelling spectroscopy 78−72070
$Pb_{1-x}Sn_xTe$, band struct. changes due to displacive phase transition, Hall coeff. meas. 80−10671
$Pb_{1-x}Sn_xTe$, basic electrons energy spectrum near mag. phase transition *(Russian)* 79−90955
$Pb_{1-x}Sn_xTe$, Cd-In diffusion, changes in elec. props. 78−91348
$Pb_{1-x}Sn_xTe$, charact. of photocond., 12-130K 78−26914
$Pb_{1-x}Sn_xTe$, charcts. of IR absorption 77−1681
$Pb_{1-x}Sn_xTe$, continuously tunable electron beam pumped laser 78−50802
$Pb_{1-x}Sn_xTe$, correlation between elec. props. and crystalline environment 77−80773
$Pb_{1-x}Sn_xTe$, cryst. growth rel. to IR detector fabrication 77−85911
$Pb_{1-x}Sn_xTe$, DH laser, gain-freq.-current relation, k.p band model 77−61951
$Pb_{1-x}Sn_xTe$ DH laser, minority carrier lifetimes and lasing thresholds 80−19031
$Pb_{1-x}Sn_xTe$, diamag. reson. *(Russian)* 78−23347
$Pb_{1-x}Sn_xTe$, diffusion of Cd, Hall effect, cond. and solubility meas. 79−69292
$Pb_{1-x}Sn_xTe$ diode laser, contact degradation due to diffusion 80−102734

lead compounds continued
$Pb_{1-x}Sn_xTe$, displacive phase transition, effect of interband hybridisation 79−33233
$Pb_{1-x}Sn_xTe$, distributed feedback DH lasers, design fabrication and characts. 77−10944
$Pb_{1-x}Sn_xTe$, effect of mag. field on thermal cond. 79−65263
$Pb_{1-x}Sn_xTe$, effective mass of holes, thermoelec. power, Hall coeff., carrier conc. 79−65371
$Pb_{1-x}Sn_xTe$, electron-irradiated, elec. and recomb. props. 79−56227
$Pb_{1-x}Sn_xTe$, electron-phonon interaction 78−71819
$Pb_{1-x}Sn_xTe$, electroreflectance, Faraday rot., elec. band struct. parameters 77−66113
$Pb_{1-x}Sn_xTe$, energy band parameters from IR Faraday rotation 78−48154
$Pb_{1-x}Sn_xTe$, energy band parameter determ. from photoluminescence. spectra in mag. field 79−11066
$Pb_{1-x}Sn_xTe$, energy gap of single crysts, comparison of indirect and direct determ. methods *(German)* 78−26812
$Pb_{1-x}Sn_xTe$, energy spectrum under hydrostatic pressure 79−65381
$Pb_{1-x}Sn_xTe$ epitaxial films, adsorption-induced accumulation layer form. on surface 80−60117
$Pb_{1-x}Sn_xTe$, epitaxial growth on $LiNbO_3$, electron diffr. and microscopy exam. 77−1331
$Pb_{1-x}Sn_xTe$, epitaxial layers, cond. *(Russian)* 77−24629
$Pb_{1-x}Sn_xTe$, epitaxial layers, In doping, donor impurity singularities, distrib. coeff. 77−80526
$Pb_{1-x}Sn_xTe$, epitaxial layers, carrier lifetime meas. 79−42559
$Pb_{1-x}Sn_xTe$, epitaxial layers, photolum. in mag. field 79−83033
$Pb_{1-x}Sn_xTe$, far IR magneto-optical meas. 79−61343
$Pb_{1-x}Sn_xTe$, Faraday effect and electron gas magnetisation, Kane two band model calcs. *(Russian)* 80−34899
$Pb_{1-x}Sn_xTe$, ferroelec. phase transition, hybridization effect *(Russian)* 79−61319
$Pb_{1-x}Sn_xTe$ film, Burstein-Moss effect, absorpt. and photocond. spectra 78−18961
$Pb_{1-x}Sn_xTe$ film, sputtered, for IR detector appl. elec. and optical props. 80−35084
$Pb_{1-x}Sn_xTe$ film hot-wall technique preparation 78−6465
$Pb_{1-x}Sn_xTe$ film on BaF_2, electron beam delineation effect on MBE growth, LEED and AES obs. 79−99434
$Pb_{1-x}Sn_xTe$ films, pure and Bi doped, polycryst., struct., elec., optical props. 79−42542
$Pb_{1-x}Sn_xTe$ films, size quantisation, optical orientation of free carriers 80−20725
n-$Pb_{1-x}Sn_xTe$, galvanomag. effects, alloy scatt., 4.2K 77−39880
$Pb_{1-x}Sn_xTe$, grown by LPE, solid-liquid tie line determ. 78−64526
$(Pb_{1-x}Sn_x)Te$, growth by sublimation technique *(German)* 77−73224
$Pb_{1-x}Sn_xTe$, growth of epitaxial layers, activation by UV and IR radiation 80−71598
$Pb_{1-x}Sn_xTe$, heteroepitaxial film, fundamental absorpt. edge and Shubnikov-de Haas effect 79−24381
$Pb_{1-x}Sn_xTe$ heterojunction lasers, instantaneous vacuum evaporation grown, threshold current density 80−5759
$Pb_{1-x}Sn_xTe$ heterostructure laser, fabrication and props. 79−10306
$Pb_{1-x}Sn_xTe$, hole effective mass near zero bandgap, IR refl. study 80−108205
$Pb_{1-x}Sn_xTe$ homojunction laser, increased freq. tuning range 77−75546
$Pb_{1-x}Sn_xTe$ IR detector, ESCA meas., surface leakage currents 77−20402
$Pb_{1-x}Sn_xTe$, impurity defused IR detector, spectral response depend. on impurity conc. *(Japanese)* 78−58036
$Pb_{1-x}Sn_xTe$, in MIS struct., tunnelling investig. of band gap and phonon energies 77−43733
$Pb_{1-x}Sn_xTe$, in MOS junction, phonon-assisted tunnelling 77−76928
$Pb_{1-x}Sn_xTe$, injection laser, use in high-resolution spectroscopy 79−76714
$Pb_{1-x}Sn_xTe$, inter- and intraband magneto-optical transitions 80−25346
$Pb_{1-x}Sn_xTe$, interband absorpt. edge for single cryst. epitaxial films 78−43948
$Pb_{1-x}Sn_xTe$ LPE film IR detector performance 80−86422
$Pb_{1-x}Sn_xTe$, LPE grown heterostructures, improved nucleation and planar interface 79−95949
$Pb_{1-x}Sn_xTe$ LPE grown heterostructures, dislocation etch pitch, interfaces 80−2023
p-$Pb_{1-x}Sn_xTe$, LPE layer, carrier conc. and mobility 79−99639
$Pb_{1-x}Sn_xTe$, large non-seeded single cryst. growth by sublimation method, and characterisation 79−78860
$Pb_{1-x}Sn_xTe$, large single crystal growth, on quartz surface, non-seeded 78−48293
$Pb_{1-x}Sn_xTe$, lattice and electronic props. and g-value 80−80161
$Pb_{1-x}Sn_xTe$, lattice instability and phonon lifetimes, neutron scatt. 78−55932
$Pb_{1-x}Sn_xTe$, lattice instability and phonon-width, comprehensive model 79−14906
$Pb_{1-x}Sn_xTe$ layers, LPE, phase diagram rel. to lattice const., distrib. coeffs. 79−37925
$Pb_{1-x}Sn_xTe$ layers, LPE growth on metal-etched substates 80−55313
$Pb_{1-x}Sn_xTe$, MBE, O_2 uptake, AES, XPS and UPS expts. 78−95227
$Pb_{1-x}Sn_xTe$, MBE, state-of-the-art 79−24450
$Pb_{1-x}Sn_xTe$, mag. and kinetic props. near ferroelec. transition 80−11160
$Pb_{1-x}Sn_xTe$, material props. and use in diode lasers, review 80−5732
p-$Pb_{1-x}Sn_xTe$, mobility meas., impurity and phonon scatt. mechanisms 78−23091
$Pb_{1-x}Sn_xTe$ monocrystal and sinter thermoelec. inhomogeneity 78−91713
$Pb_{1-x}Sn_xTe$, Mossbauer investig. of phonon softening at semicond.-semimetal transition 77−43908
$Pb_{1-x}Sn_xTe$, narrow gap, many-body interaction effects, Bloch electron scatt. lifetimes, energy renormalisation 80−49637
$Pb_{1-x}Sn_xTe$ narrow gap solid alloys, hole Fermi surface, galvanomag. and oscill. effect obs. *(Russian)* 77−69345
$Pb_{1-x}Sn_xTe$, narrow gap solid solns., mag. susceptibility and energy band spectrum 79−28276
$Pb_{1-x}Sn_xTe$, narrow gap semicond., theory of mag. susceptibility 80−93070
$Pb_{1-x}Sn_xTe$ optically pumped lasers, power output and wavelength, 4 to 30K 78−79035
$Pb_{1-x}Sn_xTe$ p-n heterostructure, VPE, struct. and electrophysical charcts. 78−10547
$Pb_{1-x}Sn_xTe$, photoconduct., photoelectromag. effect, laser intensity depend., carrier lifetimes 77−15896

lead compounds continued
$Pb_{1-x}Sn_xTe$, photoelec. props. 30 to 4.2K, temp. depend. of electron density 80−20246
$Pb_{1-x}Sn_xTe$, photomagnetic effect at low temps. 77−62960
p-$Pb_{1-x}Sn_xTe$ piezoresistance, temp. and conc. depend. *(Russian)* 79−1601
$Pb_{1-x}Sn_xTe$, polycryst. powder, low temp. prep. in PbI_2 flux 79−61524
p-$Pb_{1-x}Sn_xTe$, pressure-induced transition to zero-gap state, changes in energy band parameters 79−69413
$Pb_{1-x}Sn_xTe$, properties and use for making devices, review 78−60131
$Pb_{1-x}Sn_xTe$, reststrahlen band, reflection spectra 79−8162
$Pb_{1-x}Sn_xTe$, segregation during solidification by Bridgman technique 79−38735
p-$Pb_{1-x}Sn_xTe$, single crysts. and diodes, elec. props. under high press. 77−47809
$Pb_{1-x}Sn_xTe$, single cryst. grown from vapour, photocond. meas. 79−24016
$Pb_{1-x}Sn_xTe$ single crystals, selection using travelling solvent method *(German)* 80−2936
$Pb_{1-x}Sn_xTe$, small-gap, recomb. mech. 79−38099
$Pb_{1-x}Sn_xTe$, soft mode, ferroelec. phase transition crit. temp. and dielec. const. calcs. 77−8530
$Pb_{1-x}Sn_xTe$, soft-phonon-induced Raman scatt. 77−77209
$Pb_{1-x}Sn_xTe$ solid solutions, EPR at Te vacancies *(Russian)* 77−48050
$Pb_{1-x}Sn_xTe$ solid solution, electron scatt. by charged Te vacancies 77−69328
$Pb_{1-x}Sn_xTe$ solid solution, radiative recombination 79−52016
$Pb_{1-x}Sn_xTe$, solid-liq. phase equilib. above 750°C 79−82316
$Pb_{1-x}Sn_xTe$, soliton modulation widths for TO-phonons 77−80588
$Pb_{1-x}Sn_xTe$, surface photo-EMF under laser excitation conditions 80−6897
$Pb_{1-x}Sn_xTe$, Te-rich growth by ingot nucleation method, laser fabrication 77−77362
$Pb_{1-x}Sn_xTe$, temperature gradient LPE PbTe substrate 78−3066
p-$Pb_{1-x}Sn_xTe$, thermoelec. power, carrier conc. and temp. depend., interband scatt. 80−24957
$Pb_{1-x}Sn_xTe$, thermoelectric effects, characteristics at low temps. 80−107831
$Pb_{1-x}Sn_xTe$, VPE crystals, X-ray diffr. data interpretation 77−15712
$Pb_{1-x}Sn_xTe$, VPE growth control by EM irrad. *(Russian)* 80−34338
$Pb_{1-x}Sn_xTe$, valence band struct., Hall effect meas. 78−39016
$Pb_{1-x}Sn_xTe$, x=0.2, monocrystal, photoelectric props. of p-n structures *(Russian)* 80−70808
$Pb_{1-x}Sn_xTe$, X=0.2, monocrystal, edge of intrinsic absorpt. *(Russian)* 80−71368
$Pb_{1-x}Sn_xTe$: Mn, Mn mag. and elec. active states, mag. impurity behaviour 80−44627
$Pb_{1-x}Sn_xTe$:^{119}Sn, symm. breaking of Sn local environment, Mossbauer splitting obs. *(Russian)* 77−40166
$Pb_{1-x}Sn_xTe$:Cd, Cd diffusion obs. using Hall mobility and Cd solubility expts. 78−26584
$Pb_{1-x}Sn_xTe$:Cd, deep energy level, temp. depend. of elec. cond. 78−18994
$Pb_{1-x}Sn_xTe$:Cd, impurity photocond. spectra 80−6902
$Pb_{1-x}Sn_xTe$:Cd, long-wavelength photosensitivity shift on annealing, Cd influence 78−26912
$Pb_{1-x}Sn_xTe$:Cd, photocond., photomag. effect, carrier lifetimes 80−44658
$Pb_{1-x}Sn_xTe$:Cd, photoelec. props., surface recomb. effect 80−44659
$Pb_{1-x}Sn_xTe$:Cd(In), solid solutions, impurity states in photoluminescence spectra *(Russian)* 80−97333
$Pb_{1-x}Sn_xTe$:Ge, anomalous behaviour of impurity centres under press. *(Russian)* 80−65491
$Pb_{1-x}Sn_xTe$:In, carrier spectroscopic g-factors, magnetoresistance, temp. depend. 80−6705
$Pb_{1-x}Sn_xTe$:In, dielectric state, avalanche breakdown in strong elec. fields *(Russian)* 80−92901
$Pb_{1-x}Sn_xTe$:In, energy spectrum under combined effect of mag. field and hydrostatic press. 79−65382
$Pb_{1-x}Sn_xTe$:In, energy spectra modifications due to comp. changes and press. appl. 80−10915
$Pb_{1-x}Sn_xTe$:In, Hall const. depend. on temp., autocompensation, band gap temp. depend. explanation 79−69527
$Pb_{1-x}Sn_xTe$:In, Hall effect and photoconductivity *(Russian)* 80−103720
$Pb_{1-x}Sn_xTe$:In, high temp. Fermi level position 79−90948
$Pb_{1-x}Sn_xTe$:In, impurity influence on photoluminescence at large excitation levels *(Russian)* 80−93384
$Pb_{1-x}Sn_xTe$:In, nonequilib. metallic state *(Russian)* 79−33300
$Pb_{1-x}Sn_xTe$:In, semiconductor-metal-semiconductor transitions under press. 80−34491
$Pb_{1-x}Sn_xTe$:In, tunnelling impurity self-localisation, anomalous props. nature *(Russian)* 80−59915
$Pb_{1-x}Sn_xTe$:In, with low carrier conc., transport phenomena 80−49783
$Pb_{1-x}Sn_xTe$:In epitaxial layers, growth, elec. props., and luminesc. 80−54542
$Pb_{1-x}Sn_xTe$:In film, anomalous elec. props. 78−10477
$Pb_{1-x}Sn_xTe$:In(Ga)(Al), elec. props., dopant influence 79−51599
$Pb_{1-x}Sn_xTe/PbTe_{1-y}Se_y$ lattice-matched buried heterostructure lasers with CW single mode output 80−74386
$Pb_{1-x}Sn_xTe$-$Pb_{1-y}Sn_yTe$, p-n heterojunction, prep. and props. 79−51662
$Pb_{1-x}Sn_xTe$-PbTe, ($0 \leq x \leq 0.2$), semicond. junction laser, lasing investigation 78−10990
$Pb_{1-x}Sn_xTe$-PbTe, amorphous/crystalline heterojunction, rectification props., IR detector appl. *(Japanese)* 78−60197
$Pb_{1-x}Sn_xTe$-PbTe heterojunction, Sn diffusion and elec. effects of dislocations, elec. and metallurgical expts. 77−89839
$Pb_{1-x}Sn_xTe$-PbTe heterojunction, Sn diffusion profile, X-ray diffr. data interpretation 78−51832
$Pb_{1-x}Sn_xTe$-PbTe heterojunctions, interface recombination velocity reduction with decreasing lattice parameter mismatch 79−98370
$Pb_{1-x}Sn_xTe$-PbTe heterostructures, MBE produced on mica and $LiNbO_3$, elec. props. study 80−88629
$Pb_{1-x}Sn_xTe$-PbTe pulse laser diode, temp. tuning of modes 78−50777
$(Pb_{1-x}Sn_x)_{1+y}Te_{1-y}$ system, VPE parameters influence on epitaxial film props. 79−28229
$Pb_{87}Sn_{13}Te$, phonon dispersion, mode softening 79−42175
$Pb_xSn_{1-x}Te$, for appl. in IR detector arrays, comp. control 80−31872
$Pb_xSn_{1-x}Te$, grown by vap. transport in closed system, quality improvement 77−40341
$Pb_xSn_{1-x}Te$, oxide and Te monolayer films, Raman backscattering spectra 77−48211

lead compounds continued
$Pb_xSn_{1-x}Te$, RF sputtered films, struct., lattice parameter, stoichiometric comp., RHEED 78−38975
$Pb_xSn_{1-x}Te$, RF sputtered film IR detector, photocond. response speed improvement by annealing 79−58790
$Pb_xSn_{1-x}Te$, RF-sputtered epitaxial single-cryst. films, thermorefl. spectra 77−63476
$Pb_xSn_{1-x}Te$, thin film, oxidation, appl. of Mossbauer method 80−45410
$Pb_xSn_{1-x}Te$-PbTe p-n junction, epitaxial, elec. props. and photoresponse 78−56225
Pb_xSn_yTe, solid solns., thermoelec. power and Hall effect under hydrostatic press. 79−23990
PbSnTe(Se) Schottky barrier diode and n-p diffused junction IR detectors, comparison 80−9039
$Pb_{1-x}Sn_xTe_{1-y}Se_y$, narrow-gap solid soln., lattice parameter, energy gap and Hall mobility of carriers 79−73154
$Pb_{1-x}Sn_xTe_{1-y}Se_y$, quarternary solid solns. with const. lattice parameter, cryst. growth and characts. 80−108332
$Pb_{1-x}Sn_xTe_{1-y}Se_y$ solid solutions with constant lattice parameter, phase comp. 80−108417
$Pb_{1-x}Sn_xY$, Y=Te, Se, S, photocond. anisotropy rel. to lifetimes 78−52032
$Pb_{1-y}SnySe$, ($0 \leq y \leq 0.08$), spontaneous emission, temp. and carrier conc. depend., cathodoluminescence 78−10990
$Pb(Sr,Ti)O_3$ ceramics, modified, measurement of electrical field polarisation using automated system 79−67268
$Pb_xSr_{1-x}TiO_3$, ferroelec., with impurities, lattice dynamics 79−28061
$Pb_{0.94}Sr_{0.06}(Ti_{0.47}Zr_{0.53})O_3$-NiO, modified, dielec. and piezoelec. props. 80−11342
$Pb_{0.94}Sr_{0.06}Ti_{0.47}Zr_{0.53}O_3$, piezoelectric ceramic, stress relax., time depend. deformation 80−60899
$Pb_{0.95}Sr_{0.05}(Ti_xZr_{1-x})O_3$, solid solns., parameters of Curie Weiss law, permittivity meas. 78−15129
$Pb_xSr_{1-x}(Zr,Ti,Nb)O_3$, hydrophone ceramic, effect of one-dimensional uniaxial stress 80−80705
$Pb_{0.95}Sr_{0.05}(Zr_x, Ti_{1-x})O_3$-$Nb_2O_5$, phase coexistence range, lattice consts. 80−92680
$(Pb_{0.95}Sr_{0.05}(Zr_{0.53}Ti_{0.47})O_3)_{99\%}+Ta_2O_5(Nb_2O_5)$ piezoelectric ceramic solid soln. *(Polish)* 77−55755
$Pb_{0.95}Sr_{0.5}(Zr_{0.53}Ti_{0.47})O_3+Nb_2O_5$, optimum comp. for soft ferroelectric ceramic 77−43938
$(Pb_{0.97}Sr_{0.03})Zr_{0.51}Ti_{0.49}O_3$, ferroelec. phase transition under high press. 77−36188
$Pb_{0.95}Sr_{0.05}(Zr_{0.53}.Ti_{0.47})O_3$, low temp. internal friction in ferroelectric ceramic 77−21200
Pb_2TaFeO_6, form. reacts., thermogravimetric investig. 78−35340
$Pb_2Ta_{2-x}M_{2x}O_{7-x}$, (M=Ti, Sn Zr), oxygen deficient, form., IR spectra, dielec. const. *(Japanese)* 77−48171
Pb_2TaMnO_6, reaction of form. from oxides, ferroder. props. 80−55326
$PbTa_2O_6$, IR absorpt. spectra and diffuse Raman scatt., normal coord. anal. *(French)* 80−66198
PbTaS(Se), struct., X-ray powder diffr. meas 80−44175
PbTe 80−45236
PbTe (111), adsorption of O_2, UPS and XPS exam. 78−71962
PbTe (111), lattice vibr. amplitude anisotropy, RHEED study 80−39408
PbTe (111) epitaxial films, localised electron irrad. effects on elec. props. and O_2 sorption 80−49472
p-PbTe, absorpt. coeffs. meas. 77−24850
n-PbTe, accumulation layer, quantised surface states 80−20279
PbTe and solid solns., optimal synthesis conditions for single cryst. growth 80−100776
PbTe, asymm. strip line wall, EM wave propag. in mag. field 77−76854
PbTe, Auger recomb., photocond. decay time expts. 77−72879
PbTe, band struct., angle resolved photoemission obs. 79−33899
p-PbTe based composite material thermoelec. props. degraded by strengthening additive 79−47114
PbTe based thermoelec. materials, creep mechanisms 77−16643
PbTe, bond orbital model of band struct. 80−59853
PbTe, CDW in strong mag. fields, Peierls-type transition 80−34362
PbTe, carrier conc. inhomogeneity 78−52019
PbTe, chemisorption of O_2, room temp., UPS and XPS obs. 78−91529
n-PbTe, cold hydroextrusion, plastic deform. rel. to thermoelec. props., struct. 77−11945
PbTe, complex-composition film production method from vapour *(Russian)* 78−95702
PbTe, continuous epitaxial film, grain size, growth cond. depend. 78−26786
PbTe, crystal binding energy 79−37650
PbTe, crystallisation in constant electric field, thermoelectric parameters 77−44146
PbTe, crystallite size in epitaxial layers by X-ray diffraction rocking curves 80−20052
PbTe detector arrays, planar oxide-insulated 79−40614
PbTe, diffusion of Ag, effect of gamma irradiation 80−59515
PbTe, diffusion of Cd, Hall effect, cond. and solubility meas. 79−69292
PbTe, dispersion relation for magnetoplasma waves 79−51506
PbTe, effect of pressing and sintering, study of induced defects by SEM 80−59983
PbTe, electrochemical surface reactions 80−76389
PbTe, electron scattering interaction with coupled plasmon-polar-phonon modes 79−42536
PbTe, electron-phonon interactin induced phase transition 79−82338
PbTe, electronic struct. near band gap 77−69226
p-PbTe, energy band struct. and scattering of holes 80−10874
PbTe, energy gap and dielec. props., 77 to 373K 80−66100
PbTe, energy gap anomaly, relativistic band struct. calc. 79−4510
PbTe, energy gap temp. depend., electron-lattice interaction, dilatation effect 79−65377
PbTe, enthalpy of formation *(Russian)* 80−15267
n-PbTe, epitaxial, time dependent negative weak field magnetoresist. 78−64151
n-PbTe epitaxial film, magnetophonon and Shubnikov-de Haas oscills. 78−60234
PbTe epitaxial film, many valley semicond., band population effects, intraband magneto-optical props. 79−78007
PbTe epitaxial film, stimulated emission, absorption spectra and recombination 78−80409
PbTe, epitaxial film on fluorphlogopite, effects of annealing in Te vapour 77−80709
PbTe epitaxial films, carrier recomb. and deep levels, photocond., Hall effect, and luminesc. meas. 79−38024

lead compounds continued
PbTe epitaxial films, quantum size effect, optical meas. 80−11121
n-PbTe, epitaxial layers, elec. characts. rel. to explosive evap. in closed vol. 77−89885
PbTe epitaxial layers, orientation on different faces of $LiNbO_3$ 78−79907
PbTe, epitaxial layers, carrier lifetime meas. 79−42559
PbTe epitaxial layers, submillimetre spectroscopy 79−83048
PbTe, far IR magnetorefl., band struct. 80−76010
n-PbTe, far IR magnetotransmission and refl., dielec. function 77−52091
p-PbTe, far IR obs. of shallow bound states in high mag. fields 78−23444
PbTe, far IR spin flip reson. 79−82979
p-PbTe, Fermi surface parameters depend. on carrier density, Shubnikov-de Haas oscills. 79−42435
PbTe film, 50 μ, prep. in double quasiclosed volume 79−38745
PbTe film, (001), two-photon transition rate calc. 79−95869
PbTe film, Bi and Tl impurity dopant incorporation and diffusion during MBE growth 79−66012
PbTe film, characts. of photocond. spectra and reflectivity 77−55624
PbTe film, elec. transport props. 79−42679
PbTe film, electronic thermal cond. and thermoelec. power 80−93018
n-PbTe film, epitaxial, hot electron transport effects 77−12035
p-PbTe film, for IR magneto-optics, 8-30K 78−23543
PbTe film, ion-implantation-induced lattice defects 77−68985
PbTe film, light absorpt. 79−83043
p-PbTe film, magnetophonon effect obs. 78−23115
PbTe film, of uniformly varying thickness, photovoltaic effects 77−51774
PbTe film, on NaCl and TGS substrates, photo-EMF investig. of induced elec. inhomogeneity 77−15909
PbTe film, optical consts., support roughness effect 80−2882
PbTe film, residual conductivity 78−2595
PbTe film, struct. anal. and sensitisation 78−22982
n-PbTe film, transverse magnetoresistance oscillations, depend. on film thickness 79−65567
PbTe, film photodiodes, quantum efficiency 79−75596
PbTe films, thermal cond. and elec. props., 4.2 to 300K 79−28162
PbTe films grown from vapour, optimum conditions and elec. characts. 79−52117
n-PbTe, free carrier absorpt. and electron mobility 78−43392
PbTe, growth of epitaxial layers, activation by UV and IR radiation 80−71598
n-PbTe, Hall effect of hot electrons 77−55547
PbTe, high field drift vel. and Hall coeff. 78−26875
PbTe, high mobility polycrystalline layer, mol. beam deposition 79−83138
PbTe homogeneity region investig. in Pb-Te system, equil. consts. of quasichem. reactions 80−108405
PbTe IR diode, epitaxially grown and ion implanted, minority carrier lifetimes, efficiency 77−20411
p-PbTe, IR reflection and Faraday rotation angle meas. 77−1680
PbTe, index matching far i.r. method for static dielectric const. meas. 77−1678
PbTe injection laser, freq. tuning using press. and temp. combination 78−17978
PbTe, ion implantation induced damage and reson. levels 80−49255
PbTe, ion implanted, magneto-optical expts. *(German)* 79−28848
PbTe, ion-implanted, doping profile evaluation by Hall effect and sheet resist. meas. 78−59831
PbTe, LPE, solvent choice, equilib. in Pg-Sn-Te system 79−87589
n-PbTe, LPE layer, carrier conc. and mobility 79−99639
p-PbTe, lattice dielectric const. in far IR region, magnetotransmission meas. 79−78605
PbTe, lattice permittivity determ. by magnetoplasma waves method 78−19075
PbTe layer, spectrophotometer-type filters of highest possible performance, 2.5-40 μm 80−14438
PbTe layers, quality control of carrier conc. using Hall effect graphical representation 77−1500
n-PbTe, low temp. elec. cond. 80−20227
n-PbTe, low temperature electrical transport, Hall effect 80−84478
PbTe, MBE homostructure diode lasers with CW operation up to 100K 78−22129
p-PbTe MIS capacitors 5 μm IR detector appl. 78−52101
p-PbTe, MIS struct. inversion layer sub-bands, IR magnetoreflectance obs. 80−44731
PbTe, Magneto transport anomalies at low carrier densities, Wigner crystallisation 80−20222
PbTe, magneto-optical pinning phenomena 79−82962
PbTe, magneto-optical transitions and band parameters 79−82961
p-PbTe, magneto-optics of free and bound carriers 79−82985
PbTe, magnetoreflectance of surface space charge layers 78−52475
PbTe, microhardness meas. as function of applied load, elec. props. exam. 78−48493
PbTe, microwave magnetoplasma exam. of lattice and electronic props. 77−69364
PbTe N-type, TE figure of merit, integral form 77−24577
PbTe, NMR, chemical shift and linewidth determ. 79−19792
n-PbTe, noncubic (111) oriented epitaxial films, weak field magnetoresistance 80−75584
PbTe, nonstoichiometric, evap. and growth of epitaxial layers 80−104072
PbTe p-n junction, minority carrier lifetime, step pulse recovery 77−11995
PbTe, phase convection for effective g-factors and role of g-factors in Knight shifts 79−51473
PbTe, photoemission interpretation 80−25531
PbTe photovoltaic detector, detectivity limits 80−105709
PbTe, polycryst. film, RF sputtered, time stability 77−43758
p-PbTe, quantum oscillations in inversion layer 77−85245
PbTe, radioelectric effect in far IR 80−24967
PbTe, recombination radiation polarisation direction, two-photon selective energy valley occupation *(Russian)* 77−20924
p-PbTe, relax.-time anisotropy 77−35954
PbTe, resonant scattering, photocond. 80−6910
PbTe, semiconductor polycrystalline thin films, low-frequency 1/f noise meas. 80−15629
PbTe single crystals, growth from vapour phase under micro-gravity conditions 80−80957
PbTe, small gap, band-edge parameters 80−49594
PbTe, solidus line anal., carrier conc. 78−75806

lead compounds continued
PbTe, spin orientation under two-photon pumping 79−74000
PbTe, struct. of second valence band 77−89697
PbTe, structural transition 77−51497
PbTe substrate for MIS capacitor, C-V and G-V characts. 78−26962
PbTe, substrate in temp. gradient LPE of $Pb_{1-x}Sn_xTe$ 78−3066
PbTe surface space charge layers, far IR magnetoreflectance meas. 78−64349
PbTe surfaces, oxidation in air and thermal desorption, XPS and LEED meas. 79−47830
PbTe surfaces, Te coating, struct. and junction characts. 80−50743
PbTe surfaces, tunnelling spectroscopy in MOS and Schottky barrier junctions 80−49945
PbTe, TO phonon mode softening, sub mm spectra 78−6665
PbTe, TO phonon softening, free carriers and defects effects 78−79720
PbTe, TO-phonon mode softening, far IR Fourier transform spectroscopy 77−40248
PbTe, thermodynamic props. 77−28023
PbTe, thermoelectric alloys, phase diagrams, and imperfection chemistry 80−108422
PbTe thermoelectric materials, microstructure anal. using SEM X-ray microanalysis 80−107211
p-PbTe, thermorefl., 1.0-4-6 eV 78−76492
PbTe, thick epitaxial film, laser deposition technique 78−68629
PbTe, thick sample, atomic comp. determ., H^+ and He^+ induced X-ray anal. 79−5223
PbTe tunable laser diode IR absorption spectroscopy 79−75628
PbTe, two photon magnetoabsorption *(Russian)* 80−60553
PbTe, uncontaminated films on mica sustrates, elec. props. obs. 77−76967
PbTe, uncontaminated films prepared by mol. beam deposition, elec. props. meas. 78−15316
PbTe, undoped, nature of defects, X-ray diffr. and optical absorption meas. 77−43211
PbTe, VPE, on $LiNbO_3$, struct. and morphology obs. 80−54561
PbTe, VPE film growth under near equilib. conditions 77−32526
PbTe, VPE growth control by EM irrad. *(Russian)* 80−34338
PbTe vacuum deposited thin films, struct. and growth 79−19482
PbTe, valence level photoelectron spectra 77−27114
PbTe very thin epitaxial films, transmission and refl. spectra, 1 to 5 eV 80−7430
PbTe, wave-vector depend. of electron energy losses 78−11041
PbTe, wedge shaped film, photovoltaic effect 77−1454
PbTe, XPS investig. of valence band struct. 77−48311
PbTe:As, hole conc. control, in LPE layers 79−99640
PbTe:Bi-PbSmTe-PbTe, epitaxial laser struct., growth, p-n junction position and lasing region 79−89908
PbTe:Bi(Sb)(Cr)(Ag), thermoelec. props., thermal and elec. cond. 79−82616
PbTe:Cd, Cd diffusion obs. using Hall mobility and Cd solubility expts. 78−26584
PbTe:Cd, defect struct., Hall effect and solubility meas. 77−11570
PbTe:Fe, single crystals, state and behaviour of Fe, mag. props. 80−93080
PbTe:Ga, location, behaviour of Ga, electrophysical props. meas. 79−38016
PbTe:In, absorption spectra meas., 475-725K 77−4664
PbTe:In, electron mobility, temp.-independent part, Hall effect and elec. cond. meas. 80−92914
PbTe:In, mag. susceptibility, temp. depend., 4.2 to 200K 80−65773
PbTe:In, Shubnikov-de Haas oscillatory effects, quasilocal impurity level 80−92912
PbTe:In based solid solutions, impurity states, elec. props. 79−87054
n-PbTe:In(Cu) epitaxial films, elec. transport props. 80−75659
PbTe:Na, In, high temp. Fermi level position 79−90948
n-PbTe:Pb(Bi)(In), thermoelectric props., 300-750K 78−34851
PbTe:Ti, effect of impurities on transport props. 79−11158
PbTe:Tl, absorpt. coeff. spectral depend. 80−93370
PbTe:Tl, influence of Tl impurity states 80−20121
PbTe:Tl, thermoelectric power, elec. cond., Hall coeff. and optical absorpt. coeff. 80−39584
PbTe:Zn, defect struct., Hall effect and solubility meas. 77−11572
n-PbTe/p-$Pb_{0.8}Sn_{0.2}Te$, multicolour photodetectors *(Czech)* 79−26126
PbTe-(Pb,Sn)Te DH laser, CW operation over 1500 h at 77K 78−17950
PbTe-based solid solns., 79−23990
PbTe-based structures, zero anomaly of tunnel cond. 79−24107
PbTe-Bi_2Te_3 system cpds., powder pattern calcs. 77−43185
PbTe-CdTe heterojunctions, fabrication and characterisation *(German)* 80−89151
PbTe-CdTe(InSb) superlattices, laser deposition of multilayer heteroepitaxial structs. 80−44450
PbTe-flux, interfacial tension at boundary of fused systems 77−35797
PbTe-Ga_2Te_3, phase interaction, DTA, XPA and microstructural anal. 80−96625
PbTe-In contacts, fabrication and props. 80−60078
PbTe-InTe, solid solns., anomalies in electron mobility 77−80772
PbTe-InTe system, phase interactions and solid soln. form., physicochem. and elec. characteris. 80−104129
p-PbTe-M, M=In, Pb, Zn, Cu, barrier props. 79−7898
PbTe-metal barrier device, I-V and C-V characts., barrier energies, and depletion widths 77−85316
n-PbTe-p-$Pb_{1-x}Sn_xTe$, heterojunctions, heavily doped, current-flow mechanisms 80−96974
PbTe-$Pb_{0.82}Sn_{0.18}Te$, p-n heterojunctions, electrical and photoelectrical properties 78−39193
PbTe-$Pb_{1-x}Sn_xTe$ n-p^+ heterojunction photodetector, hot wall evaporation technique 80−65673
PbTe-$Pb_{1-x}Sn_xTe$-PbTe, DFB laser, coupling coeff. calcs. 77−14714
PbTe-$Pb_{1-x}Sn_xTe$-PbTe DH, LPE and VPE, stimulated emission 77−75526
PbTe-PbS, solid-phase solubility, use of diffusion couple 77−12602
PbTe-PbSe system, thermodynamic props. 80−11635
PbTe-PbSe(S) epitaxial layers, electron microscope contrast of misfit dislocations 77−85113
PbTe-PbSnTe heterjunction, misfit dislocations, etch pit and electron probe study 79−77926
PbTe-SnTe, solid soln. single crysts., TSM growth and elec. characts. 78−68625
PbTe-SnTe, solid soln., enthalpy of formation *(Russian)* 80−15267
PbTe-SnTe compound semiconductors, lattice instability by mm-wave magnetoplasma refl. 80−54336

lead compounds continued
PbTe-SnTe solid solns., directional solidification 77−44149
PbTe-Te, contact fusion in complex metallic systems 78−26664
PbTe-ZrO_2 (SiO_2), epitaxial MIS struct., fabrication and elec. props. 80−2472
$Pb_{1-y}Te$-$Pb_{1-x}Sn_xTe$ (x,y≤0.3), double heterostruct., LPE growth, heterointerface morphology 80−70550
Pb_xTe_{1-x} film, highly absorbant, complex index of refr. determ. method 78−54445
Pb_xTe_{1-x} film, optical consts. calc. 77−11041
$PbTeO_2$, acousto-optic interaction at high optical intensities 79−42942
$PbTe_{1-x}Se_x$, epitaxial layers synthesis, cryst. struct. perfection and elec. characts. 79−87587
$PbTe_{1-y}Se_y$:In, high temp. Fermi level position 79−90948
$Pb_{0.8}Te_{0.8}Se_{0.1}S_{0.1}$, solid solns., thermoelec. power and Hall effect under hydrostatic press. 79−23990
$Pb_{1-x}Th_xF_{2+2x}$, new solid electrolytes, conductivities and activation energies 79−28137
$Pb_{1-x}Th_xF_{2+2x}$, solid soln., anionic cond. *(French)* 78−91481
$Pb(Ti,Zr,[Fe_{1/2}Ta_{1/2}])O_3$, pyroelec. props. at transition between ferroelec. phases 78−52447
$Pb(Ti,Zr)O_3$, ceramic disc stack piezoelec. transducer, performance characts. 77−37843
$Pb(Ti,Zr)O_3$, kinetics of initial stage of sintering 77−85973
$Pb(Ti, Zr)O_3$, piezoelectric-ferroelectric ceramic, polarisation processes, X-ray obs. 80−34847
$Pb(Ti,Zr)O_3$, polycryst., orientational polarisation and phase comp. in strong field 78−27157
$Pb(Ti,Zr)O_3$, pyroelectric props., addition effects 79−33608
$Pb(Ti,Zr)O_3$, soft E(TO) phonons, and phase transitions, Raman spectra, −200 to 400°C 78−15109
$Pb(Ti,Zr)O_3$ solid solutions, phase coexistence discrepancies 80−96662
$Pb(Ti,Zr)O_3$:Fe(Mn)(Al), internal bias field and hysteresis relaxation 78−43823
$PbTiO_3$, $(PbTiO_3)_{0.9}(B_2O_3)_{0.1}$ amorphous ribbons, prep., electron and X-ray diffr. obs., dielec. const. temp. depend. 79−50993
$PbTiO_3$, amorphous, crystallisation process, DTA and Raman spectroscopy meas. 80−75161
$PbTiO_3$, anomalies in elec., photoelectric and mechanical props. 80−55051
$PbTiO_3$ ceramics, temp.-compensated, for SAW appl. 80−15355
$PbTiO_3$, channelling of 1 MeV He ions 80−39194
$PbTiO_3$, cryst., polarisation and resistivity, elec. field effects 78−64313
$PbTiO_3$, crysts., X-ray investigation of 90° domain struct. 79−15426
$PbTiO_3$, damping of soft E-symmetry phonon, Raman scatt. meas. 78−67799
$PbTiO_3$, domain struct. formation during jump motion of phase front 78−64339
$PbTiO_3$, domain struct., formation at phase transitions 79−38510
$PbTiO_3$, domain struct. form. during jump-like motion of phase boundary 79−69794
$PbTiO_3$, ferroelec., nonlinear optical susceptibility calc. 78−9409
$PbTiO_3$, ferroelec. ceramic, mech. strength 78−64332
$PbTiO_3$, ferroelec. domain boundaries, rigid body displacement of lattice 80−40079
$PbTiO_3$, ferroelec. phase, photocond. and photovoltaic effect, temp. depend. 78−95309
$PbTiO_3$, ferroelec. semicond., thermoelec. power for small polaron 77−89784
$PbTiO_3$ ferroelec. thin film, prep. by RF sputtering and dielec. props. 79−100052
$PbTiO_3$, ferroelectric ceramic, dielec., piezoelec. and elastic props., orientational contrib. 78−68468
$PbTiO_3$ ferroelectric thin films, fabrication by RF sputtering, characts. 80−40261
$PbTiO_3$ glass-ceramics, transparent, fabrication method by crystn. 77−59733
$PbTiO_3$, mechanical twinning, spontaneous polarisation shielding 79−42930
$PbTiO_3$, neutron powder profile refinement, temp. depend. 78−51476
$PbTiO_3$, O K_α X-ray emission band spectra *(Russian)* 79−15563
$PbTiO_3$, optical birefringence in low temp. region 80−93276
$PbTiO_3$, perovskite structure, semiconductor props. *(Polish)* 78−56437
$PbTiO_3$, phase transform., different kinetic types 80−71347
$PbTiO_3$, phase transition study by X-ray powder structural refinement 80−40075
$PbTiO_3$, photocond. and TSC meas. 77−15911
$PbTiO_3$, photolum. and carrier drift mobility at ferroelec. transition 80−71469
$PbTiO_3$, piezoceramics for high frequency use 78−95555
$PbTiO_3$, single cryst., He^+ backscatt. shoulder spectra struct., domain struct. 80−35048
$PbTiO_3$ single crystals, electroluminesc., elec. field, freq. and temp. depend. 78−80422
$PbTiO_3$ single crystal, channelling of He^+ ions, polarisation effects 79−99258
$PbTiO_3$ single crystals, dielectric permittivity meas. 79−99817
$PbTiO_3$, single crysts., lattice parameters and birefringence as function of temp. 79−38517
$PbTiO_3$, soft mode decay mechanism, damping parameter freq. depend. 80−54324
$PbTiO_3$, spontaneous polaris. shielding destruction by polishing and scribing 79−15427
$PbTiO_3$, struct. changes with temp. variation, rel. to elec. cond. 78−91437
$PbTiO_3$, switching, domain structure reorganisation and polarisation change 77−1645
$PbTiO_3$, tetragonal deform. of TiO_6 octahedron 77−55759
$PbTiO_3$, thermoelectric effect and ferroelectric transition 78−48123
$PbTiO_3$, uniaxial pyroelectric, nonlinear optical susceptibility 77−23705
$PbTiO_3$, vibronic theory and opt. props. 80−103939
$PbTiO_3$, X-ray interference intensity temp. depend., lattice ion vibr. *(Russian)* 80−20601
$PbTiO_3$-$CaFe_{2/3}W_{1/3}O_3$, solid solutions 78−43816
$PbTiO_3$-$KNbO_3$, ferroelec. Curie temp., theory 80−7313
$PbTiO_3$-$La_2O_3.3TiO_2$, struct. and dielec. props. 80−54200
$PbTiO_3$-$NaNbO_3$, ferroelec. Curie temp., theory 80−7313
$PbTiO_3$-$PbZrO_3$-$In(Li_{3/5}W_{2/5})O_3$, piezoelec. ceramic characteris. for surface wave filters 78−95215
$PbTiO_3$-$PbZrO_3$-$Pb(Ni_{1/3}Sb_{2/3})O_3$ solid solutions, dielec. and electromech. anomalies *(German)* 77−20800

lead compounds continued
$PbTiO_3$-$PbZrO_3$-$PbNb_{2/2}Zn_{1/3}O_3$(-$PbNb_{2/3}Co(Mg)_{1/3}O_3$) solid solutions, dielec. and piezoelec. props. 79−87393
$PbTiO_3$-$PbZrO_3$-based multicomponent ferroelec. solid solns., morphotropic transitions and comp.-temp. phase diagrams 80−55047
$PbTiO_3$-$Pb(Fe_{1/2}Nb_{1/2})O_3$ based modified ceramics, struct. and elec. props. 79−87392
$PbTiO_3$-$Pb(Fe_{1/2}Nb_{1/2})O_3$-$PbZrO_3$, with additions, exam. of electrical characteristics 80−2698
$PbTiO_3$-$Pb(Ni_{1/2}W_{1/2})O_3$ system, solid soln. form., struct., dielec. props. and thermal expansion *(Japanese)* 78−27501
$xPbTiO_3+(1-x)PbCd_{1/3}Nb_{2/3}O_3$, phase transition spread, polarisation relaxation, dielectric susceptibility *(Russian)* 80−75922
$PbTi_3O_7$, photocond. and optical transmission 78−64058
$Pb(Ti_{0.47}Zr_{0.53})O_3$, elec. cond. rel. to O_2 partial press. 77−51742
$PbTi_{1-x}Zr_xO_3$, low freq. vibrational modes and ferroelec. transitions 79−33637
$Pb(Ti_{1-x}Zr_x)O_3$, thermodynamic anal. of phase transitions 78−19431
$PbTi_xZr_{1-x}O_3$, ferroelec., electric field depend. of contour mode reson. 77−12351
$PbTi_xZr_{1-x}O_3$, piezoelectric ceramic, sound velocity temp. coefficients 77−12315
$Pb(Ti_{0.47}ZrO_{.53})O_3$, small polaron cond. mechanism, elec. cond. and thermopower meas. point defects 78−43380
$Pb_2UO_2Cl_4$ melts and mixtures, thermogravimetric determ. of uranyl cation state 80−101050
$Pb_2V_2O_7$, V-O-V bridge stretching freq. correl. with bond angle 78−74636
$Pb_3(VO_4)_2$, ferroelastic, phase transitions, boundary walls 80−107419
$Pb_3(VO_4)_2$, ferroelastic phase transition, thermodynamic theory 79−37832
$Pb_3(VO_4)_2$, low-temp. phase, cryst. data 77−39566
$Pb_3(VO_4)_2$-$Pb_3(PO_4)_3$ solid solutions, ferroelastic, dielec. consts. and birefringence meas. 78−2793
$Pb_3(VO_4)_3$, ferroelastic, dielec. consts. and birefringence meas. 78−2793
$Pb_8V_2O_{13}$, monoclinic lattice determ. and phase transitions *(French)* 79−99102
$Pb_5(VO_4)_3Cl$, vanadinite, vibr. spectra, normal coord. anal. 78−88305
$Pb_3WFe_2O_9$, form. reacts., thermogravimetric investig. 78−35340
Pb_2WMO_6, M=Cd, Mg, synthesis, struct., phase transitions 77−84715
$PbWO_2$, IR and Raman multiphonon spectra, struct. 77−90143
$PbWO_4$, ^{207}Pb mag. shielding anisotropy, Fourier transform NMR 77−90057
$PbWO_4$, doped and undoped single crysts., polarisation of luminesc. and assignments 80−76069
$PbWO_4$, EPR of radiation induced MoO_4^{3-} centres 78−80217
$PbWO_4$, growth by Czochralski method, props. 78−60566
$PbWO_4$, ionic and electronic cond. 79−91107
$PbWO_4$, photoconductivity spectral depend. 79−7856
$PbWO_4$, reflectivity, dispersion parameters and optical const. temp. depend. 77−28575
$PbWO_4$, refr. index, single crystals having scheelite struct. 78−79082
$PbWO_4$, single cryst. growth by Czochralski method and U incorporation, effective distrib. ratios, luminesc. characts. 79−42094
$PbWO_4$, thermal expansion tensor, phase transitions, X-ray diffr. obs. *(French)* 79−1515
$PbWO_4$:Mn^{2+}, zero-field splitting of Mn^{2+}, EPR 80−75531
Pb_2WO_5, phase transformation study by high temp. X-ray diffr. and differential scanning calorimetry 79−43244
Pb_xWO_3 ($0.01\leq x\leq 0.28$), tetragonal and orthorhombic bronzes, cryst. chem. data 78−42997
$Pb(WO_4)_{1-x}(MoO_4)_x$, growth and props. 80−71588
$Pb(WO_4)_{1-x}(MoO_4)_x$ mixed crystal, growth by Czochralski method, props. 78−60566
$Pb(WO_4)_{1-x}(MoO_4)_x$ mixed crystals, X-irrad., EPR and thermoluminesc. 79−15352
$Pb(Yb_{1/2}Nb_{1/2})O_3$, single cryst. growth from PbF_2-PbO-B_2O_3 77−48336
$Pb(Z,Ti,Mg,W)O_3$, low-Q ceramics, props. and transducer appl. 80−75944
$Pb(Zc,Ti)O_3$ crystal, appl. to identification of resonant frequencies of rotating beams 79−81824
$Pb(Zn,Ti)O_3$ piezoelectric electrically deformable diffraction grating 80−78963
$Pb_{1.8}Zn_{0.15}Na_{0.05}Nb_2O_{6.95}F_{0.05}$, electric cond. and dielect. props. of cathodic-sputtered films *(French)* 79−33371
$Pb(Zn_{1/3}Nb_{2/3})O_3$, cation disordered perovskite, elastic consts. and thermal expansion 80−96587
$Pb(Zn_{1/3}Nb_{2/3})O_3$, diffuse phase transition, electro-optical and dielec. obs. 79−82933
$Pb(Zn_{1/3}Nb_{2/3})O_3$, electrostriction investigation, strain gauge method 79−87395
$PbZn_{1/3}Nb_{2/3}O_3$ ferroelectric semiconductors, electro-optical and elasto-optical props., appl. to optical storage *(Russian)* 80−80749
$PbZn_{1/3}Nb_{2/3}O_3$, PZN, electro-opt., elasto-opt., opt. and photo-induced props. 78−95560
$Pb(Zn_{1/3}Nb_{2/3})O_3$, perovskite type, high-press. high temp. synthesis *(Chinese)* 78−68654
$Pb(Zn_{1/3}Nb_{2/3})O_3$ single cryst., pyroelec. props., meas. under laser beam illum. 80−66117
$Pb(Zn_{1/3}Nb_{2/3})O_3$-$PbTiO_3$-$PbZrO_3$ ceramics, HF filters appl. additives effect obs. *(Japanese)* 80−60507
$PbZnVO_4OH$, cryst. struct. refinement 79−42015
Pb(Zr,Ri)O_3:Ni-silicon rubber flexible composite pyroelectric, dielectric props. 80−80704
$Pb(Zr,Ti,Ge)O_3$, antiferro-ferroelectric transition 78−95565
$Pb(Zr,Ti,Nb)O_3$ ceramics, rel. dielec. const. and piezoelec. props. rel. to porosity 79−11388
$Pb(Zr,Ti,Sn)O_3$ ceramics, ferroelec., doped with tri- and pentavalent oxides, piezoelectric props. 78−19413
$Pb(Zr,Ti)O_2$ ceramic, surface barrier electroreflectance, hysteresis, ageing 80−80752
Pb(Zr,Ti)O_3 bimorph driven optical fibre switch 79−18502
Pb(Zr, Ti)O_3 cast tape, densification by pressing for piezoelec. devices 79−87595
Pb(Zr,Ti)O_3 ceramics, low field depoling charact. 77−8492
Pb(Zr, Ti)O_3 ceramic, appl. in electrically controllable diffr. grating for parallel polarised light refl. 77−39026
Pb(Zr,Ti)O_3 ceramic, permittivity and resonant frequency ageing, space charge field effects 77−85657
Pb(Zr,Ti)O_3 ceramic-polyvinylidene fluoride composite film, complex piezoelec. props. 78−64323

lead compounds continued
Pb(Zr,Ti)O_3, ceramic vibrator, resonant freq. temp. stability *(Chinese)* 79−47386
Pb(Zr,Ti)O_3 ceramic, substrate for In_2O_3 film, ferroelec. field effect 79−47177
Pb(Zr,Ti)O_3 ceramics, piezoelectric charcts. *(French)* 79−56727
Pb(Zr, Ti)O_3 ceramics for IR detectors, pyroelectric charcts. 79−56736
Pb(Zr,Ti)O_3 ceramic/polymer, composite systems, piezoelec. props. 79−99823
Pb(Zr,Ti)O_3 ceramic, X-ray investigation before and after polarisation *(Chinese)* 80−2712
Pb(Zr,Ti)O_3 ceramics, space charge field meas. by ferroelec. domain switching current, piezoelec. reson. freq. ageing charcts. 80−7296
Pb(Zr,Ti)O_3 ceramic, interconnected porous, props. 80−43579
Pb(Zr, Ti)O_3 ceramics, low temp. sintering, elec. and mech. props. 80−71616
Pb(Zr,Ti)O_3 ceramics with ladder type struct., prep. and props. 80−75945
Pb(Zr,Ti)O_3 ceramics, DC field sintering preparation, piezoelectric props., ageing behaviour 80−81211
Pb(Zr,Ti)O_3, dielectric thin film, geometry effect on props. *(Russian)* 77−90102
Pb(Zr,Ti)O_3, dielectric response in solid-medium high-pressure device 78−43766
Pb(Zr,Ti)O_3 disc, SH_0 waveguide spiral delay line charcts. 77−72123
Pb(Zr,Ti)O_3, doped, Goldschmidt factors and ferroelec. antiferroelec. transition 77−12332
Pb(Zr,Ti)O_3, effect of spherical pores on strength 77−70103
Pb(Zr,Ti)O_3, electrooptic ceramic *(Japanese)* 79−65840
Pb(Zr,Ti)O_3 fast transducer driving Fabry-Perot optical switch 79−86251
Pb(Zr, Ti)O_3, ferroelectric ceramics in solid matrix, high pressure effect on dielectric props. 77−16259
Pb(Zr,Ti)O_3, ferroelec. ceramic, mech. strength 78−64332
Pb(Zr,Ti)O_3, ferroelec. ceramic, axially loaded, nature of elec. field and resulting voltage 78−72468
Pb(Zr, Ti)O_3, ferroelectric ceramic discs, axial-current-mode shock depoling 79−78631
Pb(Zr,Ti)O_3, ferroic materials, fracture processes 80−79869
Pb(Zr,Ti)O_3 fibre arrays in epoxy cement, ferroelectric ceramic-plastic composites 80−81015
Pb(Zr,Ti)O_3 film, by RF sputtering in PbO vapour 78−39689
Pb(Zr,Ti)O_3 film, ferroelec. and optical props. 77−85674
Pb(Zr,Ti)O_3 film, prep. by electron beam evaporation technique 77−1809
Pb(Zr,Ti)O_3 films, ion beam sputtering, dielec. and ferroelec. props. 79−78881
Pb(Zr,Ti)O_3 films, ferroelec., ion beam deposition sputtered from multi-component targets 80−80974
Pb(Zr, Ti)O_3, formation 79−43185
Pb(Zr,Ti)O_3, fracture and deform. 80−79870
Pb(Zr, Ti)O_3 internal struct., prep. effect, ionic shadowing obs. *(Polish)* 80−11612
Pb(Zr,Ti)O_3 internally electroded multilayers, piezoelectric props., permittivity, transducers 80−80672
Pb(Zr,Ti)O_3, internally electroded with Pt, resonance behaviour 80−84701
Pb(Zr,Ti)O_3, order of ferroelec. paraelec. transition 77−12333
Pb(Zr,Ti)O_3, PCD ceramic, pyroelectric props. 80−100635
Pb(Zr,Ti)O_3 photovoltaic ferroelectric as optical memory storage medium 78−50877
Pb(Zr, Ti)O_3, piezoceramic, explosive synthesis 77−16525
Pb(Zr,Ti)O_3 piezoceramic, phase transition under shock loading *(Russian)* 77−69041
Pb(Zr,Ti)O_3, piezoceramic, nonlinear piezoeffect 79−42900
Pb(Zr,Ti)O_3, piezoelec. ceramic, coexistence of tetragonal and rhombohedral phases 77−7845
Pb(Zr,Ti)O_3, piezoelectric material, effect of processing on props. *(Polish)* 77−85655
Pb(Zr,Ti)O_3, piezoelec., compositional fluctuation and props. 78−18742
Pb(Zr,Ti)O_3, piezoelectric bimorph, quasistatic response exam. 78−43794
Pb(Zr,Ti)O_3 piezoelectric ceramic, CeO_2 additive effect on struct. and props. 79−52140
Pb(Zr,Ti)O_3, piezoelectric ceramics, low fluence neutron irrad. effects 80−92564
Pb(Zr,Ti)O_3, polarisation effect on deform. and strength, Curie pt. region 79−42902
Pb(Zr,Ti)O_3 polycrystalline ceramic, fracture and strength, surface treatment effects 80−11704
Pb(Zr,Ti)O_3, porosity-permittivity relations, depolarising factors determ. and pore effects *(Japanese)* 80−97189
Pb(Zr,Ti)O_3, prep. and reactivity from butoxide precursors 78−84749
Pb(Zr,Ti)O_3, research grade, hydrophone ceramic, effect of one-dimensional uniaxial stress 80−80705
Pb(Zr, Ti)O_3, Sc modified, sintering 77−44204
Pb(Zr,Ti)O_3, shock depoled ferroelec. ceramic, anal. of ideal response 80−60511
Pb(Zr,Ti)O_3, shock wave compressed, dielec. props. 77−48139
Pb(Zr,Ti)O_3, solid solutions, elec. and thermoelec. props. appl. *(Polish)* 77−28203
Pb(Zr,Ti)O_3 solid soln., elec. cond. and Seebeck coeff. 79−51564
Pb(Zr,Ti)O_3, synthesis from cryochem. mixtures, chem. reacts. in sublimation drying 79−11538
Pb(Zr,Ti)O_3, temp. and hydrostatic press. depend of vibr. modes, rel. to phase transforms 77−89510
Pb(Zr,Ti)O_3, tetragonal ferroelec. ceramic, 90° domain-rot. fraction after polarisation, X-ray determ. 80−75992
Pb(Zr,Ti)O_3, thermodynamic properties and formation data 80−29939
Pb(Zr,Ti)O_3, thin film evaporated on stainless steel, photovoltaic effect 79−4580
Pb(Zr,Ti)O_3 thin films, fabrication and characterisation electron-beam deposition 80−16188
Pb(Zr,Ti)O_3 thin layers, tan δ temp. dependence obs. *(Bulgarian)* 78−88259
Pb(Zr, Ti)O_3, triggered vac. gap, low-voltage firing charcts. 77−80381
Pb(Zr,Ti)O_3, X-ray anal. of phase transform. at 163K *(Ukrainian)* 77−69082
Pb(Zr,Ti)O_3, X-ray study in tetragonal-rhombohedral phase-transition composition area 79−42921

lead compounds continued
$Pb(Zr,Ti)O_3$:Ba, paraelectric ceramic, giant electrostrictive effect 79−91378
$Pb(Zr,Ti)O_3$:Ba, paraelectric ceramic, electrostrictive effect 80−80701
$Pb(Zr,Ti)O_3$:Cr_2O_3 ceramic, electrical cond. and dielectric const. meas. 80−2389
$Pb(Zr,Ti)O_3$:Cr_2O_3 ceramics, reson. freq. comp. and temp. depend. 80−70413
$Pb(Zr,Ti)O_3$:Fe(Nb) ceramic, elec. and electromechanical props., depend. on dopants 80−81212
$Pb(Zr,Ti)O_3$:La(Cd,W), electro-optical ferroelec. ceramic, secondary electron emission yield 79−91546
$Pb(Zr,Ti)O_3$:Mn ceramics, anomalous dielec. losses 79−42892
$Pb(Zr,Ti)O_3$:Nb ceramic, stress effects on ferroelec. hysteresis, macroscopic strain, US vel. 79−4778
$Pb(Zr,Ti)O_3$:Nb_2O_5(Sc_2O_3), elec. cond. investigation with and without various dopants and stoichiometry 79−11120
$Pb(Zr,Ti)O_3$:$PbTiO_3$ (up to 5%), dielec. props. and ferroelec. transitions 77−20806
$Pb(Zr,Ti)O_3$-epoxy resin composite, electromech. props. 77−8515
$Pb(Zr, Ti)O_3$-epoxy resin composite piezoelec. relax. due to ionic cond. 77−36179
$Pb(Zr,Ti)O_3$-$Pb_3Ge_5O_{11}$ ceramic, sintering conditions rel. to piezoelec., dielec. props., microstruct. 77−16252
$Pb(Zr_{0.53},Ti_{0.47})O_3$, piezoelec. ceramic, HF filter appl. *(Korean)* 79−27472
$Pb(Zr,Ti)O_3$ pyroelectric ceramics 79−47649
$PbZr_{1-x}Ti_xO_3$, paraelec. phase, first-order phase transition 77−89540
Pb_3ZrF_{10}, cryst. atomic struct. *(French)* 80−49203
Pb_3ZrF_{10}, X-ray cryst. struct. determ. *(French)* 80−33966
$PbZr_{1-x}Hf_xO_3$, crystal field distortion by impurities, PAC meas. 80−11306
$PbZrO_3$, antiferroelectricity, survey *(Japanese)* 79−65803
$PbZrO_3$ based ferroelec. ceramic, pressure-temp. phase diagrams 79−24273
$PbZrO_3$, Clausius-Mossotti formula and irreducible susceptibility *(Japanese)* 79−65802
$PbZrO_3$ crystal, structural phase transitions in very high elec. fields 80−15987
$PbZrO_3$, elec. field induced phase transitions 77−62643
$PbZrO_3$, electric field induced phase transitions, 20 to 160°C 77−43947
$PbZrO_3$, ferroelec., crystallographic shear planes as nonstoichiometric defects 80−59484
$PbZrO_3$, ferroelec. semicond., thermoelec. power for small polaron 77−89784
$PbZrO_3$, ferroelec. solid solns., atom shifts, polarisation and Curie temps. 80−100636
$PbZrO_3$, lattice distortion, X-ray diffr. profiles 79−55712
$PbZrO_3$, perovskite structure, semiconductor props. *(Polish)* 78−56437
$PbZrO_3$, perovskite type, X-ray K-absorpt. edge, chem. shift 79−91529
$PbZrO_3$, phase transitions, X-ray, dielec., and thermal anal. 80−45020
$PbZrO_3$ pyroelectric detector, low temp. behaviour, expt. 80−31869
$PbZrO_3$, struct. phase transition 79−61312
$PbZrO_3$, structural phase transition in super high elec. fields 79−33626
$PbZrO_3$, thermoelec. effect and phase transitions 78−48123
$PbZrO_3$:^{89}Zr, electron capture decay lifetime, struct. environment effects 77−28523
$PbZrO_3$:La, appl. in sub-100 ps pyroelec. detectors, 10.6 μm damage threshold meas. 80−77859
$PbZrO_3$-monocryst., elec. cond., permittivity, polarisation, para- and ferro- to antiferroelec. phase transistions 78−60402
$PbZrO_3$-Pb_2FeNbO_6-$PbTiO_3$, pyroelectric props. of ferroelec. rhombohedral transition 77−12336
$PbZrO_3$-$PbCd_{0.5}W_{0.5}O_3$, phase transitions 78−43817
1-x$PbZrO_3$-x$PbSc_{0.5}Nb_{0.5}O_3$, $0 \leq x \leq 1$, phase transitions, X-ray, dielec., and thermal anal. 80−45020
$PbZrS_3$, cryst. struct. refinement using neutron diffr. powder data 79−4294
$Pb(ZrTi)O_3$ ceramic, piezoelectric effect due to polarisation *(Polish)* 77−77151
$Pb(ZrTi)O_3$ ceramic transducer for generation and detection of unipolar stress pulses 80−64328
$Pb(ZrTi)O_3$ type piezoelectric ceramics, compressive properties 79−33612
$Pb(Zr_{0.42}Ti_{0.58})O_3$, hot-pressed piezoelec. ceramic, effect of nonferroelectric phase 77−43936
$Pb(Zr_{0.52}Ti_{0.48})O_3$, polycrystalline ferroelectric, grain-size dependent props. 80−71352
$PbZr_{0.9}Ti_{0.1}O_3$, neutron powder profile refinement, temp. depend. 78−51475
$PbZr_{0.95}Ti_{0.05}O_3$ ceramics, of ABO_3 type, dopant distrib. between A and B sites 79−42093
$PbZr_{0.95}Ti_{0.05}O_3$, impact loading, mech. and elec. response, elec. state effect 78−64317
$PbZr_{0.95}Ti_{0.05}O_3$, soft mode dielec., anomalous low temp. sp. ht. 78−14423
$PbZr_{0.95}Ti_{0.05}O_3$:oxide doped, A and B site dopant distrib., antiferroelec.-ferroelectric transition 78−34532
$Pb(Zr_{1-x}Ti_x)O_3$ ceramics, double isovalent substitution effect on piezoelectric characts. *(French)* 79−51908
$Pb(Zr_{1-x}Ti_x)O_3$, electrical conductivity and I-V charact., neutron effects 78−47781
$Pb(Zr_{1-x}Ti_x)O_3$ solid solution, piezoelectric ceramic, prop. improvement by multiple substitution 80−80702
$PbZr_{1-x}Ti_xO_3$:Nb_2O_5 ceramic, ferroelec. transitions, polarisation meas. *(French)* 80−66124
$Pb(Zr_xTi_{1-x})O_3$, anomalous photovoltaic effect 79−19625
$PbZr_xTi_{1-x}O_3$ ceramics, morphotropic phase boundary 80−81035
$Pb(Zr_xTi_{1-x})O_3$, elec. props. effect of proportional composition, morphotropic phase boundary 78−35105
$Pb(Zr_xTi_{1-x})O_3$, elec. props. temp. and composition depend. 78−47817
$Pb(Zr_xTi_{1-x})O_3$, ferroelectric energy generation by shock compression, modes 77−55757
$PbZr_xTi_{1-x}O_3$, ferroelec. phase transition under high press. 79−99833
$Pb(Zr_xTi_{1-x})O_3$ films, ion beam deposition, struct., dielec. and ferroelec. props. 80−20788
$Pb(Zr_xTi_{1-x})O_3$ films, deposition by focused ion beam sputtering 80−76177
$Pb(Zr_xTi_{1-x})O_3$, meas. of Hugoniot curve with commercial manganin stress gauges 80−70362
$PbZr_xTi_{1-x}O_3$ solid solutions, tricritical behaviour 78−80296

lead compounds continued
$Pb(Zr_xTi_{1-x})O_3$ solid solns., elec. props. near morphotropic phase boundary 79−42566
$Pb(Zr_xTi_{1-x})O_3$, temp. coeff. of resonant freq. as function of Zr/Ti composition *(Chinese)* 78−68454
$Pb(Zr_{0.47}Ti_{0.43}Sn_{0.10})O_3$:$Cr_2O_3$, ferroelec. ceramic, reversible characts. and dielectric losses *(Russian)* 78−84517
$PbZrO_3$, X-ray interference intensity temp. depend., lattice ion vibr. *(Russian)* 80−20601
x$Pb0.(1-x)B_2O_3$:Fe_2O_3, Mossbauer spectra 79−87338
$Pb_2[As_2O_5]$, paulmooreite, crystal struct., dimeric arsenite groups 80−84143
PbI_2, thermal cond., 2 to 30K, Umklapp processes and phonon boundary scatt. *(Russian)* 79−10991
$PbySn_{1-x}Se$ epitaxial film narrow band photovoltaic detectors, detection at long wavelengths 78−8443
$PdBi_2O_4$, cryst. struct. *(French)* 78−51516
PdF_2, motionally narrowed NMR line shapes, free-induction decay meas. 78−68406
$PdPb(OH)_6$, cryst. struct. determ. *(French)* 77−47419
PdS-CdS heterojunctions, photoresistive props. 80−6970
$Pn_2Nb_2O_7$, relax. phenomena, meas. of dielec. const., polarisation and sp. ht. 77−4597
$Rb_2PbCu(NO_2)_6$, incommensurate Jahn-Teller phase transitions 79−65185
Sb_2Se_3-PbSe, liq. semicond., thermal cond. meas., resistive probe method 77−15636
Si-PbS heterojunction, effect of Si substrate orientation on struct. and interface props. 80−80097
SiO_2-CaO-Na_2O-PbO system, water, alkali, acid resist., chem. durability 79−34162
SiO_2-PbO system glass, thermal capacity, temp. depend. 79−95181
SiO_2-PbO-B_2O_3-Al_2O_3-CaO-Na_2O-K_2O glaze, interaction with aluminosilicate glass-ceramics 80−84398
SiO_2-PbO-K_2O glass, reflection spectra 78−88325
$(SiTe)_{1-x}(PbTe)_x$, solid soln., mag. susceptibility meas. *(Russian)* 80−70933
$(Sn_{1-x}Pb_x)_2P_2S_6$, solid solutions, ferroelectric soft mode freq., displacive transformations 80−29701
$Sn_{1-x}Pb_xSe(Te)$ films, Mossbauer effect of ^{119}Sn, spectral characts., conc. depend. 80−103903
$Sn_{1-x}Pb_xSe(Te)$ films, oxidation rel. to annealing temp. and time, Mossbauer spectra, X-ray and microstruct. obs. 80−104311
$Sn_{1-x}Pb_xSe(Te)$ thin films, resistance to oxidation, Mossbauer study 80−39986
$Sn_{1-x}Pb_2Te$, elec. and struct. props. of epitaxial layers *(Russian)* 78−64147
$Sn_{1-x}Pb_xTe$, epitaxial layers synthesis, cryst. struct. perfection and elec. characts. 79−87587
$Sn_{1-x}Pb_xTe$, film, production under quasi-equilibrium conditions 80−45241
$Sn_xPb_{1-x}Te$ mixed cryst., cryst. growth and assessment 78−80463
SnS-PbS, phase diag. 77−36476
SnTe-PbSe, semicond. film, growth, phase composition, condensation temp. rel. to cond. type 77−28266
SnTe-PbSe mixed system layers, struct. and props. *(Russian)* 77−28082
SnTe-PbTe solid solns., defects from susceptibility meas. 77−84737
$(SnTe)_{1-x}(PbSe)_x$ films on glass-ceramics, struct. and elec. props. 77−52251
$Sr_xPb_{1-x}(Zr_{0.545}Ti_{0.455})O_3$, piezoelec. resonator, preparation and props. *(Rumanian)* 80−28402
$Tb_{1-x}Sn_xTe$, ferroelectric transition calc., effect on carrier density 77−85673
Te-Ge-Pb, Te rich, structural phase transformation concurrent with glass crystallisation, thermal evidence 79−4965
Te-PbTe system eutectics, crystn. rate effect on electrophys. props. mutual solubility effect 80−60774
$Te_{80}Ge_{12.5}Pb_{7.5}$, phase-separated system, overlapping effects of glass transition and crystn., DSC results 78−83739
$Te_{80}Ge_{15}Pb_5$, DSC sensitivity to controlled ageing in glass transition region 80−71673
$Te_{80}Si_{20-x}Pb_x$ glasses, phase separation, double T_g presence 80−88306
thermogravimetric and X-ray phase investig., synthesis by solid-phase reactions 77−21067
Tl-Pb-S system, phase diagram quasibinary Tl_2S-PbS section obs. 80−55372
Tl-Pb-Se system, quasibinary sections 77−86000
$(TlBiS_2)_{1-x}$-(2PbS)$_x$ system, phase diagram 77−36471
TlI-PbF_2 graded-index film coating technique and results 80−33265
$(Tl_{0.75}Pb_{0.25})_4Cl_5$, cation disordered phase, X-ray diffr. determ. of cryst. struct. 80−1985
$Tl_2PbCu(NO_2)_6$, incommensurate Jahn-Teller phase transitions 79−65185
Tl_2Se-PbSe system, phase equilib. 79−52181
Tl_5Te_3-Tl_4SnTe_3-Tl_4PbTe_3, phase equilib., DTA, SPA and microhardness meas. 80−96628
V_2O_5-As_2O_3-PbO, semicond. glass, electronic props. 80−88557
V_2O_5-GeO_2-PbO glasses, memory and threshold switching 78−23142
$Y_{3-x}Bi_xFe_{5-y}Ga_yO_{12}$-PbO-$B_2O_3$-$Bi_2O_3$ system, crystn. fields 78−43996
Y_2O_3-Fe_2O_3-Ga_2O_3-PbO-P_2O_3, primary crystallisation regions 77−44222
Y_2O_3-Lu_2O_3-Eu_2O_3-CaO-GeO_2-Fe_2O_3-PbO-B_2O_3 system, garnet crystn. fields 78−43995
$ZnCl_2$-$PbCl_2$, molten, viscosity coeff. meas. *(Japanese)* 79−77662
ZnO-PbF_2-SiO_2 glass, shear wave velocity and its temp. depend. *(Japanese)* 78−30702
ZnO-PbO electroluminesc. phosphors, AC field excitation green and yellow emission 77−59617
ZnO-PbO-B_2O_3, exam. of glass formation and its props. 79−8283

leak detection
acoustic emission leak detection, attenuation of elastic waves in pipelines 78−27711
air jets, free and constrained, acoustic emission, gas leak detection conditions 80−5895
air tightness inspection by gas anal. method 78−41323
airtightness, total lack of, automatic system for measurement 79−52593
airtightness criterion and effectiveness of detection 79−52590
airtightness inspection, luminescence method, sensitivity, quality and reliability improvement 79−52589
airtightness inspection, standard conditions, flow through through-defects 79−50801

leak detection continued
airtightness inspection by hydrostatic method, correcting to standard conditions 79−91898
airtightness inspection using halogen leak detector, automation 79−52595
airtightness meas., interference resistance of manometer type equipment 79−52598
airtightness monitoring, classification of high performance equipment 80−104397
airtightness of joints, foam indicator for inspection 79−52594
airtightness testing equipment, optimum accuracy 79−52591
automatic, nondestructive, design, evaluation and implementation for IC assemblies 78−53180
calibrating test leaks 78−53121
cardiac pacemaker leak testing methods 78−57133
chromatographic method of calibrating leaks 80−77800
chromatography radioactive source leak testing under dynamic flow conditions 80−3432
coarse models of capillary leakages and test leaks 79−52587
cryogenic fluid tank, leak detection device 78−37016
device for checking airtightness by parameter changes in object and medium 80−104404
EBR-II, Na-water, leak detection system 78−78484
electron capture leak tester 79−52600
equations for converting to standard conditions 79−96268
FBR, N_2O-Na leak detection system 77−38374
FFTF containment building integrated leak-rate test 80−13680
fission reactor coolant containment tightness, integral leakage rate tests 78−89956
flaw detection during leak tests, mech. treatment effects 78−60956
Freon, leak detection by decomposition products 79−66235
gas leak detection principles and practice 78−81995
general charact. and problems 79−52588
halide pickups, optimal flow rate determ. 80−48825
halogen detector with jet probe 78−89490
halogen leak test *(Japanese)* 79−93153
halogens, reduction of background effects by means of chromatographic columns 78−70110
helium mass spectrometer leak detector, design and appl. to industrial leak detection 79−63247
hermetic sealing of film products, use of $_{86}Rn^{220}$ 78−48595
improved low pressure sensitivity 79−5112
inaccessible pipes, optimised procedure using radioactive tracers 79−34217
jet type noncontact probe for halide leak detector 77−87750
joint, welded, through defects, study using vacuum bubble method of airtightness inspection 79−52599
kerosene appl. for airtightness inspection 79−52579
LMFBR, chemical leak detection, effects of NaOH in Na 80−63326
LMFBR, liquid metal to gas leak detection system 77−38375
LMFBR, water leaks in secondary cooling circuit boilers 78−86572
LMFBR diagnosis, electrochemical and physical methods 79−97787
LMFBR steam generator, acoustic detection of small leak Na-water reaction 78−29589
LMFBR steam generator, small leak detection by surface oscillation meas. during Na-water reaction 77−67789
LMFBR steam generator, small-leak Na+water reaction, dissolution rate of hydrogen 78−29545
LMFBR steam generator leak, meas. of sound produced during steam injection into Na 79−93782
LMFBR steam generators, leak detection of steam or water into sodium 79−13434
LMFBR steam generators, leak detection of water into sodium, magnetic flowmeter bubble noise monitor 80−9000
LMFBR steam generators, reliability considerations 79−22437
LMFBR steam generators, safety alarm system, water leakage detection *(Czech)* 78−33268
LMFBR steam generators, water leakage detection systems, development 80−37546
LWR primary coolant leakage detection using acoustic monitoring system 80−700
manometric tightness control, increased reliability 79−79214
mass spectrometer, increasing sensitivity by selective gas accumulation 79−6215
mass spectrometer, meas. range extension 80−73375
mass spectrometric leak detection, automation of prep. operations 79−52597
microleak, by the mass spectrometry *(French)* 77−10131
nuclear plant, steam generator heated with liquid sodium, acoustic spectra meas. *(Czech)* 78−54849
nuclear reactor containments, in-service leakage tests 79−67895
nuclear reactor leak detection system operating experience 79−9808
pacemaker battery microcalorimetric testing 80−30933
piezoelectric transducers, ultrasonic, IC aux. ccts., appl. *(Italian)* 78−42508
pipeline inspection, welding flaw detect., NDT 78−19984
pipeline leak location by coaxial test cable characteristic impedance variation 77−57317
pipelines, current state of leak detect. *(Japanese)* 79−97370
pressure changes in interconnected chambers, mathematical model 80−108678
pressure vessels, acoustic equipment for leak detection during hydraulic tests *(French)* 80−789
pressure vessels of subassemblies in LMFBR, He leak testing 77−67791
PWR, due to pressure tubes cracking, Pickering power station experience 78−82472
PWR acoustic monitoring instrumentation 78−17309
PWR acoustic monitoring instrumentation 79−89488
PWR steam generators, remote controlled TV for detection of leaking tubes *(French)* 80−791
remote leak detection for Tokamak Fusion Test Reactor 78−50403
renal dialysis membrane leak detector 77−60294
search gas testing methods, He leak detectors with mass spectrometer anal. *(German)* 80−101802
slit and crack type leaks, calc. model and results of its use 80−35490
space chamber, tracer slug leak detection 79−80627
sparking detector, using semiconductor switching diodes 80−31774
telescope for mol. flow direction detect. in large vacuum chamber 77−49735
thin film semiconductor O_2 sensor 79−52596
tightness control by IR gas method 79−66236
leak detection continued
tightness inspection, sensitivity determ. using holographic interferometry 79−36862
trapless, counter-flow mass spectrometer leak detector 79−63248
trapless, use of reversed diffusion pump 77−2662
ultrasensitive, in vacuum devices 80−47065
ultrasonic leak detector 79−39090
US, threshold sensitivity eval. criteria 80−104401
US leak detection for piping systems in reactor environment 77−61528
vacuum leak detection using liquid spray 80−234
vacuum technology, medium, high and ultrahigh, conf., Oxford, England (Apr. 1978) 79−63242
vacuum tightness monitoring in components with unclosed cavities, automatic mass spectrometer 79−52592
vacuum vessel, large, leak detection 78−74012
virtual leak, influence on pressure in high and ultrahigh vacuum systems 79−97398
water leak detector for water cooled electron microscope 78−21277
West German LWR primary system online surveillance 79−3217
D_2O, on-line infrared analyzers, CANDU report 78−82038
H_2 meter, diffusion type, Na coolant loop, LMFBR 80−68728
He leak detection in large cryogenic vessels 78−93694
He leak detector, with RF excited ion source *(Rumanian)* 80−8999
He mass spectrometer for leak detection *(French)* 77−37901
He mass spectrometer leak detection, review 77−67447
He, mass spectrometer leak detectors, probe with He-permeable membrane 80−98994
Na ionisation detector, aerosol effects on charact. 79−49243
^{133}Xe charcoal traps, simple leak tests, nuclear medicine appl. 80−104734

leakage, electrical *see electrical faults*

leakage, magnetic *see magnetic leakage*

leakage currents
bipolar cell stacks, simulation program 80−76526
CMOS ICs electrically active stacking faults, anomalous leakage currents 79−78191
electro-medical equipment, due to mains transformers, safety measures *(German)* 78−3625
electro-medical measuring equipment, protective measures *(German)* 78−3629
electromedical equipment, safety by monitoring leakage currents *(German)* 80−81749
hybrid p-i-n photodiode-FET preamplifier design for digital optical receivers *(German)* 78−33878
leakage flux calc., use of integral transforms with non-standard kernals, teaching appl. 80−31466
medical equipment safety aspects 78−11748
MHD, compensated, two channel conduction MHD pump with leakage current, obs. *(Russian)* 78−75228
MIS and MIM structures, leakage currents and conduction channels on splits 79−42664
p-n junctions, thermally assisted field emission near precipitates 78−14809
pacemaker interference, 60 Hz field and current effects 78−88769
pacemaker intermittent runaway malfunction 77−81712
satellite geomagnetic substorm charging simulation 79−96886
Si poly-oxide leakage current and conductivity reduction expts. 77−76990
thermocouples, sheathed, electrical shunting and leakage errors, model 78−4618
GaAs, with anodic oxides, leakage currents 79−38169
$GaAs_{1-x}P_x$, thermal oxide, dielec. leakage current and C-V hysteresis effects, effect of annealing 79−61772
InGaAsP avalanche photodiodes, leakage current, shot noise, quantum efficiency, gain saturation 79−67381
InGaAsP:Be, avalanche photodetectors annealing temp. effect on photolum. spectra 79−69872
Si, n^+-p junction, surface peripheral leakage currents 78−26939
SiO_2, stacked-struct. improved quality by laser annealing of Si 80−65386
ZnO resin layer leakage current in corona charging *(Japanese)* 78−24877

learning systems
see also adaptive systems; cognitive systems; self-adjusting systems
adaptive classifier *(Russian)* 77−40659
adaptive neuronlike layer net as a control learning system 79−74631
biological, sequential actions model 78−44441
biological net, effects of noise on learning velocity 79−74636
chemical dynamics applics. 77−32768
computer learning prediction systems appl. 80−108048
continuous speech recognition system for data base consultation 80−91990
fine muscular control rehabilitation using ramp threshold feedback 79−83996
large network models using the brain organisation simulation system 79−8496
McCollough effect, synaptic modification associative learning model 77−21531
neuron model as universal element for pattern recognition 77−44621
solar collectors, design and data rate requirements of computer-based sun following system 79−83573
temporal sequence memory design based on dentate gyrus anatomy 77−21508
weather forecasting, adaptive learning network approach 78−40643

least squares approximations
2γ positron annihilation radiation, polycrystalline metals, least squares fitting of angular correl. curves *(German)* 77−90214
Abel's integral eqn., least squares finite element method appl. 79−25830
Abel integral function, numerical inversion using least-squares splines 78−16753
acridine orange dye soln., dimerisation equilib., absorpt. spectra least squares anal. 79−50007
activation analysis, low-energy photon spectra, nonlinear least-squares fitting program 79−1987
aeromagnetic data, diurnal drift removal by least squares 79−53529
air pollution monitoring by pulsed lasers, numerical filters *(Japanese)* 79−43801
airborne radiometric data inversion, radioactive elements conc. mapping 78−77347
algorithm for Nth-order polynomial least-squares fits 78−24655

least squares approximations continued
alkenes, IR absorpt. curves calc. using standard fragments computer library 80−982
aquifer mineralisation field dynamics simulation, porosity estimate optimisation 77−56664
array algebra appls. 79−44702
array algebra for multilinear least squares prediction and filtering 78−69470
array algebra techniques in multilinear least squares problems 78−36296
astrometric plate reduction, least squares prediction appl. 79−40082
astronomical data reduction methods, least-squares polynomial fitting technique 80−12682
astronomy, generalisation of method of least squares 80−62028
astronomy, least-squares adjustment with probabilistic constraints 78−32352
astronomy, orbital elements, nonlinear least squares minimisation 77−33761
atmosphere, friction vel. and temp. scale from temp. and wind vel. profiles 78−81268
atmospheric particulates collected on filters, X-ray fluoresc. anal., least-squares method appl. 77−60168
atmospheric Rn daughter estimation 78−7728
atmospheric surface layer temperature extremes, probability determ. method 78−45020
atom, rel. oscillator strengths determ. by combined absorption/emission meas., Ti appl. 80−37784
atoms, $5f^N$ and $5f^N7s$ config., parametric study 80−91444
binary star orbits solution, Fourier transform method 80−26899
blood pressure automated control in dogs using microprocessor 80−81797
Bonner sphere spectrometer, least-squares technique for extracting neutron spectra 78−33366
boundary-value problems in applied mechanics, collocation least square method 77−74225
caesium hydrogen tartrate, anomalous dispersion of Cs, refined struct. from modified least squares program 78−51522
calculator program yielding confidence limits for least squares regression analysis 77−29060
calibration curve parameters for X-ray fluorescence analyzers, error estimates 79−87931
chemical analysis, multicomponent analysis computations based on Kalman filtering 80−40772
chemical data, reduction of contradictions, OH stretching frequencies in saturated alcohols 79−53966
clonal survival curves with cellular recovery, parameter fitting 77−56352
collocation method, appl. to boundary-value problems in applied mechanics 77−68434
complex dielec. and mag. props., modified von Hippel least square fit determ. 78−21179
conservation equation, numerical soln. by variational approach, mass transfer problem appl. *(French)* 80−19317
convergence of standard and damped least squares methods, Newton Raphson algorithm 77−9878
crystal atomic structure refinement, least squares programs 78−26375
crystal structure least squares refinement technique based on fast Fourier transform algorithm 78−91197
crystallographic refinement, modified least-squares formalisms for overcoming the free-atom bias 78−71632
crystallography, electron distributions, aspherical-at. least squares refinements combined with Fourier methods 78−71633
crystallography, method for optimizing relative weights 78−9909
crystallography, rigid-body least-squares molecular fit routine 77−31546
crystallography, X-ray neutron, charge deformation, vibr. smearing 78−71634
cubic bell spline sum function in least squares sense 79−12583
curve fitting by least squares criterion, with reference to exponentials and Arrhenius plots 79−17200
damped, optical system parameters optimisation *(German)* 77−68255
damped and constrained least squares method with application to gravity interpretation 79−66830
data evaluation using lognormal distribs. in least squares algorithm 79−93902
deconvolution of spectra by least-squares fitting 78−64897
diffusion equation, least-squares anal. of thick-film soln. 79−33107
Dirichlet stochastic problem *(French)* 78−89406
discrete time series spectral estimation novel aspects 77−91336
disturbed measuring systems, estimation of signal parameters, autoregressive linear models *(German)* 80−68165
dosimeter-based adjustments of fast-neutron spectra 79−54611
droplet size distribution, least squares method for fitting exptl. data 77−39329
Earth's figure and gravit. field determ., least-squares collocation method 79−48392
Earth tides, anal. of obs. *(French)* 77−87078
ECG, optimisation procedure for fixing locations of multiple dipole heart generators 77−44809
education, examination mark adjustment 79−80402
education, least squares fit, uncertainty calc. 78−86068
effective hamiltonian matrix parameter optimisation, least squares method 79−26874
elastic quadrilateral plates 79−46201
electron density mapping in mols., cyrsts., conf., Rehovot, Israel, (Apr. 1977) 78−71622
electron scattering by simple Yukawa and static pots., S-wave phase shifts 80−106374
electron-density matrix extraction from X-ray diffraction data 77−65930
elementary particle weak hadronic decays, transition amplitude determ. using least-squares anal., review 79−58956
elliptic orbit determ. by applying least squares method to observation residues *(French)* 78−40799
elliptical contact deform. between elastic solids, simplified soln. 78−55616
EM fields, approx. method for numerical studies of boundary-value problems 80−5658
equations of state, search procedure, based on step-wise least-squares technique 80−19900
equivalence relation in planar least squares inverse approximation 79−30208
ethane($-d_6$,d_3,d_1), electro-optical parameters from IR intensities, least-squares calc. 80−9584
event location by recursive least squares prediction 80−96131

least squares approximations continued
exponential clipped photon autocorrel. spectra, data anal. 79−2837
flow, Ritz-Galerkin and least squares finite element methods 79−1150
FM pressure transducer resonant diaphragm pressure-freq. characts. derivation 78−41295
force const. adjuster program for least squares fit to observed frequencies of molecules and crystals 78−91395
formaldehyde, force field calcs., damped least-squares method 80−91533
formyl fluoride ($-d_1$), IR absorption intensity anal. 78−70813
FORTRAN program, lateral absorbed dose distrib. for 25 MeV electrons appl. *(Japanese)* 78−74505
Fourier transform systems, discrete-time windows, optimum low-order 77−5631
Fredholm integral equation, free-knot spline inversion using nonlinear least squares method 79−2486
fusion regime data adjustment experience and trends 79−9881
gamma-ray peak areas observed with Ge(Li) detectors, least squares spectrum fitting method 79−85854
gamma-ray peak fitting with very low statistics 78−74529
gamma-ray spectra, environmental, eval. of standard library spectra for use in least-squares resoln. 79−9915
gamma-ray spectra, environmental, least squares method for computing nuclide conc. 79−9914
gamma-ray spectra, linear least-squares peak search algorithm 79−754
gamma-ray spectra automatic anal., using nonlinear least squares fitting 77−23362
gas (mixture), compressibility, virial coeffs., Burnett data reduction, fast least-squares method 78−47082
gas sample, spectrochem. analysis in IR, nonlinear method 78−15738
Gauss-Helmert model, singular covariances, least-squares adjustments *(German)* 80−56340
Gaussian plume model parameters determ. from diffusion-convection eqn. integration 78−81399
geodesy, foundations of least squares collocations method *(German)* 77−86748
geodesy, parameter accuracy improvement by choice and quality of obs. 79−44078
geodesy, props. of Gauss-Helmert least-squares adjustment model *(German)* 78−61309
geodesy, satellite orbital elements and station coords. determ. by least-squares collocation *(Russian)* 78−49296
geodesy, strict determ. of adjusted straight line via least squares method *(German)* 77−86751
geodesy least squares adjustment and collocation 77−90984
geodetic anomalous potential approx., choice of norm using least squares collocation 77−90985
geomagnetic lunar harmonic analysis 80−51327
geophysical time series alignment, new statistical approach using least-squares cubic splines 79−92623
global covariance function, nonhomogeneity, least squares collocation 78−3699
gravity anomaly estimation, least squares collocation 77−90983
gravity anomaly inverse problem, least-squares soln. 80−98214
gravity data handling using collocation and least squares methods 79−29870
guanidinium aluminium sulphate hexahydrate:Cr^{3+}, EPR, 295.5, 78.45, 1.61K, zero field splitting 78−68359
haemoglobin, deoxygenated, electronic term scheme using mag. susceptibility and Mossbauer data 77−44586
heat process thermal diffusivity estimation method 77−3713
hologram interferometry, sensitivity vector determ., two known object rots. 80−95840
homonuclear coupled spin system, inversion-recovery data anal. 79−33554
hot spot distribution, significance interpretation of laser produced plasma expts. 79−98945
hydrology, least squares method for statistical tolerance limit computing 78−49179
hydrometeorological process harmonic components, separation by least squares *(Russian)* 77−78246
image restoration, constrained least squares, improved computational scheme 78−82915
image restoration, least squares method 80−37961
image restoration and synthesis, Japanese activities 77−58273
image restoration by least squares method, appl. to speckle interferometric data 79−25514
impact toughness text results, cold brittleness crit. temps. determ. 80−100980
incompressible fluid flow past flat plate 77−13615
infinite elliptical cylindrical radiators array with mixed boundary conditions, sound field 78−1538
interactive curve-fitting program, for science students 77−60913
interferogram aberration evaluation program 80−13130
inverse gravity problem, unified least-squares method 77−73872
inverse scatt., Newton's method modification at fixed energy 80−73207
ionosphere incoherent scatter data, analytic partial derivatives for least-squares fitting 78−73581
ionospheric data processing, improvement of convergence of least squares method *(Russian)* 78−85700
IR spectral lines, intensities and half widths, nonlinear least squares calcs. 77−52682
joint instantaneous centre of rotation, least square analysis 79−29555
kinoform synthesis by Fresnel transform evaluation, least squared error method *(Russian)* 79−22913
Kolmogorov-Wiener least-squares filters appl. to geophys. anomalies separation 78−61580
laminar heat transfer in noncircular ducts, Schwarz-Neumann technique 77−80161
Landsat MSS points, coordinates linear lesat squares transforms for location on maps 79−2389
lattice parameter program, least squares method 79−64958
lens design, least squares fitting of Zernike's polynomials to wave aberration function 80−83660
limit of applicability, modification for large errors in independent variable 80−73301
linear least squares interpolation, numerical aspects *(German)* 77−9322
linear least squares parameters, stat. significance, student guide 80−17770
linear prediction in least-squares scheme, algorithms 80−98464
linear prediction in least-squares scheme for max. entropy spectra, Fortran subroutines 80−98465

least squares approximations continued
linear regression, least-squares eqns. derivation, appl. to g determ., for teaching 78−45450
linked-atom least-squares reciprocal-space refinement system, LALS, incorporating stereochemical restraints 78−26377
local image restoration by a least-squares method 80−14289
low-count radiation spectra, LSF processing 78−50448
macromolecular structures, struct. factor least squares refinement procedure 77−84573
mass standards, calibration by sets of weights intercomparison 78−54342
medical computing, compartmental models short parameter-fitting routine 77−82378
meteorological appls. of nonlinear least squares 78−16182
meteors, real luminosity function determ. from apparent luminosity function, least squares method 79−80231
methane, Raman intensity from electro-optical parameters, least squares refinement 79−36645
methane($-d_1,d_2,d_3$), electro-optical parameters from IR intensities, least-squares calc. 80−9584
methane ($-d_1,d_2,d_3,d_4$) Raman electro-optical parameters, overlay least squares calcs. 78−42105
minimal Gaussian basis set, for at. and mol. calcs. 80−47874
minor planets observations, least squares soln. of ill-conditioned systems 80−26747
molecular force field calcs., damped least-squares method 80−91533
molecular scattering wavefunctions, algebraic approx. 78−78780
molecular spectra, mol. consts., merging results of separate least-squares fits 78−5195
molecular spectra analysis, eval. of peak volume, position and width, computer program 80−18890
molecular valence force consts., computer program, least squares procedure 78−58656
multicomponent fluorescent mixtures, quantitative anal. of data 78−27833
multicomponent spectra, numerical anal., least squares, optimisation methods 77−56264
multiparameter discounted least squares, extrapolation 77−17792
multiple input/output data, system identification 77−37750
multivariate random vibration systems, synthesis, autoregressive-moving average model 77−84060
Navier-Stokes equations, integration, book contrib. 79−32444
Navier-Stokes equations, object in flow, H^{-1} least squares method 79−1143
neutron activation anal., gamma spectra least squares deconvolution on minicomputer, NAALSQ program 79−11853
new methods of least squares *(Japanese)* 77−64938
NMR, Voigt profile analysis, Fourier transform approach and least-squares curve fitting 77−20729
NMR bandshape, complex exchange-broadened, iterative computer anal. 79−35805
NMR fast inversion-recovery spin-lattice relax. time meas., systematic errors elimination 79−30516
NMR T_1 computation, from pulsed data, least-squares formula 78−24837
nonlinear fluid dynamic problems, least squares and finite element method soln. 79−49054
nonlinear partial differential eqn. soln. by discrete least squares 78−45474
nuclear liquid drop energy, shell correction determ. 78−12992
nuclear measurements, errors of parameters in least squares fitting procedure 78−16768
nuclear optical model parameter searches, minimisation procedures, use of derivatives 77−10379
nuclear Overhauser effect factors determ. using dynamic Overhauser enhancement with least square procedure 79−4746
nuclear scatt., least squares fitting with normalisation parameters 79−45221
objective functions, constrained minimization technique CONGAU 79−30212
optical rib waveguide with trapezoidal cross section, numerical analysis 80−96009
optimized conjugate gradient solution for least-squares equations 78−79495
overlapping spectral bands resolution 79−41198
parabolic problem exact control finite element collocation method 77−26156
partial differential eqns. of mixed type, indefinite problems 78−36807
particles in cylindrically symmetric mag. fields, least squares track fitting method 78−58896
Patterson function, three-phase invariants derivation method 79−27868
phase diagrams, optimization by least squares method 79−10915
phase diagrams optimisation by least squares method using simultaneously different types of data 78−6143
photogrammetry, least squares prediction by multiquadric and covariance functions 77−78464
photographic film response to 25 MV X-rays, sensitometric curves, relative dosimetry 80−52376
photographic zenith tube plates, new reduction method 78−73656
PIXE anal. with REX computer program 77−52714
PIXE spectra, computer code trace 77−52713
plasma diagnostics, spectral line profile calc. 79−23458
plate, thick infinite, transversely isotropic, containing circ. hole, end effects 79−27510
plate-cylinder intersection, elastic, three-dimensional anal. by boundary-point-least-squares technique 77−58558
pocket calculator program with variable precision for least square fitting of data 80−67976
polyatomic molecule vibrations, numerical soln. of nonharmonic pot. problem 77−34607
polymer lightguide attenuation coeffs. meas., data anal., accuracy 79−1005
polynomial analysis appl. to topside ionograms 77−78476
polynomials, smoothing, averaging method 80−31
polystyrene solns., correlations of network model parameters 80−106772
polystyrene solutions, light scatt., mol. parameters, computer anal. assessment 79−1766
positron lifetime spectra, anal. using DBLCON version of POSITRONFIT with nonGaussian prompt 78−33359
powder, triaxial test procedure and num. calc. method for flow props. 77−60028
powder least-squares program, POWLS 80−1892
least squares approximations continued
power curve regression equations for Ohio River, statistical computer program 78−61472
protein crystallography, min.-variance Fourier coeffs. from isomorphous replacement method 77−52938
pseudo nonlinear regression 77−64933
quartet invariants in space group P1, least-squares analysis 77−84570
quartz, irradiated, fused, crystalline, absorpt. spectra, colour centres 80−7384
quasibound state energy calc. 78−41191
radio meteor wind data, anal. using finite element approximation 78−81475
radiograph feature extraction via least squares fit to model 77−14229
radiotherapy backscatter factors for X- and γ-rays, polynomial and power law 77−2056
radiotherapy cervical intracavitary applicators, computer program for optimisation of source loading 77−13005
remanence direction from converging remag. circles 77−45182
resonance analysis of neutron transmission data, least square fitting program REFIT 80−22840
respiratory parameter interval estimation 79−48277
respiratory system, human, modelling and parameter estimation 80−12169
respiratory system, human, modelling and parameter identification 79−39444
restricted three-body problem, surface fitting of three-dimens. closed solns. 79−8800
rocks magnetic components separation, least squares methods appl. to step demagnetisation data 79−16444
rotated hamiltonians, complex-coordinate rotation and least-squares variational method 80−68075
roto-translations, method of conditioned observations 78−12531
rounding errors, least-squares parameters 78−158
Rowland circle, corrected, least-squares method derivation 80−64161
satellite-to-satellite statistical orbit determ. error analysis 78−65486
Savitsky-Golay convolution method, for least-squares fit smoothing and differentiation 79−16059
seismic data filtering and smoothing, least-squared error, stationary and nonstationary 80−4158
seismic fan shooting and least-squares analysis of non-layered anomalous vel. zones. 79−57857
seismic signal interference separation using least squares method *(Russian)* 78−15969
seismic spectra, least-squares inverse filtering and wavelet deconvolution 78−61339
seismic surface wave data inversion in source mechanism studies 77−33204
seismic traveltime data nonlinear least-squares inversion 80−4124
smoke/dust cloud temporal analysis algorithm 80−98484
source velocity meas. errors, effect on spectral parameters 79−24244
space groups, triclinic, cryst. struct. refinement by least squares 78−75607
speckle imaging phase estimation, FFT-based algorithm 79−76605
spectra, deconvolution and background subtraction by least-squares fitting with prefiltering 78−31718
spectrometer magnets, field parametrisation 79−880
spherical dome, three-dimens. elasticity soln. and edge effects 78−59306
spin-Hamiltonian parameter from EPR, data by least-squares fitting 77 1585
stagnation point flow, least square finite element soln. 77−14981
standard spectrometric source conversion peak half-width determ. 77−79499
stationary nonlinear thermal conductivity problem, least squares approach *(Russian)* 78−38172
stepwise merging of least-squares parameters 78−89319
surface area calc. by gas adsorption, progammable calculator appl. 78−15706
surveying, collocation with help of Gaussian algorithm *(German)* 79−79730
44 Tauri, δ Scuti star, periods, least-squares determ. 79−62850
tectonic plate reconstruction method, Pacific-Nazca plate evolution appl. 78−81130
TEM micrograph image restoration, of weak-phase object using computer *(Japanese)* 79−71571
thermal expansion, characterisation in minerals 79−70795
thick film diffusion experiment, introduction of weights to least squares anal. 80−49399
transient heat conduction, residual method with Lagrange multipliers 78−90630
trigonometric parallaxes, external error estimation 77−67087
turbulent boundary layer characterisation by velocity and temperature profiles *(Russian)* 78−34115
unsteady gas dynamics, least squares finite element approach 78−26134
ventilation, human, twin exponential model fitting process development 79−48284
Voigt functions, nonlinear least square algorithm 80−90900
wave front errors of minimum norm 80−48137
wavefront distortion estimate, least-square fitting to phase difference meas. 77−46689
wavefront estimation from wavefront slope meas., least-squares curve fitting model 80−106467
weighted residuals, improved finite element formulation by using least squares fit 79−52
Wiener-Hopf method for resistivity sounding filter determ. 79−92621
X-ray data, weighted method for evaluation of small angle data without desmearing 78−42851
X-ray fluoresc. anal., energy dispersive, least squares, Monte Carlo methods, mathematical anal. techniques 78−85243
X-ray fluorescence anal., energy-dispersive, appl. of mathematical techniques 79−11837
X-ray fluorescence spectra, detector response function approach 80−11989
X-ray fluorescence spectra, nonlinear least squares anal. 77−48731
X-ray line shape broadening anal., least squares method 80−63588
X-ray spectra, nonlinear least squares anal. of full-energy peaks 77−88328
2-zinc insulin, rhombohedral, cryst. struct. refinement, experience with fast Fourier least squares 78−92595
α-AlB_{12}, cryst. struct. and refinement 77−15376
BH_3CO, vibrational spectra in Ne matrices, pot. consts., bond strengths 79−45696

least squares approximations continued
BrF, $B^3\Pi(0^+) \leftarrow X^1\Sigma^+$ absorption spectrum, high-resolution anal. 79−59478
CN free radical, $A^2\Pi$-$X^2\Sigma^+$ Red system, perturbation analysis 80−87247
CO_2, dipole moment functions 80−87094
CS_2, solid, tailoring of potentials, in lattice dynamics 78−79679
Cu IV, wavelength region 700-1200 Å, extended analysis 80−99473
^{57}Fe Mossbauer spectroscopy, added precision 77−88327
Ge, resistance thermometer, low temp., approx. of calibration curve 78−45620
Ge resistance thermometry, interpolation method 80−22357
H, electron/positron elastic scatt., least squares calcs. 79−3572
N_2O, dipole moment functions 80−87094
NaCl 46 cm window optical evaluation facility 80−74526
OsO_3F_2, normal coordinate anal. in Urey-Bradley force field 79−49966
$S^{16}O_2(S^{18}O_2)$, $^1B_2$('A') state, force field for large amplitude motions 80−43023
U compounds, reduced partition function ratio calculation 77−12819
^{235}U(n,f), thermal fission, fission product decay heat evaluation by least-squares method 79−30865

leather *see materials*

Lecher wires *see high-frequency transmission lines*

Lee model
3V-particle model 78−24919
Callan-Symanzik functions and asymptotic freedom 80−73659
decay parameter calcs. for Lee-like models 77−30026
dual bootstrap models, solns. satisfying Lee-Veneziano relation 79−71729
heavy ion two nucleon transfer reactions, exact four body model 77−10426
interference terms, phases, 1/N expansion, Lee-Veneziano model 77−18247
local Galilean invariant version with renormalised interaction Hamiltonian 77−26465
low equation, solns. in no-crossing approx. 80−32012
magnetic moment calculation using Schwinger source theory 80−42350
parafield current algebra, Lagrangian quantum field theory *(Russian)* 77−13891
particle decay, measured lifetime depend. on measuring apparatus 79−22158
relativistic model in S(1,1) sector 79−71590
resonance decay interaction of three wave packets 77−67581
sequential decay processes, quantum theory 79−25896
SLAC bag method, skin- and δ-confinement *(Chinese)* 79−80757
tachyon, field model, Lee-like *(Korean)* 78−50058
V-V sector 78−24967
(π,π), scattering theory testing using Lee model 80−78325

LEED *see low energy electron diffraction*

legal protection of software *see industrial property*

legal research (computing applications) *see social and behavioural sciences computing*

legislation
air pollution, 1977 Clean Air Act amendments and industrial expansion 79−79426
air pollution meteorology, rel to 1976 USA Clean Air Act amendments 78−11989
air/water pollution detection and law enforcement 77−91263
airborne contaminants monitoring in chem. labs., USA regulations 80−12869
atomic energy, changes in West Germany *(German)* 77−71703
automotive noise legislation 79−34465
British Government transport policy criticised 78−55512
British trade weights and measures activities 80−27267
building sound insulation against aircraft noise, German federal regulation 79−90083
direct reading pen dosimeters, radiation exposure measurements, West German law, aspects *(German)* 78−5050
dynamic measurements of liquid quantities, international harmonisation 79−68840
environmental noise, study re. nuclear power plant construction 78−87194
flow measurement, using electronic equipment, legal aspects 79−68841
Health and Safety at Work Act, rel. to X-ray window shutter and collimator coupling 77−39505
industrial noise legal situation 80−12042
international metrological cooperation, legal aspects 78−89422
medical devices, safety and efficacy 77−2062
medical measurements, law *(Croatian)* 80−104797
metrological collaboration among COMECON member countries, legal foundation 78−4582
municipal noise control program development 79−74577
New York City, environmental noise codes 78−59202
noise abatement, construction and demolition sites 78−87197
noise and vibration problems 80−10084
noise consultant's position in noise abatement 80−10083
nuclear energy policies, book 77−6476
nuclear fuel accounting and rate making, regulatory issues 78−13242
nuclear fuel accounting practices at Duke Power Company 78−13244
nuclear fuel storage facility, German Government responsibility *(German)* 78−86701
nuclear generating station, waste disposal and licensing *(German)* 80−99222
nuclear material transportation, ORNL Nuclear Legislative Data Base program 80−37539
nuclear power conf., Chicago, United States, July 1979 80−794
nuclear power facility, siting, USA state laws for regulation 77−3187
nuclear power plant licensing procedures in the UK 80−27708
nuclear power plant safety, West German policy *(German)* 80−57865
nuclear power public opposition, history and effects *(German)* 80−23181
nuclear power stations, licensing procedure, public participation under Atomic Energy Act *(German)* 80−102256
nuclear reactor safety, Czechoslovak practices *(Slovak)* 80−13632
nuclear spent fuel shipping cask licensing 80−37545
Oceans 1976 conference, Washington (Sept 1976) 77−5241
offshore environmental and platform data processing from Norwegian continental shelf 79−12273
pollution problems from fertilizer manufacture 79−34450
quality control and safety, nuclear technology, basis of West German practice *(German)* 77−75004
radiation measurement system and federal regulatory agency, US 77−37713
radiation measurement system and state responsibility, US 77−37714
radiation protection European regulation in EEC countries *(French)* 79−48347
radiation protection in West Germany, standards aspects *(German)* 78−5049
radiation protection of workers, against RF fields below 300 MC/s 80−56223
radioactive waste depository in West Germany, advance payment from users, legal aspects *(German)* 79−71903
radionuclide users in Israel, surveillance and accident prevention 78−57077
radioprotection, medical regulations and standards in France *(French)* 78−48897
Safe Drinking Water Act, microbiology, QC for the Water Supply Lab., USA 79−74558
safety in nuclear power stations, statutory requirements 77−79485
safety strategy and principles in nuclear power station practice, aspects *(German)* 78−37410
solar access perspectives 79−87979
spent fuel storage and disposal and plant building and operating legislature *(German)* 80−99223
Swiss energy situation and nuclear development *(French)* 79−89491
United States Earthquake Hazards Reduction Act 79−48415
US equipment, review of BRH, FCC, CPSC, FDA and OSHA regulations 77−57311
USA, 1977 state noise restrictions 78−59203
USA, environmental noise control programs 78−59201
USA developments of energy and minerals, by means of technological innovations, federal regulations influence 80−16763
USA Quiet Communities Act (1978), implementation by Environmental Protection Agency 80−72113
vibration regulation *(Japanese)* 77−80007
waste management, legal aspects 77−88229
weather modification, international liability 79−5617
weather modification, national policy 79−20938
weights and measures, conference, Washington (1978) 80−27260
West German LWR power plant stack monitoring, legal and technical aspects 78−89988
West German nuclear fuel element factory licensing legislation *(German)* 79−89469
West German nuclear plant airborne radioactive effluent monitoring 78−89990
U mill radiological effluent and environmental monitoring guidelines 78−94153

length measurement
see also micrometry
automatic interference comparator method, interference refractometer *(German)* 78−77966
automatic optical length meas., defocusing effects *(Japanese)* 80−68174
bubbles, measurements using RF probe 80−6177
cable length, vel. and tension meas, using DBS-2 remote counting block 79−12314
capacitive transducer method, precision, procedure and instruments *(German)* 79−26024
cardiac muscle isolated preparation, determ. of segment length by mag. induction 77−48982
centre-distance meter, gear testing 80−62632
ceramic base length comparator *(Hungarian)* 79−80570
coherent-optical method, development and appl. *(German)* 77−27297
crack length meas., inductive and videoelectronic methods *(German)* 77−63866
digital instrument based on meas. of freq. differences between two quartz oscillators 79−93097
digital micrometer development and appl. 78−65902
distance between hole centres, instrum. 80−57258
end gauges, fused silica and pyroceramic, high-precision stability 79−76778
end-standards and ruled scales using laser sources *(German)* 80−86251
ends standards of length for calibration, alignment using autocollimator 79−54094
error elimination methods, optical *(German)* 78−70094
extension-nozzle ejector-transducer design 77−57313
eye axial length, using controlled weight direct contact US ophthalmological transducer 78−20239
Fabry-Perot interferometer length stabilisation using He-Ne laser radiation 77−79141
feedback monitoring, normal conditions for linear and angular measurements 79−75492
fibre optic strain gauge, arbitrarily shaped path length meas. 78−70112
fibre optical interferometers for length, temp., pressure and force meas. 80−98971
finger length meas. by ferroelectric wedge thermal transducer 77−78001
gauge block, interferometric meas. with 3.39 μm He-Ne laser 79−97346
gauge blocks, by interferometry, sources of uncertainty 79−26029
gauge blocks, errors associated with checking by interferometric methods 80−105613
gauges, microscopes with IZV-21 and IZV-23 meas. heads (USSR) 80−57257
holographic interferometry appl. *(Rumanian)* 78−49796
holographic length comparator using phase heterodynage, appl. to gauge blocks 78−58953
HTGR fuel rod length meas. and control microcomputer system 79−71942
human step length measurement apparatus 80−67271
IC photomask and wafer linewidth meas. using optical spatial coherence 80−77850
impressions in alloys, portable microscope for parameter meas. with 1 μ accuracy 77−53856
interferometer comparator error compensation 78−4587
interferometer length meas. by tunable laser 79−35817
interferometric length measurement with curved wavefronts *(German)* 80−77752
interferometric meas., secondary calibration standards *(Rumanian)* 79−40533
interferometry, heterodyne, principles and appls. *(German)* 80−68181

length measurement continued
interferometry using Ar^+ laser, wavelength stabilisation 78−33766
international standards compared *(German)* 80−36977
IR laser interferometer, length measuring, alignment using laser feedback 80−37075
laser interferometer appl., built-in system for machine tools *(German)* 80−9022
laser interferometer appl. error factors *(Japanese)* 78−8384
laser interferometer application to length meas. in production *(German)* 80−18007
laser interferometric auto-correcting system of high precision thread grinder 80−90830
laser interferometric technique, problems with environmental influences *(German)* 79−30411
laser interferometry 77−694
laser interferometry measurement system 79−6171
laser Michelson interferometer length meas. error rel. to illuminating beam form 77−26267
lasers in metrology and testing, review 77−5817
light interferometry using fractional fringes 77−71291
line standard meas. using He-Ne laser photoelectric microscope 77−82599
line standards 77−53855
linear and angular dimensions, classification and symbols for means of meas. 79−6081
linear dimension meas. means choice in terms of error levels 79−6082
linear gauge calibration measurements, automatic interference comparator appl. *(German)* 78−77847
long distance reference length, laser interferometer meas. 79−75497
long slip gauge calibration, Fabry-Perot etalon *(German)* 78−77849
manufactured part rejection validity, influence of random meas. errors 77−17947
metals and alloys, thermophysical charact., peculiarities of temp. depend., dimensional change meas. *(Russian)* 78−95868
metre, Canadian standard 79−12768
metre, new definition proposal using 88 THz stabilized He-Ne laser 80−73304
metre as standard length unit *(German)* 77−22528
microcomputer based laser interferometer for instrument graduation *(Polish)* 80−90816
ocean wave imaging and wavelength meas. by aerial photography 80−46323
optical instruments for linear dimensions meas. 80−13118
optical interferometry, wavelength stabilisation *(German)* 80−57250
optical techniques, interferometry, precision *(German)* 78−89434
paediatric radioluscent bone length meas. 78−48891
phase modulation interferometry, appls. to dimensional metrology 79−6174
photoelectric laser meas. equipment, semi-automatic 78−36966
piezoelectric material length changes laser interferometry appl., for sub-nano-meter range *(Slovak)* 78−77861
pneumatic facilities for linear dimension meas., parameter selection 78−73964
pneumatic linear dimension testing device, output pressure converted to frequency signal 80−62631
rolling mill product speed and length meas. by laser velocimeter *(German)* 79−72614
ruled steel grating system 80−13039
scale-measuring laser interferometer 77−5804
SEM linewidth meas. artifact fabrication and calibration 78−41375
small linear dimension meas., contactless laser beam diffraction method 77−22525
standard meas. procedures of GDR Bureau of Standards *(German)* 80−57246
standards, by holographic interferometry with phase heterodynage 79−6095
standards, plane-parallel gauges and spheres comparison *(Rumanian)* 78−21098
standards, temperature meas. using thermocouples and Pt resistance thermometer *(Slovak)* 78−77907
standards, time, freq. and physical measurement, unified standard 79−26038
standards 80−194
standards of time and length 77−13734
statistical observation results, uniform, conditions for obtaining 80−4688
steel gauge blocks, linear coeff. of thermal expansion *(German)* 80−68171
teaching, simple parallax expt. 78−24615
thin wires, length changes using high-temp. dilatometer 79−97380
two-colour length measurement scheme using CO_2 laser 80−99747
USSR All-Union State Standard for linear and angular meas. 77−17946
visible and IR stabilised lasers, wavelength intercomparison 77−7114
CO_2 laser wavelength standards 77−17945
CO_2 wavelength and freq. meas., speed of light determ. 77−45822
He-Ne 3.39 μm laser interferometer, length and refr. index meas. 80−68172
He-Ne laser stabilisation and performance for dimensional meas. 80−19049
Xe I wavelength standard, 147 nm resonance line stability 77−17948

length standards *see measurement standards*

Lennard-Jones and Devonshire theory *see liquid theory*

Lennard-Jones potential
(2n, n), classical small-ang. anisotropic pot. scatt. perturbation theory expression 80−1043
12-6 fluid, liq.-vap. interface, density and surface tension 79−90772
acetonitrile, mol. pair correl. functions, scatt. intensities, statistical mechs. calcs. 79−1382
acetylene, cryst., semiempirical atom-atom pots. appls. 80−100200
adsorbing walls separated by Lennard-Jones liq., Monte Carlo calc. of force 80−15363
adsorption on homogeneous solid, surface second virial coeff. 80−45558
n-alkane, adsorption energy of mols. on long-chain even n-alkane crysts., rel. to cryst. growth kinetics 78−42933
n-alkenes, n even, interaction energy at twin boundary, dihedral reentrant, salient angle effect on growth morphology 78−55876
amino acid, cryst., mol. dielec. function 79−7043
amorphous solids, vacancies and vacancy clusters, stability under relaxation 80−15005
atom+harmonic oscillator collinear collisions with attractive interactions, semiclassical theory 77−522

Lennard-Jones potential continued
atomic clusters, free energy, Becker-Doring and Lothe-Pound theory 78−22063
binary dense gaseous mixtures, struct. and thermodynamic props., molecular dynamics study 80−64866
binary fluid, molecular dynamics, critical mixing point region 80−88014
binary liquid solutions, struct. and thermodynamic props., molecular dynamics study 80−64866
binary microcluster, struct. and thermodynamics, Monte Carlo simulation 79−7736
Bose gas, hard-disc, low density, two-dimens. many-body problem 78−95195
Bose system, with Lennard-Jones interaction pair potential, zero temp. 77−39710
Brillouin scatt. and refr. index measurements 80−76035
bulk and shear modulii determinations, computer experiments on 12-6 Lennard-Jones fluid *(Spanish)* 79−60417
Chevrel-phase superconductors, lattice dynamical calcs. 79−33056
classical fluid, thermodynamic functions in liq. and vapour region 79−10910
classical fluids, correl. functions, perturbation theory for soft sphere systems 77−72536
classical Lennard Jones 6-12 fluid, surface characts., density functional theory 77−24255
cluster-Bethe model, anharmonic and nonharmonic vibr. props. of classical solid 77−43299
collinear collisions, vibr. energy transfer, exact classical and quantal calcs. 77−19014
compressed gas, radial distrib. function hard sphere model 80−69961
configuration of systems of interacting particles with minimum potential energy per particle 80−23491
coupled oscillators, quasiperiodic to stochastic transition 78−54307
crystal nucleation and symmetry, interaction pots. effect 80−34169
crystal structure from minimum energy criterion, planar molecules, molecular packing 80−24383
dense fluid, memory function model for vel. autocorrelation function and self-diffusion coeff. 79−77472
dense gases and liqs., three-body nonadditive interactions, thermodynamics props., mol. dynamics simulation 79−7435
dense Lennard-Jones fluids, solvent struct. and solvation forces between rigid particles 80−30287
dense liquids, structure at solid wall interface, NVT Monte Carlo method 79−65310
dense simple fluid near wall, density profile calc., integral eqn.−Monte Carlo comparison 80−54083
diatom, weakly bound, dissoc. energy for Morse and Lennard-Jones pots. 79−54988
diatomic mol. soln., spontaneous Raman scatt., vibr. dephasing, review 77−28568
diatomic molecule, vib.-rot. wavefunctions and matrix elements, pot. function effects 77−453
diatomic molecules, homonuclear, molecular dynamics, time-dependent statistical props. 80−44093
dibutyl sebacate, interaction parameters from submicron aerosol drop evap. obs. 79−43639
diffusion rate processes, effect of intermol. force field 77−35733
difluoromonochloromethane, parameters of Lennard-Jones 12-6, Stockmayer 12-6-3, 6-Exp, Kihary intermol. pots. 77−34711
elastic sphere, deformation and sticking to a rigid plane, mol. force effect 80−106720
equation of state for Lennard Jones fluid 79−73083
equations of state predictions, vs expt., 2-dimens. Lennard-Jones fluid 79−69223
Fermi liquid, normal, mag. ordering at absolute zero 79−38344
Fermi system, with Lennard-Jones interaction pair potential zero temp. 77−39710
fermion-boson isotopic mixture, ground state configuration, theory 80−107601
fermions, constrained variation in Jastrow method at high density, neutron system, liquid ^{3}He appls. 77−5753
finite volume statistical mechanics for highly singular two body pots., many particle interactions 77−5752
fluid, atom pairs, dynamic behaviour 80−44098
fluid, cavity-biased (T,V,μ) Monte Carlo method, computer simulation 80−92434
fluid, classical one-dimens. Lennard-Jones type, eqn. of state 80−24562
fluid, critical lengths and spinodal region 80−84045
fluid, eqn. of state, quantum corrections 78−34592
fluid, inhomogeneous, free-energy theory, using 6-12 pot. 80−10751
fluid, nonlinear viscous flow 80−24060
fluid, two-centre, perturbation theory appl. using spherically averaged reference potential 80−64860
fluid interfaces, mol. theory 77−7949
fluid with periodic boundary conditions, error in computer simulation determ. 77−15296
fluids with Lennard-Jones pot., thermodynamic props. in terms of Lebowitz variables 79−7702
p-fluoranil, ^{19}F NMR and spin-lattice relax. meas., pot. profile calc., mole. reorientation 80−29634
four term WKBJ approx., appl. to Varshni V and Lennard-Jones pot. 80−58113
freezing, statistical mechanical theory, appl. to Lennard-Jones fluid 78−47499
freezing transition, statistical mechs. theory 77−7846
gas, Lennard-Jones mols., self-diffusion coeffs. at moderate densities, mol. dynamic simulation 78−38440
gas, third virial coeffs., empirical eqns. 78−94876
gases, third virial coeff., nonadditive interactions effects calcs. 77−30122
glass, Raman spectrum calc. 78−48165
glass and glass-forming liq., viscoelastic properties, comparison with Lennard-Jones model 80−84983
glass formation in Lennard-Jones liquid, mol. dynamics method 80−38896
globular hydrocarbons, cohesive energy and Gruneisen parameter calcs. 79−19183
graphite, ^{4}He interaction and scatt. 80−60732
hard core fluid with two-Yukawa tail, appl. to Ar 80−59618
hard corrugated surface, atom scatt., threshold and Lennard-Jones reson., and elastic lifetime 78−39647
hard sphere fluid contacting soft repulsive wall, Monte-Carlo method 78−67632

Lennard-Jones potential continued
hard sphere gas, 2nd virial coeff., high temp. quantum corrections 77−76012
hard-sphere fluid, reduced density, radial distrib. function calcs. 77−3903
heavy ion collisions, classical microscopic description of particle cluster collisions 79−9533
high-temperature vapour line of Lennard-Jones pot. fluid, Monte Carlo calcs. 79−37826
HNBP, nematic, statistical mechanics, particle pots. and distrib. functions calcs. 78−2001
homonuclear diatomics, dilute gas transport props. calcs. 77−72399
hydration, hydrophobic, of nonpolar mols. in dilute aq. soln., Monte Carlo simulation 80−3314
hydration of Lennard-Jones solutes, mol. dynamics study 79−34294
inert gas, transport and equilib. props., using LJ (12-7) pot. 79−98849
inert gas absorbate-substrate system, surface phonons, superstructures 77−15676
inert gas mixture, dipole autocorrelation function, Lennard-Jones and exponential dipole pots., classical calc. 80−64665
inert gases, viscosity, expt. and derived from statistical models *(French)* 77−35302
infinite volume ground state for particle chain in one dimension 79−88888
interacting particle system with Lennard-Jones pot., Schrodinger eqn. eigenvalues 79−71292
interatomic potentials, Regge poles positions and residues, inverse power pots. 80−83439
interfaces, liq.-cryst. and liq.-rigid wall, Monte Carlo simulation 79−27896
isolated small particles, struct. stability, atomistic studies 79−77957
Lennard Jones 6-12 fluid, Pade approximant for eqn. of state 77−3905
Lennard Jones polymer, eqn. of state, collapse transition 77−19117
Lennard Jones system, nonphysical sampling distribs., Monte Carlo free energy estimation, umbrella sampling 77−26229
Lennard-Jones 9:3 adsorptive system, Percus-Yevick and hypernetted chain theories 80−20030
Lennard-Jones fluid, thermodynamic props. calc. by modified Monte-Carlo method 77−35662
Lennard-Jones gas, Ising model, critical parameters from cluster integrals 77−11297
Lennard-Jones liquid mixture, mol. dynamics, attractive term effects 77−11454
linear, tetrahedral and octahedral molecules, harmonic coeff. for Lennard-Jones pot. 79−41217
linear lattice of atoms, Lennard-Jones pot. basis, for teachers 78−61997
liquid, free-vol. distrib., dislocation like struct. 79−64972
liquid, molecular, struct., reference systems with spherical interactions 80−24337
liquid, props. of optimisation condition 78−38598
liquid, simulation by force bias and Monte Carlo methods 79−86666
liquid film, mol. dynamics simulation 77−15666
liquid mixture, binary, equimolar, static (dynamic) props., mol. dynamics calc. 80−64857
liquid mixtures, local comp., mol. dynamics calcs. 79−82133
liquid mixtures, mol. dynamics, particle mass and size depend. 78−22615
liquid mixtures, phase separation, umbrella sampling, Monte Carlo calcs. 77−35698
liquid structure, S-D periodic particle-particle/particle-mesh program P3M3DP 80−84041
liquid-vapour interface, fluid phase coexistence, Monte Carlo computer simulation 80−49349
liquids, asymptotic form of structure factor 80−33867
liquids, classical, pair pots. from inelastic neutron scatt. data, self-consistent method 78−59728
liquids, diatomic, hard and soft core, free energy difference, Monte Carlo calcs. 80−92436
low temp. gas, eqn. of state, integral eqn. and perturbation method 78−26228
matrix isolated atoms, matrix influence, theory 78−46288
MBBA, nematic, statistical mechanics, particle pots. and distrib. functions calcs. 78−2001
melting, Lennard-Jones two-dimensional systems, Monte Carlo study 80−49338
melting of two-dimens. Lennard-Jones system, appl. to Xe adsorbed monolayer 79−28071
methane, liq., mol. dynamics simulation using singularity-free algorithm 80−54116
methane, wetting of flat smooth aolid, calc. using Lennard-Jones pot. 77−89618
microdrop, energy and mol. structure, mol. dynamics method 79−11004
microdrop, pressure tensor and surface tension, mol. dynamics method 79−11005
minimum potential energy per particle configuration, one-dimens. system 78−70084
Moelwyn-Hughes parameter calc. from US data for pure liqs. and liq. alloys 80−59375
molecular dynamics, nonequilibrium, $t^{-3/2}$ long-time tail for stress-stress time correlation 80−70100
molecular dynamics simulation of a small drop 78−15719
molecular dynamics simulation of interfacial and co-existence props. at triple point of Lennard-Jones system 78−83916
molecular fluid, pair correlation function, perturbation theory 78−55799
molecular fluid perturbation theory, Pople expansion third order term, anisotropic pot. 78−79510
molecular sieves, 5A, modelling, appl. to Ar diffusion coeff. determ. *(French)* 80−54508
molecular solids, melting curves, Lennard-Jones Devonshire theory 80−65201
molecule, WKB vibr. energy level calc. 78−9057
momentum distrib., binary cluster term evaluation, 3D Lennard Jones gas, 1D hard rod gas 77−37808
monatomic gas, collision-induced light scatt. at intermediate density, integrated intensity, appl. to Ar 80−24124
monatomic liquid, short wavelength collective density excitations 77−84610
monatomic liquids, short wavelength collective density excitations, computer simulation 79−46540
monolayers, nonregistered, lateral compression effects calc., limit of compression by Lennard Jones pot. calc. 80−6641

Lennard-Jones potential continued
Mori theory evaluation, molecular dynamics simulation 80−92443
multicomponent fluid mixtures, renormalised one-chain approx. 77−11452
multipole gases, second virial coeff. meas. 80−69959
nematic liquid crystal, statistical mechanics, particle pots. and distrib. functions calcs. 78−2001
nonequilibrium, perturbation theory, time-displacement operator 77−26233
nonlinear one-dimens. lattice with Lennard-Jones potential, soliton soln. 79−54069
nonuniform fluid state, Van der Waals theory, thermodynamics, struct. and phase stability 79−77475
nonuniform one dimensional classical fluids, Lennard-Jones pot. interactions, Percus Yevick approx. and density functional calcs. 80−64864
n-octane fluid, spontaneous cavitation 80−69886
oscillator interacting via Lennard-Jones pot., collision with atom, appl. of non-integer Bessel uniform approx. 79−36733
pair potential, Percus-Yevick and hypernetted chain approx. calcs. 77−1052
Percus-Yevick eqn., orthonormal series expansion soln. 80−49065
phase separation of fluid system by spinodal decomposition, mol. dynamics computer simulation 79−10766
phase transitions in two-dimensional Lennard-Jones system, calc. 80−59621
phenol, vapour, viscosity coeff. and second virial coeff., conformity with Lennard-Jones pot. *(German)* 79−32732
plasma, real gas discharge, thermodynamic stability 80−38852
polyatomic fluid, nonassociated, vibr. relax. density depend., simple model 80−32809
polyatomic molecule, crit. consts. evaluation from intermol. force consts. 80−37844
polymer, collapse transition 77−42451
polymer chain dynamics, repulsive Lennard-Jones pot. mol. dynamics calc. 79−36805
polymer chain statics and dynamics, Lennard-Jones interaction, calcs. 80−58425
polymer chains with rigid bonds, local relax. times, mol. dynamics study *(Russian)* 80−59373
polymer fluid, static bulk props., reptation Monte Carlo method, LJ pot. 80−64868
polymer solutions, scaling theories for general interaction potentials 80−99592
polypeptides, conformational analysis, empirical pot. energy algorithm 79−50174
pressure and temp. consistent Lennard-Jones liq. 78−63647
proteins, conformational analysis, empirical pot. energy algorithm 79−50174
quantal matrix elements between unbound states, for radial Schrodinger eqn. 79−97240
rainbow scatt. props., semiclassical estimation 77−88523
Regge pole positions and residues, quantum and semiclassical calc., complex optical potentials 79−89084
satellite line shape, classical broadening theory including Doppler effect, pot. effect 79−22764
second virial coeff., closed form. 80−28084
second virial coeff. inversion for complete pot. energy functions 80−91628
second virial coefficient, functional equations 80−103442
shock wave mol. dynamics, nonsteady to steady wave transition in three-dimensional solids 80−15189
simple classical fluid, 6-12 pot., press. calcs., using integral eqn. and perturbation theory 79−4224
simple cubic lattices, coordination radii and numbers, distant neighbour potential energy contributions 79−77535
simple fluid, hard and soft core eqns. of state, termination temps. for Lennard-Jones m,n pot. 79−82306
simple fluids, hard and soft-core eqns. of state, termination temps., Kihara pot. 80−70360
simple fluids, semiempirical calcs. using perturbation theory 80−28892
simple liqs. with repulsive forces, thermodynamically selfconsistent theory 80−75139
soft discs, two-dimens. melting, phase transition boundary 80−96629
solid, amorphous, edge and screw dislocation, stability, elasticity, simulation 80−15099
solution, aq., hydrophobic apolar spheres interaction, Monte Carlo simulation 80−6335
solution, aq., hydrophobic hydration around apolar species pair, Monte Carlo simulation 80−6336
solutions, dilute, Monte Carlo free energy calcs. in isothermal-isobaric ensemble 78−92498
spinodal decomposition, of Lennard-Jones fluid, microscopic theory 79−99046
square-well+Sutherland (∞,6) fluid, perturbation theory 77−11455
statistical physics of liquids, possible modification of perturbation theory *(Russian)* 77−1056
steam, effective spherically symmetric pots., applicability to viscosity calc. 78−1779
stochastic transition in classical nonlinear dynamical system of Lennard-Jones chain 78−142
Stockmayer fluid, mol. dynamics and thermodynamic perturbation theory, mol. polarisability effects 78−71419
Stockmayer molecules, two dimens. fluid, static props., dielec. const. mol. dynamics calcs. 80−54094
testing fundamental equations of state for practical applicability 80−4684
thermodynamic properties of simple fluid in hard-sphere reference system 77−76575
transition metals, amorphous, density of electronic states, effect of struct. variation due to interatomic pot. softness 80−54597
trimer, fermion, 12-6 pot., threshold coupling const., variational calc. 78−1117
two-dimens. fluid, Percus Yevick eqn., radial distrib. function, critical point 77−76272
two-dimensional fluid, with 12-6 pot., fourth virial coeff. 78−59723
two-dimensional Lennard-Jones model, computer calc. 77−11550
two-dimensional system, velocity autocorrelation function, mol. dynamics method 79−90873
van der Waals fluid, transport props., shear viscosity calcs. 77−35738
van der Waals molecules, vibr. level spacings calc. from Lennard-Jones pot. 77−42369

Lennard-Jones potential continued
Varshni V and Lennard-Jones pots., 3rd order WKBJ eigenvalues 79−6982
water interface, mol. orientation and surface pot. at 4°C 80−15339
Yukawa fluid used as reference system in perturbation theory 80−6334
AgI surface, adsorption of water, effective pair pot. model 80−100394
Ar, dense fluid, viscosity, gaussian memory function approach 80−28904
Ar, force constant props., 12-6 pot. model 78−13563
Ar, intermediate density, collision-induced Rayleigh spectrum, second freq. moment 80−24125
Ar line broadening by at. collisions, meas. of oscillator strength of ArI lines reson. *(French)* 78−5172
Ar, liq., atomic correls., three-body interactions effects calcs. 77−84618
Ar, liq., surface properties of classical Lennard-Jones liquid *(Russian)* 79−77869
Ar, liq., variational eqn. of state and entropy 79−28070
Ar, liq. struct. factor calc., perturbation treatment using Lennard Jones (6, 12) pot. 80−10483
Ar, phase transition, anharmonic cryst.-gas transition 80−6510
Ar, solid, self consistent field calcs. of isotherms and thermodynamic props. *(Russian)* 80−10633
Ar, solid, thermodynamic props. under press., multiparametric pairwise and Lennard Jones potential calcs. 80−39316
Ar, solid-liq. transition and mech. props., modified cell theory 79−23703
Ar, thermal cond., Lennard-Jones (12-6) pot. parameters calcs. 80−28591
Ar, transport props. with Lennard-Jones (12-6) pot., distance parameter 79−55437
Ar+SF_6(tetrafluoromethane), differential scatt. cross-sections, intermol. pots. calcs. 79−89742
ArHBr, ArHCl, and isotopic forms, rot. spectra, mol. struct., mol. consts. 80−58246
As_2S_3, chalcogenide glass, effect of press. on elastic props. 80−10590
BN, hexagonal, long optical vibrs., elastic consts. from valence force consts. 78−51621
Ba-inert gas, Ba reson. lines broadening, absorpt. cross sections anal. 80−32642
Br_2, liq., entropy, computer simulation, Widom method 79−77486
Br_2, mol. dynamics of '2-Lennard-Jones centres' pair pot. liq. 79−73082
CO_2, mol. dynamics of '2-Lennard-Jones centres' pair pot. liq. 79−73082
CO_2, thermal conductivity, 400 to 1500K, vibr. internal energy calc. 79−18986
CS_2, liq. struct., mol. dynamics simulation 79−77488
CaF_2, mol. dynamics studies of superionic conductors 80−107547
$CaSO_4$, anhydrite and gypsum, phonon spectroscopy, lattice dynamical calc. 80−19889
Cl_2, liq., entropy, computer simulation, Widom method 79−77486
Cl_2, mol. dynamics of '2-Lennard-Jones centres' pair pot. liq. 79−73082
Cl_2, rot. relax. classical trajectory computation, using Lennard-Jones pot. 78−62880
Cs+He(Ne)(Ar), optical pumping, spectral line shape *(Spanish)* 79−22662
CsF+Ne, (Ar)(Kr)(Xe), sudden, body-fixed and semiclassical approx. calcs. 78−42164
$Cu_{57}Zr_{43}$, amorphous alloy, computer simulation of atomic structure 80−70125
F_2, mol. dynamics of '2-Lennard-Jones centres' pair pot. liq. 79−73082
H+HCl(HBr)(HI), elastic scatt., <50 meV, Van der Waals pot. 79−54937
o-H_2+Ar, relax. and kinetic cross sections, DWBA calc. 78−25655
H_2+Kr, differential cross-sections, diffraction undulations, anisotropic pot. calcs. 78−9223
HCl, liq. struct. simulated by a Lennard-Jones pot. 80−1917
He, 3^3D_1-2^3P_0 line, press. broadening studies by saturated absorpt. techniques 80−52939
He II, excitation spectrum and second virial coefficient calc. 80−102549
He-Ar mixture, translational IR spectrum at 165K, binary and ternary absorptances 77−68042
He+Ar mixture, collision induced absorpt. calcs. 77−6777
He+O_2, long lived collision complexes, exact classical and quantum mech. calcs. 78−33576
He+O_2, vibr. energy transfer, exact classical and quantal calcs. 77−19014
He_2, possibility of existence, Lennard-Jones pair potential 80−52869
^{3}He, liq., polarisation effect on mag. ordering, melting curve 80−80021
^{3}He, new variational wave function 79−77855
^{4}He ground state binding energy, near threshold behaviour in 2 and 3 dimens. 80−91716
^{4}He, HCP, ground-state props. 80−44389
^{4}He, liq., ground state energy and struct. 77−66051
^{4}He, liquid and solid, Lennard-Jones model at 0K, props. using Monte Carlo method 79−82401
^{4}He, superfluid, elementary excitation, structure factor and phase velocity 80−80012
^{4}He, threshold condition for forming atomic trimer 80−63741
IF_5, second virial coeff. meas., Lennard-Jones pot. determ. *(German)* 77−19658
Kr, Lennard Jones (12,6) pot. distance parameter, transport props. calc. 80−79423
Kr, molecular dynamics simulations, three effective interactions 79−69224
Kr, near solidification, 50°C, up to 6500 bar, meas. and simulation using Lennard-Jones pot. *(French)* 78−67301
Kr, thermal cond., Lennard-Jones (12-6) pot. parameters calcs. 80−28591
KrHBr, KrCHl, and isotopic forms, rot. spectra, mol. struct., mol. consts. 80−58246
LiF, He at. beam scatt., Lennard-Jones resons. and rel. displacements 77−1773
Li^*+He(Ar), Li principal series line broadening and shift, interat. pot. consts. 78−42165
Mg, spectral line broadening, by inert gas collisions 77−79580
Mg-inert gas, Mg reson. lines broadening, absorpt. cross sections anal. 80−32642
MoF_6, second virial coeff. meas., Lennard-Jones pot. determ. *(German)* 77−19658
N_2, liq., dephasing of mol. vibr. related to correl. functions 78−75523
N_2, liq., near BP, vibr. reson. energy transfer and dephasing, Raman spectra 77−6790
N_2, liq., thermodynamic props., perturbation theory with hard dumbbell reference system 80−14991
Lennard-Jones potential continued
N_2, rot. relax. classical trajectory computation, using Lennard-Jones pot. 78−62880
N_2 structural second virial coeff., intermol. pot. and mag. scatt. 80−78678
N_2, thermal conductivity, 400 to 1500K, vibr. internal energy calc. 79−18986
N_2, thermodynamic and transport props., consistent correlation using Lennard-Jones (12-6) and Buckingham (exp-6) pots. 78−91045
NaCl, aqueous soln., Lennard-Jones parameters, mol. dynamics and X-ray obs. 78−9939
Ne, equation of state determ., high temp. and pressure, computer expt. 78−75800
Ne, Lennard Jones (12,6) pot. distance parameter, transport props. calc. 80−79423
Ne, phonon dispersion relation, Gruneisen parameters at high press. 79−42179
Ne, solid, phonon-dispersion, mode Gruneisen parameters and elastic consts. 77−11651
Ne, thermal cond. Lennard-Jones (12-6) pot. parameters calcs. 80−28591
Ne-Kr, partially miscible mixture, high press. mol. dynamics using Lennard-Jones pot. 79−41929
Ne-Kr, time-dependent props. near crit. mixing point, 2000 bar, mol. dynamics calcs. 80−24580
Ne-Xe, equilibrium of coexisting phases 80−87197
Ne+Ne, (He) low pressure broadening and shift of Ne line, Lennard-Jones pot. 80−102554
O_2, structural second virial coeff., intermol. pot. and mag. scatt. 80−78678
O_2, thermal conductivity, 400 to 1500K, vibr. internal energy calc. 79−18986
OCS+He(Ar), rot. lines, collisional broadening 79−18267
PF_5, second virial coeff. meas., Lennard-Jones pot. determ. *(German)* 77−19658
Pt, diffusion energies for Pt, Ir, Au adatoms, Lennard-Jones pair pot. calcs. 79−77923
SO_2, lattice dynamics, rigid mol. model 80−44266
Sr+Ar, press. effect on Sr 4607 Å reson. line shape, width and shift 79−22653
TlI, atomic fluorescence, D_2 pressure effect on width and shift 80−99475
VCl_4, liq., struct. factor, mol. dynamics calc. 80−38898
WF_6, second virial coeff. meas., Lennard-Jones pot. determ. *(German)* 77−19658
Xe adsorbed monolayers, thermodynamic props. and lattice const., quasi-harmonic theory 79−42380
Xe, Lennard Jones (12,6) pot. distance parameter, transport props. calc. 80−79423
Xe, liq. struct. factor calc., perturbation treatment using Lennard Jones (6, 12) pot. 80−10483
Xe, mean force of two atoms dissolved in water 80−54114
Xe, physisorption on W (100), Lennard-Jones model, mol. dynamics study 80−34308
Xe, thermal cond., Lennard-Jones (12-6) pot. parameters calcs. 80−28591

lenses
see also aberrations; aspherical lenses; contact lenses; electron lenses; electrostatic lenses; focusing; magnetic lenses; photographic lenses
aberrated lens model of high-energy atm. laser propag. 78−69454
aberration weighted coeffs., belastung (strain) indicator of optical system correctability 77−46783
aberration-free lens, near focus intensity distribs. for Gaussian and const. intensity beams 77−615
aberrations, chromatic and spherical, of single glass lenses, holographic correction 79−86226
aberrations, longitudinal-chromatic and spherical, ray-tracing method estimation 78−1311
aberrations calc., third-order, modified relations using Caddington variables *(Czech)* 78−50885
aberrations determination by speckle interferometry *(French)* 79−72653
ACCOS V, commercially available optical design and anal. program 79−86230
achromatic doublet design 78−71183
achromatic triplet using holographic elements 77−58415
acoustic, broadband focusing through converging lens, linear systems approach 79−3817
acoustic, materials suitable for acoustic imaging 79−72771
acoustic, solid, pulse and freq. response anal. *(Russian)* 78−46873
acoustic, two-layer, focal plane field 77−35005
acoustic elliptic lenses, history 80−96158
acoustic field struct. in focal region of closed homogeneous lenses 77−68289
acoustic holographic lens theory and construction 78−55536
acoustic lens-filter plate, log-periodic, variation of props. with freq. 78−63256
acoustic lense-design with elliptic surfaces 80−48530
acoustic spherical compliant-tube Luneburg lens, theory 77−46842
acrylic thin sheet lens construction and performance as solar concentrator 79−62120
afocal projection optics, for laser velocimeter 80−75011
alkali halides, finished optical components, forging 77−46824
animal eye technology use in better lens and mirror design 80−28295
annular, Gaussian-beam theory 78−71185
annular, imaging improvement in type 2, scanning microscope 78−89535
annular aperture, for scanning optical microscopy, aberration and focusing props. 77−65054
annular aperture, light distrib. from diffr., aberration correction using mirror lenses *(German)* 80−69325
annular HSURIA resonators, testing with CO_2 laser, polarisation effects 80−58599
annular lens soft aperture for high power laser systems 77−72014
annular lens soft aperture for high power laser systems 77−72015
annular lenses in microscopes, imaging props., calcs. 80−22426
anti-Gaussian collimating lens, intensity uniformity 77−7167
aperture, rel. to depth of focus 78−12489
aplanetic holographic objectives, for UV photolithography 79−32031
apochromat, four-lens three-colour, glass selection for design 78−13783
apochromat optical glass development status and prospects 79−27348
apochromatic glass pair dispersion coeff. selection 79−72657

lenses continued
apochromatic pancratic objective component chromatic aberration formulae 79−76795
apochromatic pancratic objective components, primary chromatic coeffs. 80−28298
apochromats from four types of glass, components for broad spectral region 79−32026
array characts. on illuminated intensity distribution *(Russian)* 80−106591
array for extended coherent light source *(Russian)* 78−30040
array of simple lenses, for close-up imaging of documents and displays 79−36972
aspheric mirror optical systems for the infra-red 79−36983
astigmatic spectacle lenses, technological construction *(Russian)* 80−99817
astronomical doublet system resolution, random speckle structure model and expt. *(Russian)* 79−7082
automatic dioptometer with projection readout system 79−50455
automatic lens design, algorithm for accelerating convergence 80−38085
automatic lens design, pseudo-second-derivative matrix computation 79−14077
axial hologram lens with remote entrance pupil, cancellation of aberration 80−32933
axial holographic lenses, monochromatic aberrations 79−98321
axicon combined with mirrors and lenses, laser linear, annular and radial focusing 78−66856
axicon focusing of CO_2 laser beam, for optically pumped He laser plasma 79−32792
biconvex and biconcave lens combination, optical energy and spatial filter for Raman spectroscopy 79−35838
biconvex lens, MTF and wavefront aberration meas., Francon's holographic interferometry method 79−3647
bifocal, appl. to directional alignment expts. 80−46762
bifocal lens designs, marginal aberrations 78−48927
bifocus element for microscope objectives 77−41680
Bowen lens and anamorphic cameras for stellar spectrographs 80−41727
CAD, three-lens zoom system 80−43424
CAD of objectives corrected to infinity, k-stage *(Hungarian)* 79−81502
catadioptric, two-component, small zonal spherical aberration *(German)* 79−50366
catadioptric lens system, possible appl. for satellite and astronomical photography *(German)* 79−76793
catadioptric objective, development *(German)* 80−102796
catadioptric system with gradient index corrector plate 78−12096
catadioptric systems, matrix optics 79−94167
cataractous lenses, PIXE elemental anal. 80−21468
catoptric objective design, testing *(German)* 80−53400
caustic point displacement due to generalised bending, third-order approx. 80−83656
caustic surface calcs. in geom. optics, analytical illum. monitoring 77−3643
cemented doublet, 3rd order aberrations calc. 77−88889
centrally obstructed objective, resolution limit *(German)* 80−95811
centring error tolerance study *(German)* 78−33806
centring monitors design, using variable parameter system *(Russian)* 78−50883
chalcogenide glass films, kinoform optical elements and integrated optics elements prod. 77−75634
chalcogenide glass films, opt. inform. recording uses 77−75633
chalcogenide glass semiconductor film kinoform production *(Russian)* 77−14670
chirp-grating lens for guided-wave optics 79−7232
chirped grating, anal. 80−87563
chromatic aberration first-order theory, secondary spectrum correction with common glasses 78−90382
chromatic aberrations of real rays, role of each lens in optical system 80−102655
coherent Gaussian beam in laser Doppler velocimeter, interference 80−69444
coherent information processing by a pair of lenses in spherical wave illumination 80−95816
coherent optical system, impulse response for image multiplication by spatial sampling filtration 80−33126
coherent optical system, resolving power enhancement by aperture synthesis 78−25987
collimating, for GaAs laser array source package 77−84007
collimator, single element gradient index design 78−9426
coma corrector for parabolic reflector telescope off-axis guiding 80−82196
compensation for inclined beam aberrations in lens-hologram system *(Russian)* 77−19381
compensators for testing concave mirrors of astron. telescopes, design 80−28305
complex systems, higher order beam modes 77−27308
compound eyepiece development, late 17th century 77−37704
computer programs for optical design 79−36977
conference, optical production technology advances, London, England (Jan. 1977) 78−50954
conical lens, to produce large diameter openings using laser beam *(Russian)* 80−19061
conical SELFOC fibres, third order aberration coeffs., gradient-index lens design 77−27357
contact lens/spectacle system for altering retinal image movement to eye rotation relation 79−53281
convolver, generalised single-lens 78−55303
Cooke triplet, air-spaced anastigmatic quadruplet design 80−1291
Cooke triplet derivative of five-element config., design 80−33111
corneal lens, soft radius of curvature meas., using autostigmatic microscope 77−60198
coronagraph objective component surface scatt. angular distrib. obs. 80−74463
corrector lens for color television tube 79−86243
corrector lens system using wide field doublet for Cassegrain telescope *(Japanese)* 77−91427
Correlation image formation with an axicon 80−48162
correlator, wavefront propagation error effects 79−50232
cost reduction in manufacturing 80−1361
cost/tolerance relationship 79−81507
coupling from semicond laser to single-mode fibres, cylindrical lens method 79−76807
curved Fresnel surface, primary aberration contribs. 79−13913
curved zone plates and Fresnel lenses, third-order aberrations 77−72043
cylindrical, prod. of deep-image rainbow holograms 78−71061
cylindrical, rotation of parallel fan of light, matrix representation 80−38089
cylindrical gradient index lens and array radiometric props. 80−14421
cylindrical lens systems, for neutral dipoles, using electrostatic or mag. fields 77−54663
cylindrical lens systems described by operator algebra 80−38086
cylindrical Selfoc lens combination for semicond. laser/optical fibre coupler 77−79931
derivation of lens maker's equation, teaching 79−44683
design, analytic merit function based on Buchdahl's aberration coeffs. 77−755
design, and ghost focus problem in fusion lasers 79−86247
design, applied optics conf., Oakland, CA, USA (May-June 1980) 80−101661
design, least squares fitting of Zernike's polynomials to wave aberration function 80−83660
design code, CLIMB, using Monte Carlo sampling 77−3642
design computer programs, intercomparison 79−86234
design education program, desktop computer appl. 79−84922
design for laser beam shaping 78−13781
design intermediate phase approximation systems *(Hungarian)* 79−89982
design merit functions, RMS image spot size and RMS optical path difference 78−46743
design of instrument optics from basic elements 77−58418
design of lens system with extended depth of focus, Version 14 optimisation program 78−90489
design of medial copying, high aperture Distagon, photorepeater lenses 78−50888
design optimisation, Version 14 program 78−90488
design program 79−86233
design using cylindrical retractive index distribution *(Russian)* 78−74962
design via principal surface, focusing optics for laser fusion 77−3641
design with simultaneous image spot, optical path difference, diffraction MTF and Seidel abberation minimisation 80−74459
design without a computer 79−86235
designing lens system, initial phase significance *(Hungarian)* 78−50881
diamond smoothing techniques 78−50957
diffraction catastrophes, optical caustics 80−9801
dioptic, microelectronics appl. 78−46754
distortion by means of numerical transformation *(German)* 80−64132
double Gauss basic lenses, design *(German)* 80−53398
double Gaussian objective, design *(German)* 80−64134
double-layer antireflection coatings for plastic lenses, evaporation coating process 80−14491
doublet, single-radius, paraxial properties and errors correction *(Czech)* 79−76791
doublet-type eyepiece equations *(German)* 77−54767
dye laser resonator, CW, astigmatism compensation using lenses 78−29978
edge image anal., finite area sampling technique 79−22902
education, geometrical optics, lens Fourier transform properties 80−57024
education, lateral-angular magnification relationship for simple magnifier 80−57031
education, the principal plane, its pedagogic role 79−97150
electromagnetic fields, near wide angular lens and mirror systems 77−72051
electron microscope optical model, design and use 80−86534
electron-beam and photolithographic fabrication of guided-wave optical components 78−13818
ellipsoidal lens for sub keV X-ray imaging 77−26444
EM field, in focal region of wide-angular annular lens and mirror systems 78−90485
errors in thickness and reference vertex distances, statistics 78−1314
eye, cold cataract form. in young rat lens, phase separation of protein-water mixture 78−11640
eye, frog, under-corrected lens rel. to comparable aerial and underwater vision 78−7344
eye, human, aspheric curvatures 78−11642
eye, induced optical analysis fluctuation 78−35838
eye, lens pigmentation in humans rel. to UV light exposure 78−65100
eye cataractous lens, NMR study of state of water *(Hungarian)* 78−64986
eye lens, bovine, rheological analysis 77−90767
eye lens, normal and senile cataractous, PMR study of state of water 78−64987
eye lens, vertebrate, as system for study of mol. processes 77−90770
eye lens accommodation, interpositus neuron control obs. 80−21469
eye lens formation models, human 77−25423
eye lens protein, organisation in fibre cell 77−90766
eyeglass lens blanks mode from molten glass, defects elimination 77−34971
eyepieces, imaginary front focal planes, negative collection lens, design considerations 80−64139
fabrication and assembly, centration errors 80−9980
fabrications of lens blanks having reduced finishing allowances 80−74541
factor analysis methods for designing complicated optical systems 80−28303
fibre connector using low-loss lens system 78−79107
fibre lens, plastic focusing, change of ref. index profile during heat treatment process in fabricating 78−83091
fibre tip lens fabrication and smoothing 78−33923
field corrector for parabolic reflector, design method *(Chinese)* 80−85857
field corrector for paraboloid, small-field single lens 77−33344
field lens for one-step rainbow holography 79−13923
five-component wide-angle pancratic objective design 78−71190
flat image focussing spherical lens, used for Si light detector 80−91880
flat-field telecentric scanning lens design 77−58424
flatness of test glass, reading errors of interf. fringes 79−32097
flight simulator viewing, triplet lens system design 80−74457
fluids in microscopic tubes, refractometry, focal position observation 79−49273
fly's eye lens plates, superposed, image functions *(Japanese)* 77−34925
fly's-eye, 3-dimens. US image display 79−81668

lenses continued
focal length meas. error, student expt. 77−45653
focal length of thin lens under water, determ., teaching appl. 79−44676
focus and alignment sensing of a collimated light beam 78−59065
focus determ. for lens tolerancing computer program 79−86240
focus-position sensing using laser speckle 79−59785
focusing lens for laser recording with truncated Gaussian beams 79−81474
Fourier optics as approx. of Kirchoff integral, 4F path of rays with thin lenses *(German)* 79−18357
Fourier transform, design and structural charact. *(Chinese)* 79−45911
Fourier transform elements, performance of simple lenses 78−94374
Fourier transform lens, phase error model 78−71037
Fourier transform lens, spatial invariance test 80−69492
Fourier transform lens array, for shortening optical correlator length 79−59646
framing spotlight, optimizing the compound reflector 79−3766
Fresnel, acrylic, photovoltaic concentrating array appl. 79−52937
Fresnel, for solar concentration, high-efficiency 79−88003
Fresnel, manufacture digital control *(Russian)* 78−50884
Fresnel, ultrashort pulse propag. through lenses 77−58414
Fresnel condenser lens faces, nomogram for slope angle determ. 79−7193
Fresnel lens, appl. in focal reducer for stellar photometry 80−67568
Fresnel lens, colour-corrected linear convex, for solar concentration 80−45640
Fresnel lens for thin-film waveguide 78−94452
Fresnel lens in thin film waveguides 78−38075
Fresnel lenses, fabrication techniques 80−91939
Fresnel lenses, highly concentrating for solar radiation 79−94315
Fresnel lenses in BaO optical waveguides 80−96034
Fresnel optics, for concentrator solar cells 79−14088
frustrated total internal reflection element, adjustable as a function of the incidence angle of highly collimated light beams 80−96022
fundamental chromatism coefficients 78−1317
galvanometer beam-scanning rotating lens system, for laser fibre drawing 79−41463
generalised radiance propag. through lenses 79−27359
generalised ray tracing, caustic surfaces, bending and merit function for optical design 80−102612
geodesic, aberration-corrected rounded edge, profile calcs. 80−10048
geodesic, edge-rounding effects 77−7216
geodesic lens, aberration corrected, for integrated optics circuits 78−38074
geodesic lens, anisotropic and curvature losses, operation in $LiNbO_3$:Ti waveguide 80−48453
geodesic lens formation in diffusion fabricated optical waveguides 80−91937
geodesic lenses, anal. by beam propag. method 80−58686
geodesic lenses, axially symmetric, design parameters 78−83114
geodesic lenses, change of focal length as function of depth change due to fabrication errors 80−38128
geodesic lenses, spherical aberration correction and fabrication tolerances 79−27435
geodesic optical lens prod. by anisotropic etching 80−10047
geodesic optical waveguide lens analysis: comment 79−76879
geodesic thin film lenses, for integrated signal processors 78−42475
geodesic waveguide lens anal., ray tracing 78−13778
geodsic profiles for equivalent Luneburg lenses 79−76880
geometrical optics, appl. of group theory 78−25944
geometrical optics field of general optical systems 79−81503
glass active elements of pulse-periodic lasers, thermal lenses 79−89914
glass sampling, of simplex variants and of multiplets *(German)* 78−90484
graded index, design using refr. index reconstruction method 77−39013
graded index materials, optical props. meas. 79−9237
graded index rod lens applications in optical fibre communications 80−14485
gradient index fibre array, illumination intensity unevenness, theory and expt. 80−14480
gradient index fibre array development and imaging props. 80−14483
gradient index fibre array for photocopying machine 80−14482
gradient index imaging lens and system status 80−14420
gradient index imaging system theory 80−14294
gradient index lens fabrication by molecular stuffing 80−14499
gradient index optical elements and system design 80−106594
gradient index optical imaging systems, topical meeting, Rochester, USA (May 1979) 80−12851
gradient index optical lenses, use, design, fabrication and refr. meas. 78−13780
gradient index SELFOC lens, aberration improvement 80−14425
gradient index spherical lens design for selfcoupled optical pickup system 80−14427
gradient-index fibre array, unevenness of illuminance 80−69482
gradient-index fibre lens, radiometric props. 80−69481
gradient-index imaging, theory 80−69331
gradient-index optics: a review 80−69478
gradient-index rod, aberrations in multimode optical fibre devices 80−69487
gradient-index rod, appl. in optical fibre communication systems 80−69488
gradient-index rod, evaluation by imaging 80−69485
gradient-index spherical, design for optical pickup systems 80−69483
graphical ray tracing for conic surfaces 80−5683
grating lens fabrication for integrated optics 78−75004
gratings charact. control by interference pattern *(Russian)* 80−87461
grinding, as student lab. project 77−5614
guided acoustic travelling wave lens for high-speed optical scanners 79−36991
high resolving power, low distortion, technological development trends *(German)* 78−33805
high temperature solar collector with optimal concentration: Non-focusing Fresnel lens with secondary concentrator 80−35753
high-resolution holographic aplanatic objective *(French)* 77−83837
high-volume optical component tolerance/specification relationship 80−48383
hologram achromatic lens system, design using ray tautochronism principle 79−3759
hologram lens, axial, on spherical substrate with remote pupil, aberrations 80−95849
hologram lens, compensating method for spherical aberrations 77−23634
lenses continued
hologram lens system, astigmatism and coma reduction 80−53238
hologram lenses, spherical aberration compensation for short-wave shift in reconstructing radn. 77−19206
holograms as beam deflection elements, projection and collection lenses in document scanner 77−88672
holographic, interferograms 77−72045
holographic, method for wave aberrations calc. 80−28175
holographic, scanning system, lens design for hologram generation 78−50742
holographic couplers for optical fibre bundles 78−25839
holographic demonstration, comparison of real and virtual lenses 78−16599
holographic elements as lenses, optical system design 78−9425
holographic flat field lens with no first order astigmatism 77−10995
holographic Fourier transform lenses for matched-filter optical processor 79−45913
holographic generation expt. arrangement 77−83966
holographic lateral shear interferometer for differential interference contrast method 80−63947
holographic lens design techniques, 488 nm construction, 633 nm read out 79−89866
holographic lens element, astigmatism free 77−46784
holographic lens element, s and t formulae 77−46785
holographic lens image quality, estimation criteria 78−25824
holographic lens recording techniques for IR wavelengths 80−95847
holographic lenses, coherent transfer functions anal. 77−68190
holographic microscopy, lens assisted system, resolution tests 78−46539
holographic optical element, mathematical equivalence with ultra-high index lens 79−59653
holographic optical elements, third-order aberration theory and generalised aplanatic condition 80−74314
holographic reflective lenses for compact optical data processor 77−34829
holographic three-dimensional image prod., reversal method using reflective and lenticular screens 78−90403
holography, twin-image, chromatic lens system, astron. appls. 80−87346
human eye lens pigmentation in vivo, independ. of UV light exposure 77−60202
hyperbolic cone-channel condenser system 78−33811
hyperchromatic lens, expressions for first order chromatic aberrations 80−91879
illumination distribution calc. in image plane 77−31125
illumination system, lens-array, size calc. 78−59110
illumination system, optical design 80−64135
illuminator using laser light source, geometrical optical anal. *(Russian)* 78−79094
image contrast theory of electronic focus 79−13914
image formation, graphical representation for teaching 77−49539
image formation, lenslet array with periodic sampling structure 78−37964
image forming by refraction, tutorial *(Hungarian)* 77−22359
image plane irradiance caused by the natural radiation of the objective lens 78−83068
image quality criterion, second moment of diffraction point spread function 80−9818
image rotation and magnification, optical system 80−48376
image transmission, lens light-guide line 79−3789
image-forming objectives and colour filters, application and mounting *(Hungarian)* 78−9424
imaging method for data processors, lens system design 77−27261
imaging properties and OTF, Jones notation 78−25945
imaging system assessment, conference, London, England (Nov. 1976) 78−50718
immersed lenses for IR detectors, performance charact. *(Russian)* 79−27358
incoherent optical processing via spatially offset pupil masks 78−82917
individual meniscus-type lens, coarse grinding errors 79−50458
infinitely-thin-component optical system design principle 79−76794
inhomogeneous waveguide lens anal. 78−5561
integral photography, transform of 3-D image produced by lens raster 78−82921
integrated acousto-optical spectral analyser waveguide geodesic lens correction 79−50241
integrated optic spectrum analyser design and fabrication 79−72720
integrated optics thin-film waveguide lenses, progress 78−66950
intensity fluctuations behind lens, receiving aperture shape effect 80−95980
intensity fluctuations in turbulent atmosphere, with (without) central screening 79−7080
interferometer, lateral shear, using twin three-beam holograms, lens tests appl. 80−99673
interferometer, two-beam, comparison of refl. and refr. optics in condensing element 78−77968
interferometric examination of lenses, mirrors and optical systems, 3D display 80−69497
intraocular lens implant evaluation 78−81061
intraocular lenses, literature review 1976-1977 79−96707
ionosphere, chemically modified, use as lens for refracting radiotelescope 77−45312
IR heat trap field optics, compact lens-mirror system 78−55422
IR imaging and missile-borne tracker optics, selection guidelines 79−23050
IR inhomogeneity scanner for transmitting material blanks 79−32099
IR lens system, large diameter, for pyroelec. vidicon 80−19086
IR materials, high transparency, state of the art 77−27326
IR optical scanning system, narcissus effect suppression, computer results 78−59151
IR radiometer objective lens, optimal refr. index 78−29137
IR transmissive material guide, lens fabrication considerations 77−39004
Keplerian binoculars with erecting lens system 79−72662
large, simplified MTF meas. *(Japanese)* 80−33121
large-aperture condensing lenses for rainbow holograms 78−78962
laser anemometer elements, Gaussian beam transform. 79−45991
laser beam expander for short cavity dye laser 80−87532
laser beam printer scanning system with f-θ lens 80−78942
laser beam profile measurement using spatial sampling, Fourier optics and holography 79−86201
laser collimation and focusing at given distance *(Russian)* 78−29959
laser compression expts., design principles, geometrical optics theorem appl. 79−55203

lenses continued
laser diffraction-limited system, resolution, intensity, and power distribution 77−58425
laser focusing lens design for hot spot elimination 79−72658
laser focusing objectives, flare image danger reduction 79−22997
laser light source for spectroscopy, far-IR, optical coupling arrangements 80−73481
laser optics, Shiva, system, thin film coatings technology 79−7135
laser rods with negative lenses, distrib. aperture effect 78−66857
laser to fibre hybrid coupler with cylindrical lens 77−75661
LED, with self-aligned sphere lens, for efficient coupling to optical fibres 77−79939
LED coupling to optical fibres, truncated spherical lens efficiency 79−76813
lens, light scatt., appl. of random density and orientation fluctuation theory 79−62241
lens design and testing for laser systems, assets and liabilities 78−46753
lens guide, low-loss image transmission 80−91872
lens-axicon doublet illuminated by Gaussian beam, ring focal pattern 78−55421
lens-hologram optical system, monochromatic aberrations 79−3760
lens-mirror combinations with max. conc. 78−9422
lenslet-array optical device for paginal information reproduction 79−27194
light shielding characts. of lens hood, mol. scatt. calc. 78−71189
light wave propagation 80−78947
light-flux generated by single-lens illuminator, spectral composition for UV region 80−87450
linear echelon refractor/reflector solar concentrators 80−7929
linear Fresnel lens with grooves of finite size, solar radiation concentration 80−106592
liquid crystal lens cell, prep. and optical props. 79−94320
liquid surface deform. due to laser radiation thermal action, lens effect 80−33048
Luneburg guided-wave optical thin-film lens, fabrication technique and props. 80−33223
Luneburg lens, turning point of rays 80−83659
Luneburg lens index profile for planar waveguide 78−5562
Luneburg thin film lenses, formation by sputtering through circular mask 78−87132
manufacturing methods for high performance lens *(German)* 80−53482
manufacturing optical components, modern production methods 78−50960
mass production yield estimation by centering tolerance simulation 80−78941
matrix transforming incoherent optical system, using extended lens-array 79−7086
matrix treatment of primary aberrations, for optical system design 77−50622
mechanical strength, antireflection or protective film effect 78−1318
meniscus Fresnel lenses, primary aberrations 77−27328
meridional size, one eye magnification, depth perception, meridional disparity effects 79−53133
merit function, diffr. based, for automatic lens design *(Chinese)* 80−5809
micro-objective, light transmitting, fogging field glare meas. 79−75590
micro-optics testing, width meas. of slit test objects 80−64223
microlenses to improve LED-to-fibre optical coupling and alignment tolerance 80−19088
microobjectives, reflected light, image glare coeff. depend. on design parameters 80−28302
microscope, scanning, multiple traversing of the object 80−90890
microscope, wide-field objectives, image forming quality 79−35819
microwave lens for holographic imaging 80−48183
military optical system temperature effects and counter-measures 80−78938
minicomputer optical design and analysis program 79−14075
modular optical design, control of fifth-order aberrations 79−55199
monochromatic aberrations, third order, correction of four lens objective 78−87123
mounting, workshop techniques 77−27399
mounting systems, construction *(Hungarian)* 77−72050
MTF measurement, accuracy of spectral response matching 78−50721
MTF measurement, polychromatic and monochromatic assessment in far IR 78−50899
MTF measurement for lens test, light source polar intensity distrib. influence 78−50723
MTF measurement in France, ACOFAM and ACOMAT instruments 78−50727
MTF measurement via diffraction shearing with optically superimposed gratings 79−64366
MTF tolerancing computer program 80−78934
multi-element, defective surfaces, tilt meas. 78−66886
multi-lens focusing systems for energy Nd:glass lasers 78−50848
multiple lens experiment 80−82596
multiple point hologram lens array generation, appl. to micro-electronic mask making 80−95842
negative, with laser rods, distributed aperture effect 80−38046
negative system astigmatism and coma anal., third order aberration theory appl. *(Russian)* 78−30039
night vision system with refractive optics, glare characts., surface defect influence 79−32024
nodal slide, experimental and theoretical thick lens parameters comparison 80−67998
nonastigmatic spectacle, structural design parameters *(Russian)* 80−87460
nonimaging concentrators, two-dimens., with refracting optics 79−81504
nonsymmetrical optical system, matrix representation 80−64130
nontracking solar collectors, wide-angle lenses and image collapsing subreflectors 80−76603
objective, concentric, longitudinal spherical aberrations calc. method *(Russian)* 78−71184
objective, two-channel device for meas. transmission coeff. 80−106642
objective decentring modulus, probability density distrib. calc. 79−76798
objective design with reduced secondary spectrum 77−7172
objective for holographic recording devices 79−32028
objective lens manufacturing, present status and future prospects 79−94323
objective lens quality, effect on S/N ratio in scanning optoelectronic system 77−10111
objective time-varying lateral aberration meas. 79−76797
lenses continued
objectives, commercially manufactured, probability analysis of centring accuracy 78−90491
objectives, high performance, assembling technology, trends *(German)* 78−71182
objectives, tolerancing of refr. index heterogeneity 80−78948
objectives, visible and UV, for microscopes and microspectrophotometers 79−75591
objectives' two-dimensional transfer functions, holographic meas. test 79−50253
ocular design, new type, experiences from common ocular testing 79−18501
oculars of optical sights, for target and hunting guns 77−58419
ophthalmic, Schott S-1005, static fracture resist. rel. to thickness 78−81063
ophthalmic correcting cylinder axis, ophthalmometric prediction 80−98174
ophthalmic lens, choosing the base curve 79−29664
ophthalmic lens distortion display 78−7338
ophthalmic lens surface working machinery 80−28363
ophthalmic lenses, basic principles of fracture testing 79−96233
ophthalmic lenses, effectiveness against beta radiation 77−66862
ophthalmic lenses, longit. spherical aberration and its effect on visual acuity 80−99816
ophthalmic lenses, thin, chemtempered, static load strength testing 80−5812
ophthalmic lenses, thin, chemtempered, strength meas. by drop-ball testing 80−5811
ophthalmic materials evaluation 79−92426
ophthalmolscopic and vision function meas. instruments 79−96689
optical, vision sharpness corrective devices *(Hungarian)* 78−15823
optical axis designation method 80−102798
optical beam-guide lines, elec. length instability 78−46748
optical CAD, conf., San Diego, CA, USA (Aug. 1978) 79−86228
optical components testing for thermal imaging systems 78−33911
optical device performance assessment, British standards 78−50729
optical fibre connector for keyboard lens finger detection 80−19095
optical fibre coupling using graded-index rod lenses 80−91891
optical fibre excitation by lenses 79−32057
optical fibre hemispherical microlens tip fabrication for high efficiency coupling to InGaAsP laser 80−69505
optical fibre high index hemispherical microlens tip melt fabrication for coupling to GaAlAs laser 80−69506
optical glass selection for lens design 79−81496
optical relay, system design, secondary colour reduction 78−83067
optical rotation multiplier, lens-mirror reflector system *(Russian)* 78−46745
optical system design, advances and problems 79−36975
optical waveguide lenses, review *(Japanese)* 80−10019
optimised spheric and aspheric optical systems for thermal IR 79−86244
optometry, perceptual effects of low-power plus lenses in emmetropic observers 80−67084
optotransducers, electronic compensation for dirty lenses 80−68189
OTF, numerical calc. from lens design data *(Korean)* 80−19085
OTF calculation using gaussian quadrature, rel. to lens system design 78−90383
OTF quantitative image analysis, lens system evaluation 80−53481
OTF standardisation activities in Netherlands 78−50728
OTF standardisation in Japan 78−50726
OTF test standard, afocal system 79−36978
OTF testing, development and implementation of instrums. 77−19383
OTF testing, USA standards 78−50725
pancratic apochromatic objectives, variable focal length, design 80−53404
pancratic objectives, aberration stabilisation during focusing 80−102799
pancratic sights for sporting and hunting guns, design 78−71192
pancratic systems with linear and nonlinear relations between component motion, comparison 78−13782
parabolic gradient index lens, SELFOC, chromatic aberration in imaging system 80−14422
paraxial air angles between cemented surfaces, calc. 79−76799
paraxial eqn. dimensional analysis 80−74462
paraxial solves in lens design, ACCOS V program style 79−86229
pendulum controlled solar tracking system and concentrator 79−62122
perfect lens with polarisation masks, OTF 78−90380
Perspex for astronomical telescope lens manufacture 78−36458
phase conjugate adaptive optical systems, convergence 77−46688
phase plate consisting of bleached holographic lens, for noise-free coherent imaging systems 79−31817
photolithographic application 79−36976
photoresist microlens production for semiconductor lasers 78−9398
PIR-1 instrument for laser radiation divergence meas. 79−23001
planar acoustic microscope lens using Rayleigh to compressional conversion 80−87668
planar optical elements, dispersion props. 79−3811
plane parallel lenses, prep., theory 79−3761
plane plates, two sets of different physical props., energy flux splitting *(German)* 79−18500
plane step lens principle and solar energy utilisation *(Chinese)* 79−81512
plano-cylindrical Fresnel plastic lens, design and performance analysis as solar collector 80−53403
planoconvex lenses in unfolded cavity, for CW mode-locked dye laser 80−5765
plasma, unipotential, for proton beam focusing 79−41326
plastic focusing fibre for imaging appls., fabrication and characts. 77−62040
plastic gradient index lens fabrication and image evaluation 80−14426
plastic lens manufacture, mould punch surface radii calc. 77−799
plastic modular solar energy collector with reticulated foam 80−16833
plastic optical components, flexible rapid curing abrasion resistant coated film 78−66890
plastic optics, design patterns 79−32009
plastic optics for optoelectronics, moulding techniques for single, multi-element systems 78−63210
plastic rods, light focusing, prep. by two step copolymerisation of diallyl phthalate with methyl methacrylate *(Japanese)* 79−37064
plastics appls. in optical systems 79−32008
point spread modification by polarisation masks 77−65615
polycarbonate ophthalmic-prescription lens series 79−81501
polychromatic MTF measurement reproducibility 78−50719

lenses continued
polychromatic thick lens glass selection *(German)* 80−23763
precision objectives, high resolution, image-forming quality *(German)* 78−87120
prescription lenses, attenuation of diagnostic X-rays 79−92395
pressure-shaping components, glass bending monitoring 77−796
principles, w.r.t. electronics engineer appl. 77−83818
production cost reduction appl. of CAD 79−86239
production technology advances, seminar, London, England (April 1979) 80−67938
production tests for IR lenses 78−50890
projection, 35 mm cinema projections 80−87469
projection photolithography 77−58423
proof glass superposition method for testing convex spherical surfaces, errors 77−75649
pulse shaping and compression using electrooptic deflector with Fourier optical elements 80−53421
quality measurement using lateral shearing interferometer with variable shear *(German)* 80−22425
quasi-Ronchigrams for interpreting wave-front and glass-error slopes 80−37078
radial gradient-index, with zero Petzval aberration, third-order aberrations 80−69484
radial refractive index gradient optical element, off-axis aberrations 80−14423
radiation safety glasses, physical factors determining the utility 80−46067
rainbow hologram by one-step process 78−71062
ray trace program, TI59 calculator 79−32023
ray trace program for TI-59 calculator with PC100A printer 79−89985
ray tracing, generalised, caustic surfaces 79−23043
ray tracing algorithm for programmable pocket calculator 79−81508
ray tracing in general index distributions 80−14279
reflection conic, obtaining 360 degree panorama 79−86246.
refractive index gradient tolerance in optical elements 78−71179
refractive systems for IR apparatus, design *(Japanese)* 78−55428
relay optical system, derivation and appl. of Gaussian design relationships 78−94424
replicated and plastic optics, conf., San Diego, USA (Aug. 1977) 78−66961
residual wave aberration due to schlieren, diminished image quality *(German)* 77−14788
resin polishers, holders, and tools 80−33248
resonator, annular, adaptive mirror effects on performance 80−58596
restricted laser beam polar diagrams *(Russian)* 80−14381
scanning gauge for surface form meas., spherical and aspherical 79−32100
scattered light measurement for lenses and spectacle lenses *(German)* 78−46746
secondary spectrum, of thin three-lens optical systems *(Russian)* 78−57456
self-aligned sphere lens for AlGaAs DH LED *(German)* 78−38014
self-centring technique for mounting microsphere coupling lens on fibre 80−74517
SELFOC for optical fibre communication devices 78−74989
Selfoc lens, aberration improvement by glass composition and ion exchange process parameter choice 80−69486
Selfoc lens as imaging system, chromatic aberration 80−69480
Selfoc lens use in damage-free optical fibre connector 78−46829
silicone rubber, room temp. vulcanising, as variable focal length lens 78−66888
silicone-glass hybrid Fresnel lens for solar energy concentration 80−61303
simple Gaussian lens equations, content expansion and expansion of usefulness 77−42586
simple lens shape effect on image curvature 79−50368
single lens processing system, virtual Fourier transform as analytical tool 78−71036
slit image seen in total internal reflection *(French)* 80−95810
solar cell power supply, high concentration, components, design, technology and performance 80−50955
solar collector, compound parabolic type, optical and thermal design 77−23735
solar concentrator, plano-cylindrical Fresnel type, line-focusing anal., expt. 77−23732
solar concentrators, design variables, optical efficiency, heat loss coefficient and heat removal factor 80−7927
solar energy, photo-optical instrumentation, [Conf. San Diego, CA, USA Aug. 1978] 80−7926
solar energy concentrator appls. of Fresnel lenses 78−83065
solar energy concentrator designs for underdeveloped countries 79−62125
solid laser thermo-optic lens temp. distrib. and focal length calc. 79−72575
spatial filter, lens-pinhole, student laboratory apparatus appl. 79−62976
speckle interference fringes, lens aberration effects 80−105700
speckle interferometry, lens aberration effects, optical system pupil complex amplitude changes *(French)* 79−50237
speckle photography, effect of lens aberrations 78−32866
spectacle, image quality *(Russian)* 80−87463
spectacle, surface grinding and polishing, using automatic and semi-automatic machines *(French)* 80−58822
spectacle lens design, computation of unwanted sphere and cylinder in periphery 78−48928
spectacle lens inspection apparatus *(French)* 79−7235
spectacle lens test facility complex 79−39603
spectacle lenses, eye testing using screen image divider 78−57114
spectacle lenses, hard resin, comparative study of bitoric effect 80−91877
spectacle test lenses, large set 79−92427
spectrograph lenses, optical parameters 79−97440
spherical cementing fixtures for holding lenses by rigid method 80−96043
spherical glass beads in highway pavement markings, retrorefl., specular refl. 78−74837
spherical glass beads in highway pavement markings, retrorefl., diffuse refl. 78−74838
spherical lens generator, sphericity and fracture control 77−27394
spherical surface error absolute definition technique, use in interferogram analysis 79−86268
lenses continued
spherical surfaces shape deviation determ., using sphero-interferometer *(Czech)* 80−58821
spherical-cylindrical lens combination, combined 1-D image-orthogonal Fourier transform processing 80−58658
sphericity non-contact testing method *(German)* 78−5534
square Fresnel lens design for illuminating circular solar cells 78−79099
standard reference lens, for MTF equipment testing in IR 78−50898
standard reference lenses, for assessment of OTF meas. equipment 78−50897
star simulator design 78−85814
stigmats using two curved Fresnel surfaces 80−38084
strain and centering sensitivity computation in paraxial region *(German)* 79−55202
Straubel apodisation filters, equivalent passband 78−50880
stray light reduction from optical components 78−59114
superachromatic triplets, design method 80−64133
superachromatization, glass combination selection 78−1315
superposition fringes as measuring tool in optical testing 79−86267
surface acousto-optic lens, Fourier and Mellin transform props. 78−78926
surface geometry model, high-speed generating, smoothing and polishing 78−50889
surface light scattering rel. to microtopographic features 79−59639
switch constructed of graded-index rod lenses, for multimode fibre systems 79−27439
systematisation of mirror lenses according to extent of central obstruction *(German)* 80−102795
tapered microlens for optical fibre coupling, high efficiency *(Korean)* 80−43449
target and hunting gun optical sights 79−72664
teacing, lens object-image relations 78−36780
telescope, two-mirror objective systems, field lens group corrector 80−78945
Tessar-type lens, aberrations, automatic correction routine 80−58464
testing, MTF-based optical sensitivity and tolerancing computer programs 80−83686
testing, simplified Talbot interferometers 77−757
testing at 1.06 μm, using laser unequal path interferometer 78−49893
testing of long-focus optical systems, vibr. insulation of equipment 78−90543
thermal in active elements of solid lasers, focal distances meas., using Zernike interferometer 80−48268
thermo-gasdynamic control in laser beam guidance, review of developments 78−74942
thin films, lens formation, alternating elec. field effect 80−12060
thin lenses formulae for teaching purposes 79−35509
thin sheet Fresnel solar collector-concentrators, features and economic benefits 79−79402
thin three lens cemented components, performance calc. 77−75652
three layer optical waveguide for photolithographic fabrication of film lenses 77−39113
three lens cemented objectives, spherical aberration correction 77−88894
three-component objective, with telecentric ray paths and lengthened rear section, design 77−54771
three-dimensional image transmission by lens guides 79−76789
three-element lens optimisation by damped minimum method *(German)* 77−23726
three-lens cemented component calcs., reduced secondary spectrum 80−102800
time resolution of optical lenses for sub-picosec. processes 77−39012
tolerance sensitivities inclusion in merit function for lens optimisation 79−86236
tolerancing, statistical approach 79−86238
tolerancing procedure based on MTF 79−86237
transmission and MTF in 8-13 μ band 79−36982
transmissive optics for high power CO_2 lasers 78−79057
travelling wave lens, optically excited soft X-ray laser technique development 78−59016
triplet lens for fibre-optic bundle 80−14414
TV camera zoom lenses, glare characts. 79−10373
two-lens afocal compensators in high-resolution lens objectives, design 80−33125
two-lens standard phase inhomogeneity 79−14111
ultrashort pulse operations using flat lenses 78−66883
underground beam-guide lines with periodic light beam corrections 80−33196
US, three compartment variable focus 78−94499
US lens, symmetrical doublet with F 1 aperture 77−14869
US lens transmission variations and interfacial effects 78−59176
UV objectives, for submicron photolithography 79−32032
variable magnification three component system, fabrication errors 77−88895
variable-scale single-lens optical transform systems 80−58656
varifocal compensated lens for flow cells irrad. 79−27357
vision, eikonic lens design for minus prescriptions 80−46095
vision, TiO glass lenses and astigmatism of oblique rays *(Italian)* 80−56278
vision correction lens, hyperopic eye functional visual acuity at intermediate range 78−48791
visual field testing, three-channel optical system *(Spanish)* 79−24993
water soluble cryst., protective coating to aid polishing 80−33250
wave passage through lens focus, phys. course demonstration *(Russian)* 77−13550
wavefront aberration, interferometric examination techniques 80−69498
waveguide connector, detachable, for multimode graded-index optical waveguide 78−46830
waveguide lens technologies for RF spectrum analyser 77−34961
waveguide lenses, Bragg and Luneburg type 80−10050
waveguide Luneburg lenses, diffr. limited, mask synthesis for sputtering production 78−38076
waveguide optical collimator, Luneberg lenses with plane connecting waveguides 79−68446
wide-angle five-lens eyepiece 79−46027
Wolter lens component replication 80−95972
X-ray diffraction lens, image form. 77−10154
zero Petzval curvature radial gradient index lens, third-order aberrations 80−14424
zonal spherical aberrations in optical systems, correction, use of aplanatic lens 79−27360

lenses continued
zoom and multiconfiguration optimization using the indices of refraction to represent zoom modes 79−86232
zoom lens, aperture diagram *(German)* 77−39016
zoom lens, Delano and aperture diagram *(German)* 78−13779
zoom lens design by pocket calculator 78−55423
zoom null lens design for optical component and system testing 80−23811
zoom objective, displacement of individual lenses from ideal positions *(German)* 78−71186
ZTL-180 zenith telescope, objective distortion determ. from visual obs. of star pairs *(Russian)* 78−89068
CdS nonlinear lens, with variable focal length 79−81511
GaAs film optical components, prep. by MBE using Si shadow masking technique 80−28358
GaAs integrated LED/sphere-lens source for optical fibres, coupling efficiency calcs. 80−43433
Ge IR optical characteristics and performance requirements 80−48363
Ge, monocryst., for IR optics, prod. techniques and characts. 78−50873
Ge, polycrystalline thermal-imaging lens, optical requirements 80−69495
$LiNbO_3$ waveguide, form. of geodesic lenses 77−88966
$LiNbO_3$:Ti waveguide geodesic lens 77−84005
Nd:YAG laser, thermal lens effect on emission stability 80−19064
Si:B(P)(As), single cryst., transmission charects. for IR optical components 77−27325
SiC nonlinear lens, with variable focal length 79−81511

lepton-deuteron interactions
see also lepton-deuteron scattering
Coherent Tube Model for very high energy inelastic interactions of deuterons 77−18347
ed→np, dispersion approach *(Russian)* 77−22737
neutral current processes, factorisation and coupling constant determ. for νe, ed, and ν+hadron 80−27451
nucleon Fermi motion in deuteron, smearing effects, (West β correction), on expt. results. 80−32107
West correction to total cross-section of scatt. from deuterons or nuclei 77−2958
d(e,e′p)n, 500 MeV, coincidence cross section and deuteron momentum distrib. 79−67747
d electrodisintegration, Δ resonance admixtures in NN problem, OBE model 78−70373
e+d, deep inelastic scatt., nucleon structure functions 78−50036
ed, 2.3 GeV, inclusive electroprod. cross sections for final state nucleons 77−34159
ed, deep inelastic scatt., quark-parton model with logarithmic scaling violation 80−78071
ed, EM inelastic form factors, exchange current effects in electrodisintegration 79−93418
ed, elastic and inelastic scatt., quarks and dimensional scaling 77−6132
ed, strongly inelastic, in region forbidden to single nucleon scatt. *(Russian)* 77−6130
ed deep inelast. scatt., struct. function, dispersion anal. of deuteron 77−2795
ed deep inelastic scatt. at 19.4 GeV, polarised electrons, search for P violation 77−34156
ed deep inelastic scatt. cross sections, quark-parton model with broken scaling *(Russian)* 80−32109
ed→eX, polarised deep inelastic scatt., test of Weinberg-Salam model 79−22006
ed→e′NΔ, electroproduction cross section for reson. $\Delta_{3/2}$ *(Russian)* 77−67737
ed→epn, polarised deuteron disintegration, virtual nucleon density matrix formalism *(Russian)* 80−52519
ed inelastic scatt. at high momentum transfer, scaling anal. 77−26531
ed→pn, disintegration and Coulomb excitation cross sections in channelled nuclei 80−59539
ed scattering, neutron struct. function extraction, space-time descript. 78−62404
$e^-d \rightarrow e^-\pi^+nn$, $e^-d \rightarrow e^-\pi^-pp$, forward prod. of single pions in resonance region 78−37219
$e^{\pm}d \rightarrow e^{\pm}np$, polarised, parity violating asymmetry 80−78080
Ld→l′ΔX, deep inelastic scatt., isobar admixture possibility *(Russian)* 80−91095
μ+d, deep inelastic scatt., nucleon struct. functions 78−50036
$\mu^-d \rightarrow nn\nu_\mu$, neutron-neutron off shell interaction differential capture rates 79−71845
$\mu^+d \rightarrow \mu^+np$, ≤5 MeV, Coulomb break-up of deuteron and n-p off-shell effects 79−75777
$\nu(\bar{\nu})$ d, disintegration reactions, helicity flipping neutral currents, tensor coupling 77−49944
$\nu d \rightarrow \Delta_c^{++}X$, high energy charmed baryon prod. obs. 80−105881
$\bar{\nu}_e$d, evidence against axions 79−13108
$\bar{\nu}_e d \rightarrow nne^+$, cross sections, neutrino programme at ILL 79−67540
$\bar{\nu}_e d \rightarrow np\bar{\nu}_e$, cross-section calcs. 80−42440
$\bar{\nu}_e p \rightarrow ne^+$, cross sections, neutrino programme at ILL 79−67540
ed→e′pn, 1180 MeV electrons, proton distribution, neutron momentum distribution *(Russian)* 80−68652
^{2}H, weak and EM lepton reactions, exchange currents, isobaric excitations and form factors *(German)* 79−93523

lepton-deuteron scattering
see also lepton-deuteron interactions
nonscaling behaviour, p-n and d struct. functions 78−8642
nucleon structure from electron scatt., EM form factors 80−42468
nucleon structure functions from quark distrib. functions anal. of μp and μd interactions 78−50035
ed, EM form factor determ., relativistic impulse approx. 77−65158
ed, polarisation effects in presence of weak neutral current *(Russian)* 77−61291
ed, quasi-elastic scatt. and form factor of n 78−82210
ed, strongly inelastic, in region forbidden to single nucleon scatt. *(Russian)* 77−6130
ed→ed, nucleon forces, meson exchange current effects, impulse approx., review 80−57603
ed→ed*, dibaryon resonance production 80−78070
ed elastic scatt., EM form factors, relativistic harmonic oscillator model 79−54327
ed elastic scattering, neutral weak currents *(Russian)* 78−21434
ed→epn, recent developments in lepton scattering 79−80929
ed large angle elastic scatt., deuteron mag. struct. function meas. at 1.0 $(GeV/c)^2$ 77−57537

lepton-deuteron scattering continued
ed scatt., meson exchange currents for deuteron form factor 77−18290
$\nu(\bar{\nu})$d, scatt., weak hadronic neutral current struct. investig. 80−42438
ed elastic scatt. at high momentum transfer 80−82977

lepton-hadron interactions
see also lepton-hadron scattering; lepton-nucleon interactions
$(\phi^3)_6$ field theory, deep inelastic lepton-headron scatt., cut vertex theory and reciprocity relation 80−57466
angular correlations of final state leptons and hadrons, quark-gluon dynamics 79−395
asymptotic freedom and local duality 77−71518
asymptotic freedom and parton model appl. to leptonic processes 80−4959
asymptotically free theories of deep inelastic muon, and electron scatt. 78−21430
Bjorken scaling deviations, constituent quarks in nucleon 77−6089
charm changing charged current, chiral struct. anal. 77−13964
conference, lepton-hadron physics, Karlsruhe, Germany (Sep. 1978) 80−73098
conference on high energy phys. with polarised beam and target, Argonne, USA (Oct. 1978) 79−63526
deep inelastic lepton-hadron scatt., semiinclusive hadron prod., quark fragmentation function corrections, QCD 80−63013
deep inelastic lepton-hadron scatt. in massive vector gauge models 78−74262
deep inelastic muon hadron scatt. data, high energy, asymptotically free gauge theories predictions 77−49974
deep inelastic processes, QCD predictions 80−73677
deep inelastic scatt., corrections in asymptotically free field theories 77−38092
deep inelastic scatt., evidence for quarks 79−93430
deep inelastic scatt., hadron secondary average transverse momentum, comparison with e^+e^- annihilation 80−37281
deep inelastic scatt., mass corrections, asymptotically free theories 77−61297
deep inelastic scatt., proton deep structure, renormalisation group approach, review 79−85302
deep inelastic scatt., proton struct. function higher order asymptotic freedom corrections 80−105905
deep inelastic scatt., QCD event states, 3-jet events 80−52515
deep inelastic scatt., Regge behaviour, Bjorken scaling 77−244
deep inelastic scatt., review, book contrib. 80−47260
deep inelastic scatt., six-quark model of weak and EM interactions *(Russian)* 77−67658
deep inelastic scatt. and lepton pair prod., covariant parton model approach to scaling 78−21431
deep inelastic scattering, contrib. of twist-four operators, struct. functions 78−78187
deep inelastic scattering, QCD and model-independ. theory *(German)* 79−58965
deep inelastic scattering, source theory anal., polarisation 77−34160
deep inelastic scattering 80−73717
deep inelastic structure functions, moments, q^2 analyticity props. 78−78188
deeply inelastic electron scatt., QCD high energy predictions using methods of cut vertices 79−89128
duality hypothesis, predictions for Compton amplitudes 77−30388
electron deep inelast. scatt. processes, Ward identities, struct. functions *(Chinese)* 79−93431
electron-hadron interactions, P-invariance, lepton, quark anapolar moments with pol. e *(Russian)* 80−52518
electron-meson deep inelastic scatt., sea quark contrib. in 1/N 2-dimens. QCD 80−47307
fragmentation functions beyond leading order in QCD 80−13282
hadronic μ-pair prod., hadron mass corrections and parton transverse momentum 79−36034
hadronic quantum numbers beyond charm as possible source of neutrino induced trimuons 78−12903
hadrons and quarks in high energy collisions, review 79−49482
high energy hadronic collisions, similarities, universality prop., reaction mechanism 78−33090
hydrodynamical model for high-energy interactions *(Russian)* 77−229
inclusive, ξ scaling variable anal. 77−61298
inclusive, local duality and precocious scaling 77−2842
inclusive, quark and target mass effects, colour SU_3 theory 77−6090
inclusive cross sections, kinematical scaling violation 78−8671
inclusive leptoproductions, scaling violation, colour-octet model effect 79−13077
inelastic scattering, bremsstrahlung of gluous *(Russian)* 77−2839
jet anal. in lepton-hadron deep inelastic scatt. from QCD 79−40785
jet and lepton-pair production in high-energy lepton-hadron and hadron-hadron scattering 79−17729
jet production mechanism in lepton-hadron interactions, cascade and uncorrelated jet models 80−52516
Jost-Lehmann-Dyson representation, scale invariance breaking and spectral function 80−13316
large-small momentum transfer regions, transition point for s-depend. 77−30339
lepton pair production, QCD jets 80−62994
lepton-hadron hard reactions, scaling features, correlating quark rearrangement model 79−58939
multi-jet dynamics in lepton induced reactions, granular struct. calorimeter anal. 79−9350
neutral current processes, factorisation and coupling constant determ. for νe, ed, and ν+hadron 80−27451
perturbative aspects of QCD, an introduction 79−30714
perturbative QCD, recent progress 80−42418
polarised deep inelastic electroprod., QCD higher order effects, sum rule correction 79−93428
polarised deep inelastic scatt., parton transverse momenta role, struct. function, QCD evolution 80−78034
polarised electron deep inelastic scatt., asymmetry anal. 77−34158
QCD phenomenology of deep-inelastic scattering 80−73660
quantum chromodynamics, two dimens., confinement form factors, deep inelastic scatt. 77−30322
quark fragmentation functions for inclusive hadron production, Regge formalism 80−68462
scaling of inclusive form factors with respect to a generalized scaled variable 80−417
scaling violations, parton model anal. 78−62406

lepton-hadron interactions continued
scaling violations in deep inelastic lepton scatt., charm quark prod. 78−21436
structure functions, deep inelastic renormalisation group sum rules 80−22611
sum-rule for deep inelastic lepton+hadron scatt. 77−79233
symmetry principle, history of search for fundamental constituents of matter *(Polish)* 78−54588
e(μ)(ν) deep inelastic scattering, minimal mass corrections 79−30740
e^-+hadron→e^-+X, WKB calc., hadronic amplitudes in scaling region 78−41484
$e^+e^-h \rightarrow e^-X$, h=hadron, structure functions in next to leading logarithm approx., ϕ^3 field theory 80−37268
$e^-h \rightarrow e^-X$, bound states and asymptotic limits for QCD in 2-dimens. 79−71716
$e^-\pi \rightarrow e^-$+hadrons, spectator interaction effects in large $p_\perp$ deep inelastic processes 79−93427
in deep inelastic scattering, quark jet as trigger for gluon jet 80−62996
$\nu\pi^+$, semi-inclusive deep inelastic scatt., π struct. functions 79−26323
πe→πγe, dispersion relation anal. ργγ vertex 78−45971
πμ, anomalous short-range interaction anal. in $K_L^0 \rightarrow (\pi\mu \text{ atom}) + \nu_\mu$ 78−8660

lepton-hadron scattering
see also lepton-hadron interactions; lepton-nucleon scattering
Bjorken asymptotic behavior of deep inelastic scattering form factors and the general principles of field theory 79−21958
deep inelastic, from compound particle in scale-invariant quark model *(Russian)* 77−22740
deep inelastic lepton scatt., QCD perturbation theory test, review 79−326
deep inelastic scatt., higher order QCD corrections 79−97629
electron deep inelastic scattering, very high energy, correlation functions 78−74261
field theories appl. to lepton-hadron scatt. 78−74257
lepton pair prod. in processes with hadronic jets 80−27512
massive vector gauge model for deep inelastic scatt. *(Russian)* 78−89720
neutral current isobar prod., polarisation effects 77−18220
perturbative QCD, hard hadronic processes, e^+e^- annihilation, lepton-hadron deep inelastic scatt. 80−52477
polarised beam and target, review and survey of expts. and theoretical implicatons 79−67560
polarised lepton scattering, lepton and quark anapole moments *(Russian)* 79−17730
QCD perturbation theory calc. of transverse momentum distrib. in lepton-hadron scatt. 79−89163
scaling, generalised variable in parton model 77−10259
supersymmetry, field theory, fermion (meson)-meson scatt., high energy behaviour 79−295
trimuon final states, prod. mechanism model independent study, selection rules 79−93424
$U(1)\times SU_L(2)\times SU(3)$ theory, integer charge quarks, lepton hadronic processes *(Russian)* 80−86653
eπ inelastic scattering, asymptotic bounds on π form factor 78−12917
K_Le, 30 to 100 GeV, K_s regeneration, K^0 charge radius meas. 79−400
πe, 16 GeV, absolute differential cross-section meas. 79−40780
πe elastic scatt. at 50 GeV/c, π EM size 78−4862

lepton interactions *see lepton-deuteron interactions; lepton-lepton interactions; photon-lepton interactions*

lepton-lepton interactions
see also electron-electron interactions; electron-positron interactions; lepton-lepton scattering; neutrino-electron interactions; neutrino-neutrino interactions
diagonal equiv. photon density matrix 77−237
multi-jet dynamics in lepton induced reactions, granular struct. calorimeter anal. 79−9350
tauonium: $\tau^+\tau^-$, a bound state of heavy leptons 78−37194
unpolarised lepton-lepton collisions, photon 3rd struct. function, QCD implications 80−73708
$l\bar{l} \rightarrow$meson→γγ, CP nonconservation 79−58899
μe→γγ, muonic number nonconservation, pole model anal., total and differential cross sections *(Russian)* 79−80817
μe^-, 10 MeV to 10 GeV electron energy transfer, target Z/A depend. of cross section 77−30355
$\mu^+e^- \rightarrow \mu^-e^+$, $\mu^+\mu^-$, high energies μ number nonconservation, Higgs boson effects 78−45806
νl, Weinberg model, differential and total cross sections *(Russian)* 77−6112
$\bar{\nu}_l l \rightarrow$hadrons, amplitudes, cross sections, V-A theories 77−10239
T particle at 9.4 GeV, differential dispersion relations theory of l^+l^- annihilation 78−86424

lepton-lepton scattering
see also electron-electron scattering; electron-positron scattering; lepton-lepton interactions; neutrino-electron scattering; neutrino-neutrino scattering
muon scattering at Fermilab, inclusive scatt., quark models, scaling violation 80−5001
eμ, weak lepton interaction influence, weak, EM and interference ratios *(Russian)* 79−6333
eμ elastic scatt., possible weak interaction effects, Weinberg-Salam model estimates 79−75755
μμ, fourth order contrib. in gauge theory of weak interactions 77−38117
$\nu_\mu e \rightarrow \nu_\mu e$, weak and EM radiative corrections, sensitivity test 80−105880
$\nu_l l' \rightarrow \bar{\nu}_l$ processes, possible T-violation, phenomenological model of neutral currents 77−30359

lepton mass
charged leptons, mass formula, EM self energy relation to new quantum number n 80−13244
charged leptons, mass formulae from EM self energy *(Chinese)* 79−93416
chiral charge space, statistical analysis 80−42428
cosmological limitations on masses of neutral leptons 77−82800
dynamical Higgs mechanism, weak ΔI=1/2 rule, sum rules, heavy quarks and leptons 80−27442
E_6 model of unified interactions, asymptotically free, mass relations and interactions 80−73642
electron mass, calc. in left-right-symmetric model 79−26282
electron mass, truncated, gauge dependence 80−22542
electron mass operator in 2-D QED approx., radiative convections 80−4900

lepton mass continued
electron theory, chronon, charged-lepton mass formula 80−47224
electron-muon mass ratio, $SU(2)\times U(1)\times D_4$ symmetry model 79−89090
electroweak symmetry group, B-L U(1) generator and quark-lepton symmetry 80−57549
formula for mass ratios of known charged leptons *(Russian)* 79−93478
generation model from QED 80−375
grand unified model, Yukawa coupling radiative corrections, lepton and quark masses 79−97555
heavy lepton, mass determ. from inclusive hadron spectrum in dd e^+e^- annihilation 77−18304
heavy lepton decay, spin $^3/_2$, intermediate vector boson corrections 80−73761
heavy lepton mass spectra similarity with heavy quark masses 79−67508
heavy leptons, in beam dump expts. 78−66185
heavy leptons, theory 77−57582
heavy leptons as a source for dimuon events 77−54093
heavy leptons prod. via decays of heavy vector mesons 77−89774
heavy neutrino mass, cosmological upper limit from big bang model 80−8728
Higgs bosons, effects on experimental observables, and fermion mass scale 80−32061
horizontal-quantum-flavor-dynamics approach to the fermion mass spectrum in $[SU(2)\times U(1)]_{WS}\times U'(1)$ gauge 80−52474
lepton and quark spectra difference eqns., τ and toponium mass 80−22589
mass formula deriv. 79−58995
mass hierarchy in vectorlike theory with Majorana particles 77−18366
minimal O(10) grand unification, ν mass 80−57546
mixing angles of leptons in an extended Weinberg-Salam model 79−71679
muon-electron mass ratio in a semi-classical model 80−91072
neutral fermion masses, improved lower limits 77−82799
neutrino, limitation to less than 30 eV by cosmology 79−6358
neutrino mass problem, gauge hierarchy 80−90989
neutrino oscillations, mass and mixing scales 80−105823
neutrino oscillations in gargamelle experiments, limit 77−22723
neutrino rest mass, effects on Universe density perturbations spectrum and microwave background small-scale fluctuations *(Russian)* 80−109576
neutrino rest mass, implications for Universe density perturbations evolution and galaxy clusters hidden mass *(Russian)* 80−105414
neutrinos, rest mass rel. to mass density and age of Universe *(Russian)* 80−109575
O(10) theory of strong, weak and EM interactions, masses and mixing 80−13248
relativistic mass correction to spin mag. moment of moving particle 77−57213
SO(10) grand unified theory, breaking scheme and neutrino mass 80−47230
spectrum law for leptons and quarks 79−93338
stable method heavy leptons, astrophysical mass constraint, condensation in stars and galaxies *(Russian)* 80−72768
$SU(2)_L\otimes SU(2)_R\otimes U(1)$ weak model, ν mass and spontaneous P nonconservation 80−62884
$SU(2)\times U(1)$ gauge model, chiral $SU(2)\times SU(2)$ symmetry and electron mass 80−57542
$SU(2)\times U(1)$ gauge theory, μ-e mass ratio and CP violation as quantum effect 79−30691
$SU(5)\times SU(2)$ unification, horizontal symmetry due to quantised motion along internal axes 80−62905
SU(5) grand unification, strong CP violation, quark-lepton mass ratio 80−32057
SU(s) grand unification, neutrino mass and oscillations, B-L nonconservation 80−52449
unification of EM, weak and strong interactions, quark and lepton mass, quark fractional charge, baryon asymmetry 80−73637
unified gauge model based on E6 80−32053
unified weak and EM theory without scalar fields 79−75709
V-A six lepton model without the separate conservation of lepton numbers 77−87930
e, calculation from fine struct. const, muon mass, Weinberg angle 78−66180
e, moving in external EM field, radiational mass corrections 77−61226
e, self mass in QED 78−89641
e, self-mass in semiclassical limit 78−33008
e-μ mass ratio, regularisation 80−9090
e-μ mass ratio, spontaneous symmetry breaking with quaternionic scalar fields 77−61236
e-μ mass ratio 78−93825
e-μ puzzle and EM coupling const. 77−79240
e-p mass ratio, past variability limits set by quasar absorpt. line redshifts 77−61338
e^+, heavy electron, mass limits 78−8640
$e\bar{e}\nu_e\bar{\nu}_e$ mixture, transport eqns. for massive components 77−74315
heavy charged, mass determ., QED 79−9314
μ, mass from generalised Dirac eqn. 78−33011
μ-e mass quotient, modified Weinberg-Salam model calcs. *(French)* 80−82926
μ-e spontaneous mass splitting and universality 77−30302
$\mu^+\mu^-$, mass spectrum in prod. by protons on tungsten 78−89857
ν, mass and Pontecorvo oscillations 78−36879
ν, non zero mass, implications for $\gamma\gamma \rightarrow \nu\bar{\nu}$ 78−21485
$\bar{\nu}$, rest mass upper limit from ^{3}H B-decay meas. *(Russian)* 78−17144
ν mass, second-order effect in Higgs coupling 79−75716
ν masses and SO_{10} hierarchical breaking 80−22550
$\bar{\nu}_e$ mass from ^{3}H β-decay spectrum *(Russian)* 80−91159
ν_e mass from ^{3}H β-spectrum in valine molecule 80−91158
ν_μ, mass range 100 to 500 keV_s discussion 79−63570
ν_τ, grand unified field theories, mass relations and renormalisation effects 79−49436
ν_τ, mass, lifetime, decay modes and mixing angles 80−445
νμ, exptl. limits on mass and decay liftime 77−10234
$\nu\mu$, mass limits in absence of muon-lepton number conservation 78−21368
νμ mass and lifetime, exptl. limits 77−50039
$\nu\tau$, mass and number, cosmological constraints 78−45444
$\nu\tau$, mass in charmed meson decay *(Russian)* 78−62394
$\pi^0 \rightarrow \nu\bar{\nu}$, neutrino mass test 79−93406
τ, decay modes and mass 78−29325
τ, M=1.777 GeV, DELCO expt. 78−89693
τ, M=1.807 GeV, DORIS expt. 78−89765

lepton mass continued
τ, mass and coupling props. from e^+e^- annihilation studies 78−4849
τ, precise mass determ. 78−89695
$\tau \rightarrow \nu_\tau e \nu_e$, nature of τ-ν_τ-W coupling, ν_τ mass upper limit and lifetime 79−40824

lepton-nucleon interactions
see also electron-nucleon interactions; lepton-nucleon scattering; muon-nucleon interactions; neutrino-nucleon interactions
amorphous state analogy 79−54370
broken SU(6) parton model, spin depend struct. functions, deep inelastic lepton+nucleon appl. 78−428
deep inelastic hadron leptoproduction on nuclei, inclusive hadron final states 78−54741
deep inelastic lepton-nuclear scatt., final state polarisation 78−458
deep inelastic lepton-nucleon scatt., modification of Kuti-Weisskopf parton model *(Russian)* 78−17027
deep inelastic lepton-nucleon scattering, quark cascade model, struct. functions 78−25051
deep inelastic lepton-proton scatt., energy momentum sum rule approx. using QCD model 79−63439
deep inelastic scatt., renormalisation group appls. 77−57461
deep inelastic scattering, asymm. in cross section 77−38178
deep inelastic scattering and asymptotic freedom, Q^2 dependence of moments 80−82978
hadron leptoproduction, nuclear targets, quark-nucleon inclusive cross section, heavy lepton pairs 80−57607
Higgs boson production by high-energy lepton-nucleon interactions 80−27449
jet structure, cascade model and jet model 80−42471
lepton+nucleon producing polarised baryon+anything, polarisation transfer from initial to final state 77−82746
lepton-proton deep inelastic scatt., two-stage model, parton distribs. and Q^2 depend. 78−66078
lepton-Reggeon scatt. data extraction, Reggeon structure 77−6095
Melosh transformation and light cone current algebra 77−41791
nuclear matter, leptoproduced high energy particles, nuclear attenuation, hadronisation time 80−102182
nucleon internal structure, expt. evidence from lN collisions, book contrib. 80−42413
perturbative QCD corrections in inelastic Compton scattering 79−93342
polarisation, lepton and photon nuclear interactions, bremsstrahlung, pair production *(Russian)* 77−88104
quark and gluon jets, Breit frame, QCD 80−62995
quark charge meas. from deep inelastic bremsstrahlung *(Russian)* 78−41555
quark-parton model, with scaling violations, large p_T processes anal. 78−45927
quasipotential approach to deep inelastic scatt. at bound state *(Russian)* 77−49972
weak (V+A) interactions of leptons, possible existence *(Russian)* 77−74678
$l(\bar{l})N$, P-odd asymmetries in deep inelastic scatt. of polarised l and $\bar{l}$ *(Russian)* 79−49527
$lN \rightarrow l'\pi X$, semi-inclusive deep inelastic scatt. cross sections, higher twist effects 80−32105
$l^{\pm}N$, deep inelastic scatt., EM corrections to hadronic and neutral currents, systematic effects *(Russian)* 79−49526
$lp \rightarrow lX$, hadronic mass scales 77−71543
$lp \rightarrow lX$, scaling violation due to charm prod., conventional ideas 77−74691
$lp \rightarrow l'X$, weak reaction, large transverse momenta, field theories at finite temp., symm. breaking and restoration 79−399
n, structure function nonsinglet moments from deep inelastic lepton scatt., QCD 80−62980
p, structure function nonsinglet moments from deep inelastic lepton scatt., QCD 80−62980
ρ^0-electroproduction, parity violating effects 80−9178

lepton-nucleon scattering
see also electron-nucleon scattering; lepton-nucleon interactions; muon-nucleon scattering; neutrino-nucleon scattering
deep inelastic lepton scatt. in nuclei, energetic quark beam prod. 80−47304
deep inelastic nucleon constituents, parton transverse momentum, structure function 79−2976
deep inelastic scatt., quark-parton model, review 77−57545
deep inelastic scatt., SU(4) duality and quark parton models 77−61293
flavour singlet Wilson operators and coeff. functions in asymptotically free gauge theories 79−67501
neutral current effects in charged-lepton-nucleon elastic scatt., polarisation asymm. 78−33071
nonscaling behaviour, p-n and d struct. functions 78−8642
nucleon internal structure, expt. evidence from lN collisions, book contrib. 80−42413
proton-lepton deep inelastic scattering in four-quark model *(Russian)* 77−26530
quark fragmentation functions in high-p_T deep inelastic processes 77−61295
structure and fragmentation function moments, meas. and QCD predictions 80−37274
vector meson diffr. prod. cross-section calc. 77−34167

lepton production
see also electron pair production; muon production; neutrino production
$\nu_\mu N$, charged heavy muonic lepton production, explanation of Kolar events 79−9364
bremsstrahlung production of high-energy lepton pairs in QCD, gauge invariance effects 77−74650
charged heavy lepton production by nondiagonal neutral currents *(Chinese)* 79−17668
charm as possible source of prompt leptons 77−225
charmed meson $\rightarrow l^+l^-X$, model for charm fragmentation function 80−37237
charmed quark semileptonic decay, gluon corrections to charged lepton spectrum 79−75765
conference on hadron struct. and lepton-hadron interactions, Cargese, France (July 1977) 80−4473
dilepton and trilepton production in neutrino experiments *(Polish)* 78−89704
dilepton angular correlations, test for two body QCD subprocesses 80−387
dilepton charge production cross section for ν and $\bar{\nu}$, parton model 80−62966
dilepton energy bounds, form factors anal. 78−41549
dilepton prod. during hadronic collision space-time evolution, quark-parton model 79−2980
dilepton production and scaling in hadron interactions 77−50031
dilepton production in $\nu(\bar{\nu})$ reactions, bottom quark excitation contrib. 80−42439
dileptons, via resonance or continuum, momentum depend. explanation using gluons 78−58159
direct lepton generation in strong interactions, unified model, colour quark state *(Russian)* 80−82933
direct leptons in pp interactions, support for EM origin theory 77−46072
direct production in hadron-hadron collisions, interaction models, review 77−236
direct single electron prod. in $\bar{p}N$ interactions, 1.6 GeV/c 77−49994
Drell-Yan annihilation, threshold effects and quark masses 77−54076
Drell-Yan formula in QCD, lepton pair prod. 78−33025
Drell-Yan process, heavy lepton pair prod., non-scaling parton model 77−13928
Drell-Yan processes and deep-inelastic scatt., valence- and sea-quark distribs. 79−13069
Drell-Yan scaling, absorptive corrections, for initial and final hadronic state interaction 80−4950
E7 gauge model, multilepton prod. by ν, heavy leptons 77−74588
E_7 gauge model, lepton assignments and trimuon events in neutrino scatt. 79−17709
hadron+hadron interaction, Drell-Yan dynamics, lepton pair from $q\bar{q}$ collision, energy scaling breakdown 78−54610
hadron collisions, lepton and photon production, review 79−405
hadron collisions, lepton pair production, $q\bar{q}$ annihilation within same hadron, structure function anal. validity 80−57622
hadron collisions, theory and phenomenology of lepton pair production, review 78−82159
hadron induced lepton production, state of art 79−26340
hadron interactions, local thermodynamic equilibrium *(Russian)* 80−9155
hadron-hadron collisions, dilepton ang. distribs., QCD and quark model anal. 79−80801
hadron-hadron interactions, large p_T prod., parton model 77−67620
hadron-hadron interactions, lepton pair prod. 78−66138
hadronic collisions, dilepton prod., review 79−49547
hadronic collisions, inclusive lepton pair prod., invariated helicity struct. funcions anal. 79−13172
hadronic jets, extra lepton pair prod. 80−27512
hadronic lepton pair production, QCD jets 80−62994
hadronic massive lepton pair prod., theory review, Drell-Yan model 78−89752
hadronic prod. of large-P_T leptons and large-Q^2 lepton pairs 77−22810
hadroproduction, QCD test 79−17745
heavy lepton, helicity calculations for prod. in ν interactions and cascade decay 78−93870
heavy lepton bound state pair photoprod. in nuclear Coulomb field 77−6103
heavy lepton e^+e^- pair prod., two photon processes at high energy 77−71524
heavy lepton pair production by cosmic rays 79−36117
heavy lepton prod. and cascade decay 78−33059
heavy lepton production in e^+e^- annihilation, QED background 79−75706
heavy vector meson annihilation rate to lepton pairs, hadronic corrections 80−4943
heavy vector meson annihilation to lepton pairs, hadronic corrections 80−68424
high energy ν experimental physics at Fermilab, review 78−50028
high energy lepton pair prod. with pol. hadrons, P and C violations 80−99068
high energy neutrino physics, recent expt. results 80−4982
high energy neutrino-hadron collisions, dilepton mass spectrum, V-A and Weinberg interaction calcs. 79−3010
high mass dilepton prod., comparison with Drell-Yan formula in asymptotically free theories 80−4942
high-energy hadron-hadron collisions, lepton prod. with large transverse momentum, SU(6) parton model 78−89673
inclusive hadron and lepton prod. in statistical model 77−18353
jet and lepton-pair production in high-energy lepton-hadron and hadron-hadron scattering 79−17729
jet struct. in hadronic lepton pair prod. ang. energy cross section, QCD 79−75806
large Q_T transverse momentum lepton pairs and hadron jets prod., reaction mech., perturbative QCD 79−2999
lepton pair prod. struct. functions, QCD improved quark-parton model 80−73671
low-mass lepton pairs from hadron and neutrino beams, meson annihilation model 79−93401
macroscopic gauge theory of gravity, uniform gravitational collapse, lepton pair creation 78−81724
massive dileptons, hadronic prod., QCD perturbation theory test, review 79−326
massive lepton pair hadroproduction, QCD and parton model anal. 80−42421
massive lepton pair prod., constituent interchange model 78−8611
massive lepton pair prod. by polarised p, constituent spin prop. test, QCD 79−89201
massive lepton pair production as a test of models for particle production on nuclei 80−102213
massive lepton pair production at large q_T, large p_T jet props. 79−54326
massive lepton pair production in meson-nucleon collisions 79−63532
massive lepton pair transverse momentum distrib. in hadron collisions, QCD predictions 79−9391
meson resonances, low energy, narrow 78−29341
multilepton production in neutrino expts. 80−91081
neutral current effects in Berthe-Heitler pair prod. 78−33022
neutral heavy lepton signatures in ν induced dilepton events, SU(2)×U(1) model 78−70353
neutral heavy leptons decay, neutrino induced multilepton events, locality constraints 78−21411
neutrino interactions, appl. to weak interaction and nucleon struct. investigations, review 79−80823

lepton production continued
neutrino interactions, experimental results for charged and neutral current interactions and multilepton prod. 79−49512
pair photoproduction, neutral weak current consequences *(Russian)* 78−12899
pair photoproduction from protons, P violating asymmetry 80−105901
pair prod., hard-scatt., expansion 78−66091
pair prod., nonfactorisability of inclusive distribs. in nonperturbative QCD 79−13085
pair prod., structure function relns. at large-transverse momenta 79−17690
pair prod., thermal parton model 79−13075
pair production, leading logarithms technique, correl. with hard scatt. approaches 79−45072
pair production, QCD and hard-scatt. model, spin-spin asymmetries 80−63014
pair production, where the Drell-Yan picture breaks down 79−93372
pair production in hadronic collisions, parton model and scaling approach 78−82150
pair production in two-dimens. QCD 77−74644
parent-child relationship for prompt leptons and neutrinos produced in the forward direction 79−80824
photoproduction of lepton pairs in thick target, Monte Carlo simulation 78−21432
pion-quark scattering model for lepton pair production from $q\bar{q}$ annihilation 79−13056
prompt lepton sources from hadronic collisions 80−73726
prompt prod. in hadron collisions, cluster model, e/π ratios 77−2886
pseudoscalar direct lepton production mechanism *(Russian)* 77−82738
QCD, inclusive distributions in extended leading logarithms 79−13066
QCD and Feynman-x depend. of lepton pairs produced in hadron collisions 79−36036
QCD corrections at Z_0 for hadron initiated lepton pair prod., renormalisation appl. 80−86678
QCD extended leading logarithm approx. for inclusive distribs. and lepton pair prod. 80−379
QCD hard scatt. off nuclear targets 79−63444
QCD perturbation theory, high energy behaviour of jet and lepton-pair prod. 79−2932
QCD perturbation theory of hard processes in asymptotically free field theory, ϕ^3 80−13263
QCD prediction for ang. distrib. of dileptons in hadron collisions 79−26300
QCD quark-gluon plasma, hadronic prod. of leptons, photons and ψ *(Russian)* 78−89672
QCD quark-gluon plasma, hadronic prod. of leptons, photons charm and ψ 78−89669
quantum chromodynamics, hadroprod. of lepton pairs and real photons 78−50056
quark-parton model, leading proton-large p_T particle and proton-lepton pair correlations 79−353
quark-parton model relns. for dilepton and ψ meson prod. 77−82711
structure function relations, lepton pair processes at large transverse momenta 78−82214
SU(3)×U(1) model, heavy lepton prod. and decay signature 78−45900
subnuclear structure concept via dilepton prod. in hadronic collisions, historical review 79−93365
sum rules and moments for Lepton pair production cross section using Drell Yan formula 78−54611
tensor mesons, EM decay possible source of photons and leptons 79−13130
transverse momentum behaviour of hadrons, multihadron systems, and lepton pairs 79−45121
trileptonic prod. by neutrinos, book contrib. 78−78161
$D\rightarrow e+X$, anomalous electron prod. from D meson decay at $\psi(3772)$ 78−37203
$D\rightarrow K\pi l\nu$, charm-changing weak hadronic current, models 80−57585
e production in pp collisions at 53 GeV, small transverse momenta electrons 78−29367
e production in small-p_T pp interactions at 2800 GeV^2, multiparticle prod. mech., lepton-hadron relation 77−2868
$e^{\pm}$ direct prod. in pp 10-25 GeV collisions, anomalous behaviour in e/π ratio 77−14004
e^+e^- annihilation, energy bounds for charm and heavy lepton prod. 77−2810
e^+e^- annihilation, form. of forward leptons *(Russian)* 77−2811
e^+e^- annihilation, hadron and lepton prod., τ-lepton decay, $K^{\pm}$, p, $\bar{p}$ yields, quark flavours 80−73725
e^+e^- annihilation, triplet heavy leptons, charged energy fraction, anomalous $e\mu$ events 78−45897
$e^+e^-\rightarrow b\bar{b}$, single lepton spectra, coupling strengths 79−49461
e^+e^- collisions, many-lepton final states, heavy lepton families 78−45899
$e^+e^-\rightarrow e^{\pm}U^{\mp}$ or $e^{\pm}$ hadron$^{\mp}$, anomalous events, heavy lepton pair prod. and decay 78−8676
$e^+e^-\rightarrow e^{\pm}X^{\mp}$, 3.1 to 7.4 GeV, threshold behaviour of $\tau^+\tau^-$ prod. 78−70351
$e^+e^-\rightarrow e^{\pm}\mu^{\mp}$nything, effect of transverse beam polarisation on anomalous leptons 77−6102
$e^+e^-\rightarrow e\mu$ events, Higgs particle prod. 78−8644
$e^+e^-\rightarrow L^+L^-$, hadron spectra from heavy lepton decay *(Russian)* 78−12919
$e^+e^-\rightarrow L^+L^-$, heavy lepton decay, energy spectra of secondary e or μ 77−71503
$e^+e^-\rightarrow L^+L^-$, scalar model of weak interactions 77−18264
$e^+e^-\rightarrow L^+L^-X(X\rightarrow e^+e^-)$, possible heavy lepton spin determ. 77−2847
$e^+e^-\rightarrow L^+L^-\rightarrow(e^-\bar{\nu}_e\nu_L)+(\mu^+\nu_\mu\bar{\nu}_L)$, V-A and V+A model anal. 77−18262
$e^+e^-\rightarrow l^+l^-$, polarisation studies at Z^0 pole, expt. feasibility 79−97615
$e^+e^-\rightarrow\mu^+\mu^-(\tau^+\tau^-)$, cross sections, charge asymmetry, polarisation in SU(2)×SU(2)×U(1) models 79−97616
$e^+e^-\rightarrow\mu e$, intermediate heavy-lepton pairs 77−18265
$e^+e^-\rightarrow\mu e$+anything, longit. polarised beam, asymmetries, props. of heavy leptons 77−10238
$e^+e^-\rightarrow t\bar{t}$, single lepton spectra, coupling strengths 79−49461
$e^+e^-\rightarrow\tau^+\tau^-$, parity violating effects measurement 79−36057
eN, deep inelastic scatt., heavy lepton mixings, Weinberg-Salam model 80−62992
γ+hadron→lepton pair, perturbative QCD, twist-2 photon operator, parton subprocesses 80−73716

lepton production continued
$\gamma N\rightarrow l^+l^-X$, pol. γ, neutral current effect, Weinberg Salam model calcs., p violation 80−5000
$\gamma N\rightarrow l^+l^-X$, polarisation effects on P-violating asymmetry in Weinberg-Salam model 80−32055
$\gamma N\rightarrow$lepton pairs, weak neutral currents anal. 78−8670
$h_1h_2\rightarrow llX$, massive lepton pair prod., polarisation and spin effects 80−105929
L^0 prod. in pN collisions, 400 GeV/c upper limit on cross section 78−37243
L^+L^- pairs, photoprod. and decay, energy and ang. distribs. of decay leptons 77−41836
$lp\rightarrow lX$, scaling violation due to charm prod., conventional ideas 77−74691
$MB\rightarrow l^+l^-X$, meson quark struct. functions, and Drell-Yan process 79−63551
μ^-e^+ pair production in neutrino interactions in Gargamelle, associated strange particles 77−61275
μN, deep inelastic scatt., heavy lepton mixings, Weinberg-Salam model 80−62992
$\mu N\rightarrow\mu X$, broken colour gauge theory of integer charge quarks 80−13313
μN tripleton prod. calc., doubly charged Higgs boson in vectorlike gauge theory 77−61237
μp deep inelastic scatt., inclusive cross section, lepton pair EM prod. contrib. *(Russian)* 80−105904
$N+\nu\rightarrow M^0$, heavy lepton prod. and decay mechanisms cross section and coupling constant *(Russian)* 79−9365
NN collisions, lepton pair prod., $\gamma\gamma$ background of Drell-Yan process 79−13057
$NN\rightarrow l^+l^-X$, A depend. of lepton pair prod. on atomic nuclei *(Russian)* 79−49562
ν interaction, dilepton event anal. 77−30364
ν interactions, μe prod., heavy lepton decay anal. 78−33057
$\nu(\bar{\nu})N\rightarrow\mu^{\pm}e^+e^-X$, trilepton event EM and hadronic contrib. 80−409
ν reactions, dilepton events, neutral heavy lepton, rising $\sigma(\bar{\nu})/\sigma(\nu)$ 77−57523
ν-induced multilepton events, weak interaction model 78−41533
ν-nucleus reactions, lepton pair production, cross sections, transverse momenta distrib. *(Russian)* 78−54749
$\nu_\mu(\bar{\nu}_\mu)$N, heavy lepton prod. and decay, differential cross sections *(Russian)* 80−105940
ν+hadron inclusive interaction, single-lepton and dilepton prod., test of T invariance 77−34146
$\nu_\mu+Ne\rightarrow L^{\pm}$...., expt. limits on heavy lepton production 78−37197
$\nu_\mu+Ne\rightarrow\mu^-+e^++X$, possible charmed particle production 77−67645
$\bar{\nu}$N, search for μe events 77−26512
$\nu N\rightarrow\mu^-e^+X$, quark fragmentation function 77−87968
$\nu N\rightarrow\mu^-\mu^+X$, quark fragmentation 77−87968
$\nu N\rightarrow\nu'$+anything neutral current events, ν' decay modes, upper limits on mass 77−6109
$\nu N\rightarrow\nu l^+l^-$(+hadrons), lepton pair production suppression up to 10^5 GeV *(Russian)* 79−36065
$\nu_\mu N\rightarrow M^0X$, use of $\Delta\phi$ rule to disprove heavy lepton existence 79−63470
$\nu_\mu N\rightarrow\mu^-e^+$, obs. in BEBC 78−78170
$\nu_\mu N\rightarrow\mu^-e^+$, hadrons, Gargamelle picture anal., strange particles and charm prod. 77−54097
$\nu_\mu N\rightarrow\mu^-e^+$ in heavy Ne, Fermilab results, D^0 prod. and decay 78−89700
$\nu_\mu N\rightarrow\mu^-e^+X$, associated K_s^0 production 77−57528
$(\bar{\nu})\nu N\rightarrow e^-e^-e^+\mu^+K^0+7\gamma$, exptl. obs. 79−9361
$\nu p\rightarrow p2\pi^0M^0$, neutrino prod. of neutral heavy lepton in E_7 gauge model 79−17710
pair production in hadronic collisions, appl. of quark parton model 79−30715
pN, dilepton production by pol. protons, parity violating, asymmetry, Weinberg-Salam calcs. 80−42488
pN collision, 200 GeV/c, production of long-lived hadrons and leptons, antinuclei production 80−13342
pN dilepton prod. quark-parton distribs., Drell-Yan model 79−17752
pN direct prod. via hypothetical hadron and heavy lepton prod. *(Russian)* 77−46074
$Pn\rightarrow l^+l^-X$, scaling predictions, Drell-Yan model 80−73756
$\bar{p}p$, heavy lepton prod. and decay, supersymmetrical model of weak and EM interactions *(Russian)* 80−86748
pp, massive lepton pair prod., pion exchange model anal., quark parton interpretation *(Russian)* 80−82993
$\bar{p}p$, pp, Drell-Yan processes, scaling violation effects 80−382
$\bar{p}p$, pp, lepton pair prod., transverse momentum distrib., QCD calcs. to leading logarithms 80−42486
pp, $p\bar{p}$ inclusive interactions, lepton pair prod. and Drell-Yan mechanism 78−8718
pp, prompt lepton emission, 53 GeV, e/π ratio, charm particle total inclusive cross section 78−93914
$\bar{p}p$ annihilation, 2 GeV/c, search for prompt electron prod. 79−54351
$pp\rightarrow e^-$+anything, 23-62 GeV, cross section meas. 77−2877
$pp\rightarrow e^-h^+$+anything, 23-62 GeV, cross section meas. 77−2877
$pp\rightarrow e^+X$, direct prod. at 256 and 800 MeV 77−251
$pp\rightarrow l^+e^-X$, asymptotic free gauge theory calc. 77−74734
$pp\rightarrow l^+l^-X$, massive lepton pair prod., quark-gluon-parton model, scaling 79−428
$pp\rightarrow l^+l^-X$, parton density scale violations and quark-gluon correction to Drell Yan formalism 79−63560
$pp\rightarrow l^+l^-X$, QCD quark-quark correction for Drell-Yan formalism 79−75731
$pp\rightarrow l^+l^-$+hadrons, lepton pair prod. in hadronic collisions, review 80−5022
$pp\rightarrow l^+l^-x$, QCD corrections to Drell-Yan formula 80−22578
$p\bar{p}\rightarrow l$+anything, single lepton cross sections from decays of intermediate bosons 77−41868
$pp\rightarrow l\bar{l}X$, p_T behaviour and scaling violations with conventional ideas 77−74691
pp→meson+lepton pair, transverse momentum distrib. and branching ratios, proton gluon distribution 80−52537
$pp\rightarrow\mu^{\pm}e^++X$, possible charmed meson pair prod., $D\bar{D}$ cross section 78−89751
pp scatt., Drell-Yan process, quark-quark contrib. 80−73731
πN dilepton prod. quark-parton distribs., Drell-Yan model 79−17752
πp, massive lepton pair prod., pion exchange model anal., quark parton interpretation *(Russian)* 80−82993

lepton production continued
π^-p, 21 GeV, prompt e^- associated with strange particle in strong interaction, direct evidence 79−419
π^-p, 70 GeV/c, directly produced electrons from charmed D particle decay, cross sections 80−73755
$\pi^\pm$p, 18 GeV/c, prod. limits on impaired electrons or positrons 78−45967
$\pi^\pm p \to e^\pm X$, 18 GeV/c, expt. results from SLAC 78−89748
ψ hadronic prod., lepton pair ang. distribs., cross section χ contribution from πN, pN, $\bar{p}$N 80−42487
τ, production in e^+e^- annihilation, experimental evidence review 79−75758
Be+n, 300 GeV/c, $\mu^\pm\mu^\mp$ and $\mu^{\pm\mp}$ events, upper limit for charmed particle prod. 78−37245
$^{56}Fe(\nu_\mu, \mu^- + L^+ + L^0)^{56}Fe$ neutrino-induced heavy-lepton pair production at high energies and multimuon events 79−89298
$\nu N \to \mu 3eX$, radiative and hadronic production characts. 79−40771

lepton scattering *see lepton-deuteron scattering; lepton-hadron scattering; lepton-lepton scattering; photon-lepton scattering*

lepton spin and parity
beta radioactivity to V-A hypothesis, party violation 78−78133
electron mag-spin moment correction in dual vacuum polarisation model 78−54632
erratic electron nonlinear spin effects 78−93825
heavy leptons, pair production and their spin 77−2847
ME-EM field model of free electron state, spin parameters 78−29281
ME-EM field model of free electron state. mag. and electric spin momentum 78−49988
neutrino-electron mixture, spin influence on bulk viscosity 77−61223
quarks and leptons, parity and CP violation 78−74197
SU(2)*U(1) vectorlike model, heavy lepton assignments 79−40711
$e^+e^- \to \tau^+\tau^-$, parity violating effects 79−36057
$e^+e^- \to \tau^+\tau^-$, τ spin separation from two body decay energy spectra 79−49503
eN, lepton and quark anapdar moments, odd parity lepton-hadron interaction source 79−45093
ep scatt., spin effects 80−42470
$L \to \nu L \mu^+\mu^-$, heavy neutral lepton spin 79−13175
ν EM props., parity nonconservation spontaneous origin in gauge theories 78−54599
ν N in ^{7}Li, parity violating ractions 79−67543
ν_τ spin and $\tau \to \nu_\tau \pi$ decay suppression 78−21419
νe scatt., weak charge, isotopic spin 78−16974
τ, parity violation effects in e^+e^- annihilation 79−49504
τ and b-quark spin value, implications for quark and lepton theories 80−32076

leptonic decays
see also baryon leptonic decay; meson leptonic decay; muon decay
charmonium state decay, nonrelativistic and relativistic theory 78−58221
conservation laws of lepton flavours, unified gauge theories, new neutral lepton 77−54095
dimuon events, heavy lepton decay into massive ν with various spin 78−21412
exotic muon and heavy lepton decays in gauge theories 77−49939
heavy lepton, decay distribs., after prod. in transversely polarised e^+e^- annihilation 77−18261
heavy lepton, helicity calculations for prod. in ν interactions and cascade decay 78−93870
heavy lepton cascade decay in $\nu N \to \mu^-\mu^-\mu^+ + X$, gauge model 77−57526
heavy lepton cascade decay in $\nu N \to \mu^-\mu^-\mu^+ + X$ 77−57524
heavy lepton cascade decay in $\nu N \to \mu^-\mu^-\mu^+ + X$ 77−57525
heavy lepton decay, intermediate vector boson corrections 80−73761
heavy lepton decay, selection rule, $SU_2 \times U_1$ gauge model 79−49500
heavy lepton decay, source for dimuon events, appl. to e^+e^- collisions 77−54093
heavy lepton decay widths, first-order weak interaction theory 78−45899
heavy lepton pairs produced in e^+e^- annihilation leptonic decay, computer calcs. 78−21409
heavy leptons, charged, possibility of new neutrino as decay product 77−10237
heavy leptons, leptonic decay, particle energy angle distrib. 79−71775
heavy leptons weak doublet, prod. and decay, lepton mixing, lepton number nonconservation 77−54094
heavy neutral leptons→muon pairs, leptonic cascade decay 78−21407
Higgs boson, charged and trimuon events in neutrino reaction 78−21413
intermediate vector boson decay, QED and QCD radiative corrections, hadronic jets 80−73759
linear SU(4) meson σ-model, one-loop approx., spin zero mass spectrum and leptonic-decay 80−47278
massive unstable neutrinos, cosmological implications of decay modes 78−45437
minimal gauge theory of leptons, new heavy lepton, associated neutrino, muon number nonconservation 77−54096
mixing angle between ordinary and heavy leptons in a (V-A) model, constraints 78−4846
neutral heavy leptons decay, neutrino induced multilepton events, locality constraints 78−21411
parent-child relationship for prompt leptons and neutrinos produced in the forward direction 79−80824
QCD, resonance props. from sum rules 79−26301
radiative corrections to β and μ decays in $SU(2)_L \times U(1)$ models involving 2n flavors 79−40778
spin 3/2 lepton, leptonic decay, secondary lepton distrib. *(Russian)* 80−5034
$SU_4 \times U_1$ and the origin of the Cabibbo angle, charged gauge boson mixing 80−73639
$SU(2)_L \times U(1) \times SU(2)_R$ model for lepton decay and neutrino lifetime 78−62331
SU(2)×U(1) gauge theories of leptons, T violation, leptonic decay and dipole moment 79−299
unconfined unstable quark, decay characts. 77−30311
V+A theory and non-separate μ- and e-lepton number conservation 77−30367
D^0 and $\bar{D}^0$, flavour-changing neutral currents 80−22553
e decay, lifetime, charge nonconservation, paradoxes 79−6335
e^+e^-, electron type neutral heavy lepton, leptonic decays 80−52486
e^+e^- annihilation, 12-31.6 GeV, τ production and decay branching ratios, lifetime 80−78052

leptonic decays continued
e^+e^- annihilation, hadron and lepton prod., τ-lepton decay, $K^\pm$, p, $\bar{p}$ yields, quark flavours 80−73725
$F^+ \to \mu^+ \nu_\mu \bar{\nu}_F$, unconfined heavy fermion model for dimuon events in $\nu_\mu p \to \bar{\mu}\nu_F F^+ X$ 77−18269
$L^+ \to e^+ \nu_e \nu_L$, $\mu^+ \nu_\mu \nu_L$, radiative corrections to charged heavy leptons decay 78−33050
$\mu^- \to e^- \nu_\mu \bar{\nu}_e$, nucleus excitation from bound μ^- decay *(Russian)* 79−22869
$\mu^+ \to e^+ \bar{\nu}_{ce} \nu_\mu$, $\bar{\nu}$l search for muon number conservation test, neutrino expt. 80−47270
$N_e \to e^- \mu^+ \nu_\mu$, search for at PETRA and PEP energies 78−45903
ν decay in gauge theory of weak and EM processes *(Russian)* 79−22087
ν_μ mass limit in absence of muon-lepton-number conservation, unified gauge theories 78−21368
$\nu' \to \nu\gamma$, Weinberg-Salam model with neutrino mixing *(Russian)* 77−38114
τ decay, large timelike Q^2, conservation of vector current and current algebra 78−78155
τ leptonic decay mode 79−9358
$\tau \to \mu\nu_\mu\nu_\tau$, branching ratios 79−17703
$\tau \to \nu\pi / \tau \to e\bar{\nu}\nu$ branching ratio anal. for determ. of τ and ν_τ spin values 79−75757
τ rare decays and spontaneous symmetry breaking 79−9301
$\tau^- \to e^- \bar{\nu}_e \nu_\tau$, branching ratio from e^+e^- annihilation 78−78200
$\tau^+ \to e^+ + \nu_e + \nu_e$, τ^+ as a paraelectron 78−50024
$\tau^+ \to \mu^+ + \nu_\mu + \nu_e$, τ^+ as a paraelectron 78−50024
$\tau^\pm \to \nu_\tau(\bar{\nu}_\tau)\mu^\pm(\bar{\nu})_\mu(\nu)_\mu$, signals for ν_τ interactions in beam dump expt. 79−67535
W-boson prod. cross sections and hadronic jets in pp and $\bar{p}p$ collisions 78−8707
$Z \to l^+l^-$, deviations from lepton universality in renormalisable gauge models 80−91122
$Z^0 \to H^0 l^+ l^-$, leptonic decay into light Higgs boson, grand unification test 80−42381

leptons
see also electrons; heavy leptons; lepton spin and parity; muons; neutrinos; positrons
abundance of stable particles prod. in early Universe 79−44653
bootstrap geometrical approach 80−95258
bootstrap topological approach to quarks and leptons 80−95253
bound states of sub-hadronic dimens., quark lepton relation 78−54609
character, possibility of simple constituents 80−42437
Clifford algebra based unified theory for quarks and leptons 80−47228
colour model, expt. evidence 78−62350
composite heuristic model of leptons and quarks 79−93354
composite leptons and quarks, anomalous mag. moment, flavour as dynamical quantum number 80−105854
composite leptons and quarks, mag. moment 80−105896
composite model, heavy lepton+quark pair 77−49895
composite models, mag. moments of quarks, leptons and hadrons 80−32081
composite quark and lepton model 80−27473
composite quarks and leptons, mag. moments 80−91056
conference, quarks and leptons as fundamental particles, Schlamding, Austria, (Feb.-Mar. 1978) 80−17709
conservation laws of lepton flavours, unified gauge theories, new neutral lepton 77−54095
current status in elementary particle physics 79−40651
decay modes of light neutral lepton produced by neutral currents 77−6109
distribution of masses of leptons and hadrons 80−99093
division of matter, confinement of quarks and gluons *(Polish)* 80−68417
dynamical symmetry breaking in lepton models 77−5980
E6 unified gauge model, breaking patterns, quark-lepton symmetry and mass scales 78−86434
eight-lepton and eight-quark unification based on Grassmann algebra 80−105824
electron-hadron interactions, P-invariance, lepton, quark anapolar moments with pol. e *(Russian)* 80−52518
EM fine struct., Fermi weak coupling, Newtonian grav. constants, unified relation 80−101974
exotic atoms, conf., Erice, Sicily, (1979) 80−67939
Fermi-Bose couple of coloured preons, primordial QCD, leptons and quarks 80−52461
fine-structure constant, coupled Maxwell and Dirac eqns., QED 80−62894
finite spectrum relativistic wave eqn. models of quark and lepton masses 78−74130
fourth generation of quarks and leptons, mass formula 80−105876
grand unified wave function for quarks and leptons 80−91034
internal quantum numbers for quarks and leptons in bootstrap approach 80−95254
LEP, design, tests of unified field theories and quark properties, search for new quarks and leptons 80−74048
lepton number conservation, $\mu^+ \to e^+ + \gamma$, brief review 77−57516
lepton-hadron symmetry principle, history of search for fundamental constituents of matter *(Polish)* 78−54588
lepton-quark system, quantum number laws, classification of weakly interacting particles, decays 78−82138
lh theory of leptons and hadrons, unification in $GA_{4,R}$ gauge 80−86639
light neutral leptons, dynamical role in cosmology 79−35407
mass, $SU(3)_L \times SU(3)_R$ as gauge groups of weak and associated charges, symm. breaking 78−74175
mass formulae in vector-like gauge theory with Majorana particles 77−18366
minimal gauge theory of leptons, new heavy lepton, associated neutrino, muon number nonconservation 77−54096
mixing of leptons with different quantum numbers in gauge theories of weak and EM interactions *(Russian)* 78−54601
multiplicative baryon number conservation, $H \to \bar{H}$ oscill. upper limit, baryon to lepton transform. 79−298
natural lepton models for rare μ decays, doubly charged leptons 77−34143
neutral, cosmological limitations on mass *(Russian)* 77−82800
neutral, mixing model 78−4847
neutral lepton mass, lower limit determ. 77−82799

leptons continued
neutron stars, hadronic matter components, leptons and baryons *(Polish)* 79−88587
new elementary particles, quark and composite models *(German)* 80−57570
nonconservation of lepton number, $\mu \rightarrow e\gamma$, $\mu \rightarrow 3e$ 78−4798
number conservation, forbidden processes 80−68654
PETRA results for fluons, nuclear forces, t-quarks and quark-lepton symmetry 80−86731
polarised lepton-hadron scattering, lepton and quark anapole moments *(Russian)* 79−17730
preon model for hadron and lepton struct. 78−78124
properties, review from particle data group 80−67944
QCD, E_7 model, quark and lepton assignments 78−8590
QDD, quantum dath dynamics, SU(3) model for composite quarks and leptons 80−91055
quantum electrodynamics review *(Hungarian)* 78−37159
quark and lepton model constraints in SU(2)×U(1) theory 77−61238
quark-lepton mass relation in unified theory 79−97560
quarks and leptons, EM and weak interactions, flavour $SU_3 \times U_1$ gauge model 79−97554
quarks and leptons, fermion physics in terms of SU(2)×SU(1) gauge theory 78−74197
quarks and leptons, high energy and nuclear physics interface 80−41974
quarks and leptons, unification within conformal relativity 79−93343
quaternion model, gauge theory *(Russian)* 78−62315
relativistic cosmology, interactions with quarks 80−90590
relativistic kinetic gas theory, electron-neutrino system 77−5756
rishon model, topological bootstrap approach 80−78046
rishon model for quarks and leptons, topological bootstrap approach 80−78047
rishon model of quarks and leptons with double SU(2) symmetry and Dirac magnetic moments 80−82943
schematic composite model of quarks and leptons 79−93353
seven lepton model, quantum flavour dynamics, mixing angle, masses, spontaneous symmetry breaking 78−89652
SO(10) unification, composite structs., quark and lepton composite models 80−57547
solar neutrino puzzle, lepton mixing explanation 78−16373
space-time properties, unified gauge theory of gravitational and strong interactions 80−95016
spin 3/2 lepton, leptonic decay, secondary lepton distrib. *(Russian)* 80−5034
stellar gravitational collapse, neutronisation and lepton escape rel. to hydrodynamics 80−77388
structure and neutral currents 77−2788
structure model, muon nonconservation, decay and anomalous mag. moment 77−61250
structure model 80−91063
$(SU_2 \times U_1) \times S_n$ flavour dynamics, flavour number bound, n quark and n lepton generations unification 80−4907
$SU_L(4) \times U(1)$ as gauge symm. for quark, lepton quartets, weak and EM interactions, weak currents 78−74174
$SU(2)_L \times U(1)$ primitive particle model 79−40708
SU(2), unification of isospin and hypercharge, electroweak interactions of leptons 80−27439
SU(2)×U(1) gauge model, eigenvalue condition for Weinberg mixing angle, new leptons and quarks 78−41463
SU(2)×U(1) gauge models with lepton doublets and singlets, exact consequences of universality 77−54065
SU(2)×U(1) gauge theories of leptons, T violation, leptonic decay and dipole moment 79−299
SU(2)×U(1) gauge theory, lepton struct. 77−82691
SU(3) electroweak theory 80−86638
SU(5), unification of weak, EM and strong interactions, review 80−105814
SU(5) combined quark-lepton decuplets, particle families *(Russian)* 80−47217
SU(5) without symmetry constraints, unified model of quarks and leptons, conservation laws 80−101968
SU(6) exotic gauge model, lepton-quark symm., CP-violation and $\mu \rightarrow e\gamma$ decay 78−12875
SU(N) grand unification with several quark-lepton generations 80−27443
subcomponent models of quarks and leptons in SU(3) subcolour, proton decay 80−78035
subquark model of leptons and quarks, unification, currents and exotic states 80−86683
supergrand exceptional unification and quark-lepton constituents 80−91030
supergrand unification in E_8, quark-lepton assignments, symmetry breaking scheme 80−68408
supernovae, lepton-driven convection 79−84811
tumbling gauge theories with chiral fermion fields, symmetry breaking 80−99042
unified description of quarks and leptons using colour and flavour degrees of freedom 80−27445
unified field theories, proton and neutron disintegration, concepts of leptons and quarks *(French)* 80−91038
unified field theory bounds on number and masses of quarks and leptons 78−58151
unified model, mesons and numbers of quarks and leptons 78−21370
unified models of quarks and leptons, B-L conservation and B nonconservation 80−95229
unified theory of weak interactions of leptons and quarks, gauge model 80−22556
unified vectorlike gauge theory based on group SU(6) for quarks+leptons 78−4818
Universe, lepton number and neutrino species number 80−8730
V-A six lepton model, lepton no. conservation 77−87930
wave functions for bound lepton in Coulomb field of nucleus 79−94115
weak quark and lepton chiral symmetries, dynamical breaking gauge interaction 80−47215
e-μ permutation symm., lepton number conservation in gauge theories 78−4777
$e^+e^- \rightarrow$hadrons, R problem, QED and QCD corrections, quarks and leptons 80−95281
$e^-\mu^-\tau$ asymmetry, conserved currents *(Chinese)* 79−58904
μ- and e-type leptons, mixing in unified model 77−67609

leptons continued
$\mu^+ \rightarrow e^+ + \gamma$, search, lepton number conservation, brief review 77−57516
$\bar{\nu}_e e$ annihilation in Weinberg-Salam model, number of quarks and leptons *(Russian)* 80−102041

level control
ceramic suspension, ferromagnetic filtration apparatus improvement 78−11561
Cocatron, servo valve for liq. He II level control, superfluidity and supercond. applic. 78−18855
cryogenic level sensor/controller for liquid N and He 79−75536
cryostat liquid He automatic replenishment system 79−67308
GUPS-1 immersion follower gamma-level gauge 77−67412
liquid, sensor utilizing pneumatic capacitor, for process-control appls. 79−71438
liquid He non-dissipative level detector using series of capacitors 77−30158
liquid N_2, automatic level controller, transfer system for cold traps 78−24805
liquid N_2 two-level controller 80−52241
liquid nitrogen filling system, automatic 77−41620
liquid nitrogen for parametric amp. using diode sensor 78−29121
nonvacuum X-ray cryostat with liquid N level control 77−41624
tank and pipe water, US level sensor appl. 77−37845
water bath level control device 79−67283
He, liq., pump, cryogenic for long continuous running in particle accelerator *(French)* 78−32829
N_2, liq., device for level control 77−82531

level crossing (energy) *see energy level crossing*

level measurement
acoustic pulse-reflection meter, nuclear waste liquor tanks 80−86265
automatic monitoring of liquid N_2 level, in Dewar flasks 80−57309
capacitive level meter with IC convertor 79−88907
contact cryogenic fluid level sensor 80−73371
cryogenic fluid, fluidic/pneumatic level meas. 77−26310
differential thermocouple transducer for electrically insulating liquid level 77−17969
elastic waveguide slow torsional wave sensors 79−46748
electroconducting liquids, digital meas. using conversion in binary-decimal refl. code *(Polish)* 77−17949
floating level gauge for liq. He 79−2774
floating level indicator for liquid helium 79−67305
gauge checking methods and facilities 77−22526
geodetic compensator levels, systematic errors, new instrumental development *(German)* 77−2289
glass, molten design of level measuring gauge 79−29304
groundwater, using strain gauge load cells 77−21802
GUPS-1 immersion follower gamma-level gauge 77−67412
halfsecond levels, investigations using atuomatic comparator *(Russian)* 78−40675
hydrostatic levelling, automatic precision instrument for geodesy *(German)* 77−29514
hydrostatic method of level measurement *(Polish)* 80−101779
laser beam levelling of railway track, practical experience *(German)* 79−98432
level gauge reference installation for calibration 77−71294
light reflection liquid level sensor 80−82741
linearisation of scale eqn. for resonance level gauges *(Russian)* 80−68176
liquefied natural gas, level, density and temperature measurement, prediction of roll-over 80−27269
liquid, non-contact laser interferometric method *(German)* 79−12769
liquid, programmable precision digital equipment *(Hungarian)* 78−32795
liquid, transducer design 80−31709
liquid He depth gauge, level sensing circuit 77−82527
liquid He level indicator *(Japanese)* 78−12705
liquid He non-dissipative level detector using series of capacitors 77−30158
liquid level detection, audible alarm system, thermistor appl. 79−12764
liquid level detection, hot wire sensor 77−17966
liquid level measurement and regulation using megohmmeter and op. amp. *(Rumanian)* 79−40532
liquid level meter features *(Italian)* 79−169
liquid level monitor with optical coupler isolation *(German)* 78−73963
liquid level sensing using PTC thermistors 80−42209
liquid level-to-frequency converter 79−6080
liquid N_2, automatic level controller, transfer system for cold traps 78−24805
liquids, cascade transistor cct., level to freq. convertor 80−73310
LNG, automatic continuous level-gauging and temp. meas. system appl. 77−26272
manometer for liquid level stored above or below ground 78−21093
material arranged in arbitrary fashion in tank, errors in measurement of average level 80−17921
measuring cup for the blind, electronic, 50 ml indications 77−78054
nuclear gauges 80−843
ocean wind wave elevation sensor array system 80−46322
optoelectronic two-component spirit-level for whole-arm prostheses *(German)* 79−8572
pneumatic detector operational principles *(Polish)* 79−85114
potentiometric level indicator for electrically conducting substances 79−77312
PTC thermistor P310-C11, for liq. N_2 80−52247
radioisotope instrumentation, industrial appl. *(German)* 77−70245
reservoir fluid level of wave-like form, floating indicator appl. *(Russian)* 77−65018
resonance level meter, for dielectric fluids or granulated media *(Russian)* 79−88909
rivers and open channels, by anal. of random signals from surface waves 77−45205
rivers/open channels, remote sensing, cross correlation technique 78−57328
sensor for conductive liquids using array of point sensors 80−68177
settlement meas. apparatus, adjustment, based on principle of communicating vessels *(French)* 79−40538
sinter machine charging, potentiometric level detector *(Russian)* 80−90813
tank and pipe water, US level sensor appl. 77−37845
tank gauging, automatic, using density transducers 80−95067

level measurement continued
US, liquid level measurements using longitudinal, shear extensional and torsional waves 80−77757
US level detection 80−27268
US monitoring techniques using elastic strip waveguides 77−839
water, twin-wire wave height probe with calibration stabilized for changes in water conductivity 80−57280
water level short-term meas., laboratory systems 78−93654
water levels, meas. via automated tide gauging network 79−5692
water wave amplitude, surface standing, using capacitance meas. circuit 79−50833
He level detector for pumped bath 78−49843
He, liq., appl. of gas oscillation to pressurisation in storage vessel 80−57305
He liquid level indicator, small heat dissipation, made from newly developed superconducting wire *(Japanese)* 79−2775
InPb-covered manganin wire, level detector, depth gauge, demonstration of superconductivity 79−35751

level meters
see also power measurement
acoustic noise, data accumulation equipment *(Japanese)* 78−42503
acoustic noise meas. instruments, design and future developments 80−43560
audio recording peak level meter with LEDs *(Spanish)* 77−37936
cryogenic level sensor/controller for liquid N and He 79−75536
digital, programmable, for liquid level meas. *(Hungarian)* 78−32795
environmental effects on microphones and Type II sound level meters 77−62127
equivalent continuous noise level meter requirements 78−83195
floating level indicator for meas. of fluid level in reservoir *(Russian)* 77−65018
industrial noise level meter calibration procedures 77−62125
liquid, features *(Italian)* 79−169
precision, commercial instruments survey *(French)* 80−83871
sinter machine charging, potentiometric level detector *(Russian)* 80−90813
Talyvel electronic level, temp. effects *(German)* 78−45037
He level gauge, with semiconductor sensor 80−57277

levels, energy *see energy states*

levitation, magnetic *see magnetic levitation*

librarianship *see information science*

libraries
see also cataloguing
computer information, conference, London, England (Nov. 1979) 80−90599
data library for nuclear medium energy reactions 77−18765
Japanese Evaluated Nuclear Data Library, first version evaluation *(Japanese)* 78−74428
NOAA meteorological library and information services, description 80−109180
nuclear data libraries *(Spanish)* 79−36120
Royal Astronomical Society, catalogue of archives and manuscripts 78−69705
Southern Africa, astronomical archive collections 78−36473
visual science research, the place of the library 80−30711

library mechanisation
British National Meteorological Library 80−82068

library science *see information science*

LIDAR *see optical radar*

Lie groups
see also elementary particle symmetry
11-dimensional supergravity, dimensional reduction, masses from extra dimensions 79−71332
A(0,1) Lie superalgebra, Fock-type representation 80−37181
A(0,n) Lie superalgebra, Fock space representation 80−86606
affine Lie algebra $A_1^{(1)}$, explicit construction 78−89626
affine motions, flat struct. *(French)* 79−30191
algebra, matrix canonical realisations, recurrence relations 78−12533
algebras, semi-simple with centre but no outer derivation *(Japanese)* 80−68386
algebras, unusual, appls. in particle physics 80−27419
algorithm for the calculation of weight multiplicities for semi-simple Lie groups *(German)* 79−67142
analytic continuation of the Fourier Series on connected compact Lie groups 78−93511
analytic iterability of formal power series vectors *(German)* 77−53736
analytic realization theorem for transitive infinite Lie algebras *(French)* 78−28909
analytic symplectic maps, Lie series and invariant functions 77−22373
anisotropic harmonic oscillator group, quantum mech. representation 78−8262
applications *(Japanese)* 77−2511
applications *(Japanese)* 77−9851
applications *(Japanese)* 77−26132
asymptotically free models and the G_2-group 80−18072
automorphisms of Lie algebra of polynomials under Poisson bracket 77−5624
Bachlund problem, Lie algebra bundles *(French)* 80−18085
Benney's long wave eqns., Hamiltonian formalism 80−31525
Bianchi cosmologies, classification in conformal flat space times 80−56985
Bianchi model Lie groups, automorphisms 79−30313
bilocal Lie groups and solitons 77−67194
bimodular Hilbert space operators, representation theory of Lie-admissible algebras 80−37180
Bloch coherent states derivation from SU(2) van der Waerden invariant 79−3671
bonded algebra generalisation, Lie-admissible algebra source 80−37176
Bose statistics, para-, Lie superalgebra, osp(1,2n), creation and annihilation operators 80−62572
boson-fermion interacting system, coherent states on Lie groups and evolution operator 78−36932
Boussinesq equation, group theoretical approach 80−82914
broken symmetry of transformation generating general relativistic theories 80−98836
C_n algebra, 'near to minimal' canonical realisations 77−64918
canonical realisations of classical algebra 77−41453
canonical representations, representations theory, book contrib. 80−46872

Lie groups continued
Casimir invariants and characteristic identities for generators of graded Lie algebras 80−13227
Casimir invariants and vector operations 78−28911
Casimir operators of orthogonal and symplectic groups 77−71178
central limit theorem for semi-Markovian chain *(French)* 80−52127
central local limit theorem on semi-simple Lie groups *(French)* 79−71222
character of factor normal representation of connected solvable Lie group *(French)* 77−64917
characteristic identities for Lie groups 77−67181
class of representations on vector field, partial differential operators *(French)* 77−67228
classical, dimensions of irreducible representations 80−18087
classical, reduced determinantal forms 80−22533
classical and quantum mechanics, group theoretical foundations, elementary systems 79−30282
classical and quantum observables 77−74249
classical field theory, Lie-admissible struct. 80−36880
classical groups, invariant operators 79−21585
classical limit for arbitrary commutation relations in quantum theories 79−25877
classical limit for quantum theories defined by real Lie algebras 78−65807
classical limit of quantum nonspin systems 79−63134
classical mechanics, numerical methods, Newtonian, Lagrangian and Hamiltonian mechanics, book 79−63024
classical relativistic planar motion in axisymmetric EM fields 79−49064
closed systems with nonconservative internal forces, Lie admissible quantisation, hadron struct. 80−37174
cocycles, integral representation *(French)* 80−51998
coherent state representation of linear operators 78−16677
coherent states and induced representation 78−49713
coherent states and square integrable representations 79−30188
cohomological deformation of infinitesimal Lie algebras *(French)* 79−53961
cohomology of graded Lie algebras and non rational Poincare-Betti series *(French)* 80−95222
combinatorial algorithm for generating positive roots 77−2530
commutator theorems, integration of Lie algebras representations and commutation relations 77−53732
compact, relations between quantities in representation theory 77−2512
compact connected Lie groups, tensor product representation, decomposition 79−6021
compact gauge groups for unified weak and EM interactions, representations and classifications 79−22008
compact simple Lie group, Green's function, group manifold and path integral *(German)* 80−37169
compact simple Lie groups, rank 2, irreducible representations *(Chinese)* 80−68391
compact simple Lie groups of rank 2, irreducible representations of B_2 and G_2 *(Chinese)* 80−101949
complex Lie algebra with Abelian radical, derivation structure *(French)* 79−49415
complex Lie groups, connected regular compactifications, homogeneous Hopf manifolds, and bundles *(French)* 80−73617
complex semi-simple Lie algebra, parabolic subalgebra conjugacy class 77−13567
complexified SU(5) algebra, singular orbits 79−12981
composite particles and mass spectrum 79−97608
composite systems, relativistic centre of mass variable and Lie algebra of Poincare group 79−71245
conference on Lie admissible formulations, Cambridge, USA, (Aug. '79) 80−36765
conformal space-time group, invariant tensors for maximal subgroups 79−85239
conformal symm. in quantum field theory 77−65069
conformal transformations, unitary implementability 79−21965
connected, comment on conjecture of Wolf and Moore *(French)* 79−53960
connected semisimple group, nth root of element 79−93308
connected unimodular groups with discrete series, classification *(French)* 79−53958
connection set of principle bundle over 4-sphere with nonabelian Lie group, gauge transform. 78−58108
constants of motion and separable solns. in classical mechanics, group theoretical aspects 79−75332
contact Lie algebras, contraction 78−36816
contact structure, deformation of Lie algebra, of infinitesimal automorphisms *(French)* 80−62867
contact structure, Lie group actions upper bound *(French)* 79−30190
contact transformations and brackets in classical thermodynamics 80−95048
continuum mechanics, differential geometry appl. 78−12566
contracted Lie algebras, Saletan and Levy-Nahas contractions 78−73825
contraction of Lie algebra representations 79−80767
contravariant form for infinite-dimensional Lie algebras and superalgebras 80−9121
cosmic-ray eqn. of transport, steady-state, nonenergetic-source soln. 78−96366
cosmology, Lagrangian or Hamiltonian formulations, shift vector field restrictions, symmetry group 80−67923
covariant coherent states for quantized systems with nilpotent symmetry group *(German)* 78−73865
currents in Su(5) and E_7 unified gauge theories 78−54600
de Sitter groups, continuous subgroups 78−28910
deformation cohomology of truncated Lie algebra *(French)* 80−57077
deformation theory and quantisation, symplectic struct. 78−45493
deformations of representations 77−74189
derivative in special Kawaguchi space 79−30193
differential equations, first-order, infinitesimal operators of Lie group symm., algebra *(Russian)* 77−30034
diffusion equation, nonlinear, invariance props., Lie-Backlund groups 80−62596
Dirac Lorentz's equations, relativistic and nonrelativistic, maximally extensive local group of invariance 80−77946
disconnected gauge groups and the global violation of charge conservation 78−78086
discrete finite nilpotent Lie analogs: new models for unified gauge field theory 78−66025
distribution representations of Lie groups 79−17631

Lie groups continued
dual model superconformal group, isomorphic function, Fock space representations 78−74230
dual sets in associative algebras and generalized Lie algebras 80−9122
dynamic nonlinear systems containing limit cycles 78−77666
dynamic systems, deformation and quantification *(French)* 80−31598
dynamical groups, symmetries and constants of motion for electric and mag. charges 80−101945
dynamical systems, Lie and Lie-admissible symmetries 80−37179
E_7 exceptional group, calc. of 6_j symbols 78−57800
E_8 group, branching rules, Kronecker, products 80−27438
Einstein-Maxwell space-times, infinitesimal holonomy group structure, Lie algebra 80−12976
elementary structure theorems for Lie-admissible algebras 80−37175
elliptic operator, perturbation algebra 77−17774
energy-momentum tensor, effect of motions, meson field and perfect fluid 78−73903
enveloping algebras in representation theory 77−17865
equivalence of deformations and associated *-products 79−97237
Euclidean group subgroup and symmetry breaking in non-relativistic quantum theory 77−26198
Euclidean space, spherically symmetric self-dual eqns., representation theory and integration 80−77936
Euclidean Yang Mills theory, pseudoparticle parameters for arbitrary gauge groups 78−24955
Euler and Navier-Stokes eqns., group analysis in presence of rot. symmetry and exact solns. 80−8799
exceptional and orthosymplectic graded Lie algebras 79−26254
exceptional gauge groups and quantum theory 79−35983
exceptional gauge theories in 3×3 matrix formalism 78−70248
exceptional Lie algebras, quartic trace identity 79−58897
exceptional Lie groups, basic props. 77−74611
extended geometric supergravity on group manifolds with spontaneous fibration 80−31649
extension characterisation *(Italian)* 78−23
extensions of Lie graded algebras 78−4460
Fermi-Bose similarity, parafermi and parabose algebras 77−30091
fermion many-body theory based on SO(2N+1) Lie algebra of fermion operators 77−67374
fibre bundles, pseudoconvexity 77−29998
fibre bundles $P(M_4,G)$, invariant eqns. 77−17864
fibre bundles with Ricci curvature on Riemann manifolds *(French)* 79−21594
field theory, Lie-Backlund operators props. from variational derivatives 80−37159
finite affine extensions of supersymm., graded Poincare Lie algebra 78−70300
first theorem of Lie in locally convex space 78−77664
fixed points of cyclic group actions on disks 79−62994
flexible Lie-admissible algebras with nil-basis 79−54276
foliation and associated Lie algebras *(French)* 79−21521
forced harmonic oscillator, complete symmetry group 80−90705
four-parameter groups of motions acting on null hypersurfaces 77−57247
free particle, Hamiltonian mechanics, Lie theory of extended groups 80−77982
functors in Lie algebras 77−82364
Galilean groups, system quantisation 78−70
Galilean invariant Schrodinger eqn., relativistic wave eqn. derivation, Lie algebra 80−105555
Galilean supersymmetry 79−17625
Galilei relativity in Newtonian mechanics, possible Lie admissible covering 78−73838
Galilei relativity in Newtonian mechanics, possible Lie admissible algebras, addendum 79−2619
Galilei to Poincare algebra transformations 78−36793
Galileian formulation of spin, explicit realisations 80−62505
gauge field theory, loop phase factor approach, equivalence problem, space-time symm. *(Chinese)* 78−82110
gauge fields on coset spaces 78−45781
gauge groups in local field theory and superselection rules 77−18190
gauge theory classical eqns. exact cylindrically symmetric solns. from compact Lie groups *(Russian)* 80−42317
gauge theory of gravity and supergravity on a group manifold 79−21635
gauging Lie superalgebras 80−73618
Gegenbauer polynomials, generating functions from Lie group viewpoint *(French)* 77−67193
generalised brackets, appl. to Lie and Poisson algebras *(French)* 79−21520
generalised coherent states, geometrical props. 77−17873
generalised coherent states, irreducible representations of Lie groups, anal. and applications 78−62114
generalised Liouville equation from Lie derivative 80−77981
generalised superalgebras, Lie structs., Z_N+Z_N grading 78−78106
generalized Lie algebras 79−58898
generalized Lie algebras relationship to graded superalgebras 80−9123
generalized symmetries of nonlinear partial differential equations, Lie derivatives 80−4886
geometrical properties of spinor structure 80−95226
geometrical theory of contractions of groups and representations 79−58566
Gibbs fields, absence of continuous symmetry breaking in two-dimensional models of statistical physics 79−21650
gl(n,C), formal analytic continuation of Gel'fand's finite dimensional reps. 79−63381
gl(n,R) and sl(n,R), canonical realisations and Casimir operators 77−5697
GL(N), characteristic identity appls., Lie algebra generation 79−26253
global properties of systems quantized via bundles 79−75385
graded, elementary construction 78−45461
graded algebras, finite dimensional irreducible representations, appl. to (Sp(2n); 2n) 79−49074
graded Lie algebra, contraction 79−89073
graded Lie algebra, Killing form 77−29984
graded Lie algebras, generalisation of Hermitian representations 77−26129
graded Lie algebras, osp(2,1) and spl(2,1), irreducible representations 77−26130
graded Lie algebras, Wigner Eckart theorem for tensor operators 77−45984
graded Lie bundles, appl. of superspace geometry with Fermi and Bose coords. 77−26143
graded Lie groups SU(2,2/1) and OSp(1/4), finite transform. 78−57735
graded spin extension of the algebra of vol. preserving deformation 78−65855
group invariant linear partial differential operator, form, Lie transform investigation *(German)* 78−89297
group symmetries in nuclear struct., book 80−41963
hadron microstructure, de Sitter microuniverse, relativistic Hooke group and nonrelativistic quark model 80−27480
Hamilton-Jacobi eqn., symm. and separation of variables 78−32666
Hamilton-Jacobi eqn. and Lie group theory 77−57180
Hamilton-Jacobi equation, symmetry and separation of variables, normal parabolic equation *(Russian)* 79−6292
Hamilton-Jacobi equation, symmetry and separation of variables, nonparabolic equation *(Russian)* 79−6291
Hamiltonian mechanics, Lie theory of extended groups 80−77982
Hamiltonian system dynamics, symm. of basic eqns. *(Russian)* 77−30033
Hamiltonian systems and limit cycles 79−63131
harmonic oscillator, conserved quantities and symm. groups 78−28981
harmonic oscillators, complete symmetry group 80−46856
harmonics on 3-sphere, Lie group SU(2) 78−57813
Heisenberg ferromagnet, Gell-Mann and Low renormalisation group, eqn. of state 78−31033
Higgs and gauge fields, group actions on principle bundles and dimensional reduction 80−105770
higher indices of group representations 77−5622
Hochschild cohomology within transitive Lie pseudogroups, appl. to deform. theory *(French)* 77−67227
human pattern perception modelling for visual forms interactions prediction 77−5003
Hurwitz theorem generalisation and flexible Lie-admissible algebras 80−37173
Huygens principle for equations dissociating into factors 80−31581
hypergeometric functions, two-variable, Lie theory and separation of variables 80−73189
identical particle indistinguishability, field quantisation Lie algebraic approach 80−77984
induction from normal nilpotent subgroup 77−60891
infinite dimensional Lie admissible algebras, elementary particle physics 80−37177
infinite-dimensional Lie groups and quantum dynamical systems 80−8855
inhomogeneous, nonlinear representations 79−30196
Inonu-Wigner contractions of the real four-dimensional Lie algebras 78−77667
instantons and fermions in the field of instanton 79−26217
integrability of operators in Banach space 79−21523
integrable equations and differential geometry 79−75407
integral transform groups for differential operators from Lie algebras 80−4887
internal symmetry algebras, reflections, 8-component conformal spinors 80−9112
invariance algebras of Schrodinger and Dirac eqns. *(Russian)* 80−68081
invariance group instability, spacetime, group contractions and models of Universe 79−9041
invariance groups and Lagrangian theories for mech. systems 77−45689
invariant eigendistributions, semisimple Lie groups 80−12890
invariant group of KdV, MKdV or Burgers eqn., commutative Lie algebra 80−365
invariant interaction Lagrangians, mathematical theory 79−30267
invariant operators of unitary groups U(n) and SU(n) 78−8555
invariant renormalisation method for non-linear realisations of dynamical symmetries 79−108
invariants in enveloping algebras under the action of Lie algebras of derivations 79−49015
inverse scattering technique of soliton theory, Lie algebra, Poisson-Moyal bracket, rotating rigid body 77−9908
invertible matrices, with Lie- and symplectic-admissibility, struct. and classification 79−40348
irreducible components and open orbits for algebras of dimens. ≤7 *(French)* 80−18086
irreducible representations of $G_2 \supset A_2$ chain 77−5623
isolated electron pair interaction, geometry assignment by use of Lie algebra on continuous group 78−29754
isometries, 2-parameter groups, commutation properties 80−62879
isometry group representation in eigenspaces of the Laplacian *(French)* 79−21531
isometry Lie algebras, new technique for struct. anal. 78−65831
isoscalar factors, on noncanonical bases 78−81797
isotopic symmetry group in strong interactions, possible geom. origin 79−17628
Jacobi manifolds and associated Lie algebras *(French)* 78−28919
Kemmer-Duffin eqn., additional symmetry 78−89
Kepler motion, generalised, Lie groups of motor integrals 78−85831
kinematical groups and coord. transformations using light-cone frame 78−81796
Klein Gordon eqn. (1+4)-dimensional invariant expansion of soln. in orthogonal coord. system *(Russian)* 77−13875
Klein-Gordon eqn. and Poincare group 78−62292
Klein-Gordon equation, Lie-Backlund transformation group 80−68371
Korteweg de Vries equations, higher order, soliton solns., inverse scatt. problems 77−45741
Korteweg-de Vries eqn., higher order, prolongation struct., Lie algebra, soliton solns. 78−8249
Korteweg-de Vries eqn., Lie-Backlund transformation group study 80−9114
Korteweg-de Vries equation, invariances and conservation laws 79−26244
Korteweg-de Vries equation prolongation Lie algebra 80−62501
ladder operators of group matrix elements 80−31555
Laguerre polynomials generating functions *(French)* 77−71181
Langlands decompositions for parabolic subalgebras of noncompact semisimple real Lie algebras 79−58526
Langmuir solitons, prolongation struct. 79−88814
lattice systems with compact connected real Lie group config. manifold, correl. inequalities 77−33959

Lie groups continued
left invariant G-struct. on Lie group, integrability conditions *(French)* 79−71221
left-invariant differential forms and systems *(French)* 77−5620
Lie admissible algebra and nilalgebra, recent developments 78−74168
Lie admissible forces, non-self adjoint, compatible symmetry schemes 79−75696
Lie admissible formulations, math. and physical study status, strong interactions 80−37172
Lie admissible pseudo-octonion algebra deformation into octonion algebra 79−17629
Lie admissible quantisation in a self-interacting scalar field theory, deformation distribs. 78−74169
Lie algebra, sl(2,R), integration of Hamiltonian systems 78−24660
Lie algebras, finite and infinite, physics and deformation theory 77−33831
Lie algebras of vectorfields, isomorphisms and ideal struct. 79−21530
lie extensions and automorphism groups of local fields with characteristic p *(French)* 79−58895
Lie series use in studying nonlinear Hamiltonian systems 79−8811
Lie-Backlund supergroup, supersymmetry transformations *(Russian)* 79−80771
Lie-Backlund tangent transformations, conservation theorems for PDE system 77−64919
lifting Lie group actions to the cotangent bundle 79−45023
limit cycles as invariant functions of Lie groups 79−35520
linear forms of two Lie algebras 77−60893
linear groups, Casimir operators 77−2509
linearisation program for nonlinear field eqns., Lie groups 80−105784
liquid theory, classical spin system, absence of ordering 78−51402
local Lie algebra class over a manifold, automorphisms and derivations 80−366
local supersymmetry, geometric interpretation 77−38096
Lorentz and Galilei group, condition from topology and Lie group methods 78−4462
Lorentz group irreducible representations, generalised function expansion with light cone support 78−70018
Lorentz groups on skew symmetric tensor space, nonlinear realisations of direct product 78−62329
Lorentz symmetric spaces, conformal completion 77−64989
Lorentz transform. 79−97191
Mach principle, vacuum concepts, Lie group representations, Newman-Penrose method, book 80−46741
magnetic monopoles, non-Abelian, stability analysis, Yang-Mills equations 80−31987
magnetofluid, perfect, Lie invariance of stress-energy tensor 78−42671
many-spin system dynamics, group approach *(Russian)* 80−50221
matrix canonical realisations of o(m,n) group, Casimir operators 78−81795
matrix eigenvector determ. using identity spectral resolution 77−53740
matter field equation, covariant with semisimple Lie groups in general relativity 80−8876
matter field spacetimes, symm. mappings satisfying vanishing contraction of Lie deform. of Ricci tensor 79−113
maximal solvable subalgebras of gl(n,R), su*(2r), su(p,q), so*(2r), sp(2r,R) and usp(2p,2q) 77−33836
Maxwell's eqns. for free fields on compact Lie group manifold 77−49608
method of ordered operators, appl. to obtain exact solns. 79−21525
Micu-type invariants of exceptional simple Lie algebras 80−86609
Micu-type invariants of simple Lie algebras 80−12934
minimal coupling, symplectic mechanics of classical particle in Yang-Mills field 78−74136
Moyal quantum mechanics formulation and Weyl. quantisation generalisation, Lie algebras 80−17835
N-dimensional oscillator, time-depend., SL(N+2, R) symmetry group 80−46851
near canonical Hamiltonian algebras from Lie algebras 79−97537
Newton-Wigner position operator, non existence for quanta with zero mass and nonzero helicity 78−62099
Newtonian Lie-admissible equations, struct. preserving transformations 79−53969
Newtonian system statistical mechanics, Lie-admissible struct. 80−42136
nilpotency class of Lie algebras satisfying the Engel condition *(Russian)* 80−68394
nilpotent, local cohomology of enveloping algebra *(French)* 77−67190
nilpotent, structure and appls. to analysis, book 77−26133
nilpotent Lie algebra, prime spectra of an enveloping algebra *(French)* 80−8777
nilpotent Lie group, domain of holomorphy of heat-diffusion semigroup 77−49554
nilpotent Lie groups, coherent state representation 77−49618
nilpotent Lie groups, smooth functions Fourier transforms 80−99067
nilpotent Lie groups and algebras, analytic vectors and irreproducible representations 79−30195
nilpotent two step groups, hypoellipticity and differential operator solvability *(French)* 80−62868
nonassociative algebra history, Lie, Jordan and power associative algebras 80−37170
nonassociativity in particle physics and Caley-Graves' octonions 80−37171
noncommutative algebra, two point function calcs. 78−57734
noncompact Lie groups and SU(1,1), continuous spectra, coherent states 78−8548
noncompletely reducible representations of the Poincare group associated with the generalised Lorentz gauge 78−70249
nonflexible Lie-admissible algebras, struct. and classification 78−93812
nonlinear chiral fields *(Russian)* 78−28968
nonlinear evolution eqns., prolongation structs. 78−24637
nonlinear Lagrangians and spontaneous symm. breaking 78−70303
nonlinear realizations of compact and noncompact gauge groups, grand unification 80−47183
nonlinear Schrodinger equation, Lie theory calc. of invariants 80−22234
nonlinear systems of differential equations involving limit cycles and conservative Hamiltonian systems 77−78957
nonlinear wave eqns. and covariance 78−49715
nonrelativistic particle in spherical space, dynamical symmetries 79−26255
nonstationary quantum systems, SU(2) coherent states *(Russian)* 80−90693
nonuniform plasma, mode coupling, Lie operator calcs. 78−55718

Lie groups continued
normal nilpotent subgroup, induction procedure, factor systems 77−33834
nuclear collective models, moment map 80−91138
nuclearity of C^{∞} vector spaces in induced inhomogeneous Lie group representations 78−86422
O(2N) Gross-Neveu model, O(8) Dynkin diagram P_3 symmetry 80−77968
O(N), eigenvalues of invariant operators 79−71652
octonion, pseudo-alternative, and Lie-admissible algebras 79−40347
octonion algebra, unified theories with orthogonal groups 77−46005
octonion as traceless 3×3 matrices via a flexible Lie-admissible algebra 79−17630
octonion/quaternion hypercomplex numbers, nine-vectors and real world 78−37151
one-dimensional superconductivity, response functions, from renormalisation group theory 80−54829
operator hypoellipticity on nilpotent Lie groups *(French)* 79−30192
optical group Opt(3,1) and its subgroups 78−77759
optimally controlled boundary layer eqns., group fibering 79−41663
para-Bose algebra representations using single Bose field 79−49157
parafermi statistics, Lie algebraic aspects of quantum statistics 79−54045
parafermion representations of Lie-algebra chain $O_7 \supset G_2 \supset SU_3$ 78−74173
parameterised systems, dynamical groups 80−8836
partial reciprocal of Baker-Campbell-Hausdorff formula *(French)* 77−67191
particle under repulsive oscillator, Sl(3,R) complete symmetry group, Lie group 80−86602
path integral and quasiclassical asymptotic behaviour on Lie group 78−54230
Pauli's exclusion principle for strong interactions in hadrons, nuclei, and astrophysics 80−37206
perturbation theories, algebraic aspects 80−31539
Petrov G_4 types, spacelike dust cosmologies 77−57246
physics, algebras, manifolds and fibre bundles 79−44709
plethysms of finite and continuous groups, generating functions 80−31548
Poincare and Galilei groups in arbitrary dimensional spaces 78−77672
Poincare Lie algebra, Casimir operators of subalgebras 77−33835
Poisson Lie algebra deformation and quantisation 80−8854
Poisson Lie algebra deformations, quantum mechan. 77−74261
polarisation *(French)* 79−53959
polynomial algebras on Lie algebras of inhomogeneous symplectic groups *(French)* 79−53962
polynomial invariant structure in symmetrical algebra of inhomogeneous pseudo-orthogonal group *(French)* 79−30189
polynomials under Poisson brackets with canonical coords., Lie algebra *(French)* 79−71223
positive cones in enveloping algebras of finite dimensional Lie algebras 79−54280
primitive infinite Lie algebras, deformation cohomology 80−8838
projection operators for semisimple Lie groups 78−69963
projective covering group versus representation groups 80−62874
projective Lie algebra of Lorentz group, homographic transform. 78−57739
pseudo-Lie algebra, finite dimens. representations 77−60898
pseudo-Lie algebra, local solvability of nonlinear sequences 79−5965
pseudo-quartenion and pseudo-octonian Lie-admissible algebras 79−2948
pseudogroups, appl. of partial differential eqn. systems 79−25823
QFT, BRS transform. 78−93591
quantisation condition for t'Hooft monopoles in compact simple Lie groups 77−13869
quantisation of momenta and Hamiltonian 79−44775
quantum bundles, group actions, relationship to group representations 80−17837
quantum completely integrable systems connected with semi-simple Lie algebras 78−12599
quantum field Lie-admissible local powers, incompatibility with Wightman axioms and spin statistics theorem 78−93793
quantum mechanics, Heisenberg/Lie/symplectic formulations, problematic aspects 80−62497
quantum partition functions, classical limit 80−52120
quantum structures, Lie-admissible symmetry, representation theory 80−62870
quasiparticle formalism, atomic shell operators, Lie algebra 80−91414
quasirelativistic equation of motion, invariance group 79−12649
quaternionic Hilbert space and colour confinement, admissible symmetry groups 80−27458
R^{2n} function with Poisson bracket, Lie algebra *(French)* 80−46843
R-separable solutions of wave eqn. $\psi_{tt}-\Delta_3\psi=0$ 78−62293
random walk on homogeneous spaces of certain rigid type groups *(French)* 79−75320
random walks on simply connected nilpotent Lie group homogeneous spaces *(French)* 79−25977
rank 1 semisimple Lie groups, characterisation of Schwartz space, Paley-Weiner type theorem 80−4506
Rarita-Schwinger eqn., additional symmetry 78−89
real simple Lie superalgebras, finite-dimens., classification 80−57516
recurrent Lie group classification *(French)* 78−62047
reggeisation in theories with broken global symmetries, nondegeneracy of vector meson masses, non-trivial mixing 80−13236
relativisitic eqns. for massless particles, new ivariance algebras 79−58909
relativistic quantum field theory, mass splitting 77−18166
relativistic quantum mechanics, conserved four-vector currents for free particle 77−37778
relativistic wave equations, algebraic struct. Lie algebras 79−67460
relativity and deformed Lie groups 79−121
representation theory, topological methods *(Russian)* 78−54148
representations and appls., book 78−32652
residue formula to extend Roos differential forms to analytic complex Lie groups *(French)* 79−44706
Riemannian spaces, Lie derivatives and deviation eqns. 80−46876
Robertson-Walker metric, elementary particles in homogeneous isotropic universe 77−5734
scalar extensions in universal algebra *(French)* 79−53956
scalar quantum field in an external gauge field 79−97489
scalar relativistic fields, symmetry groups, with self-interaction 79−30664

Lie groups continued
in Schrodinger picture and radial matrix elements 77−2560
self dual Euclidean gauge fields, semisimple groups, Lie algebra, SU(2) and SU(3) fields 79−6278
self-adjoint systems, Lie-admissible deformation 80−101941
semi-simple algebras of rank l=2, practical form of Freudenthal formula *(French)* 78−86112
semi-simple graded Lie algebras, finite dimensional representations 79−30675
semi-simple Lie algebras, linear representation, natural topology *(French)* 79−44704
semi-simple Lie groups, Casimir operator eigenvalues, symmetric power sum expansions 80−86604
semigroup compactifications of topological groups 80−73620
semisimple, representation matrix elements and Clebsch-Gordan coeff. 79−97230
semisimple, tensor product of representation 77−64960
semisimple algebras connected with completely integrable classical systems 77−17805
semisimple graded Lie algebra (Sp(2N);2N), fourth degree Casimir operator 78−65750
semisimple groups, O(n), U(n), raising and lowering operators, infinitesimal approach 80−62875
semisimple Lie algebra, completely integrable classical system 77−74215
semisimple Lie algebras, natural topology for linear representations *(French)* 78−77665
semisimple Lie algebras highest weights 77−60888
semisimple Lie superalgebras, deformation eqns. and stability 79−93314
simple flexible Lie-admissible algebras, classification 79−75319
SL(2,C), new nonlinear realisations 79−88828
SL(2,R) dynamical Lie group, hyperbolic transforms 80−57515
SL(3,R), unitary analytic representations, hadronic Regge sequences 78−37155
SL(n,C) actions, analytic, real, on spheres and complex projective spaces 80−68382
SO(2N+1) operator representation and wave functions of fermion many-body systems 78−41227
SO(4,2), Delaunay similar elements in eccentric anomaly *(German)* 80−57507
SO(6,C), spinor representation, description of spin 1/2 polarised particles *(Russian)* 77−6053
solid state physics, octupole and hexadecapole dynamics 77−88682
soliton eqns., Lund-Regge model generalisations 79−17605
soliton eqns., path independ. care 78−24635
soliton geometrical interpretation from generation of eqns. solvable by Lie-algebraic structs. 78−24684
solitons, geom. interpretation 79−54266
solitons, pseudopotentials and Lie algebras 77−26131
solvable Lie algebras, characters *(French)* 79−44705
sp(2n,R) algebra, canonical realisations 77−60894
Sp(2n), eigenvalues of invariant operators 79−71652
SP(4) and SP(3,1) groups, unified treatment using spinor calculus 77−53797
Sp(8,R), Lorentz subgroup anal. and null plane boson realisation 78−62116
Sp(n,R), principal series of unitary representations 77−33833
Sp(n,R) discrete series, harmonic oscill. eigenstates, nuclear collective model 78−71
spatially homogeneous cosmology, dynamical degrees of freedom 79−30155
special relativity, group hypothesis, transformations with singularities 78−49655
spectroscopy and crystal physics, generating function techniques 80−44162
spherically symmetric eqns. in gauge theories for arbitrary semisimple compact Lie group 79−9289
spinor field theory, generalized spin structures on 4-D space-times 80−62564
spinor Lie derivative, geometric significance 78−65749
spinor Lie derivative, geometric significance 78−73826
step operators, Lie algebraic props. 78−62052
stochastic acceleration of particle in random pot., renormalised canonical perturbation theory 77−27233
string representation of gauge fields, chiral field topological props. 80−52410
SU_2, Pauli algebra, first order power-associative deformations 79−75400
$SU_6 \times Su_3^C$ scalars in E_7 irreps 78−36794
su(1,1) Lie algebra, multiplicity free and finite multiplicity indecomposable representations 79−283
SU(2,1), graded Lie algebra, irreducible representations 80−82913
SU(2,2) conformal group, unitary ray representations with positive energy 77−71450
SU(2,2) homogeneous symplectic manifolds, conformal Lie algebra 78−45808
$SU(2)_A R^4$, projective irreducible unitary representations 79−89075
SU(2) gauge theory instanton solns., duality condition, Lie group interpretation, quasiparticle soln. 79−6261
SU(2) instanton, physical interpretation of degrees of freedom 78−62312
SU(2) supergroups, Yang-Mills, Lie groups, chiral coeffs., Baker-Campbell-Haussdorff formula 80−68355
SU(3) group, nonlinear representations of Lie algebra 77−13570
SU(3) group irreducible representations, commutation relations *(Chinese)* 80−52434
SU(3) representation theory, connection with SU(3) particle classification schemes, Weyl character formula 77−34101
SU(n) Lie gauge group, triangular anomaly 78−29270
SU(N) unification of extra strong interactions, no-go theorem 80−32056
subalgebras of real 3 and 4 dimens. Lie algebras 77−71179
subgroups, linear, connected, in locally convex space, infinitesimal transformations 80−68381
super-convergent adiabatic invariants with resonant denominators by Lie transforms 79−1289
superalgebra generalisation, 3-colour extension of OSP (4,1) de Sitter and SU(2,2;1) Wess-Zumino superalgebras 79−330
superalgebra theory, struct. and representations 77−37716
superalgebraic approach to second quantisation 79−21654
superalgebras, Casimir invariants, calcs. 79−12976
superalgebras, generalised, Jordan- and Lie-admissibility 80−101942
superalgebras, spinor representation for Lie algebra enlargement 77−34100
superalgebras of dimension 4, classification 79−2594
Lie groups continued
superalgebras with semisimple even part *(Russian)* 79−30197
superconformal algebra, two-point and three-point Green's functions of scalar superfield 77−30280
superconformal invariant two- and three-point functions, and invariant equations in 2-D space-time *(Bulgarian)* 80−47206
supergravity, auxiliary fields 79−17315
supermanifolds, Lie superalgebras and superspace 80−9125
superspace, new class of superalgebras and local gauge groups 78−29230
supersymmetry, algebraic props., applic. to particle physics 77−87918
supersymmetry and Lagrangian field theory 77−6041
supersymmetry in de Sitter space, graded Lie algebra of generators of symmetries 79−93305
symmetry breaking perturbation technique, tensor operators 79−12975
symmetry groups of field equations for spin 1/2 79−21568
symplectic collective model, irreducible U(3) tensor interactions 80−83048
symplecton, prototype for semi-simple graded Lie algebras 77−17751
tangent bundle, Lie algebra of infinitesimal automorphisms *(French)* 79−62995
tensor operators and characteristic identities for semi-simple Lie algebras 79−35956
ternary algebras, construction of Lie algebras and superalgebras 80−24
topological solitons graded Lie algebras, appl. to obstructions for crossing defect hypersurfaces 79−42062
transform, approach to classical perturbation theory, plasma physics appl. 78−93510
transformation group and limit cycle containing nonlinear differential eqns., connection with perturbation techniques 78−20941
transformation groups for resolution of partial differential eqns., appl. to gravity, quantum mech. and heat transfer *(French)* 79−49099
transitive dynamic systems, polhode concept generalisation *(French)* 78−62065
transitive Lie pseudogroup, formal props. of normaliser *(French)* 77−67192
transitive Lie pseudogroups, normalisers *(French)* 77−67229
transitive mechanical systems, param. determ. from co-adjoint action 78−12554
Trotter limits, applic. to quantum field theory and quantum optics 80−22238
twistors and multipole moments 78−16705
two-body coordinate transform., laboratory to centre of mass coordinates 78−21345
U(3) symmetric matrices algebra applic. to π bond order calc. 80−18810
U(n) Lie group, generalized coherent states 80−362
U(p+q) and U(p,q) in U(p)×U(q) basis, matrix elements for infinitesimal operators 80−12928
U(p+q) and U(p,q) in U(p)×U(q) basis, matrix elements of infinitesimal operators 80−12929
uncertainty measure for compact Lie group, minimised for max. weight vectors 78−20996
unitary analytic representations of SL(3,R)*, operator formalism method 77−45983
unitary representations of general covariant group algebra, Lie algebra 78−58136
universal Clifford algebras, realisation and classification as associative Lie admissible algebras 80−37178
unsteady boundary layer on flat plate, analysis of self-similarity and fibering of equations by Lie group theory 77−89108
van Est theorem for groups of diffeomorphisms 78−93811
vector field Lie algebra, continuous cohomology 79−21524
vector fields tangent to sub-manifold, Lie algebra derivation *(French)* 79−53965
vector products whose components satisfy three parameter Lie algebras 79−45027
vector spaces, prehomogeneous, parabolic subgroups, local zeta functions *(French)* 80−46785
visual anal., Lie group representation, computational results 78−27939
wave eqn. in space-time, SO(4,C) group 79−12968
wave eqn. in space-time and Lie theory, Lorentz group 77−26179
wave eqns. in space-time, Lie theory and semisubgroup coords. 77−33873
weak Hamiltonian inversion in an algebra *(Spanish)* 78−54150
weight multiplicities of the exceptional Lie groups 80−9127
weight multiplicity for Lie groups, explicit formulae 77−26467
weight multiplicity for unitary groups, program 78−74166
Weinberg-Salam model, graded Lie algebra structure, derivation from lepton Lagrangian 79−49440
Weyl Lie algebra, relativistic scatt. of model particles 79−40690
Weyl Lie algebra representations as elementary particle models 79−2949
Weyl quantisation and metaplectic representation 78−49712
Wigner-Eckart theorem for an arbitrary group of Lie algebra 80−86124
wigner-Eckart theorem for graded generalized Lie algebras 79−97528
Wigner-Racuh orthogonal and symplectic groups, relationship 78−83
X-Y model; generalised, Lie algebra appl. 78−77806
Yang-Mills SU(2) eqns. in compactified Minkowski space, invariance conditions 79−63342
Yang-Mills theory, allowed supersymmetric vacuums 78−4783
$Z_2 \oplus Z_2$ graded Lie algebras and superalgebras, sequences 79−5962
zero-mass representations of Poincare supersymmetries with arbitrary spinor generators 80−99065
$\psi_{tt}-\Delta_3\psi=0$, R-separable solns. 78−4489
CaO F^+-centre, Lie group theory aspects of Jahn-Teller effect 77−20279
^{3}He, superfluid, Ginsburg-Landau region, phase equilib. in Lie group method 79−23799
^{24}Mg rotational band collectivity, shell model excitation in Sp(4, R) symmetry 80−102095
^{16}O, rotational band collectivity, shell model excitation in Sp(4, R) symmetry 80−102095

lifts
hydraulic, for domeless solar telescope *(Japanese)* 79−96914
weight handler, for piston gauge 78−8399

ligand field theory *see bonds (chemical); crystal field interactions; molecular energy levels*

light
see also airglow; optics; sunlight; zodiacal light
ballistic theory and space travel 79−80204

light continued
ballistic theory of light based on EM force laws and Newtonian mechanics 80−50
bending by Sun's gravit. field, effect on clock and local latit. corrections 78−7878
3C 279, variable quasi-stellar source, IR and visible polarimetry and photometry 78−16528
course, sound and light in the arts 77−22340
deflection by solar gravit. field, effect on meas. of Gorky latit. *(Russian)* 78−40462
deflection by Sun, principle of equivalence calcs. 78−81729
distant stars distribution, evolution seen by observer falling freely into nonrotating black hole *(Polish)* 80−26897
Einstein gravitational light deflection in astrometry 77−17359
film thickness meas. on nonplanar substrates 78−29085
fundamentals summary *(German)* 79−94145
gravitational bending, new theory of photon and energy based on two primitive particles 79−67145
gravitational bending, rel. to meas. of parallaxes of objects at cosmological distances 78−53796
gravitational bending, work of Johann Georg Soldner (1776-1834) 78−81787
gravitational bending by Sun, vars. caused by solar activity *(French)* 80−56795
gravitational deflection (Einstein effect), prospects of observation at solar eclipse (1981 July 31) *(Russian)* 80−51651
gravitational deflection in close double stars, mass meas. *(French)* 79−62753
gravitational deflection of light, meas. at 1919 May 29 solar eclipse 80−67553
gravitational focusing effect, short-wave limit imposed by lens star gravity field asphericity 79−58604
gravitational lens action by massive galaxy, QSO 0957+561 AB, flux var. and image splitting 80−27008
gravitational lens effect, appl. to twin QSOs 0957+561 A, B 80−12827
gravitational lens effect, EM wave diffr. in Schwarzschild space-time 80−90750
gravitational lens effect, evidence from double quasar (Q 0957+561) 80−27005
gravitational lens effect, focusing by slowly rotating relativistic spherical mass 80−105155
gravitational lens effect and pregalactic halo objects 80−17484
gravitational lens effect formed by spherical galaxies, multiple image prod. 80−90532
gravitational lens effect of moving black hole 77−33549
gravitational lens effect of spherically symm. mass distrib., optical scalar eqns. 77−64637
gravitational lens hypothesis, appl. to triple QSO (PG 1115+08) 80−86012
gravitational lens in double quasar 0957+561A, B due to intervening galaxy, IR obs. 80−73065
gravitational lens interpretation of QSO 0957+561 A and B, evidence from direct imaging 80−17686
gravitational lenses, high-intensification regions 79−25463
gravitational light deflection, Sun semidiameter appl. *(German)* 80−46531
gravitational mirror effect, appl. to black holes detect. *(Russian)* 78−40987
intrinsic angular momentum 79−58483
Johann Georg von Soldner and the gravitational bending of light, with an english translation of his essay on it published in 1801 79−17176
Kerr gravitational field effect on optical images 77−45480
laser beam diffraction in near and far zones, calc. 79−94274
Lorentz-invariant theory, results for red shift, light deflection, perihelion shift *(German)* 78−29030
non-classical effects in the statistical properties of light, review 80−99686
null radiation gravitation deflection by relativistic spherical masses 79−58600
photon decay in curved space-time, Hubble red shift and solar limb effect explanation 79−35606
relativistic force equation, appl. to determ. of light bending and red shift in grav. field *(Afrikaans)* 79−97270
time dependent physical spectrum 78−9317
US velocity, of liq., determ. using optical diffr. by short acoustic pulses for teaching 79−62963
wave and particle descriptions of light, equivalence, rel. to radar freq. shift 80−101692
Ag_8GeTe_6, optical props. and polymorphism 80−45082

light absorption
see also atmospheric optics; densitometry; light transmission; optical constants; optical films; optical filters; pleochroism; spectra
absorbing film-nonabsorbing substrate system optical parameters, FORTRAN code *(Rumanian)* 77−69923
additional light waves near region of exciton absorpt. and luminesc. in crystal 80−2340
adsorbed molecules, surface plasmon enhanced light absorption 80−40176
aerosol, solar radiation absorpt., visual photometric meas. technique 80−85750
aerosol absorption coeff. rel. to measurable bulk props. 77−45154
aerosol scattering and extinction coeff. simultaneous meas. in portable multipass cell 79−62588
aerosols with organic constituents, effect on fog and clouds 78−73465
aggregates, of large rigid molecules, optical absorpt. theory 77−79720
algal suspensions, light scatt. and absorpt. props., 380-720 nm 78−92604
alkali hydrides, lattice props. from interacton pot. energy function 80−100199
alkali silicate glass: Cu^+/Cu^{2+}, cpt. absorpt. rel. to impurity redox equilib. *(Japanese)* 77−12824
alloy, expt. methods, review 79−33655
alloys, substitutionally disordered, optical cond., intraband transitions 80−103933
amplitude-phase holograms, optical parameter dispersion 80−58481
anisotropically absorbing medium, polarisation nearness variation 80−1118
anthracene, in stretched polyethylene film, UV-visible and fluoresc. spectral shifts 78−62852
anthracene, single cryst., fluoresc. decay, Monte-Carlo simulation *(German)* 79−61440

light absorption continued
anthracene, structural changes induced by UV irradiation *(German)* 79−42100
antireflection coating evaluation by attenuated total refl. 77−50783
asymmetric gas-dielectric optical waveguide with wall resonances 79−7216
atmosphere, 0.63 μm attenuation and directional scatt. in droplet and cryst. clouds *(Russian)* 78−96292
atmosphere, absorpt. effects wavelength depend. rel. to anomalous gray shades in DMSP visible imagery 80−77111
atmosphere, absorpt. in 8-12 μm transparency window by fine aerosol particles *(Russian)* 78−16159
atmosphere, absorpt. in IR window due to water vapour polymers 77−45145
atmosphere, aerosol content determ. from photometric obs. of stars 78−92976
atmosphere, aerosol effect on remote sensing aerospace information 80−4101
atmosphere, aerosol extinction at 500 nm in urban and rural air at Milwaukee, USA 79−100946
atmosphere, aerosol optical attenuation statistics, spring and autumn 79−84484
atmosphere, attenuation coeffs. rel. to aerosol particle size distrib. statistical characts. *(Russian)* 78−53702
atmosphere, CO_2 laser two-freq. differential absorpt. rel. to pollutants detect. *(French)* 80−7991
atmosphere, effects on auroral brightness obs. from satellite 80−12538
atmosphere, extinction coeffs. at Wise Observatory rel. to photoelectric photometry 78−73657
atmosphere, extinction in 3.98-4.07 μm wavelength region 79−96808
atmosphere, extinction rel. to twilight visibility function of near-Sun astronomical objects 77−5321
atmosphere, haze and fog, visible and near IR attenuation 77−45153
atmosphere, in situ meas. of aerosol absorpt. coeff./extinction coeff. ratio 80−90217
atmosphere, incoherent optical propag., effects on optical/optronical systems 78−92987
atmosphere, IR absorpt. rel. to total O_3 content determ. using satellite meas. 80−77027
atmosphere, IR anomalous absorption, temp. dependence 79−34951
atmosphere, IR radiation attenuation by ice platelets 80−66141
atmosphere, light absorpt. and scatt. rel. to direct beam solar irradiance and illuminance 80−90174
atmosphere, mol. complexes presence and role in residual absorpt., light scatt. obs. 80−56607
atmosphere, molecular absorption, Lowtran 3B model 78−85690
atmosphere, near IR extinction 80−51539
atmosphere, radiation attenuation spectral struct., depend. on atmospheric surface layer turbidity *(Russian)* 78−44997
atmosphere, solar UV radiation absorpt. in mesosphere and stratosphere 80−109248
atmosphere, stellar extinction oscills. caused by atmospheric disturbances 80−56606
atmosphere, transparency meas. in Uzhgorod *(Russian)* 78−40656
atmosphere, true absorpt. rel. to polarised light transfer 80−67561
atmosphere, visible and near IR attenuation exponents up to 30 km, experimental profiles *(Russian)* 78−61558
atmosphere, water vapour absorption in 8 to 13 μm spectral region 79−39855
atmosphere aerosol absorpt. and scatt. effects rel. to satellite retrieved temp. profiles error 80−98449
atmosphere aerosol attenuation, influence on atmospheric and oceanic temp. determ. by remote sounding *(Russian)* 78−81430
atmosphere extinction, 0.65 to 2.50 μm above Mauna Kea, obs. 80−12546
atmosphere extinction, monochromatic coeffs. determ. from spectrophotometric obs. on Terskol Peak *(Russian)* 79−44246
atmosphere surface layer, statistical characts. of radiation attenuation spectral struct. *(Russian)* 78−24371
atmosphere water vapour, IR continuum absorpt. calc. *(Russian)* 78−96293
atmosphere with cloud, water vapour and CO_2 absorpt. rel. to IR radiation flux approximation 79−39854
atmospheric, contrast attenuation factors calc., for remote sensing 80−4135
atmospheric 8 to 12 μ IR emission attenuation obs. *(Russian)* 78−61556
atmospheric absorption of solar, diffuse and reflected visible radiation *(Russian)* 78−96291
atmospheric aerosol, in situ absorption meas. using reson. CW laser spectrophone 77−73860
atmospheric aerosol constituents, absorpt. coeff. rel. to imaginary refr. index 79−74956
atmospheric aerosols, absorpt. in UV *(Russian)* 78−16160
atmospheric attenuation, reson. absorption by water vap., ruby laser pulse *(Russian)* 78−49138
atmospheric degradation of electro-optical system performance 79−66805
atmospheric extinction and absorpt., effects of particulate complex refr. index and size distribs. 79−29849
atmospheric far IR laser radiation absorption, theory and expt. 77−41250
atmospheric laser beam propag., monochromatic, problems 78−92988
atmospheric NO_2 total content meas. by absorption spectroscopy *(Japanese)* 80−12469
atmospheric pressure sensing by solar occultation using wideband CO_2 absorption 79−80037
atmospheric spectral absorption of solar radiation by Denver Brown Cloud 78−16158
atmospheric transmittance model for variable-mixing-ratio absorbent gases 79−80011
atom+diatomic molecule, collinear collision, light absorption 79−76486
atomic system, hydrogenlike, polarised monochromatic laser radiation absorption in electronic transitions, DC mag. field effects 80−9563
atomic vapours, three-level system, collisional effects in saturation spectroscopy, appl. to Na 80−78579
atoms, light absorption, subtractive stimulated emission theory 79−59396
Auger recombination of carriers bound to centres involving phonons 80−107805
beam volume attenuation coeff., invalidity 80−95791
Beer-Lambert modified law calc. 78−82906

light absorption continued
beryl, channel constituents, electronic absorption spectra of Fe^{2+} 79−69863
bilevel absorber, partial differential rate eqns. 78−37950
biological structures, light absorpt. and orientation of absorpt. momenta 78−53326
Bixon-Jortner approx. limitation, coupling strength incoherence 77−57960
black surfaces, visible and near-IR meas. using calorimetric method 78−93685
blackened optical surfaces, IR absorpt. rel. to stray light reduction, spectral emittance meas. 79−61449
breather generation, inverse scatt. technique 80−78913
bulk materials, low optical absorpt. coeffs. meas., adiabatic laser calorimetry with long rod samples 79−2804
calorimetric absorption coefficient measurements using pulsed CO_2 lasers 80−9918
canted magnetic structure media, effect of light absorpt. on quadratic magneto-optic effects 77−24826
carbonized bitumen, refractive index and absorpt. coeff. as measures of structural organization 79−35811
cavitation nuclei in liquid flows, size distrib. determ. technique 77−68716
CdSe two-photon absorption, laser calorimetric obs. 80−33076
cell high-speed analysis, laser absorpt. and scatt. meas. *(German)* 78−92687
cellular anti-loss struct. as solar absorber, emittance distrib. at cell walls *(French)* 77−14890
chalcogenide glass, Urbach tail, rel. to Mott-Street model 77−47771
chemical laser window materials evaluation 77−46769
chlorophyll A low-intensity two-step absorpt. in vivo 78−35801
chloroplast thylakoid, light-induced absorbancy and scatt. changes about 520 nm rel. to struct. 78−69019
cholesteric films, absorpt. and contrast in dichroic liq. cryst. displays 80−75155
cholesteric liquid crystals optical properties, diffraction nature, review 80−70123
circular dichroism of phototransients, meas. apparatus using modulation excitation 77−46656
circular plate, optical hot spot, thermal stresses 77−11044
cirrus clouds, visible and IR absorpt. calc. from lidar and radiometer meas. 80−82060
city plume aerosol size distrib. and turbidity meas. 77−37408
classical crystal optics, lattice dynamical background, review 80−97221
clouds, droplets volume extinction coeffs. at visible and IR wavelengths 77−25750
cloudy atmosphere, radiative transfer model, solar radiation and cloud struct. 79−21016
coatings, absorptive, at normal incidence, program for TI-59 calculator 80−84793
coefficient, precise meas. of small change *(Japanese)* 80−4749
coherent propagation of light pulse, instability in reson. absorbing media *(Russian)* 77−62017
colloid, particle size distribution function, electrooptical diffusion method for determ. 80−8956
complex reaction, evaluation of first order rate constant 79−1937
compound glass rod absorption coeff. calorimetry 80−106631
cone absorption calorimeter for pulsed laser meas. 80−98980
continuum source by isolated Lorentzian lines in spectrophotometry of excited atoms 79−52667
correcting absorber selection for Si photodiodes, luminous meas. in flash photometry 79−72699
crystal optical characteristics, relax. processes exciton dispersion 80−107709
crystalline material optical absorption meas. 80−105718
crystalline optical material props., symmetries and tensorial relationships 80−108174
CW laser beam stablisation by spatially dependent absorption 79−76740
cyclotron absorption in mag. white dwarfs, theory 80−4351
degenerate four-wave mixing in absorbing media 78−71138
degenerate semiconductor photostimulated light absorption in Burnstein-Moss effect *(Russian)* 79−28706
demonstration of continuous spectrum, optical filters to audiences, students 77−45649
diamond:Sb, implanted, radiation damage and annealing study 80−100263
dichlorodifluoromethane, absorpt. meas., laser power density depend. 80−92251
dielectric, criterion for breakdown by single light pulse *(Russian)* 77−12311
dielectric film, IR surface wave selective absorpt. *(Russian)* 77−1754
dielectric mirror, temp. field during laser radiation absorpt. 80−19063
dielectric multilayer interference devices, loss mechanisms 77−83943
dielectric solid, absorpt. of laser radiation by defects in surface layer *(Russian)* 80−25497
dielectric sphere, Mie theory with spatial dispersion 79−98284
diffraction grating anomalies and energy absorpt., rel. to surface waves, general theory 78−94447
diffraction grating plasmon anomalies, energy absorpt. theory *(French)* 77−65628
diffuse scattering, statistical model, Gurevich-Kubelka-Munk theory calcs. 78−46513
diffuse solar radiation field in cloud layer *(Russian)* 79−29851
diffusion in gases, light induced atomic ground state transition absorpt. of monochromatic wave *(Russian)* 79−77335
direct-gap crystals, one-photon absorpt., Keldysh and perturbation formulas 80−20607
direct-gap semiconductor, absorpt. coeff. of light due to indirect transitions 79−91400
disordered crystal, biphonon spectra, light absorpt. coeff. and density of states, CPA calc. 80−84271
displacive ferroelectrics, connection between electron spectrum parameters and ferroelec. parameters 79−38483
DNA, natural, hypochromic effect 77−81467
DNA, soln., phase transitions, light absorption oscills. obs. 80−26197
DNA hypochromism, perturbation theory *(Russian)* 77−56339
doped cubic crystals, resonance absorption region, self-induced rot. of polarisation 80−2805
double layers of different substances, refl., transmission and absorpt. coeffs. 77−6999
light absorption continued
double-beam photometer for meas. small changes in optical absorption 80−62709
droplet motion in optical radiation field for small Knudsen number values 78−35730
Earth atmosphere, absorpt. determ. of 460 μ 78−96295
electrolytic double layer, light absorpt., electrochromic changes 78−84551
electron-ion plasma, stimulated bremsstrahlung light absorption *(Russian)* 78−87438
electrons, from heated oxide cathode, multiphoton laser absorption 80−6224
emission spectra, absorpt. method regularization 79−98250
energy absorption distrib. in material with spatially varying optical props. 77−75419
enzyme-linked immunosorbent assay, apparatus for meas. light absorbance of small vols. of liquids 80−72387
ethane, photoabsorption cross sections, 1380 to 1600 Å, at 295 and 200K 78−90181
ethidium bromide E-DNA, intercalated birefringent fibres, microspectrophotometric investig. *(German)* 80−57392
ethylammoniumtetrachlorochromate, optical absorption intensity, short-range spin correlation 80−108185
exciton ferromagnet, spin-lattice relax., light and US absorption *(Russian)* 79−7960
exciton insulator, coherence factors and transport props. 79−28291
exciton system, Bose condensation and optical props. of condensate 77−55485
ferroelectrics, absorption edge anomalies in phase transitions 80−2718
fibre attenuation and pulse dispersion due to neutron irrad. 80−58730
film, optical absorption meas. at air-film interface, within film and at film-substrate interface 79−80659
film, resonant amplification, total absorption *(Russian)* 77−7153
film absorption coefficients meas. by ATR spectroscopy 78−37073
film absorptive laser damage analysis by Weibull distrib. 80−33061
film coating, IR absorpt. meas. by laser calorimetry 78−25905
film on absorbent support, laser heating *(Russian)* 80−7441
film thickness meas., lattice absorption method *(Czech)* 77−172
filter, multilayer frustrated-total-internal-refl., spatially limited 80−96014
fine interference layers, absorpt. coeff. determ. method *(Russian)* 78−82908
fingerprint material, IR spectrum 78−78056
flashlamp in air, optical inhomogeneity due to light absorpt. heating of air 79−64299
fluorophosphate glass, optical absorpt. comparison with 3d transition elements *(French)* 79−65819
fog, droplets volume extinction coeffs. at visible and IR wavelengths 77−25750
fog, Lidar visibility meas. by Raman/aerosol ratio method 79−100953
fog hole boring with pulsed high-energy lasers 79−16662
fogs, optical probing, homogeneous particle model 79−66790
free polaron multiphoton absorpt. spectra, electron reson. coupling via longit. optical phonons 79−95347
G333.6−0.2, G298.2−0.3, compact H II regions, IR emission lines rel. to extinction 78−96522
galactic interstellar extinction law, vars. 78−85990
galactic IR sources, 3μ extinction feature identification 80−62227
galactic light extinction, A_B coeff. amplitude 80−17664
galaxies, nearby, interstellar reddening law and dust content *(German)* 80−67850
gas, laser absorpt. wave propag., shock waves 80−28597
gas, thermal fluctuations of optical absorpt., noise *(Russian)* 77−31423
gas, thermal fluctuations of optical absorpt. *(Russian)* 77−31422
gas layer, heat cond., radiation interaction in presence of band spectrum 79−55307
gaseous medium, two-photon-absorbing, polarised light propag., quantum effects 80−103107
gases, derivative spectroscopy, measurement based on 2nd derivative optical absorption spectrum *(German)* 77−21459
gases, nonmonochromatic photochemical waves, stationary propag. 77−31421
gases, self-interaction and stimulated Raman scattering effects *(Russian)* 79−3740
Gaussian beam scattering charact. at dielec. media interface 78−42275
glass, K-8, radiation coloured, msec laser pulse effects 77−16435
glass, low absorption coeff. meas., calorimetric method 77−58405
glass, transmission, reflection, absorption factors, solar radiation, calc. method 77−34918
glass absorption filters with bandpass charact. for green region *(German)* 77−34943
glass fibres, multicomponent and high SiO_2, thermal variation of attenuation 79−50390
glass laser disc interface with edge cladding glass, reflection meas. 79−27300
graded index films appl. to solar absorbers 77−62042
graded-index fibre differential mode attenuation meas. 78−1403
grains with resonant impurities, extinction cross sections theory 77−53660
HD 200775, Be star, optical and UV extinction by dust in (NGC 7023) 80−109515
heating effect due to weak intensity pulsed optical irrad. of absorbing plate 77−14658
heavy atom, parity violation in forbidden mag. transitions, chiral absorpt. of polarized light and circular dichroism in crossed DC fields 80−23370
4-n-hexyloxybenzylidene-4′-n-hexylaniline, liquid crystal, exam. of orientation order of dissolved molecules 80−44112
high pressure cell, quantitative absorpt. meas., variable thickness *(German)* 78−12769
high-silica fibre-optic waveguide, sensitivity to low-dose radiation *(German)* 78−33869
highly transparent materials, relative dominance of bulk or surface absorption by transient methods 77−52031
holographic attenuated thick gratings, anomalous absorption 78−1188
IC 3568, planetary nebula, struct. and internal extinction 80−31338
III-V semiconductors, absorpt. coeff. of light 79−69803
impurity crystal, light absorpt. max. at Brillouin zone boundary 80−55139
inert gases, electron-beam excited, transient absorpt. at XeF laser wavelenghts 80−83592

light absorption continued
inert gases, photoabsorption, local field effects, density-functional formalism 80−78766
insulator-metal multilayered structs. *(Japanese)* 79−38191
integrating cavity for small optical absorption meas. 79−12838
interference layers, absorpt. coeff. determ. 79−99961
internal field reson. struct., implications for optical absorpt. and scatt. by microscopic particles 79−10259
interplanetary ice particles, near IR absorpt. rel. to lifetime 77−29721
interstellar absorption effects in visible and UV *(Italian)* 77−87517
interstellar absorption effects on Balmer discontinuity strengths 78−89238
interstellar absorption effects on stellar absolute spectrophotometric gradients *(Russian)* 79−92752
interstellar dark nebulae, visual extinctions determ. via star counts 78−57612
interstellar dust grains, temp. fluctuations due to UV photons absorpt. 80−26938
interstellar extinction, 2200 Å extinction hump prod. by porous graphite grains 80−62228
interstellar extinction, 2200 Å feature anomalous strength in Cassiopeia-Taurus association stars 80−77469
interstellar extinction, 2200 Å feature obs. in Orion Nebula by long-slit spectroscopy 80−105297
interstellar extinction, polarisation reversal by small particles over strong resons. 79−2564
interstellar extinction at UV wavelengths, role of biochemical chromophores 80−26945
interstellar extinction rel. to H I column densities, latit. depend. effect interpretation 80−26953
interstellar extinction towards ρ Ophiuchi, rel. to large grains origin 80−41870
interstellar grains, interaction of light with small-particle system 77−74111
interstellar large globules, absorpt. meas. rel. to struct. and dynamics 80−62246
interstellar medium, total/selective extinction ratio rel. to grain growth 80−67834
interstellar Mg silicates, mid IR extinction from laboratory silicates IR optical consts. 80−31337
interstellar radiation field, attenuation rel. to K I and Na I column densities depend. on N_H 78−20872
interstellar reddening, rel. to diffuse interstellar line at 6284 Å 80−51843
interstellar reddening in near IR, new results from JHK photometry of reddened stars 80−94857
interstellar reddening in solar neighbourhood, anal. 80−62239
interstellar reddening law in Corona Austrina dark cloud polarimetric meas. 79−17050
interstellar reddening law in Taurus dark cloud complex, IR photometry results 79−8963
interstellar variable IR extinction at galactic centre, obs. 79−48909
ionic crystal, anharmonism effect on exciton peak broadening in absorpt. spectra *(Russian)* 80−97317
IR absorptiometry, gas anal., modern trends 79−8458
IR absorption mechanisms for crystals 78−80329
IR absorption of trapped line photons by dust 79−25460
IR band nonrigid rot. absorption, appl. to CO, NO, N_2O and CO_2 78−91060
IR coating with low absorpt., use for high energy laser reflector and window 79−45951
IR Doppler wind-sensing system, spaceborne, atmospheric effects 79−96828
IR extinction meas. using lidar, with CO_2 laser radiation 78−40655
IR laser energy absorpt. by atm. dust, spectrophone meas. 77−9513
IR laser window material extrinsic absorption 79−14049
IR materials, laser residual absorpt. 2 to 10 μm, review 78−25906
IR radiation spectral absorptance and transmittance, accurate modelling technique 78−91062
IR transparent materials, bulk and surface absorpt., calorimetric meas. method 79−27347
IR window materials, optical phenomena, book contrib. 78−9420
irradiated spheres, absorption centre distribution refractive index and size parameter dependence 79−50221
jacketed and cabled optical fibre low-temp. attenuation increase 80−58732
Jupiter, PH_3 absorpt. in 5 μm window 80−31243
Jupiter atmosphere, aerosol absorpt. latit. vars. from 0.6 to 1.1 μ spectrophotometry 80−46468
Kubelka-Munk system, continuous absorpt./scatt. coeff. minimising distribs. 77−50615
Lambertian cavity with dielectric window, effective absorptivity 80−38237
Langmuir films on Cu surface, surface EM wave absorpt. study 80−97359
large spherical particles, absorpt. efficiencies, approximation scheme 79−31798
laser, pulse width, meas. by two-photon absorpt. fluoresc., contrast ratio variation 79−76737
laser backscattering from turbid water-nigrosin black dye-Teflon spheres dispersion 80−1129
laser beam, modulated radiation absorpt. in liquid waveguide and sound generation 78−1539
laser beam attenuation by snowfall, characts. 80−26611
laser beam thermal blooming, stagnation and transonic effects 77−34903
laser beam with stagnant absorber region, transient thermal blooming 77−38966
laser bulk absorption homogeneity, Doppler interferometric meas. 79−14010
laser calorimetric data analysis for surface and bulk absorpt. determ. 78−25904
laser damage thresholds for mirror and window materials, 10.6 m 77−50708
laser high power CW output meas. from temp. rise of Al slab power meter 79−59739
laser light with time-varying intensity in optical medium, temp. field kinetics 78−59098
laser materials, absorpt. meas. by static profile calorimetry 78−25908
laser mirror and window absorption, reflection and transmission obs. at 10.6 μm 79−14014
laser rate calorimetry analysis with coating absorption 80−33050
light absorption continued
laser sounding method and equipment for water absorpt. and attenuation coeffs. meas. *(Russian)* 79−34998
laser window, elec. fields and power dissipation at oblique incidence 77−46746
laser window, mirror and reflector coatings, high power, materials selection 77−50735
laser window, thermal lens form. due to giant laser pulse 77−3602
laser window materials, surface and bulk absorpt., photoacoustic meas. 78−25912
lattices, FCC and BCC, optical transitions, dipole selection rules 80−97409
layer crystals, exciton absorption of light 80−70623
layered crystal, wave functions, exciton spectrum, light absorpt. *(Russian)* 80−100436
leaf optical system modelled as stochastic process 77−44877
leaves of African crop plants, optical props. rel. to photosynthesis 77−25629
leucosapphire, spectral absorpt. coeff., 1800K 78−27252
lidar observations of smoke and dust clouds at 0.7 and 10.6 μm wavelengths 78−69459
Lidar return from fogs, effect of non-uniform extinction coeff. on double scatt. contrib. 79−100952
light extinction, influence on galactic globular cluster system apparent flattening 79−48908
liquid, nonpolar, electron absorpt. of light, one- and two-photon process probabilities *(Russian)* 77−43957
liquid crystal matrix, orientational distrib. coeffs. from UV and circular dichroism meas. 80−92452
liquid refractive index meas. by ADR 77−87808
liquid surface deform. due to laser radiation thermal action, lens effect 80−33048
liquids, photoacoustic and photorefractive detect. of small absorpts., electrostrictive limits 80−108171
liquids, refractometry errors 79−67377
longitudinal permittivity crystal in strong EM field, light absorpt. and emission effect 80−15938
Lorentz gas, two-dimens., collision-induced absorption, simulation 78−46424
lossy structures, Brewster phenomena 78−5419
Lynds 134 interstellar dust cloud, visual extinction rel. to CO isotopic fractionation 80−26924
lysozyme, stepped character of thermal denaturing, optical density at 290 nm 78−15763
M82 nucleus, Brackett-line obs. rel. to visual extinction 79−25704
magnetic semiconductors, critical behaviour of electronic properties, theory 80−96861
magnetic semiconductors, electron propag., s-d model, red shift theory 77−51736
many-valley cubic semiconductor, light absorpt. by free carriers at surface 78−48200
many-valley semiconductor film, light absorpt. 79−83043
Maxwell Garnett theory, validity range 78−68507
measurement of small absorpt. coeffs., automated calorimeter and scanning Doppler interferometer 78−45680
measurement techniques for small absorpt. coeffs., using transmission, emittance and calorimetry 78−24839
medium with two types of absorpt., anomalous behaviour of intense light flux 77−88642
mesosphere, solar H Lyman-α radiation meas. rel. to O_2 density, press. and temp. profiles 78−44947
mesosphere, solar Lyman-α extinction meas. during European Winter Anomaly Campaign (1975-76) 78−45001
metal, expt. methods, review 79−33655
metal, IR absorption, contribution of conduction electron scattering 79−42971
metal, laser heating kinetics, influence of oxide film interf. effects 80−11841
metal, O_2 diffusion and dissolution effects on optical props. in radiative heating, appl. to Ti 79−65884
metal, surface roughness effect on light absorptivity 78−80314
metal absorptivity under laser radiation action, time and temp. depend. 79−95724
metal drilling with Nd lasers, absorption phenomena 78−30002
metal mirrors, diamond turned, surface, optical and laser damage characts. 77−50705
metal mirrors, dielec. enhanced, absorptance at 5.3 μm 77−50709
metal surface laser beam irrad., effective absorpt. coeff., temp. field determ. *(Russian)* 80−76108
metal target, irradiated by pulse-periodic CO_2 laser, absorpt. coeff., air breakdown effect 79−52052
metal targets, laser radiation absorption in craters 80−97386
metal-dielectric interface, p-polarised light total absorpt. by surface plasma waves 78−88373
metallic thin films *(French)* 80−60692
methane, photoabsorption cross sections, 1380 to 1600 Å, at 295 and 200K 78−90181
methyl fluoride, rot. absorpt., Stark modulation expt. 79−59396
methylammoniumtetrachlorochromate, optical absorption intensity, short-range spin correlation 80−108185
mid IR laser window materials, absorption props. 77−46770
middle atmosphere, solar UV radiation absorpt. rel. to numerical model of zonal mean circulation 80−109218
Mie scattering theory, resonances in efficiency factors for absorpt. 78−42276
mirrors, dielectric mutltilayer, reflectance under slight absorpt. conditions 80−83655
mirrors with temperature-dependent absorptance, laser-induced thermal runaway 80−91882
mitochondria, absorbance changes after ADP addition, rel. to ATP synthesis 78−27908
moist air, ion content and IR absorption 80−41493
molecular excitation processes by fluctuating light 80−9646
molecular gas, optically dense flat layer, radiation flux 78−9748
molecules, light absorption, subtractive stimulated emission theory 79−59396
molten salt, metal dilute solns., optical absorption 79−19899
Moon, 0.95 μm absorpt. strip intensity expression on colorimetric map *(Russian)* 79−44381
multilayer, dielectric reflectors, simplified description 79−89984

light absorption continued
multilayer coating preformance, thin-film volume or interface absorption effect calc. 80−33130
multilayer coatings, high-refl. or antirefl., vol., interface absorpt. and scatt. losses 80−63915
multilayer dielectric reflectors, optical props. calc. 78−30041
multilayer interference filter, calcs. allowing for weak absorption *(Russian)* 78−13812
multilayer structure devices, nonideal, computation of optical props. 80−5684
multilevel atomic system, thermally relaxing, coherent radiation reson. scatt. and absorpt. 79−81401
multimode fibres, cladding influence on light attenuation 79−76855
multipath optical cavities in saturated absorpt. expts., freq. calibration and optical delay line 77−65610
multiple optical cell for absorbance meas. of aqueous solns. 80−22450
negative light absorption by medium with selective freq. modulation of quantum oscillators 80−106501
nematic liquid crystal transducers, exam. of light absorption behaviour 79−40560
nematic-chiral-dye mixture, circular dichroism, selective light scatt. *(Russian)* 80−103944
Neptune atmosphere, UV absorpt. sources from UV albedo meas. 80−82295
neutral absorbers of NS glass, meas. of transmission when irradiated with laser radiation 80−105692
NGC 7027, planetary nebula, dust absorpt. effect on [O II] emission 80−8667
nonlinear absorbing media, ray tracing and self-focusing theory 79−27339
nonlinear optical crystals, SHG, absorpt. coeffs. and temp. variation of refr. index difference 80−14390
nonlinear optical props. of band charge carriers rel. to carrier scattering by lattice defects 80−29399
nucleic acids and their aggregates, optical activity, review, book contrib. 80−108847
ocean, absorpt. model for diurnal var. of underwater irradiances on horizontal surfaces 80−72549
ocean, clear, effective IR optical depths 79−8635
ocean, extinction profile determ. using temp. and solar radiation meas. *(French)* 79−62611
ocean, hydroptic obs. in Sargasso Sea and tropical Atlantic Ocean *(Russian)* 79−39748
ocean, in situ attenuation meas. *(German)* 79−39749
ocean, radiation attenuation index, suspended matter-distrib. estimation *(Russian)* 79−39747
ocean, radiative transfer, absorpt. and scatt. props. determ. 77−9430
ocean colour 78−61421
olivine, heavy ion irradiated, and amorphous, IR extinction rel. to interstellar dust 79−53873
opaque, semitransparent materials, Kirchhoff's second law, role of reflection or diffusion *(French)* 79−36835
ρ Ophiuchi dark cloud complex, opacity rel. to formaldehyde lifetimes 78−8080
optical absorption wave propagation in gases, struct., propag., effects 79−10629
optical coating absorption meas. by 1.06 μm laser calorimeter calorimeter 80−33066
optical component, surface evaluation techniques 79−46094
optical fibre attenuation and dispersion meas. techniques and interpretation pitfalls 78−1399
optical fibre attenuation charact. meas. by backscatter technique *(Italian)* 80−106600
optical fibre attenuation meas. instrument 78−59138
optical fibre fabrication, attenuation, packaging and interconnection properties 77−27373
optical fibre loss mechanisms, separation by graphical method 77−14806
optical fibres, basic terms, properties, uses *(Dutch)* 80−64166
optical fibres, light absorption and scatt., calorimetric meas. 78−46790
optical fibres, ultimate low-loss single-mode fibre with 0.20 dB/km loss at 1.55 micron 79−36996
optical fibres and fibre lasers, losses, approx. theory 77−27339
optical film, electric field and absorption distributions 77−601
optical films, by light intensity ratios 77−2678
optical films, optical, struct. and mechanical properties 79−76772
optical glass, absorption coeff. determ., refl. losses role 77−72100
optical glass, coloured, laser damage threshold, optical absorpt. influence 80−91830
optical glass and fibres, absorption coefficient measuremnt by calorimetric techniques *(Dutch)* 79−76774
optical glass attenuation and optical density spectral curves 79−50361
optical glass exposed to laser radiation, absorpt. coeff. temp. depend. 79−89979
optical glass irrad. with quasi-CW laser pulse, obs. of absorpt. waves 79−89952
optical isolation mechanisms 77−19288
optical material, phototransport laser damage mechanism 77−63498
optical material absorpt. meas., real time holographic interferometry 80−83569
optical materials, absorption coeff. meas., photoacoustic technique 77−26402
optical materials, laser induced damage, symposium, Boulder, USA (Sep. 1978) 80−31417
optical waveguide, multilayered, effect of material absorpt. on ray power attenuation 78−83103
oriented spheroids, magnetically oriented, expression for scattering and absorption cross sections 78−29899
Orion Nebula, H_2 emission interstellar extinction meas. 79−25668
Orion Nebula, visual interstellar extinction from search for vibrationally excited H_2 emission 78−93346
oxide film, on Ti, optical consts. and thickness determ., ellipsometric method *(Russian)* 77−81164
pair-correlated distrib. of small-spaced lossy scatterers, light propag. 80−28158
paraffin oil coatings for high power laser system components 77−88730
parallel surfaces, absorptance, reflectance and transmittance, generalised eqns. for calc. 78−42273
particle shape effect on low freq. absorpt. 80−99626
particle size dispersion, effect on IR radiation in Venus clouds 80−109384
light absorption continued
periodically stratified absorbing medium, splitting of energy flux *(German)* 77−3534
photoabsorption convection in horizontal tube, unsteady-state convection, num. investig. 80−33594
photoacoustic spectroscopy, meas. technique for low absorpt. coeffs. 78−24864
photoacoustic spectroscopy, thermoacoustic coupling effects 79−44954
photoacoustic spectroscopy in solids, phase measurement, appl. to nonradiative transitions, optical absorpt. 80−31885
photometric light attenuation systems, comparative analysis 79−12839
photoresist, Shipley AZ-1375, sensitivity and nonlinearity at 441.6 and 457.9 nm 78−90475
photosensitised reacts. in continuous chem. processes, scatt. effects 78−73057
photothermal deflection technique for absorpt. meas. in optically thin media, thermal lens effect comparison 80−105717
plane plates, two sets of different physical props., energy flux splitting *(German)* 79−18500
plant canopy light absorption model with application to wheat 78−88913
plasma polymerised ethane for laser window coatings 77−50737
plexiglass, red, gamma dose meas. by optical absorpt., elec. conductivity, and mechanical hardness 78−55045
PMMA, light absorption, laser crack development 78−68780
PMMA film, Plexiglas, penetration depth of 10.6 μm laser radiation, transmission, refl. and absorpt. meas. 79−74010
polar semiconductors, exciton-phonon interactions, optical absorpt. spectra, theory 80−49614
polarisation constants for light interaction with absorbing crystal plates 80−78765
Poley absorption magnitude 77−24813
polydisperse particulate sytems, light extinction 78−33667
polyethylene, solid-state extruded, exam. of props. 80−11669
polymer, transparent, high-temp. zone form. in laser induced mech. breakdown 77−56086
polymer clad SiO_2 fibre, ionizing radiation effect on attenuation 78−42405
polymer lightguide attenuation coeffs. meas., data anal., accuracy 79−1005
polymethine dye lasers, optical absorpt. 80−64009
polyvinyl alcohol film containing Cu^{2+} complexes, photoconductivity 80−107849
propane, and propane-N_2 gas mixture, CO_2 laser radiation absorpt. coeff. 77−58366
pulse train propagation, two-level absorber, relax. effects 79−46011
QSOs, absorpt. from clouds in emission-line regions 80−62308
QSOs, high-redshift, absorpt. line redshifts from Image Dissector Scanner (IDS) spectrometry 80−22111
quarter-wave dielectric reflector, spectral absorptance approximation 80−33131
quarter-wave mirrors, oblique incidence reflection coefficient, small absorption of layers effect 80−64140
quartz:Ge attenuator for 0.25 to 1 μm band, with attenuation coeff. up to 10^5 80−48415
quartz glass, laser breakdown and absorption, 1800-2400K 79−64296
quartz glass, spectral absorption coeff. in 2.0 to 4.8 micron region, up to 800°C 77−43985
quartz glasses, spectral adsorptance in 0.25-1.25 μ wavelength, 293-1273K temp. ranges 77−36212
quasars, props. of $Z_{abs} > Z_{em}$ systems rel. to origins of QSO absorpt. line systems 78−57682
quasars absorption line problem, optically selected high-redshift objects spectrophotometry 79−25746
quasars absorption lines origin, evidence for cosmological hypothesis 78−57684
radiation chemistry, photoabsorption data appls. 80−93778
radiation field, mean specific emission intensity, fluctuation effects *(Italian)* 79−18346
radiation field, polarized, asymptotic characts. for low absorpt., appl. to nonconservative Rayleigh scatt. 80−5686
radiative properties, parameterisation 80−56601
radiative transfer, diffusion approximation for large absorpt. 79−63170
randomly scattering light absorbing media, scale models and transmissive similarity 79−55061
rare-earth fluorides, LaF_3, CeF_3 and PrF_3, new coating materials for IR laser optical components 79−65821
reabsorption method at high optical densities for two identical tubes 80−38528
real space-time rays in absorbing media, Fermat's principle 79−3628
red variable stars, mol. absorpt. rel. to amplitude extension and amplitudes limit 79−62836
relaxation times in solid-state theory and one-dimensional molecular systems *(Russian)* 80−100640
resonance fluorescence of thin crystal films, superradiance 78−68573
Rhodopseudomonas spheroides, growth yield in light-anaerobic and dark-aerobic cultures 80−3608
rotating absorbing cylinder in light field, transverse ponderomotive effect 79−64171
rough surfaces, discontinuous films, heterogeneous materials, optical props., review 80−103935
ruby, spectral absorpt. coeff., 1800K 78−27252
ruby laser rod, absorption coeff., loss coeff. and population inversion *(Japanese)* 78−37888
Sagittarius B2, He ionising photons absorpt. by dust rel. to He abundance problem 78−49496
sapphire, natural, origin of colour 79−70794
saturable slab, steady state theory 77−68242
Schiff base azo dyes in nematic liq. cryst. hosts, order parameters, optical density meas. 80−84055
scintillation counting, liq., unified approach to counting process, stochastic model 77−3240
scintillation counting, liq., unified approach to counting process, optimising optical design 77−3241
sea, light diffusion, radiance distrib. 77−78216
sea water, hydroptic struct. variability in S. Atlantic regions *(Russian)* 78−77262
seawater, meas. technique for irradiance attenuation coefficient in a stratified ocean 80−98325
seawater off Ireland west coast, surface waters colour, UV absorbance and salinity 78−85603

light absorption continued
seawater transparency at 30 m depth in tropical Atlantic *(Russian)* 77−64307
selective surface for thermal conversion of solar energy, 80 to 200°C 77−14891
selective surfaces for high temp. photothermal conversion 78−1364
self pulsing in absorptive optical bistability, analytical description 80−78891
semiconducting plate, light absorption, temp. depend., threshold flux density 77−83937
semiconducting plate, with temp. depend. absorption coeff., heating kinetics *(Russian)* 77−54867
semiconductor, Burstein-Moss effect, photostimulated absorption of light 80−29757
semiconductor, collective excitations of electrons and holes in strong EM field and absorpt. of light *(Russian)* 78−79945
semiconductor, determ. of bulk and surface absorption coeffs., photoacoustic spectroscopy 80−4781
semiconductor, electron drag by photons during intraband absorption of light 79−51633
semiconductor, IR absorpt. and optical relax. time of free carriers 80−66206
semiconductor, nonequilibrium acoustic phonons, generation by interband light absorption 80−96607
semiconductor, optical absorpt. coeff. and minority-carrier diffusion length, differential photocurrent method of meas. 80−96896
semiconductor, optical thermal breakdown, fluctuations and wave processes 80−20587
semiconductor, p-type, intervalence-band transitions, saturation, theory 80−75997
semiconductor film, absorptance calc. 77−90207
semiconductor films, free exciton polaritons, energy dissipation 79−95870
semiconductor layer crystals, light absorption by shallow impurity centres 79−15503
semiconductor thin quantised wire, with charged defects, interband light absorption *(Russian)* 77−59593
semiconductor wire, quantised monochromatic wave absorpt., indirect transitions due to surface roughnesses *(Russian)* 79−91397
semiconductor wire, two-photon interband absorpt., quantum size effect *(Russian)* 79−95721
semiconductor with superlattice, optical phonon excitation by light absorpt., impurity photoionisation 80−44275
semiconductor-insulator structure, light refl. and absorpt. control, boundary state population rearrangement 77−69795
semiconductors, exciton light absorpt. band formation, linear and quadratic exciton acoustic photon interactions *(Russian)* 80−34368
semiconductors, intervalley electron-electron scattering effect on optical transitions 80−108267
semiconductors, magnetic, electron spectrum, light absorpt. spectrum, calcs. 80−2793
semiconductors, weakly doped compensated IR light absorption by small scale fluctuations *(Russian)* 80−66255
semiconductors, with nonspherical bands, exciton absorpt. in crossed fields 79−69432
shortwave radiation absorption by plant cover 78−16219
sieve-effect in one-component suspensions 79−22896
silica based optical fibre dopants for 1 to 1.8 μm communications 80−91930
silica glass, phosphorus containing, optical absorp. characts. of hydroxyl radicals 77−14800
silicate smokes, vapour-condensed, 800 to 130 nm extinction and interstellar extinction curve 80−82180
silicates, amorphous, IR extinction meas., rel. to interstellar dust 77−12352
single-beam two-photon absorbed light, off diagonal density matrix 78−30009
single-layer film 2.8 μm, 3.8 μm absorpt. meas. 78−90463
skin, in vivo, light absorpt. and scatt., theoretical and expt. study 80−101219
SMC, ratio between total and selective interstellar absorpt. *(German)* 80−67851
smoke aerosols, optical absorption to extinction ratio, photoacoustic determ. 80−58459
snow, light extinction at high densities *(Japanese)* 77−87028
sodium nitroprusside, isomeric molecular states generated by polarised light, Mossbauer resonance obs. 77−20781
solar atmosphere, IR opacity sources, rel. to IR continuous spectrum *(Italian)* 79−88638
solar atmosphere, model including OH continuum opacity 79−40162
solar chromosphere-corona transition region, evidence for overlying EUV continuous absorpt. 79−92738
solar collector DC reactively sputtered metal carbide and silicide selective surface props. 79−62029
solar collector stainless steel selective absorption surface props. 79−62030
solar energy materials, transparent, optical characts. investigation 80−20724
solar Lyman α radiation, atmospheric absorpt. rel. to O_2 densities 77−87010
solar photosphere, line absorpt. coeff. rel. to weak Fraunhofer lines form. depths *(Russian)* 79−44438
solar radiation absorption by water vapour, thermotidal exciting function 78−28310
solar selective surface absorption and IR emissivity calorimetry 79−62098
solar spectral lines propagating through interplanetary medium, profiles modification 79−66973
solid, temp. rise induced by laser beam 78−11025
solids, optical absorption under laser irrad. 80−34940
soot-gas mixture, in luminous flames and smoke, IR mean absorption coeffs. calc. procedure 78−91061
sound generation by laser, nonlinear theory of thermal mechanism 80−38147
spacecraft surface material performance modelling 78−4061
Spacelab launch conditions for absorption spectroscopy *(French)* 79−8791
spectrophotometer accessory for digital absorption and transmission meas. *(German)* 77−57408
spectrophotometer attachment for fused salt absorption spectrum registration 78−86353
light absorption continued
spectroscopy quantum chem. teaching, fluctuating elec. dipoles, light absorpt. 78−73802
sphere, totally reflecting, light extinction 80−95784
spherical particles, absorpt. cross-section *(Russian)* 77−83815
spherical three-layer particle cell model, effect of struct. 78−31785
spiral galaxies, internal absorpt. rel. to intrinsic flattening 80−36701
spiral galaxies, light absorpt. by interstellar dust 79−35393
spliced graded-index fibres, 11.7 km link, measured and predicted transmission characts. 80−14454
statistical properties of light, change by multiphoton absorbers with intermediate reson. 79−86208
steel, stainless, type 304, surface condition effects on IR absorptivity 79−56754
stellar radiation, allowance for IR absorpt. by atmospheric H_2O mols. *(Russian)* 78−40832
stratosphere, lidar differential absorpt. meas. rel. to O_3 vertical profile 78−11972
stratosphere, NO_2 light extinction rel. to Cretaceous-Tertiary extinctions 78−32215
stratosphere, solar radiation absorption, in O_2 Herzberg continuum, influence of O_4 and O_2N_2 dimers 78−87429
stratospheric water vapour 0.94 μ absorption cross-section obs. *(Japanese)* 80−17427
subtractive stimulated emission theory 79−59396
Sun, continuous absorption coeff. of photosphere 79−96986
superconductor, metal-insulator transition, electron pairing, effect on optical props. 80−60139
superconductor, nonlinearity of single-photon absorption near threshold *(Russian)* 78−91815
superlattice semiconductor impurity photoconductivity electron spectrum reconstruction 80−24966
superposition photometer for material absorptivity meas. 78−89522
surface polaritons, linear photon and two photon absorpt. 80−49863
TGS thin film pyroelectric detectors, far IR absorption 77−38010
thermoregulating plasma coatings, UV irrad. influence on optical parameters *(Russian)* 80−40259
thermosphere, O_2 concs. and absorpt. cross sections from EUV occultation profiles 78−28356
thin films condensed onto cold substrate, prism-film coupler for in vacuo investigation 78−24873
thin layer, weakly absorbing, radiant absorption/transmittance ratio 79−11481
thin layer absorption loss meas. by CW dye laser intra-cavity technique *(German)* 80−16113
thin walled dielec. cylinders, EM scatt. and absorpt., appl. to ice crystals 78−25795
thin-film absorption light filters 80−19101
tissue penetration depth, spectral depend., 0.35 to 1 μ 78−11714
transition elements, 3d, optical absorpt. comparison with fluorophosphate and soda-lime silica glass *(French)* 79−65819
transition metal oxides, refractive index and extinction coeff. 79−78643
translucent three-dimensional holograms, mode theory taking account of the absorption 80−91757
transparent dielectric, laser induced fracture *(Russian)* 77−51406
transparent dielectric, laser pulse energy absorption, refr. wave form. *(Russian)* 79−55167
transparent dielectric with metallic inclusions, light pulse shape effect on optical breakdown threshold 80−20588
transparent dielectric with radioimpurities, intense radiation absorption *(Russian)* 78−74939
transparent materials, absorpt. coeffs. meas., interf. effects 78−46699
transparent media, surface and bulk, photoacoustic method 77−5920
transparent media with random inhomogeneities, optical breakdown 77−59647
transparent medium with random absorbing inclusions, laser heating statistics *(Russian)* 77−28666
turbid estuarine waters, optics, approxs. and appls. 79−66712
turbid media, approx. linear relationship for optical response 78−90371
turbid media with specularly reflecting boundaries, optical props., biological appls. 77−75416
turbid medium, above reflecting surface, radiative flux *(Russian)* 79−72498
turbid water bodies, radiation absorpt. and scatt., radiative transfer eqn. solns. 79−81704
underwater light field, scatt. light influence anal. 77−64322
underwater visibility basic controlling parameters 78−36196
uniaxial crystal, macroscopic exciton luminesc. characts., high reabsorption conditions 78−19545
unpolarised monochromatic light, total absorption by crossed grating 80−106448
upper atmosphere, extinction of solar radiation 77−78546
upper atmosphere, Na absorpt. meas. rel. to daytime abundance 77−87140
Uranus atmosphere, UV absorpt. sources from UV albedo meas. 80−82295
UV radiation field in interstellar clouds, attenuation theory *(Russian)* 80−73026
vegetation canopies, solar radiation absorpt. simulation 80−104635
Venus atmosphere, IR extinction meas. from Pioneer Venus IR radiometer expt. 79−48719
Venus atmosphere, scattering layer over absorbing clouds, Venera 9 and 10 UV photometry 77−78700
Venus atmosphere, UV absorpt. rel to SO_2 vertical distrib. implications 79−101100
Venus clouds, H_2SO_4 aerosol medium IR absorpt. and extinction coeffs. 78−65526
visibility, definition, confirmation using marine optics data 80−23633
visibility in turbid media with coloured illumination 79−72489
water, absorpt. effects on underwater illumination fluctuations *(Russian)* 77−2173
water, backscatter and absorption coeffs., simultaneous determ. 80−82074
water, optical absorption coeff. 79−82992
water suspensions, radiative property measurements 80−9811
water vapour, attenuation of 10.6 μm radiation, role of $(H_2O)_2$ dimers 78−13741
water vapour absorption of CO_2 laser beam, optoacoustic detector meas. 77−9512
water vapour-N_2, absorption at CO_2 laser frequencies 79−50011
waveguide, lossy, Brewster phenomena, cut-off thickness 80−87524

light absorption continued
weakly absorbing layers, interferometric determ. of optical parameters 79−17471
weakly absorbing material calorimetric meas., theory 79−76773
zero gap semiconductor, thin layer, dielec. response 80−103635
zero-gap semiconductors, anisotropy of IR absorpt. coeff., k.p. calc. 80−97285
Ag, absorpt. coeff. temp. depend., IR, 3 to 30 μm 78−74953
Ag, ellipsoidal small particle assembly absorption spectra, optical model *(Russian)* 78−60483
Ag, granular film, anomalous light absorpt., oblique incidence 79−6205
Ag halides, formation of metallic Ag on surface, optical absorpt. calcs. 79−24791
Ag-SiO_2 composite film, optical props., appls. 77−754
AgBr polydispersed particles in unsensitised holographic emulsion, bulk attenuation and absorpt. *(Russian)* 79−2865
AgBr undeveloped photographic layer, light scattering and absorption *(Russian)* 78−37090
Ag_8GeSe_6, polymorphic transition, absorpt. coeff. meas. 78−2257
AgI large single crysts., gel and soln. growth and props. 80−35071
Al, laser radiation absorptance at 1.064μm 79−87528
AlI_3, UV absorbance, dimer-monomer dissoc. equilib., vap. press. of solid 78−13511
Al_2O_3 surface, solar radiation absorpt., comparison with Planckian black body *(German)* 77−35026
Ar III, in pulsed arc plasma, ξ, factor determ. 79−4116
Ar, oscillator strengths, determ. from self-absorption of reson. radiation 79−89641
As-Te-Cu(Ag) system glasses, absorpt. coeff. and optical band gap 79−65829
As_2Se_3 film on CaF_2, interface and bulk absorption meas. 80−35001
As_2Se_3, IR window coating, prep. and optical props. 77−50736
$As_2Se_3Ag_x$, amorphous, optical absorpt. coeff. and DC cond. 80−54699
Au, absorpt. coeff. temp. depend., IR, 3 to 30 μm 78−74953
Au, dielectric const. by multiangle reflection meas., optical props. 79−95723
Au film, laser absorpt. vs. temp., calorimetric meas. 79−98423
Au film, polycrystalline, temp. depend. of Drude absorption 79−78779
Au film on Al, reflectance and absorpt. obs. 80−7426
Au, laser radiation absorptance at 1.064μm 79−87528
Au-Cu, dielectric const. by multiangle reflection meas., optical props. 79−95723
Au-MgO cermet film, dielectric constant and selective solar absorption 78−2937
$BaSO_4$ white reflectance standard, Kubelka-Munk optical props. 77−42581
$BiF_3(I_3)$, new coating materials for IR laser optical components 79−65821
BiI_3 film, exciton-phonon interaction, optical consts., Faraday effect., permitt. 80−59884
C, amorphous grains, extinction coeffs., 0.21-340 μm, lab. meas. rel. to interstellar grains 80−73020
C particulate, airborne, photacoustic and absorption spectrum using tunable dye laser 80−4102
C smokes, vapour-condensed, 800 to 130 nm extinction and interstellar extinction curve 80−82180
C:H amorphous films, elec. cond. and optical absorpt. 80−49723
CF_3I, I laser medium, UV absorption profile modification by vibr. excitation, for fusion ignition 78−58717
CO_2, 10.6 μm reson. absorpt. behind shock front 78−42707
CO_2 absorption at 2.7 μ in atmosphere at large optical thicknesses, mechanisms *(Russian)* 78−40659
CO_2 laser beam attenuation by air discharge plasma column 80−19062
CO_2 laser Doppler system atmospheric attenuation 77−75601
CO_2 laser radiation attenuation by diffusively evaporating water aerosol 77−728
CO_2 laser radiation reson. absorpt., atm. NH_3 conc. determ. on long path 79−29904
CO_2, seeded laser mixture, photoabsorption and ionisation cross sections 77−23645
CO_2-He-N_2, absorpt. coeff. for 10.6 μm CO_2 laser radiation, 295 to 650 K 80−92252
CaF_2, laser window material, absorpt. at CO wavelengths, calorimetric meas. 78−25911
CaF_2 low-loss laser window material, surface absorpt. meas. at 2.8 and 3.8 μm 79−94267
$Ca_3Fe_2Ge_3O_{12}$ garnet, light absorpt. spectral study 80−93322
Cd_3As_2, valence band struct., optical absorpt. meas. 80−50293
$CdCr_2S_4$, hot-pressed, optical isolation appl. at 10.6 μm, intrinsic absorpt. props. 78−42368
$CdCr_2Se_4$, Mott ferromagnetic semiconductor, optical absorption edge, critical behaviour 80−97226
$CdIn_2S_4$, photoconducting semiconductors, fundamental absorption edge 80−40130
$Cd_{1-x}M_xS$ (M=Sr, Ca, Mg, Pb, Sn), solid soln., prep. and semicond. props. 80−2383
CdS, chem. sprayed film, struct. and morphology 78−72020
CdS, light-induced modulation of absorpt., rise kinetics 77−16342
CdS:Li film, optical props. 80−2886
CdS/Cu_2S, polycryst. thin film photovoltaic materials, photon loss anal., expt. determ. 80−93888
CdSe, fundamental absorpt. edge, influence of laser radiation intensity *(Russian)* 80−71445
CdSe, meas. of partial press., by optical absorption method *(Japanese)* 78−51661
CdSe, photosensitivity of elastic properties 78−92049
CdTe, 10.6 μm absorption meas. using thermal emission 77−1649
CdTe, laser window material, absorbing Te inclusions, damage threshold 77−46749
CdTe, meas. of partial press., by optical absorption method *(Japanese)* 78−51661
CdTe, single cryst. IR laser window, low absorption at 10.6 μm 78−79081
CdTe two-photon absorption, laser calorimetric obs. 80−33076
CdTe, window material with absorbing inclusions, damage thresholds 77−38971
$ClONO_2$, gaseous, light absorpt. rel. to UV photolysis mechanism at 302.5 nm 78−20031
Cr, antiferromag., EM absorpt. 79−51925
Cr film, evaporated, black selective solar absorbers, optical props. 77−34956
light absorption continued
Cr ultrafine particle selective absorption of solar energy 79−62035
Cr-Cr_2O_3, black, solar selectivity at average temps. (100 to 250°C) *(French)* 80−55899
Cr_2O_3-Cr, RF sputtered cermet film, selective black absorber 77−58399
Cs-He, new absorption/emission bands perturbed Cs transitions assignment, pot. energy curves 78−66486
Cs_2O-Ag photocathode, light absorption and photoemission 80−50510
Cu, dielectric const. by multiangle reflection meas., optical props. 79−95723
Cu target absorptivity under laser radiation action, time and temp. depend. 79−95724
Cu-Sn(Al)(Ga) reflecting surface absorpt. coeffs. at 10.6 μm 80−95984
CuCl, exciton luminesc., reabsorpt. and polariton effects 80−50430
CuCl, optical absorpt. meas., evidence against intrinsic electron-hole supercond. 80−108172
CuCl, optical absorption under press. 80−34949
$CuFeS_2$ single crystal, optical reflectivity spectrum 80−40129
CuO surface, solar radiation absorpt., comparison with Planckian black body *(German)* 77−35026
Cu_2S-CdS solar cells, optical absorption coefficient changes in Cu_2S 80−93980
Cu_2S-CdS solar cells in backwall configuration, model of photovoltaic effect 80−55861
Er, paramagnetic and antiferromagnetic states, optical absorption *(Russian)* 78−56497
EuO, light absorpt. during ferromag. reson. *(Russian)* 79−28618
Fe, laser radiation absorptance at 1.064μm 79−87528
Fe-In, superconducting Kondo alloys and alloys with strong electron-magnetic impurity interaction, EM absorpt. of light 80−39711
$Ga_{1-x}Al_xAs$-GaAs high-efficiency solar cell 79−29469
GaAs, 10.6 μm absorption meas. using thermal emission 77−1649
GaAs, absorption coefficients, method of meas. 78−83048
GaAs, deep level photoionisation, absorpt. by derivative surface photovoltage spectroscopy 79−99575
n-GaAs, electron mobility, free-carrier absorpt., and compensation ratio 79−56218
GaAs LED absorption effect on freq. characteristic 79−8189
GaP, surface polariton linear photon and two photon absorpt. 80−49863
GaS, sputtering conditions effect on film struct. and optical absorption *(Russian)* 77−12525
$Ga_{1-x}Te_x$ amorphous films, elec. cond., optical absorpt. and transparency, band gap energy 79−56335
Ge, amorphous film, optical consts. in near IR range *(Korean)* 79−8137
Ge amorphous films, self-ion bombard., electronic props. 79−28422
n-Ge, IR absorption by hot carrier 80−40087
Ge, inhomogeneously stressed, giant electron-hole drop investig. by IR absorpt. 77−39785
Ge-Al_2O_3 composite film, optical props., appls. 77−754
$Ge_{20}Bi_xSe_{80-x}$, semicond. glass, resist., thermoelec. power, optical absorpt. 80−88555
$Ge_{20}Bi_xSe_{70-x}Te_{10}$, semicond. glass, resist., thermoelec. power, optical absorpt. 80−88555
GeS, Urbach's rule, absorption edges 80−97224
$Ge_{20}Sb_{25}S_{55}$ glasses, optical props., absorption edge temp. depend. 80−2789
$Ge_{0.45}Se_{0.55}$-As_2S_3, antirefl. coating, performance at 3.8, 5.3 and 10.6 μm 77−61964
Ge_xSe_{1-x} glasses, optical props. and local struct. *(French)* 77−77162
H^- free-free absorption, target polarisation effects 79−66917
H_2O, optical properties, 250-600 nm 77−52035
H_2O, photoabsorption, Stieltjes-Tchebycheff calculations, Hartree-Fock calcs. 79−18238
H_2O_2, UV absorpt. cross sections 78−42086
HO_2NO_2, gas phase, UV and IR absorpt. cross sections 79−13733
He-Ne laser, atmospheric extinction meas. 78−40654
Hg fluid, expanded, optical absorpt., excitonic and continuum states 79−95801
Hg, vap., high density, optical absorpt. edge, density depend. 79−72985
$Hg_{1-x}Cd_xTe$, nonlinear absorption and saturation, 10.6 μm 77−746
InAs, laser excitation, photocond., optical absorpt., electron-hole scatt. 77−43661
In_2O_3:Sn coated Si, temp. depend. of 10.6 μm refl., solar selective absorber appl. 77−58398
In_2O_3:Sn solar collector selective coating resistivity obs. 79−62034
InP, compensation ratio, electron mobility and free-carrier absorpt. 80−80261
InSb, refractive index and absorpt. coeff., cryst. orientation depend. 80−60536
$In_{1-x}Te_x$ amorphous films, elec. cond., optical absorpt. and transparency, band gap energy 79−56335
KBr, absorption coeff. determ. in 10.6 μm region, laser calorimetry method 79−7186
KCl, absorpt. coeff. meas., using pulsed CO_2 laser, calorimetric method 78−18028
KCl, bulk and surface absorpt. of CO_2 laser radiation, calorimetric data analysis 78−25904
KCl, bulk and surface absorption comparison, 9.2 to 10.85 μm 80−33051
KCl, internal damage threshold for CO_2 laser pulses rel. to absorption 77−75594
KCl, laser window material, absorpt. at CO wavelengths, calorimetric meas. 78−25911
KCl low-loss laser window material, surface absorpt. meas. at 2.8 and 3.8 μm 79−94267
KCl, surface radiative absorption meas., acoustic technique 77−3596
KCl:Ca, vol. holographic grating, modulation characts. 79−94197
KCl:RbCl, $SrCl_2$, laser window material, prep., grain boundary stability 77−46774
$K_2Cr_2O_7$, acidic soln., UV absorbance standard verification 78−21092
$K_2Cr_2O_7$ acidic solns. as UV absorbance standards 77−53990
$KGaF_3$, new coating materials for IR laser optical components 79−65821
LiF dosimeter, thermoluminescence glow curves and light absorption, thermal treatment effect *(Russian)* 77−32954
LiF, thermolum. light self absorpt. obs. 79−81097
$LiNbO_3$, optical waveguides by ion implantation 80−106622
$LiNbO_3$ waveguide absorption losses, laser calorimetric meas. 79−64311
$LiNbO_3$:Ti optical waveguides, pyroelectric loss meas. 79−46046

light absorption continued
$LiNbO_3$:Ti waveguide and cryst., absorpt. loss and photorefractive index changes 80−48368
Mg-MgF_2, sputtered films, opt. props. 78−80430
$Mg+O_2$⇌$MgO+O$, shock-tube study of evap. and oxidation kinetics 80−16651
MgO-Au cermet film, selective black absorbers 77−1747
N_2, gaseous, collision-induced absorpt., temp. depend., rel. to atm. far IR transmission 79−62584
N_2, liq., photoacoustic and photorefractive detect. of small absorpts., electrostrictive limits 80−108171
NH_3, laser-induced excitation at 1076 cm^{-1} in megawatt region 80−10354
$NO^+(v=1,2)+N_2$, vibr. transfer, vibr. absorption coeff. 79−6994
NaCl, bulk and surface absorption comparison, 9.2 to 10.85 μm 80−33051
NaCl, internal damage threshold for CO_2 laser pulses rel. to absorption 77−75594
NaCl surface with adsorbed water layer, absorpt. and thickness meas. 80−16001
NaF film on CaF_2, interface and bulk absorption meas. 80−35001
NaF film on ZnSe plate, absorption coeff. ATR spectroscopy 80−35000
NaF, IR window coating, prep. and optical props. 77−50736
Na_2O-CaO-SiO_2 glass, optical absorpt. comparison with 3d transition elements *(French)* 79−65819
Ne, oscillator strengths, determ. from self-absorption of reson. radiation 79−89641
Ne superradiation propagation through reson.-absorbing positive column plasma, pulse shape change 79−4117
Ni, black, solar collector selective coatings, optical and thermal props. 79−62028
$NiCr_2O_4$, plasma-sprayed coatings, props. 77−59999
α-O_2 crystals, spin ordering effect on light absorpt. *(Russian)* 80−89029
O_2 photoabsorption cross section near Lα line, temp. depend., aeronomy appl. 77−64499
O_3 absorption coefficients for backscatter UV expt. 80−46254
O_3, in atmosphere, Chappuis-band absorpt. rel. to conc. determ. 80−77063
O_3, mesospheric, obs. of shadow on D-region in ionosphere VLF guide over Atlantic Ocean 79−58161
O_3, UV absorption, use as tracer for qualitative and quantitative flow visualisation 79−72972
PbI_2, film, reflectance meas., optical consts., humidity effects 80−34994
PbS, colloidal, light scatt. and electron microscopy 78−3379
PbTe epitaxial films, quantum size effect, optical meas. 80−11121
PbTe film, light absorpt. 79−83043
Pt black surface, solar radiation absorpt., comparison with Planckian black body *(German)* 77−35026
PtO_2, sputtered film, optical props. under H_2 reduction 80−20728
PtO_x films, electronic struct., reduction processes, photoemission, optical absorpt. and resist. meas. 80−80931
RbBr (I), optical absorpt. centre formation time meas. 80−40081
Rb_2CrCl_4, optical absorption intensity, short-range spin correlation 80−108185
SF_6, saturation absorpt. characts. at 10.53 μm CO_2 P(14) line 77−38999
SF_6, soln. in liquid Kr, resonant IR radiation, nonlinear absorpt., vibr. relaxation estimate 79−36642
S_2F_{10}, IR laser irrad., absorpt., reaction parameters 78−94241
$SSe_{22.5}$, amorphous, photo-effect on crystn. kinetics, elec. cond. obs. 79−77522
SbSI, absorption edge, elec. field effect rel. to ferroelec. props. 80−97240
Sf_6, absorpt. of pulsed CO_2-laser radiation at 140K 79−22707
Si amorphous films, laser beam annealing, optical information storage possibilities 79−87515
Si amorphous films, self-ion bombard., electronic props. 79−28422
Si, beam extinguishment device, without scatter 78−87126
Si, CVD films, polycryst., elec. and optical props., electronic density of states model 79−56332
Si, IR photoresponse at 1.15 microns 79−7864
Si, temp. depend. of Auger recomb. coeff. 80−24942
Si:H, amorphous, RF sputtered, suitability as solar cell material 80−40864
Si:H, amorphous, solar cell struct., photocurrent meas., absorpt. coeff. 80−50960
Si:H, amorphous, surface activated, photoemission spectra, minority carrier diffusion length 80−40235
Si:H amorphous, solar cell structure, optical absorption by gap states 80−94052
Si-borosilicate glass, Van der Waals interaction meas., influence of optical absorpt. 79−95273
Si-CaF_2 film, dielectric constant and selective solar absorption 78−2937
Si-MgO film, dielectric constant and selective solar absorption 78−2937
Si-SiC composite film, optical props., appls. 77−754
Si-SiO_2 interface, (001) vicinal planes, minigaps in inversion layers, far IR absorpt. meas. 80−107919
SiC smokes, vapour-condensed, 800 to 130 nm extinction and interstellar extinction curve 80−82180
$SiH_{0.16}$ amorphous films, optical props. and photocond. near optical gap 80−50443
SiH_x amorphous reactively sputtered films, optical props. 80−50444
$Si_{1-x}H_x$:Al, amorphous, co-sputtered Al modification, electronic and optical props. 80−100461
Si_3N_4, highly insulating film, current cond., CV curves, and IR absorpt. 79−38208
Si_3N_4, plasma deposition, optical absorption as control test 78−35314
SiO_2 film on Si substrate, reflectance and absorptance obs. 79−15542
SiO_2 glass, IR spectral emissivity and absorpt. coeff. at 600 to 1700K 80−16018
SiO_2 optical fibres, plastic clad, gamma-ray irradiated, signal level depend. of recovery rate 79−36997
SiO_2 optical fibres intrinsic attenuation 78−30067
SiO_2:F, silica fibres, numerical aperture and attenuation, drawing from preforms 78−1449
SiO_x, amorphous and recrystallised layer, optical props. 80−25474
$Sm_{1-x}Nd_xSe$, Nd substitution effect on lattice const., resist., and colour 79−56763
SrF_2, IR window coating, prep. and optical props. 77−50736
light absorption continued
SrF_2, laser window material, absorpt. at CO wavelengths, calorimetric meas. 78−25911
Te, evaporated deposition, absorptivity and emissivity 80−25473
Te textured thin films, prep., high solar absorptivity by multiples refl. 80−11568
TeO_2, paratellurite, optical absorpt. and refl. spectra, 80-500K, optical consts. determ. 80−50359
TiO_x antireflection coatings for solar cells, optical, struct., and compositional characts. 80−55852
TiS_2, electron energy loss spectra, dielectric function, reflectivity and absorption coefficient 79−69937
TlBr-TlI, TlBr-TlCl, KRS-5 and KRS-6 crystals, optical losses, laser calorimetric meas. 80−9973
$TlBr_{0.42}I_{0.58}$, KRS-5 crystal, 10.6 μm absorption obs. by laser calorimetry 79−50360
TlCl-TlBr, internal damage threshold for CO_2 laser pulses rel. to absorption 77−75594
$TlCl_{0.7}Br_{0.3}$, KRS-6 crystal, 10.6 μm absorption obs. by laser calorimetry 79−50360
TlI/KCl/TlI low absorpt. antireflection coatings for KCl surfaces 80−38078
VO_2, film, optical consts. and electrical props. near phase transition *(Russian)* 77−59631
VO_2 film, semicond.-metal transition, light absorption by metallic drops *(Russian)* 77−59579
V_2O_5, low dislocation density cryst. growth, opt. props. 77−63551
W-MgO cermet film, dielectric constant and selective solar absorption 78−2937
XeF* laser mixture, Ne- and Ar-rich, absorption 78−63062
YIG:Si, thermomagnetic processing and illum. effects on mag. props. *(Russian)* 77−8410
Y_2O_3 sintered pieces, optical transmittance 80−40561
$Zn_xCd_{1-x}S$, thin solid soln. films, vapour deposited, elec. and optical characts. 80−60110
ZnO-polystyrene photoreceptors sensitised by β-Cu phthalocyanine 79−17552
ZnS CVD window, IR lattice absorption, phonon assigments and image spoiling 80−33104
ZnSe, 10.6 μm absorption meas. using thermal emission 77−1649
ZnSe, coated/uncoated, effect of sand erosion 77−72037
ZnSe, laser window material, multiphonon absorpt. temp. depend., calorimetric meas. 78−25907
ZnSe, laser window material, absorpt. at CO wavelengths, calorimetric meas. 78−25911
ZnSe sputtered laser window coatings, prep. and evaluation 77−50739

light absorption spectra *see spectra*

light amplifiers *see image intensifiers*

light attenuation *see light absorption; light scattering; light transmission; optical dispersion*

light coherence
see also laser beams; lasers
AC Josephson-Fiske effect, coherence 78−88082
ambiguity function in diffraction and isoplanatic imaging by partially coherent beams 78−78925
amorphous media, light scatt., object wave and its coherence 78−25799
angular spectrum approach to diffr. of partially coherent light 77−75411
annular aperture, two point resolution limit with partially coherent light 77−88654
apodisation in coherent image form. 77−10844
apodisation problem, coherent, unified formulation 79−27187
apodization of paraxial coherent image by interposing masks in pupil plane *(French)* 80−23630
applications, seminar, San Diego, CA, USA (Aug. 1979) 80−77542
astronomical doublet system resolution, random speckle structure model and expt. *(Russian)* 79−7082
astronomical images, coherent optical processing expts. *(Russian)* 80−12675
atmosphere, light beam coherence through optically dense turbid layer 78−55300
atmosphere optics, phase correlation scale effects rel. to atmospheric imaging characts. 80−94604
atmospheric degradation of electro-optical system performance 79−66805
atmospheric optical propagation through strong turbulence 79−66802
atmospheric propagation, expt. turbulence profile and parameters 79−66801
atmospheric propagation of partially coherent radiation 78−65386
atmospheric turbulence and aerosol effects 80−82064
atmospheric turbulence structural characts., meas. using spatially limited laser beam 80−98413
atom, induced coherent emission in spatially separated light fields *(Russian)* 79−50274
atom and molecule dipole transition, transient behaviour in intense laser field *(German)* 78−66520
atom in coherent field, reson. scatt., quantum description 79−64053
atom-coupled-to-field system, coherent radiation, phenomenological theory 77−14683
atomic collisions, vel. changing, saturation spectroscopy, internal coherences 78−42245
atomic cooperative system, light scatt. spectrum, coherent-state representation, numerical results 80−23650
atomic system, photon echoes in standing-wave fields: time separation of spatial harmonics 80−9759
atomic three-level system, collisionally aided radiative excitation 79−98022
atoms, multiphoton ionisation, reson. effects, light coherence effects 80−58232
beam generation, quasi-homogeneous Gaussian sources, spatial coherence 80−48145
bilinearly distorted image linear restoration using Wiener filters 80−83557
bipolar spatial filtering, incoherent, review 80−102822
birefringent optical pulse compression 80−106437
black body radiation, anisotropy and temporal coherence 78−58904
boundary diffraction of light, formulae 79−59632
Bragg diffraction by a 3-D Gaussian ellipsoid and diffraction broadening of Mandelshtam-Brillouin scattering lines 80−55114
breather generation, inverse scatt. technique 80−78913
CH stripe laser, spatial coherence and modal struct. 80−87531

light coherence continued
chalcopyrite crystals, temp. depend. Sellmeier coeffs. and coherence lengths 79−76752
chaotic light with Lorentzian spectrum, two joint time interval distrib. 79−50269
Cherenkov radiation at resonance frequency of amplifying medium 79−22926
coherency matrix, degree of polarisation, principal idempotents 78−17859
coherent emission, caused by pulsed laser in low-density gas 79−18389
coherent multiphoton intense interactions, convergent perturbation anal. 80−1037
coherent optical spectroscopy 78−1112
coherent optics fundamentals 78−78910
coherent scattering, Gaussian beam, statistically rough surface 77−10837
coherent-radiation spectral power density unit reproduction, USSR standard 78−37957
Collett-Wolf source example 79−76783
collisional optical coherence transfer, laser spectroscopy 77−42360
colour coding of spatial freq. using incoherent optical processing 80−37956
complex degree of coherence expansion, image intensity data, object reconstruction 80−32906
complex spatial coherence meas. by sinusoidal phase modulation 80−106446
concentrator, compound parabolic, phase space conservation for incoherent propag. 80−69491
contemporary optics, book 79−81353
continuous laser radiation relative power-density distribution unit reproduction, USSR 78−37956
correlation coeffs. of planar sources and their far fields 78−66750
correlation techniques, coherent optical, review 80−43277
CW VUV radiation generation 80−58640
defocused image of periodic complex object under partially coherent illum. 77−611
defocused optical system under partially coherent illumination, apodised aperture performance 77−10847
dephasing, emitting mols. coherent oscills., appl. to I_2, optical T_1 and T_2 meas. 77−79644
depolarized double scattering, spatial and temporal coherence coupling 78−1164
Dicke model Hamiltonian, coherence props. of radiation field 78−58959
dielectric waveguide, EM field coherence 78−59145
differential detection of coherence functions and its application 80−43261
diffracting periodic structure generation by coherent beam interference 80−69570
diffraction instability of light 2π pulses, numerical anal. 79−89975
diffuse reflectance rel. to partial coherence and IR laser photogoniometric meas. 80−14283
difluoromethane far IR laser gas, CW laser pumped, gain 80−69367
directional beam generation from globally incoherent source 80−53211
directional light beams, necessity for spatial coherence, equivalence theorem 78−42398
directionality of light beams and spatial coherence 79−36834
discharge, hollow-cathode, holographic meas. of radn. coherence props. 79−76784
displacement derivative meas., image-shearing interferometric camera 80−33549
edge images, partial spatial coherence effect 79−89981
edge-ringing and edge-shifting, effects of coherence 79−36833
education, spontaneous emission and superradiance, coherence effects, semiclassical 77−82347
electro-optic laser technique for probing coherent and incoherent decay processes 77−75338
eye photoreceptor directional sensitivity, coherence and polarisation obs. 79−100610
far zone spatial coherence of statistically homogeneous plane sources 77−31066
far-field diffraction, partial coherence, primary astigmatism 79−22899
far-zone angular coherence and intensity calc. 78−8435
fast IR wavefront aberration sensor interference problems 80−74499
fibre excitation by partially coherent sources 77−790
fibre optical illuminator output speckle, smoothing methods 79−7209
fibre optics testing techniques 80−78992
fibre waveguide, chromatic signal distortion depend. on optical carrier coherence 80−1317
fibres, spatial coherence and index profiling 80−1335
finite planar source, radiant intensity and spatial coherence 77−50743
finite planar sources of arbitrary coherence states, radiance function existence 79−50208
fluorescence, nonexponential resonance decay, role of exciting light source 77−42348
focused radiation scintillations, freq. correl. by speckle interferometry 79−94153
formaldehyde-d_2 733 μm line, Autler-Townes effect in laser interacting with RF field 80−53269
four-point field coherence function, strong fluctuations of wave intensity 80−63927
four-point field coherence function meas. in laser random focusing region *(Russian)* 78−58910
four-wave mixing spectroscopy, coherent cancellation of background 80−91842
Fourier optical processor phase accuracy, coherence effects 78−90377
Fourier transform optical pulse spectroscopy, coherent transients 78−86974
Fraunhofer diffr. of partially coherent light by amplitude, phase gratings 77−46681
free electron laser, coherent states in single mode and multimode cases 80−102689
free-space propagation model for coherence-separable broadband optical fields 80−78763
gas laser spatial coherence increase, new method *(Russian)* 78−37928
gas-laser beam intensity fluctuations, spatial distrib. 79−18458
Gaussian aperture operating in partially coherent light, two-point resolution 78−78918
Gaussian beam in laser Doppler velocimeter, interference 80−69444
gaussian Schell-model planar sources, beam directionality 79−903
Gaussian-Lorentzian light, photon counting distrib. factorial moment, spatial coherence 80−83571
light coherence continued
generalised matched filters for coherent optical pattern recognition 80−99654
generalised optical theorem for partially coherent interfering beams 80−106447
generalised spherical wave mutual coherence function 78−9327
generalized Collett-Wolf sources 79−31793
generalized partial coherence of a radiation source and its far-field 78−58903
Glauber mode statistical props. 79−98326
graded-index fibre, spatial degree of coherence 80−53441
grating echoes, in Na gas, the temporally recurrent spatial ordering of at. population 79−98447
gratings without contact, Moire fringe self images, partially coherent illum. *(French)* 77−83806
holograms, reduction of coherent light requirement for viewing 77−7033
holographic coherence meter for spatial coherence of ruby laser determ. 80−9837
holographic image contrast degradation with partially coherent light reconstruction 80−102678
holographic interferometer, coherence length measurement 77−22590
holographic interferometry, double exposure, partial coherence effect *(German)* 78−82932
holographic interferometry, ruby laser coherence rel. to pumping energy 77−75440
holographic movie camera and projection system 80−78808
holography, coherence relaxation methods 78−78977
holography and coherent optics, information theory, book 80−98764
holography in partially coherent light, using Michelson interferometer 80−58480
holography through fog, coherence requirements for light source 78−58949
IC photomask and wafer linewidth meas. using optical spatial coherence 80−77850
image formalism, diffraction at straight edge, partially coherent illum., aberrations *(Chinese)* 80−43267
image formation characteristics for partially coherent light at condenser exit pupil 77−10848
image formation with coherent and partially coherent light 77−88658
image formation with paraxial coherent light *(French)* 79−31815
image of periodic complex object under partially coherent illum. 77−610
image processing, noise fluctuations and coherence 78−66771
image processing nonlinear nonmonotonic function synthesis 77−50633
image processing on-axis coherent optical feedback system 77−50631
image quality of coherently illuminated objects *(Russian)* 80−28168
image quality of diffuse objects, laser coherence influence 79−31820
image recognition by hybrid series-parallel processing *(Russian)* 77−58265
image recognition using contour transparencies *(Russian)* 77−58260
image reconstruction and partially coherent objects from mutual intensity samples 78−9333
image reconstruction using propag. law of mutual intensity 77−624
image registration and differencing by coherent optical pattern recognition 80−99648
image weak modulation detection in film grain noise with partially coherent illumination 80−77897
imagery of extended objects 80−106465
imaging of relatively strong objects in partially coherent illum., linear transfer theory 78−22091
imaging system point spread function determ. by scatt. of two monochromatic beams 80−87316
imaging system using intensity triple correlator 78−74846
in-line Fraunhofer hologram field, partially coherent illumination 77−19200
incoherent circularly symmetric source, samping theorem for complex degree of coherence *(French)* 78−79088
incoherent diffraction correlator with a holographic filter 80−37955
inhomogeneous media, coherent states and light propag., graded-index waveguide coupling 80−102625
inhomogeneous nonlinear elements, coherent frequency doubling *(Russian)* 80−5795
inhomogeneous source radiant intensity, averaged cross-spectral density concept 78−74958
injection laser, comprehensive model, current depend. of spontaneous and coherent emission 80−74361
instability of light pulses in absorbing media, resonance detuning effect *(Russian)* 79−27343
integrated speckle pattern statistics due to mixed coherent and diffused light 80−14285
intensity distrib., far field laser and partially coherent sources, comparison 78−66751
intensity distribution due to partially coherent field, Collett-Wolf equivalence theorem 79−89846
intensity fluctuation spectroscopy, of charged Brownian particles, coherent scatt. function 78−17857
intensity fluctuations and fourth-order coherence function in random media 80−78774
interference from two coherent sources, demonstration 80−4496
interference transfer function with quadratic detect., coherent illum. 80−78782
interferometer symmetry property, spatial coherence requirement 78−41346
inverse problem, evanescent waves, finite source area 77−10831
inverse problem, source reconstruction from far-field intensity data 77−10830
inverse problem for scalar planar sources radiometry and coherence, book contrib. 79−31797
inverse source problems in optics, book 79−31821
inverse source problems in optics, book contrib. 79−31822
IR source, tunable, efficient 80−5789
isoplanatic imaging, complex degree of coherence determ. 77−2691
isotropic turbulent medium, four-point coherence function of two independ. light sources 80−43263
Kirchhoff integral, cosine factor, rel. to Fourier optics *(German)* 80−18997
laser and Stokes pulses, coherent propag. in Raman active medium 77−7157
laser applications, coherence implications 77−75599
laser beam, single-pulse, spatial characts. control 78−79058
laser beam, spatially inhomogeneous, induced scatt. 80−28274
laser beam coherence and divergence *(Spanish)* 80−87424

light coherence continued
laser beam spatial coherence, turbulent distortions 77−79756
laser beam spatial coherence control by progressive US wave 80−78885
laser beam spatial coherence in a randomly inhomogeneous medium, effect of thermal nonlinearity 80−9926
laser beam transmission through fibre light guide, spatial coherence 78−71133
laser coherence length meas., for holographic appl. 77−7100
laser detection by coherence discrimination, angle-scanned interferometer as coherent energy modulator 79−58777
laser diode, spatial coherence, studied with reversing front interferometer 80−32993
laser excitation, stepwise, coherent Schrodinger vs. incoherent rate eqn. approaches 78−74871
laser light, props. 77−75408
laser low-level prolonged exposure effects on visual function 80−3714
laser operation physical principles *(German)* 79−59664
laser oscillator with Fabry-Perot resonator, spatial coherence analysis 77−79863
laser power and coherence requirements for holography 79−50260
laser radiation, measurement problems *(German)* 78−79052
laser radiation, spatial coherence degree correlation with wave vector variance 79−45985
laser radiation field, four-point coherence function meas. in turbulent atm. 80−23623
laser Rayleigh scatt., forward direction, spatial coherence deterioration, polaris. interferometry technique 77−10838
laser scattering by moving rough object, freq. spectrum 78−5418
laser single transverse mode radiation, spatial coherence 77−14733
laser sources coherence analysis, meas. system with Michelson interferometer *(Polish)* 78−33762
Lau effect, diffr. expt. with incoherent illum., appl. to Talbot interferometer, Fourier spectrometer 79−41333
Lau effect, explanation based on coherence theory 80−23619
Lau effect coherence theory explanation 80−5685
light source, low intensity, holographic determ. of spatial coherence 78−25823
linear optical system, distrib. theory as basis of postulational foundation 77−34927
linear restoration of partially coherent images, minimum mean square error 79−3637
liquid crystal, far-field coherence and radiant intensity of scatt. light 78−64372
long-distance multimode waveguide image transmission in coherent light 80−48435
lower limits of degree of coherence, limiting forms of density operator and distrib. function 80−87300
many-level molecules, unitary dynamical symmetry for superadiance, classical limit 78−9355
mask linewidth meas. effects of optical microscope operating parameters 77−37977
mask linewidth meas. with coherent optical microscope 77−37978
materials testing for vibration pattern and defect discrimination *(German)* 80−30181
matrix notation, interference, coherence and polarisation 77−38801
maximum engropy of EM fields with given degrees of coherence 78−50697
MBBA, laser radiation transmitted near isotropic transition, spatial coherence 78−18003
MBBA, light scatt. by disclinations, spatial coherence props. 77−8544
measurement, control and testing, coherent light appl. *(French)* 80−23641
medium with varying energy level populations, evolution of coherent radn. probing pulse 79−76755
methane, anharmonic molecular vibrations, coherent spectroscopy 79−18187
methanol far IR laser gas, CW laser pumped, gain 80−69367
microdensitometer performance, effective incoherence and flare tradeoff 80−77851
microscope, polarizing, with crossed polarizers, incoherent diffr. imagery 80−101838
microscope, resolution of semitransparent and π-phase annular aperture under Gaussian illum. 77−53972
modulation, consistency, classical and quantum theories of optical coherence 77−58306
modulation by US waves, partial coherence depend. on US parameters 80−58453
modulation contrast microscope, coherence theory 77−7010
molecular collisions, coherence transfer between collision partner mols. 77−71844
molecular near-resonant fluoresc. and Raman scatt. theory 79−3446
molecular optical spectroscopy, by 90° photon echo, during reson. scatt. and radiationless transitions 78−86978
molecular rotational coherence, reson. collisional exchange, time-resolved microwave obs. 80−23525
molecule in coherent field, reson. scatt., quantum description 79−64053
molecules, luminesc., photon echoes and coherence 79−31586
molecules embedded in small particles, Raman and fluoresc. scatt., incoherent results 79−41337
molecules embedded in small particles, Raman and fluoresc. scatt., coherent results 79−41338
monochromatic coherent plane wave scatt. by living cell *(Russian)* 78−48765
monochromators as tunable radiation sources in interferometry 80−23787
multifold independent partially polarised speckle fields, and coherent background, superposition statistics 78−1155
multilevel atomic system, thermally relaxing, coherent radiation reson. scatt. and absorpt. 79−81401
multilevel system, group theoretical method for coherent effects calc. 80−106502
multiphoton near-reson. ionisation, chaotic versus coherent light 78−33489
multiple imaging through nonredundant arrays 78−22095
N-level atom (molecule), coherent dynamics, two- and three-level behaviour 80−23649
NMR system, multi-level, coherent phenomena, review *(Japanese)* 79−73831
nonlinear and coherent optics, Conf., Leningrad, USSR (June 1978) 80−27027
nonlinear media, coherence oscillations, coherent state lifetime 78−66862
light coherence continued
nonlinear operator realisation, coherent optics method *(Russian)* 79−94157
nonlinear optical amplifier, coherent radiation statistical props. 80−99691
nonlinear spectroscopy, coherent background noise elimination from saturation spectrosc. signals using freq. offset pump 80−62733
objects of unequal intensity, resolution in partially coherent light 77−88647
OCR system using spatial light modulator *(Japanese)* 80−14291
optical Bloch equation, stochastic incoherences 79−68373
optical coherence modulation by two ultrasonic waves 80−1120
optical data processing extension to space-variant and nonlinear operations 78−78940
optical equivalence theorem, new type of discrete diagonal coherent state representation 78−55328
optical fibre, partial coherence propag. 77−72070
optical fibre, spatial coherence and modal struct. 80−87531
optical fibre, two-mode, temporal spreading of pulse 80−33183
optical hybrid space- and time-integrating spectrum analysis 80−48177
optical image spottiness reduction by liquid crystal screen 79−14109
optical imaging with defocusing, partial coherence effect *(German)* 77−75430
optical instrument design, partial coherence effects 80−78767
optical processing appls., beam coherence modification by transparencies 80−78769
optical processor with interference contrast microscope input 80−43281
optical ringing and incoherent resonance decay 77−24859
optical system design, advances and problems 79−36975
optical systems, entropy and neguentropy *(French)* 80−102608
optical systems evaluation, apodisation in beam propagation and image formation 77−88657
organic dye molecules, two-photon absorpt. in laser fields with arbitrary statistical characts. *(Russian)* 80−37842
OTF of quadratic detect. systems, quality evaluation 79−72504
parametric interaction with reson. medium, EM field statistics 80−1171
parametric up conversion process, coherence effect of generating radiations 79−76756
partial coherence, diffraction, bibliographic review 78−29894
partial coherence, freq. domain treatment 77−27250
partial coherence control, of light wave modulated by progressive US wave 79−76581
partial coherence studies, bibliographic review 77−27244
partial spatial coherence blur correction by postdetection image processing 80−78792
partially coherent beam intensity fluctuation calc. in turbulent atmosphere 80−78775
partially coherent image formation, bibliographic review 79−18356
partially coherent imagery, calc. method 78−90373
partially coherent imaging, edge ringing, performance function 77−46699
partially coherent light interpretation, optical theorems 80−53210
partially coherent light propagating through atm. turbulence, intensity fluctuations 79−58087
partially coherent object, coherence props. in image 77−34833
partially coherent perpendicularly polarized vibrs., anisotropic photographic recording, interferograms 80−57364
partially coherent radiation, optical heterodyne detection 80−77871
partially coherent source detection 80−47109
partially coherent source giving rise to highly directional beams 79−14070
partially coherent source in extremely strong turbulence, irradiance scintillations 79−64176
partially coherent source in turbulent atmosphere, beam propagation 80−9806
partially coherent source radiant intensity, theorems and expts. 80−78768
partially coherent sources with phase profile, Van Cittert-Zernike theorem 80−63919
partially coherent truncated bar targets, diffr. image illuminance distrib. 79−76609
partially coherent wave propagation and generalised van Cittert-Zernike theory 78−25793
particle cluster, coherent light scatt., spatial correl. function calcs. 80−99632
pattern recognition using normalised invariant moments 80−99653
pentacene, laser fluoresc. of mol., excitation bandwidth and optical dephasing 79−36679
periodic structure with coherent illum., resolution depend. on number of elements, wavelength and focal length 80−63941
phase conjugation by degenerate four-wave mixing, coherence effects 80−64101
phase determination by conjugate wave-front generation, optical coherence theory 79−7174
phase measurement anal., for microscopic radiation fields 78−17887
phase problem in astronomy, sky brightness distrib. 80−46258
phase reconstruction problem for wave amplitudes and coherence functions, book contrib. 79−31823
photoelectron counting, maximum photon antibunching in generalized coherent states 79−41358
photographic film grain noise in partially coherent imaging 80−101860
photomixer with spatially periodic photodetectors, characts., appls. 79−12852
photomixing of coherent radiation by spatially periodic photodetector 79−12851
planar sources generating same radiant intensity distribs., equivalence theorems 79−89843
plane waves, difference between polarisation and coherence 80−8805
plane waves in strongly turbulent media, two-frequency mutual coherence function 77−21907
polarisation problems, coherency matrix transform. 77−6993
polarised light, spectral analysis, polychromatic and coherent optics *(French)* 79−50209
polarising microscope, resolving power in partially coherent light 77−87819
projection printing, partial coherence 79−31834
projection system, wavelength and coherence effects 80−64136
propagation of coherent and partially coherent light 79−31790
pseudocolour density encoding, white-light, using contrast reversal 80−83560
pulse arrival time statistics in turbulent media 80−48154

light coherence continued
pulse excited multilevel system, diffr. grating effect in luminesc. 79−50272
pulse propagation, 0π pulse generation from zero-area pulse 80−48352
pulse propagation, soliton creation by chirped initial profiles 79−72632
pulse train propagation, two-level absorber, relax. effects 79−46011
pulsed coherent radiation intensity unit reproduction, USSR standard 78−37955
quantum optical field modulation concept rel. to degrees of coherence 77−83840
quantum optics, introductory lecture 78−25843
quasi-homogeneous partially coherent source, far zone range criteria 79−14069
quasi-homogeneous sources and geometrical optics 80−23620
quasicoherent light source image synthesis by phase measurable interferometry 77−58284
quasihomogeneous planar source, coherence and radiometry 78−9421
radiant intensity from planar sources of any state of coherence 79−27163
radiation laws, temporal and spatial coherence, review 77−23612
radiative transfer theory rel. to coherence theory 77−65568
radiometry, fundamental quantities and partial coherence effects 80−77838
radiometry and coherence, basic concepts 78−66745
Raman spectroscopy using powerful tunable lasers 77−53985
Raman spin-flip laser, multiply pumped, coherence effects 80−87398
random media, two-frequency mutual coherence function for pulse propagation 79−76589
randomly inhomogeneous turbulent media, spectral expansions method for optical wave propag. 80−43264
rarefied absorbing gas, coherent rad., in time separated fields 78−37938
ray optics, theory of light field, statistical optics, light meas., photometry, polarimetry 77−79748
real-time incoherent subtraction of irradiance 80−74301
resonant medium, interferograms form. by nonoverlapping pulses of coherent light 79−64191
resonantly absorbing media, instability of coherent pulse propag. *(Russian)* 77−62017
retrieval problem in coherence theory, moment estimator approach 80−95785
review of the subject 80−48140
rhodamine 6G laser with lamp pumping, spatial coherence 77−50669
rhodamine 6G water soln. laser with spatial lamp pumping, spatial coherent emission 78−82963
ring laser, coherence theory, counter-rotating laser modes 78−55387
rough surface, effects on coherence of transmitted radiation, Young's method 77−3539
ruby crystal, radiation amplification, spatial coherence 80−99737
ruby laser beam spatial coherence interferometry 79−14003
scalar wave fields of fluctuating primary planar sources, coherence and radiant intensity 78−90355
scattering object, coherently illuminated, speckle pattern statistics in diffr. field 80−63924
scintillations in weak turbulence, source temporal coherence effects 79−50223
second order coherence function, phase determ. 78−9406
second order coherence meas. using microscope and grating 77−41672
second-order coherence effects due to the superposition of two independent thermal light beams 80−23618
second-order correlation function of completely coherent field, factorisation property *(Chinese)* 79−50206
self-imaging process, partially coherent light effects *(French)* 77−23621
semiconductor junction laser, radiation coherence, interferometric analysis methods *(Polish)* 80−19065
semiconductor laser, output power and coherence length in incoherent feedback 79−98412
semiconductor laser pulse radiation, coherence rel. to Fourier hologram recording 78−50738
signal processing, time-integrating, acousto-optic 80−102641
simulation experiment 78−73810
single mode optical field, anticorrel. props. 77−83809
single-channel injection laser manufacture and characteristics 77−38893
solid laser array spatially-coherent beam formation and mode locking 78−37898
solitons in system of coherent phonons and photons 79−64291
solitons in the theory of guided lightwaves 80−58760
source coherence and far-field intensity patterns, cross spectral density function determ. 79−55053
source coherence meas. and fibre modal noise simulation by Michelson interferometer 80−48324
source-field coherence props. from radiation ang. distrib. 77−23614
space variant optical transfer with Fourier filter in extrapupilar position 77−10846
space-angle characteristics, improvement by interference method *(Russian)* 78−78909
space-variant coherent optical processing 80−102638
Sparrow limit of resolution for coherent illum., max. encircled-energy ratio 77−619
spatial coherence analysis using reversing front interferometer 78−277
spatial coherence complex degree determ. using folded-wavefront type interferometer 78−24853
spatial coherence functions phase meas., holographic method *(Russian)* 80−5703
spatial coherence meas. by correlated diffusers 80−74296
spatial distortion, post-detection, coherent optical compensation 79−98302
spatial filter correlator, coherent optical matched, for microfilm data base word recognition 80−43279
spatial filtration in coherent optics system, amplitude and phase spectra analysis *(Russian)* 80−28164
spatial pattern recognition by spectral feature classification and coherent optical correlation 80−99644
spatially coherent fields, amplitude and phase spectra synchronous detection *(Russian)* 79−44937
speckle, statistical props. of sum of two partially correlated patterns 77−83813
speckle interferometry, coherence requirements, use of thermal radiation sources 78−49891
speckle pattern statistics, partially coherent illum. effects, book contrib. 77−31070
light coherence continued
speckle pattern superposition and coherent background, statistical props. *(Chinese)* 78−90368
speckle patterns in white light images, average contrast meas. 80−9808
speckle propagation through turbulent atmosphere research progress 79−66803
speckle reduction in image plane by US modulation of spatial coherence 80−106459
speckle statistical props. and coherence aspects 80−78773
spectroscopy of high power resolution by means of photon statistics *(Spanish)* 79−21818
spectroscopy using lasers, coherent optical transients, atom, mol. and solid 77−53986
spot size estimate in diffr. pattern of scattered field 80−95789
starlight, coherence rel. to extrasolar planets detect. 77−29882
stellar holographic interferometric technique, mutual coherence function 78−53838
stimulated Brillouin scattering, Stokes radiation, spatial struct. 77−50726
storage of optical coherence, stimulated optically induced nucl. spin polaris. 80−58649
superfluorescence temporal and spatial coherence, from independ. SF beams interference obs. 80−58492
superluminescence, spatial coherence 80−99683
superposed coherent and chaotic radiation, computer simulation 80−58485
superradiant dye laser, coherence and beam geometry 78−37876
synthetic aperture radar image coherent-optical simulation 77−50632
temporal coherence rel. to optical noise, partially coherent imaging 80−102611
temporal degree of coherence bound 77−65573
tendon, rat-tail, coherent optical SHG 80−89796
p-terphenyl−pentacene, optical dephasing, optical mixing-detected ps photon echoes obs. 78−71155
thermal sources, general coherence props. 77−75408
three level absorber, two-photon transition, self-induced transparency 79−27337
three level system, coherently pumped, cooperative relax. 80−78816
three-photon vector model, resonant coherent interaction *(Chinese)* 80−43306
transparent molecular systems, optical dispersion, polarised light, depend. on coherence, radiation field 78−5294
turbid medium, infinite plane wave, mutual coherence function propag. 78−1163
turbulent atmosphere, beam props. of partially coherent curved beam waves 80−95798
turbulent flow meas., light beam coherence effect on optical method information capacity 80−1709
turbulent medium, four-point coherence function strong intensity fluctuations region 80−87319
turbulent medium, light intensity two-freq. fluctuations correl. 79−98280
turbulent medium, linear propagation of radiation, coherence length evaluation 80−48150
turbulent medium, pulsed laser radiation intensity fluctuations during thermal selfinteraction 80−102781
two photon coherent states in degenerate four wave mixing 80−5717
two-level atom in coherent monochromatic field, transmitted and fluorescent light spectra 79−49981
two-level atomic system, weak probe field absorption spectra in coherent laser field 80−23758
two-photon absorption, from polychromatic stationary radiation field, light coherence 78−74626
two-photon laser beam, breathing mode of EM field 78−46558
undulator linac, electron dynamics, coherent radiation source 78−82539
US wave, amplitude-modulated, for optical coherence reduction 79−3624
UV coherent pulse, 45 GW, for laser fusion 80−69450
vacuum UV tunable coherent radiation generation by lasers 77−54705
volume light source, spatial coherence of spontaneous radn., holographic meas. 79−98455
VUV monochromator for coherent signals *(Russian)* 79−46036
wave beam distortion by thermal self-interaction in droplet medium 80−19082
wave front mutual coherence function corrected by zonal adaptive optics 79−72490
wave propagating in turbulent medium, four-point field coherence function 79−98279
wavefront reversal, transverse enhancement of coherence of scatt. field 80−95952
white light image speckle statistical props. 80−106461
white light optical processor for edge enhancement and spectral filtering 79−76599
AlGaAs DH-injection phase-locked laser, coherence 80−102726
As_2S_3 film, optical recording, light scatt. enhancement due to coherence 80−97362
CO_2 laser Doppler system atmospheric attenuation 77−75601
CdS, attenuation of transmitted light in exciton region, polarisation, coherence, scatt. 77−69852
Cu vapour laser, coherent props., dynamic holography in VO_2 films 79−13929
GaAlAs DH laser coherent light, propagating in multimode optical fibre, speckle contrast 80−78978
GaAs, insulating, generation of far IR radiation by freq. mixing 79−50347
GaAs single-frequency injection laser, coherence of emitted radiation 79−31904
GaAs-$Al_xGa_{1-x}As$ DH laser, modulation with coherent light injection *(German)* 78−37922
GaAs-$Al_xGa_{1-x}As$ DH broad contact pulse lasers, second-order coherence props. 80−23685
GaAs-GaAlAs CW injection laser, stripe geometry DH, temporal coherence 80−38016
GaN, nonlinear susceptibility and coherence length, SHG meas. 78−25924
H, electron impact coincidence, even-odd parity coherence effects, polarisation ang. distrib. 78−9253
H_2, Raman pulse propag., 30 atm., self-induced gain/loss modulation 77−10980
HCN, laser, CW, 337 μm, spatial coherence meas. 77−3595
HCN laser, temporal coherence meas., comparison of TGS pyroelec. detector with W-C point contact diode 80−31871
HCl, anharmonic molecular vibrations, coherent spectroscopy 79−18187

light coherence continued
He, gas, fifth harmonic generation, coherent XUV light 79−46007
He-Ne laser, field distrib. and spatial coherence of superluminescence at 3.39 μ transition *(Russian)* 78−13682
He-Ne laser photon statistics variation with cavity length 80−53265
He-Ne multimode and single-mode lasers, phase locking to very high coherence degree 79−76710
He-Xe 3.51 μ laser mode competition in axial mag. field 80−63974
I_2+I_2, optical coherent transients detected by frequency-switched tunable laser 77−54762
KrF laser beam, Raman pulse compression, for fusion expts. 78−59086
$LiNbO_3$:Ti diffused channel waveguide, optical parametric amplification 80−106564
MnF_2, two-exciton many photon absorption, effect of statistical props. of light on intensity *(Russian)* 78−95589
N_2 laser, coherent radiation from unstable resonator 77−71994
Na, laser temporal coherence effects in two-photon resonant three-photon ionisation 80−32686
Na vapour doublet, dispersion free point, cooperative phased-array radiation 80−53352
Nd, multifreq. laser, coherence time meas. using bleaching dyes 80−23739
Nd:glass laser radiation, spatial coherence of fundamental and second harmonic 80−69442
Nd:YAG laser, coherence time meas. of picosecond pulser by light-induced grating method 80−53347
Ne, pulsed amplified spontaneous emission intensity, spatial and frequency distribs. 79−50270
Ne superradiation propagation through reson.-absorbing positive column plasma, pulse shape change 79−4117
S_2, selectively excited, coherence retention during rotationally inelastic collisions 77−46622
SF_6, Stokes signal amplification, effect of pump radiation incoherence 78−18015
Sr vapour, resonantly enhanced sum freq. mixing, coherence effect 77−88848
Sr vapour, vacuum UV coherent radiation generation by four-wave sum freq. mixing 79−10350
Xe three-level system, collisional effects on optical coherence 79−93954
ZnO, attenuation of transmitted light in exciton region, polarisation, coherence, scatt. 77−69852

light communication *see optical communication*

light cones
see also current algebra
0(5,1) light cone, pseudoparticle solns. to Yang-Mills theory 78−24952
asymptotic expansions of generalized functions with singularities on light cone 78−8544
bilocal operators spectral props., local operators product expansion on light cone 77−41778
canonical formalism on lightlike hyperplane, neutral scalar field, Dirac's theory 77−79214
charmed particle prod. by neutrinos, light-cone algebra 77−18274
classical Yang-Mills theory, local harmonicity of Wilson loop integral 79−75684
conformal field equations 80−46881
deep inelastic processes book contrib. 78−82222
differential scatt. cross section, influence of amplitude singularities 78−49984
electroproduction structure functions studied using light cone expansion via O_4 symm. 77−41845
EM form factors in Bjorken limit and their Fourier transforms on light cone 79−26246
EM permeability of vac. and light-cone structure 80−36879
EM two-body interaction theory 78−49739
Euclidean light cone gauge, 1/N expansions with non-isoscalar gluons 80−47169
field theory and the parton model, book contrib. 78−82220
finite normal products, perturbative Green's function method 78−86408
Fock spaces for man-zero helicity-one particles described by antisymmetrical two-tensor 77−13903
general light cone frame, from Galilei group to Lorentz group, appl. to Schrodinger-Pauli eqn. 77−61187
Green's function discontinuities across characteristic surfaces of field eqns. 79−93279
gyromagnetic ratio, light-cone formulation for arbitrary spin particles 77−13961
gyromagnetic ratio and Galilean symmetries, light cone formulation 77−13962
H space, the manifold of complex asymptotically shear free light cones 78−8292
hadron-hadron high energy scatt., Jost-Lehmann-Dyson representation, light cone singularities 78−17049
hadronic EM current, short distance scaling, R(s) behaviour as $s\to\infty$ 79−22095
hadronic structure using parton anal. of deep inelastic scattering and rel. processes 79−80803
hadrons, extended, Lorentz deformation props., O(4) and light-cone coordinate systems 80−68354
harmonic oscillators, relativistic two-body interaction, exactly soluble system 78−16955
infrared regularizations in a model gauge theory 79−30700
interacting Rarita-Schwinger field on light front 78−4786
kinematical groups and coord. transformations using light-cone frame 78−81796
left-flat space-times, null tetrad and restrictive conditions 80−62545
leptoproduction, spin-depend., light-cone model 77−2772
Lorentz group functionals, Fourier expansion in light cones 79−21604
Lorentz group in function space outside light cone, Fourier expansion 79−71246
Lorentz group irreducible representations, generalised function expansion with light cone support 78−70018
Lorentz invariant affine connection nonexistence 77−51
Mandelstam graph, deep inelastic asymptotics 79−85244
many particle prod. based on hierarchy of upper bounds 78−12891
mass corrections to scaling in deep inelastic processes 77−13929
massless propagators on light cone 78−8538
nonlinear field theory, classical solutions by inverse scatt. method 79−9272
nonlocal light cone expansion of current products, renormalisation group anal. 79−97526

light cones continued
nucleon form factors and light front dynamics *(Russian)* 77−38172
nucleonic matrix elements of local currents, Melosh transformation 77−41791
null plane fields and automodel random processes 80−32018
operator products near light cone, expansion in terms of regular bilocal operators 77−87899
optical group Opt(3,1) and its subgroups 78−77759
parton model interpretation of cut vertex formalism 80−86566
Poincare and Galilei groups in arbitrary dimensional spaces 78−77672
Poincare generators corresponding to lightlike irreducible unitarity representations 77−18193
QCD, 2-D, evidence against colour confinement 79−26293
QCD calcs., non-singlet quark struct. function 80−57464
QED, two-dimens. light cone formulation 77−57476
quantum chromodynamics, two dimens. U(N) invariant, 't Hooft bound state eqn. 77−26495
quantum field theory on cone, Green functions, diffusion kernels 77−18161
quark light-cone model, current conservation 78−21386
quark mass ratio, chiral perturbation in new key 80−37208
quasi-light-cone frame and approx. Galilean symmetries 77−13844
reduction formula and non-leptonic decays in light-front formalism 78−12911
relativistic amplitudes as wave functions, invariant diagram technique *(Russian)* 79−2957
relativistic composite particle scatt., quasipotl. approach 78−404
relativistic Hamiltonian theory, high-energy representation 78−24980
relativistic Hamiltonian theory in light like case, unitarity and causality conditions 78−78112
relativistic Hamiltonian theory on light cone, covariant formulation 79−2942
relativistic quarks; relativistic, light cone dynamics, nucleon wave function *(Russian)* 77−6085
renormalised perturbation theory, light cone expansion 80−99045
renormalised perturbation theory, operator-product light-cone expansion 77−82680
scalar field quantisation, current nonconservation 80−47220
short-distance and light-cone expansions for products of currents 79−17638
spectral function sum rules for quark and baryon fields, using lightlike charges 78−93822
structure function moment asymptotic behaviour and light cone singularities 78−4804
two-body gravidynamics 79−71683
two-dimens. light-cone coords., noncovariance of fermion fields 77−71448
weak neutral currents, light-cone algebra anal. 79−6311
Wightman function, two-point, asymptotic behaviour 80−73614
Yang-Mills 2-D theory in leading 1/N expansion 79−26242
$eN\to e\pi_s+X$, test of soft-pion theorem in inclusive pion electroprod. 79−17739
ep deep inelastic scatt., parton model 77−54077
$\nu N\to\mu N\pi$, high energy behaviour, light cone commutators, PCAC calcs. 78−37199
νp polarised cross sections, new polarised ν sum rules 77−34144
π Bethe Salpeter wave function in ladder model, light cone behaviour 77−18176
π EM form factor, dispersion theoretic study, mass, charge radius 77−67652
π electroprod., light cone dispersion sum rules, axial vector currents 78−41556
π struct., confinement scheme, light-cone gauge 78−45841
π^-p interactions, 5 and 40 GeV, inclusive struct. functions of γ, $\pi^\pm$, K^0, and Λ *(Russian)* 79−80856

light diffraction
see also holography; optical zone plates
Abbe's theory of imaging, lecture-room demonstration 78−41120
aberrated diffraction pattern obs. with computer-generated holograms 80−102681
aberrational diffraction images, computation accuracy 80−87328
aberrations, scalar diffraction theory, exact solns. 80−78778
aberrations of diffracted wave fields 78−94376
absorbing liquid, coherent light transient self-diffr., simulated thermal scatt. laser expt. 80−48361
ACCOS V program for diffraction evaluation of general optical systems 79−86231
acoustic shear waves polarisation meas. 77−35006
acoustic surface waves, laser light diffraction at solid-liquid interface 78−38127
acoustic wave, intense, in solid, divergent light beam diffracted field calc. 77−83808
acoustic waves, standing and travelling 77−600
acoustically induced, diffr. by two adjacent parallel US waves, soln. of boundary value problems 78−90358
acoustically induced optical diffusion, molecular parameter calc. 77−48144
acousto-optic deflector, anal. and design of flat transducer array 79−18527
acousto-optic deflector, bandwidth increase method 80−99861
acousto-optic frequency shifter, beam quality, heterodyne interferometry meas. 78−79127
acousto-optic interactions, light diffraction efficiency over wide wavelength interval 80−45036
acousto-optic processor, light diffr. by acoustic wave 79−76586
acousto-optical diffraction, multifrequency, in optically birefringent media 80−74300
acousto-optical phenomena in solids, review 79−18577
acoustooptic guided wave Bragg diffr., phased SAW array in $LiNbO_3$ 77−58439
acoustooptic modulator, reduction of thermal distortion of diffracted light 80−5837
acoustooptical interaction in strong field 80−95790
air bubble in water, critical angle scatt., physical optics approx. and obs. 80−9797
Airy pattern calculation by simple program run on HP 25 pocket calculator 79−72481
ambiguity function in diffraction and isoplanatic imaging by partially coherent beams 78−78925

light diffraction continued
amplitude filtering for superresolution, maximum central irradiance under energy constraint 80−91914
angular divergence from electron-beam-controlled laser, refr. and diffr. contribs. 79−59668
angular spectrum approach to diffr. of partially coherent light 77−75411
anisotropic diffraction by acoustic waves, induced anisotropy 77−50614
anisotropic diffraction by bulk acoustic waves 77−23784
anisotropic medium, by acoustic waves 77−90127
annular aperture, light distrib. from diffr., aberration correction using mirror lenses *(German)* 80−69325
annular beam profile changing by aperturing diffr. pattern 80−18991
anomalous diffraction approx. solns. for particle size remote sensing 80−17386
aperture, partially apodised, diffracted field characts. 80−48139
aperture shaping, diffracted energy spatial distrib. control, computer analysis 78−59152
apertures, multiple circular, located on circle, resolution 80−102615
apertures with Straudel Class of pupil functions, var. apodisation 80−23616
apertures with triangular and assoc. filters, variable apodisation 80−63914
apodisation filters, atm. turbulence effects on central irradiance in Fraunhofer diffr. by slit apertures 78−25796
apodisation for max. Strehl criterion and specified Sparrow limit of resolution 77−68168
apodisation for minimising intensity diffr. pattern second moment in systems with aberrations 79−81358
apodisation for minimising intensity distrib. second moment for Fraunhofer diffr. 77−31065
apodised semicircular apertures, Fraunhofer diffr. pattern 79−901
apodization, optimal, by means of coupled calc. of pupil function and shape 80−95788
arbitrary profile beam, diffr. by periodically modulated layer 80−43252
aspheric, testing in reflected light using blazed synthetic holograms 80−91881
autocollimation, resonance light scatt. by echelon *(Russian)* 77−88640
automation of real-time optical meas. of small structures 79−85115
axial patterns diffracted from optical pupils, Fourier analysis of Fabry-Perot spectrograms 79−27188
axially symmetric filters, Fresnel diffr. field, series representation 77−46696
axially symmetric filters, two-point resolution evaluation method 77−46697
band-limited angular spectrum representation of diffracted wave field 79−27162
beamed signal propagation through diffractive inhomogeneous media 77−71920
bilinearly distorted image linear restoration using Wiener filters 80−83557
biological cell diffr. pattern, Fourier optical extraction of morphological parameters 78−92749
bipolar spatial filtering, incoherent, review 80−102822
birefringent crystals, use for holographic storage of information 79−98322
boundary diffraction of light, formulae 79−59632
Bragg and Raman-Nath diffr. regimes rel. to grating thickness 78−71028
Bragg anisotropic diffraction by US waves *(Russian)* 77−10833
Bragg diffraction by a 3-D Gaussian ellipsoid and diffraction broadening of Mandelshtam-Brillouin scattering lines 80−55114
Bragg diffraction imaging systems, speckle size 78−13864
Bragg-diffraction imaging 79−64463
Bragg-diffraction imaging system with partially coherent light illumination 79−14175
causality principle 78−55295
cellular deformability, diffractometric method for meas. 80−98187
Cherenkov radiation, in spatially-periodic medium *(Russian)* 79−59623
cholesteric liquid crystal, blue phase, struct., Bragg diffr. of visible and UV light 80−59385
cholesteric liquid crystal, optically absorbing, light refl. and transmission dynamical diffr. theory 77−58954
cholesteric mixture, solid phase, spherulite textures, optical effects and mol. ordering 79−1746
cholesteryl acetate:cetyl alcohol, optical behaviour of spherulite texture 77−51314
circular aperture, diffr. of uniform and Gaussian beams, Zernike polynomials 77−61912
circular aperture, non-uniform illumination, Straubel pupil function study 79−3623
circular aperture, white light Fresnel diffr. 77−68169
circular apertures with parabolic filters, encircled energy in diffr. pattern 79−89845
circular grains, nonoverlapping, pulse jitter model 77−68173
circular particle size determ., complete histograms, diffraction spectrum anal. 79−86130
circular pupil, diffraction pattern apodisation problem 77−612
circular sector, conformal transform. use in Fraunhofer diffr. 79−76585
coherent 2π pulse diffr. instability; numerical anal. 79−89975
coherent and partially coherent light, comparison between propag. in given geometry 79−31790
coherent apodization problems, edge ringing effect 77−42495
coherent information processing by a pair of lenses in spherical wave illumination 80−95816
colloidal particles, intrinsic optical anisotropy, anomalous diffr. approx. 80−53213
communications theory, systems concepts electronic analogy *(German)* 77−3542
complex resonator with internal diaphragm, diffr. losses and field distribs., integral eqns. 80−95921
concave diffraction grating, curvilinear lines, ray path calcs. *(Russian)* 77−88958
confocal strip resonator, diffr. performance, mirror defects effect 77−19349
contemporary optics, book 79−81353
copper phthalocyanine, chlorinated, radiation damage mechanism 80−88000
coronagraph diffraction limit problems and design approaches 80−82200
coronograph, external shading disc, diffracted light intensity calcs. 77−87267
coronograph external occulting disc, diffracted light flux and reduction 78−36455
correlation filtering for increasing diffr. efficiency 80−96028
correlators, diffr. optics based, invariant to optical element shifts 80−106471
corrugated surface, Brewster affect analogues 79−13901
coupled wave diffraction, holographic grating-fringe pattern phase mismatch determ. 79−50250
cross-shaped aperture, Fresnel and Fraunhofer diffraction 80−106436
crossed Gaussian volume grating, Bragg diffr. of Gaussian beam 77−65569
crossed lamellar transmission grating, exam. of diffr. props. 78−59139
crossed slits, Fresnel and Fraunhofer diffraction 80−106436
crossed-beam volume gratings, three dimens., diffr. characts. 80−78975
crystal with defects, EM wave diffraction, Ewald dynamical theory 77−65928
cubic ferr-te garnet, diffracted light polarisation characts., spin and magnetoelastic waves 80−20614
cylindrical light beam diffr. on wideband US signal 78−50698
cylindrical light wave diffr. by complex spectral composition US 80−95939
deep dielectric gratings, light diffr., transform. props. 80−99835
defect crystal structure determination 80−103316
demonstration of continuous spectrum, optical filters to audiences, students 77−45649
demonstrations of Young's theory of diffr. 77−78938
dichromate gelatin, holographic information recording *(German)* 79−27207
dielectric coated gratings, general integral theory 78−66909
dielectric multilayer coated optical surface, diffr. and diffuse scatt. 79−50220
dielectric waveguides, optoacoustic interaction, Raman-Nath type diffr. 78−87153
diffraction gratings, theoretical method, numerical appl. 80−95786
diffraction pattern and AM sideband parallelism *(German)* 79−89854
diffractor size and shape determ. from diffracted light 78−78901
diffuse object longitudinal motion under Gaussian beam illum., laser speckle dynamic statistical props. 80−99628
diffused waveguide, corrugated section, H and E wave refl. and emission 77−34954
dimensional metrology, light diffraction patterns, technical structures *(German)* 79−30415
diode laser, mear and far field characterization 80−48242
discrete carrier holograms, diffr. efficiency 77−58299
dislocation, optical analogue of diffr. 78−38723
dispersive media, Ewald dynamical diffr. theory extinction theorem 78−66749
dispersive media, polychromatic diffraction, system theoretical approach 79−98272
DOBAMBC, ferroelec. props. 79−32884
domain lattice of transparent crystal regular birefr. regions, optical wave diffr. divergence 80−102616
dynamic self-diffraction of coherent light beams, review 80−102777
edge parameter effects, holographic method 77−34807
education, diffraction pattern display using photodiode array 78−86069
education, Fraunhofer diffr. negative order pattern, He-Ne lasers 77−78912
education diffraction pattern classroom anal., image-space method 80−51983
elastic surface wave parallel to light beam, expt. investigation 78−82904
electro-optic waveguide deflector performance characteristics 80−33213
electron microscopy, HV, accurate stigmating using optical diffr. pattern of micrograph 78−49941
elliptic umbilic diffraction catastrophe 79−50213
energy distribution of converging spherical wave for small Fresnel nos. 79−3626
energy flow lines, Maxwell eqns., interpretation of diffr. and interf. 77−34806
error reduction in radiometry by toothed apertures 79−9232
erythrocyte deformability, viscometric flow and laser diffractometric technique 78−35879
evanescent wave holograms, diffraction efficiency 79−18375
evanescent wave holography with reference Gaussian beam, diffr. efficiency theory 80−43290
Ewald extinction theorem and Green function method for semi-infinite dipole cryst. 79−23683
extended circular target, diffr. images in presence of coma 77−58250
extensometry, strain meas. appl. 79−85119
eye, human, pupil diameter and depth-of-field as meas. by laser speckle 78−15826
Fabry-Perot, and confocal resonators, comparison of diffraction formulas 78−87077
far-field diffraction, partial coherence, primary astigmatism 79−22899
ferrimagnetic single crystal layer, light diffr. by mag. bubbles *(German)* 79−56769
ferrite, light diffr. by magnetisation inhomogeneities, multiple refl. 80−2733
ferroelectric, struct. of domain boundaries, light diffr. 78−15135
ferroelectric improper, EM wave diffr. by domain walls 79−69799
ferrofluid decorated mag. domain patterns, Fraunhofer diffr., domain struct. determ. 78−6541
ferromagnetic plate, EM wave diffr. by domain walls 79−99724
fibre bundle waveguide, Fraunhofer diffr. 78−25978
fibre mode conversion analysis by diffraction theory 77−83999
fibre sizing using Fraunhofer diffraction 79−171
fibre type light shield with absorbing cladding, Fraunhofer diffr. 78−90521
field diffraction with light shadow boundary on wedge and half-plane, calc. *(Ukrainian)* 80−69324
fluid dynamics, localised optical heating, principle of meas. on flows *(French)* 77−31406
focused field, symmetry props. 80−83550
Foucault, phase edge and wire optical test 80−96046
four-wave diffraction of thick transmission gratings, analytical solutions 80−23617
Fourier optics as approx. of Kirchoff integral, Fraunhofer, diffr. *(German)* 79−18357
Fourier optics described by operator algebra 80−48163
Fourier plane signal processing for real-time meas., using Fraunhofer diffr. pattern 79−76621

light diffraction continued
Fraunhofer, diffr. integral Abbe transform, Youngian boundary wave *(Czech)* 78−29893
Fraunhofer, optical system with annular pupil, use of orthogonal polynomials 78−50714
Fraunhofer diffr. of partially coherent light by amplitude, phase gratings 77−46681
Fraunhofer diffraction, dispersion relations 79−81356
Fraunhofer diffraction, white-light, theoretical determ. of chromaticity inform. 79−72477
Fraunhofer diffraction and interference, He-Ne laser 77−60878
Fraunhofer diffraction and polarisation 79−44666
Fraunhofer diffraction in medium with uniaxial elec. anisotropy 78−1148
Fraunhofer diffraction of apertures, analogy with SSB modulation 80−48138
Fraunhofer diffraction of Gaussian beam at a straight edge 80−53205
Fraunhofer diffraction on annular aperture diaphragms *(German)* 78−33662
Fraunhofer diffraction pattern by ultrasonic phase grating with laser point source 77−79747
Fraunhofer diffraction pattern intensity distrib., apodization minimizing second moment 77−6997
Fraunhofer diffraction pattern of circular apertures with triangular apodisation filters, encircled energy 80−14277
Fraunhofer diffraction patterns, from apertures illuminated with nonparallel light 80−67983
Fraunhofer diffraction patterns, phase curvature effects 77−61914
Fraunhofer diffraction patterns, phase reversal effect 80−101691
fraunhofer diffraction patterns from apertures illuminated with nonparallel light, for teaching 79−35465
Fraunhofer diffraction patterns in Young's expt. with three holes *(French)* 77−598
Fraunhofer diffraction symmetry, series expansion of Fourier transform 79−50212
Fresnel diffr. patterns, FT analysis 77−88637
Fresnel diffraction field, anal. by quantum mech. operator method 80−5688
fresnel diffraction images of periodic objects under gaussian beam illumination 79−94148
Fresnel diffraction pattern, spatial freqs., spectral analysis *(French)* 77−58269
Fresnel images, form. of 2-D transparencies with extended periodic struct., theory 78−82920
Fresnel images of periodic transparencies of finite dimensions 79−3627
Fresnel lenses in BaO optical waveguides 80−96034
Fresnel plane interference fringe generation by correlated speckle patterns 80−106462
fused quartz, determ. of acoustic and acousto-optical parameters using acoustic interferometry 79−41532
gain measurement in optically pumped materials, diffr. effect 77−19225
Gaussian beam diffr., by periodic permittivity layer 78−33663
Gaussian beam far-field 79−81357
Gaussian beam scattering characts. at dielec. media interface 78−42275
Gaussian beams, off-axis, aberrated Fraunhofer diffr. patterns 78−66753
Gaussian laser beams, Fraunhofer diffr. by single slits 80−87298
Gaussian light beam, diffr. by plane acoustic waves at oblique incidence 80−69326
Gaussian light beam diffr. by acoustic waves 79−64173
geodesic lens, anisotropic and curvature losses, operation in $LiNbO_3$:Ti waveguide 80−48453
glassfibre reinforced composites, accumulation of fatigue damage using diffuse light transmission *(Russian)* 78−19896
graded index single-mode fibres, spot size profile independent representation, determ. 79−50380
grain boundary, optical analogue of diffr. 78−38723
grating, reflective, high efficiency, scattering types 80−99619
grating, transmission phase with deep rectangular grooves, light diffr. theory 79−10257
gravitational lenses, high-intensification regions and diffr. phenomena 79−25463
gyrotropic crystals, acoustic, light diffr. by US 79−56765
p,n-hepthyloxybenzoic acid, smectic C liq. cryst., coherent light diffr. 78−1999
high intensity light, ultrasound in nonlinear liquids 80−64270
HOBA, smectic liq. cryst., two dimensional diffr. grating due to AC electric field, pulsating diffr. 78−15148
hologram, 1-dimens., diffraction efficiency calcs. 77−68189
hologram, reflection, real image reconstruction, resolving power and diffr. efficiency 80−53237
holograms, 3-dimens., light diffr. vector eqns., Kogelnik theory *(Russian)* 78−22100
holograms, rainbow, demonstration of diffraction and interference of light *(Polish)* 80−68001
holographic attenuated thick gratings, diffr. efficiency 78−1187
holographic display of diffraction patterns, third and fifth order aberrations 80−9829
holographic interferometric anal. of boundary diffr. wave *(German)* 78−63041
holographic interferometry, nonlinear two-exposure system 77−31074
holographic interferometry, object movement generated fringe localisation analysis *(Japanese)* 78−22096
holographic interferometry used in US field investigations, theoretical analysis of light intensity distrib. 80−32903
holographic process, reference wave diffraction effects *(Russian)* 79−50256
holography, diffraction efficiency, depend. on size of developed Ag particles 78−78965
holography and coherent optics, information theory, book 80−98764
holography with evanescent waves, diffr. efficiency, TE polarisation 78−66782
holography with evanescent waves, diffr. efficiency, TM polarisation 78−66783
homogeneous medium, Gaussian light beam propag., diffr. effects described using complex-ray method 80−78770
Huygens-Fresnel integral in circular coords., asymptotic soln. 78−87013
ice crystals, diffr. theory for forward scatt. pattern *(Russian)* 80−94601
image formalism, diffraction at straight edge, partially coherent illum., aberrations *(Chinese)* 80−43267
image formation, diff. theory 80−9822
image formation, intensity distrib., theory of eikonals 77−19185
light diffraction continued
image formation in photosensitive layers on highly conductive substrates 80−43419
image intensity fluctuations in turbulent atm. after refl., Huygens-Kirchhoff principle calcs. 80−63926
image rotation and magnification, optical system 80−48376
image structure anal. using light optical diffraction *(German)* 79−72501
images of bar and edge objects, influence of optimum balanced coma 78−74850
imaging system, incoherent, diffr. images asymptotic behavior 80−1139
imaging system using intensity triple correlator 78−74846
impurity containing crystals, light diffr. by sound 79−8119
inclusions in solid, light diffr., thin lens approx. 77−79757
incoherent annulus, parabolic image motion effect 77−613
incoherent annulus object diffraction images in presence of primary astigmatism 79−22904
incoherent diffraction correlator with a holographic filter 80−37955
infrared surface with random nonuniformities, light diffr. *(Russian)* 78 58916
inhomogeneous and randomly distributed media, diffracted amplitude and intensity, statistical models *(Spanish)* 80−48151
inhomogeneous plane wave shadowing by an edge 78−90356
instrument function of spectral devices with multiple diffraction 80−37093
integrated optics deflector using chalcogenide amorphous film on graded index $LiNbO_3$ waveguide 80−48463
intense laser beam diffraction by long US wave in liquid column 78−60421
intracavity resonance asymmetries, nonlinear freq. depend. diffraction effect 80−99760
inverse diffraction problem, unique soln. 80−1123
inverse diffraction problems soln. using diffr. coeffs. 77−46698
inverse diffraction study of perfectly conducting gratings 79−94149
inverse theory of scalar diffr., eigenvalue formulation 80−102613
IR detector dimensions, rapid meas. by Fresnel diffr. *(French)* 78−89435
IR Gaussian laser beam truncated by annular aperture 79−18344
IR optical system input diffr. effects and use of spatial apodisation 78−79113
isolated surface circular defect diameter determ. based on Fraunhofer diffr. 80−73307
Jones notation, polarisation and interference effects 78−17858
Kirchhoff's unique solution, points situated outside the diffraction screen *(Spanish)* 79−59628
Kirchhoff diffraction integral validity in Fourier optics *(German)* 78−9339
Lamb wave optical detect. in fused SiO_2 80−106690
lamellar grating, reson. anomalies, analytical and numerical study using modal expansion technique 79−31791
large-aperture optical system, energy distrib. calc. in diffr. image of point 80−74305
laser, appl. to meas. of acoustic and acousto-optic props. of crystals *(Polish)* 78−76425
laser beam, diffractive ray tracing 77−27291
laser beam coherence and divergence *(Spanish)* 80−87424
laser beam diffraction, teaching approach 79−71177
laser beam diffraction focusing by sequence of irises 79−50332
laser beam transient self-diffraction in absorbing liquid 80−9927
laser beams, geometrical optics, spatial structure 78−83014
laser cavity diffraction experiment with 1-D diaphragm 80−95920
laser emission from circular inphase Gauss excited antenna aperture, Fresnel area 77−46741
laser irradiation intensity fluctuations, influence of transmitting aperture diffr. size and turbulence 79−45906
laser particle size analyser, size estimated from diffraction pattern 79−6091
laser particle size analyser, using diffraction of light by particles 79−6090
laser pulse autocorrelation by optical processing of Fabry-Perot spectrograms 80−58465
laser pulse shaping by passive optical Fourier techniques 77−10934
laser radiation intensity distrib. meas. using Bragg diffraction of light 80−64092
laser speckle produced in diffr. field, statistical props. 77−71918
laser wavefront conjugate complex prod., scatt. and diffr. in non-uniform phase film *(Russian)* 77−38973
latex, colloidal cryst., optical props. near MP 78−11562
Lau effect, diffr. expt. with incoherent illum., appl. to Talbot interferometer, Fourier spectrometer 79−41333
Lau effect coherence theory explanation 80−5685
lens design with simultaneous image spot, optical path difference, diffraction MTF and Seidel abberation minimisation 80−74459
linear systems, Fourier transforms and optics, book 79−41350
liquid crystalline grating structure *(Polish)* 77−68272
liquid crystals, cholesteric, Bragg diffraction, light Pendellosung fringes, theory 77−27830
liquid US diffraction of light, Fresnel approx. 80−48135
liquid-solid interface, acousto-optic diffr. with crit. angle incident light 78−37801
locally deformed flat boundary, numerical soln. 77−42480
locally deformed slab waveguide propagation and diffraction patterns 80−106630
low-angle scattering from coated spheres, anomalous diffr. approx., model for biological cells 77−25396
Luneberg apodization problem 80−87302
magnetic bubble fields, light diffr. 79−73904
magnetic gratings, with cylindrical and elliptical domains 79−73908
magneto-optic imaging, domain struct. obs. 77−48151
magneto-optical, by cylindrical magnetic domains *(Russian)* 79−1753
magneto-optical concentration of light, by regular domain structures *(Russian)* 79−24297
magneto-optical imaging of domain struct. in thick cryst., multiple diffr. effects 77−8552
magnon light diffr., parametrically stimulated magnons *(Russian)* 77−12368
mask, random amplitude, diffr. pattern intensity distrib., distant object imaging 77−58252
matrix notation, Jones vectors for refl., refr. and diffr. 77−34814
MBBA, nematic liq. cryst., light diffr. study of Williams domains 78−34423

light diffraction continued
metal, US surface wave vel. meas. on plane and cylindrical samples, optical methods 77−46875
metal shallow grating diffr. efficiency, Rayleigh type and surface plasmon reson. type anomalies 79−55050
metaxial optics, centred refracting systems, undiaphragmed and without aberration *(French)* 78−94369
metaxial optics, diffraction *(French)* 78−74844
methylammonium aluminium sulphate, third order elastic consts. from stress shifted reson. freqs. 78−55905
3-methylpentane-nitroethane critical binary liquid mixture, US absorpt. 80−107376
microscope, polarizing, with crossed polarizers, incoherent diffr. imagery 80−101838
microscopical and Ewald dynamical diffraction theories, refl. and transmission, spatial dispersive dielec. slab 80−83548
microspecimens, absorpt. spectra under conditions of light diffr. in elec. field, meas. methods *(Russian)* 77−36203
mirror segment, parabolic, general Fourier transforming configuration 77−46687
mode coupling by circular apertures 77−6995
Moire strain measurement method using diffraction beams, compensation of errors 80−13068
monodisperse screen shape determ. using scatt. indicatrix in Fraunhofer diffr. 78−71033
multielement acoustic array characterisation by acousto-optic diffraction 80−99911
multifrequency acoustooptic diffraction, coupled mode formulation 77−6996
multilayer spherical particle of thin concentric shells 77−46682
multiple image formation by sampling Fraunhofer diffr. patterns 78−1334
multispectral extinction data, analytic inversion in anomalous diffr. approx. 78−87016
multispectral extinction data, analytical inversion formulae compared 80−18992
muscle, cross-striated fibres, efficiency of light diffr. under stretch and isometric contract 80−85440
muscle, single skeletal fibres, laser diffr. theory 80−56110
muscle crossbridge stroke and activity revealed by optical diffr. 78−69021
nematic film, phase grating produced by shear flow induced instability 78−9945
nematic liquid crystal, hexagonal arrays 77−11478
nematic liquid crystals, light diffr. by 3D domain structs. 79−64989
nuclear track detectors, glass and plastic laser diffr. appl. to determ. of etched track parameters 80−95499
null curves, partial form, analytic props. 77−88634
object diffraction evaluation in transmission microscope, object and field stop spectrum separation *(German)* 78−92685
off-axis gaussian beam, third order spherical aberration 77−14665
off-axis gaussian beams in optical system with astigmatism and coma 78−55309
oligourethaneacrylate photopolymerised layers, production of holograms *(Russian)* 79−7102
opaque crystals, dynamical light diffr. 78−80368
open cavity, Slater method validity 80−69428
optical caustics and diffraction catastrophes 80−9801
optical coherence modulation by two ultrasonic waves 80−1120
optical diffraction analysis, in microscopy 80−32926
optical fibre, refr. index profile determ. from diffr. pattern 78−25953
optical fibres, laterally illuminated, diffr. pattern 78−50915
optical path difference meas. by double diffraction interferometer 78−24851
optical pattern recognition by diffraction pattern sampling 80−99643
optical power spectrum meas., error sources in diffr. pattern sampling 78−63030
optical ray operator method for anal. of diffraction by periodic structs. 80−43257
optical signal recording/processing, diffraction in anisotropic medium, anal. 78−90364
optical system, diffraction and aberration effects, wave optical calc. 80−83549
optical system tolerancing, encircled energy performance prediction 80−78935
optical systems with pupils of non-uniform transmittance 80−87470
optical video discs, laser read-out system, diffraction theory 79−50338
parallel plane diffr. grating with periodic structure, diffr. of plane wave 80−102620
partially coherent imaging, edge ringing, performance function 77−46699
partially coherent light, bibliographic review 78−29894
partially coherent truncated bar targets, diffr. image illuminance distrib. 79−76609
particle medium, refr. index determ. from angular, polarisation characts. *(Russian)* 77−34827
particle sizing by forward lobe scatt. intensity ratio, diffr. theory errors 78−71031
particle velocity measurement in Fraunhofer plane using double exposure holograms 79−44904
pattern recognition using optical moments from diffr. pattern 77−19184
pattern sampling, industrial appls. 80−9015
periodic amplitude grating, diffr. of wave with spatial phase modulation 79−98274
periodic interfaces of arbitrary shape 79−64174
periodic media diffr., equiv. of multiwave coupled-wave and modal theories 79−41331
periodic object single sideband Fresnel diffr. pattern studies 80−106440
periodically modulated medium, Gaussian beam diffr. close to Bragg angle 77−31063
phase distributions in images and Fraunhofer diffr. patterns prod. by non-aberrant lens 78−1172
phase gratings, Bragg regime diffraction criteria 80−48143
phase gratings, Raman-Nath regime diffraction criteria 80−48144
photolithographic mask linewidth meas. by diffraction pattern analysis 77−37960
photon energy band, low energy photon diffr. 79−78795
photothermoplastic layer, diffraction effectiveness, registration of discrete holograms *(Russian)* 79−7100
plane mirror cavity, field structure of nonstationary oscill. modes, edge diffr. effects 79−55160

light diffraction continued
plane uniformly heterogeneous wave diffr., exam. using Fraunhofer's method *(French)* 78−58901
plane waveguide, locally deformed, numerical calcs. of diffr. 77−79947
plane waves in strongly turbulent media, two-frequency mutual coherence function 77−21907
point spread function of systems with parabolic filters, effects of defocusing 78−13776
point spread function second moment as image quality criterion 80−9818
point-diffraction interferometer principles and applications 80−74530
point-source image energy centre of gravity, location accuracy, aberrations effect 79−27192
polymer, molten or amorphous, chain conform. determ. by diffr. 77−80429
polystyrene, oblique laser diffr. and reflection from surface crazes 77−47508
profile digitised diffractographic data processing 77−58276
PROM, diffr. efficiency 80−14467
pulsed holographic recording, in Fe-doped $LiNbO_3$ monocrystal *(Russian)* 77−629
purple membrane particles, freeze-fractured, protein content 77−90735
Q-switch, ultrasonic, for Nd:glass laser 80−64034
quartz, crystal growth in fluoride environment, growth features and props. 80−6373
quartz substrate, surface and bulk acoustic waves excited by interdigital transducers, optical diffr. study *(Chinese)* 78−50965
radiometric errors due to circular aperture diffr. edge effects 77−34023
rainbow phenomena and the detection of nonsphericity in drops 80−58456
Raman, by US waves, and optical heterodyning for US vel. and absorpt. meas. 79−18640
Raman-Nath diffr. as manifestation of two-ray Bragg diffr., holographic gratings 80−48147
random arrays of grains, spectral props., jitter model, comment 79−41339
random arrays of grains, spectral props., jitter model 79−45905
Rayleigh theory for diffr. at sinusoidal surface *(French)* 79−59630
real stationary ultrasonic field in liquid, temporal modulation of light beam 80−83551
red blood cell diameter meas. from He-Ne laser beam diffr. pattern 77−86582
reflecting polygonal obstacles of approx. 1 wavelength, apparent size 79−89844
reflection holographic portraits, diffraction efficiency and safety 80−37968
reflective diffraction rectangular grating with finite cond. *(Russian)* 77−75414
regularized object restoration, resolution beyond the diffr. limit 80−87324
reimaging system, out-of-field radiation analysis 78−59117
resolution of two coherently illuminated points, effect of phase angle 78−33683
resonance atom, spontaneous diffr. of light 80−91512
resonator, Gardner-Fresnel-Kirchhoff propag. algorithm 80−83621
rigorous solution on echelette with acute angle teeth *(Russian)* 79−13895
ring laser, diffraction theory, Gaussian approx. 80−53338
ring laser, gain transverse distrib. effect on diffr. splitting 77−58353
ring laser, open cavity matrix eqns. in diffraction theory 80−69429
ring laser diffraction theory, perturbation method 80−95919
rough surface, random, reflectance derived with Fresnel approx. 80−87309
rough surface speckle contrast, depend. on laser spot radius with surface height variance 79−59636
sarcomere dynamics in single skeletal muscle fibre, light diffr. spectra 78−15797
SAW, diagnostic and device appl. 77−59198
SAW oppositely propagating in optical waveguide 79−41453
SAW propagation study based on coherent light diffraction *(Russian)* 79−14172
scalar, null field approach, approximate methods 78−13657
scalar, null field approach, general method 78−13656
scalar, null field approach, inverse methods 78−13658
scalar diffraction model for small apertures *(Spanish)* 79−59629
scattered light, specification and meas. from diffr. gratings 78−78905
scattering object, coherently illuminated, speckle pattern statistics in diffr. field 80−63924
scatterplate interferometer, scalar diffraction theory 80−73432
schlieren photography, aberration and diffr. effects on resolution 77−34040
self diffraction of laser beam by liquid crystal struct. 80−5803
self-diffraction of polarised light waves in two photon absorpt. in isotropic media 80−38077
semicircular aperture, Fraunhofer diffr. 77−34810
semicircular aperture, Fraunhofer diffr. 78−46509
semiconductor, energy transfer due to dynamical self diffraction of light beams of same freq. *(Russian)* 77−58397
semiconductors, doped, light diffr. by sound 79−11404
semitransparent and π-phase annular aperture illuminated by laser beam 79−55051
serrated apertures, monochromatic light diffr. 80−43260
shaded circular apertures, encircled energy in diffr. pattern, super-resolving and apodising props. 80−95787
shadow boundary region, diffracted waves 77−65570
shadow cast by half-screen when illuminated by Gaussian beam, props. 80−28156
sieve screens, two-dimens. array, diffr.-interf. patterns, Kirchhoff approx. 78−83088
single mode fibre near- and far-field characteristics, profile-independent representation 80−58739
single slit diffraction, theory testing expt. 80−77568
sinusoidal complex object with a small phase modulation, Fresnel diffr. patterns, self-imaging 80−43256
sinusoidal interface light diffraction 79−13900
skeletal muscle fibres study 80−8096
small linear dimension meas., contactless laser beam diffraction method 77−22525
solar domain gratings, asymptotic theory 78−66910
solid bodies, optic-geometric method calc. of diffraction patterns *(Russian)* 80−91746

light diffraction continued
spatial and temporal impulse response of diffracting apertures 77−34813
speckle, dynamic props., zero-crossing study 80−63923
sphere, evanescent wave contrib. to diffracted amplitude 80−74295
spherical resonator diffraction losses, expt. meas. 78−29980
spherical surfaces, extrameridional aberrations anal., with large decentring angles 77−68181
spheroidal particles, colloidal dispersions, refractive index 80−106454
spot size estimate in diffr. pattern of scattered field 80−95789
standard sieves, Fourier transform method for verification of wire screens 77−53874
stellar occultations, diffr. theory for central spot 77−67053
stimulated emission induced by coherent crossed laser beams for conc. meas. 80−35585
straight-edged apertures, Fraunhofer diffr. analysis 79−76584
straightedge Fresnel diffraction, optical phase distrib. interferometric meas. 79−76579
strain evaluation by specimen-grating photograph electro-optical processing 77−39266
stratified medium with diffr. boundary diffuse source radiation spectral struct. *(Russian)* 77−38804
Straubel apodisation filter, rot. symmetric, circ. aperture diffr. pattern, pupil functions 79−81530
straubel apodisation filter systems, effects of defocusing on point spread function 78−25804
Straubel class of apodisation filters, diffr. field characts. 77−7198
stray light phenomena, GUERAP III Monte Carlo simulation 78−58907
stray light simulation with advanced Monte Carlo techniques 78−58906
stray radiation rejection capabilities of optical systems, GUERAP II program analysis 78−59115
striated muscle diffraction patterns, data acquisition and anal. 80−89918
strips illuminated at grazing incidence, uniform geometrical theory of diffr. soln. 80−58447
student experiment and gratings made from photographic negatives 77−17741
student experiments 80−10
surface acoustic wave diffr. of light beam propag. parallel to surface 78−66752
surface acousto-optic interaction on nonpiezoelectric substrates 79−46090
surface layer of material, refr. index meas. using diffr. method 79−30532
Talbot effect, appl. to thin film thickness meas. 78−9321
teaching, spatial filtering expts. 77−57120
teaching demonstration, TV display 77−5613
teaching demonstration of optical transforms of alphabet letters, Fraunhofer diffr. 77−57132
telescope resolution in turbulent atmosphere, diffraction limit *(Russian)* 77−25948
TEM coma-free alignment using optical diffractograms 79−21860
thermal blooming: round beam vs square beam, computer study 80−38076
thermal grid, diffr. image for turbulent flow, study of Richardson problem *(French)* 80−23993
thermal self-action problems and their compensation 80−106579
thick grating, multiwave diffr. anal. 78−9445
thick layers with regular domain structure, magnetooptical diffr. of light 80−108188
thick planar grating, Bragg diffr. of finite beams, coupled-wave theory 80−63917
thin phase variation objects under partially coherent illum., effective transfer function *(Spanish)* 79−55064
thin unbleached holograms, diffraction efficiency, relief phase modulation 78−66789
thread parameters meas., Fraunhofer diffr. coherent optics method 78−89439
transparency concept for polychromatic light *(French)* 77−79746
turbulent medium, mean diffracted rays 80−48153
two coord. deflector, anisotropic diffraction and wide band scatt. 80−91920
two dimensional grating with circular or triangular apertures 77−38802
two-beam laser interferometer, diffr. phenomena 79−63300
ultrasound, phase geometry variation analysis 80−106441
US beam effect, in homogeneous isotropic dielec. 77−599
US beam in homogeneous isotropic dielectric plate, anal. 78−82905
US beam plus amplitude grating, thick-screen diffr. theory for temporal modulation 77−50755
US beams, diffraction of perpendicular light beam 80−87629
US diffraction, appl. to US devices power meas. 77−832
US diffraction, temporal modulation by two antiparallel sound beams, thick-screen treatment 77−68256
US imaging by acousto-optic interaction in Raman-Nath diffr. regime 79−55260
US wave, spectral line calcs. and limitations of approximate solns. *(Russian)* 77−3532
US wave effect on light diffraction 80−1127
US wave superimposed with a diffuser, diffr. spectrum of transmitted light 79−89848
US waves, in optically active crystals 77−43965
vibrating laser speckle in diffr. field, dynamic statistical props. 79−22895
vibration analysis using diffraction field laser speckle dynamic statistical props. 79−76595
vision model using optical engineering theory concepts 79−96555
visualization of light propagation, hologram construction 79−81391
volume holograms in electrooptic birefr. crysts., light diffr. 79−55084
volume holograms with strong coupling, scatt. phenomena 78−33700
volume phase grating, angular depend. of width of Bragg peak 80−78811
volume phase grating, TM and TE mode diffr. efficiency, comparison 80−74507
water, light scatt. and diffraction *(French)* 79−27171
water droplets and glory formation by Airy-type diffraction 77−53191
wavefront correction in real time for atm. distortion, Bragg diffr. by acoustic wave 77−42500
wavefront reconstruction method, plane waveguide hologram coupled system 80−5708
white light diffraction patterns of amplitude and phase zone plates 80−14449
Wollaston prism type interferometer, diff. theory of image construction *(German)* 77−158
Woods anomaly angular alignment gratings 80−69503
Young's experiment with n holes, appls. *(French)* 78−42274
zonal Foucault test, diffr. effects 77−72099
Ag weakly modulated surface 77−31132
Ag-As_2S_3 sandwich structure, holographic characts., recording kinetics 78−29913
Al surface, light diffr., photon excitation of compound plasmon resonances 79−28307
$Ba_2NaNb_5O_{15}$, electrooptical diffr. by periodic domain struct. 80−40090
$Bi_{12}SiO_{20}$ electrooptic crystals, vol. phase holograms, light diffr. and nonlinear image processing 80−37972
$Bi_{12}SiO_{20}$, optically active photorefractive cryst., light diffr. by vol. holograms 79−64185
CO_2 laser Antares fusion system optical diffraction computation 80−74424
$CaCO_3$, aragonite, conical intensity distrib. 79−1747
$CaWO_4$ collinear diffr. by oppositely directed acoustic beams 80−16007
CdS, obs. of acoustically induced space charge gratings by laser diffraction 77−7203
CdS, photoconductive, obs. of high intensity sound self-defocusing 80−24972
CdS piezoelectric thin film transducers, testing via light diffr. by acoustic waves 77−23840
CdSe, phase gratings in semiconductors with one- and two-photon excitation 77−8546
CdSe, self-diffraction at induced phase lattice 77−3638
$CsAl(SO_4)_2.12H_2O$, third order elastic consts. from stress shifted reson. freqs. 78−55905
EuO film threshold characteristics in holographic and bit recording *(Russian)* 80−63944
GaAs, electron beam pumped laser, far-field radiation pattern, optical confinement effects 79−86181
GaAs, epitaxial growth and etching rate meas. method 77−35829
GaInAs, electron-pumped laser, far-field radiation pattern, optical confinement effects 79−86181
Ge surface, self diffraction of light, mechanism, rel. to nonequilib. carrier behaviour 79−72685
HF CW chemical laser amplifier with multiple pass telescope cavity, diffr. 80−19055
HF CW chemical laser with unstable telescopic resonator, diffr. effects 79−94265
α-HIO_3, optically active biaxial crystal, conical diffr. intensity patterns 79−4785
Hg_2, photoassoc., $0_u^+ \rightarrow 0_g^+$ fluoresc., Condon internal diffraction 78−78747
InSe film, photochem. production of holograms on surface *(Russian)* 79−7101
$KAl(SO_4)_2.12H_2O$, third order elastic consts. from stress shifted reson. freqs. 78−55905
KCl, diffr. by M-centres, thick plane wave hologram recording 77−7021
KCl:Ca, vol. holographic grating, modulation characts. 79−94197
α-$LiIO_3$, single crysts., light diffr. under DC field 80−11367
$LiNbO_3$, collinear light diffr. by transverse acoustic waves 77−52040
$LiNbO_3$, cryst., US vibrating laser beam diffr. *(Russian)* 78−31172
$LiNbO_3$, diffusion waveguide, acousto-optic mode conversion at surface wave freqs. *(Russian)* 78−1348
$LiNbO_3$, film lightguide, pulse signal convolution in acoustooptic interaction *(Russian)* 78−1345
$LiNbO_3$, hologram, light diffr. with electro-optical rot. *(Russian)* 78−1190
$LiNbO_3$, light diffr., elec. field effects, spatial hologram appls. *(Russian)* 77−23635
$LiNbO_3$, light diffraction from volume phase holograms 79−36860
$LiNbO_3$, optical waveguide, diffr. of modes by standing elastic surface waves *(Russian)* 78−1343
$LiNbO_3$, wedge shape cryst. optical modulation, diffr. by natural freq. US standing waves 77−75685
$NH_4Al(SO_4)_2.12H_2O$, third order elastic consts. from stress shifted reson. freqs. 78−55905
NH_4Br, dislocation influence on phase transition and light scatt. *(Russian)* 80−59648
NaCl:Ca, holographic appls., diffr. efficiency 77−54679
NaCl(:Ca) cryst., radiation colouring, amplitude-phase hologram appls., diffraction efficiency 77−68191
$Pb_5Ge_3O_{11}$, ferroelec. transition, US and elasto-optic props. 80−60527
$PbMoO_4$, diffr. modulator, two separate opposing US waves 77−3676
Si epitaxial layers, thickness meas. during deposition using diffraction *(German)* 79−97355
Si, excited by ultrashort laser pulses, self-diffr. effects 78−18022
Si, phase gratings in semiconductors with one- and two-photon excitation 77−8546
Si single crystal hologram recording time and diffraction efficiency *(Russian)* 77−58286
Sn, globular film, interf. and diffr., solar selective props. 79−4860
TeO_2 crystal multichannel acousto-optic modulator 77−39100
TeO_2, light diffr. by slow acoustic waves 80−29717
TeO_2 two coord. deflector, anisotropic diffraction and wide band scatt. 80−91920
VO_2 film based recording medium, holographic characteristics calc. *(Russian)* 79−7092
YIG, diffr. of laser radiation by parametrically excited elastic and magnetoelastic waves 78−19338
YIG, light diffr. by banded domain struct. *(Russian)* 78−15150
YIG, magnetostatic precession modes, optical investigation 78−19337
YIG, parametrically excited wave discrete structure obs., light diffr. and modulation *(Russian)* 79−95650
ZnO thin films, surface acoustic-optic interaction, diffr. 77−3685

light diffusion *see light scattering*

light dispersion *see optical dispersion*

light emitting devices
see also light emitting diodes; light sources; luminescent devices
electroluminescent cell fabrication, using ionised-cluster beam deposition and epitaxy 78−11133
film, electrolum. device appl., book contrib. 77−73176
III-V semiconductor emitters and detectors for 1.0-1.6 μ fibre-optic communications 80−10007
introduction to electroluminescence, book contrib. 77−73172
MIM tunnel junctions, roughened, photon emission, calc. 80−44738

light emitting devices continued
MOSFET, Si, voltage tunable far IR emission from inversion layers 77−12440
$As_{50}Te_{50}$, amorphous films, metal and semicond. contacts, threshold switching, IR emission 80−49831
GaAs:Si p-n light-emitting structs., soln. of general minority carrier transport eqn. 80−15597
Si p-n junction, mesoplasma formation, light-emitting properties of secondary breakdown region *(Russian)* 79−91131
SiC, phys. props. and crystal growth, rel. to appl. in electrolum. devices, book contrib. 77−77299
ZnS powder phosphors electroluminescent cells, AC electrolum. charact. *(Japanese)* 80−71489
ZnS-ZnSe mixed powders, hot-pressed polycrystalline, photolum. and electrolum. 77−32426
ZnSe film, rare earth fluoride doped, electrolum. meas. 77−16397

light emitting diodes
see also semiconductor junction lasers
2 km 20 Mb/s optical fibre transmission system 78−42437
16 and 32 Mb/s optical data links 77−68275
35 Mb/s optical fibre cable transmission using IR LED optocouplers 80−33156
acupuncture diagnostic system *(French)* 79−62397
alternative scanned light sources 80−69477
analog modulation of light-emitting diodes for optical fiber *(Japanese)* 78−90516
anthracene with powdered graphite electrodes, electrolum., ambient gas effects 77−69917
audio recording peak level meter with LEDs *(Spanish)* 77−37936
biocular magnifier design for display system viewing 79−27361
borehole probe with LED for γ-ray spectrum stabilisation 79−45552
camera character-forming display, with internal or external timing circuits 79−9251
chalcogenide glass radiator bonded, with optical guide struct., efficient coupling to optical fibres 77−39043
chalcopyrites, for electrolum. device appl., props. and technology, book contrib. 77−73175
coherence analysis of radiation, meas. system with Michelson interferometer *(Polish)* 78−33762
colour masters evaluation, using reflection coupling device *(German)* 80−95123
communication device research in Japan 77−75677
communication sources, 1 μm range, LED and laser diodes 80−48448
communication system components charact. and appl. *(Flemish)* 80−5836
communications transmitter, multipurpose IR emitters 78−30053
compatible liquid filled optical fibre, optical tick appl. 77−39060
coupling to fibre, efficiency improvement using facet radiator *(Japanese)* 77−79938
coupling to optical fibres, truncated spherical lens efficiency 79−76813
coupling to optical fibres improved using facet radiator 78−90520
coupling to spherical ended fibre, geometrical optics anal. 78−83086
CW injection lasers and LEDs for optical communications 77−7210
deep level studies, growth by time difference method at controlled vapour pressure 80−39522
deep trapping levels energy and conc. meas. *(Polish)* 78−34797
degradation, review of recent expts. 78−82970
degradation acceleration techniques 79−50320
degradation mechanisms, review 77−28630
DH, for optical communications, second harmonic distortion prediction 78−18058
DH, output power and response time, thickness depend. 79−95479
DH, top and side emission 77−79819
DH devices, interface recomb. effects on transient response 77−88722
DH devices, interface recomb. effects on transient response anal. 78−22127
diffusion lengths and near-junction luminescence-efficiency profiles from SEM scans 77−77301
digital optical fibre system, 4-level using LED, meas. at 68 Mbit/s 80−1313
digital thermometer display applic. 77−37884
displacement transmitter appl. *(Hungarian)* 78−4606
display cct., seven decade reversing counter, quadrupole mass spectrometer appl. 77−18129
electroluminescent diode, laser measurement, of semiconductor materials and devices *(Rumanian)* 78−52035
electron irrad. effect on electrolum., defects form. and quenching obs. 80−55194
end pumping, for Nd:YAG glass clad fibre laser, 1.3 μm operation 77−7120
fibre communication devices, directional couplers, atennuators, switches development 79−3782
fibre optic communication systems, sources and detectors 78−42412
fibre optic communication systems, utilisation of optoelectronic devices 80−1328
fibre optic transmission, LED coupling fine adjustment *(French)* 79−94332
fibre optics systems, technology and components *(Hungarian)* 78−66900
fibre pigtail incorporation 79−36998
fibre power calc. *(Swedish)* 79−55208
fibre-optic LED and laser source and Si photodetector development 78−42430
frequency convertor in pump system of Nd:YAG laser 77−7129
frequency measurement, using beat frequency display with LED 79−63191
glass fibre communication: introductory review, status and development *(German)* 79−89997
glass fibre long wavelength optical communication, materials and devices, review 80−99854
half-duplex optical transmission link using LED source-detector scheme 78−71214
heterojunction laser and LED reliability rel. to facet damage and nonradiative centre formation 78−5472
high efficiency, with endface extraction 79−15216
high radiance semiconductor light source for fibre optical communication 80−58653
II-VI semiconductor with wide energy gap materials *(Polish)* 79−91501
II-VI semiconductors, injection electrolum., review, book contrib. 77−73174
II-VI semiconductors appl. *(German)* 77−7745

light emitting diodes continued
III-V semiconductor, MBE and applications 78−11135
III-V semiconductors, p-n heterostructures, epitaxial growth techniques, appl. to optoelectronics, review 80−54770
information transmission appl., system components construction and operation *(German)* 79−18553
IR, industrial appl. of fibre optics 78−59123
IR emitting diodes, high radiance, analysis of radiation coupling into optical fibre 80−14473
IR emitting diodes and injection lasers, optical communication appls. 80−58563
IR line scanner, Reconofax XIII A, improved recording system using LED 79−25335
junction current, luminesc. near dislocation, surface, integral representations, appl. to LED's 78−68079
laser radiation pulse meas., based on semiconductor radiators 80−23710
light flux meas. by photometric sphere 80−253
light panel, spatial frequency analysis with incoherent optical approach 80−78779
linear brightness control, reticle illumination appl. 80−37070
linearisation by predistortion for analogue video signal transmission 78−37993
linearised LED and laser transmitters, for analogue fibre optical systems 78−46818
linearity meas. of photometric devices using two LEDs 80−17996
linearly increasing intensity light source, for photocond. lifetime meas. 77−35960
long wavelength light sources, 1.06 to 1.6 μm range, review 79−45969
LPE growth method to reduce thermal degradation of substrates, appl. to LED fabrication 80−104061
luminance meas. using photometric method *(Japanese)* 77−82584
luminous intensity and flux meas., photometric method *(Japanese)* 77−57378
luminous intensity ang. distrib. and total light flux meas. device *(Chinese)* 78−82018
matching of semiconductor sources to thin-film planar and stripe waveguides 80−64174
matrix display on miniature multi-channel pulse height analyser 78−25400
microlenses to improve LED-to-fibre optical coupling and alignment tolerance 80−19088
monitoring system for large Pb glass counter array 79−45565
near IR (1 to 2 μm) optical communications, colloquium, London, England (May 1980) 80−86040
nuclear event simulation, green LED, trigger circuit, wavelength matched to photomultiplier 77−3238
optical analogue links, evaluation of LED use 79−68395
optical communication conference, Munich (1977) *(German)* 78−33854
optical communications systems, components, review 80−87539
optical coupler, low loss, for coupling LED to fibre-optic system 80−91907
optical data transmitter, laser and LED comparison *(German)* 80−14432
optical detector time response determ. at 1.06 μm, LED source 79−89004
optical fibre, 137 Mb/s data links using LEDs, material dispersion limited operation 77−88908
optical fibre, communication link between computer units, using LED-photodiode pair 78−71224
optical fibre analogue/digital communication system with 5 MHz bandwidth *(German)* 78−30062
optical fibre communication equipment 80−43459
optical fibre communication system, source-drive optimisation 77−11007
optical fibre communication system device, review 79−76858
optical fibre light sources for 1.0 to 1.2 μm emission, review 77−38894
optical fibre sources and detectors *(Italian)* 80−69390
optical fibre system compatible, design 77−79932
optical fibre transmission system devices *(Japanese)* 80−58693
optical memory readout by superluminescent diode with integrated photodetector 80−32922
optical parameter meas. using Si, photovoltaic cell, absolute spectral sensitivity calibration, radiometry, photometry *(Chinese)* 80−86367
optical transmission evolution and development trends 79−23065
optoelectronic devices and optical imaging techniques, book 80−27059
optoelectronic devices development 80−91902
optoelectronic strain gauge, force and strain measurements giving high accuracy and resolution *(German)* 79−98673
photographic print timer, using ring of LEDs 80−77899
picture taking parameters display in amateur cameras, review 78−89578
point light sources, appls. in undergraduate expts. 77−37686
point source emitter 80−73150
precise light pulser for testing surface barrier particle spectrometer 77−79508
pulsed, for excitation of photochem. reactions in biological objects *(German)* 79−16250
pulsed imitators of laser radiation 80−23765
pulsed injection light sources, installation for meas. their characteristics 77−75640
pulsed light signal receiver 79−93216
pump for $LiNdP_4O_{12}$ laser 77−75552
pumping, Nd lasers optical transmitters appl., NPP, LNP and NAB 79−3712
pumping of miniaturized $LiNdP_4O_{12}$ lasers, single and array of dome-type LEDs 79−41395
quasi-analogue display for electronic clocks *(German)* 79−49207
quasi-digital display meters, fieldstrength and modulation appl. 77−37938
radition therapy, thin Pb sheets as tissue compensators for larger field irrad. 80−104736
red, luminance-brightness discrepancy 80−91942
red LED chips, use at temp. sensors 78−4619
reference channel nonlinearities 79−78158
reliability tests on devices for optical fibre transmission systems 80−43464
rotating prism display of multiple LED lines 79−93111
safety aspects of LED- and laser-fed cables 78−74968
safety aspects of LED- and laser-fed cables 78−74969
scintillation counter arrays, testing with computer controlled LED flashing system 77−57802
scintillation counter hodoscopes, LED test system 78−58556

light emitting diodes continued
scintillation spectrometer stabilisation using LED reference light source 80−91365
scintillation spectrometers, with LED and PIN photodiode, stabilising system 80−47821
self-aligned sphere lens, for efficient coupling to optical fibres 77−79939
SEM study of charge collection and cathodoluminesc. 80−65661
semiconductor heterostructures, elec. and optical phenomena, discrete devices, review 78−72250
semiconductor junction transceiver, for fibre optic communication 78−42410
semiconductor light sources for optical fibre transmission 77−54777
semiconductor light sources principle and appl. *(German)* 78−71108
simulator for 1.06 μm laser radiation 77−38903
spherical surface, coupling to optical fibre, efficiency 80−48416
stellar magnitude simulator, IC device 78−81742
student experiment, LED emission spectra temp. depend. 77−82348
superluminescent diode source for fibre-optic systems *(German)* 78−38013
telecommunication appl., development *(Italian)* 77−773
ternary semiconductor device applications, review 78−39207
thermal imaging system for Earth resource obs., possibility of LED use 78−93010
transient response of DH devices approx. techniques 78−68078
transmission system, semiconductor device reliability tests 80−58573
ultrasound visualisation, use of LED as short duration stroboscope 77−14863
visible spectrum LED, book 79−42428
wide-gap diode detectors of IR radiation, positive feedback 78−24863
wide-gap emitter, continuous variation of composition, emergence of luminesc. 79−11208
wideband subcarrier PFM analogue optical communications channel 77−27378
(Al,Ga)As, high radiance DH LED design for fibre optical communication 77−79963
(Al,Ga)As high-radiance double-heterostructure for optical fibre links 78−37991
Al-Ga-As, light emitting heterojunction diode, $\eta_e \approx 40\%$ *(Russian)* 77−81157
Al-Ga-As heterostruct. with confined current flow, fabrication 78−68081
AlAs-GaAs, binary heterostruct. LED, external quantum yield *(Russian)* 77−8661
AlAs-GaAs heterostructure, fabrication by selective liq.-phase epitaxy 79−15618
AlAs-GaAs LEDs, Ge or Zn-doped, mechanism of degradation 77−76911
AlGaAs electroluminescent heterostructures, LPE, appl. to LED fabrication 80−55308
AlGaAs LED pumped single-cryst. Nd-YAG fibre laser 79−59711
$Al_xGa_{1-}{}_1As$ heterojunction LED monolithic matrix fabrication 79−56301
$Al_xGa_{1-x}As$ DH laser, degradation by LED-like mechanism 77−83874
$Al_xGa_{1-x}As$ DH p-n junction, surface recomb. effects on current, luminesc. expts. 78−72246
$Al_xGa_{1-x}As$, hetero junction light-emitting diode, construction and performance characts. *(Russian)* 77−85808
$Al_xGa_{1-x}As$ heterojunction LED, fabrication by negative profiling of substrate and characts. 78−56523
$Al_xGa_{1-x}As$ heterojunction LED 79−28403
p-$Al_xGa_{1-x}As$, LED in red and IR region, multiple-pass heterostruct. 79−19653
$Al_xGa_{1-x}As$, nonlinear distortions anal. 78−37992
$Al_xGa_{1-x}As$, superlum., end pumping of miniaturized Nd:YAG laser 77−10938
$Al_xGa_{1-x}As$:N, luminescent material, appl. in optically pumped lasers and electrolum. diodes *(Japanese)* 77−44069
$Al_xGa_{1-x}As$-$Al_yGa_{1-y}As$ DH superluminesc. diode, for Nd:YAG laser pumping, room temp. CW operation 77−7122
$Al_xGa_{1-x}As$-GaAs, diode pump system for YAG:Nd^{3+} laser 79−41396
$Al_xGa_{1-x}As$-GaAs heterostructure, effect of photon recycling on diffusion length and internal quantum efficiency 77−39929
$Al_xGa_{1-x}As$-GaAs LED design and characterisation for fibre-optic communications 78−46796
p-$Al_xGa_{1-x}As$-n-$Al_yGa_{1-y}As$ junction, electrolum. spectra at high press. 77−48246
$Al_yGa_{1-y}As_{1-x}Sb_x$ heterostructure, electroluminesc., appl. to LED's 77−8663
$Al_xGa_{1-x}Sb$, LED, 1.54 μm efficient emission at 300K reproducible fabrication 79−42636
AlGaSbAs heterostructures and LED's luminesc. props. in 1-2 micron band 78−10988
Cu_2O single cryst. diodes, IR electroluminesc. 79−83034
GAP:N LED, acoustic emission study of defects 79−86799
GaAlAs DH, optically-pumped, degradation at elevated temps. 79−50295
GaAlAs, high efficiency, long-lived, for fibre optical communication 77−79940
GaAlAs LED sources for fibre optic transmission, linearity improvement using phase-shift-modulation technique 77−19403
GaAlAs, multiheterojunction, efficient power coupling with taper ended multimode fibre 79−32052
n-GaAlAs:Sn LED DH donor-level analysis, DLTS obs. 79−47040
GaAlAs-GaAs heterojunction prep., Zn conc. effect in epitaxial layer, high-power IR emission *(Spanish)* 77−39932
$Ga_{1-x}Al_xAs$, degraded DH LED, defect struct. by electrolum. topography and TEM obs. 79−60369
$Ga_{1-x}Al_xAs$ LPE crystals for DH laser, LEDs, TEM obs. of Ge, Si-doped epitaxial layers 79−1556
$Ga_{1-x}Al_xAs$, rapidly degraded LED, defect struct. of ⟨100⟩ dark lines 78−10052
$Ga_{1-x}Al_xAs$ transparent LED, optical wavelength multiplex transmission system appl. 78−30063
$Ga_{1-x}Al_xAs$:GaAs, 640 Mbit/s PCM optical fibre source, expt. 78−37998
$Ga_{1-x}Al_xAs$-$Ga_{1-y}Al_yAs$ p-n heterojunction, minority carrier lifetime, elec. characts. and electrolum. meas. 78−2554
$Ga_{1-x}Al_xP$, LPE grown, green electroluminescence 78−19571
GaAs, absolute internal quantum efficiencies of photoluminescence 77−63461
GaAs and related cpds., conf., Edinburgh, Scotland (Sep 1976) 78−3039
GaAs, dark defects attributed to dislocation loops 77−80509

light emitting diodes continued
GaAs, high speed, optical transmitter for optical communication systems 78−33844
GaAs, high speed DH superluminescent diodes, modulation characts. 77−54783
GaAs homojunction LED signal source for fibre-optic communication 78−1413
GaAs homojunction LED, mechanical stress induced degradation 80−2860
GaAs integrated LED/sphere-lens source for optical fibres, coupling efficiency calcs. 80−43433
GaAs LED, minority carrier lifetime determ. 79−42560
GaAs LED absorption effect on freq. characteristic 79−8189
GaAs, luminous intensity ang. distrib. and total light flux meas. device *(Chinese)* 78−82018
GaAs, modulation bandwidth, influence of inhomogeneous current density distrib. 80−9993
GaAs, optimum p-n junction depth, photoluminesc. method 79−4598
GaAs p^+-n diode, radiative hot carrier recomb., photoluminesc. and electroluminesc. meas. 79−38676
GaAs, quantum efficiency and nonequilibrium carrier lifetime 77−12442
GaAs:Si, LED, effect of struct., defects on quantum efficiency 79−11211
GaAs:Si grown from restricted soln.-alloy bulk, props. *(Russian)* 79−43043
GaAs:Si LED, with anti-Stokes phosphor 79−11204
GaAs:Si p-n junction, electrolum. power, injection current and temp. depend. *(Russian)* 77−16401
GaAs:Si p-n junction LED, electroluminesc. efficiency 80−71491
GaAs:Si p-n structures, speed *(Russian)* 79−43044
GaAs:Sn diode, LPE grown, electron irrad. effect on characts. 80−39667
GaAs:Te diffused LED, electron irrad. effect on characts. 80−39667
GaAs:Zn, diffused, depth profiles obs. by photoluminesc. 78−72587
GaAs:Zn, diffusion of Zn by two-temp. method, LED fabrication 80−49416
GaAs-(Ga,Al)As, DH, freq. response as function of design parameters, for optical communications 77−79941
GaAs-$Al_xGa_{1-x}As$, DH LED, self-aligned sphere lens array characteristics *(German)* 78−38014
GaAs-AlAs, heterolight diodes, mesoconstruction, output *(Russian)* 77−12441
GaAs-AlGaAs high-radiance LED for optical communication systems, power and modulation bandwidth 78−42416
GaAs-AlGaAs photoelectroluminescent diodes, characts., radiant power 80−6972
GaAs-$Ga_{1-x}Al_xAs$ double heterostructure LED and injection laser transmitters 77−68282
GaAs-$Ga_{1-x}Al_xAs$ DH LED, for optical fibre communication *(Japanese)* 80−78976
GaAs-$Ga_{1-x}Al_xAs$ red LED, 4% quantum yield *(Russian)* 77−85809
GaAs-GaAlAs DH LEDs, with thin active layer, Burrus type, internal interference in emission spectrum 78−27325
GaAs-GaAlAs DH LED, transient current trap spectroscopy 78−80049
GaAs-GaAlAs LEDs, deep levels *(French)* 78−56218
GaAs-GaAlAs superluminescent diodes for optical fibre links, modulation bandwidth 79−36993
GaAs-GaAlAs wafers, defects and degradation, transmission cathodolum. evaluation 80−65395
GaAs-GaInAs structure, dislocation struct., TEM anal., appl. as IR LED 80−70206
GaAs-GaP, red diode as pulsed reference source for photon counting systems 77−3640
$GaAs_{0.6}P_{0.4}$, deep level profile anal., double correlation technique 77−80830
$GaAs_{0.6}P_{0.4}$, CVD growth for LEDs 79−19998
$GaAs_{0.6}P_{0.4}$, deep level radiative defects detection during degradation 77−76770
$GaAs_{0.6}P_{0.4}$ LED, luminesc. investig. of degradation, deep-level form. at dislocations 77−40287
$GaAs_{1-x}P_x$ epitaxial layer prep. for electroluminescent diodes *(Czech)* 77−21032
$GaAs_{1-x}P_x$ epitaxial layers prep., photoluminesc. and electroluminesc. props. *(Czech)* 78−48233
$GaAs_{1-x}P_x$ LED, effect of band filling on emission spectra shape 78−48236
$GaAs_{1-x}P_x$, solid soln. comp. control during gas-phase heteroepitaxy 77−85091
$GaAs_{1-x}P_x$, VPE on Ge substrate, and LED characts. 78−72736
$GaAs_{1-x}P_x$:N, external quantum efficiency, press. effect 77−8655
$GaAs_xP_{1-x}$, liquid phase epitaxial growth on GaP, growth and properties for LEDs 79−47641
$GaAs_xP_{x-1}$, luminous intensity ang. distrib. and total light flux meas. device *(Chinese)* 78−82018
$Ga_{1-x}In_xAs$ epitaxial layer growth by organometallic pyrolysis, homojunction LED prep. 80−76194
$Ga_xIn_{1-x}As$ p-n junction, growth and electrolum. spectra 77−20420
$Ga_xIn_{1-x}As$:Ge LED, by LPE, radiation emitted at 1.02 μm 78−48235
GaInAsP LEDs, 1.3-1.6 μm, appl. in long haul high data rate fibre optic communication systems 80−102854
GaInAsP/InP optical sources for 1.2 to 1.4 μm wavelength region, growth and props. 79−90023
GaInAsP-InP, lattice matched, emission spectrum half width rel. to peak wavelength 80−2820
$Ga_xIn_{1-x}As_{1-y}P_y$, in compact light source 77−72041
$Ga_xIn_{1-x}As_ySb_{1-y}$, epitaxial film and DH, luminesc. props. 77−686
GaInPAs heterostructures and LED's, luminescent props. in 1-2 micron band 78−10988
GaInPAs-InP, high-efficiency 79−65545
GaN, blue LEDs, VPE *(French)* 79−28928
GaN epitaxial layers for LED, X-ray diffr. topography and cryst. characterisation 79−65336
GaN, VPE growth rate influence on elec. and luminesc. props. 80−100702
GaN:Zn, blue, yellow and green emission, temp. depend. 77−8658
GaN:Zn, electrolum. centres, rel. to growth morphology, Zn conc. and etch patterns 77−1733
GaN:Zn, low voltage LED, epitaxial layer, growth and electrolum. *(Russian)* 77−77297
GaN:Zn, MIS, I-V characts., elec. cond. mechanism 77−55614
GaN:Zn, violet bipolar LED 79−38190

light emitting diodes continued
GaN:Zn epilayers, growth parameters effect on props., device struct. 78−26975
GaP, cryst. growth for green luminesc. diode manuf. 77−40346
GaP, current/voltage and light/voltage characts. modelling 77−8662
GaP, electroluminescent diode, electron irradiated, negative resistance due to impact ionisation 77−15942
GaP electroluminescent diode struct. prep. by SSD and Czochralski methods, dynamic props. *(Czech)* 80−97425
GaP epitaxial layer appl., crystal defects influence on luminesc. obs. 79−87511
GaP epitaxial layers for yellow LEDs, prep. and props. *(Czech)* 78−48234
GaP, green, by Zn diffusion into bulk grown crystals by SSD method 77−81208
GaP, green, high efficiency, by Zn diffusion into n-LPE layers 77−80519
GaP, green, LPE growth method for mass production 77−77422
GaP, green LED, degradation, appl. of dislocation climb model 77−1125
GaP, green luminesc. efficiency, review 77−28636
GaP, ionised-cluster beam epitaxial growth on GaP and Si, characts. for LED 79−28951
GaP, LED, efficiency depend. on O_2 conc. 79−19613
GaP LED, N content by photovoltage meas. 77−11993
GaP LED, negative differential resistance and conductance associated with dielectric losses 77−63468
GaP LED degradation, effect of γ-irradiation 78−95610
GaP, LPE, LED fabrication and electroluminesc. characts. 77−28632
GaP, LPE edge-growth reduction by aux. heating in side-walls of graphite sliders 78−30848
GaP LPE layers and LEC substrates, correlation between dislocation pits 78−38706
GaP lamps, green emitting deep level photocapacitance spectra 77−69409
GaP, light emitting diode structure, effect of neutron irradiation on cathodoluminesc. 79−28843
GaP, luminous intensity ang. distrib. and total light flux meas. device *(Chinese)* 78−82018
GaP, p-i-n LED, I-V characts., electrolum., and photocond. meas. 77−20930
GaP p-n junction, capacitance-freq. dispersion and electroluminescence efficiency 78−64101
GaP, photoluminesc. distrib. meas. *(Czech)* 78−48209
GaP, red, efficiency degradation and deep level change 77−81155
GaP, red LED degradation, diffusion model 77−8657
GaP, surface treatment effect on surface recomb. vel. and leakage current 77−20410
GaP, VPE cryst., electrolum. characts. 77−28631
GaP, VPE layer structures for LED's, SEM, and TEM obs. of dislocation density reduction expt. 80−100425
GaP with S-shaped characteristic, negative resist. and red electroluminesc., expt. 78−48237
GaP:H/GaAs, amorphous film/crystal junction, optical and elec. props. 79−99611
GaP:N, epitaxial layer, determination of nitrogen concentration from cathodoluminescence spectra 78−38744
GaP:N LED, acoustic emission, NDT of dislocation motion 78−91759
GaP:N LED structures, local dopant conc. determ. using SEM cathodolum. spectra 80−101057
GaP:N VPE LED, deep level centres, DLTS studies 79−42493
GaP:S, defect struct. and tetrahedral precipitates, TEM study 80−107246
GaP:Si p-n struct., on n-$Ga_{1-x}Al_xP$ and n-GaP substrates, electrolum. spectra 79−24368
GaP:Te epitaxial layers, dopant distrib. obs. by amalgam polarography 77−39609
GaP:Zn, growth, I-V characts., electroluminesc. *(Korean)* 78−52653
GaP:Zn,O, deep-level changes associated with degradation 77−1472
GaP:Zn,O, degradation of bulk luminesc. induced by laser excitation 77−1715
GaP:Zn,O, photodiodes, high temp. emission spectra *(Russian)* 77−66545
GaP:Zn,O LED, 76K electrolum, spectrum, γ-irrad, and forward bias effects 79−78756
p-GaP:Zn,O-n-GaP:Te,N diode struct., radiative recomb. 80−7419
plGaP:Zn-electrolyte interface, electrochemical LED, luminescence obs. 80−84507
GaP:ZnO, LED, degradation, temp. and current depend. 79−87144
GaP:ZnO, neutron irrad. effects on capacitance, I-V and electrolum. characts. 77−66543
GaP-Zn,O, degradation of bulk electroluminescent efficiency 77−81156
GaSe-SnO_2 heterojunction, elec. props. and electrolum. spectra 77−59328
In-ZnSe-Pt, electrolum. spectra 78−6744
InGaAs, LED, 1.06 μm range, neutron and γ-irrad. effects 79−97433
$In_xGa_{1-x}As$, thick LPE growth, electrolum. obs. 78−60589
InGaAsP, emitting at 1.3 μm, for high-bit-rate fibre data link 78−46825
InGaAsP, high radiance CW LEDs emitting at 1.30 μm 78−22196
InGaAsP LED sources, for near-IR absorpt. meas. 80−77135
InGaAsP LED's, LPE growth, orientation depend. of incorporation of Ga, As, and Zn 78−6869
InGaAsP/InP, for graded-index fibre cables, transmission meas. in 1.2 to 1.6 μm range 80−10037
InGaAsP-InP DH LED, high temp. aged, dark-spot defects, TEM obs. 80−66300
InGaAsP-InP dual wavelength LED 80−15589
InGaAsP-InP:Mg, for high-bit-rate optical communication systems 80−5823
$In_{1-x}Ga_xP$ yellow-green LED, LPE and VPE growth 80−2281
$In_{1-x}Ga_xP$:Te,Zn, photolum. and electrolum., direct transition region 77−8659
$In_{1-x}Ga_xP_{1-z}As_z$ yellow-green LED, LPE and VPE growth 80−2281
$In_{1-x}Ga_xP_{1-z}As_z$-InP, single and multiple layer heterostruct., LEDs and lasers 78−46626
InGaSbAs heterostructures and LED's luminesc. props. in 1-2 micron band 78−10988
InP-$Ga_xIn_{1-x}As_yP_{1-y}$, DH, fabrication and operation in 1.5 μm region 78−37893
InP-InGaPAs heterojunction lasers and LEDs, 1.0 to 1.2 μm 80−74362
$PbS_{0.1}Se_{0.9}$ 4.6 μm LED, room temp., band gap and electrolum. 80−66302
light emitting diodes continued
SiC, 6H polytype, LPE growth by dipping technique for prep. by blue LEDs 77−8769
SiC (6H), blue-emitting diodes by CVD 80−97439
SiC, α-β heterojunctions, spectral characts. *(Russian)* 77−63467
SiC, blue, LPE growth 77−81228
SiC, blue-LED for stimulation of visual cells of insects *(German)* 79−39623
SiC, defect luminesc. 80−89069
SiC devices, epitaxial layer growth techniques 80−108360
SiC LEDs, current-voltage and brightness-current characts. under prebreakdown conditions 79−51667
SiC LEDs prepared by overcompensation method, photon assisted tunnelling 80−97341
SiC p-n junction, electroluminesc. 80−97343
SiC, phys. props. and crystal growth, rel. to appl. in electrolum. devices, book contrib. 77−77299
B-SiC:Al, ion implanted, elec. props. and luminesc. meas. 77−12443
α-SiC:Al diodes, ion implanted, transient characts. of electrolum. 79−24369
SiC:Al(Ga)(B) (6H) LEDs, fabrication by rotation dipping technique, electrolum. mechanisms 80−50426
SiC:B, p-n junction, LED with new low-temp. alloy 79−73582
SiC:silumin, LED, highly stable *(Russian)* 77−8183
YF_3:Yb^{3+}, Tm^{3+}, IR to blue up-converting phosphor 79−83004
$Zn_{1-x}Mg_xTe$ undoped alloys, electroluminesc. and elec. props. 80−2813
ZnO metal-semiconductor electroluminesc. diodes 79−99948
ZnS, blue, prep. and characterisation of low resistivity crystals 77−81209
ZnS, metal-semiconductor LED, injection electroluminescence 77−62992
ZnS Schottky-barrier diodes, blue light emission 79−38671
ZnS, Zn(S,Se), large single crystals, vapour growth and defect characterisation 80−25540
ZnS:Er diodes, electrolum. 79−33840
ZnS:Mn film, luminesc. of highly efficient DC diodes 77−8630
ZnS:Mn film, spectral and electro-optical props. 77−1736
ZnS:Mn Schottky diodes, reverse-biased, electroluminescence, hot electron impact excitations 80−25005
ZnS-$CuGaS_2$ n-p heterojunction, for LED appl., prep. and characterisation 79−1831
$ZnS_{1-x}Se_x$, electroluminescence with In and Au contacts, comp. depend. 77−59618
ZnSe, ageing effects 77−8660
ZnSe, electroluminescent MIS diodes, surface state density determ. 77−35993
ZnSe, hot-pressed powder LED fabrication and characts. 78−23639
ZnSe, low resistance ohmic contacts using In-Ga liquid alloy, LED fabrication appl. 80−70823
ZnSe MIS diode, blue electrolum., heat treatment effects 78−19569
ZnSe MIS diode, forward-bias electrolum. 78−23532
ZnSe MIS LED, donor density calc. from C-U meas. 78−47878
ZnSe MIS structure, photolum. and blue electrolum. obs. 77−20928
ZnSe MOS diodes, injection type electrolum. 77−59614
ZnSe MOS diodes, injection luminesc., edge emission 79−28842
ZnSe, p-n and MOS structs., blue electrolum. 77−32441
ZnSe single cryst. for LED, heat treatment effects on elec. props. 80−29406
ZnSe surface barrier diode, hot charge carriers, elec., photoelec., and electroluminesc. props. *(Russian)* 79−33841
ZnSe:Li, electroluminescence and fabrication, expt. *(Japanese)* 77−28633
ZnSe:Mn^{2+} Schottky barrier diodes, spin depend. cond. and photovoltage 79−91141
ZnSe-CdTe heterojunction, radiative recomb., electrolum. obs. 77−32445
ZnSe-CdTe(ZnTe) heterojunction, cathodolum. and electrolum. 78−6782
ZnSe-ZnTe heterojunction, prep. and props. 79−95483
ZnTe, electro- and cathodoluminesc., impurity segregation 79−43042
ZnTe, low voltage green LED, struct. double diffusion procedure 80−100697
ZnTe:P(Li), luminesc. transitions, quantum efficiency 79−1783
ZnTe-CdSe heterojunction, radiative recomb., electrolum. obs. 77−32445

light filters *see optical filters*

light intensifiers *see image intensifiers*

light interference
see also light interferometers; light interferometry; Moire fringes
acoustic sensor, fibre-optic, modulation processes 80−58771
adaptive focusing of light in inhomogeneous nonlinear medium, interf. criteria 80−99633
algorithm for fast digital analysis of interference fringes 80−73426
anisotropic grating, diffr. orders polarisation *(Russian)* 77−34818
aspheric, testing in reflected light using blazed synthetic holograms 80−91881
astronomical speckle patterns, interference, point spread function 77−22101
atmosphere, blue Moon phenomenon, due to light scatt. and mixed plate interference 77−2244
atoms, Doppler-free two-photon excitation by multiple light pulses 77−42306
atoms, Doppler-free two-photon resonances, interference fringe form. 77−42305
band-pass interference filters, $D(2HL)^m2H$ struct., transmissivity 78−83096
beat signal amplitude, influence of photoreceiver diaphragm diameter and interf. fringe width during interf. 79−7071
beat wave imaging props., in stimulated Raman scatt. medium, holographic appl. 80−5709
birefringent object film effect on interf. pattern, construction of multicapacity matched filters 80−74478
causality and classical interference and diffraction phenomena 79−55049
CBOOA, nematic, mag. field depend. of laser light scatt., interf. rings 78−26434
CBOOA, nematic phase laser light scatt., mag. field depend., crit. deform. *(Japanese)* 78−2826
cell observation, interference effects 79−84055
cholesteric mixture, solid phase, spherulite textures, optical effects and mol. ordering 79−1746
circular fringes with dark centre, form. in diffused light at infinity 78−42278
coating, thin film surface irregularities rel. to optical props. *(Russian)* 77−11047

light interference continued
coating, with narrow reflection bands, design *(Russian)* 80−43472
coherent fast IR wavefront aberration sensor interference problems 80−74499
coherent Gaussian beam in laser Doppler velocimeter, interference 80−69444
coherent radiation space-angle characteristics, improvement by interference method *(Russian)* 78−78909
composite film structures, laser micromachining, interference effects 77−88825
corundum, growth of large crystals of high opt. quality 77−34916
crack tip mixed mode isochromatic fringe patterns 80−28464
crystals, interference fringes with projection hemisphere 79−94852
decorrelated diffusers interferometer, description, exam. of interference phenomena 78−37051
demonstration of interference from two coherent sources 80−4496
dielectric bodies, stress determ. using EM waves 80−38370
dielectric interference film, with equal optical thicknesses of layers, theoretical design *(Russian)* 80−43471
dielectric multilayer interference devices, loss mechanisms 77−83943
diffracting periodic structure generation by coherent beam interference 80−69570
diffraction grating generation for integrated optics, interference method 80−48460
double slit experiment, quantum nonseparability and Bohr's complementarity principle 79−35582
dye solutions, light-induced grating form. by two independ. laser beams, DFB effect 79−94230
education, interference fringes, formation and optimisation 78−36766
education, scatter plate prod. using laser speckle, for scatter light interference expt. 79−9063
effective photon hypothesis, expt. test 77−46709
electro-optical polarisation conversion and interference tunable filters 80−102829
ellipsometer with quarter-wave compensator, multireflection interference effects 79−12841
energy flow lines, Maxwell eqns., interpretation of diffr. and interf. 77−34806
Fabry Perot spectrom., transformation of interference orders 80−263
Fabry-Perot etalon, fringes formed when unfocused, point illumination 78−86322
fibre, single-mode systems, instability due to interference and polarization effects 80−58774
fibre guide length in coherent light rel. to fringe visibility 77−34932
film, interference colours produced by white light refl. teaching paper 80−8754
film, optical consts. determ. 80−2883
film properties measurement using guided optics techniques 79−99958
filter, interference type, transmission band splitting elimination, oblique incidence 77−765
filter, narrow band interf., optical props. as function of incidence angle and polarisation 80−19102
filter characteristics and specification 78−46773
filter polychromator and narrow band rejection filter 77−72061
filter steps, wide angle interf. polarisation, made from various cryst. types 78−87156
filters, direct, quasi-telecentric and telecentric combinations with large astronomical Schmidt cameras 78−57441
fine interference layers, absorpt. coeff. determ. method *(Russian)* 78−82908
flatness of test glass, reading errors of interf. fringes 79−32097
Fraunhofer diffraction and interference, He-Ne laser 77−60878
Fresnel's interferometer parameters, determ. of, slow revolving device 80−27337
Fresnel plane interference fringe generation by correlated speckle patterns 80−106462
fringe intensity distrib. of elliptically polarised beam near critical angle 80−106449
fringe intensity distribution, demonstration using vidicon *(Polish)* 79−40340
fringe localisation, by double exposure speckle photography 78−37803
fringe phenomena, demonstrations using float glass 78−41121
fringe visibility and spacing, atmospheric turbulence effects 80−51572
fringes, separation between maxima, evaluation from difference record of interference fringes 80−62731
fringes localisation in interference by wedge 79−55055
fringes of Fresnel double mirror, localised and unlocalised, theory extended to wedge 80−67960
frustrated total internal reflection, interference enhancement 80−43253
generalised optical theorem for partially coherent interfering beams 80−106447
glass diffused and thin-film waveguides, light interf. 79−14115
gyrotropic layer, 4×4 interference matrix 79−55054
helical wave surface light beams 80−1121
hologram interference fringe bending analysis and expt. 80−106494
hologram interference fringe bending due to pre-stress in photographic emulsion 79−98318
holograms, rainbow, demonstration of diffraction and interference of light *(Polish)* 80−68001
holographic interferogram reconstruction, fringe modification 79−86140
holographic interferograms, interference anal. by analogue/digital video technique 79−86139
holographic optical element interferograms 77−72045
holography and coherent optics, information theory, book 80−98764
image subtraction through speckle modulated by Young fringes 80−95813
integrated interferometric reflector with elec. control for laser reflector 77−58490
interferometer, Doppler beats and interference fringes 79−62957
IR energy-efficient interference coatings 79−23087
IR microscope 77−74496
IR wavefront aberration sensor for high-energy laser system, interference problems 79−98422
Jones notation, polarisation and interference effects 78−17858
laser beam coherence and divergence *(Spanish)* 80−87424
laser beams, meas. of phase distrib. 79−18461
laser Doppler anemometry, instrumentation, appls., explanation using Moire patterns 77−7490
laser frequency control by spectrally depleted destructive two-beam interf. 78−74941
light interference continued
laser nonstationary generation induced interference pattern phase distortion, holographic meas. 78−58945
laser resonator gain saturation, interf. effects 80−37987
laser speckle and surface roughness 80−102622
laser vaporisation of metal film, interference effects in substrate 77−69941
layer with exponentially varying refr. index, oblique incidence of light, interf. matrix 78−55296
liquid, extinction coefficient meas. using coaxial dual channel laser system 80−73425
liquid film, thermal interf.-optical excitation of US waves 78−71794
lithium formate, optical distortion in nonlinear phase conjugation by 3 wave mixing 79−89956
localised interference fringes, teaching 80−101680
low pass interference filter for submillimetre astronomy 80−48393
matrix notation, interference, coherence and polarisation 77−38801
matrix notation, Jones vectors for refl., refr. and diffr. 77−34814
MBBA, anisotropic refr. indices from optical interference meas. 77−8538
MBBA-cholesteryl chloride mixture, liq. cryst., bubble domain texture, obs. of interference fringes 79−23520
Michelson experiment seen 90 years after first execution *(Italian)* 79−17175
microscopic interference obs. by reflection contrast 80−68248
multidither adaptive optics, speckle cancellation techniques 80−48161
multilayer interference film, mass production by roll coating *(Japanese)* 79−81577
multilayer interference filter, calcs. allowing for weak absorption *(Russian)* 78−13812
multilayered media, refl., interference theory 77−65567
multimode fibre link, modal noise 80−87536
multimode optical waveguide propagation and interference effects *(Japanese)* 78−46764
multiple-beam interference effects, Edser-Butler plate, teaching, demonstration appls. 77−41439
narrow band interference filter, spectral transmission curve meas. 78−297
nebular filters for visible astronomy 79−62746
nematic liquid crystals, refractive index and birefringence by interference method 80−96440
nonlinear crystals, interference of optical harmonics 80−64102
nonlinear interference experiments, use of dispersive phase shifter 79−50348
nonlinear interference mirror, reflection of light 80−102761
null curves, partial form, analytic props. 77−88634
optical fibres, fringe visibility for two beams from two fibres 78−33828
optical surface contract interaction zone, thickness calc. and distance meas. methodology *(Russian)* 80−99889
OTF measurement using autocorrelation method 80−58469
over-pumping energy effect, two interfering beams in nonlinear medium *(Russian)* 77−7161
partially coherent light, lecture demonstrations 80−101700
pattern electronic heterodyne recording 80−74316
pattern fluctuation statistics in turbulent atmospheric layer 78−53727
photoelastic fringe pattern analyzer, computer aided 80−38359
photoelastic fringe photography, improved photograph quality 80−27364
photoelastic stress anal. of solids, shadow and interference methods *(Russian)* 79−7352
photon antibunching enhancement by interf., polarisation effects 79−31990
photon antibunching enhancement by interf., Young's interf. expt. 79−27313
photon statistics after destructive interf. of two-photon absorbed light 80−48199
photon synchronisation effect on intensity interference *(Russian)* 80−48200
plane four-layer waveguide with diffr. grating, surface light waves 79−55250
plane parallel optical layer interference props. for radiation parameters control 80−83547
PMMA, optical interference meas. of critical crack tip displacements 78−84964
polarimeter, photoelectric, effect on accuracy of light interference in biquartz modulator 80−62713
polarised beams selective interference in crysts. with isotropic pt. 79−72484
polarizer with large entrance aperture, characts. 80−43453
positive photoresist., exposure and development, optical interf. effect 79−54208
prism optics testing for laser interferometer, interf. meas. 80−105698
N-p-propoxybenzylidene-p-pentylaniline, Williams domains, interference study 80−44114
PVC, optical interference meas. of critical crack tip displacements 78−84964
quantum theory interpretation of EM wave interference, solns. to Maxwell eqns. 77−33882
rainbow phenomena and the detection of nonsphericity in drops 80−58456
Raman and Rayleigh scatt. by optically active mol., elliptical polaris. production 77−58089
Raman scattering, reson.-prereson. interference effects, theory 77−68047
real thin films, optical consts. determ. 78−35213
reflection hologram preparation by interf. copying of transmission holograms 79−45916
resonant medium, interferograms form. by nonoverlapping pulses of coherent light 79−64191
rough surface, effects on coherence of transmitted radiation, Young's method 77−3539
scanning focus by interferometry, beam shear change 80−52301
scattering in media of various vol. concs., cooperative effects, interference interaction *(Russian)* 77−38803
semiconductor film, heteroepitaxial, on insulating substrates, characterisation, book contrib. 79−82497
semiconductor film, transparent substrate, reflectivity and transmission, surface unevenness effect 77−77310
semiconductor heterogeneity refractive index meas., interferometric method 79−6172
sieve screens, two-dimens. array, diffr.-interf. patterns, Kirchhoff approx. 78−83088

light interference continued
single mode fibre cable, 4.15 km, interf. and polarisation characts. using AlGaAs laser 79−81535
single slit diffraction, theory testing expt. 80−77568
solid state laser satellite rings, energy losses caused by diffusion, refl. in cavity 79−89911
spatial frequency determination, selected interference schemes 80−48146
spatial interference influence on amplification in stimulated scatt. 78−71149
speckle, two radially shifted patterns, interf. rings 78−90359
spectrometer, diode laser dual-beam, long-term temporal and scanning characts. 80−90902
stratified medium optical props. determ., via matrix method *(French)* 78−30070
superfluorescence temporal and spatial coherence, from independ. SF beams interference obs. 80−58492
surface velocity meas. using laser beams 78−49806
surface waveguide electrooptical deflector, high-resolution, prism model 80−48454
synchrotron radiation interference effects 80−63906
teaching demonstration, TV display 77−5613
three-beam interference images, sinusoidal complex object with phase modulation, interferometric gratings 80−53208
tilted infinite circular cylinders, extinction cross-section calc. 79−94146
transfer function, matrix theory 77−23625
transfer function with quadratic detect., coherent illum. 80−78782
transmission spectroscopy, interference fringe 78−16851
transparent film on absorbing substrate, optimum angle of incidence for monochromatic interference 80−43254
transparent materials, absorpt. coeffs. meas., interf. effects 78−46699
travelling interference pattern recording, freq. shift 77−34850
unclad optical fibre cross section defects determ. *(French)* 79−89991
VERTIVAL microscope with interference contrast equipment after NOMARSKI for gonorrhoea types classification 80−56301
volume holograms with strong coupling, scatt. phenomena 78−33700
Young's double slit experiment, modified 80−41994
Young's fringes at infinity in diffused light with dark central fringe 78−29895
Ag-AgCl emulsion, anisotropy induced by two coherent perpendicular light vibrs. 79−55196
Al_2O_3 based ceramics, ladder structures, interference phenomena explanation 78−72898
C materials, optical microscopy, reflection, interference colours, terminology 78−42871
CdS, group velocity of light and polaritons, Fabry-Perot mode analysis 77−24863
Cd_2SnO_4 selective coatings, optical absorpt. edge 78−83046
GeSe, amorphous film, optical properties 78−39620
n-InAs, hot electron temp. determ. by interference modulation of radiation 80−44610
InAs, temporary diffr. grating form. on surface 79−59801
LiCl molecular dissoc., obs. by interference method 80−40684
Li_2GeO_3 monocrystal conoscopic figure in polarised white light 79−15433
Na, 3s-5s transition, Doppler-free two-photon excitation by multiple light pulses 77−42306
Na atomic vapour, optical sum-freq.-generation interference 77−42569
$NaNO_2$, vibr. spectrum, interference effects 78−87752
Ne gas, laser induced birefr., polarised light interf. obs. 77−19368
p-Si, heavily doped contact layers on IR detectors, IR transmissivity 80−108190
Si, high-current high-dose implantation visible interf. effects 77−7743
Si:N, ion implantation, refractive index, IR spectra, ion range and straggling meas. 80−34020
Si_3N_4, reaction bonded, ladder phase, interference phenomena explanation 78−72898
SiO_2-Si system, implanted with N, P, and Te ions, reflectance spectra and interference fringes 79−23629
Sn, globular film, interf. and diffr., solar selective props. 79−4860
Sn globular film, solar selective props., effect of dielec. layer addition 79−4861
SnS_2 thin layer, far IR refractive index 80−93421
$TlSbS_2$, single cryst., spectral transmission distrib., polaris. effect, refractivity, dispersion 77−59551
VO_2 interference films, colour valencies as function of thickness and phase change *(German)* 78−56533
ZnS-Na_3AlF_6 Fabry-Perot interference filter, neutron irrad. effects on props. 79−76867
ZnS-Na_3AlF_6 multilayer dielectric optical filter, irreversible thermal effect 77−7195

light interferometers
see also light interferometry
90° phase shift beam splitter for displacement interferometer 78−87145
90° reflecting angle meas. of transparent- and opaque-materials *(German)* 78−164
achromatic interferometer, for imaging through scatt. media 79−58778
achromatic interferometer, image form. 78−16838
achromatic interferometers for white light optical processing and holography 80−53234
acoustic emission optical interfereometer and auxiliary direct viewing system 79−79217
acoustic sensor, single optical fibre interferometric 78−38161
acousto-optical fibre interferometer for reflective surface motion meas. 80−13127
adaptive optics, radial Ronchi grating lateral shear interferometer, book contrib. 79−31972
advances in optical metrology, conf., San Diego, USA, Aug. 1978 79−80565
amplitude interferometer, white light, 180 degree rot. shear astronomical appl. 78−77977
angle etalon constr., angular scale, polygon calibration appl. *(German)* 78−77852
angle interferometer with 90° range, system set-up, calibration *(German)* 78−165
angle meas. appl. *(Czech)* 78−49794
angle modulated optical signals, modulation parameter meas. *(Russian)* 78−37047
angle-scanned, as coherent energy modulator in coherence discriminating laser receiver 79−58777
angle-scanned AC and symmetrical interferometers 79−58776

light interferometers continued
anomalous dispersion by band shift method, interference max. position 79−75578
as optical test tool 79−85169
aspheric, testing in reflected light using blazed synthetic holograms 80−91881
astronomical IR instrumentation on NASA airborne observatories 78−45224
astronomical IR spatial, design and operation 78−45232
astronomical long-baseline amplitude interferometer, pupil space design 78−53832
astronomical monochromatic imaging using filters, slitless (multislit) spectrograph, and interferometers 79−8840
astronomical wide-angle Mach-Zehnder, for Na D-emission photography 77−60617
asymmetrical Fabry-Perot interferometer with feedback 79−85163
atmosphere modulation transfer function meas. equipment 80−41567
autocollimating telescope calibration, laser interferometer appl. *(German)* 78−77853
autocollimation apparatus to test manufacturing quality of aspherical mirror profile 80−10053
automatic fringe counting, independ. of signal level changes 78−58018
automatic interference comparator for precision length measurement, interference refractometer *(German)* 78−77966
automatic profile scanning, contactless *(German)* 77−87729
balanced interferometer with simply adjustable interference angle 77−71366
balloon borne interference spectrometers operation and appl. to solar UV obs. *(Japanese)* 78−57442
beam splitter phase coatings, for producing phase quadrature interferometer outputs 78−77974
beam splitters, design of high efficiency for two beam IR interferometer 78−30093
biaxial translation stage, kinematic design 77−161
birefringent element, analogue, built from polarising wide field Michelson interferometer 80−91895
birefringent fibre interferometric secondary light source 80−105702
bistable optical device development from integrated two-arm interferometer, appls. *(French)* 80−69555
bistable piezoelectric Fabry-Perot interferometer 79−97420
calibration for atomic and molecular transition wavelength meas. 79−80696
CERGA stellar interferometer, phase effect detect. and appl. to orbit of α Aurigae (Capella) *(French)* 80−36508
channel waveguide interferometric modulator for EM field detection 80−74498
chevron beam-splitter, double-pass 80−73431
chopper for deep space IR interferometer/spectrometer 78−81545
closed loop, fibre optic rotation sensor, signal detection and processing, inertial reference device 79−54111
closed-loop simple system for real-time optical phase meas. 79−63302
coaxial reference, with low mapping distortion, for testing mirrors 79−85175
coherence interferometer, for atmospheric modulation transfer function estimation *(Russian)* 79−16715
coherent optical feedback analogue computer for partial differential eqns. with inhomogeneous terms 79−76870
common path type, for obtaining variable inverted shear of object 78−4689
complex Fourier spectra, interferometric determ. 80−87327
complex refractive index of liquid dielec., at mm and sub-mm wavelength 77−82595
computer-controlled Gabry-Perot interferometer for Brillouin spectroscopy 79−40622
computer-controlled heterodyne interferometer for index gradient meas. 80−13131
computer-controlled laser interferometer 80−56294
confocal Fabry-Perot feedback system, partial differential eqn. analog soln. 80−102630
confocal interferometer light-scattering sample cell 79−6182
contactless laser interferometer sweep gauge for diamond-turned surfaces 80−73441
convection measurement, differential interferometer with achromatic $\lambda/2$ compensation 78−87419
corner cube interferometer using extended sources 77−5894
correlator with matched filtering using band-limited illumination 80−69531
counting, angle measurement in range 70° *(German)* 77−10095
creep rate determination using Michelson interferometer 78−68856
data handling in high vibration environment 80−95132
decorrelated diffusers interferometer, description, exam. of interference phenomena 78−37051
deformable mirror figure sensor control 77−19384
design, construction and interferogram processing, optical testing appl. 80−79020
design for high vibration environment 80−95131
differential heterodyne interferometer, photoinduced RI change obs. 77−3639
diffraction ballistic expt. appl., use of commercial shadowgraphic instrument 80−47093
digital, for measurement of wavelength of gas laser lines 80−37079
digital beam switch for 10.6 μm laser radar 80−102836
digital beam switch for agile beam laser radar 80−58620
digital wavemeter for CW lasers 78−89447
diode laser wavelength monitoring using fibre interferometer 80−74413
dispersive Fourier Michelson interferometer, meas. of opaque solid at 6K 79−2841
distance meas. using laser interferometer, principles and performance 78−89442
divider phase distortion compensation improvement 78−58073
Doppler, laser, error sources analysis, meas. volume structure *(Russian)* 80−27336
Doppler frequency discriminator applic. in laser velocimeter 78−26220
double arm, with US modulator, for photodetector amplitude-freq. charact. meas. 77−10112
double beam interferometer, fringe value changing 78−278
double beam interferometer for background suppression and spectral detection 80−95129
double beam Michelson interferometer meas. of small linear displacements 78−73966

light interferometers continued
double diffraction interferometer, optical path difference meas. appl. *(Japanese)* 78−82025
double grating diffraction shearing, for MTF meas. 79−64366
double grating P-polarised plane wave diffr., Fabry-Perot interferometer appl. 79−81544
double pass Fabry-Perot, for dynamic angular displacement meas. 79−49276
double-beam, background suppression technique using tailored modulation transfer functions 79−97428
double-beam interferometer, achromatic fringe pattern anomalies 79−49278
double-beam interferometer, computer analysis program 79−71520
double-frequency laser interferometric system with automatic compensation *(Chinese)* 80−27340
double-grating shearing, for real-time optical image addition and subtraction 79−55069
dual beam, autoequalisation of path length 77−157
dual laser interferometer for plasma density measurements on large Tokamaks 78−71542
dye laser, spectral selection and tuning using thin layer Fabry-Perot interferometer *(German)* 79−94242
dye laser, tuning and active mode-locking, interferometry technique 79−22982
Earth strain meas. with laser interferometer *(Japanese)* 77−81783
eigenvalue translation method for mode calculations 79−71515
electro-optical linear interferometric modulator for electromagnetic field detection 80−58782
electronic speckle pattern interferometry apparatus with multichannel data acquisition 79−80671
Fabry Perot interferometer, in laser technique for shock wave vel. meas. 77−50972
Fabry Perot spectrom., transformation of interference orders 80−263
Fabry Perot wide-band electrooptic type modulator, modulation sensitivity 79−3724
Fabry-Perot, automatic periodic alignment by microprocessor *(French)* 78−86872
Fabry-Perot, bandwidth narrowing using active element 78−4688
Fabry-Perot, basculating eigenvectors *(French)* 79−63299
Fabry-Perot, cinematographic lenses production *(Russian)* 78−37959
Fabry-Perot, coherent feedback system for information processing 77−71933
Fabry-Perot, Gaussian beam illumination, instrumental function 80−9026
Fabry-Perot, instrumental profile 79−54179
Fabry-Perot, laser mirror reflection coeff. meas. *(Russian)* 78−1237
Fabry-Perot, optically contacted, parallelism recording technique 77−18079
Fabry-Perot, performance computing, program for TI-59 calculator 79−35816
Fabry-Perot, piezoelectrically scanned, microcomputer-based data acquisition and stabilization system 80−62719
Fabry-Perot, press. scanning, 15000-30000 cm^{-1} 77−82617
Fabry-Perot, radiation pulse width meas., from solid-state meas. lasers 80−23736
Fabry-Perot, random defects in medium and mirrors 79−54180
Fabry-Perot, refractive index meas. of solids 80−52297
Fabry-Perot, resonance, phase front and polaris independence constraints 79−54176
Fabry-Perot, ruby laser frequency selection and stabilisation 80−58566
Fabry-Perot, scanning, digital stabiliser 77−10101
Fabry-Perot, stable multipass, design and anal. 78−274
Fabry-Perot, supersonic flowmeter 79−7420
Fabry-Perot, with metal gratings with nonparallel line orientation, props. 77−22595
Fabry-Perot and double etalons, as passive laser pulse shapers 77−19265
Fabry-Perot cavity, gas filled, optical bistability described by stochastic master eqn. 79−76652
Fabry-Perot cavity, optical pulse tailoring and termination by self-sweeping 80−23760
Fabry-Perot electro-optic type wide-band modulator sensitivity, surface error influence 79−50392
Fabry-Perot etalon, freq. selector in laser resonator losses *(Russian)* 77−38944
Fabry-Perot etalon, fringes formed when unfocused, point illumination 78−86322
Fabry-Perot etalon, longit. mode locking of the He-Ne laser 79−50318
Fabry-Perot etalon, method for meas. fractional part of interference order 79−67379
Fabry-Perot etalon, optical thickness error compensation 78−49889
Fabry-Perot etalon, optically contacted, stability to cosmic radiation 80−98544
Fabry-Perot etalon, tunable spatial filtering 80−58668
Fabry-Perot etalon, wavenumber calibration of Pb salt tunable diode lasers 78−45738
Fabry-Perot etalon arrangement, precision length calibration of long slip gauges appl. *(German)* 78−77849
Fabry-Perot etalon effect on laser resonator modes 78−25896
Fabry-Perot etalon plates, MgF_2 layer performance for vac. UV 77−5895
Fabry-Perot etalon with overlap bands, appl. to determ. phase difference variations in transparent object *(Russian)* 77−26394
Fabry-Perot focusing properties in multiple-beam holography system 79−13927
Fabry-Perot imaging device TAURUS for radial velocity field maps 80−82205
Fabry-Perot interference discriminator, for laser freq. stabilisation, optimisation 79−31962
Fabry-Perot interferometer, effect of zero points in light modulation *(Russian)* 79−58781
Fabry-Perot interferometer, for Raman spectrometers 78−74063
Fabry-Perot interferometer, for remote sensing rot. Raman spectrosc., background rejection method 77−71384
Fabry-Perot interferometer, lossless nonlinear 78−42375
Fabry-Perot interferometer, microcomputer stabilisation 78−74055
Fabry-Perot interferometer, multiple-zone aperture design for airglow temp. 80−82075
Fabry-Perot interferometer, optical bistability, inhomogeneous broadening, mean field approx. 80−90885
Fabry-Perot interferometer, submillimetre range, for plasma diagnostics 77−3990
light interferometers continued
Fabry-Perot interferometer, transient behaviour 78−33787
Fabry-Perot interferometer, wavefront form. by multilayered dielec. mirror 78−54449
Fabry-Perot interferometer as refractometer 80−264
Fabry-Perot interferometer data inversion algorithm 79−75604
Fabry-Perot interferometer for CO_2 laser pulse generation 78−29996
Fabry-Perot interferometer for sub ns pulse stretching and spectroscopy 77−42555
Fabry-Perot interferometer in dye laser resonator, for metrological interf. meas. 80−28250
Fabry-Perot interferometer instrumental function for short light pulses 80−105704
Fabry-Perot interferometer length stabilisation using He-Ne laser radiation 77−79141
Fabry-Perot interferometer of large Fresnel no., image profile 79−54177
Fabry-Perot interferometer photometer, for upper atmosphere daytime Li releases obs. 78−45023
Fabry-Perot interferometer response to AM light beams 78−16836
Fabry-Perot interferometers, description 80−4261
Fabry-Perot interferometers, optical bistability for homogeneously broadened two-level system 79−76653
Fabry-Perot interferometers with 20 cm^{-1} free spectral range *(Japanese)* 77−87847
Fabry-Perot interferometry of HF discharge diagnostics 78−9872
Fabry-Perot laser interferometer for plasma density meas. in unsteady flow 77−68869
Fabry-Perot multipass interferometer, wavelength scanning and mirror alignment 80−258
Fabry-Perot nonideal, instrumentation contour 79−75580
Fabry-Perot nonideal interferometer, instrum. contour 78−82027
Fabry-Perot nonlinear electro-optic device, using refl. light feedback 78−55457
Fabry-Perot nonlinear interferometer, beam profile hysteresis variations 80−86393
Fabry-Perot optical switch driven by fast $Pb(Zr,Ti)O_3$ transducer 79−86251
Fabry-Perot press. scanned three-pass interferometer 79−9238
Fabry-Perot pressure scanning interferometer, expt. construction *(Japanese)* 80−77848
Fabry-Perot pressure-scanned interferometer for nightglow meas. 77−9510
Fabry-Perot resonator with plane-parallel mirror, polaris. effects in gas lasers 80−58605
Fabry-Perot resonator with quadratically nonuniform active medium, radiation field *(Russian)* 78−46682
Fabry-Perot resonators, second-order perturbation theory 79−18451
Fabry-Perot rings, speckle, effect of freq. chirping of light from Q-switched ruby laser 79−41340
Fabry-Perot scanning, for fine structure obs. of He-Ne laser radiation 77−54749
Fabry-Perot scanning interferometer, far IR performance 80−86388
Fabry-Perot scanning interferometer, SKIF-1, for spectral-line profiles of plasma sources 79−17476
Fabry-Perot scanning interferometer with piezoelec. spacers, appl. to solar UV spectrum 80−12678
Fabry-Perot spectrometer for solar vel. field meas. 80−90333
Fabry-Perot type, focusing and beam shifting props. 79−6168
Fabry-Perot with short pulse lasers, spectral selection and analysis in dye lasers 78−46669
Fabry-Perot-interferometer imaging system for thermospheric temp. and wind meas. 80−101441
far IR interferometer for obtaining Fourier sine transform of spectrum 79−97422
far IR interferometers, self-supporting thin-film beam splitter 78−275
far IR interferometers with wire-grid beam dividers, freq. response 80−57365
far IR interferometric spectrometer, sampling comb generation and precision 80−47122
fast-scanning Fabry-Perot interferometer, reflecting surface shape determ. 79−12842
Febry-Perot interferometer, with automated data acquisition and stabilisation system 78−70180
fibre interferometer gyroscope 80−1348
fibre laser gyroscopes 77−46728
fibre optic approach to rotation sensing, active re-entrant Sagnac system 80−10038
fibre optic heterodyne interferometer for vibr. meas. in biological systems 78−77101
fibre optic interferometric sensor for acoustic detect., thermally induced optical phase effects 80−74479
fibre optic Mach-Zehnder interferometer, sensing of press. and temp. 79−72671
fibre optic Mach-Zender interferometer as mag. field sensor 80−69510
fibre optic ring interferometer gyroscope, Fresnel drag effect 78−79142
fibre optic rotating sensor, Sagnac interferometer preliminary results 80−10040
fibre optic rotation sensor, all-waveguide configuration, key element tests 80−58796
fibre optic rotation sensor with low drift 80−69530
fibre optical gyroscope, Sagnac or Fizeau effect 79−72669
fibre optical interferometers for length, temp., pressure and force meas. 80−98971
fibre optical polarisation transformer, in-line 79−72667
fibre optical ring interferometer, Sagnac-effect, sensitivity 79−50379
fibre ring gyroscope, optimum sensitivity limits 80−10039
fibre ring interferometer, optical gyro, reciprocity of birefr. single-model fibres 79−81513
fibre ring interferometer gyroscope, nonreciprocity noise, fibre dispersion meas. 80−1346
fibre rotation sensor, laboratory performance evaluation 80−1347
fibre waveguide laser interferometer 78−49892
fibre-optic interferometer gyro, thermally induced nonreciprocity 80−58665
fibre-optic microphones and hydrophones compared with conventional devices 79−72717
fibre-optic rotation sensor construction and laboratory test 79−98497
fibre-optical, beam-splitter and two-beam interferometer 77−87811
fibre-ring interferometer, rotation-sensing, polarisation analysis 79−64333

light interferometers continued
filamentary spatial filter and extended source of polychromatic light for use with interferometry in phase measurement 79−71518
filamentary spatial filter interferometer, appl. to phase meas. 78−49890
Fizeau interferometer, spherical-wave, direct phase meas. 80−95126
Fizeau wavelength meter, laser and other monochromatic sources, digital display 78−89450
FM wide-band system using optical techniques 79−64308
Fourier spectroscopy, delay compensation, sampling error reduction 79−30566
Fourier spectroscopy, far IR, spectrum distortion by multiple reflections using Michelson interferometer 80−82837
Fourier transform spectrometer based on Michelson interferometer, problems in optical measurements 79−85187
Fresnel's interferometer parameters, determ. of, slow revolving device 80−27337
Fresnel biprism or bimirror, for electron density meas. on laser-created plasma 80−48983
fringe-counting wavemeter, based on compact spherical interferometer 80−42255
frustrated total internal reflection *(French)* 77−61113
Gabry-Perot two-mirror multibeam interferometer, field and radiation reflectance, sharpness factor 80−27341
gas lasers, vibration immunity for interference work 78−5489
glass interferometer rod, inhomogeneity rel. to tempering 77−34919
grating interferometers, used in ballistic experiments 79−97426
grating lateral shear inteferometer, high efficiency 77−26391
Grubb Parson modular cube interferometer, Golay detector housing 79−26113
gyroscope, optical fibre, based on Sagnac effect, background and development *(German)* 80−48431
heterodyne, freq. shifter using multiple rotating polarisation retarders 79−6167
heterodyne, microcomputer-based automatic 79−85174
heterodyne, with RF phase reference, laser beam phase variation determ. 77−5896
heterodyne CO_2-laser interferometer with direct phase readout for meas. electron line densities in plasmas 80−1848
heterodyne interferometer, light scatt., for vibr. meas. in auditory organs 77−2073
heterodyne interferometer with improved two-channel crosstalk signal/noise ratio 77−10100
heterodyne quadrature interferometer for simultaneous measurements of plasma density along several chords 78−67416
high precision laser freq. meas., sigmameter, motionless two-channel Michelson interferometer 78−89449
holographic, for optical glass homogeneity determ. 78−90401
holographic gratings, production methods, characteristics, quality *(Korean)* 80−43289
holographic lateral shear interferometer, appl. to testing 77−7023
holographic microscopy, real time using holographic illuminating system, rotary shearing interferometer 79−81388
homodyne sub-mm interferometer for plasma diagnosis 79−32811
image-shearing camera for surface strain direct meas. 79−58773
imaging using aperture synthesis, stellar appl. 79−58244
impurity photoresistor in interferometer, threshold charact. 80−31856
inclined Fabry-Perot etalon within cavity, for ion laser freq. selection 79−55161
integrated electro-optical two arm interferometer, optical bistability expts. 79−76883
intensity autocorrelation, real-time, for picosecond, subpicosecond optical pulse display 79−17468
interference dividing prism 77−75676
internal gauge, microinterferometer IZK-61 78−89438
IR, far, computer control 77−82590
IR Fabry-Perot interferometer for astrophysics 80−8672
IR filter radiometer using selective interferometer 77−5880
IR high-resolution, using solid Fabry-Perot etalons 77−45888
IR interferometer for NDT 79−8419
IR interferometric spectrometer, slow scan, resolution and performance 80−42274
IR laser interferometer, length measuring, alignment using laser feedback 80−37075
IR laser interferometer operation and testing 80−73433
IR lateral shearing, as optical testing tools 80−68244
IR material and lens evaluation interferometer 77−39121
IR point diffraction interferometer, fabrication and use at 10.6 μm 78−86325
IR polarisation interferometer, asymmetric interferogram 79−97421
IR scanning interferometers 78−82026
IR Smartt interferometer, alignment tool for CO_2 laser fusion systems 80−74425
IR unequal path interferometer for large aperture IR window meas. 79−85170
Jamin, for interferometric saturation spectroscopy 78−74079
Jamin double-beam, two-dimens. image transmission through inhomogeneous medium 78−50706
Kosters, photoelectric determination of fringe fraction, scanning technique *(German)* 77−10096
lambdameter, improved design based on moving mirror Michelson interferometer, accuracy tests 79−63194
lamellar grating interferometer, for optical props. meas. of solids in far IR 79−58774
lamellar-grating interferometer, balloon-borne, appl. to solar brightness temp. meas. 78−85921
large angle laser interferometer for 'curved' crystal spectrometer, precision 78−77973
large aperture AC interferometer for optical testing 79−27446
large-aperture interferometer with low-resolution holographic corrector plate 80−74315
laser, for accurate positioning, built-in system for machine tools *(German)* 80−9022
laser, for displacement and vibration meas. 79−6094
laser, for length meas., error factors *(Japanese)* 78−8384
laser, for measuring beam oscill. in balance scales, construction *(German)* 77−79090
laser, for sonar echo acoustic imaging 77−58501
laser, gyromagnetic ratio of proton and fine-structure constant redeterm. 80−74253
laser, microcomputer-based, for angular displacement meas. in instrument graduation *(Polish)* 80−90816
light interferometers continued
laser, NBS system designed for seismology appl. 80−13125
laser, two-frequency for two objects movement rate meas. *(Russian)* 77−26392
laser anemointerferometer, for simultaneous velocity and density meas. 79−18976
laser beam divergence in short interferometers 77−27310
laser. calibration and measurement standard, high precision *(German)* 80−78862
laser cavity interferometer, for phase changes $<10^{-5}$Å 77−18087
laser CW digital wavemeter, moving cube-corner interferometer system 78−50840
laser Doppler velocimeter instantaneous, using fast wavelength tracking Michelson interferometer 79−7430
laser Doppler velocimeter with high resolution Fabry-Perot interferometer for supersonic vel. meas. 77−39377
laser double-beam interferometer for amplitude-phase transmission meas. in optical components 77−87815
laser feedback interferometer with phase quadrature using two-mode He-Ne laser 79−2813
laser fusion studies using polarized light interferometer 80−31855
laser homodyne multiray, for electron density determ. in high-temp. gas flows 79−86609
laser in-cavity Michelson interferometer, appl. to plasma diagnostics 79−2811
laser interferometer, 500-m base, Earth surface deform. detect. 80−105087
laser interferometer, acoustic vibration meas. 78−71253
laser interferometer, appl. to absolute vel. control of Mossbauer spectrometer 77−71715
laser interferometer, manometer applic. 77−110
laser interferometer, principles and properties *(Czech)* 79−71516
laser interferometer, prism optics testing, interf. meas. 80−105698
laser interferometer, thickness meas. in nuclear track detectors 78−86735
laser interferometer, two-frequency, small displacement meas. in LF range 79−30533
laser interferometer application to length meas. in production *(German)* 80−18007
laser interferometer for acoustic emissions meas. at high temp. and press. 78−1525
laser interferometer for detecting biological signals due to displacement *(Italian)* 78−53467
laser interferometer for meas. linear vibration report 78−86243
laser interferometer for meas. of refractive index of liquids as function of temp. 79−58780
laser interferometer for precision linear displacement meas. 80−27285
laser interferometer for routine aspheric surface testing 80−14495
laser interferometer for small angle meas., description, operation, resolution *(Chinese)* 77−49768
laser interferometer optical component parameter optimisation 77−67493
laser interferometer systems, theory and application 80−73435
laser interferometer with path difference up to 1 km, geophysical appl. 78−61616
laser interferometers, AM and FM operation and applications *(German)* 80−86389
laser microinterferometer, in laser profilograph 77−74356
laser microinterferometer limiting sensitivity and accuracy characteristics 77−79142
laser monochromator-interferometer, protable high-resolution, with multichannel electronic readout 80−33153
laser probe for measurement of vibrations of very small amplitude, in US transducers 80−73443
laser pulse shaping by nonlinear interferometers 78−59097
laser radiation wavelength meas., 3.39 μm and 0.63 μm 79−30555
laser shearing, for gas dynamic diagnostics 77−7489
laser shearing interferometer appl. to supersonic flow field meas. *(Chinese)* 79−32715
laser sliding reference interferometer for two-dimensional phase meas. 77−19280
laser stethoscope, non-contact high sensitivity, using interferometer technique *(German)* 78−69176
laser unequal path interferometer, for lens testing at 1.06 μm 78−49893
laser unequal path interferometer with electro-optical camera and minicomputer, fabrication/test appl. 80−77847
laser wavelength meter for pulsed or CW lasers, Fizeau interferometer system 78−46701
lateral shearing interferometer with variable shear appl. to lens quality meas. *(German)* 80−22425
Lau effect, diffr. expt. with incoherent illum., appl. to Talbot interferometer, Fourier spectrometer 79−41333
length meas., comparator error compensation 78−4587
length meas. by tunable laser 79−35817
length measurement, precision *(German)* 78−89434
long path Fabry Perot interferometer design for condensed phases 77−18078
long-baseline interferometer for astrometry 77−37506
Mach Zehnder CW multichannel, for plasma density radial profile measurements 79−75581
Mach-Zehnder, as optical Fourier processor, coherence effects on phase accuracy 78−90377
Mach-Zehnder, test section misalignment errors for temp. and temp. gradient meas. 78−54447
Mach-Zehnder four-framing laser interferometer system, appl. to plasma focus expt. 80−4761
Mach-Zehnder heterodyne interferometer, RF phase reference 77−26390
Mach-Zehnder heterodyne interferometer as gyroscope 77−82594
Mach-Zehnder interferometer, hook method, Ba I gf values, 7911.38 Å 78−66511
Mach-Zehnder interferometer, switch, integrated optical format 78−38084
Mach-Zehnder interferometer as basis for IR compensation phasemeter 77−39039
Mach-Zehnder interferometric optical switches for integrated astable optical multivibrator 80−87560
Mach-Zehnder interferometric switch for integrated optical multivibrators 80−53479
Mach-Zehnder interferometric waveguide modulator, polarization-independent operation 79−18552
Mach-Zender twin-wave laser interferometer for plasma diagnostics 78−4687

light interferometers continued
Martin-Puplett interferometer, use as Fourier spectrometer and for OTF meas. 78−70179
matching and coupling to plane wave limited by pinhole 79−75575
methane gas interferometer for coal mine safety 78−44423
methanol far IR laser, twin optically pumped, for plasma diagnostics 80−59306
Michelson, diaphragm scanning system 78−12764
Michelson, for holography in partially coherent light 80−58480
Michelson, laser driven, use as calibration for Mossbauer spectrometer drive systems 77−18151
Michelson, laser frequency control by spectrally depleted destructive two-beam interf. 78−74941
Michelson, mirror position control by means of capacitor probes 78−21119
Michelson, modified, for IR heterodyne detect. expts. *(French)* 77−37991
Michelson, precision balance read-off appl. 77−5809
Michelson, sequential analysis of fringes, scanning rate influence 78−77976
Michelson, wavelength intercomparison between methane and I_2 stabilised He-Ne lasers 78−87089
Michelson, with zero path difference, optical scheme props. calc. 80−262
Michelson's interferometer, instantaneous multiple use with laser light source 77−57125
Michelson asymmetric interferometer, modified He cryostat 78−74053
Michelson far IR balloon-borne for stratospheric emission spectrum obs. 79−39870
Michelson far IR interferometer for astronomical appl. 78−93118
Michelson inclined mirror interferometer, high spectral resolution, gaseous D_2O-H_2O-HDO mixture, absorpt. meas. 80−9023
Michelson interferometer, active noise compensation *(Russian)* 78−12751
Michelson interferometer, active stabilization by electrooptically tuned laser 80−86386
Michelson interferometer, cryogenic, rocket-borne, for EXCEDE II expt. 80−95133
Michelson interferometer, double-passed, influence of surface roughness on photometric setting-accuracy 78−12746
Michelson interferometer, field-widened, for meas. of vels. of shocked specimens back surfaces 77−61050
Michelson interferometer, for deform. meas. in UH vacuum system at high temps. 77−2650
Michelson interferometer, high spectral resolution, for Isaac Newton Telescope 78−4105
Michelson interferometer, modification for polarised beam interference 80−260
Michelson interferometer, optical circuit props. at zero path difference *(Russian)* 79−9241
Michelson interferometer, polarizing, for far IR and MM regions 80−73427
Michelson interferometer, residual path difference depend. on mirror setting ang. errors 80−77845
Michelson interferometer, tilt-compensated, for Fourier transform spectroscopy 79−9239
Michelson interferometer, use as selective filter for stratospheric trace gas concs. meas. 80−17408
Michelson interferometer for airborne IR obs. of interstellar media 77−73966
Michelson interferometer for airborne IR obs. of interstellar media 77−73967
Michelson interferometer for wavelength comparisons 80−98969
Michelson interferometer in laser-pistonphone for microphone calibration 77−58519
Michelson interferometer mirror, external resonator for GaAs-$Ga_xAl_{1-x}As$ injection laser 79−81455
Michelson interforometer, form. of bands of equal thickness as function of mirror and beam splitter positions 80−52298
Michelson laser interferometer, modified, for monitoring dimensional stability of fused quartz tube 79−58779
Michelson laser interferometers, noise limitations 80−82808
Michelson polarizing interferometer with optical fibre probe, high sensitivity vibr. meas. 79−7351
Michelson stellar interferometer, reconstituting nonstationary optical pattern from 2-photon correls. *(Russian)* 77−82125
Michelson stellar interferometer, seeing effects removal 77−29659
Michelson stellar interferometer for binary star obs. 79−44370
Michelson-type, for anomalous dispersion meas. *(Russian)* 79−93211
microcomputer based scanning instrument controller, for Fabry-Perot interferometer 78−93764
microinterferometer, apochromat objective, with increased resolution, surface roughness testing 79−71519
microinterferometer transducer, air-bearing, for use with universal inspection machines 78−57899
micromanometer, oil surface movement meas. using polarising interferometer 79−63263
microoptical switch, Mach Zehnder interferometer, for use with optical fibre transmission lines, exam. 78−38085
microprocessor based automatic heterodyne interferometer 80−9030
microprocessor-based interferometric data reduction system versatility 80−73439
microscope, interference, with freq. shift, for glass fibre refr. index profile meas. 80−64175
microscope, phase-locked interferometric, design and construction 78−45687
microscope interferometric attachment 79−85179
MII-4 microinterferometer for metal whisker thickness meas. 78−166
mirror fiducial system compatible with computer-controlled polishing facility 80−74539
mirror kinematic adjustment mechanism 78−59109
mirrors, semireflecting lossless, transmitted and reflected optical fields phase shift 80−46769
mobile-mirror, for measuring parameters of angular-modulated radiation *(Russian)* 80−22421
mode coupling by circular apertures 77−6995
mode locked lasers, effects of narrow-free-spectral-range etalons 80−38041
modified Michelson interferometer for hologram prod., undergraduate expt. 80−105473
modular, for dispersive Fourier transform spectrometry of gases 78−89567
modular, for dispersive refl. meas. on highly absorbing solids 78−89568
modular interferometer for FT spectroscopy in far IR 77−82629
modulated fibre ring interferometer, laser appl. 80−74506
moire stress analysis interferometer with microprocessor 80−31858
moving carriage Michelson interferometer, 1 in 10^7 laser wavelength meas. 78−89452
multi-beam, plasma particle density diagnostics, laser beam illumination 78−86324
multibeam modular interferometer design 80−18004
multichannel HCN laser interferometer for Tokamak plasma diagnostics 78−5928
multiframe laser interferometer system, meas. of rapidly varying processes 79−85166
multipass, using filamentary spatial filter 78−77975
multipath optical cavities in saturated absorpt. expts., freq. calibration and optical delay line 77−65610
multiple beam spectral analyser with thin film waveguide feed, prism radiation tap 77−34944
multiple beam/two beam combination, superposition fringes for optical testing 79−86267
multiple-beam interferometer for measuring small-amplitude mechanical vibrations 80−4759
multiple-beam reflecting interferometer, interference band profile control 80−9027
multiple-beam wedge-shaped, for high-speed laser Doppler velocimeter 80−99782
multiple-grating interferometers for hologram-forming process, MTF first-order theory 79−76632
multiturn fibre Sagnac interferometer, shot-noise-limited inertial rotation meas. 80−1349
multiwavelength testing using modified Twyman-Green interferometer 78−59169
Mylar beam splitter efficiency in far IR interferometer 78−55434
nonideal, Voigt profile parameters determ. 80−261
nonideal Fabry-Perot interferometer, instrument contour 79−63301
nonlinear, quantum fluctuations meas. in light beam 79−80672
nonlinear interferometer with Kerr cell, quantum effects 79−55193
nonlinear interferometers for laser pulse shaping 78−79051
nonlinear optical processing with Fabry-Perot interferometers containing phase recording media 80−48158
nonplanar wire polarisers for far IR 79−36989
oblique incidence interferometer for surface testing 77−26389
oblique selective Fabry-Perot etalon fabrication tolerances 79−68424
optical bench, automated scanning, remote laser interf. meas. system 78−83124
optical fibre ring interferometer, Fresnel drag in single-mode fibres 79−37035
optical fibre sensors, single-mode, polarisation effects 80−43426
optical pressure-sensing element based on interferometer, for meas. pressure of laser pulses on targets 79−35771
optical systems, modification for aspherical surface testing, design calcs. and aberration characts. 79−7236
optical workshops interferometer, description of a new interferometer *(French)* 78−58017
optoelectronic-mechanical instrum. for evaluating dynamic stress-optical coeffs. and ratio of Poisson's ratio to modulus of elasticity 80−86394
passive ring cavity optical rotation sensor, drift performance 80−1343
phase interferometer control of mode locking in gas laser 77−72009
phase locked interferometers, phase difference, surface topography measurements, transparent phase object applications 79−58775
phase shifter, broadband, for two beam interferometer 78−37968
phase-lock interference microscopy, real-time, design, appls. 79−17480
phase-locked interference microscope, design and construction 78−49894
phase-switching of a dispersive non-linear interferometer 80−82810
phase-tracking stellar interferometer, first fringe meas. 80−82215
photoelastic constants meas., precision interferometer 77−26384
photometric etalons, scatt. matrix and brightness coeffs. of MS-20, MS-14 reflectors 78−82020
picosecond optical sampling, cascade of waveguide interferometers driven by microwaves 80−99849
piezoelectric air-spaced Fabry-Perot etalon, stabilisation 77−82591
piezoelectric constant measurement, at frequencies up to 50 kHz 79−63270
plane-mirror two-beam interferometer analysis 79−2812
plasma density IF phase meas. using three-mirror interferometer 78−75414
plasma density meas. 10^{19}-10^{22} m^{-3}, and simple hydrocyanic acid 0.337 mm 78−5922
plasma density meas. by interferometer 78−55748
plasma density profiling, high speed interferometer 77−1021
plasma diagnostics, fast interferometer using N_2 laser, electron density of dense plasma 78−87489
plasma electron density and mag. field meas. by far IR polarimeter-interferometer 79−32817
point-diffraction interferometer principles and applications 80−74530
polarisation, for small dynamic deform. meas. *(Russian)* 79−9205
polarisation interferometer, construction from Michelson interferometer *(Russian)* 78−89532
polarisation ring interferometer 77−37971
polarisation Wollaston-prism interferometer fringe curvature correction 79−6170
polarised light, spectral analysis, polychromatic and coherent optics *(French)* 79−50209
polarising, mode of operation in dispersive Fourier transform spectroscopy 78−78003
polarising, using W wire grid beam divider, FIR performance 80−10012
polarization convertors for 2-freq. interferometers 80−18005
polarization interferometers, used in ballistic experiments 79−97426
polarizing interferometer, ultimate resolution, laser beam phase front radius of curvature meas. 79−88997
portable laser Doppler velocimeter for vibrating surfaces 79−68666
preprocessor, use in Earth-resources satellites 80−67430
quadrature interferometer, for plasma density meas. 78−1900
quasiquadrature interferometer for plasma density radial profile measurements, with 10-channel operation 80−70038
radial grating lateral shear heterodyne interferometer, adaptive optics appl. 80−77843
Raman laser, CW fibre, bandwidth reduction using prisms, gratings and etalons 80−53366

light interferometers continued
rapid spatially scanning IR heterodyne, for plasma diagnostics appl. 79−49275
rapid-scan polarising Michelson interferometer and InSb detector calibration 80−59305
Rayleigh, for amplitude-phase distribs. meas. of light fields 77−30200
Rayleigh, improved air refractive index meas. *(Chinese)* 77−57383
Rayleigh interferometer, two-freq., performance as refractometer and anemometer 79−75579
Rayleigh wave monitoring, simple interferometer 78−74052
real-time interferometer for optical system testing 79−85168
real-time shearing, quality factors testing appl. 80−37081
reflecting interferometer design with predetermined characteristics *(Russian)* 79−93206
ring, using optical fibre of 950 m length 77−37969
Ronchi interferometer, meas. of aberrations of non-parabolic graded-index medium 79−36843
rotating, phase shift due to Doppler effect 80−18006
rotating optical fibre ring interferometer, Fresnel-Fizeau effect 78−4685
rotation shearing interferometer, with phase compensated roof-prisms 78−77971
rotational shearing, for imaging through turbulent atm., spatial freq. resolution 78−69450
rotational shearing interferometer, 180° shear increased optical efficiency 80−47095
Rozhdestvensky interferometer with nonequal arms for anomalous dispersion measurements by the interference fringe shift *(Russian)* 78−279
Sagnac effect fibre ring gyro with electronic phase sensing 80−1350
Sagnac fibre-ring interferometer gyro with electronic phase sensing, using lasers 79−17472
satellite problems, mechanical disturbance effects on optical elements *(German)* 80−36478
scale-measuring laser interferometer 77−5804
scanning, spectral analysis of hollow cathode metal vapour ion lasers *(Japanese)* 80−9864
scanning Doppler interferometer, automated, for small absorpt. coeff. meas. 78−45680
scanning Fabry-Perot interferometer for far IR balloon astronomy 79−35093
scanning microinterferometer with correction of errors caused by overlapping 'ghost' images 80−259
scanning technique for obtaining linear fringe shift readout 78−89530
scatterplate, in uncommon path mode, for null testing 80−79015
scatterplate interferometer, energy distrib., Fourier optics approach 80−31850
scatterplate interferometer, scalar diffraction theory 80−73432
scatterplate interferometer principles, limitations and tolerances 80−73436
schlieren interferometer, 3-D vol., radiation transfer, probability model 77−87818
second-harmonic interferometers 80−101833
semiconductor etalon, optical bistability and ns modulation 80−64096
semiconductor Fabry-Perot interferometer retuning by optical excitation *(Russian)* 80−98970
semiconductor nonlinear interferometer, logical element *(Russian)* 79−49279
semiconductor thin-film nonlinear Fabry-Perot interferometer for optical pulse shaping 79−89945
servocontrolled Fabry-Perot interferometer, 3 in 10^{11} laser wavelength meas. 78−89452
Shack interferometer for optical shop use 80−73434
Shack unequal-path interferometer 78−58020
Shack unequal-path interferometer 79−54182
shearing, errors due to misaligned test section 78−93755
shearing, for aspherical wavefront testing 77−31144
shearing interferometer, holographic, description of new instrument 78−37847
shearing interferometer as filter for scattered light reduction 77−25941
shearing interferometer for dense laser prod. inhomogeneous plasma *(Russian)* 80−83994
shearing interferometer with scanned photodiode array and microcomputer for automatic transparency distortion measurements 79−80675
shock wave diagnostics using laser interferometer, appl. to Al plate 79−64814
single mode optical fibre, small phase shift meas. 80−57366
sliding reference, as wavefront analyser for diagnosing high-energy lasers 79−59740
sliding reference, as wavefront analyzer for diagnosing high-energy lasers 79−59738
Smartt interferometer as alignment tool for IR laser systems 80−33072
solar rotation induced Doppler spectral shift meas. by scanning Fabry-Perot interferometer 80−77298
space-borne interferometers, astrometry and planetary detection 80−109357
spatial filtering system 78−90515
specimen holder for transmission dispersive far IR Fourier transform spectrometry 80−86468
speckle applications to correlation and information processing 77−19189
speckle interferometer, subsystems and S/N ratio 77−41678
speckle interferometer construction, review 77−71369
speckle pattern interferometer for total plane strain field meas. 77−26388
speckle pattern TV interferometer, principle and appl. 78−58014
speckle shearing interferometer for studying aberration of optical system *(French)* 77−65616
speckle shearing interferometer using Savart plate 77−30199
spectral line profile recording, high resolution, using Fabry-Perot interferometer and monochromator 80−42268
spherical lamellar grating interferometer for airborne far IR astronomy 77−25942
spherical optical surfaces testing, shape deviation determ. *(Czech)* 80−58821
spinning IR interferometer, appl. to nonsolar planets detect. 78−85977
spring actuated parallelogram as vibr. freq. converter 78−29150
stellar interferometer with incoherent signal accumulation, sensitivity 77−25946
stellar phase-grating interferometer, appl. to double-star obs. *(Russian)* 79−101070
stellar speckle interferometer, lens-atmosphere modulation transfer function meas. 79−101078

light interferometers continued
step-height measurement, stylus-type surface texture measuring instrument calibration appl. 78−77862
stroboscopic interferometer, dynamic optical component evaluation, remote-site operation 79−85164
sub-mm-wave laser interferometer, use of low-inertia semiconductor structs. to modulate radiation 80−31848
submillimetre laser interferometer system, for plasma density meas. 77−7586
surface planarity determ., using laser source 80−31711
surface roughness, high sensitivity interferometric measurement, features of two types *(Japanese)* 78−37048
symmetry property, spatial coherence requirement 78−41346
Talbot interferometers, simplified, for lens testing 77−757
tandem etalons for intermode calibration of diode laser IR spectra 80−32982
test installation for elec. contact transducer testing 78−12683
thermal length control, for lasers and etalons 78−87056
thickness measurement in white light 79−21807
three mirror, with absorbing mirror *(Russian)* 80−257
three mirror HF laser modulator 79−3728
three-layer dielectric reflectivity standard error analysis 77−79727
time integrating acousto-optic signal processors 80−48176
tissue analysis by IR microinterferometer 79−79714
Tokamak, JET, far IR interferometer design 80−59295
tracking Michelson interferometer stability improvement *(Russian)* 78−29149
tracking system properties and advantages 79−14080
transverse-displacement interferometer, appl. to impact of y-cut quartz 78−12747
traveling Michelson interferometer with phase-locked fringe interpolation 78−89451
triangular cyclic interferometer, anal. and alignment 78−77969
triangular path inverting, for schlieren system appl. 77−34018
triple Fabry-Perot, for solar spectroscopy, instrumental profile 78−40817
tunable laser linear scan control by Fabry-Perot interferometer 79−76693
two telescope, variable baseline (13 to 19 m), 1 arc-millisecond resolution *(French)* 77−91439
two-beam, cat's-eye, for laser wavelength comparison 78−86326
two-beam, comparison of refl. and refr. optics in condensing element 78−77968
two-beam, correlation reduction of two-dimensional optical information in course of photoelectric registration 80−19000
two-beam, tuning to zero beam path difference 79−97425
two-beam, wavelength comparison to French primary standard 79−6173
two-beam corner-cube, as digital wavemeter for CW lasers 77−162
two-beam interferometers with division of amplitude, central fringe 78−16839
two-beam laser interferometer, diffr. phenomena 79−63300
two-beam mirror interferometer, accuracy, emission beam divergence effects 79−26115
two-wave interferometers for use with monochromatic source, prism components 79−35814
two-wavelength holographic for surface relief parameters meas., metrological characts. 77−26393
Twyman-Green, modified, with computer generated hologram, for testing 77−42632
unequal path interferometer, alignment and use as optical test tool 80−9031
universal interference and polarisation apparatus 78−19986
velocity sensing interferometer (VISAR) modification 79−17481
vibration dissipation using springs and viscoelastic substances *(German)* 80−17986
vibration-insensitive He-Ne laser interferometer for plasma electron density meas. 79−14610
Voigt parameters, determination using nonideal interferometer *(Russian)* 79−9240
water vapour refractive index meas. from 0.3 to 1.5 THz 77−82596
wavefront meas. control, and conjugation, adaptive optical system aspects 79−59796
wavefront sensing systems compared 79−58766
wavefront shearing, for cryogenic laser fusion target quality assessment 79−97417
waveguide interferometer using modular holographic elements 77−61116
wavelength compensated wavefront folding type, achromatic fringes from extended sources 78−32868
wavelength meter, compact static, based on Fizeau interferometer, for pulsed and CW lasers 79−36947
wavelength meter, He-Ne laser/monochromator/interferometric system 77−18086
wavemeter for CW lasers 79−26112
wedge etalons, for magneto-optic beam shifter and polarization converter 79−32054
wind tunnel water droplet size distrib. interferometer 79−80673
Zernike, three-slit, thermal lenses focal distances meas. in active elements of solid lasers 80−48268
Zernike's three-slit interferometer, Fourier optical synthesis 78−65960
zero position recording interferometer 77−71368
Zygo interferometer system 80−73437
$Al_{0.42}Ga_{0.58}As$-GaAs-$Al_{0.42}Ga_{0.58}As$, etalon, optical bistability and modulation 80−58628
Ar laser interferometer for detection of gravitational radiation 79−101076
CO_2 laser, 10 ns pulse generation, rotating mirror technique 80−33042
CO_2 laser fractional fringe interferometer with feedback stabilization, for plasma density measurements 79−75582
He-Ne $^{127}I_2$ stabilised laser source for Michelson interferometer, optical feedback obs. 80−106545
He-Ne laser, I_2-stabilised, with long path interferometer, optical feedback effect 77−9544
He-Ne laser, microtremor meas. *(Japanese)* 80−9025
He-Ne laser interferometer for US displacement meas. 77−37972
He-Ne laser two-beam interferometer phase errors *(Russian)* 79−6166
NaCl etalon used to control modelocked multiline TEA CO_2 laser 80−23713
Nd^{3+}:YAG laser frequency stability improvement using active interferometer *(Russian)* 80−64043
Si Fabry-Perot couplers for optically pumped far IR lasers 80−69404

light interferometry
see also holographic interferometry; Moire fringes
aberration evaluation program 80−13130
absolute interferometric dilatometer 77−45832
absorbing material optical consts., transmission interferometry meas. on medium-thickness films 79−78768
absorption coefficients meas., interferometric calorimetry technique 78−24839
acoustic emission detection using Michelson interferometer and laser 77−90510
acoustic emission measurement transducers, comparison of piezoelec. and optical sensors 79−14192
acousto-optic frequency shifter, beam quality, heterodyne interferometry meas. 78−79127
acousto-optical polarisation interferometry 78−32864
active mirror characterisation by heterodyne interferometry 79−59799
aero-acoustic effects in CO_2 laser discharge fast photography and interferometry obs. 79−36875
air at Ti surface, optical breakdown, interferometric investigation 80−100064
airfoil, wave drag in transonic flow, shear interferometry obs. 79−77165
algorithm for fast digital analysis of interference fringes 80−73426
alignment mechanism, testing by interferometric method 80−53454
amphibian middle ear dynamics using laser speckle interferometry 78−40198
angle meas., 30°-60° range, calibration, accuracy *(German)* 77−79051
anomalous dispersion meas. using 4-beam Rozhdestvenskii interferometer 80−68245
arc plasma, atmospheric, electron density meas. by two-wavelengths interferometry *(Japanese)* 80−38720
aspheric surface quality assurance 78−50962
aspherising layer prod., monitoring by interf. fringes in periscopic microscope 77−14820
astronomical high-resolution techniques, atm. degradation effects, book contrib. 77−33357
astronomical IR interferometry, high spatial resolution methods, speckle and aperture synthesis *(French)* 80−46405
astronomical optical intensity and speckle interferometry, review *(German)* 77−56835
astronomical optical interferometry with two telescopes *(French)* 80−46403
astronomical speckel interferometry with multiple mirror telescopes, laboratory expts. 79−80237
astronomical speckle interferogram masking, holography and phase flipping 80−109373
astronomical speckle interferometry, defocusing effects 78−40834
astronomical speckle interferometry, image reconstruction by speckle masking 77−49308
astronomical speckle interferometry, obs. using linear digicon detector 77−78648
astronomical speckle interferometry, stellar image recovery, photon noise limitations 77−49309
astronomical telescope speckle interferometry, online digital autocorrelator 78−81548
astronomy, Doppler broadening parameters and Doppler shifts meas. without spectrograph 78−20646
astrophysical applications of image restoration, conf., Bordeaux, France (Mar. 1979) 80−41935
atmospheric isoplanation measurement using speckle interferometry 78−65385
atmospheric pollutant detection, spectral interfernece correlation method 79−8727
atomic profile determ., Fourier analysis, deconvolution of Fabry-Perot interferograms *(French)* 80−48972
atomic spectral lines, unresolved components, interferometric meas. 79−98039
audio transformations in acoustical transduction based on optical principles 80−53594
automatic interference comparator, high precision linear gauge calibration appl. *(German)* 78−77847
automatic pattern processor for simple and complex interference patterns 80−13129
axially symmetric object, refr. index determ. from emerging ray directions 77−87809
axon diameter changes concurrent with action pot., crayfish, laser interferometer meas. 77−64029
Babinet compensator using white light for birefringence dispersion meas. in glass 78−27177
benzene, Raman nonlinearity characterisation by two-beam interferometry 77−38986
binary gas mass diffusivities determ. 77−62326
binary stars, obs. by speckle interferometry 80−90477
binary stars, speckle interferometric obs. with Haute-Provence 1.93 m telescope 80−90475
binary stars, unresolved, epochs of speckle interferometric obs., (1975-77) 78−73735
binary stars, visual, speckle interferometric meas. 77−78820
biological objects, electronic speckle pattern interferometry in vivo 80−109083
birefringence small retardation meas. using uniform-field Babinet compensator 79−93208
birefringent slice, isoclinics and isochromatics, speckle pattern visualization 77−2687
bonded interface defect testing by differential interferometric Stoneley wave meas. 80−76444
boundary layer turbulence, press. fluctuation meas. by optical interferometry 78−26222
Brillouin spectra, interferential spectrometry 77−178
camera window for aerial photography large interferometer for testing 78−13821
capacitative excitation of elastic oscillations 80−71862
chemical laser optical inhomogeneities, Michelson interferometric meas. 77−674
circular surface trueness testing by laser speckle photography 79−86266
clad optical fibres, nondestructive interferometric meas. of α and Δ 77−84013
colour reproduction of objects by speckle interferometry in white light 80−47094
combustion phenomena deflection mapping, speckle superposition techniques 78−44379

light interferometry continued
communication multiplexing, large path-difference white-light interferometry *(French)* 77−10842
communication system, large path diff., nonparallel light *(French)* 77−75668
complex aspheric mirror testing by phase meas. interferometry 80−74467
complex correlation function between two signals, interferometric method, with spatial filtering *(Spanish)* 79−76611
complex spatial coherence meas. by sinusoidal phase modulation 80−106446
component inspection by speckle pattern interferometry 77−37975
concave aspheric surfaces, quantitative test using Babinet compensator 79−98512
concave paraboloidal mirror, prod. method, interferogram tests 80−58823
contact lens radii and thickness meas. by interferometry 80−8118
contactless thermal expansion meas. by double Michelson interferometer 80−73317
continuous wavelength interferometry for measuring dispersion of complex refractive index 80−22423
contour slope meas. of an object, coherent optical method 78−32862
convective heat transfer coeffs. meas., refraction and end effect errors 77−71315
corner cube, dihedral angle error determ. from Twyman-Green interferogram 77−65646
correlative data processing system using semiconductor injection laser 80−74307
cotton, otpical anisotropy, multiple-beam interferometric obs. 79−8115
crack front, stress intensity factor, three dimens. speckle interferometry 77−84196
cracking metal surface deformation obs. by interference microscopy *(German)* 77−56210
crown glass, corrosion by organic acid solns., exam. of corrosion depth by interferometry *(Japanese)* 79−20237
cuvette for studying optical nonuniformities in aggressive liquids 79−2810
cylinder, rectilinearity meas. using equal chromatic order fringes 80−27286
cylindrical mirror and lens optical figure characterisation with conventional interferometer 80−78944
cylindrical thread charact. meas. by interference fringe procedure *(German)* 78−4585
data treatment in transaxial tomography, optical improvement 79−34666
defect crystal structure determination 80−103316
defocused speckle photography, topological information extraction technique 77−41676
deformation meas., interferometric method, appl. to sheet metal and transparent plastic sheets 78−75108
depth measurement of bright flat holes by means of projected fringe pattern methods 79−75583
deviation prism interferometric testing 78−30095
diameter meas., high speed noncontact light scatt. technique 77−83956
diamond turned surface production, interferometric test repeatability 80−74538
dichroism, linear and circular, Fourier transform spectroscopy-differential interferometery meas. 79−71514
dielectric film, refr. index, film thickness, phase shift and order of interference, interferometric method 78−276
dielectric film, refractive index and thickness meas. by optical method 80−82806
dielectric film or membrane, optical thickness meas. using Fabry-Perot interferometer 77−71367
dielectric relaxation spectroscopy of polar fluids in microwave region, double beam interferometry method *(German)* 80−71309
differential Fabry-Perot, for measurements of bulk particle motion fields of SAW 80−53576
differential interference contrast microscopy, computer simulation 77−53973
diffusely reflecting objects, deformation meas. by lasers, appl. of holography and speckle, review *(Japanese)* 80−9832
diffusing surface inclination determ. rel. to viewing direction, speckle photography 79−2815
digital electronic system for Fabry-Perot interferometer 78−12748
p-diiodobenzene, phase transition obs. using interferometry 78−34616
dispersive-reflection spectroscopy at liq. He temps. using Michelson interferometer 80−31910
displacement derivative meas., using multiple image shearing interferometric camera 80−33549
displacement determination in special alloys by holographic and speckle interferometric methods 78−27688
displacement meas. between reflecting surfaces with automatic interferometer 79−97354
displacement meas. by interferometers with electro-optical modulators *(Russian)* 78−12667
displacement meas. of curved surface, using laser speckle interferometry 80−31712
displacement meas. of diffuse surfaces moving with high vel., interferometric method 79−6092
displacement measurement, 3-dimens., from single image hologram, combined holographic and speckle interferometry 77−83831
distance measurement methods, recent crustal movements appl. 79−80057
distributed temperature sensor of optical path fluctuations, calibration 77−2688
Doppler beats and interference fringes 79−62957
double beam interferometer, meas. of background suppression and spectral detection 80−95130
double beam interferometric determ. of ellipsometric phase shift 78−93757
double frequency grating shearing interferometer, slope and curvature meas. 80−13126
double-beam Fourier spectroscopy with interferometric background compensation 77−38038
double-beam interferometry with optical background suppression 79−75576
double-shearing interference microscopy, appl. to optical fibres inhomogeneities *(French)* 77−54819
dual-mode optical fibre, spatial technique for modal delay difference meas. 80−78950
dye CW lasers, investigation of jet quality 79−94253

light interferometry continued
dye laser, for metrological interference measurements 80−28250
dye laser, interference metrological applications, spectral kinetic charact. *(Russian)* 79−27253
dynamic laser speckle interferometry, appl. to transient flexure 78−32861
Earth strain measurements with laser interferometer *(Japanese)* 79−25346
education, Fourier transform interferometry, visible reflectivity spectra 77−33765
elastic moduli measurement, laser-target technique, for glass, over wide temp. range 77−27497
elastohydrodynamic film thickness, meas. of artificially produced dents and grooves 80−36975
elastohydrodynamically loaded surfaces, interferometric deform. meas. 79−43532
electrochemical conc. polarisation at electrode, convectionless steady state, interferometric investig. 78−68896
electrochemistry, optical experimental methods 78−20022
electron beam impact on materials, measurement of dynamic response using laser interferometer 79−42102
electron beam pumped laser, interferometric technique for transient phase shift meas. 80−1195
electron irradiated solid, dynamic and dosimetric charact., laser and holographic interferometry obs. *(Rumanian)* 80−90886
electronic phase meas. techniques in optical testing 80−106643
electronic speckle pattern interferometry, appl. to NDT 77−74491
electronic speckle pattern interferometry, fringe contrast analysis 79−72506
electronic speckle pattern interferometry, optimal signal processing 78−16837
electronic speckle pattern interferometry, small vibr. detection and meas. 77−72253
electronic speckle pattern interferometry, small vibrations meas. 78−32865
electronic speckle pattern interferometry, vibr. phase mapping 77−5897
electronic speckle pattern interferometry, vibrating object meas., use of chopped laser light 79−85165
electronic speckle pattern interferometry for NDT 79−24702
end standards measurement, phase correction by profiling technique, gauge blocks appl. 78−73986
epitaxial magnetic film thickness meas., interferometric method 79−35675
equidensity fringe pattern lines on special film, calibration 77−18118
ether drift expts., using coupled mirrors interferometer 80−22193
Fabry-Perot, consequences of piezoelectric ceramic LF charact. 80−86390
Fabry-Perot interference ring diameter meas. using CCD linear sensors 79−93210
Fabry-Perot interference rings, focusing props. 77−58454
Fabry-Perot interferogram, determ. of far IR spectrum 79−2840
Fabry-Perot interferometer, multipassing method 78−54448
far IR 2-D plasma interferometry evaporographic and pyroelec. recording 78−5929
far IR interference filters 77−22592
far IR interferometry, (1950-76) 78−4456
far IR Michelson interferometry based on fast plasma scanning 77−31513
fast aspheric mirror figure control by profile monitor, wire tester and null lens 80−14419
fatigue crack propag., plastic wake zone effect investigated with optical interference technique 80−55502
ferrofluid, suspension, magnetodiffusion, interferometric obs. *(Russian)* 77−4946
fibre break testing by interferometry, comparison of breaking methods 77−58491
fibre diameter checking, laser interference method 78−18080
fibre index profile measurement using transverse interferogram, accuracy 78−66931
fibre optic laser gyro signal detection and processing technique 79−37037
fibre optic rotation sensor, signal detection and processing 79−37034
fibre refractive index profile calc. from transverse interf. patterns 78−74967
fibre refractive index profile meas., nondestructive transverse interference method 78−38024
fibre refractometry by interference microscopy, simplified method 79−18504
field plotting of optical fields using single-mode optical fibre 78−30097
filter, interferometric, illum. with convergent beam, spectral response optimisation *(French)* 80−99868
Fizeau, for refr. index and thickness meas. of nearly transparent films 79−17469
flame, counterflow diffusion, struct. in elec. field, interferometric obs. 80−16685
flapper-valve charact., appl. 77−24040
flatness testing by self-levelling reference plane 78−63207
flexed plate, slope and curvature contours meas. using interferometer 77−87810
fluid, effects of normal stresses, interference meas. method 78−94624
fluid flow and heat transfer visualisation *(German)* 79−86540
fluid flow patterns from speckle interference fringes 77−84346
fluid velocity measurement by speckle photography and interferometry 78−26221
Fourier interferograms, dispersive two-beam, computation 79−97424
Fourier interferograms, undispersive two-beam, computation 79−97423
Fourier spectroscopy, ghostline intensity in far IR 80−73480
Fourier transform spectroscopy, inexpensive student expt. 78−49609
Fourier-transform IR emission studies of overlayers on metal surfaces 79−67399
frequency phenomena in three-mirror laser, implications for interferometry 77−3617
frequency-variant signal waveform processing using 2-D optical processors 80−48178
Fresnel reflection coeff. of 3-phase system determ. by modulated reflectance spectroscopy and interferometry 77−82621
fringe evaluation of equidensiometric technique (for photoelasticity) 77−27495
fringe localisation region, van Cittert-Zernike theorem 78−74051
fringe position determ. accuracy improvement by photodetector signal conversion 78−58015
light interferometry continued
fringe signal generator for testing fringe shift measuring system 78−65962
functional group analysis of interferometric data from GC Fourier transform spectroscopy 80−89548
gas density meas. by multibeam interferometry 78−58016
gas dynamics, meas. using optical interferometry, review 77−35286
gas flow application of shearing interferometers 78−55706
gas laser, interferometric correction of output charact. *(Russian)* 77−79855
gasdynamic flow diagnostics by laser interferometry 77−51137
gases, compressed, refractive index meas. using Fabry-Perot interferometer *(French)* 80−14878
gases, rotational Raman spectra 77−73494
gauge block measurement, sources of uncertainty 79−26029
Gaussian beam astigmatism, meas. by Ronchi grating interferometer 79−3635
gelatinous light modulating media, dynamic deform obs. by laser interferometry 79−32072
general relativity test, precision ring laser interferometry technique 80−52117
geodesic interference distance meas. using semicond. lasers 80−77175
ghost image interferometer, anal. 78−32863
glass, index inhomogeneity, rapid interferometric determ. 79−93207
glass, small thermo-optical charact., stress coeffs. 77−31123
glass film and shell wall thickness meas., white light interferometric meas., dispersion effect 80−4757
glass microbubbles, interference fringes, forbidden zone 77−18702
graded index fibre profile determ., interferometric method 80−14481
graded index materials, optical props. meas. 79−9237
gradient index material profiles and chromatic props. 80−14409
gradient index profile measurement by Babinet fringe analysis 79−49277
grating writing, interferometric piecewise generation 77−42590
gravitational radiation detection method, elastooptical antenna, photoelastic effect 80−46947
grids of fine W wire, production, use in IR spectroscopy, polarization interferometry 80−9052
heat transfer in vertical thermal channels, interferometric simulation 79−17477
heat transfer mechanism with boiling in narrow spaces, interferometry obs. 78−94527
helical motion of rigid body, meas. by double exposure speckle method 78−16775
heterodyne, real-time digital broad-beam, for measurements of deforming surfaces 79−85173
high fringe density technique, transparent phase objects, appl. to heat transfer *(German)* 78−21212
high speed to measure effects of neutral gas density reduction on negative pulseless glow-spark transition 80−33850
high-current arc electrode vapour influence and estimation 80−70070
high-energy, IR laser component optical characterisation techniques 80−14347
high-pressure gas equation-of-state meas. 80−77810
HOBHA, smectic A to C transition, crit. biaxiality *(French)* 77−4039
holographic grating scanner with aberration corrections 77−61924
holographic image and plate substrate quality relationship 80−48193
holography, twin-image, chromatic lens system, astron. appls. 80−87346
human visual system, MTF *(Japanese)* 77−73526
hydrocarbon drops levitated in water, acoustically forced shape oscill. 79−47987
hydrophone, interferometric fibre optic, static press. sensitivity amplification 80−38094
hydrophone, optical interferometric, with homodyne detection, signal stabilization by light source tuning 80−87477
hypersonic ballistics experiment, application of laser light source 78−38433
IC 443, supernova remnant, Hα inteferometric obs. of fast filaments and high vel. gas 79−75258
image quality and wavefront profile determ. from interferograms 79−85172
image-forming reflection system testing by grazing-incidence Linnik interferometry 79−76891
image-moire method for refractive index measurement 80−22420
imaging, two-dimens., of rotating objects 78−1176
imaging through turbulence with telescope array, speckle interferometry 77−5458
impulse loaded plates, exam. of stress distribution, using Mach-Zehnder interferometer *(German)* 79−41643
in plane strain displacement near crack tip at high temp., optical meas. 79−32412
in-plane mechanical vibrs. meas. by speckle imaging, sub Å range 78−30247
in-plane stress waves in solids, mapping by laser speckles 79−27608
in-plane vibration measurement, real-time speckle interferometry with aid of liq. cryst. light valve 80−53734
inert gases, weak shock wave struct. investig. 79−94679
inhomogeneous media, optically dense, interferometric method for scatt. meas. 78−24854
interactive video image digitiser, appl. to interferogram anal. 78−58021
interference measuring devices, photodetector parameter optimisation 78−16844
interference microscope, VELOMET interphako, for optical path difference measurement 78−37054
interference microscopes, calibration standards *(Slovak)* 79−71522
interference microscopy, for colour development and phase separation 80−100976
interference microscopy for intercrystalline transport process obs. *(German)* 79−30538
interference reflection microscopy, image interpretation theory and appl. to cells 79−80677
interference-phase method of mag. field meas. in solar atm. *(Russian)* 78−65509
interference-phase method of ray vel. meas. in solar atm. *(Russian)* 78−65508
interferogram fringe pattern reduction, automated system 80−47097
interferometric examination techniques 80−69498
Interphako interference microscopy, refr. index profile determ. of light focusing rod 80−101832
IR, dual beam Fourier transform spectrometer, sensitivity improvement by using Digilab 496 interferometer 80−90910

light interferometry continued
IR absorption measurement, interference calorimetric method, effect of crystal thermo-optic props. 80−47096
IR aspherical lens and surface evaluation 77−39019
IR complex refr. index spectra, FT interferometry, errors in liquid-cell expts. 77−87814
IR emission microinterferometry for alignment of fluid bearing lubricants 78−58013
IR optical components and aspherics, 10.6 μm interferometric testing 80−74523
IR pulsed laser spectral characts. determ., interferogram display on luminesc. screen 79−10341
IR speckle interferometry, appl. to accreting young stars ang. dimensions determ. 79−44482
IR speckle interferometry, principle, performance and appl. to NML Cygni 80−31216
IR stellar speckle interferometry, modulation transfer function and evidence for log-normal statistic 79−101079
IR thermooptic coeffs. meas. of laser window materials 77−36208
irregular phase objects, dynamic interferometry, differential holography using phase conjugate refl. 80−37969
laboratory's absolute velocity meas. 80−95081
laser, diffusion of O_2, N_2, H_2 and Ar in water 77−76584
laser, fluid props. meas. 80−75018
laser, for non-contact liquid level meas. *(German)* 79−12769
laser, length changes in subnano-meter range meas. *(Slovak)* 78−77861
laser, use in analytical ultracentrifuges, background suppression of multiplexer-gated modulatable laser 80−73430
laser, using LF phase modulation, for small vertical vibration meas. 77−37970
laser beam applications, survey *(German)* 77−698
laser beam applications 77−694
laser beam contraction dynamics due to thermal transient self-focusing, high speed interferometry obs. 79−10368
laser beam divergence meas. using lateral shearing interferometry 78−13739
laser beam expander for short cavity dye laser 80−87532
laser beam interferometric wavelength measurements through post-detection signal processing 80−42254
laser beam multiplication, interferometric method *(Ukrainian)* 78−90442
laser beam propagation through turbulent atmosphere, interferometric evaluation of imaging characts. 77−88643
laser beams, high intensity, spectral purity anal. 77−88823
laser bulk absorption homogeneity, Doppler interferometric meas. 79−14010
laser coordinate control system, for program-control module *(Russian)* 78−21103
laser crystal evaluation, testing and meas. instrument 77−7226
laser diode, spatial coherence, studied with reversing front interferometer 80−32993
laser displacement meas. system for positioning of sphere and meas. roundness 79−97416
laser for vibration control and meas. *(Russian)* 78−71299
laser freq. and vel. of light meas., interference methods, accuracy 78−17997
laser frequency instability, short duration, interferometric meas. 79−3733
laser frequency meas., interferometric method based on Doppler shift 77−165
laser fusion, microballoons, wall thickness meas. using Interphako interf. microscope 78−87469
laser fusion, shadowgraph and interferometry experiments, with ten-picosecond light source 78−42824
laser fusion cryogenic target characterisation by wavefront shearing interferometer 80−74008
laser fusion target uniformity, interferometric meas. 78−47158
laser fusion targets, interferometric meas. of microsphere wall thickness variations 79−17470
laser generated plasma, expansion, pulsed mag. field effects, interferometric studies 77−58876
laser heated IR windows, interferometric meas. 77−46748
laser heterodyne detect. of slowly varying displacements 77−34019
laser interferometric auto-correcting system of high precision thread grinder 80−90830
laser interferometric profilographs for surface irregularities meas. 77−74363
laser interferometry, vibratory processes investigation appls. 77−118
laser interferometry by induced modulation of cavity field 78−49888
laser interferometry diagnosis of plasmas, review *(Russian)* 77−11409
laser interferometry in linear measuring techniques, problems with environmental influences *(German)* 79−30411
laser interferometry measurement system 79−6171
laser material nonlinear refractive index meas. by time-resolved interferometry 77−18088
laser measurement of optical, thermal and mech. props. of materials 77−74513
laser Michelson interferometer length meas. error rel. to illuminating beam form 77−26267
laser pulse duration meas. 78−50830
laser quasi-Gaussian beam geometric parameters, interf. determ. methods 79−64265
laser Rayleigh scatt., forward direction, spatial coherence deterioration, polaris. interferometry technique 77−10838
laser shearing interferometer appl. to supersonic flow field meas. *(Chinese)* 79−32715
laser single picosecond pulse, freq. sweeping and self focusing, direct streak meas. 78−25915
laser single pulse spectral distrib. meas., using Fabry-Perot interferometer and CCTV system 79−3732
laser sources coherence analysis, meas. system with Michelson interferometer *(Polish)* 78−33762
laser speckle interferometry, anal. of double aperture speckle and shearing camera techniques 79−6169
laser speckle interferometry, vibration anal. of plate and shell 77−10008
laser speckle interferometry of periodic nonsinusoidal vibrs. 77−41673
laser speckle photography, double-exposure, magnification change effect 79−40607
laser speckle photography for fluid flow vel. meas. 78−14112
laser speckle photography for in-plane displacement sign detect. 77−79140

light interferometry continued
laser speckles, bibliography (1976 to 1978) 80−82593
laser system, interferometric optical anal. 80−87401
laser system for creep measurement in pressurized tubes, in-reactor creep, reference fuel cladding appl. *(German)* 77−74925
laser velocimetry technique, for phase inhomogeneous medium, appl. to pulsed flow *(Russian)* 78−30375
laser wavelength, comparison of 2 beams, two-wave interference, book contrib. 78−9408
laser wavelength meas. with post-detection signal processing 80−105699
laser wavelength measurement, review 78−50841
laser wavelengths comparison, interference circuits analysis 80−23737
laser window materials, temp. and stress effects on refr. index 77−46771
laser-matter interactions, automatic treatment of data *(French)* 78−42830
laser-produced plasma, application of synchronised ultrashort Nd:glass laser pulse 78−42825
lateral shearing inteferometry for transparency distortion anal. 78−4684
lateral shearing interferometry for stochastic inputs, data reduction 77−26386
Lau effect-based interferometry 80−265
length meas., secondary calibration standards wavelength meas. *(Rumanian)* 79−40533
length meas. of gauge blocks, sources of random errors 80−105613
length meas. with curved wavefronts *(German)* 80−77752
length measurement from fractional fringes 77−71291
length measurement using Ar^+ laser, wavelength stabilisation 78−33766
length measurement with heterodyne interferometry *(German)* 80−68181
length of gauge block, using 3.39 μm He-Ne laser 79−97346
lens assessment techniques, polychromatic and monochromatic, in far IR 78−50899
lens sphericity non-contact testing method *(German)* 78−5534
lens wavefront aberration, interferometric examination techniques 80−69498
lenses, standard reference, for assessment of OTF meas. equipment 78−50897
leucosapphire, unique polishing features of hard crystals 80−64225
light scattering medium, spatial struct., interferometric meas. *(Russian)* 78−70181
light sources, review of options 80−47092
linear phase restitution, 10 μm *(French)* 78−12749
linear velocity meas. by YAG laser 79−26039
liquid crystal optical birefringence determ. from interference meas. 77−72551
liquid crystals, cylindrically aligned, optical characts., interferometric analysis 79−73897
liquid gas interface, deform. in inhomogeneous elec. field *(Bulgarian)* 80−54474
liquid metal column, acoustic velocity meas. across diameter 80−14527
liquid refractive index variation with temp. meas., interferometric technique 78−74050
liquids, diffusion coeff. meas. and refractive index depend. on concentration at different wavelengths 80−88346
liquids, high-press. refr. index meas. to 14 kilobars 77−49764
localisation geometry of interf. fringes in classical and holographic interferometry 79−30536
long-pathlength interferometry accuracy and noise problems 80−31860
long-radius concave optical surface curvature meas., differential technique 80−74534
lubrication of compliant bearing, study by optical interf. method 77−36711
2,6-lutidine-water thick films, interferometric obs. of crit. behaviour 80−93266
machine tool geometry inspection, appl. 77−9997
machine tool position feedback by laser interferometer 80−73438
machined part flatness and parallelism meas., contactless interferometric method 78−21208
magnetostriction measurement, small vibr. detection 78−12731
magnetostriction measurement *(Japanese)* 79−65705
magnetostrictive vibration meas., laser interferometric technique 80−37059
manometer, interferometric, method of operation 78−24808
MBBA liquid crystal wedge as a polarizing element and its use in shearing interferometry 80−53444
measurement, control and testing, coherent light appl. *(French)* 80−23641
mechanical vibration meas. optical heterodyne systems 77−13746
mechanical vibration meas. using laser *(French)* 78−67156
metal mirror, diamond turned, optical figure inspection by interferometry 78−5545
metal plate high-gradient transverse deformation interferometry 78−82024
metal surface, rough, orthogonally polarised speckle images, cross correlation, effect on fringe visibility in speckle interferometry 78−37808
metal surface inspection appl., with ground finishes 79−34216
metallic film, island surface coverage, determ. by optical interference 77−1810
metals, coated, IR surface wave interferometry 80−63913
methanol trace detection using phase fluctuation optical heterodyne spectroscopy 80−68266
Michelson interferometer technique for capacitance displacement transducer error obs. 78−54356
Michelson-Morley expt., new, verification of relativity principle in special theory of relativity, in Space Lab 80−27124
microscopic imperfection detect. on high quality surfaces using interf. patterns 77−74493
microscopy, colour schlieren technique 78−29151
microscopy, for plant cell wall and cytoplasm refr. index determ. 78−57151
microscopy, interference, surface height standard deviation on ground glass surface 79−93098
mirror, single-point diamond-turned, performance before and after polishing 80−74466
mirror reflectance meas. using multiple wave interferometer *(French)* 77−42585
mirrors, plane, spatially separated, adjustment to coplanarity, interferometric technique 80−95974
mixture chemical analysis, direct interferogram comparison of chromatography/Fourier transform IR spectra data 79−100458

light interferometry continued
Moire effect and deformation meas. in structural components *(German)* 78−88587
Moire fringe multiplication in transmitted light *(German)* 77−166
moire interferometry with white light using auxiliary compensator grating 80−31847
moire methods for contouring displacement, deflection, slope and curvature 79−80674
Moire photography, appls. of slotted apertures 77−65053
Moire technique for reading impressioned writing *(Hebrew)* 77−2690
moire techniques 79−63298
moire topography, real-time and time-resolved, in microseconds region 80−52154
Moire topography uses in medicine, radiotherapy applics. *(German)* 77−12983
monochromatic light interference meas. 78−32867
monochromators as tunable radiation sources in interferometry 80−23787
motion, combined and general forms, laser speckle interferometric obs. 78−74054
motion paths display, speckle photography, holographic reconstruction 77−18084
MTF, two-dimensional, meas. by second order speckle statistics calc. 80−63937
MTF meas. technique 77−3688
multiaperture method, strain analysis by one-beam laser speckle interferometry 79−81821
multidirectional interferograms, meas. of refr. index distrib. in interior of solid object 77−71363
multiframe, using inorganic liquid laser 77−30211
multilayer film, intrinsic and thermal stress modelling and interferometry 79−14059
multimode fibre optic interferometry, applications 80−86387
multiple beam Fizeau interference, spatial struct. 79−71517
multiple beam interferometry, polarisation doubling 79−21806
multiple-beam, meas. refractive index of solid transparent specimens 80−52299
multiplex image coding, astronomical IR speckle interferometry appl. *(French)* 80−67580
negative DC corona study in atmospheric air using Schlieren and interferometric techniques 80−49023
negative photoresist, KMR-747, transmission and refr. index 2 to 10 μm, interferometric meas. *(French)* 79−76780
negative selection, for production of uniform intensity of light 77−2685
Newtonian viscosity meas. of oil films 77−89214
NGC 604, H II region in M 33, Hβ photometry and Fabry-Perot interferometry rel. to core-halo struct. 80−85984
nitroethane/iso-octane, crit. mixture, refractive index 79−87413
Nomarski polarisation interferometry, for slope determ. of microscopic surface features 78−16840
non-optical surface topography, by oblique fringe projection from diffr. gratings 78−89437
noncontact material testing using laser energy deposition and interferometry 79−34258
noncontact material testing using laser energy deposition and interferometry 80−71846
nondestructive evaluation by laser speckle interferometry 78−60976
nonlinear optical coeffs., interf. method for relative magnitude accurate determ. 77−31115
nonlinear optical susceptibility meas. by interferometry *(Russian)* 77−61112
oil droplets, motion and optical props. by interf. method 78−67893
one-dimensional stellar and solar speckle interferometry 77−64662
optical diffuser form. of simple known statistical props., interferometric surface height determ. 78−90539
optical fibre, γ-irrad., differential interferometric meas. of refr. index changes 80−78952
optical fibre, rapid Δ meas. by refr. index tuning 78−13792
optical fibre, single layer, dimensions and refractive index meas. 77−79952
optical fibre characteristics testing, differential interferometry 80−48397
optical fibre preform rod, refractive index profile meas. by transverse differential interferogram 80−64141
optical fibres, refractive index profile meas. using thick samples, interf. pattern 77−61111
optical fibres and preforms, modified CVD, axial refr. index depression, interf. microscopy obs. 80−1319
optical films, side-illuminated, interf. pattern obs. 78−50914
optical heterodyne interferometer, appl. to surface inspection 77−90529
optical heterodyne interferometry, double, method of reducing IF 79−17475
optical heterodyning in US vel. and absorpt. meas., Raman diffr. by US waves 79−18640
optical material continuous heterogeneities, interf. meas. 78−93756
optical materials, piezo-optic coeff. determ. under static loading, interferometric and polarimetric techniques 79−4787
optical measurement technique using He-Ne stabilised transverse Zeeman laser 80−48272
optical path difference meas. by double diffraction interferometer 78−24851
optical path difference meas. by double diffraction interferometer *(Japanese)* 78−82025
optical phase modulation of light beams, Michelson interferometer meas. *(German)* 79−17473
optical screw, path difference meas. and control device, anal. of periodic errors 78−77972
optical shop computer-controlled interferometry, in-process production tool 80−74531
optical shop interferometric instrumentation as a cost-effective production tool 80−74535
optical surface mapping with quarter wavelength fringes 78−46846
optical surface meas. using FECO scanning interferometer 77−7219
optical surface modal deformation sensor for heterodyne interferometry 80−31859
optical system acceptance testing with interferometer 80−95987
optical system testing, interferogram analysis, point spread function and OTF determ. 79−76616
optical testing status and prospects 80−74529
optical transfer functions, meas. using lateral shearing interferometer with correlated diffusers 79−97419
optical window interferogram evaluation method 77−84011
light interferometry continued
optically isotropic and anisotropic materials, rapid optical method for stress-optical const. determ. 77−5899
optically transparent materials, evaluation of elastic ratio by interferometry 78−90804
optics applied to metrology, conf., Strasbourg, France (1977) 79−6159
organic compounds, nonlinear refr. index meas. by time integrating interferometry 80−102758
oxide films, corrosion resist. determ. method 79−24689
oxirane-acrylic bead, radical conc. gradient determ. by microinterferometry and microfluorometry *(German)* 79−100799
p-n junction minority carrier diffusion length meas. 80−31849
parabolic mirror testing by vibration-insensitive laser unequal path interferometer 80−74537
parabolic mirror testing during fabrication by long-wavelength interferometer 80−74536
parallel optical flat SAW meas. by reflective interferometry 79−76931
parallelicity criteria for samples studied by Fabry-Perot interf. 78−24850
partially coherent perpendicularly polarized vibrs., anisotropic photographic recording, interferograms 80−57364
particle sizing, fringe visibility in crossed beams 77−71292
path difference determ. from interference patterns 78−82028
path difference measurement on anisotropic materials 80−4758
phase changes in optical recording media, interferometric meas. 77−49769
phase locked interferometers, phase difference, surface topography measurements, transparent phase object applications 79−58775
phase measurement using interferometer with filamentary spatial filter and extended source of polychromatic light 79−71518
phase modulation, appls. to material characterisation and dimensional metrology 79−6174
phase modulation, expt. process to restore phase sign and value 78−32869
phase modulation interferometry combined with object scanning *(French)* 79−2814
phase modulation polarisation, meas. of phase differences in microscopy *(French)* 77−82593
phase problems, image recovery from Fourier transform modulus 78−82918
phase-locked interferometry 78−58022
phase-modulation interferometry, sine restoration of phase in object field *(French)* 77−79144
photoelasticity anal. by Moire method 78−51138
photometry of interference patterns, noise elimination 79−97414
piezoelectric constant measurement, at frequencies up to 50 kHz 79−63270
piezoelectric micrometer for precision movement in optical alignment applics. 77−65017
plano-plano interferometer modes, FFT computation, Fresnel numbers 80−86392
planoconvex AT-cut quartz resonator vibration displacement meas. by laser interferometry 77−37976
plasma, cylindrically symmetric refractionless, interferometric data inversion 79−90459
plasma, electron density meas. in shock generated plasma by light interferometry 80−48981
plasma diagnostics, high speed multiframe interferometry 78−1905
plasma discharge, axially symm., interferogram numerical processing 77−27717
plasma focus, electron density distrib., N_2 laser interferometric study, X-ray and neutron emission 78−87479
PMMA, destruction kinetics of intense ms loading, laser differential interferometry obs. 79−24623
polarisation interferometer, meas. of local convective heat transfer coefft. for plate calorimeter 80−82809
polarisation props., optically active samples in ring interferometers *(German)* 80−77846
polarised two-beam interferometry assessment 77−37973
polycarbonate, craze thickening mechanism during craze growth 79−91823
polyethylene terephthalate, sheet, Poisson ratio compliance consts., interferometry 77−12663
polyethylene ultradrawn fibres, Poisson ratio from Michelson interferometry 78−80596
polymer film, surface profile obs. and nature of contact by multiple beam interferometry 77−1878
precision optical element testing by phase meas. interferometry 80−74520
precision optical evaluation by phase meas. interferometry 80−74533
precision optical testing, using laser interferometers, microprocessors and computers 80−69563
pressure measurements, static or dynamic, transducer calibration 78−21159
primary mirror of large azimuthal telescope, interference testing method 77−73952
prism fabrication errors meas. by interference method 77−58494
prism figuring, optical path difference check by Hendrix interferometer 77−72094
quasi-Ronchigrams for interpreting wave-front and glass-error slopes 80−37078
quasicoherent light source image synthesis by phase measurable interferometry 77−58284
quick precision alignment of equipment, calibration against external goniometers 80−73429
radioisotope zone plate coded aperture imaging 77−40762
Ramsey fringes, saturated optical absorpt., spectroscopic appls. 77−38021
random-phase screens, deep, interferometric anal. 80−101834
real time atmospheric compensation, active optical imaging 77−49307
real time interferogram simulation by analogue device, aberration generation, CRT display 79−54181
real time linewidth meas. of tunable multiatom. CO_2 laser 78−9405
real time wavefront anal. automatic method for interferograms 79−75585
real-time digital heterodyne interferometry for optical path difference maps 80−37076
real-time heterodyne interferometry, high-performance 79−75574
redundant-spacing interferometry, image sharpness, Fourier optics 78−5427

light interferometry continued
reference marks arrangement for interferometrically recorded sedimentation, diffusion and thermal diffusion expts. 77−87813
reflective object displacement and vibration meas. *(Russian)* 79−21695
refractive index, local values in heterogeneous and homogeneous media, meas. method *(Russian)* 78−32858
refractive index automatic profiling 78−46836
refractive index field reconstruction, discontinuity effect 77−79138
refractive index field reconstruction for strongly refractive asymmetric fields 80−4760
refractive index meas., absolute interference method for solids 77−41674
refractive index measurement technique for liq. CO 79−65816
refractive index measurements using laser differential interferometer, appl. to high density plasma 77−55170
refractive index of solids, meas., Fabry-Perot interferometric technique *(Russian)* 78−82023
refractive index profiling of optical fibres 79−76816
refractive index profiling of optical fibres 79−81527
refractive index radial distrib. in light focusing rods, interf. microscopy meas. method 77−57381
refractometry, precision automatic vee block, for glass refr. index meas. 80−68243
repositioning of hologram by interferometric technique 80−23640
retinal function, laser interference fringes meas. *(German)* 77−12910
retinal resolving power meas. by laser interferometry 80−36066
retroreflector, temp. stability testing under space conditions 77−62078
retroreflector alignment, simple interferometric technique 80−95125
reversible fringe counter in laser interferometry 77−87816
review of interferometry, including holographic interferometry 78−37050
r.i. axially symmetric distrib. determ. using eikonal approx. 77−2686
rigid body, parallel displacement meas. using polychromatic speckle patterns 77−41568
ring laser interferometry, test of preferred frame cosmologies 80−77531
Ronchi interferometry appl. to large aperture flat mirrors testing 79−85171
Ronchi test, practical formulae and experimental verification 80−43490
rotary face seals, lubricated, interferometric obs. 79−20204
rotational symmetric aspheric in compensated interferometers, computer-generated-holography testing 80−33128
rough object motion measurement, real time, speckle pattern correl. 77−10098
rough surface, correlation functions determ. 78−5428
rough surface interferometry at 10.6 μm 80−86385
roughness measurement of supersmooth surfaces, using electron mirror interference microscope 79−93260
Rozhdestvenskii double-beam interferometer, interference pattern form. 80−37080
ruby, unique polishing features of hard crystals 80−64225
ruby laser beam spatial coherence interferometry 79−14003
sandwich speckle interferometry 79−30537
Savart plate interferometry for isothermal diffusion meas. 78−45678
scanning Fabry-Perot, meas. of spectral output of CW CO laser 77−27292
scanning focus by interferometry, beam shear change 80−52301
scanning interferometry approach to phase microscopy 78−45684
scanning moire topography, automatic 3-D shape meas. 77−79139
schlieren microscopy technique 77−34016
seawater density, vertical structure meas. using optical interferometry *(Russian)* 80−51569
second order coherence meas. using microscope and grating 77−41672
sedimentation phenomena of fine particles investigated by vibrational force field and interferometry 79−60086
seismic microvibration frequency analysis by 50 m interferometer 80−109276
semi-Lambertian reflecting surface, laser speckle interferometry 78−82910
semiconductor, nonlinear optical props. 80−25333
semiconductor heterogeneity refractive index meas., interferometric method 79−6172
semiconductor junction laser, radiation coherence, interferometric analysis methods *(Polish)* 80−19065
semiconductor manufacturing, interferometric method for surface deform. meas. 78−32793
seminar, San Diego, CA, USA (Aug. 1979) 80−73096
shadow-Moire time-averaged method for vibr. amplitude determ. 77−71364
shearing interferogram evaluation improvement *(German)* 80−27339
SHG, Maker fringe method, effects of beam width and wedge angle 77−72028
shock wave effects, laser interferometry 77−79145
shock-loaded solids, shear-wave particle vel., interferometer technique 79−99268
signal processing, time-integrating, acousto-optic 80−102641
silicone elastomers, dental impression materials, dimens. stability, holographic and interferometric study 80−67204
sine wave grating, linearly variable freq., production method by interferometry 80−10028
single mode fibres for optical field mapping, interf. technique 78−74966
single-mode optical fibre interferometry 80−73442
skin friction meter using viscosity balance principle for metal surfaces 77−35266
small angle meas. by constant inclination inteference *(Chinese)* 79−30419
solar granulation, one-dimensional speckle interferometry 78−45299
solar photosphere, granulation statistical properties and seeing, speckle interferometry obs. 79−88634
solar speckle interferometry calibration, atm.-lens MTF changes 79−2370
solid flaw remote sensing, laser system prod. acoustic waves, interferometric detect. 78−60975
solid surface characterisation techniques, review 78−22945
solid transparent samples, refr. index meas. by interferometry 79−95722
source coherence meas. and fibre modal noise simulation by Michelson interferometer 80−48324
space and time variables in optics and holography, interferometry in white light 77−34830
spatial coherence analysis using reversing front interferometer 78−277
spatial coherence complex degree determ. using folded-wavefront type interferometer 78−24853
spatial coherence meas. by correlated diffusers 80−74296
spatial filtering using Mach-Zehnder interferometer 77−42616
light interferometry continued
spatial frequency determination, selected interference schemes 80−48146
spatial phase resolution meas. of electro-optic modulators 77−79959
spatial power spectra estimation in speckle interferometry S/N ratio calc. 79−76608
speckle, astronomical, isoplanicity and temporal correlation meas. *(German)* 79−75116
speckle, atm. nonisoplanicity meas. using double stars 78−65387
speckle, binary stars ang. separations meas. 79−40215
speckle, interferometric measurements of binary stars 79−71065
speckle, meas. of binary stars 78−85973
speckle, mechanical guides displacement control, in meas. systems *(Czech)* 80−31852
speckle, metrology and testing by lasers, review 77−5817
speckle, stellar diameters and close binary star separation meas. *(Russian)* 78−40922
speckle, two-point, astron. appls. and disadvantages *(Russian)* 79−16840
speckle applications, review 77−83820
speckle applications in metrology *(French)* 77−67494
speckle camera and analyser for surface displacement and tilt meas. 78−32790
speckle contrast, roughness props. meas. 77−18082
speckle image for radius of curvature meas. of cylindrical surface *(French)* 77−34020
speckle interference fringes, lens aberration effects 80−105700
speckle interferometric analysis of transient phenomena 80−105701
speckle interferometric meas. of ang. diameters of asteroids Vesta and Pallas 79−35172
speckle interferometric obs. of solar photospheric granulation *(French)* 80−46523
speckle interferometry, appl. to binary stars 77−71011
speckle interferometry, astron. appls. *(French)* 80−46404
speckle interferometry, atmosphere turbulence effect ang. depend 79−101080
speckle interferometry, binary stars obs. with 1 m telescope 78−69831
speckle interferometry, book contrib. 79−75584
speckle interferometry, coherence requirements, use of thermal radiation sources 78−49891
speckle interferometry, decorrel. effects, contouring and surface roughness meas. 77−45886
speckle interferometry, decorrel. effects, machine induced strain obs. 77−45887
speckle interferometry, displacement meas. errors rel. to camera displacements during exposure 79−17479
speckle interferometry, double-exposure, with instant Polaroid film 79−221
speckle interferometry, effects of spectral bandwidths and exposure times 78−69701
speckle interferometry, focused radiation scintillations freq. correl. 79−94153
speckle interferometry, fringe visibility recovery from recorded images quantised to two levels 78−12104
speckle interferometry, image reconstruction of single stars 78−32350
speckle interferometry, image restoration by least squares method 79−25514
speckle interferometry, lens aberration effects, optical system pupil complex amplitude changes *(French)* 79−50237
speckle interferometry, meas. of astronomical objects, simulated multiple mirror telescopes 80−56716
speckle interferometry, one beam, smallest displacement 79−97427
speckle interferometry, orbital inclination and masses determ. for triple star β Persei (Algol) 80−36668
speckle interferometry, real-time meas. of vibrations and displacements *(Italian)* 78−54336
speckle interferometry, wideband, true imaging of astronomical objects 80−53226
speckle interferometry bandwidth extension using simple optical system 79−26114
speckle interferometry for looking at star surfaces 77−9675
speckle interferometry for stellar size and shape determ. 78−77491
speckle interferometry fundamentals and appl. *(Czech)* 78−29148
speckle interferometry image processing technique requiring no reference point 80−98556
speckle interferometry meas. of Pluto diameter 80−41763
speckle interferometry of binary stars, computer simulations in photon-counting mode 78−53836
speckle interferometry S/N ratio, photon counting autocorrelation mode at low light levels 79−76613
speckle measurement method, appl. to oil instrumentation *(French)* 77−71365
speckle pattern correlation, real time roughness meas. 77−18081
speckle pattern intensity and phase, second-order conditional statistics 80−37951
speckle pattern interferometer for measurement of displacements and surface tilt in stress analysis, book contrib. 79−20334
speckle pattern interferometry, electronic, using digital image processing techniques 80−87322
speckle patterns, photographic recordings, fringes generated in Fresnel plane 78−66763
speckle phenomenon fundamentals *(Czech)* 78−29147
speckle photography, defocusing problem 77−18083
speckle photography, double exposure, anal. technique 80−62718
speckle photography, effect of lens aberrations 78−32866
speckle photography, flow velocity distrib. meas. 78−67288
speckle shearing interferometry, fringe parameters 79−220
speckle topography, appl. to surface relief obs. of diffuse reflection object 79−54096
spectra calibration, using Edser-Butler bands, for teachers 79−21504
spectral-temporal effects, white-light interferometry and phase-locked pulse anal. 77−88656
spherical particle velocity and size meas., crossed-beam light scatt. interferometry 80−47011
spherical surface error absolute definition technique, use in interferogram analysis 79−86268
sphericity standards, interferometric meas. *(German)* 80−87569
standard sieves, Fourier transform method for verification of wire screens 77−53874
star cluster high resolution imaging by speckle interferometry, simulation 78−77492

light interferometry continued
star mass meas. using gravit. starlight deflection in close visual doubles *(French)* 79−62753
stars, nonsolar planets detect. via spinning IR interferometer 78−85977
static and dynamic calibration using optical interferometric techniques 79−23178
stellar interferometry, high ang. resolution obs., review 77−33355
stellar interferometry, long baseline, S/N ratio 80−26749
stellar interferometry of star cluster with prominent variable 79−84680
stellar speckle data processing method 80−17498
stellar speckle interferometry, appl. to image reconstruction of α Oriionis 77−22222
stellar speckle interferometry, atmospheric effects, laboratory simulation 79−53730
stellar speckle interferometry, lens-atmosphere modulation transfer function meas. 79−101078
stellar speckle interferometry, phase var. estimation 77−45317
stellar speckle interferometry, S/N ratio 78−12102
stellar speckle interferometry, two aperture pupil plane 79−35145
stellar speckle interferometry, wave correlation scale meas. 78−65388
stellar speckle interferometry data processing method 79−12409
stellar speckle interferometry for imaging through randomly fluctuating media 77−13248
stellar speckle interferometry lens-atm. MTF meas. 77−22103
stellar speckle interferometry on 2.5 m Isaac Newton telescope 77−22102
step height determ. by two-wavelength speckle pattern method 80−105614
step height measurement in μm range by two-ray interferometry with adjustable light wavelength *(German)* 77−82489
straightedge Fresnel diffraction, optical phase distrib. interferometric meas. 79−76579
strain analysis, Moire method, raster manufacture and copying *(German)* 77−121
strain in transparent plates 77−75865
strain measurement method using diffr. beams of diffr. beams 79−32397
stroboscopic interferometry, active mirror testing appl. 79−58782
subspeckle size changes meas. by laser-speckle photography 80−31853
subwavelength focused light beam, knife edge scanning meas. 77−75641
supergiant stars, circumstellar dust shell, stellar interferometry 79−80309
superposition fringe pattern, automated central achromatic fringe setting 78−24852
superposition fringes as measuring tool in optical testing 79−86267
surface contour and inhomogeneity testing, interf. fringe distortion with imprecise focusing 78−89531
surface deform. of opt. flats and Fizeau method for film thickness meas. 78−77970
surface displacement and strain anal. by speckle interferometry 80−14635
surface displacement and vibration meas. using laser speckle *(French)* 78−4686
surface mapping with variable sensitivity, IC manufacturing appl. 78−45592
surface roughness, high sensitivity interferometric measurement study *(Japanese)* 78−37048
surface roughness meas., speckle correlation of diffuse surface image *(French)* 77−61115
surface roughness of small-diameter channels, non-destructive inspection by replicas 77−30136
surface strain field meas. on rubber structures, optical method 77−34017
surface testing on optical element production line 77−27397
surface testing with quarter-wavelength sensitivity 78−32870
surface topography quantitative determ. by Nomarski differential interference contrast microscopy 80−73318
system test interference pattern analysis program and error elimination method 79−76894
Talbot-Schlieren interferometric method to see US waves 77−10099
techniques, Michelson, Fabry-Perot and Twyman-Green, common interferometer base 80−266
telescope arrays, large aperture, interferometric observing efficiency 79−80238
telescope with severe aberration, MTF for speckle interferometry 78−12103
temperature field measurement of axisymm. buoyant phenomena 78−89529
testplate testing interferometry in precision optical shop 80−74532
tetrafluoroethane, specific refractivity, interferometric meas. 80−95124
tetrafluoromethane, specific refractivity, interferometric meas. 80−95124
thermal conductivity and diffusivity measurement using non-steady-state method 79−50572
thermal expansion, speckle interferometric meas. apparatus 80−68170
thermal expansion at high temps., meas. via laser interferometry of two fibres 77−26270
thermal expansion meas. method 78−45676
thermal expansion ultraprecise meas. 77−71290
thermal turbulence in plane airstream, temp. fluctuation meas., interferometric method 79−7432
thermoosmotic concentration difference meas. for gaseous mixtures across membranes 79−83508
thermophysical investigation of optical inhomogeneities using laser source *(Russian)* 78−37049
theta-pinch, density, azimuthal mag. field effects, laser interferometric meas. 77−11406
thickness measurement of transparent plates, 10 to 1000 μ 79−71406
thin film thickness step gauge, Ba stearate multilayer films on EDF glass, interference colours 77−5900
thin films, unbacked, optical constants by transmission interferometry 79−78778
thin plates, plane reflecting, statically loaded, interferometric exam. of curvature and twist 78−45679
three-beam interference images, sinusoidal complex object with phase modulation, interferometric gratings 80−53208
three-dimensional display interferometry of lenses, mirrors, and optical systems 80−69497
time-resolved, with picosecond laser pulses 77−74492
time-resolved interferometry, nonlinear refr. index meas. of glasses and crystals 79−3737
time-wavelength coordinates obtained using spectrograph, time scan 80−62717
light interferometry continued
transient jet experiment, interferometry, using multiple-pulse laser light source 78−14114
transmission replica system for strain measurement 79−74323
transparent layer refr. index and thickness determ., optical interf. method 78−89528
transparent microtarget, for laser fusion, interference method 77−9012
transparent solid plates, evaluation of stress-optical coeffs. using interferometry 79−97418
transversal micro-vibration meas. on diffusing objects, real time, random moire principle 79−85123
transverse displacement of distant body, interferometric meas. 77−82488
truss joint strain meas. by modified Michelson interferometer 80−74821
tunable laser interferometry, oscillator strength meas. 80−105697
turbid media, spatial struct., light scatt. meas., interferometric study 79−54178
turbulent media interferometry 79−2816
two wave interferogram sensitivity improvement process *(French)* 80−98968
two-beam interference fringe interpolation method 80−105703
two-beam interference pattern monitoring by phase modulation 80−77844
two-beam interferometry using tapered optical fibres *(Japanese)* 77−49767
two-dimensional optical system MTF meas. by second-order speckle statistics computation 80−74304
two-wave interferometry, appl. to light pulse interactions *(French)* 77−3597
ultramicrometer technique using composite diffr. grating 78−4589
ultrasmall displacement meas. 78−57897
unsteady convection study, simultaneous velocity and interferometric meas. 79−98839
US parameter measurement and appls. to medicine 77−39184
US transducer calibration method using laser interferometry 79−23177
US wave meas. by differential interferometry 77−72120
velocity contour generation by speckle photography 77−2638
velocity measurement, using interf. effects of pair of two-freq. laser beams 77−79071
velocity of light determ., absolute wavelength meas. of CO_2 9.4μm band R(14) line 77−82485
velocity of light in vac., expt. test of wavelength independ. 77−74350
velocity-time history recording, by laser interferometer system 78−45602
vertical surface melting, heat transfer interferometric meas., convection effects 80−64339
vibration insulation of equipment for optical system performance testing 78−90543
vibration measuring system using interf. fringes TV detect. and electronic image processing 80−103004
video interferogram analysis by TV camera-microprocessor system 80−73440
viscometer, rotational interferometric, for Newtonian viscosity measurements 79−50824
viscosity measurement, falling slug method, intensity fluctuation spectroscopy appl. 78−71408
visible and IR stabilised lasers, wavelength intercomparison 77−7114
VRO 42.05.01, Hα inteferometric obs. of fast filaments and high vel. gas 79−75258
wave aberrations caused by misalignments of aspherics, and their elimination 80−33127
wave optics, partially coherent fields of illumination, pencils of rays 79−98275
wavefront analysis, automatic real-time meas. of interferograms, technique 80−9029
wavefront distortion compensation in real time 77−17219
wavefront interpretation with Zernike polynomials 80−78776
wavelength comparisons with primary Kr standard using Michelson interferometer 80−98969
wavelength measurements, review of recent developments 80−48320
wavelength stabilisation, review of decade of work in Switzerland *(German)* 80−57250
waxicons for high-power chemical lasers, interferogram analysis 80−14418
weakly absorbing layers, interferometric determ. of optical parameters 79−17471
white light interferometric microscopes 79−223
white light speckle method of experimental strain analysis 79−37255
wideband laser-interferometer gravit. radiation expt. 78−41223
Wollaston prism type interferometer, diff. theory of image construction *(German)* 77−158
X-ray mirror profile meas. machine 80−69496
Zernike, three-slit, thermal lenses focal distances meas. in active elements of solid lasers 80−48268
Zernike test, analytical aspects 77−23785
Zernike test, experimental aspects 77−23786
Zernike-Tatian polynomials for interferogram reduction 80−37077
Al alloys, optical contrast enhancement by vacuum deposited ZnTe layers 78−44301
Al plate, thermal strain meas. by one-beam laser speckle interferometry 80−103005
Al_2O_3-epoxy mechanical mixtures, stress-wave propag. model, dynamic response expts. 79−1477
Ar, laser discharge, spontaneous emission, at. line shapes, interferometric obs. 77−30816
Au, transmission interferometry, refr. index and extinction coeff. 77−69790
Bi I, excited configs., mag. hyperfine splitting factors, interferometric determ. near 200 nm 80−32852
C fibre reinforced plastic, thermal expansion, influence of resin type 78−95164
CO_2 laser fusion system optical design and analysis 80−74391
CO_2 laser multiwavelength interferometry, absolute distance meas. 79−31974
CO_2, pulsed laser, laser induced medium perturbation, time resolved interferometric obs. 78−58977
CO_2 TEA far IR laser, optimum spectral matching 79−31857
CdS, parallelicity criteria for Fabry-Perot interf. obs. 78−24850
Cu, electroplated coating, levelling kinetics, interferometric investigation *(Bulgarian)* 78−79864
Fe-Ni, interference microscopy, for colour development and phase separation 80−100976
GaS, refr. index in far IR, permitt. meas. 78−64360

light interferometry continued
He plasma chemical device, integrated electron density meas., interferometric method 79−55548
He-Ne 3.39 μm laser interferometer, length and refr. index meas. 80−68172
He-Ne commercial multimode low power laser, conversion to single mode laser 80−53325
He-Ne laser, $^{127}I_2$ saturated absorption stabilised, wavelength meas. *(Russian)* 79−22996
He-Ne laser, competitive oscillation mode frequency stabilisation *(Russian)* 79−22962
He-Ne laser freq. determ., interferometric comparison with upconverted CO_2 laser radiation 78−55395
He-Ne laser IR applications 79−94275
He-Ne laser interferometric and diffraction methods for meas. dia. of circular cylindrical wires 79−21703
He-Ne laser interferometry for vibration control and meas. *(Russian)* 78−70117
He-Ne laser stabilisation and performance for dimensional meas. 80−19049
He-Ne laser wavelength meas., stabilised by saturated absorption in I_2 80−28264
He-Ne laser wavelength stability, calibration and traceability 80−19050
He-Ne lasers, wavefront curvature and diffraction effects in high precision wavelength comparisons with a Michelson interferometer 80−99781
He-Ne two mode ring laser for interferometry 78−1260
I_2 filter structure, digital normalisation, in quasielastic light scatt. 77−13805
KBr, plate, distortions due to 10.6 μm laser irrad., interferometric obs. 78−46697
KCl, photoelastic consts. at 10.6 μm, interferometric and polarimetric meas. 78−25934
KCl plate, distortions due to 10.6 μm laser irrad., interferometric obs. 78−46697
KCl(Br)(I), single cryst., quenched, microstruct. around indentations 80−7628
(Li-K)NO_3, molten, $K^+(Rb^+)(Cs^+)(Tl^+)$ diffusion, wavefront shearing interferometric obs. 79−60535
$LiNbO_3$:Ti single mode electrooptic waveguide modulator, high-speed operation 80−91915
Mg_2SiO_4, single cryst., (010) cleavages, etch patterns and dislocations, interferometric obs. 78−2127
N_2 laser, 3371 Å, fringe visibility curve 78−46695
Na lamp, high-press. advantages of use 77−9837
NaCl 46 cm window optical evaluation facility 80−74526
NaCl, plate, distortions due to 10.6 μm laser irrad., interferometric obs. 78−46697
Nd:YAG acousto-optically mode-locked CW laser, optical spectra obs. by interferometer 79−7134
Nd:YAG mode-locked laser pulse, quadratic phase evolution direct meas., time resolved interferometry 80−48318
Ni alloys, cast, interference microscopy, for colour development and phase separation 80−100976
Ni base superalloy, fatigue crack opening load variation with meas. location 80−16425
Ni, magnetostrictive vibr. obs. by laser interferometric technique 80−66000
SF_6, trace detection using phase fluctuation optical heterodyne spectroscopy 80−68266
Se films, Ag diffusion, effect on interferometric thickness meas. 80−96695
Si guided-wave acousto-optical devices 80−102864
Si rubber as electro-optic material for optical hydrophones 80−43412
$Zn/ZnSO_4/Zn$ system, laser interferometric study of corrosion of coated and uncoated metals, technique standardisation 79−35815
^{67}Zn spectrometer, double freq. interferometer for absolute velocity calibration of piezoelectric transducer 80−37146

light meters *see photometers*

light modulation *see optical modulation*

light polarisation
see also birefringence; optical rotation; photoelasticity; polarimetry
3,3,3-trifluoropropene, struct. and vibr. spectra, IR, Raman polarisation study 80−18845
2A 0311−227, AM Herculis type binary star, IR photometry and polarimetry 80−77517
2A 0311−227, orbital period and polarisation obs. of optical counterpart 79−30151
absorbing anisotropic and gyrotropic slab between crossed polarisers, transmitted intensity patterns 80−78762
absorbing crystal plate light interaction, polarisation consts. 80−78765
accretion disc around binary star, polarisation effects in emission 79−35128
acetic acid, in cyclohexane soln., Raman scatt. near crit. stratification, temp. depend. *(Russian)* 79−11420
acetone, stimulated Brillouin scatt. wave front reversal for depolarised light 79−3743
achiral molecule, laser induced circular differential scatt., QED anal. 78−46409
achiral molecules dissolved in cholesteric liq. crysts., fluoresc. circular polarisation *(German)* 77−42350
acousto-optic polarisation modulator, use in dynamic ellipsometry, polarimetry *(Russian)* 80−14472
acousto-optical polarisation interferometry 78−32864
acridene yellow, glycerol soln., luminesc. intensity and polaris., temp. and viscosity effects 79−56833
acridine, dye solns., luminesc. spectra, conc. depend. effects 79−54885
acridine C-radical, polarised absorpt. and ESR spectra, dichroism and HF-CI calc. 78−50563
acriflavine, fluoresc. polaris., solvent effect 77−50468
acriflavine solution, fluoresc. polarisation, effect of aggregation of molecules 79−91485
active polarisation spectroscopy by combinational light scatt. *(Russian)* 78−78006
adsorbed molecule near solid surface, light scatt. calcs. 79−56069
aerosols, monodisperse, 0.1-0.4 μm, size meas. by polarisation ratio of 90° scatt. light 80−40754
alkali germanate glasses, polarised and depolarised Raman spectra, struct. 80−1936
alkali metals, two-photon ionisation with two light beams, polarisation effects 79−81190
n-alkane gases, depolarised light scatt., internal field effects 79−76471
altazimuth sky scanner optical system, polarization characts. 80−77123
Amici roof prism polarisation characteristics 79−72647
amplitude correlation mehtod for optical polarisation meas. 80−53206
analogue data processing systems, polarised modulation of light *(Russian)* 80−91884
o Andromedae, shell star, lack of linear polarisation variability 80−62157
aniline, liq., depolarised light scatt. from shear waves 80−97288
anisotropic crystal, additional light waves and boundary conditions 77−73121
anisotropic emission source, polarisation characts. meas. 78−74047
anisotropic grating, diffr. orders polarisation *(Russian)* 77−34818
anisotropic inhomogeneous medium with axial symm., mode struct. 78−18069
anisotropic media, molecular distrib. determ., using polarised absorption and emission spectroscopy 78−27298
anisotropic media, partially polarised light propag., differential 4×4 matrix calculus 79−41330
anisotropic media, polarised, depolarised scatter, anisotropy induced depolarisation 77−75412
anisotropic particles, light scatt. struct. coeff., angular depend. 80−103964
anisotropic transition layer, surface polariton spectra in presence of resonance 80−88484
anisotropically absorbing medium, polarisation nearness variation 80−1118
annular HSURIA resonators, testing with CO_2 laser, polarisation effects 80−58599
anomalous resonances in anisotropic multilayer structures 79−45902
anthracene, light polarisation depend. on energy transfer from excited to emitting mols. *(German)* 78−37677
anthracene, polarised reflection spectra, surface and vol. exciton coupling, vibronic states 78−72543
9-anthroic acid, excimer-type transition polaris. 79−50062
antiferromagnetic heavily doped semiconductors, Faraday light depolarisation in mixed mag. states 80−29726
aromatics, fluoresc. polarisation red edge effect, rot. anomaly 79−3472
atmopsheric scattering of lidar pulses, four-component polarisation meas. 78−44996
atmosphere, aerosol effects on polarisation of scatt. light from point source *(Russian)* 80−4106
atmosphere, multiple scatt. theory for dispersive media with spherical particles *(Russian)* 80−94599
atmosphere model, scatt. light intensity and polarisation degree, mol. anisotropy effect 80−77104
atmospheres, polarization and scattering 79−96814
atmospheric haze microstruct. and refr. index from scatt. light polarisation characts. *(Russian)* 79−29852
atmospheric multiple backscatt. and depolarisation obs. using lidar 78−36292
atmospheric radiance polarisation and ellipticity of multiply scatt. solar radiation 77−9457
atom, two-photon ionis. rates for circ. (linear) polarised light beams 80−43012
atom+charged particle anisotropic collision, spectral line shift and broadening, polarisation depend. 78−82695
atomic degenerate system, Doppler-free laser-induced dichroism and birefringence, linearly polarised laser 78−82711
atomic electron impact excitation, Bethe approx. modifications, impact radiation polarisation 79−31695
atomic gas with resonant levels, mag. rot. of ellipse of polarisation of propagating rad. 79−50340
atomic system, hydrogenlike, polarised monochromatic laser radiation absorption in electronic transitions, DC mag. field effects 80−9563
atomic systems, beam-foil interaction process, quantum beats, alignment and orientation obs. 80−14252
atomic vapour, f-value determ. method using stimulated electronic Raman scatt., appl. to Cs 78−82693
atoms, and ions, parity nonconservation effects 79−10086
autorotation of polarisation ellipse in nonlinear medium *(Russian)* 77−58374
axicon polarisation effects 79−45900
1-azo-bicyclo-2,2,2-octane, multiphoton ionis. spectra polaris. characts., two-photon symmetry assignment 78−74718
backscattering from water, ice or mixed phase drops 77−64426
bacteriochlorophyll absorption polarisation, in liq. cryst. cell 79−24950
Be and shell stars, Balmer line polarisation meas. 77−56995
Be shell stars, Bβ high-resolution polarisation struct. meas. by digicon spectropolarimeter 79−44485
Be stars, electron scatt. effects on emission line wings and continuum polarisation 80−17589
Be stars, mag. fields determ. via linear polarisation spectrum *(Russian)* 80−90344
Be stars, polarimetry at 1.25 and 2.2 microns 79−44484
Be-stars, intrinsic linear polarisation rel. to v sin i 77−60773
Be-stars, polarisation in extended circumstellar discs 77−56994
beam, image-bearing, nonuniformly polarized, generation of time-reversed replica 80−69459
beam sampling mirror gratings, optimal design 77−14791
beam splitter, birefringent, polarisation-independent 80−5814
beam splitters, multilayer polarised light, laboratory and factory testing 79−27428
beamsplitters, beam inherent parameters analysis 79−36999
benzene, liquid, polarised light two photon thermal blooming near UV spectra 80−66216
benzene, multiphoton ionis. spectra polaris. characts., two-photon symmetry assignment 78−74718
benzene, photoelectron ang. distrib. with linearly polarised HeI radiation 78−50580
benzene in 3-methylpentane glass, phosphoresc. polarisation and intensity, 77K 77−46588
benzoxazole, polarisation of 274 nm absorpt. system, band contour analysis 79−27043
binary and multiple stars, polarisation by Thomson scatt. in optically thin stellar envelopes 78−81655
binary mixtures, qualitative anal. using fluoresc. polarisation 79−24849
binary stars, spectroscopic and eclipsing, survey for intrinsic linear polarization 78−4288
bipolar reflection nebulae, photoelec. polarization maps 78−28742

light polarisation continued
birefringence detection system for polarisation opt. props. meas. 77−57385
birefringent element, analogue, built from polarising wide field Michelson interferometer 80−91895
birefringent object, isopachics meas. using immersion method polarisation holography 80−99672
birefringent retardation plate matrix representation 79−22894
birefringent rotating plates as modulated optical filters, polarised light meas. appl. *(French)* 77−67490
BL Lacertae-type objects, variable, IR and visible polarimetry and photometry 78−16528
blue stellar objects, from MC2 and MC3 catalogue, polarisation obs., BL Lacertae objects 79−48918
book, ellipsometry and polarised light 77−71361
borosilicate glass single-polarisation single-mode fibres 80−64205
boundary conditions in crystal optics with spatial dispersion 78−92040
trans-1,3-butadiene, multiphoton ionis. spectra polaris. characts., two-photon symmetry assignment 78−74718
3C 273, quasar, IR polarisation obs. 78−4360
canted magnetic structured materials, exciton spectra, optical props. 80−70622
α^2 Canum Venaticorum, mag. Ap star high-resolution polarisation obs. inside spectral line 78−40951
R Carinae, intrinsic linear polarisation narrow-band struct. 77−49397
η Carinae, silicate grains size distrib. rel. to linear polarisation 80−4382
η Carinae and Carina Nebula, polarimetric study 79−67043
CARS in isotropic liquid, polarisation props. 78−80334
γ Cassiopeiae, Be star, polarisation rapid vars. 80−22022
γ Cassiopeiae, Be star, rapid linear polarisation variability *(Russian)* 80−77417
γ Cassiopeiae, Hα linear polarisation in Be star 78−16425
γ Cassiopeiae, polarisation obs. rel. to circumstellar envelope model 78−40952
cataclysmic binary stars (CBS), critique of polarimetric evidence on physical parameters and orbital inclination 80−109486
VV Cephei, complex close binary, linear polarisation during 1977 elcipse 78−40995
β Cephei, linear polarisation obs. rel. to non-radial pulsations 79−40198
λ Cephei, linear polarization variability in emission line O star 78−36571
VV Cephei system, distant, in Puppis, spectral classification, UBV photometry and polarimetry 80−51810
o Ceti (Mira) at 1978 max., visible spectropolarimetry 80−94799
change of polarisation state in liquid and gaseous media *(German)* 77−88635
characterisation of materials, birefr., electro-, magneto-, elasto- and acousto-optics 77−48143
Charlier approximation in photocount statistics 80−74328
chiral compound, circular dichroism, polarisation modulated photoacoustic spectroscopy 80−18018
chiral substances, electro-optical responses, Jones matrix, meas. sytem for rot. anisotropy 80−84723
chloromethane gas, linear electro-optical effect 80−87843
chlorophylls, zero field triplet spin sublevel ordering, magnetophotoselection obs. 77−42342
cholesteric liquid cryst., opt. activity, polaris. azimuthal depend., helical chain model 77−11479
cholesteric liquid crystal, chirality determ. by circularly polarised light obs. *(Japanese)* 77−1078
cholesteric liquid crystal, imperfect, optical props. *(Russian)* 77−80420
cholesteric liquid crystal, polarised light transmission 78−9946
chromophores, circular polarisation of luminescence, book contrib. 79−5250
circular cylinders, single scatt. phase matrix, ray optics and wave theory comparison 80−102610
circular dichroism for scattering objects, examination using double-beam spectrophotometer 79−35853
circular differential photoacoustic spectroscopy 80−47114
circular polarisation of emission, magnetically induced, appl. to inorganic complexes 78−78005
circular polariser for refl. in far IR 78−79114
circular polarization of sunlight reflected from planetary atmospheres 78−28558
circularly polarised laser beam, intense, multiphoton ionis. pots. for H(He) 80−43010
circularly polarised laser light for improved visibility through mist 77−75596
circularly polarised laser radiation frequency shifting via rotating half-wave retardation plate 80−9800
circularly polarised light, right- and left-handedness, sign conventions for magneto-optical effects *(Japanese)* 78−23433
circulator, polarization-independent, configuration method 80−38095
circumstellar dust shells, Monte Carlo simulation of polarised light transfer 78−81608
circumstellar dust shells, polarisation by Mie scatt., Monte Carlo anal. 80−98650
circumstellar envelopes, Monte Carlo analysis of polarization by Thomson scattering 80−85931
close binary stars linear polarisation 77−49435
close binary systems, polarimetric determ. of revolution directions and spatial orientations 79−35309
close X-ray binary stars, ellipsoidality effects and linear polarisation in optical component 77−78898
clouds, optically thick medium, asymptotic radiance and polarisation 77−21776
coherency matrix, degree of polarisation, principal idempotents 78−17859
coherency matrix transform., comparison with Mueller calculus 77−6993
coherent light beam shifts on reflection at plane interfaces between isotropic media 80−102609
collisional polarisability effect on scatt. calcs. from dense fluids *(French)* 79−31789
colloidal dispersions, birefringence in Rayleigh and anomalous diffr. approximations 80−29710
colloidal graphite, in mag. field, optical transmission meas., polarisation depend. 78−31712
colloidal particles, interacting Brownian spheres, depolarised light scattering 79−34370
Comet Ikeya-Seki (1965 VIII), polarization reversal, grain segregation due to radiation press. 79−8881
light polarisation continued
Comet West (1976 VI), polarisation of head 80−8587
Comet West (1976 VI), radiation polarisation obs. 79−62794
compensator retardation determ. 79−26107
complete resonance Raman polarisation spectroscopy, linear and circular, modulation techniques 77−61130
composite material, sintered, microstrained state, opt. polarisation investig. 78−11476
compound optical polarisation materials for stress meas. *(Russian)* 78−87313
compressed gas, small depolarisation factor meas. method 78−32884
computer-generated polarisation holography system and reconstructed image quality 80−102677
conference, polarised light, San Diego, Calif., USA (Aug. 1976) 77−45881
conference on measurement techniques for optical fibre systems, London, England (May 1979) 79−64348
conical refraction, beam intensity distrib., using polarised light *(Russian)* 79−27172
conical refraction, of polarised light beams 80−28157
conjugate interfaces: interfaces between transparent media of the same reflection coefficient for the parallel polarization at the same angle of incidence 80−87299
continuous phase convention, extension to polarised light, impossibility 79−41335
cool stars, narrow-band polarisation effects 78−16427
cool stars, polarisation wavelength depend. 77−2426
corner cube, Jones matrix *(German)* 77−19420
corner cube, polarisation props., Jones matrices *(German)* 77−19419
correlation techniques, amplitude and intensity correls. meas. 77−154
corrugated dielectric waveguide, radiation loss calcs. for TM polarisation 80−43445
corrugated waveguide boundary, TM-polarized light diffraction, zero diffraction effect 79−64339
corrugated waveguides, effective index approach to distrib. feedback, TE polarisation 80−102859
coupled resonator model for resonant polarization conversion and anomalous beam shift *(Japanese)* 78−87133
Crab Nebula, optical linear polarization obs. from Durham 77−74126
Crab Nebula, small-scale polarisation obs. 79−25656
CRL 2688 (Egg Nebula), bipolar nebula, optical and IR polarimetry 78−36658
cube beamsplitters polarisation sensitivity, reduction by hybrid metal-dielec. coating 77−83981
cubic crystals, electro-optical effect rel. to spatial dispersion of permittivity 80−66151
cubic ferr-te garnet, diffracted light polarisation characts., spin and magnetoelastic waves 80−20614
curved 4-space interpret. of classical light propag. 77−58253
cyclic π-electron systems, magnetic circular dichroism 77−88481
CH Cygni, linear polarisation vars. rel. to circumstellar dust grains form. 78−69808
V645 Cygni (CRL 2789), bipolar nebula, O-type exciting star 78−4392
V1500 Cygni (Nova 1975), linear polarization obs. 78−36601
V1500 Cygni (Nova 1975), optical polarisation obs. 78−36622
V1500 Cygni (Nova 1975), polarimetric and photometric obs. 78−36612
V1500 Cygni (Nova 1975), UBVR Hα photometry and polarimetry 78−36611
V1500 Cygni (Nova 1975), UBVRI photometry and polarimetry 78−36614
V1500 Cygni (Nova 1975), visible-band linear polarimetry 78−36621
V1668Cygni (Nova 1978), linear polarisation obs. 80−26875
V1668 Cygni (Nova 1978), multifilter photometry and polarimetry 80−90454
Cygnus OB2 association, wavelength depend. of polarisation and interstellar birefringence 77−33577
Cygnus X-1, critique of polarimetric evidence on physical parameters and orbital inclination 80−109486
Cygnus X-1, optical polarisation orbital vars. rel. to binary system inclination 78−54077
Cygnus X-1, variable circular polarisation obs. 77−29952
Cygnus X-1 (HDE 226868), optical polarisation evidence for 78/39-day period 78−89274
Cygnus X-1 (HDE 226868), search for 78.4 day period in U-band polarisation 79−75297
Cygnus X-1 (V1357 Cygni), V-band polarisation excursions during X-ray high state 80−90578
Cygnus X-1 (V1357 Cygni), V-band polarisation vars. during X-ray high state 80−109560
daytime sky, UV light polarisation as indicator of atmospheric turbidity 78−20517
decane: pyrene (coronene), quasiline spectra, multiplet struct., freezing conditions and solvent effects 79−1786
defect crystal structure determination, light interference, diffraction and scattering 80−103316
definitions and nomenclature, for polarised light 78−29897
degenerate two level system, reson. light scatt., transient polarisation characts. 78−94382
demonstration, using rubber tubing model, classical analogy 80−77576
demonstrations with polarised light 77−45657
dense optically transparent media, third-order optical susceptibilities 77−38981
dense stars, continuum spectrum polarisation in intense mag. fields, atomic physics theory 80−105160
depolarised multispectral laser scatt., target classification 78−50846
depolarising diffusers, autocorrelation by holography *(French)* 79−31801
depolarising optical system characterisation by automated ellipsometer 78−32855
depolarization of optical emission from magnetic white dwarfs 79−97002
diatomic fragments, from triatomic mol. photodissoc., fluoresc. polarisation excitation spectroscopy 80−28054
β,β'-dichloroethyl ether-iso-octane, critical indices, allowance for light double scatt. *(Russian)* 80−60624
dielectric and absorbing nonspherical particles, scatt. and polarisation props. 77−34823
dielectric cylinder, scattered light polarisation characts. 77−75409
dielectric film, refractive index and thickness meas. by optical method 80−82806
dielectric molecular fluid, optical props., internal forces effects, theory 77−28534

light polarisation continued
dielectric multilayer coated optical surface, diffr. and diffuse scatt. 79−50220
dielectric overcoating on Al and Ag mirrors, polarisation effects 77−72055
dielectric thin film multilayer systems, polarisation effects and use in laser physics *(German)* 78−33912
dielectric waveguide, corrugated, light emission 80−96027
differential absorption at high modulation frequencies using a Fourier transform infrared spectrometer 80−95160
diffraction grating, concave, polarisation anomalies 80−69519
diffraction grating, phase difference and efficiency quotient of polarised light 77−768
diffraction grating anomalies, phase shifts and resonances 78−94446
diffraction gratings, Au, Al coatings, UV light at grazing incidence 78−87129
diffused waveguide, acoustooptic interaction efficiency of TE modes, freq. depend. 80−53455
dilute colloidal suspension, Krishnan effect, theory 77−34824
dimethyl oxalate, oriented cryst. film, polarised IR spectrum 80−29730
dipalmitoyl phosphatidylcholine vesicles, appl. of depolarised light scatt. theory from hollow spherical particles 80−45946
9,10-diphenylanthracene, luminesc. quantum yield, fluoresc. spectra polarisation effect, solvent viscosity depend. 78−27303
all-trans-diphenyltetradecaheptaene, oriented, photochem. reaction production and monitoring, reson. Raman spectroscopy 77−29020
Dirac-spinor form of Maxwell's eqns., polarised light beams in gravitational fields 78−50696
discrete deflector, matrix method anal. *(Russian)* 80−91747
discrimination techniques used in realization of acousto-optical processors 80−74310
dispersive media, theory of multiple light scatt. by spherical particles *(Russian)* 80−94599
dispersive particle sizes, from scattering and polarization meas. *(Russian)* 79−34950
DNA bases, polarised fluoresc. and estimated lifetimes, room temp. and in −125°C soln. 79−39352
DNA bases, thymine type, polarised fluoresc. in neutral aq. soln. 80−21445
DOBAMBC, polarized Raman scatt. and elec. field effects in aligned smectic phases 79−94873
doped cubic crystals, resonance absorption region, self-induced rot. of polarisation 80−2805
Doppler-free intracavity polarization spectroscopy using elliptically polarized light 80−5537
double grating P-polarised plane wave diffr., Fabry-Perot interferometer appl. 79−81544
double group theory, half-shell and two-level system, optical polarisation 78−49594
double scattering method for condensed systems parameters determ. 80−28161
dye laser, N_2 laser pumped, two wavelength outputs with orthogonal polarisations 78−50792
dye laser, pulsed, light polarisation, solvent viscosity effect 80−32977
dye pulsed laser, light polarisation with thin wedge plate in cavity 78−55394
dye soln., fluoresc. amplitude anisotropy, polarised light excited 79−85990
dye soln. tensor susceptance, reson. linearly polarised radiation, optical dye maser polarisation rot. *(Russian)* 77−58325
dye solution, polarisation of stimulated emission *(Russian)* 78−25872
dye-detergent model systems, degree of fluoresc. polarisation 78−27287
education, Brewster angle in semi-infinite dielectric moving perpendicularly to interface 80−57034
education, polar intensity profile of elliptically polarised light, comment 77−87600
electric dichroism measurement instrument with digital processing 80−82800
electric dichroism spectroscopy 78−1013
electro-optic, polarisation-conversion wavelength-selective fibre switches 80−58736
electro-optical gate for nonpolarised emission *(Russian)* 78−59132
electro-optical polarisation conversion and interference tunable filters 80−102829
electron impact excited line radiation, polarisation, long-range electron correls. effects 80−91683
electronic spectra of molecules, pure elec. quadrupole transition polaris. 80−63691
electrooptic polarization modulated injection laser 80−58591
ELLIPSA, two-photon spectroscopy method for polarisation meas. 79−6184
ellipsometer, polarisation-modulation, Fortran simulation program ELLIPS 78−271
ellipsometric characts. of optical surfaces, determ. using nanosecond laser pulses 80−101822
ellipsometry, azimuth response function, linear nondepolarising optical system 78−65957
ellipsometry, Mueller-Stokes calculus, conventions and formulas 80−102618
ellipsometry, zone theory, single zone procedures 77−82588
ellipsometry of transparent films on transparent substrates, theory 80−104007
elliptic polarization represented by the Carter and Smith charts 80−32902
elliptic retarder, expt. method for optical parameters determ. 77−88941
elliptical galaxies, polarisation by interstellar matter 78−93399
elliptically polarised beams in cubic media, self-focusing *(Russian)* 78−63156
elliptically polarised light, analysis of flow birefringence and extinction angle using U-shaped glass modulator 79−63293
elliptically polarised light, polar intensity profile calcs. 77−13526
elliptically polarised light, quantitative anal., $^1/_4$-wave plate, student expt. 78−49608
elliptically polarized Gaussian beams, nonlinear precession 80−28269
ellipticity, azimuth and system parameters linking eqns., 3-dimens. model propag. 78−50695
emergent radiation from Rayleigh atmosphere, polarisation meas. rel. to single scatt. albedo determ. 79−35117
entropy and LA fluctuations in solids, polarisation of scattered light 77−81113
eosin, fluoresc. polarisation, solvent effects 79−36678

light polarisation continued
eosin-erythrosin, soln., qualitative anal. using fluoresc. polarisation 79−24849
evanescent-wave holograms, diffr. efficiency, angular and polarisation depend. 80−48189
exciton absorption range, spatial dispersion theory *(Russian)* 79−61405
exciton luminescence, RF coherence and polarisation 78−10937
exciton resonance excitation in crystals, light scatt., polarisation, specular refl., theory 80−50356
eye photoreceptor directional sensitivity, coherence and polarisation obs. 79−100610
far IR laser intracavity polarisation modulation by CdTe AC Faraday rotation 80−58613
far IR polarising metallic cloth with periodic slits 79−14112
Faraday effect in single-mode optical fibre using injection DH laser light source 80−48245
fast ion double collision spectroscopy, polarisation obs. of emitted photons 80−16134
ferrofluid, magnetically induced polarisation, particle size determ. 77−73130
fibre, liquid core, polarisation props., bending effect 77−58440
fibre, single-mode evolution and polarisation 78−9432
fibre, single-mode systems, instability due to interference and polarization effects 80−58774
fibre fault detection using optimal time domain reflectometer 79−54173
fibre loss, dispersion and polarisation meas. by acousto-optical tunable filter 80−102855
fibre optic devices, single-mode, fractional wave devices and polarisation controllers 80−106606
fibre optic rotation sensor with low drift 80−69530
fibre optical polarisation rotator, single mode 79−76808
fibre optical polarisation transformer, in-line 79−72667
fibre Raman and Brillouin laser gains, polarisation effects 80−9887
fibre signal polarisation statistical meas. 80−99877
fibre-optic polariser, in-line, formation and props. 80−106603
fibre-ring interferometer, rotation-sensing, polarisation analysis 79−64333
fibres, noncircular core single-mode, polarisation characts. 78−94430
fibres, single-mode, subjected to tensile stress, polarisation performance 79−59808
fibres, single-polarisation, slab model, strain birefr. 79−50381
fibres characts., single-mode, VAD, long-length 80−106604
field wavefunction, analytic properties in optics 80−1138
film, magnetic depolarisation curve, influence of multiple re-emission *(Russian)* 77−28550
film, magnetic depolarisation curve, influence of multiple re-emission *(Russian)* 77−28551
filter, narrow band interf., optical props. as function of incidence angle and polarisation 80−19102
finite plane parallel atmos., polarisation studies, F_N method 79−40070
flow-birefringence, meas. using circularly polarised laser beam 79−35813
fluid, dense, light scatt., point polarisability approx., local fields, interparticle pair correls. 77−55799
fluid, dense, non-spherical mol. polarised light scatt., local fields, interparticle pair correls. 77−55798
fluids, polarisation state of light scatt. in elec. and mag. fields, symmetry indications 80−29751
fluids, simple, light scatt., particle-hole model 80−60613
fluids, viscous, local order theory and light scatt., depolarised and polarised spectra 80−45093
fluoranthene, single cryst. and in fluorene matrix, polarised absorption spectra, assignments 80−55122
fluorescein-rose bengale, soln., qualitative anal. using fluoresc. polarisation 79−24849
fluorescence, depolarisation, orientation factors, excitation energy transfer between isolated donor-acceptor fluorophore pairs 79−22740
fluorescence, polarisation anisotropy meas. via single-photon counting 77−18072
fluorescence polarisation detector for polarisation degree calc. 79−219
fluorescence solvatochromism kinetics 77−30898
foil, HeH^+ impact, dissoc., emitted light polarisation meas. 80−58361
four wave mixing, Raman spectroscopy background suppression 77−5924
frame dragging and dispersive rot., Mach's principle 77−26217
Fraunhofer diffraction and polarisation 79−44666
Fraunhofer lines and continuum, solar disc polarisation meas. 78−73688
frequency convertors for 2-freq. optical interferometers 80−18005
frequency mixing detection of polarisation modulated light 78−5433
Fresnel's interface reflection coeffs., direct reflection between parallel and perpendicular polarisations 79−94147
Fresnel coefficients of light refl. at interfaces between transparent media 80−106438
galactic centre, IR polarization due to silicate dust grains 77−9794
galactic centre, linear polarisation in near IR 78−96534
Galactic Centre, polarisation obs. at 2.2 microns 77−64850
galactic field structure and stellar polarisation 78−69869
galaxies active nuclei, continuous optical spectra and polarisation 78−57644
gas, anisotropy in strong EM field 79−98434
gas analysis by polarised coherent active Raman scatt. spectroscopy *(Russian)* 77−56295
gas concentration meas. using Raman intensity depend. on giant pulse laser polarization 80−98986
gas laser, competition between high intensity modes of different polarisation 77−58311
gas laser, induced polarisation anisotropies, direct meas. 77−19234
gas laser, linearly polarized waves, interaction with longitudinal mag. field 80−95936
gas laser, polaris. effects 80−58605
gas laser, single mode, mode polarisation in transverse mag. fields 78−22107
gas laser, theory of polarisation effects 80−23660
gas laser with internal mirrors, polarisation states 77−50701
gas laser with resonator weak phase anisotropy, output radiation polarisation 79−64264
gas lasers, single-mode in transverse mag. fields, polarisation props. 79−7167
gas multimode laser with excitation modulation, polaris. of active medium 78−82942
gas superluminescence in high-current discharge, polarisation due to Zeeman splitting 80−100060

light polarisation continued
gaseous medium, two-photon-absorbing, polarised light propag., quantum effects 80−103107
gases, light scatt., depolaris. factor meas. *(Russian)* 79−13780
Gaussian light, partially polarised, photon statistics 80−19012
GD 90, magnetic white dwarf, circular polarisation obs. 78−16409
Gegenschein, vars. in polarisation 77−71060
geocornal Lyman alpha emission, polarisation rel. to exobase H density and temp. 77−29526
geometrical optics, extension to polarised light, optics field spinor formalism 79−50210
glass, phase separated, opt. props. of elongated phases 78−27179
glass, rare-earth activated, polarised luminesc. 78−48224
glass ground surface, fissured layer effect on scatt. of polarised light 79−64172
glass laser, dynamic tuning of polarisation of radiation *(Russian)* 77−38945
glass rod amplifier, circularly polarised light to reduce self-focusing 77−58396
gloss measurements, polarisation effects 79−80662
glycerol(-d_3), single cryst., glassy, and supercooled, polarised Raman spectra, anharmonic multiphonon interactions 79−91419
grains with resonant impurities, linear and circular polarisation 77−53660
graphite intercalation compounds, KC_8 and CsC_8 polarised reflectance 78−31213
grating polariser for IR spectral region 79−55221
grating scanner meas. of stellar energy distrib., polarization effects 78−32355
grating type monochromators, spectrophotometry and colorimetry errors caused by polarisation of meas. system *(Japanese)* 80−101815
gratings, concave, mounted in Seya-Namioka monochromator, expt. charcts. 79−18526
grid polarisers for IR Fourier spectrometers 80−105724
group theoretical approach to radiation statistics 79−86129
gyroanisotropic crystal light polarisation states, Cauchy problem 80−20609
Hadamard transform image scanner, polarisation coding 77−14668
haeme proteins, inversely polarized modes in reson. Raman scatt., depolarisation dispersion curves, vibronic interactions 78−78676
halo polarization and double refraction by ice crystals 78−36283
hazes, information provision on particle size distrib. of brightness and polarisation phase functions *(Russian)* 78−44998
HD 44179 (Red Rectangle), bipolar nebula, IR polarimetry 78−36658
HD 47129 (Plaskett's star), massive O-star binary system, variable linear polarisation obs. 78−53989
HD 50896, Wolf-Rayet star, detect. of polarisation struct. across emission lines 79−97008
HD 50896, Wolf-Rayet star, linear polarisation periodic vars. rel. to binary star nature 80−72972
HDE 226868 (Cygnus X-1), long-term circular polarisation variability 79−9031
HDE 226868 (Cygnus X-1), variable linear polarisation, 1974-1975 obs. 77−9810
heavy metal vapours, optical activity as indication of electron-nucleon weak interactions *(Russian)* 77−10618
helically ruled optical filter, spherical refl. charcts. 80−64171
u Herculis, eclipsing binary, phase-locked polarization 78−4281
AM Herculis, X-ray binary, polarization obs., mag. compact star discovery 77−33569
AM Herculis (3U 1809+50), multicolour linear and circular polarisation obs. and geometrical model 78−8053
AM Herculis (3U 1809+50), polarimetry and spectrophotometry rel. to mag. field 80−94835
AM Herculis (3U 1809+50), single accretion column model rel. to optical polarisation vars. 78−57578
AM Herculis objects, linear polarisation model 78−16460
hexafluoropropene, struct. and vibr. spectra, IR, Raman polarisation study 80−18845
hexane:pyrene (coronene), quasiline spectra, multiplet struct., freezing conditions and solvent effects 79−1786
high fidelity reproduction with polarised light 79−44957
hologram grating, polarizing properties 80−69342
hologram grating, thin, transmittance type, fabrication polarisation effects *(Korean)* 78−50731
hologram quality, influence of object and reference wave polarisations 80−23643
hologram storage medium, pulsed, imaging spectrum polaris. state *(Russian)* 77−75448
holographic grating on metal with dielec. coating, polarisation anomalies 77−62058
holographic image degradation due to reflected light depolarisation 78−90398
holographic image light, object beam depolarisation effect *(Spanish)* 78−50733
holographic reconstruction of polarisation state 78−25822
holography, polarisation form reconstruction using diffuse reference beam *(French)* 77−71954
holography, TIR, polarisation influence on diffr. efficiency 78−37836
holography and optical information processing, polarised light appl. 77−46708
holography with evanescent waves, diffr. efficiency, TE polarisation 78−66782
holography with evanescent waves, diffr. efficiency, TM polarisation 78−66783
IC 5146, young star cluster, polarisation of starlight 77−5550
image spectrum in FTIROS, polarisation features 77−75439
imaging polarizer with spherical mirrors for VUV radiation 80−48375
imaging system, point spread function modification by polarisation masks 77−65615
immersed multilayers, optimum reflectance attainment for TM polarised flux 79−59627
impulse response matrix formalism for polarised light, appl. to holography 78−63045
inert gas+Li(Be^+)(Na)(Mg^+)(K)(Zn^+), collision-induced alignment, reson.-line emission polaris. obs. 80−18912
infinite cylinders, randomly oriented, extinction efficiency 80−48152
infinitely thin hollow spherical shells made of anisotropic molecules, particle scatt. factor 80−45946
influence of optical instruments 80−52290

light polarisation continued
inhomogeneous birefringent optically active medium, polarisation evolution 78−9328
inhomogeneously magnetised media, Faraday effect, polarisation plane rotation *(Russian)* 80−66154
instrument polarisation study for solar horizontal telescope 80−17492
integrated optics multilayer anisotropic structures, impedance matching effects 79−7233
integrated polariser, reduced cladding-medium, fabricated in ion-exchanged guides 80−14489
interface between transparent and absorbing medium, light refl. at 45° angle of incidence 79−31792
interface between transparent media, *p* and *s* polarisation amplitude reflectances and phase shifts 79−76578
interference fringe intensity distrib. of elliptically polarised beam near critical angle 80−106449
interference polarisation filter steps, wide angle, made from various crystals 78−87156
interference polarization filters, crystal plate orientation depend. of spectral background 80−48426
interference polarizer with large entrance aperture, charcts. 80−43453
interference polarizers on plane-parallel substrates 80−1336
interferometer, for small dynamic deform. meas. *(Russian)* 79−9205
interferometer, polarising, ultimate resolution, laser beam phase front radius of curvature meas. 79−88997
interstellar absorption bands in O, B and A stars, polarized intensities 79−8915
interstellar circular polarization, wavelength dependence, HD 183143 an exception 79−92819
interstellar grains with water ice mantles, max. linear polarisation wavelength 79−5882
interstellar linear polarisation, wavelength depend. at near IR wavelengths 80−51833
interstellar linear polarisation in 1-2.2 μ wavelength range 78−77588
interstellar medium Lyman α emission, line profile, temp. and polarisation from geocoronal absorpt. 77−67120
interstellar particle size distribution from linear polarisation calcs. 80−12787
interstellar polarisation, rel. to grain growth in dark clouds 80−67834
interstellar polarisation, reversed by small particles over strong resons. 79−2564
interstellar polarisation in irregularly fluctuating medium, statistical anal. 80−26926
interstellar polarisation rel. to grain size, polarimetric obs. of four deviating stars 80−12792
ion, multiply charged, two-electron, parity nonconservation in spectra 79−10087
ion collisions, electron capture, atomic excited state polarisation, optical detection 80−58377
IR frustrated-total-reflection polarising beam splitter 79−46047
IR laser beam polarisation flipper, mirror and prism systems 77−75586
IR polariser grid prod. process *(Russian)* 78−46795
IR sources, middle IR polarisation by dust 79−67078
IR spectrophotometers, meas. errors of polarising objects 80−86471
irregular particle scattering, meas. results versus Mie theory 78−58918
isotropic adsorbing medium boundary, light beam splitting 80−99623
isotropic medium, nonlinear refr. index, self-induced polarisation rot. 80−5802
isotropic medium with two-photon absorpt., propag. of polarised radiation 80−28290
J-dependence of intensity-dependent polarization change in atomic reson. lines 78−70775
Jones notation, polarisation and interference effects 78−17858
Jones vectors superposition, polarisation vector on Poincare sphere 78−74839
Jupiter, methane and NH_3 bands spectropolarimetry, 6800-8200 Å 79−66955
Jupiter, near IR polarisation studies 78−85899
Jupiter clouds spectropolarimetry, lines equivalent widths information content 80−31215
in Kerr metric, appls. of geometrical optics of polarisation plane rot. 77−29637
EV Lacertae, flare star, polarimetric and photometric obs. *(Russian)* 77−13368
BL Lacertae, polarisation at visible and IR wavelengths 77−9803
BL Lacertae, polarisation plane obs. rel. to light vars. periodic components *(Russian)* 79−101205
BL Lacertae type objects, linear optical polarisation study *(Russian)* 78−57640
Lamb wave optical detect. in fused SiO_2 80−106690
laser, internal mirror, polarisation mode, freq. stability *(Japanese)* 78−46675
laser, ring type, elliptically polarised oppositely travelling waves competition 78−50825
laser backscattering from dense water-droplet clouds, polarisation analysis of backscattered power 79−53513
laser based on coupled transitions with arbitrary polarization of radiation 80−78827
laser beam, depolarisation and scatt. matrices in artificial crystalline clouds *(Russian)* 77−5317
laser beam broadening and depolarization in dense water-droplet fogs 78−92981
laser beam propagating in liquid, polarization, DC elec. field influence 80−91828
laser beams, CW, in at. vap., long-range interaction 78−87110
laser cavity losses, phase polarisation method in lasing regime 80−87413
laser light, angular depolarisation and multiple scattering by water/ice clouds 80−41549
laser light polarisation, review *(Japanese)* 78−5516
laser operation physical principles *(German)* 79−59664
laser pulse scatt. by aqueous medium 77−3533
laser radiation frequency spectrum control, phase polarisation method 77−75583
laser Rayleigh scatt., forward direction, spatial coherence deterioration, polaris. interferometry technique 77−10838
laser-induced amplitude and phase gratings, effects of light polarization 79−94302
laser-induced optical activity, QED theory of multiphoton processes 79−31794
laser-Raman spectroscopy with AC differential analysis 77−38031

light polarisation continued
lateral wave amplification through reflection from active medium 78−78987
lattice relaxation and time resolved polarization of emission from localized electron with level crossing 79−4840
CW Leonis, (IRC+10216), IR C star, intrinsic polarisation origin 80−67730
Li, multiphoton ionis. at ruby laser wavelength 80−9566
lidar polarisation meas. for cloud phase discrimination 78−96269
lidar returns depolarization, scatt. from virga and source cloud 77−49169
lidar scattering from clouds at 347, 694 nm, polarisation props. 78−85689
lidar scattering from snow and ice crystals in atmosphere, polarization characts. 77−64430
lidar target calibration, backscatter refl. for circularly polarised radiation 80−102750
light polarisation measurement, modelling 77−87804
linear anisotropic crystals, acousto-optic interactions, general theory 79−99850
linear compensator for beams path difference, opt. polarisation method of stress testing 79−93204
linearly polarised light depolarisation effective ellipse phase and amplitude 80−86381
liquid, simple, depolarised light scatt., double scatt. considerations 79−87410
liquid, simple, spherical molecules, depolarised light scatt., shaped cavity theory 79−82987
liquid crystal, uniaxial, polarised fluoresc. emission, orientational distrib. function, rot. Brownian motion 78−80390
liquid crystal dynamic scatt. devices, initial molecular alignment effect on electro-optical props. *(Japanese)* 77−1655
liquid crystal image transducer, optical props. at normal incidence, off-state behaviour 80−64160
liquid crystal polarization rotator for intermodulation spatial-bandwidth reduction holography 80−53439
liquid crystal thin layer, polarised light ellipticity after passage 80−88036
liquid crystals, static and dynamic props., time depend. fluoresc. depolarisation obs. 80−29786
long-period variable stars in S.hemisphere, narrowband polarimetry 80−98666
low value rotation angles, detection and measurement *(Rumanian)* 80−22418
low-density plasma, reabsorbed radiation polarisation in mag. field 78−67426
low-intensity fluxes, polarisation meas. by photon counting 77−13795
LP 790-29, mag. degenerate star with blanketed energy distrib., spectropolarimetry 79−5815
lunar samples, surface texture from polarimetric and photometric obs. 77−60673
Lyot depolarizer in quasimonochromatic light 79−62747
β Lyrae, eclipsing binary, intrinsic linear polarisation in Hα, Hβ emission lines 77−41390
M17, dusty H II region, stellar optical polarisation meas. 78−45379
M42, far IR polarisation obs. 77−53663
M43, small diffuse nebulae in Orion complex, optical linear polarization map 80−46644
M82, optical polarisation wavelengths depend. of galaxy 80−67861
M87 jet knots, polarisation, spectroscopic and radio props. 80−12817
macromolecular relaxation time spectra rel. to luminesc. depolarisation function *(Russian)* 77−31040
macromolecular solutions, orient. in laser beam elec. field, anisotropic light scatt. 79−1768
macromolecules and colloids, apparatus for meas. electrically induced fluorescence changes 77−46662
macromolecules in dilute soln., electrically induced fluorescence polarised component change meas. 80−32863
magnetic circularly polarised emission from luminesc. mol. system, QED formalism, orientation relax. 77−46589
magnetic DA white dwarfs, spectral line and circular polarisation profiles 80−62123
magnetic fluids, light scattering and polarisation 80−60616
magnetic thin film, magneto-optical props., data reading system appl. *(Russian)* 77−1572
magneto-optical concentration of light, by regular domain structures *(Russian)* 79−24297
magneto-optical effects, simultaneous meas. rel. to polarisation ellipse 77−43975
magneto-optical relax., refl. rad. polarisation plane, monopolar mag. field pulses on solid surface 77−81086
Markarian 231, IR polarisation obs. 78−4360
Markarian 3, 231, Seyfert galaxies, optical polarisation obs. 80−90533
matching methods determ. 77−85682
matrix notation, interference, coherence and polarisation 77−38801
matrix notation, Jones vectors for refl., refr. and diffr. 77−34814
MBBA liquid crystal wedge as a polarizing element and its use in shearing interferometry 80−53444
mercurochrom, fluoresc. polarisation, solvent effects 77−14470
metal-dielectric interface, p-polarised light total absorpt. by surface plasma waves 78−88373
methane, compressed gas, apparatus for depolarisation ratio meas. of scatt. light 80−38527
methanol, optically pumped CW for IR laser lines, freq. meas. 80−58514
methanol far-IR laser, optically pumped, intracavity polarization modulation 80−23726
methyl mercaptan, CW subMM emission lines, optical pumping 80−87381
9-methylanthracene, in acetylcellulose foil, time-depend. fluoresc. anisotropy, crit. transfer distance *(German)* 78−21964
micelles, inverted containing water, hydrodynamic vol. determ. by fluoresc. polarisation 80−50892
Michelson interferometer, modification for polarised beam interference 80−260
Michelson interferometer, polarizing, for far IR and MM regions 80−73427
Michelson output coupler with one-dimensional grid, for optically pumped near MM laser 80−58555
microscope, polarizing, with crossed polarizers, incoherent diffr. imagery 80−101838

light polarisation continued
modulated-Mueller-matrix photopolarimetry [MMMP]: a technique for the study of elastic light scattering by depolarizing temporally modulated media and surfaces 80−90882
modulation of polarisation, small ang., beam in diamag. glass, by Faraday rot. *(Korean)* 78−50918
modulation of polarized light beam using piezo-optical and photoelastic modulator/chopper *(German)* 79−27395
modulation techniques to study linear, circular and vibr. circular dichroism 77−45896
modulators, photoelastic radiation polarisation, review 80−102846
molecular crystal, Brillouin scatt. intensity 79−73958
molecular crystal, principal axes of tensor of polarisability derivs., spectroscopic determ. *(Russian)* 77−85683
molecular electron impact excitation, photon-electron ang. correlation, fine/hyperfine struct. effects 78−42231
molecular fluid, optical props., intermol. forces effects, theory, appls. 77−28535
molecular fluoresc. spectrum with light quenching, spectral distrib. of polarisation 79−85989
molecular gas orientation by reson. radiation, optical detect., laser spectroscopy appl. 79−27742
molecular gases, saturation of light absorption 80−14401
molecular lasers, optically pumped, polarisation phenomena appl. 80−87384
molecular pair, fluoresc. depolarisation, using stochastic Liouville eqn. with radiative terms 80−16074
molecular single crystal, librational Raman spectra polaris., temp. depend. 79−1760
molecular systems, photoselection, orient. relax. rel. to emission mag. induced circular polarisation 78−70860
R Monocerotis, bipolar nebula, optical and IR polarimetry 78−36658
monochromatic speckle patterns, statistical props. 80−53215
monodisperse nonabsorbing particles, refractive index determ. by light scatt. *(Russian)* 77−5891
Moon, photometric and polarimetric obs., 1976 April to 1977 December 80−51677
Mueller matrix meas. of polarised light interactions, using electrooptic modulator polarimeter 80−73417
Mueller-Stokes matrix determ. using Fourier anal. 77−42496
multilayer coating design achieving a broadband 90° phase shift 80−102801
multilayer dielectric coating producing 90° phase change 79−76788
multilayer highly reflective coating design for wideband 90° phase shift 80−74464
multilayer interference polarizer, Brewster angle determ. 79−64315
multilayered structures containing anisotropy, EM wave anomalies 79−41460
multilayers, polarisation avoidance or enhancement 80−43255
multimode capillary light guide, effect on light polaris. *(Russian)* 79−37017
multiple beam interferometry, polarisation doubling 79−21806
multiplet lines emitted after beam-surface interaction, polarisation calc., time development 80−14216
naphthalene, solid, high-energy vibr. overtone spectra, local modes, intramol. relax. 79−28052
nebulae, polarisation maps obtained with electronographic camera 77−57081
nebulae M42 and M43, optical linear polarisation 78−86004
NGC 1068, Seyfert galaxy, IR photometry and polarimetry 78−54035
NGC 1275, Seyfert galaxy, IR polarisation obs. 78−4360
NGC 1275, Seyfert galaxy, radio and optical variability of nucleus 78−28793
NGC 1275 as BL Lacertae object, evidence from nucleus polarisation and variability 78−45406
NGC 1569, irregular galaxy, optical linear polarization obs. from Durham 77−74126
NGC 1999, reflection nebula, optical polarisation map and struct. 80−94856
NGC 3227, 3516, Seyfert galaxies, optical polarisation obs. 80−90533
NGC 4151, Seyfert galaxy, IR polarisation obs. 78−4360
NGC 4151, Seyfert galaxy, optical polarimetry, circumnuclear dust envelope 78−61916
NGC 654, young star cluster, polarisation of starlight 77−5550
NGC 6618, polarimetric obs. of nebula and neighbouring stars *(Russian)* 78−49491
nitrate glass: Eu^{3+} struct. reorganisation in glass transition interval, polarised luminesc. obs. 80−45141
nitrobenzene-n-hexane crit. mixture, depolarised Rayleigh linewidth meas. 77−81112
noctilucent clouds, circularly polarised light detect. 79−48568
noctilucent clouds, elliptical polarization rel. to ice crystals 78−11946
Nomarski polarisation interferometry, for slope determ. of microscopic surface features 78−16840
nonlinear active medium in Gaussian random optical field, stimulated emission statistics 80−58488
nonlinear medium, polarisation state evolution 78−50867
nonlinear optical props. of band charge carriers rel. to carrier scattering by lattice defects 80−29399
nonlinear scattering, polarisation effects, hyper-Rayleigh (Raman) scatt. 77−88858
nonmonochromatic light beam based, generalised polarisation angle method *(Russian)* 80−22419
nonspherical particles, depolarisation of scatt. radiation 77−50616
Nova Cygni 1978, interstellar polarisation obs. 78−89213
Nova Cygni 1978, spectra, polarisation, photometry and visual magnitude estimates 78−93283
Nova Monocerotis 1975 (Ariel 0620−00), linear polarisation obs. 77−13351
Nova Vulpeculae 1976, polarisation meas., reddening and distance 77−29855
OB-type southern stars, UBV, Hβ and polarisation meas. 77−26007
object's wave state of polarisation recording and reconstruction by vol. hologram 80−23636
object mutual orientation using active polarisers with tetrahedral reflectors 79−26109
ocean, optically thick medium, asymptotic radiance and polarisation 77−21776
ocean reflected and scattered radiation polarisation, utility in remote sensing 79−5498

light polarisation continued
octane: pyrene(coronene), quasiline spectra, multiplet struct., freezing conditions and solvent effects 79−1786
off-axis imaging system, polarisation dependent MTF defects 77−34837
OI090.4 and OJ−131, BL Lacertae objects 78−4359
one-quantum photoeffect, ang. photoelectron distrib. due to elliptically polarized light 79−6920
optical activity in crystals, lattice dynamical theory 80−34883
optical bistability, nonlinear polarisability model 80−37976
optical constant measurement at two incidence angle values 80−101831
optical constants, ATR meas., 2-polarisation method, accuracy, optimisation 78−45673
optical constants meas. method using polarised light refl. coeffs., accuracy 80−73423
optical fibre, current measurement appl. 80−96015
optical fibre, single-mode, single-polarisation, with refractive-index pits on both sides of core 80−99846
optical fibre birefringence measurement system, computer-controlled 79−64352
optical fibre waveguides with elliptical cores, preservation of polarisation 79−64324
optical fibres, characterisation of polarisation using automatic birefringence measurement system 79−93205
optical fibres, sandwich ribbon, measurement of polarisation props. using He-Ne laser 79−64353
optical fibres, single-mode, tension-coiled, high birefr. 80−99858
optical fibres, single-mode low birefr., prep. and polarisation characts. 79−7195
optical film, non-homogeneous, oblique light incidence *(Russian)* 79−13905
optical filters, operating principles based on energy transfer between coupled orthogonally polarised EM waves *(French)* 78−33896
optical isolators, elimination of polarisation depend., fibre communication appl. 80−5844
optical multilayer filters, non normal incidence, optical monitoring, allowable tolerances *(French)* 80−87526
optical ranger, tetrahedral reflector appl. *(Russian)* 77−27354
optical waveguide polariser with synchronous absorption 79−90002
optically active molecules, differential Raman scatt. of right and left circularly polarized light *(Japanese)* 78−17675
oriented non-spherical particles, polarisation characts. 79−81362
Orion Nebula, IR polarisation, preferential extinction in Kleinmann-Low nebula 78−4311
Orion Nebula, linear polarisation obs. 78−45392
Orion Nebula, optical linear polarisation meas. 77−45536
Orion Nebula, polarisation at 11.1 and 19.6 μm meas., aligned absorbing grains 80−36690
Orion Nebula cluster, variable stellar polarisation *(Russian)* 77−60807
Orion Nebula stars, wavelength depend. of polarisation, rel. to intracluster dust and circumstellar shells 77−78839
Orion OB 1 association stars, photometric anal. rel. to polarisation 77−82288
σ Orionis E, peculiar eclipsing binary, linear polarization obs. 78−32508
orthogonalisation properties, polarisation, of optical systems 77−58249
oscillating electric dipole contrib. to light scatt. and interpret. in terms of polarisability and hyperpolarizability 80−53212
parabolic-index fibre modes, propag. characts., linearly polarised approx. 80−78972
paramagnetic molecules in rigid isotropic medium, mag. linearly polarised emission 78−68545
parametric interaction of two waves, scatt. radiation ang. struct., amplification *(Russian)* 77−58381
parametric transformation of light polarisation in crystals 78−1153
parhelic circle, polarization model of halo phenomena 79−96819
partially coherent perpendicularly polarized vibrs., anisotropic photographic recording, interferograms 80−57364
particle medium, refr. index determ. from angular, polarisation characts. *(Russian)* 77−34827
particle size distribution parameters, estimation using forward scatt. techniques 80−36974
particles, anisotropy of optical polarisability in Rayleigh-Debye-Gans approx. 77−46685
Pauli algebraic formalism, relation between different formalisms 78−87010
p-n-pentyl-p′-cyanobiphenyl, nematic liq. cryst., Raman depolaris. ratios, order parameters 79−28733
perfect lens with polarisation masks, OTF 78−90380
periodic analysers for freq. mixing detect. of polarisation modulated light 77−45883
X Persei, V-band polarization variability 78−49455
α Persei star cluster, polarisation wavelength depend. 79−48865
perylene, α- and β-crysts. and soln., polarised reflection and absorption spectra 77−8598
perylene in paraffin, anisotropic rot. and libration 77−32417
phase-polarisation nonlinear high-resolution spectroscopy in longit. mag. field 79−41423
phase-shift sum rules for complex polarisation amplitude for photon reflections 79−69802
SX Phoenicis, simultaneous photometric and polarimetric obs. 78−49451
phonon-assisted radiative electronic transitions 79−24348
photoelasticity, matrix theory, book 79−64612
photoelasticity demonstration, colour image of stress pattern 77−13548
photoelasticity imaging using IR polariscope 79−94567
photoluminescence of solutions, decay and self-depolarisation 79−24351
photon antibunching, polaris. depend. 80−1170
photon antibunching enhancement by interf., polarisation effects 79−31990
photon echo, identification of transitions 80−78915
photon echo for small-area exciting pulses *(Russian)* 79−76766
photon helicity detection for matter/antimatter star discrimination 78−12092
physics course demonstration *(Russian)* 79−21508
PKS 0735+178, BL Lacertae-type object, brightening and linear polarisation obs. 77−22318
PKS 2155-304 (H2155−304), newly discovered BL Lacertae object, optical polarisation, spectrum and variability 80−36702
planar aromatic hydrocarbons in polymer films, polarisation data interpretations, photoselection spectroscopy appl. 80−58302
planar multilayered structure, resonant polarization conversion and beam shift 78−1438
light polarisation continued
planar waveguide, isotropic, polarisation conversion by Bragg deflection coupled mode theory 80−48461
planar waveguide, isotropic, polarisation conversion by Bragg deflection, expt. results 80−48462
plane waves, difference between polarisation and coherence 80−8805
planetary atmosphere, F_N method for polarisation studies 80−98540
planetary atmosphere, polarisation state, aerosol and Rayleigh scatt. 77−49171
planetary atmospheres, regional polarization, 1950-77 obs. of Venus 80−8570
planetary atmospheres, scatt. indicatrix and polarisation meas. via laser beam *(Russian)* 79−44365
planetary surface, dust covered, polarimetric model 79−25528
plasma interaction with laser radiation, light press. nonlinear force, polarisation influence 80−100078
plastic scintillator, degree of fluorescence light polarisation, energy depend. *(German)* 78−37677
Pleiades stars, wavelength depend. of polarisation 77−45500
PMMA, amorphous, reorientational relax., 6-165°C, polarised laser beam scatt. correlation 78−2864
Pockels cell modulator, max. depth of light modulation 80−102819
polarisation of fluorescence spectrum for enhanced resolution 77−6827
polarised photochromism in solid solutions 78−64859
polariser + crystal plate + analyser system, passage of light 80−10023
polarising beam splitter, film coatings, cemented cube 77−19422
polarizer, matching type to applic. 78−18051
polished glass surface, reflected light phase rotation 80−66147
polyacrylamide-fluorescein conjugates, fluoresc. polarisation, high press. obs. 80−20683
polyamide, aromatic, persistence length, rel. to optical anisotropy of worm-like chain 77−50577
polyatomic molecular vapour, rot. fluoresc. depolaris. 79−54889
polymer, uniaxial, fluoresc. polarisation, orientation and mol. dynamics effects 78−76516
polymer film, multiple light scatt., light depolarisation effects 77−4696
polymer film, stretched, interpretation of polarised absorption and emission spectra of molecules 78−1012
polymer solution, dil. small particles, scatt., Perrin matrix construction 77−77227
polymer solution, Perrin light scatt. matrix including mag. dipole and elec. quadrupole interactions 77−77228
polystyrene, uniaxially oriented atactic, laser Raman scattering 79−73920
polytene chromosome, stretched, stained with acridine orange, fluoresc. polarisation rel. to DNA packing 78−76995
protostellar sources, IR polarisation rel. to nearby interstellar polarisation 80−4347
pulse dispersion in a clad lens-like medium 80−53445
pulses, ~1 μsec, meas. using amplitude-digital convertor 79−17465
VV Puppis, accretion column absorpt. spectrum and polarisation 79−101176
VV Puppis, AM Herculis type binary, spectrophotometry and polarimetry 79−5860
VV Puppis, circular polarimetry in active state and evidence for two accreting poles 79−48854
VV Puppis, linear polarisation obs. in faint state 79−25643
L_2 Puppis, semiregular variable, Ca I uneven distrib. from narrowband polarimetry 80−98666
pyrazine, multiphoton ionisation spectra, circular to linear polarisation ratios, lowest ionisation pot. 78−74716
pyridine, multiphoton ionisation spectra, circular to linear polarisation ratios, lowest ionisation pot. 78−74716
pyridine solutions, degree of depolaris. in stimulated Raman scatt. 79−55184
pyrimidine derivatives, absorpt., luminesc. and polarisation spectra, electronic struct. 79−85993
QED theory of differential scatt., Raman scatt. of circularly polarised light, two chromophores model 78−9158
QED theory of differential scatt., Rayleigh scatt. of circularly polarised light, two chromophores model 78−9157
QSOs, linear polarization survey of bright objects 78−41077
QSOs, optical polarisation alignment with radio struct. 79−25751
quantum beat high-resolution polarisation spectroscopy in transmission, technique 78−58640
quarter-wave mirrors, oblique incidence reflection coefficient, small absorption of layers effect 80−64140
quartz, electrogyration effect, electric field depend. of optical activity 77−32352
α-quartz, laser Raman line polarisation meas. 77−4641
quasar 3C 273, rapid fluctuations of radio flux and circular polarisation and optical linear polarisation 77−91663
quasars and BL Lacertae objects, optical polarisation model, synchrotron radiation 77−2479
quinoline, liq., depolarised light scatt. from shear waves 80−97288
radiation field, polarized, asymptotic characts. for low absorpt., appl. to nonconservative Rayleigh scatt. 80−5686
radiative transfer equation for partially polarised light, QED derivation 77−79235
radiative transfer for polarized light, eqn. soln. method in relativistic cosmology 78−73781
radiative transfer in semi-infinite Rayleigh scattering atmosphere, exact soln. for Stokes parameters 79−35112
radiative transfer of polarized light eqns., adjoint Monte Carlo treatment 78−37799
radiative transfer problems of polarised light in presence of absorpt. soln. 80−67561
radiometer, polarisation effects meas. using partially polarized light 79−49266
rainbow polarisation rel. to droplet size and scatt. angle 79−80017
Raman and Rayleigh scatt. by optically active mol., elliptical polaris. production 77−58089
Raman scattering, electron-phonon interaction effects on polarisation 80−55088
Raman scattering, homogeneous, close to dielectric, evanescent field excitation 79−99864
Raman spectra, reversal coeff., direct scanning meas. 77−38017
Raman-luminescence problem, interference analogy and expt. discrimination by polarisation correl. 79−95764
Rayleigh scattering, anisotropic medium, 3-photon scatt. by density fluctuations *(Russian)* 78−74841

light polarisation continued
Rayleigh scattering, depolarisation ratios of cyclohexane, carbon tetrachloride and benzene 77−32387
Rayleigh-scattering absorbing atmosphere, polarised radiation intensity meas. for single-scatt. albedo determ. 80−94704
reactor amplitude determ. for single axis optical crystal systems *(German)* 79−55059
real-time image optical subtraction scheme 78−74856
reciprocity theorem, for polarised laser beams 78−79055
rectangular groove grating as IR polariser 77−3674
red supergiant stars, detect. of surrounding refl. nebulae from polarisation obs. 77−13340
reduced depth polariser for integrated optics 77−84006
reflected light, polarisation, apparatus for obs. 80−62434
reflected sunlight from Venus, polarisation, planetary atm. struct. and comp. determ. 80−36533
reflection grating polariser for IR 79−1001
reflection nebula, inhomogeneous, scatt. function for grains of silicates and ice 79−21405
reflection nebula, optical colours, polarisation, composite and mixture of nebula grains 78−16502
reflection of unpolarised light, polaris. degree, for teaching 78−24616
reflection polarisers and analysers in vac. UV, design criteria 78−55424
reflectivity, quantitative meas., undergrad. lab. expt. 78−49624
relaxation measurement in materials, using synchronously mode-locked dye lasers 79−44952
resonance medium, induced dichroism and gyrotropy 80−9971
resonant orientation of tunnelling centres, self-induced anisotropy 78−79075
resonator with conical elements, mode structure, polarisation effects 79−98411
retinoscopic and subjective refraction discrepancy, polarisation effect 79−83764
rhodamine, 6G and B, low quantum yield mol. fluoresc., polarisation, excitation energy depend. 77−50462
rhodamine 6G, blue and UV luminesc., obs. and mechanism 79−3486
rhodamine 6G, fluoresc. polarisation, solvent effects 80−32755
rhodamine 6G dye laser, degree of polaris., solvent effect 79−41375
rhodamine B, in glycerine-water mixtures mol. agglomeration effect on fluoresc. polaris. spectrum 78−25595
rhodamine-B fluoresc. polarisation, solvent effects 77−54569
rhodophorphyrin XV metal complexes, phosphoresc. polarisation 77−23517
ring gas laser interaction of elliptically polarised opposing waves 80−38044
ring interferometers, optically active samples, polarisation props. *(German)* 80−77846
ring laser, nonreciprocal effects on appl. of transverse mag. field to active medium 80−53341
ring laser, unidirectional system efficiency comparison *(French)* 79−76717
ring laser with anisotropic resonator, polarisation and freq. splitting of opposite waves 80−33037
ring Zeeman laser, interaction of modes characterized by orthogonal circular polarizations 80−48306
rotation, high sensitivity stabilisation and meas. *(French)* 77−61103
rotation of linearly polarised light by linearly polarised light in active medium 77−27248
rotator, low loss, and appl. for isolator design 77−58447
rough dielectric and rough metallic surface discrimination, specular scatter depolarisation 80−32911
rough metal surface, depolarisation of scattered light 77−71919
ruby, optically-pumped, excited-state Raman processes 79−4798
HM Sagittae, emission-line star, polarimetry, (1977 to 1978) *(Russian)* 80−36649
Saturn, atmosphere upper layers props. from polarimetry photometry and spectrophotometry *(Russian)* 78−40867
Saturn, near IR polarisation studies 78−85899
Saturn globe and rings, optical reflectance polarimetry and interpretations for B-ring 80−31248
scattering by anisotropic molecules, density depend. *(French)* 77−4652
scattering by irregular absorbing particles, polarisation and scatt. functions 80−67543
scattering matrix polaris. props., multiplicity effect, transmission and reflection 77−83807
scrambling device, for Raman spectroscopy 77−82612
scrambling using photoelastic modulator, appl. to linear dichroism meas. 78−4683
seawater sunlight polarisation, reflection, and biological effects 77−56648
second and third order nonlinear optical polarisations, general effects of cryst. symmetry and orientation 77−19358
self-diffraction of polarised light waves in two photon absorpt. in isotropic media 80−38077
SEM, polarisation contrast of cathodolum. 79−7529
semiconductor, donor-acceptor pair luminesc. polarisation with optical orientation 77−24895
semiconductor, photo-excited electron momentum distrib., hot luminesc. polarisation 77−16396
semiconductor, polarisation effects in photoconductivity, exptl. method for study 79−4581
semiconductor, spin injection, carrier polarisation, luminesc. polarisation 77−15957
semiconductor laser, ferromagnetic ordering, radiation polarisation *(Russian)* 78−9384
semiconductor laser, polarisation control, mode competition 77−75515
semiconductors, alignment and orientation of hot excitons, secondary radiation polarisation calcs. 79−65392
semiconductors polarised light nonlinear rotation 80−93268
Seyfert galaxy NGC 1068, light polarisation in nucleus 78−54046
SHG, polarisation effects 80−48350
short single-mode optical fibre polarisation effects 78−1393
single axial mode laser, degenerated by mag. field, light props. *(Japanese)* 79−64254
single mode fibre analysis and fabrication for low polarisation birefringence 80−58722
single mode fibre cable, 4.15 km, interf. and polarisation characts. using AlGaAs laser 79−81535
single mode fibre polarisation stabilisation 80−58724
single mode fibres, noncircular core influence on polarisation performance 78−37973
light polarisation continued
single mode optical fibre, polarisation modulation 80−64176
single mode optical fibre polarisation stabilisation 80−33154
single model fibres, polarisation mode dispersion 78−79128
single-mode fibre birefringence and optical activity obs. 78−1394
single-mode fibres, electro-optical polarisation control 80−91899
single-mode gas laser with slightly anisotropic resonator, output polarization stability 80−43370
single-polarisation single-mode fibre, exposed cladding fabrication 80−58725
sky intensity information content, polarisation meas. at right angles to solar direction 78−81401
slit transmission and polarisation 77−6994
soil reflection, polarised visible light photographic recording for surface moisture indications 79−53557
solar background corona, polarisation and brightness near solar minimum 78−28616
solar corona, Fe XIV 5303 Å emission line polarisation obs. during 1973, June 30 eclipse 77−49352
solar corona, green line polarisation obs. at 1973 June 30 total eclipse 79−66969
solar corona, polarisation degree of Fe XIII IR lines 77−45373
solar corona, white light polarisation during 1973 June 30 eclipse 78−20786
solar corona polarisation obs. at 1970 March 7 eclipse 77−33462
solar corona polarisation obs. during 1973 June 30 total eclipse 77−13313
solar corona white light polarisation obs. at 1973 June 30 total eclipse *(French)* 77−74027
solar coronal Fe XIV 5303 Å emission line polarisation, coronal mag. field determ. *(Russian)* 78−16389
solar coronal streamers, electron densities from K-coronameter polarisation meas. 78−4182
solar coronal transient, broadband polarimetry, importance of Hα emission 77−2389
solar inner corona polarization meas. at 1972 July 10 eclipse 77−82197
solar polarisation upper limit in mm. and far IR regions 77−49354
solar resonance line polarisation, non-mag., centre-to-limb var. 80−67678
solar resonance lines, polarisation in line core 77−29744
solar spectral lines, Stokes profiles appl. to vector mag. fields determ. 78−28611
solar spectrum, multi-dimensional non-LTE transfer of polarised radiation rel. to line profiles 78−69673
solar UV light, polarisation at solar limb 78−45302
solids of revolution, stressed state 77−14910
space-time symmetry rel. to light scatt. in elec. and mag. fields 80−29750
spatial polarisation wavefront reversal in four-photon interaction 80−9956
spatially incoherent light depolaris. by birefringent cryst. 79−98273
speckle contrast rel. to surface roughness, polarisation effect 80−43258
spectral analysis of polarised light, polychromatic and coherent optics *(French)* 79−50209
spectral apparatus, influence of polarisation on results of luminescence spectral measurements 80−31900
spectrometer polarisation corrections in reflectance spectra 77−22603
spectrometer system for investigating light polaris. dynamics in nanosecond band 79−2834
spectrophotometer IR rejection polariser system 79−63314
spectroradiometer, polarisation sensitive, methods for overcoming refl. spectra meas. problems 79−40623
spectroscopy, Doppler-free intracavity 80−52335
spectroscopy, high resolution polarisation, in strong saturation regime 79−55189
spectroscopy, high-resolution polarisation, in 10 μm region 79−6196
spectroscopy, relaxation characts. of degenerate states obs. *(Russian)* 80−27348
spectroscopy and forward scatt. in Na gas 80−52336
specular sphere scatt. radiance matrix, refl. standard for polarised beam scatt. meas. 80−74299
spheroidal particles, randomly oriented, light scatt. 80−58461
spin-dependent magneto-optical rotation for free radicals and for singlet-triplet transitions 79−10129
spinodal decomposition, polarised light scatt. 78−31380
SS 433, visible and IR photometric and polarisation obs. 79−80321
standard stars, polarisation obs. by Hatfield near IR polarimeter 79−2482
star, spherical, limb darkened, light polarisatoin from Thomson scatt. 79−58324
starlight interstellar polarisation, fluctuation theory 80−82442
stars, early-type emission-line, intrinsic and interstellar polarization components separation 79−30079
stars, early-type emission-line, intrinsic polarization interpretation 79−30080
stars, linear polarisation catalogue 77−13255
stars, linear polarisation rel. to interstellar extinction R values 77−13443
stars, polarisation meas. near N.Galactic Pole rel. to interstellar extinction 79−62814
stars, with peculiar interstellar polarisations, props. of nearby interstellar medium 77−53659
stars, zero polarisation standards list 79−40187
stars in Corona Austrina dark cloud, BV polarimetry and interstellar reddening law 79−17050
stars with intrinsic polarisation, obs. and statistical anal. *(Russian)* 77−13346
stars with IR excesses, optical emission intrinsic linear polarisation origin 78−96481
stars with nonuniform surface brightness distrib. polarised radiation 77−17549
stars within 25 pc of Sun, polarisation obs. 78−12202
stellar atmospheres and circumstellar envelopes *(Russian)* 80−17573
stellar light circular polarisation by magnetite grains, two-cloud model 77−78838
stellar radiation scattering on circumstellar clouds, circular polarisation theory 78−96428
stellar spectra, response functions for mag. lines 77−45304
Stephenson-Sanduleak 433, 1.2-2.5 μm spectroscopy, photometry and polarimetry 80−41838
stimulated Brillouin scattering wave front reversal for depolarised light 79−3743

light polarisation continued
stimulated Raman scattering gain, influence of polarisation degree 79−89965
Stokes parameters, of light beam, polarisation modulation meas. 79−21803
Stokes parameters and mag. field vector profiles *(Chinese)* 80−77386
Stokes parameters in elliptic polarisation, vector trihedron, optical element evaluation 80−53209
Stokes parameters meas., astronomical appl. 77−17381
Stokes parameters meas. 78−32854
Stokes parameters of light meas. using Fourier photopolarimeter 79−21805
Stokes relations in optically active media, macroscopic reversibility principle appl. 80−53207
Stokes vector formalism, comparison of optical and electron spin polaris. 77−27181
stress distribution, 3D, scatt. light meas. method using depolarised incident light 79−37254
strip-guides, polarisation filtering 80−102861
Sun, polarisation obs. of trans-polar coronal hole of (1973, June 39) 77−53526
sunlight, reflected, meas. from high-altitude balloon 78−61561
sunspot, radiation transfer theory rel. to broadband circular and linear polarisation 80−21964
sunspot umbrae, mag. field gradient from echelle spectrograms 77−33456
sunspots, magneto-optical effects rel. to linearly polarised intensity distribs. obs. with vector magnetograph 80−21965
sunspots, origin of broad-band circular polarisation 78−45301
superconductor Faraday effect obs. in polarising microscope 80−70892
superluminescence polarisation obs. of high-current pulsed discharge in gas with anisotropic gain 79−14515
surface polaritons in anisotropic crystals 78−87919
survey of methods for polarisation state complete determ. 77−45882
suspension of absorbing particles, simultaneous meas. of dichroism and birefringence in elec. field., photocurrent signal obs. 80−82801
synchrotron orbit radiation characts. in visible spectrum, rel. to use as radiometric standard 78−9008
synchrotron VUV and X-radiation, polarising effect of monochromators 78−66732
ζ Tauri, Be star, rapid linear polarisation variability *(Russian)* 80−77417
tetrafluoremethane, compressed gas, apparatus for depolarisation ratio meas. of scatt. light 80−38527
tetramethyl pyrazine in durene, phosphorescent mols., quantum beats in triplet states 80−58312
theoretical model for short length, single mode fibres 78−71203
thermal light with orthogonally polarised multiple-peak spectrum, intensity fluctuations 80−87303
three-dimensional objects in polarised light, refl. characts. 80−87305
three-level molecular system, cooperative evolution, transient effects of dephasing and relax. 80−28184
three-stage birefringent filter, tuning over visible region 80−58667
tilted absorbing glass plate, polarisation response rel. to polarising radiometer calibration 78−55297
time domain reflectometry, optical fibre technique 80−78959
Ton 1542, Seyfert galaxy nucleus, optical polarisation *(French)* 77−26053
total internal reflection, for s-, p-polarisations 78−42272
total reflection by multilayered struct., longit. and transverse shifts 77−75413
transfer function, matrix theory 77−23625
transition metal hexahalide complex, polarised reson. vibr. Raman spectra, electronic degeneracy effects 78−78708
transparent film on absorbing substrate, optimum angle of incidence for monochromatic interference 80−43254
transparent media interface, light refl., 45° angle of refraction 79−27164
transport process of polarized radiation in optically isotropic media 79−13899
troposphere and low stratosphere, scattered solar radiation field meas. *(Russian)* 79−16667
tunable damage-resistant polarisation rotator for UV and visible laser radiation 77−83964
twilight, Monte Carlo simulation of obs. *(Russian)* 77−33186
twilight sky polarisation during meteor showers *(French)* 77−9578
twisted anisotropic media, light propag., appl. to photoreceptors 78−63004
twisted elliptical optical fibre, polarisation coupling 80−99831
twisted single-mode fibres, polarisation optics 79−81524
twisted tape lightguides and braided cylindrical liquid-filled lightguides *(Russian)* 80−19107
two photon polarisation spectroscopy 80−9573
two-photon absorption coeff., polarisation depend. 78−80379
two-photon magnetooptic effects, theory 77−83629
two-photon spectroscopy, elliptical polarisation state alteration technique 79−40627
undulator radiation, circ. or linear polaris. generation by relativistic, helically moving particle 77−75401
uniaxial crystal plate, transmission of light in case of inclined incidence 78−1152
uniaxial liq. crystal polarised fluoresc. emission 80−80838
unstable resonator, half-symmetric, with coated rear cone, polarisation effects 80−74402
Uranus, whole-disc optical polarization meas. 77−45356
AN Ursae Majoris, nova-like variable, extremely high circular polarisation obs. 78−8018
W Ursae Majoris type eclipsing binaries, polarisation obs. 77−45489
UV discharge lamps, rotating triple-reflection polariser 78−94443
UV polariser, coating materials *(Russian)* 77−34928
vacuum UV, apparatus for circularly polarised radiation prod. 78−1310
vapours, light scatt., depolaris. factor meas. *(Russian)* 79−13780
Venus, disk, linear polarization, wavelength dependence 79−66942
Venus, Pioneer orbiter cloud photopolarimeter investigation 79−48713
Venus, scattering layers above visible clouds vertical structure 79−62775
Venus clouds spectropolarimetry, lines equivalent widths information content 80−31215
Venus polarisation, wavelength depend. obs. rel. to UV cloud model 80−82250
very rough surface, backscatt. light, polarised and depolarised components 78−63009

light polarisation continued
78 Virginis, Ap star, lines circular polarisation profiles rel. to mag. field geometry 80−51773
78 Virginis, magnetic Ap star, high resolution polarisation obs. inside spectral lines 80−51772
viscous solution, conc. depolarisation of fluoresc. *(Russian)* 77−85799
viscous solutions, fluoresc. anisotropy, conc. depend. 79−56829
vision, Macular pigment, role in polarised light detect., meas. technique 80−61560
visual detection of polarised light, human eye 80−16934
volume holograms with elec. polarisation in grating plane, 2D theory 79−72532
W3, dusty H II region, stellar optical polarisation meas. 78−45379
Walker No.67 in NGC 2264, candidate for strong interstellar circular polarisation 78−12223
waveguide, cylindrical, two-layer, light depolarisation, theory and expt. *(Russian)* 78−9454
waveguide switches and modulators, performance limitations due to polarisation 77−7175
wavelength depend. of linear polarisation in early-type stars 77−60779
weak light fluxes with slowly varying intensity detector 79−2806
whispering-gallery waves, polarisation and losses along twisted trajectories 80−9798
white dwarfs, Hα polarisation and line profiles in strong mag. fields 77−2427
white dwarfs, magnetic, source of polarised radiation 77−2428
white dwarfs, magnetobremsstrahlung and optical polarisation 77−45417
wire grid polarisers, new optical model 79−902
X-ray binaries, optical radiation polarization *(Russian)* 79−58450
X-ray binary stars, variable optical polarization rel. to black hole secondary component 78−20910
X-ray fluoresc. anal., polarised radiation excitation source 78−7314
X-ray sources, linear optical polarisation obs. *(Russian)* 77−64880
xanthene, dye solns., luminesc. spectra, conc. depend. effects 79−54885
young stars reddening and polarisation, intracluster and circumstellar dust effects 78−93199
young stellar objects, origin of polarisation 79−8911
zodiacal light, circ. polarisation 77−53474
zodiacal light, circular polarisation theory 78−96428
zodiacal light photopolarimetry, brightness annual vars. rel. to zodiacal cloud symmetry plane 78−45276
Ag mirror IR reflectance at 45° incidence, obs. 79−14074
Al mirror IR reflectance at 45° incidence, obs. 79−14074
$Al_xGa_{1-x}As$, optically magnetised, luminescence polarisation anisotropy, hysteresis effect symmetry props. 80−34982
α-Al_2O_3, additively coloured single crystal, luminescence *(Russian)* 80−55169
α-Al_2O_3, IR absorpt. spectra of OH^-, OD^-, and OT^- 80−55145
α-Al_2O_3, polarised luminescence in neutron- and proton-irradiated single crystals 80−66271
Ar, compressed gas, apparatus for depolarisation ratio meas. of scatt. light 80−38527
Ar, electron-photon coincidence obs., reson. lines, polarisation correls. 79−31697
Ar ion laser radiation, Faraday effect, polarisation plane negative rot. 79−98424
Ar, laser, ionic, with three-mirror resonator 80−23712
Ar laser resonator, effect of axial mag. field on loss increase 79−76716
Ar, light depolaris., pair-pair correlations 78−63536
Ar, liquid, depolarized Rayleigh scatt. at triple point, mol. dynamics simulation 80−60617
As_2S_3 film, hologram recording using total-internal-refl., polarisation depend. 80−106491
As_2S_3 glass, natural optical activity and related phenomena 79−95727
As_2Se_3, polarised light reflectance spectra, band struct. 78−63979
Au/Al thin film, Al diffusion studied by attenuated total reflection method 80−92722
B_2O_3-SiO_2 optical fibres, exposed cladding technique, birefr. and polarization props. 79−14094
Ba^+, inert gas atom collision, spectral line polarisation 79−13811
$BaSO_2$, suspension, light scatt., optical anisotropy determ. by polarisation ratio 79−1772
Bi atom, optical transitions, circular polarisation of light *(Russian)* 77−88420
Bi, parity nonconservation, weak electron-electron interaction, light polarisation, vapour optical activity *(Russian)* 78−55132
Bi, vapour, optical activity and HFS, neutral weak currents *(Russian)* 79−13660
$Bi_{12}GeO_{20}$, elec. field effect *(Russian)* 77−66480
$Bi_{12}SiO_{12}$, elec. field effect *(Russian)* 77−66480
$Bi_{12}SiO_{20}$ crystal, real-time holographic recording 79−72540
Br_2, organic solvent effects on Raman parameters 79−26998
CO_2 laser, with anisotropic resonator, radiation polarisation *(Russian)* 79−27309
CO_2 laser, with anisotropic resonator, output polarisation 80−28253
CO_2 laser radiation, intracavity modulation of polarization direction 80−102744
CO_2, multimode laser, fluctuating polarisation, correct use of beam splitters 77−79884
CO_2, multiple scattering contribs. to depolarisation of scattered light 80−87842
Ca II H-K and Na I D-lines, non-mag. polarisation 80−63569
Ca^+, inert gas atom collision, spectral line polarisation 79−13811
$CaCO_3$, calcite, laser Raman line polarisation meas. 77−4641
$CaCO_3$ calcite linear polarizer, role in laser technology 80−64165
$CaF_2:Eu^{2+}$, circular polarisation in luminesc. and optical orientation 78−6740
$CaF_2:Yb^{2+}$, divalent ion radiative state, magneto-optical obs. 77−69893
$CaF_2:Yb^{2+}$, luminesc. polarisation, elastic uniaxial compression effect, radiative state model 78−6739
$CaF_2:Yb^{2+}$, spectra, kinetics and polarisation of luminesc. 77−69892
$CdGeP_2$, pure and In-doped, polarisation of recombination radiation 78−19562
$CdInGaS_4$, crystal, Raman scattering spectra, polarisation meas. *(Russian)* 80−71410
CdS, attenuation of transmitted light in exciton region, polarisation, coherence, scatt. 77−69852
CdS crystals, electron-hole plasma, carrier optical orientation 80−100689
CdS platelet lasers, optically pumped, spatial and spectral distribution of laser emission 80−64032

light polarisation continued
CdS:Li, single crystals, anisotropic luminesc. centres 80−80857
CdSe, polarisation correl. of resonant Raman scatt. or hot luminesc. 80−25384
CdSe single crysts., exciton luminesc. and polarisation spectra under one- and two-photon excitation 79−65391
$CdSiAs_2$, polarisation of photoluminesc. 77−16389
CdTe:Mn^{2+}, luminesc. and magnetooptic reson., mag. field effect 80−93390
ClO_2, laser mag. reson. spectra tuned by Zeeman level crossing avoidance, perp. spectra 79−68229
ClO_2, laser mag. reson. spectra tuned by Zeeman level crossing avoidance, high-field spectra 79−76424
$Cr(CO)_6$, solid and matrix isolated, Raman spectra 79−28755
Cs atom, optical transitions, circular polarisation of light *(Russian)* 77−88420
Cs, optical reson. line electron impact excitation cross sections, polaris. 78−55244
Cs, photoelectron energy distrib. curves, depend. on light polarization 79−15591
Cs plasma in vacuum diode, pre-discharge, electron impact excitation line emission polarisation 78−47170
Cu film, diffuse optical scattering from variable roughness surfaces 80−100704
Cu-Cd-Cl stretched photochromic glass, polorisation effects 79−95729
Eu complex, with benzoylacetone, isotropic solns., Eu^{3+} luminesc. excitation spectra and polaris. spectra 79−87487
$Eu(NO_3)_3.6H_2O$, isotropic solns., Eu^{3+} luminesc. excitation spectra and polaris. spectra 79−87487
EuO, optical orientation of f-electrons, Curie temp. variation due to exchange interactions *(Russian)* 79−15431
$Eu_{0.14}Si_{0.31}O_{0.55}$ glass, optical, magnetic, and magneto-optical props., chemical clustering 79−42951
Fe, ferromag., spectral thermal emission, partial circular polarisation 78−18806
Fe, ferromagnetic, partial circular polarisation of thermal emission in mag. field 80−71387
Fe, monocryst. and polycryst., thermal emission, magneto-optic circular polarisation obs. 80−70435
Fe, tribothermoluminescence of flakes in grinding wheel, rel. to solar coronal dust radiation 78−68570
GaAs, polarisation anisotropy of hot photolum. *(Russian)* 77−90195
GaAs single-channel injection laser, polarisation characts. 80−48256
GaAs-$Al_xGa_{1-x}As$ electro-optic frequency and polarisation-modulated injection laser 80−91810
GaAs-$Al_xGa_{1-x}As$ MOS rib waveguide polarizers 80−64207
GaAs-$Al_xGa_{1-x}As$ MOS rib waveguide polariser, modulator and isolator 80−64217
ε-GaAse, optical consts. for $\perp$ and $\parallel$ light polarisation, reflectivity, interf. meas. 77−52077
GaP second order Raman spectrum, polarisation meas. 78−64368
GaP:Ni, deep traps, near IR luminesc., polarised spectra meas. 80−16077
GaP:Te, photon drag, optical rectification response meas., anomalous polarisation depend. 78−33769
GaP-GaAsP planar heterostructure strip ridged waveguide under mech. load, polarisation modulation 80−96038
GaS, infrared optical props., polarisation depend., vibr. modes 80−100658
GaSb crystals, uniaxial deform., effect on polarised luminesc. 78−10957
p-GaSb:Zn film, epitaxial, lifetime of nonequilib. carriers, determ. from circular polarisation of luminesc. 77−24898
GaSe, anisotropy effects on electroreflectance spectra at oblique incidence 77−52042
GaSe, highly excited, polarisation of luminesc. spectra and electron-hole plasma radiation 77−52169
Ge, exciton luminesc. polarisation in mag. field *(Russian)* 77−12436
GeS, orthorhombic single cryst., fine struct. in reflectivity, depend. on polarisation 79−19903
GeS_2, single cryst., IR polarised reflectivity spectra, 79−56775
$GeSe_2$, single cryst., IR polarised reflectivity spectra, 79−56775
H, beam-foil excitation of 2P-state, alignment meas. 80−14215
H, beam-foil excited, zero-field quantum beats in H_β emission, polarisation energy depend. 80−14218
H, electron impact coincidence, even-odd parity coherence effects, polarisation ang. distrib. 78−9253
H ion impact on clean Pb or Ni crystal surface, elliptic polarisation in Balmer radiation 80−35039
H lines, integrated polarisation in strong magnetic field 77−17563
H, photoionisation cross sections elec. field-induced oscills. 80−955
H-like ions, fluoresc. polarisation of Stark quenched spin-polarised beam 78−66501
H^++H, 1-7 keV, H(2s) form. and Lyman-α polarisation 80−14221
H_2, optical polarisation following electron impact 80−63831
H_2, radiation polarisation, electron-impact excited, Lyman and Werner emissions and Lyman-α 79−36681
H_2^+, polarised Balmer radiation due to scatt. from Nb surface, adsorbed O_2 effects 80−99569
H_2O, optical properties, 250-600 nm 77−52035
He, coherence meas. of light polarisation from 60 keV ions 77−71863
He, depolarisation factor *(French)* 79−82034
He, depolarising collision cross sections, quantum beat obs. 80−87203
He I, beam-foil excitation, temp. depend., linear polarisation of transitions 80−14213
He I, heavy ion impact excitation, orientation by anisotropic relax. of 4 ^1D level *(French)* 77−61844
He I beam-foil excitation, 60-180 keV, alignment production, foil temp. depend. 79−54956
He I beam-plasma discharge, optical radiation polarisation 78−67478
He I transitions, polarisation meas. using beam-foil excitation, foil tilt angle depend. 80−14212
He^- resons. in 56 to 64 eV electron collisions, autoionising states and spectral line polarisation 80−53145
He-Ne, anisotropic ring laser cavity, polarisation characts. 79−59726
He-Ne, internal mirror laser, polarisation props. of output beam 77−46744
He-Ne, single mode laser, mode polarisation in transverse mag. fields 78−22107
He-Ne, weakly anisotropic resonator laser, natural polarisation fluctuations of emission 77−79801
light polarisation continued
He-Ne gas laser, anisotropic resonator, linear polaris. freq. depend. 77−10961
He-Ne IR laser, internal modulation of polarisation 77−19350
He-Ne internal mirror lasers, polarisation in mag. field 78−17907
He-Ne laser, mag. polarised performance 77−14750
He-Ne laser light polarisation in transverse mag. field, Zeeman effect *(Dutch)* 78−29997
He-Ne laser with anisotropic cavity, fluctuations of field polaris. 79−27242
He-Ne laser with internal mirrors, mode polarisation props. 80−23672
He-Ne stabilised transverse Zeeman laser, light source for optical meas. 80−48272
He-Xe 3.51 μ laser mode competition in axial mag. field 80−63974
He^++H_2, charge transfer, appl. of atom-photon coincidence meas. 79−45829
He^++He, charge transfer, appl. of atom-photon coincidence meas. 79−45829
He^++He, interference struct., optical emission interpretation 79−45816
HeI, 3^3D-2^3P transition, light polarisation depend. on time and exciting electrons energy 80−37891
He(2s-3p transitions), beam foil spectra, emitted light polarisation, depend. on foil tilt angle 80−63786
$HgBr_2$, photofragment fluoresc. polarisation, press. depend. 80−63720
I photodissoc. ring laser, lasing regimes, emission and polarization characts. 80−48236
I_2, angular momentum transfer, elastic, inelastic collisions, orientation and polarised fluoresc. 78−90271
I_2, reson. fluoresc. obs. of rotationally inelastic collisions selection rules 77−58133
I_2+I_2, collisional energy transfer, ground and excited states, polarisation spectra 80−32805
InSb-NiSb eutectic, struct. and optical props., IR polariser appl. 80−45078
K, absolute optical electron-impact excitation functions 80−18933
K, optical reson. line electron impact excitation cross sections, polaris. 78−55244
K, stimulated electronic Raman light scatt. by mag. sublevels 78−50492
K, two photon excitation by opposing light beams, reson. lines polarisation studies 78−82705
K+He(Ne)(Ar), 0.7-80 keV, K excitation, reson.-line emission and polaris. 80−18911
KBr, colour centre form. under polarised UV irrad., dichroism in absorption spectra 80−107232
KBr:Tl, Jahn-Teller system, negative mag. circular polarisation in emission spectrum 80−20694
KCl:Pb^{2+}, inner-centre luminesc., 8 to 80K *(Russian)* 78−92112
KCl-Tl, Jahn-Teller system, negative mag. circular polarisation in emission spectrum 80−20694
KCl(Br), F-centre emission, mag. circular polarisation 80−108251
KCl(Br)(I):Ga^+, polarisation of Ga^+ centre A_T emission, temp. depend. 80−80842
KH_2AsO_4, domain struct. formation, opt. polarisation obs. 77−63381
KI:Tl, Jahn-Teller system, negative mag. circular polarisation in emission spectrum 80−20694
KI:Tl, polarised luminesc. of $(Tl^+)_2$ centres 80−71473
$KNbO_3$ half-wave voltage, electro-optic and polarisation-optic coefficients 77−40211
$La_2(SO_4)_3.9H_2O$, and isotopic forms, water librations, Raman obs. *(French)* 79−28754
Li, coherence meas. of light polarisation from 60 keV ions 77−71863
Li, two-photon ionis., many-body perturbation theory 79−22679
$Li_2(A^1\Sigma_u^+)$, state multipoles transfer following rot. inelastic He collisions, polarised emission obs. 80−5608
LiF:U^{5+}, absorption and laser-excited fluoresc. 79−99927
$LiIO_3$ crystal, nonlinear optical freq. transform. of variously polarized laser radiation 79−55181
$LiIO_3$, Raman induced Kerr effect with elliptical polarisation 78−42392
$LiKSO_4$, polarised Raman and IR reflection spectra, internal and external mode assignments 77−16293
$LiNbO_3$, anisotropic diffused optical waveguides, polarisation and spectral characts. 79−32073
$LiNbO_3$, pure and Fe doped, photorefraction kinetics under irradiation and heating 79−42934
$LiTaO_3$ platelet, electro-optical tunable filter, birefr. electro-optic cryst., light energy coupling 79−59804
Mg I, fluoresc. lines polarisation and mag. depolarisation *(German)* 77−6719
Mg, reson. line, Hanle effect, density depend. 79−6917
MgF_2, X-ray luminesc. polarisation 80−11462
$Mo(CO)_6$, polarised absorption, field effects in condensed media 78−997
N_2, Raman intensity, ab initio calc. 80−1028
NO_2, 8170-8280Å absorption spectrum, rot. struct., assignments 79−6937
NO_2, visible spectrum simplification, rot.-vibr. levels, excitation, polarisation labelling spectroscopy 80−32730
Na atom, cyclic interaction with circularly polarised laser radiation 80−78581
Na, D_1 and D_2 reson. lines, intensity dependent polarisation change 78−5163
Na, two-photon absorpt. processes, polarisation selection rules 80−9574
Na vapour, diffusion coeff. of oriented atoms in buffer gases 80−53908
Na vapour, Zeeman coherence, transient and stationary, polarisation spectroscopy 80−58212
Na_2, excited state identification by two-step polarisation labelling 79−76472
Na_2 vapour, near reson. two-photon absorption, polaris. depend. 77−79666
$NaBrO_3$, elec. field effect *(Russian)* 77−66480
NaCl:Ga^+, polarisation of Ga^+ centre A_T emission, temp. depend. 80−80842
$NaClO_3$, γ-irradiated, metastable O_2 reson. Raman scatt.,, excitation profile, polarisation meas. and decay kinetics 77−14437
NaF, M-centres, dichroim absorpt., appl. to optical waveguide polariser 79−995
NaK, $^1\Pi$ state perturbations, circular polarisation fluoresc. meas. 79−76462
NaN_3, UV irradiated, polarised optical absorpt. of F_2^+-, F-centres 77−28605
Na^*+N_2, differential quenching cross-section, polarisation effects 77−27019

light polarisation continued
Nd:glass, Q-switched laser, radiation polarisation 77−27293
Nd:glass laser with continuously tunable ps output, polaris. filter 79−22985
Nd:glass Q-switched laser emitting polarised radiation 79−45974
Nd:phosphate glass double pass amplifier with circular polarisation 77−88774
Nd^{3+}:YAG laser active element, linearly polarised light depolarisation due to thermally induced birefr. 80−106528
Ne gas, laser induced birefr., polarised light interf. obs. 77−19368
Ne, Lamb-dip structure anal., linear and helicoidal polaris. 78−25852
Ne_2, Raman spectra and polarisability 79−98107
Ni, polycryst., thermal emission, magneto-optic circular polarisation obs. 80−70435
O IV(VI), circular polarisation of light emitted in beam-foil collisions, cascade free lifetimes 78−55228
P-Se-Tl system glasses, polarisation, refr. index and dielec. const. meas. 80−20608
PLZT/TFPD thermal/flash protective lens assembly, polarised delamination investigation 80−78929
Pb atom, optical transitions, circular polarisation of light *(Russian)* 77−88420
Pb-salt tunable diode lasers, beamshaping and polarisation control props. of flexible hollow metallic rectangular pipes in mid-IR 79−76856
$(Pb_{1-x}Bi_x)_5Ge_3O_{11}$, spontaneous and induced electrogyration 79−42946
$Pb_{1-x}Sn_xTe$ films, size quantisation, optical orientation of free carriers 80−20725
Rb, circ. polarised reson. fluoresc. excited with π polarised D_2 line, 0-170 G 79−41133
Rb, Doppler-free superradiance, polarisation characts. 79−782
Rb, optical reson. line electron impact excitation cross sections, polaris. 78−55244
Rb, superrad. between degenerate levels, polaris. characts., coupled transitions 80−58493
$RbAg_4I_5$, depolarisation of light by crit. fluctuations 79−61333
RbCl(Br), F-centre emission, mag. circular polarisation 80−108251
S^-, photodetachment in mag. field 79−41143
Sb_2S_3, anisotropic cryst., optical const. determ., reflected-light polarisation 77−43960
Si film, polycryst., ellipsometric meas. *(Polish)* 78−21095
Si, reconstructed surface (111)2×1, polarization depend. of optical absorpt. spectrum 79−28396
n-Si, surface-barrier electroreflection, polarisation anisotropy 79−24295
SiO_2, vitreous, luminesc. centres, decay time and polarization props. 79−33829
SiO_2-LiO_2-Al_2O_3 glass, luminesc., polarisation degree distrib. 80−108257
SiO_2-Si film-substrate refl. polariser, operation at Hg spectral lines 77−75655
SmI, Zeeman coherence, transient and stationary, polarisation spectroscopy 80−58212
$Sm_xTb_{1-x}FeO_3$ orthoferrites, crystallo-optical props. 79−42027
SnS_2, single cryst., far IR reflectivity 79−56774
Sr^+, inert gas atom collision, spectral line polarisation 79−13811
SrF_2:Eu^{2+}, circular polarisation in luminesc. and optical orientation 78−6740
$Sr^+(^2P_{3/2})$, Penning ion, polarised emission, Hanle effect obs., radiative decay rate meas. 80−5520
$Sr^+(5p^2P_{3/2})$ alignment in $He(2s^3S_1)$+Sr Penning collisions, polarised emission obs. 80−23533
TE, current induced optical activity, polarisation plane rotation rate *(Russian)* 79−65830
TeO_2 shear wave acousto-optical device with polarisation filtering 80−106619
Tl atom, optical transitions, circular polarisation of light *(Russian)* 77−88420
Tl, electron impact excitation, threshold to 1.5 keV, 2768 Å polaris. function 77−54614
Tl, parity nonconservation, weak electron-electron interaction, light polarisation, vapour optical activity *(Russian)* 78−55132
TlBr-TlI(Cl) crystals, photoelastic moduli 80−97230
V_6O_{13}, semicond., IR vibration spectra 80−88997
W, pure and Ba covered, photo-stimulated field emission, effect of light polarisation *(French)* 80−7480
W-halogen quartz envelope lamp, polarization characteristics 80−95970
Xe, multiple scattering contribs. to depolarisation of scattered light 80−87842
XeF laser, output control by injection locking 80−74405
YAG-Ti, polarised luminescence 79−95843
Zn^++He(Ne)(Ar), 1-500 keV, Zn^+ excitation, reson.-line emission and polaris. 80−18911
$ZnGeP_2$ p-n homodiode, polarisation photosensitivity and photopleochroism spectra 80−107866
$ZnGeP_2$, polarisation of recombination radiation 78−19562
$ZnGeP_2$, single cryst., polarised light photocond., optical transparency anisotropy *(Russian)* 78−2518
ZnO, attenuation of transmitted light in exciton region, polarisation, coherence, scatt. 77−69852
ZnO, ellipsometric spectroscopy of nonpolar $(1\bar{1}00)$ surface 79−33651
ZnS:Cu, Cl, I, anisotropy of blue Cu luminesc. centres 77−81137
ZnS-Mn crystal, polarisation meas., luminesc. and Raman spectra 79−8138
ZnS-Na_3AlF_6 layer achromatic interference polarizers, design, fabrication 79−55222
ZnSe(Te), Raman-luminescence problem, interference analogy and expt. discrimination by polarisation correl. 79−95764
ZnTe crystals, secondary radiation polarization and relaxation of optical excitation 80−11399
ZnTe(Se), optical circular polarisation correl. in secondary radiation, resonant light excitation 77−69885
$ZrSe_3$, long wavelength optical phonons, Raman scatt. and IR refl. 80−34921

light propagation
see also atmospheric light propagation; guided light propagation
aberrating Gaussian beam, free-space propagation, wave eqn. solns. 78−87008
active electrooptic and magnetooptic media, matrix theory fundamentals *(Russian)* 78−63005
aerosol, plasma production by CO_2 laser beam, brightening channel 80−6272

light propagation continued
anisotropic crystals, in which dielec. tensor has components with different signs, opt. props. 79−42931
anisotropic layered media, matrix method 77−34816
anisotropic media, partially polarised light propag., differential 4×4 matrix calculus 79−41330
ballistic theory 80−4524
beam generation, quasi-homogeneous Gaussian sources, spatial coherence 80−48145
beam volume attenuation coeff., invalidity 80−95791
beam wave, propag. through weak turbulence, frequency spectra 78−78911
beamed signal propagation through diffractive inhomogeneous media 77−71920
birefringent cryst., projection dyadic treatment, for teaching 77−33789
boundary-value problem, two-point, statistical variant using Einstein-Fokker-Planck eqn. *(Russian)* 78−81924
Cherenkov radiation at resonance frequency of amplifying medium 79−22926
chirped pulse, compression, in dispersive media 78−33669
chirped steady π-pulses of arbitrary duration in lossy, exactly resonant inverted medium 79−89947
cholesteric medium, under applied mag. field *(French)* 78−80319
coherent and partially coherent light, comparison between propag. in given geometry 79−31790
coherent light beams, optical path difference, optical phase diff. meas. by polarisation technique 78−29141
coherent light pulse propag. in dielectric medium 77−31064
coherent optical systems evaluation, apodisation in beam propagation and image formation 77−88657
coherent optics fundamentals 78−78910
coherent probe light pulse, in medium with chem. reaction wave 80−61190
coherent pulse propagation, soliton creation by chirped initial profiles 79−72632
correlation coeffs. of planar sources and their far fields 78−66750
correlation velocity, in dispersive media 77−68165
correlator, wavefront propagation error effects 79−50232
crystal inhomogeneous in optical anisotropy due to stress distrib., light propag. eqns. 79−13897
crystal optics, group vel. and energy density, monochromatic wave dispersion depend., for teaching 78−25792
dielectric, isotropic, two-dimens. dielec. const. determ., wave trajectory construction 78−80276
dielectric medium, steady propag. of coherent light pulse, effect of spatial dispersion 79−72480
dielectric solids, molecular optics model, electrodynamic eqns. derivation 78−27151
dielectric tensor field determ. in weakly inhomogeneous anisotropic media 79−72492
dispersion relations with finite propagation speed 80−99606
dispersive media, theory of multiple light scatt. by spherical particles *(Russian)* 80−94599
Doppler effect in special relativity for teaching 78−24609
education, light momentum density in refracting medium, electrostriction, Peierls method 77−33772
electro-optical effect anisotropy in plane of light wavefront 79−8121
ellipticity, azimuth and system parameters linking eqns., 3-dimens. model propag. 78−50695
EM theory based on additive light velocity and gaseous ether theories 80−51
energy absorption distrib. in material with spatially varying optical props. 77−75419
eye, human, retinal spectral-response characteristics model 79−92215
Fermat principle, tutorial for physics teachers *(Hungarian)* 78−36775
focusing of light beam optimisation, in moving nonlinear media, using gradient method 80−106578
free-space propagation model for coherence-separable broadband optical fields 80−78763
Fresnel diffraction field, anal. by quantum mech. operator method 80−5688
fusion reactor advanced H-^{11}B fuel, reaction feasibility under laser compression 77−83085
gas, propag. of ultrashort light pulse in region of absorpt. line *(Russian)* 77−47141
gaseous medium, two-photon-absorbing, polarised light propag., quantum effects 80−103107
gases, self-interaction and stimulated Raman scattering effects *(Russian)* 79−3740
gases induced scattering and self-action, effect on optical radiation propagation 79−72628
Gaussian beam propagation, Fresnel-Kirchhoff integral anal. 79−45984
Gaussian beam propagation beyond the paraxial approximation 79−72476
Gaussian beam propagation in 3-layered dielec. medium *(Japanese)* 80−87306
gaussian Schell-model planar sources, beam directionality 79−903
generalised Gaussian beams in free space 78−9319
Helmholtz equation in optics, numerical soln. 78−90357
homogeneous medium, Gaussian light beam propag., diffr. effects described using complex-ray method 80−78770
Huygens' principle and Broglian waves *(French)* 79−21545
Huygens-Fresnel integral in circular coords., asymptotic soln. 78−87013
inhomogeneous media, coherent states and light propag., graded-index waveguide coupling 80−102625
inhomogeneous media, moments of field calc., in limit of saturated fluctuations 79−72497
inhomogeneous media, phase fluctuations, strong scintillations *(Russian)* 77−75417
inhomogeneous plane wave shadowing by an edge 78−90356
inhomogeneous slab, propag., rigorous soln. 78−18055
isotropic turbulence spectrum determ. from optical meas. 79−3634
in Kerr metric, appls. of geometrical optics, analytical results 77−29637
laser beam, saturation parameter from gain meas. 78−66797
laser beam propagation in particulate media, radiative transfer eqn. soln. 79−50222
laser beam propagation in thermal turbulence *(French)* 77−7007
laser beam thermal blooming, stagnation and transonic effects 77−34903
laser beam with stagnant absorber region, transient thermal blooming 77−38966
laser beams, Gaussian, geometric props. 77−19276

light propagation continued
layered reinforced plastic, light propagation for NDT 77−9024
lens systems 80−78947
lenslike medium, mode degeneracy removal by x^2y^2 term in index distrib. 77−83812
light Doppler effect, absolute spacetime theory 78−69979
linear anisotropic crystals, acousto-optic interactions, general theory 79−99850
liquids, anisotropic, light propag., intermol. correlation technique for mol. susceptibility tensor 77−58251
lossless diffraction gratings, symmetry props., time reversibility 80−48422
mechanical effects, light induced, connected with Fresnel coeffs. of drag 80−32908
microscopically inhomogeneous material, theory of optical and microwave props. 77−77161
momentum of light wave, in refracting medium, oblique refl. 77−50612
nanosecond laser pulse stretch meas. in underwater propagation 80−87426
negative correlation effect *(Czech)* 79−45901
noninertial reference system *(Russian)* 79−897
nonlinear absorbing media, ray tracing and self-focusing theory 79−27339
nonlinear electrodynamics in generalised gravitational theory 77−5727
nonlocality effects on optical phenomena in bounded solids, developments 80−93328
nonreciprocal effect, during light passage through US beam 80−106443
nonrelativistic non-Fresnel approach to light propag. in moving media 78−78904
nonsymmetric unified field theory, physical interpretation and light propag. 79−21618
ocean, irradiance in Norwegian and Barents Sea rel. to water temp. 80−31055
ocean, spatial struct. of underwater light-field fluctuations *(Russian)* 78−53656
optical barrier penetration, teaching expt. 77−67159
optical systems with large apertures, Fresnel approx. 78−66746
optical wave, log-amplitude fluctuations spectra, turbulence spectra parameters determ. 80−95797
paraxial approximation to scalar Helmholtz eqn., discrete eikonal and ray eqns. 78−90360
partially coherent source in extremely strong turbulence, irradiance scintillations 79−64176
partially coherent wave propagation and generalised van Cittert-Zernike theory 78−25793
periodic stratified medium, birefr., phase matching, X-ray lasers 77−65566
periodic stratified medium, general theory 77−65565
periodic system, suppression of filamentation of intense light beam 79−59777
photoelastic materials and crystals, geometrical optics approx. 79−898
photoelastic specimens, effect of stress gradient on propagation direction 79−45903
photoelastic stress anal. of solids, shadow and interference methods *(Russian)* 79−7352
plane wave intensity fluctuations in turbulent medium *(Russian)* 78−1156
plane wave pulses, random media propagation 78−9324
plate, rectangular, deformed, light ray propag., geometrical effects, nonclassical behaviour *(Russian)* 78−22080
polarised laser beam propag., numerical soln. of spinor Helmholtz eqn. 79−72479
polarised light radiative transfer eqns., adjoint Monte Carlo treatment 78−37799
polydisperse particulate sytems, light extinction 78−33667
pulse train propagation, two-level absorber, relax. effects 79−46011
quadratic structure functions describing random tilted phase fields 80−95799
radiation field, mean specific emission intensity, fluctuation effects *(Italian)* 79−18346
radiation patterns of mag. and elec. dipoles with arbitrary orientation 80−32886
random media, theory and appl. of wave propag. and scatt., review 77−75376
random media, two-frequency mutual coherence function for pulse propagation 79−76589
random medium, finite beam propagation 80−91748
random nonuniform medium, covariance function computation of light wave intensity 80−58463
random phase screens, probability density for intensity of plane waves 80−87317
randomly inhomogeneous media, strong fluctuations of optical beam fields 80−99634
randomly inhomogeneous medium, field intensity moments in fluctuation saturation region *(Russian)* 79−3630
randomly inhomogeneous medium, fluctuations in phase arrival angle and freq. correl. of spherical waves 80−106456
randomly inhomogeneous medium, spatially limited light beam displacement 78−5421
randomly inhomogeneous turbulent media, spectral expansions method for optical wave propag. 80−43264
randomly-inhomogeneous medium, logarithmically normal distrib. law of amplitude fluctuations *(Russian)* 77−61915
real space-time rays in absorbing media, Fermat's principle 79−3628
refractive index of empty space and scalar gravit. fields, Fresnel formula 77−30082
rotating black hole and accretion disc seen by non rotating observers 80−17606
rotating disc, light ray and particle paths 79−2670
scattering medium, stratified, narrow beam propagation theory 80−106455
scintillation meas. in turbulent propagation, detector aperture effect *(Slovak)* 80−63921
sea water, turbid, light propag. calc. from dielectric permeability algorithm *(Russian)* 78−77261
semi-infinite spatially dispersive absorbing dielectric, energy flow 77−4611
semiconductor, light pulse propag. inducing transitions between bands with different effective masses 80−34871
short wave radiation problems in inhomogeneous media, book 77−10840
skewness and probability distribs. excess coeffs. 79−50224

light propagation continued
sky appearance for observer in accretion disc of rotating black hole 80−17605
solar spectral lines propagating through interplanetary medium, profiles modification 79−66973
starlight aberration rel. to spectral type *(German)* 78−73702
Stokes relations in optically active media, macroscopic reversibility principle appl. 80−53207
supersonic boundary layers interacting with cooling wall jets, turbulent and optical characteristics 80−106792
surface wave, momentum exchange with moving atom 79−64359
thermal self-action problems and their compensation 80−106579
thin wave beam in randomly-inhomogeneous medium, ray description *(Russian)* 78−63007
transient propagation in active media, Maxwell-Bloch eqns., coherent self-focusing 78−87109
transparent anisotropic medium, ang. momentum conservation 77−50610
travelling wave amplifier, spontaneous radiation propag., spatial filtering 77−14764
turbid medium, infinite plane wave, mutual coherence function propag. 78−1163
turbulence, laboratory-generated, simulating atm. turbulence effects on optical propag. 80−9803
turbulent atmosphere, propag. of partially coherent source 80−12533
turbulent irradiance probability distrib. in saturation regime 79−76588
turbulent medium, four-point coherence function strong intensity fluctuations region 80−87319
turbulent medium, four-point field coherence function 79−98279
turbulent medium, light intensity two-freq. fluctuations correl. 79−98280
turbulent medium, meas. via optical heterodyne interferometer, two-channel crosstalk elimination 77−10100
turbulent medium, phase fluctuations 78−33668
turbulent medium, space struct. of light strong intensity fluctuations 79−98278
turbulent medium, turbulence spectrum reconstruction from time correlation function 77−19178
turbulent water optical propag., refr. index spectrum of temp. or salinity fluctuations 79−5487
tutorial, group and phase velocity Maxwell-Lorentz theory, Fermat principle *(Hungarian)* 78−36774
twisted anisotropic media, appl. to photoreceptors 78−63004
two-level resonant medium, light pulses propag. 80−64119
undersea transmission characts. of laser beam in Tago Bay, Japan 77−21782
unified wave propagation theory, tenuous random medium 78−4491
water aerosol, propagation of intense radiation at 10.6 μm 80−5692
$LiNbO_3$, electro-optical modulator, light propag. close to optic axis 79−42947

light propagation in plasma
acceleration effects in resonant interaction of laser beam and ions 80−10390
anomalous absorption, interaction of laser with laser prod. plasma 77−19734
anomalous absorption due to parametric instability of laser prod. plasma *(Japanese)* 77−43012
anomalous intense laser radiation transmission through overdense plasma 79−10671
anomalous interaction, of powerful light beam with dense plasma *(Russian)* 80−1797
backscatter from laser plasma, optical ray retracing effects 78−91133
backscattered light, nonlinear decay 79−46455
Brillouin and dielectric sidescatter of 10-μm light by a plasma 80−103156
Brillouin backscatt., Langmuir turbulence effect 77−35347
Brillouin backscatt. depend. on density scale lengths near crit. density 80−43888
charged particle propag. in parabolic intensity profile laser beam, isotope separation appl. 79−54984
collision effects on light scattering by plasmas containing ionized impurities 79−41835
collision-dominated plasma, laser scatt. intensity 80−83905
collisional magnetoplasma, self-focusing effect on filamentation instability 78−51305
collisional plasma, filamentation of laser beam, theory 77−84440
collisional plasma, mixed mode operation, cross-focusing 80−83945
column waveguide, time varying, laser beam propagation 78−94916
critical surface, enhanced stimulated Brillouin scatt. due to light refl. 80−1750
cross focusing of mixed mode operation in overdense plasma 79−94798
CW far-infrared laser scattering from a laboratory plasma ion acoustic wave 80−106974
cyclotron resonant gas breakdown with 1.22-mm $^{13}CH_3F$ laser 79−55549
degenerate 4-wave mixing in plasmas 80−24179
dense expanding plasma, laser radiation absorpt. 79−90417
dense plasma, laser scatt. 78−67408
density profile deformation and efficiency of resonance absorpt. in nonuniform plasma *(Russian)* 79−4148
discharge plasma, optogalvanic effect analysis using rate eqns. in modified Schottky formalism 79−23421
electron density meas. by far IR laser beam deflection 80−59296
EM structure resonances in inhomogeneous layers 78−30448
enhanced Brillouin scattering, Gaussian laser beam in hot collisionless plasma 79−94799
Faraday rotation anomalies in an Ne discharge in a weak magnetic field 80−38659
fluctuation of electron density, caused by nonlinear interaction of two pulsed laser beams 79−98920
focal region of intense laser beam in tenuous plasma, spatial and temporal electron and ion density variations 80−53989
focus, high density, as laser pulse clipper and optical isolator 77−65601
focused light absorpt. by spherical plasma 79−98918
focusing of low power laser beam in inhomogeneous plasma 79−73014
Fresnel drag in transversely moving dispersive media, astrophysical plasmas 79−96902
fusion target illumination reduction, enhanced stimulated Raman plasmon scatt. 77−84470
gas-laser beam intensity fluctuations, spatial distrib. 79−18458
gaseous laser target, resonant light absorpt. 77−19737
Gaussian beam conversion 78−67364
Gaussian laser beam, nonlinear self-focusing 79−27786

light propagation in plasma continued
Gaussian laser beam, transverse self-focusing and self-trapping investig., moment method 80−58652
Gaussian laser beam and stimulated Raman scatt., plasma wave excitation 77−27680
Gaussian laser beam propagation in overdense plasma, self-focusing 79−55513
glass microshell, high-power glass laser interaction 78−9804
harmonic generation in 10 μm laser-produced plasma, intensity depend. 79−55506
harmonic generation in laser prod. plasma 77−84438
high power laser pulses, localisation in plasmas 79−14554
high temperature plasma flying apart, laser radiation absorption and refl. *(Russian)* 77−27684
incoherent scattering of light by moderately hot magnetised plasma 78−5878
inert gas plasma, electron-beam produced, laser action of ionized and neutral atomic lines 80−106929
inhomogeneous birefringent optically active medium, polarisation evolution 78−9328
ion-acoustic wave excitation by two Gaussian laser beams, density profile modification 79−19006
ion-acoustic wave-CO_2 light coherent scatt. 78−34325
IR laser pulse absorption, air breakdown initiated on aerosol *(French)* 79−73021
Langmuir and ion acoustic wave coupling, turbulence spectra, light absorption 80−87902
lase light absorpt. at critical density, collective behaviour 77−43005
laser absorption, ponderomotive force, DC mag. field generation 78−38498
laser beam, elliptically shaped Gaussian, self focusing and self defocusing 79−32777
laser beam, high-power, self-focusing in fully ionised plasma 78−87451
laser beam, stimulated Brillouin to stimulated ion Compton scatt. evolution 78−42762
laser beam attenuation, 10.6 μm in elec. initiated laser-driven plasma 77−34424
laser beam filamentation in presence of longit. inhomogeneity 80−19079
laser beam filamentation in strongly ionised magnetoplasma 78−26291
laser beam focusing in plasma with linear dielectric const. variation 79−60146
laser beam in plasma waveguide, absorpt. effects, normal mode anal. 79−64871
laser beam interacting with ion-acoustic wave, filamentation instability 79−41838
laser beam propagation in plasma waveguide, normal mode anal. of oscillating Gaussian soln. 79−4145
laser beam re-entry into laser prod. plasma 79−55526
laser beam relativistic self-focusing, short-range shrinking and dielec. swelling 77−42985
laser beam self-focused in turbulent plasma, average field 80−79505
laser beam self-focusing, moment theory 79−77390
laser beam self-focusing, nonlinear absorption effect 78−79436
laser beam self-focusing, stimulated Raman and Brillouin scatt. 78−30447
laser beam stabilisation in long absorptive plasma 77−39423
laser beam transverse filamentation and self-focusing 78−67358
laser beam trapping and propagation in cylindrical plasma column 77−24093
laser beam-ion acoustic wave interaction, excitation and interference 78−34326
laser beam-plasma coupling in laser solenoid plasma 77−11351
laser beam-plasma interaction, in mag. field, breakdown, heating, trapping, fusion, diagnostics, book contrib. 77−51196
laser beam-plasma interaction nonlinear force, generalised derivation of Stamper term 79−37502
laser beams, two, collisional absorption, inverse bremsstrahlung, heating 78−26292
laser breakdown of air initiated from dust particle, laser beam shutter 79−68412
laser emission intensity reduction near solid target surface *(Russian)* 80−38681
laser energy reson. absorpt. in magnetised plasma 79−37500
laser field effect on transport coeffs. 78−67317
laser generated mag. fields, enhanced, plasma transport 78−34273
laser irradiated plasma, electron energy profile steepening, polarimetry obs. 78−34349
laser irradiated plasma, soliton generation at resonance, density modification 78−14172
laser light absorpt., deceleration and scatt. of epithermal electrons 77−84471
laser light absorpt., mag. field generation 79−10670
laser light absorpt., numerical calc. 78−75348
laser light absorpt., turbulence 78−47128
laser light absorpt. and scatt. in laser fusion plasma 78−51312
laser light absorpt. by ion acoustic turbulence in laser prod. plasma 79−4144
laser light absorpt. by short wavelength ion turbulence 77−35352
laser light absorpt. due to self-generated mag. fields 78−14170
laser light absorption, by planar plasmas, polarisation and ang. depend. 77−76096
laser light absorption, simulation 77−11347
laser light absorption and harmonic generation 78−75359
laser light absorption in high temp. plasma 77−76090
laser light absorption with self-generated magnetic field 77−24092
laser light Raman conversion, plasmon prod. 78−47125
laser light reson. absorpt. and stimulated Brillouin scatt. 78−47129
laser light resonance absorption 78−42763
laser light resonant absorpt., mag. field generation 77−15197
laser light resonant and collisional absorpt., heating, density profiles 78−38527
laser mirror plasma-optical Q-switch *(Russian)* 80−33028
laser photons, interaction with nonthermally excited plasma particles 77−47213
laser plasma, convective parametric decay instability 80−64722
laser produced plasma, laser light scatt., ang. distrib. 77−15215
laser produced plasma, wavelength effect on absorpt. and ionis. 77−27654
laser pulse self-focusing 78−34322
laser radiation, anomalous transmission through overdense plasma 78−38499

light propagation in plasma continued
laser radiation, plasma ionis. degree effect *(Russian)* 77−76098
laser radiation absorpt. in hypocycloidal pinch, heating appl. 77−27679
laser radiation absorption, by dense plasma, polarisation depend. 77−62368
laser radiation absorption by spherical plasma, geometrical optics 80−59189
laser radiation forces in magnetised plasma 77−24091
laser radiation in plasma, oscillating two-stream instability 80−92328
laser radiation interaction phenomena, review 80−43953
laser radiation nonlinear propag. 79−77389
laser radiation parametric decay into plasma waves, Thomson scatt. meas. 78−30484
laser radiation refl. and scatt. in CO_2 laser generated C plasma 77−19715
laser radiation refl. coeff. from dense plasma in anomalous absorpt. region *(Russian)* 77−15194
laser scattering from large Tokamak plasmas, signal-to-noise scaling 78−42809
laser-induced acceleration of macroparticles 80−27813
laser-pellet irradiation, two-plasmon decay instability, soliton form. role 78−1842
laser-plasma, interaction, stimulated scatt., constant mismatch effect 77−31477
laser-produced plasma, ion acceleration in presence of density profile steepening 80−14923
laser-produced plasma spherically symmetric absorption (reflection), simulation 78−51285
laser-produced plasmas, light absorpt., mag. fields and hot electron physics 77−43004
magnetic accreting neutron stars, light scatt. in strongly mag. plasma 79−62739
magnetic field generation, laser light reson. absorpt., stress tensor anal. 78−18419
magnetic field operation, in resonant absorption of light 79−73013
magnetised plasma interacting with laser, reson. enhancement of mag. radiative force 78−14166
magnetoplasma, axially inhomogeneous, laser beam self-focusing and filamentation 79−19042
magnetoplasma, laser beam self-focusing 80−102778
magnetoplasma, overdense, anomalous penetration of laser radiation, upper hybrid and whistler modes 79−77386
Mandel'shtam-Brillouin scattering, induced, from laser plasma, spectrum *(Russian)* 79−98876
metallic target, self-generated mag. fields due to laser field 79−27808
moderate-Z plasma, laser heating and ionisation in presence of strong UV and X-radiation 78−71512
multiphoton processes in plasma at equilib. 77−47212
non-uniform laser plasma, stimulated Raman light scatt. spectrum *(Russian)* 80−106926
noncooperative radiation scattering, from finite vol. of relativistic plasma *(Russian)* 79−37497
nonisothermal plasma, parametric absorpt. of laser emission *(Russian)* 77−80312
nonlinear absorption by optical mixing, temp. effects 77−15218
nonlinear electron oscillations, driven by EM wave 79−64850
nonlinear force of light press. in laser interaction with thin plasma, polarisation influence 80−100078
nonlinear inverse bremsstrahlung and heated electron distributions 80−43930
nonlinear laser forces, acting on electrons of tenuous plasma 79−41837
nonlinear pressure forces for laser radiation in plasma, experimental confirmation 80−28682
nonliner penetration of inhomogeneous beam in overdense plasma 78−22511
nonquadratic plasma waveguide, propag. of highly aberrated laser beams 77−84441
oblique incidence of laser radiation on plasma, refl. obs. *(Russian)* 79−32752
optical cavity plasma, stimulated Raman and Brillouin scatt., electrostatic and EM waves 78−34324
optical escape factor, rel. to thermalisation length 79−86611
optical mixing of two laser beams in uniform collisionless plasma 77−19711
optical transparency evaluation, line broadening effect 80−79453
optogalvanic effect, theory based on multiplication of electron within plasma 80−38741
Osterberg problem and wave propag. in inhomogeneous plasma, numerical study 80−63925
parametric back-scatt., absorptive instabilities, self-focusing effect 78−22510
parametric decay and Brillouin backscatt. instabilities, IR laser induced 77−47187
parametric decay interaction, three-wave, threshold behaviour, bounded inhomogeneous plasma 78−42746
parametric turbulence of particles emitted by a laser plasma *(Russian)* 80−53985
parylene disc, high-power glass laser interaction 78−9804
photon helicity conservation in parametric scatt. instability 77−31478
plasma, laser radiation propagation, mag. field effects *(Russian)* 77−7552
plasma critical surface, enhanced stimulated Brillouin scatt. due to light refl. 80−1750
plasmon decay, cause of anomalous light absorpt. 79−1318
plasmon scatt. by electrons in intense EM field, instability 77−72434
plastic film, laser energy transport, X-ray, ion emission, scatt. light diagnostics 77−24117
polyethylene expanding plasma, high power CO_2 laser radiation interaction 78−47138
Poynting's theorem for inhomogeneous moving media reconsidered 79−48661
pulse shaping effects on interaction processes in laser prod. plasmas 80−43946
radiation absorption in magnetoplasma, rel. to laser fusion 80−92273
Raman and Brillouin backscatt., nonlinear theory 78−47127
Raman backscattering, enhanced, of Gaussian laser beam from plasma wave 79−86566
Raman scattered light, in laser plasma, magnetic fields and line splitting *(Russian)* 79−55510
re-emission, in parametrically turbulent laser plasma *(Russian)* 79−55509

light propagation in plasma continued
reflectance, of laser pulses on laser produced plasmas 79−73015
reflectance of laser-produced plasmas, angle and polarisation depend. 78−18452
refraction into a nonlinear medium: wave profiles and hysteresis 80−43395
refractive index modulation in plasma, laser-induced 79−10668
resonance absorption, mag. field generation 77−31480
resonant absorption, mag. field generation 79−10669
resonant absorption 77−72452
resonant absorption at a rippled critical surface 79−4146
resonant CO_2 laser radiation absorption and surface instability at crit. density surface 80−48859
response to ponderomotive forces from laser pulse 77−47207
reverse field pinch, Faraday rot. diagnostics for internal mag. field 80−43976
scattering from laser produced plasma, CUPID ray tracing program 80−18990
scattering of CW Ar laser, radiation, low-temp. plasma diagnostics 78−38536
second harmonic emission spectrum, from laser produced plasma 79−90416
self focusing mechanism, current generation due to light pressure *(Russian)* 78−63571
self-focusing, of laser beam, in multiply ionized absorbing plasma 79−32776
self-focusing, short-range, due to relativistic effects on refr. index 79−10673
self-focusing of a laser beam in an inhomogeneous plasma 79−32778
self-focusing of non-Gaussian laser mode in dense plasma 78−59599
self-trapped laser beams 77−76093
self-trapping and self-focusing of elliptical laser beam in collisionless magnetoplasma 80−53991
SHG in laser plasma, review 80−53993
SHG in laser plasma *(Russian)* 79−86587
short-pulse laser backscatter from gas target 80−79454
spark, laser radiation absorpt. mechanism in deionis. stage *(Russian)* 78−22583
spark plasma deionisation stage, laser radiation absorption obs. 78−75398
specular reflection of light from laser-produced plasmas 79−37456
spherical laser plasma, classical optics and light press. 78−59601
stationary self-trapped laser beams in plasma 78−79438
stimulated bremsstrahlung of electrons, strong optical field influence 78−59623
stimulated Brillouin back-scatt. losses in weakly inhomogeneous laser-produced plasma 80−19561
stimulated Brillouin backscatter from theta pinch 78−67359
stimulated Brillouin backscattering, mag. confined plasma 78−51307
stimulated Brillouin backscattering, saturation in CO_2 laser plasma interaction 79−27787
stimulated Brillouin scatt., efficient saturation due to nonlinear ion wave decay 79−86585
stimulated Compton scatt., density inhomogeneity effects 78−30446
stimulated parametric backscattering, refl. coeff. 77−62005
thermonuclear fusion plasma, laser coupling and implosion 77−43006
theta-pinch, Scylla I-C, laser beam-plasma interaction 77−24090
third-harmonic generation in collisional plasma, self-focusing effect 77−7550
Tokamak TFR, Thomson scattering system based on two-detector spectrometers 80−32426
upper-hybrid-resonance absorption of laser radiation, magnetised plasma 77−72451
UV irradiation, boundary thickening, surface accel. *(Russian)* 77−35334
visible and UV high intensity spectral lines 79−73012
wave excitation mechanisms and harmonic generation in laser produced plasma *(Russian)* 77−11339
Wigner distribution function, transport equations, inhomogeneous dispersive medium 80−53214
Z-pinch, overdense, He plasma, laser-driven hydrodynamic perturbation, shock density struct. 79−77385
Al expanding plasma, high power CO_2 laser radiation interaction 78−47138
Al laser plasma, laser beam self-focusing, X-ray emission 79−82064
Al vapour, surrounding plane target, light propag. in plasma vapour, 10.6 μm laser 79−23435
Al(XII) and (XIII) reson. line trapping in laser-heated plasma, source distrib. diagnostics 78−42730
Ar, optical breakdown at 10.6 μm near plasma layer boundary 79−60165
Ar, plasma, shock-compressed optical props. 79−23426
CO_2 laser beam attenuation by air discharge plasma column 80−19062
CO_2 laser beam scatt. by microscopic fluctuations in plasma density 80−79574
CO_2 laser light interaction with high temp. plasma *(Japanese)* 79−82101
CO_2 laser plasma shutter, transmission cut-off time depend. on breakdown intensity 80−6259
CO_2 laser pulse temporal shaping by controlled plasma switching 79−3725
CO_2-laser (long pulse)-plasma interactions, classical absorpt. and heat conduction in low-irradiance 80−75059
CO_2-laser radiation filamentation in underdense H_2 plasma, X-ray diagnostics 80−14941
H, laser breakdown and propag., 2D-simulation 78−5921
H plasma, parametric decay instability, obs. by scatt. of laser beam from plasma 77−80309
H Z-pinch plasma, strong optical attenuation, shadowgraph meas. 78−26294
H_2 discharge plasma, laser-induced transient striations obs. 79−27785
H_2 gas target, stimulated Brillouin scatt., press. depend. 78−42764
He continuum radiation, 109 to 540 nm, meas. in arc plasma *(German)* 80−106932
He plasma, Stark shift and line broadening in 3-D stochastic laser field 78−50502
I laser, Asterix III, light-plasma interaction expt. and light pulse props. 80−53349
Na-Ne plasma, near-reson. dye laser scatt. and two-photon absorpt. 77−39459
light propagation in plasma continued
Na-seeded flame, H_2-O_2-Ar, population inversion, two-photon laser excitation 79−34307
Ne, discharge, low-press., atom densities of first excited state 80−38750
Ne glow discharge plasma, coherent on-resonance self-focusing of optical pulses 79−41427
Ne, reson.-absorpt. plasma of glow discharge positive column, Ne superradiation pulse variation 78−71489
Ne superradiation propagation through reson.-absorbing positive column plasma, pulse shape change 79−4117
Xe low threshold supersonic emission waves and effect on laser beam 79−27780

light reflection
see also mirrors; optical films
achromatic holographic optical elements 79−22917
additional light waves near region of exciton absorpt. and luminesc. in crystal 80−2340
airport control tower cab, optical design 80−58661
alkali metal vapour, reson. radiation, diffuse and selective reflection 77−50611
amplifying medium, spatially nonuniform 80−106444
amplifying region, exponential, enhanced internal refl. 78−37939
analogue model, light reflection and refraction, teaching 80−67948
analytical-geometrical calc. *(Hungarian)* 79−81355
anisotropic continuum, with anisotropic surface layer, coeff. of attenuated total reflection 80−60535
anisotropic frustrated-total-internal-refl. filter, space limited 80−102821
anisotropic layer systems, light reflection, soln. for oblique incidence *(Russian)* 77−7001
anisotropic media interface, arbitrary wave refl. and refr. 77−68170
anisotropic reflection properties of vegetated surfaces 77−82010
anisotropic semiconductors, light reflection in interband transition freq. *(Russian)* 80−88945
anthelion, form. theory, light refl. in ice crysts. in cirrus clouds 79−62583
aspheric, testing in reflected light using blazed synthetic holograms 80−91881
asteroid surface materials mineralogical characts. from reflectance spectra 78−69736
asteroids, IR reflectance spectra obs. and search for water of hydration 80−77318
asteroids, similarity of opposition effect 80−62064
astigmatic Gaussian beams in travelling-wave resonators 77−723
atmosphere, diffuse transmission and refl. rel. to emergent radiation computation method 77−87069
atmosphere, inhomogeneous, with anisotropic light scatt. and small true absorpt., refl. coeff. 79−62742
atmosphere, mol. scatt. and refl. in photon fluxes and photodissoc. rates calcs. 79−53512
atmosphere, turbid, Monte Carlo anal. of multiply scatt. lidar returns 77−25779
atmosphere, turbid, multiple scatt. effects on refl. light pulses 77−29442
atmosphere, turbulent, Huygens-Kirchhoff method, phase approx. 80−28160
atmospheric turbulence effects on echo signal of reflected optical radiation 79−8693
beam splitting device for use with smoke chamber ray optics demonstrations 80−67990
beamsplitters, beam inherent parameters analysis 79−36999
biaxial crystal plate, refl. and trans. wave amplitude 78−95573
binary stars, reflection effects evaluation, generalised approach 79−25631
black holes, detect. via gravit. mirror effect *(Russian)* 78−40987
blood, haemoglobin conc. meas. using IR reflectance 77−52860
blue-to-green reflectance ratio and lake water quality 79−53376
boundary plane between two anisotropic media, light reflection and refraction *(German)* 78−17856
Bragg diffraction grating, guided light refl., deflector appl. *(French)* 77−65621
Bragg mirror reflectance, dielectric waveguide inhomogeneity effect 80−28356
Bragg reflection in planar dielectric waveguides with periodic thickness modulation 77−79970
Bragg reflector, nonuniform, almost periodic, perturbation anal. 77−27356
Brewster's angle measurement using ordinary lab. apparatus, for high-school students 78−86097
Brewster angle determ. by dithered laser beam synchronous detection 80−73422
Brillouin scattering in reflection and transmission modes, rel. to intense acoustic flux, relation linearity test 80−45098
buffer layer theory, effect of a single layer in stack of dielectric layers 78−33800
canted magnetic structured materials, exciton spectra, optical props. 80−70622
carbon tetrachloride-perfluoroethylcyclohexane, crit. mixture, brilliant total refl. from liq.-liq. interface 79−90786
caustic, phase shift, WKB approx. 77−19166
caustics from rippling water 79−18345
chiral smectic C liq. cryst., kinematic and dynamic light scatt. from periodic struct. 79−11427
cholesteric liquid crystal, Bragg reflection of light, undergraduate expt. 77−60870
cholesteric liquid crystal, optically absorbing, dynamical diffr. theory 77−58954
cholesteric liquid crystals, apparent rotatory power *(French)* 80−50294
cholesteric liquid crystals, gamma-ray irrad. effects, dosimetry, thermography appls. *(Spanish)* 80−92457
cholesteric liquid crystals possessing a pitch gradient, reflection theory 79−91396
cholesteric liquid crysts., light reflection by crysts. with tilted molecular struct. 80−29713
cholesterin, liq. cryst., synthesis and light refl. props *(German)* 80−10497
cholesteryl chloride-cholesteryl nonanoate mixture, pitch, temp. and comp. depends. 77−39535
circular cylinders, single scatt. phase matrix, ray optics and wave theory comparison 80−102610
circular polariser for refl. in far IR 78−79114

light reflection continued
circular symmetrical reflector with laterally defocused light source, axial ray trace equations *(Russian)* 78−90365
clay soil/sand mixtures, reflectance 80−56475
clouds, light pulse reflection, height meas. *(Russian)* 80−82056
clouds, mathematical model for reflected and transmitted radiation 80−90215
coated surfaces of optical components, reflection coeff. meas. 80−28366
coating, low reflection, three layer, spectral charcts. computed 77−759
coating, refr. index calc. method refl. and transmission coeffs. 77−5890
coatings, absorptive, at normal incidence, program for TI-59 calculator 80−84793
coatings, textured, crystallites faces determ. 80−64846
coefficient meas., effect of light beam collimation 80−18003
coherent light beam shifts on reflection at plane interfaces between isotropic media 80−102609
coherent optics methods appl. to acoustic field investigations 80−106691
coherent scalar wave on medium with small scale irregularities *(Russian)* 78−22083
coherent scattering, Gaussian beam, statistically rough surface 77−10837
compound wedge cylindrical stationary concentrator, charact. 78−33815
concave gratings, blaze wavelength change 77−58448
conducting layer, light refl. theory 80−1125
conic, obtaining 360 degree panorama 79−86246
corner reflector filter, fabrication 77−14809
covered groove, optical surface wave scatt. and refl. 77−75707
critical light reflection at a plastic/glass interface and appl. to foot press. meas. 80−81681
crystal optical characteristics, relax. processes exciton dispersion 80−107709
crystal surface, light interaction effects and spatial dispersion role *(Russian)* 78−23481
crystal-vacuum interface, light reflection and transmission coeffs., additional boundary conditions 80−34870
57 Cygni, spectroscopic binary, search for anomalous refl. effect 80−17617
dark-field surface inspection using total internal reflection 80−74519
deflection effect of light reflected from moving mirror in ether theory 80−91749
diamond, identification from reflection pattern photographs 78−54481
dielectric film, refractive index and thickness meas. by optical method 80−82806
dielectric film, spatially dispersive, transmissivity and reflectivity 77−8672
dielectric interface, Gaussian beam charcts. 78−66747
dielectric interference film, with equal optical thicknesses of layers, theoretical design *(Russian)* 80−43471
dielectric mirrors, reflection and wavefront shaping, limits of coexistence 78−46747
dielectric multilayer coated optical surface, diffr. and diffuse scatt. 79−50220
dielectric plate refractive index profile determ. 79−7081
dielectric slab, transmission and refl. of Gaussian beam at oblique incidence 78−9318
diffraction image intensity fluctuations in turbulent atm. after refl., Huygens-Kirchhoff principle calcs. 80−63926
diffuse radiation emerging from semi-infinite medium, intensity accounting for inner refl. *(Russian)* 79−8637
diffuse reflectance rel. to partial coherence and IR laser photogoniometric meas. 80−14283
diffuse reflection, mutual shadowing effect classical calc. extensions 79−84666
diffuse reflection, transfer eqn. soln. 79−84660
diffuse reflection and transmission in accordance with phase function $^3/_4(1+\cos^2\Theta)$ 79−44353
diffuse reflection and transmission problem, exact soln. using Laplace transform and linear singular operators 79−35116
diffuse reflection by semi-infinite atmosphere *(Russian)* 77−82008
diffuse reflection for arbitrary phase function *(Russian)* 79−8816
diffuse reflection from rough surfaces *(Russian)* 78−74843
diffuse reflection problem, invariance principles and integral eqns. for radiation fields in plane atmosphere 80−67559
diffuse reflection problem for combination of Rayleigh and isotropic scatt., exact soln. 79−84661
diffuse reflection with radiation redistrib. in freq. and direction 78−53819
diffuse reflectors, light collection and dissemination 80−83658
diffuse solar radiation field in cloud layer *(Russian)* 79−29851
diffused channel waveguides, direct index meas. 80−87562
diffused waveguide, corrugated section, H and E wave refl. and emission 77−34954
diffusely scattering medium, refl. and transmission, Helmholtz reciprocity theorem *(German)* 77−79753
diffusing layer with Fresnel boundaries 80−1124
dihedral corner reflector, effective scattering area calculation, radiation balance method 80−48380
directional spectral reflection on plane surfaces meas. device *(German)* 78−12745
dispersive media, Ewald dynamical diffr. theory extinction theorem 78−66749
displacement at total refl., transverse and Goos-Hanchen shifts *(French)* 77−34812
distance measuring by caustics, ellipsoidal mirror with point light source system 77−42595
distributed feedback structures, hybrid modes 79−27441
double layers of different substances, refl., transmission and absorpt. coeffs. 77−6999
doubly-curved narrow-beam reflectors 79−23040
dust in thick slabs, in reflection nebulae, reflection of polarized light 79−62881
dye molecule monolayer displaced from metal surface, light refl., coupling with metal surface modes 78−48246
from Earth's surface in Rayleigh atmosphere, estimation *(Japanese)* 78−40663
Earth albedo sudden change, climatic effects 79−44241
Earth surface, relative importance of reflected and emitted flux density in 3 to 14 μm range 79−92542
Earth surface UV reflectance, meas. from airborne platform 80−98453
ebonite, nontransparent dielectric, laser emission reflection and destructive action *(Russian)* 79−74031
light reflection continued
echelette reflection characteristics in polarized radiation for an autocollimation setup 79−3787
electro-optic diffraction grating, polarisation refl. 77−3660
electrochromic ATR prism modulator 80−43440
electrode surface, anisotropy of optical props. 80−60534
electrode-solution interface, use of specular reflection methods 77−63926
electrolyte concentration meas. by portable optoelectronic convertor 78−80820
ellipsometric meas., single-element rotating-polarizer ellipsometer 80−101823
ellipsometry, azimuth response function, linear nondepolarising optical system 78−65957
ellipsometry, zone theory, single zone procedures 77−82588
ellipsometry of transparent films on transparent substrates, theory 80−104007
evanescent waves in total reflection, Raman scatt. direct recording, boundary layer obs. 80−52317
Ewald extinction theorem and Green function method for semi-infinite dipole cryst. 79−23683
exciton resonance excitation in crystals, light scatt., polarisation, specular refl., theory 80−50356
extended statistically irregular stationary surface, impulse charcts. 77−31069
eye, superposition images formed by refl. in some oceanic decapod crustacea 77−4997
Fabry-Perot nonlinear electro-optic device, using refl. light feedback 78−55457
far IR measurements, He cryostat modification for asymm. Michelson interferometer 78−74053
ferrite, light diffr. by magnetisation inhomogeneities, multiple refl. 80−2733
fibre end, reflected and backscatt. power meas., time domain reflectometer 78−70177
film, effect on light reflection, transmission and scatt. *(French)* 78−33664
film, interference colours produced by white light refl., teaching paper 80−8754
film, laser damage thresholds, effect on refl. scatt. and transmission 79−45988
filter, narrowband reflection type, charcts. calc. 77−766
flat mirror materials, specular reflectance properties and appl. 77−34917
flat plate collector energy yield increase by planar reflector, modelling appl. 78−33813
focused light ATR method, appl. to guided waves on grating 78−74992
Fourier spectroscopy, far IR, spectrum distortion by multiple reflections using Michelson interferometer 80−82837
Fresnel's classical papers, history and present appls. *(French)* 78−37800
Fresnel's eqn. for light reflection and refraction, teaching 80−101688
Fresnel's interface, reflection, transmission coeffs. transformation between normal and oblique incidence 79−72478
Fresnel's interface reflection coeffs., direct reflection between parallel and perpendicular polarisations 79−94147
Fresnel coefficients, particle approach calcs. 77−6998
Fresnel coefficients of light refl. at interfaces between transparent media 80−106438
Fresnel formulas and law of stimulated emission 80−58489
frustrated total internal reflection, interference enhancement 80−43253
frustrated total internal reflection adaptors optical consts. meas. 77−34039
frustrated total internal reflection element, adjustable as a function of the incidence angle of highly collimated light beams 80−96022
frustrated total internal reflection method for refr. index meas. 79−6165
frustrated total reflection, demonstration apparatus 77−67158
gas, anisotropy in strong EM field 79−98434
gas in boundary layer, refractive index meas. by light refl. 78−8438
gas parameter determ. using total internal reflection 77−58839
Gaussian beam at oblique incidence on plane interface of dielectrics, refl. and transmission *(Japanese)* 80−5687
Gaussian beam displacement after propag. through inhomogeneous medium 79−27175
Gaussian beam scattering charcts. at dielec. media interface 78−42275
gaussian beams, lateral shifts upon total reflection 78−1151
glass, ground, surface height and correlation length from reflection scatt. of laser light *(French)* 80−54491
glass, plane layer, 0.07 to 1000 units, reflectance and transmittance 78−17860
glass fabric laminate, nontransparent dielectric, laser emission reflection and destructive action *(Russian)* 79−74031
glass packet specimens with antisolar filler 78−90469
gloss appearance by means of moire patterns *(German)* 80−52300
Goos-Hanchen shift, ang. spectrum representation, focal shift 77−34808
Goos-Hanchen shift, phase angle correction 77−31061
Goos-Hanchen shift, reply to correction 77−31062
graphite, reflectance meas. in visible spectrum 77−77241
graphite intercalate with SbF_5 and AsF_5, optical reflectance 78−35163
graphite intercalation compounds, KC_8 and CsC_8 polarised reflectance 78−31213
graphite target in air, refl. of CO_2 laser radiation, plasma layer form. 80−25500
guided-beam splitter, refl. meas., fabrication method 80−74473
gyrotropic absorbing crystals, nonorthogonal eigenwave refl. 80−99624
helically ruled optical filter, spherical refl. charcts. 80−64171
heliostat reflected beam structure 78−90482
histological and cytological reflection contrast microscopy 80−72389
hollow dielectric lightguide fabrication defects 79−27425
hologram, reflection, real image reconstruction, resolving power and diffr. efficiency 80−53237
holograms of diffusely reflecting objects, improved efficiency 80−32939
holographic image formation modes, progress 79−50259
holographic image reconstruction in reflected light, ray inversion method appls. 78−25828
holographic plates, rear refl. elimination technique 80−73145
holographic portraits, diffraction efficiency and safety 80−37968
holography, white light refl., developer compositions compared 80−102669
homogeneous film, constriction of range reflectance and transmittance 77−75646
homogeneous plane-parallel atmosphere, unified treatment of reflected and transmitted intensities 78−85838

light reflection continued
hydrophone, multimode fibre optic, frustrated total internal reflection, testing 80−38096
hysteresis reflection and refraction of light at boundary of nonlinear medium *(Russian)* 77−62001
Iapetus, relative reflectance meas. at 1.6 and 2.2 μm 80−98607
illumination system, optical design 80−64135
image spot energy flux density distrib. for diffuse-reflection device 77−34923
image-forming reflection system testing by grazing-incidence Linnik interferometry 79−76891
imaging polarizer with spherical mirrors for VUV radiation 80−48375
incident angle of 45°C, origin of $\delta_p=2\delta_s$ relation 79−72482
inhomogeneous dielectric material, light refl. by refr. index distrib. gradient 78−25800
injection laser characteristics due to reflected optical power 79−81428
integrating sphere accessory, spectrosc. meas. of horizontal surface from above 80−86443
interface between transparent and absorbing medium, light refl. at 45° angle of incidence 79−31792
interference coating, with narrow reflection bands, design *(Russian)* 80−43472
interference reflection microscopy, image interpretation theory and appl. to cells 79−80677
interfernece filter characteristics and specification 78−46773
interferometer for 90° angle meas. of transparent- and opaque-materials *(German)* 78−164
interferometer using frustrated total internal reflection *(French)* 77−61113
internal-reflection spectroscopy 80−18019
IR bidirectional refl. distrib. function meas. for baffle and mirror materials, recording instrument 78−58012
IR optical scanning system, narcissus effect suppression, computer results 78−59151
IR solar radiance reflected from the rough sea surface *(Russian)* 79−84477
isotropic layers, thin, with rough boundary surfaces, refl. and transmission factors *(German)* 78−90354
isotropic media, light ray refl., displacement *(Russian)* 78−13659
isotropic media boundaries, energy balance 79−3625
isotropic-anisotropic media boundary, light refl. and refr., Maxwell theory *(German)* 78−87007
Jones notation, polarisation and interference effects 78−17858
Jupiter disc features spectral reflectivity, phase effect 80−98602
Jupiter sunlight refl., absorpt. bands rel. to atmospheric comp. and cloud struct. 80−56758
Kubelka-Munk system, continuous absorpt./scatt. coeff. minimising distribs. 77−50615
Lambert surface, below turbid medium, radiative flux *(Russian)* 79−72498
Lambertian cavity with dielectric window, effective absorptivity 80−38237
laminated mirrors, high refl. region width calcs. for oblique light incidence *(Russian)* 77−19382
laminates, with layers of unequal optical thickness, optical characts. *(Russian)* 77−34819
large optical components for high-power lasers, refl. and transmission meas. 79−44927
laser, torsion-effusion method, vapour press. meas., automatic data acquisition 80−52188
laser backscattering from dense water-droplet clouds, depolarisation ratio, multiple scattering 79−53513
laser beam coherence and divergence *(Spanish)* 80−87424
laser beam expander for short cavity dye laser 80−87532
laser beam reflection from sea surface, effect of water surface wavenumber spectrum 80−31121
laser cavity diffraction experiment with 1-D diaphragm 80−95920
laser mirror and window absorption, reflection and transmission obs. at 10.6 μm 79−14014
laser mirror coeff. meas., of Fabry-Perot interferometer *(Russian)* 78−1237
laser radiation freq. shifting by refl. from moving blazed grating 77−88822
laser refl. technique, contamination buildup on fusion reactor liner 77−34436
lateral wave amplification through reflection from active medium 78−78987
lateral wave structure in refl. from active medium 79−27315
latex, colloidal cryst., optical props. near MP 78−11562
leaf optical system modelled as stochastic process 77−44877
leaves of African crop plants, optical props. rel. to photosynthesis 77−25629
lidar target calibration, backscatter refl. for circularly polarised radiation 80−102750
limited light beam, nonlinear reflections and transmission 80−58624
liquid crystal displays apparatus for refl. meas. and optical characterisation 77−7222
liquid crystal field-line induced reflective interface 79−98482
liquid crystal image transducer, optical props. at normal incidence, off-state behaviour 80−64160
liquid interfacial tension meas. from scatt. light intensity 80−20012
liquid level sensor using parallel polarised light 80−82741
locally deformed slab waveguide propagation and diffraction patterns 80−106630
longitudinal static spin wave struct., magnetotropic interaction of light *(Russian)* 80−93285
longitudinally inhomogeneous running waves and their role in the nonlinear reflection and refraction of light 80−38059
lossy structures, Brewster phenomena 78−5419
low-energy photon diffraction, scatt. theory 80−43262
lunar soil, light refl. meas. rel. to brightness distrib. over lunar disc 80−17512
lunar surface reflective props. 77−33366
Mars, reflectance spectroscopy rel. to surface comp. 80−72834
Mars atmosphere, optical props. during 1971 dust storm *(Russian)* 78−93138
Mars soil photometric analogue, light refl. meas. rel. to brightness distrib. over planetary disc 80−17512
materials subject to hemispherical radn., reflecting power meas. 78−65985
matrix notation, Jones vectors for refl., refr. and diffr. 77−34814
MBBA, nematic liq. cryst., deflector based on frustrated total internal light refl. 78−50934
measurement of reflectance and transmittance, arrangement for integrating sphere *(German)* 80−31844
metal, adatom characts. depend. 78−10918
metal, surface roughness effect on light absorptivity 78−80314
metal, surface strain meas. by intensity of reflected light flux 77−17972
metal surface electrodynamics, optical refl. coeffs. and surface plasmon dispersion law 80−75619
metal-electrolyte boundary, electrodynamics in visible and near UV range, microscopic effects 80−45521
metals, multireflection cell for far IR studies 77−18075
microdensitometry, optical principles and practical solutions 80−4790
microobjectives, reflected light, image glare coeff. depend. on design parameters 80−28302
microscope image flare factor rel. to illumination system aperture 79−14083
microscopic interference obs. by reflection contrast 80−68248
microscopical and Ewald dynamical diffraction theories, refl. and transmission, spatial dispersive dielec. slab 80−83548
moderately rough surface, probability density function of refl. light intensity in far field 79−36837
monoclinic absorbing plane parallel plate, normal transmission and refl. 80−1122
moving corner reflector, special relativity testing and Doppler effect 77−37758
moving layer of scattering medium, EM radiation refl. and transmission 77−50619
multi-element interference filters using different grids, far IR characts. 78−90507
multi-layer optical system, reflection and transmission coeffs. calcs., computer program 80−66316
multicolour reflection holograms, improved image techniques 80−48184
multilayer, dielectric reflectors, simplified description 79−89984
multilayer mirrors, for X-ray and far UV radiation 78−1313
multilayer structure devices, nonideal, computation of optical props. 80−5684
multilayered media, refl., interference theory 77−65567
multilayered structure, refr. index difference between adjacent layers, meas. technique 80−101829
multilayers, ultrathin, optical characts. 80−104005
multiple reflections between clouds and surface 77−45131
multiple reflections within scattering medium, correction factor calc. 78−32888
multiple scattering theory in semi-infinite spatially heterogeneous medium *(Russian)* 78−13663
multiple-plate glass systems, spectral directional radiation characts. prediction 78−74956
multiply reflected Gaussian beams in circular cross section 79−18343
nematic liquid crystal, electrically controlled transparency based on frustrated total internal refl. 79−32074
nematic liquid crystal, total internal reflection, review 80−96445
non-redundant spectral tunnelling through periodic struct. at total refl. 78−78906
nonevacuated solar collectors with compound parabolic concentrators 79−62069
nonimaging solar concentrators for different absorber shapes 78−50895
nonlinear interference mirror, reflection of light 80−102761
nonlinear media, reflection-transmission hybrid regime, plane wave soln. *(Russian)* 77−72025
nonlinear media boundary, between transmission and total internal refl. cases 79−18470
nonlinear selection of optical radiation on refl. from stimulated Mandelstam-Brillouin scatt. mirror *(Russian)* 80−28280
nonlocality effects on optical phenomena in bounded solids, developments 80−93328
ocean surface, atm. scatt. of refl. solar radiation *(Russian)* 77−29435
ocean surface UV reflectance, meas. from airborne platform 80−98453
ocean-atmosphere system, spectral struct. of refl. solar radiation field *(Russian)* 77−33086
ocular fundus reflectometry 78−48861
opaque, semitransparent materials, Kirchhoff's second law, role of reflection or diffusion *(French)* 79−36835
opaque polished surface roughness determ., diffuse reflection method 79−49274
optical constant calculation from frustrated total internal reflection meas. 79−33658
optical constant measurement at two incidence angle values 80−101831
optical constants, ATR meas., 2-polarisation method, accuracy, optimisation 78−45673
optical constants meas. method using polarised light refl. coeffs., accuracy 80−73423
optical fibre, beam to fibre coupling with low standing wave ratio 80−99822
optical fibre, single mode, refr. index profile meas. by refl. method 78−46756
optical glass, absorption coeff. determ., refl. losses role 77−72100
optical microdevice with square law media, Gaussian beam characts. by wave optics 79−81360
optical surface contract interaction zone, thickness calc. and distance meas. methodology *(Russian)* 80−99889
optical systems with spherical and nonspherical diopters, in three-dimens. space, calc. method *(Rumanian)* 79−13898
organic semiconductor film, optical consts. by refl. and transmission, errors 77−16414
Osterberg problem and wave propag. in inhomogeneous plasma, numerical study 80−63925
paraboloid mirror with coaxial linear source, intensity distribution 80−74456
parallel optical flat SAW meas. by reflective interferometry 79−76931
parallel polarised EM waves, equal reflectance at normal and oblique incidence, dielec. const. meas. 80−1119
partial reflection, beam direction change 77−68172
particulates, frustrated total reflectance meas., interface model 77−71362
periodically stratified absorbing medium, splitting of energy flux *(German)* 77−3534
petroleum samples, extinction coeff., refractive index meas., 0.25-25 microns 79−65818

light reflection continued
phase conjugate reflection, pulsed 10.6 μm, via intracavity degenerate four-wave mixing 78−87097
phase reflection gratings, theory 79−27417
phase relations, phys. course demonstration *(Russian)* 77−13550
phase shift measurement by interferometry, complex refl. index determ., IR region *(French)* 77−87812
phase-conjugate reflection using TEM_{00} pump beam 80−48327
phase-shift sum rules for complex polarisation amplitude for photon reflections 79−69802
phonon approach, derivation of generalized Snellius law and Fresnel formulae 77−83811
photographic emulsion, cellulose base, extraordinary reflection halo *(German)* 80−42282
photographic papers, polarised light refl. 80−64127
photometric terminology for refl., transmission, scatt. and emission 77−74477
planar multilayered structure, resonant polarization conversion and beam shift 78−1438
plane absorption grating, light diffr., effect of total internal refl. 79−64330
plane parallel optical layer interference props. for radiation parameters control 80−83547
plane parallel transparent layer-inverse medium boundary, light refl. *(Russian)* 77−65574
plane plates, two sets of different physical props., energy flux splitting *(German)* 79−18500
plane-parallel plate, with spatial dispersion, light refl. and transmission coeffs. 80−88951
planetary atmosphere, diffuse refl. and transmission, soln. for three-term phase function *(Russian)* 77−13260
planetary atmosphere, transfer eqn. 80−82184
planetary atmosphere diffuse refl., adding algorithm for Markov chain radiative transfer formalism 80−21902
planetary atmospheres with rough surface, multiple scatt. and emergent radiation intensity 78−12085
planetary surface, dust covered, polarimetric model 79−25528
planets, light refl. laws rel. to photometric props. 80−67601
plasma, backscattered light, nonlinear decay 79−46455
plasma etching control using optical reflection methods 79−57127
plasma mirror refl. characts., in electron beam controlled CO_2 laser 78−59064
plastic rectilinear waveguide with core/cladding and cladding/surrounding interface *(German)* 77−34941
PMMA film, Plexiglas, penetration depth of 10.6 μm laser radiation, transmission, refl. and absorpt. meas. 79−74010
polarisation constants for light interaction with absorbing crystal plates 80−78765
polarisation degree of unpolarised reflected light, for teaching 78−24616
polarisation of reflected light, apparatus for obs. 80−62434
polished glass surface, reflected light phase rotation 80−66147
polymers, crystalline formations study, light refl. from untreated surface 77−28945
polystyrene, oblique laser diffr. and reflection from surface crazes 77−47508
pyrocarbon coatings, refl. anisotropy and struct. determ. by perpendicular incidence microellipsometer 80−101824
quarter-wave mirrors, oblique incidence reflection coefficient, small absorption of layers effect 80−64140
quarterwave multilayers, secondary refl. maxima 79−64331
quartz cylindrical fibres in regular struct., multiple frustrated total internal refl. calc. 78−83094
radiant heating, using paraboloidal reflectors 79−97392
radiative properties, parameterisation 80−56601
radiative transfer, synthetic scattering phase function 80−98541
radiative transfer diffuse refl. problem, exact soln. for semi-infinite Rayleigh scatt. atmosphere 79−35112
rainbow, physics, historical review 77−73854
Ramsey resonance, of two-level mols., in three separated fields produced by corner reflector, theory 80−74166
random transmitted and reflected waves in medium with large-scale irregularities, statistical characts. relationships 79−81364
ray reflection at dielectric-vacuum interface, exam. using Fermat's principle and evanescent waves 78−58902
Rayleigh atmosphere single-scatt. albedo, determ. from polarisation meas. 79−35117
reflecting horizontal solar collector with inclined finned tubes 79−62049
reflecting power meas. using integrating sphere 77−38037
reflection from a corner reflector moving at high velocity 79−30228
reflective coating for optical waveguides with abrupt turns 78−30059
reflective glass colour standards 80−90878
reflective light valve projector efficiency and image uniformity improvement 80−87459
reflective object displacement and vibration meas. *(Russian)* 79−21695
reflectometer, spherical, calibration of lustrous colour standards appl. *(German)* 77−18066
reflector geometrical optics design using complex coordinates 77−19380
reflectors, deep paraboloid, light intensity curves with transverse cylindrical light source, calc. *(Russian)* 80−38090
regular specular surface, theory of light refl., appl. to PAGEOS balloon 79−68363
resonance radiation, diffuse and selective reflection 77−50611
resonator, spatial field configuration with diffuse reflector 80−53344
retroreflectance measurements, unified coordinate system 80−73408
retroreflecting material metrology, errors in luminous refl., chromaticity meas. 80−68235
retroreflection from rough surfaces 79−10258
retroreflective arrays as approximate phase conjugators 79−72508
retroreflective material chromaticity meas. under nighttime geometry 80−73411
retroreflectometer, NBS reference 80−73410
retroreflector alignment, simple interferometric technique 80−95125
retroreflector photometric and goniometric accuracy 80−86375
retroreflector photometry, meas. error rel. to aperture size 80−73409
ring resonators, with counter directions linked through back refl. props. *(Russian)* 77−68233
rotation, high sensitivity stabilisation and meas. *(French)* 77−61103
rough interfaces, light reflection, scattering in homogeneous media *(French)* 79−50211
rough laser illuminated surface, no. of random point sources, RMS phase depend. 79−59635
light reflection continued
rough metal surfaces, diffuse and specular refl., empirical representation 80−87315
rough metal surfaces, empirical representation 80−87314
rough surface, random, reflectance derived with Fresnel approx. 80−87309
rough surface optical props., review 80−18996
rough surfaces, irradiance of reflected light, evaluation 77−54669
rough surfaces, reflection light, division into specular and diffuse components *(Japanese)* 80−106457
roughened spheres, ang. distrib. of reflected radiation, models analysis 77−42479
roughness and surface slope measurement, comparison of Talysurf and optical methods 80−36990
Sahel region, Africa, surface albedo vars. investigation during recent drought (1967 to 1974) 80−76981
sapphire substrate surface evaluation for SOS 77−76653
satellite retroreflector arrays, method of calculating transfer functions 80−5778
saturable reflection spectroscopy, interference phase shift 77−2696
saturable slab, steady state theory 77−68242
saturated absorption spectroscopy, optical feedback-effects suppression by phase modulation of refl. light 78−21225
Saturn B-ring, optical reflectance polarimetry interpretation 80−31248
Saturn disc centre spectral reflectivity, phase effect 80−98602
Saturn ring system, light refl. and thickness from low tilt angle photometry 79−35186
scattering layers, with different degrees of dispersity, reflecting power, theory *(Russian)* 78−82909
scattering material, transmittance and reflectance meas. by specular hemisphere method 78−58004
scattering objects, investigation using vacuum monochromator 77−74523
scintillation counting, liq., unified approach to counting process, stochastic model 77−3240
scintillation counting, liq., unified approach to counting process, optimising optical design 77−3241
sea surface, light intensity fluctuations refl. by sinusoidal waves *(Russian)* 77−13080
sea surface reflected light polarisation, utility in remote sensing 79−5498
selective refl. from atomic vapour, narrowing of level crossing curves 77−18856
semi-infinite turbid medium, intensity of exciting diffuse radiation 77−75422
semi-Lambertian reflecting surface, laser speckle interferometry 78−82910
semiconductor, IR radiation ultra-fast switching by laser-produced carriers 79−98417
semiconductor film, transparent substrate, surface unevenness and interference effects 77−77310
shadow methods, reflected, transmitted, obs. of sharp V-notched plates, under pure bending 78−90777
shadow methods for studying turbulence using reflection from a mirror in the medium 80−95801
slit image seen in total internal reflection *(French)* 80−95810
snow spectral reflectance, two-stream theory 79−88376
soil, water content estimation via total solar reflectance and spectral band ratioing 77−60479
soil reflection, polarised visible light photographic recording for surface moisture indications 79−53557
solar collector, focused, slightly curved, reflected light pattern anal. 77−23728
solar concentrating properties of truncated hexagonal, pyramidal and circular cones 78−50896
solar irradiance indicatrices of terrestrial natural surfaces and albedo effect 79−62514
solar reflecting concentrators, optical evaluation techniques 78−50893
solid laser active rod, effect of surface transition layer on laser action 79−50301
solid state laser satellite rings, energy losses caused by diffusion, refl. in cavity 79−89911
solids, effect of angular aperture and radiation polarisation of instrument on reflection coeff. 80−9020
spatially periodic media, second-order coupled-mode eqns. 78−13655
spectral transmission and reflection coeffs., USSR special standard 77−30195
spectrometer, diode laser dual-beam, long-term temporal and scanning characts. 80−90902
spectrophotometer, reference for analysis of diffuse transmittance and reflectance 77−38023
spectrophotometer, single-beam UVI, multiple reflections as source of errors 77−49788
spectroscopy, IR interference enhanced attenuated total reflection matrix technique 79−21823
specular reflectometer-spectrophotometer, NBS reference, mirror refl. meas. 80−68236
specular sphere scatt. radiance matrix, refl. standard for polarised beam scatt. meas. 80−74299
sphere, totally reflecting, light extinction 80−95784
spherical glass beads in highway pavement markings, retrorefl., specular refl. 78−74837
spherical glass beads in highway pavement markings, retrorefl., diffuse refl. 78−74838
step index fibre, pulse widths, Goos-Hanchen shift effects 77−83952
stimulated scattering by surface waves, total internal refl. conditions 77−742
Stokes relations in optically active media, macroscopic reversibility principle appl. 80−53207
stratified anisotropic media, computation method 77−19165
stray light calculations, surface refl. models 78−58905
stray light suppression in optical systems, optical design, computer analysis 78−59113
student demonstration using var. density sugar soln. 77−57134
submillimetric imaging, speckle effects and specular reflections 77−39071
substrate reflectance and medium depth effects in two-dimens. multiple scatt. expt. 78−87011
Sun glitter on sea, correl. function appl. to sea surface slope distrib. function determ. *(Russian)* 80−94611
sunlight diffuse reflection by Earth, radiation press. perturbations of near-Earth satellite 78−24444

light reflection continued
sunlight reflection by clouds, fast azimuthally dependent model 80−51532
surface, adjacency effects on imaging 79−100939
surface finish of machined surfaces, laser reflectance patterns 79−85126
surface layer, reflection related to density profile Fourier transform *(Russian)* 78−31269
surface profile from horizontal light source reflection, calc. from observed image 80−101777
surface profile from horizontal light source reflection, image calc. 80−101776
surface roughness and thin film influence on refl., transmission and scatt. of light *(French)* 77−34826
surface roughness evaluation, statistical approach 78−90367
Teflon, nontransparent dielectric, laser emission reflection and destructive action *(Russian)* 79−74031
thermal band imaging, glare in optical systems 79−32025
thermal radiation, reflection, Helmholtz reciprocity theorem *(French)* 79−7070
thermally induced index gratings Bragg refl., IR optical image conversion, thermal index changes 79−59753
thick layers, refl., transmission and brightness coeffs. 80−63918
three-dimensional objects in polarised light, refl. characts. 80−87305
time-average reflection-moire method for vibration analysis of plates 79−72863
total internal refl., Poynting vector theory, light beam shifts 80−78764
total internal reflection, boundary type soln. 78−42272
total internal reflection, focal shift, ray model 77−34809
total internal reflection, laser beam-fountain demonstration, for teachers 78−81769
total internal reflection modulator, small glancing angles 78−74987
total internal reflection whispering gallery modes, radiation damping *(Russian)* 77−75410
total reflection by multilayered struct., longit. and transverse shifts 77−75413
total reflection region, refracted beam field distrib. 79−27169
trajectories of reflected and transmitted beams in oblique tunnel effect 78−78903
transmission through reflecting cylindrical tubes, demonstration 78−73812
transmitted Gaussian laser beam, critical angle phenomena 77−27298
transparent layer, nonlinear, light reflection 79−55172
transparent materials, laser light refl. and transmission, high power densities 79−27305
transparent media interface, 45° angle of refraction 79−27164
transparent nonlinear layer, light refl. and transmission *(Russian)* 78−71142
transversely moving mirror, attempt to find freq. shift 77−30006
tunable narrow-band thin-film waveguide grating filters, performance 80−38124
turbid estuarine waters, optics, approxs. and appls. 79−66712
turbid media, approx. linear relationship for optical response 78−90371
turbulent atmosphere, fluctuations of reflected wave beam field 79−66793
turbulent atmosphere, laser radiation intensity fluctuations 77−50621
turning of beam through const. ang. by prism, for teaching 79−25805
uniaxial crystals, refl. ellipsometry nonlinear eqn. inversion 80−95120
uniaxial crystals interface, EM wave refl. and refr. laws, tensor derivation 78−71029
uniaxial media, light reflection and refraction amplitude relations *(German)* 78−90353
uniaxial media, reflection (refraction) in directions of vanishing double refraction *(German)* 79−13894
vision, common and relative components as information about illum., colour and 3-dimens. form 78−56982
visualization of light propagation, hologram construction 79−81391
water mass, nonzero subsurface 670 nm irradiance reflection of Lake Ontario 80−101387
water surface, optical pulse refl., probability characts. *(Russian)* 78−22081
wavefront reversal and short pulse generation using steady-state stimulated Brillouin scatt. 80−53381
waveguide, lossy, Brewster phenomena, cut-off thickness 80−87524
Ag film, dye monolayer effect on surface plasmons, ATR obs. 79−87001
Ag film, reflection coeff. minima and surface plasma wave dispersion curve comparison *(French)* 78−80429
Ag-MgF_2 layered system, optical excitation of surface plasma waves 78−6803
Al, etched, electronic props. of surface *(Russian)* 78−15569
Al, polished, target in air, refl. of CO_2 laser radiation, plasma layer form. 80−25500
As_2S_3 film, hologram recording using total-internal-refl., polarisation depend. 80−106491
Au film on Al, reflectance and absorpt. obs. 80−7426
$BaSO_4$ tablet, reciprocity of reflection values for geometries 45/0 and 0/45 *(German)* 80−71370
C materials, optical microscopy, reflection, interference colours, terminology 78−42871
CO_2, inverted, on-resonant phase-conjugate refl. and amplification at 10.6 μm 79−64275
CO_2, inverted, wavefront reversal, high efficiency 80−74436
CO_2 laser, with anisotropic resonator, output polarisation 80−28253
CS_2, intensity dependent total refl., ps pulses 77−14781
CdS, optical axis inversion *(Russian)* 79−24284
CdS, thermal equilib. phonon populations, acoustic intensity meas. by Brillouin scatt. intensity obs. 80−45098
Cd_2SnO_4 film, optical transmission and reflection, evaluation for solar heat collectors 77−52191
CuBr, evaporated film, magneto-optical effects on exciton bands 78−72624
CuCl, evaporated film, magneto-optical effects on exciton bands 78−72624
$Cu_{2-\delta}S$, thin films, determ. of stoichiometry from optical props. 79−60656
GaAs, laser, transverse modes, mirror reflectivity dependence 79−68404
GaAs, peculiarities of plasma region reflection, effect of surface treatment methods *(Russian)* 79−69827
GaAs, thermal equilib. phonon populations, acoustic intensity meas. by Brillouin scatt. intensity obs. 80−45098
Ge in TEA CO_2 laser cavity, wavefront reversal, high efficiency 80−74436

light reflection continued
In_2O_3 films, electron beam evaporation, elec. and optical props. *(Japanese)* 80−60784
In_2O_3, transparent electrode deposition on PLZT ceramic, elec. and opt. props. 78−74848
InSb, Auger-governed decay of laser-induced plasma, optical probing 80−76105
InSe film, photochem. production of holograms on surface *(Russian)* 79−7101
KH_2PO_4 crystal electro-optic reflection deflector 79−76861
$LiIO_3$ single crystal, surface acoustic wave parameter meas., coherent optics method 80−106691
$(NH_4)_2BeF_4$, linear and nonlinear optical props. in incommensurate phase 80−69452
Na vapour, amplified refl. by degenerate four-wave mixing using Kerr nonlinearity 78−55413
$NiCr_2O_4$, plasma-sprayed coatings, props. 77−59999
Pt films, optical props. and radiation stability 80−34999
SF_6, refl., absorpt. and transmittance depend. on irradiance at normal incidence 78−13769
Sb_2S_3, anisotropic cryst., optical const. determ., reflected-light polarisation 77−43960
Si amorphous film, anisotropic etching phenomenon, appl. as solar selective absorber surfaces 80−72054
p-Si, heavily doped contact layers on IR detectors, IR transmissivity 80−108190
Si wafer O interstitial IR absorption spectrometry, multiple reflection correction 80−55131
Si:B ion implanted layers, light refl. and transmission coeffs., computer program 80−66316
$SiH_{0.16}$ amorphous films, optical props. and photocond. near optical gap 80−50443
Si_3N_4, pyrolytic, prep. by CVD, bulk and coatings, exam. of electrical, optical and physical props. 79−95935
SiO_2 film, ion bombarded, attenuated total refl. method obs. of H capture 79−95863
SiO_2-Si, film-substrate, single reflection retarders for different Hg spectral lines 78−79122
SiO_2-Si film-substrate refl. polariser, operation at Hg spectral lines 77−75655
SnO_2, transparent electrode deposition on PLZT ceramic, elec. and opt. props. 78−74848
TlCl-TlBr, single cryst., composition determ. by reflection spectrophotometry 77−1961

light reflection spectra *see reflectivity; spectra*

light refraction
see also birefringence
aberrations of spherical surface, eqns. valid for large incidence angles 77−617
achromatic holographic optical elements 79−22917
alkali metal vapour, induced optical anisotropy in laser radiation field *(Russian)* 80−38525
analogue model, light reflection and refraction, teaching 80−67948
angular divergence from electron-beam-controlled laser, refr. and diffr. contribs. 79−59668
angular spectra of optical radiation, side wave meas. 80−69327
anisotropic media interface, arbitrary wave refl. and refr. 77−68170
anisotropic-isotropic interface, ray tracing in uniaxial and biaxial media 77−602
anomalous refraction rel. to aerological data *(Japanese)* 77−73855
apparent depth, viewing angle depend., ray tracing expts. 78−12475
aquatic eyes, retinoscopy, refractive error considerations 80−61750
aqueous solution fluorescence spectra, refr. correction 78−93766
astrometry, chromatic refr. correction tables for photoelectric stellar positions *(Russian)* 79−96889
astronomical refraction, general theory *(Russian)* 78−89045
astronomical refraction calc., theory for three-dimensional model of atmosphere 80−46260
atmosphere, anomalous refr. rel. to daytime astrometric obs. 78−24441
atmosphere, concentric solar halo display, 1974 April 14 77−2245
atmosphere, corrections to satellite laser ranging 77−75663
atmosphere, refr. angles accuracy obtained by statistical orthogonal expansion of refr. index *(Russian)* 77−70829
atmosphere, refr. index rel. to line length changes resolution by EM distance meas. ratio method 80−4143
atmosphere, refraction between synchronous satellites *(Russian)* 80−21821
atmosphere, refraction over lakes rel. to image distortion and lake monsters 80−46259
atmosphere, spectral transmission changes, refr. corrections for star colours 78−28535
atmosphere boundary layer, refr. index structural charact. *(Russian)* 80−94597
atmosphere lateral refr., elimination from astrometric absolute declinations observed by micrometric method *(Russian)* 79−96890
atmosphere layer over ice surface in Antarctica, geodetic and meteorological meas. 77−87073
atmospheric, using var. density sugar soln. 77−57134
atmospheric refraction, interactive computer graphics applied to visual image transmission 79−8689
axisymmetric optical inhomogeneities, strong refraction, calcs. 77−7009
beam broadening in randomly inhomogeneous cloudy aerosol medium *(Russian)* 78−58911
beamsplitters, beam inherent parameters analysis 79−36999
beer, in glass, apparent levels, optical illusion 77−68166
boundary plane between two anisotropic media, light reflection and refraction *(German)* 78−17856
Brewster's angle measurement using ordinary lab. apparatus, for high-school students 78−86097
caustic junctions, fine structure 77−46683
caustics from rippling water 79−18345
caustics in near field from liq. drops 78−37802
caustics method, intensity factors determ. at arched crack tip 80−19298
cholesteric prism, under applied mag. field *(French)* 78−80319
circular cylinders, single scatt. phase matrix, ray optics and wave theory comparison 80−102610
colloid, spherical particles, light refr. theory 80−23622
colloidal dispersion, spherical particle, optical turbidity and refr., particle size and relative refr. index meas. 79−92012

light refraction continued
conical, beam intensity distrib., using polarised light *(Russian)* 79−27172
conical refraction, of polarised light beams 80−28157
conical refraction in sulphur crystals 80−95792
conjugate interfaces: interfaces between transparent media of the same reflection coefficient for the parallel polarization at the same angle of incidence 80−87299
contact lens wearer diagnostic testing 80−12312
continuously varying refracting media, CUPID ray tracing program 80−18990
critical binary mixture, gravity induced gradients, optical meas. 77−4203
crystal, internal conical refraction 80−1126
dispersion zone of light-ray, deviation at boundary between two optically homogeneous media *(Russian)* 77−79744
education, light momentum density in refracting medium, electrostriction, Peierls method 77−33772
education, mirage, ray theory anal. 77−87605
ellipsoids, intrinsic, shape and configurational birefringence 80−9805
elliptic umbilic diffraction catastrophe 79−50213
Ewald extinction theorem and Green function method for semi-infinite dipole cryst. 79−23683
eye, dioptric effects of optical parameter changes, math. model, rel. to contact lenses 78−3477
eye, fish, chromatic aberration and effect on refr. state 78−64985
eye, lid closure and refractive error in macaque monkeys 78−35839
eye, rat, estimation by pattern evoked cortical potentials 77−70455
eye, refractive state of ground squirrel 80−67070
eye chromatic aberration rel. to accommodation, meas. using dynamic laser speckle pattern 80−81582
eye refractive error, simplified anal. of meridional refr. data 78−65149
eye refractive error meas. using dynamic laser speckle pattern 80−81583
eye refractive error measurement using Humphrey Vision Analyser, reliability and validity 78−61265
fibre mode analyser using refraction from oblique section 77−88952
Fresnel's eqn. for light reflection and refraction, teaching 80−101688
Fresnel drag in transversely moving dispersive media, astrophysical plasmas 79−96902
generalised ray tracing 77−27249
graded-index fibres, refracting leaky rays 78−79103
gravitational lens effect with allowance for diffraction, anal. *(Russian)* 78−32743
grazing light ray refraction in dispersion zone above optically homogeneous media interface 80−74297
homogeneous wave energy flux under conical refraction and induced gyrotropy 78−17861
hysteresis reflection and refraction of light at boundary of nonlinear medium *(Russian)* 77−62001
ice crystals, polarized halos and double refraction 78−36283
illumination system, optical design 80−64135
image rotation and magnification, optical system 80−48376
induced elliptic double refraction, separation into linear and circular components *(German)* 77−24817
inhomogeneous medium, two-dimens., light propag. problems rel. to thermogasdynamic waveguide development 80−32914
internal conical refraction of bounded light beams in biaxial crystals 79−28708
internal conical refraction theory 77−603
isotropic adsorbing medium boundary, light beam splitting 80−99623
isotropic-anisotropic media boundary, light refl. and refr., Maxwell theory *(German)* 78−87007
Jones notation, polarisation and interference effects 78−17858
laser beam propag. in evap. liq. drop medium, wind refr. 77−5322
laser beam refraction at spherical surface, distortion, geometrical optics calc. 80−95929
lens, thin, under water, focal length determ., teaching appl. 79−44676
lens image forming, tutorial *(Hungarian)* 77−22359
lens testing, simplified Talbot interferometers 77−757
limited light beam, nonlinear reflections and transmission 80−58624
liquid film, falling, 3-dimens. wave characts., laser beam refraction obs. 79−27654
lithium formate biaxial crystal, nonlinear conical refr. obs. in harmonic generation 80−23745
Lloyd's mirror, Goos-Hanchen shift at grazing incidence 77−71917
longitudinally inhomogeneous running waves and their role in the nonlinear reflection and refraction of light 80−38059
lossy liquid, for IR refr. spectrum meas. 77−2700
lunar halos, geometrical optics of formation 77−45634
marine boundary layer refractive effects in IR 79−96763
Mars, mirages, possibility of Viking lander obs. 77−29693
matrix notation, Jones vectors for refl., refr. and diffr. 77−34814
mirage occurrence conditions, ray tracing theory 78−77323
mirages, form., wave eqn. calcs. 77−33749
mirages, stratified medium light ray trajectories, educational aspects 78−69940
momentum of light wave, in refracting medium, oblique refl. 77−50612
nonlinear media boundary, between transmission and total internal refl. cases 79−18470
nonlinear medium, refr. wave profiles and hysteresis 80−43395
Novaya Zemlya effect, arctic mirage 79−80022
observable optical horizon, theory, refraction, clouds and haze effects *(Russian)* 80−4107
optical caustics from liquid drops under gravity, obs. of parabolic and symbolic umbilics 79−72485
optical glass, thermally tempered, surface stress meas. by crit. ray method 80−106766
optical radiation pressure meas. in dispersive media refractive index depend. 78−33665
optical systems with spherical and nonspherical diopters, in three-dimens. space, calc. method *(Rumanian)* 79−13898
pair-correlated distrib. of small-spaced lossy scatterers, light propag. 80−28158
phonon approach, derivation of generalized Snellius law and Fresnel formulae 77−83811
point of refraction, mathematical analysis and application *(Japanese)* 77−79743
polyvinyl alcohol, in water-ethanol mixture, processes of structure formation 80−10482
polyvinyl alcohol/vinyl acetate copolymer, in water-ethanol mixture, processes of structure formation 80−10482
light refraction continued
ponderomotive forces of light at refracting medium-vac. boundary *(Russian)* 78−22082
prism, min. ang. deviation, school corridor demonstration 78−81760
prism cut from anisotropic media, ray refr., appl. to atm. optics haloes 80−63916
Pyrex-liquid interface effect elimination in student expts. using 2-propanone/benzene mixture 77−45655
quartz, induced elliptic double refraction, separation into linear and circular components *(German)* 77−24817
radiation pressure exerted on refractive spheres *(French)* 77−61911
radiation pressure in dispersive medium, photon momentum, drag 78−33666
rainbow, physics, historical review 77−73854
rainbow phenomena and the detection of nonsphericity in drops 80−58456
rat eye refractive state 77−81493
reflection conic, obtaining 360 degree panorama 79−86246
refracted beam formation during light ray motion along optically homogeneous media interface 80−74298
refracting objectives for 8 to 13 μm 80−86421
refractive index field reconstruction for strongly refractive asymmetric fields 80−4760
ring lasers, light drag coeff. determ. 77−83810
satellite laser ranging, effect of horizontal refractivity gradients 77 25910
satellite laser tracking data, ray tracing evaluation of refraction errors 79−8588
saturable slab, steady state theory 77−68242
scattering, weak, model system 79−89849
seawater, refractive microstrcutrure from diffusive and turbulent mixing 80−8326
semiconductor prism, additional boundary conditions for photo excitons 77−69250
Snell's law, student expt. 78−36781
Snell's law for light rays in moving isotropic dielectrics 80−58458
solid state laser, refraction effects and gain meas. 79−31905
speckle motion in laser refraction, expt. obs., vision appls. 80−45879
speckle movement in laser refraction, ocular refr. determ. 80−41001
spherical surfaces, extrameridional aberrations anal., with large decentring angles 77−68181
Stokes relations in optically active media, macroscopic reversibility principle appl. 80−53207
stratified media, solns. of refraction and extinction integrals 77−27247
streaking of beam by electro-optically induced travelling lens 79−46045
structure-forming solutions, double light refraction and viscosimetry 79−94745
sunset obs. from Apollo-Soyuz, atmospheric light refr. study from space *(Russian)* 78−65383
supersonic boundary layers interacting with cooling wall jets, turbulent and optical characteristics 80−106792
teacing, lens object-image relations 78−36780
telescopes, light vergence and accommodation 78−24065
thin film glass lightguide boundary refraction expts. 80−106639
time-reversed wavefront generation by nonlinear refraction 77−34905
total internal reflection whispering gallery modes, radiation damping *(Russian)* 77−75410
total reflection region, refracted beam field distrib. 79−27169
transparent dielectric, laser pulse energy absorption, refr. wave form. *(Russian)* 79−55167
transparent media interface, light refl., 45° angle of refraction 79−27164
turning of beam through const. ang. by prism, for teaching 79−25805
uniaxial crystals interface, EM wave refl. and refr. laws, tensor derivation 78−71029
uniaxial media, light reflection and refraction amplitude relations *(German)* 78−90353
uniaxial media, reflection (refraction) in directions of vanishing double refraction *(German)* 79−13894
vision, refraction meridional differences and illum. depend., sharpness and recognition thresholds of defocused targets 80−16922
vision, spherical error of refraction, statistical anal. of biological theory of myopia 80−45881
visualization of light propagation, hologram construction 79−81391
water surface waves, optical meas. technique 77−29503
wedge deflection angle calc., approx. formula 79−32068
zoom and multiconfiguration optimization using the indices of refraction to represent zoom modes 79−86232
$AsO_{3/2}$-$BO_{3/2}$, glass, props. and struct. *(Japanese)* 77−27836
BaO-B_2O_3 glass, refraction, refractive index from 0.365 to 2.50 μm 80−88953
BaO-La_2O_3-B_2O_3, glass, refraction, refractive index from 0.365 to 2.50 μm 80−88953
$CaCO_3$, aragonite, conical intensity distrib. 79−1747
α-HIO_3, nonlinear conical refraction, second-harmonic cone 79−27329
α-HIO_3, optically active biaxial crystal, conical diffr. intensity patterns 79−4785
αHIO_3, second harmonic conical refraction 77−46758
He, underdense gas breakdown by laser pulse, backscatt. and beam refr. 78−5897
He-Ne laser demonstration of continuously varying refractive index *(German)* 80−8
Hg_2Cl_2, calomel, birefractive cryst., light spreading *(German)* 77−77168
InSb, low-power nonlinear refraction effect on laser beam propagation 80−5801
K_2O-CaO-BaO-B_2O_3, glass, refraction, refractive index from 0.365 to 2.50 μm 80−88953
$LiIO_3$ crystal, SHG, thermoelastic stresses and nonlinear refract. effect 80−74437
$LiIO_3$, irreversible double refraction in mag. field *(Russian)* 77−59560
MnF_2, magnetic, thermal, elastic refraction of light, mag. order influence on refractive index *(Russian)* 80−34880
$SbO_{3/2}$-$BO_{3/2}$, glass, struct. and props. *(Japanese)* 77−27836
Si, high-resistivity, local IR refraction and transmission 79−15429
ZnO-B_2O_3, glass, refraction, refractive index from 0.365 to 2.50 μm 80−88953
ZnO-La_2O_3-B_2O_3, glass, refraction, refractive index from 0.365 to 2.50 μm 80−88953

light scattering
see also Brillouin spectra; opalescence; Raman spectra; Rayleigh scattering; stimulated scattering
absorbing inhomogeneity molten zone, laser beam nonlinear scatt. 79−89969
absorbing-scattering layered material, light beam diffusion obs. method 78−62215
absorption spectroscopy in scattering samples using integrated optics 77−29232
achiral molecule, laser induced circular differential scatt., QED anal. 78−46409
acoustic activity in crystals, Bragg light scatt. at elastic waves *(Russian)* 77−62587
acoustic shear waves polarisation meas. 77−35006
acousto-optic multiple plane-wave scatt., explicit formalism 80−99621
acousto-optical interaction efficiency calc. 80−103940
acousto-optical modulator, geom. optics model in low scatt. efficiency limit 77−34935
acrylamide gel, spinodal line and critical point, light scatt. meas. 79−79315
F-actin, muscle, quasi-elastic light scatt. 77−64010
active and passive particles, extinction 80−102684
active particles, Lorenz-Mie scatt. theory paradox 80−74324
active particles, Lorenz-Mie scatt. theory paradox 80−102683
active polarisation spectroscopy by combinational light scatt. *(Russian)* 78−78006
adjustable single-fibre connector and output monitor *(German)* 78−38011
adsorbed molecule near solid surface, light scatt. calcs. 79−56069
adsorbed molecules at metal-solution interface, enhanced light scatt. 79−82989
aerosol, individual particle scatt. and single-burst digital correl. for wind remote meas. 79−100980
aerosol, Knollenberg light scattering counters, response characts. 79−66369
aerosol, multiple light scatt., inverse problems 79−98289
aerosol, particle size determination by light scattering, unknown refractive index 78−95957
aerosol, single droplet, size and mass meas. using electrodynamic balance 80−89535
aerosol atmosphere, MTF and PSF calcs. rel. to space-meteorological photography, multiple scatt. effect 79−66792
aerosol deflector operation at high radiation intensities 80−9922
aerosol extinction in 0.2-40 μm wavelength range, meteorological affects 80−17371
aerosol layer depth remote meas. by microwave-modulated laser *(Russian)* 78−57338
aerosol model, cigarette smoke, optical props. 79−7073
aerosol optical extinction coefficients, practical upper limits 79−72486
aerosol particle size evaluation, response function optimisation of light scatt. instruments 79−50214
aerosol particle size meas. by optical methods, review 80−40746
aerosol particle size measuring device, using spectral transparency and small angle scatt. methods 80−95069
aerosol particle sizing by laser beam Mie scatt., computer program 77−37457
aerosol particle sizing by optical scattering counters 77−21896
aerosol scattering and extinction coeff. simultaneous meas. in portable multipass cell 79−62588
aerosol scattering indicatrices under clear sky conditions in 0.55 to 2.4 μ spectral region, determ. *(Russian)* 80−94600
aerosol size distribution, meas. by combined light scatt. and centrifugation 77−10083
aerosol size distribution by inverting spectral turbidity data 80−95796
aerosol size distribution retrieval, simulated aureole data inversion in presence of multiple scatt. 79−74957
aerosols, differential scatt. coeff. to mass conc. ratio, spectronephelometer, cascade impactor obs. 80−72628
aerosols, dispersity analysis, automatic photoelec. analyser for size range 0.3-40 μm 80−57251
aerosols, high relative humidity, optical backscattering, extinction coeffs. 77−34825
aerosols, liquid and solid, size distrib. meas. by Doppler shift spectroscopy 78−33674
aerosols, Mie optical cross-sections calcs., sensitivity to size distribs. sampling errors 77−2243
aerosols, monodisperse, 0.1-0.4 μm, size meas. by polarisation ratio of 90° scatt. light 80−40754
aerosols, monodisperse, mass concentration, laser monitoring 80−98878
aerosols, scattering function determ. with telephotometer 80−105055
air bubble in water, critical angle scatt., physical optics approx. and obs. 80−9797
air pollutant particulate volume conc. determ. by atmospheric Mie scatt. method *(Korean)* 80−45835
airborne dust pollution monitor 80−55971
albumin, bovine serum, macroion soln. viscosity and diffusion, quasielastic light scatt., electrostatic interaction 79−70508
albumin, bovine serum, solutions, fluctuation transport theory 78−70057
algal suspension, light scatt. expts. and theory, ang. depend. 79−16166
algal suspensions, light scatt. and absorpt. props., 380-720 nm 78−92604
n-alkane gases, depolarised light scatt., internal field effects 79−76471
alkyl cyanobiphenyls, pretransitional behaviour, alkal chain length depend., light scatt. in isotropic phase 80−44301
amateur camera light scatt. coefficient factors 79−71559
Ambartsumyan's function for a cloudless atmosphere in the case of isotropic scattering *(Russian)* 79−39850
ammonium bioxalate monohydrate spontaneous parametric scatt. spectra, polariton wave vector and Stokes lines analysis 78−43885
amorphous media, object wave and its coherence 78−25799
anemometer signals, visibility characts., particle sizing appl. 77−42482
angular multiple scattering data, math. inversion 79−89847
aniline, liq., depolarised light scatt. from shear waves 80−97288
aniline-cyclohexane, crit. mixture with shear flow, light scatt. obs. 80−6521
anisodiametric particles, light scatt. functions 79−98286
anisometric molecules, in soln., depolarised light scattering intensity 80−45096
anisotropic ellipsoids, scatt. matrix comparable in size to light wavelength 80−1132
anisotropic ferromagnet, one-magnon light scatt., temp. depend. 77−52063

light scattering continued
anisotropic inhomogeneous medium, elastic light scatt., orientation characterization 80−83553
anisotropic media, polarised, depolarised scatter, anisotropy induced depolarisation 77−75412
anisotropic medium, inhomogeneity, orientation characterization by elastic light scatt. 80−83552
anisotropic molecules, depolarisation of scatt. light. density depend. *(French)* 77−4652
anisotropic nonconservative media, diffuse reflectance 77−7002
anisotropic particles, light scatt. struct. coeff., angular depend. 80−103964
anisotropic two layer medium, auxiliary functions *(Russian)* 77−54671
anisotropically polarisable molecules embedded in small particles, fluoresc. scatt. 79−76587
antiferromagnet, one-magnon light scatt., effect of anisotropy 79−33676
antiferromagnet, one-magnon light scatt. from metamagnetic phase effect of anisotropy 79−33678
antiferromagnet, one-magnon light scatt. from spin-flop and paramag. regions, effect of anisotropy 79−33677
antiferromagnetic insulator, light scatt. in strong mag. field 78−72523
antiferromagnetic polaritons, dispersion relation and light scatt. 77−35871
antiferromagnets, light scatt. as probe for dynamical crit. props. 79−15314
antiferromagnets, spin waves, microwave and optical expts., review 80−50081
aqueous dispersion of colloidal particles, number fluctuation meas. using light scatt. 79−96371
in aqueous polymer solutions, meas. apparatus 78−74058
Ar, light scattering, collision induced, low density limit, mol. dynamics and memory function approach 80−43841
arbitrarily shaped dielectric particles, multiple scatt. approach 80−87312
arc plasma, thermal density fluctuations, light scatt. using CW CO_2 laser and heterodyne detection 78−59677
arsenates, ferroelec. phase, E-mode splitting 78−15163
aspheric optics low scatter finishing, polishing of f/2 paraboloids 79−59855
aspherical optical surface low-scatter finishing 79−14125
asymptotic scattering efficiency of a large sphere 80−32905
atmopsheric scattering of lidar pulses, four-component polarisation meas. 78−44996
atmosphere, adjacency effects on imaging 79−100939
atmosphere, aerosol angular scatt., in situ photometric obs. 77−9492
atmosphere, aerosol content determ. from photometric obs. of stars 78−92976
atmosphere, aerosol effects on polarisation of scatt. light from point source *(Russian)* 80−4106
atmosphere, aerosol extinction at 500 nm in urban and rural air at Milwaukee, USA 79−100946
atmosphere, aerosol extinction coeff. from outgoing solar radiation meas. in O_2 0.76 μm band *(Russian)* 79−8690
atmosphere, aerosol properties rel. to solar aureole, photogrammetry 78−57315
atmosphere, aerosol size spectra from inversion of optical scatt. and spectral extinction 79−62578
atmosphere, anisotropic scatt. by artificial ice crystals *(Russian)* 77−29436
atmosphere, arrival angle statistics rel. to turbulence around solar telescope 80−26740
atmosphere, aureole phase function interp., logarithmic derivative method *(Russian)* 77−45148
atmosphere, blue Moon phenomenon, due to light scatt. and mixed plate interference 77−2244
atmosphere, diffusion effect estimation using const. transmission function 80−4100
atmosphere, directional scatt. coeffs. meas. in droplet and cryst. clouds *(Russian)* 78−96292
atmosphere, extinction at 10.6 μm CO_2 laser wavelength, from meteorological records 79−39848
atmosphere, haze microstruct. and refr. index from scatt. light polarisation characts. *(Russian)* 79−29852
atmosphere, horizontally inhomogeneous scattering layer, light intensity *(Russian)* 78−36278
atmosphere, incoherent optical propag., effects on optical/optronical systems 78−92987
atmosphere, intensity of direct and scattered UV radiation at large air masses *(Russian)* 77−49166
atmosphere, IR radiation attenuation by ice platelets 80−66141
atmosphere, large particle scatt. coeffs. approximation for total O_3 determ. 80−82091
atmosphere, light absorpt. and scatt. rel. to direct beam solar irradiance and illuminance 80−90174
atmosphere, light beam coherence through optically dense turbid layer 78−55300
atmosphere, mol. and aerosol scatt. rel. to effects of diffuse radiation on O_3 photodissoc. 80−109210
atmosphere, mol. complexes presence and role in residual absorpt., light scatt. obs. 80−56607
atmosphere, mol. scatt. and refl. in photon fluxes and photodissoc. rates calcs. 79−53512
atmosphere, mol. scatt. rel. to polarised light transfer 80−67561
atmosphere, Monte Carlo simulation of twilight obs. *(Russian)* 77−33186
atmosphere, multiple scatt. theory for dispersive media with spherical particles *(Russian)* 80−94599
atmosphere, multiple scattering effect on photodissociation 78−85692
atmosphere, multiwavelength contrast telephotometry, aerosol extinction and visibility determ. 79−66842
atmosphere, new formula relating optical parameters *(Russian)* 78−11999
atmosphere, particle optical constants and disperse aerosol comp., phase scattering function *(Russian)* 80−61898
atmosphere, propagation calcs., use of average complex refr. index 78−57314
atmosphere, scatt. aerosol effects on optical mass of real atmosphere *(Russian)* 77−2239
atmosphere, scatt. coeff. and scatt. directivity coeff. in 0-165° angle range, statistical relations *(Russian)* 77−29433
atmosphere, scatt. coeff. as function of visibility and wavelength, empirical formula 79−34944

light scattering continued
atmosphere, scatt. effects wavelength depend. rel. to anomalous gray shades in DMSP visible imagery 80−77111
atmosphere, scatt. indicatrix for large optical depth *(Russian)* 77−29440
atmosphere, scatt. of middle UV radiation from an internal source, Monte Carlo model 79−12263
atmosphere, scatt. of solar radiation refl. from ocean surface *(Russian)* 77−29435
atmosphere, scattering directivity coeff. between 0.5 and 170 degrees 77−5319
atmosphere, scattering layer with extended scattering indicatrix, radiative transfer eqn. *(Russian)* 78−40660
atmosphere, sunlight scattering, Rayleigh and Mie theory 80−56605
atmosphere, transmission and scatt. phase function, 1.9-2.3 microns, aircraft meas. *(Russian)* 77−29434
atmosphere, turbid, Monte Carlo anal. of multiply scatt. lidar returns 77−25779
atmosphere, turbid, multiple scatt. effects on refl. light pulses 77−29442
atmosphere, turbidity meas. via polarisation of UV light of daytime sky 78−20517
atmosphere, turbulent, Huygens-Kirchhoff method, phase approx. 80−28160
atmosphere, visibility reduction by sulphates in photochemical smog 77−21904
atmosphere aerosol absorpt. and scatt. effects rel. to satellite retrieved temp. profiles error 80−98449
atmosphere contaminant tele-detection apparatus using combination light scatt. spectra *(Russian)* 77−49193
atmosphere model, scatt. light intensity and polarisation degree, mol. anisotropy effect 80−77104
atmosphere optics, scatt. by mols. and particles, book 77−5323
atmospheres, polarization and scattering 79−96814
atmospheric aerosol, Barrow, Alaska 77−29386
atmospheric aerosol, use of lidars, laser rangefinders 80−51580
atmospheric aerosol above urban site, pollution monitoring by Lidar meas. *(French)* 77−25780
atmospheric aerosol extinction measurements, multiple scatt. corrections 80−98445
atmospheric aerosol particles, optical props. 78−11995
atmospheric aerosols microphysical parameters from complex optical meas. *(Russian)* 77−13123
atmospheric degradation of electro-optical system performance 79−66805
atmospheric experiments, definition weaknesses of visibility 79−8688
atmospheric extinction and absorpt., effects of particulate complex refr. index and size distribs. 79−29849
atmospheric from naturally occurring aerosols, rel. to particle size statistics, 3.8 μ meas. 78−49136
atmospheric hydrometeor backscattering cross sections, meas. at 6328 Å 78−49135
atmospheric laser beam propag., monochromatic, problems 78−92988
atmospheric models, contrast attenuation factors calc., for remote sensing 80−4135
atmospheric multiple backscatt. and depolarisation obs. using lidar 78−36292
atmospheric nonspherical aerosol particle characterisation with electrooptical nephelometry 80−77106
atmospheric optical props., appl. to satellite remote sensing of phytoplankton 80−77105
atmospheric particulates, chemical characterisation via light scatt. method 78−69533
atmospheric propagation of partially coherent radiation 78−65386
atmospheric scattering effects for high-rejection optical baffling system 78−7802
atmospheric scattering from marine aerosols, ELOS optical communications system 79−29862
atmospheric scattering meas. extension into UV using integrating nephelometer 79−74955
atmospheric seasonal extinction due to aerosol at Kottamia Observatory site 80−46253
atmospheric turbidity rel. to circumsolar radiation intensity 77−37405
atom, resonance light scattering, intensity effects 80−91511
atom in coherent field, reson. scatt., quantum description of two-level system 79−64053
atomic collisional radiation redistrib. in spectral line nonimpact region 79−22667
atomic cooperative system, light scatt. spectrum, coherent-state representation, numerical results 80−23650
atomic fluids, variable polarisability, depolarised light scatt. 79−64823
atomic levels, two-photon transitions 80−83333
atoms, reson. light scatt., collisional repopulation of at. levels 79−6907
atoms and molecules, reson. light scatt., theory of correl. meas. 78−42014
atoms interacting with polarised light, resonant Voigt effect, analysis 79−76390
aureole around UV source at finite distance 78−77320
aureole radiance field about point source in scatt.-absorbing medium 78−77319
aurora and nightglow satellite obs., contamination due to scatt. by clouds and snow 78−77385
autocollimation, resonance light scatt. by echelon *(Russian)* 77−88640
automation of real-time optical meas. of small structures 79−85115
azo pigments, dispersions in flow system, nucleation and growth kinetics meas. 77−63967
backscattering amplification during large intensity fluctuations 80−18994
backscattering technique, appl. in fibre diagnostics and attenuation meas. 80−33188
bacteria, appl. of Mie theory and cubic splines 79−36838
bacteria, diffusing and motile, light scatt. props. calc., RGD approx. accuracy 79−92193
bacteria, motile, rot.-translational models for interpretation of quasi-elastic light scatt. spectra 79−11906
bacteria, scattering pattern analysis 78−80946
bacteria E.coli strains in aq. suspension, polarisability anisotropy and aminoglycoside antibiotic effects 80−85441
bacteria species identification and conc. estimation 77−56564
bacterial migrating chemotactic bands, quasi-elastic light scatt., E. coli 78−77018

light scattering continued
bacterial motility, E. coli, struct. effects in quasi-elastic light scatt. 78−77024
bacterial movement tracking using one-dimens. fringe system 78−73299
bacteriophages T4B and T7, determ. of rotational diffusion coeff. by depolarised dynamic light scattering 80−85549
Baltic Sea, estuary region, suspension distrib. under river drifts influence *(Russian)* 80−98345
Baltic Sea inshore waters, light scatt. matrices *(Russian)* 77−29311
Barnard Loop Nebula, far UV light scatt. by interstellar dust 77−29911
Be shell stars, Hβ high-resolution polarisation struct. rel. to circumstellar envelope scatt. 79−44485
Be stars, 1.25 and 2.2 microns polarimetry rel. to electron scatt. 79−44484
Be stars, electron scatt. effects on Balmer emission lines 80−17589
bead solutions, quasielastic light scatt. in small wave vector limit 80−45088
beam broadening in randomly inhomogeneous cloudy aerosol medium *(Russian)* 78−58911
beam volume attenuation coeff., invalidity 80−95791
beam volume scattering coefficient inadequacy 77−27251
benzene, liq., light scatt. coeff. determ., absolute method 78−2868
benzene-carbon tetrachloride, mixture, mol. and Raman scatt., profile shape, conc. depend. 77−58025
benzyl benzoate, supercooled, depolarised lines in quasielastic light scatt. 80−45095
benzylidene aniline series, nematic liq. crysts., depolarised scatt. strength, free-energy, coherence length anisotropy 77−62470
bimodal systems, particle size distrib. meas., forward scatt. techniques 79−21699
binary liquid mixtures, sp. ht., light scatt., two-scale-factor universality 79−42267
binary liquid mixtures trapped in thin pores, binary crit. points *(French)* 77−59117
binary mixture in external field, crit. opalescence 78−84595
binary mixture near crit. point, singly and multiply scattered light distrib. 78−56494
biological cell analysis, high speed light scattering system 79−12042
biological cell size meas. by static light scatt. Fourier transform 80−81793
biological cell suspension, electrophoretic analysis, Doppler spectra line shape smoothing 79−84053
biological cells, backscatter depend. on membrane thickness and refr. index 79−48225
biological cells in flow system, paraxial anal. of light scatt. 79−11907
biological macromolecules, picosec. and subpicosec. relax. and dephasing, reson. light scatt. obs. 79−45876
biological material, laser stereometry light-scatt. technique, cardiac images 80−56310
biological particle structural change dynamics, rapid light scatt. meas. 79−39615
biological particles, light scatt., shell and nucleus effect on indicatrix and polarisation 79−74608
biological samples, laser scatt. obs. 79−79596
biological substances at high press. *(Dutch)* 78−27901
biological surfaces observation using laser electrophoretic light scatt. 80−41359
biological system solution, periodic conversions, optical mixing method obs. 78−96029
biological tissue, coagulation by irradiation with laser light 80−41113
biomembrane microviscosity measurement, light scatt. effects 79−39365
blazed dielectric gratings, surface wave scattering 80−48136
blood, back-scattering theory 78−77099
blood suspension aggregation in Couette flow *(French)* 80−97991
borosilicate glass, birefringent, X-ray and light scatt. study 80−103937
brain, microtubule solns., calf, dynamic laser light scattering 79−16150
breather generation, inverse scatt. technique 80−78913
brightening of disperse media, role of laser fluctuations 79−41405
broadband dielectric mirror interference coatings, scatter losses 79−50365
Brownian interacting particle system, light scatt. theory diffusion coeff., lineshape 77−27254
Brownian motion, intensity fluctuation spectroscopy applics., review 80−52129
Brownian motion, photon correlation study 78−25798
Brownian particle double scatt., Rayleigh and large dielectric sphere cases 77−10839
Brownian particles, correlations 78−82911
Brownian particles, independent, multiple light scatt. calcs. 78−22087
Brownian particles, laser light scatt., photon time-interval statistics 78−9329
Brownian particles, multiple light scattering, depolarisation ratio and linewidths 78−78913
Brownian particles solutions, diffusion effects, light scatt. theory 77−4939
Brownian polymer particles in water, multiple scatt. 78−78912
WY Caneri, eclipsing binary, scatt. in cool component atmosphere 79−92799
VY Canis Majoris, dia. meas. rel. to scatt. by dust shell 79−16974
carbon tetrachloride, liq. and plastic cryst. phases, thermodynamic props., light scatt., US propag. 78−2863
carbon tetrachloride-chloroform (methyl cyanide) solutions, anisotropic light scatt., interactions between solvent and solute mols. 78−27239
η Carinae, silicate grains size distrib. rel. to optical wavelengths scatt. 80−4382
α Carinae (Canopus), generalised Compton effect in spectrum 78−53938
cataract microstructure meas., picosecond range-gated light scatt. technique 79−8584
cavitation nuclei in liquid flows, size distrib. determ. technique 77−68716
CBOOA, smectic A-nematic transition, X-ray and light scatt. obs. 79−95129
cell analysis in flow systems, geometry for orienting flat cells 78−77161
cell average size and shape meas. light scatt. photometry compared with microscopy 79−84030
cell high-speed analysis, laser absorpt. and scatt. meas. *(German)* 78−92687
cell medically relevant class determ., scatt. light cluster anal., cervical smear tests *(German)* 78−92686
cell type recognition by multiangle laser beam scattering flow system 77−21595

light scattering continued
cellulose acetate, conc. soln. and films, light scatt. studies 80−16050
ceramic translucent systems, absorpt. and scatt. coeffs for visible light, Kubelka-Munk theory 80−60627
ceramics, nephelometer for light scatt. meas. 77−10084
chiral smectic C liq. cryst., kinematic and dynamic light scatt. from periodic struct. 79−11427
chloromethane gas, linear electro-optical effect 80−87843
chloroplast thylakoid, light-induced absorbancy and scatt. changes about 520 nm rel. to struct. 78−69019
chloroplasts, in suspension, near IR radiation dispersion *(Russian)* 78−24045
cholesteric liquid crystal, optical activity, light scatt., theory 77−36195
cholesteric liquid crystal, pseudoencapsulated film, selective light scatt. 77−16289
cholesteric liquid crystal., scatt. by fluctuation inhomogeneities *(Russian)* 78−2005
cholesteric liquid crystal *(Russian)* 79−77517
cholesteric liquid crystal thermo-optical monitor, for nonionising radiation 78−11742
cholesteric liquid crystals optical properties, diffraction nature, review 80−70123
cholesteric mixture, solid phase, spherulite textures, optical effects and mol. ordering 79−1746
cholesteryl 2-(2-ethoxy-ethoxy) ethyl carbonate, dynamics of isotropic-cholesteric transition, normal and blue phases 79−95134
cholesteryl laurate-cholesteryl caprylate (75 wt.%), polymorphic behaviour, optical, elec. and dielec. meas. 80−65208
cholesteryl oleyl carbonate, isotropic phase, polarisation of scattered light 79−78691
chromaffin granule electrophoretic mobility meas. by light scatt., effect of Ca^{2+} and Mg^{2+} 78−53357
ciliary activity obs. by laser light-scatt. spectroscopy 78−36076
circular cylinders, single scatt. phase matrix, ray optics and wave theory comparison 80−102610
circular fringes with dark centre, form. in diffused light at infinity 78−42278
circumsolar parts of sky, parabolotoroidal focones and parabolocylindrical foclines assessment 78−83064
circumsolar radiation, single and multiple scatt. contribs. 79−25325
circumstellar dust shells, Monte Carlo simulation of polarised light transfer 78−81608
circumstellar envelopes, Monte Carlo analysis of polarization by Thomson scattering 80−85931
classical crystal optics, lattice dynamical background, review 80−97221
classical fluid, collision-induced and multiple light scatt. 80−53919
classical fluid, crit. dynamics, double scatt. correction 79−42979
classical novae, light scatt. in optically thick winds 78−24516
cloud, Mie formalism, optical communication appl. 77−88651
cloud droplet spectrometry using light scatt. technique 77−41219
cloud extinction coefficient, estimation from multiwavelength lidar backscatter meas. 80−98446
cloud multiple radiation scatt., stochastic approximation 79−80012
cloud reflectance with laser beam illumination, multiple scatt. contrib. 78−85686
clouds, scatt. function in mathematical model for reflected and transmitted radiation 80−90215
clouds, scatt. intensity phase angle depend. rel. to contrast bow obs. 79−80029
clouds, thick, light pulse propag., pulse width expression for scatt. slab 80−82059
cluster of spheres, scatt. problem, soln. using Debye potentials 79−31800
coagulating dispersions, light scatt. data, Fourier inversion anal. 78−76932
COC, dynamics of isotropic-cholesteric transition, normal and blue phases 79−95134
coherent radiation beams, parameters from correlation method *(Russian)* 78−50705
coherent scattering, Gaussian beam, statistically rough surface 77−10837
coherently illuminated scattering object, speckle pattern statistics in diffr. field 80−63924
collagen, optical activity rel. to ordered aggregation 79−11899
collective plasma density fluctuations, far IR scatt. apparatus obs. 79−32818
collision-induced light scatt., moments of three-body portion 77−57961
collisional dephasing in near-reson. light scatt., non-Markovian theory 80−1045
collisional polarisability effect on scatt. calcs. from dense fluids *(French)* 79−31789
collisionally perturbed atoms, saturated near-reson. light scatt., spectral line strengths 80−23345
colloid, electro-optical characterisation methods 77−24821
colloid, electrostatically stabilised, very dilute, struct. factor scatt. vector depend. 77−36795
colloidal, concentrated dispersions, dynamic light scattering 79−15469
colloidal crystals, single, suitable for light scatt. studies, prod. technique 79−99097
colloidal particles, interacting Brownian spheres, depolarised light scattering 79−34370
colloidal particles, intrinsic optical anisotropy, anomalous diffr. approx. 80−53213
colloidal suspension of spheres, Percus-Yevick approx. 78−94368
colloids, concentrated, appl. of modern concepts in liquid state theory 80−40750
combination light scattering spectrometer temp. regulating attachment *(Russian)* 77−53987
combustion gases, light scatt. diagnostics 77−47124
Comet West (1975n), scatt. phase function of cometary dust, 0.5 to 18 μ 77−29731
Comet West (1976 VI), polarisation obs. rel. to elongated particles scatt. indicatrix 79−62794
composite media, dielec. and optical props. 78−84546
compound glass optical fibres, total and scatt. loss coefficient meas. 80−69536
conducting crystals kinematical and dynamical inelastic light scatt. 78−80368
conducting spheres, polarisability spatial extension in two body collision induced light scattering 79−98174
COOB, smectic A-nematic transition, X-ray and light scatt. obs. 79−95129
cooperative effects during scatt. in media of various vol. concs. *(Russian)* 77−38803
cooperative resonance fluorescence, photon statistics and absorption spectrum 78−42311
cornea, low-angle light scattering meas. apparatus 77−5123
coronagraph objective component surface scatt. angular distrib. obs. 80−74463
coronograph external occulting disc, scattered light flux and reduction 78−36455
correlation method for light beating spectra, entropy fluctuations of crit. mixture 77−10119
coupling of molecules to surface plasmons in resonant elastic scattering 80−20102
covered groove, optical surface wave scatt. and refl. 77−75707
critical binary mixtures, multiple light scatt. 77−48183
critical fluids, light scatt. in presence of uniform shear flow 79−78693
critical mixture, multiply scatt. light, LF spectrum 77−52125
critical mixtures, shear and critical fluctuations, instantaneous mapping of velocity gradients 80−79420
critical opalescence, multiple scatt. contrib. 79−8151
critical point, extinction coeff. 79−65889
crystal nonequilibrium thermodynamics, quasielastic light scatt., systematic anal. methodology 79−61391
crystalline clouds, artificial, light scatt. matrices *(Russian)* 77−5317
crystals, book 80−2774
crystals, meas. installation 78−4673
cumulus clouds, scattered and total solar radiation fluxes *(Russian)* 77−41169
CVD film growth probe, using inelastic light scatt. 77−40383
4-cyano-4′-octylbiphenyl, nematic-smectic-A transition, high-resolution X-ray and light scatt. study 79−73297
cyclohexane-aniline mixture, shear induced transition to mean-field crit. behaviour 80−7364
Cygnus X-1, photospheric scatt. model for optical polarisation orbital vars. 78−54077
cylinder, infinite tilted, linearly polarised incidence at arbitrary angle 80−58457
cylinder, optically active, EM wave scatt. 78−82912
cylindrical dielectric array, multiple scatt. effects in photon diffraction 80−1905
cylindrical He absorption cell, multiple scatt. effects near reson. 80−16049
cytochrome c-serotonin soln., UV effect on optical props. 80−30663
cytometry, fast flow-through, pattern recognition by light scatter meas. 79−88228
cytometry, hydrodynamic orientation of sperm heads in flow systems 78−77162
Debye generalised fluid model, dielectric relax., depolarised dynamic light scatt. 80−108156
deep water, scattering effects *(Russian)* 79−34850
defect crystal structure determination 80−103316
defect structure near phase transition pt., effect on solid props. *(Russian)* 79−37838
defocused speckle photography, tilt topology technique 77−26419
degenerate two level system, reson. light scatt., transient polarisation characts. 78−94382
dense molecular fluid, light scatt., internal field correction factor calcs. 80−25396
dense particulate system, particle size meas. device based on scatt. light 78−45006
dense scattering media, anisotropy factor 80−87307
densely distributed scatterers, picosecond pulse backscatt. 80−14281
densely distributed scatterers, pulse diffusion 79−3632
depolarised intensity, prediction from dielec. meas./theory, LRK model 77−85733
depolarised light scatt. from fluid near Benard instability 77−7371
depolarised light scatt. spectrom. double scatt. effects 79−42978
depolarised multispectral laser scatt., target classification 78−50846
depolarising diffusers, autocorrelation by holography *(French)* 79−31801
depolarising optical system characterisation by automated ellipsometer 78−32855
diamond, round brilliant cut, statistical assessment of brilliance and fire 78−90361
diamond, round brilliant cut style modifications, brilliance, sparkliness and fire 78−90362
diamond simulants, brilliance, sparkliness and fire 78−90363
p-p′-dibutyl-azoxybenzene, DIBAB, light scatt. studies *(Dutch)* 80−33885
p-p′-dibutyl-azoxybenzene, nematic liq. cryst., elasticities and viscosities, light scatt. meas. 79−4245
β,β'-dichloroethyl ether-iso-octane, critical indices, allowance for light double scatt. *(Russian)* 80−60624
dielectric, transparent, laser-induced damage, role of absorbing microinclusions, passive methods 79−31969
dielectric and absorbing nonspherical particles, scatt. and polarisation props. 77−34823
dielectric cylinder, scattered light polarisation characts. 77−75409
dielectric fibres, transversely incident beam wave scatt. 80−96004
dielectric gratings, arbitrary profiles, scatt. and guiding of EM waves 80−96005
dielectric inhomogeneous medium, refractive index profile determ. from inverse scattering 78−58914
dielectric kernel, functional differential equn. 79−32871
dielectric molecular fluid, optical props., internal forces effects, theory 77−28534
dielectric multilayer coated optical surface, diffr. and diffuse scatt. 79−50220
dielectric multilayer interference devices, loss mechanisms 77−83943
dielectric needle and disc, light scatt. using Rayleigh-Gans and Rayleigh scatt. method 79−76591
dielectric particles, statistical theory of light scatt. 80−32913
dielectric particles, variational principle for light scatt. 79−18348
dielectric plate refractive index profile determ. 79−7081
dielectric slab optical waveguide, scattering characteristics 78−87163
dielectric slab waveguide, radiation pattern determ. due to refractive index fluctuations 78−22216
dielectric slab waveguide, scatt. characts. of beam mode 79−55230
dielectric solids, molecular optics model, electrodynamic eqns. derivation 78 27151

light scattering continued
dielectric sphere, Mie theory with spatial dispersion 79−98284
dielectric spheres, resonances in radiation press., dielec. surface wave obs., and size meas. 77−58256
dielectric thin films, refractive index variation for given reflectivity, analytic soln. to synthesis problem 80−34996
diffraction grating, reflective, high efficiency, scattering types 80−99619
diffraction grating, specification and meas. of scattered light 78−78905
diffuse light scattering, mathematical modelling 80−106450
diffuse medium, reduced effective velocity of light 80−69329
diffuse quadratic surfaces, photometric representation 79−81365
diffuse radiation emerging from semi-infinite medium, intensity accounting for inner refl. *(Russian)* 79−8637
diffuse reflectance rel. to partial coherence and IR laser photogoniometric meas. 80−14283
diffuse reflection, mutual shadowing effect classical calc. extensions 79−84666
diffuse reflection problem for combination of Rayleigh and isotropic scatt., exact soln. 79−84661
diffuse scattering, statistical model, Gurevich-Kubelka-Munk theory calcs. 78−46513
diffuse solar radiation field in cloud layer *(Russian)* 79−29851
diffused waveguide, attenuation characteristics of TE modes and surface scatt. 80−5822
diffused waveguide, refractive index profile determ. by inverse scatt. theory 80−5838
diffusely scattering medium, refl. and transmission, Helmholtz reciprocity theorem *(German)* 77−79753
diffuser, weak, speckle pattern, spherical aberration effect 80−87476
diffuser for Fourier transform hologram recording 80−43285
diffuser form. of simple known statistical props. 78−90539
diffuser with pseudorandom phase sequence [hologram recording] 80−14298
diffusing glass, optically thick-layer transmission ang. distrib. 79−27179
diffusing glass catalogue and basic operational characteristics 79−46019
diffusing layers, characteristic matrices for inhomogeneous layers 78−87015
diffusing layers, characteristic matrix and general props. 78−87014
diffusing object microstructure, moire methods extension *(French)* 79−27177
diffusing surface inclination determ. rel. to viewing direction, speckle photography 79−2815
diffusing surface optical autocorrelation 80−99646
diffusion controlled reaction kinetic studies, one-step reaction case 78−35659
diffusion equation derived from space-time transport equation 80−78772
diffusion in optically finite shell, linear integral eqn. *(Russian)* 77−13236
dihedral corner reflector, effective scattering area calculation, radiation balance method 80−48380
dilute colloidal suspension, Krishnan effect, theory 77−34824
dilute gas, Boltzmann-Langevin eqn., light scatt. and density correlation function 77−11307
dioctyl phthalate, polydisperse, spectronephelometer studies 79−21797
dipalmitoyl lecithin vesicles in dil. suspension, light scatt. obs., of phase transitions 77−16915
L-α-dipalmitoyl phosphatidyl choline, monolayers, laser-ripplon scatt. at air-water interface 79−99894
dipalmitoyl phosphatidylcholine vesicles, appl. of depolarised light scatt. theory from hollow spherical particles 80−45946
disordered solids, light scatt. from configurational fluctuations 79−11428
disperse layers with loosely or closely packed particles, spectral transmission variation *(Russian)* 77−23619
disperse particles, determ. of spectrum of diameters from scattering of light 80−61169
disperse system, parameters determ. from turbidity spectrum, allowance for nonspherical particles 78−55302
disperse system of oblate particles, light scatt. functions 79−64180
disperse systems, turbidity-spectrum method, scatt. functions for nonspherical particle systems 78−20078
dispersed random prolate spheroids, light scatt. characts., for turbidity spectrum calcs. 78−25801
dispersed system, simultaneous determ. of refr. index and particle size from scattered radiation characts. 80−27335
dispersion, by small spherical particles, single process calc. *(Japanese)* 77−65578
dispersion, coagulating, light scatt. for close range struct. determ. 78−53273
dispersion relations, two dimens., phase problem appl. 80−102631
dispersions, particle size and velocity distribution, in flowing media, meas. methods *(German)* 78−34213
dispersive media, theory of multiple light scatt. by spherical particles *(Russian)* 80−94599
dispersive medium, many-photon scatt. of light by impurity centres 80−60622
dispersive medium, photon interaction models 79−82068
dispersive particle sizes, from scattering and polarization meas. *(Russian)* 79−34950
DNA, radiation induced mol. size change, electron irradiated, effect of p-nitroacetophenone 80−89807
DNA, soln., quasielastic light scattering, in AC elec. field 79−62186
DNA kinetics in soln., electron pulse radiolysis using light scatt. detect. 77−16910
DOBAMBC, ferroelectric liquid crystal film, freely suspended, polarisation, elastic consts. and viscosity meas. 79−55663
dodecylcyanobiphenyl, pretransitional behaviour of isotropic to smectic A phase transition 79−60487
Doppler scattering by ocean ripples due to acoustic and capillary waves 78−3807
double scattering method for condensed systems parameters determ. 80−28161
droplets, laser light scatt., multiplicative and additive stochastic processes 78−84596
drops of water, ice or mixed phase, backscatt. at 633 nm 77−64426
dust grain, charged, quantum approach 80−48196
dust on Mars, scattering by nonspherical particles and optical props. 79−25535
dynamical properties study using light scatt., principles spectra derivation and applics. 80−53218
E. coli, light scatt., ribosomal subunit diffusion coeffs. 80−21438

light scattering continued
Earth atmosphere, plane-parallel model appls. to multiple scattered radiation problems *(Russian)* 78−36275
EBBA liq. cryst., anisotropic light scatt. 79−78692
EBBA liq. cryst., dynamic light scatt., effect of paramag. iminoxyl radical addition *(Russian)* 77−43131
education, scatter plate prod. using laser speckle, for scatter light interference expt. 79−9063
electrolyte solutions, conc. fluctuations and light scatt. *(Russian)* 77−1758
electrolyte solutions, fluctuations rel. to acoustic relaxation and light scatt. 77−15497
electron, slow EM wave stimulation, laser radiation scatt. *(Russian)* 77−46674
electron gas, quantised in mag. field, plasma oscill., light scatt. 77−28134
electron scattering, opacity due to electron correls. 77−64634
electron-phonon system, weakly coupled, resonant light scatt. and luminescence 80−40100
ellipsoidal particles, random orientation, backscatt. cross section, in optical limit 79−18349
ellipsoids of revolution, differential and total scatt. cross sections calc. 78−37807
EM radiation in media with spatial dispersion, spatial coherence formation and polarisation increase 80−106442
emulsion, H_2O-cyclohexane-sodium dodecyl sulphate-pentanol I, light scatt. *(French)* 79−1968
emulsion, hexadecane-H_2O-butanol-Brij 96, drop dia., comp. depend. light scatt. obs. 80−45573
emulsion, hexadecane-H_2O-pentanol-Tween 60, drop dia., comp. depend. light scatt. obs. 80−45573
entropy and LA fluctuations in solids, polarisation of scattered light 77−81113
erythrocyte membrane hydraulic cond. determ., light scatt. changes 79−34528
ethanol, solns., local struct. equilib., light scatt. and IR spectra obs. 78−84564
ethanol-water-chloroform mixture, light scatt. near plait point 78−72532
ethylcellosol, aq. soln., light scatt. rel. to conc. fluctuations *(Russian)* 78−3450
exchange and dipoles coupled ferromags., light scatt. from mag. surfaces, response theory 79−42820
exciton resonance excitation in crystals, light scatt., polarisation, specular refl., theory 80−50356
excitons localised at dislocations 78−60479
exosphere, global model using optical and incoherent scatter meas. 78−36343
expanding envelopes, Lyman α quanta scattering *(Russian)* 80−67556
extinction cross sections of randomly oriented nonspherical particles 78−13661
eye, aerial image modulation lowering, contribs. of retina and eye optical system 80−81584
eye lens, light scatt., appl. of random density and orientation fluctuation theory 79−62241
eye movement measurement, laser Doppler technique 79−92322
far-field coherent, surface light probability density function on ground glass surface 79−93099
fatty acid monolayers, capillary waves, photon correlation spectroscopy, viscoelastic props. 79−75608
fatty acid monolayers, light scatt. meas. 80−89011
ferricenium complex, Franck-Condon light scatt. transitions 77−57999
ferrimagnets, one-magnon light scatt., temp. dependence, two-sublattice systems 78−31061
ferrocytochrome c, picosec. and subpicosec. relax. and dephasing, reson. light scatt. obs. 79−45876
ferroelectric crystals, polariton light scatt. freq.-angle spectra, nonlinear susceptibility interference *(Russian)* 80−92834
ferroelectric smectic-C liquid crystal film, freely suspended, two-dimensional mol. orientation fluctuations, light scatt. meas. 78−47236
ferromagnet, anisotropic, theroy of light scatt. 77−90161
ferromagnetic semiconductors, mag. excitations, light scatt. 77−63161
ferromagnetic slab, light scattering from bulk and surface spin waves, theory 80−71389
fiberglass materials, fatigue damage effects on light scatt. 79−11706
fibre, micron sized, metal or insulator 77−65571
fibre, unclad, backscattered light, approx. ray theory 77−7177
fibre attenuation meas. by backscattering method, effect of noise 80−102824
fibre connector loss evaluation by backscattering 80−58721
fibre end, reflected and backscatt. power meas., time domain reflectometer 78−70177
fibre optic glass pair quality, effective aperture and light scatt. analysis 78−90522
fibre optical ring interferometer, Sagnac-effect, sensitivity 79−50379
fibre refractive index profile nondestructive determ., backward light scatt. method 79−64306
fibre sizing using Fraunhofer diffraction 79−171
fibre sizing using light scatt., error contour charts 80−4689
fibre splice insertion loss meas., backscattering method 80−58720
fibre-optic link, splice loss evaluation by means of the back-scattering technique 79−98478
fibre-optic scattering loss dependence on launching condition, lossy-layer model 78−5577
fibres, theory of propagation, ray approach *(French)* 77−79916
fibrinogen, bovine, high energy-induced aggregation, time resolved spectra 80−61655
field wavefunction, analytic properties in optics 80−1138
film, effect on light reflection, transmission and scatt. *(French)* 78−33664
film, laser damage thresholds, effect on refl. scatt. and transmission 79−45988
film, light scatt. from interface, polaritons 79−8202
film properties measurement using guided optics techniques 79−99958
film pulsed laser damage determ., optical techniques 80−33060
filter, dispersive crystal-air, transmission depend. on scatt. layer parameters *(Russian)* 77−84002
fine-grained bleached emulsion scatt. model and expt. 80−102670
flame, containing light scatt. particles, optical props. and temp. meas. method *(Russian)* 78−56894
flat layered glass, ang. distrib. for various incidence angles 79−7079

light scattering continued
flexible polymers in soln., hydrodynamic interactions in quasi-elastic light scatt. 79−37612
flow birefringence, scattered radiation charact. 78−60418
flow birefringence and hydrodynamic boundary conditions for ellipsoid particles and Rytov dip 80−45030
flow structure, light scatt. and hot-wire anemometer expts. 78−18271
flow-oriented spheroids, light scatt., birefringence, exact and RGD approx. 77−58255
fluid, dense, depolarised light scatt. due to orientational fluctuations 77−47318
fluid, dense, depolarised light scatt. due to orientational fluctuations 77−47319
fluid, dense, light scatt., point polarisability approx., local fields, interparticle pair correls. 77−55799
fluid, dense, non-spherical mol. polarised light scatt., local fields, interparticle pair correls. 77−55798
fluid, dense, statistical mech. of stationary state fluctuations 79−54035
fluid, near liq.-gas crit. pt., local order effects on dynamic props., US and light scatt. 78−67806
fluid, simple, light scatt., gravity effects on crit. exponents determ. 80−20650
fluid, test of nonequilib. steady states statistical mech. theory 79−58623
fluid, three-body correlation determ., heterodyne coincidence spectroscopy 77−10118
fluid flow patterns from speckle interference fringes 77−84346
fluid in nonequilibrium steady state, light scatt. hydrodynamics theory 80−50354
fluid mixture near tricritical point, light scatt., mean field behaviour 80−34930
fluid near crit. point, rapid evaluation of multiple scatt. 78−84594
fluid system, quasielastic light scattering spectroscopy, bispectral anal. 80−93347
fluid with stationary temp. gradient, light scatt. 80−45097
fluid-like viscoelastic liquid, coupling of orientational and translational motions, LF depolarised (VH) scatt. 77−7642
fluids, atomic and molecular, collision induced light scatt. *(German)* 79−27057
fluids, simple, light scatt., particle-hole model 80−60613
fluids, viscous, local order theory and light scatt., depolarised and polarised spectra 80−45093
fluids with nonuniform velocity fields, light scatt., and pair correl. functions 79−61389
fly ash particles, water accretion, refract. index and accreted layer thickness 80−58462
focal plane design and optimal processing for scattered optical fields 78−78935
fog, artificial, size distrib. meas. by extinction-sedimentation inversion technique 78−37042
fog hole boring with pulsed high-energy lasers 79−16662
fogs, multiple scattering, radiative transfer iterative calcs. 79−98276
fogs, optical probing, homogeneous particle model 79−66790
forced light scatt. in interphase *(Russian)* 80−16051
Fourier analysis limitations for radiative transfer soln. in small angle scatt. approx. 80−37952
Fourier transform IR, scatter eliminated spectrometry 78−89564
Freon-113, correlation properties near phase-separation boundary, gravitational field effect 80−107410
furan, liq., US relax., light scatt. meas. 77−77231
Galaxy, starlight scatt. models rel. to diffuse galactic light interpretation 78−8118
gas, self-structure factor, kinetic modelling 79−41791
gases, light scatt., depolaris. factor meas. *(Russian)* 79−13780
gases, two-body collision induced light scatt., memory function approach and mol. dynamics 78−25658
Gaussian beam scattering characts. at dielec. media interface 78−42275
Gaussian TEM_{00} mode laser beam scatt. from surface defect, normlaization 80−48313
gels, dynamic light scattering in poor solvent 78−88318
gels, dynamic light scattering theory 78−60475
generalised optical theorem for partially coherent interfering beams 80−106447
glass, chemically strengthened, stress profile determ. using scatt. light 80−30186
glass, decomposition, phase separation processes, diffusion coeffs. determ. *(Germany)* 78−39736
glass, ground, surface height and correlation length from reflection scatt. of laser light *(French)* 80−54491
glass, liq.-phase-separated, anomalous and normal light scattering 80−20654
glass, opalescing, visible light scattering, angular depend. of intensity, correction for attenuation 79−4814
glass, plane layer, 0.07 to 1000 units, reflectance and transmittance 78−17860
glass, tempered, stress analysis, oblique incidence light scattering, birefringence *(Polish)* 80−71374
glass, undergoing phase separation and homogenisation, light scatt., kinematic theory 79−24326
glass edge cladding-glass laser disc interface, reflection meas. 79−27300
glass fibre reinforced plastic, fatigue fracture kinetics studied by diffusion scatt. of luminous fluxes 80−76446
glass ground surface, fissured layer effect on scatt. of polarised light 79−64172
glass melt, unified theory of chem. relaxation using light scattering or US absorption 79−16028
glass powder, light scatt., close particle packing 78−1161
glass surface, ground, light scatt. matrices 79−72483
glass waveguide, in-plane scatt. and loss mechanisms 80−33216
glycerol, reorientation in associated liqs. 79−77481
gramicidin A monomer-dimer states, light scatt. studies 79−92143
guided wave polaritons in thin crystals, light scatt. spectra 79−15100
gyrotropic media, diffr. of light by acoustic waves 78−72485
haemoglobin, absorpt. spectra, light scatt. method meas. *(Russian)* 78−21939
haemoglobin, in salt soln., diffusion rel. to intermol. interactions, light scatt. investig. 77−44585
haemoglobin, mutual and tracer diffusion coeffs., photon correl. obs. 80−72123
halftone or line printing, Yule-Nielsen curve fitting parameter 79−13906
hard sphere mixtures, finite angle light scatt., Percus-Yevick approx. calcs. 80−7363
light scattering continued
haze, statistical model *(Russian)* 79−34946
haze and fog, actual light scatt. coeff. calc. 79−80013
haze of arbitrary shape of nonuniform particles, forward light scatt. 77−7003
hazemeter, NBS reference, development and testing 79−75565
hazes, information provision on particle size distrib. of brightness and polarisation phase functions *(Russian)* 78−44998
HBCA liq. cryst., anisotropic light scatt. 79−78692
HD 190073, A0ep star, reson. scatt. in atmosphere rel. to struct. and vars. of Ca II lines 77−17578
Heisenberg antiferromagnet, light scatt. off surface 78−23475
heterodyne interferometer, for vibr. meas. in auditory organs 77−2073
heterogeneous plane parallel medium, multiple light scatt. calcs. *(Russian)* 78−1166
hexadecyltrimethyl-ammonium bromide, micelle form. in aq. soln., laser light scatt. 78−27825
hexanetriol 1,2,6, liq., light scatt. study of struct. relax., viscosity and dielec. relax. 79−86672
high density excited system, population instability and optical anomalies 79−28826
high-pressure cell for depolarised light scatt. from liquids *(German)* 79−21799
highly anisotropic scatt. medium, luminesc. of layer 80−100685
histone F2a solutions, effect of ionic composition of medium on struct. and effectiveness of intermol. interactions 78−48744
histone lysine-rich, laser scattering spectra 77−29095
histones H_2A and H_4, mixed solns., oligomer structs. 80−30648
holographic correlometer with phase modulation, viscous, superviscous light scatt. media study 80−74321
holographic grating with arbitrary attenuation, coupled wave theory 77−46707
holographic interferometer for studying three-dimensional optical inhomogeneities 78−87030
holography through fog, coherence requirements for light source 78−58949
homogeneous plane-parallel atmosphere, unified treatment of reflected and transmitted intensities 78−85838
human and calf lenses, light scatt. and reversible cataracts 80−56019
hydroscopic particle humidification process, electrooptic scatt. meas. 80−77107
hydrosol, artificial, influence of form of particles on light scatt. matrix *(Russian)* 78−5420
hydrosol particles in suspension, dispersivity effect on light scatt. *(Russian)* 78−68932
ice, hexagonal crystals, solar radiation scatt. 79−94150
ice crystals, light scatt. expts. *(Russian)* 80−94601
ice crystals in artificial cloud, anisotropic scattering *(Russian)* 78−40658
ice-crystal fog, aerodynamic and opt. props. 77−90648
II-VI crystals, scatt. light intensity variation under secondary illumination 79−33718
image formation by inversion of scatt. field data, expts. and computer simulation 79−89852
imaging system point spread function determ. by scatt. of two monochromatic beams 80−87316
immunochemical analysis, standardisation of light scatt. meas. 78−36081
immunochemical analysis, standardisation of light scattering meas. 77−56548
immunoglobulin, human, high energy-induced aggregation, time resolved spectra 80−61655
immunological reaction monitor using laser light scatt. 80−85463
immunology slide, darkening, Mie scatt., Maxwell Garnett theory 77−9315
immunonephelometric assays 79−84046
impurity centres, geometrical parameters determ. by scattered light method 80−2043
incoherent backscatter from rough surfaces, two-scale model re-examined 78−71013
incommensurate phase, light scatt., order parameter fluctuation *(Russian)* 80−93354
index measurement, ring method using laser diffraction structurometer *(Russian)* 78−71035
induced moments in at. and mols., polarisability density concept limitations 78−70964
inelastic, single particle excitations in many valley semiconductors 80−29749
inelastic, Stokes and anti-Stokes components correl. 78−18017
inelastic light scattering conference, Santa Monica, CA, USA (Jan. 1979) 79−95762
inert gas mixture, collision induced light absorpt., density effects 77−42258
inert gas solids, lattice dynamics, book contrib. 77−47522
infinite cylinders, randomly oriented, extinction efficiency 80−48152
infinitely thin hollow spherical shells made of anisotropic molecules, particle scatt. factor 80−45946
inhomogeneous atmosphere, double-scatt. approx. of lidar eqn. 79−29855
inhomogeneous diffuse media, reflectances and transmittances, charact. matrices 80−32915
inhomogeneous media, optically dense, interferometric method for scatt. meas. 78−24854
inhomogeneous medium, multiple scatt. near critical point, spectral comp. *(Russian)* 77−42483
inhomogeneous nonspherical object scattering 79−64179
inhomogeneous particles, geometrical optics, glory ray and rainbow 77−29430
inhomogeneous particles, scatt. cross sections calc. 80−32910
integrated optical spectrum analyzer dynamic range, waveguide scatt. effect 78−59163
integrated speckle pattern statistics due to mixed coherent and diffused light 80−14285
integrating sphere accessory, spectrosc. meas. of horizontal surface from above 80−86443
intense field QED in continuous medium, appl. to Thomson scatt. and Cherenkov radiation 80−27435
intense radiation in a liquid, propag. instability 79−10346
intensity correl. spectroscopy, spherical particle continuous distrib meas. 78−21228
intensity correlations, general theory 79−50267
intensity fluctuation spectroscopy, of charged Brownian particles, coherent scatt. function 78−17857

light scattering continued
interacting Brownian particles, light multiple scatt. by correlation spectroscopy 80−87313
interband light scattering in semimetals and semiconductors *(Russian)* 78−60485
interfacial tensions, low, meas. from light scatt. intensity by liq. interfaces *(French)* 80−20007
interferometer, scatterplate, energy distrib., Fourier optics approach 80−31850
interferometric imaging through scatt. media with achromatic interferometer 79−58778
interferometry, multimode fibre optic, applications 80−86387
internal field reson. struct., implications for optical absorpt. and scatt. by microscopic particles 79−10259
interplanetary dust, density and phase function determ. 80−109324
interplanetary dust, light scatt. function rel. to zodiacal light photometric axis 78−20727
interplanetary He, dynamical effects in 584 Å reson. scatt. 80−8509
interplanetary space, three-dimensional eqn. for zodiacal light brightness integral inversion 79−75155
interstellar, UV scatt. props. and size distrib. 80−26932
interstellar dark clouds, anisotropic scatt. and formaldehyde lifetimes 78−8080
interstellar dust around λ Orionis, scattered UV radiation obs. 80−56918
interstellar dust cloud, scattering in isotropic radiation field 79−30107
interstellar dust clouds above galactic plane, light scatt. detect. possibility 79−30124
interstellar dust in HD 200775/NGC 7023 complex, far UV albedo and phase function 80−51832
interstellar dust particles, scattering of starlight, origin and composition 79−88729
interstellar grains, interaction of light with small-particle system 77−74111
interstellar grains, UV phase function 79−97047
interstellar grains in reflection nebulae 79−53867
interstellar reflection nebulae, simplified models 78−96526
intramolecular memory effects in second-order optical processes 78−94270
inverse problem, evanescent waves, finite source area 77−10831
inverse problem, source reconstruction from far-field intensity data 77−10830
inverse problem uniqueness, scatt. object reconstruction, book contrib. 79−31824
inverse scattering in Rayleigh-Debye approx., diameter distrib. for thin circular discs 79−24840
inverse scattering in Rayleigh-Debye approx., length distrib. for thin cylinders 79−24839
inverse source problem 80−9802
inverse source problems in optics, book 79−31821
Io Na cloud, sunlight reson. scatt. as explanation for east-west asymmetries 80−36560
ion, electromagnetically confined, laser cooled, double resonance and optical pumping 80−87155
IR back-scattered from vaginal tissue, self-stabilising meas. system 80−72281
IR bidirectional refl. distrib. function meas. for baffle and mirror materials, recording instrument 78−58012
IR dispersion crystal-crystal filters, effect of particle size, layer thickness and vol. conc. on transmission *(Russian)* 77−27369
IR extinction meas. using lidar, with CO_2 laser radiation 78−40655
IR transparent materials, forward and backward scatt. data 78−59099
irradiance enhanced variance from target glint 80−5691
irregular absorbing particles, new scatt. model rel. to zodiacal light 80−67543
irregular particle scattering, meas. results versus Mie theory 78−58918
isobutyric acid-water mixtures, phase separation, light scatt. 78−84592
isobutyric acid-water mixtures, spinodal decomposition, light scatt. 77−72688
isotropic media, multiple plane wave scattering, strong acousto-optic interaction 79−76580
isotropic medium, three-photon light scatt. phenomenological theory *(Russian)* 78−83024
isotropic molecular gases, binary collision-induced light scatt., rot. Raman scatt. 80−78660
isotropic molecular gases, binary collisions induced light scatt. 80−83428
Jupiter, Lyman alpha albedo calc. from hydrocarbon and H I photochemistry 80−105194
Jupiter atmosphere, multiple scatt. calcs. rel. to refl. spectrum and atmospheric comp. and cloud struct. 80−56758
Jupiter atmosphere, scatt. model and evidence for telluric $^{12}C/^{13}C$ ratio 78−20723
Jupiter atmosphere, scatt. models for methane line profiles rel. to cloud struct. and C/H ratio 80−62067
Jupiter cloud zones, IR obs. rel. to scatt. props. 77−29712
K correlations and facet models in diffuse scattering 80−32916
Kalliroscope effect based improved light diffuser, fabrication 78−59121
KCl-$BaCl_2$ system, solid solns., phase diagram, enthalpy of soln., vibr. entropy. 78−39751
Knollenberg light scattering counters, response to doublet latex aerosols 80−37152
Kramers-Heisenberg dispersion formula, Dirac transformation generalisation 78−16960
Kubelka-Munk system, continuous absorpt./scatt. coeff. minimising distribs. 77−50615
lamellar liquid crystal, biaxiality due to oriented defects 79−41945
large anisotropic particles, dil. soln., dynamic light scatt. 77−52106
large dielectric sphere scatt., Mie theory 78−66754
large interfacial area meas. by light attenuation 78−7248
large spherical particles, absorpt. efficiencies, approximation scheme 79−31798
large transparent sphere effective extinction efficiencies using weakly collimated light 79−72487
laser aerosol deflector for energy parameters meas. 78−25916
laser anemometry and other photon correlation data, stabilized model-fitting approach 80−58622
laser backscattering from dense water-droplet clouds, depolarisation ratio, multiple scattering 79−53513
laser beam, focused, scattering by moving particles 80−48149
laser beam, multiple scatt. by radiational and advective fogs 79−100950
laser beam off-axis propag. in low visibility weather conditions, non-small-angle scatt. 80−102621
light scattering continued
laser beam scatt. by diffusing surfaces *(Chinese)* 80−1128
laser beam scattering, 1/f noise in model systems 79−98290
laser blue-green pulsed propagation through fog 79−39846
laser cloud location, microstructure of scatt. particles *(Russian)* 77−73850
laser Doppler anemometry, image form., wall scatt. effect on S/N ratio 79−89953
laser Doppler anemometry, S/N, detector influence *(German)* 77−19651
laser Doppler meas. of biological cells, scattering characts. of intersecting beams *(Russian)* 80−3874
laser echo-signal from cloud, calc. allowing for multiple scattering *(Russian)* 78−49137
laser fringe anemometers, light scatt. aspects, particle size meas. appl. 78−83020
laser heterodyne apparatus for measuring small angle scattering from particles 80−1261
laser light scatt. signal statistics 80−69328
laser measurement of optical, thermal and mech. props. of materials 77−74513
laser propagation in water, multiple scattering effects *(Japanese)* 78−78915
laser radar simulator for low scatter characts., three-mirror design 78−59118
laser radiation scattered by atmosphere, photocount distrib. 80−9921
laser Raman scattering, mol. probe of contractile state of intact single muscle fibres 80−89718
laser scattered light intensity, recurrence rate correl. 78−66760
laser speckle and surface roughness 80−102622
laser surface speed measurement by correlation, industrial paper machine test *(French)* 80−95082
laser wavefront conjugate complex prod., scatt. and diffr. in non-uniform phase film *(Russian)* 77−38973
laser-electron beam scattering, intensity differential cross-section 77−71914
latex, colloidal concentrated dispersions, dynamic light scattering 79−15469
latex, monodisperse, order-disorder phase transitions, short-range order 77−29056
latex, monodisperse, phase diagram, spectroscopic study 78−85209
latex, monodisperse, short-range order, spectroscopic study 78−85208
latex, shear waves, elastic modulus determ., light scatt. 80−58956
latex spheres in H_2O, photon correlation spectroscopy, diffusion coeffs. determ. 80−93802
layer metal particles, surface plasma oscillations 77−76765
lecithin, inelastic light scattering at second micellar formation 77−21492
lenses and spectacle lenses, scatt. light meas. *(German)* 78−46746
lidar, incoherent backscatter heterodyne, antenna parameters 79−72613
lidar observations of smoke and dust clouds at 0.7 and 10.6 μm wavelengths 78−69459
lidar probing of fogs and clouds, double scatt. approx. 78−73512
Lidar return from fogs, effect of non-uniform extinction coeff. on double scatt. contrib. 79−100952
lidar returns from clouds, double scatt. contrib. 79−5615
lidar returns from fog, doubly scatt. radiation contrib. 78−77326
lidar returns from homogeneous fogs, doubly scattered radiation effects 79−53516
lidar scattering and relative atmospheric humidity 80−77113
lidar scattering from clouds at 347, 694 nm, polarisation props. 78−85689
lidar scattering from snow and ice crystals in atmosphere, polarization characts. 77−64430
lidar target calibration, backscatter refl. for circularly polarised radiation 80−102750
light beam deflection angle determ. from holographic shear interference patterns 80−95848
light sources total luminous energy transfer, scatt. medium effect 77−65577
limiting irradiance distribution in medium of small random dielectric fluctuations, operator integro-differential equations appl. 80−5695
line formation, in expanding spherical media with partial freq. redistrib. function R_I 79−88643
line radiation transfer in heated gas, arbitrary initial conditions in kinetic eqn. 78−51051
lipid-water smectic phase, water and thermal diffusivity, light scatt. meas. 78−96031
lipoprotein, very low density, particle distrib. by intensity correl. spectroscopy 78−21228
liquid, binary, crit. conc. fluctuations, nonexponential decay, 3-methylpentane-nitroethane expt. 80−44309
liquid, comparison on interaction induced light scatt. and IR absorption 80−60561
liquid, coupling of vel. gradients to molecular orientation, light scatt. and flow birefringence anal. 80−25398
liquid, dynamic and static orientational pair correls., depolarised light scatt. 77−16321
liquid, simple, depolarised light scatt., double scatt. considerations 79−87410
liquid, simple, spherical molecules, depolarised light scatt., shaped cavity theory 79−82987
liquid, symmetric mols., anisotropic light scatt., correlation function calc. 77−12356
liquid, VH depolarised light scatt., orientational and translational motion coupling const., shear viscosity depend. 77−59584
liquid crystal, far-field coherence and radiant intensity of scatt. light 78−64372
liquid crystal, high resolution X-ray and light scatt. obs. 80−92460
liquid crystal, intensity fluctuations, model *(Russian)* 78−23478
liquid crystal, lecture on optical props. 78−35118
liquid crystal, polymeric nematic, Frank elasticity and light scatt. 77−68916
liquid crystal, scattering centres size and conc. determ. using turbidity spectrum 79−77509
liquid crystal, statistical props. of scattered light 78−27189
liquid crystal, texture, light scatt. determ. in dynamic scatt. regime 79−27913
liquid crystal cell, electro-optic props., dynamic scatt. effect 77−1080
liquid crystal cell, light scatt. distribs. 77−55772
liquid crystal cells exhibiting dynamic scatt. for light flux attenuation 80−102845

light scattering continued
liquid crystal displays with auxiliary nonlinear elements, series excitation control 77−5818
liquid crystals, scattering indicatrix determination for coherent and incoherent radiation *(Russian)* 80−64897
liquid film, free, squeezing mode relax., laser scatt. rel. to colloid interaction 78−87354
liquid interface, mol. light scatt., heat fluctuations *(Russian)* 78−23477
liquid interface, relation between mol. props. and intensity scattered 78−33671
liquid interfacial tension meas. from scatt. light intensity 80−20012
liquid light scatt. coeff. absolute determ. apparatus 78−86319
liquid mixture, near tricrit. pt., light scatt. and sum rules appl. to ethanol-benzene-water-$(NH_4)_2SO_4$ 80−34933
liquid short chain molecules, optical investig. of mol. motions 80−40123
liquid with absorbing particles, laser beam illum., refr. index change, bubbles form. 80−25334
liquid with spectral resolution of 10^{14}, registration of central peak *(Russian)* 79−4812
liquid-air interface, capillary waves, photon correlation spectroscopy 79−75607
liquid-vapour transformation, light scattering study, crit. opalescence 80−44307
liquids, collective molecular motion from depolarized light scatt. 80−60614
liquids, installation for scatt. and depolarisation meas. 79−93198
liquids, relaxation, binary collision theory 78−6000
liquids, vertical-horizontal light scatt. fine struct. and local order 77−55800
localised electron-phonon system with linear interaction, relationship between reson. light scatt. and luminesc. 78−43919
Lorenz-Mie light scatt. fine struct. 78−7242
Lorenz-Mie scattering, range of validity of Rayleigh and Thomson limits 78−66755
lossy corrugated structures, plane wave scatt., quantitative results 80−96005
low angle, multichannel meas. for environmental pollution detection 79−21061
low scatter mirror degradation by particle contamination 77−65618
low-angle, eikonal approx., for biological cell model 78−44466
low-angle scattering from coated spheres, anomalous diffr. approx., model for biological cells 77−25396
low-density fluid, scatt. intensity, irreducible spherical tensors 78−80366
low-energy photon diffraction, scatt. theory 80−43262
2,6-lutidine-water, spinodal decomposition, light scatt. obs. 78−34625
LV dynamic scatt. display liquid crystal mixtures 77−77178
Lyman α scattering in geocoronal models, effect on rocket meas. of proton fluxes 77−53273
Lyman α scattering near Venus, Venera 9 and 10 obs. 77−78703
lyotropic liquid crystal, micellar superstruct. 80−24352
macromolecular polydispersity by dynamic light scatt. and thermodiffusion 78−18816
macromolecular soln., electro-optical characterisation methods 77−24821
macromolecular solns., dilute, light scatt., Oseen's model 78−27240
macromolecular solns., light scattering, polydispersity and internal modes of motion 80−20651
macromolecular solutes, finite conc., isothermal diffusion and quasielastic light scatt. 79−82367
macromolecular solution, alternating elec. field light scatt., low angle approx. 80−84721
macromolecular solution, computer processing *(Rumanian)* 79−82990
macromolecular solution, dynamic light scatt. by flexible macromols. in fluctuating elec. field 80−84722
macromolecular solution, light scatt. in AC electric field 79−47468
macromolecular solution, quasielastic light scattering, rigid mols., theory 79−64127
macromolecular solutions, light scatt., ionic charge effects calc. 77−79714
macromolecular solutions, orient. in laser beam elec. field, anisotropic light scatt. 79−1768
macromolecule, branched, particle scatt. factor, light, computer simulation 79−64128
macromolecule monodisperse solns., macromol. length rel. to anisotropic light scatt. in elec. field 77−32391
macromolecules, conf., Prague, Czechoslovakia, (July 1976) 79−1764
macromolecules, dumbbell-shaped, alternating electric field light scatt. 80−1130
macromolecules, interacting, spherical, light scatt., conc. fluctuations, transport eqn. 79−1775
macromolecules in liq. cryst., optical changes obs. method 79−64135
macromolecules in solution, diffusion coeff. determ. by Soret effect, using optical method 77−28032
macroparticle diffusion, role of inertial effects 80−29196
magnesium alginate, light scatt., wt.-average mol. wt., charge density 77−61882
magnetic fluids, light scattering and polarisation 80−60616
magnetic semiconductor, light scatt. by magnons, appl. to $CdCr_2Se_4$ and EuTe 77−69805
magneto-optical crystals, spectra of hybrid excitations from transverse photons, excitons, magnons interactions 78−80320
many-level molecular system, light scatt., beam statistical model 78−62777
marine hydrosol scattering meas. by submerged laser nephelometer *(Russian)* 77−60418
maritime air, aerosol distribs., IR scatt. coeffs. 77−45050
Mars, atm. optical props. during 1971 dust storm 77−13274
Mars 1971 dust clouds, scatt. volume coeff. 79−84704
Mars atmosphere, aerosol characts. from isophotes 77−29699
Mars atmosphere, optical props. during 1971 dust storm *(Russian)* 78−93138
mass extinction coefficients estimated for nonabsorbing spherical aerosol particles in the geometric scattering regime 80−87310
Maxwell-Garnet theory for optical props. of heterogeneous grains 77−79750
MBBA, doping effect on cond. anisotropy and dynamic scatt. 77−40208
MBBA, laser radiation transmitted near isotropic transition, spatial coherence 78−18003
MBBA, light scatt. by disclinations, spatial coherence props. 77−8544
MBBA, liq. cryst., light scatt. and birefr. 78−22646
MBBA, nematic liq. cryst., ultrasound produced rolls, spatial coherence props. of scatt. light 78−75534
light scattering continued
MBBA, nematic liq. crysts., AC excited, dynamic light scatt., orient. fluctuations 79−1769
MBBA, secondary light scatt. in low frequency field, in dielectric state 78−48147
MBBA film, optical study of second dynamic scatt. regime *(Italian)* 78−15146
MBBA liq. cryst., anisotropic light scatt. 79−78692
MBBA liq. cryst., dynamic light scatt., effect of paramag. iminoxyl radical addition *(Russian)* 77−43131
MBBA-EBBA, controllable liq. cryst. transparency, electrooptical characts. 80−78996
medium-induced relaxation, laser pulse meas. 79−38667
medium-particle correlation effects in single scattering from particles in fluctuating medium 80−32917
melting, two-dimens., dislocation-mediated theory predictions, light scatt. use as probe 80−92651
membrane vesicle, scattering/intensity autocorrelation meas. of permeab. 77−12889
Merope reflection nebula, phase function of dust grains in UV 78−32553
metal film, structure-related optical characts. in visible and UV 77−55841
metal mirrors, diamond turned, evaporated and sputtered, surface and optical studies 78−79098
metal mirrors, diamond turned, surface, optical and laser damage characts. 77−50705
metal oxide layers, obtained by cathode and HF sputtering, light scatt. and refr. index reduction 80−29877
metal rough surface, speckle pattern statistics 77−75421
metal surface, diamond turned, finish meas. by differential light scatt. 78−5544
metal surface blistering due to deuterons, detection by laser light scatt. 78−26602
metallic mirror as complex rough surface 80−1293
metallic particles, two-phase nozzle flow into vacuum, laser scatt. 77−35194
metallic thin film, structure-related optical characteristics in visible and UV 78−35217
metallic thin films, surface plasmon light scatt. 79−87517
methane, compressed gas, apparatus for depolarisation ratio meas. of scatt. light 80−38527
methane, fluid, collision-induced light scatt. 78−68509
4-methoxy-4′-azoxybenzene, nematic liq. cryst., elasticities and viscosities, light scatt. meas. 79−4245
p-methoxybenzilidenebutylaniline, nematic, domain pattern changes in electric field 77−1079
3-methylpentane-nitroethane, correl. function near crit. mixing point 79−55893
3-methylpyridine-D_2O soln., consolute points, crit. soln. temps., light scatt. obs. 77−77230
micellar solutions, cluster size distribution for the Ornstein-Zernike correlation 80−97734
microalgae, correl. of light scatt. patterns from pure and mixed asynchronous cultures 78−44737
microcapillary gas-dielectric filled waveguide with azimuthally asymmetrical cross-section, attenuation calcs. 78−83105
microemulsion structural changes, light scatt. obs. 78−56920
microemulsions, phase diagram and homogeneity gap, light scatt. and viscosity meas. 80−16736
microemulsions, quasi-elastic light scatt. 80−108755
microemulsions, rel. to percolation phenomena 80−104467
microroughness estimation for solid surfaces, light scatt. method 77−74355
microscopic regions, photon correlation spectroscopy 79−44933
Mie coefficients, expansion coefficients of scattering indicatrix, anal. 80−18993
Mie coefficients, recurrence 77−31068
Mie modified theory for nonspherical particle scatt., validity 79−27173
Mie scattering between any two angles 77−65576
Mie scattering by sphere, numerical methods 79−50225
Mie scattering calcs., continued fractions method 78−82914
Mie scattering efficiencies, asymptotic behaviour 80−106452
Mie scattering from seeded flow, instantaneous two-dimens. conc. meas. in turbulent jet 79−41670
Mie scattering improved algorithms 80−78771
Mie theory, resonances in efficiency factors for absorpt. 78−42276
Mie theory calculations, particle sizing appl. 80−14282
Milne problem and spherical albedo, law of darkening, forward and backward scatt. effects 78−77483
mirror optical scatter meas. specification proposal 80−48390
mixture, binary, fluctuations near liq.-liq. crit. point, neutron small-ang. scatt. appl., comparison with light scatt. 79−82347
mixture, binary, off-critical, quenched, struct. functions and mobilities renormalisation 79−82343
model atmopshere, spherical harmonics and iterative methods 77−66986
modulated-Mueller-matrix photopolarimetry [MMMP]: a technique for the study of elastic light scattering by depolarizing temporally modulated media and surfaces 80−90882
modulator in high scattering efficiency regime, temporal response, algorithm 79−50377
molecular acoustics from light scattering expts. 77−52111
molecular crystal, principal axes of tensor of polarisability derivs., spectroscopic determ. *(Russian)* 77−85683
molecular crystals, scatt. from external orientation vibrations 79−95776
molecular fluid, optical props., intermol. forces effects, theory, appls. 77−28535
molecular fluid, optical scatt. dielec. screening and susceptibility fluctuations 77−90162
molecular fluids, binary mixtures, hydrodynamics eqns., VH light scatt. 78−35158
molecular light scattering, spherical tensor approach 79−72372
molecular liqs., Maxwell effect relax. timeand light scatt. line broadening 80−76040
molecular liquid-state dipoles in weak const. elec. field, orientation relaxation *(Russian)* 78−43886
molecule embedded in dielectric sphere, fluoresc. and Raman scatt. 79−76435
molecule in coherent field, reson. scatt., quantum description of two-level system 79−64053

light scattering continued
molecules adsorbed on rough surfaces, Rayleigh, Mie and Raman scatt. 80−83378
molecules embedded in small particles, Raman and fluoresc. scatt., incoherent results 79−41337
molecules embedded in small particles, Raman and fluoresc. scatt., coherent results 79−41338
molten salt, hydrodynamic correlation functions 77−31577
monatomic fluid, collision induced light scatt., correlation function, relative radial motion contrib. 80−20647
monatomic gas, collision-induced light scatt. at intermediate density, integrated intensity, appl. to Ar 80−24124
monochromatic coherent plane wave scatt. by living cell *(Russian)* 78−48765
monochromatic isotropic scattering, quadratic integrals of transfer eqn. 77−33332
monochromators for light scatt. and fluoresc. standard in colloid 80−57247
monodisperse aerosol particles, 0.627 μm scatt. from spheroidal 2 μm cladosporium and cubical 4 μm NaCl 80−9804
monodisperse nonabsorbing particles, refractive index determ. by light scatt. *(Russian)* 77−5891
monodisperse screen shape determ. using scatt. indicatrix in Fraunhofer diffr. 78−71033
monodispersion, optical extinction meas. in aerosol media, forwardscatt. corrections 78−94367
Monsanto X-500 aromatic polyamide hydrazide soln., light scatt. study 80−76038
Moon, new three-dimensional scatt. indicatrix and photometric props. 80−101538
motile spermatozoa, speed distrib. obs. 77−37061
moving layer of scattering medium, EM radiation refl. and transmission 77−50619
moving random phase screen, enhanced fluctuations 77−19171
moving rough object, laser light scatt., freq. spectrum 78−5418
moving spherical particle, scatt. by two crossed coherent plane waves 77−42478
multicomponent mixtures, tricritical behaviour, possible exptl. tests 77−47543
multilayer coatings, high-refl. or antirefl., vol., interface absorpt. and scatt. losses 80−63915
multilayer light scattering and laser gyro 78−33764
multilayer mirror surface roughness meas. roughness spectral density function, vector multilayer scatt. theory 80−58460
multilayer optical coatings, scatt. due to surface roughness, scalar theory 79−59637
multilayer thin film, optical scatt., matrix formulation 79−31804
multilayered spherically symmetric medium, scatt. problem 79−81329
multilevel atomic system, thermally relaxing, coherent radiation reson. scatt. and absorpt. 79−81401
multimode fibre waveguides, optical characts. meas. by backscatt. 80−23801
multimode telecommunications fibre scatt., geometrical analysis 77−23748
multiple reflections within scattering medium, correction factor calc. 78−32888
multiple scattering, Hovenier's exit function eqn., numerical props. 80−62054
multiple scattering, two-dimens., theory and expt. 79−31805
multiple scattering by optically thin inhomogeneous spherically symmetric planetary atmosphere 80−67600
multiple scattering on ultrasound, phase geometry variation analysis 80−106441
multiple scattering theory in semi-infinite spatially heterogeneous medium *(Russian)* 78−13663
multiplicity effect, scatt. matrix polaris. props., transmission and reflection 77−83807
multispectral extinction data, analytic inversion in anomalous diffr. approx. 78−87016
muscle, flexibility of thin filaments, dynamic light-scatt. evidence 80−41064
myristyltrimethylammonium bromide, micelle size, press. dependence, photon correlation spectrosc. 80−11953
narrow beam propagation, in stratified scattering medium 80−106455
narrow resonance structure in Mie scatt. characts. 79−7072
negative absorption objects, resonances in EM scatt. 79−64178
nematic liquid cryst., ZhK-440, transparency, electrooptical characts. 80−78996
nematic liquid crystal, DC dynamic scatt., flow direction rel. to dopant electrochem. props. 77−90130
nematic liquid crystal, dynamic light scatt., model 80−2730
nematic liquid crystal, dynamic scattering, material flow due to external electric fields 78−18543
nematic liquid crystal, orientational fluctuations causing light intensity fluctuations, spectral anal. 80−60618
nematic liquid crystal, pretransitional effects, mol. statistical calc. 77−27990
nematic liquid crystal, quasi-elastic light scatt. near instability point, dielec. regime 78−75535
nematic liquid crystal, space-time correlation function for scattered light fluctuation 80−19697
nematic liquid crystal, viscoelastic properties, spectral noise intensity of scattered laser light obs. 79−23522
nematic liquid crystal DC dynamic scatt. microscopic structure and role of dopants 77−77179
nematic liquid crystal mixture, for low voltage dynamic scatt. display 78−27184
nematic liquid crystals, field-dependent light scatt. 77−4040
nematic liquid crystals, light diffr. by 3D domain structs. 79−64989
nematic liquid crystals, light scattering centre dimensions, elec. field effect *(Russian)* 78−38619
nematic liquid crystals, role of order parameter fluctuations *(Russian)* 77−80421
nematic liquid crystals, texture, light scatt. determ. in dynamic scatt. regime 79−27913
nematic liquid crystals as optical attenuators 77−19409
nematic product dynamic scatt. characteristics in mag. field 77−77177
nematic-chiral-dye mixture, circular dichroism, selective light scatt. *(Russian)* 80−103944
nematic-cholesteric mixture with positive dielectric anisotropy, light scatt. characts. 78−75537

light scattering continued
nephelometer visual range estimates, contrast brightness theory, operational theory 80−8424
neurosecretory structure particle motion, effect of increased K^+ concs. 78−77046
neutral atoms, stimulated Coulomb interaction in external resonance field 80−83449
NGC 7000 (North America Nebula), dust scatt. of stellar continua rel. to rocket UV imagery 80−82440
nitrobenzene, liquid, electrohydrodynamic convection, laser light scatt. exam. 78−14094
nitrobenzene, steady state electroconvection, self beating laser spectroscopy 78−87408
nitrobenzene-hexane solution, double-scatt. light intensity near critical point of mixing *(Russian)* 80−55117
nitrobenzene-n-hexane, crit. mixture, multiply scatt. light, LF spectrum 77−52125
NLC inelastic light scattering by order parameter biaxial and longitudinal fluctuations *(Russian)* 80−75160
noble metal aggregated film, light scatt. 78−64423
noble metal film, modulated surface-plasmon reson. in situ meas., O_2 adsorpt., 77−77311
noctilucent clouds, circularly polarised light detect. 79−48568
nonabsorbing materials, laser radiation scatt., destructive effects *(Russian)* 78−30001
nonequilibrium harmonic chain, light scatt., temp. depend. 77−69827
nonequilibrium stationary states, light scatt., broken time reversal symm. 79−28776
nonimaging solar concentrator design, cavity enhancement by controlled directional scattering 80−45631
nonlinear molecular systems, identification by spectroscopic methods 78−29168
nonlinear scatt. in limit of ultra-strong fields 78−79067
nonlinear scattering of laser radiation by fast ion waves in plasma 80−106916
nonlinear scattering of two light beams, ultrastrong fields, differential scatt. power 80−43388
nonlinear system, kink-phonon interaction 79−73262
nonrigid polymer chains, theory of dynamic depolarised light scattering 79−3601
nonspherical particle, optical levitation for light scattering obs. 80−58455
nonspherical particle scattering, polydisperse scatt. matrix *(Russian)* 80−12543
nonspherical particles, conjugate pair, light scatt. matrices 80−32912
nonspherical particles, depolarisation of scatt. radiation 77−50616
nonspherical particles, dil. soln., light-scatt. anticorrels. 80−5693
nonspherical particles, Mueller scatt. matrices 78−90366
nonspherical particles size distrib. from scatt. meas., Mie theory 78−58909
nonstationary radiation diffusion system, iterative soln. method 79−31796
nonunitarity of scattering approx. 79−64175
nucleic acids and their aggregates, optical activity, review, book contrib. 80−108847
nylon 66 films, superstructural ordering 80−15344
Nylon 6,6 fibres, birefringence determination, using backscattered light intensity distrib. 79−42939
ocean, radiative transfer, absorpt. and scatt. props. determ. 77−9430
ocean, scatt. obs. in African upwelling region, suspended particle meas. 79−5483
ocean, scattering layer with extended scattering indicatrix, radiative transfer eqn. *(Russian)* 78−40660
ocean frontal zones, light scatt. obs. 79−2266
ocean surface with waves, radiance distrib. over surface, glitter and sky contrib. 77−21902
ocean underwater scattered light polarisation, utility in remote sensing 79−5498
octyl-cyanobiphenyl, smectic A-nematic transition, X-ray and light scatt. obs. 79−95129
p-n-octyl-p′-cyanobiphenyl, thermally addressed liq. cryst. display, light scatt. and contrast 80−34892
offset two-dimensional Gaussian beam wave, scatt. by cylinder 79−50207
oil in water microemulsion, added NaCl, light beating spectroscopy of micelles mutual diffusion coefficient 78−80793
opaque, semitransparent materials, Kirchhoff's second law, role of reflection or diffusion *(French)* 79−36835
opaque crystal, inelastic light scatt. by acoustic phonons 78−43851
opaque semi-infinite crysts., dynamical light scatt. from dielec. bulk waves, phenomenological theory, appl. to n-InSb 79−69829
open waveguide coupling problems, scattering matrix theory appl. 77−27331
optical activity of large molecules from classical scatt. theory 77−31060
optical bistability, scatt. light spectrum atomic fluctuations 78−94383
optical ceramic, KO-1, IR scatt. and brightness indacatrices meas. 78−71164
optical component, surface evaluation techniques 79−46094
optical fibre, core-cladding interface effects 77−75692
optical fibre, diameter meas., high speed noncontact light scatt. technique 77−83956
optical fibre, graded index, diameter determ. from backward scattered pattern 80−5820
optical fibre, mech. deform. meas. by light scatt. method 80−14452
optical fibre, nondestructive determ. of refr.-index profile using forward light scatt. method 79−23060
optical fibre, refr. index profile meas., scatt. pattern method 77−7178
optical fibre, refractive index and radius ratio determ. from backscatt. light 78−30049
optical fibre, side illuminated, noncircular cross section effect on forward scatt. pattern 80−33150
optical fibre, step index, scatt. from off-axis inhomogeneity, radiation loss 80−43446
optical fibre attenuation, bandwidth, and refractive index meas. methods compared 80−64190
optical fibre attenuation measurements performed by backscattering technique 80−64152
optical fibre backscatter attenuation measurements, optimised technique 80−53447
optical fibre backscattering meas., separation of power decay from imperfection contribution 79−76827

light scattering continued
optical fibre coating concentricity meas. and anal., ray theory 77—88898
optical fibre mean splice loss meas., applying backscattering method 80—19091
optical fibre scattering, ray theory 80—69528
optical fibre sinusoidal microbending loss of HE_{11}-mode in step-index fibres 78—79109
optical fibres, light absorption and scatt., calorimetric meas. 78—46790
optical fibres, step-index, scattering from arbitarily located off-axis inhomogeneity 80—58702
optical fibres and fibre lasers, losses, approx. theory 77—27339
optical films, optical, struct. and mechanical properties 79—76772
optical glass, long range refractive index fluctuations, before and after annealing 78—13772
optical glasses, light scatt. of microinhomogeneities *(German)* 78—46734
optical glory, theory, physical effects 77—60468
optical instrument light shielding characts., mol. scatt. calc. 78—71189
optical materials containing irregularities, scatt. characts. 79—3753
optical surface quality standards based on total integrated scatt. 80—48391
optical surface scattering rel. to microroughness, surface transfer function 78—58917
optical surface statistical properties and scattering angular dependence relations 79—50219
optical system for light scatt. expts. 79—76786
optical video discs, laser read-out system diffraction theory, focus error alteration influences 79—50338
optical waveguide, asymmetric dielectric-slab, beam mode scatt. characts. 80—38114
optical waveguides, light scatt. 79—10375
optically infinitely thick layer, of very low absorpt. medium, exptl. scatt. matrix. 78—1149
order parameter fluctuation spectrum, central peaks near ferroelectric phase transitions, review 79—19851
organic liquid, simple, struct. exam. and scatt. data interpret. 80—54096
organosilicon ladder polymers, struct. and phys. props., book contrib. 79—65012
oriented molecules, hyper-Raman activity from index dissymmetry in scatt. tensor 79—36650
oriented spheroids, magnetically oriented, expression for scattering and absorption cross sections 78—29899
Orion Nebula, evidence for scatt. by dust from long-slit spectroscopy in rocket UV 80—105297
Orion Nebula, optical linear polarisation meas. 77—45536
Orion Nebula, starlight scatt. by dust rel. to UV imagery 78—4326
Orion Nebula, stellar radiation scatt. by dust, contrib. to nebula UV continuous spectrum 80—90499
ζ Orionis, noncoherent electron scatt. rel. to Hα P Cygni profile 80—82365
oscillating electric dipole contrib. to light scatt. and interpret. in terms of polarisability and hyperpolarizability 80—53212
oxide single and multi-layer optical coatings, light scattering reduction and meas. 80—48381
p-n solar cell, influence of light scatt. through junction on collection efficiency 79—34436
PAA, light scatt. near cryst. to nematic transition 80—16046
paint coating directional emissivity, thickness and substrate effect, light scatt. theory 80—33437
pair-correlated distrib. of small-spaced lossy scatterers, light propag. 80—28158
parabromophenol, supercooled liq., LF region of scatt. line wing 79—65888
paramagnetic liquid, depolarized light scatt. in mag. field 80—80759
paramagnetic liquid, mag. field effect on depolarised light scatt. *(Russian)* 80—108221
parametric interaction of two waves, scatt. radiation ang. struct., amplification *(Russian)* 77—58381
partial atomic vapour pressure, meas. by forward light scatt., transverse mag. field 79—16087
partially coherent light interpretation, optical theorems 80—53210
particle charges and particle-substrate forces by optical transients 79—50218
particle cluster, coherent light scatt., spatial correl. function calcs. 80—99632
particle medium, refr. index determ. from angular, polarisation characts. *(Russian)* 77—34827
particle motion round variable luminosity source, stochastic scatt. accretion and ejection 79—44338
particle population statistical inference from scattered light 80—37950
particle shape, in laminar flow, by optical mixing *(Russian)* 79—10619
particle size analyser, using light scattering 79—6088
particle size analysis using an ultramicroscope 79—44902
particle size and velocity simultaneous meas., laser technique 78—70096
particle size dispersion, effect on IR radiation in Venus clouds 80—109384
particle size distribs. remote sensing, Rayleigh-Gans-Born approx. 79—27174
particle size distribution determ. from light scatt. extrema 78—54421
particle size distribution parameters, estimation using forward scatt. techniques 80—36974
particle size meter using laser light scatt. spectroscopy 80—77754
particle size spectrometry, use of low power gas lasers 77—78485
particle sizing by forward lobe scatt. intensity ratio, diffr. theory errors 78—71031
particle sizing by forward-scattered lobe methods, error contour charts 77—79752
particle sizing counter for in situ meas. 79—75489
particle sizing counter for in situ meas. 79—75490
particle wave scatt. 78—66764
particle with thermal halo 79—98288
particles, internal heating effects 77—23618
particles, log-normal size distrib. from laser scatt. 79—6079
particles, nearly invisible 77—23618
particles in absorbing medium, extinction 77—65575
particles in colloidal state, refr. index, theory 78—95567
particles in laser Doppler velocimeter, Mie theory 77—19167
particles in liqs., mobility meas. by optical and elec. transients 79—77303
particles in water, scattering by different shapes 78—40565
particles with embedded molecules, Raman and fluoresc. scatt. 79—64177
light scattering continued
particulate effects, over-the-horizon optical propagation in a maritime environment 80—41547
particulate material, six-beam model of radiative transfer 77—17924
particulate material, spectral reflectance, Monte Carlo model with asperity scatt. 78—37804
particulate matter suspended in water, vol. scatt. function at near-forward angles 78—55299
particulate multiple-scatt. medium, radiance prod. by laser beams 78—9325
particulate surfaces, multiple scatt. effects, planetary appls. 78—58912
n-pentane-benzene, light scatt. of liq. near crit. vaporisation state, correl. radius 79—24328
pentyl cyanobiphenyl nematogen, depolarised light scatt. 79—95790
periodic interface scattering, rigorous method derived from integral formulation 79—13896
perylene-tetracene in liquid crystal, absorption, fluorescence and polarisation, temp. depend. study *(German)* 80—18887
PET, stress induced crystallisation, X-ray and light scattering obs. 79—99083
phase autocorrelation function, scintillation behind deep random phase screen 77—79751
phase problem, zeroes of entire functions 78—29900
phase retrieval using zero information 79—76612
phase screen statistical features from scatt. data, book contrib. 79—36851
phase transformation central peaks *(Japanese)* 78—52522
phase transition points, light scatt. near points 79—15415
phenomenological theory, appl. to rough surfaces 77—14661
phenyl benzoate liq. cryst., doping effect on cond. anisotropy and dynamic scatt. 77—40208
phenyl benzoate nematic liq. cryst., dynamic scatt., alignment effects 77—40207
phosphatidylcholine monolayer vesicles, US irradiation formation, quasielastic laser light scatt., dynamics 77—48764
phospholipid vesicles, conform. change and fusion phenomenon, dynamic light scatt. obs. 78—11615
phospholipid vesicles, synthetic, phase transitions, dynamic light scatt. obs. 79—53058
photoacoustic spectroscopy, diffusion processes, light scatt. effects 80—95144
photoacoustic spectroscopy, scattered light effects 77—18099
photodissociation fluxes, tropospheric and stratospheric, Mie scatt. contrib. improved model 80—77103
photoelastic film with acoustic Love waves *(Russian)* 77—28543
photoelastic isodynes method, stress components meas. using scatt. light modulation 80—14638
photoelastic method of thermal stress determ. circumferentially grooved cylinder 80—38363
photoelasticity, three dimensional, non-destructive method for stress-state determ. using scattered light 78—90805
photographic emulsion, Callier effect, influence on image contrast 78—63017
photographic emulsions, determ. of 3-D light scatt. function of undeveloped layers *(Russian)* 79—97460
photographic film, noise diffraction spectra 80—27368
photographic image quality, scattered light effect 78—16884
photometer, differential light scatt., for rapid analysis of particles in flow, appl. to biological cells 80—77834
photometric etalons, scatt. matrix and brightness coeffs. of MS-20, MS-14 reflectors 78—82020
photometric terminology for refl., transmission, scatt. and emission 77—74477
photon correlation spectroscopy, description and applications 80—52337
photon counting and signal averaging, alternating electric field light scattering 80—95794
photon counting statistics appl. to scatt. problems 77—34864
photon merging in disperse medium, on impurity centre scatt. *(Russian)* 80—55118
photosensitised reacts. in continuous chem. processes, scatt. effects 78—73057
piezoelectric crystals, acousto-optic props. exam., light scatt. by thermal acoustic phonons 78—48144
plane waves in strongly turbulent media, two-frequency mutual coherence function 77—21907
plane-parallel layer, function of sources determ. from emitted rad. intensity eqns. *(Russian)* 77—7000
plane-parallel scattering absorbing media, approximate method for radiative transfer 78—37805
planetary atmosphere, a^m and b^m functions of anisotropic scatt. 77—56848
planetary atmosphere, light scatt. by optically thin atmosphere rel. to brightness at zenith near terminator 80—109382
planetary atmosphere, single-scatt. albedo determ. for Rayleigh-scatt. atmosphere with true absorpt. 80—94704
planetary atmosphere with isotropic scatt., radiation field 77—13232
planetary atmospheres, azimuth-independ. multiple scatt. with rough surface 78—12085
planetary atmospheres, scatt. process meas. via laser beam *(Russian)* 79—44365
planetary satellites, surface scatt. rel. to photometric obs. for solar variability detect. 80—98623
planetary spectra, anisotropic scatt. effects 77—2357
planets, light scatt. laws rel. to photometric props. 80—67601
plasma, ohmically heated, in JFT-2 Tokamak, Thomson scatt. meas. 79—50890
plasma diagnostics, electrooptically switched multipass system 77—89302
plasma diagnostics, Thomson scatt., triple grating polychromator 77—43059
plasma diagnostics using self-terminating-transition lasers 79—64923
plasma directed electron velocity meas., optimised method using laser scatt. incoherent regions 80—79561
plasma turbulence in shock waves, investigation by anal. of scattered laser light 77—3940
plasma with two ion components, meas. by collective laser scatt. 80—92388
plasma-optical emission spectrometer, inductively coupled, light scatt. effect 80—86455
plasmid DNA and DNA-histone chromatin-like complexes, conform. and soln. props. by laser light scatt. 80—55987

light scattering continued
PMMA, amorphous, reorientational relax., 6-165°C, polarised laser beam scatt. correlation 78−2864
PMMA, destruction kinetics of intense ms loading, laser differential interferometry obs. 79−24623
PMMA, destruction of microsec. time scale, tensile stresses 79−70172
PMMA, solid, mol. relax., photon correl. spectroscopy 77−90159
PMMA, submicroscopic cracking in dynamic extension, light scatt. meas. 79−70171
PMMA Doppler scatt. optical determ. of US radiation patterns 79−76930
polar semiconductor, multiphonon cascade theory of light scatt. 78−19490
polar semiconductors, resonant secondary radiation 78−31242
polarisation changes in liquid and gaseous media *(German)* 77−88635
polarisation dependent scatt. meas., using electro-optical modulator instrument 78−58010
polarisation effects in nonlinear scatt., hyper-Rayleigh (Raman) scatt. 77−88858
polarisation structure of laser pulse scatt. by aqueous medium 77−3533
polarised laser light, angular depolarisation and multiple scattering by water/ice clouds 80−41549
polarised laser light, angular scattering by water/ice clouds 80−41548
polarized radiation, transport process in optically isotropic media 79−13899
poly(2-vinyl pyridine), dil. solns., translational diffusion, chain conformation influence 80−103508
poly(γ-benzyl L-glutamate), soln. and film, light scattering study 79−66374
poly(chlorotrifluoroethylene) films, crystalline superstruct., mol. orientation, X-ray diffr., depolarised light scatt. 78−71685
poly(L-glutamic acid), texture in conc. soln. and solid films *(Japanese)* 79−90534
poly(oxyethylene glycol), texture in conc. soln. and solid films *(Japanese)* 79−90534
poly(vinyl methyl ether)-polystyrene mixture, electric field depend. of cloud point temp., laser scatt. meas. 80−6519
poly(vinylcarbazole), stress-induced crystn. from melt, optical studies 80−84113
poly-1,4-phenylene terephthalamide, in H_2SO_4, dilute soln. viscosity 78−75524
poly-2,6-dimethylphenyleneoxide, fluoresc. correction in light scatt. meas. 79−1771
poly-γ-benzyl-glutamate, conc. soln., rheology, liq. cryst. transition 79−94574
poly-γ-benzyle-L-glutamate in dioxane solution, relax. mechanisms, light scatt. spectra 80−20659
poly-(p-alkoxy-phenyl-p-acryloylbenzoates), nematic polymer, struct. determ. 79−99064
poly-(phenyl-p-acryloyloxybenzoate), nematic polymer, struct. determ. 79−99064
poly-N-vinyl imidazole solution, light scatt., viscosity and dynamic birefringence, mol. wt. obs. *(Russian)* 79−33665
polyacrylamide, aq. soln., thermodynamic props., light scatt. obs. *(Russian)* 80−71439
polyacrylamide, aq. solns., conform. changes, intermol. interactions, optical mixing spectroscopy 79−10770
polyacrylamide, gels and single chains, phase transitions and crit. behaviour 80−40759
polyacrylamide gel, network density fluctuations, crit. behaviour 77−44518
polyacrylamide gel and single chain in soln., laser light scatt. obs. near phase transitions 80−93808
polyacrylamide-water gel, translational and collective diffusion 79−52787
polyadenilic acid, semi-dil. soln., slow modes 78−53319
polyamide, aromatic, persistence length, rel. to optical anisotropy of worm-like chain 77−50577
1,4-polybutadiene, stress-induced crystn. from melt, optical studies 80−84113
polybutadiene and butadiene-styrene in tetrahydrofuran, second virial coeffs. 80−65188
polybutene-1 film, deform. mechanism, rheo-optical meas. 80−21041
polybutene-1 film, tubular-extruded, light scatt. from crystn. superstruct. 77−55796
polybutylene terephthalate, melt crystallised, solvent crystallised films and moulded bars, morpholigical obs. 80−84101
polydisperse fluid, of hard or permeable spheres, scatt. function 79−86664
polydisperse media, optical characts., approx. representation 80−63922
polydisperse particle size distrib. function, angularly scatt. light intensity profile meas. 80−13040
polydisperse particle size distrib. function determ. from angularly scatt. light intensity profile 80−98879
polydisperse particulate sytems, light extinction 78−33667
polydisperse samples, scatt. data analysis 78−50702
polydisperse spherical particles, light scatt. extremum invariants 80−9809
polydisperse suspension, two-parameter size distribs. eval. using photon correl. data 79−92011
polydisperse suspensions of inhomogeneous nonspherical particles 79−94151
polydisperse system of coarse spherical particles 79−3633
polydisperse systems, photon correlation spectroscopy, diffusion coeffs. determ. 80−93802
polydisperse-particle-size-distribution function determined from intensity profile of angularly scattered light: comments 80−87311
polydispersion, forward scatt. corrections for optical extinction meas. 79−7075
polydispersion, moments determ. of size distrib. function in scatt. 79−18347
polydispersion, size distrib. function determ. 77−10834
polyelectrolyte aqueous salt soln., inelastic light scatt. obs., conformational changes 78−60474
polyethylene, high density, film, melt growth, cryst. superstruct., small angle light scatt. 77−31602
polyethylene, mixed morphology and linear fractions, light scatt. obs. 78−2023
polyethylene, supermolecular structure, polymerisation at low pressure *(Russian)* 79−64126
polyethylene melt, cryst. kinetics during cooling, nucleation density effect 80−100181

light scattering continued
polyethylene oxide, solns. in toluene and ethyl benzene, phase equilib., struct. and thermodynamic stability *(Russian)* 79−86871
polyethylene soln., light scatt. from shish-kebab structs. 78−76482
polyethylene wax characterisation by gel chromatography, osmotic meas. and scattered light meas. *(German)* 77−86420
polyethyleneterephthalate, crystallised from thin layer melts, temp. depend. of morphology 80−54149
polyethyleneterephthalate, foil, optical microscopy and low angle light scattering 80−55210
polyisoprene-g-styrene, dil. soln., conformation, light scatt. obs. 78−91218
polymer, amorphous, bulk, structure models and exptl. methods, review 78−22671
polymer, amorphous, segmental distrib., light-, neutron- and X-ray scatt., piezooptical and dielec. meas., review 78−51444
polymer, dil. soln., light scattering charact. of thermodynamic props., solvent and mol. wt. effect 80−16717
polymer, light and Raman scattering obs. of high press. phases *(Japanese)* 80−2773
polymer, shear-induced crystallisation, optical study 78−14289
polymer, structurally inhomogeneous, light scatt. by strains, theory and expt. 80−28162
polymer, thin film with rodlike morphology, small angle light scattering, multiple scattering 78−15241
polymer blends, morphology and compatibility, X-ray and optical obs. 79−69026
polymer chains, free rotating, depolarised light scatt. spectrum calcs. 80−78731
polymer chains, helical wormlike, statistical mechanics, anisotropic light scatt. near the rod limit 80−93346
polymer coils, excluded volume parameters, light scatt. obs., graphical calcs. 80−89009
polymer crystal, in suspension, light scatt. in streaming system, dimens. characterization 79−69852
polymer film, automated light-scattering apparatus 77−53969
polymer film, melt grown, birefr. effect on polarised light scatt., phase limitation 78−10867
polymer film, multiple light scatt., light depolarisation effects 77−4696
polymer film, pressed, light-scattering, effect of birefringence *(Russian)* 77−44007
polymer film, small-angle scatt., Debye-Bueche theory treatment of multiple scatt. 80−84794
polymer films, rod-like superstruct., small-angle light scatt., vol. fraction, orient. effects 79−1795
polymer flocculation and stabilisation, concentration effects 80−45569
polymer gel, quasielastic laser light scatt. theory 79−82986
polymer glasses and melts, struct., review of expt. results 79−37636
polymer liquid-crystalline solns., struct. 80−103235
polymer mixtures, thermodynamics, review 79−1506
polymer solns., phase diagrams, pulse-induced critical scatt. 79−1490
polymer solution, anisotropy by statistical mechs. of helical worklike chains 79−99891
polymer solution, dil. small particles, scatt., Perrin matrix construction 77−77227
polymer solution, dilute, coherent scattering law, two-component description 77−51296
polymer solution, intermolecular interpenetration and entanglement, crit. concs. 79−27900
polymer solution, light scatt. for macromol. characts. in Rayleigh-Gans-Debye region 77−42452
polymer solution, Perrin light scatt. matrix including mag. dipole and elec. quadrupole interactions 77−77228
polymer solutions, conformational motions, comp. of neutron and light scatt. expts. 79−41938
polymer solutions, dilute, depolarised light scatt., solvent effects 77−20862
polymer solutions, dilute, depolarised light scatt. 79−99892
polymer solutions, dilute, intrachain dynamics and forward depolarised scatt. 78−68525
polymer solutions, microgel-containing, physico-chem. and rheological props., light scatt. obs., review *(Polish)* 78−50704
polymer solutions, moderately conc., light scatt. curves, struct. model 79−4810
polymer solutions, order, conf., Midland, USA, (Aug 1973) 79−10769
polymer solutions, quasi-elastic light scatt., slow modes 80−74271
polymer solutions, random coil, intramol. fluctuations by photon correl. spectroscopy 77−48184
polymer solutions, solvation, preferential, effect on polymer dimensions 79−10771
polymer solutions, thermodynamic props. under high press., light scatt. obs. *(German)* 78−20049
polymer solutions and gels, dynamic behaviour obs. using light scatt. 80−55727
polymer solutions and networks at equilib. swollen state, inelastic light scatt. by gel modes 78−1972
polymer solutions dilute, multiple internal light scatt. calcs. 77−77229
polymer solutions light scatt. rel. to mol. wt. distrib. function type *(German)* 79−1767
polymer system, two-phase, transparency conditions, interparticle interference effects 78−23428
polymeric gels, light scatt. intensity, network struct. effects 79−70381
polymeric glasses, amorphous object morphology, determ. by spatial filtering 77−58931
polymers, crystalline, homophase and heterophase, small-angle neutron, X-ray and light scattering, recent developments 79−10751
polymers, dilute ternary solns., mutual selective exclusion of unlike mols., light scatt. investig. 77−4922
polymers, dynamic light scattering theory 78−60475
polymers, filled, light scattering in deformation 80−11718
polymethylene, intramol. scatt. function calc. 77−38761
polymethylsiloxane-toluene gels, light scatt., compression moduli, cooperative diffusion 78−23970
polypropylene, transparent film, strain anal. by scattered-light speckle photography 79−32399
polypropylene fibres, helically twisted, small-angle light scatt. 79−1765
polypropylene film, double-exposure speckle pattern obs. of tensile deform., displacement, Poisson's ratio and stress relax. 80−84795
polyribonucleotide complexes, mag. field orientation of nematic liq. cryst. solns., light scatt. and birefr. meas. 79−82152

light scattering continued
polystyrene, diethyl malonate soln., near-crit., osmotic compressibility, correlation length, scaled functions 80−11422
polystyrene, glassy, light scattering, quenching effect 80−20649
polystyrene, in mixed theta solvent, intramol. motion, photon-correlation spectra obs. 79−77480
polystyrene, low mol. wt., conc. transdecalin soln., hydrodynamic and gel modes light scatt. obs. 79−73085
polystyrene, polydisperse, quasielectric light scatt. obs., mol. wt. and polydispersity 79−96376
polystyrene, sol, light scatt. data, Fourier inversion anal. 78−76932
polystyrene, soln. ion cyclohexane, mol. dimens. near theta point 80−54105
polystyrene charged particles in water, quasielastic light scatt. 79−24835
polystyrene coils, benzene soln., internal modes by photon beat 78−10905
polystyrene in solns., unperturbed dimensions rel. to temp., solvent composition 79−64132
polystyrene latex aq. solns., exponential clipped photon autocorrel. spectra, data anal. 79−2837
polystyrene latex particles, swollen, aggregation studied by photon correlation spectrosc. 80−66886
polystyrene mixture solutions, second virial coeff. light scatt. meas. 78−14438
polystyrene particles flocculation, light scatt. for close range struct. determ. 78−53273
polystyrene solution in benzene, laser light scatt. meas. 79−91458
polystyrene solutions, light scatt., mol. parameters, computer anal. assessment 79−1766
polystyrene solutions, ordered and disordered, particle dynamics determ. from time depend. multiple light scatt. 78−33672
polystyrene solutions, translational diffusion coeff., light-scatt. meas. 78−52519
polystyrene-benzene, dil. solns., polymer excluded volume exponent, experimental verification of n vector model for n=O 80−70104
polystyrene-benzene-methanol system, preferential solvation 79−10772
polystyrene-co-divinylbenzene microgels in dimethylformamide, diffusion coeff., viscosity and mol. wt. meas. 80−30286
polystyrene-diethyl malonate, strongly opalescent critical isochore, scattered light intensity 80−71436
polystyrene-diethyl malonate system, osmotic compressibility and correlation range near crit. point 78−6694
polystyrene-polyethylene/propylene block copolymer, micelle form. in lubricating oil 80−61171
polystyrene-polyisobutylene, solns., incompatibility, light scatt., conc. and angle depend. 77−24407
polystyrenes, in toluene 79−1773
polysulfonamide, optically active, synthesised by interfacial polycondensation, mol. wt. determ. 80−99595
polyurethane network, structural inhomogeneity by light scattering *(Russian)* 77−31605
polyurethane-polyurethane acrylate network, microinhomogeneities and props. *(Russian)* 78−51452
polyvinyl imidazolium sulphobetaine, aq. soln. props. 79−32879
polyvinylacetate and polyvinylacetate−microgels, light scatt. 80−20652
polyvinylidene fluoride film, stretched, struct. and elec. props. 79−90572
polyvinylidene fluoride films, uniaxially stretched, small-angle light scatt. 79−24377
powder, particle size distrib. meas. by spectral transparency method 78−49876
powder mixtures, diffuse reflectance, quantitative anal. 80−87308
powder particles in fluid, size distrib. anal. by light blockage principle 79−6089
powders, light scattering, close particle packing 78−1161
power detected by receiver, narrowly collimated beam backscattered by reflector in turbulent atm. 80−32918
PPT liq. cryst., anisotropic light scatt. 79−78692
propyl stearate monolayers, elasticity and viscosity determ. by laser light scatt. 77−72749
protein, high conc. soln., quasielastic light scatt. line breadth meas., diffusion coeffs. 77−1976
protein solutions, quasielastic light scatt. in small wave vector limit 80−45088
protoplasm streaming in Nitella flexilis, vel. distribs., laser Doppler spectrum 77−40684
pulse broadening in multiple-scatt. media, closed form expression 78−42277
pulsed beam wave propag. through turbulence, cloud, rain, fog 78−12000
ζ Puppis, noncoherent electron scatt. rel. to Hα P Cygni profile 80−82365
PVC, exam. of microstructure, using X-ray and light scattering 79−41983
PVC chlorinated, mol. parameters determ. 79−41974
PVC in DMF, THF solns., mol. wt., aggregation, light scatt. investig. *(Polish)* 77−28587
PVC soln., mol. wt. meas. by light scatt. photometry 79−7045
pyrometry, effect of scattered light on temp. meas. 77−26301
QSOs, scatt. rel. to optical polarisation alignment with radio struct. 79−25751
quartz, α and β phases coexistence state, elastic light scatt., birefringence 79−47412
quartz, α-β phase transition point, struct., light scatt. *(Russian)* 78−47521
α-quartz, acoustic activity, elastic wave polarisation plane rotation, Bragg scatt. of light investigation 79−65142
quartz, fundamental and second harmonic light scattering by α-β coexistence state 77−69086
quartz, fused, light scatt. by SAW on refl. and transmission 79−24288
quartz, light scattering polarisation props. at α-β phase transition 80−108220
quartz crystal, synthetic, dislocations obs. by light scatt. tomography 80−49229
quasiequilibrium sample, light scatt. and thermal radiation, phenomenological approach 80−91840
quinoline, liq., depolarised light scatt., 1-1800 bar 79−24327
quinoline, liq., depolarised light scatt. from shear waves 80−97288
radiation intensity, expansion into (a/λ) power series in electrodynamics 77−71911
radiation transfer, synthetic scattering phase function 80−74294
light scattering continued
radiation transfer in plane atmospheres, nonlinear eqns. in linear transfer problems 79−62741
radiative source function, isotropically scatt. medium, refr. index effect 77−83805
radiative transfer, anisotropic light scatt. in inhomogeneous atmosphere with small true absorpt. 79−62742
radiative transfer, diffusion approximation for large absorpt. 79−63170
radiative transfer, non-LTE, asymptotics of partial redistrib. 80−62008
radiative transfer, quasiasymptotic solns. for nonconservative scatt. in optically thin layer *(Russian)* 77−17348
radiative transfer, soln. of equation for Rayleigh's phase function by principle of invariance 79−84660
radiative transfer, synthetic scattering phase function 80−98541
radiative transfer eqn. exact soln. for semiinfinite plane-parallel isotropic scatt. atm. 79−12396
radiative transfer in semi-infinite Rayleigh scattering atmosphere, exact soln. 79−35112
radiative transfer through fog, 2D numerical soln. algorithm 78−71032
radiative transfer through turbid atmosphere, single-scatt. solution 79−16663
radiative transfer transport equation with scattering albedo $\omega_0<1$, exact soln. 79−35111
rainbow, physics, historical review 77−73854
rainbow formation in pendant drops, angular scattering 79−96816
rainbow phenomena and the detection of nonsphericity in drops 80−58456
rainbow polarisation rel. to droplet size and scatt. angle 79−80017
random media, theory and appl. of wave propag. and scatt., review 77−75376
random media causing pulse spreading and wandering 80−37942
random medium, image resolution limitation 78−37813
random phase screen, geometrical focusing, speckle effects 77−79755
random phase screen, higher order statistics 77−27253
random rough surface, exact multiple scatt. theory 79−98281
random small-angle scattering theory, dispersion coeff., MTF and contrast loss 77−68174
randomly diffusing surface, laser beam scatt., simplified statistical model *(Chinese)* 79−50217
randomly gradient fibres with irregular bends, optical mode propagation and scattering 78−1325
randomly homogeneous medium with amplitude distortions, diffuse object imaging 80−63928
randomly scattering light absorbing media, scale models and transmissive similarity 79−55061
Rayleigh atmosphere single-scatt. albedo, determ. from polarisation meas. 79−35117
Rayleigh scattering, exact soln. of diffuse refl. and transmission problem 79−35116
Rayleigh waves, diffracted intensity of scattered light calc. 78−50993
red blood cell ghosts, ang. depend. struct. 77−81475
red cell suspensions, backscatt. of light 80−41107
red supergiant stars, detect. of surrounding refl. nebulae from polarisation obs. 77−13340
reflecting power of scattering layers, with different degrees of dispersity *(Russian)* 78−82909
reflection nebula, inhomogeneous, scatt. function for grains of silicates and ice 79−21405
refractive scattering, weak, model system 79−89849
refractive spheres, radiation press. exerted *(French)* 77−61911
reimaging system, out-of-field radiation analysis 78−59117
remote probing of inhomogeneous media, Bojarski exact inverse scattering theory appl. 80−9812
resonance, two level density matrix description 78−25840
resonance atom, spontaneous diffr. of light 80−91512
resonance light scattering, spectral props. and photon correls. 80−91510
resonance scattering methods in atomic spectroscopy 80−53167
resonance scattering on 1-D cryst. and thin film *(Russian)* 78−31268
resonant optical excitation, luminesc. rel. to light scattering *(Japanese)* 80−84781
resonant scattering line, unshifted, of strong quasimonochromatic field, shape var. *(Russian)* 77−61934
retinal blood flow, laser Doppler meas. 78−69174
retinal diffusion and eye optics quality, OTF and light scatt. characterisation 80−41004
retinal spectral sensitivity to light it has scattered, human 77−9193
ring laser with methane cell, backscatt., influence on operation 79−10329
ripple structure of extinction coeff., water droplet expt. 77−34821
tRNA, conformation and intensity fluctuation spectroscopy, melting curves 78−35798
RNA solns., oriented in DC mag. field light scatt. 79−2004
rod-like macromolecules in conc. soln., basic kinetic eqn. and appl. 78−67637
rotating conducting cylinder, EM wave scatt., optical analogue of Magnus effect *(Russian)* 77−34820
rough dielectric and rough metallic surface discrimination, specular scatter depolarisation 80−32911
rough interfaces, light reflection, scattering in homogeneous media *(French)* 79−50211
rough laser illuminated surface, no. of random point sources, RMS phase depend. 79−59635
rough metal surface, depolarisation 77−71919
rough moving object, speckle 77−19172
rough object with multiple glints, amplitudes probability distrib. 78−9326
rough surface, effects on coherence of transmitted radiation, Young's method 77−3539
rough surface, exact multiple scatt., speckle contrast 80−53217
rough surface, far field polychromatic speckle, external angular dispersion effect 78−22086
rough surface light scatt., vector theory, surface plasmon effects 79−59638
rough surface small vibrs., light scatt. meas. 80−1494
rough surface speckle contrast, depend. on laser spot radius with surface height variance 79−59636
rough surface vibr. meas. by gaussian beam illumination 79−97356
rough surfaces, anisotropic, light scatt. 79−60606
rough surfaces, reflection light, division into specular and diffuse components *(Japanese)* 80−106457
rough-surface materials, laser scatt. anal. and prediction 79−72493

light scattering continued
roughness measurement using laser scanning analyser 80−36992
Royco aerosol particle counter 225, data processing system and modified system props. 80−37005
rubber, nitrite, heat ageing, light scatt. method study *(Russian)* 80−40407
rubber, with rigid filler, light scatt. by strains, theory and expt. 80−28162
rubber-epoxy resins, heterogeneity analysis, light scatt. and statistical methods 78−2024
rubbers, swollen, low-freq. dynamics, optical and mech. props. 80−43626
ruby laser elements, laser backscatt. by bulk damage zones 79−23000
salol, liq. and supercooled, VH light scatt. spectra *(French)* 77−1755
Saturn, atmosphere, scatt. model and evidence for telluric $^{12}C/^{13}C$ ratio 78−20723
Saturn B-ring, visible scatt. rel. to IR brightness obs. 80−56763
SAW, light scattering on internal refl. 78−64345
scalar diffusor autocorrelation *(French)* 78−90369
scattered light photoelasticity, appl. to determ. bottom pressure distrib. in pressed powder bed *(Japanese)* 79−75543
scatterplate interferometer, scalar diffraction theory 80−73432
scatterplate interferometer principles, limitations and tolerances 80−73436
sea, light diffusion, radiance distrib. 77−78216
sea water, multiple light scatt. rel. to dielectric permeability calc. *(Russian)* 78−77261
seawater, attenuation index meas. errors *(Russian)* 78−16041
seawater, Henyey-Greenstein indicatrixes *(Russian)* 77−60411
seawater, meas. technique for irradiance attenuation coefficient in a stratified ocean 80−98325
seawater, scattering props., statistical and physical models *(Russian)* 78−96222
seawater, transfer matrix elements of scattering medium *(Russian)* 78−36181
seawater, turbid, vol. scatt. function and light field charact. *(Russian)* 79−13902
secondary light scatt. in low frequency field, in dielectric state 78−48147
semi-infinite Heisenberg ferromagnet, macroscopic theory of response functions and appl. to light scatt. 80−20410
semi-infinite turbid medium, intensity of exciting diffuse radiation 77−75422
semiconductor, heavily doped, long range fluctuations in impurity pot. effects 80−93356
semiconductor, scattering by light by phonon zero sound 79−56145
semiconductor surface, resonance inelastic light scattering by carriers 80−20655
semitransparent structural materials, degree of blackness determ. *(Russian)* 79−27161
serum albumin, bovine, high energy-induced aggregation, time resolved spectra 80−61655
serum albumin, bovine, mutual and tracer diffusion coeffs., photon correl. obs. 80−72123
shadow device, charact., scattering medium effects, Monte Carlo calcs. 80−99630
short wave radiation problems in inhomogeneous media, book 77−10840
sickle cell anaemia sickling kinetics, multiangle laser scatt. spectrophotometer 79−79494
silica optical fibres, surface flaws obs., fracture strength 77−14793
silicate glass, comp. effect 79−99899
silicic acid sol., gel formation, characteristics of light scattering 78−53269
silicic and aluminosilicic acids, effect of increased size of scattering centres in sols 78−53270
simple fluid, light scatt. depolaris., shear viscosity meas. 77−27647
simulated microbes, suspension, size determ., teaching expts. 79−71178
single particle optical levitation to study quasi-elastic light scatt. theory 80−99620
single particle scattering, asphericity effects 79−7069
single particle scattering with focused laser beams 77−58248
single-mode optical fibres, backscattering method analysis 80−106610
single-mode optical fibres, backscattering signal anal. utilising wave optics approach 80−64151
single-particle scattering meas. with photodiode array 78−28146
skin, in vivo, light absorpt. and scatt., theoretical and expt. study 80−101219
sky brightness during 26 February 1979 eclipse, radiative transfer model 79−92588
sky radiance during total solar eclipse, model 78−40652
slab waveguide with refractive index irregularities, three dimens. scatt. patterns anal. 78−87158
slurry conc. and particle size determ., on-line light backscattering method, fibre optic appl. 79−58674
smectic C liq. cryst. film, mol. orientation fluctuations in two-dimens., light scatt. obs. 80−93355
smectic liquid crystal structural order effects of surface treatment, sample thickness, and cooling rate 78−63667
smectic mesophases, viscoelastic properties and field instabilities 79−27904
smectic-A phases, theory *(Russian)* 78−87618
smoke aerosol microstruct. and refr. index, optical determ., inversion method 80−36399
smoke aerosols, optical absorption to extinction ratio, photoacoustic determ. 80−58459
smokes, atmospheric, optical probing, homogeneous particle model appl. *(Russian)* 78−77328
Smoluchowski eqn., one-particle generalised, perturbation solution 77−27211
snow, light extinction at high densities *(Japanese)* 77−87028
soap film, light scatt., double-layer repulsion forces determ. 77−85025
soap film, light scatt., van der Waals forces determ. 77−85028
sodium alginate, light scatt., wt.-average mol. wt., charge density 77−61882
sodium bentonite, Wyoming suspension, comparison of optico-optical scattering and birefringence 80−85226
sodium copoly(ethyl acrylate-acrylic acid) copolymer, quasi-elastic light scatt. 78−35157
sodium dodecyl sulfate, micelle form. in aq. soln., laser light scatt. 78−27825
sodium dodecyl sulphate, polydisperse micellar solns., light scatt., size, shape and aggregation number calcs. 80−89531
light scattering continued
sodium dodecyl sulphate, solution, micellar, quasielastic light scattering, at low conc. limit 79−79307
sodium dodecyl sulphate NaCl aq. soln., micellar props., laser light scatt. exam. 78−92513
sodium nitroprusside, isomeric molecular states generated by polarised light, Mossbauer resonance obs. 77−20781
sodium polystyrene sulphonate in aq. soln., quasi-elastic light scatt. 80−100661
soft particles, starting from extinction efficiency factor 78−33675
soft spheroids, light scatt. matrix calc. 80−1133
soil moisture and component estimation from spectral polarisation 79−16678
soil-derived atmospheric dusts, particle absorption contributions to mass extinction coefficients 80−61896
sol-gel transition, incoherent light scatt. 79−61915
solar chromosphere, coherent scatt. rel. to S I 1807 Å and 1900 Å profiles 78−57517
solar corona, electron scatt. continuum spectrum rel. to temp. determ. 77−22169
solar prominences, photospheric radiation quasi-reson. scatt. rel. to H line emission 80−67694
solar radiation scatt. from gradient particulate atm., background noise in optical communication 79−62576
solar radiation scattering, cloud dimensions and orientation effects 77−33188
solar radiometry correction for diffuse atmospheric scatt. 79−80015
solar surge prominence, 31 May 1971, photospheric radiation scatt. rel. to electron density 77−22183
solid, molecular dynamics exam. intensity and band shape of depolarised scattered light 77−51458
solid, near phase transition, light scatt., review 80−29752
solid, reson. scatt. at impurity centres *(German)* 80−7377
solid particles in liquid dielec., charge transport 77−4329
solid state laser satellite rings, energy losses caused by diffusion, refl. in cavity 79−89911
solid surface, diffusional mass transfer exam. by light diffusion method *(Russian)* 77−7953
solids, conf., New York, USA (May 1979) 80−90611
solids, general theory 79−61324
solution, diffusion coeff. meas. by conc. gradient method and light scatt. 79−99339
solutions, fluctuation transport theory 78−70057
solutions containing dust particles scatt. meas. technique 77−37959
space-time symmetry rel. to light scatt. in elec. and mag. fields 80−29750
spatial resolution enhancement in coaxial light scatt. geometries 77−57393
spatial structure statistical charact., optical thickness, particle conc. depend. 80−5694
spatio-temporal correlation measurements, exciting light effects 79−50268
speckle, non-Gaussian, contrast variation 80−83554
speckle, non-Gaussian, correlated weak scatterers, computer simulation 80−28159
speckle, statistics from mixture of moving and stationary scatterers 78−66765
speckle intensity correlation for general scattering objects 79−89851
speckle pattern statistics, surface depend. features, book contrib. 77−31070
speckle pattern statistics for general scatt. objects, mean, covariance and power spectrum 79−31802
speckle patterns, partially developed, effect of occupation no. fluctuations 78−74842
speckle patterns in white light images, average contrast meas. 80−9808
speckle photography and holographic interferometry, scatt. geometry, topology, vector fields, theory 80−87347
spectral composition, hydrodynamic contrib. to two-time correlation functions, using nonequilibrium distrib. function 77−49703
spectral distribution of light scattered by flat, disc-shaped molecules 77−32386
spectrometer power spectrum analyser for quasielastic scatt., biological appls. *(German)* 80−12314
spectroscopy, optical heterodyning, for light scatt. spectra 79−6186
spectrum line contours in incoherent scatt. 79−88590
specular sphere scatt. radiance matrix, refl. standard for polarised beam scatt. meas. 80−74299
spermatozoa, bull, laser light-scatt. studies, orientational effects 80−89786
spermatozoa, bull, swimming speed distribs. determined by quasi-elastic light scatt. 78−44478
spermatozoa, human, motility evaluation, photon correlation meas. 80−61745
spermatozoa, swimming, quasi-elastic light-scatt. spectra 80−30760
spermatozoa flagellation, observation by depolarised laser light scatt. 80−40978
spermatozoa motility, depolarised laser light scatt. obs. 77−90749
spermatozoa motility evaluation by laser scatt. 78−48864
spermatozoa motility meas. by laser light scatt. *(German)* 79−12056
spermatozoa motility meas. by light scatt., appl. to reproduction immunology *(French)* 79−34628
sphere, totally reflecting, light extinction 80−95784
sphere crowded monolayer, multiple EM wave scatt., migration imaging film appl. 80−99627
spheres, structured, scattering problem, integral formulation 78−63010
spherical Brownian particles, interacting, wave vector dependent mutual diffusion 79−44859
spherical cells, light scatt., eikonal approx. corrections 79−57304
spherical monodisperse latexes, light scatt. matrices 79−98285
spherical objects, vector wave function theory 78−66748
spherical obstacles, small angle scatt. analysis, validity domains of approx. methods 79−72495
spherical particle, off axis Gaussian beam scatt. 77−79742
spherical particle dispersion, light scatt. and polydispersity 78−27241
spherical particle in absorbing medium, extinction 80−9807
spherical particle velocity and size meas., crossed-beam light scatt. interferometry 80−47011
spherical particles, absorpt. cross-section *(Russian)* 77−83815
spherical particles, fine structure of the Mie scattering, specific turbidity resonant structure of a_n and a_b 78−58913
spherical particles in converging beam, light scatt. 78−25802

light scattering continued
spherical three-layer particle cell model, effect of struct. 78−31785
spherical three-layer particles as cell models, light scatt. and attenuation, shell effect 78−82913
spheroidal macromolecules, solns., quasielastic light scatt. calcs. 78−43883
spheroidal macromolecules solutions, quasielastic light scatt. 79−24325
spheroidal particle, light scatt., particle parameters and orientations effect 79−50215
spheroidal particles, randomly oriented, light scatt. 80−58461
spheroids in atmosphere and ocean, scattering rel. to size distrib. determ. *(Russian)* 78−36279
spheroids in shear flow, light scatt., orientation correlation 78−76481
spherulitic materials, light scatt. theory 77−23613
spin waves in absorptive mag. material, light scatt. lineshape 78−23476
spinodal decomposition, light scattering, depend. on method of quench 78−18782
spinodal decomposition, polarised light scatt. 78−31380
spinodally decomposing system, double light scatt. 78−52516
spot size estimate in diffr. pattern of scattered field 80−95789
stack dust monitor based on particle counting and sizing 79−83683
stars, continuous spectrum, electron scattering effect *(Russian)* 79−12461
statistical theory, modified Bessel function distribs. 78−37794
stellar atmosphere, exact soln. of line scatt. intensity transfer eqn. 79−84784
stellar atmospheres, expanding, source functions for atomic and electron scatt. 77−22056
stellar envelopes, optically thin, of binary and multiple stars, polarisation by Thomson scatt. 78−81655
stellar occultations by turbulent atmospheres, heuristic scatt. model 77−37534
stellar radiation scattering on circumstellar clouds, circular polarisation theory 78−96428
step index fibre, scattering from arbitrarily located inhomogeneity 78−87161
step-index optical fibre, scattering and guided mode conversion due to spherical object, theoretical anal. 80−64153
step-index optical fibre and cable transmission characteristics 78−1404
step-index optimal fibre, scatt. and mode conversion of guided modes by spherical object 79−81558
stratified medium with diffr. boundary diffuse source radiation spectral struct. *(Russian)* 77−38804
stratosphere, aerosol and gaseous constituents from spacecraft solar extinction data, inversion retrieval 79−74961
stratosphere, scatt. profiles rel. to dust meas., (1970-1977) 78−73445
stray light, monochromators 79−32056
stray light calculations, surface refl. models 78−58905
stray light performance, surface and system scatt. characteristic specification 80−48389
stray light reduction from optical components 78−59114
stray light suppression in optical systems, optical design, computer analysis 78−59113
stray radiation analysis using first-order deterministic APART program 78−59116
stray radiation rejection capabilities of optical systems, GUERAP II program analysis 78−59115
Streptococcus mutans 10449, size determ. by laser light scatt. 80−109062
Streptococcus mutans aggregation, dextran-induced, laser light scatt. meas. 80−89729
stress distribution, 3D, scatt. light meas. method using depolarised incident light 79−37254
stress-induced crystn. from melt, optical studies 80−84113
structural phase transition points in pure and defect containing crysts., review 80−93361
structural phase transitions, quasielastic scatt. processes 80−93362
structured particles, quasi-elastic light scatt. 77−23617
styrene-isoprene block copolymers, dilute soln., conform. obs. 79−10774
styrene-p-chlorostyrene triblock copolymers in dil. soln., conform. behaviour, temp. depend. 79−90519
styrene-vinylpyrrolidone block copolymer soln., conform. props., light-, X-ray scatt. and viscometry obs. *(Russian)* 78−37779
styrol batadiene polymers, light scattering and Curie point pyrolysis, pyrolysis gas chromatography *(German)* 79−96393
submicron particle, size distrib. in colloidal suspension FODA 78−61057
submillimetric-wave laser Thomson scatt. ion temp. diagnostic implementation in Tokamak 80−59301
substrate reflectance and medium depth effects in two-dimens. multiple scatt. expt. 78−87011
sunlight, scatt. by intergalactic relativistic dust grains as source of gamma-ray bursts 79−88764
sunlight noctilucent cloud particles 78−11945
sunlight scattering intensity fluctuations from asymmetric particles 79−98282
supergiant stars, circumstellar dust shell, stellar interferometry 79−80309
superionic conductor, scattering of light and neutrons in diffusion model 78−26719
supernovae, type I, effects of line overlapping on spectra in conservative scatt. case *(Russian)* 80−105266
surface contaminant generation and bidirectional reflectance distrib. function meas. 80−14493
surface covered with multiple dielec. overlayers, IR scatt. 78−25794
surface errors rel. to optical performance, effect of mid- and high-spatial freqs. 79−59789
surface generated by diamond turning machine, physical and optical props. 80−33263
surface irregularity statistics for laser component materials 79−14057
surface light scattering rel. to microtopographic features 79−59639
surface plasmon radiation, roughness assisted, ang. distrib. 78−52521
surface ripples, role of reflectivity in light scatt. 80−20653
surface roughness and thin film influence on refl., transmission and scatt. of light *(French)* 77−34826
surface roughness measurements using optical Fourier spectrum analyzer 79−49195
surface roughness statistics, optical estimation from light scatt., review 77−61916
surface scattering of partially coherent radiation, atm. turbulence influence 78−58915
light scattering continued
surface tension of concentrated aqueous solutions of 1.1-electrolytes measured by means of Wilhelmy and laser light scattering methods 77−72745
surface tension waves, light scatt. 79−58469
surface texture and topography measurement by differential light scattering 80−36991
surface-diffused and buried waveguides, scatt. losses caused by surface imperfections 79−64332
surfactant vesicles, low-ang. light scatt. and photon correlation spectroscopy 79−79484
suspension, form-anisotropy, Rayleigh-Gans-Debye type approx. validity 79−1770
suspension, light scatt., turbidity 78−44407
suspension, particle size and concentration, determ. by light backscatter technique 78−85214
symposium, New Orleans, USA (March 1977) 78−33670
synchronous spot-scanned underwater viewing system 77−21934
tapered fibre coupler for optical pulse backscatter meas. 77−7212
TCNQ salt, K^+TCNQ^- particles, light scatt., absorpt. spectra 79−24332
TE-wave scatt. from blazed dielectric gratings 77−11005
temporal characteristics of single-scatter radiation 79−59634
tenuous particle scattering of focused laser beams 79−36836
tetracene in liquid crystal, absorption, fluorescence and polarisation, temp. depend. study *(German)* 80−18887
tetrafluoremethane, compressed gas, apparatus for depolarisation ratio meas. of scatt. light 80−38527
tetrahedral molecular fluids, collision-induced light scatt. 79−68237
thermal band imaging, glare in optical systems 79−32025
thermal halo effect, nonlinear scatt. by moving particles, symm. distortions 78−66875
thermal particles, multimode laser light scatt., photon statistics 80−99631
Thermophysical method for optical characts. determ. of scatt. medium 80−9014
thin films condensed onto cold substrate, prism-film coupler for in vacuo investigation 78−24873
thin liquid film stretching mode relax. obs. by laser intensity fluctuation spectra 79−28177
thin walled dielec. cylinders, EM scatt. and absorpt., appl. to ice crystals 78−25795
Thomson scattering, rot. Raman calibration 80−1844
Thomson scattering of light of spherical limb darkened star, polarisation prod. 79−58324
three-dimensional obstacles with complex refractive index 77−75415
three-level atoms, multitime correlations in scatt. and fluoresc. *(Russian)* 79−10065
tilted infinite circular cylinders, extinction cross-section calc. 79−94146
time interval photoelectron statistics, nongaussian scattered light 77−19177
tissue heating by laser radiation, temp. profile and scatt. determ. *(German)* 79−2099
Titan, inhomogeneous scattering model of atmosphere 79−44406
Tokamak, far IR laser collective scatt. system 80−59300
Tokamak plasma, Thomson scatt. with repetitively Q-switched ruby laser 80−59271
tough surface, effect of secondary structure 77−50620
transfer through horizontally non-uniform scattering cloud layer *(Russian)* 79−25326
transient scattering, stochastic theory of intermediate state interaction 78−13756
transonic wind tunnel laser velocimeter meas. interpretation 77−31324
transparent media inhomogeneities, laser radiation backscatt. 79−23000
transparent molecular systems, optical dispersion, polarised light, depend. on coherence, radiation field 78−5294
triangular gratings, surface wave guiding, quantitative results 80−96005
tricresylphosphate, supercooled liq., LF region of scatt. line wing 79−65888
troposphere and low stratosphere, scattered solar radiation field meas. *(Russian)* 79−16667
troposphere and stratosphere anisotropic multiple scatt. effects on solar radiation 79−80016
turbid atmospheres, path length distrib. of scattered photons 77−45147
turbid estuarine waters, optics, approxs. and appls. 79−66712
turbid media, approx. linear relationship for optical response 78−90371
turbid media, spatial struct., light scatt. meas., interferometric study 79−54178
turbid media, vol. scatt. function and light field characts. *(Russian)* 79−13902
turbid media optical meas. for biomedical appl. 79−83890
turbid media with specularly reflecting boundaries, optical props., biological appls. 77−75416
turbid medium, above reflecting surface, radiative flux *(Russian)* 79−72498
turbid water bodies, radiation absorpt. and scatt., radiative transfer eqn. solns. 79−81704
turbulence, laboratory-generated, simulating atm. turbulence effects on optical propag. 80−9803
turbulent flow inhomogeneities 77−54670
turbulent fluid, flow meas. by laser scatt. 77−35288
turbulent medium, amplification of scatt. of 0.6328 μm laser beam *(Russian)* 77−75418
turbulent mixing meas., laser light scatt. technique 77−11285
twilight in Sun's meridian, single- and multiple-scattered light dependencies, on air dispersion factor *(Russian)* 79−5612
two atom surface coupling, double reson. at plasmon freq., collective effects 80−34934
two coord. deflector, anisotropic diffraction and wide band scatt. 80−91920
two-component systems, depolarised light scatt., dilution expt. anal. 79−89850
two-dimensional scattering from a medium of finite thickness 80−5689
two-layer atmosphere with anisotropic scatt., brightness coeffs. *(Russian)* 77−17349
two-level atom, driven by reson. multimode laser, light scatt., statistical props. 80−91489
two-level atom, reson. fluoresc. spectrum of intense amplitude modulated laser light 80−91487
two-level resonant medium, light pulses propag. 80−64119

light scattering continued
two-level system, saturated lineshape, collisional and radiative damping effects 77−58124
two-state atom, near-reson. light scatt. in intense field, multiphoton treatment 80−78586
ultrashort laser pulse, scatt. by large spherical particle 79−906
unclad optical fibre cross section defects determ. *(French)* 79−89991
underwater light field, scatt. light influence anal. 77−64322
unstable resonator mirrors, diffuse scatt. effect on intensity distrib. 77−58354
upper atmosphere H Lyman α reson. emission obs. during 1973 June 30 solar eclipse 79−8901
Uranus atmosphere, scatt. models rel. to methane band-model parameters appl. to spectrum 80−98609
US wave 3D meas. in transparent solids, Doppler-shifted light scatt. technique 78−90613
UV communication based on molecular and aerosol scattering in atmosphere 79−3736
vapours, light scatt., depolaris. factor meas. *(Russian)* 79−13780
vegetation canopies, solar radiation absorpt. simulation, multiple scatt. effects 80−104635
velocimeters, S/N ratio and scatt. power, detection angle effect 77−42936
velocity measurement by light scattering techniques, digital correlation appl. 78−57916
Venus, cloud particles phase function, Mariner 10 data 79−40105
Venus, clouds, anisotropic scattering model 78−53852
Venus atmosphere, scatt. indicatrix rel. to interpretation of weak absorpt. lines 78−24481
Venus atmosphere, scatt. solar radiation in cloud layer, multiple scatt. theory inversion 79−8865
Venus atmosphere, scattered solar radiation fluxes spectral and altitude distrib. 80−62059
Venus atmosphere, scattering layer over absorbing clouds, Venera 9 and 10 UV photometry 77−78700
Venus atmosphere, SO_2 light scatt. and vertical distrib. implications 79−101100
Venus clouds, H_2SO_4 aerosol medium IR scatt. coeffs. 78−65526
Venus dust ring, scattering spectrum obs. by (Venera 9, 10) 79−75131
Venus upper atmosphere, solar Lyman α fluoresc. scatt. rel to dayglow spectrum 1250 to 1430 Å 80−77311
very rough surface, backscatt. light, polarised and depolarised components 78−63009
very-small-angle light scatt. apparatus design and performance 77−10082
vibronically coupled systems, cluster model 79−19540
virtual domain walls, dynamic struct. factor central peak correlations 79−95114
viscosity measurement method at high press. 80−69955
visibility in turbid media with coloured illumination 79−72489
visibility measurement, photometric contrast *(German)* 80−95118
vision, border enhancement, effect of scatt. light 78−11658
vision, contrast thresholds versus border enhancement, scatt. light effect 80−94213
visual instruments, optical component contamination, effect on visibility of extended objects 80−64137
visual telescope light scatt. factor meas. apparatus 79−27365
volume holograms with strong coupling, scatt. phenomena 78−33700
water, aerated, limiting detect. range in optical transmitter-receiver system 77−78461
water, backscatter and absorption coeffs., simultaneous determ. 80−82074
water, light scatt. and diffraction *(French)* 79−27171
water, turbid, spectral scatt. props. 80−72560
water droplets in mists, clouds, size, density distrib. meas., laser remote sensing technique *(Japanese)* 78−49175
water mass, inherent optical props. of Lake Ontario coastal waters 80−36337
water suspended solid analysis by single-particle scatt. 79−79435
water suspensions, radiative property measurements 80−9811
water-isobutyric acid, crit. mixture 80−24601
water-isobutyric acid (2,6-lutidine) mixtures, critically quenched, phase separation and coalescence 80−24581
water-petroleum emulsions, mean particle diameter and conc. determ. by light scatt. 80−89538
water-toluene-sodium dodecyl sulphate-butanol 1 mixture, interface light scatt., interface tension meas. 80−76039
wave field in optically soft scatt. system, propag. statistics 77−3538
wave field statistical moments in medium with large-scale inhomogeneities 80−37953
wave fluctuations in turbulent atmosphere 80−48157
wave packets in medium with spatial-time inhomogeneities, anal. *(Russian)* 77−3536
waveguide scattering problem, comparison of two perturbation theories 80−83662
waveguides with prescribed propag. consts., design 80−48419
weak diffusers with small number of correlation areas, speckle contrast 78−90370
wind velocity lidar meas. by spatial filtering 79−29901
young stellar objects, polarisation prod. by scatt. in circumstellar shell 79−8911
zenith observation, contrast reduction due to atm. extinction, calc. 79−84479
zodiacal light, circular polarisation theory 78−96428
zodiacal light, wavelength dependent model, Mie scatt. and thermal emission 78−81587
zodiacal light brightness integral, phase function isotropy, scatt. from particles *(French)* 78−45279
Ag film, surface roughness determ. from light scatt. meas. 78−5541
Ag film, surface roughness, light scatt. meas. 80−107624
Ag foil, interface with liq., oxide props., refl. and scatt. light spectroscopy 80−60702
Ag foils, surface plasma-wave reflectance and roughness-induced scatt. 80−66228
Ag halides, light scatt. ang. depend. and depolarisation, precip. defects. 77−48141
Ag particles, light scatt. spectra, size and shape effects 77−44015
Ag rough film, multiple scatt. of surface plasmons 77−48262
Ag surface, sinusoidally modulated, light emission of nonradiative surface plasmons 77−1467
Ag, surface-plasmon modulated reson. for adsorption studies 79−83045

light scattering continued
AgBr undeveloped photographic layer, light scattering and absorption *(Russian)* 78−37090
AgCl, light scatt. during photolysis 77−40565
(Al,Ga)As, laser, DH, threshold current var., optical scatt. losses 77−3588
Al mirror, with MgF_2 overcoating, reflective scatt. and reflectance meas. in vac. UV, moisture and oil vapour influence *(German)* 79−86227
Al thin films evaporated on rough quartz substrates, coherent, non-coherent analysis *(Polish)* 80−88450
Al_2O_3, corundum, impurity striation, light scatt., optical and electron microscopy meas. 78−22757
Al_2O_3, film form. by reactive HF sputtering with voltage bias 78−3045
Ar, collision induced light scatt., three- and four-body spectra 79−18260
Ar, compressed gas, apparatus for depolarisation ratio meas. of scatt. light 80−38527
Ar, fluid, collision-induced, line-shape theory and mol. dynamics 79−41921
Ar gas, two body collision induced light scatt., memory function approach and mol. dynamics 78−25658
Ar, light depolaris., pair-pair correlations 78−63536
Ar, pair polarisability determ. from collision induced light scatt. spectrum 79−13678
As_2S_3 film, optical recording, light scatt. enhancement due to coherence 80−97362
As_2Se_3, IR window coating, prep. and optical props. 77−50736
Au particles, light scatt. spectra, size and shape effects 77−44015
Au, small particles, in polyester matrix, optical scattering spectra 79−73961
Au, surface-plasmon modulated reson. for adsorption studies 79−83045
BaF_2 and fluorite large crystal, block orientation determ. from light scatt. pattern 79−50964
$BaMnF_4$, anisotropic order parameter phase fluctuations, light scatt. and thermal diffusivity meas. 80−80807
$BaSO_2$, suspension, light scatt., optical anisotropy determ. by polarisation ratio 79−1772
$BaSO_4$ white reflectance standard, Kubelka-Munk optical props. 77−42581
$BaTiO_3$, light scatt., Comes Lambert Guinier model 79−15471
Bi, optical phonon anharmonicity and melting, light scatt. study 80−60621
Bi-Sb-O-I glasses, scatt. coeffs. and acousto-optic props. 77−31121
C, paint type coating layer with spherical pigment, radiative transfer theory 80−61405
C particulate, airborne, photacoustic and absorption spectrum using tunable dye laser 80−4102
C sphere aerosol, black smoke opacity, calc. variation with particle size and refr. index 79−72488
CCl_3PCl_4, cryst., libration freqs., temp. depend., combination light scatt. and NQR obs. *(Russian)* 77−66436
CO_2 laser beam attenuation by air discharge plasma column 80−19062
CO_2, multiple scattering contribs. to depolarisation of scattered light 80−87842
CS_2, liq., light scatt. intensities, struct. models 78−60476
CS_2, liq., struct. and equilib. optical props. 80−45026
CS_2, liq. struct., mol. dynamics simulation 79−77488
CaF_2, fine-grained, forging and bulk optical props. 80−33103
CaF_2:CaO, optical scatt., absorpt. at 205 nm 80−20669
$Ca_x(PO_4)_y$, soln., coagulation effects on light scatt. obs., TEM, SEM 80−45090
Cd, photon interactions, energy role 77−36305
CdS, attenuation of transmitted light in exciton region, polarisation, coherence, scatt. 77−69852
CdS, chem. sprayed film, struct. and morphology 78−72020
CdS, collision controlled light scatt. by electrons, influence of elec. field *(Russian)* 78−64375
CdS, light scatt. by Bleustein-Gulyaev waves on refl. and transmission 79−24288
CdS, monodisperse particles form. from soln., light scatt. theory use in size estimation 80−76560
$CoCO_3$, weakly ferromagnetic, light scatt. accompanying spin system excitation by high microwave power *(Russian)* 78−2745
$Cs+Cs \rightarrow Cs_2$, inelastic light scatt. processes and mol. fluoresc. *(Russian)* 77−61787
Cu, deuteron irradiated, dynamics of radiation blistering and near-surface deuterium retention 77−84807
Cu, evaporated film, surface struct. from diffuse optical scatt. meas. 79−69381
Cu film, diffuse optical scattering from variable roughness surfaces 80−100704
Cu particles, light scatt. spectra, size and shape effects 77−44015
Cu, polished mirror, optical props. ageing 77−79912
Cu, surface-plasmon modulated reson. for adsorption studies 79−83045
CuBr(Cl)(I), LF light scatt. spectra in superionic cond. phases, ion motion obs. 80−108217
CuCl, polariton vel. direct obs. 79−28297
CuCl, propagation process of polaritons *(Japanese)* 80−24809
DyAG, crit., tricrit., and crossover phenomena, light scatt. 78−68251
DyAG, light scatt. from metamag. domains, crit. exponent determ. 77−66482
$DyPO_4$, metamagnet, phase diagrams, investigation by Faraday rot. and light-scattering technique 79−28544
EuO, ferromag. light scatt. from bulk and surface spin waves 79−28778
Eu_3S_4, inelastic light scatt., photoluminesc., anomalous vibr. 77−48229
$FeCl_2$, magnetic phase diagram, optical studies 78−88121
$FeCl_2$, metamagnet, optical determ. of thermodynamic phase diagram 78−60285
$FeCl_2$, metamagnetic transition effects 77−4513
$FeCl_2$, mixed antiferromag.-paramag. state, light scatt. in mag. field 77−40069
$Fe_{1-x}Cl_2$:Cd_x, randomly disordered, tricrit. behaviour, light scatt. 78−68255
$Fe_xCo_{1-x}Cl_2$, metamagnet, mag. phase diagram by mag. induced light scatt. 80−65883
$Fe_xMg_{1-x}Cl_2$, metamagnet, mag. phase diagram by mag. induced light scatt. 80−65883
Fe_2O_3, paint type coating layer with spherical pigment, radiative transfer theory 80−61405
Fe_3O_4 in suspension, ferromagnetic colloid, optical meas. 78−10906
$Ga_{1-x}Al_xSb$, small wave vector modes 78−75785

light scattering continued
GaAs crysts., IR light scattering and absorpt. microscopy study of dislocations 80−107249
GaAs-$Al_xGa_{1-x}As$ heterojunctions, inelastic light scatt. 79−65867
GaAs-AlGaAs heterojunction superlattices, obs. of intersubband excitations in multilayer two dimensional electron gas 80−29753
GaAs-AlGaAs heterojunction superlattices, inelastic light scatt. by two-dimens. electron gas 80−93360
GaP, cryst., characterisation by light scatt. *(Japanese)* 77−35498
GaP LEC crystal, imperfections obs. by light scatt. 78−6074
GaS(Se), optical and nonlinear optical props. *(Russian)* 79−51943
GdIG, one-magnon light scatt. with and without compensation temps. 78−31062
Ge, degenerate, scattering by light by phonon zero sound 79−56145
Ge, electron-hole drop motion, phonon wind 80−10887
Ge, electron-hole drop velocities as probe of phonons 78−68517
Ge, electron-hole drops, accel. by IR radiation field 78−95264
Ge, electron-hole drops, size distrib., light scatt. meas. 79−28292
Ge, electron-hole drops at high mag. fields 79−60721
Ge, exciton condensation, light scatt. by electron-hole drops 80−84435
Ge, impurity cloud form., anal. using heat treatment effects on light scatt. in pure crystals 80−15146
Ge, inhomogeneous stressed, electron-hole drop light scatt. and absorption 80−108212
Ge, light scattering, by pure single cryst., influence of photoexcitation 79−28780
Ge, light scattering due to microdefects 78−27248
Ge particles, homogeneously nucleated, production and props. 77−56252
Ge-Sb, meas. of electron-hole drop size by light scatt. 80−44515
Ge-type semiconductor, light scatt. from zero-sound 78−43857
H_2, gas, radiative light scatt., approx. line shapes 78−90221
$HNO_3.H_2O$, devitrification crystallisation, fast Raman and wide-line NMR obs. *(French)* 79−73915
H_2O, optical properties, 250-600 nm 77−52035
He, collision induced scattering of depolarised light 80−14118
He, light scattering spectra of gas, collision-induced scatt. 79−18137
He, liq., multiphonon boundary of excitation spectrum, neutron and inelastic light scatt. 80−92740
He, liq., review of expts. 80−54454
He, solid, theory and thermodynamic props., book contrib. 77−47646
He, underdense gas breakdown by laser pulse, backscatt. and beam refr. 78−5897
He-Ne laser, atmospheric extinction meas. 78−40654
^{3}He-^{4}He mixtures, homogeneous phase separation obs. 80−107599
^{3}He-^{4}He solutions, crit. and tricrit. exponents from light scatt. data 77−20152
^{4}He, lambda point, static and dynamic scaling phenomena 80−92739
^{4}He, liq., critical thermal cond. near λ-point, light scatt. spectrum 80−24697
^{4}He, liq., dynamic scaling near λ point 79−14977
^{4}He, superfluid, light scatt. by fluctuations in condensate near T_λ 77−11750
^{4}He, superfluid surface, spectral features of spontaneous light scatt. *(Russian)* 77−62696
Hg, optical and elec. effects during solidification 78−47502
I_2, 2-step reson. scattering, subnatural linewidths in vapour 79−76419
InS(Se), optical and nonlinear optical props. *(Russian)* 79−51943
n-InSb, stationary energy transport velocity of light scattered from bunched solid-state plasma 79−95720
K smoke particles, optical props. 480 to 620 nm, rel. light scatt. cross sections meas. 80−97293
KCl, Ba^{2+} diffusion, light scatt. meas., dipole mechanism *(Russian)* 78−22900
KCl surface texture and optical props. after forging between polished dies 80−33102
$KD_{2x}H_{2(1-x)}PO_4$ crystals, $0<x<0.98$, light scatt. by polaritons 80−96802
$K(H_{1-x}D_x)_2PO_4$ polarised impurity cluster effects in light scatt. expts. 80−29716
KH_2PO_4, central components in ferroelec. phase 78−56436
KH_2PO_4, dislocation strain decoration and static central peak 79−99263
KH_2PO_4 type crystal, H-bonded partially deuterated ferroelectrics, order parameter fluctuation spectra, central peak calcs. 79−61316
$KH_3(SeO_3)_2$, dislocation strain decoration and static central peak 79−99263
K_2SeO_4, non-zero wave vector incommensurate soft mode, light scatt. study 80−29754
Li ferrite, $Fe(Li_{0.55}Fe_{0.45})O_4$, one-magnon light scatt. with and without compensation temps. 78−31062
Li-Cr ferrite, $Fe(Li_{0.5}Fe_{0.25}Cr_{1.25})O_4$, one-magnon light scatt. with and without compensation temps. 78−31062
LiCl, polarisability bond length depend. 77−23422
LiF mech. and optical props. rel. to forging conditions 80−33101
LiF:Mg, light scatt., effect of electrostatic field 78−2823
$LiIO_3$, crysts., spontaneous parametric scattering of light by defects 80−34936
α-$LiIO_3$, light diffr. intensity, freezing effect in electrostatic effect *(Chinese)* 79−91404
$LiIO_3$, nonlinear light scatt. on cryst. defects 78−5527
$LiNbO_3$ crystals, composition determ. from parametric scattering spectra *(Russian)* 77−15595
$LiNbO_3$ interfaces, SAW reflection, light scatt. meas. 80−34286
$LiNbO_3$, light scatt. by Rayleigh waves on refl. and transmission 79−24288
$LiNbO_3$, partial waves of SAW, direct meas. by light scatt. 78−66994
$LiNbO_3$, spontaneous parametric scatt. line profile, IR absorpt. coeffs. 80−25377
$LiNbO_3$ waveguides, optical scattering phenomena 80−58786
$LiNbO_3$, y-z crystal, line shape of light scattered by SAW upon total internal refl. 79−24287
$LiNbO_3$, y-z cut, light scatt. from SAW 78−6652
$LiNbO_3$:Fe, photoinduced scatt. and bleaching effect 80−95959
$LiNbO_3$:Ti diffused optical waveguide, guided light scatt. sources 80−78966
$LiNbO_3$:Ti optical waveguide diffusion profile, AES obs. *(German)* 78−33876
$LiNbO_3$:Ti waveguide, in-plane scatt. obs. and countermeasures 80−33215
$LiTaO_3$, multidomain cryst., birefringence, Tyndall cone struct. 77−4618
$LiTbF_4$, optical study of spontaneous magnetisation at marginal dimensionality 79−73699
light scattering continued
$LiTuO_3$, light scatt. from ferroelec. domains 78−80310
MBBA, quasi-elastic light scatt. near instability point, conduction regime 77−15306
MnAs in suspension, ferromagnetic colloid, optical meas. 78−10906
N_2, compressed, depolarised light scatt., different contributing processes calc. *(French)* 78−79406
N_2, gaseous, light scatt., effects of correlation between mol. and intermolecular axis 79−50844
NH_4Br, dislocation influence on phase transition and light scatt. *(Russian)* 80−59648
NH_4Cl, transitional plasticity, light scatt. study 79−77674
$(NH_4)_2SO_4$-H_2O-ethanol-benzene, tricritical mixture, light scatt. 79−15473
Na, $^2P_{3/2}$-$^2S_{1/2}$ reson., light scatt. polarisation change 78−55144
Na atom, depolarisation obs. of near-resonant scattered light 80−52921
Na layer in upper atmosphere, lidar resonance scattering 78−36347
Na, reson. light scatt., theory of correl. meas. 78−42014
Na smoke particles, nucleation and growth, light scatt. study 80−35580
Na vapour in inert gas, effect of oxidant on optical props. 80−1736
NaCl, impurity precipitation and grain boundary diffusion 80−107567
NaCl, single cubic particles, suspended in laser beam, optical size determ. 78−33673
NaCl:Ca, light scattering coeff., effect of growing condition 78−55418
NaCl:Pb, precipitation of Pb impurity 78−48415
NaF, IR window coating, prep. and optical props. 77−50736
NaO_2-B_2O_3 glass melts, fluctuations 79−94865
Na_2O-CaO-SiO_2, glass, light scatt. rel. to heat treatment *(German)* 78−84598
$Na_2SO_4.12H_2O$ aq. soln., dodecanol additive effect near critical micelle conc. 77−73472
NaX-Se semiconductor superlattice absorpt. edge, light scatt. *(Russian)* 80−71438
Nb_2O_5 waveguide, in-plane scatt. and loss mechanisms 80−33216
Nb_2O_5-ZrO_2 sputtered thin layer structure and optical props. 79−28851
Nb_3Sn, superconducting, inelastic scattering of light 79−33390
Ne, collision-induced light scatt. of low density 77−71765
Ni powder, light scatt., close particle packing 78−1161
$NiCl_2$ aqueous solutions, autocorrelation spectroscopy 77−36796
O_3 absorption coefficients for backscatter UV expt. 80−46254
PLZT ceramic, modulator for optical communication 80−78964
PLZT ceramic;, visible light scatt. depend. on photoferroelectric space charge fields 80−80806
PLZT ceramics, electro-optic characts., w.r.t. future instrument applics. *(German)* 78−33792
PLZT ceramics, photoferroelectric image storage in antiferroelectric phase 79−47404
PLZT, controlled light scatt. 78−10909
PLZT, electrically polarised, size and conc. of light scatt. centres 77−28549
PLZT, IR laser radiation recording 78−4695
PLZT, light scatt. under switching conditions, time characts. 77−52045
PLZT, phase transitions, permittivity, birefr. and light scatt. meas. 77−81074
PLZT, time depend., switching, memory modes 77−12362
PLZT:Fe, enhancement of photochromic effect by multi-reflection scatt. 77−75632
$PbMoO_4$, acousto-optic interaction at high optical intensities 79−42942
$PbMoO_4$, SAW props. 78−63920
PbS, colloidal, light scatt. and electron microscopy 78−3379
$PbTeO_2$, acousto-optic interaction at high optical intensities 79−42942
Pt-electrolyte interface laser speckle movements related to electrode pot., H_2 adsorb. 78−40052
$Rb+Rb \rightarrow Rb_2$, inelastic light scatt. processes and mol. fluoresc. *(Russian)* 77−61787
S, liquid, polymerisation transition, anomalous light scatt. obs. 77−19861
SF_6, liq., near crit. point, optical props. meas. 77−72673
SF_6, pair polarisability anisotropy, point atom polarisability approx. calcs. 80−87244
Sb, optical phonon anharmonicity and melting, light scatt. study 80−60621
$SbCl_3$, dynamic coeff., molecular interaction effects of media *(Russian)* 77−83601
Sb_2S_3, amorphous layer, scattering of visible light, rel. to substrate temp. during deposition 79−65950
Se sphere monolayer, multiple EM wave scatt., migration imaging film appl. 80−99627
Si, beam extinguishment device, without scatter 78−87126
Si, dislocation free, C and O impurity clouds, heat treatment influence on light scatt. 80−6427
Si, light scattering due to microdefects 78−27248
Si scattering surface layer, optical props. *(Russian)* 80−11419
Si/SiO_2, adsorbed methanol, light scatt. from clusters 79−33721
SiC, CVD, polished, total integrated vac. UV scatt. 77−62029
SiC diffraction grating for vac. UV, fabrication 77−79920
SiO_2 dispersed particulates in CVD reactor, correlation with film characts. laser light scatt. meas. 80−76192
SiO_2, film form. by reactive HF sputtering with voltage bias 78−3045
SiO_2, fused, surface roughness rel. to prep. and treatment history 79−14058
SiO_2 fused fibres, radii determ. by multiwavelength laser light scatt. 80−22321
SiO_2, glassy-amorphous, light scatt. exam. 78−14281
SiO_2 glassy-amorphous system, struct. *(German)* 78−38626
SiO_2 particulates dispersed in CVD reactor, size distrib., semi-in situ obs. by light scatt. 78−27406
Sr, near reson. laser beam Rayleigh scatt., collisional redistrib. and saturation 77−57938
SrF_2, IR window coating, prep. and optical props. 77−50736
$SrTiO_3$, phonon interactions and the dynamic central peak near structural phase transition 77−81114
Ta_2O_5, film form. by reactive HF sputtering with voltage bias 78−3045
TeO_2 two coord. deflector, anisotropic diffraction and wide band scatt. 80−91920
TiO_2, paint type coating layer with spherical pigment, radiative transfer theory 80−61405
TiO_2 particles in suspension, cross section, ang. depend., particle size distrib., refr. index *(German)* 77−10835
TiO_2-Nb_2O_5 sputtered thin layer structure and optical props. 79−28851
TiO_2-ZrO_2 sputtered thin layer structure and optical props. 79−28851
Tl $GaS_2(Se_2)$, optical and nonlinear optical props. *(Russian)* 79−51943

light scattering continued
TlBr-TlI, TlBr-TlCl, KRS-5 and KRS-6 crystals, optical losses, laser calorimetric meas. 80−9973
TlCl-TlBr, KRS-5, KRS-6 crystals, optical strength pulsed CO_2 laser radiation 79−27307
TlI films, polymorphic, double epitaxy and growth on KCl, X-ray and optical obs. 79−77944
TlI, on KCl, epitaxial growth habit rel. to optical scatt. 77−50738
$TlInS_2(Se_2)$, optical and nonlinear optical props. *(Russian)* 79−51943
$TlInSe_2$ single crystals, vibr. props. by light scatt. spectroscopy 79−56804
UF_6, photodissoc. through light scatt. of UF_5 particles, influence of N_2 as collisional partner 80−95698
VO_2, light scatt. near semicond.-metal phase transition 78−60414
Xe, light scattering, in crit. region, scaling interpretation 79−46420
Xe, multiple scattering contribs. to depolarisation of scattered light 80−87842
Xe, triple light scatt. along crit. isochore 77−58838
YIG, light scatt. by parametric spin waves with longit. pumping *(Russian)* 78−43648
YIG, one-magnon light scatt. with and without compensation temps. 78−31062
YIG, optical spectroscopic exam. of ferromag. reson. *(Russian)* 77−48057
Zn, optical phonon anharmonicity and melting, light scatt. study 80−60621
ZnO, attenuation of transmitted light in exciton region, polarisation, coherence, scatt. 77−69852
ZnO, combination light scattering *(Russian)* 77−85739
ZnP_2 tetragonal crysts., light scatt. by optic phonons 80−55116
ZnTe, spin flip scatt. of laser light 77−43976
ZnTe, spin flip scatt. of laser light 77−43977
ZnTe, spin-flip plus phonon scatt., line shape and shift in peak position 79−73907

light sources
see also infrared sources; light emitting devices; photometric light sources; spectroscopic light sources
anisotropic emission source, polarisation characts. meas. 78−74047
astronomical telescope calibration, visible nd IR source, VISIR 80−36506
aureole around UV source at finite distance 78−77320
aureole radiance field about point source in scatt.-absorbing medium 78−77319
average hemispherical illum. from point source, calc. *(Czech)* 77−46778
beam generation, quasi-homogeneous Gaussian sources, spatial coherence 80−48145
binocular flicker stimulator using polarisers 78−24075
biological influences and appls. of optical radiation *(Japanese)* 78−44556
birefringent fibre interferometric secondary light source 80−105702
black body radiation, anisotropy and temporal coherence 78−58904
BNL National Synchrotron Light Source, 100 to 700 MeV booster synchrotron 79−67973
BNL National Synchrotron Light Source, 2.5 GeV X-ray ring, design status 79−68023
BNL National Synchrotron Light Source, 700 MeV VUV storage ring 79−68031
brightness measurement, standard photometric system errors 78−58005
BRV source, emission at 34 nm, absolute radiometric meas. 77−75636
calibrated piston source for optical comparison luminosity meas. 77−90603
capillary discharge, high-current, magnetogasdynamic regime 79−86628
Cepheid variable stars, simulated, for introductory astronomy course 79−44664
characteristics and parameter definition using graphical method for correct choice of compensating filters *(German)* 80−52342
Cherenkov, intense, 60 nm to IR range 79−59784
Cherenkov radiation light source in pulse radiolysis 80−42267
cinematography film flicker effect caused by AC lighting source *(German)* 80−27363
closed loop control system for light industry *(French)* 77−83941
coherence, review 80−48140
coherence and far-field intensity patterns, cross spectral density function determ. 79−55053
coherence and radiometry, basic concepts 78−66745
coherence function meas., spatial, using holographic method *(Russian)* 80−5703
coherence meas. and fibre modal noise simulation by Michelson interferometer 80−48324
coherent and incoherent light sources, spatial and temporal resolution *(German)* 77−88880
coherent radiation novel sources, book 79−27231
Collett-Wolf source example 79−76783
colour, rendering, international standards *(Russian)* 80−43423
colourephysics demonstrations for polytech. students 77−49533
COMBI SPARK, single or multiple spark gap 78−42401
commercial, illuminated scene, visual clarity, theory and expt. 78−48810
communication, conference, Amsterdam, Netherlands (Sep. 1979) 80−46733
communication channel ideal light source, high information rate 77−3541
correlation coeffs. of planar sources and their far fields 78−66750
correlative data processing system using semiconductor injection laser 80−74307
D illuminants and sources, review of use in colorimetry 78−65955
D lamp calibration for transfer standards using synchrotron radiation 78−65954
dark field magnification microphotographic illumination system 78−58025
data transmitter, laser and LED comparison *(German)* 80−14432
development support spectroradiometric system *(Japanese)* 78−45733
diffuse reflectors, light collection and dissemination 80−83658
directional beam generation from globally incoherent source 80−53211
directional light beams, necessity for spatial coherence, equivalence theorem 78−42398
directionality of light beams and spatial coherence 79−36834
discharge, electrodeless, slab-line cavity design 80−83652
discharge, evaporating-wall high-current type, pulsed press. 79−27838
discharge, hollow-cathode, holographic meas. of radn. coherence props. 79−76784

light sources continued
DORIS double storage ring, synchrotron radiation source in X-ray and UV regions 78−62668
electric lamps, historical review of development 80−9977
electronically controlled additive lamp house for optical printers 80−105732
explosion of double wire, optical flashes, photographic appl. 80−1865
far field of Gaussian beam 79−76583
fibre optic communication sources, detectors and circuits 77−27374
fibre optics communications, 1979 status and development trends 80−53408
fibre-optic communication and integrated-optics sources *(Italian)* 79−94371
fibre-optic communications source and detector props. and performance 78−22212
fibre-optic light source for curved platen illumination 78−63163
fibre-optic transmission system components *(Spanish)* 79−94348
films with selective optical properties, for enhanced output and radiation spectrum correction, appl. *(Russian)* 80−48372
finite planar sources of arbitrary coherence states, radiance function existence 79−50208
flash photography, sound triggered cct. using variable time delay 80−57414
flash trigger, sound operated 77−41717
flashbulb integrated radiance meas. rel. to max. permissible exposure 77−79911
fluctuating sources and second-order radiometry 78−50879
fluorescent lamps for colour photography, evaluation of suitability *(Japanese)* 77−26415
fluorescent source UV assessment using metameric pairs classification *(Japanese)* 77−87806
fluorescent TL tubes for sinusoidal light stimulator, flicker perception study appl. 77−86501
framing spotlight, optimizing the compound reflector 79−3766
free electron devices for light prod., history, book contrib. 79−27147
gas discharge lamps, in H, D and He, atomic light source *(German)* 79−59782
gas discharge source, nanosecond light pulses 78−22183
gas discharge tubes, effect of bulk absorpt. of radiant energy on temp. *(Russian)* 80−43422
Gaussian beam far-field 79−81357
gaussian Schell-model planar sources, beam directionality 79−903
generalised radiance uniqueness theorem 78−94365
generalized Collett-Wolf sources 79−31793
generalized partial coherence of a radiation source and its far-field 78−58903
graphic arts imaging material and laser source cost tradeoffs 80−14383
halogen lamps, KIM 9-75, relative spectral distrib. determ. 79−7189
halogen projection lamps and light fittings *(German)* 77−58408
hollow cone illumination, transfer functions in electron microscopy *(French)* 79−63327
illuminants which give prescribed tristimulus values to given object colours, design technique *(Japanese)* 78−94420
illumination with a moving light source 80−23632
illuminator for testing coordinate-sensitive photodetectors 79−72643
illuminator using laser light source, geometrical optical anal. *(Russian)* 78−79094
incandescent lamp calibration for spectral irradiance by absolute radiometers 80−102788
incandescent light bulb, conversion to X-ray tube 77−33755
incoherent circularly symmetric source, samping theorem for complex degree of coherence *(French)* 78−79088
inert gas high-current discharges, Z-pinch dynamic and radiative characts. 80−19631
inhomogeneous source radiant intensity, averaged cross-spectral density concept 78−74958
intensity distrib., far field laser and partially coherent sources, comparison 78−66751
intensity distribution due to partially coherent field, Collett-Wolf equivalence theorem 79−89846
intensity modulated sources, statistical props. of counting distribs. 79−72541
interferometry, review of options 80−47092
inverse problem for scalar planar sources radiometry and coherence, book contrib. 79−31797
inverse source problems in optics, book 79−31821
inverse source problems in optics, book contrib. 79−31822
KIM-9-75 source, controllable luminous flux regulator 77−39010
Kohler illumination using fibre optics and quartz-halogen lamp 78−58027
laboratory discharge lamp source for O_2 atmospheric bands and 0 I 5577 Å and 6300 Å lines 80−4148
laser light source in photoelec. aerosol counters *(Russian)* 79−100969
laser pump sources, efficiency of Xe and Kr arc discharges 80−64812
laser radiation parameters meas. use of injection lasers as meas. generators 80−23711
LED point light sources, appls. in undergraduate expts. 77−37686
LED point source emitter 80−73150
LED reference light source for scintillation spectrometer stabilisation 80−91365
lens array for extended coherent light source *(Russian)* 78−30040
lighting equipment, classification and terminology, new Soviet standards *(Russian)* 80−31706
line image transmission through single fibre using spectral instrums. 80−102820
linear, direct component of illumination calc. *(Rumanian)* 80−43421
luminaire with mirror cylindrical surfaces design using luminous flux balance method *(Russian)* 78−63166
luminaire with paraboloid reflectors, design, cylindrical luminous body dimensions calc. *(Russian)* 78−63165
luminaires for cinematography, development of techniques and technology *(Russian)* 80−27372
luminance standard using W halogen lamp *(German)* 79−89980
luminous field of circular source, integral characts. comparison *(Czech)* 80−53394
Lyman alpha radiation source with high spectral purity 78−13775
metal halide lighting parameters 78−21232
metal halogen, for colour rendition quality in TV *(Russian)* 79−76785
metameric white samples for testing relative UV content of light sources and daylight 79−58767

light sources continued
Michelson's interferometer, instantaneous multiple use with laser light source 77−57125
microsecond high-power light pulses, electrodynamic generation 78−22184
microsecond stratified pulsed discharge 80−87975
modulated, for dynamic investigations on optoelectronic components *(German)* 79−55197
monochromatic directed radiation, long-life He-Ne laser appl. 80−33021
multiple graybody resolution from spectrally sampled optical systems 79−76615
multiple-pulse laser source, use in transient jet expt. 78−14114
N independent sources, radiation superposition and the random flights problem 78−12467
narrow-band densitometer with pulsed-xenon illumination 77−53994
narrow-band densitometry with pulsed-xenon source 77−53993
negative correlation effect *(Czech)* 79−45901
optical communication advancements, comparison with microwave communication 79−81546
optical fibre communications development and need for standardisation *(Italian)* 79−23066
partially coherent source giving rise to highly directional beams 79−14070
partially coherent source radiant intensity, theorems and expts. 80−78768
partially coherent sources with phase profile, Van Cittert-Zernike theorem 80−63919
Penning source, continuous discharge, with 50 Å to 300 Å emission lines 79−50363
phosphor light sources, ^{147}Pm sealed sources *(Hungarian)* 80−91348
photochemical, immersion type, radiation utilisation factor calc. aspects. *(Russian)* 80−48374
photodiode array sampled light distrib. profile reconstruction *(French)* 79−30557
photographic, guide number formulae for pulsed illumination systems *(Russian)* 80−73503
photographic multimode flash trigger cct. 78−21248
photometric laboratory equipment, requirements and standards *(Slovak)* 80−17990
photostimulator for visual electrophysiology 78−35846
pinhole light source, bright and inexpensive, using optical fibres 78−83058
planar sources generating same radiant intensity distribs., equivalence theorems 79−89843
plasma focus, vac. UV emission meas. using ionisation chamber 77−80370
plasma sources of high radiation intensity 80−19084
plasma stream, supersonic dense, shock braking processes, radiation-gasdynamic obs. 80−19635
point light source, high-intensity, with adjustable light duration 78−42399
point source lighting computation using point-by-point method *(Rumanian)* 80−17987
polar intensity distribution influence on MTF meas. 78−50723
for polarimeter calibration, illuminator with adjustable polarisation 77−57380
proximity pick-ups, optical detection of light source and photoelectric cell *(Dutch)* 79−36985
psychophysical luminous efficiency *(Polish)* 80−33110
pulsed, ten-picosecond light source, shadowgraph and interferometry experiments 78−42824
pulsed coherent radiation source, 118 nm, for use in plasma diagnostics 80−106572
pulsed injection light sources, installation for meas. their characteristics 77−75640
pulsed plasma light source for vacuum UV to visible regions 77−45877
pulsed reference source, for photon counting systems 77−3640
pulsed source, formation of microsecond duration pulses 77−75638
quasi-homogeneous partially coherent source, far zone range criteria 79−14069
quasi-homogeneous sources and geometrical optics 80−23620
quasihomogeneous planar source, coherence and radiometry 78−9421
radiance spectral density meas. 79−30527
radiant intensity from planar sources of any state of coherence 79−27163
radiation fields from polygonal sources, Fock method 78−83060
radiation fluctuations from light source 80−95857
radiation flux source, in unit for measuring photodetector parameters 78−284
radiation sources for USSR state standards, 0.4-10.6 μ range 78−46739
random nonGaussian backgrounds, simulation, calc. spatial correl. function 78−79089
rectangular intensity profile source, estimate of coordinates 79−31819
reference source radiation, temp. instability and compensation methods 79−14071
reverse pinch effect cavity pulsed light source for photolysis 78−87114
safelight for Agfa 10E75 and 8E75 plates 78−74087
safelight for Agfa 10E75 and 8E75 plates 79−63318
scalar wave fields of fluctuating primary planar sources, coherence and radiant intensity 78−90355
scanned, alternative, CRT, LED and crater lamp 80−69477
sensitometric sources, photometric and radiometric calibration, tutorial 77−34044
short-arc lamp filled with rare earth halogens, light source for Super 8 cinefilm projector appl. 80−62747
silhouette photography, high-speed, of small biological subjects 78−44743
single-lens illuminator, light flux spectral comp. for UV region 80−87450
skimming discharges for pulsed gas-discharge laser preionisation, spectral characts. 80−99740
slab line cavity for excitation of electrodeless discharge tubes 77−7166
solar radiation simulator, non-axial type, reflector profile calc. *(Russian)* 78−63169
spark, with Kerr cell, construction and operation *(Russian)* 77−72042
spatial coherence meas. by correlated diffusers 80−74296
spatial coherence of low intensity source, holographic determ. 78−25823
spatial resolution of subwavelength sources from optical far-zone data, book contrib. 79−31825
spectral adaptation for receivers and light sources *(German)* 80−77837
spectral energy distribution characterisation *(German)* 77−34011
light sources continued
spectral energy standard, for stellar absolute spectrophotometry *(Russian)* 79−44372
spectral radiance calibrations, 165-300 nm, interlab. comparison 77−74478
spectrozonal light source factors in exterior photography *(Russian)* 79−40638
strobe light with variable pulse length over 22-360 Hz frequency range 80−58716
sunlight simulation, review of various light sources 80−87454
surface discharge plasma, UV pulse form. by EM shock wave front 77−58917
surface spark discharge UV light source, for H_2/F_2 laser initiation 80−78923
surface spark discharges high current, light emission props. and appls., book contrib. 79−77449
synchrotron radiation, application to EXAFS and angle resolved photoemission spectros. *(Korean)* 80−74453
synchrotron radiation, principles, prod., and research appls. *(French)* 77−68159
synchrotron radiation and its appl. *(Danish)* 79−81345
synchrotron radiation appls., characts. and sources 78−74960
synchrotron radiation facility at Orsay's ACO storage ring 77−10505
synchrotron radiation from electron storage ring, focusing condition 77−42584
synchrotron radiation from electron storage ring, focusing on single point 77−10991
synchrotron radiation from helical wiggler, orbits and fields 77−79203
synchrotron radiation from short period helical wiggler 77−79202
synchrotron radiation from superlight source *(Russian)* 77−6983
synchrotron radiation source, book contrib. 80−5421
synchrotron radiation sources and utilisation, review 78−41390
thermal radiation sources for speckle interferometry 78−49891
total luminous energy transfer, scatt. medium effect 77−65577
transition radiation optical pulse generation for optical receiver calibration *(Russian)* 77−58409
tunable, GaAs crystals with nipi superstructures appl. *(German)* 78−95064
two-coordinate measuring microscope, supplementary unit 79−75588
underwater incoherent sources, spectral emission characts. 77−82043
underwater luminaires, technical requirements *(Russian)* 80−9064
undulator linac, electron dynamics, coherent radiation source 78−82539
UV, Brown, Boveri irradiation unit, for surface sterilisation, foodstuffs and pharmaceutical industries appl. 79−62302
UV, intense vacuum light source from anti-Stokes Raman scatt., theory 80−47953
UV, low-power, with electronic chopper 78−79087
UV, miniature long lived cold cathode discharge 77−19375
UV, pulsed high-power gas-discharge lamp 79−18496
UV, tunable generation in $KB_5O_8.4H_2O$ at 1966Å 77−68238
UV, vac., 50 MeV electron synchrotron with cyclotron preaccel. 77−61641
UV, vacuum, high resolution and picosecond-time-scale, anal. 78−9411
UV, water sterilisation unit design and appl. 79−57713
UV and IR radiation effects on eyes, safety measures *(Japanese)* 78−35881
UV and IR rays, effect on skin, safety measures *(Japanese)* 78−35882
UV high power μs light source for photodissoc. laser pumping 77−27295
UV high-intensity narrow-band light source, 3130 Å, for photolysis expts. 78−22185
UV light source in 20 to 100 nm range *(French)* 79−71537
UV radiation, accurate measurement techniques 78−37954
UV radiation sources modelling, upper atmosphere appl. 80−1288
UV radiometric standards at NBS 77−38011
UV sources for curing 78−88443
UV vacuum spectrofluorimeter design for luminescience meas. from thin films 79−71538
vacuum UV, apparatus for circularly polarised radiation prod. 78−1310
vacuum UV, He condensation pump for supersonic gas jet 79−93155
vacuum UV radiation scales, plasma blackbody lines and synchrotron radiation 78−1309
vacuum UV source using inert gas supersonic jets 77−75639
visual acuity charts, suitable illumination sources 80−12079
volume light source, spatial coherence of spontaneous radn., holographic meas. 79−98455
VUV spectral irradiance calibrations, method and appl. 80−87452
waveguide, superluminal radiator theory *(Russian)* 80−64156
working position illumination, factors affecting good vision and efficiency *(Spanish)* 80−3638
Ar cascade arc, wall-stabilised, calibration of radiation detectors in VUV 79−80679
Ar lamp, pulse-operated, for VUV irrad. *(Russian)* 78−75453
CaH, in RF-excited heat pipe oven, efficient arc source 78−63162
Cd discharge, low-press., high current, intensity in middle UV 78−50878
H, UV light source for plasma diagnostics, 121.5-121.6 nm *(Russian)* 78−25942
H-He arc lamp, 60-360 nm, calibration 78−87117
H_2 stabilised arc as vacuum UV radiation standard for 600 to 900 Å 78−66879
He, hollow-cathode type discharge, spectroscopic obs., laser light source appl. 80−59335
He-Ne lasers, standard wavelength sources 78−74957
He-Ne stabilised transverse Zeeman laser, light source for optical meas. 80−48272
^{198}Hg electrodeless lamp, Ar lines 531 to 561 nm 78−42396
Kr, UV light source for plasma diagnostics, 121.5-121.6 nm *(Russian)* 78−25942
MgH, in RF-excited heat pipe oven, efficient arc source 78−63162
Mo, prep. by powder metallurgy technique, appl. in lighting industry 80−29904
Na lamp, high-press. advantages of use in interferometry 77−9837
Na light source, for undergraduate laboratory 79−35479
Na vapour, two-photon resonant fifth harmonic generation 80−53374
Rb optical pumping light source 79−46023
Sr vapour, vacuum UV coherent radiation generation by four-wave sum freq. mixing 79−10350
T, radioactive source in sensitometer for astron. photographic photometry *(French)* 77−13246
W and W-Re alloy, prep. by powder metallurgy technique, appl. in lighting industry 80−29904

light sources continued
W incandescent filament, light flux fluctuations, limiting factors in photoelectric meas. 80−13136
W ribbon-filament temperature lamps, radiation error estimation 80−64128
Xe and Ar flashlamps for vacuum UV radiation 80−106590
Xe, arc, wall-stabilised, dynamic analysis, radiation transport 80−44066
Xe flash lamp in photographic sensitometer, for daylight, W illum. simulation 78−29192
Xe lamp operating in pulsed regime, Soviet-made DKSSh ultrahigh-pressure, spectral characts. 80−48371
Zr ribbon filament lamp, calibrated source for IR radiometer 80−83653

light transmission
see also light absorption; optical filters
8.5 m IR imaging system performance in degraded atmospheres 77−19445
45 Mb/s fibre-optic transmission system performance 77−27376
absorbing anisotropic and gyrotropic slab between crossed polarisers, transmitted intensity patterns 80−78762
absorbing gases with variable mixing ratios, transmittance model 77−23616
absorbing material optical consts., transmission interferometry meas. on medium-thickness films 79−78768
aerosol, H_2O-droplet, CO_2 laser beam clearing process, transmission function ratios 78−88919
agitated dispersion, breakage and coalescence processes, obs., data reduction 77−90645
airborne particulate detection by metal-coated Nuclepore filters 77−37463
alkali metal anions and trapped electrons formed by evaporating metal-ammonia solions which contain cryptands 79−100340
anthracene, polariton effects in transmission and absorpt. spectra in thin crysts. 77−20886
anthracene, ultrathin films on fused quartz and sapphire 80−59812
anthracene films, optical props., comparison between free and optical contact mounting 80−89079
apodisation for max. encircled energy with specified over-all transmittance 77−34835
aqueous fog form. in shock tube 80−19531
atmosphere, $^{18}O^{16}O$ Schumann-Runge bands transmission rel. to photodissoc. and O_3 prod. 80−94559
atmosphere, absorpt. coeff. for line with Voigt profile *(Russian)* 77−64429
atmosphere, aerosol content determ. from photometric obs. of stars 78−92976
atmosphere, const. transmission function appl. to diffusion effect estimation 80−4100
atmosphere, diffuse transmission and refl. rel. to emergent radiation computation method 77−87069
atmosphere, extinction at 10.6 μm CO_2 laser wavelength, from meteorological records 79−39848
atmosphere, inhomogeneous, with anisotropic light scatt. and small true absorpt., transmission coeff. 79−62742
atmosphere, IR spectral transmission data in fog from Electro-Optical Test Facility modelling 80−90218
atmosphere, IR transmission rel. to total O_3 content determ. using satellite meas. 80−77027
atmosphere, IR transmissivities cooling rate in standard atmosphere 80−26609
atmosphere, IR transmissivities for H_2O vapour, CO_2 and O_3 78−11998
atmosphere, IR transmittance, meas. and calc. 77−64431
atmosphere, laser transmission, anomalous effects during August, 1976 at Farnborough, England 79−39862
atmosphere, solar UV transmission calc. down to 28.7 altitude 79−62575
atmosphere, spectral transmissivity, rel. to direct beam solar irradiance and illuminance 80−90174
atmosphere, spectral transmittance sensitivity to line and meteorological parameters 80−26610
atmosphere, transmission and scatt. phase function, 1.9-2.3 microns, aircraft meas. *(Russian)* 77−29434
atmosphere, transmittance functions generated by numerical methods 80−98455
atmosphere, transparency, meas. on Maidanak mountain during autumn and winter (1977 to 1978) *(Russian)* 80−72627
atmosphere, transparency meas. in Uzhgorod *(Russian)* 78−40656
atmosphere, water droplets size distrib. in mist, vol. extinction coeff. at visible and IR wavelengths 77−37287
atmosphere IR transmission at Mauna Kea, determ. from obs. of H Paschen α in P Cygni and other OB-type stars 80−62156
atmosphere IR transmittance spectrum, 2.8 to 14 μm 80−85743
atmosphere transmission, 1923 to 1957, from Smithsonian Astrophysical Observatory pyrheliometric meas. 80−17374
atmosphere transmittance, algorithm accuracies 80−101429
atmosphere with cloud, transmission functions band averaging for IR radiation flux 79−39854
atmospheric IR transmission spectra, high resolution field meas. and computer code calc. 79−66798
atmospheric transmission meas. using IR lasers and Fourier spectroscopy 77−70885
atmospheric transmissometer/radiometer for electro-optical sensor evaluation 77−70884
atmospheric transmittance, profile depend., line parameter vars. 78−77322
atmospheric transmittance model for variable-mixing-ratio absorbent gases 79−80011
bandpass interference filters, peak transmittance 79−46053
beamsplitters, beam inherent parameters analysis 79−36999
Beer-Lambert modified law calc. 78−82906
biaxial crystal plate, refl. and trans. wave amplitude 78−95573
bidirectional reflectance and transmission for optical diffusers use in space projects 78−36438
binary composites, percolation effects and sum rules in optical props. 79−69801
binary liquid mixture heated from above, convective instability, optical meas. 77−42823
biphenyl, phase transitions at 40 and 16K, transmitted light intensity meas. 78−51663
biphenyl-d_{10}, phase transitions at 38 and 24K, transmitted light intensity meas. 78−51663
black liquid water, total transmittance of solar radiation 79−34441

light transmission continued
bubble chamber fluid, thermal turbulence, optical distortion effect 77−3221
bubble swarms, light transmission 77−79749
bubbly flow, void fraction meas. by light attenuation technique derivation of transmission rate reln. *(Japanese)* 80−48795
cabled fibre, temp. effect on transmission loss and pulse delay distortion 78−1407
camera lens photographic chromaticity, spectral transmission curves analysis 80−31925
carbonaceous hard insulating film, phys. props. 77−39752
$Cd_xHg_{1-x}Te$, vertically grown crysts., effects of growth speed on comp. variations, transmission spectra 79−55684
ceramic crystalline materials, IR transmission, review 78−55417
ceramics, transparent ferroelectric, composition selection for appl. in light modulators *(Russian)* 80−91869
characteristics of optical fibres measurement, alignment chuck design 78−30090
cholesteric liquid crystal, gyrotropy, depend. on thickness of layer 77−40204
cholesteric liquid crystal, incident angle dependence calc. 78−43834
cholesteric liquid crystal, optically absorbing, dynamical diffr. theory 77−58954
cholesteric liquid crystal, polarised light transmission 78−9946
cholesteryl chloride, depolarised light transmission, microstructural changes 78−22647
cholesteryl chloride-cholesteryl crotonate, polarised light transmission, DC elec. field effect 77−77173
cholesteryl crotonate, depolarised light transmission, microstructural changes 78−22647
clouds, mathematical model for reflected and transmitted radiation 80−90215
cloudy atmosphere, radiative transfer model, solar radiation and cloud struct. 79−21016
coated substrate, transmittance and reflectance, film refr. index meas. 78−56534
coating, low reflection, continuously varying refr. index, transmission curves 78−25947
coating, refr. index calc. method refl. and transmission coeffs. 77−5890
coating, thin film surface irregularities rel. to optical props. *(Russian)* 77−11047
coatings, absorptive, at normal incidence, program for TI-59 calculator 80−84793
colloidal graphite, in mag. field, optical transmission meas., polarisation depend. 78−31712
communication system, 800 Mb/s optical transmission expt., using single mode fibre 77−88917
communications theory, systems concepts electronic analogy *(German)* 77−3542
contact lenses, hydrogel 79−11918
crystal-vacuum interface, light reflection and transmission coeffs., additional boundary conditions 80−34870
crystalline slab of point molecules, dielec. theory 80−97222
Curculionidae head capsule transmission of long-wavelength light, rel. to visual cues 77−64030
cyanobiphenyls, physical props., appl. to Kerr cells 79−19142
cylindrical optical fibre transmission and guided mode behaviour 80−28348
cylindrical-mirror confocal resonator design with high transmissivity region *(Russian)* 80−14361
dark filter, integrated transmission coeff. meas., zonal method 77−34953
demonstration of continuous spectrum, optical filters to audiences, students 77−45649
β,β'-dichloroethyl ether-iso-octane, critical indices, allowance for light double scatt. *(Russian)* 80−60624
didymium glass filters for spectrophotometer wavelength scale calibration 80−43417
dielectric film, spatially dispersive, transmissivity and reflectivity 77−8672
dielectric interface, Gaussian beam characts. 78−66747
dielectric interference film, with equal optical thicknesses of layers, theoretical design *(Russian)* 80−43471
dielectric laser mirror production with variable transmissivity *(Russian)* 80−14362
dielectric layer, transmission of laser radiation, phase and intensity distribs. *(Russian)* 77−88821
dielectric slab, transmission and refl. of Gaussian beam at oblique incidence 78−9318
diffraction patterns for optical systems with pupils of non-uniform transmittance 80−87470
diffuse reflection and transmission in accordance with phase function $^3/_4(1+\cos^2\Theta)$ 79−44353
diffuse reflection and transmission problem, exact soln. using Laplace transform and linear singular operators 79−35116
diffusely scattering medium, refl. and transmission, Helmholtz reciprocity theorem *(German)* 77−79753
diffusing glass, optically thick-layer transmission ang. distrib. 79−27179
disperse layers with loosely or closely packed particles, spectral transmission variation *(Russian)* 77−23619
dispersive media, Ewald dynamical diffr. theory extinction theorem 78−66749
distributed feedback structures, hybrid modes 79−27441
DODCI dye dissolved in glycerine, time delayed picosecond pulse transmission obs. 80−48355
domain lattice of transparent crystal regular birefr. regions, optical wave diffr. divergence 80−102616
double layers of different substances, refl., transmission and absorpt. coeffs. 77−6999
dusty IR Test-1 lidar obs., transmission meas. 80−99625
dye concentration meas. for cardiac output determ., error due to nonuniform distrib. 77−36979
dye passive switch for Nd laser pulses, transmission coeff. depend. on power density 77−23686
electrohydrodynamics, relax., inversely normalised frequency, rel. to Prandtl number 79−23369
EM sensor window materials, particulate erosion 80−38080
epoxy, for interference filter, γ-radiation effects on transmission 79−64297
eye, cataractous lens, optical transmission at 430 nm and blue field entoptoscopy 80−45883

light transmission continued
Fabry-Perot etalon, optically contacted, stability to cosmic radiation 80−98544
Fabry-Perot interference filter props. for oblique incidence illum. *(French)* 79−81545
far IR multi-element interference filter, generalised treatment 80−33174
ferrite spinels, dielec. permeability tensor and transmittance, transition to single lattice struct. *(Russian)* 79−87465
fibre cable transmission and strength improvement technology 80−28347
fibre taper couplers, diameter and slope meas. by light transmission technique 77−88905
fibre transmission, dispersion, and strength characteristics 79−37021
fibre transmission experiments, 100 Mb/s and 400 Mb/s PCM signals 77−88918
fibre-optic component polished end degradation in storage 79−32064
filament waveguides for signal transmission in far IR region *(Czech)* 80−96017
film, computational algorithm for optical consts. determ. 78−72617
film, effect on light reflection, transmission and scatt. *(French)* 78−33664
film, optical and elec. props. in situ determ. during deposition 77−59341
film, optical const. determ. from meas. of normal incidence reflectance and transmittance 77−85825
film, optical consts. determ. 80−2883
films, in situ meas. in ultrahigh vac. at low temp., optical reflectivity and transmissivity, DC resistivity, Au appl. *(French)* 78−39617
filter, dispersive crystal-air, depend. on scatt. layer parameters *(Russian)* 77−84002
filter, interference type, transmission band splitting elimination, oblique incidence 77−765
filter fabrication, reducing variation in transmission band location 77−14816
filter transmission coeff. zonal nonuniformity 79−32063
filters, low transmission meas. 79−85158
filters, multielement reciprocal grid interf., far IR transmission charact. 77−46789
flame propagation in long tubes, ducts investig., fibre optic technique 77−31404
flat layered glass, ang. distrib. for various incidence angles 79−7079
fluorescence angiography, colour and black and white, use of interference filters 78−48856
fluorescence spectrometry, beam splitter and cell window errors 80−31897
fluorite crystal windows, transmission in vac. UV region, heat treatment effect 77−31137
fog, laser light nonlinear transmission 80−1256
Fresnel's eqn. for light reflection and refraction, teaching 80−101688
Fresnel's interface, reflection, transmission coeffs. transformation between normal and oblique incidence 79−72478
Fresnel coefficients, particle approach calcs. 77−6998
gas, inhomogeneous layer, transmission calc. for spectral line with Voigt profile 80−59164
gas in applied elec. field, IR transmission modulation *(French)* 78−50912
Gaussian beam at oblique incidence on plane interface of dielectrics, refl. and transmission *(Japanese)* 80−5687
Gaussian laser beam, transmitted field at total internal reflection 78−13654
glass, coloured, toughening process, spectral charact. 80−43416
glass, for interference filter, γ-radiation effects on transmission 79−64297
glass, high-transmission, least-squares method for extinction coeff. determ. 78−90470
glass, IR transmitting, as optical material in passive systems, preparation and characterisation 79−23034
glass, plane layer, 0.07 to 1000 units, reflectance and transmittance 78−17860
glass, transmission, reflection, absorption factors, solar radiation, calc. method 77−34918
glass fibre reinforced plastics, ageing by boiling in water, effect on physicomech. props. 80−60892
glass filter simulating CIE spectral tristimulus value $\bar{z}(\lambda)$, spectral transmittance 78−30037
glass high-temperature transmission/wavelength characteristics *(French)* 79−7188
glass packet specimens with antisolar filler 78−90469
glass transmission and other props. 80−84712
glass-ceramics, transparent, microstruct. and props. 78−59960
glasses, high vol. low cost, as solar reflectors, compositions and weathering effects 80−106589
gradient index fibre array, transmittance analysis 80−14478
graphical ray tracing for conic surfaces 80−5683
greasy films on glass, due to everyday handling, effect on optical transmittance 80−27329
heterogeneous gas layer, method of calculating transmission *(Russian)* 77−27255
hollow light guides, dielectric-type, light transmission characteristics, minimum losses *(Russian)* 79−98503
homogeneous film, constriction of range reflectance and transmittance 77−75646
homogeneous layer, transmission and refl. coeffs., integral eqn. *(German)* 78−82907
homogeneous plane-parallel atmosphere, unified treatment of reflected and transmitted intensities 78−85838
illuminating fibre bundles, improved charact. due to glasses type VS 1637 and VO 720 80−102844
inhomogeneous atmosphere, interpolation method for rapid calc. of transmittance *(Russian)* 79−29850
inhomogeneous diffuse media, reflectances and transmittances, charact. matrices 80−32915
inorganic glasses, IR transmitting materials, appl. in 1 to 6 μm range, mech. props., review 79−4250
interfaces having non-sharp boundaries *(Russian)* 77−79745
interference coating, theoretical design, with two narrow spectral transmission bands *(Russian)* 79−72666
interference filter, V(λ), design appl. to visual system MTF evaluation 79−76843
interference filters, multilayer, design method 80−48396
interference microscope, VELOMET interphako, for optical path difference measurement 78−37054
interfernece filter characteristics and specification 78−46773
light transmission continued
IR inhomogeneity scanner for transmitting material blanks 79−32099
IR lens production tests 78−50890
IR radiation spectral absorptance and transmittance, accurate modelling technique 78−91062
IR transmissive material guide 77−39004
IR transmissive waveguide, flexible, meas. of propagation 77−88924
isotropic layers, thin, with rough boundary surfaces, refl. and transmission factors *(German)* 78−90354
Jupiter, atmosphere, $^{12}CH_4(^{13}CH_4)$ ν_4 band, line parameters, 7.7 micron transmission 78−85894
large optical components for high-power lasers, refl. and transmission meas. 79−44927
laser diode and transmitter unit lifetime tests *(German)* 78−37883
laser mirror and window absorption, reflection and transmission obs. at 10.6 μm 79−14014
laser radiation wavelength meas. using material spectral transmission curves 79−76738
laser Rayleigh scatt., forward direction, spatial coherence deterioration, polaris. interferometry technique 77−10838
latex, colloidal cryst., optical props. near MP 78−11562
layer with exponentially varying refr. index, oblique incidence of light, interf. matrix 78−55296
leaf optical system modelled as stochastic process 77−44877
leaves, chlorophyll A low-intensity two-step absorpt. in vivo 78−35801
lenses and optical materials, transmission and MTF in 8-13 μ band 79−36982
limited light beam, nonlinear reflections and transmission 80−58624
liquid crystal image transducer, optical props. at normal incidence, off-state behaviour 80−64160
liquid crystal lens cell, prep. and optical props. 79−94320
liquid crystal T-cell light transmission rel. to angle of incidence 79−27426
longitudinal static spin wave struct., magnetotropic interaction of light *(Russian)* 80−93285
low-energy photon diffraction, scatt. theory 80−43262
macromolecules, mol. wt. meas., light transmission meas. 78−17828
MBBA, laser radiation transmitted near isotropic transition, spatial coherence 78−18003
MBBA, liq. cryst., electrohydrodynamic instability, fluctuation of light transmission meas. 77−11468
MBBA, nematic, EHD instabilities, director-fluctuation autocorrelation and power spectrum 79−41944
MBBA, nematic, EHD instabilities, director-fluctuation second moment 79−41943
MBBA, nematic liq. cryst., secondary dynamic scatt. mode, light transmission and microscopic obs. 79−4246
measurement of reflectance and transmittance, arrangement for integrating sphere *(German)* 80−31844
measurement techniques for small absorpt. coeffs., using transmission, emittance and calorimetry 78−24839
meniscus collimator viewfinder, optimisation of mirror light transmission coeffs. 80−74469
metal island film, two-dimens. distrib. system, optical refl. and transmission calcs. 79−4862
metal-dielectric interference filters in transmitted light 80−96013
metallic thin film filters for long-wavelength IR, transmission curves 77−31136
metallic thin films, free-electron, optical props., theory including electron surface scatt. 80−29817
$MgSiO_3$, Mg_2SiO_4, vapour condensed, mid IR optical props. 80−31337
micro-objective, fogging field glare meas. 79−75590
microcantilever electrostatic deflection system for transmission optical modulator array 80−87512
microscopic interference obs. by reflection contrast 80−68248
microscopical and Ewald dynamical diffraction theories, refl. and transmission, spatial dispersive dielec. slab 80−83548
monochromator stray light transmission meas. and evaluation 77−38030
monoclinic absorbing plane parallel plate, normal transmission and refl. 80−1122
moving layer of scattering medium, EM radiation refl. and transmission 77−50619
multi-element interference filters using different grids, far IR charact. 78−90507
multi-layer optical system, reflection and transmission coeffs. calcs., computer program 80−66316
multidielectric film, optical control by method of static ratios *(French)* 77−69993
multilayer interference filter, design and construction 79−46052
multilayer oxide correcting coatings, u.v. transmission cutoff 77−760
multilayer structure devices, nonideal, computation of optical props. 80−5684
multilayer superlattice stacks, very thin nonideal, wavelength variation of transmissivity, refl. 80−100701
multilayers, ultrathin, optical charact. 80−104005
multiple-plate glass systems, spectral directional radiation charact. prediction 78−74956
1,2-naphthalocyanine-rare earth ion complexes, electronic excitation deactivation mechanism 79−85988
natural illumination of Earth's surface in European USSR 77−78422
negative photoresist, KMR-747, transmission and refr. index 2 to 10 μm, interferometric meas. *(French)* 79−76780
nematic liquid crystal, effect of ultrasound on orientation, light transmission meas. *(French)* 77−59067
nematic liquid crystal display, twisted, ang. and voltage depend. of light transmission, two-layer model 80−76006
nematic liquid crystal twisted layer 78−68476
nematic liquid crystals, light transmission exam., positive and negative dielectric anisotropy 77−43141
nematic liquid crystals, light transmission meas. 80−88025
nematic product dynamic scatt. characteristics in mag. field 77−77177
nematic twisted layer, off-state transmission 79−82948
neutral absorbers of NS glass, meas. of transmission when irradiated with laser radiation 80−105692
nitrocellulose fibres, polarised light study 80−80736
non-redundant scanning, high efficiency freq. modulation, of light beam in half space 78−78907
non-redundant spectral tunnelling through periodic struct. at total refl. 78−78906
nonlinear media, reflection-transmission hybrid regime, plane wave soln. *(Russian)* 77−72025

light transmission continued
objective lenses, two-channel device for meas. transmission coeff. 80−106642
ocean, bottom nepheloid layers and bottom mixed layers, on continental shelf off Oregon 78−16027
ocean, hydroptic obs. in Sargasso Sea and tropical Atlantic Ocean *(Russian)* 79−39748
ocean, meas. in N.Arabian Sea 77−91144
ocean analysis by Beer's law, daylight irradiance meas. 77−21800
ocean transparency field, statistical relationships with hydrological and biological charact. *(Russian)* 79−88361
ocean waters, Pacific, irradiance and beam transmittance meas. 79−48491
optical channel transmission calc., matrix method 78−18033
optical coatings, algorithms for determ. of reflectance and transmittance 79−98271
optical cuvette, high temp., for transmission spectra meas. over 2-13 μm, 300-1600K ranges 79−2839
optical fibre, secondary coating rel. to transmission loss 80−58704
optical fibre, timing extraction in optical transmissions 79−10397
optical fibre, transmission charact. of graded-index fibres with lossy outer layer 78−55437
optical fibre, transmission meas. without disturbing integrity 77−72076
optical fibre low-loss transmission achievement and utilisation 77−27381
optical fibre preform, high-silica, OH-ion distribution by light transmission profiles 79−14121
optical fibre transmission loss and pulse delay distortion before and after cabling 78−1406
optical fibres, multilayered dielectric 77−42615
optical film, non-homogeneous, oblique light incidence *(Russian)* 79−13905
optical filters, diffractive, prepared by reactive sputter etching, microfabrication and evaluation 79−90008
optical microdevice with square law media, Gaussian beam charact. by wave optics 79−81360
optical system, cryogenic and contamination effects 80−38113
organic semiconductor film, optical consts. by refl. and transmission, errors 77−16414
oscillating beam spectrometer for organic thin film transmission 80−18022
oxazine dyes, orientation of $S_1 \rightarrow S_n$ transition moments, continuous ps photometry 79−10152
PAA, nematic liq., cryst., light transmission in high elec. field grad. 79−19150
parallel surfaces, absorptance, reflectance and transmittance, generalised eqns. for calc. 78−42273
periodically stratified absorbing medium, splitting of energy flux *(German)* 77−3534
petroleum samples, extinction coeff., refractive index meas., 0.25-25 microns 79−65818
photochromic glass, Ag halide type, photobrown, transmittance meas. at environmental extremes 79−46020
photographic film grain size and transmittance influence on fluctuation and diffraction spectra *(German)* 80−4788
photometric terminology for refl., transmission, scatt. and emission 77−74477
photoresist, negative, as phase profile material for near IR, IR spectrophotometric meas. 78−37953
photosensor multilayer structure transmittance calc. 77−38008
photothermoplastic layers, optical transmission function, charge carrier drift effects *(Russian)* 79−3661
plane plates, two sets of different physical props., energy flux splitting *(German)* 79−18500
plane transmission diffraction grating in convergent beam 79−72693
plane-parallel plate, with spatial dispersion, light refl. and transmission coeffs. 80−88951
planetary atmosphere, diffuse refl. and transmission, soln. for three-term phase function *(Russian)* 77−13260
planetary atmospheres with rough surface, diffuse refl. and transmission laws 78−12085
plant leaves, spectra of nonlinear optical effects *(Russian)* 78−48829
plant leaves, spectral transmission coeff. changes, nonlinear optical effect 79−57707
plume opacity related to particle mass concentration and size distribution 79−74566
PMMA, rain erosion behaviour, exam. 78−53001
PMMA film, Plexiglas, penetration depth of 10.6 μm laser radiation, transmission, refl. and absorpt. meas. 79−74010
PMMA-d_8 ductile plastic optical fibre cables with improved visible and IR transmission 78−46834
polarisation constants for light interaction with absorbing crystal plates 80−78765
poly-γ-benzyl-L-glutamate, monolayers, struct. studies, IR, ATR, and TEM obs. 80−44396
polyacetylene films, doping investigation, insulator-metal transition, optical transmission meas. 80−103729
polyalkali photocathode films, photoelectron emission depth rel. to thickness 79−83106
polyamide-polyurethane, enamel lacquer, far IR transmission, encapsulation of optical devices 79−55194
polyethylene mixtures as IR filters, transmission charact. 77−39020
polymer impregnating soln. concentration meas. by transmission photometer *(Russian)* 77−73484
polysiloxane urethane as optical cement, transmission 0.2 to 6.2 μm 77−7163
polyvinyl acoustal, enamel lacquer, far IR transmission, encapsulation of optical devices 79−55194
pulsed lamps for laser systems, bulb transmittance changes 80−5740
quartz, cultured cryst., vacuum UV transmittance before and after electron irrad. 78−83044
quartz fibres, liquid core tetrachloroethylene filled, transmission loss meas. at 3.39 μm 79−81532
quartz high-transmittance antirefl. film, vacuum-etched 80−74449
quartz in metamorphic rocks, transmission spectra rel. to c-axis fabrics anal. 80−101456
radiation induced transmission loss in optical materials 79−94306
radiative properties, parameterisation 80−56601
radiative transfer, synthetic scattering phase function 80−98541
random inhomogeneous media, Lagrangian and Euler description *(Russian)* 77−3537
light transmission continued
random small-angle scattering theory, dispersion coeff., MTF and contrast loss 77−68174
random transmitted and reflected waves in medium with large-scale irregularities, statistical charact. relationships 79−81364
randomly scattering light absorbing media, scale models and transmissive similarity 79−55061
retina, frog, near IR transmission of rods rapid light-induced changes 79−74658
retinal spectral sensitivity to light it has scattered, human 77−9193
rhabdomere transmittance decrease due to blue light, rel. to desensitisation of peripheral photoreceptors 78−64993
rotation, high sensitivity stabilisation and meas. *(French)* 77−61103
rough surface, effects on coherence of transmitted radiation, Young's method 77−3539
rubeanic acid, in ethanol and water solns., UV transmission filter charact. 77−3679
sailcloth, optical transmission charact., telescope dome slit cover appl. 77−83936
Saturn ring system, light transmission and thickness from low tilt angle photometry 79−35186
scattering material, transmittance and reflectance meas. by specular hemisphere method 78−58004
scattering objects, investigation using vacuum monochromator 77−74523
sea spray and coastal aerosol effects on transmission 79−39861
seawater transmission props. for underwater laser communication 80−33069
semiconductor, IR radiation ultra-fast switching by laser-produced carriers 79−98417
semiconductor, sound-induced anomalous transmission of light below plasma edge 78−68475
semiconductor film, laser-induced transmittance oscills. and struct. phase transitions 79−87516
semiconductor film, transparent substrate, surface unevenness and interference effects 77−77310
semitransparent structural materials, degree of blackness determ. *(Russian)* 79−27161
SF_6, buffered, 10.6 μm transmission props. for nanosecond pulses 80−58644
shadow methods, reflected, transmitted, obs. of sharp V-notched plates, under pure bending 78−90777
silicone resin clad fibre technology, optical and mech. props. 80−28349
slit transmission and polarisation 77−6994
smoke aerosols, optical absorption to extinction ratio, photoacoustic determ. 80−58459
smoke particle size and conc. meas., three-wavelength light transmission technique 79−79438
solar collector glazings, effective beam rad. incidence angles for determ. of diffuse rad. transmittance 80−94112
solar collector selective coating microstructure rel. to processing parameters and optical props. 79−62033
solar glazing hemispherical transmittance props. 79−52957
solar radiation penetration of Indian Ocean waters, calc. 79−2278
Solc birefringent filter, transmission spectrum calc. 79−55052
spatially periodic media, second-order coupled-mode eqns. 78−13655
spectral transmission and reflection coeffs., USSR special standard 77−30195
Spectrofloat glass, theoretical anal. of optical transmission and refl. props. 77−90120
spectrophotometer, photometric scale calibration using fluorite 1200-800 cm^{-1} transmission 79−12837
spectrophotometer, reference for analysis of diffuse transmittance and reflectance 77−38023
spectrophotometer, SF-26, stray radiation level during 280 to 350 nm region operation 80−101852
spectrophotometer accessory for digital absorption and transmission meas. *(German)* 77−57408
spectrophotometer for colour and UV/vis. range, Pye Unicam SP8-100 78−93768
spectrophotometry, semi-transparent metallic thin films as transmittance standards 77−53991
star simulator lightguide test instrument and method 79−27422
stearic acid-based, layer periodic structure, prep. and optical props. 77−69199
step-index optical fibre and cable transmission characteristics 78−1404
submarine communication lightguide cable design and manufacture 79−37027
sunglasses, commercial, UV and IR windows, transmission meas. 0.3 to 0.85 μm 77−36915
surface roughness and thin film influence on refl., transmission and scatt. of light *(French)* 77−34826
tellurite glass, Cu^{2+} and Ni^{2+} doped, band-pass filters for 550 to 616 nm, transmission charact. 78−71166
textured surface, reflectance and transmission props. 78−1165
thermoplastic enamel lacquer, far IR transmission, encapsulation of optical devices 79−55194
thermoplastics, wideband optical transmission meas. 79−76771
thick layers, refl., transmission and brightness coeffs. 80−63918
thick planar films, index-profile meas., transmission technique 80−33230
thick planar films, transmission method for index meas., modal effects 80−102862
thin films, optical transmittance and reflectance, bulk optical props. determ. 80−88954
thin films, unbacked, optical constants by transmission interferometry 79−78778
thin films, vac. deposited, mass change, optical transmittance, and reflectance, simultaneous meas. apparatus 79−75501
thin layer, weakly absorbing, radiant absorption/transmittance ratio 79−11481
through reflecting cylindrical tubes, demonstration 78−73812
trajectories of reflected and transmitted beams in oblique tunnel effect 78−78903
transmission spectrophotometry in visible and UV regions, standardisation 77−53989
transparent conductors, figure of merit 77−1741
transparent materials, laser light refl. and transmission, high power densities 79−27305
transparent nonlinear layer, light refl. and transmission *(Russian)* 78−71142
turbid atmosphere, transparency charact. calc. 78−81407
turbid media, approx. linear relationship for optical response 78−90371

light transmission continued
turning of beam through const. ang. by prism, for teaching 79−25805
two-phase bubbly flow, void fraction meas. by laser beam attenuation technique, theory *(Japanese)* 79−50779
two-phase bubbly flow, void fraction meas. by laser beam attenuation technique, expt. *(Japanese)* 79−50780
two-phase bubbly flow, void fraction meas. by laser beam attenuation technique, meas. accuracy determ. *(Japanese)* 79−50781
two-phase systems, mean specific surface area, light transmission meas. *(German)* 78−89431
ultrathin metal film, evaporation cryostat for elec. and optical meas. under ultrahigh vac. 77−87769
underground optical cable transmission meas. 78−50942
undersea transmission characts. of laser beam in Tago Bay, Japan 77−21782
underwater laser beam transmission characts. in Tago Bay *(Japanese)* 77−21797
uniaxial crystal plate, transmission of light in case of inclined incidence 78−1152
vacuum UV coatings reflectance and transmission, depend. on wavelength 79−46030
vacuum UV optics, reflecting coatings and transmitting filters, review 79−46029
Venus atmosphere, results of solar flux radiometer expt. aboard Pioneer Venus multiprobe mission 79−48718
Voigt profile, fast calculational algorithm, line-by-line transmittance 78−7767
water, aerated, limiting detect. range in optical transmitter-receiver system 77−78461
waveguides, bent hollow metal, low-loss optical transmission 77−88904
window, composite vacuum-tight, for IR and visible observations, strength and IR transmission 80−48406
yeast cell IR spectrum, effect of membrane components 77−70433
yeast cells in suspension, vacuole detect. by transmittance radiometry 80−26418
Ag film, granular, transmission and reflection spectra, validity of sum rule 80−97358
Ag granular film, plasma reson. absorpt. by incident light 79−28850
Ag halide optical fibres, extrusion, visible and IR transmission 80−58829
Ag halide polycrystalline fibre, 10.6 μm transmission loss obs. 80−64197
Ag ultrafine particles evaporated on glass, optical transmittance meas. 79−78772
Ag-SiO_2, coevaporated films, neutral density filters for near IR radiation 79−72673
β-AgI thin film, exciton spectrum 80−55216
AgPd, dil. alloys, electronic states, virtual bound states model test *(French)* 77−62809
Al_2O_3, integrally coloured oxide films on Al, optical properties 80−93420
α-Al_2O_3, single crystal transmission and reflectance IR phonon spectra, polariton dispersion 80−66170
Al_2O_3, transparent hot-pressed, transparent and translucent properties 80−60533
Ar, oscillator strengths, determ. from self-absorption of reson. radiation 79−89641
As-Ge-Se and As-Ge-Se-Sb glasses, IR transmission and acousto-optic props. 77−27327
As-S glassy film, photobrightening effect 80−11498
As-Se, amorphous film, kinetics of photo-induced processes *(Russian)* 79−69896
As-Se amorphous film, optical props. change under high-power light pulse action 79−47534
As-Se and As_2S_3 films, electron-stimulated changes in optical props. and dissolution rate 80−29709
As-Se system, chalcogenide vitreous semiconductors, darkened films, thermal and optical bleaching, light transmission obs. 80−50447
As-Se-Te, laser induced crystn. kinetics 77−76317
$As_4Sb_2Se_9$ glassy semiconductors, electronic props. 80−103712
AsSe film, light-induced light absorption changes 77−73181
Au black solar absorber, struct. comp. and optical props. 78−27339
Au discontinuous film, optical transmittance, effect of island morphology 78−84673
Au film, granular, transmission and reflection spectra, validity of sum rule 80−97358
Au film, self-supporting, thermotransmission meas. 1.8 to 3.5 eV 78−27343
Au film growth, optical and elec. prop. meas. during deposition *(French)* 77−70007
Au, films, optical props. meas. rel. to electron surface scatt. theory 80−29818
Au-Pd dil. alloys, electronic states, virtual bound states model *(French)* 77−62809
BaF_2, optical ceramic, hot pressing in vacuum, rel. to spectral transmission 78−52730
Bi film, refractive index determ. using Rayleigh-Lowe refractometer 80−7427
Bi-Sb-O-I glasses, 500-550 nm transmission and acousto-optic props. 77−31121
$Bi_{1-x}Sb_x$, far IR transmittance meas. *(Russian)* 77−44006
$Bi_{12}SiO_{20}$, use in incoherent-to-coherent optical image convertor of transmission type 79−94340
$Bi_{12}SiO_{20}$:Nd, light absorpt. and transmission spectra, photoluminescence spectrum, optical absorpt. coeff. 79−74001
$Bi_8T_7S_5$, thin crystal, optical consts. from transmissivity spectra, classical oscillator anal. 77−1748
C foil, ion irrad., crystallographic transform. 79−55794
C foils, forward photoemission and transmittance meas. 80−25516
CO_2, transmission functions for 15 μm band, calc. and expt. *(Russian)* 77−64428
CO_2-N_2-He, coefficient of optical amplification behind an axisymmetric shock wave *(Russian)* 77−89153
$Ca_{10}(PO_4)_6(OH)_2$, synthesis and characterisation in dense polycryst. form 77−4749
$Cd_xHg_{1-x}Te$ films, epitaxial growth, optical, elec., and photoelec. props. 79−11512
CdO-SnO_2 DC reactively sputtered films, elec. and optical props. 80−103763
CdO-SnO_2 film, DC reactively sputtered, transparent electrode props., optimum sputtering conditions 80−11116
light transmission continued
CdO-SnO_2 film, DC sputtering prep., visible and near IR transmission, resist. 78−88049
CdO-SnO_2 film, prep. by RF sputtering, elec. cond. and transparency 80−7492
CdS, attenuation of transmitted light in exciton region, polarisation, coherence, scatt. 77−69852
CdS, electron-hole liquid, non-equilib. transmission spectroscopy meas. 77−20883
CdS film, high cond., high transmittance, growth by evaporation method, and characterisation 77−77386
CdS, plastically deformed, electronic transport and optical props. 79−73508
CdS, spontaneous and stimulated emission from electron-hole plasmas 77−69241
CdS-ZnS(CdSe), film, light transmittance spectra, comparison with Schott GG 495 glass filter 78−33838
$CdS_{1-x}Se_x$, graded comp. semicond., tunable narrow-band filter, 5130 to 3700 Å 77−31128
Cd_2SnO_4 film, optical transmission and reflection, evaluation for solar heat collectors 77−52191
Cd_2SnO_4 film, sputter deposition and characterisation 79−43146
CdTe, electron-beam-controlled transmission of 10 μm radiation 79−81466
CdTe sputtered films, deposition conditions effects on struct. and props. 77−43452
$Cd_{1-x}Zn_xS$, RF sputtered electro-optical film for data storage and display 78−83047
CoO-containing glass, effects of γ-rays, electron beam and neutron flux on transmissivity *(Japanese)* 77−73156
Cr ultrafine particle selective absorption of solar energy 79−62035
Cr/Au layered films, microstruct. and interdiffusion during ageing, 423 to 573K 79−46965
Cu film, complex impedance, IR transmission and refl. meas. 79−78216
Cu light pipe, submm. wave transmission, and refl. of surfaces 50-10 cm^{-1} 78−18050
Cu-Pd dil. alloys, electronic states, virtual bound states model test *(French)* 77−62809
CuBr, evaporated film, magneto-optical effects on exciton bands 78−72624
CuCl, evaporated film, magneto-optical effects on exciton bands 78−72624
CuCl, optical microscopic, X-ray diffr. and elec. resist. studies at high press. 80−11051
$CuGaTe_2$ film, flash evaporated, growth and optical props. 79−95296
$CuGaTe_2$, refr. indices meas. 80−93259
$CuInSe_2$, refr. indices meas. 80−93259
$CuInTe_2$, refr. indices meas. 80−93259
Cu_2S epitaxial films, reactive sputtering prep. and electronic props. 79−78885
Cu_2S, rel. to band models of Cu_2S-CdS heterojunctions *(Japanese)* 78−23154
$Cu_{2-\delta}S$, thin films, determ. of stoichiometry from optical props. 79−60656
Cu_xS, layers produced by reactive RF sputtering, struct., elec. and optical props. 79−90908
$EuO_{1-\Delta}$, thin film, Faraday effect dispersion and transmission, 0.5-1.1 μ, 20.4 and 77K, anion vacancies 79−19945
$GaAs_{1-x}Sb_x$, narrow-gap film on wide-gap GaAs, energy gap grading, optical transmission meas. 77−20943
GaP, growth and props. of LPE layers on Si substrates 78−6864
$GaS_{1-x}Te_x$, solid soln., single cryst., crystallography and optical props. 79−55711
GaSe, thin layers, far IR refractive index 80−80799
Ge amorphous film, crystn. front velocity during scanned laser crystn. 80−107662
Ge, electron-beam-controlled transmission of 10 μm radiation 79−81466
Ge film, amorphous to crystalline transform. 77−20206
Ge, free carrier, intervalence band indirect absorpt., at high optically created carrier densities 79−42961
Ge, monocryst., for IR optics, prod. techniques and characts. 78−50873
Ge optical windows, contaminated by NH_3, CO_2, CO, HCl, methane, cryocooled, IR transmission 79−32007
Ge-As-Se IR transmitting glass composition, prep. and props. 80−69474
GeS, thin layer cryst., far IR transmission spectra 79−56870
GeS_2, single crystal, far IR transmission 80−80800
$Ge_{100-x}S_x(Se_x)(Te_x)$, amorphous film, effect of alloying chalcogen atom on elec. cond., optical transmission and ESR 79−78101
$GeSe_2$ chalcogenide film, struct. changes due to laser induced transmittance oscill., SEM obs. 78−6240
$GeSe_2$ film, glassy, self-controlled laser-beam chopping effect 78−60528
$GeSe_2$ film, light induced transmittance oscillations 77−81171
$GeSe_2$ film, light-induced light absorption changes 77−73181
H_2, Raman pulse propag., 30 atm., self-induced gain/loss modulation 77−10980
H_2O, liquid, far IR optical consts. meas. with optically pumped laser 80−40082
Hg, optical and elec. effects during solidification 78−47502
$Hg_{1-x}Cd_xTe$, narrow-gap semiconductor, high intensity IR transmission limit 80−7361
IN_2O_3:Sn, RF magnetron sputtered film, elec. and optical props. 80−104065
In film, evaporated, resist., Hall effect and light transmittance, use as semitransparent electrode 77−39966
In films, vacuum deposited, growth conditions effect on elec., optical, and structural props. 79−78215
n-InAs, hot electron temp. determ. by interference modulation of radiation 80−44610
InAs IR filter properties, operational characts. of antireflection coatings 79−14107
InAs, narrow-gap semiconductor, high intensity IR transmission limit 80−7361
In_2O_3 film, conductive, transparent, optimal reactive sputtering conditions for prep. 79−95295
In_2O_3, films, activated reactive evaporation technique of prep. 80−80989
In_2O_3 films, electron beam evaporation, elec. and optical props. *(Japanese)* 80−60784
In_2O_3, reactive ion plating onto insulating substrates, and elec. and optical props. 79−87588
In_2O_3, thin film, sputter deposition form., optical and elec. props. 80−60123

light transmission continued
In_2O_3, transparent electrode deposition on PLZT ceramic, elec. and opt. props. 78−74848
In_2O_3:Sn, films, activated reactive evaporation technique of prep. 80−80989
In_2O_3:Sn, transparent conducting films, prep. by $InCl_3$ thermal decomp., transmittance, resistivity 79−33944
In_2O_3:Sn film, RF sputtered, effect of O_2 press. during deposition on props. 78−19664
In_2O_3:Sn films, prep. at low deposition temps. by ion-beam sputtering, elec. and optical props. 79−66004
In_2O_3:Sn films, pure and doped, prod. by ion plating, elec. and optical props. 80−2488
In_2O_3:Sn transparent cond. films, hydrolysis deposition, elec. and optical props. 79−43144
In_2O_3-SnO_2, magnetron RF sputtered electro-optical film for data storage and display 78−83047
InSb, Auger-governed decay of laser-induced plasma, optical probing 80−76105
InSb, narrow-gap semiconductor, high intensity IR transmission limit 80−7361
$In_xSi_yO_z$, thin film, sputter deposition form., optical and elec. props. 80−60123
$In_{1.9}Sn_{0.1}O_3$ laser-damage-resistant transparent conductive coatings, appl. in Pockels cells 79−50333
$In_{2-x}Sn_xO_{3-y}$ thin films, optical transmission and elec. resist. 77−69926
KBr film, oblique incidence transmission spectra for polarised extreme UV radiation 78−39614
KCl film, oblique incidence transmission spectra for polarised extreme UV radiation 78−39614
KH_2PO_4 crystal, and deuterated cpd., optical meas. of phase transition point by domain obs. 77−40187
La_xS_y, stoichiometry and opt. props. during hot pressing 78−23653
LiF, refractive index, effect of ageing, wavelength range 460-1000 nm 80−84707
$LiNbO_3$ crystal, elec. cond., optical quality, impurity depend., space charge pyroelectric field compensation 79−64295
$LiNbO_3$ transparency with vacuum-deposited electrodes *(Russian)* 78−60422
LiO_2-Al_2O_3-SiO_2, glass containing ZrO_2, cryst. process 80−103253
$MgAl_2O_4$, composition rel. to ceramic microstruct. form., light transmission 79−43188
MgF_2 refractive index and extinction coefficient meas., 115 to 400 nm 79−78640
Mn film, refractive index determ. using Rayleigh-Lowe refractometer 80−7427
$NH_4H_2PO_4$, crystal, and deuterated cpd., optical meas. of phase transition point by domain obs. 77−40187
Na_3AlF_6, effect of temp. var. on light transmission 78−79136
NaF-SrF_2-CrF_3, glass transition, crystn. and melting temps., optical transmission *(French)* 80−64910
$NaSbSe_2$ films, struct., photoelec. and opt. props. 78−51834
Ne, oscillator strengths, determ. from self-absorption of reson. radiation 79−89641
NiO (111) platelets, antiferromag. S domains, optical obs., spin flop 80−54915
$NiSO_4$, aq. soln., UV transmission filter characts. 77−3679
PLZT ferroelectric display electro-optical props. *(Russian)* 79−9211
Pb bismuthate glass, IR transmission props., density 79−74127
PbF_2-AlF_3 glass, optical props., crystn. and thermal expansion 80−48367
PbI_2, exciton spectra depend. on strong excitation, crystal transmission 79−69433
PbS, low carrier conc., prep. and props. 77−39846
PbTe very thin epitaxial films, transmission and refl. spectra, 1 to 5 eV 80−7430
Pt films, optical props. and radiation stability 80−34999
$RbAg_4I_5$, depolarisation of light by crit. fluctuations 79−61333
RbCN, molecular motion and ordering from dielec. and Raman techniques 79−73932
S, single liq. droplet, optical transmission and elec. resist. changes on polymerisation 77−35460
SF_6, 10.4 μm laser pulse transmission 78−14128
SF_6, refl., absorpt. and transmittance depend. on irradiance at normal incidence 78−13769
Se, red amorphous film, textural change, thermal and photo effects 78−63951
Se spheres embedded in polymer matrix, electrophotographic film, optical props. 78−83055
Se, vitreous, darkened films, thermal and optical bleaching, light transmission obs. 80−50447
$Se_{75}Ge_{25}$, obliquely deposited amorphous films, photo-induced optical effects 79−56871
Si amorphous film, optical props., electronic states 80−25475
p-Si, heavily doped contact layers on IR detectors, IR transmissivity 80−108190
Si, interband and free carrier absorpt. consts. at high-level photoinjection 79−38514
Si wafer processing, CO_2 laser heating dynamics 80−76106
Si:B ion implanted layers, light refl. and transmission coeffs., computer program 80−66316
Si:B(P)(Sb), single cryst., transmission characts. for IR optical components 77−27325
$SiH_{0.16}$ amorphous films, optical props. and photocond. near optical gap 80−50443
Si_3N_4, pyrolytic, prep. by CVD, bulk and coatings, exam. of electrical, optical and physical props. 79−95935
SiO amorphous film, optical transmittance and reflectance, bulk optical props. determ. 80−88954
SiO evaporated film, dielec. function 8 to 33 μm, spectrophotometric and refl. meas. 80−80883
SiO_2, film, transmission, photocond. and band gap meas. 79−73540
SiO_2 films, microporous, sintering effects, IR ATR, transmission investigs. 79−66031
SiO_2 films, Si-rich, amorphous Si region obs. 80−84400
SiO_2 wideband dielectric mirror production, spectral transmission 79−76897
SiO_2-Ta_2O_5, plane optical waveguide, fabrication by reactive sputtering 78−71221
Sn, globular film, interf. and diffr., solar selective props. 79−4860
SnO_2 film, pure and Sb doped, transparent cond., prop., characts., stability, struct. *(Japanese)* 78−47889

light transmission continued
SnO_2, reactive ion plating onto insulating substrates, and elec. and optical props. 79−87588
SnO_2, transparent conductive film, prep. by magnetron sputtering and elec., optical and structural props. *(Japanese)* 79−8247
SnO_2 transparent electrodes, effect of Sb doping on elec. and optical props. *(Korean)* 77−1749
SnO_2, transparent electrode deposition on PLZT ceramic, elec. and opt. props. 78−74848
SnO_2:Sb, transparent cond. film prep. by thermal decomp. of Sn salt of organic acid *(Japanese)* 77−90269
SnO_2:Sb, transparent cond. films, hydrolysis deposition, elec. and optical props. 79−43144
SnS_2 thin layer, far IR refractive index 80−93421
SrF_2, thin film, optical props., spectral dependence, 460-1000 nm 80−76094
Ta_2O_5, plane optical waveguide, fabrication by reactive sputtering 78−71221
TiO_2 wideband dielectric mirror production, spectral transmission 79−76897
Tl halide single crystals, spectral transmission meas. 77−59581
TlBr, electromodulation spectroscopy of excitons 79−73444
TlCl, electromodulation spectroscopy of excitons 79−73444
VO_2 single cryst. film, ion-irrad., 'splitting' of semicond.-metal transition 80−11053
V_3Si superconductor film, Fourier and laser spectroscopy comparison in far IR-sub. mm. range 79−93237
YAG:Nd crystal, orientation influence on thermally induced birefringence *(Chinese)* 80−88958
$Y_{3-2x}Ca_{2x}Fe_{5-x}V_xO_{12}$ single cryst., Faraday effect and opt. props. 77−1660
Y_2O_3 sintered pieces, optical transmittance 80−40561
$Zn_{1-x}Cd_xS$, graded comp. semicond., tunable narrow-band filter, 4272 to 4584 Å 77−31128
$ZnGeP_2$, synthesis, characts., applic. to laser windows *(French)* 78−80467
ZnO, attenuation of transmitted light in exciton region, polarisation, coherence, scatt. 77−69852
ZnO-$Al_2O_3SiO_2$, transparent glass-ceramic, microstruct., physical props., crystallisation ht. treatment depend. 78−80506
ZnS CVD IR window, optical and physical characteristics 80−106620
ZnS, effect of temp. var. on light transmission 78−79136
ZnS-Ag, broad band visible heat reflecting mirror 77−39017
ZnS-MgF_2 mixtures, triple-layer broad band antireflection coatings 79−32011
ZnS-MgF_2/MgF_2 double-layer antireflection coatings, transmittance meas. 79−36967
ZnSe, electron-beam-controlled transmission of 10 μm radiation 79−81466

light velocity
coordinate transformations of the absolute space-time theory 79−67157
correlation velocity, in dispersive media 77−68165
diffuse medium, reduced effective velocity of light 80−69329
distant synchrony and the one-way velocity of light, thesis of conventionality 79−67153
extraterrestrial test, speed of light independence of source vel. 78−8241
Fizeau effect, theory, expt., and Zeeman meas., for teaching 78−24597
frequency dependence, as cosmic test for photon rest mass and Maxwell's eqns. 77−45708
frequency shifts for light having traversed moving prism *(Spanish)* 77−88638
geometry of the space of events hypothesis 77−53713
gravitational potential of source, Laplace's deduction of differential aberration *(German)* 78−57838
invariance, three-temporal Lorentz transformation 79−44717
isotropy of light velocity convention, teaching 80−101689
nonlinear electrodynamics in generalised gravitational theory 77−5727
relativity, clock signal, light signal synchronisation, one-way light velocity meas. 80−42055
relativity, special, dilatational degree of freedom, six-dimensional space V_6 80−57088
Romer, Ole, determ. of hesitation (velocity) of light *(Danish)* 77−57140
simultaneity, distant, conventionality, standard synchronisation 80−77612
special relativity, secondary-school course not relying on historical approach 78−86096
speed of light independence of source vel. extraterrestrial test 78−8241
ultrahigh velocities in special relativity, superspace concept 79−88802
vacuum, quantised space, special relativity and relativistic field theories 80−82869
variations in light velocity due to motion of earth 78−24666

light velocity measurement
beat frequency method, using internal laser modes 80−41992
clock retardation, absolute space, and special relativity 79−67156
current status *(Chinese)* 79−97342
demonstration apparatus using two dollar rotators 80−77578
education, undergraduate expt. 79−9060
ether wind first-order expt. with stabilised lasers 77−5665
feedback and optical transients for light velocity meas. in transparent media 77−109
fibre optic wink-around expt. 80−90628
Foucault's method modification, student laboratory expt. 79−40327
Foucault's rotating mirror method for meas. speed of light 80−67996
frequency determination of laser light by interferometric comparison, speed of light derivation 78−55395
interferometric technique, absolute wavelength meas. of CO_2 9.4μm band R(14) line 77−82485
laser application in speed of light and wavelength determ. 80−42190
laser freq. meas. and determ. of C, review 78−81952
Marinov's expt., comment on ang. distrib. of background radiation 78−32673
Mossbauer meas., isotropy 80−95026
nuclear timing technique 80−90637
one-way velocity meas., determ. of Earth's absolute velocity 79−44924
one-way velocity of light, and light signal synchronisation 80−82644
relativistically moving light source, vel. of light meas., depend. on light source vel. 77−82486
rotating axle expt., oscilloscopic and absolute 'coupled-shutters' variants 80−68234

light velocity measurement continued
special relativity, meas. by stable clocks 78−54185
student experiment using TV ghost 77−13561
unsteady convection study, simultaneous velocity and interferometric meas. 79−98839
wavelength independence of velocity of light in vac., expt. test 77−74350
He-Ne laser IR applications 79−94275
He-Ne methane stabilised laser, confirmation of speed of light value 299,792,458 m/s$_{air}$ 80−37002

light water *see water*

lighting
see also floodlighting; street lighting
airport control tower cab, optical design 80−58661
average hemispherical illum. from point source, calc. *(Czech)* 77−46778
Candela, radiometric definition appraisal *(German)* 78−32845
chemiluminescent disposable lighting device based on oxalate esters 80−11488
chromatic adaptation effects and colour appearance at various illum. levels *(Japanese)* 78−92628
cinematograph luminaire systems, statistical eval. *(Russian)* 79−89030
colour changes due to distance and lighting, direct assessment using Natural Colour System 78−57004
commercial large-scale laser displays using path-controlled galvanometers 77−17963
effectiveness, ESI meter application 80−22417
equipment and services, 1979 video yearbook 79−14197
equivalent sphere illumination, maximum contrast sensitivity publication proposal, advantages 79−9235
equivalent sphere illumination meas., new instrument features 79−9243
fibre optical illuminator output speckle, smoothing methods 79−7209
fibre optics commercial developments, 1978 state of art 79−3776
film copying techniques, colour *(German)* 80−62751
glare source position and BCD brightness relationships under uniform field brightness, expt. *(Japanese)* 80−35889
illuminance at reflex-reflector, photometer for performance meas. 78−45668
illuminants which give prescribed tristimulus values to given object colours, design technique *(Japanese)* 78−94420
illumination engineering, contributions of luminous surfaces *(Rumanian)* 80−4750
illumination engineering measurements using photometry and spectroradiometry 80−22416
illumination meters, metrological requirements *(Hungarian)* 80−17997
illumination system, optical design 80−64135
illuminators light distribution indication method for computerised illumination projecting *(Hungarian)* 80−27333
light meters and their appl. *(German)* 78−8434
luminous fields, integral charact. meas. *(Czech)* 79−40604
luminous flux distrib. in room, electrical analogy 80−33266
metal casting workplace lighting, vision problems, Swedish report *(Swedish)* 77−77896
office complex design, with solar power utilisation, up to 70% energy savings 80−40831
optical systems, luminance determination by critical flicker fusion apparatus *(Japanese)* 77−75645
photometry in circumferential field, spectrum charact. *(Polish)* 78−29136
point source lighting computation using point-by-point method *(Rumanian)* 80−17987
radar precipitation maps as lightning indicators 78−85652
reflection factor for walls, floors and ceilings, determination *(German)* 79−27165
relief objects on plane, brightness and illumination charact. calc. 79−904
retroflectors and retroflective material luminous intensity coeffs. meas. using photometry 77−74479
return stroke models 80−77050
shape factors determ., luminous flux transfer meas. 77−31147
small subjects, basic lighting 77−41709
solar illumination after dark, orbiting mirror appl. 78−33816
spectral eye fatigue, school lighting effects 80−76732
static interruptor cct., triac, thermostatic and lighting control appl. *(Italian)* 78−73984
studio, control system for cinematography, ring power supply system appl. *(Russian)* 79−2863
sunlight for building interior lighting, sun tracking concentrators 77−62043
technical meteorology, technical and commercial appls. *(German)* 80−46231
temperature increase and skin sensation under strong lighting *(Japanese)* 78−44557
thyristor feeding devices type TPU, TV, cinematographic light sources appl. *(Russian)* 79−58816
TV studios, metal halogen light sources for colour rendition quality *(Russian)* 79−76785
veiling reflections and reflected glare from glossy paper, lighting conditions for visual comfort 80−76733
vision, brightness subjective evaluation rel. to object and adaptation luminances *(Japanese)* 78−44509
visual luminance difference threshold, Holladay's principle *(Japanese)* 78−65000
visual target discrimination rel. to colour of illumination 79−53135
working position illumination, factors affecting good vision and efficiency *(Spanish)* 80−3638
InAsSb/GaSb broad-spectral-band IR detector, backside-illum. heterostructure approach 80−73450

lightning
aircraft skin, lightning damage simulation 78−87575
analogous gliding linear discharge over dielectric surface, obs. 80−38826
artificial, return stroke rise speed meas. method *(French)* 80−51493
artificial triggering, expt. study 80−8414
ball, energy condensation, comparison with exciton droplet *(Russian)* 80−107712
ball, evidence, charact. and existing theories *(German)* 77−2220
ball and bead lightning, new theory *(French)* 78−92884
ball lightning, appl. of transmission line model for fireball plasma formation 78−59702
ball lightning, chem. mechanism model 78−28287
ball lightning, elec. charge explanation 80−56572

lightning continued
ball lightning, elec. discharge into sand layer expts., erosion-discharge model 78−81322
ball lightning, forms and energy density 80−98402
ball lightning, maximum energy liberation 79−16615
ball lightning, observations, theories, review 79−92577
ball lightning, plasma bunch description, stationary state, energy supply, occurrence 78−44969
ball lightning, quantum mech. theory *(German)* 78−16082
ball lightning, radiation, electrical and magnetic props. 80−77086
ball lightning, radiation emission, cluster plasma 77−2219
ball lightning, report freq. during 1651-1978 period 79−48552
ball lightning, theory, high density plasma with high binding energy 78−32153
ball lightning, theory *(Russian)* 78−40608
ball lightning, turbulent plasma sphere, rel. to confinement in fusion reactor 80−32516
ball lightning, vacuum bubble model 77−9468
ball lightning 78−88900
ball lightning as EM energy 77−5307
ball lightning correl. with solar activity, comment 77−81972
ball lightning correl. with solar activity, comment 77−87017
ball lightning event, video tape recording 77−66969
ball lightning explanation by water electrolysis and combustion 78−69436
ball lightning in Holland rel. to solar activity 77−21840
ball lightning origin of luminescing sphere in S-shaped bend, model verification 77−37307
book 78−16139
book 78−53713
charact. survey, w.r.t. atmospherics and meteorology 80−51470
clear air triggered lightning, movie film obs. 80−90166
cloud seeding method for lightning triggering 78−3880
cloud-to-ground discharges, radar cross section meas. 77−2279
conductivity charges in cloud and energy losses 80−61867
current, elec. field strength anal. *(Russian)* 79−88402
currents meas. in Italy, results of statistical survey *(German)* 79−12187
DC source in continuously var. conductivity, electric and magnetic fields 77−49140
detection by satellite monitoring 79−92559
direction finding at close range, VHF method 80−98481
direction to lightning channel, mag. direction finding method 80−77078
discharge, elec. field strength at ground level, calc. *(German)* 78−28254
discharge processes, VHF technique for space-time mapping 78−85721
discharges, NO production in troposphere 77−17189
discharges, parameters, protection of electrical systems 80−94590
discharges to ground, charge structure analysis 79−79938
DMSP data from lightning flash detection 79−16593
electric fields time and amplitude props. near lightning in VLF, LF and HF bands 77−78352
electrical processes associated with single stroke 77−21828
electrons heating in lower ionosphere by horizontal lightning discharges 80−90283
electrostatic charges meas. and localisation, neutralised during lightning flashes 80−77097
EM emission of vertical lightning discharges causing D-region electron heating 77−25818
EM fields radiated from lightning return stroke, Maxwell eqns. exact soln. appl. 78−73442
EM radiation, properties 79−58038
energy dissipation in return stroke channel 78−28280
energy estimates, survey 79−100925
expanding return stroke channel diameter and shock waves 77−70751
flash counter and interval recorder 78−88928
flash counters, for ground flash density meas. 80−51552
Florida lightning return stroke electric fields, 200 km propagation 77−25754
flux induced voltage transients on low loss transmission lines, aircraft lightning threats 79−36814
French research *(French)* 80−46225
frequency rel. to ground topography *(French)* 78−3845
frequency versus time plots, rels. to hail cloud identification and hail suppression *(Chinese)* 77−66968
ground flashes at Port Moresby, Papua New Guinea 80−67393
ground wave atmospherics generated by lightning return strokes, initial peaks, model 80−61876
ground-flash multiple-stroke discriminator cct. 78−81446
HF and VHF radiation produced by intracloud lightning discharges, temporal struct. 80−17337
HF effects assoc. with lightning discharge 79−88456
ice clouds, lightning discharges rel. to ice particles rapid orientation and alignment changes 80−17330
incidence prediction and effects in electrical systems, obs. 79−39789
intracloud lightning discharge processes, radiation field wave forms 79−84386
intracloud lightning discharges, inclination 78−73440
ionisation in power station plumes, effect on natural lightning 78−88909
Japanese winter thunderstorms hazard to aircraft, abnormal charact. 77−5309
Kennedy Space Center, unusual lightning flash 79−20953
leader stroke model, electric field strength computation *(Czech)* 79−5554
leader-stoke velocity, significance for lightning and long sparks 77−76234
lightning points, frequency of impact calculations, for selected and arbitrary objects *(German)* 79−79923
location and ionospheric refl. heights from two-station mag. field meas. 79−70845
location of flashes to ground rel. to precipitation 77−45087
long arc simulated lightning attachment testing using 150 kW Tesla coil 80−70074
magnetic component of induced lightning voltage, calculation, supplement *(French)* 78−73419
magnetosphere examination of VLF whistler pulse analysis 80−17441
main discharge theories, review 78−32132
mechanism types and biological effects 78−49081
multiple-stroke flashes, S.African storms 79−34921
multipulse lightning discharge oscillogram scanning camera 78−61588
New York City blackout (1977 July 13) economic and social costs 79−24894

lightning continued
nonlinear electron acoustic waves, discharges in gas, book contrib. 77−80395
optical radiations, simultaneous obs. from above and below clouds 80−85698
panoramic lightning recorder, operational use for aviation weather support 77−78482
peak current meas. and recording device results *(Japanese)* 80−46288
photoelectric detector for daytime lightning 78−57336
photographic obs. from Space Shuttle 79−58078
photographs, daylight time-resolved 79−20954
physical mechanisms, present and future research *(French)* 80−82015
Poland, frequency of lightning rel. to ground topography *(French)* 77−73781
prebiotic atmosphere, N fixation 79−58096
precipitation observed immediately after lighting, within thundercloud 80−77055
radar echoes and simultaneous elec. field changes 79−84372
radial expansion of lightning channels and shock wave form 80−12530
radiation fields, of multiple return stroke lightning 78−3885
radiation spectrum, effect of pulse interval statistics 77−53135
radio emission, Maxwell's eqns. soln. 77−29403
radio emission from lightning, comments 78−24342
randomised modification experiment, statistical anal. 77−2218
ratio of cloud to cloud-ground flashes in thunderstorms 78−3870
recording with modified cine sound camera 79−21058
registration by multichannel counter, with digital display 80−51570
research methods and problems *(German)* 79−12186
return stake, channel current modelling 77−78351
return streamer, EM radiation 79−8652
return stroke channel, transmission line model, computer soln. 78−85644
return stroke elec. and mag. fields, obs. in Florida 80−31096
return stroke generation of ground-wave atmospherics, statistical simulation 78−44967
return stroke lightning, current and vel. 79−25306
return stroke radius estimation 78−3862
return stroke wave forms fine struct. 79−39800
return strokes, EM radiation simulation, tortuosity effects 79−8672
return strokes, latitude dependence 80−67394
return strokes, temporal struct. of HF and VHF emissions 77−33136
RF radiation generation, elec. field var. obs. 80−98401
rotating camera obs. in Northern Poland 77−91185
satellite link, crosspolarisation model 78−11961
satellite links at 20 and 30 GHz, crosspolar phase variations on satellite-Earth path, meas. 77−81957
shielding against direct lightning strokes, theory 78−88899
Singapore, soldier killed by lightning strike 78−44949
slashes on seismic records caused by electrical bursts 77−86794
small spark form. mechanism 78−18469
source directions, 34 MHz interferometry 79−79939
Space Shuttle lightning current distrib., circuit modelling and exptl. verification 78−49293
and spark discharge leader-stroke velocity comparison 78−94947
static electrification hazard, review 78−28283
stationary camera photographic obs. 77−91184
stepped leader, electrodynamics, anal. *(French)* 78−28255
stepped leader, spark gap+parallel R-C network simulation 77−17155
stepped leader theories, comparisons 78−32133
stepped leader theories, review 79−25320
stepped leaders, electric field production 77−37301
stroke current electric fields study 78−3860
stroke current meas. using optical fibre cable and optoelectronic conversion, rocket launched 78−92930
stroke current measurement, automatic observation system *(Japanese)* 77−29506
stroke current obs., at isolated high tower *(Japanese)* 78−40641
strokes, artificial, experimental station in France *(French)* 80−61841
strokes to Earth per km^2 per year, CIGRE count (since 1962) *(German)* 78−40606
superbolts, detect. by Vela satellites 77−73811
superbolts detect., criticism of comment 79−20921
superbolts rel. to positive current lightning distrib. 78−57254
suppression by chaff seeding, comments and reply 77−53139
suppression by chaff seeding, further comments 77−53140
survey of research, definitions, unresolved problems 80−61868
theory of the main discharge of lightning *(French)* 78−92887
thermoluminescent dosimetry measurement of radiation 80−36361
thunder measurements, thunder duration rel. to strike pt. *(Russian)* 80−56532
thunderstorm VHF emission, rel. to three-dimens. motion 80−46218
thunderstrom observed by radar, depolarisation rel. to precipitation 80−51453
transmission line model with general vels. 77−33156
triggering lightning by pulsed laser 80−72626
tropical, unducted VLF energy as possible source of midlatit. VLF emission and electron precip. 77−21980
tropical regions, atm. noise data 80−61875
tropical thunderstorms, cloud to ground and intracloud discharge 80−85705
tropospheric lightning correl. with thermospheric gravity waves 79−84557
UHF atmospherics, emissions from lightning discharge considered as plasma 78−61497
UHF radiation meas. from lightning, 2200 MHz 79−62558
ULF electric and magnetic fields 78−7731
unusual flash photograph with double ground termination 77−56720
upward lightning stroke parameters *(German)* 78−57237
VHF direction finder studies 79−20928
visual obs. from space 79−96850
VLF atmospheric disturbance flux, intra-group structure 80−56683
VLF atmospherics, spectral parameters random scatt. 78−49095
VLF atmospherics meas. at San Miguel, Argentina, rel. to thunderstorms 79−39799
VLF spectral characteristics of K-field changes, expt. 77−2217
what it is, how it happens, effects, and protection 79−48536
wind profile in subcloud layer of thunderstorm from lightning photographs 77−87013
CO production 79−70836
CO production in electric discharge 79−96786
N fixation by lightning 80−90147
lightning continued
N fixation in instantaneous linear discharges, variable energy input effect 79−20952
N fixation in lightning channels, theory 80−90148
NO, production by lightning, shock and channel heating methods 80−72581
NO_x production in lightning 77−56677
N_2O production in electric discharge 79−96786
lightning conductors *see lightning protection*
lightning protection
see also surge protection
air gap between electrodes, conducting body and space charge effect on breakdown 79−50919
book 78−16139
book 78−53713
cathodic protection using lightning conductors connected with diodes, for metals and concrete reinforcements 79−52418
dielectric stimulated arcs in lighting-arrestor connectors, substantial lowering of breakdown voltage 79−99013
discharges, parameters, protection of electrical systems 80−94590
French research *(French)* 80−46225
fusion reactor, JT-60, grounding system pot. rise during lightning strike, anal. 80−102314
general principles 79−48536
photovoltaic terrestrial systems, protection from lightning effects 80−89648
power overhead lines, overvoltage calc., pseudo-random number generator appl. *(Polish)* 77−24234
research methods and problems *(German)* 79−12186
shielding against direct lightning strokes, theory 78−88899
shielding angle, granite Polish Tatra ridges *(Polish)* 78−40604
survey of research, definitions, unresolved problems 80−61868
tower, insulation flashover probability calc. *(Russian)* 77−55180
lightning rods *see lightning protection*
limit, elastic *see elastic limit*
limit cycles
autocatalytic reaction system, sustained oscills., deterministic and stochastic theories 78−95922
autonomous dynamic systems, limit cycles and one parameter transformation groups 78−49641
bifurcation and nonequilibrium phase transitions of limit cycles and multiperiodic flow 78−24759
bifurcation and nonequilibrium phase transitions of limit cycles and multiperiodic flows in continuous media 78−81937
biological statistical mechanics, ensemble methods 79−66437
bounded medium, nonlinear parametric reson., limit cycle solns. 80−19071
brain wave model, existence and external stimulation effect 78−3464
brain waves, limit cycle model, Frohlich's model 77−73520
channel, straight (buckled), two-dimens. flow, stability anal. 78−59490
chaotic behaviour, self and mutual interaction 80−46789
chemical network, nonlinear oscills., transformation group symmetry treatment 77−32771
chemical oscillations, reaction systems with exactly evaluable limit cycles 79−66262
dissipative systems, limit cycles and constants of motion 79−35555
dynamic nonlinear systems containing limit cycles 78−77666
dynamical system, limit cycles and symmetries 80−62462
entrainment by periodic external excitation 77−61020
Frohlich brain wave model, limit cycle stability, enzyme-substrate reaction 78−44490
Hamiltonian systems and limit cycles 79−63131
intestinal electrical rhythms model, stability of entrainment conditions for RLC coupled Van der Pol oscillators 77−56361
invariance theorem *(French)* 78−36813
invariant functions of Lie groups 79−35520
Lorenz model, intermittency, first limit cycle-second strange attractor transition 80−31674
nonlinear diffusion-reaction with autocatalysis and saturation law, single perturbation approach 80−35502
nonlinear systems of differential equations involving limit cycles and conservative Hamiltonian systems 77−78957
olfactory bulb model, spatial and temporal charact. freqs. of interactive neural masses 77−25476
perturbation theory, quasi-periodic motion, asymptotic expansion method 80−17877
plasma, nonlinear mode coupling model eqns., topological struct. 78−75304
plasma-electron beam system, high-power, relax. oscillations 80−64744
reactors, chem., relaxation oscills. 79−39120
retarded Josephson eqn., critical limit cycles 79−1644
smooth vector fields, geometrical generalization of relation between limit cycles and symms. 78−54163
stable limit cycles of vector fields, new negative criteria 78−57756
symmetric, bifurcation to asymmetric limit cycle, simple model 80−57080
synergetics, introduction and appls. 79−26019
thermal fluctuation of self oscillating reaction system under periodic external force 80−50828
transformation group and limit cycle containing nonlinear differential eqns., connection with perturbation techniques 78−20941
limited space charge accumulation
see also Gunn effect; negative resistance effects; space-charge limited devices
amorphous insulator film, high-field cond. 79−56320
polyethylene terephthalate film, elec. cond. and space charge accumulation 80−10998
semiconductor, basic shape of Gunn domain using $\mathcal{J}$ operator 77−55535
GaAs LSA diodes, current controlled LPE for optimum doping profiles 78−35318
Ge, electron heating by nonuniform elec. field, I-V characteristics 77−47825
InP, relaxation LSA mode obs. 77−8102
Si_3N_4, amorphous insulator film, high-field cond. 79−56320
ZnSe surface states, electron interaction characterisation, by low energy electron transmission photovoltaic modulation 79−60896
limiters
see also microwave limiters
frequency-selective, for correction of speech sound track defects *(Russian)* 79−27486

limiters continued
with level independent phase shifts, for H_2 maser tuning 77−19223
selective limiter-amplifier, high phase-amplitude stability 78−4632
vacuum arc plasma, fault current limiter mode, temp. distrib. diagnostics 78−9851
InSb power limiter for CO_2 TEA laser 77−38935

limiting circuits *see limiters*

linear accelerators
see also collective accelerators; electrostatic accelerators
5 MeV electron accelerator modulator charging system 79−13563
accelerating system, RF adjustment 78−78523
accelerator complex for relativistic multicharged ions, Wideroe and cyclotron accelerator 79−54655
ALFA, electron pulse stretcher to increase Frascati Linac duty factor, feasibility study 80−23237
Amsterdam 500 MeV high duty factor electron scatt. facility, status report 80−23191
applications in applied physics 77−38461
Argonne superconducting heavy ion linac 77−38459
Argonne superconducting heavy-ion linac, initial operation and recent development 79−67985
asymptotic lower exit emittance limits, mechanism 79−72003
Bates Linac, projects and improvements 80−23192
beam breakup instability in linear accelerators, theoretical model 79−72031
beam charge meas. with toroid monitors at Bates Linac 80−14026
beam coasting off axis, electrostatic potential and field 77−38796
beam energy spread, cancellation by current loading 78−9007
beam loading, reactive and resistive, effects on efficiency 78−9006
beam loss monitoring by long radiation detector 77−88310
beam profile scanner, medical appls. 80−101267
beam trajectories through einzel lens for linear accelerator ion source *(Japanese)* 80−18718
BEVALAC, high purity radioactive beam prod. 79−72129
biomedical, 4 MV, use for whole-body irrad. 80−109001
biomedical, field separation between lateral and anterior fields, dose distrib. 80−94336
Birmingham dynamitron accelerator appl. to nuclear fuel radiography using Be target 77−81452
BLIP at AGS beam transport 200 MeV line 78−25362
BNL linear accelerator development 77−38484
bremsstrahlung spatial distribution in water and water-iron by 22 MeV electron bombardment, meas. with activation detectors 77−57754
bremsstrahlung yield produced by 4 MeV linear electron accelerator calc. rel. to hazard in radiolysis 79−76181
Brookhaven 200 MeV proton linear accelerator 79−31245
Brookhaven accelerator-reactor breeder concept 77−54294
Brookhaven National Laboratory Linear accelerator reactor, system study *(Japanese)* 79−93801
bunch shape meas. and double drift harmonic buncher 77−38471
buncher, high efficiency for injection 77−38472
buncher cavity, resonant at 1st and 2nd harmonic of ANL low beta linac 79−72134
calibration monitor with a memory 80−3821
calibration using Si diode detector, high-energy photon dosimetry 78−24143
cancer therapy facility, microprocessor based control system 78−40398
CANDU Th advanced fuel cycle, accelerator breeder concept 79−45393
cavity anal., evaluation of LACC program 78−90000
cavity code, based on finite element method 78−33307
CERN, 50 MeV proton linac injector, performance 79−67972
CERN, status of 50 MeV linac project 77−38451
CERN 50 MeV linac, accelerating structure 77−38452
CERN 50 MeV linac, beam emittance meas. in matching 77−38479
CERN 50 MeV linac, beam optics 77−38477
CERN 50 MeV linac for proton synchrotron, operation and modification 77−38442
CERN linac, computer control system 77−38480
CESR control system, interface hardware 79−72069
CESR injection linac, electron beam modulator, design, performance 77−83374
charged particle beam, short pulse detect. by reverse-current method 79−63856
Clinac-18 radiotherapy accelerator, dosimetry of 10 MV X-rays 77−21631
closely-coupled cavity chain, unit cell reson. freq. meas. method 77−83179
CN-Van de Graaff at Frankfurt, upgrading 77−75009
collective effect linear accel. in presence of strong axial mag. field 77−83165
collective effects for particle acceleration 77−38495
collective ion accel. program at Maryland, electron ring and linear beam methods 77−83168
compact standing-wave electron linac with RF drive system using 3 dB hybrid junction 79−72030
compendium of accelerators used in research, 1976 77−5609
computer interface for a linear accelerator 80−51226
computerised dosimetry calcs., linear accelerator electron beam parametrisation 79−83945
conference on nuclear physics with EM interactions, Mainz, Germany (June 1979) 80−22145
control computer for Chalk River electron test accelerator 78−90004
CPS at CERN, pulse to pulse modulation, extraction modes, beam intensity 77−83277
cryogenic booster linac, heavy ion beam dynamics in chopper, buncher, mag. lenses 77−67919
Daresbury facility tandem, elec. power provision 77−83153
Darmstadt electron Linac, developments and results 77−83183
Darmstadt linear accelerator, detector system and performance of elec. scatt. system 78−70680
Darmstadt linear accelerator electron scatt. facility, beam transport and spectrom. 78−70679
Darmstadt linear accelerator electron scatt. facility, data processing 78−70681
Darmstadt linear accelerator high resolution scatt. facility 78−70653
depth dose curve improvement, Monte Carlo calcs. 79−20681
deuteron accelerator, two freq., for high power neutron generator, expt. 78−78540
deuteron Linac, 35 MeV, intense neutron source for fusion material anal. 77−83423

linear accelerators continued
deuteron linac, Brookhaven Accelator-based Neutron Generator 77−38465
deuteron linac as neutron generator for materials irradiation and fusion reactor investigation 77−34486
deuteron linac for high intensity neutron source 77−38464
deuteron linear for fusion reactor ignition 79−71991
drift tube array, meas. of alignment error by hot wire method *(Japanese)* 77−61638
Dubna heavy ion synchrophasotron facility 79−72125
Dynagen IV, compact high intensity neutron generator 77−86603
electrically conducting surface coating, of linear induction accelerator tube, beam losses and coating inhomogeneity 78−5066
electron, 20 GeV, intercomparison of high-energy accelerator field dosimetry 78−25331
electron, 2 GeV, monochromatic annihilation γ-ray beam prod. 77−50322
electron, 40 MeV, therapeutic and research appl. 79−57752
electron, 600 MeV, Saclay, 40000 hrs. of operation, recent improvements *(French)* 79−688
electron, activities at Amsterdam 77−82918
electron, ALIN accelerator, waveguide system *(French)* 79−9925
electron, ELV-1 accelerator for industrial use 77−30679
electron, equipment and methods *(Russian)* 79−13562
electron, for medical use, qualitative charact. calc. of deceleration photon pencil *(French)* 80−12282
electron, for pulse radiolysis, correl. between radiation absorbed dose and elec. parameters 77−34482
electron, health physics aspects of 20- to 40-MeV LINAC operations 79−45482
electron, high energy low running cost linac, proposed design *(Japanese)* 78−78516
electron, high-current injector 78−70655
electron, high-duty cycle, 500 MeV, electron scatt. facilities 79−72036
electron, irrad. system for photon activation anal. 77−63992
electron, klystron self excited oscillator with short time delay microwave pulse 77−6578
electron, medical, industrial and nuclear appl. 77−38473
electron, multisection, freq. charact. calc. method 79−13560
electron, pion production and appls. *(Japanese)* 78−78533
electron, prebuncher design calcs. 79−54624
electron, precise control for pulsed X-ray radiography *(Japanese)* 78−35944
electron, pulsed, giving 20 ps 300 A electron pulses, radiation chem. appl. *(Japanese)* 78−80754
electron, radioisotope production, review *(Japanese)* 78−78534
electron, regulations, standards, and guidelines for use in medical radiation therapy 79−53258
electron, status, uses, 500 MeV 100 kW linac design *(Japanese)* 78−78514
electron 35 MeV accelerator at Univ. of Tokyo *(Japanese)* 79−26786
electron 60 MeV CW accelerator using conventional standing wave linac 77−38507
electron acceleration, in two-conductor struct. by EM wave 79−26788
electron accelerator, 35 MeV, Tokyo, Univ. *(Japanese)* 79−54620
electron accelerator, asymmetric focusing coils, beam dynamics by 3-D model 78−17450
electron accelerator, computer prediction and diagnosis of failures of systems 79−693
electron accelerator, dose monitoring system 78−92710
electron accelerator, efficiency of calorimetric method 79−6778
electron accelerator, high-current, for optical pumping of gases 80−32544
electron accelerator, high-current, high pulse, inductive energy storage 78−46189
electron accelerator, linear, for 1-mA average current, 10 μsec duration 80−68978
electron accelerator, linear highfrequency, hazard factors and conditions for safe operation *(Czech)* 80−52794
electron accelerator, reduction in energy spread of nanosec. relativistic beam 80−5397
electron accelerator, two-section, two-component beam energy distrib. 80−9435
electron accelerator for split 25 MeV microtron 77−23319
electron accelerator powered by laser beam, parameter estimates 77−83167
electron accelerators, development for industry and medicine, review 79−45481
electron accelerators, elimination of electron multipacting in supercond. structs. 78−9004
electron beam, intense, ns, production in linear accelerator, space charge and radiation field effects 78−70654
electron beam, intense, transient radial motion 80−9434
electron beam collimation in SL 75 accelerator, electron therapy appl. 80−41204
electron beam diode, repetitively pulsed 79−76164
electron beam photon contamination obs. 79−59285
electron bunching, optimum phase energy distrib. determ. 77−379
electron CW 820 MeV normal conducting accelerator 77−38503
electron gun voltage supply, using pulse transformer 77−75007
electron guns, high-current, laminar beam formation 78−74516
electron linac design for pion radiotherapy 77−83138
electron linac transient operation 77−83163
electron linear accelerator, development and present status, review *(Chinese)* 79−54625
electron linear accelerators, freq. control methods *(Chinese)* 79−54619
electron polarised source, injection gun for Stanford linear accelerator 79−76242
electron pulsed high current nanosecond accelerator 78−826
electron radiation processing applications 77−54370
electron scattering experiments, detection system of proportional chambers, scintillation and Cerenkov counters 80−52809
electron supercond. accel., 3 MeV, design and status 79−72009
electron test accelerator, computer control of beam transport system 78−25359
Electron Test Accelerator, graded-β, modelling of high energy portion of proton linac 77−38467
electron Van de Graaff, digital beam-intensity meter and fluence programmer 77−54378
electronuclear fuel producer, linear accelerator driven design 79−81063

linear accelerators continued
electrostatic 160 kV, 200 mA dc accelerator for high 14 MeV neutron yield 77−83421
EM conservative fields, canonical formulation 78−33310
EM field in cavity, calc. by MESSYMESH computer program 77−38462
EM fields in resonance systems used in charged-particle accelerators 80−37641
emittance meas. unit for 100% duty factor Linac injector beams 77−38490
energy doubling using coupled cavities *(Russian)* 78−70652
ETA, electron gun injector 79−76157
ETA gun, beam dynamics calc. with EBQ code 79−72023
ETL electron accelerator, energy increased up to 40 MeV by improvement of klystron efficiency *(Japanese)* 78−78515
Fermilab, acceleration development 77−38478
Fermilab, H^- injection linac, operation and uses 79−71989
Fermilab cancer therapy facility, status report after $2^1/_2$ years operation 79−79628
Fermilab linac, microprocessor-based preaccelerator control system 77−38481
ferrite-filled waveguide, chopped electron beam, self-accel. theory 77−54660
field control in standing wave structure at high average beam power 77−38486
filtering of the six-dimensional phase volume of a beam in a linear ion accelerator 79−67994
fissile and fertile material, non-destructive testing 77−74917
fissile fuel breeding for nuclear fuel cycle 79−49814
fission fuel breeder appl. 79−81059
fission product transmutation using linear accelerator for protons of 0.5 to 1.5 GeV 78−13268
fission reactor driven and regenerative systems, U and Th fuel cycle 79−81064
fission reactor fuel breeding 79−81062
fission reactor fuel enrichment, and waste disposal, appl. 79−67980
FMIT accelerating struct. design 79−76160
FMIT accelerator vacuum system 79−71993
FMIT deuteron accelerator, proposed RF system 79−67981
FMIT deuteron linac, Alvarez section geometry choice 79−72130
FMIT neutron source, energy spectra and yields, fusion reactor mat. development appl. 80−32552
FN tandem accelerator, telemetry component tests 77−83156
Frascati, annihilation photon beam prod. 77−83438
Frascati linac, feasibility study of electron pulse stretcher to increase duty cycle 79−72135
free electron devices for light prod., history, book contrib. 79−27147
functional generator of controlling voltage of energy modulator for injector 80−68975
Fusion Materials Irradiation Test Facility, high flux neutron source for material development 80−32551
fusion reactor ignition appl. 79−71992
GELINA, electron linac, neutron time of flight meas. appl. 78−90002
GSI heavy ion research facility, two step linear accelerator, appls. 77−19041
Gyrocon, efficient relativistic high power VHF generator 80−13990
Hanford FMIT linear accelerator, high energy beam transport 79−76159
Harwell, 136 MeV electron linac 80−863
Harwell 136 MeV electron linac, slow neutron production, optimisation calcs. 79−41048
Harwell linac, small angle neutron scatt. 80−19675
Harwell linac II total scatt. spectrometer, calibration using Ni diffr. data 78−86725
heavy element linear accelerators *(Japanese)* 79−36436
heavy ion, alternating phase focusing 77−38476
heavy ion, Argonne, development and production of supercond. resonators 79−36435
heavy ion acceleration, spiral loaded cavities 77−38455
heavy ion accelerator, ring compressor magnetic field distortion by disconnected multiturn coils 78−66436
heavy ion beam linac, 12.5 MHz, for ion beam fusion 79−76158
heavy ion boosters for electrostatic tandems 78−33328
heavy ion experiments at UNILAC *(German)* 78−66435
heavy ion facility, target production 80−23213
heavy ion fusion, linear accelerator facilities at Argonne 78−50327
heavy ion linear accelerator, Munich, 50 kW transmitter, power stage design 77−83175
heavy ion low and medium energy accelerators, recent design advances 79−67984
heavy ion post accelerator at Munich 77−83150
heavy ion post accelerator test section, operation experiences 77−83149
heavy ion research facilities, Darmstadt *(German)* 77−67916
heavy ion superconducting booster, split ring resonator 77−83126
heavy ion-nucleus reactions, use of accelerators *(Norwegian)* 79−13316
heavy particles, development at Kharkov Inst., Ukrainian SSR *(Russian)* 79−22503
heavy-ion, linear induction accelerator for fusion power application 77−38483
heavy-ion 300 kV accelerator design 77−75010
heavy-ion accelerators, book contrib., review 78−90003
heavy-ion booster, Stony Brook project 77−83125
heavy-ion simulated neutron damage facility at ORNL 77−75011
heavy-ion superconducting linac, alternating phase focusing 77−3194
heavy-ion superconducting linac, design of re-entrant cavities 77−6580
Heidelberg, heavy ion 3 MV postaccel., first operational year review 79−72002
Heidelberg heavy-ion postaccelerator with spiral resonators 79−13558
HF struct., standing waves in strip transmission line *(German)* 78−50420
high average current, initial operating parameters 77−38466
high current beam stability 79−72001
high current linear ion accelerators utilizing electron neutralization 79−72016
high gradient proton linac, high energy accel. structs. 77−83144
high intensity beam profile monitors for the LAMPF primary beam lines 79−72154
high power, low energy electron linac, radiation processing appl. 79−45472
high-current 100% duty factor accelerating columns at Chalk River 77−38468
high-current pulsed linear ion accelerators, insulated drift tube 78−50417
hollow-beam accelerator, with phase focusing, limiting current 79−18065
incompatibility theorem, stability and focusing 77−3195
induction linacs, efficiency calcs. 80−99357
injection system beam dynamics, computer simulation 80−13989
injection system of Elektronika linear accelerator, triode gun anode modulation 79−67978
integrator for use in bombardment experiments 79−18092
ion acceleration in evacuated drift tube geometry 77−61637
ion accelerators and their use for controlled thermonuclear reactions, review *(German)* 79−67933
ion accelerators for fusion ignition, neutron resistant ceramic insulator development 80−37639
ion beam neutralisation in transverse mag. field 78−78513
ion beams, intense, production and postaccel. in magnetically insulated gaps 80−74041
ion beams from pulsed linear accelerator for inertial fusion 78−50325
ion linacs, permanent magnet quadrupoles, development 77−38494
ion linear accelerator, synchronous phase focusing, standing wave continuous interaction *(Russian)* 77−38444
ion linear accelerator development for neutron radiotherapy 79−20654
ion transport in linear accelerators by electron neutralisation 80−58014
iris loaded waveguide relativistic electron beam interaction, electron energy distrib. space charge effects 78−46190
Japanese, state of development 77−38449
Japanese accelerator facilities, current status and KEK 12 GeV synchrotron 79−72041
Kal'mar-1 pulsed electron accelerator, relativistic electron beam for fusion 80−32543
Karlsruhe supercond. proton linear testaccelerator, performance characteristics 79−72006
KEK, 750 keV beam line construction 77−38438
KEK, 750 keV beam monitoring 77−38439
KEK 20 MeV injection linac, operational behaviour 77−38441
KEK injector linac development 77−83146
KEK projector operation 77−38437
Kharkov linear electron accelerator for obtaining beam of quasichromatic linearly polarized photons, 2-crystal goniometric setup 80−68976
LAMPF, effect of perturbation in low-β proton accelerating structures 77−34485
LAMPF, medium energy particle beams, biomedical appl. 79−53216
LAMPF, Monitor remote handling system update 80−68979
LAMPF, quadrupole field aberrations, source of emittance growth 77−38508
LAMPF, secondary beam line phase space meas. and modelling 79−72157
LAMPF, status 77−18715
LAMPF, status 77−38447
LAMPF, status of injector complex 77−38440
LAMPF, time resolved beam energy meas. 79−71995
LAMPF beam dynamics, PARMILA computer model 77−38504
LAMPF H^+ beam chopper 79−72158
LAMPF linac, Monitor remote-handling system, status, improvements and accomplishments 79−71997
LAMPF line D fast deflector system 77−38501
LAMPF line D fast kicker system, operating experience 79−72010
LAMPF line-D fast deflector system 77−83157
LAMPF mineral-insulated magnet experience 79−31248
LAMPF muon beam characts., surface and cloud beam polarisation 79−71994
LAMPF primary beam line protection system 79−72014
LAMPF radiation effects facility, total neutron flux, energy spectrum, meas. and calc. 77−23331
LAMPF standard data-acquisition system 79−89534
large aperture contact ionized Cs^{+1} ion source for an induction linac for fusion 79−76229
laser electron accelerator, mechanism 79−81103
LASL Van de Graaff accelerator, nondestructive assay of fissile nuclear material 77−83182
leakage radiation characts., 18 MeV, clinical linear acceleration 79−5379
linac cavities, field theoretical approach to stabilisation 78−33309
LINAC-ESR spectrometer, modification for irrad. food anal. 79−52699
linacs, heavy-ion superconducting 77−83141
linacs for protons and heavy ions, loss reduction 77−83120
linacs for radiation therapy, physical characts., marketing parameters and ideal accelerator 79−53226
LLL 14 MeV neutron source facility, ion source and accelerator development 77−38491
low beta accelerating system for heavy ions 79−72005
low energy (250 keV, 2.5 mA) for neutron production 80−99354
low energy low beam system for materials studies 79−85834
low energy proton accelerator, voltage or energy calibration using (p,γ) reaction 77−50316
low-energy linac structure for PIGMI 77−83147
LWR fuel enrichment and prod. using 1-3 GeV proton accelerator 79−13497
LWR fuel regeneration and waste transmutation using proton linac 80−63365
LWR fuel regeneration by linear accelerator reactor 80−32336
macroparticle acceleration, megagauss fields 80−47789
magnetic linac as driver for impact fusion, design 79−67983
magnetically insulated linac driven by multistage Marx generator for multi-GeV beams 77−30680
magnetically insulated pulse power driven 78−5045
Mainz 300 MeV linear accelerator, energy loss system of electron scatt. facility 78−58524
MAX, a continuous electron accelerator system 80−23189
MEA 500 MeV electron linac, 140 MeV chemistry facility 80−37640
medical accelerators, neutron dose equivalent rate obs. 79−70643
medical electron accelerator, radioactive and toxic gas production 80−94378
membranes in pulsed electron beam, temp. and ultimate load calcs. 79−45484
meson beam line at Rutherford Lab. using SNS 79−74758
meson factories, status and survey in 1977 77−83161
Mevatron 60, X-ray accelerator for medical appls. 80−21530
microparticle accelerator and charged particle source description 78−41373

linear accelerators continued
microprocessor applications in upgrading accelerator controls 77−83173
microwave, transient behaviour of high-current relativistic electron beam 80−32541
microwave cavity, transient response 79−72027
microwave linear accelerators, systematic patient-dose errors 79−92387
MIT Bates Linac, progress report 77−14278
MITE, long self-magnetically insulated power transport expts. 79−90471
modular variable energy post accelerator linac 78−33327
MP tandem at Rochester, heavy-ion transmission meas. 77−83154
muffin tin cavity, computer calc. of EM fields 79−9923
muffin tin struct., transverse shunt impedance of deflection waves *(French)* 80−5396
muffin-tin structure, deflecting modes *(French)* 79−45469
multipactor effect, microwave cavity anal. 79−76175
multiple rabbit, target system for tandem Van de Graaff accelerator 77−54385
Munich heavy ion postaccelerator 79−22500
Munich heavy ion postaccelerator 79−72004
MUSL-2, 6-pass microtron using superconducting linac, operating experience 79−72042
MUSL-Z, 6 pass microtron using superconducting linac, operating experience 80−23196
nanosecond beam dynamics in linear electron accelerator 80−86996
nanosecond electron beam, particle dynamics in linear accelerator 79−26787
National Synchrotron Light Source, vac. system 79−81106
NDT appl. 78−40009
NDT application in industrial products inspection 80−81267
Netherlands National Institute for Nuclear and High Energy Physics, exptl. programme *(Dutch)* 77−46475
neutron dose levels of 8 MeV linear accelerator and 18 MeV betatron used in radiotherapy *(German)* 78−69221
neutron production by electron linear accelerator beam *(Japanese)* 78−78532
neutron production from 10 MV linac used in high-energy photon-radiotherapy 77−16995
neutron spectral meas. in intense photon field of high-energy X-ray therapy machine 78−24133
NIIEFA linear accelerator−flaw detectors for nondestructive inspection of atomic power plant equipment 79−47856
NIMROD 70 MeV injector, 665 keV pre-injector 77−38435
nondestructive inspection appl. 79−41046
NUMATRON project, high energy heavy ion facility, design, performance 78−62665
Osaka University linac 79−72028
particle dynamics computer modelling, alternating phase focusing LINAC *(Russian)* 80−23234
particle tracing simulations 79−71999
particle trajectory distortion by strong focusing fields 80−83228
permanent quadrupole magnets 77−38498
Philips SL/75-20, 18 MV photon beam, fast and slow neutron contamination 78−65127
photon beam characts. of 20 MV accelerator for radiation therapy appls. 80−26430
photon beam fast neutron contamination obs. 79−59284
picosecond pulse electron linac, design and manufacturing *(Japanese)* 80−5395
PIGMI, 250 kV proton injector system 79−45467
PIGMI, accelerator control system 79−45475
PIGMI, linear pion generator, mechanical technologies 79−72008
PIGMI, linear proton accelerator, mechanical description 79−45474
PIGMI program at LASL, proton linac development for medical appl. 79−45471
PIGMI prototype, linear pion generator, initial performance 79−72007
pion beam, hydraulic servomechanism for shifting range 77−83358
pion conversion target for Saclay electron linear accelerator 77−54384
plasma waveguides appl. as accelerating structures 80−9438
prebuncher design calculations for 150 MeV electron linac 79−68075
proton, accelerating structure of meson factory 77−38482
proton, appl. to reactor fuel breeding 78−29630
proton, electron and H^- accelerators, USSR Radiotechnical Institute developments 77−38448
proton, electron and ion [conference, Ontario, Canada (Sept. 1976)] 77−38445
proton, high energy, possible use of quadrupoles with permanent magnets 77−23320
proton, increase of beam radius and image ellipsoid 77−65360
proton, ion sources and injector development 77−38470
proton, non-destructive bunch length monitor 77−376
proton, optimum particle bunching 78−5068
proton, source of neutrons for radiotherapy 77−81569
proton, with variable phase focusing, calc. parameters 77−46426
proton accelerating mechanisms in vacuum diodes, induced radioactivity 79−97470
proton accelerator, parameter errors, theory 77−30678
proton accelerator, with quadrupole RF focusing, URAL-15 78−82543
proton accelerators, struct. reson. 77−83158
proton beam cooling channel for injection into linear accelerator 80−68973
proton dynamics in linear accelerator with variable phase focusing, space charge effect, simulation 79−13561
proton high current appl. in nuclear power 77−38450
proton high power accelerators for fissile material spallation breeding 77−83162
proton injection into a large amplitude space charge wave 79−71990
proton linac, KEK preinjection accelerating column 77−38436
proton LINAC−injector I-2 operation for several users 79−45480
proton linear cavity, calc. methods for field distrib. 77−38505
proton pion generator for medical applications, beam dynamics 77−38475
proton pion generators for Medical Applications 77−38474
proton radiography beam line establishment at Fermi National Accelerator Laboratory 78−65121
proton-pion generator for medical irradiations, mechanical fabrication 77−38496
pulse amplifier with digital gain control 80−68977
pulse amplitude instability meas. apparatus 78−82537
pulsed electron gun with Ta cathode, for linear accelerator *(Russian)* 79−9924
'Pulsed ferrite core tests for 50-ns linear induction accelerator' 79−690
linear accelerators continued
pulsed linear accelerators for inertial fusion driver appls. 80−13842
pulseline driven neutralised linear ion accelerators, longit. instabilities 80−78459
Pulserad 445W, a compact high-power beam generator 79−76172
quadrupole lenses, magnetically hard, for ion drift tubes 79−3261
quasi-static drift tube accelerating structs. for low speed heavy ions 78−82542
radiation free linac of meson or neutron generaton type 77−38502
radiation therapy simulator and linear accelerator meas. and control by microprocessor 77−40902
radiotherapeutic linear electron accelerator NEPTUN-10p 78−88744
radiotherapy, dose levels due to neutrons 77−13008
radiotherapy, high-energy accelerators, mixed photon-neutron field meas. 80−51267
radiotherapy, linear accelerator, 5.5 MeV Neptune phys. characts. of beam *(French)* 77−29196
radiotherapy, linear accelerator neutron sources and characts. 80−51239
radiotherapy, Mevatron 20, compact high-output linear accelerator 78−28035
radiotherapy, SL 75-20 accelerator, neutron and gamma doses in entrance mazes of treatment rooms 80−85500
radiotherapy, use as simulator 78−3581
radiotherapy, use factors 77−9275
radiotherapy 4 MeV rot. accelerator, medical usage factors for radiation protection 77−64139
radiotherapy accelerator neutron leakage survey 80−51269
radiotherapy accelerator primary beam neutron contamination 80−51268
radiotherapy Clinac-18, satellite digital display 78−3599
radiotherapy electron accelerator neutron prod. 80−51240
radiotherapy high-energy linear accelerator photon beam exit design for neutron prod. minimisation 80−51242
radiotherapy moving-strip technique, comparison of ^{60}Co unit and Varian 4 and 10 MV linear accelerators 77−70553
radiotherapy neutron leakage characts. rel. to room shielding 80−51273
radiotherapy treatment verification and recording using small computer 77−81554
radiotherapy with electrons, up to 20 MeV, phys. aspects 80−85474
reactor fuel enrichment by proton accelerator 79−13498
reflex triode, unidirectional ion generation and geometric focusing 79−76235
relativistic electron beam accelerator, FX-75, 1-D coaxial transmission line model, FXPULSE program 78−58506
relativistic electron beam destruction and equilibrium in mag. guide 79−76171
relativistic electron storage device, phase free cavity resonator+mag. mirrors 77−83172
relativistic heavy ion accelerator description and applications *(German)* 78−78522
relativistic high current nanosecond electron beam, transverse instability 77−83180
resonant frequencies and quality factor meas. for accelerating struct. with plane symmetry *(French)* 77−30676
resonator sensor for the parameter of charged-particle beams 80−68991
RF, low cost struct. for electron and proton linacs 77−88293
RF accelerating structures, improved reference cavity design for freq. tracking 77−83176
RF cavities with cylindrical symm., evaluation by computer program SUPERFISH 77−18714
RF cylindrical cavity, evaluation by computer code SUPERFISH 77−38463
RF high power supply for Chalk River 100% duty factor Alvarez linac 77−38487
RF linac cavities, microprocessor based control 79−71996
RF quadrupole beam dynamics 79−71986
RF structures as high duty factor structures for e^+e^- storage rings 77−38469
RF superconducting resonators for booster linac 79−54623
RILAC, variable freq. heavy ion linac 77−38454
S-band standing wave accelerators, effective shunt impedance 77−38492
S-band standing wave with on-axis couplers, mechanical design 77−38493
S-band subharmonic prebuncher for picosecond single electron pulse *(Japanese)* 80−78460
Saclay 600 MeV electron linac, present and future operation 80−23190
Saclay 600 MeV linear accelerator, facilities and expts. 77−61636
Saclay linac, 500 MeV intense positron source 79−72171
Saclay linac, flexible dialogue using computer control room 77−38499
Saturne, improvement in 20 MeV beam brightness 77−38500
self-magnetic insulation in vacuum for coaxial geometry 78−78520
SEM with electron energies up to 5 MeV 79−80728
Sendai 1.5 GeV linac electron accelerator with pulse-beam stretcher ring 80−23188
shielding, local absorber in accelerating section to reduce radiation level 80−83229
short pulse accelerators, resistive wall coating's parameter determ. 80−63418
simulation, code PARMILA, longitudinal tuning of low energy linac portion of LAMPF 77−83159
SL 75-20, clinical results with 79−48332
SLAC, beam containment electronics operational experience 77−83466
SLAC, control and monitoring system, use of microprocessors, cost 77−83177
SLAC, electron beam spectrum monitor using synchrotron light 79−72146
SLAC, microwave beam position monitors 77−38488
SLAC, polarised electron gun, operating experience 77−83396
SLAC 3 km accelerator, single bunch beam loading 77−83160
'SLAC beam, feedback system for steering and energy correction in beam switchyard 79−93852
source definition for head shielding requirements in linear accelerators, effect on room shielding design 80−46068
space uniform quadrupole focusing 79−71998
stabilizing resonator of high-power klystron self-oscillator for microwave supply system of linear accelerator 80−42878
stable particle motion in accelerator with solenoid focusing 79−72000
standing wave high gradient accelerator struct. 77−83143
standing wave high gradient structure, design concept 78−50423
standing wave triperiodic structure for 10 MeV medical accelerator 77−10498
Stanford superconducting heavy ion linac, reentrant cavities 77−83124

linear accelerators continued
Stony Brook supercond. heavy-ion linac, current status 79−67986
superconducting, electron acceleration charact. 77−83178
superconducting accelerator structs. for medium energy protons 77−83151
superconducting cavities for heavy ion LINAC, beam tests and phase locking 77−26896
superconducting heavy-ion, hybrid solenoid as focusing element 77−38460
superconducting heavy-ion resonator, microprocessor based feedback system 77−88292
superconducting linac with MUSL-2, a second microtron 77−83198
superconducting linear accelerator, comparison of short muffin tin structs. *(French)* 78−33330
superconducting Nb split-ring resonator as heavy-ion accelerating struct. 77−26895
superconducting proton-linac, Karlsruhe, 1.8K cooling circuit 79−58707
superconducting quadrupole magnet design for ion beam fusion linac 79−36433
superconducting quadrupole magnets for Karlsruhe proton linac 77−26889
superconducting resonators, ion acceleration at 4.4K 77−34483
superconducting slow-wave structures for accelerators 77−38458
superconducting split-loop resonator as heavy ion accelerating element 77−26894
superconduction linac recyclotron at Stanford, initial performance 77−83145
superHILAC, MINUS3 general purpose data acquisition system 79−93901
superHILAC, operation information 77−38453
superHILAC, Wideroe pre-accelerator 77−38457
tandem, 16 MV, Legnaro, description of facility 78−25352
tandem 1.2 MeV accelerator at Giessen polarisation facility 77−65359
tandem Pelletron, calibration of 90° analysing magnet 77−57777
teaching experimental nucl. physics, undergraduate course 77−30
theoretical physics at Kharkov Inst., Ukrainian SSR *(Russian)* 79−12558
Therac 6 linear accelerator, computer controlled evaluation for X-ray therapy 79−5363
Therac 6 linear accelerator, field elongation effects on depth-dose curves, central-axis output of X-rays 79−5361
three-stage MP accelerator upgrade program at BNL 77−83142
tissue-maximum ratio expression fitted to Varian Clinac-6 and Clinac-4 accelerators 78−24148
TOF pulsed neutron diffraction of liquids using electron linac, CCl_4 appl. 78−18504
Tohoku 300 MeV LInac, energy compressing system 78−74515
Toshiba LMR-16, X-ray depth-dose charact. 79−62369
transformer, 3 MV, for PFL pulse charging 79−76173
transmission line, charged internally switched configurations for electron acceleration 79−72024
travelling wave accelerator, beam loading effects 77−377
travelling wave linac., magnetic-gun igniter for controlled thermonuclear fusion 80−91238
TW drift-tube structure for CERN SPS acceleration system 77−38517
two stage linear accelerator, H ion beam optics 79−36438
ultrahigh-power ion accelerator, pulsed, operating regimes 80−78462
undulator linac, electron dynamics, coherent radiation source 78−82539
UNILAC, Darmstadt, heavy-ion research 77−67917
UNILAC, Darmstadt, kinetic energy of ^{86}Kr accelerated ions, recoil proton technique 78−58527
UNILAC, heavy ion collisions up to 10 MeV/nucleon review of recent developments 78−50194
Unilac, prestripper accelerator 77−38456
Unilac, stripper section 77−38485
Unilac beam diagnostic system 77−38489
Unilac heavy ion accelerator, development and status 77−38446
Unilac heavy-ion RF accelerator 77−57775
Unilac injector for stable elements 77−34481
Unilac status report 77−83140
Van de Graaff, 10 MV, digital data telemetry system 77−83155
Van de Graaff, proton beam resolution improvements 77−75008
Varian 18 MeV, transvaginal cone electron beam technique 80−21531
Varian 6 MV CLINAC-6X accelerator, beam charact. 78−3582
Varian Clinac 18/10, use of polystyrene filters for electron energy modification 80−56168
Varian Clinac 4 MeV linear accelerator, radiation from U collimators, and shielding 78−24135
very cold neutrons from linac-cold moderator system 80−27842
waveguide bunchers, nonlinear anal. 77−378
waveguide RF power manifold, resonantly coupled 77−38497
Wideroe-based heavy ion preaccelerator for the SuperHILAC 79−71987
X-radiation, primary and leakage, attenuation in concrete 79−63823
X-ray beam, 4 MeV linear accelerator, dosimetric aspects in radiation therapy 80−17140
X-ray beam characteristics, 25 MV, from a 35 MeV linear accelerator 79−25110
X-ray beam energy at off-axis points, calc. technique for correct. 80−81742
X-ray beams, off-axis beam quality change 80−78461
π factories, multidisciplinary role 78−21791
π production and properties, LAMPF linear proton accelerator *(French)* 80−63417
π^- clinical facilities, linear accelerator selection 79−20645
B^- ion beam acceleration in EN tandem 77−26912
Be^- ion beam acceleration in EN tandem 77−26912
^{48}Ca tandem accelerated beam 77−79496
Fermilab, H^- ion program 77−38506
H^- ion short bunch shaping at entrance of accelerator, calcs. 79−700
H^- ion source, 50 mA for accelerator injection, beam quality and reliability 79−72172
H_2 generator, resonator tuning methods 77−88294
^6Li vector polarised source at Heidelberg EN tandem 77−65371
Na vapour charge exchange cell 77−38542
Nb superconducting C-band cavities for linear accelerator appl. 79−36432
Nb_3Sn disc loaded waveguide, for linear accelerator appl., fabrication and props. 77−26892
spiral resonators, independ. phased, postacceleration and bunching of 150 MeV ^{58}Ni 77−34484

linear algebra
see also determinants; eigenvalues and eigenfunctions; matrix algebra; tensors; vectors
*-algebra classical moment problem generalisation, relativistic quantum theory appl. 77−54039
array algebra for multilinear least squares prediction and filtering 78−69470
CG method generalisation, linear and nonlinear problem appl. 79−30243
Cholesky-conjugate gradient method, incomplete, for iterative soln. of systems of linear eqns. 78−28932
classical mechanics, canonical formalism, Bose type classical Hamilton algebra, phase space variables 78−54170
conformal mapping technique for plate vibrs. on elastic foundation 78−79251
density matrix characterisation, geometric and other methods comparison 79−6001
dynamical system, connectance, increasing no. of degrees of freedom 78−81831
EM permeability of vac. and light-cone structure 80−36879
Euler's theorem on rigid-body motion, matrix theoretic proof, for teaching 79−62964
flow, Couette, statistical linear algebraic model 78−47002
four-velocities in quantum theory, K-space 78−49720
Gauss and Mainardi-Codazzi eqns. generalisations, appls. to quantum and classical mechanics 78−62092
gyroscopic system, linear, damped, modal anal., appl. to satellite 78−63275
heat pipe, heat transfer agent flowrate through porous wick, approx. calc. method 78−75197
Hermitian, antiHermitian and unitary operators, basic props. for quantum mechs. appl. 78−54113
Hilbert space decomposition and W-A determinant factorisation in linear transport theory 77−67189
hyperbolic conservation laws, Glimm scheme for solving, deterministic version 78−20972
infinite equation system of plane wave diffraction on periodic array, reduction *(Ukrainian)* 77−67205
Kirkwood-Salsburg operator, spectral props., connection with Mayer-Montroll eqns. 77−74307
Lie algebra, class of representations on vector field, partial differential operators *(French)* 77−67228
linear equation solution, out-of-core assembly in FORTRAN IV subroutines 79−30213
linear response theory and area preserving mappings, review 78−62174
N-level system, generator of completely positive dynamical semigroups 78−45513
noisy exponential decays, algebraic anal. for on-line computer anal. 77−67415
non-self-adjoint linear operators, bivariational bounds 77−49569
oil-bearing layer with input parameter correction, discrete dynamic model 80−83778
operator equations, convergence rates of variational solns. 77−33
optical image matrix transforming system 79−7086
optical imager, linearly degraded, iterative restoration 80−95807
optical images, linearly degraded, iterative restoration, reblurring procedure 80−99640
orthocomplemented subspaces of nondegenerate partial inner product spaces 78−32647
orthonormalisation method, appl. to j-j coupling of fermions in single j-shell 78−81922
paired summation eqns. with legendre associated function kernels, effective solution 79−84968
partial differential equations, multidimensional, fast implicit iterative soln. method 78−93519
penalty function techniques for constraint definition, error analysis 77−41467
perturbed energies, 2nd order, coupled HF iterative procedure, geometric approx. 79−9991
planar wave diffr., soln. from knife-edge grid with complex period struct. 79−72467
plane wave set, orthogonalised, construction method, bound states 79−25894
quantum field theory, conformal-invariant, composite field operators 78−81886
quantum fields, exponential momentum-space growth, generalisation of local commutativity 78−21013
quantum statistical mech., correlation inequalities hierarchy, relation to equilib. states 78−21064
reconstruction from projections, uniqueness and resolution, book 79−43989
representation of linear operators in L^2 spaces, generalised matrices 78−62095
resistance of anisotropic medium, geometric effects 79−28331
resolvent operator expansion 77−49551
simultaneous linear eqns., topological soln. 80−31483
spin-1/2 models, on square lattice, sublattice renormalisation transformations 78−65878
temperature field, heat transfer problems, linear algebraic soln. method 78−59281
tube, circ., entrance region, mass transfer, asymptotic expansion soln. 78−87392
turbulence, fractal approach, attractors and dispersion 78−46943
turbulence, Lorenz attractor struct. 78−46944
turbulence dynamical systems approach, Navier-Stokes eqns. and strange attractor 78−46942
two- and three-dimensional magnetostatic problem program packages 79−41276
two-density matrix, N-representability, rels. between necessary conditions 79−6000
von Neumann algebra, unbounded derivations and invariant states 78−45456

linear combination of atomic orbitals calculations *see LCAO calculations*

linear differential equations
acoustic wave propagation in isotropic viscous weakly compressible medium, eqn. limits problem *(French)* 80−8808
active electrooptic and magnetooptic media, matrix theory fundamentals *(Russian)* 78−63005
asymmetric top rotational Brownian motion and electric polarisation calc. 80−15949

linear differential equations continued
atom recombination, heterogeneous, Smith-Linnett theory, H_2 appl. 77−48634
baroclinic equatorial motions, nonhomogeneous eqn. 78−49098
biological model mathematically exact soln. by Laplace transform *(German)* 79−1991
Blasius profile, eigenvalues determ. using Riccati transform. method 77−65731
boundary layer equations with self-induced pressure, anal. for $M_\infty=1$ case 79−86458
boundary value problem for linear partial differential eqns., approx. soln. *(Russian)* 77−57170
Cauchy problem, linear eqns. with const. coeffs., absolute instability, 3-dimens. 79−12622
cell growth appl. of time-optimal control theory 77−40638
cone with arbitrary surface deviations in supersonic gas flow, aerodynamic characts. 77−19620
confined solutions of multidimensional inversion equations 78−77678
conserved densities, Hamiltonian systems 80−90682
continuum mechanics, macroscopic determinancy principle corollaries *(Russian)* 78−77714
Cosserat viscoelastic inversion problems, models *(German)* 77−84166
coupled, second-order, hybrid soln. method 80−94968
coupled second order eqns., adiabatic expansions of solns. 79−71226
degenerative parabolic eqns., first boundary problem *(Russian)* 77−22374
diffusion, finite element method appl. *(French)* 77−78965
diffusion of O_2 facilitated by haemoglobin and myoglobin 77−48747
earthquake model, nonstationary, identification, nonlinear filtering approach 79−5458
education, linear differential eqns. with polynomial appl. Schrodinger eqns. 77−49522
extended Graetz problem, approx. soln. by orthogonal collocation 77−89118
Falkner Skan eqn., exact soln. 79−98680
Feynman integrals, holonomic character and local monodromy struct. 77−54038
Feynman integrals, singularity struct. study using micro differential eqns. 78−74123
first-order, optimum integration operators 77−78962
forced second order eqns., nonoscillatory solns. 77−17775
fourth order, numerical soln., finite difference formulae for boundary value problems 78−73856
functional equations of neutral type with periodic coeffs., stability *(Russian)* 77−60903
hard rods and spheres, radial distrib. function, differential difference eqns. in Percus-Yevick approx. 79−18701
Helmholtz equation in Euclidean 2-space, symmetries 77−17781
Helmholtz homogeneous equation, numerical soln. methods *(German)* 78−90337
Hill's equation determination from spectrum, necessary and sufficient conditions 77−9853
holonomic quantum fields, deformation model 79−25907
holonomic quantum fields, model 79−25908
holonomic quantum fields, model 79−25909
holonomic quantum fields, Riemann-Hilbert problem on complex sphere 79−25910
holonomic quantum fields 79−25911
hydrodynamic type equation, asymptotic fundamental system construct., thermally stratified plane Poiseulle flow *(German)* 77−902
hyperbolic mixed boundary value problem, soln. existence, uniqueness, hydraulics appl. *(German)* 78−93514
hyperbolic partial differential equation, reciprocity rels. 77−37732
inhomogeneous integral representations of particular integrals 78−45465
integration using Runge-Kutta-Nystrom algorithm *(German)* 78−8235
iterative numerical solution method for second order linear differential eqn. with two strong singularities *(German)* 77−30000
ladder operators of group matrix elements 80−31555
linear two point boundary value problems, reduction to Cauchy systems 78−54158
local two-body interaction, first order linear eqns. 78−45516
magnetostatics, integral equations 79−72453
matrix differential equation, rotations as solns., for teachers 78−62021
motion in spherically symmetric force fields, vector consts. differential eqn. 78−85833
multibody system equations of motion, computer-aided formulation *(German)* 78−39
multiterm linear recursion relations 77−29992
multivalent binding to substrate, linear differential equations in chemical equilibrium calculations 80−30279
mutlicompartment analysis, direct estimation of parameters, appl. to drug conc. 77−44580
neural membrane two-factor two-mode model 78−7330
non-conservative systems, dynamics 77−2538
non-self-adjoint linear operators, bivariational bounds 77−49569
nonequilibrium processes, eqns. of motion derivation 77−13696
nonlinear eqns., linear correspondents 78−20949
nonlinear network noise anal., algorithm *(German)* 77−88997
nonlinear periodic waves stability in plasmas 80−38615
nuclear reactor system fixed end-point problem suboptimal control, appl. *(Japanese)* 78−33259
numerical solution of linear elliptic and parabolic partial differential eqns. with boundary singularities 78−41142
oscillations, free damped, differential eqn. soln., teaching appl. 79−62950
partial, canonical forms of some completely integrable systems 77−67214
partial, multidimensional inversion formalism as compatibility condition 79−84961
partial, system with constant coeffs., Cauchy problem 77−67215
partially cavitating hydrofoil, linearised theory, singularity method *(Japanese)* 78−14050
periodic coefficients, stability conditions, energy expressions *(German)* 77−53746
periodic coefficients with small modulation, solution techniques 78−87155
periodic solns. of eqns. with maxima *(Russian)* 79−12571
relativistic fluids, partial differential eqns., hodograph transformations 77−955
renal medulla solute cycling model soln. by Laplace transforms 77−40694

linear differential equations continued
Riccati method for difficult eigenvalue problems 77−64937
Riccati transformations for eigenvalues of eqns. with separated boundary conditions 77−38
Riccati transforms., eigenfunctions of linear differential eqns. with separated boundary conditions 77−64936
rods, generalised conjugate analogy for arbitrarily curved rods 77−49588
second order, const. coeffs., two linearly independ. solns., change of variable 77−13546
second order, symm. and separation of variables *(Russian)* 78−65752
second order, symm. and separation of variables *(Russian)* 78−73828
second order eqns. with periodic coeff. *(Russian)* 79−58528
second order linear partial differential eqns. of math. phys., integration by separation of variables *(Italian)* 78−81798
second order nonhomogeneous, oscill. type behaviour of solns. 78−32662
second-order, solutions, eigenvalues and eigenfunctions 77−9852
Seidel's process for linear eqns. with non-negative elements *(Ukrainian)* 78−54165
self-adjoint differnetial eqns. in finite elasticity for small superimposed deforms. 77−78982
shape of drop on inclined plane, analysis 78−79856
singulary perturbed evolution eqns. in Banach space 77−64924
solar energy, photosynthetic conversion in agricultural systems, incremental model 79−70457
solution of $dy/dx=(a_1x+b_1y+c_1)/(a_2x+b_2y+c_2)$ 78−77641
special functions for phase integral approx. 79−75321
stability criteria for time-dependent flows 78−79305
Stokes multipliers for a class of ordinary differential equations 80−12891
structural dynamics problem soln., generalised Euler method 79−46245
symmetry, algebraic classification *(Russian)* 77−74193
symmetry and separation of variables, book 78−36798
systems with periodic coeffs., stability determ., numerical method 77−2535
Szebehely equation in celestial mechanics, modification 78−24447
third order eqn., soln. zeros *(Italian)* 77−29989
time-dependent polynomial Hamiltonians, nonlinear transform. 79−40395
total dynamic characteristics of meas. facilities, limit error estimation 78−77841
turbulent flows with coherent structs., theory of mixing mechanism 79−7369
two nonlinearly coupled variables, space and time evolution, special solns. 77−78960
with variable algebraic coeffs., Laplace transforms appl. *(Czech)* 78−86115
vector-matrix differential eqn., convergence of assoc. eigenfunction expansions 78−69965
vibrations of parametrically excited systems 79−80425
Si, epitaxial film, dopant incorporation model 79−99228

linear integrated circuits
amplifier, high input/low output impedances, nucleonics appls. 80−5451
analogue ohmmeter circuits, design, review 78−37031
automatic camera lens focusing, using optolinear chip 78−54480
CMOS 77−41653
environmental thermometer, using ICs and Si transistor 79−67300
monolithic implantable CW Doppler US flowmeter appls., blood flow meas. 78−11749
photoelectric luxmeter design *(Rumanian)* 80−17993
TEM image and electron energy loss spectrum display by self-scanned linear Si photodiode arrays 80−68330
temperature transducer, two-terminal, operation and characts. 77−10021
two-channel amplifier section with common negative feedback loop 78−9042

linear motors
asynchronous motor drive system, for rotating optical components inside vac. system 80−102874
blood intermittent pump with linear motor drive *(German)* 79−5401
electric and magnetic fields calc., Green and influence functions appl. *(Russian)* 77−53745
EM travelling wave linear induction, long cond. cylinder 78−46484
graphics plotter using linear step motors 79−93127
induction, fluid flow induced in liquid metals, investigation 80−43800
slide drive system for optical machining 80−1366
$CeCo_5$ hard magnets, appl. *(German)* 77−80966

linear network analysis
basilar membrane, electrical model giving displacement 77−90810
block graph structural number, determ. by cut-set method *(Polish)* 77−33829
Blumein circuits, transient anal., for effective operation of UV lasers 77−68230
geometrical representation for teaching 78−12513
Maxwell's equations, numerical soln. by transmission line and lumped network models 80−27147
optical receiver noise analysis, time-domain impulse response technique 77−68280
T-network for Schrodinger equation, unreal components *(German)* 77−53792

linear network synthesis
retina receptor layer current spatial distribution, frog, electrical model 77−40666

linear programming
absorbed dose, bounded estimate using linear programming 78−37452
adsorption isotherms for heterogeneous substrates, improved CAEDMON program 79−77895
antireflection coating design 78−5537
biomedical pion$^-$ radiation, uniform depth-dose distrib. technique and cell survival obs. 80−17139
combined elastoplastic and limit analysis via restricted basis linear programming 79−68595
combined sewer system detention storage, real-time control algorithm 77−37281
concrete slab, reinforcement optimisation by linear programming 77−89022
diffusion, approx. soln., linear programming, regularisation 78−32775
education, linear programming, introduction and appl. to simple cct. 80−73136
elastic contact stress minimisation by contour design 78−63396
elastic plane frame anal., second-order 77−39231
elastoplastic arches, shakedown anal. 78−51091

linear programming continued
energy system modelling, New Zealand appl. 80−76590
environmental systems control, transient finite element and linear programming method 79−57497
intracavity implant therapy, appl. of linear programming to dose optimisation 80−72329
inverse gravity problem, linear programming appls. 78−28331
inverse gravity/mag. problem, appl. of linear programming, basic numerical techniques 79−53581
Lithuanian water resource distrib. optimisation, informational preconditions *(Russian)* 79−92555
lung ventilation-perfusion ratio resolution of inert gas data 77−12943
moment problem, density functions, linear programming formulation 80−53620
multicomponent fluorescent mixtures, quantitative anal. of data 78−27833
multicomponent spectra, resolution by multiple regression and linear programming 79−74443
national energy policy anal. and planning models 80−101071
nuclear optical model parameter searches, minimisation procedures, use of derivatives 77−10379
nuclear reactor, multizone, reactivity and power shape control, optimisation method 77−6529
optimal composite sheets, fixed upper bound on number of layers 78−30177
optimal control of 1-D linear distributed parameter systems with cost functionals 78−59257
optimal plastic design of circular plates, linear programming appl. 78−42539
optimal water distribution systems design 78−61457
pattern recognition, mathematical programming techniques 78−92523
plastic anal. of thin-walled beams of open cross section, finite-element model 80−74767
polycrystalline metals plastic stress-strain relations computation 77−22419
porcelain techno-economic form. by linear programming 78−39721
Pourbaix diagrams, calc. using modified linear programming technique 79−10919
regional wastewater management systems, chance constrained approach 79−57513
regional water quality management, goal programming approach 79−57514
reinforced concrete deep beams, optimal force transmission 78−34009
reservoir design and management, SESLP model 79−2314
reservoir management for irrigation, chance-constrained linear programming 79−2317
respiratory mechanical behaviour lumped parameter models evaluation using simplex algorithm 80−89783
SAW filter design optimisation 79−32154
SAW filter design using linear programming technique *(Japanese)* 77−23839
sensitivity theory, general nonlinear algebraic equations with constraints 78−21086
space vehicle family selection for space study programs 79−8790
spacecraft trajectory optimal correction, pulse count constraint, combinatorial method 77−64598
spatially-varying image degradation compensation 77−58275
super modified simplex, appl. to flame spectrophotometry 78−3397
transport, problems, estimation of moments 77−71281
water shortage and supply, Israel, long-run policy for agriculture 78−61454

linear rectification *see rectification*

linear rectifiers *see rectifiers*

linear systems
acoustic radiation and scatt. anal., use of linear system theory 77−75729
acoustic signals, matrix formulation of coherence rel. to unwanted signals removal 77−46831
acoustic system identification, from multiple input/output data, comment and reply 78−83179
aerodynamic stability of Timoshenko bar, time- and space-harmonic balance *(German)* 80−83812
bilinear systems, unconstrained, optimal control 77−10464
catheter pressure meas., transducer smearing correction using microprocessor based discrete deconvolution 80−67275
conservative, energy flux for plane waves 78−12574
continuous-time, varying environment, state estimation methods 79−12581
damped linear systems, vibr. 79−18790
deconvolution, for detn. of input from output data, thermokinetics appl. 78−12699
dynamic system, optimal transfer impulse function calc. *(Polish)* 77−53753
frequency response of complex lumped parameter linear systems 78−5610
generalised backward substitution method of soln. 79−63008
instrument mechanism analysis, error statistics *(Hungarian)* 78−49823
kinetic equation for a linear dynamic system with Poisson parameter fluctuations 80−31675
linear systems with nonwhite parameter fluctuations, differential anal. 79−85082
mean square response to nonstationary random excitation 80−57085
measurement, dynamic errors calc. 77−5796
medical US, linear-filter model for signal transmission process 80−17026
microdensitometer flare, methodology for quantifying 80−52293
monochromator, total spread function description of props. 80−19100
multiple parameter system vibrations and stability, book 78−93532
non-conservative systems, dynamics 77−2538
nondelta-correlated parameter fluctuations, statistical anal. 80−95036
optimal control of 1-D linear distributed parameter systems with cost functionals 78−59257
oscillation due to external parametric random perturbations *(Russian)* 79−17207
oscillatory system response to shock impact *(Russian)* 79−9096
parallel-connected transducer systems, integral parameters determ. 77−17939
parametric, time delays, optimality, control coordination and entropy *(French)* 77−9161
process dynamics investigation using time-varying models 77−41099
randomly perturbed systems, mean-square stability 77−9870

linear systems continued
respiratory system, human, modelling and parameter estimation 80−12169
respiratory system, human, modelling and parameter identification 79−39444
response to square wave force, transients, teaching appl. 80−31467
single process integral parameter meas. method 77−5792
solution by modified Stone finite element method *(French)* 79−41279
spectral anal. of systems with multiple inputs and outputs, comment 79−17344
stability of motion rel. to part of variables *(Russian)* 78−86144
stable structure maximax response estimates compared 79−68626
statistical analysis of system acted upon by Poisson processes 80−57196
stochastic, moment and cumulant functions *(Russian)* 78−32759
stochastic, with non-white fluctuations of parameters, differential description *(Russian)* 79−145
stochastic Green's function mean value Dyson eqn. approx. anal. *(Russian)* 77−74201
stream-well-aquifer system groundwater flow anal., linear system models 78−77289
structures' greatest maximum response analysis 78−38241
time varying systems, stability anal. 78−37
vibrating, damped, of finite degrees of freedom, numerical solution 78−24656
Volterra kernel estimation of bilinear systems, cross correlation algorithm 79−80919
Volterra stochastic integral eqns. of second order, anal. of dynamic system of variable inertia 77−57166
weakly coupled linear systems, block iterative LU solution technique 77−60941

linear vibrations *see vibrations*

linearisation techniques
see also piecewise-linear techniques
AC potentiometer, self-balancing, nonlinear servomechanism design *(Russian)* 78−70156
automatic blood pressure meas., device for linear press. change in cuff 77−48902
automatic piecewise linear approximation of yield function in ideal plasticity 77−46929
characteristics of Si p-n junction, linearisation of 77−53904
chemical analysis, for Beckman LB-1 CO_2 analyser 77−29215
computerised tomography spectral artifact correction 78−35953
diffusion flames, appl. of quasi-linearisation techniques 79−20368
digital thermocouple cold junction compensation methods *(Italian)* 78−37002
digital thermometer sensor nonlinearity correction *(Russian)* 79−26054
Duffing oscillator, statistical linearisation approx. method for nonlinear stochastic processes 77−17790
four-arm bridge measuring circuits with linearised characteristics *(Russian)* 79−12820
galvanomagnetic semiconductor voltage and current transducers, Gauss effect compensation 78−77892
illumination measurement appl., digital linearisation using microprocessors *(German)* 78−77961
ion-specific electrode output volt. linearisation 78−35991
materials analysis spectrophotometer with linear output 78−86344
matrix Riccati eqn., quasi-linearisation, iterative approx. 78−57871
multi-input nonlinear system statistical anal. by optimal linearisation *(German)* 78−64918
muscle mechanics in isometric contraction, linear approx. 77−73535
nonlinear stochastic differential equations, approx. soln. by statistical linearization method, variational procedure 77−17789
nuclear reactor optimal shutdown control, quasilinearisation and numerical soln. *(Korean)* 79−89395
periodic system induced oscillation and rotation analysis 77−37753
photoelectric scanning microscope output linearisation 77−5905
positron annihilation, pulsed distrib. from expt. data, parameter reconstruction 78−41290
pure harmonic tide in canal, eqns. of motion quadratic resistance term linearisation 78−69369
radiative transfer, transient temp. of body, surface radiation and convection 77−80054
radiography, straight-line tomography 78−35934
remote sensing, Planck spectral distrib. eqn. linearisation for selective radiant temp. mapping 77−56750
strain gauge transducer compensation linearisation by shunt resistors 78−12688
tail-wheel struct. of light aircraft, large deflection anal. using incremental linearisation 78−83272
thermal transducer, contact, dynamic characs. normalisation *(Russian)* 77−13748
thermistor temperature indication linearizing circuits 79−49230
thermistor thermometer bridge network charact. linearisation *(German)* 78−86271
transducer response linearisation using programmable multifunction module 78−45604
Warren-Averbach method averaging *(German)* 77−58922
water network anal. using sparse matrix and successive linearisation methods 78−85614
wedge compensator, operating nonlinearity elimination 79−32065
Pt resistance thermometer calibration charact. linearisation methods *(Russian)* 78−70123
Pt thermometers, circuit description *(German)* 78−200
Pt-Rh resistance thermometer temp. convertor for nonlinearity error correction *(Russian)* 78−70124

lines (telephone) *see telephone lines*

linewidths (spectral) *see spectral line breadth*

linguistics
contrastive, P-struct. C-struct. grammar 78−69959
intelligent communication device, design parameters 77−52928
Japanese, consonant perturbations, and vowel articulation by adjacent segments *(Japanese)* 78−92655
Japanese kinki dialect, anal. and perception of two-mora word accent types *(Japanese)* 78−92659
Japanese vowels, multivariate anal. of estimated vocal tract area functions *(Japanese)* 79−27469
subglottal air pressure and vocal-fold tension, indirect assessment of contrib. to changes of fund. freq. in English 78−92650
Telugu vowels, acoustic-phonetic features 79−18666

linguistics, computational *see computational linguistics*
linguistics, language *see linguistics*
linkages (electric connectors) *see electric connectors*
linking *see joining processes*
links, telecommunication *see telecommunication links*
Liouville equation
see also Vlasov equation
aromatic hydrocarbon soln., delayed fluoresc., mag. field effect, excimer form. 77−14479
aromatic radical ion recomb., mag. field modulation, Liouville eqn. soln. 77−28995
atom+diatom, vibr.-translational energy transfer, self-consistent and stochastic treatment 77−83693
atoms, eqn. of motion-Green's function and config. interaction methods comparison, appls. 80−47841
Brownian fluid affected by potential, Maxwell-Boltzmann distrib. in infinite-time limit 80−105573
Brownian motion, Fokker-Planck eqn. deriv. from generalised kinetic eqns. 78−36936
Cauchy problem, T-ordered exponentials, appl. to quantum mech. 77−17832
Cauchy problem for Liouville eqn., global solns. in case of singular initial data 80−4509
Cauchy problem general solutions for Liouville eqn. 79−84942
chemically induced spin polarisation, finite element method, stochastic-Liouville eqn. 79−64018
CIDEP theory, stochastic-Liouville vector model with asymptotic soln. 78−66567
CIDN(E)P, infinite elements, in variational soln. of stochastic-Liouville eqn. 79−94014
classical and quantum statistical mech., common Liouville space 78−32758
classical Liouville operators, eigenvalue problems 77−26228
collisionless molecular multiphoton processes, rate eqns. 79−98173
constrained systems, statistical mechanics, generalized canonical approach 78−48743
continuum theory, nonlocal, using kinetic theory, stress, energy density *(Japanese)* 78−32677
convolutionless master equation, perturbation expansion 78−70047
correlation function, long time asymptotic behaviour, influence of waves on relax. processes *(Chinese)* 80−59195
correlation functions, two-time, in Liouville space, calc. 79−44795
DC resistivity as functional of generalised dynamical susceptibilities, solid state model 79−28330
density matrix equation, macroscopic cell representation and optimal choice of projectors by variational principle 77−74321
difference analogues to nonlinear partial differential eqns., reducible to linear eqns. 79−25831
dissipative system, rel. to description in quantum statistical mechanics 78−16725
dynamical inverse problem for phase-space density 79−97305
Enskog quasiparticle, non-Hamiltonian dynamics 80−101750
EPR spectra of stable radicals, slow molecular motion study, review 80−25212
F-region dynamics, Sturm-Liouville problem 77−13149
fluctuations, dynamic theory, Liouville operator and eqn. anal. *(Russian)* 79−6051
fluid, rotational and translational diffusion, stochastic Liouville eqn. formalism 79−64971
general relativistic statistical mechanics, BBGKY hierarchy and Boltzmann eqn. 79−63127
generalised Liouville equation from Lie derivative 80−77981
generalized Liouville equation, entropy, and dynamic systems containing limit cycles 79−21648
Goursat problem regular solns. 80−105795
Hamiltonian systems, integrability, Liouville theorem *(Russian)* 80−22191
Heisenberg eqns. on C* algebra of quasilocal observables, boson and fermion systems 78−57854
higher monotonicity properties of certain Sturm-Liouville functions 78−57750
inverse Liouville problem, quasi-particle dynamics from a given kinetic eqn. 80−101749
Jupiter, magnetosphere, particle flux ang. distrib. in rot. system 77−9700
kinetic theory, formal struct. 77−13683
kinetic theory, irreversibility, Liouville eqn. in Gell-Mann-Goldberger limit 77−61005
liquids, simple, elementary-excitation dispersion relation 77−31816
magnetised plasma, Vlasov theory coherent state approach 80−64675
many body problems, real time Green's function 78−57855
master equation for coupled systems, deriv. from Liouville eqn. 79−85060
master equations, discrete, approx. methods for stationary solns. 77−22480
membrane, passive transport through open membrane, multicomponent system, statistical-mech. theory 78−67261
molecular collisions, stochastic reductions, projection operator formalism forced oscill. model 77−65521
molecular emission spectra, in presence of strong driving field, stochastic Liouville eqn. 79−59503
molecular inelastic collisions, reduced Liouville eqn. 78−33569
molecular pair, fluoresc. depolarisation, using stochastic Liouville eqn. with radiative terms 80−16074
molecular vibrational relaxation and dephasing in condensed phases, non-Markovian theory 79−41224
molecules, eqn. of motion-Green's function and config. interaction methods comparison, appls. 80−47841
Moon, tidal effect in rot. theory 77−13259
N interacting particle canonical distrib. from kinetic theory 80−105569
non-conservative description of evolution in physics *(French)* 79−97328
nonlinear eqns., linear correspondents 78−20949
nonlinear transport, in Burnett order, theory 78−49778
phase properties and time fluctuating solns. 78−24724
phase space and Liouville theorem of classical statistics, relativistic analoga 80−27184
phase space quantization of the linearly damped harmonic oscillator 79−35627
piecewise continuous eigenfunctions, extension of theorem of orthogonality 80−31541

Liouville equation continued
pyrene-N,N-dimethylaniline system, radical ion pair geminate recomb., mag. field modulated, Liouville eqn. 77−86302
quantisation using correspondence principle and gauge invariance 78−4509
quantum, renormalised, simplified derivation 77−57275
quantum-mechanical scatt. for particle in field of variable scatterers, soln. of stochastic Liouville eqn. 78−140
radical ion pair geminate recomb., polar solvents, mag. field modulated, stochastic Liouville eqn. 77−86302
reacting fluid mixture, kinetics, BBGKY hierarchy in arrangement channel quantum mechanics 79−70299
reacting hard sphere dynamics, Liouville eqn. for condensed media 79−70298
relativistically invariant generalised quantum kinetic eqn., Liouville eqn. basis 78−54299
relaxation phenomena, general treatment 78−44398
scattering and dynamics, classical and quantum statistical mechs., unified treatment 78−45522
single-parameter quasi-Liouville system periodic soln. sets *(Russian)* 78−73833
solutions of generalised eqn., density matrices 78−27739
spatially extended systems, stochastic Liouville eqn. rel. to generalized master eqn. 78−45581
spectra of Liouville operators 77−9952
spectral and scattering inverse problems 79−17282
spectral simulation via finite elements, variational method and stochastic-Liouville eqn. 79−85157
spin echo expts. for diffusion in bounded heterogeneous media, stochastic Liouville eqn. 80−54992
step-type interparticle interaction, Liouville operator 77−33927
stochastic dynamical systems, kinetic eqn. derivation based on cumulant function props. 80−12995
stochastic Liouville equation, generalised, nonMarkovian and memoryless master eqns. 78−24737
Sturm Liouville inverse discrete problem, different spectral data *(French)* 79−53964
Sturm-Liouville discrete inverse problem, algorithms *(French)* 79−49022
superalgebra in (0,1) integration of supersymmetrical Liouville eqn. *(Russian)* 80−101947
superoperator perturbation theory, applic. to mag. field effects on delayed fluoresc. 77−30913
superoperator perturbation theory of density operators of generalized Liouville eqns. 77−26235
system theoretic representation of mechanical systems 79−17342
systems theoretic representation of mechanical systems, stochastic interpretation 79−17343
thermodynamics, second law, classical derivation 79−21682
thermostat-subsystem contact, density matrix, exact kinetic eqn. 79−85068
weakly relativistic statistical mechanics, choice of measure and Liouvilles eqn. 80−46956

lip microphones *see microphones*

lipid bilayers
alkane solubility modified by elec. field 80−97874
n-alkanes, adsorption into bimolecular lipid layers 80−88435
anaesthetics, general, site of action, X-ray and neutron diffr. and solubility data 78−77008
artificial membranes, excitable and ion-selective, review of axon and bilayer membrane props. 77−86451
artificial membranes, pancuronium inactivation of alamethicin-induced conductance 79−39189
asymmetry, dipole pot. meas. 77−4984
bacteriorhodopsin containing, photoelectric activity investigation by focused laser beam scanning 79−16148
bacteriorhodopsin generated photocurrents on planar bilayer membranes 80−51050
bilayer membranes, ion transfer parameter calcs. 79−53053
biomembranes, lipid-protein interactions, flexoelectric effects 78−92600
biomembranes, piezo-effect, background conductivity and filtration coeffs. 79−57598
Biophysical Society, 23rd annual meeting, conf., Atlanta, USA (Feb. 1979) 79−34468
black hydrocarbon, in aqueous medium, change in tension due to pot. diff. 77−25304
black lipid film stability, interfacial props. effects 78−15798
black lipid membranes, permeability of cyclic nucleotides 79−39376
black lipid membranes and bilayer vesicles in solution, thermodynamic stable states anal. 80−45856
byotropic liquid crystalline and other lamellar phases in lipid-water systems 78−92592
capacitance, voltage depend., harmonic response to AC excitation with DC bias 77−4983
cation-phospholipid-induced shape changes in lipid bilayer couple 80−108855
cerebroside-lipid mixed films, surface viscosity 79−74601
charge transfer in thin membranes, steady state, discrete models 77−16913
cholera toxin effect, formation of ion transport channels in bilayers containing gangliosides 78−88702
cholesterol model 78−56953
chromophore energy transfer 79−62200
conductance fluctuations and ionic pores, review 77−90752
conductivity of membranes of different surface charge in presence of tetra-alkylammonium salts 77−21489
current pulse-induced voltage variations in bilayer membranes, apparatus 80−94420
curvature elasticity, vesicle shapes 77−21493
curvature elasticity 79−48222
curved membrane, flexoelectric polarisation at blocked flip-flop 79−100582
cyanine-dye adsorption, spectrophotometric and elec. correls. 80−85358
cytochrome b_5 rotational diffusion, influence of lipid physical state 79−83693
cytochrome c interaction with bilayer phospholipid membranes 78−69001
cytochrome c interaction with phospholipid membranes 77−25384
dielectric constant and refr. index calc. 77−29105

lipid bilayers continued
dielectric constant of phospholipid bilayer rel. to ion permeability 80−81364
diffusion transport modelled by dimeric β-cyclodextrin complexes, cryst. struct. anal. 78−80838
1,2-dimyristoyl-sn-glycero-3-phosphoserine multilayers, phase transitions, temp. depend., ellipsometric study 80−108846
dioleoyl-phosphatidylcholine/dipalmitoyl-phosphatidylcholine bilayer membranes, phase transitions 79−39367
dipalmitoyl lecithin bilayer, ^2H NMR in liq. cryst. and gel phases 79−92173
dipalmitoyl lecithin vesicles in dil. suspension, light scatt. obs., of phase transitions 77−16915
dipalmitoyl lecithin-water system, lyotropic liq. cryst., pretransitional effects, PMR second moment meas. 78−91234
dipalmitoyl phosphatidyl choline, deuterated gel phase lipid bilayer, neutron scatt. sudy 79−43829
dipalmitoyl phosphatidylcholine, conformational nonequivalence of chains 1 and 2 79−16133
dipalmitoyl phosphatidylcholine, gel and liquid crystalline phases, deuterium mag. resonance obs. 79−91308
dipalmitoyl phosphatidylcholine(-cholesterol) aligned multilamella lipids, elastic props., Brillouin spectra 79−5255
dipalmitoyl phosphatidylcholine containing $CaCl_2$, monodomain sample phase behaviour birefr. obs. 79−83712
dipalmitoyl phosphatidylcholine monodomain samples with varying concs. of water and other ingredients, prep. 78−15780
dipalmitoyl phosphatidylcholine vesicles, appl. of depolarised light scatt. theory from hollow spherical particles 80−45946
dipalmitoyl-lecithin, NMR dispersion of layers dispersed in D_2O 79−48223
dipalmitoyl-phosphatidylcholine bilayer membrane, melting point rel. to electrostatic field 78−92602
1,2-dipalmitoyl-sn-glycero-3-phosphocholine multilayers, phase transitions, temp. depend., ellipsometric study 80−108846
dipalmitoylphosphatidylcholine, changes in vol. mag. susceptibility at the phase transition 80−76770
diphenylhexatriene, quantitation of hindered rotations by differential polarised phase fluorometry 79−16128
dipolmitoyl phosphatidylcholine lamellar phases and bilayer phase transitions, structural parameters 78−64948
discrete charge effect, dipicrylamine anions surface absorption 79−16159
dodecanate/decyltrimethylammonium micelles, type II mesophase, bilayer struct., NMR spectra study 80−75149
double electric layer at aqueous soln. interface with surface-active ions 77−36872
dynamic molecular organization 79−39364
dynamic response on simultaneous exposure to two anaesthetics 78−35809
egg lecithin membranes, magnetic anisotropy obs. 79−20520
elastic modulus freq. depend. 78−48762
elastic properties, effect of oxidation and hydrolysis 79−92165
elastic props. changes on exposure to different agents, elec. and chem. 80−81548
elasto-viscous properties, model for biomembranes 80−30671
electrical breakdown 80−81552
electrical breakthrough of bilayer lipid membranes 79−70531
electrical conductivity in presence of proteolytic enzymes and substrates 78−15779
electrical properties, effect of stress factors 79−92161
electrical strength fall after UV irrad. 78−69002
electrolyte-membrane-electrolyte, freq. depend. of capacitance and cond., model 77−21488
electrophoretic mobility 79−79479
erythocyte membranes, complement proteins interaction, ESR 79−100584
erythrocyte membranes, human, elec. cond. characts., ghosts and lipid bimol. membranes 77−9180
fluorescence decay, direct meas. apparatus *(French)* 77−5116
fluorescence polarisation, meas. apparatus *(French)* 77−9307
fluorescence polarisation decay theory 78−20138
Forster energy transfer problem in 2D, analytic soln. 80−26195
galvano-static regime of non-steady process 78−64963
glycerol monooleate bilayers, photoinitiated mediated transport of OH^- and H_3O^+ 79−88059
gramicidin A channel cation flux interaction 78−56957
gramicidin A channel struct., elec. meas. with lipid bilayer membranes 78−15783
gramicidin channel structures, charact. of succinyl derivatives 79−8484
gramicidin channels, interaction of countercurrent cation fluxes 79−70528
head group, orientational order and rotational diffusion, NMR, obs. 80−21451
hydrocarbon chain tilt differences between hydrated bilayers 80−51038
hydrocarbon chains, conformational anal. 80−81532
hydrophobic interactions, lipid-protein binding, thermodynamics, book contrib. 79−16129
hydrophobic ion current noise, autocorrel. anal. 80−30676
hydrophobic ion electrostatic interactions 78−27904
hydrophobic ion interactions, inner volt. clamping method 78−28129
hydrophobic molecule distribution in artificial membrane, 4-dimethylaminochalcone fluoresc. 77−16912
inhalation anaesthetics, effect on conductivity and time of adhesion 79−53070
interaction forces in zone of contact 78−53345
intervesicular lipid transfer, direct fusion of phospholipid vesicles, kinetic basis comparison 78−96034
intracellular membrane microviscosity, rat liver and hepatoma 27 80−30675
intramembrane potential jump meas. by potentiodynamic method 80−81778
ion channel formation in artificial lipid bilayer membranes by synthetic peptides 77−90750
ion transport, induced, limiting stages 77−36878
ion transport modification by 2,4-dichlorophenoxyacetic acid 79−83710
ion-conducting channels appearance at phase-transition temp. 79−70530
ionic channel formed by gramicidin A, membrane distortion 79−92164
K^+ transport modification by 2,4-dichlorophenoxyacetic acid 79−83709
lamellar liquid crystalline system, rheological props. 79−23289
lamellar liquid crystalline systems, probe mol. orientation, linear dichroism 77−90718

lipid bilayers continued
lateral mobility in multibilayer membranes 80−40975
lecithin, reaction kinetics of radicals, OH, e_{aq}^- 79−11886
lecithin bilayer, ion-induced changes in head group conform, ^{31}P and ^2H NMR 78−3452
lecithin bilayer force meas. and modification 77−56346
lecithin bilayers, density and mol. interactions 78−80837
lecithin bilayers, orientation and rot. freedom of fluoresc. probes 77−44583
lecithin bilayers, spontaneous form. at air-water surface 79−74603
lecithin bimolecular leaflets, incorporated fluoresc. probes, PMR 77−90734
lecithin cryst. growth rel. to mol. bilayer props. 78−31780
lecithin liposomes, binding sites for $Fe(CN)_6^{3-}$ ions, PMR obs. 79−79481
lecithin liposomes, negatively charged, rate of interaction with ferricytochrome c 77−16914
lecithin membranes, artificial, rheological and viscoelasic props. 80−26252
lecithin membranes, mag. susceptibility anisotropy, phase contrast microscope obs. 78−92601
lecithin monolayer model, equilib. and metastable states 77−60188
lecithin translational diffusion, pulsed NMR 77−9176
lecithin-cholesterol interaction, hydrocarbon chain length and unsaturation effects, Raman spectra 77−64012
lecithin-deoxycholate mixed micelles, surface curvature and mobility, PMR study 80−21452
lecithin-water systems, bilayer connecting passages 78−96028
lecithins, L_α phase, shear-induced biaxiality 78−95997
lens formation, appl. of alternating elec. field 80−12060
lethicin, membrane, elastic props., in direction perpendicular to membrane plane 79−57602
lipid membranes, orientational phase transitions with mol. config. change 78−14444
lipid-water smectic phase, forced Rayleigh scatt. 78−14278
liposomal membrane permeability, radioresist. 78−80919
liposome phasic transitions, use of hydrophobic fluoresc. probes 78−96021
liposomes, interactions with mammalian cells, review, book contrib. 79−5261
liposomes, nanosecond relax. processes 79−8477
liquid crystal, lyotropic, form. in biological systems 77−86454
liquid crystal physics appl. to functions of biological membranes 79−53051
liquid crystals, lipid, parabolic focal conics and polygonal defect arrays 79−37618
mechanosensitive ionic channel, model of reception and macromolecular rearrangement, effect of deform. 79−79564
melamine resin, as water containing embedding medium for electron microscopy 78−92764
membrane, black, adsorpt. of phloretin 79−34504
membrane bilayers, quasitwo dimens., theoretical models 80−76713
membrane buried charges, virial expansion 79−16158
membrane electron density profiles, determ. method on an absolute scale 79−16358
membrane incremental resistance unaffected by anaesthetics 79−83718
membrane stabilisation by polymer resins 79−57288
membrane voltage transients from photo-isomerising azo dye 79−92166
membrane-bound enzymes, lipid requirement 79−20521
membranes, ionic displacement current 79−34503
membranes, static, dynamic current response effect of local anaesthetic 77−52750
N-methyl acetamide, Na^+, Mg^{2+} binding to carbonyl O, lipid membrane permeation mechanisms 79−16134
mirochondrial lipid components of rat liver, Ca^{2+} transport system 78−64966
mitochondrial lipid ability to form bilayers, effect of temp. 77−36879
mixtures, phase transitions, phase diagrams, theoretical model 80−8032
model phospholipid membrane, structural changes, aggregation 79−66451
molecular forces between and within lipid membranes 80−51051
molecular motion determ. using periodic pattern photobleaching 79−34719
molecular theory of lipid membrane order 79−66452
monolayer, backfolding, SCF theory 79−8451
multilayer system, fluid membrane steric interaction, free energy of interaction 78−44463
myelin sheath, thickness irregularities distrib., paracryst. struct. 77−12892
nerve action pot., lipid bilayer local phase transition 80−89744
nigericin action, dimer mechanism 78−24048
NMR, D relax. rates and mol. dynamics 80−26206
nonlinear electric effects studied by harmonic anal. 78−24188
nonpolar molecules, adsorption into lipid bilayer membranes 80−61517
nystatin induced conductance increase, evidence against channel form. 77−44598
organisation and mobility using D-NMR and spin label EPR as probes 77−44600
orientational long-range order, phase transition, coherence lengths 78−92593
oxidation of lipids coupled with NAD.H oxidation by atm.O 77−36875
paraffin chain dynamics, ang. correl. function decay by multiple rot. pot. diffusion 80−3569
permeability behaviours, steady-state, induced by cyanine dyes 80−85357
permeability modification by drugs 78−69026
permeability of flat membrane in presence of vesicles of sarcoplasmic reticulum 77−21490
permeation of water mols. meas. using fluoresc. quantum yield solvent-isotope effect 79−34710
phase changes and determination methods *(Czech)* 80−3599
phase transition, cholesterol effect 80−85361
phase transition, cluster model, appl. to bilayer mol. passive permeation and struct. relax. 78−53346
phase transitions, cell membrane model 78−35808
phase transitions model 78−44460
phosphatidyl choline bilayers, interaction of chlorophyll-a with β-carotene, fluoresc. quenching 79−20506
phosphatidyl ethanolamine, charge distrib., dipole moment, CNDO calcs. 78−80840
phosphatidylcholine, lateral mobility of bound amphipathic apolipoprotein ApoC-III 80−97884

lipid bilayers continued
phosphatidylcholine bilayer endothermic transitions, Raman difference spectroscopy 78−40119
phosphatidylcholine bilayers, artificial, interaction with C-reactive protein 80−3579
phosphatidylcholine bilayers, fluidity changes and phase transitions, intramol. excimer fluoresc. obs. 80−85342
phosphatidylcholine hydration, adsorpt.-desorpt. isotherm and PMR 78−15781
phosphatidylcholine membranes, interaction of colchicine, spin-label study 77−86455
phosphatidylcholine vesicle sizing by TEM 79−70722
phosphatidylserine vesicles, sonicated, Ca-induced fusion, temp. depend. 79−92172
phospholipid, 1,2-dilauroyl-DL-phosphatidylethanolamine, X-ray diffr. anal., crystallogrpahy, bond lengths 77−44590
phospholipid, one- and two-component, main phase transition, Landau phenomenological theory 80−97872
phospholipid, US relax. spectra in transition zone 79−92169
phospholipid bilayer, ^{1}H NMR study of valinomycin conformation 80−40958
phospholipid bilayer, artificial, incorporation of fragmented sarcoplasmic reticulum, elec. phenomena 79−96524
phospholipid bilayer, Gramicidin antibiotics effect on Raman spectra 77−66798
phospholipid bilayer, hydrated, monoclinic (ripple) phase, thermodynamic model 79−70532
phospholipid bilayer containing chlorophyll a, photo-oxidation of water 77−16917
phospholipid bilayer melting transition, thermodynamic fluctuations, ion permeability, statistical mechanics model 78−73140
phospholipid bilayer membrane modified by valinomycin, volt. fluctuations 78−31777
phospholipid bilayer membranes, NMR and molecular motion 77−48767
phospholipid bilayer membranes, voltage depend. channel form. by colicin K 79−8490
phospholipid bilayer surface binding centre heterogeneity, hydrophobic mol. distrib. 77−56344
phospholipid bilayers, carbonyl groups dynamics, ^{13}C chem. shift anisotropy obs. 80−85326
phospholipid bilayers, low temp. transition from fluid state 80−97871
phospholipid bilayers, selectively deuterated, neutron diffr. study of mol. struct. 78−24036
phospholipid bilayers, struct. dynamics from deuterium spin-lattice relax. time meas. 79−79485
phospholipid bilayers, van der Waals interactions, total potential curves 78−77006
phospholipid cell membranes, at mol. resoln., introduction 80−104841
phospholipid membrane, polar head motion, NMR and EPR linewidth study using $TCNQ^{-}$ ion-radical *(French)* 80−45865
phospholipid membranes, artificial, lamellarity determ. by photometric phase-contrast microscopy 79−39368
phospholipid membranes, conductivity changes on exposure to HF EM field 79−79483
phospholipid mixtures, phase transition anal. by high sensitivity differential scanning calorimetry 77−40637
phospholipid topological aysmm., in biomembranes, review 77−90736
phospholipid vesicle surface charge equilib. distrib., effect of non-electrostatic factors 80−30672
phospholipid vesicles, conform. change and fusion phenomenon, dynamic light scatt. obs. 78−11615
phospholipid vesicles, hydrostatic press. 80−56000
phospholipid vesicles, NMR determs. of maleic acid permeation coeffs. 79−83711
phospholipid vesicles, surface charge equilib. distrib., calc. method 78−96019
phospholipid vesicles, surface charge equilib. distrib., calc. results 78−96020
phospholipid vesicles, synthetic, phase transitions, dynamic light scatt. obs. 79−53058
phospholipid vesicles charge asymmetry obs. 79−62202
phospholipids, ^{31}p NMR, slow-motional lineshapes for very anisotropic rot. diffusion 80−5644
phospholipids, direct obs. of hydrocarbon chain tilt angle 79−34481
phospholipids, synthetic, ionic permeability in region of phasic transition 79−53052
phosphorylation in simple lipid and chloroplast ATP synthetase system 79−92298
photoelectric effects in membranes containing Schiff bases of retinal *(Japanese)* 78−7322
photosynthetic reaction centre functional reconstitution in planar lipid bilayers 80−97881
phytanic acid, in phospholipid bilayers, struct., order parameters, liq. cryst. transition, entropy 79−83713
phytol in phospholipid bilayers, struct., order parameters, liq. cryst. transition, entropy 79−83713
pigmented, photoelec. and magneto-orientation effects, review 77−48766
planar, interaction of Ca^{2+} with negative lipids, solvent effect 77−77871
planar, lateral diffusion meas. using fluoresc. correl. spectroscopy 77−36884
planar, light guide effect, bilayer spectrosc. appls. 79−29509
planar lipid bilayers as light guides, elec. field induced scatt. 80−48148
planar multibilayers, spin label study of nystatin and amphotericin B action 77−29108
planar systems, asymm. charge distribs. 77−29104
pore size distrib., exactly solvable two-dimens. biomembrane model 78−31783
protein membrane multilayers, thickness depend. of props. 80−89726
protein-lipid interaction, appl. of surface tension meas. 79−24940
protein-lipid interaction in membrane bound Na^{+}, K^{+}-ATPase, spin label anal. 79−11902
protein-lipid interactions, in bilayer membranes 79−5254
purple membrane asymm. struct., X-ray diffr. data anal. 77−73512
purple membrane topography of Halobacterium halobium 79−48211
Raman studies of biomembranes, phospholipid-d, as nonperturbing components 78−53330
receptor function of glycophorin and concanavalin A receptor 78−48764
review of current ideas 77−32878
rhodopsin and other proteins in artificial lipid membranes 77−90730
rhodopsin-containing bilayer membranes, light-induced transmembrane channel form. 77−52784
saddle splay instability, crit. elastic modulus 78−44462
saddle-splay elasticity and mol. asymmetry 78−92594
single-ion channels in unmodified membrane at phase transition temp. 80−45559
smectic lipid bilayer, in cryst. matrix, phase transition 80−21453
sodium decyl sulphate/water/decanol/Na_2SO_4, lyotropic mesophase, mag.-oriented, X-ray diffr. obs. 80−1921
solvent-depleted membrane prep. from conc. lipid solns. 78−53347
sphingomyelin bilayer systems, monolayer coupling, choline methyl proton line width 78−35807
sphingomyelin-cholesterol interaction in oriented bilayers, X-ray diffr. exam. 77−44603
spin probes EPR partitioning between lipid and aq. phases 79−79455
spin-labelled, pure, EPR lineshape evidence of phase transitions 78−69004
structural constitution and function *(German)* 79−5256
structural order of lipids and proteins, fluoresc. anisotropy data eval. 80−97873
structure, X-ray refl. phases from oriented model membrane systems 78−96022
surfactant vesicles, low-ang. light scatt. and photon correlation spectroscopy 79−79484
synthetic voltage-dependent cation-selective transmembrane channel characterisation 78−77009
teaching demonstration using molecular membrane model 77−57117
thermal excitations, propagating vibr. modes detect. by light beating spectroscopy 77−48762
thermal structural rearrangements obs. 79−92163
thermotropic transitions of phospholipid membranes, effects of bivalent cations and proteins 77−48765
α-tocopherol in phospholipid bilayers, struct., order parameters, liq. cryst. transition, entropy 79−83713
tumour cells, differences in fluidity between bilayer halves of plasma membranes 79−16164
two-dimensional conductor applic. *(Russian)* 78−23190
US effects on cond. and capacitance, 1 MHz 78−77082
vesicles, theoretical shapes under conditions of increasing membrane area 79−24960
vesicular artificial membrane struct., effect of protein-lipid interaction 77−25385
vesicular membranes, gangliosides orientation, ^{1}H NMR, viscometric and ultracentrifugation obs. 79−92162
virus envelopes, plasma membranes, review, book contrib. 79−5257
voltage-dependent capacitance in bilayers made from monolayers 78−27903
water and thermal diffusivity in lipid-water smectic phase, light scatt. meas. 78−96031
Ca-Na channel of cell, reconstruction in lipid bilayer 77−25404
K^{+} ion transport inducing compound identification in mitochondria and bilayer lipid membranes 78−31788
K^{+} permeability of mitochondrial and artificial bilayer membranes 78−53365

liquefaction of gases
air, from Cailletet and Pictet to microkelvin 79−40
air, optimum operating conditions 77−61075
air, use of energy chart for study of liquefaction process 79−69238
cryogenic microhead 79−95150
expansion turbines, review 77−5847
flow calorimeter for condensable gases, low temp. and high press., design and eval. 80−37033
flow calorimeter for condensable gases, low temp. and high press., computer program prediction and exptl. data comparison 80−37034
liquefaction shock waves, shock tube expt. study 80−19439
miniature cryogenic liquefier, heat exchange characts. 77−67440
natural gas, design of evaporators *(Russian)* 77−68589
organic fluids, liquefaction shock wave obs. 77−51484
superconducting magnet circulation cooling system based on He liquefaction apparatus 78−57992
superconducting magnet Large Coil Program, He liquefier-refrigerator and distrib. system 78−50398
thermodynamic analysis *(Russian)* 79−82325
He, automatic multirange liquefaction plant 80−57306
He liquefier, trouble shooting and repairing record *(Japanese)* 77−67439
He purifier for small laboratory liquefier 77−17990
He, withdrawal from liquefier 79−67306
^{85}Kr extraction, occupational doses in gas liquefaction industry 78−15905
N_2, optimum operating conditions 77−61075
N_2-Kr-Xe, liquefaction, retention of ^{85}Kr from fission exhaust gases, separation technique *(German)* 80−27753
O_2, isotopically enriched, prep. and storage under press. 79−29620
O_2-^{85}Kr-Xe, liquefaction, retention of ^{85}Kr from fission exhaust gases, separation technique *(German)* 80−27753

liquid alloys
see also liquid metals
actinide, thermodynamic props. 77−55366
Al-Si (2.4 wt.%), liq. fluidity, solid-liq. coexisting zone *(Japanese)* 80−15175
alkali metal-H, mol. orbital approach, solvation energies 77−4201
alloy melt, impurity conc. field model, growth by Czochralski method *(Russian)* 80−75191
alloy melt, temperature distribution during cryst. growth by Czochralski method *(Russian)* 80−75192
alloys, liq., composition determination during electron bombardment furnace fabrication, X-ray emission spectrography *(French)* 78−3427
amalgams, mixing, excess entropy, vibr. contrib. *(Russian)* 79−51263
association, effect on thermodynamic behaviour of alloy melts *(German)* 78−20050
atomic position correlations, nearly free electron approx. 77−39529
atomic transport props., review 77−1248
binary, atomic order effects, statistical mechanics and fluctuation theory 78−14263
binary, calc. of triplet correlation function on basis of thermodynamic quantities for solute atoms 80−49087
binary, classification on basis of average atomic order effect 78−14269
binary, concentration fluctuations and struct. factors 77−47322
binary, electrode pot., rel. to intermetallic compound content 78−9940

liquid alloys continued
binary, including transition metal, ht. of formation, prediction model 77−56246
binary, influence of associate formation on thermodynamic quantities 79−66329
binary, interatomic forces, thermodynamic props. and alloying 77−47324
binary, kinetic crystallisation diagrams, given finite diffusion coeff. *(Russian)* 80−40341
binary, stability against conc. fluctuations, pair interaction energy 77−47323
binary, surface tension, compressibility and surface segregation 78−67889
binary, viscosity coeffs. by Enskog theory 80−1920
binary alloy melts, assoc., liquidus curve calcs. *(German)* 79−20352
binary alloys, calc. of electromigration forces and resistivities 79−82572
binary alloys, excess viscosity 77−55380
binary ferro alloys, crystallisation under forced mixing in ingot mould *(Russian)* 79−52192
binary melt, spherical particle growth, morphological stability 80−29943
binary melts, appl. of quasichem. method of cluster components *(Russian)* 77−80623
binary melts, short-range order, X-ray and neutron scatt. *(German)* 78−14272
binary metallic melt, deviation from the Kopp law, specific heat *(Russian)* 80−39305
binary metallic systems, rule for surface enrichment 80−75406
binary substitution solution, molten thermodynamics 79−11559
binary with strong chem. interactions, surface tension model 77−15665
boiling, bubble growth dynamics, electron-beam vol. heat source 77−47565
brass, calorimetric investigation of thermodynamic props. 79−52172
brass, liquid, thermodynamic props. *(German)* 80−66482
chemical diff. coeff. meas. 77−1249
complex melt, processes taking place during vaporisation *(Russian)* 79−73298
composition determination during electron bombardment furnace fabrication, X-ray emission spectrography *(French)* 78−3427
concentration fluctuations, nucl. quadrupole spin relax. 78−91975
conference, Bristol, England (July 1976) 77−47297
crystallisation, under conditions of temp.-conc. convective mixing of liq. nucleus, impurity distrib. *(Russian)* 80−40342
crystallisation front interaction with turbulent alloy melt stream, heat exchange *(Russian)* 80−74708
diffusion coefficient, determ. from meas. of elec. resist. 77−55375
dilute, partial interference functions of solutes 79−19139
dilute binary alloys, conduction electron scatt. cross section and component effective charges *(Russian)* 77−8082
dilute ternary liq. alloy, heteroatomic solute, thermodynamic partial pair struct. factory, sticky hard sphere 79−32867
electromigration, driving force, pseudopot. calc. 77−55373
electromigration, driving force expression 78−51714
electromigration direction reversal in selected alloy systems 77−55374
electron charge transfer in transition-metal and rare-earth alloys 77−1388
entropies of binary alloys, ab initio calcs. 77−47599
ferrous eutectic liquids, exam. of structures 78−71668
geometrical model, soft sphere static approx. eqn. of state 78−42892
Gibbs energy interaction parameters with O_2 and N_2 79−56961
Hall effect sign, cond. and thermoelec. power calcs., tight binding model 77−47798
heat of formation, model predictions 78−35351
highly resistive, temp. depend. on elec. resist. 78−91657
inductive stirring, melt vel. 77−73250
internal energy, chem. pot., critical consts. 78−34422
liquid alloys, positron annihilation due to vacancy trapping, simplified model *(Russian)* 80−71511
magnetic properties, review 79−51741
melts, of a congruently melting substance, single struct. model 80−103233
metal, liquid crystallisation, fluidity resistance effects *(Russian)* 77−55957
metal-insulator transition, review 77−1367
metallic, binary, O_2 activity coeff. 77−4925
metals and alloys, gas diffusion coefficients, stationary method determ. *(German)* 79−10974
molten, compound-forming, vol. of mixing, conc. depend. 80−103484
molten metallic system, contribution to sign inversion of effective charge *(Czech)* 78−60656
multicomponent alloys, partial struct. factors in the long wavelength limit 78−22633
multicomponent system, higher-order partial struct. factors 77−47339
neutron diffraction, struct. investigations of melts and amorphous substances *(German)* 80−44108
NMR, of liq. metals and alloys, review 78−2755
nuclear quadrupole relaxation 78−15050
oxide solubility 77−72692
partial structure factors, higher-order 77−31572
partial structure factors, square well pot. calcs. 77−51300
penetration mechanism, in WC-Co sintered hard alloy 78−60619
photoelectron spectroscopy, electronic structure 77−48321
physical chemistry, conf., Konigstein, Germany (Mar. 1976) 77−1059
quadrupole relaxation rate temp. depend 80−88884
quenching device, electronic, piston and anvil liquisol apparatus 78−23905
rare earth, thermodynamic props. 77−55366
semiconducting liquid alloys, anomalous thermodynamic props., theory 80−49287
semiconductor, metal-nonmetal transition model 77−1368
stability and structure, pseudopotential calcs. *(German)* 80−38913
steel, 20A, melt, tube blanks, mech. props., statistical determ. 79−29316
steel, graphite dissolution, segregation and diffusion *(Russian)* 78−11201
steel, liquid bath, shooting methods for projecting buoyant alloy additions, expt. and mathematical eval. 77−21047
steel, molten, heat loss during solidification hydrodynamic eqns., hardening front kinetics *(Russian)* 80−55385
steel, molten, spectrochem. anal. 79−16096
steel, molten, wettability of aluminosilicate refractories 79−82415
steel, molten interfacial tension in phase boundary molten $CaO-SiO_2-Al_2O_3-CaF_w2$ slag *(Czech)* 78−63908

liquid alloys continued
steel, nonmetallic inclusion behaviour simulation by multiple phase medium eqn. *(Russian)* 78−94965
steel, Si-Mn, melt, surface tension *(Russian)* 78−43212
steel, stainless, dissolution kinetics of Ti *(Russian)* 80−34193
steel-$(MnO-SiO_2-ZrO_2)$ slag system, molten, interface, wetting angles, surface tension *(Czech)* 79−19432
structure, thermodynamic and transport props., book 78−51406
structure and thermodynamic props., ab initio calcs. 77−84621
ternary, atomic order effects, statistical mechanics and fluctuation theory 78−14263
ternary and higher order, activity coeff. of nonmetallic solutes 80−107433
thermodynamic ab initio calcs. 77−47602
thermodynamic properties, review *(German)* 78−18794
thermodynamic props. rel. to struct. 77−1237
thermoelectric power measurement apparatus 79−40591
three-component melts, enthalpies of form. *(Russian)* 79−51277
transition metal alloys, elec. resist. using t matrix 77−31988
transition metal alloys, thermoelectric power 78−91675
transition metals, liq. and amorphous, elec. transport 77−51720
transition metals and alloys, elec. resistivity, Hall coeff., mag susceptibility 78−95280
transition metals and their alloys, review of struct. 77−51304
US treatment of melts *(Russian)* 77−44259
vapour pressure, pseudopot. and Gibbs-Bogoliubov calcs. 78−83935
Wood's alloy, liq. enthalpy effects when solute is added 80−39314
Ag-Au, liquid, surface tension *(Japanese)* 79−19431
Ag-Bi, liq. alloys, thermodynamic investigation 80−70428
Ag-Bi(Pb), melt, Ag crystal growth, transition from round to face forms *(Russian)* 79−28906
Ag-Cu, liquid, surface tension 78−43217
Ag-Ge, liq. eutectic, neutron diffr. determ. of struct. 77−51302
Ag-Ge, liq. eutectic, struct. by neutron diffr. 78−18537
Ag-Ge, neutron diffr. investig. of pair correl. function, coordination numbers 77−35467
Ag-Ge, surface tension exam., sessile drop method *(French)* 77−20162
Ag-Ge, thermodynamics and short range order, mass spectra meas. 79−52740
Ag-Ge, viscosity, temp. depend. *(French)* 78−59964
Ag-Ge eutectic alloy, heat capacity meas. over temp. range 800-1200K *(French)* 80−88331
Ag-Ge liquid alloy, small angle neutron scatt. 79−64982
Ag-In melt system, conc. depend. of component and impurity diffusion coeffs., radioactive isotope method *(Russian)* 80−107454
Ag-In(Sn)(Pb)(Bi)(Sb), liquid alloy, thermoelectric powder and magnetic susceptibility 77−8076
Ag-Li, solid and liquid alloys, calorimetric investigation of mixing enthalpy *(German)* 78−52773
Ag-O system, melt, blow hole form. during solidification 79−43238
Ag-Sn, liquid alloys, thermodynamic props. *(Japanese)* 80−108396
Ag-Sn(Sb), liquid alloys, anomalous behaviour of electrical resistivity and thermoelectric power 77−11901
Ag-Te, calorimetric study at high temp. 79−61893
Ag-Tl, eutectic liquid alloy, structural features, interatomic interaction *(Russian)* 79−77494
Ag-Zn, liquid, thermodynamic props. *(German)* 79−87615
Ag-Zn, molten, EMF meas. of activities using ZrO_2 solid electrolytes *(Japanese)* 80−88339
$Ag_{0.285}Li_{0.715}$, partial interference functions, short range chem. order effects 79−7541
Al alloy melts, centrifugally atomised, granule size distribution 79−100080
Al alloys, liquid, kinematic viscosity temp. depend., porosity, H solubility, supercooling *(Russian)* 80−54425
Al alloys, molten, determination of H content, using electrochemical probe 79−11843
Al base alloys, contact reactions with Fe group metals 78−60879
Al melt, Ti alloy dissolving, reaction zone formation, component interaction *(Russian)* 80−54377
Al-Au melt, Si solubility *(Russian)* 77−66024
Al-Bi(In)(Pb), monotectic system, rapid cooling from melt, effect on struct. *(Russian)* 79−70053
Al-Cu, liq. alloys, surface tension meas. *(French)* 78−18875
Al-Cu, liq. alloys, with zero superheat, fluidity 80−70289
Al-Cu, liq. diffusion coeff. meas. using temp. gradient zone melting 78−26710
Al-Cu, melt near solid-liquid interface, diffusion during crystallisation *(German)* 79−29046
Al-Cu, molten, showering cryst. form. in mould cooled from top *(Japanese)* 80−66498
Al-Cu, partially solidified, viscosity and struct. *(Japanese)* 79−14950
Al-Cu alloy, nonstationary mass transfer in front of moving phase boundaries in normal freezing *(German)* 77−44238
Al-Cu dilute alloys, vein closing mechanism in fluidity tests 80−84924
Al-Cu eutectic melts, struct. determ. *(Russian)* 77−80408
Al-Cu liquid alloys, rapid quenching prep. of metastable solids, apparatus *(German)* 79−28990
Al-Cu-Fe, liquid, mag. moment and transition from mag. to nonmag. state 79−24132
Al-Cu-Fe alloys, exam. of constitution and mag. props. *(German)* 78−52206
Al-Ga-Ge, enthalpy of form., direct reaction calorimetry, 713-1230K *(French)* 79−66336
Al-Ga-In, liq. alloys, excess Gibbs functions 633 to 1173K 78−60655
Al-Ge, enthalpy of form., direct reaction calorimetry, 713-1230K *(French)* 79−66336
Al-La, thermodynamic interaction in liquid phase *(Russian)* 78−44080
Al-Mg, liquid alloy energy of soln. pseudopotential calcs. *(Russian)* 79−66330
Al-Mg-Si liquid alloy, exam. of thermodynamic props at 780-820°C *(Czech)* 79−91626
Al-Mn(Fe)(Co)(Ni), liquid alloys, thermodynamic charact. calc. *(Russian)* 78−27475
Al-Ni alloys, solid and liq. mag. susceptibility, 600-1650°C *(Russian)* 80−15685
Al-Ni solid, liquid mixture, diffusion processes *(Russian)* 80−107563
Al-Ni(Si), liquid, thermodynamic props. 79−91619
Al-Pb(Sn), surface tension, size effect *(French)* 80−15341
Al-Si, and Al-Si-Na eutectic melts, struct. determ. *(Russian)* 77−80408
Al-Si, compressibility and struct. factors at zero wavevector 79−23515

liquid alloys continued
Al-Si, liq. alloy, chem. diff. coeff. determ. 77−1249
Al-Si, molten, Na determ. using β-Al_2O_3 probe 77−48714
Al-Si (16 wt.%) melt, fivefold twinned Si cryst. growth, crytallographic study 80−2942
Al-Si melt, microheterogeneity *(Russian)* 80−103238
Al-Si melts, hypoeutectic, eutectic, hypereutectic structural factors, atomic radial distrib. functions *(Russian)* 79−73091
Al-Si melts, spreading behaviour on Fe 80−84345
Al-Si melts, struct. factors, at. distrib. curves, thermodynamics, neutron diffr. study *(German)* 80−19687
Al-Si(Mn)(Ti)(Cr)(Ni)(Cu)(Fe), liq., dissoln. and diffusion of alloying components, 700-1000°C *(Russian)* 80−15275
Al-Sn, liq. alloy, chem. diff. coeff. determ. 77−1249
Al-Sn liquid alloys, heats of mixing and activities calcs. 79−42264
Al-Sn(Ag) liquid alloys, diffusion of Ge, mechanism *(Russian)* 80−15276
Al-Sn(Ag)(Cu)(Au), liquid alloys, exam. of Si diffusion *(Russian)* 79−28118
Al-Ti, molten, showering cryst. form. in mould cooled from top *(Japanese)* 80−66498
Al-Zn, liq. solutions, thermodynamic properties *(Polish)* 80−49380
Al-Zn, physical props. study by electrodiffusion method *(Czech)* 77−84956
Al-Zn melt, electrotransfer *(Russian)* 77−66034
Al_cMg_{1-c}, vols. and entropies of mixing, calc. 80−75363
Au-Ag, liquid alloy, surface energy meas. by const. temp. method on solid alumina 78−6208
Au-Al, liq. alloy, thermodynamic activities and enthalpies 80−19960
Au-Co, ^{59}Co NMR studies 79−95660
Au-Co, liq. alloys, partial struct. factors 80−1919
Au-Co, liquid alloys, struct. determ. by X-ray diffr. 78−6006
Au-Co, molten, US vel. meas., compressibility and partial struct. factors determ. 77−69045
Au-Co melts, struct., compressibility, X-ray and neutron diffr. 77−11614
Au-Cs, liq. alloy, mag. susceptibility rel. to ionic charact. 77−1536
Au-Fe, thermodynamic mixing effects, mass spectroscopic meas. evaluation *(German)* 77−59123
Au-Ge-Si, influence of struct. on elec. resist. of glass forming alloys 80−65518
Au-M, liq. alloys, M=Ga,In,Sn,Sb,Te, ΔG^E of mixing, exptl. determ. 77−4920
Au-M, liq. alloys., M=Ga, Bi, activities of Ga and Bi, ht. of mixing 77−4921
Au-Si, liq. alloy, thermodynamic activity meas. by Knudsen-cell mass spectrometry *(French)* 80−10684
Au-Si, melt, thermodynamic study of phase diagram *(French)* 78−27482
Au-Si eutectic melt, wetting of quartz 77−31840
Au-Sn liquid alloys, Sn activity *(Japanese)* 78−6901
Au-Sn(Bi)(Ga)(Ni), elec. resist. in liquid and solid state *(Russian)* 79−51549
Au-Te, thermodynamic props., calorimetric meas. 78−20051
Au-Zn, liq., thermodynamic props. *(German)* 80−49386
Au-Zn, molten, EMF meas. of activities using ZrO_2 solid electrolytes *(Japanese)* 80−88339
Au(Ag)(Cu)-Sn liquid, optical reflectivity spectra of virtual bound states 80−89021
Au_xGe_{1-x}, ang. distrib. of positron annihilation 77−55848
$Au_{77}Ge_{13.5}Si_{9.4}$, heat of crystn. and viscous behaviour 80−75166
AuSi, wetting and reactions on α-Al_2O_3 77−85022
$Au_{1-x}Si_x$, liquid, elec. resistivity as function of temp. and comp. 79−56188
$Au_{81}Si_{19}$, optical refl., 0.5 to 6 eV, hall coeff. and elec. resist. 80−29755
$Au_{1-x}Sn_x$ liq./solid alloy, resist. and percolation 80−6804
Ba-Mg, liq. alloys, thermodynamic activities determ. 80−50604
Bi-Cd, Hall coeff., up to 360°C 78−14711
Bi-Cu, molten, struct., cold neutron scatt. in region of small momentum transfer 77−39527
Bi-Cu, molten, struct., thermal neutron diffr. meas. 77−39526
Bi-Cu melts, struct., neutron scatt., conc. of segregated regions calc. 77−39528
Bi-In, Hall coeff., up to 360°C 78−14711
Bi-Mn, dil. liq. alloy, static and dynamic props. of localised Mn moments 79−82755
Bi-Pb-Hg, liquid, surface tension and density *(Russian)* 77−55418
Bi-Pb-Sn, molten metallic system, contribution to sign inversion of effective charge *(Czech)* 78−60656
Bi-Sb, melts, interdiffusion, long capillary method and electron probe obs. 77−89563
Bi-Sb-Te melt, Sb and Te distribution coeffs. during crystallisation *(Russian)* 80−93472
Bi-Sn, Hall coeff., up to 360°C 78−14711
Bi-Sn melt structure, radial distrib. function of atoms, anal. *(Russian)* 80−14995
Bi-Sn(Pb), liq., conc. and temp. depend. nucl. relax. rates meas. 78−19357
Bi-Te(Se), diamag. susceptibility, semicond./metal behaviour 78−14927
Ca-Ag(In), liquid alloy, thermodynamic exam 78−75848
Ca-Mg, liq. alloys, thermodynamic activities determ. using modified Ruff method *(German)* 80−11631
Ca-Zn liquid alloys, thermodynamics 79−52173
Cd, surface plasmons at inhomogeneous liq. metal/dielec. interface, second dispersion branch 77−32059
Cd-As, liq. alloys, thermodynamic props. and cpd. formation 77−1238
Cd-Bi, US vel. and thermophysical props. meas., 500-1000K 78−38778
Cd-In-Sb, liq. alloy, Cd thermodynamic activities, Gibbs free mixing enthalpy *(German)* 80−45279
Cd-In-Sb, liq. alloys, thermodynamic activity of Cd between 833 and 953K *(German)* 80−45278
Cd-Pb-Bi-Sn system, ternary liq. alloys, thermodynamic props. 78−51701
Cd-Pb(Sn)(Bi) alloy, molten, EMF meas. of liquid separation 78−39747
Cd-Sb, hard-sphere struct. factors 77−51301
Cd-Sb, liq., thermoelec. power meas. 79−40591
Cd-Sn-(Pb), (0.03 to 0.10 at.% Cd), Cd activity coeffs., interaction parameters, EMF depend. on temp. 80−49383
Cd-Zn binary systems, melts, elec. resist., 0-700°C 80−65517
Cd-Zn-Hg, comp. and temp. depend. of Hg VP, activity, free energy and enthalpy *(Russian)* 77−20087
Ce-Co, charge transfer effect 78−94967
liquid alloys continued
Ce-Cu, charge transfer effect 78−94967
Ce-Cu, liquid, normal spectral emissivity 80−103506
Ce-Ga (Al)(In)(Sn)(Pb)(Bi)(Zn) liquid, solubility and thermodynamic props. *(Russian)* 78−19717
Ce-Sn, liq., elec. resistivity negative temp. coeff., CPA calcs. 79−42515
Co alloy, dil., liquid, thermodynamics 77−20086
Co-Al, band model of high temp. magnetism 78−26809
Co-Ca, liq. alloy form. kinetics *(French)* 80−96652
Co-Fe(Ni)(Cr), liquid, N activity coefficient 77−72699
Co-Ga, band model of high temp. magnetism 78−26809
Co-Ga liquid and solid alloys, elec. resistivity at high temps., partial struct. factors 80−6806
Co-Ge, structure studied by X-ray diffr. *(Russian)* 79−77493
Co-Mn-Sn liquid alloy, magnetic props. *(German)* 79−87235
Co-Ni, thermoelec. power and elec. resist. meas. 77−51719
Co-Ni (5 to 95 at.%), paramag. props., 800-1800°C *(Russian)* 77−55660
Co-Si, liquid alloy, optical charact. *(Russian)* 77−24810
Co-V, magnetic susceptibility and electronic struct. 80−39738
Co-Zn melt, Zn activity determ. *(German)* 78−19715
Co_5Ge_3, solid and liquid, physicochemical props. and structure 80−39548
Cr binary substitutional solutions, thermodynamics 80−54410
Cr-Ge liquid and amorphous alloys, struct. props., cond., viscosity, surface tension *(Russian)* 80−54119
Cr-Ni(Co)(Fe), liquid, N activity coeff. 77−72699
Cr-rare earth alloys, liquid phase, topology in diagrams of state *(Russian)* 80−54121
Cs-Au, electronic struct., effects of short-range order 77−15755
Cs-Au, exptl. evidence for ionic elec. transport 77−51534
Cs-Au, liq., molar vol. meas. 80−59546
Cs-Au, liq. alloys, ionic conductance 77−1251
Cs-Au, liq. ionic alloy, elec. props. 79−99338
Cs-Au, liquid, metal-insulator transition, mag. susceptibility, Knight shift, theory 80−44672
Cs-Au liq. alloy, formation of localised electronic states, NMR obs. 80−93201
Cs-Au(Sb), liq. alloys., mag. susceptibility and electronic struct. 77−1537
Cs-Sb(Au), liq., metal-nonmetal transition and change in electronic and mag. props. 77−51790
Cs-Tl(Hg), elec. resist. meas. 77−51717
CsAu, molten, equimolar, structural evidence of ionic nature 80−64882
CsAu, optical absorpt. in liq. and solid 79−61397
$Cs_{1-x}Au_x$, metal-nonmetal transition, electronic theory 78−79930
Cu alloy, binary liquid, activity meas. 77−20085
Cu alloys, liq. and solid, positron trapping 78−48255
Cu alloys, molten, gas content meas., reduced pressure test *(Chinese)* 80−81390
Cu alloys, thermal cond. and elec. resistivity 80−103661
Cu, viscosity 77−4138
Cu-(Sn-)Ti melts, wetting of SiC 78−68664
Cu-Ag, diffusion-limited evaporation for const. comp. film prep. 77−21038
Cu-Ag, dil. molten alloy, Ag activity determ. by two-component evap. *(Japanese)* 77−48395
Cu-Ag, liquid alloy, solubility and activity of O_2 79−29028
Cu-Ag(Pb)(Bi)(Ag-O)(Bi-O)(Si-S), stirred at different speeds under press., evaporation of Ag, Pb, Bi, S 77−47555
Cu-Al-Co liquid alloys, constant Co-content of 5 wt.%, mag. props. *(German)* 80−88720
Cu-Al-Fe, dil. liq. alloy, localised mag. state interactions *(German)* 77−1539
Cu-Al-Mn liq. alloys, susceptibility behaviour 80−93077
Cu-Al(Ga)(In) alloys, elec. cond., temp. and conc. depend., model interpret. and alloy struct. *(Russian)* 80−88528
Cu-Fe(Co)(Ni), liquid, surface tension *(Japanese)* 79−19431
Cu-Ga(Gd), mag. susceptibility, diamagnetism 78−72326
Cu-Ge, hard-sphere struct. factors 77−51301
Cu-Ge, liq. alloy, thermodynamic activity meas. by Knudsen-cell mass spectrometry *(French)* 80−10684
Cu-In, solubility and activity of O 77−43331
Cu-In liquid alloy, thermodynamic props., potentiometric exam. *(French)* 77−59126
Cu-In liquid alloys, heat of form meas. *(Korean)* 77−9116
Cu-M, M=Al,Cd,In,Ga,Zn, magnetic susceptibility, comp. and temp. depend., melting effects 78−52202
Cu-M-O ternary alloys, thermochem. calcs. 80−85209
Cu-Ni, liq., surface conc. profile and surface energy 80−84350
Cu-Ni, melt, accel. by shock wave treatment, crystallisation *(German)* 77−86022
Cu-Ni-O, liquid alloy, thermodynamic study by EME method *(Japanese)* 78−15367
Cu-Ni-S, molten, thermodynamic props. 80−104122
Cu-Ni-Sn, liq. alloy, calc. and anal. of mixing enthalpies *(German)* 80−44325
Cu-Ni-Sn, liq. alloy, mixing enthalpies determ. using a SETARAM high temp. calorimeter *(German)* 80−44324
Cu-Ni-W melt, solubility of W, primary solidification 78−19726
Cu-O (0.05 to 0.1 wt.%) liquid alloy, deoxidation kinetics by rotating graphite cylinders 80−61084
Cu-O-Zn dilute liquid alloy, Zn-O interaction parameter 80−55694
Cu-Pb, surface tension, size effect *(French)* 80−15341
Cu-Pb (Fe), liq., thermodynamic props. *(Polish)* 80−89199
Cu-Pb liquid alloys, exam. of O diffusivity at 1430K using electrochemical cell 78−51713
Cu-Pb-O, liquid, dil. alloy, O_2 activity, 1100 to 1200°C 80−25662
Cu-S, liquid, oxidation kinetics, by CO_2 77−28986
Cu-SO_2 system, melt, blow hole form. during solidification 79−43238
Cu-Sb melt, eutectic struct. by neutron diffr., isotopic substitution 78−47233
Cu-Si, melt, enthalpy of formation at 1370K 80−26042
Cu-Sn, self-diffusion of Sn, correl. with other props. *(Russian)* 79−23764
Cu-Sn, thermodynamics of Cu and Sn solns. using copper β-alumina solid electrolyte, 800-1100K 80−107502
Cu-Sn (25 wt.%), liq., struct. from thermodynamic and diffr. studies 80−6350
Cu-Sn binary system, wettability and interaction between solids and liqs. *(Japanese)* 80−92760

liquid alloys continued
Cu-Sn liquid alloy, surface energy meas. by const. temp. method on solid alumina 78−6208
Cu-Sn liquid alloys, thermodynamic meas. 78−52765
Cu-Ti-Al(Ga)(Au)(In)(Ag)(Ni), wetting of Al_2O_3, alloying effects 80−107617
CuGa alloys with Mn impurities, liq., elec. resistivity 79−51545
$Cu_{1-x}Ga_x$ liquid alloys, elec. resistivity 79−47073
$Cu_{0.85}Ni_{0.15}$, 3d bandwidths, photoelectron spectrum 77−4286
Fe alloy, molten, N_2 diffusion, effect of Si, P, Al and B *(German)* 77−20099
Fe alloys, complex, diffusivity and solubility of N_2 at 1600°C 77−39684
Fe base melt, thermodynamic props. *(Russian)* 77−55363
Fe, cast, anodic polarisation in slag melt *(Russian)* 80−45513
Fe, pig, liquid gas bubble form. at nozzles, acoustic exam. 78−52723
Fe-Ag-Cu melts, phase interface props., Cu influence *(Russian)* 79−51261
Fe-Al, liquid, N solubility, AlN precipitation 79−11630
Fe-Al liquid alloys, apparatus for viscosity meas. *(Czech)* 80−29103
Fe-As, liquid alloy, density and surface free energy *(Russian)* 78−11204
Fe-As melts, influence of Sn, Si, Mn and Cr additions on surface tension and density *(Russian)* 80−15337
Fe-As melts, surface tension, density, adsorption *(Russian)* 80−92757
Fe-As-Su-Si (Cr)(Mn) melts, As and Sn distrib., Si, Cr, and Mn influence *(Russian)* 80−16274
Fe-B, liq., mag. susceptibility meas. 80−75740
Fe-based, C solubility, donor-acceptor mechanism 80−49365
Fe-based solns., liq., diffusion of N 78−75862
Fe-bearing binary, substitutional liq. and solid solns., statistical thermodynamics 80−11630
Fe-C, C content effect on short-range order struct., X-ray diffr. obs. 80−6351
Fe-C, levitated drops, carburisation and decarburisation in CO-CO_2 gas mixture, exam. of reaction kinetics 78−85053
Fe-C, pre-eutectic melt, struct. anomalies *(Russian)* 77−28794
Fe-C, struct., neutron and X-ray diffr. meas. 77−51306
Fe-C liquid alloys, Si and C transfer from SiO-CO gas phase 80−55655
Fe-C melt, graphite cryst. growth rate rel. to supersaturation *(German)* 77−55940
Fe-C melt, mag. susceptibility and short range order, 900-1800°C 78−84382
Fe-C melt structure, X-ray diffr. study *(Russian)* 80−19685
Fe-C melts, C oxidation by CO_2, kinetics *(Russian)* 80−40680
Fe-C melts, short-range order, neutron scatt. obs. *(German)* 78−71669
Fe-C molten alloy, short range order *(Russian)* 79−90521
Fe-C-S-Mg melt, S and Mg effect on graphite growth shape 79−38817
Fe-C-(P)(S), drops, oxidation kinetics in oxidizing slags 78−11153
Fe-C(Si)(Mn)-S melt, S evaporation *(Russian)* 78−19716
Fe-Co, X-ray diffr., struct. determ. *(Russian)* 77−80409
Fe-Co melt, volumetric characts., molar volume conc. depend. density *(Russian)* 80−33873
Fe-Co-Ni, solubility of H, 1400 to 1800°C 77−1231
Fe-Co(Ni)(Cr), liquid, N activity coefficient 77−72699
Fe-Cr (Mn)(Ni)(Si), liquid diffusion of H_2 *(German)* 78−14487
Fe-Cr melts, ultrasonic propag. and isothermal compressibility using pulse-phase method *(Russian)* 79−51202
Fe-Cr-C, lqiuid, reduction of Cr_2O_3 by dissolved C 78−6877
Fe-Cr-Ni liquid alloy, N_2 soln. and TiN precipitation 78−6931
Fe-Cr-Ni melts, S solubility and solid soln. precipitation *(Russian)* 80−15251
Fe-Cr-Ni-Mn-Mo, liquid, N_2 solubility 78−44087
Fe-Cr-Ni-Mo-V, Mo and V effects on segregation *(German)* 77−55942
Fe-Cr-Ti(Al) liquid alloys, thermodynamical anal. of O_2 solubility *(Russian)* 80−92676
Fe-Cu liquid alloy, heats of mixing, mixing entropies *(Russian)* 80−65224
Fe-Ga (up to 50 at.%), elec. resist., 1200-1800°C *(Russian)* 78−6341
Fe-Ga-C melts, thermodynamics and C solubility *(Russian)* 80−39292
Fe-Ge, liquid alloy, thermodynamic mixing function determ. by mass spectrometric meas. 79−29025
Fe-Ge melts, struct. determ. 79−41940
Fe-Hl (Si) (Ti) (V), molten, gaseous O_2 absorption 80−11836
Fe-Ni, liq. alloy, electrochem. meas. of O, thermodynamic props. at 1873K 80−30244
Fe-Ni, solid and liquid, determ. of activities for temp. range 1500-1900K, using mass spectroscopy 79−11558
Fe-Ni, thermochem. props. 77−59755
Fe-Ni liquid alloy, physical and chemical props. deviations from Raoult's law *(Russian)* 78−95729
Fe-Ni melt, short-range order, m.p. to 1750°C *(Russian)* 78−94966
Fe-Ni-Al, liq. alloys, N solubility and AlN precipitation 80−11648
Fe-Ni-Cr melts, O solubility *(Russian)* 80−15250
Fe-Ni-Ge, liquid alloy, H_2 thermodynamic interaction, solubility *(Russian)* 78−11202
Fe-Ni-Mn melt, thermodynamic dissolution of O_2 *(Russian)* 78−27473
Fe-Ni(Co), liquid, activity meas. by transportation method *(Japanese)* 79−4949
Fe-Ni(Co), solid and liq., paramag. susceptibility and electron struct., 800-1800°C *(Russian)* 80−25081
Fe-Ni(Cu)(Al)(Si) liquid alloys, thermodynamic characts. calc. *(Russian)* 80−15264
Fe-O-V melts, phase equilib. *(Russian)* 80−16273
Fe-Si, liq. alloys, surface tension, sessile drop method meas. *(French)* 78−84029
Fe-Si (0-6 wt.%) melts, viscosity *(Russian)* 80−15285
Fe-Si alloys, liq., refractive index, absorpt. coeff., elec. cond. 78−43830
Fe-Si melts, high Si, O solubility *(Russian)* 80−15252
Fe-Si-C, liquid alloy, activity of Si and C *(Russian)* 78−11203
Fe-Si-C melt, Si and C activity *(Russian)* 77−55364
Fe-Si(Ge)(Al), paramag. props. *(Russian)* 77−66247
Fe-Sn liquid alloy, conc. depend. of enthalpy of form., conc. depend. *(Russian)* 78−44081
Fe-V-C melts, electron struct., mag. susceptibility meas. *(Russian)* 78−47729
Fe_xGe_{1-x}, ang. distrib. of positron annihilation 77−55848
$(Fe_{0.5}Ni_{0.5})$-Co, solid and liq., paramag. susceptibility and electron struct., 800-1800°C *(Russian)* 80−25081
$(Fe_{0.5}Ni_{0.5})_{1-x}Co_x$, paramag. susceptibility, 1000-1800°C *(Russian)* 77−16040
FePC molten and amorphous alloys, struct. factors 80−79674

liquid alloys continued
Ga and alloy high-temp. couplants for acoustic transducers 79−14195
Ga liquid spreading over Ag thin film, kinetic eqn. *(Russian)* 80−59376
Ga-Bi liquid binary mixtures, phase separation under press. 80−34183
Ga-Cu liquid alloy, solubility and activity of O_2 77−59122
Ga-Cu(Tl)(In), liq., mag. susceptibility *(Russian)* 78−6513
Ga-Ge, enthalpy of form., direct reaction calorimetry, 713-1230K *(French)* 79−66336
Ga-Ge-Zn ternary alloys, thermodynamic props., EMF meas. 80−81033
Ga-In, liq., O diffusion coeff., thermodynamic activity and solubility 78−38860
Ga-In, repetitive pulses electron emission 79−24416
Ga-Pb, liquid alloy, thermodynamic activity determ. using Knudsen method *(German)* 79−34008
Ga-Sn alloys, compressibility, US velocity meas. *(Russian)* 77−59060
Ga-Te, alloys, liq., thermodynamic functions, struct. 78−40075
Ga-Te, thermodynamic props. 80−35567
Ga-Zn(In)(Ta)(Sn)(Bi)(Pb), liquid binary alloys, magnetic susceptibility *(Russian)* 77−24671
GaIn, liq. alloys quad. relax. rates, 3-particle correls., ^{71}Ga and ^{115}Sn 77−12272
Ge, molten binary, struct. and charact. of interatomic interaction, X-ray diffr. meas. *(Russian)* 77−1070
Ge-Ce liquid alloys, enthalpies of mixing, exothermal effects *(Russian)* 80−34192
Ge-Co, liq., enthalpy of formation meas. 80−30267
Ge-Cu, liquid, solubility of O_2 at 1373K, in equilibrium with GeO_2 78−44109
Ge-Fe, liq., enthalpy of formation meas. 80−30267
Ge-Ga liq. alloys, thermodyn. props. 78−26695
Ge-Mn, liq., calorimetric investigation of heats of mixing, and entropies of mixing 79−95165
Ge-Ni, liq., enthalpy of formation meas. 80−30267
Ge-Sb liq. alloys, SRO 78−22632
Ge-Sn, liq. alloys, thermodyn. props. 77−51518
Ge-Sn(In) melts, short-range order, radial atomic distrib. functions 79−86673
Ge-Te, As-Te, Ge-As-Te molten systems, metal-semicond. transition, cond. obs. *(German)* 77−1457
Ge-Te, liq. alloy, heat of formation, 1030-1150K 77−1943
Ge-Te alloy, liq., magnetic susceptibility 79−87232
Hg, liq. and dil. liq. amalgams, elec. cond. and thermoelec. power 77−55511
Hg-Cd liq. amalgam, elec. cond. and thermoelec. power meas. 77−59273
Hg-Cd(-Te), partial vapour pressure, determ. for volatile component by static method 80−37150
Hg-In, liq., positron annihilation meas. 78−43955
Hg-In, liq. alloy, chem. diff. coeff. determ. 77−1249
Hg-In, positron studies, trapping at solute-vacancy complexes 78−31271
Hg-In-Bi, liquid alloy, elec. resist. *(Russian)* 79−51544
Hg-In(Tl)-Zn, liquid alloys, thermodynamic props., 25 to 75°C *(German)* 77−73259
Hg-K, liquid, structure factors, X-ray scatt. *(Japanese)* 80−54122
Hg-Na, liquid, structure factors, X-ray scatt. *(Japanese)* 80−54122
Hg-Tl, liq., positron annihilation meas. 78−43955
Hg-Tl, liq. alloys, struct. from thermodynamic props. *(German)* 77−1066
Hg-Tl, liq. alloys, struct. from elec. cond. 77−1067
Hg-Tl alloys, compositional depend. of positron annihilation 79−99973
Hg-Zn(In)(Pb), dil. liq. amalgams, expanded, cond. at high temps. and press. 77−20287
In alloys, ^{117m}Sb nucl. spin relax., quadrupolar interaction 78−39437
In alloys, $^{117}Sb^m$ nucl. quadrupole relax. rate, systematical trends 79−73849
In alloys, concentration fluctuations, nucl. quadrupole spin relax. 78−91975
In-Bi, PAC of ^{111}Cd 77−4584
In-Ga liquid alloy, low-resistance ohmic contacts in ZnSe, LED fabrication appl. 80−70823
In-Hg, Knight shift of ^{115}In, temp. and conc. depend. 79−47343
In-Hg amalgam, EMF meas. of $In/InCl_3$/amalgam cell and thermodynamic quantities 79−33999
In-Hg amalgam, thermal and electric cond., temp.-conc. depend. 78−43349
In-Hg liquid alloy, activities meas. 77−86351
In-Pb, liquid alloy, thermodynamic activity determ. using Knudsen method *(German)* 79−34008
In-Sb, mag. susceptibility, MP to 1000°C, anomalies due to electron-ion interaction 77−20546
In-Sb alloys, liq., spin relax. of ^{117}Sb and ^{115}Sn 77−16216
In-Sb liquid alloy, calorimetric investigation, rel. to association equilibrium *(German)* 77−16862
In-Sb liquid alloy, mixing enthalpy, temp. depend. *(German)* 80−84298
In-Sn liquid alloy, 2-butanol vapour adsorption, effect on surface tension and surface comp. 79−14981
In-Sn-Sb, liquid state, structure of eutectic alloy 78−42890
In-Sn(Pb), liq., conc. and temp. depend. nucl. relax. rates meas. 78−19357
In-Te, nucl. spin relax. of ^{117}Sb 77−52004
In-Te alloys, liq., transport props. interpret. using effective-medium theory 77−76806
In-Tl liquid alloy, thermodynamic props. and struct. *(German)* 77−48400
In-Zn, liq., Zn activity meas. by Knudsen torsion-effusion method 79−10950
In-Zn binary system, melts, elec. resist., 0-700°C 80−65517
$In_{1-x}Sb_x$, liquid, nucl. quadrupole relax. of Sb, time depend. PAD meas. 77−43899
K-Cs solution, activity and saturated vapour press. of Cs, reson. line absorpt. obs. 77−51509
K-Rb, liq., elec. resistivity, temp. depend. 78−39084
K-Rb, liq., form factors and transport coeffs., pseudopot. perturb. theory 80−44561
K-Rb(Cs), resistivity calc. using general model pseudopot. 77−55506
K-Tl, elec. resist. meas. 77−51717
Li-Ag, density, compressibility and diffr. data 77−47336
Li-Bi, sorption of tritium, appl. as thermonuclear reactor material 77−1301
Li-Cd, elec. resist. and Knight shift 80−75537
Li-H, mol. orbital approach, solvation energies 77−4201

liquid alloys continued
Li-In, liquid alloy, elec. resist., Knight shift of ^{115}In and ^{7}Li nuclei 79−11352
Li-Mg, liq., elec. transport props. and phase diagram 78−23070
Li-Mg, liq. alloy, thermoelec. power and elec. meas. 77−47788
Li-Mg, liquid alloys, thermodynamic investigation *(German)* 79−91630
Li-Mn, form factor effects, pseudopotentials resist. calc. 80−103608
Li-Na, conc. fluctuations and struct. factors 78−30534
Li-Na, liq. alloy, thermoelec. power and elec. resist. 77−47788
Li-Na, short-range order, neutron diffr. obs., near crit. composition 78−22639
Li-Na liquid binary mixtures, phase separation under press. 80−34183
Li-Pb, liq. alloy, enthalpies of mixing, calorimetric study *(German)* 80−2170
Li-Pb, thermodynamic study using Knudsen effusion mass spectrometry 80−24578
Li-Pb liquid alloys, elec. resistivity, negative temp. coeff. 80−88527
Li-Pb liquid compound forming alloy, entropy of mixing 80−88328
Li-Sb(Bi), thermodynamic props., 355-600°C 78−34634
Li-Te alloys, liq., electrochem. investig. of thermodynamic props. 77−1244
Li-Tl(In)(Bi), liquid alloys, calorimetry study *(German)* 80−25664
$Li_{1-x}Pb_x$, metal-nonmetal transition, electronic theory 78−79930
Mg-Bi, far IR reflectivity meas. 77−52105
Mg-Bi, thermodynamic study vapour pressure measurement by transpiration 78−44395
Mg-Bi (30 at.%), molten, short range order and partial struct. factor, neutron and X-ray diffr. 78−9941
Mg-Bi alloy, liq., far IR reflectivity rel. to possible transport processes 78−2827
Mg-Bi melt; X-ray and neutron diffr., conc. depend., correl. number and nearest neighbours 80−49091
Mg-Ca(Sr)(Ba), thermodynamic characts. *(German)* 77−59757
Mg-Cd melts, atomic struct., short range order and melting *(German)* 78−14273
Mg-In liquid solns., EMF and calorimetric meas. 80−55359
Mg-Sn, melt, assoc., liquidus curve calcs. *(German)* 79−20352
Mg-Sn melt, density and free surface energy *(Russian)* 77−66074
Mg-Sr, liq. alloys, thermodynamic activities determ. 80−50604
Mg-Tl liq. systems thermodiffusion of Tl 77−11717
Mn-Cu(Ni), melt solubility and activity of S *(Russian)* 77−25012
Mn-Cu(Sn), liquid alloys, thermochemistry 79−56962
Mn-Fe-C, melts, activities of Mn at 1673K 80−50597
Mn-Fe-Si-C, melts, activities of Mn at 1673K 80−50597
Mn-Ge (5 to 90 at.%) liquid alloy, electrical resistivity *(Russian)* 77−55509
Mn-N, liquid, N soln. 79−99321
Mn-Sb(Sn)(In), liq., elec. resist. meas. 77−51721
Mn-Si, liq. alloys, equilibria between $MnO-SiO_2-CaO-MgO$ slags 80−10639
Mn-Si, liq. thermodynamic props., rel. to alloy form. 77−7875
Mn-Si, vapour-pressure meas. using torsion effusion method 79−42215
Mn-Si-C, melts, activities of Mn at 1673K 80−50597
Mn-Si(C), melt, activation determ. by vapour press. meas. 80−16279
$Mn_{0.6}Ni_{0.4}$, liq., soln. enthalpies of C and Mn, enthalpy determ. for graphite-diamond transform. and Mn_5C_2 form. 78−59945
Na-Cd, mag. susceptibility, diamagnetism 78−72326
Na-Cs, conc. fluctuations, X-ray transmission meas. 77−47329
Na-Cs, liq., thermopower 78−23074
Na-Cs, liq. alloy, thermoelec. power and elec. resist. 77−47788
Na-Cs, struct. factor, free energy of mixing, and electrochem. pot., thermodynamic calc. 80−96436
Na-Cs, struct. factors, X-ray transmission diffr. expts. 77−47337
Na-Cs melt, density and molar volume *(Russian)* 78−15357
Na-Cs solution, saturated vapour pressure of Cs over solution 78−26688
Na-Ga, mag. susceptibility and elec. cond. *(Russian)* 80−29522
Na-Ga liquid alloy, thermodynamic props. 79−37854
Na-Ga liquid alloy, thermodynamic props. of mixing derivation method 80−54385
Na-H, mol. orbital approach, solvation energies 77−4201
Na-In, dilute soln., thermodynamic props. 77−89553
Na-K, collective excitations, mol. dynamics calc. 80−28895
Na-K, dynamical struct. factor calc. 78−22634
Na-K, electron theory of chemical potential and activity *(Japanese)* 77−72702
Na-K, liq., static struct. factors 78−63664
Na-K, liq. alloy, electronic correl. functions calcs. 78−63663
Na-K, liq. alloys, electromigration driving force expression 78−51714
Na-K, liquid alloy energy of soln. pseudopotential calcs. *(Russian)* 79−66330
Na-K, partial structure factors, square well pot. calcs. 77−51300
Na-K, third-order partial struct. factors 77−47339
Na-K alloys, liq., thermal conductivity, NaK_2 formation 78−10416
Na-K liq. alloy, Moelwyn-Hughes parameter calc. from US data 80−59375
Na-K liquid alloy, self and mutual diffusion coeff. 78−22877
Na-K liquid alloy, small angle X-ray scatt. study, conc.-fluctuation structure factors 80−54120
Na-K liquid alloys, struct., X-ray and neutron diffr. meas. 80−107041
Na-K liquid alloys, triplet correlation functions and thermodynamics, solute partial structure factor 80−64881
Na-K-Cs alloys, liquid contact material, phase diagram calcs. 78−6145
Na-K(Cs), liq., form factors and transport coeffs., pseudopot. perturb. theory 80−44561
Na-K(Rb)(Cs), resistivity calc. using general model pseudopot. 77−55506
Na-Li, liq., Knight shift calc. by multiple scatt. Xα method 80−54961
Na-Rb, liq. alloys, electromigration driving force expression 78−51714
Na-Se system, liq., thermodynamic props. 80−21319
Na-Sn liq. alloys, thermodynamic props. by EMF meas. with $\beta-Al_2O_3-Ba_2$ electrolytes 79−19379
Na-Te, chemical pot. and resist. 77−55232
Na-Te system, liq., electrochem. determ. of thermodynamic props. rel. to temp. 77−1245
Na-Tl, liq., elec. resist. meas. 77−51717
Na-Tl, mag. susceptibility, diamagnetism 78−72326
$Na_{1-x}Bi_x$, metal-nonmetal transition, mag. susceptibility meas. 79−82525
$Na_{1-x}Sb_x$, liq., mag. susceptibility 78−14926
Nb-K melts, thermodynamic characts., elec. resistivity, single parameter rigid sphere calcs. *(Russian)* 80−34410
liquid alloys continued
Ni base melt, thermodynamic props. *(Russian)* 77−55363
Ni-Al, diffusion coeff. differences, rotating-disc determ. 80−39330
Ni-Al, melt, short-range order and microinhomogeneity, rel. to NiAl form. 77−35466
Ni-Au-Fe, activity of iron at 1573K 77−70328
Ni-Co, liquid, activity meas. by transportation method *(Japanese)* 79−4949
Ni-Co, solid and liq., paramag. susceptibility and electron struct., 800-1800°C *(Russian)* 80−25081
Ni-Co-Mo-Al-Cr, melt, effect of Al, Cr on O_2 activity, electrochemical determ. 79−11556
Ni-Cr (Mo)(W) melts, N_2 diffusion *(Russian)* 78−18812
Ni-Cr(Co)(Fe), liquid, N activity coeff. 77−72699
Ni-Cu, liq., activity meas. of O_2 by EMF method *(Japanese)* 80−54408
Ni-Ge, density and surface energy temp. depend., 1000-1700°C *(Russian)* 77−15662
Ni-Ge, liq. alloy, thermodynamic activity, mass spectrometric determ. *(German)* 78−20052
Ni-Ge alloys, liq., integrated emissivity, electric resistivity 78−43155
Ni-O, liquid alloys, surface tension and wettability of Al_2O_3 *(Japanese)* 79−99398
Ni-P, molten alloy, struct., X-ray scatt. 78−22640
Ni-Si liquid alloys, thermodynamic props., enthalpy of mixing *(Russian)* 80−34207
Ni-Si melt, ultra acoustic study *(Russian)* 78−15613
Ni-V, magnetic susceptibility and electronic struct. 80−39738
Ni-Zn liquid alloys, Zn activity obs., 1100 to 1300K 78−40072
Ni-Zn melt, Zn activity determ. *(German)* 78−19715
Ni_5Ge_3, solid and liquid, physicochemical props. and structure 80−39548
Ni_xGe_{1-x}, ang. distrib. of positron annihilation 77−55848
No-Ni alloy, integral emissivity in range 1200 to 1700°C 77−43357
Pb-Ag, liquid alloy, exam. of thermodynamic props. using solid oxide galvanic cell 78−75851
Pb-Bi, liquid alloy, chemical and intrinsic diffusion coeffs., exam. *(German)* 78−83987
Pb-Bi alloy, liq., thermal cond. and elec. resistance up to 900°C 77−47785
Pb-Bi alloy, vapour press., meas. using transpiration method, thermodynamic props. determ. 78−3365
Pb-Bi eutectic alloy flow rate meas. apparatus 77−79412
Pb-Bi eutectic melt, in contact with Cu, mutual indentation *(Russian)* 77−59853
Pb-Bi liquid alloy, Pb and Bi diffusivities, temp. and conc. depend. *(German)* 80−84311
Pb-Bi molten alloys, density, surface tension, temp. depend. 77−69147
Pb-Fe(Cu), liq., thermodynamic props. *(Polish)* 80−89199
Pb-Li liq. alloy internal spectral shifter and energy converter for laser fusion reactor 79−49841
Pb-Pd, liq. alloy activity by effusion method *(German)* 79−29023
Pb-Sb, liq. alloy, Pb thermodynamic props. *(Czech)* 80−29925
Pb-Sb molten alloys, oxidation and drossing *(German)* 79−74313
Pb-Sn, melt viscosity rel. to phase equilib. *(Russian)* 79−69272
Pb-Sn (20wt.%), eddy current study of solidification 80−104141
Pb-Sn-Hg amalgam, liq., thermodynamic props. *(Russian)* 77−66624
Pb-Sn(-Sb), surface tension liquidus temp. to 550°C *(Korean)* 79−90848
Pb-Tl viscosity, comp. and temp. depend., up to 500°C 79−65233
Pb-Tl-Cd(Sn) melt, short-range order struct. 80−49088
Pb-Zn, liquid phase immiscibility determ., DTA 78−64523
$Pb_{1-c}-Li_c$ (As)(Ag)(In)(Sn)(Sb)(Te)(Au)(Tl)(Bi), liquid alloys, local fluctuations and quadrupolar relaxation 80−66060
Pd-Al(Si) melts, appl. of quasichem. method of cluster components *(Russian)* 77−80623
Pd-Au-Si, influence of struct. on elec. resist. of glass forming alloys 80−65518
Pd-Ni(Co)(Cr), liquid alloys, enthalpy of form. *(Russian)* 77−56244
Pd-Ni(Si), melt, struct. and physical-chemical props., thermodynamic props. *(Russian)* 78−18536
Pd-Si, liq., mag. susceptibility 78−95415
Pd-Si(−Cu), glassy, liq. and cryst., mag. and elec. props. 77−66249
Pd-Te liquid alloys, thermodynamic activities *(German)* 79−29022
Pd-Ti liquid alloy, mass spectrometric study of high temp. thermodynamic stability 78−15369
$Pd_{77.5}Cu_6Si_{16.5}$, heat of crystn. and viscous behaviour 80−75166
$Pd_{0.8}Si_{0.2}$ alloy, short-range order, comparison with amorphous state 77−1069
$Pd_{82.5}Si_{17.5}$, struct. compared with amorphous state, X-ray diffr. 77−24275
Pr-Al liquid alloys, atomic interactions, thermodynamic props. *(Russian)* 80−39307
Pt-Pd (Co)(Su)(Al)(Si) melts, surface tension and density *(Russian)* 80−39388
Rb-Cs, electron theory of chemical potential and activity *(Japanese)* 77−72702
Rb-Cs, liq., elec. resistivity, temp. depend. 78−39084
Rb-Hg liquid amalgams, thermodynamic props. determ. from conc. cell EMFs 77−1246
Rh-Cu(Si), melts, surface props. *(Russian)* 78−26750
Sb-Sn melt, electrotransfer *(Russian)* 77−66034
Sb-Te(Se), diamag. susceptibility, semicond./metal behaviour 78−14927
Se-Na, and Se, liqs., elec. resistivity and phase separation 79−82573
Se-Tl-S alloys, liq., dielectric relax. and elec. cond. 80−108150
Se-Tl(Bi)(Sb), liquid alloys, vapour phase effect on activity determ. *(German)* 79−43210
SeTe liquid alloy, effect of branched chain polymers on bond equilib. 80−24348
Si-Mn(Fe)(Co)(Ni), liquid alloys, thermodynamic charact. calc. *(Russian)* 78−27475
Sn-Ag liquid alloys, thermodynamic study by solid-oxide galvanic cell 79−20031
Sn-Al melt, reaction with Nb for protective coating prod. *(Russian)* 79−70221
Sn-Bi, atomic self-motions *(Rumanian)* 78−47226
Sn-Bi, US vel. and thermophysical props. meas., 500-1000K 78−38778
Sn-Cu film, spreading kinetics on Nb substrate in vacuum, 700 to 800°C *(Russian)* 77−80680
Sn-Ge(Au), liquid alloy, exam. of activity and heat of mixing, using mass spectrometry 78−51706
Sn-In dil. liq. alloy, electrodiffusion and electroconvection, effective diffusion coeff., apparent effective valence 78−87802

liquid alloys continued
Sn-Pb, liquid alloy, thermodynamic activity determ. using Knudsen method *(German)* 79−34008
Sn-Pb, refining by fractional solidification 79−61536
Sn-Pb (26%), liq. eutectic alloy Seebeck coeff. 80−84463
Sn-Pb (38.1 wt.%), self-diffusion coeff. of Sn, 466 to 786K 77−69106
Sn-rare earth , dil. liq., elec. resist. and mag. susceptibility 78−43350
Sn-Sb dil. liq. alloy, electrodiffusion and electroconvection, effective diffusion coeff., apparent effective valence 78−87802
Sn-Sb molten alloys, thermodynamic study *(Korean)* 78−31383
Sn-Se, melt, density, kinematic viscosity, struct., 900-1400K 78−14395
Sn-Te, molten, elec. cond. and phase diagram 80−84454
Sn-Te alloy, liq., magnetic susceptibility 79−87232
Sn-Te liquid alloy, thermodynamic meas. 77−73271
Sn-Zn, molten, struct. investig. by neutron diffr. 79−4233
Sn-Zn eutectic, liq., appl. to drilling of steel, cutting conditions rel. to tool parameters *(Russian)* 79−34187
Sn-Zn melts, plasticising action in deform. hardening of medium C steel 80−55415
Sr-Y, phase diag. *(Russian)* 77−59745
Ta-W TV-10 alloy, thermal expn., 1146-2288K 78−43148
Te-Co(Cr)(Au)(Ag), dil. liq. alloy, elec. cond. at high temp. and press. 78−87959
Te-In alloys, direct reaction calorimetric study, 737 to 1340K *(French)* 80−49382
Te-Sb, liq., elec. cond. 78−84186
Te-Se, electrotransfer of Se 77−11716
Te-Tl, eutectic liquid alloy, structural features, interatomic interaction *(Russian)* 79−77494
Te-Tl, liquid alloy, thermodynamic investigation, enthalpy of form. and phase diagram 77−59756
Te-Tl liq. systems, thermodiffusion of Tl 77−11717
Te-Tl system, thermodynamic investigation, enthalpy of form. at elev. temps. 78−52774
Te-transition metal, dilute, elec. resist., cond. electron conc. 77−15814
Th-Pb, liquid alloy, thermodynamic props. *(Russian)* 77−25011
TiC-base alloys, anomalous phase flaky precipitation *(Japanese)* 78−48401
Tl-Bi(Sb), mag. susceptibility, MP to 1000°C, anomalies due to electron-ion interaction 77−20546
Tl-Cd-Sb, liq., Cd vapour pressure and thermodynamic functions *(Russian)* 79−51247
Tl-Se, liquid mixtures, press. effect on two-phase region 80−75347
Tl-Sn-Bi, liquid alloy, thermodynamic props. *(Russian)* 79−10968
Tl-Te, mag. susceptibility 77−51880
Tl-Te, miscibility gap 79−10952
Tl-Te alloy, liq., bond equilib. theory for electronic props., thermochemistry 77−89365
Tl-Te system melts, conc. depend. of surface tension 79−37904
U-Mo(Re), high temp. phase diagram, thermodynamic props. of refractory metal solutes in liquid U 77−25022
W-Ni liquid alloys, sintered, coarsening of W grains, exam. 78−56598
Y-Ni, liquid alloys, enthalpy struct. *(Russian)* 78−27474
Y-Si melts, enthalpy of formation and dissolution, microinhomogeneous struct., interatomic interactions *(Russian)* 80−34206
Zn-Bi, liquid, inconsistent conjugated liquidus 80−76232
Zn-Bi(Sn), specific elec. resist., temp. and conc. depend., 20-800°C 79−82571
Zn-Ca, liquid alloy, exam. of thermodynamic props., using EMF method *(Russian)* 79−34003
Zn-Cd alloys, liq. and solid, ultrasound speed and compressibility meas. 80−102941
Zn-Cd liquid alloy, activity meas. by transportation method *(Japanese)* 78−35358
Zn-Cd liquid/Fe-Ni-Al mag. powder, effective viscosity of composites *(Russian)* 80−54424
Zn-Ga liquid soln., thermodynamic props. determ., invariant method appl. 77−59742
Zn-In-Cd soln., liquid, thermodynamic props. 79−83176
Zn-Pb melt, immiscible component distrib. in crossed EM fields *(Russian)* 77−48396
Zn-Pb(Bi), surface tension, size effect *(French)* 80−15341
Zn-Sn-Hg amalgam, liq., thermodynamic props. *(Russian)* 77−66624

liquid crystal devices
A/D conversion, parallel real-time, using liq. cryst. light valve 80−53451
acoustic image detector with nematic liquid cryst., expt. on resolution 78−46871
acoustic imaging with nematic liquid crystals *(French)* 80−69617
acousto-optical image and hologram convertor using nematic liq. crysts. 80−76002
acoustooptical image convertor 78−18062
active optical devices, seminar, San Diego, CA, USA (August 1979) 80−101664
alignment by O_2 RF plasma exposed solid surfaces 77−76307
alignment on plasma-synthesized polymer films 77−76308
alignments of director using submicrometre periodicity gratings 78−63666
anthraquinone pleochroic dyes in liq. cryst. soln., photostability, appl. to liq. cryst. displays 80−88961
bibliography of liquid crystals, 1976 79−19146
bistable element array generation by liquid crystal light valve and optical feedback 80−48442
bistable optical spatial device using direct optical feedback 79−18535
calorimeter, radiation characts. 77−71327
cell, with pretilt angle, electro-optical props. *(Japanese)* 78−43837
cells, pretilt influence on capacitance voltage depend. 78−83724
cholesteric films, absorpt. and contrast in dichroic liq. cryst. displays 80−75155
cholesteric layer-semiconductor layer systems, auto-oscill. behaviour *(Russian)* 77−43971
cholesteric liquid crystal non-ionising radiation monitor, response charact. 79−2818
cholesteric liquid crystal panel, energetic sensitivity, as IR registrator *(Russian)* 79−89995
cholesteric liquid crystal photographic plate, for images in IR, extreme characts. *(Russian)* 79−89994
cholesteric liquid crystal resonator for distrib. feedback dye laser, theory 79−31956
cholesteric liquid crystal thermo-optical monitor, for nonionising radiation 78−11742

liquid crystal devices continued
cholesteric liquid crystal visualisation of microwave fields 78−58031
cholesteric sheet heat detector thermographic photographic characterisation of US intensity patterns 80−106689
cholesteric-nematic liq. cryst. mixtures, electro-optic charact., light scatt. modes *(Japanese)* 78−79527
cholesteryl nonanoate-MBBA, liq. cryst. mixture, two colour display device 80−70116
colour filter, electrically controlled 78−83113
colour generating, by optical birefringence, special electrodes 77−68911
computer-controlled liquid-crystal transparency array *(Russian)* 77−58430
conference, Minneapolis, MN, USA (June 1979) 80−77535
conference on liquid crystals, Bordeaux, France (Jul. 1978) 79−86677
Controlled phase transparencies in coherent-optical systems performing Walsh and Hilbert transformations 78−50931
cyanobiphenyl liquid crystal IR modulator expts. 80−102837
cyanobiphenyls, physical props., appl. to Kerr cells 79−19142
p-cyanophenol mixtures, p-alkylbenzoates twisted nematic effect, appl. to digital display prep. 79−82947
dichroic dyes, guest-host interactions, colour switching 77−51312
dielectric waveguide, flow detection using UHF EM field pattern display 80−104378
differential calorimeter dosimeter for nonionising radiation 79−70649
diffraction grating, light diffraction phenomenon *(Polish)* 77−68272
digital multimeter, hand-held instrument 77−74423
digital optical processing, optical parallel logic device and half-adder cct. 79−94364
digital voltmeter appl. *(German)* 78−21165
display, electrothermo-optic effects obs. 77−11469
display, for real-time multichannel optical spectral analysis 78−38042
display, nematic, low melting phenylcyclohexances appl. 77−84652
display, twisted cells, mol. orientation 77−27818
display, twisted nematic, control and elimination of disclinations 77−68912
display, with dichroic dye guest, field-induced colour switching 80−1327
display device, dichroic dyes for guest-host interactions 77−59554
display elements, principles and applications *(German)* 80−86277
display mechanism, smectic cryst., electrically induced scatt. texture and elec. reversal 78−83725
display properties, effect of (+)-4-n-alkylphenyl-4′-(4″-methylalkylbenzoyloxy)benzoates 78−1997
display technique 78−51419
display using dichroic I polarising element 77−46807
displays, appl. of liq. cryst.-rubber dispersion 77−27821
displays, optical characterisation appratus 77−7222
displays, twisted nematic, review of recent advances 79−99056
displays and surface thermography, synthesis and props. of chiral alkylcyano-biphenyls (and p-terphenyls) 77−27820
displays with auxiliary nonlinear elements, series excitation control 77−5818
dye laser oscillator and amplifier in liq. cryst. matrix, anisotropic props. 80−74355
dynamic data display on large screen by brightness enhancing system 77−58462
dynamic scattering, initial molecular alignment effect on electro-optical props. *(Japanese)* 77−1655
edge enhancement of optical images, by Fourier transform optical system 78−33680
electrically controlled transparency based on frustrated total internal refl. 79−32074
electro-optic switch, four-port, for unpolarized fibre light 80−58715
electro-optic valve testing using laser light *(French)* 80−28311
electro-optical applications, review 77−43136
electro-optical modulators for two-dimensional data processing 78−79141
electrooptical filter, teaching expts. 77−41434
electrooptical switches, teaching expts. 77−41434
EM radiation monitor 77−79514
feedback optical system using liquid crystal light valves 78−66924
fibre optic switch based on nematic liq. cryst. film 79−64334
field induced twisted structure with quasihomeotropic boundary conditions, electro-optic behaviour 78−60424
field-line induced reflective interface 79−98482
fluorescent display, utilising elec. field induced cholesteric-nematic transition 78−16781
fluorescent shutter, fast, based on guest-host interaction 78−83092
holographic reader-copier development and speckle suppression 79−81395
holographic recording materials and devices, book contrib. 78−25838
hybrid aligned nematic cell as multicolour display 77−4624
hybrid field-effect liquid crystal light valve, sensitometry control 80−23788
hybrid field-effect liquid-crystal light valve, optical data processing performance 80−99860
image convertor, incoherent to coherent, hybrid optical processors appl. 80−33166
image convertor, incoherent-coherent based on semicond.-insulator struct. 80−28342
image convertor, with memory effect 79−23711
image intensifier, reflective ultra-LV, using liq. cryst. twisted nematic effect 77−7190
image processing, digital, parallel logic device and half-adder circuit 80−10027
image transducer, input device for coherent optical processor, phase response 79−23051
image transducer, normal incidence, on-state optical performance 80−99852
image transducer, optical props. at normal incidence, off-state behaviour 80−64160
image transducer, performance effects of liquid crystal thickness 80−102838
image transducer, real-time, response time 78−74845
image transducer, spatial frequency spectrum temporal meas. 79−76810
incoherent-coherent image transducer for real time correl. 77−27262
indicator, for the velocity of fluids 77−55108
indicator of variable light-reading angle 78−57932
information display technology, symposium, San Francisco (1978) 79−9209
information storage electro-optical props. of cholesteric liquid crystal mixtures *(Rumanian)* 79−78657
IR modulator properties 78−25970

liquid crystal devices continued
IR video camera at 10 μm, using liq. cryst. thermooptical convertor and scanning polarimeter 79−94326
IR visualizer, cholesteric liq. cryst., wide dynamic range 77−79955
joint transform correlator performance rel. to wavefront modulator characteristics 80−102651
layer stabilisation additives 77−76305
lens cell, prep. and optical props. 79−94320
light deflector 79−59814
light flux attenuators, use of liq. cryst. cells exhibiting dynamic scatt. 80−102845
light modulator using piezoelectric effect 80−83679
light valve, appl. to real-time optical data processing 78−83102
light valve, fast photoconductor coupled 79−59805
light valve, in-plane vibr. meas. by real-time speckle interferometry 80−53734
light valve, light-modulated 79−14098
light valve, nonlinear optical processing in real time 80−87338
light valve, optical feedback in incoherently illuminated systems 80−87336
light valve for coherent optical data processing 78−38041
light valve operation and appls. 78−46826
light valve-image tube hybrid device for data processing 77−72083
light valves, appl. to real time image subtraction 78−33677
light valves for active feedback optical processor 78−22204
LV dynamic scatt. display liquid crystal mixtures 77−77178
matrix-addressable controlled transparency, spatial modulation in holographic memory recording 79−10401
MBBA, deflector based on frustrated total internal light refl. 78−50934
MBBA nematic liq. cryst. cell, quasihomeotropic orientation induced by PTFE deposited on SiO surface 79−90525
MBBA-EBBA, controllable liq. cryst. transparency, electrooptical charcts. 80−78996
MBBA-EBBA mixtures, quinone and hydroquinone doped, dynamic scatt., elec., electro-optical props. 79−37616
MBBA-PCB (41 wt.%)+pleochroic dye, electrothermo-optic effect, optical storage device appl. 78−87611
S-(+)-4-2′-methylbutyl phenol, cholesteric derivatives, appl. in display devices 79−19145
microprobes, non-perturbing, based on cholesteric crystals 78−16791
miniature battery-operated digital voltmeter with liquid crystal display *(German)* 79−80601
MIS photosensitive high resolution struct., spatial light modulation with liq. cryst. 80−96026
modulation transfer function comparison for photographic lenses with liquid crystal cells *(Russian)* 79−89025
molecular orientation, effect of deposition of SiO_2 films *(French)* 79−10789
mosaic liquid crystal controlled transparency for holographic store data input *(Russian)* 79−94182
multicolour device, Poincare sphere analysis 77−85690
multiplexed liquid cryst. display, use of cholesteric-nematic phase change 80−107408
multiplexed twisted nematic displays, liq. cryst. material design 79−90533
nematic, low tilt angle alignment, on evap. SiO layer, compatible with frit sealing 77−68910
nematic cell, light scatt. distribs. 77−55772
nematic cell, twisted, Leslie threshold field verification 77−84638
nematic cell structures for light deflection *(Japanese)* 77−39051
nematic cells, spatial resolution and phase retardation in inhomogeneous elec. fields 80−44118
nematic crystal operation, display appl. *(Italian)* 79−46553
nematic display, thin film process to improve off axis viewing 79−4239
nematic display device, generation of arbitrary colour 80−5815
nematic display devices, with twisted and tilted arrangements, guest-host interactions 80−34891
nematic dynamic scattering display, flow direction rel. to dopant electrochem. props. 77−90130
nematic layer as active element for acoustic information transform. 77−20824
nematic liquid cryst., ZhK-440, transparency, electrooptical charcts. 80−78996
nematic liquid crystal adjustable access couplers for fibre-optic switching 80−33217
nematic liquid crystal display, capacitative anal. 77−43969
nematic liquid crystal display, twisted, ang. and voltage depend. of light transmission, two-layer model 80−76006
nematic liquid crystal light modulator, scanning mode of operation 80−33200
nematic liquid crystal matrix display, scanning capability improvement 77−55770
nematic liquid crystal transducers, dynamic scatt., pre-excitation 80−88021
nematic liquid crystals, temp. dependent props., twisted nematic displays 79−32901
nematic mixture, for low voltage dynamic scatt. display 78−27184
nematic mixtures, extended range, for appl. in electro-optic devices 78−83728
nematic reversely pretilted cell, conformation of molecular orientation 80−59388
nematic twist cell, dynamic props., voltage depend. 80−70117
nematic twisted layer, off-state transmission 79−82948
nonlinear acoustics 8th symposium, conf., Paris, France, July 1978 80−33277
p-n-octyl-p′-cyanobiphenyl, thermally addressed liq. cryst. display, light scatt. and contrast 80−34892
one-dimensional Fourier hologram line data recording scheme *(Russian)* 79−22912
optical attenuators using nematic liquid crystals 77−19409
optical fibre temp. probe rel. to thermometry and dosimetry of heat 80−98204
optical logic with variable-grating-mode liquid-crystal devices 80−106613
optical modulator, time depend. of conductivity under dynamic scatt. conditions 80−64178
optical shutter, applic. of guest-host interaction 78−74988
optically active binary liquid crystal thermometry 79−42952
organic surfactants for liquid crystal orientation control 78−91251
orientation, of liquid crystal on obliquely evaporated SiO film 77−69190
orientational bistability, nematic storage effects 80−70112
liquid crystal devices continued
PCB, nematic liq. cryst., US imaging, convertor, acousto-optical effect 78−59218
p-n-pentyl-p′-cyanobiphenyl, nematic phase, mapping of acoustical fields 79−91402
photoactivated liquid crystal light valves, CdS film, pure and Al doped 78−60162
photoconductivity controlled liq. cryst. light valve for reconstruction of long wave holograms 77−79787
photoconductor reflective light intensifiers, sensitivity to imaging light 77−42598
photosensitive MIS structure in contact with nematic liq. cryst., light spatial modulation 80−48436
picture taking parameters display in amateur cameras, review 78−89578
polarization rotator for intermodulation spatial-bandwidth reduction holography 80−53439
pretilted liquid crystal structure formation and props. 77−76306
pretilted nematic structure, colour control by elec. field 77−73127
Q-switched pulse stretching by intracavity nonlinear ellipse rot. 78−17991
real-time image optical subtraction scheme 78−74856
real-time moving object tracking by optical correlation, using liq. cryst. image transducer 79−32035
real-time nonlinear optical signal processing with liquid crystal light valves 79−76868
real-time optical processing using the liquid crystal light valve 80−63936
response time improvement 79−76806
review of applications *(Polish)* 78−30537
scattering indicatrix determination for coherent and incoherent radiation *(Russian)* 80−64897
screen, coherent optical image spotty structure reduction 79−14109
self diffraction of laser beam by liquid crystal struct. 80−5803
semiconductor-liquid crystal interface props. *(Rumanian)* 78−83723
smectic A liquid crystal, scattering textures, appl. to display device 78−91236
smectic C liquid crystals, ferroelec., fundamentals and display appl. 80−79676
smectic displays, thermo-optic and elec. field effects *(French)* 78−91223
spatial filters, tunable, in optical signal convertors 78−50930
spatial light modulator, for optical data processing, 1978 state of art and development trends 79−7201
spatial light modulator using phase transition type liquid crystal *(Japanese)* 78−79119
spatial light modulators for coherent optical computing, performance evaluation 79−89989
surface alignment treatment giving controlled low angle bit 77−19871
surface temp. meas. using contact thermometer, field meas. by liquid crystals *(German)* 79−58686
T-cell light transmission rel. to angle of incidence 79−27426
temperature meas., jet stagnation point heat transfer on plate 78−18327
thermal field measurements, liq. cryst. improved technique 80−216
thermography, in breast pathology *(French)* 78−7420
thin-film waveguide with liq. cryst. boundary modulation of refr. index, mode switching 80−23800
three-dimensional multiplane liquid crystal matrix *(Russian)* 77−9995
total radiation monitoring using liquid crystals and thermoluminescence 80−3819
translucent screens, resolution 80−28335
transparency, liq. cryst. controlled, 128×128 element capacity, for hologram recording 79−50254
transparency, liq. cryst. controlled, information optical recording in microholograms 79−10406
twist cell, flow patterns 80−49094
twisted nematic display with cholesteric dopant, transmission characteristic temp. depend. compensation 80−103934
twisted nematic displays, electro-optical props., solute effects 77−1072
twisted nematic layer, light transmission 78−68476
twisted nematic layer, transmission characts. 77−1653
twisted nematic liq. cryst. matrix display, two-frequency 100-line addressing 79−54119
twisted nematic liquid crystal cell, off-ninety degree, electro-optical colour effect 77−77172
twisted nematic liquid crystal-fibre optic modulator for display 79−72718
US field visualisation by nematic-cholesteric mixed cell 78−1524
US transducer, liq. cryst. cell for US visualisation *(German)* 78−79179
US visualisation using liquid-crystal film 80−5893
variable tilt smectic A electro-optic effect giving stored colours 78−51415
VHF field thermoindication, linearity *(Russian)* 79−1391
visual perception tester, road safety appl. *(French)* 77−36930
visually evoked response test goggle system using liquid crystal shutters 79−79676
waveguides for integrated optics 77−34960
InO_3:Sn transparent conducting films, homeotropic orientation of liquid crystals *(Russian)* 80−108181
SiO coatings for nematic alignment, surface struct. effects 77−39726

liquid crystal phase transformations
4-octyl-4-cyano-biphenyl, nematic to smectic A phase transition texture changes, thermoelectrooptic effect 80−49098
A to C transition, mol. polar bond model 77−51478
acoustic emission, appl. to defect dynamics study 78−91232
p′-acryloyloxyozoxybenzenes, substituted 79−1494
p-alcoxybenzilidene butylaniline, mag. anisotropy and polymorphism *(French)* 77−76532
alkali alkanoates, phase relationships and thermal behaviour branching effects 78−43111
4-n-alkoxy-4′-cyanodiphenyldiacetylenes, synthesis and mesomorphic props. 79−82148
4-n-alkoxy-4′-cyanostilbenes, synthesis and mesomorphic props. 79−82148
4-n-alkoxy-4′-cyanotoluenes, synthesis and mesomorphic props. 79−82148
trans-p-n-alkoxy-α-methyl cyanophenyl cinnamates, elastic consts. and orientational order parameters 80−44244
n-alkoxy-α-methyl-p′-cyanophenyl cinnamate, orientational order, tricrit. behaviour 79−27907
1-(4-alkoxy-benzoyloxy-phenyl)-2-(4′-pentylphenyl)-ethanes, synthesis and mesomorphic props. 79−90536

liquid crystal phase transformations continued
p,p′-n-alkoxyazoxybenzene homologous compounds, isotropic-nematic, DC Kerr constants 78−27185
alkoxyazoxybenzenes, isotropic-nematic transitions, RI, orientational relax. times 77−24390
p-alkoxybenzal-p′-ethoxyaniline, even-odd effect and chain config. 79−50989
p-n-alkoxybenzoic acids, mol. arrangement in cryst., nematic, and smectic C phases 79−32889
4(4′-n-alkoxybenzoyloxy)benzylidene-4″-aminophenols, synthesis and mesomorphic props. 79−90546
alkoxybenzylidenaminobenzonitriles, elec. field and press. induced transitions, transparency and texture 77−43317
N-(4-n-alkoxybenzylidene)-4′-alkylanilines, smectic-B to H transition, B-phase struct. 79−94896
N,N′-bis(p-alkoxybenzylidene)-α,α′-bi-p-toluidines, nematic phase, synthesis, thermodynamic props., gas-liq. chromatographic anal. 79−90763
4-n-alkoxybenzylidene-4′-methylalkylanilines, chiral nematic cryst., mesorphic behaviour and binary systems 78−2000
N-4-alkoxybenzylidene-4′-n-alkylanilines, smectic F phases 79−94891
p-alkoxybenzylidene-p-n-alkylanilines, thermotropic mesophases, proton spin-lattice relax. 78−91968
p-alkoxybenzylidene-p-n-butylanilines, optical and mag. anisotropies in liq. cryst. phase, thermal variations of order parameter *(French)* 79−82149
4′-n-alkoxybiphenyl-4-carboxylic acids, 4-(2′-methylbutyl)phenyl esters, smectic phases 79−86684
6-alkoxynicotinic acid, liq. cryst., prep. and transition temp. 77−27811
4″-n-alkoxyphenyl biphenyl-4-carboxylates, liq. cryst. props. 79−82150
4-alkoxyphenyl-4′-alkylbenzoates, mesomorphic props., terminal alkyl chain length effect 80−88024
p-alkoxyphenylazo-p-phenylesters, polymorphism, calorimetry *(French)* 78−51650
p-alkoxyphenylazody-p′-phenylesters, mesomorphis, synthesis and transition temps. *(French)* 77−27815
n-alkyl 4′-n-alkoxybiphenyl-4-carboxylates, smectic C and tilted smectic B phases 79−32888
n-alkyl 4′-n-alkoxybiphenyl-4-carboxylates, smectic polymorphism, X-ray diffr. and miscibility meas. 79−27912
alkyl cyanobiphenyls, pretransitional behaviour, alkal chain length depend., light scatt. in isotropic phase 80−44301
4-n-alkyl-4′-cyanobiphenyls, Raman spectra in solid state, polymorphism of mesogenics 79−82964
4-alkyl-4′-cyanostilbenes, liq. cryst., prep. and transition temps. 77−27823
4,n-alkyl-4′-cyanotolanes, and related compds., homologous series, mesomorphic transition temps. 77−27991
4′-n-alkyl-4-cyanobiphenyls, elasticity, orientational order, and nematic-isotropic transition 77−84643
4′-n-alkyl-4-cyanobiphenyls, press. effect on liq. cryst. phase transitions 79−95138
alkyl-cyano-biphenyls, nematic to isotropic phase transition, volumetric studies 79−86878
alkyl-cyano-biphenyls (and p-terphenyls) and related cmpds., chiral, synthesis and liq. cryst. props. 77−27820
alkyl-cyanobiphenyl homologues, isotropic-nematic phase, optical Kerr effect 80−91866
p-n-alkyl-p′-n-alkoxytolanes, hydrostatic pressure effects, phase transitions *(French)* 78−14448
4′-n-alkylbiphenyl-4-carboxylic acids, 4-(2′-methylbutyl)phenyl esters, smectic phases 79−86684
4-4-n-alkyloxybenzoyloxy-benzylidene-4′-cyanoanilines, reentrant nematic and smectic phases 80−88308
N-4-n-alkyloxybenzylidene-4-n-alkylanilines, smectic polymorphism, calorimetric study 80−88307
(+)-4-n-alkylphenyl-4′-(4″-methylalkylbenzoyloxy)benzoates, optically active, synthesis and effect on liq. cryst. display props. 78−1997
2-4-n-alkylphenyl-5-(4-n-alkyloxyphenyl)-pyrimidines, smectic polymorphism, calorimetric study 80−88307
amphiphilic nematic with optically active compounds, cholesteric states and twisting power 78−63846
p-anisalaminoazobenzene, acoustic relax. in nematic phase 77−1184
aromatic esters derived from naphthalene, liqs. cryst. props. 78−47235
aryl esters, cyano-substituted, liq. cryst. props. 77−27822
aryl p-fluoroalkoxybenzoates, synthesis and mesomorphism 78−91243
aryl p-fluoroalkylbenzoates, synthesis and mesomorphism 78−91243
azoxy-4,4′(di-undecyl α-methyl cinnamate), refr. index at 2nd order smectic A to C phase transition 79−19357
azoxy-4,4′-(di-undecyl α-methylcinnamate), smectic A to smectic C phase transition, optical tilt angle meas. 78−95141
p-azoxyanisole, depend. of phase transition temp. on thickness 78−26669
p-azoxyanisole, nematic eqn. of state, incorporating short-range orient. order. 77−55237
BBOA, polymorphism, radiothermoluminescence and differential scanning calorimetric study 80−24570
BBOA, pretransitional shear viscosity divergence near smectic A-smectic B transition 79−33077
BBOA, smectic liq. cryst. glass-supercooled transition and Debye temp., ^{57}Fe Mossbauer effect 80−54999
BBOA, thermal diffusivity meas. by forced Rayleigh scatt. 78−76483
benzazoles, liq. cryst., prep. and transition temp. 77−27811
benzene-hexa-n-alkylanoates, disc-like molecules, miscibility studies of mesophases 80−19696
benzylidene aniline series, nematic liq. crysts., coherence length anisotropy above isotropic to nematic transition 77−62470
benzylideneanilines, ordered smectic phases, X-ray diffr. meas. 77−89375
benzylideneanilines, thermal parameters for cryst.-mesophase and cryst.-cryst. transitions 77−11679
binary mixture phase separation, statistical theory 77−4188
binary mixtures, phase transitions, entropy, relation to smectic plane tilt angle 80−65203
biomembrane phase transitions 78−35808
biphenyl mixtures with cholesteryl chloride, static and dynamic electro-optical props., cholesteric-nematic transition 80−100646
biphenyl-p-ethylbenzoate, high press. mesomorphic and polymesomorphic transitions 78−18750
biphenylbenzoates, synthesis, mesomorphic, and thermodynamic props. 80−44117
biphenyls, cholesteric blue phases, struct. and props. 80−103243
4-biphenylyl 4″-n-alkoxybenzoates, smectic liq. crysts., transition temps., DTA 78−75815

liquid crystal phase transformations continued
bis-4-n-alkylphenyl tetrafluoroterephtalates, synthesis and mesomorphic props. *(French)* 79−86679
bis-4-nalkyltetrafluorophenyl tetrafluoroterephtalates, synthesis and mesomorphic props. *(French)* 79−86679
bis-(4,4′-n-alkoxybenzylidene)-1,4-phenylenediamines, smectic polymorphism up to 3 kbars, differential thermal anal. 79−55873
butoxybenzylidene-aminobenzonitrile, crystalline and liq. cryst. states, low freq. spectra 78−34437
N-n-butoxybenzylidene-n-butylaniline, US propag. near nematic-smectic A transition, mag. field effect 80−39266
N-p-butoxybenzylidene-p-n-octylaniline, smectic A-B transition, birefringence pretransitional behaviour 80−15226
n′-n-butyl-n-methoxyazoxybenzole, specific heat anomaly and isotropic liquid to nematic liquid cryst. transition *(Russian)* 77−62624
butyloxybenzylidene octylaniline, liq. cryst., phase transitions, calorimetric obs. 80−103466
butyloxybenzylidene octylaniline, liq. cryst. film, smectic B-A transition, mech. meas. 80−79918
4-n-butyloxyphenyl-4′-nonyloxybenzoate, edge dislocations in smectic C mesophase 78−91231
caesium perfluorooctanate, thermodynamically independent nematic amphiphilic mesophase obs. 79−95126
carrier mobility anisotropy at nematic-smectic transition *(Japanese)* 77−43605
CBNA, nematic-isotropic transition at high press., turbidity meas. 80−92655
CBOOA:nitroxide, liq. cryst. phase transition study by electron spin relax. *(French)* 79−55874
CBOOA, acoustic emission at liq. cryst. transitions prod. by thermo-optically excited defects 79−95137
CBOOA, dynamic crit. neutron scatt. obs. near smectic-A nematic phase transition 78−79752
CBOOA, isotropic, nematic, smectic-A phases, Brillouin scatt. 80−11421
CBOOA, liq. cryst.-isotropic transition at high press., P-V-T eqn. of state 79−95135
CBOOA, mag. aligned, smectic A-nematic transition, US absorpt meas. 78−95137
CBOOA, nematic phase laser light scatt., mag. field depend., crit. deform. *(Japanese)* 78−2826
CBOOA, nematic to smectic A transition, high resolution X-ray scatt. exam. 78−94984
CBOOA, nematic-smectic transition, singularities, elastic const. var. 77−39537
CBOOA, smectic A, nematic and isotropic phases, surface tension 77−39539
CBOOA, smectic A to nematic phase transition, crit. neutron scatt. 78−95135
CBOOA, smectic A-nematic, interf. rings and bend elastic constant 78−26434
CBOOA, smectic A-nematic transition, X-ray and light scatt. obs. 79−95129
CBOOA, smectic-A reentrant nematic transition under press., X-ray obs. 80−59637
CBOOA, smectic-A-nematic and nematic-isotropic transitions, vol. behaviour 77−39666
CBOOA, twist viscosity and mech. props. near smectic A-nematic transition 78−95136
CBOOA, US absorpt. and dispersion at nematic-smectic-A transition 79−82287
CBOOA, US attenuation near nematic-smectic A transition 78−87773
CBOOA, with cholesterol decanoate, short range smectic A order in nematic phase, NMR meas. 77−28475
CBOOA/4-cyanobenzylidene-4′-n-octyloxybiphenyl mixture, reentrant nematic phases 79−41953
cellulose acetate, solvent effect on lyotropic mesomorphicity 80−70121
chiral smectic A to C transition, electroclinic effect 77−39668
chiral smectic A-C* transition, elec. susceptibility and electroclinic coeff. 79−28089
chiral smectic A-C* transition, elec. susceptibility and electroclinic coeff. 79−28088
chiral smectic critical behaviour near phase transformation point between two ferroelectric phases *(Russian)* 80−44124
chiral smectic liquid crystal, A-C phase change, electroclinic effect 79−42224
p-chlorobenzylidene-p-n-pentylaniline, metastable phases formed by rapid cooling of mesophase, IR and Raman spectra and DSC obs. 80−34919
cholesteric, Brillouin scatt. in isotropic phase 78−2867
cholesteric, field induced nematic texture, nucleation of focal-conic domains 78−34430
cholesteric, ordering mechanism *(Russian)* 77−68921
cholesteric, phase transitions and critical phenomena *(Russian)* 79−4407
cholesteric, with temp. hysteresis 77−84902
cholesteric blue phase, BCC struct., theory 80−59380
cholesteric defect struct. near smectic A transition 79−46559
cholesteric helix period, mag. field strength depend. near phase transition to smectic A *(Russian)* 78−59754
cholesteric layer-semiconductor layer systems, auto-oscill. behaviour *(Russian)* 77−43971
cholesteric liq. crysts., isotropic phase, pretransitional viscosity 80−84312
cholesteric liquid cryst., guest mol. fluoresc. in scatt. state 80−63698
cholesteric liquid crystal, bubble domain texture, obs. of forming process 78−26431
cholesteric liquid crystal, microstruct. rel. to optical props. 78−47240
cholesteric liquid crystal, US velocity, temp. depend. 77−11637
cholesteric liquid crystal film, optical rotating power near cholesteric to smectic A transition 78−10865
cholesteric liquid crystals, mixtures, hysteresis, bistability effects under elec. fields 78−42907
cholesteric liquid crystals, viscosity coeff. at smectic-cholesteric transition 79−77791
cholesteric nonanoate, US attenuation near cholesteric to smectic A transition 79−28091
cholesteric textures, confocal, optical and electro-optical props. *(Russian)* 77−80419
cholesteric-nematic phase change, threshold voltage for electro-optic effect 79−91405
cholesteric-nematic phase transition, boundary induced 77−76533
cholesteric-nematic transition, helix stepped unwinding *(Russian)* 79−90548

liquid crystal phase transformations continued
cholesterilcinamate, low press. phase transition temp. change, relative transparency *(Russian)* 78−2242
cholesteryl 2-(2-ethoxy-ethoxy) ethyl carbonate, dynamics of isotropic-cholesteric transition, normal and blue phases 79−95134
cholesteryl acetate, phase transitions and solid polymorphs 78−2255
cholesteryl acetate-cholesteryl octanoate system, phase transitions, thermoanalytical microscopy obs. 79−55871
cholesteryl acrylate, mono- and polymer, liq. cryst. order 78−9942
cholesteryl caproate, isothermal crystn., spherulites growth rate, optical microscopy obs. 79−32892
cholesteryl chloride, depolarised light transmission, microstructural changes 78−22647
cholesteryl chloride-cholesteryl crotonate (75:25% wt.) mixture, cholesteric-nematic transition field effect temp. depend. 78−75813
cholesteryl chloride-cholesteryl pelargonate mixture, cholesteric-nematic transition 78−91244
cholesteryl crotonate, depolarised light transmission, microstructural changes 78−22647
cholesteryl decanoate, cholesteric pitch near smectic-A transition meas. 77−7856
cholesteryl decanoate, NMR spectroscopy of blue phase 79−4236
cholesteryl decanoate, optical activity in blue phase 80−100641
cholesteryl esters, kinetics of cholesteric/blue phase transform. 79−95140
cholesteryl esters, liq. crysts., P-T diagrams up to 5000 kg/cm^2 78−2003
cholesteryl esters, phase transitions, volumetric behaviour, dilatometric obs. 77−59106
cholesteryl laurate, crystallisation kinetics and phase transitions, differential scanning dilatometric obs. 79−69230
cholesteryl laurate-cholesteryl caprylate (75 wt.%), polymorphic behaviour, optical, elec. and dielec. meas. 80−65208
cholesteryl linoleate, dielec. props., phase transitions rel. to temp. 79−33592
cholesteryl methacrylate, mono- and polymer, liq. cryst. order 78−9942
cholesteryl myristate, density of smectic, cholesteric, blue, isotropic phases 78−42897
cholesteryl myristate, high press. mesomorphic and polymesomorphic transitions 78−18750
cholesteryl myristate, polymorphism of blue phase, DTA and microscopy meas. 79−37819
cholesteryl myristate, press. depend. of cholesteric pitch near cholesteric-smectic A phase transition 77−68918
cholesteryl myristate, smectic A-cholesteric transition, tricritical behaviour, DTA and DSC study 80−65206
cholesteryl nonanoate, high press. mesomorphic and polymesomorphic transitions 78−18750
cholesteryl nonanoate, liq. cryst.-isotropic transition at high press. 79−95135
cholesteryl nonanoate, polymorphism of blue phase, circular dichroism at high-press. 79−37821
cholesteryl nonanoate, polymorphism of blue phase, DTA and microscopy meas. 79−37819
cholesteryl nonanoate, polymorphism of blue phase, optical rot. and refl. 79−37820
cholesteryl nonanoate (decanoate), effect of cholesteryl alkanoyl esters on red-green transition temp. 80−19924
cholesteryl oleate, isotropic phase, shear viscosity, logarithmic divergence 78−26668
cholesteryl oleate (linoleate), solid-solid transition, glass transition, cryst. nucleation temps., DSC obs. 78−34604
cholesteryl oleyl carbonate, high-purity, prep. for thermal radiography and phase transitions, appl. in thermal radiography 77−15311
cholesteryl oleyl carbonate, isotropic phase, polarisation of scattered light 79−78691
cholesteryl oleyl carbonate, isotropic phase, shear viscosity, logarithmic divergence 78−26668
cholesteryl oleyl carbonate, press. depend. of cholesteric pitch near cholesteric-smectic A phase transition 77−68918
cholesteryl p-acryloyloxybenzoate, mono- and polymer, liq. cryst. order 78−9942
cholesteryl pelargonate, liq. cryst. phase transitions *(Russian)* 79−37818
cholesteryl vinyl succinate (fumarate), polymer+monomer systems, liq. cryst. phase states 79−1494
cholesterylalkanoates, liq. cryst., optical anisotropy and struct. ordering *(Russian)* 78−87616
cholesterylpelargonate, cholesteric-smectic A transition, metal-supercond. analogue 79−23712
COC, cholesteric liq. cryst., positron lifetimes and phase transitions 80−59383
COC, cholesteric-smectic-A transition, press. depend., optical meas. 77−47556
COC, dynamics of isotropic-cholesteric transition, normal and blue phases 79−95134
COC, prep., cryst. state, and mesophases 79−95143
COC test of tricriticality 80−10648
collagen fibrils as examples of smectic A biological fibres, transition to smectic C phase 77−90721
colloidal solution, flow alignment, transition from isotopic to nematic phase 80−84060
conference, Kent, Ohio, USA (Aug. 76) 77−27808
conference on smectic and lyotropic liq. crysts., Trento, Italy (Jan. 1978) 78−91222
COOB, acoustic emission at liq. cryst. transitions prod. by thermo-optically excited defects 79−95137
COOB, sheared liq. crystal, near T_{A-N}, optical response 79−94895
COOB, smectic A-nematic transition, X-ray and light scatt. obs. 79−95129
COOB, solid state dimorphism and cryst.-smectic transition, Raman study 80−45063
copolyethylene terephthalate-p-oxybenzoate, nematic phase, thermodynamics 78−91427
CPB, nematic temp. range broadening by nonmesogenic solute 77−47559
critical fluctuations, shear flow effects 77−20045
crystal-smectic and smectic-nematic transitions, Lennard-Jones and Devonshire model extension 79−94883
cyano Schiff bases, high press. reentrant nematic bilayer smectic-*A* transition 79−28087
4-cyano-4′-alkyltolans, prep. and transition temp. 77−31588

liquid crystal phase transformations continued
4-cyano-4′-n-pentylbiphenyl, refr. index meas. and isotropic-nematic phase transition study, surface plasmon technique 80−84282
4-cyano-4′-octylbiphenyl, nematic-smectic-A transition, high-resolution X-ray and light scatt. study 79−73297
4-cyano-4′(n-amyl)-diphenyl, isotropic phase, induced molecular orientation relaxation time, Kerr effect *(Russian)* 80−19699
4-cyano-4′-octyloxybiphenyl, nematic-smetic-A transition, optical birefr. temp. coeff. 78−47505
cyano-biphenyl, nematic liq. crysts., director fluctuation quenching by mag. field *(French)* 78−87613
cyano-biphenyl LC alignment on obliquely evaporated SiO_2 films 80−79677
4-4′-cyano-octyl-biphenyl, smectic A liq. cryst., elec. field effects, capacitance meas. 78−91237
4-4′-cyano-octyloxy-biphenyl, smectic A liq. cryst., elec. field effects, capacitance meas. 78−91237
p-cyano-p′-pentylbiphenyl/p-pentylbenzoic acid, mixture, induced smectic phase, dielec. props. 80−6498
4-cyanobenzoyloxy-4′-pentylstilbene, nematic, smectic A, and orthogonal smectic B phases 80−64890
cyanobenzylidene octyloxyaniline, director bend mode behaviour near nematic to smectic-A phase transition 78−1985
n-pcyanobenzylidene-p-n-octyloxyaniline, liq. cryst., proton FFT of aromatic and alkyl motions 77−15302
N-p-cyanobenzylidene-p-n-octyloxyaniline, smectic-A liq. cryst., nematic pretransitional mech. effects 77−11481
N-p-cyanobenzylidene-p-octyloxyanilene, second order nematic-smectic-A phase transition 77−72681
cyanobiphenyl, surface tension, meas. near nematic-isotropic transition temp. 78−43219
4-cyanobiphenyl derivatives, deuterated, transition temp. meas., comparison with normal compounds 78−14449
cyanobiphenyl liquid crystal IR modulator expts. 80−102837
cyanobiphenyls, 80CB and its mixtures with 7CB, orientational order and elastic consts. 78−91245
cyanobiphenyls, isotropic phase, pretransitional behaviour, optical and elec. Kerr effects 79−10928
4-cyanophenyl 4-n-pentyloxybenzoate, electrical Kerr effect studies 80−25339
4-cyanophenyl-3-methyl-4-(4-n-alkylbenzoyloxy) benzoates, mesomorphic props. 79−94888
2-p-cyanophenylazo-S-akloxypyridines, synthesis, phase transition temps., and dielec. props. 79−86876
4-cyanotetrafluorophenyl 4-n-alkylbenzoates, synthesis and mesomorphic props. *(French)* 79−86679
cybotactic nematic mesophase, X-ray scatt. 80−92454
cyclohexane derivatives, mesophases obs. *(French)* 78−59747
trans-1,4-cyclohexane-di-4′-n-alkoxybenzenes, synthesis and mesomorphic props. 79−94887
trans-1,4-cyclohexane-di-n-octyloxybenzoate, struct. of smectic phases, X-ray diffr. meas. 79−86702
decylammoniumchloride and bromide, lyotropic nematic struct. 78−51410
p-decyloxbenzylidene p′-amino 2-methyl butyl cinnamate, smectic A to C transition, Landau theory 77−84906
decyloxybenzoic acid, vibr. bands., IR dichroism, phase change effects *(Russian)* 78−15174
p-n-decyloxybenzoic acid p-n-hexyloxyphenyl ester, dielec. permittivity in nematic and smectic phases 79−32899
deoxycholic acid, lyotropic and thermotropic phase transitions, clathrate form. 80−49341
deuterated compounds, molecular order and conformation changes in phase transitions 78−47237
4,4′-di(p,n-alcoxybenzylideneamino) biphenyls, smectic polymorphism, dilatometric exam. *(French)* 77−51480
4,4′-di(p,n-alcoxybenzylideneamino)diphenyls, X-ray diffr. study of smectic polymorphism *(French)* 77−76299
4,4′-di-n-acyloxydiphenyldiacetylenes, synthesis and mesomorphic props. 79−82148
p,p′-di-n-butylazobenzene, high press. mesomorphic and polymesomorphic transitions 78−18750
diarylethanes, bromo- or cyano-substituted, mesomorphic props. 79−90535
α,ω-diarylperfluorpolienes, X-ray spectra, phase transition temp. depend., struct. and mesomorphic props. *(Russian)* 78−38621
dibenzoate-TBBA, polar smectic A to non-polar smectic A transition line 79−82324
dicyano compounds, synthesis and dielec. props. 79−86685
dielectric relaxation at phase transitions 79−28090
diffusionless first order based on Landau-Ginzburg eqns. 78−30734
p,p′-dihexyloxyazoxybenzene-fluorobenzene, solute orientational order, NMR obs. 77−84627
dimer-forming compounds, nematic to isotropic transition 79−28085
dipalmitoyl lecithin vesicles in dil. suspension, light scatt. obs., of phase transitions 77−16915
dipalmitoyl lecithin-water system, lyotropic liq. cryst., pretransitional effects, PMR second moment meas. 78−91234
dipalmitoyl phosphatidylcholine, gel and liquid crystalline phases, deuterium mag. resonance obs. 79−91308
discotic mesophases, solute-solvent interactions, effect on phase transition 80−10490
distribution function of anisotropic liq., integral eqn., quasi-chem. approx. *(Russian)* 78−6147
p,p′-disubstituted phenyl thiolbenzoates, synthesis and props. 77−15308
DOBAMBC, and DOBAMBCC, chiral smectic C liq. cryst., dielec. consts., electroclinic effect 78−94980
DOBAMBC, chiral smectic, ferroelec., press. and solute effects 80−103920
DOBAMBC, chiral smectic phases, pyroelectric and dielec. props. 79−91380
DOBAMBC, dielec. dispersion at ferroelec. smectic A-smectic C transition 79−91385
DOBAMBC, dielec. props. near ferroelec. smectic A to C transition 80−45015
DOBAMBC, ferroelec. props. 79−32884
DOBAMBC, polarized Raman scatt. and elec. field effects in aligned smectic phases 79−94873
DOBAMBC, smectic, ferroelec. transition mechanism obs. by X-ray scatt. 79−77515

liquid crystal phase transformations continued
DOBAMBC, smectic A and ferroelec. smectic phases, ^{13}C NMR study 80−75153
DOBAMBC, smectic A to C transform., birefringence and optical rotary power 78−75812
dodecylamine ($-NH_2$)/H_2O_2 and deuterated cpd., liquid crystal, phase relationships, isotope effects 79−19358
dodecylcyanobiphenyl, pretransitional behaviour of isotropic to smectic A phase transition 79−60487
p-n-dodecyloxy benzoic acid, liq. cryst. phase transition, thermal studies 78−71843
p-ndodocyloxy benzylidene p-azophenyl aniline, smectic phases, mol. order, EPR study 80−79693
double spin $^1/_2$ lattice gas model, phase diagrams 77−20521
dye laser, tunable, dye dissolved in liq. cryst., second order phase transform. 80−43328
EBBA: nitroxide, mol. reorientation in nematic and isotropic phases, EPR study *(French)* 79−91297
EBBA, binary systems with non-nematic solutes, phase transition behaviour and ^1H NMR anal. 80−34174
EBBA, containing $FeSnO_3$ particles, Mossbauer study of Brownian motion 79−95691
EBBA, crystallisation and melting of metastable solid crystalline phases 78−2240
EBBA, liq. cryst., Raman and calorimetric evidences for existence of three solid modifications 77−77207
EBBA, metastable phases formed by rapid cooling of mesophase, IR and Raman spectra and DSC obs. 80−34919
EBBA, nematic, linear and nonlinear relaxations of fluid dynamical motion 77−31585
EBBA, nematic-isotropic transition, birefringence anomaly at clearing pt. 79−46788
EBBA, nematic-isotropic transition at high press., turbidity meas. 80−92655
EBBA, orientational order in glassy and nematic phases, IR dichroism meas. 80−64891
EBBA, phase transition enthalpies, 1 bar to 2.5 kbar 78−75814
EBBA, polymorphism, radiothermoluminescence and differential scanning calorimetric study 80−24570
EBBA, rapid cooling and mag. field effects on NMR relax. and thermal behaviour 79−82321
EBBA-aromatic hydrocarbon systems, solute size and shape effect on nematic-isotropic equilib. 79−23710
EBBA-non-mesogenic binary liq. cryst. system, two-phase premelting, NMR obs. *(Russian)* 78−30743
EBBA-polymer systems, phase diagrams 79−23709
EBRA, nematic, EPR investig. 80−108077
EEBAC-TBBA, mixed liq. cryst., layer thickness of smectic-B phases 78−38822
electro-optic cholesteric-nematic transition, and memory effect *(Russian)* 77−84911
electro-optical effects, charact. wave number, boundary effect of flow *(Japanese)* 77−20828
enantiomers, discrimination using liq. crystalline solns., IR rot. dispersion meas. 79−16064
enantiotropic nematic reentrant behaviour at atmospheric pressure in a pure compound 79−69233
EOBC, liquid crystal phase transforms., Raman obs. 78−87774
esters, incidence of smectic liq. cryst. phases, effects of mol. framework changes 77−27819
trans-4-ethoxy-4′-alkanoyloxyazobenzenes, nematogenic liquid crysts., birefr., order parameters, vol. changes during nematic-isotropic transitions 78−59742
ethoxy-hexyltolane, orientation-statistical props. studies by optical methods *(Russian)* 79−77518
ethoxy-octyltolane, orientation-statistical props. studies by optical methods *(Russian)* 79−77518
ethoxyhexyltolan, Raman spectra, molecular conformational instability, internal field effects 80−54127
ethoxyoctyltolan, Raman spectra, molecular conformational instability, internal field effects 80−54127
ethyl-(methoxybenzylidene-amino)cinnamate, low freq. dielec. constant meas. in cryst. and liq. cryst. phase 78−91226
ethyl-p-azoxybenzoate, far IR and Raman spectra, smectic polymorphism 80−76022
eutectic mixtures, glassy transition, DTA obs. 79−4405
ferroelectric, crit. exponents 77−80607
ferroelectric helicoidal smectic-C liq. cryst. dynamics 79−1396
ferroelectric liquid crystals, kinetics of spontaneous polarisation *(Russian)* 79−8101
ferroelectric liquid crystals, soft mode dynamics 77−7852
and ferroelectric struct. development, theory 77−66018
field-induced nematic-cholesteric relax., hysteresis behaviour of texture 77−84900
fluorescent liquid crystal-display, utilising elec. field induced cholesteric-nematic transition 78−16781
Freedericksz transitions in twisted nematics with surface tilt 78−71671
hard rod fluid, rotational and liquid-crystalline phase transitions, 1-D model 80−54090
hard-particle fluids, general scaled-particle-like descriptions 80−103231
hard-particle fluids, general y-expansion-like descriptions 80−107032
HBAB soln. in CBOOA, re-entrant nematic phase 79−14674
HBHA, synthesis and smectic B-smectic B transition 77−15562
HBPA, smectic liq. cryst. glass-supercooled transition and Debye temp., ^{57}Fe Mossbauer effect 80−54999
HBT, mag. susceptibility and anisotropy, smectic, nematic, isotropic phases 78−18748
HBT, quenching effects, DSC, DTA, X-ray diffr. and microscopic obs. 78−22833
helicoidal ferroelectric smectic A-smectic C phase transition, low freq. polarisation fluctuation spectrum 79−95714
n-heptyl cyanobiphenyl, namatic-isotropic transition, orientational order parameter temp. depend. 78−27201
4′-n-heptyl-4-cyanobiphenyl, nematic, mag. field depend. of birefringence and order parameter 77−76534
p-p′-n-heptyl-cyanobiphenyl-isotropic solute systems, nematic-isotopic phase transformation, volumetric study 80−92653
p-n-heptylhydroxybenzylidene-p'-n-butylaniline, phase transition study from 22 to 80°C 79−14679
4,4′-di-heptyloxyazoxybenzene, diffuse X-ray scatt. near smectic C-nematic transition 79−95139
liquid crystal phase transformations continued
heptyloxyazoxybenzene, liq. cryst., pretransition behaviour, volumetric study 77−69076
4-4′-di-heptyloxyazoxybenzene, liq. cryst.-isotropic transition at high press. 79−95135
p-n-heptyloxybenzylidene-aminofluorenone/COOB mixtures, dynamic twist viscosity near polycrit. points 79−95133
p-n-heptyloxybenzylidene-p-aminobenzoic acid, smectic C to nematic transition 79−33076
N-p-heptyloxybenzylidene-p-heptylaniline, dislocations obs. in smectic A and C mesophases 78−91230
heptyloxylbenzoic acid, isotropic phase, light scatt., ultrasonic vel. and absorpt. meas. 78−48189
4-n-heptyloxyphenyl 4-n-hexydexybenzoate, freezing polarisation, electret effect *(Polish)* 80−10496
hexyl-azoxybenzene, twist viscosity and mech. props. near smectic A-nematic transition 78−95136
4-n-hexyloxybenzilidene-4′-n-propylaniline, liq. cryst. phases, thermal and structural studies 78−1989
4-n-hexyloxybenzylidene-4′-n-propylanilene, smectic S_H and S_m phase structs. 79−14673
p-n-hexyloxybenzylidene-p-aminobenzoic acid, phase transitions, X-ray diffr. and DSC meas. 79−86877
N-p-hexyloxybenzylidene-p-toluidine, optical props., density, and order parameter in liq. cryst. phases 79−55657
p,n-hexyloxybenzylideneamino-p′-chlorobenzene, liq. cryst., sp. ht. meas. 78−22831
HOAB, effect of smectic C struct., on dielectric relax. 79−19140
HOAB, liq. cryst. phase transitions, specific ht. meas. 79−33075
HOAOB, isotropic-nematic transition, supercooling and nucleation, interface dendrites 78¬42896
HOBA, isotropic phase, Brillouin scatt. spectra, hypersound data determ. 79−91453
HOBACPC, chiral smectic C liq. cryst., dielec. consts., electroclinic effect 78−94980
HOBHA, smectic A to C transition, crit. biaxiality *(French)* 77−4039
HxBPA, DSC and X-ray diffr., 170-380K 77−15314
HxBPA smectic phases, X-ray diffr. and Raman spectra 78−6012
image convertor, liq., cryst., with memory effect 79−23711
n-indecyl-p-azoxy-α-methyl cinnamate, dislocations obs. in smectic A and C mesophases 78−91230
instability, azimuthally-oriented, produced by elec. field, near nematic-smectic transition *(Russian)* 77−4041
internal field anisotropy changes, order parameter determ. by optical methods 79−86711
isotropic phase, self-focusing stability of laser beam 80−99812
isotropic phase NMR, critical orientational order fluctuations 77−55236
isotropic to nematic phase transition, rel. to universality in percolation problem 77−79045
isotropic-nematic liquid crystal phase transition, theory including mol. orientation correlation 78−47508
isotropic-nematic phase transition, first order, bifurcation approach to theory 77−35677
isotropic-nematic phase transition, van der Waals theory 77−31757
isotropic-nematic transition, mean-field theory, thermodynamic props. 77−24391
isotropic-nematic transition, model, mol. shape, vol. effects on orientational ordering 78−30741
isotropic-nematic transition, Onsager's orientational order theory 78−79750
isotropic-nematic transition, pretransition effects study, optical method of determ. of crit. indices *(Russian)* 78−63847
isotropic-nematic transition, substrate surface effects *(German)* 77−31759
isotropic-nematic transition, tricritical behaviour 78−75817
Landau point crit. exponents to order ε^2 78−41259
lattice gas model, double spin 1/2, for mag. annealed binary alloy and nematic mixture 77−66342
lattice models showing liquid-liquid crystal phase transitions 79−95128
lecithin bilayers, density and mol. interactions 78−80837
lecithin surface films, equilib. and metastable states rel. to use as biological model 77−60188
light generation at impurity atoms in ferroelectrics and LC, fluctuation effects *(Russian)* 80−91767
lipid bilayers, cholesterol model 78−56953
lipid bilayers, long-range order, phase transition, coherence lengths 78−92593
lipid membranes, orientational phase transitions with mol. config. change 78−14444
lipid phase transition, cluster model, appl. to bilayer mol. passive permeation and struct. relax. 78−53346
lipid-water systems, byotropic liquid crystalline and other lamellar phases 78−92592
liquid crystals, deuterated, dueteron mag. resonance mol. odering, conformational changes 80−34789
liquid crystals, structure and dynamics, neutron diffr. studies 78−94972
lithium perfluoro-octanoate-water, liquid crystal, ^{19}F multipulse NMR obs. 80−34795
lyotropic, phase diagrams and NMR solubilised mols. effect on struct. 77−84628
lyotropic liq. cryst., phase transitions *(Japanese)* 77−20060
MBAB:cholesteryl chloride, thickness depend. of threshold elec. field for instabilities 79−32896
MBAB-chiral cpd. mixture, cholesteric, helical screw sense and pitch determ., Grandjean-Cano method *(German)* 77−80609
MBBA: 4-methoxybenzaldehyde, pure and doped, nematic-isotropic transition temps., appl. to purity control 79−55872
MBBA:diacetylferrocene, nematic glass-supercooled nematic transition, Mossbauer temp. obs. 79−95687
MBBA, Brillouin scatt. in isotropic phase 78−2867
MBBA, dynamic critical behaviour in NLC above nematic-isotropic transition 80−49096
MBBA, electronic spectra 78−52530
MBBA, high freq. EHD instabilities, temp. depend. 79−94879
MBBA, isotropic phase, Brillouin scatt. spectra, hypersound data determ. 79−91453
MBBA, isotropic phase, light scatt., ultrasonic vel. and absorpt. meas. 78−48189
MBBA, isotropic-nematic transition, birefringence for tricrit. exponents 79−37816

liquid crystal phase transformations continued
MBBA, laser radiation transmitted near isotropic transition, spatial coherence 78−18003
MBBA, liq. cryst.-isotropic transition at high press., P-V-T eqn. of state 79−95135
MBBA, metastable phases formed by rapid cooling of mesophase, IR and Raman spectra and DSC obs. 80−34919
MBBA, mol. alignment, comparison of exptl. data at high press. with mean field theory predictions 79−99075
MBBA, mol. dynamics near nematic-isotropic liq. cryst. transition *(Russian)* 78−84495
MBBA, nematic, nonlinear effects, in elec. and mag. fields 77−24263
MBBA, nematic liq. cryst., cylindrical domain struct. thermal excitation, optical obs. 79−73097
MBBA, nematic liq. cryst., mol. order and motion, EPR study 77−76298
MBBA, nematic liq. cryst., nonlinear optical amplification above Frederiks transition 80−95937
MBBA, nematic liq. cryst., nonlinear optical processes near Freedericks transitions 79−69011
MBBA, nematic liq. cryst. isotropic phase, phase-conjugate refl. by degenerate four-wave mixing 80−43389
MBBA, nematic-isotropic pretransition regions, ±15K, volumetric obs. 77−76535
MBBA, nematic-isotropic transition, birefringence anomaly at clearing pt. 79−46788
MBBA, nematic-isotropic transition, intermolecular forces, IR N_2O mol. probe obs. 80−29155
MBBA, nematic-isotropic transition, isothermal compressibility and thermal expansion coeff. meas. 79−99301
MBBA, nematic-isotropic transition at high press., turbidity meas. 80−92655
MBBA, orientational order in glassy and nematic phases, IR dichroism meas. 80−64891
MBBA, polymorphism, positron annihilation obs. 78−72632
MBBA, proton spin-lattice relax. in crit. regime 80−80631
MBBA, pure and mixed with bezene (chlorobenzene), nematic-isotropic transition, US absorpt., visual hysteresis 80−54355
MBBA, shear modulus and viscosity relax. near isotropic-nematic phase transition *(Russian)* 77−39543
MBBA, solid, NMR and thermal behaviour, cooling and mag. field effects 78−76336
MBBA, specific heat anomaly and isotropic liquid to nematic liquid cryst. transition *(Russian)* 77−62624
MBBA, US propag., nonlinear effects 77−59069
MBBA, volume meas. and phase transitions at high press. 79−90764
MBBA liquid crystal, premelting detected by spin probes, effect of spin probe size 79−46563
MBBA nematic liq. cryst. systems, orientational order rel. to solute size, shape 77−4565
MBBA-cholesteryl chloride mixture, mol. orientation during mag. field induced cholesteric-nematic transition 79−28086
MBBA-EBBA mixtures and MBBA, thin and mol. films, between Hg electrodes, I-V characts. 79−11253
MBBA/EBBA binary liquid crystal mixture, US absorpt. and vel. dispersion, phase transition and alignment effects *(Korean)* 80−29121
MBBA/n-hexane mixtures, isotropic-nematic transition, transient optical Kerr effect study 79−82323
mean field theory of model anisotropic pot. of rank >2 79−60268
mean-field equations, phase diagrams 78−18751
melting behaviour, proton NMR spectra 78−15044
mercury carboxylates, phase transitions, DTA 79−90759
mesogenic compounds with smectic F phase, succession order of smectic mesophases *(French)* 79−19143
mesogens, chiral, transition temp. 78−2241
mesomorphic mixtures, binary phase diagrams, thermodynamic props., diamag. anisotropy 78−95139
mesomorphic state formation mechanism and molecular struct. correlation 80−54128
methoxy-amyltolane, orientation-statistical props. studies by optical methods *(Russian)* 79−77518
p-methoxy-benzoate-p-n-pentylbenzene, isotropic phase nematogen optical Kerr const. 80−78919
p-methoxy-p′-alkyl tolanes, Raman scatt. in isotropic, nematic, and solid phases *(French)* 77−15309
p-methoxybenzilidenebutylaniline, nematic, domain pattern changes in electric field 77−1079
p-methoxybenzoate-p′-n-pentyl benzene, slow non-critical mol. reorientation in isotropic phase 80−84062
p-methoxybenzylidene-p′-alkyl anilines, Raman scatt. in isotropic, nematic and solid phases *(French)* 77−15309
methylene-bridged liquid crystals, homologous series, mol. struct. effects on mesomorphism 77−47347
microscopic theory of the first order phase transitions in liquid crystals *(Chinese)* 79−60486
mixture phase equilibria and transition temperatures 78−63845
molecular and phenomenological theories, book contrib. 79−60491
molecular crystal, action of external forces on mesogenic struct. form. 80−2147
molecular crystal, conditions of existence as mesogenous system 79−60488
molecular crystal, unidimensional struct. instability charge under torsional force, liquid cryst. transition *(Russian)* 78−87776
molecular model with ordered liq. columns *(Russian)* 79−19152
molecular orientational distrib., statistical mechanical stability 79−94880
molecular structure effect on mesomorphism, lateral substituents 78−51411
molecular-statistical theory of translational transitions, taking account of short-range order *(Russian)* 77−15564
monomer-dimer system with attractive interactions on square lattice, nematic ordering 80−79681
Mossbauer isomer shift at phase transitions, book contrib. 79−87352
multiplexed liquid cryst. display, use of cholesteric-nematic phase change 80−107408
N-(4-alkoxybenzylidene)-4′-n-alkylanilines, Raman spectra in solid state, polymorphism of mesogenics 79−82964
nematic, finite crystal SCF method *(Russian)* 77−89528
nematic, Maier-Saupe lattice model, stochastic model method simulation 77−43129
nematic, nonlinear effects, in elec. and mag. fields 77−24263

liquid crystal phase transformations continued
'nematic' amphiphilic liquid crystalline mesophases, thermodynamic stability 79−95126
nematic and isotropic phases, flow alignment and flow-induced phase transitions 77−15565
nematic and smectic phases, X-ray diffr. studies, review 80−100166
nematic bend-splay elasticity near the nematic-smectic-A transition 80−24360
nematic binary mixture, smectic phase form. 78−26670
nematic crystal, phase transitions in Landau's theory 80−29158
nematic eutectic-forming binary system, melting behaviour 77−89526
nematic homologous series, even-odd effect in Kerr effect 77−43970
nematic isotropic transition temp., effects of mol. struct. 77−84903
nematic liq. crystal spin-relaxation, composite Markov process, rot. reorientation and director fluctuations 77−62471
nematic liquid cryst., orientational acoustic nonlinearity 80−34143
nematic liquid cryst., tricritical behaviour near transition to isotropic fluid *(Russian)* 80−15001
nematic liquid cryst., two-dimensional, Monte Carlo simulation 80−100168
nematic liquid crystal, acoustic attenuation anomaly above clearing point 78−75816
nematic liquid crystal, anisotropic interfacial interactions with substrate 78−75532
nematic liquid crystal, cluster variational const.-coupling theory, thermodynamic props., nematic-isotropic transition 77−24265
nematic liquid crystal, critical US absorption 79−65174
nematic liquid crystal, eqn. of state, incorporating short-range orient. order 77−55237
nematic liquid crystal, intermol. forces, in anisotropic mean field, hard spherocylinder model 77−35468
nematic liquid crystal, isotropic phase, light scatt., ultrasonic vel. and absorpt. meas. 78−48189
nematic liquid crystal, Merck 389, polymorphism, radiothermoluminescence and differential scanning calorimetric study 80−24570
nematic liquid crystal, order parameter fluctuations and anomalous sound propag. just above clearing point, critical dynamics 80−15224
nematic liquid crystal, static and dynamic behaviour at transition to isotropic state 77−35678
nematic liquid crystal, surface structural crit. point 78−91247
nematic liquid crystal, surface tension, pre- and post-transitional effects 79−77511
nematic liquid crystal, twisted, phase transition like instability in static samples with surface induced tilted alignments 78−26667
nematic liquid crystal, two-dimensional, Kosterlitz-Thouless phase transitions 79−7680
nematic liquid crystal film, with two free surfaces, mol. orientation 78−47238
nematic liquid crystal mixtures with low-freq. dielec. relax., phase behaviour 78−91246
nematic liquid crystal-isotropic liquid phase transition, fluctuations effect *(Russian)* 79−86879
nematic liquid crystals, orientation fluctuations in high mag. field, quenching, birefringence effects 80−64892
nematic liquid crystals, sound attenuation, near clear point, microscopic derivation 78−34605
nematic liquid crystals, twofold orientations and hysteresis props. 79−82146
nematic liquid crystals subject to EM fields, continuum theory 80−33876
nematic mesophase, mode-coupling theory near clearing point 77−89377
nematic mixtures, binary, induced smectic phases, X-ray diffr. obs. 78−94987
nematic ordering, dimer model calcs. 77−27817
nematic ordering and phase transition, Wulf Rocco model extension 77−84626
nematic phase, pretransitional effects, mol. statistical calc. 77−27990
nematic phase, validity of Landau approx. 77−27989
nematic reentrant mesophases, phase diagrams 80−103467
nematic temperature range broadening by nonmesogenic solute 77−47559
nematic to cholesteric transition, elec. field induced, transient phenomena of relax. 78−75811
nematic to cholesteric transition, light induced *(Russian)* 78−14452
nematic to isotropic transition, effect of quasispherical and chainlike solutes 80−65202
nematic to isotropic transition, orientation order effect, Maier-Saupe model 77−84650
nematic to smectic C phase transition, renormalisation group anal. 80−34173
nematic to smectic-A transition, anisotropic crit. props. of de Gennes model 78−43110
nematic-bilayer smectic A reentrant transition, thermodynamic model 79−95130
nematic-chiral-dye mixture, circular dichroism, selective light scatt. *(Russian)* 80−103944
nematic-cholesteric field-induced relax. time, phase transition temp. depend. 79−86874
nematic-cholesteric mixture, helical pitch, depend. on composition 78−42899
nematic-cholesteric mixture, surface boundary conditions influence on transition *(Russian)* 79−23705
nematic-cholesteric mixtures, spiral pitch temp. depend. *(Russian)* 80−19700
nematic-isotropic, complex shear viscosity 77−39667
nematic-isotropic, thin slab Brownian particle fluid *(French)* 77−27829
nematic-isotropic mixture, dielec. props., phase diagram 78−52424
nematic-isotropic phase equilibria, Flory-Huggins theory appl., heat of transition 77−4187
nematic-isotropic phase equilibria in binary mixtures containing rigid rod solutes 79−86873
nematic-isotropic phase transition, Monte Carlo calculation 77−43316
nematic-isotropic phase transition and short range orientational order 77−27832
nematic-isotropic phase transition at high press., thermodynamics *(Russian)* 78−87778
nematic-isotropic phase transition character, molecular bending fluctuations critical growth *(Russian)* 80−79919
nematic-isotropic transition, chain flexibility, flexible chain in rigid rod solvent 79−4400

liquid crystal phase transformations continued
nematic-isotropic transition, correlation functions, Cotton-Mouton coeffs. 80−15228
nematic-isotropic transition, Landau theory breakdown 79−99302
nematic-isotropic transition, lattice model, semiflexible chain solutes 79−10927
nematic-isotropic transition, lattice model for hard core mols. with flexible tails 78−38818
nematic-isotropic transition, lattice model for hard core mols. with semiflexible tails 78−38819
nematic-isotropic transition, mean-field lattice model, meta- and unstable states 78−38817
nematic-isotropic transition, nature, field renormalisation group formalism study 78−87775
nematic-isotropic transition, permanent dipoles effect 77−20054
nematic-isotropic transition, renormalisation groups calc. 78−59937
nematic-isotropic transition, structural parameters *(German)* 80−15003
nematic-isotropic transition, thermodynamic props. calc. 80−103464
nematic-isotropic transition in mixtures, phase separation and diffusive instabilities 80−29156
nematic-isotropic transition temp., polarisability anisotropy depend. 78−38614
nematic-isotropic transition temp. depend. on anisotropy of C-X bond polarisability for terminal substituents 77−20058
nematic-smectic A, nonlinear elastic behaviour 77−35679
nematic-smectic A(C) phase transitions, contribs. to viscosities from order parameter fluctuations 79−60489
nematic-smectic A(C) transitions, NMR spin-lattice relax. time 80−71222
nematic-smectic A phase transition, sound attenuation and dispersion 79−82286
nematic-smectic A phase transition renormalisation group approach to crit. dynamics 80−10646
nematic-smectic A transition, Meyer-Lubensky model 80−19694
nematic-smectic A transition, orientational fluctuation effect 80−6496
nematic-smectic A-smectic C Lifshitz point 77−69077
nematic-smectic transition in an aligned rod system 79−77729
nematic-smectic-A, appl. of crossover calcs. for supercond. phase transitions 78−80098
nematic-smectic-A(C), Landau-Ginzburg mean field theory 77−27992
nematic-smectic-A phase transition, mean field theory 77−24393
nematic-smectic-A transition, hydrodynamic theory, and acoustic props. 79−77731
nematic-smectic-C phase transition fluctuations, ring model 77−24392
nematic-smectic-C transition, density and director fluctuations effects 79−55875
nematic-smetic A-smetic C polycrit., point, expt. and Landau theory 77−80608
nematic-solid, and nematic-liq., up to 3 kbar, transition enthalpy, entropy, vol. changes 77−20051
nematic/smectic A/smectic C triple point, Landau theory 79−95142
nematics, binary mixture, dil., thermodynamic props., statistical model 79−94882
nematics, uniaxial and biaxial, formed by non-cylindrically symm. mols., computer simulation 80−79680
nematogenic solutions, binary, Van der Waals theory 79−27916
nematogens, enthalpy of fusion 78−22645
nematogens, incompatible, induced smectic mesomorphism 78−1983
4-nitrophenyl 4-n-octyloxybenzoate, electrical Kerr effect studies 80−25339
4-nitrophenyl 4-n-pentyloxybenzoate, electrical Kerr effect studies 80−25339
4-nitrophenyl 4-octyloxybenzoate, smectic-A and nematic phases, dielectric meas. 79−23516
4-nitrophenyl-4′-alkoxybenzoates, incommensurate smectic A phase 80−10647
4-nitrophenyl-4-octyloxybenzoate, nematic and smectic-A phase, dielec. meas. 78−60392
NMR expts., state-of-the-art 78−75820
NOBAMBC, chiral smectic phases, pyroelectric and dielec. props. 79−91380
p-nonyloxy benzoate p-butyloxyphenol, smectic A to smectic C transition, crit. ang. fluctuations, Rayleigh scatt. obs. 79−95131
p-nonyloxybenzoate p-butyloxyphenol, smectic A to smectic C transition, crit. fluctuations, Rayleigh scatt. obs. 78−95140
p-n-nonyloxybenzylidene-p-aminobenzoic acid, phase transitions, X-ray diffr. and DSC meas. 79−86877
8OCB, nematic-smectic A transition, impurity effects 78−47507
7-8-OCB mixture, nematic-smectic A transition, impurity effects 78−47507
p-n-octadecyloxybenzoic acid, thermal props. 77−47345
p-octoxybenzoic acid:cholesteric nonanoate, mag. field induced cholesteric→nematic transition Raman spectra 77−27988
4-n-octyl-4′-cyano-diphenyl, appl. in detection of graphite powder particles by optical microscopy 80−9034
4′-n-octyl-4-cyanobiphenyl, interlayer elastic const. meas. close to smectic-A to nematic transitions 77−80606
4′-n-octyl-4-cyanobiphenyl, smectic bilayers, press. effects, phase diagrams *(French)* 78−10177
octyl-cyano-biphenyl, elastic props. near smectic-A nematic transition 79−23704
octyl-cyano-biphenyl, nematic and smectic-A phase, dielec. meas. 78−60392
octyl-cyano-biphenyl, smectic-A and nematic phases, dielectric meas. 79−23516
octyl-cyanobiphenyl, elastic props. near nematic-smectic A transition 78−59756
octyl-cyanobiphenyl, smectic A-nematic transition, X-ray and light scatt. obs. 79−95129
octylcyanobiphenyl, crit. heat. capacity near nematic-smectic A transition 80−100323
octylcyanobiphenyl, second sound propag. and smectic response function, forced Rayleigh scatt. obs. 79−86693
p-n-octyloxy benzylidene-p-toluidine, mol. order, EPR VAAC probe 80−70114
4′-n-octyloxy-4-cyanobiphenyl, smectic bilayers, press. effects, phase diagrams *(French)* 78−10177
trans-p-n-octyloxy-α-methyl-p′-cyanophenyl cinnamate, mag. and elec. birefr. in isotropic phase 80−80744
4-n-octyloxybenzoyloxy-4′-cyanostilbene, re-entrant polymorphism, nematic-smectic A-nematic-smectic A, X-ray study 80−34172
liquid crystal phase transformations continued
4-octyloxybenzoyloxy-4′-cyanostilbene, enantiotropic reentrant nematic behaviour at atmos. press. 79−60490
N-p-octyloxybenzylidene-p-toluidine, optical props., density, and order parameter in liq. cryst. phases 79−55657
octyloxycyanobenzylidene, smectic A, anomalous ordering, Landau-Peierls system 78−30538
octyloxycyanobiphenyl, nematic-smectic A transition, heat capacity study 80−88033
octyloxycyanobiphenyl, nematic-smectic-A transition sp. ht. 79−42225
octyloxycyanobiphenyl, twist viscosity and mech. props. near smectic A-nematic transition 78−95136
4-n-octyloxyphenyl 4-n-pentyloxybenzoate, permittivity, microwave dielectric relaxation 80−80671
4″-n-octylphenyl-4′-n-octylbiphenyl-4-carboxylate, orthogonal smectic B to tilted smectic B (smectic H) transition 79−94881
OOBPD, smectic, DTA obs. of phase transitions to 3 kbar 79−23708
ordered continuously degenerate systems, props. 79−93040
organic compounds, high-press. expansivity determ. by piezo-thermal anal. 77−72705
orientationally ordered liquids, Helmoholtz free energy, generalised van der Waals theory 80−44119
orientationally ordered two-dimensional fluid phase, existence, mol. dynamics calcs. 79−73095
oxtyloxycyanobiphenyl, nematic-smectic-A transition, high-resolution 80−10649
p-(p-ethoxybenzylidene) amino benzonitrile, positron annihilation exam. 79−19149
PAA, appl. of integral eqn. for ang. distrib. function *(Russian)* 78−6147
PAA, homologous series, isotropic phase, mol. self diffusion by spin echo method 80−44109
PAA, isotropic phase, Brillouin scatt. spectra, hypersound data determ. 79−91453
PAA, isotropic phase, light scatt., ultrasonic vel. and absorpt. meas. 78−48189
PAA, isotropic-nematic phase transition, optical microscopic obs. 79−69230
PAA, isotropic-nematic transition, mean-field theory, thermodynamic props. 77−24391
PAA, isotropic-nematic transition, supercooling and nucleation, interface dendrites 78−42896
PAA, light scatt. near cryst. to nematic transition 80−16046
PAA, liq. cryst., solid-state polymorphism obs. 77−4200
PAA, methyl deuterated, soft-mode dynamics, proton NMR 78−79749
PAA, nematic, nonlinear effects, in elec. and mag. fields 77−24263
PAA, nematic to isotropic liquid cryst. transform. at high press. *(Russian)* 77−4191
PAA, nematic-isotropic phase transition, US meas. 79−90761
PAA, nematic-isotropic pretransition regions, ±15K, volumetric obs. 77−76535
PAA-di, nematic liquid crystal, NMR data, appl. of Landau-de Gennes theory 80−64893
paradiheptyloxyazoxybenzene, mol. cryst., characts. of mesomorphic transition to smectic phase 79−14920
paradiheptyloxyazoxybenzol-d, dynamics of smectic-nematic liq. cryst. phase transiton *(Russian)* 78−55938
paradiheptyoxyazoxybenzol, low press. phase transition temp. change, relative transparency *(Russian)* 78−2242
PEBAB, nematic, EPR investig. 80−108077
p-pentoxybenzilidene alkylaniline, mag. anisotropy and polymorphism *(French)* 77−76532
pentyl cyanobiphenyl, laser and electric field induced Kerr effect 80−84061
pentyl cyanobiphenyl nematogen, depolarised light scatt. 79−95790
4-n-pentyl-4′-cyanobiphenyl, isotropic, optical and electrical Kerr effect 79−32886
4-n-pentyl-4′-cyanobiphenyl, mol. alignment, comparison of exptl. data at high press. with mean field theory predictions 79−99075
4-n- pentyl-phenylthiol-4′-alkoxybenzoate, homologous series, specific heat meas., nematic-smectic-A tricritical point 80−15227
4-n-pentyl-phenylthiol-4′-n-octyloxybenzoate, smectic A-smectic C phase transition, high-resolution X-ray study 80−79921
4-n-pentylbenzenethio-4′-n-alkoxybenzoates, birefr., crit. behaviour near smectic A-C transition 80−80745
4-n-pentylbenzenethio-4′-n-octyloxybenzoate, liq. cryst. phase transitions, press. and temp. depend. 79−77730
pentyloxy-cyanobiphenyl, liq. cryst., laser and electrical Kerr effect 78−68477
4,4′-di-n-pentyloxyazoxybenzene, anomalous smectic mesomorphism, calorimetric and optical texture obs. 79−77505
N-4-n-pentyloxybenzylidene-4-n-hexylaniline (50.6), unclassified smectic phase 80−75157
4-pentylphenyl-4′-benzoyloxybenzoate/TBBA system, smectic A_1-smectic A_2 transition, X-ray diffr. obs. 80−44303
4-n-pentylphenyl-4′-n-octylthiobenzoate, smectic-C phase, undulation instabilities, microscopic obs. 77−68919
4-n-pentylphenylthiol-4′-n-octyloxybenzoate, sp. ht. and crit. behaviour of liq. cryst. phases 78−67816
4-n-pentylphenylthiol-4-n′-octyloxybenzoate, birefringence, crit. suppression 78−76422
phenyl 4-benzoyloxybenzoates, influence of lateral substitution on liq. cryst. props. 79−4242
phenyl 5-alkoxypicolinates, synthesis, phase transition temps., and dielec. props. 79−86876
phenyl 6-alkoxynicotinates, synthesis, phase transition temps., and dielec. props. 79−86876
phenylcyclohexanes, alkylamino substituted, synthesis and mesomorphic props. 80−44120
p-phenylene bis (p-substituted benzoates), cryst.-nematic transition, mol. struct. effects, DTA 78−47504
phenylene derivatives, effect of substitution on liq. crystalline props. 80−70113
phenylthiobenzoate derivatives, thermodynamic and mesomorphic props. 77−11678
phosphatidylcholine bilayer endothermic transitions, Raman difference spectroscopy 78−40119
phosphatidylcholine bilayers, fluidity changes and phase transitions, intramol. excimer fluoresc. obs. 80−85342
phosphatidylcholine dispersion, phase transitions obs. with interference refractometer 78−44459

liquid crystal phase transformations continued
phospholipid membrane thermotropic transitions, effects of bivalent cations and proteins 77−48765
physics of transitions, introduction 78−26660
phytanic acid, in phospholipid bilayers, struct., order parameters, liq. cryst. transition, entropy 79−83713
phytol in phospholipid bilayers, struct., order parameters, liq. cryst. transition, entropy 79−83713
plasma low density lipoproteins, human, size and surface effects rel. to phase transitions 78−3446
plasma low-density lipoprotein, human, molecules organisation of central core 77−90722
plate-like solute in mesomorphic solvent, effect on isotropic-nematic transition temp. 77−59104
poly(γ-benzyl-L-glutamate), in benzene soln., cholesteric liq. cryst. props. 79−94889
poly(azomethines), thermotropic mesophases *(French)* 79−77507
poly(n-dodecyl L-glutamate), thermotropic polymorphism, low-angle X-ray diffr. *(French)* 78−34601
poly(p-phenylene terephthalamide), liq. cryst. phase transition *(Chinese)* 79−65175
poly (γ-benzyl-l-glutamate)-dioxane system, periodic struct. under elec. field 78−47234
poly-γ-benzyl-glutamate, conc. soln., rheology, liq. cryst. transition 79−94574
poly-γ-benzyl-L-glutamate, mag. oriented liq. cryst. solns., order parameter 77−15305
poly-γ-benzyl-L-glutamate, soln., liquid crystal transitions anal. 80−65207
poly-γ-benzyl-l-glutamate solns., mesomorphic re-entrance phenomena 79−99074
poly-γ-benzyl-L-glutamate solutions, calorimetric study of fusion of liquid cryst. struct. 79−53022
poly-γ-benzyl-L-glutamate-dichloroethane in conc. soln., mol. assoc., electro-opt. investig. 78−1973
poly-p-aminobenzhydride terephthalamide in dimethyl sulphoxide soln., rheological study 80−43683
polydisperse solution of rodlike particles, isotropic-nematic phase transition, Onsager theory 80−100324
polyethylene terephthalate-p-oxybenzoate, nematic→isotropic transition loss 80−44300
polymer, linear, liq. cryst. state prediction using Flory's model of phase transitions *(Russian)* 77−43318
polymer liquid-crystalline solns., struct. 80−103235
polymer solution, nematic helix-coil transtition model 79−94870
polymeric liquid crystals structurally related to 4-alkoxyphenyl-4′-alkoxybenzoates, nematic phase 79−60267
polymeric mesophases, discotic phases, optical microscopy obs. 79−41951
polymeric thermotropic liq. crysts., mesogenic elements and flexible spaces in main chain 79−60269
polymoprhic properties, impurity effects 79−10930
polypeptide in conc. soln., mol. assoc., electro-opt. investig. 78−1973
polypeptides, electric field-induced phase transition 80−24571
polypeptides, helical, conc. solns., rheological behaviour and liq. cryst. order 80−83771
polyphenylene terephthalamide in H_2SO_4-H_2O system, phase equilib., possibility of liq. cryst. formation 79−73314
positive dielectric, pretransitional domains, Kerr effect and orientational relax. 77−77171
potassium alkanoates, phase transitions, differential scanning calorimetry 77−43319
potassium laurate-1-decanol-water mixtures, biaxial nematic phase obs. 80−107409
potassium palmitate-water bilayer, lamellar liq. cryst. polymorphism, NMR and birefringence 79−60270
premelting, high resolution NMR 78−26671
pretransitional behaviour, nonlinear optical obs. 77−51483
trans-p-n-propoxy-α-methyl-p′-cyanophenyl cinnamate, high press. mesomorphic and polymesomorphic transitions 78−18750
N-p-propoxybenzylidene-p-pentylaniline, orientational order in glassy and nematic phases, IR dichroism meas. 80−64891
p-quinquephenyl, melting data and liq. cryst. transitions 79−55869
re-entrant nematic phase, orientational order, electron reson. study 80−103242
reentrant nematic, oriented, capillary shear flow 80−49344
reentrant nematic-smectic A phase transition, Landau theory 79−28084
reentrant-transition, nematic to bilayer smectic-A, under high press. 77−84905
refractive index near smectic-A/smectic-C transition, orientational order 80−24572
review, book contrib. 77−39544
review of phases and phase transitions 78−2006
rigid-rod fluid, thermodynamic props., crit. points and transitions 78−73919
rod system, nematic ordering 79−60271
rubidium n. alkanoates, long-chain, phase transformations, in melt, DTA obs. 77−76536
Schiff's base compounds, double axis, Siamese Twin type liq. crysts., thermal and X-ray obs. 80−39312
Schiff's bases, deuterated, transition temp. meas., comparison with normal compounds 78−14449
Schiff's bases, mesomorphic, two-component system, tricritical nematic-smectic A point 77−51482
Schiff's bases, nematic phys. props. 79−99057
Schiff base compounds, cholesteryl esters, mesomorphic behaviour 78−1994
Schiff base compounds, p-n-alkoxybenzaldehydes condensed with p-bromoaniline, transition temp. 78−42898
Schiff base esters, mesomorphic behaviour 78−1993
second order transition, liquid-cryst. ordering *(Russian)* 78−34606
second-order phase transitions, Landau thoery, group-theoretical arguments 80−29154
self diffraction of laser beam by liquid crystal struct. 80−5803
p-sexiphenyl, solid-smectic and smectic-nematic transitions 79−82322
sitosteryl esters, mesomorphic props. 79−90539
size and surface effects 77−15555
smectic, Lifshitz point in H-T phase diagram between A, C and modulated C phases 77−84904
smectic A→C second order phase transition, symm. changes and dipole orderings 78−2238

liquid crystal phase transformations continued
smectic A and C phase and A-C phase transitions, diffuse-cone model 79−41952
smectic A and C phase occurrence, mol. struct. 78−6008
smectic A and C phases, classification of defects 78−26433
smectic A and isotropic phases, Brillouin scatt. 77−8591
smectic A liquid crystal, EHD instability and elec. cond. anisotropy *(Russian)* 78−59753
smectic A to C, crit. behaviour in mag. field 78−6148
smectic A to C phase transition, phenomenological model 79−1495
smectic A to C transition, effect of chiral solute 77−24389
smectic A to nematic phase transition, critical dynamics 79−1493
smectic A to smectic A phase transition 79−69229
smectic A to smectic C phase transition, mean field model 78−95142
smectic A to smectic C phase transition of first kind 78−71844
smectic A to smectic C transition, separate order parameter for layer thickness and optical tilt angle 80−19923
smectic A-C transition, ferroelec. liq. cryst., soft modes 79−55653
smectic A-nematic phase transform., liq. cryst. binary mixture, birefringence study 80−59638
smectic A-nematic transition, defect model 79−14916
smectic A-nematic weak first order transition 77−59105
smectic A-smectic C transition, model 79−90762
smectic B-E and H-VI phase transitions, symmetry changes and crit. behaviour 78−2243
smectic C* liquid crystal under press. *(French)* 79−99061
smectic C phase, with second order transition to smectic A, molecular tilt, zigzag model 78−94986
smectic C phase and smectic C-smectic A transition, induced dipole model 79−90527
smectic C to smectic A transitions, exptl. evidence 77−89527
smectic C with induced helical struct., ferroelectric props. and spontaneous polarisation, C→A transition 80−54123
smectic F materials 78−51651
smectic film, two-dimens. melting, dislocation-mediated theory predictions, light scatt. use as probe 80−92651
smectic helixing crystal, dielec. props., temp. and freq. depends. *(Russian)* 78−60380
smectic layers with tilted molecules, solid and fluid phases 80−96444
smectic liquid cryst., long range order excim. *(Russian)* 79−1392
smectic liquid crystal, electric field induced Lifshits point 78−71674
smectic liquid crystal, electro-optical reversible memory effect *(Russian)* 78−31174
smectic liquid crystal, homeotropic to confocal texture transformation *(Russian)* 78−18548
smectic liquid crystal, polymorphism, mol. struct. effects 77−47348
smectic liquid crystal structural order effects of surface treatment, sample thickness, and cooling rate 78−63667
smectic liquid crystals, chiral polarised electric field induced tricritical point 78−10176
smectic mesophases, viscoelastic properties and field instabilities 79−27904
smectic mesophases of binary mixtures, isobaric phase diagrams, non-ideal behaviour *(French)* 79−95141
smectic mixtures, thermodynamic phase diagram 77−62623
smectic order in cholesteric mesophase *(Russian)* 79−95145
smectic-A-smectic-C transition, model of tilted mols. in planar layer 78−79751
smectic-B to smectic-E, orientational intermol. pot. calcs. 79−4406
smectic-C film, mol. orientation fluctuations in two-dimens., light scatt. obs. 80−93355
smectic-nematic phase boundary, elliptic, thermodynamic anal. 79−99300
sodium undecanoate/water system, lyotropic liq. cryst. struct. change due to polymerisation of amphiphilic component 80−59386
sodium valerate, mesophase, self-diffusion and spin-lattice relax. 79−69008
solid-liquid transitions, symmetry and thermodynamic states, review 80−10493
solid-to-smectic B phase transition, defect model 77−7855
stilbene, depend. of phase transition temp. on thickness 78−26669
surface-aligned film, nematic-isotropic crit. thickness, Landau-de Gennes theory 77−4189
TBAA, synthesis and smectic B-smectic B transition 77−15562
TBBA, dielec. const. in cryst. and smectic phases 79−78607
TBBA, metastable phase, thermodynamic props., differential scanning calorimetry meas. 78−94985
TBBA, phase transitions involving ordered biaxial phases, X-ray diffr. study 79−95136
TBBA, smectic A-nematic transition, cybotactic cluster form., X-ray obs. 78−95138
TBBA, smectic C to A phase transition, neutron diffr. exam. 78−91428
TBBA, smectic C to smectic A transition, crit. exponent, neutron diffr. obs. 78−95143
TBBA, smectic liq. cryst., polarised Raman spectra, 90-300K, 0-400 cm^{-1} 77−12383
TBBA, smectic phases, orientational order, ^{14}N NQR and double NMR obs. 78−94974
TBBA, smectic phases, rot. viscosity, phase transitions 77−80418
TBBA, smectic polymorphism *(French)* 77−35470
TBBA, temp. depend. of deuteron NMR splittings in nematic and smectic phases 79−32898
TBBA, US absorpt. and dispersion at nematic-smectic-A transition 79−82287
TBBA mesophases, mol. orientational order 79−37619
TBBA/4-n-pentylphenyl-4-(4-cyanobenzoyloxy)benzoate, mixture, possibility of smectic A-smectic A transition 79−95132
TBBA/n-hexyl-4′-n-dodecyloxy-biphenyl-4-carboxylate, mixtures, orthogonal smectic B to tilted smectic B (smectic H) transition 79−94881
TCOOB, smectic A and C liq. cryst., A-C phase transition, diffuse-cone model description 79−86674
TDOBAMBCC, chiral smectic C liq. cryst., dielec. consts., electroclinic effect 78−94980
p-terephthal-bis-aminocinnamate, smectic phases, orientational order, ^{14}N NQR and double NMR obs. 78−94974
terephthal-bis-n-alkylaniline, homologous series, prep. and mesomorphic props. 78−26436
terephthal-bis-p-p'-butylaniline, pretransitional anomaly, US obs. 78−75818
terephthalylidene-bis-4-n-alkylanilines, smectic F planes 78−42902

liquid crystal phase transformations continued
terephthalylidene-bis-(4-n-alkylanilines), smectic polymorphism, calorimetric study 80−88307
terminal polar liq. cryst., amines and nitriles, binary mixtures, induced phases 79−90765
p-n-tetradecyloxy benzoic acid, liq. cryst. phase transition, thermal studies 78−71843
thermal parameters, transition temps. and latent heats 78−22832
thermotropic systems of rodlike molecules with orientation-depend. interactions 80−33883
α-tocopherol in phospholipid bilayers, struct., order parameters, liq. cryst. transition, entropy 79−83713
transition points determination via AC conductance meas. 77−55341
translational order, effect of dipole-dipole interaction 77−84910
trifluoromethyl liquid crystals, effect of mol. struct. on mesomorphism 78−51414
triphenylene, hexasubstituted, thermotropic mesophases 79−86681
triphenylene hexa-n-dodecanoate, mesomorphic polymorphism 79−41950
TTF derivatives, smectic and nematic, for liq. cryst. device appl. 80−54124
TV screens, use of cholesteric-nematic phase transitions *(Chinese)* 80−79922
twisted nematics, evidence for hexagonal phase 78−34602
two dimensional model, structure, transition to smectic and cryst. phases 77−7857
two-dimensional fluid of overlapping ellipses, nematic ordering 78−34424
undecylazoxymethylcinnamate, crit. angular fluctuations above second order smectic-A to smectic-C transition 77−4190
unified Landau theory, for nematic, smectic-A and smectic-C phases 77−55238
unified model for bulk smectic-A, nematic and isotropic phases 80−79692
US expts. and phase transitions 79−46571
virtual nematic-isotropic transitions, depolarised Rayleigh scatt. 78−51652
viscosity, anomalous properties near $N \rightarrow S_A$ transition point *(Chinese)* 80−84052
viscosity-pressure behaviour rel. to transition pts. 79−23707
volume change, differential scanning dilatometric obs. 79−69230
water-in-dodecane microemulsions, dielec. study of phase transition 79−28668
water-in-dodecane microemulsions, struct. transitions in liq. cryst. phase, dielec. props. 79−28669
X-ray and light scattering obs., high resolution 80−92460
xylideneaniline-p′-benzonitri 80−44328
CBOOA, smectic A order parameter meas. and crit. scatt. near smectic A⇄nematic phase transition 77−84649
LC-440, shear modulus and viscosity relax. near isotropic-nematic phase transition *(Russian)* 77−39543
Li soaps, n.C_{13}-n.C_{20}, phase transition temps. and enthalpies, DSC obs. 80−45544
MBBA, nematic-isotropic transition, compressibility-press. relations obs. 77−51481
MBBA+optically active substance, pretransition optical rotation in isotropic phase *(Russian)* 80−92657
Ni complex, bis-[4-(n-butyl)-styryl-dithiolato] Ni nematic complex, IR absorption 80−49342
$Ni(CN)_2$-dodecylamine, lamellar paraffinic system, phase transitions, wide-line NMR obs. *(French)* 80−44929
4n-octyl-4′-cyano-biphenyl, liq. cryst., density, and rel. change at phase transitions determ. 77−80605
TBBA, liq. cryst., evidence for cybotactic cluster pretransition formation, X-ray diffr. meas. 78−10179

liquid crystals
see also cholesteric liquid crystals; liquid crystal phase transformations; nematic liquid crystals; smectic liquid crystals
acenaphthylene, anisotropic mesophase during refluxing carbonization 78−14274
acoustic storage effect 78−94992
aerodynamic heating test, use of melting liq. crysts. 79−77299
aggregation in membranes, fluctuation-induced interactions in liquid crystals 77−90732
alignment, appl. of submicrometer struct., using STEM and X-ray lithography 79−15844
alignment, use of SiO_2 critical surface tension anisotropy 79−86676
alignment by amphiphilic monolayers 79−37614
alignment films prod. by RF plasma beam technique 80−76198
alignment on surfaces, double evaporation for surface prep. 77−11464
p-alkanoyl-benzylidene-p'-aminoazobenzenes, liq. cryst., proton mag. relax., self-diffusion 77−84632
alkoxy-cyanobiphenyls, isotropic phase, Cotton-Mouton effect 80−16013
p-alkoxy-phenyl-p-acryloyloxy benzoate polymers, mesomorphic struct. 80−38905
alkoxybenzenes, 4-substituted, liq. cryst. intermediates, prep. 78−51409
alkoxybenzoic acids, liq. crystal, solid phase, methyl group C_3 reorientation, proton spin relax. 77−1071
p-alkoxybenzylidene-alkylanilines, solid state, nucl. spin-lattice relax. 78−64294
p-alkoxybenzylidene-p-alkylaniline, liq. crysts., ^2H NMR, aliphatic and chain conformation 79−14670
p-alkoxyphenylazody-p′-phenylesters, mesomorphis, synthesis and transition temps. *(French)* 77−27815
4-n-alkyl-4′-cyanobiphenyls, deuteriated, improved synthesis 79−32893
4-n-alkyl-4′-cyanobiphenyls, synthesis method from biphenyl 80−79684
4-alkyl-4′-cyanostilbenes, liq. cryst., prep. and transition temps. 77−27823
3-nalkyl-6-(4-n-alkyloxy-phenyl)-1,2,4,5-tetrazines, stable dyestuffs with liq. cryst. props. 80−19693
alkyl-cyanobiphenyls, isotropic phase, Cotton-Mouton effect 80−16013
4-alkylbenzoyl chlorides, liq. cryst. intermediates, syntheses 79−90540
amines, liq. cryst., low transition temp., incorporating biphenyl ring system 79−94892
aminoacidic side chain-liquid crystalline polymers, synthesis physicochem. props., struct., optical anisotropy *(Russian)* 79−23521
amphiphilic, ESR using TCNE as spin probe, feasibility 78−75548
amphiphilic compounds, phase diagrams 79−1389
amphiphilic solvent effect on hydrolysis of benzylidene t-butylamine N-oxide 79−100355
amphiphilic systems, review 79−99062

liquid crystals continued
amphiphilic-polymer liquid crystal, NaCl conc. influence on struct., X-ray diffr. study 80−44126
anisotropic fluid, diffusion, EPR spin exchange and nuclear spin relax., theory 80−34753
anisotropic liq. ang. correl. functions, memory function approach, Mori theory and extended diffusion eqn. 80−10489
anisotropic molecular fluids, local elec. fields 77−59545
anisotropic system, computer simulation, energy and specific heat temp. depend. 78−9947
anthracene, mesophase formation during carbonisation under pressure 77−44182
aromatic copolyamide solns., conformational energy and mesomorphic character *(French)* 79−99066
aromatic free radical, D quadrupole splittings, ENDOR and TRIPLE reson. obs. 77−51989
aromatic hydrocarbons, melting behavior and role of free radicals and molecular site in producing mesophase pitch 79−90523
aryl esters, cyano-substituted, liq. cryst. props. 77−27822
azobenzenes, p-acryloyl- and p-methacryloyl-oxy-p′-substituted, monomers and polymers, liq. cryst. props. 79−99065
azobenzenes, substituted, isotropic, nucl. spin-lattice relax. 79−23519
azoxybenzenes, p-acryloyl- and p-methacryloyl-oxy-p′-substituted, monomers and polymers, liq. cryst. props. 79−99065
azoxybenzenes, substituted, isotropic, nucl. spin-lattice relax. 79−23519
benzene-hexa-n-alkanoates, disc like mols., highly ordered lamellar liquid crysts. 78−14279
benzene-hexa-n-alkanoates and benzene mixture, disc-like mesogens, thermotropic mesophases 79−86699
benzene-hexa-n-alkylanoates, disc-like molecules, miscibility studies of mesophases 80−19696
benzoate derivatives, m-cyano or m-halogeno synthesis and mesomorphic props. 78−1990
biaxial order parameters, NQR determ. 78−59750
bibliography, 1975 literature 78−18544
bibliography, 1976 79−19146
bibliography for 1977 80−41973
bilayer membrane dynamics, combination of Rouse model and Marcelja liq. cryst. theory 79−100581
biology, liq. crysts. in living and dying systems, review 77−44602
biomembrane systems, dynamical mechanical spectroscopy, mol. interactions 77−29109
biomembranes, lipid-protein interactions, flexoelectric effects 78−92600
biomembranes, struct. and energy characts., appl. with liq. cryst. *(Chinese)* 79−16163
birefringence measurement, high resolution apparatus 79−2803
bis-(4′-n-alkoxybenzal)-2-chloro-1,4-phenylenediamines, liq. cryst., improved preparation technique 78−75541
BOBOA, deuteron mag. reson. of mol. order and dynamics 77−35469
bromobenzene, in EBBA, ^1H NMR and NQR of D, geometric struct. 78−17689
bubble domains in liquid crystal *(Japanese)* 78−22413
2-butyl-7-(1-oxopentyl)-9,10-dihydrophenanthrene, mesomorphous, cryst. struct. determ. *(French)* 77−4095
p-n-butyl-p′-heptanoyloxyazoxybenzene oriented on NaCl MgF_2 coated NaCl, surface phenomena and IR spectra 80−79678
caesium perfluoro-octanoate/D_20, NMR of ^2D nuclei, response to three-pulse sequences in inhomogeneous B_0 field 79−42861
caesium perfluoro-octanoate/D_2O, NMR of ^2D nuclei, response to three-pulse sequence in homogeneous B_0 field 79−42860
carbonaceous mesophase, disclinations 77−43147
carbonaceous mesophase, formation at lower temps. 79−90524
carbonaceous mesophase, twist disclinations 79−95010
carbonaceous mesophase and disc-like liquid crystals 80−79687
carbonaceous mesophase spherules, new mol. arrangement in mag. field, orientation behaviour 79−94869
carbonisation under pressure, mesophase formation 77−44182
CBOOA, deuteron mag. reson. of mol. order and dynamics 77−35469
CBOOA, with cholesterol decanoate, short range smectic A order in nematic phase, NMR meas. 77−28475
cell for investigation of IR spectra of liquid crystals 79−93238
cell membrance studies 79−29508
cellulose acetate, solvent effect on lyotropic mesomorphicity 80−70121
central rigid cores, mesogenic power, depolarised Rayleigh scatt. study 80−89012
chain ordering properties, theoretical foundations 80−38907
chlorobenzene in EBBA, ^1H, D NMR and NQR, geometric struct. 78−17689
5α-cholestanes, molecular geometry polarisation factors and mesomorphic phases *(French)* 77−84647
cholesteryl benzoate, crystallographic data, rel. to mesogenic state 79−77590
cholesterylbenzoate, substituent effects on mesomorphic props. 77−11465
cholesterylcinnamate, substituent effects on mesomorphic props. 77−11465
coalescence of emulsion droplets, influence of liq. cryst. on van der Waals pot. 77−12834
coaxial DTA cell for study of liquid crystalline transitions at elevated pressures 77−22564
coke, anisotropic spheres obtained during needle coke form., struct. obs. 77−63573
collective molecular motion from depolarized light scatt. 80−60614
colloid and surface chemical aspects 78−9950
conference, Bordeaux, France (Jul. 1978) 79−86677
conference, International Crystallography Congress, Warsaw, Poland (Aug. 78) 79−23481
conference, Kent, Ohio, USA (Aug. 76) 77−27808
conference, Krusevac, Yugoslavia, Sept. 1978 79−56104
conference on smectic and lyotropic liq. crysts., Trento, Italy (Jan. 1978) 78−91222
continuous symmetry groups 79−32902
copoly(ethylene terephthalate)-p-oxybenzoate solns., polymer mesophases, optical microscopy obs. 79−99067
copolymer globule model, orientationally-ordered liq. cryst. state *(Russian)* 80−59389
copolymer mesophases, scaling laws 79−94872
correlations, short-range, rel. to anisotropic hard-rod fluid model 79−86675
crystal-smectic and smectic-nematic transitions, Lennard-Jones and Devonshire model extension 79−94883

liquid crystals continued
4-cyan-phenyl esters of 4'-N-alkoxycinnamic acids, liq. cryst., refr. indices, optical anisotropy 79−28704
4-cyano-4'-alkyltolans, prep. and transition temp. 77−31588
4-cyano-4'-octylbiphenyl, nematic-smectic-A transition, high-resolution X-ray and light scatt. study 79−73297
cyano-biphenyl LC alignment on obliquely evaporated SiO_2 films 80−79677
4-cyanobiphenyl derivatives, deuterated, transition temp. meas., comparison with normal compounds 78−14449
cyanobiphenyls, isotropic phase, pretransitional behaviour, optical and elec. Kerr effects 79−10928
4-cyanophenyl esters, of 4'-n-alkylcinnamic acids, birefringence 79−64991
cyclohexane, plastic and liquid crystal phase, rot. correl. func. by Raman spectroscopy 80−23403
decyloxybenzoic acid, vibr. bands., IR dichroism, phase change effects *(Russian)* 78−15174
defects, electron microscopy, conf., Nancy, France (May 1978) *(French)* 79−41915
defects, struct., optical, electron microscopy *(French)* 79−46567
depolarised Rayleigh scatt., review 77−40256
deuterated, deuteron mag. resonance mol. ordering, conformational changes 80−34789
deuterated nitroxide radical probe, synthesis and appls. *(French)* 78−76314
p,p'-di-n-alkoxyazoxybenzene series, C_1-C_7, submillimetre wave absorpt. investig. 80−34910
α,ω-diarylperfluorpolienes, X-ray spectra, phase transition temp. depend., struct. and mesomorphic props. *(Russian)* 78−38621
dichroic dyes for guest-host interactions 77−59554
dielectric anisotropy meas., over wide freq. range 79−33594
dipalmitoyl lecithin bilayer, mol. tilt, X-ray diffraction obs. in gel phase 80−84059
dipalmitoyl lecithin dihydrate, phase transforms., 20 to 70°C, X-ray diffr. obs. *(French)* 78−91436
dipalmitoyl lecithin-water system, lyotropic liq. cryst., pretransitional effects, PMR second moment meas. 78−91234
dipalmitoyl phosphatidylcholine, gel and liquid crystalline phases, deuterium mag. resonance obs. 79−91308
disc-like molecular structure, props. and industrial appl. *(French)* 79−90549
disclinations *(French)* 79−41947
discotic mesophases, solute-solvent interactions, effect on phase transition 80−10490
dissipative structures in turbulent movement *(Russian)* 78−55808
dithiolato nickel complexes with aliphatic substituents, synthesis and mesomorphic props. 77−84646
DOBAMBC, ferroelec. liq. cryst., helical struct., elec. field depend. *(Japanese)* 80−38910
dye laser action in liq. cryst. 77−14705
EBBA, liq. crysts., thin layers, addition of iminoxyl radicals, effect on elec. cond. *(Russian)* 78−67641
EBBA liq. cryst., anisotropic light scatt. 79−78692
EBBA liq. cryst., orient. of dissolved acetone investig., NMR 77−1605
eddy currents *(Russian)* 77−39541
effective one-body pots. for orientationally anisotropic fluids 77−55235
EHD instabilities, director relax. time depend. on wave number near WD pt. *(Japanese)* 79−32700
EHD instabilities, electric Nusselt no. *(Japanese)* 78−18356
elastic continuum theory *(Chinese)* 80−79697
electrically induced fluorescence polarised component change meas. 80−32863
electro-optical phenomena in lyotropic liquid crystals 80−107050
electro-optical properties, dynamic scatt. effect 77−1080
electro-optical props. and applications to displays 77−77174
electrodynamic instabilities, principle of conservation of moment of momentum study 79−46566
electrohydrodynamic instability, splay mode near Williams domain point *(Japanese)* 78−9952
electromag. oscill., four modes per freq., evanescence waves 78−14276
encapsulated, colour transition temp. rel. to gamma dose 77−38547
EPR spectra of spin probes, line broadening 77−12203
p-p-ethoxyphenylazo phenyl heptanoate, mesogenic compounds, thermal stabilities, packing coeffs. and mol. packings 79−46558
ethyl 4-(4'-methoxybenzylideneamino)cinnamate, mesomorphic compound, cryst. struct. and binding energy 77−80494
Euclidean invariance, spontaneous breaking, long range ordered media, defect, config. classification 78−59748
eutectic mixtures, glassy transition, DTA obs. 79−4405
ferrocene derivatives, exhibiting mesomorphic props., synthesis, appl. in Mossbauer spectroscopy 77−31589
ferroelectric, low freq. lattice vibrs. and pseudospin modes, instabilities struct. phase transitions 78−15108
ferroelectric, review of props. 77−85667
ferroelectric liquid crystals, kinetics of spontaneous polarisation *(Russian)* 79−8101
ferroelectric phases, mag. material analogy 77−11467
ferroelectric struct. development, theory 77−66018
film, imaging of US in air 80−38166
flexoelectricity, microscopic interpretation 77−32339
four wave mixing and relaxation effects *(Chinese)* 80−53351
free energy, slowly varying orientational order parameters *(Russian)* 78−75533
free energy derivation *(Chinese)* 80−79696
generalised Suzuki formula application *(Chinese)* 80−107045
1-glyceryl 1-octanoate-water-CsCl, Cs^+H_2O interaction in lamellar phase, NMR quadrupole splitting and chemical shift 80−50209
hard rod lattice model, nearest neighbour attraction, cryst. ordering 77−80411
HBCA liq. cryst., anisotropic light scatt. 79−78692
p-heptyl-p'-cyanobiphenyl, refractive index, dielec. const., mag. susceptibility, orientational ordering *(Dutch)* 80−33884
hexagonal, developable domains 80−92453
hexatic, nonlinear hydrodynamic props., theory 80−100169
p-n hexyloxy benzylidine-p-toludine, elec. cond. and dielectric constant in solid phase 79−61293
hydrocarbon chains, stability of lyotropic phases 80−24359
hydrodynamic instabilities and neutron scattering 79−50990
hydroxypropyl cellulose in conc. aq. soln., mesophase struct., colour 77−19870

liquid crystals continued
IC technology appl., obs. of localised cond. regions in SiO_2 film 77−1507
inhomogeneous birefringent optically active medium, polarisation evolution 78−9328
instabilities in liq. crysts. with tilted orientation 77−27826
interacting dimers on the simple cubic lattice as a model for liquid crystals 80−42154
interface total reflection and surface wave obs. 80−108292
internal field anisotropy changes, order parameter determ. by optical methods 79−86711
isotropic, Brillouin scatt. 77−8591
isotropic, compressibility and thermal expansion anomalies, appl. to MBBA 77−43138
isotropic, statistical props. of scattered light 78−27189
isotropic and nematic, with positive dielec. anisotropy, EHD instability *(Russian)* 77−31594
isotropic phase, self-focusing stability of laser beam 80−99812
isotropic phase, surface induced ordering, birefringence obs. 80−14998
isotropic phase NMR, critical orientational order fluctuations 77−55236
lamellar liquid cryst. phases, form. at liquid-liquid interface, rheological props. 79−99063
lamellar liquid crystal, biaxiality due to oriented defects 79−41945
lamellar liquid crystals as biomembrane models, ^2H NMR study of A. laidlawii membrane 77−86456
laminar, counterion condensation, soln. of Poisson-Boltzmann eqn. for two parallel charged plates 79−87849
laminar-turbulent flow transition, fluctuation correlations *(Japanese)* 77−14988
Landau crit. point, mean-field theory, scaling theory and crit. exponents to second order in ε^2 79−4395
laser and pulsed electric field Kerr effect 77−40210
laser self-focusing, effect of spatially dispersed nonlinearity 80−38908
lattice models showing liquid-liquid crystal phase transitions 79−95128
layer, effect of substrate surface on mol. alignment 77−7663
layer, thin, symmetry defects and solitons, topological classif. 80−107044
lecithin membranes, mag. susceptibility anisotropy, phase contrast microscope obs. 78−92601
L_α-lecithin multilayers, shear-induced biaxiality near solid surfaces 78−24035
lecithin/ethylene glycol and lecithin/water systems, lyotropic liq. crysts., X-ray diffr. and microscopic obs. 79−60266
lecithins, L_α phase, shear-induced biaxiality 78−95997
light scattering, far-field coherence and radiant intensity analysis 78−64372
light scattering, intensity fluctuations, model *(Russian)* 78−23478
lipid bilayers, long-range order, phase transition, coherence lengths 78−92593
lipid bilayers, saddle-splay elasticity and mol. asymmetry 78−92594
lipid lamellar liquid crystalline systems, orientation studies of probe molecules by linear dichroism 77−90718
lipid liquid crystals, parabolic focal conics and polygonal defect arrays 79−37618
lipid-water systems, byotropic liquid crystalline and other lamellar phases 78−92592
liquid crystals, cylindrically aligned, optical charact., interferometric analysis 79−73897
liquid crystals, subcritical region, vortex penetration length, cct. behaviour 79−55662
liquid lamellar liquid crystalline system, rheological props. 79−23289
lithium perfluoro-octanoate-water, liquid crystal, ^{19}F multipulse NMR obs. 80−34795
lithium perfluoro-octanoate-water system, liq. cryst. struct., self-diffusion, NMR 78−15036
lyo-mesophases, induced chem. shift, NMR obs. 79−33548
lyotropic, ^{23}Na NMR quadrupole splittings, elec. double layers 78−76345
lyotropic, C_{18} mono-cis-unsaturated soaps, X-ray diffr. and EPR meas. Monte Carlo simulation 78−94981
lyotropic, chemical shift anisotropy obs. of $^{19}F^-$ 80−20478
lyotropic, containing Cs^+, ^{133}Cs NMR, chemical shift anisotropies 78−79525
lyotropic, counterion binding, NMR, ion condensation model 80−1922
lyotropic, formation of mesophases in presence of water, biological implications 77−86454
lyotropic, micellar superstruct., light scatt. 80−24352
lyotropic, NMR line shapes, free induction decay, Jeener echoes 77−63291
lyotropic, orientation in mag. field, glass interface effects 79−1390
lyotropic, parabolic focal conic struct., disclination/dislocation relation 79−27909
lyotropic, partially ordered matrix for EPR of dimethyldithiocarbamate 77−77103
lyotropic, phase diagrams and NMR, solubilised mols. effect on struct. 77−84628
lyotropic, sodium dodecyl sulphate NaCl aq. soln., micellar props., laser light scatt. exam. 78−92513
lyotropic, structure rel. to amphiphilic structure 78−51416
lyotropic liquid crystal properties, biological aspects *(Japanese)* 77−70407
lyotropic liquid crystals formed by phosphated polyoxyethylene surfactants, n-hexane, water, rheological props. meas. 77−54947
lyotropic mesophase, ^6Li, ^7Li, and ^{23}Na NMR, metal ion-polar head group interaction 79−4243
lyotropic mesophase, mag.-oriented, X-ray diffr. obs. 80−1921
lyotropic mesophases as defects in binary mixtures 77−31586
lyotropic phases, water orientation, ^{17}O and ^2H NMR 78−27905
lyotropic systems, NMR of dissolved cations and D_2O molecules 79−22732
macromolecular liquids and solutions, statistical thermodynamics 78−18528
macromolecules in liq. cryst., optical changes obs. method 79−64135
materials science, phys. and mech. props. 80−25538
MBBA, isotropic, surface-induced ordering 80−108176
MBBA, liq. crysts., thin layers, addition of iminoxyl radicals, effect on elec. cond. *(Russian)* 78−67641
MBBA, refractive index, dielec. const., mag. susceptibility, orientational ordering *(Dutch)* 80−33884
MBBA liq. cryst., anisotropic light scatt. 79−78692
MBBA-EBBA mixtures, quinone and hydroquinone doped, dynamic scatt., elec., electro-optical props. 79−37616

liquid crystals continued
mean field equation, systematic soln. 77−76300
mean field theory of model anisotropic pot. of rank >2 79−60268
mean-field equations, phase diagrams 78−18751
medium for detection of small objects in optical microscopy 80−9034
melting, use in aerodynamic heating test 79−77299
mesocarbon microbead, heat treatment under high pressure 77−28736
mesogenic compounds, thermal stabilities, packing coeffs. and mol. packings 79−46558
mesogenic materials, tails or smear effects in X-ray diffr. photographs 80−96438
mesomorphic mixtures, binary phase diagrams, thermodynamic props., diamag. anisotropy 78−95139
mesomorphic state formation mechanism and molecular struct. correlation 80−54128
mesophase, investigation of possible cpds. by mol. orientational correl. in isotropic phases 77−84637
mesophase pitches, Raman spectroscopy 79−91416
metal/liquid crystal interface, elec. double layer, statistical equilib. state 80−40708
N-methacryloil-ω-aminolauric acid cholesterol ester, liq. cryst. polymers, copolymers, structuring *(Russian)* 79−55665
p-methoxy-XY-p′-alkyl tolanes, mol. struct., packing coeffs., and thermal stability 78−95046
microscopic model of structural organisation, mol. dynamics method 80−10492
microstructural EHD model of continuous medium 77−42731
molecular, relaxation eqns. for mean orientation *(Russian)* 77−11483
molecular crystal, action of external forces on mesogenic struct. form. 80−2147
molecular electronics appl. 80−6355
molecular geometry, orientational order and melting 79−37810
molecular model with ordered liq. columns *(Russian)* 79−19152
molecular order and dynamics, high resolution neutron scatt. study 79−50991
molecular order induced by cell walls, exptl. results 78−1996
molecular ordering from incoherent quasi-elastic neutron scatt. 79−4241
molecular orientation, effect of deposition of SiO_2 films *(French)* 79−10789
molecular orientational distrib., statistical mechanical stability 79−94880
molecular reorientation correlation times, librational model 78−1968
molecular reorientation on C_∞ group 77−1053
molecular spectroscopy, conference, Wroclaw, Poland (Sept. 1977) 78−62951
moleculear liquids and liq. crysts., theory of irreversible processes 80−54125
Mossbauer radiation scatt. by condensed matter, review 79−78596
multicomponent system of nonspherical molecules, statistical thermodynamics in quasichemical approximation *(Russian)* 78−5995
multipulse NMR line narrowing, appl. to solids and liq. crysts. 78−72424
naphtha tar pitch, mesophase formation during carbonisation under pressure 77−44182
nematic/smectic A/smectic C triple point, Landau theory 79−95142
neutron scattering techniques in applied research, medium-flux research reactors 79−13514
p-nitrophenyl p-n octyloxy benzoate, elec. cond. and dielectric const., in solid phase 79−61293
NMR in biaxial and uniaxial liq. crysts. 78−75552
NMR magic echo by sample reorientation 80−103899
NMR of ^{13}C, high-resolution spectra 79−38388
NMR spin-lattice relax. time near phase transitions 80−71222
NMR technique, dipole coupling of ^{13}C NMR 79−99073
nonlinear, use of dissipation functions 80−84054
nonylphenol diethylene glycol ether-water-p-xylene system, liquid crystal stabilization of multiple emulsions 79−16046
OBPA, liq. cryst., proton spin-lattice relax., freq. cut-off effect 77−20738
p-n-octadecyloxybenzoic acid, thermal props. 77−47345
octaphenylcyclotetrasiloxane, mesophase form., neutron diffr. obs. 78−91224
p-octoxybenzoic acid:cholesteric nonanoate, mag. field induced cholesteric→nematic transition Raman spectra 77−27988
p-n octyloxy benzylidine-p-toludine, elec. cond. and dielectric constant, in solid phase 79−61293
optical birefringence determ. from interference meas. 77−72551
optical properties, lecture 78−35118
optical properties, Poincare sphere analysis 77−85690
order parameter measurement, phys. chem. lab. expt. 80−36818
ordering and theory of mol. dispersion forces and pair pots. 80−64886
orientating action of solid substrates, on liq. cryst. layer exam. 80−44111
orientation, on obliquely evaporated SiO film 77−69190
orientation at interfaces 78−1992
orientation mol. ordering determ. by Raman scatt. *(Russian)* 79−19153
orientational distrib. coeffs. for liq. cryst. matrix 80−92452
orientational order parameter, optical birefr. meas., polarisation field problems 80−79688
orientationally ordered two-dimensional fluid phase, existence, mol. dynamics calcs. 79−73095
orienting action of US related to theorem of minimum entropy production 79−77498
PAA, isotropic, nucl. spin-lattice relax. 79−23519
PAA, refractive index, dielec. const., mag. susceptibility, orientational ordering *(Dutch)* 80−33884
N-pentanol-Na-N-octanoate-water system, partial molar enthalpies 78−75543
4-n-pentyl phenyl-4(4-pentyl benzoyloxy)3-chlorobenzoate, flexoelectric and dielec. relax. behaviour 78−94979
pentyloxy-cyanobiphenyl, liq. cryst., laser and electrical Kerr effect 78−68477
phases and phase transitions, review 78−2006
phenanthrene, mesophase formation during carbonisation under pressure 77−44182
phenomenological hydrodynamic model, rel. to macroscopic behaviour *(Polish)* 77−51311
phenomenological models of liquid crystal state, electrohydrodynamic models 80−24354
phenyl 4-benzoyloxybenzoates, influence of lateral substitution on liq. cryst. props. 79−4242
liquid crystals continued
p-phenylene bis (p-substituted benzoates), cryst.-nematic transition, mol. struct. effects, DTA 78−47504
phosphatidylcholine bilayers, fluidity changes and phase transitions, intramol. excimer fluoresc. obs. 80−85342
phospholipid bilayers, carbonyl groups dynamics, ^{13}C chem. shift anisotropy obs. 80−85326
phospholipid membranes, orientational order and integral protein struct. 80−45862
photoelectrochemical evolution of O_2 using manganese chlorophyll-liquid crystal electrode 79−83719
phthalozine, oriented in lyotropic mesophase, proton NMR spectra 79−82886
physical properties, account of discovery *(Dutch)* 77−62473
physical props. and analysis, liquid chromatography and purity improvement 79−14682
physical props. and sample prep., book 80−105444
physics, topology theory appl. *(Russian)* 80−8770
physics of liquids, book 79−60245
piezoelectric solution, thermodynamic treatment 79−32903
pitch, mesophase form. under reduced press. 77−63571
pitch, solubility 78−67831
plasma low density lipoproteins, human, size and surface effects rel. to phase transitions 78−3446
poly(γ-benyl-D-glutamate) liquid crystal, orientation in magnetic field, NMR study *(Japanese)* 77−72550
poly(γ-benzyl-D-glutamate), liq. cryst., tactoidal shell defects 78−22642
poly(γ-benzyl-L-glutamate) solns., osmotic press. in isotropic and anisotropic phases 79−94886
poly(p-phenylene terephthalamide), liq. cryst. phase transition *(Chinese)* 79−65175
poly-1,4-phenylene terephthalamide, in H_2SO_4, dilute soln. viscosity 78−75524
poly-γ-benzyl-L-glutamate, ^{131}Xe orientation, NQR quadrupolar splitting 79−4741
poly-γ-benzyl-L-glutamate, γ-methyl-L-glutamate solns. in p-Cresol-$CDCl_3$ mixed solvent system, NMR 79−91303
poly-γ-benzyl-L-glutamate, lyotropic liq. cryst., crosslinking in mag. fields, aligned orientation form. 77−43137
poly-γ-benzyl-L-glutamate, lyotropic liq. cryst., trifluoroacetic acid effect on viscoelasticity, susceptibility 77−84644
poly-γ-benzyl-L-glutamate, mag. oriented liq. cryst. solns., order parameter 77−15305
poly-γ-benzyl-L-glutamate, sidechain order parameters, ^2H NMR meas. 80−1923
poly-γ-benzyl-L-glutamate solution orientation of liq. cryst. domains, IR spectroscopy *(Russian)* 77−62477
poly-γ-benzyl-L-glutamate solutions, calorimetric study of fusion of liquid cryst. struct. 79−53022
poly-γ-benzyl-L-glutamate-dioxane liq. cryst., orientational order temp. depend., diamag. susceptibility 77−47966
poly-γ-methyl-L-glutamate solns. in p-Cresol-$CDCl_3$ mixed solvent system, NMR 79−91303
poly-n-benzamide, lyotropic liq. cryst., structural orientation *(Russian)* 77−31593
poly-N-benzamide, lyotropic liq. crystals, viscosity anisotropy 80−10693
polyesters, thermotropic, quiescent crystn. 80−38937
polyisocyanides, solns., struct. and acidification 80−19915
polymeric, struct. and morphology, theory 79−69025
polymeric mesophases, discotic phases, optical microscopy obs. 79−41951
polymeric thermotropic liq. crysts., mesogenic elements and flexible spaces in main chain 79−60269
polymoprhic properties, impurity effects 79−10930
polyoxyethylene dodecyl ether/water system, lamellar liq. cryst., solubilized hydrocarbon effect on struct. and dislocation pattern 79−94885
polypeptide lyotropic liq. crystals, van der Waals-Lifshitz forces 77−84624
polystyrene latex, ordered monodisperse, lyotropic liq. cryst., mech. props. 79−98676
polyvalent mesogenic struct., synthesis and mesomorphic props. *(French)* 80−6357
potassium palmitate-d_{31}, spin-lattice relax., chain position and temp. depends. 78−68405
potassium palmitate-water bilayer, lamellar liq. cryst. polymorphism, NMR and birefringence 79−60270
potassium soaps, heterogeneity of chain lengths, factor in lyotropic polymorphism 78−59746
PPT liq. cryst., anisotropic light scatt. 79−78692
properties rel. to molecular structure 78−55807
protonated multiple quantum transitions, excitation detection, Fourier transform multiple quantum NMR 80−31819
pseudo-groups applied to symmetry and defects ordered media 80−10541
pyrene central core, discotic mesophase potentiality, isobaric phase diagram method 79−36680
quinoxaline, oriented in lyotropic mesophase, proton NMR spectra 79−82886
refractive index anisotropy, meas. using different methods *(French)* 77−16274
review, book contrib. 77−39544
review, cyclobiphenyl compounds, crystal display 80−67962
review, history of development, props., appls. *(Chinese)* 79−32905
review, mol. struct. and dynamics, effect of chem. constitution anal. 77−43149
review of props. and characts. 78−18546
review of structure and properties 77−43134
rigid rod adsorption, long-range dispersion interactions, appl. to lyotropic molecules 80−29265
rotary motion about short axis, dielectric and splay viscosity meas. 77−43145
rotation and diffusion, neutron scattering obs., book contrib. 77−89573
rubidium n. alkanoates, long-chain, phase transformations, in melt, DTA obs. 77−76536
scattering centres size and conc. determ. using turbidity spectrum 79−77509
scattering indicatrix determination for coherent and incoherent radiation *(Russian)* 80−64897
Schiff's bases, deuterated, transition temp. meas., comparison with normal compounds 78−14449
Schiff base liq. crysts., multicomponent, phase diagrams and metathetic reactions 79−56965
semiflexible macromolecule soln. liquid crystalline ordering 78−94963

liquid crystals continued
short rod fluid, short range correl. and orientational energy 78−1978
singularities, investigation by homotopic topology methods *(Russian)* 77−69140
sodium decanoate-n-decanol-H_2O system, lamellar G-phase, orientational-order, EPR investigation 80−24355
sodium dodecylsulfate−H_2O system, X-ray anal. 80−1926
sodium octanoate-decanol-water system, struct. of C phase using electron microscopy 77−47341
sodium pentadecyl sulphonate, lyotropic liquid crysts., X-ray study of domain structure *(Russian)* 77−62469
sodium undecanoate/water system, lyotropic liq. cryst. struct. change due to polymerisation of amphiphilic component 80−59386
solid state, ^{14}N NQR spectra 79−61260
solid state polymorphism, differential scanning calorimetry obs. and IR and Raman spectra obs. 80−55094
spiral-like, struct., PMR of dissolved mols. 78−1981
static and dynamic properties, time depend. fluoresc. depolarisation obs. 80−29786
structural and optical props., neutron and X-ray diffr. obs. 80−24323
structure, properties, applications *(Italian)* 79−82145
structure and dynamics, neutron diffr. studies 78−94972
surface, atomic processes, book contrib. 79−60605
surface alignment treatment giving controlled low angle tilt 77−19871
surface alignment using polynuclear metal complexes 80−1924
surfactant-water liquid crystal phases, review 80−28913
symmetry and thermodynamic states, review 80−10493
symmetry of materials, transformation of coords. in constitutive eqn. 80−53621
TBBA, new cryst. phase, calorimetric meas. 79−51254
technological appls., role in biological systems *(Croatian)* 79−10788
tensor field of weak inhomogeneous orientational ordering *(Russian)* 78−67640
terminal polar liq. cryst., amines and nitriles, binary mixtures, induced phases 79−90765
terphenylene mesophase, X-ray diffr. meas. 79−41946
tetramethylammonium perfluorooctanoate-water, lamellar lyotropic liq. cryst., neutron diffr. struct. obs. 80−64888
texture, light scatt. determ. in dynamic scatt. regime 79−27913
textures, deform. and struct.-order, review 77−43135
theory, phenomenological and microscopic approaches connection 79−4248
thermooptical effects used to visualise EM fields 80−62723
thermotropic, formation, dynamic approach 78−47239
thermotropic, NMR relax., review 78−39436
thermotropic, struct., two-dimens. order, and symm. props., review 79−86698
thermotropic, X-ray diffr. obs. of struct. 79−27905
thin films, disjoining pressures isotherms *(French)* 79−99401
thin layer, polarised light ellipticity after passage 80−88036
three-dimensional order, differences compared to solid cryst. 78−83727
three-level lattice system with quadrupole type interaction, analogue of Ising model 78−29063
1,3,5-tribromobenzene mesophase, spiral-like, struct., PMR of dissolved mols. 78−1981
1,3,5-trichlorobenzene mesophase, spiral-like, struct., PMR of dissolved mols. 78−1981
triphenylene, hexasubstituted, thermotropic mesophases 79−86681
triphenylene core, discotic mesophase potentiality, isobaric phase diagram method 79−86680
triphenylene derivatives, hexasubstituted, disc-like cpd., mol. conform. and arrangement, semiempirical calcs. 80−107048
triphenylene esters, crystalline arrangement of disc like compounds 79−99175
triphenylene hexa-n-dodecanoate, mesomorphic polymorphism 79−41950
twisted cells, mol. orientation 77−27818
two-dimensional systems, order parameter from chemical shift anisotropy patterns 80−80624
undecylenate, mesogenic compounds, thermal stabilities, packing coeffs. and mol. packings 79−46558
uniaxial, polarised fluoresc. emission, orientational distrib. function, rot. Brownian motion 78−80390
uniaxial liq. crystal polarised fluoresc. emission 80−80838
uniaxial rotator in N-fold cosine pot., correlation functions, neutron incoherent scatt. law 78−9970
uro-porphyrin I octa-n-dodecyl ester, discotic phase 80−103240
US and laser cavitation phenomena 80−87633
US expts. and phase transitions 79−46571
van der Waals forces in liq. crysts. with large dielec. anisotropy 77−15317
VHF field thermoindication, linearity *(Russian)* 79−1391
viscosimeter for three coeffs. of viscosity of liq. crysts. meas. 79−4095
water-cetyltrimethylammonium bromide-haxanol system, ^{13}C NMR, catalysis in micellar and liq. cryst. phases 79−61909
water-in-dodecane microemulsions, struct. transitions in liq. cryst. phase, dielec. props. 79−28669
water-in-oil microemulsions, structural relaxation by thermal current anal. 80−107049
X-ray scattering, small-angle, data interpretation *(Russian)* 78−59752
X-ray scattering experiments, sample cell system with very highly stabilised temp. 77−13830
X-ray structural analysis, computer program for analysing exptl. data 78−1956
78−18749
Cs perfluoro-octanoate, amphiphilic liq. cryst., ^{19}F multipulse NMR study 78−76328
DPM-4, electroviscous effect 79−69010
NH_4 perfluoro-octanoate, amphiphilic liq. cryst., ^{19}F multipulse NMR study 78−76328
$Ni(CN)_2$-dodecylamine, lamellar paraffinic system, phase transitions, wide-line NMR obs. *(French)* 80−44929
TBBA, liq. cryst., evidence for cybotactic cluster pretransition formation, X-ray diffr. meas. 78−10179

liquid drop model (nuclear) *see nuclear liquid drop model*

liquid films
see also adsorbed layers; helium films; liquid helium; superfluidity; surface tension
absorbance ratios, of thick films, IR spectra determ. 78−48710
acetone, condensation in presence of instabilities, photographic study 78−10180

liquid films continued
alkali metal anions and trapped electrons formed by evaporating metal-ammonia solutions which contain cryptands 79−100340
annular, thickness meas. techniques 80−31439
annular climbing film flow dispersion models 78−83473
aqueous film, plane-parallel symmetrical, stability, non-spreading oil droplet effect 80−107620
binary mixture vapour condensation, forced-free convection, finite difference treatment 78−5741
binary mixtures, film boiling, theory 77−84912
black foam films stability, review 80−104463
boiling, bubble nucleation and venting 78−30153
boiling, destabilisation in liq.-liq. systems 78−94588
boiling, heat conduction and radiation from flat plate *(German)* 79−72789
boiling, heat transfer peculiarities 78−90656
boiling, laminar, with chem. react. on catalyst surface, model 80−45553
boiling, post-dryout heat transfer, review 79−1094
boiling, transition type, in forced convective flow, boundaries meas. 79−27499
boiling crisis, surface material thermophys. props. influence, data correl. 80−5923
boiling instability, during quenching in subcooled water *(French)* 79−46167
boiling liquid films (mm), critical thickness for destruction *(Russian)* 77−80611
boiling liquid thin film rupture, heat-transfer surface state effect 78−55552
boiling mechanism during burnout phenomena in subcooled two-phase water flows 78−94529
boiling mode, disperse, of cryogenic liqs., heat transfer and modified Reynolds model 80−5924
boundary layers, struct. and thermodynamic peculiarities 80−88408
breakdown, numerical anal. 79−46285
butyloxybenzylidene octylaniline, liq. cryst. film, smectic B-A transition, mech. meas. 80−79918
capillary rise, contact angle and film jumps 77−66076
carbon tetrachloride-acetone (chloroform) mixtures, film boiling on elec. heated horizontal wire, atm. press. 77−20061
carboxymethylcellulose, aq. soln., hydrodynamics of falling liquid film *(Russian)* 79−64715
carrier mediated transport theory, survey of applications 77−89113
cholesteric liquid crystal coatings, superimposed left- and right-handed, peak refl. and colour gamut 80−74472
cholesteric liquid crystal on Al evaporated surface, thermal emissivity study *(Japanese)* 77−35732
cholesteryl oleate, thin film, disclination morphology *(Russian)* 77−62474
classical fluid structure near solid substrates 78−63655
condensate film flow on finned surfaces, heat transfer, heat exchanger design 78−75038
condensation enhanced by surface forces, optimum condenser tube fin geometry 78−75039
condensation inside pipes, heat transfer, general correlation 79−46312
condensation of laminar film on helical elliptical cylinders, governing eqns. soln. 78−9689
condensation of moving vapour on horizontal cylinder, exptl. dependences 80−58892
condensation of vapour in elec. field, heat exchange intensification 79−86331
confining substrate for micron thick liquid films, semicond. films 80−96722
continuous film flow, range of existence 77−39273
continuous flow squeeze film, load-bearing capacity 78−87306
convective coupled heat transfer, Nusselt no. computation, laminar fluid film 78−59398
cooling, from single hole and hole row, free stream turbulence effect 79−46310
counter-current two-phase flow, annuli, rod bundles, liq. film behaviour, flooding 78−59452
counter-current two-phase flow in tube, liq. film waves and flooding 78−18345
cryogenic and ordinary liquids on vertical surface, film boiling heat transfer 80−48555
cryogenic liquids on flat horizontal surfaces, film boiling heat transfer 80−48553
cumene, films, thin, wetting, rheological characts. determ., capillary method 78−51788
decane, film flow calc., effect of temp. and press. gradients in conical capillaries 79−55416
n-decane, films, thin, wetting, rheological characts. determ., capillary method 78−51788
deposit of liq., response of quartz crystal microbalance 79−30422
dielectric liquid, film condensation, heat transfer enhancement in elec. field 78−55551
dipalmitoyl lecithin bilayer, mol. tilt, X-ray diffraction obs. in gel phase 80−84059
Disjoining pressure of thin layers of binary solutions 78−15716
dispersion, close-packed, two-dimens., gravity effect on thin film drainage 79−86486
disruption, variation in minimum thickness rel. to capillary forces 79−65297
DOBAMBC, ferroelectric liquid crystal film, freely suspended, polarisation, elastic consts. and viscosity meas. 79−55663
drainage, withdrawal and postwithdrawal drainage with inertial effects, unified treatment 77−23932
draining, vertical column of drops approaching interface, shape 79−32725
draining deformation between rigid sphere and gas-liquid interface 77−66078
dryout in an SGHWR rod bundle, exptl. and calc. comparison 79−3192
dye liquid layers, fluorescence angular distribution, evanescent wave excitation 79−51996
dynamic behaviour, surface mobility effects 80−88409
dynamics and wave propagation 80−19464
education, soap film on wire frame in zero gravity, variation problem branching 79−9057
EHD coupled minimum film boiling in dielec liqs. 77−42921
elastohydrodynamic film form. between rubber cylinder and glass plate 77−28910
electrolyte layer, convection onset condition 79−14492

liquid films continued
emulsion, films, thinning vel. and lifetime, surfactant in continuous and dispersion phases 77−84306
emulsion films, thinning vel., surfactant in continuous and disperse phases 77−84305
entrained, thickness, effect of surface induced gradual viscosity increase 78−83488
entrapped liquid lenses at elastomer-glass interface, formation and geometry 77−85021
equilibrium dispersed-ring water vapour flows, liq. distrib., film paramters and hydraulic resist. 80−24079
ethanol-water mixture, saturated, min. film boiling temp. on horiz. stainless steel and Cu surfaces 78−90692
evaporating, heat transfer model 78−30154
evaporating, interline heat sink capability, optical and thermophysical props. depend. 78−71276
falling, 3-dimens. wave characts., laser beam refraction obs. 79−27654
falling, laminar, evaporation model 79−46305
falling, laminar, gas adsorpt. with zero order react. in entrance region 80−64652
falling, theory of mass transfer 79−65309
falling, wave struct., linear stability problem and Orr-Sommerfeld eqn., expt. 78−38343
falling film, linear stability theory, applicability 77−23938
falling film, thickness meas., statistical props. 79−12708
falling film, vol. profiles in hydrodynamic stabilisation zone from non-parallel sided slot 80−53748
falling film flow, equivalence of spatial and temporal formulations for linear stability 77−19589
falling film flow, spatially growing three dimens. wave, annular-froth flow transition 78−14071
falling film rewetting 78−75906
falling films, nonisothermal flow *(German)* 78−83439
falling laminar liq. film, transport augmentation by surface waves 78−71343
ferroelectric smectic-C liquid crystal film, freely suspended, two-dimensional mol. orientation fluctuations, light scatt. meas. 78−47236
flow, cellular convection 77−68588
flow, down vertical cylinder, linear hydrodynamic stability 77−19588
flow, down vertical surface, minimum thickness, Mikielewicz-Moszynski eqn. 77−47652
flow, meniscus shape theory, Navier Stokes eqn. 78−38270
flow, wave parameter meas., local electrical cond. method 77−51141
flow affected by streaming turbulent gas *(Russian)* 79−14386
flow down inclined plane, deflection toward underside 79−18867
flow down inclined plane, stability, anal. quadrature by differentiation method 79−90219
flow down vertical or inclined surface, surface tension effects 80−106778
flow of annular climbing film, tracer dispersion 79−64751
flow of falling films, surfactant effects 77−89093
flow of film preheated to boiling 77−62244
flow of stratified gas-liquid film, equns. of motion 79−37376
flow of viscous fluid down vertical cylinder surface, long waves 77−75928
flow on porous vertical plate surface, suction and injection effects 80−53849
flow on vertical plate, hydrodynamic stabilisation *(Russian)* 77−35117
flow on vertical wall 77−62237
flow over horiz. smooth tubes 78−38273
flow over rot. disc 78−38342
flow speed measurement, electromagnetic pipeline system 80−79417
flowing concurrently with air in horiz. duct, flow pattern 80−43774
flowing down inclined plane with heat transfer, interfacial shear, stability 79−37290
flowing on pipe wall, gas absorption rates 79−94696
fluid interfaces dynamics and instability, conf., Lyngby, Denmark (May 1978) 80−31423
fluorocarbon refrigerant, film boiling heat transfer from heated plate 79−55380
foam breakdown, syneresis, drainage rate rel. to time 80−11954
formation and thinning 80−39391
free binding liquid film, mean velocity distrib. meas. by laser Doppler velocimeter 80−38508
free coating of surface, effect of angle 79−46892
free film, stabilised with ionic surfactants, EHD 78−87403
freely flowing liquid film, cooling, heat transfer, turbulent transport model calcs. 80−64560
fuel film, combustion behind shock wave, heat and mass transfer in turbulent boundary layer *(Russian)* 78−71401
gas absorption, into accelerating thin falling liq. film on inclined surface 78−93632
gas bubble formation dynamics 80−24083
gas diffusion through surfactant films, interfacial resistance 80−39385
gas entrained, combined plane parallel flow, linear and nonlinear stability 80−33655
gas mixture, binary, condensation in boundary layer flow, numerical method 79−1236
gas-liquid film interface stability behind slipping shock wave front *(Russian)* 78−55630
gas-liquid mixture, entrained downward flow in vert. channel 79−94704
gas-liquid two phase flow film thickness, tube four rectangle obstacle, expt. 78−87377
gas-liquid two phase flow film thickness, tube ring obstacle effects, expt. 78−87376
gas-streamlined liquid film, quasiharmonic motion development in vertical flow 77−55014
gravity wave, liquid with superficial film and diffusion effect *(French)* 78−75156
heat and mass transfer during vapour absorpt. 78−63427
heat transfer, and film breakdown in subcooled falling film 78−34121
heat transfer and film breakdown in falling film with nucleate boiling 78−34122
heated horizontal channel, heat transfer and dry patch formation 80−64554
hexadecane, boundary viscosity using blow-off method 79−23383
hexane, film flow calc., effect of temp. and press. gradients in conical capillaries 79−55416
highly viscous fluid emerging from slit onto plate, flow development and meas. 80−59142
homogeneous surface, hysteresis of contact angle 78−51793

liquid films continued
horizontal elliptical conduits, turbulent film evaporation and condensation 79−1182
hot surface quenching rate, countercurrent single- and two-phase flow effects 78−59451
hydrocarbon layer, influence on laser-induced surface damage 78−60533
hydrodynamic contacts, films, elastic properties 80−88239
hydrodynamic stability of liquid films and jets, effect of soluble surface-active substances 80−6027
hydrodynamics, generalized equations, nondeformable surfaces 80−10224
hydrodynamics and heat transfer expts. *(German)* 78−18305
hydromagnetic squeeze film between porous circular disks with velocity slip 80−74997
impermeable film on liquid surface, persistence in presence of disturbance 77−31839
infinite plate, thin liquid film evaporation, surface temp. and heat transfer 80−64346
instability and rupture 80−34279
instability on surface of rot. sphere 80−59006
insulating layer, cellular deformation mechanism, charge flux *(French)* 80−70507
interaction of fast-moving drop with liq. film surface *(Russian)* 79−64756.
interfaces, liq.-liq., in isolation and in interaction, review 77−47651
irregular wavy flow of a liquid film down a vertical plane 80−106808
irrigating films, laminar, entry zone length for vertical plate wetting 80−53742
laminar falling liquid films, mass transfer with heat transfer and interfacial shear 80−80033
laminar film, condensation on underside of inclined flat plate 79−50700
laminar film boiling of binary liquid mixture, heat transfer rates *(German)* 77−7398
laminar film condensation from moving vapour, with suction 78−59459
laminar film condensation on vertical surface with heat generation 79−72786
laminar flow, absorption with chem. reaction 77−42929
laminar liquid film in vertical flow down solid surface, coherence *(German)* 78−22322
laminar liquid film moving along sloping surface, hydrodynamics 77−7365
laminar liquid films, dependence of temp. variation of film substance viscosity 79−41686
laminar liquid flow around plate, boundary-value problem soln. for generalised diffusion eqn. 77−7366
laminar non-Newtonian falling liquid films, dynamics 79−7393
latex suspension liquid film flow, local thickness meas. 79−4070
liquid crystal, dislocation-mediated theory of two-dimens. melting predictions, light scatt. use as probe 80−92651
liquid crystal, imaging of US in air 80−38166
liquid crystal films, disjoining pressures isotherms *(French)* 79−99401
liquid film, laminar, stability, mass exchange and heterogeneous chem. reaction effects 77−75990
liquid film condensation on vertical wall, linearised stability anal. 79−55381
liquid films on horizontal tubes, combined boiling and evaporation 79−81882
liquid metal, film, turbulent flow down vertical wall under gravity, heat transfer 78−59396
long waves on film flow down inclined uneven wall 78−42623
2,6-lutidine-water, fluid film, crit. phenomena, scaling, law of corresponding states 79−90787
2,6-lutidine-water, fluid film, crit. temp. shift, crossover temp., coexistence curve amplitude, fluid-boundary interaction 79−90788
2,6-lutidine-water thick films, interferometric obs. of crit. behaviour 80−93266
magnetic liquid film flow in mag. field, laminar regime 78−34203
MBBA, homeotropic nematic layer, torsional shear flow in normal elec. field 79−82155
MBBA, nematic film, with two free surfaces, EHD flow 79−98817
meniscus profile, contact angle, differential interference method 79−56039
meniscus-film-vapour equilibrium, generalised Young equation at low or zero contact angle 79−65298
metal, supercooling, electron diffraction study *(French)* 79−7676
methanol-cyclohexane, crit. temp. and coexistence-curve determ., optical meas. 77−7952
MHD film flow, porous-walled squeeze film, slip effect in transverse field 79−77262
MHD flow on vertical surface, viscous lifting and drainage 78−18348
MHD gravity-capillary waves in liq. film falling by permeable bed 78−67277
micro-polar fluid, on flat surface, effect of couple stresses on unsteady drainage 77−14985
microcontinuum theory for elastohydrodynamic inlet zone of line contact, lubricant film 77−50998
microemulsion, struct. description of liq. particle dispersion, ultracentrifugation and small ang. neutron scatt. obs. 79−5184
microscopic film, with deformable interface, rate of thinning, calcs. 78−43220
mineral oil, finite amplitude equilib. waves on surface of nonvertical falling film 77−19614
mixture, shallow, laser separation, thermal mechanism 80−5925
mixtures, decomposition into components by thermal action of continuous laser irradiation 79−19362
molecular forces, theory 78−40087
molten cladding film relocation following HCDA, large wave dynamics 78−17365
multi-layered liquid films, instability 79−1158
multicomponent mixtures, mass transfer, penetration depths 79−42286
multilayered liquid films, wave motion, governing eqn. 79−10580
nematic, critical splay-bend deform. numerical anal. 77−58957
nematic liquid crystal, ZLI-207, electro-opt. props. *(Russian)* 77−43967
nematic liquid crystal film, mol. dynamics *(Russian)* 79−27903
nematic surface aligned film, nematic-isotropic crit. thickness, Landau-de Gennes theory 77−4189
nematic suspended films under AC and DC fields 77−11470
Newton black film, line tension, determ. by cnt. bubble method 80−88406
Newton black films, line tension determ. by diminishing bubble method 80−88407
Newton black soap film, interaction forces, contact angles 79−77870

liquid films continued
Newtonian liquid, coating on to rotating roll 79−41692
Non-Newtonian falling film, hydrodynamic entrance length 77−58743
non-Newtonian falling film, Taylor diffusion of solute 77−39317
non-Newtonian fluid, rot. liq. film, free surface instability 79−37294
non-Newtonian fluid film flow along vertical oscillating plate *(German)* 78−59431
non-Newtonian fluids, lubrication, elastohydrodynamic, between two rot. cylinders 78−83435
non-Newtonian incompressible liquid film, surface waves 80−43748
non-Newtonian laminar falling liq. films with smooth wave free gas-liq. interface, heat transfer 79−7389
non-Newtonian liquid, shock-induced spreading of film between two colliding surfaces 77−7419
nonisothermal liquid film, nonlinear dispersive surface waves 80−33617
nucleate boiling suppression 78−75055
oil, Newtonian viscosity meas. by two optical methods 77−89214
oil, spreading on water, rel. to surface contamination 79−43795
oil film crossflow around cylinder, local heat transfer 79−98711
oil films, thickness meas. by neutron imaging, and scattering, exam. of flow props. 79−15815
optoacoustic spectroscopy using pulsed dye laser for micron thick film 80−42265
paraffin oil coatings for high power laser system components 77−88730
poly-γ-benzyl-L-glutamate, monolayers, struct. studies, IR, ATR, and TEM obs. 80−44396
polyacrylamide soln., films, hydrodynamics *(Russian)* 77−31338
polydimethylsiloxane, non-pure, dielec. behaviour 80−29672
polymer continuous flow squeeze film, load-bearing capacity 78−87306
polymer melts and solutions, foam stabilisation *(French)* 80−21323
polymer solution, elastic, load bearing capaicty of squeeze film flow 80−103051
potassium palmitate-water bilayer, lamellar liq. cryst. polymorphism, NMR and birefringence 79−60270
pseudoplastic liquid film, wave motion 79−32583
pulmonary surfactant film, surface dilatational viscosity obs. 79−62278
quasiviscous fluid, thin film flow over surface of rotating nozzle 77−54965
quenching temperature, 0.03-1.3 MPa, base material thermal props. depend. 78−94587
rare earth ions in aq. solns., optoacoustic spectroscopy using pulsed dye laser for micron thick film 80−42265
restricted withdrawal of vertical cylinders from quiescent liquids, numerical treatment 77−72756
ripple flow, stat. characts. 77−7408
rod bundle dryout, liq. film, droplet entrainment and deposition 78−13204
roll waves, small amplitude, behaviour in turbulent liquid films *(German)* 78−94756
rotating cylinder in gravitational field, liq. film motion, steady soln. 78−83411
rotating disc apparatus, thin-film, minimum irrigation density determ. 77−47125
rotating disc flow regimes 78−1671
rotating radial pipe with liq. film, Coriolis effect, film width and vaporisation 79−18955
on rotating surface, hydrodynamics and heat exchange, entrance section influence, interface frictional forces 79−86433
rupture in laminar and turbulent lubrication, inertia forces effect 80−74813
saturated liquid, boiling onset, film boiling transition, crit. heat flux densities *(Russian)* 78−83234
saturated liquids, nucleate boiling, thin film breakdown 80−48695
silicone liquid film, cond. currents obs. 79−91062
silicone oil thin films, convective heat transfer, surface tension effect 78−94681
simple fluids, small strain oscillatory squeeze film flow, polymeric liquids 80−92765
slug formation, horizontal and inclined pipes, gas-liq. flow model 78−14083
smectic C liq. cryst. film, mol. orientation fluctuations in two-dimens., light scatt. obs. 80−93355
smectic liquid crystals, octylcyanobiphenyl asymmetrical and symmetrical structure *(French)* 77−35473
soap, contact angles, thermodynamic description 78−47639
soap, Newton black, contact angle meas. 78−47640
soap built-up multilayers, defect visualisation by optical microscopy 77−59186
soap film, light scatt., double-layer repulsion forces determ. 77−85025
soap film, light scatt., van der Waals forces determ. 77−85028
soap film in a wedge, expts. for teachers 79−17169
soap film simulation of phase changes, catastrophes 79−62974
soap films as analogue for minimum path and minimum area problems 77−17740
solution film adsorbed on cryst. surface, NMR investig. 77−8426
squeezing mode relaxation of free liq. film, laser scatt., rel. to colloid interaction 78−87354
stability adjacent to supersonic boundary layers 77−930
steam, film condensation in tube, heat transfer, vibr. effect 78−51044
steam condensation heat transfer on below-freezing pt. surface 78−75042
steam-water, flow characts. at high press. 78−94805
steam-water mixture, upward flow in tube, liq. film-core mass transfer, liq. distrib. 78−75189
steam-water mixture, with high vap. content, annular flow, heat transfer, press. loss 78−75193
subcooled film boiling heat transfer from spheres 78−51047
surface deformation under charge *(French)* 77−31848
surface deformation under charge flux *(French)* 77−31847
surface structure, mol. dynamics simulation 77−15666
surface tension driven instability of flow down heated incline 79−27620
surface waves under charge flow *(French)* 77−31849
swirling water bells 79−50733
tetradecane, wetting on solid substrates, disjoining pressure isotherms 78−51794
tetramethyltetraphenyltrisiloxane film, DC-704, on Ge, Al and KRS-5, IR refl. spectra anal. 77−59630
thickness and stability, on nonplanar surfaces 80−10755
thickness calc. of film on rough surface *(Russian)* 79−77061
thickness meas. using laser based fluorescence technique 79−49201
thickness measurement, conductometric method 80−77751
thickness measurement, of thin liquid films on inaccessible surfaces 79−30412
thickness measurement, using excited fluorescence in dye solns., report 78−81945
thin, break-up due to mass transfer intensity in absorption 80−80032
thin falling liquid films in tubes, 'dry patch' stability 80−53747
thin film, evaporation and breakdown driven by shear stresses 80−38410
thin films, role of disjoining pressure in equilib. and flow 79−14984
thin films with extensive evaporation, heat transfer *(German)* 80−99920
thin free films, stabilised with ionic surfactants, dynamics 78−87416
thin liquid film flows, boiling crisis models 80−74710
thin liquid film stretching mode relax. obs. by laser intensity fluctuation spectra 79−28177
thin liquid films in emulsions, contact angles 80−92761
thin nonplane liquid films, existence and stability 80−92764
three-phase contact, perimeter expansion rate, theory 78−22937
transient thermocapillary flow in thin liquid layers 80−92226
tube, vertical, steam generating annular flow, dry-out position prediction, computer model 78−59447
turbulent, heat transfer predictions for nonsheared and sheared films 77−15024
turbulent falling liq. film, gas absorpt. 79−50714
turbulent flow over vertical surfaces, heat transfer, friction factor 77−42819
turbulent liquid film, gas absorpt. accompanied by first order reactions 79−69327
turbulent water film, with different initial flow conditions and high temp. gradients, heat transfer 78−90862
two-phase flow, annular, crit. heat flux, swirl effect 80−10113
two-phase flow with condensed liq. particles, heat transfer to wall with solid condensate layer 79−86426
two-phase liquid film flow, hydrodynamic and heat transfer in downward annular motion 77−89190
US wave generation, thermal interf.-optical excitation 78−71794
van der Waals forces calcs. using Lifshitz theory 77−72755
vapour absorption, combined heat and mass transfer 79−19430
vapour condensation on vertical surface, laminar flow in film condensate 78−75057
velocity profile, instantaneous, of wavy fluid film 78−79299
velocity profiles, optical method of meas. *(French)* 80−6170
vertical wall, large amplitude surface wave 78−14030
viscoelastic fluid film, flow along conical rotor 78−1697
viscoelastic squeeze films, effect of normal oscill. and fluid inertia 78−67224
viscoplastic liquid film, shaking off flat surface 79−14362
viscoplastic liquid film on vertical vibr. wall, with slip, shaking loose 78−59371
viscous, between two nearly parallel walls, temp. distrib., convection effects 80−83801
viscous drainage, over naturally permeable wall, steady-state film profile 77−27509
viscous drainage, over permeable wall, Navier-Stokes eqn. 77−31278
viscous fluid film, approx. eqns. for long nonlinear waves 78−38346
viscous fluid layer, solitary waves *(Russian)* 77−51070
viscous liquid film instability under the influence of an adjacent gas flow 80−92110
volatile liquid droplets, impaction on hot liquid surfaces 77−39330
volatile liquids, boundary viscosity, meas. by blowoff method 79−11006
water, between muscovite sheets, permittivity change meas. method, 20-70°C 80−55009
water, coalescence times of H_2S and CO_2 bubbles 77−42899
water, evaporation on heated surfaces, heat transfer characts. 78−59269
water, films, thin, wetting, rheological characts. determ., capillary method 78−51788
water, flow behaviour and effect on cocurrent air flow, press. distrib. along rigid wavy structures 77−55029
water, high-pressure gases effect on stability of liq. film 77−85026
water, hot, film, wavy laminar flow down vertical plate at high surface tension numbers 79−94587
water, IR spectra, thin layer between quartz plates 79−56773
water, liq.-like layer between ice and substrate, model, appl. to wire regelation and particle migration 79−46893
water, on slightly rough quartz surface, ellipsometric thickness meas., error estimation 78−32856
water film crossflow around cylinder, local heat transfer 79−98711
water film on Fe surface, stability 80−75408
water film on Teflon surface, boiling heat transfer 79−90124
water film shape on mosaic surface of solid *(Russian)* 79−51395
water films, subcooled, flowing down vertical tube, heat transfer 80−79318
water films vaporisation in rot. pipes 79−14228
water jet, round, impinging, heat transfer in interference zone of film flow along wall 77−58750
water subcooled films on horizontal tubes, heat transfer correlation 79−77114
waves, influence of mass transfer *(Russian)* 79−64677
waves, travelling, gravity-capillary, on liq. film surface falling past permeable bed 78−87351
wedge, forced-convection film boiling, boundary layer flow 79−46366
wetting, kinetics of rupture 79−56045
wetting, on solid surfaces, isotherms of disjoining press., meas. methods 78−51804
wetting, thickness on rough substrates 79−56044
wetting tension depend. on meniscus curvature, adjacent liquid film disjoining press. isotherm 80−2247
Al, electron diffr. 78−83721
Ar film, phase transition phenomena 77−62741
H_2-N_2-Ar, two-phase flow film boiling, in vap. generator, heat transfer 78−75190
He, superfluid, anal. of film boiling 80−10716
^{3}He-^{4}He mixture superfluid thin film, third sound vel. calc. 80−107602
^{4}He superfluid, subcooled, Kapitza resistance of Al 79−23794
^{4}He, superfluid, transient heat transport 80−10715
^{4}He, superfluid healing length and density, ring diagram approx. 80−54452
^{4}He, superfluid saturated liq., recovery heat flux from silent and noisy film boiling states 79−72784
Hg, droplets, film boiling 78−14453
KCl, aqueous film on Hg, secondary electrocapillary effects, interfacial tension and entropy 77−55420

liquid films continued
N_2, liquid, film boiling heat transfer coeff. for vertical surfaces 80−48556
N_2, liquid film boiling heat transfer, orientation effect 80−48554
N_2, transient pool boiling, premature transition to stable film boiling 79−81709
N_2-O_2-Ar saturated air vapour mixture, film mixed condensation, comparison with water vapour 77−11780
Pb, electron diffr. 78−83721
Pb, supercooled liquid thin films, liq. struct. factor determ. by STEM 80−10487
Sn-Cu film, spreading kinetics on Nb substrate in vacuum, 700 to 800°C *(Russian)* 77−80680
Xe adsorbed on graphite (0001) surface, monolayer liquid and solid struct. 80−65400

liquid flow coaxial cables *see coaxial cables*

liquid He *see liquid helium*

liquid helium
see also helium films; liquid helium-3; liquid helium-4; liquid helium sound propagation; ripplons; vortices
boiling, critical heat fluxes, effect of cylindrical heater dimensions 79−35756
boiling, cryogenic liquids, investigations on heat transfer 79−60494
boiling, vapour bubble growth rate 77−24397
boiling, vapour bubble growth rate 77−24398
boiling on surfaces, heat transfer coeff. 78−9545
boiling tube hydraulic resistance and burnout expt. 80−24085
book, liquids and their props., mol. and macroscopic treatise 78−87604
bubble boiling, heat exchange regimes 80−23879
bubble growth consts. calc. 77−35680
bubble-type boiling crisis on various surfaces 77−11682
cell model, generalised, incorporating strong spatial correls. 77−55403
cell model, generalised for strong spatial correls. 77−57276
charged surface, current instability theory *(Russian)* 80−29243
charged surface stability *(Russian)* 77−35791
charged surface vibrations in metal approx. *(Russian)* 80−10718
condensed He phases, book 79−99377
conference, Erice, Italy (June 1977) 78−59985
conference on dynamical critical phenomena, Geneva (Apr. 1979) 80−27040
contact cryogenic fluid level sensor 80−73371
cooling experiments, large-scale, using Helitex test facility 79−63232
cooling system, forced flow, for superconducting magnet, numerical anal. of heat-induced transients 80−82773
cooling unit, continuous flow liq. He, for Mossbauer expts. 77−33992
cryogenic He cycles, minimal losses due to thermodynamic irreversibility 80−86320
cryopump for 1 MV accelerator, cryogenic supply and boil-off removal 79−72011
cryopumping panel, liquid He cooled, appl. in vacuum deposition system 78−56581
cryostat, for use in dispersive Fourier transform spectroscopy 79−54135
cryostat, with refrigerator, for superconducting magnet 79−58733
cryostat as zero mechanical work thermal pump for superconducting AC machines 79−58717
cryostat for metal and insulating material thermal conductivity meas. *(Croatian)* 77−26302
cryostat liquid He automatic replenishment system 79−67308
cryostat system for gas sorption meas. at 12-150K 78−32823
cryostats and storage containers, safety aspects 79−58730
cyclotron reson. with surface electrons *(Russian)* 77−59319
density correlation function and dynamic transient exponents at and above T_λ 79−51325
depth gauge, level sensing circuit 77−82527
dewar, temp. profile 77−41621
dewar, wide-aperture, heat analysis and reduction of evaporation rate 79−58743
dewar prod. using stainless steel 78−16801
dielectric breakdown voltages, anomalous polarity effect 80−2695
drift mobility, conduction band energy, of excess electrons 77−4348
electric discharges at low temps., appl. to elec. insulation for supercond. cables 77−27757
electrical breakdown characts. 79−91364
electrical resistivity expts. in He II environment using computerised facility 80−31799
electrical strength, breakdown voltage depend. on electrode configuration 80−7293
electron bound states on surface 79−28166
electron bubble tunnelling below surface 79−86945
electron fluid, two-dimensional, collective modes 77−80661
electron sheet on liquid surface, liq. to cryst. transition 79−42341
electron solid on surface, phonon-ripplon coupling 79−42337
electron solid on surface, self-consistent Debye-Waller factors 80−84337
electron-charged surface, nonlinear wave propag., theory 78−67879
electron-ripplon scattering, adiabatic approach *(Russian)* 77−80660
electrons localised at surface, cyclotron freq. shift *(Russian)* 80−6582
electrons outside liq. He surface, Hamiltonian for one-dimensional Coulomb field 77−43764
EPR of negative ions field emitted into sample 77−47636
equation of state calc. of T_c, P_c, V_c 78−2228
evaporation loss minimisation during expansion and transfer 77−30166
fault diagnosis and repairing of He liquefier *(Japanese)* 77−67439
fibreglass nonmagnetic He cryostat construction 79−67309
film, acoustic wave phase velocity meas. using CW feedback technique 78−83187
film, superfluidity and the two dimensional XY model 79−28498
films, review 78−60002
first and second sound generation by optical pumping of immersed Ge cryst. 80−6581
floating level gauge 79−2774
floating level indicator 79−67305
flow characts. of forced-flow Nb_3Sn conductors for toroidal-field coils 79−58741
flow in rot. cryostat, temp. distribs., thermodynamics 78−34666
free convection heat transfer in supercritical He 80−79296
free surface, book 80−2227
fusion reactor cooling, distrib. system for Large Coil Test Facility 78−55001
fusion reactors, Large Coil Test Facility, liq. He cooling system 80−102321

liquid helium continued
Hamiltonian of interaction with quantised EM field 79−46853
heat transfer and hydraulic drag in turbulent flow in circular tube 80−14821
heat transfer by natural convection to liquid contained in high-speed rotating frame 79−58720
heat transfer from heated plate 79−63235
heat transfer in centrifugal acceleration fields, free convection and boiling regimes 77−89604
heat transfer in supercritical He, non-bulk Prandtl and Reynolds numbers 78−22346
high-field carrier transport at pre-breakdown and breakdown regions 80−25305
interface with $Ce_2Mg_3(NO)_{12}$, effect on spin-lattice relax. 80−66011
interface with freshly cleaved solid, phonon pulse refl. 79−60573
interface with NaF, freq. of emitted phonons 79−55978
intermolecular correlation effects on liquid props. determined by X-ray diffraction 77−27799
intermolecular potential, accurate empirical 79−68291
ion mobility 78−2324
ionic impurities in fluids, press. induced struct. transition 78−51770
itinerant ferromagnetism, of two dimensional systems 77−24666
Kapitz resistance at boundary with metallic slab, heat transport and Boltzmann eqn. 77−62730
Kapitza conductance, acoustical mismatch 77−76637
Kapitza resistance, heat transfer rel. to adsorbed monolayer *(Russian)* 78−51758
Kapitza resistance and phonon refl. at liq.-solid interface 79−86941
Kapitza resistance on freshly cleaved surfaces 78−63923
laminar free convection heat transfer, analytical study 79−23311
level gauge, with semiconductor sensor 80−57277
level indicator *(Japanese)* 78−12705
level indicator with small heat dissipation, made from newly developed superconducting wire *(Japanese)* 79−2775
Lichtenberg figures at cryogenic temperatures *(German)* 77−82536
metal-liquid He interface, electron-phonon interaction, thermal boundary resistance 78−67899
multiphonon boundary of excitation spectrum, neutron and inelastic light scatt. 80−92740
narrow channel flow and heat transfer characts., void fraction in steady and transient states 78−55000
neutral excitation currents study 79−55953
nonlinear cyclotron resonance of localised surface electrons *(Russian)* 77−59318
nucleate boiling in centrifugal accel. field, heat transfer and flux 78−94538
nucleate pool boiling, heat flux and press. effect on heat transfer 79−14235
orthopositronium decay, press. up to 140 atm. 77−39713
Pellam's He paradox, quantitative explanation 77−39711
phase transition, fluctuational character *(Russian)* 77−47633
phonon coupling of two-dimens. Wigner cryst. with second surface sound *(Russian)* 80−92756
piston pumps, double-acting, for cryogenic He 79−58716
plane surface layer, density profiles and pair correlation asymptotics *(Russian)* 80−88371
pool boiling, charact. curve 77−46887
pool boiling, nucleate and film, in sat. liq. 78−18854
pool heat transfer, in high centrifugal accel. field 77−15034
positronium and electron bubbles, density-functional theory 80−80016
pump, cryogenic, for long continuous running in particle accelerator *(French)* 78−32829
pump, design and construction, appl. in supercond. mag. system 77−45849
purifier for small laboratory liquefier 77−17990
radial distrib. functions and structural parameters 79−55640
Rayleigh-Benard expt., freq. locking and turbulence onset 79−90255
reciprocating circulation pump for withdrawal of liquid He from liquefier 79−58745
refrigeration cycle using two circuits, comparison with Claude cycle 77−17993
refrigerator, performance for different operational modes and flow impedances, 4.4 to 16K 79−58736
refrigerator/liquefier for CERN 400 GeV Super Proton Synchrotron 79−58737
rotating cryostat, design and tests 77−26309
short range order parameters, from information theory 78−83730
solid-liquid He, interface, Kapitza resist. and phonon scatt. 79−55983
solid-liquid He interface, tunnelling as mechanism of anomalous Kapitza resist. 79−55982
stability loss mode of charged He surface 77−20149
superconducting bolometer operation obs., high-speed superconducting bolometer appl. 80−57368
superconducting generator appl., aspects *(French)* 77−26304
superconducting magnet circulation cooling system based on He liquefaction apparatus 78−57992
superconducting magnet coolant, dielec. tracking 78−92022
superconducting magnet Large Coil Program, He liquefier-refrigerator and distrib. system 78−50398
superconducting magnet transfer lines, for cooldown or warmup 79−63234
superconductivity appl. in Czechoslovakia *(Croatian)* 77−28282
supercritical, dielec. breakdown 79−65796
supercritical, forced convective heat transfer meas. 77−27523
supercritical, heat transfer in turbulent tube flow 78−30287
supercritical, natural convection heat transfer 78−94694
supercritical, reciprocating pump for forced flow 78−41317
supercritical He, pool heat transfer, in high centrifugal accel. field 77−15034
supercritical He refrigerator, recovery time after thermal upset 77−17992
superfluid, flowing hydrodynamics of vortex generation 77−1272
superfluid, sealing via PTFE ring 78−4625
superfluid, universal relations among crit. amplitude, calc. up to order ϵ^2 for systems with continuous symm. 77−17936
superfluid film, very thick, electrohydrodynamic instability 79−51382
surface, 2D electron plasma, RF absorpt., parallel pumping *(Russian)* 78−22911
surface, collective excitation spectrum of electron Wigner cryst. *(Russian)* 77−47647

liquid helium continued
surface, collective excitations and electrodynamic behavior in three layer structure 78−60079
surface, cyclotron reson. of two-dimens. electrons *(Russian)* 80−88374
surface, electron gas struct. 79−65400
surface, electron liq., high freq. cond. electron correlation effects 80−107589
surface, electron-ripplon spectrum in mag. field normal to surface *(Russian)* 80−49444
surface, escape rate of two-dimensional electrons, around 1K 79−46856
surface, escape rate of two-dimensional electrons 79−28165
surface, hot electrons *(Russian)* 78−87832
surface, image-pot.-induced surface states, in strong elec. and mag. fields 78−946
surface, liquid-crystal transition in two dimensional electronic system 80−88303
surface, local disorder, for IR transmittance meas. 80−75395
surface, localised electron states 78−60007
surface, macroscopic electron lattice formation 79−77861
surface, parametric excitation of electrons *(Russian)* 79−37892
surface, parametric excitation of electrons in mag. field 79−51389
surface, quasi-one dimensional electron chain instability, string-zig zag transition *(Russian)* 80−65335
surface, two-dimens., electronic cryst., dynamic props. in strong mag. field *(Russian)* 80−92755
surface, two-dimens. Wigner cryst., electron-ripplon reson. anomalies *(Russian)* 80−92754
surface, two-dimensional electron gas, CDW 80−65476
surface, two-dimensional electron gas, cyclotron reson. 79−60566
surface electron high freq. cond., electron system heating, I-V charcts. *(Russian)* 80−29244
surface electron layer, parametric excitation of collective modes 77−15928
surface electron liquid, vel. autocorrel. time from spectral line broadening 77−20146
surface electron mobility, 0.02 to 1K 79−55985
surface electron states, two-dimens. cryst. form. 78−60006
surface electron system, liq. to cryst. phase transition *(Russian)* 80−6593
surface electrons over macroscopic periodic struct. *(Russian)* 79−10997
surface state electron lifetime, rel. with chemical potential of electron liquid 79−78028
surface tension, quick meas. method 78−43208
surface with trapped electron, parallel mag. field effect on interband transition 78−87835
thermodynamic and thermophysical props. calc. using HEPROP computer program 80−6529
time depend. effects above convection, Rayleigh-Benard expt. using local probe 79−7718
transient heat transfer, static coolant 78−75049
transient heat transfer, temp. meas. with μs response time 78−71270
two body potential, theory 79−69305
two-dimensional system, electronic props., conf. Berchtesgaden, Germany (Sept., 1977) 78−60177
two-phase mixture, circulation using jet pumps 80−82771
ultra cold neutron prod. rate in external liq. He source 78−70678
US subharmonic responses 80−33327
vapour formation and heat transfer in supercond. magnet cooling channels 79−32197
vertical plate, laminar natural convection heat transfer, supercritical CO_2 and He 80−64544
Wigner 2-dimensional lattice, on surface, reson. linewidths 79−86949
Wigner crystal on liq. surface, cond. *(Russian)* 80−6594
withdrawal, from liquefier 79−67306
H atoms on liquid He surface, interaction and bound states 79−18131
He at low temp., discharge voltage anal. 77−89341
He II film boiling, heat transfer prediction 80−33424
He II system for refrigerating Spacelab scanning IR telescope 79−54141
He:Xe, 0.04-0.1 g cm^{-3}, vac. UV absorpt. spectra, Wannier impurity states 77−77232
He-I, liquid, Taylor vortex instability in Couette flow 79−98683
He-I in capillary channels, forced convection boiling heat transfer 80−48707
^{4}He, liquid groundstate, pairing function, numerical calc. 79−4441
He(2^3S) bubble in liq. He, phenomenological model 77−20147
Si-liquid He interface, refl. of high frequency phonons, role of phonon focusing 77−80691

liquid helium-3
see also fermion systems; superfluid helium-3
acoustic impedance, transverse, Landau theory 78−51778
acoustic impedance, variational theory 79−42334
adsorbed layer on graphite, NMR relax. times below 4.2K 78−38898
adsorbed monolayers, dipolar anisotropy effects in spin relax 77−7940
adsorbed monolayers on Grafoil, NMR, low coverage 78−91503
adsorbed monolayers on solid Ne, desorption heat capacity 79−51383
adsorbed on Grafoil, ground state, thermodynamic anal. 79−19421
adsorbed on Grafoil, NMR relax. times 79−28171
adsorbed on graphite, mag. props., 2-D gas behaviour 78−47631
adsorbed on solid Ne, desorption heat capacity 79−4452
adsorbed on superfluid ^{4}He surface, ripplons and heat conduction meas. 80−49459
binding energy, variational calcs. by Pandharipande's method 80−101752
binding energy and effective interactions, variational calcs. 80−107596
binding energy calcs., Pandharipande method 79−65269
Born-Green-Yvon eqns. for strongly interacting Fermi systems 79−71363
capillary confinement for refrigeration and liquid control in zero gravity 78−43198
Chakravarty-Woo eqn., extension and appl. to liq. ^{4}He, liq. ^{3}He, and nucl. matter 80−68124
collective quantum fields for many body systems, appl. to BCS, ^{3}He and type II superconductors *(German)* 79−35917
conference on many-body theories, Trieste, Italy (Oct. 1978) 80−22135
confined in Al_2O_3 and Pt powders and Grafoil, NMR expts. 79−51371
continuous flow cryostat, for polarised targets 80−52240
cooling by double bundle nucl. demagnetisation refrigerator atom to 0.4 mK 79−49236
critical fluid, ratio of sound dispersion to attenuation 79−55826
cryostat with automatically refilled condensation stage 77−17996
cryostats for different refrigerating capacities 79−58749

liquid helium-3 continued
density, of normal fluid, 2-29 bar 79−82408
density matrix, one-body, and momentum distrib. calc. for ground state 77−85008
density matrix and spin-depend. correlations 79−73369
dielectric constant, static, near liq.-vapour crit. point 78−56016
diffusive heat flow and sum rules in the hydrodynamic limit 78−56012
dilution refrigerator, ^{3}He circulating, with more than one mixing chamber 77−30153
dilution refrigerator, multiple mixing chamber 80−37042
dilution refrigerator, with two mixing chambers 77−61073
dynamic form factor, particle density, spin density correlation, RPA calcs. 79−46873
dynamic properties, neutron scatt. studies, review 79−50972
dynamic structure function, in impulse approx. 77−7934
dynamical structure factor and elementary excitations 79−33142
electron and positronium bubbles, density profiles 79−55952
electron escape from image-potential-induced surface states 80−49440
electron spectra of localised electrons above surface *(Russian)* 80−29241
electron surface barrier, density depend. determ. 77−1270
electrostatic image force depend. on spatial dispersion, energy spectrum *(Russian)* 80−107593
elementary excitation, neutron scatt. study 79−46874
elementary excitations, density and spin density, zero sound mode, press. depend. RPA model calcs. 80−59749
elementary excitations, RPA model using extended Landau theory 78−14527
energy expectation value, test of Wu-Feenberg and F_2 approximations 79−40873
EPR of negative ions, antiferromagnetic transition possibility *(Russian)* 80−15322
equation of state and crit. exponents near liq.-vapour crit. point 80−24707
equations of state, 3.3 to 14K *(Russian)* 78−83912
exact Green function eqns., extraordinary phases 77−47642
exchange model, antiferromagnetic exchange field, susceptibility-specific heat ratio *(French)* 80−80019
exchange model 80−88387
extended Fermi-hypernetted chain scheme, Landau parameters calc., transport coeffs., Jastrow theory 77−41529
Fermi quantum crystals, melting curves low temp. anomalies rel. to neutron stars 78−24757
fermion hypernetted chain approx., optimal correlation functions 80−24822
fermions, constrained variation in Jastrow method at high density, neutron system, liquid ^{3}He appls. 77−5753
ferromagnetism, surface induced 78−79844
film, adsorbed on graphite, nucl. mag. susceptibility below 4.2K 77−20155
film, multilayer adsorbed, in restricted geometries, book contrib. 79−99391
film, ordered, finite size effect, crit. parameters and three-state Potts model 77−31836
film, submonolayer and multilayer, adsorbed on Grafoil, pulsed NMR study 80−49456
first sound attenuation under press. *(Russian)* 80−10730
fluctuation contribution to sound vel. and damping above superfluid transition temp. 80−15324
free surface, book contrib. 80−2231
free-surface density profile and tension 79−33147
ground state, Fermi-hypernetted chain methods, convergence props. 78−16727
ground state and low excited states, book contrib. 79−60564
ground state energy of fermion liquid 77−85010
ground state in Kirkwood superposition approx. 77−15650
ground state of polarised and unpolarised fluid, Monte Carlo calcs. 80−92748
ground-state properties, variational method using Fermi hypernetted-chain approach 77−35781
group theoretical interpretation of phases, gauge field topology *(Russian)* 77−37786
heat capacity anomalous near transition, 0.8-20 mK 80−15326
hydrodynamic modes, macroscopic dispersion relations, two fluid model 78−10242
hydrodynamic modes, microscopic dispersion relations, transport coeffs. 78−10243
hyperfine enhanced nuclear cooling using $PrNi_5$ powder, demagnetisation expt. 79−44909
inelastic neutron scatt. under pressure, zero sound mode nature 79−55998
inhomogeneous many-body system integral equations 80−22732
interface with Ag, thermal boundary resist. from 0.4 to 10 mK 79−56000
interface with antiferromagnet, anomalous thermal behaviour and nucl. spin relax. 79−56002
interface with $Ce_2Mg_3(NO_3)_{12}.24H_2O$, Kapitza resistance around the mK, effect of ^{4}He impurity 79−55999
interface with $LiF:Mg^{2+}$, dislocation struct. of deformed crysts. 79−69112
interface with nonmagnetic solid, Kapitza resist., quantum perturbation treatment 80−88385
interface with sapphire, heat transfer at very low temp. 79−56003
ion injection, optimal positioning of field emitters 80−24700
ion mobilities in normal and superfluid phases 79−65280
ion mobility, temp. and freq. depend. 80−70493
ion mobility 78−51773
ion motion in normal and superfluid states 77−66054
Kapitza conductance of Cu sinter in contact, heat flow model calc. 80−10728
Kapitza resistance, anomaly near Neel temp. of $Cu(NH_3)_4SO_4.H_2O$ 77−69139
Kapitza resistance, size effect 77−62698
Kapitza resistance at magnetic salt boundary *(Japanese)* 78−51780
Kapitza resistance of $Ce_2Mg_3(NO_3)_{12}.24H_2O$/He system, appraisal of expt. results 79−51414
Kapitza resistance of interfaces with Pb, Cu, Al and Ni, 0.3-1.4K 77−24475
Kapitza thermal resistance and tunnelling states of atoms, theory 77−85046
kinetic theory of normal Fermi liquids 78−87841

liquid helium-3 continued
Landau Fermi liquid theory and low temp. props., book contrib. 79−99386
light scattering, review of expts. 80−54454
localised electron states, cyclotron reson. above surface *(Russian)* 80−6587
long-range order Hartree-Fock states with different magnetic properties 79−42476
longitudinal zero-sound dispersion, thermal cond., and Landau F_2 78−2327
low and ultralow temp. cryogenic coolers for space missions 80−77790
low temperature props., review 79−37896
magnetic Kapitza cond. calc. for ^{3}He/ordered Heisenberg ferromagnet system 79−51415
magnetic susceptibility in Grafoil at ultralow temp. 78−79843
magnetically polarised state, prep. and obs. 79−46870
melting, specific heat, entropy, latent heat 78−75904
melting curve shifts due to pore condensation 80−54469
melting pressure temperature scale 77−22557
microdroplets momentum transfer in collisions with Xe and CO_2 beams 79−50113
momentum distrib., Fermi-hypernetted-chain theory 80−82716
momentum distribution, theoretical 78−51776
monolayer, quantum tunnelling, NMR linewidth 77−39720
monolayer, sp. ht., low-density phase modification produced by substrate changes 77−76642
monolayer adsorbed on Grafoil, phase determ. by sp. ht. meas. 77−11764
monolayer systems, book contrib. 79−99390
Monte Carlo simulation of many-fermion system 78−12644
nearly ferromagnetic Fermi systems, temp. depend. of spin susceptibility 79−8008
negative ion mobility 79−55996
negative ion motion in normal and superfluid phases 78−38900
negative ion structure in normal liq. phase 79−86953
negative ionic mobility, absence of non-linearity at low temp. 79−28167
negative ions, ESR obs. 79−60582
neutron inelastic scatt. studies of elementary excitations 79−65275
neutron inelastic scattering, zero sound and spin-fluctuation peaks 78−79836
neutron scatt. meas. 79−46860
neutron scattering, book contrib. 80−2230
neutron scattering, dynamical form factor, RPA calc. 77−7938
neutron scattering, inelastic, 0.7K, 10 and 20 bars, wavevector transfers 78−71899
NMR and ion mobility experiments 78−91505
NMR detection with SQUID 79−67368
nonlinear positive ionic motion in normal phase, equiv. of temp. and vel. depend. 79−86952
nonlocality in ^{3}He-^{3}He interatomic potls. 77−26593
normal, dynamical structure factor and elementary excitations 79−99384
normal and superfluid, acoustic props. 79−46875
nuclear refrigeration by Cu adiabatic demagnetisation 79−67315
nuclear spin relax. in confined geometries 79−51372
nuclear spin relaxation normal ^{3}He in contact with mag. substrate 78−43200
optimised Jastrow correlations for Fermi liquids 80−32223
ordered ferromagnet interface magnetic Kapitza conductance, surface spin wave effects 79−99406
overdamped modes and transport 78−56011
pair condensation, variational theory using correlated basis functions 80−32220
paramagnon exchange and quasiparticle interaction 79−95231
phase diagram, press. and mag. temp. coordinates meas. 79−30469
pionic ^{3}He liquid, X-ray energies, Lorentzian widths, relative intensities 78−46470
Poisson brackets, nonlinear hydrodynamics eqns. in condensed matter physics 80−54296
polarisation effect on mag. ordering, melting curve 80−80021
polarisation potentials, viscosity, thermal cond., spin diffusion 80−88389
polarisation potentials and elementary excitations 78−91502
portable ^{3}He cryostat for space appls. 77−22077
positive ion mobility 78−10244
positive ion mobility 78−22923
positive ion mobility in normal and superfluid phases 79−4449
positive ion mobility meas. 79−55995
positive ion nonlinear behaviour, expt. and parameterless theoretical prediction comparison 79−14978
positive ionic mobility, press. and temp. depend. 78−91504
positive ionic mobility of normal phase, 3-100 mK 78−18863
pressure cell for neutron scatt. 78−14246
radial distribution function for hard-sphere fermions, zero and finite temps. 78−14530
rotons and solidons 79−95228
shear viscosity and thermal cond., s- and p-wave approx. 79−1535
significant structure theory, thermodynamic props. 78−51774
simple quantum liquids, Jastrow variational wave functions, for nuclear matter, liquid ^{3}He and ^{4}He 80−22729
sound propag. at elevated densities, 0.35 to 1.4K *(Russian)* 80−92741
sound propagation, transition from first sound to zero sound 77−89609
spin fluctuation peak obs. by inelastic neutron scatt. 80−49447
spin polarisation, rapid melting of polarised solid 79−46872
spin polarised, quantum fluid *(French)* 79−46862
spin polarised, thermodynamical nuclear orientation 79−46879
spin relaxation to paramagnetic centres, in surfaces at very low temps. 79−33552
spin-zero-sound solns. of the quasi-particle Boltzmann equation 79−77856
SQUID NMR techniques, appl. to liquid ^{3}He 79−26093
strongly polarised, from rapid melting of polarised solid 80−70495
superfluid transition temp. calcs. 80−103530
surface, cyclotron resonance of localised electrons above surface *(Russian)* 78−14533
surface energy calc. 77−85011
surface ferromagnetic instability, attraction to solid substrate 79−46863
surface ferromagnetic instability, reinforcement due to attraction between ^{3}He and wall 79−51373
surface ferromagnetism, possibility in confined geometries 77−69137
surface fluctuation influence on free energy, surface tension *(Russian)* 80−92746
surface induced ferromagnetism, pulsed NMR expts. on ^{3}He admixed with C particles 79−51362
surface magnetism, in contact with dielec. surface, thermodynamics 80−54460
surface tension, density profile, variational calcs. 78−67882
surface tension, quasiparticle theory for normal liq. 79−56012
surface tension and density profile at 0K 79−55997
surface tension in ground state, variational calc. 77−7935
susceptibility measurement, by double bundle nuclear demagnetisation refrigerator 78−93692
target for scatt. expts. 78−70663
thermal conductivity, boundary resistance at low temp., heat flow model calc. 80−10120
thermal conductivity at very low temps., press. depend. 80−92742
thermal contact with Pd sinter down to 0.4 mK, anomalous Kapitza boundary conductance 79−69312
thermodynamics below Debye temp., thermal capacity temp. depend. *(Russian)* 79−10999
transverse acoustic impedance meas., 0.015-1.0K 77−59167
triple point, 180° rule violation criteria, thermodynamic stability 77−7841
US dispersion and attenuation near liq.-gas crit. point 78−38897
variational calculations for liquid ^{3}He, Jastrow-type methods 79−77854
variational wave function 79−77855
viscosity coefficient, T-approx. *(Russian)* 79−21655
viscosity of normal and superfluid phases 79−51357
zero sound *(Russian)* 79−95240
zero sound lifetime, neutron inelastic scatt. study 80−65329
zero sound suppression by mag. field *(Russian)* 78−59995
zero sound with velocity less than Fermi velocity *(Russian)* 80−92747
π^3He, liquid, K X-ray transition energies and Lorentzian widths 80−78727
$Ce_xLa_{2-x}Mg_3(NO_3)_{12}.24H_2O$, magnetically diluted thermometer for sp. ht. meas. 79−17420
^{3}He/solid interface, refl. of transverse zero sound *(Russian)* 80−70492
interface with $CuK_2(SO_4)_2.6H_2O$, thermal boundary resist. from 8.5 to 110 mK 79−56001
Si-^{3}He interface, phonon reflection 78−84043

liquid helium 3-4 mixtures
^{3}He bound states on ion bubbles in liq. ^{4}He 78−2329
acoustic modes in superleak waveguide filled with superfluid ^{3}He-^{4}He soln. *(Russian)* 79−90842
adiabatic demagnetisation of ^{3}He in ^{4}He *(Dutch)* 77−61072
adsorbed film, systematic exptl. study 80−107603
Benard instability and thermal meas. above and below T_λ 79−56009
Benard instability near λ-temperature 80−34268
bound impurity pair effect on surface tension *(Russian)* 80−65332
capillary waves and second sound, mag. excitation 79−60594
characteristics, theory in mag. field *(Russian)* 78−59999
charged interface, ripplon softening 80−34269
concentrated, ^{3}He spin diffusion expts. 78−34671
concentration susceptibility near superfluid transition 78−18865
concentration susceptibility near superfluid transition 79−56006
convection in dil. solns. of ^{3}He superfluid ^{4}He 80−107600
critical and tricritical dynamics, renormalisation group calc. 80−29239
critical and tricritical exponents from light scatt. data 77−20152
critical dynamics, diffusion const. and thermal cond. along λ line 77−47644
density matrix, hydrodynamic eqns. of ^{3}He-superfluid ^{4}He mixture 77−35790
differential osmotic press. meas. of conc. suscept. near lambda curve and tricritical point 79−73371
dilute, ^{3}He atoms in superfluid ^{4}He, ground state props., variational calc. 79−73372
dilute, ^{3}He excitations, calc. 79−7730
dilute, absorpt. and scatt. expts. 77−20153
dilute, ballistic phonons, transition to second sound 78−10249
dilute, nucleation and stratification induced by press. at low temp. *(Russian)* 78−34672
dilute, number density calc. 78−43205
dilute, second sound vel. and absorpt. 77−20154
dilute, second sound velocity 78−63898
dilute ^{3}He-^{4}He mixtures, ^{3}He superfluidity 79−19420
dilute solution, ^{3}He excitation spectrum at zero temp. 79−60592
dilute solution, grand partition function ground state energy determ., ^{3}He conc. depend. 80−49455
dilute solution, mag. susceptiblity 77−7939
dilute solution, second-sound damping meas. 79−73370
dilute solution, sp. ht., ^{3}He quasiparticle excitation spectrum 78−71901
dilute solutions, dielec. model of roton interactions 78−55998
dilution refrigeration system, choice of tube lengths and diameters 80−57308
dilution refrigerator, condensation stage 77−45852
dilution refrigerator, manipulation of sample in mixing chamber 78−41318
dilution refrigerator, mixing chamber for single cycle expts. 78−41315
dilution refrigerator, process anal. 79−93150
dilution refrigerator, with superfluid ^{4}He circulation 80−57304
dilution refrigerator without pumped ^{4}He bath 77−45853
dilution refrigerators, ^{3}He circulation cycle with continuous heat exchangers, 2 mK production 79−67313
dynamic behaviour, appl. of holographic interferometry technique 78−51781
entropy of transfer for 6.4% soln. 79−56013
equation of state and crit. exponents near liq.-vapour crit. point 80−24707
equimolar mixture, excess volumes *(Russian)* 80−39380
evaporation and condensation meas., weak coupling model anal. 79−51366
evaporation and condensation mech. 79−65283
evaporation and condensation mechanism 79−77858
excess molar volume, temp. depend., 1.5-14K *(Russian)* 77−62700
excitation spectrum, exptl. studies using neutron inelastic scatt. 77−59170
excitation spectrum, neutron inelastic scatt. study 79−46877
excitation spectrum and quasiparticle interactions, perturbation theory 78−10250
excitations, review 78−60000
film, many body approaches to liquid-vapour transition 78−51783

liquid helium 3-4 mixtures continued
film, superfluidity precipitous onset 79−23802
film, thermodynamic theory 77−4238
film, third sound meas. using TOF techniques 79−51381
film, tricritical behaviour in vicinity of walls 79−51387
film superfluidity and phase separation 79−77857
films, 2-D interface excitation spectrum 80−96718
films, thickness calc. from dielec. const. data *(Russian)* 79−11003
first and second sound interaction, hydrodynamic approx. *(Russian)* 77−69142
free surface, book contrib. 80−2231
ground state configuration of isotopic mixture, theory 80−107601
heat of transport, anomalous cooling power of dilution refrigerators 80−37045
heat transfer between Ce salts and dilute ^{3}He below 50 mK 79−51413
heat transfer with solids below 100 mK 80−24701
holographic obs. of diffusion waves 79−60595
homogeneous phase separation obs. 80−107599
interface, charge induced ripplon softening and dimple crystallisation 79−28170
interfacial tension near tricrit. point 78−2330
interfacial tension near tricritical point 77−69141
interfacial tension of phase separated mixtures under press., 0.3-0.7K 79−51367
ion trapping at crit. interface 79−65285
ion trapping at tricritical point, depend. on temp. and elec. field 79−7729
Kapitza resistance at Au interface, dynamic meas. 79−28188
Kapitza resistance of $Ce_2Mg_3(NO_3)_{12}.24H_2O$/He system, appraisal of expt. results 79−51414
kinetic coefficients, thermodynamic props., hydrodynamic, acoustic and spin wave propag. *(Russian)* 78−18867
light scattering, review of expts. 80−54454
low and ultralow temp. cryogenic coolers for space missions 80−77790
mass diffusion coeff. meas., 0.55-1.05K 78−47630
mobility of ions trapped on vortex lines 77−7919
molar volume meas. at pressures up to 100 atm., 1.5-4.2K *(Russian)* 77−35785
multiple positive ionic mobility, in normal ^{3}He contaminated with ^{4}He 79−46876
neutron inelastic scatt. studies of elementary excitations 79−65275
neutron scattering, book contrib. 80−2230
NMR and ion mobility experiments 78−91505
normal solution, size effect influence on capillary mass transport *(Russian)* 80−70497
nuclear relaxation of polarised ^{3}He diluted by liquid ^{4}He at 4K in low mag. fields 79−51365
nuclear spin relaxation, anomalous, near lambda transition 80−54463
nuclear spin relaxation, anomalous 78−79849
nucleation of superfluidity and phase separation 78−43204
osmotic and mag. props., review *(French)* 80−10733
osmotic pressure along phase separation curve 77−89613
osmotic response function near tricrit. point, meas. method 78−2331
periodic inhomogeneities, excitation in external mag. field parallel to temp. gradient 80−88392
phase changes near absolute zero, holographic interferometry 78−38905
phase diagram and conc. susceptibility near tricritical pt. 79−56005
phonon velocity in dilute solns. 79−23803
positive ion mobility, wetting-nonwetting transition analogy 80−103532
positive ion mobility 78−10244
positive ion mobility in dil. soln. of ^{4}He in ^{3}He 79−33151
positive ion mobility in normal liq. ^{3}He, effect of ^{4}He 79−60589
positive ion structure in ^{3}He rich mixture, ^{4}He halo around ion 78−18864
positive ions in ^{3}He rich liq. He, shell model 79−56007
preferential adsorption of ^{4}He onto Vycor glass 78−84023
pressure release superleak sound modes, U-tube sound 80−54453
quantised vortex lines and lifetime of negative ions trapped by vortices 78−84022
quantum solutions, separation of opposite charges, dipole complex form. *(Russian)* 80−6588
quantum statistics, hard sphere model 77−89614
rotating solution, vibrating disc meas. *(Russian)* 77−24464
second sound, quantised vortex creation at constrictions, excitation model 80−44383
second sound absorpt. and vel., phonon-^{3}He interactions 77−31835
singular surfaces theory and sound propag. 77−47643
sound attenuation, crit., HF, near T_λ 79−95241
sound propag. near superfluid transition and tricritical point 79−65284
sound propagation near superfluid transition 78−79848
specific heat at λ transition, universality 78−51782
specific heat meas. near λ transition, universality test of α and α' 79−51364
spin diffusion in tricritical region along coexistence curve 77−15654
spin diffusion under press. 78−56018
spin waves and zero sound possibility, ^{3}He in superfluid ^{4}He degenerate solution *(Russian)* 77−35789
stability and stratification of quantum liq. mixture 80−59754
structure factor determ. 79−60591
superfluid, ^{3}He supercritical states contrib. to thermodynamics *(Russian)* 79−65282
superfluid, early stages of spinodal decomposition, calc. 80−20004
superfluid, fifth sound mode 80−75398
superfluid, normal density at elevated press. *(Russian)* 79−90841
superfluid, roton spectrum, calc. *(Russian)* 77−4240
superfluid, second sound attenuation and dissipation processes, 1.3-2.0K *(Russian)* 79−42335
superfluid, second sound velocity, influence of spin 77−80676
superfluid, Tomonaga model, 3-D analogue *(Russian)* 78−71900
superfluid ^{3}He, in ^{3}He superfluid ^{4}He solns., mag. phases 80−59755
superfluid ^{3}He-^{4}He mixtures, two-phase sound 79−86958
superfluid ^{4}He-^{3}He solns., second sound vel. and absorpt. 79−56008
superfluid film, adsorbed on Vycor substrate, superfluid mass and transition temp. 79−51385
superfluid fraction, density near λ point, oscillating disc method 77−43404
superfluid He II, pulsed NMR investig. of ^{3}He flow vel. 77−59171
superfluid injection dilution refrigerator, process anal. 79−97394
superfluid phase transition, universality and scaling laws 77−11763
superfluid phase transitions at container walls 79−56014
superfluid solution, dil., low temp. props., book contrib. 80−15330
liquid helium 3-4 mixtures continued
superfluid solution, second sound velocities *(Russian)* 79−33150
superfluid solution, sound vibrations in narrow channels *(Russian)* 78−79851
superfluid solutions, nonlinear sound interaction 80−34267
superfluid thin film, third sound vel. calc. 80−107602
superfluid transition nucleation, coherence length effects 77−66069
superfluid transition onset props. 77−35786
superfluid transition temp., Green's function calc. method 77−72735
superfluid-^{3}He, dil. soln., ^{3}He quasiparticle interaction, conc. depend. 77−15655
surface tension, quasiparticle theory for normal dil. soln. of ^{4}He and in ^{3}He 79−56012
thermal conductivity on λ line, conc. depend. for low ^{3}He conc. 77−51567
thermal diffusion ratio near λ transition, onset of heat flush 77−35787
thermal transport coeffs. near lambda line 78−22926
thermal transport near lambda line 79−56004
thermal transport near tricrit. point 79−51363
thermal transport properties near and below superfluid transition 79−60590
third and fourth sound, Doppler shift 78−56017
transport properties, near superfluid transition and tricritical point 80−29242
tri-critical phenomena, Callan Symanzik study of $\lambda\phi_3{}^4+g\phi_3{}^6$ theory 77−35788
tricritical crossover exponent 77−4239
tricritical dynamics and λ-line behaviour, model 77−39719
tricritical mixture universality under press. 80−103533
tricritical normal phase, ion mobility 78−79850
tricritical point, thermal conc. gradients, thermal diffusion ratio 77−76640
two-dimensional mixtures, phase diagram of dil. classical X-Y model 79−60593
US propagation near tricritical point 77−59169
viscosity behaviour props. *(Russian)* 80−44382
weak bound state for ^{3}He quasiparticles in dil. ^{3}He-He II mixtures 78−22925
He II-^{3}He, ^{3}He diffusion coeff., order parameter relax., second sound 78−30808
He II-^{3}He, roton lifetime from neutron inelastic scatt. meas., 1.27-2.15K 79−56011
He II-^{3}He dilute mixture, ^{3}He phase transition 77−80677
He II-^{3}He dilute mixtures, scatt. function S_{33} (q,ω) 79−56010
He II-^{3}He solns., in strong mag. field *(Russian)* 78−18866
^{3}He bound state, surface pot., heats of vaporisation 77−1274
^{3}He, quasi particles in superfluid ^{4}He, dispersion law, under pressure *(Russian)* 79−42336
^{3}He quasiparticle excitation spectrum and second sound vel. meas., dil. soln. of ^{3}He in superfluid ^{4}He 80−24708
^{3}He, two-dimensional, in ^{4}He film, sp. ht. meas. 80−39382
^{3}He-^{4}He, superfluid, spin waves *(Russian)* 79−95240
^{3}He-^{4}He film, adsorbed on graphite, nucl. mag. susceptibility below 4.2K 77−20155
^{3}He-^{4}He mixture films, unsaturated, third sound and decay of persistent currents obs. 80−75402
^{3}He-^{4}He mixtures, rotating, ion trapping on vortex lines 79−28169
^{3}He-He II dilute solution, fourth sound velocity 80−70498
^{3}He-He II soln., magnetokinetic effects 79−19419
^{4}He effective interaction in dilute ^{3}He soln., low temp. 80−10734
^{4}He impurity at. and ion interaction and mobility, in solid or liq. *(Russian)* 78−18868
^{4}He-^{3}He, fifth sound 79−60569

liquid helium-4
see also boson systems; superfluid helium-4
λ-transition, renormalisation-group theory 80−143
acoustic impedance meas. by acoustic surface waves 79−77848
adsorbed film, density profile 78−10252
adsorbed monolayer struct., neutron scatt. 77−7942
adsorption cryostats, high cooling power, temp. below 0.7K 77−17995
anharmonic effects in US propagation near λ transition 80−96707
atomic scattering at free surface 78−56003
atomic trimer formation, threshold condition 80−63741
binary boson mixtures, thermodynamics ground state 79−35630
binding energy, variational calcs. by Pandharipande's method 80−101752
binding energy calcs., Pandharipande method 79−65269
binding energy of ^{3}He atom near surface 79−77853
boil-off reduction for cryostats and cryopumps 77−30157
boiling, heat transfer crises 79−94466
Bose condensate density temp. depend., rel. to supercond. *(Russian)* 79−33140
Bose-Einstein condensate near lambda point 77−15645
boundary resistance at low temp., heat flow model calc. 80−10120
Chakravarty-Woo eqn., extension and appl. to liq. ^{4}He, liq. ^{3}He, and nucl. matter 80−68124
condensate fraction, low temp. and density calcs. 78−43196
condensation, momentum, correlation function 80−46966
condensed phase, long-range order of one- and two-body density matrices 80−10726
conference on many-body theories, Trieste, Italy (Oct. 1978) 80−22135
cooling to 0.43K 78−16802
correlation function, variational calcs., hard-sphere, Coulomb, ^{4}He, nucl. Yukawa fluids 77−76638
corresponding states, quantum, mech. law 79−55945
Coulomb gas, 2-dimens., dissociation at low temp. 77−31748
coupled field theory, classical perturbation theory appl. 78−57799
critical and tricritical dynamics, renormalisation group calc. 80−29239
critical attenuation of sound in restricted geometries meas. 80−29235
critical dynamics and fluctuation-dissipation theorem 79−40467
critical thermal cond. near λ-point, light scatt. spectrum 80−24697
cryostat, miniature continuously filled 78−41316
cryostat design for supercond. tunnelling study *(Spanish)* 80−73347
crystallisation wave detection, solid-liquid boundary oscillation spectra *(Russian)* 79−90844
cyclotron reson. of hot electrons 80−88377
density correlation function calc. near T_λ in symmetric planar-spin model 77−4232
density matrix, one-body, and momentum distrib. calc. for ground state 77−85008

liquid helium-4 continued
dielectric breakdown across epoxy insulation 78−62658
dielectric constant meas. 77−20143
dimple lattice of electrons on surface, struct. 79−99380
distribution functions within hypernetted-chain approx. 80−24696
droplet, charged, in ^{4}He vap., He^+ mobility, 1.3-2.0K 79−32734
droplets, surface energy, tension, thickness 78−84015
dynamic scaling, possible breakdown at lambda point 78−91498
dynamic scaling deviation 77−31820
dynamic scaling near lambda point 80−15321
dynamic scaling near T_λ 80−34264
dynamic structure, neutron diffr. determ. 77−11749
dynamic structure factor, 2.5K, inelastic neutron scatt. study 79−55647
dynamic structure factor, neutron scatt. meas. 79−46545
dynamic structure factor function, surface contrib. 77−47634
effective pair potential, 4.2K, from inelastic neutron scatt. data 79−50980
electron effective mass localised above liq. ^{4}He surface, cyclotron reson. meas. *(Russian)* 77−11756
electron mobility at surface, 1.17-2.7K 77−39712
electron surface barrier, density depend. determ. 77−1270
electrostatic image force depend. on spatial dispersion, energy spectrum *(Russian)* 80−107593
energy density fluctuation, at fixed wavevector, max. below T_c 79−69225
equations of state, 3.3 to 14K *(Russian)* 78−83912
excitation spectrum, exchange effects 78−10236
excitations produced by impinging ^{4}He atomic beam 78−10241
excited states, variational calcs. 80−80017
film, adsorbed on graphite substrate, layering and thermal cond., heat capacity and vapour press. meas. 79−51386
film, energy spectrum and specific heat, superfluidity 77−15656
film, hypernetted chain generalised eqn. optimal solns. 80−75396
film, ordered, finite size effect, crit. parameters and three-state Potts model 77−31836
film, saturated superfluid, on rough surfaces, persistent currents in presence of third-sound reson. 77−20156
film, superfluid, third sound attenuation, 0.1-200 Hz 77−20159
film adsorbed on graphite, transition temp., entropies, internal energies and heats of desorption 80−2238
film on solid H, film transfer velocity, Van der Waals interaction *(Russian)* 80−54465
first sound nonlinear wave distrib. *(Russian)* 80−107588
flow boiling in vertical channels, visualisation 77−42938
form factors, inelastic neutron scatt., observability of Beliaev terms 78−51764
fourth order structure and Raman scattering 79−56801
free convection at supercritical pressures 78−26745
free surface, binding energy of spin-polarised H atom 80−34277
free surface, crit. behaviour near λ point 80−2228
freezing, density and entropy, 0.1 to 0.82K 77−7925
Galilean presymmetry and quantisation of circulation 77−35772
ground and low excited state struct., pair-pair correlation function 80−24694
ground state, self consistent description of long- and short-range correlations 80−107592
ground state, self-consistent description of long-range and short-range correlations 80−70491
ground state, wavefunctions 80−10724
ground state and low excited states, book contrib. 79−60564
ground state condensate fraction 77−20145
ground state energy, analytical treatment of hypernetted-chain and Percus-Yevick eqns. 79−30359
ground state from HNC and BBGKY eqns., elementary diagram effects 80−24693
ground state in Kirkwood superposition approx. 77−15650
ground-state energy, perturbation corrections 77−7918
heat capacity of liquids and dense gases at low temps. *(Russian)* 80−65324
heat transfer for nucleate pool boiling, crit. heat flux 77−31823
heat transfer in narrow cooling channel below 4.2K 77−30170
heat transport and critical slowing down near Rayleigh-Benard instability in cylindrical containers 77−84253
HF crit. attenuation, 0.55-1.7 GHz 79−55958
HF sound scatt. near λ-transition *(Russian)* 77−59165
hydrodynamic theory, variational methods 79−42331
image-potential-induced surface states, broadening of inter-subband transitions 78−43194
impulse approx. inadequacy for hard core potl. 77−15646
impurities, surface bound states, quantum and classical liquids 78−18859
inhomogeneous many-body system integral equations 80−22732
integrated polarised Raman scatt. intensity calcs., Jastrow ground state 80−50342
interacting phonon beams, freq. up-conversion 79−55975
interface with Bi, transient heat transfer 77−85123
interface with $LiF:Mg^{2+}$, dislocation struct. of deformed crysts. 79−69112
interface with NaF, phonon propagation 78−14526
interface with NaF, phonon reflection 79−55979
interface with NaF, phonon transmission in both directions 79−28164
interface with solid, phonon transmission and Kapitza resist. 79−65271
interface with solid ^{4}He, phonon transmission using heat pulse technique 79−56035
interface with superfluid ^{4}He, temp. jumps across phase boundary 79−51334
ion injection, optimal positioning of field emitters 80−24700
irreducible cluster expansion for the logarithm of the s-particle density matrix of a many-boson system 79−21657
isotopic purification 77−35769
Jastrow wave function optimisation 79−7719
Kapitza conductance, meas. using supercond. current comparator, appl. to Evanohm 77−41645
Kapitza heat-transfer model, liq. ^{4}He-solid interface 80−107591
Kapitza resistance between solid and liquid ^{4}He, macroscopic calc. 77−11754
Kapitza resistance of interfaces with Pb, Cu, Al and Ni, 0.3-1.4K 77−24475
Kaptiza resistance meas. using transient temp. response 77−59164
kinetic energy per atom, struct. factor anal. from neutron scatt. data 77−69126
lamba transition free energy in Feynman's model *(French)* 78−71895

liquid helium-4 continued
lambda point, light scatt. props., static and dynamic scaling phenomena 80−92739
lambda transition, microscopic theory, thermodynamic potential 79−73365
lambda-tight In rings, simple demountable device for fixing 77−30160
Lennard-Jones model at 0K, props. using Monte Carlo method 79−82401
light scattering, near T_λ 80−29238
light scattering, review of expts. 80−54454
liquid-solid boundary, capillary sound motion, Kapitza resistance *(Russian)* 80−92737
localised electron states, cyclotron reson. above surface *(Russian)* 80−6587
localised ion states, effective mass, binding energy, surface displacement 80−84333
long range order, extended boson matter density matrices 80−22731
magnetic field-induced temperature changes 78−57960
melting kinetics, sound transmission at liq.-solid interface 80−92734
microdroplets momentum transfer in collisions with Xe and CO_2 beams 79−50113
mobility of ions trapped on vortex lines 77−7919
monolayer, multicritical behaviour from triangular lattice gas model 77−74328
monolayer, solidification, theory 77−20158
monolayer, triangular Ising model, phase diagram 78−10631
monolayer adsorbed on Grafoil, phase determ. by sp. ht. meas. 77−11764
monolayer systems, book contrib. 79−99390
neutral excitation current above 1K 79−86940
neutron scattering dynamic struct. factor, saturated vap. press. 78−42878
neutron scattering study in low momentum transfer region 79−46546
nuclear target with remote handling for TRIUMF cyclotron 78−25364
nucleate boiling crisis in supercond. magnet cooling channels 79−32196
nucleation of freezing by positive ions 77−84893
order parameter relax. near T_λ, HF first sound meas. 79−55960
pair distribution function in composite boson approach, exclusion principle effect 77−11753
paired phonon model at low temp., condensate fraction 80−80018
pairing energy 78−2323
phase transitions, positive and negative ion mobilities meas. 78−87833
phonon dispersion curve from entropy meas. down to 0.75K 77−7922
phonon dispersion relation, low-momentum, press. depend., US velocity meas. 77−47635
phonon dispersion relation, thermal expansion meas. 77−7924
phonon excitation, long-wavelength, series expansion 80−88372
phonon temp. depend. above and below T_λ, neutron scatt. meas. 79−55973
phonon-phonon interactions, review 77−55410
Poisson brackets, nonlinear hydrodynamics eqns. in condensed matter physics 80−54296
positive impurity ion struct., modified theory 77−39714
positive ion mobility, with large He I halos 77−43400
positive ions, struct. 79−4440
positron self-trapping 77−62697
pulsed perturbation relaxation, intense short heat pulse passage, compression wave propagation *(Russian)* 79−82400
purity, upper limit for conc. of potential dissolved contaminants 80−39373
quartz-liquid ^{4}He interface, saturation effects in phonon reflection 80−92736
quasiparticle model, finite temp. 77−39715
Rayleigh linewidth meas. 78−14522
Rayleigh-Benard experiment *(French)* 80−80013
rotating, second sound attenuation in presence of const. supercritical heat flow *(Russian)* 77−55409
second and third virial coeffs., meas. from 2.6 to 27.1K 79−37808
second layer film on graphite, liquefaction 78−47632
second sound, quantised vortex creation at constrictions, excitation model 80−44383
short range order parameter 78−83712
simple quantum liquids, Jastrow variational wave functions, for nuclear matter, liquid ^{3}He and ^{4}He 80−22729
single particle occupation probability and one body density matrix, of quantum fluids 77−4233
solid-liquid interface mobility under 1 MHz sound wave *(French)* 80−100373
solidification at room temp. under high press. 79−82413
solvent effect on $(^4He)_2$, $(^3He)_2$ dimers and ^{3}He-^{4}He mixture 79−41120
sound velocity in dense hard sphere Bose liq. 79−69308
sound velocity temp. variation, microscopic theory 77−35776
spatial correlations and elementary excitations in many-body systems 80−22730
spatial order, temp. depend. 80−39374
specific heat, isobaric 78−18788
specific heat, low-density phase modification produced by substrate changes 77−76642
static struct. factor and pair correls., neutron diffr. study, 1.00 to 4.27K 80−80010
static structure factor and pair correlation function, at saturated vapour press. 80−64878
statistical mechanics of bosons with attractive interaction 79−12717
structure factor, excitation spectrum, ground state momentum distrib. 78−79833
structure factor, momentum transfer meas. 78−22912
structure factor meas. at 10K 79−51322
structure factor meas. in range 5.5 to 7K 80−80011
structure factors, static and dynamic, quantum conserving approx. 79−51321
supercritical, free convection heat transfer, 4.2-25K, 3-35 atm. 77−23961
supercritical, turbulent pipe flow, heat transfer by Melik-Pashayev technique 80−74860
supercritical coolant in cryostat, for meas. on superconductors 77−30155
supercritical He I, heat transfer to turbulent flow 80−69631
supercritical HeI, heat transfer to turbulent pipe flow 80−64348
superfluid, boundary-value problem for confined He 77−39707
superfluid, density temp. depend. in restricted geometry, oscill. U-tube technique 77−35774
superfluid, film, persistent current stability 77−7923

liquid helium-4 continued
superfluid, film, third sound long pulse propag. 77−20148
superfluid, generalised two-fluid eqns., canonical form. 77−20144
superfluid, ion escape from vortex rings at press. up to 2.5 MPa 77−31821
superfluid, lambda-tight ruby valve for He transfer 77−30159
superfluid, light scatt. by fluctuations in condensate near T_λ 77−11750
superfluid, maximum roton vel. obs. 77−31818
superfluid, neutron probing 77−43102
superfluid, pair condensation 77−1271
superfluid, phonon dispersion at long wavelengths and low temps. 77−11752
superfluid, polarisation pots. and elementary excitations at low temps. 77−15643
superfluid, precision second sound meas. 77−15648
superfluid, properties in zero gravity, appl. as cryogen on spacecraft 77−31822
superfluid, rotating, mutual friction parameters, crit. region meas. 77−15647
superfluid, rotating, superfluid vel. distrib. in intervortex regions *(Russian)* 77−43398
superfluid, roton energy determ. from neutron diffr. exam. 77−24458
superfluid, roton interactions 77−7926
superfluid, roton-roton interactions and excitations at large wavevectors 77−28058
superfluid, solidification on Grafoil, nucleation 77−28062
superfluid, sp. ht. of interacting Bose systems at low temps. 77−15651
superfluid, temp. depend. of mutual friction force near λ-point *(Russian)* 77−35778
superfluid, tensile strength and visible US cavitation 77−7920
superfluid, thermal expansion coeff., scaling and universality near superfluid transition 77−7927
superfluid, thermodynamic props., review 77−39708
superfluid, thermodynamic props. determ. from sound velocity data 77−15649
superfluid, transformation of first sound into second sound *(Russian)* 77−11755
superfluid, two-dimensional, roton spectrum 77−11751
superfluid, vortex ring energy and momentum for large core radius 77−4231
superfluid, vortex ring transition 77−4234
superfluid, vortex tangle dynamics, turbulence theory 77−35777
superfluid bath for supercond. magnets 77−30188
superfluid film, crit. vel. 77−7941
superfluid film, excitation spectrum, neutron scatt. 77−7942
superfluid film, kinetic thinning 77−35793
superfluid film, thinning in persistent flow 77−35792
superfluid transition, singular behaviour of mass conductivity in superleak 77−28059
superfluid-normal transition, inverse temp. expansion, quantum lattice model 79−55950
superfluidity, conditions for existence, phase fluctuation spectrum, Thomas-Kuhn sum rule 77−39709
superfluidity breakdown, expt. test of Landau's theory 77−24459
surface, ^{3}He atom scatt., reflection coeff. meas. 77−15644
surface, hot carrier mobility 78−59988
surface, hot electron theory 78−22915
surface, hot electrons theory 79−42329
surface, interaction with atomic H, Euler Lagrange eqn. 79−77850
surface electron interaction with EM radiation *(Russian)* 80−54449
surface electron mobility due to electron-ripplon interaction *(Russian)* 77−35770
surface excitations, theory 78−22918
surface structure 78−87837
surface warm electrons, non-Ohmic transport, scatt. mechanisms 77−20142
thermal conductivity, 3.3 to 20K, meas. in guarded parallel plate apparatus 77−22553
thermal quenching behaviour for a formvar-coated composite superconductor 79−61633
thermally induced oscills. in cryogenic apparatus 78−67875
thermodynamic props. at 0.7K, boson system anal. 77−4230
thermodynamic temp. meas. by noise thermometry at various vapour pressures 80−27298
thermodynamics below Debye temp., thermal capacity temp. depend. *(Russian)* 79−10999
three-particle correlations, new form for variational calcs. 78−84018
transient heat transfer, from bare Cu surfaces 79−72785
transients in critical dynamics of He^4 79−40513
trimer binding in two dimensions 79−69306
two-dimens., excitation spectrum and thermodynamic props. 79−86959
two-dimensional, ground state 80−49438
US attenuation and dynamical scaling near T_λ 77−24460
US finite amplitude wave propag. 80−80024
vaporisation critical point region, p-ρ-T data *(Russian)* 80−88373
vapour pressure controller 78−16900
variational ground-state energy, perturbation corrections 77−69132
variational Monte Carlo calcs. with three body correl. 80−96711
variational wave function, three-body correlations 78−87834
viscosity and positive ion mobility near melting transition 78−10240
viscosity behaviour near superfluid transition 77−89605
viscosity behaviour props. *(Russian)* 80−44382
viscosity near superfluid transition under press. 79−55959
wave equation of particle density operator, sound vel. 77−53830
X-ray scattering, inelastic response function 77−55406
Cu-liquid ^{4}He interface, time depend. of anomalous Kapitza conductance 79−56066
^{4}He I, stable microscopic bubbles and evaporation-condensation resonance 78−91381
He I liquid, temp. fluctuations 79−19414
He II, ion velocity shift in vortex resonance 77−35771
He II, motion in rapidly rotating bucket 77−31817
He, liquid, short-wave surface excitation study using electron gas nonlinear I-V characts. *(Russian)* 80−10717
He-H_2 mixtures, isobaric sp. ht. 78−18788
He-II, critical heat flux for narrow Sn films 79−23795
^{4}He, adsorpt. and sp.ht. in 0.2 μm Nuclepore filters 77−35773
^{4}He film, specific heat near Tλ 77−80664
^{4}He, liq., hard-sphere roton interaction, transition temp. calculated 78−51767

liquid helium-4 continued
^{4}He, normal liq., collective excitations, neutron inelastic scatt. study 80−107590
^{4}He, superfluid, Bose-Einstein condensation, interacting boson theory without anomalous propagators 77−33942
^{4}He, superfluid, dispersion of roton second sound 77−31819
^{4}He, superfluid saturated liq., recovery heat flux from silent and noisy film boiling states 79−72784
interface with heated Au thin film, at 0.1K, temp. for large values of energy flux 79−55981

liquid helium sound propagation
see also second sound; zero sound
^{4}He, superfluid, one phonon excitation spectrum and interaction pot. 80−54455
bubble formation mechanism, on surface of deformed crystal *(Russian)* 78−85066
film, sound modes of two-dimensional electron gas 77−69145
films, crit. attenuation at 9 GHz 77−4241
first sound response, nonlinear, at 1, 3 10 MHz 79−46858
superfluid, acoustic turbulence, first and second sound kinetic eqn. soln. *(Russian)* 78−43193
superfluid ^{3}He-^{4}He mixtures, two-phase sound 79−86958
superfluid ^{4}He, fifth sound, vel. meas. 80−39377
superfluid Fermi system, Bose spectrum, hydrodynamic action functional *(Russian)* 78−14534
superfluid He, transformation of first sound into second sound *(Russian)* 77−11755
superfluid variational and reciprocity principles 77−72727
superfluidity, model Hamiltonian, rel. to first sound speed 80−44377
He, film, superfluid props. 80−34270
He, films, inhomogeneities 77−76641
He II, asymmetry phenomenon *(Russian)* 78−22913
He, sound transmission at liq. solid interface, probe of melting kinetics 80−92734
^{3}He, first sound attenuation under press. *(Russian)* 80−10730
^{3}He, fluctuation contrib. to sound vel. and damping above superfluid transition temp. 80−15324
^{3}He, liq., polarisation potentials and elementary excitations 78−91502
^{3}He, mag. A_1 phase, macroscopic dynamics 77−7929
^{3}He, normal, diffusive heat flow and sum rules in the hydrodynamic limit 78−56012
^{3}He, normal, overdamped modes and transport 78−56011
^{3}He, normal and superfluid, acoustic props. 79−46875
^{3}He, sound propag. at elevated densities, 0.35 to 1.4K *(Russian)* 80−92741
^{3}He, superfluid, A and B phases, US props. 79−65278
^{3}He, superfluid, A phase, theory of sound propag. 78−38896
^{3}He, superfluid, acoustic shear impedance meas. 77−11759
^{3}He, superfluid, B-phase, first-sound attenuation and viscosity 80−75401
^{3}He, superfluid, dynamic orbital effects, US propag. and viscosity, book contrib. 80−2235
^{3}He, superfluid, fourth sound Helmholtz resonator study 79−51359
^{3}He, superfluid, hydrodynamic modes interaction, sound propag. and spin waves *(Russian)* 79−37897
^{3}He, superfluid, order parameter, sp. ht., mag. props., sound propag., hydrodynamic props., book contrib. 79−99388
^{3}He, superfluid, second viscosity and attenuation of fourth and second sound near transition temp. 77−31830
^{3}He, superfluid, size effect influence on fluid density and transition temp., fourth sound meas. 80−80022
^{3}He, superfluid, sound propag. and kinetic coeffs., book contrib. 80−2237
^{3}He, superfluid anisotropic A-phase, nonlinear sound interactions *(Russian)* 77−11761
^{3}He, superfluid B-phase, acoustic shear impedance 79−51343
^{3}He, superfluid B-phase, HF sound propag. meas. 80−88391
^{3}He, superfluid B-phase, sound dispersion and neutral superfluids with BCS pairing at T=0 79−51345
^{3}He, transition from first sound to zero sound 77−89609
^{3}He-^{4}He, dilute, phonon absorpt. and scatt. expts. 77−20153
^{3}He-^{4}He, phonon vel. 79−23803
^{3}He-^{4}He film, third sound meas. using TOF techniques 79−51381
^{3}He-^{4}He mixture, HF crit. sound attenuation near T_λ 79−95241
^{3}He-^{4}He mixture, pressure release superleak sound modes, U-tube sound 80−54453
^{3}He-^{4}He mixture, superfluid fraction, density near λ point oscillating disc method 77−43404
^{3}He-^{4}He mixture, superfluid solution, sound vibrations in narrow channels *(Russian)* 78−79851
^{3}He-^{4}He mixture films, unsaturated, third sound and decay of persistent currents obs. 80−75402
^{3}He-^{4}He mixture near tricritical point, thermal diffusion ratio and thermal conc. gradients 77−76640
^{3}He-^{4}He mixture superfluid thin film, third sound vel. calc. 80−107602
^{3}He-^{4}He mixtures, propag. conditions and vels. for first, second and fourth sound, singular surfaces theory 77−47643
^{3}He-^{4}He mixtures, sound propagation near superlfuid transition 78−79848
^{3}He-^{4}He mixtures, sound propag. near superfluid transition and tricritical point 79−65284
^{3}He-^{4}He mixtures Doppler shift in third and fourth sound 78−56017
^{3}He-^{4}He solution, first and second sound interaction, hydrodynamic approx. *(Russian)* 77−69142
^{3}He-^{4}He solution, in mag. field, characts., theory *(Russian)* 78−59999
^{3}He-^{4}He superfluid solution in superleak waveguide, acoustic-modes *(Russian)* 79−90842
^{3}He-He II degenerate soln., kinetic coefficients, thermodynamic props., hydrodynamic, acoustic and spin wave propag. *(Russian)* 78−18867
^{4}He and ^{3}He-^{4}He mixtures, superfluid, fifth sound mode 80−75398
^{4}He, anharmonic effects in US propagation near λ transition 80−96707
^{4}He, Bose-Einstein condensate near lambda point 77−15645
^{4}He, critical attenuation of sound in restricted geometries meas. 80−29235
^{4}He dynamic scaling and US attenuation near superfluid transition point 78−84016
^{4}He, film, saturated superfluid, on rough surfaces, persistent currents in presence of third-sound reson. 77−20156
^{4}He film, superfluid, complete decay of persistent currents, pulsed third sound TOF expts. 79−51378
^{4}He film, superfluid, dynamics 80−59748

liquid helium sound propagation continued
^{4}He film, superfluid, third sound attenuation, 0.1-200 Hz 77−20159
^{4}He film, third sound, two-dimens. hydrodynamics and elementary excitations 79−7721
^{4}He, film adsorbed on Grafoil, onset and third sound vel. meas. 80−44388
^{4}He, HF crit. attenuation, 0.55-1.7 GHz 79−55958
^{4}He, HF sound scatt. near λ-transition *(Russian)* 77−59165
^{4}He, Kapitza heat-transfer model for boundary with solid 80−107591
^{4}He, liq., acoustic impedance meas. by acoustic surface waves 79−77848
^{4}He, liq., nonsuperfluid, low momentum transfer neutron scatt. study 79−46546
^{4}He, liquid, first sound nonlinear wave distrib. *(Russian)* 80−107588
^{4}He, liquid-solid boundary, capillary sound motion, Kapitza resistance *(Russian)* 80−92737
^{4}He, λ point, US absorption, dynamic scaling 80−44380
^{4}He monolayer superfluid films, third sound modes, superfluid solitons 79−10998
^{4}He, normal liq., collective excitations, neutron inelastic scatt. study 80−107590
^{4}He, order parameter fluctuation critical attenuation near critical temp., first sound 80−2229
^{4}He, order parameter relax. near T_λ, HF first sound meas. 79−55960
^{4}He, pressurized, attenuation and dispersion of first sound near superfluid transition 78−14524
^{4}He, pulsed perturbation relaxation, intense short heat pulse passage, compression wave propagation *(Russian)* 79−82400
^{4}He, singular behaviour of mass conductivity in superleak at superfluid transition 77−28059
^{4}He, sound vel. temp. variation, microscopic theory 77−35776
^{4}He, sound velocity in dense hard sphere Bose liq. 79−69308
^{4}He, superfluid, attenuation of fourth sound 79−51332
^{4}He, superfluid, concave energy spectrum of very low wave numbers 79−4438
^{4}He, superfluid, continuum theory based on classical theory of irreversible processes 80−29236
^{4}He, superfluid, excitation spectrum, Bogoliubov theory 79−7722
^{4}He, superfluid, fifth sound 79−60569
^{4}He, superfluid, fifth sound 80−88379
^{4}He, superfluid, film, third sound long pulse propag. 77−20148
^{4}He, superfluid, film and bulk, superflow in very long glass-capillaries 79−65273
^{4}He, superfluid, first and second sound contribs. to thermal flux 77−59164
^{4}He, superfluid, flows, healing and relax., first, second and fourth sound 78−47617
^{4}He, superfluid, fourth sound vel. under press. 78−2322
^{4}He, superfluid, fourth sound vel. and attenuation 79−86942
^{4}He, superfluid, fourth sound propag. and flow props. in very long capillaries 80−44384
^{4}He, superfluid, fourth sound phenomenon under adiabatic and isothermal conditions 80−100369
^{4}He, superfluid, fourth sound attenuation 80−100370
^{4}He, superfluid, fourth-sound-like propagation in grafoil-filled resonators 80−34263
^{4}He, superfluid, physical acoustics 77−51561
^{4}He, superfluid, precision second sound meas. 77−15648
^{4}He superfluid, pressure release sound modes 79−51331
^{4}He, superfluid, pressure release superleak sound modes 80−54453
^{4}He, superfluid, quasiparticle sound velocity, temp. depend., imperfect Bose gas picture 78−51761
^{4}He, superfluid, resonant nonlinear mode conversion 78−79831
^{4}He, superfluid, sound absorption, theory *(Russian)* 77−89607
^{4}He, superfluid, sound conversion phenomena at free surface, acoustic coeffs. 80−96709
^{4}He, superfluid, sound pulse amplitude meas. method sound transform. at free surface 80−54451
^{4}He, superfluid, temp. depend. of sound vel. 79−33139
^{4}He, superfluid, thermodynamic props. determ. from sound velocity data 77−15649
^{4}He, superfluid, third sound pulses in doubly connected systems 79−55956
^{4}He, superfluid, threshold first sound amplitudes for vortex line generation 79−55970
^{4}He, superfluid, two- and three-dimens., energy spectrum and phase vel. 80−70489
^{4}He superfluid, wave processes, in parallel channels, with different degrees of damping *(Russian)* 78−91496
^{4}He, superfluid, wave process propag. in flow, new related phenomenon 79−51330
^{4}He superfluid film, adsorbed on Al_2O_3 powder, surface tension sound 80−24691
^{4}He, superfluid film, compressible and layered, third sound 80−65325
^{4}He superfluid film, fifth sound 79−60570
^{4}He, superfluid film, solitons at low temps., Korteweg-de Vries eqn. 80−96717
^{4}He, superfluid film, third sound propag. and attenuation *(Russian)* 80−92733
^{4}He superfluid film, unsaturated, direct obs. of third-sound mass displacement waves 78−30804
^{4}He, US attenuation near λ line under high press. 79−55972
^{4}He, US finite amplitude wave propag. 80−80024
^{4}He, wave equation of particle density operator, sound vel. 77−53830
^{4}He-^{3}He, fifth sound 79−60569

liquid lasers
see also dye lasers
actinide in organic soln., nuclear pumping 78−5470
benzene, Raman laser as efficient excitation source for stimulated Raman scatt. 79−18480
complex molecules, solns., stimulated emission by simultaneous 2-freq. excitation *(Russian)* 78−13701
complex molecules in solns., picosecond generation, spectral polarisation characts. *(Russian)* 77−10918
cryogenic active media as Raman lasers, stray transverse stimulated emission 78−25927
DFB film laser, wavelength control by elec. field 77−3616
emission kinetics of solutions of complex organic compounds for pumping with linearly polarised radiation *(Russian)* 77−83872
hydroacoustic perturbations of active medium 79−94229
inorganic for high-speed photography and multiframe interferometry 77−30211
molecular laser, optically pumped, development 78−13732
nitrobenzene, Raman laser as efficient excitation source for stimulated Raman scatt. 79−18480
nitromethane, Raman laser as efficient excitation source for stimulated Raman scatt. 79−18480
organic compound solution laser, miniature broadband type LOS-3 79−3706
organic compound solution lasers, polarisation diagrams *(Russian)* 77−88721
pyridine, vibr. reson. lasing threshold, complex form. and solvent effects *(Russian)* 77−75507
Raman laser, IR, high-power tunable 79−7140
rare earth lasers, book contrib. 80−53306
rare earth metal inorganic soln., nuclear pumping 78−5470
CS_2, Raman laser as efficient excitation source for stimulated Raman scatt. 79−18480
Er^{3+} in $SeOCl_2$ solvent, Racah and Judd-Ofelt parameters in laser liqs. 80−106516
Er^{3+}:$POCl_3$:$ZrCl_4$, radiative transition probabilities 77−8617
$Eu^{3+}+UO_2^{3+}$ solution, nuclear pumped liq. lasers, LASL program 80−64011
N_2, delay of broadband-pumped stimulated Raman gain 79−50351
N_2 high power tunable liq. Raman laser, for spectroscopy 80−48277
N_2, laser action due to stimulated Raman scatt., nonmonochromatic pump radiation 79−64284
N_2 liquid high-power tunable Raman lasers and applications 77−54709
N_2 liquid IR Raman laser with unstable resonator 79−31957
N_2 liquid Raman laser with slowly relaxing active medium, radiation divergence 79−98352
N_2, possible active media in high-power Raman lasers 80−19028
N_2, tunable Raman laser based on third Stokes component 78−50859
Nd^{3+} in $Nd(NO_3)_3$(tributylphosphate-d_{27})$_3$, soln. luminesc., stimulated emission *(Russian)* 78−33734
Nd^{3+} in $SeOCl_2$ solvent, Racah and Judd-Ofelt parameters in laser liqs. 80−106516
Nd:$POCl_3$-$SnCl_4$, laser parameters and physicochem. props. 77−14709
Nd^{3+}:$POCl_3$:$ZrCl_4$, radiative transition probabilities 77−8617
Nd^{3+}:$POCl_3$-$SnCl_4$, liquid laser material, luminesc. centres conc., temp. depend. 79−50287
Nd^{3+}:$POCl_3$-$SnCl_4$, liquid laser material, luminesc. centres changes, crystn. process effects 79−50288
Nd^{3+}:$POCl_3$-$SnCl_4$, relaxation oscillations with high power spikes obs. 78−42331
Nd^{3+}:$POCl_3$-$ZrCl_4$ free-running liquid laser, design and performance 77−14706
$Nd^{3+}+UO_2^{3+}$, solution, nuclear pumped liq. lasers, LASL program 80−64011
O_2, possible active media in high-power Raman lasers 80−19028
$Pm^{3+}+UO_2^{3+}$ solution, nuclear pumped liq. lasers, LASL program 80−64011
Pr^{3+} in $SeOCl_2$ solvent, Racah and Judd-Ofelt parameters in laser liqs. 80−106516
Pr^{3+}:$POCl_3$, fluoresc. and lifetimes of excited states 80−71466
$Th^{3+}+UO_2^{3+}$ solution, nuclear pumped liq. lasers, LASL program 80−64011

liquid metal embrittlement
α-brass, liquid metal embrittlement, eval. by quasistatic crack propag. technique 79−29262
ductile metals in liquid metal environments, embrittlement and brittle fracture, exam. 78−60766
Incoloy 800, corrosion and carburization in liquid Na up to 973K 79−47841
Incoloy 800, effect of liquid Na on creep and rupture props. 79−47775
literature survey 79−15798
metallic systems, liq. metal embrittlement mechanism, Rebinder effect *(Russian)* 79−34186
metals, liquid metal embrittlement, mechanism 79−43495
micromechanisms of crack growth, review 80−108637
review 79−29272
review 80−3257
steel, stainless, liq. Li corrosion rate expressions, 600-1000°C 80−93682
steels, types SS41, SB42, SM50A, STK55, liq. Zn embrittlement *(Japanese)* 80−81164
Zircaloy-2, Cd metal embrittlement in 300-340°C 77−16747
Al, liquid metal embrittlement by Ga 78−64653
Al single crystals, effect of environment on liquid-metal embrittlement, stress corrosion cracking and corrosion fatigue 78−64676
Al single crystals, liq. metal embrittlement by Ga 80−7675
Al-Bi(Cd)(Pb)-Ti, containing low-melting pt. inclusions, mech. props. 80−93632
Al-Zn-Mg (6.27, 2.94 wt.%), single crystals, effect of environment on liquid-metal embrittlement, stress corrosion cracking and corrosion fatigue 78−64676
Cu-Al (5.5, 7.3, 6.3 and 2.5 wt.%), Hg embrittlement under cyclic loading 77−86225
Fe, Armco, fracture in liq. metals, Rebinder effect *(Russian)* 79−29266
Fe, cast, liquid metal embrittlement, eval. by quasistatic crack propag. technique 79−29262
Ni, single crysts., H and liq.-Hg embrittlement 80−25862
Zn alloy, liquid metal embrittlement, eval. by quasistatic crack propag. technique 79−29262
Zn, liquid metal embrittlement 78−64653
Zn, liquid metal embrittlement 79−83375
Zn, single crystal, crack growth in contact with liq. Hg and Ga 79−87757

liquid metals
see also electron energy states of liquid metals; liquid alloys; mercury (metal)
3d bandwidths, photoelectron spectrum 77−4286
acoustic wave velocity calc. within limits of hard sphere model *(Russian)* 78−43072
activity coefficient of nonmetallic solutes in liquid metals and binary alloys 78−52766
Al, effect of treatment on dissociation of solid solns. of alloys *(Russian)* 78−15353
alkali, reactions with refractory metals and oxides, relevance to reactor technology 80−85173

liquid metals continued
alkali liquid metals, US absorption due to electrons and phonons 79−28046
alkali metal, law of corresponding states, microscopic basis 77−47539
alkali metal, liq. struct., from 1st-principles pseudopot. calc. 79−41941
alkali metal, salt solns., phase equilib., and chem. 78−73040
alkali metal, thermoelectricity, optimised model pot. calcs. 78−2467
alkali metal liq. binary systems, thermodynamic props. at high temps. 80−15262
alkali metal technology development, high-temperature experimental plants *(German)* 77−10461
alkali metal-H, mol. orbital approach, solvation energies 77−4201
alkali metal-molten salt mixtures, thermal EMF calcs., Rice and Pitzer models 78−20057
alkali metal-solid metal interfaces, chemistry and physics 77−51576
alkali metals, calc. of enthalpy of soln. of nonmetals and elec. resist. 77−55225
alkali metals, crystalline and alkaline, eqns. of state, zero compression isotherms *(Russian)* 80−103446
alkali metals, density, enthalpy, up to 1500 bars 77−84821
alkali metals, elec. resist., exchange of correlation effects 77−1403
alkali metals, equations of state and density meas. installation 77−43307
alkali metals, internal energy, chem. pot., critical consts. 78−34422
alkali metals, liq., collective excitations and short-range order 78−63665
alkali metals, liq., electrical resistivity and thermoelec. power, Harrison's method 79−78066
alkali metals, liq., self-diffusion coeffs. calcs. 78−2274
alkali metals, liquid, O_2 pot. and O_2 distrib. coeffs. between alkali and struct. metals 80−65231
alkali metals, liquid, thermoelectric power, optimised model pot. calcs. 80−29391
alkali metals, nonlocal harmonic model potential, appl. to elec. props. 80−6802
alkali metals, resist. and struct. factor, temp. depend. 77−62466
alkali metals, soln. chemistry as elucidated from elec. resist. studies 77−52636
alkali metals, solubility and solns. of nonmetals 77−51505
alkaline earth, pseudo-Gruneisen parameter, temp. depend. 77−7873
Ashcroft and Schaich, and Gyorffy theories equivalence 79−60693
atomic radial distrib. curve anal. *(Russian)* 80−14996
atomic transport props., review 77−1248
boiling, mag. field effect on bubble growth 79−32217
boiling in heated annular channel with blockage, FBR core, partial failure 77−42108
boring of steel in metallic melts *(Russian)* 78−56736
Born-Green equation stability for effective pair pot. in dense liqs. 77−51292
Brillouin scattering from reflections of surface ripples 78−48188
bulk modulus, calc. using press. fluctuation in microcanonical ensemble 80−2106
cathodes, nanosec. discharge form. in H_2 atmosphere 78−87578
cavitational bubble collapse and erosion intensity in constant mag. field *(Russian)* 80−60987
charge density fluctuations in surface layer *(Russian)* 80−15580
chemical physics of liq. state, book 77−31574
classical fluid model, neutralising negative background density 78−22621
clean metal magnetoresistance in solid and liquid phases *(Russian)* 80−107767
cluster ion energy spread from molten metal, charge exchange 80−37922
cohesive energy density, surface and interfacial tension and heat of mixing 77−55431
collective modes in classical monoatomic liqs., coherent neutron scatt., book contrib. 77−89371
column, acoustic velocity meas. across diameter 80−14527
compressibilities, surface tension at melting temp. 78−91370
compressibility, long wavelength limit of liquid struct. factor 78−67633
compressibility calc. by struct. factor *(Russian)* 78−59847
conductivity calculation with regard for nonlinearity of electron-ion interaction screening *(Russian)* 78−43351
conductivity meas. by rot. mag. field method, viscosity effect *(Russian)* 77−57349
conference, Bristol, England (July 1976) 77−47297
contact angle, on polycryst. Al_2O_3, surface energy meas. 78−6209
continuous casting, solidification process, convective heat transfer, anal. 78−84789
convection analysis, w.r.t. Prandtl number and relative roughness *(Czech)* 77−7389
cooling, solidification, new technique 77−36493
coordination numbers, calc. in microinhomogeneous struct. model *(Russian)* 80−38902
core polarisation and struct., model potentials and simulation methods 79−77492
corrosion resistance of fission reactor structural materials *(Czech)* 77−50245
crystal melt interfacial free energy calc. from exptl. radial distrib. function data 79−10926
crystallisation, fluidity resistance effects *(Russian)* 77−55957
d-band metal force fields 79−33051
Debye temp. determ. from US vels. and thermodynamic data 79−99289
density determ. by X-ray diffr. *(Russian)* 78−75529
density measurements 0-2000°C automatic device using γ-ray transmission 79−87787
density of states and effective medium approach 77−76717
diffraction model, critical test, elec. resistivity of amorphous and liq. metals 78−84191
diffusion, electrotransport and thermotransport 77−55371
diffusion, isotope effect determ. using radioisotopes 79−95191
diffusion mechanisms and coeff. determ. *(Russian)* 80−34215
diffusion of Hg and Cd 77−84955
diffusivity and solubility of oxygen, electrochem. obs. using solid oxide electrolytes 80−59669
dipole dipole-dispersion coeffs. calcs. 80−70109
disordered systems, mode softened unified theory 79−55637
droplets, electrostatic metallic spray theory 77−25317
eddy current response to solidification in one dimension 80−104140
effective interatomic potential from struct. data 78−47232
effective interionic interaction, many particle effects *(Russian)* 77−39530
effective interionic potentials 78−91221
electrical conductivity, role of multiparticle effects *(Russian)* 79−91015
liquid metals continued
electrical conductivity of disordered systems, tight binding approx. in Kubo formalism 79−60778
electrical resistivity calcs. 77−85190
electrical resistivity in short mean free path regime 79−56184
electroconductivity, effect of multiparticles interionic correls. *(Russian)* 79−28333
electroconductivity in mag. field *(Russian)* 78−39085
electromagnetic confining, centering and guiding *(French)* 80−24103
electromigration driving forces, linear-response theory 77−55372
electron correlations, evidence 78−55805
electron momentum density, correlations and ionic potentials, appl. to Al 78−60052
electron states, esp. opt. and mag. props., review 78−2882
electron transport, nonlocal pseudopot. calc., appl. to Cd 77−1404
electronic states, optical theorem, multiple scatt. theory 80−49578
electronic structure in muffin-tin model 77−69219
electronic theory of thermodynamics and struct., summer school lecture series 80−6353
electrons in fluids, conf., Banff, Alberta, Canada, (5-11 Sept. 1976) 77−89680
embrittlement, review 79−29272
embrittlement 79−15798
embrittlement and brittle fracture, of ductile metals in liquid metal environments, exam. 78−60766
embrittlement of Armco Fe, Rebinder effect *(Russian)* 79−29266
embrittlement of cast Fe, brass, Zn alloys, eval. by quasistatic crack propag. technique 79−29262
embrittlement of engineering materials 79−52421
embrittlement of metals 79−43495
embrittlement of Zn 78−64653
enthalpy meas. up to 2100K 80−4715
entropy, electron component *(Russian)* 79−23747
entropy of fusion and activation energy for self-diffusion 79−28121
environment for Ti ductility testing at 700-900°C *(Russian)* 77−52537
equation of state and triplet and higher correlations in long wavelength limit 77−11453
equation of state parameters rel. to Earth core energetics 77−15536
expanded fluid metal transport coeffs., temp. and press. depend., Enskog theory 78−6170
fast reactors, Na purification system for primary and secondary loops 79−45344
Fe, melt, wettability of CaO-MgO refractory *(Russian)* 78−10257
field ion sources 78−65999
film boiling, thermodynamic superheat limit rel. to Leidenfrost temp. 79−55325
film in electric field, instability *(Russian)* 77−89203
flow, and energy characts., in linear induction MHD pump *(Russian)* 77−47104
flow, in open channel, MHD regulation, armature reaction calc. *(Russian)* 77−47107
flow, inert gas bubble dynamics, simplified model 77−15098
flow, laminar thermal boundary layers, variable thermal cond. 79−59962
flow at high Hartmann no. in variable area ducts, nonuniform mag. field effect 78−30363
flow at high temperatures through circular pipes, connection mechanism *(Spanish)* 79−37315
flow in curved channels under transverse mag. field, transition and turbulent flows 80−79396
flow in tube in mag. field, turbulent transfer coeff. *(Russian)* 78−75220
flow in tubes, turbulence, heat transfer, thermogravitation effect 78−71315
flow measurement, using EM flowmeter with nonuniform mag. field *(Russian)* 77−47122
flow near wall, turbulent heat transfer coeff. 77−35142
flow rate measurement for metals with poor contact resistance 79−41778
flow rate regulators for liq. metal systems, MHD or mechanical *(Russian)* 78−75229
flow redistribution using const. mag. fields *(Russian)* 79−1261
flow velocity measurement, using EM system, vel. profile effects on output voltage *(Russian)* 78−45600
fluid flow during blast furnace tapping, mathematical model 78−85117
forced convection in metals with variable thermal cond. and capacity 79−37310
fragmentation following reactor core meltdown accident, contribution of collapsing vapour bubbles 80−755
fusion system, imploding liq. metal liner, rot. electron beam stabilisation 77−74994
galvanomagnetic properties obs., measuring cell construction 77−5866
gas diffusion coefficients, stationary method determ. *(German)* 79−10974
gas inclusions, bubble release dynamics, mag. field effects *(Russian)* 77−3865
gas injection, X-ray cinematrographic obs. 79−49360
gas-liq. metal two-phase two-component heat transfer, review 79−1239
gas-liquid metal reactions, mixed transport control 77−72709
geometrical model, soft sphere static approx. eqn. of state 78−42892
Hall effect, theory 78−23073
Hall effect sign, cond. and thermoelec. power calcs., tight binding model 77−47798
Hall effect theory 77−47797
heat capacity near melting point, vacancy mechanism of melting 80−10641
heat pipe flow, low temp. region, effect of compressibility, friction and evaporation 77−47066
heat transfer bibliography 78−63425
heat transfer criterial eqns. anal. 79−68707
heat transfer in closed conduits 77−47016
heat transfer with gas bubbled through *(Russian)* 80−38395
HF expansion of memory function 77−15301
Hg, hot-film vel. meas. in MHD duct flow 80−75009
high-temperature chemical processes, review, book contrib. 77−40545
impurity atom diffusion, hard sphere fluid model calcs. *(Russian)* 80−49089
incipient boiling press. signal and evaporation coeff. meas. 79−77734
incipient boiling superheats, heat flux effects 80−74697
individual and collective atomic motion, inelastic neutron scatt. and computer simulation 77−55226

liquid metals continued
inertial confinement fusion reactors, liquid metal protection schemes for first wall 79−76118
infiltration in medium with interconnected pores, during passage of elec. current 80−100033
ingot forming from melt, liq. containment by EM field 80−35120
ingot solidification and shrinkage cavity form., model *(Russian)* 77−16566
integrated density of states, expression in Roth's effective-medium approx., generalisation of Friedel formula 79−99467
interatomic forces and thermodynamic props., hard-sphere model 77−47321
interatomic interaction potential, rel. to structure factor *(Russian)* 79−69006
interface heat transfer of horizontal co-current liquid metal-H_2O stratified flow 80−92131
interface phenomena *(French)* 79−43632
interionic effective potentials determ. from expt. data 77−47338
ion bombardment, adaptation of ion microprobe 77−49805
ionic transport coefficient calculation *(Rumanian)* 79−60533
isothermal compressibility, harmonic pot. model calc. 79−14870
isothermal compressibility and eqn. of state at m.p. 80−79673
jet disintegration by electric pulse, powder and granule prod. 79−33968
jets, 3D fluid flow model induced in ladles or holding vessels 80−10278
jets, breakup in mag. field *(Russian)* 78−47062
kinetic equation for electrons for strong ion-ion interaction 77−35908
Knight shift, nonlocal pseudopot. calc. 78−91965
laminar convective heat transfer along cylinder 77−914
laminar flow in curved channels, transversely applied mag. field, flow anal. 80−59116
lattice model, metal-nonmetal transition, eqn. of state, phase diagrams 77−69220
lattice model, parameters for supercritical region 79−64983
liquid metal, electronic density of states, pseudopotential calcs. 80−70578
liquid metal film, turbulent flow down vertical wall under gravity, heat transfer 78−59396
LMFBR, equipment design, Na-NaK engineering handbook 79−97815
LMFBR, yield characts. of short-lived fission products in Na heat-transfer agent 78−66338
LMFBR boiling acoustic detection sensitivity, PFR commissioning expts. 79−13452
LMFBR coolant flow monitoring by balanced outlet temp. signals 79−13393
LMFBR core orificing computer code 79−9681
LMFBR debris bed simulation expt., in-reactor expt. 79−13404
LMFBR fuel subassembly temp. noise prediction, Monte Carlo approach 79−13392
LMFBR Na vapour bubble collapse detection by acoustic emission 79−13451
LMFBR Na-cooled 7-rod bundle acoustic and temp. noise obs. 79−13391
LMFBR post-accident containment, time-resolved penetration of liquid Na into limestone concrete 79−93787
LMFBR principles and potential advantages 79−81072
LMFBR steam generator leak, meas. of sound produced during steam injection into Na 79−93782
LMFBR steam generators, leak detection of steam or water into sodium 79−13434
LMFBR structure materials in liquid Na, capsule type creep tester *(Japanese)* 80−108653
LMFBR subassembly local boiling detection by outlet temp. fluctuation analysis 79−13390
LMFBR subchannel coolant flow behind blockage, temp. noise obs. 79−13389
LMFBR surveillance technique development 79−13448
LMFBR wire-wrapped subassemblies, Na boiling behaviour 79−31031
Lorentz number, Wiedemann-Franz ratio 80−80243
Lorenz number and thermal cond., apparatus for meas. 77−51716
low-density metallic fluids, review of continuous metal-nonmetal transition 77−51787
magnetic model 80−88719
magnetic susceptibility rel. to theories of electronic structure 77−1536
mean spherical approx., particles interacting with damped oscill. pot. 77−55221
measurement technique using Archimedes' Principle 78−22784
melt atomising unit, gasdynamic parameters 77−63576
melts, of a congruently melting substance, single struct. model 80−103233
meltspinning, theoretical anal. of ribbon thickness formation 80−104143
metal, liq., tight binding theory of transport props., Ishida-Yonezawa approx. for single-band model 78−84190
metal-insulator transition, review 77−1367
metal-insulator transition induced by expansion 78−2529
metallic systems, liq. metal embrittlement mechanism, Rebinder effect *(Russian)* 79−34186
metals, amorphous and liquid, electronic states, average spectrum 80−49579
MHD, high Hartmann number flows in ducts with conducting walls 80−33689
MHD, rectangular duct flow with opposite walls conducting and insulating 80−33688
MHD, review of flow problems and cellular motion 78−83498
MHD, temp. pulsation cross correlation coeffs., in longitudinal mag. field *(Russian)* 77−65815
MHD flow in periodic EM field, turbulent stresses calc. *(Russian)* 78−47056
MHD flow of liquid metal plane layer, industrial furnace appl. *(Russian)* 78−5817
MHD flow velocity structure, in nonuniform const. mag. field *(Russian)* 78−75215
MHD generator channel, liquid metal piston dynamics, math. model *(Russian)* 80−74996
MHD in EM trough creating azimuthal and axial forces *(Russian)* 79−1259
MHD induction pump channel press. loss, laminar liq. metal flow friction losses *(Russian)* 78−75224
MHD laminar flow, longitudinal dynamic effects determination for Na, Al, Sn and Hg *(Rumanian)* 80−64792
MHD pump, performance indices channel geometry *(Russian)* 78−5821
MHD rotation, vel. meas. by vane type sensor *(Russian)* 77−47123

liquid metals continued
microparacrystals in physics, review *(German)* 79−27933
microstructure and dynamics, summer school, Aleria, Corsica, France (Sept. 1977) 80−6339
mixing and refining in EM chute 79−77284
mixing volumes, pseudopotential method 79−37846
model potential, exact. soln. of mean spherical approx. 79−82144
Moelwyn-Hughes parameter calc. from US data for Cu, Ag, Zn, Cd, Hg, Al, Ga, In, Sn, Pb, Bi 80−59375
molten core debris contact with Na, particulate debris bed formation expt. 79−13405
monatomic liquid metals, interatomic pair pots., numerical calcs. 79−55649
Na, dynamic struct. factor, two body interaction pot. sensitivity 78−67638
Na, local boiling behind local flow blockage, simulated LMFBR fuel subassembly 78−54842
natural convection in liquid metal in annulus 78−30294
neutron diffraction, struct. investigations of melts and amorphous substances *(German)* 80−44108
neutron scattering, book contrib. 79−60232
NMR, of liq. metals and alloys, review 78−2755
NMR-PAD of ^{71}Ge, ^{78}Br in liq. metal targets 77−59465
noble metals, elec. resist., temp. depend. data 80−51967
noble metals, muffin-tin pot. model, electronic density of states determ. 77−51645
NQR rel. to viscosity 77−1615
nuclear quad. relax. rate temp. depend. calcs. 77−12273
nuclear quadrupolar relax. rate 78−48076
nuclear quadrupole relaxation, Sternheimer antishielding and fluctuating elec. field gradients 77−55726
nuclear quadrupole relaxation 78−15050
nuclear reactor, fuel element array, temp. distrib. for turbulent liq. metal flow 78−13203
nucleation undercooling meas. in small drops 77−7851
one dimensional shouldered hard-sphere fluid, struct. factor 78−34417
one-component high density plasma at intermediate wave numbers, collective excitations 78−67314
optical properties by spectroscopic ellipsometry, review 80−103929
optimised cluster expansion, struct. function evaluation 80−49085
orbital magnetic susceptibility of conduction electrons, pseudopotential calc. 78−76217
oscillations in liquid metals, vel. correl. function 77−58940
pair correlation function, self-consistent calcs. for simple fluids 77−1061
pair potential, self-consistent calcs. for simple fluids 77−1062
periodic fluid transients in cylindrical ducts with transverse magnetic fields 79−27708
perturbation theory extension to dense partially ionised plasmas 80−75500
photoelectron spectroscopy, electronic structure 77−48321
physical chemistry, conf., Konigstein, Germany (Mar. 1976) 77−1059
plasma arc heating, equilib. in gas-melt system *(Russian)* 79−37512
plasma valve design with liq. metal cathodes, high-power conversion/switching appls. 78−9865
plastic deform. and fracture obs. by acoustic emission of Zn single crysts. in metal melt *(Russian)* 78−56737
plugging indicator, liquid Na impurity deposition rate obs. 79−13557
polymer model, approx. eqn. for average distance between atoms calc. *(Russian)* 77−15293
polyvalent, electrical resistivity by harmonic model potential 80−54668
polyvalent, influence of pair pots. on struct. 80−28909
polyvalent, struct. factors with shoulder 80−19686
positron annihilation studies, book contrib. 79−99977
pseudopotential study of electronic props. 80−20149
pure, surface tension and electron density 78−51803
purification and thermodynamics, possibilities in space environment 79−46816
radial distrib. function and thermodynamic characts., interparticle interaction pot. *(Russian)* 80−49086
radiation loops, use of Ti alloys as structural materials 78−72958
rare earth, liquid, divalent electrical resist. 79−38039
rare earth, liquid, trivalent, electrical resist. 79−42514
rare earth metals, entropies 77−69100
rare earths, heavy, mag. susceptibility meas. 80−75740
rare earths, resistivity 80−24865
reactor coolant interaction, vapour film collapse expts. 79−13474
reduced density metals, screening, struct. and elec. resist. 78−19016
refining by fractional solidification 79−61536
resistivity, struct. factor calcs. 78−51962
resistivity as function of press., nearly-free-electron model 78−84192
resistivity expression, electron kinetic eqn. 80−48857
review of research, phys. aspects, Knight shift, elec. resist. *(Dutch)* 77−76557
run-off is elec. field, undamped waves 79−90271
SCF method for struct. and dynamics calcs. of simple classical liqs., appl. to Rb 77−51303
second-order thermal boundary layer 79−77106
self diffusion coeff. determ. using radial distrib. function 80−15280
self-diffusion coefficient, rel. to type of liquid 77−11715
self-diffusion mechanism and coeffs. calc., model *(Russian)* 77−15610
simple, resistivity at MP, general model pseudopot. method 77−55508
simple metal, entropies and struct. factors 77−7656
simple metals, elec. resist. and thermoelec. power calc. 77−76788
simple metals, solid and liq., electronic struct., mag. susceptibilities calc. 78−52204
sintered composite-liq. metal interaction, mass transfer eqn. approx. soln. 78−67262
solid-liquid interfacial energy 79−42396
solidification interface shape during continuous casting 79−15656
solubility of H rel. to that in solid phase *(Russian)* 80−65222
solubility of rare gases 77−51506
sound vel. meas., pulse-echo overlap technique 80−99906
space metal growth, mathematical model predictions from melt props. 78−84786
specific heat determ. in tunnel theory 79−33095
specific heat eqn. for high temp. 77−51510
spectrometer for soft X-ray emission studies of liquid metals and metallic vapours 80−73564
spherical particles production, equal-sized, controlled disintegration of free jets 80−7515
spin-orbit coupling and resistivity 77−85189

liquid metals continued
spin-orbit interactions effect on mag. susceptibility, effective pseudohamiltonian 80−29299
spreading on solid substrate 77−51575
steel, alloy, Fe-C-Si-S, liquid, desulphurisation with CaO, exam. of reaction mechanisms 78−80742
steel, interaction with Al_2O_3:Zr ceramic 80−104305
steels, types SS41, SB42, SM50A, STK55, liq. Zn embrittlement *(Japanese)* 80−81164
strong binding model, electronic density of states, Green's function calcs. *(Russian)* 80−70111
structural micro-inhomogeneity, Brownian motion studies *(Russian)* 80−92426
structure, harmonic approx. model 77−47331
structure, perturbation calcs. using Percus-Yevick equation 78−42889
structure, thermodynamic and transport props., book 78−51406
structure and dynamical properties 79−55648
structure and interatomic interaction, pseudopotential method 80−107042
structure and thermodynamic props., ab initio calcs. 77−84621
structure determ. by hard sphere model of repulsive interatomic pot. 79−55650
structure factor asymptotic form 77−7651
structure factor modelling using quasi-crystallised model *(Russian)* 80−54118
structure factor of system with shouldered hard sphere potential 77−43127
structure factor shoulders and interatomic pot. rel. to electron theory 77−7658
structure factors, higher order distrib. functions 77−51299
structure singularities *(Russian)* 78−79521
supercooled melt, dendrite growth morphology *(Japanese)* 78−11216
supercooling, on homogeneous crystn. *(Russian)* 80−19914
supercritical fluid metals, metal-insulator transition, quantal percolation method 79−56129
surface, atomic processes, book contrib. 79−60605
surface dipole layer and surface tension 80−70505
surface energy, relation with melting temp. and Fermi wavelength 77−51571
surface energy calc. in model of discrete positive charge *(Russian)* 78−38911
surface entropy using hard-sphere model 79−37906
surface instability, in elec. field, new type 79−64634
surface ion density, nonmonotone, perturbative discrete ion introduction into jellium 78−72222
surface layer structure, rel. to neutron refl. on boundary *(Russian)* 78−1976
surface plasmons at inhomogeneous liq. metal/dielec. interface, second dispersion branch 77−32059
surface properties, hard-sphere and square-well models 80−19684
surface props., thickness and energy, functional anal. for semi-infinite Fermi systems 80−52600
surface tension, appl. to calc. of surface free energy of solid at MP 77−31866
surface tension, critical temp. and temp. coeff. *(German)* 77−35800
surface tension, review of theory 79−77866
surface tension, temp. depend. *(Russian)* 80−15336
surface tension and critical props. 79−28176
surface tension and width, density functional theory 80−103537
surface tension measurement apparatus 80−59759
surface tension temp. depend. 77−4248
surface wave excitation, parametric, by alternating AC elec. field 79−23375
thermal convection suppression by distributed automatic regulator *(Russian)* 78−30364
thermal press. coefficients and sp. ht. 79−65207
thermoelectric power, pseudopotential calc., groups IIB, IIIB, and IV 80−59959
thermoelectric power 79−65450
thermoelectric power measurement apparatus 79−40591
thermoelectricity, expt. methods review 79−65451
thermophysical properties meas. by submicrosecond-pulse-heating method 80−52220
thin film, supercooling, electron diffraction study *(French)* 79−7676
tight-binding model, effective medium approx. 77−15756
transition metal, 3d, density of states of d-band, heat of vaporisation 78−95253
transition metal, amorphous and liq. state, simulated model 79−14733
transition metal, electronic states densities from struct. and entropy data 77−1347
transition metals, 3d, effect of d-band on heat of vaporisation and sp. ht. 77−76539
transition metals, 3d, thermodynamic and electronic props., Percus-Yevick eqn. soln. *(Japanese)* 77−76579
transition metals, and their alloys, elec. resist. using t matrix 77−31988
transition metals, electrical transport 79−38040
transition metals, liq., multiple scatt. calcs. of resist. 78−76039
transition metals, liquid, thermal volume expansion, MP to BP 79−90802
transition metals, muffin-tin pot. model, electronic density of states determ. 77−51645
transition metals, struct., rel. to amorphous state struct. 77−51323
transition metals, structure factors, calc. of temp. coeff. of resistivity, one component plasma model 79−32881
transition metals, thermodynamic characts. calc. *(Russian)* 80−15264
transition metals, thermoelectric power 78−91675
transition metals and alloys, elec. resistivity, Hall coeff., mag susceptibility 78−95280
treatment by high-temp. gas stream, math. model, applic. to nitriding *(Russian)* 78−53016
turbulent heat fluxes, channel flow, nucl. reactor appl. 77−42035
turbulent heat transfer, Nusselt no. calcs. 77−31304
turbulent heat transfer characts. 78−42602
turbulent natural convection in liq. metals in narrow cell *(French)* 78−94701
turbulent temperature fluctuations, in heated pipe flow, theory 77−84246
two phase flow, gaseous phase redistrib. in strong mag. field 79−37410
two-phase MHD flow in strong mag. field 79−23368
two-phase solid-liq. melt regime, thermodynamic props. eqns. 77−55342

liquid metals continued
UMFBR molten core debris and core containment material interactions 79−13469
vaporisation in arc heated gas stream, model 79−46795
vapour pressure, pseudopot. and Gibbs-Bogoliubov calcs. 78−83935
on vibrating solid surface, equipment for investigating interaction at US freqs. 77−51589
viscosity, calc. using microinhomogeneous struct. model *(Russian)* 80−15284
viscosity anal. 78−91468
viscosity determination by oscillating vessel method *(Japanese)* 80−70439
viscosity meas. by torsional oscillation method, crucible size effect 77−51139
viscosity measurement apparatus 80−59759
viscous flow due to high overheating, quasipolycrystalline model 80−70110
wetting of refractory oxide single crysts. *(Russian)* 77−43408
wire, thermomigration through a solid in thermal gradient, force model 78−67870
Ag, nuetron diffr. investig. of pair correl. function, coordination numbers 77−35467
Ag, viscosity, temp. depend. *(French)* 78−59964
Al, atomic radial distrib. curve anal. *(Russian)* 80−14996
Al, bulk modulus, calc. using press. fluctuation in microcanonical ensemble 80−2106
Al, calc. of neutron scatt. law 77−47330
Al, charge density fluctuations in surface layer *(Russian)* 80−15580
Al, Compton profiles for liq. and solid phases 79−91519
Al, density fluctuations, neutron scatt. anal. 80−70349
Al, density fluctuations 78−55806
Al, diffusion and dissolution of alloying components, 700-1000°C *(Russian)* 80−15275
Al, diffusion interaction with solid W *(Russian)* 78−26735
Al, diffusion of W under low gravity *(Russian)* 78−22875
Al, dislocation behaviour at melting, HV electron microscope in-situ obs. *(Japanese)* 77−43216
Al, dissolution of Co and Fe, kinetics, 700-900°C *(Russian)* 77−59119
Al, dissolution of Fe and Fe alloys *(Japanese)* 78−71858
Al, electron correlations, evidence 78−55805
Al, electron diffr. 78−83721
Al, electron momentum density, correlations and ionic potentials 78−60052
Al, energy moments and longit. freq. dispersion 79−60262
Al, Fermi momentum, for solid and liq. phases, temp. variation, Compton scatt. obs. 80−50451
Al, film, bleaching possibility by laser pulse, liq. metal-insulator transition 77−43498
Al, interaction potential 77−58945
Al, kinematic viscosity temp. depend., porosity, H solubility, supercooling *(Russian)* 80−54425
al, liq., sticky hard sphere pot., stuct., function evaluation 80−33869
Al, liq. struct. factor, 680 to 840°C, neutron diffr. study 79−46552
Al, liquid, dynamical struct. factor 78−71667
Al, liquid, dynamical struct. factor calc. 80−64880
Al, liquid, structural details, molecular dynamics calcs. *(Russian)* 80−64879
Al, longit. current spectra calc. 79−82143
Al melt, adhesive props. on Ti and graphite, 300 to 1200K *(Russian)* 77−15663
Al, melt density, temp. depend. *(Russian)* 79−69174
Al melt-NaF filter material interaction mechanism *(Russian)* 80−108743
Al, melting, existence of before and after effects, neutron scatt. 77−84895
Al, metallic materials diffusion rate, meas. apparatus 79−86913
Al, model pseudopotential 78−91582
Al, molecular dynamic simulation of static and dynamic structural factors *(Russian)* 79−69005
Al, molten, determination of H content, using electrochemical probe 79−11843
Al, molten, dissoln. kinetics and diffusion coeffs. of Fe, Co and Ni 80−59666
Al, molten, Na determ. using β-Al_2O_3 probe 77−48714
Al, molten, showering cryst. form. in mould cooled from top *(Japanese)* 80−66498
Al, molten, struct. factors, at. distrib. curves, thermodynamics, neutron diffr. study *(German)* 80−19687
Al, molten, thermal expansion meas. to 1300K 80−65254
Al, molten, viscous flow, H dissolution temp. depend. X-ray anal. 79−91628
Al, momentum density of electron 78−6309
Al, pair correl. function, Monte Carlo calc., with pseudopot. 77−15300
Al, pair interaction pot., struct. factor calcs. 77−51298
Al, phase form. and diffusion interaction with W-Re alloy, under weightlessness *(Russian)* 78−22876
Al, pure, surface tension meas. *(German)* 77−35799
Al, radial distrib. function calc., pseudopot. method *(Russian)* 79−19138
Al, reaction kinetics with B_4C 80−84344
Al, resist. and thermo-electric power using corrected parameters of Shaw model 79−19566
Al, second and fourth order moments temp. depend. 77−72545
Al, short range order amongst cond. electrons 80−107040
Al, short-wavelength density fluctuations 79−46550
Al, spreading behaviour on Fe-Si 80−84345
Al, spreading kinetics on Ni 80−24717
Al, structure factor and radial distrib. function, neutron diffr. 77−47334
Al, thermodynamic props., pseudopot. calc. *(Russian)* 79−46549
Al, US effect on graphite wetting 79−15629
Al, viscosity 600-1000°C *(Russian)* 77−59133
Al, wettability of ZrO_2 melt 77−89619
Al, wetting of fused silica 77−15664
Al, wetting of MgO-Al_2O_3-ZrO_2 refractory 78−22936
Al, X-ray diffraction analysis 79−4232
alkali metals, liquid, internal energy, heat of mixing, entropy, dielectric function 80−88340
Am, vap. press., 1200-1600K, heats of vap. and La mixing 80−15232
Ar loaded K heat pipe performance characteristics 78−89934
Au, electron-ion pseudopot., form factor, liquid elec. cond., phonon dispersion 78−34785

liquid metals continued
Au, field emitted ions, energy distrib. 79−61501
Au, ion source fabrication and emission characts. 80−68995
Au, local pseudopotential, phonon frequencies, binding energy and liq. metal resist. calc. 77−20216
Ba, density meas. at intermediate temps., method employs Archimedes' Principle 78−22784
Ba, high-purity solid and liq. phases, elec. resist. and thermopower meas. 77−47799
Ba, solubility of Ti *(Russian)* 78−80513
Ba, thermophysical properties, up to 1800K 78−30767
Be, containerless melts in terrestrial and space environment, thermodynamic props. calc. from solidification and cooling curves 79−70052
Bi, diffusion of Sb, 713-853K *(Russian)* 77−15611
Bi, effect on short time strength of Nb based alloy *(Russian)* 77−25186
Bi, elec. cond. and assoc. optical scattering 78−76040
Bi, electrical resistivity with spin-orbit scatt. 78−64018
Bi, environment for wear resistance testing of carbon steels and Armco iron *(Russian)* 77−59941
Bi, fused, solubility of GaP, thermodynamics, rel. to epitaxial growth 78−34721
Bi, liq., collective motions, cold neutron scatt. obs. 78−67639
Bi, liq., in fused alkali chloride binary mixtures, electrocapillary phenomena 77−40553
Bi, liq., in fused KCl-KBr mixtures, electrocapillary phenomena 77−40554
Bi, liquid, field ion source emission characts. 80−74059
Bi, liquid, interference functions by double hard sphere model 80−49090
Bi, max. mol. fraction solubility of O 80−6527
Bi, molten, density, surface tension, temp. depend. 77−69147
Bi solid and liquid, positron annihilation temp. depend. 80−108296
Bi, struct. factor, interat. interaction pot., X-ray diffr. obs., 280-800°C *(Russian)* 78−14270
Bi, UPS, optical densities of states 80−2924
Bi, US vel. and thermophysical props. meas., 500-1000K 78−38778
Ca, density meas. at intermediate temps., method employs Archimedes' Principle 78−22784
Ca, elec. resist. and thermopower, meas. at melting temp. 79−99524
Cd, electron energy states calc. *(Russian)* 79−4506
Cd, interference function temp. depend. from X-ray diffr., elec. resist. calc. 77−47332
Cd, liq., X-ray diffr. meas. and interatomic interaction pot. calc. *(Russian)* 78−59735
Cd, Percus-Yevick eqn., perturbation treatment, struct. factor 77−7641
Cd, resist. and thermo-electric power using corrected parameters of Shaw model 79−19566
Cd, small-ang. X-ray scatt., at. microgrouping depend. *(Russian)* 78−14271
Cd, US vel. and thermophysical props. meas., 500-1000K 78−38778
Ce, 4f electron susceptibility temp. depend. 80−20378
Ce, liquid, resist. and thermoelec. power, t-matrix calc. 78−26840
Ce, struct., neutron diffr. meas. 77−51305
Ce, surface and volume props., flow props., surface layer thickness *(Russian)* 80−59760
Co, amorphous and liquid, density of electronic states 79−23881
Co, amorphous and liquid states, electronic states and transport 79−99474
Co, contact reaction with graphite 80−15342
Co, density of states of d-band, heat of vaporisation 78−95253
Co, liquid, Hall effect, band struct. and exchange scatt. 80−80250
Co, liquid, N solubility depend. on added elements, mechanism *(Russian)* 80−65223
Co melt, struct. charact. time depend. in X-ray studies *(Russian)* 80−24350
Co, N activity coeff. 77−72699
Co, NMR in paramagnetic and ferromagnetic states, crit. nucl. relax. 79−56622
Co, near-order struct., X-ray scatt. meas. 77−55231
Co, soft X-ray band spectra 77−52199
Co, struct. factor and isothermal compressibility 77−11462
Co, struct. factor and radial distrib. curves, X-ray determ. *(Russian)* 77−31580
Co, thermoelec. power meas. 77−35928
Co, viscosity, up to 2100K, vibr. method 78−38866
Cr, N activity coeff. 77−72699
Cr, N_2 absorption at high temps., Cr-N phase diagram, solubility-temp. relation *(Japanese)* 79−43201
Cs, corrosion of SrO-Al_2O_3-B_2O_3-SiO_2 glass 77−16706
Cs, eqn. of state meas. 80−19905
Cs, equations of state determ. 80−24564
Cs, fluid, metal-nonmetal transition and mag. interactions 80−49602
Cs fluid, metallic and nonmetallic, mag. props. 80−44799
Cs, liquid, meas. of density at high temp. and pressures 78−55903
Cs, liquid, neutron diffr. struct. anal., density and viscosity temp. depend. 80−6352
Cs, radial distribution functions calc. at 100°C 78−22638
Cs, relativistic model pseudopot., appl. to elec. resist. calc. in liq. phase 78−51866
Cs, resist. and thermo-electric power using corrected parameters of Shaw model 79−19566
Cs, specific heat meas., at temp. up to 1700K under pressure 78−51696
Cs, struct. factors, X-ray transmission diffr. expts. 77−47337
Cs, T_c, P_c, V_c, from eqn. of state 78−2228
Cs, vapour press., thermodynamic functions determ., Knudsen-effusion radiotracer method 78−26678
Cs-CsCl, liq. mixture, enthalpy of fusion, Gibbs energy of mixing and excess entropy 80−19947
Cs-NH_3, Cs-ND_3, solns., US absorption, metal-nonmetal transition 79−69194
Cu, absorption of gaseous O_2 78−51686
Cu, defects at thermal equilib. and melting, positron annihilation meas. 77−76391
Cu, deoxidation kinetics using CO 78−44403
Cu, deoxidation mechanism by reducing gas mixture *(Japanese)* 77−52638
Cu, determ. of Ag activity by two component method *(Japanese)* 78−11547
Cu, diffusion coeffs. of ^{124}Sb, ^{113}Sn, ^{110m}Ag and ^{195}Au 79−95196
Cu, diffusion of Tl, Ir, Pb and Bi *(Japanese)* 78−59962
Cu, droplets, surface tension meas., 1000 to 1330°C 77−62711

liquid metals continued
Cu, effective interionic interaction, pseudopot. method *(Russian)* 77−84622
Cu, effective interionic pots. determ. from expt. data 77−47338
Cu, electronic spectrum 77−51646
Cu, impurity diffusion of Ru, In, Sn, Sb *(Japanese)* 78−10204
Cu, Krasko-Gurskii model potential, test of validity 80−39485
Cu, liq., deoxidation rates by CO_2-CO gas mixture *(Japanese)* 80−89394
Cu, liq., normal spectral emissivity meas., 1376 to 1687K 80−10687
Cu, liq., surface tension rel. to temp., surface enthalpy, entropy 78−38912
Cu, liquid, dissolved O below 0.02 wt.% effect on surface tension 80−107618
Cu, liquid, impurity diffusion, shear cell assembly meas *(French)* 80−75375
Cu, liquid, oxidation kinetics, by CO_2 77−28986
Cu, liquid, struct. factor, neutron diffr. meas. and Monte Carlo calc. 80−38903
Cu liquid, thermodynamic study of O_2 80−88342
Cu liquid, wetting of W surface, depend. on preliminary surface treatment *(Russian)* 80−35388
Cu liquid/liquid CuS, miscibility gap *(German)* 80−49370
Cu melts, induction stirred, electrochemical deoxidation 78−39718
Cu, molten, O_2 absorption, surface tension driven flow effect 78−6199
Cu, pure, surface tension meas. *(German)* 77−35799
Cu, solubility of S, Se and Te 77−21096
Cu, surface tension meas. with levitated metal droplets, influence of oscill. amplitude 78−51798
Cu, thermal cond. and elec. resistivity 80−103661
Cu, viscosity 77−4138
Cu, X-ray diffraction analysis 79−4232
Dy, mag. susceptibility, elec. resistivity 80−20377
Eu, electrical resistivity of solid and liquid phases, thermopower, melting temp. 80−59955
Eu, liquid, resist. and thermoelec. power, t-matrix calc. 78−26840
Fe, absorption of gaseous O_2 78−51686
Fe and alloys, C solubility, donor-acceptor mechanism 80−49365
Fe, C saturated, interfacial tension determ. between graphite by buoyancy meas. *(German)* 80−34273
Fe, contact reaction with graphite 80−15342
Fe, diffusion of alloying elements *(Russian)* 78−79791
Fe, diffusion of O_2, Ar, H_2 *(Russian)* 77−55369
Fe, dissolution mechanism of C *(Russian)* 79−51264
Fe, effect of C, O, S, P additions on viscosity *(Russian)* 77−59134
Fe, eqn. of state in Earth's core conditions 77−73694
Fe, H_2 diffusion *(German)* 78−14487
Fe, homogeneous nucleation of CO bubbles 77−60106
Fe, in heterogeneous equilib. with CaO, MgO, Al_2O_3, SiO_2, calcs. *(Russian)* 77−59093
Fe, liq., struct. model, mol. dynamics calc. 79−50994
Fe, liq., thermodynamic data *(German)* 80−40328
Fe, liquid, alloying element effect on H_2 diffusion *(Russian)* 79−69270
Fe, liquid, at Earth outer core conditions, Gruneisen γ function determ. 79−84186
Fe liquid, C saturated, decarburization by CO_2, effect of S 79−11726
Fe, liquid, Hall effect, band struct. and exchange scatt. 80−80250
Fe, liquid, N solubility and AlN precipitation 79−11630
Fe, liquid, N solubility depend. on added elements, mechanism *(Russian)* 80−65223
Fe, liquid, reactions of CO, CO_2, with dissolved O and C, equilibria 78−44397
Fe, liquid, viscosity meas., temp. depend. *(German)* 77−55377
Fe, liquid and amorphous states, electronic states and transport 79−99474
Fe, mag. neutron scatt. at small momentum transfer caused by spin fluctuations 77−47968
Fe, molten, diffusion of V, Co, Mb *(Japanese)* 77−51531
Fe, molten, impurities effect on viscosity 78−95172
Fe, N activity coeff. 77−72699
Fe, near-order struct., X-ray scatt. meas. 77−55231
Fe, O_2 diffusivity, meas. by EMF method 78−14494
Fe, optical and electronic props., temp. depend., 20, 1400 and 1600°C 79−87412
Fe, reaction kinetics with B_4C 80−84344
Fe, short-range order, comparison with amorphous state 77−1069
Fe, short-range order struct., O impurity influence *(Russian)* 80−38901
Fe, soft X-ray band spectra 77−52199
Fe, struct. factor and isothermal compressibility 77−11462
Fe, struct. factor and radial distrib. curves, X-ray determ. *(Russian)* 77−31580
Fe, structure factor near transform. to amorphous solid, X-ray diffr. *(Russian)* 77−31579
Fe, surface tension meas. with levitated metal droplets, influence of oscill. amplitude 78−51798
Fe, thermoelec. power meas. 77−35928
Fe, transfer of Si from gas phase to molten Fe in blast furnace 77−4930
Fe, viscosity, up to 2100K, vibr. method 78−38866
Fe, wettability of ZrO_2 melt 77−89619
Fe, wetting of MgO-Al_2O_3-ZrO_2 refractory 78−22936
Fe-O system, thermodynamics of viustite-haematite alloy melt *(Russian)* 80−65249
$Fe_{40}Ni_{40}B_{20}$, molten, jet streaming, planar and cylindrical, instabilities rel. to glassy alloy casting 80−35129
Fr, properties from melting point to 7500K, prediction *(Russian)* 80−44296
GA, liq., electrode metal-solvent interaction rel. to elec. double layer struct., adsorpt. 78−61023
Ga, 1/f noise 78−64073
Ga and alloy high-temp. couplants for acoustic transducers 79−14195
Ga, Brillouin scatt. obs. 77−24858
Ga, effective pair pot. and thermodynamical props. 77−47600
Ga, effective pair potential and entropy *(French)* 78−14267
Ga, elec. resist. calc., 19 and 35°C, using calc. and expt. struct. factors *(Russian)* 78−56124
Ga, electrodiffusion conc. of impurities 80−54414
Ga, electron work function meas., dynamic capacitor method 77−39919
Ga, embrittlement of Al 78−64653
Ga, field ion microscopy using mag.-sector atom probe, ionisation characts. 79−43106
Ga, heating of glass substrate, surface temp. of substrate 79−97390

liquid metals continued
Ga, high-intensity scanning ion probe with submicroscopic spot size 79−54225
Ga, interference function temp. depend. from X-ray diffr., elec. resist. calc. 77−47332
Ga ion source, emission characts. obs. 80−62810
Ga ion source, high intensity, emission characts. 80−80950
Ga, Knight shift of ^{69}Ge 77−12271
Ga, liq., electron transfer of rare earth metal impurities *(Russian)* 77−59132
Ga, liq., nucl. acoustic reson. Knight shift, rel. to spin-lattice relax. 78−19351
Ga, liq. optical density of states, low-energy photoemission meas. 77−77341
Ga, liq. particles-He(N_2)(CO_2)(air), nonequilib. Laval nozzle flow calib., numerical soln. 77−75967
Ga, liq.-solid transition, collective mode dynamics, quantum corrections 77−15554
Ga liquid, contact angle with Nb and Zr substrates 79−77864
Ga, liquid, field ion source emission characts. 80−74059
Ga, liquid, field ionisation, surface temp. and elec. field depend. 79−78849
Ga liquid metal field emission ion source, characts. 80−108326
Ga liquid metal ion source, energy distrib. meas. 80−95493
Ga, liquid point anodes, field-ion emission 80−2928
Ga, liquid., supercooled, dynamics 79−27902
Ga, melt, adhesive props. on Ti and graphite, 300 to 1200K *(Russian)* 77−15663
Ga, neutron diffr. room temp. to 1303K, struct. model 78−51405
Ga, nuclear quadrupole relax. rate for ^{69}Ga, 20-150°C, calc. 77−36151
Ga solid and liquid, positron annihilation temp. depend. 80−108296
Ga, solubility and activity of O_2 77−59122
Ga, struct., X-ray diffr. obs. 77−84619
Ga, struct. factor, short range repulsive forces 78−75528
Ga, supercooled, double hard sphere model 77−43128
Ga, surface tension, low-temp. H_2 plasma influence, elec. double layer form. 79−33160
Ga, thermal props. at high temp. 80−75536
Ga, tracer diffusion studies using metallic ^{67}Ga 80−24629
Ga, viscosity, 370-1800K 77−1254
Ga, X-ray diffr., 323 and 203K *(French)* 77−84575
Ga, X-ray diffr. exam. of struct. at 203 and 323K *(French)* 78−14268
Ga-Ag interface, γ-phase interlayer growth, two-dimens. electron diffr. 79−19487
Gd, liquid, resist. and thermoelec. power, t-matrix calc. 78−26840
Gd, mag. susceptibility, elec. resistivity 80−20377
Gd, thermal diffusivity, conductivity and elec. cond. 110 to 2100K 79−42516
Ge, wetting of β-SiC 77−85016
H_2, electron kinetic eqn. with exchange, elec. resist. 79−15131
H_2, struct. and forces 78−22636
^{3}H meter for Na coolant systems 79−9690
He, mag. susceptibility, elec. resistivity 80−20377
Hf, liquid, viscosity at melting point, free energy *(Russian)* 80−92699
Hg, air jet injected horizontally, physical behaviour 77−3857
Hg, Brillouin scatt. obs. 77−24858
Hg, diffusion of Al, diffusion coeff. meas. 80−24627
Hg, droplets, film boiling 78−14453
Hg, effect on grain boundary fracture of Al bicrystal 77−36690
Hg, electrode metal-solvent interaction rel. to elec. double layer struct., adsorpt. 78−61023
Hg, electron density of states at 20 and 200°C 77−15754
Hg, electron energy states calc. *(Russian)* 79−4506
Hg, expanded, Knight shift interpretation in terms of electronic struct. and transport 77−43895
Hg, expanded, thermodynamic and electron transport props. 79−23938
Hg, expanded fluid, opt. gap, KKR band calcs. 77−1354
Hg, expanded fluid, optical props. 79−19902
Hg, expanded fluid, thermoelec. power near crit. point 79−23951
Hg, expanded liq., band model for electronic struct. 77−89690
Hg, expanded liq., electronic props. 77−55477
Hg, flow, unsteady stagnation, heat transfer through laminar, incompressible boundary layer 80−1584
Hg, flow and energetic characts. in linear induction MHD pump *(Russian)* 77−3882
Hg, flow in transverse mag. field, laminar and transition, channel wall effects 78−63500
Hg, liq., elec. cond. and thermoelec. power meas. 77−59273
Hg, liq., self-diffusion coeffs. by radioactive tracer technique 80−49392
Hg, liquid metal flow in curved channels, transversely applied mag. field 80−14829
Hg, liquid structure, X-ray diffr. obs., 173-473K 80−14997
Hg, long wavelength limit, triplet and higher correls., Percus-Yevick eqn., perturbative anal. 79−37613
Hg, nucl. spin relax. and quadrupolar relax. mech. 78−64292
Hg, nuclear quadrupole relax. rate for ^{201}Hg, −35 to 80°C 77−36151
Hg, partial vapour pressure, determ. for volatile component by static method 80−37150
Hg, quad. relax. of ^{202}Tl impurities 77−16215
Hg quadrupole relaxation rate temp. depend 80−88884
Hg, soft-sphere equation of state 79−55863
Hg, sound vel. near metal-nonmetal transition, up to 1600°C and 2000 kg/cm^2 80−39222
Hg, struct., X-ray diffr. obs. 77−84619
Hg, supercritical, elec. cond., four electrode method 80−62685
Hg, supercritical vap., semicond. model 77−51154
Hg, surface plasmon dispersion 77−62978
Hg, T_c, P_c, V_c, from eqn. of state 78−2228
Hg, thermophys. props. rel. to clustering in liqs. 77−1065
Hg, turbulent annular flow 77−19602
Hg, turbulent flow on stabilising thermal section, temp. fields and heat transfer 80−19366
Hg, X-ray diffraction analysis 79−4232
In, diffusion coeff. determ. of P, mathematical model, numerical method 79−23754
In, diffusive interaction with solid Cu *(Russian)* 78−95156
In, direct pair correl. function 78−38613
In, electrodiffusion conc. of impurities 80−54414
In, interatomic interaction potential, rel. to structure factor *(Russian)* 79−69006

liquid metals continued
In, liq., X-ray diffr. meas. and interatomic interaction pot. calc. *(Russian)* 78−59735
In liquid, contact angle with Nb and Zr substrates 79−77864
In, melt, adhesive props. on Ti and graphite, 300 to 1200K *(Russian)* 77−15663
In, Nernst-Ettingshausen effect in solid and liq. states *(Russian)* 78−6353
In, nuclear quadrupole relax. rate for ^{115}In, 170-650°C 77−36151
In, O_2 activity from electrochemical meas. 80−104123
In, PAC of ^{111}Cd 77−4584
In, resist. and thermo-electric power using corrected parameters of Shaw model 79−19566
In, small-ang. X-ray scatt., at. microgrouping depend. *(Russian)* 78−14271
In, solubility and activity of O 77−43331
In, struct. factor, Percus-Yevick equation perturb. treatment, square-well pot. approx. 78−75530
In, surface tension, low-temp. H_2 plasma influence, elec. double layer form. 79−33160
In, thermal conductivity meas. in Spacelab, design and terrestrial testing of measuring cell *(German)* 80−57303
In, thermal props. at high temp. 80−75536
Ir, thermophysical props. at temps. up to 7000K 80−103497
K cathode, liq., in Ar arc, cathode erosion rate estimation *(French)* 80−44056
K, density, at near critical temp. 80−103407
K, density meas. up to 1800K and up to 100 atm. 77−43264
K, equation of state, press. and entropy along melting curve 77−47540
K heat pipe, heat transport characteristics, transverse mag. field effects 79−37127
K, liq., density, 1640-2030K, 36.1-100.2 atm 78−91369
K, liq. elec. resistivity calcs. 78−79974
K, liquid, electrical resistivity, effect of inter-electron interactions *(Russian)* 77−24546
K, liquid, interionic interaction theory, pseudopotential calcs. *(Russian)* 80−79675
K, liquid, shear waves, molecular dynamics 80−44096
K, liquid, thermoelectric power, optimised model pot. calcs. 80−29391
K, liquid cathode arc in AR atom., plasma prod. and parameters, cathode sheath model 77−4003
K, mean spherical approx. and effective pair pots. 80−70099
K, pair correl. function and ion-ion pot. 79−50982
K, paracrystalline BCC lattice evidence 79−41942
K, radial distribution function, Monte Carlo calcs. 77−55230
K, reaction with Cu_2O and CuO 79−66277
K, resist. and thermo-electric power using corrected parameters of Shaw model 79−19566
K, short-wavelength density fluctuations 79−46550
K, stagnant, mag. field infuence on boiling 77−47096
K, struct. factors, X-ray transmission diffr. expts. 77−47337
K, T_c, P_c, V_c, from eqn. of state 78−2228
K, thermal expsn. coeff. for high temp. 78−75853
La, liquid, resist. and thermoelec. power, t-matrix calc. 78−26840
La, liquid, viscosity from 940 to 1220°C *(German)* 79−28123
La, solubility, heat of mixing and vaporisation of Am, 1200 to 1600K 80−15232
La, struct., neutron diffr. meas. 77−51305
La, surface and volume props., flow props., surface layer thickness *(Russian)* 80−59760
La:Eu^{2+}, liquid, γ-ray spectra observation of exchange interaction 80−84672
Li, ^{7}Be impurity control, fusion reactor appl. 80−32466
Li, air contamination effect on compatibility with Mo, TZM, Nb, stainless steels, Ni, Hastelloy N 78−25285
Li, compatibility with ceramics 77−44387
Li, Compton profiles in liq. and solid states 79−87520
Li, cooling system of fusion reactor, corrosion inhibition by Al addition 80−108646
Li, corrosion of Nb-Zr-O alloys *(Russian)* 78−31567
Li, corrosion of refractory oxides 77−44378
Li, corrosion resistance properties of Fe alloy containers 79−47815
Li, density of states in K excitation spectra of solid and liq. phases 78−19601
Li, diffusion in KSiAl doped W wire, effect on recrystallisation *(German)* 78−64644
Li, effect on short time strength of Nb based alloy *(Russian)* 77−25186
Li, electron energy states calc. *(Russian)* 79−4506
Li, entropy and enthalpy of solution of H 78−51692
Li, getter for efficient particle removal from Tokamak 77−38411
Li, getter for Tokamak reactors, thermal and dynamic flow props. of falls 77−38412
Li, ISSEC selection for fusion reactor 80−57950
Li, impurity monitoring and control system for fusion reactor 80−32465
Li, in contact with steel, mutual indentation *(Russian)* 77−59853
Li, in fusion reactor, estimate of diffusion coeff. of Pb 79−93828
Li, in laser fusion plant, systems for protective Li falls 79−85785
Li liq., deuteron activated, shielding 80−99286
Li, liq., elec. resistivity and thermoelec. power, orthogonalisation hole pseudopotential calc. 80−29376
Li, liq. and solid states, γ-ray Compton profiles 77−48269
Li liq. blanket, T removal by Y for fusion reactor recovery 80−95434
Li, liq. cooled pulsed fusion reactor blanket heat transfer, numerical calc. 78−94141
Li, liquid, transverse flow around tube bundle, heat transfer 80−64537
Li, nucl. spin-lattice relax. of β-emitter ^{8}Li 77−51985
Li, paracrystalline BCC lattice evidence 79−41942
Li, penetration into Nb-O at 400°C, effect of O content 79−11719
Li, pure and containing dissolved Ni, reaction with rare earth oxides 79−66276
Li, resist. and thermo-electric power using corrected parameters of Shaw model 79−19566
Li, resistivity, thermoelectric power, Harrison nonlocal pseudopot. calcs. 78−23069
Li, short-wavelength density fluctuations 79−46550
Li, solubility of Fe, Cr, and Ni, effects of nonmetallic impurities 79−77760
Li, solubility of Li_2C_2, for fusion reactor appls. 80−13840
Li, solubility of Li_2O, determ. by fast neutron activation 79−42252
Li, solubility of Li_2O by neutron activation anal. 78−11601

liquid metals continued
Li, solubility of LiD 78−2259
Li, solvent for LiN, LiH, LiD, elec. resists. meas. 77−47786
Li, temp. and density depend. of struct., improved pseudopot. theory 79−14669
Li, thermophys. props. rel. to clustering in liqs. 77−1065
Li, trapping efficiency for 20 keV tritium ions 77−50290
Li, X-ray scatt. factor, solid state effect 80−70163
Lu, elec. resist. up to 1800°C, rel. to elec. struct. 78−39083
Lu, struct. factors, high temp. X-ray diffr. obs. 79−7544
Mg, diffusion and thermal diffusion of Fe, Si and Al, obs. using unidirectional solidification 78−30772
Mg, infiltration kinetics into porous Ti 78−60595
Mg, Percus-Yevick, eqn., perturbation treatment, struct. factor 77−7641
Mg, vaporisation from inductively stirred melt, meas. and prediction 78−51659
Mn, contact reaction with graphite 80−15342
Mo, elec. resist., melting pt. to boiling pt., temp. depend. 80−96839
Mo, exptl. determ. of crit. data 78−75531
Mo, liquid, spectral emissivity and brightness-temp. meas. at MP 77−43356
Mo, liquid and solid, thermophysical props. 78−75808
Mo, up to 4300K, thermophysical measurements 78−43136
N solubility, droplet weighing method 79−86889
NH_3-metal, soln., thermophysical props., review 79−77758
Na, atomic self-motions *(Rumanian)* 78−47226
Na, boiling, LMFBR safety, seven pin bundle expts., flow patterns, two-phase press. drop 77−88241
Na boiling acoustic emission burst detection in parasitic noise 79−3214
Na boiling detection technique tests, FFTF capabilities 79−13395
Na boiling expts. ref. to fast reactor safety *(Italian)* 79−9764
Na, boiling hazard in LMFBRs *(French)* 80−78402
Na, compatibility with ceramics 77−44387
Na, Compton profiles in liq. and solid states 79−87520
Na cooled power reactor noise analysis for malfunction diagnosis 79−13450
Na, decarburisation effects on Cr-Mo steel 77−16619
Na, diffusion coefficient for model potentials through mean square displacement 80−70098
Na, effect on atomistic diffusion in alloys 77−7899
Na, effect on austenitic stainless steel mech. props. 79−20150
Na, effect on corrosion and creep of stainless steels, 873 and 973K 77−57722
Na effect on fatigue crack growth in pressure vessel steel 77−8997
Na, effective interionic potentials 78−91221
Na, elec. cond., role of multiparticle effects *(Russian)* 79−91015
Na, elec. resist. temp. depend. 77−85190
Na, electrical resist. temp. depend. calc. 77−55507
Na, electron correlations, evidence 78−55805
Na, electronic structure, optical absorption 79−38566
Na entropy and enthalpy of solution of O(N)(C)(H) 78−51692
Na, eqn. of state and thermodynamic props. at high temp. and density 79−55902
Na, eqn. of state meas. 80−19905
Na, equation of state, press. and entropy along melting curve 77−47540
Na, equations of state determ. 80−24564
Na, evaporation from capillary-porous struct., capillary restriction in initial stages 80−107609
Na, fast reactor coolant, boiling in circular pipe, single-bubble model 77−10466
Na, HF expansion of memory function 77−15301
Na, heating modular steam generators, pressure and temp. loading in breakdown situation *(Czech)* 78−50264
Na, impurity conc. meas. by automatic plugging indicator 78−17283
Na in 7-pin bundle, LMFBR safety, KNK II driver zone 77−88246
Na, in EBR-II sodium systems, control of oxygen, hydrogen and tritium impurities 79−93696
Na, incipient boiling in the presence of a mag. field 79−37411
Na, incipient superheat meas., expt. and physical parameter effects 78−18289
Na, inelastic thermal neutron scatt., interatomic pots. calc. 78−42891
Na, interaction with stainless steel fuel cluster sheath, effect on porosity development 77−71651
Na, ions in liquid, Born-Oppenheimer pot. derivative, Monte Carlo calcs. 80−54117
Na, LMFBR safety, flow rundown expts. in seven pin bundle 77−88240
Na, linear induction pump development *(Russian)* 78−94839
Na, linear pot. and elec. resist., calcs. 80−65519
Na, liq., coolant in fission reactor, degassing of Xe invest. using Na loop 77−34410
Na, liq., elec. resistivity calcs. 78−79974
Na, liq. and solid states, γ-ray Compton profiles 77−48269
Na, liq. sphere, in UO_2 infinite medium, heat transfer problem, temp. profile 77−75783
Na, liq.-vapour transition at low press. 77−39669
Na, liquid, electrical resistivity, effect of inter-electron interactions *(Russian)* 77−24546
Na, liquid, entropy calc. using phonon theory of liquids 80−39310
Na liquid, interionic interaction theory, pseudopotential calcs. *(Russian)* 80−79675
Na, liquid, natural convection from plane surfaces, LMFBR design, review 80−37417
Na, liquid, self-diffusion coeff., 127°C, from mol. dynamics data 77−76585
Na, liquid, shear waves, molecular dynamics 80−44096
Na, liquid, thermoelectric power, optimised model pot. calcs. 80−29391
Na, liquid metal slug flow, transfer function of temp. fluctuations 78−46133
Na MHD generators, optimisation for maximum electrical efficiency, output and power factor *(Rumanian)* 80−64793
Na, MHD induction machine, duct local flow charact. at large EM interaction parameter *(Russian)* 78−5818
Na, mean spherical approx. and effective pair pots. 80−70099
Na, molten chlinak extraction of K_2, in LMFBR 80−27702
Na, O_2 content determ. by ceramic probes, manufacture and props. 77−54308
Na, optical conductivity 77−63425
Na, paracrystalline BCC lattice evidence 79−41942
Na, pool boiling heat transfer, liq. head effects 78−89951
Na pool fuel vapour and aerosol transport in HCDA 79−13455
Na, radial distribution functions calc. at 100°C 78−22638

liquid metals continued
Na, resist. and thermo-electric power using corrected parameters of Shaw model 79−19566
Na, resistivity, thermoelectric power, Harrison nonlocal pseudopot. calcs. 78−23069
Na, short-wavelength density fluctuations 79−46550
Na, small-leak Na+water reaction in LMFBR steam generator, dissolution rate of hydrogen 78−29545
Na, solubility of NaH, and elec. resist. of Na-NaH and Na-Na_2O solns. 79−14934
Na, struct. factor, transport props. 78−22620
Na, struct. factors, X-ray transmission diffr. expts. 77−47337
Na, superheated, LMFBR safety, formation of critical boiling nuclei 77−88242
Na, superheated flow in pipe, single bubble slug expulsion 78−672
Na, T_c, P_c, V_c, from eqn. of state 78−2228
Na temperature fluctuation in single-pin-heated blocked annular channel 78−78439
Na test loop boiling, acoustic detection expts. 79−13487
Na, thermocouple transfer function and flow velocity meas. by temp. noise 79−13394
Na, thermodynamic activity of C, continuous method of determ. 77−56306
Na thermodynamic props. for reactor safety analysis 79−13478
Na, thermophys. props. rel. to clustering in liqs. 77−1065
Na transient boiling in single-pin annular channel under loss of flow 78−89933
Na, transport coeffs., static struct. factor calcs. 77−7643
Na, velocity autocorrelation function and freq. spectrum 79−27892
Na, velocity autocorrelation from memory function, hard-sphere and square well pots. 80−28893
Na, working fluid in AC cond. pump, performance charact., freq. depend. *(Japanese)* 80−13092
Na-H, mol. orbital approach, solvation energies 77−4201
Na-K, rotationally stabilized liquid liner implosion for fusion plasma production 77−23274
Na-NaK engineering handbook, purification, heaters, coolers, radiators 80−27045
NaK matural convection under transverse magnetic field 80−69827
Nb, liq., spectral emissivity and brightness-temp. meas. at MP 77−43356
Nb, liq. and solid, enthalpy meas. by levitation calorimetry 80−103499
Nb, O_2 solubility investigation *(Russian)* 79−55889
Nd, surface and volume props., flow props., surface layer thickness *(Russian)* 80−59760
Ni, absorption of gaseous O_2 78−51686
Ni, amorphous and liquid states, electronic states and transport 79−99474
Ni, contact raction with graphite 80−15342
Ni, contact reaction with B_4C-Ti(V)(Cr) 80−55707
Ni, contact reaction with graphite 80−15342
Ni, crystallographic orientation relationships in coalescing sintered W spheres 80−45249
Ni, diffusion of O_2, Ar, H_2 *(Russian)* 77−55369
Ni, distribution coefficient of Ir, Os, Rm between liquid and solid phase, zone fusion *(French)* 77−77374
Ni, effective interionic pots. determ. from expt. data 77−47338
Ni, electronic density of d-states, hard-sphere model and tight-binding approx. calc. 79−15065
Ni, liquid, Hall effect, band struct. and exchange scatt. 80−80250
Ni, liquid, N solubility depend. on added elements, mechanism *(Russian)* 80−65223
Ni melt, struct. charact. time depend. in X-ray studies *(Russian)* 80−24350
Ni, migration into WC-Ni hard alloys, sintered, with uneven binder metal distrib. 78−35336
Ni, molten, mag. small-angle scatt., persistent spin fluctuations 79−11288
Ni, N activity coeff. 77−72699
Ni, N_2 diffusion *(Russian)* 78−18812
Ni, near-order struct., X-ray scatt. meas. 77−55231
Ni, neutron scatt. and atomic dynamics 77−55233
Ni, neutron scatt. and atomic dynamics 78−22637
Ni, O_2 diffusivity, meas. by EMF method 78−14494
Ni, reaction kinetics with B_4C 80−84344
Ni, soft X-ray band spectra 77−52199
Ni, spreading over α-SiC single crystals 79−86962
Ni, struct. factor and isothermal compressibility 77−11462
Ni, struct. factor and radial distrib. curves, X-ray determ. *(Russian)* 77−31580
Ni, structure factor at 1873K 79−77490
Ni, surface tension meas. with levitated metal droplets, influence of oscill. amplitude 78−51798
Ni, thermoelec. power meas. 77−35928
Ni, viscosity, up to 2100K, vibr. method 78−38866
^{61}Ni, paramag. solid and liq. phases, nucl. spin relax. and Knight shift 78−76327
Ni(s, 1)+NiO(s)+NiX_2O_4 (X=Al, Ga), chem. potential and solubility of O_2 80−92679
O_2 bomb calorimeter modification for liquid metal reaction enthalpy meas. 79−201
Pb, ^{113,117m,125}Sn diffusion coeff. meas. *(Ukrainian)* 80−10690
Pb, As and Sn distrib., Si, Cr and Mn influence *(Russian)* 80−16274
Pb, collective excitations, neutron inelastic scatt. obs. 80−75148
Pb, dynamic struct. factor, slow neutron scatt. obs. 80−28908
Pb, effective interionic potentials 78−91221
Pb, elec. resist., temp. depend., calc. 78−14701
Pb, electrical resistivity, 300-1050K 80−24868
Pb, electrical resistivity with spin-orbit scatt. 78−64018
Pb, electron diffr. 78−83721
Pb, evaporation in shock compression release waves *(Russian)* 78−18761
Pb, evaporation under action of laser beam, recoil press. behaviour 80−25501
Pb, filament production, ejection of molten metal through nozzle, jet stability *(Japanese)* 78−52719
Pb, HF expansion of memory function 77−15301
Pb, ISSEC selection for fusion reactor 80−57950
Pb, liq., dynamic scatt. functions, 300 and 600°C, neutron scatt. study 79−50983
Pb, liq., elec. resist. calcs., pseudopot. depend. 80−96840

liquid metals continued
Pb, liq., elec. resistivity, 600-860K 79−56180
Pb, liq., sticky hard sphere pot., stuct. function evaluation 80−33869
Pb, liq., wetting of Ge surface rel. to cryst. orientation 78−43211
Pb, liq., wetting of Si surface in H_2+HCl 78−43210
Pb, liquid, US wave velocity *(Japanese)* 79−60438
Pb, mag. relax. of excited ^{207}Bi 77−16217
Pb, melt density, temp. depend. *(Russian)* 79−69174
Pb, melting, existence of before and after effects, neutron scatt. 77−84895
Pb, melts, effect on fracture stress of Armco iron *(Russian)* 77−21246
Pb, molten, density, surface tension, temp. depend. 77−69147
Pb, molten, struct. factors, tetrahedral concs., neutron diffr. study *(German)* 80−19688
Pb, molten, thermal expansion meas. to 1300K 80−65254
Pb, neutron diffr. meas. of pair and direct correl. functions 77−55229
Pb, paracryst. struct., coordination statistics calcs. 77−1063
Pb, relativistic model pseudopot., appl. to elec. resist. and phonon spectra calc. 78−51866
Pb, short range order amongst cond. electrons 80−107040
Pb, short-wavelength density fluctuations 79−46550
Pb, stream interaction with N_2 jet in metal powder prod. 79−43170
Pb, struct. factors, neutron diffr. 78−18538
Pb, supercooled liquid thin films, liq. struct. factor determ. by STEM 80−10487
Pb, surface tension liquidus temp. to 550°C *(Korean)* 79−90848
Pb, thermal conductivity meas. in Spacelab, design and terrestrial testing of measuring cell *(German)* 80−57303
Pb, thermophys. props. rel. to clustering in liqs. 77−1065
Pb, UPS, optical densities of states 80−2924
Pb, vapour press., meas. using transpiration method, thermodynamic props. determ. 78−3365
Pb, viscosity, comp. and temp. depend., up to 500°C 79−65233
Pb, viscosity, hard sphere diameter, interionic potential 79−77797
Pb, wetting of β-SiC 77−85016
Pd, elec. resist., temp. depend. data 80−51967
Pd, electrical resist. calc. using muffin-tin pots. 77−69287
Pd, liq., energy bands and electronic density of states, resistivity 78−34755
Pd, liquid and solid, thermophysical props. 78−75808
Pd, mag. susceptibility 78−95415
Pd, Percus-Yevick equation, perturbation theory calcs. 78−75515
Pr, struct., neutron diffr. meas. 77−51305
Pr, surface and volume props., flow props., surface layer thickness *(Russian)* 80−59760
Pt, thermodynamic characterisation, by isobaric expansion meas. 80−103494
Pt. Percus-Yevick equation, perturbation theory calcs. 78−75515
Pu, hard-sphere model, phys. prop. meas. interpret, adjacent solid phase implications 77−19866
Rb, coherent scatt. function calc. 78−22635
Rb, coherent scatt. function calc. 78−42875
Rb, coherent scatt. function anal. by self consistent field method 79−55651
Rb, computer-simulated, search for atomic vacancies 77−84620
Rb, cryst. nucleation and growth, mol. dynamics calcs. 79−74144
Rb, current-fluctuation spectra, mode-coupling theory 79−4231
Rb, density fluctuations from mol. dynamics simulations 80−100161
Rb, density functions, SCF method, coherent scatt. function 78−18527
Rb, dynamic struct. factor 78−30533
Rb, dynamical struct. factor 78−38612
Rb, effective interionic pots. determ. from expt. data 77−47338
Rb, effective interionic potentials 78−91221
Rb, elec. resist. temp. depend. 77−85190
Rb, electrical resist. temp. depend. calc. 77−55507
Rb, eqn. of state meas. 80−19905
Rb, equation of state, press. and entropy along melting curve 77−47540
Rb, equations of state determ. 80−24564
Rb, equilib. props., self consistent field methods calcs. 79−10767
Rb, expanded fluid, struct., Monte Carlo study 78−83720
Rb, expanded liq., struct. factor up to 1400K, 200 bar 77−47335
Rb, HF expansion of memory function 77−15301
Rb, higher order struct. functions in long wavelength limit, improved perturbation approx. 79−37606
Rb, kinetic model, dynamic struct. factor 79−10768
Rb, kinetic theory of self motion, memory function of vel. autocorrel. function calc. 80−14986
Rb, liq., dynamic struct. factor, two-relax. time model 77−1068
Rb, liq., pair interaction pot., thermodynamic, neutron diffr. calcs. 77−11463
Rb, liq., phonons, collective modes calcs. 78−2218
Rb, liquid, expanded, eqn. of state, transport up to 1700°C, 400 bar 80−2136
Rb, liquid, shear viscosity correlation function 78−47460
Rb, liquid, shear viscosity coeffs., model calcs. 78−47549
Rb, liquid, vel. correl. function, memory function calcs. 80−49081
Rb, long wavelength collective motion 78−38601
Rb, long wavelength limit, triplet and higher correls., Percus-Yevick eqn., perturbative anal. 79−37613
Rb, mode coupling theory of simple classical liquids 79−55630
Rb, model, derivation of vel. autocorrelation function from incoherent scatt. function 79−77491
Rb, mol. dynamics data, test of Born-Green eqn., pair pots. determ. 77−1057
Rb, nuclear spin relax. of 13.9 msec ^{88m}Y 77−12270
Rb, resist. and thermo-electric power using corrected parameters of Shaw model 79−19566
Rb, self-consistent calc. of coherent scatt. function 77−51308
Rb, shear wave modes and velocity correl. spectra 78−63654
Rb, short-wavelength density fluctuations 79−46550
Rb, simple classical liq., long-time anomalies suppression 80−24339
Rb, simultaneous meas. of density, elec. cond., absolute thermopower up to 1400°C and 400 bar 77−1402
Rb, static struct. and electronic transport props., pseudopotential calc. 79−7543
Rb, struct. factor, improved perturbation anal. of Percus-Yevick eqn. 77−58942
Rb, struct. factor determ. by neutron diffr. up to 1400K and 200 bar 77−1064
Rb, structure and dynamics, SCF calcs. 77−51303
Rb, T_c, P_c, V_c, from eqn. of state 78−2228

liquid metals continued
Rb, transverse correlations in simple liqs., effective field approach 79−82135
Rb, van Hove's dynamical structure factor for classical liquids 79−55631
Ru, liq., spectral emissivity and brightness-temp. meas. at MP 77−43356
Sb, fused, solubility of GaP, thermodynamics, rel. to epitaxial growth 78−34721
Sb, liq., self-diffusion, long capillary method obs., using radioactive Sb 77−89564
Sb, liq., thermoelec. power meas. 79−40591
Sb, liquid, solubility and activity of O_2 *(German)* 79−90793
Sb, max. mol. fraction solubility of O 80−6527
Sb, struct. model, using interference functions *(German)* 77−58946
Se, liq. struct. factor determ. rel. to short-range correlations 77−1060
Sn, ^{113,117m,125}Sn diffusion coeff. meas. *(Ukrainian)* 80−10690
Sn, atomic self-motions *(Rumanian)* 78−47226
Sn, collective motions, struct. factors calcs. 77−76295
Sn, diffusion and electrotransport of impurities meas. 77−51535
Sn, diffusion coeff. of ^{113}Sn, ^{124}Sb, ^{110}Ag, and ^{195}Au 80−96676
Sn, distribution functions, 232 to 870°C 77−4035
Sn, elec. resist. calcs., 232, 450 and 650°C, using calc. and expt. struct. factors *(Russian)* 78−56124
Sn, electrodiffusion conc. of impurities 80−54414
Sn, electron energy states calc. *(Russian)* 79−4506
Sn, environment for wear resistance testing of carbon steels and Armco iron *(Russian)* 77−59941
Sn, friction of C steels and Fe, Rebinder effect *(Russian)* 79−29269
Sn, in contact with Fe, Fe distrib. on thermal cycling *(Russian)* 80−16562
Sn, interference function temp. depend. from X-ray diffr., elec. resist. calc. 77−47332
Sn, liq., wetting of Ge surface rel. to cryst. orientation 78−43211
Sn, liq., wetting of Si surface in H_2+HCl 78−43210
Sn liquid, contact angle with Nb and Zr substrates 79−77864
Sn, liquid, electron transfer of rare earth impurities *(Russian)* 78−95278
Sn, liquid, impurity diffusion, shear cell assembly meas *(French)* 80−75375
Sn, liquid, interference functions by double hard sphere model 80−49090
Sn, liquid, thermal diffusivity and cond., 1000 to 1900°C, flash laser method *(French)* 79−99525
Sn, liquid, US wave velocity *(Japanese)* 79−60438
Sn, Lorenz number and thermal cond. meas. 77−51716
Sn melt fragmentation on quenching in n-pentadecane and water 79−15706
Sn, molten, struct. factors, tetrahedral concs., neutron diffr. study *(German)* 80−19688
Sn, molten, struct. investig. by neutron diffr. 79−4233
Sn, molten, thermal expansion meas. to 1300K 80−65254
Sn, molten drops, gas evolution on quenching 78−39818
Sn, molten rotating stream, vortical filament generation during solidification *(Russian)* 78−88460
Sn, optical props., 0.62-3.7 eV 80−75996
Sn, optical props. by spectroscopic ellipsometry, review 80−103929
Sn, pair interaction pot., struct. factor calcs. 77−51298
Sn, pure, surface tension meas. *(German)* 77−35799
Sn, quad. relax. of ^{114}Sb impurities 77−16215
Sn, second and fourth order moments temp. depend. 77−72545
Sn, small-ang. X-ray scatt., at. microgrouping depend. *(Russian)* 78−14271
Sn, soln. of InP, InAs, vapour phase partial press. 78−34610
Sn, stream interaction with N_2 jet in metal powder prod. 79−43170
Sn, structure factor meas. by X-ray diffr., interaction pot. *(Russian)* 77−7655
Sn substrate for CVD of Si polycrystal 78−64479
Sn, surface tension liquidus temp. to 550°C *(Korean)* 79−90848
Sn, thermotransport of solutes and NFE calc. of electronic heats of transport 77−55376
Sn, US vel. and thermophysical props. meas., 500-1000K 78−38778
Sn, viscosity meas. *(Italian)* 79−19137
Sn, wetting of β-SiC 77−85016
Sn, X-ray diffraction analysis 79−4232
Sn:^{114}Sb, PAC, mag. moment of 8$^-$, 210 μs state of ^{114}Sn 77−26609
Sr, density meas. at intermediate temps., method employs Archimedes' Principle 78−22784
Sr, elec. resist. and thermopower, meas. at melting temp. 79−99524
Sr, soln. in liq. Na., elec. resistivity, conc. depend. 78−84188
Sr, solubility of Ti *(Russian)* 78−80513
TE, small-ang. X-ray scatt., at. microgrouping depend. *(Russian)* 78−14271
Ta, electrical resistance temp. depend. in solid and liq. states, 2200-4200K 78−10415
Ta, heat capacity, 10^8-10^9 K s^{-1} pulsed heating, (2-4)×10^3K 78−14473
Ta, melt, thermal expn., 1146-2288K 78−43148
Ta, static struct. factor 77−19865
Ta, up to 7500K, thermophysical measurements 78−43136
Tb, mag. susceptibility, elec. resistivity 80−20377
Te, elec. cond. in metallic region, calc. using modified Ziman theory *(Russian)* 77−66149
Te, liquid, classical fluid model, neutralising negative background density 78−22621
Te, liquid, localized impurity states, paramag. susceptibilities 78−64185
Ti, density of states of d-band, heat of vaporisation 78−95253
Ti, elec. resist., melting pt. to boiling pt., temp. depend. 80−96839
Ti, liq., spectral emissivity and brightness-temp. meas. at MP 77−43356
Ti, liquid, viscosity at melting point, free energy *(Russian)* 80−92699
Ti, molten, reson. model calc. of elec. resist. 78−84189
Tl, electrical resistivity, 300-1050K 80−24868
Tl, mag. relax. of excited ^{207}Bi 77−16217
Tl, Nernst-Ettingshausen effect in solid and liq. states *(Russian)* 78−6353
Tl, O_2 activity from electrochemical meas. 80−104123
Tl, resist. and thermo-electric power using corrected parameters of Shaw model 79−19566
Tl, struct. factor, Percus-Yevick equation perturb. treatment, square-well pot. approx. 78−75530
Tl, thermal props. at high temp. 80−75536
Tl, UPS, optical densities of states 80−2924
Tl, viscosity, comp. and temp. depend., up to 500°C 79−65233

liquid metals continued
U, hard-sphere model, phys. prop. meas. interpret., adjacent solid phase implications 77−19866
UO_2-Na contact interface temp., effect of internal radiation 79−13477
V, elec. resist., melting pt. to boiling pt., temp. depend. 80−96839
V, liq., spectral emissivity and brightness-temp. meas. at MP 77−43356
V, liquid, viscosity at melting point, free energy *(Russian)* 80−92699
V, thermophysical props. at temps. up to 7000K 80−103497
W 79−42280
W, chemically driven grain growth during sintering in liquid Ni 79−61532
W, containerless melts in terrestrial and space environment, thermodynamic props. calc. from solidification and cooling curves 79−70052
W, density at onset of sharp fall in elec. cond. 79−33026
W, elec. resist., melting pt. to boiling pt., temp. depend. 80−96839
W, molten drop break up in gas flow, surface drag, capillary excitation *(Russian)* 80−100024
Y, electrical resistivity of solid and liquid phases, thermopower, melting temp. 80−59955
Yb, liquid, resist. and thermoelec. power, t-matrix calc. 78−26840
Zn, electron energy states calc. *(Russian)* 79−4506
Zn, hot galvanising of Fe, Fe-Zn compound form. *(French)* 79−20275
Zn, interference function temp. depend. from X-ray diffr., elec. resist. calc. 77−47332
Zn, liq., NMR and relax. 79−8061
Zn, liq. Knight shift, temp. depend. 78−80232
Zn, liquid, US wave velocity *(Japanese)* 79−60438
Zn, liquid, viscosity determination by oscillating vessel method *(Japanese)* 80−70439
Zn, melt density, temp. depend. *(Russian)* 79−69174
Zn, molten, struct. investig. by neutron diffr. 79−4233
Zn, molten, surface tension, positive temp. coeff. 77−72751
Zn, reaction with solid Cu 77−9127
Zn, reaction with WC-Co, lamellar struct. form. 79−33964
Zn, resist. and thermo-electric power using corrected parameters of Shaw model 79−19566
Zn, structure factor, 460 to 650°C, by neutron diffr., elec. resist. temp. coeff. 77−47333
Zn, surface tension, temp. depend. *(Russian)* 80−15336
Zn, thermal conductivity meas. in Spacelab, design and terrestrial testing of measuring cell *(German)* 80−57303
Zn, X-ray diffraction analysis 79−4232
Zr, liquid, viscosity at melting point, free energy *(Russian)* 80−92699
ZrC-Ni, refractory-liquid metal, interfacial reactions, C effect, electron microprobe analysis 77−12829

liquid oscillations
see also liquid waves
autooscillations, azimuthal wave type, rot. Couette flow stability loss 77−75882
Bering, Chukchi and East Siberian Seas, mean sea level vars. 77−17144
boiling, sustained and transient, inlet subcooling effect on flow instabilities 78−94809
boiling loop in low-pressure operation of BWR at PNC Japan, stability anal. 78−8894
bubble stagnation depth in vertically oscill. liq. column viscous effect 77−42901
bubbles motion dynamics 80−38483
BWR coolant oscillatory flow perturbations, altered transverse momentum transport 79−608
capillary fluids rot. in cylindrical vessel, free oscill. *(Russian)* 77−27542
carbon tetrachloride drops falling through H_2O, surfactants rel. to deform., oscill. *(French)* 80−66880
cavitation bubble in liquids with polymer additives, small pulsations 77−68647
cavity in solid body, effect on solid body control device motion *(Russian)* 78−14031
charged liquid, parametric surface wave excitation by AC elec. field 79−23375
complex cavity containing liquid, appl. of finite difference method *(Russian)* 77−72227
compressive and tensile wave propagation in fluid column 79−18901
confined vortex oscillator, mathematical model 78−14104
container subjected to forced pitching oscillation, liquid motion, nonlinear anal. 80−96270
controlled vibratory movement under near-zero gravity conditions 78−14119
convection in vibr. layer of fluid heated from above 79−86424
convective stability of weakly cond. liq. in electrostatic field *(Russian)* 77−27601
cooling, in oscillating liquid-filled cylinders 80−10117
cross flow effects in oscillating boundary layers 77−42802
cryogenic liquid in straight tube, forced oscillations *(Russian)* 79−97393
cylinder, circ., oscillating in turbulent water flow, press. fluctuations 79−59995
cylinder, two-dimensional, oscillating in shallow water, hydrodynamic forces and moments 78−38269
cylinder oscillating in viscoelastic fluid, secondary flow 79−60037
damping, hydraulic torsional vibration damper *(Russian)* 80−92164
double structures of steady streaming in the oscillatory viscous flow over a wavy wall 79−94636
doubly connected free liq. surface acted upon by surface tension forces 77−80682
drop, oscillating, immersed in 2nd fluid, induced flow field streaming 78−59454
drop of viscous liquid, in immiscible liquid, normal-mode anal. of oscillations 80−74932
droplets, forced vibr., Raman scatt. obs. 80−34929
droplets, oscillating, in stationary liquid phase, behaviour 78−1718
drops in immiscible liquid, intermittent elec. field heat transfer augmentation 78−94872
duct flow with oscill. plate, numerical soln. 79−50794
duct with abrupt enlargement, transonic flow, self-excited oscills., model calcs. 80−28522
dusty fluid, flow past wavy moving wall 80−96299
dusty fluid flow past plate, small amplitude oscillations 80−14792
dusty viscous flow due to torsional vibrations of a circular disc 80−28548

liquid oscillations continued
elastico-viscous MHD fluctuating flow past porous plate, heat transfer 79−90342
eustatic sea level changes and continental platform subsidence mechanisms 77−21718
external flow, oscillating, struct. and development of turbulent boundary layer 80−19353
ferrohydrodynamics, mag. relax. models 79−94706
ferroliquid, magnetoelastic oscills. 79−94639
ferromagnetic fluid rotating about vertical axis, convective instability of layer 79−27698
film, ripple flow, stat. characts. 77−7408
film boiling crisis, surface material thermophys. props. influence, data correl. 80−5923
flow between two oscillating discs 77−39355
flow in U-tube manometers, effect of drag reducing polymer additives 80−64584
flow past vertical porous plate with constant suction, free convection effect, correction to earlier paper 77−27594
fluctuating boundary layer in a rotating fluid with variable suction 79−50718
fluctuating flow past a cylinder at high frequencies 80−1518
fluctuating free convection flow on horizontally magnetised plate 80−33683
fluid force on oscillating disc in a still fluid 80−14724
fluid structure vibr. eigenvalue problems, finite elements, modal methods 80−96269
fluid-structure coupling problem soln. using boundary-integral eqn. method 77−54920
forced oscillations in large vessels of circulatory system, dog's arterial blood flow anal. 78−85329
forced oscillations in rotating stratified liquid 78−63478
forced oscillations of an enclosed rotating fluid under a uniform magnetic field 79−32688
free liquid surface oscillations, gas bubble motion 80−100025
free oscillation in a rotating spherical shell 80−19409
free oscillation of liquids through a tube with abrupt changes in flow sections, damping ratio calc. 79−77149
free oscillations in U-tube, slip boundary conditions *(Russian)* 80−79338
free surface on simple fluid between cylinders undergoing torsional oscills. 77−35152
gas bubbles in vibrating liq., selective bubble drift *(Russian)* 79−14456
gas vibrations in tubes under action of periodically varying pressure 79−94718
Gentilly-1 steam mains, hydrodynamic oscills., acoustic anal. 79−97771
gravity waves, propag. in two liquids separated by membrane *(French)* 78−87355
harbours, reson. in closed L-shaped channel 77−78190
heavy viscous rotating fluid system, normal oscillations *(Russian)* 79−14417
n-heptane, self-excited thermoacoustic oscills. in heat transfer 78−79186
Holocene eustatic sea level change, British Isles 78−65333
hydraulic lines, wave phenomena, coupled vibrations in bending and branching lines 80−14778
hydraulic lines, wave phenomena, freq. characts. between press. and flow rate 79−32669
hydrocarbon drops levitated in water, acoustically forced shape oscill. 79−47987
hydrodynamic oscillations in Gentilly-I steam mains by inertial analysis 78−89944
immersed bodies in buoyant fluid, steady state oscills. 77−15052
impinging free shear layers, self sustained oscillations, book contrib., review 80−19466
incompressible liquid oscills. in variable cross section viscoelastic tube due to pulsating press. 80−31519
inertial oscillations of rotating fluid in rigid axisymm. container 78−1673
inviscid liquid, spherically oscillating, force acting on particle and bubble 77−35222
Lake Huron, Saginaw Bay, Georgian Bay and North Channel, gravit. oscills. 77−60435
lake level vars. recorded by bottom sediments 77−66936
laminar boundary layer, small amplitude oscillation development, stability characts. 80−48674
laminar boundary layer on body in simple harmonic motion, three dimens. unsteady flow 77−27507
liquid, in vessel, vibr. amplitude determ., structural damping and surface tension applied to stress anal. 80−19417
liquid metal, unsteady channel flow with transversely applied mag. field 77−84328
liquid-to-gas surface, dynamic behaviour in near weightlessness *(Russian)* 77−68611
measurement technique for oscillations in isochronous containers 80−53899
MHD oscillatory flow past impulsively started porous limiting surface, variable suction 79−86518
MHD stratified flow between oscillating disks, boundary layers 80−28570
miscible, viscous, incompressible fluids, oscillatory pressure gradients, anal. 78−38405
mixture, binary, oscillatory convective instability, thermodynamic anal. 78−94753
non-Newtonian fluid, convection, stationary, vibr. instability 79−94683
nonlinear forced oscillations in closed tube, functional eqn. continuous solns. 79−72948
nonlinear instabilities, filtering in fluid dynamic eqns. 79−41667
nonlinear liq. column oscills. in manometer, theory and expt. 78−90922
nonlinear wave effects in a closed tube 79−90332
ocean, S.Sicily Basin eigenperiods rel. to 'Marrubbio' phenomenon 77−53062
ocean, time averaged drag on obstacle or floor in oscill. flow 77−65748
ocean, wind-induced turbulence energy distrib. rel. to mixed layer evolution *(Russian)* 80−94529
ocean inertial oscills. from current meter data near Oregon coast 77−41047
ocean inertial oscills. radiation damping, wind mixed layer turbulence 79−39730
oscillating vessel with liquid containing compressible sphere, finely disperse inclusion motion 80−74963

liquid oscillations continued
oscillatory hydromagnetic free convection flow past an infinite vertical flat plate with suction 79−32687
parametrically excited nonlinear chain, stochastic oscills. *(Russian)* 79−55363
particle free fall in oscill. liqs., eqn. of motion 77−3859
particle motion induced by liq. oscills. 77−35210
periodic MHD oscillations, stability, perturbation theory 80−83858
pigment dispersion rheology, kinetic model, expt. results 79−7361
pipe flow, curved pipes, fully developed oscillatory flow 80−83846
pipe flow, curved pipes, oscillatory flow development 80−79400
pipe flow with high viscosity, acoustical streaming and thermal effects 77−15122
plane jet, stability and autooscillations from channel anal. 80−100018
plate oscillation effect on horizontal free convection flow 77−75904
polyethylene melt, high density, oscillating flow during extrusion, model anal. 80−100016
polymer solutions, drag-reducing, in U-tube 79−1217
polymeric liquid, steady shear flow, parallel superposition of oscillatory motion 79−18919
postglacial sea level changes, W.Newfoundland, rel. to ^{14}C age of Robinson's Head moraine 78−20401
pseudo-periodic flow in U-shaped tube, stability anal. 79−98809
pulsatile flow of immiscible liq., stability of interacting cylindrical liq. jet 78−83444
pulsation effect on mass transfer inside drops *(French)* 78−55686
Rayleigh-Benard convection, time depend. vel., turbulence transition 77−3824
reversed flow characteristics due to jet issuing from dead end channel *(Japanese)* 80−100021
Rivlin-Ericksen viscoelastic fluid, unsteady flow through confocal elliptic cylinders 79−37354
rolling motion of sphere on plane boundary 77−3834
rotating cylindar partially filled with liquid, oscillations of free liq. surface *(Russian)* 77−68594
sea level changes before and after 1961 and 1968 earthquakes at Hyuganada, Japan 77−17042
second-order fluids, oscillatory free convection from infinite horizontal cylinder 77−72332
self excited oscillations, impact of liquid jet against plane barrier 79−32545
self-oscillations during spiral flow, loss of stability 77−80171
self-sustaining oscills. of flow past cavities, review 78−94645
shell of revolution immersed in liquid, freq. distribution function 80−69587
shell-fluid system, steady periodic motions appearance *(Ukrainian)* 77−31240
sinusoidal oscillations, forces on cylinders near plane boundary 77−42855
solar energy collector system using regenerative oscills. in water columns 79−23188
source flow of conducting fluid between parallel discs 80−99986
spherical shell moving in acoustic medium, transient response 77−35067
stability of flow between two rotating cylinders, effect of thermal diffusion 78−18308
steady streaming over infinite plate 80−19125
Stokes problem, effects of free convection on oscillatory flow past infinite porous vertical limiting surface 80−109348
straight ducts of arbitrary cross section, oscillatory and steady flow 80−48801
stratified medium, rotating, small oscillations, internal waves 77−68664
streaming in vicinity of plate possessing propagating longitudinal strain wave 80−87758
sub-Rayleigh oscill. convection 80−87774
suction controlled boundary layer flow, perturbation caused stability loss 77−75886
surface elevation produced by oscillatory press. distrib. in uniform translation on surface 77−47027
surface oscillations, viscosity and surface tension relax. effects 77−62266
suspension, oscillating parallel flow in channel 77−68677
thermoacoustic vibrations of subcritical press., vibrs. onset mechanism 77−47026
thixotropic fluid, shear flow, oscillatory Couette flow, apparent viscoelasticity 79−90288
torsional oscillations of a non-Newtonian fluid with a free surface 79−94682
tube, forced gas (liq.) oscills. linearised treatment 79−50744
turbulent boundary layer structure at smooth solid wall *(Russian)* 77−58667
turbulent boundary layers in oscillating flow with a mean adverse pressure gradient *(French)* 79−77085
turbulent flow, press. fluctuation spectrum, elastic boundary compliance effect 78−63422
turbulent subcooled flow, transient radial heat transport effects 77−42834
two-phase flow instability in parallel channels 78−94810
two-phase systems, thermally induced flow oscillations investig. 77−42907
U-tube manometers, Navier-Stokes equations solution and expt. verification *(Japanese)* 80−6142
unsteady viscous flow near axisymmetric stagnation point on circular cylinder 79−23302
US resonance driving of ellipsoidal oscillations of liquid drops 77−31164
vapour generator, two-phase flow dynamics 78−94808
vertical surface with suction, oscillatory flow, free convection effects 80−53865
vibrations and stability in nonlinear systems with one degree of freedom, book contrib. 80−1530
vibrations source characteristics, placed in liq. layer *(Russian)* 78−75154
vibratory liquid-gas mixture, nonlinear resonance expt. *(Ukrainian)* 78−90811
vibrosource, characts. in liq. layer 79−81905
viscoelastic fluid in oscillating pipe, effect on flow rate 79−60031
viscoelastic fluid layer heated from below, vertical periodic oscillations, convection, overstability 80−48755
viscoelastic liquid, boundary layer anal. of oscillating cylinder flows 77−65771
viscoelastic liquid layer, electrohydrodynamic instability 80−14832
viscous flow around cylinder *(French)* 77−905
viscous flow in oscillatory spherical annuli 79−32542
viscous fluid in toroidal tube, oscillations 80−79253
viscous fluid under cyclic deform., self-heating, hydrodynamic thermal explosion 80−58993
viscous incompressible heat generating flow past porous plate with free stream oscillations, laminar free convection 79−37311
viscous incompressible heat generating flow past porous plate with free stream oscillations, laminar free convection 79−37312
wall with one-way heat flow, vertical inclined cavity stack 79−3899
water, forces on sinusoidally oscillating cylinder, parametric study 79−32547
water jet, penetration through water surface, high-speed photography 78−42693
water outflow from collapsible tube 77−89202
water-air two phase flow, oscillatory flow instabilities 80−83833
water-fluidised bed, viscosity meas. by oscills. damping 78−59475
wave, periodic, long, deform. over gently sloping bottom 78−90921
wave-induced oscillations in harbours of variable depth 79−4023
wedge oscillations in confined vesicle *(Russian)* 80−43651
H_2O channel flow, heat transfer from cylinder oscill. in cross flow 79−55386
^4H, superfluid, thermally induced flow oscillations 79−82404
He, aspect ratio, effect on time depend. flow above convection 79−7718
He II rotating, Poisson brackets and continual dynamics of vortical lattice *(Russian)* 79−73359
He, thermally induced oscills. in cryogenic apparatus 78−67875
^4He, solid, nucleation in Vycor under press., superfluid oscills. near melting press. 79−51388
^4He, superfluid film, saturated, oscills. induced by persistent circulation 77−47637
^4He superfluid film, two-reservoir, oscills. below 1K, damping 78−14535
^4He, superfluid vortex lattice collective oscills. *(Russian)* 78−51759
N_2 thermisiphon, flow oscills. 77−23960

liquid permeability *see permeability*

liquid phase epitaxial growth
buried heterostructure laser, DH multilayer LPE growth on etched substrate, optical read-out appls., longitudinal mode operation 80−99749
cassette for batch growth of layers 77−77424
constant growth rate conditions, for growth from cooling static solution, exam. 78−56051
covalently bonded materials, surface reconstruction effects, review 77−89669
decamethylene polyester, epitaxial crystn. on aromatic hydrocarbon substrates 79−61521
dopant segregation during liq. phase electroepitaxy, theory and expt. 80−54384
dotriacontane polyester, epitaxial crystn. on aromatic hydrocarbon substrates 79−61521
edge-growth reduction, by aux. heating of graphite slider side-walls 78−30848
ferrite films, hexagonal, growth by LPE 78−3062
ferrite spinel films, LPE growth and props., SIMS, X-ray diffr., and spin wave reson. obs. 80−34323
ferrites, hexagonal and spinel, growth on nonmag. spinel substrate by isothermal dipping LPE 77−12552
ferrites, LPE growth and characterisation 78−68640
film property control, regression eqns. 79−33200
from solution in melt, crystn. theory 80−16204
$Ga_{1-x}Al_xAs$ LPE growth: composition control and growth rate analysis 79−95946
Ga(AsP) on GaAs, LPE, growth with Ge and Sn solvents, phase diags. 78−88434
GaInAsP quaternary alloys, orientation effects in LPE growth 78−92203
garnet, bubble film, LPE growth reproducibility 79−1830
garnet bubble film LPE with high Pb content 79−38750
garnet double layer prod. for magneto-optical devices, LPE 77−21043
garnet ferrites 77−89673
garnet film, Bi substituted, LPE growth 77−1798
garnet film, Ga and Ge substituted, mag. prop. control during LPE growth and processing 78−68638
garnet film, growth rate depend. of growth-induced anisotropy 78−14992
garnet film, LPE technique, difficulties and advantages 79−28958
garnet film containing Lu, Curie temp. and flux spin-off, melt comp. effect 77−85515
garnet film LPE growth, for bubble memory appl., review, book contrib. 79−70009
garnet film preparation, single-crystal, for magnetic bubble domain appl. 78−60588
garnet films, isolated steps, rate analysis of growth parameters 80−10805
garnet films, oxidic high temp. solns. struct. 80−10808
garnet films, thermally induced substrate fracture 78−68639
garnet films 180° capped double layer LPE film, bubble wall states coding 80−34716
garnet layers, growth kinetics and struct. as functions of cryst. lattice parameter mismatch 80−6677
garnet layers, growth rate depend. on supercooling, induced striation expt. 79−24453
garnet LPE, liquidus temp. and growth-dissoln. kinetics 79−51028
garnets, bubble domain memory appls., growth requirements 77−20660
garnets, LPE growth, using horizontal dipping, exam. of growth kinetics 78−60039
growth rate calc., from GaP and GaAs LPE data 79−19485
growth rate calcs., comparison with GaP experimental results 79−52134
heterostructures for integrated optics 77−39112
hexamethylene polyester, epitaxial crystn. on aromatic hydrocarbon substrates 79−61521
horizontally dipped LPE film, inhomogeneities, spin wave reson. meas. 79−91298
III-V compounds, Stefan problem, exact soln. describing growth rate with linear cooling 80−59411
III-V pseudobinary compound, growth and phase equilib. in vertical rotating LPE reactor *(French)* 77−77430
III-V semiconductor compounds for optical devices in 1.0-1.6 μm region, crystal growth by LPE and CVD 79−43161
III-V semiconductor heterostructures, growth and dissolution kinetics by LPE 80−49543
III-V semiconductor solid soln., doping with groups II and IV *(Russian)* 77−80705

liquid phase epitaxial growth continued
III-V semiconductors, electroliquid epitaxy, role of electrotransport 79−56095
III-V semiconductors, impurity distribution, during epitaxial growth from liq. phase 80−88443
III-V semiconductors, p-n heterostructures, epitaxial growth techniques, appl. to optoelectronics, review 80−54770
III-V semiconductors prep. *(Czech)* 80−89131
integrated optical circuits, selective LPE 78−6868
layer growth from undercooled melts, numerical model 80−6665
layer thickness and growth efficiency calcs. 79−51453
macromolecules, epitaxial crystallisation, review 79−42409
magnetic bubble materials, review 80−50153
magnetic garnet films, for magneto-optic appls., substituted rare earth garnet substrate crystals 78−31351
model layer thickness calc. 79−19484
molecular beam mass spectrometry, in situ anal. of minor gaseous species 80−52357
multi-layer, furnace design and fabrication *(Japanese)* 80−108366
multicomponent systems, electroepitaxy, theoretical model 80−65396
multilayer, technique 78−31345
multiple layers, apparatus using centrifugal forces 77−77433
oriented thin film mosaic, growth using stochastic distrib. of minute pinholes 80−7509
Peltier-induced, in semiconductor films, composition control 78−48343
Peltier-induced, in semiconductor films 78−48342
periodic structures, props., prep., use 78−51982
perturbations propagation, surface, large-amplitude 79−37929
photocathode structures, TEM obs. of dislocations generated 80−100241
polycaprolactone, epitaxial crystn. on aromatic hydrocarbon substrates 79−61521
polyesters, epitaxial crystallisation, on organic and inorganic substrates 78−91565
polyethylene, epitaxial crystallisation, IR investig., macromol. struct. changes 77−35493
polyethylene azelate, epitaxial crystn. on aromatic hydrocarbon substrates 79−61521
polyoxyethylene, epitaxial crystallisation, IR investig., macromol. struct. changes 77−35493
polyoxymethylene, kinetics of epitaxy and over-growth on needle-like single crystals 78−14291
polyoxymethylene film, epitaxial crystallisation from soln. 77−7984
polypropylene, isotactic, epitaxial crystn. on alkali halide surface 78−26787
polyurethanes, epitaxial crystallisation, IR investig., macromol. struct. changes 77−35493
polyvinylidene fluoride vinyl fluoride copolymer, epitaxial crystallization 79−65005
pure melt batch production in sliding apparatus 78−44028
rare earth garnet prep., novel Li_2MoO_4-$R_2(MoO_4)_3$ flux system 77−48359
rare earth garnets, prep. and props. book contrib. 80−44193
rare earth iron garnet single crystal films, synthesis and props., reviews 78−48013
rare earth iron garnets, (Ca,Ge)-substituted, flux growth in regular soln. approx. 79−78907
review of growth and appl. 78−22966
ripple wavelength, morphological stability theory 78−34725
saturated solution evaporation, crystallisation by epitaxial nucleation *(French)* 77−35831
semiconductor, ion-implanted regrowth by LPE 79−69121
semiconductor binary compounds, LPE, book contrib. 77−12553
semiconductor laser material requirements, liq. heteroepitaxy of solid solns., review 77−14718
sliding boat method for high purity LPE growth, GaAs FET buffers appl. *(Japanese)* 79−28955
source materials, for LPE, weighing method 80−66439
Stefan problem, exact soln. describing growth rate of binary III-V compounds with linear cooling 80−59411
substrate holder 78−92207
substrate material, nonmag. flux growth and suitability of $ZnGa_2O_4$ single crysts. 78−44000
superalloy, laser melted, epitaxial resolidification 77−90491
temperature gradient meas. using W-graphite thermocouple 80−25584
ternary component solution, liquid and solid comp. variations during LPE growth 79−99445
TGS, on Ag film, saturated soln. evaporation, crystallisation by epitaxial nucleation *(French)* 77−35831
TGS-d, TGSe-d, single cryst. films, IR transmission spectra *(French)* 78−72742
thermal degradation of substrates, reduction method, appl. to LED fabrication 80−104061
thermodynamics of phase transition intensity in crystn. processes *(Russian)* 78−38636
thermoelectric recrystallisation, epitaxial film growth rate 80−100424
two-dimensional computer analysis of LPE 79−95286
urea mixed and adsorption mixed crystals and epitaxial growth from solns., tracht and habit *(German)* 80−38973
vapour-liquid-solid growth mechanism *(Russian)* 80−107074
volume-controlled film growth 78−88432
wipingless method *(Japanese)* 78−27422
zone recrystallisation with moving temp. gradient, LPE kinetics *(Russian)* 77−48354
Ag epitaxial growth, on W-ribbon substrate, in UHV, cryst. orientation determ. by etching *(German)* 79−65994
AgCl, epitaxial overgrowth on AgBr sheet crystals 79−19988
(Al,Ga)As/GaAs, LPE grown heterostructures, X-ray diffr. exam. of interfacial elastic strains 78−72019
Al-Ga-As heterostruct. with confined current flow, fabrication 78−68081
Al-Ga-As heterostructure formation by LPE 77−32517
Al-Ga-Sb ternary phase diagram, calc., DTA and LPE expts. 80−29931
AlAs-GaAs heterostructure, fabrication by selective liq.-phase epitaxy 79−15618
AlGaAs electroluminescent heterostructures, LPE, appl. to LED fabrication 80−55308
AlGaAs, heteroepitaxial waveguides for image transmission *(Russian)* 77−11037
AlGaAs heterojunction laser, lightwave sources and detectors 80−64068
AlGaAs, LPE layers, growth initiation and cathodoluminesc. irregularities 79−87010
AlGaAs p-n diodes, I-V characts., tunnelling 80−100510

liquid phase epitaxial growth continued
(AlGa)As-GaAS DH lasers prep. by new LPE technique 77−40358
AlGaAs-GaAs, DH laser material, singular instabilities of LPE growth surface 77−24969
(AlGa)As-GaAs, large area high efficiency solar cell fabrication, LPE process 77−36410
AlGaAs-GaAs transverse mode stabilised plano-convex waveguide laser made by single step LPE 80−48274
$Al_{0.3}Ga_{0.7}As$:Te(SN), impurity effects on interface morphology of LPE films on corrugated GaAs substrates 78−88435
$Al_{1-x}Ga_xAs$, transient-mode LPE on GaP 78−72746
$Al_xGa_{1-x}As$ and GaAs planar local struct. synthesis by LPE 79−56097
$Al_xGa_{1-x}As$ DH laser, with constricted active region, fabrication and characts. 78−37895
$Al_xGa_{1-x}As$ DH laser, rake-line form. in LPE growth, doping effects 80−2287
$Al_xGa_{1-x}As$, electron mobility illumination, compensation, space charge regions, carrier scatt. 80−70691
$Al_xGa_{1-x}As$, epitaxial growth, orienting substrates effects 77−43444
$Al_xGa_{1-x}As$, epitaxial growth from limited vol. melt 79−70005
$Al_xGa_{1-x}As$, epitaxial layer crystn. from soln. in melt, diffusion limited 78−35321
$Al_xGa_{1-x}As$, growth of high-resistivity layers by liquid-phase epitaxy 79−70008
$Al_xGa_{1-x}As$, growth of uniform epitaxial layers 77−40393
$Al_xGa_{1-x}As$, LPE, cathodoluminesc. obs. 78−68565
$Al_xGa_{1-x}As$, LPE, effect of doping on interface morphology 77−81231
$Al_xGa_{1-x}As$ layer, LPE, graded bond gap solar cell, composition profile, Rutherford backscatt. 78−76612
$Al_xGa_{1-x}As$ layers, graded band gap, growth and properties 79−60645
$Al_xGa_{1-x}As$, monolithic optical integration for new devices 77−75714
$Al_xGa_{1-x}As$ semi-insulating film, growth and elec. props. 77−44179
$Al_xGa_{1-x}As$ solid soln., epitaxial layer growth on GaAs by zone recrystallisation with temp. gradient 77−16510
$Al_xGa_{1-x}As$ thick epitaxial layer production, by zone recrystn. in temp. gradient 79−15619
$Al_xGa_{1-x}As$ thin graded band-gap layers, isothermal LPE growth 80−34325
$Al_xGa_{1-x}As$, VPE and LPE growth, electron mobility 79−91165
$Al_xGa_{1-x}As$, waveguide heterostruct. epitaxial growth with gradual composition change 79−42416
p-$Al_xGa_{1-x}As$:Ge layer on GaAs substrate, Hall and elec. cond. meas., Hall mobility 80−2402
$Al_xGa_{1-x}As$:Zn epitaxial layers, composition and Zn carrier conc. 80−25585
$Al_xGa_{1-x}As$-GaAs, heterojunction, interface width, AES obs. 80−20290
$Al_xGa_{1-x}As$-GaAs multilayers, using addition of GaCl vapour and new boat struct. 79−33950
AlGaAsP(Sb), compositional grading by LPE 80−10844
AlGaAsSb LPE growth, lattice-matched to GaSb, characterisation 80−60794
AlGaAsSb, photodiode, lattice-matched to GaSb 79−71527
$Al_yGa_{1-y}As_{1-x}Sb_x$ LPE phase diagram 78−11137
$Al_yGa_{1-y}As_{1-x}Sb_x$, LPE, strain effects near miscibility gap, importance 79−7759
$Al_xGa_{1-x}AsZn$-GaAs solar cells by LPE, open circuit voltage, fill factor 80−101108
$Al_xGa_{1-x-y}In_yAs$, LPE on InP, solid-liq. equilib. calcs. 78−84083
$Al_xGa_{1-x}P$-GaP structure, double heterostruct. light modulator appl. 79−28963
AlGaSb, growth and characts. for 1.0-1.8 μm heterojunction devices 78−6870
$Al_xGa_{1-x}Sb$, compositional var. during LPE growth using ternary phase diagram 77−59761
$Al_xGa_{1-x}Sb$, solid soln., epitaxial layer growth from liq. phase 77−85089
$Al_xGa_{1-x}Sb$, surface flatness depend. on LPE condition 79−15042
$Al_xGa_{1-x}Sb$:Zn(Si)(Ge)(Sn)(Pb), doping of solid solns. during LPE *(Russian)* 77−85087
$Al_xGa_{1-x}Sb$-Pd contacts, struct., preparation elec. props. 80−65684
$(AlSb)_x(GaSb)_{1-x}$, solid soln., phase diagram of Ga-AlSb-GaSb 77−40392
Au, electroless deposition, epitaxial initial growth with microtwinning 77−8771
Au-GaAs Schottky barrier diode, X-band applications 77−8192
(Ba,Pb)$Al_{12}O_9$, LPE growth 79−100064
Ca, Ge-substituted garnet, LPE growth atm. effects on bubble props. 77−20655
$Cd_xHg_{1-x}Te$, epitaxial growth from stoichiometric melt, crystn. and diffusion 80−75475
$Cd_xHg_{1-x}Te$, solubility in Hg, rel. to LPE 78−35359
CdSe, LPE growth on ZnTe, characterisation of heterojunction 77−4745
CdTe, in CdTe-$CdCl_2$ system 78−35323
CdTe, optical waveguide, fabrication by LPE using boat-slide technique 77−63570
CdTe, solubility in Hg, rel. to LPE 78−35359
CdTe:Cl, LPE from $CdCl_2$ soln., elec. props., defects 80−39689
CdTe/$Hg_{1-x}Cd_xTe$ multilayers, LPE growth 80−80104
CdTe-In system, equilib. phase diagram and liq. phase epitaxial growth of CdTe from In soln. *(Japanese)* 80−71634
Co ferrite, growth on fine acicular γ-Fe_2O_3 particles 80−29871
Cu, epitaxial electrocrystallisation, substrate imperfections effect 78−18921
Cu ferrite films, Mn-, Ni- and Al-substituted, LPE growth 80−96752
Cu film, on W substrate, cementation, vac. deposition, and electroplating, growth characts. 79−95291
$CuFe_2O_4$, LPE grown, domain struct. rel. to tetragonal distortion 78−92205
p-$CuGaS_2$, on n-ZnS, heterojunction prep. and characterisation 79−1831
Cu_2S, epitaxial layers grown from liq. soln. RHEED obs. 78−91558
$Er_3Al_{5-x}O_{12}$ spectroscopic props. 80−93419
$(Eu,La,Ca)_3(Fe,Ga,Al)_5O_{12}$ film, LPE growth and induced orthorhombic anisotropy 77−20652
$(Eu,Lu)_3Fe_5O_{12}$, submicron bubble films on rare earth-Ga garnet substrates, prep. and mag. props. 78−91909
$Eu_{3-x}Ca_xSi_xFe_{5-x}O_{12}$, bubble film, LPE growth induced anisotropy 77−20659
$(EuLu)_3(FeAl)_5O_{12}$, film epitaxial growth on Gd_3GaO_{12} substrate, mag. props. 80−65402
EuTm-CaGe, magnetic FE garnet film, LPE growth and composition 78−23634

liquid phase epitaxial growth continued
$EuTm_2Fe_5O_{12}$ film , CaGe substituted, LPE growth kinetics 78−31349
(Ga,Al)As, LPE growth of multilayered struct., explanation for meniscus lines on surfaces 77−76681
(Ga,In)(As,P) DH lasers, 1.55 μm, low-threshold current densities 80−1221
Ga, diffusion coeff. of As at 720°C during LPE growth 80−54419
Ga-Al-As(Sb) solid soln., liquidus surface in ternary phase diagram, simplex lattice method 77−7847
Ga-Al-As(Sb) system, ternary phase diagrams, method for determ. of liquidus surfaces 77−28787
Ga-Al-Sb, liq. phase epitaxy, phase diagram, X-ray microanal. 79−19491
Ga-As-P solid soln., liquidus surface in ternary phase diagram, simplex lattice method 77−7847
Ga-As-P system, ternary phase diagrams, method for determ. of liquidus surfaces 77−28787
Ga-In-As solid soln., liquidus surface in ternary phase diagram, simplex lattice method 77−7847
Ga-In-As system, ternary phase diagrams, method for determ. of liquidus surfaces 77−28787
Ga-In-As-Sb system LPE layers, pseudoquaternary phase diagram 78−10293
GaAS-AlGaAs LPE layers, defects formed by oxygen in ambient gas *(Japanese)* 77−70009
GaAlAs based heterojunctions, integrated optics appl., technology advancements *(Slovak)* 80−33226
(GaAl)As, DH laser, LPE growth, meniscus lines as nucleation sites 77−15706
GaAlAs, heterostruct. formed by LPE, growth and dissolution kinetics 79−99439
(GaAl)As, LPE, GaAs dissolution kinetic in undersaturated isothermal solns. in Ga-Al-As system 80−80106
(GaAl)As system, automated system for growth of multilayered structs. by LPE 79−38752
GaAlAs/GaAs, n-p-n heterojunction transistor, elec. props. 79−87149
GaAlAs-GaAs heterostructure laser fabrication 77−42538
GaAlAs-GaAs heterostruct. solar cells, Al, P, Zn incorporation by LPE *(French)* 79−24899
GaAlAs-GaAs lasers, channelled substrate, prepared by combination of organometallic pyrolysis and LPE 80−99745
$Ga_{0.65}Al_{0.35}As$ epitaxial layer on GaAs, two-dimensional lattice mismatch parallel to interfacial boundary 79−51439
$Ga_{0.65}Al_{0.35}As$, LPE growth, wave morphologies on surface 77−40396
$Ga_{0.7}Al_{0.3}As$ epitaxial film, inclusion-generated dislocation clusters 77−89445
$Ga_{0.7}Al_{0.3}As$-GaAs n-n heterojunction, LPE, rectification 80−49888
$Ga_{0.9}Al_{0.1}As$, nucleation morphologies on $Ga_{0.65}Al_{0.35}As$ surfaces grown by LPE 78−15323
$Ga_{1-x}Al_xAs$, appl. of theory of electroepitaxy of multicomponent systems 80−65396
$Ga_{1-x}Al_xAs$ DH laser, LPE surface protective coating 78−35320
$Ga_{1-x}Al_xAs$ film, with x=0.23 and 0.37, grown by linear cooling, thickness comparison with GaAs 78−87892
$Ga_{1-x}Al_xAs$, growth mechanism and morphology on channelled substrates 79−28960
$Ga_{1-x}Al_xAs$ heterostructure, LPE prep., growth and dissolution kinetics, thermodynamic and kinetic models 80−75456
$Ga_{1-x}Al_xAs$ integrated optical waveguide LPE 77−75703
$Ga_{1-x}Al_xAs$ LPE crystals for DH laser, LEDs, TEM obs. of Ge, Si-doped epitaxial layers 79−1556
$Ga_{1-x}Al_xAs$, LPE growth and characterisation 80−50566
$Ga_{1-x}Al_xAs$, LPE layer thickness depend. on soln. comp. 78−10295
$Ga_{1-x}Al_xAs$, LPE layers, grown under const. cooling rate conditions, cryst. composition 78−39710
$Ga_{1-x}Al_xAs$ LPE layers, comp. and refr. index, ellipsometry meas. 79−87011
$Ga_{1-x}Al_xAs$, liquid and solid comp. variations during LPE growth 79−99445
$Ga_{1-x}Al_xAs$, Peltier LPE, absence of electromigration of As and Al 77−81230
$Ga_{1-x}Al_xAs$ transverse mode DH laser with inbuilt plano-convex waveguide 80−48296
$Ga_{1-x}Al_xAs$:Si, LPE, phase diagram, Hall effect meas., carrier conc., donor ionisation energies 77−72803
$Ga_{1-x}Al_xAs$:Si p-n junction, doping in LPE, elec. and luminesc. props. *(Czech)* 78−47851
$Ga_{1-x}Al_xAs$-GaAs, heteroepitaxial layers on GaAs(001), misfit dislocation asymmetry 77−47694
$Ga_{1-x}Al_xAs$-GaAs, high efficiency solar cell, isothermal etchback-regrowth method 77−59701
$Ga_{1-x}Al_xAs$-GaAs injection laser, branching waveguide coupler fabrication by LPE 78−63202
$Ga_{1-x}Al_xAs$-GaAs LPE multilayer heterostructure photovolt. solar cells, fabrication and performance 79−48128
$Ga_{1-x}Al_xAs$-GaAs p-n and p-p-n heterojunction solar cells, high efficiency, prep., eval. and characters *(Japanese)* 80−61342
$Ga_xAl_{1-x}As$, LPE, charge carrier conc. distrib. *(Russian)* 78−52694
$Ga_xAl_{1-x}As$, LPE, GaAs solubility in Ga-Al alloys investig. 78−52690
$Ga_xAl_{1-x}As_x$ photodetector diode on GaAs substrate dark currents, tunnelling, energy gaps, effective masses 80−70805
$Ga_{1-x}Al_xAs_{1-y}P_y$ layer of uniform composition grown on GaAs by LPE, temp. diff. method appl. 79−23864
$Ga_{1-x}Al_xAs_{1-y}P_y$-GaAs quaternary heterojunction strains and IR laser diode performance 78−9385
GaAlAsSb/GaSb alloys, prep. and optoelectronic device appl. 80−25587
GaAlAsSb-GaSb low bandgap solar subcell for high efficiency multibandgap convertors, LPE growth 80−93927
$Ga_{1-x}Al_xP$ varigap structs., crystallation 80−80993
$Ga_{1-x}Al_xSb$, LPE growth and phase diagram *(French)* 77−24974
$Ga_{1-x}Al_xSb$ p-n homojunction LPE and photovoltaic effect obs. *(French)* 78−64108
$Ga_{1-x}Al_xSb$ variable-gap p-n struct., selective photoelec. effect 77−76912
GaAs (111) substrate, and homoepitaxial layers, characterisation by divergent X-ray beam diffr. 78−31352
GaAs, and its alloys, as integrated optics materials, book contrib. 79−64362
GaAs and related cpds., conference, St. Louis, MO, USA (Sept. 1978) 80−8737

liquid phase epitaxial growth continued
GaAs, back etching and growth by liq. phase epitaxy, surface morphology obs. 80−29287
GaAs, current controlled LPE for optimum doping profiles in LSA diodes 78−35318
GaAs, deep levels rel. to growth conditions 79−28314
GaAs, epitaxial growth for microwave devices *(French)* 77−48360
GaAs, epitaxial layer, surface morphology 79−90852
GaAs epitaxial layers, from mixed Ga solns., C solubility 80−15392
GaAs epitaxial layers on polycryst. GaAs substrates, LPE growth charcts. 80−75471
GaAs FET, continuous growth of LPE double layers 78−64487
GaAs FET buffers, high purity LPE growth by sliding boat method *(Japanese)* 79−28955
GaAs FET double layer production, study by sliding boat method *(Japanese)* 79−66014
GaAs film, growth kinetics for step-cooling LPE technique 77−40395
GaAs film, thickness comparison with $Ga_{1-x}Al_xAs$, for layers grown by linear cooling 78−87892
GaAs film grown on O-implanted GaAs substrate, elec. props. 78−2592
GaAs, gaseous impurity source and effect on purity 79−28959
GaAs, growth mechanism and kinetics 78−34726
GaAs, heteroepitaxial layers on Si substrates by LPE 79−1832
GaAs, LPE, charge carrier conc. distrib. *(Russian)* 78−52694
GaAs, LPE, temperature instability effect, report 80−66446
GaAs LPE buffer layers for MESFET appls. 80−29887
GaAs LPE from Ga soln., carrier conc., growth condition depend. 80−71584
GaAs, LPE growth, electric current controlled, on n^+ and semi-insulating substrates 77−73240
GaAs, LPE growth 78−18924
GaAs, LPE growth from supercooled soln., thickness uniformity 80−54547
GaAs, LPE growth of high purity layers by sliding boat method 78−76610
GaAs, LPE growth on O-implanted GaAs substrates, surface morphology 77−28732
GaAs, LPE growth surface, singular instabilities 77−24969
GaAs, LPE in graphite boat, total ionised impurity density 77−12550
GaAs LPE in situ etchback calibration 79−83114
GaAs, LPE layers, ambient O_2 effect on defects and elec. props. 77−76683
GaAs, LPE layers, outdiffusion of recomb. centres from substrate during growth 80−39466
GaAs, LPE layers, voids and depressions in facet and terrace growth 78−38974
GaAs LPE on polycrystalline Mo 79−43157
GaAs, LPE with $AsCl_3$-saturated Ga/As solns. 78−63953
GaAs, layer growth by electroepitaxy, thickness profiles 79−4486
GaAs layers, electroepitaxy and thermal LPE growth, defect struct. and electronic characts. 80−2290
GaAs layers, grown by electroepitaxy and LPE, surface morphology 79−19478
GaAs layers, LPE from Au-Ge-Ni melts, elec. props. of Ni/Au-Ge/GaAs contacts obs. 77−77437
GaAs layers, LPE growth, graphite boat construction 78−31348
GaAs layers and p-n junctions grown by current-controlled LPE, elec. characts. 78−6436
GaAs, liquid-phase electroepitaxial growth kinetics, Peltier effect and solute electromigration 79−42401
GaAs, MESFET structure, buffered, LPE growth 80−40271
GaAs MM-wave and sub MM-wave receiver elements, Schottky-barrier resistive mixer devices 80−11558
GaAs, multilayer liquid phase epitaxy, transition to faceting 80−96750
GaAs, multiple layer LPE growth by controlled supercooling of Ga soln. 77−77429
GaAs, O^+ implantation, effect on LPE growth and elec. props. 80−24477
GaAs, optical integrated circuits appl. 77−65644
GaAs, Peltier induced growth kinetics of LPE 78−64485
GaAs, Peltier LPE, absence of electromigration of As and Al 77−81230
GaAs pure and Se-doped, photoluminescence at dislocations, band gap electronic levels 79−99926
GaAs, residual impurities and deep levels, FET fabrication 79−28964
GaAs Schottky-barrier diode submicron layer LPE reactor 77−77439
GaAs, semi-insulating, LPE growth for FET buffer layers 79−66015
GaAs, smooth, thin layers on nominally oriented substrate 78−44030
GaAs, solar cell, thin film, prep. by Peeled Film Technology 79−29472
GaAs, substrate for epitaxial growth, backscatt. anal. of surface prep. and anodic oxidation 77−25175
GaAs, synthesis by molten salt electrolysis 78−64486
GaAs, temp. difference growth under controlled vapour press., screw dislocations 77−35561
GaAs, transient-mode LPE on InP 78−72746
GaAs, undoped epitaxial layer growth from nonstoichiometric solns., O_2 contamination sources 80−108362
GaAs, wave morphologies on surface 77−40396
GaAs, X-ray topographic studies of defects 77−62772
GaAs:Cr, semiinsulating, LPE and elec. props. 77−44178
GaAs:Cr semi-insulating substrate, photoluminescence obs. of surface degradation during LPE growth 78−6865
GaAs:Fe, LPE, phase diagram 77−16509
GaAs:Fe LPE layers, negative resist. effects and deep acceptor model 77−72929
GaAs:Ge, LPE, on semi-insulating GaAs, film-substrate interface characterisation 78−72017
GaAs:Ge, LPE growth, Ge incorporation 78−27423
GaAs:Ge(Sn), LPE layer growth, impurity effect on terrace form. 79−95288
GaAs:Mn epitaxial layers, fabrication and electrical props. 77−80859
GaAs:P films, epitaxial growth from melt with components introduced by ion bombardment 77−21044
GaAs:Se, LPE growth, Ga-As-Se phase diagram 79−1849
GaAs:Se ohmic contacts, pulsed electron beam annealing donor density, mobility 80−65678
GaAs:Si, current-controlled growth, segregation and amphoteric behaviour 78−31346
GaAs:Si, thick LPE layer growth and characterization 77−12511
GaAs:Si LPE layers, surface morphology, substrate misorientation, initial supercooling effects 80−34329
GaAs:Si(Cr), LPE, spiral growth patterns, dopants role 77−72800

liquid phase epitaxial growth continued
GaAs:Sn, dopant segregation during liq. phase electroepitaxy 80−54384
GaAs:Sn, doping characts. during LPE 79−10866
GaAs:Sn, influence of growth process in doping profile and mobility profile during LPE 79−70000
GaAs:Sn, LPE, growth rate and temp. depend. of impurity incorporation 78−3063
GaAs:Sn, LPE layers, electronic props., depend. on Sn incorporation 78−87883
GaAs:Sn, selective LPE, orientation dependent growth, luminesc. 77−12551
GaAs:Sn, solubility and point defect-dopant interactions, LPE growth 79−90688
n-GaAs:Sn-p-GaAs:Ge-p-$Al_xGa_{1-x}As$:Ge heterostructure solar cells, LPE growth techniques 80−66977
GaAs:Te, LPE, Te induced defects, rel. to growth conditions 78−6067
GaAs:Zn, diffusion during LPE, impurity gradients and annealing effects 80−29882
GaAs:Zn, Se, double doping during LPE, exam. of elec. cond. and Hall effect 79−4923
GaAs:Zn epitaxial layers, composition and Zn carrier conc. 80−25585
GaAs:Zn(S), LPE, and doping characts. 79−33948
GaAs/AlGaAs integrated twin guide injection lasers prepared by LPE, coupling coeff. and coupling length meas. 79−81458
GaAs-(Ga, Al)As heterostructure transmission photocathode, characts. *(French, English)* 78−52616
GaAs-(GaAl)As channelled substrate buried heterostruct. injection laser, fabrication 77−7087
GaAs-(GaAl)As DH lasers, automated LPE growth, CW reliability tests 80−20804
GaAs-$Al_xGa_{1-x}As$, DH laser, lateral current confinement by reverse biased junction 77−58339
GaAs-$Al_xGa_{1-x}As$ buried-heterostructure lasers, current injection confinement, MBE/LPE hybrid technique 80−74374
GaAs-$Al_xGa_{1-x}As$ epitaxial layer heterointerface, toroidal defect obs. 79−77933
GaAs-$Al_xGa_{1-x}As$ heterojunctions, LPE grown, 2D electron gas obs. 79−99606
GaAs-$Al_xGa_{1-x}As$ structures for DH lasers *(Polish)* 79−4922
GaAs-AlGaAs DH, improved LPE growth, lasing characts. 77−81229
GaAs-AlGaAs DH laser, improved lifetime by defects reduction during LPE 77−75547
GaAs-AlGaAs DH laser, wipinglass method *(Japanese)* 78−48304
GaAs-AlGaAs DH layers, tapered growth by wipingless LPE 77−66594
GaAs-AlGaAs LPE layers, baking effect on surface morphology 78−14625
GaAs-AlGaAs photoelectroluminescent diodes, characts., radiant power 80−6972
GaAs-Au Schottky barrier diodes, fabrication using LPE 77−40357
GaAs-element systems, solidus curves calc. for liq. phase epitaxy technology 77−8768
GaAs-$Ga_{0.7}Al_{0.3}As$ channelled substrate buried heterostructure injection lasers 77−38932
GaAs-$Ga_{1-x}Al_xAs$, DH, improved LPE growth method 77−4746
GaAs-$Ga_{1-x}Al_xAs$, optically pumped ring laser fabricated by LPE over chemically etched channels 77−10958
GaAs-$Ga_{1-x}Al_xAs$, LPE growth for solar cells 77−77427
GaAs-$Ga_{1-x}Al_xAs$ half-ring laser, fabrication by LPE over chemically etched channels 77−684
GaAs-$Ga_{1-x}Al_xAs$ laser, low threshold room temp. embedded DH, fabrication and characts. 77−681
GaAs-$Ga_{1-x}Al_xAs$ LPE wafer stress-free dislocation generation 77−75527
GaAs-$Ga_{2.2}Al_{0.8}As$:Be, LPE, diffusion of Be into GaAs substrate 80−103517
GaAs-$Ga_xAl_{1-x}As$ CW stripe geometry laser fabrication and performance 77−38933
GaAs-$Ga_xAl_{1-x}As$ double heterojunction laser structures, LPE growth with double source method 79−28962
GaAs-$Ga_xAl_{1-x}As$ DH laser wafers, active layer inhomogeneities 79−74106
GaAs-GaAlAs, DH laser material, LPE grown, obs. of melt carryover 78−91553
GaAs-GaAlAs, inverted-ridge-waveguide DH injection laser with current and lateral optical confinement LPE growth 77−75540
GaAs-GaAlAs DH CW laser, growth by Peltier effect induced LPE 77−48357
GaAs-GaAlAs double heterostructures for CW injection lasers, LPE growth 79−31931
GaAs-GaAlAs heterostructures, Peltier effect *(Polish)* 78−6861
GaAs-GaAlAs LPE layers, DH material, TEM obs. of crystal defects 78−6241
GaAs-$Ge_{1-x}(GaAs)_X$ n-p heterojunctions, hydrostatic press. effect on elect. and photoelectric props. 80−20304
$GaAs_{1-x}P_x$ heterostructure, LPE prep., growth and dissolution kinetics, thermodynamic and kinetic models 80−75456
$GaAs_{1-x}P_x$ layer, growth by isothermal LPE 77−40398
$GaAs_xP_{1-x}$, liquid phase epitaxial growth on GaP, growth and properties 79−47641
GaAsSb/GaAlAsSb DH lasers, growth and props. 80−69412
$GaAs_{1-x}Sb_x$, cryst. growth by steady state LPE 78−44032
$GaAs_{1-x}Sb_x$, LPE,phase diagram meas. 77−20047
$GaAs_{1-x}Sb_x$ layer on GaAs, dislocation density reduction by improved LPE growth method 80−76202
$GaAs_{1-x}Sb_x$ on GaAs, LPE growth of GaAs 79−61519
$GaAs_{1-x}Sb_x$ ternary phase diagram, LPE, band gap and elec. props. 77−55896
$GaAs_xSb_{1-x}$, lattice-matched LPE growth in InP substrates 79−42402
$GaAs_xSb_{1-x}$ solid solution epitaxial layer, morphology and defect structure 77−1330
$GaAs_ySb_{1-y}$, miscibility gap, rel. to LPE 79−33090
$GaAs_{1-x-z}Sb_xP_z$, continuous comp. grading, use as secondary substrate 77−31913
$GaAs_xSb_yP_{1-x-y}$, continuously graded comp. layers 77−24970
$(GaAs)_{1-x}(ZnSe)_x$, LPE growth, resist., Hall effect and cathodoluminesc. meas. 77−28270
$Ga_yIn_{1-y}As_xP_{1-x}$-InP heterostructure, lattice matching and cryst. perfection 78−6437
$Ga_{0.47}In_{0.53}As$, LPE growth and characterisation 80−10845
$Ga_{0.47}In_{0.53}As$, photodetector applications 80−95140
$Ga_{1-x}In_xAs$:Mn grown by LPE, elect. props. 80−100541

liquid phase epitaxial growth continued
$Ga_xIn_{1-x}As$, cryst. growth on (100) InP by LPE 78−56591
$Ga_xIn_{1-x}As$, on (111)B InP, LPE growth, characterisation of high purity lattice 80−104082
$Ga_xIn_{1-x}As$ on InP, lattice matched LPE film growth and characts. 78−72033
$Ga_xIn_{1-x}As$, substrate orientation effect on liq.-solid distrib. coeffs., 600-700°C 80−2278
$Ga_xIn_{1-x}As$:Ge LED, by LPE, radiation emitted at 1.02 μm 78−48235
$Ga_xIn_{1-x}As$-InP, lattice matched LPE film growth and characts. 78−15320
GaInAsP, diffusion-limited growth in LPE 80−10842
GaInAsP layers on InP substrate, conditions for lattice matching in LPE growth 78−6866
GaInAsP on InP substrate, epitaxially grown, fabrication of avalanche photodiode 78−37071
GaInAsP on InP substrate 79−90023
GaInAsP/InP DH lasers, with (100) substrate, 1.2-1.5 μm, LPE growth conditions 79−15617
GaInAsP/InP DH lasers emitting at 1.3 μm, growth and characts. 80−64057
GaInAsP/InP DH stripe geometry lasers emitting at 1.3 μm 80−69410
GaInAsP/InP DH lasers, 1.3 μm wavelength, LPE growth and characterisation 80−69411
(100)GaInAsP/InP DH lasers, 1.5-1.6 μm wavelength, two phase soln. LPE technique using anti-meltback layer 80−99750
GaInAsP/InP lasers, LPE grown, effect of p-doping on carrier lifetime and threshold current density 80−99726
GaInAsP-InP buried stripe DH laser, fabrication using meltback method and CW operation 79−3708
GaInAsP-InP DH laser, LPE and wet chem. etching techniques for integration 79−98388
GaInAsP-InP DH lasers, LPE growth and operational characts. 80−53313
GaInAsP-InP DH injection lasers prep. by LPE, 1.11-1.67 μm operation 80−53321
GaInAsP-InP double heterostructure laser, prep. by LPE growth and laser operation 77−3590
$Ga_xIn_{1-x}As_yP_{1-y}$, LPE layers, growth and characterisation 78−38983
$Ga_xIn_{1-x}As_yP_{1-y}$/GaAs structure, LPE growth and lattice consts. matching conditions 80−59822
$Ga_xIn_{1-x}As_yP_{1-y}$-GaAs substrate, lattice matching 79−90901
$Ga_xIn_{1-x}As_yP_{1-y}$-InP, rib-waveguide injection lasers 79−59710
$Ga_xIn_xAs_yP_{1-y}$-InP substrate, lattice matching 79−90901
$Ga_yIn_{1-y}As_xP_{1-x}$, LPE growth 80−66440
GaInAsSb/GaSb DH lasers, 2 micron CW operation at 80K 80−53291
$Ga_{1-y}In_yAs_xSb_{1-x}$, LPE on GaSb, miscibility gap in liq. phase and lattice mismatch 80−15404
$Ga_xIn_{1-x}P$, LPE producing coherent interface, model 77−59229
$Ga_xIn_{1-x}P$ solid soln. epitaxial layers, stabilisation of composition 78−18933
$Ga_xIn_{1-x}P$ solid solns., isothermal liq. epitaxy 80−60793
Ga_xIn_xP, with GaP saturation source wafer *(Polish)* 78−23633
$Ga_{1-x}In_xP_yAs_{1-y}$/InP DFB injection laser, one-step LPE 80−58575
$Ga_{1-x}In_xSb$, LPE on GaSb by stepwise grading and characterisation 78−72745
$Ga_xIn_{1-x}Sb$, growth by LPE 78−27421
$Ga_xIn_{1-x}Sb$, LPE, growth by vertical dipping method and elec. props. 77−85949
GaP, current controlled LPE from finite volume melt 80−20805
GaP, epitaxial growth from Sb and Bi melts 79−52131
GaP epitaxial growth from solution in melt, crystn. theory 80−16204
GaP, epitaxial layer perfection, effect of dislocation loops in GaP substrate 78−30843
GaP, epitaxial layers, anisotropy of growth rate from soln. in melt 78−35322
GaP epitaxial layers, stable growth conditions, by molten salt electrodeposition on Si and GaP substrates 79−20000
p-GaP, epitaxial layers grown from liq., overcompensated, doping levels 78−91353
GaP, GPE layers, nonradiative dark regions along surface ripples 77−59600
GaP, green LED mass production 77−77422
GaP, growth and props. of LPE layers on Si substrates 78−6864
GaP, growth of epitaxial layers from limited of melt-soln. 78−19676
GaP, heteroepitaxial deposition on GaAs, Sn solvent inclusion, surface morphology *(German)* 79−28968
GaP, LED fabrication and electroluminesc. characts. 77−28632
GaP, LPE at 650°C from In solvent, low Si contamination 78−80480
GaP, LPE layers, comparison of growth rates with theoretical predictions 79−52134
GaP LPE layers, low temp. growth from In solvent 79−56924
GaP, LPE layers high purity, invest. *(German)* 78−31353
GaP, LPE solvent choice, equilib. in In-Ga-P system 79−87589
GaP layers, LPE growth, elec. props., residual impurities 79−38202
GaP on GaAs, LPE, growth with Ge and Sn solvents, phase diags. 78−88434
GaP, solubility in fused Sb, Bi, thermodynamics, rel. to epitaxial growth 78−34721
GaP, two-stage vapour/liq. epitaxial growth on Si 78−3054
n-GaP:In, LPE from In solvent, dislocation density reduction by doping 78−18919
GaP:N, N doping profiles in GaP grown by LPE, cathodoluminesc. data 79−23631
GaP:Sn, LPE growth from Sn soln., elec. resist. and Hall coeff. meas. 78−2593
GaP:Te on GaAs, LPE growth fron Sn, exam. of impurity band conduction effects 79−11249
GaP:Zn, doping from gas phase during LPE 80−55312
GaP:Zn, Sn doped epitaxial layers, Hall const., hole mobility and conc. 80−15143
GaP:Zn, Te, epitaxial layers, determ. of Zn conc. 79−77614
GaP:Zn, thermodynamics of Zn doping by liquid phase expitaxy 78−83832
GaP-GaAlP-GaP, lattice-matched, LPE layer growth under P vapour pressure and reduced O_2 contamination 79−51445
$(GaP)_x(ZnSe)_{1-x}$, solid solution, reaction of Zn with Se during Czochralski growth and LPE 79−8238
GaSb, electroliquid epitaxial growth 80−89160
GaSb high-purity and doped layers grown by LPE and VPE methods 78−6863

liquid phase epitaxial growth continued
p-GaSb−n-$Ga_{1-x}Al_xSb$, photodiode, LPE, spectral response, quantum efficiency 78−47850
$(Gd,Tm,Y)_3(Fe,Ga)_5O_{12}$ LPE garnet thin films, magnetocrystalline anisotropy 80−93147
Ge, growth conditions and doping level influence on impurity distrib. ratio 77−12516
Ge, ion-implanted amorphous layers, melting model for pulsing-laser annealing 79−56080
Ge p-n junction, high-grade, temp. gradient zone melting in production 77−4747
HgCdTe photodiodes formed by double-layer LPE 80−104078
HgCdTe-CdTe photodiode, 1.33 μm, grown by LPE, phys. props. 80−107892
$Hg_{0.60}Cd_{0.40}Te$, LPE growth from Te-rich soln. 80−7508
$Hg_{0.6}Cd_{0.4}Te$ LPE layer growth from Te-, Hg-, and HgTe-rich solns., comparison 80−76199
$Hg_{1-x}Cd_xTe$ epitaxial layers, elec. props. 80−96910
$Hg_{1-x}Cd_xTe$, LPE current controlled 80−40272
$Hg_{1-x}Cd_xTe$, LPE growth and characterisation 80−50565
$Hg_{1-x}Cd_xTe$-CdTe photodiodes, backside-illum., LPE growth and thermal noise characts. 79−40610
$Ho_{0.7}Er_{0.3}FeO_3$, crystn. on seeds, layer morphology 78−72041
$Ho_3Fe_5O_{12}$:Pb film, grown from fluxed metals by LPE 77−24972
In-As-P solid soln., liquidus surface in ternary phase diagram, simplex lattice method 77−7847
In-As-P system, ternary phase diagrams, method for determ. of liquidus surfaces 77−28787
In-Ga-As-P, phase diagram rel. to lattice matched LPE 78−39708
In-Ga-P ternary system, low temp. phase diagram rel. to epitaxial growth 80−84916
In-In-P-GaP, liquidus surface obs. 78−22829
InAs, soln. in liq. Sn, vapour phase partial press. meas., rel. to LPE 78−34610
InAsSb/GaSb broad-spectral-band IR detector, backside-illum. heterostructure approach 80−73450
$InAs_{1-x}Sb_x$ on GaSb, LPE growth 80−29293
$InAs_{1-x}Sb_x$-InAs stepwise-graded struct., steady-state LPE, etching, investig. 77−21042
$InAs_xSb_yP_{1-x-y}$, quaternary layers lattice matched to InAs substrate 78−3065
(InGa)As film, growth kinetics for step-cooling LPE technique 77−40395
InGaAs, LPE, diffusion-limited step-cooling technique, layer thickness and composition 80−84402
InGaAs-$In_{1-x}Ga_xAs_yP_{1-y}$ DH laser, LPE fabrication, electroluminesc., lasing characts. 79−3709
InGaAs-InP heterojunction detector for 1.0-1.7 μm wavelength range 78−49895
$In_{0.53}Ga_{0.47}As$, growth on (100)-oriented InP, from supercooled solution 79−70001
$In_{0.53}Ga_{0.47}As$, incorporation of Ga during LPE growth on (111)B and (100)InP substrates 78−91557
$In_{0.53}Ga_{0.47}As$, interband magnetoabsorption study, quasi-Ge model application 80−50304
$In_{0.53}Ga_{0.47}As$, LPE growth on (100) InP, for field assisted photocathode appl. 78−15318
$In_{0.53}Ga_{0.47}As$ p-i-n photodiode-FET photoreceiver for 1.0 to 1.7 μm wavelength optical fibre communications systems 80−58794
$In_{0.53}Ga_{0.47}As$, phase diagram at 650°C and LPE growth of lattice-matched layer 79−96009
$In_{0.53}Ga_{0.47}As$-InP heterostructure, LPE growth 80−11582
$In_{1-x}Ga_xAs$, LPE, electron mobility and max. drift vel., microwave device appls. 77−77431
$In_{1-x}Ga_xAs$, LPE growth on InP substrate, quasi grown layers, photoluminescence meas. 79−23862
$In_{1-x}Ga_xAs$, LPE layer on InP substrate, phys., elec. and optical props. 78−39235
$In_{1-x}Ga_xAs$ layer on InP, misfit dislocation free, LPE growth 80−108364
$In_{1-x}Ga_xAs$, on InP substrate, comp. latching phenomenon and lattice mismatching effects 79−28961
$In_xGa_{1-x}As$, LPE growth on GaAs 79−61519
$In_xGa_{1-x}As$, thick LPE growth, electrolum. obs. 78−60589
$In_xGa_{1-x}As$:Si, p-n junction form. in LPE layers, In content effect on inversion temp. 77−4266
$In_xGa_{1-x}As$:Zn, lattice matching to InP, LPE growth conditions 80−70541
InGaAsP, anodic oxidation, refractive indices 80−97601
InGaAsP DH lasers with etched reflectors, fabrication, current density 80−64050
InGaAsP, epitaxial layer, defect evaluation by cathodoluminescence 80−2866
InGaAsP, high radiance CW LEDs emitting at 1.30 μm 78−22196
InGaAsP, LPE, diffusion-limited step-cooling technique, layer thickness and composition 80−84402
InGaAsP, LPE growth, orientation depend. of incorporation of Ga, As, and Zn 78−6869
InGaAsP, LPE growth on InP, influence of lattice mismatch on surface morphology 79−1553
InGaAsP, LPE growth techniques influence on composition 79−52130
InGaAsP, LPE growth, impurity depend. of distrib. coeff. 80−10843
InGaAsP, LPE grown, impurity effect on surface morphology 80−29291
InGaAsP LPE heterostructs., interface grading, Auger depth profile 80−103585
InGaAsP, lattice matched, LPE growth on (100) InP, for 1.15-1.31 μm spectral region 78−64483
InGaAsP:Sn(Te)(Zn), LPE growth, influence of growth-solution dopants on distrib. coeffs. 79−47640
InGaAsP/InP, DH laser, 1.5 μm, with optical waveguide structure, fabrication 79−72587
InGaAsP/InP, native oxide stripe laser 79−68405
InGaAsP/InP phototransistors, fabrication by LPE, photodetectors 80−95139
InGaAsP-InP DH laser, 1.55 μm, low temp. LPE growth for room-temp. CW operation 80−64045
InGaAsP-InP DH lasers, perturbed InP growth, photoluminesc. study 80−106518
InGaAsP-InP lattice-matched heterojunction, LPE growth and characterisation 77−21041

liquid phase epitaxial growth continued
InGaAsP-InP lattice matched DH, growth by two-phase supercooled soln. technique 78−10296
InGaAsP-InP layers, grown by LPE techniques, lattice const., bandgap, thickness and surface morphology meas. 80−59818
$In_{0.8}Ga_{0.2}As_{0.5}P_{0.5}$, LPE growth 80−11557
$In_{1-x}Ga_xAs_{1-y}P_y$ layers on InP substrate, LPE growth, quaternary phase diagram, and band gaps 79−42403
$In_{1-x}Ga_xAs_yP_{1-y}$ DH laser, low threshold current density, near equilibrium LPE growth 80−19040
$In_{1-x}Ga_xAs_yP_{1-y}$, LPE growth on InP (100), lattice matched composition 78−87881
$In_{1-x}Ga_xAs_yP_{1-y}$, traps in device quality n- and p-type material 80−10999
$In_{1-x}Ga_xAs_yP_{1-y}$/InP 1.5 μm room-temp. CW laser fabrication and operation 80−64070
$In_{1-x}Ga_xAs_yP_{1-y}$-InP DH lasers, fabrication and performance 78−5500
$In_{1-x}Ga_xAs_yP_{1-y}$-InP DH laser on InP (100) substrate 78−29965
$In_xGa_{1-x}As_yP_{1-y}$ layers on InP, LPE and opt. props. characteris. 79−28849
$In_xGa_{1-x}As_yP_{1-y}$ photodetector diode on InP substrate dark currents, tunnelling, energy gaps, effective masses 80−70805
InGaAsSb, LPE growth, and appl. in GaSb/AlGaAsSb/InGaAsSb/AlGaAsSb/GaSb DH 80−16205
$In_{1-x}Ga_xAs_{1-y}Sb_y$, on (111)B-oriented InAs, growth conditions and lattice matching 77−24973
$In_xGa_{1-x}As_ySb_{1-y}$ laser, nonequilibrium carrier recombination, luminesc. study 80−50431
$In_{0.3}Ga_{0.7}P$, N free and implanted, photoluminescence study 80−97322
$In_{1-x}Ga_xP$, compositional inhomogeneity 80−88444
$In_{1-x}Ga_xP$, epitaxial growth from melt, optimisation of growth conditions 79−52132
$In_{1-x}Ga_xP$, epitaxial growth on GaAs substrate, formation of intermediate layers 80−2304
$In_{1-x}Ga_xP$ LEDs and electron-beam-pumped lasers 80−2281
$In_{1-x}Ga_xP$, LPE, conditions, reacts. in In-Ga-P system 79−11525
$In_{1-x}Ga_xP$, solid soln., evaporation of P during LPE 79−95948
$In_{1-x}Ga_xP$:N(Te), composition depend. of bound state luminesc. transitions 78−39595
InGaPAs LPE layers, compositional inhomogeneity, photoluminesc. obs. 80−75451
InGaPAs, LPE-grown on (001)-InP, lattice mismatch study using X-ray double-cryst. diffr. 79−99440
$In_{1-x}Ga_xP_{1-y}As_y$ lattice-matched epitaxial layers, LPE growth on GaAs(100), characterisation 80−75465
$In_{1-x}Ga_xP_{1-z}As_z$ DH lasers, multiple LPE, lattice matching 77−77421
$In_{1-x}Ga_xP_{1-z}As_z$ LEDs and electron-beam-pumped lasers 80−2281
$In_{1-x}Ga_xP_{1-z}As_z$ LPE DH laser with multiple thin layer active region 77−83887
$In_{1-x}Ga_xP_{1-z}As_z$ near IR DH laser, constant temp. LPE, external grating cavity 77−75550
$In_{1-x}Ga_xP_{1-z}As_z$, room temp. visible heterojunction lasers 78−5501
$In_{1-x}Ga_xP_{1-z}As_z$ single thin active layer visible spectrum heterostruct. lasers 78−63120
$In_{1-x}Ga_xP_{1-z}As_z$:Zn, x∼0.12, z∼0.26, LPE, DH lasers, tunnelling involving defects 77−65594
$In_{1-x}Ga_xP_{1-z}As_z$-$In_{1-X}Ga_XP_{1-Z}As_z$ visible spectrum multiple-quantum-well heterostruct. lasers 80−106537
$In_{1-x}Ga_xP_{1-z}As_z$-InP, LPE heterojunctions, lattice matching and dislocations 78−23150
$In_{1-x}Ga_xP_{1-z}As_z$-InP, single and multiple layer heterostruct., LEDs and lasers 78−46626
$In_uGa_{1-u}P_vAs_{1-v}$-InP, LPE, lattice matching, phase 80−54350
InGaSb, LPE growth characteristics, substrate surface contamination dependence 80−39470
InP (111) substrate, and homoepitaxial layers, characterisation by divergent X-ray beam diffr. 78−31352
InP, current controlled LPE growth 77−77428
InP, current-controlled LPE growth, Peltier cooling at In-InP interface 77−8770
InP, effects of baking time on purity and morphology 78−6862
InP, expt. studies on meltback morphology 78−31347
InP film, on (100) and {111} substrates *(Slovak)* 79−15037
InP grown by LPE, method for free In removal from surface 80−84860
InP in vertical reactor, construction and expt. data *(Slovak)* 77−28081
InP, LPE, high purity, use of baking to reduce Si contamination 78−72744
InP, LPE, solvent choice, equilib. in In-Ga-P system 79−87589
InP, LPE grown, impurity effect on surface morphology 80−29291
InP, LPE growth 80−11557
InP, LPE growth on GaAs, etching and electron probe anal. 79−11526
InP layer growth method, model validity evaluation *(Slovak)* 80−54535
InP layers, grown by LPE from supercooled solns., thickness meas. 78−10307
InP layers, LPE growth from undercooled melts, numerical method 80−6665
InP n^+-p-p^+ homojunction solar cells, high efficiency, LPE layer growth, photolithographic fabrication 80−93929
p-InP, prep. of single and bi-crysts., epitaxial layer and polycryst. films 77−81211
InP preparation, for integrated optics appl. *(Slovak)* 80−33225
InP, soln. in liq. Sn, vapour phase partial press. meas., rel. to LPE 78−34610
InP substrates, control of thermal degradation in LPE growth with PH_2 partial pressure 79−33949
InP surface decomposition prevention in LPE growth 80−96749
InP, surface morphology 77−62771
InP, terracing of LPE growth, doping effects 80−10846
InP, thermal degradation and its control in LPE growth 79−100343
InP very high purity LPE layer growth 78−3061
InP:Be, LPE, Be distrib. coeff., carrier conc. 79−90694
InP:Sn, LPE growth from Sn soln., elec. props., 80 to 300K 79−11250
InP-$Ga_xIn_{1-x}As_8P_{1-y}$ systems, for optical devices in 1 to 1.6 μm region, LPE growth *(Japanese)* 79−28956
InP-$Ga_xIn_{1-x}As_yP_{1-y}$ DH, LEDs and lasers, fabrication and operation in 1.5 μm region 78−37893
InP-$Ga_xIn_{1-x}P_yAs_{1-y}$ heterostruct. lasers, growth and characterisation 80−23691
InP-GaInAsP buried heterostructure lasers of 1.5 μm region, fabrication and characts. 80−74388

liquid phase epitaxial growth continued
InP-$In_{1-x}Ga_xAs_yP_{1-y}$-InP 1.53 μm single-mode CW ridge-waveguide laser 80−64072
InP-$In_{1-x}Ga_xP_{1-y}As_y$, LPE for optoelectronic devices *(German)* 79−95280
InP-$In_{1-x}Ga_xP_{1-z}As_z$ heterostructure laser, single and multiple quantum-well, liquid-phase epitaxial growth 80−38031
InSb, impurity distribution, during epitaxial growth from liq. phase 80−88443
InSb, LPE growth characteristics, substrate surface contamination dependence 80−39470
$K_3Li_2Nb_5O_{15}$ films for optical waveguides epitaxial growth and characterisation 80−79016
$KNdP_4O_{12}$, laser waveguide, fabrication by LPE 79−36925
$KNdP_4O_{12}$ laser waveguide, epitaxial growth 79−91597
$LiBi_xNd_{1-x}P_4O_{12}$ waveguide laser layer epitaxially grown on $LiNdP_4O_{12}$ substrate 80−23709
$Li_{0.5}Fe_{2.5-x}Al_xO_4$ ($0 \leq x \leq 0.68$) films, LPE 80−29884
$Li_{0.5}Fe_{2.5}O_4$, LPE growth on spinel substrate crystals, ferrimagnetic resonance exam. 78−76613
$Li_{1-x}Na_xNbO_3$, LPE, growth and temp. coeff. of SAW velocity 78−43227
$Li(Nb,Ta)O_3$ solid solution, LPE growth of thin film waveguides on $LiTaO_3$ substrates 79−41467
$Li(Nb,Ta)O_3/LiTaO_3$, multi-layer optical waveguide fabrication by LPE 80−71605
$LiNbO_3$, LPE on $LiTaO_3$ substrate, using Li_2O-V_2O_5 flux 78−44031
$LiNbO_3$:Na structure field stability limits, LPE film growth, SAW velocity 80−80102
$LiNbO_3$:Na^+(Co^{2+},Zr^{4+}) films, LPE growth from Li_2O-V_2O_5 flux, X-ray and acoustic characterisation 80−15383
$Li(Nb_{1-x}Ta_x)O_3$, $0 \leq x \leq 1$, LPE thin film growth on $LiTaO_3$ substrate, lattice mismatches, meas. of temp. depend 79−56087
(Lu, La, Y, Ca)$_3$(Ge, Fe)$_5O_{12}$, temperature compensated high mobility bubble garnet, LPE and props. 77−20656
Mg $(Fe,In)_2O_4$:Pb,Pt film, LPE 77−77436
$MgFe_2O_4$, LPE growth, film quality, mag. meas. 78−11136
$(Mn_xSn_{1-x})Fe_2O_4$ thin film LPE on Bridgman grown Zn_2TiO_4 substrate 79−100065
Mo, electrocrystallisation from fused salts, growth rate, and struct. 77−77438
$NdAl_3(BO_3)_4$, LPE for thin film miniature lasers 79−74101
$Nd(Ga,Cr)_3(BO_3)_4$, cryst. growth by LPE, Nd^{3+} fluorescence, lattice constants 80−29883
NdP_5O_{14} single crystals grown from polyphosphoric acids, morphology control 80−15395
Ni electrodeposition, surface-stress phenomena at start 80−35542
Ni electrodeposition on Cu (001), three-dimens. epitaxial crystallites, TEM image contrast 80−88457
$NiFe_{2-x}Al_xO_4$, stress-induced anisotropy in LPE grown single cryst. films, domain struct. 79−28238
$NiFe_2O_4$, LPE growth, film quality, mag. meas. 78−11136
$Ni_{1-x}Zn_xFe_2O_4$, LPE growth, film quality, mag. meas. 78−11136
Pb, underpotential adsorption, cathodic deposition, on Ag(111) and (100) *(German)* 80−108363
$Pb_{1-x}Hg_xS$ epitaxial films, electroless deposition and struct. props. 79−90915
$Pb_{1-x}Sn_xSe$ layers, growth conditions correl. with morphology 80−104079
$Pb_{1-x}Sn_xSe(Te)$ epitaxial layers, growth, phase diagram, p-n junctions, optical, elec. props. 78−44029
PbSnTe/PbTe inverted heterostructure mosaics, long wavelength, energy gap-Fermi level temp. depend. 79−85182
$Pb_{0.8}Sn_{0.2}Te$, LPE layers, carrier conc. variation with annealing and growth temp. 77−39878
$Pb_{0.8}Sn_{0.2}Te$-PbTe p-n heterojunction, prep., elec. and photoelec. props. 79−51664
$Pb_{1-x}Sn_xTe$, grown by LPE, solid-liquid tie line determ. 78−64526
$Pb_{1-x}Sn_xTe$ LPE film IR detector performance 80−86422
$Pb_{1-x}Sn_xTe$, LPE grown heterostructures, improved nucleation and planar interface 79−95949
$Pb_{1-x}Sn_xTe$ LPE grown heterostructures, dislocation etch pitch, interfaces 80−2023
$Pb_{1-x}Sn_xTe$ layers, LPE, phase diagram rel. to lattice const., distrib. coeffs. 79−37925
$Pb_{1-x}Sn_xTe$ layers, LPE growth on metal-etched substates 80−55313
$Pb_{1-x}Sn_xTe$ optically pumped lasers, power output and wavelength, 4 to 30K 78−79035
$Pb_{1-x}Sn_xTe$, temperature gradient LPE, PbTe substrate 78−3066
$Pb_{1-x}Sn_xTe$-$Pb_{1-y}Sn_yTe$, p-n heterojunction, prep. and props. 79−51662
$Pb_{1-x}Sn_xTe$-PbTe heterojunctions, interface recombination velocity reduction with decreasing lattice parameter mismatch 79−98370
PbTe, LPE, solvent choice, equilib. in Pg-Sn-Te system 79−87589
PbTe:As, hole conc. control, in LPE layers, plasma reflectivity and thermoelec. probe meas. 79−99640
PbTe-$Pb_{1-x}Sn_xTe$-PbTe DH, LPE and VPE, stimulated emission 77−75526
PbTe-PbSnTe heterjunction, misfit dislocations, etch pit and electron probe study 79−77926
$Pb_{1-y}Te$-$Pb_{1-x}Sn_xTe$ (x,y≤0.3), double heterostruct., LPE growth, heterointerface morphology 80−70550
$(PrGdYb)_{3-x}Bi_x(FeAl)_5O_{12}$ system, LPE growth and magnetooptical props. 79−65842
Sb, epitaxial growth, of electrodeposits on oriented single cryst. surfaces of CU, electron diffr. study 79−66016
Sb, epitaxial growth of electrodeposits on oriented single crystal Au and Ag 78−43267
Si buried-grid fabrication by LPE 79−78906
Si, epitaxial layer grown by saturated Sn melt undercooling, morphology 78−22969
Si, heteroepitaxy, refractory oxides as substrates *(French)* 77−44181
Si, ion-implanted amorphous layers, melting model for pulsing-laser annealing 79−56080
Si, ion-implanted layers, epitaxial regrowth by laser beam and flash annealing 80−100420
Si junction diodes, fabrication by LPE on Si:B substrates, and characts. 80−80363
Si, LPE from Sn melt, kinetics 78−19675
Si, LPE from Sn melt by dipping 78−6871
Si, LPE growth from supersaturated Sn melt 78−56592
Si LPE layers, dopant distrib., meltback effects 79−69151

liquid phase epitaxial growth continued
Si, LPE using Ga_xAl_{1-x} solvent 77−36411
Si laser annealed, nonequilibrium solubility and segregation 80−84296
a-Si, laser induced crystallisation mechanism, epitaxial regrowth 80−84962
Si layers on metallurgical-grade polycryst. substrates, characteris. 79−28967
Si, slip dislocation nucleation during laser annealing 80−84179
Si solar cells, metallurgical-grade, fabrication by epitaxial growth or direct diffusion 80−101104
Si:Ga, LPE growth on Si substrate, melt-back approach 78−80481
Si:Ga, LPE on Si, technique and characterisation 79−38751
Si-Au-P system, partition coeff. of P, temp. depend. 79−43158
SiC, 6H polytype, LPE growth by dipping technique for prep. by blue LEDs 77−8769
SiC, epitaxial film, effect of impurities on polymorphism during growth 80−15414
SiC epitaxial layers, energy distrib. in photolum. spectra, influence of synthesis conditions 79−52009
SiC epitaxial layers, growth techniques 80−108360
SiC, for blue LEDs 77−81228
β-SiC, polytype stability, $\alpha \rightarrow \beta$ phase transformation during growth 78−6028
p^+-$Si_{1-x}Ge_x$-nSi junction diodes, lattice misfit effects on I-V characts. 80−70804
$(Sm,Lu)_3Fe_5O_{12}$, submicron bubble films on rare earth-Ga garnet substrates, prep. and mag. props. 78−91909
$(Sm,Y)_3(Fe,Ga)_5O_{12}$, epitaxial mag. layer, LPE, growth rotation rate, effect on props. 78−56053
SmCaGe garnet LPE bubble film, coercivity, thickness depend. 78−68324
$(SmLu)_3(FeAl)_5O_{12}$, film epitaxial growth on $Gd_3Ga_5O_{12}$ substrate, mag. props. lattice mismatch 80−65402
$Sm_{0.3}Lu_{0.2}Tm_{0.2}Y_{1.45}Ca_{0.85}Fe_{4.15}Ge_{0.85}O_{12}$, LPE growth, saturation magnetisation, collapse field, bubble diameter 78−95703
$(SmYCa)_3(FeGe)_5O_{12}$ epitaxial layer, growth kinetics and struct. as functions of cryst. lattice parameter mismatch 80−6677
$Sm_{0.1}Y_{1.9}CaFe_4GeO_{12}$, LPE growth, saturation magnetisation, collapse field, bubble diameter 78−95703
$(SmY)_3(FeGa)_5O_{12}$, on $Gd_3Ga_5O_{12}$, growth kinetics, 920-980°C 78−3064
$Sm_{0.4}Y_{2.6}Fe_{3.8}Ga_{1.2}O_{12}$, LPE. improved method of stirring 78−68641
$Sm_{0.4}Y_{2.6}Ga_{1.1}Fe_{3.9}O_{12}$, LPE, growth rate anisotropy and kinetic coeffs. of vicinal faces 78−51846
SnTe, LPE, solvent choice, equilib. in Pb-Sn-Te system 79−87589
$SrFe_8Al_4O_{19}$, thin film LPE growth and mag. props. 80−80992
$SrSO_4$, surface crystn., on $BaSO_4$, isotope exchange and electron microscopy study 80−34332
$SrSo_4$ epitaxy, on $BaSO_4$ from aqueous solns. mechanisms of growth 79−56093
Tl, underpotential adsorption, cathodic deposition, on Ag(111) and (100) *(German)* 80−108363
W, heteroepitaxial deposits with (110) orientation by molten salt electrolysis 78−47683
(Y, Eu, Yb, Ca)$_3$(Ge, Fe)$_5O_{12}$, bubble film, LPE on $Gd_3Ga_5O_{12}$, mismatch and faceting 77−20657
$(Y,Eu)_3(Fe,Ga)_5O_{12}$, LPE growth from molybdate fluxes, bubble props. 78−68322
$(Y,Gd,Yb)_{3-x}Bi_x(Fe,Al)_5O_{12}$, garnet single cryst. film, possible bubble appl. 78−6552
$(Y,Gd,Yb)_{3-x}Bi_x(Fe,Al)_5O_{12}$, LPE, for magneto-optical appls. 78−48341
$(Y,Re)_{3-x}Ca_xGe_{5-x}Ge_xO_{12}$, garnet films, LPE growth for bubble memory appls. 77−11813
$(Y,Sm,Ca)_3(Fe,Ge)_5O_{12}$ epitaxial films, mag. props., growth condition effects 80−97124
$(Y,Sm,Lu,Ca)_3(Fe,Ge)_5O_{12}$ bubble magnetic garnet film, LPE grown, props., $CaCO_3/GeO_2$ molar ratio influence 80−50152
$(Y,Sm,Lu,Ca)_3(Ga,Ge,Fe)_5O_{12}$, film growth and mag. props. for bubble-memory appl. 79−87297
$(Y,Sm,Lu,Tm,Ca)_3(Fe,Ge)_5O_{12}$, epitaxial garnet film, temp. depend. mag. props. 80−39825
$(Y,Sm,Lu)_3(Fe,Ga)_5O_{12}$, LPE mag. film, suitability for 1 to 3 micron bubble devices 78−68323
$(Y,Sm)_3(Fe,Ga)_5O_{12}$, garnet LPE films, growth rate anisotropy 80−54558
YAG, solubility in solvent $PbO_{-x}PbF_2$, phase form. in system Y_2O_3-Fe_2O_3-PbO-PbF_2-B_2O_3 78−95247
YAG:R^{3+}, R=Nd, Er, (Er, Ga), LPE and luminesc. 78−64408
$(YBiSmCa)_3(FeGe)_5O_{12}$ epitaxial layer, growth kinetics and struct. as functions of cryst. lattice parameter mismatch 80−6677
$(YEu)_3(FeGa)_5O_{12}$, monocrystalline films, uniaxial magnetocryst. anisotropy 77−8766
$Y_3Fe_{5-x}Ga_xO_{12}$ grown from solution, prep. and props. *(German)* 78−52691
$Y_3Fe_{5-x}Ga_xO_{12}$ layers, current-induced soln. growth 77−48358
$Y_3Fe_5O_{12}$ LPE growth on $Gd_3Ga_5O_{12}$ substrates, substrate orientation effect 80−66438
$Y_3Ga_xFe_{1-x}O_{12}$, film growth conditions rel. to memory element props. 77−66399
$Y_3Ga_xFe_{5-x}O_{12}$ film, growth kinetics of film with cylindrical mag. domains 77−1577
YIG, double layer struct., LPE growth from molybdate and Pb borate fluxes 80−39827
YIG film, Ca, Ge-substituted, having mag. bubbles, LPE growth 78−31350
YIG, film, LPE, annealing-induced relief of compressive misfit strain 78−2386
YIG, garnet, high temp. solns., shear viscosity meas., rel. to LPE 80−10697
YIG grown from solution, prep. and props. *(German)* 78−52691
YIG, La- and Ga-substituted, inhomogeneous epitaxial films, spin wave reson. 79−99773
YIG:Co film, influence of stress induced anisotropy on domain struct. 80−100605
YIG:La,Ga, film, LPE-grown, Ga incorporation, depend. of magnetisation on growth rate 80−84627
YIG:La,Ga film, uniaxial anisotropy, variation along growth direction 77−28416
$Y_{3-x}La_xFe_{5-y}Ga_yO_{12}$ film, horizontally dipped LPE grown, FMR, anisotropy field obs. 79−78449

liquid phase epitaxial growth continued
$(YSmCa)_3(FeGe)_5O_{12}$ mag. bubble garnets, ion implantation induced stress influence on props. 79−91274
YSmCaFeGe, mag. garnet films, segregation of Ca and Ge in LPE growth 80−29959
$(YSmCa)_3(FeGe)_5O_{12}$ LPE films, optimum growth conditions for low coercivity 78−95499
$(YSmCa)_3(FeGe)_5O_{12}$ LPE film, growth and coercivity 79−4707
$(YSmCa)_3(FeGe)_5O_{12}$ films, mag. bubble props. 79−74107
$(YSmCaLu)_3(FeGe)_5O_{12}$, bubble film inhomogeneity, spin wave reson. meas. 80−44439
$(YSm)_3(FeGa)_5O_{12}$ film, LPE on $Gd_3Ga_5O_{12}$, interface processes, horizontal chipping obs. 80−49552
$(YSm)_3(FeGa)_5O_{12}$, growth rate anisotropy and kinetic coefficients of vicinal faces 78−63954
$Y_{2.6}Sm_{0.4}Fe_{3.8}Ga_{1.2}O_{12}$, garnet films, LPE growth, mag. anisotropy field control 77−69642
$Y_{3-y}Sm_yFe_{5-x}Ga_xO_{12}$ film, LPE process exam. by induced striation 77−69643
$Y_{3-y}Sm_yFe_{5-x}Ga_xO_{12}$ film, LPE growth induced mag. anisotropy 78−2709
$Y_{3-y}Sm_yFe_{5-x}Ga_xO_{12}$ grown from solution, prep. and props. *(German)* 78−52691
$(Y_{1.5}Sm_{0.3}Lu_{0.3}Ca_{0.9})(Fe_{4.1}Ge_{0.9})O_{12}$, growth reproducibility, static bubble props. 77−16130
$(YSmLuCa)_3(FeGaGe)_5O_{12}$, reproductibility in bubble garnet LPE growth 78−92204
YSmLuCaFeGe garnets, growth and temp. characts. of small bubbles 78−80183
$(YSmLuCa)_3(FeGe)_5O_{12}$, LPE growth, growth reproducibility of bubble props. 78−92208
$(YSmLuCa)_3(FeGe)_5O_{12}$ films, mag. bubble props. 79−74107
$(YSmLuCa)_3(FeGe)_5O_{12}$, double layer struct., LPE growth from molybdate and Pb borate fluxes 80−39827
$(YSmLuCa)_3(FeGe)_5O_{12}$, epitaxial films, LPE grown, annealing effects on mag. anisotropy 80−66548
$(YSmLuCa)_3(GeFe)_5O_{12}$, LPE low defect density films, prep. for mag. bubble device fabrication 79−87590
YSmLuCaGeIG, mag. props. and defects, depend. on B_2O_3 conc. on growth in PbO-B_2O_3 solvents 78−68321
YSmLuCaGeIG films, epitaxial growth with 3 μm magnetic bubbles 79−61518
Zn electrodeposition, on Zn and Al single crysts., from H_2SO_4 bath, SEM obs. *(Japanese)* 80−93502
Zn film deposition on Al, TEM and electron diffr. obs. 80−75460
Zn, on Cu single cryst. planes, electrocrystn. under influence of asymm. AC 77−28731
Zn_3As_2, solubility in Bi, LPE on $(Cd_xZn_{1-x})_3As_2$ 78−35324
$Zn_{1-x}Cd_xTe$ p-n junctions, process, elec. props. 77−7981
$ZnFe_2O_4$, LPE growth, film quality, mag. meas. 78−11136
ZnS, epitaxial growth, appl. to electronic devices, review *(Japanese)* 80−55281
ZnS-$CuGaS_2$ heterodiodes, LPE, emission spectra 79−33335
ZnSe, from Zn-Ga soln., characts. 79−28965
ZnSe, LPE growth on ZnTe, characterisation of heterojunction 77−4745
ZnSe layers, LPE growth from Zn-Ga soln., photoluminesc. 79−56840
$ZnSnAs_2$, LPE in open tube system 78−92206
ZnTe, LPE growth on ZnSe, characterisation of heterojunction 77−4745

liquid semiconductors
see also electron energy states of liquid semiconductors
alkali metal-based liquid semiconductor alloys, struct. and electronic props. 78−2403
alloys, anomalous thermodynamic props., theory 80−49287
binary alloy, metal-insulator transition induced by density changes 78−2529
bonding and transport properties 79−90950
chalcogen-based liquid semiconductor alloys, struct. and electronic props 78−2403
chalcogenide semiconductors, elec. cond. freq. depend., hopping cond. contrib. 77−76856
conductivity meas. by rot. mag. field method, viscosity effect *(Russian)* 77−57349
conference, Cambridge, MA, USA (Aug. 1979) 80−41933
electrical conductivity and thermo-EMF meas., quartz cells, specimen holders 77−74439
electrons in fluids, conf., Banff, Alberta, Canada, (5-11 Sept. 1976) 77−89680
elemental semiconductors, model pseudopotential, band struct. calcs., liquid semicond. resistivity calcs. 80−20075
Hall conductivity in random-phase model 80−65599
Hall effect measurement 80−65594
Hall effect obs., measuring cell construction 77−5866
with ionic character, mag. susceptibility 77−1536
melts, estimate of positional component of entropy of fusion, cluster model 77−55349
metal-insulator transition, review 77−1367
metal-nonmetal transition model 77−1368
metallic conductivity at high temp. 80−49832
neutron scattering, book contrib. 79−60232
NMR and metal-nonmetal transition 77−51973
with pseudogap, mag. susceptibility 77−1536
random field parameters and pseudopotential calc., amorphous, liquid and glassy semiconductors 80−29316
randomly shifted bands model for semiconductor-metal transition 78−79929
reflectance data and model densities of states 80−50364
resistivity temperature dependence, meas. apparatus for 10^{10} Hz freq. region 78−21169
structure of semiconds. in noncryst. states, diffr. investigations review 77−72559
switching effect, V-I characts. in strong elec. field 77−87787
Te, liquid, structure metallic constituent calcs. hard sphere model *(Russian)* 80−24349
thermoelectric power 79−65450
Tl-Te melt system, semicond., Hall effect 78−56164
Ag-Te, liq., struct. and elec. props. 80−49083
Ag_2S, liquid, ionic and electronic cond., thermoelec. power 80−39329
$AgSbSe_2(Te_2)$, exam. of kinematic viscosity of melts, and short range ordering 79−1383
Ag_2Se, liquid, ionic and electronic cond., thermoelec. power 80−39329

liquid semiconductors continued
Ag_2Te, changes in elec. cond. and thermoelec. power at melting point 79−15147
Ag_2Te, elec. cond. at high temps. and pressures 79−11119
Ag_2Te, liquid, ionic and electronic cond., thermoelec. power 80−39329
$AgTlSe_2$ and AgTlSe, elec. cond. and thermoelectric power, doping effects, rel. to pseudogap model 78−2506
AlSb, molten, temp. depend. of vel. of sound and adiabatic compressibility 77−27944
AlSb-Bi system, molten, enthalpy change due to mixing *(German)* 79−86892
AsSe, molten semicond., pseudogap, elec. cond. and optical absorption meas. 77−8160
As_2Se_3, liq., semicond.-metal transition at high temp. and press. 77−51784
As_2Se_3, molten semicond., pseudogap, elec. cond. and optical absorption meas. 77−8160
As_2Se_3, solid and liq., elec. cond. meas. 77−28185
As_2Se_3, struct., investigation using neutron diffr. meas. 79−23514
As_2Se_3, struct. determ. in amorphous and liq. state using EXAFS meas. 77−89366
As_2Se_3, temp. depend. of 10^{10} Hz elec. cond. 77−4388
As_2Se_3-As_2Te_3, solid and liq., elec. cond. meas. 77−28185
As_2Se_3-As_2Te_3, thermoelec. power and elec. cond. near metallic cond. transition 78−10486
$As_2(Se_{1-x}Te_x)_3$ semiconducting glasses, solid and liquid, thermal cond. 80−6574
As_2Te_3, liq., neutron diffraction study 79−77485
As_2Te_3, solid and liq., elec. cond. meas. 77−28185
As_3Te_3, thermoelec. power and elec. cond. near metallic cond. transition 78−10486
Au-Cs, liq. alloy, mag. susceptibility rel. to ionic charact. 77−1536
Bi-Se, fused, mag. susceptibility, temp. and conc. depend. 77−36052
Bi-Te, fused, mag. susceptibility, temp. and conc. depend. 77−36052
Bi-Te(Se), diamag. susceptibility, semicond./metal behaviour 78−14927
Bi-Te(Se), liq. chalcogenides, elec. cond. and mag. susceptibility 79−51578
Bi_2Te_3, liq. semicond., thermal cond. meas., resistive probe method 77−15636
Cd_3As_2 and $CdAs_2$, molten, thermal expansion and atomic bond strength parameters 80−65257
CdTe, mag. susceptibility at 20-1400°C 77−12085
Cs-Au, liq. alloys, ionic conductance 77−1251
Cu-Te, liq., struct. and elec. props. 80−49083
Cu_3AsS_4 and Cu_3SbS_4, thermal cond. in solid and liq. phases, 300 to 1100K, thermoelec. Q-factor 80−19997
$CuGaTe_2$, exam. of kinematic viscosity of melts, and short range ordering 79−1383
$CuInSe_2$-$CuInS_2$, melts, viscosity, elec. cond., density composition prop. graphs 79−14948
$CuInTe_2$, exam. of kinematic viscosity of melts, and short range ordering 79−1383
Ga-As system, phase equilib., Krupkowski model *(German)* 78−95132
Ga-Te, liq., compressibility and US velocity meas. 77−51426
Ga-Te, mag. susceptibility 77−51881
Ga-Te, reflectance, 0.65-3 eV, comp. depend. 78−72549
Ga-Te liquid alloys, mag. susceptibility 77−59383
GaAs, liq., semicond.-metal transition at high temp. and press. 77−51784
GaP(As), liquid interaction parameters determ., 580-670°C 80−65197
GaSb, molten, temp. depend. of vel. of sound and adiabatic compressibility 77−27944
GaSb-Bi system, molten, enthalpy change due to mixing *(German)* 79−86892
GaTe-SnTe, melt, temp. and composition dependence of elec. cond. and thermo EMF 79−95430
Ga_2Te_3, liq., elec. resistivity meas. up to 30 kbar 79−38070
Ge, liquid, surface tension exam., sessile drop method *(French)* 77−20162
Ge-Se liquid solutions, glass-forming, viscosity 77−66036
Ge-Te, As-Te, Ge-As-Te molten systems, metal-semicond. transition, cond. obs. *(German)* 77−1457
$GeSe_2$, struct., investigation using neutron diffr. meas. 79−23514
$GeSe_2$-As_2Se_3-Sb_2Se_3, elec. cond. over wide range of temp. 80−88564
$Ge_{0.08}Se_{0.92}$, molten semicond., pseudogap, elec. cond. and optical absorption meas. 77−8160
Ge_xSe_{1-x} melts, short-range order change with comp. and temp., anomalous density behaviour 77−11676
GeTe, neutron diffraction study 79−77485
In-Te, liq., nucl. spin relax. of ^{117}Sb 77−52004
In-Te, mag. susceptibility 77−51881
In-Te, molten thermodynamic props. determ. by EMF method 77−51504
In-Te, reflectance, 0.65-3 eV, comp. depend. 78−72549
In-Te alloys, atomic struct., X-ray diffr. meas. 79−41934
In-Te alloys, transport props. interpret. using effective-medium theory 77−76806
In-Te liquid alloys, mag. susceptibility 77−59383
InP, fused, SRO structure changes on heating 77−89367
InP(As), liquid interaction parameters determ., 580-670°C 80−65197
InS(Se)(Te), fused, charge transfer nature 77−89757
InSb, molten, temp. depend. of vel. of sound and adiabatic compressibility 77−27944
InSb-Bi system, molten, enthalpy change due to mixing *(German)* 79−86892
InTe, In_2Te_3, molten III-VI semiconductors, SRO 77−65945
InTe-SnTe, melt temp. and composition dependence of elec. cond., and thermo EMF 79−95430
In_2Te_3, liq., elec. resistivity meas. up to 30 kbar 79−38070
Li alloys, electronic struct., resistivity and thermoelec. power 77−51753
Li-Au(Hg)(Tl)(Pb)(Bi), liq. semicond., electronic struct., resist. and thermoelec. power meas. 77−47712
Mg-Bi, far IR reflectivity meas. 77−52105
$Na_{1-x}Bi_x$ liq. alloys, metal-nonmetal transition, mag. susceptibility meas. 79−82525
Ni-Te, liq., struct. and elec. props. 80−49083
Pb-S melt, absolute thermo-emf obs. 77−85251
Pb-Te, molten mag. susceptibility, conc. and temp. depend. 78−80121
S, eqn. of state determ., crit. props. and mol. comp. 80−49336
S-Se(Te)(Tl), bonding energies and entropies, mag. susceptibility meas. 80−49082
Sb-Te, fused, mag. susceptibility, temp. and conc. dependence 77−36052

liquid semiconductors continued
Sb-Te(Se), diamag. susceptibility, semicond./metal behaviour 78−14927
Sb_2S_3-SnS, Sb_8S_3-As_2S_3, fused mixtures, resistivity 77−80815
Sb_2Se_3, liq. struct. anal., neutron diffr. study 78−79519
Se, correlation between switching and struct. 77−69388
Se, electrical cond. transition at high temp. and press., Anderson localisation *(Russian)* 77−1462
Se, electronic transport props. at sub- and supercritical conditions 77−51788
Se, electronic transport props., equation of state, to 1900K and 1800 bars 80−65574
Se, eqn. of state determ., crit. props. and mol. comp. 80−49336
Se, estimate of self-diffusion coeffs. from viscosity data 77−55370
Se, liq. and amorphous, struct. by pulsed neutron diffr. using an electron LINAC 77−51307
Se liquid, pure and I doped, DC cond. and thermoelectric power *(French)* 79−56223
Se, liquid-crystal phase transition, elec. cond. changes 79−33310
Se, mol. structure, local atomic arrangement at intrinsic bonding defects 80−59374
Se, pure and I doped, DC cond., temp. depend. *(French)* 77−69322
Se, pure and I doped, thermopower, temp. depend. *(French)* 77−69360
Se, Raman scatt. meas., comparison with amorphous Se spectra 80−50328
Se, Raman spectra, crystn. processes 80−60608
Se, review of continuous metal-nonmetal transitions 77−51787
Se, US rel. temp. depend., melting effects 78−38782
Se:Cd dilute liquid, perturbed ang.-correl. meas. of motional-correl. time 79−41930
Se-Te, liq., localised impurity states, mag. susceptibility of Co and Mn solutes 77−51882
Se-Te alloys, liq., electronic props., mag. susceptibility meas. 79−95567
$Se_{1-x}Te_x$ systems, amorphous and liq. states, short range order, neutron scatt. study 80−49124
Se_xTe_{1-x} system melts, bonding system change obs. using density meas. 77−11456
Se_xTe_{1-x}, thermoelec. transport at mobility edge 80−49787
Si, dissolution of quartz, effect of C, rel. to melt growth 80−70414
Si, liq., mag. susceptibility and diamag.-paramag. transition at melting pt. 78−95415
Si, liq., sound vel. meas. 79−77684
Si, reaction kinetics with B_4C 80−84344
Sn-S melt, absolute thermo-emf obs. 77−85251
Te, elec. cond. at high temps. and press. 77−55592
Te, estimate of self-diffusion coeffs. from viscosity data 77−55370
Te, liq., elec. resistivity meas. up to 30 kbar 79−38070
Te, mag. susceptibility, temp. depend. 78−47943
Te, Raman spectra, crystn. processes 80−60608
Te, semicond.-metal transition at high temp. and press. 77−51784
Te, US rel. temp. depend., melting effects 78−38782
Te-Se, resist. meas. under high press. 77−51791
Te-Se liquid mixtures, sound vel. meas., adiabatic compressibility determ. 80−65161
Tl-S melts, Hall effect 77−85239
Tl-Te, reflectance, 0.65-3 eV, comp. depend. 78−72549
Tl-Te, resist. meas. under high press. 77−51791
Tl-Te alloys, atomic struct., X-ray diffr. meas. 79−41934
Tl-Te liquid alloys, mag. susceptibility 77−59383
$Tl_2S(Se)$, molten III-VI semiconductors, SRO 77−65945
TlSe, Tl_2Se, Tl_2Se_3, liq., diffusion coeff. of Sn, Ag and Tl *(Russian)* 77−28030
Tl_2Se_3, elec. cond. and thermoelectric power, doping effects, rel. to pseudogap model 78−2506
$Tl_{66}Se_{34}$, thermoelectric figure of merit meas. 77−28202
Tl_xSe_{1-x}, liquid semiconductor, diamagnetism and paramagnetism, dangling bond paramag. centres, mag. susceptibility obs. 80−44797
$Tl_2SeAs_2Te_3$, temp. depend. of 10^{10} Hz elec. cond. 77−4388
Tl_2Te, liq., elec. resistivity meas. up to 30 kbar 79−38070
Tl_2Te_3, exam. of electrical props., density and viscosity, for solid or liquid states 79−95431
Tl_2Te_3, exam. of electrical props., in solid, liquid state 80−54686
Tl_2Te_3 melt, impurities effect on surface tension polytherm and adsorption obs. 77−7947
Tl_2Te_3:Ag(Sn), effect of dopant on electrical props., density and viscosity, for solid or liquid states 79−95432
Tl_xTe_{1-x}, rigid band behaviour, elec. cond. and thermopower 77−35845
Tl_xTe_{1-x}, thermodynamic evidence against large scale fluctuations in composition in heterogeneous transport models 77−28172
V_2O_5 containing melts, activation energy of electron mobility and electronegativity 77−35971
V_2O_5 type liquid semiconductor, elec. props. control, by O_2 partial press. *(Russian)* 78−72142
Zn_3As_2 and $ZnAs_2$, molten, thermal expansion and atomic bond strength parameters 80−65257
$ZnGeAs_2$, elec. cond. in solid and liq. state 77−11912

liquid-solid transformations *see solid-liquid transformations*

liquid structure
see also classical theories of fluid structure; long-range order; quantum theories of fluid structure; short-range order; X-ray diffraction examination of liquids
α,β-β-trifluoroacetonitrile, liq.-liq. transition rel. to mol. motion, NMR study 80−70383
acetic acid, dil. soln., dielectric polaris., linear correlation factor 78−6624
acetic acid, Rayleigh-Brillouin scatt., 20-115°C, viscoelastic theory anal. 79−28774
acetone-toluene-tetrachloromethane, mol. interaction and thermodynamic props. 80−71935
acetonitrile, in dilute CCl_4 soln., far IR spectra and mol. dynamics models 79−99876
acetonitrile, liq., $CD_3C^{15}N$, neutron diffr. 77−11460
acetonitrile, liq. struct., RISM equation calc. 78−71665
acetonitrile, mol. pair-correl. function, X-ray and neutron diffr. 78−26420
acetonitrile, Raman spectral study of aq. soln. struct., H-bond effects 77−88454
acetonitrile, soln., high press., mol. reorientation, correl. times, depolarised Rayleigh scatt. obs. 80−29748
acetonitrile-carbon tetrachloride solns., rot. and vibr. relax., Rayleigh and Raman scatt. 77−66513
liquid structure continued
acetonitrile-d_3, liq., intermol. ^1H spin-lattice relax. and pair-diffusion 79−99781
acetonitrile-toluene-benzene, mol. interaction and thermodynamic props. 80−71935
acoustic levitation technique appl. 79−44906
acoustic parameters and density determ. using piezoelectric transducer *(Russian)* 78−49799
acriflavine solution, fluoresc. polarisation, effect of aggregation of molecules 79−91485
acrylonitrile, NMR and relax. props., liq.-liq. transition rel. to mol. motion 80−70382
alcohol-alkane dilute system, electron solvation, picosecond spectral obs. 77−44573
alcohol-H_2O solutions, structure, luminesc. probe obs. 78−84636
alcohols, aliphatic, dilute aqueous solns., excess partial molal heat capacities 79−57280
alcohols, liq. mol. rot., deuteron relax. obs. 77−8432
alcohols, vapour and liq. IR spectra, bandwidth, directional mol. rot., H-bonding 79−78661
aliphatic chains, mol. orientation correls. with squalane in soln., depolarised Rayleigh scatt. *(French)* 79−65885
alkali chlorides, aq. soln., ion-solvent and solvent-solvent interactions, X-ray obs. 80−44107
alkali halide solns. with H_2O and D_2O, struct. and O isotope fractionation 78−22629
alkali halide solutions, tetrahedral hydration of ions from Raman bands obs. 78−55804
alkali halides, ion hydration numbers in aq. solns., mol. dynamics calcs. 77−62464
alkali halides, molten, ionic radii and X-ray diffr. patterns 78−59732
alkali halides, molten, mode coupling theory of charge fluctuation spectrum 80−92451
alkali halides, molten, struct. determ. by X-ray scatt. 78−87609
alkali metal, from 1st-principles pseudopot. calc. 79−41941
alkali metal halide, melt, estimation of struct. models by comparing vol. parameters 77−89368
alkali metal iodide (bromide), molten, struct. by X-ray diffr. 77−4033
alkali metal-ammonia solns., metal-insulator transition, h.f. and u.s. props. 77−1369
alkali metal-based liquid semiconductor alloys, struct. and electronic props. 78−2403
alkali metals, calc. of enthalpy of soln. of nonmetals and elec. resist. 77−55225
alkali metals, liq., collective excitations and short-range order 78−63665
alkali metals, resist. and struct. factor, temp. depend. 77−62466
alkali nitrites, molten, combination scatt. spectra, freq. shifts, jumps at melting, line widths *(Russian)* 77−40241
alkaline earth halides, thermodynamic and structural props., computer simulation 78−75849
alkaline earth nitrites, molten, combination scatt. spectra, freq. shifts, jumps at melting, line widths *(Russian)* 77−40241
n-alkane, polymer, liq., mol. arrangement, computer model 80−92446
n-alkane chains, pure liq. and solns., small angle neutron scatt., ang. depend. 79−1384
alkane chains in liquids, rot. and torsional dynamics, Riemann tensor theory 80−54084
n-alkane liquids, molecular orientational correlations 79−19131
n-alkane mol. config. in melt and cyclohexane soln., small-angle neutron diffr. 78−55800
alkanes, liq., mol. struct., selective deuteration and IR vibr. spectra 80−96432
alkanes, liq. state rot. dynamics for nonrigid 4-, 5-, and 6-bond chains 79−99054
alkanes, liquid, chain reorientation, Brownian dynamics simulation, comparison of models 80−49067
alkanes, mixtures, order, enthalpy of mixing, calorimetric obs. *(German)* 78−18773
1-alkanols, liq., H-bond order temp. depend. from Hildebrand rule 80−7838
alloy, binary, classification on basis of average atomic order effect 78−14269
alloy, binary or ternary, atomic order effects, statistical mechanics and fluctuation theory 78−14263
alloy, dil., partial interference functions of solutes 79−19139
alloy, thermodynamic props. rel. to struct. 77−1237
alloys, partial structure factors, square well pot. calcs. 77−51300
alumino-silicate melt, Monte Carlo calc. of ionic struct. 79−60256
amorphous metals, struct., harmonic approx. model 77−47331
amorphous solid, supercooled liquid-glass transition region, short-range order, simulation 80−44127
aniline-phenol, liq., US vel., adiabatic compressibility, H-bonded complex form. 77−35635
aqueous non-electrolytes, US velocity measurement, adiabatic compressibility studies 78−87605
aqueous nonelectrolytic soln. microheterogeneous struct., X-ray diffr. study 78−87608
aqueous solns., max. density temp., structural interpretation 77−58933
aqueous solns., max. density temp., structural interpretation 77−58934
aqueous solution, hydrophobic interaction, simple solute, one-dimens. model 79−37601
aqueous solutions, Monte Carlo simulation, convergence of new algorithm 78−63649
aqueous-organic mixed solvent structure, solvation, cation exchange *(Dutch)* 79−83500
associated liq., US absorpt. and hole theory 78−10124
associated liquid radial correlations, comparison of Monte Carlo and Ewald mol. dynamics calc. methods 80−14984
associated liquids, correl. between dielec. and acoustic relax. times 78−9925
associated solution, characteristic sums method in stat. theory 80−10480
associated solutions, H bonding and anomalous saturation 78−52426
asymptotic form of structure factor 77−7651
atom/molecule effective volumes and electron correls. in one- and two-electron systems 77−3286
autocorrelation function spectrum of the velocity of a molecule in a liquid *(Russian)* 79−7534
benzene, deuterated, neutron diffraction by electron LINAC 79−50974
benzene, liq., vibr. excitons, reson. energy transfer and local struct., IR spectra 77−75145
benzene, mean free path meas., US relax. 80−59585

liquid structure continued
benzene, numerical exam. of a neutron quasielastic scattering 78−9938
benzene binary liquid mixtures, US study of mol. interaction 77−15494
benzene X-ray diffr. pattern and liq. models using C-H group scatt. factors 78−6004
benzene-chloroform mixture, reorientational motion and intermolecular interaction by Raman spectroscopy 77−24839
benzene-hexafluorobenzene, mixtures, dielectric relax. and US absorpt. 77−12307
benzenes, substituted, dense liq., mol. reorientation and shear viscosity 77−4213
benzenes, substituted, dielectric absorpt. and NMR 78−88251
benzyl benzoate, supercooled, depolarised lines in quasielastic light scatt. 80−45095
bifurcation of solutions with crystalline symmetry 77−7650
binary alloy, atomic position correlations, nearly free electron approx. 77−39529
binary alloy, dil., partial interference functions, short range chem. order effects 79−7541
binary alloys, calc. of triplet correlation function on basis of thermodynamic quantities for solute atoms 80−49087
binary fluid of charged hard spheres, radius-ratio effects 77−7649
binary liquid, crit. conc. fluctuations, nonexponential decay, 3-methylpentane-nitroethane expt. 80−44309
binary liquid mixtures, excess Gruneisen parameter and intermolecular interactions 77−20082
binary liquid solutions, struct. and thermodynamic props., molecular dynamics study 80−64866
binary liquid solutions, surface cluster functions 78−67631
binary liquid system, colligative prop., composition diagram *(Russian)* 79−14663
binary mixture, rel. to viscosity isotherm classification *(German)* 77−28033
binary mixture, viscosity, Panchenkov model calcs. *(German)* 77−31797
binary mixtures of optically anisotropic molecules, depolarized Rayleigh scatt. 80−40122
biphenyls, cholesteric blue phases, struct. and props. 80−103243
book 79−60245
borate glass melts, struct. determ. using graph theory 79−64980
Born-Green equation stability for effective pair pot. in dense liqs. 77−51292
Bose fluid, quantum conserving approx. of static and dynamic struct. factors, normal ^{4}He liq. appl. 79−51321
boson systems, correlation function, variational calcs. with healing constraint 77−76638
Brownian particles, angular velocity autocorrelation function 77−27932
n-butane, liq., temp.-depend. free vol. 79−99052
n-butane, trans or gauche, solute mol., solvent mol. distrib. 80−96433
n-butane in nonassociated solvents, intermol. struct., superposition approx. and two-cavity model 78−71656
t-butanol-water, X-ray scatt. intensity composition depend., soln. struct. 78−6005
t-butyl alcohol, aq. solns., US relax. freqs., clathrate-hydrate model 78−30704
t-butyl alcohol, struct. determ. from vibr. spectra, H-bonding and heat of mixing *(Russian)* 78−3368
tert-butyl alcohol in nonpolar solvents, liq. struct. from dielectric studies 80−38894
butyloxybenzylidene octylaniline, two- and three-dimensional smectic B liq. cryst. film, long range order 80−96442
carbon tetrachloride, liq. struct. by neutron diffr. 79−73089
carbon tetrachloride, liq. struct. by pulsed neutron diffr. 79−69004
carbon tetrachloride, mol. struct. factors, X-ray diffr. 77−76291
carbon tetrachloride, struct., oscill. amp., neutron diffr. study 79−46544
chalcogen-based liquid semiconductor alloys, struct. and electronic props. 78−2403
charged hard sphere fluids, meas. spherical model 78−18524
charged particles, two-component liquid, in equilib. with vapour, surface dipole layer and surface tension 80−70505
chemical physics of liq. state, book 77−31574
chloroform, dense liq., mol. reorientation and shear viscosity 77−4213
chloroform, X-ray diffr., struct. of mol. in liq. 78−26421
chloroform. liquid, RIMS calc. of struct. 79−37610
chloroform-d_1, and isotopic forms, liq., neutron diffr. obs. 79−32878
chloroform-d, neutron diffr., struct. of mol. in liq. 78−26422
chloroform-ethanol solns., light scatt. spectra, conc. fluctuations, assoc. complex form. 77−40254
chloromethane, rot. dynamics, far IR spectra 77−19864
classical fluids, correl. functions, perturbation theory for soft sphere systems 77−72536
collective modes in classical monoatomic liqs., coherent neutron scatt., book contrib. 77−89371
colloid, hard sphere solvent struct. effects on particle interactions 78−7237
computer simulation on molten ionic salts, review 79−19130
conference on neutron inelastic scattering, Vienna, Austria (Oct. 77) 79−41912
coordination numbers, calc. in microinhomogeneous struct. model *(Russian)* 80−38902
covalent elements, cohesion in condensed phases, corrections to simple Huckel approx. 78−59779
covalent elements, cohesion of σ and π bonds in condensed phases, simple Huckel approx. 78−59778
critical fluid, local order effects on dynamics near liq.-gas pt., US and light scatt. 78−67806
cryolite, molten, struct. charact. by IR spectroscopy and splat cooling *(French)* 79−69835
cyclohexane, liq. and soln., Raman scatt. for vibr. and rot. relax. 79−82969
cyclohexanol, US relaxation at 0.5 to 45 MHz 78−59868
Debye generalised fluid model, dielectric relax., depolarised dynamic light scatt. 80−108156
decalin, liq. and glass mol. motion, kinematic and electrodynamic solns. 80−25293
decanol, dynamic mol. struct. in cyclohexane-d_{12}, ^{13}C NMR 78−33519
dense electrolytes, semiempirical analytic theory for pair correlation function 77−27800
dense fluid, square-well pot. mols., struct. factor, transport props. 78−22620
dense fluids, solvation forces between two solids 80−64855
liquid structure continued
dense liquids, structure at solid wall interface, NVT Monte Carlo method 79−65310
deuterated nitroxide radical probe, synthesis and appls. *(French)* 78−76314
dextrans, branched, in soln., cross-section factor correction in small-angle X-ray scatt. data 80−84048
diatomic-like mol. fluid, with isotropic rot. diffusion quasielastic neutron scatt. 77−47312
dibenzenechromium, cryst. and soln., dynamic struct., NMR expts. 77−15328
dichloromethane, liq. dynamics, neutron inelastic scatt. 78−71664
dichloromethane, liq. state dynamics, models 79−73087
dichloromethane, mean free path meas., US relax. 80−59585
dichloromethane, mol. struct. factors, X-ray diffr. 77−76291
dielectric liquid, bubble creation in high elec. fields, explained in terms of struct. 79−91370
diffraction data neutron and X-ray 79−46538
1,1-difluoroethylene, rot. dynamics far IR spectra 77−19864
dilute fluid mixtures, spherical mols., struct. and permittivity 80−92433
dilute polar fluid, electron solvation, picosecond spectral obs. 77−44573
dilute ternary liq. alloy, heteroatomic solute, thermodynamic partial pair struct. factory, sticky hard sphere 79−32867
p-dioxane, aq. soln., excess molar heat capacities, 298.15K, US vel. obs. 80−6523
1,4-dioxane, liq., reorientational correl. times from light scatt. 77−32385
dioxane, Raman spectral study of aq. soln. struct., H-bond effects 77−88454
p-dioxane-water mixtures, adiabatic compressibilities and sound vels., temp. depend. 79−28044
dipolar fluids, equilib. statistical mechanics, struct., dielec. and thermodynamic props. 80−6345
disorder parameter-pseudo-Gruneisen parameter relation 78−34411
dynamic and static orientational pair correls., depolarised light scatt. 77−16321
EBBA, isotropic phase, order fluctuations, self-diffusion, and rot. motion, proton spin relax. meas. 79−87328
education, possible excitations, ball bearing model 77−45642
effective pair potential from static struct. factor data 78−75521
ELDOR obs. for discriminating rot. and transl. correl. times in liqs. 77−1619
electrolyte, Debye-Huckel ionic atmosphere, number density of ions 79−29369
electrolyte, polarisable dielectric spheres model, struct. around ions in soln. rel. to ionic solvation and activity coeff. 79−29368
electrolyte, soln. and cryst. *(German)* 80−80804
electrolyte, solutions, 1-1 and 1-2, extended mean spherical approxs. 79−4216
electrolyte aq. solns., IR librational bands, struct. making and breaking 78−56476
electrolyte solns., aq., water struct., differential IR spectral investig. 77−52651
electrolyte solution, anion-cation couple, role in struct. 79−37604
electrolyte solution, conc. aqueous, struct. determ. using pulsed NMR methods 78−38605
electrolyte solution, primitive model, using modified BBGY integral eqn. 79−99049
electrolyte solution, second moment condition of Stillinger and Lovett 77−90609
electrolyte solution structure, (1952-1977) 78−26417
electrolytes, aq. soln., molecular dynamics simulation 80−54097
electrolytic solution, thermodynamics and correlation functions 80−24132
electron diffraction 78−83686
electron diffraction pattern evaluation, single beam microdensitometer 80−86370
electrons in fluids, picosecond chromodynamics 79−35850
electrostatic interactions and the structure of water, conf. Brussels, Belgium (1972) 78−26413
1,2-ethanediol, aq. soln., proton NMR study of H-bonding 79−78545
ethanol$_{(l)}$, hydroxyl proton chem. shift, density and temp. effects 77−1607
ethanol-H_2O mixture, liq. US vel., −80 to 20°C, 1-5 MHz 78−59933
ethyl alcohol, solution, struct. determ. from vibr. spectra, H-bonding and heat of mixing *(Russian)* 78−3368
ethylene-propylene copolymer, melt struct., X-ray diffr. obs. *(Russian)* 79−23533
excess number and charge functions 78−18525
ferrocene, cryst. and soln., dynamic struct., NMR expts. 77−15328
fluctuating local structure, Fokker-Planck type eqns. 79−64966
fluid interfacial stress and struct., gradient theories 79−19428
formaldehyde-water, heuristic intermol. pot. function, ab initio MO calcs. 78−33566
formic acid, liq., microdynamic behaviour, struct., nucl. spin-lattice relax. 77−76270
furan, mean free path meas., US relax. 80−59585
gas-liquid surface of mol. fluids, mol. dynamics computer simulations 80−39387
glass-forming melts, anionic constitution 78−2011
glycerol, aq. soln., proton NMR study of H-bonding 79−78545
glycerol, Mossbauer and neutron scatt. 80−20559
glycerol, supercooled, Mossbauer effect and model of mol. motion 78−64301
glycerol, supercooled liq., dynamical struct. factor, Mossbauer spectroscopy 78−27126
glycerol, supercooled liq., mol. motion, Mossbauer effect, Rayleigh scatt. obs. 77−73099
Hamaker constants, struct. effects, dispersion forces calcs. 78−43215
hard rod system, initially ordered, one-dimens., mol. dynamics computer simulations 78−71658
hard sphere fluid, in contact with soft repulsive wall, struct. calcs. 78−1967
hard sphere fluid theory applic. to liq. particle dispersions 77−9129
hard spherocylinders, dumbbells and spheres, equations of state, theory 79−50970
hard spherocylinders and spheres mixtures, Monte Carlo study 80−49073
heavy water neutron diffraction by electron LINAC 79−50974
heptane, liq., Raman scatt. at high-press., chain kinking 79−87429
heterocyclic compounds in dilute solutions, dielectric relax., microwave technique 78−84520

liquid structure continued
hexadecane, liq., Raman scatt. at high-press., chain kinking 79−87429
n-hexadecane, pure liq. and solns., small angle neutron scatt., ang. depend. 79−1384
hexane, liq., Raman scatt. at high-press., chain kinking 79−87429
hexanetriol 1,2,6, liq., light scatt. study of struct. relax., viscosity and dielec. relax. 79−86672
n-hexatriacontane, pure liq. and solns., small angle neutron scatt., ang. depend. 79−1384
hydration, anionic, press. effect, neutron diffr. obs. of $NiCl_2$(^{7}LiCl) heavy water solns. 80−30212
hydration, hydrophobic, of nonpolar mols. in dilute aq. soln., Monte Carlo simulation 80−3314
hydrocarbon liquid, residual energy and entropy, rel. to liq. and mol. structs. 78−71869
hydrogen-bonded liquids, HF, H_2O, NH_3, computer simulation, intermolecular potentials 80−38890
hydrophobic effect, dil. soln. struct. and thermodynamic props., semi-empirical model 78−20060
hydrophobic interaction, solubility and solvent struct. changes 78−83705
hydroxylic solvents, dielec. consts., effect of non H-bonding solutes 77−48673
hydroxypropyl cellulose in conc. aq. soln., mesophase struct., colour 77−19870
imidazoline nitroxide radical, H-bonding with H donors, NMR, DNP and spin lattice meas. 79−15971
immiscible mixtures, variational theory 79−27885
independent structure model, inert gases critical point, liquid-vapour equilib., second virial coeff. *(Spanish)* 77−4031
independent structure model, vibr. and translational degrees of freedom *(Spanish)* 77−4027
inert gases, liquid phase mixtures, dipole autocorrelation function, IR absorpt. spectra obs. 80−28903
inhomogeneous fluid, pair and density correl. functions 79−27887
integral eqn. with approximation of direct correl. function in pot. rigid core region 77−84611
integral equations, numerical solns. new method 80−28896
interfaces, liq.-cryst. and liq.-rigid wall, Monte Carlo simulation 79−27896
intermolecular correlation effects on liquid props., determined by X-ray diffraction 77−27799
intermolecular nucl. relax. by translational and rot. diffusion, effect of pair correl. functions *(French)* 79−19794
iodomethane, liq. (liq. mixtures), vibr. relax. and reorientation, symmetric C-H bending mode 1st overtone 78−62884
ion structure in fluids, Atkins model revision 77−7921
ion-water interactions, survey of diffr. studies 80−24347
ionic liquid, binary, mode coupling theory of charge fluctuation spectrum 80−92451
ionic liquids, hypernetted chain eqn., Newton Raphson soln. 80−49071
ionic liquids, S-D periodic particle-particle/particle-mesh program P3M3DP 80−84041
ionic liquids, struct. determ., summer school lecture series 80−6349
ionic liquids, structural props., review 80−96430
ionic solution in molecular polar solvent, stat. mech. 78−30527
ionic solutions, struct., neutron diffr. technique study 79−10787
ions in dipolar solvent, potential of mean force, linearised hypernetted chain approx. calcs. 78−55798
isopropyl alcohol-carbon tetrachloride, mixture, dielec. const., two-sided estimate 79−42262
kinetic theory, equilib. and non-equilib. props., book contrib. 79−60246
Lennard Jones liquid, simulation by force bias and Monte Carlo methods 79−86666
2-Lennard-Jones centres pair pot., thermodynamic and struct. props. 77−58939
Lennard-Jones fluid, critical lengths and spinodal region 80−84045
Lennard-Jones fluid, phase separation by spinodal decomposition, mol. dynamics computer simulation 79−10766
Lennard-Jones fluid, two-centre, perturbation theory appl. using spherically averaged reference potential 80−64860
Lennard-Jones liquid, free-vol. distrib., dislocation like struct. 79−64972
Lennard-Jones liquid mixtures, equimolar, mol. dynamics, struct. and thermodynamic props. 78−18517
Lennard-Jones liquids, S-D periodic particle-particle/particle-mesh program P3M3DP 80−84041
Lennard-Jones solutes, hydration, mol. dynamics obs. 79−34294
light nuclei liquids, neutron diffraction exam., dynamical corrections for structural factor determ. 79−99034
light scattering spectra, struct. and dynamical information 80−55105
liquid binary mixtures, proton mag. relax. and mol. motion 77−28471
liquid crystals, lyotropic, counterion binding, NMR, ion condensation model 80−1922
liquid metals, strong binding model, electronic density of states, Green's function calcs. *(Russian)* 80−70111
liquid metals, surface layer structure, rel. to neutron refl. on boundary *(Russian)* 78−1976
liquid-vapour interface, pair correl. function at triple pt., Monte Carlo method 80−10753
liquid/solid interface, mol. dynamics simulation of struct. 78−26764
local order and vertical-horizontal light scatt. fine struct. 77−55800
local order theory characterisation by vectors tensors, internal energy density multipolar expansion 80−49070
macromolecular solutions trapped in small pores, statistics 77−39524
macromolecule liquid, translational friction coeffs. of rigid, symm. top mols. 80−6003
macromolecules, polydispersity in nonlinear electric methods, nonlinear dielec. effect formulas derived 78−59730
maleic acid, acid slats, melts, H_2 bonding, IR, NMR investigs. 79−65859
MBBA, isotropic phase, order fluctuations, self-diffusion, and rot. motion, proton spin relax. meas. 79−87328
mean spherical approx. and effective pair pots. 80−70099
mean spherical model approx. 78−75514
medium cluster model, vapour press. isotope effects, mol. orientation effect 77−72542
medium cluster model, vapour press. isotope effects 77−65943
melting, dislocation generation, anharmonicity and solitons 78−79746
melts, of a congruently melting substance, single struct. model 80−103233
metal, classical fluid model, neutralising negative background density 78−22621
liquid structure continued
metal, conference, Bristol, England (July 1976) 77−47297
metal, effective interatomic potential from struct. data 78−47232
metal, effective interionic potentials 78−91221
metal, effective interionic pots. determ. from expt. data 77−47338
metal, electronic theory of thermodynamics and struct., summer school lecture series 80−6353
metal, model potential, exact soln. of mean spherical approx. 79−82144
metal, phys. chem., conf., Konigstein, Germany (Mar. 1976) 77−1059
metal, polymer model, approx. eqn. for average distance between atoms calc. *(Russian)* 77−15293
metal, structure, perturbation calcs. using Percus-Yevick equation 78−42889
metal, structure determ. by hard sphere model of repulsive interatomic pot. 79−55650
metal, structure factor shoulders and interatomic pot. rel. to electron theory 77−7658
metal, structure singularities *(Russian)* 78−79521
metal, surface ion density, nonmonotone, perturbative discrete ion introduction into jellium 78−72222
metal, thermal press. coefficients and sp. ht. 79−65207
metal, viscosity anal. 78−91468
metallic liquids, resistivity, struct. factor calcs. 78−51962
metallic melts, viscous flow due to high overheating, quasipolycrystalline model 80−70110
metals, atomic radial distrib. curve anal. *(Russian)* 80−14996
metals, core polarisation and struct., model potentials and simulation methods 79−77492
metals, d-band, force fields 79−33051
metals, electron correlations, evidence 78−55805
metals, interatomic interaction potential, rel. to structure factor *(Russian)* 79−69006
metals, lattice model, parameters for supercritical region 79−64983
metals, liq., dipole dipole-dispersion coeffs. calcs. 80−70109
metals, liq., structure and dynamical properties 79−55648
metals, liquid, structural micro-inhomogeneity, Brownian motion studies *(Russian)* 80−92426
metals, polyvalent, struct. factors with shoulder 80−19686
metals, radial distrib. function and thermodynamic charact., interparticle interaction pot. *(Russian)* 80−49086
metals, struct. factors, elec. resist. calcs. 77−85190
metals, structure and interatomic interaction, pseudopotential method 80−107042
metals, structure factors, higher order distrib. functions 77−51299
metals, viscosity calc. using microinhomogeneous struct. model *(Russian)* 80−15284
metals and alloys, book 78−51406
metals and alloys, geometrical model, soft sphere static approx. eqn. of state 78−42892
metals and alloys, struct., and thermodynamic props., ab initio calcs. 77−84621
methane, dil. aqueous soln., Monte Carlo calcs. on struct. 79−32874
methane, in alkane soln., ^{13}C nucl. spin-spin relax., for mol. correl. times 79−95661
methane, liq., medium cluster model, vapour press. isotope effects 77−65943
methane, liq., medium cluster model, vapour press. isotope effects, mol. orientation effect 77−72542
methane, liq., mol. dynamics calcs. 77−19857
methane, liq., temp.-depend. free vol. 79−99052
methane, mol. dynamics simulation using singularity free algorithm 80−54116
methanol, pure liq. and soln., Raman and IR intensity, polymerisation degree *(French)* 79−28740
methanol solns., IR spectroscopic detection of free lone-pair groups or terminal methanol mols., PMR 79−19869
methanol-ethanol mixture, dielectric const. composition depend. rel. to struct. effects 79−11378
methanol-H_2O, liq., zero-angle X-ray scatt., conc. depend. 79−27897
methyl bromide, liq., NMR relax., anisotropic mol. reorientation 78−2764
methyl halides, orientational dynamics, local coherence 77−27805
methyl iodide, dense liq., mol. reorientation and shear viscosity 77−4213
methyl iodide, liq., expt. comparison with rough sphere rot. diffusion model 78−30532
methyl iodide, liq., vib. relax., A_1 Raman bands 77−40220
methyl rotator in isotropic fluid, motional asymm. determ. from ^{13}C spin dynamics 77−69718
2-methyl-1-propanol, liq. struct. at 20°C 79−32873
methylene bromide-d_0-d_2, liq., nucl. spin-lattice relax., rot. correl. times 77−59476
3-methylpentane-nitroethane, correl. function near crit. mixing point 79−55893
microemulsion type systems, implication for struct. of percolative cond. model 79−100452
microparacrystals in physics, review *(German)* 79−27933
micropolar effects in liquids, charact. evaluation under rotating electric field *(Polish)* 79−55638
microstructure and dynamics, summer school, Aleria, Corsica, France (Sept. 1977) 80−6339
mixed ion-dipole system, binary distribution function calcs., dipole orientations *(Russian)* 80−79664
mixture, binary, fluctuations near liq.-liq. crit. point, neutron small-ang. scatt. appl. 79−82347
mixture, excess Gibbs free energy, quasilattice local composition model, phase equilib. 78−31681
mixture, near tricrit. pt., light scatt. and sum rules, appl. to ethanol-benzene-water-$(NH_4)_2SO_4$ 80−34933
mixture, strongly nonideal, vap.-liq. equilib. data correlation eqn., heat of mixing 78−30763
mixtures, long wavelength limits of third and higher order structure factors 77−4029
model liquid, velocity autocorrelation function, spectra anal. 79−90512
modified cell theory, thermodynamic props. 79−19133
molecular dynamics of liqs., neutron scatt. and computer simulation 78−63650
molecular dynamics thought experiments 80−1910
molecular fluid, hard-core triatomic, Monte Carlo simulations 80−38880
molecular fluid, pair correlation function, perturbation theory 78−55799
molecular fluid mixtures, equilibrium props. 80−64867
molecular fluids, coupling of rotation and translation 80−38892

liquid structure continued
molecular fluids, diatomic, struct. and dynamics 80−38889
molecular fluids, free energy, computer simulation and quantum corrections 80−28905
molecular fluids, translational motion, Mori three variable theory and mol. dynamics simulation 78−63651
molecular liquid, anisometric, light scatt. obs. of orientational pair correlations 77−36252
molecular liquid, interval normalisation of neutron diffr. data 77−35441
molecular liquid, non-stoichiometric complex formation, thermodynamic equilib. consts. 77−21406
molecular liquid, orientation dependent distrib. function from NMR relax. data 77−20737
molecular liquid, reference systems with spherical interactions 80−24337
molecular liquid, reorientation PAC, nonadiabatic effects 77−12274
molecular liquid, short chain molecules, optical investig. of mol. motions 80−40123
molecular liquids, depolarised light scatt., flow birefringence and local order 80−45094
molecular reorientation, conditional pair distrib. function, irreducible expansion, symmetries 77−47317
molecular reorientation correlation times, librational model 78−1968
molecule torsion angle fluctuation, correl. time for three bond chains 79−55624
molten salt, mol. dynamics simulation, of liquids with ionic interaction 80−54097
molten salt, nucl. quadrupolar spin-lattice relax., microscopic liq. dynamics 79−91313
molten salt, possibility of plasmon mode obs., struct. dynamics 80−10477
molten salt model, mean spherical approx. 78−63662
molten salts, IR, Raman, EPR and NMR spectroscopy, review *(French)* 79−69832
monatomic liquids, short wavelength collective density excitations, computer simulation 79−46540
monoatomic liquids, quasi-crystalline structure, role of vacancies in dynamics 80−92438
2(4)-monooxopyrimidines, gaseous, matrix, soln., tautomeric equilib., IR and UV absorpt. spectra 80−58256
Monte Carlo calc., long-range dipolar interactions in computer simulations of polar liquids 78−87603
Mori formalism for far IR and microwave absorption 77−24833
multicomponent alloys, partial struct. factors in the long wavelength limit 78−22633
multicomponent liquid surface, single particle distrib. 77−35458
multicomponent mixture, number-conc. struct. factors 78−18526
multicomponent mixture, viscosity, Panchenkov model calcs. *(German)* 77−31797
multicomponent system, higher-order partial struct. factors 77−47339
multicomponent systems, higher-order partial struct. factors 77−31572
neopentane, liq. struct. by X-ray diffr., −17-150°C 79−27898
neopentane, mol. motion in cryst., liq. and plastic phases, neutron scatt. obs. 78−6021
neutron diffraction, book, with emphasis on technical aspects 79−60225
neutron diffraction investigations, book contrib. 79−60230
neutron diffraction of liquids using electron linac, CCl_4 appl. 78−18504
neutron diffraction spectrometer, resolution and luminosity study for liquid on amorphous samples anal. 78−87591
neutron diffraction studies at high momentum transfer 79−46525
neutron scattering, book contrib. 79−60232
neutron scattering conference, Gatlinburg, TN, USA (June 1976) 79−41910
nitrates of monovalent metals, molten, NO_3^- ion struct., pulsed neutron diffr. obs. 78−22631
p-nitroaniline, Raman spectra, mol. struct. in molten state 79−91435
nitroxyl radical rotation in liquids, ESR, dielec. relax. 77−28447
non-rigid molecules in condensed phases, liquid struct. effects on chem. reactions and conform. changes 80−40725
noncentral intermolecular interactions, struct. contrib., perturbation method and partition function separation 80−24341
nonelectrolyte aqueous solns., X-ray diffr. meas. of struct., scatt. curves 79−10785
nonelectrolyte aqueous solutions, lattice model approach 79−32876
nonelectrolyte solutions, liq. theory, review, book contrib. 77−39523
nonelectrolyte-water, X-ray scatt. intensity composition depend., soln. struct. 78−6005
nonelectrolytes, aqueous, excess heat capacity, H bonding 78−3362
nonpolar fluid, permittivity, Kerr const., in terms of at.-at. correlation functions 77−36200
nuclear magnetism of liquid systems in the Earth field range, review 80−50206
nucleic acids, bases and base pairs, water struct. in soln., Monte Carlo simultion 80−76709
octane, liq., Raman scatt. at high-press., chain kinking 79−87429
1-octanol, dielec. consts., solvent struct., effect of H bonding solutes, chain length 77−48674
1-octanol-H-bonding solute system, chain assoc., dipole correl. theory, dielec. const. anal 77−48675
1-octanol-nonhydroxylic solvent complexes, H bonding, assoc. consts., elec. dipole moments, dielec. consts. 77−48672
oligobutenes, critical mol. weight for liq.-like behaviour 77−63704
one dimensional shouldered hard-sphere fluid, struct. factor 78−34417
optimised cluster expansion, struct. function evaluation 80−49085
organic ionic melts, novel class of liquids 77−35463
organic liquid, simple, struct. exam. and scatt. data interpret. 80−54096
organic liquid mixtures, excess free vol. US vel. meas. 77−51294
organic liquids, polar and nonpolar, entropies of vaporisation 78−26676
organic N bases, solutions in organic solvents, IR spectra and struct. 79−38534
Ornstein-Zernike eqn., rel. to pair pots. calc. 77−1054
pair correlation function, self-consistent calcs. for simple fluids 77−1061
pair correlation function errors, dilute hard sphere approx. 78−79514
pair correlation function of the liquid-vapour interface 79−55633
pair distribution functions, extrapolation method 77−58938
pair potential, Percus-Yevick and hypernetted chain approx. calcs. 77−1052
pair potential, self-consistent calcs. for simple fluids 77−1062
pair potentials, from inelastic neutron scatt. data, self-consistent method 78−59728
pair potentials determ., formulation of extended Born-Green eqn. 77−1057

liquid structure continued
paraffin, liq., electron mobility, mol. struct. depend. 77−4350
paraffins, solid and liquid, diamagnetic susceptibility 78−14923
partial structure factors, freq. modulated X-ray diffr. 77−35440
n-pentane-benzene, light scatt. of liq. near crit. vaporisation state, correl. radius 79−24328
Percus-Yevick approximation, thermodynamically consistent analogue *(Russian)* 77−84603
Percus-Yevick eqn., construction based on equilib. BBGKY system 80−1911
phenol-aniline (quinoline) (pyridine), liq., US vel., adiabatic compressibility, H-bonded complex form. 77−35635
polar liquid, integrated absorpt., microstruct. effect *(French)* 78−10823
polar liquids, solns., mol. rot., kinetics 77−51984
polar-polar liquid mixture, significant structure model applic. to dielec. const. correl. 77−8487
polar/nonpolar mixtures, pot. of mean force, approx. theories, clustering of solute mols. 78−26401
poly-1-olefin melts, viscous flow activation energy, melt struct. 77−7654
polyacids, unsaturated carboxylic, in organic solvents, hydrogan bonding, structurisation *(Russian)* 78−71666
polyatomic fluid, local dynamics, spectroscopic studies, summer school lecture series 80−6343
polydimethylsiloxanes, liq., proton spin relax., mol. motion, network form. 79−15369
polyelectrolyte solution, neutron scatt. 79−77484
polyelectrolytes, weakly charged, collapse in poor salt free soln. 80−44091
polyelectrolytes in soln., electrostatic persistence length rel. to unified theory 78−95932
polyethylene, electron diffr. radial distrib. 77−4032
polyethylene, melt struct., X-ray diffr. obs. *(Russian)* 79−23533
polyethylene glycol solns., US vels. rel. to struct. 77−72655
polyethylene imine, oligomers, solns., linear struct., props. *(Russian)* 79−50177
polymer, soln., freely jointed chain, with excluded vol. interaction, Monte Carlo studies 80−10475
polymer chain in bulk and soln., elastic, coherent small-angle neutron scattering 77−80428
polymer liquid-crystalline solns., struct. 80−103235
polymer melt, cross-links effect on struct. 79−41928
polymer melt, entangled, reptation 78−22669
polymer melt, quasielastic incoherent neutron scatt., Q^4-depend. broadening 77−47327
polymer melt, review of expt. results 79−37636
polymer melt, rheology and mol. struct. 78−63405
polymer melt inside small pores, chain conform. *(French)* 79−90516
polymer melts, defect fluctuations, reptation, Monte Carlo investig., NMR autocorrel. function 77−3499
polymer soln., colloid stability near repulsive wall 80−21326
polymer solns., supermol. struct. determ. from scattered light spectrum *(Russian)* 79−32880
polymer solution, diffusion, viscosity and dynamic struct. factor, dynamic scaling theory 79−64977
polymer solution, quasimonomers, concept and appl. to polymer statistics 79−41931
polymer solution, scaling laws for correlations, rel. to mag. variables 77−47326
polymer solutions, long chain immersed in shorter chains, end-to-end dist. 79−1387
polymer solutions, moderately conc., light scatt. curves, struct. model 79−4810
polymer solutions, random coil, intramol. fluctuations by photon correl. spectroscopy 77−48184
polymer solutions light scatt. rel. to mol. wt. distrib. function type *(German)* 79−1767
polymer systems, phase dualism, gas-, liq.-like, appl. to compression effects 79−1388
polymeric liquids, constitutive eqn. with factorised memory function 80−70105
polymers, random coil, radial distrib. function calcs. 80−44101
polymers, self-consistent field approximation, BBGY and Kirkwood calcs. *(Russian)* 79−64981
polymers, short range order, amorphous and liquid, ideal peak method calcs. 80−28900
polyolefine, liq., memory effect 80−103268
polystyrene, diethyl malonate soln., near-crit., osmotic compressibility, correlation length, scaled functions 80−11422
polysulphone, glass and melt, PVT props., glass transition 79−14911
polytetramethylene glycol, short range order, amorphous and liquid, ideal peak method calcs. 80−28900
polyvalent metals, influence of pair pots. on struct. 80−28909
polyvinyl alcohol, in water-ethanol mixture, processes of structure formation 80−10482
polyvinyl alcohol/vinyl acetate copolymer, in water-ethanol mixture, processes of structure formation 80−10482
polywater, discovery, production and appls. 78−30529
propane, liq., temp.-depend. free vol. 79−99052
1,2-propanediol, aq. soln., proton NMR study of H-bonding 79−78545
1-propanol, X-ray diffr. study of struct. at −25°C 77−55227
protein solutions, small-angle neutron scatt. using time of flight method, spectrometer 79−1371
PVC, suspensions, melts, rheological props. rel. to struct. 79−3983
pyrene-3-sodium sulphonate solubilised in didodecyldimethylammonium bromide-benzene inverted micelles 80−3417
pyridine, liq. and in CCl_4 soln., depolarised Rayleigh scatt. 79−51973
pyridine, mean free path meas., US relax. 80−59585
pyrrole, liq. and nonaq. solns., ^{14}N NQR, ^1H line shape anal. 78−6598
quantum fluids, deep inelastic behaviour of dynamic struct. function 77−69129
quantum liquid mixture, stability and stratification 80−59754
quasi-crystalline model, asymptotic behaviour of radial distrib. function 77−68906
quasi-crystalline model, asymptotic oscills. of radial distrib. function 78−9935
radial distribution function and structure factor, struct. diffusion model 78−51403
radial distribution function peaks and coord. numbers 77−76271
radial distribution functions, for liqs. and amorphous substances, analytical computation method 80−24301

liquid structure continued
Raman spectra of liq. phase weak H-bonds, short range order and anharmonicity effects 78−64357
rare earth metals, structure factors, calc. of temp. coeff. of resistivity, one component plasma model 79−32881
rare earth metals 77−76294
Rayleigh scattering investig. of mol. motion and orientational correl. time *(French)* 77−1687
real liquids, quenched to glassy state, struct., one dimens. Ising model appl. 80−54134
reduced density metals, screening, struct. and elec. resist. 78−19016
rhodamine dyes, methanol-water solns., triplet state EPR spectra, aggregation, mol. orientation 77−48031
rigid molecules, dil. soln. in decalin, mean librational freqs. 80−6479
RISM equation, soln. for diat. symmetric mols. 79−90508
ruthenocene, cryst. and soln., dynamic struct., NMR expts. 77−15328
salol, liq., supercooled, relax. kinetics, optical Kerr effect obs. 77−84613
salts, partial struct. factors from small-angle neutron scatt. 79−60258
SCF method for struct. and dynamics calcs. of simple classical liqs., appl. to Rb 77−51303
Se, two-fluid relaxation model rel. to US absorpt. 78−2202
semiconducting liquid alloys, anomalous thermodynamic props., theory 80−49287
semiconductors in noncrystalline states, diffr. investigations review 77−72559
significant liquid structure theory, liquid-vapour transition, reduced eqn. of state for real fluids 79−32869
significant structure theory, critical pt. exponents calc. 77−7837
silicate melt, cavities in random close packed struct., applic. as model exam. 78−55802
silicate melt, Monte Carlo calc. of ionic struct. 79−60256
silicates, molten, stat. interpret. of Masson theory *(French)* 80−49078
silicates, molten, with high and medium Si contents, stat. theory *(French)* 80−49079
simple fluids, dynamics, history of inelastic neutron scatt. determ. 79−46539
simple fluids, fluctuation expressions for nonequilib. distrib. functions in adiabatic flows 80−92441
simple ionic liquids, struct. and dynamics, review 79−60243
simple liquid, dynamical structure factor and Green's functions 79−4228
simple liquid, new integral eqn. for struct. calcs., interparticle pot. reconstruction 78−5999
simple liquid free energy and radial distrib. function expansion rel. to fundamental system 78−26402
simple liquids, internal pressure and cohesive energy density, Gruneisen parameter 80−88007
simple liquids, simplified WCA theory 80−84042
simple metal, entropies and struct. factors 77−7656
sodium dodecylsulfate−H_2O system, X-ray anal. 80−1926
sodium oleate, frozen soln., NMR study of phase transitions 79−56617
soft-core Yukawa fluid, Ornstein-Zernik equation soln. 80−54091
solute molecules in 1-dimensional fluid, forces due to solvent struct. 79−73080
solute-solute-solvent interaction, dielec. behaviour problems, review 80−25298
solute-solute-solvent interactions, introduction to symposium in Vienna, Austria (1978) 80−26098
solution, aq., hydrophobic apolar spheres interaction, Monte Carlo simulation 80−6335
solution, aq., hydrophobic hydration around apolar species pair, Monte Carlo simulation 80−6336
solvated ion dynamics, kinetic dielectric decrement, microscopic theory 80−7801
solvated ion dynamics, mol. theory, fluid struct. and ionic mobility 80−7800
solvent, at polarisable interfaces, mol. models, review 80−59359
square-well potential liquid, struct., transport props. 77−7643
stability limit at low temp. 79−7539
statistical functions of far IR absorpt. spectra, survey *(French)* 78−39534
statistical mechanical models in X-ray and neutron diffraction data interpret 77−31551
steel, nonmetallic inclusion behaviour simulation by multiple phase medium eqn. *(Russian)* 78−94965
sticky hard sphere pot., struct. function evaluation 80−33869
Stockmayer molecular fluid, 2-dimens., permittivity and dynamic props. 80−103910
structural diffusion model, and struct. correls. 77−72540
structure factor for simple liquids, asymptotic form 80−33867
structure factor of system with shouldered hard sphere potential 77−43127
styrene isoprene multiblock copolymers, microstruct. and dil. soln. props. 78−42885
styrene-p-chlorostyrene triblock copolymer, dil. soln., conform. behaviour, comp. depend. 78−42886
sulphophthalein dyes in aq. soln., reson. Raman spectra 79−89678
surface, free, charged, isolated, exptl. study of deform. *(French)* 80−88240
surface density variation, Bose hard-sphere fluid model 77−20163
surface of molten salt, Fowler model, electroneutrality correction 79−28174
surface tension and width, density functional theory, appl. to liq. metals 80−103537
Te, liquid, structure metallic constituent calcs. hard sphere model *(Russian)* 80−24349
ternary liquid mixtures, molecular interaction and thermodynamic props. 78−59861
tetra-n-pentylammonium salts, molten, thermodynamic props., cation struct. 79−55639
tetrabutylammonium halides, solutions in organic solvents, IR spectra and struct. 79−38534
tetrachloromethane, liq. struct. and dynamics 80−79669
tetrachloromethane, liq. struct. temp. depend., X-ray meas. 79−77478
tetracosane melt, Brillouin spectroscopy obs. of struct., 65-250°C 79−55642
tetrafluoromethane, compressed fluid ang. momentum relax., NMR 78−19354
tetrafluoromethane-inert gas, compressed fluids, ang. momentum relax., NMR 78−19355
thermodynamically self-consistent theories, radial distrib. function, functional derivative 80−92435
thiophene, mean free path meas., US relax. 80−59585
transition metal, electronic states densities from struct. and entropy data 77−1347
transition metals, struct., rel. to amorphous state struct. 77−51323
transition metals, structure factors, calc. of temp. coeff. of resistivity, one component plasma model 79−32881
transition metals and their alloys, review of struct. 77−51304
trichloracetonitrile, IR dispersion, complex refractive index and permittivity, time correl. function 80−45057
trichloroethane, CH_3-stretching modes, Raman spectra reson. energy transfer obs. 78−48162
trichloromethane, liq., radial pair distrib. function determ. 79−77476
trichloromethane, mol. struct. factors, X-ray diffr. 77−76291
triethylenediamine, aq. soln., stimulated Raman scatt., struct. enhancing solute 78−27222
triplet correlations, book contrib. 79−60251
US velocity, repulsive exponent, Rao's and Kuczera's relations 80−79878
van der Waals forces, many-particle correl. attenuation *(Russian)* 77−27798
velocity-autocorrelation function from neutron scatt., comparison with Ar, H_2 data 77−1058
vibrational dynamics using picosecond Raman techniques 80−52325
vibrational energy relax. of excited probe mol., density fluctuation interaction 78−63653
vibrational modes, direct and indirect modes, reson. energy transfer, population decay 78−48162
vibrational relaxation, appl. of Bogoliubov's relaxation time hierarchy idea *(Russian)* 77−15297
virial coefficients for hard rectangular parallelepipeds and cubes on simple cubic lattice 79−97308
viscous flow mechanism, simple liquids, Ree Eyring theory extension 77−31794
Viton A fluoroelastomer-EPDM blends, melt viscosities 77−7781
water, boundary conditions for numerical simulation, book contrib. 79−60247
water, coherent Raman ellipsometry, vibr. stretching region and liq. struct. obs. 80−93341
water, collision-induced far IR absorpt., depolarised Rayleigh scatt. 77−81100
water, compressibility modulus 78−75701
water, cooperative effects importance in computer simulation calcs. 80−28906
water, dielectric constant of bonded lattice model 78−23386
water, effects of dimethylsulphoxide, Raman and IR spectral study 80−14143
water, free surface, metastable effects associated with press. pulse refl. 80−6463
water, group freqs. appl. 79−98057
water, H-bond networks, percolation process 79−69001
water, heat capacity and structure, isomerisation reaction role 79−33097
water, I^- charge transfer to solvent spectra, water struct., solvated electron 77−50447
water, in quartz pores, H^- excess mobility IR spectroscopic study 79−51955
water, lattice fluid model on 2D quadratic lattice 79−93056
water, liq., H bond distrib., Monte Carlo simulation calcs. 80−54106
water, liq., Monte Carlo simulation, convergence of new algorithm 78−63649
water, liq., NMR proton spin-lattice relax. and shear viscosity press. depend., −15 to 10°C 77−40144
water, liquid, zeroth order random network model 79−68993
water, models of surface layer based on autoadsorption and surface entropy in 20-50° temp. range 77−28065
water, Monte Carlo simulation 80−54113
water, Monte Carlo simulation of struct. and thermodynamic props. 80−88017
water, Monte Carlo-Metropolis computer simulation, convergence characts. 80−10485
water, optical consts., 400-5000 cm^{-1}, 1, 16, 27, 39 and 50°C, rel. to intermol. struct. 77−66469
water, physical props., two-state model approach 80−75144
water, pot. energy function appl. to ice lattice energy 79−73125
water, relax. compressibility and heat capacity 80−92580
water, review *(French)* 78−26424
water, simulation, Monte-Carlo method, 1 g cm^{-3}, 300K, using Rahman Stillinger ST2 pot. 77−51290
water, solutions in organic solvents, IR spectra and struct. 79−38534
water, solvent, structure, ESR spin probe obs. 77−59460
water, struct. changes due to hydration of monat. ions, in stoichiometric mixtures, thermodynamic props. 78−7225
water, struct. effect of small additions of nonelectrolyte, dielec. const. obs. 78−9937
water, structure, liq. theory, review, book contrib. 77−39525
water, structure and motion at high pressure 78−87606
water, structure and props., minimal basis set description 80−6347
water, supercooled, sound vel. dispersion, struct. relax. effect, Brillouin scatt. obs. 80−107375
water, supercooled, US vel. and attenuation *(French)* 79−90730
water, temp. of maximum density, solute effects and partial molal expansibility 77−24256
water and dil. aq. solns., statistical mech., book contrib. 79−60250
water and saturated monatomic alcohol mixtures, effects of chlorides on struct. 79−86840
water liq., struct. relax. time in 2-state model, 0-100°C 80−1914
water structural relax. times, model comparison 80−54108
water-2-propanol, density, US vel. meas. 78−18529
water-carbon tetrachloride soln., fundamental H_2O IR spectrum, liq. struct. 80−23419
water-dioxane mixtures, compressibility, density, US vel. rel. to temp., conc., struct. *(German)* 77−43263
water-polystyrene spheres (highly charged), solid- and liq.-like phases, soft core liq. theory 77−63963
water-urea-valeric acid systems, sound vel. and liquid structure *(Japanese)* 77−1177
water-water, pair pot. near H bonded equilib. config., amorphous and crystalline solid and liq. 80−64946
X-ray diffraction, frequency modulated, for multi-element disordered system struct. 77−72525
acetone-d_0, d_6, Raman spectral study of aq. soln. struct., H-bond effects 77−88454

liquid structure continued
Ag chalcogenide melts, changes in short-range order struct. during heating 79−50973
Ag, nuetron diffr. investig. of pair correl. function, coordination numbers 77−35467
Ag-Ge, liq. eutectic, neutron diffr. determ. of struct. 77−51302
Ag-Ge, liq. eutectic, struct. by neutron diffr. 78−18537
Ag-Ge, neutron diffr. investig. of pair correl. function, coordination numbers 77−35467
Ag-Ge liquid alloy, small angle neutron scatt. 79−64982
Ag-Te, liq., struct. and elec. props. 80−49083
Ag-Tl, eutectic liquid alloy, structural features, interatomic interaction *(Russian)* 79−77494
AgBr, molten, Monte Carlo computer simulation 78−26426
$AgNO_3$, molten, X-ray diffr. structural anal. 78−42887
$AgSbSe_2(Te_2)$, exam. of kinematic viscosity of melts, and short range ordering 79−1383
Al, atomic radial distrib. curve anal. *(Russian)* 80−14996
Al, density fluctuations, neutron scatt. anal. 80−70349
Al, density fluctuations 78−55806
Al, dislocation behaviour at melting, HV electron microscope in-situ obs. *(Japanese)* 77−43216
Al, electron diffr. 78−83721
Al, energy moments and longit. freq. dispersion 79−60262
Al, interaction potential 77−58945
Al, liq., short-wavelength density fluctuations 79−46550
Al, liq. struct. factor, 680 to 840°C, neutron diffr. study 79−46552
Al, liquid, dynamical struct. factor 78−71667
Al, liquid, dynamical struct. factor calc. 80−64880
Al liquid, molecular dynamic simulation of static and dynamic structural factors *(Russian)* 79−69005
Al, liquid, structural details, molecular dynamics calcs. *(Russian)* 80−64879
Al, melting, existence of before and after effects, neutron scatt. 77−84895
Al, molten, struct. factors, at. distrib. curves, thermodynamics, neutron diffr. study *(German)* 80−19687
Al, pair correl. function, Monte Carlo calc., with pseudopot. 77−15300
Al, pair interaction pot., struct. factor calcs. 77−51298
Al, radial distrib. function calc., pseudopot. method *(Russian)* 79−19138
Al, second and fourth order moments temp. depend. 77−72545
Al, short range order amongst cond. electrons 80−107040
Al, structure factor and radial distrib. function, neutron diffr. 77−47334
Al, thermodynamic props., pseudopot. calc. *(Russian)* 79−46549
Al, X-ray diffraction analysis 79−4232
Al-Cu eutectic melts, struct. determ. *(Russian)* 77−80408
Al-Si, and Al-Si-Na eutectic melts, struct. determ. *(Russian)* 77−80408
Al-Si, compressibility and struct. factors at zero wavevector 79−23515
Al-Si alloys, molten struct. factors, at. distrib. curves, thermodynamics, neutron diffr. study *(German)* 80−19687
Al-Si melt, microheterogeneity *(Russian)* 80−103238
Al-Si melts, hypoeutectic, eutectic, hypereutectic structural factors, atomic radial distrib. functions *(Russian)* 79−73091
$AlCl_3$, aq. solns., order phenomena, X-ray diffr. obs. 80−1915
$AlCl_3$ aqueous soln., quasi-elastic neutron scatt. study 78−26425
$Al(NO_3)_3$, aq. soln., X-ray diffr. obs. 77−72541
Ar, aqueous soln., dil., energy and struct., pair pot. energy function, Monte Carlo calc. 80−54107
Ar, asymptotic oscills. of radial distrib. function quasi-crystalline model 78−9935
Ar, liq., pair potential, Percus-Yevick and hypernetted chain approx. calcs. 77−1052
Ar, liq., quasi cryst. model, radial distrib. function 79−19135
Ar, liq., reduced hard core dias. from compressibility, viscosity and freezing data, Lindemann laws 77−39521
Ar, liq., short range order parameter 78−83712
Ar, liq., struct. determ. by X-ray diffr., pair pot. calcs. 78−6003
Ar, liq., surface thickness, near triple point, using surface tension data 79−99400
Ar, liq. nuclei, thermodynamic props. mol. dynamics calc. *(Russian)* 77−47325
Ar modified droplet model, mean droplet interaction below T_c 80−70363
Ar, mol. dynamics calc. 77−19857
Ar, solid-liq. transition and mech. props., modified cell theory 79−23703
Ar, transverse current correl. functions 79−77489
Ar, velocity autocorrelation from memory function, hard-sphere and square well pots. 80−28893
Ar-HCl, liq. density fluctuations, far IR absorpt., neutron scatt. mol. dynamics calc. 78−19461
^{36}Ar, liq. dynamic struct. factor, 120K, press. depend., quasi-elastic NDEMAT 79−50981
As-S, melt struct., orientation birefr., viscosity, refr. index, and density 80−84713
AsI_3, molten, X-ray intensity curve, short-range order 77−4034
As_2Se_3, struct., investigation using neutron diffr. meas. 79−23514
As_2Se_3, struct. determ. in amorphous and liq. state using EXAFS meas. 77−89366
As_2Te_3, neutron diffraction study 79−77485
Au, electron-ion pseudopot., form factor, liquid elec. cond., phonon dispersion 78−34785
Au-Co, liq. alloys, partial struct. factors 80−1919
Au-Co, liquid alloys, struct. determ. by X-ray diffr. 78−6006
Au-Co alloys, molten, US vel. meas., compressibility and partial struct. factors determ. 77−69045
Au-Co melts, struct., compressibility, X-ray and neutron diffr. 77−11614
Au-Ge-Si, influence of struct. on elec. resist. of glass forming alloys 80−65518
B_2O_3, molten, BO_3 triangles in boroxyl rings and random networks, Raman intensity investig. 80−45058
$BaCl_2$, molten, struct. determ. by neutron diffr. 78−42883
Bi, liq., collective motions, cold neutron scatt. obs. 78−67639
Bi, liquid, interference functions by double hard sphere model 80−49090
Bi, struct. factor, interat. interaction pot., X-ray diffr. obs., 280-800°C *(Russian)* 78−14270
Bi-Cu alloys, molten, struct., thermal neutron diffr. meas. 77−39526
Bi-Cu alloys, molten, struct., cold neutron scatt. in region of small momentum transfer 77−39527
Bi-Cu melts, struct., neutron scatt., conc. of segregated regions calc. 77−39528
Bi-Se, fused, mag. susceptibility, temp. and conc. depend. 77−36052

liquid structure continued
Bi-Sn melt structure, radial distrib. function of atoms, anal. *(Russian)* 80−14995
Bi-Te, fused, mag. susceptibility, temp. and conc. depend. 77−36052
Bi_2O_3-$Mo(W)O_3$ melts, electrophys. props. 77−89817
Bi_2O_3-$SiO_2(GeO_2)$, melt struct. model 80−33870
Bi_2O_3-$Si(Ge)O_2$ melts, phys. props. 77−89566
Br_2, liq. struct. factor by neutron diffr., wavelength depend. 77−89370
Br_2, neutron diffr., evaluation of effective pair pot. 78−75527
Br_2, struct., theory and computer simulation 78−59734
Br_2, struct., X-ray diffr. obs. 78−59733
Br_2-Ar liquid mixture, vibr. relax., 1-D mol. dynamics study 79−73079
CO, liq., ^{13}C NMR for mol. diffusion and spin-rot. interaction, 0-1.73 kbar 79−99777
C_2O_3, liq., mol. conform. and orientation correlation 79−32877
C_3O_2, liq., neutron diffraction studies at high momentum transfer 79−46525
CS_2, in alkane soln., ^{33}S NMR linewidth for mol. correl. times 79−95661
CS_2, liq., light scatt. intensities, struct. models 78−60476
CS_2, liq., S partial struct. factor, 20°C, from X-ray and neutron diffr. data 77−80407
CS_2, liq., struct. and equilib. optical props. 80−45026
CS_2, liq. struct., mol. dynamics simulation 79−77488
CS_2, X-ray scatt., reference-site-interaction model, intermol. pot. function 77−11459
CSe_2, liq., partial struct. factor, neutron diffraction meas. 80−79672
$CaCl_2.6H_2O$, liq., structural order 80−33871
CaF_2, molten, struct., electrolyte 'general primitive model' prediction test 80−28902
CaO-Al_2O_3 melts, density, atm. comp. effect 78−22624
CaO-SiO_2, molten binary, X-ray exam. of struct. 78−38610
CaO-SiO_2-MnO molten mixtures, struct. and phys. props. *(French)* 80−24635
CaO-SiO_2-MnO systems, melts, elec. cond., struct. *(French)* 79−51287
Cd, interference function temp. depend. from X-ray diffr., elec. resist. calc. 77−47332
Cd, liq., X-ray diffr. meas. and interatomic interaction pot. calc. *(Russian)* 78−59735
Cd, Percus-Yevick eqn., perturbation treatment, struct. factor 77−7641
Cd, small-ang. X-ray scatt., at. microgrouping depend. *(Russian)* 78−14271
Cd-Sb, hard-sphere struct. factors 77−51301
$CdCl_2$, aq. soln., Raman spectrum, local order 78−84563
$CdCl_2$, aq. solns., sound absorpt. and relax. phenomena 80−49311
CdTe, mag. susceptibility at 20-1400°C 77−12085
Ce, struct., neutron diffr. meas. 77−51305
Ce-Co, liq., charge transfer effect 78−94967
Ce-Cu, liq., charge transfer effect 78−94967
Ce-Ni liq., X-ray diffr. exam. of struct. 77−62465
CeO-SiO_2, molten and glassy state, X-ray diffr. determ. of struct. *(Japanese)* 78−9936
Co melt, struct. charact. time depend. in X-ray studies *(Russian)* 80−24350
Co, near-order struct., X-ray scatt meas. 77−55231
Co, struct. factor and isothermal compressibility 77−11462
Co, struct. factor and radial distrib. curves, X-ray determ. *(Russian)* 77−31580
Co-Ga liquid and solid alloys, elec. resistivity at high temps., partial struct. factors 80−6806
Co-Ge, liq. alloy, structure studied by X-ray diffr. *(Russian)* 79−77493
$CoCl_2$, electronic absorpt. spectra and coord. in cryst., soln. and melt 79−38570
Co(II)-containing aq. electrolyte soln., nucl. mag. relax., hydration shell *(Russian)* 80−54966
$Cr(H_2O)_6Cl_3$, aq., solute structuring 77−15298
$Cr(NO_3)_3$, aq. soln., X-ray diffr. obs. 77−72541
Cs, liq., short range order parameters, from information theory 78−83730
Cs, liquid, neutron diffr. struct. anal., density and viscosity temp. depend. 80−6352
Cs, radial distribution functions calc. at 100°C 78−22638
Cs, struct. factors, X-ray transmission diffr. expts. 77−47337
Cs_2, liq. struct. factor determ. rel. to short-range correlations 77−1060
CsAu, molten, equimolar, structural evidence of ionic nature 80−64882
CsCl(Br)(I), molten, structural props., computer simulation 77−84616
$CsNO_3$, molten, X-ray diffr. structural anal. 78−42887
Cu, effective interionic interaction, pseudopot. method *(Russian)* 77−84622
Cu, liquid, struct. factor, neutron diffr. meas. and Monte Carlo calc. 80−38903
Cu, X-ray diffraction analysis 79−4232
Cu-Al(Ga)(In) alloys, elec. cond., temp. and conc. depend., model interpret. and alloy struct. *(Russian)* 80−88528
Cu-Ge, hard-sphere struct. factors 77−51301
Cu-Sb melt, eutectic struct. by neutron diffr., isotopic substitution 78−47233
Cu-Te, liq., struct. and elec. props. 80−49083
$CuBr_2$, highly conc. aqueous soln., local ordering, extended X-ray absorb. fine struct. spectra 78−79520
$CuBr_2(Cl_2)$, aq. soln., structural transition, neutron diffr. study 80−64872
CuCl, molten, ionic liquid description from NMR meas. 77−24257
CuCl, molten, struct. and transport props. 79−19134
CuCl, partial struct. factors, hard-sphere model calc. 77−15299
$CuCl_2$, aq. soln., Raman spectrum, local order 78−84563
$CuCl_2(Br_2)$, aq. solns., EXAFS meas. 80−60714
$CuGaTe_2$, exam. of kinematic viscosity of melts, and short range ordering 79−1383
$CuInTe_2$, exam. of kinematic viscosity of melts, and short range ordering 79−1383
$Cu(NO_3)_2$, aq. soln., Raman spectrum, local order 78−84563
DCl, liquid, on coexistence line, light scatt., orientational correlation function 80−20632
D_2O, atom pair correlation functions, X-ray, electron and neutron diffr. data 77−80406
D_2O, atom-atom and mol. correlation functions, electron diffr. 77−80405
D_2O, liq., mol. rot., deuteron relax. obs. 77−8432
D_2O, liquid water, structural relax. times, model comparison 80−54108
D_2O, molecular dynamics anal. by inelastic neutron scatt. 77−35462
D_2O, struct., temp. effects, neutron diffr. obs. 77−72544

liquid structure continued
D_2O, struct. at press. 79−60253
D_2O-H_2O, IR absorption spectra, statistical charact., continuous model of liq. struct. confirmation 78−6671
Fe and alloys, C solubility, donor-acceptor mechanism 80−49365
Fe, liq., struct. model, mol. dynamics calc. 79−50994
Fe, near-order struct., X-ray scatt. meas. 77−55231
Fe, struct. factor and isothermal compressibility 77−11462
Fe, struct. factor and radial distrib. curves, X-ray determ. *(Russian)* 77−31580
Fe, structure factor near transform. to amorphous solid, X-ray diffr. *(Russian)* 77−31579
Fe-C, pre-eutectic melt, struct. anomalies *(Russian)* 77−28794
Fe-C, struct., neutron and X-ray diffr. meas. 77−51306
Fe-C melt, mag. susceptibility and short range order, 900-1800°C 78−84382
Fe-C melt structure, X-ray diffr. study *(Russian)* 80−19685
Fe-C molten alloy, short range order *(Russian)* 79−90521
Fe-Co, X-ray diffr., struct. determ. *(Russian)* 77−80409
Fe-Co melt, volumetric charact., molar volume conc. depend. density *(Russian)* 80−33873
Fe-Ge intermetallides, melt struct. rel. to growth mechanism 77−84681
Fe-Ge melts, struct. determ. 79−41940
Fe-Ni melt, short-range order, m.p. to 1750°C *(Russian)* 78−94966
Fe-Si intermetallides, melt struct. rel. to growth mechanism 77−84681
Fe^{3+}-Fe^{3+} distances, in aq. NO_3^- and ClO_4^- solns., from small-ang. X-ray diffr. maxima 78−42880
$FeCl_3$ aq. soln., quasi-elastic neutron scatt. 79−37607
$FeCl_3$, nonaq. solns., solvent-solute interactions, Mossbauer investig. of equilib. consts. 79−1729
$FeCl_3$, solns. and hydrated melts, complexes form., X-ray diffr. obs. 80−24342
$Fe(ClO_4)_3$, soln., struct., X-ray scatt. obs. 78−34421
$Fe(NO_3)_3$, aq. soln., Fe (III) hydration shells, X-ray diffr. 79−29337
$Fe(NO_3)_3$ conc. aq. solns., and nonahydrate melt, struct., X-ray scatt. investig. 77−31576
FeO-Fe_2O_3-SiO_2 system, molten, struct. using high temp. X-ray method *(Japanese)* 80−14992
FeO-Fe_2O_3-SiO_2 system, molten, struct. by high temp. X-ray diffr. 80−49084
FeO-SiO_2, molten, X-ray diffr. exam. of struct. 79−46543
$Fe_2(SO_4)_3$, aq. soln., solute struct. by X-ray scatt., Fe(III) sulphate complexes 79−32875
Ga, elec. resist. calc., 19 and 35°C, using calc. and expt. struct. factors *(Russian)* 78−56124
Ga, interference function temp. depend. from X-ray diffr., elec. resist. calc. 77−47332
Ga, liq., struct., X-ray diffr. obs. 77−84619
Ga, neutron diffr. room temp. to 1303K, struct. model 78−51405
Ga, struct. factor, short range repulsive forces 78−75528
Ga, X-ray diffr. exam. of struct. at 203 and 323K *(French)* 78−14268
Ga-Te, alloys, liq., thermodynamic functions, struct. 78−40075
GaIn, liq. alloys quad. relax. rates, 3-particle correls., ^{71}Ga and ^{115}Sn 77−12272
Ge alloys, molten binary, struct. and charact. of interatomic interaction, X-ray diffr. meas. *(Russian)* 77−1070
Ge, molten, struct. factors, tetrahedral concs., neutron diffr. study *(German)* 80−19688
Ge, rel. to acoustic vel. and adiabatic compressibility, temp. depend., MP to 1400K 77−15498
Ge-Sn(In) melts, short-range order, radial atomic distrib. functions 79−86673
Ge-Te, As-Te, Ge-As-Te molten systems, metal-semicond. transition, cond. obs. *(German)* 77−1457
$GeBr_4$, liq., reference interaction site model and struct. 80−70106
$GeCl_4$, liq. struct., oscill. amp., neutron diffr. study 79−46544
$GeCl_4$, liq. struct. by neutron diffr. 79−73089
GeO_2 melts, density, viscosity, struct., at high and low press. 79−87431
$GeSe_2$, struct., investigation using neutron diffr. meas. 79−23514
GeTe, neutron diffraction study 79−77485
H bond dynamics in soln. 78−84573
H_2, corresponding states, quantum, mech. law 79−55945
H_2, liq. slow neutron scatt. rel. to intermol. excitations, analyt. model 77−58941
H_2, metallic, ground-state energies of liq. and solid phases, variational and Monte Carlo methods 80−70502
H_2, metallic, struct. and forces 78−22636
H_2, vibr. population relax. in gas and fluid 80−29775
H_3BO_3, aq. soln., dielec. props. and struct. 77−89369
HBr, liquid, on coexistence line, light scatt., orientational correlation function 80−20632
HCl, liq. struct. simulated by a Lennard-Jones pot. 80−1917
HCl, liquid, on coexistence line, light scatt., orientational correlation function 80−20632
HCl, liquid, struct. and mol. dynamics studied using intermolecular force models 80−83445
HF, computer simulation of struct. and dynamics, assoc. system 79−86667
HF, liquid, Monte Carlo simulations 79−64967
HF, liquid, struct. and props., intermol. pot. function calcs., basis set depend. 79−82134
$(HF)_2$, intermol. force model, rel. to liq. struct. 78−78773
H_2O, and aq. solns., IR spectral investigations of assoc. 79−65847
H_2O, atom-atom and mol. correlation functions, electron diffr. 77−80405
H_2O, empirical potential model EPEN/2, parameterisation testing 79−54933
H_2O, $H_2{}^{18}O$, D_2O, low freq. Raman spectra, isotope shifts, ice-like struct. 79−28732
H_2O, high-press. props. and struct., mixture model 77−84612
H_2O, liq. struct. factor, neutron diffr. meas. 79−46547
H_2O, modified droplet model, mean droplet interaction below T_c 80−70363
H_2O, molecular dynamics anal. by inelastic neutron scatt. 77−35462
H_2O, n-state configurational excitation model, diagnostic thermodynamic props. 80−10481
H_2O, solvent properties, electrochem. adsorpt. of tetraethylammonium bromide from H_2O, D_2O solns. 79−83459
H_2O, struct. and dynamics, simulation using central force pots. 78−38607

liquid structure continued
H_2O, supercooled, longit. proton relax. times, press. and temp. depend. 77−85598
$H_2{}^{16}O$, $H_2{}^{18}O$, isotope fractionation, H-bonds, force consts., liq. water struct. 77−76288
H_2O_2 aq. solns., struct. and dielec. props. 78−63659
$(H_2O)_2$ dimer intermolecular pot., liq. struct. mol. dynamics simulation 78−71657
HOD, IR spectra in D_2O, combination vibr. 80−9609
He, accurate empirical intermol. pot. 79−68291
He, density correlation function and dynamic transient exponents at and above T_λ 79−51325
He, dynamic struct. factor function, surface contrib. 77−47634
He, radial distrib. functions and structural parameters 79−55640
^{3}He, dynamic structure function, in impulse approx. 77−7934
^{3}He, dynamical structure factor and elementary excitations 79−33142
^{3}He, Jastrow wavefunction, hypernetted chain method 80−17866
^{3}He, normal, dynamical structure factor and elementary excitations 79−99384
^{3}He, superfluid B-phase, textures and NMR, theory 77−39717
^{3}He-^{4}He, excitation spectrum and quasiparticle interactions, perturbation theory 78−10250
^{3}He-^{4}He mixtures, structure factor determ. 79−60591
^{4}He, fluid struct. factor meas. in range 5.5 to 7.0K 80−80011
^{4}He, fluid structure factor meas. at 10K 79−51322
^{4}He, ground-state energy, perturbation corrections 77−7918
^{4}He, Jastrow wavefunction, hypernetted chain method 80−17866
^{4}He, Lennard-Jones model at 0K, props. using Monte Carlo method 79−82401
^{4}He, liq., dynamic struct. factor, 2.5K, inelastic neutron scatt. study 79−55647
^{4}He, liq., dynamic structure, neutron diffr. determ. 77−11749
^{4}He, liq., nonsuperfluid, dynamic struct. factor, neutron scatt. meas. 79−46545
^{4}He, liq., short range order parameters, from information theory 78−83730
^{4}He, liq., static struct. factor and pair correls., neutron diffr. study, 1.00 to 4.27K 80−80010
^{4}He, liq., static structure factor and pair correlation function, at saturated vapour press. 80−64878
^{4}He, liq., two-dimensional, ground state 80−49438
^{4}He, liquid, fourth order struct. and Raman scatt. 79−56801
^{4}He, nonsuperfluid liq., neutron scatt. dynamic struct. factor, saturated vap. press. 78−42878
^{4}He, normal and superfluid, short range order parameter 78−83712
^{4}He, normal and superfluid, spatial order, temp. depend. 80−39374
^{4}He, normal liq., collective excitations, neutron inelastic scatt. study 80−107590
^{4}He, normal liq., static and dynamic struct. factors from quantum conserving approx. 79−51321
^{4}He, struct. factor, excitation spectrum, ground state momentum distrib. 78−79833
^{4}He, structure factor, momentum transfer meas. 78−22912
^{4}He, superfluid, density regions, λ transition and roton physical picture 79−82402
^{4}He, superfluid, dynamic struct. factor, temp. depend. 78−95197
^{4}He, superfluid, elementary excitation, structure factor and phase velocity 80−80012
Hf complex, with N-benzoyl N-phenyl hydroxylamine, mol. reorientation in soln. 77−16218
Hg, liq., struct., X-ray diffr. obs. 77−84619
Hg, liq., themoelec. power from X-ray diffr. struct. at −30 to 290°C 79−46551
Hg liquid, quadrupole relaxation rate temp. depend 80−88884
Hg, liquid structure, X-ray diffr. obs., 173-473K 80−14997
Hg, long wavelength limit, triplet and higher correls., Percus-Yevick eqn., perturbative anal. 79−37613
Hg, X-ray diffraction analysis 79−4232
Hg-K, liquid, structure factors, X-ray scatt. *(Japanese)* 80−54122
Hg-Na, liquid, structure factors, X-ray scatt. *(Japanese)* 80−54122
Hg-Tl, liq. alloys, struct. from thermodynamic props. *(German)* 77−1066
Hg-Tl, liq. alloys, struct. from elec. cond. 77−1067
$HgCl_2$, partial struct. factors in mol. fluid model 78−22628
Ho, struct. factors, high temp. X-ray diffr. obs. 79−7544
I_2 liq., static structure factor, neutron diffraction 80−103236
$_xI_{1-x}$ mixtures, high-temp. solids and melts, struct., thermodynamic props., Raman spectra obs. 80−66174
In, direct pair correl. function 78−38613
In, interatomic interaction potential, rel. to structure factor *(Russian)* 79−69006
In, liq., X-ray diffr. meas. and interatomic interaction pot. calc. *(Russian)* 78−59735
In, small-ang. X-ray scatt., at. microgrouping depend. *(Russian)* 78−14271
In, struct. factor, Percus-Yevick equation perturb. treatment, square-well pot. approx. 78−75530
In-Sn liquid alloy, 2-butanol vapour adsorption, effect on surface tension and surface comp. 79−14981
In-Sn-Sb, liquid state, structure of eutectic alloy 78−42890
In-Te alloys, atomic struct., X-ray diffr. meas. 79−41934
InP, fused, SRO structure changes on heating 77−89367
K, liq., paracrystalline BCC lattice evidence 79−41942
K, liq., short-wavelength density fluctuations 79−46550
K, mean spherical approx. and effective pair pots. 80−70099
K, pair correl. function and ion-ion pot. 79−50982
K, radial distribution function, Monte Carlo calcs. 77−55230
K, struct. factors, X-ray transmission diffr. expts. 77−47337
K^+ salts, diamag. ion solvation in methanol soln., NMR relax. obs. 78−56389
K-ethylamine-ethylenediamine, soln., ion-pairing and EPR 79−78502
K-Rb, liq., form factors and transport coeffs., pseudopot. perturb. theory 80−44561
KBr, liquid inelastic neutron scatt. obs. from short wavelength charge fluctuations 78−47487
KBr, molten, charge fluctuations, neutron diffr. anal. 79−42198
KBr-LiBr, liq. mixture, struct. and diffusion 80−24344
KCl, aq. soln., zero-angle X-ray scatt., 25°C, conc. depend. 78−83713
KCl, melt, mol. dynamics simulation 80−54097
KCl, molten, pair and triplet distrib. functions by mol. dynamics simulation 79−90520

liquid structure continued
KCl, molten, rot. ordered ion distrib., mol. dynamics simulation 78−22630
KF-BeF_2, and BaO-SiO_2 systems complex ionic liquids, corresponding-state principle *(Japanese)* 77−56245
KI-KCl(CsI) melts, X-ray diffr. struct. determ. 79−41925
KNO_3, molten, X-ray diffr. structural anal. 78−42887
K_2O-CaO-Al_2O_3-SiO_2 glass, exam. of liquid phase separation phenomena 79−4417
K_2SO_4, molten, struct. analysis using X-ray scatt., correl. with cryst. struct. 80−10486
La, struct., neutron diffr. meas. 77−51305
$LaCl_3$, aq. soln., H_2O coordination of metal ion, X-ray diffr. 79−69000
Li, liq., paracrystalline BCC lattice evidence 79−41942
Li, liq., short-wavelength density fluctuations 79−46550
Li, temp. and density depend. of struct., improved pseudopot. theory 79−14669
Li, X-ray scatt. factor, solid state effect 80−70163
Li^+ salts, diamag. ion solvation in methanol soln., NMR relax. obs. 78−56389
Li-Mg, liq., elec. transport props. and phase diagram 78−23070
Li-ND_3, near liq.-liq. crit. point, conc. fluctuations, neutron diffr. long wavelength thermodynamic limit 79−10948
Li-NH_3 solution, small angle X-ray scatt. meas. 79−14667
Li-Na, short-range order, neutron diffr. obs., near crit. composition 78−22639
Li-Na alloy, conc. fluctuations and struct. factors 78−30534
LiBr, liq., ionic motion study using memory functions 80−10484
LiCl, frozen soln., NMR study of phase transitions 79−56617
LiCl-KCl, molten mixture, struct., diffusion, cond., mol. dynamics calc. 80−64871
LiF-BeF_2, and MgO-SiO_2 systems, complex ionic liquids, corresponding-state principle *(Japanese)* 77−56245
$LiNO_3$, molten, X-ray diffr. structural anal. 78−42887
$LiNO_3.3H_2O(D_2O)$, crysts. and melts, density, mol. vol., thermal coeff. of expansion, rel. to struct. 80−15270
Li_2SO_4, molten, and molten Li_2SO_4-Na_2SO_4 mixtures, struct. anal. by X-ray diffr. 78−63660
Mg, Percus-Yevick, eqn., perturbation treatment, struct. factor 77−7641
Mg SiO_3 melt, instantaneous struct. simulated by mol. dynamics 80−84049
Mg-Bi (30 at.%), molten, short range order and partial struct. factor, neutron and X-ray diffr. 78−9941
Mg-Bi melt; X-ray and neutron diffr., conc. depend., correl. number and nearest neighbours 80−49091
$MgCl_2$, aq. soln., ^{25}Mg NMR, longit. relax. rates 79−91309
$MgCl_2$ aq. soln., quasi-elastic neutron scatt. 79−37607
$MgCl_2$, aq. solns., X-ray diffr. study 79−37608
$MgCl_2$, molten Raman spectrum, $MgCl_4^{2-}$ and polynuclear complexes equilib. 77−1669
$MgCl_2$-alkali metal chloride system, solid and molten states, struct. props., Raman spectra 80−76011
$MgCl_2CaCl_2$, aq. soln., hydration, X-ray diffr. 77−43126
$Mg(NO_3)_2$, aq. soln., ^{25}Mg NMR, longit. relax. rates 79−91309
$Mg(NO_3)_2$, aq. soln., ionic coordination by X-ray diffr. 79−29338
MgO-SiO_2, molten binary, X-ray exam. of struct. 78−38610
Mn-Si intermetallides, melt struct. rel. to growth mechanism 77−84681
Mn-Zn series, aqueous solutions, equilib. props. struct. 79−61894
$MnCl_2$, molten, struct. anal. by X-ray diffr. 78−63661
MoF_5, mol. and electronic struct., vitreous, liq., and tetrameric states, ^{19}F NMR obs., mol. mobility 80−34787
N_2, liq., atom pair pots., X-ray diff. 80−100158
N_2, liq., computer-simulated ang. correlations and rot. motion 77−11461
N_2, liq., simulation of atomic and quadrupole interactions, predictions 77−11457
N_2, liq., struct. factor, short-wavelength neutron scatt. obs. 80−44105
N_2, liq. struct., thermal neutron diffraction 79−46542
N_2, liquid, mol. correl. functions, effective pair pot. evaluation 80−10476
N_2+$H_2(D_2)$, vibr. relax. in liquid phase 79−847
N_2+O_2, molecular fluid mixtures, equilibrium props. 80−64867
NH_3, assoc. mols., struct. and dynamics, atom-atom pots., gas, solid and liq., props. 80−23487
NH_3, mol. correlation functions 77−62459
NH_3 vapour, supercrit. and subcrit. 80−59162
NH_4Cl, aq. soln., dynamical props., mol. dynamics simulation 80−1918
NH_4Cl, aq. soln., struct. props., mol. dynamics simulation 79−82142
$NH_3(D_3)$, longitudinal proton and deuteron relaxation rates, press. and temp. depend. 80−44941
NH_4NO_3 conc. aqueous soln., X-ray scatt., NO_3^--H_2O interactions 78−42881
$(NH_4)_2SO_4$, aqueous soln., SO_4^{2-}-H_2O interaction, X-ray scatt. 79−77479
NO_3^- in aqueous electrolyte solution, vibr. relax. theory 79−94862
N_2O, pure liq., mol. motion, anisotropic interaction 80−24345
Na, atomic self-motions *(Rumanian)* 78−47226
Na, effective interionic potentials 78−91221
Na, inelastic thermal neutron scatt., interatomic pots. calc. 78−42891
Na, ions in liquid, Born-Oppenheimer pot. derivative, Monte Carlo calcs. 80−54117
Na, liq., paracrystalline BCC lattice evidence 79−41942
Na, liq., short-wavelength density fluctuations 79−46550
Na, mean spherical approx. and effective pair pots. 80−70099
Na, radial distribution functions calc. at 100°C 78−22638
Na, struct. factors, X-ray transmission diffr. expts. 77−47337
Na, velocity autocorrelation from memory function, hard-sphere and square well pots. 80−28893
Na^+ salts, diamag. ion solvation in methanol soln., NMR relax. obs. 78−56389
Na-Cs, struct. factor, free energy of mixing, and electrochem. pot., thermodynamic calc. 80−96436
Na-Cs, struct. factors, X-ray transmission diffr. expts. 77−47337
Na-Cs alloys, conc. fluctuations, X-ray transmission meas. 77−47329
Na-Ga alloy, rel. to mag. susceptibility and elec. cond. *(Russian)* 80−29522
Na-K, liq., static struct. factors 78−63664
Na-K, liq. alloy, electronic correl. functions calcs. 78−63663
Na-K, partial structure factors, square well pot. calcs. 77−51300
Na-K, third-order partial struct. factors 77−47339
Na-K alloy, collective excitations, mol. dynamics calc. 80−28895
Na-K alloy, dynamical struct. factor calc. 78−22634
Na-K alloys, liq., thermal conductivity, NaK_2 formation 78−10416

liquid structure continued
Na-K liquid alloys, struct., X-ray and neutron diffr. meas. 80−107041
Na-K liquid alloys, triplet correlation functions and thermodynamics, solute partial structure factor 80−64881
Na-K(Cs), liq., form factors and transport coeffs., pseudopot. perturb. theory 80−44561
Na-NH_3 solution, small angle X-ray scatt. meas. 79−14667
Na_3AlF_6, molten *(French)* 77−51297
$NaAlSi_2O_6$, jadeite, melt, changes in viscosity and struct. at high press. 77−29290
$NaAlSi_3O_8$, albite, melt, viscosity and struct. changes at high press. 79−29754
NaCl, aq. soln., isothermal compressibility, hydration parameters, up to 350°C and 10^3 kg cm^{-2} 78−10112
NaCl, aqueous soln., Lennard-Jones parameters, mol. dynamics and X-ray obs. 78−9939
NaCl aqueous soln., mol. dynamics simulation, central force model 80−49077
NaCl, frozen soln., NMR study of phase transitions 79−56617
NaCl, liq. surface, Fowler model, electroneutrality correction 79−28174
NaCl, molten, dynamical struct. factors 78−47228
NaCl solution, ionic hydration for cations 77−62460
NaCl-KCl(CsCl) melts, X-ray diffr. struct. determ. 79−41925
$NaCo(CO)_4$, soln., ion sites, cryptand C221 doping effects 80−70102
NaF-BeF_2, and CaO-SiO_2 systems, complex ionic liquids, corresponding-state principle *(Japanese)* 77−56245
$NaNO_3$, aqueous soln., X-ray diffraction, radial functions and positional correl. 80−79665
$NaNO_3$, molten, X-ray diffr. structural anal. 78−42887
Na_2O-CaO-Al_2O_3-SiO_2 glass, exam. of liquid phase separation phenomena 79−4417
Na_2O-SiO_2 melts, cryoscopic struct. study 80−14994
NaOH water solution, struct. props. of disordered systems, Raman spectral study 77−4631
Na_2SO_4, molten, and molten Li_2SO_4-Na_2SO_4 mixtures, struct. anal. by X-ray diffr. 78−63660
Na_2WO_4, molten, struct. by X-ray radial distribution anal. 78−83717
$Na_2W_2O_7$, molten, struct. anal. 79−41927
$NdCl_3$, aq. soln., H_2O coordination of metal ion, X-ray diffr. 79−69000
Ne, effective pair pot. from perturbation approach 77−68908
Ne, higher order structure factors and their inverses 79−55646
Ne, liq., short range order parameter 78−83712
Ne, liquid, higher order struct. functions in long wavelength limit, improved perturbation approx. 79−37606
Ne, mol. dynamics calc. 77−19857
Ne, neutron scatt. determ. of dynamic struct. factor, generalised hydrodynamic anal. 80−54103
Ne, radial distrib. functions and structural parameters 79−55640
Ne, struct. factor, improved perturbation anal. of Percus-Yevick eqn. 77−58942
Ne-Kr, time-dependent props. near crit. mixing point, 2000 bar, mol. dynamics calcs. 80−24580
Ni, liquid; structure factor at 1873K 79−77490
Ni melt, struct. charact. time depend. in X-ray studies *(Russian)* 80−24350
Ni, near-order struct., X-ray scatt. meas. 77−55231
Ni, neutron scatt. and atomic dynamics 77−55233
Ni, neutron scatt. and atomic dynamics 78−22637
Ni, struct. factor and isothermal compressibility 77−11462
Ni, struct. factor and radial distrib. curves, X-ray determ. *(Russian)* 77−31580
Ni-Al, melt, short-range order and microinhomogeneity, rel. to NiAl form. 77−35466
Ni-P, molten alloy, struct., X-ray scatt. 78−22640
Ni-Te, liq., struct. and elec. props. 80−49083
$NiCl_2$, aq. soln., diffusion and struct. 78−14488
$NiCl_2$, aq. soln., Ni^{2+} coordination from extended X-ray absorption fine struct. 80−1913
$NiCl_2$, aq. soln., partial struct. factors in long wavelength limit 78−47231
$NiCl_2$ aq. soln., quasi-elastic neutron scatt. 79−37607
$NiCl_2$, aq. soln., Raman spectrum, local order 78−84563
$NiCl_2$, aq. soln., structural transition, neutron diffr. study 80−64872
$NiCl_2$, aq. soln., viscosity meas., struct. props. 78−75863
$NiCl_2$ aqueous solution, hydration of Ni^{2+} 78−79518
$NiCl_2$ solution, ionic hydration for cation 77−62460
$NiCl_2$-D_2O solution, hard-sphere model 77−62461
$NiCl_2(Br_2)$, aq. solns., EXAFS meas. 80−60714
$Ni(NO_3).6H_2O$, Ni(II) coordination in aq. soln., EXAFS 77−85837
O_2, liq., vibr. energy relax., 53-96K 79−77477
O_2, liq. struct., thermal neutron diffraction 79−46542
O_2, liquid, mol. correl. functions, effective pair pot. evaluation 80−10476
O_2, modified droplet model, mean droplet interaction below T_c 80−70363
O_2, mol.-dynamic study of struct., dynamics 80−96467
O_3-O_2 mixture, significant struct. theory appl. to phase separation 77−51503
α-$PVW_{17}O_{40}^{5-}$, α_2-$P_2VW_{17}O_{12}^{8-}$, aq. soln., hydrodynamic radii from ESR line width 79−78504
Pb, collective excitations, neutron inelastic scatt. obs. 80−75148
Pb, effective interionic potentials 78−91221
Pb, electron diffr. 78−83721
Pb, liq., dynamic scatt. functions, 300 and 600°C, neutron scatt. study 79−50983
Pb, liq., dynamic struct. factor, slow neutron scatt. obs. 80−28908
Pb, liq., short range order parameters, from information theory 78−83730
Pb, liq., short-wavelength density fluctuations 79−46550
Pb, liq., sticky hard sphere pot., struct. function evaluation 80−33869
Pb, melting, existence of before and after effects, neutron scatt. 77−84895
Pb, molten, struct. factors, tetrahedral concs., neutron diffr. study *(German)* 80−19688
Pb, neutron diffr. meas. of pair and direct correl. functions 77−55229
Pb, paracryst. struct., coordination statistics calcs. 77−1063
Pb, rel. to temp. depend. of elec. resist., calc. 78−14701
Pb, short range order amongst cond. electrons 80−107040
Pb, struct. factors, neutron diffr. 78−18538
Pb, supercooled liquid thin films, liq. struct. factor determ. by STEM 80−10487
Pb, viscosity, hard sphere diameter, interionic potential 79−77797

liquid structure continued
Pb-Tl alloy, inferred from comp. and temp. depend. of viscosity, up to 500°C 79−65233
Pb-Tl-Cd(Sn) melt, short-range order struct. 80−49088
PbO-Fe_2O_3 melt, used for growth of LPE garnet films, struct. and cond. 80−10808
PbO-SiO_2, melt, elec. cond. and struct. 80−88020
PbO-SiO_2, melt, polymer equilibria 80−88019
Pd, liq., Percus-Yevick equation, perturbation theory calcs. 78−75515
Pd-Au-Si, influence of struct. on elec. resist. of glass forming alloys 80−65518
Pd-Ni(Si), melt, struct. and physical-chemical props., thermodynamic props. *(Russian)* 78−18536
$Pd_{82.5}Si_{17.5}$, X-ray diffr., compared with amorphous state 77−24275
Pr, struct., neutron diffr. meas. 77−51305
Pr-Al liquid alloys, atomic interactions, thermodynamic props. *(Russian)* 80−39307
$PrCl_3$, aq. soln., H_2O coordination of metal ion, X-ray diffr. 79−69000
Pt, liq., Percus-Yevick equation, perturbation theory calcs. 78−75515
Pu, hard-sphere model, phys. prop. meas. interpret, adjacent solid phase implications 77−19866
Rb, coherent scatt. function calc. 78−22635
Rb, density fluctuations from mol. dynamics simulations 80−100161
Rb, density functions, SCF method, coherent scatt. function 78−18527
Rb, dynamic struct. factor 78−30533
Rb, dynamical struct. factor 78−38612
Rb, effective interionic potentials 78−91221
Rb, expanded liq., struct. factor up to 1400K, 200 bar 77−47335
Rb, higher order struct. functions in long wavelength limit, improved perturbation approx. 79−37606
Rb, liq., current-fluctuation spectra, mode-coupling theory 79−4231
Rb, liq., dynamic struct. factor, two-relax. time model 77−1068
Rb, liq., pair interaction pot., thermodynamic, neutron diffr. calcs. 77−11463
Rb, liq., short-wavelength density fluctuations 79−46550
Rb, long wavelength limit, triplet and higher correls., Percus-Yevick eqn., perturbative anal. 79−37613
Rb, model, derivation of vel. autocorrelation function from incoherent scatt. function 79−77491
Rb, static struct. and electronic transport props., pseudopotential calc. 79−7543
Rb, struct. factor, improved perturbation anal. of Percus-Yevick eqn. 77−58942
Rb, struct. factor determ. by neutron diffr. up to 1400K and 200 bar 77−1064
RbBr, liq., dynamic density fluctuations, diagonalized relax. theory 78−47230
RbBr, molten, dynamical struct. factor calc. 78−22627
RbCl, molten, struct., mol. dynamics study 77−47328
$RbNO_3$, molten, X-ray diffr. structural anal. 78−42887
S, eqn. of state determ., crit. props. and mol. comp. 80−49336
S, polymerisation transition, anomalous light scatt. obs. 77−19861
S-Se(Te)(Tl), liq. semicond., bonding energies and entropies, mag. susceptibility meas. 80−49082
SF_6, liq., depolarised light scatt., dipole-induced dipole effect 77−12395
SF_6, liq., near crit. point, optical props. meas. 77−72673
SO_2 liquid, short range orientation effects, vibr. Raman spectra 80−2759
Sb, struct. model, using interference functions *(German)* 77−58946
Sb-Te, fused, mag. susceptibility, temp. and conc. depend. 77−36052
$SbCl_3$, liquid, neutron X-ray diffraction pattern and models 80−38893
$SbCl_3$ liquid, X-ray and neutron diffraction study at 80°C 79−4230
$SbCl_3/AlCl_3$ molten mixtures, Raman spectra 80−93305
$SbCl_5$-$NbCl_5$, melt and solid-soln. Raman spectra, $SbNbCl_{10}$ dimer *(German)* 77−4645
SbI_3, molten, X-ray intensity curve, short-range order 77−4034
Sb_2Se_3, liq. struct. anal., neutron diffr. study 78−79519
Se, correlation between switching and struct. 77−69388
Se, eqn. of state determ., crit. props. and mol. comp. 80−49336
Se, liq. and amorphous, struct. by pulsed neutron diffr. using an electron LINAC 77−51307
Se, liq. struct. factor determ. rel. to short-range correlations 77−1060
Se, liquid, chain molecule struct. exam. by time-of-flight pulsed neutron diffr. 77−55228
Se, liquid and amorphous, struct. modelling using Monte Carlo method 80−59391
Se, liquid-glass transition, P-V-T relations 77−24387
Se, mol. structure, local atomic arrangement at intrinsic bonding defects 80−59374
Se, Raman scatt. meas., comparison with amorphous Se spectra 80−50328
Se, Raman spectra, crystn. processes 80−60608
Se, ring-chain transition, disordered chain model 78−59943
Se, US rel. temp. depend., melting effects 78−38782
Se:Cd dilute liquid, perturbed ang.-correl. meas. of motional-correl. time 79−41930
Se:Te, liq., viscosity, impurity effect, chain length role *(French)* 78−51717
$Se_{1-x}Te_x$ systems, amorphous and liq. states, short range order, neutron scatt. study 80−49124
Si, molten, struct. factors, at. distrib. curves, thermodynamics, neutron diffr. study *(German)* 80−19687
Si, molten, struct. factors, tetrahedral concs., neutron diffr. study *(German)* 80−19688
$SiCl_4$, liq. struct., oscill. amp., neutron diffr. study 79−46544
$SiCl_4$, liq. struct. by neutron diffr. 79−73089
$SiCl_4$-$TiCl_4$, liq. struct., oscill. amp., neutron diffr. study 79−46544
SiO_2, molten, struct., X-ray radial distrib. anal. 78−67651
SiO_2-Al_2O_3-CaO-MgO, liq. silicic and slag, struct, density, surface tension *(Polish)* 78−83711
SiO_2-basic oxide system, struct. model 80−54109
Sn, atomic self-motions *(Rumanian)* 78−47226
Sn, collective motions, struct. factors calcs. 77−76295
Sn, distribution functions, 232 to 870°C 77−4035
Sn, elec. resist. calc., 232, 450 and 650°C, using calc. and expt. struct. factors *(Russian)* 78−56124
Sn, interference function temp. depend. from X-ray diffr., elec. resist. calc. 77−47332
Sn, liquid, interference functions by double hard sphere model 80−49090
Sn, molten, struct. factors, tetrahedral concs., neutron diffr. study *(German)* 80−19688
Sn, molten, struct. investig. by neutron diffr. 79−4233
Sn, pair interaction pot., struct. factor calcs. 77−51298
Sn, second and fourth order moments temp. depend. 77−72545
Sn, small-ang. X-ray scatt., at. microgrouping depend. *(Russian)* 78−14271
Sn, structure factor meas. by X-ray diffr., interaction pot. *(Russian)* 77−7655
Sn, X-ray diffraction analysis 79−4232
Sn-Bi, atomic self-motions *(Rumanian)* 78−47226
Sn-Pb (38.1 wt.%) alloy, rel. to Sn self-diffusion, 466-786K 77−69106
Sn-Se, melt, density, kinematic viscosity, struct., 900-1400K 78−14395
Sn-Zn, molten, struct. investig. by neutron diffr. 79−4233
$SnCl_2$-AlkAlCl$_4$ melts (Alk=Li, Na or Cs) 79−99874
$SnCl_4$, liq. struct., oscill. amp., neutron diffr. study 79−46544
$SnCl_4$, liq. struct. by neutron diffr. 79−73089
$SnCl_4$-$TiCl_4$, liq. struct., oscill. amp., neutron diffr. study 79−46544
$SrAg_2I_4$, Raman and autocorrelation spectra, solid and soln. 79−38532
$SrBr_2$, aq. solns., EXAFS meas. 80−60714
$SrCl_2$, aq. soln., Raman spectrum, local order 78−84563
$SrCl_2$, liq., dynamic struct. factors, computer simulation 79−37611
$SrCl_2$, molten, struct., electrolyte 'general primitive model' prediction test 80−28902
$SrCl_2$, partial static structure factors, velocity autocorrelation functions 78−91219
TE, small-ang. X-ray scatt., at. microgrouping depend. *(Russian)* 78−14271
Ta, molten, static struct. factor 77−19865
Tb, struct. factor and compressibility, rel. to metal-nonmetal transition 78−2529
Te, liquid, classical fluid model, neutralising negative background density 78−22621
Te, liquid, meas. of viscosity, density and surface tension *(French)* 78−91371
Te, Raman spectra, crystn. processes 80−60608
Te, US rel. temp. depend., melting effects 78−38782
Te-Tl, eutectic liquid alloy, structural features, interatomic interaction *(Russian)* 79−77494
$TiCl_4$, liq. struct., oscill. amp., neutron diffr. study 79−46544
$TiCl_4$, liq. struct. by neutron diffr. 79−73089
$TiCl_4$-$SiCl_4$($SnCl_4$), liq., beat effects, neutron diffr. studies 80−38897
Tl, struct. factor, Percus-Yevick equation perturb. treatment, square-well pot. approx. 78−75530
Tl-Te alloys, atomic struct., X-ray diffr. meas. 79−41934
$TlNO_3$, molten and aqueous soln., Raman spectra 79−78673
U complex, tetrakis(dipivaloylmethanato)uranium IV, in CS_2 soln., ^1H NMR, intromol. rearrangement 79−19784
U, hard-sphere model, phys. prop. meas. interpret., adjacent solid phase implications 77−19866
UO_2, ionic model partial struct. factors, radial distribs. 77−84617
UO_2, struct. differences between ionic and molecular fluid models 78−26423
VCl_4, liq., struct. factor, mol. dynamics calc. 80−38898
VCl_4, liq. struct. by neutron diffr. 79−73088
$VOCl_3$, liq. struct. by neutron diffr. 79−73088
$VW_5O_{19}^{4-}$, aq. soln., hydrodynamic radii from ESR line width 79−78504
Xe, radial distrib. functions and structural parameters 79−55640
Y-Si melts, enthalpy of formation and dissolution, microinhomogeneous struct., interatomic interactions *(Russian)* 80−34206
Zn, interference function temp. depend. from X-ray diffr., elec. resist. calc. 77−47332
Zn, molten, struct. investig. by neutron diffr. 79−4233
Zn, structure factor, 460 to 650°C, by neutron diffr., elec. resist. temp. coeff. 77−47333
Zn, X-ray diffraction analysis 79−4232
Zn^{2+}-H_2O clusters, solvation, Monte Carlo simulation 80−44102
$ZnBr_2$, aq. solns., EXAFS meas. 80−60714
$ZnCl_2$, aq. soln., Raman spectrum, local order 78−84563
$ZnCl_2$, aq. soln., structural transition, neutron diffr. study 80−64872
$ZnCl_2$, glassy and liq, EXAFS obs. of struct., comparison with vitreous GeO_2 80−70133
$ZnCl_2$-$CdCl_2$ melt, Raman spectra, struct. anal. 79−38549
$ZnCl_2$-LiCl(NaCl)(KCl)(CsCl), molten, US velocity, thermodynamic quantities and struct. *(Japanese)* 80−88270
$ZnCl_2$-$ZnBr_2$ melt, Raman spectra, struct. anal. 79−38549
$Zn^{2+}.CO_2$-H_2O clusters, solvation, Monte Carlo simulation 80−44102

liquid surface waves *see surface waves (fluid)*

liquid theory
see also classical theories of fluid structure; equations of state of liquids; quantum theories of fluid structure
acetone, vibr. dephasing theories, test using selective coherent ps. Stokes scatt. 80−59609
acetonitrile, electrolyte solns., IR and Raman spectra interpretation, CN-stretching region 79−73941
acetonitrile, in dilute CCl_4 soln., far IR spectra and mol. dynamics models 79−99876
acetonitrile, in liq. phase, Ramon band profiles, calc. using IR intensities 80−2741
acetonitrile, mol. pair correl. functions, scatt. intensities, statistical mechs. calcs. 79−1382
adhesive hard sphere fluids, clustering phenomena, theory of freezing 79−7533
adsorbing walls separated by Lennard-Jones liq., Monte Carlo calc. of force 80−15363
adsorption isotherm for study of interfacial and biological phenomena 77−59207
adsorption of polymer at surface of simple solvent 77−20166
alcohols, H-bond system, liq., high-press. effect 80−49080
alcohols, liq., picosec. mol. dynamics and electron localisation 79−46548
alkali halides, crit. consts., dense gas formulation 79−23700
alkali halides, molten, crit. consts. calc., dense gas formulation 80−44100
alkali metal, law of corresponding states, microscopic basis 77−47539
n-alkane-dimethylsiloxane mixtures, shear viscosity press. depend., applicability of hard sphere model 78−30775
alkanes, diffusive Langevin dynamics of model systems 79−86671
n-alkanes, numerical method for mol. dynamics 77−27804
alloy, binary, concentration fluctuations and struct. factors 77−47322
alloy, binary, interatomic forces, thermodynamic props. and alloying 77−47324

liquid theory continued
alloy, binary, stability against conc. fluctuations, pair interaction energy 77−47323
alloy, binary liq., viscosity coeffs. by Enskog theory 80−1920
alloy, binary or ternary, atomic order effects, statistical mechanics and fluctuation theory 78−14263
alloy, thermodynamic ab initio calcs. 77−47602
angular velocity correlation, from angular position correlation functions of molecules in liq. 79−86660
anisometric molecules, in soln., depolarised light scattering intensity 80−45096
anisotropic fluid, diffusion, EPR spin exchange and nuclear spin relax., theory 80−34753
anisotropic micropolar fluid theory 80−31515
anisotropic molecular fluids, local elec. fields 77−59545
anormal fluids, saturated liq. densities, four-parameter corresponding state theory 79−33066
aqueous electrolyte solutions, refr. index, Tamman-Tait-Gibson model 78−10863
aqueous electrolyte solutions, vel. correls., improved representation 80−59360
aqueous mixtures, lower crit. soln. pt. theory 79−4415
aqueous non-electrolytes, excess internal pressure and Gruneisen parameter behaviour 80−88015
aqueous solution, hydrophobic interaction, simple solute, one-dimens. model 79−37601
aqueous solutions, Monte Carlo simulation, convergence of new algorithm 78−63649
associated liquids, mechanism of structural dielectric relaxation 80−107034
associated solution, characteristic sums method in stat. theory 80−10480
asymmetric electrolytes, mean spherical model, chem. pot. of ions 78−27781
atom pairs, dynamic behaviour, in Lennard-Jones and simulated Rb fluids 80−44098
atom-glasses, hard sphere model of glass transition 79−4399
atomic liquids, shear viscosity determ. by nonequilib. mol. dynamics 80−79971
atomic self-motions, in simple liquids *(Rumanian)* 78−47226
benzene, equation of state studied using statistical theory results 80−84276
benzene, vib. relax. and Raman line widths 77−32359
Bernal holes, size statistics 80−33892
binary and ternary systems, pred. of isothermal vapour-liquid equilibria, heat of mixing, viscosity 77−31761
binary collision approximations to space-time memory functions 80−14987
binary fluid, molecular dynamics, critical mixing point region 80−88014
binary fluid system, Onsager coeffs., steady state soln. for Benard convection 80−64851
binary hard-sphere mixture, mutual isothermal diffusion Onsager reciprocity relations effect 78−30773
binary liquid mixture, diffusivity from simple kinetic model 79−23752
binary liquid mixtures, cell mol. theory for calc. of thermodynamic props. *(Spanish)* 79−68991
binary liquid mixtures, dispersion interactions, struct. effects 79−46535
binary liquid mixtures, first order transitions, pseudo-critical slowing down 79−55627
binary liquid mixtures, vibr. and rot. relax., crit. point effects 79−50969
binary liquid mixtures, viscous flow props., mol. thermodynamic theory 78−2280
binary liquid solutions, surface cluster functions 78−67631
binary liquid systems, apolar-apolar and polar-apolar, significant structure theory, appl. 80−1909
binary liquids, dynamical correlations, fourth moment of current and appl. 79−14664
binary mixture of hard spheres and square-well molecules, quantum corrections to eqn. of state 80−6338
binary mixtures, excess surface tension calc. and theories of solns. 78−91508
binary mixtures, hole theory in quasichemical approx., excess function formulae *(Spanish)* 79−68992
binary mixtures theory in quasichem. approx., hole theory and thermodynamic functions *(Spanish)* 77−72534
binary molten salt, charge and mass fluctuations in hydrodynamic limit *(French)* 77−31573
binary molten salt mixture, excess free energy of mixing, conformal ionic soln. theory 77−1230
binary solution, equilibrium distrib. function *(Russian)* 79−1377
book, liquids and their props., mol. and macroscopic treatise 78−87604
book 79−60245
Born-Green equation stability for effective pair pot. in dense liqs. 77−51292
Born-Green-Yvon eqn., deduction involving ang. distrib. function 80−64863
bromoethane, liq., relative mol. orientation appl. of nucl. mag. relax. data 79−41933
Brownian motion and NMR spin relax., book 78−15054
Brownian particle, freq.-depend. friction coeff. in fluid near crit. pt. 78−73929
bulk viscosity, inverse power pot. 78−91466
butane, flexible chain molecules, momentum space diffusion eqns. 80−75142
n-butane, intermol. pair correls., RISM integral eqn. 78−63656
carbon tetrachloride, equation of state studied using statistical theory results 80−84276
carbon tetrachloride, optical props. under press., molecular polarisability depend. on thermodynamical state 78−80312
cavity model, refr. index and density, permittivity *(French)* 79−78642
charged fluid, gas-liq. transition theory 79−82327
charged hard sphere fluids, meas. spherical model 78−18524
charged hard spheres, distrib. function, mean spherical approx. 79−4222
charged hard spheres, pair correlation function, mean spherical approx. 79−4223
charged hard spheres in neutralising background, radial distrib. function 77−33936
charged hard spheres in uniform neutralising background, Monte Carlo and perturbation theories 77−55223
charged hard-sphere fluid, electrified interface pot., extended mean spherical approx. calcs. 80−84502

liquid theory continued
charged particles in continuous dielectric medium, free energy, hard core pot. effects 79−37600
chemical physics of liq. state, book 77−31574
chemically reacting dense fluid, Enskog theory 78−35667
2-chloro-2-nitropropane, far IR-microwave estimation of binary collision approx. 80−55095
chloroform-carbon tetrachloride mixture, Lennard-Jones pots., mol. dynamics calcs. 78−34418
classical, coherent and incoherent scatt. functions, Maxwell relax. time 77−76283
classical fluid, crit. dynamics, double scatt. correction 79−42979
classical fluids, triplet correls. and moments of current correl. functions 79−14666
classical fluids in crit. region, generalised perturbation theory 79−77474
classical hard rod fluid in external field, equilib. state 77−27801
classical Lennard Jones 6-12 fluid, surface characts., density functional theory 77−24255
classical liq., kinetic theory, dynamical struct. factor calc. 78−21050
classical liq., sum rules and at. correlations, appl. to Ar 77−76282
classical liquid, metastable supercooled state, props. 78−55796
classical liquid, $S_s(q,\omega)$ incoherent scatt. function 77−24254
classical liquids, dynamic correl. functions 78−26412
classical liquids, in equilib., mol. theory, integral eqns. 77−39522
classical liquids, kinetic model, dynamic struct. factor 79−10768
classical liquids, kinetic theory for coherent scatt. function 78−42875
classical liquids, microdynamics, book contrib. 79−60248
classical liquids, mode-coupling effects on transverse current memory function in dynamical region 78−83706
classical liquids, vel. correl. and relative diffusion 78−14262
classical simple liquids, memory function, dynamical struct. factor, current-current correl. function 78−26411
cluster expansion for fluids with long-range interactions 80−92440
cluster identification, computer expts. on systems of particles 78−59725
coexistence curve of liquid system with global eqn. of state 79−1487
cohesive energy density, surface and interfacial tension and heat of mixing 77−55431
collective modes in classical monoatomic liqs., coherent neutron scatt., book contrib. 77−89371
collective molecular motion from depolarized light scatt. 80−60614
collective motion, limits of classical hydrodynamics from Brillouin neutron scatt. for simple liqs. *(German)* 77−24258
colloid, excess press., calc. and expt. 77−86386
colloids, concentrated, appl. of modern concepts in liquid state theory 80−40750
computer modelling of matter, conf., Anaheim, USA (March 1978) 80−51954
concentrated aqueous electrolyte solutions, transport props. *(German)* 78−80750
condensation, cluster model, excluded volume effect 79−10932
condensation, vacancy theory, cell model calcs. 77−55224
cooperative atomic motion in simulated two dimensional liquid 79−90513
correlation function, long time asymptotic behaviour, influence of waves on relax. processes *(Chinese)* 80−59195
correlation functions, mono- and multi-molecular, for liquids and solutions *(French)* 79−50971
correlation functions and their relationship with experiments, summer school lecture series 80−6340
Coulombic system, statistical mechs., eqn. of state in restricted primitive model 77−7644
Coulombic systems, HNC and RHNC eqns. for restricted primitive model 78−67630
coupled molecular rotational diffusion and conform. change 78−22613
critical binary mixtures, sound propag., mode coupling theory, validity breakdown 80−65159
Debye generalised fluid model, dielectric relax., depolarised dynamic light scatt. 80−108156
dense, quadrupolar, hard sphere fluid, integral eqn. approx. 78−63652
dense classical liquid, struct. factor, long range pot. 78−47224
dense dipolar hard sphere fluid, integral eqn. theory 77−76278
dense fluid, collective modes and neutron scatt. 80−92442
dense fluid, electronic struct., cluster effects 79−95305
dense fluid, new description of random stacks *(French)* 78−79512
dense fluid, statistical mechanics of mol. motion 78−38603
dense fluid, with square-well + hard core pot., equilib. props., quantum corrections 79−27891
dense fluid transport phenomena, generalised moment method 80−33866
dense fluids, HF kinetic sum rule 77−27803
dense fluids, relative motion of atomic pairs investigated in short-time regime 80−96426
dense fluids, statistical mechanics, using hard sphere model 80−59364
dense fluids, translational motion, modified Fokker-Planck eqn. 78−75517
dense gas, transport coeffs. density expsn., logarithmic terms 78−34250
dense gas transport calcs., Rice Allnatt theory 77−76590
dense gases and liqs., three-body nonadditive interactions, thermodynamics props., mol. dynamics simulation 79−7435
dense hard core system, transport coeffs., entropy 77−62656
dense liquids and their mixtures, mol. dynamics, numerical algorithm 80−28890
dense molecular fluid, light scatt., internal field correction factor calcs. 80−25396
dense simple fluid, equilib. props., 3-body forces effects 77−76273
density fluctuations in classical and quantum liquids, general theory 79−35628
depolarised Rayleigh scatt., nonlorentzian behaviour, 3-variable theories *(French)* 80−25395
diatomic liquids, hard and soft core, free energy difference, Monte Carlo calcs. 80−92436
diatomic mol. soln., spontaneous Raman scatt., vibr. dephasing, review 77−28568
diatomic molecules, homonuclear, molecular dynamics, time-dependent statistical props. 80−44093
diatomic molecules, homonuclear, molecular dynamics, translation-rotation coupling 80−44094
o-dichlorobenzene, liq. mixtures, excess vols. and eqns. of state 77−29036
dichloromethane, liq. state dynamics, models 79−73087
dielectric fluid near critical point, effect of elec. field *(Russian)* 77−62647

liquid theory continued
dielectric kernel, functional differential equn. 79−32871
dielectric liquid, bubble creation in high elec. fields, explained in terms of struct. 79−91370
dielectric relax. time rel. to single particle correl. time 80−97193
diffusion of particle, in hard sphere liq., translational, mol. theory 79−42288
diffusion rate processes, effect of intermol. force field 77−35733
dilute fluid mixtures, spherical mols., struct. and permittivity 80−92433
dilute solution, associated, lattice model, chem. equilib. laws 79−82139
dilute solutions, Monte Carlo algorithm for preferential sampling near solutes 77−51287
dilute systems of dipoles and dipolar charged particles, Mayer resummation method 78−83710
dipolar fluid, ion-ion distrib. function 78−83704
dipolar fluid mixtures, dielec. const. calcs. 79−64969
dipolar fluids, equilib. statistical mechanics, struct., dielec. and thermodynamic props. 80−6345
dipolar fluids, integral eqn. approximation 79−86669
dipolar fluids, theory 79−37602
dipolar hard sphere solvent with charged hard spheres, hypernetted chain approx. 80−61130
dipolar hard-sphere system, pair correl. function calcs. 77−89362
dipolar liquid, far IR absorpt. rel. to Mori continued fraction for autocorrel. function 78−2875
dipolar liquid time-variation of dispersion and absorption of third-order electric polarisation, mol. relax. times 80−60487
dipolar liquids, hypernetted-chain eqn., perturbation theory soln. 80−49072
dipolar media, 0-10^{12} Hz freq. polarisation, dipole-dipole interaction effects 79−59525
dipolar mixtures, pair distribution function 79−86668
dipole, spherical, steadily rot., dielec. friction 78−87600
dipole fluid theory in hypernetted chain approx. *(Russian)* 80−14988
dipole in polarizable fluid, effective field 77−76280
dipole solvation, one polar mol. dissolved in 499 moderately polar particles 78−47221
direct correlation function, factorisation 80−96427
direct correlation function of liq. from Ornstein-Zernicke eqn. 77−47314
disordered systems, mode softened unified theory 79−55637
droplets nucleation in finite systems, theory and computer simulation 80−26038
dynamic critical exponents, inequalities 80−79662
dynamic structural correlations and van Hove's correlation function for liquids 78−94958
dynamical correlation functions of classical liquids 79−1381
dynamical struct. factor and velocity autocorrelation function, appl. to classical one-component plasma 78−71430
electric double layer, at charged planar interface, hypernetted chain approximation appls. 79−60912
electrical double layer theory, modified Poisson-Boltzmann equation 78−94955
electrical double layer theory, through Born-Green-Yvon eqn. 80−35539
electrical double layers, repulsive electrostatic interaction, statistical mech. theory 80−92432
electrolyte, polarisable spheres model 78−56898
electrolyte, screened Coulomb interaction range, double layer problems 78−27765
electrolyte, spherical nonlinear Poisson-Boltzmann theory Debye-Huckel linearisation 80−35538
electrolyte soln. grand canonical ensemble Monte Carlo method 80−54092
electrolyte solution, Brownian dynamics approx., time evolution and transport props. 79−37604
electrolyte solution, primitive model, using modified BBGY integral eqn. 79−99049
electrolyte solution, radial distrib. functions, symm., in pot. theory 78−34410
electrolyte solution, two-dimens., theory 77−86323
electrolyte solutions, thermodynamics, transport props., semi-phenomenological approach including short range forces 80−3353
electrolytes, aq. solns., ion-solvent interactions, transport props. *(German)* 78−79790
electrolytes, Blum's theory, derived conclusions involving Helmholtz free energy, correlation functions 77−48651
electrolytes, osmotic coeffs., mean spherical approx. refined model 79−1965
electrolytic aqueous media, ion-pairing, hard sphere model 80−96428
electronic density of states in one-dimens. dense fluid, Katz-Rice calc. 80−20063
electronic structure, structured medium approx. 80−84421
electrostatic interactions in liquid state, effect on frontier orbitals and chem. reactivity 80−84046
equilibrium correlation functions with various potentials, mol. dynamics expts. *(Spanish)* 79−90502
equilibrium theories of simple liquids, review 80−38887
ethanol, aq. soln., conc. fluctuations, shear and longit. relax., Brillouin scatt. and pulse techniques 78−71792
ethylene, condensation, zero point energy shift, isotope effects 78−95147
excess enthalpy of liquid mixtures 79−23733
exchange processes, two-dimensional NMR spectrosc. investig. 80−25218
expanded fluid metal transport coeffs., temp. and press. depend., Enskog theory 78−6170
Fermi system, extended, energy expectation value per particle, lack of $O(A^{-1})$ contribution in Iwamoto-Yamada expansion 78−60081
film, mol. dynamics simulation of surface struct. 77−15666
flexible mols., constrained dynamics computer simulation 80−92437
fluid, hard sphere, nonspherical mols., dielectric const., Monte Carlo simulation 78−23385
fluid, rough sphere, kinetic theory, density fluctuations 78−131
fluid interfacial stress and struct., gradient theories 79−19428
fluid mixtures, analytic and perturbation theories 78−18516
fluid mixtures, unified mol. theory, statistical thermodynamics 77−31570
fluid near critical point, spin-lattice relaxation time 80−80630
fluid of partially rough spheres, translational and rot. diffusion coeffs. 78−26404
fluid phase coexistence in liquid-vapour interface, Monte Carlo simulation 80−49349
fluid surface correlations, density profiles 78−6196
fluid with nearly spherically symmetric molecules, thermodynamic perturbation theory 80−14985
liquid theory continued
fluid with triangular-well potential, eqn. of state, quantum corrections 79−69222
fluid-like viscoelastic liquid, coupling of orientational and translational motions, LF depolarised (VH) scatt. 77−7642
fluids, one and two dimensional, hydrodynamics, viscosity, heat conductivity, kinetics *(Russian)* 80−79972
fluids, perturbation theory and thermodynamic props., CRIS model 80−92430
fluids, perturbation theory and thermodynamic props., inverse power and 6-12 pots. 80−92431
fluids, perturbation theory and thermodynamic props. 80−92429
fluids with nonuniform velocity fields, light scatt., and pair correl. functions 79−61389
fluoromethanes, condensation, zero point energy shift, isotope effects 78−95147
Fokker-Planck equation for non-Markovian system 77−47313
Fokker-Planck fluid of symmetric top mols., orientational relax. 78−5996
free asymmetric rotors, classical system, second rank tensors, ang. correl. functions 80−64865
free energy, charged hard sphere system, restricted primitive model 79−27890
free energy, of electrolyte, due to Coulombian and hard core pots. 79−23748
free energy calcs., mixed liquids, local mole fractions consistency 78−83702
freezing, Van der Waalsian theory 78−22821
fused hard sphere fluids, equations of state, virial coeffs., Monte Carlo simulation 80−54095
fusion of liquids with spherical- and linear-like mols. 79−82318
gas-liquid surface of mol. fluids, mol. dynamics computer simulations 80−39387
gases in liquids, Henry's constants, modified Pierotti theory 79−51259
generalised hydrodynamics, review 77−14973
glass forming liquids, vol. relax. 80−96429
glass transition, soft-sphere model, mol. dynamics study 80−49343
glass-forming liquids, relax. times, temp. depend. 78−83924
glass-forming materials, ion activation, energy parameters determ. 80−24634
glycerol, liq., effective Debye temp., temp. depend., quasi-cryst. model 77−4209
group contribution mol. model of liqs. and solns., thermodynamic props. 77−58932
Gruneisen parameter rel. to Rao's acoustical parameter 80−92581
halogenobenzenes, dipolar liquid, far IR absorpt. rel. to Mori continued fraction for autocorrel. function 78−2875
hard core diatomic system, pair correl. functions, Monte Carlo and RISM calcs. 77−72537
hard core fluid with Yukawa tail, eqn. of state 80−24330
hard core with attractive part reference pot., perturbation expansion 77−19856
hard diatomic fluid mixtures, dense, orientational struct., Monte Carlo study 78−34415
hard dumbbell fluids, RAM and BLIP function theories 80−79658
hard dumbbell molecules, reference pot., perturbation theories, spherical reference systems 80−28898
hard heteronuclear dumb-bell fluid, thermodynamic props., eqn. of state 78−38599
hard nonspherical molecule fluids, mixtures, conformal theory 79−94860
hard oblate spherocylinders, Monte Carlo virial coeffs. 78−26400
hard particle fluids, short range solvation forces 80−38885
hard polyatomic molecular fluid, virial press., Monte Carlo method 77−89357
hard rod fluid, phase transitions, rotational and liquid-crystalline, 1-D model 80−54090
hard rod system, improved lattice model, nematic and isotropic phases 80−33882
hard rod system, initially ordered, one-dimens., mol. dynamics computer simulations 78−71658
hard rods, attractive interactions, scaled particle theory 80−82735
hard sphere, surface tension, compressibility, bulk modulus press. coeffs. and Rao's acoustical parameter 80−80027
hard sphere fluid near hard wall, diffusion coefficient, mol. dynamics simulation 80−64858
hard sphere fluid struct. near hard wall 79−23511
hard sphere gas, H-theorem for Enskog kinetic eqn. 77−68905
hard sphere liq., dil. impurity diffusion coeff., quasihydrodynamic approx. and simulation 80−49066
hard sphere mixture, nonadditive dias., perturbation theory, double reference system 78−38597
hard sphere mixtures, finite angle light scatt., Percus-Yevick approx. calcs. 80−7363
hard sphere mixtures, with negatively nonadditive diameters, scaled particle theory 78−71654
hard sphere model, computer built, for simulation of cryst.-melt interface 77−20165
hard sphere solvent, dense, solute test hard sphere kinetic energy relax. 80−33864
hard sphere system, high densities, Kirkwood eqn., variational principles 77−65942
hard sphere system in equilibirum 80−86225
hard sphere system in equilibrium, two-dimens. hard disk system 80−107033
hard sphere system in three dimens., thermodynamic props. 80−86226
hard spheres in thermal eqn., time correlation functions in low-density limit 80−64859
hard spheres mixtures, equations of state for calc. thermodynamic props. 80−84301
hard spheres with square-well attraction, Percus-Yevick eqn. soln. 79−37599
hard spherocylinder fluid, mol. dynamics simulation 78−5997
hard spherocylinder fluid, Monte Carlo calcs. 78−91208
hard spherocylinder fluid, props., blip function theory 78−91207
hard spherocylinders and spheres mixtures, Monte Carlo study 80−49073
hard- and soft-core equations of state 79−55635
hard-core fluid, struct. of shock wave front, mol. dynamics study 78−1970
hard-core fluid with Yukawa tail, eqn. of state, Monte Carlo results 78−26410

liquid theory continued
hard-disc fluids, long-time correlation effects on displacement distributions 79−27894
hard-disc mixture, mol. dynamics simulation, self-diffusion coeffs. 77−89356
hard-disc system, expt. model for melting transition 78−43100
hard-particle fluids, series representation of eqn. of state 80−6337
hard-sphere fluid, interacting with wall, virial coeffs., in surface tension 79−23808
hard-sphere fluid, kinetic theory of self-diffusion 79−4225
hard-sphere fluid, modified nonlinear Enskog eqn., entropy function 78−63526
hard-sphere fluid, near a wall, surface tension, approx. method calcs. 78−59724
hard-sphere fluid, shear viscosity, nonequilib. molecular dynamics calcs. 79−68996
hard-sphere fluid, three particle interaction with wall 78−47223
hard-sphere fluid, translational correl. functions, stochastic theory 77−84608
hard-sphere fluid, viscosity and self-diffusion coeffs. 78−51716
hard-sphere fluid density, near ideal wall, Percus-Yevick rel. to superposition approx. 77−27802
hard-sphere fluid/soft wall interface, nonuniform fluid in external field 78−34413
hard-sphere fluids, dipolar and quadrupolar, radial distrib. functions, perturbation theory 78−59727
hard-sphere liquid, glass transition, computer mol. dynamics simulation 77−11674
hard-sphere liquid, shear viscosity, from nonequilib. mol. dynamics 79−19132
hard-sphere suspension, viscosity, direct inter-macromolecular interactions effects 79−95199
hard-sphere system, liquid-solid transition, chem. pot. calcs. 80−54088
hard-sphere system, with square well attraction, Percus-Yevick theory 77−43123
hard-sphere-like mixtures, soln. of Ornstein-Zernike eqn. 77−4028
Helmholtz free energy of triangular well fluid, Barker-Henderson perturbation theory 79−4218
n-heptadecane, short-chain mol. liq., statistical thermodynamics 79−73084
heteronuclear hard dumbbells, eqn. of state derivation 77−30085
n-hexane, optical props. under press., molecular polarisability depend. on thermodynamical state 78−80312
high density fluid states, fluctuating free-vol. anal. of soft-core model 78−75516
high-density fluid-perturbation theory, based on inverse 12th power hard-sphere reference 79−99042
highly viscous liquids, nuclear magnetic spin relaxation, high-freq. translational jitter 79−51874
hole theory rel. to US propag. 78−38775
homonuclear diatomic mols., force-torque correls. 80−87196
homonuclear diatomics, dense fluids, transport props. 78−75519
hydrocarbons, thermodynamic props., multiparameter conformal solution theory 78−18796
hydrodynamic boundary conditions and radii, appl. to rot. rough sphere friction with chloroform 78−9926
hydrodynamic interactions and pair correl. functions on reaction kinetics, dynamic effect 80−97684
hydrodynamic singularities and the renormalization group 79−54063
hydrogen-bonded liquids, HF, H_2O, NH_3, computer simulation, intermolecular potentials 80−38890
hydrophobic solutions molecular properties, one dimensional soluble models 79−46536
immiscible mixtures, variational theory 79−27885
independent structure model, vibr. and translational degrees of freedom *(Spanish)* 77−4027
inert gas, simple classical fluids, density functional theory, localised excess electron states 79−55641
inert gas liquid mixtures, collision induced absorpt. 77−4638
inhomogeneous charged fluids, density functional theory, rel. to molten salts surfaces 80−79660
integral eqn. with approximation of direct correl. function in pot. rigid core region 77−84611
integral equations for liquids, systematic series formation 78−14264
integrand of free volume for fluid described by Kihara potential of spheric core 80−1908
interatomic and intermolecular forces, summer school lecture series 80−6342
interface tension, density-gradient term in free energy near crit. temp. 77−89617
interface with vapour, kinetic eqn. at mean field level 79−37905
intermolecular free-length determination in liquids at cryogenic temp. 79−82131
intermolecular potentials, coulombic and multipolar, 2-dimens. mol. dynamics simulation 78−75520
internal rotation barrier, IR spectral linewidths meas. 78−72507
ion mobility, long wavelength fluctuations effect 79−77786
ion solvation, in polar media, continuous charge distrib. model, quantum mech. calcs. 78−68913
ion-dipole mixed system, dipole-dipole distrib. function for electrolytic soln. *(Russian)* 77−35459
ion-dipole mixtures, ion-ion distrib. function 78−83704
ionic and multipolar liq., thermodynamic perturbation theory 77−47316
ionic fluids, pair correl. functions, self-consistent Ornstein-Zernike approx. 77−84605
ionic fluids, pair distrib. functions, self-consistent Ornstein-Zernike approx. 77−84606
ionic hard-sphere solution, in polar hard-sphere solvent, cond. functions 79−99045
ionic liquid, long wavelength modes, space-time correlation functions 78−9772
ionic liquids, collective modes 79−55636
ionic liquids, hypernetted chain eqn., Newton Raphson soln. 80−49071
ionic mobility theories, continuum and stochastic models, comparison with conductance data 80−44345
ionic salt, Monte Carlo simulation using multipole series *(Russian)* 77−62339
ionic solution, charged square well model, virial osmotic coeffs. 79−4217
ionic solution, in mol. polar solvent, charged sphere model, statistical mechs. 78−71655
ionic solution theory, variational approach 77−7645
liquid theory continued
ionic solutions, elec. field statistics 78−87601
ionic system, computer simulation, boundary conditions distorting effects 79−50968
ionic systems, weakly screened, evaluation of convolution integrals appearing in integral eqn. describing pair correlations 80−84044
isomerisation dynamics, in liquid solutions, statistical mechanics, transition state approx. 78−60999
isopropyl alcohol-carbon tetrachloride, mixture, dielec. const., two-sided estimate 79−42262
isotropic nonpolar fluid, elec. quadrupole density 78−94956
itinerant oscillator model, anal. for dielectric relax. and incoherent neutron scatt. 79−90509
kinetic theory, equilib. and non-equilib. props., book contrib. 79−60246
kinetic theory models of density fluctuations, memory functions 80−38886
kinetic theory of dense fluids, derivation, transport coeffs., soln. of kinetic eqn. by moment method 79−54032
kinetic theory of dense fluids, generalised Chapman-Enskog soln. 79−54033
Kirkwood instability, mean field theory 80−84043
Laplace molecular pressure and internal pressure, rel. to capillary theory formulas 77−25303
Lennard Jones 6-12 fluid, Pade approximant for eqn. of state 77−3905
Lennard Jones fluid simulation, liq.-vap. surface density profile, fluctuation effects 77−89355
Lennard Jones liquid, simulation by force bias and Monte Carlo methods 79−86666
Lennard Jones system, nonphysical sampling distribs., Monte Carlo free energy estimation, umbrella sampling 77−26229
Lennard-Jones 12-6 fluid, liq.-vap. interface, density and surface tension 79−90772
Lennard-Jones 12-6 system, triple pt. props., mol. dynamics simulation 78−2231
Lennard-Jones 9:3 adsorptive system, Percus-Yevick and hypernetted chain theories 80−20030
Lennard-Jones (100) crystal-liquid interface, structure 78−91284
Lennard-Jones and Stockmayer pot. parameters, crit. evaluation, correl. methods 78−1966
Lennard-Jones chain, stochastic transition in classical nonlinear dynamical system 78−142
Lennard-Jones dense fluid, radial distrib. function, explicit eqn. 80−49068
Lennard-Jones diatomics system, vel. autocorrelation functions 78−9931
Lennard-Jones fluid, 2-D, radial distrib. function, integral eqn. perturbation theory 78−26409
Lennard-Jones fluid, 6-12 pot., press. calcs., using integral eqn. and perturbation theory 79−4224
Lennard-Jones fluid, dense, memory function model for vel. autocorrelation function and self-diffusion coeff. 79−77472
Lennard-Jones fluid, equation of state 79−73083
Lennard-Jones fluid, hypernetted-chain eqn. of state 78−67800
Lennard-Jones fluid, nonequilibrium molecular dynamics, $t^{-3/2}$ long-time tail for stress-stress time correlation 80−70100
Lennard-Jones fluid, self-diffusion 78−43163
Lennard-Jones fluid, thermodynamic props. calc. by modified Monte-Carlo method 77−35662
Lennard-Jones fluid, two-centre, perturbation theory appl. using spherically averaged reference potential 80−64860
Lennard-Jones fluid, vel. autocorrel. functions calcs. 77−58944
Lennard-Jones fluid in contact with Lennard-Jones wall, interfacial density profile 78−67901
Lennard-Jones liq., press. and temp. consistent, approx. theory, Helmholtz free energy 78−63647
Lennard-Jones liq., time correlation functions attenuation *(Russian)* 79−60244
Lennard-Jones liq. mixtures, mol. dynamics calc. 78−55794
Lennard-Jones liquid mixture, mol. dynamics, attractive term effects 77−11454
Lennard-Jones liquid mixtures, equimolar, mol. dynamics, struct. and thermodynamic props. 78−18517
Lennard-Jones liquid mixtures, local comp., mol. dynamics calcs. 79−82133
Lennard-Jones liquid mixtures, mol. dynamics, particle mass and size depend. 78−22615
Lennard-Jones mixture, binary, equimolar, static (dynamic) props., mol. dynamics calc. 80−64857
Lennard-Jones molecules, dilute gas, density fluctuations, dynamic struct. factor 79−99044
Lennard-Jones pot. liquid, high-temperature vapour line using Monte Carlo methods 79−37826
Lennard-Jones system, 2- and 3-dimens., crit. point parameters, quantum corrections 79−4227
Lennard-Jones system, cryst. nucleation kinetics 77−62615
librational reorientation, sum rules 78−71659
linear hard core fluid as limit of lattice fluid 80−38882
linear molecule liquids, computer simulation and theory, review 78−38604
linear molecules, forced rot. diffusion, nonlinear aspects 79−90503
liquid, simple, transport coeffs. and internal energy relation, hard sphere model 77−76284
liquid, thermal response to weak external field, molecular dynamics 78−71660
liquid-glass transition, free volume approach, thermodynamic behaviour 80−1940
liquid-vapour co-existence, dipolar hard sphere fluid, Monte Carlo method 79−99293
liquid-vapour interface, pair correl. function at triple pt., Monte Carlo method 80−10753
liquid-vapour interface and stability rel. to spinodal decomposition, Cahn-Hilliard theory departure 79−77752
liquid-vapour interface nature, non uniform classical fluids statistical mechanics 79−77468
local order theory characterisation by vectors tensors, internal energy density multipolar expansion 80−49070
long wavelength collective motion 78−38601
long-time anomalies suppression in classical simple liq., Ar(Rb) appls. 80−24339
longitudinal modes, transverse modes and vel. correls. 79−94858
luminescent system, orientation factor in conc. effects due to nonradiative energy transfer 80−25425

liquid theory continued
macromolecular, solutions, mol. orientation, time-depend. torque, rot. diffusion eqn. 78−68471
macromolecular chain dynamics model interpret. of dielec. relax. data 77−52014
macromolecular dynamics, constraint dynamics, computer simulation 78−9932
macromolecular liquids and solutions, statistical thermodynamics 78−18528
macromolecular solns., stress and heat flux in dumbbell soln. 79−68999
macromolecular solution, flexible mols., mol. models for mech. props. 79−59957
macromolecular solution, quasielastic light scattering from rigid mols. 79−64127
macromolecule, rigid, in soln., depolarised Rayleigh spectroscopy 79−94119
macromolecule liquid, translational friction coeffs. of rigid, symm. top mols. 80−6003
magnetic reson. lineshape, with slow mol. motion, asymptotic method, strong collision limit 77−48063
mathematical models of disordered systems, book 80−1878
mean spherical approx., particles interacting with damped oscill. pot. 77−55221
mean spherical approx., thermodynamic props. 77−80401
mean spherical approx. for arbitrary hard ions and dipoles, soln. for electrolytes 79−1380
mean spherical model for hard ion and dipoles, thermodynamics and correlations 80−103230
medium cluster model, vapour press. isotope effects, mol. orientation effect 77−72542
medium cluster model, vapour press. isotope effects 77−65943
melting, vacancy theory, cell model calcs. 77−55224
memory function, influence of collective modes on single-particle motion 77−68749
memory function, self-consistent theory, incoherent scatt. law. 77−89360
memory functions, microscopic theory, generalised Langevin equation 80−49076
memory functions for ang. motions 80−59358
metal, effective interatomic potential from struct. data 78−47232
metal, effective interionic interaction, many particle effects *(Russian)* 77−39530
metal, effective interionic potentials 78−91221
metal, effective interionic pots. determ. from expt. data 77−47338
metal, entropy of fusion and activation energy for self-diffusion 79−28121
metal, eqn. of state and triplet and higher correlations in long wavelength limit 77−11453
metal, interatomic forces and thermodynamic props., hard-sphere model 77−47321
metal, model potential, exact soln. of mean spherical approx. 79−82144
metal, mol. motions from NQR, viscosity and sound damping 77−1615
metal, surface entropy using hard-sphere model 79−37906
metal, thermal press. coefficients and sp. ht. 79−65207
metal, viscosity anal. 78−91468
metallic glass, heat of crystn. and viscous behaviour 80−75166
metallic glass, stability, hole theory of liquids appl. 80−100174
metallic glasses, transport properties, applicability of liq. metal theory 79−56179
metals, Ashcroft and Schaich, and Gyorffy theories equivalence 79−60693
metals, HF expansion of memory function 77−15301
metals, isothermal compressibility and eqn. of state at m.p. 80−79673
metals, surface properties, hard-sphere and square-well models 80−19684
metastable liquid, instability and freezing, theory 78−18746
methane, aq. soln., Monte Carlo simulation of isothermal-isobaric ensemble 78−30531
methane, condensation, zero point energy shift, isotope effects 78−95147
methane, liq., mol. dynamics calcs. 77−19857
methane, liq. and gas, mol. dynamics simulation, thermodynamic props., struct. factors, etc. 79−50976
methanol, liq., simulation using modified intermol. dimer pot. function 80−32629
methanol, vibr. dephasing theories, test using selective coherent ps. Stokes scatt. 80−59609
methyl cyanide ($-d_3$), vib. dephasing, Raman obs. 77−59566
methyl iodide, liq., Raman meas. of transversal angular velocity correlation function 79−87422
methyl iodide, liquid, rough sphere rot.-diff. model, relax. times 77−15294
methyl iodide, vib. relax. and Raman line widths 77−32359
methylcyclohexane, dense liq., self-diffusion and viscosity 80−15278
microfluids, heat conduction 79−72776
microstructure and dynamics, summer school, Aleria, Corsica, France (Sept. 1977) 80−6339
mixed ion-dipole systems, binary distrib. functions *(Russian)* 77−80404
mixed ion-dipole systems, rot. diffusion, statistical theory *(Russian)* 77−80403
mixture, of dense simple fluids, bulk viscosity, hard spheres appl. 80−14982
mixture, of hard convex body fluids, accurate eqn. of state 80−6484
mixtures, binary interaction consts., thermodynamic props. 79−41917
mixtures, intermol. forces effect on phase diagram and excess props., perturbation theory 80−39287
mixtures, perturbed hard chain theory, thermodynamic props., appl. in chem. technology 79−34343
mixtures, phase equilibrium, augmented Van der Waals theory 78−79737
mixtures, thermodynamic props., mol. theory 78−18515
mode-coupling theory for simple classical liqs. 78−42876
model liquid, velocity autocorrelation function, spectra anal. 79−90512
modified cell theory, thermodynamic props. 79−19133
modified cell theory of the liquid state 80−24338
Moelwyn-Hughes parameter calc. from US data for pure liqs. and liq. alloys 80−59375
molecular acoustics in fluids, time correlation functions 77−51451
molecular assembly, iterational soln. to integrodifferential eqn. 79−77473
molecular dynamic simulation, event scheduling 80−49069
molecular dynamics, computer simulation, orientation space representation 77−76276
liquid theory continued
molecular dynamics, high speed computation of correl. functions 77−7648
molecular dynamics, principles and appls., summer school lecture series 80−6341
molecular dynamics computer simulation, multiple time-step methods 78−47220
molecular dynamics method in statistical physics, dense media, review 80−18895
molecular dynamics of rough sphere fluid, specific kinetic models 77−58936
molecular dynamics simulation, partial press. evaluation 78−71663
molecular dynamics simulation of a small drop 78−15719
molecular dynamics simulation of dense gases, test particle motion 78−9930
molecular dynamics simulation of rigid polyatomics, singularity free algorithm 77−76277
molecular fluid, dielec. const. and equilib. props., interaction site cluster theory 77−84614
molecular fluid, hard-core triatomic, Monte Carlo simulations 80−38880
molecular fluid, optical scatt. dielec. screening and susceptibility fluctuations 77−90162
molecular fluid, spherical harmonic formalism, thermodynamic props. 79−27886
molecular fluids, angular pair correl. function, second order perturbation theory 79−86662
molecular fluids, coupling of rotation and translation 80−38892
molecular fluids, diatomic, struct. and dynamics 80−38889
molecular fluids, free energy, computer simulation and quantum corrections 80−28905
molecular fluids, Lennard-Jones interaction site, RISM theory applications 79−46532
molecular fluids, ref. system selection and average Mayer-function perturbation theory 80−38891
molecular fluids, RISM eqn., cluster theory for site site pair correl. functions 79−7536
molecular liquid, depolarised Rayleigh-Brillouin spectra, theory 79−69850
molecular liquid, mean squared torque and mean squared force, interaction energy spherical harmonic expansion 80−54093
molecular liquid, non-stoichiometric complex formation, thermodynamic equilib. consts. 77−21406
molecular liquid, orientation dependent distrib. function from NMR relax. data 77−20737
molecular liquid, orientational correlations 80−6346
molecular liquid, reorientation PAC, nonadiabatic effects 77−12274
molecular liquid, thermodynamic functions, interaction site model calc. 78−71661
molecular liquid, vibr. correl. function, dephasing and depopulation 79−99048
molecular liquid-state dipoles in weak const. elec. field, orientation relaxation *(Russian)* 78−43886
molecular liquids, corrected Enskog theory, transport props. 77−72538
molecular liquids, generalised mean field theory, thermodynamic props. 80−6332
molecular liquids, glass transition temp., press. depend. 80−49135
molecular liquids, IR absorpt. lineshape, orientation density fluctuation effects 78−48171
molecular liquids, IR spectra, calc. involving vibr. and reorientational relax. 78−48170
molecular liquids, thermodynamic perturbation theory, equilib. props. 79−64976
molecular liquids, vibr. dephasing and reson. energy transfer 78−18519
molecular liquids, vibr. line broadening, Zwanzig-Mori theory and quasi-elastic processes 78−27221
molecular liquids and solids, dissipation functions, conservation laws 77−45817
molecular motion, translational itinerant oscillator, probability density functions 78−59726
molecular motions in liquids, review and anal., hydrodynamics 80−59356
molecular orientation, cooperative, rel. to OH proton chem. shift 78−1974
molecular orientational motions, time-dependent distribution functions, pictorial representation, correlation functions 80−55021
molecular relaxation, statistical treatment, review 77−51284
molecular relaxation processes, symposium, London, England (Dec. 1976) 80−56993
molecular reorientation, autocorrelation functions 77−80400
molecular reorientation, conditional pair distrib. function, irreducible expansion, symmetries 77−47317
molecular reorientation, dielec. friction theory 78−87599
molecular reorientation, extended rotational diffusion models, unified treatment, review 77−27797
molecular reorientation, orientational autocorrelation functions, appl. to rot. Brownian motion 78−18520
molecular reorientation in fluids, stochastic differential eqns. 79−82132
molecular reorientation on C_∞ group 77−1053
molecular rot. diffusion const., mode-coupling theory 77−62458
molecular rotation and reorientation, microscopic and hydrodynamic contrib. 79−1379
molecular rotational averages, 3-dimens., tensor calc. 78−26406
molecular solvation, in polar media, continuous charge distrib. model, quantum mech. calcs. 78−68913
molecular theory of fluids, integral eqn. equivalence 79−86670
molecular vel. correl., form of freq. spectrum 77−15295
molecular vibration dephasing, hydrodynamic model 79−64968
molecular vibrational energy relax. rate 78−17764
molecule torsion angle fluctuation, correl. time for three bond chains 79−55624
moleculear liquids and liq. crysts., theory of irreversible processes 80−54125
molecules, nonrigid, orientational correlation times, tensor correlations 79−4220
molecules with internal rot., forced diffusion, correlation function 77−80402
molten metals, impurity atom diffusion, hard sphere fluid model calcs. *(Russian)* 80−49089
molten salt, ionis. equilib. instability of weakly-ionised 3-component plasma 80−10877
molten salt mixtures, transport props. *(German)* 78−80750
molten salt model, mean spherical approx. 78−63662

liquid theory continued
molten salts, compressibility hard sphere calcs. 77−51295
molten salts, density and charge fluctuations 79−55645
molten salts, transport processes by ionic dynamics, mass depend. 78−22616
monatomic fluid, collision induced light scatt., correlation function, relative radial motion contrib. 80−20647
monatomic liquid, short wavelength collective density excitations 77−84610
monatomic liquid metals, interatomic pair pots., numerical calcs. 79−55649
monatomic liquids, kinetic theory of self motion, memory function of vel. autocorrel. function 80−14986
monatomic liquids, short wavelength collective density excitation 78−30528
monolayer mobile adsorption, 2-D hard disc model, perturbational method 78−38932
monomer-dimer system with attractive interactions on square lattice, nematic ordering 80−79681
Mori theory evaluation, molecular dynamics simulation 80−92443
multicomponent electrolyte systems, velocity correl. coeffs. 78−85167
multicomponent fluid mixtures, renormalised one-chain approx. 77−11452
multicomponent system of nonspherical molecules, statistical thermodynamics in quasichemical approximation *(Russian)* 78−5995
N-particle system, Brownian dynamics with hydrodynamic interactions 78−91209
Na, dynamic struct. factor, two body interaction pot. sensitivity 78−67638
nematic liquid crystal, molecular dynamics, self-diffusion and structure 77−65946
nematic liquid crystals, equation of state, anistropic props., perturbation theory 78−67645
neopentane, molecular dynamics simulation of rough spheres 79−82137
neutron incoherent scatt. functions, non-Gaussian corrections 78−42874
non-uniform fluids, statistical mechs., spinodal decomposition and crit. interface 79−68998
nonadditive hard spheres, scaled particle theory, positive nonadditive solns. 78−79515
n-nonane, short chain mol. liquid, statistical thermodynamics 79−64974
nonelectrolyte aqueous solutions, lattice model approach 79−32876
nonelectrolyte solutions, liq. theory, review, book contrib. 77−39523
nonergodic hard parallel squares, with Maxwellian vel. distrib., mol. dynamics calcs. 80−100156
nonpolar fluids, Hamaker consts. and principle of corresponding states 78−11543
nonpolar liquid, electron absorpt. of light, one- and two-photon process probabilities *(Russian)* 77−43957
nonpolar liquids, b.p. calc. using London eqn. for dispersion energy 79−95148
nonpolar liquids, soft nonspherical repulsions, effect on props. 77−68903
nonpolar liquids, surface tension, geometric model 79−86963
nonpolar molecule substituting polar mol. in mol. dipole lattice, dielectric alignment 77−89359
nonpolar polarisable fluids, effective field of a dipole, rel. to mol. polaris. 80−79659
nonrelativistic scattering, quantum statistical theory 77−4030
nonspherical molecules, rot. and translational motion, modified Fokker-Planck equation 78−75518
nonuniform fluid state, Van der Waals theory, thermodynamics, struct. and phase stability 79−77475
nonuniform simple hard-sphere fluid, interface props., statistical mech., perturbation theory 77−84607
normal liquids, quantum field theory 78−91213
n-octane fluid, spontaneous cavitation 80−69886
one-component high density plasma at intermediate wave numbers, collective excitations 78−67314
one-component molecular solution, excess electron diffusion 78−52043
one-dimensional fluid, triangular well pot., perturbation theory 77−35455
one-dimensional system, with exponentially repulsive interactions, statistical mechanics 79−55629
open binary mixtures, fluctuation theory, entropy prod. and energy dissipation *(German)* 78−64879
optical oscillator strengths and excitation energies in liquids, solids and mols. 78−6648
order parameter model, appl. to dielec. relax. 80−108151
order parameter model, vol. and enthalpy relax. 80−88008
ordering absence in real liquids, appl. to nematic liquid crystals 78−51402
organic liquid, simple, struct. exam. and scatt. data interpret. 80−54096
organic ternary liquid systems, intermolecular interaction, US vel. meas. 80−79879
orientation autocorrelation functions of spherical Brownian particle 77−7646
orientational correlation functions for dipolar and induced dipolar absorpt. in far IR 77−11451
orientational dynamics of non-rigid three-bond chains 79−7537
orientationally ordered two-dimensional fluid phase, existence, mol. dynamics calcs. 79−73095
Ornstein-Zernike eqn., rel. to pair pots. calc. 77−1054
Ornstein-Zernike eqn. with Yukawa closure for a mixture of spherical molecules 79−27893
Ornstein-Zernike equation with Yukawa closure, mean spherical model 77−76275
Ornstein-Zernike theory of classical fluids at low temps. 78−9934
oscillations in liquid metals, vel. correl. function 77−58940
PAA, nematic, equation of state, anistropic props., perturbation theory 78−67645
packing densities for liquids, solutions and random assemblies and spheres 77−58937
pair correlation function, self-consistent calcs. for simple fluids 77−1061
pair correlations, asymptotic decay, Percus-Yevick eqn. solns. 77−47311
pair distrib. functions, modification of regular solution theory 78−67829
pair potential, Percus-Yevick and hypernetted chain approx. calcs. 77−1052
pair potential, self-consistent calcs. for simple fluids 77−1062
pair potentials determ., formulation of extended Born-Green eqn. 77−1057
paired ion model, conductance-conc. function 79−37603
particle rotation and translation in fluid with spin 77−72539

liquid theory continued
n-pentane, optical props. under press., molecular polarisability depend. on thermodynamical state 78−80312
Percus-Yevich equation, perturbation treatment, liq. structure factors 77−7641
Percus-Yevick eqn., orthonormal series expansion soln. 80−49065
Percus-Yevick equation, numerical calc. of crit. exponents 78−91212
Percus-Yevick equation, perturbation theory calcs. 78−75515
Percus-Yevick equation, square-well pot., perturbation version 78−63648
Percus-Yevick theory, liq.-gas phase transition 78−38824
perfluorocyclobutane, dense fluid, self-diffusion, shear viscosity, density, and temp. depend., NMR 77−36152
permittivity, dipolar hard sphere fluid, interaction-graph theory 79−51898
perturbation theory, props. of optimisation condition 78−38598
perturbation theory and triangular well pot. 77−47310
perturbation theory for soft core pot., radial distrib. function 80−6333
phase behavour of multicomponent fluids, method of pseudocomponents 77−59094
picosecond intramolecular dynamics in solution, Fokker Planck eqn. 80 28891
picosecond molecular dynamics and electron localisation 79−46548
polar fluid, thermodynamics and thermodynamics perturbation theory 79−41919
polar fluid of heteronuclear molecules, dielectric const. 78−84514
polar fluids, continuum theory thermodynamics 80−31691
polar fluids, fluctuations and inequalities 79−7538
polar fluids, intermol. and thermodynamic potentials, angle-depend. pot. 78−22618
polar fluids, intermol. and thermodynamic potentials, preaveraged pot. 78−22617
polar fluids, pair correl. functions, self-consistent Ornstein-Zernike approx. 77−84605
polar fluids in elec. fields, statistical mechanics 80−54085
polar liqs. permittivity, computer simulation with hard sphere point dipole pot. 80−103911
polar liquid, computer simulation, thermodynamic props., diffusion coeffs. 79−90507
polar liquid, rel. to dielec. props. in far IR range 77−85639
polar liquid solns., H bonding, dielec. theory, apparent dipole moment, chem. model 77−48671
polar liquids, elec. polarisation theory 77−4596
polar liquids, thermodynamics, electrostatic approximations using Onsager model 80−55693
polar mol. rot. relax., dielectric friction, Onsager cavity model 80−64664
polar solvent, nonlocal screening, spatial correls. calcs. 80−59361
polar systems, structure, effect of boundary conditions, Onsager models 80−44095
polar-nonpolar mixtures, pot. of mean force 79−90510
polar/nonpolar mixtures, pot. of mean force, approx. theories, clustering of solute mols. 78−26401
polarisable and deformable molecule liquid, polarisation models, dynamic and ensemble averages 79−99043
polarisable fluid, effective field of dipole 79−7540
polarisable fluid containing charged particles, mol. dynamics theory 78−91214
polarisable hard sphere fluid, thermodynamic props. 79−42277
poly-1-olefin melts, viscous flow activation energy, melt struct. 77−7654
polyatomic fluid, nonassociated, vibr. relax. density depend., simple model 80−32809
polyatomic fluid mixtures, thermodynamics, phase equilib. calcs. 79−1485
polyatomic fluids, generalised hydrodynamics 77−1055
polyatomic molecule in solution, vibr. population relax. model 78−17756
polydisperse fluid, of hard or permeable spheres, scatt. function 79−86664
polyelectrolyte, 1-1 soln., excluded vol. theory, Khun statistical segment basis 78−83716
polyelectrolyte soln., counterion condensate around line charge as δ-function, nonlinear Poisson-Boltzmann theory 80−85184
polyelectrolytes, appl. of Poisson-Boltzmann eqn. 79−77483
polyelectrolytes, translating, electrolyte friction theory 80−29194
polyelectrolytes in soln., electrostatic persistence length rel. to unified theory 78−95932
polyethylene glycol solns., US vels. rel. to mol. kinetic theory 77−72655
polyglycidyl methacrylate, soln., mol. dynamics, by spin mark method *(Russian)* 79−60260
polymer chain dynamics, in soln., computer simulation 78−83718
polymer chain in solution, mol. dynamics obs. 80−5643
polymer gelation, statistical mech. model, site-band correl. 79−34368
polymer single chain in soln., dynamical scaling exponent, renormalisation along the chain 79−10786
polymer solution, conc., rheological props., rod-like mol. model 78−75114
polymer solution, configurational props. of model lattice chains under varying solvent conditions 77−89364
polymer solution, diffusion, viscosity and dynamic struct. factor, dynamic scaling theory 79−64977
polymer solution, excluded volume and intrinsic viscosity plots 77−89363
polymer solution, light scatt. aniotropy by statistical mechs. of helical worklike chains 79−99891
polymer solution, osmotic pressure, correlation functions, in grand canonical formalism 80−100159
polymer solutions, internal viscosity, in poor solvents, self-entanglements *(French)* 79−4229
polymer solutions, thermodynamics, Flory-Huggins lattice theory appls. 77−40574
polymeric liquids, Hamaker consts. and principle of corresponding states 78−11543
polymeric liquids, rheology and kinetic theory, review 78−38611
polymers, amorphous high, surface tension temp. depend., appl. of significant liquid struct. theory 80−44394
polymers, connection between Yvon-Born-Green and Kirkwood hierarchies in SCF approx. 78−42882
polymers in poor solvent, loop expansion of irreducible diagrams 80−100160
primitive model electrolytes, grand canonical Monte Carlo calculations 80−92427
primitive model electrolytes, symmetrical, canonical Monte Carlo calcs. 80−92428
principle of corresponding states, dynamic props. 77−89358

liquid theory continued
pure fluids, augmented van der Waals theory 78−18518
quantum-defect theory of heats of formation and struct. transition energies 78−55830
quasi-crystalline model, asymptotic behaviour of radial distrib. function 77−68906
quasi-crystalline model, asymptotic of radial distrib. function 79−55628
radial distribution function and structure factor, struct. diffusion model 78−51403
radial distribution functions, method of reducing termination errors 80−24332
radical pairs recombination probability in liqs., HF mag. field, reson. effect 80−93737
Raman band profile, vibr. dephasing and intermolecular interactions 80−60556
Raman band shapes in liq., rot.-vibr. coupling effect for reorientation 78−72491
randomly stirred fluid, large-distance and long-time vel. correls. calcs. 77−89361
randomly stirred fluids, energy spectra 79−41923
rare gases, liquid, long wavelength limit of liquid struct. factor, compressibility 78−67633
reacting spheres, Enskog theory of transport processes 78−35668
reaction dynamics in liqs., generalised Langevin eqn. method, chemical relax. 79−91908
real fluids, static and dynamic crit. phenomena, theory, summer school lecture series 80−6344
reference hypernetted chain equation, derivation 80−59363
relationship with paracryst. theory *(German)* 77−39552
relaxation in liquids, binary collision theory 78−6000
relaxation processes and spectra in liqs. and dense gases 77−58935
review of present understanding of liquid phase 77−7653
rigid assemblies of spheres, creeping flow translational resistance 80−54086
rigid sphere model and evaluation of surface tension of liquids 79−56040
rod-shaped molecules, restricted rot. diffusion, time correl. functions 80−79655
rotational diffusion in solvents with large characteristic lengths 79−73329
rotational relaxation, molecular hydrodynamics, long time tails 80−59357
rough hard spheres treatment of tracer diffusion 78−87798
rough sphere, rot. in bath of spheres, microscopic boundary layers 78−18521
rough sphere fluid, computer simulation comp. to stochastic models 79−82138
rough sphere fluid, mol. dynamics simulation 79−82137
rough sphere fluid, translational and rot. motion, particle roughness depend. 78−26403
rough sphere fluids, rot. correls. 78−34412
salt, molten, surface tension calcs., Fowler model modification 78−67888
scaled particle model for mixtures of hard spheres with nonadditive diameters *(German)* 79−10765
scaled particle theory for non-additive hard spheres 79−60252
scaled particle theory results for dense mixtures of convex shaped mols. 78−1969
SCF method for struct. and dynamics calcs. of simple classical liqs., appl. to Rb 77−51303
semiclassical model of vibr. energy relax. in simple liqs. and compressed fluids 80−33865
semiclassical statistical mechanics, mean field effective pair pot. 80−54087
semiclassical statistical mechanics, nonperturbative incorporation of quantum effects 79−64819
shear viscosity via periodic nonequilib. mol. dynamics 77−62660
shear wave modes and velocity correl. spectra 78−63654
sheared polymer melt, birefringence build up and relax. Lodge's rubberlike liquid model 77−54946
short-range interactions mediated by a solvent with surface adhesion 78−71973
short-range interparticle interaction potential, thermodynamic perturbation theory 77−43124
significant liquid structure theory, liquid-vapour transition, reduced eqn. of state for real fluids 79−32869
Simha-Somcynsky hole theory, eqns of state eval. of polyolefin melts 79−37807
simple classical fluid, new theory 79−99051
simple classical liquids, kinetic theory, formal justification for memory function approx. 78−87598
simple classical liquids, memory functions 79−55626
simple classical liquids, ternary correlation function, Bogolyubov method *(Russian)* 80−38888
simple classical liquids, vel. autocorrel. spectrum 79−4226
simple fluid, Coleman-Noll eqn., appl. hereditary partial differential eqn. 77−35454
simple fluid, correls. near phase transition 78−9928
simple fluid, struct. and thermodynamics, Monte Carlo calcs. 80−59365
simple fluids, hard and soft-core eqns. of state, termination temps., Kihara pot. 80−70360
simple fluids, light scatt., particle-hole model 80−60613
simple fluids, semiempirical calcs. using perturbation theory 80−28892
simple liqs. with repulsive forces, thermodynamically selfconsistent theory 80−75139
simple liquid, dynamical structure factor and Green's functions 79−4228
simple liquid, mol. dynamics study of effect of nonadditive interparticle interactions on transfer props. 77−43360
simple liquid, self-diffusion and viscosity near MP, hard sphere model *(Russian)* 77−66035
simple liquid free energy and radial distrib. function expansion rel. to fundamental system 78−26402
simple liquid intermolecular interaction, extremal values 78−87602
simple liquid with twelfth inverse power potential, density depend. of effective mass 77−68904
simple liquids, collective motion 80−24329
simple liquids, corresponding states correls. and triple point solid vol. 80−92649
simple liquids, dynamical current correls., damping functions 77−47320
simple liquids, thermodynamic props. and solubility parameters 78−2265
simple liquids, transverse mode, Maxwell relax. time 78−22622
simple soft core liquids, vel. correl. functions calcs. 79−94857
single-particle motion in a fluid, kinetic theory 79−41922
liquid theory continued
slip boundary condition, rough sphere ang. vel. correlations, hydrodynamic anal. 77−51286
Smoluchowski eqn., one-particle generalised, perturbation solution 77−27211
Smoluchowski equation, with Coulomb pot., appl. to fluoresc. quenching 78−73051
Smoluchowski equation with Coulomb pot., time-depend., soln. 78−73050
soft core model, self diffusion, glass transition 78−67634
soft potential, mean spherical model, hard core perturbation 80−24340
soft spheres binary mixtures, equilib. and non-equilib. radial distrib. functions 80−49074
soft-sphere dense fluid, bulk viscosity, nonequilib. and equilib. mol. dynamics calcs. 80−79663
soft-sphere melting transition, phase coexistence props., mol. dynamics calcs. 79−10909
soft-sphere mixture viscosity, nonequilib. mol. dynamics 80−19680
solid sphere system, struct. parameters optimisation, radial distrib. function *(Russian)* 77−72535
solute molecules in 1-dimensional fluid, forces due to solvent struct. 79−73080
solute transport in porous media, statistical theory 80−28899
solution, electronic excited state transport, Green function soln. 79−68994
solution, Gibb's excess energy, thermodynamic restrictions on analytic expression 78−27817
solution ionisation, induced ion pair separation, Coulomb cage pair 79−11811
solutions, dynamic orientational correlation functions, coupled translational-rot. diffusion model 77−84604
solvated ion dynamics, mol. theory 78−35695
solvation of large dipoles, mol. dynamics study 79−77470
solvent mediated interactions−solute size effects and predictions of mean field theory 78−75513
solvent structure, at polarisable interfaces, mol. models, review 80−59359
solvent structure, in particle interactions, short range forces 78−83709
solvent structure in particle interactions, asymptotic regime 78−83708
sorbitol, relax. processes, optical probe obs. 79−47430
spectral linewidth, vibr. dephasing and gas-liq. crit. density fluctuations 79−51954
spherical Brownian particles, interacting, wave vector dependent mutual diffusion 79−44859
spherical molecules, depolarised light scatt., shaped cavity theory 79−82987
spherical particles, hydrodynamic interaction, translational, rot. and translational-rot. diffusion 78−26405
spinodal curve, exptl. verification 79−55625
spinodal decomposition, of Lennard-Jones fluid, microscopic theory 79−99046
square well+hard core fluid, quantum corrections 79−7535
square well fluid, eqn. of state well width depend., Monte Carlo calc. 80−64853
square well molecule system, below triple point, Yvon-Born-Green eqn. soln. 79−32872
square-well+Sutherland (∞,6) fluid, perturbation theory 77−11455
square-well fluid, eqn. of state and thermodynamic props. 77−7834
square-well fluid, using corrected integral eqns. 78−79511
square-well fluid, viscosity below critical density, molecular dynamical calcs. 80−79661
square-well liquids, equation of state, acoustic properties 79−99270
square-well potential liquid, struct., transport props. 77−7643
stability limit at low temp. 79−7539
statistical mechanics of nonspherical mols., hard-core models 77−51288
statistical physics of liquids, possible modification of perturbation theory *(Russian)* 77−1056
Stockmayer and Lennard-Jones pot. parameters, crit. evaluation, correl. methods 78−1966
Stockmayer fluids with dipoles and quadrupoles, spherical harmonic coeffs., dielec. const. and Kerr factor calcs. 80−84678
Stockmayer molecular fluid, 2-dimens., permittivity and dynamic props. 80−103910
structure factor asymptotic form 77−7651
structure factor extrapolation into low-angle scatt. region 77−51289
structure of the BBGKY hierarchy near phase transition 80−88013
supercooled liquid, long wavelength density fluctuations 79−90515
superionic conductors, hard sphere fluid model 80−44363
surface, atomic processes, book contrib. 79−60605
surface energy of simple liq., nonadditivity contrib. 78−18874
surface of molten salt, Fowler model, electroneutrality correction 79−28174
surface response to intense laser pulse, hydrodynamic anal. 77−24468
surface tension, kinetic tunnel model 78−56022
surface tension, statistical mechanical theory 79−82414
surface tension and width, density functional theory, appl. to liq. metals 80−103537
surface tension at triple point, and bulk modulus, theoretical relationship 78−47638
surface tension of hard sphere fluid, wall 79−73081
symmetric molecular simple liq., anisotropic light scatt., correlation function calc. 77−12356
symmetric top molecule, angular velocity correlation function, from angular position correlation functions 79−86661
Te, liquid, structure metallic constituent calcs. hard sphere model *(Russian)* 80−24349
tetrahedral mol. fluids, collision induced light scatt. intensity 80−103955
thermodynamic properties of simple fluid in hard-sphere reference system 77−76575
thermodynamic props. in terms of Lebowitz variables 79−7702
thermodynamic results for simple fluids with various pots. *(Spanish)* 77−72533
thermodynamic stability and crit. points, comparison with ferromagnets 78−16766
thermodynamically self-consistent theories, radial distrib. function, functional derivative 80−92435
thermodynamics, Riemannian geometric model, appl. to pure fluid 80−17910
time-dependent pair distrib. function, const. accel. approx. 80−59362
topological cell model in two dimens., correl. functions 79−41924
transition metal, amorphous and liq. state, simulated model 79−14733

liquid theory continued
transition metal, electronic states densities from struct. and entropy data 77−1347
transverse correlations in simple liqs., effective field approach 79−82135
triangular well potential, optimised cluster theory 80−70101
triangular-potential fluid, Zwanzig's perturbation theory, appl. to thermodynamic props. 79−41920
trichloromethane-d_1, in nonpolar solvents, vibrational and rotational relax. 79−10182
triethylamine/alcohol mixtures, AB interactions and sound vels. theory 78−18706
triethylamine/phenol mixtures, AB interactions and sound vels. theory 78−18706
triplet correlations, book contrib. 79−60251
trypsin inhibitor, mol. dynamics, computer simulation 78−9932
two fluids model of simple liquid 79−37605
two-centre Lennard-Jones liquids, free energy, perturbation theory 80−79656
two-component molecular solution, excess electron diffusion 78−52043
two-dimensional Born-Green-Yvon and other integral eqns. 77−89354
two-dimensional fluid, with 12-6 pot., fourth virial coeff. 78−59723
two-dimensional itinerant oscillator model testing by molecular dynamics 79−32868
two-dimensional square well fluid, anal. eqns. for compressibility factor 79−77664
two-dimensional system of diatomic mols., time correl. functions 78−9929
two-molecular-weight liquid, universal reduced glass transition temp. 80−38895
universal intermolecular interactions, semiempirical pot. derivation using continual model assumptions *(Russian)* 79−90514
unsymmetrical electrolytes, highly charged hard sphere model, HNC approx. 78−23969
validity, agreement with pertinent experimental fact 80−38881
Van der Waals, space correlation functions of particle numbers and energy densities *(Russian)* 78−1971
van der Waals fluid, transport props., shear viscosity calcs. 77−35738
van der Waals liq., statistical theory of viscoelastic relax. 77−68907
Van Hove correlation function, convolution approximation 79−82136
vapour pressure, temp. depend. two-parameter eqn. based on kinetic theory of fluids 77−89520
vapour-liquid equilib., perturbation theory of convex end mol. fluids 79−90769
velocity autocorrelation from memory function, hard-sphere and square well pots. 80−28893
velocity autocorrelation function, longitudinal modes and tranverse modes in liquids 78−94954
velocity autocorrelation function, modified Alder-Wainwright model 77−51293
vibr. energy relax., nonMarkovian effects 80−74230
vibrational dephasing, polyat. mols. in condensed phases, intermol. energy exchange mechanism 78−74737
vibrational relax., line widths, intermol. forces dephasing 77−47315
vibrational relaxation in liqs., hydrodynamic theory 77−35734
virial series divergence for hard discs and spheres at closest packing 79−94859
viscosity, simple kinetic model 78−55793
viscosity mechanism, in simple liquids and gases, interrelation *(Russian)* 78−67846
viscous flow mechanism, simple liquids, Ree Eyring theory extension 77−31794
viscous fluids, local order theory and light scatt., depolarised and polarised spectra 80−45093
viscous liquids, relax. processes, optical probe obs. 79−47430
water, and ionic dissoc. products, polarisation model 78−91216
water, cooperative effects importance in computer simulation calcs. 80−28906
water, force bias Monte Carlo simulation 79−77487
water, Ising lattice model with directional bonding, renormalisation group study 80−28894
water, liq., internal press. isobars, anomaly short-range order influence 77−65944
water, liq., Monte Carlo simulation, convergence of new algorithm 78−63649
water, long range forces in mol. dynamics calcs. 78−79517
water, Monte Carlo simulation of isothermal-isobaric ensemble 78−30530
water, optical props. under press., molecular polarisability depend. on thermodynamical state 78−80312
water, random network model, entropy calc. 80−64870
water, random network model, liq. and ice polymorphs enthalpy and heat content 80−64869
water, simulation, Monte-Carlo method, 1 g cm^{-3}, 300K, using Rahman Stillinger ST2 pot. 77−51290
water, single-particle motions 79−1385
water, structure, liq. theory, review, book contrib. 77−39525
water, structure, theory based on quasi-component distrib. functions 78−38606
water, Van der Waals interaction, Kramers-Kronig eqn. with full spectral data vs. oscillator model approx. 78−5998
water and dil. aq. solns., statistical mech., book contrib. 79−60250
water interface, mol. orientation and surface pot. at 4°C 80−15339
water liq., struct. relax. time in 2-state model, 0-100°C 80−1914
water-ethanol mixtures, hydrophobic interaction, scaled particle theory 78−22625
Yukawa fluid, fluid-solid interface 80−38883
Yukawa fluid, hard planar wall interactions with exponential tail, mean spherical approx. 80−38884
Yukawa fluid used as reference system in perturbation theory 80−6334
zero sound, in classical liq., excitation, damping, memory function approach 78−67771
Zwanzig perturbation expansion convergence, free energy 77−76274
Al, longit. current spectra calc. 79−82143
Ar, current fluctuation spectra 78−42888
Ar, dense fluid, viscosity, gaussian memory function approach 80−28904
Ar, depolarised Rayleigh scatt., mol. dynamics calcs., fluid density effects 80−24123
Ar, diffusion coefficient for model potentials through mean square displacement 80−70098
Ar, fluid, light scatt., collision-induced, line-shape theory and mol. dynamics 79−41921

liquid theory continued
Ar, fluid, vel. autocorrel. functions calcs. 77−58944
Ar, hole theory, compressional viscosity and vibrational relaxation 80−70311
Ar, liq., atomic correls., three-body interactions effects calcs. 77−84618
Ar, liq., compressed, excess electron mobility theory 80−80338
Ar, liq., elastic modulus and stress relaxation 79−19304
Ar, liq., equation of state studied using statistical theory results 80−84276
Ar, liq., mol. vel. correls. 77−19862
Ar, liq., numerical anal. of density fluctuations 78−21051
Ar, liq., numerical anal. of transverse current correl. 78−21052
Ar, liq., quasi cryst. model, radial distrib. function 79−19135
Ar, liq., reduced hard core dias. from compressibility, viscosity and freezing data, Lindemann laws 77−39521
Ar, liquid, binary non-additive particle interaction, self diffusion and at. motion, mol. dynamics method 80−59372
Ar, liquid, depolarized Rayleigh scatt. at triple point, mol. dynamics simulation 80−60617
Ar liquid, vel. correl. function, memory function calcs. 80−49081
Ar, longitudinal modes, transverse modes and vel. correls. 79−94858
Ar, mol. dynamics calc. 77−19857
Ar, neutron incoherent scatt. functions, non-Gaussian corrections 78−42874
Ar, relative motions in molecular dynamics investigation 80−92439
Ar, solid-liq. transition and mech. props., modified cell theory 79−23703
Ar, surface properties of classical Lennard-Jones liquid *(Russian)* 79−77869
Ar, transverse correlations in simple liqs., effective field approach 79−82135
Ar, transverse current correl. functions 79−77489
Ar, transverse mode, Maxwell relax. time 78−22622
Ar, Van Hove correlation function, convolution approximation 79−82136
Ar, velocity autocorrelation function and freq. spectrum 79−27892
Ar-He, liq. soln., sound vel., perturbation theory *(Russian)* 77−47512
Ar-He(Kr)(Ne), solubility in Ar, and related functions, three-body forces 79−10776
$BaCl_2$ aq. soln., vel. correls., time integral calcs. 80−59360
Br_2, mol. dynamics of '2-Lennard-Jones centres' pair pot. liq. 79−73082
Br_2-Ar liquid mixture, vibr. relax., 1-D mol. dynamics study 79−73079
t-butyl chloride, dipolar liquid, far IR absorpt. rel. to Mori continued fraction for autocorrel. function 78−2875
CO_2, mol. dynamics of '2-Lennard-Jones centres' pair pot. liq. 79−73082
CS_2, liq., electronic optical Kerr effect, subpicosec. optical gating 79−46548
CS_2, liq., props. from allowed light scatt. spectra 80−25364
^{13}C spin relaxation time field-depend., time-depend. correlation times 79−61247
$CaCl_2$ aq. soln., vel. correls., time integral calcs. 80−59360
Cl_2, mol. dynamics of '2-Lennard-Jones centres' pair pot. liq. 79−73082
Cl_2, mol. liquid, mean squared torque and mean squared force, interaction energy spherical harmonic expansion 80−54093
Cu, liq., electronic structure, structured medium approx. 80−84421
CuCl, partial struct. factors, hard-sphere model calc. 77−15299
D_2O, US excess absorption and compressional viscosity, temp. depend., hole theory 77−4157
F, hard sphere model with attractive interactions 80−96434
F_2, mol. dynamics of '2-Lennard-Jones centres' pair pot. liq. 79−73082
Ga, liq. supercooled, double hard sphere model 77−43128
Ga, liquid, effective pair potential and entropy *(French)* 78−14267
H-bonded species, in soln., vibr. relax. model 78−84559
H_2, liq. slow neutron scatt. rel. to intermol. excitations, analyt. model 77−58941
H_2, metallic, struct. and forces 78−22636
HCL, fluid states, mol. dynamics simulation 80−79671
HCl aqueous soln., H^+ mobility, 15, 25, 40°C, up to 5000 atm 78−10207
HCl liq., time correlation function, computer simulation 80−79670
HCl, liq. struct. simulated by a Lennard-Jones pot. 80−1917
HCl, polar liqs. models, mol. polarisability effect 80−92444
HF, computer simulation of struct. and dynamics, assoc. system 79−86667
HF, liquid, Monte Carlo simulations 79−64967
HF, polar liqs. models, mol. polarisability effect 80−92444
H_2O, struct. and dynamics, simulation using central force pots. 78−38607
H_2O, surface tension and energy, Fowler model 80−10754
He, liquid, surface state electron lifetime, rel. with chemical potential of electron liquid 79−78028
^3He, radial distribution function for hard-sphere fermions, zero and finite temps. 78−14530
Hg, electrical and thermodynamic props. in metal-semicond. transition range 80−20144
$HgCl_2$, partial struct. factors in mol. fluid model 78−22628
K, pair correl. function and ion-ion pot. 79−50982
KCN, liq., mol. dynamics computer simulation 78−38609
KCl, molten, rot. ordered ion distrib., mol. dynamics simulation 78−22630
Kr, monolayer, on graphite (0001) liq. state model appl. 77−69185
LiBr, liq., ionic motion study using memory functions 80−10484
LiBr, liq., transport processes by ionic dynamics, isotope substitution, mass enhancement 78−22616
LiCl aq. soln., vel. correls., time integral calcs. 80−59360
LiCl-RbCl, molten, Chemla effect, mol. dynamics simulation, self exchange vel. 80−79967
N_2, dephasing of mol. vibr. related to correl. functions 78−75523
N_2, liq., ang. freq. autocorrelation function for mol. oscillator 79−90511
N_2, liq., simulation of atomic and quadrupole interactions, predictions 77−11457
N_2, liq. and glassy state, spin density and current correl. functions, computer simulation 79−14661
N_2, liquid, mol. correl. functions, effective pair pot. evaluation 80−10476
N_2, mol. liquid, mean squared torque and mean squared force, interaction energy spherical harmonic expansion 80−54093
N_2, thermodynamic props., perturbation theory with hard dumbbell reference system 80−14991
NH_4Cl, aq. soln., dynamical props., mol. dynamics simulation 80−1918
Na, diffusion coefficient for model potentials through mean square displacement 80−70098
Na, effective interionic potentials 78−91221
Na, HF expansion of memory function 77−15301

liquid theory continued
Na, liq., equilib. props., self consistent field methods calcs. 79−10767
Na, liq., transport coeffs., static struct. factor calcs. 77−7643
Na, liquid, entropy calc. using phonon theory of liquids 80−39310
Na, velocity autocorrelation function and freq. spectrum 79−27892
Na-K alloy, collective excitations, mol. dynamics calc. 80−28895
NaCl aq. soln., vel. correls., time integral calcs. 80−59360
NaCl, liq. surface, Fowler model, electroneutrality correction 79−28174
NaCl molten salt, collective dynamical props., mol. dynamics calc. 77−76292
Nb-K melts, thermodynamic characts., elec. resistivity, single parameter rigid sphere calcs. *(Russian)* 80−34410
Ne, higher order structure factors and their inverses 79−55646
Ne, mol. dynamics calc. 77−19857
Ne-Kr, partially miscible mixture, high press. mol. dynamics using Lennard-Jones pot. 79−41929
Ni, liq., electronic density of d-states, hard-sphere model and tight-binding approx. calc. 79−15065
$NiCl_2$ aqueous solution, hydration of Ni^{2+} 78−79518
O_2, liquid, mol. correl. functions, effective pair pot. evaluation 80−10476
O_3-O_2 mixture, significant struct. theory appl. to phase separation 77−51503
Pb, effective interionic potentials 78−91221
Pb, HF expansion of memory function 77−15301
Pb, paracryst. struct., coordination statistics calcs. 77−1063
Pu, hard-sphere model, phys. prop. meas. interpret., adjacent solid phase implications 77−19866
Rb, density functions, SCF method, coherent scatt. function 78−18527
Rb, effective interionic potentials 78−91221
Rb, Fokker-Planck eqn. for non-Markovian system 77−47313
Rb, HF expansion of memory function 77−15301
Rb, liq., computer-simulated, search for atomic vacancies 77−84620
Rb, liquid, vel. correl. function, memory function calcs. 80−49081
Rb, self-consistent calc. of coherent scatt. function 77−51308
Rb, shear wave modes and velocity correl. spectra 78−63654
Rb, transverse correlations in simple liqs., effective field approach 79−82135
RbBr, molten, density and charge fluctuations 79−55645
SF_6, dissolved in O_2 and Kr, cryogenic liqs., mol. motions, IR and Raman spectra 79−69823
SF_6-N_2O solution, IR and Raman rot. correl. functions, expt. and theory 79−46541
$SrCl_2$, liq., dynamic struct. factors, computer simulation 79−37611
$TlNO_3$, molten, Tl^+ self-diffusion coeff., 230-330°C 78−22878
$TlNO_3$-$LiNO_3$(KNO_3) mixtures, molten, surface tension, regular solution theory 78−71903
U, hard-sphere model, phys. prop. meas. interpret., adjacent solid phase implications 77−19866
UO_2, struct. differences between ionic and molecular fluid models 78−26423
Xe, monolyaer, on graphite (0001), liq. state appl. 77−69185

liquid-vapour transformations
see also boiling; condensation; evaporation; liquefaction of gases
acetone-benzene(cyclohexane), vap.-liq. equilibria 78−30745
acetone-chloroform-methanol system, multicomponent vapour-liquid equilibrium, direct integration of Gibbs-Duhem eqn. 79−23714
acoustic levitation technique, for phase transition studies and props. of liqs. 80−43565
alcohol-solvent, associated, excess free energy and enthalpy of mixing 78−31680
alcohols, vapour-liq. equilib. and heats of mixing, simplified group method anal. 80−96637
alkanes, vapour-liq. equilib. and heats of mixing, simplified group method anal. 80−96637
alloys, spinodal decomposition, review 80−96657
aniline+cyclohexane critical mixture, gravity-induced concentration gradients 77−28004
asymmetrical Ising model, phase transitions 80−17891
benzene, soln., light deflection, near crit. point, due to gravitational effect 78−2818
benzene-carbon tetrachloride-cyclohexane system at atmospheric pressure, isobaric-liquid equilib. data 79−46793
benzene-cyclohexane, vap.-liq. equilibria 78−30745
benzonitrile-isooctane mixture, dielec. const. near consolute point, temp. and freq. depend. meas. 80−71292
binary and ternary systems, pred. of isothermal vapour-liquid equilibria, heat of mixing, viscosity 77−31761
binary heterogeneous vapour-liquid equilibrium, student experiment demonstrating miscibility effects 77−82352
binary lattice gas, crit. phenomena, cluster expansions and transcriptions 80−4670
binary liquid mixtures, spinodal decomposition, review 80−96657
binary liquid mixtures nonidealities, optimal representation 79−42248
binary liquid-vapour equilib. data, numerical anal. 78−26675
binary mixtures, hydrostatic and external field effect, anal. 80−19929
binary mixtures, liquid-vapour equilib. data, internal consistency, automatic checking method 80−54364
binary mixtures, near critical, metastable, phase separation and nucleation and drop growth, rate eqns. 80−65232
binary mixtures an and liquid-gas transitions, model for coupling between molecule polarisation and order parameter 78−22823
binary mixtures near critical state, gravitational distrib. of thermodynamic props. *(Russian)* 80−88241
binary vapour mixtures, simulation of unsteady state behaviour of dephlegmation 79−7285
binary vapour-liquid equilibrium data, determ. and correlation 78−87781
binary vapour-liquid equilibrium experiments, design of experiments 78−14440
binary vapour-liquid equilibrium experiments, parameter estimation and consistency tests 78−14439
blurred phase transitions, effect of external factors *(Russian)* 79−19364
Bose system, with Lennard-Jones interaction pair potential, zero temp. 77−39710
n-butanol-1,1,2,2-tetrachloroethane, isobaric vapour-liquid equilibria at atmospheric pressure 79−51246
carbon tetrachloride, drops, on brass surface, Leidenfrost pt., press. effect 78−87784
carbon tetrachloride, surface study, ellipticity coeff., ellipsometric method 80−84343
catastrophe theory, appl. to eqn. of state for gas-liq. transition 77−59092

liquid-vapour transformations continued
catastrophe theory, implications for press., density and temp. 79−55864
charged fluid, gas-liq. transition theory 79−82327
chemically irreversible systems, liquid-vapour equilibrium *(Russian)* 78−3369
chemically reacting system, thermodynamics of liq.-vapour equilib. *(Russian)* 77−63947
chloroalkanes, vapour-liq. equilib. and heats of mixing, simplified group method anal. 80−96637
chloroform, crit. dynamics, nuclear relax. 78−75805
chloroform, drops, on brass surface, Leidenfrost pt., press. effect 78−87784
chloroform, liq., crit. fluctuations, proton spin relax. obs. 78−19358
clean metal surface physics, review 77−15659
conducting liquid, effect of metal-insulator transition on crit. state 80−20089
critical fluids, non-Newtonian effect and normal stress effect 80−49396
critical liquid, spectra linewidth, vibr. dephasing and density fluctuations 79−51954
critical phenomena experiments, gravity effects in fluids near the gas-liquid critical point 79−58667
critical point in 3.3 dimensions 79−7684
critical props. for pure liqs. and mixtures 80−65213
critical state conditions *(Russian)* 78−47496
dense media, Q-branch Raman scattering impact theory, collisional rotational relaxation, line broadening 79−98104
dielectric fluid, Debye absorption at crit. liq.-vapour transition 80−100322
diffusion, in critical region, appl. of E.V. Tolubinskii's integral method *(Russian)* 77−24378
dimethylsulphoxide-water-0.9 m $NaClO_4$, salt effect on vap.-liq. equilib. 79−51245
1,4-dioxane-1,1,2,2-tetrachloroethane, isobaric vapour-liquid equilibria at atmospheric pressure 79−51246
dipolar hard sphere fluid, Monte Carlo method for co-existence curve 79−99293
disperse annular flow, crit. heat transfer, liq. distrib. 79−32209
droplet model for gas above T_c and the metastable phase 78−34608
dynamic scaling and crit. point universality of fluids 80−88297
electrolyte, free surface structure, single ion hydration energies 78−26752
electrolyte, weak volatile, multicomponent aqueous solns., vapour liquid equilibria 79−51243
empirical description of liq. vapour crit. region, from coexistence data 77−27973
equation of state, nonanalytic, modification for low density limit, appl. to ethylene 79−46779
equilibria, generalised method for calc. and prediction at high press. 78−87780
equilibria prediction with aid of computer, Wilson and NRTL equations assessment 79−86883
equilibrium, appl. of differential tensimetrical titration to study *(Russian)* 80−54363
equilibrium, cell design for use below 300K and to 9 MPa press. 80−62821
equilibrium, hard-sphere equation of state 77−4181
equilibrium data reduction by maximum likelihood 79−51244
equilibrium theory, data and correlation 79−33081
ethane, coexistence curve diameter singularity, phase boundary position *(Russian)* 79−65179
ethane, gas-liquid crit. pt. region, depolarised light scatt. 78−34612
ethane, liq.-vap. coexistence curve, interferometric meas. 79−99303
ethane, liquid-vapour coexistence curve, neutron transmission exam. *(Russian)* 78−79758
ethane-n-butane-n-hexane, vap.-liq. equilib. behaviour, visual cell, for 48.3-143.5°C, up to 7619 kPa 79−46790
ethane-propane, binary mixture near crit. point, conc. fluctuation decay rate, spectrosc. obs. 77−81108
ethyl ether, nucleation press. for bubble form., dissolved N_2 effect 77−51486
ethylene, gas-liquid crit. pt. region, depolarised light scatt. 78−34612
Fermi system, with Lennard-Jones interaction pair potential zero temp. 77−39710
field-theory renormalization and critical dynamics above T_c: helium, antiferromagnets, and liquid-gas systems 78−87767
flat plate solar collector performance with fluid phase change 79−62052
flow problems, phase conversions 77−89532
fluid, ion mobility, effect of long-wavelength fluctuations 80−49393
fluid, near liq.-gas crit. pt., local order effects on dynamic props., US and light scatt. 78−67806
fluid density bibliography, temp. range exceeding 40K 80−51980
fluid phase equilibrium data, qualities of models for evaluation, representation and prediction 79−14921
fluids with polar, quadrupolar, octupolar mols., thermodynamics, vapour-liq. equilibria 78−95127
free volume, hypothesis about integrand in prediction of equilibrium *(Spanish)* 79−90767
Freons, C51-12, 113, drops, on brass surface, Leidenfrost pt., press. effect 78−87784
gas-liquid surface of penetrable sphere model, surface energy and tension 77−4249
gases, mass transfer, mag. field effects 78−63535
glasses, spinodal decomposition, review 80−96657
hard sphere fluid, Ornstein-Zernike eqn. with Yukawa closure 79−99050
hard sphere fluid, with Yukawa tail interaction 79−99304
heat of evaporation and liq.-vapour equilib., appl. to real substances 79−4409
n-hexadecane-acetone, noncritical interface near crit. end point, surface tension meas. 79−69322
high pressure, quantitative description 79−1486
high pressure experimental technique 79−42227
high pressure vapour-liquid equilibrium, phenomenological description 78−91415
high pressure vapour-liquid equilibrium quantitative description 79−14923
II-IV-V_2 semiconductors, equilib. between vapour phase and stoichiometric melt 77−11681
inert gas fluid, localised excess-electron states, quasilocalisation 80−44529
inert gas liquid independent structure model, critical point, liquid-vapour equilib., second virial coeff. *(Spanish)* 77−4031

liquid-vapour transformations continued
inhomogeneous fluid in rigid container, equilib. states stability 80−44392
interface, liq./vap., free energy theory 80−10751
interface struct. from uniformity of chemical pot. 79−60241
interface structure near hard wall 80−14983
interfacial density profiles by integral eqn. approach 77−35682
ions, mol. clustering, gaseous-condensed state, nucleation and solvation 80−28129
Ising model, spin-1 asymmetric, liquid-gas transition exam. 79−42212
isobutene, droplet nucleation from crit. gas-phase+positive ions 79−39222
isothermal, excess Gibbs free energy, general calc. method 77−89552
kinetics, pressure jump relax. method *(German)* 80−29159
lattice gas model, nonsingular diameter without particle-hole symmetry 80−88311
lattice gas model, three phase eqns. of state 78−22818
Lennard Jones fluid simulation, liq.-vap. surface density profile, fluctuation effects 77−89355
Lennard Jones system, nonphysical sampling distribs., Monte Carlo free energy estimation, umbrella sampling 77−26229
Lennard-Jones 12-6 fluid, liq.-vap. interface, density and surface tension 79−90772
Lennard-Jones fluid, phase separation by spinodal decomposition, mol. dynamics computer simulation 79−10766
Lennard-Jones pot. fluid, location of phase transition using reduced vol. 79−37826
light induced, crit. parameters *(Russian)* 77−11685
light scattering study, crit. opalescence 80−44307
liquid stability, effect of elec. field on limits 77−31764
liquid-high pressure vapour equilibrium, quantitative description 78−79736
liquid-vapour interface, fluid phase coexistence, Monte Carlo computer simulation 80−49349
liquid-vapour interface, struct. at 110K, Monte Carlo method, for Ar-like fluid 80−54477
liquid-vapour interface and stability rel. to spinodal decomposition, Cahn-Hilliard theory departure 79−77752
liquidons and gasons, continuity of state historical controversies 80−12882
LOCA, blowdown phase separation mechanics effect on containment pressure response 79−93771
meniscus, nonmonotonic motion, in asymmetric theory of scale transforms. *(Russian)* 77−28066
l-menthol, vap., homogeneous nucleation, high-temp. Becker-Doering theory predictions 78−67820
metal, critical temp. determ. by exploding wires method, liquid metal enthalpy 78−6149
metal, equation of state, isentropic expansion method 78−91414
metal damage by intense EM radiation, kinetic mechanism 77−20167
metal-H, phase transitions 80−50631
methane, fluid, electron mobility, density and temp. effects 80−10351
methane, thermal diffusivity within 0.001K of critical temp., Rayleigh scatt. obs. 78−34607
methane-ethane liq. mixture, phase equilib., heat of mixing, vol. change, data evaluation 80−15233
2-methoxyethanol-1,1,2,2-tetrachloroethane binary system, isobaric vapour-liquid equilib. data 79−46792
2-methoxyethanol-chlorobenzene binary system, isobaric vapour-liquid equilib. data 79−46792
methylcyclohexane-1,1,2,2 tetrachloroethane binary system, isobaric vapour-liquid equilib. data 79−46792
methylcyclohexane-chlorobenzene binary system, isobaric vapour-liquid equilib. data 79−46792
methylethylketone-butanol-water-isobutadiene quaternary system, isobars of liq.-vapour and liq.-liq. equil. *(German)* 79−33079
methylfluoride, anomalous behaviour of proton chemical shift in gas-liquid crit. region 78−39419
microclusters, computer simulation of nucleation and thermodynamics, mol. dynamics and Monte Carlo 78−51656
microdrop-gas phase equilib. in small system, mol. dynamics 78−95146
microheterophase state, characteristic time and size *(Russian)* 78−18740
mixture, crit. points, analogy with pure fluids 78−67819
mixture, excess Gibbs free energy, quasilattice local composition model, phase equilib. 78−31681
mixture, strongly nonideal, vap.-liq. equilib. data correlation eqn., heat of mixing 78−30763
mixtures, high-press. vap.-liq. equilib., phenomenological description, review 78−30737
mixtures, liquid-vapour equilibrium, thermodynamic props. using modified Redlich-Kwong eqn. of state 77−36775
mixtures, showing phase splitting, modified Wilson eqn., phase equilib. prediction 80−96636
mixtures, vapour-liq., equilibria, fugacity coeff. calc., pseudocritical method 77−27972
molecular dynamics of clustering near gas-liq. phase transition 78−47509
molecular fluid, computer simulation of liquid-vapour surface 80−54478
molecular vibr. freq. shift during gas-soln. phase change, intermolecular interaction pot. 77−23487
molecular vibr. freq. shift during gas-soln. phase change, Onsager-Bottcher model 77−23488
multicomponent mixtures, phase envelopes and crit. points calc. 80−54337
multicomponent mixtures, vapour-liquid equilibria predictions, statistical thermodynamic approach 77−55335
multicomponent vapour-liquid equilibrium, direct integration of Gibbs-Duhem eqn. 79−23714
natural gas mixtures, simulated, enthalpy and phase equil., correl. with modified Starling eqn. 80−61127
neopentane, critical, electron mobility, gravity effect 78−91738
NMR shielding constant, cusp-type anomaly in fluid crit. region 78−39411
non-Ising-like effects, eqn. of state, renormalisation group calc. 80−84286
nucleation, mol. dynamics theory 78−75803
nucleation theory and first order phase transition dynamics near critical points 80−84284
organic binary mixtures, with weak charge transfer interactions, thermodynamic props. 80−54360
organic compounds, crit. temps. correl. with boiling pts. 78−91421
pair correlation function of the liquid-vapour interface 79−55633
n-pentane-benzene, light scatt. of liq. near crit. vaporisation state, correl. radius 79−24328
pentane-benzene solution, vapour-liquid equilibrium study, vaporisation critical state *(Russian)* 80−79931
Percus-Yevick theory 78−38824
phase diagrams, renormalised one-chain approx., square mound reference system 77−11663
phase equilibria calculation possibilities *(German)* 79−33067
phase equilibrium, derivation and extension of UNIQUAC eqn. 79−14933
phase equilibrium, systems with components of very different volatility, total press. static method meas. 79−14922
physical-math. model, nonequilib. conds., interface and transport kinetic props. 77−62631
polyatomic substances, thermal eqns. of states *(French)* 78−91413
porous element under phase conversion and vap. superheat, steady and transient operation 77−7442
propane, saturated and compressed liq., sp. ht. 79−86898
propane, vapour-liquid and vapour-solid equilib. data, mass spectroscopic tracer pulse chromatography 80−37115
propylene, equation of state for gas-liq. transition, catastrophe theory 77−59092
pure component liquid-vapour transition, two component decorated lattice gas model 79−35650
pure components, liq.-vapour equilib. and thermodynamic props. using modified Redlich-Kwong eqn. of state 77−36775
quantum crossover effect in gas-liquid phase transition 77−7839
quantum mechanical effects, theory 80−103452
radiation-induced vaporisation of liquids, manifestation of spirodal singularities 80−2152
Rayleigh scattering linewidth near pt., simple fluid, gravity effect 77−85735
Rayleigh scattering near crit. pt., nonzero beam diameter and gravity effect 77−85737
Rayleigh scattering near crit. pt., nonzero beam diameter effect 77−85736
Redlich-Kwong, eqn. of state, modified parameters, appl. to vapour-liquid equilib. 77−39659
resonant field influence on critical parameters 77−84914
scaling equation of state derived from the pseudospinodal 80−44286
semimetal, excitonic phase and gas-liquid transition in strong mag. field 79−4514
significant liquid structure theory, liquid-vapour transition, reduced eqn. of state for real fluids 79−32869
simple fluid near crit. point, homogeneous phase sp. ht. at const. vol. 78−71832
simple fluids, order-parameter fluctuations near crit. point, Ornstein-Zernike theory 78−34416
simulation of statistical systems, homogeneous nucleation *(Russian)* 78−83934
singularity in coexistence curve diameter, non-Ising like effects 80−79929
spherical gas bubble, in nonNewtonian liquids, growth by solute diffusion 78−34677
spinodal decomposition dynamics, generalised diffusion eqn., numerical soln. 78−10193
square-well fluid, nonclassical crit. behaviour 80−44291
statistical kinetic theory, heat and mass transfer 77−20044
steam, crit. region, universality, revisions and corrections to scaling 78−38810
steam, saturated and superheated, up to 800°C, equation of state 79−14908
steam-water mixtures, reversible adiabaticity equations 79−12751
supersaturated vapour, critical clusters, theory and Monte Carlo simulation, review 80−82734
supersaturated vapour nucleation on photoexcited mols. 77−76540
surface tension, review of theory 79−77866
ternary system, bubble pt. equilib. compositions determ. from dew pt. meas. 79−77733
thermodynamic stability criterion for orthobaric volumes *(Russian)* 78−51644
thiophene- or benzene-light alcohol binary system isobaric liquid-vapour equilibrium *(Spanish)* 79−77738
transition metals, thermophysical data at high temps., submicrosecond-pulse-heating method 80−103459
trifluoromethane, dielectric const. near critical point 79−15394
US velocity in crit. region water 80−59582
Van der Waals' model, gas-liquid phase transition 78−14445
Van der Waals fluid near critical pt., transport props. 79−46537
vapour pressure, between triple and crit. pts., predictive eqn. 78−30744
vapour pressure, rel. to liq. internal press., statistical mech. 79−33094
vapour pressure, var. with temp. up to critical conditions 77−31760
vapour pressure curves for pure substances in terms of conic sections 80−44304
vapour-gas bubbles, phase-transition effects associated with oscillations 80−6133
vapour-liquid coexistence and correlations in interface 80−65212
vapour-liquid equilibria, and intermol. forces, semi-empirical approach 80−54359
vapour-liquid equilibrium, generalised one-parameter Redlich-Kwong eqn., mixtures 78−34589
vapour-liquid equilibrium, supercritical components, standard state fugacities 80−15230
vapour-liquid equilibrium, T-x meas. by semi-micro method 78−87782
water, drops, on brass surface, Leidenfrost pt., press. effect 78−87784
water, free surface struct., single ion hydration energies 78−26752
water, isentropic decompression from crustal and mantle press., thermodynamics 79−79769
water cluster evidence from phase transition changes in IR mol. absorpt. coeff. 79−10100
water in critical region, thermal cond. results analysis 77−89599
water-methanol (n-propanol), binary mixtures, nucleation 80−44305
Ar, liq., critical exponent, η, X-ray scatt. 80−92660
Ar, liq., surface properties of classical Lennard-Jones liquid *(Russian)* 79−77869
Ar, liquid, surface study, ellipticity coeff., ellipsometric method 80−84343
Ar, liquid surface thickness near crit. point 80−34180

liquid-vapour transformations continued
Ar, liquid-vapour interface, surface of tension near triple point, theory 80−100375
Ar, nucleation, thermodynamics 78−14454
Ar, pair correlation decay rate exponent, small-angle X-ray scatt. obs. 77−76293
Ar-Ne mixture in critical region, renormalised one-chain approx. 77−11452
As, elec. cond. and density meas., crit. parameters 77−47562
Au, vapour press. determ. above 3000K, by pulsed-electron-beam meas. 77−15567
CO_2, gas-liquid crit. pt. region, depolarised light scatt. 78−34612
CO_2, isentropic decompression from crustal and mantle press., thermodynamics 79−79769
CO_2, Rayleigh linewidth, vap. near crit. pt., gravitationally induced effects 79−82035
CO_2, specific heat, meas., near crit. point 77−51490
CO_2, two-scale factor universality near crit. point 78−55936
CO_2, vapour-liquid and vapour-solid equilib. data, mass spectroscopic tracer pulse chromatography 80−37115
CO_2, viscosity near liquid-vapour transition point 80−2189
CO_2-2,2-dimethylpropane, liquid, -vapour equili., 220 to 300K and 6.7 MPa 80−62821
Cs, dense plasma near saturation line elec. cond. 80−38559
Cs, liquid-vapour coexistence curve and critical exponent β 77−76538
$CuCl_2$-water solution, Nd-glass laser radiation induced vaporisation, press. history 80−2153
D-T fusion fuel, liquid-vapour equilib., Raoult's law 79−67947
H-T fusion fuel, liquid-vapour equilib., Raoult's law 79−67947
H_2 and isotopes, 4 to 30K 77−72674
p-H_2, liq.-vap. phase equilib., surface tension *(Russian)* 79−65178
H_2-Ar, liq.-vapor equilib. 83 to 141K, to 52 MPa 79−42226
H_2-N_2, liquid-vap. equilib., 63-110K and up to 57 MPa 79−55881
HBr, triple-point temp. and pressure, vapour pressure of liquid to 205K 79−7683
HCl, proton spin-lattice relax. time near liq.-vapour critical point 79−73842
HCl-H_2O, p-V-T relations up to 773K and 1500 bars 78−43096
H_2S, proton spin-lattice relax. time near liq.-vapour critical point 79−73842
He, dense gas, positive ion excess, ion-induced droplets 79−14925
He, microscopic gas-liquid like phase transition around positron 77−43322
^{3}He, equation of state and crit. exponents near liq.-vapour crit. point 80−24707
^{3}He, US dispersion and attenuation near liq.-gas crit. point 78−38897
^{3}He-^{4}He film, many body approaches to liquid-vapour transition 78−51783
^{3}He-^{4}He mixture, equation of state and crit. exponents near liq.-vapour crit. point 80−24707
$HfCl_4$-CsCl melt, equilib. phase diagram and vapour press., equilib. reaction 77−66764
Hg, expanded liquid, US vel., density depend. 78−43073
Hg, liq.-vap. interface, density profile near triple point, X-ray refl. 78−75821
Hg, liquid-vapour coexistence curve and critical exponent β 77−76538
KCl, molten, vapour-liq. interface, mol. dynamics model 80−54362
Li-LiH liq.-vap. equilib., activity coeff. 80−103468
Li-LiH system, H isotope solubility thermodynamic singularities 80−81356
N_2, viscosity near liquid-vapour transition 79−77799
N_2-Ar-O_2, liq. vap. equilib. prediction using cubic eqn. of state 78−18737
N_2-Ar-O_2 system, vapour-liq. equilib. 80−54358
N_2-O_2, vap.-low. equilib., mag. field effect 78−91429
NH_3-ethylene (propylene) mixtures, crit. curves at high-press. 79−23715
NH_3-water system, vapour-liquid equilib., thermodynamics 79−42246
N_2O_4-HNO_3-H_2O dissociating system, surface tension at liquid-vapour boundary *(Russian)* 78−47643
N_2O_4-NO mixtures, attainable superheating temp., depend. on NO conc. *(Russian)* 77−72140
Na, liq.-vapour transition at low press. 77−39669
Na vapour heat pipe performance rel. to nozzle discharge theory 78−75033
Ne, dielectric constant near liquid-vapour critical point 80−50252
Ne-H_2 mixture, liquid vapour phase equilib., sound vel., compressibility, thermodynamic perturbation theory obs. *(Russian)* 80−39306
O_2, gas, vibr. Raman spectrum, anomalous behaviour near crit. point 78−55179
SF_6, gas-liquid crit. pt. region, depolarised light scatt. 78−34612
SF_6, liq., near crit. point, optical props. meas. 77−72673
SF_6, long-range correlation length near liquid-vapour transition, Rayleigh scatt. 77−8593
SF_6, two-scale factor universality near crit. point 78−55936
SmS-GdS system, crit. effects and phase equilibria 79−7692
Xe, gas-liquid crit. pt. region, depolarised light scatt. 78−34612
Xe, liq.-vap. crit. exponents, NMR 78−18759
Xe, liquid-vapour coexisting densities, nonlinear crossover, scaling corrections 77−84913
Xe, ortho-positron quenching rate critical slowing down near gas-liquid transition 77−24907
Xe, positronium formation in Xe gas near crit. pt. 79−86091
Xe sound propag., near crit. point, theoretical anal. 77−69046
Xe, two-scale factor universality near crit. point 78−55936
$ZrCl_4$-CsCl melt, equilib. phase diagram and vapour press., equilib. reaction 77−66764

liquid waves
see also capillary waves; ocean waves; surface waves (fluid)
accompanying waves of a ship, explicit approx. from slender body theory *(French)* 78−59408
air flow separation over water waves 77−11208
aniline, liq., depolarised light scatt. from shear waves 80−97288
autooscillations, azimuthal wave type, rot. Couette flow stability loss 77−75882
Baie des Chaleurs, Gulf of St. Lawrence, waves rel. to sediments distrib. 77−64257
barotropic nondivergent shelf waves on Ghana continental shelf 78−44837
barotropic waves, large amplitude, interaction with ambient shear flow, critical modes 77−80175

liquid waves continued
Benjamin-Ono equation, internal wave solitons, linear stability 80−53802
Blasius boundary layer, sound and Tollmien-Schlichting waves 79−10578
boundary layer, laminar to turbulent transition, Tollmien Schlichting wave development *(French)* 78−38285
Boussinesq type eqn., reduction to modified Hirota eqn. 80−8804
Burgers' equation for nonlinear shallow water waves, Galerkin method soln., expansion of B-splines 78−87352
capillary wave form. on gravity water waves, model eqn., surface tension, viscosity 78−83421
capillary waves, interaction between current and wave decay 77−62265
Caspian Sea, short internal waves in near-surface thermocline *(Russian)* 78−81231
Cauchy problem for nonstationary surface waves of perfect liquid *(French)* 79−27652
caustic region, nonlinear theory for shallow water waves 77−11211
charged particle beams in liqs., elastic wave excitation, microscopic bubble acoustic emission 80−43516
S.China Sea, satellite obs. of internal wave refr. 77−64298
cnoidal, mass transport, in boundary layer second approx. 77−15049
cnoidal waves, linear stability anal. 77−68612
conducting fluid, run-off is elec. field, undamped waves 79−90271
continuously-stratified fluid of finite depth, nonstationary wave development *(Russian)* 77−39322
Couette flow, instability of longitudinal convection rolls 78−26122
counter-current two-phase flow, annuli, rod bundles, liq. film behaviour, flooding 78−59452
counter-current two-phase flow in tube, liq. film waves and flooding 78−18345
couple stress effects on wave prop. in elastic layer immersed in infinite liquid 79−1126
cylindrical waves in variable depth water 78−40578
deep water waves prod. by local disturbance 77−72314
deepwater, nonlinear, evolution of continuous wave train 78−5756
dense fluid, hydrodynamics, high freq., small wavelength 77−19860
diffraction theory appl. to free floating and moored rigid structs. 79−7321
dissipation and forces on perforated caisson breakwater 77−73760
disturbance wave speed, in conduits conveying aerated water 77−27581
double boundary layers in standing interfacial waves, mass transport velocity 77−3835
duct, horizontal, slugging onset 80−10296
Earth core, internal waves 77−91082
edge waves over trench-ridge topography adjoining straight coastline 78−44838
elastico-viscous fluid, compressible, nonperiodic wave propag. 80−43724
energy extraction by submerged reson. ducts, 2-dimens. anal. 79−50743
evanescent internal waves in rotating stratified liquid *(French)* 78−38356
exterior linear elliptic problem, numerical method, appl. to 2-dimens. wave resistance 80−28485
external disturbance transformation into boundary layer waves 80−28523
falling film flow, spatially growing three dimens. wave, annular-froth flow transition 78−14071
film, falling, wave struct., linear stability problem and Orr-Sommerfeld eqn., expt. 78−38343
film, flowing concurrently with air in horiz. duct, flow pattern 80−43774
film, free, squeezing mode relax., laser scatt. obs., rel. to colloid interaction 78−87354
film, influence of waves on mass transfer *(Russian)* 79−64677
film, ripple flow, stat. characts. 77−7408
film, thin free, stabilised with ionic surfactants, dynamics 78−87416
film flow of viscous fluid down vertical cylinder surface, long waves 77−75928
finite, amplitude disturbance, hydraulic jumps, extension of Rayleigh's approach 80−69854
finite amplitude water waves, wave action conservation eqn. 80−1612
finite depth fluids, exact one- and two-periodic wave solns. 80−53797
finite depth fluids, N-soliton soln. of higher order wave eqn. 80−48724
finite depth water with immersed vertical boundaries, surface waves 79−77151
flagellar propulsion, hydrodynamic anal. 79−53072
floating torus, analysis of oscillations due to incident waves 78−22356
flood wave propagation in channels with storage areas, diffusion eqn. 79−25277
fluid 2-component mixtures, stability conditions and wave speeds 78−30344
fluid filled viscoelastic tube, nonlinear waves, mathematical anal. 79−55395
fluid-solid dynamic interactions and wave forces, numerical treatment 79−3944
forced standing wave instability in viscous stratified fluid, stratosphere quasibiennial oscill. simulation 79−55396
forced water waves, 2-D anal. *(Chinese)* 79−18904
forces exerted on submerged circular cylinders in deep waves 80−28520
forward diffraction of Stokes waves by a thin wedge 80−92167
freesurface breakdown in rot. liq., wavelets 78−59402
gravitationally unstable propagation, rot. and streaming effects 79−37293
gravity waves, finite amplitude, in deep water, instabilities, superharmonics 78−38349
gravity waves, finite amplitude, in deep water, instabilities, subharmonics 78−38350
gravity waves, nonlinear Schrodinger eqn. exact solns. 79−77147
gravity waves, weakly nonlinear, long, on two-layer fluid 78−83419
gravity-capillary waves with edge constraints 79−68732
hot surface quenching rate, countercurrent single- and two-phase flow effects 78−59451
hydraulic lines, wave phenomena, coupled vibrations in bending and branching lines 80−14778
hydraulic lines, wave phenomena, freq. characts. between press. and flow rate 79−32669
hydraulic pressure wave propagation in plastically deforming pipe, rel. to reactor HCDA 78−8876
immersed parallel-plate duct, wave tank expts. 79−52873
immiscible incompressible fluids, interfacial convective instability, diffusional exchanges, adsorption-desorption processes 80−70504
immiscible liquid layers, Kelvin-Helmholtz instability, nonlinear wave packets 79−46289
inclined open channel, stability of permanent roll waves 80−64629

liquid waves continued
incompressible irrot. flow, water waves and Korteweg-de Vries eqns. 80−69850
inert binary mixtures, weak wave evolution, Burger's eqn. 78−90924
inertial damping collocation approx. for uncoupling fluid-struct. interaction problems 79−27655
inertial wave and flow struct. for disturbances at low Rossby number 78−22360
inertial waves frequency in rotating sectored cylinder 77−47031
infinite depth water with immersed vertical boundaries, surface waves 79−77150
inhomogeneous liquid, waves due to bottom displacements in presence of floating plates *(Russian)* 77−68606
instability zones due to acoustic pulse striking a vortex sheet on a supersonic stream 79−64689
interaction between short surface waves and long internal waves 80−48723
internal 1st class waves and Sommerfeld radiation cond. *(French)* 77−72311
internal Kelvin waves in fjord lake, obs. 78−73411
internal solitary waves in stratified flows, cubic and quadratic nonlinearity 80−69856
internal wave diffraction by vertical half plane in rotating basin *(French)* 77−68603
internal wave generation in stratified fluid collapse *(Russian)* 80−74942
internal waves, bispectra calcs. 80−53800
internal waves, generated by local disturbances in stratified fluid *(Russian)* 79−16480
internal waves, radiation by sources in exponentially stratified flow *(Russian)* 77−64300
internal waves at interface between two heavy liquids 80−14718
internal waves at interface of two water media of different densities *(Polish)* 78−38352
internal waves generated by travelling disturbance in two-layer sea *(Russian)* 78−16031
internal waves in stratified fluid, tank wall effect 80−53799
ionic liquid, long wavelength modes, longitudinal, microscopic theory 77−89239
ionic liquid, long wavelength modes, space-time correlation functions 78−9772
ionic liquid, long wavelength modes, transverse, microscopic theory 77−89238
irregular wavy flow of a liquid film down a vertical plane 80−106808
jet, circ., free shear layer transition wave development 78−94643
jet, controlled break-up, droplet prod. by imposed flow perturbation 77−68667
Keller's solitary wave, capillary force effect 77−72313
Kelvin wave diffraction from rotating channel with infinite and semi-infinite barrier 79−46331
kinematic waves, several examples *(German)* 77−72310
Korteweg-de Vries equation, recurrence phenomena of soln. 77−35153
Lake Suwa, wind driven currents, obs., numerical calcs. *(Japanese)* 77−37254
laminar to turbulent boundary layer transition, Orr-Sommerfeld eqn. eigenvalues, series representation 78−38280
linear waves, asymptotic behaviour and wave patterns construction *(Czech)* 80−69
liquid film, wave parameter meas., local electrical cond. method 77−51141
liquid film hydrodynamics and heat transfer expts. *(German)* 78−18305
liquid film stability adjacent to supersonic boundary layer 77−930
liquid flow in viscoelastic tube, wave propag. 78−9714
long water waves, stable eqns. 77−58707
long waves on film flow down inclined uneven wall 78−42623
lorenz attractor behaviour in a continuously stratified baroclinic fluid 80−83806
Love waves, propgation and attenuation in elastic solid-liquid-isotropic solid medium 80−17811
lubrication, cavity-fluid interface, wavy interface anal. 77−55059
magnetic fluid with intrinsic ang. momentum, one-dimensional nonstationary waves 80−33690
magnetohydroelectric waves in fluid dielectric 79−27703
MBBA, electrohydrodynamic instabilities, power spectra and autocorrel. in flow transitions 77−68914
MBBA, nematic liquid crystals, wave number spectrum of dissipative structures 80−38904
MHD, solitary fluid transients in rectangular ducts with transverse mag. fields 79−77288
MHD gravity-capillary waves in liq. film falling by permeable bed 78−67277
mixtures, miscible (immiscible) fluids, in closed horizontal (vertical) ducts 77−62263
molten cladding film relocation following HCDA, large wave dynamics 78−17365
momentum flux in monochromatic waves of large amplitude *(Russian)* 77−31317
monochromatic waves, obliquely incident on plane beach, instabilities 80−17275
multilayered liquid films, wave motion, governing eqn. 79−10580
non-rigid bed, water wave attenuation 80−69851
nonlinear internal wave solitons, Calogero-Moser-Sutherland N-body problem 79−27679
nonlinear internal waves, turbulence, numerical anal. 80−14721
nonlinear internal waves in channels 78−63442
nonlinear long waves on liq. layer adjacent to gas stream 77−11203
nonlinear propagation of wave-packets on fluid interfaces 77−47032
nonlinear shallow water waves, deformation, disintegration into solitons 77−84266
nonlinear shallow water waves, second order terms contrib. 77−15045
nonlinear water waves generated by an accelerated circular cylinder 79−72905
nonlinear wave groups in deep water, evolution eqns. 79−98742
nonlinear wave packets propagation, finite depth effects 79−48510
oblique instability of periodic waves in shallow water 78−63418
ocean, acoustic phase modulation by first-mode directional internal wave 77−62089
ocean, internal gravity waves, rel. to low-freq. acoustic fluctuations 77−50809
ocean, internal waves instability rel. to turbulence generation *(Russian)* 78−16022
liquid waves continued
ocean, waves rel. to rhomboidal lattice struct. on sandy beaches 77−37178
ocean, weak turbulence of internal waves *(Russian)* 77−33089
ocean internal wave obs. temperature measurement array 77−5380
ocean internal waves, damping by rough bottom *(Russian)* 78−24293
ocean internal waves, Gaussianity 77−60386
ocean internal waves, influence on sound propag. 77−14837
ocean internal waves, reson. interaction 77−45010
ocean internal waves, vertical vel. modulation of underwater sound phase 77−46852
ocean long waves, scattering at estuaries bordering continental shelf 77−78191
ocean wave height determ. by synthetic aperture radar imagery 77−70845
oceanic short-period internal gravity waves, nonstationary features rel. to thermocline oscills. *(Russian)* 78−16024
opto-acoustic antenna, floating, acoustic field statistical characts., surface waviness depend. *(Russian)* 78−1536
oscillating water column wave-energy device 79−39274
parallel flow normal modes in inviscid stratified fluid with propagation at infinity 80−24071
pipe flow, turbulence struct., wave model 77−58649
pipeline hydrodynamical resistance reduction by dynamical effects *(Ukrainian)* 79−32670
pipes, hydraulic, with nonlinear boundaries, transient waves 80−43722
piping conveying swirling liquid, free harmonic wave propagation 77−84187
plane waves, group vel. in inhomogeneous media *(Russian)* 78−5755
plates, fixed vertical in waves, hydrodynamical characteristics *(Japanese)* 79−68734
power absorption, by two independently oscillating bodies 79−52874
propulsive wave hydrodynamics 79−46330
protein solution, propagation of surface shear waves 79−77146
pulsating laminar compressible flow in cylindrical pipe with through flow 77−80216
quasiperiodic flow between rot. cylinders, second charact. mode visualisation 80−28519
quinoline, liq., depolarised light scatt. from shear waves 80−97288
refraction, lab. expts. 78−38355
regular wave interactions with body in canal, wave power absorption appl. 80−96271
resistance of ship with finite beam at low Froude numbers 77−75927
resonance in harbour, combined finite element boundary integral eqn. method 79−2633
ripple growth to swell, ang. momentum conservation explanation 80−56478
ripples, generation by parametric subharmonic reson. with sound waves 77−46849
ripples, wind-generated, gravity waves effects, Doppler meas. 77−62264
ripples on carrier waves, distrib. and steepness 80−72548
river, tidal wave propag., nonlinear model 79−5512
Rossby waves, refraction at plane interface 77−68610
Rossby waves, topographically induced, laboratory expts. and theory 77−64289
Rossby waves in parallel flow, nonlinear critical level evolution 79−27621
rotating fluids, Rossby and Kelvin waves, open boundary conditions 80−61810
sea, recording and analysing technique *(Italian)* 77−29458
sea waves, rel. to sideband struct. of scatt. sound in upward-refr. ocean 77−46847
second class internal waves and edge effects *(French)* 77−65747
semi-infinite horizontal liquid layer with free boundaries, heat convection waves 77−11187
shallow water, numerical computation of steep gravity waves 80−1615
shallow water in polygonal bottomed tank, wave motion, initial condition influence 79−50746
shallow water solitary waves, shelves and Korteweg-de Vries eqn. 80−92166
shallow water theory, solitary wave interactions 79−68728
shallow water waves, Backlund transformations as canonical transformations 78−81855
shallow water waves with quasi-periodic boundary conditions, eigensolutions of elliptic problem 80−83804
shallow water-wavess, generalised inverse scatt. problem, solitons 77−3833
shell of revolution immersed in liquid, freq. distribution function 80−69587
ship oscillation, wave-generated, numerical methods *(French)* 78−30216
ship waves, shallow water 77−11169
shoaling of finite-amplitude surface waves on water of slowly-varying depth 80−69853
short wave generation by cylinder oscillating at liquid interface 78−79331
slug formation, wave instability effects 78−14085
small amplitude, generation by obstacle placed beneath free surface of running stream of infinite depth 78−38345
small-amplitude internal waves due to an oscillatory pressure 79−72906
solid particle suspension, wave propagation *(French)* 79−46361
solitary water wave amplitude, in slowly varying channel 77−39302
solitary wave diffraction in water, amplitude and direction determ. 78−22361
solitary wave stability in shallow water 79−90270
soliton, dimensioned profile for propagation *(French)* 77−35155
soliton interaction in liq. with gas bubbles *(Russian)* 79−14419
soliton shallow water waves strong interaction in channel 78−46989
solution branching in wavy flow problem of viscous liquid with free boundary 80−14760
stability of a plane soliton to infinitesimal two-dimensional perturbations 78−83420
standing waves, large amplitude on deep water, numerical computation 80−24042
stationary oblique breaking wave, laboratory surfboard testing 77−15050
steadily progressing shallow water waves, high order cnoidal wave theory 79−94638
steady gravity-capillary waves on deep water, weakly nonlinear waves 79−77153
steep progressive gravity wave, rounded crest, transcendental eqn. 77−56643
stratified fluid, internal wave solitons, numerical computation 78−59410

liquid waves continued
stratified fluid, nonlinear reson. waves interaction 78−83418
stratified fluid, wave motion during flow around submerged body 79−77213
stratified fluid density interface, wind-wave interaction 77−62291
stratified fluid flows, transient solns. 77−35196
stratified fluid layer, propagative thermal excitations *(French)* 80−33590
stratified fluid with free surface, near field disturbance due to slender body 78−59443
stratified liquid, internal waves generated by local disturbances 79−86485
stratified liquid, plane internal waves during flow around a source-sink system *(Russian)* 77−68659
stratified liquid flow around submerged body, wave motion *(Russian)* 79−14453
stratified medium, rotating, small oscillations, internal waves 77−68664
stratified rotating liquid, waves energy relations *(Russian)* 77−27575
supercritically flowing water, upstream propagation of waves *(German)* 79−68727
surface gravity wave reflection in variable depth water 77−15051
surface waves and internal waves interaction 79−10576
surface waves on water, soliton solns. of Davey-Stewartson eqn. for long waves 78−38351
symmetric finite-amplitude rotational waves, streamfunction soln. 77−41044
three-layer flow, explosive reson. wave interactions 79−64680
Tollmien Schlichting wave, two-dimens., flat plate downstream flow field 78−38357
Tollmien-Schlichting waves, sound field 78−18090
topographic planetary waves, resonant interactions, continuously stratified fluid 78−36186
transient axisymmetric wave motions due to sources in presence of surface tension 77−72312
tsunami risk, estimation via stochastic model 77−21685
turbulence theory, review 80−4536
turbulent air/water wavy interfaces, statistical anal. using computer 77−924
turbulent shear flow, struct., water wave interaction 77−47028
two-layer fluid, dispersion relns. for internal waves *(French)* 77−68602
two-layer fluid, finite depth, solitary waves, exact stationary wave soln. to Whitham eqn. 78−22355
two-layer shallow water flow, internal and surface waves, numerical anal. 80−19472
two-phase flow, an.. of induced vibral in horizontal piping system 77−80215
underwater ridge, wave guide properties for surface waves 80−96268
unsteady long wave reflection from walls of rotating channel 77−3832
unsteady ship waves *(Russian)* 78−16032
upstream long waves in shallow channels with running water 77−25726
variable depth water, wave propag. eqns., derivation 77−15048
Venice lagoon inlets, maximum waves forecasts computation *(Italian)* 77−37205
viscoelastic layer, flow down inclined plane, finite amplitude long wave stability 79−37365
viscoelastic tube, viscous fluid wave propag., asymptotic formulae and numerical results 79−34595
viscous film, nonlinear stability w.r.t. side-band disturbances 77−75887
viscous fluid flow down inclined plane, development of roll waves 78−75160
viscous fluid flow in pipeline, wave mechanism for control *(Ukrainian)* 78−1675
viscous incompressible liquid, wave generation by radially symm. press. on free surface 78−26133
viscous liquid boundary layer, nonlinear wave growth in perturbed flow, stability 78−34107
vortex ripples 77−27544
water, capillary-gravity waves, nonlinear modulation 77−11206
water, deep, direct variational anal. of oscillatory irrotational waves *(Italian)* 78−83415
water, electronic instrument for precise meas. 78−86294
water, finite depth, half-immersed circ. cylinder, long-wave behaviour of virtual mass 80−83810
water, finite depth, half-immersed cylinder, virtual mass, integral equation method 80−87783
water, forces on sinusoidally oscillating cylinder, parametric study 79−32547
water, hot, film, wavy laminar flow down vertical plate at high surface tension numbers 79−94587
water, long wave propag. over water of lowly varying depth 77−49073
water, microwave holographic imaging 78−37861
water, response of porous elastic bed 78−67208
water jets, waves 78−5775
water of variable depth, conf., Canberra, Australia (July 1976) 78−40572
water surface roughness rel. to air flow *(Russian)* 77−70669
water wave, partial reflection by nonuniform adverse currents 79−64681
water wave diffr. and radn., numerical methods, book contrib. 78−59412
water wave diffraction by 3-D bodies, hybrid element method 78−38344
water wave generation by wind, airflow separation 77−70734
water wave initial value problem *(German)* 79−77155
water wave packet evolution, Schrodinger and Korteweg-de Vries eqn. models 79−72902
water wave propag., long-period, finite difference-element integration scheme 78−75157
water wave propag. over circular shoal, parabolic eqn. method 80−14717
water wave reflexion by permeable barrier 80−14716
water wave stability, linear theory approach 77−51068
water waves, discontinuous Steklov problem 79−98739
water waves, hybrid element method appl. 80−10258
water waves, Mach reflection from wall *(Polish)* 77−70684
water waves, nonlinear, instability to infinitesimal long-wave perturbations 78−5757
water waves, steep, surface tension effects 79−55398
water waves, viscous attenuation of mean drift 77−58710
water waves in closed channels approaching Kelvin-Helmholtz instability 77−89136
water waves in narrow channels: faster capillary waves 79−18905
water waves in varying depth, classical problems 78−38354
water waves reflection and refraction by shear currents 78−32117
wave energy dissipation by turbulence *(Chinese)* 79−81908

liquid waves continued
wave generating apparatus for a given wave spectrum *(Russian)* 79−77142
wave generator model, traction force determ., Navier-Stokes liquid motion description 79−77152
wave power absorption by oscill. body, efficiency 77−921
wave resistance due to vessel near solid walls *(Russian)* 77−55013
wave-guides, slowly-varying, acoustic and liquid wave propag. 78−4490
wave-induced oscillations in harbours of variable depth 79−4023
wind generated, flow field meas. using submerging hot wire probes 77−7483
wind waves calc. 79−14418
He II rotating, Poisson brackets and continual dynamics of vortical lattice *(Russian)* 79−73359
^{4}He flow, slow thermal wave *(Russian)* 78−56005
K, liquid, shear waves, molecular dynamics 80−44096
Na, liquid, shear waves, molecular dynamics 80−44096
$SrCl_2$, liq., dynamic struct. factors, computer simulation 79−37611

liquids
for generalities only; for specific aspects see appropriate headings see also liquid structure; liquid theory; solutions
cryogenic liquids, technique for producing uniformly charged drops 77−49733
oil, slurries, ultrasound assisted filtration 78−94504
refractometer laser detector for anal. of liquids 80−101830
US propag. velocity meas., biomedical optical computer appl. 80−28392
weightless liquid systems, acoustic manipulation in space 77−49716

LISP
physics and astronomy appls. *(Polish)* 78−61749

list processing
plasticity problem soln. by symbolic computer processing of formulae 80−17803

list processing languages *see list processing*

literature
American contemporary fiction, world view, influence of physics 79−58517
Indian scientific and technical Journals critical evaluation 80−94906
nuclear spectroscopy publications produced in USSR 80−22186
romantic movement in Denmark, influence in H.C. Oersted *(French)* 78−69955
science publication growth and assoc. problems 78−8209
scientific papers, refereeing system 77−33719
world's scientific journals, subject composition 80−36757

literature reviews *see reviews*

lithium
see also nuclei with .....
abundance determ. in weak-G band giant stars 78−53948
abundance in cosmic rays, balloon borne telescope meas. 78−40785
abundance in Luna 24 soil samples 80−67590
abundance in tektites and impact glasses 80−61799
abundances in stellar atmospheres *(Russian)* 77−64748
adion-surface interaction energy, density formalism calcs. for Al and W surfaces 78−68069
adsorption, of methyl groups, complex form., STO calcs. 77−9124
adsorption of O on (100), cluster models, ab initio HF LCAO theory 78−71978
adsorption on MgO, AES, LEED, work function, and secondary electron emission meas. 80−44407
aggregated deposit, optical props., 1-6 eV 77−66549
anharmonic props., temp. depend. 79−19340
anharmonicity and low temp. phase struct., neutron diffr. study 80−107105
anodic behaviour in aq. LiOH solns. 78−39941
in arc discharge, unipolar, influence on axial distrib. of Tl atoms 80−19656
arc lamp, heat-pipe, as spectroscopic source 80−102787
Ashcroft pseudopotential, unified study of props. 80−39239
atmospheric tracking of Li release by photometer, upper atm. daytime neutral winds obs. 79−39871
atom, 1s2s2p config. nonrelativistic energy *(Russian)* 77−75048
atom, 2P level lifetime, at. beam-laser expt. *(Russian)* 77−79575
atom, $2s^22p$ double Auger rate 80−99489
atom, $2s^2sp$ and $1s2s^2$ decay rates many-body perturbation theory calc. 79−59376
atom, $3d^2D$ level, lifetime meas., fast-beam spectroscopy 77−61714
atom, 4^2D state, fine-struct. splitting, level-crossing spectroscopy 77−83552
atom, ^2P-state, hyperfine structure, UHF and PHF methods calcs. 79−36517
atom, ^2S ground state calc. using Hylleraas-type wavefunctions 78−33418
atom, absorpt. spectra, high mag. field, quasi-Landau reson. 78−90109
atom, and isoelectronic sequence, correlated and HF electron density differences 78−46275
atom, and isoelectronic series, photoionisation resons. characts., Z depend. 77−50412
atom, and isoelectronic series, Z=10-100, L-shell energy struct. and level classification 78−55129
atom, Auger and autoionisation spectra, collisional excitation mechanisms 77−19042
atom, autoionisation spectrum, theory *(Spanish)* 79−89647
atom, autoionising states, config. decays and excitation energies 78−13475
atom, beam foil spectra, coherence meas. of light polarisation from 60 keV ions 77−71863
atom, beam-foil populations, charge state distribs., independent electron model 77−19035
atom, cooperative cascade emission 78−78659
atom, core excited states, generalised Brillouin theorem multiconfig. method 77−67993
atom, correlation energies, Hartree-Fock Hamiltonian 78−41965
atom, damping const. in acetylene-air flame, Lorentz collisions, mag. field effects 80−66805
atom, dipole (quadrupole) polarisabilities, shielding factors, using hydrodynamic analogy 80−52905
atom, dipole oscill. strength distribs., sums 78−21975
atom, dipole oscill. strength sums, dipole-dipole and dipole-quadrupole van der Waals consts. 78−9127
atom, doublet open-shell restricted SCF eqns. 79−59350

lithium continued
atom, doublet state, ionis. pots., electron affinities, using electron propagator 79−63933
atom, doubly excited states, fine and hyperfine struct. of $1s2s2p^4P^o$ state 79−3370
atom, doubly excited states, Hartree-Fock energy 79−22613
atom, effective potentials, energy levels 80−106263
atom, elastic electron scatt., momentum-transfer cross sections 79−25777
atom, electron affinity, model pot. SCF and CI calcs. 77−38609
atom, electron affinity, variation-perturbation approach 77−54513
atom, electron elastic scatt., differential cross-section, local optical pot. calcs. 77−10760
atom, electron elastic scatt., two-pot. eikonal approx. calcs. 80−99573
atom, electron excitation cross section calc., Born approx. with Slater wave functions 80−69243
atom, electron impact excitation, 15-190 eV, generalised oscill. strengths, differential cross sections 80−23556
atom, electron impact excitation, 2nd order pots. method calcs. 78−13608
atom, electron impact excitation cross sections, Vainshtein approx. 78−25721
atom, electron impact excitation of autoionis. state, ejected electron intensity 78−5352
atom, electron impact excited high-l Rydberg states 77−65535
atom, electron impact reson. transition excitation, unitarised distorted-wave polarised-orbit model 78−25710
atom, electron impact total excitation cross section, first order exchange approx. 79−31692
atom, electron scatt., elastic, adiabatic exchange approach 79−31684
atom, electron scattering, second-order pot. method calcs. 79−72419
atom, electronic excitation cross-section determ. method 77−540
atom, emission obs. using modified graphite furnace at. absorpt. spectrometer 78−31727
atom, even-parity core-excited ^2P states, accurate CI calcs. 79−54782
atom, excitation energy calc., improved virtual orbitals in extended basis function space 77−46491
atom, excited state lifetime var. along isoelectronic series, HF cal. *(French)* 77−46538
atom, excited-state lifetime meas. using disc-shaped heat-pipe oven 80−52941
atom, fine and hyperfine structure of $1s2p^2\ ^4P^e$ state, using configuration-interaction wavefunctions 79−3369
atom, Gaussian basis sets, uniform quality, ab initio calcs. 78−5116
atom, ground state, HFS 80−91699
atom, ground state, Li^+ electron capture cross sections 10-60 keV 80−48084
atom, ground state, optimised one-electron wave function 77−38597
atom, ground state, radially correl. wave functions 77−75066
atom, ground state static polarisability and hyperpolarisability, numerical SCF method 79−36567
atom, ground state wavefunction, SCF HF calc. 78−90070
atom, HFS, unrestricted and projected Hartree-Fock methods 79−63924
atom, hyperfine coupling, in ground and excited states, Green's function calcs. 77−6692
atom, hyperfine splitting and isotopic shift, Doppler-free two-photon spectroscopy 79−36592
atom, in diatomic mol., nuclear magnetic shielding LCAO MO functions and gaussian expansion calcs. 79−36548
atom, inelastic Feshbach resons., quasi projection operator calc. 80−58395
atom, isoelectronic sequence, radiative transition probabilities calcs. 77−83544
atom, isoelectronic series, model potential field, pseudopotential calcs. 79−59339
atom, isoelectronic series, quartet states, HF and CI calcs. 78−17582
atom, isotope shift in 2^2P states and spatially resolved laser-induced fluoresc. 80−14103
atom, K-edge photoabsorpt. cross section 79−10080
atom, kaonic X-rays meas., strong interaction widths, shifts, yields 77−58210
atom, lifetime measurement of D-states, by time resolved resonance fluorescence 79−63965
atom, lifetime of $1s2p^2\ ^2P$ state, radiative autoionisation 78−78665
atom, long range and temp. depend. interaction with Re surface, theory 80−59802
atom, lowest $^2P^0$ and $^4P^0$ states, variational Hylleraas-type wavefunction 79−10023
atom, microwave fine-struct., Rydberg states 78−13451
atom, min. basis of Slater-transform-Preuss functions 79−59343
atom, model pots., STO calcs. 77−408
atom, motional Stark effect in high mag. field 79−63958
atom, multiphoton ionis. at ruby laser wavelength 80−9566
atom, multipole polarisabilities, shielding factors calc., hydrodynamic analogy to quantum mechs. 77−68134
atom, muonic X-ray intensities in low-Z elements and their hydrides 80−9761
atom, optical beam foil spectra, relative level populations 80−23540
atom, optical beam-foil spectra, relative level population 80−14207
atom, optical oscill. strengths calcs. 80−91495
atom, optimised one-electron wave functions 77−38598
atom, perturbed Hartree-Fock wavefunctions for ^2S and ^2P states 79−10033
atom, photoexcitation of high levels, reson. radiation at 670.7 nm 79−783
atom, photoionis., one-electron pseudopotential calc. 79−18166
atom, photoionisation, depolarisation effects 77−83663
atom, photoionisation, two- and three-photon, calc. methods comparison 78−956
atom, photoionisation cross section meas. at 2P level 78−58637
atom, positron scattering, second-order pot. method calcs. 79−72419
atom, positronium formation in highly excited states, first Born approx. 80−58420
atom, pseudospectral dipole oscillator strength distribs. 78−50503
atom, quantum mech. energy spectra calc. using trajectory integrals 78−21838
atom, quartet states, absolute term values, CI calcs. 78−58596
atom, quartet states, transition energies, oscill. strengths, CI calcs. 78−58597
atom, resonance spectral lines, Stark broadening and shift 77−75097
atom, Rydberg state quantum defects, semiclassical calc. 77−38621

lithium continued
atom, s^2S and 2^2P states, spin-optimised SCF general spin orbitals 78−82617
atom, S and D state electron impact excitation, emission line intensity obs. 80−23560
atom, saturated three-step resonance ionisation spectroscopy 79−81189
atom, SCF electron-gas local-spin-density model including correlation 80−9488
atom, SCF ion improved virtual orbitals, excited configs. calcs. 77−10585
atom, seeded flames, excitation, laser radiation absorpt., sound vel., opto-acoustic effects obs. 80−43345
atom, seeded in acetylene-air flame, optoacoustic pulses, energy transfer from laser excited atoms 78−25490
atom, selective two-step photoionisation and isotope separation 77−71783
atom, spin magnetic moment densities, spin density functional method calcs. 77−67969
atom, two photon ionisation in presence of one photon ionisation, cross section calc. 80−83327
atom, two-photon ionis., many-body perturbation theory 79−22679
atom, two-photon ionization spectra 80−23382
atom+inert gas, quenching cross sections of alkali n^2P states, 5-100 eV 79−76505
atom ^2S, $^2P^0$ and ^2D autoionising states, positions and widths 79−26944
atom triple-dipole energy calcs. using pseudo spectral theory 78−46418
atom-positron bound states, CI-Hylleraas calcs. 77−10603
atomic beam, laser excited, surface ionis. of Ta and Re, quantum yield 79−87540
atomic beam, spin-polarisation by dual-freq. optical pumping 80−43003
atomic beam mag. reson., Ramsey patterns of field depend. transitions 77−71767
atomic beam probing of plasma, for electron density profile 78−63590
atomic cluster with attached H_2 molecule, MO study 79−76541
atomic clusters, equilib. struct. *(German)* 78−29874
atomic clusters, studied by quadrupole mass analyser 77−71900
atomic electron collision cross sections 77−42410
atomic electron scatt., polarised orbitals method modification 79−22835
atomic emission spectra in 10 to 25 nm range excited by electron-atom collision *(Russian)* 77−83526
atomic energy levels of isoelectronic series, semiempirical prediction 79−72243
atomic excited state lifetimes, differential meas. using atomic ionoluminesc. 79−13672
atomic resonant lines, wing intensities after inert gas perturbation 78−37596
atoms, classical many-body collision model incorporating Heisenberg and Pauli principles 80−63511
atoms, dispersion energy consts., dipole oscill. strength, refractivity 77−50492
atoms, laser excitation and ionisation, autoionising states obs. 77−61699
atoms, photoexcitation and ionisation cross sections, Stieltjes-Tchebycheff procedure 78−17633
atoms and ions, excited in single gas collisions, high-resolution Auger spectra 80−9717
Auger line shape KVV, energy band theory 79−43074
Auger widths of core levels calc. using diagrammatic many-body technique 77−43544
Auger widths of core levels using renormalised many-body perturbation theory 79−74033
band structure, cryst. pot. of BCC phase 77−89693
band structure, MAPW method, asymptotic behaviour of Fourier coeffs. 77−24510
batteries, high energy, solid state electrode materials 80−55836
battery, organic electrolyte secondary type, corrosion-resistant materials 79−100387
battery characts. *(German)* 79−66404
battery solid electrolyte evaluation 79−29465
battery with dissolved S and THF electrolyte, capacity, rate and rechargeability 79−100510
BCC, coherent twin boundaries and interatomic pots. 78−51558
BCC, modified tensor force model for lattice dynamics 77−35644
BCC crystal, elastic constants, thermal expansion and bulk modulus 80−6452
binding energy and atomic radius calc., effect of nonlocalised charact. of pseudopot. *(Russian)* 78−18575
binding energy and equilib. struct., pseudopot. calc. *(Russian)* 79−47037
blanket coolant for Tokamak reactor, flow resist., MHD effects 78−66423
in brines in SW.Bolivia, chemical composition and distribution 79−48479
cells, electrochemistry of amorphous V_2S_5 80−76626
cells, Pb compounds as cathode materials evaluation 78−11525
chain, linear, ab initio calcs., cryst. orbital method 79−37659
chemisorption of jellium, simple model 79−60625
chemisorption of O_2, KVV Auger spectrum of oxidised Li 77−55454
chemisorption on GaAs, charge injection into space charge layers 80−100496
classical plasma frequency in long-wavelength limit, quantum correction 80−107728
cluster, chemisorption of H, ab initio HF calcs. 77−76670
cluster, density functional calcs. 77−8031
cluster and microcrystal, matrix isolated, optical absorpt. spectra, photolysis and plasmon absorpt. 79−89820
clusters, dissociation chemisorption of H_2, ab initio SCF-MO calcs. 79−77918
coating on MgO secondary emitter, increasing of emission efficiency 78−2960
Compton defect 77−73183
Compton profile, expt., one dimens. Fourier transform 77−73187
Compton profiles in liq. and solid states 79−87520
concentration determination using nuclear track techniques 80−95504
concentrations in McDermitt Caldera, in Nevada and Oregon, geological survey 79−48478
corrosion in alkaline soln. 77−73367
cross-relaxation processes, polarised β-active nuclei 80−60431
crystal and electronic props., Hartree-Fock calcs. 79−60698
density of states, AES meas. 77−36325
density of states in K excitation spectra of solid and liq. phases 78−19601

lithium continued
deposits and potential, Quebec and Atlantic Provinces, in Canada, report 79−48481
determination, in terrestrial, meteoritic and lunar samples, rel. to cosmochemical processes 78−12111
diamond: Li, ion implantation doped, IR photocond. 80−20249
diamond:Li, electron transport character 80−92917
diamond:Li, ion implantation, Hall effect and elec. cond. meas. 80−15526
diamond:Li, ion implantation, investigation of Li^+distrib. 79−77630
diffusion, in Mo, mechanism 78−84007
diffusion in CdTe, 300°C 77−43383
diffusion in Ge single cryst., effects of ultrasound 77−69119
diffusion in Mo, W, vacancy mechanism *(Russian)* 80−70472
diffusion in silicate glasses, ion-microprobe determ. 78−53649
diffusion in WO_3 thin film, appl. of AC techniques 80−70468
dislocation behaviour, rel. to temp. between 90 and 300K 80−88146
disordered system, ab initio cryst. orbital calcs. 77−47715
elastic constants of ^{6}Li and natural Li, temp. and press. depend. 78−30692
elastic free energy meas., rel. to localised soft mode theory for martensitic transforms. 78−10159
elastic scattering amplitudes, for high energy electron scattering, by ionised atoms, numerical calcs. 80−49057
electric cells, future uses, production, and advantages 80−35659
electrical resistivity, data tables, 1-2000K 79−78072
electrical resistivity, non-alkali-metal behaviour 79−60793
electrical resistivity, soln. of Boltzmann transport eqn. 78−39090
electrical resistivity, temp. depend., anharmonic effects 78−76045
electrical resistivity, temp. depend., free energy approx., anisotropic continuum dispersive model 77−43557
electrical resistivity and thermal resist. calcs. 79−91016
electrical resistivity measurement by eddy current decay method *(Korean)* 80−27275
electrochemical behaviour, in propylene carbonate, SEM study *(French)* 78−56899
electrochemical injection kinetics into WO_3 film, LF AC meas. 80−57339
electrode, cycling behaviour in $LiAsF_6$-methyl acetate solns. 78−27769
electrode, electron microscopy, photoelectron spectroscopy, surface anal. *(French)* 80−50859
electrode, passivation layer, in $LiClO_4$-propylene carbonate solution, composition *(French)* 80−11899
electron density redistribution on passing from atom to cryst. *(Russian)* 77−66103
electron emission induced by low energy light ions 79−61482
electron microprobe local anal. of light elements, ultrasoft X-ray spectroscopy 80−99027
electron potentials and wave functions *(Russian)* 78−47688
electronic impact excitation, energy level calcs. *(Chinese)* 80−83488
electronic structure and lattice const. determ. using orthogonalised modulated plane wave method *(Ukrainian)* 79−42436
electronic thermal cond. in metal and dil. alloys 78−47764
energy and elastic constants 80−59435
energy reserves of D-T fusion, Li resources, recovery costs 78−46162
exchange current in LiCl-KCl eutectic melt at 400°C for Li-S secondary cells 80−93867
exploding wire plasma, ionisation and radiation dynamics simulation 78−83606
Fermi surface and quasiparticle props., density functional approx. 80−96771
film, adsorption on Mo (112) surface, LEED and contact pot. method 80−10794
film, band struct., appl. of extended rigorous cellular method 78−52055
film, optical absorpt. spectra, rel. to phase struct. 77−4651
film, XPS lineshapes, many body processes 78−39663
film exposed to methanol, identification of methoxide species by He(I) photoelectron spectra, MO calcs. 80−83417
film temp. depend. of K X-ray emission edge 77−32472
fine structure, 3^2D state, level crossing meas. 79−13832
fine-structure transition probability, semiclassical multichannel scatt. matrix 80−37854
first Landau spin parameter, transmission ESR obs. 77−20703
flow stability of liquid Li thin films on inclined surface 79−22458
fusion blanket, isotopic exchange equilib. for H and D 79−49845
fusion hybrid reactor blankets, constant power, Li control 79−85791
fusion reactor blanket, thermoelectric MHD 79−50806
fusion reactor blankets, chemical processing 80−32512
fusion reactor blankets, experimental model studies 77−71694
fusion reactor Li activation, laser fusion progress *(German)* 80−52783
fusion reactor Li liq., deuteron activated, shielding 80−99286
fusion reactor materials, neutron experiments for data testing 78−5023
fusion reactor T breeding blanket, T, removal from liq. K and Li by sorption onto Y 78−66411
fusion reactor wall, microexplosion of pellet, energy deposition 78−54890
fusion reactors, liquid Li, safety anal. and support facilities 80−63380
G and K-type giant stars, Li abundances 80−41819
galactic Li abundance, rel. to cosmic-ray nucleosynthesis and extragalactic matter infall rate 79−17084
gamma-ray buildup factors 80−27822
glass:Li, depth distrib. meas. using ^{7}Li(p,n)^{8}Be 77−35582
grain boundary energy calcs. 77−27892
graphite Li-intercalated, theory of order-disorder phase transitions 80−19908
ground state of solids, spin density functional method, binding energy, compressibility 80−65477
Gruneisen parameter temp. var. for BCC struct. 78−6137
heat carrier in loops, phase transition process, temp. field 79−55867
heat pipes, for thermionic convertors using Li and K working fluids 79−48153
helicon-phonon interaction for parallel wave propagation 78−64054
hyperfine interactions from β-ray spectra of recoil nuclei polarised by fast polarised beams 77−28502
ICF reactors, liquid Li 80−32431
implantation in Nb, depth profiling using ^{7}Li(p,n) reaction 77−80534
impurity and conduction electron scatt. at 4.2K *(Russian)* 77−35931
impurity in Al nuclear reactor fuel tubes, proton activation determ. 80−27741
interatomic function from phonon-dispersion curves and Heine-Abarenkov-Shaw optimised model pot. 79−19185
intercalated atoms, host lattice strain effects 80−88082
lithium continued
intercalation compound with $CrPS_4$, phys. props. 79−19788
ion beam source, negative, polarised, Heidelberg EN-Tandem accessory 78−33356
ion implantation in Ag, V, Si, and Al, depth profiles and sputtering anal. by optical spectra 77−35579
ion implantation of Si, charcts. for thin film solar cell use *(Korean)* 77−51812
ion scattering, from Ni surfaces, expts. and computer simulation 77−63511
ion soft X-ray laser, 199 Å, autoionising state effect 77−34876
ion source for mass spectrometer calibration 77−41727
ion source using surface ionisation process 80−68999
ions, 65 to 500 keV, stopping power and straggling in H_2, He, CO_2, N_2, O_2, Ne, Ar, Kr, and Xe 79−3529
isoelectronic sequence, 1s3s3p $^4p^0$ state, Hartree-Fock function, third-order energy 78−37569
isoelectronic sequence, appl. of first order model pot. for optical dipole transitions 78−25474
isoelectronic sequence, correlated and HF electron density differences 78−46275
isoelectronic sequence, doubly-excited states, relative ordering 79−31424
isoelectronic sequence, electron impact ionisation cross section 80−91688
isoelectronic sequence, Hartree-Fock eqns., perturbation calcs. 79−6846
isoelectronic sequence, ionization equilib. balance, solar and stellar atms. appl. 79−36587
isoelectronic sequence, oscill. strengths 77−3309
isoelectronic sequence, photoionisation cross section, core polarisability effects 77−57944
isoelectronic sequence, pot. energy relationships 79−22584
isoelectronic sequence, quartet states hyperfine consts., Hartree-Fock and CI calcs. 78−919
isoelectronic sequence, self-consistent relativistic density-functional theory 80−91441
isoelectronic sequence, theoretical oscillator strengths *(French)* 77−34586
isoelectronic sequence, transition probabilities, relativistic effects calcs. 77−27028
isoelectronic sequence of three electron atoms, pair correlation study 80−74096
isoelectronic sequences, screening constants, ground and excited states 78−62701
isoelectronic series, dipole polarisability, numerical Coulomb approx. 80−43199
isoelectronic series, doubly excited states, Hartree-Fock energy 79−22613
isoelectronic series, electron impact, inner shell excitation cross-sections 79−59580
isoelectronic series, hard-core pseudopotentials and struct. maps 80−44168
isoelectronic series, Hartree-Fock line strengths 78−9122
isoelectronic series, ionisation pot. relativistic corrections calc. 77−46484
isoelectronic series, relative contribution of excitation-autoionisation process 79−45850
isoelectronic series, relativistic pseudopot. appl. in HF calcs. 80−27960
isoelectronic series, transition moments, exchange and core polarisation effects 77−54531
isoelectronic series, wave functions, effective pots. and energy values 79−68182
isotope abundance, spectrographic determ. *(Chinese)* 79−68325
isotope separation by plasma centrifuge, static charcts. anal. *(Japanese)* 80−5326
isotopic comp. determ., using coincident meas. of complementary particles in ^{6}Li(p,α) and ^{7}Li(p,α) 79−5201
isotopic composition in LiCl, determ. by mass spectrometry 80−66899
kaonic X-ray spectra, strong interaction widths 77−10796
Keweenawan rhyolites, anomalous Li content 79−84252
Knight shift volume depend. 80−84663
laser, 207 Å, proposal for construction 80−43324
lasing on Balmer-α line of shock tube generated plasma ions 77−58317
lattice dynamics, cubic metal, Sharma-Joshi model, correl. exchange effects 80−10613
lattice dynamics, microscopic theory using Bloch wavefunctions 77−35648
lattice dynamics, phenomenological model 77−20017
lattice dynamics, temp. depend., 110-424K 77−20033
lattice stability, comparison of BCC and FCC struct. in tight-binding calc. 77−51632
lattice vibration modes, phenomenological calc., mon-central force model 78−38791
liquid, ^{7}Be impurity control, fusion reactor appl. 80−32466
liquid, air contamination effect on compatibility with Mo, TZM, Nb, stainless steels, Ni, Hastelloy N 78−25285
liquid, compatibility with ceramics 77−44387
liquid, diffusion in KSiAl doped W wire, effect on recrystallisation *(German)* 78−64644
liquid, elec. resistivity and thermoelec. power, orthogonalisation hole pseudopotential calc. 80−29376
liquid, electron component of entropy *(Russian)* 79−23747
liquid, electron energy states calc. *(Russian)* 79−4506
liquid, entropy and enthalpy of solution of H 78−51692
liquid, Fe alloy containers corrosion resistance properties 79−47815
liquid, fusion reactor blanket, removal of T 80−95434
liquid, fusion reactor Li cooling system, corrosion inhibition by Al additions 80−108646
liquid, getter for efficient particle removal from Tokamak 77−38411
liquid, getter for Tokamak reactors, thermal and dynamic flow props. of falls 77−38412
liquid, in laser fusion plant, systems for protective Li falls 79−85785
liquid, ion bombardment via modified ion microprobe 77−49805
liquid, ISSEC selection for fusion reactor 80−57950
liquid, nucl. spin-lattice relax. of β-emitter ^{8}Li 77−51985
liquid, O_2 pot. and O_2 distrib. coeffs. between alkali and struct. metals 80−65231
liquid, paracrystalline BCC lattice evidence 79−41942
liquid, penetration into Nb at 400°C, effect of O_2 79−11719
liquid, pure and containing dissolved N_2, reaction with rare earth oxides 79−66276
liquid, resist. and thermo-electric power using corrected parameters of Shaw model 79−19566

lithium continued
liquid, resistivity, thermoelectric power, Harrison nonlocal pseudopot. calcs. 78−23069
liquid, short-wavelength density fluctuations 79−46550
liquid, solubility of Fe, Cr, and Ni, effects of nonmetallic impurities 79−77760
liquid, solubility of Li_2C_2, for fusion reactor appls. 80−13840
liquid, solubility of Li_2O, determ. by fast neutron activation 79−42252
liquid, solubility of Li_2O by neutron activation anal. 78−11601
liquid, solubility of LiD 78−2259
liquid, solvent for LiN, LiH, LiD, elec. resists. meas. 77−47786
liquid, thermophysical properties rel. to clustering 77−1065
liquid, transverse flow around tube bundle, heat transfer 80−64537
liquid, trapping efficiency for 20 keV tritium ions 77−50290
liquid and solid states, γ-ray Compton profiles 77−48269
liquid cooled pulsed fusion reactor blanket heat transfer, numerical calc. 78−94141
liquid effect on short time strength of Nb based alloy *(Russian)* 77−25186
liquid impurity monitoring and control system for fusion reactor 80−32465
local orbital energy bands using Kohn-Sham and near Hartree-Fock exchange 78−30866
low-temperature plasma atomic level population density computation 78−71461
lunar samples, Li and halogen contents 77−60638
M-type supergiants, Li abundance in atmospheres *(Russian)* 80−72950
magnetic property volume depend., Knight shifts, electron spin response 80−88729
magnetic susceptibility, 3.7-294K *(German)* 78−68156
main-sequence stars, Li, Be and B abundances rel. to envelopes hydrodynamical instabilities 78−93202
martensitic phase transformation in single cryst., US attenuation and vel. measurements 80−75358
martensitic phase transitions, and phase diagrams at moderate press. 78−72775
mechanical ideal strength, pseudopot. model calcs. 79−77670
melt, corrosion of refractory oxides 77−44378
melt, in contact with steel, mutual indentation *(Russian)* 77−59853
melt, interaction with Ti-O alloys *(Russian)* 78−11396
melting at high pressures, thermodynamics 78−91426
melting thermodynamics *(Russian)* 78−71840
mesic atom, X-ray radiation anisotropy, suppression coeffs. *(Russian)* 78−22058
mesoatoms, π^-, μ^-, K^-, p^- atoms, energy spectra, wave functions *(Russian)* 78−55264
metallic, obs. of intrinsic spin-lattice relax. of conduction electrons 78−10774
metallic compressibilities, general pseudopotential approach 80−54631
microwave Faraday effect, relation to CESR 79−99855
MIM struct., electron-phonon interaction function investigation by microcontact spectroscopy 79−95108
molecular laser, optically pumped, review 80−58519
molecule, circular polarisation of emission, influence of nucl. hyperfine interactions and elastic collisions 80−9635
molecule, collisional depolarisation and rot. energy transfer, laser-induced fluoresc. obs. 80−9698
molecule, dissoc. energy 77−14602
molecule, dissoc. energy 77−14603
molecule, ground state, determination and use of molecular α values in MSXα calcs., MTXα$_R$ meth. 79−10032
molecule, isotope fractionation, two step photoionization, due to Ar laser beam 78−25631
molecule, Li_2, Li_3(g), thermochem. props. 77−21410
molecule, pot. energy curves, bound states 77−88409
molten, estimate of diffusion coeff. of Pb 79−93828
molten , corrosion of Nb-Zr-O alloys *(Russian)* 78−31567
natural isotope ratio, spectroscopic determ. *(Russian)* 78−23996
NMR, thermal mixing rate calc. 78−10795
nuclear double resonance, cross relax. rates between ^{7}Li and ^{6}Li 77−40153
nuclear target, evaporation preparation 80−23224
occurrence in flint clay and related rock types in United States, preliminary survey 79−48475
optical constants, Kramers-Kronig anal., 0.5-10.7 eV 77−40201
optical properties by spectroscopic ellipsometry, review 80−103929
ores in Horse Spring Formation Miocene rocks, Clark County, Nevada, report 79−48474
ores in United Kingdom, brief assessment 79−48476
ores resource evaluation, United States Geological Survey role 79−48477
p-i-n struct. in Ge, Li ion drift thermal profile 77−51813
pacemaker battery similarities and differences 77−81737
particle size distrib. meas. by SEM 80−101775
Pauli susceptibility meas. by CESR method 79−42735
Pauli susceptibility meas. by CESR transmission 79−61217
pegmatite ores in Tanco mine area, SE.Manitoba, in Canada, exploration methods 79−48577
pegmatite ores in Western Superior Province, in Canadian Shield, distribution and petrogenesis 79−48480
phonon cross-over, model 79−60445
phonon dispersion, calc. using electron fluid model 78−75738
phonon dispersion curve crossing in (ξ00) direction 78−38795
phonon dispersion curve crossing in [ξ00] direction 77−59078
phonon frequency, liquid electrical resist. and interionic pair potential 78−10140
phonon limited resistivity struct. depend., Umklapp scatt., elastic consts. 80−88532
phonon spectra, variable-form pot. calcs. 78−2209
phonon spectral density, pseudopotential calcs. 80−39234
phonon spectrum, calc. from band structure 78−6134
photostimulated thermal diffusion in Si using concentrated solar rays 77−51544
plasma, dense, in arc, elec. and heat conds., two-probe diagnostics 80−38560
plasma, elec. cond. at 12.5-50 MPa, (7-50)×10^{3}K 80−64685
plasma, electrode pot. layer characts., surface ionisation and Schottky effects 77−15260
plasma, exploding wire, holographic interferometry, self pinching, charge density 79−77436
plasma, fully ionized dense, hollow cathode arc, V-I characts. and other props. 79−14627
lithium continued
plasma, ion density, soft X-ray absorpt. obs. 77−1015
plasma, low-temp. nonequilib. plasma flux, ionis. rate const. 77−47143
plasma, nonequilib., excited levels populations meas. *(Russian)* 77−62349
plasma, spectrum profiles, line broadening parameters at different intensities 78−86820
plasma conductivity, effect of elastic electron scatt. by at. excited states 78−42715
plasma jet, moving, and discharge, ion sound dissemination 80−38707
plasmon dispersion effect in (e,2e) process with atomic electron knockout 80−2904
plasmon linewidth, k-dependent, anomalous behaviour explanation, interband transitions 78−47721
plasmon satellite struct. in (e,2e) process 80−96809
point contacts, current-voltage characts. at liq. He temps. 80−39663
polarised intense Li-ion source proposal 79−63853
precipitates in MgO, orientation relationship and struct. 79−82342
precipitation of $Al(OH)_3$ from solutions containing lithium ions, X-ray diffr. pattern and comp. determ. 80−76502
primary batteries, cathodic props. of metallic oxysalts 80−3502
primary cells with Ag_2SeO_4 and Ag_2TeO_4 as cathodes, performance determination 79−52918
proton activiation analysis of B and Li local levels in minerals, rocks and ores 79−74477
pseudopotential wavefunctions calc. 77−43542
quartz:Ti^{3+} (Li), ENDOR 77−90067
reactions with dissolved salts in fusion reactor regime 80−32464
red cell membrane, Li transport in manic depressives 80−61525
reduction of Al_2O_3, Y_2O_3, Si_2O_3, in Li vapour, 1800-2500K, thermodynamics 77−90595
requirements for fusion power plants, survey 79−45401
reserves, estimates of economically recoverable resources for nuclear fusion appls. 80−52788
resources, conf., Corning, USA (Oct. 1977) 79−48473
resources, Yellowknife area, in NW.Canada, report 79−48482
resources and potentials, NW.Ontario, Manitoba, Saskatchewan, in Canada, estimation 79−48483
Righi-Leduc and Hall coeffs. meas., 2 to 120K 77−66156
screening of light impurities 77−85177
second virial coeffs., Konowalow MCSCF potential calcs. 80−23312
secondary cells, solid cathode, Li closoboranes as electrolytes 80−108794
Soft X-ray emission edge self absorption and effect of exciting voltage 77−90220
soft X-ray spectra, phonon broadening calc. 77−63526
solar white light flares, Li prod. in chromosphere and photosphere 77−71092
solenoid, partially disintegrated superhigh field, for fusion reactor *(Russian)* 77−7584
solution in methylamine, NMR investig. of metal-nonmetal transition 77−40142
spallative origin of Li in weak G-band stars 80−51752
spectral lines intensity and plasma parameters dependence on Li additive 80−73478
spin susceptibility and volume dependence 79−95569
sputtered excited states, secondary photon emission, role of transition probability 80−102483
sputtering, kinetic energies of sputtered excited atoms 80−66373
steel, stainless, liq. Li corrosion rate expressions, 600-1000°C 80−93682
structure stability 77−8015
submonolayer film, on W (011) or Mo (011), disordering, LEED obs. *(Russian)* 77−89655
surface (100), electronic states calc. by mixed-representation method 77−20399
surface characterization of film growth by SEM, EDS and ESCA 80−81240
surface energy, self-consistent calc. including ion pot. perturbation effect 77−8166
surface relaxation in CESR, evidence of spin lattice character 79−28615
surfaces, Van der Waals forces computation 79−15204
thermal resistivity, ideal, free-electron approx. 77−51724
thermalised positron annihilation, photon emission and spectator electron recoil, short range electron correl. determ. 80−50456
thermodynamic props. at high press. *(Russian)* 78−47536
Tokamak breeding blankets, T breeding perform. comparative eval. 80−95398
trap for liquefied Ar purification, ionisation chamber appl. 80−47814
Tunguska event, 1908, egregious theory involving Li meteorite nuclear explosion 79−21229
twin boundaries, computer simulation 80−39109
vacancy form. energy, math. model 77−51369
vacancy formation energies calc. 79−82197
vacancy formation energy calcs., electron density functional method 80−19801
valence band Auger spectra, surface effect 80−80915
vapour, absorpt. spectra 79−21509
vapour, coherent two photon reson. third and fifth harmonic VUV generation 79−72627
vapour, fluoresc., scan of $2^2S \rightarrow 6^2P$ transition using freq. summed UV radiation 79−55182
vapour, laser beam photoionisation, cross-section obs. by absorpt. spectroscopy 77−71782
vapour, multiphoton absorption, space-charge ion detect. 79−54827
vapour, two-photon coherent propag., third harmonic generation 78−30020
wire, NMR line shape, eddy current effect in presence of self-diffusion 80−54955
wire, optical meas. of laser detonated shock meas. 78−42798
X-ray absorption and emission edges, one-electron and many-body effects 80−25484
X-ray edge spectra, phonon broadening 77−77279
X-ray emission, incomplete phonon relax. calc. 77−52202
X-ray emission and absorpt. edges, temp. depend. 78−31282
X-ray emission spectrum, one-electron band approx. calcs. 78−80437
X-ray inelastic scatt. for $k \gtrsim 2k_F$ plasmon dispersion relation 79−15557
X-ray K-edge transitions, band theory 77−16426
X-ray scatt. factor, solid state effect 80−70163
X-ray spectra, temp. broadening 77−69936
X-ray threshold, improved compatibility relations 77−8684
X-ray threshold, K edge, exchange effects 77−4702
X-ray threshold anal. 78−31281

lithium continued
XPS core line asymmetries in muffin tin approximation 79−69953
zero-temperature equation of state, statistical model with density gradient correction 80−15215
AgBr:Li^+, correlated diffusion of impurities, nuclear spin relax. meas. 80−108094
AgBr:Li^+, impurity induced IR absorpt. 80−7386
AgBr:Li^+, local mode freqs., Green's function calc. 80−39237
AgBr:Li^+, time-depend. infrared absorpt. due to Li-localised mode 79−8133
AgCl:Li^+, impurity effect on plasticity 78−14398
Al_2O_3:Li, TSEE, Li doping effects 80−80953
Ar:Li^+, interstitial interaction energy calc. 78−38692
Be:Li, ion-implanted, interstitial props. 79−37876
Be:Li, lattice location of implanted ^6Li, ion beam channelling study 79−37730
Be-Li-V, phase diagram, metallurgical aspects for fusion blanket use 80−32467
BeO:Li, ceramics, thermally stimulated exoelectron emission *(German)* 79−100028
in C stars, Li I line form. 78−65615
$CaCO_3$:Li, CO_3^{3-}-Li^+ centre, irradiated synthetic single crystal, bond angle and wave function 77−81006
$CaCO_3$:Li, synthetic calcite, $(CO_3Li)^{2-}$-Li^+ defect after X-irrad., EPR study 80−75852
CaF_2:Gd^{3+}, Li^+, elec. field gradient at nuclei on orthorhombic sites, vs. elec. zero-field splitting 79−87070
CaO:Li, thermally quenched, generation of Li^0 centres 80−50382
CaS:Bi^{3+},Li^+ phosphor, luminescence of associated centres *(French)* 80−40155
$CaSO_4$:Tm, Li, mixed field TLD 77−9263
CdS:Li, anisotropy of the absorption by impurity centers in hexagonal crystals 78−88343
CdS:Li, Auger excitation mech. of 1.6-2.0 micron luminesc. band 79−8184
CdS:Li, complex luminescence centres, recombination-stimulated conversion 80−108268
CdS:Li, donor-acceptor interactions, photochem. reactions *(Russian)* 77−40285
CdS:Li, electrodiffusion of shallow donors, photocurrent, TSC, and exciton luminesc. meas. 80−79992
CdS:Li, green edge luminesc., complex nature of centres 80−60671
CdS:Li, luminescence bands, photocurrent spectra *(Russian)* 80−60677
CdS:Li, nature of recombination centres responsible for 0.95 μm luminesc. band 77−69908
CdS:Li, photocond. characts., electron and hole traps obs. 77−8140
CdS:Li, photoconductivity, luminescence, radiative and radiationless transition mechanisms 78−10948
CdS:Li, single crystals, anisotropic luminesc. centres 80−80857
CdS:Li, subjected to elec. fields, drift of defects 80−6558
CdS:Li, TSC and optical photocurrent quenching spectra, Auger excitation of recomb. centres 79−33294
CdS:Li, thermochemical changes in microstructure of anisotropic centres, polarisation modulation method meas. 79−38027
CdS:Li chemically deposited filter, elec. props. 80−11113
CdS:Li film, chemical bath deposited, photocond. and optical props. 80−2426
CdS:Li film, optical props. 80−2886
CdS:Li film, photocond., effects of annealing, S vacancies, and O_2 adsorption 78−34854
CdS:Li lattice, location of implanted Li atoms 80−6428
CdS-Li, hexagonal crystl., orientation degeneracy of anisotropic centres, dichroism of impurity photocond. 79−73981
CdSe:Li, reson. Raman and Brillouin scatt., elastic exciton-defect scatt. 80−80788
CdTe:Li, acceptor states study by donar acceptor pair excitation luminesc. 80−100683
CdTe:Li, excitation spectrum of Li acceptor and valence band parameters 79−28795
Cr_3O_4:Li, elec. cond. and thermo-EMF 80−20231
CsBr(Cl)(I):Li, optical absorpt. investig. of F_A-centres 77−44029
CsF:Li, F-centres, saddle-point configuration, molecular model parameter 80−107234
GaAs:Li diffused, lattice imperfections, TEM 77−80521
GaAs:Si, Li, IR absorpt., microstruct., charge compensation 80−107565
GaSb:Li, dopant behaviour 77−51696
Ge:Li, determ. of drift parameters of Li 78−17509
Ge:Li, diffusion study using $^6Li(d,\alpha)$ reaction 79−5202
Ge:Li, dislocation free, anomalous transmission of X-rays *(Russian)* 77−15286
Ge:Li, long wavelength photoconductivity spectrum 77−43641
Ge:Li, shallow defects, PTIS meas. 80−24971
Ge:Li, supersaturated solid solns., decomp., surface impurity content 78−51681
Ge:Li, thermal cond., 0.4-20K, Li valley-orbit splitting 79−15111
Ge:Li,O, EPR and piezospectroscopy 80−25338
Ge:Li-O, donor complex EPR and photoelectron piezoelectric spectra, dynamic tunnelling 79−1711
Ge(Li) commercial coaxial large-volume detectors, time characts. 78−9029
Ge(Li) detector, Monte Carlo photon transport simulation 79−81122
$H+Li_2$, collinear reactions, SCF correl. diagram for Li_2H form. 77−70292
$H+Li^{3+}(Be^{4+})(B^{5+})(C^{6+})$, charge transfer cross sections, distorted wave Born approx. 79−72415
H^-+H_2(He)(Li), 50-150 keV, scatt. angle of neutral H 78−5340
n-H_2+Li^+, rot. excitation, 150-750 eV 79−45805
$He+Li^+$, 2 to 5 keV, ejected electron profile variation with impact angle 78−37729
$He+Li^+$ autoionisation, electron spectra 80−91653
$He(^1S_0)$+Na(Li) radiative Penning ionis., photoionis. cross section depend. of continuum radiation 77−19034
hexamethylphosphoramide:Li glass, metallic condensation of Wannier-Mott impurity states 78−2420
I_2:LI, doping effect on elec. cond., semicond. props. 80−49732
KBr:Li, ENDOR of F_A(Li) centre meas., 4.2 and 1.8K 77−63320
KBr:Li, F_A centres, optical detection of ESR 79−99793
KBr:Li, low temp. radiation hardening mechanism, single halogen interstitials as hardening agent, Ha annealing 79−23634
KBr:Li, low temp. radiation hardening mechanism, dislocation-halogen interstitial interaction 79−23635

lithium continued
KBr:Li, paraelectric reson. meas. 77−36190
KBr:Li, radiative recomb. of localised excitons 78−72605
KBr:Li^+, electronic struct. of $(V_Ke)_{Li}$ 78−95269
KBr(Cl):Li^+, far IR props. of lattice resonant modes, hydrostatic press. effects 77−28574
KCl:Li, 9.4 GHz pulse paraelec. reson. at zero elec. field 77−81076
KCl:Li, $(F_2^+)_A$ centres, optical props. 80−89026
KCl:Li, ⟨111⟩ off centre Li^+ under biaxial stress, bistable tunnelling 78−15090
KCl:Li, additively coloured, luminesc. material for IR region *(Russian)* 78−15209
KCl:Li, F_A-centre optical absorpt., estimate using symmetry-adapted wave functions 80−11448
KCl:Li, K band of F_A centre, perturbation treatment 78−76016
KCl:Li, microwave modulation by paraelec. reson. *(Russian)* 77−20809
KCl:Li, self-induced resonant optical rotation 79−65831
KCl:Li, tunable CW IR lasers using F-centres 77−88725
KCl:Li, tunable IR lasers with F_A(II) and F_B(II) colour centres 78−90420
KCl:Li, X-irrad., F_A centres, thermolum. studies 80−80878
KCl:Li,H optical and EPR exam. of H centre, $(LiH)^+$ absorpt. spectra 79−99920
KCl:Li $(F_2^+)_A$ centres, tunable CW laser action 80−87399
KCl:Li F_A(II) centre laser, pumped by flashlamp-pumped dye laser 80−102737
KCl:Li^+, coherent excitation by EM and acoustic waves, induction and echo signal study 78−67773
KCl:Li^+, defect induced tunnelling states, depend. on strain, pot. model calcs. 79−69865
KCl:Li^+, off to on centre defect transitions under hydrostatic press. 78−15199
KCl:Li^+, phonon generation by EM excitation, mechanism 80−2129
KCl:Li^+, press. tuning of motional behaviour in shallow off-centre pots. 79−78718
KCl:Li^+, restricted interstitial motion of $H_A(Li^+)$ centre, ESR and uniaxial stress expts. 77−48053
KCl:Li^+, shape of pot. energy well of impurity 79−23692
KCl:Li^+, single-pulse excitation of paraelectric induction and echo signals 80−80732
KCl:Li^+ F_A (II) colour-centre laser, mode locking and tunable picosecond IR pulse generation 80−43364
KCl(Br):Li^+, localised impurity modes, static lattice distortion effect 77−47530
KF:Li, F_A-centre optical absorpt., estimate using symmetry-adapted wave functions 80−11448
KF:Li^+, shape of pot. energy well of impurity 79−23692
$KTaO_3$:Li, ferroelec. transition and atomic motions, ^7Li NMR study 80−75872
$KTaO_3$:Li, polarised cluster stabilisation by Li defects, polar glass form. 79−91342
$KTaO_3$:Li, susceptibility extrinsic peak, dielectric const. meas. 79−11394
Li^+,Na^+:KCl(RbCl), F_A(II) to F_B(II) centre crystals, CW laser oscill. with extended tuning range 80−32997
Li clusters, DIM pot. energy hypersurfaces, stationary points 78−25763
Li core excited even parity ^2P states, fluoresc. 80−69100
Li, cryst. wave function deter., muffin-tin method 80−65436
Li cylindrical lens for high energy particle focusing, aberrations 77−14649
Li, highly excited states, electronic struct., oscillator strengths and resons., HF calcs. 77−46506
Li I, autoionising levels, electron impact excitation, ejected electron spectrum 78−9259
Li I, doubly-excited $^4P^0$ terms calcs. 78−9100
Li I, II, absorption spectra in grazing incidence region, 215-160 Å 78−5164
Li I, spectra calcs., fine struct., transition energies 77−42260
Li I 6708 Å twilight emission enhancement following rocket release 77−53255
Li I (2p-4d, 4f, 4p) line broadening in electrolytic plasma *(French)* 78−1892
Li I and Li II, beam-foil excited, 70-400 keV, relative initial populations 80−14211
Li I isoelectronic series, transition probabilities, oscill. strengths, lifetimes, branching ratios 78−33470
Li I laser, 207 Å, oscillator strengths 80−83598
Li I to Li III, beam-foil obs. of 2000-5500 Å spectra 80−9548
Li I to Ne VIII isoelectronic sequence, quartet spectra, Hylleraas method calcs. 80−9524
Li I to Ne VIII isoelectronic sequence, term level diagrams of doubly excited states 80−14093
Li I-like spectra, energy struct., accurate semiempirical formulae 79−49970
Li II, electron impact excitation, distorted wave approx. 80−91689
Li II, ground-state electron impact excitation strengths, close-coupling calcs. 80−23561
Li II, III, X-ray lasers pumped with synchroton radiation and low-energy photons 79−41371
Li III, electron ionisation cross sections of excited atoms and ions 80−43186
Li metal for battery industry, sources and preparation 80−97781
Li, one-electron calcs. of X-ray absorpt. and emission, jellium model 78−56543
Li plasma dynamic laser, using supersonic nozzle, population inversion, excitation cross section 78−50760
Li^-, core excited bound states in beam foil expts., CI calcs. 80−78559
Li^-, core-excited bound states 80−91468
Li^-, electron affinity, model pot. SCF and CI calcs. 77−38609
Li^-, optical transition between bound states, beam-foil spectrosc. obs. 80−91476
Li^-, photodetachment cross-sections and multipole polarisabilities, extended asymptotic model 78−42028
Li^- positron complex, ground and excited states theoretical studies 80−42934
Li^+, ^3P and ^3S states, fine (hyperfine) struct., dye laser saturation spectroscopy, beam expt. 80−58169
Li^+, 2^2S_1 metastable state radiative lifetime, fluoresc. meas. 80−42999
Li^+, $2(^{1,3}S)$ excited states, dynamic polarisabilities 77−34772
Li^+, $2(^{1,3}S)$ excited states and ground state, dynamic polarisabilities, van der Waals force consts. 77−34773

lithium continued
Li^+, 2p3d $^{1,3}L^0$ doubly excited state, soln. of Hartree-Fock eqns. 77−75072
Li^+, amorphous target impact, 100 keV, electronic stopping power, models comparison 78−2180
Li^+, at. fine struct. and HFS, meas. by Doppler tuned hyperfine spectrosc. 79−81292
Li^+, autoionising, and quasibound states, Feshbach calcs. 77−54505
Li^+ diffusion and ion-neutral interactions, laser sounding of upper atmosphere *(French)* 80−82115
Li^+, doubly excited autoionis. resons., laser prod. plasma absorption spectra obs. 77−50392
Li^+, dynamic multipole polarisability, functional calcs. 78−74595
Li^+, dynamic polarisability calc. 77−14599
Li^+, elastic form factors, correlated two-electron-core pots., closed form expressions 79−68195
Li^+, electron correl. effects, ang. and radial, in momentum space 77−88399
Li^+, electron impact excitation, cross-sections, modified Oppenheimer approx. 78−82843
Li^+, electron scatt., inelastic Feshbach resons., quasi projection operator calc. 80−58395
Li^+, few parameter two-electron wavefunction of ground state 77−75051
Li^+, ground state energy via correl. wave function calc. 77−23439
Li^+, H_2O affinity, ab initio SCF calcs. 80−58125
Li^+, hydrated, polarisation model, review 80−54115
Li^+ hydration, ab initio MO calcs., fractional charge model 77−34547
Li^+, imaginary frequency mutipole polarisability and long-range dispersion consts, functional calcs. 78−74596
Li^+ injection into cortical glia demonstrating glial-neural interaction 77−36905
Li^+, isoelectronic series, electron correlation and Coulomb hole in momentum space 78−86793
Li^+, low energy ion scatt. from clean Ni (110) surface 80−104026
Li^+ mobilities in gases *(Japanese)* 79−60101
Li^+, mobility and clustering in Ar gas 77−84389
Li^+ mobility in He 300K, interaction pot., drift tube meas. 77−76026
Li^+, mobility in N_2 and CO_2, obs. using injected-ion drift tube mass spectrometer 78−1784
Li^+, n=4 resonances, complex rot. meas. calcs. 79−97995
Li^+, numerical Hartree-Fock calc. of $1s^2$ ground state 79−81155
Li^+, pair polarisability, ab initio SCF MO energies 78−70741
Li^+, polarised state electron excitation, electron-photon coincidence 77−6930
Li^+ quantum defects rel. to angular momentum, nuclear charge, Coulomb-Born approx. method *(Japanese)* 77−50534
Li^+, reson. line regularities in plasma Stark widths and shifts 80−43881
Li^+, S autoionising states, appl. of at. reson. theory 80−23329
Li^+, S-autoionising states, energy calcs. 79−36520
Li^+, three-particle atomic system, binding energy, Faddeev method calcs. 77−57858
Li^{2+}, electron impact, mutual ang. and energy distribs. near ionis. threshold 79−64108
Li^{2+}, electron impact ionisation, electron ang. momentum exchange 78−78820
Li^{2+}, electron scatt. near ionis. threshold, ang. momenta 79−31698
$^6Li^+$ enrichment, countercurrent electromigration cell containing molten NH_4NO_3 78−47547
Li:NH_3, soln., free MHD convection near horizontal cylinder *(Russian)* 77−7467
Li/H_2O, surface complex form., obs. using photoelectron spectra 79−69359
Li/He heat pipe, start-up power, heat transport, thermal regulation 80−53615
Li/Li_2 supersonic nozzle beam characts. by spectroscopic techniques 78−55255
Li/Li^+/$M_yV_{1-y}S_2$ cells (M=Fe, Cr), effect of metal substitution of Li intercalation 79−100395
Li/Na ratio upper limit for novae 79−101156
Li/O_2, surface complex form. obs. using photoelectron spectra 79−69359
Li/SO_2 cells, DTA, safety studies 80−81428
Li/SO_2 cells, safety studies, DTA of constituents 80−16795
Li/SO_2 cells, safety studies, kinetics of Li-organic solvent exothermic reactions 80−72030
Li/$SOCl_2$ cells, high rate discharge characts. 80−72021
Li/$SOCl_2$ hermetic primary cells, effect of type of C on performance 80−35661
Li/$SOCl_2$ primary cell, cyclic voltammetric and coulometric obs. of $SOCl_2$ reduction 80−30440
Li/$SOCl_2$ primary cells, $SOCl_2$ reduction mech. in supporting electrolyte 80−108792
Li/Sb(Cu) interface, CESR meas. 78−80218
Li/TiS_2 cell with solvate melt, discharge characts. and lack of rechargeability 80−72022
Li-$AgCrO_4$ pacemaker cell construction 77−81739
Li-Al-FeS, high temp. battery, ceramic powder, as electrode separators 79−61966
Li-D equation of state under extreme conditions, solid state to plasma region 80−69976
Li-FeS_x molten salt battery, anodic corrosion rate of candidate current collector metals 79−100512
Li-FeS_x molten salt battery, anodic corrosion rate of candidate current collector metals 79−100513
Li-H, liq. and solid, mol. orbital approach, solvation energies 77−4201
Li-HN_3 solns., metal-insulator transition 77−1369
Li-He, oscill. strength, for induced dipole transitions, pot. energy curves 77−75100
Li-I_2, primary battery, self-discharge rates using microcalorimeter 79−61963
Li-I_2 pacemaker cell end-of-life characteristic approximation 80−30937
Li-I_2 power cell accelerated discharge test for battery longevity model 80−30938
Li-Kr, oscill. strengths, for induced dipole transitions, pot. energy curves 77−75100
Li-LiH, evaporation diagram at high liq. phase hydride concs. 77−35681
Li-LiH liq.-vap. equilib., activity coeff. 80−103468
Li-LiH system, liquid Li, dilute solns., equilib. H press., solubility, heat of soln., CTR materials 77−14266
Li-LiH system, vaporis. diagram in region of immiscibility of liq. phase 78−43113
Li-LiH two-phase equil. system, vaporis. diagram at high temps. 80−19926
Li-like atoms, $^4S^e$ doubly excited states, orbital config. assignment 79−41118
Li-like ions, electron impact excitation, config. and parentage mixing effects 77−58176
Li-like ions, fine struct. in $1s2p^2\ ^4P$ and $1s2s2p\ ^4P^0$ states 78−66471
Li-like ions, multiply charged, laser plasmas, 1.5-15 Å 78−13462
Li-like ions, partial photoionis. cross-sections and radiative recomb. rate coeffs. 80−52951
Li-like multiply charged ions, spectra, radiative corrections 79−98015
Li-methylamine soln., metal-nonmetal transition, electron and nucl. spin-lattice relax. 79−87306
Li-MnO_2 batteries development, Sanyo, with high energy densities 80−85272
Li-ND_3, near liq.-liq. crit. point, conc. fluctuations, neutron diffr. long wavelength thermodynamic limit 79−10948
Li-NH_3, conc. solns., elec. cond. and thermoelec. power 79−19640
Li-NH_3 concentrated solution, NMR relaxation of ^7Li 80−108084
Li-NH_3 solution, metal-nonmetal transition, US absorption coeff. 77−51443
Li-NH_3 solution, small angle X-ray scatt. meas. 79−14667
Li-NH_3 system, inhomogeneous, numerical simulations of Hall effect 77−43551
Li-$SOCl_2$ battery for implantable cardiac pacemakers 80−30939
Li-$SOCl_2$ cells, discharge reaction mechanisms 79−100504
Li-$SOCl_2$ hermetic D cells, effect of $Li_2B_{10}Cl_{10}$ and $Li_2B_{12}Cl_{12}$ on performance 80−12000
Li-Si, electrode pot., Li utilisation determ. 80−81427
Li-TiS_2 cell, electrochemical pot. spectroscopy, thermodynamic props. meas. 79−100426
Li-TiS_2 storage batteries *(German)* 80−12001
Li^+-$(H_2O)_n$, complex struct., coord. numbers 79−7049
Li^+-affinities of methylamine, ab initio SCF calculations 80−102443
Li^+-affinities of NH_3, ab initio SCF calculations 80−102443
Li^+-amide, assoc. in aq. soln., potentiometric obs. 77−29005
Li^+-H_2O complex, charge transfer theory, Mulliken population, ab initio calc., multiconfiguration scheme 80−106392
^6Li-loaded liquid scintillators with pulse-shaped discrimination 79−59310
$Li+C^-(O^-)(F^-)(Cl^-)$, negative ion stripping, at. beam form. 77−6926
$Li+CH_3I(CCl_4)(CH_3NO_2)$, mol. beam kinetics 77−28978
$Li+Cl_2$ (SF_6) (dichlorofluoromethane) *(German)* 78−92485
$Li+Cl_2(Br_2)$, ion pair form., double differential cross sections, 8-30 eV 78−11507
$Li+Cl_2(Br_2)(ICl)$, product mag. deflection slotted disc velocity analysis 77−16806
Li+doubly charged ions, electron capture excitation, theoretical predictions in fusion plasma 80−63810
$Li+F_2(Cl_2)(NO_2)$, $4^2S_{1/2}$ excited atom crossed beam collisional ionisation 79−64087
$Li+F_2(HF)$, electron transfer reactions, semiempirical pot. energy surfaces calcs. 78−73022
Li+H, superthermal collisions, photon and positive ion prod. 78−78788
$Li+H_2$, exponential gap relation, rot. inelasticity 80−78693
$Li+H_2$, inelastic collision, ab initio pot. energy surface 79−10055
$Li+H_2$, LiH form. at Mo surface, mass spectroscopic obs. 77−66771
$Li+H_2$, rot. and vibr. transitions, close-coupling calcs. 77−58136
$Li+H_2$, vibr. excitation, rotationally sudden calcs. 79−22797
$Li+H_2O \rightleftharpoons LiOH+H$, equilib. consts., ab initio SCF and CEPA calcs. 78−3361
$Li+H^+$, electron capture cross sections 79−86061
$Li+H^+$, Li core excitation cross section, correlation and reorganisation effect 80−87215
$Li+H^+(H_2^+)(He^+)(He^{2+})(He_2^+)$, excited state form. obs. 80−9686
$Li+H^+ \rightarrow Li^+(X)+H(nl)$, (X=$1^1S$, 2^1S, 2^3S and nl=1s, 2s, 2p) continuum distorted wave method calc. 80−1062
$Li+HF \rightarrow LiF+H$, pot. energy surface, SCF and CI calcs. 80−71904
Li+H(He) 78−9127
Li+He, direct excitation of Li I (nl) levels in keV collisions 78−90280
Li+He, elastic scatt., fine-struct. transition cross sections, eigenphase formulation 78−25651
Li+He, gas-phase collisions, intermediate and high velocities, excitation 80−32822
Li+He, intermol. forces, ab initio VB calc. using nonorthogonal basis set 80−23490
Li+He, $P_{1/2\text{-}3/2}$, fine-structure transition probability, semiclassical multichannel scatt. matrix 80−37854
Li+He, press. broadening, line shifts 78−5290
Li+He (methane), collisional excitation, prompt decay line energy, projectile Auger spectrosc. 79−85941
$Li+He^{2+}$, collisions, soft X-ray emission obs. 80−83591
$Li+He^{2+}$, electron capture, ionis. cross section, low-vel. $He^+(3l)$ production, X-ray production 79−22822
Li+He(Ne), 2s→2p excitation cross sections, model pot. calcs. 77−58152
Li+He(Ne), excitation cross sections, Li I resonance line emission and polarisation 77−61846
Li+He(Ne), inelastic collisions, Baylis-Gombas pseudopot. appl. 77−58151
Li+He(Ne)(Ar), Li collision-induced alignment, reson.-line emission polaris. obs. 80−18912
Li+He(Ne)(benzene), relative level excitation, orbital ang. momentum quantum number depend. 78−25688
Li+inert gas, Doppler and collisional broadening, correls. 77−14530
Li+inert gas, fluoresc. reson. line broadening 77−6734
Li+inert gas atom, low energy, excitation, emission cross sections and polarisation fractions 80−37867
Li+inert gas collisions, electron loss cross-section meas. *(French)* 78−86941
Li+$KFeS_2$, electrochemical reaction, in situ Mossbauer spectra study 79−100397
$Li+Li_2 \rightleftarrows Li_3$, rovibronic symmetry correlation 78−92461
Li+LiH, collinear reactions, SCF correl. diagram for Li_2H 77−70292
$Li+Li^*(H^*)$, resonant ionisation, cross section and ionisation probability 80−63785
Li+Li(Be), London coeffs. for long range interaction, CI variation-perturbation method 78−5310
$Li+N_2$, vibr.-rot. relax., optical pot. method 78−62886
$Li+N_2^+$, 50-1000 eV, crossed beams, electron transfer and excitation 80−14226

lithium continued
$Li+N_2(H_2)(O_2)$, excited atom quenching, semi-empirical model 78−1065
$Li+Na^+$, direct and charge exchange scatt., differential scatt. cross-sections meas. 78−42158
Li+Ne, autoionising Ne levels excited in 5-10 keV collisions 78−22017
$Li+O_2$, semiempirical pot. surfaces, dynamical considerations 79−11766
$Li+SnCl_4(PCl_3)(SF_6)$, product mag. deflection slotted disc vel. anal. mol. beam kinetics 77−25250
$Li+TiS_2$, intercalation chemistry and electrochemical energy storage 79−100541
Li^++Ar, interaction pot. of $X^1\Sigma$ state, CI calc. 79−50100
Li^++Ar, up to 70 keV, symmetric (antisymmetric) reson. charge transfer cross sections *(Korean)* 78−50636
Li^++CO, 4-7 eV, final rot. state distrib., small ang. depend. 79−68300
Li^++CO, differential cross-sections, ab initio CI vibrotor pot. energy surface calcs. 78−46421
Li^++CO, pot. energy surface, equilib. distance, SCF calcs., correl. effects 77−3430
Li^++CO, rot. excitation, ab initio CI pot. energy surface, classical mech. and coupled states calcs. 78−25665
Li^++CO, rot.-vibr. energy transfer, 1-10 eV, calc. 79−45799
Li^++CO_2, collisional excitation, quasiclassical trajectory calcs. 80−83467
Li^++CO_2, rot. vibr. energy transfer, 1 to 10 eV, many body theory 80−28093
Li^++$CO_2(N_2O)$, vibr. excitation, time of flight meas. 77−79682
Li^++$CO(CO_2)(N_2O)$, vibr. excitation, 70 to 1500 eV 78−82824
Li^++$CO(N_2)$, differential cross-sections, classical trajectory calcs. 78−29841
Li^++ether(thioether)(amide), pair pots., ab initio LCAO SCF MO calcs. 80−58184
Li^++H_2, dissoc., multiple scatt. theory 78−21999
Li^++H_2, dissociative collision, H_α, H_β emission prod. 77−75093
Li^++H_2, elastic scatt. and rot. excitation, multistate semiclassical orbital method 79−27058
Li^++H_2, exponential gap relation, rot. inelasticity 80−78693
Li^++H_2, quasiclassical approx. for scatt. amplitude, rot. degrees of freedom *(Russian)* 77−79676
Li^++H_2, rot. energy transfer, power scaling law 79−54942
Li^++H_2, rot. excitation dynamics, quasi-classical phase space density functions 77−88532
Li^++H_2, rot. inelastic scatt., body frame partitioning approx. calcs. 80−23527
Li^++H_2, sudden approx. of Cross, computational tests, cross section factorisation, scatt. phenomena 80−58352
Li^++H_2, vibr.-rot. excitation at intermediate energies 79−3534
Li^++H_2 78−9234
Li^++H_2 (j=0), rot. alignment, state-selected differential and integral rotationally inelastic cross sections 80−37863
Li^++H_2 (ortho, para), rot. excitation and ang. depend. transition probabilities, time of flight spectra 80−23517
Li^++H_2O, ab initio GTO calc. of vibr. intensity changes of spectroscopic parameters 78−58583
Li^++$H_2(D_2)(O_2)(N_2)$, vibr. excitation cross sections, 100-1200 eV 79−27077
Li^++$H_2(N_2)$, ion-molecule forces, generalised electron gas Drude model appl. 79−98183
Li^++H^+, charge transfer and ionisation, total cross sections for production of Li^{2+} determ. 80−91657
Li^++He, 10-50 keV, mol. promotion, many-electron aspects 79−50124
Li^++He, <5 keV, autoionised electron spectra 80−32823
Li^++He, electron gas model, polarisation inclusion 78−37699
Li^++He, excitation, optical emission line shapes 80−18820
Li^++He, interaction pot., direct determ. from gaseous ion mobility 77−10720
Li^++He, Li excitation mechanisms, Auger and autoionisation spectra 77−19042
Li^++He, quasimol. study of collisions in 0.3-50 keV range 77−88529
Li^++He collisions, K-shell vacancy sharing, ab initio LCAO-SCF, CI calcs. 77−19054
Li^++He collisions, Li-K shell excitation, autoionisation spectra meas., total cross sections 77−19053
Li^++He(Ne), slow collision, ionis. obs. 79−10194
Li^++$Hg(6^3P_1)$, excitation, optical polarisation fractions and mag. sublevels obs. 78−50619
Li^++inert gas, elastic differential scatt., diffr. effects 77−511
Li^++K, differential scatt. cross section, electronic excitation via. rot. coupling in LiK^+ 78−13579
Li^++K, rot. coupling, Fraunhofer diffraction effects 77−65526
Li^++Li, charge exchange, relative differential cross-sections 79−81273
Li^++methane, single collision, time delayed autoionisation spectra 78−1067
Li^++methane, vibrational excitation, time of flight measurements 79−45826
Li^++N_2, (0.5 to 1.0 keV) energy loss spectra, ionisation, electronic and vibro-rot. transitions 77−14541
Li^++N_2, rot-vibr. transitions, semiclassical calc. of cross sections 79−22798
Li^++N_2, rot. and vibr. inelastic collisions, trajectory calcs. rel. to previous data 78−62878
Li^++N_2, rot.-vibr. energy transfer, 1-10 eV, calc. 79−45799
Li^++$N_2(CO)$, comparison with classical small-ang. pot. scatt. theory 80−1043
Li^++Na, charge exchange, generalised Rosen-Zener model 77−50497
Li^++Na, charge transfer and elastic scatt., two state model 78−58805
Li^++Na, direct and charge exchange scatt., differential scatt. cross-sections meas. 78−42158
Li^++Na→Li+Na^+, electron transfer collisions time independ. quantum theory with nonorthogonal basis and R-matrix propag. 79−89769
Li^++Ne, autoionising Ne levels excited in 5-10 keV collisions 78−22017
Li^++Ne, low energy, ionisation, total cross-section meas. 77−54606
Li^++Ne collisions, vel. dependence of Ne 2s and 2p, vacancy production, electron spectroscopy 80−58344
Li^++SF_6, mode selective vibr. excitation 80−58351
Li^++X, X=H, H_2, He, C, N, O, cross-section, closure-Born approx. 78−66630
Li^{l+}+$H(H_2)$, (q=1-3), electron capture and loss cross sections 78−42187
lithium continued
Li^{2+}+Li^{2+}(H), two-body dispersion interaction, freq. depend. multipole polarisability, variational calc. 80−37758
Li^{3+}+He, electron capture and impact-ionis. cross sections, Monte Carlo calcs. 79−27083
Li^{3+}+He(C)(Ne), K-shell charge transfer cross sections, Bates-Born formalisms 79−45834
Li^{3+}+methane, (Ne), (Ar), inner shell electron capture cross-sections 79−76510
Li^{n+}+Ar(Si)(Ne), K-shell ionisation of atom, projectile charge state depend. 77−34743
Li_1^+, potential energy curves, exchange and ion-multipole interactions, vibrational energy levels 79−98175
Li_2, $^3\Sigma_g^+$-$^3\Sigma_u^+$ excimer emission, ab initio calcs. 80−91608
Li_2, A-X band intensity distrib. Franck-Condon calcs. validity 77−65511
Li_2, $A^1\Sigma_u^+$ state, radiative lifetime 77−27104
Li_2, $A^1\Sigma_u^+$ state, vibr. energy levels calcs. 77−83566
Li_2, ab initio pseudopotential for FSGO calcs., bond length 77−75043
Li_2, and anion, electronic struct., spin-unrestricted, spin-restricted SCF HF calc. 78−90331
Li_2, and isotopic variants, low-lying X-B transition freq. calc. 78−90180
Li_2 and Li_2^+, Li 1s hole states calc., dissoc. Auger electron energies 77−23443
Li_2, $B^1\Pi_u$, pot. energy curve, MC SCF approx. calcs. 77−38618
Li_2, bond orbital model, model pot. approach 79−49923
Li_2, charge distrib. anal. rel. to Berlin's binding and antibonding regions 79−6875
Li_2, core-excited states, theoretical and experimental investigation 78−37655
Li_2, electron binding energies calcs. 78−86768
Li_2, electron impact, vibr.-rot. excitation by slow electrons, multiple scatt. calcs. 78−13617
Li_2, electron scatt., effective pot. calcs. 80−53131
Li_2, emission circ. polaris., hyperfine coherence and elastic collisions effect 79−3471
Li_2, floating spherical Gaussian orbital, Hartree-Fock-Roothaan and pseudopot. calcs., comparison 78−46262
Li_2, gerade excited electronic states, pulsed optical-optical double reson. spectroscopy, laser medium 79−81220
Li_2, Hellman pseudopot. calcs., dissoc. energy, ionis. pot., bond length 77−10577
Li_2, isotope separation, by two-photon ionisation, ionisation pot. determ. 78−70950
Li_2, laser, continuous, optically pumped 78−87046
Li_2, lowest $^1\Pi_g$, $^1\Pi_u$, $^3\Pi_g$, $^3\Pi_u$ states 77−54517
Li_2, MCSCF and CI calcs. 80−95526
Li_2, MCSF accurate pot. energy curves for $^3\Sigma_u^+$ and $b^3\Sigma_g^+$ states, level crossing 77−50369
Li_2, magnetic susceptibility and anisotropy calc. *(French)* 78−37559
Li_2, mol. polarisability, correlation corrections in finite-field method 77−71889
Li_2, mol. struct. 2-electron integral evaluation by Multipole Expansion of Diatomic Overlap 78−908
Li_2, nucl. spin-spin coupling, scanning MO HF LCAO calc. 79−50045
Li_2, optical-optical double reson., $^1\Sigma_g^+$ state mil. consts. 80−53027
Li_2, optically pumped CW dimer lasers 80−14322
Li_2, polarisability, generalised London formula for dispersion coeff. 78−82662
Li_2, pot. energy surface, half-projected HF model 79−36564
Li_2, potential curve calc. using MTXα_R method 77−10593
Li_2, radiative lifetimes of $B^1\Pi_u$ states, model pot. calcs. 78−46397
Li_2, relativistic Dirac-Fock multiconfig. SCF calcs. 80−99456
Li_2 SCF polarisability, polarisation potentials 79−89602
Li_2, spectroscopy and structure, triplet excimer continuum emission 80−32769
Li_2 spin-coupled theory of mol. wavefunctions, mol. struct. and props. 77−50337
Li_2, total SCF energy estimation from orbital energies 79−63908
Li_2, triplet absorpt. bands, 6215-5875 Å, after two-photon excitation 79−50035
Li_2, valence-shell MO calc. with pseudopot. 78−907
Li_2, $X^1\Sigma_g^+$ and $A^1\Sigma_u^+$ states, electronic struct. and spectra 79−89615
Li_2^+, electronic struct., ab initio calcs. 77−34553
Li_2^+, $^2\Sigma$ and $^2\Pi$ state pot. energy curves, two-centre model 79−26906
Li_2^+, core-core interaction potential calc. 78−25645
Li_2^+, dissoc. energy, laser photodissoc. determ. 78−70950
Li_2^+, FSGO calcs. with model pots. 78−33413
Li_2^+, nonadiabatic coupling matrix elements by Hellmann-Feynman theory and HF 80−83263
Li_2^+, photodissoc., effective cross-sections calcs. 79−86014
Li_2^+, Simons-type pseudopots. calcs. 78−5120
Li_2^+, $X^2\Sigma_g^+$, $^2\Sigma_u^+$, $A^2\Pi_u$ and $^2\Pi_g$ states, electronic struct. vibr. spectra, ab initio calcs. 79−36507
$^7Li_2$, $B^1\Pi_u$-$X^1\Sigma_g^+$ band system, absorpt. and laser fluoresc. spectra 79−68256
Li_2+H, superthermal collisions, photon and positive ion prod. 78−78788
Li_2+inert gas, collision induced transition rate consts., two-laser spectrosc. 80−9629
Li_2+inert gas, energy and ag. momentum transfer, polarised laser fluoresc. obs. 79−31590
Li_2+K_2→2KLi, equilib. const., enthalpy change 78−25750
Li_2+Li, collisional depolaris. and rot. energy transfer, laser-induced fluoresc. 79−13794
Li_{2n}, (n=1, 2, 3), stable cluster configs., ionisation pots., binding energies, vibr. freqs., al initio SCF and CEPA calcs. 80−14265
Li_3 and Li_3^+, ΔE SCF ionis. and excitation energies, transition functional method 77−88404
Li_3, BO hypersurface and vibronic states, coupled electron pair approx. 78−94203
Li_3, binding energy, Wigner-Seitz pot. calcs. 77−83512
Li_3, electronic struct., SCF and SCF-CI calcs. 80−87044
Li_3, geom. struct. and binding energy, diatomic-in-molecules 78−74785
Li_3, multibody and stability considerations, small clusters 78−90333
Li_3, potential energy surface and config., RHF CI calc. 77−34562
Li_3, spin density, Gaussian basis set 78−33427
Li_3, spin populations, restricted Hartree-Fock calcs. 77−57906
Li_3^-, ab initio pseudopotential for FSGO calcs., bond length 77−75043
Li_3^-, electronic struct., SCF and SCF-CI calcs. 80−87044
Li_3^+, ab initio pseudopotential for FSGO calcs., bond length 77−75043
Li_3^+, electronic struct., SCF and SCF-CI calcs. 80−87044
Li_4, geom. struct. and binding energy, diatomic-in-molecules 78−74785

lithium continued
Li_4, MCSCF and CI calcs. 80−95526
Li_4, plane configs., ab initio SCF calc., rel. to condensation *(French)* 77−4062
Li_n, equilibrium struct., effect of p-functions *(German)* 79−89823
$Li_2(A^1\Sigma_u^+)$, dye laser excited, collision induced dissociation 79−91920
$Li_2(A^1\Sigma_u^+)$, state multipoles transfer following rot. inelastic He collisions, polarised emission obs. 80−5608
$Li_2(B^1\Pi_u)$+inert gas, laser-excited collision-induced dissoc. 79−79232
$Li_2(B^1\Pi_u)$+inert gas, rot. inelastic collision, classical trajectory calc. 78−1054
LiH, resonance Raman scatt. *(Russian)* 78−52503
Li^+H_2, elastic of rot. excitation, semiclassical treatment 79−31657
$LiNbO_3$, thin-film electrooptic modulator, optimal charcts. 79−10405
LiO_2, reactions with Mo in fusion blanket feasibility tests 80−26055
$Li(^2P)$, quenching cross-sections, energy depend. 79−63952
$Li^+(^1S)$, correlation energy calc. of at. in spherical box 79−97984
$Li(^2S)$, open shell polarisation propagator, for doublet-doublet transitions calcs. 80−27939
^6Li, appl. of four-body atomic Faddeev eqns. 79−59569
^6Li, D substitute effect in inertially confined fusion with low T inventory 78−58403
^6Li, determination using nuclear track techniques 80−95504
^6Li enrichment, isotope separation in rotating plasma *(Japanese)* 79−41248
^6Li glass scintillators, appl. as neutron detector, problems and consequences 79−9968
^6Li ion depth profile meas. by deuteron induced reactions 77−19978
^6Li, nuclear mag:spin-lattice relaxation times 78−86889
^6Li, surface anal. using ^6Li ion beams 79−5211
^6Li tensor polarised beam prod. and calibration 78−46199
$^6Li/^7Li$ abundance ratio, meas. using isotope ratio mass spectrometer 77−88601
$^6Li/^7Li$ ratio in C stars, low-energy spallation model 78−40927
$^6Li^+$, confined ions, density distrib., laser scanning meas. 79−81303
$^6Li^+$, hyperfine structure, Doppler-tuned ion beam laser spectroscopy 79−89627
$^6Li^{35}Cl$, electronic ground state, first vibration state lifetime, MBER meas. 79−86023
$^6Li^*+^7Li^*$, laser-induced Penning and associative ionisn., $^{13}Li_2^+$ enrichment 78−58796
^7Li, HFS using Doppler-tuned HFS spectroscopy 79−13831
^7Li I and Li abundances towards ζ Persei and ϵ Aurigae 78−49494
^7Li, level-crossing method for HFS and at. lifetimes 78−66678
^7Li, nuclear polarised ions, grazing incidence refl. from Cu surface 79−64077
^7Li, prod. in nova explosions 78−57555
^7Li selective excitation, by intracavity nonlinear absorpt. in CW dye laser 79−866
$^7Li_2$ $A^1\Sigma_u^+$-$X^1\Sigma_g^+$ band system anal. 77−83565
$^7Li+H_2$, electron capture collisions, 0.2 to 3 keV 77−6925
$^ALi^+$, A=6,7, $2^3{}_1$-2^3P, dye laser saturation spectroscopy 80−18821
Li^*+He(Ar), Li principal series line broadening and shift, interat. pot. consts. 78−42165
Li^*+He(Ne)(Ar)(H_2)(N_2), thermal, high-Rydberg Li behaving as ion core 78−22004
$Li^*(2^2P_J)+H_2(D_2)$, collision induced quenching and fine struct. transition rate coefficients meas. 80−74221
$Li^*(2^2P_J)$+He(Ne)(Ar)(Kr)(Xe), collision induced fine struct. transition rate coefficients determ. 80−74220
$Li^+(2^3P)$, electron impact excitation, absolute 548.5 nm emission cross-section 79−10209
$Li(2^2P_{1/2,3/2})$, laser induced flame chemistry, saturated mode fluoresc. meas. 80−89491
Li(2p)+H_2(N_2), Li(2p) excitation, alignment and orientation obs. 80−63794
MgF_2:Li^+, atom transport, diffusion and ionic cond. meas. 80−107492
MgF_2:Li^+, defect struct., theory 77−47472
MgO, Li precipitates orientation and struct. *(French)* 79−86888
MgO:(Li), polycrystn., internal friction *(German)* 80−59577
MgO:Li, $[Li]^0$ defect, high temp. and ionisation induced effects 78−34509
MgO:Li, $[Li]^0$ defect, stress induced optical dichroism 78−35179
MgO:Li, $[Li]^0$ defects, magneto-optical props. 77−12365
MgO:Li, enhancement of elec. cond. by oxidation 80−44600
MgO:Li, hole processes in photostimulated luminesc., electron emission, X-ray irrad., ESR relaxation 79−69889
MgO:Li, impurity-induced UV luminesc. 79−83037
MgO:Li, internal friction, mech. and dielec. relax. *(German)* 80−34135
MgO:Li, mech. deformed crysts., imprinting of slip bands using Li impurities 80−59473
MgO:Li, oxidation and reduction up to 1700K, defect prod. 79−39013
MgO:Li, TEM studies 79−29069
MgO:Li, thermally generated $[Li]^0$ defects, valence compensation 79−77598
MgO:Li^+, precipitation, dislocation obs. by TEM *(French)* 79−51163
MgO:Li^+, quenched, elec. polarisation, thermal depolarisation and dielectric loss meas. 79−1738
MgO:Li^+ short-wave luminesc. V-centre electron recomb., impurity effects *(Russian)* 77−20921
MnO_2:Li, Zn^{2+} ion specific adsorpt. kinetics, ^{65}Zn γ-ray scintillation investig. 80−70529
Mn_3O_4:Li, elec. cond. and thermo-EMF 80−20231
MoO_3:Li, elec., catalytic props. 78−60122
N_2+Li^+, inelastic scatt., initial rot. and vibr. excitation effects 77−14543
N_2+Li^+, rot. polarisation, spectator model 77−30970
NO+Li^+, vibr. excitation cross sections 79−54946
NaBr:Li^+, lattice relaxation around tetragonal and rhombic defects 79−95110
NaCl:Li, U-centres, HFS consts., g-factor, EPR spectra 80−39869
NaCl:Li^+, lattice relaxation around tetragonal and rhombic defects 79−95110
NaF:Li, combined suppressive and extinction writing, using $M(M_A)$ centres 77−7164
NaF:Li, pulsed double nucl.-nucl. reson. *(Russian)* 78−10804
NaF:Li^+, substitutional impurities, defect props. of (001) and (011) surfaces 77−47443
Ne+Li^+, autoionising level excitation, electron spectra 77−14554
Ni+H^+($^4He^{2+}$)(O)(Li), K-shell ionis., impact parameter depend. 77−83707
lithium continued
NiO:Li^+, finely divided catalyst, low-temp. doping 79−51128
$NiPS_3$-Li, chemical and electrochemical intercalation *(French)* 78−38679
phonon frequencies, depend. on atomic mass, cross-over of [ζ00] branches 79−14901
RbCl:Li, tunable CW IR lasers using F-centres 77−88725
RbCl:Li, tunable IR lasers with F_A(II) and F_B(II) colour centres 78−90420
RbCl:Li F_A(II) centre laser, pumped by flashlamp-pumped dye laser 80−102737
RbCl:Li^+, new off-centre defect system, studied with dielec. techniques under hydrostatic press. 79−19834
RbF:Li, F-centres, saddle-point configuration, molecular model parameter 80 107234
Si: Li, absorpt. and luminesc. transitions involving exciton excited hole states 79−78038
Si:H,Li, amorphous, DC electrical conductivity, absorption edge and IR meas., role of H 80−54694
Si:H,Li, amorphous, photoluminescence obs. 80−66280
Si:Li, amorphous, elec. cond. and thermopower 79−73537
Si:Li, amorphous, implantation effects on elec. props. 80−49716
Si:Li, amorphous, interstitial doping by in-diffusion and implantation and elec. characterisation 78−26585
Si:Li, amorphous, thermopower and cond. meas. 79−69142
Si:Li, amorphous, vac. evaporated, doping, transport and optical props. 80−49715
Si:Li, bound exciton complexes associated with Li, photolum. meas. 79−28823
Si:Li, bound-exciton excited states, uniaxial anal. 80−71475
Si:Li, defect electronic struct. and config., semi-empirical calc. 80 107739
p-Si:Li, dislocation free, minority carrier lifetime, effects of heat treatment *(Japanese)* 79−65492
Si:Li, EPR in mechanically affected sampler 78−39385
p-Si:Li, electrolytical doping, depth-profile anal. 79−77623
Si:Li, electron-phonon scatt., in intermediate conc. region 80−65180
Si:Li, evaporated amorphous film, doping by in-diffusion 79−51127
Si:Li, luminesc., stress effects on donor exciton satellites 77−85786
Si:Li, luminesc. of bound exciton and bound multiexciton complexes 79−28821
Si:Li, nonrandom strain, EPR of thermally excited donors 78−43629
Si:Li, phonon conductivity, phonon reson. scatt. effects 79−19407
Si:Li, photolum. of bound exciton and bound multiexciton complex, Zeeman effect 80−108265
Si:Li, piezospectroscopic studies of bound multiexciton complexes 80−16006
Si:Li, precipitation centres, elec. cond., Hall effect meas. 78−48417
Si:Li, strongly doped, piezoresist., gas-liq. type transition 77−43600
Si:Li, thermal cond., low temp. phonon scatt., internal strain effects 80−96706
Si:Li ion implanted, channelling and random equivalent depth distrib. 80−100293
Si:Li n^+-p solar cells, electron beam irrad. damage 80−94000
Si:Li P/N type solar cells, irradiation obs. 79−66406
Si:Li radiation detector, influence of distrib. of drift temp. on props. 77−3234
Si:Li X-ray detector, escape peaks and internal fluoresc., general geometry case 77−18150
Si+$Li^{+1,2,3}$, K-shell ionisation depend. on projectile charge state 77−34743
Si(Li), 2D position sensitive detector with 100 μm resolution 79−45544
Si(Li) detectors, escape peak losses 80−27383
Si(Li) electron spectrometer with superconducting transporting magnets 80−27376
SiO_2:Li^+, surface crystn. of fused SiO_2 by ion implantation and annealing 80−89383
So-Li, diffusion-induced defects, X-ray triple cryst. diffractometry 80−2213
T breeding performance eval., multigroup neutron and photon transport calc. 80−13831
T prod. meas. in Li metal sphere using new methods of neutron source strength determ. 78−74470
TaS_2, 2H polytype, Li intercolation kinetics PAC hyperfine spectrosc. 79−87337
TaS_2-Li intercalation compound, CDW's and superlattice patterns 77−47746
V_2O_5:Li, elec. cond. and thermoelec. power meas. 80−10987
α-V_2O_5:Li, far IR absorption spectra meas. 77−73158
ZnO:Li, band-edge emission obs. 77−20933
ZnO:Li, effect of LiOH mineraliser on struct. and optical props. 77−8737
ZnO:Li, electron irrad., F^+ centre, photosensitivity of e.p.r. spectrum 77−1594
ZnO:Li, luminesc. donor-acceptor pairs, exchange broadened optically detected EPR spectra 78−23373
ZnO:Li, optically detected ESR, donor-acceptor pairs, line broadening 78−80256
ZnO:Li single crysts., photo-induced AC impedance meas., photodielec. effect 78−52034
ZnSe:In, Li, binding energy of excitons bound to donor-acceptor pairs, electron-phonon coupling 77−4689
p-ZnSe:Li, LPE layers, photocapacitance and photocond. meas. 79−99572
n-ZnSe:Li, semicond. selective pair luminesc., excited impurity state investigation 79−61439
ZnSe:Li, shallow acceptor excited states, luminescence spectra, Rydberg energy 79−78750
ZnSe:Li diodes, electroluminescence and fabrication, expt. *(Japanese)* 77−28633
ZnSe:Li(Na)(Ga) doped and pure cryst., donor-acceptor bands 80−11465
ZnTe:Li, binding energy of shallow acceptors from photoluminesc. excitation spectra for donor-acceptor pairs 79−95809
ZnTe:Li, bleaching by green laser radiation 77−62015
ZnTe:Li, diffusion investigation by SEM and TEM 80−10706
ZnTe:Li, donor-acceptor pair excitation and recomb., photoluminesc. obs. 80−20691
ZnTe:Li, electron-phonon interactions in Raman scatt. 80−60594
ZnTe:Li, electronic Raman scatt., mag. field depend. 79−73928

lithium continued
ZnTe:Li, electronic Raman scatt. and IR absorpt. spectra of shallow acceptors 79−73978
ZnTe:Li, fluorescence spectra meas. 78−10949
ZnTe:Li, impurity segregation during short annealing and quenching, SEM, TEM and elec. meas. 80−10676
ZnTe:Li, ion implanted and annealed, photoluminesc. meas. 78−15208
ZnTe:Li, Li in Te precipitates, diffusion during thermal anneal 80−39358
ZnTe:Li, O, Hagemark theory, O modification isoelectronic trap 80−75517
ZnTe:Li, spin-flip acceptor scatt., transition selection rules, gyromagnetic ratios 79−61380
ZnTe:Li, Zeeman splitting of ground and excited acceptor states, selective pair luminesc. 80−84780
ZnTe:Li high purity, acceptor bound and free exciton states 79−99941

lithium alloys
dilute, impurity and conduction electron scatt. at 4.2K *(Russian)* 77−35931
dilute binary alloy, residual resistivity 77−1406
liquid semiconducting alloys, electronic struct., resistivity and thermoelec. power 77−51753
mutual alloying behaviour of the elements straddling the line Li-Mg-Cu-Au in the long periodic table 78−84769
Ag-Li, solid and liquid alloys, calorimetric investigation of mixing enthalpy *(German)* 78−52773
$Ag_{0.285}Li_{0.715}$, liq., partial interference functions, short range chem. order effects 79−7541
Al-Cu-Mg-Li alloy extrusions, microstruct., embrittlement and fracture props. 80−60965
Al-Li, ageing mechanism, metastable δ' phase and stable δ phase precip. *(Russian)* 77−8858
Al-Li, annealing of vacancies and ageing, resist. and TEM obs. 77−21172
Al-Li, cold worked neutron irrad. alloys, He bubble behaviour, microstruct. changes 77−54359
Al-Li, diffusion coeff. determ. during hydriding *(German)* 79−29288
Al-Li, dil., quenched and irrad., recovery, resist. and internal friction obs. 78−52848
Al-Li, dil. alloy, cold-worked, annealing spectrum 78−39801
Al-Li, dilute substitutional alloy, impurity Knight shift and electric field gradient 80−44940
Al-Li, Fermi surface impurity scatt. 79−56114
Al-Li, microvoid form., gaseous impurity atom effects, positron annihilation study 80−49275
Al-Li (10 at.%), struct. changes on annealing, 25-500°C, Li atoms role 80−35183
Al-Li (1.3 wt.%), prismatic dislocation loop rows due to precipitation *(Japanese)* 79−52220
Al-Li (2.8 wt.%), ageing in US field, precip. hardening *(Russian)* 80−29968
Al-Li (6.72 at.%), δ' coherent solvus determ. on ageing at 20 to 200°C, X-ray scatt. 77−25056
Al-Li ageing, δ-$'$-phase precip., effect of quenching conditions *(Russian)* 78−19761
Al-Li alloy, thermal anal. of precipitation 78−15417
Al-Li alloys, precipitating, annealing spectrum 78−31429
Al-Li solid soln., decomposition exam. by secondary ion ion emission *(Russian)* 78−68696
Al-Li system, δ' coherent miscibility gap determ. by small-angle X-ray scatt. 77−77483
Al-Li-Mg, estimation of isothermal sections of phase diagram 79−11567
Al-Li-Mg system, isothermal sections comput. 78−6896
Al-Li-Mg-Be alloys, phase composition of surface films, oxidation protection mechanism *(Russian)* 80−65417
Al-Li-Mn (2.8, 0.3 wt.%), recrystallised sheet, fracture behaviour, SEM and TEM study 80−97566
Al-Mg-Li, subboundary brittleness due to horophilic Na *(Russian)* 77−21244
Al-Mg-Li alloy, 01420, surface layer props. *(Russian)* 78−80674
Al-Mg-Li alloy, metastable S$'$-phase, struct. *(Russian)* 80−103291
Al-Mg-Li alloy 01420, riveted, low-cycle fatigue strength 80−30097
Al-Mg-Li-Si system, phase diag. *(Russian)* 78−80515
Al-Mg-Li-Zr alloys, struct., mech. props. 79−24498
Al-Si-Li system, Al-rich, phase comp., limits of solid solubility *(Russian)* 77−21097
Al-Zn-Mg-Li alloys, effect of Li on thermal props. 79−24515
AuLi, vibr. freq. determ., IR spectra, matrix depend. 77−75146
Ca-Li-Mg, isothermal section calc. 79−29034
IrLi and Ir_3Li, cryst. struct. 77−11506
K_2Li^+, equilib. geom. and dissoc. energy, pseudopot. calc. 78−94329
$LiAl_{1-x}In_x$, thermal expansion, comp. depend. 78−22869
Li Al, electronic struct., mol. cluster calc. 78−14649
Li-Ag, liq., density, compressibility and diffr. data 77−47336
β-Li-Al, lattice parameters, density, defect struct. 80−24440
Li-Al, sorption of tritium, appl. as thermonuclear reactor material 77−1301
Li-Al, T-recovery from fusion reactor blankets 78−58455
Li-Al alloy electrode performance, effects of metal additives 78−23953
Li-Al electrode performance In and Mg surface additives effect 80−40698
Li-Al system, Li solubility and chem. diffusion in Al, electrochem. study 80−107432
Li-Al-Mg alloy electrodes, polarisation behaviour and struct. 79−43588
Li-Au, electron diffusion thermoelectric power calc. 77−28161
Li-Au(Hg)(Tl)(Pb)(Bi), liq. semicond., electronic struct., resist. and thermoelec. power meas. 77−47712
Li-B (0-60 at.%), density, elec. resist. and Hall coeff. 78−39089
Li-B alloys, Li extraction and determ. using potentiometric titration 79−48016
Li-Bi, molten, sorption of tritium, appl. as thermonuclear reactor material 77−1301
Li-Bi, thermodynamic props., 355-600°C 78−34634
Li-Cd, phys. props. of liq. phase and LiCd solid cpd. 80−75537
Li-H, liq. and solid, mol. orbital approach, solvation energies 77−4201
Li-In, liquid alloy, elec. resist., Knight shift of ^{115}In and ^7Li nuclei 79−11352
Li-LiH(D)(T), decomposition in $(\alpha+\beta)$ field 79−15652
Li-Mg, BCC, mag. susceptibility var. with temp. *(Russian)* 77−51878
Li-Mg, liq., elec. transport props. and phase diagram 78−23070

lithium alloys continued
Li-Mg, liq. alloy, thermoelec. power and elec. meas. 77−47788
Li-Mg, liquid alloys, thermodynamic investigation *(German)* 79−91630
Li-Mg, Mathiessen's rule, elec. and thermal deviations, impurity scatt. 80−88536
Li-Mg, positron annihilation and charge transfer 78−31274
Li-Mg, X-ray Compton scatt. 77−16421
Li-Mn liquid alloys, form factor effects, pseudopotentials, resist. calc. 80−103608
Li-Na, liq., concentration fluctuation and structure factor 78−30534
Li-Na, liq., short-range order, neutron diffr. obs., near crit. composition 78−22639
Li-Na, liq. alloy, thermoelec. power and elec. resist. 77−47788
Li-Na liquid binary mixtures, phase separation under press. 80−34183
Li-Pb, liq. alloy, enthalpies of mixing, calorimetric study *(German)* 80−2170
Li-Pb, quasi-ionic, thermodynamic props. using EMF meas. 78−51705
Li-Pb, thermodynamic study using Knudsen effusion mass spectrometry 80−24578
Li-Pb eutectic alloys for fusion reactor solid breeder blankets, reactions with water 80−102297
Li-Pb liquid alloys, elec. resistivity, negative temp. coeff. 80−88527
Li-Pb liquid compound forming alloy, entropy of mixing 80−88328
Li-Pb-cooled blanket for tandem mirror fusion reactor, neutronic anal. 80−99273
Li-Pd, phase diagram and mag. props. 77−90321
Li-Pd (60 to 75 at.%), phase diagram and cryst. struct. of $LiPd_2$ phase *(German)* 79−51055
Li-Pt, phase diagram for comp. range 0-40 at.% Pt, mag. and elec. props. *(German)* 80−84912
Li-Rh-H system, intermetallic cpds. and phase relationships, cryst. struct. 78−44084
Li-SAP alloys, T recovery from fusion reactor blankets 78−58455
Li-Sb, thermodynamic props., 355-600°C 78−34634
Li-Si, eval. as negative electrodes for Li-FeS_2 cells, thermodynamic props. 77−16547
Li-Sn, phase relationships between Li_7Sn_2 and LiSn 79−78933
Li-Te alloys, liq., electrochem. investig. of thermodynamic props. 77−1244
Li-Tl(Al), equiatomic, B-32 superstruct. instability in absence of many-particle interactions 77−58972
Li-Tl(In)(Bi), liquid alloys, calorimetry study *(German)* 80−25664
$Li_2Ag_{2-x}In_x$, optical props., struct., energy bands, interband transitions 78−72539
LiAl, anomalous elec. resistivity near critical composition 80−103673
LiAl, β phase thermodynamic props., chem. diffusion coeff., electrochem. meas. 80−39308
7LiAl, cryst. growth, Stockbarger method, struct. and homogeneity 80−89137
LiAl, elastic moduli and Debye temp., US meas. 79−91724
LiAl, NMR relax. investig. of ^7Li self-diffusion 77−12217
β-LiAl, optical dispersion, room temp. reflectance spectra 80−66195
LiAl, pseudopotential method and ordering problem 77−35500
LiAl, semimetallic, B32 struct., electronic props. 78−56062
LiAl single crystals, growth by Tamman technique 80−66422
LiAl, transport props., rel. to semimetallic band struct. 80−88581
LiAl/FeS, battery system research developments at ANL 80−61323
LiAl/FeS experimental cells with molten salt electrolyte, self-discharge behaviour 80−104501
LiAl/FeS_x cell with negative electrode prep. by powder metallurgy, performance 80−26130
LiAl(Si)/$FeS(S_2)$ battery developments for electric vehicle propulsion and load levelling appls. 80−61325
Li_5B_4 form., thermodynamic considerations 79−56959
Li_5B_4, molecular and electronic struct. 80−20107
$Li_2Cd_{2-x}In_x$, optical props., struct., energy bands, interband transitions 78−72539
$LiCd_{1-x}Tl_x$, intermetallic, X-ray and Knight shift meas. of ^{205}Tl and ^{113}Cd 79−42851
LiIn, elastic moduli and Debye temp., US meas. 79−91724
LiIn, electrical resist. and thermal expansion temp. depend., 30 to 400°C, vacancy form. 77−24547
LiIr, struct. and props. exam. 78−92245
Li_2K^+, equilib. geom. and dissoc. energy, pseudopot. calc. 78−94329
LiMg, ordered, local density of states and local environment 79−82509
LiNa, ground and excited states, model pseudopot. calcs. 77−75069
$LiNa^+$, equilib. geom. and dissoc. energy, pseudopot. calc. 78−94329
LiPb alloy, compound-forming, vol. of mixing, conc. depend. 80−103484
$Li_{1-x}Pb_x$, liq., metal-nonmetal transition, electronic theory 78−79930
Li_yPdH_x, production and cryst. props. *(German)* 77−43176
Li_yPtH_x, production and cryst. props. *(German)* 77−43176
$LiRh_3$, cryst. struct. 77−11506
LiTl, pseudopotential method and ordering problem 77−35500
LiZn, elastic moduli and Debye temp., US meas. 79−91724
Mg-Li, complex energy band, l-depend. pseudopot. 78−84124
Mg-Li dil. alloys, effect of alloying on Fermi surface, de Haas-van Alphen effect meas. 77−76732
Mg-Li dil. alloys, effect of alloying on Fermi surface, pseudopot. model 77−76733
Mg-Li-Al, phase diag. *(Russian)* 77−59746
Mg-Li-Al (31, 1 at.%), heat treated, precipitation 80−40364
Mg-Li-Ga(Ge)(In)(Tl)(Pb), phase diagram, isothermal cross section *(Russian)* 80−20900
Mg-Li-Sn system in Mg-rich region *(Russian)* 77−52289
Mg-Li-Sn-Al, investigation in Mg rich region *(Russian)* 78−15364
Na-Li, liq., Knight shift calc. by multiple scatt. Xα method 80−54961
Na-Li (19.2 wt.%), elec. resistivity, immiscibility region 79−1593
Na_2Li^+, equilib. geom. and dissoc. energy, pseudopot. calc. 78−94329
NiNaK, mol., intersection of pot. energy surfaces, ab initio calcs. 79−36557
Pb-Li alloys, ^3H breeding blanket for fusion reactor, ^2H solubility 80−18626
Pb-Li liner for fusion reactor, with controlled implosion 79−49860
Pb-Li liq. alloy internal spectral shifter and energy converter for laser fusion reactor 79−49841
$Pb_{1-c}Li_c$, liquid alloys, local fluctuations and quadrupolar relaxation 80−66060
Pb_4Li, eutectic, ISSEC selection for fusion reactor 80−57950

lithium compounds
see also lithium alloys
β-eucrypite, glass-ceramics, internal stresses 79−15770
β-spodumene, glass-ceramics, internal stresses 79−15770
acetate dihydrate, nearly free methyl rotors, rot. energy states, nucl. reson. props. 80−34784
acid oscalate, neutron inelastic scatt. spectra in 2200-200 cm^{-1} range 80−70327
air enthalpy meas. by LiCl humidity sensors 80−90858
alkali metal-rare earth oxides, $MLnO_2$, Ln=Y or Gd, synthesis and physicochem. props. 77−48216
alkanoates, phase relationships and thermal behaviour branching effects 78−43111
aluminosilicate glass, formation of glass-ceramic in $LiCl_3$ vapour 77−16536
aluminosilicate glasses, containing Cu and halogen impurities, ESR spectra 80−66027
ammonium tartrate monohydrate, dielec., EPR *(Japanese)* 77−85550
ammonium tartrate monohydrate elastic props., piezoelec. reson. method meas. 77−63370
B_2O_3-Li_2O-LiCl, ionic conductor, IR refl. Raman study 80−66173
benzoate-DMSO, cryst., nitrobenzene anion radical impurity, EPR 77−1597
binding energy of Li^+ with −NCO, −CO, −COO−, O, N, and −CN, ab initio SCF calcs. 77−50352
borides, prep., structs., book contrib. 78−47304
n-butyl-lithium, intercalation with transition metal chalcogenophosphates, possible appl. in Li to batteries 80−71446
calibo glass:Eu^{3+}, Ho^{3+}, energy transfer 78−76510
closoboranes as electrolytes in Li solid cathode cells 80−108794
convolution of ps optical signals 80−58629
disilicate glass, radiation induced centres, EPR exam. 78−35033
efficient intensity modulator 78−22190
eucryptite-cordierite binary system, sintering of polycrystalline bodies *(Japanese)* 77−12588
ferrite, electrical cond., thermoelectricity, magnetoresistance meas. 78−19039
ferrite, $Fe(Li_{0.55}Fe_{0.45})O_4$, one-magnon light scatt. with and without compensation temps. 78−31062
ferrite, ferromag. reson., linear elec. field shift 79−1716
ferrite, film, magnetic circular and linear dichroism, temp. depend. 79−69815
ferrite, fine particle, for arc plasma spraying mm-wave phase shifter 78−64469
ferrite, linear electric field effects in mag. anisotropy and ferromag. reson. 80−65854
ferrite-Bi_2O_3, phase diagrams and sintering conditions 79−52141
ferrites, conditions for obtaining high-density one-phase mag. ceramic 79−52141
ferrites, MW dielectric losses, causes and reduction *(Chinese)* 80−75930
formate, active spectroscopy, under conditions of double-w-k-resonance *(Russian)* 78−33777
formate, and deuterated, polaritons, spontaneous parametric light scatt. 77−90150
formate, Fermi reson. of optical phonons with two particle state zone, interference effects *(Russian)* 77−90149
formate, isotope exchange during crystallisation from aqueous solns. 78−18569
formate, mixing of Nd laser radiation for coherent picosecond source, 350 to 680 nm 78−13762
formate, optical phonons, small oscillator strength meas. from frequency-angular polariton spectra 80−92629
formate, UV radiation prod. by freq. doubling 77−743
formate biaxial crystal, nonlinear conical refr. obs. in harmonic generation 80−23745
formate cryst., 90° phase matching 80−58634
formate crystal, dehydration, influence of hydrostatic press., ^7Li NMR 78−2758
formate crystal, optical phase configuration 78−5524
formate monohydrate, elec. props. 79−87371
fusion reactor blanket solid Li compounds, removal of bred T 80−32513
germanate crystals and glasses, struct. and stability, IR spectra meas. 80−64911
graphite intercalation compound, LiC_6, ^7Li NMR *(French)* 78−35050
graphite intercalation cpd., C_6Li, charge distrib. 78−34743
graphite intercalation cpd., C_6Li energy band struct. 78−30861
graphite intercalcation compounds, prep. from Na-Li melts *(French)* 80−2970
halides, cohesive energies, effect of three body interactions 77−76516
halides, elastic constants, temp. derivatives at constant volume 80−59549
halides, F-band energies extended ion model, variational method 78−60086
halides, moments of phonon spectrum from sp. ht. data 77−35649
intercalation compounds with graphite, nucl. relax. times 80−44947
intercalation cpd., NMR 77−90048
intercalation with graphite, Raman scatt. study 80−88999
ionic conductors, review 77−84979
(Li^+,-) model calcs., correl. between electron affinity and dipole moments 77−57857
LiF, TLD material, nonlinear response to mixed dose rates 79−5372
$^6LiH_3(SeO_3)_2$, absolute atomic arrangement rel. to spontaneous polarisation, neutron diffr. study 80−15067
LiH, cubic, vibronic struct. and anisotropy of excitons, refl. and edge luminesc. spectra 78−23523
α-$LiIO_3$ powders, temp. depend. of electro-acoustic echo 80−66115
$LiNb0_3$ wedge waveguide apodised interdigital transducer evaluation 77−27451
$LiNbO_3$:Fe(Cu), photorefractive recording of volume holograms 78−37849
$LiNbO_3$, elec. quadrupole coupling const. of ^{93}Nb, cross relaxation processes, polarised β-active nuclei 80−60431
$LiNbO_3$ single-mode planar waveguides for integrated optics, fabrication *(Korean)* 80−43448
lithium acetate dihydrate, γ-irrad., methyl radical, ENDOR, line-shape model appl. 79−73853
lithium ammonium tartrate, ferroelectric and ferroelastic transitions, Brillouin scatt. meas. 79−33716
lithium ammonium tartrate, piezoelec., proper ferroelastic transition 78−2812

lithium compounds continued
lithium ammonium tartrate dihydrate, ferroelectric-elastic phase transition, theoretical model and expt. *(Russian)* 80−75961
lithium ammonium tartrate monohydrate, isostructure with lithium potassium tartrate monohydrate: Mn^{2+}, EPR obs. 80−29607
lithium ammonium tartrate monohydrate, Raman spectra, anomalous low-lying response 80−2746
lithium ammonium tartrate monohydrate, spontaneous shear strain, X-ray obs. 78−56433
lithium ammonium tartrate monohydrate, struct. phase transitions, light scatt. meas. 79−95774
lithium formate monohydrate, temp. depend. Raman spectra, H bonds 78−6673
lithium hydrogen phthalate monohydrate, X-ray cryst. struct. determ. 79−14791
lithium potassium tartrate monohydrate: Mn^{2+}, isomorphism with lithium ammonium tartrate monohydrate, EPR obs. 80−29607
lithium thallium tartrate, single cryst., thermal cond. at low temps. 79−33125
lithium thallium tartrate, sp. ht., 0.3 to 25K, second-order ferroelec. transition 80−59674
lithium thallium tartrate monohydrate, paraelectric phase structure by neutron diffraction data 79−19238
melt-crystal interface temp. meas. during crystallization of melts 79−44908
microwave optical radiation modulator using $LiNbO_3$ crystal resonator 77−27353
nylon 6-Li halide mixtures, viscoelastic behaviour, stress relaxation 80−58995
nylon 6-LiCl mixtures, DC cond. and struct., Lill effects 80−44149
optical waveguide channel branches 80−58811
oxalate hydrate, proton spin-lattice relax., 180° flips and diffusion of water mol. 77−15327
perfluoro-octanoate-water, liq. cryst., ^{19}F multipulse NMR obs. 80−34795
polyisoprene, struct. regularity and crystn. 80−103269
salt electrolyte submillimetric absorption obs. 80−60611
sitall coatings in Li_2O-Na_2O-CaO-SiO_2 system, heat treatment effects on tech. characts. 78−84853
soaps, n.C_{13}-n.C_{20}, phase transition temps. and enthalpies, DSC obs. 80−45544
sodium decylsulphate-Li_2SO_4-decanol-H_2O system, lyotropic liq. cryst., high resolution NMR 79−4243
solid electrolyte, synthesis and characterisation, secondary cell appl. *(French)* 80−72034
solid electrolyte materials, review of crystal and electrochem. props. 80−107524
solid electrolytes, review 77−84980
superionic conductors, prep. 80−71610
TCNQ salt, Li^+TCNQ^-, extrinsic and intrinsic mag. susceptibility 78−43556
tetramethylaminelithium(0), $Li(CH_3NH_2)_4$, existence, conduction- and localised-electron spin reson. 80−66035
transition metal oxides, Li incorporated, topochem. reactions, chem. prep. and characterisation 80−61115
trisoxalatoferrate complexes, Mossbauer studies of electronic relax. phenomena 80−44973
zeolite inclusion complexes, LiA.$LiNO_3$ and LiX.$LiNO_3$, ^7Li NMR motional line narrowing 79−56618
$LiTbF_4$, NMR shift tensors, temp. and field depend. 79−38391
Ag-LiF, alternating plasma-dielec. five layer system, ATR angular spectra 79−19943
$AlCl_3$-LiCl, molten mixtures, specific cond. meas., comp. and temp. depend. 80−15279
β-AlO_3-(Na,Li)$_2O$, NMR, Raman and IR spectra, and X-ray diffr., heat treatment induced changes 80−107508
β-Al_2O_3-(Na,Li)$_2O$, first-order quadrupole NMR obs. of cation distrib. and ion motion 80−108113
β-Al_2O_3-(Na,Li)$_2O$, ionic motion obs. using NMR and internal friction 80−108099
β-Al_2O_3-(Na,Li)$_2O$ and β-Al_2O_3-(K,Li)$_2O$, ionic cond. and Raman spectra 80−107509
β-Al_2O_3-(Na,Li)$_2O$ solid electrolyte, Li motion and activation obs. using ^7Li NMR 80−108100
β″-Al_2O_3-Li_2O, ionic cond. at room temp. 80−107513
β-Al_2O_3-Li_2O, low temp. dielec. susceptibility meas. 79−82911
β-Al_2O_3-Li_2O, low-energy excitation spectra, localised modes 80−59606
β-Al_2O_3-Li_2O, Raman scatt. from $^6Li^+$ and $^7Li^+$ ions 79−28766
β″-Al_2O_3-Li_2O, single cryst. Raman scatt., cond. mechanism and cryst. struct. 80−66209
β-Al_2O_3-Li_2O, sp. ht., 0.1-1 K, evidence for localised low-energy excitations 78−34632
β-Al_2O_3-Li_2O, thermal cond. below 300K 77−24454
β-Al_2O_3-Li_2O, with mobile ion species, dielec. relax. 79−91351
β-Al_2O_3-Li_2O-Na_2O, solid electrolytes, elec. props., stability 77−84978
β-Al_2O_3-Li_2O-Na_2O, spin-lattice relaxation and Li motion 80−70451
β-Al_2O_3-Na_2O-Li_2O, ^7Li NMR 79−15361
Al_2O_3-Na_2O-Li_2O, phase transformations during firing 80−3036
β-Al_2O_3-Na_2O-Li_2O, struct. determ. by powder neutron diffr. 79−46623
β″- Al_2O_3-Na_2O-Li_2O (8.85, 0.75 wt.%) pressing powders, prep. by spray drying 80−40294
β-Al_2O_3-Na_2O-Li_2O membranes from Na-S cells, failure anal. 80−12003
Al_2O_3-Na_2O-LiO_2 (8.8, 0.75 wt.%) exam. of Na^+ resistivity as function of temp. grain size model 78−80654
Al_2O_3-SiO_2-Li_2O, coordination number study by AlK_α fluorescence X-ray spectra *(Japanese)* 77−73190
β-Al_2O_3.Li_2O, low temp. sp. ht., tunnelling states and diffusion theory 77−43345
$Al(PO_3)_3$-LiF system glasses, microhardness and US vel. 79−99274
$Al(PO_3)_3$-NaF-LiF glasses, mixed-alkali effect 80−19715
n-alkanoates, long-chain, thermal and phase props. 77−62619
B_2O_3-Li_2O glass, absorption spectra of S_2 mols. 79−24337
B_2O_3-Li_2O-Fe_2O_3, prep. by quenching methods, exam. of microcrystalline precipitates of Li_2O-Fe_2O_3 *(French)* 79−20019
B_2O_3-Li_2O-Li Cl(F)(I)(Br), vitreous, ionic cond. of Li *(French)* 79−90823
B_2O_3-Li_2O-LiCl, X-ray irradiation, EPR of Cl_2^- colour centres *(French)* 79−47333
B_2O_3-Li_2O-LiCl glass system, exam. of ionic conductivity of Li *(French)* 78−51730
B_2O_3-Li_2O-LiCl glasses, solid electrolyte, NMR meas. 80−29208

lithium compounds continued
[(100-x)B_2O_3.xLi_2O]$_{98}$.2CdO, glass, X-ray irrad., EPR study of Cd^+ centres *(French)* 78−43638
$Ba_{0.725}Sr_{1.775}Li_xNb_{5-x}Ti_xO_{15}$, solid soln., prep., struct., dielec. props. *(French)* 77−69782
$BaTiO_3$, photorefractive effects and light-induced charge migration 80−69447
BeF_2-LiF, thermodynamically predicted miscibility gap 78−11209
BeF_2-LiF molten mixtures, mass transport, chronopotentiometry 77−21391
BeO-P_2O_5-Li_2O glass, gamma irrad., cation modifier effect on radiation centre formation 80−40720
BeO_2-Al_2O_3-SiO_2-LiF system glass, role of fluoride cations during crystn. 79−65176
$Bi_{12}SiO_{20}$ crystal, piezoelec. and SAW props. 80−75949
β-$Li_xV_2O_5$ bronzes, thermochemical study 80−55691
CLi_3, desorption from graphite expt., ionis. pot. 79−34392
C_3Li_4, structure calculations 78−5364
CaO-Li_2O-Al_2O_3-SiO_2:Nd^{3+}, CaO enriched, laser-type glasses, spectroscopic behaviour 78−60497
CaO-Li_2O-B_2O_3, calibo glass, $Dy^{3+}\rightarrow Ho^{3+}$ non-radiative energy transfer, diffusion limited relaxation 79−65925
CaO-Li_2O-B_2O_3:Dy^{3+} glass, optical excitation energy transfer from $Dy^{3+}\rightarrow Nd^{3+}$ 79−15515
CdF_2-LiF, liquid mixture, enthalpy of mixing 78−48684
$CdLi_2(PO_3)_4$, cryst. struct. determ. *(French)* 77−4069
CdS-$LiNbO_3$ monolithic two-dimensional Fourier transformer 79−72516
CdS-$LiNbO_3$ structure, acoustoelectric interaction of surface waves with inhomogeneously distributed free carriers 77−43668
$CoCl_2$-LiCl-glycerin-water system, Co^{2+} ion coordination transition, spectral investig. 79−42953
CoO-Li, dislocation spacing effect on high-temp. creep 78−35444
$CsLi_{0.5}(Al,Fe)_{1.5}F_6$ pyrochlore, Mossbauer contrib. to exam. of cationic order *(French)* 80−93224
$Cs_2LiFe(CN)_6$, struct., phase transformations, temp. depend. Raman spectra 79−11416
$CsLi_{0.5}Fe_{1.5}F_6$ pyrochlore, Mossbauer contrib. to exam. of cationic order *(French)* 80−93224
$CsLiSO_4$, crystal structures of I and III phases, twins 80−70181
$Fe(Li_{0.5}Fe_{1.5-x/8}Mn_{x/8})O_4$ $0\leq x\leq 2$ spinel system, X-ray diffr. anal. of loss of order on Cr substitution 79−73178
Fe_5LiO_8, magneto-crystalline anisotropy, magnetoelectric effect interpretation *(French)* 79−47316
Fe_5LiO_8, magnetoelec. effect interpretation by magneto-cryst. anisotropy *(French)* 79−33515
α-Fe_2O_3-Li_2O, structural and thermal phase behaviour from mag., spectral and thermal studies 80−2673
FeS Li_2S−Cu_2S system, Mossbauer spectra and lattice parameters 79−78584
Ge:Li, Cu p-n junctions, current stimulated LiCu complex formation, photocurrents 80−107897
GeO_2-Li_2O glass, Raman spectra, struct. and crystn. 80−92463
H+LiF, laser-induced nonadiabatic collision process, classical model 80−97701
$HgLi_2(PO_3)_4$, cryst. struct. determ. *(French)* 77−4069
InAs/$LiNbO_3$ structure, SAW generated transverse acoustoelectric voltage, image scanning and signal processing appl. 80−49826
InSb/$LiNbO_3$ acoustoelectric convolver, gap-coupled, for IR imaging device 78−94492
InSb-$LiNbO_3$ SAW convolver, efficient struct. realisation, Hall mobility meas. 80−83705
KCl:LiCl 79−72713
KF:LiF, photodichroic, real time recording medium, for optical spectrum analyzer 78−71174
KF:LiF, photodichroic real-time recording medium, for optical spectrum analyser 78−66878
KF:LiF photodichroic crystals as adaptive spatial filters 79−72713
KF:LiF photodichroic spatiai light modulator for joint Fourier transform correlation 80−106617
$K^2H_2PO_4$ electro-optic shutter natural birefringence compensation by β-$LiIO_3$ monocrystal 79−55247
$KLi_3Ca_7Ti_2(Si_6O_{18})_2F_2$, baratovite, cryst. struct. determ. by X-ray diffr. 77−76382
$K_6LiFe_{24}S_{26}Cl$, Mossbauer spectra and lattice parameters 79−78584
$K_{2.89}Li_{1.55}Nb_{5.11}O_{15}$, elastic and piezoelec. props. 79−15403
$K_3Li_2Nb_5O_{15}$ films for optical waveguides epitaxial growth and characterisation 80−79016
$K_3Li_2Nb_5O_{15}$ optical waveguides fabricated on sapphire by RF sputtering 79−98488
$K_xLi_{1-x}NbO$ films, epitaxial growth by melting on $K_{1.5}Bi_{1.0}Nb_{5.1}O_{15}$ substrate 79−33204
$K_xLi_{1-x}NbO_3$, epitaxial growth of single-cryst. films on $K_2BiNb_5O_{15}$ substrate by RF sputtering 79−15041
$KLi(Pt(CN)_4).2H_2O$, cryst. struct., polarised emission obs. 78−52538
$KLiSO_4$, ^7Li NMR, spin-lattice relax. *(Chinese)* 80−39884
$KLiSO_4$, phase transition, lattice parameter variation with temp. 78−79767
$KLiSO_4$:Cr; optical activity characts. cryst.-chem. exam. 78−95569
$K_{0.75}Li_{0.25}TaO_3$, press. depend. of impurity soft modes, low energy Raman scatt. meas. 78−2852
$KLi[Pt(CN)_4].2H_20$, energy band calcs. 77−39780
$K_5NdLi_2F_{10}$, high yield luminesc., potential miniature Nd laser 79−1784
$K_2O.3MoO_3.3H_2O$, fibrillar crysts., morphology and struct. 78−63959
$K_5PrLi_2F_{10}$:Pr^{3+}, emission spectroscopy, ionic interaction 79−83015
$LICr_{0.99}Fe_{0.01}O_2$, layer oxide, dimensionality of mag. interactions, Mossbauer study *(French)* 78−23377
$LIFe_5O_8$, absolute struct. and space group determ. by electron microscopy 77−62454
LIOT, release from CTR, radiological dose calc. 78−78511
LaF_3-BaF_2-ZrF_4-LiF, glassy transition, refr. index, density and molar refr. 80−1937
(Li,Na,Cu,Zn) ferrites, nonceramic synthesis, electrochem. investig. 78−35339
(Li,Na,K) $(Nb,Ta)O_3$, pseudo-binary and ternary systems quenched metastable glassy and cryst. phases 80−29935
(Li, Na)NbO_3 ceramic, dielectric and electromechanical props. 77−40183
(Li,Na)NbO_3, polycryst. disc, temp. and time dependent dielec. props. 77−81060
(Li,Na)VO_3, struct. systematics 79−55719
lithium compounds continued
Li,K/PO_3,F system, low melting point comp., solvent for InP electrodeposition 79−28079
Li,Na/PO_3,F and Li,K/PO_3,F systems, low melting-point comps. for electrodeposition appl. 79−43662
Li,Na/PO_3,F system, low melting point comp., solvent for InP electrodeposition 79−28079
Li aluminosilicate glasses, variation of refractive index during ion-exchange diffusion from molten salts *(Russian)* 77−28539
Li complex, butene-2-cis Li^+, intermolecular interaction energy, PCILO calc. 77−34572
Li complex, $Li_4W_2(CH_3)_{8-x}Cl_x.4THF$, quadrupole bond stability, crystallographic investig. 77−58193
Li complexes $((C_2H_2X_2)_2Li)^n$ where X=S, O, binding and orbital energies, biological systems ab initio calc. 80−102442
Li compounds, electronic structure, configs., energy, bonding, of small mols. and complexes 78−13420
Li ferrite, cladding on plastic foil, thermal deform. *(Polish)* 80−30002
Li ferrites, nuclear spin echo excitation on subharmonics, and multiple freq. *(Russian)* 80−60454
Li ferrites, porous, porosity effect on saturation of magnetisation 80−108036
Li H^-, mol. orbital calcs., diffuse functions for basis sets, electron affinity 78−25436
Li IO_3, parametric generation of nanosec. high-power pulse, tunable over 0.74-1.85 μm 79−18484
Li matrix ferrites, coercivity, synthesis, thermostability control 80−80569
Li^+ ion complexes with HF, H_2O, and NH_3 solvent molecules, structural and electronic props. calc. 77−57873
Li/TiS_2($TiSe_2$)($Ti_{1-t}S_2$), electrochem. obs. of Li intercalation 80−61216
Li-Al-Cl system, thermodynamic props., phase equilib. 80−89211
Li-Al-borophosphate glass, activated with Ag, in-reactor dosimetry *(Russian)* 77−83113
Li-Co ferrite, mag. anisotropy induced by thermomag. treatment, ionic order effect, magnetostriction meas. 80−103830
Li-Cr ferrite, $Fe(Li_{0.5}Fe_{0.25}Cr_{1.25})O_4$, one-magnon light scatt. with and without compensation temps. 78−31062
Li-ferrite, ultrafine powders, prod. by cryochemical, freeze drying, spray drying or soln. techniques 80−55336
Li-graphite intercalation compounds, synthesis, elec. and optical props. 79−74108
Li-H_2O(ethylene) 78−66465
Li-La phosphate glass, Nd, Cr activated, Nd luminesc. quantum efficiency meas., Nd-Cr nonradiative transfer 80−66296
Li-$La_{1-x}Nd_x$ phosphate glasses, stimulated emission spectroscopy of $^4F_{3/2}$ to $^4I_{11/2}$ and $^4F_{3/2}$ to $^4I_{13/2}$ transitions 79−38573
Li-LiH, evaporation diagram at high liq. phase hydride concs. 77−35681
Li-LiH liq.-vap. equilib., activity coeff. 80−103468
Li-LiH system, H isotope solubility thermodynamic singularities 80−81356
Li-LiH two-phase equil. system, vaporis. diagram at high temps. 80−19926
Li-LiH_x system, vaporization diag. 78−43113
Li-Na ferrite powders, props. rel. to Fe_2O_3 chem., thermal, mech. historical 79−11539
Li-Nd-La phosphate glass, nonradiative losses, pulse periodic stimulated emission and luminesc. 77−83878
Li-Nd-La phosphate glass active elements, laser characts., comparison with Nd:YAG 80−33002
Li-pyrographite intercalation cpds., synthesis and elec. resist. 79−91601
Li-Rh-H system, intermetallic cpds. and phase relationships, cryst. struct. 78−44084
Li-Ti ferrite, microwave props. 77−40082
Li-transition metal dioxide intercalation compounds, mag. props., decomposition effects 80−25075
Li-Zn ferrite, magnetic props., effect of V_2O_5 addition *(Japanese)* 77−28415
Li-Zn ferrites, (Li, Zn, Ti, Cr substituted), Mossbauer spectrometry, effect of supertransferred hyperfine fields and relaxation *(French)* 80−80654
Li^+-ligand complexes, NMR appl. ^7Li chemical shifts, expt. and ab initio studies 80−63670
Li^+-rich borate glasses, ionic cond. and activation energy 80−107561
Li+LiH, collinear reactions, SCF correl. diagram for Li_2H 77−70292
$Li_{0.5}Fe_{2.5}O_4$, microwave material, mag. props., review 79−33504
Li_2, $A^1\Sigma_u^+$-$X^1\Sigma_g^+$ band system transition dipole moments and radiative lifetimes, model pot. calcs. 78−9160
(Li-Cs)NO_3, molten, internal cation mobility meas. 79−60534
(Li-K)NO_3, molten, $K^+(Rb^+)(Cs^+)(Tl^+)$ diffusion, wavefront shearing interferometric obs. 79−60535
(Li-Rb)NO_3, molten, internal cation mobility meas. 79−60534
LiAl ferrite, substituted ferrospinel, spin configuration determ. *(Russian)* 77−32162
LiAl, transport props., rel. to semimetallic band struct. 80−88581
LiAl-NaAlCl$_4$-$MoCl_5$ thermal battery test results 79−29459
LiAl-NaAlCl$_4$-$MoCl_5$ thermal battery evaluation and optimisation 79−29458
$LiAlCl_4$, fast ionic conductor, thermodynamic and phase props. 80−89211
$LiAlCl_4$, solid and liq., ionic cond., 25-180°C 77−20114
$LiAlCl_4$, solid and molten electrolyte, thermodynamic stability 80−107447
$Li_{0.5}Al_{2.5-t}Cr_tO_4$,($0\leq t\leq 0.25$), cryst. struct. 79−60319
$LiAlF_4$, dissoc. enthalpies, mass spectrometric determ., heat of form. 80−97720
$LiAlF_4$, struct. pot. energy surface, Li^+ migration, ab initio LCAO SCF calcs. 80−23305
Li_3AlF_6-AlF_3, liquid-solid and liquid-liquid enthalpy of mixing meas. 77−40569
$LiAl_xFe_{5-x}O_8$, IR spectra, ionic ordering in absence of fine struct. 77−8583
$Li_{0.5}Al_xFe_{2.5-x}O_4$, polycrystalline, ferromag. reson. absorpt. curves, stress effects *(Russian)* 77−20713
$Li_{0.5}Al_xFe_{2.5-x}O_4$, polycrystalline ferromagnetic reson. theory applicability limits *(Russian)* 77−55709
$Li_5Al(Ga)O_4$, ionic cond. depend. on moisture, potential humidity sensors 79−65248
$LiAlH_4$, ab initio calc. of geom. struct., charge distrib., bonding and pot. energy surfaces 80−18796
$LiAlH_4$, molar heat capacity, thermodynamic props., 10 to 300K 80−44329

lithium compounds continued
Li_3AlH_6, molar heat capacity, thermodynamic props., 10 to 300K 80−44329
$LiAlO_2$ coating, on 316 stainless steel, corrosion protection of molten carbonate fuel cell gas seal 79−39293
$LiAlO_2$, fine particle size, heat treatment synthesis, molten carbonate fuel cell appl. 80−21395
$LiAlO_2$, fuel cell electrolyte matrix, prep. and struct. charact. 78−80488
$LiAlO_2$, matrix support material for molten carbonate fuel cell, thermal stability, effects of different environments 80−50952
α-$LiAlO_2$, NMR study of Li^+ motion 79−42863
β-$LiAlO_2$, reindexing X-ray powder diffr. pattern 79−51069
$LiAlO_2$ solid breeding banket, low temp. T cyclic purging 79−59256
$LiAl_5O_8$, ordered single cryst., struct. determ. *(French)* 80−15074
$LiAl_5O_8:Cr^{3+}$, fluoresc. and excitation spectra, zero phonon lines 79−33785
$LiAl_5O_8:Cr^{3+}$, primary and stimulated photon echo generation 79−10364
$LiAl_5O_8:Cr^{3+}$, self-induced transparency and light echo *(Russian)* 77−62016
$Li_{0.5}Al_{2.5}O_4$, spinel struct. magnetodielectrics, free energy of form. 79−83493
Li_5AlO_4, additives and moisture effect on ionic cond. 80−107523
Li_5AlO_4, α and β phases, NMR study of Li^+ motion 79−42863
Li_5AlO_4, ionic cond., effects of Li_2SO_4 addition, moisture, and LiOH 79−99362
Li_5AlO_4, ionic conduction, environment effects 77−76600
β-Li_5AlO_4, microcryst., neutron irrad., ^3H diffusion studies, fusion blanket appl. 80−18627
Li_5AlO_4, NMR relaxation by paramag. impurities 79−42866
Li_5AlO_4 pure and doped ionic conductivity increase obs. 78−14506
$LiAlSiO_4$, and $LiAlSi_2O_6$, ionic cond. 77−1256
$LiAlSiO_4$, β-eucryptite, one-dimens. Li ionic cond. 77−84982
$LiAlSiO_4$, β-eucryptite, one dimens. co-operative Li diffusion 78−2294
$LiAlSiO_4$, β-eucryptite, heating effect on domain struct. 79−66078
$LiAlSiO_4$, β-eucryptite one-dimens. fast ion cond., temp. depend. of cryst. struct. 80−107191
β-$LiAlSiO_4$, cryst. growth from high temp. LiF-AlF_3 soln. 78−31317
$LiAlSiO_4$, crystalline, glass and glass-ceramic form, effect of composition changes, substitutions and press. on ionic cond. 78−43172
β-$LiAlSiO_4$, eucryptite, temperature-compensated cuts for SAW devices 78−60018
β-$LiAlSiO_4$, eucryptite, one-dimensional ionic conductor, neutron scatt. study 80−49361
$LiAlSiO_4$ glass-ceramics, percolative ionic cond. 77−76605
β-$LiAlSiO_4$, superionic cond., NMR relax. 77−12220
β-$LiAlSiO_4$, superionic cond., ionic cond. and NMR line narrowing 79−42306
$LiAlSiO_4$:Cu, β-eucryptite solid electrolyte, Cu^{2+} EPR obs. of ion exchange props. 80−108056
$LiAlSi_2O_6$, IR refl. spectra dispersion anal. 79−99877
$LiAlSiO_4$, β-eucryptite, superionic conductor, order-disorder transition, microwave impedance obs. 79−14966
α-$LiAmO_2$, prep. and crystallographic data *(French)* 78−47290
Li_xAmO_{1+x}, after-effects of ^{241}Am α-decay, ^{237}Np Mossbauer spectra obs. 79−61271
$LiAsF_6$, cryst., elec. cond. 80−34232
Li_3AsO_4, electronic struct. of AsO_4^{3-} clusters 79−65417
$Li_3AsO_4:CrO_4^{3-}$, EPR, 4.2K, cryst. field parameters 79−28586
Li_5B_4, cryst. struct., X-ray and neutron diffr., and NMR 79−23571
$LiBF_4$, $LiHBF_3$, spin-spin coupling and T_1 in non-aq. solns. 77−23512
$LiBF_4$, nonrigid mol. struct. and stability, ab initio calcs. 80−83259
$LiBF_4$, thermal decomposition, equilib. decomposition press. and enthalpy of form. 79−91983
$LiBH_4$, ab initio calc. of geom. struct., charge distrib., bonding and pot. energy surfaces 80−18796
$LiBH_4$, comparison of potential surfaces, calculated ab initio and semiempirical CNDO/2 scheme 79−41112
$LiBH_4$, H bridged system, floating spherical Gaussian model 80−78518
$LiBH_4$, non-rigid complex molecule, ab initio calcs. of pot. energy surface and geometric struct. 77−6678
$LiBH_4$, pot. surface and geometry, ab initio calcs. 78−86771
$LiBH_4$, struct., pot. surface, ab initio calcs. 79−41092
$LiBO_2$, Czochralski growth 78−19657
$LiBO_2$-In_2O_3, phase composition, mag. props, elec. cond. 80−55365
LiB_4O_7, crystal growth from undercooled melt 77−52248
$Li_2B_2O_4$-$LiFe_5O_8$ glass, rapidly quenched, mag. and ferrimag. props. 80−75744
$Li_2B_2O_5$ glass, phase separation 79−41965
$Li_2B_4O_7$, Czochralski growth 78−19657
$Li_2B_4O_7$, ferroelectric glass, phase transition, permittivity, electrochromism, photochromism 80−80719
$Li_2B_4O_7$, heat low controlled growth during crystallisation 79−65014
$Li_2B_4O_7$ TLD, comparison of two commercially available types 79−81094
$Li_2B_4O_7$ thermoluminescent dosimeters, high dose characteristic 78−35966
$Li_2B_4O_7$:Ag TLD, fast neutron dosimetry 78−94163
$Li_2B_4O_7$:Cu, Ag, as thermoluminescence dosimeter *(Japanese)* 78−31906
$Li_2B_4O_7$:MN bulb dosimeters, nonuniversality of TL linear energy transfer response 79−97948
$Li_2B_4O_7$:Mn, gamma ray response 80−23153
$Li_2B_4O_7$:Mn, TLD phosphor, γ-induced sensitisation and residual thermolum. 79−28844
$Li_2B_4O_7$:Mn, thermolum. response to pions 80−101270
$Li_2B_4O_7$:Mn TLD phosphor, additivity of α and γ response 79−9891
$Li_{4+x}B_7O_{12+x/2}$ Cl, solid solns., ionic cond. rel. to struct. and chemical bonding *(French)* 78−2295
$Li_{4+x}B_7O_{12+x/2}$Br, solid. solns., ionic cond. rel. to struct. and chemical bonding *(French)* 78−2295
$Li_{4+x}B_7O_{12+x/2}$Cl, solid electrolyte, NMR meas. 80−29208
$Li_4B_7O_{12}Cl$, cryst. struct. and ionic conductivity 77−84690
$Li_4B_7O_{12}Cl$, new solid electrolytes, conductivities and activation energies 79−28137
$Li_4B_7O_{12}Cl(Br)$, Li^+ mobility, isotropic cond. *(French)* 77−1258
$(Li_2B_4O_7)_{1-x}(WO_3)_x$ dipolar glass, space charge injection, thermally stimulated depolarisation currents 80−66103
$Li_2B_4O_7.xWO_3$ (x=0 to 1 mol.) glass, random elec. dipole, cooperative phenomena 79−28693

lithium compounds continued
$LiBaAlF_6:Eu^{2+}$, luminesc., band emission and line emission 79−28810
$LiBaF_3:Cr^{3+}(Mn^{2+})(Fe^{3+})(Co^{2+})(Ti^{3+})$, EPR, spin Hamiltonian parameters 79−65718
$LiBaF_3:Mn^{2+}$, having inverse periodic struct., ENDOR study 80−97162
$LiBa_3Nb_3(Ta_3)(Sb_3)Ti_5O_{21}$, insertion of Li, X-ray and neutron diffr. study *(French)* 78−91324
$Li_2Ba_4O_7$ non-universality of TL-LET response, effect of high-temp. TL 80−99348
$LiBaPO_4$, vibrational spectra and cryst. struct. 78−39536
$LiBeF_3$, $LiBe_2F_4$, molten, self-diffusion of Li 80−54417
$LiBeF_3$, pot. energy surface, struct., stability and internuclear distances, ab initio calc. 80−58147
Li_2BeF_4, melting systematics at high press. 77−51475
Li_2BeF_4, molten, thermal diffusivity meas. at 470-700°C 77−82525
Li_2BeF_4-Na(K)BF_4, phase diagram 77−21119
$LiBeH_3$, ab initio calc. of pot. surfaces and geometry 79−10024
$LiBeH_3$, H bridged system, floating spherical Gaussian model 80−78518
$LiBeH_3$, pot. surface, struct., ab initio calcs. 77−88385
LiBe(Mg)(Ca), $^2\Sigma^+$ and $^2\Pi$ states, mol. binding energy curves 80−58189
Li_3Bi, evaluation as electrode material, electrochem. expts., 360-600°C 78−11526
$LiBi(MoO_4)_2$, acoustooptic characteristics 79−8118
$LiBi_xNd_{1-x}P_4O_{12}$ waveguide laser layer epitaxially grown on $LiNdP_4O_{12}$ substrate 80−23709
LiBr absorption, solar air conditioning system, low and high temp. cycles 80−81425
LiBr absorption air conditioner, solar powered, computer-aided performance predictions 79−62134
LiBr, aqueous soln., NO_2^- impurity anions, temp. quenching of luminesc. *(Russian)* 77−1714
LiBr, Compton profile anisotropies 79−27044
LiBr, dil. aq. solns., conductance at 25°C 77−69105
LiBr film, electron emission under metastable He and Ne atom impact 80−20747
LiBr, in anhydrous acetone, elec. conductance at high press., Shedlovsky method 78−53219
LiBr, liq., ionic motion study using memory functions 80−10484
LiBr, liq., transport processes by ionic dynamics, isotope substitution, mass enhancement 78−22616
LiBr, pair pot., dipole moment, polarisability tensor, bond length depend., finite field SCF calcs. 80−58127
LiBr, shock adiabatic, nonparametric equation of state 78−10121
LiBr soln., conductance and viscosity, temp. and concentration depend. 80−6531
LiBr solution, EPR of O_2^- luminesc. centres, 4.2K *(Russian)* 79−15339
LiBr, XPS, satellite of Br 4s line 78−56556
$LiBr:Cu^{2+}(Ni^{2+})(Co^{2+})(Fe^{2+})(Mn^{2+})$, optical absorpt., charge transfer spectra 80−2797
LiBr-Al_2Br_6 soln. in toluene, conduction mechanism 80−6870
LiBr-KBr, liq. mixture, struct. and diffusion 80−24344
LiBr-LiF-KBr-KF, fused, miscibility gaps 79−82348
Li_2Br_2, UPS of dimeric mol., expt. and Xα calc. 80−9640
$LiBrO_3$, radiation damage, XPS obs. 80−29844
LiC_{12}, intercalation cpd., electronic struct. calcs. 80−70613
LiC_6, band struct., density of states and Fermi surface props. 79−37982
LiC_6, intercalated, charge-transfer and non-rigid-band effects 80−44496
LiC_6, intercalated graphite, band struct. determ. by angle-resolved photoemission 80−45203
LiC_6, intercalation compound with graphite, sp. ht. meas., 4-300K 80−44332
LiC_6, intercalation compound, electronic struct., XPS meas. 80−59850
LiC_6 intercalation cpd., synthesis method and reflectivity spectrum 79−15600
LiC_6, intercalation cpd., electronic struct. calcs. 80−70613
LiC_6, prep. from Na-Li melts *(French)* 80−2970
LiC_6, Raman spectrum, rigid band model anal. 79−4800
LiC_6, spatial distribution of valence electrons 79−37983
LiC_x, lamellar cpds. with graphite, EPR studies 80−44902
LiC_x, lamellar cpds. with graphite, ^{13}C NMR studies 80−44936
Li_2C_2, heat of formation, at. absorpt. spectrometric determ. *(Russian)* 78−15699
Li_2C_2 solubility in Li, for fusion reactor appls. 80−13840
$LiCH_5$, H bridged system, floating spherical Gaussian model 80−78518
LiCL, band struct. calc. by mixed LCAO and OPW method 77−8019
LiCN, electron density distrib., SCF mol. orbitals calcs. 78−9058
LiCN, vibr.-rot. spectra, model with two large-amplitude coords. 78−5196
LiCNS, ether solns., dimer struct. and force consts., IR and Raman spectra 79−72442
$Li(CO)_n$ (n=1,2,3,4,5,6,8), semiempirical CNDO calcs., solvation struct. 78−82649
Li_2CO_3, decomp. and ferritisation, effect of initial Fe_2O_3 content 77−52269
Li_2CO_3, molten, IR emission spectra *(Japanese)* 78−19469
$^7Li_2CO_3$, and $^6Li_2CO_3$, polycryst., low freq. IR and Raman bands assignments 79−42970
$^7Li_2CO_3$, and $^6Li_2CO_3$, polycryst., Li-O Raman bands 79−42969
LiCa, laser chemiluminesc. 80−93759
Li_2CaUF_8, X-ray single cryst. struct. determ. 79−77574
LiCd ferrite, dielec. const. and loss meas., 50-10^6 Hz 77−77135
$LiCdBO_3$, cryst. struct., X-ray determ. 79−19226
$LiCdBO_3$ triclinic cryst. struct., X-ray and Patterson function anal. 80−39055
$LiCdSiO_4$, X-ray cryst. struct. determ. 77−80458
$LiCdVO_4$, luminesc. spectra in visible region, vanadate group 78−43921
LiCl (Br), aqueous solutions, IR absorpt. ν_1 (CN) band parameter temp., conc. study *(Russian)* 80−80801
LiCl, and LiBr, glassy aq. solns., Raman spectra, rel. to amorphous ice and liq. water 79−47423
LiCl, aq. soln., ^7Li spin-lattice relax. time, 5-65°C 77−48075
LiCl, aq. soln., density, isothermal compressibility, 293.15K, up to 200 MPa 80−44243
LiCl aq. soln., vel. correls., time integral calcs. 80−59360
LiCl, aqueous, proton, deuteron and ^7Li relax. times, mol. motion obs. 79−28632
LiCl aqueous glass, X-irradiated, localised electron optical, IR and photoconductivity spectra 78−73064
LiCl, aqueous soln., high precision viscosity meas. 80−10695

lithium compounds continued
LiCl aqueous soln., ion-water clusters, electronic struct., Compton profile 78−47227
LiCl, aqueous soln., NO_2^- impurity anions, temp. quenching of luminesc. *(Russian)* 77−1714
LiCl, aqueous soln., self consistent wavefunctions, HFS Xα pot. in cluster model, Compton profile calc. 79−78783
LiCl aqueous solns., dynamical props. by ultrasonic propag. meas. 80−76517
LiCl, aqueous solution at 298.15K, isentropic compressibility 78−22783
LiCl, charge transfer and pair polarisability anisotropy 80−43173
LiCl, colloidal suspension, radiowave dielec. dispersion 80−11311
LiCl, Compton profile anisotropies, charge and momentum distrib., LCAO-SCF-MO calc. 79−3500
LiCl, concentrated aqueous soln., IR absorpt. to high press. and temps. 80−80803
LiCl, deuterated aq. glasses, pulse radiolysis, trapped electron reactions 79−24804
LiCl, deuterated aqueous glasses, pulse irrad., trapped electron yield 79−20385
LiCl, dil. aq. solns., conductance at 25°C 77−69105
LiCl, effective core potentials, all-electron calcs. 78−62704
LiCl electrolyte influence of lasing props. of rhodamine G solutions 80−91788
LiCl, electron irrad., F-centre emission 78−60501
LiCl, electron momentum distrib. and Compton profiles 79−13631
LiCl film, electron emission under metastable He and Ne atom impact 80−20747
LiCl, frozen soln., NMR study of phase transitions 79−56617
LiCl glass, aqueous, neutral matrix for EPR studies of radiation damage to biomols. 79−96632
LiCl glycerol solns. quadrupole interactions, nucl. mag. relax., correl. time determ. 77−14449
LiCl, ground state pot. energy curve, improved ab initio effective core pot. calc. 80−32625
LiCl, hypersonic relaxations studied by Brillouin light scatt. techniques, viscoelastic effects obs. 80−83375
LiCl in H_2O, complexity investigation using US method 80−33326
LiCl in water+tetrabutylammonium tetraphenylborate in nitrobenzene systems, electrolyte dropping electrode investig. 77−25279
LiCl, Li isotopic comp. determ. by mass spectrometry 80−66899
LiCl, microcrystal, melting, mol. dynamics simulation 80−65199
LiCl molecular dissoc., obs. by interference method 80−40684
LiCl, molten, struct. anal. by X-ray diffr. 78−94961
LiCl, neutron irradiated, EPR exam. 78−76309
LiCl, photoelectron spectra using Zr Mζ, Al Kα and other X-ray lines, photoionis. cross sections ratios 77−90246
LiCl, polarisability bond length depend. 77−23422
LiCl, press. shifts of F-centre hyperfine interaction parameters 78−79957
LiCl, radiation effects on decay time of F-centre emission 80−93381
LiCl, refr. index, 300-700 nm., temp. coeff., 100-580K *(Russian)* 78−15142
LiCl, rot. excitation by electron impact, calc. cross sections 78−66670
LiCl single crysts., γ-irrad., thermolum. meas. 80−80880
LiCl, solar cooling of buildings appl., using open water evaporation 79−57463
LiCl solution, EPR of O_2^- luminesc. centres, 4.2K *(Russian)* 79−15339
LiCl, spectral interference in at. absorption spectroscopy in C tube atomiser *(Japanese)* 79−48018
LiCl, thermolum., order of kinetics 80−89074
LiCl, thin film, crystal-vacuum (100) surfaces, mol. dynamics computer simulation 80−34288
^{6}LiCl, aq., temp. depend. spin-lattice relax. and nuclear Overhauser effect 77−1613
^{7}LiCl, heavy water soln., anionic hydration, 1 bar and 1 kbar, neutron diffr. obs. 80−30212
LiCl:Ag, fluoresc. and UV absorpt. spectra 80−80844
LiCl:Ag, luminesc. anal. using synchrotron radiation 79−38639
LiCl:Ag film, EPR and optical exam. of Ag impurity centres 77−85562
LiCl:Cd, EPR of anisotropic Cd_F^+ centres, similarity to Z-centres 77−77101
LiCl:Cu^+, 3d→4p transitions, near UV absorpt. spectrum assignment 78−27272
LiCl:Cu^+, luminescent centre, cluster MO calculation of energy levels 78−64411
LiCl:Cu^+, MO calc. of luminesc. Cu^+ centres 79−38609
LiCl:Cu^{2+},$(Ni^{2+})(Co^{2+})(Fe^{2+})(Mn^{2+})$, optical absorpt., charge transfer spectra 80−2797
LiCl:F^-,$(Br^-)(I^-)$, anion impurities substitution, energies of soln., association and migration 78−83831
LiCl:Fe, defect struct., Mossbauer spectra and X-ray diffr. obs. 80−7237
LiCl:Na (K,Rb,Cs,Ag), theoretical and experimental study of partition coeffs. of isovalent impurities 79−65111
LiCl:Ni^{2+}, EPR meas. of Ni^{2+} vacancy dipoles 79−28594
LiCl:Ni^{2+}, first order induced Raman scatt. from Ni^{2+} and cation vacancies 77−48169
LiCl:V(Cr)(Mn)(Fe)(Co)(Ni)(Cu), electron transfer absorption bands 79−95810
LiCl-$AlCl_3$, molten mixture, vap. pres. meas. 78−87779
LiCl-$AlCl_3$, phase diagram determ. by DTA and X-ray anal. *(Japanese)* 78−92250
LiCl-D_2O, aq. 10 M glass, optical absorpt. spectra after X-irrad., electron scavenging efficiency 79−83476
LiCl-D_2O glass, trapped and quasifree electrons optical transitions, bound-continuum character 78−6660
LiCl-KCl, analysis of reduction waves of Ti ion in chronopotentiometry of K_2TiF_6 *(Japanese)* 78−20025
LiCl-KCl, molten mixture, struct., diffusion, cond., mol. dynamics calc. 80−64871
LiCl-KCl eutectic, anodic corrosion rate of candidate current collector metals for Li-FeS_x battery 79−100512
LiCl-KCl eutectic melt, impedance meas. of Ni/Ni(II) electrode reaction *(Japanese)* 79−100392
LiCl-KCl eutectic mixture, purification, effect of impurity ions *(Japanese)* 78−40108
LiCl-KCl molten eutectic mixture, PbS solubility product and Li_2S solubility 80−54387
LiCl-KCl:Cu^+, fused eutectic, diffusion and surface effects, chronopotentiometry *(French)* 78−11524
lithium compounds continued
LiCl-KCl:Ln^{n+}, fused eutectic, electrolytic behaviour *(Japanese)* 79−16009
LiCl-KCl:Th^{n+}, fused eutectic, electrolytic behaviour *(Japanese)* 79−16009
LiCl-Li_2O-B_2O_3 system of vitreous electrolytes *(French)* 78−27767
LiCl-LiF molten eutectic mixture, PbS solubility product and Li_2S solubility 80−54387
LiCl-$LiNO_3$-H_2O, mixed salt solutions, apparent and partial molal volumes 77−9114
LiCl-NaCl mixed crystals, Au decoration study of solid-melt interface, phase separation 80−15026
LiCl-NaCl-$AlCl_3$ melt, elec. cond., 800 to 1200K *(Japanese)* 80−24633
LiCl-NaCl-$AlCl_3$ ternary melt, density as function of temp. and composition, meas. by macrometric method *(Japanese)* 79−42130
LiCl-$PbCl_2$, molten, struct. anal. by X-ray diffr. 78−94961
LiCl-RbCl, molten, Chemla effect, mol. dynamics simulation, self exchange vel. 80−79967
LiCl-rhodamine B-H_2O solutions, absorpt. pH, electric conductance 77−27079
LiCl-$ZnCl_2$, molten, US velocity, thermodynamic quantities and struct. *(Japanese)* 80−88270
LiCl-$ZnCl_2$, molten, US absorption coeffs. and bulk viscosity coeffs. *(Japanese)* 80−88271
LiCl+$NaNO_3$, apparent and partial molar volumes in aq. soln. 78−44396
Li_2Cl^+, mass spectra, struct., stability, expt. and theory 77−554
Li_2Cl^+, triplet polarisability, ab initio MO calc. 79−98244
Li_2Cl_2, UPS of dimeric mol., expt. and Xα calc. 80−9640
$Li_nCl^{(n-1)+}$, energy cluster expansion convergence 80−91715
LiCl(Br) aqueous solutions, tetrahedral hydration of ions, Raman obs. 78−55804
LiCl(Br)(I), diamag. ion solvation in methanol soln., NMR relax. obs. 78−56389
LiCl(Br)(I), glassy aqueous soln., LF region Raman spectra 80−84729
$LiClO_4$, diamag. ion solvation in methanol soln., NMR relax. obs. 78−56389
$LiClO_4$, organic solns., complex permittivity meas., dielec. relax. spectrum *(French)* 78−27154
$LiClO_4$, radiation damage, XPS obs. 80−29844
$LiClO_4$, solutions in amides and esters, structure *(French)* 80−7343
$LiClO_4$-$CsNO_3$($RbNO_3$)(KNO_3)($KClO_4$)($RbClO_4$)($CsClO_4$), binary melt, Raman spectra, polarised line width, temp. depend. 78−84578
$LiClO_4$-propylene carbonate solution, composition of passivation layers on Li electrode *(French)* 80−11899
$LiClO_4.3D_2O$, hexagonal, piezoelec., electro-optic, dielec., elastic, thermoelastic props., space groups 78−76388
$LiClO_4.3H_2O$, absolute sign of piezoelec. d_{33} and pyroelectric p_3 coeffs. 78−43793
$LiClO_4.3H_2O$, hexagonal, piezoelec., electro-optic, dielec., elastic, thermoelastic props., space groups 78−76388
$LiClO_4.3H_2O$, pyroelec. and piezoelec. coeffs., struct. refinement 78−18602
$LiCl_2.H_2O$ activated polyvinyl alcohol film, thermochromism *(Russian)* 79−91415
$LiCoO_2$, XPS of low spin Co (III) 78−31300
Li_xCoO_2, cathode material for batteries of high energy density 80−101089
$LiCoPO_4$, flux growth 79−83113
β_{II}-Li_2CoSiO_4, disordered struct., twinning description 80−39017
β_{II}-Li_2CoSiO_4, X-ray cryst. struct. determ. 80−15062
LiCr ferrite, elec. resist., thermoelec. power and Nernst-Ettingshausen meas. near compensation point 78−10487
$LiCr_xFe_{5-x}O_8$, IR spectra, ionic ordering in absence of fine struct. 77−8583
$LiCrO_2$, EPR of Cr^{3+} ion, g-factor and effective mag. moment 77−73073
$LiCrO_2$, evaporation, as a corrosion product in compatability experiment of Li_2O pellets with Fe-Ni-Cr alloys, mass spectrometric study 79−73301
$LiCrO_2$, two-dimens. mag. order, neutron powder diffr. obs. 80−44805
$LiCrO_2$, two-dimens. mag. props. rel. to cryst. struct. 80−75776
$LiCrO_2$, two-dimensional antiferromag., mag. props. *(French)* 78−23251
Li_2CrO_4, electron irrad., reduced species form., XPS 79−11498
Li_2CrO_4-K_2CrO_4, phase diagram determination by DTA and X-ray diffr. 78−31391
$Li_2Cr_2O_7.2H_2O$, cryst. struct. 79−32980
$LiCrS_2$, noncollinear magnetic order and spin wave spectrum in presence of competing exchange interactions 80−65834
$Li_xCr_yV_{1-y}S_2$, Mossbauer and mag. studies 79−73869
$LiCrX_2$, X=S, Se, EPR meas., g-factors, effective mag. moments, and dipolar shifts 79−8043
LiCs, Hellman pseudopot. calcs., dissoc. energy, ionis. pot., bond length 77−10577
$LiCsSO_4$, thermal and dielec. props. 80−34860
$LiCsSO_3.2H_2O$, cryst. struct. *(French)* 80−24412
$LiCuCl_3$-$2H_2O$, ^{7}Li NMR lineshape 77−48061
$LiCuCl_3.2H_2O$, antiferromagnet, symm. of field-induced phases, mag. space groups 77−32166
$LiCuCl_3.2H_2O$, antiferromagnetic relax., autocorrel. function time evolution 77−59464
$LiCuCl_3.2H_2O$, EPR linewidth and relax., effect of antisymmetric exchange 77−59448
$Li_2Cu_5(Si_2O_7)_2$, cryst. struct. and proposal of new values for effective ionic radii of Cu^{2+} 79−4276
Li(D,T), prep. via exchange reaction 77−9109
LiD, appl. of microscopic and model theories of lattice dynamics of nonmetals 78−59871
LiD, cubic cryst., exciton-phonon interaction and exciton anisotropy 78−72083
LiD, deformable-ion model and lattice dynamics 77−47514
LiD, excitons and exciton-phonon interaction, refl. spectra meas. 4.9 to 5.3 eV 77−44019
LiD, isotope exchange reactions, equilib. consts., adiabatic correction, electron correl. effects 78−88626
LiD, lattice dynamics, effect of long-range three-body forces 77−89507
LiD, long-range three centre potentials, influence on lattice dynamics 80−96605
LiD, luminesc. of free and localised excitons, UV, X-ray and electron irrad. luminesc. 79−87483
LiD, phonon dispersion, microscopic calc. 79−42188

lithium compounds continued
LiD plasma, laser-irrad., inverse bremsstrahlung energy absorption 79−37521
LiD, resonance Raman scatt. *(Russian)* 78−52503
LiD, resonant Raman scattering in crystals with self-trapping excitons 80−7344
LiD, single cryst., reson. zero-phonon exciton luminesc., polariton emission 78−52564
LiD, soln. in liq. Li, elec. resist. 77−47786
LiD solubility in liquid Li 78−2259
^{6}LiD advanced fuel, fusion dynamics reactivity coeffs. 77−23296
^{6}LiD, new material for polarised targets for pol. neutron prod. *(French)* 80−68987
^{7,7}LiD, cryst., cohesive energy, force const., lattice freq., Debye temp., Gruneisen parameters, calc. 78−91293
LiD:Mg^{2+}, two peaks in ionic thermocurrent curves 77−31807
LiD:Mg^{2+}, X-irrad., dielec. loss 80−55024
LiD:Rh, EPR spectra of Rh centres, UV-irrad. cryst. 79−65724
$LiDyF_4$, NMR rotation spectra, transferred hyperfine interaction 77−85590
$LiErF_4$, cryst. field parameters, mag. susceptibility meas., 0.3 to 100K 80−60214
$LiErF_4$, EPR studies, lowest levels of rare-earth ions, submillimetre freq. 80−39865
$LiErF_4$, low-temp. mag. susceptibility, evidence of antiferromag. ordering 78−23249
$LiErF_4$, NMR rotation spectra, transferred hyperfine interaction 77−85590
$LiErF_4$ powder, ^{19}F NMR 77−48067
$LiErF_4$, spectroscopic anal. Er^{3+} polarised absorpt. spectra, cryst. field parameters 79−95756
$LiEu(PO_3)_4$, vibr. spectra 80−34905
$LiEu(SO_4)_2$, cryst. struct. 78−67695
LiF, ^{4}He scatt., selective adsorption induced intensity maxima 78−72667
LiF, ^{7}Li and ^{19}F double NMR, existence of single nuclear dipolar spin temp. 78−35065
LiF, 3 MeV electron induced, F, F_2, F_2^+, R_1, R_2 and F_2 colour centre obs., IR spectra obs. *(Russian)* 77−48210
LiF, 63 meV He atom scatt., single Rayleigh phonon interaction 78−80447
LiF (TLD-100), behaviour for doses up to 10 Mrad 77−5084
LiF (TLD-100), pre-irradiated, non-irradiation induced TLD 78−48242
LiF (TLD-100), thermoluminescent glow peaks 78−35211
LiF (TLD-100), thermoluminescent response to 0.1-5 keV electrons 79−95852
LiF (001), adsorption of H_2, molecular orbital calc. 78−87878
LiF (001), elastic and inelastic scatt. of He and Ne, selective adsorption 77−66564
LiF (001), H and D beam scatt., specular bound state reson. struct. 79−52069
LiF (001), He adsorpt., theory of selective adsorpt., azimuthal and polar dependent intensities 79−60624
LiF (001), He elastic scatt., hard corrugated surface model, GR Method 77−85863
LiF (001), He scatt., corrugated wall model, GR method 77−63520
LiF (001), He scatt., hard corrugated surface model, calc. methods 77−16447
LiF (001), He scatt., sudden approximation accuracy, coupled channel calcs. 79−4873
LiF (001), multiple Debye-Waller effects at selective adsorption in atom-surface scattering 80−76126
LiF (001), scatt. of He(Ne), sudden decoupling approxs. 78−64437
LiF (001), scatt. of Ne, coupled channel calcs., symmetry appls. 78−92156
LiF (001), surface phonon obs. in He atom inelastic scatt. 80−80927
LiF (001) surface, coeff. of thermal expansion (parallel to surface) 77−59129
LiF, (001) surface, He and Ne inelastic resonant scatt. assisted by phonons 77−73201
LiF (100), elec.-mech. coupling of dislocations 78−75676
LiF, (100) face, surface layer and dislocation etch pits 77−19962
LiF (200) Bragg peak, Mossbauer diffraction meas., calibration 79−82897
LiF, ATR IR spectrum from rough surfaces 77−20850
LiF, ab initio SCF MO energy, dipole moment and polarisability 80−1085
LiF, adsorbed on Ag photocathode, work function decrease 79−78824
LiF, adsorbed on GaAS (110), adsorpt-desorpt. processes and phase transitions 78−2361
LiF, aggregation, microcryst. form., IR spectra obs. 78−46331
LiF, alkali halide crystals, defect state change during electrolysis 78−95057
LiF, alkali ion implantation, migration, segregation, effect on optical props. 80−100269
LiF and dimer, Li 1s ionisation pot. calc., Li 1s XUV absorpt. spectrum 77−23443
LiF, anharmonic cryst. of order λ^4, self-energy of phonons, approximate numerical results 79−55843
LiF, anisotropic Compton scattering using synchrotron radiation 80−60703
LiF, annealing effects on thermoluminescence, dipoles and dimers 77−12452
LiF, appl. as X-ray monochromator for high-angle double-cryst. diffr. 77−43111
LiF, appl. of variable-path X-ray Laue diffr. meas. technique 77−31555
LiF, appl. to calibration of Mossbauer diffr. expts. 78−24906
LiF, band struct. and charge densities, intersecting spheres model 80−49591
LiF, band structure, use of two-centre approx. with Hartree-Fock eqns. 77−76726
LiF, behaviour of nucl. spins near highly polarised paramag. centres 77−77127
LiF bicrystal, high-angle tilt boundary and edge dislocation intersection effects 80−79836
LiF bicrystals, intergranular fracture due to single slip 78−34520
LiF binary molten salt sytems with NaF, KF, CaF_2, BaF_2, elec. cond. *(Japanese)* 77−76588
LiF, Bragg diffraction, anharmonic contributions, Mossbauer study 78−76359
LiF, bulk and (001)-surface equal-time vibr. correlation function 78−47655

lithium compounds continued
LiF, CESR of dendritic metal phase precip. 77−24744
LiF, calc. of third- and fourth-order elastic constants 79−10891
LiF, cation motion energy parameters, dielectric relax. meas. 78−30784
LiF cell, for X-ray struct. investigations 80−64829
LiF, ceramic, characts. on pressing in vacuum and in air 78−52734
LiF, channelling of MeV H^+ and He^+, zero dose meas. 78−18689
LiF, charged dislocations, comprehensive deform. effects on charge, elec. field 79−14815
LiF, cleaved cryst., electrification mechanism 78−19126
LiF, cluster calcs., unrestricted HF approach 78−84117
LiF, coherent freq. tunable radiation generation in F-centres, 0.6 to 1.26 μm range 79−36902
LiF, coherent radiation generation in F_2-centres 78−50782
LiF, cohesion energy, compressibility and density, ab initio calc. 77−72648
LiF compact, particle size rel. to pore characts. 78−60631
LiF, compressed crystals, inhomogeneous elec. field due to piezoelectric effect 80−55044
LiF, Compton profile interpretation to give ionic deform. and bonding 77−40301
LiF, Compton profiles, anisotropies 80−20730
LiF, condensation and evaporation in monomers, dimers and trimers, mol. beam method *(German)* 77−85052
LiF, cross relaxation of β-active ^{8}Li nuclei *(Russian)* 80−103895
LiF, cross relaxation processes, polarised β-active nuclei 80−60431
LiF, cryst., laser induced plasma at surface 80−79531
LiF, cryst., laser irrad., electron emission 80−80948
LiF, cryst., triboluminesc. spectra 80−66312
LiF, cryst., ultrasonic attenuation along (111) and (110) directions 78−63813
LiF crystal, contact damage obs. by cathodoluminesc. 80−71728
LiF crystal, dislocation movement study with new chem. polish 78−15614
LiF, crystal, electron emission under uniaxial compresssion 80−7483
LiF crystal, gamma irradiated, shear stress depend. on oriented dipoles conc. 79−28013
LiF crystal, plastically deformed, elec. field distrib. on surface meas. 77−31716
LiF crystal, thermoluminescent dosimetry measurement of radiation near lightning strokes 80−36361
LiF crystal, tunable laser via F_2^+, F_2^--centres, 0.88 to 1.25 microns 77−75529
LiF crystal active element for colour-centre laser, thermal strain anal. 80−91804
LiF, crystal fracture induced surface charge, elec. signal meas., double elec. layer approx. 80−44254
LiF crystal windows, transmission in vac. UV region, heat treatment effect 77−31137
LiF crystal with F_2^+ centres, periodic pulsed tunable laser, Nd laser second harmonic excited 80−38021
LiF crystals, in pile irradiation, nucl. reactions 78−29463
LiF crystals, mirror chips, in contact with liq. phase, ellipsometric investigation 80−11516
LiF crystals, relation of struct. and bond type to slip geometry 80−88165
LiF crystals, X-ray irradiated, luminescence during release of pressure 79−65939
LiF, crysts. containing rigid dislocation forest, mech. props. 79−99212
LiF curved crystal spectrograph, diffraction efficiency calc. method 80−79630
LiF, damage by UV laser radiation, avalanche ionization mechanism 80−76110
LiF, defect state model for localised excitations 77−43529
LiF, defects of electron irradiated single crystals *(Russian)* 77−47488
LiF, deform. mech. map. 77−81298
LiF, deformed, influence of surface on density of edge components of dislocations 77−31670
LiF, deformed by conc. loading, X-ray beam scattering *(Russian)* 78−35430
LiF, deformed in liquid He, penetration of He, dislocation effects 77−20131
LiF, desorption of ^{4}He, comparison with quantum statistical theory of flash desorption 80−44410
LiF, diffr. scatt. of H_2 and D_2, quasiclassical trajectory method 77−36332
LiF, diffusion of O_2, high-temp. 77−84988
LiF, dil. aq. solns., conductance at 25°C 77−69105
LiF, dilute paramagnet, ^{8}Li-^{6}Li cross relaxation *(Russian)* 79−4747
LiF, dislocation creep, creep deform. predictions 78−19815
LiF, dislocation distrib., after deform. *(Russian)* 78−22732
LiF, dislocation distrib. on surface parallel to Burgers vector 79−65090
LiF, dislocation dynamic props., investigation by impact loading *(Russian)* 78−85069
LiF, dislocation internal friction, orientation depend. 78−48439
LiF, dislocation mechanism of electrification during cleavage 77−24353
LiF, dislocation mobility near fast-moving crack tip 78−47389
LiF, dislocation structure, influence of variable deform. temp. 80−70211
LiF dispersing crystal, X-ray source, synchrotron-like intensities, EXAFS expts. 78−86398
LiF dosimeter, radiothermoluminescence dosimetry of 10 MeV electrons *(Italian)* 77−81582
LiF dosimeter, thermoluminescence glow curves and light absorption, thermal treatment effect *(Russian)* 77−32954
LiF dosimeter energy response to high energy electrons <30 MeV, Monte Carlo calc. 77−86637
LiF, dosimeter material, thermolum. non-linear response to sequential irrad. at different dose rates 79−1793
LiF dosimeters for high energy electrons, Monte Carlo calc. of energy dependence 77−46421
LiF, dynamic strength, cryst. orientation effects 78−39846
LiF, ESR study of interstitial atomic H centres 79−56609
LiF, effect of impurity traces on physical props. 77−12450
LiF, effect of valence state on X-ray Compton line shapes 77−8682
LiF, elastic and rot. excitation cross sections for electron scatt. 78−46446
LiF, elastic const. data, quadratic fit for elastic modulus temp. depend. 78−14397
LiF, elastic electron scatt. intensity, rel. to electron density distrib. 78−1079
LiF, electrification by plastic deform. 79−33334

lithium compounds continued
LiF, electrification of crystals by cleavage 78−60189
LiF, electron elastic scattering, by highly polar mols., chem. bond effects 78−9248
LiF, electron elastic scatt. cross sections 78−50641
LiF, electron elastic scatt., differential cross-sections, effective range theory 80−83485
LiF, electron impact, elastic scatt., model, static and static exchange calcs. 78−94321
LiF, electron impact fragmentation, in mass spectrometer, porous barrier obs. 77−75313
LiF, electron irrad., transport of valence band holes, optical absorpt. obs. 79−99188
LiF, electron irradiated, mech. characts. 78−26595
LiF, electron momentum distrib. and Compton profiles 79−13631
LiF, electron scatt., orthogonalisation and model exchange pots. calcs. 80−23552
LiF, electron scatt., quasiclassical close-coupling approximation 79−81280
LiF, electron scattering; differential cross sections, three part hybrid method 80−58381
LiF emitter, secondary electron emission study 78−27356
LiF, estimation of activation parameters in sclerometric tests 80−66625
LiF, evaporated film, thermally stimulated exoelectron emission rel. to thermolum. 79−47602
LiF, evaporated film, UPS, valence and cond. band struct. 77−63528
LiF, Ewald method, convergence of reciprocal lattice sums 77−11834
LiF, exoelectron emission and radiation dosimetry *(Japanese)* 79−83110
LiF, exposed to US waves, dislocation multiplication in original stage 78−47383
LiF, exposed to ultrasoft X-rays, thermal luminesc. and electron emission 79−8192
LiF, F centre study by mol. SCF calcs. 80−44530
LiF, F_2^- mag. reson. absorpt. spectrum 77−73079
LiF, F-centre, excited state, optical absorption 77−20267
LiF, F-centre electronic struct. determ. using LCAO method, appl. of cubic harmonic expansion 77−20268
LiF, F-centres, defect electron struct., extended-ion model calcs. 80−59907
LiF film, ATR spectrum, reson. between longit. phonons and substrate surface polaritons *(Russian)* 77−32384
LiF, film, characteristic energy loss and secondary electron spectra *(Japanese)* 78−15266
LiF film, contamination by 1 MeV proton bombardment, backscatt. obs. 77−11811
LiF film, electron emission under metastable He and Ne atom impact 80−20747
LiF film, electronic excitations, inelastic electron scatt. spectra 77−32479
LiF film, guided wave excitation by fast electrons 79−24384
LiF film, intrinsic stress meas. 80−71696
LiF film, refractive index as function of time, ATR meas. 79−65940
LiF film, secondary emission yield, primary electron ang. of incidence effects 78−2961
LiF film, surface phonons and thickness variation, EELS meas. 80−92774
LiF films, polycrystalline and single-cryst., comparative study of phonons by electron spectroscopy 80−25505
LiF, fluorine K absorpt. spectra using APS technique 79−99986
LiF, fracture in mag. field 78−59855
LiF, ground and excited state props., local density formalism 78−10349
LiF, ground state, pot. curve, determination and use of molecular α values in MSXα calcs., MTX$\tilde{\alpha}_R$ meth. 79−10032
LiF ground surface, structure features of dull layer 77−54763
LiF, γ-irrad. induced defects, positron capture and annealing obs. 80−60707
LiF, γ-irrad. pure and Mg-doped, phonon scatt. and interstitial clusters 80−70254
LiF, γ-irradiated, chemilum. during dissolution *(Russian)* 78−80427
LiF, γ-irradiated, Huang diffuse scattering of neutrons 80−10544
LiF, γ-irradiated crysts., dislocation retardation centre 79−95051
LiF, H_2 scatt. from surface, qudrupole interaction and rot. transitions 79−74041
LiF, H(He)-surface bound states, surface averaged pot. energy function 77−11789
LiF, hardening under dynamic load, grain boundary effect 77−12674
LiF, hardness anisotropy obs. 79−79085
LiF, hardness increase mode, effect on dislocation mobility 79−51114
LiF, He and H beam scatt., semiempirical determ. of atom-surface interaction 78−72676
LiF, He at. beam scatt., Lennard-Jones resons. and rel. displacements 77−1773
LiF, He at. scatt., bound state reson. data anal. 78−39644
LiF, He scatt., bound state reson. calc. 77−1779
LiF, heteronuclear mag. spin system relaxation in many pulse NMR expts. 80−93203
LiF, high temp. depend. of thermal expansion coeff., interatomic pot. approach 78−95166
LiF, high-energy particle bombard., F-centre creation, optical meas. and model 77−47497
LiF, high-temp. behaviour of elastic moduli, comparison with MgO and CaO 77−11621
LiF, IR filter, elimination of near from far IR, Brewster angle refl. *(French)* 79−3772
LiF IR window refractive index var. with temp., −180° to +200°C obs. 79−14052
LiF in TLD, energy response to neutrons 77−29210
LiF, influence of neutron irrad. temp. on F-aggregate centre form. 78−72561
LiF, ion and electron emission following ion impact 80−100729
LiF, irrad. at pile temp., higher F aggregate centres produced during thermal annealing 77−43212
LiF, irradiated and plastically deformed, thermoluminesc. defect centres 77−1740
LiF, irradiated at 20K, deformation under stress *(French)* 79−90715
LiF, irradiated at room temp., stored energy 80−79839
LiF, Kα-satellites of F^- *(German)* 79−28864
LiF, kinetic energies of sputtered excited atoms 80−66373
LiF, kinetics analysis of stress relaxation 80−65136
LiF, Knoop microhardness anomaly on (001) planes 79−38942
LiF, LCAO calc. of Compton profiles 79−95871

lithium compounds continued
LiF, large unit cell semiempirical mol. orbital approach to props. of solids 79−87037
LiF, laser action of M-centres at 700 nm 78−82972
LiF, laser irrad., Li^+ emission, time and energy characts. 80−100710
LiF, laser window material, surface and bulk absorpt., photoacoustic meas. 78−25912
LiF, laser-irrad., emitted electrons and positive ions delay 80−29830
LiF, load relaxation studies 79−79016
LiF, low-energy electron impact rot. excitation, close-coupling calc. 77−58187
LiF, M-centre vibronic absorpt. spectra, elec. field, method of moments 78−27186
LiF, M-centres, quadratic Stark effect, differential electroabsorption spectra 77−66526
LiF, manifestation of local vibrs. of dislocations in IR spectra 78−88339
LiF mech. and optical props. rel. to forging conditions 80−33101
LiF, mech. excitation, luminesc. electron emission, friction, static electrification, meas. method *(German)* 77−24904
LiF, microcrack propagation and plastic strain 80−81187
LiF, microcryst. and polymers, IR absorpt. 77−63412
LiF microcrysts. matrix isolated in Ar, IR absorpt. by aggregated and isolated samples 77−55782
LiF, microindentation, dislocation rosette generation 77−27936
LiF, mid IR laser window material, absorption props. 77−46770
LiF, molten, charge fluctuations, collective dynamics, from IR reflectivity 78−67841
LiF, molten, polaritonic spectra 79−23908
LiF, monitoring of stress relaxing profile using shorted guard-ring quartz gauge 79−58680
LiF monocrystal, impact damage, influence of particle props. 80−30120
LiF, mosaic single-cryst. film, electron diffr. reflection intensities, precision meas. 79−94851
LiF, multiplication of screw dislocations during deform., yield stress depend. 77−24321
LiF, muon Coulomb capture ratio 78−62959
LiF, N^+ and Ne^+ irradiation, MO X-ray intensity meas. 78−82831
LiF, NMR, thermodynamic effects of RF pulse pair on system with two spin species 77−66433
LiF, NMR exam. of point defects generated in (n,γ)-reaction *(Russian)* 78−60347
LiF, Ne atom scatt., test of scatt. model on expt. data 79−28877
LiF, neutron irrad., F-centres prod., hyperfine structure constants *(Japanese)* 77−69729
LiF, neutron irradiated, ESR of Li metals *(Japanese)* 79−82858
LiF, neutron ns. slowing down time, expt. obs. 78−58319
LiF, neutron-irrad., X-ray diffr. profiles 77−84803
LiF, non-universality of TL-LET response, effect of batch composition 80−16106
LiF, non-universality of TL-LET response, effect of high-temp. TL 80−99348
LiF, nucl. dipolar mag. ordering, dipole-dipole interactions, review 77−85475
LiF OH-stabilised F_2^+-centre laser, appl. to intracavity laser spectroscopy 80−32999
LiF oligomers, struct., stability SCF and CEPA-PNO calcs. 78−78640
LiF, one electron props., SCF-Xalpha scattered wave method 80−83279
LiF, optical damage threshold anisotropy, polarised laser radiation 77−16433
LiF, photoelectron spectra using Zr Mζ, Al Kα and other X-ray lines, photoionis. cross sections ratios 77−90246
LiF, photostimulated thermolum. as UV radiation dosimeter 77−16984
LiF, picosecond generation on F_2^+ colour centres, induced mode synchronisation *(Russian)* 80−64033
LiF, picosecond laser-induced breakdown at 5321 and 3547 Å, freq. depend. 77−63495
LiF, plasic deform., cleavage-crack propag., X-ray topography 77−39625
LiF, plastic deform. and dielec. losses 78−19410
LiF, plastic strain accompanying local rise in surface temp., of natural shear *(Russian)* 80−6411
LiF, possible fusion reactor material, gamma-rays from 14 MeV neutron scatt. in extended samples 77−57739
LiF, pot. curve, one-config. Hartree-Fock-Roothaam calc. for force consts. 78−82627
LiF, powder energy distrib. of TSEE 77−12504
LiF, premelting elec. cond., heat capacity 78−91445
LiF, prep. and dosimetric props. of new highly sensitive form 79−22483
LiF, press forged, mech. and optical props. 80−38079
LiF, pulsed dielectric breakdown, mech. stress photoelasticity obs. *(Russian)* 78−2800
LiF, pulsed RF radiation produced by scratching *(Russian)* 78−19607
LiF, pulsed-laser-induced damage, role of avalanche multiplication and multiphoton absorpt. 80−48316
LiF, R core exciton thermotransmission and absorpt. spectra, line shapes, forbidden and allowed excitons 79−73968
LiF, RF spectra, spin interactions and moments, mol. beam elec. reson. meas. 77−18912
LiF, radiation damaged, proton and $^4He^+$ channelling, F-centre production, optical absorpt. meas. 78−79656
LiF, radiation induced voids, formation on dislocations 80−15159
LiF, Raman spectra and vibrational modes of V_K centre meas. 78−80338
LiF, refractive index, effect of ageing, wavelength range 460-1000 nm 80−84707
LiF, restored thermoluminescence mechanism 78−19580
LiF, seeded in supersonic beam, vibr. relax. 78−37716
LiF, selective adsorption of He, band struct. effects 79−73402
LiF, self-shielding factors for TLD-600 and TLD-100 in isotropic flux of thermal neutrons 77−6638
LiF, self-trapped exciton, ODMR spectra 79−28286
LiF, sensitised TLD phosphor, photon energy dependence 80−78498
LiF, shock wave, precursor decay, stress threshold 77−4156
LiF, single cryst., impression creep 78−6986
LiF single cryst. with vac. deposited Bi film, surface failure induced by laser impulse *(Russian)* 77−35585
LiF, single crystal, dislocation generation, beneath static and rolling contact with sphere 78−87671
LiF, single crystal, neutron and gamma irradiation, SEM and Bragg profile anal. 80−15158
LiF single crystal, void disappearance 78−55864

lithium compounds continued
LiF single crystals, dislocation motion and generation on plate impact 79−95011
LiF single crystals, exam. of void morphology effects on their disappearance kinetics 79−10843
LiF single crystals, glide band sources, work hardening 80−34126
LiF single crystals, stepwise creep, 300K, in dislocation depletion conditions, thermal cycling effects *(Russian)* 77−15484
LiF single crystals, visible superradiance of excited F_2-centres 79−33733
LiF single-layer film 2.8 μm, 3.8 μm absorpt. meas. 78−90463
LiF, slip anisotropy under neutron irrad. and external stress, orientation of defects 77−31674
LiF, slip band steady-state expansion, dislocation vel. theory 77−24320
LiF, small-angle boundary migration in steady creep state 77−39624
LiF, space charge distribution meas. in solid dielectrics 80−50271
LiF, Stark effect, M-centre absorpt. bands 78−84614
LiF, static SIMS, mol. rearrangement, cluster formation 78−64440
LiF, strain hardening curve correlation with slip band nucleation stress spectra 80−70217
LiF, strained, mean mobile dislocation velocity 78−18657
LiF, stressed state and dynamics of dislocations near tip of fast growing crack 77−62541
LiF, strong reorientation resulting from creep, X-ray obs. 79−100228
LiF, supersonic seeded molecular-beam, vibr. relax. 78−17761
LiF surface, diffractive scatt. of H atoms, meas., Debye temp. and Morse pot. determ. 80−76124
LiF surface, He atom inelastic scatt., phonon coupling 80−71554
LiF surface, He elastic scatt., high-energy approx. 79−65965
LiF, surface lattice dynamics, Green function approach 77−31865
LiF TLD, accuracy of megavolt. radiation dosimetry 77−81574
LiF TLD, anal. of energy response to high energy electrons 77−52882
LiF TLD, comparison with BeO 80−26357
LiF TLD, plastic deform. effects on thermolum. sensitivity, rel. to handling technique 77−16988
LiF TLD, press. deform. and recovery 77−8668
LiF TLD, re-estimation of absorbed doses below 1 rad using UV bleaching 77−16992
LiF TLD, use as thermal neutron detector 78−21821
LiF TLD 100, TLD phosphor, γ-induced sensitisation and residual thermolum. 79−28844
LiF, TLD 100, thermolum. peaks anal. 77−44073
LiF TLD disc response to ^{131}I and ^{125}I, influence of thyroid geometry 78−73250
LiF TLD materials, influence of composition on sensitivity to high energy electrons 77−40775
LiF, TLD materials, kerma for monoenergetic neutrons, theory, expt. comparison 77−5086
LiF TLD phosphor, γ-irrad. induced sensitisation, UV effects 80−108286
LiF TLD phosphor, incompatibility of sensitisation and dose re-estimation 78−40340
LiF TLD phosphor, residual thermoluminescence effect on sensitisation 80−108287
LiF, TLD phosphor, Z_3 centre, thermolum. and optical absorption spectra 79−24374
LiF TLD response to high-energy X-rays and electrons rel. to ^{60}Co photons 78−40332
LiF TLD-100, thermolum. response to 5 to 30 keV electrons effect of annealing atm. 77−86638
LiF, TLD-100, thermoluminesc. emission spectra meas. 78−84667
LiF, TLD-100, thermolum., glow curve kinetics 78−84668
LiF TLD-100, thermoluminesc., kinetics and trapping parameters, dose depend. 80−2872
LiF, TLD-100, trapping centres, optical absorpt. spectra defect and thermolum. mechanism models 80−50436
LiF TLD-100 material, long term recycling characts. 78−11737
LiF TLD-100 phosphor, sensitisation mechanism study, thermolum. glow peak intensity obs. 80−55202
LiF TLD-700, Harshaw, effect of sample size and batch origin on thermal neutron sensitivity 78−40342
LiF TLDs, response to ^{99m}Tc γ-rays 80−89854
LiF, thermal and athermal plasticity *(Russian)* 79−11685
LiF, thermal cond., Umklapp process 80−39367
LiF, thermal cond. press. depend. 77−15641
LiF, thermal cond. under press. meas. 78−30802
LiF, thermal expansion, rapid increase near melting point 77−51521
LiF, thermal expansivity determ. at high press. 78−79787
LiF, thermal phonon scatt. by low angle grain boundaries 78−67795
LiF, thermal phonon-dislocation interaction, thermal cond. and ballistic phonon propag. meas., 0.03-25K 79−95226
LiF, thermally stimulated exoemission, radiation defects and adsorpt. centres 78−11087
LiF, thermocyclic stress effects in corrosive-media, electrochem. polarization applic. *(Russian)* 78−11356
LiF, thermolum., formulation of sensitisation based on simple two-step reaction rate model 78−39610
LiF, thermolum., trapping mechanism based on Z-centres 80−76089
LiF, thermolum. dosimeter, neutron damage, displacement and ionis. fractions of fast neutron kerma 78−30669
LiF, thermolum. light self absorpt. obs. 79−81097
LiF, thermolum. response to pions 80−101270
LiF, thermoluminescence, γ-radn.-induced sensitization and supralinearity 79−91507
LiF thermoluminescence induced by 13.8 and 81 meV diffr. neutrons 77−56481
LiF, thermoluminescence mechanisms following gamma irradiation 77−59625
LiF, thermoluminescence response to gamma rays 77−59626
LiF, thermoluminescence intensity depend. on heating rate and deep trap 78−56527
LiF, thermoluminescence mechanism, extension of Mayhugh-Christy model 78−80425
LiF, thermoluminescent dosimeters, high dose characteristic 78−35966
LiF thermoluminescent dosimeter, high and low temperature response to X-rays 79−22492
LiF thermoluminescent dosimeters, response to ground-level cosmic-ray background 79−59265
LiF thermoluminescent detectors, survey 80−68964
LiF, thermostimulated exoemission, adsorbed layer effects 78−11085
LiF thin film boundary influence on IR spectrum 77−40243
lithium compounds continued
LiF, thin insulating film, lattice parameter meas. by electron microscope 77−65940
LiF thin layers, effect of LET on thermolum. props. 78−73255
LiF tile and sheet for thermal neutron shielding *(Japanese)* 78−74510
LiF, tunable CW lasers using F_2^+ centres for 1.26-1.48 and 0.82-1.07 μm bands 78−79023
LiF type surface, He scatt., selective adsorption intensities, attractive corrugated wall model 79−28874
LiF, US attenuation, 4.2 to 300K 77−47513
LiF, UV visible absorpt. by laser calorimetry, wavelength modulation spectroscopy 78−66876
LiF, ultra-microhardness testing for vacuum deposited film and bulk specimen 78−79910
LiF, ultralow loss optical fibre material, loss mechanism 80−78920
LiF, V_k and F centres, efficiency of formation, temp. depend. 79−7600
LiF, V_k-centre generation, temp. depend. 78−18644
LiF, V_t centre (F_3^{2-}) identification, ESR spectrum anal. 80−7164
LiF vapour system, fragmentation in mass spectrometer ion source 78−70944
LiF, vibrational contribution to surface thermodynamic functions 77−47659
LiF, vibrational surface modes of (001) unrelaxed face, shell model 77−43420
LiF, viscous drag of dislocations, internal friction, 4.2-300K 77−11566
LiF, viscous drag of dislocations exam., using mobility of individual dislocations 79−14814
LiF with stable F_2 centres, F_2^+ colour centre generation accumulation, tunable laser production *(Russian)* 80−28238
LiF, $X^1\Sigma^+$ state, many-body effects, HF STO calcs., diagrammatic perturbation theory 77−50355
LiF, X-irradiated cryst., luminesc. during press. release 80−20722
LiF, X-ray integrated intensities in Bragg and Laue geometries 77−31553
LiF^-, ground and excited states, ab initio calcs. single config. and multiconfig. SCF calcs. 80−52873
^6LiF, nonluminous, and $CaSO_4$:Tm powders mixture thermoluminesc. response to thermal neutrons 77−73588
LiF:Be(Mg), Maxwell-Wagner relax. induced by impurity clouds around dislocations, ionic thermocond. meas. 80−7281
LiF:Co^{2+}, solid soln. decomp., precip. of new phase, electron microscope expt. 79−11619
LiF:Co^{2+}, X-ray and electron microscope obs. of CoF_2 precip. morphology 77−31777
LiF:Co(Mg), nucl. acoustic reson. 77−8445
LiF:Fe, dispersed ions, absorber Mossbauer spectra 78−15077
LiF:Fe, Mossbauer study of Fe precipitates 79−91327
LiF:Fe^{3+}, optical absorpt., 200-750 nm 78−39576
LiF:H, neutron irrad., ENDOR meas. 79−11356
LiF:Hg^{2+}, electrolytic colouration 78−75665
LiF:In, optical absorption effects of ion implantation 80−70239
LiF:Mg, dependence of optical absorpt. on temp. during X-ray irrad. 80−66237
LiF:Mg, effects of grain size on thermolum. and thermally stimulated exoelectron emission 79−15536
LiF:Mg, geometrical parameters of impurity centres by scattered-light method 80−2043
LiF:Mg, light scatt., effect of electrostatic field 78−2823
LiF:Mg, origin of dislocations *(Russian)* 77−15425
LiF:Mg, role of impurity-vacancy pairs in thermolum. 79−8195
LiF:Mg, slip band struct. changes with temp. 78−47390
LiF:Mg, TLD-100, thermolum. phosphor, photolum. and absorpt. spectra, thermolum. mechanisms 80−97321
LiF:Mg, thermal annealing effects on sensitivity and fading of dosimeter 78−82522
LiF:Mg, Ti, luminesc. increase by O implantation 78−64412
LiF:Mg, Ti TLD long-term annealing at 400°C, radiation and thermally induced damage, recovery 77−5085
LiF:Mg, X-irrad., colour centres, ESR and UV asborpt. meas. 80−108069
LiF:Mg, X-irrad. induced sensitisation mechanism, optical absorpt. spectra 80−60637
LiF:Mg, X-irradiated, thermoluminesc. of Z_3-centres 78−15236
LiF:Mg, X-irradiated, Z_1-centre exam. 77−68968
LiF:Mg, X-ray irrad., trapping processes, Z-centres and dipoles, two models 80−49222
LiF:Mg, Z_2- and associated Z-centres, elec. cond., ionic thermocurrent, and optical absorpt. meas. 80−107229
LiF:Mg,Ca detectors, variation of parameters of thermally stimulated luminesc. 79−6793
LiF:Mg,Ti, (TLD-100), optical bleaching of defect centres 79−19911
LiF:Mg,Ti, defect states, ESR and ionic cond. study 80−108058
LiF:Mg,Ti, optically induced dichroism of Z_2-centres 79−28710
LiF:Mg,Ti, thermolum. related Z-centres, optical absorpt. bands 78−23540
LiF:Mg,Ti, thermoluminesc. activation energies 79−74009
LiF:Mg,Ti crystals, Z_3-centres, correlation of thermoluminescence and optical absorption 80−45154
LiF:Mg cryst., Mg electron colour centers 80−100229
LiF:Mg dosimetric cryst., light-sum storage during linear stage 79−8194
LiF:Mg^{2+}, deformed in ^3He and ^4He, dislocation struct. characteristics 79−69112
LiF:Mg^{2+}, TLD-100, precipitation reactions and ionic cond. 77−56479
LiF:Mg^{2+}, TLD-100, solution treatment temp. and ageing effects 77−56480
LiF:$Mg^{2+}(CO^{2+})$, X-ray induced UV absorpt., band shapes, F- and Z-centers 77−20889
LiF:Mg(Ag), electron spin-lattice relax. of V_k-centre 78−95518
LiF:Mg(Co), flow stress changes during precipitation 80−92594
LiF:Mg(Eu)(Co)(Si)(O), elec. cond., influence of impurity ion 79−7709
LiF:Na^+ H_A-centre struct., hyperfine interaction 78−79611
LiF:Ni, dislocation behaviour in diffusion zone, Cottrell clouds *(Russian)* 80−70212
LiF:OH, neutron irrad., interstitial H-centres, ESR obs. 80−93175
LiF:OH crystals, X-irradiated, H centres formation and annealing 80−54226
LiF:OH:Mg, γ-irrad. induced oxyhydryl complexes 80−92555
LiF:OH^-, electron irrad., F_2^+ centre stabilisation 80−54231
LiF:OH^-, IR spectra 80−20676
LiF:Si, injection electrolum., fields up to 10^4 V cm^{-1} 77−12445
LiF:Ti, EPR exam., superhyperfine interactions 78−31107

lithium compounds continued
LiF:Ti, thermoluminesc., effect of plastic deform. 79−33853
LiF:Ti, thermoluminesc. dosimetry appl. 79−38683
LiF:U, Mn, EPR of Mn^{4+} centre, g-values and hyperfine struct. 77−12192
LiF:U, X- and γ-irrad., EPR of U^{5+} centre, charge compensation mechanism 77−90030
LiF:U, X-ray and γ-ray irrad., EPR of U^{5+} centres 79−91295
LiF:U_3O_8, X- and γ-irrad., U^{5+} luminesc. molecular centres, optical and ESR expts. 77−48224
LiF:U^{5+}, absorption and laser-excited fluoresc. 79−99927
LiF-AlF_3, ion-molecule equilibria studied by mass spectrometric method, heats of dissoc. and form. calc. 80−104479
LiF-AlF_3, mixture at 1293K, thermodynamic function 80−104134
LiF-AlF_3-Na_3AlF_6-Al_2O_3 system, phase equilibrium, X-ray diffr., DTA, quenching, optical microscopy study 80−50610
LiF-$Al(PO_3)_3$ glass, phase decomp., X-ray diffr. and IR spectra study 80−30003
LiF-BeF_2, and MgO-SiO_2 systems, complex ionic liquids, corresponding-state principle *(Japanese)* 77−56245
LiF-BeF_2, molten, corresponding state principle with MgO-SiO_2 and appl. 79−11589
LiF-BeF_2, molten, self-diffusion coeff. of F *(Japanese)* 77−47610
LiF-coated Ag grating, p-polarised reflected light intensity, reson. anomalies 77−3665
LiF-ethylene complex, ab initio calcs. of bonding 78−29745
LiF-He interface, absence of anomalous Kapitza resistance 78−63923
LiF-Li_2O, F-aggregate centres *(Russian)* 78−64394
LiF-Li_2O-Al_2O_3-P_2P_5 glass, ionic cond., transport numbers determ. 79−28143
LiF-$Li_2O.SiO_2$, activities rel. to liquidus comp. 77−28797
LiF-LiCl-LiBr, molten, H electrochemical extraction, appl. to fusion reactor blanket processing 78−53217
LiF-LnF_3 (Ln=Y, La, Yb) binary liquid mixtures, thermochemistry 80−45538
LiF-MgF_2, high-pressure phase relations rel. to mixed oxide zone of Earth mantle 77−37193
LiF-MgF_2, ionic conductivity increase rel. to point defect cone 77−72717
LiF-NH_2 adduct, mol. consts., ab initio SCF LCAO MO calcs. *(French)* 78−13423
LiF-NaF-KF molten mixture, diffusivity and solubility of H_2 78−34640
LiF-NaF-KF-K_2GeF_6-GeO_2 fused mixture, for electrodeposition of Ge powder 80−2979
LiF-NaF(KF)(CaF_2)(BaF_2), densities of binary molten salts *(Japanese)* 79−7644
LiF-$NaPO_3$-MeF_x (Me=Mg, Ca, Al) glasses, IR spectroscopy study 80−16042
LiF-OH, γ-irrad., colour centre lasing at 0.84-1.13 μ at 300K 80−5739
LiF-PTFE TLD performance, influence of heating element design 78−25333
LiF-polytetrafluorethane thermolumin. dosimeters, absorbed dose assessment 80−95470
LiF-UF_4, molten binary mixtures, viscosity meas. 80−65270
LiF+Ar, polarisation cross section, close-coupling calcs. 80−69214
LiF+Ar, polarised rot. selected mol., high resolution differential cross section 77−27147
LiF+Ar, polarised rot. state-selected cross sections, anisotropic intermol. pots. 79−72398
LiF+Ar(Kr), anisotropic system intermol. pot. determ. 77−58121
LiF+inert gas atom, interaction anisotropy, Van der Waals forces 79−6985
LiF+UO_2^+, optical absorpt. spectra 77−81129
LiF_2, protection from biological overgrowths 78−18034
LiF_2:Ni^+, compressed D_{4h} cluster, g_{zz}-g_0 value 77−80756
$(LiF)_n$, 'polymers', aggregation, microcryst. form., IR spectra obs. 78−46331
Li_2F^+, mass spectra, struct., stability, expt. and theory 77−554
Li_2F_2, struct., force fields and normal mode freqs., ab initio calcs. 80−83260
Li_2F_2, struct., internuclear-distances and mean amplitude of vibr. determ. by electron diffr. 80−69252
Li_2F_2, UPS of dimeric mol., expt. and Xα calc. 80−9640
Li_3F_3, isotopically substituted, IR freq. and intensity patterns 78−21926
LiF(:Mg), shock waves in ⟨111⟩ direction, elastic precursor amplitudes 80−54314
LiF(Br), fast Li^+ ion stopping, chem. bonding effects 77−27929
LiF(LiF^-), electron affinity and dipole moment, ab initio calc. 78−41938
LiF(TLD-600), unannealed, fading for thermal neutrons and γ-rays 80−83225
LiF(001), ethanol-covered, atomic H scatt. 77−31905
LiF(001), He scattering, semiclassical treatment 77−20977
$Li_{0.5}Fe_{2.17}Al_{0.33}O_4$:Co, single cryst., domain struct., mag. annealing effect depend. on induced anisotropy 78−68290
$Li_{0.5}Fe_{2.5-x}Al_xO_4$ ($0 \le x \le 0.68$) films, LPE 80−29884
$Li_{0.5}Fe_{2.5-x}Cr_xO_4$, mag. anisotropy, ferromag. reson. meas. 77−69542
$Li_{0.5}Fe_{2.5-x}Cr_xO_4$ press. depend. of anisotropy consts. 80−65865
$Li_{0.5}Fe_{1.25}Ga_{1.25}O_4$, ferrimag. with local canted struct. thermal expansion anomalies 79−73762
$Li_{0.5}Fe_{1.32}Ga_{1.18}O_4$, temp. depend. on mag. moments, neutron diffr. data *(Russian)* 77−28371
$Li_3Fe(MoO_4)_3$, paramag. props., 90-800K *(French)* 80−39734
$LiFeO_2$, ion ordering, transition state cluster model, electron diffr. 77−47547
$LiFeO_2$, quadrupole splitting in Mossbauer ^{57}Fe spectrum, geometric anal. and computer simulation 79−1730
$LiFe_5O_8$, elec. props. 77−80641
$LiFe_5O_8$, enantiomorphic crystals, electron microscopy 77−84602
$LiFe_5O_8$, hysteresis and other mag. props. rel. to microstruct., TEM investig. 77−20636
$LiFe_5O_8$, material loss and high-temp. phase transition 78−64534
$LiFe_5O_8$, microstruct. and magnetic props., electron microscope obs. 79−87290
$LiFe_5O_8$, second order magnetoelectric effect 77−66409
$LiFe_5O_8$, spinel, mixed cond. using four-point DC techniques 79−60877
$LiFe_5O_8$, vacuum annealed, tetragonal γ-phase obs. with TEM 80−11661
$Li_{0.13}Fe_{2.87}O_4$, acoustic spin wave dispersion branch, exchange const., neutron scatt. study 79−47266

lithium compounds continued
$Li_{0.5}Fe_{2.5}O_4$, antiphase domains, broadened X-ray diffr. line anal. 78−26578
$Li_{0.5}Fe_{2.5}O_4$, domain struct. in (110) and (111) plates, Faraday effect meas. 79−61180
$Li_{0.5}Fe_{2.5}O_4$, effects of low-melting additive on struct. and dielec. props. 77−85494
$Li_{0.5}Fe_{2.5}O_4$, ht. treatment conditions effect on superlattice formation 77−84922
$Li_{0.5}Fe_{2.5}O_4$, LPE growth on spinel substrate crystals, ferrimagnetic resonance exam. 78−76613
$Li_{0.5}Fe_{2.5}O_4$, linear elec. field shift of ferromag. reson. field 79−78530
$Li_{0.5}Fe_{2.5}O_4$, magnetic domain walls, mobility 80−2600
$Li_{0.5}Fe_{2.5}O_4$, magneto-optical Kerr effect, reflectivity spectra 80−66157
$Li_{0.5}Fe_{2.5}O_4$, magnetooptical spectra, polar Kerr rotation, dielectric tensor elements spectra 80−40091
$Li_{0.5}Fe_{2.5}O_4$ milled ferrite powder, substruct. and sinterability 80−84894
$Li_{0.5}Fe_{2.5}O_4$, neutron-irrad., mag. spectra *(Russian)* 77−44092
$Li_{0.5}Fe_{2.5}O_4$, phase transitions during reduction 80−55642
$Li_{0.5}Fe_{2.5}O_4$, polar Kerr rotation spectra, 2-5.7 eV, comparative study with YIG 79−47413
$Li_{0.5}Fe_{2.5}O_4$ Ru substitution effect on struct. and mag. props., and max. solubility determ. 80−75364
$Li_{0.5}Fe_{2.5}O_4$, slow neutron polariser, by single cryst. (222) refl. 80−49052
$Li_{0.5}Fe_{2.5}O_4$, spinel ferrite, prep. by thermal treatment of spray-dried formates, scanning electron microscope examination 79−24482
$Li_{0.5}Fe_{2.5}O_4$, spinel struct. magnetodielectrics, free energy of form. 79−83493
$Li_{0.5}Fe_{2.5}O_4$, superexchange interactions, three-sublattice anal. 79−61095
$Li_{0.5}Fe_{2.5}O_4$, temp. depend. of mag. moments, neutron diffr. data *(Russian)* 77−28371
$Li_{0.5}Fe_{2.5}O_4$, uniaxial anisotropy energy, elec. field depend. 78−68346
$Li_{0.5}Fe_{2.5}O_4$-Bi_2O_3(V_2O_5) systems, phase diagrams, sintering conditions 78−35366
$Li_{0.5}Fe_{2.5}O_4$-$CuFe_2O_4$-$MnFe_2O_4$, structural characteristics and mag. props. of solid solutions 77−35696
$Li_{0.5}Fe_{2.5}O_4$-$CuFe_2O_4$-$ZnFe_2O_4$, order-disorder transition, quadratic transformation *(French)* 78−76447
$Li_{0.5}Fe_{2.5}O_4$-LiNb(Ta)O_3, in situ composite growth, phase diag., melting relns. 77−21132
$Li_{1-x}Fe_{5-x}O_8$:Co, single cryst., domain struct., mag. annealing effect depend. on induced anisotropy 78−68290
Li_5FeO_4, additives and moisture effect on ionic cond. 80−107523
Li_5FeO_4, compatibility of Fe-Ni-Cr alloy with Li_2O pellets, mass spectrometric study of Li_5FeO_4 evaporation 79−8385
Li_xFeOCl, intercalation cpd., cryst. struct. 78−51512
$(Li_{0.5}Fe_{2.5}O_4)_{0.8}(CuFe_2O_4)_{0.2}$, struct., magnetic props., rectangular hysteresis loop 77−20645
$LiFePO_4$, cryst. struct. by neutron diffr. 78−43003
$LiFeS_2$, magnetic hyperfine interactions, Mossbauer spectra and mag. susceptibility meas. 80−29658
Li_2FeS_2, Mossbauer spectra and lattice parameters 79−78584
Li_xFeS_2 ($0 < x \le 2$) cathodic system, chem. and electrochem. studies 80−85188
$Li_xFe_yV_{1-y}S_2$, Mossbauer and mag. studies 79−73869
$Li_{0.17}Fe_{2.17}Zn_{0.66}O_4$, ferrimag. with local canted struct. thermal expansion anomalies 79−73762
LiGa ferrite, substituted ferrospinel, spin configuration determ. *(Russian)* 77−32162
$Li_{0.5}Ga_{0.85}Cr_{1.625}O_2$ spinel, tetrahedral coordination of Cr^{3+} ion, electronic spectra, X-ray and neutron diffr. *(French)* 79−65031
$LiGaCr_4S_8$, 1:1 ordering on tetrahedral sites, IR spectra obs. *(German)* 78−6669
$Li_{0.5}Ga_{0.095}Fe_{1.55}O_4$ ferrites, linear magnetostriction in weak field, 150 to 300K *(Russian)* 77−80983
$Li_{0.5}Ga_xFe_{2.5-x}O_4$, polycrystalline, ferromagnetic reson. theory applicability limits *(Russian)* 77−55709
$Li_{0.5}Ga_xFe_{2.5-x}O_4$, superexchange interaction parameters, Mossbauer spectra obs. 77−51899
$LiGaO_2$, light scatt. *(German)* 79−28730
$LiGaO_2$, Raman scatt., optical modes determ. 79−15463
$LiGaO_2$, single crystal ionic conductor, migration losses 77−80643
$LiGaO_2$:Fe, phosphor, luminesc. 78−92108
$LiGaO_2$:Fe IR emitting phosphor preparation and props. 78−6789
$LiGa_5O_8$:Cr^{3+}, antisymmetric exchange interaction, EPR study 79−47331
$LiGa_5O_8$:Cr^{3+}, fluoresc. and excitation spectra, zero phonon lines 79−33785
$Li_{0.5}Ga_{2.5}O_4$, spinel struct. magnetodielectrics, free energy of form. 79−83493
$Li_{0.5}Ga_{2.5}O_4$-$CuCr_2O_4$ system, phase diagrams, IR spectra, Cu^{2+} electronic spectra *(French)* 78−51461
Li_5GaO_4, additives and moisture effect on ionic cond. 80−107523
$LiGaO_2.6H_2O$, cryst. struct. *(French)* 78−42967
$LiGaO_2.8H_2O$, X-ray powder diffr. data *(French)* 80−39033
$Li_2Gd_4(MoO_4)_7$, ferroelec. and paramag. props. 78−39517
$LiGd(MoO_4)_2$, defect struct. and phase transitions 79−28697
$LiGd_3(MoO_4)_5$, single crysts., cryst. growth, optical props. 80−60763
$Li_2Gd_4(MoO_4)_7$, Czochralski growth, struct. and optical props. 78−27397
$Li_2Ge(GeO_3)_2(OH)_2$, cryst. struct. determ. 79−90629
Li_2GeO_3, acoustic props., intrinsic piezoeffect, US absorpt. coeffs. *(Russian)* 80−29692
Li_2GeO_3, components of elastic, piezoelec. and permittivity tensors meas. 77−8518
Li_2GeO_3, melt-grown single crysts., polar twins, piezoelec. meas., etching behaviour 79−32999
Li_2GeO_3 monocrystal conoscopic figure in polarised white light 79−15433
Li_2GeO_3 piezoelectric glass ceramic, recrystallisation, pyroelectric response, permittivity 80−80703
Li_2GeO_3, pure, and Si- and Mg-doped, impurity effects on elastic and piezoelec. props. 79−47388
Li_4GeO_4, Mg_2GeO_4, Li_3PO_4, structural relns. *(French)* 77−47433
Li_4GeO_4-Zn_4GeO_4, solid electrolyte system, phase diagram 80−66489
LiH (D), single crystals, electronic excitations, review *(Russian)* 78−72574
LiH, ab initio pseudopotential for FSGO calcs., bond length 77−75043
LiH, adsorption of H_2, on (100 surface), FSGO calcs. *(German)* 79−33196

lithium compounds continued
LiH, adsorption of He, ab initio calc. 78−38952
LiH, and $LiBH_4$, muonic X-ray intensities in low-Z elements and their hydrides 80−9761
LiH, antiferromagnetism, neutron diffraction study, appl. to polarised targets 79−68065
LiH, bond orbital model, model pot. approach 79−49923
LiH chains, long-range Coulombic contribution to direct space LCAO CO matrix elements 78−37774
LiH, closed liquid Ar circuit for electron irrad. at 90K *(French)* 78−62214
LiH, cluster cryst., extended HMO calc. of defects 79−51521
LiH, correlated potential energy curve, correlation hole concept, restricted Hartree-Fock solutions *(Spanish)* 80−14081
LiH, correlation energy, perturbation calc. using Gaussian-type geminals 79−10042
LiH, correlation energy calc. by many-body diagrammatic perturbation theory 78−9087
LiH, cryst., Compton profile, position space anal. 79−47536
LiH, cryst., specific heat at const. vol., isotopic modifications effects 80−103490
LiH, crystalline, surface struct., quantum mechanical ab initio calc. 77−1281
LiH crystals, temp. effects on X-ray scattering factors in LCAO calcs. 80−10454
LiH, cubic cryst., exciton-phonon interaction and exciton anisotropy 78−72083
LiH, defect form. at low temp., EPR, thermolum. and TSC study 80−107222
LiH, density matrix, factor X-ray struct. factor 78−67692
LiH, dipole moments and transition moments, semi-rigorous bounds, error limits 78−78635
LiH, direct optimisation of orbitals for multiconfiguration self-consistent field theory by unitary transformations 80−63544
LiH, directional Compton profiles for mol. simulation of crysts. 77−30931
LiH, directional Compton profiles 79−4867
LiH, EPR line shape of Li colloids created by γ-irrad. 77−77097
LiH, effect of surface hydrolysis to LiOH on IR absorption, X-ray luminesc. and EPR spectra 80−60660
LiH, elec. struct. by spin-adapted vector method 79−54777
LiH, electric dipole polarisabilities and hyperpolarisabilities, perturb. theory calcs. 78−17563
LiH, electron binding energies calcs. 78−86768
LiH, electron correl., double SCF method, mol. dissoc. energy 78−17575
LiH, electron elastic scattering, by highly polar mols., chem. bond effects 78−9248
LiH, electron scatt., low energy, multichannel variational calcs., static exchange approx. 80−83483
LiH, electron scatt., orthogonalisation and model exchange pots. calcs. 80−23552
LiH, electron scattering, iterative static exchange method 80−53155
LiH, electronic distribution functions and correl. holes, theory 78−17562
LiH, electronic struct., equation of state, insulator-metal phase transition 79−33234
LiH, electronic struct., valence bond orbital method appl. 80−106268
LiH, electronic struct. and equation of state up to 100 Mbar 77−1361
LiH, electronic structure SCEP theory calcs. 77−10579
LiH, energy functional, direct minimisation in LCAO-MO density matrix formalism 78−5118
LiH, excitons, reflection, cathodolum. and photocond.-excitation spectra 78−10989
LiH, excitons and exciton-phonon interaction, refl. spectra meas. 4.9 and 5.3 eV 77−44019
LiH, F-center, dynamic and NEDOR polarisation meas. *(French)* 77−28481
LiH, F-centres, dynamic nucl. polarisation, solid effect meas. *(French)* 77−81028
LiH, finite-field method calcs., dipole moment gradients, polarisability gradients and elec. field effects 77−88589
LiH, force const. evaluated in first order of perturbation theory 77−34781
LiH, form. on polycryst. Mo membrane, from diffusing gases, mass spectrometric obs. 77−66771
LiH, formation and annihilation of Li colloids and H bubbles 80−107228
LiH, Fourier transforms of Compton profiles 79−83050
LiH, gamma-ray buildup factors 80−27822
LiH, ground state, pot. curves, MTXα_R method 80−5482
LiH, half-projected HF scheme, stability conditions 77−61676
LiH, Hartree-Fock density matrix equation, soln. 77−14339
LiH, Hellman pseudopot. calcs., dissoc. energy, ionis. pot., bond length 77−10577
LiH in diffuse interstellar clouds 78−93361
LiH, insulator-metal transition press. calc. 78−34769
LiH, ionic cond., thermocurrent and photocond., defect and electronic props. 77−15621
LiH, ionic polarisability in cryst. lattice, quantum mech. model 79−47384
LiH, isotope exchange reactions, equilib. consts., adiabatic correction, electron correl. effects 78−88626
LiH, isotopic species, $A^1\Sigma^+ \rightarrow X^1\Sigma^+$ bands 78−42091
LiH, iterative natural orbitals for CI using perturbation theory 79−79549
LiH, kaonic X-ray spectra, strong interaction widths 77−10796
LiH, kaonic X-rays meas., strong interaction widths, shifts, yields 77−58210
LiH, laser irradiated, single/multiphoton dissociation, ab initio theory 78−17735
LiH, lattice dynamics, effect of long-range three-body forces 77−89507
LiH, lattice energy calc., teaching 78−16595
LiH, layers and solid, localised HF orbitals 78−9076
LiH^-, pot. energy curves, electron affinity, spectroscopic consts. 78−5129
LiH, $LiHe^+$ and $LiHe_2^+$ systems, ab initio SCF LCAO calcs. of stability and spectroscopic consts. 77−71748
LiH, limited MC SCF calcs. 79−36537
LiH, linear chain, ab initio calcs., cryst. orbital method 79−37659
LiH, linear response function, diagonal ARPA calcs. 78−74594
LiH, liq., density and surface tension, 982-1280K 80−59548
LiH, liq., surface tension investigation, 964-1300K 80−70503
LiH, luminesc. of free and localised excitons, UV, X-ray and electron irrad. luminesc. 79−87483
LiH, mag. domains and nucl. mag. ordered phases, antiferromag. and ferromag. neutron diffr. obs. 80−50051
LiH, mag. ordering in nucl. antiferromag. state, neutron diffr. obs. 79−65654
LiH, many body perturbation theory fourth order calc. of correl. energy 80−14087
LiH, many electron Green's function calcs. optical pot. 80−58126
LiH, many-body Green's function, electronic mol. props. 78−25417
LiH, mol., vibr. quantum numbers of rotating vibrator 79−85949
LiH, mol. elec. polarisabilities and dipole moments calcs. 78−41976
LiH, mol. electronic momentum distrib. functions and correl. holes in p-space 79−97978
LiH, mol. polarisability, correlation corrections in finite-field method 77−71889
LiH, mol. struct. 2-electron integral evaluation by Multipole Expansion of Diatomic Overlap 78−908
LiH molecule, fast electron elastic scatt. intensity calcs. 77−3459
LiH, molecule, floating spherical GO calcs of electron momentum distribs. and Compton profiles 77−30933
LiH, motion and relax. of free excitons, luminesc. spectra 79−43037
LiH, NMR shielding consts. and mag. susceptibilities, coupled HF with extended GTO basis 80−5480
LiH, neutron diffr. evidence of nuclear antiferromagnetism 79−61066
LiH, nucl. antiferromag. struct., neutron diffr. and dynamic polarisation *(French)* 78−88226
LiH, nucl. dipolar mag. ordering, dipole-dipole interactions, review 77−85475
LiH, nuclear antiferromagnetism, dynamic nuclear polaris., NMR 79−1724
LiH, nuclear antiferromagnetism studied by neutron diffr. 79−11358
LiH, nuclear ordered ferromag. and antiferromag. phases, neutron diffr. study 80−50052
LiH, numerical calc. of one-electron props. from SCF-Xα-SW calcs. 77−6688
LiH oligomers, struct., stability SCF and CEPA-PNO calcs. 78−78640
LiH, one electron props., Xα multiple scattering wave functions 80−42945
LiH, one electron props., SCF-Xalpha scattered wave method 80−83279
LiH, optical parameters of localised centres at high hydrostatic press. 78−10943
LiH, pairwise correlated GVB model, multiconfig. overlap approx. calcs. 79−31408
LiH plasma, phase transition 78−42710
LiH plasmas, magnetic mirror confinement decay measurement 79−46470
LiH, polarisabilities and dipole moment derivatives, virial theorem calcs. 77−57865
LiH, positron affinity, ab initio LCAO MO SCF calc. 78−82870
LiH, pot. curve, one-config. Hartree-Fock-Roothaam calc. for force consts. 78−82627
LiH, relativistic Dirac-Fock multiconfig. SCF calcs. 80−99455
LiH, relativistic Dirac-Fock multiconfig. SCF calcs. 80−99456
LiH, resonant Raman scattering in crystals with self-trapping excitons 80−7344
LiH, rot. excitation by electron impact, calc. cross sections 78−66670
LiH, SCF ab initio calcs. with noninteger Slater orbitals 77−26969
LiH, STO calcs. 79−6847
LiH, STP basis sets, energies calc. 77−3262
LiH, self-diffusion of Li and H ions 78−59974
LiH, separated electronic pair functions, direct minimisation of energy functional, LCAO-MO SCF, density matrix formalism 79−31392
LiH, single cryst., reson. zero-phonon exciton luminesc., polariton emission 78−52564
LiH, single crysts., refl. photolum., cathodolum., and photocond. meas. 77−52186
LiH, solid, anion and neutron diffusion, NMR relax. and linewidth obs., Schottky disorder 80−15815
LiH, solid, mag. susceptibility calc. 77−85412
LiH, solid. Hartree-Fock energy band calc. using OPW method 80−10856
LiH, soln. in liq. Li, elec. resist. 77−47786
LiH, spectroscopic consts., FSGO calcs. 77−6758
LiH, spin-coupled theory of mol. wavefunctions, mol. struct. and props. 77−50337
LiH, state selected rot. transition integral cross section, laser fluoresc. obs. 80−63770
LiH, UV induced luminescence 77−85784
LiH, valence band struct., XPS exam. 79−69416
LiH, variation-perturbation minimal Gaussian geminal basis sets correl. energy calc. 78−78629
LiH, variational Hylleraas-type wavefunction, correl. 78−9082
LiH, variational time-dependent H-F calcs. in pseudopot. framework 77−10588
LiH, $X^1\Sigma^+$ and $A^1\Sigma^+$ states, hybrid pot. energy curves, dissoc. limits 77−79669
LiH, $X^1\Sigma^+$ ground state, spectroscopic and pot. functions, method for combining spectroscopic data 79−45782
LiH, $X^1\Sigma^+$ states, many body effects, diagrammatic perturbation theory 77−79547
LiH, zero temp. phases, high density props. 78−75725
LiH^+, FSGO calcs. with model pots. 78−33413
LiH^+, PNO-CI and CEPA calcs. of electron correl. effects 77−34561
LiH^+, spin densities, SCF and CI calcs. 79−3362
LiH^+, spin-extended Hartree-Fock ab initio calculations for small radicals 78−70746
LiH^{3+}, LCAO method, improvement by directed variation of exponential parameters 79−41101
LiH^{3+}, pot. energy curves for 2pπ and 3dδ excited states 78−29756
^{6,7}LiH, cryst., cohesive energy, force const., lattice freq., Debye temp., Gruneisen parameters, calc. 78−91293
^{7}LiH, $A^1\Sigma^+$ state, vibr. levels, radiative and nonradiative lifetimes 78−66604
^{7}LiH, $A^1\Sigma^+$-$X^1\Sigma^+$ bands, radiative transition probabilities calcs. 78−66603
^{7}LiH, radiative transition probability, from pot. curves, $B^1\Pi$ curve calc. 78−78752
LiH:Ca^{2+}, two peaks in ionic thermocurrent curves 77−31807
LiH:Ce, thermolum., appl. as X-ray detectors 79−6794

lithium compounds continued
LiH:LiF, luminesc. of free and localised excitons, UV, X-ray and electron irrad. luminesc. 79−87483
LiH:Rh, EPR spectra of Rh centres, UV-irrad. cryst. 79−65724
LiH-NH_3(ethylene)(acetylene), struct. and props., SCF ab initio calcs. 80−106250
LiH+Ar, rot. energy transfer, power scaling law 79−54942
LiH+Ar, rot. transition cross-section, 0.8 eV 79−36742
LiH+Ar, rotationally inelastic cross-sections, state resolved, determ. 78−13577
LiH+HCl(DCl), rot. inelastic collisions, sudden theories 79−98201
LiH+HCl(DCl), state-to-state rot. inelastic cross sections, new laser fluoresc. technique 79−98200
LiH+H→Li+H_2, linear LiH_2 pot. energy surface, MCSCF functions optimisation 77−67960
LiH+He, rot. inelastic collisions, ab initio pot. energy surface calcs. 80−87208
LiH+He, rot. inelastic collisions, dynamics 80−87209
LiH+He, rot. inelastic collisions, state-to-state cross sections determ. 80−87210
LiH+He, rot. inelastic collisions, rigid shell models 80−99545
LiH+LiH, interaction energy, multipole anal., charge overlap, orientation and bulk props. 77−34715
LiH+LiH(CO_2)(H_2)(N_2), intermol. forces, multipole results validity, charge overlap effects 79−89730
LiH+Te exothermic solid-state reaction, ion backscatt. obs. 78−20064
$(LiH)^+$+meson system, ground and 1st excited state pot. surfaces, quantum mech. calc. 78−5377
^{7}LiH+HCN, rot. inelastic collision, energy transfer 80−87211
LiH_2 and LiH_2^+ binding energies, LiH_2 ionis. pot. and form. heat 79−94042
LiH_2, quantum mech. pot. surface, power series expansions 77−34577
LiH_2^+, ab initio pseudopotential for FSGO calcs., bond length 77−75043
$(LiH)_3$ complex, SCF interaction energy nonadditivity 80−91437
LiH_6^+, AB_6, non-transition element complexes, shapes and other props. 78−82647
Li_2H, form., SCF correl. diagram for low-lying linear and bent states 77−70292
Li_2H, Li_2H^+, binding energies, ionisation pot., mass spectrometric determ. 77−65546
Li_2H, natural orbital contour diagrams and occupation nos. for form. and dissoc. 79−18107
Li_2H^+, ab initio pseudopotential for FSGO calcs., bond length 77−75043
Li_2H^+, equilib. geom. and dissoc. energy, pseudopot. calc. 78−94329
$LiHCd(Ge_5O_{15})$, cryst. struct. determ. by X-ray diffr. 77−76381
$LiHCd_4(Ge_5O_{15})$, cryst. struct., comparison with natural rhodonite 78−30600
LiH(D), elastic constants, lattice dynamics and phonon dispersion 78−30711
LiH(D), electrical conductivity, effect of isotopic composition of H 79−15150
LiH(D), isotope effect on Wannier-Mott exciton levels 80−103633
LiH(D), second-order Raman spectra 79−47443
LiH(D):Rh, EPR of axial impurity complex 77−40123
LiH_2F hypothetical crystal, existence, total energy calc., pseudopot. calc. 78−2442
LiHH, pot. function by trial function method 77−6699
LiHH system, pot. surfaces, nonempirical GO calcs. 77−42374
$Li_{1-x}H_xIO_3$, cryst. growth from soln. and phys. props. 77−31634
$Li_{1-x}H_xIO_3$, dielec. behaviour, Raman and IR spectra 77−32357
$Li_{1-x}H_xIO_3$, piezoelectric props., space charge effects 78−6637
$LiH_2(LiD_2)(LiT_2)$, pot. surfaces, fundamental freqs. and thermodynamic functions 80−69205
$Li_2H(Li_2D)(Li_2T)$, pot. surfaces, fundamental freqs. and thermodynamic functions 80−69205
LiHLiH array, Mott transition mag. analog, Hamiltonian for paramagnetic-diamagnetic transition 79−95565
LiH^-(LiH), ab initio ground-state pot. energy curves, electron affinities 78−41946
$Li(H_2O)^+$, coherent X-ray scatt. profile calcs. 77−61765
$Li(H_2O)^+$, config. ab initio GAUSSIAN 70 calcs. 79−49939
LiH_2O^+, geom., electronic struct. FSGO model calcs. 78−82614
$Li^+(H_2O)_n$, (n=1,2,3,4,6), FSGO-pair-pot. calcs. *(German)* 80−74277
$Li(H_2O)_3ClO_4$, Li sites determ., using method based on bond-strength calcs. 79−7514
LiH_2PO_3, nonlinear and linear optical props. 80−48330
LiH_2PO_3, P-H bond dipole direction, nonlinear optical coeffs. meas. 80−69253
LiH_2PO_3, Raman and IR spectra of transverse and longitudinal modes *(French)* 80−60573
$LiHSeO_3$, and deuterated analog, vibr. spectra 79−24311
$LiHSeO_3$, X-ray cryst. struct. determ. 80−28966
$LiH_3(SeO_3)_2$, ferroelec., absolute atomic arrangement and spontaneous polarisation, neutron diffr. study 80−59442
$LiH_3(SeO_3)_2$, IR and Raman spectra, internal modes, intra- and inter-H-bond tunnelling 78−43853
$LiH_3(SeO_3)_2$:Mn^{2+}, single crystal, EPR 78−72396
$LiH_3(SeO_3)_2$:VO^{2+}, ferroelectric, 298K, EPR 79−51846
$LiHe^+$, from LiT β-decay, pot. energy curves 78−56910
$Li_{1-x}Hf_{2-x}Ta_x(PO_4)_3$, new solid ionic conductors 77−35953
$LiHoF_4$, crit. behaviour of mag. suscept. 79−33465
$LiHoF_4$, cryst. field parameters, mag. susceptibility meas., 0.3 to 100K 80−60214
$LiHoF_4$ crystal melt growth, comparison of Czochralski and Bridgman-Stockbarger methods 80−60765
$LiHoF_4$, dipolar-coupled Ising ferromag., submillimetre ferromag. and paramag. reson. 77−69697
$LiHoF_4$, EPR studies, lowest levels of rare-earth ions, submillimetre freq. 80−39865
$LiHoF_4$, NMR rotation spectra, transferred hyperfine interaction 77−85590
$LiHoF_4$, NMR shift tensors, temp. and field depend. 79−38391
$LiHoF_4$, spectroscopic anal., Ho^{3+} polarised absorpt. spectra, cryst. field parameters 79−95756
$LiHoF_4$, uniaxial dipolar ferromag. crit. behaviour 79−61149
$LiHoF_4$, uniaxial dipolar ferromag., critical behaviour, mag. susceptibility meas. 80−80528
LiI aqueous solution, US study of apparent molar compressibility 78−10125
LiI complexes, ionic cond., electrochem. props. 77−60072
LiI crystal, emission spectra under UV-light excitation at 77K 78−92110
LiI crystal, irradiated at low temps., optical absorption spectra 80−45123
LiI, dil. aq. solns., conductance at 25°C 77−69105
LiI, electron-mol. beam collisions, autoionising states, electronic spectra *(Russian)* 78−22023
LiI hybrid IC pacemaker, reliability, experience 77−81736
LiI in acetone, press. effects on Walden products, ion-solvent interactions 80−3398
LiI, Mossbauer charge density of $^{129}I^-$ 79−61275
LiI powered pacemaker types evaluated 77−81738
LiI, reactor irrad., absorpt. spectra 79−65902
LiI UV photodissoc. cross section, reson. ionis. Li detection 80−63719
$Li^{129}I$, Ar matrix isolated and cryst., Mossbauer verification of distortion overlap 77−63325
LiI:α-Al_2O_3, model for fast ionic cond. 79−77811
LiI:Pb, absorpt. spectra of Pb^{++} centres 80−76058
LiI:Tl, absorpt. spectrum obs. 80−50378
LiI-WO_3 solid-state electrochromic cell, fabrication and charact. *(Japanese)* 80−84717
Li_2I_2, UPS of dimeric mol., expt. and Xα calc. 80−9640
α-$LiIO_3$, ^{7}Li NMR, spin-lattice relax., spurious reson. *(Chinese)* 80−39884
$LiIO_3$, ^{7}Li nuclear spin-lattice relax. meas. 78−10796
$LiIO_3$, 5.3 μm down-conversion, IR source appls. *(German)* 78−90452
$LiIO_3$, active spectroscopy of polaritons, interf. of direct and cascade processes *(Russian)* 77−38982
$LiIO_3$, $AgGaS_2$, IR radiation two-stage conversion, high sensitivity detector appl. 79−59761
α-$LiIO_3$, attenuated total reflection spectra of anisotropic surface polaritons 78−87919
$LiIO_3$ CW intracavity upconverter using Ar laser, noise props. 80−64099
$LiIO_3$, circular dichroism and UV absorpt. spectra, optical activity 77−20879
$LiIO_3$, cross relax. in two-spin system, inhomog. broadened line 78−88218
α-$LiIO_3$, cryst. growth of high piezoelec. and optical quality 78−31313
α-$LiIO_3$, cryst. growth by conc. convection of soln. 78−72716
$LiIO_3$ crystal, coherent antiStokes Raman scatt. by polaritons 79−36961
$LiIO_3$ crystal, noncollinear stimulated Raman scatt. using parallel pump beam 80−78912
$LiIO_3$ crystal, nonlinear optical freq. transform. of variously polarized laser radiation 79−55181
$LiIO_3$, crystal, parametric superluminescence in ps band 80−11469
$LiIO_3$ crystal, SHG, thermoelastic stresses and nonlinear refract. effect 80−74437
$LiIO_3$ crystal elastic, piezoelec., dielectric and acoustic props. 79−46740
$LiIO_3$, crystal gyrotropy, meas. in IR region 80−88957
$LiIO_3$, crystal inside Nd:$YA1O_3$ pumping laser, 0.9 W Raman oscillator operation 77−62004
$LiIO_3$ crystal inside cavity of 1064 nm YAG:Nd^{3+} laser, optical SHG *(Russian)* 80−28272
α- $LiIO_3$, crystal struct. refinement, corrected thermal parameters 77−4092
$LiIO_3$ crystals with optical freq. conversion, IR detect. charact. 77−87832
$LiIO_3$, crysts., spontaneous parametric scattering of light by defects 80−34936
α-$LiIO_3$, DC effects on transmitted light *(Chinese)* 78−10869
α-$LiIO_3$, defects decorated by space charge, X-ray topography study *(Chinese)* 80−107204
α-$LiIO_3$, depolarisation current, dielectric const. relaxation behaviour *(Chinese)* 80−88905
α-$LiIO_3$, dielectric constant and elec. cond. of single crystals *(Chinese)* 77−77134
$LiIO_3$, difference freq. generation tunable under dispersive phase-matching conditions 78−46726
α-$LiIO_3$, dislocation etching 78−18653
α-$LiIO_3$, dislocation struct. 77−1132
$LiIO_3$, dispersion of cubic nonlinear susceptibility meas. 79−76747
$LiIO_3$, elastic wave leakage across gap between piezoelectrics 78−6204
$LiIO_3$, electrogyration coeff. meas. 79−19859
α-$LiIO_3$, energy band struct., nonlinear optical absorpt. obs. 79−64277
α-$LiIO_3$, Fermi resonance in surface polariton spectra *(Russian)* 80−71423
$LiIO_3$, freely oscillating Nd:glass freq. doubling, phase matching 77−14780
$LiIO_3$, freq. conversion of CW chem. HF laser radiation 78−30023
$LiIO_3$, freq. tunable single ultrashort light pulse generation 77−79896
$LiIO_3$, freq. up-conversion, spontaneous parametric noise 77−75622
$LiIO_3$, generation of tunable CW IR radiation by difference freq. mixing 77−3623
α-$LiIO_3$, hexagonal cryst , vibrs. and force consts. 79−69220
$LiIO_3$, high power Raman oscillator, shared resonator config. 77−88853
$LiIO_3$, IR radiation parametric upconversion with pulsed ruby and CW Ar lasers 77−72026
$LiIO_3$, IR radiation generation, difference freq. mixing of N_2 and dye laser laser radiation 78−37942
α-$LiIO_3$, in electrostatic field, X-ray double cryst. spectrometric investigation *(Chinese)* 78−67666
$LiIO_3$, influence of injected protons on cond. 77−69115
$LiIO_3$, intracavity freq. doubling of Nd:YAG laser long pulse emission 80−102736
α-$LiIO_3$, ion migration polarisation phenomena, current correlation function *(Chinese)* 80−6539
$LiIO_3$, irreversible double refraction in mag. field *(Russian)* 77−59560
$LiIO_3$, KD_2PO_4 doubler and KH_2PO_4 mixer crysts. mW 213 nm source based on Nd:YAG laser 79−55178
$LiIO_3$, laser accessory for freq. doubling 78−46725
α-$LiIO_3$, lattice consts. variation due to electrostatic field *(Chinese)* 78−83787
α-$LiIO_3$, light diffr. intensity, freezing effect in electrostatic effect *(Chinese)* 79−91404
$LiIO_3$, mixing of Nd laser radiation for coherent picosecond source, 350 to 680 nm 78−13762
$LiIO_3$, multistage conversion of pump energy into low-freq. radiation 78−30022

lithium compounds continued
$LiIO_3$, NQR freq. temp. depend., phonon spectra interpretation 77−12226
α-$LiIO_3$, neutron diffr. intensity enhancement under DC field, investig. 80−10462
$LiIO_3$, noncollinear SHG, background-free meas. of picosecond laser pulse time behaviour 79−59758
$LiIO_3$, noncollinearly phase matched SHG 77−46754
$LiIO_3$, nonlinear cryst., difference freq. generation by superposed beams, vector matching effects *(Russian)* 77−62014
$LiIO_3$, nonlinear cryst., use for ps reson. spectroscopy, stroboscopic method *(Russian)* 77−83930
$LiIO_3$, nonlinear crystals, interference of optical harmonics 80−64102
$LiIO_3$, nonlinear light scatt. on cryst. defects 78−5527
$LiIO_3$, nonlinear optical activity *(Russian)* 79−45994
$LiIO_3$, optical parametric oscillator, Nd laser pumping 77−744
$LiIO_3$, parametric convertor of IR radiation, angular and spectral characts. 79−64282
$LiIO_3$ parametric convertor, appl. to cancellation of optical inhomogeneities in Nd:glass laser 80−33049
$LiIO_3$, parametric oscillator, tunable IR ultrashort pulse prod. 77−3629
$LiIO_3$, parametric oscillator, stimulated Raman scatt. competition 78−18016
$LiIO_3$, parametric scatt. at interface between two media *(Russian)* 79−59767
$LiIO_3$, parametric superluminesc., picosec. spectroscopy 79−55187
$LiIO_3$, phase transitions obs. by DTA, heat treatment, X-ray diffr. *(Chinese)* 78−2249
$LiIO_3$, piezoelec. coated with semicond. film, Bleustein-Gulyaev wave amplification 79−61309
α-$LiIO_3$, piezoelec. mat. for acoustooptic cells, piezoelectric transducers 78−95575
$LiIO_3$, piezoelectric transducer, acoustic field distrib., Bragg diffr. method 80−97231
$LiIO_3$, polarisation effect in piezoelectric executing longitudinal vibs. 79−1741
α-$LiIO_3$, positron annihilation meas. 78−19597
$LiIO_3$, possible separation of direct and cascade processes in active combination scatt. Raman spectroscopy 78−13764
α-$LiIO_3$, pot. energy distrib. and force const. variations with temp. 80−79894
$LiIO_3$, pulse-period parametric oscillator, tunable 0.63 to 3.4 μm, for nonlinear spectroscopy 78−59083
$LiIO_3$, Raman induced Kerr effect with elliptical polarisation 78−42392
$LiIO_3$ Raman oscillator, high-average-power, employing shared resonator config. 78−30013
$LiIO_3$, Raman spectra and phase transitions 77−16316
α-$LiIO_3$, Raman spectra behaviour in electrostatic field *(Chinese)* 80−7333
$LiIO_3$, Raman-induced Kerr effect 77−40227
α-$LiIO_3$, refr. index, temp. coeff., 285-700 nm, 320-500K *(Russian)* 77−66473
$LiIO_3$, SHG of ps pulses, freq. tuning 77−50724
$LiIO_3$, second harmonic optical coeffs. based on highly deformed oxygen-octahedra model of $(IO_3)^{-1}$ *(Chinese)* 77−75608
$LiIO_3$, simultaneous stimulated Ramam scatt. and optical freq. mixing 79−86210
$LiIO_3$, simultaneous stimulated Raman scatt. and optical freq. mixing using three-mirror config. 80−48342
α-$LiIO_3$, single cryst., opt. and physicochem. props. 77−8566
α-$LiIO_3$ single crystals, electrical conduction and dielectric behaviour *(Chinese)* 78−30783
$LiIO_3$, single crystals, Raman induced Kerr effect 79−7185
α-$LiIO_3$ single crystals, research work, review *(Chinese)* 79−69782
α-$LiIO_3$ single crystal, enantiomorphism 79−95725
$LiIO_3$ single crystal, DC field effect, neutron diffr. enhancement *(Chinese)* 80−44077
$LiIO_3$ single crystal, surface acoustic wave parameter meas., coherent optics method 80−106691
α-$LiIO_3$, single crysts., light diffr. under DC field 80−11367
$LiIO_3$, spectral phase-matching props. for SHG 77−83922
α-$LiIO_3$, statistical theory of relaxation current and low-freq. dielectric dispersion 78−60391
$LiIO_3$, Stokes and antiStokes scatt. by LF polaritons 77−77202
α-$LiIO_3$, surface defect layer struct. due to mechanical working *(Russian)* 80−100238
$LiIO_3$, surface polariton spread length by modified DCIR method *(Russian)* 79−73566
α-$LiIO_3$, surface polariton spectroscopy, frustrated total reflection method *(Russian)* 80−49628
α-$LiIO_3$, temp. depend. studies of Raman spectra of polaritons in region of phase transition 78−76467
$LiIO_3$, transverse gap elastic waves, expt. 80−59576
α-$LiIO_3$, two-photon absorption spectra, energy struct. anal. 80−99785
$LiIO_3$, US wave tunnelling across piezoelectric gap 78−87857
$LiIO_3$, UV radiation prod., freq. doubling of N_2 laser pumped dye laser output 77−743
$LiIO_3$, visible and UV refr. indices 78−19439
$LiIO_3$, Z-cut, temp. coeff. of delay for SAWs 77−76654
$LiIO_3$, Z-cut cryst., appl. as wide band transducer in US pulse-phase interferometer 77−14868
α-$LiIO_3$:Cr^{3+}(Fe^{3+}), zero-field splitting const. calc. 77−51709
α-$LiIO_3$:Cr^{3+}(Fe^{3+}), hyperfine interactions, RF discrete saturation of EPR lines 78−48032
α-$LiIO_3$:Cr^{3+}(Mn^{2+})(Fe^{3+}) and radn. induced defects, EPR spectra *(German)* 78−84480
α-$LiIO_3$:Cr^{3+}(Ni^{2+})(Mn^{3+}), absorption spectra, impurity environments 78−27275
α-$LiIO_3$:Fe^{3+}, local environment and superhyperfine interactions by RF discrete saturation 77−85554
$LiIO_4$, radiation damage, XPS obs. 80−29844
$LiIO_4.2/3H_2O$, and $LiIO_4$, dynamics of IO_4^- vibr. in lattice 79−42157
$LiInCr_4S_8$, 1:1 ordering on tetrahedral sites, IR spectra obs. *(German)* 78−6669
α-$LiIn(MoO_4)_2$, high-temp. form., X-ray cryst. struct. determ. 80−107183
$LiInO_2$, prep., props. and struct. 80−35517
$Li_6In_2O_6$, ion mobility, NMR meas. *(French)* 79−65240
$Li_6In_2O_6$, pseudo-two-dimens. electrolytic solid, Li ion mobility, NMR study *(French)* 80−34235
$LiInS_2$, blue-band emission 80−76062
lithium compounds continued
$LiInS_2$, ionic cond., galvanic cell meas. 77−47616
$LiInS_2$, prep., props. and struct. 80−35517
$LiInS_2$, single cryst. growth by directional solidification, photoluminescence meas. 79−61514
$Li_2IrCl_6.xH_2O$, hyperfine spectra of mag. ordered state at very low temp., Mossbauer meas. 77−69744
Li_4IrH_4, and Li_4IrH_6, struct. and props. exam. 78−92245
LiK, Hellman pseudopot. calcs., dissoc. energy, ionis. pot., bond length 77−10577
$Li_{1-x}K_xI$, intrinsic optical absorpt. spectra 78−23500
$Li_2K(IO_3)$ in $LiIO_3$-KIO_3 system, lattice parameter, equilib. and metastable phase diagram *(Chinese)* 80−7538
$LiKSO_4$, polarised Raman and IR reflection spectra, internal and external mode assignments 77−16293
$LiKSO_4$, sulphate ion optical and spectroscopic props., cryst. environment effect 77−40224
$LiKSO_4$, thermal and dielec. props. 80−34860
$LiKSO_4$, uniaxial crystal, pyroelectric, thermal expansion, phase transition 80−19966
$(Li_{0.5}La_{0.5})_xBa_{1-x}TiO_3$, cryst. struct., dielec. and IR spectral meas. 79−46614
$LiMSO_4$, M=Li, Na, K, Li_2SO_4-$ZnSO_4$, ht. capacity and ht. of transform. 78−26690
$Li_xM_yV_{1-y}S_2$ (M=Fe, Cr) physical props., effect of metal substitution of Li intercalation 79−100395
$Li_{16-2x}Mg_x(GeO_4)_4$, $0<x<4$, synthesis, resistivity and structure 78−18831
Li_2MgGeO_4, high temp. modif., struct. derivation *(French)* 77−47433
$LiMgP_{1-x}V_xO_4$, luminesc. spectra in visible region, vanadate group 78−43921
$Li_{16-2x}Mg_x(SiO_4)_4$, $0<x<4$, synthesis, resistivity and structure 78−18831
Li_2MgSiO_4-Li_2ZnSiO_4, form. of solid soln. *(Japanese)* 77−25037
$LiMgVO_4$, luminesc. spectra in visible region, vanadate group 78−43921
$Li_{0.5(1-x)}Mn_x\ Fe_{2.5-0.5}O_4$, rectangular hysteresis loop, microstruct. form. 77−12718
$LiMnCrF_6$, ferrimagnetic, magnetic props. *(French)* 79−1668
$Li_{0.5}Mn_{0.15}Fe_{2.35}O_4$ ferrite cores with rectangular hysteresis loops, pulse parameters, effect of Fe_2O_3 heat treatment 80−60370
LiMnSc ferrites, role of intergranular microstresses in control of coercive force 77−20640
$Li_xMn_{1-x}Se$, anomalies obs. in mag. and elec. props. 77−69509
$Li_2Mn_xTi_{1-x}O_3$, EPR exam. of antiferromag. props. 78−15015
LiMnZn ferrites, elementary coupling energy to lattice of Mn^{3+} ions, depend. on T_c 77−69534
$LiMn[BO_3]$, X-ray cryst. struct. determ. 79−42034
Li_2MoO_4, electronic struct., XPS and X-ray emission spectra 77−42336
Li_2MoO_4, Li_2MoO_7, $Li_2Mo_3O_{10}$ and $Li_2Mo_4O_{13}$, thermodynamic props. 77−12822
Li_2MoO_4-$R_2(MoO_4)_3$, flux system for garnet prep. 77−48359
$Li_xMo_6S_{8-y}$ electrodes, thermodynamic and transport props. 80−66963
LiN, soln. in liq. Li, elec. resist. 77−47786
LiN_2, geom., electronic struct. FSGO model calcs. 78−82614
LiN_3, evidence for N_3^- from static and dynamic props. 78−60465
LiN_3, ionic nature, quadrupole splitting, mag. field depend., N^{3-} electron cloud deform., NMR 80−50210
LiN_3, low temp. method for single cryst. growth 79−74077
LiN_3, polycryst., IR active lattice vibr., optical consts. 77−77185
Li_3N, catalyst, form. of cubic BN from hexagonal BN *(Japanese)* 80−54374
Li_3N, defect props. and ionic transport 80−107486
Li_3N, defect struct., quartet state paramag. centres, EPR meas. 79−42837
Li_3N, diffusion processes and struct. NMR study 80−108090
Li_3N, electron density study using Compton scattering 80−79750
Li_3N, existence of N^{3-} ion in cryst. struct. 79−7583
Li_3N, heat capacity 5 to 350K, thermochem. props. to 1086K 78−92500
Li_3N, IR and Raman spectra and lattice dynamics 78−48177
Li_3N, interstitial sites and anharmonic thermal vibrs. in cryst. struct., ionic cond. mechanism 80−107190
Li_3N, ionic cond., annealing, trans- and intercryst. resist. 78−43176
Li_3N, ionic conductivity obs. 78−14507
Li_3N, ionic conductor, single cryst. defect struct. anal. data reduction and struct. refinements, 153-678K 79−32988
Li_3N, ionic hopping model, NMR relax. data anal. 80−92714
Li_3N, ionic transport mechanism and defect props. 80−107528
Li_3N layer structure with fast ion cond., ^6Li NMR obs. of diffusion 80−108102
Li_3N, NMR exam. of ion diffusion 79−19397
Li_3N, optical absorpt. coeffs., exciton creation, optical anisotropy 79−95796
Li_3N phonon spectra and lattice dynamics 77−59580
Li_3N, photoluminesc. props. 80−50414
Li_3N, single cryst., ionic conductivity 77−72711
Li_3N single crystal and sinters, Li ion conduction 80−70449
Li_3N single crystals, Czochralski growth, exam. 78−56574
Li_3N, sinter prep. and Li ionic cond. props. 79−99361
Li_3N, superionic conductor, local ionic motion, anisotropic dielec. behaviour 78−87817
Li_3N, superionic conductor, cryst. growth and struct., phys. props., book contrib. 79−42308
Li_3N, superionic conductor, far IR absorption, temp. and isotope effects 79−51969
Li_3N thin film, vacuum evaporation on WO_3, retarded deposition 80−108351
Li_3N, vaporisation, studied by Knudsen effusion method 80−92662
Li_3N, Watson sphere model, Madelung energy calc. 79−99112
Li_3N:H, ionic cond., nuclear reaction anal. 80−34454
Li_3N:H, ionic cond. 79−42305
Li_3N-LiBr(Cl)(I) quasibinary cuts, fast ionic cond. props., 25 to 400°C 80−107527
Li_6NBr_3, $Li_{13}N_4Br$, ionic transport 79−73336
LiNC, electron density distrib., SCF mol. orbitals calcs. 78−9058
LiNC, metal atom motion, WKB calcs. 78−82623
LiNC, mols. with polytopical bond, spatial distrib. and motion of Li 78−66533
LiNC, struct. vibr. states and pot. energy calcs. 78−86776
LiNC type molecules, Born-Oppenheimer approx. applicability 80−32603

lithium compounds continued
LiNC⇌LiCN, isomerisation energy/barrier correlation, rel. to HNC(BNC) 80−50840
$LiND_4SO_4$, ^7Li and ^2D NMR exam. of high-pressure phase 79−11396
$LiND_4SO_4$, dielec. pyroelec., and thermal props. 80−60509
$LiNH_3^+$, geom., electronic struct. FSGO model calcs. 78−82614
$LiNH_3^+$, $LiNH_2$, Li_2NH, localised orbital anal., bond props. 77−6676
Li_2NH, ionic cond. from −30 to 105°C 79−86922
$LiN_2H_5BeF_4$, hysteresis loop, protonic cond. model *(French)* 77−32320
$LiN_2H_5BeF_4$, linear and nonlinear optical props. *(French)* 78−33778
$LiNH_4PO_3F$, cryst. struct. *(French)* 78−34475
$LiNH_4SO_4$, atomic struct. exam. 79−37678
$LiNH_4SO_4$, DC elec. cond. 80−88603
$LiNH_4SO_4$, dielec. pyroelec., and thermal props. 80−60509
$LiNH_4SO_4$, ferroelect. and press. induced phase transitions 79−38473
$LiNH_4SO_4$, ferroelectric phase transition, lattice parameters and thermal expansion coeffs. 80−40074
β-$LiNH_4SO_4$, lattice modes and phase transition, polarised Raman meas. 77−20859
$LiNH_4SO_4$, low temp. antiferroelec. III phase, X-ray cryst. struct. determ. 79−42036
$LiNH_4SO_4$, nonlinear opt. props. including SHG 78−76396
$LiNH_4SO_4$, nuclear spin lattice and effective proton relaxation, phase transitions 80−54965
$LiNH_4SO_4$, phase transitions, temp. depend. of NMR, spontaneous polarisation, birefringence and SHG 78−10191
$LiNH_4SO_4$, phase transitions and phys. props. 78−76399
$LiNH_4SO_4$, press.-temp. phase diagram, NMR and SHG meas. 78−23690
$LiNH_4SO_4$, thermal props. near high temp. phase transition 78−19428
$LiN_2H_5SO_4$, single cryst., refr. indices, birefringence, optic axes orientation 77−90125
$Li(N_2H_5)SO_4$, thermal diffusivity exam. 78−63886
$LiNH_4SeO_4$, nonlinear opt. props. including SHG 78−76396
LiNO, four electron three centre bonding units, ab initio valence bond calcs. 80−27949
$LiNO_2$, Raman spectra, 18-493K, polycryst., comparison with other nitrites 79−87425
$LiNO_3$ cell, power capacity assessment 79−34428
$LiNO_3$, electron irrad. damage, XPS obs. 78−64444
$LiNO_3$, electronic struct., relative energies, iterative EH calcs. 77−38615
$LiNO_3$ in N,N-dimethylacetamide, Raman, IR and US relaxation studies 80−50315
$LiNO_3$, melt, NO_3^- ion struct., pulsed neutron diffr. obs. 78−22631
$LiNO_3$, mol. struct. ab initio calcs. 79−26884
$LiNO_3$, molten, X-ray diffr. structural anal. 78−42887
$LiNO_3$, Raman spectroscopic study of NO_3^- component with temp. 78−76458
$LiNO_3$ soln., Raman spectral studies of NO_3^- motion and interaction 78−92067
$LiNO_3$, soln. in organic liq. or D_2O, Raman lineshape, solvent-solute interaction 78−76448
$LiNO_3$ solns. coagulation of omphoteric latex sols, reversibility and specific ion effects 80−45567
$LiNO_3$ solution cathodic gas evolution rate rel. to electrode material *(Russian)* 80−26020
$LiNO_3$, spectral interference in at. absorption spectroscopy in C tube atomiser *(Japanese)* 79−48018
$LiNO_3$ waveguide, planar structure for integrated optics, props. *(Czech)* 80−96018
$Li^+NO_3^-$ ion pairs and hydrated ion pairs, MO calcs., matrix isolation data 78−46267
$^{6,7}LiNO_3$, cryst. vibr., Raman and IR spectra 79−15445
$LiNO_3$-$Cd(NO_3)_2$ molten mixtures, electrical conductance, non-Arrhenian behaviour 78−43158
$LiNO_3$-$NaNO_3$-$AgNO_3$, molten salt mixture, excess thermodynamic props. and US vel. *(French)* 77−31720
$LiNO_3$-$NaNO_3$(KNO_3), solid eutectic mixtures, Raman, IR spectra, line shifts, widths 77−55793
$LiNO_3.3H_2O$, cryst. struct., X-ray determ. 77−80470
$LiNO_3.3H_2O$, crystallisation kinetics 79−4264
$LiNO_3.3H_2O$, neutron diffr. studies at 120 and 295K, H bond studies 80−88099
$LiNO_3.3H_2O(D_2O)$, crysts. and melts, density, mol. vol., thermal coeff. of expansion, rel. to struct. 80−15270
$LiNO_3.3H_2O(3D_2O)$, density, thermal apansion coeff., isotope effect 78−87733
$Li(Na,K)CO_3$, therm. anal. and X-ray diffr. study *(French)* 79−46630
LiNa, and anion, electronic struct., spin-unrestricted, spin-restricted SCF HF calc. 78−90331
LiNa ferrite, effect of sintering temp. on oxidation kinetics, conductivity meas. 77−21298
LiNa, Hellman pseudopot. calcs., dissoc. energy, ionis. pot., bond length 77−10577
$LiNa^+$, FSGO calcs. with model pots. 78−33413
$Li_{1-x}Na_xBr(I)$, intrinsic optical absorpt. spectra 78−23500
$Li_{0.04}Na_{0.1}Fe_{2.5}O_4$, $Li_{0.3}Na_{0.2}Fe_{2.5}O_4$, ferrites, form., X-ray, chem. and mag. anal. 77−36424
$Li_{0.5-x}Na_xFe_{2.5}O_4$, Na_2CO_3 effects on ferrite formation 78−27458
$Li_{1-x}Na_xNbO_3$, LPE, growth and temp. coeff. of SAW velocity 78−43227
$(Li_{0.63}Na_{0.37})_2O.2SiO_2$, short range struct. by pulsed neutron scatt. 80−59396
$Li(Nb,Ta)O_3$ solid solution, LPE growth of thin film waveguides on $LiTaO_3$ substrates 79−41467
$Li(Nb,Ta)O_3/LiTaO_3$, multi-layer optical waveguide fabrication by LPE 80−71605
$LiNbO_2$:Ti SAW acousto-optic modulators for integrated optics 79−90032
$LiNbO_3$, 3-D waveguide, efficient SHG, phase matching 77−7156
$LiNbO_3$, 3.39 micron HeNe laser radiation, difference freq. mixing and SHG 77−83928
$LiNbO_3$ 400 MHz saw filters 79−23158
$LiNbO_3$, acoustic characts. meas. of Z-cut single crysts. by acousto-optical method 79−3867
$LiNbO_3$ acoustic conversion, piezoelect. surface wave behaviour at discontinuities 77−31198
Y-Z $LiNbO_3$, acoustic effects of filamentary defects 80−75314
$LiNbO_3$ acoustic waveguide, nonlinear interaction of elastic waves with reson. *(Russian)* 78−6206

lithium compounds continued
$LiNbO_3$, acoustically tuned optical filter, electrostatic field effect 77−58443
$LiNbO_3$, acousto-optic interaction with surface waves, for image scanning 77−3673
$LiNbO_3$ acousto-optic memory correlator 77−88992
$LiNbO_3$, acousto-optic interaction, phase grating production 79−41454
$LiNbO_3$, acousto-photorefractive effect 77−88878
$LiNbO_3$, acousto-photorefractive effect for acousto-optic memory correlator 78−71248
$LiNbO_3$ acoustoelectric memory correlator struct. for scanning of optical images 80−74632
$LiNbO_3$, acoustooptic interaction, unguided light deflection via SAW 77−8543
$LiNbO_3$, acoustophotorefractive effect, appl. at acousto-optic memory correlator 78−15145
$LiNbO_3$ acoustophotorefractive memory correlator enhancement 79−55080
$LiNbO_3$, acoustophotorefractive effect, phenomenological theory 79−78649
$LiNbO_3$, aluminum-coated YZ, measurements of SAW attenuation 80−74619
$LiNbO_3$, amorphous ribbons, prep., electron and X-ray diffr. obs., dielec. const. temp. depend. 79−50993
$LiNbO_3$, anisotropic, waveguide, guided-radiation mode interaction in off-axis propag. 79−76839
$LiNbO_3$, anisotropic diffused optical waveguides, polarisation and spectral characts. 79−32073
$LiNbO_3$, anisotropic multilayer waveguide for electro-optical modulator, propag. characts. *(Italian)* 78−50904
$LiNbO_3$, anisotropic planar waveguide, TE to TM mode conversion *(Russian)* 77−11039
$LiNbO_3$, anisotropy and phase velocities of prop. of elastic waves 79−1478
$LiNbO_3$, anomalous photovoltaic effect and photocond. 78−52449
$LiNbO_3$, anomalous photovoltaic effect and photocond. 79−38122
$LiNbO_3$, anomalous photovoltaic effect obs., Anderson method 80−88595
$LiNbO_3$, anomaly in elec. resist. 78−68030
$LiNbO_3$ appl. in optical bistable devices, electro-optical multivibrator operation 80−58674
$LiNbO_3$, appl. in sub-100 ps pyroelec. detectors, 10.6 μm damage threshold meas. 80−77859
$LiNbO_3$, asymm. phononlines, IR refl. analysis 78−27197
$LiNbO_3$ balanced bridge modulator/switch with ion-etched slot 79−89993
$LiNbO_3$, band struct. and spontaneous polarisation calcs. 78−95261
$LiNbO_3$ birefringent crysts., holographic writing, image polarisation characts. storage 77−61926
$LiNbO_3$ blazed grating electro-optic deflector development 77−42627
$LiNbO_3$, blocking effect, backscatt. method *(Chinese)* 79−90708
$LiNbO_3$ branching waveguide, optical TE-TM mode splitter 80−96033
$LiNbO_3$, broadly tunable repetitive picosecond parametric oscillator, freq. conversion 78−66866
$LiNbO_3$, bulk, Ti-diffused integrated optical spectrum analysers, H implantation effects, pot. uses 80−43486
$LiNbO_3$, bulk wave generation near SAW reson. by interdigital transducers 80−33402
$LiNbO_3$, channel waveguide to single-mode fibre high-efficiency flip-chip coupling 80−99833
$LiNbO_3$, chemical, struct. and physical props., book contrib. 79−69783
$LiNbO_3$, chemical control of optical damage, due to laser beams 78−38056
$LiNbO_3$, cleaved, crystallographic and electrooptic props. 80−59575
$LiNbO_3$, collinear light diffr. by transverse acoustic waves 77−52040
$LiNbO_3$, comparative frustrated total refl. and Raman scatt., fundamental mode freq. and phonon dispersion 77−28579
$LiNbO_3$, complex conjugate wavefront generation via degenerate four-wave mixing 80−48329
$LiNbO_3$ computer-controlled IR parametric oscillator source 77−19365
$LiNbO_3$ computer-controlled Nd:YAG-pumped parametric oscillator 77−54758
$LiNbO_3$ continuously tunable parametric oscillator and amplifier, for remote SO_2 meas. 78−77365
$LiNbO_3$ corrugated optical waveguide, electrooptic scanning of coupled light 78−38050
$LiNbO_3$, cryst., US vibrating laser beam diffr. *(Russian)* 78−31172
$LiNbO_3$ crystal, different interdigital electrode struct., electric field distrib. obs. 78−76433
$LiNbO_3$ crystal, elec. cond., optical quality, impurity depend., space charge pyroelectric field compensation 79−64295
$LiNbO_3$ crystal acousto-optical tunable filter 77−19434
$LiNbO_3$ crystal and ruby lasers in difference freq. laser, tunable MM range emission 80−5764
$LiNbO_3$, crystal defects, X-ray diffr. topographic study *(Chinese)* 80−84173
$LiNbO_3$ crystal in laser resonator, thermo-optical effect *(Chinese)* 80−106546
$LiNbO_3$ crystal two-stage electrooptic deflector 80−106625
$LiNbO_3$, crystallisation from solution in borate, vanadate and tungstate melts 79−1820
$LiNbO_3$ crystals, activated by $3d^n$ ions, enhancement of polarisation echo 79−38439
$LiNbO_3$ crystals, composition determ. from parametric scattering spectra *(Russian)* 77−15595
$LiNbO_3$ crystals, electro-optical feedback system, polarisation control on single-mode optical fibres 80−91899
$LiNbO_3$ crystals, grating phase shift determ., holographic techniques 79−50250
$LiNbO_3$ crystals, in Nd^{3+}:YAG laser cavity, AM of optical second harmonic 80−78908
$LiNbO_3$ crystals, low temp. polarisation reversal 79−61322
$LiNbO_3$ crystals, polaron character of colour centres 80−2013
$LiNbO_3$ crystals, SHG, temperature phase-matching curve hysteresis 80−91852
$LiNbO_3$ crystals, velocity and propag. loss meas. of surface shear waves 80−74581
$LiNbO_3$ crystals with optical freq. conversion, IR detect. characts. 77−87832
$LiNbO_3$, crysts., elec. field influence on hypersonic wave propag. 80−44668

lithium compounds continued
$LiNbO_3$, Czochralski grown single crysts., cellular interface and struct. due to constitutional supercooling *(Chinese)* 79−51026
$LiNbO_3$ Czochralski grown single crystals, facetted and nonfacetted growth sections, growth striae *(Chinese)* 80−64940
$LiNbO_3$, damping of elastic waves at 36.5 GHz 77−39632
$LiNbO_3$, damping of LF elastic vibrs., internal friction meas. 79−28043
$LiNbO_3$ deflector, use in streak camera of approx. 100 ps resolution 79−18533
$LiNbO_3$ delay line, bulk wave generation due to nonlinear interaction of SAW 79−42359
$LiNbO_3$, difference freq. generation of submm. waves *(Russian)* 77−10981
$LiNbO_3$, difference freq. radiation of IR radiation, high efficiency 77−19363
$LiNbO_3$, diffr. effects from very narrow surface wave transducers 78−22240
$LiNbO_3$ diffused optical waveguide, with exponential profile, metal-clad and dielec. overlay effects 78−46755
$LiNbO_3$, diffused waveguide as Bragg electro-optic modulator 77−34955
$LiNbO_3$ diffused waveguides, optical insertion loss meas. 78−38054
$LiNbO_3$ diffused waveguides, SHG *(Russian)* 79−59770
$LiNbO_3$, diffused waveguide for acoustooptical signal processing 79−90029
$LiNbO_3$ diffused waveguide, induced diffr. grating, integrated optics applications 79−98511
$LiNbO_3$, diffusion of Ti, surface acoustic waveguide formation 77−79998
$LiNbO_3$, diffusion of Co, Ni, Zn and Cu and its effect on acoustic velocity 77−84847
$LiNbO_3$, diffusion of alkali metals and self-diffusion 77−84989
$LiNbO_3$, diffusion waveguide, acousto-optic mode conversion at surface wave freqs. *(Russian)* 78−1348
$LiNbO_3$ directional coupler waveguide for travelling wave optical modulator 80−96035
$LiNbO_3$, dispersion law of polaritons, refr. index in IR, and Raman spectra meas. 78−27232
$LiNbO_3$, dispersion law and temp. depend. of polariton damping constant 79−95779
$LiNbO_3$, dispersion of quadratic optical susceptibility *(Russian)* 77−3635
$LiNbO_3$, doped, photorefr. and photovoltaic effects 77−38835
$LiNbO_3$ doped with transition metal oxides, absorption spectra temp. depend. 77−90176
$LiNbO_3$, double-pass config., parametric generation of single picosecond tunable pulses 80−19067
$LiNbO_3$, doubly resonant intracavity SHG of 1153 nm radiation with stabilization on HFS components of $^{127}I_2$ 80−33077
$LiNbO_3$ $\Delta V/V$ waveguide SAW propagation obs. and modal analysis 78−38128
$LiNbO_3$, effect of spontaneous polarisation on thermionic emission 78−35245
$LiNbO_3$, electric-field induced microscopic struct. changes, modulated X-ray diffr. detect. 78−47296
$LiNbO_3$, electro-optical modulator/switch, switched directional coupler principle 77−7191
$LiNbO_3$ electro-optical total internal reflection diffraction industrial modulators and deflectors 77−19436
$LiNbO_3$, electro-optic cryst., photo-induced electron and hole transport holographic method for determ. 79−28375
$LiNbO_3$, electro-optical modulator, light propag. close to optic axis 79−42947
$LiNbO_3$ electro-optic phase modulator for unpolarised laser beam 79−50403
$LiNbO_3$ electro-optic deflector based streak camera, 20 ps resolution 79−85189
$LiNbO_3$, electroacoustic interaction obs. 77−11966
$LiNbO_3$, electroacoustic echo excitation with aid of surface waves 77−14834
$LiNbO_3$, electroacoustic correlation memory effect 78−88001
$LiNbO_3$, electroacoustic coeffs. 79−69564
$LiNbO_3$, electromigration in ion bombardment 78−26601
$LiNbO_3$ electrooptic light modulator 78−1349
$LiNbO_3$ electrooptic phase modulator, axial mode locking of CW Nd^{3+}:YAG ring laser 78−50835
$LiNbO_3$ electrooptic phase modulator, freq. shift device for optical range 78−59147
$LiNbO_3$ electrooptic crystal, dynamic holographic light beam conversion, geometric factors 79−13928
$LiNbO_3$ electrooptic device, interdigitally electroded, acoustic reson. 80−19097
$LiNbO_3$ electrooptic switches used in Nd^{3+}:YAG lasers, contrast and configs. 80−33012
$LiNbO_3$ electrooptic crystal voltage-induced birefr. obs. for very high resist. meas. 80−73386
$LiNbO_3$, electrooptic photorefractive crysts. for optical information processing 80−74313
$LiNbO_3$, electrostatic probe for absolute measurement of SAW amplitude 79−50543
$LiNbO_3$, energy band struct., nonlinear optical absorpt. obs. 79−64277
$LiNbO_3$, exciton migration, laser time-resolved spectra obs. 79−69861
$LiNbO_3$ fast-response broad-band electrooptic elements for laser beam control systems 79−89944
$LiNbO_3$, ferroelec., cathodlum. spectral and temp. depend. 78−84665
$LiNbO_3$, ferroelec., displacive type phase transition, far IR reflection spectra 80−71339
$LiNbO_3$, ferroelec., phonon dispersion relations, neutron inelastic scatt. meas. 78−56435
$LiNbO_3$, ferroelec. crysts. for electrooptic and nonlinear optics, optical inhomogeneities, review *(Japanese)* 77−65613
$LiNbO_3$, ferroelec. glass *(Japanese)* 79−65840
$LiNbO_3$, ferroelec. phase, soft vibr. modes, far IR refl. meas. 79−87407
$LiNbO_3$, ferroelec. phase, phonon dispersion relations and lattice dynamics calcs., comparison with expt. 80−49319
$LiNbO_3$, ferroelectric devices for optical systems 78−90473
$LiNbO_3$, ferroelectric, anomalous photovoltaic effect 79−7861
$LiNbO_3$, ferroelectric transitions, thermally stimulated electron emission meas. 80−25534
$LiNbO_3$, Fi diffused, single-mode waveguide, comparison of bending losses in integrated optical circuits 80−83684

lithium compounds continued
Y-Z $LiNbO_3$, filamentary defects visualisation at wafer inspection stage 80−75315
$LiNbO_3$, film, Lamb waves near. crit. freq. study *(Russian)* 78−52039
$LiNbO_3$, film lightguide, pulse signal convolution in acoustooptic interaction *(Russian)* 78−1345
$LiNbO_3$ film on Al_2O_3, optical guided wave mode conversion by Love waves 79−46055
$LiNbO_3$, finite amplitude SAW distorted rippling profiles, optical probing obs. 80−34287
$LiNbO_3$, finite difference anal. of SAW 80−75423
$LiNbO_3$, for reflective dot array pulse compression filters 80−74623
$LiNbO_3$, Fourier transform Ir spectroscopy of vibr. states at high temp. 80−97256
$LiNbO_3$, freq. conversion of CW chem. HF laser radiation 78−30023
$LiNbO_3$, freq. depend. of TO phonon decay parameter, and phonon-phonon interaction mechanisms 77−59084
$LiNbO_3$, freq. up-conversion, spontaneous parametric noise 77−75622
$LiNbO_3$ geodesic lens fabrication by single-point diamond turning 80−33239
$LiNbO_3$ glass, quenched, ionic cond., appl. as solid electrolyte 79−1522
$LiNbO_3$ graded-index planar waveguide, $As_{40}Se_{50-x}S_xGe_{10}$ film strip-loaded 78−74965
$LiNbO_3$ grating-tuned picosecond IR source with CdSe down-conversion 80−74435
$LiNbO_3$, growth from melt and charact. *(Chinese)* 80−54155
$LiNbO_3$, guided wave devices, use of ferroelectric materials, review 78−38048
$LiNbO_3$, γ-irradiated and annealed, elastic and piezoelectric props. 78−2807
$LiNbO_3$, heteroepitaxial growth on MgO by RF sputtering, SHG 79−27323
$LiNbO_3$, high freq. plane acousto-optical light modulators *(Russian)* 78−79106
$LiNbO_3$, hologram, light diffr. with electro-optical rot. *(Russian)* 78−1190
$LiNbO_3$, hologram form. in external elec. field, transient energy transfer 78−22098
$LiNbO_3$, hologram indexing with tunable pulsed laser source 79−94186
$LiNbO_3$, hologram recording by photorefr. effect 77−83830
$LiNbO_3$, hologram recording, γ radiation effect 80−78812
$LiNbO_3$, hologram storage, book contrib. 78−25834
$LiNbO_3$, hologram storage depend. on envelope field, space charge field 80−78801
$LiNbO_3$, holograms stored by photorefractive effect, reading and optical erasure 78−90390
$LiNbO_3$, holographic storage at high temp., optical damage relax. 77−14677
$LiNbO_3$, holographic storage, expt. confirmation of theory for electro-optic crysts. in steady-state case 79−86136
$LiNbO_3$, holographic storage, beam coupling and light amplification, expt. compared with theory for electro-optic crysts. 79−86137
$LiNbO_3$, holographic storage, effects of nonstoichiometry and Fe-doping 80−69344
$LiNbO_3$, holographic storage and retrieval 80−99669
$LiNbO_3$, hyper-Raman scatt. *(Russian)* 78−87102
$LiNbO_3$, IR parametric oscillator source for remote air pollution monitoring 77−21936
$LiNbO_3$, IR reflectivity spectra and phonon self-energy effect 77−63413
$LiNbO_3$, IR reflectivity temp. depend. 78−27202
$LiNbO_3$, imaging of photorefractive effects by double cryst. X-ray refl. topography 78−39521
$LiNbO_3$, in-diffused Y-cut, optical switching device using leaky surface wave 79−23090
$LiNbO_3$, induced refl. and transparency increase *(Russian)* 78−59094
$LiNbO_3$, influence of spontaneous polarisation on photoelec. emission 79−28898
$LiNbO_3$ interfaces, SAW reflection, light scatt. meas. 80−34286
$LiNbO_3$, interfacial polarisation effects 79−60538
$LiNbO_3$, internal CW parametric upconversion 78−42376
$LiNbO_3$ intracavity upconvertor for IR detect., limits to low noise equivalent power operation 80−74430
$LiNbO_3$, inverse Raman scatt. by polaritons 78−23434
$LiNbO_3$, ion beam etching, for SAW refl. struct fabrication, role of redeposition 77−56123
$LiNbO_3$, ion implanted, acoustic model of SAW delay lines *(French)* 78−55540
$LiNbO_3$, ion-bombardment erosion of single cryst., prep. for TEM exam. 79−38996
$LiNbO_3$, ionic grouping theory of electro-optical and nonlinear optical effects of crystals *(Chinese)* 78−27183
$LiNbO_3$, LF sound attenuation, internal friction 78−63804
$LiNbO_3$, LPE on $LiTaO_3$ substrate, using Li_2O-V_2O_5 flux 78−44031
$LiNbO_3$, laser accessory for freq. doubling 78−46725
$LiNbO_3$ laser beam/SAW mode conversion 79−46056
$LiNbO_3$, laser induced optical damage, pyroelec. contrib., electrostatic obs. 78−37935
$LiNbO_3$, laser induced optical inhomogeneity in external electric field 79−95730
$LiNbO_3$, laser-induced optical damage, electrostatic obs. 78−18030
$LiNbO_3$, layered acoustic waveguide, group delay time, temp. coeff. var. 78−83152
$LiNbO_3$ layers, Li out-diffused, SHG phase matching temp. variation 80−69455
$LiNbO_3$, leaky SAW and guided light Bragg interaction, theoretical anal. 78−72484
$LiNbO_3$ lenses, diamond-turned aspheric geodesic waveguide lenses 80−58804
$LiNbO_3$, $LiNbO_3$:Fe, holography in ferroelectrics 78−90394
$LiNbO_3$, $LiNbO_3$:Fe, dynamic holography and optical image processing 79−94194
$LiNbO_3$, $LiNbO_3$-Fe, photorefraction in ferroelectrics rel. to electro-opt. effects 78−92048
$LiNbO_3$, light diffr., elec. field effects, spatial hologram appls. *(Russian)* 77−23635
$LiNbO_3$, light diffraction from volume phase holograms 79−36860
$LiNbO_3$, light emission from surface on heating or cooling 78−64416
$LiNbO_3$, light induced ultrasonic wave velocity change, refractive index 80−97236
$LiNbO_3$, light modulator with interdigital electrodes, operating charact. 78−90511

lithium compounds continued
$LiNbO_3$, light scatt. by Rayleigh waves on refl. and transmission 79−24288
$LiNbO_3$, line acoustical waves anal. 78−34692
$LiNbO_3$, line acoustic wave device 80−5854
$LiNbO_3$, linear thermal expansion coeffs. meas., room temp. to 250°C 78−55416
$LiNbO_3$, long wavelength phonons, low temp. lifetime 78−18710
$LiNbO_3$, low freq. Raman scatt. spectra of polaritons, photographic recording 79−73952
$LiNbO_3$ low-loss high-coupling volume mode 79−51409
$LiNbO_3$, luminesc. props., Li/Nb ratio effect 80−97323
$LiNbO_3$, magnetoelectric susceptibilities, phenomenological rules for computation 80−55068
$LiNbO_3$, mechanism of hologram writing, expt. 77−19212
$LiNbO_3$, microfabrication by ion-bombardment enhanced etching 78−76779
$LiNbO_3$, monocryst., thermoemission, anomalous zone bending *(Russian)* 77−55860
$LiNbO_3$, monodomain ferroelec. cryst., secondary electron emission coeff. 78−11032
$LiNbO_3$, monolithic filter operating at 220 MHz 77−42671
$LiNbO_3$, Mossbauer radiation modulation by coherent US excitation 79−61277
$LiNbO_3$, multistage conversion of pump energy into low-freq. radiation 78−30022
$LiNbO_3$, Nd laser radiation, difference frequency generation in rectangular mm waveguide 79−18479
$LiNbO_3$, Nd:YAG laser pumped, parametric oscillator, picosecond IR pulse generation 78−71151
$LiNbO_3$, non-centrosymm. crystal, hyper-Raman scatt. obs. 78−94409
$LiNbO_3$, nondirectional glow under laser irrad. 78−52575
$LiNbO_3$, nonlinear cryst., use for ps reson. spectroscopy, stroboscopic method *(Russian)* 77−83930
$LiNbO_3$, nonlinear crystals, interference of optical harmonics 80−64102
$LiNbO_3$, nonstationary intracavity stimulated Raman scatt. by polaritons 79−18473
$LiNbO_3$, OH^- groups effect on dielec. and optical props. of single crysts. 77−12327
$LiNbO_3$, OH^- ion conc., PMR calibration method, IR determ. *(German)* 77−55712
$LiNbO_3$, OH^- ion incorporation, mobility and optical absorpt. 77−35583
$LiNbO_3$, opposed interaction of acoustic waves 77−24360
$LiNbO_3$, optical absorption of hole centres, polaron model 80−97314
$LiNbO_3$, optical consts. determ. by background stimulated Raman scatt. 80−48336
$LiNbO_3$, optical damage induced by X-irradiation 77−20814
$LiNbO_3$, optical damage effects 77−40186
$LiNbO_3$, optical damage in doped and undoped ferroelectric, mechanism 78−95570
$LiNbO_3$, optical diffusive waveguide, profile determ. *(Russian)* 77−42622
$LiNbO_3$, optical material, thermal expansion, 60-300K 78−33791
$LiNbO_3$, optical parametric oscillator, for IR linear absorpt. spectroscopy 79−7180
$LiNbO_3$ optical parametric oscillator, depend. on pump laser beam quality 79−23019
$LiNbO_3$, optical parametric oscillator threshold parameters and linewidth control 79−81480
$LiNbO_3$, optical parametric amplifier 79−81481
$LiNbO_3$, optical parametric oscillator, down-conversion using GaSe, $AgGaSe_2$, 4 to 18 μm 79−86215
$LiNbO_3$ optical parametric oscillator, synchronously pumped, design and operation 80−14388
$LiNbO_3$, optical phonon modes and anharmonic couplings 78−60466
$LiNbO_3$, optical rectification in external resonator 78−13748
$LiNbO_3$, optical stability to laser pulse, 1.54 μm 79−3734
$LiNbO_3$, optical strength, surface layer influence 78−50843
$LiNbO_3$, optical strength anisotropy, excitation of second harmonic 79−69923
$LiNbO_3$, optical wave reflectance *(Japanese)* 78−87012
$LiNbO_3$, optical waveguide, Ti diffusion, XPS 77−11014
$LiNbO_3$ optical waveguide, Bragg interaction of leaky and Rayleigh waves 77−23783
$LiNbO_3$ optical waveguides, elimination of Li_2O out-diffusion waveguide 77−65641
$LiNbO_3$, optical waveguide, anisotropic planar, acoustooptic interaction 77−68273
$LiNbO_3$, optical waveguide, diffr. of modes by standing elastic surface waves *(Russian)* 78−1343
$LiNbO_3$ optical waveguides, electrooptic modulation and switching, recent progress 78−50945
$LiNbO_3$ optical waveguide, tuning characts. of parametric interactions 79−3779
$LiNbO_3$, optical waveguide fabrication, closed tube control of out-diffusion 79−10419
$LiNbO_3$, optical waveguide, coupling length adjustment by loading a metal film 79−23055
$LiNbO_3$ optical waveguide, diffused with mag. garnet film top layer, non-reciprocal props. 79−41444
$LiNbO_3$ optical waveguide, beam-to-waveguide coupler 79−90003
$LiNbO_3$ optical waveguide, acoustooptic interaction efficiency of TE modes, freq. depend. 80−53455
$LiNbO_3$ optical waveguides, Ag-Li and Tl-Li ion exchange effects 80−58791
$LiNbO_3$ optical waveguide surface, acoustooptical interaction for TE modes, metallisation effect 80−69541
$LiNbO_3$, optical waveguides by ion implantation 80−106622
$LiNbO_3$, optically active centres, form. by electron and γ-irrad. 78−18642
$LiNbO_3$ out-diffused and in-diffused waveguides, WKB analysis of guided and semileaky modes 79−27416
$LiNbO_3$ parametric generator, producing high power tunable ps visible and IR pulses, spectroscopy appl. 79−46003
$LiNbO_3$, parametric mixing of SAW in 20 to 100 MHz range 79−86279
$LiNbO_3$, parametric oscillator, Nd:YAG laser pumped 77−46767
$LiNbO_3$ parametric oscillator, 4 to 12 μm tunable down-conversion in GaSe 78−66865
$LiNbO_3$ parametric oscillator-amplifier system, grating tuned 79−3747

lithium compounds continued
$LiNbO_3$, parametric phonon echo obs. 80−59588
$LiNbO_3$, parametric superluminesc., picosec. spectroscopy 79−55187
$LiNbO_3$, partial waves of SAW, direct meas. by light scatt. 78−66994
$LiNbO_3$, partially clamped single cryst., secondary pyroelectricity, electrostatic meas. 79−82927
$LiNbO_3$, partially clamped single cryst., tertiary pyroelectricity, electrostatic meas. 79−82928
$LiNbO_3$ periodic laminar struct., optical SHG *(Japanese)* 77−72029
$LiNbO_3$, phase and amplitude relations between fundamental and second harmonic SAW 77−69157
$LiNbO_3$, phase holograms fixation kinetics 79−81393
$LiNbO_3$, phase modulator, use in multimode integrated optical bistable switch 78−79145
$LiNbO_3$, phased SAW array, acoustooptic guided wave Bragg diffr. 77−58439
$LiNbO_3$, phonon heat conduction of single crysts. by quantum acoustic method 77−11748
$LiNbO_3$, photocond. induced by N_2 laser *(Japanese)* 78−2521
$LiNbO_3$, photoelasticity tensor, including piezoelectrooptic interaction correction, Brillouin scatt. 77−24820
$LiNbO_3$, photoinduced grating contrib. to acoustic wave vel. 77−77154
$LiNbO_3$, photoinduced birefringence obs. 78−15144
$LiNbO_3$, photoinduced surface storage of SAW patterns 80−74309
$LiNbO_3$, photorefractive process sensitivity *(French)* 77−31124
$LiNbO_3$, photorefractive medium, hologram form. theory 77−68185
$LiNbO_3$, photorefractive, optical information storage 78−33708
$LiNbO_3$, photorefractive effect sensitivity 78−43833
$LiNbO_3$ photorefractive reversible optical memory *(Russian)* 78−58943
$LiNbO_3$, photorefractive sensitivity, dependence on impurity Fe^{2+}/Fe^{3+} ratio, EPR and APR data 79−73893
$LiNbO_3$ photorefractive crystals for computer interfaced optical memory system, hologram characterisation 80−58475
$LiNbO_3$, photosensitive electro-optical materials for holographic data storage *(French)* 77−31077
$LiNbO_3$, photovoltaic current, temp. and spectral depend. 78−47828
$LiNbO_3$, photovoltaic effect, latent-image formation kinetics, electrophotography appl. 78−84246
$LiNbO_3$, picosecond IR-continuum generation by 3-photon parametric amplification 80−23746
$LiNbO_3$, piezoceramic, elastic normal wave propagation, phase transitions *(Russian)* 80−40067
$LiNbO_3$, piezoelec., SAW interaction with secondary electrons 80−80708
$LiNbO_3$, piezoelectric powder, RF dynamic polarisation echo obs. 77−16254
$LiNbO_3$, piezoelectric stress const. determ. by impact loading technique 77−69778
$LiNbO_3$, piezoelectric layer, non-crystalline characteristics after ion implantation *(French)* 77−73117
$LiNbO_3$ piezoelectric fibre vibrations 78−31156
$LiNbO_3$, piezoelectric surface wave velocity, flexural biasing state influence 79−56730
$LiNbO_3$, piezoelectric plate resonator, acoustic correl. 79−76929
$LiNbO_3$ piezoelectric coeff. and permittivity meas., small-sample method 80−15981
$LiNbO_3$ piezoelectric plate, direct and indirect elastic wave excitation *(Russian)* 80−34858
$LiNbO_3$, piezoelectric material for electrostatic voltage sensors *(Japanese)* 80−105632
$LiNbO_3$ planar HF acousto-optic modulator construction and expts. 79−76863
$LiNbO_3$, planar lightguide, optical mode interaction with standing elastic surface waves 80−99836
$LiNbO_3$, planar optical waveguide, SHG in angle-matched conditions 79−41422
$LiNbO_3$ planar waveguide, light beam switching and modulation using built-in dielectric channel 77−88967
$LiNbO_3$ planar waveguide, light beam switching and modulation using built-in dielec. channel 78−46840
$LiNbO_3$ planar waveguide, refractive index rel. to Ti diffusion *(Russian)* 78−59120
$LiNbO_3$ planar waveguide mode conversion and intensity modulation 79−10410
$LiNbO_3$, polariton excitation for tunable coherent far IR generation 79−31982
$LiNbO_3$, polydomain, nonstoichiometric crysts., elastic, piezoelec., dielec. constants. 77−8513
$LiNbO_3$, powder, polarisation echo, repetitive read out effect 79−82913
$LiNbO_3$ powder, RF field depend. of memory echoes 79−8095
$LiNbO_3$, pure, two-photon photorefractive recording 78−31220
$LiNbO_3$, pure and Fe doped, photorefraction kinetics under irradiation and heating 79−42934
$LiNbO_3$, pure and Fe doped, photorefraction, effect of external elec. field and light intensity *(Russian)* 79−56766
$LiNbO_3$, pure and Fe doped, photorefraction, temp. and light intensity depend. 80−50288
$LiNbO_3$ pure and Fe doped, IR induced acousto-photorefractive memory effect 80−80746
$LiNbO_3$, pure and Fe doped, two-photon photorefractivity 80−80753
$LiNbO_3$, pyroelectric induced optical damage 78−52446
$LiNbO_3$, radiation induced heating by thermal neutrons, meas. of temp. 79−4337
Y-Z $LiNbO_3$, radiation patterns of bulk acoustic modes from finite interdigital transducer 80−43491
$LiNbO_3$, Raman line phonon relative intensities *(German)* 77−59582
$LiNbO_3$, Raman scatt. intensities, photorefractive index change effects 78−84590
$LiNbO_3$, Raman spectra temp. depend. 77−40239
$LiNbO_3$, Raman spectra and dielec. props. near Curie point 79−38530
$LiNbO_3$, reduced, electron Hall mobility, photo-Hall meas. 77−8121
$LiNbO_3$, reduced, photovoltaic effect and holographic recording mechanisms 79−69556
$LiNbO_3$, reduced cryst., photovoltaic effect, appl. to holographic recording *(Russian)* 79−51635
$LiNbO_3$, ref. index, stoichiometry effects 77−59549
$LiNbO_3$, refr. index, equal-deflection method, UV laser rad. 78−29145
$LiNbO_3$, refractive index, temp. depend. over 300 to 620 nm *(Russian)* 78−56451
$LiNbO_3$, resonator transverse modes, effects of anisotropy 78−5609
$LiNbO_3$, return pump parametric oscillator 78−9414

lithium compounds continued
$LiNbO_3$, reversed polarity layer at positive domain surface, heat-induced, etching investig. 77−63383
$LiNbO_3$, ridge struct. fabrication by CF_4 plasma etching 80−28357
$LiNbO_3$, SAW, delay line for acoustoelectric integrating correlator 77−88990
$LiNbO_3$, SAW, suppression of harmonic generation by ZnO thin-film loading 80−84355
$LiNbO_3$, SAW convergence props. 80−24726
$LiNbO_3$, SAW conversion to bulk plate modes in shallow gratings 80−1385
$LiNbO_3$ SAW device, obs. of bulk waves and surface waves through side planes of several cuts 78−71238
$LiNbO_3$, SAW excitation and propagation patterns, frequency translated holographic obs. 77−80690
$LiNbO_3$ SAW filter bulk wave suppression by triangular metal film overlay 77−23830
$LiNbO_3$, SAW generation, use of analytical calc. for semi-infinite piezoelec. 78−51809
$LiNbO_3$, SAW in uniform layered medium, metallic gratings and grooved arrays 79−81596
$LiNbO_3$ SAW plate convolvers at 1 GHz 80−1382
$LiNbO_3$, SAW propag., effects of He ion implantation 80−75421
$LiNbO_3$, SAW propag. velocity meas. 80−92003
$LiNbO_3$ SAW propagation, temp. coeffs., piezoelectric coupling *(French)* 78−35093
$LiNbO_3$, SAW propagation losses due to surface roughness 78−38926
$LiNbO_3$, SAW propagation and scatt., finite difference anal. 80−20595
$LiNbO_3$, SAW refl. from metal dot arrays 78−13867
$LiNbO_3$, SAW reflection from conducting strips 80−5853
$LiNbO_3$ SAW resonator design with Al metallisation 77−39147
$LiNbO_3$ SAW-CdS bulk wave piezoelectric coupling 77−23845
$LiNbO_3$, SHG, refr. index induced optical inhomogeneity effect 80−9951
$LiNbO_3$, SHG in external optical resonator, He-Ne laser radiation 79−27326
$LiNbO_3$, SHG of 260 THz ^{20}Ne laser, absolute freq. meas. in visible 79−93104
$LiNbO_3$, SHG of ps pulses, freq. tuning 77−50724
$LiNbO_3$ sensor for elec. hygrometer *(Japanese)* 80−95103
$LiNbO_3$, shock loaded above Hugoniot elastic limit, elec. and mech. response 78−19411
$LiNbO_3$, shock-wave compression, 2.4-44 GPa 80−34139
$LiNbO_3$, single cryst. growth and phys. props. *(Japanese)* 79−65018
$LiNbO_3$, single crystal, dielectric const., dispersion, loss tangent and susceptibility 77−16245
$LiNbO_3$, single crystal, exam. of microhardness using static indentation 79−52517
$LiNbO_3$ single crystals, brittle, deform. during static indentation 79−87714
$LiNbO_3$ single crystals, growth from melt, Czochralski method *(Chinese)* 80−76171
$LiNbO_3$ single crystals grown by automatic diameter control, power striations *(Chinese)* 80−81080
$LiNbO_3$ single crystals, wetted-die growth technique 80−97426
$LiNbO_3$, spectral phase-matching props. for SHG 77−83922
$LiNbO_3$, spontaneous elec. breakdown 77−66458
$LiNbO_3$, spontaneous parametric light scatt. characts. meas., 1000-4000 cm^{-1} 77−8640
$LiNbO_3$, spontaneous parametric scatt. line profile, IR absorpt. coeffs. 80−25377
$LiNbO_3$, spontaneous polarisation, low temp. meas. 80−75921
$LiNbO_3$ sputtered layers, on $LiTaO_3$, optical waveguide props. 77−11012
$LiNbO_3$, strength of nonlinear interaction between collinear surface acoustic waves 80−33295
$LiNbO_3$ substrate, covered with metal or quartz powder, dynamic SAW reflecting struct. 80−74565
$LiNbO_3$ substrate, fabrication and props. of double-layered polycrystalline CdS 78−64480
$LiNbO_3$ substrate, $Pb_{1-x}Sn_xTe$-PbTe heterostructures produced by MBE 80−88629
$LiNbO_3$ substrate, struct. and morphology of VPE PbTe layer 80−54561
$LiNbO_3$ substrate, Ti in-diffusion, planar optical waveguides construction *(Czech)* 79−41452
$LiNbO_3$ substrate for optical ICs, performance obs. *(Japanese)* 79−86265
$LiNbO_3$ substrate for InSb films, prep. and props. 80−35093
$LiNbO_3$ substrate for 4-bit digitally driven integrated optical amplitude modulator for data processing 80−53476
$LiNbO_3$ substrates, optical waveguides and waveguide components development *(Czech)* 80−19090
$LiNbO_3$ substrates for integrated passive optical rotation sensors using guided waves, developments 80−58781
$LiNbO_3$, surface acoustic wave device, obs. of bulk waves by freq. shifted holography 77−19505
$LiNbO_3$, surface acoustic waves power densities approximation 77−79987
$LiNbO_3$, surface elastic wave propag. in piezoelec. plate, elec. screening effect *(Russian)* 79−14999
$LiNbO_3$, surface wave anal. using orthogonal functions 78−51810
$LiNbO_3$, surface waves, perturbation anal. of attenuation and dispersion 78−47653
$LiNbO_3$ surfaces, ion and electron bombard., photoelectron spectroscopy and electronic props. 80−71559
$LiNbO_3$ TE-TM mode convertor, using collinear acoustooptic interaction 77−19407
$LiNbO_3$, tapped SAW delay line, coupling with CdS bulk wave 77−1289
$LiNbO_3$, temp. coeff. of freq. determ. 80−75316
$LiNbO_3$, temp. dependence of Raman scattering 77−16297
$LiNbO_3$, thermal and spectral variations in the photovoltaic current in ferroelectrics 78−91719
$LiNbO_3$, thermionic emission characts. 80−104034
$LiNbO_3$, thermoelastic stress distribution in single cryst. pulling by Czochralski technique 78−63681
$LiNbO_3$, thin crystal plates, specific directions of plane elastic waves 79−82281
$LiNbO_3$, third order nonlinear optical difference frequency generation 78−22176

lithium compounds continued
$LiNbO_3$ three-dimens. optical waveguide, parametric difference freq. generation 80−48335
$LiNbO_3$, Ti diffused, mirror type optical branch and switch 78−33834
$LiNbO_3$, Ti diffused, planar waveguide, leaky mode propag. 78−87149
$LiNbO_3$, Ti diffused, optical waveguide isolator using electrooptic branching waveguide 79−18532
$LiNbO_3$, Ti diffused, optical directional couplers, characts. 80−33145
$LiNbO_3$, Ti diffused optical waveguides, efficient prism-coupling 79−46089
$LiNbO_3$, Ti diffused optical waveguide, ferrolectric domain inversion 79−94338
$LiNbO_3$, Ti diffused planar waveguide, WKB approx. for refr. index profile determ. 78−30086
$LiNbO_3$, Ti diffused slab waveguide, mode control by doping 77−88903
$LiNbO_3$ Ti diffused single-mode waveguide coupling to single-mode fibre 79−81547
$LiNbO_3$, Ti diffused waveguide, active Y-junction switching devices 79−23091
$LiNbO_3$, Ti diffused waveguide, refr. index and thickness precise determ. 79−41446
$LiNbO_3$, Ti diffused waveguide, leaky mode loss coeffs., calc. 80−19094
$LiNbO_3$, Ti diffusion and characts. of graded-index lightguide 79−27433
$LiNbO_3$ Ti-diffused C-plate waveguide with metal cladding, buffer layer effects 78−25956
$LiNbO_3$, Ti-diffused strip waveguide, appl. in balanced bridge modulator switch 78−63201
$LiNbO_3$ Ti-diffused waveguide for cutoff modulator 80−9991
$LiNbO_3$, transient parametric generation of far IR radiation 79−94293
$LiNbO_3$, transition metal doped, photovoltaic and photorefractive effects, origin 77−20364
$LiNbO_3$, transition metal doped, photovoltaic effects, spectroscopic investigation 77−20365
$LiNbO_3$, transition metal doped, photoferroelectric phenomena and optical storage 79−42577
$LiNbO_3$ transparency with vacuum-deposited electrodes *(Russian)* 78−60422
$LiNbO_3$ travelling wave optical waveguide modulator, 10 GHz bandwidth 78−59134
$LiNbO_3$, trigonal crystal, optical heterodyne detection using collinear acousto-optic interaction 78−66927
$LiNbO_3$, trigonal crysts., anisotropy of linear electrooptic effect 80−34894
$LiNbO_3$, tunable IR sources, parametric oscillators and difference freq. generation 78−59030
$LiNbO_3$, tunable parametric oscillator, remote air pollution detect. appl. 78−59089
$LiNbO_3$, tunable parametric Raman laser utilizing polaritons 79−41418
$LiNbO_3$, twinning systems produced by plastic compression 77−1135
$LiNbO_3$, two properly aligned crysts., narrow-band tunable IR pulse prod. 78−42382
$LiNbO_3$, two-photon absorption spectra, energy struct. anal. 80−99785
$LiNbO_3$, two-photon and X-ray induced Nb^{4+} and O^- small polarons, ESR and optical absorpt. 78−76306
$LiNbO_3$ UHF SAW filters using group-type unidirectional interdigital transducers 78−59252
$LiNbO_3$, uniaxial pyroelectric, nonlinear optical susceptibility 77−23705
$LiNbO_3$, use as surface acoustic wave devices 78−91525
$LiNbO_3$, valence band UPS and partial p and d density of states 80−71560
$LiNbO_3$ very high throughput damage resistant waveguide modulator 80−58788
$LiNbO_3$, vitreous, anomalous dielectric behaviour and reversible pyroelectricity 77−85658
$LiNbO_3$, vol. holograms, photorefr. recording dynamics, multiple storage 77−38834
$LiNbO_3$, vol. hologram recording and reconstruction 78−9349
$LiNbO_3$, vol. phase hologram for coherent beam structural conversion 79−59656
$LiNbO_3$ volume holographic grating as spatial-freq. selector for tunable dye laser 80−53240
$LiNbO_3$, volume phase hologram erasure 78−42301
$LiNbO_3$, wave front convolution in 4-wave interaction with nonlocal nonlinear media *(Russian)* 79−86205
$LiNbO_3$ waveguide, corrugated, electro-optic scanning of light diffr. from grating output coupler 78−63172
$LiNbO_3$ waveguide, diffusion of Ti, exam. by electron probe anal. and X-ray diffr. 78−47588
$LiNbO_3$ waveguide, diffused, 2nd harmonic generation 79−14041
$LiNbO_3$ waveguide, diffusion fabricated, angular variation calcs. using mode propag. consts. 80−69540
$LiNbO_3$ waveguide, electrooptic surface prism laser deflector 80−87492
$LiNbO_3$ waveguide, form. of geodesic lenses 77−88966
$LiNbO_3$ waveguide, holographic writing technique based on multiphoton photorefractive processes 77−38824
$LiNbO_3$ waveguide, horn struct. and thin film optical switch 77−88968
$LiNbO_3$ waveguide, planar electro-optic prism array beam splitter 80−64209
$LiNbO_3$, waveguide, single-mode planar and rigid type electro-optic waveguide modulators, design 77−11029
$LiNbO_3$ waveguide, thin-film optical filtering using acoustooptic interaction 79−81572
$LiNbO_3$ waveguide, Y-cut, for fabrication of wideband guided-wave acousto-optic Bragg deflector 80−74510
$LiNbO_3$ waveguide absorption losses, laser calorimetric meas. 79−64311
$LiNbO_3$, waveguide and modulator form. by ion implantation 80−48469
$LiNbO_3$, waveguide form. technique, using organometallic soln. diffusion sources 78−38099
$LiNbO_3$, waveguide formation using organometallic solns. as diffusion sources 80−23810
$LiNbO_3$ waveguide modulators and switches, Ti-diffused, fabrication on directional coupler principle 80−83678
$LiNbO_3$ waveguides, diffused channel, multimode and single mode, direct index meas. 80−87562
$LiNbO_3$ waveguides, optical scattering phenomena 80−58786
$LiNbO_3$ wedge, apodized ID transducer, radiation conductance 78−38164
$LiNbO_3$, wedge fabrication for line acoustic wave propag., using cleavage method 78−30818
$LiNbO_3$, wedge shape cryst. optical modulation, diffr. by natural freq. US standing waves 77−75685

lithium compounds continued
$LiNbO_3$ X-cut plate shear transducer, direction of displacement 78−51031
$LiNbO_3$, X-ray determ. of piezoelec. coeff. 77−8511
$LiNbO_3$, X-ray diffr. study of lattice dynamics parameters *(Russian)* 79−65156
$LiNbO_3$, X-ray diffuse scatt., temp. depend., 20 to 750°C 79−37800
$LiNbO_3$, X-ray photovoltaic effect and its correl. with ESR 79−82639
$LiNbO_3$, XPS and UPS from surface defects 80−76136
$LiNbO_3$, XPS core line intensities, electron escape depth 79−100025
$LiNbO_3$, Y-Z, Rayleight-wave reflection from groove 79−51408
$LiNbO_3$, Y-Z, SAW scatt. from groove 78−60019
$LiNbO_3$, Y-Z cut, surface to bulk mode wave conversion, at interfaces ang. spectrum meas. 78−47652
$LiNbO_3$, Y-cut, waveguide form. by Ti diffusion, refr. index and electrooptic coeffs. 79−14114
$LiNbO_3$ Y-cut four-mode waveguide, generalised parameters describing acoustooptic interaction 80−91924
$LiNbO_3$, y-z, x-z and $41^1/_2$-x cuts, SAW SHG, laser probing 77−31153
$LiNbO_3$, y-z crystal, line shape of light scattered by SAW upon total internal refl. 79−24287
$LiNbO_3$, y-z cut, light scatt. from SAW 78−6652
$LiNbO_3$, YZ-cut, coated with SiO_x thin film, SAW props. 80−84356
$LiNbO_3$ Z-cut crystals, bit and holographic recording, electric field control *(Russian)* 77−42512
$LiNbO_3$:$^{57}Fe^{2+}$, Mossbauer spectroscopy 77−20782
$LiNbO_3$:$^{57}Fe^{2+}$ Mossbauer spectra, EFG axis 77−20760
$LiNbO_3$:$3Li_2O.Nb_2O_5$ eutectic, dielectric props. 79−1743
$LiNbO_3$:Co, optical props. 78−64383
$LiNbO_3$:Cr^{3+} glass, roller quenched, crystn. kinetics 80−44143
$LiNbO_3$:Cu, holographic grating, for electro-optical laser beam modulation 77−3672
$LiNbO_3$:Cu^{2+}, EPR and optical spectra 80−20453
$LiNbO_3$:Cu(Fe), light induced charge transport, photovoltaic effects, impurity states 80−80317
$LiNbO_3$:Fe, anomalous bulk photovoltage effect, Jahn-Teller mechanism 77−28218
$LiNbO_3$:Fe, anomalous photovoltaic effect in polarised light *(Russian)* 80−34484
$LiNbO_3$:Fe, bulk photovoltaic effect in ferroelecs. 79−15181
$LiNbO_3$:Fe, calc. of photorefraction *(Russian)* 78−90474
$LiNbO_3$:Fe, characts. for holographic storage appls. 77−23630
$LiNbO_3$:Fe, dynamic hologram recording, high speed memory appl. 77−83835
$LiNbO_3$:Fe, dynamic optical storage 78−33706
$LiNbO_3$:Fe, efficient hologram recording using Nd:YAG laser pulses 79−55081
$LiNbO_3$:Fe, elec. resist., temp. and conc. depend. 80−80275
$LiNbO_3$:Fe, electrically accessible Lippmann hologram memory 77−88663
$LiNbO_3$:Fe, electro-optic cryst., light induced charge transport, holographic obs. 80−70747
$LiNbO_3$:Fe, electron irrad., photoinduced charge transfer and hologram recording 79−36859
$LiNbO_3$:Fe, electron spin relaxation study, Mossbauer effect, mag. and crystal field effects 80−39902
$LiNbO_3$:Fe, exoelectron emission in pyroeffect regime 80−76158
$LiNbO_3$:Fe, ferroelec. semiconductors, anomalously high photovoltage 77−69378
$LiNbO_3$:Fe, ferroelectric, treated in Li_2CO_3, formation of Fe^{2+} state, Mossbauer effect 78−92003
$LiNbO_3$:Fe, hologram recording, photorefr. effect time depend. *(Russian)* 77−7032
$LiNbO_3$:Fe, hologram writing, beam coupling and transport length in bulk photovoltaic effect 79−94190
$LiNbO_3$:Fe, hologram nondestructive readout using different recording and readout wavelengths 80−14302
$LiNbO_3$:Fe, holography appl., comparison with $KNbO_3$, w.r.t. recording and erasure sensitivity *(Russian)* 80−78795
$LiNbO_3$:Fe, holographic recording and thermal fixing, invest. of mechanisms 80−78810
$LiNbO_3$:Fe, impurity valence state charge on X-ray irrad., Mossbauer meas. 80−7235
$LiNbO_3$:Fe, impurity charge states after UV irradiation 80−60462
$LiNbO_3$:Fe, induced optical inhomogeneity, refr. index and short-circuit photocurrent meas. 79−69806
$LiNbO_3$:Fe, influence of anomalous photovoltaic effect on exoelectron emission 79−28374
$LiNbO_3$:Fe, intensity enhanced bulk photovoltaic effects 79−19616
$LiNbO_3$:Fe, intrinsic field effect, photoelectric emission study 79−69961
$LiNbO_3$:Fe, laser induced optical damage 78−95572
$LiNbO_3$:Fe, lattice-strains induced by light, X-ray topography 77−76458
$LiNbO_3$:Fe, local photodeformation 79−42932
$LiNbO_3$:Fe, local photodeform. and photorefraction 80−16003
$LiNbO_3$:Fe, Mossbauer spectra quadrupole doublet asymmetry 80−44960
$LiNbO_3$:Fe, nonlinear image processing in 3-dimens. hologram 80−14303
$LiNbO_3$:Fe, optical damage induced by laser light, X-ray irrad., carrier mobility effects 79−33657
$LiNbO_3$:Fe, optical damage, Fe ion conc., EPR and optical spectra evaluation 79−42933
$LiNbO_3$:Fe, optical damage depend. on temp., press., and applied elec. field *(Japanese)* 79−81498
$LiNbO_3$:Fe, origin of photoelectrons and conc. of point defects 77−43645
$LiNbO_3$:Fe, phase hologram storage and fixing, review 77−19210
$LiNbO_3$:Fe, photocond. and photorefractive effects 79−38124
$LiNbO_3$:Fe, photoinduced Rayleigh scatt. and bulk photovoltaic effect 79−38554
$LiNbO_3$:Fe, photoinduced refractive index discontinuities at surface 80−75999
$LiNbO_3$:Fe, photoinduced scatt. and bleaching effect 80−95959
$LiNbO_3$:Fe, photorefractive recording of vol. holograms 77−637
$LiNbO_3$:Fe, photorefractive effects under external elec. field 77−23723
$LiNbO_3$:Fe, photorefractive effect in a ferroelectric 78−92047
$LiNbO_3$:Fe, photorefr., surface recombination 79−56759
$LiNbO_3$:Fe, photorefraction, γ-irrad. influence, polarisation-optic and holographic obs. 80−11359
$LiNbO_3$:Fe, photovoltaic effect and charge transport mechanism 79−38123

lithium compounds continued
$LiNbO_3$:Fe, polarization echo signals amplification *(Russian)* 78−43780
$LiNbO_3$:Fe, pulsed photorefr. process for hologram recording 80−53235
$LiNbO_3$:Fe, pure and doped, photocond. and dark cond. 80−29439
$LiNbO_3$:Fe, recording dynamical holograms in crystals with photovoltaic effect, nonstationary energy exchange *(Russian)* 79−31842
$LiNbO_3$:Fe, refractive index change induced by light irrad. *(Japanese)* 79−65824
$LiNbO_3$:Fe, spontaneous polarisation reversal and photorefractive effect 78−31163
$LiNbO_3$:Fe, state of impurity Fe cation, nucl. gamma reson. study 80−40014
$LiNbO_3$:Fe, temp. depend., electron cond., holography appl. 78−14731
$LiNbO_3$:Fe, thermally activated trapping caused by small polaron formation 77−20259
$LiNbO_3$:Fe, two different phase holographic recording processes, expt. 77−19211
$LiNbO_3$:Fe, unipolar Malter emission under pyroelectric effect conditions 80−29862
$LiNbO_3$:Fe, used for holographic storage 79−98322
$LiNbO_3$:Fe, volume phase holographic storage 78−82929
$LiNbO_3$:Fe, white-light image processing 80−87321
$LiNbO_3$:Fe, X-ray and γ-ray irradiation effects on Fe charge state, Mossbauer study 80−40013
$LiNbO_3$:Fe (0.05%), hologram recording γ radiation effect 80−78812
$LiNbO_3$:Fe crystal, transient optical storage 80−9838
$LiNbO_3$:Fe crystal conductivity and photoinduced birefringence obs. *(Russian)* 78−60151
$LiNbO_3$:Fe crystals, volume hologram storage; exam. of material 78−37848
$LiNbO_3$:Fe crystals, reflection hologram recording 79−10272
$LiNbO_3$:Fe electro-optic crystal holographic storage data error probability 80−43304
$LiNbO_3$:Fe holographic information storage material 78−55321
$LiNbO_3$:Fe monocrystal, pulsed holographic recording *(Russian)* 77−629
$LiNbO_3$:Fe photosensitive electro-optical crystals for image storage display and processing 77−19215
$LiNbO_3$:Fe spatial holograms, ageing mechanism and thermal fixing *(Russian)* 80−74311
$LiNbO_3$:$Fe^{2(3)+}$, X-ray absorpt. 80−108299
$LiNbO_3$:Fe^{3+}, electrooptical effect, charge transfer mechanism, defect. pair form. 79−38519
$LiNbO_3$:Fe; photorefraction for holographic recording, thin hologram diffr. efficiency 79−55086
$LiNbO_3$:Fe(Cu), photorefractive centres, optical absorption, EPR and Mossbauer spectra meas. 77−32403
$LiNbO_3$:Fe(Cu)(Co), pure and doped, nonlinear excitation, multiphoton photorefractive process 79−36950
$LiNbO_3$:Fe(Nb), SHG, phase-matching temp., impurity influence 80−69463
$LiNbO_3$:He, ion implantation, optical waveguide form., refr. index changes 78−46762
$LiNbO_3$:He^+, ion implanted SAW guides, air-gap Si convolver data 78−42500
$LiNbO_3$:M, (M=Cr,Mn,Fe,Co,Ni,Cu), absorpt. spectra, 0.3-2.0 μm *(Russian)* 77−20898
$LiNbO_3$:Mn, photorefractive sensitivity, holographic and photocurrent investig. 77−24581
$LiNbO_3$:Na structure field stability limits, LPE film growth, SAW velocity 80−80102
$LiNbO_3$:Na^+ (Co^{2+}, Zr^{4+}) film, improvement in temp. stability and SAW device appl. 80−75939
$LiNbO_3$:Na^+(Co^{2+},Zr^{4+}) films, LPE growth from Li_2O-V_2O_5 flux, X-ray and acoustic characterisation 80−15383
$LiNbO_3$:Ni optical absorpt. spectra 80−71450
$LiNbO_3$:NiO, appl. in DC direct reading electro-optic voltmeter with high input resist. 78−245
$LiNbO_3$:phosphor, piezoelec., interaction with SAW, excitation of electrolum. 79−60615
$LiNbO_3$:Rh, Czochralski-grown oxide crystals, fluid-flow effect on gas-bubble entrapment 80−84121
$LiNbO_3$:Ti, BiTm ferrite garnet coated, nonreciprocal optical waveguide system *(Russian)* 77−42623
$LiNbO_3$:Ti, broad-band travelling wave waveguide modulator 77−39036
$LiNbO_3$:Ti, coupled waveguided TE/TM mode splitter 80−64142
$LiNbO_3$:Ti, diffused, optical channel waveguides, Bragg switch 78−75002
$LiNbO_3$:Ti, diffused strip waveguide, refractive index changes, two-dimensional distrib. 79−86254
$LiNbO_3$:Ti, dopant conc., refr. index profile rel. to integrated optics 78−5583
$LiNbO_3$:Ti, electro-optic multichannel waveguide deflector 77−42607
$LiNbO_3$:Ti, electro-optic waveguide modulator, temp. stabilisation 78−50926
$LiNbO_3$:Ti, electrooptical modulator and switch *(French)* 78−30074
$LiNbO_3$:Ti, graded-index optical waveguides, mode dispersion characts. 79−3770
$LiNbO_3$:Ti, in-diffused waveguide, integrated bistable optical device development 78−75001
$LiNbO_3$:Ti, in-diffused waveguide, acousto-optical meas. of optical field profiles 79−23054
$LiNbO_3$:Ti, in-diffused waveguides, optical damage thresholds 79−46033
$LiNbO_3$:Ti, integrated bistable optical device using Mach-Zehnder interferometric optical waveguide 79−59843
$LiNbO_3$:Ti, planar and channel optical waveguides, anisotropic diffusion expts. 80−64200
$LiNbO_3$:Ti, planar optical waveguides, processing and props. 80−78965
$LiNbO_3$:Ti, two mode waveguide coupler electrooptical switch 77−83961
$LiNbO_3$:Ti, Y-cut thin film waveguide, acousto-optical deflector, electro-optical modulator *(Russian)* 77−39115
$LiNbO_3$:Ti 3-dB optical waveguide mode convertor using chirped gratings, power transfer 80−79014
$LiNbO_3$:Ti active branching waveguide modulator 77−19392
$LiNbO_3$:Ti branched waveguide amplitude modulator 77−39037
$LiNbO_3$:Ti channel waveguide high-speed cutoff modulator 80−64195
$LiNbO_3$:Ti cleaved, waveguide, attenuation coefficient and coupling loss 78−74975
$LiNbO_3$:Ti diffused, optical waveguide, fabrication problems *(Japanese)* 80−33256

lithium compounds continued
$LiNbO_3$:Ti diffused optical waveguide, guided light scatt. sources 80−78966
$LiNbO_3$:Ti diffused optical waveguide, efficient tapered gap prism coupling 80−78967
$LiNbO_3$:Ti diffused strip waveguide, optical insertion losses 78−74985
$LiNbO_3$:Ti diffused strip waveguide, optical propag. losses and coupling losses 80−58664
$LiNbO_3$:Ti digitally driven integrated optics amplitude modulator 80−58808
$LiNbO_3$:Ti electro-optic TE-TM mode convertor structure 80−64215
$LiNbO_3$:Ti electro-optic branching waveguide, characts. 80−83681
$LiNbO_3$:Ti in-diffused optical waveguide fabrication 79−76892
$LiNbO_3$:Ti in-diffused waveguide, refractive index profile calc. from measured coupling angles 80−78954
$LiNbO_3$:Ti layers, detection by harmonic generation of SAW 77−80688
$LiNbO_3$:Ti narrow ridge optical waveguides and electro-optical, ion-bombardment-enhanced etching 80−38133
$LiNbO_3$:Ti optical waveguides, suppression of LiO_2 out-diffusion 77−50749
$LiNbO_3$:Ti optical waveguide, technique for suppressing Li_2O out-diffusion 78−18040
$LiNbO_3$:Ti optical waveguides, fabrication and waveguiding props. 78−30091
$LiNbO_3$:Ti optical waveguide diffusion profile, AES obs. *(German)* 78−33876
$LiNbO_3$:Ti optical waveguide directional coupler type modulator 78−66951
$LiNbO_3$:Ti optical waveguide, SHG with 25% conversion efficiency 78−94432
$LiNbO_3$:Ti optical waveguides, elec. field tuning of SHG, phase-matching condition 79−41412
$LiNbO_3$:Ti optical waveguide electrooptic devices polarisation independ. directional coupler switch and wavelength filters 80−58783
$LiNbO_3$:Ti optical waveguides and crystals, absorption loss and photorefractive index changes 80−58787
$LiNbO_3$:Ti optical waveguides, Ti diffusion process and control, waveguide characts. 80−58790
$LiNbO_3$:Ti optical waveguide, surface wave mode conversion, static strain-optic effect 80−87561
$LiNbO_3$:Ti phase-matched waveguide electro-optic TE⇄TM mode convertor 80−58749
$LiNbO_3$:Ti planar and channel waveguides, appl. of Li_2O compensation technique 78−74976
$LiNbO_3$:Ti planar and channel optical waveguides, Ti diffusion coeff. meas. 80−19096
$LiNbO_3$:Ti planar waveguide, edge coupling to GaAlAs DH laser diode 80−87559
$LiNbO_3$:Ti single mode electrooptic waveguide modulator, high-speed operation 80−91915
$LiNbO_3$:Ti single-mode optical waveguide, fabrication by sequential combination of Ti diffusion and masked ion-implantation 80−58785
$LiNbO_3$:Ti single-mode waveguides, losses due directional changes 80−58789
$LiNbO_3$:Ti strip waveguide, SHG 80−102773
$LiNbO_3$:Ti thin film acousto-optic deflector 77−75698
$LiNbO_3$:Ti waveguide, diffused, Mg diffusion effects on characts. 78−66905
$LiNbO_3$:Ti waveguide, precise determ. of refr. index 78−94442
$LiNbO_3$:Ti waveguide, integrated bistable Fabry-Perot resonator fabrication 79−41459
$LiNbO_3$:Ti waveguide, in-plane scatt. obs. and countermeasures 80−33215
$LiNbO_3$:Ti waveguide, operation of geodesic lens, anisotropic and curvature losses 80−48453
$LiNbO_3$:Ti waveguide, ps signal processing with planar, nonlinear integrated optics 80−64208
$LiNbO_3$:Ti waveguide geodesic lens 77−84005
$LiNbO_3$:Ti waveguide for lightwave communications and data processing systems 79−37052
$LiNbO_3$:Ti waveguide laser diode end-fire coupling 79−94368
$LiNbO_3$:Ti waveguide thin film electrooptic Bragg modulator, bistable optical element 80−10034
$LiNbO_3$:Ti waveguide and cryst., absorpt. loss and photorefractive index changes 80−48368
$LiNbO_3$:Ti waveguide directional coupler switches, optically-induced cross-talk 80−48417
$LiNbO_3$:Ti waveguide electro-optic TE⇄TM mode converter-wavelength filter 80−64210
$LiNbO_3$:Ti Z-cut crystals, Ti diffusion process parameters 80−102849
$LiNbO_3$:transition metal, photorefr. effect, 1.5-4.0 eV 77−28213
$LiNbO_3$/CdS integrated optical half adder circuit 79−76877
$LiNbO_3$/YIG/GGG magneto-optical waveguide, semileaky thin film, for modulator appl. 77−62055
$LiNbO_3$-3(Li_2O).Nb_2O_5 eutectic, anomaly in elec. resist. 78−68030
$LiNbO_3$-$Ca(NbO_3)_2$, cryst. growth in baked mixture, Seignettoelec. phase *(Russian)* 79−47395
$LiNbO_3$-CdO, CdO addition effect on sintering 79−83157
$LiNbO_3$-CdS, layered structure, acoustoelectric surface current kinetics 78−43232
$LiNbO_3$-CdS, layered struct., transverse acoustoelectric effect 79−69567
$LiNbO_3$-CdS, layered structure, transverse acousto-electric current 80−44669
$LiNbO_3$-CdS layer structure, temp. depend. of acoustoelectric current 79−7867
$LiNbO_3$-CdS separated medium convolver, illumination effects 77−72766
$LiNbO_3$-CdS system, expt. investigation of nonlinear Rayleigh wave interaction 80−102946
$LiNbO_3$-CdSe, piezoelec.-semicond. layer struct., acoustic-wave-induced increase in cond. 77−59307
$LiNbO_3$-CdSe layer structure, SAW absorpt., elec. field effects 80−65355
$LiNbO_3$-CdSe structure, electroacoustic effects and signal convolution 80−10098
$LiNbO_3$-gap coupled Schottky diode memory correlator, grating coupled optical imaging 80−64143
$LiNbO_3$-Ge, acoustooptic modulator for CO_2 lasers 78−42365
$LiNbO_3$-Ge acousto-optic modulator for 10.6 μm CO_2 laser 80−99776
$LiNbO_3$-Ge acoustooptic modulator *(Japanese)* 80−69542
$LiNbO_3$-InSb amplifier production, role of protective films 78−95220
lithium compounds continued
$LiNbO_3$-InSb layer structures, fabrication and use in SAW amplification 79−41540
$LiNbO_3$-InSb struct., electroacoustic interaction temp. depend. 79−69336
$LiNbO_3$-liquid-CdS-liquid-$LiNbO_3$ structure, acoustic wave propag. and amplification 77−42654
$LiNbO_3$-$NaNbO_3$-$SrNb_2O_6$, pseudo-ternary system, DTA, heat treatment and X-ray diffr. obs. *(Chinese)* 79−52175
$LiNbO_3$-Ni, layered structure, mag. control of surface elastic waves 77−20666
$LiNbO_3$-p-Si, frequency doubling of the two-pulse and three-pulse echoes in surface acoustic waves 79−69335
$LiNbO_3$-pn-diode airgap convolver struct. optical scanner using single SAW pulse 80−64144
$LiNbO_3$-Si, acoustoelec. SAW phase shifter 78−13866
$LiNbO_3$-Si, acoustoelectronic memory, effect of band-bending 80−70771
$LiNbO_3$-Si acoustically-matched surface elastic wave transducer 78−90623
$LiNbO_3$-SiO_2:Fe_2O_3 glasses, Li^+ ion cond. 80−107471
$LiNbO_3$-SiO_x-InSb-SiO_x monolithic acoustoelectronic amplifier with pulsed power supply 79−56269
$LiNbO_3$-Si(CdTe) structure, acoustoelectronic interaction between SAW and transverse drift current 77−69424
$LiNbO_3$-Si(Ge) layer struct., acoustoelectronic phenomena 77−55556
$LiNbO_3$, Li_2O diffusion for chemical control of laser induced optical damage 78−46693
$LiNbO_4$, dispersion of vibrational excitations, Raman scatt. 78−84588
Li_7NbO_6, ion mobility, NMR meas. *(French)* 79−65240
Li_7NbO_6, pseudo-two-dimens. electrolytic solid, Li ion mobility, NMR study *(French)* 80−34235
$Li_x(NbO)_4Nb_{30}O_{90}$, struct. and ionic cond. 79−65246
$Li_{0.5}NbS_2$, supercond. props., alkali cation and topotactic solvation influences 79−87180
$Li(Nb_{1-x}Ta_x)O_3$, $0 \leq x \leq 1$, LPE thin film growth on $LiTaO_3$ substrate, lattice mismatches, meas. of temp. depend 79−56087
$LiNb_{1-y}Ta_yO_3$, Czochralski growth and basic props. 77−63556
$LiNb_{1-y}Ta_yO_3$, Czochralski grown, refr. index, 5893-10600 Å, and zero birefr. 78−31166
$LiNb_xTa_{1-x}O_3$ stripe waveguides, fabrication, physical and optical props. 78−38055
$LiNbO_3$:Fe, anomalous photovoltaic effect and diffraction efficiency *(Russian)* 79−15190
LiNd phosphate glass, spectral and generation props. 77−1700
$Li_3Nd_2(BO_3)_3$, cryst. struct., X-ray diffr. meas. 78−10028
$LiNd_{0.3}La_{0.7}$ phosphate glass, stimulated emission characts. 79−18426
$LiNd_{0.5}La_{0.5}P_4O_{12}$ laser, stabilised dual-polarisation oscill. 77−54723
$LiNd(MoO_4)_2$, defect struct. and phase transitions 79−28697
$LiNd(PO_3)_4$, crystallisation from $LiPO_3$ flux, exam. of optical props. *(German)* 79−11401
$LiNd(PO_3)_4$ laser with external and Fabry-Perot resonators, 1.05, 1.32 μm CW oscill. 80−23693
$LiNdP_4O_{12}$ (LNP) laser, optical transmitter appl., properties and LED pumping 79−3712
$LiNdP_4O_{12}$, CW laser oscill., near 1.32 μm 77−61957
$LiNdP_4O_{12}$ efficient miniature laser pumped with GaAlAs laser diode 80−32994
$LiNdP_4O_{12}$ electroluminescent diode pumped miniaturized laser for optical transmission system 79−41395
$LiNdP_4O_{12}$, glass clad, slab waveguide laser 78−46625
$LiNdP_4O_{12}$ glass-clad rectangular waveguide, laser performance 80−32996
$LiNdP_4O_{12}$, grown by top seeded pulling technique, possible laser material 80−25542
$LiNdP_4O_{12}$ laser, fluoresc. and oscill. characts. at 1.317 μm 78−5473
$LiNdP_4O_{12}$ laser, fluctuations in bath of strong Gaussian noise 79−55166
$LiNdP_4O_{12}$ laser, intensity fluctuations due to external perturbations 79−81437
$LiNdP_4O_{12}$ laser, LED and semiconductor laser pumped 77−75552
$LiNdP_4O_{12}$ laser, relaxation oscillations and mode spectra, high density pumping effect 80−69396
$LiNdP_4O_{12}$ laser, spontaneous phase locking obs. 78−83005
$LiNdP_4O_{12}$, laser emission cross sections, fluorescence spectra, radiative lifetimes, quantum efficiency 80−23694
$LiNdP_4O_{12}$ laser material, optical props. and crystal growth *(Japanese)* 79−27259
$LiNdP_4O_{12}$ laser material, crystal growth and optical props. 79−41386
$LiNdP_4O_{12}$ miniaturised lasers for optical communication systems *(Japanese)* 79−27278
$LiNdP_4O_{12}$, simultaneous oscillations of different transitions in lasers 79−22927
$LiNdP_4O_{12}$, single crysts. flux growth and cryst. morphology, solubility curve 79−43124
$LiNdP_4O_{12}$ single crystal growth, study of Li_2O-Nd_2O_3-P_2O_5 phase diagram 80−25668
$LiNdP_4O_{12}$, single-transverse-mode slab waveguide laser, characts. 79−55141
$LiNdP_4O_{12}$ stable miniature laser with compact resonator, single mode operation 79−50305
$LiNdP_4O_{12}$ substrate, growth of $LiBi_xNd_{1-x}P_4O_{12}$ waveguide laser layer 80−23709
$Li_{0.45}Ni_{0.1}$, $Fe_{2.45}O_4$, sintering, mag. props., rare earth oxide additive effects *(Japanese)* 77−66602
Li_3Ni, densified polycrystalline, use in solid state batteries 79−86921
$Li_2Ni_2(MoO_4)_3$, paramag. props., 90-800K *(French)* 80−39734
$Li_2Ni_2Mo_3O_{12}$, cryst. struct. and struct. type systematics 77−72587
$LiNiO_3$, surface dendrite occurrence, growth condition-depend. 80−2316
Li_xNiPS_3, antiferromag., mag. props. and ionic mobility, NMR meas. 79−24223
Li_xNiPS_3, ionic conductivity, activation energies, NMR study 79−28138
$Li_xNi_{1-x}0$ ($x=0$ to 0.03), solid soln. effect of Li on densification during sintering 80−25638
LiO, struct., spectra, SCF MO calcs. 78−17559
LiO_2 fusion reactor blanket, Monte Carlo anal. of asymmetric effects 78−74464
LiO_2, molecule, vibronic interaction in low-lying states, model calc. 80−32603
LiO_2 pellets, sintered, exam. of microstructure 78−72749
LiO_2 pellets, T release due to recoil process 79−85767
LiO_2 sintered pellets, neutron irradiated, T release 78−5014

lithium compounds continued
LiO_2, T breeding performance eval., multigroup neutron and photon transport calc. 80−13831
LiO_2-$2SiO_2$, glass, devitrification with ageing 78−79536
LiO_2-$2SiO_2$, reaction with NaCl-kCl melt, X-ray, IR exam. 80−55706
LiO_2-Al_2O_3-SiO_2, bonding of Si-O exam. by X-ray emission spectra 78−52594
LiO_2-Al_2O_3-SiO_2, anal. of composition by IR reflection spectra 80−40783
LiO_2-Al_2O_3-SiO_2, glass containing ZrO_2, cryst. process 80−103253
LiO_2-Al_2O_3-SiO_2-TiO_2:Sn^{3+}, ESR and X-ray phase anal. 79−99752
LiO_2-CaO-SiO_2 phase equilibria 78−64528
LiO_2-Na_2O-CaO-SiO_2 glass-ceramic coating, high temp. effects on steel substrate 79−61776
LiO_2-Na_2O-MgO-TiO_2-Al_2O_3-SiO_2, exam. of specific heat and thermal conductivity *(Russian)* 79−55898
LiO_2-SiO_2 glass ceramic mineralogy 80−60826
LiO_3, up-conversion of signal from thermal source 80−9938
Li_2O (LiOLi, LiLiO), struct., spectra, SCF MO calcs. 78−17559
Li_2O, additive in ZnO sintering 78−80497
Li_2O, Ar^+ implantation, depth distrib. by proton backscatt. 78−51577
Li_2O, C atom conc. profile determ. by proton backscattering 78−10079
Li_2O, cation diffusion, NMR obs., MgO and LiF doping effects *(German)* 77−20112
Li_2O, cation diffusion NMR investigation up to 800°C 80−108092
Li_2O, coexistence of rhombohedral and cubic form, X-ray study 80−1980
Li_2O compensation technique, appl. to $LiNbO_3$:Ti planar and channel waveguides 78−74976
Li_2O, effect on props. of PbO containing cryst. glass 80−24637
Li_2O, effect on viscosity of PbO containing crystal glasses 80−19973
Li_2O, elastic electron scatt. intensity, rel. to electron density distrib. 78−1079
Li_2O gas carried fusion reactor blanket, neutronics and photonics 77−67880
Li_2O, heat capacity 306 to 1073K 79−10965
Li_2O in liquid Li, solubility determ. by neutron activation anal. 78−11601
Li_2O, in phosphate or silicate glass, effect on thermooptic props. 78−18029
Li_2O, lattice energy calc. 78−79556
Li_2O, Li^+ ion self-diffusion coeff., sectioning technique 80−15296
Li_2O, mass-spectrometric study of vaporization of solid and thermochemistry of gas 79−10940
Li_2O, microspheres for gravity flow bed fusion reactor, fabrication research 80−32468
Li_2O, neutron irrad. effects, optical absorpt. spectra 80−75271
Li_2O, neutron irradiated, ESR of F^+, O^-, H^0 and colloidal Li centres 78−2737
Li_2O out-diffusion waveguide elimination in $LiNbO_3$ and $LiTaO_3$ 77−65641
Li_2O packed bed blanket, T transport 80−37612
Li_2O pellets, neutron irrad., microstruct. and Vickers mircohardness meas. 79−8339
Li_2O pellets, neutron irradiated, temp. distrib. 80−86968
Li_2O pellets, sintered, reaction with Mo and Ho alloys 79−47913
Li_2O pellets, sintered, neutron irradiated, ESR study 80−92566
Li_2O pellets, thermal neutron flux distrib. inside and outside 80−47700
Li_2O, porosity, dependence on thermal diffusivity and thermal conductivity, 200-900°C 80−92726
Li_2O, segregation at grain boundaries in ZnO 78−64513
Li_2O single cryst., $^6Li(n,\alpha)^3H$, 2.7 MeV triton recoil range 80−63372
Li_2O, single crystal synthesis using vacuum fusion technique 80−71585
Li_2O, single crysts., growth by floating zone method 79−43139
Li_2O sintered pellets, reaction with 316 stainless steel, Incoloy 800, Hastelloy X-R, Inconel 600 and pure Ni 79−39137
Li_2O solid state breeding blanket for controlled thermonuclear reactors *(Japanese)* 79−9869
Li_2O solubility in liquid Li, determ. by fast neutron activation 79−42252
Li_2O Tokamak breeding blankets, T breeding perform. comparative eval. 80−95398
Li_2O^-, electronic struct. and config., ab initio SCF study 79−85898
Li_2O-$2SiO_2$ glass, alkali motion ionic thermocurrent study, polarised impurity-vacancy dipole relaxation study 79−77806
Li_2O-$2SiO_2$ glass, DTA study, Kissinger plot 80−84084
Li_2O-$2SiO_2$ glass, ionic cond. under DC potential 79−28134
Li_2O-$3SiO_2$ glass, crystallization 79−74141
Li_2O-(Al_2O_3)-SiO_2 glass-ceramic, crystallisation mechanism 79−90559
Li_2O-Al_2O_3, rapidly quenched glasses, Li ion cond., elec. cond. 80−100346
Li_2O-Al_2O_3-Cr_2O_3 system, subsolidus equilibria 80−60843
Li_2O-Al_2O_3-GeO_3, glass, interdiffusion coeffs. of Li and Na 80−88369
Li_2O-Al_2O_3-P_2O_5:V^{4+}, glass exam. of ESR spectrum of V^{4+}, optical spectra, and structure 78−88180
Li_2O-Al_2O_3-SiO_2, glass ceramic form. obs. using positron annihilation 77−7762
Li_2O-Al_2O_3-SiO_2, glassy and polycryst., interdiffusion coeffs. for ion exchange 78−26738
Li_2O-Al_2O_3-SiO_2, glass ceramic, elastic props. at high press., US meas. 78−83863
Li_2O-Al_2O_3-SiO_2, glass, study of elastic props. 80−104205
Li_2O-Al_2O_3-SiO_2, kinetics of glass-ceramic formation, by modified broken total internal reflection method 77−36444
Li_2O-Al_2O_3-SiO_2, phase separation of initial stages of sitallisation 80−88053
Li_2O-Al_2O_3-SiO_2, with refractive index gradient, produced by ion exchange diffusion, exam. of refractive index and concentration changes 79−4782
Li_2O-Al_2O_3-SiO_2 ceramic, chem. resist. and struct. 79−61756
Li_2O-Al_2O_3-SiO_2 glass, crystn. aggregation and migration of ion-implanted Ag 77−55240
Li_2O-Al_2O_3-SiO_2 glass, He migration, struct. effects 77−55389
Li_2O-Al_2O_3-SiO_2 glasses, Tb^{3+}($^5D_3$) luminesc., cross-relax. quenching *(Russian)* 79−33836
Li_2O-Al_2O_3-SiO_2 glasses, viscosity, thermal expansion, glass transform. temp., and refr. index 79−42282
Li_2O-Al_2O_3-SiO_2 glass, aq. corrosion 79−61753
Li_2O-Al_2O_3-SiO_2 glass ceramic, fracture initiation, influence of temperature and composition 79−100246
Li_2O-Al_2O_3-SiO_2 glass-ceramic, near-zero thermal-expansion heat treatment effect in fracture behaviour 80−66537

lithium compounds continued
Li_2O-Al_2O_3-SiO_2 glass, crystallised, grain size and internal strain 80−103259
Li_2O-Al_2O_3-SiO_2 system glass melts, alkali ions interdiffusion coeffs., conc. depend. 79−65231
Li_2O-Al_2O_3-SiO_2:Cu, Cu film self-generation for low-expansion IR laser mirrors 79−14127
Li_2O-Al_2O_3-SiO_2:Cd^+, glass, ESR study 80−103879
Li_2O-Al_2O_3-SiO_2-TiO_2 system glasses, Raman spectra obs. of glass-ceramics form. 80−60825
Li_2O-Al_2O_3-SiO_2(P_2O_5):Cd^+ glasses, γ-irrad., EPR study 80−84639
Li_2O-Al_2O_3-$4SiO_2$, glass-ceramic, tensile creep and high temp. fracture 78−52914
Li_2O-Al_2O_3(Ga_2O_3)(Bi_2O_3), quenched glasses, crystn. and ionic cond. 80−33899
Li_2O-B_2O_3, crystalline and glassy, thermolum. meas. 77−16406
Li_2O-B_2O_3 glass, conductivity, permittivity, and dielectric loss obs., mixed isotope effect 78−95182
Li_2O-B_2O_3 glass struct. study using ^{10}B NMR 80−84658
Li_2O-B_2O_3 glass system, 4-coordinated B atomic fraction determ. 78−94999
Li_2O-B_2O_3 glasses, fast ion transport 80−107470
Li_2O-B_2O_3 glasses, low Li_2O content, ^7Li NMR study 80−84657
Li_2O-B_2O_3:Cr^{3+} glass, absorpt. spectra, Fano antireson. and vibronic Lamb shift 80−71458
Li_2O-B_2O_3:Eu^{3+} glass, laser induced fluoresc. line narrowing, struct. 79−38613
Li_2O-B_2O_3:Mn^{2+} glass, fine struct. parameter distribs., EPR meas. 80−11256
Li_2O-B_2O_3:Tl^+(Pb^{2+})(Bi^{3+}) glass, optical basicity, variation with probe ion and comp. 80−2800
Li_2O-B_2O_3-Fe_2O_3 glass, Mossbauer expts., 85-500K 78−80260
Li_2O-B_2O_3-P_2O_5, glass, mech. and elec. props 80−84228
Li_2O-B_2O_3-SiO_2 glass systems, phase separation effect on the diffusion processes 78−26734
Li_2O-B_2O_3-WO_3 glass, photochromic and electrochromic props. 79−28787
Li_2O-BaO-Al_2O_3-SiO_2-xTiO_2 glass, X-ray spectra, Ti ion electron config. *(Russian)* 77−8674
Li_2O-BaO-SiO_2 glasses, elec. cond., room temp. to 450°C 80−107473
Li_2O-based mixed oxides, ionic cond., effects of moisture and LOOH on elec. and struct. props. 79−69283
Li_2O-BeO-SiO_2, X-ray diffr. exam. of phase equilibrium 78−80522
Li_2O-Bi_2O_3, rapidly quenched glasses, Li ion cond., elec. cond. 80−100346
Li_2O-CaF_2 melts, component activities *(Russian)* 77−60104
Li_2O-Cr_2O_3-SiO_2 system, phase equilibria 79−78944
Li_2O-Fe_2O_3-Pr_6O_{11}(Er_2O_3)(CeO_2)(Eu_2O_3), Hall effect and magnetoresist. 78−34849
Li_2O-Fe_2O_3-siO_2 glass, struct. and crystallisation behaviour 78−83738
Li_2O-Ga_2O_3, rapidly quenched glasses, Li ion cond., elec. cond. 80−100346
Li_2O-GeO_2 glass, struct., Raman scatt. obs. 80−1936
Li_2O-GeO_2 glass, synthesis, Ge coordination state 77−24271
Li_2O-GeO_2-Ga_2O_3, glass, electrode props., dissolution kinetics 80−89387
Li_2O-GeO_2-SiO_2, refractive index and density 79−51926
Li_2O-Li_2SO_4-B_2O_3 vitreous electrolytes, ionic cond. and Raman spectra *(French)* 80−24656
Li_2O-LiCl-B_2O_3 system, fast Li^+ ion vitreous superconductors, EPR study *(French)* 80−11269
Li_2O-LiF-B_2O_3 glasses, fast Li^+ conduction 80−79984
Li_2O-LiF-B_2O_3-Li_2SO_4 glasses, DC cond. and secondary struct. relax. 80−107469
Li_2O-LiX-B_2O_3 glass, X=halogen, high anionic cond. of new solid electrolytes 80−107546
Li_2O-MgO-Al_2O_3 system, subsolidus phase equilibria 80−81036
Li_2O-MgO-Al_2O_3-SiO_2 glass scintillator for pulsed neutron detection 80−87019
Li_2O-Na_2O-B_2O_3-Al_2O_3-SiO_2 glass, Young's modulus and density, ion exchange effects 80−84982
Li_2O-Na_2O-B_2O_3-SiO_3, exam. of metastable phase separation region 78−88450
Li_2O-Na_2O-P_2O_5, heat of soln. *(Japanese)* 79−34350
Li_2O-Na_2O-P_2O_5 glasses with oxide additions, eval. as membranes for chem. sources of current *(Russian)* 79−96338
Li_2O-Na_2O(K_2O)-SiO_2 glass, heat of mixing *(Japanese)* 78−10195
Li_2O-Nd_2O_3-P_2O_5 glass, physicochem., spectral, luminesc. and stimulated emission props. 77−54715
Li_2O-Nd_2O_3-P_2O_5 phase diagram, $LiNdP_4O_{12}$ single crystal growth 80−25668
Li_2O-Nd_2O_3-P_2O_5 ultraphosphate glasses, Nd^{3+} conc. quenching of luminesc. effect 79−19931
Li_2O-NiO-O_2, phase diagram and mag. props. of $Li_xNi_{1-x}O_{1\pm y}$ 78−48380
Li_2O-P_2O_5 glass, ESR of VO^{2+} ions 80−100610
Li_2O-P_2O_5:Cd^+ glass, γ-irrad., EPR study 80−84639
Li_2O-SiO_2, cation interdiffusivity, electrochem. determ., 1100-1350°C 78−47544
Li_2O-SiO_2, corrosion behaviour in aq. solns. of Al compounds 80−66679
Li_2O-SiO_2, glass ceramics, phase transformation processes 80−3025
Li_2O-SiO_2 based glasses, high field cond. and ionic jump processes 78−38873
Li_2O-SiO_2 glass, bulk crystn., SEM and optical microscope studies 80−44142
Li_2O-SiO_2 glass, crystn. and phase separation, positron lifetime and annihilation lineshape meas. 78−23550
Li_2O-SiO_2 glass, crystallisation and phase separation 79−10803
Li_2O-SiO_2 glass, crystallisation study 79−90567
Li_2O-SiO_2 glass, cryst. nucleation, test of classical nucleation theory 80−1939
Li_2O-SiO_2 glass, protonated, field-driven guest proton redistrib. 80−107474
Li_2O-SiO_2 glass, suitability of small angle neutron scatt. for struct. determ. 78−22663
Li_2O-SiO_2 glass, thermotransport props. 80−79985
Li_2O-SiO_2 glass, water content effect on crystal nucleation and growth 79−55670
Li_2O-SiO_2 glass ceramic, aligned, prep. by hot extrusion and microstruct. 77−32552
Li_2O-SiO_2 glasses, crystn. kinetics from amorphous X-ray scattering study 80−38919

lithium compounds continued
Li_2O-SiO_2 glasses, Li self-diffusion, mass spectrometric method 80−79982
Li_2O-SiO_2-GeO_2 digermanosilicate glass, Raman study of structure 79−77524
Li_2O-SiO_2-P_2O_5 glass ceramic fibres, heat treatment, crystn., tensile strength 80−84995
Li_2O-SiO_2(-TiO_2) glass, crystn., kinetic study using differential scanning calorimetry 80−44138
Li_2O-Ta_2O_5 system phase diagram 79−47668
Li_2O-TeO_2 glass, radiational EPR centres, struct. model *(Russian)* 77−28426
Li_2O-TeO_2 glass, struct. and props. *(Japanese)* 79−32917
Li_2O-TeO_2 glasses, struct., IR reflection spectra 78−68516
Li_2O-TeO_2 glassy system, struct. recomb. model 80−19707
Li_2O-TiO_2, pseudobinary phase rotations, DTA and X-ray anal. 80−108411
Li_2O-TiO_2-Al_2O_3-SiO_2 glass, γ-irrad., struct. position of Ti, EPR study 80−84644
Li_2O-V_2O_5-Al_2O_3 melts, soln. of Al_2O_3 single crystals 80−20910
Li_2O-ZnO-P_2O_5, exam. of chemical durability, glass transformation temp. 79−20221
Li_2O, fund. optical absorpt. edge, number of displaced atoms from $^6Li(n,\alpha)^3H$ reaction 78−51594
Li_2O_2, ab initio geometry, vibr. freqs., ionis. pots., and force consts. 77−65421
Li_2O_2, gas, thermochem. props., mass spectra study 79−47957
Li_2O_2, thermal decomposition and heat capacity 301 to 566K, enthalpy 80−3322
Li_2O_3, treatment of ferroelec. $LiNbO_3$:Fe, Mossbauer effect 78−92003
Li_3O, gas, thermochem. props., mass spectra study 79−47957
(Li_2O-Al_2O_3-SiO_2):Fe_2O_3, glass, pyroceramic form., colour centres, magnetochem. investig. 77−16537
($LiO_{1/2}$-$NaO_{1/2}$)-$2SiO_2$ glass, alkali motion ionic thermocurrent study, polarised impurity-vacancy dipole relaxation study 79−77806
LiOH, $^1A'$ pot. energy surface, diatomics-in-mols. method calcs. 79−36566
LiOH, anodic oxidation of Cu amalgam at room temp. 79−61865
LiOH, electron distrib. of OH^- 78−75973
LiOH, fundamental vibr. freqs. 79−98068
LiOH, geom. and electronic struct., ab initio SCF calc. 79−76331
LiOH, hydrolysed surface of LiH, effect on IR absorption, X-ray luminesc. and EPR spectra 80−60660
LiOH, ionic conduction, environment effects 77−76600
LiOH, NMR study, motional narrowing 79−42863
LiOH, potential energy surface, diatomics-in-molecule method 79−63929
LiOH, spectral interference in at. absorption spectroscopy in C tube atomiser *(Japanese)* 79−48018
$LiOH^-$, electronic struct. and config., ab initio SCF study 79−85898
^{6,7}LiOH, LiOD, polycryst., Raman active modes and isotopic effects 79−87424
$Li^+(OH_2)_2$, 3-body pots., SCF energy partitioning calcs. 80−18953
LiOH(D)(T), thermal decomposition rates 530-690K, activation energy and enthalpy meas. 80−3321
LiON, four electron three centre bonding units, ab initio valence bond calcs. 80−27949
LiOO, struct., spectra, SCF MO calcs. 78−17559
$(Li_2O)_{1-x}U_{1.4}W_{4.6}O_{18}$, $0 \leq x \leq 0.4$, crystallographic identification, paramag. props. *(French)* 79−46633
$19Li_2O.19Al_2O_3.62SiO_2$ glass, ionic cond. meas. 79−33110
$Li_2O.2GeO_2$, powder Raman spectra, compared with digermanosilicate glass 79−77524
$Li_2O.2SiO_2$ ceramics unidirectionally solidified, porosity *(Japanese)* 79−38816
$Li_2O.2SiO_2$, ceramic, prep. of oriented microstructure by unidirectional solidification of melts 80−71614
$Li_2O.2SiO_2$, directionally solidified, thermal and mech. props. *(Japanese)* 80−16295
$Li_2O.2SiO_2$ glass, kinetics of crystal nucleation, effect of Pt and other impurities 78−88440
$Li_2O.2SiO_2$ glass and glass-ceramic, fatigue props. in various environments 79−91820
$Li_2O.2SiO_2$ glass and glass ceramic, Auger electron signal decay, crystn. effects 80−25503
$Li_2O.2SiO_2$ melt, bubble form. during unidirectional solidification *(Japanese)* 79−70057
$Li_2O.2SiO_2$, polycrystalline, oriented, fabrication by unidirectional solidification from melt *(Japanese)* 78−31371
$Li_2O.2SiO_2$, prep. from film forming soln. 80−60811
$Li_2O.2SiO_2$, short range struct. by pulsed neutron scatt. 80−59396
$100(Li_2O.2SiO_2).3B_2O_3(3Na_2O)(3MgO)(3Al_2O_3)(3SiO_2)(3P_2O_5)$, directionally solidified, thermal and mech. props. *(Japanese)* 80−16295
$Li_2O.3MoO_3.5.7H_2O$, fibrillar cryst., IR and NMR investig. of water bonding 77−12370
$Li_2O.3MoO_3.5.7H_2O$, fibrillar crysts., morphology and struct. 78−63959
$Li_2O.nAl_2O_3(7.3\text{-}n)SiO_2$, metastable solid soln., Al^{3+} vacancy incorporation 77−12593
$Li_2O.nB_2O_3$ (n=6, 4, 3), heat of soln. *(Japanese)* 77−77802
$LiPO_3$, cryst. struct. determ. *(French)* 77−4071
$LiPO_3$, crystn. mechanism from melt 80−44139
$LiPO_3$, form. from dihydroorthophosphate dehydration, reaction thermodynamics 79−52643
$LiPO_3$, melt viscosity *(Russian)* 77−43362
$LiPO_3$, vitreous, microhardness 80−25864
$LiPO_3$-$Al(PO_3)_3$:Ag glass, ionic motions, thermally stimulated depolarisation study 79−65239
$LiPO_3$-Li_2SO_4, new Ag^+ and Li^+ ion glass conductors, glass transition, Raman spectra *(French)* 79−47094
$LiPO_3$-LiX(X=I, Br, Cl) glass, ionic cond. *(French)* 79−99365
Li_3PO_4, Auger lineshape determ. by numerical integration background subtraction 79−74469
γ-Li_3PO_4, cryst. struct. of synthetic analog of lithiophosphatite 79−37688
Li_3PO_4, Li_4GeO_4, Mg_2GeO_4, structural relns. *(French)* 77−47433
Li_3PO_4, solid, low energy photoelectron spectra 78−95656
Li_3PO_4:CrO_4^{3-}, EPR, 4.2K, cryst. field parameters 79−28586
$Li_{x+2}P_xO_{3x+1}$, polyphosphate, melting and crystallisation 80−70376
$LiPO_3.Al(PO_3)_3$:U, vibronic excitation, absorption and emission spectra 78−52524
$(LiPO_3)_x.H_2O$, existence of high- and low-temp. cryst. forms, X-ray diffr. data 79−19179

lithium compounds continued
Li_7Pb_2, fusion reactor breeding material, reaction with H_2O 80−13830
Li_7Pb_2, T breeding fusion blanket with boiling water coolant 80−99274
Li_7Pb_2, T breeding performance eval., multigroup neutron and photon transport calc. 80−13831
Li_7Pb_2 Tokamak breeding blankets, T breeding perform. comparative eval. 80−95398
$LiPbPO_4$, vibrational spectra and cryst. struct. 78−39536
$Li_3Pr_2(BO_3)_3$, cryst. struct. 78−87655
$LiPr(SO_4)_2$, X-ray diffr. cryst. struct. determ. 79−14786
α-$LiPr(WO_4)_2$, single cryst., X-ray diffr. cryst. struct. anal. 80−33976
$LiR(WO_4)_2$, R=La-Sm, triclinic modification, cryst. struct. 80−33976
$LiRF_4$, (R=Tb, Dy, Ho, Er, Yb), paramag. phase props., basal plane anisotropy and cryst. field parameters 77−69486
$LiRF_4$, R=rare earth, laser matrices prep. and characterisation 77−24945
$LiRF_4$, R=rare earth, low-temp. magnetically ordered states 77−63098
$(Li_{0.5}R_{0.5})TiO_3$, distorted perovskite struct. 78−83791
LiRb, Hellman pseudopot. calcs., dissoc. energy, ionis. pot., bond length 77−10577
$Li_{1-x}Rb_xI$, intrinsic optical absorpt. spectra 78−23500
$LiRbSO_4$, order-disorder phase transitions with many-minimum potential, thermodynamic props. 80−96623
$LiRbSO_4$, X-ray cryst. struct. determ. 80−33982
$LiReO_4$, ^{187}Re HQR freq. temp. depend. 80−25245
$LiReO_4$, IR matrix-isolation spectra 80−87108
$LiReO_4$, thermodynamic activity in $LiReO_4$-$CsReO_4$ system, mass spectra meas. 80−2174
$LiReO_4.2H_2O$, ^{187}Re HQR freq. temp. depend. 80−25245
Li_2S, cation diffusion NMR investigation up to 800°C 80−108092
Li_2S, solubility in LiCl-KCl and LiCl-LiF molten eutectic mixtures 80−54387
Li_2S-Al_2S_3, prep., phase props. and elec. cond. 79−96010
Li_2S-GeS_2, glass forming region, struct. and ionic cond. 80−88358
Li_2S-P_2S_5-LiI, ionic cond. meas. from room temp. to glass transition temp. *(French)* 80−88355
LiSCN in N,N-dimethylacetamide, Raman, IR and US relaxation studies 80−50315
Li_2SO_4, Auger lineshape determ. by numerical integration background subtraction 79−74469
Li_2SO_4 based solid electrolytes, FCC phase transport mechanism studies and uses 80−107525
Li_2SO_4, electron irrad. damage, XPS obs. 78−64444
Li_2SO_4, fast ion conductors, X-ray diffr., neutron diffr., and Brillouin scatt. study 80−107170
Li_2SO_4, high temp. fast ion cond. phases, neutron diffr. obs. of struct. 80−107512
Li_2SO_4, IR absorpt. spectra, polymorphism, site group approx. and SO_4 stretching mode 78−52510
Li_2SO_4, liq. and plastic crystalline phases, Brillouin scatt. 79−99897
Li_2SO_4, molten, and molten Li_2SO_4-Na_2SO_4 mixtures, struct. anal. by X-ray diffr. 78−63660
Li_2SO_4, molten, Brillouin spectra, refr. index meas., hypersonic vel. 78−68523
Li_2SO_4, optical fibres, material dispersion 79−27377
Li_2SO_4, solid, low energy photoelectron spectra 78−95656
Li_2SO_4 solid electrolyte plastic deformation and thixotropy obs. 78−79660
Li_2SO_4, triboluminescence and cryst. fracture dynamics 80−50437
Li_2SO_4, UPS, expt. methodology aspects 77−90245
Li_2SO_4:$Na^+(K^+)(Mg^{2+})(Zn^{2+})(Cd^{2+})(Al^{3+})$, monoclinic-cubic transform., effect of impurities 79−52744
$LiSOCl_2$ battery undersea applications 80−45658
$LiSO_3F$, cryst. struct. determ. 78−26509
$Li_2SO_4.D_2O$, ^2D resonance lineshape of exchange spin-1 pair 78−2751
$LiSO_4.H_2O$:Cr^{3+}, single cryst., EPR and optical absorpt. spectra 80−39855
$Li_2SO_4.H_2O$, $^6Li/^7Li$ and H/D substituted, IR and Raman spectra, vibr. and librational modes 77−85716
$Li_2SO_4.H_2O$, electrocaloric cooling effect, low temp. behaviour of primary pyroelectric coeff. 78−39506
$Li_2SO_4.H_2O$, far IR spectra, H_2O flipping motion, lattice modes 80−84258
$Li_2SO_4.H_2O$, linear pyroelectric, temp. depend. of polarisation 79−99821
$Li_2SO_4.H_2O$, X-ray diffr., IR and Raman spectra, internal optic modes, mol. dipole model 77−76493
Li_3Sb, evaluation as electrode material, electrochem. expts., 360-600°C 78−11526
Li_3Sb, mixed conducting electrodes, kinetic parameters determ. 78−14772
$LiSbO_3$.1/6LiF, dielec. spectroscopy study, 100 Hz to 10 MHz, 238 to 417K *(German)* 80−108144
$LiScO_2$:Bi^{3+}, luminesc., vibr. struct. 79−33790
$LiScO_2$:Fe^{3+}, Mossbauer exam. of relaxation behaviour of Fe^{3+} 77−1620
$LiScS_2$, crystal struct. determ. by X-ray powder diffr. 80−49205
Li_2SeO_4, electronic struct. of SeO_4^{2-} clusters 79−65417
$Li_x(Si,Al)_{12}(O,N)_{16}$, α′-Sialon ceramics, prep. and characterisation 78−84750
$Li_{2.33}Si$, cryst. struct. and electrochem. anal. *(German)* 80−88132
$LiSiO_4$, pure and doped ionic conductivity increase obs. 78−14506
Li_2SiO_3, Czochralski growth and charact. 79−91577
Li_2SiO_3 glass pH meter electrode performance *(German)* 80−40695
Li_2SiO_3, IR and Raman spectra, normal coord. anal. of unit cell vibrs. 77−81090
Li_2SiO_3, melt-grown single crysts., polar twins, piezoelec. meas., etching behaviour 79−32999
$(Li_2SiO_3)_x$, bond length variations, mol. orbital study 78−26500
$(Li_2SiO_3)_x$, cryst. struct. 77−35519
Li_2SiO_4, piezoelectric glass ceramic, recrystallisation, pyroelectric response, permittivity 80−80703
$Li_2Si_2O_5$, and Li_2SiO_3, ionic cond. 77−1256
$Li_2Si_2O_5$ glass, steady state crystal nucleation rate 79−90564
$Li_2Si_2O_5$ glass, steady state crystal nucleation rate 79−90565
$Li_2Si_2O_5$, laminated cryst., IR spectra, dispersion anal. 77−1675
$Li_2Si_2O_5$, pyroelectric glass-ceramics 80−75950
$Li_2Si_2O_5$-Li_2SO_4 glasses, electrical cond. and Raman study of struct. *(French)* 79−65482
$Li_2Si_2O_5$-TiO_2 glasses, struct. and crystn. investigation using Raman spectra 80−38918
Li_4SiO_4, interfacial polarisation effects 79−60538

lithium compounds continued
Li_4SiO_4, ordered, cryst. 80−19752
Li_4SiO_4-Li_3PO_4, ionic cond. enhancement by Li_3PO_4 addition 77−7893
Li_4SiO_4-Li_3PO_4 solid solns., Li ion cond., struct. and comp. effects 77−89575
LiSiON, allotropes, powder diffr. obs. *(French)* 78−63726
Li_8SnO_6, ion mobility, NMR meas. *(French)* 79−65240
Li_8SnO_6, pseudo-two-dimens. electrolytic solid, Li ion mobility, NMR study *(French)* 80−34235
$LiSnS_2$, Li intercalation effects on electronic struct. 79−78004
$Li_2Sr(CO_3)_2$, phase diagrams *(French)* 78−95033
$LiSrPO_4$, vibrational spectra and cryst. struct. 78−39536
LiT, ^{3}He distrib. 78−30661
LiT, retention and distrib. of ^{3}He NMR studies 79−69153
$Li^+(TCNQ)^-$, low temp. EPR of impurity reson. 77−85548
Li^+TCNQ^-, optical absorpt. spectra of small particles 78−19505
$LiTaO_2$ and SiO_2/$LiTaO_3$ struct., Rayleigh waves, piezoelectric leaky surface waves, temp. depend. 79−46905
$LiTaO_3$, ^{181}Ta NQR spectra, 77K to room temp. 79−38401
$LiTaO_3$, acoustics surface wave propag., temp. coeffs., piezoelectric coupling *(French)* 78−35093
$LiTaO_3$, anomalous polariton dispersion near Curie temp. 77−80743
$LiTaO_3$, appl. in sub-100 ps pyroelec. detectors, 10.6 μm damage threshold meas. 80−77859
$LiTaO_3$, asymm. phonon lines, IR refl. analysis in paraelec., ferroelec. phases 78−27197
$LiTaO_3$, characterisation as holographic storage materials 78−29909
$LiTaO_3$, complex conjugate wavefront generation via degenerate four-wave mixing 80−48329
$LiTaO_3$, compound optical crosspoint with low crosstalk 78−33915
$LiTaO_3$, crystallographic features and domain struct. 78−34498
$LiTaO_3$ crystals for commercial SAW TV IF filters, fabrication 80−80961
$LiTaO_3$, crysts., elec. field influence on hypersonic wave propag. 80−44668
$LiTaO_3$, Czochralski growth technique, light guide prod. by Nb diffusion *(German)* 80−20783
$LiTaO_3$, Czochralski-grown oxide crystals, fluid-flow effect on gas-bubble entrapment 80−84121
$LiTaO_3$, displacive ferroelectric, effective charge determ. 80−97212
$LiTaO_3$, electric field gradients and isomer shift ^{181}Ta 78−39453
$LiTaO_3$ electro-optical total internal reflection diffraction industrial modulators and deflectors 77−19436
$LiTaO_3$, electro-optic cryst., photo-induced electron and hole transport holographic method for determ. 79−28375
$LiTaO_3$, electro-optic guided-wave A/D convertor, high speed 80−33234
$LiTaO_3$, electroacoustic interaction obs. 77−11966
$LiTaO_3$, electroacoustic coeffs. 79−69564
$LiTaO_3$, far IR complex refl. coeff. and refr. index, dispersive Fourier transform meas. 79−2841
$LiTaO_3$ fast electro-optic deflector, arbitrarily shaped optical pulsed generation 80−53421
$LiTaO_3$, ferroelec., displacive type phase transition, far IR reflection spectra 80−71339
$LiTaO_3$, ferroelec., IR high temp. amplitude-phase spectroscopy 79−35860
$LiTaO_3$ film, pyroelectric effects, origin 78−88258
$LiTaO_3$, finite amplitude SAW distorted rippling profiles, optical probing obs. 80−34287
$LiTaO_3$, for substrate used in fabrication of SAW Butterworth contiguous filters 79−68493
$LiTaO_3$, Fourier transform Ir spectroscopy of vibr. states at high temp. 80−97256
$LiTaO_3$ glass, quenched, ionic cond., appl. as solid electrolyte 79−1522
$LiTaO_3$ glass-ceramics, transparent fabrication by crystn. of aluminosilicate glasses 77−59734
$LiTaO_3$, guided wave devices, use of ferroelectric materials, review 78−38048
$LiTaO_3$ high-temp. ferroelec. transition, soft mode IR reflectivity spectroscopy 79−33692
$LiTaO_3$, IR reflectivity spectra and phonon self-energy effect 77−63413
$LiTaO_3$, interdigital transducer on piezoelectric half space, spectrum of emanating acoustic waves 80−79044
$LiTaO_3$, ionic grouping theory of electro-optical and nonlinear optical effects of crystals *(Chinese)* 78−27183
$LiTaO_3$, low freq. Raman scatt. spectra of polaritons, photographic recording 79−73952
$LiTaO_3$, magnetoelectric susceptibilities, phenomenological rules for computation 80−55068
$LiTaO_3$, monolithic filter operating at 230 MHz 77−42671
$LiTaO_3$ monolithic pyroelectric array, IR detectors 80−77857
$LiTaO_3$, multidomain cryst., birefringence, Tyndall cone struct. 77−4618
$LiTaO_3$, multimode electro-optical 2×2 crossbar switch 78−55473
$LiTaO_3$, near ferroelec. transition, elasticity, photoelasticity 78−88268
$LiTaO_3$ optical modulator, temperature compensated, feedback control method 77−42611
$LiTaO_3$, optical phonon modes and anharmonic couplings 78−60466
$LiTaO_3$ optical waveguides, Ag-Li and Tl-Li ion exchange effects 80−58791
$LiTaO_3$ optical waveguide, Ag-Li ion exchange 80−91888
$LiTaO_3$, paraelectric phase, soft vibr. modes, far IR refl. meas. 79−87407
$LiTaO_3$, photoelastic consts., Brillouin scatt. 77−28546
$LiTaO_3$, photorefractive sensitivity, holographic and photocurrent investig. 77−24581
$LiTaO_3$, picosecond study of colour centre translocation 80−40144
$LiTaO_3$, piezoelectric resonator characterisation 78−95550
$LiTaO_3$, planar waveguide, leaky mode propag. 78−87149
$LiTaO_3$ platelet, electro-optical tunable filter, birefr. electro-optic cryst., light energy coupling 79−59804
$LiTaO_3$, primary pyroelec. effect, lowest order mode contrib. 78−15103
$LiTaO_3$, propagation of SAW, arbitrary cut *(Japanese)* 80−92769
$LiTaO_3$, pyroelectric detector, temperature noise and dielec. loss 77−17975
$LiTaO_3$, quadratic optical susceptibility dispersion crystal struct. 79−18478
$LiTaO_3$, Raman spectra and dielec. props. near Curie point 79−38530
$LiTaO_3$, refr. index, equal-deflection method, UV laser rad. 78−29145
$LiTaO_3$, refr. index distrib. after surface lapping, theory 78−72479
$LiTaO_3$, rotated Y-cut, SH and Rayleigh surface waves 79−46910
$LiTaO_3$ rotated Y-cuts for SAW launching 79−56060

lithium compounds continued
$LiTaO_3$ SAW delay line with −70 dB spurious responses 77−31182
$LiTaO_3$ SAW substrate minimal diffraction cuts 78−33934
$LiTaO_3$, single cryst. growth and phys. props. *(Japanese)* 79−65018
$LiTaO_3$, single cryst. prep. for surface acoustic wave device appls. *(Japanese)* 80−60772
$LiTaO_3$, single crysts., Czochralski growth for SAW device appl. 79−33922
$LiTaO_3$, single crysts., temp. depend. of diffuse X-ray scattering intensity 79−61318
$LiTaO_3$, spontaneous elec. breakdown 77−66458
$LiTaO_3$ substrates, LPE growth of $Li(Nb,Ta)O_3$ solid soln. thin film waveguides 79−41467
$LiTaO_3$ substrates, optical waveguides and waveguide components development *(Czech)* 80−19090
$LiTaO_3$ surface skimming bulk wave theory 79−56064
$LiTaO_3$, surface wave anal. using orthogonal functions 78−51810
$LiTaO_3$ temperature-stable shallow bulk acoustic wave devices 79−55293
$LiTaO_3$, thin crystal plates, specific directions of plane elastic waves 79−82281
$LiTaO_3$ thin plate temperature characteristics 77−39141
$LiTaO_3$, Ti diffused, electrooptic diffraction modulation 79−10381
$LiTaO_3$, time depend. phase inhomogeneity compensation via degenerate four-wave mixing 80−53353
$LiTaO_3$, transition metal doped, photovoltaic and photorefractive effects, origin 77−20364
$LiTaO_3$, trigonal crysts., anisotropy of linear electrooptic effect 80−34894
$LiTaO_3$, uniaxial ferroelec., polariton dispersion relations 77−20249
$LiTaO_3$, uniaxial pyroelectric, nonlinear optical susceptibility 77−23705
$LiTaO_3$, used in 2 Gbit/s electro-optic modulator for visible lasers 79−86262
$LiTaO_3$, vitreous, anomalous dielectric behaviour and reversible pyroelectricity 77−85658
$LiTaO_3$, wave front convolution in 4-wave interaction with nonlocal nonlinear media *(Russian)* 79−86205
$LiTaO_3$, waveguide, single-mode planar and rigid type electro-optic waveguide modulators design 77−11029
$LiTaO_3$, X-ray diffr. study of lattice dynamics parameters *(Russian)* 79−65156
$LiTaO_3$, X-ray diffuse scatt., temp. depend., 20 to 750°C 79−37800
$LiTaO_3$ zig-zag reflection interferometric light modulator 78−90527
$LiTaO_3$:Cr (III), radiationless relax., heat-pulse meas. technique 77−36277
$LiTaO_3$:Cu, waveguide with periodic electrodes, mode conversion 78−33840
$LiTaO_3$:Cu waveguide, electro-optic control of radiation loss in off-axial propagation 80−23789
$LiTaO_3$:Cu(Fe), light induced charge transport, photovoltaic effects, impurity states 80−80317
$LiTaO_3$:Fe, electro-optic cryst., light induced charge transport, holographic obs. 80−70747
$LiTaO_3$:Fe crystal, holographic storage process 80−32942
$LiTaO_3$:M, optical damage of transition-metal-doped ferroelectric 78−95571
$LiTaO_3$:Ti, diffused waveguide prep., parameters determ. 80−14465
$LiTaO_3$:Ti waveguide modulator structs., high optical power capabilities 77−39023
$LiTaO_3$/CCD hybrid focal plane, IR imaging and detection, crosstalk 80−77856
$LiTaO_3$/SiO_2 SAW device, thermal stress effects of acoustic surface waves in layered media *(Japanese)* 79−98573
$LiTaO_3$-$CaZrO_3$, struct. and dielec. props. 78−80298
$LiTaO_3$-$NaTaO_3$-$KTaO_3$, quenched metastable glassy and crystalline phases 79−61568
$LiTaO_3$-SiO_2-Al_2O_3, transparency in relation to microstruct. 78−53005
$LiTaO_3$-SiO_3, temp. compensated SAW device fabrication 79−76923
$LiTa_3O_8$, H-form cryst. struct. 79−60325
M-$LiTa_3O_8$, neutron diffr. obs. 78−18599
$Li_{1-x}Ta_3O_{8-x}F_x$ (x=0,0.25,0.5), structural studies by full profile refinements of Guinier-Hagg X-ray film data 79−23584
$Li_{0.33}TaS_2$, supercond. props., alkali cation and topotactic solvation influences 79−87180
Li_xTaS_2 and Li_xTiS_2, chem. diffusivity of Li at 30°C 80−59737
$Li_{1+y}Ta_{1.5y}Ti_{6y}O_3$ ($0 \leq y \leq 0.028$), non-stoichiometric phase, crystallographic and dielec. props. 80−75212
$LiTaI_3$, ferroelec. crysts. for electrooptics and nonlinear optics, optical inhomogeneities, review *(Japanese)* 77−65613
$LiTb_4$, $LiTb_{0.5}Y_{0.5}F_4$ and $LiTb_{0.25}Gd_{0.75}F_4$, Faraday rotation, optical absorpt. spectra and refr. index 78−72542
$LiTbF_4$, cryst. field parameters, mag. susceptibility meas., 0.3 to 100K 80−60214
$LiTbF_4$, dipolar-coupled Ising ferromag., submillimetre ferromag. and paramag. reson. 77−69697
$LiTbF_4$, EPR studies, lowest levels of rare-earth ions, submillimetre freq. 80−39865
$LiTbF_4$, ferromag., spontaneous magnetisation at marginal dimensionality 77−24683
$LiTbF_4$, ferromag., susceptibility, sp. ht., renormalisation group theory test 77−16087
$LiTbF_4$, mag., optical, magneto-optical behaviour 78−68484
$LiTbF_4$, mag. props., crit. behaviour at marginal dimensionality 80−54906
$LiTbF_4$, magnetisation near crit. pt., temp. and field depend. 79−38337
$LiTbF_4$, NMR rotation spectra, transferred hyperfine interaction 77−85590
$LiTbF_4$, optical study of spontaneous magnetisation at marginal dimensionality 79−73699
$LiTbF_4$, Tb^{3+} absorption spectra, 4000 to 25000 cm^{-1} 78−72550
$LiTbF_4$, uniaxial dipolar ferromag., critical behaviour, mag. susceptibility meas. 80−80528
$LiTbF_4$, uniaxial ferromag., nonuniversal props. in dipolar crit. region 77−24703
$LiTbS_2$, long and short range order 78−38667
$LiTb_{0.5}Y_{0.5}F_4$, mag. susceptibility, dilution effect on critical behaviour of dipolar uniaxial ferromagnet 80−34635
$LiTb_{0.5}Y_{0.5}F_4$, uniaxial dipolar ferromag., critical behaviour, mag. susceptibility meas., effect of Y^{3+} dilution 80−80528
$LiTe_3$, cryst. struct., X-ray and neutron diffr., Te displacements 77−47399
Li_2TeO_4, cryst. struct. *(French)* 78−6041

lithium compounds continued
Li_4TeO_5, crystl. struct. anal. by Patterson and Fourier synthesis *(French)* 79−4273
Li_3ThF_3, cryst. struct. comment on coordination polyhedra for ThF_9 group 79−69083
Li_3ThF_7, cryst. struct. 78−63702
Li_3ThF_7, $LiThF_5$, $LiTh_2F_9$, $LiTh_4F_{17}$, flux growth 77−85919
$Li_2Th_5F_{22}.LiOH$, cryst. struct. determ. and refinement 79−73142
LiTi ferrite, Mossbauer study, relax. and supertransferred hyperfine fields 80−39941
LiTi, substituted ferrite, cation distribution, Mossbauer, X-ray, neutron diffr. study 80−28975
$LiTi_2O_4$, prep., characterisation and supercond. props. 77−40010
$LiTi_2O_4$, press. depend. of supercond. transition temp. meas. 77−12050
$LiTi_2O_4$, single-phase, prep., crystal struct. and superconducting transition characts. 80−50583
$Li_{1-x}Ti_{2-x}O_4$, struct. phase transition and thermal expansion 78−14465
$Li_{1+x}Ti_{2-x}O_4$, high temp. spinel-Ramsdellite transform. 80−70407
Li_2TiO_3-MgO (20 to 40 at.%), order-disorder transitions, DTA and X-ray anal. 79−29050
$Li_2Ti_3O_7$, channel-structured superionic conductor, anisotropic conductivity 80−6546
$Li_2Ti_3O_7$ growth by Bridgman-Stockbarger technique 80−25548
$Li_2Ti_3O_7$, Li^+ ion conductor, X-ray cryst. struct. determ. 79−46604
$Li_2Ti_3O_7$, NMR data for new ionic hopping rate prefactor expression, superionic conductor 78−47559
$Li_2Ti_3O_7$, NMR data for new ionic hopping rate prefactor expression, superionic conductors 78−47560
$Li_2Ti_3O_7$, superionic cond., ionic cond. and NMR line narrowing 79−42306
$Li_2Ti_4O_9$, preparation, cryst. struct. determ. 78−75646
$Li_{2.6}Ti_xO_4$, superconducting, upper critical field, paramag. limiting effects 77−8251
$LiTiS_2$, intercalation complex, band struct., tight-binding calc. 79−95323
$Li_{1-y}Ti_{1+y}S_2$, intercalation chemistry and electrochemical energy storage 79−100541
Li_xTiS_2, ($0 \leq x \leq 3$), intercalation in TiS_2, possible electrochem. cathode 80−19772
Li_xTiS_2, alkali ion ordering, X-ray study 80−107165
Li_xTiS_2, electrochemically intercalated, ion ordering, X-ray diffr. meas. 80−44177
Li_xTiS_2 electrodes, thermodynamic and transport props. 80−66963
Li_xTiS_2, intercalation cpd., Li ordering, electrochem. obs. 78−59795
Li_xTiS_2, Li ordering in intercalation battery, theory 79−77580
Li_xTiS_2, struct. determ. by neutron diffraction 80−54196
LiTiZn ferrites, elec. resist., mag. props., effect of Bi addition 78−95474
LiTiZn microwave ferrites, effects of Mn and Bi additives, expt. *(German)* 77−28411
$LiTmF_4$, ^{169}Tm NMR spectrum, hyperfine field parameters, and cryst. field calcs. 77−12213
$LiTmF_4$, local mag. field at ^{19}F rel. to paramag. susceptibility, NMR meas. *(Russian)* 77−81023
$LiTmF_4$, spectroscopic anal., Tm^{3+} absorpt. spectra, cryst. field parameters 79−95757
$LiTmF_4$, spin density parameters at ^{19}F nuclei 78−68001
$LiTmF_4$, strongly isotropic Van Vleck paramag., nucl. spin interaction *(Russian)* 80−34792
$LiTmF_4$, Van Vleck paramag., mag. reson. on uniaxial and uniform compression *(Russian)* 79−61243
$LiTmF_4$ Van Vleck paramagnet, electron and nuclear spin-lattice relaxation of Er^{3+} ions 79−95643
$LiTmF_4$, van-Vleck paramagnet, giant magnetostriction *(Russian)* 80−103872
$LiTmF_4$:rare earth, EPR spectra, elec. field effects, cryst. field interactions 80−71176
$LiTuO_3$, light scatt. from ferroelec. domains 78−80310
$LiUF_5$, LiU_4F_{17}, flux growth 77−85919
$LiUO_3$, EPR and mag. susceptibility, temp. depend. 79−33451
Li_2UO_4, cryst. struct., X-ray diffr. obs. 78−34485
Li_2UO_4, energy transfer, cryst. struct. and chemical composition effect 80−108248
Li_4UO_5, energy transfer, cryst. struct. and chemical composition effect 80−108248
$Li_2UO_2Cl_4$ melts and mixtures, thermogravimetric determ. of uranyl cation state 80−101050
$Li_xUO_2F_2$, $0 \leq x \leq 2$, use in electrochemical batteries 80−50858
$Li_xV_{1-y}Fe_yS_2$, intercalated battery cathode material, Mossbauer studies 80−44984
$LiVO_3$, cryst. struct. 78−6043
$LiVO_3$:Cr^{5+}, study of ESR spectra 80−80601
LiV_2O_5, needle cryst. form. by reduction of molten Li_2O-V_2O_5, semicond. props. *(Japanese)* 78−3030
β-$Li_{0.27}V_2O_5$, heat of form. and sp. ht., 450 to 900K 80−61129
Li_3VO_4, enthalpy of formation 79−99333
Li_3VO_4:CrO_4^{3-}, EPR, 4.2K, cryst. field parameters 79−28586
$Li_xV_{12}O_{30}$, oxygen bronze synthesis and thermal props of single crysts. 77−84717
$Li_xV_2O_5$ ($0.1 < x < 1.0$), phase relationship in ambient temperature system 80−20912
β-$Li_xV_2O_5$ bronze, thermodynamics of ordering 80−84302
$Li_xV_2O_5$, catalytic behaviour in decomp. of isopropanol, 186-300°C 78−11553
β-$Li_xV_2O_{5-y}$ bronzes, thermodynamic props. by coulometric titration 80−34209
$Li_{0.8}VOCl$, magnetic, optical and electrical props. 79−95402
$LiVS_2$, intercalation cpd., NMR 77−90048
$Li_2VS_2(Se_2)$ based topochemical cells, low voltage behaviour 79−92069
Li_xVSe_2, intercalation cpds., electron chem., ionicity 80−89501
$Li_{0.33}WO_3$, supercond. and special phonons, neutron scatt. obs. 80−15643
Li_2WO_4, high press. modifications, IR spectra *(German)* 78−23459
Li_2WO_4, liq. mixture, mixing enthalpy with WO_3 at 801, 950°C 79−10949
Li_2WO_4-WO_3, phase relns. 77−48407
Li_3WO_4:U^{6+}, luminescence meas. 77−32432
Li_4WO_5, IR, Raman, luminesc. spectra meas., cryst. struct. investig. 77−52074
Li_4WO_5:U^{6+}, vib. fine struct. in luminesc. spectra 77−8620
Li_xWO_2/Li_yTiS_2 cyclable organic electrolyte cell, using 2 intercalation electrodes 80−76625
Li_xWO_3, atom motion 78−75874
lithium compounds continued
Li_xWO_3, band struct., XPS meas. 77−59667
Li_xWO_3, electrochem. and chem. Li incorporation, cryst. struct. 80−88131
Li_xWO_3, electrochromic characteristics 78−6653
Li_xWO_3, electrochromism, potentiostatic and galvanostatic meas. 78−43835
Li_xWO_3, Vegard relationships, lattice parameter versus composition, X-ray and chem. anal. 79−23582
Li_2WO_4(IV), cryst. struct. rel. to wolframite-type struct. 80−92505
$Li_x(WO)_4W_{30}O_{90}$, struct. and ionic cond. 79−65246
Li_2W0_4, type II polymorph. crys. struct. determ. 80−15073
LiX,(X=F,Cl,Br,I), UPS, expt. methodology aspects 77−90245
LiX-alcohol mixtures, (X=Cl, Br, ClO_4), OH(OD) vibr. bands in sat. solns. and crysts. 77−8564
$LiY_{1-x}Er_xF_4$, structure, constitution and melting behaviour 77−39665
$LiY_{0.416}Er_{0.5}Tm_{0.067}Ho_{0.017}F_4$, Stockbarger single cryst., charact. of solidification behaviour 77−24948
$LiYF_4$, chem. laser window material 77−46769
$LiYF_4$, ESR spectra of non Kramers ions, elec. field influence 80−103884
$LiYF_4$, elastic consts. and acoustic symm. 80−15182
$LiYF_4$, electron-irrad. induced defects, optical and EPR study, impurity effects 80−66238
$LiYF_4$, prep. and crystal grwoth for laser appls. 77−55879
$LiYF_4$ UV reflectance, transmission and photoluminescence obs. 79−15488
$LiYF_4$, UV window and coating materials, two-photon absorpt. coeffs. 79−59734
$LiYF_4$:Ce, tunable UV laser at 325, 309 nm, KrF laser excitation 80−38022
$LiYF_4$:Ce^{3+}, UV laser at 325 nm, stimulated emission obs. 79−72574
$LiYF_4$:Dy^{3+}, spectrum, Stark struct. 77−85756
$LiYF_4$:Dy^{3+}(Yb^{3+})(Er^{3+}), ESR, nonlinear effect of elec. field 80−2635
$LiYF_4$:Er^{3+}, ESR spectrum, higher order Zeeman effects 79−99766
$LiYF_4$:Er^{3+}, magnetocaloric behaviour, cryst. field theory 77−4520
$LiYF_4$:Ho, 750 nm laser oscill., flashlamp and dye laser pumping 78−9386
$LiYF_4$:Ho laser, TEM_{00} mode and Q-switched operation 80−74395
$LiYF_4$:Ho^{3+}, optical absorpt. and luminesc. spectra 79−4844
$LiYF_4$:Nd^{3+}, pulsed free running laser action at 1053, 1046 nm, passive mode locking *(French)* 78−79048
$LiYF_4$:Nd^{3+}(Er^{3+})(Tm^{3+}), VUV fluorescence and tunable coherent sources from 1650 to 2600 Å 77−688
$LiYF_4$:Nd^{3+}(Er^{3+})(Tm^{3+}), vacuum UV excitation studies 78−80381
$LiYF_4$:Pr, NMR meas. of hyperfine const. of Pr^{3+} excited state 80−88895
$LiYF_4$:Pr^{3+}, laser, blue light emission, room temp. operation 77−38899
$LiYF_4$:Pr^{3+}, mag.-dipole transitions obs. in fluoresc. 80−11451
$LiYF_4$:Pr^{3+}, polarized absorpt. and fluoresc. spectra, 10 to 300K, energy levels and live intensities 79−95836
$LiYF_4$:Pr^{3+}, spectroscopic determ. of ground config. energy levels 80−34969
$LiYF_4$:rare earth, EPR spectra, elec. field effects, cryst. field interactions 80−71176
$LiYF_4$:Tm_3 XeF pumped, excimer excited storage laser 80−33003
$LiYF_4$:Tm^{3+}, cryst. field parameters, appls. 77−20277
$LiYF_4$:Tm^{3+}, vacuum-UV excitation spectra 78−80381
$LiYF_4$:Yb^{3+} Ho^{3+}, sensitised anti-Stokes luminesc., theory 77−66537
$LiYF_4$-HO^{3+}, 1.392, 1.673 and 3.914 μm stimulated emission, laser cascades 80−9886
$LiYFd_4$:Er^{3+}, optical spectra and multifreq. stimulated emission 79−56818
$LiY(MoO_4)_2$, X-ray cryst. struct. determ. 80−107124
$LiYO_2$:Nd^{3+}, absorption and luminesc. spectra, energy level diagram 77−63441
$LiYSiO_4$, cryst. struct. determ. 77−58997
$LiY_{1-x}Tb_xP_4O_{12}$, and $LiY_{1-x}Eu_xP_4O_{12}$ phosphors, prep. and fluoresc. 77−48219
$Li_6Yb(BO_3)_3$, cryst. struct. determ. 78−18621
LiYbF:Ho^{3+}, active medium for Nd laser freq. convertor, cascade stimulated emission 80−102727
$LiYbF_4$:Ho^{3+}, laser converter for 2.06 μm radiation, Nd primary laser 79−18427
LiZn ferrite, dielec. const. and loss meas., 50-10^6 Hz 77−77135
LiZn ferrite, Mossbauer study, relax. and supertransferred hyperfine fields 80−39941
LiZn ferrospinel, sequence of mag. transforms. *(Russian)* 78−19252
LiZn ferrospinels, mol. field. coeff. conc. depend. 80−97114
LiZn, substituted ferrite, cation distribution, Mossbauer, X-ray, neutron diffr. study 80−28975
Li_2ZnCl_4, conc. aq. solns., ionic hydration and secondary dielec. relax. 79−24882
$Li_{0.2}Zn_{0.6}Fe_{2.2}O_4$, ferrite, mag. ordering at low temp. *(Russian)* 77−32171
$Li_{0.44}Zn_{0.09}Fe_{2.47}O_4$, ordering, elect. of V_2O_5 additions 77−35532
$Li_{0.5-z/2}Zn_xFe_{2.5-z/2}O_4$, field magnetisation and susceptibility 79−82762
$Li_{0.5(1-x)}Zn_xFe_{2.5-0.5x}O_4$, cryst. struct., neutron and X-ray diffr. obs. *(Russian)* 77−31645
$Li_{0.5(1-x)}Zn_xFe_{2.5-0.5x}O_4$, canted spin struct., neutron diffr. study 78−68175
Li_2ZnGe, single cryst. growth, by normal freezing method, X-ray diffr. study 79−28908
$Li_{12}Zn_2(GeO_4)_4$ LISICON system, Li ionic conductivity *(Chinese)* 80−88350
$Li_{14}Zn(GeO_4)_4$, crystal struct. and ionic conductivity 78−51728
$Li_{14}Zn(GeO_4)_4$, LISICON, AC meas. of ionic cond., 298 to 573K 80−107526
$Li_{16-2x}Zn_x(GeO_4)_4$, $0 < x < 4$, synthesis, structure and resistivity 78−18831
$Li_4Zn(GeO_4)_4$, ionic cond. 79−55922
$Li_4Zn(PO_4)_2$, cryst. struct. determ. 77−15386
$Li_{16-2x}Zn_x(SiO_4)_4$, $0 < x < 4$, synthesis, structure and resistivity 78−18831
γ_{II}-Li_2ZnSiO_4, flux growth *(Japanese)* 79−95917
Li_2ZnSiO_4, tetahedral struct., polymorphic α-β transform. kinetic obs. and method 79−90778
γ_{II}-Li_2ZnSiO_4, X-ray cryst. struct. determ. 80−15061
$Li_{14}ZnTa_4O_{18}$:Eu, fluorescence and cryst. symm. 77−24886
$LiZnVO_4$, high press. spinel modification, vibr. spectra 78−35124

lithium compounds continued
$LiZnVO_4$, luminesc. spectra in visible region, vanadate group, and high-press. phase 78−43921
$LiZn[BO_3]$, X-ray cryst. struct. determ. 79−42034
$Li_2Zr(MoO_4)_3$, X-ray cryst. struct. determ. 80−88125
Li_2ZrO_3, thermal decomposition, enthalpy of formation 298.15K 78−61003
Li_4ZrO_4, thermal decomposition, enthalpy of formation 298.15K 78−61003
Li_8ZrO_6, thermal decomposition, enthalpy of formation 298.15K 78−61003
$Li_{1-x}Zr_{2-x}Ta_x(PO_4)_3$, new solid ionic conductors 77−35953
^6LiD, polarised target material, DNP 80−87007
^6LiD sphere, T prod. under 14 MeV neutron irradiation 79−59254
^6LiH shielding for NaI gamma spectrometer, neutron background reduction 78−90012
$^7Li_2O$, β-radiation detected NMR of ^8Li obs., double freq. irradiation, $^{7,8}Li$ hyperfine struct. anomaly 78−91994
$^7Li_2S$, β-radiation detected NMR of ^8Li obs. double freq. irradiation, $^{7,8}Li$ hyperfine struct. anomaly 78−91994
^7LiF, TLD, supralinearity meas. using ^{60}Co source 78−82534
^7LiH, radiative lifetimes for vibr. levels of $B^1\Pi$ state 78−78753
^8Li, in $LiTaO_3$, multiple quantum NMR transitions obs., quadrupole moment determ. 77−73090
$Li_3[B_3O_8(OH)_2]$, interplanar distances atomic coordinates, temp. corrections 79−82192
$Li[Mn_2]O_4$ spinels, crystallographic, electronic and mag. props. *(German)* 79−60324
$Li[Ni_{0.5}Mn_{1.5}]O_4$, magnetisation and magnetostriction, fields up to 11 kOe, 4-160K *(Russian)* 78−19304
$Li_2[Pt(CN)_4].3H_2O$, DC elec. cond. props. 79−51582
$LifaO_3$, optical waveguides, elimination of Li_2O out-diffusion waveguide 77−65641
$LinBO_2$, adjacent to thermally oxidised Si, SAW attenuation obs. of semicond. surface props. 79−87131
lithium ammonium tartrate monohydrate ferroelastic phase transition *(Japanese)* 79−77747
$LixTiS_2$, mechanism of Li intercalation, optical and X-ray studies 79−100394
MgF_2:LiF crystal, defect struct., anelastic and dielec. relax. meas. 77−27938
$Mg(NO_3)_2$-RNO_3 (R=Li, Na, K), thermogravimetric anal. of dehydration processes *(Japanese)* 80−66791
MgO:LiF, accretive recrystallisation during hot pressing 77−36421
MgO-LiCl, solution under hydrothermal conditions, exam. of phase equilibria 79−8292
MnF_2:LiF, anelastic relax. of Li^+-Li^+ split interstitial defect 79−77678
NH_3-lithium halide complex, ab initio calcs., Li bond rel. to H bond 77−14343
$NH_4^+ + LiH(H^-)$, substitution and abstraction reactions, ab initio calcs. 77−48624
NH_4LiSO_4, ferroelec., PMR line shape and spin-lattice relax. 78−88205
NH_4LiSO_4, high press. phase, point group symmetry 79−51039
NH_4LiSO_4, I-II phase transition in improper ferroelec., hydrostatic press. effects 78−84533
NH_4NO_3-$LiNO_3$-NH_4Cl-water system, cond. and viscosity *(French)* 79−51286
$(Na,Li)NbO_3$, ceramics, electrophys. and struct. props. near morphotropic transition 78−2816
$(Na,Li)NbO_3$ ceramic, optimum prep. conditions and characterisation 78−3079
Na_3AlF_6-LiF-CaF_2-AlF_3-Al_2O_3, electrolyte, exam. of phase equilibria, review 79−11590
$NaBF_4$-$LiBF_4$(LiF), phase diagram 77−21119
NaCl:LiCl, melt, semiperiodic closed growth lamellae on crystal-melt interface 78−67668
NaF:LiF, γ-irrad., colour centre form., reflectance and thermolum. meas. 79−55739
NaI-LiI, phase diagram 77−21119
$Na_{5-x}Li_xErSi_4O_{12}$, solid electrolytes for Na/TiS_2 cells, synthesis, characts. and utilisation 80−107518
$Na_{1-x}Li_xNbO_3$, dielec. const. and X-ray diffr., for Curie temp. and phase diagrams 78−72768
$Na_{1-x}Li_xNbO_3$ mixture, ferroelec.-paraelec. transitions, dielec. props. meas. 80−66125
$NaLiSO_4$, anhydrous, struct. relationships w.r.t. fast ion cond. 80−107188
$Na_{2-x}Li_xSiO_3$, long-period superstructure 77−55269
$NaLiZrSi_6O_{15}$, zektzerite, silicate mineral with six-tetrahedral-repeat double chains 78−63719
Na_2O-Li_2O-Al_2O_3, local electrode current density and flow decoration 80−100935
Na_2O-Li_2O-NiO-Fe_2O_3-B_2O_3-SiO_2 glasses, thermally stimulated cond. studies of trapping centres 79−78113
Na_2O-Li_2O-β-$Al_2O_3.H_2O$, water mol. vibrs., IR and Raman spectra 80−89006
$Na_2O.Li_2O.Al_2O_3$, comp. and props. for use in Na-S battery 79−87745
Ni-ferrite powders, form. in presence of Li_2SO_4-Na_2SO_4 molten salts, prep. and characts. 80−84869
$Ni_{1-x}Li_xO$, $0.01 \leq x \leq 0.08$, mag. susceptibility in region 80 to 800K *(Russian)* 78−2664
NiO and lithiated NiO, thermally grown, electrochemical capacitance variations 80−29475
NiO:Li_2O-ZnO p-n heterojunction, contact resist., effects of water vapour 80−34506
$Pb_{2-x}Ba_xLi_{0.5}Nb_{1.5}O_6$, elec. resistivity, Curie temp., x=0-0.15, 50-350°C 78−2478
$PbLi(PO_3)_3$, cryst. struct. determ. *(French)* 77−80463
PbO-B_2O_3-Li_2O melt, activity of PbO 77−11708
PbO-B_2O_3-SiO_2-Li_2O-ZrO_2-CdO(CoO)(CuO), glass enamel, chemical durability, microstruct., CuO, CdO and CoO addition effects 79−29256
PbO-B_2O_3-SiO_2-Li_2O-MgO(CaO)(ZnO)(Al_2O_3)(TiO_2)(ZrO_2), glass enamel, heat treated, chemical durability, MgO, CaO, ZnO, Al_2O_3, TiO_2, ZrO_2 addition effects 79−29255
$RbIO_3.2LiIO_3$, crystal struct. refinement, Li atom localisation in I atom presence, cell parameters 79−77585
$Rb_2LiMO_xF_{6-x}$, M=Nb or Mo, high press. transforms. *(German)* 77−89400
$RbLiSO_4$, field induced ferroelec. phase 79−78633
$RbLiSO_4$, successive struct. transitions, X-ray diffr. 80−10521
$RbLiSO_4$, thermal and dielectric props., ferrielectricity 79−28688
lithium compounds continued
Rb_2O-Li_2O-P_2O_5 glasses, Raman and far IR spectra, vib. at cation site, struct. 78−60435
SiO_2-Al_2O_3-B_2O_3 $LiO_2.Na_2O$, exam. of optical props. 78−88277
SiO_2-Al_2O_3-B_2O_3-LiO_2, exam. of optical props. 78−88277
SiO_2-Al_2O_3-Li_2O glass ceramic, crystn., microstructures rel. to conditions 80−11638
SiO_2-Al_2O_3-Li_2O:$TiO_2(ZrO_2)$,Fe_2O_3, pyroceramic glass, coloration, absorpt. spectra obs. 77−8615
SiO_2-B_2O_3-Li_2O-Al_2O_3 (28, 2, 1 wt.%) glass, dielec. const. at 3 GHz 80−93233
SiO_2-Li_2O, glass, layers near surface, anal. using SIMS 80−88041
SiO_2-Li_2O, phase separation detection 77−1890
SiO_2-Li_2O glass, bonding of Si-O exam. by X-ray emission spectra 78−52594
SiO_2-Li_2O-Al_2O_3-K_2O:Ag_2O(-CeO_4) (-Sb_2O_3), surface resist. meas. 80−44700
SiO_2-Li_2O-K_2O-ZnO-P_2O_5, glass ceramic, phase changes and crystn. processes 80−7562
SiO_2-Li_2O-K_2O-ZnO glass ceramic, prep., phase transformations and physical props. 80−45299
SiO_2-Li_2O-Li_2SO_4, glass-forming region, struct. and ionic cond. 80−84320
SiO_2-LiO_2-Al_2O_3 glass, luminesc., polarisation degree distrib. 80−108257
SiO_2-$LiTaO_3$ structure, SAW propag. characts., thermal strain effects 79−19440
SiO_2-RO-Na_2O-Li_2O (RO=MgO, CaO, SrO) glass-ceramic coating, optimisation of props. by selective oxide action 80−55552
SiO_2-ZnO-Na_2O-Li_2O, glass-ceramic coating, optimisation of props. by selective oxide action 80−55552
SiO_2-ZrO_2-Al_2O_3-CaO-Na_2O-K_2O-Li_2O, chemical resistant glass for glass fibres 80−21128
SiO_2-ZrO_2-Li_2O-Na_2O based crystallisable glasses composition and properties 80−50731
$SnCl_2$-$AlkAlCl_4$ melts (Alk=Li, Na or Cs) 79−99874
$Sn_{2.8}Li_{1.6}Mg_{1.6}O_8$, four layer close packing, cryst. struct. determ. *(French)* 80−28999
$Sn_{2.8}Li_{1.6}Sn_{1.6}O_8$, four layer hexagonal close packing, cryst. struct. determ. *(French)* 80−28999
Sr_2LiReO_6, new seignettomagnets and ferroelectrics 78−19425
$Sr_4NaLiNb_{10}O_{30}$, electro-optic, pyroelec., dielec. and piezoelec. props. *(Chinese)* 79−69810
$Sr_4NaLiNb_{10}O_{30}$, single cryst. growth, Czochralski method *(Chinese)* 79−74078
SrO-Li_2O-Al_2O_3-SiO_2:Tb^{3+} glass, energy transfer, luminesc. efficiency under UV, neutron and charged-particle excitation 79−95822
TeO_2-Li_2O glass:Nd^{3+}, highly doped, spectroscopic props. and CW laser action *(French)* 79−41385
TeO_2-V_2O_5-Li_2O, glass, IR spectra of crystalline phases 79−38536
$TlNO_3$-$LiNO_3$(KNO_3) mixtures, molten, surface tension, regular solution theory 78−71903
V_2O_5-Fe_2O_3-Li_2O ternary system, charge compensation of Fe ions, Mossbauer obs. 78−52410
WO_3-LiF, electrochromic display struct., efficiency and humidity depend. 79−81540
WO_3-LiF, glass film compositions, electrochromism *(Russian)* 79−28721
WO_3-LiF system, on glass substrate, electrochromism of glass film compositions 80−29720
$YLiF_4$:rare earth, spin-lattice relax. and nuclear polarisation *(Russian)* 79−8049
Zn-Li silicates, cryst. struct. and phase transform. 79−65036
$ZnCl_2$-LiCl, molten, density meas. *(Japanese)* 79−19383
$ZnCl_2$-LiCl, molten, viscosity, 260 to 560°C *(Japanese)* 77−51537
$ZnCl_2$-LiCl fused mixture, transport number determ. of Li^+ and Zn^{++} at 398°C *(French)* 79−69286
$ZnCl_2$-LiCl melt, viscosity meas. by oscillating cylinder method *(Japanese)* 80−10696

lithospace *see Earth crust*

lithosphere *see Earth crust*

liver
125 I-TAN excretion and liver visualisation in the rat 77−56456
acoustic attenuation coefficient slope for liver tissue, statistical estimation from refl. US signals 80−46000
acoustic attenuation slope for in vitro liver samples, spatial correl. props. 79−57702
acoustic parameters of freshly excised tissues of Sprague Dawley rats, freq. depend. 77−86573
alcohol dehydrogenases, yeast and horse-liver, composition differences 78−40116
amino acid transport in γ-irrad. rats, hormonal control 78−65099
amino acids, induced transport in rat liver after whole-body γ irradiation 77−9232
angiographic methods for the diagnosis and therapy of liver diseases *(German)* 80−56211
artificial kidney and liver, wearable, fundamental studies, long-term blood filtration efficiency of nuclepore membrane filter with pore-size of 0.6 mu 79−44051
artificial liver support, affinity chromatography systems 78−7538
artificial liver support, detoxifying enzymes bound to artificial carrier for extracorporeal appl. 79−25160
artificial liver support, equilibrium props. of removal of protein-bound substances 79−20709
artificial liver support, physico-chemical aspects of removal of protein-bound substances 79−20710
beta irradiation effects from tritiated water, mouse 79−57719
bile acid hepatobilary kinetics, compartmental model validity 80−30971
biliary ductal system, status demonstating ability of ultrasonography and computerised tomography 79−92310
blood effective flow meas. by fractional clearance of ^{198}Au-colloids 79−66547
bovine, metals determ., in water and organic materials, flameless atomic absorpt. spectrometry with wire loop atomiser 80−45586
bovine, PIXE and neutron activation anal. 80−56199
cancer therapy, appl. of ^{90}Y 80−17098
carcinoma, VX2, improved detectability in the rabbit with contrast enhancement in computerised tomography 80−98118
cattle, concs. of ^{210}Pb and ^{210}Po 80−30904
cell contacts and surface, effect of raised osmotic press. 77−56354
cell nuclei structural change in the physiological pH interval 79−79492

liver continued
cell proliferation and failure of X-radiation to produce hepatomas in rats 79−25050
cells of regenerating liver, specific resistance and electrophoretic mobility 77−25402
cellular survival after single and fractionated exposures to UV light 77−56439
cirrhosis, nuclear medicine, evaluation of 1D profile scans with a whole body counter 80−51213
cirrhosis detection, accuracy of US diagnosis 80−30802
computed tomography of liver, comparison with nucl. medicine scans 80−17109
computed tomography of liver and biliary tract 80−17108
computer aid for diagnosing pancreatic, hepatic and gastric diseases by pancreatic function test 77−4611
computer-aided diagnosis of liver disease using nonlinear stochastic modeling techniques 78−36024
computerised tomography rel. to radionuclide imaging and grey scale US 77−52864
cytochromes, conc. in the liver at different stages of adaptation to cold 79−62196
DC excitation of the liver cell 77−56565
DNA dynamics, single-clipped photon correl. obs., mouse 77−48748
drug action, intermittent, mathematical model 77−2983
drug-metabolising enzymes, rel. to circulating hormones after whole- and partial-body irrad. 78−48840
echohepatograms in children, computer analysis 79−57728
echotomographic aspects of structs. of intrahepatic vessels and ducts 77−90868
electrogenesis and Ca balance obs., rate 79−57608
electron microscopic anal. of liver acinus, double embedding technique 80−3885
electron microscopic diagnosis using clinical pathology liver and kidney samples, computer assisted 80−85485
EPR spectral anal., γ-irradiated liver and hepatoma samples 79−92289
fat content assessment by photon scattering technique 78−24124
free radical centres, appearance in mouse liver tissue on low temp. oxidation 78−69013
functional reserve capacity meas. by organ-reflectance spectrometry *(Japanese)* 80−94313
gamma camera and computer technique for absolute meas. of radioactivity 79−25087
gamma camera scans, clinical evaluation of computer processing 79−29579
gamma irradiated rats, simulatable liver transport system 78−65098
gamma irradiation, struct. rel. to functional alterations of UDPG-dehydrogenase 78−15873
gamma-camera images, improvement using physiological gating mechanism 80−98065
giant cell formation after ^{45}Ca administration, desert gerbil 79−92299
glycoproteins extraction during tissue preparation for electron microscopy 79−25167
growth protein metabolism and turnover, radiotracer obs. 79−88062
hepatecomy partial, using a high power ND-YAG-laser *(German)* 77−44734
hepatic assist improved hemoperfusion sorbents and plasma filtration system 78−48939
hepatic elimination, statistical mechanics 79−96503
hepatic lesions, improvement in visualisation with upright views 78−24129
hepatic mass evaluation, relationship of ultrasonography, nuclear medicine and computerised tomography 80−17092
hepatitis-BS antigen antibody, quantitative radioimmunoassay 77−13036
hepatobiliary agent ^{99M}Tc-pyrodixal leucine, pharmokinetic and imaging studies 79−29597
hepatobiliary disorder scintiscanning, evaluation of ^{131}I labelled ioglycamic acid 80−36072
hepatobiliary dynamic flow study using technetium-99M p-isopropylacetanilidoiminodiactic acid-tin 79−53217
hepatobiliary functional scintillation recording, review *(German)* 80−30874
hepatobiliary imaging, clinical evaluation of ^{99m}Tc-(p-butyl) iminodiacetic acid *(Japanese)* 80−67236
hepatobiliary imaging, evaluation of ^{99M}Tc pyridoxal-phenylalanine, studies expt. 78−31893
hepatobiliary imaging, evaluation of ^{99M}Tc pyridoxal-phenylalanine clinical tests 78−31894
hepatobiliary imaging, use of ^{99M}Tc-pyridoxylidene glutamate scanning in jaundiced adults and infants 79−5339
hepatobiliary imaging agent assessment, importance of uptake and retention indices 79−83911
hepatobiliary imaging agents in rats, pharmocokinetics 79−79637
hepatobiliary scintigraphy, characts. of ^{99m}Tc-E-HIDA *(Japanese)* 80−81729
hepatobiliary study of liver-transplant patients, ^{99m}Tc diethyl-iminodiacetic acid rel. to ^{131}I rose bengal 80−3793
hepatocellular disease diagnosis, computer quantification of spleen/liver ratio 79−83909
hepatocytes, adhesive strength of ultrastructural elements 79−57682
hepatoma, dog, evaluation of 3 imaging instruments 80−17074
histopathological information obtained from US tissue signatures and microscopy of biopsy samples 80−51195
image analysis of rat liver histological sections 77−4649
imaging, comparison of scintigraphy, US and computerised tomography scanning 80−17105
intracellular membrane microviscosity, rat liver and hepatoma 27 80−30675
intrahepatic lithiasis detection, sequential scintiphotography with ^{99m}Tc pyridoxylideneglutamate 80−72309
ion movements during energy-linked mitochondrial structural changes, rat 80−12065
laser irradiated white rats, temp. changes dynamics 79−57594
laser surgery actual state 77−40729
leveen shunt, technique for testing shunt patency 79−57763
magnetic susceptibility measurement, living rats 80−72391
mass estimation from γ-camera images, computer assisted method 79−83908
membrane, potential, in situ, effect of speed of liquid flow 78−48772
membrane alternations after X-irrad., normal and vitamin E deficient ducklings 80−41139
membrane protein-lipid complexes, spatial organisation obs. 79−70529
liver continued
membranes, mouse, X-irrad., dose-rate effects 80−94293
metastases, γ-scan accuracy for detect., comparative study with grey scale ultrasonography *(French)* 80−104741
metastases diagnosis, conf., Brussels, Belgium (Nov.-Dec. 78) 80−82568
Micro-Videomat, use in light microscopic liver diagnosis 77−78013
microsomes, γ-induced lipid peroxidation and membrane-bound enzymes 80−104660
mitochondria, isolated, SEM obs. 79−34516
mitochondria in bilayer lipid membranes, Ca^{2+} transport system study 78−64966
mitochondria interaction with some cationic dyes, spectroscopic study 77−52752
mitochondrial, Ca^{2+} transport, effect of cations on temp. sensitivity 78−11621
mitochondrial membrane, outer, candidate for the permeability pathway 79−74602
mitochondrial protein synthesis in rat liver, radiation-induced alterations 78−80925
molecular replacement method, a new translation function 77−19820
Mossbauer spectrometry of Fe in hepatic and splenic tissues 80−81544
motion corrected hepatic scintigraphy, objective clinical evaluation 78−65111
neonatal jaundice detection, serum bilirubin conc. rel. to skin reflectance 79−92328
neutron activation analysis, bovine liver matrix 78−28050
NMR observations, pulsed, spin-lattice relax. values 80−94171
NMR of rat liver homogenate ^{23}Na, effects of alkali cations 77−12893
NMR relaxation behaviour in living and ischemically damaged tissue 77−12895
Novikoff hepatoma ascites cells, irrad. effects, dose-response obs. 78−3560
Novikoff hepatoma ascites cells, irrad. effects 78−7389
nuclear imaging, comparison of conventional rectilinear and multiplane tomographic scanning 80−17106
nuclear medicine, dynamic studies with ^{99m}Tc labelled S colloid, processing 80−41169
nuclear medicine, respiratory motion in supine and upright positions 80−30858
nuclear medicine conference, Karlovy Vary, Czechoslovakia (May, 1979) 80−12840
nuclear medicine studies, automated interpretation 80−8164
nuclear resonant scattering, new technique for in vivo meas. of hepatic Cu 77−9245
nuclear-medical diagnosis, the use of ^{123}I *(German)* 78−28061
paramagnetic properties of liver tissues and transplantable hepatomas 77−86459
parenchyma, expt. rheology *(German)* 78−7377
pathology characterisation, clinical appl. of a US attenuation coeff. estimation technique 80−76813
pattern recognition techniques, appl. to discrete clinical data 77−5738
percutaneous transhepatic cholangiography and endoscopic retrograde cholangiopancreaticography 79−92333
perfusion, normal and partially hepatectomized rat, in vivo meas. using ^{99m}Tc S colloid 79−79636
physiological compartment tracer flow modelling and digital imaging 80−101257
pictorial pattern recognition applied to morphometric cytology 79−25179
PIXE analysis of human blood and liver tissue for Cu, Zn and Fe 79−53291
PIXE application to trace element analy. 77−48975
PMR relaxation, effect of Fe content 79−39355
polyribosome distribution in regenerating livers of irradiated adrenalectomised rats 78−7398
porta hepatis irradiation 79−20661
proton spin-lattice relaxation time study, adult newt tissues 79−20515
radiation injury leading to interphase cell death in rat liver, in vivo repair 77−52850
radiation response by experimental tumours with markedly different growth charact. 78−53454
radiation-induced DNA breaks rejoining capacity obs. in senescent mice 78−69148
radiocolloid liver images polar reference texture 78−73241
radioimmunoassay for carcinoembryonic antigen as adjunct to radioisotope scan 79−100720
radioisotope clearance, automatic meas. 79−34644
radioisotope scanning agents, comparison of ^{113m}In-phytate, ^{99m}Tc-phytate and ^{113m}In-colloid 79−96650
radionuclide imaging, computer tomography, and gray-scale ultrasonography of the liver 77−52864
RBE of cyclotron fast neutrons and γ-rays for late hepatic injury in rats 80−108975
retention of $^{237}Pu+^{239}Pu$ in mature beagles 78−96095
RNA, messenger, synthesis in rat livers, ionising radiation and partial hepatectomy effects 79−92144
scintiangiography, technical aspects 78−20259
scintigraphy, intercomparison of computer assisted image processing and display methods 79−53234
scintigraphy, optimisation of analogue-circuit motion correct. 79−39472
scintigraphy, pattern recognition 80−8157
scintiphotography, clinical value optimisation 79−88169
signal processing of broadband pulsed US meas. of attenuation of soft tissues 78−77094
sorbent perfusion systems, characterisation of solute removal 78−44689
spleen and liver colloid take up ratio in diagnosis and treatment of diffuse hepatic disease 80−41203
steatosis, ^{133}Xe retention rel. to biopsy 80−17069
stochastic ESR analysis of rat liver and hepatoma mitochondrial lipids 78−76984
subtraction scintigraphy with ^{67}Ga-citrate and ^{99m}Tc-colloid in the diagnosis of intrahepatic masses 80−104752
tissue characterisation using reflected US signals, variance reduction 79−48307
tissue constituents, EPR absorpt. obs. 77−90727
tissues and cell nuclei, cooperative charact. of the denaturing process 79−57593
transcapillary exchange and solute removal by the liver, distributed model, self-similar soln. 79−34524
tritiated water, effects on mouse liver rel. to age 79−43967
tumour regrowth after irradiation in rat hepatoma 79−92292
US and hepatic metastases 78−73179

liver continued
US backscatter from human tissue, depend. of freq. and protein/lipid content 80−45960
US diffraction analysis in the investigation of liver desease 80−30803
US in the detection of chronic liver disease 79−48295
US local lesions in rabbit kidney, liver, and testicle, threshold obs. 77−81527
US propagation speed distrib. in soft tissue, reconstruct. 77−48850
US reflected signals, estimating acoustic attenuation coeff. slope 80−5876
US scattering, quantitative meas. 80−45959
US scattering from tissues 79−48310
US scattering struct., theoretical modelling 80−89785
US signals in diffuse liver disease, computer anal. 80−67173
US thresholds for structural changes in the mammalian liver 79−48287
USA-scan quantitative anal. of normal and cirrhotic liver 77−64109
volume determination by US scanning 80−17034
volume measurement by emission computerised tomography 80−12230
X-irrad. induced changes in glycogen, phosphorylase and glucose-6-phosphatase activity, guinea pig 80−51173
X-irradiation effect on tyrosine aminotransferase activity circadian rhythm, mouse 80−41121
X-irradiation effect on vitamin E deficient rat liver mitochondrial ATPase and cytochrome C ocidase 79−34511
Cd conc. in kidney and liver, neutron activation anal., organ depth determ. 80−72321
Cd measurement by neutron capture γ-ray anal. 78−15885
Cd trace detection in human liver by neutron activation analysis 79−79632
Cd, transportable system for in vivo meas. 79−39496
Cs accumulation in rat livers, effects of altered thyroid states 78−24136
Fe overload, non-invasive diagnosis, SQUID appl. 80−101244
Fe stores meas. technique, nuclear resonant scatt. 79−83914
HTO, effect of continuous intake on liver chromosomes of mice 77−25518
I images isolated, using spatial-freq. encoding 79−39485
O_2 diffusion and chemical reaction in biological tissues 77−44615
PO_4 transport in mitochondria and submitochondrial particles 78−27913
^{31}P NMR studies of isolated rat liver cells 78−61150
T content in organs, and DNA of rat liver cells, after doses of tritiated food, protein or water 80−56226
T radiation dose absorbed in rat organs, after feeding with organically bound T 80−51262
^{178}Ta radiopharmaceuticals for lung and liver imaging, rat expts. 80−51254
^{99M}Tc labelled diethyl-acetanilido-iminodiacetate, a new hepatobiliary agent 77−90874
^{99m}Tc-hepatobiliary agents, absorbed dose estimation 80−72330

livestock *see farming*

living systems
see also biocybernetics; brain models; extraterrestrial life; physiological models
bacteriophage φX174 DNA, possible message from extraterrestrial intelligence 79−53738
bio- and neurocybernetic models of the living being 79−53018
biophysics of living organisms communities in natural state, pollution effect 77−73503
biosphere, atmospheric effects, symposium (Mainz, Germany, 11-14 July 1977) 78−73461
biota as modulator of atmosphere 78−73517
dynamic processes on Earth, extraterrestrial causes, rel. to extinction of life 78−92820
enzyme catalyzed reactions with positive feedback, existence of stable limit stables 79−96289
heart adaptation to large loads structural changes simulation 79−5258
information processing studies, association and self-repair models *(Japanese)* 78−44443
neural net discrete model synthesis *(Russian)* 77−36910
non-chemical life-form, crystalline physiology model 77−90978
nonequilibrium linear behaviour, enzyme-mediated multidimensional inflection points 80−72122
organisation level comprehension, SYSTEMA approach *(French)* 77−9163
origin of life, review of problems 80−4111
review of ecology and systematics (book) 80−67945
self-organising, analysis, bionic aspects *(Russian)* 77−52732
stochastic and deterministic time delays in living systems 80−30636
thermodynamic and informational aspects of life, model 77−1974
C_3O_2 polymers in primitive atmosphere rel. to living systems genetic code 79−83690

load (electric)
see also load dispatching; load regulation; load shedding; power station load
MHD convertor, pulsed, limiting energy generated, load characts. depend. 78−42833
power overhead lines, current carrying capacity determ. 77−84126
pulsed, Tokamak fusion test reactor, AC distribution system 78−54963
small village solar electrification economics 79−57387

load control *see load regulation*

load dispatching
environmental dispatch simulation and emission dispersion modelling 78−32221
real-time urban power dispatch with ambient air quality constraints 79−57542

load regulation
electric utility load management, thermal storage systems appls. 80−16845
energy storage options, Na/S battery development program at GEC 80−61327
fusion reactor neutral beam injection, comparison of series and shunt regulation for power supply 77−23271
levelling, Li-FeS_2 batteries appl., ANL program with industrial participation 79−48113
off-peak power storage system, thermal, high efficiency, for utility appl. 79−48188
peak-shaving battery plants, 100 MWh, Zn-Cl_2 79−48119
power system that includes wind energy generators, model based 80−61256
pulsed MHD convertor, threshold energy characts. for elec. power production with resistive load 78−1908

load regulation continued
satellite solar cell panel monitoring by ground station telemetry 79−62003
underground pressurised saturated hot water storage for peak lopping appls. 80−76653
utility energy storage, Li-Si alloy/FeS cells appl., research and development at Atomics International 79−48115

load shedding
superconducting magnetic energy storage applic. 78−25360

lobes (distribution) *see antenna radiation patterns*

local moments in dilute systems
actinide alloy, resistivity temp. depend. due to localised spin fluctuations 77−8083
actinide elements, cpds. and alloys, mag. props., review 79−4649
actinide metallic systems, magnetism 80−7076
alloys, local moment formation, nonequivalent orbitals model 80−11164
alloys, mag. ordering of localised spins 77−1541
alloys, magnetic localisation and charge oscillations 80−75781
Anderson model, asymmetric, renormalisation-group approach, static props. 80−44802
Anderson model, ground state, var. trial function approach 80−59913
Anderson model, impurity pair interactions, local moment form., var. method 80−92854
Anderson model, symm., renormalisation-group approach, static props. 80−44801
Anderson model for dilute magnetic alloys, static suscept., functional integral approach 80−50050
conduction electron scatt. by mag. impurities, asymm. effects 77−62916
Curie-Weiss susceptibility of local moments 78−80128
de Haas-van Alphen wave shape anal., electronic props., appl. to dil. mag. alloys 78−84127
degenerate Anderson model, Fermi liq. theory 79−19715
degenerate d-electron alloys, dilute, local moment and ferromagnetic state formation 79−51748
dilute alloy, method of orthogonal operators 79−33254
disordered linear chain, exchange probability distrib., Hubbard model 78−10641
ferromagnetic alloys, disordered crystalline and amorphous, dipole field distribution 80−25101
ferromagnetism, itinerant electron theory, local moment approach, review *(Japanese)* 80−25071
ferromagnetism onset, mag. inhomogeneity 80−75774
Hubbard model, doubly degenerate, functional integral approach 79−99711
indirect exchange between local moments, cyclotron reson. effect 77−40051
itinerant electron antiferromagnetic matrix, local moments, spin Hamiltonian 80−34626
itinerant magnets, band struct., mag. props. and local moments 80−70929
itinerant to local moment magnetism transition with comp. 77−72984
Kondo coupling, hyperfine and exchange interactions 79−65647
linear conductor, localized mag. moment formation and one and two impurity sites 80−50087
local magnetisation, Kondo-like deviations from free spin behaviour 80−44800
localised states and local moments, theory, review 79−23935
localising pseudopotentials for local moments and certain virtual bound states 78−34959
low temperature nuclear orientation investigation 80−15825
magnetic alloys, dil., relaxational paramag. absorpt. of RF power *(Russian)* 79−65645
magnetic alloys, dil., transition metal hosts, props. review 78−84417
magnetic impurities and Kondo effect, theoretical model 79−33455
magnetism conference, Freudenstadt and Bad Nauheim, Germany (March and April 1978) 79−24121
metal, CESR and inhomogeneous broadening due to local moments 79−99769
metal, indirect coupling between localised mag. moments by narrow band electrons 80−70942
metal, supercond. as probe of mag. state of local moments 77−20491
metal-insulator transition and local moment-formation, spin-density functional approach 80−65451
metallic system, interaction between local moments 77−1540
metals, ESR of localised moments 80−71153
metals, indirect mag. coupling between local moments 78−52207
metals, localised mag. moment magnitudes of transition or rare earth impurity, Anderson model 80−25086
metals, localised moment interaction, Alexander-Anderson model, perturbation expansion 80−29524
metals, review of early work on Anderson model 78−72327
metals, spin and charge polarisation around mag. impurities 80−75714
metals, spin- and charge-density oscillations 77−11886
metals, with mag. impurities, kinetic exchange interaction, Curie-Weiss high temp. susceptibility 79−33457
nearly magnetic impurities in non-mag. host 78−2647
quasi-localised spin system, mag. excitations, neutron scatt. studies 80−44838
random collinear states, Gaussian internal mol. field distrib. 77−16016
rare earth metals, indirect exchange between localised moments *(Russian)* 79−87237
rare-earth impurities in s-p hosts, self-polarization hyperfine fields 79−33456
semiconductor, doped, indirect interactions between localised mag. moments 77−66296
semiconductors, doped, local spin-density-functional method, appl. to metal-insulator transition 80−96789
semiconductors, indirect exchange interaction between localised moments 80−93079
semiconductors, localised magnetic moment of transition metal impurities 80−60192
superconducting dilute mag. alloys, effects of indirect coupling upon nucl. spin-lattice relax. 77−80874
transition metal alloy disordered host, actinide impurity localised magnetism 77−51883
transition metal alloys, local environment and mag. props. 78−64187
transition metal alloys, origin of states, doubly degenerate orbitals 79−78311
transition metal based alloy, resistivity temp. depend. due to localised spin fluctuations 77−8083

local moments in dilute systems continued
transition metal binary alloys, local environment and mag. props., effect of disorders 77−63085
transition metal-actinide dilute alloy, disordered occurrence of localised magnetism, CPA calc. 77−63096
transitional alloys, local moment formation 78−43562
variational method for mag. impurities in metals 80−103814
Wolff model, thermodynamic props., local moments in dil. alloys, var. method 80−65781
A-Mn, dil., mag. susceptibility and single impurity effects 78−64186
Ag, electronic and mag. structure calcs. of mag. impurities 80−80213
Ag-Dy(Er), cryst. field and spin exchange parameters, susceptibility and ESR expts. 77−40129
Ag-Fe alloy, local moment system, low. temp. susceptibility, Mossbauer effect meas. 77−43810
Ag-Gd(Tb)(Tm), thermopower, crystal field and interaction effects 77−66158
Ag-Mn, dilute spin glass, AC susceptibility and ESR meas. 79−7968
Ag-Mn film, supercond. proximity effect and pair breaking, normal state mag. interactions 77−63035
Ag-transition metal, dil., mag. impurities, electronic struct., KKR-Green's function calc. 80−65783
AgPd alloys with Mn and Fe impurities mag. susceptibility 79−73677
Al-Ce, very dil., low temp. sp. ht. 79−51745
Al-Cr (Mn), magnetic susceptibility, single impurity and interaction effects 77−63093
Al-Cu-Fe, liquid, mag. moment and transition from mag. to nonmag. state 79−24132
Al-Mn, dil., magnetisation, 2-0.01K 79−4652
Al-Mn, NMR investig. of spin density oscills. around Mn impurities 77−4570
Al-Mn(Cr), dil. alloys, single impurity and interaction effects in susceptibility 77−8269
Au alloys, dil., conduction electron-local moment interactions using dHvA waveshape anal. 79−77981
Au-Co, dil. alloy, de Haas-van Alphen obs. of spin dependent scatt. by mag. pairs 77−32007
Au-Co, electron scatt. by mag. impurity pairs, de Haas-van Alphen obs. 77−66162
Au-Cr, dil., elec. resist., generalised phase shift anal. of Kondo effect 80−75556
Au-Cr, dil. alloys., elec. resist., deviations fro Matthiessen's rule 80−75541
Au-Er, dil., EPR at 100 mK to 1K 80−66028
Au-Fe, competing interactions in FCC alloys 78−95453
Au-Fe, dil., local mag. moments, neutron scatt. study 79−61058
Au-Fe alloys, spin-orbit electron scatt. near percolation limit, anomalous Hall effect meas. 79−73492
Au-Gd, dil., crystal-field splitting of localised Gd^{3+} moments, ESR obs. 79−82869
Au-Gd, fine struct. splitting, magnetisation meas. 79−56498
Au-Gd(Tb)(Tm), thermopower, crystal field and interaction effects 77−66158
Au-Gd(Y), dil., conduction electron-local moment exchange interaction meas. 80−60191
Au-Mn, dil., ^{52}Mn γ-ray anisotropy down to 3 mK, Kondo and relax. effects 77−81034
Au-Mn, dil., nuclear orientation of recoil implanted ^{52}Mn 78−43716
Au-Mn(Cr)(Fe), spin glass state and Kondo effect, nucl. orientation of ^{54}Mn 78−6514
Au-Yb, dil., EPR at 100 mK to 1K 80−66028
Au-Yb, NMR investig. of anisotropic cond. electron exchange 77−63309
Au-Yb alloys, dil., nucl. reson. of ^{173}Yb local moments 79−65763
Bi-Mn, dil. liq. alloy, static and dynamic props. of localised Mn moments 79−82755
Cd-Cr, dil., estimates of s-d interaction from supercond. transition temp. and mag. susceptibility 78−43561
Cd-Mn dil. alloys, single cryst., low temp. mag. anisotropy 77−59386
$Cd_{1-x}Mn_xTe$, indirect exchange interaction 80−97087
$Cd_{1-x}Mn_xTe$, spin-orbit coupled bands, indirect exchange interaction via electrons 80−34407
(Ce, La)Al_3, near stabilisation of Ce moment upon dilution 79−91209
Ce compounds, Kondo coupling, hyperfine and exchange interactions 79−65647
Ce impurity Kondo system, crystal field effects on thermopower and Kondo effect 77−66163
Ce-alloys, abnormal ordered Kondo lattice 78−47947
$CeCu_2Si_2$, local mag. moments, neutron scatt. study 79−61058
$Ce_x(La_yY_{1-y})_{1-x}Al_2$, local mag. moments, neutron scatt. study 79−61058
$CePd_3$, dil., local mag. moments, neutron scatt. study 79−61058
Co-V, solid and liq., mag. susceptibility and electronic struct. 80−39738
$(Co_{1-x}Fe_x)_2Y$, substitutional Fe atoms effect on mag. and elec. props., paramagnon scatt. 77−36054
CoS_2 and $CoSe_2$, local mag. moments, spin fluctuation theory 79−65687
Cr-Co (up to 8 at.%), antiferromagnetic, resist. minimum, Kondo effect by pairs of Co atoms 80−39566
Cr-Co alloys, dil., with local mag. moments, Neel temps. 79−73713
Cr-Fe, dil., magnetisation, Fe local moments 80−60215
Cr-Fe, low conc. alloys, coexistence of itinerant antiferromagnetism with paramagnetism 78−84386
Cr-Fe(Co) alloys, dil., exchange interactions 77−47986
CrCo, dil., low temp. specific heat meas., 1.5 to 4K 80−60328
$Cr_{1-x}Mo_xCo$, $x \lesssim 0.25$, antiferromag., nucl. mag. relax. 78−6590
$Cr_{1-x}V_xCo$, localised mag. moment of Co impurity 78−27014
$Cr_{1-x}V_xCo$, mag. state of Co impurity, NMR exam. 78−27100
$Cr_{1-x}V_xCo$, $x \lesssim 0.5$, antiferromag., nucl. mag. relax. 78−6590
Cu, electronic and mag. structure calcs. of mag. impurities 80−80213
Cu-Al-Mn liq. alloys, susceptibility behaviour 80−93077
Cu-Fe, dil., local mag. moments, neutron scatt. study 79−61058
Cu-Fe, dil. alloy, anomalous thermoelec. power, sensitivity to defects, annealing effect 77−51728
Cu-Fe (1.2 at.%), Fe moment and lattice distortion, neutron scatt. meas. 79−24133
Cu-Fe alloy, dil. dynamic susceptibility around T_k, satellite nucl. spin-lattice relax. time meas. 77−4573
Cu-Fe alloy, local moment system, low temp. susceptibility, Mossbauer effect meas. 77−43810
Cu-Fe alloys, Kondo system, Cu-Fe, static and dynamic susceptibilities, hyperfine studies 77−63090
local moments in dilute systems continued
Cu-Fe group, dil., NMR satellite data calc., struct. of mag. impurities 80−103894
Cu-Fe(Mn), interaction between local moments 77−1540
Cu-Mn, dil., Kondo deviations of Mn electron spin relax. and g-factor, NMR meas. 79−51747
Cu-Mn, dil., local mag. moments, neutron scatt. study 79−61058
Cu-Mn, exchange-coupled localised moments, Korringa relaxation rate 80−75851
Cu-Mn dilute alloys, local moment fluctuations, NMR meas. 77−63091
Cu-Ni(Fe)(Mn)(V), dil., local mag. moments and Kondo effect, theoretical model 79−69651
Cu-transition metal, alloys, satellite NMR study, lineshifts and splitting 80−34786
Cu-transition metal, dil., mag. impurities, electronic struct., KKR-Green's function calc. 80−65783
CuCr(Fe)(Mn), dil., anisotropic hyperfine coupling, NMR study 80−65784
Fe dilute alloys, itinerant 3d electron spin density oscills. around solute atoms 77−72978
Fe-Ge amorphous films, conversion electron Mossbauer spectra, mag. moments 77−16231
Fe-Si, spin- and charge-density oscillations 77−11886
γ-Fe-transition metal alloy, mag. moment in FCC d-metal lattices *(Russian)* 78−72337
Fe-V alloys, Mossbauer study, hyperfine field effect on formation of local moments 78−27134
Fe_2-Mn-Al alloys, Fe-rich, disordered, local moments on Fe and Mn 77−43811
$(Fe_{1-x}Mn_x)_3Al$, local Mn moment distrib., neutron scatt., nucl. spin echo *(Russian)* 77−12091
FeOOH:Cl(F), quadrupole interaction, Mossbauer spectra 80−15895
Gd in CsCl type alloys, exchange between localised 4f and cond. electrons 77−63279
$Gd_{0.99}Ho_{0.01}(Rh_{1-x}Fe_x)_2$, spin echo meas. on ^{165}Ho, quenching effect of Fe substitution 78−48079
$Gd_xLa_{1-x}Al_2$ ($x<0.05$), Hall effect measurements 80−44569
$Gd_xY_{1-x}Al_2$ ($x<0.05$), Hall effect measurements 80−44569
$Hg_{1-x}Mn_xSe$, spin-orbit coupled bands, indirect exchange interaction via electrons 80−34407
$Hg_{1-x}Mn_xTe$, indirect exchange interaction 80−97087
$Hg_{1-x}Mn_xTe$, spin-orbit coupled bands, indirect exchange interaction via electrons 80−34407
InAs:Mn, NMR, magnetoresist., Hall effect and mag. susceptibility meas. 78−26888
InSb:Mn, NMR, magnetoresist., Hall effect and mag. susceptibility meas. 78−26888
Ir-Fe, dil., local magnetisation, Mossbauer meas. 80−66091
(La,Ce)Al_2 and (La,Gd)Al_2, magnetic impurity effect on thermal cond., normal and supercond. states 77−63027
(La,Gd)Al_2, reverse Kondo alloy, transport props. at finite mag. field 80−6812
(La,Th)-Ce, dilute alloys, mag.-nonmag. transition of impurity moments, environment effects 77−40034
La-Eu(Gd), EPR investig. of local moment, correl. with supercond. props. 77−63282
La-Gd, exchange-coupled localised moments, Korringa relaxation rate 80−75851
La-P-Ce, NMR investig. of anisotroptic cond. electron exchange 77−63309
$LaBe_{13}$-Er(Dy), dil., ESR, crystalline elec. field splitting, exchange parameters 78−52348
$La_{1-x}Ce_xB_6$, Kondo system, low-field impurity susceptibility, 0.03 to 8K 77−63095
$La_{80-x}Gd_xAu_{20}$, amorphous dil. alloy, RKKY interaction, magnetisation meas. 77−32207
$La_{3-x}V_xS_4:Gd^{3+}$ localised moment-conduction electron interact., ESR obs. 78−88183
$(La_{1-x}Y_x)_{1-y}Ce_yAl_2$, resistivity meas., Kondo temp. enhancement 77−62917
$La_{3-x}\square_xS_4:Gd^{3+}$, indirect mag. interaction *(Dutch)* 77−63277
$La_{3-x}\square_xS_4:Gd^{3+}$, localised moment-cond. electron interactions, EPR data interpretation 77−63280
LiZn ferrospinels, mol. field. coeff. conc. depend. 80−97114
Lu-Gd, dil., positive exchange Kondo system, magnetisation and resist. 78−68158
Lu-rare earth metal alloys, dil., elec. resist. 79−82578
$LuCo_2$, paramag., field induced mag. density localisation 77−72999
Mg-Mn, cryst. field and spin parameters, transmission ESR obs. 77−40130
Mg-Tb(Dy)(Ho)(Tm), dil., macroscopic shape effect due to quadrupole orientation, magnetostriction and thermal expansion meas. 80−60396
$Mg_{1-x}Er_x$, cryst. field interactions, neutron scatt. spectra 80−50048
MnO, paramag., μ^- spin rotation at O site 77−20785
Mo-Fe, local magnetisation from Mossbauer meas. 77−20549
Mo-Fe alloy, local moment system, low temp. susceptibility, Mossbauer effect meas. 77−43810
$Mo_{1-x}Re_xCo$, mag. state of Co impurity, NMR exam. 78−27100
Nb-Mo-Fe, dil., local environment and mag. props. 78−64187
$Nb_{50}Ni_{50-x}Fe_x$, amorphous alloy, mag. interactions 78−95432
$Nb_{50}Ni_{50-x}Fe_x$, magnetically dil. glass, 3d moments, mag. susceptibility and magnetisation meas. 79−95574
$NbSe_2$:Fe, local moment form., mag. susceptibility meas. 79−82756
$NbSe_2$:Mn, Kondo effect, mag. ordering and superconductivity 77−62915
β'-Ni-Al-Fe, mag. impurity states, resist. meas. 77−55519
Ni-Cr, dil. alloy paramag., μ^- relax. 77−24776
Ni-Mn alloy, mag. moment distribs. and environmental effects, neutron scatt. obs. 80−60247
Ni-Ti (2wt.%) alloy, polarised neutron diffuse scatt. 77−36057
Ni-V, solid and liq., mag. susceptibility and electronic struct. 80−39738
Ni-V(Nb)(Ta)(Si)(Ge), dil., mag. props. at elevated temps. 77−63089
Ni_3Al-Fe, Fe effect on Mossbauer effect study 77−32298
β'-$Ni_{48}Al_{52}$, 3d transition metal impurities, elec. resist. meas., local moment formation 77−69295
$(Ni_{1-x}Fe_x)_{1-\delta}S$, anisotropic spin glass, mag. props. 80−39793
$(Ni_{1-x}Rh_x)_{99}Mn$, ferromagnetic, NMR study of local environment effect, Mn moment reversal 80−7192
$Ni_{0.97}Ru_{0.03}$, mag. form factor and moment distrib., obs. using polarised neutrons 78−68171

local moments in dilute systems continued
$(Ni_{1-x}Ru_x)_{99}Mn$, ferromagnetic, NMR study of local environment effect, Mn moment reversal 80−7192
$NpPd_{3-x}Rh_x$, Mossbauer spectra, hyperfine interactions and mag. ordering 77−20783
PbTe:Fe, single crystals, state and behaviour of Fe, mag. props. 80−93080
Pd, muon end depolarisation, hyperfine anomaly 77−28503
Pd-Co, nuclear orientation expt., Co impurity in singlet Kondo state 77−63296
Pd-Co(Ni), dil. local orbital moment evidence 77−20299
Pd-Fe, del. alloy, Mossbauer obs., 0.018-300K 77−69740
Pd-Fe, dil. alloy, conduction electron polarisation at 0.1K, μ^+SR 77−20784
Pd-Fe alloy, NMR of ^{27}Al meas. 77−12215
Pd-Fe(Mn), dil., depend. of neutron small-angle scatt. intensities on appl. mag. field and temp. 79−11291
Pd-H-Gd, dil., ESR exam. of low temp. region of phase diagram, and electronic props. 80−29930
Pd-Mn, dil. alloy, giant moment at very low temp. 78−88094
Pd-Mn, dilute, paramag. diffuse neutron scatt. 77−63094
Pd-Mn, nuclear orientation expt., Mn impurity giant moment 77 63296
Pd-Mn (1-10 wt.%), mag. ordering, influence on resistivity 80−75557
Pd-Mn alloy, NMR of ^{27}Al meas. 77−12215
Pd-Mn(Fe), mag. ordering phenomena, neutron scatt. obs. 80−44812
Pd-Ni alloy, ferromagnetism, local moments, susceptibility, magnetisation and Curie temp. *(Russian)* 78−88115
Pd-transition metal, dil., itinerant versus localised magnetism 78−64188
$(Pd_{1-x}Au_x)_{0.99}Co_{0.01}$, mag. hyperfine interaction for impurity Co atoms *(Russian)* 80−7078
PdCo, ferromag., nucl. mag. relax. 78−6590
$Pd_{0.98}Fe_{0.01}Gd_{0.01}$, ferromag., Pd-Gd exchange const. and Pd polarisation, neutron scatt. meas. 80−25122
PdH_x-Fe, dil., Kondo system, local moment hyperfine studies, Mossbauer expt. 80−39908
$PdH_xFe_{0.003}$, Kondo system, local moments, hyperfine fields, Mossbauer study 80−80478
$Pd(M_nCo)$, giant moments, Mossbauer study of ^{57}Fe 80−44969
$(Pd_{1-y}M_y)_{100-x}Fe_x$, M=Ag, Rh, exchange-enhanced alloys, mag. ordering 79−61050
Pt-Fe, competing interactions in FCC alloys 78−95453
Pt-transition metal, dil., mag. susceptibility and NMR meas. 78−39290
Rh-Fe, competing interactions in FCC alloys 78−95453
Rh-Pd, mag. moment of Ni, Co, Fe, Mn and Cr impurities 78−95416
Rh-Pd-Co(Fe), dil., local environment and mag. props. 78−64187
Ru-Fe, dil., local magnetisation, Mossbauer meas. 80−66091
Sc-Dy(Er)(Tb), dil. alloy, high field magnetisation 78−56292
SnTe:Mn, NMR shift meas. 80−97154
SrO:Ni^{2+}, EPR line splitting rel. to Jahn-Teller coupling and soft localised mode 80−66022
TaS_2:Fe, local moment form., mag. susceptibility meas. 79−82756
$TaSe_2$:Fe, local moment form., mag. susceptibility meas. 79−82756
Tc-Fe, dil., local magnetisation, Mossbauer meas. 80−66091
Tc-Fe dilute alloys, supercond. and mag. props. 80−29494
$(Ti_{1-x}V_x)_2O_3$ spin glass, mag. props., metallic antiferromagnetism 79−82791
$(Ti_{1-x}V_x)_2O_3$, O<x<0.1, magnetisation and mag. moments 80−65772
$Ti_{1-x}V_xSe_2$, mag. susceptibility, 4.2-300K 80−60188
$(U_xTh_{1-}x)S(Te)$ solid solns., electronic struct., mag. susceptibility and elec. resist. obs. 77−20551
$V_{1-x}Fe_x$, low temp. sp. ht. and mag. props. 80−2548
$V_{1-x}Fe_xH_n$, low temp. sp. ht. and mag. props. 80−2548
$V_{1-x}Fe_xO_{2-x}F_x$, mag. susceptibility *(German)* 79−78305
VO_2, metal-insulator transition, electron correls. and spin dimerization, thermodynamical study 80−70615
W, resistivity min., thermoelectric anomaly correlation 78−2468
Y-Ce, Kondo system, spatial extent of Ce moment, neutron diffr. meas. 78−68159
$Y_{1-x}Er_x$, cryst. field interactions, neutron scatt. spectra 80−50048
$Y(Fe_xCo_{1-x})_2$, compositional dependence of Co's mean mag. moment, local environment model anal. 78−43560
$Y_3Fe_{5-x}Sc_xO_{12}$, local spin struct., Mossbauer obs. 77−32305
Yb impurity Kondo system, crystal field effects on thermopower and Kondo effect 77−66163
$YbCu_2Si_2$, local mag. moments, neutron scatt. study 79−61058
Zn-Mn(Cr), dil, mag. anisotropy, Hartree-Fock calcs. 80−11162
Zr-Mn (up to 0.3%), high-magnetic field magnetisation and magnetoresistance 78−10652
$Zr_{40}Cu_{50}Fe_{10}$, magnetically dil. glass, 3d moments, mag. susceptibility and magnetisation meas. 79−95574
$Zr_{40}Cu_{60-x}Fe_x$, electronic and mag. props. 77−8271
$Zr_{40}Cu_{60-x}Gd_x$, magnetically dil. glass, 4f moments, mag. susceptibility and magnetisation meas. 79−95575
$Zr_{40}Cu_{60-x}M_x$, (M=Gd, Tb, Fe or Mn), amorphous alloy, mag. interactions 78−95432
$Zr_{40}Cu_{50}Mn_{10}$, magnetically dil. glass, 3d moments, mag. susceptibility and magnetisation meas. 79−95574
$Zr_{40}Cu_{60-x}Tb_x$, magnetically dil. glass, 4f moments, mag. susceptibility and magnetisation meas. 79−95575

localised electron states
see also Anderson model; charge-ordered states; charge transfer states; Wigner crystal
2,4-hexadiyne-1, 6-diol, bis(p-toluene sulphonate), dark-current meas. 80−15520
4f substances, electronic props. at config. crossover 77−47775
actinide compounds, neutron scatt. studies 80−75716
actinide metals, Coulomb ten U and 5f electron excitation energies calc. 77−11867
actinide metals and intermetallics, localised versus itinerant character of 5f electron states 77−28138
actinides, 3d X-ray spectra, 4f and 5f states 78−84681
actinides, self-consistent relativistic muffin-tin calc., atomic vol. and bulk modulus Ac-Am 78−72065
actinides, struct. props. rel. to F electrons 78−83951
adsorbate, photoelectron core level spectra calc. 77−85896
adsorbed molecules, photoelectron line shapes, vibr. excitation and hole delocalisation effects 79−95905
alkali halide, polarisation energy for core states 80−10903
alkali halide crystal, defect formation in thermal equilibrium state of self-localised exciton 80−44205

localised electron states continued
alkali halide crystal, hole localisation at two halogenide ions, polaron theory *(Russian)* 77−69268
alkali metals, positive muon spin rotation frequency, Knight shift meas. 79−38421
alkaline earths, positive muon spin rotation frequency, Knight shift meas. 79−38421
alkane:toluene, radiolysis at 77K, luminesc., excited singlet toluene form., energy transfer mechanism 77−16846
alkanes, electron localisation and solvation, radical ion theory 78−87936
alloy, disordered, DC conductivity temp. depend. meas. in off-diagonal CPA 77−28153
alloy, ferromag., local density of one-magnon states, cluster-Bethe-lattice approximation 77−32181
alloy, random binary, Anderson localization, equation-of-motion method 79−42482
alloy, X-ray self-absorpt. spectroscopy method for unoccupied valence states obs. *(Russian)* 77−81175
alloys, local density of states and local environment 79−82509
amorphous compound semiconductor, thermoelectric power and transport models 78−10482
amorphous covalent semiconductor, random two-band Weaire model, localisation theory 77−15788
amorphous material, trap-controlled transient current injection theory 77−47772
amorphous Schottky barrier, capacitance-voltage meas., localised density of states determ. 80−49900
amorphous semiconductor, charge transport behaviour, model 79−91048
amorphous semiconductor, cond. mechanism and localised states *(Japanese)* 80−84467
amorphous semiconductor, electronic properties and localised states, review 77−62871
amorphous semiconductor, gap states electronic behaviour 79−87098
amorphous semiconductor, local order as determined by electronic and vibrational spectroscopy 79−37627
amorphous semiconductor, local rearrangement mode model for pair and single particle localised states 77−76773
amorphous semiconductor, localised gap states, hopping cond. and chem. bonding 78−23052
amorphous semiconductor, localised gap states, variable range hopping, susceptibility and EPR 77−72866
amorphous semiconductor, screening effects in Poole-Frenkel cond. 77−43606
amorphous semiconductor, wave packet propagation in random struct. at crit. energy 78−26855
amorphous semiconductor film, density of localised band tail states, transient photoconductivity 77−15898
amorphous semiconductor or insulator, optical absorption 77−90167
amorphous semiconductors, covalent, localised electronic states, Hubbard model calcs. 77−89732
amorphous semiconductors, doping effect and nature of localised states 78−14696
amorphous semiconductors, gap states, electronic behaviour 78−2452
amorphous semiconductors, localised gap states, chemical trends 78−39067
amorphous semiconductors, mobility gap, phononless hopping 77−55527
amorphous semiconductors, optically induced metastable paramag. state, optical absorpt. and ESR meas. 77−40113
amorphous solid, abnormal bonding and electronic states in forbidden energy gap 78−51942
amorphous solid, two-band model, Thorpe-Weaire type, localisation near band edges 78−23050
amorphous system, cluster effective lattice method, mag. and electron props. 77−66242
amorphous system, Schrodinger equation with random pot. 79−65414
amorphous system, theory of electron localisation 77−1391
amorphous tetrahedrally bonded solid, theory of fluctuations and localized states 78−10405
Anderson localisation, mean field theory and ε-expansion 80−80203
Anderson localisation and recursion method 78−84167
Anderson localisation in presence of off-diagonal disorder 77−85179
Anderson localisation problem, anal. of time depend. of randomly specified wavefunction 77−47761
Anderson localisation problem, numerical results 78−23040
Anderson model, wavefunctions on long finite random chains 78−47726
Anderson model for disordered systems, electron localisation, spatial extension of wavefunction 77−80752
Anderson transition in three dimensions, crit. strength of disorder 77−59256
anthracene, single cryst. with photoinduced local centres, luminesc. 79−61433
band tailing due to zero-point vibrs. in perfect cryst. 79−28267
benzene, solid, electronic struct., XPS 77−73213
binary alloy, electron localisation, self-consistent theory *(French)* 78−60088
binary alloy, random, wavelength localisation 78−34795
binary alloy, self-consistency theory *(French)* 79−42480
binary alloy model, 2D disordered system, chain-like localisation 78−91646
binary alloy type of disorder, numerical study of localisation 78−64009
biphenyl crystals, electronic and vib. states, cryst. field mixing, two-photon spectra 77−59603
bipolarons, localised, in ionic crystals 78−67957
Boltzmann electron gas in Gaussian random potential, mean field approach 80−107721
bond-type disorder system, electrical cond. and electron localization calcs. 78−2475
book, current topics in material science 80−46747
bound s-state energies for static screened Coulomb pot. 77−18771
cancellation effects in localised theories 80−84445
Cayley tree, diffusion 79−69473
chain with light emitting ends, radiative lifetime, recombination kinetics 80−108260
chalcogenide glass, localised gap states, Mott-street model 79−37968
chalcogenide glass, localised states role in cond. in high elec. fields 77−76841
chalcogenide glass, optical transitions and electronic struct., review 77−76741
chalcogenide glasses, field effect, localised states and electronic transport 77−66187

localised electron states continued
chalcogenide glasses, localised states calc. rel. to contact capacitance and field effect 79−11090
chalcogenide glasses, optical versus transport processes. 80−84449
charge density distortions and lattice dynamics, appl. to Nb 78−30714
charge ordered state and collective excitations 77−28136
charge ordered state and mag. collective excitations 77−35876
charge-ordered crystal, electronic excitation spectra, pair correl. effects 77−72829
chemisorbed atoms, atomic and extra-atomic relax. and IR catastrophe in core spectra 77−48304
chemisorption on Ni (001), electronic struct., KKR model calcs. 78−56200
condensed media, electron localisation and solvation, radical ion theory 78−87936
correlation effects in hopping transport theory, applic. to cond. and thermal EMF *(Russian)* 78−23079
covalent semiconductor, Hall effect, hopping cond. and nature of local orbitals 77−72872
covalent solid, struct. props. and valence force fields, non-empirical calc. 77−1096
critical binding of particle moving in given pot., renormalisation group theory 77−66135
d-band metals and alloys, s-d hybridisation 78−91644
dark current relax., barrier cond. mech. 80−6904
de Haas-van Alphen effect, role of quasilocal levels 79−69398
degenerate centres in crystals, possibility of direct orbital ordering 77−62872
dense gas, of dipolar mols., electron localisation, density fluctuation, mol. orient. 78−38446
diamond, hard conducting C ion implanted layer, resistivity 77−15974
diamond, linewidth of GR2-8 transition 78−60488
1,4-dibromonaphthalene, substitutionally disordered, energy localisation, optical and ODMR spectra of triplet Frenkel excitons 80−54996
disorder at surfaces and interfaces, effect on electronic props. 78−26932
disordered alloy, electron localisation, temp. depend. 80−80219
disordered alloy, short range order effect on electron states 77−15732
disordered electronic system, scaling theory of localization and non-ohmic effects in two dimensions 80−44539
disordered electronic systems, near two-dimens., noncompact σ models and existence of mobility edge 80−92860
disordered Fermi systems, in two dimensions, interaction effects 80−75655
disordered materials, effect of electron correlation 77−31982
disordered materials, electronic hopping transport 80−39580
disordered materials, thin films and wires, resist. and localisation 80−44537
disordered media, inhomogeneous transport, continuum theories 77−20283
disordered one-dimensional conductors, interacting electron thermodynamics *(Russian)* 80−54679
disordered one-dimensional systems, electron localisation, and solitary waves in Ginzburg-Landau (ϕ^4) field theory 78−14646
disordered semiconductor, mobility edge exam. by new perturbation theory 78−47790
disordered solids, electronic props., numerical methods 80−44538
disordered system, Anderson localisation, numerical study *(Japanese)* 78−30890
disordered system, conductivity and mobility edge, square and diamond lattice calc. 78−43347
disordered system, Coulomb gap, Monte-Carlo simulation 78−84168
disordered system, electron localisation 80−29359
disordered system, fluctuations of localised wave function 77−15783
disordered system, four dimens., electron density of states determ. 78−72057
disordered system, four-dimensional, electrons 77−8039
disordered system, local moments and localized states, theory, review 79−23935
disordered system, low-freq. cond. due to variable range hopping, cluster approx. 80−92886
disordered system, Mott localisation criterion validity 77−76772
disordered system, one-dimens., density of states and wavefunction shape, periodic boundary condition influence 80−80223
disordered system, reson. Raman scatt. 80−2772
disordered system in mag. field, frequency dependence of conductivity tensor, theoretical investigation 80−70725
disordered system with n orbital per site, Lagrange formulation, hyperbolic symm., Goldstone modes 80−80222
disordered systems, asymptotic behaviour of recursion method 79−65413
disordered systems, bond-type, elec. cond., effects of fluctuations of transfer energies 77−80757
disordered systems, Coulomb gap computer simulation 79−51465
disordered systems, elec. transport mechanisms 79−69483
disordered systems, electron localisation and classical solns. in Ginzburg-Landau field theory 78−56108
disordered systems, localisation using random series, Anderson transition for extended states 80−44542
disordered systems, optical energy transfer 78−92105
disordered systems, simplified treatment of energy levels 77−76774
disordered systems, site-diagonal and off-diagonal, electron localisation, numerical study 80−44541
disordered systems, size of localisation domain 77−15787
disordered systems, static. cond. at zero temp. and localisation of states 77−51715
disordered systems, two dimensional, localisation of p-electrons 77−15784
disordered systems, two-dimensional, optical conductivity calcs. 77−11865
dispersive media, localised states of Wannier exciton type, bound state energy 77−43506
donor-acceptor pair lines, broadening due to potentials of ionised impurities 79−51522
dynamic effects of localised nearly degenerate electronic states 78−6338
edge dislocation, extended Huckel theory 78−18999
electrical conductivity freq. depend. in disordered system two site model *(Russian)* 80−54666
electron emission, atomic screening model for solid-state effects 77−73194
electron gas, screening of proton 77−1382
electron liquid, static struct. factor, short-range correl. and Wigner crystn. 77−39795
localised electron states continued
electron localisation and mobility edge, spin glass problem 78−52283
electronic density of states, cluster Bethe lattice method, appl. to amorphous III-V semiconds. 77−11868
electronic elementary excitations in far UV, core level exciton and core hole polarisation 78−39032
electronic localised state at edge dislocations, parabolic dispersion law *(Russian)* 80−65479
electronic phase transition accompanied by valence change, effect of damping and hybridisation of f-electrons 77−24520
electronic transitions, optical dephasing times and line shape functions 78−35162
elemental semiconductors, hybridisation effect on dislocation electronic states 78−51936
energy spectrum of current carriers, cryst. with electron ordering *(Russian)* 77−62848
ethane, excess electron localisation, density effects 77−31970
f-band metals, mode softening and lattice instability under press. 77−51833
Falicov-Kimball model, electronic phase transition 80−20108
Fermi glass, elementary excitation exam. 78−56086
Fermi glass, theory for localised electrons 77−39807
ferricyanide, X-ray spectral study of electronic struct. 77−28652
ferrocyanide, X-ray spectral study of electronic struct. 77−28652
ferrocyanide ion, electronic struct. and related props., calc. by SCF Xα-scattered wave method 77−15809
ferromagnetic semiconductor, autolocalised electron states 78−51924
ferromagnetic semiconductor, surface localised low energy electron-magnon states *(Russian)* 80−88734
field emitted electrons, effects of band struct. on energy distrib. 77−24932
filament, condenson energy and mass 78−91637
finite chain, with random dil. impurities, localisation characts., amplitude anal. 80−96825
fluid, effect of disorder on electron mobility and localisation 77−89682
glass systems, electronic props. 79−42495
glasses, electron scavenging, hopping controlled time-depend. reaction rates 80−108723
Hartree-Fock band theory, Mott-Hubbard condition for electron localisation 79−73417
heavily doped semiconductor, density of eigenvalues, localisation, general disordered system 78−56109
HEED, Bloch waves, corresponding atomic and mol. orbitals 79−27880
n-hexane, liquid, ground state energy of excess electrons 78−68976
HF orbitals for mol. clusters, layers and solids 78−9076
highly ionised atoms, L-shell refilling rate in solid 77−12469
HMPA:alkali metal, density of states in band gap, EPR and optical correlations 79−61201
homopolar cryst., anharmonic props. and nonlinear electron-lattice interaction *(Russian)* 77−51691
homopolymers, ESCA methods, core levels of simple homopolymers 78−88673
hopping conduction, correl. effects 77−89762
rel. to hopping conduction exponential band tail, calc. method 79−87100
hopping conduction in disordered insulator, continuous-time random walk model 80−96863
hopping conductivity and thermopower, percolation and effective medium theory 79−78103
hopping transport kinetic theory, localised state separation, Pauli master eqn. 80−80276
hybridization effect on phase transitions in the Falicov-Kimball model 78−91617
II-VI and III-V compounds, Compton line shapes of atoms 77−44080
III-V semiconductor, amorphous, electronic local density of states, cluster Bethe lattice method 77−11868
III-V semiconductor, d core levels, electron-hole interaction 77−11880
III-V semiconductor, localised defects, one-electron pseudopot. 77−24533
ilvaite, electron delocalisation obs. in Mossbauer spectrum 79−33581
ilvaite, Fe temp. depend. oxidation states, electron hopping, Mossbauer spectra, X-ray diffr. obs. 78−2779
ilvaite, temp. dependent electron delocalization, Mossbauer spectra 79−11361
impurities, elec. dipole moment and local fields 79−90992
impurity band, localisation criteria 80−20114
impurity electron level position depend. on interaction with bands, Wannier representation calcs. 80−54653
inert gas crystal, bound self-localised hole states assoc. with lattice distortion 77−24530
inert gas fluid, localised excess-electron states, quasilocalisation 80−44529
inert gas solid, delocalisation probability of interstitials 79−7801
insulator, disordered, charged impurity states, Lloyd model 80−29360
insulator, in inhomogeneous elec. field, localized states in forbidden band 77−8060
insulators, noncryst., electron density captured at traps, liberated to conduction band 78−87946
intermediate valence, three-site, six-electron, even-parity model 80−20125
intermediate valence, three-site, six-electron model, variational calc. 80−20126
intermediate valence compounds, mag. susceptibility and sp. ht., mean-field theory of periodic Anderson model 78−47937
Invar, electronic structure, influence of temp., X-ray photoelectron study 77−28681
Invar, XPS of valence electrons, temp. effects, 122-580K *(Russian)* 77−8727
ionic and partially ionic solids, electron-lattice interaction 77−20274
ionicity, Pauling's and Phillips' comparison by empirical LCAO band theory 78−51464
Kondo alloys in supercond. proximity, localised bands 78−10613
Kovar, effect of magnetic electrons on atomic interactions 77−43820
lattice relaxation and time resolved polarization of emission from localized electron with level crossing 79−4840
layer materials with stacking faults, fine structure splitting of ground state excitons 77−51665
linear chain, arbitrary number of impurities, analytic conditions 78−2443
liquid, self-localised electron states *(Russian)* 80−2366
liquid rare earth metal, mag. susceptibility rel. to theories of electronic structure 77−1536

localised electron states continued
local moments and localised states, review of early work on Anderson model 78−72327
localisation in ionized and excited states, conf. 77−30750
many body systems, Anderson model, localisation phenomena, state variable randomness, perturbation theory 80−29297
many-valley semiconductor, Mott transition, critical carrier conc. 77−47747
metal, cond. electron polarisation, magnetisation densities, neutron mag. form factors 77−72981
metal, d-band, generalized pseudopotential theory, density functional formulation 78−10389
metal, electric surface impedance 78−88017
metal, plasmon dispersion effect in (e,2e) process with atomic electron knockout 80−2904
metal, plasmon satellite struct. in (e,2e) process 80−96809
metal, screening energies in photoelectron spectroscopy of localised electron levels 77−1781
metal, US attenuation, quantum oscills. with dislocations under press. *(Russian)* 80−88273
metal, X-ray self-absorpt. spectroscopy method for unoccupied valence states obs. *(Russian)* 77−81175
metal surface chemisorption theory, electron localisation, surface interactions 80−84376
metal with incomplete shell, spin-depend. final-state interactions in core photoelectron spectra 77−20981
metal with incomplete shell, spin-depend. final-state interactions in core photoelectron spectra 77−20982
metal-insulator contact, electron tunnelling and its role in contact electrification 80−2453
metal-semiconductor interface, disordered, supercond. 80−20347
metal-semiconductor junction layer charge migration with localised state participation *(Russian)* 80−49913
metal/PbI_2/metal struct. reson. and inelastic tunnelling 80−44739
metallic actinide compounds, localised cryst. field states, neutron inelastic scatt. obs. 78−14697
metallic glass, conduction electrons interacting with tunnelling states 79−15137
metallic glasses, ferromag., Mossbauer investigation of electronic struct. 78−92009
metals, electronic struct. and magnetism, review 80−70573
metals and alloys, APS, multiple scatt. approach using muffin-tin pot. 80−25490
methanol, dry-electron localisation, impurity trapping, solvated electron rate consts. 79−1990
3-methylpentane glassy matrix, localised electrons, cavity model 80−107743
minimal metallic cond., localisation scaling theory *(Russian)* 80−103671
mixed crystal, semi-infinite, local electronic states, CPA extension 79−65401
mixed valence compounds, charge-orbital ordering 78−39069
mixed valence cpds., electron-hole symmetry, phase diagrams, and lattice props., periodic Anderson model 80−15481
mixed valence impurity model, Fermi liq. theory, Ward identities 80−34401
mixed valence model, spinless, coherent-hybridisation states and virtual-bound states 80−107749
mixed valence model, spinless, isolated f-level problem 80−107750
mixed-valence systems; short-range-order model 79−78049
mobility edge, analogy with spin glass problem 77−85164
molecular crystals, shallow traps, spin triplet population temp. depend. 77−1371
molecular simulated cryst., diatomic mol. directional Compton profiles 77−30931
molecular solid, electronic struct., polarisation fluctuations effect 77−72833
molecular solid, isotopically-mixed, electronic excitation localisation, off-diagonal disorder effects 79−99503
molecular solid, localisation of mol. ion or exciton states 79−47048
MOS inversion layer, 2-dimens. disordered electron systems in strong mag. fields 77−76930
Moss insulators and polymeric chains, similarities w.r.t electronic correl., AMO method *(French)* 80−24775
Mossbauer ^{57}Fe spectra, ferrous charact., cryst. field interactions 80−108133
Mott excitons in crossed fields 77−4299
Mott insulator, magnetism and charge ordering 79−60751
Mott insulator electronic struct. review 78−18963
Mott insulator superconductor transition, Bari model, tricrit. behaviour and phase diagrams 78−14876
Mott insulator susceptibility 79−78302
Mott problem, in 1D-disordered system *(Russian)* 77−8038
Mott transition, spin glass description 79−65386
MTHF, localised excess electrons, semicontinuum models 78−73129
multilayer assembly, freq. depend. cond., electron transitions between localised states 77−43699
naphthalene: pentacene, intermol. interaction dynamics and optical dephasing 80−64112
naphthalene, in naphthalene-d_8, Anderson-Mott transition model for excitation transport 80−96812
naphthalene, in naphthalene-d_8, energy trapping from localised states 80−100440
narrow band metals, extra-atomic relax., X-ray spectra 77−36312
neutron scattering from localised electronic excitation, theory 79−4539
nickel phthalocyanine, ohmic and space-charge-limited currents in vacuum ambient 77−20323
non-stoichiometric phase, physico-chemical props. 80−29532
noncrystalline materials, optical props., lecture 78−27263
nuclear relaxation under ESR saturation conditions 77−8451
off-diagonal disorder 77−20258
one dimensional disordered system, cond. and electron localisation 80−103658
one-dimensional Bloch electrons, binding by external fields 77−89681
one-dimensional conductor, phonons effect on localisation and electro-cond. 78−6362
one-dimensional crystal, electron problem in uniform elec. field 77−20280
one-dimensional disordered lattice, classical diffusion of localised excitations 78−72114
localised electron states continued
one-dimensional disordered system, electron density distrib. *(Russian)* 77−11877
one-dimensional disordered system, numerical expt., Coulomb gap *(Russian)* 77−31932
one-dimensional random system, localisation length 78−10406
one-dimensional solids, energy transfer processes, optically detected electron spin coherence meas. 79−19808
one-dimensional strongly disordered conductor, localisation of electrons *(Russian)* 79−78046
one-dimensional system, energy and charge transport theory *(German)* 80−15506
one-dimensional system, fluctuations and localisation 77−35883
one-dimensional Tomonaga model, localisation and delocalisation 77−89735
one-electron approximation, effect of correls. and defects 78−63960
optical absorption spectra evolution for localisation in trapping and solvation 77−90173
orbital charge ordering in crysts. 77−35884
organic donor-acceptor compounds, incomplete charge transfer stability 78−30883
orthogonality catastrophe due to local electron interaction, overlap integral, Anderson theorem in general case 78−67962
orthogonality catastrophe for a system of interacting electrons 79−1576
Peierls dielectric, one dimensional, selftrapped excitations in Peierls-Frohlich state *(Russian)* 80−54678
perovskite oxides, ferroelec., point defects and elec. props. 79−42533
perturbed crystals in kq representation, in presence of uniform mag. field 78−30856
$(perylene)_3TCNQ$, prep. and spectra, electron-mol. vib. coupling 77−16290
phase transition with valency change, sound vel. renormalisation *(Russian)* 78−79963
phosphides of Cu,Ag,Zn,Cd,Ga,In, d-electron participation in chem. bonds 77−28682
photoconductivity and autoionisation calc., impurity states 80−44648
photoelectron spectra, collective effects, relax. and localisation of hole levels 80−52950
photoelectron spectra, localised and delocalised calcs. 80−63709
photoemission from localised states, model, fractional spin polarisation 78−92172
polar fluid, improved model of long range electron solvent interaction of localised electron 77−90710
polyacene quinone radical polymers, elec. props. described by variable range hopping model 80−44588
polyacrylonitrile, AC conduction mechanism, freq. and temp. depend. *(Japanese)* 80−54706
polydiacetylene cryst., electronic struct. change at phase transition, Raman spectra 78−2833
polydiacetylene-toluenesulphonate, photocond. meas., 0.62-3.1 eV 80−70757
polyene, infinite, electronic states under local perturbation 77−57878
polyene, linear, band gap calcs. 77−31969
polyethylene 2,6-naphthalate, AC conduction mechanism, freq. and temp. depend. *(Japanese)* 80−54706
polyethylene disordered chains, electron localisation 78−87945
polymer, amorphous, excess charges, band gap levels and elec. props. 78−23053
polymer, conjugated and saturated chain, electronic struct., review 80−59860
polymer, core levels, ESCA expts. 78−14302
polymer, electronic struct., polarisation fluctuations effect 77−72833
polymer, linear, struct. disordered, electron localisation 80−29359
polymer metal contact, charge transfer and contact charge spectroscopy 80−65680
polymer metal contact, charge transfer and contact charge spectroscopy 80−65681
polynaphthol film, semicond., trap depth and trapping cross section from TSC curves 79−51700
propane, excess electron localisation, density effects 77−31970
1-propanol, dry-electron localisation, impurity trapping, solvated electron rate consts. 79−1990
protons, fast, charge states, capture into and loss from bound states 77−43257
pseudopotentials for local moments and certain virtual bound states 78−34959
quantum particle in one-dimensional potentials with incommensurate periods 80−34345
quasi-local level, line shape induced by impurity 80−100441
quasi-one dimensional conductor, electron density of states, influence of disorder 77−28091
radiative and nonradiative recomb. at metal ions, core struct. effects, review 79−4834
random binary alloy, self-consistent theory of localisation 78−34805
random impurity system, density of states tails, fluctuations and mobility edges 78−67983
random lattice, with purely off-diagonal disorder, electron localisation 80−49672
random lattice with off-diagonal disorder, absence of Anderson's transition 78−30889
random lattices, localisation theory 78−6336
random potential, electron localisation, random walk analogue 80−107733
random potentials insufficient to localise all electronic states in 1-dimens. 79−42481
random systems, localisation 80−80218
rare earth alloys, mixed-valence effect, limiting model of dilute alloy 77−47768
rare earth compound, valence fluctuation type, replicate core level XPS probe 80−25521
rare earth compounds, magneto-optical effects rel. to 4f electron excitation energies, XPS 77−52222
rare earth compounds, mixed-valence systems spatial correlations of rare-earth ions 79−19560
rare earth compounds, Raman light scatt., phonons and valence fluctuations, review 77−63415
rare earth dodecaborides, mag. susceptibility temp. depend., 90-1200K 80−20374
rare earth ion, R^{3+}, relativistic mag. form factors, Dirac-Fock calc. 77−40037
rare earth ions, Dirac-Fock exam. of electronic props. 79−56106

localised electron states continued
rare earth metal, lattice dynamics and scatt. reson. 78−59872
rare earth metal, s-core levels multiplet splitting, exchange correl. 78−10407
rare earth metals, d-band occupancy rel. to cryst. struct. 77−35510
rare earth metals, excitation energies, 3d electrons, relativistic calcs. 80−20109
rare earth metals, optical props., review 77−40259
rare earth metals and compounds, electronic phase transition 77−47773
rare earth monobismuthides, LCAO calc., electronic struct. *(Russian)* 77−39777
rare earth orthotitanates, $RTiO_3$, metallic and semicond. elec. and mag. props. 79−38068
rare earth orthovanades, $LnVO_4$:R^{3+}, R=Nd, No, Tm, Sm, Dy, Er, Eu, Tb, electronic struct. and spectra of VO_4, RO_8 clusters 78−10953
rare earth trichlorides, magnetic phonon splitting, Raman spectra 77−52099
rare earths, 3d X-ray spectra, 4f and 5f states 78−84681
rare earths, excitation energies for 4f electrons, relativistic calc. 78−72117
rare earths, struct. props. rel. to F electrons 78−83951
rare earths and their cpds., XPS satellites, screening of 3d holes 78−76586
rare earths cpds., Fano-resonances, surface and bulk effects in photoemission 80−97405
rare-earth oxides, absorption spectra and energy levels of trivalent ions 77−63420
rare-earth oxides, energy levels of trivalent ions 77−62874
resonance Raman scattering, appl. to ultrafast dephasing and relax. obs., phonon scatt. effects 80−7337
resonance Raman scattering in systems with localised carriers 80−7356
resonant phonon scatt. at trigonal Jahn-Teller centres 77−66010
resonant Raman scattering in systems with localised electron states, theory 79−15455
ruby:Cr^{3+}, diffusion of localised optical excitations and trap emission 77−24887
ruby, optical energy storage and retrieval 77−73165
secondary radiation spectrum of localised electrons interacting with nonequilib. vibrs. 80−2778
semiconductor, amorphous, electronic states, effect of local rearrangement modes 78−47696
semiconductor, amorphous, non-polaronic, cond. and thermopower near band edge 80−49719
semiconductor, amorphous or disordered, cond. mechanisms, model of medium-range comp. disorder 78−79994
semiconductor, barrier cond. mechanism, effects due to emptying of local levels by electric field 79−65468
semiconductor, core level spectra, electronic polaris. effects 79−90985
semiconductor, disordered, absorption edges, temp. depend. 77−77160
semiconductor, disordered, with soft Coulombic aperture, screening and absorpt. of long EM waves *(Russian)* 78−23001
semiconductor, donor levels, anomalous press. effects, Hall const. meas. 77−51693
semiconductor, doped, coexistence of insulating and metallic electronic phases 79−65385
semiconductor, excitation spectrum and optical props. in field of standing EM wave and homogeneous field 78−91625
semiconductor, ferromagnetic, with mag. impurities, low-energy localised states *(Russian)* 79−19543
semiconductor, layered, DC hopping cond. due to stacking disorder and electron localisation 77−47819
semiconductor, local level parameters from thermally stimulated excitation curves, influence of variations of rate of heating 80−6769
semiconductor, lone-pair, localised gap states valence alteration model 77−8040
semiconductor, XPS, core electron line shapes 78−11082
semiconductor nonhomogeneous, dimens. localisation of electrons *(Russian)* 78−19000
semiconductor or semimetal, screened and localised impurity states in 'optical' and exciton insulators *(Russian)* 77−62870
semiconductor-dielec. superlattice, high freq. electromagnetic response 78−19073
semiconductors, compensated and amorphous, hopping cond. and density of localised states 77−89763
semiconductors, elementary excitations in disordered systems with localised electrons, polarons *(Russian)* 80−49632
semiconductors, many-valley, localised impurity states with low binding energy 80−24835
semiconductors, many-valley, magnetic electron fluctuon states spin direct interactions 80−29364
semimetal, XPS, core electron line shapes 78−11082
shielded point defect potential well calcs. using Poole-Frenkel effect 80−20122
solid electrolyte, mobility paths for MI_4^{-3} clusters, ab initio electronic struct. calcs. 80−70458
solid state systems, electron localisation and spectra 79−15110
solid-electron interaction, nature and consequences 78−72230
solid-state theory, introduction, book 79−33215
spatially disordered system, two-dimens., localisation and conductivity exam. 78−18998
specific heat capacity, singularity at Anderson-Mott transition 80−34381
spectroscopy using synchrotron radiation 77−20882
spectrum of one electron Hamiltonians with impurities 79−1578
spin chain impurity zone fine struct. *(Russian)* 80−6787
spin-dependent correlated atomic pseudopotentials 80−107686
spin-phonon interaction, dynamic screening by carriers, effect on paramag. relax. times 77−16150
square lattice, electron localisation with site-diagonal and off-diagonal disorder 79−73472
Stark ladders in finite crystals 77−24540
structurally disordered systems, with diagonal and off-diagonal disorder in non-orthogonal basis set, numerical study 79−69387
substitutionally disordered, energy localisation, optical and ODMR spectra of triplet Frenkel excitons 80−54996
sulphides, of Cu,Ag,Zn,Cd,Ga,In, d-electron participation in chem. bonds 77−28682
superconducting localised state near dislocation, influence of impurities 80−10917
superconducting transition temp. enhancement by localised states, band struct., electron-phonon interaction 78−47902
localised electron states continued
superconductivity-ferromagnetism coexistence in two-band model *(Russian)* 80−84539
superconductor with magnetic impurities, EM penetration depth 77−66225
supercritical fluid metals, metal-insulator transition, quantal percolation method 79−56129
TCNQ, electron-mol. vib. coupling 77−15782
TCNQ alkali salt, spin-Peierls transition 80−29395
TCNQ complexes, Qn(TCNQ)$_2$, NMePh.TCNQ, and Li^+TCNQ^-, rel. to extrinsic and intrinsic mag. susceptibility 78−43556
TCNQ salt, $(TMA^+)_3(I_3^-)(TCNQ^-)_2(TCNQ^0)$, struct., phys. props. and lattice distortion evidence 78−6305
TCNQ salts, complex, with symmetric and asymmetric donors, transport and mag. props. 78−6315
TCNQ salts, electron localized and band motion, IR spectra 77−66487
ternary semiconductors, defect tetrahedral crystals, band structure 77−11850
p-terphenyl:pentacene, optical coherence and resonance decay 77−24859
p-terphenyl, hopping cond. among localised states 80−70861
p-terphenyl film, polycryst., charge carrier transport and DC cond. 80−70858
tetracene, hopping cond. among localised states 80−70861
tetracene, noncryst., localised valence states in forbidden gap 78−72113
tetracene, polycrystalline layer, hopping transport in localised states 79−65569
tetrahedral crystal, electron localisability by LCAO band theory, Pauling ionicity 77−47776
tetrahedrally coordinated solids, charge distrib., localised mol. orbitals 79−23560
tetramethylaminelithium(0), $Li(CH_3NH_2)_4$, existence, conduction- and localised-electron spin reson. 80−66035
tetramethylsilane, liquid, ground state energy of excess electrons 78−68976
theory of localisation in condensed matter, electrons, phonons and magnons 80−10905
tight-binding chains, off-diagonal disorder, density of states, localisation length 78−88247
transition matrix elements based on local atomic environment 77−39758
transition metal, 3d, energy parameter, Auger spectra, quasi-atomic behaviour 77−20966
transition metal, 3d, localised moments, detection by electron energy loss spectra 77−69949
transition metal, 3d, s-core levels multiplet splitting, exchange correl. 78−10407
transition metal, 3d, superatomic relax. and positions of inner levels 78−11069
transition metal, diffusion of C, electronic state effect *(Russian)* 77−1264
transition metal, itinerant-localised electron model for magnetism 78−14918
transition metal, lattice dynamics and scatt. reson. 78−59872
transition metal borides, charge state of B, core electron binding energies *(German)* 78−10391
transition metal chalcogenide, possible anionic clusters and mixed valence effects 78−43333
transition metal complexes, A_2MX_6, d-electron config., effects on phase transitions 77−35687
transition metal compounds, localisation of electrons, review 80−49650
transition metal compounds, phonon anomalies due to d-band effects, electron-phonon matrix elements 78−30720
transition metal hydrides, electronic struct., heat of formation, single particle lifetimes, Dingle temp. meas. 78−51923
transition metal interfaces 77−59313
transition metal ion system, multiplet and cryst. field split photoemission spectra 77−66577
transition metal sulphides, electronic struct. from X-ray emission spectra 77−28661
3d-transition metal-metalloid cryst. and glassy alloys, electronic struct. from magnetisation and Mossbauer meas. 80−29363
transition metals, 3d, core electrons, Sternheimer shielding-antishielding factor 80−39534
transition metals, 3d, electron impact excited soft X-ray spectra, resonances and many body effects 80−50468
transition metals, alloys, and cpds., XPS asymmetry of core electrons and electronic struct. parameters 80−93460
transition metals, double d-band model, delocalisation of electrons 77−76743
transition metals, itinerant and localised d-electrons, positron annihilation data 80−93428
transplutonium element symposium, Baden-Baden, Germany (September 1975) 77−28974
transport eqn. for system of localised states *(French)* 77−72845
transport equation in system of localised electron states *(French)* 78−56141
2,2,4-trimethylpentane, liquid, ground state energy of excess electrons 78−68976
trinitrofluorenone-polyvinylcarbazole, freq. depend. photocond. 77−8141
two-dimensional electron system in strong mag. field, Anderson localisation 77−15929
two-dimensional impurity bands, carrier-density dependence of activation energies associated with hopping 80−88561
two-dimensional localisation, real-space scaling study 79−65416
two-dimensional random potential, localisation of particles 79−60672
two-electron bond-orbital model of tetrahedrally coordinated solids 77−8000
vacancy-impurity scattering, complex dispersion law 78−87957
valence fluctuations, power spectrum 78−47742
valence model, local mixed, exact limit 77−51705
very large bonded systems, local formalism 77−4313
vibronic systems with localised electrons, reson. Raman scatt., hot luminesc. 79−38616
Wigner condensation, localisation of electrons in a magnetic field 79−60752
Wigner glass, effect of coexistence of random potential and electron-electron interaction 79−56169
Wigner instability, Mott's $T^{1/4}$ law as evidence 77−80751
X-ray photoelectron spectral characterisation of solids *(French)* 77−36367
zero-component classical field, electron localisation and statistical mechanics 78−30855

localised electron states continued
Ag, Auger $M_{4,5}$-VV spectrum, quasi-atomic final states 78−72688
Ag halides, localised MO treatment of fractional bonding 77−58970
Ag halides, valence and cond. states, UPS, temp. depend. 77−20997
Ag particles embedded in dielec. KCl medium, search for maximum metallic resist. 80−107756
Ag-As-Te glasses, elec. props. *(Russian)* 77−85211
Ag-Cu, optical spectra, 0.5-6 eV, d-band struct. 77−48168
Ag_n, n=7,10,13,19, atom clusters, local density of states, Xα scattered wave calcs. 78−18989
AgBr sensitized photolayer, overall spectra of local electronic levels 79−23933
AgCl(Br), thermal shifts in energy level separations, ESCA 77−8723
AgN_3, optical absorpt. spectra, and photoemission, electron band scheme 79−100015
Al, film, granular, transition to localisation, elec. resist. 80−70877
Al, granular supercond., normal state cond. 80−88529
Al, vacancy electron density, local electronic struct. theory 79−1580
Al-3d transition metal, dil., localisation of additional screening charge 79−47051
Al-Zn changes in inner-electron binding energies during ageing, electronic spectra study 77−28816
AlAs-GaAs LEDs, Ge or Zn-doped, mechanism of degradation 77−76911
AlF_3, localised electronic levels, thermoluminesc. and thermally stimulated current exam. 78−11001
AlH_3, I-V and relax. characts. in dark cond. 77−85235
AlH_3, localised states spectrum, photosensitivity 79−78135
AlH_3, photo-and thermochem. reactions, 200-350K, UV Induced local states 78−31667
AlN, effect of valence states on X-ray Compton line shapes 77−8682
Al_2O_3, noncrystalline films, opt. and elec. props. 77−51627
β-Al_2O_3-Na_2O, colour centre ESR by localised tunnelling states 80−108073
AmO_2, XPS of core and valence states obs. 77−48314
Ar, cryst., luminesc., absorpt. spectra, free, self-localised excitons coexistence *(Russian)* 78−31231
Ar, valence electron distrib., pseudopotential calcs. 80−2335
As-Se amorphous system, photocond. props. 80−88587
As-Se-Tl system, chalcogenide glasses, NMR spin-lattice relax. time meas. 79−95671
AsI_3, photopolarisation, photoelectret state, electron-hole transitions 77−12300
As_2S_3, amorphous, band-to-band luminesc., electronic band states 79−61432
As_2S_3 and As_2S_3-Sb_2S_3 system glasses, long-term photocond. relax. 77−76874
As_2S_3 film, evaporated, switching effects 80−96952
As_2S_3 glass, localised paramag. states, As_4S_6, As_4S_4 units, mol. analogue models 78−60087
As_2S_3 thin glassy films, hole drift mobility, interaction with deep localised levels 80−11117
As_2S_3 vitreous, Ag, Cu, Sn and Ge impurities infleunce on electrophys. props. 77−76826
As_2S_3:Ag, vitreous, doping influence on photolum. at 77K 77−77293
$As_2S_3(Se_3)$, vitreous, photostimulated light absorpt. 77−77221
$As_xS_{100-x}(Se_{100-x})$, localised states density near valence band edge *(Russian)* 80−103638
AsSe, molten semicond., pseudogap, elec. cond. and optical absorption meas. 77−8160
As_2Se_3, amorphous, transient hole transport props., trap controlled hopping model 77−47820
As_2Se_3, amorphous radiative interband recombination 80−66286
As_2Se_3, glass, density of optically induced localised paramagnetic states 78−52354
As_2Se_3, molten semicond., pseudogap, elec. cond. and optical absorption meas. 77−8160
As_2Se_3:Al, glassy, energy spectrum of deep localized states, thermal dielectric relaxation 78−15088
As_2Se_3-As_2Te_3, vitreous, localised states role in cond. in high elec. fields 77−76841
As_4Se_5Ge, glass, light irrad. induced changes in optical and elec. props. *(Japanese)* 78−68031
As_2Te_3, chalcogenide glass film, charge screening length 79−23974
As_2Te_3, glassy, field depend. elec. cond. and localised states role 77−76829
$As_xTe_{90-x}Ge_{10}$, $As_{35}Te_{55}Ge_{10-x}Si_x$ glasses, elec. and optical props., comp. depend. 77−24555
$As_{30}Te_{48}Si_{12}Ge_{10}$, chalcogenide glass film, charge screening length 79−23974
Au-3d transition metal alloys, UPS study, localised states 80−93449
Au-Ag, optical spectra, 0.5-6 eV, d-band struct. 77−48168
Au-Cu, optical spectra, 0.5-6 eV, d-band struct. 77−48168
β-B, rhombohedral, AC cond. meas., 150 to 300K, hopping cond. mechanisms 80−15521
β-B, rhombohedral, localised states charact., review, book contrib. 78−47728
BN, chem. bonding and electronic struct., AES and SIMS meas. 80−50512
B_2O_3, chem. bonding, electronic struct., ESCA, Auger, and SIMS spectra 80−50512
BaF_2, XPS, core-electro peaks, satellite and loss structs. 77−66571
$BaMnF_4$, luminesc., emission from localised traps 79−33777
$Ba_2NaNb_5O_{15}$, ferroelectric, local states, thermoluminesc. study 80−60690
$BaTiO_3$:^{89}Zr, electron capture decay lifetime, struct. environment effects 77−28523
Be, anisotropy, theoretical investigation by K-emission, APS, and Compton profiles 78−63970
Bi, film, oxidation, UPS, valence band, cond. band and 5d core states 77−20995
Bi, solid and liq., core-level line shape, high-resolution XPS meas. 77−59668
Bi-Sb alloy film, rel. to amorphous nature, AC and DC cond. and Hall coeff. obs. 80−11114
BiI_3, excitonic shifts of quasiatomic optical core to cond. band transitions, UPS obs. 78−11079
BiI_3, photopolarisation, photoelectret state, electron-hole transitions 77−12300
$Bi_{86}Sb_{14}$:Te, single crystal, dispersion of magnetoplasma waves *(Russian)* 80−70739

localised electron states continued
BiTeI-SbTeI, solid solns., phase diagrams, photocond., elec. props. 79−38125
BkO_2, XPS of core and valence states obs. 77−48314
C, elec. cond. at low-temp. as function of freq., hopping cond. between localised states 79−23965
CC NiO, amorphous, charge transport in band tails 78−76026
CaF_2, XPS core electron peaks, satellite and loss structs. 77−66571
CaF_2:Eu^{2+}, second order perturbation in vibronic system 78−30893
CaSe:Pb^{2+} phosphors, luminesc., refl., emission, and excitation spectra 79−11456
$CdCr_2Se_4$, optical absorption due to transitions between bands and local levels 79−38537
$Cd_{0.93}Cu_{0.07}Cr_2Se_4$, single cryst., ferron formation 79−7848
$Cd_xFe_{3-x}O_4$, cond. mechanism, collective electron description 77−4588
CdS, localised level anal. from generation-recomb. noise spectra 78−14777
CdS, powder, mechanically induced localised states in energy gap 80−2354
$CdSiP_2$, electronic struct., X-ray spectroscopic investigation 80−108300
CdTe, amorphous, photocond., effective density of localised states 77−28210
CdTe:Cl, semi-insulating, impurity photocond. spectra, local state distrib. in band gap 80−107865
CeAs, XPS for electronic struct. determ. 79−33888
$CeCl_3$, doubly degenerate phonon states, mag. field dependent splitting 77−16320
$Ce(Cu,Ni)_2$, pseudobinary phases, struct. and mag. props. rel. to Ce valence 78−6032
$CeCu_2Si_2$, tunnelling anomalies due to intermediate valence phenomenon 77−62873
CeN, XPS for electronic struct. determ. 79−33888
CeP, XPS for electronic struct. determ. 79−33888
CeP_5O_{14}, photoemission spectra, 4f, 5p and 5s giant reson. enhancement 78−95660
$CePd_3$, mixed-valence, 3d and 4d core levels, XPS study 80−89111
$CePd_3$, tunnelling anomalies due to intermediate valence phenomenon 77−62873
$CeRh_{3-x}Pd_x$, electronic and cryst. struct. comparison, catalytic behaviour 78−84398
CeSb, XPS for electronic struct. determ. 79−33888
$CeSn_3$, low temp. mag. behaviour, press. induced valence change 77−63078
Cf_xO_y, XPS of core and valence states obs. 77−48314
CmO_2, XPS of core and valence states obs. 77−48314
Co, Co alloys, electrical resistivity and specific heat meas., anomalies rel. to thermally excited states 80−6809
$Co_2Ga_{2-x}Fe_x$, elec. resist., temp. and mag. field depend., mag. contrib. 80−96846
$CoS_2(Se_2)$, core-level and valence-band XPS 80−93450
Cr alloy, localised magnetic moments in band antiferromagnets, impurity interactions *(Russian)* 80−54888
$CrTe_{1-x}Se_x$ (Sb_x), Curie temp., high press. and doping effects *(Russian)* 77−12125
Cs-Au liq. alloy, formation of localised electronic states, NMR obs. 80−93201
$Cs_3BiSbBr_9(Cl_9)$, ^{121}Sb Mossbauer chem. shifts, optical reflectance spectra, solid state band populations 77−40162
Cu atom in bulk, local density of states 79−37947
Cu, $L_3M_{4,5}M_{4,5}$ and $M_{2,3}M_{4,5}M_{4,5}$ Auger line shapes, independent electron calc. 77−63500
Cu on Ag (001), ultrathin film electronic states calc. 78−6318
Cu, positive muon spin rotation frequency, Knight shift meas. 79−38421
Cu-As-Se glass, localised states exam. *(Russian)* 78−34806
CuBr, UPS, temp. depend., dynamic hybridisation 77−20998
$Cu_{0.67}Cr_{1.78}Se_{2.67}Br_{1.34}$, ferrons and mag. and elec. props. 79−7846
CuH, electronic struct., heat of formation, single particle lifetimes, Dingle temp. meas. 78−51923
$Cu_{0.75}VS_2$, cryst. struct. and phys. props. *(French)* 78−14328
D_2O, effect of phase density on ionisation process and electron localisation 77−89731
Eu chalcogenides, paramagnetic, optical orientation of 4f electrons 77−69799
Eu+t_2, high press. Mossbauer spectra, interconfig. charge fluctuations 77−63341
$EuCu_2Si_2$, XPS studies, valence band, 4-f region 78−6831
$Eu_{0.25}La_{0.75}Rh_2$, high press. Mossbauer spectra, interconfig. charge fluctuations 77−63341
EuO, nonstoichiometric film with excess EU, effect on elec. resist. and Curie temp. 79−8204
EuO:Eu, doped ferromag. semicond., carrier density and mag. susceptibility rel. to M-S transition 77−72820
$EuO_{1-x}N_x$, ferromag. semicond., elec. and mag. props. *(French)* 78−79993
EuO(S), ferromagnetic electronic structure, absorption, thermoreflection and thermotransmission spectra *(French)* 80−97300
$Eu_3O_4(S_4)$, mixed valence system, inelastic light scatt., photoluminesc. 77−90145
$EuRh_{2-x}Pt_x$, intermediate-valance state, XPS obs. 77−28687
Eu_3S_4, inelastic light scatt., photoluminesc., anomalous vibr. 77−48229
Fe 2p states in Fe and Fe alloys, XPS 78−52625
Fe complexes, S-bridged binuclear, orbitally dependent exchange 77−24688
Fe, effect of valance state on X-ray Compton line shape 77−8682
Fe, electronic structure, influence of temp., X-ray photoelectron study 77−28681
Fe, excitation of 1s core-level photoelectrons with synchrotron radiation 78−19632
Fe-Al compounds, X-ray emission investig. of electron localisation in valence zone *(Russian)* 77−48277
Fe-O compounds, MO cluster calc. of charge densities and elec. field gradients 77−76783
FeB and Fe_2B, multiplet splitting of ESCA Fe 3s core levels 80−29847
$Fe_{70}Cr_{30}$, disordered, X-ray spectra study of electronic struct. 77−77324
FeF_2, electronic struct., charge density and elec. field gradient, MO cluster calc. 77−51704
FeF_3 film, elec. cond. mechanisms 79−99649
FeF_3 film, localised electronic states effect on elec. cond., MIM struct. meas. 80−20328
FeF_3, thin film, optical absorpt. meas., electronic transitions from localised states in forbidden band 79−15546

localised electron states continued
Fe_3O_4, magnetic after-effect by valency fluctuations assoc. with cond. transition 77−8365
Fe_3O_4, magnetite, charge order-disorder and metal-insulator transition 77−20241
Fe_3O_4, SCF X_α calcs. of one-electron energy levels 78−47727
Fe_xO, wustite, width of d-level final-state struct. obs. in XPS 78−19633
FeS_2, core-level and valence-band XPS 80−93450
GaAs, 3d core level spectra, electronic polarisation effects 80−6765
GaAs (110), oxidation, 3d core level binding energy, multiple bonds 78−35543
GaAs (110), oxidation, 3d core level binding energy, single bonds 78−35544
n-GaAs, electronic transition scheme via radiative centres 77−69905
GaAs, piezoelectric constant due to bond bending, electron redistribution effect 79−38457
GaAs, Schottky diode, trap levels, admittance spectroscopy 79−51672
GaAs, self-consistent localised electronic struct. 79−42445
GaP, 3d core level spectra, electronic polarisation effects 80−6765
GaP, core levels, chem. shift and relaxation energy, temp. dependence 80−39520
GaP, core levels, temp. depend. of conduction band and core exciton energies 80−24828
GaP, line shape and symmetry analysis of core-level electroreflectance spectra 77−8600
GaP:O, optical transitions via deep levels, phonon interaction 78−87939
GaP:O, optical transitions via deep levels, cross section temp. depend. 78−87940
GaSb, 3d core level spectra, electronic polarisation effects 80−6765
GaSe, core level excitation effects, synchrotron radiation UPS study 80−40234
GaSe, core-level photoemission anisotropy 78−11076
GaSe, layered, DC hopping cond. due to stacking disorder and electron localisation 77−47819
GaSe MSM struct., inelastic tunnelling investigation of lattice dynamics, electron-phonon interaction 80−20330
GaSe, photocond., influence of stacking disorder 80−2422
Gd in CsCl type alloys, exchange between localised 4f and cond. electrons 77−63279
Gd, magneto-optical Kerr effect in UV region, 4f excitations and binding energy 77−52127
$Gd_{0.67}La_{0.33}P_5O_{14}$, photoemission spectra, 4f, 5p and 5s giant reson. enhancement 78−95660
Ge, amorphous, Cayley trees appl. 79−65373
Ge, amorphous, Mott's parameters for hopping cond., effect of annealing 77−69324
Ge, amorphous film, annealing, effect on localised states 79−4535
Ge amorphous films, high elec. field cond. and magnetoresist. at 4.2K 80−49748
Ge amorphous films, self-ion bombard., electronic props. 79−28422
Ge, effect of valence state on X-ray Compton line shape 77−8682
a-Ge, elastoresistive effects 79−60838
Ge, electron states associated with core region of 60° dislocation 78−39057
Ge film, amorphous, high field effects, 100-300K 77−24563
Ge, self-consistent localised electronic struct. 79−42445
Ge surface, Cl chemisorption, cluster calc. by iterative EHT 77−32062
n-Ge:As closely compensated, photolum. of charge carriers localised in trails of density of states 77−77294
Ge:Sb, amorphous, electronic transport props. 80−44589
Ge-Mo amorphous semicond.-granular metal film system, elec. transport and thermopower 77−76984
Ge-Se glasses, radiative localised centres, photoluminesc. 79−83025
Ge-Si, electronic structure, short-range order effects, calc. 80−92861
Ge-SiO_2-p^+Si tunnel junctions, for determ. of AC cond. of amorphous Ge 77−24608
$GeSe_2$ glass, photoluminesc. spectrum, rel. to cryst. forms 77−55819
$Ge_{0.08}Se_{0.92}$, molten semicond., pseudogap, elec. cond. and optical absorption meas. 77−8160
Ge_xSe_{1-x}, amorphous semicond., elec. props. 78−84219
Ge(100) surface electronic state localisation, layer density of states calcs. 80−6931
H_3BO_3, chem. bonding, electronic struct., ESCA, Auger, and SIMS spectra 80−50512
H_2O, crystalline ice, localised excess electrons yield studied as function of dose rate 80−97712
H_2O, liq. and ice, localised excess electrons, semicontinuum models 78−73129
He, liquid, nonlinear cyclotron resonance of localised surface electrons *(Russian)* 77−59318
He liquid surface, localised electron states 78−60007
^{3}He liquid, electron spectra of localised electrons above surface *(Russian)* 80−29241
^{4}He, electron localisation, mobility in dense low temp. gas 80−92247
Hg, expanded fluid, optical props., localisation of electronic states 79−19902
Hg-Xe solid films, optical absorpt., localised states 79−61452
Ho, soft X-ray APS of 4f states 77−24911
In film, polycrystalline optical transitions from d core states 77−85827
In, outer core d level linewidths determ. using synchrotron radiation 77−44118
InP injection laser, strong mag. field effect on emission 77−58329
InSb, elec. cond. in intense mag. field, freeze out, hopping 77−20338
n-InSb, galvanomag. props. at low temp., carrier localisation, metallic impurity cond. 77−28195
n-InSb, spin flip Raman scatt. from electrons in localised donor states 77−3630
InSe, core-level photoemission anisotropy 78−11076
K, core thresholds, inelastic electron scatt. spectra meas. 79−95359
K, pseudowavefunctions calc. 77−43542
KBr:Ag, formation of electron centres and self-localised holes, ESR exam. 78−91947
KCl:Ag(Tl), formation of electron centres and self-localised holes, ESR exam. 78−91947
KCl:Tl, neutron scattering from localised electronic excitation, theory 79−4539
$KCoF_3$, XPS of band struct. 77−11851
$KCuF_3$, XPS of band struct. 77−11851
$KFeF_3$, XPS of band struct. 77−11851
$KMnF_3$, luminesc., emission from localised traps 79−33777
$KMnF_3$, XPS of band struct. 77−11851
localised electron states continued
$KNiF_3$, XPS of band struct. 77−11851
$K_2Pt(CN)_4Br_{0.3}.3H_2O$, Krogmann salt, non-empirical localised orbital cal. of electronic struct. 78−91636
$K_2Pt(CN)_4Br_{0.3}.xH_2O$, transport props. x depend., CPA calc. of screened random pot. 77−39828
$KZnF_3$, XPS of band struct. 77−11851
La, electron impact excited soft X-ray spectra, resonances and many body effects 80−50468
La, low temp. P-T diagram 77−47550
$LaCoO_3$, Mott isolator, paramag. props., calc. 80−93071
La_2O_3, 4f states of La, diagram lines in L-spectrum obs. 77−20959
$La_{1-x}Pb_xMnO_3$, spin polarised XPS and UPS, elec. struct. 77−8717
$La_{1-x}Sr_xCrO_3$, x=0-0.2, AC and DC cond., 77-1300K, hopping of polarons 78−2477
Li, Auger widths of core levels calc. using diagrammatic many-body technique 77−43544
Li, plasmon satellite struct. in (e,2e) process 80−96809
Li, pseudowavefunctions calc. 77−43542
Li_3AsO_4, electronic struct. of AsO_4^{3-} clusters 79−65417
LiCl aqueous glass, X-irradiated, localised electron optical, IR and photoconductivity spectra 78−73064
LiCl-D_2O, aq. 10 M glass, optical absorpt. spectra after X-irrad., electron scavenging efficiency 79−83476
LiF, defect state model for localised excitations 77−43529
LiF, effect of valence state on X-ray Compton line shapes 77−8682
LiF film, electronic excitations, inelastic electron scatt. spectra 77−32479
LiH, layers and solid, localised HF orbitals 78−9076
Li_2O-BaO-Al_2O_3-SiO_2-xTiO_2 glass, X-ray spectra, Ti ion electron config. *(Russian)* 77−8674
Li_2SeO_4, electronic struct. of SeO_4^{2-} clusters 79−65417
$LuCoO_3$, spin-state equilib. 77−12087
Mg-Bi alloy, liq., far IR reflectivity rel. to possible transport processes 78−2827
Mg-Cu alloy, electronic struct., X-ray emission obs. 77−16428
Mg-Ga(Ge), electronic struct., X-ray spectra *(Russian)* 77−48279
$MgAl_xSc_xFe_{2-x-y}O_4$, X-ray spectra Mossbauer spectra, electronic struct. of Fe and Sc 77−28647
MgF_2, localised electronic levels, thermoluminesc. and thermally stimulated current exam. 78−11001
MgF_2, XPS, core-electron peaks satellite and loss structs. 77−66571
MgO, effect of valence state on X-ray Compton line shape 77−8682
MgO, valence electron distrib., pseudopotential calcs. 80−2335
MgO-CaO-FeO(Fe_2O_3)-Al_2O_3-SiO_2 glass, X-ray spectra Fe ion electron config. *(Russian)* 77−8674
$MgSiP_2$, electronic struct., X-ray spectroscopic investigation 80−108300
$Mg_2V_2O_7$, elec. props. and EPR meas. 79−11114
MnAs, high spin state electron config. *(Japanese)* 77−43812
$MnAs_{0.925}P_{0.075}$, low spin state electron config. *(Japanese)* 77−43813
$MnAu_2$, helical antiferromagnetic compound, optical props. and electronic struct., visible and IR obs. *(French)* 80−45101
$MnS_2(Se_2)$, core-level and valence-band XPS 80−93450
Mo, calc. using SCF-Xα-SW method 77−15797
Mo, electron states, localised and itinerant features using mixed-basis representation of crystalline wave functions 79−60748
MoO_4^{2-}, valence level electron struct. by XPS 77−4712
$MoSe_{2-x}$, transport meas. and band structure 77−69361
N_2, solid, self-localisation of high frequency triplet excitations *(Russian)* 79−8176
ND_3, effect of phase density on ionisation process and electron localisation 77−89731
NH_3, dense vapour, electron localisation 80−44558
NH_3, liq., localised excess electrons, semicontinuum models 78−73129
Na, Auger widths of core levels calc. using diagrammatic many-body technique 77−43544
Na, core thresholds, inelastic electron scatt. spectra meas. 79−95359
Na, plasmon satellite struct. in (e,2e) process 80−96809
Na, pseudowavefunctions calc. 77−43542
NaBr(:I), exciton ionisation and decay, photoluminesc. in elec. field 77−44046
NaCl, interatomic Auger processes 77−85892
NaCl, valence electron distrib., pseudopotential calcs. 80−2335
NaCl:Ag, formation of electron centres and self-localised holes, ESR exam. 78−91947
$NaMnCl_3$, antiferromagnet, exciton self-localisation luminesc. and excitation spectra *(Russian)* 80−11456
Na_2O-B_2O_3-SiO_2-As_2O_3(As_2O_5) glasses, DC and AC resist., bipolaronic hopping cond. 80−88558
Na_xVS_2, Na_xVSe_2, charge density waves, electron localisation 79−47038
Na_xWO_3, ($0.22 \leq x \leq 0.84$), ^{183}W NMR, electronic struct. near metal-semicond. transition, Knight shift 78−48063
Na_xWO_3 bronze, XPS of W 4f levels 78−95648
Na_xWO_3, core level photoelectron spectra, final state effects 80−50509
Na_xWO_3, cubic, final-state effects in XPS 77−90251
Na_xWO_3, metallic, XPS, initial and final states, WO_3 binding energy 79−95898
Nb, binding energies and chemical shifts *(French)* 77−44541
Nb, charge density distortions and lattice dynamics 78−30714
Nb-Al_2O_3 composite, semicond. films, cond. on localised states 77−24628
$Nb_3Al_{0.8}Ge_{0.2}$, supercond., sp. ht. meas., rel. to band density of states 77−28296
NbO, binding energies and chemical shifts *(French)* 77−44541
NbO_2, binding energies and chemical shifts *(French)* 77−44541
NbO_2, rutile phase, energy levels, momentum density, and Compton profile, embedded cluster model 80−50453
Nb_2O_5, binding energies and chemical shifts *(French)* 77−44541
Nb_2O_5, partly reduced, mag. and elec. props. 77−43593
$Nd_{1-x}Sr_xCoO_3$, Anderson transition, elec. cond. meas. 77−51786
Ni, (001) surface, local density of states, asphericity of pot. and charge transfer, ab initio self-consistent calcs. 79−15064
Ni compound, $[Ni_3(CO)_6]_n^{2-}$, n=1,2, one-electron states in polynuclear carbonyls 79−95358
Ni, core level excitation effects, synchrotron radiation UPS study 80−40234
Ni, electronic structure, influence of temp., X-ray photoelectron study 77−28681
Ni, photoemission spectra, valence band and core level satellite due to excitation of d electron 80−97408

localised electron states continued
Ni-Au alloy, electronegativity and core electron binding energy shifts of Au 77−15346
$Ni(CO)_4$, bonding, shakeup energies, and shakeup intensities for photoelectron spectra 80−50528
$Ni_{1-x}Co_xS_2$, elec. cond., thermoelec. power and optical meas. 80−59986
$Ni_{1-x}Co_xS_2$, elec. transport and semicond.-metal transition 80−10985
$NiS_2(Se_2)$, core-level and valence-band XPS 80−93450
NpO_2, XPS of 5f electrons 77−73216
NpO_2, XPS of core and valence states obs. 77−48314
OsO_4^{2-}, valence level electron struct. by XPS 77−4712
Pb and compounds XPS 77−44118
Pb film, polycrystalline, optical transitions from d core states 77−85827
Pb granular film, Josephson coupled, resistive transition 80−88683
Pb, granular film, superconducting, Josephson-coupled, role of clusters in localisation 80−39716
Pb-Te, molten mag. susceptibility, conc. and temp. depend. 78−80121
PbI_2, cryst., photocond., energy gap localised level obs. 78−43443
PbI_2, excitonic shifts of quasiatomic optical core to cond. band transitions, UPS obs. 78−11079
PbI_2 film, photolyzed, refr. index change 78−11010
PbI_2, TSC meas., localised levels in energy gap, depend. on purity and history 77−15856
$Pb_{1-x}In_xTe$, $0.01 \leq x \leq 0.2$, elec. cond., Hall coeff. liquid He temp. 78−47815
$Pb_{1-x}Sn_xTe$:In, tunnelling impurity self-localisation, anomalous props. nature *(Russian)* 80−59915
$PbTiO_3$, photocond. and TSC meas. 77−15911
$PbZrO_3$:^{89}Zr, electron capture decay lifetime, struct. environment effects 77−28523
Pd on Ag (001), ultrathin film electronic states calc. 78−6318
Pd, photoemission spectra, valence band and core level satellite due to excitation of d electron 80−97408
Pd-Ag alloys, photoelectron spectra of core electrons 79−100021
Pd-Ag(V), H mobility and solubility, appearance pot. spectra obs. 80−55231
Pd-Au alloy, electronegativity and core electron binding energy shifts of Au 77−15346
Pd-H sytem, electronic struct. of H, mol. cluster and pseudojellium models 80−24832
PdH, electronic struct., heat of formation, single particle lifetimes, Dingle temp. meas. 78−51923
Pr, localised 4f shell breakdown under press. 80−70411
$Pr_{1-x}Sr_xCoO_3$, Anderson transition, elec. cond. meas. 77−51786
Pt, 5d band structure effects on line shapes and intensities of core electron excitations 78−92177
Pt compound, $[Pt_3(CO)_6]_n^{2-}$, n=1,2, one-electron states in polynuclear carbonyls 79−95358
Pt, core level excitation effects, synchrotron radiation UPS study 80−40234
Pt-Au alloy, electronegativity and core electron binding energy shifts of Au 77−15346
Pt-Cu, ESCA study 80−2923
Pt-Ni alloys, XPS d bands and core levels 77−32498
$PtCl_3Pt(NH_3)_4$, Magnus' Green Salt, extended localised holes charge distrib. 77−55496
PuO_2, XPS of 5f electrons 77−73216
PuO_2, XPS of core and valence states obs. 77−48314
PuP, electronic ground state, neutron diffr. 77−15789
RbCl(Br)(I), thermal shifts in energy level separations, ESCA 77−8723
ReO_4^-, valence level electron struct. by XPS 77−4712
Sb-S-I system crystals and glasses, adhesion levels, TCE spectra 77−24529
SbI_3, photopolarisation, photoelectret state, electron-hole transitions 77−12300
SbSI-BiSI, solid solns., phase diagrams, photocond., elec. props. 79−38125
$(Sb_2S_3)_{0.95}(Na_2S)_{0.05}$, condensate, local states and switching effect 80−20336
Se, amorphous layer, localised states in band gap 80−59928
Se film, amorphous, density of localised states 78−34742
Se, glassy, localised electronic states, photoluminesc. and ESR studies 80−65501
Se, liquid, electrical cond. transition at high temp. and press., Anderson localisation *(Russian)* 77−1462
Se, trigonal single crystal, dark current relax., barrier cond. mech. 80−6904
Se-Te-Sb glasses, electronic transport 80−88579
Si, 2p hole core level spectra, electronic polarisation effects 80−6765
Si, amorphised by ion implant., localised states and cond., irrad. and heat treatment, doping 80−39529
Si, amorphous, electronic struct. and optical dielec. function, LCAO calc. 79−42478
Si, amorphous, glow discharge deposited, mobility edge calc. 80−80220
Si, amorphous, hydrogenated, electronic density of states determ. from Schottky diode meas. 80−49907
Si amorphous, ion implantation, negative magnetoresist., localised mag. states 80−70731
Si, amorphous, rel. to transport results, interpretation 80−80260
Si amorphous film, rel. to hole carrier transport 80−2500
Si, amorphous film, TSC, density of localised states distrib. 80−65587
Si amorphous films, self-ion bombard., electronic props. 79−28422
Si, core levels, chem. shift and relaxation energy, temp. dependence 80−39520
Si, core levels, temp. depend. of conduction band and core exciton energies 80−24828
Si, dangling bonds, EPR, localised states and unpaired electrons on microcrack surfaces 78−52351
Si, electron states associated with core region of 60° dislocation 78−39057
Si film, amorphous, effects of annealing of gap states 78−72115
Si, glow discharge deposited, optical spectra, reflectance, dielectric function and oscillator strength 80−11492
Si, impurity states, localised orbital approach 80−92851
Si inversion layers, high field magnetocond. 77−32020
Si inversion layers, magnetocond. in ground Landau level, defect diffusion in Wigner cryst. 77−39914
Si, inversion layers, magnetic localisation of electrons 78−43481
Si, pure and heavily doped, 2p core levels and core exction binding energy, photoemission obs. 78−76583
Si surface, Cl chemisorption, cluster calc. by iterative EHT 77−32062

localised electron states continued
Si:Au surface, electronic props. 77−66194
Si:H, amorphous, mobility edge position using continuous random network model for struct. 80−44544
a-Si:H, depletion width determ. by analytical model 80−100445
Si:H,B, amorphous, field effect and thermoelec. power 80−96924
Si:H,Li, amorphous, DC electrical conductivity, absorption edge and IR meas., role of H 80−54694
Si:H amorphous sputtered films, optical gap, IR absorpt. meas. 80−50320
a-Si:H:F, depletion width determ. by analytical model 80−100445
Si:H(F), amorphous, Schottky barrier profiles, depletion region width 80−49871
Si:Li, amorphous density of localised states from position of Fermi energy at zero temp. 79−69142
Si:O, semi-insulating polycryst. film, cond. through localised and extended states 77−28268
Si:P, amorphous, CVD, substitutional doping, electronic props. 79−23923
Si:P, CVD amorphous film, electronic density of states 79−46993
Si:P, heavily doped, metallic region, resist. decrease due to ESR 77−16178
Si:P,B, amorphous, localised level density 79−56168
Si:P amorphous films, doping and annealing effects on localized states, ESR meas. 79−38380
$Si:P^+$, Zeeman energy transfer at surface layer 80−11247
Si:Sb, amorphous, electronic transport props. 80−44589
$Si\text{-}As_2Se_3Ge_4$ heterojunction, elec. props. 78−6434
$Si\text{-}SiO_2$ interface, unwanted effects of ions in SiO_2 layers, review 80−92985
$Si\text{-}SiO_x$ interface, localisation in inversion layer due to states in gap of oxide 77−12012
$Si_{1-x}B_x$:H, amorphous films, thermopower and cond. for mixed band and broad tail state cond. 80−49786
$Si_{12}Ge_{10}As_{30}Te_{48}$, vitreous, localised states role in cond. in high elec. fields 77−76841
$Si_xGe_{1-x}O_2$, $0 \leq x \leq 1$, XPS and UPS, electronic struct. 77−48318
Si_3N_4, amorphous, charge transport in band tails 78−76026
SiO_2, core levels, chem. shift and relaxation energy, temp. dependence 80−39520
SiO_2, core levels, temp. depend. of conduction band and core exciton energies 80−24828
SiO_x thin film dielec., in MIM struct., interfacial props. rel. to non-stoichiometry 80−80399
Sm metal, XPS evidence for weak surface divalent component 77−39808
SmB_6, mixed valence cpd., EPR and heat capacity obs., metal-semicond. behaviour 80−20456
SmB_6, valence mixing, XPS 77−21000
SmB_6, XPS of 4f-levels, Sm^{2+}/Sm^{3+} valence ratio 77−63537
$SmCo_5$, electronic struct., X-ray photoelectron spectra 77−20992
$Sm_{1-x}Gd_xS$, phase transition temp. depression by mag. field, hybridisation 77−62828
SmS, electronic config., Mossbauer spectra meas. 77−16228
SmS, metallic, optical refl. investig. of valence fluctuations 77−63428
SmS, mixed valence states at surface 77−20398
SmS, nonorthogonal orbitals in intermediate valence 78−43323
SmS, phase diagram in p-T plane, theory 79−28278
Sm_3S_4, magnetic susceptibility and valence fluctuations 77−8266
Sm_3S_4, mixed valence system, inelastic light scatt., photoluminesc. 77−90145
$Sm_{1-x}Y_xS$, CPA calc. of rare-earth impurity, valence change 77−63096
$Sm_{1-x}Y_xS$, electronic config., Mossbauer spectra meas. 77−16228
Sn film, polycrystalline, optical transitions from d core states 77−85827
Sn, outer core d level linewidths determ. using synchrotron radiation 77−44118
n-SnO_2, high resist., photoelectronic processes 78−60157
$SnS_2(Se_2)$, optical transitions from d core levels 80−45105
SrF_2, XPS core-electron peaks, satellite and loss structs. 77−66571
$Sr_2Fe_xRu_{1-x}O_4$ solid soln., Mossbauer spectrosc. study 80−50235
TTF-TCNQ, transport props. of dynamically disordered chains 78−72137
1T-TaS_2, pure and cation-doped, charge carrier localisation 80−44597
TaS_2(1T) pure and doped, electrical, structural and mag. props. 79−78141
TaS_2(1T) pure and doped, Mott and Anderson localisation, commensurate phase transition 80−39641
Te, dislocations influence on galvanomag. props. 80−54722
Th, local model pseudopotential applic. to lattice dynamics 77−39646
Th, XPS of 5p level, screening and configuration interaction effects 80−54633
ThF_4, 5d X-ray spectra, degree of localisation 78−88382
ThH_2:Er^{3+}, EPR of Er localised electron mag. states, Kondo effect 80−25202
Th_4H_{15}:Er^{3+}, EPR of Er localised electron mag. states, Kondo effect 80−25202
ThO_2, 5d X-ray spectra degree of localisation 78−88382
Ti, X-ray emission spectra, $K\beta_{1,3}$ line width and $K\beta_5$ band 78−2946
TiC, TiC_6^{20-} cluster electron state, MS $X\alpha$ calculations 77−8037
TiC_x, single cryst., core level shifts, valence band struct., ESCA 77−32499
TiO_2, core levels, cryst.-field splitting, X-ray emission study 80−66328
TiO_2:Ta, Ti^{3+}-Ti^{3+} exchange interaction *(French)* 77−89945
TiO_x, X-ray emission spectra, $K\beta_{1,3}$ line width and $K\beta_5$ band 78−2946
Ti_2O_3, IR refl. spectra, IR active phonons, Ti 3d electronic effects 78−35145
Tl, core level binding energies, UPS obs. 80−66388
TlCl, UPS, valence band struct., dynamic hybridisation 77−20999
$Tl_2SeAs_2Te_3$, amorphous semicond., nuclear spin-lattice relaxation by localised electronic states, modification by spin diffusion 78−52372
TmSe, metallic, optical refl. investig. of valence fluctuations 77−63428
UAs and UPd_4, localised cryst. field states, neutron inelastic scatt. obs. 78−14697
β-UD_3, electronic props., metallic character 80−6693
UO_2, 5d X-ray spectra degree of localisation 78−88382
UO_2, electronic distributions by X-ray spectroscopy 80−97407
UO_2, electronic struct. and Coulomb correl. energy, XPS and bremsstrahlung spectra 80−55272
UO_2, localised versus itinerant 5f electrons exam., reflectivity meas. 79−19905
UO_2, Mg $K\alpha$ and He(II) photoelectron spectra, origin from multi-configurational Dirac-Fock calcs. 80−66387

localised electron states continued
UO_2, U_2O_5, U_3O_8, and UO_3, bonding and valence obs. by ESCA and EPR 77−28696
UO_2, uranyl cpds., X-ray photoemission spectra obs. of electronic struct. 77−28695
UO_{2+x}, possible anionic clusters and mixed valence effects 78−43333
UO_3, 5d X-ray spectra degree of localisation 78−88382
UPd_3, crystalline electric field levels of U, neutron scatt. exam. 78−60267
USb, localised versus itinerant 5f electrons exam., reflectivity meas. 79−19905
USb, UPS and XPS, surface oxidation 80−7465
$(U_xTh_{1-x})S$, metallic, 5f virtual bound states, elec. resist. and mag. susceptibility meas. 77−28363
$(U_xTh_{1-x})Se$, metallic, 5f virtual bound states, elec. resist. and mag. susceptibility meas. 77−28363
$(U_xTh_{1-}x)S(Te)$ solid solns., electronic struct., mag. susceptibility and elec. resist. obs. 77−20551
V, and its cpds. with light elements, surface state, XPS investigation 78−11070
V, effect of valence state on X-ray Compton line shape 77−8682
V oxides, XPS and AES study, electron correl. effects, semicond.-metal transition 80−7467
V, supercond., soft modes, d-electron localisation 78−14872
V-Ti-C, high temp. carbide form., electron microscopy study 80−89228
$V_{1-x}Fe_xO_{2-x}F_x$, mag. susceptibility *(German)* 79−78305
V_2O_5, core levels, cryst.-field splitting, X-ray emission study 80−66328
V_2O_5, electronic and band struct. and spectra, CNDO CI cluster method 79−11091
V_2O_5-CuO-BaO glass, unpaired electron localisation, ESR study 80−66026
V_2O_5-P_2O_5 glass, splat-cooled, EPR of V^{4+}, polaron hopping and carrier localisation 77−28436
V_2O_5-P_2O_5 glasses, anomalous cond. mechanism 77−76832
V_3Si, X-ray emission spectra, XPS 77−48278
W (001) surface with adsorbed Cs, core-level photoemission anisotropy 78−11076
W, electronic states, localised and itinerant features using mixed-basis representation of crystalline wave functions 79−60748
W-Fe spin glass, optical props. and electronic states 80−20412
W-Re amorphous alloys, phase-slip and localisation diffusion lengths 80−107747
WF_6, electronic structure, SCF-Xα-SW calcs. 77−26974
WO_3 amorphous layers, electrochromic absorpt. depend. on crystallinity and electron localisation 77−59589
WO_4^{2-}, valence level electron struct. by XPS 77−4712
W(001), surface density of states for directional photoemission spectroscopy 77−20396
YIG, thermoreflectance spectra 80−20616
YVO_4, soft X-ray APS study of empty electron states, VO_4^{3-} cluster model 80−25488
YVO_4:Eu, cluster electron struct., X-alpha calc., emission spectra 78−2898
YbAg, mag. susceptibility, thermally excited interconfiguration crossover 77−16042
$YbAl_3$, XPS studies, valence band, 4-f region 78−6831
YbAu, mag. susceptibility, thermally excited interconfiguration crossover 77−16042
YbCu, mag. susceptibility, thermally excited interconfiguration crossover 77−16042
$YbCu_2Si_2$, tunnelling anomalies due to intermediate valence phenomenon 77−62873
YbZn, mag. susceptibility, thermally excited interconfiguration crossover 77−16042
Zn, core levels, cryst.-field splitting, X-ray emission study 80−66328
Zn, oxidation, MVV Auger spectra, line shape, relax. energies 77−73195
$Zn_xFe_{3-x}O_4$, cond. mechanism, collective electron description 77−4588
ZnO ceramic varistors, trapping by localized states, effect on dielec. and elec. props. *(Russian)* 79−28671
ZnO sensitized photolayer, overall spectra of local electronic levels 79−23933
ZnSe 79−38457
ZnSe and ZnSe:Sb, photoconduction under Nd laser irrad., local level distrib. 77−55580
ZnSe, self-consistent localised electronic struct. 79−42445
$ZnSiP_2$, electronic struct., X-ray spectroscopic investigation 80−108300
Zr-Ni alloys, energy spectra, X-ray emission obs. *(Russian)* 78−19604
$Zr_{0.9}Fe_{0.1}V_2$, NMR and mag. susceptibility 78−95527
ZrO_2:^{89}Zr electron captive decay lifetime, struct. environment effects 77−28523
$Zr_{0.99}Pt_{0.99}V_2$, NMR and mag. susceptibility 78−95527
$ZrRh_{3-x}Pd_x$, electronic and cryst. struct. comparison 78−84398
ZrV_2, NMR and mag. susceptibility 78−95527

localised modes in crystals *see lattice localised modes*

localised states, electron *see localised electron states*

locomotives
see also electric locomotives; motorcoaches; railways
acoustic noise propagation models, railway track 80−48500
British passenger trains, noise meas. and prediction 80−14516
ground noise, underground systems 80−48490
ground vibration, propagation pathway modelling 80−48491
ground vibrations, propagation and wayside effects 80−48489
high speed trains, noise annoyance 77−68313
high speed trains, role of aerodynamic noise in wayside levels 78−13851
noise emission of passing trains 77−68310
noise measurement, acoustic telescope appls. 79−94426
noise measurements, stationary locomotive in-cab 79−14155
service evaluation tests, AMTRAK Northeast corridor, noise meas. 80−48506
urban railway vehicles with sound absorbing wheel systems, noise emission reductions *(German)* 79−50508
wayside noise, high-speed trains 80−48497
wheel temperature in railroad service, effect of brake shoes 80−93660
wheel/rail noise research 80−48496
H-fuelled railway motive power systems 80−40923

loggers *see data loggers; recorders*

logging (recording) *see recording*

logic, formal *see formal logic*

logic arrays *see cellular arrays*

logic CAD
fault trees, methodology for computer-aided construction, nuclear system appl. 78−37412

logic circuit elements *see logic devices*

logic circuits
see also combinatorial circuits; emitter-coupled logic; flip-flops; formal logic; integrated logic circuits; logic devices; magnetic logic; probabilistic logic; sequential circuits; threshold logic; transistor-transistor logic
control circuits, for optical shutter 77−3678
CRO, control system for sweep signal *(Italian)* 78−77882
delay lines, multichannel remotely programmable 77−10560
ECG arrhythmia simulator for monitor testing 78−61270
error monitoring, correction cct. for electronic clocks 78−73970
extremal value indicator using glow-discharge thyratrons 77−17967
guided wave optical devices, using electrooptical switches and modulators, to perform logic and computation 78−38089
Josephson logic circuits, nonlinear current injection switching 79−11269
NMR pulsed, automatic trigger pulse logic for pulse programmer 80−47084
nuclear radiation pulse counter control cct. *(Spanish)* 80−95508
nuclear reactor safety-channel trip comparator, fail-safe logic elements 77 65277
particle track chamber, semi-automatic meas. instrum. register for camera photograph reduction 78−78575
phase angle averages computed using digital phase detection 78−21163
programmable NIM-standard logic unit 77−6657
teaching apparatus, evaluation of PASCO scientific digital mini-modules 77−57126
Pr wire thermal cond. automatic meas. device 78−54362

logic design
see also computer architecture; logic CAD; roundoff errors
optical signal receivers, optimal and nonoptimal, logical structs. efficiency comparison, simulation *(Russian)* 78−71041
scanning cytophotometer controller design method 78−31920
Swiss watch and clock industry, microprogrammed counter logic *(French)* 80−8963
truth-table look-up optical processing utilizing binary and residue arithmetic 80−69334

logic devices
see also fluidic logic; logic gates; threshold elements
laser logic elements, transients during switching *(Russian)* 80−23697
MB DC-SQUID, crit. current mag. modulation, logic device appl. 78−84371
optical logic with variable-grating-mode liquid-crystal devices 80−106613
optical processing, optical parallel logic device and half-adder cct. 79−94364
optical using nonlinear coherent coupler 80−58630
R-S latch, mag. approach to upset prediction 77−18710
semiconductor lasers, triggerable, light-coupled logic appl. 80−74360
superconducting, conference, Stanford, Calif., USA (Aug. 1976) 77−28272
Swiss watch and clock industry, microprogrammed counter logic *(French)* 80−8963
thin-film laser logic elements, charact. and limiting capability optimisation *(Russian)* 79−18431

logic gates
CMOS, for diffusion pump monitoring 77−5855
electro-optic devices, guided wave, for logic and computation 78−66946

logic testing
CROs, plug-in type used for spectrum and logic analysis, timers, computer interfaces 77−41648
fluidic element nonstationary flow meas. by laser Doppler velocimeter with frequency tracker *(Japanese)* 78−55707
oscilloscope eight channel store accessory cct. *(German)* 78−45607
Swiss watch and clock industry, microprogrammed counter logic *(French)* 80−8963

long-range order
see also order-disorder transformations
A15 superconductors, effects of material parameters on H_{c2} 79−61005
trans-p-n-alkoxy-α-methyl cyanophenyl cinnamates, elastic consts. and orientational order parameters 80−44244
p-alkoxybenzylidene-p,n-butylanilines, IR absorpt. spectra, elec. field effects, orientational order parameter determ. by IR dichroism 80−80778
p-alkoxybenzylidene-p-aminocyanoanilines, IR absorpt. spectra, elec. field effect, orientational order parameter determ. by IR dichroism 80−80777
p-alkoxybenzylidene-p-n-butylanilines, optical and mag. anisotropies in liq. cryst. phase, thermal variations of order parameter *(French)* 79−82149
alkylcyanobiphenyls, far IR absorpt. in nematic and isotropic phases, order parameter determ. *(French)* 80−50330
alloy, AB type, equilib. props. by Markovian simulation 78−91302
alloy, binary, conc., with short and long range order, computer simulation of diffusion 78−30778
alloy, binary, elec. resist. depend. on LRO, SRO and composition, inhomogeneous order effects 79−60781
alloy, binary, magnetic, interface struct., Monte Carlo simultion 80−60317
alloy, binary, ordering, residual resist. in CPA *(Russian)* 77−24545
alloy, binary, simultaneous mag. and spatial long-range order 77−69491
alloys, AB stoichiometry, mean field theory of ordering 78−2233
alloys, binary, ferromagnetism and spatial long-range order 80−60159
alloys, binary ordered, residual resist., s-d hybridisation effect 80−39559
alloys, binary with long and short range order, electron energy spectrum calcs. *(Russian)* 79−99471
alloys, DO_{22} and $L1_0$ superstructures, atomic ordering, multicluster approx., order-disorder transition 80−38990
alloys, substitutional, electrical resist., long and short range orders effect 80−107761
p-n-amyloxybenzoic acid, refr. index and orientational order parameter, temp. depend. 79−90537
binary, segregating alloy, theory of surface effects 79−19435
binary alloy, ordered BCC to disordered FCC transition 77−43327
binary disordered alloy with long range order, elec. cond., single band model 77−28154
binary ordering alloy, theory of surface effects 79−19434

long-range order continued
binary substitutional alloy, with long range order, electron energy spectrum *(Russian)* 78−84121
binary substitutional alloy with long range order, electron energy spectra *(Russian)* 78−75974
1,3-bisdiphenylene-2-phenyl allyl benzene complex, free radical, EPR, antiferromag. long range ordering 79−47335
brass, creep of β and β' phases, influence of order *(French)* 79−38921
β-brass, phonon spectra pseudo potential calcs. rel. to long range order and composition *(Russian)* 79−99279
p-n-butoxybenzoic acid, refr. index and orientational order parameter, temp. depend. 79−90537
N-(p-butoxybenzylidene)-p-pentylaniline, refr. index and density in nematic and isotropic phases 79−90538
N-(p′-butoxybenzylidine)-p-n-octylaniline, order parameters in nematic and smectic phases, X-ray diffr. meas. 79−94874
CDW, one-dimensional, commensurability pinning versus impurity pinning 79−11075
CDW structure, incommensurate, phase fluctuations, Coulomb effects and long-range order 77−43524
cholesteryl decanoate, NMR spectroscopy of blue phase 79−4236
cholesteryl m-fluorobenzoate, NMR spectroscopy of blue phase 79−4236
cholesteryl nonanoate, cyclohexanone admixture effect on mesophase order parameter, refr. index meas. 80−100165
COC, cholesteric-smectic-A transition, press. depend., optical meas. 77−47556
colouring problem on randomly occupied lattice, critical conc. existence for long range order 80−80519
copper formate.4D_2O, field-induced antiferromag. order above T_N 78−84389
Coulomb systems, absence of long-range order with long-range potentials 80−70157
cyano-biphenyl cpds., nematic, mag. susceptibility and order parameters 79−86709
4-cyanobiphenyl/4-cyano-p-terphenyl liq. cryst. mixture, order parameters of dissolved dyes 80−100167
cyanooctylbiphenyl, smectic A phase, X-ray diffr. study 80−79690
deformable jellium model, long-range order HF-type orbitals 80−2349
deformable-jellium model, self-consistent long-range order in terms of non-plane-wave HF states 79−19533
p-dioxane, aq. soln., excess molar heat capacities, 298.15K, US vel. obs. 80−6523
p-dioxane-water mixtures, adiabatic compressibilities and sound vels., temp. depend. 79−28044
disordered transition alloys, generalized perturbation calcs. of ordering energies 77−4282
distribution of dissimilar atoms among interstices of various types, appl. to isotopic ordering *(Russian)* 78−67706
EBBA, IR absorpt. spectra, elec. field effects, orientational order parameter determ. by IR dichroism, bend elastic consts. 80−80778
EBBA, mematic, orientational order, effect of hexa-n-alkoxy-triphenylene disc-like solutes 80−79682
EBBA, orientational order in glassy and nematic phases, IR dichroism meas. 80−64891
EBBA, Tsvetkov parameter, temp. depend. 80−88035
electron irradiation effects on kinetics of order-disorder transformations 80−34056
Euclidean invariance, spontaneous breaking, long range ordered media, defect, config. classification 78−59748
extended lattice VB theory, long range order spin pairing 80−52136
FCC alloy, long range mag. order 77−63215
fermion one-dimensional many-body system, SCF approx. 77−62699
fermion system, long-range order Hartree-Fock states with different magnetic properties 79−42476
ferroelectric, rel. to photon condensation effect in phase transition 77−68201
ferroelectric, relaxation processes in Ising model, cluster approx., complex dielectric const. *(Russian)* 80−11352
ferromagnet, dislocation effects on phys. props. at $T \neq 0K$ *(Russian)* 77−8378
ferromagnetic binary alloy, short-range and long-range ordering 78−76206
ferromagnets and antiferromagnets, one-dimens., thermodynamically stable long-range order *(Russian)* 79−27946
ferrous alloys, phase transforms. and ordering, Mossbauer spectroscopy 77−12619
garnet, pretransition phenomena and long-range ordering 79−99151
glasses, polymerised, statistical thermodynamics, short and long range props. 77−27834
graphite, disorder, Raman scatt. and luminesc. 78−23460
graphite intercalation compound $C_{24}K$, order-disorder transition, X-ray study 80−33922
hard-sphere solid, disordered, lattice energy 79−23542
Heisenberg ferromagnet, nearly one- and nearly two-dimensional, long-range order, upper bound for magnetisation 78−34947
Heisenberg linear chains, dimerisation, variational localised-site cluster expansions 79−60670
Heisenberg multi-quadratic isotropic model, LRO, phase transf., exchange interactions *(Chinese)* 80−88756
N-p-hexyloxybenzylidene-p-toluidine, optical props., density, and order parameter in liq. cryst. phases 79−55657
HOAB, chain ordering model 80−24357
honeycomb extended lattice VB theory, long range order spin pairing 80−52136
Hubbard model, off-diagonal long-range order 77−28118
IBPBAC, order parameters in nematic and smectic phases, X-ray diffr. meas. 79−94874
α-In_2Te_3. I phase, order-disorder transform. for DO_{22} struct., thermodynamic study 80−70155
interfaces, co-segregation of metallic and non-metallic impurities 80−60868
Ising 2D regular model, frustration effects 80−39784
Ising antiferromagnet, BCC, in mag. field, Monte Carlo calcs. 78−31032
Ising chain with several phase transitions, Monte Carlo simulation, changes in long-range order 79−12732
Ising ferromagnets, correlation decay, zero-field susceptibility, mass gap 80−50116
Ising model, with long-range interactions, dynamical props. 80−100593
itinerant electron ferromagnetic alloys, magnon energy, effect of ordering 79−7986

long-range order continued
liquic crystals, orientational order parameter, optical birefr. meas., polarisation field problems 80−79688
liquid crystal, refractive index near smectic-A/smectic-C transition, orientational order 80−24572
liquid crystal, tensor field of weak inhomogeneous orientational ordering *(Russian)* 78−67640
liquid crystalline phases, Lennard-Jones and Devonshire model extension 79−94883
liquid crystals, internal field anisotropy changes, order parameter determ. by optical methods 79−86711
liquid crystals, mean field theory of model anisotropic pot. of rank >2 79−60268
liquid crystals, thermotropic, struct., two-dimens. order, and symm. props., review 79−86698
liquid-vapour interface, struct. at 110K, Monte Carlo method, for Ar-like fluid 80−54477
long period stacking variants, stability in pairwise interaction model 79−94956
lyotropic liquid crystal, struct. rel. to amphiphilic structure 78−51416
lysozyme, aq. solns., H_2O ordering, NMR relax. investig. 79−62171
magnetic materials, transparent, optical studies of phase transitions 77−66481
magnetic superconductor, thermodynamics of magnetism and supercond., mol. field theory 80−34668
magnetic system, interactions, spirals and phase transitions with and without long range order 80−60350
magnetic ternary alloys, statistical theory of electrical resistivity 78−87969
MBBA, IR absorpt. spectra, elec. field effects, orientational order parameter determ. by IR dichroism, bend elastic consts. 80−80778
MBBA, nematic, flexibility gradient of fatty acid spin labels, EPR study 80−71181
MBBA, nematic, mag. susceptibility and order parameters 79−86709
MBBA, orientational order in glassy and nematic phases, IR dichroism meas. 80−64891
MBBA, Tsvetkov parameter, temp. depend. 80−88035
MBBA-d_{13}, nematic phase, mol. order and director fluctuations, ^{2}D NMR meas. 79−90529
melting and freezing, computer simulation of simple systems using array processor 80−54353
Merck nematic phases, ZLI 1052 and ZLI 389, mag. susceptibility anisotropy and order parameter 79−86704
mixed crystal, coexistence of different spin structures, computer simulation 77−8276
mixed valence systems, Falicov-Kimball model, mag. short- and long-range order 80−15480
mixed-chain silicates, new ordering schemes 79−99142
mobility edge, analogy with spin glass problem 77−85164
modulated structures, review 79−94929
molecular crystals, struct. disorder effect on optical props. 77−90165
nematic liquid crystals, continuum theory of disorder, comparison with lattice models 80−54126
nematic mesophase, statistical model, orientational order parameters 80−28910
nonlinear cooperative system, kinetic Ising model in Bethe approx. 77−13709
4′-n-octyl-4-cyanobiphenyl, chain ordering model 80−24357
N-p-octyloxybenzylidene-p-toluidine, optical props., density, and order parameter in liq. cryst. phases 79−55657
one-dimensional conductors, Peierls instability, dynamics, structural energy, pseudopot. calc. 80−54676
one-dimensional disordered systems, electron transmission and wave propag. 80−24907
one-dimensional system, phase fluctuations, disorder, nonlinearity 80−54331
ordered alloys, rational and irrational long period struct. 79−95175
ordered overlayers, on FCC metal surface, electronic struct. calcs. 79−60906
ordered regions near macroscopic defects and percolation phase transform. in crystals *(Russian)* 80−92665
oxide, non-stoichiometric, pretransition phenomena and long-range ordering 79−99151
PAA, Tsvetkov parameter, temp. depend. 80−88035
pair correlation splitting in phases with long range order 79−15109
PAP, Tsvetkov parameter, temp. depend. 80−88035
Permalloy, order-disorder transform. and magnetic props. obs., by neutron diffraction method *(Slovak)* 79−4963
phenyl benzoate and thiobenzoate, 4,4′-disubstituted, mag. susceptibility anisotropy and order parameter 79−86704
phytanic acid, in phospholipid bilayers, struct., order parameters, liq. cryst. transition, entropy 79−83713
phytol in phospholipid bilayers, struct., order parameters, liq. cryst. transition, entropy 79−83713
plasma, classical two dimensional one-component, Monte Carlo simulation, solid-liquid phase study 79−94814
poly-γ-benzyl-L-glutamate, sidechain order parameters, ^{2}H NMR meas. 80−1923
polyethyleneterephthalate, ordering, thermal pretreatment at vitrifying temp. effect *(German)* 79−65006
polymer glasses and melts, struct., review of expt. results 79−37636
pretransition phenomena and long-range ordering 79−99151
N-(p-propoxybenzylidene)-p-pentylaniline, refr. index and density in nematic and isotropic phases 79−90538
N-p-propoxybenzylidene-p-pentylaniline, orientational order in glassy and nematic phases, IR dichroism meas. 80−64891
pyrographite, surface struct., amorphisation, secondary electron spectra and AES 79−43077
quantum field theory, external field depend. anal. 77−10165
p-quinquephenyl, nematic, mag. susceptibility and order parameters 79−86709
random impurity effects 78−95061
random system, absence of long range order, classical X-Y model 77−30103
rare earth oxide film, short-range order to long-range order transition 78−10288
rare earth ternary compounds, coexistence of superconductivity and long-range magnetic order 79−11264
singlet ground state system, mag. props. 80−44850
smectic A to smectic C transition, separate order parameter for layer thickness and optical tilt angle 80−19923

long-range order continued
smectic B, liq. cryst., bond orientational long-range order 79−10790
smectic liquid cryst., long range order excim. *(Russian)* 79−1392
sodium decanoate-n-decanol-water system, lamellar G-phase, orientational-order, EPR investigation 80−24355
solid solution, free energy extrema characterised by two long-range order parameters *(Russian)* 77−76576
solid solution, ordering, characterisation by long range order parameters *(Russian)* 79−1489
solid solutions, BCC, SRO and LRO 77−43178
solid solutions binary, order-disorder transitions, long range order parameter and chemical potential 80−6487
spinel compounds, 1:3 octahedral order, order-disorder transition, review 80−88079
squaric acid, two-dimens., phase transition, elastic neutron scatt. 78−6155
stepped ordering in binary solid solutions 78−67807
superconducting film, off-diagonal long-range order, observability of decay 77−59352
superconductor, neutron effects 78−52121
surface waves, inhomogeneous liq.-vap. interface, origin 78−75158
TANOL, linear chain antiferromagnet, long-range order, magnetisation, PMR 78−23266
TBBA, order parameters in nematic and smectic phases, X-ray diffr. meas. 79−94874
p-terphenyl, long range order at phase transition, neutron diffr. exam. 77−1228
α-tocopherol in phospholipid bilayers, struct., order parameters, liq. cryst. transition, entropy 79−83713
transition metal, chemisorption of ordered atomic layers, HF Green's function formalism and phase shift technique 80−24733
transition metal-metalloid amorphous alloys, mag. props. review 78−52300
TTF-TCNQ, short-range and long-range order of phason clusters 77−35874
two dimensional system of electrons in uniform neutralizing positive background, absence of cryst. order 80−103610
two-dimensional lattice, ordered phase form. by elastic stress relax. at antiphase boundaries *(Russian)* 79−14817
two-dimensional nonscalar system, dynamics of symmetry-breaking long-ranged order 77−20613
type II superconductor, A15 struct., electronic density of states and T_c changes with atomic ordering 78−91800
water, in quartz pores, H^- excess mobility IR spectroscopic study 79−51955
X-Y model, spin 1/2, determ. by variational method 78−72322
AgCd-AgMg(AgZn), quasibinary alloys, phase relations 79−8273
Ag_3Mg, long-period ordered, struct., high resolution electron microscopy obs. 79−94960
Ag_3Mg, ordered, rational and irrational long period struct. 79−95175
Ag_3Mg, two different types of long-period ordered alloys, characterisation by high resoln. electron microscopy 80−49181
Al superconducting film, transition to zero vorticity, long-range topological order 80−93039
Al-Cu-Ni, vacancy ordering, electron microscope and electron diffr. obs. 79−27954
Al-Er, dil., supercond., order parameter dynamics and collective modes, pair tunnelling meas. 79−56409
Au-Fe, long range mag. order 77−63215
AuCu II, rational and irrational long period struct. 79−95175
$Au_3Zn(Cd)$, long-range ordered, periodic antiphase domain boundary struct., X-ray diffr. obs. 79−95028
C films, surface struct., graphitisation, secondary electron spectra and AES 79−43077
$CeFe_2$, H_2 absorption effect on mag. props. and struct. 77−40045
Co complex, $Co(C_5H_5NO)_6(ClO_4)_2$ and $Co(C_5H_5NO)_6(BF_4)_2$, $S=^1/_2$ XY magnet, sp. ht. below 1K 77−55682
Co-P, amorphous electrodeposited foils, struct. characterisation by X-ray scatt. 79−77932
$Co_xZn_{1-x}Rh_2O_4$ spinel, crit. conc. for long range mag. order, expt. evidence 79−47239
Cr, lattice dynamics, improved Fielek model 80−59598
$CsLi_{0.5}(Al,Fe)_{1.5}F_6$ pyrochlore, Mossbauer contrib. to exam. of cationic order *(French)* 80−93224
Cu complex, 1,2-ethanediammonium tetrachlorocuprate, layered struct. mag. susceptibility 80−7094
Cu-Al (21 at.%) transition state, tempered and quenched alloy *(French)* 80−55392
Cu-Au, long-range ordered, periodic antiphase domain boundary struct., X-ray diffr. obs. 79−95028
Cu-Au (50 at.%), ordered, influence of elastic stresses on mech. props. *(Russian)* 78−92298
Cu-Au alloys, vacancy and divacancy migration activation energies, elec. cond. meas. 80−88140
α-Cu-Ni-Zn-Pb, fire cracking and ordering *(German)* 78−60760
Cu-Zn, rheological study of crystallographic order on creep *(French)* 80−97548
$(Cu_xAn_{1-x})_2AsO_4(OH)$, olivenite-adamite solid soln., ordering 78−42962
CuAu, order-disorder transform., band theory for internal energy 79−19539
CuAu type structures, interstitial atom redistrib. in octahedral and tetrahedral interstices *(Russian)* 77−55280
Cu_3Au, alloys, superlattice-fringe imaging theory, images formed from two beams 80−79649
Cu_3Au, deformation twinning 77−63717
Cu_3Au, elec. resistivity, temp. depend. 79−47078
Cu_3Au, electrical resistivity and LRO, energy gap formation in Fermi surface 80−88533
Cu_3Au, long-range order parameter from electron micrograph thickness fringes 77−65938
Cu_3Au, neutron irrad., displacement cascades, direct obs. method 80−107335
Cu_3Au, ordered and disordered, cavitation induced erosion 77−16743
Cu_3Au-$Cu_3Pd(Pt)$, quasibinary system, order-disorder transform., superlattice form. 80−2159
$Cu_3Au(-xCo)$, x=0.64 and 1.5 at.% Co, LRO 78−18584
Cu_3Ga, interpretation of diffuse contours in electron diffr. *(French)* 79−19377
Cu_3Ga, transition state between long range order and short range order, model, computer simulation *(French)* 80−49371
long-range order continued
$Cu_{1/2}In_{1/2}Cr_2S_4$, transition from long-range to short-range mag. ordering 77−36087
$CuIn_5S_8$, sulphospinel electron diffr. and electron microscopy study, order-disorder transform obs. 80−88080
$Cu(NO_3)_2.2^1/_2H_2O$, long-range ordered state, mag. props. 78−39417
$Cu(NO_3)_2.2^1/_2H_2O$, singlet ground state system, mag. props. 80−44850
$Cu_{83}Pd_{17}$, Cu^+ (Au^+) ion-bombarded, displacement cascades and disordered zones, TEM studies 80−15167
$CuSeO_4.5H_2O$, $CuSO_4.5H_2O$ and $CuBeF_4.5H_2O$, linear-chain antiferromag., mag. phase transition investig. 77−55684
$Dy_{1.2}Mo_6S_8$, low temp. heat capacity anomaly rel. to antiferromag. transition in supercond. state 80−25044
Dy_2O_3-ZrO_2 phase diagram and long range ordering 80−93542
ErO, vac. deposited films, struct. changes due to annealing 79−77741
ErO_x films, phase transforms. 77−62784
$ErRh_4B_4$, superconductivity destruction at onset of long-range mag. order 77−76994
$EuCrO_3$, long term mag. ordering, antiferromagnetic resonance study *(Russian)* 80−54953
$(Fe, Co, Ni)_3V$, control of ordered struct. and ductility 80−21029
$(Fe,Ni,Co)_3V$, long-range ordered alloy for fusion reactor appl. 80−32481
Fe-Al, Mossbauer study of ordering *(Japanese)* 79−19822
Fe-Al-C alloys, C migration and mag. aftereffect, mag. permeab. disaccommodation and long-range order meas. 79−8020
Fe-Al(25 at.%), mag. anisotropy induced by plastic deform., dislocations, long-range order 77−4544
β-Fe-Be, pseudotwinning and pseudoelasticity 79−96056
Fe-Co, long range order, neutron powder diffr. meas. 79−42243
Fe-Co, partially ordered, elec. cond. 78−91663
Fe-Co, surface comp. and surface segregation 80−34280
Fe-Co alloy, atomic ordering phenomena, neutron diffr. obs. *(Russian)* 77−81254
Fe-Co-Cr, Cr effect on struct. of ordering 78−35407
Fe-Co-Si, BCC solid soln. interchange energies, high temp. neutron diffr. 80−29166
Fe-Co-V(-Ni), annealing effect on microstruct. rel. to mag. and mech. props. 80−89267
Fe-Co(Al), B_2 superlattices, point defect investigations 78−47357
Fe-Cr-Co martensite, ordering and segregation *(Russian)* 79−20052
Fe-Ni (31 at.%), austenitic, ageing, absence of at. order 77−11502
$Fe-Ni_3$, hyperfine field, variation with atomic order 79−7953
Fe-Ni-Al, Curie temp. depend. on ordering, antiferromag. ordering *(Russian)* 79−61101
γ-Fe-Ni-Mn alloys, spin glass state, short and long range order investigation 80−65808
Fe-Pt (22-24 at.%) austenite, long range order parameter, temp. depend. 80−40353
Fe-V (10 to 50 at.%), solid soln., tempered, exam. of long and short range order, using Mossbauer effect *(Russian)* 79−29105
FeAl, order parameter, atomic scattering factor, thickness fringes in electron micrographs 79−10832
Fe_3Al, alloys, superlattice-fringe imaging theory, images formed from two beams 80−79649
Fe_3Al, Cu^+ (Au^+) ion-bombarded 80−15167
Fe_3Al, electrical resistivity and LRO, energy gap formation in Fermi surface 80−88533
Fe_3Al, long-range order parameter from electron micrograph thickness fringes 77−65938
$FeGa_2O_4$, magnetic props. by Mossbauer effect, neutron diffr. and magnetisation meas. 77−43918
$Fe_{40}Ni_{40}P_{14}B_6$ metallic glass, ferromag. reson., spin waves, thermal ageing and long-range order effects 80−25214
Fe_3O_4, optical cond. anisotropy calcs. below Verwey transition 80−50289
Fe_3Pt austenite, long range order parameter, temp. depend. discussion 80−97481
$Ga_{0.67}Cr_2S_4$, semiconducting thiospinelide, spin glass type mag. ordering *(Russian)* 80−50123
$Gd(Cu_{1-x}Gd_x)$, pseudobinary alloy, mag. susceptibility and elec. resist. at low temp. 80−34602
$Gd_{1.2}Mo_6S_8$, low temp. heat capacity anomaly rel. to antiferromag. transition in supercond. state 80−25044
$GdNi_2H_4$, effect of H_2 absorption on struct. and mag. behaviour 78−10685
^4He, liquid, condensed phase, long-range order of one- and two-body density matrices 80−10726
KH_2PO_4, Green's function theory of ferroelec. phase transition 77−85669
$KMnF_3$, precursor order and Raman scatt. near displacive phase transitions 80−45061
$K_xWO_{(3+y)}$, direct imaging of ordering 77−11511
LaB_2C_2, ordering of B and C atoms in struct. 80−96481
$LiTbS_2$, long and short range order 78−38667
Mg base Laves phase alloys, long period struct. classical lattice gas model method 79−94957
Mg_3Cd, disordering under electron irrad. in electron microscope 78−83849
$Mn_{1.11}Al_{0.89}$, unit cell parameters, temp. depend. 79−55697
MnF_2, magnetic, thermal, elastic refraction of light, mag. order influence on refractive index *(Russian)* 80−34880
Mo, lattice dynamics, improved Fielek model 80−59598
Mo-permalloy, magnetic permeability and order form. kinetics under annealing, conc. depend. 77−8356
NH_4Cl, Raman scatt. of light on limiting and nonlimiting dipole vibr. 80−11402
NI_3Al, structural order and homogeneity, X-ray, mag. susceptibility and Mossbauer meas. 77−63663
Na-Fe fluorophosphate glass, EPR and Mossbauer resonance study 80−15838
$NaNO_2$, antiferroelec. phase, struct. anal. by neutron diffraction 80−24410
$Na_xV_2O_5$ β-phase single cryst., phase transitions EPR meas. 78−95514
Nb-H, modulated ordering, elastic free energy theory 79−94945
NbD_x, x=0.55 to 0.88, deuteron and ^{93}Nb mag. resonance, β-α transitions 77−20721
Nb_3Ga, comp. and LRO effects on supercond. T_c 77−39992
Nb_3Ga, supercond. crit. temp. and struct., heat treatment and stoichiometry effects 77−43769
Nb_2O_5-TiO_2, splat cooled, crystallization and ordering 77−68953

long-range order continued
$3Nb_2O_5.8WO_3$, circular diffuse scattering studied by 1 MV high resolution electron microscopy 80−59350
Nb_3Sn, powder metallurgically produced, microstruct. characts. 80−89233
Nb_3Sn, supercond. props. and struct., neutron irrad. dose depend. 77−15985
Nd_3S_4 chem. and mag. structures, neutron diffr. obs., ferromag. long-range order *(German)* 78−10654
Ni-Al system, ordering and instability of β phase near martensitic transform. *(Russian)* 80−45304
Ni-Al-Fe system, order-disorder phase transform., Gorskii-Bragg-Williams approx. *(Russian)* 79−29048
Ni-Cr (33.3 at.%) alloy, ordering after US deform., microhardness and elec. resist. meas. *(Russian)* 79−20113
Ni-Cr-W(Mo)(Ti)(Al), long range ordering of matrix of complex heat resistant alloys *(Russian)* 77−77509
Ni-Fe-Nb (Mo), magnetic alloy, TEM and X-ray obs. *(Chinese)* 80−24401
Ni-Mo, short range order considerations and development of long range order 77−16574
Ni-Nb amorphous alloy, transformation to crystalline state, ion emission microscope study *(Russian)* 79−82158
Ni_3Al, temp. depend., 25-1000°C 77−27849
Ni_3Fe alloys, low-temperature specific heat, long and short range order effects 80−100339
Ni_3Fe, magnetocryst. anisotropy, annealing temp. depend. 80−103828
Ni_3Fe, Mossbauer spectra, X-ray anal. comparison 78−10810
Ni_3Fe, single crysts., long range order degree influence on strain hardening *(Russian)* 80−11660
Ni_3Fe, superlattice dislocations, compression induced mag. anisotropy 77−85443
Ni_3Fe, X-ray diffraction investig. of order-disorder transform. *(Russian)* 77−70043
$Ni_3(Mn,Cu)$, ordering kinetics, neutron diffr. and elec. resist. meas. *(Russian)* 77−47379
Ni_3Mn, order-disorder transform. *(Russian)* 77−59776
Ni_4Mo, order-disorder phase transform., X-ray diffr. *(Russian)* 79−1855
Ni_4Mo, statistically homogeneous ordering, computer-simulated field ion images 78−9991
Ni(111), chemisorbed CO, adsorption sites and long range order, vibr. spectra 79−46946
Pd-Fe (25-55 at.%) alloy, rel. to mag. struct. *(Russian)* 77−90085
Pd-H_x, model possibilities for the 50K transition 79−8299
Pd-Ti, hydrogenation, lattice spacings, microhardness and mag. susceptibility meas. 79−77557
$Pd_{50}Fe_{37.5}Co_{12.5}$, elec. resist., depend. on composition, relative magnetisation and long-range order *(Russian)* 79−56189
Pr, soft mode excitation behaviour under press., long range order 80−39838
$Pt_{50}Fe_{12.5}Co_{37.5}$, elec. resist., depend. on composition, relative magnetisation and long-range order *(Russian)* 79−56189
$Pt_{37.5}Pd_{12.5}Co_{50}$, elec. resist., depend. on composition, relative magnetisation and long-range order *(Russian)* 79−56189
$Pt_{12.5}Pd_{37.5}Fe_{50}$, elec. resist., depend. on composition, relative magnetisation and long-range order *(Russian)* 79−56189
$RbCaF_3$, precursor order and Raman scatt. near displacive phase transitions 80−45061
$Rb_2Co_cMg_{1-c}F_4$, random two-dimens. Ising antiferromag., unstable mag. long-range order, neutron scatt. obs. 80−44839
Se-Te solid solutions, ordering, diffuse X-ray scatt. 77−65965
$SrCl_2$, superionic, quasielastic neutron scatt. 78−79504
$Sr_2Fe_xRu_{1-x}O_4$ solid soln., Mossbauer spectrosc. study 80−50235
$SrTiO_{3-x}$, anion deficiency and anion vacancy ordering 78−51532
$SrTiO_{3-x}$, long-range order of empty anion positions 78−22708
Ta-D system, thermodynamic stability of Ta_2D, rel. to long-range order parameters *(Japanese)* 78−15376
Ta_2D_{1+x}, phase relations in terms of long-range order 79−38808
Ta_2H, ordered, distortion-induced superstruct. modulation, from X-ray scatt. 80−49186
$Tb_{1.2}Mo_6S_8$, low temp. heat capacity anomaly rel. to antiferromag. transition in supercond. state 80−25044
$ThFe_3$, H_2 absorption effect on mag. props. and struct. 77−40045
Ti-Al (40 wt.%), TiAl plate dissolution 79−66055
Ti_3Al-(Mo) (0.5 at.%), ordering, Mo effects 77−28841
TiN_x, cryst. and internal structs., electron diffr. and microscopy 77−27861
V_3Au, effect of atomic ordering on XPS of valence bands 77−52224
V_2D, elec. resistivity studies of order-disorder phenomena 79−78961
V_2D, ordered, distortion-induced superstruct. modulation, from X-ray scatt. 80−49186
V_2D, single crystal, superstructure modulation and long range order, X-ray obs. 78−71712
V_3Ga, parameter variations determ. and correls. with supercond. T_c 77−11504
V_3Ga, structure effects on supercond. props. and electron spectrum *(Russian)* 77−80862
V_2H, elec. resistivity studies of order-disorder phenomena 79−78961
V_2H, long-range order and β to β' transition, X-ray scatt. obs. 79−95160
VI_2, mag. struct., long- and short-range order and Mossbauer spectroscopy 80−65803
V_3Si, neutron irrad., neutron diffraction studies 78−88076
W (001), chemisorption of H, HF Green's function formalism and phase shift technique 80−24733
$W_xNb_yO_z$ ordering of atom string, cluster model 77−68959
$(Y_{3-x}Ca_x)(Fe_{2-x}Sn_x)(Fe_3)O_{12}$, long and short range magnetic order 79−38419
$YbFe_xMo_6S_8$, singularities in mag. and supercond. props. 79−51710
Zr_3Al, deformed and irrad., lattice defects obs., superlattice dislocations and defect clusters 80−107261
$Zr_{1-x}S$, short- and long-range ordering of vacancies, rel. to supercond. transition temp. 77−19945

long tailed pair *see differential amplifiers*

loop antennas
current loop radiation pattern in inhomogeneous plasma column 77−76102
cylindrical tissue models excited by loop antenna 79−39446
electron plasma wave radiator and detector, exptl. obs. 77−51198
Fresnel region mag. field intensity meas. accuracy 77−79132
measuring loop antenna characteristic improvement 78−49174

Lorentz transformation
acceleration in Lorentz transformation, teaching 80−90639
active Lorentz transformations, consequence of lack of invariance 79−84951
active Lorentz transformations, consequence of lack of invariance, reply 79−84952
affine connections in special relativity and Lorentz transforms. 79−2626
Bethe-Salpeter eqn., Lorentz deformation 79−54246
bilinear spinors and space-time, field eqns. of motion 77−22647
charges in EM field, generalised covariant Hamiltonian formulation 80−46794
classical spin and the Lorentz group, a correlation 79−5979
Clebsch-Gordan expansion for Lorentz group in n dimensions 77−5626
clock hypothesis of Einstein 79−58537
conformal transformations in spinor space-time 79−30674
consistency, kinematic, for teaching 78−24608
contraction of metric standards 80−82638
covariance and basic inertial frame, non-invariance of rest mass 80−22194
covariant quantum equations in curved spacetime, Lorentz covariance and tachyons, book contrib. 79−44725
derivation, necessary suppositions 77−30007
derivation from first postulate of special relativity 77−42
diffraction, invariant properties *(Russian)* 77−82470
Dirac spinor amplitudes, calc. by complex Lorentz transforms. and trace calculus 80−42322
discrete special relativity, bases 77−71208
education, group theory of covariant harmonic oscillators, interacting quarks 78−61970
education, Lorentz transformation and causality condition 78−7
education, Maxwell's eqns., Lorentz and conformal covariance, normal transformation rules 78−49589
education, rotations, Lorentz transformations, and arbitrary axes 79−97155
education, self-inverse form of Lorentz transformation 77−82345
Einstein's spectral relativity, Lorentz's rod contraction-clock retardation ether theory, possible equivalence 78−49654
EM transmission structures, relativistic foundation and network formalisms 80−58446
evanescent EM wave behaviour under Lorentz transformation 79−22880
extended inertial frames and Lorentz transformation 77−44
extended relativity, T-violation and new particle 80−37182
fibre bundles $P(M_4,G)$, invariant eqns. 77−17864
fine-grained one-particle distribution function, invariance under transformation 79−80433
finite Lorentz transformations in quantum field theory 77−45976
finite Lorentzian distance space-time singularity theorem *(French)* 78−62075
fluxoid motion for Lorentz transform law with EM fields 80−67954
four-vector operators from unitary representation of Lorentz transformation 78−49720
gas, energy and momentum transformation, for teaching 78−24618
gauge theory monopole solns. Poincare group algebra representation 78−16925
general relativity, quantum field theory, vierbein formalism 80−22263
general relativity, tetrad formulation, weak conservation law covariant consequences 80−17848
generalised, in general relativity, and behaviour of physical quantities at R- and T- region boundary *(Russian)* 78−49725
geometrical and mechanical method 77−30008
ghost-field formalism, spin 3/2 and 2 fields, EM interaction 78−70315
Gonzalez-Gascon effect, comment 77−33863
gravit. and EM wave flux compared 78−29027
gravitational interaction of spin-1/2 particles, Lorentz invariant theory 80−22257
group theoretical condition of Lorentz and Galilei groups 78−4462
hadron jet prod., Lorentz deformation 80−27420
hadronic jet phenomenon and Lorentz deformation 80−105806
hadrons, extended, Lorentz deformation props., O(4) and light-cone coordinate systems 80−68354
helicity reversion of circularly polarized EM evanescent wave 78−32696
Higgs mechanism and the inverse Einstein-Infeld-Hoffman problem 79−63100
homogeneous 16-vertex model, symm. group Lorentz similarity transformation interpretation 79−9300
homogeneous transform., general form. 78−86151
internal Lorentz basis for two-particle states 80−31499
invariance of quantum field theories 78−21317
k-calculus approach and the generalized Lorentz transformations 79−17212
Kepler problem, Lorentz and anti-de Sitter group 78−36817
Kerr-Schild metric, Maxwell-Hamilton-Jacobi-, and Dirac-eqns. Minkowski covariance 77−64977
kinematic consistency 77−33734
Klein Gordon lattice field eqn. in 4-D space-time, Lorentz covariance 78−54184
Lie group Sp(8,R), Lorentz subgroup anal. and null plane boson realisation 78−62116
Lie theory, nonlinear transforms. 79−97191
light clock, special-relativistic slowing of clock rates 80−77613
Liouville eqn. basis of relativistically invariant generalised quantum kinetic eqn. 78−54299
local field theory, universal singular functions 78−32969
local supersymmetry, geometric interpretation 77−38096
locally conserved currents and energy-momentum tensor 77−60889
Lorentz group in function space outside light cone, Fourier expansion 79−71246
Lorentz group in oscillator realisation 78−77755
Lorentz group O(2,1), coupling of continuous representations 79−49078
Lorentz groups on skew symmetric tensor space, nonlinear realisations of direct product 78−62329
lorentz invariance from classical particle paths in quantum field theory of electric and magnetic charge 79−49431
Lorentz invariant e.m. current paradox, soln. 77−51
Lorentz invariant multiparticle amplitudes, massive particle relativistic kinematics, spinor amplitudes 78−41156
Lorentz transformations, derivation by Ives, review 80−4523

Lorentz transformation continued
lorentz-invariant spin-1/2 equation for the representation (1,1/2) ⊕ (1/2,0) ⊕ (0,1/2) ⊕ (1/2,1) 80−42334
magnetic and electric charge quantum field theory, Lorentz invariance 78−33010
massless Euclidean Thirring field, four point Schwinger function, Lorentz group invariant forms *(German)* 80−90980
massless fields as unitary representations of the Poincare group *(German)* 79−89056
massless particle fields, arbitrary spin, Lorentz transformation laws *(French)* 80−62823
Maxwell's equations as one quaternion eqn., appl. to wave propag., for teaching 78−54133
Maxwell-Boltzmann statistical distrib. function, Hsu's space-light transformations, agreement with Lorentz results 80−17858
modern atomic and nuclear physics (book) 80−11
monopoles, elec. and mag., without strings, heuristic pot. theory, teaching approach 79−5931
non Euclideans Lorentz transformations and special relativity 79−97194
nonequilibrium relativistic strain tensor, rigid disc relativistic rotation *(Russian)* 80−22195
nonlinear field theory, classical solutions by inverse scatt. method 79−9272
nonlinear vector product, appls., teaching 79−44668
nonzero mass quantum field theory, Lorentz (Poincare) transformation laws 78−37123
O(3,1) Lorentz group, generating functions, integrity bases *(French)* 80−105803
O(p,q) generalised groups, finite subgroups 80−47209
photon, Dirac-like eqn., transform. props. 79−58914
photon, stochastic phase space kinematics 79−2649
physical system, model of space-time from set theory concepts 80−82660
Poincare group contraction and high energy effects 77−65119
Poincare group representations for relativistic extended hadrons 79−89099
Poincare $IO_{3,1}$, coordinate transforms. and centraliser subalgebra, algebra Casimirs 79−6295
Poincare-invariant motion equations for arbitrary spin particles *(Russian)* 79−2964
pre-Schwinger model, Lorentz transforms. if operator solns. 80−47171
proper time interval transformations 78−32669
QCD, two-dimens., Lorentz invariance 79−67504
QED, and Abelian gauge theory, Lorentz boosts on observable and ghost particle states 78−66061
QED, Lorentz invariance, nonphysical variation 78−93828
quantum chromodynamics in two-dimens., Lorentz invariance 79−93339
quantum fields in Lorentz basis 80−86565
quark processes, interaction with hadronic sea 80−37236
quaternion equations *(Russian)* 77−41481
quaternions and subluminal and superluminal Lorentz transformations, book contrib. 79−44724
relativistic Hamiltonian mechs., position variables 80−27123
relativistic harmonic oscillators and hadronic struct., 1st year graduate quantum mechs. 78−61971
relativistic motion in a plane, teaching 80−101686
relativistic semigroup, Lorentz group and tachyons *(Russian)* 77−82801
relativistic time transformations for noninteracting physical processes 80−48
relativistic two fermion equations, Lorentz, parity and charge conjugation invariance 80−90976
renormalised Thirring model, massless scalar field in 2-space-time dimensions 79−12929
rotations in space-time 79−97190
Rutherford scattering with radiation reaction, Lorentz-Dirac eqn. soln. for opposite point charges 78−55289
school demonstration model *(Danish)* 78−20923
self-inverse form, for teaching 79−25808
six-dimensional space-time, contradiction of Thomas precession 80−31500
soliton, non-topological, non-Abelian internal symmetry in 3+1 dimensional space-time, quantisation, collective coord. and Lorentz covariant methods 80−47199
space-time reflections, Dirac 4-spinor transform. 77−57187
spin-orbit coupling, classical derivation 79−53971
spinor operators of Weiss-Zumino type and their irreducible components 79−71602
spinor theory via involutions, Lorentz group representation appl. 80−86607
string moving in uniform static external field, 2-D space-time surface 80−57087
SU(2) gauge fields, classification 78−70281
supergravity, geometry of superspace, vector-spinor matter 78−49744
superluminal, imaginary quantities problem in extended relativity 80−52020
superluminal, quantum mechanics of spin-1/2 tachyons 77−5693
superluminal boost in x-direction in complex Minkowski space, tachyonic connections 80−105497
superluminal frames and tachyons, introductory review, generalised Lorentz transform. derivation 78−69983
superluminal frames and tachyons, introductory view, book contrib. 79−44719
superluminal Lorentz transformations, imaginary units, motion of tachyon 80−86082
superluminal transformations, generalised Lorentz transforms. 78−73844
supersonic flow, Lorentz-like coord. transform. 79−37348
tachyon magnetic monopoles, existence in 6 dimens. space, superluminal transforms. in Dirac theory 78−54183
tachyon theories 78−54581
tachyons, Lorentz group and relativistic semigroup *(Russian)* 77−82386
tachyons, quaternionic formulation superluminal transformation, in complex space-time 79−53973
tachyons, role in strong interaction field theory 79−9353
tachyons and bicharacteristics, reply to comment 78−49656
teaching, acoustic and ballistic situations 78−24623
Thirring and Schwinger spinor field models, correct Lorentz transformation formula 78−12837
Thirring model of massless scalar field, conformal transformations 80−52428
Thomas precession, geometrical kinematical origin 79−6
three temporal, theoretical reliability 79−35550
three-temporal, light speed invariance 79−44717
Lorentz transformation continued
three-temporal transform. possibility 79−97192
time-like reflections 78−32671
timelike lines, mapping 78−32670
transverse contractions of moving bodies 78−69980
two gravitating particle system, covariant model 80−8865
two-dimensional QCD, Lorentz invariance 80−37216
undergraduate teaching, matrix representation of arbitrary boosts 80−17760
unified, quaternionic form 80−46799
unified Lorentz transformations, complex rot. in four dimens. space 78−73846
unified model for description of subluminal and superluminal objects 78−73845
unified theory of matter, fundamental idea 77−60929
vector formulation, as student introduction to special relativity *(Italian)* 78−12447
vector laws of physics, reformulation 80−68036
vector product formulation of special relativity and electromagnetism 80−105496
wave eqn. in space-time and Lie theory, Lorentz group 77−26179
wave equations, first-order relativistic, relationship between Lorentz and Foldy-Wouthuysen transformations 77−30252
Weyl tensor diagonalisation, Lorentz transformation of gravitational superenergy flux 79−134
Wigner rotations and associated matrices for Dirac particles 77−2761
K_S^0 decays and Lorentz invariance 79−26250

Lorenz number
alkali metals, ideal thermal resist. and Lorenz number due to conduction electron-phonon scatt. 80−29377
alkaline earth metals Wiedemann-Franz law deviations 78−39086
kinetic equation, iteration soln. 77−43564
liquid metal, Lorenz no. and thermal cond., apparatus for meas. 77−51716
metal, thermal resist. calc., role of electron diffusion over Fermi surface 77−62894
metal, transport coeffs. in strong mag. field, Wiedemann-Franz law and Mott rule 77−69303
metals, liq., Wiedemann-Franz ratio 80−80243
narrow band semiconductor, transport phenomena electron energy spectrum *(Russian)* 79−51616
phonon inelastic interband scatt. in transport effects 77−43552
semiconductor, Seebeck and Hall coeffs. Lorenz number, anisotropy, theory *(German)* 80−65608
semimetals, degenerate, heat conduction, thermal EMF, Lorenz number anisotropy at low temp. 80−75549
spin glass, low temp. Lorentz number 79−19567
spin glasses, elec. resist., thermal resist. and thermopower 80−65542
steel, N27Yu2T2B, elec. and thermal cond., 4.2 to 200K, Wiedemann-Franz law *(Russian)* 79−78076
thermal props. at high temp. 80−75536
thermophysical measurements, sample shape determ. 79−30457
transition metal, Lorenz number and high-temp. interband transitions 78−26844
transition metal, thermal and electrical conductivity at high temperature, interpretation of temp. depend. 77−35912
Wiedemann-Franz law in semiconductor and metal glasses 79−65422
Ag film, thermal and elec. cond., Lorenz no. 78−43487
Ag, low temp. resist. and thermoelec. ratio, electron-electron scatt. contrib. 80−70670
Al, low temp. resist. and thermoelec. ratio, electron-electron scatt. contrib. 80−70670
As, reduction in Lorenz number due to inelastic scatt. of charge carriers 79−19610
Au, low temp. resist. and thermoelec. ratio, electron-electron scatt. contrib. 80−70670
Cd_3P_2, thermomagnetic transport effects obs. 77−15883
Co, thermal diffusivity meas., 300 to 1000K, Lorenz number determ. 80−29384
Cu alloys, liq., thermal cond. and elec. resistivity 80−103661
Cu, liq., thermal cond. and elec. resistivity 80−103661
Cu, low temp. resist. and thermoelec. ratio, electron-electron scatt. contrib. 80−70670
Cu powder, sp. ht. cond. and sp. elec. cond. meas., Wiedemann Franz Lorenz law *(German)* 80−92872
Fe, thermal cond., elec. resist., Lorenz number and magnetisation, crit. behaviour 77−4521
Hf, thermal diffusivity meas., 300 to 1000K, Lorenz number determ. 80−29384
In, liq., thermal props. at high temp. 80−75536
In, thermal cond. in solid and liq. phases, Wiedemann-Franz law 80−39554
K, electron-electron scattering, elec. resistivity, thermal cond., thermoelec. power and Lorenz function 79−95382
K, low temp. resist. and thermoelec. ratio, electron-electron scatt. contrib. 80−70670
NbC_x, thermophys. props. 77−89600
Pb-Bi alloy, liq., thermal cond. and elec. resistance up to 900°C 77−47785
Rb, transport props. and electron-electron scatt. 79−73490
RuO_2, thermal conductivity meas., rel. to elec. cond. 80−65317
Sn, liq., Lorenz number and thermal cond. meas. 77−51716
Sn, Lorenz function and horizontal and vertical components of thermal resist. 79−65427
Sn_xPg_{1-x}, thermal cond. and Lorenz function 78−51966
Tl, liq., thermal props. at high temp. 80−75536
VN-CrN solid solutions, thermal cond., Lorentz number 80−15317

Loschmidt number *see constants*

loss angle
see also dielectric losses
ceramics, granular, electrophysical props. depend. on porosity, temp., solid-phase props. 77−69764
PA6, loss factor rel. to fatigue strength *(Polish)* 77−28904
viscoelastic material, complex dynamic moduli and loss angles 77−68451
Bi-NbO_2-Bi system, Schottky barrier effects in transport and dielec. props. 80−29486
$Cd(NO_3)_2$, phase transition, SHG, optical and dielec. meas. 80−71334
CeF_3 film, in MIM struct., dielec. props. *(Czech)* 80−25309
Si oxide film, porous Si layer oxidation, dielec. props. 80−55556

loss angle, dielectric *see dielectric losses*

loss-angle measurement
absolute meas. using toroidal cross capacitor 78−93736
automatic dielcometer for polymers dielec. relax. meas. 77−45864
capacitor, by three-voltmeter minicomputer multibridge system *(Russian)* 78−70159
capacitor loss-angle and capacitance checking cct. 77−61085
complex dielectric constant meas. of thin foils in mm-wave region, method *(German)* 79−58755
dielectrics, microwave cavity resonator bridge method 77−37914
extended standing wave method, for low dielec. loss meas., permittivity, loss angle calc. *(Japanese)* 77−45869
ferroelectrics, dielec. props. in vicinity of phase transition, microwave method 78−74022
insulation loss-angle and capacitance test trolley *(Russian)* 77−10041
loss angle/permittivity meas. as function of temp. at 9-10 GHz 77−82559
open resonator methods for microwave permittivity meas. 80−15942
solid dielectric props. meas. with superconducting resonators 78−21180
two plate capacitor with aerostatic electrode regulation for precise determination of capacitor loss factor *(German)* 78−74021

loss measurement
amorphous alloys 79−73776
components of (30-100) Hz and (1-10) kV, Schering bridge amplifier system appl. *(Bulgarian)* 77−61083
composite superconductor, multifilament, AC loss meas. apparatus 77−22576
compound glass optical fibres, total and scatt. loss coefficient meas. 80−69536
conference on measurement techniques for optical fibre systems, London, England (May 1979) 79−64348
digital loss meter in mechanical oscillating systems *(Russian)* 79−60079
digital meter for inductance coil parameters meas. 78−12718
EHV choke coil measuring bridge *(German)* 77−18047
electrical steel sheets, specific core loss meas. using analogue wattmeter *(German)* 80−13099
epoxy/E-glass continuous fibre composite type 3M Scotchply, complex moduli, comparison of meas. with estimated bounds 80−93590
feedthrough waveguide resonator Q-factor meas. 77−10053
fibre-optic cable manufacture, testing, and installation *(German)* 78−33863
flat plate solar collector efficiency and heat loss characteristic meas. 79−62064
heat loss from heat receiver assembly, of fixed-mirror solar concentrator 79−52905
lossy waveguide attenuation and phase meas. 77−26343
magnetic circuit loss meas. by warming/cooling method 77−57368
microwave cond. of materials, by resonance input impedance method *(Czech)* 77−26326
multimode step index optical fibres, effect of lossy outer layer, optical links appl. 79−18540
optical, of multi-mode fibres, non-destructive method 80−69550
optical fibre cable vibration characteristics, fibre strain and optical loss meas. 80−99870
optical fibre connector loss evaluation by backscattering 80−58721
optical fibre insertion loss measuring set for field use 79−64357
optical fibre joint loss measurements with OTDR 79−64354
optical fibre loss, dispersion and polarisation meas. by acousto-optical tunable filter 80−102855
optical fibre loss estimation using backscatter technique, time domain reflectometry theoretical assumptions 80−74508
optical fibre loss measurement, mode elimination 79−50375
optical fibre loss measurement using enhanced sensitivity nondestructive method 78−66895
optical fibre splice insertion loss meas., backscattering method 80−58720
optical fibre systems, effect of system parameters on joint loss 79−50435
optical fibre total loss spectra, precise meas., automatic meas. system 80−64169
optical fibres, backscattering method for attenuation and connection insertion loss meas, anal. 80−58675
optical fibres, effects of different modal filters 79−50439
optical fibres, insertion loss meter and reflectometry of prepared fibre ends 79−64358
optical fibres, multimode, loss and mode-conversion parameter meas. principle 78−22192
optical fibres, observation of cascade effect for splices 79−50436
optical loss, precision loss measurement of photoelectric pulse signals using microcomputer 80−13142
optical mean splice loss meas., applying backscattering method 80−19091
optical transmission characts. meas., Tektronix digital radiometer/photometer appl. *(French)* 79−89000
optical waveguide, loss measurement, nondestructive, using three prisms 80−106596
pacemaker battery internal loss characterisation calorimeter 80−30934
polyester/E-glass chopped fibre composites types PPG SMC-R25 and PPG SMC-R65, complex moduli, comparison of meas. with estimated bounds 80−93590
polyester/E-glass hybrid chopped/continuous fibre composite type PPG XMC-3, complex moduli, comparison of meas. with estimated bounds 80−93590
power loss of mag. materials under sinusoidal flux conditions 80−86348
radiation loss of optical waveguide, polariser with anisotropic cladding obs. *(Japanese)* 78−18047
sky-wave mixed-path loss computation, piecewise homogeneous ground models appl. 79−66774
solar collector thermal performance test procedures 79−62066
solar flat plate collector cover system and absorber heat loss rel. to angle of incidence 79−62068
solar receiver radiative loss and eye hazard evaluation by Net-Radiometer 80−89673
spectral loss meas., automated, optical fibres 79−23074
stored beam energy loss to vacuum components, particle bunch simulation meas. at PETRA 77−83258
superconducting magnet, device for energy loss meas. 79−71489
superconducting magnet, pulse loss and voltage meas., elec. method 77−37949
superconducting magnets, analogue digital double integration joulemeter 80−57325

loss measurement continued
superconducting wire, coil simulation, class and instability meas. 79−71487
superconducting wire 80−37050
technique, and appl. to PVC, 10-90 kHz 77−86235
Fe-Si, power loss and permeability meas. by means of Hall probes and stochastic ergodic correl. 80−86350
Nb_3Sn, multifilament superconductors, AC losses 79−60979
Si-Fe sheet, magnetic loss, instrument design *(Rumanian)* 77−79131
V_3Ga multifilament superconductors, AC losses 79−60979

losses
see also dielectric losses; eddy current losses; heat losses; loss angle; magnetic leakage
acoustic plane wave reflection, existence of Stoneley waves as loss mechanism 79−50498
acoustic waveguides, damping of normal and surface waves, depend. of vel. on losses 79−14135
alkali lime germanosilicate GRIN fibre prep., losses and geometrical props. 80−69560
alkali-$PbSiO_3$ optical fibres, high aperture, double-crucible preparation 78−1450
anisotropic optical waveguides of $LiNbO_3$ type, guided and semileaky modes 79−18530
arc, heat exchanges between electric arc and electrodes, dependence on electrode material and cooling conditions *(French)* 80−19655
asymmetric three-layered slab waveguide, leaky TE modes 80−43447
asymmetric-slab optical waveguide losses due to refractive index inhomogeneities 78−1381
cabled fibre, temp. effect on transmission loss and pulse delay distortion 78−1407
chemical laser, electronic phototransition, with thermal initiation by shock wave 80−53283
combined superconductors, losses under nonisothermal conditions, cooling effects 79−87218
composite superconductor, multifilament, longit. and transverse field losses 77−28308
composite superconductor, multifilamentary, self-field losses 77−28315
composite superconductor, power increase at current close to crit. current, expt. meas. 77−28314
corrugated dielectric waveguide, radiation loss calcs. 79−41461
corrugated dielectric waveguide, radiation loss calcs. for TM polarisation 80−43445
corrugated waveguide leaky modes, anomalies of dielec. coated gratings *(French)* 77−79969
cosine^4 losses in photographic lens example demonstrating 79−97456
curvilinear multimode optical waveguide statistical tolerance calc. 78−1361
cylindrical optical fibre transmission and guided mode behaviour 80−28348
cylindrical-mirror confocal resonator design with high transmissivity region *(Russian)* 80−14361
dielectric rectangular waveguides for integrated optics, bending losses 78−63205
dye laser, double wavelength operation using gratings at grazing incidence 80−53317
electro-optical light modulator with small nonactive losses 80−78981
EM field of moving wire calc., parallel to infinite conducting slab 80−18959
energy losses in magnetically soft materials, determ. *(Russian)* 79−8014
externally coupled resonator-filter (ECRF), loss minimizing 79−41542
fibre, single-mode, numerical aperture effects 80−69548
fibre cable and chuck connector optical and mech. props. *(German)* 78−33862
fibre joints, losses causes and reduction *(Norwegian)* 77−14801
fibre lightguide transmittance, approx. calc. 79−55228
fibre optic connectors, theory and design 80−38122
fibre optic measurement system based on near IR SiO_2 fibre Raman laser 79−23070
fibre optical cable, low loss 79−18546
fibre to fibre coupling loss due to displacement, separation, misalignment, automatic measuring technique 79−32036
fibre-optic connector manufacture and insertion loss 79−90035
fibre-optic index-difference dispersion and bending loss/wavelength relationships 78−1367
fibre-optic link, splice loss evaluation by means of the back-scattering technique 79−98478
fibre-optic scattering loss dependence on launching condition, lossy-layer model 78−5577
flexible hollow waveguide, IR light propag., optical losses 77−19389
fusion-welded optical fibre splice loss expts. 79−37023
gas-dielectric optical waveguide, general azimuthal asymmetry, loss evaluation 80−53453
geodesic lens, anisotropic and curvature losses, operation in $LiNbO_3$:Ti waveguide 80−48453
glass, high GeO_2, zero material dispersion wavelength and waveguide props. 80−58733
glass fibre, loss, mechanically induced periodic bends effect 77−3668
glass fibre waveguide, losses below 1 dB/km 78−50936
glass fibres, multicomponent and high SiO_2, thermal variation of attenuation 79−50390
glass waveguide, in-plane scatt. and loss mechanisms 80−33216
glass-fibre waveguides, dependence of overall losses on coupling-in angle of radiation 79−98504
graded index fibre optical loss meas. using dummy fibre 80−5819
grating mirrors, periodic mode losses and optimal geom. characts. *(Russian)* 79−27434
heavy-current cabled and soldered multifilament superconductor AC losses 79−32808
image contrast loss in presence of chromatic magnification difference, numerical estimate 80−95823
interference polarizer with large entrance aperture, characts. 80−43453
Josephson tunnel junctions, high frequency losses 78−88083
lamellar gratings, power losses 80−38091
laser, homogeneously broadened with constant loss, optimum output efficiency 80−74403
laser amplifier with spatial filters, graphoanalytic determ. of energy parameters 80−48322
lasers, homogeneously broadened CW type with nonsaturating lasers, optical extraction characts. 80−91770

losses continued
lens, gradient-index rod, aberrations in multimode optical fibre devices 80−69487
lens, gradient-index rod, appl. in optical fibre communication systems 80−69488
lens guide, low-loss image transmission 80−91872
low-loss graded-index fibre, 3 km and 10 km preform design and modified CVD method 80−58746
magnetron cylindrical sputtering system, end losses 79−47628
metal-clad diffused optical waveguide propagation losses 77−84000
methylundecanhydride hardened phenol formaldehyde resin, hardening kinetics and mech. losses 80−66520
MHD generators, open-cycle, losses effect on charact. 77−68876
MHD generators, technique for boundary layer voltage loss determ. 77−72507
micro-optic directional coupler, aberration losses 80−48395
microstrip waveguide, theory of radiated waves using asymptotic wave diffr. theory 79−18339
microwave losses from nonlinear resonant interaction in inhomogeneous plasma 79−94793
monomode optical fibre dimensions, dispersion, and losses *(German)* 78−33866
multicomponent ring transducers, mechanical loss resistance calc. technique 78−38166
multifilamentary composite superconductor power losses 79−30507
multifilamentary composite superconductors, coupling losses in outer normal layers 79−99667
multifilamentary superconductors with alternating twist, losses in transverse pulsed fields 79−30508
multimode focusing fibre with random bends, optical power loss 79−7214
multimode step index fibre, excess loss due to outer layer 78−9430
multimode W-type optical fibre launching and connection characteristics 78−1376
optical blazed waveguide corrugations, loss coeffs. 77−34948
optical compound glass fibres, silicone and glass clad, medium loss 80−69533
optical curved single-mode fibres, radiation loss meas. 78−74984
optical directional coupler with lapped multimode fibres, charact. 80−91892
optical fibers, graded-index, wavelength dependence of differential group delay and appl. to fibre-link characterization 79−50440
optical fibre, bend loss radiation 80−33187
optical fibre, doubly clad W-type, microbending losses 77−88899
optical fibre, graded index, connectors and splices, transmission loss estimation 79−18550
optical fibre, graded index, wave eqn. for propag. fields 80−58757
optical fibre, helically deformed, radiation loss calcs. 77−786
optical fibre, jacketed, hydraulic pressure depend. of losses 78−63175
optical fibre, joint and connector losses *(French)* 78−55464
optical fibre, losses due to fibre cross section variations 78−71226
optical fibre, low-loss graded index, produced by double crucible technique 80−48449
optical fibre, microbending eqns., exact time-dependent, solns. 80−87530
optical fibre, modified CVD prep., optical and mechanical props. reproducibility 80−69535
optical fibre, multimode, graded index, mode conversion coeff. meas. method 80−99820
optical fibre, multimode, optical loss changes caused by hydraulic pressure 79−41440
optical fibre, origin of temp. dependence of attenuation 79−46073
optical fibre, radially inhomogeneous, surface wave propag., bulk loss and dispersion influence 78−33892
optical fibre, single fibre separate connectors 77−88939
optical fibre, single mode, normalised freq., depend. of splice losses 78−55444
optical fibre, single-mode, dependence of optical losses on bending effects 79−50417
optical fibre, single-mode, misalignment and bend losses 79−10411
optical fibre, single-mode splices, loss anal. 77−75667
optical fibre, step index, scatt. from off-axis inhomogeneity, radiation loss 80−43446
optical fibre bandwidth limitations and bend losses 80−87553
optical fibre butt-joining to Ti-diffused $LiNbO_3$ waveguide 79−76812
optical fibre cable, single-mode, cabling and splicing loss increase charact. 79−81522
optical fibre cable attenuation and input and output efficiency 80−14469
optical fibre cables, single mode, random bend losses, power spectrum estimation from spectral losses 78−87143
optical fibre cables, single-mode and parabolic-index multimode, random-bend loss 80−78951
optical fibre cables using reverse-lay unit-core struct., with attenuation <3 dB/km 79−46072
optical fibre coating structure for microbending loss minimisation 80−28346
optical fibre communication advances, materials and techniques 80−102853
optical fibre concatenated connectorized cables, transmission losses 79−46071
optical fibre coupling using graded-index rod lenses 80−91891
optical fibre evolution, low-loss 80−69532
optical fibre link leakage induced by non-destructive methods 78−42450
optical fibre loss mechanisms, separation by graphical method 77−14806
optical fibre mode losses, coupled power eqns. 79−10376
optical fibre parameter measurement using optical time domain reflectometer 80−58755
optical fibre propagation, leaky-mode radiation field computation *(German)* 78−33867
optical fibre ribbons, loss meas. using calorimetry 78−87127
optical fibre second generation systems, 1300 to 1600 nm 80−64163
optical fibre splices, loss and output numerical aperture meas. 78−42403
optical fibre splices, parabolic-profile, loss model 79−23058
optical fibre splicing characteristics and techniques 78−46798
optical fibre technology and information transmission props. *(German)* 80−10010
optical fibre total dispersion and loss minima 80−91929
optical fibre waveguide, length influence on total losses 79−59836
optical fibre waveguide, low loss, ionizing radiation effect on attenuation 80−38112
optical fibre waveguide, low loss, radiation induced transmission loss behaviour 80−38111

losses continued
optical fibre waveguides and cables, microbending losses, depend. on numerical aperture 80−96025
optical fibre waveguides with large-diameter core and low optical losses, prod. technology 80−14463
optical fibres, Al coated, empirical formula for induced excess loss 79−46074
optical fibres, arbitrary-index profile, bending loss of propag. modes 78−66896
optical fibres, coated, strain-induced excess loss 79−50418
optical fibres, coated single-mode, bending losses 78−71209
optical fibres, compound glass, total loss decomposition into absorpt. and scatt. loss 80−53437
optical fibres, deformation of cable sheath by bending in plastic range, loss anal. 80−43477
optical fibres, excess loss due to coated resin shrinking at low temp. 80−43476
optical fibres, graded index, low temp. dependence of loss increase due to nylon jacket shrinkage, optimum cable unit 80−64182
optical fibres, graded index, splice loss/mode conversion relationship 79−64321
optical fibres, graded noncircular multimode, attenuation const. of leaky modes 80−33160
optical fibres, graded-index, differential mode attenuation meas. 78−71198
optical fibres, leaky mode behaviour, with non-circularly refractive index profile 77−62045
optical fibres, meas. method of connection loss using steady-state power distrib. 79−46084
optical fibres, multimodal double-layer with random axial bends, losses 79−90025
optical fibres, multimode, excess loss caused by lossy outer layer 77−58434
optical fibres, multimode, universal tunnelling coeff. 78−66922
optical fibres, multimode graded index, cladding loss effect 78−50927
optical fibres, multimode W-type, power flow numerical soln. 80−78955
optical fibres, non-circular graded index, leaky modes 79−1003
optical fibres, number of gaps allowable 79−14110
optical fibres, plasma augmented vapour deposition 80−69561
optical fibres, reversible photobleaching of radiation-induced losses 79−94356
optical fibres, single mode, curvature and microbending losses 79−27418
optical fibres, single- and multimode, fundamental mode signal transmission 78−42442
optical fibres, single-mode, fusion splice loss anal. 80−64181
optical fibres, single-mode, splicing and bending losses 79−18505
optical fibres, single-mode dispersion-free long-span, pulse broadening meas. 80−53417
optical fibres, single-mode step-index, practical microbending loss formula 79−81534
optical fibres, step-index, excess loss dependence on parameters, expt. 78−66936
optical fibres, two dimens., microbending theory, role of nonadjacent mode coupling 79−27415
optical fibres, ultimate low-loss single-mode fibre with 0.20 dB/km loss at 1.55 micron 79−36996
optical fibres, water diffusion, measured changes with time in OH absorpt. 79−46082
optical fibres and fibre lasers, scatt. and absorpt. losses, approx. theory 77−27339
optical fibres and fibre resonators, steady-state losses 77−27338
optical fibres development, polymer clad, for communication use 80−69546
optical fibres with arbitrary-index profile, splice loss evaluation 78−90499
optical fibres with bends, singly and doubly clad, excess losses 79−14104
optical graded-index fibres, refracting leaky rays 78−79103
optical graded-index multimode fibres, launch depend. loss in short lengths 78−90495
optical isolators for semiconductor laser, in laser-to-fibre coupling module 80−48267
optical leaky dielectric waveguide, planar hollow structure, eigenmode analysis 80−78973
optical link, 11.7 km spliced fibres, measured and predicted transmission charact. 80−14454
optical multimode fibre, mode conversion coeffs. and mode dependent losses meas. 79−10377
optical multimode fibre, splice loss and mode conversion 80−99830
optical multimode fibres, loss mechanisms of leaky skew rays 77−39054
optical multimode step index fibre, excess loss due to outer layer 77−58441
optical multimode strip-waveguides made by thick film technology, loss meas. 79−59846
optical multimode three-layer fibre waveguides, mode attenuation 79−59835
optical multimode W-type fibre, periodi bending loss 79−76848
optical multimode W-type fibre transmission charact., intermediate layer effect 78−90497
optical parabolic fibres, mode depend. attenuation 77−72059
optical parabolic index fibre, modal dispersion characteristics, lossy cladding effect 79−18515
optical planar waveguides, Ti diffused $LiNbO_3$ and $LiTaO_3$, leaky mode propag. 78−87149
optical power, in thin-film waveguide, theory and expt. 80−106640
optical receiver system, narrow-field, spherical aberration effect on radiation power losses 80−28299
optical S-shaped transition between offset straight waveguides, length optimisation 78−46838
optical single mode fibers, microbending loss evaluation, core index profile effects 80−48412
optical single mode fibres, arbitrary index, microbending loss evaluation 80−48411
optical single-mode fibres, low-loss, arc fusion splicing 80−53489
optical single-mode fibres, simplified bending loss formula 79−59800
optical single-mode fibres, splice loss, Gaussian field approx. 79−94354
optical strip waveguide directional coupler, leaky-wave 78−38058
optical surface-diffused and buried waveguides, scatt. losses caused by surface imperfections 79−64332
optical systems, losslessness, vectorial treatment 80−83558
optical transmission line, loss compensation using distributed gain amplifier 77−14811

losses continued
optical waveguide, asymm. three-layer, radiation losses due to discontinuities 80−53446
optical waveguide, bent multimode, loss calcs., geometric optics method 79−37013
optical waveguide, diffused, attenuation characteristics of TE modes and surface scatt. 80−5822
optical waveguide, multilayered, attenuation and tunnelling coeffs. for leaky rays 78−38002
optical waveguide, multilayered, effect of material absorpt. on ray power attenuation 78−83103
optical waveguide, weakly guiding three layer slab, attenuation coeff. 78−5567
optical waveguide bending losses, coherent mode coupling 78−38060
optical waveguide corner bends, mode conversion for integrated optics 77−42594
optical waveguide in chalcogenide glass film, low bending losses 77−79978
optical waveguides, graded-index anisotropic, WKB analysis of guided and semileaky modes 79−27416
optical-fibre loss for high-speed drawing 79−14095
pair-correlated distrib. of small-spaced lossy scatterers, light propag. 80−28158
parabolic-index slabs and fibres with bent axes, radiation losses 78−46758
parasitic mode losses in cylindrical cavities with beam ports 77−83271
phosphosilicate glass fibre waveguide, possibility of near IR operation 78−50935
photorecombination reactions initiated by shock wave, light amplification *(Russian)* 80−38011
piezoceramic SAW propagation loss reduction by hot pressing 78−2356
piezoelectric transducers, input electrical impedance expression, internal loss correction 78−53101
polyethylene waveguide, O-type, loss characts. at 337 μm 80−33175
polyethylenepolyamine hardened epoxy resin, hardening kinetics and mech. losses 80−66520
pseudocolour density encoding, white-light, using contrast reversal 80−83560
quartz fibres, liquid core tetrachloroethylene filled, transmission loss meas. at 3.39 μm 79−81532
quartz glass, hydroxyl-free, for low-loss fibre waveguides, γ-irrad. effects 78−13773
radiation from optical waveguides: leaky-mode interpretation 79−32039
rhodamine laser, induced losses in active medium during incoherent excitation *(Bulgarian)* 79−10297
ring Zeeman laser, interaction of modes characterized by orthogonal circular polarizations 80−48306
ruby ring laser with forced mode locking 80−95915
SAW reflective-array-compression filters, nonsynchronous scatt. loss 78−71246
self-filtering multilayer S-waveguides with absorption and radiation losses 80−38102
semileaky thin-film optical waveguide mode filter radiation-coupling loss 77−88953
silica fibres, contamination with furnace drawing, losses 77−42634
single fibre optic cable connector losses 78−46802
single mode and graded-index multimode fibre cable random bend losses 80−58741
single-fibre separable connector insertion loss characteristics 77−23770
single-mode fibre cabling for low-loss communication 80−53467
single-mode fibre joint losses calc. 78−74980
single-mode fibre tapered velocity coupler performance 79−55246
single-mode optical fibre microbending loss and pulse distortion analysis 78−1395
solar cells, stacked multibandgap monolithic multijunction struct., loss evaluation, optimum performance 80−93928
solar collector with stationary spherical reflector and tracking absorber, characts. 77−54773
solid laser, multimode, with modulated resonator losses, radiation intensity fluctuations 80−74367
sound transmission meas. 77−19486
spatial filtering, nonlinear medium, loss formation 80−53357
spectrometer efficiency, S/N ratio formula 80−31881
spherical resonator diffraction losses, expt. meas. 78−29980
step-index optical fibre and cable transmission characteristics 78−1404
superconducting cables for PF and TF coils, losses and transient field effect 78−62635
superconducting magnets, pulsed, hysteretic and mechanical loss calcs. 79−80649
superconducting multifilamentary composites, transverse elec. cond. 77−24648
superconducting wire, AC losses *(Japanese)* 78−84364
superconductor, composite, energy dissipation, expt. and theory 77−85386
superconductor, standard measurement techniques for determ. of props. 79−69622
three layer vibration absorbing structures, temp. characts. of loss factors 79−64395
transmission loss characteristics of optical fibres under hydrostatic pressure 80−99869
transversely inhomogeneous slab, modal wave propag. with gain or loss variations 80−48122
type II superconducting slab, AC losses in small mag. field of sinusoidal wave form 78−47920
type II superconductor, cylindrical, rotating in mag. field, dissipation determ. 77−28309
type superconductor with field-dependent surface barrier, AC losses 79−87216
unbiased nuclear reactor core *(Russian)* 77−61493
unstable resonators with rounded edges, mode losses 78−79039
voltage loss calc. using special sliderule *(Russian)* 77−53869
waveguide, graded-index surface or buried, realized by ion exchange in glass 80−69499
waveguide, hollow-core rectangular, propagation losses at 10.6 μm for distributed feedback appl. 80−38101
waveguides, metal, hollow, multimode IR laser losses 79−23076
wavelength division multiplexer using optical fibre pieces 80−91917
Ag halide optical fibres, extrusion, visible and IR transmission 80−58829
Ag halide polycrystalline fibre, 10.6 μm transmission loss obs. 80−64197

losses continued
AlGaAs buried heterostructure lasers, gain and absorpt. spectra meas. 80−91792
B_2O_3-SiO_2 low-loss single mode fibres, design, fabrication and transmission characts. 78−71199
CO laser, water-sealed, efficiency increase by reducing resonator losses 80−64081
CO pulsed laser, stimulated emission dynamics, transition lines for isotope enrichment 80−48225
p-GaAs-$Al_{0.3}Ga_{0.7}As$, cladded dielec. waveguide, loss meas. using Raman scatt. 79−81539
Ge, amorphous film, high freq. cond., AC loss 80−49792
GeO_2-B_2O_3-SiO_2 optical fibres, optical transmission loss as function of drawing conditions 79−32038
He-Ne laser, cavity losses, phase polarisation method in lasing regime 80−87413
$In_xGa_{1-x}As$ epitaxial layer, waveguiding at 1.06 μm, losses 78−18052
$LiNO_3$ waveguide, planar structure for integrated optics, props. *(Czech)* 80−96018
$LiNbO_3$ diffused waveguides, optical insertion loss meas. 78−38054
$LiNbO_3$, Fi diffused, single-mode waveguide, comparison of bending losses in integrated optical circuits 80−83684
$LiNbO_3$, Ti diffused waveguide, leaky mode loss coeffs., calc. 80−19094
$LiNbO_3$ waveguide absorption losses, laser calorimetric meas. 79−64311
$LiNbO_3$:Ti cleaved, waveguide, attenuation coefficient and coupling loss 78−74975
$LiNbO_3$:Ti diffused strip waveguide, optical insertion losses 78−74985
$LiNbO_3$:Ti diffused strip waveguide, optical propag. losses and coupling losses 80−58664
$LiNbO_3$:Ti optical waveguides, pyroelectric loss meas. 79−46046
$LiNbO_3$:Ti waveguide and cryst., absorpt. loss and photorefractive index changes 80−48368
$LiTaO_3$ optical waveguide, Ag-Li ion exchange 80−91888
$LiTaO_3$:Cu waveguide, electro-optic control of radiation loss in off-axial propagation 80−23789
Na_2O-B_2O_3-SiO_2 glass, Rayleigh scattering losses 79−99893
Na_2O-B_2O_3-SiO_2 glass, low-loss GRIN fibres, double-crucible prod., loss and bandwidth meas. 80−69559
Nb, superconducting, AC losses surface effects 77−28313
Nb-Ti superconducting multifilamentary composites, high current, effect of matrix on losses 77−24649
Nb-Ti superconducting multifilamentary wires, high B losses 77−24650
Nb-Ti-Zr, superconducting wire, coil simulation, class and instability meas. 79−71487
Nb_3Ge, hysteretic losses in parallel AC and DC mag. fields 79−87217
Nb_2O_5 waveguide, in-plane scatt. and loss mechanisms 80−33216
Nb_3Sn, AC losses, surface effects 78−64171
Nb_3Sn multilayered supercond. power line conductors, elec. props. and growth morphology 77−28325
NbTi in Al composite superconductor, AC losses and crit. current 77−28310
NbTi multifilament superconductor, AC loss reduction by low twist rates 77−12057
NbTi-Al-(Cu-Ni) multifilamentary composite supercond. wire, stability, AC losses 77−76998
$(Nb_{1-x}Zr_x)_3$ Sn, bronze-processed tape, AC losses between 5 and 16K 79−82727
P_2O_5-SiO_2 clad low-loss monomode fibres for 1.2 to 1.6 μm, modified CVD prep. 80−48479
Si-SiO_2-$Si_xO_yN_z$ waveguide model *(Russian)* 79−10374
SiO_2 optical fibres, plastic clad, gamma-ray irradiated, signal level depend. of recovery rate 79−36997
SiO_2:GeO_2 single-mode optical fabre fabrication 79−46050
SiO_2:GeO_2-P_2O_5 graded-index fibre, spectral loss characts. in long wavelength band 79−59811
SiO_2-GeO_2 cored optical fibre with borosilicate cladding, loss mechanisms 77−62072
SnCaV garnet polycrystal, ferrimag. resonance loss rel. to grain size 77−85581
ZnO piezoelectric films, RF planar-magnetron sputtered, characterisation 80−96751

loudness
see also acoustic intensity measurement
acoustic reflex, in animals, influence on loudness of pulsed pure tones 78−92647
acoustic reflex, loudness, summation and critical bandwidth 77−2009
acoustic reflex, statistically based measure and relation to stimulus loudness 77−32907
artificial speech, loudness function for reference equivalent meas. 80−79068
audibility and effective loudness of sirens and speech in automobiles 77−16935
binaural summation of the loudness of pure tones 78−92638
comfortable loudness levels for pure tones and speech 78−65050
community noise, scaling of loudness, noisiness and annoyance 77−11086
complex sounds, loudness as function of standard stimulus and number of components 79−5296
continuous judgement by category as rating of road traffic noise *(Japanese)* 78−83170
critical bandwidth in patients with acoustic neuroma 80−16953
critical bandwidth in presbycusis 80−16955
detection probability of continuous signal parameter change evoking blurred change of loudness 80−41054
dichotic chords, effects of signal intensity and noise on pitch mixture 78−3501
difference limens and the subjective scale of loudness 80−41046
dynamic difference limen determ., loudness discrimination for varying intensity sounds *(Japanese)* 80−97942
fans, loudness rating programme 79−24930
filtered N-wave sonic booms, subjective loudness and annoyance 79−50505
growth depend. on excitation pattern skirts 78−61195
hearing, comparison of monaural and binaural discrimination of intensity and freq. 77−86511
hearing, comparisons between different types of stimuli 78−20186
hearing, detection of combined differences in freq. and intensity 78−35863
hearing, intensity perception, roving-level discrimination and resolution and bias edge effects 77−86509

loudness continued
hearing, loudness discomfort level and acoustic reflex threshold for speech stimuli 80−76762
hearing, loudness discomfort level and acoustic reflex threshold for normal and sensorineural hearing-impaired subjects 80−76763
hearing, loudness enhancement and decrement in four paradigms 80−51119
hearing protectors, meas. of real-ear attenuation, SABS 572 1973 80−53581
impact sound loudness meas. *(Japanese)* 79−98546
infrasound, subjective annoyance due to environmental pollution *(Japanese)* 80−35805
intensity resolution and relation to loudness matching 80−108908
judgment for continuous and interrupted pure tones, effect of psychophys. method 80−76760
loudness perception, for short-duration tones in masking noise 78−65047
minimized sonic boom waveforms, subjective loudness 79−16221
model of creation of sound sensation varying with time 80−41053
modulated tones, hearing in comparison to continuous tones *(German)* 80−94219
monaural intensity processing, nonlinear-algebraic approach 78−57012
N-wave sonic booms, subjective loudness tests 79−16220
narrowband noise pulses 80−38194
noncombination of pitch and loudness in multidimensional scaling 78−40193
perception of signals of monotonically changing sound pressure 77−64044
pipe organ, loudness, plenum combinations 79−18628
pipe organ, loudness, single notes 79−18629
precise perceptibility of original loudness through electroacoustic playback *(German)* 77−21535
quarry blast waves, simulated, subjective loudness 79−72751
sensorineural hearing loss effect on loudness discomfort level 79−96577
speech, bimodal cues 80−10090
speech perception, use of comfortable listening levels, effect of loudness level 79−2078
statistical prediction of vibr. distrib. and random noise in higher level region *(Japanese)* 79−1023
steady sounds, mathematical theory 79−53154
subjective loudness and its physical correlate 77−64037
subjective loudness measurement, affecting auditory factors *(Japanese)* 80−85409
temporally variable sounds, procedure for loudness calc. 78−3508
tone sequences ABAB, min. level and freq. differences for perceptual fission 77−56384
tones, AM, dependence of fluctuation strength on sound parameters *(German)* 79−34569
traffic noise, meas. by L_{eq} and L_{α} *(Japanese)* 79−1024

loudspeakers
accuracy of reproduction determ., w.r.t. ear props. *(German)* 80−106703
acoustic display effects, computer calcs. 80−14524
acoustic imaging, impulsive sound method 79−10431
acoustic measurement limitations *(German)* 79−37105
acoustic power response monitor 80−87674
Acoustic Research AR9, performance tests 79−81669
Advent 1 system, review of performance 79−81670
artificial head system, transmission errors causes and improvements *(German)* 80−106700
artificial heads with stereophonic intensity signals, directional effects *(German)* 80−106701
B and W DM2, JBL L50, Infinity Q Junior, comparative test *(German)* 79−64476
bimorph element using piezoelectric ceramic props. and manufacture *(Japanese)* 80−53597
cabinet panel vibrations meas. 77−54827
cabinet reflection effects 79−64451
Cerwin-Vega 12TR system, review of performance 79−81671
characteristics calculation, appl. FEM to coupled structural-acoustic radiation system 80−83691
concert halls, hearing impressions of loudspeaker reproductions and orchestras *(German)* 78−94485
cone, vibration analysis using finite elements method *(Japanese)* 79−18660
cones, effect of voice-coil and surround on vibration and sound pressure level 80−96172
conference halls, mathematical model of insonification rel. to speech intelligibility *(French)* 78−13857
damping materials, behaviour in loudspeaker units *(Spanish)* 79−46146
design for domestic conditions *(Italian)* 80−91960
diaphragm development, composite, B-Ti, by physical vapour deposition *(Japanese)* 80−58883
diaphragm using carbon rinforced olefin polymer, with high specific modulus flexural rigidity and loss factor *(Japanese)* 80−53596
dipole radiator systems, operational principles 80−38207
directivity, meas. in ordinary rooms 80−87681
directivity of loudspeaker and subjective hearing event *(German)* 78−79174
domestic room acoustics, speaker positioning for optimum frequency response 77−54845
driver parameters, time domain measurement implemented with digital computer 79−59901
driver phase response and crossover network design 80−87686
efficiency determ. method 78−51028
elastically supported circular plate, sound radiation 79−41507
flame acoustic radiation rel. to flame loudspeakers 78−59227
forced oscillations, for respiratory impedance meas. 77−37079
free-field meas. in normal room using digital signal processing 78−66995
free-field system, compensating cct. for system function of an acoustic transmission system *(Japanese)* 80−53566
frequency response measurement in echo chamber *(German)* 77−75762
group delay distortions in electroacoustical systems 78−69105
Grundig SL 1000 with stove-pipe design, nominal load of 50W *(German)* 79−81679
hi-fi, with passive and active units, 4/8 ohm output *(German)* 79−64475
high-impedance low quality microphone using small 8 Ω loudspeaker *(Spanish)* 80−96173
high-power unit with 4 component loudspeakers *(German)* 79−86314

loudspeakers continued
honeycomb structure cone, with low distortion, MS series, Mitsubishi Electric's development 80−14536
horn, anal. of acoustic radiation by finite element method 80−96171
infinite baffle simulation with small loudspeaker enclosure 78−55531
interaction with room resonances, absorption, stereo reception appl. *(Italian)* 78−51005
lateral, phantom sources generated by two loudspeakers, localisation 77−54849
LF horn-loaded, specification of moving-coil drivers 80−28404
living room loudspeaker performance problems *(German)* 79−90081
Lowther Classic 400 *(German)* 79−64474
magnetic fluid influence on design parameters 80−38206
measurement, by application of digital techniques 77−68345
medium-scale live concert sound reinforcement system requirements 80−92012
moving coil temp. meas. systems *(Hungarian)* 80−106698
oscillating circular plate, axial field, meas. and anal. 77−7235
outdoor classical music sound reinforcement systems compared 80−92011
outdoor environment, loudspeakers positioning for assisted reverberation effect 78−13825
phase inverter loudspeaker system, design using nonlinear optimization method *(Japanese)* 79−18659
piezoelectric, using high polymer film *(German)* 77−62128
polar diagram variation with freq. and speaker directivity 79−98587
polyvinylidene fluoride foil appls. *(German)* 78−22243
power matching with amplifiers *(Japanese)* 79−90106
radiation patterns effect on stereo imaging and clarity 79−64401
real-time room-acoustic analyzer using tone burst signal from loudspeaker *(Japanese)* 80−10087
reproduction at home, charact. and problems *(German)* 79−72755
reverberation chamber design, construction, loudspeaker performance measurement appl. *(Italian)* 78−26013
reverberation problems in enclosed auditoria *(German)* 78−87204
ripple tank wave generator, using loudspeakers, student demonstration 77−78915
signal displacement meas., optical method 78−51023
sound amplifying systems in halls, model *(French)* 79−37090
sound diffusion systems, fundamentals calc. *(Spanish)* 79−3855
sound power measurement *(Spanish)* 79−3871
sound power measurement using type 4205 power source 80−1392
sound quality, perceived, investigated by multivariate techniques from experimental psychology 79−68536
sound quality, subjective and objective data correl. *(Japanese)* 77−75766
sound reinforcement systems, concert hall, Nippon Budokan Hall *(Japanese)* 80−64291
spectral analysis, constant-Q, using chirp Z transform, impulse-response measurements 79−64407
subjective evaluation tests of audio perception thresholds from front and rear *(Polish)* 79−55288
surround stiffness, fund. reson. freq. *(Japanese)* 80−92009
system amplitude and phase response rel. to driver alignment on baffle 80−92010
system group and phase delay requirements 80−92014
technology, state-of-the-art review *(German)* 79−50559
three-way systems, proposals for correct combinations *(German)* 79−32171
US amplifier for directly driving solid-dielectric capacitance speakers 80−19186
vented alignments, providing fourth order responses 77−68356
vented box loudspeaker analogue model using operational amplifiers 80−92015
vibrating shell and closed cavity model, finite element analysis 80−69622
vibration characteristics of moving coil and supporting piece *(Japanese)* 77−62101
Walsh loudspeaker and high-power film cylindrical tweeters *(German)* 79−50558

Love waves
attenuation across Pacific Ocean, 15-110 s periods 77−9353
Black Sea basin, crustal struct. from Love and Rayleigh waves dispersion *(Russian)* 78−28192
Bonin Is. earthquakes, two-parameter scaling of source spectra 77−73642
Brillouin scattering by Love waves, theory 80−66212
China, seismic surface wave study of crust and mantle 80−104916
composite, layered, Love wave diffr. by stress-free crack in plane interface 80−33501
dispersion curves for stressed stratum in isotropic elastic media 78−57169
dispersion eqns. in transversely isotropic layer on istropic elastic material 79−14308
dispersion in continuously stratified layered Earth 79−20760
dispersion in semi-infinite medium with inhomogeneous layers 77−49031
Earth stretching approx. 77−73664
Earth upper mantle, inversion of surface wave dispersion data with random errors 77−73681
elastic surface waves propag., charact. for SAW filters, book contrib. 80−1378
excitation of surface waves propag. along cylindrical surface 80−102907
frequency eqn. for waves under initial stresses 79−29714
Great Basin of Nevada and W Utah, struct. from seismic surface waves 78−73336
hypoelastic half space, transverse elastic waves in medium with material boundary 79−1133
hypoelastic stratified solid with material boundary 78−30225
infinite strip with surface step, transmission, reflection and diffraction 79−88260
initial stress effects in isotropic elastic incompressible medium 79−98655
inversion of wave data for vel. and anelasticity 79−8604
isotropic half-space with layer of incompressible material, Love wave propagation 80−23929
Japan area, surface wave group vels. 77−56603
magnetoelastic Love waves by interaction with carrier waves in layered composite 79−28577
magnetoelastic surface wave propagation in laminates 80−38322
magnetoviscoelastic solids under initial stress, surface waves 79−84140
mantle of Europe and Eurasia, inferences from higher mode seismic data 80−72436

Love waves continued
Mediterranean area, surface wave and seismotectonic studies 77−37151
microseisms obs. at New York Rayleigh and Love wave characts., geologic control 80−26462
mode conversion, shear, Lamb and Rayleigh waves, demonstration 80−101687
mode conversion of continental margin 77−40986
near-field Love waves synthesis by exact ray method 79−79750
normal mode propagation in oceanic struct. rel. to Sn transverse component 77−56583
oceanic Lg phase search 79−25203
Oroville earthquake, California, 1975 August 1, surface wave constraints on source parameters 77−56579
Pacific crust surface wave dispersion 77−56604
Pacific upper mantle regionalized shear vel. models from Love and Rayleigh wave dispersion 79−53321
perturbation matrix method for propag. in irregular stratification 77−73869
phase vel. determ. of fundamental Love and Rayleigh waves 77−37148
photoelastic film, fluctuations of acoustic waves and light scattering *(Russian)* 77−28543
piezoelectric medium, Love wave propagation *(Russian)* 77−69039
poroelasticity, Love wave propagation 79−98653
propag. in bodies with initial strains *(Ukrainian)* 79−30258
propagation across a step (ocean-continent transition), by finite elements 80−72437
propagation in 3-dimens. structures, finite element techniques 80−21631
propagation in heterogeneous medium between semiinfinite homogeneous elastic media 79−18767
propagation in viscoelastic medium, effect of initial stresses 79−14299
propagation on an ellipsoidal Earth 77−37152
reflection and transmission coeffs. in media with lateral inhomogeneities 77−37156
resonant excitation, acoustic wave passage through gap between piezoelectrics coated with insulating films 79−28187
scattering matrix for continental margin, theory 78−20360
seismic, application of phase-matched filters 79−92602
seismic long-period waves dispersion obs., shield-like upper mantle struct. 77−56608
seismic Love waves, possible mode conversion at continental margin 78−73314
seismic phase velocity and attenuation, simultaneous inversion over continental and oceanic paths 79−92488
seismic strong ground motions, Love wave contribs. 79−88302
seismic surface wave data inversion in source mechanism studies 77−33204
seismic surface waves dispersion curves, partial derivatives calc. *(Russian)* 79−34764
seismic wave anelastic attenuation lateral var. across Pacific 79−84123
seismic waves azimuthal anisotropy, physical model 78−65186
seismic waves scattering matrix for continental margin model 78−48982
SH wave equation soln. for scattered field near plane boundary 77−86788
SH wave propag. in medium with step-shaped discontinuity 77−56602
SH waves in infinite monoclinic crystal plate with initial stress 77−86789
SH waves in multilayered, laterally heterogeneous media, dispersion eqn. 77−73645
SH-waves, propag. in nonhomogeneous internal stratum between two elastic media 78−32016
slowly varying layered media, propagation 77−37153
stratified elastic solid, transverse surface waves in medium with material boundary 79−1135
in stratified magnetoelastic solid with material boundary, amplitudes and phase vels. 78−32015
strong simple harmonic motion in isotropic layer over isotropic elastic material 79−23239
surface wave props. in frictionally bonded layer 80−21630
surface waves in vertically inhomogeneous elastic halfspace with horizontal inhomogeneity 77−52998
surface waves initial phase and phase vel. from 1968 Jan. 29 Shikotan earthquake 78−92793
surface waves on layer-coated cylinder 78−2354
surface waves propag. in crystalline media 78−2350
thermoelastic surface waves in micropolar elastic solid medium 77−72206
thin film with periodic surface corrugation 79−14130
Thomson-Haskell method extension to non-homogeneous spherical layers 77−9362
transmission through laterally varying structure 77−56592
viscoelastic media, surface wave propagation 78−42555
YIG, anisotropic elastic waveguide normal-mode anal., appl. to Rayleigh-Love wave mode converter 79−23113
YIG, ferromag. film on nonmag. substrate, magnetoelastic wave propag. 79−99744

low energy electron diffraction
acetylene, chemisorption on Pt (111), ethylidyne group form., LEED and ELS obs. 78−73075
adlayer-induced LEED beams near order-disorder transitions, Monte Carlo study 79−82438
adsorbed atom interaction, LEED exam. 78−95237
adsorbed inert gas layers, LEED apparatus 77−47306
adsorbed layer, superelastic electron scattering *(French)* 78−56039
adsorbed overlayer, order-disorder transition, Ising model, LEED superlattice beam intensity distrib. 80−65371
adsorption on Pt electrode surface, struct. and comp. exam. by LEED and AES 79−70342
AES-LEED system, three-grid type *(Japanese)* 79−55618
alkali halide film, low energy electron scatt. 78−26928
alkali metal submonolayer film, on W (011) or Mo (011), disordering, LEED obs. *(Russian)* 77−89655
n-alkanes, conduction band struct., LEED, secondary electron emission and UPS study 80−70601
amino acid monolayers and ordered films on Cu, surface struct. LEED 78−38968
angle of incidence determ. using fluorescent display photographic technique 78−75508
anisotropic vibration effects 78−71650
apparatus, using high-tension source, construction 78−38591
low energy electron diffraction continued
apparatus for low energy in scatt. spectroscopy, LEED and AES *(Japanese)* 80−20746
Au film growth on Si(100), LEED and X-ray texture anal. 79−99452
automatic LEED spot tracing method 80−10467
beam intensity measurement by photographic method, use of Vidicon camera 77−7638
benzene, chemisorption on (111) surface of Pt, LEED and Auger spectroscopy obs. 78−30823
benzene, epitaxial film, on metal (111) substrates, surface struct., LEED obs. 79−86969
benzene film, on metal substrate, surface struct. using LEED 79−77879
benzene on Ni(100) and (111), chemisorpt., LEED and high resoln. electron energy loss spectra 78−6224
blanking resistive heating for Auger spectroscopy and LEED using retarding field analyzer 78−54509
chain method of LEED/MEED intensity analysis for NaCl type structure 80−20018
chemisorbed O_2 effects, CH formation 78−18902
chemisorption structures, complex interpretation 77−89652
crystallography of clean surfaces and chemisorbed species 77−24470
Cu, adsorption of CO, on (110), LEED, surface pot., IR spectra 77−66092
cyclohexane, monolayers and thin crystals grown on Pt (111), LEED obs. 77−59230
Debye model, high temp. limit 77−1207
defect surface structures, LEED studies, review 77−80685
defects role, review 78−14551
diatomic surfaces, LEED/MEED intensity calcs. 80−44083
diffractometer, high-resolution 77−4025
disorder theory, appl. to Au (101) 79−4463
disordered crystal surface, diffuse LEED pattern, correl. between statistics and multiple diffr. 79−4461
disordered overlayer, model calc. 78−84074
disordered overlayers, diffuse LEED intensities, multiple scatt., theory 79−4476
elastic and inelastic slow electron scatt. in solids 79−90857
electrode-electrolyte interface, solid film props., review of expt. techniques 77−77780
electron stimulated desorption, LEED system 78−14567
electronic surface resonances and crystal surface structure 78−71648
epitaxy, growth modes, exp. techniques, book contrib. 80−49558
ethylene, chemisorption on Pt (111), ethylidyne group form., LEED and ELS obs. 78−73075
extinction rules, cluster-embedded chain method 78−94952
faceted surfaces, investigation by slow electron diffraction 80−100377
ferromagnets, spin polarised LEED, calc. 79−99686
Fourier transform deconvolution procedure, multiple scatt. effects 79−32862
Fourier transform deconvolution procedure, multiple scatt. effects 80−6322
Fourier transform-deconvolution procedure, LEED data anal., multiple scatt. effects 79−41913
Fourier transform-deconvolution procedure, LEED data anal. multiple scatt. effects 79−41914
Frenkel exciton formation in LEED theory of mol. crystals 78−38592
gas-surface interactions, mol. beam apparatus 78−72675
graphite, adsorbed Kr, Ar, overlayer-substrate spacing, LEED determ. 80−103579
graphite, Ar monolayer, adsorpt. isotherms LEED geometry and intenstiy meas. 79−65316
hydrocarbons, adsorbed on Ru(001), characterisation by electron-stimulated desorpt. 78−71958
ice, epitaxial film, on metal (111) substrates, surface struct., LEED obs. 79−86969
ice, film, on metal substrate, surface struct. using LEED 79−77879
II-VI semiconductors surface struct., LEED and AES *(Japanese)* 78−22943
III-V semiconductor, surface protection by KCl layer, obs. 77−89628
inelastic scattering of low energy electron beams by surface vibrs., nature of image force 78−91527
intensity dynamics of slow-electron diffr. patterns 78−10267
intensity meas. using video camera and video tape recorder 79−73074
intensity measurement by photographic method with digital image processing, appl. to Si (111) surface 79−60234
Kikuchi pattern, contrast change due to plasmon excitation 78−34686
Laue-case Kikuchi pattern, contrast behaviour, in refl. diffr. 78−1963
liquid nitrogen cooler, for specimen manipulator of LEED-AES experiment *(Japanese)* 78−45639
magnetic surface props., polarised electron scatt. study 80−93160
MBE, obs. by LEED-AES *(Japanese)* 78−91564
measurements of spectra *(Japanese)* 79−37595
metal, image pot. and LEED intensity above beam threshold 80−44084
metal, surface relax. from LEED, Fourier transform-convolution method 79−4459
metal, surface relaxation determ. from LEED via transform method, appl. to W 77−43419
metal, surface-resonance fine struct. in LEED intensity profiles 77−39518
metal adsorbed molecules, low-energy electron inelastic scatt. 79−46526
metal surface barrier, transmission and reflection of low-energy electrons 78−18507
metal-InP contacts, intermediate adsorbed layer effect on electronic props. 80−39674
metallic surface, anisotropic contrib. to optical pot., in electron spectroscopy, theory 80−44086
metals, chemisorption of gases, book 79−69370
model for LEED one-electron potential 77−31567
molecular crystal, LEED, Frenkel exciton influence, diagram formalism 78−47217
molecular crystal, LEED differential cross-section, Frenkel excitons effects 78−51398
molecular crystal, LEED specular beam intensity, bulk Frenkel exciton effects 78−51399
naphthalene, epitaxial film, on metal (111) substrates, surface struct., LEED obs. 79−86969
naphthalene, films, on metal substrate, surface struct. using LEED 79−77879
one-dimensional crystal, surface pot. influence on electron refl. intensities 77−63506

low energy electron diffraction continued
n-paraffins, monolayers and thin crystals grown on Pt (111), LEED obs. 77−59230
n-paraffins, thin crysts. and monolayers on Ag(111) surface, LEED 79−11014
peak widths, analogue of Fabry-Perot etalon 80−28887
phase of diffracted wave calc. 78−71647
photographic-vidicon camera method for intensity meas. 79−37596
phthalocyanine monolayers and vapour-grown films, surface struct., LEED 77−35830
planar scattering matrix props., multiple scatt. of electrons by infinite lattice plane 77−76265
polarised electrons, symmetry 79−60233
polarised LEED using a GaAs spin polarised electron source 78−83693
polarised low energy electron scattering from solids and liquids, temp. effects 78−71649
polarized, appl. of GaAs spin-polarized electron source 80−69000
polyethylene, conduction band struct., LEED, secondary electron emission and UPS study 80−70601
potential barrier, surface, electron reflection and transmission coeffs., Schrodinger eqn. 80−87998
pulse-counting LEED instrum. 80−37133
random distributed steps at interfaces and surfaces, quantitative LEED evaluation 78−63912
reconstructed surfaces 78−95214
reliability factors in LEED calcs. 80−49058
retractable rear viewing LEED/Auger spectroscopy system 80−57434
rotation diagrams for surface struct. anal., appl. to W 78−38917
Rydberg states, existence and detection via LEED 78−56198
semiconductor, cubic, tetrahedral and layered structs., review 77−85032
semiconductor, tetrahedrally coordinated, review of surface struct., chem. and spectroscopy 80−59764
semiconductor surface, atomic geometry, ELEED meas. 79−51399
single-layer scattering matrix, efficient calc. scheme 77−58930
single-reflection layer scatt. theory 80−49059
slow electron diffraction, from thin crystal struct., theory *(Russian)* 80−64843
solid surface characterisation techniques, review 78−22945
solid surfaces, problems *(Japanese)* 78−43222
solid surfaces props. characterisation, structural, chemical and electronic *(Italian)* 80−49467
solid-electron interaction, nature and consequences 78−72230
spin-dependent features in LEED intensity curves, model calcs. on W (001) 78−34685
spin-polarised, symm. props. 80−96420
spin-polarized, time reversal and spatial symmetries 80−87999
steel, austenitic stainless, oxidation of (100)-plane, LEED-AES obs. *(German)* 78−68841
stepped surface exam., cf RHEED 77−72762
surface (100), atomic struct., angle-resolved XPS, LEED and ISS investigation 80−10765
surface and interface struct., book contrib. 79−42358
surface barrier resonances and intensity-energy profiles, model calcs. 78−42870
surface characterization, by LEED, tutorial 79−68986
surface crystallography, past and present 78−14253
surface crystallography, reliability 79−37910
surface crystallography, review 78−83691
surface crystallography 77−80686
surface crystallography 79−42349
surface crystallography and bonding, book contrib. 80−24724
surface defect struct. determ., book contrib. 77−62726
surface lattice vibrations, interaction with low-energy electrons 78−30820
surface magnetism, investigation by LEED *(Japanese)* 78−43627
surface resonance band structure, lateral surface struct., determ. method 78−68067
surface science, conf., York, England (March 1977) 78−14540
surface step densities, two-dimens. random probability model 80−80036
surface struct. anal., review of LEED crystallography 79−14656
surface struct. determ., multiple scatt. theory based FORTRAN computer programs, book 79−86971
surface structure, clean and with adsorbed monolayers 77−24469
surface structure, coherence length and transfer width in LEED and mol. beam diffr. 79−42347
surface structure, distribution of defects, LEED 80−44402
surface structure, LEED intensity meas., reliability determ. 80−92424
surface structure, LEED reliability determ. 80−49474
surface structure by Rutherford backscattering and LEED 79−82419
surface structure derivation, data averaging, objective approach 77−15668
surface structure determ., accuracy-limiting factors 80−75127
surface structure determ., reliability factor 77−35802
surface structure determ. by LEED intensities anal., transform deconvolution method 77−62717
surface structure determination, comparision of rel. intensities of diffraction beams 80−54082
surface structure of solids and adsorbates by LEED 78−94953
surface structure refinements, via reliability factors for surface crystallography 77−59193
surface structure studies, review *(Russian)* 79−14994
surface structure study by LEED, dynamic installation 80−44399
surface studies, review 79−10764
surfaces with hexagonal symm., anal. of two-dimens. superstructs. obs. by LEED and RHEED 79−23817
techniques, double modulation method and photographic technique 80−75128
theoretical advances 78−83688
transition metal oxides, UPS, LEED and AES studies of mol. adsorption 79−4480
unified computation scheme of LEED, combined space method 78−9919
universal ultrahigh vacuum manipulator for LEED camera 77−43121
UPS, angle-resolved, in modified LEED system 78−15293
vacuum system for LEED-AES system with sample transfer capability 77−7639
Varian movable Faraday cup assembly, CEM addition for ang. resolved UV spectroscopy 77−44130
vicinal surface, system of regularly spaced steps *(French)* 80−49060
vidicon-based system, instrument response functions 79−90500
water at interfaces, mol. struct. and dynamics, LEED-Auger obs. 77−31873

low energy electron diffraction continued
WO_3, (100) and (111) layers, electron stimulated desorption of O^+, LEED obs. 79−23840
Ag (110), adsorption of O_2 and CO-O_2 interaction, ellipsometry-LEED expts. 78−91542
Ag (110), ethylene-O_2 interaction, LEED and AES obs. 80−89520
Ag (110), struct. and effect of surface roughness on LEED intensities 77−24471
Ag (110), surface relax., LEED results anal. by convolution-transform method 77−89624
Ag (110), surface struct., LEED determ., const. momentum transfer averaging 79−42350
Ag (110) surface, adsorption and surface structural chemistry of Na and Na+O_2 77−31883
Ag (110) surface, clean and Na dosed, chemisorption and surface reactivity of NO 77−31882
Ag (111), adsorpt., coadsorpt., and reactivity of Na and NO 78−38948
Ag (111), adsorpt.-desorpt. props. and surface struct. chem. of Cl 77−89648
Ag (111), adsorption of acetic and propanoic acids, LEED obs. 80−80073
Ag (111), clean or Na-covered, adsorpt.-desorpt. props. of Br_2 78−38944
Ag (111), epitaxially grown on mica, surface defect struct., LEED study 80−80038
Ag (111), incommensurate Xe overlayer, dynamical calc. of LEED 78−30828
Ag (111), ordered and damaged surfaces, O_2 adsorption, O_2+CO interaction 78−14583
Ag (111), Xe monolayer adsorption obs. 77−1307
Ag (111) surface, Ar ion bombardment, effect on struct. and reactivity, ellipsometry and LEED meas. 77−59192
Ag (331), adsorpt.-desorpt. props., coadsorpt. and surface struct. chem. of O_2 and Cl_2 78−34711
Ag {110}, surface struct. re-exam. 77−85029
Ag, adsorbed on Si (111), electronic and cryst. struct., Schottky barrier form. obs. 78−84091
Ag, adsorption of Cl_2 on low index surfaces, energetics and structures 79−87000
Ag, cluster growth and nucleation on Mo (100), UHV-SEM, AES/(RHEED or LEED) obs. comparison 78−63956
Ag, deposition on Si(100) surface, LEED and AES meas. 77−35833
Ag epitaxially grown film, on Au (111), twin form., LEED detection 80−88442
Ag film, epitaxial growth on Pd, AES and LEED obs. of growth modes and substrate influences *(French)* 80−84408
Ag film, initial stages of growth on Si (111) 7×7, LEED, AES and UPS expts. 78−38988
Ag film, vacuum deposited on NaCl, microstructure and orientation, surface condition influence 79−82486
Ag film, vacuum deposition on Pb (111), substrate diffusion effects, RHEED, LEED, AES 80−65410
Ag film growth on KCl, LEED, AES meas. 77−35834
Ag monolayer on (111)Si surface, Schottky barrier, interface electronic nature and epitaxy 79−77934
Ag, spherical crystal, Bragg case, Kikuchi patterns 77−84599
Ag-Ni solid solution, reversible surface segregation, radioactive tracer, LEED, and AES expts. *(French)* 77−69155
Al, (001) and (110) surfaces, LEED intensities 77−47656
Al (100), inelastic LEED at beam emergence condition 78−83690
Al (100) surface, prep. and props. of Pb and Sn monolayers 79−15018
Al (110), surface relax., LEED results anal. by convolution-transform method 77−89624
Al (111), LEED Kikuchi pattern, contrast change due to plasmon excitation 78−34686
Al (111), oxidation, initial stages, LEED anal. 80−80082
Al (111) adsorption of O_2, possible ordered struct. 80−44412
Al (111) and (100) surfaces, initial interaction with O_2, LEED and AES meas. 79−83383
Al, (111) surface, adsorbed O, surface struct., LEED and SEXAFS data 80−92782
Al, adsorption of O_2, AES, XPS, and LEED obs. 79−46938
Al, chemisorption of O, site determ. by LEED 80−39421
Al, initial interaction of O with single cryst. faces, LEED, AES and work function study 80−84392
Al surface, (111), interlayer spacing, LEED data anal. 80−54484
Al surface, obs. of positron Bragg refl. 80−103221
Al/GaAlAs, film, epitaxial growth on (100) GaAs by hot vac. deposition and characterisation 79−56085
Al-O (100), extended appearance potential fine struct. anal., LEED study 80−50467
Ar, adsorbed on graphite, orientational ordering of incommensurate monolayers, LEED obs. 78−95233
Ar, monolayer, adsorbed on graphite, lattice spacing and isosteric heat below 50K, LEED obs. 80−34303
Ar monolayers, on graphite, condensation and compression, high resolution LEED obs. 79−77906
Au (100), characterisation of reordered and normal surfaces by LEED, AES and EELS 78−34687
Au (100), disordered, diffuse LEED intensities obs. 79−4462
Au (101), disordered surface, diffuse LEED intensities statistical disorder theory 79−4463
Au (110), (1×2) and (1×3) superstructures, LEED study 80−20024
Au (110), electron spin polarisation in LEED 78−83692
Au (110), reconstructed surface, LEED anal. 79−77878
Au (111), relativistic effects on LEED intensities 79−7737
Au, (320) and (311) surfaces, Pb adsorption, LEED and AES obs. 79−86998
Au, adsorption of Xe and CO on (100) 77−15691
Au, condensed layers on Si (111), AES obs. of very first stages of condensation 78−14633
Au epitaxy on W (110), LEED and AES 77−69198
Au film, epitaxial growth on Ag(111) surface, LEED meas. 78−14632
Au film, epitaxially grown, struct., LEED, AES, resist. and X-ray diffr. analysis 77−59223
Au film, on Si (100) substrate, growth and struct., LEED and AES obs. 79−51457
Au film growth on Mo (110) surface, AES, LEED, thermal desorption study 80−80130
Au, spin-polarised LEED from low-index surfaces 78−14556
Au surface, chemisorption of I, AES and LEED study 80−100405

low energy electron diffraction continued
Au-Si interface, critical Au-film thickness obs. for room temp. interfacial reaction 80−75390
Au(III) and polycrystalline surfaces, O_2 adsorption, LEED, AES and energy loss spectra 80−34310
$AuPb_2$, epitaxial layer, formation during Pb absorpt. on Au, LEED, AES study of $Au/AuPb_2$ interface 78−71988
Au(110), spin polarised LEED 78−18508
Ba film, deposited on W (100), struct. determ. using LEED 79−90902
BaO coating, on W cathode, struct. transforms., LEED obs. 78−11061
BaO epitaxial films, cathode poisoning due to O_2, CO_2, and S, surface anal. 79−42600
BaO film, depend. of struct. on thickness 78−2391
BaO, film, initial struct., field electron emission microscopy and LEED determ. 79−11033
BaO film on W surface, struct. of crit. nuclei in heterogeneous crystn., LEED and FEM 77−11817
BaO films on Ir, thermionic props., Auger, LEED, and emission microscopy 79−43089
BaO, single cryst. on Ir, chemical structural effects examination 78−14790
BaO, surface pot. meas., cond. band edge, electron affinity, LEER 77−24606
$BaTiO_3$ (001), LEED and UPS studies 80−100747
Be (0001) surface, work function and purity, AES, LEED and photoelectron spectra meas. 78−68606
Be film, on W (110), growth mode, work function, thermal desorption, and struct. 80−75477
Bi (0001), chemisorption of O_2, LEED, AES and electron loss meas. 79−77908
Bi film, on Si(111) substrate, MBE deposition kinetics 80−10817
C, adsorbed on Fe(100), adsorbate coverage determ. by LEED, AES and XPS 80−103566
CO adlayers, on Cu(100) and Cu(111), struct., LEED pattern reinterpretation 79−28209
CO adsorbed layers, on W (210), surface struct., LEED obs. 79−82449
CO, adsorbed on Ni and Cu(100) surfaces, LEED study of c(2×2) struct. 79−86983
CO, adsorbed on Pd (210), inclined bonding config., electron stimulated desorption and LEED obs. 80−39430
CO, adsorbed on stepped Ni, thermal decomposition, LEED, AES, thermal flash desorption study 78−71984
CO, chemisorbed on Ni{001}, LEED study of mol. orientation in c(2×2) struct. 79−86982
CO_2, on Rh(110), chemisorpt., surface struct. chemistry, electron-impact props. 78−6225
CaO (100), surface struct., LEED study 80−39396
CaO, (100) surface struct. using LEED meas. and rumpled ionic models 80−20019
CaO epitaxial layer, on Mo, secondary electron emission, struct. effects, LEED and AES expts. 78−2959
Cd (0001), oxidation, LEED and AES obs. 79−87756
Cd deposited layers on Ti (0001), LEED and AES determ. of struct. 77−72804
Cd deposited layers on Ti (0001), LEED and AES determ. of structure 77−76688
CdS, clean surface, AES and LEED exam. 80−10762
CdS, surface electronic struct., slow electron reflection, total current spectroscopy *(Russian)* 80−54759
CdS(Se)(Te), evap. onto electron bombarded NaCl substrates, epitaxial growth and characts. 79−28948
CdSe ($11\bar{2}0$), surface electronic struct. and chem. struct. 78−14788
CdTe surface, sputter cleaning and dry oxidation, XPS and LEED study 80−108618
Co (0001), adsorption and reactivity of NO, LEED, AES, and thermal desorption study 80−80090
Co (0001), chemisorption of O_2, surface oxidation and CO oxidation 79−60631
Co (0001) surface, LEED and AES meas. 77−31857
Co (0001) surface, LEED meas. 77−59188
Co (100), clean and C-covered, LEED-Auger expts. 78−38921
Co ($10\bar{1}2$), struct. and CO chemisorption obs. 79−4474
Co {001} surface, LEED struct. anal. 78−47645
Co, chemisorption of O, LEED anal. of Co{001}c(2×2)-O struct. 78−91546
Co, martensitically transforming, state of surface 78−43223
Co, surface structure in HCP and FCC bulk phases 78−51807
CoO (100), surface struct., LEED anal. 80−15352
CoO (100), surface struct., LEED study 80−39396
CoO, surface layer spacing relax., electrostatic argument 79−46901
Co($10\bar{1}2$), surface struct. of non-unique planes, LEED obs. 79−99402
Cr (100), adsorption of O_2 and initial oxidation at room temp. 80−20034
Cr, (100) surface, clean ($\sqrt{2}\times\sqrt{2}$)R45° struct. 80−2255
Cr (111) face, oxidation, LEED and RHEED meas. *(French)* 78−39955
Cs monolayer on Cu(111), dilution of electron gas by O adsorption, plasmon energy losses 79−47036
Cu (001), electronic surface barrier resons., LEED study 80−39651
Cu (001), surface barrier struct., LEED study 80−65354
Cu (001), surface potential energy barrier model, LEED, intensity profiles 78−64089
Cu (100), adsorpt. of CO, UV and X-ray photoelectron spectra, LEED 78−56037
Cu (100), adsorpt. of O and S, ang. resolved AES and LEED 78−18908
Cu (100), chemisorption of CO, vibr. excitations and struct., EELS and LEED study 80−39437
Cu (100), coadsorption of Pb and Bi, LEED and AES meas. 79−15017
Cu (100), N adsorption, LEED, data averaging, objective approach 77−15668
Cu, (100) single crystal surface oxidation 80−11846
Cu (100) surface, interaction with O_2, AES, EELS, LEED and work function studies 80−24731
Cu (100) surface crystallography, LEED I-V profile anal. 80−75415
Cu (110), adsorption of CO, electron energy loss vibr. spectra and LEED obs. 79−77902
Cu, (110) surface, contraction determ. by LEED intensity anal. 79−73385
Cu (110) surface, O_2 and N_2O interactions, CO reaction with adsorbed O_2, LEED study 80−6635

low energy electron diffraction continued
Cu (111), adsorpt.-desorpt. props. and surface struct. chem. of Cl 77−89648
Cu (111), chemisorpt, of CO on differently prepared surfaces 78−6223
Cu (111), chemisorption of CO, IR spectra, LEED, and surface pot. meas. 80−39438
Cu (111), interaction of O_2 and N_2O and reaction of CO with adsorbed O_2, AES, LEED and ellipsometric meas. 79−65317
Cu (111), LEED crystallography and reliability indices 80−54081
Cu, (111), low-energy positron diffr. 80−70511
Cu (111), vicinal stepped surface obs., LEED vs. RHEED 77−72762
Cu, (111) and (100) surfaces, Sn segregation 78−14554
Cu (111) surface, structural determ. using reliability factor proposed for LEED 78−43224
Cu (210) surface, adsorption of O_2, LEED and AES meas. 78−71998
Cu adsorption of O_2, N_2O on (100) surface, reaction with CO 80−103583
Cu, adsorption of Pb on stepped and low index surfaces, LEED, AES and desorption anal. 79−46942
Cu, chemisorption on low-index and stepped surfaces, LEED, AES and UPS obs. 80−84391
Cu epitaxially grown film on Au (111), twin form., LEED detection 80−88442
Cu film, superstructs. caused by O adsorption 79−33179
Cu film, vacuum deposition on Pb (111), substrate diffusion effects, RHEED, LEED, AES 80−65410
Cu films on Ru (0001), growth, struct. and electronic props. 79−77958
Cu surface, (001), O_2 adsorption effect on surface barrier, LEED study 80−84378
Cu surface, obs. of positron Bragg refl. 80−103221
Cu surface (100), adsorption of O_2, LEED study 80−100408
Cu surfaces, O_2 adsorbed, exam. of structure by LEED, O_2 pressure-temp. diagram *(Japanese)* 78−79884
Cu vicinal surfaces, LEED study, S, O and Pb adsorption effects 80−103575
Cu-Al, surface segregation during adsorption and low pressure oxidation *(French)* 78−75932
Cu-Au, surface anal. by LEED and AES 77−69153
Cu-Au(Pd), surface structures, LEED obs. 80−10761
Cu-Ni (110), adsorption of CO and H_2, UPS, thermal desorption, AES,and LEED study 80−80087
Cu-Ni alloy surfaces, chemisorption of CO, LEED, AES, thermal desorption, and work function meas. 79−90879
Cu-Pd, surface struct. from LEED and AES meas. 79−77882
Cu-Pd alloy, (100) and (110) surfaces, LEED patterns 77−85031
Cu(100), adsorption and incorporation of O_2 78−56042
Cu(100), adsorption of Xe monolayers, thermodynamics and kinetics, LEED and AES obs. 79−99423
Cu(311), measurements of intensities as function of energy 77−89623
Cu(311) surface, struct. determ. by multiple scatt. calcs. of LEED intensities 78−56028
EuO (100), disordered, LEED and electron spectroscopy 79−28178
EuO (100), surface struct., LEED study 80−39396
f.c.c. crystals, layer by layer LEED and 2-dimens. space group symmetry 77−1280
Fe (001) surface, clean, LEED anal. 77−43411
Fe (001) surface, initial reaction with water vap. 77−69173
Fe (100), adsorption of Br_2, AES, LEED, work function, and thermal desorption study 80−15375
Fe (100), adsorption of carbon tetrachloride, AES, LEED, work function, and thermal desorption study 80−15376
Fe (100), adsorption of Cl_2, AES, LEED, work function, and thermal desorption meas. 79−82465
Fe (100), adsorption of I_2, AES, LEED, thermal desorption, and work function study 80−15374
Fe (100), adsorption of tetrabromomethane, AES, LEED, work function, and thermal desorption meas. 80−39422
Fe (100), equilib. surface segregation of dissolved C, N and S 77−62723
Fe (100) and (111) surfaces, chemisorption of CO, CO_2, acetylene, ethylene, H_2 and NH_3, LEED and thermal desorption 78−71996
Fe, (100) surface, S segregation and 2D compounds precipitation *(Japanese)* 80−35188
Fe (11O), coadsorption of K and 0_2, XPS, UPS, AES, and LEED study 80−80084
Fe (110), adsorption and decomposition of ammonia, LEED, AES, UPS, work function and desorption meas. 79−69345
Fe (110), adsorption of C, N, O, S, CO, NO and C_2H_2, UPS and LEED/Auger meas. 77−72773
Fe (110), adsorption of K, LEED, AES, UPS and XPS meas. 79−77919
Fe (111) surface, S segregation, LEED, AES and work function changes 80−15350
Fe {001} surface, determ. of c(2×2) structure of S, LEED 77−85063
Fe {110}, atomic struct., LEED anal. 80−88410
Fe, adsorption of CO and O_2 79−15003
Fe, atomically clean, N_2 treatment, corrosion inhibition 78−19954
α-Fe, BCC, LEED intensity spectra of (100), (110) and (111) surfaces *(German)* 77−31854
Fe epitaxial growth on Cu(111), supersaturation and mode of growth, LEED and AES exam. 78−18929
Fe, oxidation of (001) surface, first monolayer at. struct. 78−34706
Fe, single cryst., segregation behaviour of S, O and P at (100) surface 80−100841
Fe surface, (111) and (100), adsorpt. and decomp. of NH_3 78−40077
Fe surface, H_2 chemisorption LEED, UPS, thermal desorption spectroscopy, work function meas. 78−14566
Fe surfaces, adsorption, segregation and reactions of non-metal atoms, LEED and AES obs. 80−59783
Fe-Cr alloy, (100) and (110) surfaces, lateral lattice spacings, simultaneous LEED and AES 77−20174
Fe-Cr alloy, (100) and (110) surfaces, initial oxidation stages, simultaneous LEED and AES obs. 77−20175
Fe-Si (1%), LEED-Auger exam. of ($1\bar{1}0$) surfaces 78−71915
Fe(001), adsorption of CO, random occupation of adsorption sites, LEED exam. 78−63930
Fe(111), single cryst. surface, chemisorption of N_2, NH_3 and H_2, photoelectron spectra and LEED meas. 77−66087
$Ga_{0.5}Al_{0.5}Sb$, surface cleaning by sputter-etch technique 77−48560
GaAs, (001) vicinal stepped surface obs., LEED vs. RHEED 77−72762
GaAs, (100), comp. and struct. of differently prepared surfaces, LEED and AES 78−91524
GaAs (100), VPE, role of Cl, LEED, RHEED, and AES obs. 77−1327

low energy electron diffraction continued
GaAs (100) surface struct. determ. by LEED, UPS, and EPR 80−49475
GaAs (110), adsorpt.-desorpt. processes and phase transitions in alkali halide adsorbed layers 78−2361
GaAs (110), atomic struct. of clean and As covered surfaces, LEED study 80−49476
GaAs (110), comparison of LEED intensities for chemically polished and cleaved surfaces 78−18884
GaAs, (110), correl. of short-range order and sputter dose, using vidicon-based LEED system 79−83082
GaAs (110), LEED intensities, dynamical calc. 79−77462
GaAs (110), order-disorder interaction with O_2, LEED anal. 80−75445
GaAs (110), semidynamical renormalised forward scatt. technique for LEED anal. 79−77877
GaAs (110), struct., elec. props., effects of illumination, O_2 absorpt., electron bombard. *(French)* 78−34690
GaAs (110), subsurface atomic displacements, evidence from LEED/CMTA analysis 78−38920
GaAs (110), subsurface atomic displacements, LEDD exam. 78−71912
GaAs (110), surface and near-surface atomic struct., LEED 78−91515
GaAs (110), surface struct., LEED and AES study, comparison of MBE and ion bombard. surface prep. 80−54496
GaAs (110), with Al or Ga overlayers, interfacial electron states, UPS and LEED obs. 80−80377
GaAs (110) clean surface, internal pot., interplanar spacing 77−89627
GaAs (110) surface, atomic geometry from elastic LEED intensities 77−20170
GaAs, (110) surface, bond angle and lengths of rearranged As and Ga atoms 78−71918
GaAs (110) surface, O_2 interaction, order-disorder effects, LEED, UPS anal. 80−6634
GaAs, chemisorption of Cs, isobars, LEED and loss spectroscopy meas. 77−4262
GaAs, chemisorption of O_2, effect of surface index and atomic disorder AES, LEED and optical ellipsometry 79−60638
GaAs, electronic surface structure Cs(Rb)(Na) adsorpt. processes, AES, LEED, EELS, study 78−68068
GaAs, epitaxially grown (001), (111) and ($\bar{1}\bar{1}\bar{1}$) surfaces, LEED, AES, photoemission 78−38924
GaAs on GaAs and Ge, epitaxy, mechanism, effect of substrate surface struct. 77−51614
GaAs, substrate for homoepitaxy, vicinal surfaces characterisation 77−20207
GaAs surface, during vapour phase epitaxial growth, characterisation techniques and meas. *(French)* 77−1817
GaAs, surface studies during MBE growth 79−90899
GaAs surfaces (110) and (111)As, UPS and LEED 78−91514
GaAs VPE growth, in situ surface anal. 79−95937
GaAs(110), surface struct., kinematical LEED calcs. 77−85034
GaAs($\bar{1}\bar{1}\bar{1}$)As surface, 3 states, comp., struct., surface states and O_2 sticking coeffs. 77−66080
GaP (100), prep. of negative electron affinity surface by Cs adsorption 80−10768
GaP, adsorption and desorption of Cs, LEED, AES, and photoemission meas. 80−70532
GaP, surface cleaning by oxidation and heating, characterisation for electron emitter appl. 78−35548
GaSb, adsorption and desorption of Cs, LEED, AES, and photoemission meas. 80−70532
GaSb-Pb junction, Ar ion bombard. effect on tunnelling props. 80−54783
Ge (100), surface structure and chemical state 77−15670
Ge (110) surface, sublimation of deposited GeS film, LEED meas., structural transitions 77−59195
Ge, (111) cleavage face, struct. changes, LEED and Auger spectroscopy study 79−95249
Ge, order-order type phase transition at surface *(Russian)* 77−39728
Ge, reconstructed (001)2 x 1 surface structure, LEED intensity calcs., dimer model variations 79−77875
Ge, surface structure, LEED and spot photometric meas. 79−23811
Ge, vicinal surface obs. 78−14561
GeS, (001) surface struct., LEED expt. 78−84034
Ge(100) surface, Ar ion bombarded, determ. of atomic steps, LEED 78−63913
H, adsorbed on transition metal surfaces, charge density oscills., LEED pattern anal. 79−42389
$Hg_{0.8}Cd_{0.2}Te$ surface, sputter cleaning and dry oxidation, XPS and LEED study 80−108618
Hg_2Cl_2, surface composition, electron impact, mass spectrometry, AES and LEED meas. 79−60607
HgTe surface, sputter cleaning and dry oxidation, XPS and LEED study 80−108618
In ultrathin films on TbTe and Te, prep. and characterisation 77−7995
InP (110) surfaces, cleaved and polished-sputtered-annealed, LEED and AES study 80−103550
InP, photoemission and LEED meas., minority carrier diffusion length 77−69959
InP surface, interaction with Cl, electron spectroscopic obs. 78−56036
InSb (110), clean, O_2 adsorption, AES, LEED, RHEED and field effect meas. 80−49501
InSb (110), ion bombard. effect on surface struct. and electronic props. 80−6923
InSb (110), surface struct. by elastic LEED, comparison with GaAs(110) and ZnTe(110) 80−80040
InSb (110) surface, LEED and surface conductivity during gas adsorption 77−62760
InSb (110) surface, LEED intensity dynamical anal. 80−88412
InSb (110) surface struct. determ. by LEED, UPS, and EPR 80−49475
InSb, (111) surface, anal. by low energy ion scattering spectroscopy, LEED and AES *(Japanese)* 80−20746
InSb, electronic surface struct., Cs(Rb)(Na) absorpt., AES, LEED, EELS study 78−68068
InSb(111) surface, oxidation props., LEED and surface cond. meas. 78−15559
Ir (100), chemisorption of acetylene, benzene and ethylene, geometric and electronic effects 77−55457
Ir (100), superstructure from LEED meas. 79−73259
Ir (100)-1×1 surface struct. and reconstruction kinetics, LEED, UPS and work function meas. 79−90851
Ir (110), adsorption of CO, O_2, H_2, N_2, ethylene and benzene 78−38961
Ir (110), chemisorption of CO, preexponential factor and desorption energy 78−71963
Ir (110), chemisorption of O_2, sorption and dissoc. kinetics 79−33186
Ir (110), chemisorption of O_2, AES, LEED, thermal desorption mass spectra, and contact pot. difference meas. 79−77901
Ir (110), O adsorbed, surface struct. anal. using hybridisation model 80−44423
Ir (110), unreconstructed and constructed surface, LEED obs. 79−77880
Ir (110) 1×2 reconstructed surface, struct. study by LEED, reliability factor anal. 80−39399
Ir (110) and (111) surfaces, Debye temps., LEED meas. 79−60619
Ir (110)-(1×2) reconstructed surface, LEED expts., test of struct. models 79−56050
Ir (111), ($\sqrt{3}\times\sqrt{3}$)30° S overlayer struct., LEED obs. 80−15365
Ir (111), oxidation, combined LEED/UPS obs. 78−19955
Ir (111) surface, chemisorption of O_2, dynamics, LEED meas. 77−59211
Ir (111) surface, structural anal. of (2×2) O overlayer 80−2264
Ir, chemisorption of CO on clean and oxidised (110) surfaces 79−11015
Ir, chemisorption of H_2, adsorption and desorption kinetics, struct. of overlayer 80−84367
Ir, chemisorption of NO, chemisorptive bonding and reaction 77−51596
Ir surface, (110), unreconstructed, determ. of atomic arrangement by LEED 79−14990
Ir surface, chemisorption of H_2 and hydrocarbons, LEED, AES, and thermal desorption meas. 77−1297
Ir(110), adsorption of O, structure of c(2×2)O overlayer 79−19463
Ir(111), chemisorption of O_2, LEED-Auger expts. 77−20191
Ir(111) surface, electron beam induced desorption and dissociation of chemisorbed CO, LEED and AES 78−56043
Ir(111) surfaces struct. 77−85040
K, adsorbed on Fe(100), adsorbate coverage determ. by LEED, AES and XPS 80−103566
KCl, LEED-AES study of oriented adsorption of TCNE 77−62737
Kr, epitaxial monolayer on graphite, second order phase transform. obs. by LEED 77−76687
Kr, solid monolayer on graphite, commensurate to incommensurate transition, LEED data 80−80079
La, adsorbed monolayer on W (112) face, LEED and contact pot. difference meas. *(Russian)* 77−1316
La submonolayer film, on W (011) or Mo (011), disordering, LEED obs. *(Russian)* 77−89655
LaB_6 (001) surface, struct., initial oxidation, XPS, UPS, LEED, AES, work function meas. 79−99403
LaB_6, (001) surface struct., XPS, LEED meas. 78−63909
LaB_6 (100), (110), and (111), surface structs. and work functions 80−70512
LaB_6 (100) surface, O_2 adsorption, UPS and LEED study 80−49519
LaB_6 (210) surface, work function, struct. and chemisorpt. stability, XPS, UPS and LEED 80−65344
LaB_6, clean and oxidised (100) surface, LEED, AES, work function, evaporation meas. 78−71989
LaB_6, surface (100), atomic struct., angle-resolved XPS, LEED and ISS investigation 80−10765
LaB_6:C, AES, LEED and energy-loss spectra study of C layer on (100) surface 77−62715
$LaNi_5$, surface segregation induced by O_2, LEED and AES exam. 79−11009
Mg (0001) face, incipient oxidation, EELS and LEED studies 80−81237
MgO (001), LEED Kikuchi pattern, surface state reson. 78−83689
MgO (001) cleavage face, LEED Kikuchi pattern, surface reconstruction 78−84038
MgO (100), surface struct., LEED study 80−39396
MgO, adsorption of Cs and Li, AES, LEED, work function, and secondary electron emission meas. 80−44407
MgO, Kikuchi pattern intensity, angular and temp. depend. 78−2349
MgO, surface layer spacing relax., electrostatic argument 79−46901
MnO (100), surface struct., LEED study 80−39396
Mo (001), surface struct. determ. using LEED 79−42351
Mo (001) surface struct., LEED anal. 80−34282
Mo (100), adsorption of CO_2 and trimethylamine, adsorbed O effect, LEED and AES obs. 80−39443
Mo (100), adsorption of O_2, AES, LEED, work function, and desorption meas. 80−6654
Mo (100), adsorption sites of CO, electron stimulated desorption and LEED meas. 80−49516
Mo (100), chemisorption of H, phase changes, LEED obs. 79−77911
Mo (100), early stage condensation of Cu and Ag, comparison with W (100) 80−80072
Mo (100) surface, phase transition exam. of LEED 77−55433
Mo (110), oxidation exam. of LEED 78−92402
Mo (112) surface adsorption of Li film, LEED and contact pot. method 80−10794
Mo, adsorption and dissoc. of CO on (100) surface, comparison with carburised surface 77−15689
Mo, coadsorption of O_2 and Cs, struct., emission props., thermal stability 80−66878
Mo film, characteristics of elastic reflection of slow electrons 79−14657
Mo, surface struct. changes due to ionic bombardment *(Russian)* 77−1775
Mo:C (110) surface, segregation, precip. and desorpt. of C, AES and LEED study *(French)* 80−103480
MoS_2 (2H), surface struct. determ. by dynamical LEED 77−43415
MoS_2 (2H), surface struct. and interplanar separation by LEED 77−59191
MoS_2, adsorption of Cs and O_2, LEED, Auger and work function meas. 78−71994
MoS_2, clean surface, AES and LEED exam. 80−10762
MoS_2, surface electronic struct., slow electron reflection, total current spectroscopy *(Russian)* 80−54759
Mo(001), clean and H chemisorbed, atomic displacements, LEED obs. 80−70514
Mo(100), adsorpt. of CO, LEED, AES, study 78−87873
N_2 adsorbed layers, on W (210), surface struct., LEED obs. 79−82449
NH_3, epitaxial film, on metal (111) substrates, surface struct., LEED obs. 79−86969
NH_3, film, on metal substrate, surface struct. using LEED 79−77879
NO, chemisorbed on Pt(100), vibr. spectra, electron energy loss, LEED and Auger investig. 79−90866
Na (110), Na_2O (111) surface comp., LEED obs. 77−72761
NaCl (100), adsorption of Xe, AES and LEED meas. 77−11792

low energy electron diffraction continued
NaCl (100) surface perturbations during LEED investig. *(French)* 77−28069
Na_xWO_3, cubic single cryst., LEED/Auger obs. 78−19614
Na_xWO_3, x=0.6 and 0.8, surface characts. 80−39392
Nb (110) and (750), interaction with O_2, LEED, AES, SIMS, and EELS obs. 80−44408
Nb, adsorption of O_2, continuous meas. of surface pot. variations using mirror electron microscope 77−47680
Nb, adsorption of O_2 and N_2, on (100) planes, LEED-AES obs. 77−69186
$NbSe_2$ (2H), surface struct. determ. by dynamical LEED 77−43415
$NbSe_2$ (2H), surface struct. and interplanar separation by LEED 77−59191
$NbSe_2$, adsorption of Cs and O_2, 200-300K 78−26767
Nd film, on W(100), struct., electronic and dynamic props. *(Russian)* 77−76702
Ni (001), adsorbed S, crystallography by LEED, appl. of iso-intensity map method 79−19128
Ni (001), adsorpt. of S, multiple binding sites and diffusion, photoelectron spectra and LEED struct. 77−66569
Ni (001), adsorption of N_2, c(2×2) struct. form 80−80083
Ni (001), structural parameters and interplanar spacing by LEED averaging 77−11771
Ni (001), surface barrier struct., LEED anal. 80−20023
Ni (001), surface potential energy barrier model, LEED, intensity profiles 78−64089
Ni (001) and (001)c(2×2)S adsorbed, electronic surface resonances by LEED 79−24051
Ni (001) surface, adsorbed N_2, p(2×2) struct., LEED and AES study 80−54515
Ni (001)-c(2×2)-Te, atomic surface struct. using LEED, compared with MeV ion scatt. 79−56904
Ni (100), adsorption of C, LEED struct. anal., substrate distortion 80−6637
Ni (100), adsorption of CO, EELS and concomitant surface anal. 80−7453
Ni (100), adsorption of O_2 and reduction of surface oxide by H_2 80−108741
Ni (100), adsorption of water $(O_2)(H_2)(CO)$, combined XPS/LEED/SIMS exam. 79−83075
Ni (100), chemisorption of NO, LEED, AES, UPS, and thermal desorption study 80−39449
Ni (100), clean surface and with chemisorbed O, rapid LEED intensity meas. 80−44420
Ni (100), dissociative chemisorption and mol. adsorption of NO 80−65373
Ni (100), initial oxidation process, angle-resolved AES and LEED obs. 79−52463
Ni (100), initial oxidation, electron energy loss spectra, LEED, AES, and work function meas. 79−61795
Ni (100), interaction with methane, diffusion of deposited C, AES-LEED study 79−99418
Ni (100), phase of diffracted wave calc. 78−71647
Ni (100) surface, adsorption of H_2, LEED, work function meas. and thermal desorpt. obs. 79−23843
Ni (100) surface, ang. resolved Auger emission and LEED Kikuchi intensities at 850 eV 80−66340
Ni, (100) surfaces, Si-, P- and Cl-chemisorbed, LEED and angle-resolved AES obs. 79−95258
Ni (100)-c(2×2)CO, surface struct., LEED meas. 80−6647
Ni (100)-p(2×2)C, decomp. of formic acid and adsortion/desorption of H_2, CO, and CO_2 79−91995
Ni (100)c(2×2)CO structure, dynamical LEED expts. 78−34710
Ni, (100)p(2×2)O and (100)c(2×2)O surfaces, struct. and vibrs. of adsorbed CO 78−2375
Ni (110), adsorption of O_2, obs. by electron microscopy, AES and LEED *(French)* 77−62732
Ni (110), chemisorption of H_2 and O_2 77−24470
Ni (110), chemisorption of N_2, mol. and dissociative mechanisms 80−39431
Ni (110), effect of surface O on catalytic and chemisorptive behaviour, LEED and AES 77−85066
Ni (110), NO chemisorption and dissoc. 77−15695
Ni (110), polarised LEED study of magnetism 80−71102
Ni (110), S and O adsorbed, surface struct. anal. using hybridisation model 80−44423
Ni (110), surface relax., LEED results anal. by convolution-transform method 77−89624
Ni, (110) and (111) surfaces, oxidation exam. at room temp. by combined SIMS-AES/LEED method 79−20241
Ni, (110) surface, methane interaction kinetics, AES-LEED-ellipsometry 77−62756
Ni, (110) surface, S adsorbed layer struct. from anal. of LEED pattern 79−73407
Ni (111), adsorption of acetylene and ethylene, surface structs., LEED and AES obs. 79−60636
Ni (111), adsorption of CO and O, LEED and low-energy ion scatt. investigation 79−65324
Ni (111), adsorption of H_2, LEED intensity spectra, 173K 79−28192
Ni (111), adsorption sites of CO using IR reflection-absorption spectroscopy and LEED 79−69355
Ni (111), adsorption sites of CO, LEED, AES, thermal desorption, work function, and IR system meas. 79−77903
Ni (111), C monolayer phase condensation, LEED and AES obs. 79−46960
Ni (111), chemisorption and reaction of NH_3, LEED, desorption and photoemission expts. 80−59799
Ni (111), chemisorption geometry of H, LEED, thermal desorption, and work function meas. 80−39433
Ni, (111), chemisorption of H, geometry, order and disorder 79−65311
Ni (111) surface, adsorption of Cl, LEED, AES, work function and flash desorption meas. 77−85069
Ni (111) surface, with O_2, Se, S and Te adsorbed layers, bonding geometry and electronic struct. 79−77909
Ni, adsorption of ethylene at room temp., surface complex vibr. from electron energy loss spectroscopy 79−73404
Ni, CO adsorbed mols. on (100), bonding struct., vibr. excitations 77−15687
Ni, c(2×2)O superstructure, angle resolved photoemission from chemisorption induced states and LEED spectra 77−85898

low energy electron diffraction continued
Ni, coadsorption of Pb or Sn iwth P or C, AES study 80−54521
Ni dissolution of C through (110) surface, LEED and AES meas. 78−63932
Ni, epitaxial film on NaCl, struct. and purity 78−72047
Ni, epitaxial growth, on NiO(100), by low pressure hydrogen reduction *(French)* 80−11578
Ni film, ferromagnetic (100) and (110), energy bands, surface state to LEED state transition 79−1630
Ni film, surface properties and photoelectron spin polarisation 78−14782
Ni, H chemisorption, order-disorder transitions on (111) surface, LEED observation 78−47668
Ni, spin polarisation in LEED 77−43696
Ni stepped surface, morphology exam. by LEED and ARS 78−71913
Ni surface, (110), O_2 adsorption, LEED and ion scatt. study 80−84386
Ni surface, S and O_2 covered, polycrystalline, initial sticking coeff. of H_2, LEED and AES 78−63937
Ni-Cu diffusion couple surface, epitaxial, AES, CO chemisorption and LEED 77−31891
Ni-Fe, (100) surface, O interaction, LEED and XPS studies 79−82437
NiO (001), surface layers, sublattice magnetisation temp. depend., LEED exam. 78−27018
NiO (100), antiferromag., LEED calcs. of exchange refls. 78−14949
NiO (100), surface struct., LEED study 80−39396
NiO (100) surface, dynamical LEED calc. 77−62721
NiO (100) surface, LEED expt. and calc. down to 60 eV 80−92767
NiO (100) surface, sulphurisation by H_2S, AES, LEED, RHEED structural study *(French)* 78−64888
NiO, (100) surface interaction with SO_2, electron diffr. and Auger spectrosc. obs. *(French)* 80−97728
NiO (111) surfaces, antiferromag., mag. scattering by polarised LEED, spin polarisation effect in theory 80−29529
NiO, surface layer spacing relax., electrostatic argument 79−46901
NiO, surface sublattice magnetis., temp. depend., determ. using low energy electron exchange scatt. *(Japanese)* 77−55700
Ni(001), adsorbed c(2×2)-CO, struct. by LEED, self-consistent scatt. pot. 80−70536
Ni(001) surface, p(2×2) and c(2×2) O superstructure, angle resolved photoemission from adsorbates 78−23585
Ni(001) surface N adsorption due to ion beam irrad., surface struct. LEED study *(Chinese)* 80−84364
Ni(100), chemisorption of unsaturated hydrocarbons, LEED and AES obs. 77−31904
Ni(110), ferromag., surface magnetisation, polarised LEED expt. 80−97118
Ni(110)(2×1)C surface, kinetics of D_2 desorption, LEED and AES meas. 77−47683
Ni(111), adsorpt. of CO, absolute coverage determ., AES and LEED 77−76661
Ni(111), adsorption of acetylene, evolution of adsorber species, rel. to vibr. spectra 78−95952
Ni(111), chemisorption of H_2, geometry, LEED anal. 79−28200
Ni(111), coadsorption of CO and H_2, surface carbide influence, vibr. electron energy loss obs. 79−52772
Ni(111) surface, adsorption of H_2 at low temps., LEED meas. 78−56045
O, adsorbed on Fe(100), adsorbate coverage determ. by LEED, AES and XPS 80−103566
O adsorbed on Ni (111), order-disorder transition 79−82447
Pb (100) and (110) surfaces, oxidation and sulphidation, LEED and XPS obs. 78−20070
Pb, epitaxial growth on Ag (111) and Cu (111) LEED, RHEED, AES study 78−84090
Pb monolayer, double layer with Sn, growth on Al (111), struct. 80−70567
Pb ultrathin films on PbTe and Te, prep. and characterisation 77−7995
PbS, surface defect annealing *(Russian)* 77−47658
PbS, surface optical phonons, anal. of LEED results 79−69339
$Pb_{0.8}Sn_{0.2}Te$ surfaces, oxidation in air and thermal desorption, XPS and LEED meas. 79−47830
$Pb_{1-x}Sn_xTe$ film on BaF_2, electron beam delineation effect on MBE growth, LEED and AES obs. 79−99434
PbTe surfaces, oxidation in air and thermal desorption, XPS and LEED meas. 79−47830
Pd (100), adsorption struct. of CO, LEED and high-resolution EELS study 80−20037
Pd (110) surface, adsorption of S, characterised by LEED *(French)* 80−88422
Pd (111), adsorpt. of NO, LEED, UPS, and thermal desorpt. expts. 77−69179
Pd (111), adsorpt. of O_2 and NO, LEED, photoelectron spectra and thermal desorpt. expts. 77−69180
Pd (111), chemisorption of Cl_2, LEED, AES, thermal desorption, and work function meas. 80−75444
Pd (111), interaction with O_2, EELS, AES and LEED obs. 79−86985
Pd surface, chemisorption of CO, IR spectroscopic evidence for localised site adsorption 78−47669
Pd-Ag (Cu) alloys, epitaxial growth and surface characterisation 78−14638
Pd-Si structure, epitaxial silicide growth, LEED and AES study 80−103590
Pd(001), adsorpt. of CO, LEED, electron energy loss spectra study, surface struct. effect on weak chemisorpt. bonding 78−71987
Pd(110) surface, adsorption of Xe, LEED study 80−6633
Pt (100), adsorbed Cs layer, surface struct., LEED anal. 77−89654
Pt (100), adsorption of acteylene or ethylene , intermolecular forces and kinetics of adsorption 78−75930
Pt (100), adsorption of H_2S, intermolecular forces and kinetics of adsorption 78−75930
Pt (100), adsorption of NO, 40-400°C LEED, AES, XPS and UPS obs. 77−35820
Pt (100), CO or C_2N_2 adsorpt. induced backscatt. enhancement 77−90227
Pt (100), superstructure from LEED meas. 79−73259
Pt (100) (5×20) and (1×1) surfaces, stability and reactivity, adsorption of H 80−75434
Pt (100) chemisorption of acetylene and benzene, LEED, AES, HPS and temp. programmed dehydrogenation exam. 77−55456
Pt (100) surface, chemisorption of acetylene and benzene, AES, UPS, LEED and flash dehydrogenation 77−59216
Pt (100) surface, LEED intensity spectra, double diffr. model 77−31858

low energy electron diffraction continued
Pt (100) unreconstructed surface, CO chemisorption 78−38962
Pt (110), acetylene adsorption, desorption and surface dissoc. 77−62749
Pt (110), surface structs. during S adsorption, LEED pattern interpretation model 77−69184
Pt (110) reconstructed surface, LEED-AES study, O_2 treatment effect 80−39398
Pt (111), adsorbed H_2 and O_2 interaction investig. 77−55461
Pt (111), adsorption of acetic and propanoic acids, LEED obs. 80−80073
Pt (111), adsorption of NO, EELS, thermal desorption, LEED, and AES study 80−80086
Pt (111), at. steps role in H interaction 77−15690
Pt (111), chemisorption of Cl_2, LEED, AES, thermal desorption, and work function meas. 80−75444
Pt (111) and (100) superlattices formed by dissociative adsorption of HI, LEED, AES, and thermal desorption studies 80−55715
Pt (111) and Pt (S)-12(111)X(111)surfaces, adsorption of 0, thermal desorption, AES, XPS, and LEED study 80−70534
Pt (111) stepped surface, adsorption of O_2, CO, C_2N_2 and ethylene 78−71992
Pt (111) surface, of CO, LEED, desorption and work function meas. 77−72781
Pt (111) surface, relax., dynamical LEED calcs. 77−59196
Pt (111) surface, surface struct. and bonding of (2×2) acetylene overlayers, LEED analysis 77−85067
Pt (997) surface, partial facetting, He beam scatt. and LEED study 80−103547
Pt, adsoprtion of H, electrode surface exam. by LEED and AES 77−47665
Pt, adsorption and desorption of O_2 on (110) surface, thermal desorpt., LEED/AES obs. 77−72788
Pt, adsorption of hydrocarbons, on (111) surface, LEED intensity obs. 77−51592
Pt, adsorption of O_2, AES, LEED and thermal desorption spectroscopy exam. 78−79891
Pt, adsorption of O_2, surface struct. depend., LEED, AES, and electron energy loss spectra 79−46934
Pt electrode (100), (111), polycryst. surfaces, comparison of electrochem. activity 78−61015
Pt film, growth on amorphous Si:H, AES and LEED study 80−88447
Pt, hydrocarbon reactions catalysed by surfaces with variable kink concs., surface O_2 effects 80−35576
Pt, low index surface, O_2 reduction exam. using LEED and AES 79−70343
Pt, spin-polarised LEED from low-index surfaces 78−14556
Pt, stability and struct. of high Miller index forces in vacuum and with adsorbed C and O 77−76651
Pt, stepped surface, adsorpt. and decomp. of NO and NH_3, LEED, AES, and thermal desorption expts. 78−38943
Pt surface, adsorption of H_2, rel. to electrocatalysis 78−38935
Pt, surface struct. and electronic props., CO_2, O_2 and H_2 chemisorption, LEED, AES 77−1300
Pt:C, C layer formation on (111) surface, temp. depend., LEED, AES study 78−71911
Pt-$SrTiO_3$ (100) interface, struct. and electronic props., AES, LEED, EELS, and UPS study 80−24986
Pt(S)-[9(111)×(111)] face, adsorption of O_2, flash desorption, LEED and AES obs. 77−69182
Pt(100) surface, clean and Cs covered, LEED intensity spectra, τ-matrix interpretation method 77−15673
Pt(111), adsorption of Br, irreversible order-disorder transition, LEED AES, thermal description and work function meas. 79−69361
Pt(111), adsorption of NO, anal. of adsorption processes and surface reactions, vibration spectroscopy 78−87868
Pt(111), LEED, quantitative anal. 80−44085
Re (10$\bar{1}$0), surface struct. 80−75414
Re, adsorpt. of CO on basal (0001) and stepped |14(0001)×(10$\bar{1}$1)| planes 78−14594
Re, O_2 adsorption, effect of struct. defects, steps and kinks 80−29269
Re, polycryst. and (0001) single cryst., ethylene and acetylene adsorption 78−38947
Re vicinal faces, adsorption of O_2, mirror electron microscopy, LEED and AES obs. 79−65323
Rh (100) surface, structural determ. using reliability factor proposed for LEED 78−43224
Rh, (100) surface struct. determ. 77−69152
Rh (110), chemisorption of CO and NO, LEED, AES, XPS, UPS, and desorption obs. 79−77899
Rh (110), S adsorbed, surface struct. anal. using hybridisation model 80−44423
Rh (110), S-adsorbed, LEED crystallographic determ. of struct. 80−44422
Rh (110) surface structure, LEED exam. 78−87853
Rh (111), adsorption of O_2, AES, LEED, and thermal desorption mass spectra meas. 79−77900
Rh (111), catalytic reaction between adsorbed O_2 and H_2, LEED obs. 79−52773
Rh (111), chemisorption of CO, thermal desorption mass spectrometry and LEED meas. 79−77917
Rh (111), chemisorption of H_2, thermal desorption spectra and LEED obs. 79−86989
Rh (111), chemisorption of CO and CO_2, high resolution EELS, thermal desorption, and LEED study 80−44419
Rh (111), chemisorption of water, effect of adsorbed O, H, or CO, LEED and thermal desorption meas. 80−75435
Rh (111), chemisorption of acetylene and ethylene, EELS, LEED and thermal desorption mass spectrometry 80−80057
Rh (111), co-adsorption of H_2 and CO segregation of co-adsorbed species 80−65361
Rh (111), coadsorption of O_2 and H_2 below 140K 80−29276
Rh (111), interaction with O_2, thermal desorption spectra, AES and LEED obs. 79−51428
Rh (111), LEED crystallography and reliability indices 80−54081
Rh (111) and (100) surfaces, chemisorption of H_2, O_2, CO, CO_2, NO, C, ethylene, acetylene, LEED, AES and thermal desorption meas. 78−38951
Rh, (111) surface, chemisorbed O_2, catalytic reaction between adsorbed O_2 and gaseous H_2 79−83503
Rh, (111) surface struct. study 79−14987

low energy electron diffraction continued
Rh (755), (331), chemisorption of H_2, O_2, CO, CO_2, NO, C_2H_4, and C_2H_2, LEED and TDS obs. 79−65318
Rh, adsorpt. of CO and H_2, on (111) surface, 2-dimens. phase separation 80−107634
Rh(100), adsorption of H_2S, (2×2) surface struct., LEED anal. 79−99426
Rh(111), surface geometry, vibrational props., Debye temp., LEED study 78−87852
Ru (0001) surface, adsorption and desorption of NH_3, effects of electron beam 78−38955
Ru (001), adsorption of CO, IR spectra, LEED, and thermal desorption meas. 80−70533
Ru (001), adsorption of H_2S and S, LEED, UPS, AES, and thermal desorption meas. 79−99420
Ru (001), coadsorption of O_2 and CO, uptake and flash desorption meas. 80−39450
Ru (001), dissociation of adsorbed H_2S, chemisorption and electronic struct. of S layer 79−79292
Ru (001), geometric struct. of chemisorbed CO, LEED obs. 79−51429
Ru (10$\bar{1}$0), adsorption of NO and CO 77−72783
Ru (10$\bar{1}$0), dissociative adsorpt. of NO, LEED and AES expts. 77−90642
Ru (101), O_2 chemisorption, CO+O_2 interaction 77−73471
Ru (11$\bar{2}$0), adsorption of O_2, H_2, and CO, ellipsometry-LEED study 80−103570
Ru (~001) stepped surface, O_2 chemisorption, LEED and AES obs. 80−11947
Ru(001), adsorpt. of cycloparaffins, LEED, ESD study 78−87872
Ru(001) surface, adsorption of CO, IR spectra and LEED 79−37914
Ru(101), chemisorption of CO, surface structural chemistry and electron impact props. 77−1312
S, adsorbed on Fe(100), adsorbate coverage determ. by LEED, AES and XPS 80−103566
S-metal interactions 80−55710
Se surface, (10$\bar{1}$0) and (1$\bar{2}$10), LEED study *(French)* 79−14991
Si, (001) and (111), geometrical and electronic struct., review 80−80039
Si (100), intensity-energy spectra 77−47653
Si (100), struct., LEED study, atomic arrangement model 78−71922
Si (100), vicinal, LEED obs. of stepped surface 80−59773
Si (100) (2×1) clean surface, struct. using averaged LEED 77−59194
Si (100) surface, LEED meas. 78−60016
Si (100) surface, models of (2×1) surface struct., quasidynamical calc. of LEED intensities 78−71921
Si (110) surface, chemisorption of H, UPS spectra meas. and LEED 77−20186
Si (111), 2×1 reconstructed, self-consistent anal. 78−91518
Si (111), adsorpt. of Cs, LEED, work function and thermal desorpt. 78−14590
Si (111), Cl_2 chemisorption, ang. resolved UPS and LEED meas. using Vidicon intensity processor 78−71972
Si (111), cleaved, geometrical struct., LEED expts. 78−91517
Si (111), impurity stabilised by Te deposition, atomic arrangement, LEED exam. 77−11770
Si (111), ion bombard., struct. changes, AES obs. 80−79842
Si (111), nitridation, AES and LEED results 80−80041
Si, (111) 2×1 surface, LEED theory and expt. 79−46895
Si, (111) 7×7 surface, adsorption of Al, electron energy loss spectroscopy and LEED 77−43432
Si (111) 7×7 surface, H_2S interaction, LEED and AES 78−38966
Si (111) 7×7 surface states, comparison with low-energy electron loss spectroscopy 79−60891
Si (111) (7×7) surface structs., LEED anal. and energy minimisation calcs. 80−49478
Si (111) clean surface, internal pot., interplanar spacing 77−89627
Si (111) surfaces, 2×1 to 7×7 struct. transition during annealing, LEED obs. 79−42352
Si (111) surfaces, cleaved, electronic structure following Al adsorption 80−75610
Si (111) surfaces, geometric struct., LEED obs. 80−49479
Si (111)/Au deposit, 2-dimens. condensed phase characterisation 77−69181
Si adsorbed on W(100) face, LEED, dynamic props. 77−89634
Si, adsorption of O_2, early stages, AES, LEED, and XPS obs. 79−46937
Si, Cs adsorption, (100)2×1 surface, LEED 77−62747
Si film, on W (100), struct. and work function, LEED meas. 77−66096
Si, intensity dynamics of slow-electron diffr. patterns 78−10267
Si, order-order type phase transition at surface *(Russian)* 77−39728
Si, periodic stepped structure, on vicinal planes, LEED obs. 80−24725
Si, pure and with adsorbed Al(Au), thermal expansion and at. vibr. singularities 77−89635
Si, reconstructed (001)2 x 1 surface structure, LEED intensity calcs., dimer model variations 79−77875
Si, surface (100)(1×1)H struct., LEED study 78−67910
Si, surface self-diffusion, investigation by slow electron diffr. method *(Russian)* 78−51808
Si, surface structure, LEED and spot photometric meas. 79−23811
Si, surface structures after pulsed laser annealing, LEED obs. 80−54494
Si surfaces, amorphous, hydrogenated, and monocryst., AES and LEED, comparative study *(French)* 80−44398
Si, vicinal surface struct., LEED exam. 79−60611
SiC (6H) (000$\bar{1}$), Ar^+ ion bombard., defect form., LEED obs. 79−69165
SiC, radiation defect annealing, recovery of LEED maxima 80−65075
SiC, surface defect annealing, following Ar ion and electron irrad. 80−7603
SiC, surface defects due to Ar ion bombardment, 100-1000 eV 80−6445
α-SiC(6H), electron bombardment, formation of defects on (000$\bar{1}$) surface 80−19844
α-SiC(6H), radiation defect distrib. anisotropy near (000$\bar{1}$) surface, LEED study 80−96577
Si(001)2×1 surface, struct. determ. by LEED 79−19438
Si(100), (1×1)H struct., averaged LEED 77−62720
Si(100) (1×1)H surface structure, LEED meas. 78−14602
Si(110), clean surface structural transitions, LEED obs. 78−6203
Si(111) 7×7, surface struct., theory and expt. 77−85033
Si(111) 7×7 surface struct., LEED seventh order diffr. beams interpretation 77−62716
Si(111) 7×7 surface struct., LEED intensity calc. 78−34683
Si(111)(7×7) surface models, LEED anal. 80−75418

low energy electron diffraction continued
Si{001}2×1 reconstructed surface, atomic struct., LEED intensity analysis 77−28068
Sn, monolayer, double layer with Pb on Al (111), layer growth, struct. 80−70567
SnTe surfaces, oxidation in air and thermal desorption, XPS and LEED meas. 79−47830
Sr submonolayer film, on W (011) or Mo (011), disordering, LEED obs. *(Russian)* 77−89655
Sr submonolayers adsorbed on Mo crystal, LEED and contact pot. study 80−2271
SrO epitaxial layer, on Mo (110), secondary electron emission and struct., LEED and AES expts. 78−2958
$SrTiO_3$, (100), LEED and UPS studies 80−100747
$SrTiO_3$ (100) surface, struct. and electronic props., AES, LEED, EELS, and UPS study 80−24986
$SrTiO_3$ (111), surface struct., electronic props., LEED, AES, UPS study, photoelectrochem. cell anode appl. 78−84035
$SrTiO_3$ photoelectrolytic electrodes, defect surface states obs. 78−14815
$SrTiO_3$, surface defects, electronic struct., LEED, AES, UPS study 78−84273
surface atoms, Debye temps. determ. during field evaporation and LEED 80−39406
TaS_2 (2H), surface struct. and interplanar separation by LEED 77−59191
Te coating of PbTe surfaces, struct. and junction characts. 80−50743
Te(10$\bar{1}$0), surface struct. 80−88411
Te(1$\bar{2}$10) face, epitaxial growth of Se, LEED and AES meas. 77−1328
Th (111), struct., Debye temp., and oxidation, LEED and AES obs. 77−89625
Ti (0001), chemisorption of CO, LEED struct. anal. 78−71964
Ti (0001) surface, oxidation, LEED and AES meas. 77−31851
Ti, chemisorption of N_2 on {0001}, at. underlayer form. 77−15693
TiO_2 (100), chemisorption of H_2, O_2, and H_2O, electron spectroscopy, evidence for Ti^{3+} photogeneration 78−38940
TiO_2, (110) and (100) surfaces, LEED and electron spectra 77−72757
TiO_2 (rutile), (001) and (110) faces, UPS and LEED obs. 80−45206
TiO_2-Ni (100) interface, electronic props., struct., comp., chemical bonding 80−84499
TiS_2, single-reflection layer scatt. theory 80−49059
Tl, epitaxial growth on Ag (111) and Cu (111), LEED, RHEED, AES study 78−84090
UF_4 optical interference layers, electron-beam decomposition 78−34541
UIr_3, (100) surface reconstruction, LEED, AES, electron energy loss spectra study 78−75918
UO_2 (~100), vicinal surfaces, LEED and AES expts. 79−4464
V_2O_5 and lower oxides, defect structures and related props. 80−59454
V_2O_5 and lower oxides, electronic, optical, structural and surface props., review 80−88120
W (001), adsorption of N_2, effect on LEED electron spin polarisation and intensity profiles 80−65377
W (001), anal. of surface barrier struct. using LEED data 78−84037
W (001), disordered CO and O_2 overlayer effect on electron spin polarisation in LEED 79−60632
W (001), double diffr., spin polaris. effects 79−64963
W (001), electron spin polarisation and intensity in LEED, temp. depend., 1000-300°C 79−14989
W (001), electronic surface reson. band struct. and lineshapes, LEED meas. 79−82655
W (001), LEED, 20 to 150 eV, electron-spin polarisation 78−51400
W (001), LEED spectra, expt. rel. to theory 78−84039
W (001), ordered CO overlayer effect on electron spin polarisation in LEED 79−60633
W (001), spin-depend. features in LEED intensity curves, model calcs. 78−34685
W (001), surface relax., LEED rotation diagrams 79−28180
W (001), surface relax. determ. using LEED rot. diagrams 78−38917
W (001), surface resonance band fine struct. in LEED 78−47844
W (001), surface structure, LEED anal. 78−38919
W (001) (1×1) surface contraction using LEED intensity anal 80−6606
W (001) clean surface displacive phase, long-range inhibition by N 80−2266
W (001) face, surface contraction, LEED exam. 77−43412
W (001) surface, high resolution LEED, threshold effects 77−51581
W (001) surface, spin polarisation in LEED, theoretical predictions 77−31855
W (001) surface, spin polarisation and temp. effects in refl. diffr. 78−18881
W (001) surface with adsorbed S, struct. and effect on CO adsorption 79−86981
W (011), adsorption of Ag, LEED, AES, and work function meas. 79−86990
W (100), adsorpt. of acetylene, room temp., electron spectroscopy obs. 79−7749
W (100), adsorption of Cl_2, LEED and AES study 79−90878
W (100), adsorption of O_2, AES, desorption, LEED and work function obs. 77−1317
W (100), adsorption of O_2, surface struct. and thermally stimulated reaction 77−55451
W (100), adsorption of Zr, AES, LEED, thermal desorption, and work function meas. 80−39444
W (100), chemisorption of Hg, AES, LEED, work function and thermal desorption expts. 78−34709
W (100), chemisorption of H, phase changes, LEED obs. 79−77911
W (100), coadsorption of Zr and O_2 at high temp. 80−6653
W (100), early stage condensation of Cu and Ag, comparison with Mo (100) 80−80072
W (100), H adsorbate low energy electron vibrational excitation 80−84375
W (100), LEED intensities, temp. depend., surface struct. phases and surface Debye temp. 80−39395
W (100), reconstruction in presence of O half monolayer, struct. props. 80−44421
W (100), specular scattering of polarised low energy electrons 79−60233
W (100), surface reconstruction kinetics in presence of O half-monolayer 80−65375
W (100) photocathode, monitoring of Cs and O_2 coadsorption 77−55862
W (100) surface, phase transition exam. by LEED 77−55433
W (110), chemisorption of CO, LEED, XPS and Auger meas. 77−89647
W (110), O adsorption, adatom interaction energies, Monte Carlo calc. 78−71948
W (110), O chemisorbed, island form. and condensation 80−49517
W (110), O_2 and WO_2 adsorption by LEED AND AES 80−34317
W (110), order-disorder transform. in chemisorbed O, theory compared with LEED data 79−7748
W (110) and (111) surfaces, KCl adsorption-desorption behaviour 80−75442
W (110) surface, adsorbed monolayer of CO, LEED meas. 77−59213
W (110) surface, adsorbed Pd, growth, struct., stability, desorption 80−59794
W (110) surface, adsorption of O_2, LEED, AES and thermal desorption meas. 78−38957
W, (110) surface, conduction electron interaction with diffracting electrons *(Russian)* 80−79643
W (110) surface defect. exam., LEED obs. 79−82421
W (110)-O chemisorbed layer, island size determ., response function and substrate struct., LEED meas. 79−42414
W (111), O_2 and CO adsorption, angle resolved electron stimulated desorption, LEED and AES 80−6645
W (111), adsorption of O_2, AES, LEED and electron stimulated desorption obs. 79−46935
W (112), adsorption of La, contact pot. difference, LEED and field emission microscopy *(Russian)* 78−14618
W {001}, displacive surface phases formed by H_2 chemisorption, LEED study 80−49520
W {001} (1×1)→($\sqrt{2}\times\sqrt{2}$)R45° surface struct. transition, LEED, AES, and work function meas. 79−42348
W {001}($\sqrt{2}\times\sqrt{2}$)R45°, low temp. surface struct., space group determ. by LEED 77−85037
W {110}, chemisorption of β-N_2, underlayer mechanism 80−39432
W, adsorption and early stages of condensation of Ag and Au on single cryst. surface 78−6212
W, adsorption of O_2, N_2 and CO, on (100) planes, LEED-AES obs. 77−69186
W, chemisorpt. of O_2, island form., adatom interactions 79−46922
W clean {001}-(1×1) surface, struct. determ., dynamical and exptl. LEED results 78−14560
W crystal-atom and W(001) surface, low-energy positron diffraction, theoretical study 80−84034
W epitaxy on W(110) substrate, work function meas., LEED investigation 80−80103
W, LEED and electron microscopic investigs., review *(Hungarian)* 77−47654
W, low index surfaces, spin polarisation, intensity profiles 77−62722
W, O chemisorbed layer, phase transitions, coverage effects 78−79879
W, secondary electron emission rel. to LEED 78−84689
W, spin polarised LEED, energy and ang. distrib. *(German)* 80−49468
W stepped surface, O adsorption and desorption obs. 77−47675
W surface, (100) adsorbed N_2, vibr. spectra, bonding struct., LEED study 80−84387
W, surface struct. changes due to ionic bombardment *(Russian)* 77−1775
W, surfaces (100) and (110), adsorbed O electron stimulated desorption, combined method using LEED and AES 79−33181
WC_x, (3×5) struct. on W (110) surface, at. beam diffr. and scatt., surface characteris. 79−78819
W(001), surface state resonance exam. above vacuum level 78−30965
W(100), clean thermally induced c(2×2) surface struct. 77−62714
W(100), I adsorption at room temp., LEED and AES study 80−84389
W(110), adsorpt. of Xe, 77 to 90K, LEED study 79−42382
W(110), Cs and O_2 coadsorption, surface anal. 77−89656
W(111), chemisorption of ethane, AES and LEED pattern exam. 79−15005
W(210) surface, surface struct. for adsorbed CO and N_2 79−15009
W{001} (1×1) surface structure, pseudo-relativistic LEED calcs. and R-factor anal 80−70510
W{100} surface, co-adsorption of Cu and O_2, AES, thermal desorption, LEED and work function meas. 78−38950
Xe adsorbed on Cu, NaCl, stepped and disordered surfaces, two-dimens. phase transformations 80−103580
ZnO 10$\bar{1}$0 surface, reaction of O_2, AES, LEED, EPR, desorpt., surface cond. and work function expts. 78−95950
ZnO (0001) and (000$\bar{1}$) polar surfaces, 6-fold LEED patterns 78−71920
ZnO (10$\bar{1}$0), LEED anal. of atomic geometry 77−69149
ZnO (10$\bar{1}$0), surface struct. from LEED anal., matrix inversion method 79−46897
ZnO (10$\bar{1}$0) and (11$\bar{2}$0) surface, atomic geometry from elastic LEED intensities 77−20170
ZnO, nonpolar surface, interaction with CO and CO_2, thermal desorption, AES, EELS and LEED obs. 79−65321
ZnO on Zn (0001), oxide film growth, at. and electronic struct. 78−15587
ZnO, polar (000$\bar{1}$) surface, annealing and Ar^+ bombard. effects on conductivity, LEED obs. 79−51653
ZnO, prismatic surface, O_2 interaction obs. 77−31899
ZnS, clean surface, AES and LEED exam. 80−10762
ZnSe (100) surfaces, surface states meas. *(Japanese)* 79−99599
ZnSe (110), LEED intensity anal. and electron spectroscopy 77−43678
ZnSe, evap. onto electron bombarded NaCl substrates, epitaxial growth and characts. 79−28948
ZnSe(110), surface struct., kinematical LEED calcs. 77−85034
ZnTe (110) surface, elastic LEED anal. 79−86967
ZnTe (110) surface struct. determ. by LEED, UPS, and EPR 80−49475
Zr, (0001) surface struct., HCP phase, LEED study 80−20017

low gravity experiments *see zero gravity experiments*

low induction loss *see loss angle*

low-pass filters
acoustic, muffler for small two-cycle engines 79−18585
Butterworth, oceanographic data appl. 79−16704
ECG linear filtering artifacts 77−44810
EMG filtered signal in isometric muscle contraction, S/N ratio anal. *(German)* 77−81490
Fourier spectroscopy, delay compensation, sampling error reduction 79−30566
integral pulse freq. modulator, spectral props., heart-rate variability meas. 77−90951
interference filter for submillimetre astronomy 80−48393
interference filters for Tokamak plasma diagnostics 80−64783

low-pass filters continued
linear filter appl. to evoked pot. data 79−84032
nonrecursive, based on analogue delay device, for mass spectrometer ion multiplier 78−92541
numerical digital filter for on-line processing of wind tunnel data *(French)* 80−19537
optical filter, using Polaroid film type H32 for GaAs beam 78−33853
recursive of high contrast images 80−91754
semiconductor magnetophonon oscillations, separation by low-pass-filtering autocompensation 78−2499
spectroscopy, noise reduction by low pass filter for DC signal, appl. chlorophyll-a fluoresc. 80−87249
US low-pass spatial filtering 79−47869

low-temperature physics *see cryogenics*

low-temperature production
see also Joule-Thomson effect; magnetic cooling; refrigeration
0.5K, by pumping ^{3}He 77−10029
astronomical instrumentation cooling problems for space platform use 78−16298
circulating cryogenic systems, cooling time for laminar and turbulent flow 77−5849
closed-cycle cryocoolers, design trade-offs w.r.t. appl. 80−52242
closed-cycle refrigerator at 4.5K, features, improvement 78−93704
continuous flow cooling unit, for the cryostat 80−31761
continuous flow unit, for Mossbauer experiments, 4.2 to 300K 80−31954
cooled satellite telescopes, control of contamination due to cryogenic cooling 80−31209
cryocooler, microminiature size, scaling laws 78−93701
cryocooler for supercond. instruments, requirements 78−93710
cryocoolers, closed-cycle, design problems 78−93705
cryogenerators, thermally activated closed-cycle regenerative 79−58742
cryogenics, a critical review 78−89485
cryopump, refrigerator cooled 20K, with adsorption panels 77−30172
cryosurgery, self-contained apparatus 80−56271
cryosurgical applicator, temp. distrib. reproducibility 79−39589
cryosurgical instruments, open and closed circuit supplies compared 79−39592
dilution refrigeration, history from 1951 79−41
dilution refrigeration, practical design of heat exchanger 78−41314
dilution refrigeration with continuous countercurrent heat exchanger, theory 77−30152
dilution refrigerator, ^{3}He circulating, with more than one mixing chamber 77−30153
dilution refrigerator, anomalous cooling power, heat transport of ^{3}He-^{4}He solutions 80−37045
dilution refrigerator, concentric heat exchanger 79−21756
dilution refrigerator, multiple mixing chamber 80−37042
dilution refrigerator for neutron expts. 77−30151
dilution refrigerator with double mixing chamber system 78−81978
dilution refrigerator with sintered Ag powder heat exchangers, millikelvin range 77−30154
electrocaloric refrigeration, for 4 to 15K 79−80624
electrocaloric refrigeration for 4-20K range 78−93703
evacuated chamber with specimen cooling via a mechanical switch [for optical measurements] 79−35765
fusion reactor research appls. 79−49840
galvanothermomagnetic refrigerating element, cooling mechanism *(Russian)* 77−26308
Leiden dilution refrigerator, lowest temp. and temp. gradient in counterflow capillary calc. 77−2660
low temperature He compressor *(Japanese)* 77−53918
neutron four-circle diffractometer, cooling down to 3.9K 77−27789
nuclear demagnetisation refrigerator, microprocessor controller 80−37043
nuclear demagnetisation refrigerator, two stage *(Japanese)* 80−47063
nuclear demagnetisation refrigerator, two-stage 80−52244
nuclear spin system, ultra low temp., nuclear adiabatic demagnetisation *(Japanese)* 79−12807
pyroelectric substance, adiabatic depolarization under cryogenic conditions 80−55045
refrigeration cycle using two circuits, comparison with Claude cycle 77−17993
refrigeration fundamentals, system development 78−93697
refrigeration technology for superconductors 77−82529
refrigerator, 300 W 1.8K for superconducting RF particle separators 77−18770
refrigerator, closed-cycle, 4.5K, for supercond. susceptometer 78−93707
refrigerator, closed-cycle, 4.5K, mag. and vibration characts. 78−93706
refrigerator, closed-cycle, for supercond. electronic systems, design 78−93711
regenerative refrigerators, closed-cycle, for cooling small supercond. devices, concept 78−93698
silica gel for low temp. regenerator of cryogenic refrigerator 77−17994
SQUID appls. portable refrigerator 80−27313
stainless steel dewar prod. 78−16801
Stirling cryocooler, milliwatt refrigeration at temps. 3 to 4K 79−67307
superconducting tunnel-junction refrigerator 80−57311
supercritical He refrigerator, recovery time after thermal upset 77−17992
thermoelectric cooling devices, maximum refrigerating capacity determ. 80−86318
tunable diode laser, operating temp. production, stability 78−33745
ultra low temp. generation and meas. *(Japanese)* 78−45635
vapour pumping system, for liquid cryostat, 4.2 to 300K 78−81980
CaF_2, achievement of negative temp. *(French)* 78−74009
He cooling systems, large, review of hydrodynamics and heat transfer 79−204
He II, flow through porous plugs, space cooling system appl., plug characts. 78−49842
He liquefiers and refrigerators, cryogenics of Sulzer, Switzerland 80−82769
He refrigerator, gas bearing turbine with dynamic gas bearings 79−35754
He unit requirements, for superconductive energy appl. in USA 78−89999
^{3}He circulating dilution refrigerator with two mixing chambers 77−61073
^{3}He, continuous flow cryostat, for polarised targets 80−52240
^{3}He/^{4}He dilution refrigerator, temp. inhomogeneity in glass mixing chamber 79−17429

low-temperature production continued
^{3}He-^{4}He, combined, dilution refrigerator, manipulation of sample in mixing chamber 78−41318
^{3}He-^{4}He, dilution refrigerators, ^{3}He circulation cycle with continuous heat exchangers, 2 mK production 79−67313
^{3}He-^{4}He, mixing chamber for use in dilution refrigerator, single cycle expts. 78−41315
^{3}He-^{4}He dilution refrigerator, with superfluid ^{4}He circulation 80−57304
^{3}He-^{4}He dilution refrigeration system, choice of tube lengths and diameters 80−57308
^{4}He, liq., cooling to 0.43K 78−16802
^{4}He, superfluid, properties in zero gravity, appl. as cryogen on spacecraft 77−31822
N_2, liq., boiling, cryogenic, heat transfer rel. to sinusoidal elec. field 77−72135
N_2, liquid, computer design and optimization of cryogenic refrigeration cycle 79−58750
N_2 vapour columns, cryogenic, complex flow 78−34119
$PrBe_{13}$, nuclear demagnetisation, prod. of μK temps. 77−17987

low-temperature techniques
see also cryostats; refrigeration
3-channel far IR detector based on coded Si;B, Ge:B, n-GaAs photoresistors 80−101839
absolute temperature stabilizer, below lambda point, the adritron 79−21757
aerosol detector, in cryogenic systems 78−81986
alloy selection for cryogenic resistors with low temp. coeff. 80−98922
apparatus volumetric calibration by cryogenic Xe gas transfer 78−93653
Araldite, high vacuum sealant at liq. N_2 temp. 80−57319
atmosphere organic pollutants, cryogenic sampling and gas chromatography determ. 78−81468
atmospheric gases, cryogenic conc. technique for PIXE anal. 79−53005
autodyne, for low-temperature measurements up to 400 MHz 77−13755
automatic multirange He liquefaction plant 80−57306
automatic thermal cycling apparatus, for superconductive thin film devices 78−37014
back diode amplifier, use at low temp. 80−57324
biaxial stress production at low temp. 78−45609
biological frozen hydrated bulk specimens instrumentation and specimen prep. for electron beam X-ray anal. 78−57142
biological SEM, comprehensive freezing, fracturing, and coating system 80−76883
biological SEM and X-ray microanalysis 79−74818
biological specimen complex permittivity meas. bench for 2-10 GHz at 77-300K *(Russian)* 77−32966
biological specimen rapid freezing under controlled and reproducible conditions 78−57139
biological specimens, low-temp. TEM, radiation damage, review 78−57147
breakdown voltage, of gaseous N_2 and air, from normal to cryogenic temps. 78−59692
C-impregnated glass thermometer *(Chinese)* 79−30479
calorimeter for meas. heat capacity in 4 to 370K range 80−105647
calorimetric system for temp. range 3-300K, with on-line computer 78−4620
calorimetry, automatic data acquisition system *(German)* 77−37898
capacitance thermometer for low-temp. measurements, bridge detector circuit 79−54132
cell for X-ray diffuse scattering studies up to 5 kbar and down to 77K 80−86336
chemical reaction apparatus, automatic, for low temp. inert atmosphere system 78−93695
chromatography, gas, conc. device 80−85235
circulating cooling system, based on commercial 6.3 helium liquefier 78−57961
clamp cell for elec. conductivity measurements down to 77K 80−37047
closed-cycle cooling system, at UPM Cryogenic Facility, Saudia Arabia 79−71459
closed-cycle mech./adsorption refrigeration for cryogenic device appl. 78−93708
coaxial cables, vacuum feedthrough to low-temp. apparatus 77−79101
cold finger, for cryosurgery, heat transfer characts. *(Russian)* 77−22556
compact low-temperature fixed point device 79−35761
compression, elastic, uniaxial, of single crysts. at low temps., device 78−49809
conduction cooling device for low temp. phosphorimetry 80−90855
conference, Grenoble, France (Aug. '78) 79−51462
constant volume gas thermometer for temps. 4-300K *(French)* 77−133
conversion electron Mossbauer spectroscopy down to 4.2K, applications to thin film and surface studies 78−84504
coolant transfer, four-fold coaxial corrugated piping 79−21758
cooling of mm- and submm-wave Josephson receiver, closed-cycle refrigerator 78−93709
counterflow gas-liquid helium heat exchanger with copper grid 80−17947
coupling for vent gas cooled transfer lines 78−81983
cryo current comparator, toroidal, as DC ratio standard 79−88977
cryo-ultramicrotomy and myofibrillar fine struct., review 78−53592
cryochemical techniques, prod. of ultrafine ceramic powders 80−55336
cryocoagulator for uterine contraction promotion and bleeding suppression 79−39591
cryocooler for supercond. devices, conf., Boulder, CO, USA (1977) 78−93696
cryocoolers for superconductive electronics 79−26058
cryocurrent comparators, ring cavity elements, field attenuation 77−144
cryofixation of tissue specimens studied by cooling rate measurements and scanning electron microscopy 80−94430
cryogenic container, cylindrical estimation of steady state heat link 79−35750
cryogenic cryst., apparatus for cryostat transfer and deform. 79−2773
cryogenic flange connection 79−71460
cryogenic flow measurement, transfer standards 79−68888
cryogenic fluid tank, leak detection device 78−37016
cryogenic fracturing, appl. to metal surface layer struct. investig. 77−30219
cryogenic free-precession ^{3}He magnetometer using a SQUID 79−6153
cryogenic insulation, thermal cond. meas. 79−30484
cryogenic liqs., floating level gauge 79−2774

low-temperature techniques continued
cryogenic liquid, bubble population density meas. on immersed heated surface 77−30169
cryogenic liquids, technique for producing uniformly charged drops 77−49733
cryogenic pressure regulator 78−57963
cryogenic pressure-vacuum valve 78−37020
cryogenic refrigerators for fusion research 79−679
cryogenic sorption trap for high-vacuum system protection 79−88963
cryogenic system, thermally driven acoustic oscillation, stability limit 80−8992
cryogenic target containing liquid He, H_2 and D_2 79−68111
cryogenic vacuum feedthrough, with isolated shield, DC to 6.5 GHz 79−67324
cryogenic-vacuum chamber, shaft seal method for rotation transmission 77−26314
cryogenics, a critical review 78−89485
cryogenics, general review 80−31770
cryoirrigator, stomatological, for tissue destruction 77−21654
cryophotoaggregation, bimetallic cluster, transition metal atom nucleation, review 80−53182
cryoprobe, for medical surgery 80−56274
cryopump, appl. in science and technology 79−63252
cryopump system, for use in HV centre terminal of tandem Van de Graaff 79−63253
cryopumped hydrogen cluster beam source 79−63258
cryorefrigerator, double-stage for cooling to 10K on a 4-circle diffractometer 80−98919
cryosorption pump, porosity of solid gas layers *(Japanese)* 80−20031
cryosurgery, clinical appl. 80−12295
cryosurgical probe, heat transfer coeff. within cavity formed by tip 80−36188
cryotumourectomy control with LF impedance meter 77−25591
cryoultramicrotome sections, reproducible spreading device 80−21585
cryoultrasonic surgical instrument 77−78027
crystal, low temp. spectrophotometry *(Russian)* 79−40635
crystal absorption meas. using system response corrector 78−86347
crystal growth, apparatus for growing low-temp. single crysts. 79−4908
DC potentials in low temp. ccts., superconducting chopper amplifier for meas. 77−26306
densimeter, mag. suspension, for meas. on fluids on cryogenic interest 77−10031
density of refrigerated hydrocarbon liqs., meas. by capacitance method 77−26273
Dewar flasks, automatic monitoring of liquid N_2 level 80−57309
dewar utilising foam resin insulation for light scatt. expts. *(Japanese)* 78−29108
Dewar vessels for liq. N_2, foam plastic, manufacture, heat insulation test *(Japanese)* 78−37023
Dewars, vacuum space saving via simple valve seal 77−5851
diamond anvil cell, variable temp., for polycrystalline X-ray studies to 2K 78−1951
dichrograph for measuring magnetic circular dichroism in 200 to 850 nm region 80−101806
dielectric constant gas thermometry, 4-27K, and eqn. of state of He 79−63222
dielectric loss meas., expts. on polymers, 0.1-10 GHz, 2.2-4.2K 77−24786
dielectric loss meas., spacer material for supercond. cable, method using supercond. reson. cavity 77−8501
dielectric loss measurement in polymeric solids using superconducting microwave resonators, 2.2 to 15K 79−67316
differential scanning calorimeter 80−86311
digital thermometer, for 4 to 300K range 80−4709
dilatometer based on mechanotron for meas. linear expansion coeff. 80−105639
dispersive-reflection spectroscopy at liq. He temps. using Michelson interferometer 80−31910
DRON-0.5 X-ray diffractometer, low-temp. attachment 78−343
DTA apparatus for use in martensitic transform. studies at low temp. 79−49237
dual pilot operated valve for switching the flow of a cryogenic liquid 80−98918
elastomer seal, easily demountable, for cryogenic appl. 79−207
electric breakdown characts. of cryogenic liqs. 79−91364
electric resistance high precision meas. and control of metal samples 78−54403
electrical contact, at He temperature, to evaporated Au film in Si detector 78−37019
electrical contacting method, Au wire-semiconductor, spark welding, for elec. meas. *(German)* 79−49215
electrical feedthrough for gas pressures up to 10 kbar and low temps. 80−31787
electrical residual resistivity and thermal conductivity coeff., comparison of max. values as parameter of metal purity 79−65431
electrical resistivity expts. in He II environment using computerised facility 80−31799
electron accelerator cryogenic equipment for point defects in solids research *(French)* 77−132
electron irrad. of LiH at 90K, closed liquid Ar circuit *(French)* 78−62214
electron microscope, high resolution, obs. at liq. He temps. 80−86517
electron microscope, HV, in-situ elec. resistivity meas. 80−101893
electron microscope, JEOL JEM 100C, low temperature specimen stage and transfer system 78−32945
electronic level sensor/controller for liquid N and He 79−75536
epoxy, Stycast 1266, very low temp. thermal conductivity and optical props. 78−55992
EPR cavity matching device for use at low temperatures 78−54420
EPR Dewars containing liq. N_2, bumping elimination 79−40600
EPR multipurpose cavities, 1.6-1300K appl. 78−8430
EPR spectra, inexpensive quick-freeze technique 80−9012
EPR spectrometer attachment for studying materials in 120 to 350K. $1\text{-}10^4$ atm. range 80−105686
EPR X-band and Q-band spectrometers, liquid He cooling units 77−2675
experimental reactor facilities, irrad. devices, cold neutron sources *(French)* 77−131
fatigue test machine, low-cycle, far sheet material bending to −196°C 80−55616
film thickness meas., quartz thickness monitor 77−79052

low-temperature techniques continued
film thickness meas., quartz thickness monitor 78−41275
floating level indicator for liquid helium 79−67305
flow calorimeter for condensable gases, low temp. and high press., design and eval. 80−37033
flow calorimeter for condensable gases, low temp. and high press., computer program prediction and exptl. data comparison 80−37034
flow of liq. N_2, hot-wire anemometric meas. 77−31409
flux pump supply, using inductive current transfer 78−12704
freeze-fracture electron microscopy freezing method evaluation by low temp. X-ray diff. 78−57145
Freon 14, roto-vibr. mol. laser, low-temp. performance 80−9871
gas flow measurement method 79−4093
gas stream cooling method used in X-ray diffraction 78−219
gas thermometer, parameter calc. allowing for actual state of He 80−105641
gas thermometer, small, const. vol., sensitivity and linearity at low temps. 79−63223
gas-cooled current leads, for superconducting magnets 80−37056
glass-ball packing, thermal insulation props. *(German)* 77−27463
graphite thin film low-temp. thermometer 77−49734
grating spectrometer, liquid He cooled, for far IR astronomical obs. 79−66925
gravitational-wave antenna, small, cryogenic, meas. at 1.5K 79−21646
gynaecological cryogenic treatment apparatus 79−57807
heart muscle cells, paraffin-embedded, cryofracture, SEM and TEM obs. 78−57148
heat capacity determ., modified heat pulse method, 0.2-4.2K range 78−21143
heat capacity measurement, of metals under pressure 78−81979
heat detector, temps. close to absolute zero *(Russian)* 79−6130
heat exchanger, transient performance of extended surfaces 77−30168
heat filters for bolometers cooled to very low temperatures 80−52315
heat flux rectifiers 79−58751
heat pipe, heat and mass transfer 77−13758
heat pipe, mathematical model including transport-opposing body forces 79−41552
heavy ion irrad. of low temp. target, device 77−23327
hemispherical dielectric permittivity cell for low temps. 78−70161
high pressure production at low temps., review 78−12709
high vacuum, HV bushings, for cryogenic appl. 78−81977
high vacuum evaporation system with low-temperature substrate for superconducting meas. 78−84716
high-pressure optical cell for Raman scattering at low temps. 79−49247
high-pressure temperature meas. in liquid He region 80−31748
hybrid cooler for space flight appl. 78−89484
hydraulic single-bellows valve use at 1K in dilution refrigerator 78−225
hydrostatic liquids for obs. of NMR of ^1H at high press. and low temp. 79−2801
inertial confinement fusion target fabrication system operable inside room-temp. chamber 80−106152
internal friction meas. system using one-crystal composite oscillator 77−42789
ion source cooling attachment using liquid N_2 for MI-1305 mass spectrometer 80−105744
ionic mobility measurement, of cryogenic liquids, pulsed spacecharge technique 77−74420
IR cell, low temp. for use with hydrated films 79−6193
IR detectors, trends in low-temp. thermal and photon detectors *(Russian)* 80−72778
IR opaque heat shield with high thermal conductance for use in changing mag. fields 77−74408
IR radiation thermometer, −10 to +600°C range, solid-state, features *(German)* 77−82513
IR sensor, spinning cryogenic, integrated thermal/structural/optical evaluations 78−82040
irradiation calorimeter for simultaneous, low-temperature measurements of energy release and of resistivity recovery in irradiated metals 80−31756
jet pumps, circulation of the two-phase mixture 80−82771
Josephson-effect voltage-standard instrument, features 78−93729
Kapitza conductance, meas. using supercond. current comparator, appl. to Evanohm 77−41645
Kerr cell for measurements of Kerr effect in liquids down to 77K 80−52199
lambda tight cement, for low temp. techniques 79−35752
lambda-tight In rings, simple demountable device for fixing 77−30160
lanthanum diluted cerium magnesium nitrate magnetic properties at milli Kelvin region *(Japanese)* 77−71331
laser, low-temp. ruby, with optical delay line inside resonator, cooling system 79−36922
level detector for liq. He, using series of capacitors 77−30158
level sensor, for liq. N_2, PTC thermistor P310-C11. 80−52247
LF dielectric measurements using time-domain technique, 20 Hz to 10 kHz 80−57329
Lichtenberg figures at cryogenic temperatures *(German)* 77−82536
linear expansion coeff. measurements in 4 to 80K range using differential dilatometer 80−17922
liquefied gas, cold loss minimisation during transfer and storage 77−30165
liquid He dewar, heat anal., reduction of evaporation rate 79−75533
liquid He level indicator *(Japanese)* 78−12705
liquid He level meas., capacitive level meter with IC convertor 79−88907
liquid He stage, for scanning electron microscope 80−9073
liquid He-cooled MOSFET preamplifier, for use with astronomical bolometer 77−61123
liquid N_2 transfer valve 77−136
liquid N_2 two-level controller 80−52241
liquid nitrogen cooler, for specimen manipulator of LEED-AES experiment *(Japanese)* 78−45639
liquid nitrogen filling system, automatic 77−41620
low frequency acoustic thermometry in the range 4.2-20K with implications for the value of the gas constant 79−30477
low temp. meas. in high magnetic field 77−30171
low voltage meas. in DC cct. at liquid He temp. 77−37919
low-boiling compound separation by low-temp. gas chromatography 79−70397
magnet spectrometer, QQDDQ Big Karl, cryopump system 79−63257
magnetic refrigerators, small, to pump heat from He temp. to above 10K 78−93702
magnetic safety valve 80−8966

low-temperature techniques continued
magnetic specimen stage, liq. He, investigation of ferromag. domains in $CrBr_3$ 80−103855
magnetic temperature scale, for 2K to 30K range 77−5850
magnetic thermometry, depend. of AC mag. susceptibility on magnitude of meas. field 80−241
magnetic thermometry, to below 1 mK, with La diluted $Ce_2Mg_3(NO_3)_{12}.24H_2O$ 79−30469
magneto-optical spectroscopy, mag. field modulation apparatus 77−34032
magnetometer, for magnetocrystalline anisotropy meas. from 4 to 300K 77−2673
magnetometer, for meas. of mag. props. of whiskers 79−63284
magnetothermal conductivity measurement for selected metals, 4 to 20K 79−67317
manostat, stable automatic pressure controller, use of thin polyester film 79−35700
matrix isolation spectroscopy of sputtered products, apparatus 77−26407
Matsushita C resistance thermometers, heat capacity below 1K 78−65934
mechanical press for Mossbauer spectroscopy at low temps. 78−21803
mechanical test device, for metals and alloys electric current effect, 4.2-300K 80−66719
mechanical testing devices for high and cryogenic temps. 78−7137
melt-spinning device for eutectic glassy alloy prod. 80−100825
metal atom reactions, cryogenic techniques and matrix isolation spectroscopy 77−9080
metal hollow O-ring seal, for UHV and cryogenic use *(Japanese)* 80−22374
metallic thermal connectors for use in nuclear refrigeration, elec. resist. meas. 78−224
metallography, modified installation IMASh-5S-65 80−21229
metals, specific heat meas. method of low temperatures and high pressures 80−52246
meter, digital, 4 to 300K, with Ge pickups 80−31747
meter-controller for 1.5-300K range 77−45840
MHD generator, RB and Cs applicability *(Hungarian)* 80−3526
microprocessor-controlled gas chromatograph, low temp. range extension 78−3395
microspectrofluorometry design of cold chamber 78−57144
microwave spectrometer, moderate press., 4.2-295K, for paramag. reson. appl. 78−266
mixing chambers for dilution refrigerators 79−58703
moire strain analysis in cryogenic environments 79−77029
molecular spectroscopy at low rot. temps., appl. of composite wall hollow cathode source 77−19376
Mossbauer effect measuring installation for pressure at low temp. 77−77129
Mossbauer experiments, efficient continuous flow He cooling unit 77−33992
Mossbauer meas. of ^{83m}Kr implanted in Al 78−35071
Mossbauer spectroscopy, conversion electron, cryogenic proportional He counter 80−69010
moving coil linear variable differential transformer for displacement meas. at liquid helium temps. in strong magnetic fields 78−54415
multi-layer insulation with thermal cond. below 0.1 μW/cmK 77−30161
multihole SQUID, miniature, with preset point contact, sensitivity 77−37952
multilayer insulation, simple struct. insulating material props. for low temp. appl. 80−57307
multilayer insulation thermal cond., accel. temp. field method in low temp. investig. 77−30162
multiple superconducting energy doubler accelerator magnets, series operation 77−83214
myocardial tissue, shock-frozen, preservation as shown by cryo-ultramicrotomy and freeze-fracture studies 78−53593
neodymium ethyl sulphate enneahydrate, mag. susceptibility, 2-27K, appl. as mag. thermometer 79−63224
NMR, double sample cell technique for mag. susceptibility meas. in solid ^3He 79−63225
NMR double-tuned pickup for cryogenic flow meas. 77−13756
NMR field cycling method for obs. of low temp. tunnelling in molecular solids 79−65755
NMR thermometry at ultra-low temperatures 77−17985
noise thermometry, using Josephson junctions 79−21752
nuclear magnetic order determ. using low-temperature techniques *(French)* 80−5062
nuclear susceptibility thermometry using enriched ^{119}Sn 80−4710
Nuclepore filters, characterization measurements 80−86324
nylon-quartz fibre support for low temp. mag. suscept. meas. 78−65947
optical chamber with fixed pressure, use of liquefied gases 80−57358
optical chamber with fixed pressure up to 16 kbar, single-window, 1.5-300K 79−35770
optical cryogenic illuminator 80−105652
orbiting astronomical telescopes, IR detector cryogenic cooling requirements 78−96400
organic compound luminescence spectrometer attachment for recording at liquid N_2 temp. 79−67394
phase equilibrium study cell, 220-300K and up to 6.7 MPs 80−62821
phthalocyanine, quasiline emission spectra using low temp. laser luminesc. spectrosc. *(Czech)* 80−86445
physics and meas. *(Japanese)* 78−45636
physiomechanical testing, low temperature, temp. control for tests in liquid coolant vapours 80−81260
piezogalvanomagnetic effects measurement in semicond. at low temps., apparatus with stabilised dynamic load 77−67458
point defect concentration monitoring during low-temp. irradiations and anneals 80−7741
portable self-contained refrigerants transfer system, for use with supercond. magnet dewars 80−8993
powders, semiconducting, exam. of freeze drying rate in cryochemical prep. method 78−52706
pressure cell for neutron scatt. from liq. ^3He 78−14246
pressure cells and hydraulic press working down to 10 mK 79−63229
pressure transducer, high-resolution, operating at liquid He temps. 79−58735
pressure transducers, suitability discussion 77−30130
proton filter, polarised, for polarisation of slow neutrons 79−63238
provisional 1976 temperature scale between 0.5K and 30K *(French)* 79−63231
PTFE seal for superfluid He 78−4625
pulsed NMR thermometry below 0.1K 77−5852
pyrometer, total-radiation, UNT-74 apparatus for checking, 20° to 300°C 79−67387
quartz thermometer, with FET oscillator 78−81967
quenching techniques and devices 80−76291
quick access sample system for low temp. K-band ESR and ENDOR 80−57352
Raman spectroscopy of crystals, sample holder 78−86342
rapid low-temp. dielectric meas. method 79−12818
rectangular resonator for observation of double electron-nuclear resonance in 3 cm range 80−98956
reference temperature device, 0.015 to 0.21K, based on superconducting phase transitions 80−17948
refractometer for inert gas refr. index meas. 77−57382
refrigerator with double nuclear stage for research on superfluid ^3He 79−58704
research activity, natural gas liquefaction, Hungary *(Hungarian)* 77−67443
resistance thermometer, GaAs p-type, for meas. under strong mag. fields *(Russian)* 78−89477
resistance thermometer, suitability of Ti-Be-Zr base glassy alloy as active element 77−82532
resistance thermometers, for 4.2 to 100K range 78−223
resistance thermometry, use of C black loaded field plotting paper 77−74404
resistive pickup based on Ge-Si solid soln. layer on ceramic 79−88953
resistive SQUID thermometer, theory 79−21753
rotatable sample holder with voltage readout, for low-temp. CW US expts. 78−13873
sample holder for electron probe analysis of Na and K in minerals *(French)* 80−85248
sample holder using thermal cycling to reduce stress 79−49238
sample orienting device with 2 degrees of freedom for galvanomagnetic meas. 78−81958
screw-fastened joints for thermal contact at low temperatures 79−35760
seal, electrically-insulating high-pressure seal for use at cryogenic temps. 77−41633
seal for high press. and low temps., simple closure 78−4626
sealing nylon chambers for use at low temp. 79−6131
SEM, appls., techniques and specimen prep., review 78−54510
SEM chamber attachment for fracturing and coating frozen biological samples 78−69260
SEM with cryo-unit, rapid prep. technique for highly water-swollen membranes 79−89047
semiautomatic bridge for high-precision DC resistance measurements on pure metals at low temperatures 79−35788
semiconductor piezogalvanomagnetic effects at low temp., meas. installation 77−41625
shuttle heat transfer in plastic displacers at low speeds 78−93700
silica (metallised) gels, thermal cond., 10-200K, cryogenic appls. 78−79828
single crystal strong uniaxial compression apparatus 78−57973
skeletal muscle bulk specimen, quantitative X-ray microanal. of diffusible ions 78−57143
soldering superconducting wire to cryogenic leads, simple repeatable method 80−4728
solid cryogens usage in space research instrumentation *(French)* 77−134
solidified gas constant-volume thermal conductivity meas. cell 80−31739
sorption pump, design of cheap pump 79−63255
specific heat meas., 4.2 to 90K, USSR special standard 77−31207
specific heat meas. at low temps. via adiabatic calorimeter 77−41614
spectrophotometer, SPECORD UV VIS, low-temp. device 78−21229
spectrophotometer UR-10 attachment for investigation of small objects at low temps. 79−21822
spectroscopy techniques, review *(Japanese)* 78−291
Speer C resistance thermometer, magnetoresist. effect 78−4624
spin glass film, quench-condensed, apparatus for measurement of initial paramagnetic susceptibility 79−54160
SQUID, for Earth's mag. field meas. using magnetotelluric sounding technique 78−96322
SQUID arrays, for mag. field meas., geophysical, biomedical appls. 78−32830
SQUID detector appl. in biomagnetism, techniques 78−96061
SQUID NMR meas. at low-temp., improved technique 78−54417
steel, high-speed, low temp. mag. cycling effects on ferromag. struct. 80−100928
STEM, obs. of single heavy atoms, in frozen biological specimens 80−89921
stimulated Raman scatt. Dewar cell for biomedical appls. 80−99799
strain gauge for cryostatic temp. 78−24782
Stycast-1266, mechanical props. at low temps. 80−57286
superconducting Al heat switch and plated press-contacts 78−54377
superconducting alloy films prod. by implantation of light-element ions 78−64161
superconducting fast-response thin-film probe, for detection of second-sound shock waves in superfluid He 79−63237
superconducting magnet, device for energy loss meas. 79−71489
superconducting magnet Large Coil Program, He liquefier-refrigerator and distrib. system 78−50398
superconducting switch for large heat flow below 50 mK 78−54376
superconducting thermometer, low temp. stabilisation appls. *(German)* 78−86250
superconducting wire, coil simulation, class and instability meas. 79−71487
superconductive device to provide reference temps. below 0.5K 79−63220
superconductive fixed points for temperatures above 0.5K 79−63221
superconductive temperature fixed point device, prep. and calibration 80−82770
superconductors, meas. of small changes in calorimetric props. using direct difference technique 77−33988
superconductors, test facility for dynamic stress effects 77−77698
superfluid He bath for supercond. magnets 77−30188
superfluid plug, control device for He coolant 80−82774
supersonic flow electronic transition lasers, low-temp. and high-pressure, pulsed blowdown and electron gun facility 79−59723
TCNQ salt, $Qn(TCNQ)_2$, Heisenberg antiferromag. chain for low temp. thermometry and cooling, EPR expts. 79−63217
Teflon superleaktight gasket seals for use at low temps. 78−16806

low-temperature techniques continued
TEM, analytical, contamination reduction using liq. N_2 cold trap assembly 80−101056
TEM, struct. determ. of frozen, hydrated, cryst. biological specimens 78−57146
temperature control for mech. meas. under light ion irrad. 78−86278
temperature error of some low-temp. thermometers magnetic field effects 79−12802
temperature measurement, via Krion 1-2 instrument 78−222
temperature production in 20-63K range using solid N 78−221
temperature reference standard for use below 0.5K, SRM 768 80−27303
temperature sensors, Pt-100, stability and calibration 20-273K range *(German)* 77−79094
tensile testing, strain gauge for testpiece deform meas. at low temp. 78−7118
thermal capacity, heat transfer meas. instrument for mK region *(French)* 79−1097
thermal conductance measurement apparatus, for insulating mechanicl supports 80−82772
thermal conductivity meas., differential method and expts. on Al_2O_3:Mn 79−63227
thermal conductivity meas. for discs of arbitary shape, method demonstrated on type II supercond. 79−63228
thermal conductivity meas. under uniaxial compression 80−105653
thermal conductivity of low-temperature fluids, meas. using guarded parallel plate apparatus 77−22553
thermal contact, to unmodified carbon resistors 78−37015
thermal cycling apparatus, for testing Ge thermometer stabilities 77−61066
thermal noise thermometer with supercond. quantum magnetometer *(Czech)* 80−220
thermal probe for semiconductor cond. type determ. 77−37900
thermal radiation shield, for cryogenic apparatus, thermodynamic optimisation 78−81982
thermocouple, W-Re, calibration 77 to 290K 77−57324
thermodynamic temperature meas. using noise and nuclear orientation thermometers, comparison, 0.011-0.05K 79−63218
thermoelectric coolers, fast transient response of novel Peltier junctions 78−21141
thermoelectric coolers, numerical anal. of transient behaviour 78−21140
thermoelectric effects, low-temperature measurements, undergraduate lab. project 78−54119
thermometer characteristics in strong mag. fields 78−37005
thermometers, C film resist., manufacture and performance 77−37883
thermometry around 10 mK using 1/8 W C resistors 77−135
thermometry below 1.5K 77−57332
thermometry between 0.5 and 30K 80−42225
thermometry temp. scale based on H_2 and He 78−206
thermosiphon, liquid N_2, flow oscills. 77−23960
thermovacuum system, thermal system design for temp. range 173-373K 79−35764
tissue dispersions, unglycerinated, freeze-etching by appl. of oil emulsion technique 78−53594
tissue surfaces cryofixation for electron microscopy 79−53294
tissue temperature simulation in cryosurgery 80−85355
transformer-rectifier flux pump power supplies performance anal. 78−12703
triple point temp. of Ar and O_2 realised by calorimetry 79−12806
UHF spectrometer for NQR studies at liquid N_2 temp. 80−13114
ultra low temp. generation and meas. *(Japanese)* 78−45635
ultrahigh vacuum and cryogenic feedthrough, with 48 pins 79−97399
ultrathin cryo-section stabilization by freeze-drying 78−54349
vacuum chamber in cryogenic environment, H_2 and He press. meas. 78−77925
vacuum feedthroughs, coaxial and multipin, cryogenic performance 80−8995
vacuum seal, demountable, for low temp. conditions 77−45857
vacuum seal, demountable, operating at low temps. 77−67445
vacuum tight heat bridge, for use at temperatures below 0.1K 78−37018
vaporising coolant enthalpy for cryodevice initial cooling *(Russian)* 78−70130
variable-temperature apparatus for detect levels in Si semiconductor wafers 79−88951
vascular occlusion treatment by cryothrombectomy and cryovenectomy 77−78026
voltage measurement, to ±15 nV, CMOS analogue gates at low temp. 79−35776
von Hippel's method, AC resistivity meas., Eccosorb HF-2050, 100-320K, 500-2000 MHz 77−32314
water cryofilm, on specular and diffusing surfaces, bidirectional reflectance 78−88274
whisker crystals uniaxial deformation, at He temperatures in magnetic field, mechanical displacement transformers design 80−50788
wind tunnel, cryogenic induction-driven, preliminary tests *(French)* 79−27730
X-ray diffraction at high press., liquid He cryostat 77−11442
X-ray diffractometer for work with actinide metals and compounds 80−316
X-ray horizontal axis θ-θ diffractometer with cryostat *(French)* 77−84575
X-ray photography at low temps., using powder camera 79−58099
X-ray topography, specimen stage with vacuum chamber *(Japanese)* 79−35901
zero mechanical work thermal compressor or pump, in high speed rotating frame 78−57962
Al, anodised, cryogenic material, IR reflectance 79−71458
Ar, liq., magnetic field-induced temperature changes 78−57960
BF_3, boiling/condensation heat transfer props., cryogenic appls. 78−79192
^{10}B enrichment by low-temp. exchange in $BF_3.SO_2$ system *(Japanese)* 78−55251
Be, low temp. elec. and thermal cond. in mag. field, use as heat switch 77−35923
BeCu pressure clamp cell, for low temp. specific heat and magnetisation meas. 80−17956
C film bolometer detection system with <0.1 μs response time 79−63226
C film resistor, high sensitivity temp. sensor, 1-10K 77−13757
C glass resistance thermometry, comparison of characts., stability and construction with Ge resistance thermometry 77−22558
C powder magnetisation thermometry for very low temps. 79−63219

low-temperature techniques continued
C resistance thermometers, determination of magnetoresistance in liquid He temp. range 80−31752
C resistors for low temp. thermometry 80−86308
C resistors for temp. meas. in low temp. reactor irradiation expts. 77−45848
CC He, liq., withdrawal from liquefier 79−67306
CH_4 triplet point temp. meas. at 90.6861K 79−26060
CO, boiling/condensation heat transfer props., cryogenic appls. 78−79192
CdSb resistance thermometer, characts. of cryogenic temps. 79−21760
$CePd_3$-Er, dil., low field mag. susceptibility, electro-nuclear effects, rel. to thermometry 80−60189
Cu resonant cavity RF loss reduction by cryogenic cooling 78−93761
Cu/Au+0.03 at.% Fe, thermocouple characteristics, in mag. field at low temps. *(Russian)* 78−54365
Cu-constantan cryogenic thermometer and temp. controller *(Czech)* 79−26056
Ga, thermal contact agent for low temperatures 77−49731
GaAs semiconducting resistance thermometer for low temp. measurement 0.3 to 350K range 79−58687
$Gd(PO_3)_3$, mag. susceptibility, 2-27K, appl. as mag. thermometer 79 63224
Ge and Ge-diamond bolometers operated at 4.2, 2.0, 1.2, 0.3; 0.1K, design and construction 80−77868
Ge cryogenic bolometer, for 20 to 500 μm spectral region 78−70187
Ge detectors, use at low temps. 77−65398
Ge IGFET cryogenic temp. operation 79−69604
Ge resist. thermometers, characts. from 1 to 35K, ISU mag. temp. scale 78−81970
Ge resist. thermometers, stability test at 20K 78−81971
Ge, resistance thermometer, low temp., approx. of calibration curve 78−45620
Ge resistance thermometer appls. below 0.1K 78−73999
Ge resistance thermometry, comparison of characts., stability and construction with C glass resistance thermometry 77−22558
H beam, low temp., direct determ. of temp. and density 80−14875
H storage by use of cryoadsorbents 80−45783
H_2 atoms trapping and thermal detection using superconducting magnet of low temp. 80−73396
H_2 storage using cryoadsorbents, 65 to 150K, comparative evaluation 79−74548
H_2 targets, liq., prep. of Lawsonite end plates for working spaces 77−67926
H_2 triple, boiling and 17K equilib. points realization, cryostat and method 80−27314
H_2 uniform solid spheres production, apparatus 77−74409
He cooling systems, forced flow, numerical anal. of heat-induced transients 80−82773
He level detector for pumped bath 78−49843
He level gauge, with semiconductor sensor 80−57277
He, liq., appl. of gas oscillation to pressurisation in storage vessel 80−57305
He liquefier, trouble shooting and repairing record *(Japanese)* 77−67439
He liquefiers and refrigerators, cryogenics of Sulzer, Switzerland 80−82769
He, liquid, temp. control by manostat 79−35757
He, liquid, withdrawal from liquefier using reciprocating circulation pump 79−58745
He liquid level indicator, small heat dissipation, made from newly developed superconducting wire *(Japanese)* 79−2775
He purifier, automatic 79−58738
He purifier for small laboratory liquefier 77−17990
He refrigerated and liquefiers, optimisation for larger superconducting systems 80−8994
He technique for superconductivity *(Croatian)* 77−28282
He transfer line, oscillation damper 80−37041
He valve, tank, pressure gauge and whistle-indicator *(Czech)* 77−61069
He-cooled LWIR spectrometer for exo-atmospheric airglow measurement, calibration 79−97450
^{3}He dilution refrigerator for neutron diffr. exam. of nucl. antiferromag. order 79−58701
^{3}He gas thermometer secondary standard for 0.5 to 40K 80−82762
^{3}He melting curve obs. by Pomeranchuk cooling 79−7731
^{3}He superfluid transitions, thermometry 77−65038
^{4}He, liq., magnetic field-induced temperature changes 78−57960
^{4}He superfluid fountain pump 78−59987
In solder joints, thermal conductance at low temps. 77−30150
InPb-covered manganin wire, level detector, depth gauge, demonstration of superconductivity 79−35751
KCl:OH, mag. field-independent capacitance thermometers 78−4623
^{85}Kr radioactive waste gas recovery system using cryogenic distillation 77−54331
LiN_3, low temp. method for single cryst. growth 79−74077
N_2, liq., decanting siphon using self-opening valve 80−57310
N_2, liq., device for level control 77−82531
N_2, liq., magnetic field-induced temperature changes 78−57960
N_2 supply, liquid, to vacuum installations 80−31762
N_2-Kr-Xe, liquefaction, retention of ^{85}Kr from fission exhaust gases, separation technique *(German)* 80−27753
NO, boiling/condensation heat transfer props., cryogenic appls. 78−79192
NaF:OH, mag. field-independent capacitance thermometers 78−4623
Nb SQUID point-contact operation in very low-power cryocooler 78−93699
Nb_3Sn, cryostabilised conductor cooling system for Large Coil Program 78−50393
NbTi split coil superconducting magnet system, for Mossbauer spectroscopy and susceptibility meas. 79−71486
NbTi-Cu, supercond. composite, use in temp. and heat transfer coeff. meas. 80−77780
Ni-Cr foldfoil strain gauge, for cryogenic anal. of supercond. structs. in high mag. fields, fusion reactors 78−54947
O_2-^{85}Kr-Xe, liquefaction, retention of ^{85}Kr from fission exhaust gases, separation technique *(German)* 80−27753
OCS, roto-vibr. mol. laser, low-temp. performance 80−9871
Pd+Cr+Ru/Au+Fe thermocouple, for temp. meas. in 2-200K range 77−26293
Pt resistance standard capsule thermometer, for 13.81 to 273.15K, two-point calibration 79−206

low-temperature techniques continued
Pt resistance standard low-temp. thermometer checking methods 78−37006
Pt wire NMR thermometer for ultralow temp. down to 0.55 mK 78−89478
Pt-Co resistance thermometer, for low temp. appl. 78−73994
Si cell for precise measurement of thermal expansion, results for Cu, NaF 80−37027
Si diode, thermometric props. in temp. range 4.2-300K 77−17998
Si diode thermometer, anomalous behaviour, 11 to 16K 79−35738
Si diodes as low temperature sensors *(German)* 80−31744
Si linear thermometer, superconducting transition temp. meas. 77−57330
n-Si:P, etched, high sensitivity temperature sensor, 1-10K 77−13757
Si(Li) detector, cooling system with liq. N_2 *(Rumanian)* 79−85867
Si(Li) electron spectrometer with superconducting transporting magnets 80−27376
^{117}Sn, ^{119}Sn, low temp. NMR thermometry 80−82775
T, low-temp. gas target fast neutron prod. facility 77−30691
U atomic motion on thin C substrate, low-temp. obs., biomolecule marking appl. 79−25176

LPE *see liquid phase epitaxial growth*

LS coupling *see Russell-Saunders coupling*

LSA *see limited space charge accumulation*

LSI *see large scale integration*

lubrication
see also friction
adhesive wear of lubricated contacts 80−16491
articular cartilage, asymptotic theory for thin layers with appl. to knee joint 78−44537
articulation mechanical properties and physical aspects of lubrication *(French)* 79−34591
articulations, global anal. *(French)* 79−34592
asymptotic approximation to class of regular perturbation problems 78−18258
Auger electron spectroscopy of wear surfaces formed in lubricant testing machine 77−40452
automatic, advantages 78−27646
average flow model, appl. to lubrication between rough sliding surfaces 80−16497
bearing and frictional material, current state of prod. and development trends review 78−19902
bearing materials, rolling, steel, WC and Si_3N_4, effects of high temperature operation 80−21124
bearing surface with area-distributed isotropic roughness 78−18256
bearings, strength and damping coeffs. of lubricating oils, vibration diagnostics *(Russian)* 80−97592
boronised coating on steel, sliding and abrasive wear, corrosion resist. 78−11428
boundary conds. and cavity-fluid interface, review 77−55058
boundary friction study by ultramicrosclerometry, dislocation generation 80−34131
boundary layers influence on friction, effects of adding MoS_2 80−21125
boundary lubricated surfaces, wear initiation 79−34157
boundary lubrication characteristics, of lubricants used in cold rolling of steel, SEM 80−85068
brass, fractional wear, effect of alloying and metal oxide compounds *(Russian)* 78−31541
breakdown and exhaustion, during diamond-abrasive polishing 79−96196
bronze, Al, wear on 13% Cr steel in presence of aviation fuel 80−11781
bronze P, friction with steel, boundary lubrication conditions, element conc. anal. of films 78−85001
bronze-on-steel contact, lubricated, effect of zinc di-n-butyl dithiophosphate on wear 79−20219
cavity-fluid interface, wavy interface anal. 77−55059
circumferentially ground rough disc, elastohydrodynamic lubrication 78−64708
coatings for wear and lubrication 79−19494
compliant bearing, study by optical interf. method 77−36711
compliant bearing lubrication, finite element model minimisation algorithm 78−63400
composite material deposition by electrolysis *(French)* 77−73375
composite materials, water lubrication, wear studies 80−60984
contact, frictionally heated, thermoelastic deform. 80−83764
cutting fluid, hydrolysed polyacrylonitrile based, operational characteristics 80−89359
cutting fluids testing rel. to tool wear, thin layer activation technique 80−55619
cutting oil performance, test machine 80−11848
cylinder contact with visocelastic lubricant, friction 78−7056
cylinders in elastohydrodynamic contact, lubricant layer thickness and resistance to rolling 80−96236
of cylindrical surfaces with Rivlin-Ericksen fluid *(French)* 77−80126
debris dent effect on elastohydrodynamic lubrication 78−64709
deformation broaching of difficult-to-form metals 80−108473
delamination wear, macroscopic effects 80−35343
drag reduction of an oscillating flat plate with an interface film 80−10268
dry film, parylene (vacuum deposited polymeric coating) appl. 80−108607
EHD contacts, asperity interactions 79−20215
elastohydrodynamic contact, rheological model 80−33544
elastohydrodynamic contact, shear rheological behaviour at high press. 80−35342
elastohydrodynamic contact optimisation 78−79288
elastohydrodynamic contacts, ellipsoidal solids subjected to Hertzian contact stress, surface deform. 77−35097
elastohydrodynamic lubrication, 2-D random surface model for asperity contact 80−66675
elastohydrodynamic lubrication, low elastic moduli material, elliptical contact 79−90198
elastohydrodynamic lubrication, non-Newtonian effects of volume relaxation 80−103009
elastohydrodynamic lubrication at high press., mineral oils between disks 78−34094
elastohydrodynamic lubrication at high press., non-Newtonian behaviour 79−46350
elastohydrodynamic lubrication of elliptical contacts for materials of low elastic modulus 79−20214
elastohydrodynamic traction, granular behaviour 80−103008
lubrication continued
elastohydrodynamic traction, non-Newtonian thermo-viscoelastic, from combined slip and spin 80−103043
elastohydrodynamics, solns. to steady-state problems 77−35107
elastomers in contact with regularly spaced sliders, frictional dynamics 79−20213
ester-type, thin film test for meas. of oxidation and evaporation 80−40626
extrusion, benefit of vibrations 78−51135
Fe, cast, mechanism of boundary lubrication with zinc dithiophosphate 79−79120
Fe sintered material, operating performance, effect of polymer and graphite lubricant additives 80−11785
ferrofluids, magnetic liquid vacuum seals 79−63244
ferrography of polymer form. under lubricated nibbing contact 77−21292
film, thickness meas. using laser based fluorescence technique 79−49201
film rupture in laminar and turbulent lubrication, inertia forces effect 80−74813
film temp. and traction, rel. to solidification and glass transition temp. 79−28041
fluid film, press. distrib. between axially oscillating parallel circular plates in magnetic field 78−19904
fluid film lubrication, velocity profile meas., using ZnS phosphorescent tracer method 78−94866
fluid-film flows, of differential fluids of complexity n dimensional approach, lubrication theory appl. 80−16492
four ball test re-examination for lubricants 78−60964
Fourier emission IR microspectrophotometer for surface anal., lubrication problem appls. 80−13162
free boundary problem in hydrodynamic lubrication including surface tension 80−19542
friction, lubrication and wear, review of papers published 1974 to 1976 79−15806
friction boundary *(German)* 77−86190
friction pair with low vel., friction microgeometry influence on $\mu(a_s)/\mu(a_k)$, slip-stick amplitude 78−26091
gas lubricated manometer, effective area calculation for free-piston 78−93714
glass transition, light scattering study 79−29228
glass transition rel. to elastohydrodynamic lubrication 79−29227
graphite as lubricant at UO_2/Zircaloy interface of operating fuel pin 79−67857
graphite fluoride, chemical reactivity, rel. to lubrication appl. 79−66349
hard ellipsoid sliding on rubber, orientation effects, theory 77−86188
high loaded contacts, influence of press. and temp. on effective viscosity during lubrication *(German)* 77−46974
hip joint prostheses 78−40413
hip prostheses, expt. study of friction and lubrication 80−17189
hydrodynamic, roughness effect 79−20207
hydrodynamic contacts, films, elastic properties 80−88239
hydrodynamic fundamental problem solns. for related nonlinear system 79−59946
hydrodynamic in precision pivot bearings *(Polish)* 79−91803
hydrodynamic lubrication, free boundary problem, variational inequalities 80−62475
hydrodynamic lubrication, turbulence field study 79−1255
hydrodynamic lubrication of rough surfaces, two-dimensional Reynolds roughness 79−1919
hydroextrusion under hydrodynamic lubrication conditions *(Russian)* 79−38852
hydromagnetic squeeze film between porous circular disks with velocity slip 80−74997
isothermal one dimensional problem in contact hydrodynamics, correct formulation 79−86387
joints, human, elastohydrodynamic lubrication 78−44522
journal bearings, performance, turbulent lubrication theory using frictional law appl. 79−98695
journal motion on oil film, partition method anal. 79−68662
knee joint replacement, lubrication mechanism model 79−74790
laminar lubrication with Reynolds roughness, general theory 79−90196
large Reynolds number, 2-D hydrodynamic lubricating theory *(Russian)* 78−59368
liquid continuous flow squeeze film, load-bearing capacity 78−87306
liquid layer appl. using rubber roller, nip flow operations anal. 78−71310
liquid props. review, viscoelasticity and lubrication 79−7356
liquid-friction bearing tester, description and improvements over existing designs 80−64503
lubricant evaluation, using four ball friction machine 80−25951
lubricant vapour pressure and evap. rate in vacuum, determ. using ambient press. meas. 78−29123
lubricants, four-ball test specimens mag. orientation and effect on total test time 78−80700
lubricants, viscosity and density determ. up to 150°C and 150000 psig 77−59940
lubricated load-bearing surfaces pitting mechanism, Zeta potential effects 79−87761
machine bearings, turbogenerator, with hybrid hydrostatic hydrodynamic lubrication, behaviour in laminar and turbulent conditions *(Italian)* 80−81208
materials and lubrication media, for frictional pairs, choice by energy criteria *(Russian)* 78−31541
mechanism, by surrounding gas molecules in adhesive wear 79−42143
metal-metal metal-polymer sliding, wear mechanisms, review 79−70174
metals, antiwear action of Zn di-n-butyl phosphate 80−11782
metals, in sliding contact, glow discharge effect 79−83333
metalworking, role of friction, and energy saving in deep drawing 80−76271
microcontinuum theory for elastohydrodynamic inlet zone of line contact, lubricant film 77−50998
micropolar lubricant, characts. in hydrostatic step seal and externally pressurised conical step bearing 77−86189
microtransducer for elastohydrodynamic lubrication expts. 80−37048
mineral oil lubricants, behaviour in line contact and oscillatory movement *(Spanish)* 79−98671
mineral-fibre composites, matrix lubrication for increased fracture and cracking resistance 77−8798
Mossbauer spectroscopy appl. to friction, lubrication and wear studies 80−40547

lubrication continued
motor oils, use of polymeric additives to increase viscosity index, exam. of mechanism 78−95816
nearly viscometric glide bearing fluid *(German)* 79−81830
Ni, friction props. of surface films in air and high vacuum 78−60850
Nichrome-silicate glass-CaF_2 multicomponent self-lubricating coating, prep. by plasma spraying, and props. 80−40604
non-Newtonian fluids, lubrication, elastohydrodynamic, between two rot. cylinders 78−83435
non-Newtonian lubricant, frictional behaviour 79−87736
non-Newtonian lubricant hydrodynamic theory *(German)* 78−79341
nonNewtonian lubricant, bubble behaviour 78−56786
nuclear reactor components, lubrication, friction system in liquid Na and Ar 79−59176
oil, ageing parameter determ. by IR spectroscopy *(German)* 80−27360
oil, HF combined mag. treatment *(Russian)* 79−15682
oil, lubricating, radn. effects and radn. dosimetry appl. 80−2069
oil film formation, techniaues 80−97597
oil films, thickness meas. by neutron imaging, and scattering, exam. of flow props. 79−15815
oil seal, static contact shape and kinetic behaviour 80−97598
oil-cooling baffled shell-and-tube heat exchanger expt. 78−83395
oils, antiwear props. determ. method in tests on friction machines 78−60915
optomechanical device frictional elements, solid lubricant tests 79−52388
particle-fluid mixture, lubrication flow 79−64600
perfluoro polyether, vacuum behaviour 79−63254
perfluoro polyethers, props. and use in vacuum appls. 78−70136
phosphate ester, electrical prop. rel. to lubrication 79−38150
phosphate esters, scuffing resistance 79−38990
plasma spraying utilisation in research work 79−83117
plastic, antifriction, self-lubricating, behaviour at elevated temps. in friction process 77−86192
point contact elastohydrodynamic lubrication, surface deform. calc. 78−18255
point contact problem, finite element anal. 78−1613
point contacts, elasticity effects 79−52379
polymer, microporous, lubricant supply charact. 78−64711
polymer electrophoretic coating, effect of silicone additive on electrophys. props. *(Russian)* 79−15615
polymer-containing metal-filled lubricant, tribological study on steel 80−104301
polymer-polymer and metal-polymer sliding wear mechanisms, review 79−70174
polyorganosiloxane fluids, temp. determ. in friction zone accompanying breakdown, using TV *(Russian)* 80−7688
porous bearings, linearised turbulent lubrication eqn. 79−87741
porous boundaries, Reynolds eqn., generalised form. 80−87803
porous composite slider bearing, hydrodynamic lubrication 78−39915
pressure distribution and gap shape in a one-dimensional elastohydrodynamic contact 79−94526
pressure meas. at solid-lubricant interface, strain and deform. meas. techniques with diaphragms, comparison *(French)* 79−30453
protective coatings, role in mechanical failure prevention, conf., Caithersburg, USA (Oct. 1975) 77−21327
PTFE-metal interaction, X-ray photoelectron spectroscopy obs. 80−11788
Reynolds equation, asymptotic soln. 79−14369
Reynolds equation, numerical soln. with slip boundary conditions and large bearing number 79−90197
Reynolds equation at very low spacing, compressible, numerical soln., factored implicit scheme, mag. recording appl. 80−92183
rotary face seals, lubricated, interferometric obs. 79−20204
rough surfaces, lubrication theory, derivation of Reynolds equation 79−14355
rubber, graphite filled performance assessed against steel structures under water lubrication conditions 80−21123
rubber cylinder against glass plate, elastohydrodynamic lubricant film form., expt. and theory 77−28910
rust prevention in lubricants, test method 78−15635
self-excited vibrations in lubricated friction 80−58984
self-modelling discharge of compressible fluid in bulk machines, initial parameter determ. *(Russian)* 79−77026
sheet galling, development of quantitative test 78−92433
signature response, for friction and wear 80−40541
silicone oil, props. determ. by harmonical shear vibr. *(German)* 78−67164
silicone oil drop spreading on horizontal surfaces 80−2250
silicone oils, environmental stress cracking of polyethylene due to liq. viscosity 77−4863
sintered materials, operating performance, effect of polymer and graphite lubricant additives 80−11785
sliding bearings, effect of solid surface lubricant interaction on load carrying capacity 79−20206
sliding contact seal, thermoelastic instabilities 78−18257
sliding surfaces temperature meas., stationary and non-stationary meas. *(German)* 80−23975
soft metal used as solid lubricant, compatibility effects 77−21291
solid lubricating coatings, tribopolymerized, formation and behaviour 78−35528
solid lubrications dynamics, obs. using Micro Contact Imager 78−85002
steam turbine lubricating oil, filter separators and centrifuges eval. for effects on props. 78−3283
steel, alloy, friction surface and lubricant nature, effect on adsorption and temp. stability of lubricant layers 78−15544
steel, bearing, type AISI 52100, tricresyl phosphate treated, Auger anal. 79−52413
steel, contact fatigue life of S-P type extreme pressure additive lubricated surfaces 79−47780
steel, contact rapid meas. tech. for electrical contact resistance applied to lubricant additive studies 77−16698
steel, friction and wear during hot forging 80−89358
steel, mechanism of boundary lubrication with zinc dithiophosphate 79−79120
steel, mild, two sandblasted interfaces, tangential displacement, contact press. and lubricating film distrib. effect 80−16484
steel, mild and type EN31, eval. of cold rolling oils and boundary lubrication characts. by SEM 80−85068
steel, scoring and scuffing on lubricated sliding surfaces, Mossbauer study 80−7690

lubrication continued
steel, sheet structural changes during rolling influence of lubricants on friction and wear 78−95815
steel, water accelerated fatigue, lubricant additive effects 78−64710
steel, wear testing in oils containing organosulphur cpds., XPS obs. of surface comp. rel. to wear 77−36668
steel against Al_2O_3, elastohydrodynamic contact, lubricated by naphthenic hydrocarbon, IR meas. of surface temp 79−15807
steel bearing, surface-ground, residual stress fatigue property comparison 80−60975
steel mild, ground/sandblasted interfaces, tangential displacement, contact press. and lubricating film distrib. effect 80−16484
steel/Al sliding system, tribological behaviour, effect of temp., atmos., load and geometry *(German)* 79−34158
steels, self lubricating composite, frictional props., Ag-Cu-Zn-Cd lubricant 78−11340
striated rough surface, applicability of modified Reynolds eqn., math. verification 78−11347
surface analysis, appl. to lubrication problems, review *(French)* 80−45616
surface analysis, spectroscopic methods *(French)* 80−26095
surface friction meas. *(German)* 79−68668
surfaces meas., sliding *(German)* 80−14643
synovial joints, three layer model, incompressible fluid+linear elastic solid, natural lubrication 77−70490
testing, test machine 80−76452
thermal elastohydrodynamic anal. of flats 78−15547
thermal elastohydrodynamic inlet zone, refined model 79−51198
thin film, viscous, between two nearly parallel walls, temp. distrib., convection effects 80−83801
traction prediction in elastohydrodynamic contacts 78−63394
tribology, material aspects in manufacturing processes 80−81210
tribopolymerised lubricants, mechanism of action, SEM expts. 79−29226
TU-20 turbine oil, 4-methyl-2,6-ditertiarybutylphenol determ., using IR spectrophotometry *(Polish)* 80−13161
tunnelling spectroscopy, appls., review 78−92588
turbogenerator bearing oil film damping and stiffness coefficients determ. for dynamic behaviour stability study *(Italian)* 80−106762
turbomolecular pumps with corrosion resistant oil 77−87776
turbomolecular vaccum pump, grease lubrication of bearings 79−80630
turbulent, eqn. derivation using friction law 79−98694
uncompressed viscous plastic lubricant, in bearing with temp. depend. viscosity, nonfixed motion *(Russian)* 79−50672
unequal surface temp. effect on heat transfer in lubrication problems 80−53613
vacuum techniques, applications of perfluoropolyethers *(Japanese)* 78−229
viscoelastic fluid lubrication, slider-bearing config., non-Newtonian normal stresses 80−69753
viscoelastic lubricants in human joints 79−57699
viscoelastic lubricants reln. to human joints 79−39430
viscous liquid laminar flow in gap, nonstationary Reynolds differential eqn. *(German)* 77−58641
viscous plastic lubricant, nonlinear effects on stability of bearing tenon movement *(Russian)* 79−32393
wcrn ball, metallographic micro prep. method 78−3274
wear, lubricated, contrib. to theory 80−88257
wear debris examination, oil anal. techniques, appl. to plain bearing materials study 80−97596
wear tests with plastic lubricants, friction machine attachment 78−3273
worn surfaces, lubricant additive effects, AES appl. 77−44445
zinc dialkyldithiophosphate surface film, prep. and nature 80−104300
zinc stearate lubricant, admixed, effect on Fe sintered compact, shrinkage and mech. props. 80−45402
zinc stearate lubricant effect on Fe powder compact, apparent density, mixing, and friction 80−45403
Al alloy granules, lubricants for rolling 80−60980
Al boundary lubrication, inelastic electron tunnelling spectroscopic study 80−70302
Au contact surface by plasma-deposited thin films of fluorocarbon polymer 80−89157
Au, friction props. of surface films in air and high vacuum 78−60850
$(CF_x)_n$ rubbed films applied to different finished surfaces, obs. 79−83332
Cd film, dry lubrication on C steel, tribological behaviour 80−89364
Cu, friction props. of surface films in air and high vacuum 78−60850
Cu pin-on-disc friction and wear under boundary lubrication, dissolved O_2 effect 80−76365
Cu surface, interacting mechanisms with organic sulphides rel. to friction and lubrication behaviour 80−45546
Cu-steel and Cu-brass system, realisation of selective transport mode with friction, effects of normal stresses 79−87735
Fe alloy granule reinforced Cu M2 wear resistance in rubbing with lubrication 80−16490
Fe, friction props. of surface films in air and high vacuum 78−60850
Fe powder compact, apparent density, mixing, and friction, zinc stearate lubricant effect 80−45403
Fe sintered compact, shrinkage and mech. props., admixed zinc stearate lubricant effect 80−45402
Fe surface, interacting mechanisms with organic sulphides rel. to friction and lubrication behaviour 80−45546
FeO compacted powder, effect of wall groove orientation and wall lubricants, on WC wall friction 78−23831
MgO single crystal, absorbed fluid effect on rolling contact deform. 78−64719
Mo sintered composite, MoS_2 containing, friction and wear props. 80−11786
MoS_2 film, sputtered, solid lubricant, morphological growth 77−35825
MoS_2, $MoSe_2$, texture and lubricating props. 77−44368
MoS_2, RF sputtered, solid lubricant on mild steel, morphology 78−6239
MoS_2, RF sputtered layers with variable stoichiometry, lubrication props. 80−40557
MoS_2, RF sputtered lubricant, wear life, sputtering parameter effects 80−40558
MoS_2 solid lubricant, antifriction and elec. props. depend. on oxidation temp., dopant influence 80−108584
$MoS_2(Se_2)(Te_2)$ coatings, growth kinetics and friction coeffs. 77−16731
$MoSe_2$ lubricant, synthesis by Mo+Se vapour reaction, process kinetics 79−33942
$MoSe_2$, lubricating coatings, texture, prep. by $Se_{(g)}$+Mo 78−53018

lubrication continued
$NbSe_2$ solid lubricant, antifriction and elec. props. depend. on oxidation temp., dopant influence 80−108584
Ni-Cr-Mo-V steel disc, rolling contact fatigue and residual stress on contact surface 77−32671
Ni-Mo-MoS_2 composite, Mo alloying effect on physicochem. interactions 80−7692
Si wafers, saw damage reduction in lubricant environment 80−108585
TaS_2, texture and lubricating props. 77−44368
Ti alloys, lubrication by chloroparaffins, friction and wear *(Russian)* 80−93657
UO_2 pellets-graphite-Zircaloy cladding, evaluation of graphite lubrication 80−32342
WS_2 solid lubricant, antifriction and elec. props. depend. on oxidation temp., dopant influence 80−108584
WSe_2, lubricant, prep. by self-propagating high-temp. synthesis, technological characts. 78−35338

Luder's bands
α-brass, single crystal, obstacle strength variation during stress relaxation 78−68723
Hartmann layers, current content 77−72366
herringbone specimen weld stresses rel. to heat-affected zone rigidity 79−29130
Inconel 718, plastic deform., accelerated evolution of H_2 77−36594
steel, alloy, Ni-Cr-Mo, exam. of transformation behaviour 78−76718
steel, C (0.1-1.15 wt.%), fatigue under reversed tension-compression stresses, photoelasticity investig. *(German)* 78−31493
steel, low C, ferritic, static yield prop. changes during fatigue cycling 77−52427
steel, low C, structural, AE rel. to crack tip plasticity *(Japanese)* 79−66150
steel, low C and alloy, serrated flow and thermomechanical treatment *(Korean)* 80−30026
steel, mild, Luders band front 78−3168
steel, mild, Luders bound front, elastoplastic anal. by finite element method 78−3169
steel, stainless 304L, plastic deform., accelerated evolution of H_2 77−36594
steel, yield point charact., grain size effect *(German)* 78−72810
Zircaloy, annealed, neutron irradiated, inhomogeneous deform. behaviour 80−85014
Al alloy 5086, plastic deform., accelerated yielding of H_2 77−36594
Al alloy 7075, serrated flow and thermomechanical treatment *(Korean)* 80−30026
Al bicrystals, isoaxial, fatigue crack initiation in grain boundary affected regions *(Japanese)* 80−89338
Al, plastic deform. and prominent cross slip ⟨100⟩ oriented single crystal 78−19851
Al-Mg (5 wt.%), serrated flow 79−43343
Al-Ni-(Mg) (6, 0.3 wt.%), fine grained, Luders' band deform. 77−77527
Cu single cryst., drawing deform. band form., axial orientation force meas., X-ray pole figure determ. *(Japanese)* 78−76710
Cu-Ge (8 wt.%), anelastic effect due to deform. twins *(Japanese)* 79−20095
Cu-Ni-Al (5, 2.5 at.%), precip. hardening *(Japanese)* 80−71663
Cu-Si (6.5 at.%) alloy, easy glide deform., obs. and mechanism 77−8887
Fe, Luder's band form. high speed camera obs. 80−16410
Fe, polycrystalline, exam. of Luders deformation 78−84893
Fe whiskers, elongation induced struct. distortion, X-ray topographic investig. 77−85121
α-Fe, yield point behaviour for extremely inhomogeneous deformation *(German)* 80−55453
Fe-Ni-C alloy, austenitic, pre-deform. effects on TRIP *(Japanese)* 77−8890
Ni, plastic deform., accelerated, evolution of H_2 77−36594
Si, deformed crystal, Czochralski and float zone growth, Luder's bands 79−79025
Zr_3Al, $L1_2$ phase yield strength 78−19811
Zr_3Al, ordered, strengthening by fast neutron irrad. 78−84838

Ludwig-Soret effect *see diffusion in solids*

luminance *see brightness*

luminescence
see also cathodoluminescence; chemiluminescence; electroluminescence; fluorescence; fluorescent screens; ionoluminescence; luminescence of gases; luminescence of liquids and solutions; luminescence of solids; luminescent devices; phosphorescence; phosphors; photoluminescence; sonoluminescence; stimulated emission; superradiance; thermoluminescence; triboluminescence
atom ejected by ion beams from metallic targets, continuous emission spectra *(Russian)* 78−55140
bacteria, calorimetric study of growth 77−25378
bacterial luminescence, yellow light, Photobacterium fischeri 77−66802
bacterial single cells, bioluminesc. obs. 80−108860
bacteriorhodopsin of purple membrane of H.halobium cells 77−36890
benzoxazole, aromatic derivatives, spectral luminesc. and lasing props. rel. to electronic struct. 80−99519
bifurcated fibre luminometer for inaccessible or hazardous location 80−62712
bioluminescence, reaction rate theory, review 77−90716
bioluminescence determination of extracellular ATP in native platelet-rich plasma 77−25615
bioluminescence field in ocean, meas. by moving linear sensor 79−20732
bioluminescence of firefly larva, circular polarisation 80−94441
bioluminescence of lantern fish, Myctophidae, in response to light intensity by visual monitoring 77−16953
candoluminescence spectrophotometry, flame technique for trace metal anal. 78−61093
circularly polarised, from model molecular system 80−63705
conference, luminescence, Paris (July 1978) 79−33755
coordination compounds, chemistry, electronic excitation, luminesc. methods 79−54880
decay curve simulation, finite breadth light pulse excited *(Hungarian)* 80−11473
decay time evaluation, computer programs, student expts. 77−26115
dye laser applications 79−55130
electronic line profile, narrowing and oscill. *(Russian)* 79−56859
emitting species spatial distrib. 79−83009
fast light phenomena, detection and analysis *(French)* 80−13133
fireflies, bioluminesc. spectra 80−35821

luminescence continued
laser spectroscopy, atom and mol. interactions, conf., Zarogoza, Spain (June 1979) 80−27041
LED, meas. using photometric method *(Japanese)* 77−57378
low intensity spectra recording, amplifier *(German)* 77−37904
low temperature luminescence spectroscopy using pulsed dye laser *(Czech)* 80−86445
macromolecular relaxation time spectra rel. to luminesc. depolarisation function *(Russian)* 77−31040
macromolecule, torsional oscills., HF, investig., polarised luminesc. method *(Russian)* 77−31039
magnetic circularly polarised emission from luminesc. mol. system, QED formalism, orientation relax. 77−46589
molecular electronic spectra, pure elec. quadrupole transition polaris. 80−63691
molecular luminescence, conf., Minsk, USSR (May 1977) 79−54878
molecules, luminesc., photon echoes and coherence 79−31586
moving acceptors, direct energy transfer, decay law 80−89045
multichannel time analyzers for luminescence spectroscopy 79−85185
multicomponent analysis by synchronous luminesc. spectrometry 78−73089
multiparticle system, effects of powerful coherent radiation on spontaneous emission *(Russian)* 78−46554
nuclear operators single $\hbar\omega_0$ and models of luminescence centres, operators 79−78749
picosecond luminescence detection using type II phase-matched freq. conversion 77−31024
polarized emission, mol. theory by quantum field theory 77−83633
pulse excited multilevel system, diffr. grating effect in luminesc. 79−50272
quantum yields, absolute, chem. actinometric meas. 78−32892
radioluminescence, spectrometer system for investigating light polaris. dynamics in nanosecond band 79−2834
radioluminescence spectra, distortions in one-quantum statistical method anal. *(Russian)* 77−67508
radiolyoluminescence, appl. to dosimetry of ionising radiation 79−62374
in Raman spectroscopy, FM technique 77−57412
recombination decay kinetics in diffusion approx. in presence of particles pair correlation 78−80398
research, survey of new trends 79−47503
resonance energy transfer, donor excimers effect 79−95825
ring laser, luminesc. effects on beat signal *(Russian)* 77−54742
second order optical processes, stochastic theory 79−94201
semiconductor-metal structure, luminesc. due to photoinduced injection 78−10939
spectroscopy, refractive index correction, quantum efficiencies calc. 80−86444
spectrum recording monochromator wavelength reference marker generator 78−58050
spontaneous emission, 2 particle system in strong reson. field *(Russian)* 77−50646
standardisation in spectrophotometry and luminescence meas., conf., Gaithersburg, USA (Nov. 1975) 78−32846
stilbene derivatives containing 2-pyrazoline and 1,3,4-oxadiazole groups, spectral-luminescent props. 80−7394
thin layer chromatography, luminesc. meas. methods 78−53305
thin layer chromatography, luminescence quantitation, solvent effects 78−53306
transient emission spectra, observability in theory 78−55199
two-chromophore systems, circularly polarised luminescence 80−63705
two-phase inhomogeneous media, cylindrical geometry 79−23377
weak light fluxes with slowly varying intensity detector 79−2806
worldwide research survey 78−10986
Ca^*+HCl, reaction performed under high resolution, luminescence obs. 80−95662
H ions, grazing incidence collision with surface, Balmer radiation, elliptical polarisation 78−86804
He condensed spark discharge, integrated luminosity, pulsed longit. mag. field 77−76233
$OH(A^2\Sigma^+)$ form. during H_2O photodissoc., luminesc. spectrum 79−57270
Sr^*+HCl, reaction performed under high resolution, luminescence obs. 80−95662

luminescence chambers *see scintillation chambers*

luminescence of gases
aerodynamic isotope separation technique based on vel. slip in freejet expansions 80−19441
air, light flash excited by γ-ray source, electric field effect 79−14514
air, luminous emittance of neutron beam 78−86567
air flow glow discharge, voltage, current oscills. 79−55585
airtightness inspection, luminescence method, sensitivity, quality and reliability improvement 79−52589
automatic meas. of SO_2 and oxides of nitrogen, optical technique *(Dutch)* 80−3565
2-(4-biphenylyl)-5-phenyloxazol, vapour, electron beam excited luminesc. *(Russian)* 78−82780
combustion products, Raman scatt., fluoresc. interference 78−15728
9-cyanoanthracenes-N,N-dimethylaniline, fluoresc. exciplex emission in gas phase 79−68250
1,4-di(2-(5-phenyloxazolyl))benzol, vapour, electron beam excited luminesc. *(Russian)* 78−82780
2,5-diphenyl-1,3,4-oxadiazole, vapour, spectral, fluoresc., photochem. and laser props. 80−106344
2,5-diphenyl-1,3-oxazole vapour, spectral, fluoresc., photochem. and laser props. 80−106344
2,5-diphenylfuran vapour, spectral, fluoresc., photochem. and laser props. 80−106344
emission spectroscopy for gases excited by products of neutron nuclear reactions 80−26074
finite cylindrical volume, effective luminesc. time 79−77334
isoquinoline, radiationless transitions, internal conversion, energy depend. 78−94272
light flash excited by γ-quantum pulse without direct visibility of source 78−69457
luminous flares, heat of radiation calcs. *(German)* 80−68154
measurement by rotation of spectral lines, optical system *(Russian)* 77−53913
methanol, HF laser irrad., visible luminesc. 77−46593
POPOP vapour, spectral, fluoresc., photochem. and laser props. 80−106344

luminescence of gases continued
pyrimidine, vapour, phosphoresc. 80−83408
quinoline, radiationless transitions, internal conversion, energy depend. 78−94272
smear samples, simple and rapid meas. of α-rays using air luminesc. 80−106243
spectrometer for examining emission spectra of gas mixtures produced by α-particles 79−35852
superluminescence polarisation obs. of high-current pulsed discharge in gas with anisotropic gain 79−14515
p-terphenyl vapour, spectral, fluoresc., photochem. and laser props. 80−106344
vibrational relaxation rate meas. by delta *(Russian)* 77−68074
Ar, excitation by pulsed electric discharge, luminescence obs., time resolved spectra meas. 80−102482
Ar gas, high press., recombination luminescence in scintillation induced by alpha particles 78−50441
CO in Venus' atmosphere nighttime luminescence spectra 77−78702
CO_2, HF laser irrad., visible luminesc. 77−46593
CO_2 nighttime luminescence, Venera 9 and 10 spectroscopic obs. in Venus atmosphere 77−78701
CO_2-N_2, high temperature gas diagnostics by spectral remote sensing, 700-1350K 78−74002
Ca_2, new ground state, photolum. obs. vibr. consts., dissoc. energy 80−5576
Cl_2 partially dissociated, recomb. reaction freezing in supersonic nozzle, chemiluminescence *(Russian)* 77−52644
Cs-He, new absorption/emission bands perturbed Cs transitions assignment, pot. energy curves 78−66486
p-fluorobenzaldehyde, vap., high-resolution electronic emission spectrum assignments 78−78742
H, diffusion coeff., in H_2, luminesc. intensity meas. 80−103098
HBr, vibrationally excited, chem. prod. for CW laser using CW supersonic mixing HF chem. laser 80−1196
He^++acetylene-d_0($-d_2$), CH^+(CD^+), A-X luminesc., in near-thermal charge exchange 78−50632
$He(2^3S)+H_2O(H_2S)$, energy transfer processes, reaction products, UV and visible obs. in flowing afterglow 78−85138
$Hg_2(Hg_3)$, violet emission, formation and decay kinetics, luminesc. time resolved spectra 79−76464
$HgNH_3$*, excited complex photosensitised luminesc. and fluoresc. phase shifts 78−33535
NH_3, HF laser irrad., visible luminesc. 77−46593
NO, automatic meas., luminescence appls. *(Dutch)* 79−88041
NO concentration meas. in gas mixtures, chemiluminescence method *(Russian)* 79−16094
N_2O, electron impact excitation, ionisation, emission spectrum 77−50469
N_2O+N_2, vibroluminesc., V-V transfer consts., quadrupolar transition moment, IR spectra 79−10112
Na gas diffusion induced by resonance light field 80−53918
P_4, vap., oxidation, chemiluminesc., reduced press. system 77−32795
PbO, vapour, photoluminescent decay, a(1) state 78−58745
SF_6 gas, CO_2 TEA laser-excited, slow intermol. redistrib. of vibr. energy 80−53039
SO_2, automatic meas., luminescence appls. *(Dutch)* 79−88041
SiF_4, interaction with strong IR field, instantaneous luminescence 79−18232
Xe electroluminescence, electron resonance trapping, temp. effects 78−14130

luminescence of inorganic solids
actinolite, optical spectra obs. 77−40284
alkali aluminometaphosphate glass, $MPO_3.Al(PO_3)_3$:U (M=Li,Na,K), vibronic excitation, absorption and emission spectra 78−52524
alkali borate binary glass, energy storage behaviour studied by thermoluminesc. 80−50432
alkali chloride:Mn^{2+} luminesc. spectra and decay *(German)* 77−48234
alkali cyanides, mol. excitons, X-ray excited emission spectra obs. 80−66287
alkali earth halides, solid soln. spectroscopy, investigs. by F. Klement *(Russian)* 80−8767
alkali halide: monovalent cation, recomb. luminesc. (V_K+e)$_A$-type emission 77−28615
alkali halide: O^{2-}, photoluminesc. spectra, phonon using struct. *(Russian)* 78−2912
alkali halide: S_2^-, laser-excited spectra and reorientation of S_2^- 77−28563
alkali halide:Cu^+, absorpt., emission and lifetime data, temp. depend. 77−4671
alkali halide:Cu^+(Ag^+), high press. studies of luminesc. phenomena 79−43017
alkali halide:Cu^+(Ag^+), luminesc. spectra and lifetime, high-press. effects 78−35194
alkali halide:Eu^{2+} phosphor, explosive loading method form., spectra, luminesc. characts. *(Russian)* 78−35212
alkali halide:In, high press. studies of luminesc. phenomena 79−43017
alkali halide:O_2^-, frozen soln., impurity luminesc., zero-phonon lines interpretation 79−87488
alkali halide:Sn^{2+}, V_c^--centres, vacancy induced splitting of excited states, Sn^{2+} structure 78−51931
alkali halide:Sn, excited states producing polarised type A emission from Sn centres 78−10945
alkali halide:Tl^+-like ions, triplet state lifetime, hyperfine interaction 80−2844
alkali halide, activated, luminesc. and stored light sum 78−6738
alkali halide, activated crystal, absolute quantum yield of stored light sums *(Russian)* 79−56851
alkali halide, chalcogen^{2-} vacancy centres, absorpt. and fluoresc. spectra 78−48204
alkali halide, dynamics of nonrelaxed and self-trapped holes *(Russian)* 80−80607
alkali halide, F-centre, stabilisation process in first colouring stage 79−19246
alkali halide, molecular model for F_A(II)-centre emission process 77−28616
alkali halide, rel. between thermoluminescence and X-ray induced luminesc. 79−28830
alkali halide crystal, activator centres, excited state transitions, bleaching dynamics 79−4527
alkali halide crystals, activated, physical phenomena and optical data processing appl. *(Russian)* 80−80819

luminescence of inorganic solids continued
alkali halide crystals, deformation spectroscopy, dislocation interactions with electron and hole centres 78−10983
alkali halide crystals, X-ray irradiated, luminescence during release of pressure 79−65939
alkali halide crysts., photoemission on mech. stimulation, mechanism *(German)* 77−85819
alkali halide crysts., triboluminesc. spectra 80−66312
alkali halide F-centres, cation vacancy model, rot. mechanism 77−76393
alkali halide phosphors, Ag-doped, luminesc. rel. to formation of complex compounds *(Russian)* 80−11454
alkali halide phosphors, Pb^{2+}(Sm^{2+}) doped, luminesc. props., press. effects to 140 kbar 77−40278
alkali halide phosphors, Tl doped, press. effect on emission spectra at low temps. 77−85771
alkali halide salt solid solns., Stokes losses for crystalline vibr. in impurity O_2^- anions luminescence spectra *(Ukrainian)* 79−43012
alkali halide surface light emission, 10.6 μm laser pulse irradiation *(Russian)* 78−27352
alkali halides, colour centres and radiation-tunnel transition 79−4846
alkali halides, coloured, light amplification at activator centres 80−2795
alkali halides, cryst., optical emission following pulsed 10.6 μ irrad. 79−28847
alkali halides, emission band of F-centre 80−76071
alkali halides, emission spectra of O_2^- and NO_2^- centres at high hydrostatic press. 78−10943
alkali halides, ion-induced luminesc.c. effect of CN radical impurity 77−16402
alkali halides, irradiated, formation of Z centre 80−103326
alkali halides, luminesc. induced by ion impact, −160 to 200°C 77−8654
alkali halides, luminesc. polarisation and low-temp. photoinduced orientation change in O_2 and S_2 mol. centres 78−6735
alkali halides, luminescence excited by vacuum UV lasers 78−10941
alkali halides, luminescence of Tl^+-like centres, Ga^+-centre polaris. effect 79−33806
alkali halides, luminescence quenching by defects produced by electron irradiation *(French)* 77−26378
alkali halides, M-centre, lifetime data for excited state 78−35193
alkali halides, rare earth ion doped, optical props., review 79−15492
alkali halides, solid soln. spectroscopy, investigs. by F. Klement *(Russian)* 80−8767
alkali halides, spectra of O_2^-, S_2^- and NO_2^- mol. ions, electron-phonon interaction 77−52174
alkali halides, Z_1-centres, peculiarities of thermolum. 80−103999
alkali halides F-centre luminescence and lifetime, review 79−11442
alkali halides with NaCl structure, F-centre emission and relaxed excited state 79−42060
alkali hexahalogeno compounds: $ReCl_6^{2-}$($ReBr_6^{2-}$), low symm. splittings in vibronic spectrum due to phase transitions 80−55161
alkali iodides, free exciton reson. luminesc. lines 77−77272
alkali metal complex vanadates, $M^+_3M^{3+}(VO_4)_2$, $M^+_2M^{4+}(VO_4)_2$, M^{3+}=Sc, La, B, Al, Ga, In, M^{4+}=Ti, Zr, Sn, phosphors 77−48217
alkali metal halides, F-centre luminesc. rel. to cryst. chemical parameters 80−29780
alkali metal halides, X-ray induced colour centre and halogen aggregate form. 80−96565
alkali metal hexahalogenostannate: $ReBr_6^{2-}$, vibronic transition $\Gamma_7(^2T_{2g})\rightarrow\Gamma_8(^4A_{2g})$, intensity distrib. 80−45142
alkali metal metaphosphate glass:Nd^{3+}, luminesc. and lasing *(Russian)* 77−46724
alkali metal-rare earth oxides, $MLnO_2$, Ln=Y or Gd, synthesis and physicochem. props. 77−48216
alkali phosphate glass:Nd^{3+}, laser material evaluation 77−54715
alkali-alumino-phosphate:U, rontgenoluminesc. and fluoresc., radiative transitions obs. 80−103977
alkaline earth dimens., heteronuclear, matrix-isolated, laser photoluminesc., van der Waals ground state 79−41192
alkaline earth fluorides, F-centre annealing and intrinsic luminesc. 79−65937
alkaline earth fluorides, luminescence excited by vacuum UV lasers 78−10941
alkaline earth glasses, $45RO.5Al_2O_3.50P_2O_5$, (R=alkali earths), electron beam irrad., exam. of charge accumulation and light-sum kinetics 79−4336
alkaline earth glasses, RO-Al_2O_3, -P_2O_5, R=Mg, Ca, Sr, Ba, exam. of electron beam irradiation effects 79−4253
alkaline earth halides:Eu^{2+}, fluorescence lifetime and quantum efficiency for 5d→4f transitions 80−100681
alkaline earth halides, rare earth ion doped, optical props., review 79−15492
alkaline earth oxide:Cu phosphors, electroluminesc. 77−32440
alkaline earth oxide, photon multiplication and secondary electron-hole pairs generation *(Russian)* 80−66262
alkaline earth oxides, luminescence excited by vacuum UV lasers 78−10941
alkaline earth oxides and fluorides, F-centre luminesc. rel. to cryst. chemical parameters 80−29780
alkaline earth oxides photoluminescent spectra of surface states 79−47505
alkaline earth tetraborates, doped, radiothermoluminesc. detectors, dosimetric characts. 77−61665
aluminate:Ce^{3+}, hexagonal, luminesc. rel. to host lattice structure 78−6776
aluminate:Eu^{2+}, Mn^{2+}, efficiency of $Eu^{2+}\rightarrow Mn^{2+}$ energy transfer, struct. effects 77−8629
aluminate phosphors, energy transfer models 79−43019
aluminates:Ce^{3+}, luminesc. exam. 78−56513
aluminates:Mn, Eu, red Mn^{2+}-luminesc. 79−61420
aluminophosphate glass:Mn:Mg(Sr), optical props. H_2O effects 77−28600
amorphous semiconductor, defect chemistry and states in gap, models 79−38030
amorphous semiconductor, electronic properties and localised states, review 77−62871
amorphous semiconductors, doped, electronic props. 78−19030
amorphous semiconductors, photogeneration of charge carriers and recomb. 77−81147
amorphous semiconductors, photoluminesc. props. 79−56862
amorphous solids, electron-phonon interactions, fluoresc. line broadening and spectral diffusion 78−84655

luminescence of inorganic solids continued
anodic oxide films on Al, heat treatment effect on photoluminesc. props. 77−28610
anodic oxide films on Al, photoluminesc. obs. 77−1729
anomatic hydrocarbon high density excitation effects on fluoresc. 79−1782
anthracene, γ-irradiation influence on defects, luminesc. study *(Russian)* 80−55185
anthracene, single cryst. with photoinduced local centres, luminesc. 79−61433
anthracene film, effect of struct. on luminesc. quenching *(Russian)* 80−7411
antiferromagnetic garnet, absorpt. and luminesc. spectra, cryst. field and exchange interactions 77−73154
aqueous glass, γ-radiolysis, photolysis of trapped electrons, quasi-free electron IR absorpt., luminesc. 77−21401
aqueous glasses, mixed solute, luminesc. following laser excitation of trapped electrons 78−31666
biexciton luminescence, influence of free excitons on profile 77−4684
borate glass: $UO_2^{2+} \rightarrow Ho^{3+}$, energy transfer processes 78−10969
borate glass:Er^{3+}, $^4I_{13/2}$ level relax. 79−87476
caesium uranyl propionate, low temp. absorpt., luminesc. spectra, intermol. interactions 80−2830
calcium halophosphate, thermostimulated luminesc., mech. milling effects *(Russian)* 78−76537
calibo glass:Eu^{3+}, Ho^{3+}, energy transfer 78−76510
calibo glass:Eu, Br, quantum efficiency of non-radiative energy transfer 79−33832
CdS:Cu, V, photoluminescence spectra 79−83027
CdS, green edge luminescence spectrum, temp. depend. 80−108274
ceramic materials, thermoluminesc. dating, comparison of results 80−84791
chalcogenide glass, charged dangling bond model reassessment 77−72813
chalcogenide glasses, Luminescence, temp. depend. rel. to nonradiative transitions 80−71485
chalcogenide glasses, optical versus transport processes. 80−84449
chalcogenide glasses, radiative recomb. obs. as efficient luminesc. 78−2914
chalcogenide semiconductors, optical and elec. props., comparison with SiO_2 78−6721
chalcopyrites, for electrolum. device appl., props. and technology, book contrib. 77−73175
chamber calibration using ruby R_1 luminescence line shift, 80 to 550K 78−86284
charge transfer complex high density excitation effects on fluoresc. 79−1782
corundum, vac. UV luminesc. spectra *(Russian)* 77−24903
crystal luminescence, polariton mechanism, reabsorption, spatial dispersion effects, boundaries *(Russian)* 80−55186
cubic crystals, III-V and II-VI, luminesc. polarisation and hot-exciton orientation and decoupling 78−6733
decay curve recording of crystals and glasses, stroboscopic installation 77−74512
DH, nonequilib. carrier distrib., local excitation of active region, influence of diffusion of luminesc. 79−73574
1,4-di(triphenyl lead)diacetylene, phosphoresc. spectra, triplet state 79−47490
1,4-di(triphenyl tin)diacetylene, phosphoresc. spectra, triplet state 79−47490
diamond:B, thermoluminesc., TSC, correlation meas. 78−88369
diamond, dynamic Jahn-Teller distortions at trigonal optical centres 79−87069
diamond, electroluminescence, thermoluminesc., photocurrents 79−38675
p-diamond, electroluminescence 78−15229
diamond, frictional anisotropy, cathodoluminesc. study 80−35340
diamond, GR1 and UV band, fine struct. 80−20678
diamond, GR1 band, E to T state transitions coupled to e vibrs. 77−12430
diamond, GR defect, high resolution optical spectra after electron irrad. 78−56515
diamond, impurity centres, vibronic spectra, Van Hove singularities, quasi-local vibrs. 77−85782
diamond, ion implanted, p-i-n structure, double injection of carriers 79−11214
diamond, irradiated, optical study of TR12 and 3H defects 77−85772
diamond, Jahn-Teller coupling at neutral vacancy 80−71453
diamond, N9 and ND1 energy levels, electron irrad. photocond. obs., thermolum. 78−6324
diamond, natural, cathodoluminescence of defects *(French)* 80−34988
diamond, natural, defect struct., recent obs. by new methods 78−30628
diamond, natural, free exciton luminesc. line shape 80−40165
diamond, natural, N3 luminesc. decay time 78−76520
diamond, natural, subthreshold defect formation due to electron irrad., cathodoluminescence study *(Russian)* 80−45152
diamond, natural, thermoluminescence, phosphorescence, defects, low temp. 78−11000
diamond, natural type-IIb, single dislocations, cathodoluminescence obs. by STEM 80−80871
diamond, optical absorption and luminesc. spectra, review 80−2848
diamond, planar defects, in {100} planes, electron microscopy 77−11569
diamond, polarised cathodoluminescence in near IR, from platelet defects 77−48253
diamond, pseudo-Jahn-Teller effects in H3 vibronic spectrum 77−90182
diamond, semicond., energy band struct., elec. and optical props., review 77−35862
diamond, semiconducting, GR1 cathodoluminescence, fine struct. 78−68566
diamond, synthesis on nondiamond substrate, electron diffr. and luminesc. exam. 77−76344
diamond, synthetic, doped electroluminescence exam. 78−6783
diamond, synthetic, electroluminescence excitation mechanism, role of defects 78−52581
diamond, synthetic, external crystal morphology, SEM obs. 79−73078
diamond, synthetic semiconductor, IR spectroscopy and cathodoluminesc. *(Ukrainian)* 79−78758
diamond, van Hove singularities, absorpt. and luminesc. electronic-vibr. spectra 80−70639
diamond, vibronic bands at 2.498 eV (H4), 2.417 eV and 2.536 eV, absorpt. and luminesc. under stress 77−85758
diamond cathodoluminesc. at dislocations 79−47524

luminescence of inorganic solids continued
diamond crystal, deep centres, changes in Van Hove singularities in vibronic spectra 77−8645
diamonds, synthetic, polarised infra-red cathodoluminescence 80−89073
diamonds, topographically identifiable sources of cathodoluminescence 77−55836
direct gap semiconductors, exciton energy determ., electron beam excited luminesc. 79−38680
direct gap semiconductors, gain spectrum of electron-hole liquid 80−66279
direct semiconductor, exciton luminescence in longitudinal optical photon sideband, formation time 79−61438
dosimeter glass, radiophotoluminescence intensity change by intense laser light 80−89050
electroceramics, thermoluminescent and dosimetric characts. 79−8196
electroluminescence, principles and appls. 77−40288
electron-hole droplet reson. radiation, radiative decay of surface plasmons *(Russian)* 77−62841
electron-hole plasma condensation, in supersaturated gas of free excitons 77−69242
exciton condensation, light scatt. by electron-hole drops 80−84435
exoemission phenomena, TSC, thermionic emission, book contribution 80−80954
F centre luminescence polarisation, stress induced, temp. dependence 79−56857
F-centre electron levels, temp. depend. shift calcs. 77−28599
F-centres, struct., quantum optics, laser spectra 77−52147
feldspar, thermolum., anomalous fading, thermolum. dating 78−10999
ferroelectrics, O-octahedric, cathodlum. spectral and temp. depend. 78−84665
ferroelectrics, triboluminescence on piezo-electrification of surfaces during fracture 80−29815
fibreglass, mechanoluminescence during monoaxial stretching 78−68742
fluoride:Pr^{3+}(Tm^{3+}), photon-cascade emission quantum yield calc. 77−4669
fluoride, Mn^{4+} activated, configurational co-ordinate model, predictive use 79−19918
fluorides, thermoluminescent glow-peak shapes 77−28639
fluorophosphate glasses, rare-earth activated, luminesc., bonding 78−64415
fluorphlogopite, synthetic, luminesc. props. 78−19579
GaAs-$Ga_{1-x}Al_xAs$ DH crystals, <110> oriented dark line defects 77−80510
n-GaP, quasidirect radiative recombination of free holes at neutral shallow donors 78−64410
gelatin in nuclear photoemulsion, effect of pulsed elec. field on physical and mech. props. *(Russian)* 78−869
germanate glass: Tb^{3+}, luminesc. props. 79−33798
germanate glass:Bi^{3+}, time-resolved spectra, radiative and nonradiative processes 79−47501
germanate glass:Bi^{3+},Eu^{3+}, time resolved spectra for Bi-Eu energy transfer 79−33748
germanate glass:Nd^{3+}, spectral behaviour under narrow-line excitation 79−33747
GG GaS_e indirect exciton exam. 78−39029
glass:Eu^{3+}, spectroscopic props. of excited states of ions, laser induced fluorescence line narrowing meas. 79−38641
glass:Nd^{3+}, $^4I_{11/2}$ level population, absorpt. and relax. rate meas. 77−36290
glass:Nd^{3+}, ED-2 glass, spectral behaviour under narrow-line excitation 79−33747
glass:Nd^{3+}, ED-2 laser glass, transition probabilities and quantum efficiency 77−58330
glass:Nd^{3+}, line narrowed fluorescence spectra and site dependent transition probabilities 79−38640
glass:Nd^{3+}, spectral props. *(Chinese)* 80−60645
glass:Nd^{3+},Cr^{3+}, nonradiative energy transfer from Cr to Nd, optical pumping efficiency improvement 80−33001
glass:Nd, fluoresc. decay data from minicomputer-operated spectroscopy equipment 77−74526
glass:Nd, laser material, population inversion depend. on pump pulses 77−23679
glass:Nd laser materials, intensities of optical transitions 77−689
glass, ageing use, photothermal processing, sorptive and luminescence props. *(Polish)* 78−11250
glass, colour centre form. by UV irrad., afterglow, thermolum. and EPR obs. 78−10047
glass, coloured, for short wavelength cutoff filters, fluoresc. data 79−61411
glass, conduction and valence bands props., review 77−66106
glass, electron migration and spectral relax., random-walk model 80−80280
glass, fluorescence linewidth, anomalous of impurity ions, theory 80−50404
glass, rare-earth activated, polarised luminesc. 78−48224
glass with nonequivalent optical centres, decay rate averaging 79−8178
glasses:Nd^{3+}, energy transfer processes, radiative transitions *(Chinese)* 79−61431
glasses, elec., mag., and optical props., conference, Troy, NY, USA (Aug. 1979) 80−105417
glasses, non-radiative recombination at valence-alternation pairs 80−89048
graphite, and Raman scatt. 78−23460
halophosphate phosphors, radiation stability, recomb. processes effect *(Russian)* 80−7424
hexamethylolmelamine, doped, phosphoresc., crystallinity, cross-linking and H-bonding effects 79−73984
highly photoexcited semiconductors, picosec. luminesc. spectrosc. 79−47517
hot electron distribution functions, expts., review 78−27231
hot luminescence and relaxation processes in resonant secondary emission 78−52549
II-VI compounds, electron energy radiation damage threshold meas., EPR and luminesc. 77−84799
II-VI luminophore, broad fluoresc. bands, spectral distrib. of emission probability 77−8653
II-VI semiconductor:Co^{2+}, IR luminesc., local density of phonon states 79−33778
II-VI semiconductor, charged dislocation motion during plastic deform. 79−82233

luminescence of inorganic solids continued
II-VI semiconductor, resonant secondary emission spectra, relax. of energy and polarisation 80−93331
II-VI semiconductors, highly excited blend type involving free particle scatt. 79−38648
II-VI semiconductors, impurity and defect centre energy states, luminesc. meas., review 80−55150
II-VI semiconductors, injection electrolum., review, book contrib. 77−73174
II-VI semiconductors, radiation effects, optoelectric props. control 80−25458
III-V multilayer structure, as-grown, assessment of defects by differentiated cathodolum. topography 80−59819
III-V semiconductor, acceptor levels, anisotropy of Zeeman splitting and polarization of luminesc. in mag. field 79−24365
III-V semiconductors, electrolum. and related props., book contrib. 77−73173
III-V semiconductors, optical transitions, effect of perturbed k-selection and gap shrinkage 80−66257
III-V semiconductors, radiative recomb., optical evaluation review 80−60647
III-V semiconductors, radiative recomb. and related phenomena, conference, Prague, Czechoslovakia (Sept. 1979) 80−51940
III-V semiconductors epitaxial structures as wide-gap substrates, minority carrier diffusion length determ. by photoluminesc. 80−103992
inelastic biexciton-biexciton collision, effect on radiative recombination of biexcitons 79−15529
inert gas:Eu(Sm), absorpt. and emission spectra, phonon sidebands 79−43021
inert gas, solid, electron impact excited, exciton recomb. spectrum, temp. variation 78−48239
inert gas crystal, exciton-phonon interaction, absorption and luminesc. data *(Russian)* 77−62831
inert gas crystal, lattice vibrs. and radiative transitions of implanted ions *(Russian)* 80−69098
inert gas crystals, excitons exam. 78−51898
inert gas solid, electronic struct. of self-trapped excitons 79−19525
inert gas solid, VUV luminesc. from excitons 79−43020
inert gas solids, benzene doped, energy transfer processes, excitons, photoemission, luminescence spectra 77−69886
inert gas solids, luminesc., self-trapped exciton 79−38605
inhomogeneously broadened systems, spectral-spatial diffusion 77−77280
interstellar grains, luminesc. emission 79−8967
Invar, photon emission from sputtered atoms, obs. of apparent local thermodynamic equilib. in excitation 78−72672
ion-surface collisions, luminesc. accompanied by ion implantation 80−60683
ionic compounds, electron irrad., broad band radioluminesc. 77−32446
ionic crystal:transition metal, excitation and trapping at impurity sites 79−33776
ionic crystal, electron beam excited, luminesc. and cond. of nonideal degenerate electron-hole plasma 78−10488
ionic crystal, fundamental luminescence at high ionisation levels *(Russian)* 80−103985
ionic crystal containing self-localising excitons, cathodolum. 78−6785
ionic crystals, exposed to ultrasoft X-rays, thermal luminesc. and electron emission 79−8192
ionic crystals, luminesc. of free and self-trapped excitons 79−33757
IR absorpt. and luminesc. spectra 80−55079
junction current, luminesc. near dislocation, surface, integral representations, appl. to LED's 78−68079
KBr, γ-irradiated and additively coloured, chemiluminescence origin *(Russian)* 77−32453
laser diode, spontaneous emission linewidth, calcs. 77−10927
laser diode luminescence, heterostructure defect influence *(Russian)* 77−54712
lattice relaxation and time resolved polarization of emission from localized electron with level crossing 79−4840
leucosapphire, phosphorescence, decay obs., impurity effects *(Russian)* 79−15530
leucosapphire crystal, kinetics of radioluminescence flare-up *(Russian)* 77−12439
LiH, cubic, vibronic struct. and anisotropy of excitons, refl. and edge luminesc. spectra 78−23523
loess-formed quartz silt thermoluminescence and dating *(Chinese)* 78−57226
low voltage excitation materials *(Japanese)* 77−73169
lunar plagioclase, luminesc. cause and significance 77−60674
Lyman-α emission from proton bombard. of Si, Cu, Ge, Mo, Ta, Pt surfaces 79−91503
manganese minerals, photoluminesc., cryst. field theory *(Russian)* 78−84654
matrix isolated species, mag. circ. dichroism and mag. circularly polarised luminesc. 78−46379
metal, laser irradiated, optical and electronic emissions *(French)* 80−2919
metal, photon emission from inert gas-surface impact 78−11059
metal, surface plasmon light emission due to low energy electron irrad. 80−34997
metal, visible region emission associated with deformation and destruction *(Russian)* 77−12453
metal cathode, electrically stressed surface elec. phenomena, electrolum. and breakdown with medium gap spacings 80−20710
metal film, electroluminescence mechanism *(Russian)* 79−47523
metal film, luminescence, electron beam excited *(Russian)* 79−47526
metal oxide:U^{6+}, luminesc. sensitivity to vibrational fine structure 78−6772
metal oxides, mixed, luminesc., of U^{6+} 79−33765
metal surface, luminesc. due to equilib. excitation of electrons by laser radiation 80−7399
metallic cathodes, electroluminescent impurities causing vacuum breakdown, obs. 78−84660
metallic film, phonon fluorescence stimulated by laser radn. 79−87504
metals, luminescence of electron irrad. surfaces 79−65934
metaphosphate glass: Ag dosimeter, optical absorpt. and radiophotolum., effect of temp. 78−40333
metaphosphate glass: Nd^{3+}, Yb^{3+}, luminesc., energy transmission and migration between Nd^{3+} and Yb^{3+} 80−66297
metaphosphate glasses, $n(M_2O.P_2O_5).(1-x)Y_2O_3.xTb_2O_3.3P_2O_5$, M=Li, Na, K, excitation and emission spectra 80−40150
metaphosphate glasses with Ag activator, radiophotoluminesc. 79−38596
MIM cathode, local electron emission and electroluminescence patterns obs. 80−108327
mineralogy, appl. of cathodolum. microscopy and spectrometry 77−69919
minerals, physical theories for origin of colour 78−69323
minerals, thermoluminesc. dating, error sources 78−11006
minority carrier recombination at surfaces, dislocations and microdefects, luminesc. evaluation 78−6769
mixed fluoride crystals, nucl. radiation effects 80−80831
molybdates, alkaline earth, U activated, scheelite struct. luminesc. props. vibr. modes and quenching temp. 80−60651
neutron scintillating glasses activated by Ce^{3+}, luminesc. 79−38668
nitrate glass: Eu^{3+} struct. reorganisation in glass transition interval, polarised luminesc. obs. 80−45141
NMR under optical pumping conditions 80−25253
nonmetal, impurity optical absorption and emission, anharmonic effects 78−56503
nonuniform broadening profile, optical excitation migration effects 78−48215
obsidian, Lipari and Teotihuacan origin, Mossbauer, magnetisation, X-ray diffr. and fluoresc. study 80−46173
optical fibre, neutron and gamma induced transient absorpt. and luminesc. 80−58763
optical glass, luminescence spectra of Fe^{3+} ion *(Polish)* 79−69886
orthovanadates, rare earth activated, spectroscopic props. 77−16363
oxalic acid dihydrate, pulsed excitation of luminesc. 78−27326
oxide:U^{6+}, struct. sensitivity of luminesc. 77−90187
oxide glass:Cr^{3+} absorption and emission 78−6774
oxide glasses:Sm^{3+}, optical transitions 79−61430
oxide semiconductor crystals, with forbidden energy gap, review of spectroscopic props. 78−2876
oxides, excited states of F-centres 78−64006
p-n junction, luminesc. due to photoinduced injection 78−10939
p-n structure, variable-gap, current-voltage and spectral charact 79−7885
p-type epitaxial layer, thermalisation of electron-hole plasma, photolum. meas. 78−80408
p-type semiconductor with GaAs band struct., hot luminesc. 78−39601
Peierls dielectric, one dimensional, selftrapped excitations in Peierls-Frohlich state *(Russian)* 80−54678
phonon spectroscopy, phonon pulse spatial, spectral and temporal evolution 78−34580
phonon spectroscopy, phonon pulse spectral distrib. 78−34579
phosphate glass: Nd^{3+}, miniature laser with high ion conc., luminesc. characts. 80−19038
phosphate glass: UO_2^{+}, Sm^{3+}, energy transfer from UO_2^{+} to Sm^{3+} 79−78732
phosphate glass:Ce^{3+},Tm^{3+}(Tb^{3+}), temp. depend. of energy transfer $Ce^{3+}\rightarrow Tm^{3+}$, $Ce^{3+}\rightarrow Tb^{3+}$ 77−24882
phosphate glass:Nd^{3+}, giant laser pulse-induced luminesc., spectral shape temp. depend. *(Russian)* 77−19257
phosphate glass:Nd^{3+}, highly conc., electron energy deactivation and transfer *(Russian)* 80−29802
phosphate glass:Nd^{3+}, spectral behaviour under narrow-line excitation 79−33747
phosphate glass:Nd^{3+}(Yb^{3+}), nonresonance interaction parameters of rare earth ions, luminescence kinetics obs. *(Russian)* 78−31246
phosphate glass:Sb^{3+},Dy^{3+}, fluorescence and energy transfer obs. 78−6778
phosphate glass:Tb^{3+}, luminesc. props. 79−33798
phosphate glass:Tm^{3+}, eigenstates and radiative transition probabilities calcs. 77−77265
phosphate glass:Yb^{3+}, excitation migration in inhomogeneous line profile, energy gap depend. 80−7407
phosphate glass:Yb^{3+}, impurity centres, migration of excitations, math. modelling 78−48225
phosphate glass:Yb^{3+}, luminesc. band struct., chronoscopic study at 4.2K 80−60663
phosphate glass:Yb^{3+}, migration of electronic excitations, manifestation in reson. luminesc. 77−8642
phosphate glass, Nd^{3+} frequency selection by monochromatic laser excitation at resonant transition *(Russian)* 79−78747
phosphate glass Mn^{2+}, luminesc. colour change 80−7392
phosphate glasses, fading mechanisms 79−95851
phosphate laser glasses, review 80−9888
phosphor:Sm^{3+}(Eu^{3+}), rel. band intensities in luminesc. spectra *(Russian)* 77−48238
phosphor, EL-590 M type, electroluminesc. excitation by SAW, nonlinear effects 80−16104
phosphor model system, thermal quenching, QMSCC calcs. 79−78731
phosphors, cathodoluminesc. investig., appl. to cathode ray tube screening 80−108282
phosphors, thermoluminescence, UV dosimetry 80−853
photographic emulsion, luminescence rel. to latent image 80−73498
photographic emulsion microcrystals luminescence, effect of adsorbed Ag ions *(Russian)* 77−69912
photon emission from sputtered atoms, obs. of apparent local thermodynamic equilib. in excitation 78−72673
picosecond interactions, book contrib. 77−65057
plagioclase:Mn^{2+}(Fe^{3+}), ligand field bands of impurity luminesc. centres and their site occupancy 78−88350
plastic scintillators, specific luminescence, semi-empirical expression 77−57820
PMMA, X-ray irrad., thermoluminescence emission, exam. of kinetic order 79−43046
point defects in crystals, book 77−47442
polar semicond., impurity pseudopotential screening, absorption and emission energies 79−15121
polar semiconductor, electron-hole liquid, electron-phonon interactions 80−6739
polyethylene, thermoluminesc. spectrum *(German)* 78−76538
polymer, uniaxial, fluoresc. polarisation, orientation and mol. dynamics effects 78−76516
polypropylene; thermoluminesc. spectrum *(German)* 78−76538
polystyrene, thermoluminesc. spectrum *(German)* 78−76538
quartz:Cu, glassy and cryst., luminesc. centres 77−4679
quartz:Mn, X-ray and thermally stimulated luminesc. *(Russian)* 78−84626
quartz, alpha particle induced radiation defects, EPR and thermoluminescence study 80−20461

luminescence of inorganic solids continued
quartz, crystalline, thermolum. sensitivity, proton and gamma induced 77−90205
quartz, electron capture by impurity ions, cross sections eval. using thermolum. data 79−95855
quartz, luminescence centres at 396 and 280 nm 80−103996
quartz, natural, thermoluminesc. glow curves and spectral characts., γ-ray effects 78−2927
quartz, photoelectric and photoluminescent props. in fundamental absorpt. region 78−39596
quartz, thermally excited state relax., acoustic and EM pulse obs. *(Russian)* 77−40293
quartz, thermoluminesc., sensitivity, heat treatment effects 77−59622
quartz, thermoluminescence, superlinear accumulation of light sum *(Russian)* 79−52030
quartz, thermoluminescence output intensity depend. on γ- and ξ-irrad. temp. 77−59623
quartz, thermoluminescence sensitivity change due to stress 77−59627
quartz glasses of various grades, natural luminescence and lattice vacancies *(Russian)* 77−28625
rare earth activated phosphors, for low press. fluoresc. lamps, luminesc. characts. 78−10960
rare earth cobalticyanides, $R(Co(CN)_6)n.H_2O$, (R=La to Lu), optical spectra 78−39566
rare earth complexes, formation and props., book contrib. 80−43204
rare earth compound:Ho^{3+}(Er^{3+}) phosphors, active layer effective thickness calc. *(Russian)* 79−43039
rare earth compound, crystal field and Slater parameters and coordination 78−6771
rare earth double orthophosphates with alkali metals, conc. depend. of luminesc. props. 80−100673
rare earth double orthophosphates with alkali metals, spectroscopic obs., struct. and chem. nature 80−100674
rare earth gallium borates, high temperature crystallisation, composition, struct., props. 80−40253
rare earth garnets, cryst. field parameters for R^{3+} ions, exchange charge model 78−47747
rare earth germanates, R_2O_3-GeO_2 system cpds., physicochem. characts. 80−97469
rare earth laser materials, linear conc. quenching of luminesc. 79−31908
rare earth luminescence, relaxation phenomena, book contrib. 77−32439
rare earth niobates, pyrochlore structure, synthesis and props., 79−11533
rare earth niobates, with fergusonite struct., model of energy transfer processses 77−4670
rare earth orthovanadates:Eu^{3+}, ligand field parameters 78−2453
rare earth orthovanadates, covalency, chemical bonding and opt. spectra 77−80442
rare earth oxyhalides: Eu^{3+}, fluorescence spectra obs. *(French)* 80−89042
rare earth oxyhalides and oxysulphides, thermochromic luminescent mats. *(Russian)* 78−48230
rare earth oxymolybdates and oxytungstates, R_2MO_6, spectroscopic props. and crystallochem. laws 77−36215
rare earth oxysulphides:Eu^{3+}, luminescence decay 78−15214
rare earth oxysulphides, R_2O_2S:(Eu^{3+})(Tb^{3+})(Pr^{3+}), branching ratios for fluoresc. 79−33807
rare earth oxysulphides and oxyhalides, Tm^{3+}, Tb^{3+}, Eu^{3+} activated, thermochromatic luminophors, lumines. spectra rel. to temp. 79−56849
rare earth pentaphosphates:Ce^{3+},Tb^{3+}, energy transfer between dopants, excitation spectra, laser appls. 78−10961
rare earth phosphates:Eu^{3+}, vac. UV luminesc.-excitation spectra 77−85774
rare earth phosphates:Eu, electronic-vibr. spectra rel. to struct. 79−56850
rare earth stoichiometric cpds., reson. energy transfer 79−99930
rare earth tetracyanoplatinates, energy transfer from linear stacks of donors 78−68546
rare earth titanates, pseudoperovskite struct., nonlinear spectral and luminesc. characts. 80−29771
rare earth vitreous dielectric, electronic energy transfer to impurity OH^-, luminesc. kinetics *(Russian)* 79−47509
rare earths, trivalent, 5d states charge transfer and intershell spectra, separation and overlap 78−10966
rare gas, crystal, quasi-atomic and quasi-molelcular exciton states *(Russian)* 80−103628
rubidium uranyl propionate, low temp. absorpt., luminesc. spectra, intermol. interactions 80−2830
ruby:Cr^{3+}, diffusion of localised optical excitations and trap emission 77−24887
ruby:Cr, lifetimes of laser-induced population density gratings, comparison with fluoresc. lifetimes 79−64276
ruby, anisotropic 29 cm^{-1} phonon capture *(Russian)* 80−6471
ruby, Cr^{3+} ions excitation rel. to optical detect. of 10^{12} Hz acoustic phonons 77−36272
ruby, cryst., lasing action, spectrum, luminesc. spectrum effects *(Russian)* 78−13716
ruby, energy diffusion distance, upper limit within fluoresc. lifetime 80−29789
ruby, energy migration and transfer to N-line traps 79−83006
ruby, energy transfer time const. between single Cr^{3+} and Cr^{3+} pairs 79−38627
ruby, excited state spin-phonon interaction, time resolved spectroscopic exam. 78−19549
ruby, fluoresc. R-lines appl. to press. calibration, ambient and low temps. meas. 77−18106
ruby, fluoresc. spectrum, appl. to glass transit fluid press. determs. 77−26321
ruby, fluorescence line narrowing, energy transfer studies 78−84642
ruby, ground state of Cr(III) pai 79−33782
ruby, heat-pulse induced energy transfer, time-resolved optical spectroscopy 77−24456
ruby, high energy phonon spectroscopy 78−83893
ruby, implantation temperature meas. using impurity luminesc. 79−52012
ruby, induced absorpt., radioluminesc., thermoluminesc., Cr^{3+} conc. depend. *(Russian)* 77−90206
ruby, luminescence, absorption of R and N lines, effect of mag. field 80−60550
ruby, luminescence, red emission intensity at various temps., mag. field depend. 77−32423
luminescence of inorganic solids continued
ruby, nonequilibrium luminesc. of hot electrons, nonradiative transition probability 77−32436
ruby, optical energy storage and retrieval 77−73165
ruby, optical hole burning, Stark and pump-probe studies 80−48356
ruby, optical pumping, bottlenecked 29 cm^{-1} phonon spectral width 77−12425
ruby, optically excited, diffusion of bottlenecked 29 cm^{-1} phonons 80−6472
ruby, optically induced two-phonon processes connecting ^2E states 80−25443
ruby, phonon bottleneck effect, 29 cm^{-1} phonons 78−68562
ruby, phonon spectrum of high energy heat pulses generated in thin metal films 77−20140
ruby, phosphorescence, decay obs., impurity effects *(Russian)* 79−15530
ruby, piezo-spectroscopy of exchange coupled Cr^{3+} pairs 79−33783
ruby, quantum efficiency, photoacoustic meas. 80−73472
ruby, radiation-induced optical processes, impurity effects 80−66310
ruby, radiative spectral transfer, time resolved fluoresc. 78−2900
ruby, red thermoluminesc. *(Russian)* 79−56868
ruby, resonance radiation transfer and nonequilibrium phonons *(Russian)* 78−80418
ruby, resonantly trapped 29 cm^{-1} phonons, spectral diffusion 78−92113
ruby, spatial diffusion of weakly bottlenecked 29 cm^{-1} phonons, quasi-stationary techniques 79−73996
ruby, spin dependency of optical feeding into $\bar{E}(^2E)$ metastable doublet 79−28812
ruby laser, generation, amplification of high power picosecond pulses depend. on superluminescence 80−53305
ruby R_1 zero phonon line, resonance fluoresc. meas. 80−89055
sapphire, luminesc. of F centre 79−73990
sapphire, neutron bombard., F-centre fluorescence, photoluminescence 80−100676
sapphire, optical detection of acoustic phonons at THz freqs. 80−75320
sapphire, phosphorescence, decay obs., impurity effects *(Russian)* 79−15530
sapphire, pure and doped, luminesc. centres 79−33791
scintillating glasses, effects of temp. on pulse height and cond. 77−10547
secondary photon emission from sputtered excited neutrals, thermal excitation model anal. 79−4878
semiconductor, biexcitons, one-photon radiative recomb. 80−70621
semiconductor, bound excitons, review, book contrib. 80−44519
semiconductor, cathodoluminescence meas. of minority carrier lifetime, appl. to GaP 78−19572
semiconductor, direct band-gap, polariton emission spectrum, exciton kinetics influence 78−14676
semiconductor, direct-gap, oscillator strengths for electron-hole complexes (A^0X) 77−35869
semiconductor, due to exciton-electron scatt., calc. 77−16379
semiconductor, effect of surface space charge region 78−43939
semiconductor, electron-hole liquid, prod. and props. at low temp. 79−82527
semiconductor, ferroelectric props., paraelec. phase transition, cathodoluminesc. *(Russian)* 78−23535
semiconductor, high intensity photoexcitation, hot electrons and phonons 78−26905
semiconductor, highly excited states, ps spectroscopy 77−48245
semiconductor, jumps and sustained oscillations in polarisation in light oriented electron and nucl. spin systems *(Russian)* 77−85619
semiconductor, luminescence in presence of intense laser field 79−38621
semiconductor, non-radiative de-excitation of deep centres 79−38644
semiconductor, optical absorption and emission by impurities, phonon-electron interaction 78−56502
semiconductor, optical orientation of electrons, surface quality effects 79−11466
semiconductor, optical props. under intense laser fields 78−72513
semiconductor, p-type luminesc. parameters, reabsorpt. influence 79−95826
semiconductor, photo-excited electron momentum distrib., hot luminesc. polarisation 77−16396
semiconductor, photoexcitation phenomena, low density 78−27319
semiconductor, quenching of luminesc. by charged defects 78−23531
semiconductor, radiative spectra from hot photocarriers 78−31249
semiconductor, recomb.-enhanced defect reactions 77−51377
semiconductor, single-quantum radiative recomb. of biexcitons due to biexciton-exciton interactions 80−96793
semiconductor, STEM spectroscopic techniques for simultaneous electronic and defect obs. 80−100145
semiconductor, variable-gap, photoluminesc. 78−48222
semiconductor, wurtzite-type, emission lineshape of excitonic mols., polariton states 77−20918
semiconductor alloys, reson. light scatt., luminesc. and Raman spectra 79−38615
semiconductor electrode, electrolum. due to hole injection from electrolyte 77−20926
semiconductor film, electron spin orientation in quantum size effect conditions 78−68575
semiconductor layer structure, laser-induced photolum. and collective effects *(Russian)* 79−95830
semiconductor layers, direct gap, optical compensation profiling 77−76450
semiconductor structures, s-type switching at high current densities 77−20417
semiconductors, amorphous, luminescence 80−80862
semiconductors, electron beam or optically excited, quasi-equilib. approx. 80−84779
semiconductors, exciton and domain luminesc., book 80−82588
semiconductors, II-VI cpds., dislocation motion obs. by SEM in cathodolum. *(Japanese)* 79−46666
semiconductors, intervalley electron-electron scattering effect on optical transitions 80−108267
semiconductors, light absorption, amplification and luminescence, saturation effects *(Russian)* 78−13771
semiconductors, p-type, mag. oscills. of momentum distribution of hot photoexcited electrons *(Russian)* 80−2854
semiconductors, PH luminescence band profile 80−20702
semiconductors, photoluminescence in crossed electric and magnetic fields 79−11464
semiconductors, recombination processes, review 79−38088

luminescence of inorganic solids continued
semiconductors, resonant Raman scatt. from exciton-polaritons *(Japanese)* 80−50349
semiconductors, spin orientation by optical pumping, review 79−38410
semiconductors, thermally stimulated conductivity luminescence, defect levels, traps, book contribution 80−80296
semiconductors, thermally stimulated relaxation processes, book contribution 80−80295
β-SiC, optical quenching of luminesc., acceptor ionisation energy 80−55178
silica glass:Nd^{3+}, laser-spectroscopic method, for studying solids with nonuniform spectral broadening *(Russian)* 79−40630
silicate galss:Eu^{3+}, fluoresc. linewidth variation, electron-phonon coupling 78−19531
silicate glass: Cr^{3+}, optical props., 88-273K, energy levels in crossing region 78−6709
silicate glass: Er^{3+}, $^4I_{13/2}$ level relax. 79−87476
silicate glass:Tb^{3+}, photoluminesc. and optical absorption spectra 79−19919
single crysts. and thin films, absorpt. edge temp. depend., gap energy changes 79−42991
small-polaronic glass, dynamics of optically induced props. 80−49630
sodium uranyl acetate (deuteroacetate) 80−2830
sphalerite, hydrothermal single crysts., feasibility of optical methods for quality control 80−89065
spin-lattice relax. in triplet state of PO_2^- centres, pulsed photoexcitation 79−95644
steel, stainless, photon emission from sputtered atoms, obs. of apparent local thermodynamic equilib. in excitation 78−72672
steel, trace element UV emission, spectrochem. anal. *(French)* 80−71997
superionic conductors, transitions, structures, dynamics and spectra, review 79−60549
surface analysis, quantitative, using ion-induced secondary ion and photon emission 77−86423
tellurate perovskites, $M_2^{2+}Y^{2+}TeO_6$, M=Ba,Sr,Ca,Cd, Y=Ba,Sr,Ca,Cd,Zn,Mg, luminesc. on activation by Eu^{3+}, Tb^{3+}, Dy^{3+}, Er^{3+} 79−4838
tellurite glass:Nd^{3+}, spectral behaviour under narrow-line excitation 79−33747
tellurite glass:Tm^{3+}, eigenstates and radiative transition probabilities calcs. 77−77265
ternary metal oxides, DC electrolum. 77−77300
thermally stimulated luminescence application, radiation dosimetry, book contribution 80−80882
thermally stimulated relaxation in solids, transport phenomena, book 80−77553
thermoluminescence, supralinearity *(Japanese)* 78−31263
thermoluminescence, traps and emission centres 79−24373
thermoluminescent phosphors, thermolum. induced by 254 nm UV photons 80−55204
thin organic crystals, electrolum., detection and determ. of spatial distrib. 79−19937
transition metal complexes, excited states geometrical parameters, Franck-Condon anal. 77−27047
transparent dielectrics, with inclusions, laser-induced stresses 79−28012
tremolite, optical spectra obs. 77−40284
tungstate phosphors, thermoluminesc. and afterglows 79−38681
tungstates:Eu, electronic-vibr. spectra rel. to struct. 79−56850
tungstates, U activated, scheelite struct. luminesc. props. vibr. modes and quenching temp. 80−60651
tungstates, U-doped, perovskite struct., luminesc. quenching, QMSCC calcs. 80−71470
uniaxially compressed crystal, exciton molecule radiation *(Russian)* 80−108264
uranates, luminesc. 79−33765
uranyl complexes, fluoresc. state, rel. to electronic struct. *(Russian)* 78−5274
uranyl salts, cryst., multiphonon relax. 80−15208
ureilite meteorites, fluorescent accessory phases in carbonaceous matrix 79−40143
UV laser possible pumping by synchrotron radiation, NaCl:I(Br) luminesc. 78−66835
vacuum UV laser possibility for crystals pumped by X-ray synchrotron radiation 79−41387
vanadates, closed-shell tetroxo-complex triplet levels, luminesc. meas. 79−69874
variable gap semiconductor, photolum. emission and excitation spectra 78−76526
wide-gap semiconductors, distant donor-acceptor pairs, electroluminesc. effects 79−99944
zinc blende-type hosts, Co^{2+} impurities Huang-Rhys number rel. to props. of host lattice 79−83018
zircon, natural and synthetic crysts. Hf and Tb activated, capture centres and luminescence mechanism *(Russian)* 77−28626
ZnS:Mn,Cu, thin-film phosphors, LV DC electroluminescence 79−11472
Ag film, sputtering, photon emission enhancement compared with sputtering rate 79−78815
Ag, film and polycryst. samples, low energy electron irrad., visible and UV emission 78−2921
Ag halide, crystals and photographic emulsions, luminescence parameters at 77K 79−24787
Ag halide, visible luminescence obs. at or below 77K 80−108263
Ag halide emulsions, primitive and $AgNO_3$-digested, IR luminescence obs. at 77K 80−103983
Ag halide microcrystals, low-temp. triboluminescence 77−87861
Ag halide microcrystals, pulsed luminescence expts. 79−24786
Ag, implanted Li atoms, depth profiles and sputtering anal. by optical spectra 77−35579
Ag polycrystal, luminesc. spectra due to slow electron bombard. 78−10995
Ag, surface and volume plasmon light emission due to low energy electron scatt. 80−40177
Ag, surface plasmon light emission induced by fast electrons on modulated surface 78−80424
AgBr, Bose-Einstein condensation of triplet excitons 77−44057
AgBr, connection between the topography of luminescence centres and the latent image *(Russian)* 80−62785
AgBr, decay of proposed Bose-Einstein condensed excitons 78−15221
AgBr, EPR of excitons, detected in X-ray excited luminesc. spectra at 4K 77−55732

luminescence of inorganic solids continued
AgBr, electron simulation, luminescence and hidden image formation *(Russian)* 79−47515
AgBr, electron-hole liq. and biexciton pocket, luminesc. obs. 78−15216
AgBr, excitonic mol. recomb., photoluminesc. 77−8633
AgBr excitonic mols., time-resolved luminesc. line obs. 77−69888
AgBr film coatings, luminesc. props. for H_2 and other reduction sensitisation 79−61886
AgBr, highly excited, time resolved luminesc., recomb. of excitonic mols. 77−69889
AgBr, indirect near edge emission, 1.5-50K 77−16380
AgBr, luminesc. band shape of free excitons, at high exciton density, calc. 77−81148
AgBr luminescence/wavelength relationship visible and near IR spectra *(Russian)* 80−50422
AgBr microcrystals, spectrally sensitised, luminesc., effect of hydrophobic organic compounds 80−97331
AgBr, new shoulder in luminesc. spectra, triplet excitons 80−20706
AgBr, one-phonon sidebands, rel. to anal. of 4.4K neutron scatt. data 77−39643
AgBr, photoluminesc. study of excitons in high mag. fields 80−80843
AgBr, radiative recomb. of indirect excitons at high concs. 78−6732
AgBr, shoulder in luminesc. spectra due to triplet excitons 79−15525
AgBr, time resolved luminesc. spectra at high excitation density 79−78751
AgBr:Cl, exciton-phonon interaction, reson. Raman scatt. vs photolum. 80−29798
AgBr:$Cu^+(Cu^{2+})$, luminesc., ion interactions 77−66534
AgBr:I, activator luminesc., energy model 79−28808
AgBr:I, isoelectronic trap 79−43016
AgBr:I, refilling of recombination centres during thermal stimulation 78−10464
AgBr:I emulsion, photocond. and luminesc. at −186°C, rel. to incident light intensity 78−64063
AgBr:I^-, emission spectra at 4.2K 79−4841
AgBr(I) crystals, luminesc. of individual monocrystals *(Russian)* 80−301
AgBr(I) microcrystals, photocond. and luminesc. 78−26904
AgBrI microcrystals, luminescence spectra 79−19935
AgCl, and Br doped, EPR of excitons, detected in X-ray excited luminesc. spectra at 4K 77−55732
AgCl, cryst. luminesc. and photovoltaic effect kinetics 78−64391
AgCl, electron simulation, luminescence and hidden image formation *(Russian)* 79−47515
AgCl, luminesc. excited by UV radiation at 80K *(Russian)* 78−31256
AgCl, luminescence fatigue, adsorbed Ag atoms 80−66281
AgCl luminescence/wavelength relationship visible and near IR spectra *(Russian)* 80−50422
AgCl, optically detected EPR of excited states rel. to luminesc. 77−12256
AgCl, photoconductivity and photoluminesc., 6.8 to 80K, exciton and valence band states 77−43644
AgCl, single cryst., optical, acoustic and acousto-optical props. *(Czech)* 78−76417
AgCl, theory and measurement 79−19934
AgCl:$Cd^{2+}(Pb^{2+})(Mn^{2+})$, recombination processor, radioluminescence 78−2915
AgCl:$Cu^+(Cu^{2+})$, luminesc., ion interactions 77−66534
AgCl:Ni, optically detected double resonance, radiative recombination electron traps 80−20518
AgCl-AgI, mixed cryst., trap distrib., thermolum. 78−68568
$AgGaS_2$, electroluminesc., mechanism *(Russian)* 77−69918
AgGaSe, direct gap semicond., exciton energy at 300K from reabsorption of luminesc. 79−78728
$AgGaSe_2$, reabsorpt. of excitonic luminesc. in direct band gap semiconds. 77−63469
Ag_2HgI_4, preparation, optical and luminescence spectra 80−104064
AgI, connection between the topography of luminescence centres and the latent image *(Russian)* 80−62785
β-AgI, exciton luminesc. of 2H and 4H polytypes 77−85783
AgI large single crysts., gel and soln. growth and props. 80−35071
β-AgI, luminesc. of 2H- and 4H-polytypes 80−2843
Ag_2O, exciton luminesc. spectra, mag. field influence 80−80860
Ag_2S sols, red-IR photoluminescence obs. at 77K 80−103982
$AgUO_2(NO_3)_3$, fluoresc. decay rates, temp. depend. 80−25429
(Al,Ga)As DH lasers, superlinear emission characts., negative resist. obs. 80−95895
Al anodisation, 'flaw-free' film growth and luminesc. characterisation 78−15605
Al, anodisation, intensity of luminesc. and film thickness 78−80413
Al, Ar^+ ion bombard., photon and secondary ion emission, single cryst. struct. effect 77−59660
Al, continuous UV emission under inert gas ion bombard. 78−84664
Al electrochemical electrode, oxide film growth accompanied by luminesc. 79−57236
Al, galvanoluminescence during anodisation in non-dissolving electrolytes 79−52680
Al, galvanostatic anodising of high purity samples, galvanolum. obs. 77−90488
Al, galvanostatic anodising of high purity sheet, galvanolum. obs., cryst. orientation effect 77−90489
Al, implanted Li atoms, depth profiles and sputtering anal. by optical spectra 77−35579
Al, ion bombarded, photon and ion emission, simultaneous meas. 78−15276
Al, oxide covered, tensile deform. in high vac., particle and photon emission 78−39672
Al-Al_2O_3:Mn-electrolyte, yellow electrolum. during anodisation of Al-Mn (1 wt.%) 77−63464
Al-Al_2O_3-electrolyte, electroluminesc., nondestructive electronic avalanche 78−68563
Al-Mg-Zn, O_2^+ ion bombard., SIMS and photon emission spectra, local thermodynamic equilib. model 80−20751
Al-Mn, anodisation, intensity of luminesc. and film thickness 78−80413
Al-oxide-electrolyte system, luminesc. spectra *(Russian)* 78−76539
Al-SiO_2-Au, thin layer struct., electroluminesc. *(French)* 78−76531
AlAs-GaAs, heterostructure electroluminesc. characts., active region electron density depend. 77−12446
AlAs-GaAs monolayer crystal, two-photon absorpt. spectrum 78−52589
AlAs-GaAs multipass heterostructure, spectral and ang. charact. of luminesc. 77−20418

luminescence of inorganic solids continued
AlAs-GaAs multipass heterostructures, external quantum efficiency of luminesc. 77−20419
AlAs-GaAs:Ge double heterojunctions, efficiency of radiative recombination 77−77286
AlF_3, localised electronic levels, thermoluminesc. and thermally stimulated current exam. 78−11001
(AlGa)As DH, proton-striped, proton-induced defects, photoluminesc. study 80−48251
AlGaAs DH, temp. depend. of intensities and times of radiative transitions 79−38660
AlGaAs DH stripe geometry lasers, spontaneous radiation, carrier conc., and threshold current, luminesc. meas. 79−36898
AlGaAs electroluminescent heterostructures, LPE, appl. to LED fabrication 80−55308
AlGaAs heterojunctions, nonradiative recomb. vel. estimate from edge luminesc. props. 80−65668
AlGaAs heterojunction photocell with luminesc. wavelength converter 80−108800
(AlGa)As heterostruct., proton irrad., photoluminesc. 80−29808
AlGaAs, LPE layers, growth initiation and cathodoluminesc. irregularities 79−87010
AlGaAs layer, epitaxial, grown from pre-heated Ga soln., photolum. study 78−39591
p- (AlGa)As:Zn, MBE grown, elec. props., shallow junction solar cell use 79−91175
AlGaAs-GaAs heteroepitaxial wafers, Mg doping, surface morphology and photoluminesc. props. laser applics. 77−3591
AlGaAs-GaAs heterostructures, luminescent characts., efficiency and radiative lifetime conc. depend. 80−55151
$Al_xGa_{1-x}As$ DH, origin of $n \simeq 2$ injection current, photolum. expts. 78−14799
$Al_xGa_{1-x}As$ DH lasers, deep-level luminesc. 79−65913
$Al_xGa_{1-x}As$ DH p-n junction, surface recomb. effects on current, luminesc. expts. 78−72246
p-$Al_xGa_{1-x}As$, DH under optical orientation conditions, diffusion of spin labelled electrons 77−8189
n-$Al_xGa_{1-x}As$, epitaxial, photolum. emission and excitation spectra 78−76526
$Al_xGa_{1-x}As$ epitaxial diode, neutron and γ-irrad. effects on cathodolum. in SEM 79−11473
$Al_xGa_{1-x}As$ film, hot photoluminescence spectrum, polarisation depend. 78−31254
$Al_xGa_{1-x}As$ grown by organometallic VPE, luminesc. efficiency 79−78892
$Al_xGa_{1-x}As$, hetero junction light-emitting diode, construction and performance characts. *(Russian)* 77−85808
$Al_xGa_{1-x}As$, indirect, exciton-phonon coupling, photolum. meas. 79−47511
n-$Al_xGa_{1-x}As$, ion implanted films, optical and luminesc. props. 80−60699
$Al_xGa_{1-x}As$, LPE, cathodoluminesc. obs. 78−68565
$Al_xGa_{1-x}As$ MBE layers, ionized beam doping, elec. and optical characts. 79−37721
$Al_xGa_{1-x}As$, optically magnetised, luminescence polarisation anisotropy, hysteresis effect symmetry props. 80−34982
$Al_xGa_{1-x}As$, organometallic VPE growth, and characterisation 79−78899
$Al_xGa_{1-x}As$, p-n homojunction, hot carrier recomb., overheating luminesc. 78−92122
$Al_xGa_{1-x}As$, pure and Ge doped, shallow acceptor photoluminescence 80−76064
$Al_xGa_{1-x}As$, solid soln., synthesis by ion implantation Al^+ ions 78−38741
$Al_xGa_{1-x}As$, VPE growth and characterisation 78−35315
n-$Al_xGa_{1-x}As$, variable-gap solid solns., diffusion length, photolum. meas. 79−38659
p-$Al_xGa_{1-x}As$:Be layer, MBE growth, Be doping and diffusion, elec. and optical props. 77−51397
$Al_xGa_{1-x}As$:Cr, deep level props. 79−69465
$Al_xGa_{1-x}As$:Cr, exptl. verification of Cr^{2+} models of photoluminescent transitions 78−27320
$Al_xGa_{1-x}As$:Cr, high resist. film, photolum. and photocond. meas. 78−72596
$Al_xGa_{1-x}As$:Cu, variable-gap semicond., impurity props., carrier recomb. 80−96907
$Al_xGa_{1-x}As$:Ge(Te)(Zn), photo- and cathodolum., comp. depend. *(Russian)* 77−48215
$Al_xGa_{1-x}As$:N, ion implantation, in situ annealing photoluminesc. obs. 80−10567
$Al_xGa_{1-x}As$:N, luminescent material, appl. in optically pumped lasers and electrolum. diodes *(Japanese)* 77−44069
$Al_xGa_{1-x}As$:N, photolum. excitation spectra 77−63451
$Al_xGa_{1-x}As$:N, photoluminesc. and optical absorpt. spectra of N impurity bound-excitons 79−47496
$Al_xGa_{1-x}As$:N^+, (x=0.58), laser annealing of optically active impurities, photolum. charact. 80−20682
$Al_xGa_{1-x}As$:O-n-GaAs heterojunction for MIS device, capacitance voltage meas. 79−87157
$Al_xGa_{1-x}As$:Sn(Te)(Ge), anneal-induced defects, photoluminesc. obs. 79−61422
$Al_xGa_{1-x}As$-GaAs heterostructure, effect of photon recycling on diffusion length and internal quantum efficiency 77−39929
$Al_xGa_{1-x}As$-GaAs heterostructure photoluminesc., origin of large dark spots 77−85763
$Al_xGa_{1-x}As$-GaAs heterostructures, nonradiative large dark spots exam. 78−23149
$Al_xGa_{1-x}As$-GaAs heterostruct., varizonal, parameter determ. by photoluminescence method *(Russian)* 80−108291
$Al_xGa_{1-x}As$-GaAs quantum-well heterostruct., exciton in recomb. 80−103990
p-$Al_xGa_{1-x}As$-n-GaAs heterojunction solar cells, optical characts. study 77−24609
$Al_yGa_{1-y}As_{1-x}Sb_x$ heterostructure, electroluminesc., appl. to LED's 77−8663
$Al_xGa_{1-x}N$ epitaxial layers, growth and props. 79−11522
$Al_{2x}Ga_{2(1-x)}O_3:Cr^{3+}$, luminesc., lifetime, 77 and 4K, struct., energy transfer 79−28798
$Al_{2x}Ga_{2(1-x)}O_3:Cr^{3+}$, luminesc., lifetimes 79−33784
$Al_xGa_{1-x}P$, LPE, crystallographic obs. and electrolum. 80−88445
luminescence of inorganic solids continued
$Al_xGa_{1-x}P$, photoluminescence excitation spectra, bound excitons, Al conc. depend. 80−20687
$Al_xGa_{1-x}P$(:Zn), solution-grown single crysts., photo- and electrolum. at 77K 79−52004
AlGaSb, growth and characts. for 1.0-1.8 μm heterojunction devices 78−6870
p-$Al_xGa_{1-x}Sb$ epitaxial layers, cathodoluminescence. investig. for varying x *(Russian)* 77−20931
$Al_xGa_{1-x}Sb$, LED, 1.54 μm efficient emission at 300K reproducible fabrication 79−42636
$Al_xGa_{1-x}Sb$, photolum. intensity increase due to composition variation 79 15528
$Al_xGa_{1-x}Sb$, solid soln., depend. of forbidden-band width on composition 78−39602
$Al_xGa_{1-x}Sb$ solid solns., freq. dependences of form of luminesc. spectra 80−40160
$Al_xGa_{1-x}Sb$, soln.-grown, photolum. 80−71476
AlGaSbAs heterostructures and LED's luminesc. props. in 1-2 micron band 78−10988
$Al_xGe_{1-x}Sb$, photolum. spectra 78−95602
AlN, epitaxial film growth by MBE, physical and optical props. 80−2293
AlN, excitation, luminescence, reflection spectra in fund. absorpt. region 78−10956
AlN film on Si and Ge, growth, struct. and props. 77−55468
AlN, impurity-doped film, cathodoluminescence spectra 79−83038
AlN, luminesc. excitation spectrum and band struct. 80−84783
AlN:Mn, vol. and surface excited luminesc. 79−38630
AlN:Mn(Eu), luminescence at high excitation levels with and without doping 77−1721
AlN:O, influence of O on luminesc. excitation spectrum in interband transition range 77−8644
AlN:O, thermolum. mechanism, 80-420K 79−78761
AlN:O, UV spectra of deep impurity centres, radiative recombination 79−87490
$AlNbO_4$, diffuse refl. and luminesc. spectra 78−56516
α-Al_2O_3, additively coloured single crystal, luminescence *(Russian)* 80−55169
Al_2O_3 and double oxides, photon multiplication and secondary electron-hole pairs generation *(Russian)* 80−66262
Al_2O_3 anode film, galvanoluminesc. during pulsed excitation 79−74006
Al_2O_3, anodic oxide films, luminesc., breakdown and colouring 78−19528
Al_2O_3, cathodic luminesc. of oxide covering on Al electrode in electrolyte soln. 77−69915
α-Al_2O_3, complex glow spectra, improvement of fractional glow technique, thermally stimulated exoelectron emission 79−65984
α-Al_2O_3, crystal defects from X-ray irradiation, F-centres, X-ray luminesc. obs. 80−55176
α-Al_2O_3, defects in unirradiated cryst., optical absorpt. spectra 79−61409
Al_2O_3 film, anodic, luminesc. during growth on high purity Al 77−48589
Al_2O_3, γ-irrad., hole centres, luminesc. and EPR obs. 77−32256
Al_2O_3, optical props. of F-centre 79−43003
α-Al_2O_3, polarised luminescence in neutron- and proton-irradiated single crystals 80−66271
α-Al_2O_3 recombination luminescence excitation by synchrotron radiation 79−95841
α-Al_2O_3, recombination luminescence mechanism 80−71477
Al_2O_3, sintered, residual stress meas., piezospectroscopic technique 78−52704
Al_2O_3 TLD phosphor for gamma-rays 77−6637
Al_2O_3, thermoluminescence, in H_2O vap. atm., temp. depend., time decay *(Russian)* 77−44074
Al_2O_3, thermoluminescence, effect of heat treatment following gamma irradiation 77−59624
Al_2O_3, thermoluminescence, optical bleaching/stimulation effects following irrad. 78−43940
Al_2O_3, UV dosimetry grade, thermolum. glow curves and emission spectra, 90-500K 78−72615
Al_2O_3:Cr photoexcited crystals, cooperative thermoluminescence quenching *(Russian)* 80−80881
$Al_2O_3:Cr^{3+}$, ruby, reson. scatt. and trapping of 29 cm^{-1} acoustic phonons 80−93403
α-Al_2O_3:Er(Cr), crystal defects from X-ray irradiation, F-centres, X-ray luminesc. obs. 80−55176
Al_2O_3:Eu, surface luminesc. centres excitation characts. 78−52560
Al_2O_3:Mg, pure and doped, recombination luminesc. spectra 79−83021
β-Al_2O_3:Mn(Co)(Ni), absorpt. and emission spectra, mag. susceptibility 79−87471
Al_2O_3:Ni, γ-irrad., thermoluminesc. 78−2925
Al_2O_3:Si, Ti, pure and doped, luminescence, optical absorpt. and colour centres 79−87501
Al_2O_3:Si,Ti photostimulated thermolum., and appl. to UV dosimetry 78−53511
Al_2O_3:Si thermoluminescent phosphor, annealing characts. and nature of traps 77−85817
α-$Al_2O_3:V^{3+}$, near IR spectra, line lifetime, 2, 10, 77K 78−10972
α-$Al_2O_3:V^{4+}$, emission spectrum, Jahn-Teller effect in $^2T_{2g}$ and ^2E_g states 79−83007
Al_2O_3-$La_2O_3:Eu^{3+}$ system, optical and struct. exam. 77−4674
β-Al_2O_3-Na_2O:Cr, absorpt. and emission spectra, mag. susceptibility 79−15495
β-Al_2O_3-Na_2O:Fe, coordination site, oxidation state, Mossbauer, absorpt., emission spectra, mag. susceptibility meas. 78−68431
Al_2O_3-$P_2O_5:Nd^{3+}$ glass, high Nd conc., spectroscopy and lasing obs. 78−46609
Al_2O_3-SiO_2 glass ceramic, surface streaks and blisters, UV fluoresc. study 80−84347
$AlPO_4:Fe^{3+}$, luminesc. emission and excitation spectra 79−69873
$3Al_2S_3$.$La_2S_3:Ho^{3+}$, radiative and multiphonon relax. 79−33794
$Al_2SiO_4F_2$, topaz, thermolum. props., dosimeter appl. 78−35957
$Al_2TeO_6:U^{6+}$, luminesc. spectrum 79−56845
$AlVO_4$, luminesc. spectrum 79−56846
$Al_2(WO_4)_3$:Cr(Eu), and undoped crystals, luminesc. obs. 80−89047
Ar, condensed, luminescence decay under α- and β-particle excitation 79−38678
Ar, cryst., luminesc., absorpt. spectra, free, self-localised excitons coexistence *(Russian)* 78−31231

luminescence of inorganic solids continued
Ar, liquid and solid, absorpt. and luminesc. spectra of self-trapped excitons 79−65893
Ar, optical absorpt. and luminesc. spectra, obs. of relaxed exciton states 77−52082
Ar:Eu, matrix isolated, obs. of Stokes and anti-Stokes vibrational sidebands in emission spectra 77−73164
Ar:$O_2(N_2)$, long-wave UV luminesc. *(Russian)* 78−88347
ArO, in doped inert gas matrix, photoluminesc. 79−31579
As chalcogenides, deep levels, photoluminesc. and photocond. 80−70641
As, photoluminescence, bulk and sputtered thin films 80−25457
As-Se glasses, low temp. photocond., complementary nature of photocond. and photolum. 80−49808
As_2S_3, amorphous, band to band radiative recomb. 80−25435
As_2S_3, amorphous, band-to-band luminesc., electronic band states 79−61432
As_2S_3, amorphous, charged defect pair photolum. meas. 80−16078
As_2S_3, amorphous, luminesc. and optically detected ESR, photoinduced struct. change 80−50399
As_2S_3, amorphous, quantum efficiency and fatiguing behaviour of luminesc. processes 80−7402
As_2S_3, amorphous, time resolved spectroscopy of valence alternation pair luminesc. 80−50400
As_2S_3, amorphous, time resolved luminesc. 80−66288
As_2S_3, amorphous, time-resolved photolum., spectrosc. 79−24360
a-As_2S_3, luminescence with short decay time 78−2906
a-As_2S_3, time-resolved photoluminescence study 80−89057
As_2S_3:Ag, vitreous, doping influence on photolum. at 77K 77−77293
As_2S_3:B glass, impurity effect on photoluminesc. and optically induced EPR 79−65918
As_2S_3:Fe glass, photolum. and ESR, Fe impurities as non-radiative recomb. centres 80−29788
As_2S_5, amorphous, struct., vibr. and electronic spectra 80−64908
$As_2S_3(Se_3)$, X-ray induced paramag. states and luminesc. 78−95520
As_2Se_3, amorphous, defect states, exptl. study. 80−54645
As_2Se_3, amorphous radiative interband recombination 80−66286
a-As_2Se_3, doped film, photoluminescence intensity and lineshape study 80−50448
As_2Se_3 glasses, impurity effect on photoluminesc. and optically induced EPR 79−65918
a-As_2Se_3, luminescence with short decay time 78−2906
As_2Se_3, neutrality of luminescence centres 78−88356
As_2Se_3:In, amorphous, photoluminesc. fatigue, metallic additive effect 79−61434
As_2Se_3:Tl, hole transport, photoluminesc. and photoinduced ESR 79−8183
$As_{50}Se_{50}$ and $As_{20}Se_{80}$ semicond. glasses, densified, photoluminesc., inelastic deform. effect 80−66293
Au discontinuous film, electroluminescence obs. 80−103998
Au film, electron emission and electroluminesc. 77−90257
Au, film and polycryst. samples, low energy electron irrad., visible and UV emission 78−2921
Au, ion bombardment-induced photon emission as function of target temp. 80−100698
Au polycrystal, luminesc. spectra due to slow electron bombard. 78−10995
Au-ZnO-In metal-semicond. diode, electrolum. spectra 79−99948
AuBr, spectra and luminesc., 100 to 200K *(Russian)* 77−69911
$AuBr_3$, spectra and luminesc., 100 to 300K *(Russian)* 77−69911
AuCl, luminesc., excitons 80−2839
α-Al_2O_3, thermoluminescent trap stability, 450 to 1400°C 79−24372
BCl_3, visible fluoresc., IR laser induced, acousto-optical effects *(Chinese)* 79−78733
BH_x, photoluminesc. spectra 80−2815
BN external crystal morphology, SEM obs. 79−73078
BN, phosphided, spectra of products 77−12418
B_2O_3 glasses, thermolum., additives effect 78−27337
B_2O_3-SiO_2:Ce glasses, radiation resistance mechanism, optical absorpt. and luminesc. obs. *(Polish)* 79−86825
BP, cryst. growth from Cu-fluxed melt, and characterisation 77−85920
Ba luminate:Eu, effect of non-stoichiometry on luminesc. 78−68550
$BaAl_{12}O_{19}$:Mn, phosphor, vac. UV excitation spectra, appl. to gas discharge display 80−2816
$BaBr_2$:Sm^{2+}, radiationless coupling, $4f^5$5d band effects, spectra 77−8627
$BaBr_2$:Sm^{2+}, spectra, ^5D states, Lauer-Fong formula and SCC model 79−15513
$BaCaLu_2F_{10}$, site occupancy from excitation and emission spectra *(French)* 77−81145
$Ba_{15}Ca_{27-x}Nd_xAl_{31}Be_{27}F_{231+x}$, $0 \leq x < 8$, optical props. and vitreous domain 79−65820
$Ba_2CaTe_{1-x}W_xO_6$, tungstate luminescence 77−69904
Ba_2CaUO_6, luminescence and energy migration 79−4837
$BaCl_2$, Sn-activated, luminescence studies 80−108246
$BaCl_2$:Pb, absorption and emission spectra *(Russian)* 78−23527
$BaCl_2$:Pb crystal phosphor, emission spectra 80−66298
$BaCl_2$:Sm^{2+}, radiationless coupling, $4f^5$5d band effects, spectra 77−8627
$BaCl_2$:Sm^{2+}, spectra, ^5D states, Lauer-Fong formula and SCC model 79−15513
BaClF:Sm^{2+}, energy levels, optical props. 78−84631
BaClF:Sm^{2+}, radiative and radiationless transition rate meas. using tunable pulsed dye laser 77−24891
BaF_2, barrier instability in strong elec. fields 79−69522
BaF_2, thermoluminesc. and F-centre annealing, after neutron irrad. 80−7422
BaF_2:Cm(Bk), fluorite-struct., self-luminesc. 78−27309
BaF_2:Er^{3+}, fluoresc., importance of defect clustering 79−33827
BaF_2:Er^{3+}, fluoresc. spectra of charge compensated cryst., multiphonon and energy transfer relax. 79−87496
BaF_2:Er^{3+}, single-site multiphonon and energy transfer relax. 78−52547
BaF_2:Gd^{3+} film, Gd^{3+} luminesc. spectrum and kinetics 78−6763
BaF_2:Pb^{2+}, band struct., Jahn-Teller effect, UV luminesc. and optical absorpt. spectra 80−66243
BaF_2:Sm^{2+}(Tm^{2+}), vibronic spectra and dynamics of impurity-contaiing lattice 79−1787
BaF_2:Tb^{3+}, cubic Tb^{3+} centres, energy level and cryst. field parameters 77−52181
BaFBr, X- and γ-irrad., thermolum. and optical absorpt. spectra 79−95857
BaFCl crystals, F-centres, X- and γ-irradiation, thermoluminescence and optical absorption spectra 80−45155
BaFCl, luminesc. and ionic conduction 79−28829
luminescence of inorganic solids continued
$BaGd_4Si_5O_{17}$, cell consts., luminesc. of various rare-earth activators 80−93376
$Ba_{1-x}Mg_xSO_4$:Eu^{3+} phosphor, thermolum. charact. 77−90203
$BaMnF_4$, luminesc., emission from localised traps 79−33777
$BaMoO_4$, luminesc. props. 80−11459
$Ba_2NaNb_5O_{15}$, ferroelec. phase, thermally stimulated light flashes, surface elec. props. effects 79−73885
$Ba_2NaNb_5O_{15}$, ferroelectric, local states, thermoluminesc. study 80−60690
$BaNd_2(MoO_4)_4$, luminescence spectra 80−84161
BaO-B_2O_3 glass, Mn^{2+}→Nd^{3+} energy transfer, fluoresc. obs. 77−8621
BaO-B_2O_3: UO_2^{2+}, Eu^{3+} glass, nonradiative energy transfer 77−59602
BaO-B_2O_3:UO_2^{2+}, Nd^{3+} glass, radiative and nonradiative energy transfer 78−60508
BaO-B_2O_3:UO_2^{2+}→Er^{3+} glass, energy transfer 78−2895
BaO-Nd_2O_3-P_2O_5 ultraphosphate glasses, Nd^{3+} conc. quenching of luminesc. effect 79−19931
BaO-P_2O_5 glasses, Cu^+ ion electromigration at 400°C, luminesc. meas. 77−76610
BaO-P_2O_5(SiO_2) glasses, Nd^{3+} luminesc. quenching by transition metal and rare earth ions 80−25449
$Ba_3(PO_4)_2$ phosphor, ionisation of capture centres, thermolum. spectra 80−11487
$Ba_3(PO_4)_2$, recomb. luminesc. mechanisms 80−2874
$Ba_3(PO_4)_2$:Eu, X-ray phosphor, study of emission and trapping centres 79−8197
BaR_2O_4, luminesc. on activation by Eu^{3+}, Nd^{3+}, Eu^{3+}-Tb^{3+} 77−52156
BaS:Bi phosphors, polycrystalline, effect of grain size on thermolum. 79−61446
BaS:Cu, thermoluminesc. and decay 78−80426
BaS:Cu phosphor, photo- and electro-luminescence 79−43030
BaS-CaS:Cu phosphors, X-ray diffr. and fluoresc. spectra 80−40148
$BaSO_4$, barytes, with large magnitude of emitted light, thermolum. curves 78−88368
$BaSO_4$, natural barite, thermoluminesc. glow curves after γ-ray irrad., low doses 77−63471
$BaSO_4$ natural barites, mech. of thermolum. 79−78763
$BaSO_4$, with small retrapping factor, thermolum. glow curve 77−52188
$Ba_3SiAl_{10}O_{20}$, Ce^{3+} activated, X-ray diffr. and luminesc. props. 80−49199
$Ba_5SiO_4Br_6$:Eu, blue emitting X-ray luminescent material for intensifying screens *(French)* 80−66260
$BaTiO_3$ ceramics, grain boundary pot. barriers, cathodoluminesc., electron probe anal. 80−2864
$BaTiO_3$, intrinsic luminesc. 80−71467
$BaTiO_3$, light emission during repolarisation 77−36299
$BaTiO_3$, pure and Fe doped, X-ray induced luminesc. 79−69885
$BaTiO_3$, pure and Fe doped, ferroelec., switching and electrolum. 80−76079
$BaTiO_3$, single cryst., dielec. breakdown and electroluminesc. 78−2917
$BaTi(PO_4)_2$, cryst., luminesc., struct. interpretation 79−47489
$Ba_2TiSi_2O_8$, luminescence of TiO_5 group, decay time, IR and Raman spectrosc. 80−2819
$BaWO_4$ crystals, X-irradiated, EPR, TSC and thermoluminescence spectra meas. 79−1791
$BaWO_4$, single cryst. growth by Czochralski method and U incorporation, effective distrib. ratios, luminesc. charact. 79−42094
$BaWO_4$:Mo, P, thermoluminesc. traps, EPR meas. 77−90032
BaY_2F_8, energy transfer from Eu^{2+} to trivalent rare earth ion 79−91490
$BaY_4Si_5O_{17}$, cell consts., luminesc. of various rare-earth activators 80−93376
Ba_2ZnS_3:Mn, luminescent props. 77−77292
$BaZrO_3$, cryst. growth and thermoluminesc. *(Russian)* 78−23604
$Ba[Pt(CN)_4].4H_2O$, polarised time-resolved emission spectra 79−33811
Be, foil, ion bombardment, secondary photon emission, ion energy depend. 80−97346
BeF_2:Eu^{3+} glass, luminesc. of Eu^{3+}, transition probabilities 80−80845
BeF_2:Eu^{3+} glass, struct., Monte Carlo simulations 80−96448
BeF_2:Pr^+, glass, optical homogeneous linewidths 80−7395
BeF_2-KF-CaF_2-AlF_3:Nd^{3+} (Er^{3+}) glass, multiphonon relax., fluoresc. obs. 78−15219
BeF_2-KF-CaF_2-AlF_3-EuF_3 fluoroberyllate glass, Eu^{3+} fluoresc. linewidth 80−66285
BeO, ceramic, sintered, thermoluminesc., EPR, emission spectra, energy level diagram 77−81163
BeO, ceramic, thermolum. glow curves 79−47527
BeO, ceramic and single cryst., EPR-ENDOR study of [Li]° centre 77−85569
BeO ceramic TLD, operational charact. and problems 77−42216
BeO discs, thermally stimulated exoelectron emission and thermolum. sensitisation 78−35277
Bi complex, $BiCl_7^{4-}$ in HCl aq. soln., photolum. excitation spectral characts. by stroking method *(Russian)* 79−78753
Bi^{3+} activated phosphors, luminesc. charact. 80−2849
$Bi_2Al(Ga)_4O_9$, fluoresc. and X-ray data 78−80403
$Bi_2Al_4O_9$, luminesc. expts. 80−60656
$Bi_{12}GeO_{20}$:Dy(Ho)(Er), luminesc., emission and excitation spectra 80−103975
$Bi_4Ge_3O_{12}$ crystals, doped with Dy^{3+}, Ho^{3+}, Er^{3+}, Tm^{3+}, Yb^{3+}, growth, spectral and laser props. 80−45115
$Bi_4Ge_3O_{12}$, temp. depend. luminesc. meas. 77−20910
$Bi_4Ge_3O_{12}$:Er^{3+}, host-sensitised energy transfer, laser time resolved spectroscopy 79−83013
$Bi_4Ge_3O_{12}$:Nd^{3+} and $Bi_4Si_3O_{12}$:Nd^{3+} crysts., absorpt. and luminesc. spectra, 4.2-300K 80−34957
BiI_3, charcts. of low-temp. photoluminesc. 77−8646
BiI_3, doped, IR photolum. and EPR spectra 78−19558
BiI_3 single crystals, refl., absorpt. and photoluminesc. spectra, exciton transitions 77−52164
$Bi_{12}SiO_{20}$:Nd, light absorpt. and transmission spectra, photoluminescence spectrum, optical absorpt. coeff. 79−74001
$Bi_{12}SiO_{20}$:Nd, single cryst., photoluminesc. meas. *(Russian)* 78−23519
$Bi_2W_2O_9$, energy transfer and luminesc. props. 80−55177
$Bi_2W_2O_9$:Mo(Eu), energy transfer and luminesc. props. 80−55177
CC GaP, improvements in synthesis, solute diffusion (SSD) growth and characterisation 79−65992
$(CH_4)NMnCl_3$, nearly-one-dimensional cpd., energy migration rel. to impurity trap behaviour 77−55811
$(CH_3)_4NUO_2(NO_3)_4$, fluoresc. decay rates, temp. depend. 80−25429

luminescence of inorganic solids continued
CO, cryst. at 5K, absorpt. and emission spectra, exciton interpretation 79−87481
CO, matrix isolated, vibrational energy migration, vibr. fluoresc. obs. 79−91486
CO-Ar, cryst. at 5K, absorpt. and emission spectra, exciton interpretation 79−87481
CO-Ne, cryst. at 5K, absorpt. and emission spectra, exciton interpretation 79−87481
C_3PbCl_3, single crysts., X-ray and photoluminesc., and reflection spectra 77−69896
Ca halophosphate luminophors, grinding influence on thermolum. 79−95854
Ca halophosphates, thermoluminesc., defects *(Russian)* 79−56869
$CaCO_3$, Akiyoshi stalactite, thermoluminescence and ESR dating comparison 78−88807
$CaCO_3$, calcite, tunnelling afterglows and retrapping 77−69902
$CaCO_3$, calcite, X-ray irrad., luminesc. and dielec. loss decays 77−12431
$CaCO_3$, Iceland spar natural crystals, optical charact. 77−10988
$CaCO_3$, luminesc. under N_2 laser excitation, and appl. to archaeological dating 80−60685
$CaCO_3$, thermoluminesc. spatial distrib. using image intensifier technique 80−47115
CaF_2, barrier instability in strong elec. fields 79−69522
CaF_2, doped, colour centre form. by UV irrad., afterglow, thermolum. and EPR obs. 78−10047
CaF_2, doped and gamma irrad., high temp.-peak in thermoluminescence 80−50434
CaF_2, EXAFS, intrinsic UV luminesc. excitation spectra 78−52567
CaF_2, hot pressed, dielectric, optical props. 79−56720
CaF_2, kinetics of thermoluminesc. buildup 79−65936
CaF_2, optical detection of acoustic phonons at THz freqs. 80−75320
CaF_2, phototransfer of thermoluminesc. peaks 79−83040
CaF_2, thermolum., F-centre annealing after neutron irrad. at 20K 79−55787
CaF_2, thermoluminesc. and F-centre annealing, after neutron irrad. 80−7422
CaF_2:Ce, Stark struct., phototransitions, g-factors 78−67995
CaF_2:Ce,Mn, heavily-doped phosphor, cathode-ray irrad., energy transfer 79−87509
CaF_2:Cm, fluorite-struct., self-luminesc. 78−27309
CaF_2:Co, X-irrad., luminesc. spectra 79−28801
CaF_2:Dy, TLD-200, thermolum. phosphor, photolum. and absorpt. spectra, thermolum. mechanisms 80−97321
CaF_2:Dy dosimeter crystals, γ-irrad. dose effect on thermoluminesc. response 77−64135
CaF_2:Dy^{3+}, fluoresc. spectra, A-centres and B-centres, Stark levels 80−25428
CaF_2:Dy^{3+}, high temp. fluorescence using Ar^+ and N_2 lasers 78−56514
CaF_2:Dy^{3+}, thermolum., associated luminesc. centres and traps 77−28638
CaF_2:Dy(Ho)(Pr)(Tb), V_k-centre recomb. kinetics, phosphoresc. 77−55817
CaF_2:Dy(Mn), thermolum. induced by monoenergetic parallel beam 81 MeV diffr. neutrons 77−52883
CaF_2:Er, γ-irrad., photostimulated luminesc. meas. 77−66538
CaF_2:Er^{3+}, fluoresc. spectra of charge compensated cryst., multiphonon and energy transfer relax. 79−87496
CaF_2:Er^{3+} laser fluoresc. of Er^{3+} sites, defect equilibria 78−6748
CaF_2:Eu, CaF_2:Eu,Mn(Gd), single crystal predisintegration phenomena, SEM cathodolum. obs. 80−59502
CaF_2:Eu, thermolum. in presence of lanthanide impurities 80−2870
CaF_2:Eu, X-ray luminesc. 79−99933
CaF_2:Eu^{2+}, circular polarisation in luminesc. and optical orientation 78−6740
CaF_2:Eu^{2+}, energy transfer to luminesc. centres, pulsed excitation obs. 77−85781
CaF_2:Eu^{2+}, photoluminesc. mag. circ. polaris. 80−89056
CaF_2:Eu^{2+}, short high-energy pulse induced X-ray luminesc., anomalous kinetics 77−59608
CaF_2:Eu^{2+}, Sm^{2+}, relaxed resonance acoustic phonons in vibronic anti-Stokes luminescence *(Russian)* 80−93404
CaF_2:Eu^{2+}, tunable optical detection and generation of THz phonons 79−65149
CaF_2:Eu^{2+}, X-ray excited luminesc., $^5D_0$-$^7F_1$ transition 80−2842
CaF_2:Eu^{2+}, X-ray induced luminesc. kinetics, energy transfer processes 79−8181
CaF_2:Gd^{3+}, Mn^{2+}, photo- and radioluminesc. investig. of intracentric energy transfer 77−16378
CaF_2:Gd^{3+} evaporated film, struct. of impurity centres, substrate temp. effects 79−99943
CaF_2:Gd^{3+} film, Gd^{3+} luminesc. spectrum and kinetics 78−6763
CaF_2:Ho^{3+}, fluoresc., relative intensities, lifetimes 78−27296
CaF_2:Ho^{3+}, site-selective spectroscopy 80−29791
CaF_2:Mn, CaF_2:Eu,Mn, single crystal predisintegration phenomena, SEM cathodolum. obs. 80−59502
CaF_2:Mn, low temp. X-irrad., Mn centres, optical absorpt. and emission props. 80−60635
CaF_2:Mn^{2+},Yb^{3+}, efficient luminesc. energy transfer from Mn^{2+} to Yb^{3+} 78−19536
CaF_2:Mn^{2+},Yb^{3+}, luminescent energy transfer efficiency obs. 78−6777
CaF_2:Mn(Co)(Ni), X-irrad., thermolum. 80−60686
CaF_2:Na, single cryst., X-irrad., optical absorpt. and thermoluminesc. 80−34952
CaF_2:Na, tunable room temp. laser action of M-centres, luminesc. and absorpt. spectra 79−31907
CaF_2:Pb^{2+}, band struct., Jahn-Teller effect, UV luminesc. and optical absorpt. spectra 80−66243
CaF_2:Pr^{3+}, laser selective excitation and energy transfer 79−38612
CaF_2:Pr^{3+}, multisite system, laser selective excitation and energy transfer 78−84634
CaF_2:Sm^{2+}, luminesc. spectra, vibronic wing, 2K 79−8182
CaF_2:Sm^{2+}, phonon spectrum of thermal pulses by fluorescence 79−95860
CaF_2:Sm^{2+}, pseudo-Jahn-Teller effect 79−69476
CaF_2:Sm^{2+}(Eu^{2+}), cubic crysts., vibronic spectra, induced dichroism method 77−81131
CaF_2:Tb^{3+}, cubic Tb^{3+} centres, energy level and cryst. field parameters 77−52181
CaF_2:Tb^{3+}(Eu^{3+}), one- and two-photon luminesc. excitation spectra 79−83023

luminescence of inorganic solids continued
CaF_2:Tm^{2+}, vibronic spectra and dynamics of impurity-contaiing lattice 79−1787
CaF_2:U, γ-irrad., EPR and luminesc. studies of U^{5+} and U^{6+} centres 79−51854
CaF_2:Yb^{2+}, cryst., stress polarisation of luminesc. and emitting states struct. 77−69897
CaF_2:Yb^{2+}, divalent ion radiative state, magneto-optical obs. 77−69893
CaF_2:Yb^{2+}, luminesc. polarisation, elastic uniaxial compression effect, radiative state model 78−6739
CaF_2:Yb^{2+}, spectra, kinetics and polarisation of luminesc. 77−69892
CaF_2:Yb^{3+}, Er^{3+}, and CdF_2-CaF_2:Yb^{3+}, Er^{3+}, IR to visible upconverting system 77−44035
CaF_2-SrF_2-BaF_2:Gd^{3+}, luminescence spectrum of Gd^{3+} ion and solid solution region obs. 78−84638
CaF_2-YF_3:Nd^{3+}, selective excitation of activator centres, time resolved luminesc. 78−15223
CaF_2-YF_3:Nd^{3+}, spectral migration of electronic excitation, selective laser excitation *(Russian)* 78−80417
CaF_3:Ho^{3+}, laser excited fluoresc. rise and decay meas., expt. 80−22448
CaI_2:Pb(Mn), recomb. processes, luminesc. charact. *(Russian)* 80−25450
$CaLaBO_4$, crystallographic and Pb^{2+} luminesc. data 79−32971
$CaLaGaO_4$:Eu^{3+},Bi^{3+}, luminesc. influenced by struct. transition 78−6773
$CaLaGaO_4$:Eu^{3+}(Bi^{3+}), luminesc. of α- and β-phases 77−90186
$CaLa_{1-x}Gd_xGaO_4$, $(0 \leq x \leq 1)$, Gd^{3+} luminescence and cationic distrib. *(French)* 79−78734
$CaLa_4(SiO_4)_3O$:Nd^{3+}, spectra, stimulated emission 77−85755
$CaMoO_4$, luminesc. efficiency, temp. and high-press. 78−23507
$CaMoO_4$:Na(Y), pure and doped, luminesc. props., emission decay time 79−95835
CaO, chemisorption of O_2, adsorboluminescence from surface F-centres 80−20723
CaO, electron irradiated, photocond. and luminesc. meas., F-centre electronic struct. determ. 78−6409
CaO, electron irradiated, symmetry assignment of new point defect 78−31261
CaO, electronic struct. calc. of F-centre, absorpt. and luminesc. bands 77−62859
CaO F-centre luminesc. and PMDR 79−95832
CaO, luminesc. single cryst., sharp IR absorpt. lines 77−1704
CaO, photoionisation of F-centre, luminesc. and photocond. meas. 80−66270
CaO, single cryst., tribolum. obs. 79−52031
CaO, undoped and Cl-, F- or Al-doped, X-ray and UV luminesc., electron-hole recombination processes *(Russian)* 78−76528
CaO:Ag (Au), electroluminesc. meas. 80−40162
CaO:Bi^{3+}(Pb^{2+}), impurity centres vibronic spectra, lattice dynamics and electron-phonon interactions 80−7396
CaO:Ce,Gd phosphors, trap distrib., phosphoresc. decay charact. obs. 80−29773
CaO:Ce^{3+}, Gd^{3+}, sensitization of Ce^{3+} luminesc. by Gd^{3+} 80−97326
CaO:Cu(Ag)(Au), thermoluminesc., following UV excitation, 290-500K 77−40292
CaO:Eu,Tb phosphor emission under X-ray excitation 79−52011
CaO:Eu^{3+}, influence of crystal field on luminesc. *(Russian)* 80−80834
CaO:Eu(Tb), phosphor, isothermal decay 80−55156
CaO:F(Cl)(Al), phosphon, luminesc., electron-hole recombination processes 79−65919
CaO:Mn phosphor, surface radical recomb. and cathodoluminesc. *(Russian)* 78−6787
CaO:Y phosphor, chemical instability, thermoluminescence study 79−38682
CaO-Li_2O-Al_2O_3-SiO_2:Nd^{3+}, CaO enriched, laser-type glasses, spectroscopic behaviour 78−60497
CaO-Li_2O-B_2O_3, calibo glass, $Dy^{3+} \rightarrow Ho^{3+}$ non-radiative energy transfer, diffusion limited relaxation 79−65925
CaO-Li_2O-B_2O_3 calibo glass, diffusion limited energy transfer from $Tb^{3+} \rightarrow Ho^{3+}$ 78−31235
CaO-Li_2O-B_2O_3:Dy^{3+} glass, optical excitation energy transfer from $Dy^{3+} \rightarrow Nd^{3+}$ 79−15515
CaO-Li_2O-B_2O_3:Er, Tb, calibo glass, nonradiative energy transfer 78−19541
CaO(S):Pb^{2+}(Bi^{3+}) 77−73166
$Ca(PO_3)_2$:Eu^{3+}, amorphous, phonon-assisted site-to-site electronic energy transfer, fluoresc. line narrowing obs. 77−81140
$Ca(PO_3)_2$:Eu^{3+}, anomalous spectral props. 79−38614
$Ca_2P_2O_7$:Sb, (Sb,Mn), luminesc., activation, colour centres *(Russian)* 78−92123
$Ca_2P_2O_7$:Sb(,Mn), luminesc., colouration 80−2828
$Ca_3(PO_4)_2$:Sb,(Sb,Mn), luminesc., activation, colour centres *(Russian)* 78−92123
β-$Ca_3(PO_4)_2$:Sb(,Mn), luminesc., colouration 80−2828
$Ca_5(PO_4)_3F$:Nd^{3+}, luminesc. and absorpt. spectra, line shift and broadening 77−4678
$Ca_5(PO_4)_3F$:Nd^{3+}, optical fluorescence intensity and cryst. field parameters 78−52570
$Ca_5(PO_4)_3F$:Nd^{3+} site symmetries, EPR and spectral obs. 78−6571
$Ca_{10}(PO_4)_6(OH)_2$, UV induced thermolumin. glow peak obs. 80−29814
$Ca_{10}(PO_4)_6(OH)_2$:Mn, thermoluminesc. 77-500K, X-irrad. at 77K *(French)* 78−15234
$Ca_5(PO_4)_3OH$ prod. by hydrothermal synthesis, thermolum. props. 80−2877
$Ca_5(PO_4)_3OH$:Mn, synthesized by hydrothermal method in CaO-P_2O_5-H_2O, thermoluminescence study rel. to starting mixture 78−95612
$Ca(Pt(CN)_4)5H_2O$, transition energy tuning from 3.3 to 1.4 eV 79−61436
CaS, atomic and mol. centres of O, ESR and luminesc. methods *(Russian)* 80−84764
CaS, colour centres and photoluminesc., flash stimulation bands *(Russian)* 77−20923
CaS phosphor, deep capture centres obs. 78−10951
CaS, phosphor, tunnel luminescence *(Russian)* 78−72577
CaS, phosphors, hole recombination luminescence *(Russian)* 78−72576
CaS, polycryst., cathodoluminesc. of point defects 79−78759
CaS:Bi, Tm, phosphor sensitisation mechanism, energy transfer 78−60507
CaS:Bi,Dy phosphors, thermoluminesc. 77−69921
CaS:Bi phosphors, UV dosimetry by thermolum. 80−55199

luminescence of inorganic solids continued
CaS:Bi^{3+}, Pd^{2+}, phosphor, electroluminesc., brightness and mechanism 77−48248
CaS:Bi^{3+},Na^{+}(Li^{+}) phosphors, luminescence of associated centres *(French)* 80−40155
CaS:Ce, Na, photon sidebands in emission and excitation spectra, pseudolocalised vibrs. 79−28800
CaS:Ce, Na phosphor, photoluminescence and excitation spectra 80−89049
CaS:Cu, colour centres, optical and thermal depths determ. 80−66275
CaS:Cu, colour centres and photoluminesc., flash stimulation bands *(Russian)* 77−20923
CaS:Mn,Ce, phosphor, fluoresc. spectrum, fine struct., $^4T_{1g}(^4G)\rightarrow{}^6A_1(^6S)$ transition 80−45130
CaS:Nd, Cu, phosphor, electroluminesc., spectral charact. 79−19936
CaS:Pb^{2+} phosphors, luminesc., refl., emission, and excitation spectra 79−11456
CaS:Pd phosphors, trap and luminescent centre location, photo-, thermo- and electroluminescence studies 80−71482
CaS:Tb,Eu phosphors, fluoresc. spectra under X-ray excitation 80−16083
CaS:Zn phosphor, photoluminesc. meas. 77−20913
CaS:Zr, Gd phosphors, thermoluminesc., trap distrib., activator effects 78−2929
CaS:Zr phosphors, photoluminesc. 79−28806
CaS:Zr phospors, photoluminesc. 79−28805
CaS-Bi, Mn, phosphors, thermoluminesc., phosphoresc. 78−2928
CaS-Pb,Mn, phosphors, thermoluminesc. and fluoresc. spectra 78−64396
CaS(O), Eu^{2+} to Eu^{3+} charge transfer 78−72403
$CaSO_4$ phosphors:Ce(Eu)(Dy)(Tm), gamma-irradiated valency conversions in rare-earth ions 80−55198
$CaSO_4$, thermoluminesc. spectra, X-irrad. effect 78−35210
$CaSO_4$ with rare-earth and Y dopants, ESR, thermolum. correlation studies following gamma irradiation 77−59628
$CaSO_4$:Bi, cryst. growth, luminesc. props. 77−58993
$CaSO_4$:Ce(Eu) phosphors, fluorescence spectra, thermolum. glow curve 80−2879
$CaSO_4$:Dy, α and γ thermoluminescence response comparison 79−85814
$CaSO_4$:Dy, Cd-covered TLD, thermal neutron dosimetry 77−90912
$CaSO_4$:Dy, competing deep trap model for thermoluminescence 79−83039
$CaSO_4$:Dy, cryst. growth from soln., thermoelec. and thermoluminesc. props. 79−56923
$CaSO_4$:Dy, γ-ray induced sensitization, competing trap model 80−2881
$CaSO_4$:Dy, high exposure UV response and sensitisation 79−91506
$CaSO_4$:Dy, phosphor, X-irrad., thermoluminesc., role of Na_2SO_4 as charge compensator 79−78764
$CaSO_4$:Dy, photo-stimulated thermolum., for high-exposure dosimetry 77−9262
$CaSO_4$:Dy, phototransferred TL studies 80−80875
$CaSO_4$:Dy, TLD during irrad. by γ-rays, X-rays, electrons, ambient atm. effect 78−19578
$CaSO_4$:Dy, TLD-900, thermolum. stability at low radiation doses 80−101272
$CaSO_4$:Dy, thermolum. origin, test of model on $CaSO_4$:Eu 77−85813
$CaSO_4$:Dy, thermolum., studies for dosimetry 79−29634
$CaSO_4$:Dy, thermoluminescent glow peaks, post γ-irrad. annealing study 80−89077
$CaSO_4$:Dy photostimulated luminesc. for radiation dosimetry 77−90910
$CaSO_4$:Dy ribbon, dosimetric props. study 80−63395
$CaSO_4$:Dy sintered pellets, thermolum. response 80−93411
$CaSO_4$:Dy Teflon TLD discs, graphite-mixed, for beta dosimetry 77−86639
$CaSO_4$:Dy thermoluminescence sensitivity and glow curves, 700° to 1300°C 79−85815
$CaSO_4$:Dy-KBr thermolum. phosphor, thermal neutron detect. by activation 80−32581
$CaSO_4$:Dy(Tm), thermolum. thermolum. phosphor, photolum. and absorpt. spectra, thermolum. mechanisms 80−97321
$CaSO_4$:Dy(Tm) thermoluminescent props. of non-commercial phosphors 78−58550
$CaSO_4$:Mn, phosphor, thermoluminesc., low energy ion excitation 77−55838
$CaSO_4$:Sm phosphors, X-ray induced fluorescence and phosphorescence 80−55179
$CaSO_4$:Sm phosphors, X-irrad., thermoluminesc., charge compensation effects 80−97351
$CaSO_4$:Tm, Li, mixed field TLD 77−9263
$CaSO_4$:Tm and nonluminous ^{6}LiF powders mixture, thermoluminesc. response to thermal neutrons 77−73588
CaS(Se):Eu^{2+}, emission and excitation spectra obs. 80−55162
CaSe: Sn^{2+}, dimer centre, emission and excitation spectra, temperature quenching *(French)* 79−99937
CaSe:Pb, luminesc. and EPR props. of Pb centres 80−55168
$CaSo_4$:Mn trap depth, thermolum. meas. 77−36301
$Ca_{1-x}Sr_xF_2$:Er^{3+} mixed crystal, luminesc. transition, inhomogeneous line broadening calc. 80−97332
$CaTaRO_6$, (R=La, Nd, Gd, Sm, Er, Lu), synthesis and physicochem. props. 79−52139
$CaWO_4$, luminesc. efficiency, temp. and high-press. 78−23507
$CaWO_4$ phosphor, interaction between intrinsic and impurity emission 79−8198
$CaWO_4$, phosphors, energy storage, afterglow decay and thermolum. meas. 77−12422
$CaWO_4$, single cryst. growth by Czochralski method and U incorporation, effective distrib. ratios, luminesc. charcts. 79−42094
$CaWO_4$, type selfactivated luminophors, nature of optically active centres 77−69880
$CaWO_4$:Eu^{3+}(Sm^{3+}), energy transfer after red edge excitation 78−52552
$CaWO_4$:Mo, P, thermoluminesc. traps, EPR meas. 77−90032
$CaWO_4$:Na(Y), pure and doped, luminesc. props. 79−95835
$CaYAlO_4$:Nd^{3+}(Er^{3+}), absorpt. and luminesc. spectra 77−69901
$CaY_2Ge_3O_{12}$:Nd, energy levels and laser action, fluoresc. meas. 79−81438
$Ca_3Y_2Ge_3O_{12}$:Eu^{3+}, garnets, prep., struct., luminesc., absorpt. spectra, Eu^{3+} localisation 77−69884
$CaY_2Mg_2Ge_3O_{12}$:Nd^{3+}, optical absorpt. and fluoresc. intensities 80−29793
$CaY_4(SiO_4)_3O$:Nd^{3+}, absorpt. and luminesc. spectra 77−85755

luminescence of inorganic solids continued
$CaZrO_3$:Pb^{2+}, UV luminescence temp. depend., three-level model 77−4683
$CaZrO_3$:Pb^{2+} (Bi^{3+}) and related Pb^{2+}(Bi^{3+})-actuated hosts, cryst. struct. effects on luminesc. 77−16376
Cd complex, Cd (II) halide with 8-aminoquinoline, cryst., photolum. 77−52152
$CdBr_2(I_2)$, Mn activated, electron-phonon interaction, lattice vibr. effective energies *(Russian)* 78−59911
$Cd_xCa_{1-x}MoO_4$, intrinsic hole centres EPR study, thermoluminescence and thermal decay 79−99957
$CdCl_2$:Cu, optical props. 78−43918
$CdCl_2$-$CdBr_2$, solid soln., luminesc., optical absorpt. 78−19538
CdF_2, MnF_2 or rare earth fluoride doped, elec. cond. and electroluminesc. 79−87508
CdF_2, pure, thin powder layers, electrolum. 79−56865
CdF_2, rare earth doped, multicoloured electroluminesc. 79−78755
CdF_2:Er^{3+}, selective monochromatic excitation of $^4S_{1/2}$-$^4I_{15/2}$ transition *(French)* 77−85765
CdF_2:Er^{3+}, Tm^{3+}, evidence for $Er^{3+}\rightleftharpoons Tm^{3+}$ energy transfers, fluoresc. expts. 80−60655
CdF_2:Eu^{3+}, electroluminescence spectra from 400 to 700 nm *(Russian)* 77−69916
CdF_2:Eu^{3+}, luminesc., charge transfer states 79−33799
CdF_2:Eu^{3+}, luminesc. spectra conc. and annealing depend. 79−65917
CdF_2:Eu(Gd), impurity and intrinsic electrolum. 77−36298
CdF_2:Eu(Gd)(Nd), semicond., symmetry of optical centres, optical and elec. props. 77−59592
CdF_2:Mn, thermolum., recomb. processes 78−15237
CdF_2:Mn,Y, in MIS struct., blue-green electrolum. 79−52025
CdF_2:Mn films, electroluminesc. meas. *(French)* 79−11471
CdF_2:NaF thin films, electroluminescence obs. at 77K *(French)* 80−80866
CdF_2:R^{3+}, cooperative luminescence influenced by symmetry of centres 78−6791
CdF_2:Sm^{3+}, photoconverted, thermally stimulated relax. 80−84476
$CdGa_2S_4$, interpretation of thermolum. and TSC meas. 78−27336
$CdGa_2S_4$, photoluminesc. and photocond. meas. 78−60159
$CdGa_2S_4$:Ag(In), photoluminesc. and photocond. meas. 78−60159
$CdGeP_2$, polarisation of luminescence emitted 77−69909
$CdGeP_2$, recombination radiation 78−19562
$CdGeP_2$:In, photolum. spectra and kinetic coeffs. 79−19927
$CdGeP_2$:In, recombination radiation 78−19562
n-$Cd_{0.3}Hg_{0.7}Te$, recomb. levels 79−91076
CdI_2 (Br_2), cathodoluminescence, 300 and 80K *(Russian)* 79−78760
CdI_2, layered cryst., photoluminesc., and reflection spectra obs. 78−6726
CdI_2, luminesc., relaxed excitonic states 79−33758
CdI_2, polytypism and luminesc. *(Russian)* 78−56520
CdI_2, thermoluminesc. of traps *(French)* 79−4856
CdI_2, with cation or anion impurities *(Russian)* 78−2913
$(CdI_2)_x(PbI_2)_{1-x}$, layered cryst., photoluminesc., and reflection spectra obs. 78−6726
$(CdI_2)_x(PbI_2)_{1-x}$, reflection and luminesc. spectra obs. 77−8648
$CdIn_2$:Cr, photocond. and photoluminesc. spectra 77−28214
$CdIn_2S_4$, impurity centres, photoluminesc. and photocapacitance data on config.-coordinate diagrams 78−10938
$CdIn_2S_4$, photoluminesc. spectra anal. by method of moments 77−12433
$CdIn_2S_4$, photoluminesc., reson. Raman scatt. 78−48179
$CdIn_2S_4$, photoluminesc., thermal quenching and recomb. centres 79−24362
$CdIn_2S_4$, single cryst., oscill. behaviour of photocurrent and luminesc. 78−10501
$CdIn_2S_4$ single crystals, recombination process and localised levels 80−93383
$CdIn_2S_4$:CO^{2+}, site symmetry, spectral meas. 79−78729
$CdIn_2S_4$:Cr, absorpt. and photoluminesc. spectra, Cr conc. depend. 79−78712
$Cd_{1-x}Mg_xTe$:Al, donor-acceptor pair and self-activated luminesc. 77−52161
$Cd_{1-x}Mg_xTe$:P, luminescence centres, photoluminesc. meas. 78−31236
$Cd_{1-x}Mn_xTe$, exchange induced ionization of bound excitons, luminesc. meas. 80−97328
$CdMoO_4$, luminesc. efficiency, temp. and high-press. 78−23507
$Cd_2Nb_2O_7$, photolum. and carrier drift mobility at ferroelec. transition 80−71469
CdP_2, polarised spectra of IR absorption and emission of single crysts., oscillatory states *(Russian)* 77−28583
CdP_2:Bi,Zn, photolum. and photocurrent stationary charcts. 78−27317
CdP_2:Cu, photoluminescence and photocond. charcts., interimpurity recomb. of carriers 77−8637
$Cd_xPb_{1-x}I_2$, photoluminescence comp. and energy depend., band gap 77−44045
CdS, and CdS:Li, photoconductivity, luminescence, radiative and radiationless transition mechanisms 78−10948
CdS, anti-Stokes excited crystals, luminescence band at 12K 79−19922
CdS, Auger effects in donor acceptor pair spectra 80−20707
CdS, Auger excitation mech. of 1.6-2.0 micron luminesc. band 79−8184
CdS, Auger interaction between luminescence centres and donor-acceptor pairs 77−63458
CdS, biexciton fluoresc. line shape 77−44059
CdS, biexciton levels, luminescence-assisted two-photon spectra 80−29795
CdS, biexcitonic luminesc. for allowed and forbidden polarisation 77−44040
CdS, cathodolum. in red and exciton regions, surface treatment influence 77−77303
CdS, compensated, charcts. of Auger excitation spectra of photoluminesc. and photocurrent 77−90194
CdS, condensation of optically excited carriers, electron-hole-liquid phase diagram 77−31950
CdS crystals, doped with groups III and VII elements, self-activated emission, modelling *(Japanese)* 78−31247
CdS crystals, electron-hole plasma, carrier optical orientation 80−100689
CdS crystals, radiative recombination, high excitation rates 80−108269
CdS, deep level IR luminescence, origin 80−20704
CdS, deform. effects on exciton excitation spectra 78−35191
CdS, dislocation effects on radiative recombination processes 79−8186
CdS, dislocation emission, photoluminesc. spectra 80−16084
CdS, dislocation structural optical absorpt., plastic deformation *(Russian)* 80−34959

luminescence of inorganic solids continued
CdS, doped laser mechanism and output study 80−43340
CdS, edge emission spectra alteration by uniaxial stress *(Russian)* 78−72486
CdS, electron and hole trapped centres, EPR, photoluminescence, photoconductivity study 80−108071
CdS, electron-hole condensate, luminesc. obs. *(Russian)* 78−19552
CdS, electron-hole liq., effect of excited electron states lifetime on gain spectra 77−85748
CdS, emission and transmission spectra, excitonic mols. effect 77−44062
CdS, emission lineshape of excitonic mols., polariton states 77−20918
CdS epitaxial layers on sapphire, exciton struct. of absorpt., photoluminesc. and photocond. spectra 80−89027
CdS, excitation spectroscopy, relation between I_2 bound exciton line and CdS excitonic molecule line 80−40153
CdS, exciton cathodoluminesc. of semicond. with surface pot. barriers 78−88366
CdS, exciton condensation, photoluminesc. spectra 80−25448
CdS, exciton luminescence, surface recombination, space-charge-layer effects 78−80410
CdS, exciton optical and luminescence spectra characts. near dislocation slip bands 80−45111
CdS, exciton resonant secondary emission spectrum temporal evolution 79−51499
CdS, exciton-LO phonon interactions under high excitation and temp. conditions 77−69899
CdS, excitonic mol. emission, strain induced splitting 77−44060
CdS, fine struct. of two-photon absorption, luminesc. meas. 77−24893
CdS, free-exciton multiphonon luminesc. 78−6741
CdS, group velocity of light and polaritons, refl. and luminesc. spectra 77−24863
CdS, high intensity excited, exciton reflection spectra, reflection struct. 80−20692
CdS, high-energy electron irrad., photoluminescence spectra, course of annealing 77−90198
CdS, highly excited cryst., biexciton, impurity transition and electron-hole plasma 79−15092
CdS, highly photoexcited, picosec. luminesc. spectrosc. 79−47517
CdS, IR stimulated edge emission 77−59613
CdS, impact ionisation of excitons, photocond. and photolum. meas. 79−56266
CdS, influence of Lamb US waves on exciton spectra *(Russian)* 80−7374
CdS, influence of surface annihilation of excitons on cathodolum. meas. 77−20937
CdS, ion implantation effect on luminesc. and cryst. damage 78−6758
CdS, kinetics of recomb. radiation 78−31243
CdS, Lamb US wave induced luminesc., green edge radiation *(Russian)* 79−91509
CdS laser irrad. native defect formation, influence on photoelectric props., IR luminescence *(Russian)* 80−11039
CdS, local cathodolum. of single crysts. under colour contrast conditions in SEM 79−8191
CdS, low temp. IR-induced flash of green edge luminescence 77−63457
CdS, luminesc. and gain spectra of two-photon excited excitons 79−33815
CdS, luminesc. data. statistical anal. *(Russian)* 78−68559
CdS, luminesc. from heavy ion tracks 78−88365
CdS, luminesc. of I_2 bound exciton and excitonic mol. 79−91492
CdS, M_1-M_2 luminesc. band, assignment to exciton-impurity complexes 77−8649
CdS, magnetoreflectance and magnetoluminesc. of A exciton 78−39597
CdS, multiphonon reson. Raman scatt. and exciton-phonon luminesc. 77−16319
CdS, multiphoton cross-section determination by means of luminescence experiments 80−93377
CdS, neutron and fast electron irrad., local centre form., TSC and photoluminesc. meas. 78−87719
CdS, neutron irradiated, intrinsic defects 78−51599
CdS, nonequilibrium electron-hole plasma, optical orientation of carriers *(Russian)* 78−2904
CdS, ps decay kinetics of luminesc., streak camera obs. 79−78752
CdS, psec time resolved spectroscopy, electron-hole plasma 79−47500
CdS, pure and Cl doped, stimulated emission due to indirect band-band transitions 80−7376
CdS, recomb. radiation of electron-hole liq., quantum oscills. *(Russian)* 77−36293
CdS, reflectance, transmittance and luminesc. spectra, light group vel. near exciton reson. *(Russian)* 77−69857
CdS, reson. scatt. of exciton-polaritons second emission under monochromatic excitation 77−1717
CdS, resonant scatt. of exciton polaritons by LO and acoustic phonons 79−95760
CdS, reversible threshold modification of luminesc. spectrum by uniaxial compression 79−38662
CdS, single cryst., bound excitons in surface layers, luminesc. obs. 79−28294
CdS, single cryst., laser emission following single-photon excitation *(Russian)* 78−37889
CdS, single cryst., surface treatment effects on photoluminesc., struct. and optical props. *(Russian)* 78−15224
CdS, single crystal, subnanosecond light pulse generation by laser radiation pumping 79−64234
CdS single crystal growth by sublimation *(Japanese)* 78−11093
CdS single crystals, depend. of radiative props. on equilib. carrier density 79−19932
CdS single crystals, Roentgenoluminescence, exciton interactions *(Russian)* 80−2853
CdS, single crysts., US luminesc. obs. 80−76092
CdS sintered film, photolum. and recomb. photocurrent noise spectra 78−6743
CdS, size effect of dense electron hole systems 80−7413
CdS, spatial diffusion of excitons under intense excitation 77−44061
CdS, spectral anal. of luminesc. of high density excitons 79−11451
CdS, spectroscopic study of local centre interaction, change with external illumination 80−80323
CdS, spin-polarised electron-hole liquid, theory 78−43307
CdS, stimulated and spontaneous emission from degenerate electron-hole plasma at 300K 80−29762
CdS, streamer luminescence 78−6762

luminescence of inorganic solids continued
CdS, stress-induced photolum. bands, photocond., rel. to dislocation electron states 80−25447
CdS, superluminescence due to pulsed X-rays, 170 and 295K 78−42338
CdS, temp. depend. of edge emission band shape 77−20934
CdS thin films, growth and evaluation for fabrication of high performance photovoltaic solar cells 80−93501
CdS, three-photon absorpt. coeff. determ. by nonlinear luminesc. expt. 80−14384
CdS, time-resolved spectra of spontaneous luminesc. from high density electron-hole plasma 80−40156
CdS, two-photon-excitation, tunable laser emission, luminesc. processes 80−55127
CdS, up-conversion and optical storage, spatially modulated band struct. 78−64397
CdS, with group III or VII dopant, self-activated emission 77−16371
CdS:Ag, orange luminesc. at 77K and induced impurity photoconductivity 79−43035
CdS:Ag phosphor, mechanism of trap ionisation by elec. field, Gudden-Pohl flashes 79−74007
CdS:Cl, heavily doped, fluoresc. spectrum upper threshold calculated 78−52568
CdS:Cu, diffusion doping, photolum. 79−91493
CdS:Cu, Fermi level position, luminesc., and photosensitivity, electron irrad. effects *(Russian)* 78−14652
CdS:Cu, IR photolum. at 10K 79−28824
CdS:Cu, photocurrent, elec. field effect on recombination processes *(Russian)* 80−100484
CdS:Er^{3+}, spectra of different emission centres *(Russian)* 77−16356
CdS:Ga crystal cathodoluminescence, SEM analysis 80−97349
CdS:In(Cl) concentration quenching mechanism of luminescence 80−97336
CdS:In(Ga)(Al), cathodolum. on diffusion front 77−32447
CdS:Li, complex luminescence centres, recombination-stimulated conversion 80−108268
CdS:Li, donor-acceptor interactions, photochem. reactions *(Russian)* 77−40285
CdS:Li, luminescence bands, photocurrent spectra *(Russian)* 80−60677
CdS:Li, nature of recombination centres responsible for 0.95 μm luminesc. band 77−69908
CdS:Li, pure and doped, green edge luminesc., complex nature of centres 80−60671
CdS:Li, single crystals, anisotropic luminesc. centres 80−80857
CdS:Li, TSC and optical photocurrent quenching spectra, Auger excitation of recomb. centres 79−33294
CdS:$Li^+(N^+)(Ne^+)(P^+)$, ion-implanted, edge emissions 77−77274
CdS:Li(Cu), pure and doped, electrodiffusion of shallow donors, photocurrent, TSC, and exciton luminesc. meas. 80−79992
CdS:Mn(Co), intensity and spectral distrib. of luminescence *(Russian)* 77−16392
CdS:N, P, As, Sb, Bi photoluminescence obs. 78−10965
CdS:Na, Hagemark theory, green edge emission line intensity 80−75517
CdS:Ni, elec., photoelec. and luminesc. props. *(Russian)* 78−84259
CdS:Ni, elec., photoelec. and luminesc. props. 79−95828
CdS:P, implanted, photoluminesc. and electroreflection spectra *(Russian)* 78−52544
CdS-based phosphor, microstruct. and luminesc. efficiency 78−10959
CdS-Co^{2+}, IR spectrum, 4.2K, electron-phonon interaction effect on emission spectrum 78−27270
CdS(Se), with dislocations, optical props. 79−83001
$CdS_{1-x}Se_x$, chem. comp. and luminescence obs. 80−80869
$CdS_{1-x}Se_x$, mixed cryst., electron-hole drops and plasma, luminesc. obs. *(Russian)* 78−92119
$CdS_{1-x}Se_x$ mixed crystals, free excitons, disorder effects 80−34365
$CdS_{1-x}Se_x$, mixed crystals, deformation effects on free excitons 80−76073
$CdS_{1-x}Se_x$ single crysts., photocond. and excitonic luminesc. under high laser excitation 78−23127
CdS_xSe_{1-x} mixed crystals, exciton spectra 78−92131
CdS(Se)(Te):Co^{2+}, IR luminesc. quenching, Co^{2+} level position, ionisation energy 80−16079
CdS_xTe_{1-x}, emission spectra at high excitation levels *(Russian)* 79−74004
CdS_xTe_{1-x}, low temp. photoluminesc. *(Russian)* 78−43931
p-CdSb, photoconductivity and absorpt. in submm region, electroluminesc. 77−32046
CdSe, deep dislocation levels, TSC and luminesc. obs. 77−8050
CdSe, electron irrad., edge emission 80−25461
CdSe, exciton-phonon luminesc. 77−16319
CdSe, free-exciton multiphonon luminesc. 78−6741
CdSe, high intensity excited, exciton reflection spectra, reflection struct. 80−20692
CdSe, highly photo-excited, time-resolved luminesc. spectra, 1.8K 78−35197
CdSe, kinetics of recomb. radiation 78−31243
CdSe, low resist., mech. for nonradiative recombination of carriers, photoluminesc. and photocurrent characts. 78−19092
CdSe, luminesc. of high density electron-hole plasma at elevated temps. 80−20696
CdSe, magnetoreflectance and magnetoluminesc. of A exciton 78−39597
CdSe, monocryst. layers and bulk specimens, spectral comp. of impurity luminesc. 77−16364
CdSe, optical gain spectra, exciton collision processes and electron-hole plasma 79−28814
CdSe, oriented single-crystal films, edge luminescence at high excitation levels 77−1720
CdSe, pico-second time depend. of luminesc. line due to exciton-exciton collision 78−39587
CdSe, picosecond time-resolved luminesc. spectra 79−93890
CdSe, plastically deformed, luminescence line 0.96 eV 78−10950
CdSe, polar semiconductor, collisions between hot excitons and hot electrons 80−7415
CdSe, polarisation correl. of resonant Raman scatt. or hot luminesc. 80−25384
CdSe, psec time resolved spectroscopy, electron-hole plasma 79−47500
CdSe, pure and In-doped epitaxial growth on ZnTe (111), and characterisation 78−14631
CdSe, radiative recomb. process, P-band, 2-psec time resolution 79−24346
CdSe, recombination mechanism at dislocations, photoluminescence 80−103993

luminescence of inorganic solids continued
CdSe, reson. absorpt. of coherent IR radn. by acceptors, photocurrent and emission spectra 79−73974
CdSe single crysts., exciton luminesc. and polarisation spectra under one- and two-photon excitation 79−65391
CdSe, single crysts., luminesc. of electron-hole plasma 80−60675
CdSe:Cl(In), photoluminesc. props. near fund. absorpt. edge, impurity conc. effects 79−52003
CdSe:P, effect of P on edge luminesc. 78−64399
CdSe:P(Zn), single crystals, luminesc. 79−87493
$CdSiAs_2$, polarisation of photoluminesc. 77−16389
$CdSnP_2$, luminescent props. *(Russian)* 78−35201
$CdSnP_2$:Cu, deep centres, emission transitions, polarisation *(Russian)* 78−84650
CdTe, average number of phonons emitted in optical transition 77−8614
CdTe crystals, exciton luminescence spectra rel. to shallow impurity conc. 80−97335
CdTe, electron-hole liquid formation in pure and doped crystals, luminesc. study *(Russian)* 80−55184
CdTe, excitation spectra, resonant Raman scatt. versus hot electron effects 79−38645
CdTe, growth from Te-rich soln. by travelling heater method, cond. and luminesc. 77−40351
CdTe, high-resistivity, irradiation effects on carrier transport and trapping process 78−2164
CdTe, low temp. luminesc. *(Russian)* 79−91497
CdTe, luminescence and reflect. investig. of excitons, stress and Zeeman splitting 77−40281
p-CdTe, nondoped, heat treatment in vacuum, dissoc. obs. effects on struct. and props. *(Japanese)* 80−60662
CdTe optical applications, review 77−42580
p-CdTe, photocond., photoluminesc., spectral studies 80−88593
n-CdTe, photolum., plastic deform. effects 79−15509
CdTe, recombination radiation due to high-density excitons 80−93392
CdTe, undoped and donor-compensated, cathodoluminesc. of 1.4 eV bands 77−40291
CdTe, vapour-phase-grown, cathodoluminesc. study 80−76086
CdTe, Yb^{3+} implantation, nonstoichiometry effect 77−15440
CdTe:Cl, electron irrad., defects 80−25460
CdTe:Cl, heavily doped, elec. and photoluminesc. investig. of defect interactions 77−39603
CdTe:Cl, interaction of impurities and lattice defects, changes in elec. props. and photoluminesc. 77−4685
CdTe:Cr^{2+}, absorpt. and luminesc. of $Cr^{2+}(d^4)$, cryst. field theory interpretation 79−83000
CdTe:Fe(Ni), luminesc. and refl. spectra, high temp. annealing effects 80−24472
CdTe:In, lightly- and heavily-doped, cathodoluminesc., temp., injection level and freq. depend. 78−52584
CdTe:In, pure and heavily doped, electron-hole liq. form., luminesc. spectra 80−10884
CdTe:Li(Cl), acceptor states study by donar acceptor pair excitation luminesc. 80−100683
CdTe:Mn^{2+}, luminesc. and magnetooptic reson., mag. field effect 80−93390
CdTe:Mn(Fe)(Ni), exciton refl., photoluminesc., and mag. suscept. meas., influence of impurities 77−39787
CdTe:V,Cr, optical props. meas. 79−73969
CdTe:Xe, anomalous Xe^+ ion implantation defect introduction, cathodolum. obs. 77−62554
CdTe:Yb, exciton emission, cathodoluminescence 78−39033
n-CdTe-electrolyte solar cells, interface changes during operation, AES, electrolum. and electroreflectance meas. 79−100525
CdTe(Se):Co, impurity luminescence no phonon line depend. on temp., Debye temp. 80−66273
$CdWO_4$, luminesc. efficiency, temp. and high-press. 78−23507
CdZnS thin films, growth and evaluation for fabrication of high performance photovoltaic solar cells 80−93501
$Cd_{1-x}Zn_xS$ heteroepitaxial single-cryst. layers, photoluminesc. props. 80−100692
Ce^{3+} impurities in cubic crystals, 5d→4f radiative transition probability calc. 80−71474
$CeBO_3:Tb^{3+}$, vacuum UV excitation spectra and quantum efficiencies 79−28811
$Ce_xLn_{1-x}P_5O_{14}$, UV luminescence lifetimes obs. 78−6775
$CeP_5O_{14}:Gd^{3+}$, EPR and emission spectra *(French)* 77−69686
Cl_2, matrix isolated, Zeeman effect and magnetically polarised luminesc. 78−46379
Cr, ion bombard. induced photon and secondary ion emission in O_2 atmosphere 77−90231
Cr, photon emission due to Ar^+ ion bombard., adsorbed and recoil-implanted O effect 80−80872
Cr^{3+}, electronic states interactions with crystal odd vibrs., R-lines vibr. recurrences 78−84639
Cs halides, electronic struct. of self-trapped excitons magneto-optic props. 79−33805
Cs halides:H, luminesc. of interstitial atomic H 80−103986
CsBr, irradiated with ultrasoft X-rays, thermolum. meas., surface energy losses 77−16408
CsBr, luminesc., mag. circ. polaris., self-trapped excitons, EPR 79−33805
CsBr, luminesc. polarisation for free and bound excitons 78−10942
CsBr, self-trapped excitons, magneto-optical props., 1.3-50K 80−49606
CsBr:Cl(F), luminescence investig. of F_H-centre lifetime 77−20917
CsBr:Cu, polarisation study of tetragonal Cu^{2+} aggregate centres 78−39590
CsBr:Cu^-, excitation and absorpt. spectra 80−108255
CsBr:Cu^+, X-ray irrad., thermoluminesc. 80−16107
CsBr:NO_2^-, luminesc. centre polarisation and reorientation *(Russian)* 78−76529
CsBr:O_2^-, Stokes' losses on cryst. vibrs. in luminesc. spectra of mol. centres *(Russian)* 77−55827
CsBr:O_2^- centres, luminesc., polarisation temp. depend. 78−87943
CsBr:Pr, absorpt. and fluoresc. spectra, crystal field 78−2885
CsBr:Th, absorpt., excitation, fluorescence spectra 79−43032
CsBr:Tl, emission bands, press. effect 79−33789
CsBr(Cl):Cu^+, γ-irradiated, thermolum. emission 80−104001
CsBr(I), single crysts., polarisation of luminesc. and reorientation of NO_2^- centres 79−95823
$CsCaCl_3$:Pb, and undoped crystals, photolum. and thermolum. meas. *(Russian)* 77−85767
luminescence of inorganic solids continued
$CsCa_{0.95-x}Mg_xEu_{0.05}F_3$, blue luminesc. obs. 77−32428
CsCl, electron beam excited luminesc., phase transition effects 77−85810
CsCl, F- and F_H-centres, luminesc. meas. 78−10397
CsCl, luminesc. in vac. UV range above and below phase transition temp. 80−93399
CsCl:Ag phosphor, spectral charact., optical range 77−1724
CsCl:Cu^+, X-ray irrad., thermoluminesc. 80−16107
CsCl-AgCl, spectral luminesc. charact., optical range 77−1724
CsCl(Br)(I):NO_2^-, vibronic and reson. Raman spectra of BCC cryst. 79−87468
CsF, EPR of self trapped exciton and MCd meas. 77−48091
$Cs_2GeF_6:Mn^{4+}$, magnetically circularly polarised emission and MCD of vibronic lines 77−16377
CsI based powdered phosphors and screens possible appl. in X-ray radiography and fluorography 79−6245
CsI, F- and F_H-centres, luminesc. meas. 78−10397
CsI, intrinsic UV, correl. with V_k plus F-centre config. of self trapped excitons 78−75998
CsI, luminesc., mag. circ. polaris., self-trapped excitons 79−33805
CsI, pure, influence of strain on photolum. 79−15527
CsI, pure and Na(Tl)-doped, luminesc. from bound excitons, UV absorpt. and EPR 77−77282
CsI, self-trapped excitons, magneto-optical props., 1.3-50K 80−49606
CsI:NO_2^-, luminesc. centre polarisation and reorientation *(Russian)* 78−76529
CsI:Na, electronic struct. and luminesc. 80−16080
CsI:Na, localised excitons, absorption and emission 77−32425
CsI:Na, photoluminescence spectra and lineshapes anal., exciton energies 77−77281
CsI:Na, self-trapped exciton emission polarisation 80−49607
CsI:Na, UV irrad., thermoluminesc. 79−28846
CsI:$Na^+(K^+)$, luminesc. processes 80−103989
CsI:Tl, crystallophosphor, luminesc. charact., temp. and conc. depend. 80−55175
CsI:Tl, emission bands, press. effect 79−33789
CsI:Tl, gamma-scintillation growth front, external elec. field effect 80−34984
CsI:Tl, luminescence yield depend. on orientation of fast electron beam *(Russian)* 77−8665
CsI:Tl X-ray phosphor, spectral charact. 79−8172
CsI:Tl^+, Jahn-Teller split luminesc., high press. study 78−52565
CsI:Tl(Na), light yield under charged-particle bombardment 80−93409
CsI(Br):Mn phosphors, luminesc. spectra 77−59610
CsI(Br)(Cl):Tl, $[X_2^-]$ centre dynamic props. 79−65730
Cs_2MX_6(M=Se, Te, X=Cl, Br), $\Gamma_4^-(^3T_{1u})$ state, Jahn-Teller effect, luminesc. obs. 80−60650
$CsMnBr_3:Nd^{3+}$, nearly 1-dimens. cryst., emission spectrum, extensive energy transfer 79−15516
$CsMnCl_3(Br_3)$, rare earth doped, energy transfer, emission spectra obs. 80−20684
$CsMnCl_3.2H_2O$, antiferromag. insulator, self-trapping of excitons 80−70619
$CsMnCl_3.2H_2O$, luminesc., electronic excitations localisation *(Russian)* 79−87492
$CsMnCl_3.2H_2O$, nonequilibrium magnon population obtained by optical pumping *(Russian)* 80−11457
$CsMnCl_3.2H_2O$, quasi-one-dimensional antiferromag., luminesc. enhancement in mag. field *(Russian)* 79−91487
$CsMnF_3$, exciton migration, excitation and luminesc. study *(Russian)* 80−66264
$CsMnF_3$, exciton-magnon interactions in optical transition, absorpt. and emission spectra meas. 80−70981
$CsMnF_3$, magnon absorption and luminesc. 80−7400
$Cs_2NaBiCl_6$, optical props. 78−68549
$Cs_2NaEuCl_6$, mag. dipole transitions $^5D_3 \rightarrow {}^7F_4$, interpretation 79−42505
$Cs_2NaTbCl_6$, emission spectra, mag. dipole transitions assignments 78−23505
$Cs_2NaTbCl_6$, mag. circ. polarised emission, MCD, $^7F_J \rightleftarrows {}^5D_4$ transitions 77−77242
$Cs_2NaTbCl_6$, Tb^{3+} $^5D_4 \rightarrow {}^7F_J$ transitions, mag. and elec. dipole intensities 78−76033
$Cs_2NaYCl_6:Bi^{3+}$, luminesc., cryst. growth, Stockberger method 79−8174
$Cs_2NaYCl_6:Bi^{3+}$, luminescence props., emission and excitation spectra 80−108262
$Cs_2NaYCl_6:Re_3Tm$, fluorescence, two-step blue up-convertors 78−95603
$Cs_2NaYCl_6:Tb^{3+}$, emission spectra, mag. dipole transitions assignments 78−23505
α-$CsNd(PO_3)_4$, single cryst. struct. and spectral-luminescent props. 80−96490
$CsPbBr_3$, $CsPbCl_3$, ionic semiconductors, electronic and optical props. 79−38594
$CsPbBr_3$, electronic and optical props. 80−25414
$CsPbCl_3$, electronic and optical props. 80−25414
$CsPbCl_3$, electronic struct. and optical props. in fundamental absorpt. region 80−93367
$Cs_2SnCl_6:ReCl_6^{2-}$, luminesc. and absorpt. spectra, relax. processes 77−85779
$Cs_2SnCl_6:UO_2Cl_4^{2-}$, luminesc., vibronic anal. 79−33767
$CsSrCl_3$:Pb, luminesc. spectral distrib., transitions identification *(Russian)* 77−40276
$CsSrCl_3$:Tl, absorpt. and luminesc. spectra 78−72586
$Cs_2TeCl_6:Re^{4+}$, vibronic transitions progressions, intensity distrib. 79−78735
$Cs_2TiF_6:MnF_6^{2-}$, $^4A_g \rightleftarrows {}^2E_g$ transition of Mn^{4+}, absorpt., emission, linear and MCD, MCE 78−10929
$Cs_2UO_2Cl_4$, fluoresc. decay rate of pure and impure cryst. 79−47487
$Cs_2UO_2Cl_4$, low-lying excited electronic levels, fluoresc. decay meas. 79−47491
$Cs_2UO_2Cl_4$, luminesc. spectra of cryst., polarised, vibr. anal. 79−73983
$CsUO_2(NO_3)_3$, fluoresc. decay rates, temp. depend. 80−25429
$Cs_2ZrCl_6:Os^{4+}$, multiple state luminesc. 78−72584
$Cs_2ZrCl_6:Re^{4+}$, cryst., mag. circularly polarised emission 77−28613
$Cs_2ZrCl_6:UO_2Cl_4^{2-}$, luminesc., vibronic anal. 79−33767
$Cs_2[Pt(CN)_4].H_2O$, polarised emission, correlation to cryst. struct. 79−19917
Cu cathode, electrically stressed, broad area, surface elec. phenomena, electrolum. K-spot radiation identification with electron emission 80−20711
Cu cathode, electroluminesc. from semicond. impurities on surface 77−90200

luminescence of inorganic solids continued
Cu, dislocation mechanism of luminescence during fracture 79−24376
Cu, excited state formed by B^+ impact, light emission coeffs. 78−64417
Cu, film and polycryst. samples, low energy electron irrad., visible and UV emission 78−2921
Cu, hot cathodoluminescence study, electron-hole recombination 80−93410
Cu, ion bombardment-induced photon emission as function of target temp. 80−100698
Cu, photon emission from inert gas-surface impact 78−11059
Cu target, bombardment by Ar^+-ion beam, luminosity spectrum 79−4884
$Cu_{1-y}Ag_yInS_{2(1-x)}Se_{2x}$, lattice consts. and band gap variations 79−78000
$Cu_{1-y}Ag_yInS_{2(1-x)}Se_{2x}$ pentenary alloy system, appl. to photovoltaic solar energy conversion, cathodolum. determ. of band gap 80−35680
$CuAl_5S_8$, cryst. growth, struct., and fluoresc. 77−48328
CuBr, biexciton luminesc. 77−44056
CuBr, dispersion of multicomponent exciton polaritons, hyper-Raman emission spectra 80−20096
CuBr, emission spectra after two-photon excitation, Raman scatt. 79−47518
CuBr, excitonic mols., two photon generation 77−43511
CuCl, biexciton luminesc. 77−44056
CuCl, biexciton luminesc., subnanosecond time resolved spectroscopy 77−73167
CuCl, biexciton luminescence and two photon Raman emission, polarisation props. 78−80406
CuCl, biexcitons, two-photon absorption and luminesc. 77−43513
CuCl, Bose-Einstein condensation of biexcitons 79−56138
CuCl crystal resonant Raman scatt. and luminescence competition *(Japanese)* 80−80770
CuCl, decay time mas. of biexcitonic photoluminesc. 78−10935
CuCl, direct creation of high biexciton density at K=0, two-photon absorpt. and emission spectra 79−33727
CuCl, donor-acceptor recomb. spectra 80−45131
CuCl, emission spectra after two-photon excitation, Raman scatt. 79−47518
CuCl, exciton luminesc., reabsorpt. and polariton effects 80−50430
CuCl, excitonic mol. luminesc. spectra, picosecond time anal. 78−52548
CuCl, excitonic molecules, secondary emission under two-photon reson. excitation 80−11468
CuCl, excitonic mols., ps time resolved luminesc. spectra 77−16383
CuCl, excitonic mols., two photon generation 77−43511
CuCl, H^+ irrad., luminesc., high density excitons in particle tracks 79−47020
CuCl, luminesc. and Raman processes under reson. two-photon excitation 79−33796
CuCl, luminesc. and reson. Raman scatt. of excitonic mols. 79−33814
CuCl, luminesc. from Bose-condensed state of biexcitons 79−23905
CuCl, luminesc. of excitonic mols. 80−2817
CuCl, luminesc. spectra, excitonic mol. reson. two phonon excitation 78−19514
CuCl, phonon interaction of excitonic molecule 80−50316
CuCl, picosecond spectroscopy of secondary radiation from resonantly excited excitonic molecules 79−15461
CuCl, polariton effects in resonant Raman scatt. 78−10881
CuCl, ps. luminesc. spectra, resonantly excited excitonic mols. 78−19555
CuCl, psec time resolved spectroscopy, excitonic mols. 79−47500
CuCl, Raman and luminesc. processes under reson. two-photon excitation of excitonic mol. 79−8143
CuCl, relaxation of excitonic molecules generated by two-photon excitation, forward Raman scatt. 78−2838
CuCl, reson. Raman scatt. and luminesc. of biexcitons 79−38618
CuCl, reson. Raman scatt. and luminesc. due to excitonic mols. 79−91425
CuCl, reson. Raman scatt. and luminesc. under two-photon excitation 79−95765
CuCl, resonant emission, lifetime of excitons 77−69887
CuCl, resonantly excited excitonic molecules, time resolved spectroscopy 78−92109
CuCl, time resolved exciton-biexciton transitions, UV excitation, luminescence spectra 79−69883
CuCl, time-resolved study of induced absorption due to exciton-biexciton transitions 79−38658
CuCl, two-photon absorpt. and luminesc., biexcitons 80−11434
CuCl, two-photon reson. Raman scatt. and luminesc. of excitonic mols. 79−28819
$CuGaS_2$, crystal growth and luminesc. *(Japanese)* 78−23515
$CuGaS_2$, direct gap semicond., exciton energy at 300K from reabsorption of luminesc. 79−78728
$CuGaS_2$, reabsorpt. of excitonic luminesc. in direct band gap semiconds. 77−63469
$CuGaS_{2-2x}Se_{2x}$, mixed crysts., luminesc. spectra 77−63454
$CuGaSe_2$ crystals, I_2 vapour transport grown, luminesc. spectra 78−88349
p-$CuGaSe_2$, electrolum. obs. 77−32444
$CuGaSe_2$, evidence of donor-acceptor type transition 80−93375
$CuGaSe_2$, photoluminesc. spectra at 76K 79−38655
$CuGaSe_2$ single crystals, elect. and optical props. for solar cell appl. 80−10981
$CuGaSe_2$ thin films, on GaAs substrates, structural and elec. props., photoluminesc. meas. 79−65564
CuI, photolum., effect of heat treatment temp. 77−52151
CuI, single crysts., growth and optical props. 80−93470
$CuInS_2$, cathodolum. spectra, heat treatment and electron irrad. effects 78−10996
$CuInS_2$, optical and elec. phenomena 78−39605
Cu_2O, evidence of competitive phenomenon between 0.72 μm and 0.93 μm luminesc. 78−27310
Cu_2O, exciton luminesc. spectra, mag. field influence 80−80860
Cu_2O, ortho and para exciton lifetime meas. 80−6730
Cu_2O, positive and negative photomemory, IR luminesc. spectra, illum. effect 79−69557
Cu_2O, residual conductivity, role of vacancies, photoluminesc. and photocond. 77−15901
Cu_2S-CdS heterojunction diodes, barrier model estimated from photovoltage and cathodoluminesc. spectra 79−78165
Cu_2S-Ga_2S_3 alloys, cryst. growth, struct. and fluoresc. 77−48328
Cu_xS film for Cu-Cd-S solar cell, cathodolum. spectrum rel. to prod. method 79−56866

luminescence of inorganic solids continued
Cu_xS, photon and electron excitation phenomena 79−7865
Cu_3SbSe_4, cathodoluminesc., 90-298K 77−40290
p-Cu_2Sn-n-ZnS heterojunction, I-V characts., photocond. and electrolum. 78−72251
Dy^{3+} activated vanadates, photoluminesc. meas. 77−77277
DyP_5O_{14}, luminesc. spectra 77−52155
$Dy_2[Pt(CN)_4]_3.21H_2O$, phase transitions, X-ray study and spectroscopic study 79−60506
Er^{3+} doped phosphors, IR excitation and absorpt. and emission spectra *(Russian)* 79−52021
ErAG, rare earth impurity, spectral probe of stoichiometry variations 77−85790
ErAlG:Ho, Tm, Et⇄Ho and Er⇄Tm energy transfer, fluorescence meas. 78−27305
ErGG, rare earth impurity, spectral probe of stoichiometry variations 77−85790
ErP_5O_{14}, single cryst., radiative and non-radiative transitions 79−19920
$Er_2SiO_5:Ho^{3+}$, single cryst., luminesc. and stimulated emission 77−69895
$Er_2[Pt(CN)_4]_3.21H_2O$, phase transitions, X-ray study and spectroscopic study 79−60506
Eu complex, $(Et_4N)_3$ $[Eu(NCS)_6]$, Eu^{3+} ion site symm. 78−84656
Eu complex, benzoylacetonate, energy transfer at high pressures 78−52541
Eu complex, benzoyltrifluoro-acetone-chelate, refr. index determ. of fluoresc. films 80−40175
Eu compounds tetrahedral, ligand struct., rel. to luminesc. spectra satellite intensity *(Russian)* 78−72603
Eu double metaphosphates with alkali metals or H, luminesc. props. 80−100675
Eu monochalcogenides, anti-Stokes luminesc. 78−60515
Eu, monochalcogenides, multiphonon inelastic light scatt. 77−90144
Eu^{2+} activated phosphors, luminesc. efficiency, temp. and high pressure 78−23508
Eu^{2+}, broadband luminesc. in fluorite struct. crysts. 79−65923
Eu^{2+} doped microcrystals, unusual optical emission 79−73992
Eu^{2+} impurities in cubic crystals, 5d→4f radiative transition probability calc. 80−71474
$Eu_2B_5O_9Cl(Br)$, synthesis and characterisation 80−39039
$EuGa_3(BO_3)_4$, luminesc. spectra, local symmetry of rare earth ion determ. 80−16095
$Eu_xLa_{1-x}Ta_7O_{10}$, polycryst., luminesc. and excitation spectra 80−60659
$EuNa_2Mg_2(VO_4)_3$, disordered, thermal quenching of luminesc. 80−71472
EuO, anti-Stokes luminesc., magnon assisted 78−31252
Eu_2O_3-Gd_2O_3-Ta_2O_5 system at 25, 50 and 75 mole.% Ta_2O_5, cross section investig. 77−12607
Eu_2O_3-R_2O_3-Ta_2O_5, R=La, Gd, Y, quasibinary cross sections 77−90333
Eu_2O_3-Sc_2O_3-Ta_2O_5 system, orthotantalate section, X-ray diffr. and luminesc. obs., conc. depend. 80−54205
Eu_2O_3-Y_2O_3-Ta_2O_5, struct., phase form., luminesc. and X-ray diffr., obs. *(Russian)* 78−6765
Eu_2O_2S, cooperative optical absorption obs. in luminesc. excitation spectra 78−27308
$Eu_3O_4(S_4)$, mixed valence system, inelastic light scatt., photoluminesc. 77−90145
EuP_5O_{14}, 4f-level press. depend., fluorescence exam. 77−72841
EuP_5O_{14}, luminesc. of Eu^{3+}, transition probabilities 80−80845
EuP_5O_{14}, luminesc. spectra 77−52155
Eu_3S_4, inelastic light scatt., photoluminesc., anomalous vibr. 77−48229
$Eu_xSr_{1-x}O$, ferromag. ordering and photoluminesc. 77−66313
$Eu_xSr_{1-x}S$, ferromag. ordering and photoluminesc. 77−66313
$Eu_xSr_{1-x}S$, magneto-optical redshift in absorpt. and photoluminesc., mag. short-range order 80−71388
$EuTi_{1.5}W_{0.5}O_6$, Stark sublevels in mag. suscept. and luminesc. 77−51876
EuX, X=chalcogen, antiStokes luminesc. 77−63455
Fe, ferromagnetic, partial circular polarisation of thermal emission in mag. field 80−71387
Fe flakes, light flashes, tribo-induced discharge luminesc. rel. to astrophys. 80−25471
Fe, surface contamination due to polishing, determ. by luminescent-discharge spectrometry *(French)* 79−52839
Fe_2O_3, semicond. anode in aq. electrolyte, electrolum. and electrochem. 80−76080
$Fe_3[Co(CN)_6]_2.12H_2O$ struct. dehydration fluorescence and IR studies 80−28976
GGG, GGG-ErGG, rare earth impurity, spectral probe of stoichiometry variations 77−85790
(Ga,Al)As:Si(Ge), epitaxial layers, radiative recomb., compensation, cathodolum. study 80−66307
Ga complex, photoluminesc. spectra, $\pi\rightarrow\pi^*$ and charge transfer L→M transitions, Stokes shift 78−64407
n-GaAS epitaxial film, radiative recomb. under influence of mech. stresses 80−66291
GaAS, photoluminescence in polycrystalline samples at 5K, possible solar cell material 79−99929
GaAS, semiinsulating, heat treatment effects 78−6382
GaAlAs DH laser diodes, catastrophic degradation 79−50290
(GaAl)As DH laser wafer, photoluminesc. improvement with buffer layer 80−64014
(GaAl)As, DH lasers, degradation mechanisms, temp. depend. 78−66825
GaAlAs DH lasers, proton-bombard., nonradiative recomb., luminesc. time-response meas. 79−98371
GaAlAs, luminescence circular polarisation, electron optical orientation resonant variation *(Russian)* 80−84782
GaAlAs p-n heterostructures, current-flow mechanisms, luminesc. spectra 80−20298
GaAlAs, SEM defect study, transmission cathodoluminescence 79−64964
GaAlAs:Zn recombination radiation drift, charge carrier photon induced drift in varigap semicond. 80−50418
GaAlAs-GaAs double heterostructure, interfacial recomb. velocity, photolum. meas. 78−68075
$Ga_{0.5}Al_{0.5}As$-GaAs(:Ge) DH structure, minority carrier lifetime and internal quantum efficiency of surface-free GaAs 79−43013
$Ga_{1-x}Al_xAs$ DH catastrophically degraded laser, TEM obs. of defects 80−32989
$Ga_{1-x}Al_xAs$, degraded DH LED, defect struct. by electrolum. topography and TEM obs. 79−60369
$Ga_{1-x}Al_xAs$, electrolum. study using high-gain image intensifier 80−55193

luminescence of inorganic solids continued
$Ga_{1-x}Al_xAs$, epitaxial, radiative deep states 80−76061
$Ga_{1-x}Al_xAs$, hot electron distrib. meas. and calc. 78−27318
$Ga_{1-x}Al_xAs$ LPE layer photoluminescence obs. *(Polish)* 77−77268
$Ga_{1-x}Al_xAs$ n-p_3-p_2-p_1-p_0 struct., degradation electrolum. 80−50428
$Ga_{1-x}Al_xAs$, photoluminescence, deep level trap emission capture 80−29805
$Ga_{1-x}Al_xAs$ structures, STEM and scanning deep level transient spectroscopy in defect centre anal, cathodoluminesc. techniques 80−103642
$Ga_{1-x}Al_xAs$:Si, Si determ., spectrochem. method, photoluminesc. spectra, Hall effect meas. *(German)* 77−77851
$Ga_{1-x}Al_xAs$:Si p-n junction, reemission effects 78−15230
$Ga_{1-x}Al_xAs$:Si p-n junction, doping in LPE, elec. and luminesc. props. *(Czech)* 78−47851
$Ga_{1-x}Al_xAs$-GaAs heterojunctions grown by metallorganic CVD 80−15599
$Ga_{1-x}Al_xAs$-GaAs solar cells, photoluminesc. characterisation 80−3512
$Ga_{1-x}Al_xAs_{1-y}P_y$-GaAs heterojunctions, light-induced misfit dislocation motion, photoluminesc. and X-ray diffr. meas. 79−11200
$Ga_{1-x}Al_xN$ heteroepitaxial films, photoluminesc., cathodoluminesc. 80−66292
$Ga_xAl_{1-x}N$, epitaxial film, cathodoluminesc. 80−25469
$Ga_xAl_{1-x}N$ film, growth and props. 78−39702
$Ga_{1-x}Al_xP$, LPE grown, green electroluminescence 78−19571
$Ga_{1-x}Al_xP$:N epitaxial films, ion implanted, cathodoluminescence study 80−60684
$Ga_{1-x}Al_xSb$ p-n structure, variable-gap, elec., photoelec. and electrolum. props. 77−11996
$Ga_{1-x}Al_xSb$ p-n structure, variable-gap, electroluminescence 78−52582
Ga(As,P):N, isoelectronic impurity states, long-range, short-range model 80−75524
GaAs, ambient-enhanced photoluminesc. props., mol. adsorption and gas-flow effect 79−99925
GaAs amorphous film/GaAs crystal junction, optical and elec. props. 79−99611
GaAs, Auger recombination, luminesc. meas. 77−85850
n-GaAs, Auger transitions, nonlinear extrinsic luminesc. study sublinear emission 79−95833
GaAs, carrier lifetime, radiation induced changes, edge luminesc. spectra 77−8664
p-GaAs, circular polarisation of hot luminesc. 78−52572
GaAs, complex luminesc. centres at 1.20 and 1.30 eV 77−16386
GaAs, deep radiation centres from heat treatment, γ-irrad., deform., probability of nonradiative electronic transitions 80−50408
GaAs, degraded layer form. by annealing, photolum. obs. of defects 78−10968
GaAs diode, quantum efficiency and nonequilibrium carrier lifetime 77−12442
GaAs, donor and acceptor concs. determ. by optical method 78−19525
n-GaAs, donor-acceptor pair recomb., isolated-pair model revisited 79−28825
GaAs, donor-acceptor type complex, mag. field splitting of photolum. line 79−15512
GaAs, doped with Group IV elements, etching, electron spectra, cathodoluminesc. study of inhomogeneities 77−11556
GaAs, electroluminescent study of irrad. induced struct. damage, athermal annealing 80−108280
p-GaAs, electron minority carrier diffusion lengths 80−29807
GaAs, electron-exciton collision influence on luminescence line profile due to bound excitons 80−29800
GaAs, electron-hole liquid form., luminesc. 79−33804
GaAs, electron-spin relaxation and recomb. kinetics, time-resolved luminesc. study 80−108074
n-GaAs, electronic transition scheme via radiative centres 77−69905
GaAs epilayers, high-quality, sharp-line transitions due to donor-acceptor recomb. 78−6768
GaAs, epitaxial, nonequilibrium carrier relax., recombination radn. 80−7416
GaAs, epitaxial film, photon transfer of excitation of nonequilibrium carriers, radiative recomb. 77−8639
GaAs epitaxial films on strongly doped substrate, basic parameter meas. utilising magnetoresist. and SEM techniques under cathodoluminesc. conditions 80−65728
GaAs epitaxial layer, comparison of compensation ratios determ. by photolum. and elec. methods 79−28818
GaAs epitaxial layer, photoluminesc. defect complex 80−29804
GaAs epitaxial layers, electronic surface props., photoluminesc. exam. 77−20901
GaAs, epitaxial layers, high density electron-hole plasma luminesc. 78−19537
p-GaAs epitaxial layers, electron-hole plasma, quantum effects in magnetoluminesc. 78−72591
GaAs, epitaxial layers, multiexciton complex bound to neutral acceptors, photoluminesc. obs. 79−87503
GaAs excited by HV pulses, stimulated emission and luminesc. obs. 79−59704
GaAs, excited luminescence, influence of IR illumination 80−76072
GaAs, exciton effects in photocond., photoluminesc. 80−96797
n-GaAs, exciton luminescence, excitation intensity depend. 78−52554
GaAs FET structure, sharp line photolum. spectra 78−72248
GaAs, film, radiative relax. time, nonequilibrium carriers 78−84657
GaAs, gamma and electron irrad. defect formation depend. on interface, luminescence study 80−34057
GaAs, γ- and electron irradiation, influence on recomb. characts. near surface 80−71478
n-GaAs, heat treated, origin of 1.41 eV emission band, photolum. expt. 78−72579
n-GaAs, heavily doped, non-linear extrinsic luminesc., role of Auger recombination 79−52010
GaAs heterolaser, active layer, photoluminesc., temp. depend. *(Russian)* 79−10310
GaAs, highly deformed samples, absence of dislocation-induced luminescence 79−4835
GaAs, holes optical orientation, luminesc. 80−25452
GaAs homoepitaxial interface, thermal degradation 77−11988
GaAs homojunction LED, mechanical stress induced degradation 80−2860
n-GaAs, hot electron distrib. function with LO phonon kink, photoluminesc. 79−19925
GaAs, hot electrons and exciton-electron collision under external elec. field 78−43928
luminescence of inorganic solids continued
GaAs, hot photoluminescence spectrum, polarisation depend. 78−31254
GaAs, hot photoluminescence depolarisation in mag. field, 0.4 eV energy state electron lifetime *(Russian)* 80−16086
GaAs, hot photoluminescence spectrum on pumping across the L-valley *(Russian)* 80−103984
n-GaAs, IR luminesc. emitted by travelling acoustoelec. domains 78−27329
n-GaAs, IR luminescence from acoustoelectric domains 77−55822
n-GaAs, IR luminescence of acoustoelectric domains 78−31258
GaAs, impact ionisation of excitons 79−38079
GaAs, impurity anal. by photoluminescence *(Japanese)* 77−24888
n-GaAs, impurity interaction and donor-acceptor recombination 80−16094
GaAs, indirect band edge, determ. by quantum-well bandfilling 78−92120
GaAs injection laser, intensified luminesc. *(Russian)* 78−90416
GaAs injection lasers, amplified luminesc. 80−2824
n-GaAs, interband transition times, luminesc. depolarisation obs. *(Russian)* 79−33831
n-GaAs, intrinsic emission intensity, role of local centres in determ. of conc. depend. 78−39599
n-GaAs, intrinsic luminescence intensity, effect of 0.94, 1.0, 1.2 and 1.3 eV radiative centres 78−23517
GaAs, ion bombarded, defect distrib., photolum. meas. 77−20920
GaAs, ion etching, effects on optical props. and lattice disorder 78−83122
n-GaAs, ion implanted films, optical and luminesc. props. 80−60699
GaAs, LED, absolute internal quantum efficiencies determ. 77−63461
n-GaAs, LPE, impurity compensation photolum. and free carrier conc. meas. 77−62558
GaAs LPE buffer layers for MESFET appls. 80−29887
GaAs, LPE layers, ambient O_2 effect on defects and elec. props. 77−76683
GaAs LPE layers, dopant tracing of terrace growth 78−75948
GaAs laser material, secondary dislocation climb during optical excitation 78−75672
p-GaAs, linear polarisation of hot photoluminescence 79−38661
n-GaAs, low energy photolum., 77K, deep centre obs. 77−69877
GaAs luminesc. emitted as a result of carrier heating 77−52185
GaAs, luminesc. emitted by deep centres, illumination-induced change in internal quantum efficiency 79−91495
GaAs, luminescence by laser excitation, photocarrier thermalisation and polariton kinetics 77−66533
GaAs, luminescence due to deep centres, annealing effect on quantum efficiency 77−55825
GaAs, luminescence during streamer discharge *(Russian)* 77−55835
n-GaAs, luminescence emitted from deep centres, γ-irrad. induced changes in internal quantum efficiency 80−20701
GaAs, luminescence emitted from deep centres, plastic deform. effect on internal quantum efficiency 80−60672
GaAs, MBE, growth temp. depend. and characts. 79−28946
GaAs, MBE, undoped, growth and characterisation 80−10836
GaAs MBE epilayers, photoluminesc. and elec. characterisation 80−11500
p-GaAs, MBE grown, As_2 and As_4 effects on photolum. 80−103974
GaAs MOS and Schottky systems, electromodulated reabsorption of luminesc. 79−15524
p-GaAs, magnetoluminesc. of cond. band to acceptor transition 77−1716
GaAs, melt grown, improve elec. and luminesc. props. after short time heat treatment 77−63452
n-GaAs, melt-grown, stoichiometry, photolum. obs. 78−72583
GaAs, minority carrier diffusion length, reabsorbed radiation effect 77−28191
n-GaAs, non-Maxwellian electron distribution function, from electric field-depend. photolum. spectrum 79−11450
GaAs, nonlinear extrinsic luminescence 78−84645
GaAs, nonlinear light absorpt., photoluminesc. meas. 77−66528
GaAs, O^+ implantation, energy levels, photoluminesc. 80−24838
GaAs on $Ga_xAl_{1-x}As$, electron scatt., cathodoluminesc., loss spectra 80−104023
GaAs p^+-n diode, radiative hot carrier recomb., photoluminesc. and electroluminesc. meas. 79−38676
GaAs, photocarrier thermalisation by laser excitation spectroscopy 78−31250
n-GaAs, photolum., rel. to n-InP 77−40272
GaAs, photolum. intensity degradation caused by excitation-enhanced oxidation 78−15205
GaAs, photoluminescence, deep level trap emission capture 80−29805
GaAs, photoluminescence, electron-acceptor, from non-Maxwellian distrib. of photo-excited electrons 80−45138
GaAs, photoluminescence, electron gas coding influence in ion-bombarded layers 80−108272
GaAs, photoluminescence at low temp., free exciton recomb. mechanisms *(Russian)* 77−32438
GaAs, photoluminescence and resonant Raman spectra, press. depend. 78−31251
GaAs, photoluminescence intensity rel. to heat treatment in S vapour *(Russian)* 78−48216
GaAs, photoluminescence intensity of cleaved surface, ambient gas influence 78−88345
GaAs, photon transfer of excitation of nonequilib. carriers, conc. profile and relax. time 77−69907
GaAs, polar semiconductor, collisions between hot excitons and hot electrons 80−7415
GaAs, polarisation anisotropy of hot photolum. *(Russian)* 77−90195
GaAs, polariton fluoresc., spatial and spectral features 79−33760
GaAs, prep. of thin films by ionised-cluster beam deposition, photolum. meas. *(Japanese)* 80−25596
GaAs, psec time resolved spectroscopy, electron-hole plasma 79−47500
GaAs pure and Se-doped, photoluminescence at dislocations, band gap electronic levels 79−99926
GaAs, radiative yield improvement by laser annealing 80−45128
GaAs, recombination radiation, anomalous temp. depend. 80−2847
n-GaAs, recombination scheme for $h\nu_m \approx 1.0$, 1.2 and 1.3 eV luminesc. bands 77−69906
GaAs, reson. polariton fluoresc. obs. 77−85785
GaAs, SEM defect study, transmission cathodoluminescence 79−64964
GaAs, semi-insulating, thermal conversion, Hall effect and luminesc. meas. 78−6405
GaAs, spin-depend. recomb., photoluminesc. obs. 80−60666

luminescence of inorganic solids continued
GaAs, spontaneous luminesc. due to high density electron-hole plasma under nano- and picosecond pulse excitation 80−40157
GaAs, stimulated and spontaneous emission from degenerate electron-hole plasma at 300K 80−29762
n-GaAs substrates, ion implanted, compensation 78−75680
GaAs surface, Ar ion bombardment induced photon emission, rel. to target temp. 78−72612
GaAs thin layers, MBE, growth conditions and phys. props. *(German)* 80−55307
GaAs, two-photon 1.06 μm absorption coeff., absolute meas. 78−19527
GaAs, two-photon absorpt. spectrum, band gap luminesc. 78−10888
n-GaAs VPE layers, Hall mobility, effect of Cu contamination, photolum. expts. 80−54810
GaAs VPE layers for FET devices, impurity characterisation 80−29491
GaAs, VPE on Ge substrate, and characterisation 78−72736
n-GaAs vapour phase epitaxial film electrophysical props. rel. to growth temp. *(Russian)* 80−49961
GaAs, weakly excited, luminesc. from exciton polaritons, based on exciton-electron collisions 79−83020
GaAs: Si(Te), radiative recomb. *(Russian)* 79−91499
GaAs:Be, ion implanted, elec. profiling and optical activation expts. 77−89457
GaAs:Be, ion-implanted, photolum. spectra, effects of implantant depth distrib. 78−27293
GaAs:Be,Se VPE layers, ion implanted, donor-acceptor pair radiative recomb. 79−91489
p-GaAs:Be layer, MBE growth, Be doping and diffusion, elec. and optical props. 77−51397
GaAs:Be(C)(Ge)(Sn), MBE layers, photoluminesc. 80−29803
GaAs:C, Zeeman effect of effective mass acceptor, polarised luminesc. 79−4541
GaAs:Co VPE layers, bound-exciton luminesc., Zeeman anal. 79−95818
GaAs:Cr, 0.84 eV no-phonon luminesc., fine struct. and origin 80−103980
GaAs:Cr, exptl. verification of Cr^{2+} models of photoluminescent transitions 78−27320
GaAs:Cr, fine structure in cathodoluminescence spectrum 78−56524
GaAs:Cr, intracenter radiative transition in Cr^{2+} ions 79−11463
GaAs:Cr, luminesc. stress splitting, 4.2K 78−84627
GaAs:Cr, luminescence and absorption spectra, temp. depend. of fine structure 80−6779
GaAs:Cr, Mg, ion implanted, elec. meas. and optical activation studies 79−86806
GaAs:Cr, O, effect of O in photoluminesc. meas. 80−29799
GaAs:Cr, origin of sharp near IR transitions 80−10913
GaAs:Cr, photoluminescence in strong electric fields 80−108270
GaAs:Cr, semi-insulating, i.r. induced modulation of cathodoluminescence, and specimen current 77−1737
GaAs:Cr, semi-insulating, Zeeman studies of 0.839 eV emission 80−103987
GaAs:Cr, Si, deep centre photoluminescence spectra 78−95601
GaAs:Cr, surface and bulk recombination parameter determ. from photoluminesc. spectra 77−55820
GaAs:Cr, VPE growth, carrier conc. profiles, photoluminescence spectra 79−74099
GaAs:Cr photoluminesc. meas. 78−6761
GaAs:Cr semi-insulating substrate, photoluminescence obs. of surface degradation during LPE growth 78−6865
GaAs:Cr semi-insulating wafer, heat treatment technique for no thermal conversion 80−100857
GaAs:Cr(O), mechanism of thermal quenching of luminesc. and photocurrent stimulation 77−55821
GaAs:Cr(W), deep trapping centre exam. by thermally stimulated capacitor discharge method and luminesc. 77−55495
n-GaAs:Cu, contaminated single cryst., deep level photoluminesc. model 78−68554
GaAs:Cu melt grown, 1.36 eV band luminescence studies, edge emission 79−87510
n-GaAs:Ge, film, substrate temp. depend. of Ge incorporation during MBE 80−76196
GaAs:Ge, ion-implanted, photoluminesc., deep emission centres 80−34965
GaAs:Ge, LPE, on semi-insulating GaAs, film-substrate interface characterisation 78−72017
GaAs:Ge, vap. grown, diatomic complex donor and acceptor model 78−80003
GaAs:Mg, photoluminesc. temp. depend., 4.2-293K 77−69878
GaAs:Mg ion implanted, photoluminesc. and annealing characts. 77−16361
GaAs:Mg(Be)(Cd)(Zn), implanted, low temp. photolum. spectra 78−39583
GaAs:Mn, LPE layer, near band edge photoluminescence, 2K, low excitation intensities 78−48218
GaAs:Mn, photoluminesc., emission props. and radiative mechanism 79−56842
GaAs:O, electrolum., photolum., negative differential resist. rel. to recomb. processes 80−66304
GaAs:O, field depend. of radiative recomb. 80−20700
GaAs:O, optical characterisation of deep O implants 77−55294
GaAs:P films, epitaxial growth from melt with components introduced by ion bombardment 77−21044
GaAs:S, LPE growth, photoluminescence spectra at liquid N_2 temps. 79−33948
GaAs:Se cathodoluminescence decay obs. with SEM and streak camera, 90 to 300K 80−97348
GaAs:Si, accelerated growth rate effect on MBE, Hall mobility and photolum. meas. 80−104067
GaAs:Si, epitaxial layers, photo- and cathodoluminesc. 77−77285
GaAs:Si, influence of stoichiometry on recomb. processes 80−93396
GaAs:Si, ion implanted, photoluminesc. 79−69887
n-GaAs:Si, ion implanted and/or annealed, As vacancy form., photolum. line 77−27875
GaAs:Si, LED, effect of struct., defects on quantum efficiency 79−11211
n-GaAs:Si, thermally treated, photolum., acceptor levels obs. 79−38587
GaAs:Si, thick LPE layer growth and characterization 77−12511
GaAs:Si encapsulated with AlN, Si_3N_4 layers, photolum., annealing effects 80−20681
GaAs:Si layers, MBE growth, elec. and optical props., doping characts. 80−10819

luminescence of inorganic solids continued
GaAs:Si p-n junction, electrolum. power, injection current and temp. depend. *(Russian)* 77−16401
GaAs:Si p-n junction LED, electroluminesc. efficiency 80−71491
GaAs:Si p-n structure, radiative recombination region 78−52071
GaAs:Si(Ge) LPE layers, luminesc. props. rel. to substrate quality 78−52583
n-GaAs:Si(Te), radiative transitions induced by modest annealing, photoluminesc. spectra 80−55158
GaAs:Si(Te)(S), vapour phase epitaxial grown layers, photoluminesc. and emission spectra 80−29774
GaAs:Sn, 1.39 eV luminescence, injection level depend., freq. response and thermal quenching 78−19529
n-GaAs:Sn, photoluminesc. spectra 79−43031
GaAs:Sn, selective LPE, orientation dependent growth, luminesc. 77−12551
GaAs:Sn, Te, luminescence props. 79−52017
GaAs:Sn epitaxial layer, electronic props. and epilayer-substrate interface props. 77−89886
n-GaAs:Te, 0.93-0.99 eV luminesc. band characts. 78−19560
n-GaAs:Te, heavily doped, interband luminesc. intensity, heat treatment effect 78−72593
GaAs:Te, impurity cond., microcathode-luminesc. investig. 77−8666
n-GaAs:Te, vibr. props. of 1.0, 1.2 and 1.3 eV luminesc. centres 77−55823
GaAs:Te influence of fluctuations of impurity pot. on Burstein-Moss effect 78−48240
GaAs:Te(Cd)(Mg)(B), ion implant depth distribs., AES and glow discharge optical spectroscopy meas. 80−65028
GaAs:V, ion implanted, luminesc., level splitting 80−97338
GaAs:W^{2+}, radiative transitions, photoluminesc. obs. 80−108271
p-GaAs:Zn, diffusional doping, photoluminesc. in mag. field 77−16384
GaAs:Zn, distribution of radiative recombination efficiency 79−78725
GaAs:Zn, heavily doped, photolum. obs., above gap 80−29796
p-GaAs:Zn, luminescent, ion doped MBE growth 80−44436
GaAs:Zn films, VPE growth and photoluminesc. props. 79−38642
GaAs:Zn MBE layers, ionized beam doping, elec. and optical characts. 79−37721
GaAs/(Ga,Al)As, DH laser diode, electroluminescence near 1 eV 80−60682
GaAs-(GaAl)As epitaxial layers and DH lasers, deep centre 1.02 eV luminesc. 78−80387
GaAs-$Al_xGa_{1-x}As$ DH laser structures, high-resolution composition profiling with photolum. 78−71101
GaAs-$Al_xGa_{1-x}As$ DH lasers, MBE grown, substrate temp. effect on current threshold 80−48243
GaAs-$Al_xGa_{1-x}As$ heterostruct., photon recycling, diffusion length and lifetime determ. 79−47499
GaAs-$Al_xGa_{1-x}As$ multilayer, photoluminesc., electron spin orientation 80−25453
GaAs-AlAs, epitaxial struct. with alternate layer comp. modulation, fabrication and characterisation 77−1322
GaAs-AlAs layered films, MBE prep., struct., rel. to optical props. 79−77950
GaAs-AlAs multilayer heterostructure laser, power and photoelectroluminescence characts. 80−53297
GaAs-AlGaAs photoelectroluminescent diodes, characts., radiant power 80−6972
GaAs-Au, quenching of exciton luminesc. by surface elec. field 80−29801
GaAs-Cu:Tl, cathode luminescence spectra, Hall effect, cryst. defects 80−76087
GaAs-disperse metal film, photoluminesc. at interface 78−26953
GaAs-$Ga_{1-x}Al_xAs$ red LED, 4% quantum yield *(Russian)* 77−85809
GaAs-$Ga_{1-x}Al_xAs$-$Ga_{1-y}Al_yAs$ n^+-i-n heterostructure, electroluminesc. characts., 80 to 330K *(Russian)* 79−28404
GaAs-$Ga_xAl_{1-x}As$ DH laser material crystal cathodoluminescence, SEM analysis 80−97349
GaAs-$Ga_xAl_{1-x}As$ heterostructure, depend. of efficiency of radiative transitions on composition 78−2909
GaAs-$Ga_xIn_{1-x}P$ heterostruct., MBE layers, photolum. props., assessment as laser struct. 80−20705
GaAs-GaAlAs, DH laser material, LPE grown, obs. of melt carryover 78−91553
GaAs-GaAlAs DH LEDs, with thin active layer, Burrus type, internal interference in emission spectrum 78−27325
GaAs-GaAlAs DH lasers, optical studies of defects and degradation 78−18654
GaAs-GaAlAs DH lasers, strain-enhanced luminesc. degradation, photoluminesc. obs. 80−69392
GaAs-GaAlAs wafers, defects and degradation, transmission cathodolum. evaluation 80−65395
GaAs-GaP heterostructure, radiative recomb. under influence of mech. stresses 80−66291
GaAs-insulator film interface, evidence for growth-induced damage from photolum. expts. 78−75953
GaAs-Si_3N_4 system, photoluminesc. edge line *(Russian)* 79−4852
GaAs-ZnSe system, heterovalent solid solns. of substitution, prep. and investig. 77−24553
$GaAs_{1-x}P_x$, hot photoluminescence spectrum, polarisation depend. 78−31254
$GaAsAl_xGa_{1-x}As$ heterostruct., anomalous elec. and optical characts. 80−2865
$GaAs_{0.6}P_{0.4}$ LED, luminesc. investig. of degradation, deep-level form. at dislocations 77−40287
$GaAs_{0.6}P_{0.4}$:N, isoelectronic tape by ion implantation and CO_2 laser annealing 80−24464
$GaAs_{0.6}P_{0.4}$:$Zn^+(Ar^+)$, ion-implanted, thermal degradation of mechanical surface perfection and surface photolum. 77−77271
$GaAs_{1-x}P_x$, $0 \leq x \leq 1$, evidence for common nature of certain deep-level radiative centres 78−6767
$GaAs_{1-x}P_x$, bound exciton, luminesc. reson. excitation 79−95840
$GaAs_{1-x}P_x$ epitaxial films, VPE grown, photolum. spectra 79−73997
$GaAs_{1-x}P_x$ epitaxial layers prep., photoluminesc. and electroluminesc. props. *(Czech)* 78−48233
$GaAs_{1-x}P_x$, indirect-gap, evidence for exciton localization by alloy fluctuations, photolum. 80−66276
$GaAs_{1-x}P_x$, mol. beam epitaxial growth, cryst. quality, composition investig. *(Japanese)* 77−55895
$GaAs_{1-x}P_x$, N implantation, characterisation by photolum. and channelling 80−54262

luminescence of inorganic solids continued
$GaAs_{1-x}P_x$, N^+ implantation photoluminesc. props. 77−68987
$GaAs_{1-x}P_x$, N^+ implantation, annealing props. 77−68988
$GaAs_{1-x}P_x$, solid soln., synthesis by ion implantation P^+ ions 78−38741
$GaAs_{1-x}P_x$, structural defects, optical props. effect 80−55208
$GaAs_{1-x}P_x$:N, 0.6<x<1, photoluminesc., comp. depend. 78−52546
$GaAs_{1-x}P_x$:N, doping using inonised beam in MBE, photolum. meas. 78−47400
$GaAs_{1-x}P_x$:N, film, optical absorpt. from photoluminesc. meas. 78−92134
$GaAs_{1-x}P_x$:N, Koster-Slater model and N-states 78−47732
$GaAs_{1-x}P_x$:N, LED, external quantum efficiency, press. effect 77−8655
$GaAs_{1-x}P_x$:N, N isoelectronic trap, model calc. of N_Γ and N_x electronic states 78−10398
$GaAs_{1-x}P_x$:N, photoluminesc. and optical absorpt. spectra of N impurity bound-excitons 79−47496
$GaAs_{1-x}P_x$:N, photolum. and electrolum. study of N isoelectronic traps 80−89061
$GaAs_{1-x}P_x$:N, upper branch of N isoelectronic trap., photo- and electrolum. expts. 77−63462
$GaAs_{1-x}P_x$:N epitaxial layers, absorption and photolum. spectra meas. 77−24894
$GaAs_{1-x}P_x$:N heterojunction, N_x and N_Γ bound states, high-press. effects on electroluminesc. meas. 77−11870
$GaAs_xP_{1-x}$ epitaxial film nonlinear light absorpt., photoluminesc. meas. 77−66528
$GaAs_xP_{1-x}$, liquid phase epitaxial growth on GaP, growth and properties 79−47641
$GaAs_{1-x}P_x$(Te), bound exciton stress depend., piezoluminescence, photoluminescence 80−80206
$GaAs_{1-x}Sb_x$, ($x \leq 0.05$), band gap, temp. depend., from edge photolum. meas. 80−71486
$GaAs_{1-x}Sb_x$ undoped epitaxial layers, photoluminesc. meas. 80−20703
$GaAs_xSb_{1-x}$, epitaxial layer, struct. defects rel. to luminesc. 78−72040
$GaAs_xSb_{1-x}$-GaAs epitaxial films and multilayer heterostruct., SEM obs. under cathodolum. conditions 79−11023
$(GaAs)_{1-x}(ZnSe)_x$, LPE growth, resist., Hall effect and cathodoluminesc. meas. 77−28270
$(GaAs)_x(ZnSe)_{1-x}$ single crystal, visible cathodoluminesc. spectra 80−20716
GaInAs-InP, growth by low-pressure metalorganic CVD 80−71595
p-$Ga_xIn_{1-x}As$, Auger recomb., theory and luminesc. expts. 78−56518
$Ga_xIn_{1-x}As$ p-n junction, growth and electrolum. spectra 77−20420
GaInAsP-InP, lattice matched, emission spectrum half width rel. to peak wavelength 80−2820
$Ga_xIn_{1-x}As_{1-x}P_x$ film, energy band struct., photolum. meas. 79−7784
n-$Ga_xIn_{1-x}As_{1-y}P_y$, photoluminesc. of epitaxial films; isovalent substitution 80−16097
$Ga_xIn_{1-x}As_yP_{1-y}$, LPE layers, growth and characterisation 78−38983
$Ga_xIn_{1-x}As_ySb_{1-y}$, epitaxial film and DH, efficiency 77−686
$Ga_xIn_{1-x}P$, real struct. exam. by electron microscopy and channelling 78−2143
$Ga_xIn_{1-x}P$, undoped liquid epitaxial layers, effect of heat treatment on photoluminescence 78−60512
$Ga_xIn_{1-x}P$, with indirect band struct., radiative recomb. of free excitons, cathodolum. meas. 77−90202
$Ga_xIn_{1-x}P$:N layers, LPE growth, luminesc. and direct exptl. obs. of band struct. effects 77−52157
GaInPAs heterostructures and LED's, luminescent props. in 1-2 micron band 78−10988
$Ga_xIn_{4-x}PyAs_{1-y}$, In rich bulk single crysts. growth from melt via gradient freeze method, and characterisation 78−68618
$Ga_{1-x}In_xSb$:Zn(Te), photolum. and stimulated emission obs. 78−72595
$Ga_{1-x}In_xSe$, energy bands near absorpt. edge, transmission and photoluminesc. spectra 79−83022
$Ga_{1-x}In_xSe$, layered, luminescence and photocond. obs., two-photon excitation 78−76521
GaN and GaN:Zn epitaxial layers, doping effect on cathodoluminesc. 77−20935
GaN, epitaxial, cathodolum., 78-300K 78−19575
GaN epitaxial films, cathodoluminesc. spectra 80−71496
GaN, epitaxial layer, characts. from cathodoluminesc. 78−35208
GaN epitaxial layers, exciton cathodolum. *(Russian)* 78−76543
GaN epitaxial layers, exciton cathode luminesc. 79−65933
GaN film, preparation by pyrolysis of $Ga(CH_3)_3$ in NH_3, cathodoluminesc. 77−4691
GaN, luminesc. centres 80−93405
GaN, photoluminesc. characts. for 35 implanted elements 77−24884
GaN, photoluminesc. spectra, energy distrib. 80−97339
GaN, polarised electroluminescence emission, microstructure investigations 80−97344
GaN, VPE growth rate influence on elec. and luminesc. props. 80−100702
GaN, VPE on sapphire, and characterisation 78−2387
GaN:Al, VPE grown, luminesc. and elec. props. depend. on doping conc., bound excitons 80−20688
GaN:As(P), implanted single cryst. film, cathodolum. 78−60523
GaN:P, photoluminesc. 79−78730
GaN:Zn, cathodolum. obs., recomb. model 79−11474
GaN:Zn, cathodoluminesc., photocapacitance 79−38679
GaN:Zn, epitaxial layer, effective electroluminesc., blue regime *(Russian)* 77−77302
GaN:Zn, LED, blue, yellow and green emission, temp. depend. 77−8658
GaN:Zn, low voltage LED, epitaxial layer, growth and electrolum. *(Russian)* 77−77297
GaN:Zn, n-i struct., anomalous luminesc. 80−80865
GaN:Zn, polarised electroluminescence, mag. field intensity depend. *(Russian)* 79−91502
GaN:Zn, temp. and press. depends., electrolum. 78−19567
GaN:Zn, VPE grown, optical cross sections, photoluminesc. and optical absorpt. meas. 80−55160
GaN:Zn, VPE growth, photoluminesc. rel. to doping conditions 80−55159
GaN:Zn epilayers, growth parameters effect on props., device struct. 78−26975
GaN:Zn epitaxial films, luminesc. spectra separation into individual bands by impurity absorpt. region excitation 79−74002
GaN:Zn LED, electrolum. centres, rel. to growth morphology, Zn conc. and etch patterns 77−1733
$GaNbO_4$, diffuse refl. and luminesc. spectra 78−56516
β-Ga_2O_3, doped, photolum., emission centres struct. 78−52557
luminescence of inorganic solids continued
β-Ga_2O_3, pure and doped samples, UV luminesc. obs., 5 to 300K 78−80396
β-Ga_2O_3:Cr, temp. depend. of luminesc. characts. *(Russian)* 77−28621
GaP, camel's back induced stabilisation of electron-hole liquids 79−19524
GaP, complex form of donor energy levels, optical spectra anal. 78−23045
GaP, donor-acceptor pair spectra, electron-phonon interactions 79−38631
GaP, donor-acceptor pair luminesc., excitation spectroscopy 80−25440
GaP, dopant dislocations, scanning electron micrographs, cathodoluminesc. 78−91340
GaP, electrolum. study using high-gain image intensifier 80−55193
GaP, electron-hole drop, luminesc. 79−33812
GaP, electron-hole liq., cathodolum. spectra meas., 4.2-20K 77−63470
GaP, electron-hole liquid obs. by luminesc. spectra 77−51668
GaP, electron-hole liquid, emission band from time-resolved spectra 78−43938
GaP, electron-hole liquid props., luminescence at high excitation intensity 79−69882
GaP, electron-hole plasma photolum. obs. 78−52559
GaP, electron-hole plasma luminesc. 79−38651
GaP, epitaxial layer, carrier recomb. at dislocations 77−20932
GaP epitaxial layer, crystal defects influence obs. 79−87511
GaP, epitaxial layers, dislocation recomb., SEM cathodoluminescence studies 79−42558
GaP, epitaxial struct., cathodolum. in SEM 78−10991
GaP, first order Mott transition of exciton gas 78−76535
GaP, frozen-in pt. defects annihilation 79−99949
GaP, GPE layers, nonradiative dark regions along surface ripples 77−59600
GaP, green cathodolum. from cryst. defects, SEM, TEM study 80−80870
GaP, green luminesc. efficiency, review 77−28636
GaP, growth and props. of LPE layers on Si substrates 78−6864
GaP, impurity interaction on excited acceptor states, luminesc. excitation spectra 79−15517
n-GaP, ion implanted films, optical and luminesc. props. 80−60699
GaP, LEC crystal, cathodolum. and photolum. around dislocations 78−84663
GaP, LPE, cathodo- and electrolum., residual impurity and struct. defect effects 78−19570
GaP, LPE, LED fabrication and electroluminesc. characts. 77−28632
n-GaP, LPE, minority carrier bulk lifetime and diffusion coeff. meas. 77−11932
n-GaP, LPE, non-radiative recombination 78−19565
GaP, LPE layer for LED, photoluminesc. distrib. meas. *(Czech)* 78−48209
GaP, luminesc. emission band, electron-hole liquid 77−69245
GaP, luminesc. from electron-hole drops, 2 to 77K 79−11454
GaP, mol. beam epitaxial growth, cryst. quality composition investig. *(Japanese)* 77−55895
GaP, Mott transition of exciton gas, cathodoluminesc. 79−33845
GaP, non-radiative recombination and structural defects 78−19566
GaP p-n junction, capacitance-freq. dispersion and electroluminescence efficiency 78−64101
GaP, powder, electroluminesc. excitation by SAW, nonlinear effects 80−16104
GaP, radiative and non-radiative recombination around dislocations 78−19576
GaP, rare earth doped, photolum. and elec. props. *(Russian)* 78−52545
GaP, red LED degradation, diffusion model 77−8657
GaP, spectral depend. of O photoneutralisation cross-section near threshold, and band gap 79−1788
GaP, stabilisation of electron-hole liquid by camel's back 80−6740
GaP, VPE cryst., electrolum. characts. 77−28631
GaP:Bi,N, photoluminesc., electroluminesc., 4.2 to 300K, excitons and hole traps 80−108275
GaP:Bi(N), luminesc. decay kinetics 79−38646
GaP:Ce(Dy)(Pr) epitaxial films, photoluminesc. spectra 80−66294
GaP:Co, deep levels, IR photoluminesc., stress effects 80−55163
GaP:Co, optical spectra and Zeeman anal. of Co 3d^7 state 80−66247
GaP:Co(Ni), photolum. excitation spectroscopy 80−80841
GaP:Cr, ESR of doubly ionised Cr acceptor and IR luminesc. 78−56374
GaP:Cr, origin of sharp near IR transitions 80−10913
GaP:Cu, deep levels, photoluminesc. and optical cross sections 79−38653
GaP:Dy, photolumines. spectra 79−52015
GaP:Fe, current-voltage characteristics, p-i-n diodes, absorpt. double injection methods 79−65407
GaP:Fe^{2+}, absorpt. and luminesc. spectra 77−16388
GaP:Fe^{2+}(Co^{2+})(Ni^{2+}) d→d luminesc. spectra 80−7414
GaP:H/GaAs, amorphous film/crystal junction, optical and elec. props. 79−99611
GaP:N, appl. of temp. modulated photolum. induced by photoexcitation technique 78−95605
GaP:N, bound excitons, low temp. photoluminesc. thermal quenching 77−48228
GaP:N, Cd(Zn),(C), interimpurity recomb., acceptor binding energies 78−34796
GaP:N, electron-hole liq., luminesc. obs. 80−25438
GaP:N, epitaxial layer, determination of nitrogen concentration from cathodoluminescence spectra 78−38744
GaP:N, excited states of excitons bound to NN_i pairs, fluoresc. obs. 77−44039
GaP:N, luminesc. from electron-hole drop 79−33813
GaP:N, phonon satellite intensity distrib. in luminesc. spectrum 77−55832
GaP:N, photoluminesc., temp. depend., exciton recombination mechanism 78−88355
GaP:N, photoluminescence, temp. modulated 79−38623
GaP:N, radiative recomb. from electron-hole drops, impurity induced transition 78−19547
GaP:N, radiative recomb. of electron-hole liq. 79−73442
GaP:N, spin dependent exciton recombination at N_2 isoelectronic traps 77−69734
GaP:N, temp. modulated photoluminesc. 77−55818
GaP:N, temp.-modulated photoluminesc., phonon assisted tunnelling process 78−23511
n-GaP:N,O,S,C end, dielec. const. from S-C donor acceptor pair spectra 79−65788

luminescence of inorganic solids continued
GaP:N LED structures, local dopant conc. determ. using SEM cathodolum. spectra 80−101057
GaP:N(N,O) epitaxial struct., luminesc. study of degradation during heat treatment 80−45139
GaP:Ni, absorpt. and luminesc. spectra 79−42996
GaP:Ni, deep traps, near IR luminesc., polarised spectra meas. 80−16077
GaP:Ni, optical and EPR study of two-electron-trap state 79−73806
GaP:Ni, VPE GaP, Ni detection 78−15212
GaP:O, impurity concentration determ. by donor-acceptor luminescence 78−6090
GaP:O, optical transitions via deep levels, phonon interaction 78−87939
GaP:O, optical transitions via deep levels, cross section temp. depend. 78−87940
GaP:S, effects of uniaxial stress on luminesc. 79−78739
GaP:S(Se), donor bound exciton excited states 80−66284
GaP:S(Se)(Te), pot.-depend. g-values and quenched diamag., props. of donor states 77−62861
GaP:S(Se)(Te), pot.-depend. g-values and quenched diamag., pseudoacceptors D^0, X 77−62862
GaP:Zn, growth, I-V characts., electroluminesc. *(Korean)* 78−52653
GaP:Zn, luminesc., acceptor-bound multiple excitons 80−11476
GaP:Zn, O, influence of impurity-absorbed illumination on luminesc. 80−93395
GaP:Zn,O, Auger coeff. from luminesc. decay and Hall effect 77−48226
GaP:Zn,O, Auger coeff. from luminesc. efficiency and Hall effect 77−48227
GaP:Zn,O, degradation of bulk luminesc. induced by laser excitation 77−1715
GaP:Zn,O, epitaxial p-n junction, IR electroluminesc. exam. *(Russian)* 78−35207
GaP:Zn,O, kinetics of X-ray luminesc. 78−10984
GaP:Zn,O, photodiodes, high temp. emission spectra *(Russian)* 77−66545
GaP:Zn,O p-n junctions, electron irrad. effect on electrolum., defects form. and quenching obs. 80−55194
p-GaP:Zn,S, spin polarisation of donors and acceptors in mag. field, optical and microwave study 80−93393
GaP:Zn(Mg)(Cd), multiple bound excitons, photoluminesc. obs. 79−95837
GaP-GaAs, amorphous film/crystal junction, optical and elec. props. 79−99611
GaP-ZnSe solid solutions, spectral studies *(Russian)* 79−91498
GaP_xAs_{1-x}, N doped, alloying induced shift between excitation and luminesc. of N bound exciton 79−52013
GaP_xAs_{1-x}:N, luminesc. of N bound state excitons, local-environment effects 80−100691
$(GaP)_x(ZnS)_{1-x}$ solid solutions, X-ray fluorescence spectra, photoluminescence *(Russian)* 79−74003
GaS, anti-Stokes photon replica emission under two photon excitation 77−52175
GaS, electrolum. and electroabsorpt., 77K 77−48247
GaS, luminescence excited by high-intensity two-photon pumping 77−44038
GaS two-photon absorpt., cond. and luminesc. meas. 77−52166
Ga_2S_3-La_2S_3-Nd_2S_3:Nd^{3+} chalcogenide glass, Nd^{3+} emission and absorption spectra, nonradiative relax. 77−40268
GaS_xSe_{1-x}, indirect exciton spectrum and phase transition, luminesc. and absorption spectra 79−8160
GaS_xSe_{1-x}, recomb. radiation intensity, temp. depend. *(Russian)* 79−33830
$3Ga_2S_3$.La_2S_3:Ho^{3+}, radiative and multiphonon relax. 79−33794
GaSb and alloys, struct. defect, photoluminesc. 80−25459
GaSb, Auger recombination, luminesc. meas. 77−85850
GaSb, bound excitons at doubly ionisable acceptors 79−42459
GaSb crystals, uniaxial deform., effect on polarised luminesc. 78−10957
GaSb high-purity and doped layers grown by LPE and VPE methods 78−6863
p-GaSb, hot exciton luminesc., LO phonon Raman scatt. 80−11474
GaSb, interaction of exciton recombination with LO phonons 79−38647
p-GaSb, interband optical pumping, optical detection of EPR 77−28483
GaSb, inversion of Γ and L conduction bands under uniaxial stress, photoluminescence meas. 79−33229
GaSb, photolum., electrolum. meas. in p-n junction, temp. influence 78−72594
GaSb, photolum. spectra under hydrostatic press. 79−19930
GaSb:Fe, shallow acceptor level, electrical meas. 79−11087
GaSb:Sn, p-n junction, electroluminesc. and photoluminesc. 80−66306
p-GaSb:Te, effective radiative recombination centre nature, photoluminescence spectra 79−90998
n-GaSb:Te, heavily doped, electron-hole recomb., photoluminesc. spectra 78−84644
n-GaSb:Te, heavily doped, spontaneous radiative recomb. vel., photoluminesc. spectra 79−11458
GaSb:Te, indirect gap photolum. 80−29797
p-GaSb:Zn film, epitaxial, lifetime of nonequilib. carriers, determ. from circular polarisation of luminesc. 77−24898
GaSb-$Ga_{1-x}In_xSb$ p-n heterojunction, electrolum. spectra and elec. props. 77−12444
$GaSb_{1-x}As_x$, disorder-enhanced Auger recomb. 79−43014
GaSe, additional IR electrolum. band obs. at 77K 78−72607
GaSe, cathodolum., 115 and 285K 79−87512
GaSe, deep free and constrained excitons and biexcitons, collective interactions *(Russian)* 80−66282
GaSe, direct exciton excited state hot luminescence, band struct. props. 80−55183
GaSe, electron beam excited free exciton luminesc. 79−19940
GaSe, exciton, excitation-induced absorption and luminesc. 78−60516
GaSe, exciton luminesc. kinetics, intermediate electron-hole states 80−93389
GaSe, exciton spectra at 4.2K rel. to layer struct. 77−16336
GaSe, exciton-phonon quasibound states, photocond. and luminesc. study 80−96800
GaSe, highly excited, polarisation of luminesc. spectra and electron-hole plasma radiation 77−52169
GaSe, highly excited photoluminesc. exciton-exciton and exciton-carrier scatt. 77−48244
GaSe, interlayer interaction and exciton spectra study 77−52165
GaSe, luminesc. emitted by electron-hole plasma 77−85795
luminescence of inorganic solids continued
GaSe, luminesc. from exciton-electron and exciton-exciton collisions 77−52168
GaSe, luminescence and absorpt. spectrum in region of high-energy resonance 77−44044
GaSe, luminescence excited by high-intensity two-photon pumping 77−44038
GaSe, magnetoluminesc. at 4.2K 79−61345
GaSe, optical excitation, excitonic spectra, stimulated luminesc. 80−40132
GaSe, optical orientation and alignment of free excitons, on resonant excitation *(Russian)* 77−90196
GaSe, photolum. decay 79−15518
GaSe, photolum. under strong optical excitation 79−24364
GaSe, photoluminescence between 4.2 and 40K 78−10974
GaSe, polarized exciton luminesc. 78−6734
GaSe, population dynamics and spin relax. of excitons 77−66122
GaSe, radiative decay of direct and indirect excitons 78−10975
GaSe, radiative transitions, cathodoluminescence 78−10997
GaSe, reson. light scatt., luminesc. and Raman spectra 79−38615
GaSe, spontaneous and stimulated emissions due to exciton-electron and exciton-exciton collisions 77−32421
GaSe, triplet indirect bound exciton, level anticrossing effect on magnetolum. 79−47513
GaSe, two-photon absorpt., cond. and luminesc. meas. 77−52166
GaSe-SnO_2 heterojunction, elec. props. and electrolum. spectra 77−59328
$GaSe_{1-x}S_x$, polytypes, exciton gap energies, luminesc. study 80−54611
GaSe(Te)-SnO_2 spray heterojunction, electro-optical props. 78−64102
$GaSe_{0.9}Te_{0.1}$, undulation spectra associated with acceptor complexes 78−80392
$GaSe_{1-x}Te_x$, energy bands near absorpt. edge, transmission and photoluminesc. spectra 79−83022
$GaSe_{1-x}Te_x$ layered crystal, photoluminesc. meas. 77−1725
$GaSe_xTe_{1-x}$, solid solns., exciton luminesc. 78−10992
Gd complex, benzoylacetonate, energy transfer at high pressures 78−52541
Gd^{3+} in host lattices, energy transfer from sensitizer to activator 79−38628
$GdAlO_3$:Cr^{3+}, mag. field effects on fluoresc. 80−2850
$GdAlO_3$:Er^{3+}, $^4S_{3/2}$ to $^4I_{9/2}$ transition laser action, optical and luminescence spectra 80−16082
$GdBO_3$:Eu^{3+}(Tb^{3+}) and $GdBO_3$:Bi^{3+},Eu^{3+}, vacuum UV excitation spectra and quantum efficiencies 79−28811
GdB_3O_6:Bi^{3+}, Tb^{3+}, energy transfer from sensitiser to activator, intermediate role of Gd^{3+} 80−50389
$GdBr_3$, frozen aq. soln., fluoresc. and absorpt. spectra 79−43022
$GdCl_3$, frozen aq. soln., fluoresc. and absorpt. spectra 79−43022
$Gd(ClO_4)_3$, frozen aq. soln., fluoresc. and absorpt. spectra 79−43022
$GdCl_3.6H_2O$, thermal decomp., X-ray emission luminesc. *(Japanese)* 80−55763
GdF_3:H films, H, F profiles meas. by sputter-induced optical emission 78−47407
$Gd_3Ga_5O_{12}$:Nd^{3+}, growth, stimulated emission, spectral props. 78−95593
$Gd_3Ga_5O_{12}$:Nd^{3+}, optical absorpt. and fluoresc. intensities 80−29793
$Gd_2Gi_2O_7$:Nd^{3+}, spectroscopic props. 77−69866
$Gd_2(MoO_4)_3$, ferroelec.-ferroelastic, photolum. and photocond. meas. 80−84768
GdNbTiO$_6$:Eu^{3+} emission under UV excitation 78−6770
Gd_2O_3:Eu^{3+}, luminesc., rel. to crystallographic data 79−33793
Gd_2O_2S:Tb, recomb. processes and emission spectra *(Russian)* 78−6797
Gd_2O_2S:Yb^{3+},Ho^{3+}, anti-Stokes emission band assignments, energy transfer mechanism 77−40277
$GdPO_4$:Dy^{3+}, Bi^{3+}(Sb^{3+}), energy transfer from sensitiser to activator, intermediate role of Gd^{3+} 80−50389
Gd_2S_3, resonance excitation of Nd^{3+}, luminescence, absorption spectra *(Russian)* 80−50381
β-Gd_2S_3:Nd^{3+}, spectroscopic props. from absorpt., photoluminesc. and excitation spectra 80−34968
$(Gd_{1-x}Tb_x)_2O_2S$ phosphor, concentration quenching of Tb^{3+} luminesc. 80−29785
$GdVO_4$:Eu^{3+}, absorption and fluoresc. spectra, SU(2) chain *(French)* 78−28912
$GdVO_4$:R^{3+}, R = Nd, No, Tm, Sm, Dy, Er, Eu, Tb, electronic struct. and spectra of VO_4, RO_8 clusters 78−10953
$Gd_xZr_{1-x}O_{2-x/2}$:Tb^{3+}(Eu^{3+}), energy transfer, luminesc. 79−51999
Ge, amorphous, elec. and opt. props., review 78−23094
Ge, biexciton and trion existence, photolum. *(Russian)* 80−16088
Ge, compressed electron hole plasma, luminesc. 78−72592
Ge, cyclotron resonance and radiative recomb. with laser excitation, book contrib. 80−11472
Ge, deform. of laser induced electron-hole drops under high magnetic fields *(German)* 78−23027
Ge, direct gap recombination, at high excitation level and low temp. 79−38650
Ge, doped, electron-hole drops, low-temp. photolum. spectra obs. 77−69900
Ge, electron hole drop diffusion const., hysteresis effect determ. 79−23902
Ge, electron hole drop recombination spectrum, low energy tail 77−59612
Ge, electron-hole correlation density depend., in electron-hole liq., under uniaxial stress 79−15090
Ge, electron-hole drop binding energy, optical threshold studies 79−38652
Ge, electron-hole drop deform., accel. and luminesc. under influence of radiation press. 77−47739
Ge, electron-hole drop emission kinetics, effect of nonequilib. phonons, 4.2K 78−14674
Ge, electron-hole drop formation, nucleation phenomena 79−33240
Ge, electron-hole drop luminescence at high mag. fields 79−65390
Ge, electron-hole drop luminesc., phonon wind induced anomalous depend. at low mag. fields 80−34980
Ge, electron-hole drop motion 80−6744
Ge, electron-hole drop recombination radiation due to heat pulse action *(Russian)* 80−16087
Ge, electron-hole drop velocities, excitation wavelength depend. 78−88358
Ge, electron-hole droplet cloud form., phonon wind, luminesc. obs. 80−45136
Ge, electron-hole droplets, transient photoluminesc. intensities 78−88353

luminescence of inorganic solids continued
Ge, electron-hole droplets, luminesc. and absorpt. lineshapes, RPA theory 80−49613
Ge, electron-hole droplets in high stress limit 78−10369
Ge, electron-hole droplets distrib., and phonon wind 80−103629
Ge, electron-hole drops, Auger recomb. 77−48240
Ge, electron-hole drops, inflammation radiation under action of ultrasound *(Russian)* 79−7788
Ge, electron-hole drops, kinetics of spatial distrib. *(Russian)* 78−43312
Ge, electron-hole drops, motion in low mag. fields 79−23904
Ge, electron-hole drops, photoluminesc. kinetics 78−23524
Ge, electron-hole drops, US absorpt. and recomb. radiation, 1.8 to 3.5K 77−31954
Ge, electron-hole drops at high mag. fields 79−60721
Ge, electron-hole gas and liq. coexistence 78−14668
Ge, electron-hole liq. thermalisation between mag. field split valleys 80−25444
Ge, electron-hole liquid, luminesc. under infinite uniaxial compression 78−87915
Ge, electron-hole liquid, strain-confined 78−10355
Ge, electron-hole liquid, strain-confined 80−6745
Ge, electron-hole luminesc. and transport props. 77−48241
Ge, electron-hole-droplet cloud, photoluminesc. of laser excited surface, phonon wind 78−84146
Ge, electron-hole-liquid, de Haas-van Alphen-like oscills. in luminesc. line shape 79−60720
Ge, exciton condensate and electron-hole droplet, metastable state, effect of illumination and high-frequency heating 79−15097
Ge, exciton condensation, microwave breakdown, luminesc., book contrib. 80−11471
Ge, exciton energy gap and LA and LO momentum-conserving phonon energies 79−90965
Ge, exciton gas, entropy ionisation, luminesc. meas. 78−35196
Ge, exciton luminesc. polarisation in mag. field *(Russian)* 77−12436
Ge, exciton recombination with emission of single phonon, luminesc. replicas, detect. and anal. 79−60728
Ge, HF breakdown of excitons effect on kinetic of electron hole droplets *(Russian)* 77−59260
Ge, heavily doped and compensated, photoluminesc. exam. 78−2902
p-Ge, hot-hole relax. rates by saturation spectroscopy 77−65611
Ge, indirect excitons, photoexcitation spectra, 2.0-2.6 meV 77−44051
Ge, influence of dislocations on free-exciton lifetime 78−60064
Ge, ion bombardment-induced photon emission as function of target temp. 80−100698
Ge, luminescence circular polarisation in mag. field, Landau levels paramag. splitting 77−32435
Ge, luminescence kinetics and electron-hole drop motion 77−77288
Ge, luminescence line shape of free exciton, electron-hole droplet binding energy 77−44041
Ge, luminescence meas., presence of trions, molecules and excitons above Mott density 77−80737
Ge, mag. field luminesc. lifetime, quantum oscills., phonon wind effects 80−93385
Ge, magnetoluminescence of electron-hole liq. 80−29790
Ge, magnetostriction of electron-hole drop 77−85540
Ge, microwave exciton breakdown and luminesc., under one- and two-photon excitation 77−31955
Ge, Mott distortion of the electron-hole fluid phase diagram, luminesc. meas. 79−42457
Ge, nonequilibrium charge carrier-mag. field interaction electron-hole drops, recombination *(Russian)* 80−75511
Ge, nonuniformly deformed, electron-hole drop density depend. on size *(Russian)* 80−20092
Ge, nucleation anal. of electron-hole drops 77−69243
Ge, ODMR using luminescence of electron-hole drops *(Russian)* 77−90072
Ge, optically stimulated, electron-hole drops and appearance of dense plasma *(Russian)* 77−4688
Ge, phase diagram of electron-hole fluid in low temp. photoexcited semicond. 77−69237
Ge, phonon-assisted exciton emission, temp. depend. of relative integrated intensities 77−1375
Ge, photoluminesc., high excitation intensities, direct and indirect gap transitions 77−12429
Ge, photoluminesc. decay from electron-hole drops 77−66532
Ge, plasma excitation, ultrafast optical props. 78−31248
Ge, pure, large, electron hole drops, microwave heating and evaporation 79−28287
Ge, pure, magnetic phase transition between electron-hole drops and free-excitons 78−6278
Ge, pure and doped, electron-hole drops net charge, photocond. and photoluminesc. 79−38589
Ge, recombination luminesc. spectra from hot and cold carriers in electron-hole drops 79−38608
Ge, shallow impurities, excited states, population and lifetime *(Russian)* 79−51532
Ge, size distrib. of electron-hole drops, kinetics of recomb. 79−28292
Ge, size effects in small electron-hole drops 79−82530
Ge, strain-confined electron-hole liq. 77−47738
Ge, strain-confined electron-hole liquid, lifetime and radiative efficiency vs density 79−38000
Ge, strain-narrowing of luminesc. line from excitons 79−24356
Ge, stressed, α_1 and α_3 electron-hole droplet luminesc. 79−28820
Ge, stressed, metal-insulator transition, luminesc. 80−20695
Ge, stressed, recombination luminescence from hot carriers in electron-hole droplets 78−6754
Ge, stressed cryst., props. of strain-confined electron-hole liquid 79−7787
Ge, strong microwave field effect on electron-hole drops, luminescence kinetics 79−87047
Ge, surface energy effect on electon-hole drop luminesc. 77−48239
Ge type semiconductor, interimpurity zero-phonon radiative transitions 78−15222
Ge, ultra high vac. cleaved, photolum., role of intrinsic surface states 78−52571
Ge, ultra-pure electron-hole drop condensation nucleation phenomena 77−47744
Ge, uniaxially deform., electron-hole drop flight, photolum. max. press. depend. 78−10977
Ge, uniformly stressed, density and binding energy of electron-hole droplets, photolum. meas. 78−60062
n-Ge:As, heavily doped, luminesc. from electron-hole drops 77−81144

luminescence of inorganic solids continued
Ge:As, recomb. of donor bound excitons, luminesc. intensity decay 80−25441
n-Ge:As closely compensated, photolum. of charge carriers localised in trails of density of states 77−77294
Ge:As(Bi), donor bound exciton luminesc. and absorpt. 80−29777
n-Ge:As(Sb), moderately heavily doped, electron-hole drops photoluminesc. 80−7417
Ge:B(Al)(Ga), shallow acceptor spectral line intensities 80−88517
Ge:B(Al)(Ga)(In)(Tl), binding energy, excited state spectra, photolum., semi-empirical short range pot. 80−44534
Ge:In (Sb) and pure cryst., kinetics of strain-confined large electron-hole drop and its clinging exciton system 80−75508
Ge:P, bound-exciton luminesc. and absorpt. 79−87469
Ge:Sb, electron-hole drop lifetime, quenching temp. influence 80−59889
Ge-Sb, far IR emission stimulation by impact ionisation 80−66301
Ge-Se, glassy, photoinduced photolum. fatigue *(Russian)* 78−60520
Ge-Se glass system, effect of changes in local surrounding of atoms on optical props. *(Russian)* 78−80414
Ge-Se glasses, radiative localised centres, photoluminesc. 79−83025
GeO_2 based glasses, absorpt. and emission of Ho^{3+} 79−11439
GeO_2, hexagonal and glassy, X and γ-irrad., thermolum. and paramag. centres 77−63472
$GeO_2:Pr^+$, glass, optical homogeneous linewidths 80−7395
GeS, exciton luminescence 78−52555
GeS, low temp. photoluminesc. 77−77287
GeS orthorhombic layer crystals, photolum. spectra 80−2851
GeS_x glass, chem. struct. effects 77−63460
Ge_2S_3-Ge_2Se_3, glass, photoluminesc. spectra, solid soln. form. *(Russian)* 78−23525
GeSe, low temp. photoluminescence 77−77287
$GeSe_2$ glass, photoluminesc. spectrum, rel. to cryst. forms 77−55819
$GeSe_2$, glassy, powdered and bulk, fatigue of photolum. 80−80855
$GeSe_2$, glassy and single-cryst., photoluminesc. at 77K 77−63456
$GeSe_2$, glassy photoinduced photoluminescence fatigue 79−28827
$GeSe_2$ powdered crystalline, photoluminescence intensity under continuous excitation 80−71480
$GeSe_2$, single crysts., 3 polymorphic forms, DTA, photolum., IR and Raman sepctroscopy 80−33923
$Ge_{1-x}Se_x$, photolum. and optical props. meas. 77−20908
Ge_xSe_{1-x}, amorphous, excitation spectra of photolum. fatigue and creation of paramag. centres 80−50402
Ge_xSe_{1-x} glasses, defect states, photoluminesc. and ESR obs. 79−61418
α-Ge_xSe_{1-y}, photoluminescence and fatigue effects 78−84648
$Ge_{1-x}Si_x:Ga_2As$, interimpurity radiative recombination, composition depend. 79−11465
glass:Nd_3 for lasers, luminesc. absolute quantum efficiency 77−34893
glass:Nd^{3+}, kinetic description of excitation spectra 78−68557
$Hg_{0.7}Cd_{0.3}Te$, 17 to 77K, photo- and cathodoluminesc. 78−52569
n-$Hg_{1-x}Cd_xTe$, far IR recomb. radiation in elec. field, acceptor states 77−16399
n-$Hg_{1-x}Cd_xTe$, far IR recomb. radiation with applied elec. field 78−27324
$Hg_{1-x}Cd_xTe$, near band-gap photoluminesc., bound exciton luminesc. obs. 80−103973
$Hg_{1-x}Cd_xTe$, photolum. and optical pumping 80−50424
Hg_2Cl_2, single cryst., luminesc. 397 nm band props. 77−66529
HgI_2, emission spectra in highly excited state 77−52167
HgI_2, low temp. luminesc. spectra by holographic spectroscopy 79−33820
HgI_2, phonon-assisted recomb. of free electron-hole pair 78−23521
HgI_2, red, liminesc. and Raman scatt., biexcitons and exciton-phonon interactions 79−61424
HgI_2, red, luminesc., excitation spectra on M-band 79−28822
HgI_2, red, reson. Raman scatt. and luminesc. 78−84579
HgI_2 X-ray luminesc., emission band charact., use as X-ray detectors 77−55815
HgI_2:Ag, trapping effects, TSC, photocond. and photolum. meas. 77−32023
$HgMoO_4$, luminesc. efficiency, temp. and high-press. 78−23507
α-HgS, band gap shrinkage, cathodolum. under very strong excitation 77−85146
HgS, cathodoluminescence, evidence of donor-acceptor type transition 77−24902
α-HgS, cinnabar, donor-acceptor transitions, cathodolum. meas. *(French)* 77−48250
α-HgS, cinnabar, photolum. meas. 79−19929
α-HgS, cinnabar, reson. Raman effect and luminesc. meas. 80−50338
HgS, cinnabar powder, 1.65 eV pair recomb., thermal quenching and total light decay 78−27330
α-HgS, green cathodoluminesc., impurity effects 78−2924
α-HgS, natural, yellow emission 78−68567
III-V alloys, disorder-enhanced Auger recomb. 79−43014
In complex, photoluminesc. spectra, $\pi \rightarrow \pi^*$ and charge transfer L→M transitions, Stokes shift 78−64407
In-ZnO-Al metal-semicond. diode, electrolum. and photoluminesc. spectra 79−99948
$In_{1-x}Al_xP:Bi(N)(Zn,O)$ radiative recombination at isoelectronic centres 79−52027
InAs and solid solutions, recombination mechanisms of excess carriers, luminesc. obs. 80−97337
p-InAs, Auger recomb., theory and luminesc. expts. 78−56518
n-InAs, cathodoluminescence, radiative recomb. of hot carriers 77−8667
n-InAs, edge luminescence band, shape depend. on degree of doping, band gap 80−7405
InAs, electron beam excitation, luminesc. and stimulated emission 77−16339
InAs, epitaxial, laser action mechanisms with electron beam excitation 80−28240
InAs, heavily doped, Burstein-Moss effect and near-band-edge luminesc. 79−47525
InAs, photoluminescence exam. 79−28809
n-InAs, recomb. of nonequil. charge carriers at high photoexcitation levels 77−44053
n-InAs:Te(Sn), heavily doped, cathodoluminescence, doping effect on luminesc. band position and spectral profile 80−45153
$InAs_{1-x}Sb$, disorder-enhanced Auger recomb. 79−43014
$InAs_{1-x}Sb_x$, epitaxial film, carrier recomb., elec. and optical props. 79−15164
InBr, metastable exciton emission, electron excitation mechanism 77−66546

luminescence of inorganic solids continued
InGa-GaSe interface, microplasma electrolum. at 300K 79−11469
InGaAs-$In_{1-x}Ga_xAs_yP_{1-y}$ DH laser, LPE fabrication, electroluminesc., lasing characts. 79−3709
p-$In_{0.53}Ga_{0.47}As$:Zn on InP, elec. and optical props. 80−75662
$In_{1-x}Ga_xAs$, LPE layer on InP substrate, phys., elec. and optical props. 78−39235
$In_xGa_{1-x}As$, heteroepitaxial, MBE grown, props. 78−84328
$In_xGa_{1-x}As$, MBE layers on InP substrates, elec. props., photoluminesc., X-ray and Auger obs. 79−51450
$In_xGa_{1-x}As$ multilayer struct., photoluminesc. and X-ray spectroscopic microprobe analysis 77−4687
$In_xGa_{1-x}As$, thick LPE growth, electrolum. obs. 78−60589
$In_xGa_{1-x}As$:Si p-n structs., electrolum. spectra, 77 to 300K 80−93408
InGaAsP, bandgap energy by electroreflectance and photoluminesc. spectra 80−107700
InGaAsP DH, luminesc., quantum efficiency determ. 80−108273
InGaAsP, epitaxial layer, defect evaluation by cathodoluminescence 80−2866
InGaAsP, quaternary alloy, physical props. *(Japanese)* 80−15449
InGaAsP, with and without InP cladding layers, low photolum. regions 79−33754
InGaAsP:Be, avalanche photodetectors annealing temp. effect on photolum. spectra 79−69872
InGaAsP-InP DH laser, optical gain meas., low-intensity luminesc. and absorpt. spectra 79−98356
InGaAsP-InP DH LED, high temp. aged, dark-spot defects, TEM obs. 80−66300
InGaAsP-InP DH lasers, perturbed InP growth, photoluminesc. study 80−106518
$In_{1-x}Ga_xAs_{1-y}P_y$ layers on InP substrate, LPE growth, quaternary phase diagram, and band gaps 79−42403
$In_{1-x}Ga_xAs_yP_{1-y}$, DH laser material, spatially resolved photolum. characterisation and optically induced degradation 79−47486
$In_{1-x}Ga_xAs_yP_{1-y}$ DH laser, low threshold current density, near equilibrium LPE growth 80−19040
$In_xGa_{1-x}As_yP_{1-y}$ layers on InP, LPE and opt. props. characteris. 79−28849
$In_xGa_{1-x}As_ySb_{1-y}$ laser, nonequilibrium carrier recombination, luminesc. study 80−50431
InGaP-GaAs junction, effect of elastic strain on energy band gap and lattice parameters 79−24057
$In_{0.3}Ga_{0.7}P$, N free and implanted, photoluminescence study 80−97322
n-$In_{1-x}Ga_xP$, direct-gap semiconductor, cathodoluminesc., electron irrad. effects 80−108283
$In_{1-x}Ga_xP$, epitaxial film, cathodolum. obs., recomb. mechanisms 78−72613
$In_{1-x}Ga_xP$, epitaxial growth on GaAs substrate, formation of intermediate layers 80−2304
$In_{1-x}Ga_xP$, LPE, on $GaAs_{1-y}P_y$, photo- and cathodolum. 78−19559
$In_{1-x}Ga_xP$ luminesc. props. from cathodoluminesc. and electroluminesc. meas. 80−2281
$In_{1-x}Ga_xP$, solid soln. film, photoluminesc. meas. 78−27321
$In_{1-x}Ga_xP$, temp. depend. of forbidden band width, photoluminesc. meas. 78−19556
$In_{1-x}Ga_xP$:Bi(N)(Zn,O) radiative recombination at isoelectronic centres 79−52027
$In_{1-x}Ga_xP$:N_2, N-trap bound states, photoluminesc. and absorption data 77−1719
$In_{1-x}Ga_xP$:N(Te), composition depend. of bound state luminesc. transitions 78−39595
$In_{1-x}Ga_xP$:Te,Zn, photolum. and electrolum., direct transition region 77−8659
$In_{1-y}Ga_yP$-GaAs heterojunction, VPE, energy band gap and lattice parameter, lattice mismatch effects 78−95345
InGaPAs LPE layers, compositional inhomogeneity, photoluminesc. obs. 80−75451
$In_{1-x}Ga_xP_{1-y}As_y$ lattice-matched epitaxial layers, LPE growth on GaAs(100), characterisation 80−75465
$In_{1-x}Ga_xP_{1-z}As_z$ luminesc. props. from cathodoluminesc. and electroluminesc. meas. 80−2281
$In_{1-x}Ga_xP_{1-z}As_z$ solid solution, radiative transitions 79−11476
$In_{1-x}Ga_xP_{1-z}As_z$, stimulated yellow-green emission under electron excitation, 80K 79−33846
$In_{1-x}Ga_xP_{1-z}As_z$ thin well in InP p-n junction, confined carrier luminesc. and laser modes 78−13703
$In_{1-x}Ga_xP_{1-z}As_z$ well in InP, tunnel injection into confined particle states 78−19130
InGaSbAs heterostructures and LED's luminesc. props. in 1-2 micron band 78−10988
InI, photoluminesc., Raman scatt. 79−38593
In_2O_3-SnO_2-CdTe:P, p-n homojunction solar cell, elec., photovoltaic props., photoluminescence 80−81463
n-InP, (110) surfaces, photolum. intensities in vac. and gas ambients 79−61412
InP, acceptor excited states, luminesc. spectra 80−16091
InP, ambient-enhanced photoluminesc. props., mol. adsorption and gas-flow effect 79−99925
InP, bulk grown, selective spectroscopy, acceptor level studies 80−29778
InP, deep level electron traps, emission and capture props. 80−29806
InP, exciton localisation at impurity pairs 79−37999
InP, excitons bound to neutral donors in VPE layers, luminesc. and absorpt. obs. 79−42460
InP films, organometallic VPE grown, props. 80−96753
InP, growth and props., Zn acceptor obs. 79−1822
InP growth from soln. and LEC, photolum. and elec. meas. 79−87575
InP, luminesc. emitted as a result of carrier heating 77−52185
InP, luminescence, hot electron effects 80−66277
InP, model for ~1.10 eV emission band 80−66289
n-InP, photolum., evidence for low surface recomb. vel. rel. to n-GaAs 77−40272
InP, photolum. depend on surface treatment 79−78727
InP, photolum. meas. using diamond-anvil press. cell 80−108256
InP, photoluminesc. of epitaxial films, isovalent substitution 80−16097
InP, photoluminescence at dislocations, band gap electronic levels 79−99926
InP, photoluminescence intensity of cleaved surface, ambient gas influence 78−88345
InP, polar semiconductor, collisions between hot excitons and hot electrons 80−7415
InP, press. depend. of direct absorption edge 80−93365

luminescence of inorganic solids continued
p-InP, single cryst. and epilayers, photoluminesc. 77−81211
InP substrate, LEC-grown, defect evaluation by cathodoluminescence 80−2866
InP, synthesis solute diffusion grown, elec. props., photoluminesc., etch pit profiles 79−4914
InP, VPE growth for MESFET's 80−103602
InP:Bi, isoelectronic impurity states, emission and absorpt. obs. 79−42491
InP:Bi, uniaxial stress effect on free and Bi-bound excitons 79−56854
InP:Fe, deep levels 79−56166
InP:Fe, Fe acceptor charge states, photolum., absorpt. and ESR meas. 77−36123
InP:Te(S), heavily doped, dislocation imaging using transmission cathodoluminesc. 80−29023
p-InP:Zn, vapour grown, prep. and props. 80−54268
InP:Zn heavily doped X-ray topography, cathodolum., and TEM obs. 79−99197
InP-CdS heterojunction, injection electrolum. 78−23153
InP-electrolyte struct., field effect of photoluminesc. 79−99928
InP-$Ga_xIn_{1-x}As_{1-y}P_y$ heterojunctions, energy band diagram 77−16400
InP-$In_{1-x}Ga_xP_{1-z}As_z$, valence band discontinuity, quantum well luminesc. 79−91483
InP(100) undoped homoepitaxial films grown by MBE, photoluminesc. props. 80−2809
InSB, impact ionisation, influence of external mag. field on recomb. radiation and I-V characts. 79−56864
InSb, absorpt. saturation by nonequilib. electron-hole plasma, luminesc. 78−9418
InSb, electron spin levels resonant excitation, photolum. 80−25454
n- InSb, hot electron energy relax. in quantizing mag. fields 78−31259
InSb, interaction of exciton recombination with LO phonons 79−38647
n-InSb, Landau emission spectra, influence of bakcground radiation 78−43935
InSb, overheating luminescence, carrier generation-recomb. equilib. shift in elec. field 77−44068
InSb p-n junction, minority carrier injection in mag. field, recomb. radiation obs. 80−11078
n-InSb, photoluminesc. in crossed EM fields *(Russian)* 77−24892
n-InSb, photoluminescence exam. 79−28809
InSb, prep. of thin films by ionised-cluster beam deposition, photolum. meas. *(Japanese)* 80−25576
InSb, reabsorbed radiative recomb. and photon recycling 80−76076
InSb-oxide-electrolyte interface, electroluminesc. in anodic oxidation *(Russian)* 77−90201
InSe, excitonic absorpt. edge 78−88352
InSe luminescent film, production and characterisation *(Russian)* 78−39581
InSe, optical props. near fundamental absorption edge 77−12434
$InTa_{1-x}Nb_xO_4$ system, structural and luminescent props. 80−84769
$(In_2Te_3)_x$-$(Hg_3Te_3)_{1-x}$, photoelec. and luminesc. props. 77−39889
K film, splitting of surface plasmon emission spectra 79−99954
K halide, Yb^{2+} activated, X-ray and intracentre luminesc. 78−6737
K salts, spectral refl. changes and luminesc. during 2-10 keV proton bombardment, implications for Io 79−96950
$KAlSi_3O_8$:rare earth ion, glass, nonradiative energy transfer and fluoresc. quenching 77−20905
$K_5Bi_{1-x}Nd_x(MoO_4)_4$ solid soln., growth, spectroscopic and laser props. 78−2901
KBr, barrier instability in strong elec. fields 79−69522
KBr, cation defects creation mechanism 80−75224
KBr, decay and time resolved emission spectra from σ-excitons produced by heavy-ion irradiation 80−89071
KBr, excitation of thermolum. near liq. He temp. 80−40171
KBr, F-centre lifetime, perturbation effects, luminesc. meas. 80−108252
KBr, F-centre luminesc., MCD effects 78−39598
KBr, F-centre radiative lifetime meas. near 65K 80−25439
KBr, heavy ion irrad., σ and π exciton emission spectra, 4.2K 78−76534
KBr, interaction between F- and α-centres, luminesc. meas. 79−73988
KBr, irrad., colour centres and thermolum. 77−85815
KBr, m-crocryst. powders coloured in electrodeless discharge, reflectance spectra, thermolum. 78−15238
KBr, optical conversion, luminesc. and colour centre formation 79−24354
KBr, photoluminescence under pulsed UV laser excitation 77−77289
KBr, S centres, luminesc. and photochemistry *(German)* 77−44055
KBr, self-trapped exciton form. via thermally induced defect reactions 80−60687
KBr, spectral distrib. of triplet to singlet luminesc. of F_2 centre 77−59601
KBr, thermolum. and reactions of freed interstitial and trapped hole centres 78−23538
KBr whisker, X-irrad., defect form., thermolum. and ionic cond. obs. *(Russian)* 78−84666
KBr, with Frenkel cation defects, EPR and thermolum. of V_F, V_2-centres 78−10769
KBr, X-irrad., F-centre role in thermoluminescence 80−20720
KBr, X-irradiated, thermally stimulated and tunnelling luminescence spectra, temp. varied 78−72606
KBr:Ag, mag. field effect on luminesc. of paired Ag^- ions 78−27313
KBr:Br_2^-, triplet luminesc. kinetics, 0.4-4.2K 79−87482
KBr:Eu(Yb), electron-irrad., photostimulated luminesc., ionic processes 78−52561
KBr:Ga^+, luminescence decay times, fluorescence kinetics, 1.6-300K 79−33825
KBr:I, energy transfer due to excitons and holes under host sensitization 79−15526
KBr:I, luminesc., exciton and hole migration to I^- sites 79−38626
KBr:I^-, OH^-, luminesc. of interstitial atomic H 80−89062
KBr:In^+, type A long-wave luminesc., polarisation obs. 78−10944
KBr:In^+, emission lifetimes, temperature dependence 79−78745
KBr:Li, radiative recomb. of localised excitons 78−72605
KBr:Li:(Na^+), electronic struct. of $(V_K e)_A$ 78−95269
KBr:NO_2^-, Na effect of Na^+ impurity on self-trapped hole *(Japanese)* 78−67982
KBr:Na, exciton-like state disturbance in radioluminesc. *(Russian)* 77−85805
KBr:Na, X-irrad., luminesc. from self-trapped excitons 77−28614
KBr:No_2^-, effects of Mg, Ca, Sr, Ba, Pb impurities on vibrational constants of NO_2^- ion 77−20035
KBr:PO_2^-, phosphorescence, triplet state sublevels, mixing 80−25446

luminescence of inorganic solids continued
KBr:Pb, luminesc. spectra obs. 78−95604
KBr:Pb; A-luminesc ., 8-80K 80−2836
KBr:Sr^{2+},Cu^{+}, thermolum. response, extension of two-step reaction model 80−89075
KBr:Tl, 480K thermal glow peak, Tl^{+} centres 80−108284
KBr:Tl, A-emission, line shapes and relative efficiencies 79−83011
KBr:Tl, electroluminescence, spectra and quantum yield activator conc. depend., cond. changes 80−89070
KBr:Tl, Jahn-Teller system, negative mag. circular polarisation in emission spectrum 80−20694
KBr:Tl, luminesc., decay model for A_T and A_X emissions 80−93379
KBr:Tl, thermoluminesc. excited by UV radn. and X-rays 79−87513
KBr:Tl excitation in fund. absorpt. region, luminesc. and thermolum. 80−50433
KBr:Tl^{+}, Jahn-Teller split luminesc., high press. study 78−52565
KBr(Cl), X-ray irrad., tunnelling recomb. luminesc. 80−2873
KBr(Cl):Tl, visible emission, temp. depend. 78−60511
KBr(Cl)(I), electron-spin memory and magnetic-circular-dichroic effects in F-centre luminesc. 80−29794
KBr(Cl)(I):O_2^{-} centres, luminesc., polarisation temp. depend. 78−87943
KBr(Cl)(I):Tl^{+}, recomb. luminesc. kinetics 77−16366
KBr(I), photostimulated recomb., electron spin polarisation 80−60673
KCN, F-centre emission spectrum 77−12420
KCN, F-centres, optical props. 78−2892
KCN, optical F centres and phase transitions 78−56504
$K_{2(1-x)}Ca_xSO_4$:Tl^{+} phosphor, thermolum. characts. 77−90203
KCl (Br) crystals, thermally stimulated luminescence accompanying recombination of V_F and F centres 80−55201
KCl, absence of energy transfer between F- and M-centres 79−99935
KCl absorption and emission of F_A(Li) centres under hydrostatic pressure 78−92117
KCl, cryst., colour centres, ionic cond., X-ray effects, thermoluminesc. *(Russian)* 78−6056
KCl, F_3-centre quartet state, IR emission spectra 78−43930
KCl, F-center pairs, light excitation, mag. field and resonance effects on absorption bands 78−92094
KCl, F-centre luminesc., MCD effects 78−39598
KCl, gamma irrad. relationship between thermolum. and deform. luminesc. 79−19942
KCl, γ-irradiated, photo- and thermoluminesc., F-centre interstitial recomb. 77−44036
KCl, luminesc. excitation spectra of F-aggregate centres, 400-900 nm. *(Russian)* 78−10980
KCl, luminesc. of Z_4 centres 79−24355
KCl, luminesc. under 10.6 μm laser pulse irrad. *(Russian)* 77−16381
KCl, M-centres, F-centre sensitised luminesc. 77−4681
KCl, m-crocryst. powders coloured in electrodeless discharge, reflectance spectra, thermolum. 78−15238
KCl, pure and Pb^{2+}-doped, X-irrad., quenching effects on thermal glow curves 78−27333
KCl, S centres, luminesc. and photochemistry *(German)* 77−44055
KCl, self-trapped exciton luminesc. 77−48225
KCl single crystals, F-band absorpt. and thermolum. under DC field and X-ray irrad. 79−65910
KCl, spectral distrib. of triplet to singlet luminesc. of F_2 centre 77−59601
KCl, thermal annealing of F, V_2-, V_3-centres *(Russian)* 80−54229
KCl, thermoluminesc., halogen and alkali impurity effects 80−97352
KCl, tunnelling recombination between neutral Ag atoms and V_k centres 79−61442
KCl, undoped, or In- or Eu-doped, injection electrolum., fields up to 10^4 V cm^{-1} 77−12445
KCl, with colour centres, laser stimulated luminesc. 78−6749
KCl, with Frenkel cation defects, EPR and thermolum. of V_F, V_2-centres 78−10769
KCl, X-irrad. induced deform. effects, glow curves *(Russian)* 79−52022
KCl, X-irradiated, formation of cation defects 78−91359
KCl, X-irradiated, thermally stimulated and tunnelling luminescence spectra, temp. varied 78−72606
KCl, X-ray irrad., thermoluminescence, TSC and thermal stability 79−95859
KCl:Ag, hole capture radius, scintillation luminesc. obs. *(Russian)* 78−39582
KCl:Ag, thermoluminesc. meas. using high impedance DC amplifier 79−99955
KCl:Ag, X-irrad., thermoluminesc. study of Ag centres 80−80874
KCl:Ag,Tl, cryst. high-press. energy transfer, sensitised luminesc. 77−36281
KCl:AgCl, tunnelling-recombination luminesc. 78−88354
KCl:Ag(Cu), strong IR luminescence obs. of Ag_F^0 centres 78−6736
KCl:Ag(In)(Tl), excitation in fund. absorpt. region, luminesc. and thermolum. 80−50433
KCl:Au^{-}, fluorescence, stress and mag. field depend., Jahn-Teller effect and relax. processes 77−48220
KCl:Ba(Sr), Z-centre, luminesc. and absorpt. spectra obs. 80−49221
KCl:Ca, optical studies of Z_4 centres 79−24336
KCl:Ca, thermolum. and optical absorpt. spectra of Z_1 centres 79−52029
KCl:Ca^{2+}, Z_1-centre thermolum. 80−80879
KCl:Cu, EPR, optical absorpt. and luminesc. investig. of anisotropic Cu_F^0 centres 77−20893
KCl:Cu,Tl, plastic deform., charge exchange of hole centres *(Russian)* 77−11876
KCl:Eu, luminescence and absorption of color centres in RbCl:Cu and KCl:Eu crystals 78−92118
KCl:Eu^{2+}, γ-irrad., photostimulated low temp. recomb. luminesc. 80−11435
KCl:Eu^{2+}, radiationless processes 78−80391
KCl:Eu^{2+}, zero phonon lines, time-resolved fluoresc. spectra 77−77269
KCl:Eu^{2+} crystals, photostimulated afterglow investigation at room temp. 80−108259
KCl:I, luminesc. at low temp. 80−2818
KCl:I^{-}, H, fluorescence of interstitial H-centres 79−73987
KCl:Li, additively coloured, luminesc. material for IR region *(Russian)* 78−15209
KCl:Li, X-irrad., F_A centres, thermolum. studies 80−80878
KCl:Li(Na), M_A-centre, decay 77−77278
KCl:NO_2^{-} (O_2^{-}), Stokes' losses on cryst. vibrs. in luminesc. spectra of mol. centres *(Russian)* 77−55827

luminescence of inorganic solids continued
KCl:Na, thermoluminescence peaks cleaning using optical bleaching 77−81162
KCl:Na^{+}, self trapped excitons, optical absorption and emission 77−43503
KCl:PO_2^{-}, phosphoresc. and PMDR spectra, electronic and vibr. states 79−65768
KCl:PO_2^{-}, photo-orientation, spectrosc. and ODMR obs. 80−29772
KCl:Pb, 420 nm A-emission band *(Russian)* 79−56852
KCl:Pb, luminesc. spectra obs. 78−95604
KCl:Pb, photolum. in A band region, spectral and time decay anal. 79−33823
KCl:Pb, photoluminesc. induced by Suzuki-like occlusions, ionic thermocond. 79−33808
KCl:Pb, thermoluminesc. meas. using high impedance DC amplifier 79−99955
KCl:Pb^{2+}, decay of luminescence emission 78−39593
KCl:Pb^{2+}, γ-irrad., rel. to props. 78−31262
KCl:Pb^{2+}, highly doped, state of dispersion of Pb^{2+} 77−1144
KCl:Pb^{2+}, inner-centre luminesc., 8 to 80K *(Russian)* 78−92112
KCl:Pb^{2+}, origin of 420 nm emission band 77−40279
KCl:Sm^{2+}, spectra, ^5D states, Lauer-Fong formula and SCC model 79−15513
KCl:Sn, pure and doped, thermoluminesc. and luminesc. decay 79−83041
KCl:$SnCl_2$, photostimulated hole recombination luminesc. *(Russian)* 80−80833
KCl:$SnCl_2$, Sn^{+} centres, polarised luminesc. and EPR 79−65076
KCl:$SnCl_2$, X-ray irrad,, polarised luminesc. and EPR study of Sn^{3+} centres 80−39868
KCl:Sr, M-centre photoluminesc. *(Russian)* 78−84649
KCl:Sr, thermally pre-treated, glow curves 80−25470
KCl:Sr crystal, Z_4 colour centre, luminesc. study 80−64993
KCl:Sr^{2+}, X-irrad., thermolum., impurity aggregation, trapping centre form. 78−88367
KCl:Sr^{2+}, X-irradiated, thermolum. decay, effect of impurity aggregation 77−85814
KCl:Sr^{2+},Cu^{+}, thermolum. response, extension of two-step reaction model 80−89075
KCl:Sr(Ca), thermoluminescence and colour centre thermal stability in irradiated sample 78−43941
KCl:Tl, 375 nm emission band 79−95834
KCl:Tl, 475 nm emission, attributed to Tl^{+} dimer 78−39611
KCl:Tl, effective cross sections ratio of charged and neutral centres for holes and electrons *(Russian)* 79−28319
KCl:Tl, electroluminescence, spectra and quantum yield activator conc. depend., cond. changes 80−89070
KCl:Tl, low-temp. ionisation of activator, photoexcitation, in region of interzone transitions *(Russian)* 79−28320
KCl:Tl, temp. depend. of cathodolum. *(Russian)* 80−80868
KCl:Tl, thermal glow of trapped electron and hole centres 79−78762
KCl:Tl (0.003 to 0.27 mol.%), electrolum. 80−71490
KCl:Tl phosphors, heavily doped, luminesc. obs. 77−32427
KCl:Tl_2^{+}, decay modes of 3000 Å emission band 77−73168
KCl:Tl^{2+}, hole mechanisms of H- can F-centre production, thermolum. obs. 77−16407
KCl:Tl^{2+}, Na, X-irrad., activator-impurity association *(Russian)* 77−85761
KCl-Ba, X-ray irrad. cryst., thermoluminescence spectra 80−20719
KCl-$BaTiO_3$, composite cryst., F-centres, thermoluminesc., DC field and X-irrad. effects 78−2926
KCl-CuCl solid solution supersaturated, precipitation, impurity aggregation 80−29174
KCl-KBr mixed crystals, thermolum. studies 80−11486
KCl-KBr:Tl^{+}, cryst., luminesc. and excitation spectra 77−66535
KCl-Mg, thermolum. of Z-centre, optical absorpt. 80−55203
KCl-$SrCl_2$, photoluminescence of Z_4-centre and associated Z type colour centre *(Russian)* 79−4851
KCl-Tl, Jahn-Teller system, negative mag. circular polarisation in emission spectrum 80−20694
KCl(Br), F-centre emission, mag. circular polarisation 80−108251
KCl(Br), triplet state lifetime of F_2 centre, mag. field effect 78−35177
$KCl_{0.5}Br_{0.5}$:Ca, X-ray irrad., Z_1-centres, thermoluminesc. and optical absorpt. meas. 80−16108
KCl_xBr_{1-x}, mixed crystals, thermolum. and optical absorption studies 80−104000
KCl(Br)(I), electronic struct. of self-trapped excitons calc. 77−39784
KCl(Br)(I):Ga^{+}, polarisation of Ga^{+} centre A_T emission, temp. depend. 80−80842
KCl(Br)(I):In^{+}, Jahn-Teller split luminescence, high press. study 78−52565
KCl(Br)(I):Tl, emission spectra, press. effects 78−23509
KClIn, absolute quantum output of low-inertial energy transmission *(Russian)* 77−32429
$K_2Cr_2O_7$, closed-shell tetroxo-complex triplet levels, luminesc. meas. 79−69874
$K_2Cr_2O_7$, luminesc., vibr. anal. 79−38620
$K_5Eu(MoO_4)_4$, electric dipole transition cross section and effective site symmetry of Eu^{3+} 78−52556
KF(Cl)(Br), mag. props. of relaxed excited state of F-centre, vibronic theory 78−60502
KH_2PO_4, electrophotoluminescence obs. 79−47521
KI, edge emission of excitons 77−59606
KI, edge luminesc. under UV excitation 77−77273
KI, electron irrad., polariton effects in reson. emission 79−33843
KI, exciton diffusion, luminesc. quenching, meas. 4 to 77K 77−32433
KI, F-centre luminesc., MCD effects 78−39598
KI, free exciton-F^{-} centres interaction, electron excited emission 79−83036
KI, growth time of π emission in picosecond range 80−76067
KI, intrinsic luminesc. quenching, by X-ray induced coloration 78−19539
KI, luminesc. due to free excitons, line shapes 79−33803
KI, luminesc. lines due to n=2 free exciton state of Wannier series 80−29776
KI, luminesc. polarisation for free and bound excitons 78−10942
KI, mag. circular dichroism in luminesc. of F-centres 77−20919
KI, polariton effects in resonant emission 78−76533
KI, quenched, absorpt. and emission spectra, α-centres 80−11442
KI, recomb. luminesc. of H-centre and F-centre electrons *(Russian)* 78−80402

luminescence of inorganic solids continued
KI, self trapped exciton form. time at $^1\Sigma_u^+$ state under pulsed electron beam in ps range 80−97347
KI, self-trapped exciton form. via thermally induced defect reactions 80−60687
KI, spectral distrib. of triplet to singlet luminesc. of F_2 centre 77−59601
KI, surface, 420 nm band laser-stimulated emission, V_2 centres 78−84633
KI, zero phonon and LO phonon assisted luminesc. of free excitons 79−28799
KI:Eu, electron-irrad., photostimulated luminesc., ionic processes 78−52561
KI:Eu^{2+}(Sr^{2+})(Mn^{2+}), elec. field effect on mech. of recomb. 78−80397
KI:I_2^-, triplet luminesc. kinetics, 0.4-4.2K 79−87482
KI:In^+, luminesc. decay, excited state symm. and g-value 79−99922
KI:In(Tl), type A long-wave luminesc., polarisation obs. 78−10944
KI:Pb^{2+}, absorpt., excitation and luminesc. spectra 78−19519
KI:S_2^-, Stokes' losses on cryst. vibrs. in luminesc. spectra of mol. centres *(Russian)* 77−55827
KI:S_2^- centres, luminesc., polarisation temp. depend. 78−87943
KI:Se_2^-, reson. secondary emission, total spectrum *(Russian)* 78−19551
KI:Sn^{2+}, luminesc. 79−33817
KI:Sn^{2+}, red emission, mag. field effect on radiative decay time 79−33818
KI:Sn^{2+} luminesc. decay, excited state symm. and g-value 79−99922
KI:Tl, activated crystal, induced recombination emission *(Russian)* 78−48214
KI:Tl^+, A_T emission, mag. circular polarisation, WKB approx. for non-radiative transition rate 80−55180
KI:Tl, $(Tl^+)_2$ centre luminesc. 78−84632
KI:Tl, A_T emission, linear polarisation, appl. of semi-classical WKB formalism 80−45134
KI:Tl, cryst., induced recomb. emission 79−4845
KI:Tl, decay of fast component of impurity luminesc. excitation in A-absorption band *(Russian)* 80−84767
KI:Tl, electron-hole and V_k-Tl recomb., TSC and thermolum. study *(French)* 80−34461
KI:Tl, emission and excitation spectra, press. effects 79−83028
KI:Tl, emission bands, press. effect 79−33789
KI:Tl, Jahn-Teller system, negative mag. circular polarisation in emission spectrum 80−20694
KI:Tl, phosphor, press. effect on emission spectra at low temps. 77−85771
KI:Tl, polarised luminesc. of $(Tl^+)_2$ centres 80−71473
KI:Tl, X-ray phosphor, influence of different factors on emission intensity 79−8171
KI:Tl^+, luminesc., time depend. polaris. 79−33810
KI:Tl^+ type phosphor, press. effects on triplet relaxed excited states, quadratic Jahn-Teller interaction 78−23510
KI:Tl(In) and KBr:In, A-luminescence spectra and polarisation, Jahn-Teller minima 77−20914
KI(Br), irradiated at room temp., thermolum. and F-centre thermal stability 78−84669
KI(Br), X-irradiated cryst., luminesc. during press. release 80−20722
$KLi(Pt(CN)_4).2H_2O$, cryst. struct., polarised emission obs. 78−52538
$KMgF_3$:Eu^{2+}, Zeeman absorpt. and luminesc. spectra *(Russian)* 77−69872
$KMgF_3$:Ni, Co, emission from Ni-Ni and Ni-Co pairs, exchange coupling const. 79−33788
$KMgF_3$:Ni, Ni-Ni pair optical spectra 80−45042
$KMgF_3$:Ni^{2+}, absorpt., MCD and emission spectra 79−51953
$KMgF_3$:Sm^{2+}, luminesc. spectra 4.2, 77 and 295K and Zeeman spectra, 4.2K 77−81146
$KMgF_3$:Yb^{3+}, cryst. field parameters, optical, EPR spectra, spin-lattice relax. time 77−51950
$KMnCl_3$, rare earth doped, energy transfer, emission spectra obs. 80−20684
$KMnF_3$, antiferromag., multi-magnon luminesc. sidebands 78−76525
$KMnF_3$, antiferromag. cryst., luminesc. enhancement in mag. field, exciton model *(Russian)* 77−48214
$KMnF_3$, exciton and exciton-magnon emission 79−33779
$KMnF_3$, exciton dynamics by time resolved emission spectroscopy 80−54615
$KMnF_3$, luminesc., emission from localised traps 79−33777
$KMnF_3$, stress-induced phase transition, optical props. meas. 77−20067
K_2MnF_4, quadratic layer antiferromag., intrinsic emission obs. 77−20906
K_2MnF_4-Ni^{2+}, and undoped, magnon spectra, Raman, far IR and fluorescence meas. 77−20573
KNO_3, and KNO_2, fused, electrolum. 79−99945
K_2NaAlF_6:Cr^{3+}, ^2E_g-$^4A_{2g}$ phosphoresc. spectrum, vibr. struct. 79−47494
K_2NaGaF_6:Cr^{3+}, magneto-optical study of $^2T_{1g}$, $^4T_{2g}$, ^2E_g-$^4A_{2g}$ transitions 80−71384
$(K_{1-x}Na_x)_2SO_4$:Tl^+ phosphor, thermolum. characts. 77−90203
$KNbO_3$, single cryst., dielec. breakdown and electroluminesc. 78−2917
$K_6Nb_6Si_4O_{26}$, luminesc. bands, Stokes shift, rel. to crystal struct., stacking faults 80−34974
$K_8Nb_{14}Si_4O_{47}$, luminesc. bands, Stokes shift, rel. to crystal struct., stacking faults 80−34974
$K_5NdLi_2F_{10}$ (KNLF), spectroscopy and lasing 80−5737
$K_5NdLi_2F_{10}$, high yield luminesc. 79−1784
$K_5Nd(MoO_4)_4$, spectral and struct. props. *(Russian)* 79−52020
$KNdP_4O_{12}$, determ. of fluoresc. quantum efficiency and laser emission cross sections 80−48264
K_2O-B_2O_3, glass, PbO-activated, luminesc. and excitation spectra *(Russian)* 78−10979
K_2O-B_2O_3 glass, γ- and UV- irrad., thermodecolorisation and thermolum. 80−20721
K_2O-BaO-GeO_2:Bi^{3+}, Nd^{3+}, absorpt. and excitation spectra, fluoresc. 77−90183
K_2O-BaO-SiO_2:Nd^{3+} glasses, absorption and fluoresc. spectra, density 80−25417
K_2O-GeO_2:tb^{3+}, Yb^{3+} glass, luminesc, cooperative sensitization correlated with Rayleigh scatt. intensity 78−52573
$K_5PrLi_2F_{10}$:Pr^{3+}, emission spectroscopy, ionic interaction 79−83015
$K_{1.75}Pt(CN)_4.1.5H_2O$, Raman scatt. and luminesc. studies 80−25394
K_2PtCl_6:Os^{4+}, multiple state luminesc. 78−72584
K_2PtCl_6:Os^{4+}, sharp line luminesc. band at 10K, vibr. assignment 78−95600
K_2SnCl_6:$ReCl_6^{2-}$, (K_2PtCl_6:$ReCl_6^{2-}$), luminesc. and absorpt. spectra, relax. processes 77−85779
$K_2UO_2Cl_4$, fluoresc. decay rate of pure and impure cryst. 79−47487
luminescence of inorganic solids continued
$K_5(UO_2)F_9$, optical spectra, vibr. freqs. calcs. *(Russian)* 78−31205
$KUO_2(NO_3)_3$, fluoresc. decay rates, temp. depend. 80−25429
$K_2UO_2(NO_3)_4$, fluoresc. decay rates, temp. depend. 80−25429
KYF_4, KY_2F_7, KY_3F_{10}, Er^{3+} and Yb^{3+} doped, IR excitation curves for visible luminesc. 79−33795
KY_3F_{10}:Eu^{2+}, luminescence 79−78746
KY_3F_{10}:Eu^{3+}, fluoresc. intensity, 77 to 4K, cryst. field parameters of Eu^{3+} 78−72580
KY_3F_{10}:Eu^{3+}, fluoresc. decay, radiative and nonradiative transition probabilities 78−72581
KY(Gd)O_2:R^{3+}, R=Eu, Nd, Sm, Dy, Tb, activator effect 77−48216
$KZnF_3$, Cu^{2+} and Mn^{2+} exchange interactions, luminesc. line temp. depend. 79−69480
$KZnF_3$:Mn^{2+}, Cu^{2+}, exchange coupled, luminesc. props. 79−33781
$KZnF_3$:Ni^{2+}, absorpt., MCD and emission spectra 79−51953
$KZnF_3$:Ni^{2+}, mechanism of conc. quenching of fluoresc. from T_{2g} of Ni^{2+} 77−59605
$KZnF_3$:Ni^{2+}, temp. depend. of luminesc. 79−83016
$KZnF_3$:Yb^{3+}, cryst. field parameters, optical, EPR spectra, spin-lattice relax. time 77−51950
Khu_3F_{10}:Eu^{3+}, site occupancy from excitation and emission spectra *(French)* 77−81145
Kl:Tl, excitation in fund. absorpt. region, luminesc. and thermolum. 80−50433
Kr, liquid and solid, absorpt. and luminesc. spectra of self-trapped excitons 79−65893
Kr:N_2O, cryodeposited film, exciton-enhanced KrO excimer luminescence 77−36288
Kr:N_2O, photoluminesc. from KrO (^1S) excimers 78−68544
KrO, in doped inert gas matrix, photoluminesc. 79−31579
Li_2UO_4, energy transfer, cryst. struct. and chemical composition effect 80−108248
$LaAlO_3$:Tb^{3+}, cathodo- and photoluminesc. 77−12448
$La_2Be_2O_5$:Nd^{3+}, optical absorpt. and fluoresc. intensities 80−29793
$La_2Be_2O_5$:Nd^{3+} (Pr^{3+}), cryst. growth, spectral and laser properties in $^4F_{3/2}$→$^4I_{11/2}$ and $^4F_{3/2}$→$^4I_{13/2}$ transitions 80−80853
$LaBr_3$:Np^{3+}, energy level anal., polarised absorpt. and fluoresc. spectra 80−76056
$LaBr_3$:Pr^{3+}, laser-induced fluoresc. line-narrowing, hyperfine struct. and Zeeman effect 77−85789
$LaBr_3$:U^{3+}, luminesc., fluoresc. lifetimes 79−33768
LaCl-Pr(Dy)(Sm), mech. for X-ray luminesc. and thermolum. 79−8170
$LaCl_3$:Nd^{3+} radiation upconversion, 1.06 to 0.873 μm 78−19530
$LaCl_3$:Np^{3+}, energy level anal., polarised absorpt. and fluoresc. spectra 80−76056
$LaCl_3$:Np^{3+}, phonon-induced relax. in excited optical states, linewidth temp. depend. meas. 80−100688
$LaCl_3$:Pr^{3+}, hyperfine Zeeman effects, fluorescence line-narrowing technique 77−62881
$LaCl_3$:Pr^{3+}, Nd^{3+}, single cryst., optical double reson. excitation, energy transfer and transform. 77−69891
$LaCl_3$:Pr^{3+}, second order Zeeman hyperfine effect *(French)* 77−52162
$LaCl_3$:Pr^{3+}, Zeeman second-order effects, fluoresc. line narrowing technique 80−16103
$LaCl_3$:U^{3+}, cryst., spectrum anal., cryst. field parameters 80−76057
LaF_2:Pr^{3+}, ultraslow optical dephasing for $^3H_2$-$^1D_2$ transition 79−64290
LaF_3, VUV luminescence, conference, Moscow, USSR (Apr. 1978) 80−62378
LaF_3:Ce^{3+}, UV fluoresc. potential tunable laser 2760 to 3220 Å 78−15206
LaF_3:Dy^{3+}, $^4F_{9/2}$ and $^4I_{15/2}$ levels, radiative decay rates 79−61415
LaF_3:Dy^{3+}, high temp. fluoresc., Dy^{3+} G-level emission 78−27295
LaF_3:Dy^{3+}, laser excited fluoresc., lifetimes meas. 79−24353
LaF_3:Er^{3+}, optically excited, direct-process spin-lattice relaxation 80−93378
LaF_3:Er^{3+}, spin-lattice relax. meas. in excited $^4S_{3/2}$ state by purely optical method 79−19923
LaF_3:Eu^{3+}, absorpt and laser fluoresc. spectra 77−52159
LaF_3:Ho^{3+} single crysts., multiphonon relax., fluoresc. obs. 79−47495
LaF_3:Ho^{3+}(Dy^{3+}), laser excited fluoresc. rise and decay meas., expt. 80−22448
LaF_3:Nd^{3+}, laser-excited fluoresc., self-adsorpt. 78−15210
LaF_3:Nd^{3+}, luminesc. decay times 80−2811
LaF_3:Nd^{3+}, radiative transition rates of Nd^{3+}, Judd-Ofelt theory 79−33753
LaF_3:Nd^{3+}, vacuum UV luminesc. *(Russian)* 78−64414
LaF_3:Nd^{3+}(Er^{3+})(Tm^{3+}), VUV fluorescence and tunable coherent sources from 1650 to 2600 Å 77−688
LaF_3:Pr^{3+}, anomalous luminesc. decay, phonon reson. trapping and bottlenecking 79−43023
LaF_3:Pr^{3+}, fluoresc., time resolved excitation technique 79−95820
LaF_3:Pr^{3+}, laser-induced fluoresc. line narrowing 77−40280
LaF_3:Pr^{3+}, Nd^{3+}, fluorescence linewidth and energy transfer 77−8635
LaF_3:Pr^{3+}, optical free induction decay meas. of low temp. dephasing 79−46009
LaF_3:Pr^{3+}, optical transition, spin decoupling and magic angle line narrowing 80−28286
$LaGaS_3$:Ce^{3+}, phosphor, luminesc. props. 80−103979
$La_2MgSn_{1-x}Ti_xO_6$, luminescence and energy transfer 77−28619
$LaNbO_4$, Raman scatt. and fluoresc. spectra 80−20625
$LaNbO_4$:Eu^{3+}, single cryst., photoluminesc. obs., vibronic transition dichroism 77−69890
$La_{1-x}Nd_xP_5O_{14}$, Nd^{3+} luminesc. anomalously weak quenching 77−75533
$La_{2-x}Nd_xTi_2O_7$, luminesc. and absorpt. props. 79−65928
La_2O_3:Eu(Tb)(Tm), powder layer, electrolum., comparison with Y_2O_3 and Y_2O_2S 77−20927
La_2O_3-Al_2O_3-SiO_2:Sm^{3+}, luminesc. selective laser excitation line narrowing 80−25434
LaOCl:Sm^{3+}, conc. quenching of X-ray and UV-excited luminescence *(Russian)* 77−55829
La_2O_2S:Eu, high press. effect on luminesc. efficiency and lifetime, charge transfer absorpt. 80−66266
La_2O_2S:Eu_3 slow phosphoresc., high press. study 80−80839
La_2O_2S:Eu^{3+}, luminesc., excitation spectra, cooperative phonon sidebands 79−33771
La_2O_2S:Tb, cathodoluminesc. efficiency changes due to processing, XPS meas. of surface changes 79−99951
La_2O_2S:Tb, recomb. processes and emission spectra *(Russian)* 78−6797

luminescence of inorganic solids continued
La_2O_2S:Tb based barrier layer phosphors, prep. and cathodum. props. in penetration phosphors 77−1738
$La_2O_2S:Yb^{3+}$, charge transfer type luminesc. 79−33797
$La_2O_2S:Yb^{3+},Er^{3+}$, IR excited visible luminesc. of Er^{3+} 78−2910
$La_2O_2S:Yb^{3+},Ho^{3+}$, anti-Stokes emission band assignments, energy transfer mechanism 77−40277
$LaPO_4$:Bi, fluoresc. props., blue emission mechanism 79−52002
$LaPO_4:Yb^{3+}$, charge transfer type luminesc. 79−33797
$La_{1-x}Pr_xP_5O_{14}:Pr^{3+}$, fluorescence spectrum 79−83014
$La_2S.3GaS_3:Ho^{3+}$, fluoresc., visible and IR spectra assignments 77−52150
$La_2S_3.3Ga_2S_3:Er^{3+}$ glass, fluoresc., and possibility of lasing 78−23514
$LaSiO_3F(Cl)(Br)$, phosphor host, luminesc. and struct. props. 78−48212
$La_{1-x}Tb_xOBr$ phosphor, concentration quenching of Tb^{3+} luminesc. 80−29785
Li disilicate glass, radiation induced centres, EPR exam. 78−35033
Li-La phosphate glass, Nd, Cr activated, Nd luminesc. quantum efficiency meas., Nd-Cr nonradiative transfer 80−66296
Li-Nd-La phosphate glass, nonradiative losses, pulse periodic stimulated emission and luminesc. 77−83878
$LiAl_5O_8:Cr^{3+}$, fluoresc. and excitation spectra, zero phonon lines 79−33785
$Li_2B_4O_7$:Cu, Ag, as thermoluminescence dosimeter *(Japanese)* 78−31906
$Li_2B_4O_7$:Mn, thermolum. response to pions 80−101270
$LiBaAlF_6:Eu^{2+}$, band emission and line emission 79−28810
$LiCdVO_4$, luminesc. spectra in visible region, vanadate group 78−43921
LiCl, electron irrad., F-centre emission 78−60501
LiCl, radiation effects on decay time of F-centre emission 80−93381
LiCl single crysts., γ-irrad., thermolum. meas. 80−80880
LiCl, thermolum., order of kinetics 80−89074
LiCl:Ag, fluoresc. and UV absorpt. spectra 80−80844
LiCl:Ag, luminesc. anal. using synchrotron radiation 79−38639
$LiCl:Cu^+$, luminescent centre, cluster MO calculation of energy levels 78−64411
$LiCl:Cu^+$, MO calc. of luminesc. Cu^+ centres 79−38609
LiD, cubic cryst., exciton-phonon interaction and exciton anisotropy 78−72083
LiD, luminesc. of free and localised excitons, UV, X-ray and electron irrad. luminesc. 79−87483
LiF (TLD-100), pre-irradiated, non-irradiation induced TLD 78−48242
LiF (TLD-100), thermoluminescent glow peaks 78−35211
LiF (TLD-100), thermoluminescent response to 0.1-5 keV electrons 79−95852
LiF, annealing effects on thermoluminescence, dipoles and dimers 77−12452
LiF, coherent radiation generation in F_2-centres 78−50782
LiF, cryst., triboluminesc. spectra 80−66312
LiF crystal, contact damage obs. by cathodoluminesc. 80−71728
LiF dosimeter, thermoluminescence glow curves and light absorption, thermal treatment effect *(Russian)* 77−32954
LiF, effect of impurity traces on physical props. 77−12450
LiF, irradiated and plastically deformed, thermoluminesc. defect centres 77−1740
LiF, M-centre vibronic absorpt. spectra, elec. field, method of moments 78−27186
LiF, mech. excitation, luminesc. electron emission, friction, static electrification, meas. method *(German)* 77−24904
LiF, non-universality of TL-LET response, effect of batch composition 80−16106
LiF, photostimulated thermolum. as UV radiation dosimeter 77−16984
LiF, prep. and dosimetric props. of new highly sensitive form 79−22483
LiF, restored thermoluminescence mechanism 78−19580
LiF TLD, plastic deform. effects on thermolum. sensitivity, rel. to handling technique 77−16988
LiF TLD, press. deform. and recovery 77−8668
LiF, TLD 100, thermolum. peaks anal. 77−44073
LiF TLD materials, influence of composition on sensitivity to high energy electrons 77−40775
LiF TLD phosphor, γ-irrad. induced sensitisation, UV effects 80−108286
LiF TLD phosphor, incompatibility of sensitisation and dose re-estimation 78−40340
LiF TLD phosphor, residual thermoluminescence effect on sensitisation 80−108287
LiF, TLD phosphor, Z_3 centre, thermolum. and optical absorption spectra 79−24374
LiF TLD-100, thermolum. response to 5 to 30 keV electrons effect of annealing atm. 77−86638
LiF, TLD-100, thermoluminesc. emission spectra meas. 78−84667
LiF, TLD-100, thermolum., glow curve kinetics 78−84668
LiF TLD-100, thermoluminesc., kinetics and trapping parameters, dose depend. 80−2872
LiF, TLD-100, trapping centres, optical absorpt. spectra defect and thermolum. mechanism models 80−50436
LiF TLD-100 phosphor, sensitisation mechanism study, thermolum. glow peak intensity obs. 80−55202
LiF TLD-700, Harshaw, effect of sample size and batch origin on thermal neutron sensitivity 78−40342
LiF, thermolum., formulation of sensitisation based on simple two-step reaction rate model 78−39610
LiF, thermolum., trapping mechanism based on Z-centres 80−76089
LiF, thermolum. light self absorpt. obs. 79−81097
LiF, thermolum. response to pions 80−101270
LiF, thermoluminescence, γ-radn.-induced sensitization and supralinearity 79−91507
LiF thermoluminescence induced by 13.8 and 81 meV diffr. neutrons 77−56481
LiF, thermoluminescence mechanisms following gamma irradiation 77−59625
LiF, thermoluminescence response to gamma rays 77−59626
LiF, thermoluminescence intensity depend. on heating rate and deep trap 78−56527
LiF, thermoluminescence mechanism, extension of Mayhugh-Christy model 78−80425
LiF with stable F_2 centres, F_2^+ colour centre generation accumulation, tunable laser production *(Russian)* 80−28238
LiF, X-irradiated cryst., luminesc. during press. release 80−20722
LiF:Mg, effects of grain size on thermolum. and thermally stimulated exoelectron emission 79−15536
luminescence of inorganic solids continued
LiF:Mg, role of impurity-vacancy pairs in thermolum. 79−8195
LiF:Mg, TLD-100, thermolum. phosphor, photolum. and absorpt. spectra, thermolum. mechanisms 80−97321
LiF:Mg, Ti, luminesc. increase by O implantation 78−64412
LiF:Mg, X-irradiated, thermoluminesc. of Z_3-centres 78−15236
LiF:Mg,Ca detectors, variation of parameters of thermally stimulated luminesc. 79−6793
LiF:Mg,Ti, defect states, ESR and ionic cond. study 80−108058
LiF:Mg,Ti, thermolum. related Z-centres, optical absorpt. bands 78−23540
LiF:Mg,Ti, thermoluminesc. activation energies 79−74009
LiF:Mg,Ti crystals, Z_3-centres, correlation of thermoluminescence and optical absorption 80−45154
LiF:Mg dosimetric cryst., light-sum storage during linear stage 79−8194
$LiF:Mg^{2+}$, TLD-100, solution treatment temp. and ageing effects 77−56480
LiF:Si, injection electrolum., fields up to 10^4 V cm^{-1} 77−12445
LiF:Ti, thermoluminesc. dosimetry appl. 79−38683
LiF:Ti, thermoluminesc., effect of plastic deform. 79−33853
$LiF:U_3O_8$, X- and γ-irrad., U^{5+} luminesc. molecular centres, optical and ESR expts. 77−48224
$LiF:U^{5+}$, absorption and laser-excited fluoresc. 79−99927
LiF-Li_2O, F-aggregate centres *(Russian)* 78−64394
LiF(TLD-600), unannealed, fading for thermal neutrons and γ-rays 80−83225
$LiGaO_2$:Fe, phosphor, luminesc. 78−92108
$LiGa_5O_8:Cr^{3+}$, fluoresc. and excitation spectra, zero phonon lines 79−33785
LiH (D), single crystals, electronic excitations, review *(Russian)* 78−72574
LiH, cubic cryst., exciton-phonon interaction and exciton anisotropy 78−72083
LiH, defect form. at low temp., EPR, thermolum. and TSC study 80−107222
LiH, effect of surface hydrolysis to LiOH on IR absorption, X-ray luminesc. and EPR spectra 80−60660
LiH, excitons, reflection, cathodolum. and photocond.-excitation spectra 78−10989
LiH, formation and annihilation of Li colloids and H bubbles 80−107228
LiH, LiD, single cryst., reson. zero-phonon exciton luminesc., polariton emission 78−52564
LiH, luminesc. of free and localised excitons, UV, X-ray and electron irrad. luminesc. 79−87483
LiH, motion and relax. of free excitons, luminesc. spectra 79−43037
LiH, optical parameters of localised centres at high hydrostatic press. 78−10943
LiH, UV induced luminescence 77−85784
LiH:LiF, luminesc. of free and localised excitons, UV, X-ray and electron irrad. luminesc. 79−87483
LiH-LiF(Cl), mixed cryst., thermolum., appl. as X-ray detectors 79−6794
LiH(D), resonant Raman scattering in crystals with self-trapping excitons 80−7344
LiI crystal, emission spectra under UV-light excitation at 77K 78−92110
$LiIO_3$, crystal, parametric superluminescence in ps band 80−11469
$LiInS_2$, blue-band emission 80−76062
$LiMgP_{1-x}V_xO_4$; luminesc. spectra in visible region, vanadate group 78−43921
$LiMgVO_4$, luminesc. spectra in visible region, vanadate group 78−43921
LiN_3, evidence for N_3^- from static and dynamic props. 78−60465
Li_3N, photoluminesc. props. 80−50414
Li_3N, superionic conductor, cryst. growth and struct., phys. props., book contrib. 79−42308
$LiNbO_3$, exciton migration, laser time-resolved spectra obs. 79−69861
$LiNbO_3$, light emission from surface on heating or cooling 78−64416
$LiNbO_3$, luminesc. props., Li/Nb ratio effect 80−97323
$LiNbO_3$, optically active centres, form. by electron and γ-irrad. 78−18642
$LiNbO_3$, spontaneous elec. breakdown 77−66458
$LiNbO_3$, spontaneous parametric light scatt. characts. meas., 1000-4000 cm^{-1} 77−8640
$LiNbO_3:Cr^{3+}$ glass, roller quenched, crystn. kinetics 80−44143
$LiNbO_3$:phosphor, piezoelec., interaction with SAW, excitation of electrolum. 79−60615
LiNd phosphate glass, spectral and generation props. 77−1700
$LiNdP_4O_{12}$ laser, fluoresc. and oscill. characts. at 1.317 μm 78−5473
Li_2O-Al_2O_3-SiO_2 glasses, Tb^{3+} ($^5D_3$) luminesc., cross-relax. quenching *(Russian)* 79−33836
Li_2O-B_2O_3, crystalline and glassy, thermolum. meas. 77−16406
Li_2O-$B_2O_3:Eu^{3+}$ glass, laser induced fluoresc. line narrowing, struct. 79−38613
Li_2O-Fe_2O_3-SiO_2 glass, struct. and crystallisation behaviour 78−83738
Li_2O-Nd_2O_3-P_2O_5 ultraphosphate glasses, Nd^{3+} conc. quenching of luminesc. effect 79−19931
Li_2SO_4, triboluminescence and cryst. fracture dynamics 80−50437
$LiScO_2:Bi^{3+}$, luminesc., vibr. struct. 79−33790
$LiTaO_3$, spontaneous elec. breakdown 77−66458
$Li_3WO_4:U^{6+}$, luminescence meas. 77−32432
$Li_4WO_5:U^{6+}$, vib. fine struct. in luminesc. spectra 77−8620
$LiY_{1-x}Eu_xP_4O_{12}$ phosphor, prep. and fluoresc. 77−48219
$LiYF_4$ UV reflectance, transmission and photoluminescence obs. 79−15488
$LiYF_4:Ce^{3+}$, laser transition at 325 nm, large fluoresc. linewidth 79−72574
$LiYF_4:Ho^{3+}$, optical absorpt. and luminesc. spectra 79−4844
$LiYF_4:Nd^{3+}(Er^{3+})(Tm^{3+})$, VUV fluorescence and tunable coherent sources from 1650 to 2600 Å 77−688
$LiYF_4:Pr^{3+}$, mag.-dipole transitions obs. in fluoresc. 80−11451
$LiYF_4:Pr^{3+}$, polarized absorpt. and fluoresc. spectra, 10 to 300K, energy levels and live intensities 79−95836
$LiYF_4:Pr^{3+}$, spectroscopic determ. of ground config. energy levels 80−34969
$LiYF_4:Yb^{3+}$, Ho^{3+}, sensitised anti-Stokes luminesc., theory 77−66537
$LiYFd_4:Er^{3+}$, optical spectra and multifreq. stimulated emission 79−56818
$LiY(Gd)O_2:R^{3+}$, R=Eu, Nd, Sm, Dy, Tb, activator effect 77−48216
$LiYO_2:Nd^{3+}$, absorption and luminesc. spectra, energy level diagram 77−63441

luminescence of inorganic solids continued
$LiY_{1-x}Tb_xP_4O_{12}$ phosphor, prep. and fluoresc. 77−48219
$Li_{14}ZnTa_4O_{18}$:Eu, fluorescence and cryst. symm. 77−24886
$LiZnVO_4$, luminesc. spectra in visible region, vanadate group, and high-press. phase 78−43921
Lisd4UO$_5$, energy transfer, cryst. struct. and chemical composition effect 80−108248
$LuAlO_3:Er^{3+}$, $^4S_{3/2}$ to $^4I_{9/2}$ transition laser action, optical and luminescence spectra 80−16082
$LuAlO_3:Nd^{3+}$, spectral-generation characts., expt. and theory *(Russian)* 77−7090
$Lu_3Al_5O_{12}:Er^{3+}$, absorpt., luminesc., stimulated emission 77−32402
$LuF_3:Ce^{3+}$, UV fluoresc. potential tunable laser 2760 to 3220 Å 78−15206
$LuF_3:Nd^{3+}(Er^{3+})(Tm^{3+})$, VUV fluorescence and tunable coherent sources from 1650 to 2600 Å 77−688
$Lu_2O_2S:Eu_3^+$, luminesc., excitation spectra, cooperative phonon sidebands 79−33771
$Lu_2O_2S:Yb^{3+}$, charge transfer type luminesc. 79−33797
$LuPO_4:Yb^{3+}$, charge transfer type luminesc. 78−64392
$LuPO_4:Yb^{3+}$, charge transfer type luminesc. 79−33797
$Lu_{2-x}Si_2O_7:Eu_x$, synthesis and spectroscopic study 80−84846
$LuVO_4:Eu^{3+}$, absorption and fluoresc. spectra, SU(2) chain *(French)* 78−28912
$LuVO_4:R^{3+}$, R=Nd, No, Tm, Sm, Dy, Er, Eu, Tb, electronic struct. and spectra of VO_4, RO_8 clusters 78−10953
$Lu_2(WO_4)_3$:Cr(Eu), and undoped crystals, luminesc. obs. 80−89047
$LuYScO_3:Er^{3+}(Tm^{3+})(Ho^{3+})$, thermolum. meas. 80−97354
$Mg_{(S)}+Ne^+$, O-dependent photon emission 79−1810
$MgAlO_4:Cr^{3+}$, exchange parameters of Cr^{3+} pairs, optical and EPR meas. 77−69282
$MgAl_2O_4$, γ-irradiated crystal, TSC, thermoelec. power, thermolum. and afterglow 80−75583
$MgAl_2O_4$, spinel, γ-irrad. effect on optical absorpt. and thermolum. spectra 77−85759
$MgAl_2O_4$, spinel, vac. UV luminesc. spectra *(Russian)* 77−24903
$MgAl_2O_4:Cr^{3+}$, exchange parameters determ. from emission and luminesc. excitation spectra 77−52160
$MgAl_2O_4:Cr^{3+}$, luminesc. spectrum, N-lines *(German)* 77−16382
$MgAl_2O_4:Cr^{3+}$, N-lines and Cr^{3+} pairs 78−2896
MgF_2, cryst., Roentgenoluminesc., exciton emission *(Russian)* 78−95609
MgF_2 crystal, $M(D_{2h})$ centre absorption and emission spectra obs. 79−19910
MgF_2, localised electronic levels, thermoluminesc. and thermally stimulated current exam. 78−11001
MgF_2 long-persistence cathode-ray screen, phosphoresc. decay into second-order components 77−20907
MgF_2, nonactivated, X-ray luminesc., 80−2832
MgF_2, transient absorption and luminesc. following electron beam excitation 77−69920
MgF_2, X-ray luminesc. polarisation 80−11462
MgF_2:Mn, X-ray luminesc. yield temp. depend. 77−4680
MgF_2:Mn(Co), photoluminesc. due to X-rays, colour centre thermal breakdown 79−24359
$MgF_2:Ni^{2+}$, temp. depend. of luminesc. 79−83016
MgO, cathodoluminesc. at dislocations 79−47524
MgO, chemisorption of O_2, adsorboluminescence from surface F-centres 80−20723
MgO, cryst. short-wave luminesc. V-centre electron recomb., impurity effects *(Russian)* 77−20921
MgO crystal, contact damage obs. by cathodoluminesc. 80−71728
MgO crystal cathodoluminescence, SEM analysis 80−97349
MgO, defect centres, thermolum. examination 78−15235
MgO, deformation induced damage, effect on optical props. 77−77258
MgO, direct-response UV TLD 77−13010
MgO doped powder phosphors, photo- and thermostimulated luminesc. obs. *(Russian)* 80−66263
MgO, electron irradiated, luminescence, radiative recombination kinetics 80−7421
MgO, electronic excitations and luminescence, review *(Russian)* 78−72575
MgO, exciton luminesc. spectrum, fine struct. 80−20715
MgO, F centre luminesc., effects of uniaxial stress and ODMR 80−20690
MgO film, vacuum deposited on NaCl-type alkali halides, struct. characterisation 79−82490
MgO, γ-irrad. polycryst., isothermal luminesc., recomb. of electron from F_s^+ centres 80−34985
MgO, light emission during adsorpt. and desorpt. of O_2 78−38949
MgO, local loss of stoichiometry caused by plastic deform., cathodoluminesc. spectra 78−35209
MgO, photoluminesc. during mechanical deform. 80−60665
MgO powder, vacuum UV induced thermoluminesc. in Γ-irradiated and non-irradiated samples 77−36302
MgO, pure and doped, luminesc. of free and relaxed excitons 79−74008
MgO, pure and doped crysts., X-ray stimulated luminesc. 79−28802
MgO, single cryst., thermolum. for UV dosimetry 77−16986
MgO, single cryst., tribolum. obs. 79−52031
MgO, single crystal, thermolum. meas. *(Japanese)* 78−19577
MgO, single crystal, thermal and optical stimulation processes of V-centres *(Japanese)* 80−11485
MgO, single crystals, compressed, SEM exam. of cathodoluminescence 78−56525
MgO, thermoluminescence mechanism 79−15538
MgO:Al, and nominally pure single crystal, thermally stimulated luminesc. rel. to temp., and EPR *(Russian)* 80−84789
MgO:Al, MgO:Sn, exciton, electron hole energy transfer 78−10998
MgO:Al(Li)(F)(Sn), hole processes in photostimulated luminesc., electron emission, X-ray irrad., ESR relaxation 79−69889
MgO:Be epitaxial layers, vacuum UV luminescence 80−11480
$MgO:Cr^{2+}(V^{2+})$, coupling of T_{1u} and T_{2u} vibr. to $^2E_g \rightarrow {}^4A_{2g}$ transition 77−63453
$MgO:Cr^{3+}$, $^4T_{2g}$ excited level of Cr^{3+} 78−43920
$MgO:Cr^{3+}$, axial centres, EPR and fluoresc. meas. 78−2731
$MgO:Cr^{3+}$, broad band luminesc., relaxed level and emission processes 78−31234
$MgO:Cr^{3+}$, emission and excitation spectra 80−93387
$MgO:Cr^{3+}$, no-phonon lines associated with broad band emission *(French)* 77−52163
$MgO:Cr^{3+}$, optical excitation transfer 80−97325
$MgO:Cr^{3+}$, site symmetry of Cr^{3+}, polarised luminesc. meas. 77−12426
MgO:Fe, cathodolum. after plastic deform. 79−95849
MgO:Li, oxidation and reduction up to 1700K, defect prod. 79−39013
MgO:Li(Al)(F), impurity-induced UV luminesc. 79−83037
$MgO:Ni^{2+}$, near IR luminesc. from isolated and exchange-coupled Ni^{2+} ion pairs, temp. depend. 80−93382
$MgO:Ni^{2+}$, single crystal, thin film, near IR luminescence *(Russian)* 79−28807
$MgO:Ni^{2+}$, temp. depend. of luminesc. 79−83016
MgO:S, cathodoluminesc. spectrum *(Russian)* 80−55197
MgO:Sn, exciton, electron hole energy transfer 78−10998
MgO:Sn(Al), luminescent crystals, exciton, electron hole energy transfer 78−10998
MgO-Al_2O_3 spinel crysts., thermolum. spectra 79−65938
MgO-Al_2O_3-P_2O_5 system glass, heat treatment of aluminium metaphosphate influence on thermolum. 80−108285
MgO-Al_2O_3-$SiO_2:Ce^{3+}$ glass scintillator, energy transfer, luminesc. efficiency under UV and charged-particle excitation 79−95821
MgO-NH_4F-GeO_2:Mn phosphor, luminance. spectra due to UV irrad., 26-294°C 79−83005
MgO-P_2O_5-Al_2O_3-$3P_2O_5$ glass, absorpt. shift, electron and hole traps, thermolum. meas. 79−65897
$Mg(Pt(CN)_4)7H_2O$, transition energy tuning from 3.3 to 1.4 eV 79−61436
$MgS:Ce^{3+}$ phosphors, emission and excitation spectra *(French)* 80−93380
$MgS:Eu^{2+}$, emission and excitation spectra obs. 80−55162
Mg_2SiO_4:Tb, TLD material, UV induced thermolum. and phosphoresc. 78−92707
Mg_2SiO_4:Tb, thermolum. phosphor, photolum. and absorpt. spectra, thermolum. mechanisms 80−97321
Mg_2SiO_4:Tb TLD, response to X-ray and electron irrad. 79−3285
$Mg_4Ta_{2-x}Nb_xO_9$, luminescence, model of niobate and tantalate centres 77−16373
$MgUO_4$, emission and excitation spectra 79−83012
$MgUO_4$, energy transfer, cryst. struct. and chemical composition effect 80−108248
$Mg_3(VO_4)_2$, luminesc. spectra in visible region, vanadate group 78−43921
$MgWO_4$, luminesc. and capture centres *(Russian)* 78−52543
$MgWO_4$, luminesc. efficiency, temp. and high-press. 78−23507
$Mg_xZn_{1-x}Te$, high purity, luminesc. and band gap 78−68553
$Mg[Pt(CN)_4].7H_2O$, high press. tuning of optical transitions 79−28813
Mn complex, $[Mn(urea)_6](UO_4)_2$, thermal expansion coeff., crystal field parameters, phosphoresc., absorv., excitation spectra 78−43932
Mn complex, Mn amine, luminesc. spectra *(French)* 79−51997
Mn complex, $MnCl_2$ with 3,5-lutidine hydrochloride, cryst. 77−52153
Mn complex, $MnCl_2$.3,5-lutidene hydrochloride complex, photoluminesc. and photoexcitation 78−92106
Mn complex, papaverine hydrochloride with $MnCl_2$, cryst. 77−55812
Mn complex, with 4-benzylpyridine hydrochloride, photoluminesc. props. 80−89044
Mn complexes, verification of laws of luminesc. of solids 78−60506
Mn complexes, with pyridine, excitation luminesc., ligand field effect 77−48213
Mn minerals, photoluminesc. 79−95829
Mn^{2+} in crystals with different site symmetries, luminesc. spectra 78−80400
Mn^{2+}, in nearly tetrahedral clusters, ^4E levels, orbit-lattice interaction and Jahn-Teller effect, spectra obs. 80−24860
$Mn_xCd_{1-x}Se$ single crysts., photoluminesc., composition depend. 80−80854
$MnCl_2$-lutidine HCl complex, photoexcitation, photoluminesc. 78−27301
$MnCl_4$, fine struct. of Mn^{2+} lines 79−33780
MnF_2, antiferromag., multi-magnon luminesc. sidebands 78−76525
MnF_2, fluorescence props. 79−73994
MnF_2, one-magnon luminesc. sidebands of excitonic transition 78−60517
MnF_2, radiation damage, optical absorpt. and luminesc. expts. 78−2161
MnF_2, two-exciton light absorption, with four-photon excitation *(Russian)* 78−35186
$MnF_2:Eu^{3+}(Er^{3+})$, fluorescence props. 79−73994
$MnF_2:Ni^{2+}$, IR fluoresc., field depend., exchange energy 78−68543
MnF_2:Zn, shift and broadening of optical transitions 79−38579
MnF_6^{2-}, $A_2^IM^{IV}F_6$ hosts, luminesc., IR and Raman spectra, 5K, assignments 77−20904
MnP_2, nonequilibrium luminesc. and relaxation processes, 25 to 300K *(Russian)* 78−80415
Mo, bombardment by 1 to 30 keV ions, emitted radiation spectral comp. *(Russian)* 77−81159
Mo, broadband optical emission for heavy ion bombardment 77−28635
Mo, excited state formed by B^+ impact, light emission coeffs. 78−64417
Mo, ion bombard., ion and photon yields, CO adsorption effect 80−89098
Mo, ion impact, radiative spectrum of sputtered particles *(Russian)* 79−91504
Mo, photon emission from inert gas-surface impact 78−11059
N_2 crystals, luminesc. and biexcitons 79−69893
N_2 film, on metal or sapphire substrates, luminescence and nonradiative energy transfer to surfaces 80−97350
N_2 in Ar matrix, luminesc. lifetime 79−36690
N_2, luminesc., multiphonon-assisted energy transfer 79−47498
N_2, solid, cathodoluminesc. 77−28634
N_2, solid, electron impact excited, luminesc. spectra 77−48252
N_2, solid 79−19939
N_2, solid and matrix isolated mol., triplet state spectra *(Russian)* 80−5574
N_2, vacuum UV luminesc., 8K 78−10958
N_2:N, dynamically induced electronic transitions of matrix isolated atom 78−63825
$NH_4Br:Cu^+$, luminesc., orientation phase transition 80−100687
NH_4Br:Tl, absorption, excitation and fluorescence spectra 79−33824
NH_4Br:Tl, and pure crystals, luminesc., VUV irradiated at 80K *(Russian)* 80−84763
$(NH_4)_2Cd_2(SO_4)_3:Mn^{2+}$, UO_2^{2+}, luminesc., vibr. modes 79−38629
NH_4Cl:Tl, phosphoresc. decay rates obs., pretreatment effects 79−4853
NH_4NO_3, intrinsic electroluminescence obs. 78−80420
NH_4SO_4, intrinsic electroluminescence obs. 78−80420
$NH_4UO_2(NO_3)_3$, fluoresc. decay rates, temp. depend. 80−25429
NO+O, in Ar matrix, chemiluminesc. 78−35688

luminescence of inorganic solids continued
Na, chemisorption of halogens, surface chemiluminesc., MO description 79−43048
Na film, slow electron bombarded, light radiation 80−40168
Na salts, spectral refl. changes and luminesc. during 2-10 keV proton bombardment, implications for Io 79−96950
$Na_{56}(AlO_2)_{56}.(SiO_2)_{136}:Eu^{3+}$, Y-type zeolite, emission spectrum at room temp. 79−83017
$Na_6Al_6Si_6O_{24}$, zeolite, luminescence and coloration *(Russian)* 78−72578
$Na_4Al_3Si_3O_{12}Cl$:Br,Ge, sodalite, reflectance and luminescence obs. 79−4839
$Na_8Al_6Si_6O_{24}F_2(Cl)(Br)(I)$, sodalite, luminescence and coloration *(Russian)* 78−72578
$Na_6Al_6Si_6O_{24}(NaX)_{2n}$, X=Cl, Br or I, sodalites, thermal destruction of colour centres *(Russian)* 80−84169
$Na_3Al_6Si_6O_{24}X_2$, optically erasable colouring and luminesc. *(Russian)* 77−85801
$Na_8Al_6Si_6O_{24}.Cl(Br)(I)$, cathodochromic sodalites, coloured crysts., tunnel and recomb. luminesc., temp. depend. *(Russian)* 80−66261
NaBr, lifetime of colour centres 78−92115
NaBr powder coloured in electrodeless discharge, reflectance spectra, thermoluminescence props. 78−6796
$NaBr:Cu^+$, luminesc. and lifetimes, press. depend. 79−33809
$NaBr:Eu^{2+}$,Ho^{3+}, single cryst., cluster luminesc. centres *(Russian)* 77−20922
NaBr:Pb, absorpt. and emission spectra of Pb centres 79−78717
$NaBr:Tl^+$, emission spectra, excitation in A-band 78−15218
NaBr(:I), exciton ionisation and decay, photoluminesc. in elec. field 77−44046
NaBr(I), optically activated F→F′ centre conversion in mag. field 80−108253
$NaBrO_3$, cryst., mechanoluminesc. spectra 80−97355
$NaBrO_3$, single crystals, thermolum., optical absorpt., X-ray effect 79−95858
$NaCaVO_4$, luminesc. spectra in visible region, vanadate group 78−43921
$Na_3Ce_{1-x}Tb_x(PO_4)_2$, UV excitation, emission spectra 79−38595
NaCl, absorpt. spectra, influence of elec. field 80−2794
NaCl, barrier instability in strong elec. fields 79−69522
NaCl, bi-exciton luminescence possibility 80−40167
NaCl, cryst., triboluminesc. spectra 80−66312
NaCl, electron and ion beam excited luminesc. spectra 79−52026
NaCl electron excited luminescence yield orientational depend. 80−40169
NaCl, exciton luminesc. obs. 77−12449
NaCl, excitons at $L_{II,III}$ absorption edge of Cl^-, decay characts. thermolum. meas. 77−28121
NaCl, F_3-centre quartet state, IR emission spectra 78−43930
NaCl, influence of coloration on intrinsic luminesc. 78−80399
NaCl, irradiated, at 80K, thermolum. processes 80−34990
NaCl, irradiation-induced energy transfer from bulk to surface, luminesc. meas. 78−92132
NaCl, luminesc. singlet from triplet self-trapped excitons 79−99936
NaCl, luminesc. under 10.6 μm laser pulse irrad. *(Russian)* 77−16381
NaCl, m-crocryst. powders coloured in electrodeless discharge, reflectance spectra, thermolum. 78−15238
NaCl, microcryst. powder, isothermal stability of colour centres, thermolum. glow curve 79−15535
NaCl, migration of nonrelaxed holes, self-trapping, ESR and luminesc. obs. *(Russian)* 80−66033
NaCl, optical conversion, luminesc. and colour centre formation 79−24354
NaCl particle, luminesc. duration rel. to time in CO_2 laser beam focal zone 80−34983
NaCl, photoluminescence under pulsed UV laser excitation 77−77289
NaCl preirradiation effect on proton channelling, thermoluminescence study 80−19860
NaCl, pure, indoped, luminesc. obs. 77−32412
NaCl, pure and doped, 20K X-ray irradiation, thermolum. and recovery processes 80−93412
NaCl, self-trapped exciton form. via thermally induced defect reactions 80−60687
NaCl, thermoluminesc. and optical absorpt., simultaneous DC field and X-irrad. 79−99956
NaCl, tunnelling recombination between neutral Ag atoms and V_k centres 79−61442
NaCl:Ag, absorpt. spectra, influence of elec. field 80−2794
NaCl:Ag, diffusion parameters of hot holes created by ionising radiation 78−47800
NaCl:Ag, electroluminescence spectra 78−2918
NaCl:Ag, excitation in fund. absorpt. region, luminesc. and thermolum. 80−50433
NaCl:Ag, irrad. with synchrotron radiation, thermolum. light-sum spectrum of L absorpt. edge of Cl^- 79−15540
NaCl:Ag, thermolum. light sum storage by ultrasoft X-rays 77−20939
NaCl:Ba, X-irrad., Z_1-centre prod., thermolum. obs. 78−75663
NaCl:Br, host-sensitized luminesc., energy transfer due to excitons and holes 79−38590
NaCl:Ca, microhardness and thermoluminescence, hardness-quenching temp. variation 80−29813
NaCl:Ca, X-irradiated, Z_1-centre form. kinetics, thermolum. investig. 77−4693
NaCl:Ca, Z_1 centre thermoluminescence study 80−16109
$NaCl:Ca^{2+}$, X-ray induced luminescence 78−23516
NaCl:Ca(Mg), X- and gamma-irrad., thermostimulated electrons and luminesc. 79−91505
NaCl:Cu, UV absorpt., emission, excitation spectra, Cu^- centres 77−81127
NaCl:Cu, X-irrad., thermoluminesc., F-centres 79−33849
$NaCl:Cu^+$, luminesc. and lifetimes, press. depend. 79−33809
$NaCl:Cu^+$, X-irrad., thermoluminesc. centre, EPR anal. 79−43045
$NaCl:Cu^+$, X-ray irrad., role of Cu^+ in thermoluminesc. 78−56526
$NaCl:Ga^+$, polarisation of Ga^+ centre A_T emission, temp. depend. 80−80842
NaCl:I, UV laser generation by optical pumping 78−82973
$NaCl:MgCl_2$ (0.1 mol.%), thermoluminesc. glow curves, temp. distrib. and trapping centres 78−48241
$NaCl:Mn^{2+}$, radiation-induced colouring, room temp. kinetics 79−55736
$NaCl:Mn^{2+}$, thermolum. spectra, mechanisms 80−80873
$NaCl:Mn^{2+}$, X-irrad., thermoluminesc. and EPR 79−61444
$NaCl:Mn^{2+}$, X-ray irradiated, thermolum. and EPR 77−81161

luminescence of inorganic solids continued
$NaCl:O_2^-$, excitation and absorpt. spectra at 2K, O_2^- excited state field 79−56843
NaCl:Pb, γ-irrad., centres in thermoluminescent emission 77−85816
NaCl:Pb, luminesc. spectra obs. 78−95604
$NaCl:Pb^{2+}$, decay of luminescence emission 78−39593
$NaCl:Pb^{2+}$, emission spectra obs., and luminesc. centre model 77−36286
NaCl:Tl, deformed phosphors, thermoluminesc., impurity conc. effects 77−63473
NaCl:Tl, luminesc. yield, effect of fast electron channelling 78−84646
NaCl(:Ca), irrad. at room temp., stored energy rel. to thermolum. 80−10574
NaCl(Br), X-ray or UV irradiated, cation defects creation mechanism 80−75224
NaCl(Br):Tl, emission spectra, press. effects 78−23509
NaCl(F), irradiated at room temp., thermolum. and F-centre thermal stability 78−84669
$NaClO_3$, cryst., mechanoluminesc. spectra 80−97355
$NaClO_3$, X-irrad., thermal stability of radiation damage products 79−34324
NaF, F_3^+-centre decay by optical free induction 78−68555
NaF, gamma irrad., colour centre stimulated emission, threshold pump power, tuning range 79−73971
NaF, M-centre vibronic absorpt. spectra, elec. field, method of moments 78−27186
NaF, two-photon absorpt. cross sections of N_1 and F_3^+ centres 79−73991
NaF, with colour centres, laser stimulated luminesc. 78−6749
NaF, X-irrad., colour centres and thermolum. 80−84790
NaF:LiF, γ-irrad., colour centre form., reflectance and thermolum. meas. 79−55739
NaF:Mn, role of Mn^{2+} in thermolum. 80−97353
NaF:U, luminesc. spectra, Vibr. struct. 80−80840
NaF:U, single crystals 78−72588
$NaF:U^{6+}$ luminesc. spectrum obtained using chronospectroscopic method and phase spectra 79−54199
$NaGdO_2:Tb^{3+}$, obs. of efficient luminesc., UV excitation 78−43922
NaI and $NaI:Tl^+$, intrinsic and impurity induced luminesc., exciton diffusion 77−16367
NaI, exciton luminesc., characteristics near absorption edge 78−88363
NaI, exciton-phonon polarisation interaction *(Russian)* 78−35195
NaI, luminesc. polarisation for free and bound excitons 78−10942
NaI, motion of free excitons and their self-localisation 80−2342
NaI, pure and Tl doped, luminesc. mechanism effects on scintillation response to ions 77−48255
NaI, resonant Raman scattering in crystals with self-trapping excitons 80−7344
NaI, single cryst., reson. zero-phonon exciton luminesc., polariton emission 78−52564
NaI, thermal dissoc. of photoproduced excitons at UV band edge, recomb. luminesc. obs. 80−50412
$NaI:Cu^+$, luminesc. of isolated V_K-centres 78−84641
NaI:Tl, fluoresc. excited by γ-rays, a student laboratory expt. 79−97143
NaI:Tl, scintillation excitation mechanism 80−2857
$NaI:Tl^+$, luminescence spectrum, excited states of monomer centre 77−66536
$Na_3La_{1-x-y}Ce_xTb_y(PO_4)_2$, optical props. *(French)* 80−103991
$Na_3La_{0.98}Eu_{0.02}(VO_4)_2$, luminesc. spectrum 77−4673
$NaLaO_2:Pr^{3+}$, obs. of efficient luminesc., UV excitation 78−43922
$Na_3La(PO_4)_{1.9}(VO_4)_{0.1}$, luminesc. spectrum 77−4673
$Na_3La(VO_4)_2$, luminesc. spectrum 77−4673
$NaLnO_2:Bi^{3+}$, (Ln=La, Gd, Sc), luminesc., vibr. struct. 79−33790
$NaMgF_3$, defects induced by X- and vacuum UV irrad., optical and elec. study 80−107319
$NaMgF_3:Eu^+$, Zeeman absorpt. and luminesc. spectra *(Russian)* 77−69872
$NaMgF_3:Sm^{2+}$, luminesc. spectra 4.2, 77 and 295K and Zeeman spectra, 4.2K 77−81146
$NaMnCl_3$, antiferromagnet, exciton self-localisation luminesc. and excitation spectra *(Russian)* 80−11456
$NaMnCl_3$, antiferromag. insulator, self-trapping of excitons 80−70619
$NaNO_2$, cryst., delayed fluoresc., triplet excitons, dopant effects 78−10963
$NaNO_2$, fine struct. in luminesc. spectra in UV region 77−59607
$NaNO_2$, hot luminesc. 78−6722
$NaNO_2$, hot luminescence 78−10976
$(NaNO_3\text{-}Mg(NO_3)_2):Nd^{3+}$, glass, cryst., absorpt. luminesc. spectra, term struct. of Nd^{3+}, bonding 77−8624
$Na_2NdPb_6(PO_4)_6Cl_2$, self-activated mini-laser material, quantum yield determ. 79−33773
$Na_2Nd_2Pb_6(PO_4)_6Cl_2$, high-Nd conc. laser material, oscillator strengths and laser effect 79−55140
$Na_2O\text{-}3SiO_2$ glass, high-temp. thermolum., colour centre absorpt. 80−16110
$Na_2O\text{-}Al_2O_3\text{-}B_2O_3\text{-}SiO_2\text{-}AgBr(Cl)$, photochromic glass, exam. of role of O and Cu ions, using luminescence spectra 79−4849
$Na_2O\text{-}Al_2O_3\text{-}P_2O_5$:Eu glasses, fluorescence line narrowing meas. *(French)* 80−34975
$Na_2O\text{-}B_2O_3$ glass, $Eu^{3+}\rightarrow Nd^{3+}$ diffusion-limited energy transfer, quantum efficiency 78−31238
$Na_2O\text{-}B_2O_3\text{:}PbBr_2$ glasses luminescence damping kinetics *(Russian)* 77−16393
$Na_2O\text{-}B_2O_3\text{-}SiO_2$:Yb(Tb), luminesc. cooperative processes, glass struct. and comp. effect 80−16101
$Na_2O\text{-}BaO\text{-}SiO_2:Nd^{3+}$ glasses, absorption and fluoresc. spectra, density 80−25417
$Na_2O\text{-}CaO\text{-}SiO_2\text{:}UO_2$, energy spectrum of UO_2 ions, fluoresc. and absorption spectra 77−66531
$Na_2O\text{-}P_2O_5\text{-}Y_2O_3\text{-}Tb_2O_3$ glass, conc. quenching of luminesc. in disordered system with dipolar interaction 80−89059
$Na_2O\text{-}SiO_2$ glass, tunnelling recomb. luminesc. 80−2875
$Na_2O\text{-}SiO_2$ glasses, elementary electronic excitations, refl., luminesc., and photoemission meas. 80−84778
$Na_2O\text{-}TeO_2:Ho^{3+}(Er^{3+})(Yb^{3+})$, luminesc. quenching by OH and OD *(Russian)* 79−28839
$NaPO_3:Eu^{3+}$, luminesc. of Eu^{3+}, transition probabilities 80−80845
$Na_2(Pt(CN)_4)3H_2O$, transition energy tuning from 3.3 to 1.4 eV 79−61436
$Na_2S:Mn^{2+}$, polycrystalline, EPR and luminesc. of Mn^{2+} 78−27082
$Na_2S_2O_3$ digested AgX emulsions, red-IR photoluminescence obs. at 77K 80−103982

luminescence of inorganic solids continued
Na_2SiO_2-CaO glass, thermostimulated and tunnel luminesc. 80−45157
$NaY(Gd)O_2:R^{3+}$, R=Eu, Nd, Sm, Dy, Tb, activator effect 77−48216
$NaY_{1-x}Sm_xF_4$, luminesc. expt. suggesting Sm^{3+} ion pairing 80−76065
$NaZnGeO_4:Mn$, electrolum., ionisation domains 80−84787
$Na_2ZrGeO_5:Eu^{3+}$ crystals, luminescence spectrum 79−47604
$Na_4[UO_2(CO_3)_3]$, vibr. and low temp. optical spectra, rel. to U recovery from oceans 79−73939
Nb, broadband opt. emission on heavy ion bombardment 77−28635
Nd crystals, determ. of fluoresc. quantum efficiency and laser emission cross sections 80−48264
Nd glasses, GLS-1 and GLS-22, luminesc. band, forced transition cross sections, laser meas. 80−40152
Nd glasses, luminesc. obs. by chronospectroscopic technique 79−11467
Nd^{3+} activated laser matrices, luminesc. quantum efficiency, conc. depend. 79−27263
Nd^{3+} ions in solids, anti-Stokes effects 78−80405
Nd:glass, luminesc. quantum yield meas., relative method *(Russian)* 78−35203
Nd:silicate glass, resonance laser excitation, inhomogeneously broadended emission spectra 80−66295
Nd^{3+}:glass, fluoresc. line narrowing, hole burning and ion-ion energy transfer 79−89912
Nd^{3+}:glass, kinetic description of excitation spectra 78−68557
Nd^{3+}:glass, laser induced fluoresc. line narrowing, site depend. 79−33819
Nd^{3+}:glass, laser props., uncorrelated inhomogeneous broadening of 1.06 μm band induced luminesc. quenching 79−31914
Nd^{3+}:glass, multitype opt. centres 78−68558
Nd^{3+}:glass based on alkali metal metaphosphates, luminesc. and lasing *(Russian)* 77−46724
Nd^{3+}:glass luminesc. band profile deform. under free-oscillation conditions 80−71487
$Nd^{3+}:LaCl_3$, laser-induced fluoresc., hyperfine structs. 80−100677
$Nd^{3+}:LaCl_3$, laser-induced fluoresc. energy transfer effects 80−100678
Nd^{3+}-Yb^{3+}:glass, excitation transfer, selective filling of levels in inhomogeneous contour 77−69898
$NdAl_3B_4O_{12}$, self-activated mini-laser material, quantum yield determ. 79−33773
$Nd(Ga,Cr)_3(BO_3)_4$, cryst. growth by LPE, Nd^{3+} fluorescence, lattice constants 80−29883
$Nd_xLa_{1-x}P_5O_{14}$, Nd^{3+} stoichiometric materials, luminesc., conc. quenching 78−27315
$Nd_xLa_{1-x}TaO_4$, polycryst. optical centres, thermodynamic equilib., 1600-1700K *(Russian)* 77−68970
Nd_2O_3, transmission and luminesc. spectra 79−65929
Nd_2O_3-Al_2O_3-SiO_2 glass, exam. of spectroscopic and luminescent props. 78−88364
Nd_2O_3-SiO_2 glass, exam. of spectroscopic and luminescent props. 78−88364
Nd_2O_3-Y_2O_3-As_2O_5 glass, spectroscopic props., rel. to possible appl. in lasers 78−84624
NdP_5O_{14}, fluoresc. decay times meas. 79−8187
NdP_5O_{14}, fluoresc. lifetime meas., IR and photoacoustic spectroscopy 80−60652
NdP_5O_{14} laser, flashlamp excited, emission cross section at 1.32 μm 79−59701
NdP_5O_{14}, laser materials, linear conc. quenching of luminesc. 79−31908
NdP_5O_{14}, laser site-selection time-resolved spectroscopy 78−76524
NdP_5O_{14}, luminesc. excited by LED radiation 79−24366
NdP_5O_{14}, self-activated mini-laser material, quantum yield determ. 79−33773
NdP_5O_{14} single crystals, fluoresc. decay times, excitation density effect 80−7390
NdP_5O_{14}, spectral line intensity anal. 78−43888
Nd_3PO_7, prep. and luminesc. props. 80−34964
$Nd_4P_2O_{11}$, $^4F_{3/2}$−$^4I_{11/2}$ transition 80−34964
$NdTa_7O_{19}:Nd^{3+}(^4F_{3/2})$, fluorescence intensity and lifetime rel. to mini laser prod. *(French)* 77−71988
$Nd_2Ti_2O_7$, transmission and luminesc. spectra 79−65929
$Nd_xY_{1-x}P_5O_{14}$, conc. quenching 79−61435
$Nd_xY_{1-x}P_5O_{14}$, fluorescence quenching 77−69903
$Nd_xY_{1-x}P_5O_{14}$, fluoresc. conc. quenching, decay rate consts. 78−64404
$Nd_xY_{1-x}P_5O_{14}$, fluoresc. energy transfer and radiationless relax. 79−38625
Ne, liquid and solid, absorpt. and luminesc. spectra of self-trapped excitons 79−65893
Ne, solid, doped with Xe and benzene, energy transfer 77−32416
Ne, solid, lattice relax. model of n=1 exciton emission 79−47492
Ne, solid, quasi-line emission in transitions between excited states *(Russian)* 79−91494
Ne:Ar(Kr)(Xe), luminesc. in vacuum-UV excitation of guest atoms by free and relaxed excitons 79−15519
Ne:H, exciton states and L_α,L_β emission 80−93372
Ne:O_2 (N_2), long-wave UV luminesc. *(Russian)* 78−88347
Ne:Xe(Ar), electronic relax. cascades in Wannier and Frenkel type exciton states 79−33759
Ni, bombardment by 1 to 30 keV ions, emitted radiation spectral comp. *(Russian)* 77−81159
Ni, ion bombard., ion and photon yields, CO adsorption effect 80−89098
Ni, oxide covered, tensile deform. in high vac., particle and photon emission 78−39672
Ni, photon emission due to Ar^+ ion bombard., adsorbed and recoil-implanted O effect 80−80872
O_2, chemisorbed on metal films, active sites, chemiluminesc. and vacuum microbalance obs. 78−22950
OH^- vibr. dipole field and ion-pair processes with rare earth ions 79−38624
P, amorphous, red, photolum. props. and band gap 80−50403
PLZT, opt. spectra and luminesc. 78−76508
P_2O_5-glass, diffusion of Cu^+, fluoresc. meas. 78−59980
P_2O_5-K_2O-CdO-Na_2O glass:Nd^{3+}, highly doped, spectroscopic props. and CW laser action *(French)* 79−41385
P_2O_5-R_2O_3-M_2O(M′O), (M=alkali metal, M′=alkaline earth, R=Y or rare earth), metaphosphate glass phosphors, fluoresc. props., activation conc. effect 80−89058
$POCl_3$-$SnCl_4$: Tb^{3+}, Sm^{3+}, lifetime and quantum yield of fluoresc. emission 77−20909
Pb halides, above-edge cathodolum. from metastable excitons 78−6786

luminescence of inorganic solids continued
Pb, ion bombardment-induced photon emission near melting point 80−100699
$PbBr_2$, cryst., red luminesc. at low temps. *(Russian)* 78−92125
$PbBr_2$, metastable exciton emission, electron excitation mechanism 77−66546
$PbBr_2$, red luminesc., absorpt. spectra 80−2831
$PbBr_2$, single cryst., photolum. meas. 77−69882
$PbBr_2(Cl_2)$, light sensitive material, regularities in exciton states 77−20885
$PbCl_2$, blue emission 78−23518
$PbCl_2$, metastable exciton emission, electron excitation mechanism 77−66546
$PbCl_2$, single cryst., photolum. meas. 77−69882
$PbCl_{2-2x}Br_{2x}$, luminesc. and reflection spectra *(Russian)* 80−84762
β-PbF_2, single cryst., photolum. meas. 77−69882
$PbF_2:Tb^{3+}$, cubic Tb^{3+} centres, energy level and cryst. field parameters 77−52181
PbFBr, single cryst., photoluminesc. 77−16375
PbFCl, single cryst., photoluminesc. 77−16375
$Pb_5Ge_3O_{11}$ crystal, ferroelec., luminesc. under pulse polarisation switching conditions 77−1735
PbI_2 (2H), angular depend. magnetoluminesc. 79−43029
PbI_2 (2H), layer cpd., band parameter determ. 79−95332
PbI_2 (2H), photolum. spectrum, in strong photoexciton mixing region 78−48223
PbI_2, cryst., photochem. phenomena investig. *(Russian)* 78−35204
PbI_2 crystals, exciton condensation, excitation and luminesc. study 80−55182
PbI_2 direct gap semiconductor, exciton lifetime and condensation threshold, luminescence spectra 80−34981
PbI_2, emission spectra, 80K, high excitation intensity effects at different pump wave lengths 77−52170
PbI_2, exciton spectra depend. on strong excitation, crystal transmission 79−69433
PbI_2 film, highly excited, oscillator strength of excitons, absorpt. and emission spectra 78−76001
PbI_2, first-order 2H-4H polytype transition, exciton spectroscopic study 80−59647
PbI_2 laminar semicond., phase transition of first kind by exciton spectroscopy *(Russian)* 79−82334
PbI_2, layered cryst., photoluminesc., and reflection spectra obs. 78−6726
PbI_2, luminescence excited by high-intensity two photon pumping 77−44038
PbI_2, metastable exciton emission, electron excitation mechanism 77−66546
PbI_2, multiphoton cross-section determination by means of luminescence experiments 80−93377
PbI_2, photoexciton interaction, luminescence spectra, polariton dispersion diagram 80−93397
PbI_2, photolum. and reflectivity temp. depend., cryst. anisotropy effect on electron-phonon interaction *(Russian)* 78−15225
PbI_2, photoluminesc. spectra, generation of stimulated radiation 77−8647
PbI_2, single cryst., luminesc., photocond. and absorpt. after thermal treatment 79−56855
PbI_2, temp. depend. of electron-hole drop emission *(Russian)* 77−16394
PbI_2, three-photon absorpt. coeff. determ. by nonlinear luminesc. expt. 80−14384
PbI_2 two-photon absorpt. cond. and luminesc. meas. 77−52166
$PbMg_{1/3}Nb_{2/3}O_3$, carrier mobility and photoluminesc. near ferroelec. transition *(Russian)* 78−2813
$PbMg_{1/3}Nb_{2/3}O_3$, photolum. near ferroelec.-paraelec. phase transition 80−16100
$PbMg_{1/3}Nb_{2/3}O_3$, photolum. and carrier drift mobility at ferroelec. transition 80−71469
$PbMoO_4$, colour study from absorption, fluorescence and thermoluminesc. exam. 78−31245
$PbMoO_4$, defect electron centres after X-irrad. 79−55738
$PbMoO_4$, doped and undoped single crysts., polarisation of luminesc. and assignments 80−76069
$PbMoO_4$, near-edge absorpt. band, fluoresc. and photocond. 77−44017
PbO single crystals, current-voltage characts., electrolum. *(Russian)* 80−2863
PbO, single crysts., exciton and impurity luminesc. 80−60674
PbS, molecule, vibr. anal., in neon matrix *(Russian)* 79−10094
PbS-$(PbSO_4)_x$(PbO.$PbSO_4)_y$ heterosystem, cathodoluminescence spectra 79−24370
$PbS_{1-x}Se_x$ thin film, stimulated emission, temp. depend. 80−66232
PbSe film, stimulated photoluminesc. characts. meas., room temp. 77−90193
PbSe, photoluminesc. spectra and stimulated emission, effect of temp. 77−8638
PbSe, X-ray diffr. exam. of struct., and luminescence props. 80−55209
$Pb_{1-x}Sn_xSe$ epitaxial layers, radiative and nonradiative recomb. processes 80−60670
$Pb_{1-x}Sn_xSe$ solid solns., photoluminesc. spectra, energy band parameter determ. 80−71484
$Pb_{1-y}Sn_ySe$, ($0 \leq x \lesssim 0.08$), spontaneous emission investigated 78−10990
$Pb_{1-x}Sn_xSe(Te)$ epitaxial layers, growth, phase diagram, p-n junctions, optical, elec. props. 78−44029
$Pb_{1-x}Sn_xSe_{1-y}Te_y$ optically pumped heterojunction laser with matched gratings, photolum. obs. 79−89909
$Pb_{0.78}Sn_{0.22}Te$, $Pb_{0.91}Sn_{0.09}Se$, radiative and nonradiative recombination 80−80849
$Pb_{0.78}Sn_{0.22}Te$:In epitaxial layers, dislocation density, Hall effect, conductivity, photoeffects 80−25024
$Pb_{0.9}Sn_{0.1}Te$, situated in quantizing magnetic field, photolum. spectra 79−71461
$Pb_{1-x}Sn_xTe$, ($0 \leq x \lesssim 0.2$), spontaneous emission investigated 78−10990
$Pb_{1-x}Sn_xTe$, energy band parameter determ. from photoluminescence. spectra in mag. field 79−11066
$Pb_{1-x}Sn_xTe$, epitaxial layers, photolum. in mag. field 79−83033
$Pb_{1-x}Sn_xTe$ films, size quantisation, optical orientation of free carriers, polarisation props. of luminesc. 80−20725
$Pb_{1-x}Sn_xTe$ solid solution, radiative recombination 79−52016
$Pb_{1-x}Sn_xTe$:Cd(In), solid solutions, impurity states in photoluminescence spectra *(Russian)* 80−97333
$Pb_{1-x}Sn_xTe$:In, impurity influence on photoluminescence at large excitation levels *(Russian)* 80−93384

luminescence of inorganic solids continued
$Pb_{1-x}Sn_xTe$:In epitaxial layers, growth, elec. props., and luminesc. 80−54542
PbTe epitaxial film, stimulated emission, absorption spectra and recombination 78−80409
PbTe epitaxial films, carrier recomb. and deep levels, photocond., Hall effect, and luminesc. meas. 79−38024
PbTe, recombination radiation polarisation direction, two-photon selective energy valley occupation *(Russian)* 77−20924
PbTe, spin orientation under two-photon pumping 79−74000
$PbTiO_3$, photolum. and carrier drift mobility at ferroelec. transition 80−71469
$PbTiO_3$ single crystals, electroluminesc., elec. field, freq. and temp. depend. 78−80422
$PbWO_4$, doped and undoped single crysts., polarisation of luminesc. and assignments 80−76069
$PbWO_4$, single cryst. growth by Czochralski method and U incorporation, effective distrib. ratios, luminesc. characts. 79−42094
$Pb(WO_4)_{1-x}(MoO_4)_x$ mixed crystals, X-irrad., EPR and thermoluminesc. 79−15352
Pr^{3+}-based IR quantum counters, photon avalanche 79−97431
$PrCl_3$, spectral energy transfer 78−19550
PrF_3, spectral energy transfer 78−19550
$Pr_{0.2}La_{0.8}F_3$, fluorescent line narrowing, time depend. effects 78−31244
$Pr_xLa_{1-x}P_5O_{14}$, laser emissions, fluoresc. 79−72572
PrP_5O_{14}, laser emissions, fluoresc. 79−72572
$PrVO_4$, energy levels, opt. and NMR meas. 78−80226
$Pr_xY_{1-x}P_5O_{14}$, laser emissions, fluoresc. 79−72572
Rb_2AgCl_3 luminesc., absorpt. and excitation spectra 77−12424
RbBr, self trapped exciton form. time at $^1\Sigma_u^+$ state under pulsed electron beam in ps range 80−97347
RbBr, suprapure, thermolum. glow and emission studies at room temp. 80−7423
RbBr:I^-, OH^-, luminesc. of interstitial atomic H 80−89062
RbBr:O_2^- centres, luminesc. polarisation temp. depend. 78−87943
RbBr-Ag, mag. field effect on luminesc. of paired Ag^- ions 78−27313
$RbCa_{0.95-x}Mg_xEu_{0.05}F_3$, green luminesc. obs. 77−32428
RbCl, undoped and Sn doped, γ-irrad. crysts., thermolum. and emission, 300 to 560K 79−15539
RbCl:Ag, phosphor, luminesc., absorpt. and excitation spectra 77−12424
RbCl:Ag(Cu), strong IR luminesc. obs. of Ag_F^0 centres 78−6736
RbCl:Ca^{2+}, thermolum. and optical absorption studies 80−104002
RbCl:Eu, electron-irrad., photostimulated luminesc., ionic processes 78−52561
RbCl:Eu, γ-irrad., thermoluminesc., EPR meas. 78−84670
RbCl:Eu, luminescence and absorption of color centres in RbCl:Cu and KCl:Eu crystals 78−92118
RbCl:I, H, fluorescence of interstitial H-centres 79−73987
RbCl:Mg, γ-irrad., thermoluminesc. 79−47528
RbCl:Tl, origin of 3.55 eV emission band 80−7401
RbCl(Br), cation defects creation mechanism 80−75224
RbCl(Br), F-centre emission, mag. circular polarisation 80−108251
RbI, edge emission of excitons 77−59606
RbI, edge luminesc. under UV excitation 77−77273
RbI, electron irrad., polariton effects in reson. emission 79−33843
RbI, intrinsic luminesc. quenching, by X-ray induced coloration 78−19539
RbI, luminesc. spectra induced by pulsed Ne^+ and electron beams and X-rays 80−80851
RbI, photostimulated recomb., electron spin polarisation 80−60673
RbI, zero phonon and LO phonon assisted luminesc. of free excitons 79−28799
RbI:Pb^{2+}, luminescence under B-band excitation 78−35192
RbI:Tl, emission and excitation spectra, press. effects 79−83028
RbI:Tl, emission bands, press. effect 79−33789
$Rb_2InOH(SeO_4)_2.H_2O:Eu^{3+}$, synthesis and luminesc. 79−91488
$RbMg_xMn_{1-x}F_3$, impurity induced fluorescence, thermal depend. 77−85776
$RbMnCl_4$, quadratic layer antiferromag., intrinsic emission obs. 77−20906
Rb_2MnCl_4, rare earth doped, energy transfer, emission spectra obs. 80−20684
$RbMnF_3$, antiferromag., multi-magnon luminesc. sidebands 78−76525
$RbMnF_3$, antiferromagnetic resonance, optical detection, luminescence 80−7174
$RbMnF_3$, exciton and exciton-magnon emission 79−33779
$RbMnF_3$, radiation damage, optical absorpt. and luminesc. expts. 78−2161
$RbMnF_3:Er^{3+}$, absorption, emission, excitation and lifetime meas. 80−71460
$RbMnF_3$:Fr, pure and doped, unirradiated and electron irrad., energy transfer 80−108254
$RbMnF_3$:Ni, antiferromag., exchange splitting of $^3T_{2g}E$ state, fluorescence meas. 77−12419
$Rb_2SnCl_6:ReCl_6^{2-}$, luminesc. and absorpt. spectra, relax. processes 77−85779
$Rb_2TeCl_6:Re^{4+}$, vibronic transitions progressions, intensity distrib. 79−78735
$Rb_2UO_2Cl_4$, fluoresc. decay rate of pure and impure cryst. 79−47487
$RbUO_2(NO_3)_3$, fluoresc. decay rates, temp. depend. 80−25429
$ReBr_6^{2-}$, in cubic crysts., luminesc. spectra and relax. processes 78−68552
$ReCl_6^{2-}$ doped in various host lattices, luminesc. spectra and vibr. struct. 79−43024
Rh(III) complexes, luminesc. rise time meas. by wavelength shifter 80−50390
Ru complex, Ru(2,2′-bipyridine)$_3Cl_2$-$6H_2O$, photocond., optical absorpt. and fluoresc. 77−80807
S_2, matrix isolated, chemilum. in solid Ar 79−47529
$SRF_2:Er^{3+}$, laser excitation of single ion and clustered ion sites 77−69879
SbSI, photolum. spectra in ferroelec. phase, 600-800 nm., 14-100K 80−71468
$ScBO_3:Tb^{3+}$, vacuum UV excitation spectra and quantum efficiencies 79−28811
Sc_2O_3 and double oxides, photon multiplication and secondary electron-hole pairs generation *(Russian)* 80−66262
$ScVO_4:R^{3+}$, R=Nd, No, Tm, Sm, Dy, Er, Eu, Tb, electronic struct. and spectra of VO_4, RO_8 clusters 78−10953
$Sc_2(WO_4)_3$:Cr(Eu), and undoped crystals, luminesc. obs. 80−89047
Se, exciton luminesc. in trigonal form 79−33802
luminescence of inorganic solids continued
Se, glassy, localised electronic states, photoluminesc. and ESR studies 80−65501
Se, glassy, pure and K-doped, photolum. and optically induced ESR 80−50398
Se, trigonal, cathodolum. at 10K *(German)* 78−2923
Se, trigonal, indirect exciton ground states, photoluminescence 79−24361
Se, trigonal, luminesc. identification of indirect transition 80−55189
SeO_4^{2-} ions in aqueous solns. of halides at 4.2-290K *(Russian)* 77−28624
Si, amorphous, elec. and opt. props., review 78−23094
Si, amorphous, glow discharge deposited photolum. decay 78−72590
Si, amorphous, glow discharge, fatigue effect in luminesc., recovery by annealing 80−50416
Si, amorphous, glow discharge produced, defect creation, high optical excitation 80−97327
Si, amorphous, hydrogenated, photolum., heating effects 78−15204
Si, amorphous, hydrogenated, spin depend. photoluminesc. 78−72589
Si, amorphous, luminesc. of diode structures 77−8656
Si, amorphous, mag. field depend. of luminesc. 79−43034
Si, amorphous, phonon interaction in luminescence 78−43927
Si, amorphous, photoluminesc. spectra from 77K to room temp. 77−20916
Si, amorphous, photoluminesc. and radiative lifetimes 79−61419
Si, amorphous, photoluminescence, fast radiationless recombination 79−99939
Si, amorphous, radiative and non-radiative tunnelling, photoluminesc. decay meas. 79−83026
Si, amorphous, radiative recomb. obs. as efficient luminesc. 78−2914
Si, amorphous, spin depend. recomb., luminesc. and light induced ESR 80−50393
Si, amorphous, time resolved photoluminesc. near band gap 80−25445
Si, amorphous, time-resolved ODMR and luminesc. 80−25254
Si amorphous film, optical props., electronic states 80−25475
Si, amorphous film, plasma-deposited, photoluminesc. and EPR meas. 79−4864
Si, annealed, photoluminesc. anal. of defects 80−80836
Si, Auger recomb. coeff. meas. using laser excitation 79−38654
Si, biexcitons, photoluminesc. spectrum exam. 78−47705
Si, bound exciton lifetimes for acceptors 77−80738
n-Si, bound excitons and bound multiexciton complexes, excitation spectra 80−96792
Si, bound multiexciton complexes, luminesc. 80−10888
Si, CW laser annealed, defect luminesc. 80−50388
Si, characterisation by photoluminescence method *(Japanese)* 78−80404
Si, characterisation by photolum. method *(Japanese)* 79−38638
Si, correl. between photolum. spectra and impurity conc. 78−23513
Si, deformed, recomb. radiation from electron-hole drops and free excitons 77−8641
Si, diamagnetism of excitons and biexcitons, recomb. spectra *(Russian)* 80−7412
Si, dislocation luminesc. obs. 78−15217
Si, dislocations, luminesc. spectra *(Russian)* 77−90197
Si, donor bound excitons and bound multiexciton complexes 77−40282
Si, electron beam irrad. at 31 GeV, polarised photon emission *(Russian)* 80−29811
Si, electron irradiated, photolum. due to interstitial complex 77−44048
Si, electron-hole drop luminescence, hysteresis effect and surface energy 78−2907
Si, electron-hole droplet luminesc., laser excitation threshold meas. 79−33821
Si, electron-hole droplet spatial distrib., luminesc. obs. 80−49615
Si, electron-hole droplets nucleation at swirl defects 79−15095
Si, electron-hole drops, Auger recomb. 77−48240
Si, electron-hole drops, near and far IR emission spectra 77−48242
Si, electron-hole drops, nonequilib. paramagnetism 80−6749
Si, electron-hole drops, nucleation, time resolved luminesc. spectroscopy 78−6280
Si, electron-hole drops, nucleation, luminesc. threshold obs. 79−33822
Si, electron-hole drops, thermodynamical parameter determ. from luminescence data 80−2845
Si, electron-hole drops radius, luminesc. meas. 80−50415
Si, electron-hole liquid, free excitons, biexciton gas, luminesc. 80−6750
Si, electron-hole liquid, spatial condensation of strain-confined excitons and excitonic mols. 78−39592
Si, emission spectra, excitons bound to isoelectronic trap 79−33772
Si exciton luminescence in mag. field or under uniaxial stress 78−27322
Si, exciton-impurity complexes, emission spectra, Zeeman splitting *(Russian)* 78−64413
Si, exciton-plasma Mott transition, luminescence spectra 77−62836
Si, excitonic molecules, thermodynamics, luminesc. 80−25442
Si, excitons and electron-hole drops, phonon assisted luminescence lineshape 79−99942
Si, excitons and electron-hole liquid, luminesc. 80−6746
Si, fast electron irradiated, models of luminescence centres, role of interstitials 77−81153
Si, fast neutron and ion irradiation, radiative recombination centres 77−81152
Si, free exciton luminesc. band, resolved splitting 79−73995
Si, free excitons, drift and diffusion, luminesc. obs. 80−84434
Si, H_2^+ irrad., annihilation of free excitons, inelastic scatt. by SiH_4 mols., photolum. obs. 78−19561
Si, high purity, exciton lifetime, temp. depend., photoluminesc. meas. 80−44508
Si, highly doped and highly exerted, Auger coeffs., radiative band to band recomb. lifetime meas. 77−85764
Si, hydrogenated amorphous, laser annealing, photolum. spectra 80−100713
Si, IR emission under α-irrad. *(Russian)* 77−85811
Si, implanted Li atoms, depth profiles and sputtering anal. by optical spectra 77−35579
Si, impurity content characterisation, exciton luminesc. 80−60653
Si, intrinsic, phonon replicas of electron-hole liq. luminesc. line 79−28831
Si, intrinsic, radiative recombination probability *(German)* 79−61441
Si, intrinsic, two-phonon assisted free exciton recomb. radiation 78−2922
Si, intrinsic semiconductor, radiative recombination probability *(German)* 78−95608
Si, inversion layers, far IR emission from hot electrons 78−30995
Si, ion implanted films, optical and luminesc. props. 80−60699
Si, irradiated, nature of 0.97 eV A band luminesc. 77−44049

luminescence of inorganic solids continued
Si, LO and TO phonon assisted free exciton luminesc. 79−33833
Si, luminesc., simultaneous kinetics of drops and excitons during drop formation 77−48222
Si, luminesc. emitted as a result of carrier heating 77−52185
Si, luminescence of multiparticle exciton-impurity groups 79−83003
Si, MOSFET, voltage tunable far IR emission from inversion layers 77−12440
Si, MeV region O^+ implantation, induced luminesc. spectrum 78−6788
Si, neutron transmutation doping, photoluminesc. characterisation 80−11453
Si, non-equilib. orientation of electrons in electron-hole droplets in mag. field *(Russian)* 77−36294
Si, nonequilib. electron-hole system, gas-liq. phase diagram *(Russian)* 77−43509
Si, nonradiative deexcitation in O_2 atmos., using differential meas. of excited state lifetime 78−2920
Si, nonradiative recombination and luminesc. 79−33770
Si, phonon-assisted exciton emission, temp. depend. of relative integrated intensities 77−1375
Si, photoluminescence of electron-hole drops under uniaxial stress 79−91491
Si, photoluminescence of thermal donors after annealing 79−87499
Si, photon emission due to Ar^+ ion bombard., adsorbed and recoil-implanted O effect 80−80872
Si, piezospectroscopic effect on zero phonon luminescence lines 80−50406
Si, plastically deformed, hot-exciton luminesc. as function of strain 78−88361
Si, polarisation of recombination radiation from multiparticle exciton-impurity complexes, induced by uniaxial deform. *(Russian)* 79−78754
Si, proton irradiated and annealed, hydrogen containing radiative recomb. centres 77−24896
Si, pure and doped amorphous photolum. meas. 77−36285
Si, radiative recomb. centre accumulation due to high temp. electron irrad. 80−93394
Si, radiative recombination involving silane mols. 79−73998
Si, recombination luminescence, electron-hole drop, excitons orientation in mag. field 78−88362
a-Si, resonant and non-resonant luminesc. changes theory 80−50410
Si, Si_3N_4 and SiC, ion bombard. induced light emission 77−48257
Si, sputtering by Ar^+ ions, energy depend. of excitation 79−56906
Si, swirl defects, gettering effects, obs. by photoluminesc. meas. 78−84623
Si type semiconductor, interimpurity zero-phonon radiative transitions 78−15222
Si, uniaxial stress effects and excited states for multiple bound excitons 78−6281
Si, uniaxially deformed, photoluminesc., biexcitons *(Russian)* 77−59611
Si, uniaxially stressed, excitonic molecule emission spectra, electron valley degeneracy effects 80−60669
Si: Li, absorpt. and luminesc. transitions involving exciton excited hole states 79−78038
Si:Al, bound exciton and bound multiexciton complexes, electronic structure, luminesc. obs. 79−56139
Si:Al, bound exciton and multiple bound electron luminesc., fine struct. 77−48221
Si:Al, localised exciton bound to isoelectronic trap 80−66283
Si:As(Li)(P), luminesc., stress effects on donor exciton satellites 77−85786
Si:As(Sb)(Bi)(P), luminescence associated with transitions from bound exciton excited states 78−23534
Si:B, bound many-exciton complexes, luminescence spectra, mag. props. 80−103994
Si:B, bound multiexciton luminesc., recomb. kinetics 79−38591
Si:B, impurity conc. from photoluminesc. anal. 78−63785
Si:B, many-body exciton-impurity complexes, stress depend. of photolum. meas. 79−28833
Si:B, photolum. of heavily doped p- and n-type 80−20708
Si:B,In, sharp line series in near-band-edge photolum. 80−16092
n-Si:B,P, radiative recombination at thermal defects, luminescence centre electron struct. 79−91496
Si:B recombination emission polarisation of bonded multiple-exciton complexes in mag. field *(Russian)* 78−2905
Si:B(Al)(Ga)(In)(Tl), high resolution recomb. radiation, investigation, electron excited 78−15233
Si:B(Al)(Ga)(In)(Tl), binding energy, excited state spectra, photolum., semi-empirical short range pot. 80−44534
Si:B(Ga), even-parity acceptor excited states, bound exciton two hole transitions 77−85793
Si:B(P), uniaxially stressed, impurity-assisted intervalley scatt., photoluminesc. obs. 80−34979
Si:B(P)(Sb), multiparticle impurity complexes *(Russian)* 78−72601
Si:C(O), photoluminescence spectra, radiation damage investig. 77−28620
Si:Ga, luminescence fine struct. from bound exciton and multiexciton complexes 77−32430
Si:Ga(Al), edge luminesc. spectra of acceptors, multiexciton complexes 78−56517
Si:H, amorphous, defect creation and H evolution 80−50392
Si:H, amorphous, defect photoluminesc. meas. 80−97334
Si:H, amorphous, defect states, luminesc. and ESR obs. 80−76075
Si:H, amorphous, effect of gap state density on photocond. and photolum. 79−91096
Si:H, amorphous, excess carrier thermalisation and recomb., luminesc. decay and photocond. 80−50397
Si:H, amorphous, geminate recombination model for photoluminescence decay 80−71481
Si:H, amorphous, glow discharge deposited, laser annealing 80−49104
Si:H, amorphous, light-induced ESR and photoluminesc., dangling bonds with positive correl. energy 80−50161
Si:H, amorphous, luminesc., band tail states and thermalization 80−25455
Si:H, amorphous, radiative recomb. by diffusion and tunnelling, photocond. quantum efficiency 80−50394
Si:H, amorphous, radiative recomb. and luminescent processes 80−55152
Si:H, amorphous, rehydrogenation, photoluminesc. recovery 78−72571
Si:H, amorphous, temp. depend. of photolum. 80−89063
Si:H, amorphous and crystalline, hydrogenation and dehydrogenation, luminesc. spectra 80−11477
luminescence of inorganic solids continued
Si:H, amorphous sputtered, excitation spectra and photoluminesc. 80−50396
Si:H, Cl(F), amorphous, photocond., dark cond. and photoluminesc. 80−49802
Si:H, ion-implanted, photoluminesc. spectrum 80−45129
a-Si:H, spin defect and recombination influence on electronic transport 80−50409
Si:H,F,O amorphous, plasma deposited, comp. and optical props. 80−50441
Si:H,Li, amorphous, photoluminescence obs. 80−66280
Si:H,P, amorphous, heavily hydrogenated, high gap state densities 80−49803
Si:H amorphous, plasma-deposited, luminesc. decay 79−73989
Si:H amorphous film, sputtered IR vibr. spectra and photolum., effects of partial evolution of H 80−44413
Si:H amorphous films, optoelectronic behaviour depend. on impurity incorporation during plasma deposition 80−49804
Si:H amorphous sputtered film, photoluminesc., photocond. 80−20729
Si:H film, amorphous, bombarded, defects, luminesc. and ESR meas. 80−34977
Si:H sputtered amorphous film, luminesc. and non-radiative decay 80−50395
Si:In, bound exciton photolum. obs. 78−95607
Si:In, capture cross section of excitons on neutral In impurities, photoluminesc. decay 78−6760
Si:In, obs. of long lifetime lines in photolum. 79−47512
Si:In, photoluminesc., In acceptor excited level 79−47506
Si:In,P, photoinduced IR absorpt. and luminesc. 79−33828
Si:K, bound exciton luminescence in mag. field *(Russian)* 80−108278
Si:Li, bound exciton complexes associated with Li, photolum. meas. 79−28823
Si:Li, bound-exciton excited states, uniaxial anal. 80−71475
Si:Li, luminesc. of bound exciton and bound multiexciton complexes 79−28821
Si:Li, photolum. of bound exciton and bound multiexciton complex, Zeeman effect 80−108265
Si:O,H amorphous, plasma-deposited, electronic and struct. props. 80−50391
Si:O,H amorphous, time resolved luminesc. 80−66288
Si:P, acceptor bound multiexciton complex recomb., shell model, luminesc. line splitting 78−6275
Si:P, amorphous, CVD, defect compensation 80−54644
Si:P, bound exciton and multiexciton complex struct., luminesc. obs. 77−81138
Si:P, bound multiexciton complexes, shell model 77−31953
Si:P, excitation density depend. of cathodoluminesc. from bound multiexciton complexes 78−72609
Si:P, exciton complexes bound to impurities, resolved fine structure 77−62843
Si:P, exciton two-electron luminesc., temp. and impurity-conc. depend. 78−39585
Si:P, heavily doped, electron-hole droplets, photolum. obs. 1.5 to 80K 77−36289
Si:P, heavily doped, IR bound-exciton luminesc. spectra 78−15211
Si:P, heavily doped, origin of photoluminesc. 79−56856
Si:P, impurity band states calc. and photoluminesc. meas. 77−8046
Si:P, impurity conc. from photoluminesc. anal. 78−63785
Si:P, ion-implanted and unimplanted, laser annealing, photoluminesc. study 80−2049
Si:P, luminesc. lines, multiexciton complexes and unaixial stress 78−92114
Si:P, luminescence circular polarisation, emission by many exciton complexes 80−93398
Si:P, metallic, heat treatment effects, EPR and photoluminesc. 77−77262
Si:P, model for exciton bound to donor pair, photolum. data anal. 79−51498
Si:P, photolum. obs. of donor pairs 79−52014
Si:P, photoluminesc. associated with impurity clusters 79−38656
Si:P, satellite of bound excitons, transient decay 80−11466
Si:P, uniaxially deformed, multiparticle impurity complexes, luminesc. spectra *(Russian)* 79−4854
Si:P bound multiexciton complexes, expt. evidence for shell model 78−39036
Si:P heavily-doped, photoluminescence 78−72572
Si:P(B), multiple-particle exciton-impurity complex form. *(Russian)* 78−43925
Si:P(B), recombination spectra of bound multiexciton complexes, Zeeman splitting *(Russian)* 79−38526
Si:Sb(As)(P), bound excitons and bound multiexciton complexes for shallow donors, luminesc. meas. 79−24363
Si:Tl, optical absorption and photolum. of bound exciton 78−88359
Si-H, amorphous, plasma-deposited, H evolution and defect creation 80−44914
Si-H, amorphous, sputtered, photolum. obs. 80−80856
Si-H, RF sputtered amorphous alloy, influence of Ar press. on elec. props. and photoluminesc. 79−91585
Si-H amorphous film, reactively sputtered, prep. and props. 79−78889
Si-SiO_2 electrode, electronic cond., luminesc obs. 80−61111
Si-type, semiconductor, interimpurity radiative recomb. with phonon cooperation 77−16385
α-SiC, 6H, excited states, photoluminesc. efficiency 78−39604
SiC, 6H polytype, LPE growth by dipping technique, electroluminesc. meas. 77−8769
SiC (15 R), polytype, many valleyed polar semicond., electron-hole-liquid, obs. from excitation and time delayed spectra 79−28289
SiC (6H), blue-emitting diodes by CVD 80−97439
SiC, (6H), radiation damaged, luminesc. 80−25462
α-SiC (6H) laser excited thermostimulated luminescence light sum dose depend. *(Russian)* 80−16111
α-SiC, afterglow stimulated by IR radiation *(Russian)* 80−89066
SiC, cathodoluminescence, comparison with other materials 78−92130
β-SiC, cubic, conduction band minima location and shape determ. 77−85141
SiC, cubic, electron-hole liq., luminesc. obs. 78−31239
α-SiC, deep centre levels, IR photoluminescence 77−16387
SiC, donor exciton satellites, multiple bound excitons 77−11857
SiC, epitaxial layer polytypism 77−62781
SiC epitaxial layers, energy distrib. in photolum. spectra, influence of synthesis conditions 79−52009

luminescence of inorganic solids continued
SiC, epitaxial layers, growth processes 77−85105
p-SiC, inequivalent sites of IR luminescence centres *(Russian)* 77−1722
SiC, influence of plastic deform. on struct. of photoluminesc. spectra 77−55824
SiC, laser Raman spin-flip scatt. from excitons, luminesc. 80−80786
SiC, luminesc., electron-hole drop 79−38606
SiC, mechanoluminesc., Mn impurities role 78−39612
SiC p-n junction, electroluminesc. 80−97343
SiC p-n junctions, electrolum. spectra and kinetics 80−66305
SiC, phys. props. and crystal growth, rel. to appl. in electrolum. devices, book contrib. 77−77299
SiC polytypes, electrolum. in anodic oxidation, band model *(Russian)* 80−50429
SiC polytypes, free exciton luminesc. meas., phonon energies 80−80852
SiC, power, electroluminesc. excitation by SAW, nonlinear effects 80−16104
SiC reverse biased p-n junctions, prebreakdown violet luminesc. 80−7420
SiC, spin-flip scatt. of laser light from photoexcited excitons 80−93330
SiC, surface luminesc. in presence of anodisation 78−52579
SiC, thermolum. excited by light outside fundamental absorpt. region 79−24375
B-SiC:Al, ion implanted, elec. props. and luminesc. meas. 77−12443
SiC:Al,N, blue cathodolum. spectra obs. 78−19574
SiC:Al(B)(Ga), 4H-, 6H- and 3C-polytypes, melt growth and photoluminesc. 77−24885
SiC:Al(Ga)(B) (6H) LEDs, fabrication by rotation dipping technique, electrolum. mechanisms 80−50426
4H-SiC:B, very slow decays of luminesc., 2-300K 77−1718
β-SiC:B p-n junction, IR electroluminesc. spectrum 77−44067
β-SiC:Ga, donor-acceptor pair emission 77−4682
4H-SiC:Ga(Al), photoluminesc. spectra 77−66530
n-SiC:N, O, cathodolum. spectra meas. 78−19573
SiC:N(Al)(Ga) (6H), photoluminesc., site-depend. donor and acceptor levels 79−61421
α-SiC:Sc, quasiline luminesc. spectrum 77−4686
SiC:Tb(Sc), various polytypes photolum. meas., identification of 4H and 6H polytypes 77−63459
Si_xC_{1-x}, amorphous, photoluminesc., comp. depend. 78−68541
α-SiC(6H), two stage transitions, nonlinear absorpt., thermoluminesc. method 80−7425
a-$Si_{1-x}H_x$, oxygenated thin film, sputtered, elec. cond. and optical props. 79−15239
Si_3N_4, encapsulant for annealing of GaAs, photolum. and AES evaluation 78−27657
Si_3N_4 layers, on GaAs, encapsulation, low-energy ion beam sputtering 79−78882
Si_3N_4-GaAs, layer struct., near-edge surface luminesc., temp. depend. 79−69434
Si_3N_4-GaAs structure, photoluminesc. and collective effects 78−6727
SiO_2, amorphous, intrinsic defects, photoluminesc. 79−78740
SiO_2, amorphous, optical and elec. props., comparison with chalcogenide semiconds. 78−6721
SiO_2, amorphous and crystalline, with O vacancy, cathodolum. meas. 77−24901
SiO_2, amorphous and cryst., neutron irrad. and unirrad., intrinsic defect photolum. 80−50401
SiO_2 coatings on SiO_2 substrate, cathodoluminescence spectra, electron irrad. 80−76085
SiO_2, encapsulant for annealing of GaAs, photolum. and AES evaluation 78−27657
SiO_2, exciton study, luminescent centres as exciton detectors 80−66278
SiO_2, film, diode expt. for detecting photoluminescence and excitons 79−73540
SiO_2, fused, ion beam induced luminescence 80−40166
SiO_2, intrinsic luminescence 80−16098
SiO_2 layers in LSI cct. device, cathodoluminesc. obs. 80−80867
SiO_2, thermoluminescence, in H_2O vap. atm., temp. depend., time decay *(Russian)* 77−44074
SiO_2 undoped film, cathodoluminescence *(Russian)* 80−40164
SiO_2, vitreous, grown from vapour, gamma ray irradiated, ESR and thermoluminescence exam. 78−88189
SiO_2, vitreous, luminesc. centres, decay time and polarization props. 79−33829
SiO_2, vitreous, neutron irrad., luminescence nature and ESR signals correl. 79−43038
SiO_2, vitreous, non-bridging O centre, optical props. and energetic struct. 80−34976
SiO_2, vitreous, photoelectric and photoluminescent props. in fundamental absorpt. region 78−39596
SiO_2, vitreous, pure and Ge doped, luminescence centres at 396 and 280 nm 80−103996
SiO_2:Ag, cryst. and glassy, X-ray induced EPR and luminesc. centre 80−65043
SiO_2:Ag, fused, crystalline, luminescence centre props. 78−10954
SiO_2:Nd^{3+} films, cathodoluminesc. 80−20717
SiO_2-LiO_2-Al_2O_3 glass, luminesc., polarisation degree distrib. 80−108257
SiO_2-Si, cathodoluminesc. and AES rel. to struct. 78−43937
p-Si_2Te_3, photoelectric props., luminesc., hole lifetime and trapping 77−39892
Sm_3S_4, mixed valence system, inelastic light scatt., photoluminesc. 77−90145
$SmTi_{1.5}W_{0.5}O_6$, Stark sublevels in mag. suscept. and luminesc. 77−51876
Sn, ion bombardment-induced photon emission near melting point 80−100699
SnI_2, layered cryst., photoluminesc., and reflection spectra obs. 78−6726
SnI_2, single crysts. and film, optical props. 77−32437
SnO_2, correl. between simultaneous thermally stimulated cond. and thermlum. transients 79−91073
SnO_2 defective crystals, exciton-impurity complex luminescence spectra *(Russian)* 79−65926
SnO_2, exciton luminescence spectra, absorpt. spectra 80−89064
SnO_2, photoluminesc., 77-185K, recomb. model 78−80395
SnO_2, rare earth ion doped, luminesc. and charge compensation 78−76532
SnO_2, semiconductor, photoluminescence, depend. on lattice temp. and excitation intensity 80−45137
SnO_2:Eu film, RF cosputtering, cryst. site of Eu, cathodolum. obs. 77−7987
luminescence of inorganic solids continued
SnO_2:Eu powder phosphor, prep., low energy electron excitation 78−39608
SnO_2:Eu^{3+}, luminesc. and charge compensation 77−28618
SnO_2-Cu_xS-ZnS:Mn,Cu-Al_2O_3-Al, light-emitting struct., cond. and electrolum., heat treatment 80−97345
$Sn_2P_2S_6$, illumination effect on soft mode and dielectric props., luminesc. study *(Russian)* 80−50420
p-SnTe, cathodoluminescence and Fermi level hole effective mass 80−25467
SrB_2O_4:Eu^{2+}, luminesc. of high-press. phases 80−100680
$SrCl_2$, in-activated, luminescence studies at 77 and 300K 80−108247
$SrCl_2$:Cm(Bk), fluorite-struct., self-luminesc. 78−27309
$SrCl_2$:K^+(Na^+)(Rb^+) X-irradiated, recomb. luminesc. between trapped electron and self trapped holes 77−73162
$SrCl_2$:Pb^{2+}, intracentre luminesc. *(Russian)* 77−16395
$Sr_{1-x}Eu_xB_2O_4$, luminesc. props. 80−34972
$Sr_{1-x}Eu_xB_4O_7$, luminesc. props. 80−34972
$Sr_{1-x}Eu_xB_6O_{10}$, luminesc. props. 80−34972
SrF_2, neutron irrad., role of F-centres in thermoluminesc. 79−19941
SrF_2, optical detection of acoustic phonons at THz freqs. 80−75320
SrF_2, thermoluminesc. and F-centre annealing, after neutron irrad. 80−7422
SrF_2:Cm, fluorite-struct., self-luminesc. 78−27309
SrF_2:Dy(Ho)(Pr)(Tb), V_k-centre recomb. kinetics, phosphoresc. 77−55817
SrF_2:Er^{3+}, fluoresc. spectra of charge compensated cryst., multiphonon and energy transfer relax. 79−87496
SrF_2:Eu^{2+}, circular polarisation in luminesc. and optical orientation 78−6740
SrF_2:Eu^{2+}, phonon spectroscopy, phonon pulse spatial, spectral and temporal evolution 78−34580
SrF_2:Eu^{2+}, spectral, spatial and temporal phonon spectroscopy, new spectrometer 78−83892
SrF_2:Eu^{2+}, tunable optical detection and generation of THz phonons 79−65149
SrF_2:Gd^{3+} film, Gd^{3+} luminesc. spectrum and kinetics 78−6763
SrF_2:Na, γ-irrad. cryst., spontaneous and induced colour centre emission 79−7131
SrF_2:Na, tunable room temp. laser action of M-centres, luminesc. and absorpt. spectra 79−31907
SrF_2:Pb^{2+}, band struct., Jahn-Teller effect, UV luminesc. and optical absorpt. spectra 80−66243
SrF_2:Sm^{2+}, interconfig. luminesc., spectral and kinetic characts., appls. 77−4677
SrF_2:Sm^{2+}, interconfig. luminesc. spectra, vibronic wing 79−24358
SrF_2:Sm^{2+}, pseudo-Jahn-Teller effect 79−69476
SrF_2:Sm^{2+}, spectra, ^5D states, Lauer-Fong formula and SCC model 79−15513
SrF_2:Sm^{2+}(Tm^{2+}), vibronic spectra and dynamics of impurity-contaiing lattice 79−1787
SrF_2:Tb, and pure, UV induced processes 77−32452
SrF_2:Tb^{3+}, cubic Tb^{3+} centres, energy level and cryst. field parameters 77−52181
SrFCl, thermolum. and optical absorption spectra 80−66309
$Sr_2Gd_{1-x}Tb_xGaO_5$, Gd^{3+}→Tb^{3+} energy transfer, emission and excitation spectra *(French)* 80−84770
$SrLaBO_4$, crystallographic and Pb^{2+} luminesc. data 79−32971
SrO, electronic struct. of F-centre 78−30887
SrO, luminesc. band edge, 4-6.5 eV, optical absorpt., photoluminesc., cathodoluminescence, photocond. obs. 80−50411
SrO, neutron- or proton-irrad., F^+ centre fluoresc. yield and lifetime, 5 to 140K 80−55181
SrO, proton, neutron irradiated, fluorescence from anion vacancies, F^+ centre model 78−48221
SrO, single cryst., tribolum. obs. 79−52031
SrO:Pb^{2+}(Bi^{3+}), impurity centres vibronic spectra, lattice dynamics and electron-phonon interactions 80−7396
SrO-Li_2O-Al_2O_3-SiO_2:Tb^{3+} glass, energy transfer, luminesc. efficiency under UV, neutron and charged-particle excitation 79−95822
SrO(S):Pb^{2+}(Bi^{3+}) 77−73166
$Sr_2R_2O_4$ luminesc. on activation by Eu^{3+}, Nd^{3+}, Eu^{3+}-Tb^3 77−52156
SrS:Cu, phosphor, photolum. meas. 78−80393
SrS:Cu, phosphor electroluminescence characts. 79−33838
SrS:Hf, phosphor fluoresc. spectra, host lattice defect 77−12416
SrS:Hf phosphor, activation energy and freq. factor calcs. from glow curves 77−12451
SrS:Hf^{4+} phosphors, phosphorsc. decay curve 77−63450
SrS:Nd, phosphorescence decay, trapping levels 80−104003
SrS:Zr(Zr,Mn), yellow and red fluoresc. mechanism 77−32419
$SrSO_4$, celestite, colouring mechanisms 79−82998
$Sr_3SiAl_{10}O_{20}$, Ce^{3+} activated, X-ray diffr. and luminesc. props. 80−49199
$SrTiO_3$, photolum. and carrier drift mobility at ferroelec. transition 80−71469
$SrTiO_3$, semicond. anode in aq. electrolyte, electrolum. and electrochem. 80−76080
Sr_2TiO_2:Eu, synthesis, luminesc. of materials 79−11534
$SrWO_4$, single cryst. growth by Czochralski method and U incorporation, effective distrib. ratios, luminesc. characts. 79−42094
TR^{3+} ion excited state population depend. on lattice on IR excitation. *(Russian)* 80−50425
Ta, (111) surface, 100 eV electron bombardment, adsorbed mol. luminesc., coherent bremsstrahlung *(Russian)* 78−31290
Ta, bombarded by Cs^+, transient emission of continuous photon spectrum by cathodic sputtering products 79−74046
Ta-Ta_2O_5-ZnS:TbF_3-Au thin films, MIS struct., DC electrolum. obs., Poole-Frenkel effect 78→88038
Ta_2O_3, cathodic luminesc. of oxide covering on Ta electrode in electrolyte soln. 77−69915
Ta_2O_5, thermoluminesc., in H_2O vap. atm., temp. depend., time decay *(Russian)* 77−44074
Tb^{3+} in rare earth ion cryst. field in YF_3 struct., spectra 78−19563
$TbAlO_3$:Nd^{3+}, absorpt. and luminesc. spectra 79−91470
TbF_3:Sm^{3+}, induced visible emission of Sm^{3+} 80−97330
$TbGa_3(BO_3)_4$, luminesc. spectra, local symmetry of rare earth ion determ. 80−16095
$Tb_xLa(Y,Gd)_{1-x}$.DAM.Sal_3, DAM=diantipyrylmethane, luminesc. *(Russian)* 77−55830
Tb_2O_3-P_2O_5-MO system glasses, (M=Mg, Ca, Sr, Ba or Pb), photoluminesc. under X-ray excitation 80−89060

luminescence of inorganic solids continued
$Tb(OH)_3$, exciton dynamics within an inhomogeneously broadened line, luminesc. spectra 80−50407
$Tb(OH)_3$, sign of energy dispersion of one dimens. excitons, time resolved spectroscopy 77−1377
TbP_5O_{14}, IR absorpt. and luminesc. spectra 80−55079
TbP_5O_{14}, luminesc. spectra 77−52155
$Tb_xY_{1-x}PO_4$, H_2 VUV laser excitation, fluoresc. decay characts. 78−60510
$Tb_{0.8}Yb_{0.2}(PO_3)_3$, cooperative sensitisation of luminesc., order-disorder transition effect 77−36283
$Tb_2[Pt(CN)_4]_3.21H_2O$, phase transitions, X-ray study and spectroscopic study 79−60506
$Te_{39}As_{36}Si_{17}Ge_7P_1$ amorphous film, electroluminescence from on state 79−8188
TeO_2-Li_2O glass:Nd^{3+}, highly doped, spectroscopic props. and CW laser action *(French)* 79−41385
Th, O_2 adsorpt., and oxidation, electron-induced luminesc. expts. 78−38946
$ThBr_4$, luminesc. conversion of efficiency on α- and β-particle irrad. *(French)* 77−77296
$ThBr_4$:U^{4+}, IR luminesc., zero phonon lines 79−33769
$ThBr_4$:U^{4+}, single cryst., absorpt. and emission spectra 77−90174
ThO_2, pure and Tb^{3+} doped, impurities effect in absorboluminesc. and photoluminesc. 79−38597
ThO_2, temp. programmed desorpt. and photoluminesc. of surface states 79−73399
ThO_2:Pr^{3+}, luminesc., calcination temp. and excitation process depend. 79−33749
$ThOF_2$:Ce,Tb, photolum. obs. 77−77270
Ti, photon emission due to Ar^+ ion bombard., adsorbed and recoil-implanted O effect 80−80872
n-TiO_2, crystal, in aqueous soln., electrochemistry and electrolum. meas. 78−48665
TiO_2, exciton luminescence spectra, absorpt. spectra 80−89064
TiO_2 pigments in commercial polyethylene, luminesc. props. and photoactivity 79−83008
TiO_2, semicond. anode in aq. electrolyte, electrolum. and electrochem. 80−76080
n-TiO_2-electrolyte interface, electrolum. obs. 79−47520
TlBr, hot-exciton effects, luminesc. excitation spectra 77−32434
TlBr, two indirect excitons decay to direct and indirect excitons 77−44058
TlBr:I, isoelectronic donor, broad-band photoluminesc. meas. 77−8636
TlBr(Cl), light sensitive material, regularities in exciton states 77−20885
TlCl, hot-exciton effects, luminesc. excitation spectra 77−32434
TlCl powder and solution, luminesc. obs. 77−32427
TlCl, two indirect excitons decay to direct and indirect excitons 77−44058
TlCl-TlBr mixed cryst., impurity-induced self-trapping of holes and minority-ion percolation 78−64398
$Tl_2Cl_2Br_2$, excitation of luminesc. by AC elec. field 79−38670
$TlGaS_2$, optical and photoelec. props. 77−55571
$TlR(MO_4)_2$, R=Eu, Dy, Er; M=Mo, W, luminesc. *(Russian)* 78−48229
$TlR(MoO_4)_2$, (R=Eu, Dy, Er), fluoresc. spectra at 77, 300K 79−56848
$TlR(WO_4)_2$, (R=Eu, Dy, Er), fluoresc. spectra at 77, 300K 79−56848
Tm^{3+}, in oxide glasses, multiphonon relax. rates and fluoresc. lifetimes 77−77266
U containing minerals, luminescence spectra, chemical bond effect 78−72597
U, sputtered atoms, laser fluorescence spectroscopy 80−66359
UO_2^{2+}, excited, in liq. and glassy media, luminesc. decay processes, temp. activation 79−91978
UO_2^{2+} luminesc., excited states anal. 79−33766
UO_6^{6-} group, in perovskite type hosts, luminesc. var. with chem. environment 77−16374
UO_6^{6-} in oxides, excitation and emission transitions involved in green luminesc. obs. 77−16372
UO_6^{6-}, octahedral uranate group, charge transfer transition and luminesc. 80−97324
UO_n^{6-2n} ion in cryst. matrices, luminesc. 78−84640
$UO_2(NO_3)_2$, mechanoluminesc., cryst. size depend. 79−38685
$UO_3.HCONH_2.0.5H_2O$, prep., cryst. struct. and charact 80−29010
^{238}U complex, α-induced defects, vibronic luminesc. band fine struct. 79−87489
V (d^3) in II-VI semiconductors, absorption and luminesc. spectra 78−15203
V, implanted Li atoms, depth profiles and sputtering anal. by optical spectra 77−35579
W, bombardment by 1 to 30 keV ions, emitted radiation spectral comp. *(Russian)* 77−81159
W, broad band optical emission for heavy ion bombardment 77−28635
WO_3, semicond. anode in aq. electrolyte, electrolum. and electrochem. 80−76080
WO_6^{6-}, in lattice electronic struct., luminesc. ab initio calcs. 78−6337
Xe, cryst., X-ray and photoluminesc. 79−87480
Xe, crystal, edge hot emission, free exciton luminesc. *(Russian)* 79−15520
Xe, crystalline, photoluminesc. lifetime meas. 78−19548
Xe, crystalline, polariton effects, reflectivity, absorpt., and resonant luminesc. spectra calcs. 80−20095
Xe film, decay times meas. of 1750 Å intrinsic luminesc. band 77−59619
Xe, luminesc. from self trapped excitons (excimers) 79−1785
Xe, solid, self-trapped exciton emission bands 80−20697
Xe, solid, synchrotron irradiation pulse excitation photoluminesc. decay, exciton generation 78−6746
Xe:N_2O, photoluminesc. from XeO (^1D) excimers 78−68544
(Y,Gd)BO_3:Eu^{3+}, phosphor, vac. UV excitation spectra, appl. to gas discharge display 80−2816
Y, X-ray fluorescence of L_α spectrum *(Russian)* 77−63491
YA-O_3:Er^{3+}, pulsed laser action, $^4S_{3/2}$ to $^4I_{9/2}$ transition laser action, optical and luminescence spectra 80−16082
YAG crystal with rare earth ion impurities, active medium reson. pumping method for Nd laser freq. conversion 80−1206
YAG, rare earth impurity, spectral probe of stoichiometry variations 77−85790
YAG, transient colour centres caused by UV radiation 77−84744
YAG, traps, energy spectra, X-irrad. effects and thermoluminesc. *(Russian)* 77−20940

luminescence of inorganic solids continued
YAG, undoped and Ce^{3+}-doped, cathodolum. intensity and decay time, 10-480K 79−99952
YAG:Ce phosphors, luminesc. efficiency, prep. and dopant effects 80−45151
YAG:Ce^{3+}, excited-state absorpt. meas., tunable laser model system 79−42994
YAG:Ce^{3+}, photoluminescence excitation energy, crystal field and temp. effects 80−11460
YAG:Ce^{3+} luminesc., efficiency reduction after annealing 79−61443
YAG:Ce^{3+}(Eu^{3+})(Gd^{3+})(Tb^{3+}), cathodoluminesc. efficiency rel. to activator conc. 80−11479
YAG:Cr, optical detection of phonons 80−92630
YAG:Cr^{3+}, absorption and luminesc., spectra, Cr conc. depend. 77−12435
YAG:Cr^{3+}, radiation colour centres, absorpt. and thermolum. spectra 78−48206
YAG:Eu^{3+}, reson. fluoresc. spectra, showing multiple Eu^{3+} sites 80−2812
YAG:Ge^{3+}, excited state absorpt. loss, 5d→4f rare earth lasers 78−90417
YAG:Ho^{3+}, spectroscopy, stimulated emission 80−93374
YAG:Mn, impurity-induced O^- colour centres, absorpt. and fluoresc. spectra 77−1709
YAG:Nd, with improved fluoresc. lifetime of $^4F_{3/2}$ state 77−687
YAG:Nd^{3+}, Ce^{2+}, sensitisation, luminesc., absorpt. and emission spectra *(Russian)* 78−10982
YAG:Nd^{3+}, energy transfer between Nd^{3+} ions, laser-excited time-resolved site-selection spectroscopy 79−95839
YAG:Nd^{3+} crystal, zero-phonon linewidths, in $^4I_{9/2} \rightleftarrows {}^4F_{3/2}$ luminesc. band calc. 79−28834
YAG:R^{3+}, CRT and X-ray phosphor lattice-activator energy transfer model 78−6792
YAG:R^{3+} R=Nd, Er, (Er, Ga), LPE and luminesc. 78−64408
YAG-Ce^{3+}(Eu^{3+})(Tb^{3+})(Gd^{3+}), cathodolum. intensity, temp. depend., comparative study 79−99953
YAG-Ti, polarised luminescence 79−95843
$YAl_3(BO_3)_4$, thermolum. anal. 79−87514
$YAl_3B_4O_{12}$:Bi^{3+}, luminesc., vibr. struct., energy transfer 79−38584
$Y_3(Al_{1-x}Ga_x)_5O_{12}$:Nd, fluoresc. energy transfer and radiationless relax. 79−38625
$Y_3(Al_{1-x}Ga_x)_5O_{12}$:$Nd^{3+}$, time-resolved site-selection spectroscopy, energy transfer 80−2814
$YAlO_3$:Cr^{3+}, fluorescence R-lines anisotropy, effective Hamiltonian parameters 77−16368
$YAlO_3$:Nd^{3+} biaxial laser cryst., anisotropy of spectral characts. 79−50303
$YAlO_3$:Yb^{3+}, absorption and luminescence spectra, electron-phonon resonances, Stark splitting *(Russian)* 80−20674
$Y_3Al_5O_{12}$:Nd^{3+}, luminesc. spectra dependence on press. *(Russian)* 77−52183
$Y_3Al_5O_{12}$:Yb^{3+}(Nd^{3+}), one-phonon satellites in luminesc. spectra, rel. to effective phonon density 78−6730
YBO_3:Bi^{3+},Eu^{3+}, vacuum UV excitation spectra and quantum efficiencies 79−28811
YE+AG:Er^{3+}, laser material, radiative and nonradiative transitions, conc. quenching 77−16391
YErAG:Er^{3+}, $^4I_{11/2}$ to $^4I_{13/2}$ laser transition cross section, luminesc. energy 77−79833
$Y_{1-x}Eu_xP_3O_9$ phosphor, prep. and fluoresc. 77−48219
YF_3:Er^{3+}, Yb^{3+}, IR excitation curves for visible luminesc. 79−33795
YF_3:Nd, Ce, energy transfer between 5d electronic states 80−2808
YF_3:Nd^{3+}(Er^{3+})(Tm^{3+}), VUV fluorescence and tunable coherent sources from 1650 to 2600 Å 77−688
YF_3:Tm, Nd, energy transfer between 5d electronic states 80−2808
YF_3:Yb,Er, IR to visible light conversion, effect of temperature on efficiency *(Russian)* 77−28628
YF_3:Yb,Er, IR to visible radiation transform., limit yield *(Russian)* 79−28838
YF_3:Yb,Er, limit efficiency of transformation of IR to visible radiation 80−29784
YF_3:Yb^{3+}, Tm^{3+}, IR to blue up-converting phosphor 79−83004
YGG, YGG-ErGG, rare earth impurity, spectral probe of stoichiometry variations 77−85790
$Y_3Ga_5O_{12}$:Nd^{3+}, energy transfer between Nd^{3+} ions, laser-excited time-resolved site-selection spectroscopy 79−95839
$Y_3Ga_5O_{12}$:Nd^{3+}, $YGaO_3$:Nd^{3+}, spectroscopic characts. 77−12427
$Y_3Ga_5O_{12}$:Tb^{3+}, fluoresc. and absorption spectra 77−32422
$Y_3Ga_5O_{12}$:Tb^{3+}, luminesc. 77−48251
$(Y_{0.8}Gd_{0.2})AlO_3$:Er^{3+}, spectroscopic props. 77−85791
$Y_{1-x-\epsilon}Gd_xNd_\epsilon ScO_3$, crystal, absorption, luminescence, stimulated emission spectra 78−15220
$YNbTiO_6$:Eu^{3+} emission under UV excitation 78−6770
Y_2O_3 and double oxides, photon multiplication and secondary electron-hole pairs generation *(Russian)* 80−66262
Y_2O_3, autolocalised excitons *(Russian)* 79−19523
Y_2O_3, electron and hole migration distances determ. 78−19526
Y_2O_3, film, anodic glow in Y-Y_2O_3-electrolyte system 77−12447
Y_2O_3, rare earth activated, cathodolum., use of internal reference 77−44071
Y_2O_3, thermoluminesc., in H_2O vap. atm., temp. depend., time decay *(Russian)* 77−44074
Y_2O_3, vacuum UV luminesc., excitation by X-ray synchrotron radiation 79−8168
Y_2O_3:Eu, fluoresc., cathodoluminesc. and thermal quenching 79−47488
Y_2O_3:Eu, surface luminesc. centres excitation characts. 78−52560
Y_2O_3:Eu sintered slice, DC electroluminesc., impact excitation 79−47522
Y_2O_3:Eu^{3+}, absorpt. spectra, fluoresc., electron beam excitation 78−92093
Y_2O_3:Eu^{3+}, cubic, laser-induced polarised fluoresc., Stark levels and cryst. field parameters 79−95838
Y_2O_3:Eu^{3+}, quantum yield in candoluminescence process by low energy H^+ ion bombard. 79−65930
Y_2O_3:Eu(Tb)(Tm), powder layer, electrolum., comparison with La_2O_3 and Y_2O_2S 77−20927
Y_2O_3:Tb^{3+}(Dy^{3+}), conc. quenching of X-ray and UV-excited luminesc. *(Russian)* 77−55829
Y_2O_3:Zr^{3+}, F-centre charge state, ESR and thermally stimulated luminesc. obs. 80−60418
YOCl:Yb,Er, anti-Stokes luminesc., temp. depend. *(Russian)* 78−6764
YOCl:Yb^{3+}, Er^{3+}, anti-Stokes luminesc., 4.2 to 293K 77−59609

luminescence of inorganic solids continued
YOF:Tb^{3+}, conc. quenching of X-ray and UV-excited luminesc. *(Russian)* 77−55829
$Y(OH)_3$:Tb^{3+}, excited state relax., ns time resolved spectroscopy 77−61140
Y_2O_2S:Eu, high press. effect on luminesc. efficiency and lifetime, charge transfer absorpt. 80−66266
Y_2O_2S:Eu, phosphor, temp. meas. by line shift method 77−13750
Y_2O_2S:Eu phosphor, luminescence saturation effects due to N_2 laser and cathode-ray excitation 80−40151
Y_2O_2S:Eu^{3+}, luminesc., excitation spectra, cooperative phonon sidebands 79−33771
Y_2O_2S:Eu(Tb)(Tm), powder layer, electrolum., comparison with La_2O_3 and Y_2O_3 77−20927
Y_2O_2S:Tb, cathodoluminesc. efficiency at low electron energy 78−6790
Y_2O_2S:Tb, cathodoluminesc., nonlinear depend. on activator concs. 79−8190
Y_2O_2S:Tb, cathodoluminesc. efficiency changes due to processing, XPS meas. of surface changes 79−99951
Y_2O_2S:Tb, recomb. processes and emission spectra *(Russian)* 78−6797
Y_2O_2S:Tb^{3+},Eu^{3+}, energy transfer mechanism 78−6793
Y_2O_2S:Tb^{3+}(Pr^{3+}), enhancement of cathodolum. efficiency 79−69891
Y_2O_2S:Yb^{3+}, charge transfer type luminesc. 79−33797
Y_2O_2S:Yb^{3+},Ho^{3+}, anti-Stokes emission band assignments, energy transfer mechanism 77−40277
YPO_4 phosphor, ionisation of capture centres, thermolum. spectra 80−11487
YPO_4:Ce(Tb), luminesc. and optical spectra 79−65921
YPO_4:Yb^{3+}, charge transfer type luminesc. 78−64392
YPO_4:Yb^{3+}, charge transfer type luminesc. 79−33797
$YP_{0.99}V_{0.01}O_4$, luminesc. spectra in visible region, vanadate group 78−43921
δ-Y_2S_3:Nd^{3+}, spectroscopic props. from absorpt., photoluminesc. and excitation spectra 80−34968
Y_2SiO_5:Ho^{3+}, single cryst luminesc. and stimulated emission 77−69895
$Y_3Si_2O_8Cl$; Ce phosphor, prep. and luminescence props. 78−52740
$YSiO_3F(Cl)(Br)$, phosphor host, luminesc. and struct. props. 78−48212
$Y_{1-x}Tb_xAl_3B_4O_{12}$ phosphors, cathodoluminesc. 77−73177
$Y_{1-x}Tb_xP_3O_9$ phosphor, prep. and fluoresc. 77−48219
$Y_2Ti_2O_7$:Nd^{3+}, spectroscopic props. 77−69866
Y_6UO_{12}, energy transfer, cryst. struct. and chemical composition effect 80−108248
YVO_4, luminesc. spectra in visible region, vanadate group 78−43921
YVO_4 phosphor, ionisation of capture centres, thermolum. spectra 80−11487
YVO_4, pure and Bi^{3+} doped, absorpt. and emission props., excitons 79−38592
YVO_4:Er^{3+}, Yb^{3+}, IR excitation curves for visible luminesc. 79−33795
YVO_4:Eu, cluster electron struct., X-alpha calc., emission spectra 78−2898
YVO_4:Eu, fluoresc., cathodoluminesc. and thermal quenching 79−47488
YVO_4:Eu^{3+}, absorption and fluoresc. spectra, SU(2) chain *(French)* 78−28912
YVO_4:Eu^{3+}, absorpt. spectra, fluoresc., electron beam excitation 78−92093
YVO_4:Eu^{3+}, laser site-selection spectroscopy investigation 78−68556
YVO_4:Eu^{3+} phosphor, cathodoluminesc. and photon statistics 77−59621
YVO_4:Eu^{3+}(Er^{3+}), energy transfer, laser time-resolved spectroscopy 78−27306
YVO_4:Nd^{3+}, absorption and fluoresc. spectra of laser states 77−38900
YVO_4:Nd^{3+}, fluoresc. lifetime of $^4F_{3/2}$ state 79−87494
YVO_4:R^{3+}, R=Nd, No, Tm, Sm, Dy, Er, Eu, Tb, electronic struct. and spectra of VO_4, RO_8 clusters 78−10953
Y_2WO_6, new structural type, unit cell, space group, fluorescence spectra 79−1420
Y_2WO_6:Eu, noncontinuum model for energy transfer 79−33800
Y_2WO_6:Eu^{3+}, luminesc., rel. to crystallographic data 79−33793
Y_2WO_6:U^{6+}, luminesc. 77−55816
Y_6WO_{12}:Eu^{3+}, crystal struct., fluorescence spectra, exam. 78−52558
$(Y_{0.80}Yb_{0.19}Er_{0.01})F_3$ phosphors, IR to visible conversion 78−48210
$Y_{1-x-y}Yb_xEr_yOCl$, Er ion excited state decay and population *(Russian)* 80−100694
$(Y_{0.80}Yb_{0.19}Ho_{0.01})F_3$, IR to visible conversion 78−48210
$Y_2[Pt(CN)_4]_3.21H_2O$, first order phase transform., spectroscopic and thermodynamic anal. 78−38829
$Y_2[Pt(CN)_4]_3.21H_2O$, phase transitions, X-ray study and spectroscopic study 79−60506
Yb monochalcogenides, multiphonon inelastic light scatt. 77−90144
Yb^{2+}, broadband luminesc. in fluorite struct. crysts. 79−65923
Yb^{3+} doped phosphors, IR excitation and absorpt. and emission spectra *(Russian)* 79−52021
Yb:glass, luminesc., low temp. energy transfer 80−2837
Yb^{3+}:phosphate glass, relation between absorption and equilib. luminesc. spectra 77−85754
YbP_5O_{14} and $Yb_{0.9}Tb_{0.1}P_5O_4$, IR absorpt. and luminesc. spectra 80−55079
(Zn, Cd, Hg)S:Cu,In, electroluminesc. temp. depend. 77−1732
(Zn,Cd,Hg)S:Cu,In, electroluminesc., brightness waves 77−59616
(Zn,Cd)S:Cu,Al, luminesc. efficiency deterioration due to surface oxidation by $(NH_4)_2Cr_2O_7$ thermal decomp. 80−29810
(Zn, Hg)S:Cu, Cl, effect of superposition of two sinusoidal fields and freq. on electroluminesc. 78−39606
$(Zn,Mg)_3(PO_4)_2$:Mn^{2+}, cathodoluminescence obs. 80−71492
Zn, radiative emission from sputtered atoms, geometry depend. 77−28669
$ZnAl_2O_4$:Cr^{3+}, N-lines and Cr^{3+} pairs 78−2896
$Zn_3(BO_3)_2$:Sm^{3+}, photoluminescence obs. *(Spanish)* 79−73986
$Zn_4B_6O_{13}$:Tb^{3+}, fluoresc. and thermophosphoresc. spectra *(Spanish)* 77−90188
ZnCdS:Ag screen, electron beam excited, light emission spectra 80−25466
$Zn_xCd_{1-x}S$, bound-exciton lines, compositional fluctuation-induced broadening 80−2846
$Zn_xCd_{1-x}S$ epitaxial layers, elec. resist. and luminescence obs. 78−19540
$Zn_xCd_{1-x}S$, forbidden band width, exciton refl. and luminesc. meas. 78−10947
$Zn_xCd_{1-x}S$, graded single crysts., laser or electron beam excited, luminesc. 77−85792
$Zn_xCd_{1-x}S$ monocrystal, optical and nonlinear optical characts. *(Russian)* 79−98442
$Zn_xCd_{1-x}S$:Cl, Cu^+(Ag^+), high pressure luminesc. 78−19533
luminescence of inorganic solids continued
$Zn_xCd_{1-x}S$:Cu, photoluminesc., Birman effect *(Russian)* 79−28837
$Zn_xCd_{1-x}S$:Cu, photoluminescence 80−29783
$Zn_xCd_{1-x}Te$, absorpt. edge luminesc. on high-intensity excitation 78−6745
$Zn_xCd_{1-x}Te$, relaxation processes, emission spectra *(Russian)* 78−72598
$ZnCr_2O_4$, antiferromag. spinel, absorpt. and luminesc. spectra 80−66225
ZnF_2:Mn, thin films, electroluminescence, brightness voltage characts. hysteresis 80−20709
p-$ZnGeP_2$, photoluminescence of crystals with varying comp. and dopants 77−32431
$ZnGeP_w$, recombination radiation 78−19562
$ZnIn_2S_4$ (I) film, one-packed polytype, resist., photocond. and luminesc. 79−1608
$ZnIn_2S_4$ film, photoluminesc. and photocond. 78−52677
$ZnIn_2S_4$, photoluminesc., reson. Raman scatt. 78−48179
$ZnIn_2S_4$, recomb. process of photoexcited carriers 77−44042
$ZnIn_2Se_4$, luminescence spectra, recomb. processes and energy level scheme 77−1726
$Zn_{1-x}Mg_xTe$ alloy, luminesc. in green and blue and cathodolum. efficiency *(French)* 77−21019
$Zn_{1-x}Mg_xTe$ alloys, high purity, metallurgical and analytical methods of prep. 80−40247
$Zn_{1-x}Mg_xTe$ alloys, LED appl., elec. props. 80−2813
ZnO, band gap depend. on energy of zero-point vibrs., luminesc. obs. 79−73436
ZnO, biexciton levels, luminescence-assisted two-photon spectra 80−29795
ZnO, change in exciton-phonon mechanism due to defects 78−71804
ZnO, diffusion of excitons due to scatt. by optical phonons, photoluminesc. 77−24521
ZnO, electron-hole liq., optical gain meas. 77−85794
ZnO, electron-hole recombination emission, temp. depend. and phonon repetitions *(Russian)* 79−15521
ZnO epitaxial film, ionized-cluster beam and reactive ionized-cluster beam deposition, cathodolum. characterisation 80−16202
ZnO epitaxial film, UV luminesc. due to one-, two-photon excitation, laser possibility 79−11468
ZnO epitaxial film on Al_2O_3 substrate, recombination radiation in intense single photon excitation 80−7410
ZnO epitaxial layers, rel. between elec. and photoluminesc. props. and their deposition conditions 79−95530
ZnO, excited states of bound excitons, photoluminesc. obs. 80−44513
ZnO, exciton luminesc., 16 to 77K 80−97329
ZnO, excitonic mol. emission, strain induced splitting 77−44060
ZnO, excitonic molecule transitions, M-band emission 79−78742
ZnO film, prep. by reactive ionized cluster beam deposition, and characterisation 80−10829
ZnO, green luminesc. band, UV irrad. photocond. and quantum yield 77−36284
ZnO, hexagonal spot pattern production with light source and electron beam 77−69148
ZnO, highly excited, biexciton states, M-band luminescence 79−78744
ZnO, ion implantation effect on luminesc. and cryst. damage 78−6758
ZnO, low energy cathodolum., surface effects 78−60522
ZnO, luminescent, phonon detection by shallow electronic trap states 79−14902
ZnO, multiparticle exciton complexes, luminesc. spectra *(Russian)* 80−16090
ZnO phosphor fired with Zn, luminesc. in green and red region 80−66265
ZnO, phosphors, emission spectra, impurity effects 77−32420
ZnO phosphors, origin of UV emission 78−64400
ZnO powders, UV luminesc. spectral distrib., comparison with single crysts., excitons role 80−55167
ZnO, pure and rare earth doped, photo- and electroluminesc. 79−28803
ZnO, red, electronic and opt. props., electrographic props. 77−57419
ZnO, self-activated phosphor, band width and shift, temp. depend. 77−8623
ZnO, single cryst., photo- and thermoluminescence 80−66311
ZnO, single cryst. and film, visible and near IR spectra *(Russian)* 77−52133
ZnO, single cryst. growth in ZnO-H_2-H_2O-O_2 vapour, morphology, electrophys. and opt. props. 78−52649
ZnO, stimulated two-photon emission from excitonic molecules 79−28815
ZnO, two-photon-excitation, tunable laser emission, luminesc. processes 80−55127
ZnO, Zeeman splitting of A1-exciton emission lines, k-linear term effects 78−52563
ZnO:Ce(Sm) phosphors, electrolum. 79−99946
ZnO:Ce(Tb) phosphors, electrolum. brightness, voltage and freq. depend. 80−60681
ZnO:Cu, excited state, zero phonon lines in emission and Zeeman spectra 79−38026
ZnO:Dy(Nd)(Sm), phosphor, electroluminesc., photoluminesc. spectra 78−80421
ZnO:Dy(Yb)(Nd)(Sm)(Pr)(Gd)(La)(Er), electrolum. brightness, field strength and freq. depend. 80−100696
ZnO:Er, phosphors, photo- and electroluminesc. 77−12428
ZnO:Er,Ag, photoluminescence and electroluminescence 78−27327
ZnO:La phosphor, electrolum. brightness waves, −168 to +85°C 78−52580
ZnO:Li, effect of LiOH mineraliser on struct. and optical props. 77−8737
ZnO:Li, luminesc. donor-acceptor pairs, exchange broadened optically detected EPR spectra 78−23373
ZnO:Li(Na), band-edge emission obs. 77−20933
ZnO:Nd, electrolum. brightness waves, 93 to 363K 79−33839
ZnO:Pr(Gd)(Er), phosphors, photoluminesc. and electroluminesc. spectra 79−11457
ZnO:Yb(Nd)(Pr)(Sm), electro- and photoluminesc. 79−83024
ZnO-GeO_2-MnO-B_2O_3 wideband cathodoluminescent phosphor 80−55196
ZnO-PbO electroluminesc. phosphors, AC field excitation green and yellow emission 77−59617
ZnO-TeO_2 glass, Ho^{3+} or Er^{3+} doped, visible green emission 79−15523
(ZnO-ZnS)Cu:I, double band electroluminophors, form., props. 78−19568
$Zn_4O(BO_2)_6$:Tb, phosphoresc. study *(Spanish)* 80−16105

luminescence of inorganic solids continued
ZnP_2, cathodoluminesc. 4.2 to 200K 79−52028
ZnP_2, monoclinic, cathodoluminesc. spectra exam. 79−15534
ZnP_2, polarised spectra of IR absorption and emission of single crysts., oscillatory states *(Russian)* 77−28583
Zn_3P_2, photoluminesc. spectra 79−87502
Zn_3P_2, thermoluminescence glow curve method for radiation induced traps 80−60689
$Zn_3(PO)_2$, thermoluminescence glow curve method for radiation induced traps 80−60689
ZnPz, trapping levels, TSC and thermolum. meas. 79−15115
ZnS, additively coloured or neutron irradiated, near IR emission 77−90199
ZnS, cathodolum. emission spectra, exciton lines 80−76084
ZnS crystals, luminescence kinetics, centre discrimination exam. 78−15215
ZnS crystals in electrolyte, electrolum. and elec. props. 80−93407
ZnS, current and refractive index oscills. in electric fields due to barrier instability 79−91372
ZnS, decomposition in H_2 atmosphere, electron-hole mechanism *(Russian)* 77−16409
ZnS, electrolum. phosphors, surface phenomena occurring during ageing *(Russian)* 79−33842
ZnS, electroluminesc. and photoluminesc. spectra, fine struct. *(Russian)* 78−84661
ZnS, electroluminescent emission, UV excitation after effects 80−45144
ZnS, electroluminophor, ageing rate, voltage effects *(Russian)* 78−84662
ZnS electroluminophors, ageing effects *(Russian)* 78−15231
ZnS, epitaxial film, CVD growth, photolum. spectra *(French)* 77−36403
ZnS, excited phosphor, IR stimulation and quenching of luminesc., review *(Russian)* 80−11455
ZnS films, electrolum., bistable excitation 80−93406
ZnS, green-blue luminesc. charcts., model of luminesc. centres 79−73999
ZnS, high temp. annealing effects on photoluminescence 78−19564
ZnS, interaction between charged dislocations and luminesc. centres *(Russian)* 79−56860
ZnS, interimpurity high press. luminesc. 78−19532
ZnS ion beam etching, topographic changes, amorphisation, luminescence study 80−76078
ZnS, ion implantation effects on luminesc., thermo-EMF 80−88178
ZnS, low voltage cathodoluminescence 78−52585
ZnS, low-temp. trap anal. thermally stimulated luminesc. model extension 80−80877
ZnS, luminesc. data. statistical anal. *(Russian)* 78−68559
ZnS, luminescence of M-centre 80−29779
ZnS phosphor, deep capture centres obs. 78−10951
ZnS phosphor, exciton struct. in luminesc. excitation spectra 77−52176
ZnS, phosphor, voltage depend. of electrolum. brightness 80−45148
ZnS phosphors, Gudden-Pohl effect, temp. depend. and decay rate 77−44070
ZnS phosphors, Gudden-Pohl effect, field ionis. of trapping centres 77−73170
ZnS phosphors, synthesis under unidirectional pressure and roasting in vacuum 77−32547
ZnS, photoluminesc. quenching by weak alternating field 77−85778
ZnS, plastic deform. induced luminesc., dislocations role *(Russian)* 78−10985
ZnS platelets, cathodolum. analysis using STEM 78−32950
ZnS, polarisation of self-activated luminesc. 77−73159
ZnS, post field recomb. in pulsed electrolum. 80−71488
ZnS, powder phosphor, IR-induced changes in emission spectra 78−80389
ZnS powder phosphors electroluminescent cells, AC electrolum. charcts. *(Japanese)* 80−71489
ZnS, prebreakdown electrolum., domain form. and negative resist. effects 80−84788
ZnS, rare earth activated phosphor, scintillation mechanism *(Russian)* 78−48231
ZnS Schottky-barrier diodes, blue light emission 79−38671
ZnS, self activated emission, spin depend. donor acceptor pair recombination, ODMR exam. 79−42870
ZnS, self-activated, IR sensitivity 78−6742
ZnS, self-activated, orientation of luminesc. centre 78−27307
ZnS, self-activated, trap distrib. and photoelectronic effect due to UV, IR and visible excitation 77−36282
ZnS, shallow traps, thermolum. glow curves obs. 79−91508
ZnS, single cryst., radiation emission, stimulation by IR light *(Russian)* 77−66542
ZnS, single crysts. excited by laser beam and elec. field, streamer luminesc. and photolum. obs. 80−34986
ZnS, single electron excitation study, cathodoluminescence image contrast using STEM 80−89072
ZnS striated platelets, SEM studies of local variations in cathodolum. 78−15232
ZnS, surface, work function and luminesc. phenomena, effect of H,H_2,O and O_2 adsorpt. 78−10538
ZnS, temp. depend. of edge emission band shape 77−20934
ZnS thin films, effect of fabrication parameters on electroluminescence and related props. *(Japanese)* 80−76083
ZnS type lattices, luminescence, constants, temperature dependence, activation energies 79−99923
ZnS:^{90}Sr, continuously acting luminous solid for photoelec. meas. over 300-800 nm range 79−3757
ZnS:(Cu, Cl), electroluminesc., voltage effect on ageing rate 79−95848
ZnS:Ag, Al and ZnS:Cu, Al, LV cathodoluminesc. 79−33844
ZnS:Ag, Al(Cu), trap parameters, thermostimulated luminesc. and cond. meas. *(Russian)* 77−72868
ZnS:Ag, cryst. struct., electron traps and glow curves 79−61437
ZnS:Ag, electroluminesc., surface barriers *(Russian)* 78−2919
ZnS:Ag, luminesc. efficiency deterioration due to surface oxidation by $(NH_4)_2Cr_2O_7$ thermal decomp. 80−29810
ZnS:Ag, phosphor, luminesc. of surface glow centres 80−29782
ZnS:Ag, phospors, nature of fluorescent centres and traps 79−91484
ZnS:Ag, photon counting statistics of cathodoluminesc. light emission 79−24371
ZnS:Ag, single crystal, ionisation mechanism of field trapping centres 80−45156
luminescence of inorganic solids continued
ZnS:Ag,Al, computer calc. of band model for luminesc. and photocond. *(Russian)* 78−52542
ZnS:Ag,Cl, embedded in HBO_3-glass matrix, blue electrolum. 80−55195
ZnS:Ag,Sm, recomb. centre interaction, luminesc. quenching 78−10946
ZnS:Ag phosphors, luminesc. of glow surface centres *(Russian)* 79−28836
ZnS:Al,Cu(Ag)(Au) phosphors, luminesc. excitation spectra and exciton struct. 80−55164
ZnS:Al(Te) phosphors, luminesc. excitation spectra and exciton struct. 80−55165
ZnS:Au, phosphor, 'blue' and 'green' centre form. *(German)* 79−38665
ZnS:B, new luminesc. centre 79−38635
ZnS:Cl, self-activated, blue emission band 79−38633
ZnS:Cl, shape of self-activated cathodoluminesc. band 80−34987
ZnS:Cl^-, $Cu^+(Ag^+)$, phosphor, high press. effect on thermoluminesc. 78−64419
ZnS:Cr^+, Fe^{3+}, luminesc., cond. and paramag. centre conc. parameters 78−6724
ZnS:Cr^{2+}, excitation spectrum of IR emission 77−12421
ZnS:Cu, Al phosphors, mechanism of IR stimulated and quenching 77−69881
ZnS:Cu, Br based electroluminesc. cells, light, const. field effects on electroluminesc. 78−84658
ZnS:Cu, Cl, I, anisotropy of blue Cu luminesc. centres 77−81137
ZnS:Cu, Cl, Mn film, AC electrolum. 80−60680
ZnS:Cu, Cl luminophor, photoluminesc. and struct. props. 77−32414
ZnS:Cu, Co, deep traps and stationary luminescence *(Russian)* 78−48227
ZnS:Cu, electroluminesc. spectra fine struct. 79−95847
ZnS:Cu, Er, Na, phosphor, mechanism of sensitisation effect of Cu and Na ions 77−16369
ZnS:Cu, Gudden-Pohl effect, flash kinetics 79−24367
ZnS:Cu, H, double band phosphor, electrolum., −100 to +100°C 78−10987
ZnS:Cu, halogen, electroluminescent cells, visible light and DC voltage effects on ageing 77−69914
ZnS:Cu, Mn DC electroluminescent powder panels, bulk and junction effects 80−89068
ZnS:Cu, Pb, phosphors, ruby laser stimulated time delayed emission spectra 77−69874
ZnS:Cu, polycryst. electret, electroluminesc. light flash character *(Russian)* 77−55833
ZnS:Cu, polycryst. phosphor, excitation storage, recombination barrier participation 78−27316
ZnS:Cu,Al, anisotropy of blue-Cu luminescence centres 78−64390
ZnS:Cu,Al phosphor, shallow hole traps 78−31237
ZnS:Cu,Cl, electrolum. brightness wave, effect of square pulses 77−52184
ZnS:Cu,Cl phosphor, effect of charged imperfections on electrolum. 77−32443
ZnS:Cu,Cl(Br)(I), green luminesc., interimpurity phototransitions investig. *(Russian)* 77−66541
ZnS:Cu,Er,Cl film, ageing and forming, DC electroluminesc., impact excitation 79−47522
ZnS:Cu,Pb film, sublimated, pulse electrolum. meas. *(Russian)* 77−85806
ZnS:Cu,Pt phosphors, photoluminesc., thermoluminesc. 78−43915
ZnS:Cu 79−24350
ZnS:Cu AC electroluminescent patterns and polytypic transformations 78−6784
ZnS:Cu crystal, powder, epitaxial film, luminescence anomalous thermal 80−76077
ZnS:Cu phosphor, electric field quenching of photoluminesc. and flashlike rise in luminesc. 78−2911
ZnS:Cu^{2+}, Jahn-Teller effect, stacking faults and formation of polytypes, absorption and emission spectra 77−4660
ZnS:Cu(Cl), electroluminesc. and photoluminesc. spectra, fine struct. *(Russian)* 78−84661
ZnS:Cu(Pb), phosphor, photocapacitive effect, Gudden-Pohl effect 79−65520
ZnS:Er diodes, electrolum. 79−33840
ZnS:Er^{3+}, ion-implanted, annealing, cathodolum. obs. 80−2868
ZnS:Er^{3+}, luminesc. centres with cubic symmetry 79−38636
ZnS:Eu^{3+}, origin of red fluoresc., occurrence of rare earth oxysulphide inclusions *(French)* 77−69875
ZnS:Fe, luminesc. and ESR investigations 80−2822
ZnS:In, polarisation of deep centre electroabsorpt., effect of random electric fields 77−48148
ZnS:In, recombination emission by optically detected magnetic resonance 80−66272
ZnS:Mn, AC thin film electroluminesc., filamentary emission and memory effect 79−38672
ZnS:Mn, AC thin-film electrolum. devices, electrolum. efficiency profiles 79−65931
ZnS:Mn, Cu powder devices, DC electroluminesc. 79−38674
ZnS:Mn, electrolum. film, direct impact excitation of Mn centres 77−24900
ZnS:Mn, phosphor, surface changes following interaction with H *(Russian)* 78−72602
ZnS:Mn, self-activated and Mn^{2+} emission, high press. action 80−16093
ZnS:Mn, spectral distribution and decay times of the luminescence of Mn^{2+} on different lattice sites 79−78743
ZnS:Mn electroluminescent films, amplification factor during electric field excitation, population inversion *(Russian)* 79−78757
ZnS:Mn film, AC electrolum., memory effect 78−15228
ZnS:Mn film, AC electrolum., memory effects 79−38673
ZnS:Mn film, current conduction and light emission, physical mechanism 78−14840
ZnS:Mn film, electroluminescence theory 79−11470
ZnS:Mn film, emission centres of DC electrolum. 78−68564
ZnS:Mn film, luminesc. of highly efficient DC diodes 77−8630
ZnS:Mn film, spectral and electro-optical props. 77−1736
ZnS:Mn film device, laser modulation of electrolum. 78−52576
ZnS:Mn film in SnO_2-ZnS-Cu_xS-ZnS:Mn-Al_2O_3-Al struct., electrolum. 79−33837
ZnS:Mn films, photoluminesc. and electroluminesc., excitation mechanism of luminesc. centres 79−11459
ZnS:Mn on SnO_2/glass transparent conductive base, surface morphology effects on electroluminesc. *(Russian)* 78−48238

luminescence of inorganic solids continued
ZnS:Mn Schottky diodes, reverse-biased, electroluminescence, hot electron impact excitations 80−25005
ZnS:Mn-H atom systems, surface physiochem. changes, radical recombination luminesc. investig. 79−56863
ZnS:Mn^{2+}, $^4T_1$ excited state, absorpt., MCD, Jahn-Teller model 78−43907
ZnS:Mn^{2+}, Jahn-Teller effect in fluorescent level 78−52566
ZnS:Mn^{2+} phosphors, luminesc. excitation spectra and exciton struct. 80−55164
ZnS:Mn(Al)(Te), luminesc., exciton struct. 79−33801
ZnS:Ne, implanted single crysts., photolum. and bombardment effect, thermolum. curve obs. 80−55166
ZnS:Ni, IR luminesc. and absorpt. spectroscopy 80−108261
ZnS:Pb, blue luminesc., photoexcited EPR spectrum 80−108070
ZnS:Pb, luminescence, polaris. emission 79−38634
ZnS:Pb phosphor, electrolum. brightness, temp. depend. 77−48249
ZnS:Pb phosphor, ionisation mechanism of field trapping centres 80−45156
ZnS:Pb phosphor mech. of elec. field liberation of electrons from traps 78−72616
ZnS:Pb^{2+}(Mn^{2+}), high press. luminesc., localised excitations 78−19534
ZnS:RF_3 film, AC electrolum., memory effects 79−38673
ZnS:RF_3 in Ta-Ta_2O_5-ZnS:RF_3-Au struct., electrolum. and cathodolum. meas. *(French)* 77−16398
ZnS:Tb_2 Cu(Ag) phosphors, luminesc. props. 80−100690
ZnS:Tb^{3+}, NdF_3 film, vac. deposited, electrolum. energy transfer 80−2861
ZnS:Tb^{3+}, sputtered film, DC electroluminesc. and host-excited photoluminesc., Tb^{3+} content depend. 77−85807
ZnS:TbF_3, photoelectroluminescence, effect of electron-hole pairs 78−27328
ZnS:Te, single crysts. grown from Te soln., photolum. props. 79−52005
ZnS:Tl(Al)(Zn), UV spectra of donor-doped single crysts. 77−12404
ZnS:Tm^{3+}, charge compensation and polytypism influences on fluorescence 80−89051
ZnS:Tm(Er)(Nd) phosphors, optical scintillation mechanism 79−56867
ZnS-based phosphor, microstruct. and luminesc. efficiency 78−10959
ZnS-BiOCl, electroluminesc. heterojunction phys. props. 77−66198
ZnS-CdS system, IR luminesc. and absorpt. centres, donor-acceptor pair model 77−44043
ZnS-CdS:Ag, Ni, Co, thermoluminesc. glow curves 78−95611
ZnS-CdS:Ag, Ni, Co phosphor, thermoluminesc. 77−66547
ZnS-CdS:Ag, phospors, nature of fluorescent centres and traps 79−91484
ZnS-CdS:Ag(Cu), cryst. struct., electron traps and glow curves 79−61437
ZnS-CdS:Tm,Ni, recomb. centre interaction, luminesc. quenching 78−10946
ZnS-Cu, comet shaped electroluminesc. lines 78−52578
ZnS-Cu, polycryst., influence of alternating elec. field and UV light on struct. defects, electrolum. expts. 79−43041
ZnS-$CuGaS_2$ heterodiodes, LPE, emission spectra 79−33335
ZnS-Mn crystal, polarisation meas., luminesc. and Raman spectra 79−8138
ZnS-Mn sublimated phosphor films, annealing effects *(Russian)* 78−43949
ZnS-O, single cryst., fast neutron irrad., optical props. 78−27331
ZnS-ZnO, solid solns., edge emission and exciton spectra *(Russian)* 77−24899
ZnS-ZnSe mixed powders, hot-pressed polycrystalline, photolum. and electrolum. 77−32426
(ZnS-ZnSe):Cu, H systems, electrolum. 77−4690
$ZnS_{1-x}Se_x$, electroluminescence with In and Au contacts, comp. depend. 77−59618
$ZnS_{1-x}Se_x$:Cu,Br ceramic, current oscills. and electrolum. under high elec. fields 79−38677
ZnS_xSe_{1-x}, VPE, characterisation of defect centres by photoelectronic meas. 80−10914
ZnS_xSe_{1-x}, VPE on CaF_2 substrate, in flowing H_2, growth and characterisation *(French)* 80−107678
ZnS_xSe_{1-x}:Fe, photolum. meas. 79−19921
ZnS_xSe_{1-x}:Mn(Cu), luminesc. obs. 78−60519
ZnS(Se)(Te):Co, impurity luminescence no phonon line depend. on temp., Debye temp. 80−66273
ZnS(Se)(Te):Co^{2+}, IR luminesc. quenching, Co^{2+} level position, ionisation energy 80−16079
ZnS(Se)(Te):Cr^{2+}, absorpt. and luminesc. of $Cr^{2+}(d^4)$, cryst. field theory interpretation 79−83000
ZnSe, band-edge photoluminesc., far-below band-gap excitation 80−76063
ZnSe, blende type struct., luminesc. under high excitation 79−19928
ZnSe, blue photoluminesc. excited with strong laser radiation 80−93391
ZnSe, cubic monocrystal, electron-phonon interaction, low temp. luminesc. *(Russian)* 80−25451
ZnSe, direct gap semicond., exciton energy at 300K from reabsorption of luminesc. 79−78728
ZnSe, donor-acceptor pair emissions charact. *(French)* 80−108249
ZnSe, electroluminesc. exam. high voltage pulses 79−15533
ZnSe electroluminescent diode, ageing effects 77−8660
ZnSe, epitaxial, organometallic CVD, on GaAs, and photolum. 79−8249
ZnSe, epitaxial layers, close-spaced technique, preparation and optical props. 79−47637
ZnSe epitaxial layers, organometallic CVD prop., growth kinetics and luminescent props. 79−51458
ZnSe, exciton emission, halfwidths, thermal and optical activation energies obs. *(French)* 80−66268
ZnSe film, MBE and resistivity 79−100059
ZnSe film, rare earth fluoride doped, electrolum. meas. 77−16397
ZnSe, grown from Ga soln., near band-edge luminesc. 79−69881
ZnSe, Gudden-Pohl effect, release of electrons from traps 80−45149
ZnSe, impact ionisation electroluminesc. 77−44066
ZnSe layers, LPE growth from Zn-Ga soln., photoluminesc. 79−56840
ZnSe, low resist. single crysts., radiative recomb. mechanism, photolum. and electrolum. 78−6744
ZnSe, luminesc., hot electron effects 80−66277
ZnSe, luminesc., reson. Raman scatt. due to excitonic mols. 79−33816
ZnSe, MBE growth, elec. and optical props. 80−75462
ZnSe MIS diode, blue electrolum., heat treatment effects 78−19569
ZnSe MOS diodes, injection type electrolum. 77−59614
ZnSe MOS diodes, injection luminesc., edge emission 79−28842

luminescence of inorganic solids continued
ZnSe, near band edge photoluminescence, electron-hole recombination 80−80835
ZnSe, optically detected mag. reson., donor g-factor 77−69732
ZnSe, optically pumped stimulated emission at 4580 Å, near band edge luminesc. 78−71105
ZnSe, photoexcited hot electrons at 2K, photolum. meas. 79−78741
ZnSe, photolum. and blue electrolum. in MIS structs. 77−20928
ZnSe, reabsorpt. of excitonic luminesc. in direct band gap semiconds. 77−63469
ZnSe, relaxation processes in Raman scattering and exciton luminescence under resonant excitation 80−25386
ZnSe, reson. absorpt. of coherent IR radn. by acceptors, photocurrent and emission spectra 79−73974
ZnSe, resonance Raman scatt., exciton-polariton luminescence *(Russian)* 80−97287
ZnSe, single cryst., electron-hole drops, boundary luminesc. *(Russian)* 78−80412
ZnSe, single cryst. film, MBE, quality obs. using photoluminesc. 77 77419
ZnSe single crystal, exciton photolum. and refl. spectra, 4-90K *(Russian)* 77−66540
ZnSe surface barrier diode, hot charge carriers, elec., photoelec., and electroluminesc. props. *(Russian)* 79−33841
ZnSe, thermally treated crystals, photoluminesc. 80−60661
ZnSe:Ag, low-temp. photolum. meas. 77−20912
ZnSe:Al, thermally stimulated transients, new approach 79−38086
ZnSe:Al single crysts., photoluminescence spectra *(Russian)* 77−28627
ZnSe:Al(Ga)(In), single cryst., doping, blue luminesc. 78−39584
ZnSe:Al(Mn), elec. and luminesc. props. 77−39844
ZnSe:B(F), ion implantation, photocond. and cathodoluminesc. meas. 78−26586
ZnSe:Co, optical props. in near IR 78−43924
ZnSe:Cr^+, Fe^{3+}, luminesc. cond. and paramag. centre conc. parameters 78−6724
ZnSe:Cr^{2+}, excitation spectrum of IR emission 77−12421
ZnSe:Cu, Al, single cryst., low-voltage red cathodolum. 78−80423
ZnSe:Cu, Cl, high press. luminesc. 78−19532
ZnSe:Cu, I, ceramic, electroluminesc., electric field induced switching effect under illum. 77−1460
ZnSe:Cu, I ceramic, injection electroluminesc. of p-n microjunctions 80−40163
ZnSe:Cu, luminescence and diffusion behaviour of Cu impurities 78−35188
ZnSe:Cu,Al, LV cathodoluminesc. 79−33844
ZnSe:Ga(As), edge luminesc. 80−20699
ZnSe:I, I vapour transport prep., conductive and photolum. cryst. 79−100035
ZnSe:In, Li, binding energy of excitons bound to donor-acceptor pairs, electron-phonon coupling 77−4689
ZnSe:In, single crysts., new vapour phase growth method, elec. cond. props. and photoluminesc. spectra 79−19982
ZnSe:In films, MBE growth, doping effect on photoluminesc. 80−10818
n-ZnSe:Li, semicond. selective pair luminesc., excited impurity state investigation 79−61439
ZnSe:Li diodes, electroluminescence and fabrication, expt. *(Japanese)* 77−28633
ZnSe:Li(Na), shallow acceptor excited states, luminescence spectra, Rydberg energy 79−78750
ZnSe:Li(Na)(Ga) doped and pure cryst., donor-acceptor bands 80−11465
ZnSe:Mn thin film, AC electrolum. 79−47519
ZnSe:Mn^{2+}, Jahn-Teller effect in fluorescent level 78−52566
ZnSe:Mn-n-GaAs, single cryst. substrate low threshold DC electrolum. 77−63465
ZnSe:Mn(Al)(I), Schottky diode, direct impact excitation of luminescent centres 79−7900
ZnSe:N, ion implanted cond. type conversion on annealing *(Korean)* 78−18668
ZnSe:Na, characterisation of edge emission 78−27312
ZnSe:Ni, evidence for exciton binding at Ni impurity sites, photolum. excitation spectrum 80−45135
ZnSe:Ni, photolum. excitation spectroscopy 80−80841
ZnSe:Pb, luminescence photocond. 79−38634
ZnSe-BiOCl, electroluminesc. heterojunction phys. props. 77−66198
ZnSe-CdTe heterojunction, radiative recomb., electrolum. obs. 77−32445
ZnSe-CdTe(ZnTe) heterojunction, cathodolum. and electrolum. 78−6782
ZnSe-ZnTe heterojunction, prep. and props. 79−95483
$(ZnSe)_x(CdTe)_{1-x}$, low temp. photoluminesc. *(Russian)* 78−43931
ZnSeCu, double comet shaped electroluminesc. 78−52577
$(ZnSe)_{1-x}(GaAs)_x$ solid solns., photoluminescence spectra 80−40159
$ZnSe_{1-x}S_x$, luminescence, polaris. emission 79−38634
$ZnSe_xS_{1-x}$, melt grown, 10K, band edge photoluminesc. 78−84628
ZnSe(Te), photolum. excitation spectra of tightly bound holes, valence band contrib. 80−50658
ZnSe(Te), Raman-luminescence problem, interference analogy and expt. discrimination by polarisation correl. 79−95764
p-$ZnSiAs_2$:Au(Tl)(S), photoluminesc., radiative recombination 77−24883
Zn_2SiO_4:As,Mn, enhanced luminesc. stimulation, 20-320K *(German)* 77−20900
Zn_2SiO_4:Mn, energy storage effect and retrieval 80−100684
Zn_2SiO_4:Mn, phosphoresc. decay into second-order components 77−20907
Zn_2SiO_4:Mn film, electron beam depth-dose functions, cathodoluminesc. 80−2867
Zn_2SiO_4:Mn phosphor, luminesc. saturation under intense vac. UV irrad. 79−56841
Zn_2SiO_4:Mn phosphor, efficiency enhancement by $AlPO_4$ substitution 80−11452
Zn_2SiO_4:Mn^{2+}, quantum yield in candoluminescence process by low energy H^+ ion bombard. 79−65930
$ZnSiP_2$, effect of crystal growth method, on physical props., effect of doping on physical props. *(German)* 79−52094
$ZnSiP_2$ monocryst., impurity induced photoluminescence *(Russian)* 79−4850
$ZnSiP_2$, photocond. and photolum. spectra, optical anisotropy 78−72200
$ZnSiP_2$ Schottky diode, electrolum. under forward and reverse bias conditions 77−63466
p-ZnSnAs, LPE, electronic struct. obs. by laser excited photolum. 80−60654
p-$ZnSnP_2$, photolum. anisotropy, 77K 78−19557

luminescence of inorganic solids continued
$ZnSnP_2$-$ZnSiP_2$, heterocombination simultaneous crystallisation 78−60560
ZnTE, MBE growth, elec. and optical props. 80−75462
ZnTE, relaxation processes in Raman scattering and exciton luminescence under resonant excitation 80−25386
p-ZnTe 79−43028
ZnTe, band parameters from bound exciton, donor-acceptor pair excitation luminescence 78−92111
ZnTe, blende type struct., luminesc. under high excitation 79−19928
ZnTe crystals, polariton effects in luminesc. 80−103988
ZnTe crystals, secondary radiation polarization and relaxation of optical excitation 80−11399
ZnTe, dominant acceptors, annealing and quenching 80−24463
ZnTe, donor acceptance pairs, photoluminesc. excitation spectra *(Japanese)* 78−64409
ZnTe, donor-acceptor-pair excitation spectroscopy 80−25456
p-ZnTe, doped and pure, photoluminesc. and photocond. spectra 77−55826
ZnTe, edge luminesc. excited by electron bombard. 80−66308
ZnTe, elec., SEM and TEM studies of impurity segregation during long annealing 80−30001
ZnTe, electro- and cathodoluminesc., impurity segregation 79−43042
ZnTe, electron-phonon coupling, donor-acceptor pairs selective excitation 80−11475
ZnTe, excited acceptor, donor states, luminesc. 78−72604
ZnTe, exciton localisation at impurity pairs 79−37999
ZnTe, excitonic complexes, stress splitting of luminesc. lines 77−4672
ZnTe, extrinsic luminesc., bands, temp. injection level, and freq. depend. 80−20714
ZnTe, free-exciton emission band under high-intensity photoexcitation 79−73993
ZnTe, high purity acceptor bound and free exciton states 79−99941
ZnTe, high quality p-type cryst., predominant acceptors 78−60504
ZnTe, I_4 bound exciton, magneto-optical meas. 77−20836
ZnTe, ion implantation defect introduction, cathodolum. studies 80−75250
ZnTe, irradiation induced radiative centers obs. 80−66290
ZnTe, luminescence spectra struct. surface and volume polaritons *(Russian)* 80−16089
ZnTe, magneto-optical effect, I_2 bound exciton 77−12432
ZnTe, optical identification of substitutional acceptors by low temp. photoluminescence 79−99940
ZnTe, photoluminesc., donor and acceptor excited states 79−38622
ZnTe, pure and P(As) doped, shallow-acceptor, donor, free-exciton, and bound-exciton states 80−60667
ZnTe, radiative recombination involving free particle scatt. 79−38648
ZnTe, Raman scatt. and exciton luminesc. under reson. excitation 79−38617
ZnTe, real structure effect on luminescence and absorption spectra, dislocations 80−16085
ZnTe, refined, undoped, Cu acceptor, optical absorption and photoluminesc. meas. 80−34970
ZnTe, relax. processes at high excitation levels, Bose-Einstein condensation of excitons 78−48219
ZnTe, relax. times of secondary radiations, circular polarisation correlation 79−28816
ZnTe, relaxation processes, emission spectra *(Russian)* 78−72598
ZnTe, reson. secondary radiation 79−99886
ZnTe, SEM and luminesc. study of Li segregation 79−38657
ZnTe, secondary emission, transient behaviour under band-to-band excitation 80−108266
ZnTe, single cryst., electron-hole drop conc. *(Russian)* 79−11460
ZnTe, temp. depend. of Raman scatt. and exciton luminesc. spectra 78−39586
ZnTe, unalloyed, mechanism of radiative transitions 80−50405
ZnTe:Ag, real structure effect on luminescence and absorption spectra, dislocations 80−16085
ZnTe:Al,Cl, photolum., complex acceptor, ionization energy 80−20693
ZnTe:As(Li), donor-acceptor pair excitation and recomb., photoluminesc. obs. 80−20691
ZnTe:As(P)(Li), binding energy of shallow acceptors from photoluminesc. excitation spectra for donor-acceptor pairs 79−95809
ZnTe:Au, impurity identification and characterisation, capacitance, luminescence and IR absorption 80−60639
ZnTe:Cu, doping behaviour, SEM in cathodoluminesc. and photoluminesc. exam. 79−65927
ZnTe:Cu, elec. and optical identification of persistent acceptor 79−60764
ZnTe:Li, diffusion investigation by SEM and TEM 80−10706
ZnTe:Li, impurity segregation during short annealing and quenching, SEM, TEM and elec. meas. 80−10676
ZnTe:Li, Zeeman splitting of ground and excited acceptor states, selective pair luminesc. 80−84780
ZnTe:Li(Cl)(Al)(In), ion implanted and annealed, photoluminesc. meas. 78−15208
ZnTe:O, Ne or Al implantation, electronic and optical parameters of O-related centre 78−6399
ZnTe:O,Zn, dual ion implantation, luminesc. spectra obs. 78−87697
ZnTe:P, excitations spectra of donor-acceptor pair photoluminesc. 78−23522
ZnTe:P, pure and doped, electron and exciton excited states of neutral donor 80−34393
p-ZnTe:P, semicond. selective pair luminesc., excited impurity state investigation 79−61439
ZnTe:P(As), ion implanted, cathodoluminescence emission spectrum 80−108281
ZnTe:P(Li), luminesc. transitions, quantum efficiency 79−1783
ZnTe-CdS(Se)(S_xSe_{1-x}) heterojunctions, prep. and electrolum. charact. 77−24610
ZnTe-CdSe heterojunction, radiative recomb., electrolum. obs. 77−32445
ZnTe-ZnSe(CdSe), LPE growth, elec., photoelec. and luminesc. meas. 77−4745
ZnTe(:In), single cryst. film, MBE, quality obs. using photoluminesc. 77−77419
ZnTe(Se), optical circular polarisation correl. in secondary radiation, resonant light excitation 77−69885
$Zn_3(VO_4)_2$, luminesc. spectra in visible region, vanadate group 78−43921
$ZnWO_4$, luminesc. and capture centres *(Russian)* 78−52543
$ZnWO_4$, scintillation charact. 80−66256

luminescence of inorganic solids continued
$ZnWO_4$:Ni^{2+}, luminescence rel. to Ni concn. 79−24352
Zr, photon emission due to Ar^+ ion bombard., adsorbed and recoil-implanted O effect 80−80872
Zr, photon emission from inert gas-surface impact 78−11059
ZrF_4:Eu^{3+} glass, luminesc. of Eu^{3+}, transition probabilities 80−80845
ZrF_4-BaF_2-NdF_3 glass, vitreous domain, prep. and optical props. 78−27304
ZrO_2, stabilized, thermal barrier coating system, spectral emission and absorpt., 300 to 1590K 79−24672
ZrO_2 TLD using stabilised single cryst., for high gamma doses 77−56476
ZrO_2, thermolum., UV and γ-ray effects 78−2930
ZrO_2, thermoluminesc., in H_2O vap. atm., temp. depend., time decay *(Russian)* 77−44074
ZrO_2, Y_2O_3-stabilised, X-irrad., thermoluminesc. 77−48259
ZrO_2-Y_2O_3:M^{3+}, M=transition metal, X-ray luminesc. 77−44063
$ZrS:O_4$, X-irradiated, trapping and emission centres, thermolum. meas. 80−89076
ZrS_3, photolum. from excitons 80−66274
$ZrSiO_4$, X-irrad., trapping and emission centres, OH^- ion contribution 80−80876
$ZrSiO_4$, zircon, (sand), thermolum., UV and γ-ray effects 78−2930
$ZrSiO_4$, zircon, thermoluminesc. glow curve and spectrum 79−33847
$Zr(SiO_4)_{1-x}(OH)_{4x}$, synthetic hydroxyled zircon, influence of OH^- on thermoluminescent emission *(French)* 78−6795

luminescence of liquids and solutions
acetophenone, highly purified, luminesc. props. 80−32764
3- and 4-acetylamino-N-methylphthalimide, in alcoholic solns., phosphoresc. decay laws 78−17709
2-acetylanthracene, soln., excitation spectra rel. to recording wave length *(Russian)* 77−12438
2-acetylanthracene solutions, excitation spectra rel. to absorption spectra, 77-300K 79−85970
acetylenic hydrocarbons, cyclohexane soln., structureless fluoresc. 80−5575
achiral molecules dissolved in cholesteric liq. crysts., fluoresc. circular polarisation *(German)* 77−42350
acridene yellow, glycerol soln., luminesc. intensity and polaris., temp. and viscosity effects 79−56833
acridine, dye solns., luminesc. spectra, conc. depend. effects 79−54885
acridine, methanol soln., edge excitation red shift, excited state proton association 79−18228
acridine orange, solvent effect on fluoresc. polaris. 79−41191
acridine orange in ethanol, soln., excited single state lifetimes, aggregates, visible luminesc. spectra, conc. depend. 80−55172
acriflavine, fluoresc. polaris., solvent effect 77−50468
acriflavine solution, fluoresc. polarisation, effect of aggregation of molecules 79−91485
aequorin, Ca^{2+}-induced luminesc., inhibition by anaesthetics 78−76985
aequorin, light emission rel. to Ca^{2+} conc., Ca-independ. component 77−48750
aequorin luminescence during activation of single isolated smooth muscle cells 79−88064
albumin, human serum, assoc. solns., excited state deactivation, flash photolysis obs. 79−54895
albumin, human serum, interaction with luminol. chemilum. and fluoresc. 77−21471
albumin, human serum, kinetics of eosin-sensitised photochemilum. of solns. 78−68991
albumin-unsaturated fatty acid binding kinetics, fluoresc. anal., rel. to struct. lability of biomembranes 78−15755
alcohol solutions, fluoresc. damping curves in reson. quenching by one-photon counting method 78−10978
alcohol-H_2O solutions, structure, luminesc. probe obs. 78−84636
alkali halide=O_2^- soln., phonon wings in luminescence spectra *(Ukrainian)* 79−52001
alkali halide aq. solns. with O^{2-} anion impurities, luminescence spectra regularities *(Russian)* 77−69876
alkali halides, aq. solns. with extrinsic O_2^- ions, spectral props. *(Russian)* 78−6766
alkali halides, gamma and additively coloured, dissolving in pure water, lyoluminesc. mechanism 80−100693
alkali metal cation pairs, lumiensc. with dichromate anion 80−83409
amino acids, technique for study of radiation in induced free radicals using lyoluminesc. 77−29230
4-amino-4′-nitrostilbene, thermal motion of prolate luminescent molecules in solvents with different viscosities 79−83029
6-amino-7-hydroxy-4-methylcoumarin solutions, additions effect on fluoresc. 80−2833
2-amino-7-nitrofluorene, in binary solvent soln., time-resolved fluoresc. spectroscopy 79−36680
3-amino-N-methylphthalimide, in polar-nonpolar solvent mixture fluorescence band struct. 78−15213
3,4-amino-N-methylphthalimide, intermolecular orientational relax. 'upwards', fluorescence spectra displacement *(Russian)* 79−78748
4-amino-N-methylphthalimide, reversible induced absorpt. spectra in binary solvents 79−98117
4-amino-N-methylphthalimide-decalin-n-propanol, translational relax. kinetics, luminesc. obs. 79−8180
aminobenzoic acid, aqueous and dioxane solns. with nonfluoresc. impurity, fluoresc. and pH *(Russian)* 77−83635
4-aminomethylphthalimide-decalin-n-propanol, electronic spectra of 3-component solns., temp. depend. 79−4822
4-aminophthalimide, soln. in n-propanol, fluoresc., orient. relax. of solvent 79−24357
4-aminophthalimide soln., fluoresc. nanosec. kinetics, dielec. relax. 79−78737
3-aminophthalimide-ethanol soln., luminesc. quantum yield, photoacoustic method 77−86335
2-aminopurine, in viscous soln., fluoresc. quenching, emission, intensity and reson. transfer *(German)* 80−91599
2-aminopurine, triplet state, elec. dipole moments 79−22742
5-aminopyrimidine, triplet state, elec. dipole moments 79−22742
aminoquinoline derivatives, solvent effect on absorpt. and fluoresc. spectra 79−59494
t-amyl alcohol+m-aminoacetophenone, in soln., fluoresc. and absorpt. spectra, excimer form. 78−78737
8-anilinenaphthalene-1-sulphonic acid, edge excitation red shift, temp. depend. 77−6849

luminescence of liquids and solutions continued
8-anilino-1-naphthalenesulfonic acid, fluoresc. probe mol. in mixed solvent 79−45746
anthracene, aromatic solvents, two-photon absorption cross section meas. by energy migration 77−58204
anthracene, excimer fluoresc. lifetime and quantum yield in soln. 77−6834
anthracene, excimer form. in soln. and cryst., fluoresc. study 79−45759
anthracene, fluorescence spectra in aq. and surfactant solns. 77−83639
anthracene, in acethylcellulose, fluorescence, time dependent emission anisotropy *(German)* 78−94279
anthracene, in cyclohexane soln., triplet state decay consts. by sampling flash apparatus 79−51998
anthracene derivatives in soln., fluoresc. and laser parameters 79−27251
anthracene-2-methyltetrahydrofuran, glassy solution, site-selective impurity phonon coupling 77−81142
anthracene-N,N-diethylaniline exciplex, intersystem crossing 77−30905
anthracene/trans, trans-2,4-hexadiene-exciplex, fluoresc. rel. to photodimerization 77−3401
anthracenes, in soln., triplet-triplet fluoresc. 79−59501
anthracenophanes, fluoresc. and photoisomerisation 79−33781
anthraquinone in pentane solvent, sublevel phosphorescence spectra, molecular distortion 80−74190
9-anthroic acid, excimer-type transition polaris. 79−50062
apomyoglobin-arylaminonapththalenesulfonate system, fluorescent behaviour 79−39359
aqueous soln., ion luminesc. quenching by electron transfer 78−76511
aqueous solution fluorescence spectra, refr. correction 78−93766
arene, photophysics, functionalised micellar assembly, phosphoresc. and triplet Ag^+ enhancement 78−95598
aromatic compounds, subpicosecond states, fluoresc. spectroscopy in liquids 79−45758
aromatic esters, in ethanol, luminescence spectra, phosphoresence and fluorescence 79−54899
aromatic hydrocarbon, quenched with Ag^+ in ethanol, triplet state form. 79−11801
aromatic hydrocarbon acceptor, energy-deficient, and tetrathiafulvalene donor systems, electrogenerated chemiluminesc. 79−20372
aromatic hydrocarbon in soln., excited electronic state vibr. relax., time resolved fluoresc. 80−48024
aromatic hydrocarbon-dicyanobenzene, aq. micellar soln., fluoresc. quenching mechanism 79−50063
aromatic hydrocarbon-N,N-dimethylaniline, aq. micellar soln., fluoresc. quenching mechanism 79−50063
aromatic hydrocarbons, aqueous micellar soln., triplet state room temp. phosphoresc., hydrophillic quenchers 78−9181
aromatic hydrocarbons, ethanol-KI solns., fluoresc. affected by I^- 79−13749
aromatic hydrocarbons, excimer decay dynamics, rate const. rel. to solvent 78−58729
aromatic hydrocarbons in soln., low quantum-yield mol. fluoresc. 77−58063
aromatic hydrocarbons in soln., mag. field effects on delayed fluoresc., perturbation theory applic. 77−30913
aromatic molecule, electronic excitation energy degradation, electronic-vibr. spectrum 77−488
aromatic-molecules, conformeric fluoresc. and phosphoresc., rotation of chromophoric fragments around single chemical bonds 77−68068
Na^+,K^+-ATPase preparations, tryptophan fluoresc. 77−21477
auramine O, fluoresc. efficiency, solvent viscosity effects at high press. 78−9188
2-azaanthracene in heptane, benzene and ethanol, max. intensity of fluoresc. on axis of cylindrical cell *(Russian)* 77−55814
azulene, soln., laser-excited $S_2 \rightarrow S_1$, $S_1 \rightarrow S_0$ emission and $S_2 \rightarrow S_n$ absorption 79−10131
azulene in cyclohexane, relax. time of first excited electronic singlet state 77−6825
BBOA, polymorphism, radiothermoluminescence and differential scanning calorimetric study 80−24570
1,2-benzanthracene, monomer and excimer fluoresc. in soln., triplet-triplet annihilation and mag. field depend. 78−78738
1,2-benzanthracene, secondary reson. radiation and hot energy transfer, soln. luminesc. 80−87167
1,2-benzanthracene in soln., luminesc. and vibr. relax. 79−52007
benzene, fluoresc. quantum yield in soln., dipole-dipole interaction 78−25598
benzene, soln., fluoresc., quenching in pulsed proton and alpha particle irrad., radiation quality effects 80−66259
benzene in dilute cyclohexane solution, fluoresc. quenching on pulsed proton irrad., temp. depend. 80−21307
benzil triplet-anisole, reversible exciplex form., phosphorescence, photostationary and transient obs., simulation 78−9182
benzophenone-Eu complex, triplet-triplet energy transfer, viscosity and temp. depend. 79−87847
Benzophenones, substituted solvent independence of radiative rate constant 77−30904
3,4-benzpyrene, monomer and excimer fluoresc. in soln., triplet-triplet annihilation and mag. field depend. 78−78738
biacetyl, aq. solns., fluoresc., phosphoresc. 77−3395
bilirubin, anomalous solvent shift effect and phosphoresc. 77−30899
bilirubin, soln. luminesc. 79−31572
biphenyl, carbonyl derivatives, absorpt. and luminesc. spectra, solvent effects and triplet lifetimes 77−24889
9-bromoanthracene, fluoresc. and phosphoresc. spectra 77−14480
Bronian rotational motion-effect on anisotropic props. of absorpt. and luminesc. from excited states 79−93978
bulk solution temperature effect on sonoluminescence intensity 80−76090
carbazole, in presence of KI, decay functions of triplet state of fluoresc. and phosphoresc. 78−66590
2-carbethoxy-5-chloro-7-aminoindole, soln., liq. scintillator, UV excitation, energy transfer and quenching 78−64395
carbohydrate solutions, irradiated, lyoluminesc. and carbohydrate peroxy radical reactions 77−48665
carbon tetrachloride, liq., luminesc. on giant ps. pulse irrad., spectral and time characts. *(French)* 78−88348
carbon tetrachloride-$GaCl_3$-Nd^{3+} nontoxic liquid phosphor system, synthesis 80−55157
cetyltrimethylammonium bromide and chloride aqueous micelle, fluoresc. showing coexistence of rod-like and globular struct. 79−61910

luminescence of liquids and solutions continued
chemiluminescence, step expts., analytical treatment of diffusion and electron transfer 78−27763
chemiluminescence in soln., energy transfer 79−11479
chlorophyll, fluoresc. decay time depend. on luminesc. and excitation wavelengths 79−66447
chlorophyll, transfer of electronic excitation energy from monomer to dimer *(Russian)* 78−27289
chlorophyll a, fluoresc. decay rate obs., inhomogeneous struct. and relax. time effects 79−86007
chlorophyll a, phosphoresc., triplet state, photochem. reacts. *(Czech)* 78−78842
chlorophyll a and b, assoc. solns., excited state deactivation, flash photolysis obs. 79−54895
chlorophyll fluorescence quenching by β-carotene 77−52735
chlorophyll mixed associates, intermol. interaction, energy transfer, luminesc. and absorpt. spectra 78−64924
chlorophyll pigments, aggregated forms in soln., spectral-luminesc. characts. *(Russian)* 78−23529
chlorophyll solutions, photolum. of singlet O_2 78−80831
chlorophyll-a, soln., luminesc. spectrum, impurity bands *(Russian)* 77−88493
chlorophyll-a, spectral props. of liquid crystal solutions 78−27291
chlorophylls, luminesc. analysis of triplet states *(Russian)* 78−27288
chloroquinolines, photophys. behaviour, substituent and solvent effects 80−106342
chromone, solns., pH dependent fluorescence spectra, pK_a and tautomerism 79−59506
chromophore emission spectra, exciting wavelength depend., hydroxylated solvent reorientation 78−76514
complex molecules, solns., stimulated emission by simultaneous 2-freq. excitation *(Russian)* 78−13701
conference, Szeged, Hungary (Aug. 1976) 78−27279
coronene, in ethanol soln., external heavy atom effect on triplet state, phosphorescence meas. 79−18231
coumarin, aqueous solution, fast neutron irrad., dosimetry appl. 78−44613
coumarin 1, multiphoton cross-section determination by means of luminescence experiments 80−93377
coumarin 6-diethylamine, fluoresc. induced by laser, vibr. relax. 79−26984
coumarin deriv. solns., mol. struct. effects on luminesc. and lasing characts. *(Russian)* 77−83873
coumarin laser dyes, in methanol, ethanol, and water, fluoresc. lifetimes meas. 79−27252
cresyl violet, luminesc. quantum yield standard for red, calorimetric obs. 80−190
cresyl violet, rot. diffusion, picosec. saturation spectrosc. obs. 80−5634
cryptocyanine, soln., $S_2 \rightarrow S_0$ fluoresc. 78−13541
cryptocyanine, solns., fluoresc. lifetime, viscosity depend. 79−59497
cryptopleurine derivatives, absorpt. and fluoresc. obs. of photodecomp. processes, dye laser relevance 80−55686
crystal violet, fluoresc. efficiency, solvent viscosity effects at high press. 78−9188
crystal violet, soln., picosec. relax., wavelength depend. 79−99921
cyanine dye sensitisers, J-aggregate formation, spectral changes of UV bands 77−70318
cyanine dye sensitisers, J-aggregates, meso substituents effect on mol. assoc. 77−70320
cyanine dyes, solns., excited states, duration meas. 77−65503
4-cyanobiphenyl and 4′-alkyl- or 4′-alkoxy-substituted liq. cryst. derivatives, soln., absorpt. and fluoresc. spectra 80−87164
cytidine monophosphate, aq. soln., spectra, 300-450 nm, polarisation study 78−96015
cytidylyl-3′,5′-cytidine, aq. soln., spectra, 300-450 nm, polarisation study 78−96015
3,6-diacetylamino-N-methylphthalimide, in alcoholic solns., phosphoresc. decay laws 78−17709
dialkylanilines, p-substituted, twisted internal charge transfer excited state form. 79−22683
diarylalkane, in isooctane soln. triplet excimer form., phosphoresc., delayed fluoresc., triplet-triplet absorption 78−25597
diarylethylene, luminesc. spectra and rot. isomerism 79−85991
3,4,9,10-dibenzpyrene, hexane soln., UV fluoresc. line-narrowing two-photon site selective excitation 77−88484
9,10-dibromoanthracene, fluoresc. and phosphoresc. spectra 77−14480
dicarbonitrile-anthracene solutions, absorpt. and emission spectra, solvent influence 80−43083
dichloromethylene, radical, emission and excitation spectra, in Ar matrix 77−34657
dicyanoanthryl-naphthyl, intramol. exciplex, fluoresc. quenching by pyridine (γ-picoline), triple exciplex form. 79−50061
1,1-diethyl-2,2′-dicarbocyanine iodide, solns., fluoresc. lifetime, viscosity depend. 79−59497
diethylamine, liq., Raman scatt. following optical excitation, vibr. relax. 79−26984
dimesitylboranes, phenyl substituted, absorption and emission 78−27311
dimethyl POPOP, multiphoton cross-section determination by means of luminescence experiments 80−93377
3,8-dimethyl-2-azaanthracene in heptane, benzene and ethanol, max. intensity of fluoresc. on axis of cylindrical cell *(Russian)* 77−55814
4-dimethyl-amino-4′-nitrostilbene, in EBBA, nematic ordering influence on fluoresc., temp. depend. *(German)* 79−81235
4-dimethylamino-4′-nitrostilbene, thermal motion of prolate luminescent molecules in solvents with different viscosities 79−83029
4-dimethylamino-4′-nitrostilbene in solvent fluorescence lifetime meas. by picosecond optical amplification 79−81227
p-dimethylaminoacetophenone, ps reversible isomerisation kinetics, O_2 quenching obs. 79−5133
9,10-dimethylanthracene, conc. solns., fluoresc. quenching by anthracene and derivatives 78−17711
1,5-dimethylnaphthalene, fluoresc. quenching by cyclic azoalkanes, micelle system probe 80−35578
2,6,dimethylpyrazine, PMMA soln., fluoresc. and phosphoresc. quantum yield and lifetime, 20-120 kbar 79−54902
1,4-bis(2,5-dimethylstyryl)benzene, lasing charact. on UV N_2 laser excitation 80−32979
dimethylsulphoxide, $Eu^{3+} \rightarrow Pr^{3+}$ and $Eu^{3+} \rightarrow Er^{3+}$ non-radiative energy transfer 79−47510
dinaphthylalkanes, triplet-triplet annihilation of excimers in soln. 78−86904

luminescence of liquids and solutions continued
dioxane solutions, radioluminescence quenching in mixtures of solvents *(Russian)* 80−55192
9,10-diphenyl anthracene, cyclohexane soln., solute excited state form. kinetics in pulse radiolysis 79−79263
diphenyl styryl pyrazoline-active electrolyte system, electrochemiluminesc. spectral shift 77−20929
9,10-diphenylanthracene, luminesc. quantum yield, fluoresc. spectra polarisation effect, solvent viscosity depend. 78−27303
1,6-diphenylhexatriene soln., light quenching effect on fluoresc. band shape 79−98148
2,5-diphenyloxazole, phosphoresc., 77K, solvent effect 78−42118
diquinolyl cyanomethane, fluoresc. quantum yields, viscosity effects 80−60646
dissolution of solids, installation for luminescence meas. *(Russian)* 79−93202
DMSO:Cr^{3+}, Nd^{3+}, energy transfer and migration, donor-acceptor interaction, phosphoresc. quenching conc. depend. 78−64403
DNA bases, thymine type, polarised fluoresc. in neutral aq. soln. 80−21445
DNA in soln., mol. wt. determ. by fluctuation spectroscopy 77−10800
donor excimers, effect on resonant energy transfer *(Russian)* 78−76530
dye molecule, excited, thermal rotations and relaxation of vibr. energy 79−81231
dye molecules, dissolved, influence of environment on luminesc., intense laser excitation 78−84622
dye molecules, long wavelength conc. shift in luminesc. 79−64032
dye soln., fluoresc. amplitude anisotropy, polarised light excited 79−85990
dye solns., two-component, before-relax. energy transfer and absorpt. spectra overlap 78−27285
dye solution, fluoresc. yield, photoacoustic determ. method 78−42117
dye solution, luminesc. quenching, pulsed photoacoustic detection technique 77−85780
dye solution, mol. fluctuation distrib. function 79−36692
dye solution, nonlinear fluoresc. meas., two-photon pumping by low power laser 80−48037
dye solutions, dil., fluoresc. decay time determ. 78−68540
dye solutions, light-induced quenching of spontaneous and stimulated emission *(Russian)* 78−27290
dye solutions, liq. scintillation counting, rel. to colour quenching ability 79−1790
dye solutions, mixed, energy transfer and conc. depolarisation of fluoresc. 78−25583
dye solutions, mixed, fluoresc. conc. quenching, sensibilisation 79−24347
dye solutions, picosecond flash photolysis and very fast processes 80−30249
dyes, fast mode-locking, IR fluoresc. and laser action obs. 80−102717
dyes, fluoresc. conc. depolarisation, during intense excitation *(Russian)* 77−65507
dyes, S_2-S_0 luminesc. for picosec. excitation 79−87506
dyes, substituted methane, press. effs. on viscosity-depend. fluoresc. 77−34672
EBBA, nematic, ordering parameter temp. depend. 79−23517
EBBA, polymorphism, radiothermoluminescence and differential scanning calorimetric study 80−24570
EHD sonoluminescence, visible, due to collapse of cavity in liquid 80−45158
electrochemiluminescence reactions, background electrolyte effects *(Russian)* 78−7209
electrochemiluminescent organic dyes and new type of laser 77−678
energy transfer, between ions in solutions under conditions of n-pair formation 79−4843
eosin, fluoresc. polarisation, solvent effects 79−36678
eosin, in glycerine-water mixture, excitation and emission peaks, concentration shifts 78−33540
eosine^{2-}, in dimethylsulphoxide, transition metal ionic associations, fluoresc. quenching 77−73163
erythrosin, aq. soln., polarisation of fluoresc. spectra, aggregation of mols. 78−31227
ethylbenzocarbazole, soln., luminesc., effect of electronic excitation energy vibr. 80−55174
ethylene, dye laser probing of C_2 radicals, IR intense field photolysis 77−16851
europium B-diketone chelate solns., fluoresc. quenching by appl. voltage, display devices appl. 79−87497
excitation energy transfer in multi-component luminescent solutions 78−84621
filter, luminescent, efficiency for Nd:glass lasers 80−1213
flavin aqueous solns., fluorescence quenching by iodide ions, temp. and viscosity effects 77−34673
fluid, radio band pulse radiation due to spark initiated cavity dynamics, sonoluminescence *(Russian)* 80−66313
fluorene, in ethanol soln., external heavy atom effect on triplet state, phosphorescence meas. 79−18231
fluorescein, fluoresc. quenching by rose bengal 79−78726
fluorescence energy transfer in the rapid-diffusion limit 79−92151
fluorescence polarisation meas. at high press. 78−66576
fluorescence quantum yield measurements, real, observed and mol. parameters, ref. soln. standards 78−32898
fluorescence solvatochromism kinetics 77−30898
fluorescent dye medium, short laser pulse superposition, numerical anal. 79−31891
fluorescent intensity analysis, absorption and self-absorption quenching effects 77−37693
fluorescent solutions, quantum yields, optoacoustic determ. 77−12415
fluorocarbon liquid prebreakdown light emission obs. 80−15963
Forster kinetics breakdown, low-viscosity liq., time-depend. rate const. 79−86033
glycerine solutions, fluoresc. damping curves in reson. quenching by one-photon counting method 78−10978
glycerol-D_2O:Tb^{3+}, Nd^{3+} soln. and frozen glass, energy transfer 78−60509
hexamethyl indatricarbocyanine iodide-ethanol soln., luminesc. quantum yield, photoacoustic method 77−86335
hexamethylbenzene charge-transfer complexes, heavy atom effect on radiative and radiationless transitions 78−25607
hydrodynamic electrochemiluminescence cell 80−45506
7-hydroxy-2-methylchromone, solns., pH dependent fluorescence spectra, pK_a and tautomerism 79−59506
7-hydroxycoumarin, absorpt. and emission spectra, ionic forms 78−21955

luminescence of liquids and solutions continued
7-hydroxylepidone, solns., multiple fluoresc. emission 78−33547
indigo derivatives, fluorescence decay times, meas. by synchroscan streak camera 80−84759
indocyanine green fluoresc. spectrum in blood and other solvents, rel. to angiography 78−28057
indole, aq. alkaline soln., charge transfer, luminesc. obs., 77 and 300K 79−69876
indole soln. containing histidine, fluoresc. rel. to soln. pH 80−2826
inner filter effects in front face and total refl. fluoresc. 78−88357
intermolecular relaxation effect on soln. luminesc. spectra under powerful excitation 79−85985
intermolecular relaxation spectroscopy 79−95844
9-iodoanthracene, picosecond fluoresc. lifetimes, thermally activated $S_1 \rightarrow T_n$ intersystem crossing 80−28045
4-isocyanate-trans-stilbenes, donor substituted, anisotropic fluoresc. in low viscosity solvents *(German)* 80−93401
2-isopropoxyphenyl-N-methyl carbamate, fluoresc. and phospheresc. in solns. 79−61426
isotropic rigid solutions, polarisation of fluorescence 78−31228
isotropic solutions, fluorescence emission anisotropy, time depend. 80−7391
ketocyanines alcohol solns., spectral-luminesc. props. 80−2835
ketyl radical+benzophenone, triplet-doublet energy transfer, viscosity and mag. field effects 77−71850
lanthanides complexes with L-histidine, intermolecular energy transfer, influence of metal-to-ligand ratio 80−32763
lanthanides in molten $LiNO_3$-KNO_3, transition probabilities in absorpt. and fluoresc. spectra 79−50085
laser dyes, fluoresc. efficiency and standards 78−35205
lepidopterene exciplex, luminesc. intramolecular anthracene-ethylene exciplex, mol. geometry-fluoresc. relationship 78−58728
lifetime measurement, using CW laser beat noise as multifreq. modulated source 77−57406
light quenching of mol. fluoresc. spectrum, spectral distrib. of polarisation 79−85989
lipid systems, anti-oxidant action mechanism determ. by chemiluminesc. 77−56330
liq. scintillator, UV excitation, energy transfer and quenching 78−64395
liquid, electron-hole interactions and double proton transfer, picosec. laser obs. 79−45773
liquid crystal, uniaxial, polarised fluoresc. emission, orientational distrib. function, rot. Brownian motion 78−80390
liquid crystals, static and dynamic props., time depend. fluoresc. depolarisation obs. 80−29786
lubricant film thickness meas. using laser based fluorescence technique 79−49201
lyoluminescence meas. by photon counting system 79−97441
macromolecules, thermal rotations of mols. in soln. mol. wt. depend. 79−13847
macromolecules in dilute soln., electrically induced fluorescence polarised component change meas. 80−32863
malachite green, luminesc. decay kinetics on ps time scale 79−19916
malachite green+rhodamine 6G, in low viscosity solvent, ps time resolved energy transfer 78−70910
mannose lyoluminescence dosimetry in photon and fast neutron beams 78−15902
MBBA, nematic, ordering parameter temp. depend. 79−23517
MBBA, uniaxial, orientational order, polarised fluoresc. meas. 79−55655
mercurochrom, fluoresc. polarisation, solvent effects 77−14470
metal chloride aqueous solns. with NO_2^- impurities, luminesc., absorpt. and Raman spectra *(Russian)* 77−36291
N-methacryloil-ω-aminolauric acid cholesterol ester, liq. cryst. polymers, copolymers, structuring *(Russian)* 79−55665
methine dyes, spectral props., solvent effects 80−69181
9-methylanthracene, solubilisation in water by hypercoiled polymethacrylic acid 80−91591
2-methylchromone, solns., pH dependent fluorescence spectra, pK_a and tautomerism 79−59506
1-methylindole-n-butanol (ethyl acetate), soln., ground state complex form., fluoresc. spectra, Stoke's shift origin 80−58299
N-methylphthalimide in ethanol soln., gain and induced absorpt., struct. props. 77−24890
1-methylpyrene, fluoresc. quenching by Cu^{2+} in micellar system, general kinetic model 80−32753
micellar dye soln., energy transfer 80−45581
micellar solutions, fluoresc. quenching rel. to aggregation numbers 79−34364
micellar system, naphthalene as fluoresc. probe 78−95599
micelle forming detergent solutions, fluoresc. quenching by O_2, dynamic parameters and solubility charact. 79−83513
micelle-confined molecules reaction, diffusion-controlled, luminesc. quenching, excimer form. 80−50890
migration mechanism of approaching particles, energy transfer, luminesc. quenching study 80−100343
molecular pair, fluoresc. depolarisation, using stochastic Liouville eqn. with radiative terms 80−16074
molecular radiative rate consts., solvent depend. 78−66587
di-molybdenum cyclopentadienyl tri-carbonyl, dual luminesc., ps pulse excitation 80−32754
3-monomethylamino-N-methylphthalimide solns., fluoresc. and excitation spectra 79−61425
multicomponent luminescent system, nonradiative transfer of electronic excitation energy 79−28804
multicomponent solutions, solvatofluorochromism kinetics, orientation-concentrational relax. 77−65506
naphthalene, fluoresc. and phosphoresc., singlet/triplet excimers conform. difference 77−14469
naphthalene ($-d_8$), gamma irradiated soln., fluoresc. mag. field depend., spin correls. 77−44492
naphthalimide derivatives, solutions, lasing charact. in green spectral region, photostability 80−32978
1,8-naphthoilene-1′,2′-benzimidazole-phenylimide of 4-aminonaphthalic acid luminophor mixture *(Russian)* 79−47514
1-naphthyl methacrylate-9-vinylanthracene copolymer, time-resolved fluoresc. spectra 78−80401
1-naphthylamine, anisotropic rot., red edge transition moment, fluoresc. 77−10699
β-naphthylamine, soln., fluoresc., photochem. quenching, excitation wavelength depend. 77−50470

luminescence of liquids and solutions continued
β-naphthylamine-cyclohexane soln., luminesc. quantum yield, photoacoustic method 77−86335
nematic liq. cryst. with luminesc. impurity, luminesc. and absorpt., order parameter determ. 79−4240
nematic liquid crystal, Merck 389, polymorphism, radiothermoluminescence and differential scanning calorimetric study 80−24570
nonlinear luminesc. quenching kinetics, high excitation power 79−56834
1,3,5,7-octatetraene, UV, visible, and fluoresc. spectra and assignments, evidence for ^1A_g state 78−33518
OEBBA, polarised luminesc. 77−24897
organic compounds, electrochemiluminesc. excitation via generator producing bipolar voltage pulses 77−28629
organic compounds as active media in lasers *(Russian)* 80−38015
organic laser dyes, electrochemiluminescence, electrochem. oxidation, reduction 77−70304
organic liquid scintillator, γ-irrad., energy transfer and quenching 77−8622
organic matter dissolved in seawater, fluoresc. spectra *(Russian)* 77−13083
organic molecules in solution, electronic energy level shift estimation 79−54919
oxypyrenetrisulphonate anion, aq. soln., ps time depend. fluoresc. depolaris. obs. rot. diffusion determ. 77−81139
perfluorocarbons, γ-irrad. solns., mag. field effect on fluoresc. 80−55677
perylene, organic soln., picosec. fluoresc. for rot. diffusion 79−56839
perylene in EBBA, nematic ordering influence on fluoresc., temp. depend. *(German)* 79−81235
perylene in paraffin, anisotropic rot. and libration 77−32417
perylene-tetracene, in liq. cryst., temp. depend. of absorption and fluoresc. *(German)* 80−18887
phenyl methacrylate copolymers, photoluminescent behaviour 80−25432
9-phenylanthracene, fluoresc. lifetime and quantum yield in solns. 77−6834
2-phenylindole, in viscous soln., fluoresc. quenching, emission, intensity and reson. transfer *(German)* 80−91599
pheophytin a and b, assoc. solns., excited state deactivation, flash photolysis obs. 79−54895
pheophytin solutions, photolum. of singlet O_2 78−80831
photoluminesc. decay time, donor conc. effect 80−66299
photoluminescence of solutions, decay and self-depolarisation 79−24351
photoluminescence quantum yield of primary light absorbers and nearest neighbours 77−52148
phthalamide derivatives, solutions, excitation spectra rel. to absorption spectra, 77-300K 79−85970
phthalic anhydride and halogen derivatives, phosphorescence spectra *(Japanese)* 78−48217
phthalimide, soln., excitation spectra rel. to recording wave length *(Russian)* 77−12438
phthalimide acetyl derivatives in polar solvents, luminesc. kinetics and phosphoresc. quenching 80−18885
phthalimide derivative-tetramethyldiaminodiphenylmethane exciplexes, luminesc. props. 77−68070
phthalimide derivatives, solns., ultrafast mol. relax. 79−85984
phthalimide derivatives, solutions, lasing characts. in green spectral region, photostability 80−32978
phthalimide P derivatives 79−56836
phthalimide solutions, fluoresc. optical quenching by ruby laser rad. *(Russian)* 77−12437
phthalimides, solns., solvent effects on absorpt. spectra and fluoresc. 77−34650
phthalimides, spectrum luminesc. props., laser generating capacity and generation features *(Russian)* 79−31897
pigment associations, conc. effects, luminesc., absorpt. spectra and dichroism obs. 80−1007
pinacyanol, solns., fluoresc. lifetime, viscosity depend. 79−59497
polarised fluorescence in elec. field, mol. props. deriv. for solns. and suspensions 80−84785
poly-1-naphthyl methacrylate, time-resolved fluoresc. spectra 78−80401
poly-1-vinylnaphthalene solution, time-resolved fluoresc. spectroscopy, excimer form. and dissoc. 79−38637
poly-2,6-dimethylphenyleneoxide, fluoresc. correction in light scatt. meas. 79−1771
poly-N-vinylbenzocarbazole, soln., luminesc., effect of electronic excitation energy vibr. 80−55174
poly-N-vinylcarbazole, soln., picosecond time-resolved fluoresc. by pulse radiolysis 80−28122
polyacrylamide-fluorescein conjugates, fluoresc. polarisation, high press. obs. 80−20683
polyaromatic hydrocarbons, n-alkane solvent effect on low temp. fluorescence spectra 77−36274
cis-polybutadiene and butadiene-styrene copolymer mixture, effect of temp. on phase composition 79−96005
polycyclic aromatic hydrocarbons, alternant and nonalternant, fluoresc. quenching by nitro cpds. *(German)* 78−21967
polyenes, linear, radiative rate consts., environmental effects 79−72348
polymer chains with rigid bonds, local relax. times, mol. dynamics study *(Russian)* 80−59373
polymers containing carbazole units, optically active, fluoresc. props. 78−84647
polymethacrylic acid, dye-tagged, electrically oriented solns., fluoresc. polaris. changes 78−76523
polymethine dye solutions, photochem. transformations and short-wavelength luminesc. 80−100686
polymethine dyes, excited mols., photoisomeric transformations 79−87854
polymethine dyes, mol. struct., lasing props. 79−3693
polyphenyls, fluoresc. and sensitization props. 79−38599
polyribonucleotides, dye tagged, aqueous solns., elec. induced fluoresc. changes 80−85346
polystyrene photophysical behaviour, solvent effect obs. *(Spanish)* 79−57267
polystyrene solution, time-resolved fluoresc. spectroscopy, excimer form. and dissoc. 79−38637
polyvinylbenzocarbazole, weak solution, intramolecular energy transfer by singlet and triplet excitons 80−34971
polyvinylcarbazole, fluoresc., photooxide quenching, exciton migration effects 79−56830
polyvinylcarbazole, weak solutions, intramolecular energy transfer by singlet and triplet excitons 80−34971

luminescence of liquids and solutions continued
porosity and pore size measurement using soln. of luminescent material flowing around sorbent granules 80−53850
porphin ($-d_2,d_4,d_6,d_8,d_{10},d_{12},d_{14}$), nonradiative transition probabilities, deuteration effects 79−3485
porphyrin solns., quenching of excited states by nitro-cpds., donor-acceptor interactions 78−2899
protein: Eu^{3+}, luminesc. spectra and binding centres 78−15754
protein, radical limiting conc. on UV irrad. at 77K, effect of luminesc. quenchers 80−30662
protein chromophores, fluoresc. props., use in macromol. equilib. struct. mobility investigs. 79−64130
protein-lipid model systems, chemiluminesc. on exposure to formalin 77−56329
proteins, fluoresc., equilib. structural mobility *(Russian)* 78−76986
proteins, triplet state energy transfer 78−20143
proteins, UV irradiated, luminesc. quenching, EPR and absorpt. spectra 78−15768
ps reversible isomerisation kinetics, O_2 quenching obs. 79−5133
pyrazine, PMMA soln., fluoresc. and phosphoresc. quantum yield and lifetime, 20-120 kbar 79−54902
pyrene, emission from triplet state in electrochemical at low temps. 77−77307
pyrene, fluorescence spectra in aq. and surfactant solns. 77−83639
pyrene, in cyclohexane soln., triplet state decay consts. by sampling flash apparatus 79−51998
pyrene, monomer and excimer fluoresc. in soln., triplet-triplet annihilation and mag. field depend. 78−78738
pyrene solutions, emission spectra 77−30910
pyrene-3-sodium sulphonate solubilised in didodecyldimethylammonium bromide-benzene inverted micelles 80−3417
pyrene-diethyl aniline in acetonitrile-toluene, triplet exciplex state in pulsed laser photolysis 77−16836
pyronin dye, use as fluorescent indicator of energetic state of mitochondria 77−66790
quenching agents and temp. effects *(Russian)* 78−15227
quenching due to approaching particles transferring energy *(Russian)* 78−43933
quinine bisulphate, aq. soln., abs. fluoresc. quantum efficiency, optoacoustic determ. 78−16849
quinoline, in binary solvents, phosphorescent and fluorescence 80−7409
radiationless energy transfer between ions in solutions 79−10140
radiationless energy transport in ion pairs in assoc. soln. 79−56835
rare earth complexes, formation and props., book contrib. 80−43204
rare earth ions in soln., absorpt. and fluoresc. spectra, book contrib. 80−45112
retinals, prod. and quenching of singlet oxidation 80−35840
rhodamine 101, quenching of emission in methanol and latex particle suspensions 80−3374
rhodamine 4C, in ethanol soln., rot. relax. time using ps. spectroscopy technique 80−1013
rhodamine 6 Zh solution, radiant transport effect on luminesc. duration 80−103995
rhodamine $6G_2$ molecules in solution, photoluminescence study, fluorescence decay time 80−80832
rhodamine 6G, associated, in polyvinyl alcohol film and soln., emission, room temp. 79−54896
rhodamine 6G, blue and UV luminesc., obs. and mechanism 79−3486
rhodamine 6G, delayed fluoresc. of simple associates in polar and nonpolar solvent mixtures *(Russian)* 78−48185
rhodamine 6G, electronic energy transfer from S_2 state to BBOT in soln. 78−88346
rhodamine 6G, fluoresc. polaris. spectra in glycerol soln. 79−76458
rhodamine 6G, fluoresc. polarisation, solvent effects 80−32755
rhodamine 6G, in glycerine-water solns., anti-Stokes fluoresc., conc. quenching 79−24349
rhodamine 6G, in methanol, fluoresc. lifetime meas. 78−29811
rhodamine 6G, in organic solvent, hot luminesc. 79−4842
rhodamine 6G, micellar soln., aq., fluoresc. decay for rot. diffusion const. 79−11826
rhodamine 6G, orientated relax. times, streak camera meas. 80−14168
rhodamine 6G, soln., hot luminesc. and vibr. relax. 79−22752
rhodamine 6G, solns., delayed fluoresc. of simple associates 79−56847
rhodamine 6G aqueous solution, surfactant effect on fluoresc. intensity *(Japanese)* 77−42536
rhodamine 6G associates, spectroscopic evidence of luminesc. *(Russian)* 77−48233
rhodamine 6G ethanol soln., absorpt. and luminesc. spectra using picosecond excitation 80−106351
rhodamine 6G in dimethylsulphoxide, concentrational red shift and luminesc. spectra 80−83426
rhodamine 6G polar solution, conc., temp effect on spectral props. 79−87505
rhodamine 6G soln., delayed annihilation fluoresc., external heavy at. effect 79−99931
rhodamine 6G soln. in ethanol, luminesc. liq., pump radiation conversions to enhance laser efficiency 80−48293
rhodamine 6G solns., picosec. kinetics of emission 79−76685
rhodamine 6G-alcohol, two-photon luminesc. intensity, appl. to picosecond pulse meas. 78−71134
rhodamine B, 6G, spectra of lowest excited singlet states 79−81424
rhodamine B, in glycerine-water mixtures mol. agglomeration effect on fluoresc. polaris. spectrum 78−25595
rhodamine B and 6G, fluoresc. decay time meas. in different solns. 80−9637
rhodamine B in ethylene glycol, fluoresc. decay meas. via modulated gain spectroscopy 80−63699
rhodamine B lactone, dual fluoresc., solvent polarity depend. 77−3394
rhodamine B-ethanol soln., luminesc. quantum yield, photoacoustic method 77−86335
rhodamine C and 6G, strong base solns., electronic spectra, temp. depend. 79−85987
rhodamine dye, intercombination conversion rate consts. from triple quenching by 1,4-diphenylbutadiene 79−956
rhodamine dye solns., amplified spontaneous emission 79−45941
rhodamine dye solutions, additional heavy atom effects on triplet state transitions *(Russian)* 77−85800
rhodamine dye solutions, vibr. relax. in S_1-state 77−6826
rhodamine dyes, phosphoresc. quantum yields determs. 79−8179
rhodamine G solutions, LiCl and $NaClO_4$ electrolyte influence on its lasing props. 80−91788

luminescence of liquids and solutions continued
rhodamine R derivatives, water (heavy water) detergent solns., luminesc., lasing 79−56836
rhodamine solns., anti-Stokes fluorescence 78−27284
rhodamine solns., short-wavelength luminesc. 79−78738
rhodamine solutions, quenching of two-photon fluoresc. and stimulated anti-Stokes emission 79−72619
rhodamine Zh, isomer separation, identification and emission efficiencies *(Russian)* 77−83871
rhodamine-B, fluorescence decay meas. via modulated gain spectroscopy 79−64025
rhodamines, 5G, 6G, B, 3B in ethanol soln., luminesc. quenching by photoirradiation 80−87168
rhodamines in ethanol soln., gain and induced absorpt., struct. props. 77−24890
riboflavin in various solvents, absorpt. spectra, relative quantum yields, electronic transitions 77−52149
ribonuclease T_1 in soln., phosphoresc. at 293K *(Japanese)* 77−44595
rose bengal, excited state orientational relax., in protic and aprotic solvents 78−46383
rose bengale, fluoresc. polaris., solvent dipole moment effect 78−25596
rubrene, electrochemilum. by DC, highly organised EHD convection obs. 80−71499
rubrene, electrogenerated chemilum., production of excited states by direct heterogeneous electron transfer 79−20371
rubrene, soln. in benzonitrite, electrochem. luminesc. 77−77776
rubrene radical cation reduction at n-ZnO electrode, triplet state formation, luminesc. 77−16825
ruthenium trisbipyridyl ions in surfactant solns., excited state decay kinetics 80−83407
saccharides, lyoluminescence dosimetry 77−52881
scintillator systems, liq., organic, energy transfer, fluoresc. intensity-max. solvent depend. 78−21966
Smoluchowski equation, with Coulomb pot., appl. to fluoresc. quenching 78−73051
sodium fluorescein dil. soln., luminesc. absolute quantum yields, thermal blooming method 78−72582
sodium fluorescein-rhodamine B, energy transfer in luminescent mixed solutions 80−103976
sodium lauryl sulphate-3,3'-diethylthiacarbocyanine iodide-rhodamine-6G, soln., premicellar region, energy transfer 80−20685
sodium polystyrene sulphonate, dye-tagged, electrically oriented solns., fluoresc. polaris. changes 78−76523
sodium tetraphenylborate soln., electrolyte, steady state electrochemiluminesc. 79−57250
spatially inhomogeneous gain saturation due to amplified spontaneous emission 77−42534
trans-stilbene, fluoresc. decay, picosecond anal. 79−31569
trans-stilbene, soln., lifetime and anisotropic fluoresc., viscosity effects *(German)* 80−106352
Stokes shift, rel. to stat. broadening of electronic bands of solns. 77−71837
styrene (-d_3, d_5, d_8), fluoresc. quantum yields and lifetimes, 298 and 77K 79−59500
styrene-phenylacetylene copolymer, fluoresc. emission, energy redistrib. 78−39580
terbium chelate solns., fluoresc. quenching by voltage appl. 79−87498
ternary solutions, spectral relax. of fluoresc. 79−65920
p-terphenyl, cyclohexane soln., solute excited state form. kinetics in pulse radiolysis 79−79263
p-terphenyl, fluoresc. quenching by 4-aminobenzophenone in different dielec. const. solvents *(German)* 79−83030
p-terphenyl solns., mag. field effects on scintillation pulse shape, ion pair recomb. 77−16835
tetrabutylammonium tetrahalomanganate, phosphoresc. lifetimes in fused salts and solids 78−72573
tetracene in liq. cryst., temp. depend. of absorption and fluoresc. *(German)* 80−18887
1,2,4,5-tetracyanobenzene, CT complex in micellar soln., fluoresc. and photolysis study 79−61911
3,6-tetramethyldiamino-N-methylphthalimide soln., hot luminesc. and vibr. relax. 79−22752
3,6-tetramethyldiamino-N-methyphthalimide, in organic solvent, hot luminesc. 79−4842
N,N,N',N'-tetramethylparaphenylenediamine, recomb. fluoresc., elec. field quenching 78−92107
tetramethylpyrazine, PMMA soln., fluoresc. and phosphoresc. quantum yield and lifetime, 20-120 kbar 79−54902
s-tetrazine in n-hexane, picosecond time-resolved fluoresc., vibr. relax. 80−48025
thionine in sodium lauryl sulphate micellar solns., absorpt. spectra and fluoresc. yield, local dye conc. depend. 80−106343
TMPD, 2,2,4-trimethylpentane, fluoresc. quenching by elec. field, above photoionis. threshold 78−33539
toluene, fluoresc. quantum yield in soln., dipole-dipole interaction 78−25598
toluene-d_8, soln., fluoresc. quantum yields, temp. and deuteration effects 77−3396
total luminescence spectroscopy, mixture anal. appl., practical values 78−56927
TP-C-DMP, new bifluorophoric laser dye with intramolecular energy transfer, lasing characts. 78−74899
TP-CSC-DMP, bifluorophoric mol. ultrafast intramolecular energy transfer 78−74900
transfer of electronic excitation energy between like mols. in soln. *(German)* 78−21965
triethylamine, gas (soln.), fluoresc. quenching by 'inert' perfluoromethylcyclohexane 78−46438
triphenylene-d_{12}, in ethanol soln., external heavy atom effect on triplet state, phosphorescence meas. 79−18231
trypsin, photoluminescence after UV irradiation *(German)* 79−92137
tryptophan, aq. alkaline soln., charge transfer, luminesc. obs., 77 and 300K 79−69876
tryptophan, aq. soln. charge transfer, luminesc. obs., 77 and 300K 79−69875
D-tryptophan, soln., excitation spectra rel. to recording wave length *(Russian)* 77−12438
tryptophan residue in horse liver alcohol dehydrogenase, room-temp. phosphoresc., temp. and enzymic complex form. effects 80−61512
tryptophan soln. containing histidine, fluoresc. rel. to soln. pH 80−2826

luminescence of liquids and solutions continued
di-tungsten cyclopentadienyl tri-carbonyl, dual luminesc., ps pulse excitation 80−32754
two-photon excited molecular fluorescence, in optically dense media 78−33534
tyrosine fluorescence at 345 nm in proteins lacking tryptophan 79−39360
umbelliferone, excited states, in ethanol-water soln., absorption and emission spectra 79−13763
uniaxial liq. crystal polarised fluoresc. emission 80−80838
uranine, intercombination conversion rate consts. from triplet quenching by 1,4-diphenylbutadiene 79−956
uranyl solns. in perchloric acid, radioluminesc. due to self-alpha-radiation of U^{238} *(Russian)* 77−55831
vesicular phospholipid membranes dispersion, luminescence spectra of Eu complexes 79−79478
viscous solution, conc. depolarisation of fluoresc. *(Russian)* 77−85799
viscous solutions, fluoresc. anisotropy, conc. depend. 79−56829
water, sonoluminescence spectrum in visible region *(French)* 79−33855
water containing dissolved gases, sonoluminesc. theory 77−85818
xanthene, dye solns., luminesc. spectra, conc. depend. effects 79−54885
xanthene dye, solute-solvent hydrogen bonding and temp. effects on internal conversion 77−3402
xanthene dyes, phosphorescence and orbital nature of triplet state *(Russian)* 77−85797
xanthene dyes in n-alcohols (ethylene glycol) (glycerol), rot. relax., time-resolved fluoresc. depolaris. obs. 80−58300
xanthione, solns., triplet state quenching by ground state xanthione 78−42180
xanthione in benzene, second excited singlet state, ps spectra 77−3399
p-xylene-d_{10}, soln., fluoresc. quantum yields, temp. and deuteration effects 77−3396
$AgNO_3$ soln., visible luminescence obs. at or below 77K 80−108263
Ar jet, supersonic, electron beam-excited, continuous VUV emission spectrum origins 79−6964
Ar, liq., recomb. and self-trapped exciton luminesc., free electron dynamics, excited states 80−25463
Ar, liq., recomb. luminesc. 78−60521
Ar, liquid, triplet state of self-trapped exciton states, evidence of existence, luminescence meas. 78−72608
Ar saturated solutions, NO_3^- effects on spectral distribution and intensity of sonoluminescence 80−76091
Bi^{3+}, in soln., luminesc., halide ion effects 78−35187
Cr complex, $[Cr(NCS)_{6-n}(DMSO)_n]^{n-3}$, phosphorescence spectra, decay times 78−10970
1,3-diphenylpropane, in isooctane soln., monomer phosphoresc., low binding energy triplet excimer not obs. 78−25597
Dy complex, acetoacetic ether, luminesc. spectral band intensities, solvent effects *(Russian)* 78−84653
Dy^{3+}, in soln., non-radiative transitions as Forster's energy transfer to solvent vibrations 80−1014
$Dy^{3+}+O_3(SO_5^{2-})(SO_2)$, in H_2SO_4 soln., electrochemiluminesc. emitters quenching by electrolysis products 79−1794
Er^{3+}, luminesc. sensitisation by Yb^{3+}, in liq., efficiency *(Russian)* 78−90116
Er^{3+}:Yb^{3+} in liq. media, luminesc. cooperative sensitisation 80−2827
Eu complex, with benzoylacetone, isotropic solns., Eu^{3+} luminesc. excitation spectra and polaris. spectra 79−87487
Eu ion based liquid phosphors, using aprotonic solvents 80−20686
Eu ions, solvent effects on band intensities *(Russian)* 77−55828
Eu^{3+}, in soln., non-radiative transitions as Forster's energy transfer to solvent vibrations 80−1014
Eu^{3+} soln., luminesc. quantum yield spectral depend. 80−2838
$EuCl_3.6H_2O$-$NdCl_3.6H_2O$($HoCl_3.6H_2O$), in DMSO soln., $Eu^{3+}\rightarrow Nd^{3+}$ (Ho^{3+}) radiationless energy transfer 80−5499
$Eu(NCS)_3$ solns., luminesc. quenching of Eu^{3+}, charge transfer states 77−90190
$Eu(NO_3)_3.6H_2O$, isotropic solns., Eu^{3+} luminesc. excitation spectra and polaris. spectra 79−87487
H-bond complex formation, enthalpy change due to electronic excitation, spectroscopic determ. 78−92496
H_2, vibr. population relax. in gas and fluid 80−29775
HCl:Bi^{3+} solution, characts. of luminesc. spectra, 82 to 130K *(Russian)* 79−28835
HCl:Bi^{3+} solution, kinetics and struct. of luminesc. spectra *(Russian)* 77−77290
HCl-Bi^{3+} soln., luminesc., quantum yield and lifetime *(Russian)* 79−33834
HgI_2, aq. soln., luminesc. after high energy electron pulse radiolysis 77−32793
$I_2(B^3\pi_{o^+u})$, ps excitation, in CCl_4 soln., ultrafast decay and spectrum 78−9184
Kr, liq., recomb. and self-trapped exciton luminesc., free electron dynamics, excited states 80−25463
Kr, liquid, triplet state of self-trapped exciton states, evidence of existence, luminescence meas. 78−72608
LiBr, aqueous soln., NO_2^- impurity anions, temp. quenching of luminesc. *(Russian)* 77−1714
LiCl, aqueous soln., NO_2^- impurity anions, temp. quenching of luminesc. *(Russian)* 77−1714
LiF, γ-irradiated, chemilum. during dissolution *(Russian)* 78−80427
Mn complexes, with pyridine, excitation luminesc., ligand field effect 77−48213
Mn^{2+}, in soln., non-radiative transitions as Forster's energy transfer to solvent vibrations 80−1014
$MnCl_2$ in soln., luminesc., strong vibronic coupling 79−65922
MnX_2 solns., (X=Cl, Br, I), heavy at. effect on rate consts. of radiative and non-radiative transitions 79−78736
N_2-CO-OCS, liq. mixture, vibr. energy relax. and exchange, laser induced fluoresc. obs. 78−70905
Na-fluorescein, glycerol-alcohol soln., luminesc. decay time, conc. depend. 80−34960
NaCl, gamma-irradiated, aquoluminescence spectra in presence of activators 77−69913
NaCl, γ-irradiated, F→M phototransformation, effect on aquoluminescence 80−7418
NaCl:Tl^+, γ-irrad., aquoluminesc. obs. 80−2856
Nd ion based liq. phosphors, using aprotonic solvents 80−20686
Nd^{3+} in $Nd(NO_3)_3$(tributylphosphate-d_{27})$_3$, soln. luminesc., stimulated emission *(Russian)* 78−33734
O, singlet, photosensitised luminesc. in soln. 77−70309

luminescence of liquids and solutions continued
O_2 in chloroform and carbon tetrachloride solns., sensitized luminesc. 80−32762
O_2, liq., photoluminesc., dimer effects 78−31233
O_2 singlet in solns., luminesc. duration following pulsed laser excitation 80−76070
O_2 singlet-state luminesc. in energy transfer from dissolved pigments 79−54886
$POCl_3:Pr^{3+}$, fluoresc. and lifetimes of excited states 80−71466
$POCl_3:ZrCl_4:Nd^{3+}(Er^{3+})$, radiative transition probabilities within 4f configs. 77−8617
$POCl_3$-$SnCl_4$, Sm^{3+} fluoresc. quenching temp. depend., near reson. interaction 79−65915
$POCl_3$-$SnCl_4:Nd^{3+}$, liquid laser material, luminesc. centres conc., temp. depend. 79−50287
$POCl_3$-$SnCl_4:Nd^{3+}$, liquid laser material, luminesc. centres changes, crystn. process effects 79−50288
$POCl_3$-$ZrCl_4:Yb^{3+}$, Er^{3+}, energy transfer from Yb^{3+} to Er^{3+}, agglomeration formation 78−64405
$PO(SCN)_3:Nd^{3+}$ solns., spectroluminesc. props. 77−16362
Pb^{2+}, in soln., luminesc., halide ion effects 78−35187
$Pm^{3+}:POCl_3$-D_2O soln., absorption and fluoresc. spectra *(French)* 77−66514
$Re_2Cl_8^{2-}$, in acetonitrile and dichloromethane solns., 300K, emission spectra and lifetimes 79−59447
Rh complexes, Rh(III) halopentaammines, solns., luminesc. and excited state lifetimes, photoaquation 79−8175
Ru complex, electrogenerated chemiluminesc., production of excited states by direct heterogeneous electron transfer 79−20371
Ru complex, Ru(II)-polypyridine, excited charge transfer states, multiple emissions 79−3468
Ru complexes, $[Ru(bipy)_n(pq)_{3-n}]^{2+}$ mixed-ligand, electronic absorpt. and emission spectra meas. 80−71441
Ru complexes, luminescent, non-radiative pathways in solvents 77−3393
Ru complexes, $Ru(bipy)_3Cl_2.6H_2O$ and $Ru(bipy\text{-}d_8)_3Cl_2.6H_2O$, soln. electronic excitation energy, deactivation determ. 80−55173
SeO_4^{2-} ions in aqueous solns. of halides at 4.2-290K *(Russian)* 77−28624
Tb complex, acetoacetic ether, luminesc. spectral band intensities, solvent effects *(Russian)* 78−84653
Tb complexes, intermol. energy transfer to Eu complexes in aq. soln. 80−25426
Tb complexes, intermol. energy transfer to Eu complexes in aq. soln. 80−25427
Tb^{3+}, aqueous soln., radioluminescence intensity conc. depend. 80−87055
Tb^{3+}, bound to benzene-carboxylic acid derivatives, emission intensity 79−18230
Tb^{3+}, in $POCl_3:SnCl_4$, $^5D_3 \rightarrow {}^5D_4$ transition, solvent depend. 79−22644
Tb^{3+}, luminesc. sensitisation by Yb^{3+}, in liq., efficiency *(Russian)* 78−90116
$Tb^{3+} \rightarrow Nd^{3+}(Ho^{3+})$, diffusion limited energy transfer in DMSO soln., fluoresc. obs. 79−61428
Tb^{3+} soln., luminesc. quantum yield spectral depend. 80−2838
$Tb^{3+}:Yb^{3+}$ in liq. media, luminesc. cooperative sensitisation 80−2827
$Tb^{3+}+O_3(SO_5^{2-})(SO_2)$, in H_2SO_4 soln., electrochemiluminesc. emitters quenching by electrolysis products 79−1794
$TbCl_3.6H_2O$-$PrCl_3.6H_2O(ErCl_3.6H_2O)$, in DMSO soln., $Tb^{3+} \rightarrow Pr^{3+}(Er^{3+})$ energy transfer mechanism 80−5498
Tl^+, in soln., luminesc., halide ion effects 78−35187
TlCl powder and solution, luminesc. obs. 77−32427
UO_2^{2+}, excited, in liq. and glassy media, luminesc. decay processes, temp. activation 79−91978
UO_2^{2+} in aq. solns., luminescence quenching by metal ions 78−39588
UO_2^{2+} in aq. solns., luminescence quenching by H_2O mols. 78−39589
UO_2^{2+} in aqueous solution, time resolved luminesc. for lifetime, $U_2O_4H^{4+}$ exciplex 79−61417
UO_2^{2+}, in $HClO_4$ soln., photoluminesc. intensity, conc. depends. of uranyl and H^+ 77−68069
Xe, liq., α-particle and electron excited luminesc., time depend., specific ionisation density effect 80−71495
Xe, liq., recomb. and self-trapped exciton luminesc., free electron dynamics, excited states 80−25463
Xe, liq., recomb. luminesc. 78−60521
Xe, liquid, triplet state of self-trapped exciton states, evidence of existence, luminescence meas. 78−72608
$Y_2O_2S:Tb^{3+}(Eu^{3+})$ temp. and viscosity depend. of colour coords. 80−40149
Yb^{3+}, in dessicated (nondessicated) and protonated (deuterated) solvents, photoluminesc. energy degredation 78−19544
Yb^{3+}, in soln., non-radiative transitions as Forster's energy transfer to solvent vibrations 80−1014
Zn-porphin(-d_4,d_8,d_{12}), nonradiative transition probabilities, deuteration effects 79−3485
Zn-tetraphenylporphine/metal electrode, photocurrent generation mechanism 78−76868

luminescence of organic solids
acetone, γ-irrad., isothermal luminesc. decay, temp. depend. 79−66322
acetophenone in toluene glass, quasi-line phosphoresc. spectra 77−69883
5-acetyl-5H-benzo[b]carbazole-5H-benzp[b]carbazole, singlet-singlet energy transfer *(German)* 80−93402
acridene-toluene-phenol, luminescence of complexes with hydrogen bonding at 4.2-77K 79−87486
adamantane, plastic cryst., radio- and photothermoluminesc. *(Russian)* 79−11477
adamantane, plastic cryst., thermolum. curves 80−2876
2-adamantanone, absorption and fluoresc., high-press. 77−52113
adenine film, polycryst., energy conversion processes, quantum yields, 4 to 10 eV 80−88589
L-alanine:Cr^{3+}, X-irrad., thermoluminesc., ESR, UV photobleaching 77−9104
alkane:toluene, radiolysis at 77K, luminesc., excited singlet toluene form., energy transfer mechanism 77−16846
alkyl ammonium halide:Tl phosphors, exciton absorpt. spectra 79−28782
trans-bis(N-1alkyliminodiacetato)-chromate(III) complexes, luminesc. spectra 80−1020
ammonium tartrate, triboluminescence and cryst. fracture dynamics 80−50437
anils, cryst., high-press. optical effects 78−31170

luminescence of organic solids continued
anthracene:2-chloroanthracene, electrolum., voltage- and freq.-brightness characts., dopant conc. depend. 78−2916
anthracene:2-hydroxyanthracene, site-selective photochem., fluoresc. spectra at 3K 78−80756
anthracene:2-hydroxyanthracene cryst., site selective photochem. change, fluoresc. obs. 77−40273
anthracene:9-vinylanthracene, electroluminesc. at room temp. 79−15532
anthracene: 1-chloroanthracene, electrolum. meas. 78−84659
anthracene: tetracene, singlet exciton trapping mechanism, fluoresc. mag. field modulation obs. 77−77267
anthracene:acridine, electroluminesc. exam. 77−63463
anthracene:acridine(carbazole), fluoresc., structural traps for singlet excitons 78−19542
anthracene:rhodamine, triplet exciton density, isotope substitution effect, in weak mag. field 77−90184
anthracene:tetracene, crysts., triplet kinetics model *(German)* 79−4518
anthracene:tetracene, delayed fluorescence excitation spectra 78−39594
anthracene:tetracene, fluorescence decay with X-irrad., energy transfer by excitons 77−20915
anthracene:tetracene, nonlinear quenching of fluoresc. 79−65924
anthracene:tetracene, singlet exciton fission, fluoresc. in mag. field 79−69877
anthracene:tetracene, upper excifed vibronic states optically pumped energy transfer matrix fluoresc. 78−76512
anthracene:tetracene (pentacene), effect of elec. field on fluoresc. *(Russian)* 78−56521
anthracene:tetracene crysts., mag. field modulation of scintillation under α-irrad. 77−48256
anthracene, α-particle tracks, excited states, creation and evolution 78−43934
anthracene, γ-irradiated, temp. depend. of photolum. *(Russian)* 78−56511
anthracene, and related derivatives, fluoresc. and photoreactivity 77−48668
anthracene, cryst., exciton aggregate possible form. under intense optical pumping, fluoresc. spectra 80−84772
anthracene, cryst., fluoresc. spectra, press. tuning 77−28612
anthracene, cryst., heat pulse propag., exciton condensation, time-resolved fluoresc. spectra 80−84771
anthracene, cryst., polariton luminesc. 80−84775
anthracene, electron irrad., creation and evolution of excited states, scintillation obs. 78−92128
anthracene, evaporated films, fluoresc. 77−85777
anthracene, excimer form. in soln. and cryst., fluoresc. study 79−45759
anthracene, excitation and propagation of phonons, luminesc. meas. *(Russian)* 78−35202
anthracene, excitation spectra of exciton fission in organic crystals 78−92116
anthracene, exciton sounding of α-particle induced radiation defects 77−12423
anthracene, film substruct., vacuum deposited, low temp. luminesc. *(Russian)* 78−15226
anthracene, fluoresc., site selection spectroscopy, 2-300K 77−1731
anthracene, fluoresc. from (001) surface and sub-surface excitons 79−33763
anthracene, fluoresc. spectra and decay curves, 4-300K, reabsorpt. in cryst. *(German)* 78−68561
anthracene, high exciton conc., low temp. fluoresc. *(Russian)* 77−28623
anthracene, hot luminesc. in solid matrix at 4.2K, intramol. thermal bath 79−85999
anthracene, in n-paraffin matrices, luminesc. spectra, depend. of inhomogeneous broadening *(Russian)* 79−10145
anthracene, in stretched polymer film, mol. distrib. determ. 78−27298
anthracene, isotopically mixed cryst., exciton dynamics 80−29329
anthracene, lifetimes of exciton-polariton luminesc. 79−33761
anthracene, light polarisation depend. on energy transfer from excited to emitting mols. *(German)* 78−37677
anthracene, liq. chromatography, sublimation, zone refining, exciton fluoresc., mobility meas., melt grown crystal 79−38736
anthracene, luminesc. spectra, exciton-phonon interaction, triplet exciton bands 79−65387
anthracene, noncryst. solid, excimers, time resolved fluoresc. obs. 79−52006
anthracene, nonlinear fluorescence quenching 78−52562
anthracene, photon-emitting singlet excitons spatial distrib. 79−83009
anthracene, pure and doped, singlet exciton diffusion lengths, fluoresc. quenching by dye 78−43923
anthracene, reflectivity and fluoresc. of (001) surfaces, sub-surface exciton states 79−15508
anthracene, reson. Raman emission and hot luminesc. *(Russian)* 79−61377
anthracene, Shpolskii spectra, vibronic struct., fluoresc. *(German)* 79−22754
anthracene, single cryst., fluoresc. decay, Monte-Carlo simulation *(German)* 79−61440
anthracene, single cryst., X-ray radiation damage, delayed fluoresc. meas. *(Japanese)* 79−37736
anthracene, single cryst. triplet excitation form. 79−69437
anthracene, singlet and triplet excitons as probes for photochem. reactivity 79−74406
anthracene, singlet exciton annihilation kinetics 79−19926
anthracene, singlet exciton fission, fluoresc. in mag. field 79−69877
anthracene, singlet exciton fission, prompt and delayed fluoresc. mag. field depend., temp. effects 78−52540
anthracene, structural defect, photolum., γ-irrad. and temp. depend. *(Russian)* 79−28797
anthracene, structural imperfections and delayed fluorescence 78−68551
anthracene, temperature independent intersystem crossing 78−39030
anthracene, thick crystals, excitation spectrum of fluorescence 80−76068
anthracene, thin surface layer, delayed fluoresc. obs., surface trap influence 77−77291
anthracene, triplet energy migration in polystyrene matrix, rate meas. 78−35185
anthracene, triplet excitons, phosphoresc. and delayed fluoresc. excitation spectra 78−63986
anthracene, UV irrad. effects on fluoresc. emission at room temp. 79−83019
anthracene, with pentracene and tetracene impurities, laser-pulse-excited luminesc. 80−7408

luminescence of organic solids continued
anthracene crystal, resonance secondary emission, Raman scatt. in exciton absorpt. region *(Russian)* 80−40120
anthracene crystal, singlet-triplet exciton annihilation 78−31240
anthracene crystals, α-particle induced scintillation, mag. field effects 80−40161
anthracene crystals, basal dislocations, fluoresc. spectra and etching obs. 77−84755
anthracene crystals, local biexciton formation, luminesc. spectra *(Russian)* 78−2428
anthracene crysts., nonlinear fluorescence quenching, recomb. of free excitons 80−7397
anthracene in 2 methyl-THF glass, low temp. fluoresc. bandshape, excess energy effects 78−76509
anthracene isotopic mixed crystals, exciton spectra 79−38602
anthracene Langmuir film, lightly substituted, electrolum., photolum. and electroabsorption 80−20726
anthracene single cryst., Frenkel exciton spectra at dielectric and conducting layer interfaces 80−44510
anthracene single crystals, effect of γ-irrad. on photolum. *(Russian)* 80−2852
anthracene with powdered graphite electrodes, electrolum., ambient gas effects 77−69917
anthracene-Au interface, energy transfer 77−85775
anthracene-dimethylpyromellite-imide, CT complex, reaction yield detect. double reson., delayed fluoresc. quenching *(Russian)* 78−88230
anthracene-dimethylpyromellitimide CCT crystals, mag. field effect on fluorescence 78−19543
anthracene-phenanthrene-tetracyanobenzene, CT-cryst., mini-excitons and lattice dynamics, ESR, optical and Raman spectra 80−60406
anthracene-PMDA, charge transfer cryst., 2K, zero-phonon lines, singlet spectra 78−23484
anthracene-PMDA crysts., phosphorescence blue shift of charge transfer config. 77−36278
anthracene-pyromellitic dianhydride complex, optical and photoelectric props. *(Russian)* 80−15570
anthracene-tetracene amorphous films, host-guest energy transfer 78−60505
anthracene-tetracenebenzene, triplet excitons annihilation, mag. reson. sign reversal 79−65769
anthracene-trinitrobenzene complex, neat and mixed cryst. and glass opt. spectra 77−40274
anthracene/TCNB, charge-transfer cryst., fluoresc., 1.2-300K, mobile triplet excitons 78−43913
anthracenes, long-lived luminesc. in solid state *(German)* 78−23528
anthraquinone, site selective sublevel phosphoresc. spectra in octane or hectane soln. 79−69878
aromatic compounds, in n-paraffin cryst., luminesc. characts. 79−3480
aromatic compounds in benzene polycrystalline host, active N_2 induced chemilum., 77K 80−60691
aromatic compounds luminesc. polarisation, quasilines and bands in Shpolskii spectra *(Russian)* 79−31592
aromatic esters, phosphoresc. and fluoresc. spectra in organic matrices 80−32756
aromatic hydrocarbons, doped mol. crysts., singlet host exciton nonradiative heterofission 77−28122
aromatic hydrocarbons, $S_0 \rightarrow T_1$ phosphoresc. under Shpolskii effect conditions 77−83643
aromatic hydrocarbons, Shpolskii systems, key and hole rule test, fluoresc. 77−42347
aromatic impurity molecule, internal conversion processes 78−82776
aromatic media, electron excitation, delayed fluoresc. 79−52024
aromatic molecules in clathrates, Raman and phosphoresc. spectra 79−36647
aromatic rigid soln., luminesc. exchange promotion kinetics 80−50387
aromatic scintillators radioluminesc. yield *(French)* 78−52574
aromatic-molecules, conformeric fluoresc. and phosphoresc., rotation of chromophoric fragments around single chemical bonds 77−68068
ATP content meas. in single red blood cell, using firefly bioluminescent reaction with optical instrument 79−79695
azomethines, photochromic, intramol. proton phototransfer sensitisation, organic cation energy transfer 78−53230
azulene, Shpol'skii matrix, $S_2 \rightarrow S_1$ fluoresc., spectral anal. 77−18956
azulene in naphthalene mixed cryst., $S_2 \rightarrow S_1$ fluoresc., vibr. anal. 78−66586
benzaldehyde, and deuterated forms, in p-xylene, 4.2K, $n\pi^*$ phosphoresc. assignments 78−9197
benzaldehyde in toluene glass, quasi-line phosphoresc. spectra 77−69883
benzaldehydes, in mixed cryst., T_1/T_2 interstate interactions, modulation polaris. phosphoresc. spectra, 4.2K 78−9185
benzene, cryst., vibronic spectra using 2-photon fluoresc. excitation 79−47493
benzene, deuterated mixed crysts., phonon assisted trap-trap triplet energy migration, 0K limit, phosphoresc. obs. 77−48218
benzene, isotopic mixed crysts., triplet excitation energy transfer theory 77−28611
benzene, isotropically mixed crysts., singlet and triplet exciton percolation theory 78−26818
benzene, luminesc. yield spectra in VUV 79−36685
benzene, mixed deuterated crysts., triplet energy transfer mechanism 77−16365
benzene, solid, fluoresc. decay times and quantum yields, rel. to vap. phase 80−55154
benzene, solid and isolated in rare-gas matrices, spectroscopic study 79−3455
benzene cryst., electron irrad., phenylcyclohexadienyl radical form., absorpt. and fluoresc. spectra study 80−89035
benzene in 3-methylpentane glass, phosphoresc. polarisation and intensity, 77K 77−46588
benzene phenol crystal, asymmetry of phonon side bands, absorption, luminesc. and specular spectra 77−1730
benzene-d_0,-d_6, phosphoresc., Boltzmann population and spin-lattice relax., decay processes 78−31230
benzene-d_6:benzene-d_0, phonon side bands of specular optical transitions 78−26649
benzened_6:phenol, phonon side bands of specular optical transitions 78−26649
benzil, cryst., phosphoresc. kinetics rel. to spin-lattice relax. 79−87485
benzil crystals, mol. triboluminesc. meas. 80−40172
1,2-benzocoronene, phosphoresc. and ODMR meas. 79−18220
luminescence of organic solids continued
1,12-benzoperylene in n-alkane, zero-phonon lines in luminesc. spectra 78−56512
benzophenone: diphenylmethylene, mixed cryst., emission and absorpt. spectra, 2-30K, excitation-phonon coupling 79−99900
benzophenone, cryst., phosphoresc. spectra and decay time, temp. depend. 79−87479
benzophenone, migration of triplet excitons, EPR profiles and phosphoresc. decay data 80−84641
benzophenone, triplet exciton absorpt. lines 79−38563
benzophenone in toluene glass, quasi-line phosphoresc. spectra 77−69883
benzophenones, in host crysts., triplet state PMDR, phosphoresc. spectra, transitions mechanisms 77−46585
p-benzoquinone, mixed crysts., PMDR and thermal modulation spectroscopy, electron-phonon interaction 77−32297
2,1,3-benzothiadiazole, EPR of phosphorescent state 77−8405
2-benzoylpyridine, mol. cryst. triplet state selective photoexcitation, phosphoresc. spectra and microwave-optical double reson. 79−15507
2-benzoylpyridine, triplet states, phosphoresc. and ODMR 79−38603
2-benzoylpyridine crystals, optical spectra of lowest triplet state 80−16081
1,12-benzperylene, in benzene, 77K, quasi-line luminesc. spectra obs., Shpolskii's method 77−69894
1,2-benzpyrene, butyl bromide solid soln., phosphoresc. line struct. obs., vibr. assignments 77−58075
1,2-benzpyrene, in cyclohexane, 77K, quasi-line luminesc. obs., Shpolskii's method 77−69894
betamethylnaphthalene in $C_{10}D_8$, exciton percolation and coherence 77−59258
biphenyl:fluoranthene(pyrene)(chrysene), triplet and singlet transport rate ratio 79−56832
biphenyl, luminesc. yield spectra in VUV 79−36685
biphenyl, luminescence spectrum intensity distribution 79−3476
biphenyl crystals, electronic and vib. states, cryst. field mixing, two-photon spectra 77−59603
biphenyl glutarate polymer, resonant Raman spectra and fluoresc. 77−24830
bis(p-toluene sulphonate) diacetylene, partially polymerised, defect-induced absorpt. and fluoresc. 77−44030
bisphenol-A-diglycidyl epoxy, light emission under high elec. field, compared with photolum. 80−25465
bone polychrome fluorescence labelling and photomicrography 80−89821
calcite, luminescence spectral anal. of polycyclic aromatic hydrocarbon impurities 80−71483
carbazole, crystalline, room temp. afterglow 78−27314
carbazoles, luminescence, $AgNO_3$ heavy atom effect, donor-acceptor interaction *(German)* 78−84651
carbazolyl substituted diacetylene monomer cryst., ODMR and triplet state kinetics 78−76355
cellulose-PAN copolymer, luminesc., ageing effect 78−64401
charge-transfer crystals, long lived emission 79−33752
1-chloro-9,10-anthraquinone crystal, electronic structure of lowest triplet state *(Japanese)* 79−8158
2-chloroanthracene:acridine, electrolum. at 300K 79−15531
p-chlorobenzaldehyde in methylcyclohexane, matrix perdeuteration effects on $^3\pi\pi^* \rightarrow S_0$ phosphoresc. 77−20903
p-chlorobenzene, and deuterated forms, in p-dibromobenzene and p-dimethoxybenzene, 4.2K, $\pi\pi^*$ phosphoresc. assignments 78−9197
chlorophyll, fluoresc. detection of triplet state kinetics 77−30903
chlorophyll, singlet-triplet optical resonance in solid soln. 77−52741
chlorophyll a and analogues, triplet state, phosphoresc. polaris. 79−39358
chlorophyll in leaves and algae cells, phosphorescence obs. 79−92142
chlorophyll-a, crystalline film, energy levels and carrier generation by photocond. and fluoresc. 77−16909
chromophores, $^1O_2$, annihilation luminesc., in polymer matrices 77−88488
chrysene, butyl bromide solid soln., phosphoresc. line struct. obs., vibr. assignments 77−58075
citric acid monohydrate, triboluminescence and cryst. fracture dynamics 80−50437
coal, Raman scatt. and luminesc. 78−23460
complex mixtures in solid-state matrices, dip shape saturation effects on nonuniformly broadened spectra 79−95799
copper (I)-butyrate, dimorphism, X-ray diffr. and fluoresc. *(German)* 79−51090
copper porphin, Zeeman expt. on phosphoresc. triplet and quartet states 79−33786
copperporphin, metastable quartet state radiative decay 80−23453
coronene, butyl bromide solid soln., phosphoresc. line struct. obs., vibr. assignments 77−58075
coronene, in cyclohexane, 77K, quasi-line luminesc. spectra obs., Shpolskii's method 77−69894
coronene-rhodamine 6G, energy transfer in PMMA matrix, fluoresc., temp. depend. 78−13539
cyanine dye monolayer/p-chloranil crystal, charge carrier injection rate const. determ., energy transfer vs. charge transfer method 79−83031
9-cyanoanthracene:perylene, exciplex emission 78−60513
9-cyanoanthracene, cryst., excimer emission, spectra, photochem. and multiphonon processes 78−10914
9-cyanoanthracene, luminesc., excimeric species 78−84637
9-cyanoanthracene, metastable crystal, red excimer emission 78−6757
9-cyanoanthracene, quenching of solid state photodimerisation reaction by cryst. doping 78−68547
9-cyanoanthracene excimer emission, in glassy and cryst. matrices 79−11445
cyclohexane crystals, luminesc. emitted at 55 cm^{-1} near phase transition point 77−52180
decane: pyrene (coronene), quasiline spectra, multiplet struct., freezing conditions and solvent effects 79−1786
deuteronaphthalene:β-deuteromethylnaphthalene crystal, asymmetry of phonon side bands, absorption, luminesc. and specular spectra 77−1730
di-isobutyl kitone, γ-irrad., isothermal luminesc. decay, temp. depend. 79−66322
3,5-di-tert-butyl-4-hydroxybenzylidenemalononitrile, excited-state proton transfer, cryst. and mol. struct. 78−84630
diacetylene, luminesc. and ODMR spectra 79−38604
dianthronylidene ethane, luminescent excimer geometries, intermol. shift 78−27294
diarylethylene, luminesc. spectra and rot. isomerism 79−85991

luminescence of organic solids continued
dibenzene-naphthalene, relax. time of vibr. levels of ground state *(Russian)* 77−44054
1,2,5,6-dibenzocoronene, phosphoresc. and ODMR meas. 79−18220
dibenzofuran:anthracene, cryst., prompt fluoresc., temp. depend., trap effects *(German)* 80−93400
dibenzofuran, cryst., phosphoresc. spectra and ODMR meas. 80−11470
dibenzofuran, cryst., prompt and delayed spectra, purity *(German)* 77−28622
dibenzofuran-fluorene, mixed cryst., phosphoresc. spectra and ODMR meas. 80−11470
p-dibromobenzene, cryst. electronic and vibr. energy transfer and relax. 78−31229
4,4′-dibromodiphenylether:benzophenone-d_{10}, optical decay constants, photoexcited triplet state near level anticrossing field 78−80250
1,4-dibromonaphthalene:octafluoronaphthalene, absorpt. and phosphoresc. spectra, intermol. reson. 79−33764
1,4- dibromonaphthalene, highly disordered quasi-one-dimens., excitation transport 80−34961
1,4-dibromonaphthalene, k-k scatt., exciton dephasing time-resolved phosphoresc. obs. 80−11458
1,4-dibromonaphthalene, substitutionally disordered, energy localisation, optical and ODMR spectra of triplet Frenkel excitons 80−54996
1,4-dibromonaphthalene, triplet-triplet exciton annihilation in quasi-1-dimens. cryst. 78−27297
9,10-dichloroanthracene, cryst., singlet-triplet absorpt. spectra, delayed fluoresc. 77−8619
9,10-dichloroanthracene, mag. field effect on exciton processes and photodetrapping 77−4668
p-dichlorobenzene-p-dibromobenzene, mol. cryst., intermol. mixing of electronic states 77−85768
p-dichlorobenzene-p-dibromobenzene, solid soln., local struct. and triplet energy migration 78−60489
p-dichlorobenzene-p-dibromobenzene mixed crysts., triplet exciton migration, time resolved emission spectroscopy 80−89052
4,4′-dichlorobenzophenone, cryst., X-traps, rel. populations, elec. field effect 77−12414
4-4′ dichlorobenzophenone, triplet exciton absorpt. lines 79−38563
4,4′-dichlorobenzophenone single crysts., mutual annihilation of triplet excitons, 1.5 and 4.2K, phosphoresc. obs. 80−80850
2,3-dichloroquinoxaline, in tetramethylbenzene cryst., sublevel phosphoresc. spectra 78−70863
1,1′-diethyl-2,2′-cyanine iodide, neat and mixed crysts., visible absorption and emission spectra assignments 77−1692
diethylammonium manganese chloride, antiferromag., low temp. luminesc. spectra, magnetoelastic effect 80−2810
3,3′-diethyloxadicarbocyanine iodide, lasing and photoisomerisation, conc. and temp. effects 77−7081
dimethyl sulphoxide, UO_2^{2+} γ-irrad. frozen solns., radiothermolum. and temp. deactivation *(Russian)* 79−33854
dimethylammonium manganese chloride, antiferromag., low temp. luminesc. spectra, magnetoelastic effect 80−2810
9,10-dimethylanthracene, Shpolskii spectra, vibronic struct., fluoresc. *(German)* 79−22754
dinaphtho-(2′,3′:1,2);(2″,3″:6,7)-pyrene, triplet state, phosphoresc. and ODMR obs. 79−27013
diphenyl:(benzophenone, naphthalene), triplet exciton diffusion, phosphoresc. obs. 78−10964
diphenyl:naphthacene, relax. times of ground electronic state vibrational levels 79−19907
diphenyl:naphthalene, benzophenone, phosphoresc., triplet diffusion excitons 78−63985
diphenyl:pyrene, self induced transparency under nonreson. excitation, luminesc. and stimulated emission 80−11436
diphenyl:pyrene, stimulated emission at 0-0 transition, 4.2K 80−11437
1,3-diphenyl-5-(p-chlorophenyl)-2-pyrazoline, singlet excitation energy migration in cryst. and glassy states 79−95831
diphenylanthracene, fluoresc., site selection spectroscopy 2-300K 77−1731
diphenylene sulphide, phosphoresc. vibronic struct., solvent heavy at. effect 78−17710
ditetraethylammonium manganese bromide $^4T_1$ excited state, absorpt., MCD, Jahn-Teller model 78−43907
DNA, luminescence, excitation wavelength depend. in UV/VUV region 78−31768
durene:fluoranthene(pyrene)(chrysene), triplet and singlet transport rate ratio 79−56832
dye molecules adsorbed on Ag, Au and Cu films, absorpt. and luminesc. study 80−103981
dyes in rigid matrices, solvent reorientation relax. effect on luminesc. 79−43009
electrogenerated chemiluminescence, estimation of triplet energies, possibilites and restrictions 80−34992
energy transfer between 5d electronic states 80−2808
epoxy resin, electroluminesc. 78−56522
epoxy resins, strain anal. by fluoresc. meas. *(French)* 79−47846
erbium ethylsulphate, cryst. laser-excited fluoresc. intensity 79−33751
10,10′-ethanediylidenedianthrone, fluoresc. efficiency, mol. geom. effects in two cryst. structs. 77−18953
ethyl substituted ammonium halides, exciton absorpt. spectra 79−28782
extrinsic molecular crystal, luminesc. spectra, relax. of vibr. levels 79−87484
fatty acids, anisotropic layers, multipole emission, energy transfer, classical theory 77−8625
ferroelectrics, triboluminescence on piezo-electrification of surfaces during fracture 80−29815
film scintillators for extended UV response Si detectors 80−86412
films, X-ray induced luminesc. and optical absorpt. rel. to γ-induced free radicals 77−5033
flavins, phosphoresc. props., solvent effects 77−12885
fluoranthene, in rigid glass, S_1 and S_2 fluoresc. 77−3403
fluorene:benz(f)indan(anthracene), single cryst., γ-irrad. rel. to luminesc. decay 77−12417
fluorene:dibenzofuran, mixed cryst., dipole-forbidden guest-host energy transfer 79−38585
fluorene:pyrene-d_{10}, exciton-guest, triplet-triplet annihilation, impurity traps effects 80−25433
fluorene:pyrene-d_{10}, single cryst., host-guest triplet pairs, mag. field effect 80−60649
fluorene, cryst., phosphoresc. spectra and ODMR meas. 80−11470
fluorene, electroluminesc. *(Russian)* 78−92129

luminescence of organic solids continued
fluorene, lowest singlet state, exciton band struct. calc. 78−63983
fluorene, near 6K, two-photon excitation spectrum, g-exciton states location 78−64393
fluorene, single cryst., dielec. matrix suspension, electroluminesc. 80−2862
fluoresc. decay time and emission spectra obs. *(Spanish)* 77−69873
formaldehydes, (deuterated), A^1A_2 state, photoluminesc. in low temp. matrices, vibr. relaxation 79−50070
formylstyrene copolymers, luminesc. *(Russian)* 79−56861
glass, rigid, electron-cation recombination; charge distrib. simulation and luminesc. kinetics 80−2855
glasses, hole burning, fluoresc., struct. 79−31588
glycerol-D_2O:Tb^{3+}, Nd^{3+} soln. and frozen glass, energy transfer 78−60509
glycine sulphate:L-alanine, unirradiated, optical spectroscopy of scintillations 80−80863
glyoxal-d_0, -d_2, triplet kinetics, microwave-saturation recovery and MIDP obs. 77−71823
guest/host mixed crystal systems, thermally activated intermolecular effect of deuteration on guest phosphoresc. 79−43010
1-halonaphthalenes, lowest triplet state, spin sublevels decay, internal heavy atom effects 79−95819
2,4-hexadyne-1,6-diol-bis-p-toluene sulphonate, partially polymerised single crystal, fluoresc. 78−6756
hexamethylolmelamine, doped, and condensation resin, room temp. phosphoresc., thermal transforms. 80−45132
hexane:pyrene (coronene), quasiline spectra, multiplet struct., freezing conditions and solvent effects 79−1786
hexaphenylcarbodiphosphorane, cryst. struct., triboluminesc., polymorphism effects 79−61447
hydrocarbon, long chain single cryst., carrier transport meas. 80−6874
hydroxypyridines, phosphoresc. emission, polarisation and lifetimes 78−31232
II-VI compounds, transition metal ion activated, vibronic struct. in absorption and luminesc. 78−6729
4,5-iminophenanthrene, polymorphism, X-ray diffr. and photoluminesc. obs., 77 to 300K 77−63449
impurity crystals, press. effect on shift of zero-phonon lines 79−95824
2-indanone, single cryst., ODMR and phosphoresc. of $^3n\pi^*$ state 79−78570
indeno[2,1-a]indene, in glassy media, phosphoresc., heavy atom effects 80−55153
indole, aq. alkaline soln., charge transfer, luminesc. obs., 77 and 300K 79−69876
indole, in PMMA matrix, high press. luminesc. 78−84629
indoles, in glassy hydrocarbons, complexation vs. aggregation, absorption and fluoresc. obs. 79−98132
1-iodonaphthalene-perfluorated naphthalene solid soln., sensitised phosphoresc., site selection method, Dexter's theory 79−4836
ion-surface collisions, luminesc. accompanied by ion implantation 80−60683
isoquinoline, fluoresc., phosphoresc. and H bonding 77−79647
isoquinoline luminesc. in polymeric media at high press. 79−13756
ketones, mol. cryst., interband transitions, triplet-triplet absorptions 79−11452
lepidopterene exciplex, luminesc. intramolecular anthracene-ethylene exciplex, mol. geometry-fluoresc. relationship 78−58728
Lexan polycarbonate, thermolum. radiation-induced EPR of free radicals and track etchability 79−76295
luminescence, $AgNO_3$ heavy atom effect, donor-acceptor interaction *(German)* 78−84651
luminophores, luminesc. under action of atomic H *(Russian)* 79−8177
mannose, increased lyoluminescence response on storage 79−25112
methiodides of nitrogen heteroaromatics, frequencies of multiple charge transfer bands 79−94009
12-methoxypyridine, phosphoresc. emission, polarisation and lifetimes 78−31232
9-methylanthracene, Shpolskii spectra, vibronic struct., fluoresc. *(German)* 79−22754
methylcyclohexane:styrene-d_0, -d_3, -d_5, d_8, fluorescence meas., 77K 78−25606
methylcyclohexane, γ-irrad., isothermal luminesc. decay, temp. depend. 79−66322
methylcyclohexane glass, γ-radiolysis, electron tunnelling from matrix trapped biphenyl ions 79−29379
methylcyclohexane glasses, γ-irradiated in presence of naphthalene, isothermal luminesc. 80−93388
methylene phenanthrene cryst., delayed fluoresc., mag. field effect, sense depend. 77−73160
5-methylindole, in PMMA matrix, high press. luminesc. 78−84629
3-methylpentane, γ-irradiated, isothermal luminescence in presence of aromatic solutes at 77K 78−76519
3-methylpentane glass, γ-radiolysis, electron tunnelling from matrix trapped biphenyl ions 79−29379
3-methylpentane glasses, γ-irradiated in presence of naphthalene, isothermal luminesc. 80−93388
mixed crystals, energy transfer 78−76515
molecular crystal, coherent pairing of excitons in reson. EM field, biexciton spectra 77−47736
molecular crystal, delayed fluoresc., anisotropic spin relax. effects 79−61416
molecular crystal, exciton scatt. by lattice defects, absorpt. line shape 79−38576
molecular crystals, intermolecular interactions, spectroscopic studies, review 80−103958
molecular crystals, optical spin alignment, phosphoresc. *(Russian)* 78−84652
molecular crystals, thermal modulation spectroscopy, electron-phonon interaction 77−32392
molecular organic crystals, triexcitons, theory 79−33787
molecular solid, intermolecular interactions, laser induced phonon probe 80−79891
molecular solids, substitutionally disordered, Anderson localisation of mol. excitons 77−89733
naphthacene, thermoluminesc., exam. at liquid N_2 temp. 77−4692
1,2-naphthacoronene, phosphoresc. and ODMR meas. 79−18220
naphthalene:β-chloronaphthalene, reaction rate constants of triplet excitons 78−80407
naphthalene:β-methylnaphthalene, impurity phosphoresc. centres *(Russian)* 77−81151

luminescence of organic solids continued
naphthalene:β-naphthyl-n-biphenyl-ethylene, relax. time of vibr. levels of ground state *(Russian)* 77−44054
naphthalene:β-naphthyl-n-biphenyl-n-biphenylyl ethylene, relax. times of ground electronic state vibrational levels 79−19907
naphthalene: quinoxaline, anisotropic spin lattice relax. of triplet mols. in high mag. field 77−81141
naphthalene:anthmacene, singlet exciton energy transfer dynamics, time resolved spectra 79−83032
naphthalene:anthracene, cryst. energy transport and luminesc. at room temp. and 4.2K 79−56828
naphthalene:anthracene, pure and doped, delayed fluoresc. *(French)* 80−80846
naphthalene:anthracene, two-photon picosec. excitation, sensitised fluoresc. kinetics 79−47516
naphthalene:benzofuran, luminescence spectra and intensity, 1.6-77K 79−87477
naphthalene:indole, luminescence spectra and intensity, 1.6-77K 79−87477
naphthalene:quinoxaline, spin-lattice relax. of triplet states of high mag. fields 79−19933
naphthalene:thionaphthalene, luminescence spectra and intensity, 1.6-77K 79−87477
naphthalene, 2-methylnaphthalene and anthracene doped, single cryst., sensitised fluoresc. 78−68548
naphthalene, $^1B_{2u}$ supertransfer, exciton percolation, fluoresc. spectra obs. 77−55482
naphthalene, β-naphthol impurity mol. distrib., spectral obs. *(Russian)* 79−82253
naphthalene, and deutero derivatives, fluoresc., absorpt. spectra under Shpolskii conditions 80−2825
naphthalene, cryst., fluoresc. spectra, press. tuning 77−28612
naphthalene, cryst., luminesc., excitons, phase aspects 79−56838
naphthalene, cryst., singlet exciton interactions, prompt fluoresc. decay 78−60500
naphthalene, cryst., singlet exciton interactions fluoresc. decay 79−47027
naphthalene, crystalline, singlet exciton diffusion coeff. meas., fluorescence quenching anal. 78−67945
naphthalene, doped, fluoresc., impurity centre struct. depend. *(Russian)* 77−48231
naphthalene, electron excitation energy transfer efficiency, temp. depend. *(Russian)* 77−52182
naphthalene, exciton migration, variable range cluster model 79−33762
naphthalene, fluorescence decay induced by electron pulse, exciton interactions 77−16403
naphthalene, in stretched polymer film, mol. distrib. determ. 78−27298
naphthalene, isotopic mixed cryst., phospheresc., photoselection of pure initial triplet states 78−35189
naphthalene, long range exciton percolation, superexchange, energy denominator 77−28609
naphthalene, mag. effects on delayed fluoresc. at high and low triplet exciton density 77−8634
naphthalene, microcryst. and evaporated film, excimer emission 80−2823
naphthalene, multiphoton excitation 79−61414
naphthalene, nonlinear fluorescence quenching 78−52562
naphthalene, pure and doped, exciton-phonon luminesc. 80−84773
naphthalene, singlet and triplet excimer interactions, exciton resons. 80−95535
naphthalene, triplet exciton annihilation and triplet spin relax. 80−29792
naphthalene, triplet exciton annihilation at high triplet densities 79−37996
naphthalene, triplet excitons, phosphoresc. and delayed fluoresc. excitation spectra 78−63986
naphthalene, vibronic fluorescence spectrum, intensity distribution 79−3477
naphthalene β-chloronaphthalene, optically induced detrapping of triplet excitons 79−28828
naphthalene anthracene doped, decay times and diffusion coeffs. of singlet excitons, under press. 77−20911
naphthalene cryst., anthracene doped, fluoresc., two-photon excited 78−68560
naphthalene crystal, inclined dimers as model for quenching centres 77−42237
naphthalene crystal, vibronic spectra at 1.6K, two-photon fluoresc. excitation 77−59604
naphthalene crysts., nonlinear fluorescence quenching, recomb. of free excitons 80−7397
naphthalene in $C_{10}D_8$, exciton percolation and coherence 77−59258
naphthalene in various crystals, luminesc. and stimulated emission on laser irrad. *(Russian)* 77−48236
naphthalene mixed crystal, Nh_8/Nd_8, phosphoresc., energy transfer model 79−38600
naphthalene mixed crystal, time resolved excitation migration, triplet and singlet critical concs. 79−78010
naphthalene-betamethylnaphthalene, mixed cryst. ($C_{10}H_8/C_{10}D_8$), luminesc., test of excitation transport model 79−65914
naphthalene-d_4(d_8) crystal, with isotopic impurities, Rashba effect, luminescence spectra, impurity states 80−29768
naphthalene-d_8:β-methylnaphthalene -d_{10}, phonon side bands of specular optical transitions 78−26649
naphthalene-d_8:naphthalene, betamethylnaphthalene, $^1B_{2u}$ naphthalene exciton percolation kinetics, exciton coherency 79−33750
naphthalene-h_8, and -d_8 mixed crystals, phosphoresc. excitation spectra of clusters 78−43914
naphthalene-TCPA charge transfer triplet states, electron-phonon coupling 79−38601
naphthalene-tetrachlorophthalic anhydride charge-transfer cryst., electronic states 77−32415
naphthalene-triethylamine exciplex, effect of dipolar molecules on quenching curves 78−52551
naphthalenes, phonon satellite narrowing in local exciton luminesc. *(Russian)* 79−47507
1,8-naphthoilene-1′,2′-benzimidazole-phenylimide of 4-aminonaphthalic acid luminophor mixture *(Russian)* 79−47514
2-naphthol-toluene-phenol, luminescence of complexes with hydrogen bonding at 4.2-77K 79−87486
napthhalene-benzophenone mixed crysts., phosphoresc., emitting centres 79−61427
nicotinamide co-enzymes, reduced, phosphorescence obs. at −196°C 79−79471
α-NPO in polystyrene, 77K phosphorescence *(Russian)* 78−27286

luminescence of organic solids continued
nucleic acids and related compounds, photoemission rel. to absorpt. and luminesc., 120 to 250 nm 77−81466
octaethylporphin in Al-Ag sandwich cell, electroluminesc. 77−59615
octafluoronaphthalene crystalline complexes with naphthalene and durene, triplet exciton emissions 80−84760
octane: pyrene(coronene), quasiline spectra, multiplet struct., freezing conditions and solvent effects 79−1786
1,3,5,7-octatetraene, lowest excited singlet state, dipole forbidden character 79−27024
organic compounds, inductive-resonance energy transfer, heterogeneous electron level broadening *(Russian)* 78−23530
organic donor-acceptor solns., triplet-triplet energy transfer under Shpolskii effect conditions 79−64031
organic molecular crystals, phosphoresc., optical spin alignment 79−95827
organic molecules in Shpolskii matrices, phosphoresc. site selection spectrosc., ODMR 79−36687
organic photoconductor, electric field-induced fluoresc. quenching 80−34967
organic solid, motion of localised excitations 77−31961
orthorhombic crystals, triboluminescence and piezoelectric behaviour 79−95861
palladium porphin, Zeeman expt. on phosphoresc. triplet and quartet states 79−33786
[2.2]paracyclophane, delayed luminesc. in cryst. and rigid glass solns. 79−15510
n-paraffin crystal matrices, organic impurity molecular fluoresc., effect of heat pulses 78−88360
pentacene, narrow band laser excitation, fluoresc. decay, optical free induction, dipole moment 78−21956
pentacene films, luminesc., struct. 80−11461
pentacene in naphthalene (p-terphenyl), mol. mixed crysts., optical dephasing and vibronic relax. 80−95957
pentacene in p-terphenyl, intermolecular interactions, laser induced phonon probe 80−79891
pentacene-d_0, -d_{14}, in p-terphenyl-d_0, mixed cryst., photon-echo relax. 77−72034
perylene, cryst., fluoresc. at low temp. 78−27299
perylene, cryst., fluoresc. spectra, time-resolved, excimer and excitons 79−78724
perylene, excimer form. process, ps laser fluoresc. obs. 79−11448
perylene, excitation spectra of exciton fission in organic crystals 78−92116
perylene, exciton fission in excimer forming cryst., fluoresc. 79−15511
perylene, fluoresc., exciton fission in excimer forming cryst. dynamics 79−61423
perylene, hot luminesc. in solid matrix at 4.2K, intramol. thermal bath 79−85999
perylene, intermolecular interactions, laser induced phonon probe 80−79891
α-perylene crystal, emission spectra, temp. variation and pair states 78−27300
perylene crystal, molecular exciton system, resonance Raman and fluorescence studies, dynamical effects 80−66169
perylene in n-alkane, zero-phonon lines in luminesc. spectra 78−56512
perylene in n-heptane cryst., polarised fluoresc. 80−1017
perylene-N,N-dimethylaniline exciplex, effect of dipolar molecules on quenching curves 78−52551
PET, photoexcited, thermolum. and carrier detrapping mechanism 79−61445
PET, uniaxially drawn, comparison of polarised fluorescence, polarised Raman and IR dichroism measurements 79−99084
[2.2]phanes in glass matrices, transanular π-electron interaction, emission spectra 79−36682
phenanthrene:anthracene, cryst., triplet-triplet annihilation, shallow traps effect, 77-293K 79−11446
phenanthrene:anthracene, delayed fluores. of cryst. in mag. field 79−52023
phenanthrene, mol. cryst., thermolum. build-up 78−27334
phenanthrene, two-photon excitation spectra, exciton-phonon and intramol. vibronic coupling 80−84774
phenanthrene-d_{10}, oriented in biphenyl, triplet zero-field splittings, conc. depend. 78−2773
phenanthridinic spiropyran photocoloration mechanism 79−83487
phenanthrolines, in Shpolskii matrices, phosphoresc. spectra 78−94276
phenazine, substitutionally disordered, energy localisation, optical and ODMR spectra of triplet Frenkel excitons 80−54996
phenylacetylene, phosphorescence polarisation, intramolecular heavy atom effect 78−52550
phthalic anhydride and halogen derivatives, phosphorescence spectra *(Japanese)* 78−48217
phthalocyanine, in n-alcanes and polyethylene, absorpt. and fluoresc. spectra, 4.2 and 77K 78−976
phthalocyanine, metal-free, singlet-triplet fusion rel. to carrier photogeneration 77−36276
phthalocyanine, metal-free, solid, fluoresc., lifetimes temp. depend., polymorphic modification 78−80388
phthalocyanine, quasiline emission spectra using low temp. laser luminesc. spectrosc. *(Czech)* 80−86445
phthalocyanine, x-metal-free, photogeneration and fluoresc. quenching theory 79−65513
phthalocyanine, X-metal-free in polyvinylacetate, elec. field induced fluoresc. quenching, carrier photogeneration 78−48207
piperidine-$MnBr_2$ complexes, substituted, excitation spectra, ligand field theory 77−27103
plastic scintillator, degree of fluorescence light polarisation, energy depend. *(German)* 78−37677
plastic scintillator excited by ^{60}Co γ-rays, absolute radioluminesc. yield meas. 80−2829
plastic scintillators, bistilbenes used as mixers of luminesc. spectra 77−23373
plastic scintillators, radioluminesc. absolute output following ^{60}Co γ-ray irrad. *(Russian)* 78−92124
platinum phthalocyanine single cryst., triplet state Zeeman effect, phosphoresc. 78−6747
PMA, phosphorescence depolarisation, segmental relax. time 78−95606
PMMA, phosphorescence depolarisation, segmental relax. time 78−95606
PMMA crosslinked by dimethacryloxymethylanthracene, radiothermoluminesc. *(Russian)* 78−73068

luminescence of organic solids continued
poly(N-vinylcarbazole) film, fluoresc. and phosphoresc., energy transfer mechanism 80−16112
poly-N-epoxypropylcarbazole layers, optical and photoelec. props. 77−39896
poly-N-vinyl carbazole, pulsed laser excitation, time resolved fluoresc., 80−89041
poly-N-vinylcarbazole:2,4,7-trinitrofluorenone, fluoresc. kinetics, stroboscopic meas. 79−11443
poly-N-vinylcarbazole, in polymer film, excimer fluoresc., high press. effects 80−34966
poly-N-vinylcarbazole film, triplet-triplet energy transfer, chemiluminesc. 78−43944
poly-N-vinylcarbazole-biacetyl, triplet exciton quenching, exciton trapping model 80−66267
poly-p-xylylene films, carrier traps, X-ray induced TSC, thermolum. and dielec. loss study 80−88570
polyacenaphthalene, glassy soln., fluoresc. yield, polarisation and decay., temp. depend. 80−89043
polyacenaphthalene-methylmethacrylate copolymer 80−89043
polybutylene terephthalate film, photoluminesc. exam. 78−48213
polycyclic aromatic hydrocarbons, matrix isolated, quasilinear Shpol'skii fluoresc. spectra 78−9189
polyethylene, γ-irrad., electrolum., 77K 77−32442
polyethylene, γ-irradiated, luminesc. in warming and cooling 77−32450
polyethylene, high density, thermolum. and its oxidation effects 77−77305
polyethylene, low-density, α-irrad., thermolum. mechanism biphenyl anions influence 80−2880
polyethylene, oxidised, origin of high temp. anomalous luminesc. 77−85812
polyethylene, space charge effect on local electric breakdown 77−69773
polyethylene, space charge injected from electrode at low temps., luminesc. obs. 80−25464
polyethylene terephthalate, photoexcited, thermoluminescence field quenching 78−43942
polyethylene terephthalate, TSC and thermolum. due to electron detrapping by local mol. motions 80−96898
polyethylene terephthalate film, photoluminesc. exam. 78−48213
polyethylene-2,6-naphthalate fluorescence, transparency decay, possible appl. as polymer scintillators *(Chinese)* 79−93870
polyethylene-terephthalate, field-controlled photogeneration and carrier trapping 80−25285
polymer, carrier trap study by X-ray induced TSC and thermoluminescence *(Japanese)* 80−54713
polymer, photoradiative processes in free radical form. *(Russian)* 79−57269
polymer, thermolum. rel. to mol. relax. 78−11003
polymer, thermoluminescence data numerical anal., glass-rubber transition temp. spread 77−52189
polymer films, carrier transport meas. 80−6874
polymer orientation measurement, in solid, by spectroscopic techniques, mech. anisotropy 78−75558
polymers, space charge behaviour and luminescence at 77K 79−99947
polymethine dyes, secondary luminesc. 79−99934
polymethinium dye, excitonic fluoresc., absorpt. trapping spectra 78−27302
polymethyl acrylate, phosphorescence depolarisation studies of relaxation effects 78−56685
polymethyl methacrylate, subthreshold luminesc. 80−93414
polymonochloroparaxylylene film, photoluminesc. exam. 78−48213
polynitramines, solid cyclic, luminesc. meas. 77−32424
polyoxymethylene, irrad., thermoluminesc. above room temp. 80−2871
polyparaxylylene film, photoluminesc. exam. 78−48213
polypeptide hormones, conformations, ODMR investig. 78−76356
polypeptide hormones, folding, ODMR and phosphoresc. 79−20518
polyphenyls, fluoresc. and sensitization props. 79−38599
polystyre, irrad, thermoluminesc. 78−2931
polystyrene, electron trap depth distribs., thermolum. data 78−11002
polystyrene, end group modified, chain dynamics studied by fluorescence depolarization 80−19724
polystyrene, thermoluminescence glow curves, quenching and isothermal decay plots 77−48258
polystyrene, X-ray irrad., thermoluminescence emission, exam. of kinetic order 79−43046
polyvinylcarbazole, exciton migration, luminesc. and quenching *(Russian)* 77−36275
polyvinylcarbazole, fluoresc., photooxide quenching, exciton migration effects 79−56830
polyvinylidene fluoride, TSC and thermoluminescence, reln. to molecular motion *(Japanese)* 80−55200
porphin in host n-alkane crystals, phototautomerism, IR spectral obs. 80−34963
porphyrins, solid solns., phosphoresc. rel. to solvent heavy ats. *(Russian)* 77−40286
protein interaction with nucleic acids and sugars, studied by luminesc. 79−34476
PVC, film, uniaxially stretched, effect of mol. orientation on anisotropy of Young's modulus 77−86076
PVC, ozonized, decomposition of peroxides, chemilum. meas. 78−68893
PVC film, uniaxially stretched, mol. orientation, polarised fluoresc. investig., deform. mechanism 77−52440
pyrazine, electronic energy transfer to metal surface, classical image dipole theory 80−97318
pyrene, luminescence of free and self-trapped excitons 80−108250
pyrene, perylene doped, decay times and diffusion coeffs. of singlet excitons, under press. 77−20911
pyrene, triplet state, excitonic energy transfer, phosphoresc. and delayed fluoresc., 2 to 300K 80−84776
pyrene cryst., delayed fluoresc., mag. field effect, sense depend. 77−73160
pyrene crystals, anomalous emission excited near absorption edge 80−100682
pyrene in diphenyl cryst., luminesc. polaris. to induce radn. at O-O transition freq. *(Russian)* 79−38663
pyrene-PMDA complex, electron-phonon interaction, phosphoresc. 78−48208
pyrene-triethylamine exciplex, effect of dipolar molecules on quenching curves 78−52551
pyridine-$MnBr_2$ complexes, substituted, excitation spectra, ligand field theory 77−27103

luminescence of organic solids continued
pyridinium tetrachloromanganate II, luminesc. spectra, expt. and calcs. *(French)* 78−10967
pyrimidine derivatives, absorpt., luminesc. and polarisation spectra, electronic struct. 79−85993
quinazoline, in n-pentane (isooctane) Shpolskii matrices, luminesc. props., vibr. struct. 79−22739
quinoline, fluoresc., phosphoresc. and H bonding 77−79647
quinoline complexes with proton donors in triplet state, phosphorescence spectra 77−48230
quinoline in alcoholic glasses, induced fluoresc. 79−33775
quinoxaline in Shpolskii-type hydrocarbon matrices, vib. struct. of electronic spectra 77−85773
rhodamine 6G, electronic spectra, intermol. interactions effect *(Russian)* 77−48237
rhodamine 6G, in rigid matrix, conc. effects in spectra 80−83347
rhodamine 6G, on surface of stilbene cryst., sensitised luminesc., energy migration 79−56831
rhodamine 6G, quantum efficiency of intercombination conversion to triplet state by sensitised phosphoresc. *(Russian)* 77−85798
rhodamine 6G doped polyurethane film, fluoresc., photoinduced effects 77−1727
rhodamine dye polar frozen solns., luminesc. broadening 80−2834
Rochelle salt, mechanoluminescence and crack mobility, charge prod. during fracture 78−88370
rubrene film, excited complex with charge transfer, fluoresc. obs. of mag. reson. *(Russian)* 77−8454
Shpolskii multisite luminesc. spectrum deconvolution, vibr. struct. anal. 80−58304
shrimp, midwater, cryptic bioluminescence 80−3890
sodium 4-biphenylcarboxylate, room temp. phosphoresc., student demonstration 77−29
sodium naphthalate, room temp. phosphoresc., student demonstration 77−29
sodium salicylate, UV convertor layer, fluoresc. props. *(French)* 77−4676
sodium salicylate, vac. UV scintillators, characteristic props. at 253.7 nm 79−71525
sodium uranyl acetate, fluoresc., circ. dichroism 79−38598
spectra of diffuse reflection and photoluminesc. *(Russian)* 79−11447
spectrometer attachment for recording at liquid N_2 temp. 79−67394
stilbene:rhodamine-6Zh, luminesc. of adsorbed mols., excitonic energy transfer to surface 78−31255
stilbene, adsorbed rhodamine 6Zh, mol. cryst., role of excitonic and radiative mechs. of energy transport 80−108276
trans-stilbene, cryst., triplet excitons, $S_0 \rightarrow T_1$ transition 78−76518
trans-stilbene, in glassy media, phosphoresc., heavy atom effects 80−55153
stilbene, single cryst., triplet excitons, delayed fluorescence 78−63988
stilbene, single cryst. under pulsed electron excitation, triplet exciton luminescence and opt. absorpt. 79−7838
styrene-methacrylic acid copolymer, ionomer radiothermoluminesc. 79−95856
styrene-phenylacetylene copolymer, fluoresc. emission, energy redistrib. 78−39580
sugar, cryst., triboluminesc. kinetics 77−8669
sugar, mechanical relax. time, determ. from tribolum. 77−1173
sugar, mechanoluminesc., cryst. size depend. 79−38685
sugar, triboluminesc. kinetics 77−77306
sugar, triboluminescence and cryst. fracture dynamics 80−50437
sugar crystal, triboluminesc. kinetics and mech. relax. 77−73178
sugar crystals under stress, fracture-initiation time from triboluminesc. 77−59065
tartaric acid, triboluminescence and cryst. fracture dynamics 80−50437
p-terphenyl, cryst., double injection and electrolum. 80−97342
p-terphenyl, cryst., exciton phosphoresc. at 300K 80−108277
p-terphenyl, cryst., highly excited states decay, mag. field effects 78−10962
p-terphenyl, single cryst., delayed fluoresc., mag. field depend., 130-300K 79−69879
p-terphenyl, triplet exciton annihilation and triplet spin relax. 80−29792
p-terphenyl, vac. UV scintillators, characteristic props. at 253.7 nm 79−71525
p- terphenyl cryst., low lying single state 80−97320
tetraalkylammonium tetrahalometalates, opt. lifetimes rel. to thermal transitions 77−28608
tetrabenzo[a, cd, j, lm]perylene evaporated film, crystn., time depend. as function of purity 80−88449
tetrabutylammonium europium yttrium isothiocyanate, conc.-depend. electron-phonon coupling, and self-quenching 80−60657
tetrabutylammonium tetrahalomanganate, phosphoresc. lifetimes in fused salts and solids 78−72573
tetracene:pentacene, exciton migration, picosec. meas. 78−15207
tetracene:pentacene, pressure-induced phase transition, mag. field effect on guest fluoresc. 79−33083
tetracene:pentacene, thermally activated heterofission, fluoresc. 77−85787
tetracene, cryst., fluoresc. decay time, synchrotron radiation excitation 77−4675
tetracene, cryst., prompt fluoresc., mag. field depend. 77−85788
tetracene, cryst., solid-state transitions, Raman spectra, prompt fluoresc. in mag. field 79−99865
tetracene, cryst., triplet exciton pair kinematics, diffusion model, prompt fluoresc. decay 78−79931
tetracene, disordered, vapour deposited on glass substrate, fluoresc. and energy transfer 80−84761
tetracene, excimer luminesc. spectra, 4.2-300K 79−87478
tetracene, fluoresc. time decay, exciton interaction depend. 77−8618
tetracene, fluorescence, effect of weak external electric field *(Russian)* 78−80416
tetracene, optical obs. of charge transfer 78−35199
tetracene, photoluminescence spectra, 4.2-300K, phase transition and excitons 79−4847
tetracene, press.-induced phase transition, fluoresc. mag. field depend. 77−1728
tetracene, single cryst., exciton interactions, ps laser pulse intensity depend. 77−63448
tetracene, singlet exciton fission and fluorescence, mag. field depend. 78−39026
tetracene, spatial distrib. of electrolum. and recomb. process 79−19938

luminescence of organic solids continued
tetracene, thin cryst., electrolum. detection and determ. of spatial distrib. 79−19937
tetracene, triplet exciton diffusion and double photon absorpt., delayed fluoresc. obs. 77−36287
tetracene, unrelaxed fluoresc., direct picosecond obs. 80−89046
tetracene in alcoholic glasses, laser-induced hole burning mechanisms, zero-phonon fluoresc. 78−43912
tetracene surface states, electric field effects, exciton-charge carrier interactions *(Russian)* 80−24989
1,2,4,5-tetrachlorobenzene, exciton migration and trapping, X-trap phosphoresc. 79−1780
tetrachlorobenzene, in durene, 1.6K, $S_1 \sim\!\!\rightarrow T_1$ relax. mechanism, Zeeman phosphoresc. and PMDR obs. 77−30912
1,2,4,5-tetrachlorobenzene, in durene host, phosphoresc., cross-relax. between spin levels 78−9186
1,2,4,5-tetrachlorobenzene, localised excitations thermal promotion to exciton band, impurity states effect 78−52539
1,2,4,5-tetrachlorobenzene, mol. cryst., coherent 1-dimens. exciton transport and impurity scatt. 78−14666
1,2,4,5-tetrachlorobenzene, mol. solid, heat pulses, phonon-induced delocalisation of trapped excited triplet states 80−89053
tetrachlorobenzene, pure and doped crysts., triplet exciton trapping, phosphoresc. spectra 77−85766
1,2,4,5-tetrachlorobenzene, triplet energy transfer in substitutionally disordered system 79−52000
1,2,4,5-tetrachlorobenzene, triplet state spin-lattice relax. in cryst. and matrix isolated mol. 79−11449
tetradecane, with tetra-4-tert-butylphthalocyanine impurity mols., luminesc. 77−18965
1,4,5,8-tetrahydroxyanthraquinone, selective excitation, luminescence of long-wavelength component of multiplet 79−3478
N,N,N′,N′-tetramethyl-p-phenylenediamine, TMPD, glassy soln., photoionisation, recombination isothermal luminesc. *(French)* 77−16404
tetramethylammonium manganese chloride, energy migration rel. to impurity trap behaviour 77−55811
tetramethylbenzene: 2,3-dichloroquinoxaline, sublevel phosphoresc. spectra 78−70863
tetramethylpyrazine-d_{12}, photoexcited triplet state, in durene, phosphoresc., spin coherence and quantum beats 78−76517
s-tetrazine-benzene, mixed cryst., 2K, lifetime limited photochem. hole burning 78−9183
TGS:L-alanine, unirradiated, optical spectroscopy of scintillations 80−80863
TGS, switching induced electrolum. 79−38669
TGS, thermoluminesc. near Curie temp., effect of DC elec. field 79−33848
thymine film, polycryst., energy conversion processes, quantum yields, 4 to 10 eV 80−88589
toluene-1-hexene(1-pentene), radiolysis at 77K, fluoresc., energy transfer processes 78−20037
toluidinonaphthalenesulphonate, room temp. phosphoresc., isomer effects 79−61429
trialkylammonium, iodides, absorpt. and luminesc. spectra of self-localized excitons 80−97340
triethylenediamine, plastic cryst., thermolum. curves 80−2876
2,4,5-trimethylbenzaldehyde, in durene, cryst., photochem. and photophys. processes 77−60092
triphenylene, triplet state, MIDP and T-S excitation spectrosc. 79−81233
triphenylene in Shpolskii matrix, orientation, ESR and fluoresc. spectra 79−36688
triplet exciton dynamics, kinetic model 78−67948
trypaflavine, on silica gel, luminesc. quenching, activator location effects 77−52172
tryptophan, aq. alkaline soln., charge transfer, luminesc. obs., 77 and 300K 79−69876
tryptophan, aq. soln. charge transfer, luminesc. obs., 77 and 300K 79−69875
uranyl acetates, cubic crysts., optical spectra fine struct. 77−1693
uranyl propionates, cubic crysts., optical spectra fine struct. 77−1693
N-vinylcarbazole-1-vinylnaphthalene copolymer, triplet-triplet annihilation carrier photocurrent, delay fluoresc. 78−2513
xanthone, in n-pentane, heat pulse induced delayed phosphorescence 80−83404
xanthone in host crysts., triplet state PMDR, phosphoresc. spectra, transition mechanisms 77−46585
xanthone in n-hexane, 77 and 4.2K, phosphoresc. spectra, triplet lifetime 78−21957
p-xylene, isotopically mixed cryst., phosphoresc. triplet state, ESR and MIDP obs. 77−58071
ytterbium etiophorphyrin, electronic energy transfer with porphines and metalloporphyrins, luminesc. 77−474
zinc chlorophyll b, triplet state population at 4.2K, magnetic field effects 77−30915
zinc porphin, in n-alkane crystals. at 4.2K, Zeeman spectra for Jahn-Teller instability 78−27256
zinc porphin in n-octane, population hole-burning using triplet reservoir 79−87491
$AgGaSe_2$, two-photon absorpt. and short pulse stimulated recombination 80−89054
Al_2O_3 anodised film, surface impregnated by organic phosphors, fluoresc. spectrum *(Japanese)* 80−55170
CdS laser radiation under excitation by pulsed bremsstrahlung X-rays 79−91467
CdS(Se), magnetooptic study of P line at high excitations, biexciton binding energy values 78−48220
Cu complex, bis(triphenylphosphine) phenanthroline copper (I), luminesc. spectra, decay times 80−60648
1,6-di-(N-carbazolyl)-2,4 hexadiin, cryst. struct., luminesc., γ-ray polymerisation 78−18629
Eu complex, europium benzoyltrifluoroacetane chelate layers, fluorescence lifetime changes induced by variable optical environments 80−93386
Eu complex Eu dibenzoylmethane chelate with piperidine, vibronic and IR spectra 79−82981
Eu complexes, luminesc. spectra, electronic-vibr. transitions 77−52171
Eu piperidinium salts, emission spectra, ligand field symmetries 79−61413
Ir(III) complex, cis-dichlorobis(1,10-phenanthroline) iridium chloride, luminesc. excited states, solvent effects 80−97319

luminescence of organic solids continued
Mg porphyrins, additional ligands deuteration effect on luminesc. charcts. 79−99932
Mn^{2+}, in nearly tetrahedral clusters, ^4E levels, orbit-lattice interaction and Jahn-Teller effect, spectra obs. 80−24860
Mo_3 oxidation, IR emission spectrosc. obs. 78−68942
Nd^{3+} in glass and cryst. hosts, fluoresc. branching ratios 78−29956
$NdAl_3(BO_3)_4$, luminescence and lasing charcts., solubility 79−31910
Si, photoluminescence of annealed cryst., defect anal. 79−87500
UO_2 complexes, cubic crysts., low temp. optical spectra *(Russian)* 78−92083
Y_2O_3, formation and changes in point defects, EPR, optical transitions and thermolum. spectra 78−2118
Y_2O_3 sintered body, blackness study thermoluminescence anal. *(Japanese)* 78−23541

luminescence of solids
see also luminescence of inorganic solids; luminescence of organic solids
activated crystal, electron excitation energy transfer, collective coherent phenomena 77−90189
activated crystals, electronic excitation energy transfer efficiency, inverse transfer effects 78−2897
activated crystals, influence of temp. on energy transfer 79−28323
additional light waves near region of exciton absorpt. and luminesc. in crystal 80−2340
adhesive bonds breaking under high vacuum, light and electron emission, spectral comp. obs. 80−55190
amorphous and liquid semiconductors, conference, Cambridge, MA, USA (Aug. 1979) 80−41933
amorphous semiconductors, luminescence and absorption spectra calcs. 79−99938
anisotropic crystal, diffusion of excitons due to scatt. by optical phonons, Stokes line 77−24521
anthracene-Au interface exciton luminescence Frenkel exciton metallic quenching *(Russian)* 80−50421
anthracene-quartz interface exciton luminescence, Frenkel exciton metallic quenching *(Russian)* 80−50421
band shapes, Poisson distrib. moments 80−25419
benzene, in inorganic frozen solns., structured phosphoresc. spectra 77−65504
Bethe random lattice, spectral diffusion, total conductance distribution probability 80−8928
bistability and anomalies in absorption and resonance scattering of intense light 79−95803
bombardment induced light emission, chem. effect 77−28672
cathodluminescence measurement techniques 78−41354
cathodoluminescence analysis in SEM 78−32949
cathodoluminescence phosphor efficiencies, rel. to other material props. 77−81158
chain with light emitting ends, radiative lifetime, recombination kinetics 80−108260
configurational co-ordinate model, predictive use 79−19918
correlative transitions in relaxing systems, nonequilib. density matrix method *(Russian)* 80−50419
CRT display unit for weak luminesc. investig. 78−12763
crystal luminescence, effect of internal Raman scatt. *(Russian)* 78−60518
decay kinetics, jump mechanism case *(Russian)* 77−85796
diffusion-drift problem with plane symm. 77−8652
dilute systems, donor fluorescence at high trap concentration 80−71479
disordered molecular system, exciton percolation, book contrib. 77−36297
disordered system, phonon assisted energy transfer 79−38610
disordered systems, fluoresc. energy transfer, conc. depend. 80−50413
disordered systems, time dependent spectral transfer, Monte Carlo calc. 80−11464
donor fluorescence, t-matrix analysis 80−100679
donor-acceptor energy transfer, quantum statistical calcs. 77−1713
donor-acceptor energy transfer, quantum theory of temp. depend. *(Russian)* 77−73161
donor-acceptor energy transfer, reabsorpt. mechanism 79−78041
donor-acceptor pair lines, broadening due to potentials of ionised impurities 79−51522
donor-acceptor pair luminesc. band maximum position 77−52177
dynamic multiphoton processes as criteria for luminesc. of electronically excited centres 80−11463
electron+phonon system, weakly coupled, reson. light scatt. and luminesc. 77−12374
electron beam irradiated crystals, apparatus for optical parameters meas. *(French)* 77−26378
electron excitation energy transfer between molecules, theory, including reabsorpt. *(Russian)* 78−10981
electron recombination kinetics, Debye-Edwards law 79−87495
electron-phonon system, weakly coupled, resonant light scatt. and luminescence 80−40100
electron-vibrational transitions in presence of several minima of adiabatic potentials 77−81150
electronic excitation energy transfer, electron-vibr. transitions *(Russian)* 77−48232
electronic excitation energy transfer in activated crysts., math. modelling 79−38028
electronic states determ. using synchrotron radiation 77−20882
emission spectra and phonon relax. 77−77279
energy percolation is multicomponent solids 77−31972
energy transfer, unified model, arbitrary Franck-Condon offset and temp. 79−1781
energy transfer and two-centre optical transitions in OH^- and rare earth double-doped solid 80−7398
energy transfer models 80−76074
excitation spectra, automatic analysis 77−52154
excited-state decay for strongly interacting donors 77−8651
exciton luminescence, RF coherence and polarisation 78−10937
exciton luminescence spectra, surface polaritons and Brewster waves *(Russian)* 79−43033
exciton-photon interaction, exciton absorpt. lineshape, polariton and wave models 79−38564
excitonic molecule, Bose condensation, optical response 77−43512
excitonic molecules, Bose-condensed, emission spectrum, polariton effect 77−11856
excitonic molecules, secondary radiation, optical orientation effects 79−83010

luminescence of solids continued
excitonic molecules, theory, luminescence spectra of crysts., biexcitonic states classification 77−69238
excitons, condensation effects, review 78−2427
excitons, resonant secondary radiation, hot luminesc. *(Russian)* 79−52018
excitons and related states, conf., Tomakomai, Japan (Sept. 1975) 77−43510
F-centres, relaxed excited state, spin polarisation, saturated optical pumping 79−15522
fluorescence and absorption spectra, zero-phonon impurity lines, temp. broadening 77−8643
fluorescence detected circular dichroism, direction dependent opt. activity of photoselection 77−36279
fluorescence in prescence of traps, general theory 80−11478
Frenkel excitons, kinematical interaction at light absorption and luminesc. 78−10359
glass fibre reinforced plastics, stress luminescence, volume resistivity effects *(Japanese)* 78−43943
heavily doped semiconductor, interimpurity radiative recomb. 78−31253
high density excited system, population instability and optical anomalies 79−28826
hot luminescence and relaxation processes 79−38619
hot luminescence and reson. Raman effect of impurity centres 77−81149
impure crystal, sensitiser radiation quenching by activators, influence of collective phenomena 77−44052
impure substance, excitation migration effect on luminesc. spectrum with inhomogeneous broadening 80−60676
impurities in solids, absorption and emission spectra, bandshapes, moments 80−45122
impurity absorption and fluorescence spectra, quadratic electron-phonon interaction and impurity-ion band shape 78−6731
impurity atom fluoresc. radiation, intensity correlation, low temp. limit 80−80847
impurity atom in solid, reson. fluoresc., transient spectrum, intensity, and intensity correl. 80−84777
impurity atoms in solids, photon antibunching in reson. fluorescence 79−43025
impurity centres, migration of excitations, under inhomogeneous broadening conditions, math. modelling 78−48225
impurity centres, theory of time depend. of resonant secondary emission specta 78−92082
impurity luminescence, effects of reson. laser radiation on O-O line 78−6728
impurity radiative transitions, hydrostatic press. effects 79−38632
incoherent resonance decay and coherent optical ringing from coherently prepared electronic states 77−10698
inelastic light scattering conference, Santa Monica, CA, USA (Jan. 1979) 79−95762
ion beam induced light emission, review 79−95850
ion bombardment-induced photon emission, spectral features, mechanisms band struct. depend., review 77−44072
ion induced optical emission for surface and depth profile analysis 79−4333
ionic crystals, lattice defects, conference, Canterbury, England (Sept. 1979) 80−105420
ions in solids, time resolved fluoresc. line narrowing 79−38611
Jahn-Teller effect, equal coupling to ε and τ_2 vibrs., Γ_8 quartet 78−2454
Jahn-Teller system, lattice relax., photo-absorpt.-luminesc. polarisation correl. 77−51708
kinetics, WKB calcs. 79−33810
lanthanide ion fluorescent probes, spectroscopic obs. system 78−11573
lecture on luminescence and luminescent devices 78−27323
line profile, microscopic theory 79−28832
line shapes, for impurities, quantum-mechanical moments 78−72566
local heating, quantum transitions in coupled electron-vibr. system 79−15514
localised centres, reson. scatt. and absorpt. *(German)* 79−65848
localised centres in strong EM fields, multiquantum transitions 78−10936
localised electron-phonon system, second order optical processes, stationary response 78−43916
localised electron-phonon system, second order optical processes, transient response 78−43917
localised electron-phonon system with linear interaction, relationship between reson. light scatt. and luminesc. 78−43919
lone-pair semiconductor, defects, valence-alternation model and new directions 80−54646
microspecimens photo-, X-ray and thermally stimulated luminescence obs., installation for specimens ≥0.8 mm 80−57381
molecular chain, radiative lifetime of solitons. theory *(Russian)* 77−66539
molecular crystal, coherent 1-dimens. exciton transport and impurity scatt. 78−14666
molecular crystal, disordered, transport of energy of electron excitations 77−40283
molecular crystal, mixed, electronic energy dispersive diffusion in impurity band 79−69458
molecular crystal, sensitised luminesc. calc. for trapping models using momentum-space theory of exciton transport 80−11447
molecular crystal, Stark modulation of Lorentzian line shapes, Fourier anal. 77−1691
molecular crystal, surface exciton levels, radiation corrections 80−34962
molecular crystal with impurities, nonequilib. phonon excitation by laser pumping *(Russian)* 79−38664
molecular crystals, disordered, incoherent, electronic energy transfer in impurity band 80−75525
molecular crystals, triply-excited impurity centres, effect of acoustic wave on phosphorescence 78−27115
molecular fluoresc., phosphoresc., and ODMR line narrowing in solids 80−43084
molecular solid, disordered, exciton migration, dynamical approach 79−65916
molecular solids, Raman, fluoresc. and nonlinear props. 79−33702
molecular system, electron excitation energy transfer *(Russian)* 77−36292
non-equilibrium phonon distrib., in cryst., spectral line shape theory 80−60530
noncrystalline materials, optical props., lecture 78−27263
nondegenerate semicondcutor, three exciton radiative recomb. producing biexcitons 78−39603
luminescence of solids continued
nonequilibrium free carrier distrib. in EM wave field, luminesc. intensity and IR scatt. cross section 79−69888
nonequilibrium thermodynamics of luminescent processes in solids 80−50435
nonlinear luminescence quenching at high pumping levels, microscopic theory 80−89040
nonradiative quenching of hot luminesc. in F centres 80−11467
nonresonant energy transfer interactions, randomly distrib. mols. in lattice, numerical anal. 77−8626
nonresonant transfer of energy between impurities in solids 78−23520
optical no-phonon impurity lines, influence of local and quasilocal vibrations on thermal broadening 78−30717
paramagnetic molecules in rigid isotropic medium, mag. linearly polarised emission 78−68545
particle-surface collisions, optical emission obs. 77−36300
percolation model, one-dimens., spectral diffusion 78−80411
perfect crystals, low-temp. exciton luminesc. 79−56826
phonon-assisted radiative electronic transitions 79−24348
phonon-assisted radiative transfer 77−90192
phosphor, rare earth activators, sensitized luminesc., computer simulation 78−6723
phosphor adsorbates, luminesc. quenching, activator location effects 77−52172
phosphor recombination after glow build-up 77−8628
phosphors, quantum efficiency meas. for UV, visible, cathode ray and X-ray 77−41699
photoacoustic measurement of absolute quantum efficiencies 79−19924
photogeneration and fluoresc. quenching theory, appl. to x-metal-free phthalocyanine 79−65513
photographic recording device based on oscillographic delayed-coincidence method 77−38025
photoluminescence, radiationless relax. of excitation energy *(Russian)* 77−32418
polar semiconductors, resonant secondary radiation 78−31242
polycrystalline solids, Zeeman spectra 78−68487
pre-breakdown luminescence in dielectrics, intensification of underexposed photographs 77−24793
predictability of luminesc. props. 79−47504
quantum and radiant efficiency meas. methods, standard materials 78−32899
quantum EM processes, population var. and natural radiative decay *(Russian)* 77−32343
quenching, hopping mechanism, kinetics 80−7406
quenching parameters, donor-acceptor exchange mechanism 80−2840
radiative and nonradiative recomb. at metal ions, core struct. effects, review 79−4834
radiative electronic transitions of impurities, effects of hydrostatic press. 80−11446
rare earth activated phosphors, chemistry and physics, book contrib. 80−55187
rare earth luminescence from intensity meas. on powdered phosphor screens self-concentration quenching mech. determ. 79−69880
recombination interactions, unimolecular processes, diffusion-limited kinetics 78−6794
recombination kinetics 79−47502
relaxation between systems with equidistant levels *(Russian)* 78−23526
resonance light scattering, statistical aspects 78−80323
resonance light scattering and hot luminesc. of self-trapping excitons 80−93336
resonance Raman scattering and luminescence of excitons in self-trapping process 80−20689
resonant secondary emission, time depend. spectra 79−52019
resonant secondary emission components classification, theory applic. to expt. 80−93339
resonant secondary emission theory 79−38615
resonant secondary emissions by impurities in crysts. 80−93335
resonant secondary radiation of excitons strongly interacting with phonons 79−60724
resonant secondary radiation of excitons weakly interacting with phonons, theory 78−31241
review, conduction band behaviour, defects and impurity centres *(Chinese)* 79−33835
review, progress over past 25 yrs. 79−28840
second order optical processes, intermediate state interaction stochastic models 77−48243
second order optical processes, stochastic models of intermediate state interaction, stationary response 77−85769
second order optical processes, stochastic models of intermediate state interaction, stationary response 77−85770
selective excitation of probe in luminesc. technique development for chem. analysis 80−40797
semi-infinite direct-gap semiconductor effect of reabsorbed recomb. rad. 78−95312
semiconducting solid solutions, optical transitions, review 78−2908
semiconductor, bound exciton recombination, phonon replicas 79−38649
semiconductor, broad-band, meas. setup with GDM 1000 grating double monochromator 78−21226
semiconductor, direct-gap, polariton luminesc., under strong excitation conditions, exciton gas model 77−8650
semiconductor, donor-acceptor pair in elec. field, anomalous Stark shift of ground state energy 79−19564
semiconductor, donor-acceptor pair luminesc. polarisation with optical orientation 77−24895
semiconductor, effect of free carriers on exciton luminescence 78−48226
semiconductor, high-conc. exciton and biexciton emission 78−6725
semiconductor, hot carrier phenomena, optical obs. 79−95845
semiconductor, impurity interaction and donor-acceptor recombination 80−16094
semiconductor, impurity study by visible and far-infrared laser spectroscopy 77−74524
semiconductor, luminescence, coherent conversion of excitons and photons to biexcitons *(Russian)* 79−47508
semiconductor, luminescence emitted from excited acceptor-donor complexes subject to external electric field 77−66544
semiconductor, magneto-optic effects due to optical alignment of electrons and nuclei 78−6654
semiconductor, multiphonon recombination processes 79−38643
semiconductor, narrow-band, heterogeneous chemiluminesc., ionisation mechanism of excitation 80−50438

luminescence of solids continued
semiconductor, optical parameters in strong EM field, effects of finite wavelength of light 77−44050
semiconductor, optical phonon generation on intraband absorpt. of EM radiation *(Russian)* 77−48235
semiconductor, optical props. under intense laser field 79−43040
semiconductor, phonon fluorescence stimulated by laser radn. 79−87504
semiconductor, photoluminescence, deep level recombination temp. depend. 79−47497
semiconductor, polariton dispersion change by virtual biexciton form. under laser irrad. 79−38607
semiconductor, radiative recomb. at donor-acceptor pairs, majority impurity config. average calcs. 80−40154
semiconductor, recombination radiation mag. depolaris., spin level quadrupole splitting of lattice nuclei *(Russian)* 79−38666
semiconductor, resonance secondary radiation emission, theory 78−60452
semiconductor, spin injection, carrier polarisation, luminesc. polarisation 77−15957
semiconductor, spin-depend. luminescence of donor-acceptor pairs 77−48223
semiconductor, strong electron-lattice interaction, review *(Japanese)* 80−49664
semiconductor, TEM/SEM observations comparing diffr., elec. and luminesc. contrast from dislocations 78−38714
semiconductor, temp. modulated photolum. induced by photoexcitation 78−95605
semiconductor, two stage model for deep level capture 78−10396
semiconductor, variable band, recomb. radiation polarisation oscills. in mag. field *(Russian)* 77−77283
semiconductor, variable-gap, with high band-gap gradient, charact. of radiative recomb. 79−56858
semiconductor crystals, with high quantum efficiency, minority carrier lifetime meas. *(Japanese)* 80−54711
semiconductor crysts., polarisation of emitted pair radiation 77−52173
semiconductor electron-hole pair creation and migration 77−77304
semiconductor film, cubic, polarisation of edge luminesc. arising from quantum size effect calc. 77−16390
semiconductor film, donor-acceptor pairs, polarisation of recomb. radiation in presence of quantum size effect 79−11462
semiconductors, Auger and radiative recombination of acceptor bound excitons 79−47023
semiconductors, exciton condensation and electron hole liquids, state-of-the-art 80−49625
semiconductors, heavily doped, compensated, long wavelength recomb. radiation 80−7403
semiconductors, high density excitons and biexcitons, recomb. radiation bands profiles, time depend. 80−45140
semiconductors, luminesc. parameters, absorpt. parameter effects *(Russian)* 78−80419
semiconductors, optical props. under press., book contrib. 80−84715
semiconductors, radiative recomb., book contrib. 80−84784
semiconductors, variable-gap, photoluminesc. under transient excitation conditions 80−20698
sensitised anti-Stokes luminesc., theory 77−66537
single crystal impurity luminesc. attenuation in Raman spectra using Cu vapour laser 79−15467
solid solutions, inhomogeneity and site selective impurity-phonon coupling effects 78−84625
solid state spectroscopy using synchrotron radiation, book contrib. 80−7375
spectral transport, time-dependent, Monte Carlo study 79−33826
spectrally inhomogeneous media, nonreson. transfer of excitations, temp. depend. 80−80859
spectroscopy using Weierstrass sphere geometry 77−49777
statistics 79−33756
substitutionally disordered material, impurity band triplet energy transfer 79−51513
superlinear filling of traps in crystals due to competition during irradiation 79−33850
superradiance in solid state physics, review 79−51988
thermal quenching of luminesc. for linear and derivative nucl. operators 77−8631
thermoluminescence and TSC, evaluation of model, reliability of trap depth determ. 77−32451
time resolved spectroscopy using new laser techniques 77−79162
transition quasilinear spectra of resonant secondary emission *(Russian)* 80−16102
transition rates in single $\hbar\omega$ models 79−33774
transparent dielectric, nondirectional glow under laser irrad. 78−52575
trap dynamics rel. to minimum entropy prod. *(French)* 77−77263
triboluminescence kinetics in crysts. 77−77306
tunnelling during excitation of electroluminescence 78−43936
two-dimensional crystals, exciton-exciton and exciton-electron interactions in luminesc. spectra 77−52179
uniaxial crystal, macroscopic exciton luminesc. charact., high reabsorption conditions 78−19545
up-conversion and excited state energy transfer in rare earth doped materials, book contrib. 77−36296
variable-gap semiconductors, anal. of drift of recombination radiation 80−16096
vibrational relaxation of molecules in condensed media, survey, book contrib. 77−36295
vibronic systems with localised electrons, reson. Raman scatt., hot luminesc. 79−38616

luminescent devices
see also fluorescent screens; phosphors; scintillation counters
CRT display unit for weak luminesc. investig. 78−12763
display tube, vacuum, scaling decade circuit 77−18754
electroluminescent, photoconductive image intensifier parameters *(Russian)* 78−42421
heterostructures, multipass, external quantum efficiency of luminescence 77−20419
hydrodynamic electrochemiluminescence cell 80−45506
lecture on luminescence and luminescent devices 78−27323
m.i.m. structure, light emission, by inelastic electron tunnelling 77−1734
radiation crack detection, use of luminescent convertors 78−53125
review, progress over past 25 yrs. 79−28840
rubrene thin layer and flow cells, steady DC electrogenerated chemilum. 80−55205
solar cell greenhouse collector 77−761

luminescent devices continued
AlAs-GaAs multipass heterostructure, spectral and ang. charact. of luminesc. 77−20418
AlAs-GaAs multipass heterostructures, external quantum efficiency of luminesc. 77−20419
Au/ZnSe:Mn/n-GaAs low threshold thin film DC electrolum. cell, pulse-excited charact. 80−76081
GaAs MOS structure, white light emission obs. 78−76148
n-Ge-ZnSe:Mn^{2+}-$In_{2-x}Sn_xO_{3-y}$ thin film electrolum. cell with low-threshold voltage 80−84786
InSb, overheating luminesc., appl. as large-area light emitter 77−44068
SnO_2-Cu_xS-ZnS:Mn,Cu-Al_2O_3-Al, light-emitting struct., cond. and electrolum., heat treatment 80−97345
ZnS:Cu, Br based electroluminesc. cells, light, const. field effects on electroluminesc. 78−84658
ZnS:Mn AC thin film devices, domain electrolum. 80−66303
ZnS:Mn AC thin film electrolum. device, filament behaviour 80−20712
ZnS:Mn co-deposited electrolum. thin film device, phys. and elec. characterisation 80−20713
ZnS:Mn film device, laser modulation of electrolum. 78−52576
ZnS:TbF_3 film between semicond. Y_2O_3 layers, bright green electrolum. 80−2859
ZnSe-GaAs thin film DE electroluminescent cell with 20 V threshold voltage 78−76141
ZnTe-CdS(Se)(S_xSe_{1-x}) heterojunctions, prep. and electrolum. charact. 77−24610

luminophors *see phosphors*

luminors *see phosphors*

lumped parameter networks
US transducer lumped wideband equaliser design optimisation 79−46159

lunar atmosphere *see extraterrestrial atmospheres; Moon*

lunar geology *see lunar rocks and minerals*

lunar rocks and minerals
adsorption of methanol and water on soil 15081,2, microcrystallinity determ. 77−87292
ages, rel. to early chronology of Moon and collisional history of solar system 77−60640
aluminous mare basalt obtained by Luna 16, petrology and mineralogy 80−41737
analysis, neutron activation, using standard reference materials as multielement irrad. standards 78−80815
ancient magnetic field intensity determ. from NRM and surface field meas. 77−37530
ancient regolith, record of solar and galactic radiations 77−60695
anorthosite 15415, isotope and age spatial distrib. from stepwise degassing data 79−34967
anorthosite from Luna 20 landing site, petrographic investigation and high-voltage electron microscopy 77−60631
anorthositic breccia, Luna 20 sample, petrology *(German)* 77−45329
Apollo 11, 12 and 15 basalts and regolith, anal. of var. in Al, Mg and Si abundances 78−16320
Apollo 14 soil, high silica glasses, evidence for silicic lunar volcanism 77−5468
Apollo 15 fines, ^{40}Ar intercept values and young apparent ^{40}K-^{40}Ar ages 77−29669
Apollo 16 'melt sheet' chemistry, age and Rb/Sr systematics 77−17389
Apollo 17 drill core samples, low Ti mare basalts 77−71022
Apollo 17 KREEPy basalt, rock type intermediate between mare and KREEP basalts 77−87286
Apollo and Luna samples, surface texture from polarimetric and photometric obs. 77−60673
Apollo-17 drilled sample major and trace elements in grain size fractions, U, Co, La, Fe, Ge, Cd *(German)* 80−51673
armalcolite, synthetic, stability as function of press. and O_2 fugacity 77−64275
basalt, chemical comp. rel. to Moon bulk comp. and terrestrial basalt 77−60636
basaltic liquids, Fe and Mg distrib. 79−35158
basaltic magmatism and bulk comp., major and heat-producing elements 78−7891
basaltic magmatism and bulk comp., siderophile and volatile elements 78−7892
basalts, chemical differentiation by gravit. separation of quenching crysts. 77−60649
basalts, expt. crystallization at low press., Fe gain and loss problems 77−87293
basalts, redox state 78−77217
basalts from Mare Crisium, mineralogy 78−65519
Bench Crater meteorite, member of new subgroup of carbonaceous chondrites 78−65573
bonded particles, gas interaction effects 77−37523
boulder shadow temp. and duration from shaded soil sample thermoluminescence 77−33372
breccia, $^{40}Ar/^{39}Ar$ dating of plagioclase clasts, rel. to early lunar differentiation 78−65514
breccias, magnetization origin, thermal overprinting 78−61760
breccias from Apollo 16, ages, comp. and depths rel. to pre-Imbrian craters and basins 79−53739
charged particle track anal., thermoluminesc. and microcratering studies 77−60665
chemical changes at impact-induced phase transitions 77−60662
chemical composition from albedo and colour index 77−87296
Chernier Crater, lava-like material nature and origin 78−81569
classification of lunar rcks and glasses by multivariate statistical technique 77−41336
classification of rocks and glasses using the G-mode central method 80−101535
complex magnetic susceptibility rel. to viscous remanent mag. 79−29999
conductor-like behaviour of photoemitting dielectric surface 79−101046
core samples, technique for thermal cond. meas. 80−72781
cosmic ray exposure ages and burial depths from cosmogenic Xe ratios 77−57661
cosmic ray fossil tracks rel. to long term composition changes 77−60552
cosmic ray induced fission of heavy nuclides, influence on apparent ^{238}U fission track ages 79−40047
cosmic ray interactions, nature and composition of species formed 77−41334
cosmogenic isotope concs. in lunar samples rel. to past solar activity 78−61828
detrital zone in Shorty Crater cores, age estimation 79−2494

lunar rocks and minerals continued
dielectric props. of lunar and planetary surfaces 77−60678
differential photoelectric charging of nonconducting surfaces in space 79−25439
dust, electrostatic transportation by localised photoelectric charging at sunset terminator 77−45330
dust, LEAM response to electrostatically charged microparticles 79−58259
dust and mass transport on lunar surface 80−8558
dust far UV reflectivity, comparison with moon far UV albedo 77−37513
dust sample 61501, light rare gases abundances in primary particles *(French)* 80−51674
electrical conductivity rel. to thermocline 77−60687
elemental abundances, implications from sputtering rates of minerals 80−61797
Fahrenheit crater ejecta, emplacement at Luna-24 site 80−8564
far IR radiation with rocks 77−60666
felspathic liquids, origin 77−60650
ferrobasalts from Mare Crisium, Luna 24 soil samples 78−32371
ferromagnetic resonance studies, sample quality effects 79−70971
fines, gaseous Rn accumulation and circulation 77−60668
fines, implantation of rare gases 77−60672
fires, rare gas diffusion as bubbles 79−48695
Fra Mauro basalts, origin, rel. to Mg_2SiO_4-Fe_2SiO_4-$CaAl_2Si_2O_8$-SiO_2 system phase relations 78−65512
front-side mare fillings, effect on lunar moments of inertia differences 78−45247
gabbroic anorthosite sample, thermal and deform. history, shock melting 78−65517
gabbros from Mare Crisium, anal. of Luna 24 soil 78−32370
gardening process, by meteoroid impact cratering *(Japanese)* 77−91452
geochemical mapping by orbital gamma-ray spectroscopy 77−25953
glass clod, Ti rich, at Oceanus Procellarum, implications 79−70970
glass globules, origin of shapes 80−62048
glass spheres formation on lunar surface by impact melting 77−60661
grains, catalytic action for prod. of high mol. wt. glycerides 78−3333
grains surface chem., solar wind sputtering effects 78−77501
heavy-ion tracks, etchable ranges 77−30734
high-energy particle interactions, gamma-ray production, simulation 78−16318
high-silica glass inclusions, in olivine of Luna 24 samples 78−32368
highland melt rock suite 78−81568
highland rocks, indigenous siderophiles content 80−8562
highland rocks, radiometric dating rel. to stratigraphy 77−60645
highland samples, chemical element correls. rel. to Moon bulk comp. 77−60637
highlands rocks, origin and comp. and effects of meteorite bombardment 80−109381
igneous events in lunar evolution 77−87294
igneous rocks, normative composition and classification 79−44382
igneous rocks, supercooling on lunar surface, review of analogue information 77−60652
ilmenite, cell dimensions and antiferromag. 77−21764
Imbrian-age highland volcanism, Gruithuisen and Mairan domes 78−77504
Imbrium ejecta, petrology rel. to lunar stratigraphy 77−60641
impact ejecta, props. rel. to ages of Serenitatis, Imbrium and Orientale events 77−60642
impact microcraters, diameter to depth ratio dependence 80−94765
internal composition, from density model consistent with topographic, gravit., librational and seismic data 77−45332
ion beam analysis 80−62089
KREEP basalt evolution and Sm-Nd age 80−12686
KREEP origin 80−4279
KREEP-basalt formation ages, radioactive dating 78−32372
large-scale chemical variation, results from orbital gamma-ray data 78−12123
lavas, effusion rate and rheology 77−60654
logical searching of the lunar data, FORTRAN program incorporating Boolean search capabilities 79−2491
Luan 16 and 20 samples, mineralogy and petrochemistry *(German)* 77−41326
Luna 16 and 20 samples, ^{40}Ar-^{39}Ar dating 77−22125
Luna 16 and 20 samples, major and trace element anal. *(German)* 77−41327
Luna 24, Mare Crisium core sample return and analysis 77−29673
Luna 24 basalt age rel. to crater density data 77−22119
Luna 24 basalts, irrad. history and $^{40}Ar/^{39}Ar$ age determ. 80−82245
Luna 24 core, fragment mineralogy and petrology 80−82243
Luna 24 core sample, solar flare exposure and thermolum. obs. 80−82246
Luna 24 core sample L24125, optical excitation spectroscopy 80−82244
Luna 24 core samples, separation and distrib. 80−82241
Luna 24 drill core soil samples, depositional history 79−88608
Luna 24 landing area, regional basalt types from remote spectral refl. meas. 77−22118
Luna 24 soil samples, metal and phosphide phases 80−82242
Luna 24 soil samples, metallic phases anal. 78−32367
Luna-20 pyroxenes, cation distrib. and exsolution as chronological indicator of thermal history 78−45246
Luna-24 regolith column, particle track based irradiation and accretion history 78−45244
magnetic field, shock effects and remanence in hypervel. impact expt. 79−29755
magnetic field of Moon determined from fines 80−36526
magnetic fields in early solar system, recorded in lunar rocks, meteorites and planets 79−5765
magnetisation due to hypervelocity impact, lab. simulation 77−91115
magnetism of sample 10017135, application of new palaeointensity method 80−36527
mare and highland soils, elements distrib. 78−12114
mare basalt magmas, compositions and characts. 77−45333
mare basalt petrogenesis, comment 77−87295
mare basalt petrogenesis, review of expt. studies 77−13258
mare basalt petrogenesis 77−60647
mare basalt petrogenesis and interior composition 77−60694
mare basalt suite 78−77500
mare basalts, absolute time scale of mare form. and filling 77−60646
mare basalts, comparison with terrestrial mid-ocean ridge basalts 79−16424
lunar rocks and minerals continued
mare basalts, crystal chemistry, mineralogy and petrology 77−45334
mare basalts, Fe^{2+} reduction by S loss 77−9681
mare basalts two-stage generation model 77−60648
mare basalts with high Ti content, opaque oxide mineral crystallization 79−66933
Mare Crisium, radar-detected subsurface interface as buried regolith 79−16848
Mare Crisium, view from Luna 24, conference, Houston, Texas (1977, December 1 to 3) 80−17710
Mare Crisium gabbroic and basaltic fragments, opaque mineral chemistry 78−32369
mare grounds relative spectral reflectivity 80−12695
metallic fragment, dendritic struct. *(Russian)* 77−67050
metallic fragment, from Mare Foecunditatus, struct. and comp., meteoritic origin *(Russian)* 77−9682
meteorite flux recent temporal changes, from lunar sample data 79−2534
microcrater and accretionary grain populations, development from lunar surface and Apollo samples obs. 80−94732
microcrater and accretionary grain populations, temporal development under meteoroid and solar wind bombardment 80−94731
microcraters density, rel. to micrometeorites and solar flare particles in and out of ecliptic 77−29737
Mossbauer spectra, assessment of results 77−60655
neutron activation analysis of lunar samples and primary matter 78−7890
North Ray Crater soil (Apollo 16), surface props. 77−87287
olivine, petrologic data from crystallised silicate melt and other inclusions 77−2146
olivine dominated upper mantle, implications on development of Moon of fission origin 77−41335
olivine fractionation equations for basaltic and ultrabasic liquids 79−20818
olivines, Luna 16 samples, cryst. struct. rel. to terrestrial olivines *(German)* 77−41324
Orientale basin ejecta, radial thickness vars. 78−89088
orthopyroxene from anorthosite 15415, crystal structure and thermal history 78−53842
outcrop of bedrock, possibility at Fossa Recta, Lunokhod-2 data 78−24475
palaeomagnetism, origin 78−93132
particle track record of lunar regolith history 77−33369
petrology and early development of crust 77−37517
plagioclase, luminescence cause and significance 77−60674
plutonic rocks, suite of materials depleted in trace siderophile elements 79−62766
pyroxenes from planetary basalt, silicate mineralogy study 80−72802
Q-values in 3000-5000 range 77−60682
quartz, impact structs., peak shock press., X-ray diffr. investig., lunar rock bombard. appls. 78−7002
radar backscatter properties, rel. to dielectric props., density and surface slopes 77−53438
raw materials for space manufacturing, comparison of terrestrial practice and lunar availability 77−87233
ray material, origin and darkening 78−12119
regolite, Fe reduction on heating in vacuum, XPES spectra 80−41740
regolite, XPS 79−21206
regolith, dynamics rel. to irradiation and accretion of solids in space 77−60562
regolith, elements volatilisation from solid particles 77−9680
regolith, EM sounding during Apollo 17 SEP expt. 79−62768
regolith, fine particulate Fe *(Russian)* 78−89089
regolith, IR spectra, Salyut 4 obs. in 3.5-7 μ range 78−69716
regolith, Luna 16 and 20 samples, electron microscope examination *(German)* 77−45328
regolith, Luna 16 and 20 samples, high voltage electron microscopy of 0.1-10 μ grain fractions *(German)* 77−41325
regolith, Luna 16 and 20 samples, mineralogy, crystal struct. and elec. cond. *(German)* 77−41323
regolith, metallography of Fe particles *(Russian)* 78−16321
regolith, physical charact. and dynamics 77−60660
regolith, reduction of Fe, Ti, Si when heated in H atm., X-ray photoelectron spectra 79−25527
regolith, secondary electron emission charact, determ. method 80−12687
regolith density meas., review 78−16317
regolith fine fraction, Luna-24 slow positron probe 80−26762
regolith from Mare Crisium, chem. comp. determ. 79−62767
regolith interaction with lunar exosphere, Monte Carlo simulation methods 80−67588
regolith light element chemistry of Apollo 12 site 78−65515
regolith microbreccias $^{15}N/^{14}N$ ratio indicating ancient solar wind composition 80−62046
regolith mixing extent 80−8561
regolith particles, size distrib. rel. to Rosin's law 78−45248
regolith particles in Earth's atmosphere, variation in chemical composition in surface layers *(Ukrainian)* 80−12685
regolith radioactivity in Mare Crisium, orbital and laboratory estimates comparison 80−62045
regolith reprocessing by cratering, erosion of material layer which loses charact. props. 80−62053
regolith samples from Luna-24, element abundance determ., neutron activation obs. 80−67597
regolith samples from Luna-24, X-ray diffr. and thermogravimetric obs. 80−67598
remanence in lunar rock fragments and fines from Luna 16 and 20 77−22123
returned samples, radiometric ages rel. to lunar chronology 77−60644
review, crystal chemistry, petrology and geochemistry 77−45327
ringed impact basin ejecta deposits, correl. with far-side magnetised regions 80−36521
rock samples from craters, comparison with samples from Manicouagan Impact Structure, Canada *(French)* 79−88355
Rosiwal Principle appl., solar wind implanted species, grain size dependence 77−29667
sampling techniques for interplanetary particles 78−57459
siderophile elements deficiency rel. to fission from Earth origin 77−60693
siderophile elements indigenous abundances in lunar highlands, rel. to lunar origin 79−5767

lunar rocks and minerals continued
silicate magmas, liquid immiscibility in K_2O-FeO-Al_2O_3-SiO_2 system 77−13076
silicate rocks and minerals, instrumental neutron activation anal. 78−20548
silicates, electronic absorpt. spectra, transition metal ions presence 77−60657
soil, ^{40}Ar excess, retrapping mechanism 77−60671
soil, comparative modal petrology and phase chem. of >20 μm and <20 μm fractions 79−84688
soil, Fe and Ti bands in glass fraction 77−49320
soil, from mare and highland areas, element abundance anomalies 78−49349
soil, light refl. meas. rel. to brightness distrib. over lunar disc 80−17512
soil, near IR refl. coeff., Luna 24 obs. *(Russian)* 77−73983
soil, particle size distrib. anal., Rosin's law 77−78682
soil, particle size distrib. at Luna 16 and Luna 20 landing sites 77−53437
soil, relationship between surface chemistry and albedo, Auger electron spectroscopy 77−60677
soil, shock effects on magnetism 77−60675
soil, surface refl. characts. for radar, obs. from Luna spacecraft 80−72798
soil and gabbroic fragment from Mare Crisium, ^{87}Rb-^{87}Sr age 78−40850
soil column from Luna-24, grain size separates from particle track anal. 80−67599
soil electrostatic transport, terminator configuration model 79−35157
soil from Luna 24 drill cores, rare gas elemental and isotopic ratios 80−26760
soil grains, surface related component of Fe metal 79−16851
soil grains from Luna 24 drill core samples, surface exposure duration 80−67592
soil grains surface composition, comparison of results of Auger and ESCA spectroscopy 78−32366
soil physical props. of Luna 20 sample 77−33365
soil properties, effects of sample selection process 77−29665
soil sample separation and distrib. from Luna 16 and 20 missions 77−22121
soil samples from Luna 24, inert gas element and isotope composition 80−67593
soil samples from Luna 24 and Apollo 16, natural radioactivity meas. 80−67595
soil samples from Luna-24, N_2 abundance neutron activation obs. 80−67594
soil samples from Luna-24, radioactivity and cosmic ray dose rate, thermolum. obs. 80−67596
soils, ^{14}C abundance in solar wind 77−5407
soils, effect of annealing temp. on reactivity towards adsorbed water 77−60632
soils, exotic component rel. to global radioactive crust 77−60643
soils, IR spectra compared with astrophysical IR features 80−26728
soils, Li abundance in Luna 24 soil samples 80−67590
soils, mineral comp. determ. from spectral behaviour of albedo 79−21207
soils, simple molecules presence, appl. to Mercury surface mols. 78−16324
solar wind, inert gas abundance, 500 Myr ago from lunar dust anal. *(German)* 80−51637
solar wind effects, in-situ meas. review 80−77556
solar wind effects on surface chemistry of lunar grains, reply 79−12374
solar wind interactions with surface grains, O^{n+} role 80−62050
solar wind sputtering, chemical and isotopic fractionation 78−61762
solar wind sputtering, comments 78−61763
solar-wind exposure effects in the lunar soil, review 79−75070
solute partitioning, diffusive isothermal, in layered material 77−16896
space weathering effects, microprobe studies 77−60725
spacecraft exploration results, review 77−2356
stratigraphy, basic principles 77−60690
surface chemistry, weighted-filter imaging technique appl. to X-ray fluoresc. data 78−12124
surface dust movements, evidence and causes 77−60667
surface layers, dielectric const. and temp. gradient from 2 and 6 cm brightness distrib. 78−81572
surface material, heavy isotope enrichment due to solar wind sputtering 79−87538
surface material, props. from optical obs. 78−12130
surface materials, interaction with exospheric atmosphere 78−49351
thermal conductivity prediction of heterogeneous mixture, digital simulation technique 78−87247
thermally metamorphosed agglutinate from Apollo 16 soil 77−37529
thermoluminescence measurement apparatus, lunar samples and meteorites appl. 77−13803
trace element nondestructive anal. using proton microprobe 78−64911
troilite, ^{34}S enrichment mechanism, appl. to lunar soil 80−77303
upper lunar crust, lithification and structure densities 77−60681
volatile trace elements determ. by RNAA 79−44276
volcanic ash, terrestrial vs. extraterrestrial 77−2134
X-ray anal. of microcrystallite nucleation and detection threshold 80−890
$^{39}Ar/^{40}Ar$ dating of rock fragments from Mare Crisium 78−65513
C chemistry of lunar soil samples from Luna 16 and 20 77−22122
Ca, isotope fractionation on Earth and other solar system materials 79−20835
Fe content via Mossbauer studies, Luna 16 and 20 samples 77−22124
Fe, first order shock induced mag. transitions characts. and discrimination from TRM 78−64205
Fe particles, FMR study, effective linewidth method 78−95523
Fe-group nuclei, energy spectrum from lunar soil samples 77−53353
FeOOH stability on lunar surface 77−33371
H, O, Si isotope systematics in soil and rocks 77−60676
He, Ne and Ar isotopes and ^{236}U prod. by solar cosmic ray protons, rate calc. 77−17311
^{3}He content meas., method for solar flare cosmic ray proton flux determ. 80−98576
Hf, determ. in silicate rocks, meteorites and lunar samples by neutron activation 78−20547
K-rich globules in Luna 20 soil, SEM obs. 80−67591
$KAlSi_3O_8$, orthoclase, impact structs., peak shock press., X-ray diffr. investig., lunar rock bombard. appls. 78−7002
Li and halogen contents, in soils, breccias and rocks 77−60638
Li and halogens determ., rel. to cosmochemical processes 78−12111
^{53}Mn meas. in lunar soil, evidence for cosmic ray modulation absence during glacial period 79−80129
O isotope abundance in Luna 16 and 20 soil 77−22120
O preferential sputtering, rel. to metallic Fe prod., element fractionation and trace element enrichment 77−29666
S contents, neutron capture gamma-ray spectroscopy 80−94728
S distribution in rocks rel. to C lontent 78−4123
Ti rich basalt geology of Oceanus Procellarum, Flamsteed region 80−105183
TiO_2 distrib. over surface from anal. of Mikhail's photometric catalogue *(Russian)* 78−73661
Zr, determ. in silicate rocks, meteorites and lunar samples by neutron activation 78−20547

lunar seismology
Apollo data, processing methods 80−51676
Apollo lunar surface science stations shutdown 78−57425
Apollo seismic network results, lunar seismicity, structure and tectonics 77−60679
basin-forming impacts, global seismic effects 78−12122
deep moonquakes, HF teleseismic events and transient lunar phenomena 77−60684
deep moonquakes, tidal triggering 79−66938
density model consistent with topographic, gravit., librational and seismic data 77−45332
high frequency teleseismic events, shallow moonquakes 77−71027
mantle, seismic vels. rel. to constitution 78−85866
microseismic background, observing possibilities 78−16319
moonquake data anal. from Apollo stations 77−71028
moonquake mechanisms rel. to tidal stresses 77−78685
multiple scattering role in formation of seismogram coda 79−25205
periodicity rel. to lunar sidereal period 78−53844
rock Q-values in 3000-5000 range 77−60682
seismic energy transmission in intensively scatt. environment, diffusion eqn. 77−73685
surface reflections use in lunar seismograms 78−65504
theoretical problems, conf., Aug. 1978, Caracas, Venezuela 80−51400
thermal history, present state and tectonics, fission origin model 80−98582
tidal stresses rel. to moonquakes 78−40848
velocity structure of shallow crust 80−26761
viscosity models rel. to seismic Q-values 77−60680
wave propagation in highly scattering medium, diffusion approach 77−86804

lunar structure
see also lunar rocks and minerals; Moon
Apennine Mountains, possible batholith 77−37528
Apennines and regional surroundings, isostatic state 78−77503
Apollo seismic network results, lunar seismicity, structure and tectonics 77−60679
basin-forming impacts, seismic effects on global struct. 78−12122
blocky craters rel. to megaregolith 80−62051
convection and lunar thermal history 79−84690
core, formation, history and energetics 79−84694
core dynamo, rel. to superheavy elements 78−65521
core formation in terrestrial planet, appl. to Moon 80−17514
core radius and density rel. to moment of inertia determ. improvement 78−24477
crater morphology and size relation 77−41332
craters, floor fractured, morphologic classes 77−37516
craters, rel. to standard crater curve for Mars and possible new time scale 77−33391
craters on farside, volcanic events after impact 78−65516
crust, seismic vel. structure 80−26761
crust and mantle, differential evolution rel. to initial $^{143}Nd/^{144}Nd$ ratio 79−35156
crust differentiation, evidence from trace element abundances 77−60651
crustal evolution, major impact processes contrib. 77−60658
crustal tectonics, relation to internal evolution 78−12116
crustal tidal stresses rel. to lineaments 78−89087
density, vol. distrib., theoretical anal. 80−8567
density model consistent with topographic, gravit., librational and seismic data 77−45332
density structure, max. entropy inversion 80−67602
differentiation, rel. to two-stage model for mare basalts generation 77−60648
differentiation of rocks in early history, KREEP basalt Sm-Nd systematics 80−12686
elastic lunar lithosphere, strength and rigidity rel. to present-day mantle convection 77−37532
EM induction studies, effects of magnetometer data errors 79−96932
far-side magnetised regions, correl. with ringed impact basins 80−36521
force function, third and higher harmonics rel. to peculiarities of translatory-rotatory motion *(Russian)* 80−90349
fossil bulge to explain gravity field anomaly 80−56733
gardening process, by meteoroid impact cratering *(Japanese)* 77−91452
geologic evolution of terrestrial planets 77−53442
global radioactive crust, evidence from exotic component in soils 77−60643
global tectonics, following tidal despinning 77−60698
global tectonics, of Mercury and the Moon 78−12128
grabens structural anal. rel. to shallow crustal struct. 80−31221
gravitational field model, harmonic anal. 80−72799
gravity determinations, implications for struct. 77−60653
gravity field, harmonic anal. rel. to press. and uncompensated loads 77−87290
gravity field, mass point model rel. to surface features 77−87289
highlands crust 80−109381
homogeneous model, rel. to deep moonquakes tidal triggering 79−66938
Imbrium sculpture and lunar basin radial texture, evidence for sedimentary origin 77−37526
Imbrium stratigraphy, petrological aspects 77−60641
impact basin rings formation theory 78−61766
impact crater size-frequency distrib., age determ. 77−60659
impact craters modification, role of rim slumping 79−84689
impact craters struct. from gravity models 77−64674
impact erosion 78−57476
intercrater plains on Moon and Mercury, origin and relative ages 78−12117

lunar structure continued
interior, struct. and thermal evolution rel. to mag. field 78−12115
interior composition and mineralogy determ., effects of basalts differentiation by crysts. gravit. separation 77−60649
internal structure evolution, calc. 77−82137
landform degradation evidence from crater depth/diameter relations 77−37536
large impact structures, numbers and isostasy rel. to average crustal viscosity 78−12120
lava flow effects on crater populations 77−37514
Letronne-Montes Riphaeus region, tectonic pattern of mare ridges 79−66935
light plains, different ages 78−81571
lithosphere from EM sounding data 78−24474
mare basalts derivation and petrogenesis rel. to internal struct. 77−60647
mare basins vertical movements, rel. to emplacement, tectonics and thermal history 79−80250
Mare Crisium, radar-detected subsurface interface stratigraphic correlation 79−16848
Mare Crisium, regional stratigraphy and geological history 78−61765
mare domes, classification and origin 80−77305
Mare Serenitatis, elec. cond. anomaly detect. by Lunokhod 2 and Apollo 16 magnetometers 80−56730
Mare Serenitatis multiringed basin, struct. and selenology 80−77304
marginal zone relief maps from stellar occultation obs. *(Russian)* 77−73984
Maria Serenitatis and Crisium, orbital radar evidence for subsurface layering 78−85868
mascon basins: lava filling, tectonics and origin, review 80−98583
mascon maria, evidence for isostasy 77−37524
moment of inertia and gravity field, study of Earth-Moon system 80−105184
moments of inertia, origin of differences 78−45247
Moon thermal history, effects of chemical stratification 78−65522
morphological considerations of local convection processes, selenological history *(Japanese)* 78−20660
Necho, farside crater morphology and structure 80−41739
Orientale basin, comparison with Caloris basin on Mercury 78−12121
palaeomagnetism, pole positions rel. to lunar core dynamo processes 78−93132
regolith reprocessing by cratering, erosion of material layer which loses charact. props. 80−62053
regolith Ti distribution, orbiting γ-ray expt. 80−17510
relief and selenoid deform., harmonic anal. 80−72800
review 80−4278
Rima Sirsalis magnetic anomaly 80−36524
ringed basin formation mechanics 79−16850
seismic energy transmission in intensively scatt. environment, rel. to lunar struct. determ. 77−73685
seismic waves scattering, diffusion theory rel. to struct. 77−86804
selenodesy using satellites 79−66835
selenodetic investigations in USSR, bibliography (1928 to 1975) 79−88609
solar wind ion bombardment, lunar surface modification 80−109325
surface, Luna 16-24 3 cm radar obs. 80−77302
surface, photogeologic data rel. to ages of Serenitatis, Imbrium and Orientale events 77−60642
surface features, absolute heights from photographs, computer processing technique *(Russian)* 80−109380
surface origin and evolution 77−60691
surface structure forecast, based on thermal conditions 78−77502
surface unit definition and characterization using remote sensing 78−28551
tectonic pattern of Cruger/Rima Sirsalis-Rima De Gasparis area 78−65520
tectonic zone structures and activity 79−66937
thermal history, present state and tectonics, fission origin model 80−98582
topography, harmonic anal. 77−60634
Tycho secondary craters, morphology and ejecta deposits 77−29670
upper lunar crust, lithification and structure densities 77−60681
viscosity models rel. to seismic Q-values 77−60680
volcanism, and heliogenic model of planet origin *(French)* 77−64671
volume distribution of density 79−70972
Fe and Ti surface distrib., orbital γ-ray spectra 80−94727
Fe core, heating by superheavy elements, possible evidence from Fe meteorites 79−48742

lung
see also pneumodynamics
acoustic input impedance of excised dog lungs 79−5309
acoustic instrumentation and characterisation of lung tissue 78−44575
acoustic lung ducts, sound wave propagation obs. 77−12981
acute pulmonary failure, treatment with extracorporeal oxygenation 78−7539
adaptive analogue tracker for automatic meas. of lung parameters 77−48911
aerosol decay in human lung during breath holding 79−66480
airway network geometry, noninvasive inference from broadband lung reflection data 79−29560
airway smooth muscle, contracted, hysteresis, dog expts. 80−81634
airway smooth muscle mech. alterations in canine asthmatic model 79−100648
airway transepithelial elec. pot. in vivo, species and regional diffs. 80−98208
albumin flux, differential permeability of endothelial and epithelial barriers, sheep expts. 80−81553
algorithm for rib extraction in chest X-rays for pneymoconiosis detect. 78−31904
alveolar epithelium transport of albumin and sucrose, conc. diff. effect 80−67329
alveolar macrophage number, index of effect of radiation on lungs 78−31869
alveolar macrophages, effect of X-irrad. in mice 80−98024
alveolar membrane, role of bulk fluid flow in protein permeability, dog 77−52814
alveolar surface tension in excised lungs 79−92257
animals, small, nose-only inhalation exposures to $^{106}RuO_4$, system 80−41346

lung continued
arterial hypertension meas., Bubble Ultrasonic Resonance Pressure method 79−92313
arteries, small, pulmonary, elasticity in the cat 80−108942
artificial, controlling factors for O_2 transfer through bubbles 78−53568
artificial, O_2 exchange in silicone rubber capillaries 79−44060
artificial 'membrane lung' 77−78051
artificial lungs 77−25601
asbestos minerals nature and paragenesis 77−81876
atelectatic, mechanism of decreased blood flow 80−45931
automated pulmonary function test apparatus for space shuttle 78−31912
Bayer map evaluation in ^{57}Co-bleomycin scintigraphy *(Japanese)* 80−72319
beta irradiation of beagle dogs, early lung damage indicators 80−17018
beta-emitting particles, fraction of energy absorbed, rat obs. 80−104641
blood flow, quasi 1 dimensional unsteady fluid flow eqns. study 80−3691
blood flow, spatial distrib. in dogs with PEEP ventilation 80−72191
blood flow estimation, Ljung's algorithm sensitivity 80−56107
blood flow in isolated perfused dog lung lobes, effect of oedema 80−97975
blood flow redistrib. in PEEP ventilated dogs 80−8083
blood oxygenators, 1977 view of progress and problems 78−36064
blood perfusion, regional, assessment by continuous intravenous infusion of ^{81M}Kr 79−39477
body plethysmograph and pneymatic differentiator, static and dynamic testing 78−28150
breathing movement dynamics, human fetus 80−3707
bronchial angiography in the staging of bronchogenic carcinoma 80−46007
bronchial elasticity and air flow, mathematical anal. 80−45942
bronchial epithelium, population average dose from Rn pollution 79−70485
bronchial epithelium tissue, technique for high sensitivity α autoradiography 80−17210
bronchogenic cancer, small cell, undifferentiated, role of radiation therapy in treatment 80−67226
bronchogenic carcinoma among former U mine workers at Port Radium, Canada 80−89802
bronchopulmonary lavage 78−15910
bronchoscopic tumour localisation, small radiation detector probes, scintillation and semiconductor detectors 80−61676
burdens of low-energy photon-emitters, interlaboratory comparison of techniques for meas. 79−20671
cancer, early detect. with laser fiberoptic bronchoscope *(German)* 79−12024
cancer, interstitial brachytherapy, 20 year experience 80−72302
cancer, U miners, rel. to radiation exposure time distrib. 79−79605
cancer rel. to Rn in dwellings 80−89870
carcinogenesis induced by inhaled high-fired oxides of Pu and Be 78−96077
carcinogenic effect of localised fission fragment irrad., rat expts. 80−81656
carcinogenicity of inhaled air-oxidised $^{239}PuO_2$, rat obs. 79−66492
carcinoma, extended fractionation radiation therapy study 80−72305
carcinoma treatment, combined local irrad. and corynebacterium parvum 78−65091
cardiovascular system, mathematical models and identification problems 80−89780
cell nuclei, estimation of mean caliper diameter 79−25165
cells, mouse, radiosensitivity, in vitro colony method obs. 80−101230
chest photofluorograms, recognition of vessel shadows *(Japanese)* 79−57761
chest photofluorograms automated interpretation using AISCR-V3 software system 79−88183
chest photofluorograms recognition of vessel shadows for automated meas. and classification system 77−81566
chest radiograph nodule detection system 80−8140
chest radiographs, computed detection of nodules 80−8172
chest radiographs, hybrid optica-electronic processing appl. 79−74754
chest radiographs, processing of large numbers, problems 80−8138
chest radiography, introduction to physiological aspects 79−25071
chest X-ray images, fundamental study on automated meas. of changes *(Japanese)* 79−29615
chest X-ray images, recognition of eature points by sequential decision process model *(Japanese)* 79−39480
chest X-ray lung region subimage automated extraction for pneumoconiosis opacities detection 79−88182
chromosome aberrations induced in Syrian hamster lung cells by inhalid $^{238}PuO_2$-ZrO_2 particles 77−56440
chronic obstructive pulmonary disease detection, airway resistance model 79−96603
circulation, density dilution method appl. to obs. of fast osmotic fluid shifts 80−104781
coal-workers pneymoconiosis, optical digital approach to pattern recognition 78−40389
coiled tube blood oxygenation 78−40422
complex bioelectric impedance terminal instrumentation system for meas. 78−48853
computed tomography, pots. in radiation therapy treatment planning 79−88174
computerised tomography, resource sharing computer hierarchy for 3D image reconstruct. 80−26345
computerised tomography in pulmonary nodule diagnosis 80−17110
death due to inhalation of β-emitters, probability estimation 80−89801
deflation, large-deform. anals. of strains in excised lobes, dog 80−3689
degassing, evaluation of 2 methods 80−101294
densitometer, 3D, using CdTe detectors for diagnosis and evaluation of pulmonary edema 77−44749
density, Compton scatt. meas., multiple photon interactions 80−67146
diagnostic capability of computer-aided tomography in the thoracic region *(German)* 79−39498
dolphin, lung collapse and intramuscular circulation during diving 80−81643
dose distribution calculation method for bone- and lung-equivalent material, diagnostic X-rays *(German)* 80−61704
dose distribution effect on induction of expt. lung cancer by alpha radiation 79−16254
dose in half body radiotherapy, determ. by computerised tomography 80−104763
dynamic boundary surface detection 77−78019

lung continued
elasticity in regional and diffuse pulmonary fibrosis 80−30742
electrode for PN_2O and PO_2 anal. in blood and gas 79−62412
electron microscopy of lung rapidly frozen under controlled physiological conditions 79−39619
endothelial cell nuclei from human lung, mean caliper diameter estimation 79−29679
epithelial cells, type 2, proliferative response after X-rays and fission neutrons 80−108974
esophageal multiprobe for temp. ECG, and heart and lung sound meas. 79−57791
esophageal multiprobe for temperature, ECG and heart and lung sounds measurements 78−77146
extracorporeal blood oxygenators, safety and efficacy 78−77153
extracorporeal processing devices, review, book contrib. 80−12308
extravascular lung thermal vol., reappraisal as meas. of pulmonary oedema 80−97867
fast-neutron therapy, in vivo meas. of lung corrects. 77−13007
fibrosing disease diagnosis, histological section SEM and energy-dispersive X-ray microanalysis 80−72314
finite element model for macroscopic deform. 80−108945
fissionable radionuclides in rat lung, visualisation using neutron induced autoradiography 78−28055
fluid transport in pulmonary oedema, hybrid computer simulation 78−27915
fluorescence bronchoscopy, use for localisation of small lung tumours 77−86580
FONAR scans of patients with cancer 79−62327
gas exchange functions of lungs, digital computer simulation *(Russian)* 79−2092
gas transport model, derived from human anatomical data 77−5020
gas trapping mechanism model in excised lungs 79−96604
gradient pattern coding appl. to meas. of pneumoconiosis in chest X-rays 79−34632
gravitational deformation, excised canine lungs, linear elasticity soln. 80−30747
haemodynamic responses to lobar venous occlusion, dog 80−30743
haemodynamics, quasi one-dimens. unsteady nonlinear fluid flow eqns. soln. 80−41104
health aspects of canadian uranium mining 79−88140
health hazards from minerals 77−86732
heart-lung machine, thermocontrol device with remote control 79−48374
hemithoracic irradiation, late biochemical changes in the rat lung 77−5053
histological sections, techniques for studying radionuclides 80−56315
hybrid optical-digital radiography-based system for lung disease detect. 78−11753
hybrid optical-electronic system for estimating pulmonary venous pressures from routine chest radiographs 78−44657
hyperthermic radiosensitisation of thermotolerant tumour cells in vitro 79−74600
imaging small pulmonary ischemic lesions after radioactive CO inhalation 77−2035
industrial atmosphere submicroscopic asbestos fibre evaluation 79−74585
inert gas absorption, closed lung system study 80−30969
inert gas elimination studies without mixed venous partial pressures 80−26250
inert gas exchange, steady state, for compartmental model 80−26249
inhalation carcinogenesis of high-fired $^{238}PuO_2$ in rats 78−28009
inhalation carcinogenesis of high-fired $^{239}PuO_2$ in rats 77−21576
inhalation carcinogenesis of high-fired $^{244}CmO_2$ in rats 80−21502
inhalation of transuranium oxides, aerosol prod. by gas phase neutralisation of acidic droplets 80−26427
inhalation toxicology of $^{238}PuO_2$ and $^{239}PuO_2$ in Syrian gold hamsters 77−86552
inhaled ^{239}Pu, removal from beagle dogs by bronchopulmonary lavage and chelation therapy 77−9270
inhaled $^{239}PuO_2$, effect on lung lipids 77−25510
inhaled radioactive particles, mammals, guide to prognosis for survival 77−16956
inhaled radioactive particles, removal, by lung lavage, review 78−3618
instrumental neutron activation analysis studies of tissues from patients with pulmonary diseases 80−21535
interactive graphics for lung vol. determination 77−77985
interface for pulmonary exploration by real-time treatment of curves obtained by transthoracic impedance 79−34686
interstitial fluid space compliance, estimation in isolated perfused rabbit lung 80−104605
intrapulmonary haematocrit maldistrib., effect on O_2, CO_2, inert gas exchange 80−8033
intrapulmonary shunt, influence of cardiac output 80−8086
irradiation, specific early fine struct. changes 78−31859
irradiation effects on immune function in patients with carcinoma 79−16251
irritant receptions and afferent C-fibres, stimulation prostaglandins 77−12930
ischemic lesion, experimental, after inhalation of a diffusible radioaerosol, imaging 77−37047
KHT sarcoma cells, effect of intercellular contact on radiation sensitivity 80−30801
laser fibre optic bronchoscope for optical fluoresc. localisation of early lung cancer 78−48921
laser fluorescence bronchoscope for occult lung tumor localisation 80−30832
lesions evaluation, comparison of ^{67}Ga-citrate, ^{111}In-bleomycin and ^{99m}Tc-citrate 80−94327
lipid extract of lung surfactant, IR studies 79−24941
lymph transport increase without heart failure after coronary ligation in sheep 80−67122
lymphocytes, peripheral, function in dog, impairment by chronic pulmonary ^{144}Ce irradiation 79−88135
macroscopic deformation, finite element model 80−89781
magnetic field meas., comparison between two methods 80−104712
magnetopneumographic measurement, localised-fluid, freeze-dried lungs 80−104714
magnetopneumography, analytic methods 80−104713
mean caliper diameter of lung nuclei determ. 80−98189
membrane of lung surface, indentation on an elastic half space 79−20522
metastases, artificial, of the EmT6 tumour radiation response 77−12977
metastases of the Lewis lung carcinoma, artificial, enhanced tumour cell radiosensitivity 77−12978
metastases prevention by lung irrad. 77−37021
microvascular filtration, comparison of characts. in isolated and intact lungs, dog expts. 80−97974
microvascular response to haemorrhagic shock, resuscitation and recovery 80−3674
microwave reflection and transmission meas. for pulmonary diagnosis and monitoring 78−28031
Monte Carlo calcs. of external detector response to photon source in phantom's lungs 80−8132
mouse lung tumour growth delay by bleomycin with 2.45 GHz local hyperthermia 79−83894
muco-ciliary transport mechs. 80−97956
mucociliary tracheal clearance vel., radiological method for determ. 80−104727
neonatal pulmonary assist membrane oxygenator, toward the development 79−25159
neutron dose changes caused by inhomogeneities, correct. factors 79−39511
neutron-telecobalt combined therapy, investigations on tumour reaction of lung cancer 79−20642
NMR zeugmatographic imaging of heart and lungs 80−17053
nuclear imaging, gated and cinematic perfusion imaging, dogs with expt. pulmonary embolism 80−17071
nuclear medical imaging, estimates of radiation absorbed doses from radioxenons 80−101269
nuclear medicine conference, Karlovy Vary, Czechoslovakia (May, 1979) 80−12840
numerical modelling of the human lungs 78−80911
O_2 and CO_2 exchange and cardiopulmonary control interaction model, duck 80−3600
oedema diagnosis by a surgically noninvasive microwave technique 80−61659
oedema of intact dogs, meas. by transthoracic γ-ray attenuation 80−81787
oscillating helix membrane lung employing O_2 perfused inner capillaries 78−44712
parachyma described as a prestressed compressible material 77−90837
parenchyma, elastic props., pressure-volume hysteresis effect on large blood vessels 80−41084
parenchyma, expt. study of anisotropic props. 78−31842
parenchyma, math. model 80−108940
parenchyma irradiated by inhaled $^{238}PuO_2$ particles, collagen localisation, Syrian hamsters 80−72252
parenchymal deformation in excised canine lung lobes, rot. corrected strain analysis 80−41087
pathologic changes following single and multi-fraction irrad. 78−3553
pathologic effects of neutron and photon exposures of lung and spinal cord, rabbit expts. 80−41126
pathological lung gases anal. by special redox gas sensors *(German)* 78−85440
pathology, appl. of PIXE 80−61691
percutaneous cricothyroid bronchography *(Dutch)* 80−85471
perfusion images, effect of particle number 77−37049
peribronchial fluid pressure rel. to vascular and airway press. and interstitial oedema 80−97971
perimicrovascular fluid pressure estimation in isolated perfused dog lung lobes 80−30750
photon altenuation in tissue substitutes rel. to lung Pu assessment 79−16307
proportional multidetector intended for the functional study of the lungs *(French)* 77−37035
pulmonary arterial blood flow dynamics, nonlinear anal. 78−44527
pulmonary arterial pressure, noninvasive estimation in dogs using ^{133}Xe images 80−41184
pulmonary artery blood pressure analysis algorithm 78−40376
pulmonary blood flow, spatial distrib. in dogs in increased force environments 78−92664
pulmonary blood flow distrib., effect of altered pulmonary arterial compliance 78−44553
pulmonary capillary blood flow in dogs, atraumatic measuring 78−7552
pulmonary circulation, human, behaviour, during head-up tilt 79−39433
pulmonary clearance of S. aureus after inhalation of $^{144}CeO_2$ or $^{239}PuO_2$, mouse expt. 80−36013
pulmonary disorders, use of ^{67}Ga 79−57771
pulmonary dysfunction, detect. method using acoustic transmission 77−37031
pulmonary edema, early, quantitative diagnosis 77−77981
pulmonary embolism resolution rates assessed by serial positron imaging 80−3789
pulmonary function anal. using ^{133}Xe *(German)* 77−21600
pulmonary gas exchange data, on-line acquisition 78−28100
pulmonary gas exchange model *(French)* 79−8516
pulmonary gas transfer, aspects of on-line digital integration 78−20325
pulmonary hila, 55° posterior oblique tomography 80−41189
pulmonary infiltration, interactive radiographical anal. 77−21625
pulmonary nodules, use of computerised tomography in diagnosis 79−29582
pulmonary oedema, quantitative elec.-impedance plethysmography 78−31951
pulmonary physiology, pathology, and ventilation-perfusion studies 79−29613
pulmonary radiograph interpretation, review of models used 80−36089
pulmonary sheet flow, effect of blood rheology on haematocrit distrib. 79−79572
pulmonary testing, vitality of proper training, technique 78−24170
pulmonary thromboembolism new percutaneous caval filter device 77−48925
pulmonary vascular interdependence in isolated dog lobes, continuum mechs. anal. 80−3671
pulmonary vascularity automated diagnosis from chest roentgenograms 77−60248
pulmonary vascularity computerised texture features rel. to catherisation parameters 80−8154
radiation dose to the lungs from ventilation studies with ^{133}Xe 78−24146
radiation dose-response, early, an ultrastruct. 78−35890
radiation dose-response curves, hazard function method of resolution 79−66556

lung continued
radiation effects, canine, relative effectiveness of fast neutron and ^{60}Co γ-ray irradiation 80−3737
radiation-induced pulmonary fibrosis after inhalation of beta-emitting radionuclides, beagle dogs 79−25049
radioactive microspheres for localised irrad. of lung tissue, production and props. 78−53445
radiographic chest film, pre-operative, rel. to post-operative management 80−51207
radiographical visibility and sharpness of lung struct. at 90, 140 and 350 kV 80−98124
radionuclide and chemical pollutants, pulmonary effects *(French)* 80−8102
radionuclide imaging, history 80−42035
radionuclide imaging, technique for contralateral subtraction 80−41207
radionuclide venography, simplified approach 77−5068
radionuclide venography and lung scanning 80−3791
RBE of neutrons for control of artificial pulmonary meatastases 77−81536
regional differences, effects of body position and respiration 79−25073
respiratory mass-spectrometer appls. 79−62383
respiratory muscle EMGs, digital computer technique for anal. 78−28102
respiratory parameter measurement with mass-spectrometer 79−62382
rheological properties of excised rabbit lung stiffened by repeated hyperinflation 80−41078
roentgen-videographically recorded displacements of implanted markers, calcs. of lung translation, rotation and strains 78−31843
roentgenfilm densitometry rel. to linear lung expansions 79−25074
scinticamera type lung monitor for assessment of low energy photon-emitters 79−25067
scintigrams, observation of changes by means of crosscorrel. 78−80961
scintiphotography of lungs with dry aerosol, generation and delivery system 78−24126
shape during normal gravity and weightlessness, radiographic comparison, human 80−67260
shear modulus and pleural membrane tension, improved meas. 80−30746
small cell carcinoma, low dose elective brain irrad. 80−67253
smoking, effects on regional, lung differences, radiological study 79−25075
solubility of inert gases in homogenates of canine lung tissue 80−46117
sound transmission in a lung, expt. obs. 78−28149
sputum viscoelasticity, meas. using conventional dynamic and raised cosine pulse methods *(Japanese)* 80−67132
SQUID fluxgate magnetometers, magnetopneumographic meas. 80−104711
static mech. behaviour 77−36993
static mechanical behaviour 77−36993
stereological parameters of lung tissue, computer anal. 78−73280
strain variations in excised lobe of canine lung, finite-element anal. 79−8517
stretch receptors intrapulmonary and extrapulmonary, dynamic response in the dog 78−20194
structure and elasticity, 3-dimens. modelling 77−36992
structure and elasticity, 3D modelling 77−36992
sublobar atelectasis and regional pulmonary blood flow, pig expts. 80−81633
surface US tissue signature 80−45957
surfactant early release following lung irrad. of alveolar type II cells 80−94291
surfactant film from rabbit lung, surface dilatational viscosity obs. 79−62278
T content in organs, and DNA of rat liver cells, after doses of tritiated food, protein or water 80−56226
thermal enhancement of effectiveness of γ-radiation for reproductive death induction 79−34509
tissue elasticity, constitutive eqn. 79−96595
tissue micrograph computer processing approach 80−8123
tomographic imaging, evaluation of image quality 77−86607
tomographs, conventional, use of neuristic search to find lung boundaries 78−73240
tracheal ciliary beat, improved device for freq. recording 80−109070
tracheal epithelium, dog, interdependence of Na^+ and Cl^- transport 80−61519
tracheal muco-ciliary transport, theoretical and expt. study 80−97958
tracheal mucosa, canine, interaction between Na^{2+} and Cl^- transport 79−88060
tracheal mucus gel props., changes induced by divalent cations 80−51142
tracheobronchial clearance of inhaled particles in man 80−8080
transaxial image recon struction, ultra high-speed, of heart, lungs, and circulation 79−34633
transient inert gas exchange in compartmental models 80−26251
transmission densitometry, modified method 80−36091
transuranic elements lung burden, in vivo meas. at CRNL 77−77993
transvascular fluid shifts in zone I lungs, rabbit obs. 80−101198
tumour diagnosis, contribs. of radioisotopes *(French)* 77−70519
tumour induction in RFM mice after localised X- or neutron irrad. 80−72260
tumourigenesis from particulate sources of ^{147}Pm β-radiation 80−72247
tumourigenic hazard of particulate α-activity in Syrian hamster lungs 80−41133
US measurement of pulmonary haemodynamics 78−35902
US tissue characterisation for the lung 77−40717
vascular interdependence in excised dog lobes 80−97976
vascular permeability after microemboli, effect of platelet depletion, sheep obs. 80−97972
velocity distribution and pressure drop characts. in human lung model 79−96602
vessel pressure-diameter behaviour, pigs, effect of parenchyma and length changes 80−67116
volume measurement from supine portable chest radiographs 80−81703
whole body counter, optimisation studies 79−2132
whole body irradiation, late biochem. changes in the rat lung 77−56432
X-irradiation, single dose, sequence of histological changes, mouse obs. 80−98019
X-radiation interaction with inhomogenous media, Monte Carlo study 79−8531
CO diffusion in dog lungs, effect of static or slowing flowing blood 80−30970
CO, single breath diffusing capacity, theoretical anal. 80−67328

lung continued
$^{144}CeO_2$, effects of repeated inhalation exposure, mouse obs. 80−104676
$^{144}CeO_2$, repeated inhalation exposure of mice, retention and dosimetry 80−109034
$^{244}CmO_2$, mobility in bronchially intubated rat 80−30967
^{60}Co, inhaled, long-term clearance 79−79663
$^{253}Es(NO_3)_3$, inhaled by rats, late effects 80−30781
Fe loss from asbestos fibres in pulmonary tissue, obs. 79−74825
^{192}Ir, estimation of long-term biological elimination 79−70642
^{95}Nb, inhaled by beagle dogs, deposition and retention 78−35959
Pu, acute inhalation, estimate of early mortality and morbidity 78−96079
Pu, biological solubility in the rat after inhalation 78−96096
Pu burdens in Austrian residents 80−109042
Pu dose to lung and bone from contaminated soils, statistical uncertainties 80−109028
Pu in lungs, X-ray counting efficiencies 78−85391
Pu in pronghorn antelope near a nuclear fuel reprocessing plant 80−30906
Pu in vivo assay methods 79−20674
Pu isotopes, maximum permissible inhalation values 79−70640
$^{238}PuO_2$ particle inhalation, pulmonary tissue local dose computation 79−92385
$^{239}PuO_2$ inhalation, rat pulmonary connective tissue modification by internal α-irrad. 79−92302
$^{238}PuO_2$, factors affecting mobility in rats 79−12003
$^{239}PuO_2$, in vivo solubility in the rat lung 78−28093
$^{239}PuO_2$, inhaled by baboons, toxicity and translocalion 79−2109
$^{239}PuO_2$ aerosol inhalation exposure, miniature swine 79−11976
$^{239}PuO_2$ in lung cells, freq. of α-particles 78−69151
Rn daughters exposure rel. to lung cancer incidence 78−96080
^{222}Rn daughter dosimetry in Syrian golden hamster lung 79−16304
$^{106}RuO_4$ in the lung, invivo meas. and dosimetry *(English, French, Russian)* 78−53515
T radiation dose absorbed in rat organs, after feeding with organically bound T 80−51262
^{178}Ta radiopharmaceuticals for lung and liver imaging, rat expts. 80−51254
^{99M}Tc lung imaging kit, impurities 77−56469
^{99M}Tc-labelled lung imaging agents, quality control 78−28069
U stored in lung, comparison of meas. detectors 78−28090

lutecium *see lutetium*

lutetium
see also nuclei with .....
atom, α-particle impact K-shell ionisation, 40 to 110 MeV 78−17752
atom, even config., parametric calcs. 78−82631
atom, K-shell X-ray energy, excitation mode depend. 79−26926
atom, valence orbitals, Dirac-Fock scheme, direct and indirect relativistic effects 78−41969
atom, X-ray emission spectra, L-shell satellite, $L_2M_4 \rightarrow M_4M_4$ transition 77−79565
band structure, influence of relativistic effects 78−75991
binding energies for metal and 4d, 4f atomic levels from XPS data 79−15586
Compton profiles, electronic configurations 80−11501
crystal surface study from refl. electron energy loss spectra obs. 80−20742
diffusion of H, hopping process 80−24673
electric fields gradient, at ^{181}Ta substitutional atoms, pressure dependence 78−52385
electron irradiated, defect annealing, recovery spectra 79−23648
electron irradiation effect at low temps. 77−43249
electron-irradiated, low-temp., recovery 78−6102
EXAFS, white lines, interatomic distances 77−40302
Hall coefficient meas., 80 to 1000K 80−49694
lattice dynamics, heat capacity, thermal expsn. 79−86857
liquid, elec. resist. up to 1800°C, rel. to elec. struct. 78−39083
liquid, struct. factors, high temp. X-ray diffr. obs. 79−7544
liquid, trivalent, electrical resist. 79−42514
magnetic form factor, field-induced, polarised neutron technique meas. 77−72998
nuclear quadrupole alignment and low temp. systematics of elec. field gradients of $^{176}Lu^m$ and ^{177}Lu 79−78565
point defect production during electron irrad. at low temp. 80−49273
quadrupole interactions, nuclear quadrupole alignment of ^{177}Lu 78−48090
specific heat from 1.6 to 18K, electronic coeff., Debye temp. at 0K 79−7700
superconductivity at 200 kbar and 20 mK 77−47916
thermophysical properties at high temps., exam. *(Russian)* 79−28105
X-ray absorption discontinuity, spectroscopic anal., energy separation of orbitals 78−76557
X-ray emission spectra, calc. by the relativistic APW method 79−78792
Co:Lu, nuclear orientation meas., hyperfine field 77−32308
Fe:$^{169}Tm(^{175}Lu)$, radiation-damage evolution influence on hyperfine interaction 80−6793
Fe:Lu, nuclear orientation meas., hyperfine field 77−32308
Li I, IR emission spectrum, extended anal. 78−62747
Lu I, 5d6s6p-config., laser spectrosc. investig. 80−69096
Lu I, 5d6s(^{3}D)6p$^2D_{3/2}$ state, Stark effect, level crossing obs. 77−75098
Lu III, 6s $^2S_{1/2}$-6p $^2P^o_{1/2,3/2}$ transition, relativistic oscillator strengths, influence of core polarisation 80−58132
Lu V, spectrum anal., 500-2100 Å 79−26920
Lu-H, effect of low-temp. electron irradiation 77−43249
Lu-Mn, relative activity ratios in natural UO_2 reactor fuel 78−58347
$Lu_2Fe_4Si_9$ and $LuFeSi_3$, cryst. struct. and mag. suscept., temp. depend. *(Russian)* 78−34957
^{A}Lu, A=175,176, 5d6s^2$^2D_{3/2}$-5d6s6p$^4F_{3/2}$ transition, isotope shift and hyperfine struct. 80−83309
^{71}Lu, L_2M_3 electric quadrupole transition detect., L X-ray spectrum 77−3294
^{175}Lu, muonic, nuclear spectroscopic ground state quadrupole moments from X-rays 79−98252
^{176}Lu, hyperfine struct. and isotope shift of 605.5 nm line by laser spectroscopy 79−41137
$^{176}Lu/^{175}Lu$ isotopic ratio, eval. of neutron temp. in Oklo natural reactors *(French)* 80−21766
Ni:Lu, nuclear orientation meas., hyperfine field 77−32308

lutetium alloys
rare earth alloys, mag. phase diagram 78−10684

lutetium alloys continued
Ag-Lu, dil., virtual bound states, transport props. obs. 80−70667
Al-Lu, dil., transmission ESR expts. 77−20704
Au-Lu, dil., virtual bound states, transport props. obs. 80−70667
$Dy_{0.9}Lu_{0.1}Al_2$, hyperfine field, NMR spectra 80−15811
Fe-Lu amorphous films, mag. props., Mossbauer effect and magnetisation meas. 79−69701
Ga-Ni-R, (R=Dy, Ho, Er, Tm, Lu), struct. determ. by X-ray powder method *(Ukrainian)* 80−39001
Gd-Lu, Curie temp. and saturated mag. moment, nonmag. solute effects 78−39301
$(La_{.993}Lu_{.007})_{1-x}Gd_xRu_2$, exchange enhanced supercond., compensation effect on H_{c2} 77−4474
Lu-Fe, amorphous alloy film, spin reson. meas. 78−68389
Lu-Fe amorphous alloy film, mag. props. 77−16121
Lu-Gd, dil., positive exchange Kondo system, magnetisation and resist. 78−68158
Lu-Gd, positive exchange const. Kondo system, resistivity meas. 78−47775
Lu-H, effect of low-temp. electron irradiation 77−43249
Lu-H, electronic sp. ht. 80−49378
Lu-H alloy, influence of H on low temp. sp. ht. 78−38854
Lu-Hf, elec. field gradient at ^{175}Hf nuclei aligned at low temps. 79−82884
Lu-Ir, dil., elec. field gradient at ^{193}Ir, Mossbauer meas. 80−66090
Lu-Mn alloy, mag. props. and effect of H_2 absorpt. 78−19250
Lu-rare earth, dil., cryst. fields 78−80127
Lu-rare earth, dil. alloy cryst. field determ. 78−10651
Lu-rare earth metal alloys, dil., elec. resist. 79−82578
Lu-rare field, dil. alloy, cryst. field parameter determ. 78−10650
$LuAl_2$, sp. ht. and thermal props., 5 to 300K 77−43342
$LuAl_2$-Er(Dy)(Nd), dil., EPR and mag. susceptibility 80−15797
$LuBe_{13}$, lattice spacings and susceptibilities 80−65778
$LuBe_{13}$-Er, dil., ESR, crystalline elec. field splitting, exchange parameters 78−52348
$LuCo_2$, anomalous high-field magnetisation 78−47958
$LuCo_2$, high-field magnetisation, Fermi liquid model 79−11303
$LuCo_2$, mag. interactions, effects on moments *(Rumanian)* 79−15296
$LuCo_2$, paramag., field induced mag. density localisation 77−72999
Lu_2Co_{17}, single cryst., magnetostriction const. temp. depend., 78 to 300K 79−51836
LuCoAl, mag. props. 78−2659
$LuFe_2$, crystal field interaction contribution to specific heat 80−39788
$LuFe_2$, electronic heat capacity coeffs. 80−39787
$LuFe_2$, $ErFe_3$-$LuFe_2$ (10, 90 wt.%), mag. props., 80-1300K *(Russian)* 80−75750
$LuFe_2$, ferromag., magnetisation density, neutron diffr. study 80−60217
$LuFe_2$, ferromagnetic cpds., mean field exchange consts., Stoner itinerant model calcs. 80−50084
$LuFe_2$, mag. props. changes upon H_2 absorpt. 80−71270
LuFeAl, scatter order cpd., mag. props. 77−51891
$LuFe_4Al_8$, mag. props. 78−52250
LuIr:Gd influence of cryst. field on EPR 78−52346
$LuIr_2$, ESR of Nd^{3+} and Gd^{3+} 77−85564
$LuIr_2$-Nd^{3+}, dil., ESR, hyperfine crysts. of ^{143,145}Nd, g-factor, crystalline field splitting 78−52349
Lu_5Ir_2, cryst. struct. 80−96473
$LuMn_2$, Lu_6Mn_{23}, H_2 absorption effect on mag. props. 77−89931
$LuNiSi_3$, mag. susceptibility, 80-1200K *(Russian)* 77−66281
Lu_5Pt_4, isotypic with Pu_5Rh_4, X-ray cryst. struct. refinement anal. 79−4271
$LuRh_2$, ESR of Nd^{3+} and Gd^{3+} 77−85564
$LuRh_2$-Nd^{3+}, dil., ESR, hyperfine crysts. of ^{143,145}Nd, g-factor, crystalline field splitting 78−52349
$Pr_{10}Lu_{40}Ag_{50}$, amorphous, mag. props. 80−60182
Tb-Lu, mag. ordering temps., susceptibility meas. 80−25136
Th-Lu (1 at.%), Heisenberg exchange, residual resist. meas. 80−75558
$Tm_{1-x}Lu_xZn$, third-order mag. susceptibility, quadrupolar effects 79−99674

lutetium compounds
see also lutetium alloys
diphthalocyanine, solid-state anion migration in anodic oxidation 80−60994
ferrite aluminates, prep. 77−85970
LuF_3:Tm^{3+}(Nd^{3+})(Er^{3+}), vacuum-UV excitation spectra 78−80381
$BaCaLu_2F_{10}$, site occupancy from excitation and emission spectra *(French)* 77−81145
$CaLu_2S_4$, cryst. struct., space group *(French)* 77−80479
$Dy_{0.7}La_{0.3}FeO_3$, reorientational phase transitions, influence of La^{3+} ions 80−7108
$(Eu,Lu)_3(Fe,Al)_5O_{12}$ film, epitaxial, increased domain wall velocities, due to orthorhombic anisotropy 77−20653
$(Eu,Lu)_3Fe_5O_{12}$ epitaxial film, induced orthorhombic anisotropy 77−69640
$(Eu,Lu)_3Fe_5O_{12}$, epitaxial film, orthorhombic mag. anisotropy 78−19290
$(Eu,Lu)_3Fe_5O_{12}$, submicron bubble films on rare earth-Ga garnet substrates, prep. and mag. props. 78−91909
$(Eu,Lu)_3Fe_5O_{12}$:Ga(Al)(Ca,Ge), bubble material, dynamic characterisation, comparison between transport and FMR methods 80−39833
$(EuLu)_3(FeAl)_5O_{12}$, film epitaxial growth on Gd_3GaO_{12} substrate, mag. props. 80−65402
$(EuLu)_3Fe_5O_{12}$, Ga, Al or (Ca,Ge) substituted, mag. props. and growth of 2 μm bubbles 78−91910
$Eu_{2.9}Lu_{0.1}Fe_5O_{12}$:Si magnetoresistance meas. 79−78120
$(Gd,Lu)_3(Fe,Mn,Al)_5O_{12}$ epilayer with orthorhombic anisotropy, domain wall vel. 78−52322
$Ho_{1.15}Lu_{0.05}Mo_6S_8$, long range mag. order in supercond. state 79−65653
KF-LuF_3, phase analysis 78−44101
$KLu(WO_4)_2$:Er^{3+}, room temp. stimulated emission obs. 80−106527
$KhuF_{10}$:Eu^{3+}, site occupancy from excitation and emission spectra *(French)* 77−81145
La-Sm-Lu iron garnet film grown as NdGaG substrates, mag. props. 80−44888
$(LaLuSm)_3(GaFe)_5O_{12}$ bubble garnet film, coercivity 79−78459
$(Lu,Bi)Fe_5O_{12}$, magneto-optic colour effects 78−23308
$(Lu,Er)_3Al_5O_{12}$:Er^{3+}, stimulated emission 77−52135
(Lu, La, Y, Ca)$_3$(Ge, Fe)$_5O_{12}$, temperature compensated high mobility bubble garnet, LPE and props. 77−20656
$(Lu,Yb)_3Al_5O_{12}$:Yb^{3+}, stimulated emission 77−52135
Lu porphyrin complexes, luminesc. 77−18958

lutetium compounds continued
LuAG, electrostatic model of cryst. field 80−59945
LuAG:Nd^{3+}, cryst. field anal. 78−64013
$LuAlO_3$, single crysts., EPR *(Russian)* 77−63267
$LuAlO_3$, single crysts., prep. and phys. props., X-ray struct. anal. 79−4298
$LuAlO_3$:Er^{3+}, $^4S_{3/2}$ to $^4I_{9/2}$ transition laser action, optical and luminescence spectra 80−16082
$LuAlO_3$:Nd^{3+}, spectral-generation characts., expt. and theory *(Russian)* 77−7090
$Lu_3Al_5O_{12}$:Er^{3+}, 3 μm stimulated emission at room temp. 77−42541
$Lu_3Al_5O_{12}$:Er^{3+}, 3-μm crystal laser functional scheme, stimulated emission 80−43339
$Lu_3Al_5O_{12}$:Er^{3+}, absorpt., luminesc., stimulated emission 77−32402
$Lu_3Al_5O_{12}$:Er^{3+}(Ho^{3+}), stimulated radn., electron-phonon interaction *(Russian)* 77−8605
$Lu_3Al_5O_{12}$:Ho^{3+}, stimulated emission at low temps. 80−106526
$Lu_3Al_5O_{12}$:Ho^{3+}(Er^{3+}) sensitized stimulated emission at 3 microns 80−53302
LuB_{12}, mag. susceptibility, 90-1200K 80−50032
$LuBO_3$:Fe^{3+}, ESR spectra, lattice parameters 80−93170
$LuBe_{13}$:Er(Dy)(Gd), ESR, crystalline field single ion effects 78−84481
$LuBiTe_3$, prep., elec. props., and crystallographic date 80−59981
Lu_2C_3, superconductivity 79−73621
$Lu_{3-x}Ca_xFe_{5-x}Si_xO_{12}$ film on $Ca_3Ga_2Ge_3O_{12}$, mag. bubble props. 77−28418
LuCl, visible emission spectra, detection and characteris. 79−6963
$LuCl_3$, aquo complex form., in aq. chloride soln., coord., X-ray diffr. obs. 79−64975
$LuCl_3$, pyramidal struct. and force field coeffs., electron diffr. obs. 78−9250
$Lu(ClO_4)_3$, osmotic coeffs. 80−45556
$LuCoO_3$, spin-state equilib. 77−12087
$LuCrO_3$:Er^{3+}, doping effect on ^{53}Cr NMR in domain walls 80−71219
LuF, $^1\Pi$ hyperfine struct. parameters, bonding 77−58036
LuF, electro-vibr. levels mol. consts., global fit *(French)* 77−3339
LuF, mol. electronic states, 3000-6500 Å *(French)* 77−23502
LuF_3, mol. consts., kinetic consts. and L-approx. methods 80−18839
LuF_3, mol. force, compliance and Coriolis consts. 79−31726
LuF_3:Ce^{3+}, UV fluoresc. potential tunable laser 2760 to 3220 Å 78−15206
LuF_3:Nd^{3+}(Er^{3+})(Tm^{3+}), VUV fluorescence and tunable coherent sources from 1650 to 2600 Å 77−688
LuF_3:Tm, Nd, energy transfer between 5d electronic states 80−2808
$LuFe_2B_2$, compounds with $CeAl_2Ga_2$ structure type *(Ukrainian)* 79−32970
$Lu_3Ga_5O_{12}$:Nd^{3+}, cryst. field anal. 78−64013
LuH, $^1\Sigma$ state, Dirac-Fock one-centre calcs. 80−23301
LuH_2, electronic struct., optical studies, 0.2-5 eV, 4.2-340K 79−78005
LuH_2, electronic struct., photoelectron spectra study 80−50527
LuH_2, lattice thermal expansion and point defect form. energy 77−51524
LuH_2, synchrotron XPS obs., rel. to theory for metal dihydrides 80−55275
$LuH_{2.05}$, Compton profiles, electronic configurations 80−11501
$(Lu_{1-x}Ho_x)Rh_4B_4$, interaction between superconductivity and magnetism 79−38248
$Lu_{1-x}Ho_xRh_4B_4$, supercond., phase diagrams and upper crit. fields 80−2531
Lu_3InO_6, high press. synthesis, cryst. struct. 77−68955
$Lu_2Ir_2O_7$, pyrochlore, sp. ht. below 20K, Debye temp. 80−65241
$LuMO_6X_8$ (X=S, Se), supercond., sp. ht., 1 to 14K 79−51720
$Lu_xMo_6Se_8$, supercond., mag. props., 0.7 to 295K 77−32113
Lu_2O, atomisation energies and stand. ht. of formation 77−54622
Lu_2O_3, binding energy from XPS data 79−15586
Lu_2O_3, EXAFS and chemical shift 77−81176
Lu_2O_3, elec. cond. and dielec. const., 400-1180K 79−56224
Lu_2O_3, XPS, charging effects on core-level binding energies 79−24409
Lu_2O_3-K_2O_3 (K=Ho, Er, Tm, Yb, Y), crystn. by Verneuil method 80−40254
LuOOH, $Lu(OH)_3$, growth from gel on ageing, X-ray diffr. patterns 80−24386
Lu_2O_2S:Eu_3^+, luminesc., excitation spectra, cooperative phonon sidebands 79−33771
Lu_2O_2S:Eu^{3+}, luminesc. props., charge transfer effects 78−15214
Lu_2O_2S:Yb^{3+}, charge transfer type luminesc. 79−33797
$LuOs_3B_2$, supercond. and mag. props. 80−97028
LuP(As)(Sb)(Bi), coupling between Gd 4f electrons and conduction electrons, EPR linewidth 78−52347
$LuPO_4$, IR and Raman spectra 80−34904
$LuPO_4$:Eu^{3+}, vac. UV luminesc.-excitation spectra 77−85774
$LuPO_4$:Gd^{3+}, zircon struct. EPR investig., rel. to radiation resistance 80−97138
$LuPO_4$:Pb^{3+}, EPR, hyperfine interactions 80−108050
$LuPO_4$:Sc, Gd^{3+} EPR spectrum, satellite resonances 78−2734
$LuPO_4$:Yb^{3+}, charge transfer type luminesc. 78−64392
$LuPO_4$:Yb^{3+}, charge transfer type luminesc. 79−33797
$LuPO_4$-$Pb_2P_2O_7$, solubility curves for high temp.-melts for growth of single crysts. 78−95687
$LuRh_4B_4$, cryst. struct., X-ray diffr. 77−89423
$LuRh_4B_4$, high supercond. transition temp. 77−89893
$LuRh_4B_4$, magnetic and electrostatic props., NMR study 80−93195
$LuRh_4B_4$, superconducting and normal state props. 79−73632
$LuRhO_3$, elec., mag. and photoelectrochemical props. 80−96925
LuS_n, high-temp. vaporisation and thermodynamics 79−73325
Lu_2S_3, XPS, binding energies 79−15586
Lu_3S_4, high-temp. vaporisation and thermodynamics 79−73325
Lu_3S_4, XPS, binding energies 79−15586
$(Lu_{1-x}Sc_x)_2V_2O_7$, prep., cryst. chem. and chem. anal. 79−41986
Lu_2Se_3, elec. resist., thermoelectromotive force, temp. depend., 300 to 1400K *(Russian)* 78−84243
$Lu_2(SeO_4)_3.8H_2O$, thermal decomp. and IR spectra 80−3319
$Lu_{2-x}Si_2O_7$:Eu_x, synthesis and spectroscopic study 80−84846
$Lu_2Si_2O_7$, crystal struct. of X form, polymorphism under press. *(French)* 77−47430
$Lu_2Si_2O_7$, IR and Raman spectra, internal and external modes 79−61365
$Lu_2Si_2O_7$, polymorphism under press., cryst. struct. 77−35692
$Lu_4Si_2O_7N_2$, lattice consts., X-ray diffr. anal. 80−28986
$Lu_xSn_xMo_6S_8$, supercond. props. 80−97023
LuTb garnet film, scratch-modified mag. domain patterns 78−48007

lutetium compounds continued
$Lu_{0.75}Th_{0.25}Rh_4B_4$, high supercond. transition temp. 77−89893
$LuVO_4:Eu^{3+}$, absorption and fluoresc. spectra, SU(2) chain *(French)* 78−28912
$LuVO_4:Eu^{3+}$, ligand field parameters, computed from fluoresc. and absorption data 78−2453
$LuVO_4:R^{3+}$, R=Nd, No, Tm, Sm, Dy, Er, Eu, Tb, electronic struct. and spectra of VO_4, RO_8 clusters 78−10953
$Lu_2V_2O_7$, physical props. 78−39320
$Lu_2V_2O_7$, prep., cryst. chem. and chem. anal. 79−41986
$Lu_2V_2O_7$, pyrochlore struct., mag. props. 78−72335
$LuVo_3$, phase transitions and Jahn-Teller distortions 79−28548
$Lu_2(WO_4)_3$:Cr(Eu), and undoped crystals, luminesc. obs. 80−89047
Lu_2WO_6, growth from soln. in melt 77−1806
$LuYScO_3:Er^{3+}(Tm^{3+})(Ho^{3+})$, thermolum. meas. 80−97354
$(Lu_{1-x}Y_x)_2V_2O_7$, prep., cryst. chem. and chem. anal. 79−41986
$(Sc_xLu_{1-x})_2V_2O_7$ 80−29547
$(Sm,Lu)_3Fe_5O_{12}$, submicron bubble films on rare earth-Ga garnet substrates, prep. and mag. props. 78−91909
$(SmLu)_3(FeAl)_5O_{12}$, film epitaxial growth on $Gd_3Ga_5O_{12}$ substrate, mag. props. lattice mismatch 80−65402
$Sm_{0.3}Lu_{0.2}Tm_{0.2}Y_{1.45}Ca_{0.85}Fe_{4.15}Ge_{0.85}O_{12}$, LPE growth, saturation magnetisation, collapse field, bubble diameter 78−95703
$(SmLuYCa)_3(FeGe)_5O_{12}$ film, ion implant profile 79−78477
$Tb_2Lu_1Fe_5O_{12}$ film, magnetostriction meas. using double cryst. X-ray diffractometry 78−84468
$Tm_{0.82}Lu_{0.18}VO_4$, elastic consts. at 9 GHz 77−62576
$Tm_{1-x}Lu_xVO_4$, Jahn-Teller system, thermodynamic properties, internal stress effects 80−59679
$(Y,Eu,Lu,Ca)_3(Fe,Ge)_5O_{12}$, bubble memory chip, dynamic conversion comparison with $(Y,Sm,Lu,Ca)_3(Fe,Ge)_5O_{12}$ 78−68319
$(Y,Lu)_3(Fe,Sc)_5O_{12}$ LPE layer, exchange stiffness coeffs., 30-300K 79−78464
$(Y, Sm, Lu, Ca)_3(Fe, Ge)_5O_{12}:Ne^+$, film, S=1 bubbles dynamic props., temp. depend. 77−20658
$(Y,Sm,Lu,Ca)_3(Fe,Ge)_5O_{12}$, bubble memory chip, dynamic conversion comparison with $(Y,Eu,Lu,Ca)_3(Fe,Ge)_5O_{12}$ 78−68319
$(Y,Sm,Lu,Ca)_3(Fe,Ge)_5O_{12}$ garnet film coercivity, new annealing method 78−84459
$(Y,Sm,Lu,Ca)_3(Fe,Ge)_5O_{12}$ bubble magnetic garnet film, LPE grown, props., $CaCO_3/GeO_2$ molar ratio influence 80−50152
$(Y, Sm, Lu, Ca)_3(FeGe)_5O_{12}$ LPE films, factors affecting coercivity 79−91267
$(Y,Sm,Lu,Ca)_3(Ga,Ge,Fe)_5O_{12}$, film growth and mag. props. for bubble-memory appl. 79−87297
$(Y,Sm,Lu,Cu)_3(Fe,Ge)_5O_{12}$, ion implanted, hard bubble suppression 80−11238
$(Y,Sm,Lu,Tm,Ca)_3(Fe,Ge)_5O_{12}$, epitaxial garnet film, temp. depend. mag. props. 80−39825
$(Y,Sm,Lu)_3(Fe,Ga)_5O_{12}$, LPE mag. film, suitability for 1 to 3 micron bubble devices 78−68323
$(YEuLuCa)_3(FeGe)_5O_{12}$ film, stable state of bubbles containing Bloch lines 78−76281
$Y_xLu_{1-x}Ir_4B_4$, supercond., magnetism and metastability 80−29501
$(YLuSmCa)_3(FeGe)_5O_{12}$ garnet film, bubble domain expansion, fuzzy wall struct. 80−71128
$(YLuSmCa)_3(GeFe)_5O_{12}$ bubble garnet film, coercivity 79−78459
$(YLuSmCa)_3(GeFe)_5O_{12}$ garnet films, bubble expansion saturation vel., sampling optical photography 80−75820
$(Y_xLu_{1-x})_2V_2O_7$ semiconducting ferromag. pyrochlore, mag. props. 80−29547
Y_2O_3-Lu_2O_3-Eu_2O_3-CaO-GeO_2-Fe_2O_3-PbO-B_2O_3 system, garnet crystn. fields 78−43995
$(YSmCaLu)_3(FeGe)_5O_{12}$, bubble film inhomogeneity, spin wave reson. meas. 80−44439
$(YSmLuCa)_3(FeGaGe)_5O_{12}$, reproductibility in bubble garnet LPE growth 78−92204
$(YSmLuCa)_3(FeGe)_5O_{12}$, mag. props. and growth of 2 μm bubbles 78−91910
$(YSmLuCa)_3(FeGe)_5O_{12}$, LPE growth, growth reproducibility of bubble props. 78−92208
$(YSmLuCa)_3(FeGe)_5O_{12}$ films, mag. bubble props. and LPE conditions 79−74107
$(YSmLuCa)_3(FeGe)_5O_{12}$ film, bubble propagation direction effects on high frequency bias margin 79−78480
$(YSmLuCa)_3(FeGe)_5O_{12}$, double layer struct., LPE growth from molybdate and Pb borate fluxes 80−39827
$(YSmLuCa)_3(FeGe)_5O_{12}$, bubble material, dynamic characterisation, comparison between transport and FMR methods 80−39833
$(YSmLuCa)_3(GeFe)_5O_{12}$, garnet film, refractive index dispersion 78−88273
$(YSmLuCa)_3(GeFe)_5O_{12}$, LPE low defect density films, prep. for mag. bubble device fabrication 79−87590
$YSm_{0.5}Lu_{0.7}Ca_{0.8}Ge_{0.8}Fe_{4.2}O_{12}$ film, magnetic bubble propagation with 8 μm period ion implanted propagation patterns 79−78475
YSmLuCaGeIG, mag. props. and defects, depend. on B_2O_3 conc. on growth in PbO-B_2O_3 solvents 78−68321
YSmLuCaGeIG films, epitaxial growth with 3 μm magnetic bubbles 79−61518
$(YSmLu)_3(FeGaSc)_5O_{12}$, submicron mag. bubble garnet 80−54929

Luxemburg effect *see ionospheric electromagnetic wave propagation*

Lyapunov methods
artificial satellite, spin-stabilised, nutation damping *(Russian)* 77−64626
asymptotic stability of unsteady inviscid stratified flows 80−83832
autonomous system instability, sufficient criteria, Lyapunov instability *(Russian)* 79−17210
axisymmetric flow stability 79−23300
Boltzmann eqn., stability anal. by Lyapunov functionals 78−29069
catalytic pellet, isothermal n-order decomposition reaction, steady state stability anal., topological degree and Lypunov method 80−30280
celestial mechanics, stabilisation of Kepler's problem 78−24445
characteristic exponents and stochasticity 80−59177
characteristic numbers and Kolmogorov entropy, stochasticity of dynamical systems 80−59178
corrected gyrocompass asympotic stability *(Russian)* 79−10457
differential equations, almost-diagonal systems, Lyapunov functions construct., iterative process *(Russian)* 77−57168
diffusion, nonlinear, stability 78−8366

Lyapunov methods continued
diffusion-reaction problem, nonlinear, dissipative structs., stability anal. 79−1938
dissipative dynamical system, iterative transitions between periodic and turbulent 78−62159
dissipative dynamical systems, ergodic problem, numerical approach 79−88878
elastic plate, stability via Lyapunov's Second Method 77−54914
entropy, nonequilib., Lyapunov variables, ergodic props. of classical systems 79−2739
Euler column Lyapunov stability analysis 78−71285
flexible damped satellites, Liapunov stability anal., comparative study 79−37148
Freidrichs model, Lyapunov function evaluation 78−73876
geophysics, analytic continuation of function for Earth surface *(Russian)* 79−35008
hyperbolic system, simple wave growth, charact. shock instability, fluid appl. *(French)* 77−68623
hyperelastic bodies, Lyapunov stability sufficient criteria 79−12604
infinitesimal steady motions, stability exchange *(German)* 79−41751
lumped system in conflict with environment, Liapunov type design 79−57498
lunar librational stability, effect of external disturbing torques 77−71021
macromolecular systems, self-reproducing, stability and selection 79−96507
mechanical systems, follower load type, time invariant functionals 80−77609
MHD equilibria, stochastic stability 79−77414
multidimensional systems oscillations of mechanical systems that do not become linear when the parameter vanishes 80−68032
nonequilbrium steady states, irreversible processes, Lyapunov functions 80−95049
nonhamiltonian systems with one degree of freedom, forced periodic motion *(Russian)* 78−20959
nonlinear oscills. of round plate, difference eqn. approx., Lyapunov methods *(Russian)* 77−39259
nonlinear systems, asymptotic stability, geom. props. of Lyapunov functions *(German)* 78−87286
one dimensional distributed parameter system parameter and state estimation, heat conduction experimental result *(Japanese)* 80−83727
parameter identification and adaptive control, applic. to nuclear reactor systems 80−22970
periodic surface scatt., existence theorems *(Russian)* 78−73890
perturbed motion stability anal. *(Russian)* 78−16640
plane restricted three body problem, asymptotic solns. *(Russian)* 77−22049
ring laser, beat regime with resonator freq., existence, stability 79−50326
rotating cantilever, stability and instability conditions, Lyapunov function method *(Russian)* 80−36840
satellite attitude control system, gyrodampers appl. 78−96379
satellite under aerodynamic torque, total stability anal. 77−56805
self-gravitating system of N parallel plane sheets, Kolmogorov entropy 79−80562
self-oscillating mode origination in nonequilib. magnetised plasma 79−86568
spacecraft detumbling, using movable telescoping appendages 77−54868
stability in the presence of several resonances *(Russian)* 77−71203
stability of constant Laplace solutions of the unrestricted three-body problem 80−68030
stability of motion, approx. Lyapunov function definition *(Russian)* 78−62068
stability of motion on a ring *(Russian)* 80−42052
stochastic control system, integral inequalities 79−17341
stochastic differential eqns. and differential inequalities 77−5641
symmetric gyroscope motion, differential eqns. stabilisation procedure including perturbing torques 80−4244
three rigid bodies problem, particular solns. for translational motion *(Russian)* 80−61999
two-phase interface and free surface equations in groundwater flow 79−48527

M-centres
alkali halide, CW lasing of F_2^+-centres, 0.9-2 μm 78−29957
alkali halide crystals, binding energy of F_{e+}', M_{e+}' and R_{e+}' centres, positron trapping 79−69460
alkali halide crystals, capture and annihilation of positrons at M- and R-centres *(Russian)* 77−85829
alkali halide crystals, computer-generated polarisation holography 78−46538
alkali halide crystals, tunable CW IR lasers using F_A(II), F_B(II), M and F_2^+ centres 77−88725
alkali halide photodichroic crystals use for coherent opt. data processing 77−68248
alkali halides, doped, F-centre accumulation efficiency temp. depend. 77−76394
alkali halides, M-centre, lifetime data for excited state 78−35193
alkali halides, photodichroic, as optical processing elements 78−83056
alkali metal halides, F-centre luminesc. rel. to cryst. chemical parameters 80−29780
alkaline earth oxides and fluorides, F-centre luminesc. rel. to cryst. chemical parameters 80−29780
CaF_2:Na, Stark effect on Na disturbed F_2-centres 77−69279
ionic cryst. positron-containing M-centre, struct. 80−49220
laser, mode-locked F_2^+ centre, use for distortionless propagation of 5 psec-wide pulses in fibres 79−94358
laser, pulsed F_2 centre, tunable in 1.1 to 1.26 μm range, spectral charcts. 80−91805
optical waveguides, slab-type, mode coupling via dichroic absorpt. of M centres 80−33178
BaF_2, undoped and U-doped, neutron irrad., absorpt. band attributed to F_2- centres 80−7380
BaF_2:U, absorption band spectra following neutron irrad. 80−29763
CaF_2:Dy crystal with M centre, antiresonance line, mag. field effect 80−55138
CaF_2:Na, tunable room temp. laser action of M-centres, luminesc. and absorpt. spectra 79−31907
CaF_2:Y, absorpt. spectra, radiation defect formation energy, F to M centre conversion kinetics 79−65079
CaO, ODMR and spin coherences in phosphorescent state of exchange-coupled F^+-centre pairs 79−87336

M-centres continued
CaS phosphor, deep capture centres obs. 78−10951
GaP crystals, radiation defects, TSC obs. 80−65588
KBr photochromic materials, F→M transform., electrostatic field control of optical information recording *(Russian)* 80−48370
KBr:H^+(H_2^+), absorption bands, V_4- and M-centres 77−48204
KCl, absence of energy transfer between F- and M-centres 79−99935
KCl, absorption spectra of F-aggregate centres, 2K 77−48207
KCl, additively coloured photochromic crystals, spectral sensitivity *(Russian)* 80−91871
KCl, diffr. by M-centres, thick plane wave hologram recording 77−7021
KCl, F_2 centres triplet state, radiative and nonradiative decay 79−11438
KCl, F_2-centre triplet-triplet transition at 685 nm, MCD obs. *(French)* 77−63433
KCl, gamma irrad. relationship between thermolum. and deform. luminesc. 79−19942
KCl, luminesc. excitation spectra of F-aggregate centres, 400-900 nm. *(Russian)* 78−10980
KCl, M-centres, F-centre sensitised luminesc. 77−4681
KCl, perturbed M-centre triplet state, M-F centre exchange mechanisms 79−69884
KCl, photoconductivity during F→X transition *(Russian)* 77−43663
KCl, radiative tunnel transitions in negatively charged colour centre systems 80−49655
KCl:Li, $(F_2^+)_A$ centres, optical props. 80−89026
KCl:Li $(F_2^+)_A$ centres, tunable CW laser action 80−87399
KCl:Li(Na), M_A-centre, decay 77−77278
KCl:Na^+, CW laser action of $(F_2^+)_A$-centres, tunable from 1.62 to 1.91 μm 80−32998
KCl:Pb^{2+}, pure and doped, electrolytically coloured, elec. cond. and optical absorpt. meas. 80−100668
KCl:Sr, M-centre photoluminesc. *(Russian)* 78−84649
KCl(Br), triplet state lifetime of F_2 centre, mag. field effect 78−35177
KCl(Br):OH^-, electron irrad., F_2^+ centre stabilisation 80−54231
KCl(Br)(I) with alkali and halogen impurities, colour centre deformation induced nonradiative decay 80−7387
KF F_2^+-centre laser, picosecond pulse generation 1.24 to 1.45 μm, mode locking 79−89925
KF, F_2+-centre excited-state absorption spectrum, rel. to H_2^+ model 80−16066
KF, tunable CW laser, using F_2^+ centres for 1.26-1.48 and 0.82-1.07 μm bands 78−79023
KF:Pd^{2+}, pure and doped, two-step photoionisation, laser-active F_2^+ centre form. 79−963
KI(Br), irradiated at room temp., thermolum. and F-centre thermal stability 78−84669
LiF, 3 MeV electron induced F, F_2, F_2^+, R_1, R_2 and F_2 colour centre obs., IR spectra obs. *(Russian)* 77−48210
LiF, coherent freq. tunable radiation generation in F-centres, 0.6 to 1.26 μm range 79−36902
LiF crystal with F_2^+ centres, periodic pulsed tunable laser, Nd laser second harmonic excited 80−38021
LiF, electron irrad., transport of valence band holes, optical absorpt. obs. 79−99188
LiF, irrad. at pile temp., higher F aggregate centres produced during thermal annealing 77−43212
LiF, lasing action, room temp. obs. 78−82972
LiF, M-centre vibronic absorpt. spectra, elec. field, method of moments 78−27186
LiF, M-centres, quadratic Stark effect, differential electroabsorption spectra 77−66526
LiF OH-stabilised F_2^+-centre laser, appl. to intracavity laser spectroscopy 80−32999
LiF, picosecond generation on F_2^+ colour centres, induced mode synchronisation *(Russian)* 80−64033
LiF single crystals, visible superradiance of excited F_2-centres 79−33733
LiF, Stark effect, M-centre absorpt. bands 78−84614
LiF, thermostimulated exoemission, adsorbed layer effects 78−11085
LiF with stable F_2 centres, F_2^+ colour centre generation accumulation, tunable laser production *(Russian)* 80−28238
LiF:OH^-, electron irrad., F_2^+ centre stabilisation 80−54231
LiF-Li_2O, F-aggregate centres *(Russian)* 78−64394
MgF_2 crystal, M(D_{2h}) centre absorption and emission spectra obs. 79−19910
MgF_2, M-centre, dissoc. kinetics after pulse electron irrad. 79−7601
MgF_2, primary pair of radiation defects, energy of form., colour centre conversion rates *(Russian)* 78−6055
NaBr, lifetime of colour centres 78−92115
NaCl, gamma irradiated, optical bleaching of colour centres, F-aggregate centre form. 79−95813
NaCl, γ-irradiated, F→M phototransformation, effect on aquoluminescence 80−7418
NaCl, M-centre prod. processes, in-beam studies, 15-95°C 79−55737
NaCl, M-centre statistical prod. meas. 80−15097
NaCl plates, γ-irrad., optical absorption spectra, hologram recording samples 78−17878
NaCl, transient infrared absorption of bound polarons 78−91642
NaCl(F), irradiated at room temp., thermolum. and F-centre thermal stability 78−84669
NaF, computer generated polarisation hologram 77−61923
NaF crystal M-centre storage element, photosensitive characteristics 79−14067
NaF, dichroim absorpt., appl. to optical waveguide polariser 79−995
NaF, excess electron colour centre obs. 77−16343
NaF, F_2^+-like colour centre, room temp. stable, CW laser, 0.99-1.22 μm tunable 80−69399
NaF, M-centre vibronic absorpt. spectra, elec. field, method of moments 78−27186
NaF, M-centres, quadratic Stark effect, differential electroabsorption spectra 77−66526
NaF, photodichroic, direct-writing M-centre, Hurter-Driffield curves 77−4662
NaF, reversible optical storage element using M-centre polarisation 78−94416
NaF, Stark effect, M-centre absorpt. bands 78−84614
NaF, X-irrad., colour centres and thermolum. 80−84790
NaF:Li, combined suppressive and extinction writing, using M(M_A) centres 77−7164
NaF:LiF, M/M_A-centre photodichroic props., for holographic spatial filter 77−7011
M-centres continued
NaF:Mn^{2+}, two-step photoionisation, laser-active F_2^+ centre form. 79−963
NaF(Cl):OH^-, electron irrad., F_2^+ centre stabilisation 80−54231
RbCN, ferroelasticity and F- and M-centres absorpt. 79−87475
$RbNgF_3$, radiation defect F,M,R-centre absorpt., emission, excitation spectra 79−43000
SrF_2:Na, tunable room temp. laser action of M-centres, luminesc. and absorpt. spectra 79−31907
ZnS, luminescence of M-centre 80−29779
ZnS phosphor, deep capture centres obs. 78−10951
ZnSe, deep centres, photolum., photocapacitance and photocurrent expts. 78−39053

M-regions *see Sun*

Mach number
see also acoustic wave velocity; shock waves
capillary discharge, with evaporable wall, plasma parameters axial distrib. *(Russian)* 78−75280
concave corners, Whitham theory of shock-wave diffr. 80−100012
hypersonic blunt-slender cones, artificially induced boundary layer transition 80−28496
hypersonic shock tunnel, development for aerospace simulation 79−41777
Navier-Stokes equations, Lighthill's theory to non-adiabatic cases 78−83372
near-wake for slender cone, Mach number depend. of laminar transition 77−62277
nonlinear one-dimensional waves in near-sonic flows 79−41701
nonstationary oblique reflections, actual isopycnics and numerical expts. 79−41712
Prandtl-Meyer function soln., hybrid computer method 77−11164
scaling law, for helicopter rotor noise 78−83167
separated two-phase flow, pressure drop and sonic vel. 80−106840
shock tube flows, unsteady non-equilibrium, discretisation of boundary layer terms, computation at Mach 10 80−14742
shock tubes, use of fast-acting valves, shock wave formation, max. Mach number 80−24052
sonic boom, nonlinear propag., including asymm. effects, numerical soln. program 77−72326
subsonic base pressure fluctuations on axisymmetric blunt-based body, Mach no. depend. 80−19423
subsonic turbulent boundary-layer flow, compressibility effects 77−62268

Mach principle *see cosmology; space-time configurations*

machine bearings
air bearing and diamond machine design for optics 80−1365
air bearing for precision linear displacement 80−105637
ball bearing surface CVD coating expts. 79−83366
conical step bearing, externally pressurised, characts. of micropolar lubricant 77−86189
elastic hydrostatic sliding bearing, forced vibrs. of vertical rotor 79−18798
elastomeric bearings, high-capacity, laminated, finite-element anal. 80−96197
fatigue testing, Weibull distrib. statistical interference 79−52473
flywheels, development of low loss magnetic bearings, for energy storage appls. 80−30566
flywheels, performance of retainerless bearings for vehicular energy storage appls. 80−30567
friction meas., thermal load and wear props. *(German)* 79−81826
grinding and polishing of optical glass, semiautomatic machines kinematics *(Czech)* 78−63208
high-precision ball bearings, new method of calc. 79−30445
hydrostatic bearing, pressure regulator device, behaviour anal. 78−93668
journal bearing, hydrodynamic lubrication including surface tension free boundary problem 80−19542
journal bearings, performance, turbulent lubrication theory using frictional law appl. 79−98695
linear motion gas bearing for Fourier spectrometers 80−31893
lubricant wear debris examination, oil anal. techniques, appl. to plain bearing materials study 80−97596
lubricating oils, strength and damping coeffs., vibration diagnostics *(Russian)* 80−97592
nearly viscometric glide bearing fluid *(German)* 79−81830
optical diamond turning air-bearing spindle and eddy-current motor 80−5851
rigid rotor in elastic ball bearings, free oscillations *(Russian)* 79−18773
rotating machinery subharmonic vibration diagnosis 79−3971
rotating mirror deflector design cost/performance tradeoffs 77−58485
rotating mirror laser beam TV scanner, development programme *(Japanese)* 80−74369
rotating system balancing in uninterrupted operation 78−90746
spherical bearings with stone pillow blocks, friction and wear *(French)* 79−18832
steel bearing balls, exoelectron emission for surface fatigue wear testing 78−39960
turbogenerator, with hybrid hydrostatic hydrodynamic lubrication, behaviour in laminar and turbulent conditions *(Italian)* 80−81208
turbogenerator bearing oil film damping and stiffness coefficients determ. for dynamic behaviour stability study *(Italian)* 80−106762
turbomolecular pump, development and use 79−63251
wear resistant coatings, impulse discharges treatment *(Russian)* 79−1917
Al alloy-mica particle composite, cast prep. and mech. props., bearing appl. 80−71613

machine insulation
bar insulation in stator winding of large turbogenerator, inspection using microwave defectoscope 80−35474
epoxy mica generator insulation, dielectric stress conc. influence on voltage endurance 78−15094
volts-per-bar and flashover, causal mechanisms and preventive measures 80−92408

machine oriented languages
CRETA 74, improvement of PAL 11 A assembler for IML syntax implementation 78−33406

machine protection
nuclear power stations, turbogenerator overspeed protection, reliability study, design *(French)* 77−3156
turbogenerators, H_2 cooled, heating-up detect. by gas stream chromatography and mass spectrography *(French)* 79−48024

machine testing
200 kW vertical axis wind turbine, preliminary test results 80−66928
acoustic noise meas. standards and reference sources *(French)* 78−83185
electric equipment testing laboratory, movable, type ETL-35, design *(Russian)* 80−95088
electroacoustic, analytic and diagnostic equipment 78−63249
homopolar generator, fast discharge machine, design, fabrication, testing, for fusion reactor 78−54952
nuclear power station outages, turbine-generator reliability assurance through large scale test facilities 77−3151
rotating machine flaw detection, acoustic signature analysis and time-domain techniques 79−50525
Savonius rotor, aerodynamic performance testing in wind tunnel 80−61266
signature analysis systems with Fourier analyzer 78−87195
stroboscopes appl. 78−55453
vertical axis wind turbines 80−66929
vibration testing and dynamic balancing 80−23971
water-bath US coupling and piece-part testing methods *(German)* 79−74317
wind generator, vertical axis, 1 kW, using steel reinforced fibreglass blades 79−61940
wind turbine generator, 5 kW, with automatic load matching device, field testing 79−70418

machine theory
eddy current problems, three dimensional, soln. *(Japanese)* 79−81325
EM field analysis, numerical techniques for conformal transformation 78−74816
linear induction MHD machine, elec. cond. body motion in mag. field *(Russian)* 77−7468
magnetic field calc., saturable, by finite element method, using scalar magnetic potential 77−38773
magnetic fields, quasi-stationary, finite element anal. 78−94356
optimum design, interactive method of soln. 79−17204
rectangular conductor in slot, transient field anal. using Bubnof-Galerkin method *(Polish)* 77−54643
spiral vibration of rotating shaft rubbing against interference element *(German)* 78−87252
superconducting, heat transfer in rotating windings, free convection in cryo-fluid He-I modelling 78−26745
viscous liquid flow through annular clearance over rotating inner cylinder 80−64626

machine tools
see also numerical control
acoustic noise, power press, relationship between force waveform and sound radiation 80−74596
afocal projection measuring system, moire fringe techniques, large lathes, milling machine appl. 77−71295
angle measurement, automatic testing of precision dividing heads *(German)* 80−82740
astronomical optical surface shaping automation methods 79−84675
cemented carbide tools coated with HfN and TiC, machining evaluation 79−29253
chip geometry and cutting forces 80−93629
computer-controlled machine tool for diamond-turned surface accuracy improvement 80−1367
computerised control for diamond-turned surface finish 79−98517
cutting element rectilinearity testing, laser beam appl. *(German)* 77−44419
cutting fluids testing rel. to tool wear, thin layer activation technique 80−55619
cyanided, wear characts. 78−48542
diamond turning precision machine tool system 80−69568
diffraction grating ruling engine with piezoelec. control 78−83128
diffusive wear, effect of magnetic fields, cutting tools 80−60985
floating-collar saw, moving-load stability of circular plate 77−46863
framework rigidity meas., holographic interferometry *(German)* 77−7040
geometry inspection using laser interferometry 77−9997
grinding and polishing of optical glass, semiautomatic machines kinematics *(Czech)* 78−63208
grinding wheel life modelling, group method of data handling 80−58987
hyperboloid lens manufacturing technique 80−96039
length meas. international standards compared *(German)* 80−36977
metrological gratings, multisectional linear, production technique 77−3686
noise, determ. of sound performance for multi-position machines *(German)* 80−43523
noise and vibration reduction method 79−50506
noise control, conf., W.Lafayette, IN, USA (Apr/May 1979) 80−43526
noise control, power hacksaw machines 79−68482
noise meas. techniques 77−31172
optical aspheric rotationally symm. surface generation, computer control 77−27395
part displacement meas. using holographic interferometry 78−9348
polisher, controlled, for optical fabrication 78−75006
polishing and grinding, semiautomatic, kinematic ratios calc. *(Czech)* 78−79146
polishing of optical surface, computer control 77−23787
position feedback by laser interferometer 80−73438
positioning system using laser interferometer *(German)* 80−9022
precision, floor vibration isolation 80−43522
reactor fuel pin diameter meas., sectioning cutoff saw adaptation 79−9748
small grinding and polishing tool control by computer 79−98516
spark erosion machine for cutting X-ray-aligned dielectric crystals 79−80592
spectral analysis of vibration data, failure prediction 80−79048
vibration stability assessment method 78−87316
vibration-damping plug for noise reduction 80−43525
vibratory tools, hand-arm energy dissipation and accel. levels 78−96116
wear resistance, accelerated testing *(Russian)* 80−40543
CO_2 laser appl. 77−40517

machine windings
see also rotors; stators
superconducting, heat transfer in rotating windings, free convection in cryo-fluid He-I modelling 78−26745
turbogenerator, water/oil cooled type TVM-300, stator winding vibration tests *(Russian)* 77−9886

machine windings continued
turbogenerators type TVV-800-2, endwinding vibration tests *(Russian)* 77−9885
wound wires, enamel insulated, elongation plus flexibility 80−20999

machines, electric *see electric machines*

machining
see also cutting; electrolytic machining; electrolytic polishing; electron beam machining; grinding; laser beam machining; spark machining
adsorption-sensitive fracture processes, control and appl. 77−52468
alloys, machining damage, depth of surface layers determ. 80−85094
angle synchronous contact sensing for noise investigations, anal. of gear wheels machining errors appl. *(German)* 79−68477
brass, magnetoabrasive machining, optimum conditions 80−30172
brittle material, wear, acoustic emission obs., effect of ion aggregates in Rebinder-Westwood environment 78−48536
chip formation, frictional interactions between chip and rake face 79−52387
chip-formation process control 79−63319
diamond machined optical surface specification 80−48472
diamond tool bit machining, comparison with conventional optical process 80−69569
electroerosion machining, steel surface damage by supersonic plasma flow 79−32780
ferrites, Mn-Zn, effect on magnetisation curves obs. *(Japanese)* 77−21295
glass, wear, acoustic emission obs., effect of ion aggregates in Rebinder-Westwood environment 78−48536
glass-ceramic machinable, machining techniques 78−77881
high strain rate processes, review 80−84864
information criterion for selecting the number of points in workpiece monitoring 79−67274
ion beam sputtering, appl. to surface machining 80−30129
lathe during metal removing, automatic vibration control systems reviews *(Russian)* 78−70118
linear motor slide drive system for optical machining 80−1366
magnetic bubble device large-area ion milling from small sources 79−75510
metal cutting, separation process tool tip, fracture detection, acoustic emission method *(Japanese)* 80−1388
metals, abrasive finishing with refractory carbide micropowders, surface struct. 80−11842
milling spherical surfaces 80−64222
NC diamond turning system evolution 80−1369
nonuniqueness of machine process 78−39932
ophthalmic lens surface working machinery 80−28363
optical diamond turning and precision engineering 80−1364
optical elements, diamond turning 77−27400
optical precision machining, seminar, San Diego, USA (Aug. 1978) 80−1363
optical precision machining commercialisation for military economy 80−1371
optical surface programmed aspherisation accuracy rel. to tool size 79−72727
precision machining in optics, conf., San Diego, California (1976) 77−42637
residual stress measurement, bending deflection and stress source methods *(French)* 79−34265
roughness of machined surfaces, on-line meas. technique using He-Ne laser *(German)* 80−33014
roughness parameter measurement, profilograph needle radius of curvature and finely machined surfaces 77−53859
steel, austenitic stainless type 304N, machining induced deformation transformation, mag. evaluation 79−83195
steel, stainless, smoothing for plastic pre-straining of material cut by turning *(Russian)* 80−60911
steel, type 4340, machining by TiC-coated high speed steel tool 78−11435
steel C60, machined, surface morphology, struct., SEM, topographic investigs. *(German)* 77−73372
strain rate predictions in chip formation zone, work material flow stress props., cutting conditions 77−70277
surface, mech. and corrosion props. improvement using US energy *(Rumanian)* 79−15821
surface layer structure determ. using Barkhousen noise probe *(German)* 79−24710
tension test with neck triaxiality reduction 78−7159
tools, chip geometry and cutting forces 80−93629
US lapping, of conical surfaces 78−44235
Al alloy, drilling accuracy *(Japanese)* 79−100181
Al alloy fatigue cracked alloy 7075 T6, repair machining and inspection of components 78−80689
AlB_2 flake reinforced composites, prep., props. rel. to aspect ratio, book contrib. 78−48366
Ar^+, 30-cm multipole sputtering electron-bombardment ion source, design and characts. 77−87870
Be, machining damage, SEM exam. 78−39990
Fe, degree of charging of surfaces polished by TiC and synthetic diamond micropowders 78−60880
Fe-Cu-C sintered porous materials, machinability 80−66457
GeTe, machining effects on electrophys. props. 77−86199
$LiTaO_3$ monocrystal lapping and precision machining characteristics *(Japanese)* 79−80593
Mn-Al-C, permanent magnet, mag. props., machinability 77−85505
Mo, surface machined, struct., electron diffr., TEM *(German)* 77−73371
Ni plated aspheric metal mirror fabrication for IR optical systems 80−14497
PuN, fabrication and high-temp. thermodynamic and transport props. 77−28774
Ti, degree of charging of surfaces polished by TiC and synthetic diamond micropowders 78−60880
Ti-Al-Cr-Mo, type VTZ-1, machinability, using different abrasive materials *(Russian)* 80−97593
Ti-Al-Mo, type VT14, machinability, using different abrasive materials *(Russian)* 80−97593
Ti-Al-V-(Sn), surface finishing effect on internal stresses, X-ray study *(German)* 79−34210
TiB_2-TiC(20 wt.%), sintered, US machining 77−21325
WC-Co hard alloys, machined with polycryst. superhard materials, surface struct. using X-ray photoelectron spectroscopy 80−25919

macromolecular configurations
acetylcholine receptor protein structure 80−85339
acrylonitrile Na methallylsulphonate copolymer electrolytes in dimethylformamide, gel permeation chromatography appl. 80−21345
acrylonitrile-MMA copolymers, sequence distrib. determ. by NMR 77−14622
F-actin, struct. changes in living muscle fibres, polarised UV fluoresc. microscopy 80−67037
adenine-uracil polynucleotides, alternating, premelting, melting, postmelting transitions 79−57574
adenovirus hexon, three dimensional structure from electron microscopy, computer modelling 80−35833
adrenocorticotropic hormone polypeptide chain left helical conform., aqueous soln. 77−70414
adsorbed chain structure, Monte-Carlo simulation *(Russian)* 77−19122
adsorbed macromolecules, conform. and thermodynamics at liq./solid interface 77−11782
adsorption of macromolecules at plane surface, computer rel. to real expts. *(Russian)* 79−56077
alanine, oligomer, vibr. spectra rel. to polymeric form 79−83695
albumin, adsorbed layers on polystyrene, contact angle meas. 80−61508
amino acid, cryst., mol. dielec. function 79−7043
aminoacidic side chain-liquid crystalline polymers, synthesis physicochem. props., struct., optical anisotropy *(Russian)* 79−23521
anthramycin-DNA adduct, proposed struct. 80−30658
antibodies, conformation in presence and absence of antigen, small angle X-ray studies 79−11890
aromatic copolyamide solns., conformational energy and mesomorphic character *(French)* 79−99066
p-aromatic poly(amide hydrazide), dimethyl sulphoxide solvent, dynamic birefringence, conform., viscosity *(Russian)* 78−39525
aromatic polyamides, rigid and nonrigid, ultrahigh modulus fibres 79−95992
Na, K-ATPase membrane prep. struct. characts. studied by paramag. probes 78−64930
Na^+,K^+-ATPase preparations, tryptophan fluoresc. 77−21477
Azotobacter ferredoxin, struct. of Fe-S clusters at 4.0 Å resolution 79−57575
bacteriophage FI-5$^+$, struct. in intact state 79−70513
bacteriophage S shape determ. from small-angle X-ray scatt. 79−39347
bacteriorhodopsin, anomalous amide I IR absorpt. rel. to alpha helices distorted struct. 80−12058
bacteriorhodopsin, effect of high press. on absorpt. spectrum and isomeric composition 80−67041
bacteriorhodopsin, purple membrane struct., Halobacterium halobium 78−15782
bacteriorhodopsin orientation in Halobacterium halobium, selective proteolysis investig. 78−77010
bacteriorhodopsin proton pump, elec. demonstration of rapid light-induced conform. changes 77−44597
basic pancreatic trypsin inhibitor, methyl group PMR, 360 MHz 78−27887
biological macromolecule, high resolution struct. determ. by electron microscopy 80−89717
biological macromolecule observation using CTEM and STEM with negative staining 80−85561
biological macromolecules, conformation studied by calorimetry, review 80−97870
biological macromolecules, struct. determ. by diffr. 79−94932
biological polymers, importance of chiral purity in self-reproduction of organisms 77−36864
biological structure studies, neutron scattering from soln. of macromols. 77−16906
biomembrane, phase changes and determination methods *(Czech)* 80−3599
biomolecular systems, computer simulated modelling 79−88049
biomolecular systems, topographic analysis in FORTRAN IV 79−88050
biomolecule computer graphics, protein and nucleic acid conform. 77−36865
biomolecule recognition model, stereochem. enhancement of specificity 77−81461
biomolecules, ZDO method for very large mols., low computer time 77−14356
biopolymer, electronic-conformation interactions 80−3588
biopolymer, local mode resonance enhancement in Raman spectra 77−77204
biopolymer chain, uniform, elastic, possible conformational states 80−37913
biopolymer chains, intramol. reacts., enzyme catalysis appl., review 80−40953
biopolymer molecular dynamics and structure, fluorescence spectroscopy 77−60329
biopolymer thermodynamic props. in helical and coiled state, 4 to 400K, calorimetry 78−20140
biopolymers, circular dichroism, optical rotatory dispersion, conformational anal., review 77−3497
biopolymers, electro-optical changes, chem. and rotational contribs. 80−85352
biopolymers, X-ray struct. study using synchrotron radiation and multichannel detector 78−47210
biostereochemical modelling, interactive computer graphics, appl. to DNA-protein interaction 78−88693
bis(methylthio)alkanes, model compounds of polythioethers, vibr. spectra 80−58430
bisphenol A polycarbonate, end-cap ratio and mech. props. of block copolymer 78−91266
block copolymer chain conformations 80−69282
block copolymers, morphology rel. to stress/strain props., deform. hardening effect, birefringence meas. 77−48501
bovine carbonic anhydrase, γ-ray perturbed directional correl. obs. of conform. change, active site ^{111}In ions 79−83700
branched macromolecule, particle scatt. factor, light, computer simulation 79−64128
branched polymer molecules, second virial coeff., chain length effects calcs. 78−37775
Brownian motion entropy calc. 77−34791
butadiene styrene elastomers, cross-linked, mech. relax. behaviour *(German)* 80−84986
butadiene-nitrile elastomers, high temp., and press. chem. transformations *(Russian)* 79−52659

macromolecular configurations continued
butadiene-styrene block copolymer, containing free polybutadiene mols., viscoelastic behaviour 77−56015
N-tert-butylacrylamide-styrene copolymers, struct., composition, IR, DTA investigs. *(Polish)* 79−31751
butyryl cholinesterase of horse serum, quaternary struct. obs. 79−57570
C1q of human complement, neutron scatt. obs., conformational calcs. 80−81537
β-casein, adsorption kinetics, surface denaturation 79−79460
β-casein, molecular structure of adsorbed film 79−79462
κ-caseins of cow and sheep, secondary structures 78−96001
cellulose, conform. states and IR dichroism calcs. 80−55986
cellulose, nitrated, strength, deform. and disintegration, influence of stable free nitroxyl radicals 80−11717
cellulose, struct. and conform. props. of cotton fibre grown from γ-irrad. seed 77−81539
cellulose acetate-dimethylphthalate gel, mech. props., substitution effect *(Russian)* 79−23291
cellulose triacetate I, mol. and cryst. struct., parallel chains 78−30548
cellulose trinitrate, in soln., gel-like aggregate form. rel. to configuration 77−31036
chain configuration-dependent props., review 77−38758
chain molecule in solutions, finite concentrations, different solvent conditions, simulation 79−45872
chain mols., conformational transition kinetics 80−83339
chain networks, static and dynamic entanglements, contrib. to equilib. shear modulus 80−28126
chains confined to strips or tubes 77−61883
chaotic branched macromolecules, struct. simulation, parameters calcs. *(Russian)* 80−69283
chondroitin-4-sulphate biopolymer, adsorption on adsorbed collagen 79−79459
choroplast 16S rRNA gene, sequencing of 3′-terminal 79−70518
chromatin, neutron scatt. rel. to higher order struct. 79−11894
chromatin, nucleosomal arrangement DNA, histones and non-histones, review 79−79464
chromatin, reversible conformational transition obs. 79−62179
chromatin structure and thermal denaturation profiles 77−12881
chromatin subunits, in glycerol/sucrose solns. containing various D_2O/H_2O mixtures, neutron scatt. study 79−11893
chymotrypsin-like proteins, gamma irrad. induced struct. changes 77−44594
chymotrypsin-like proteins, gamma-irrad., inactivation rel. to struct. changes 77−56341
collagen, 3-dimens. struct., rel. to props. of connective tissue 80−67038
collagen, axial arrangement of α-chains, intramolecular polar and apolar interactions 78−27891
collagen, enzyme- and alkaline-soluble, optical rot. dispersion and circular dichroism 77−70411
collagen, helical and coiled, thermodynamic values, 4 to 300K 77−25379
collagen, interpretation of small-angle X-ray diffr. using α1 chain primary struct. 77−66792
collagen, polarisation, contribution of permanent and induced dipole moments, elec. birefringence 80−85351
collagen and muscle elastic moduli rel. to phonons, Brillouin sectra 77−52824
collagen biopolymer, adsorption on solid surfaces 79−79459
collagen molecular organisation and connective tissues props. 80−97858
collagen structures, piezoelec. effect, in rel. to mol. struct. 80−41100
collagen triple helical struct. study using Fourier transform 78−7318
collagne fibrils, rat tail tendon, quasi-hexagonal mol. packing model 80−30660
collodion, film, IR spectrum, vibr. assignments, chain config. 77−34789
computer modelling of matter, conf., Anaheim, USA (March 1978) 80−51954
computer simulation techniques for mol. theory verification 78−13633
conference, Dublin, Eire (July 1977) 79−55012
conformational props. rel. to spatial electron density determs., computer simulations 78−70763
cooperative reaction between simple synethetic macromolecule, rel. to chain length *(Russian)* 77−63911
copolymer globule model, orientationally-ordered liq. cryst. state *(Russian)* 80−59389
copolymer model with alternating spins, kinetics 80−9768
copolymers, alternating block, prep. by polycondensation, mol.-mass distrib. parameters *(Russian)* 78−73042
cross-sectional area per chain: a useful structural parameter for polymer characterization 78−86984
crystal structure refinement, by simultaneous minimisation of energy and R factor 79−7517
cytochrome c, metal substitution effect on mol. struct. and functional props. 79−53037
cytochrome c adsorbed on different carriers, conformation study 79−53029
cytochrome c oxidase, coupled to proton pump in mitochondria 77−25406
cytochrome c oxidase, macromolecular struct., electron microscopy and image anal. 80−89716
cytochrome c oxidase, struct. of cytochrome a_3-Cu_{a3} couple, NO binding studies 80−67039
deoxy ferrous haemoglobin, Fe atom distortion, pseudo-Jahn-Teller effect 80−55984
deoxyhaeme model, semiempirical calcs., EM props. rel. to electronic config. and Fe-plane distance 78−53324
dextran fractions, production, characterisation and solution properties 80−59368
diacetate-nitrocellulose, long period struct., 180-265°C, X-ray diffr. obs. *(Russian)* 79−24556
N,N-diethylacrylamide, cross-linked copolymer, improved mech. props. 80−61091
L-β-3,4-dihydroxyphenyl-α-alanine with L-glutamic acid, polymers and copolymers, synthesis and conform. 79−33996
dimensions, mean square end-to-end distance, Monte Carlo calcs. 79−68337
dinucleoside monophosphates, conformational anal. by nuclear Overhauser effects 79−20509
dinucleoside monophosphates, struct. and conform. in aq. soln., Raman spectra 78−78847
dipalmitoyl phosphatidylcholine, conformational nonequivalence of chains 1 and 2 79−16133
dipeptide, struct. and bonding, ab initio calcs. 79−53039

macromolecular configurations continued
DNA, A and B structs., non-standard conforms. of sugar ring 78−80827
DNA, B form conformations, double-helix and side-by-side models, X-ray diffraction 80−78735
DNA, calf-thymus and superhelical PM2 aq. solns., electro-optic obs. of γ-irrad. damage 80−85452
DNA, circular superhelical, X-ray diffr. at 300-10000 Å resolution 77−9168
DNA, conformation changes, soft modes 77−29097
DNA, conformation of native molecule, influence of solvent struct. 80−30655
DNA, double-helical model, sedimentation coeff., X-ray scatt. 77−14629
DNA, double-stranded, ^{13}C NMR obs. 80−69281
DNA, entropy nature of B-A transition 79−92130
DNA, gamma-ray effects on hydration, PMR of frozen and liq. solns. 78−27900
DNA, helix-coil transition model 77−52734
DNA, improved definition of A and B forms, atom-atom potential functions method 78−96000
DNA, length measurement, appl. of random flight theory 78−35799
DNA, mammalian, organisation of repeated nucleotide sequences in replicons 77−73506
DNA, monodisperse, rod-like mols., transient elec. dichroism 78−94344
DNA, mutations, quantum theory, proton transfer by dynamic interactions 77−77868
DNA, phase transition, ψ transition of single coils 80−26200
DNA, polymorphism, X-ray diffr. and computerised model building study 78−27894
DNA, possible conformations calcs. 80−76705
DNA, RF II ΦX174, melting profiles 78−24027
DNA, supercoiled torsional stress and local denaturation 80−72131
DNA, supercoiling, elastic model 78−15767
DNA, supercoiling 78−31766
DNA, synthetic, duplexes in soln., struct., dynamics 79−57574
DNA, Tetrahymena, viscoelastic meas. 79−100570
DNA, torsionally stressed, transitions between B- and Z-conformations, theoretical anal. 80−94166
DNA, X-ray diffr. from side-by-side model 80−35835
DNA B-form, closer definition of struct. from X-ray diffr. and energetic criteria 80−81533
DNA conformation, influence of intermol. interactions 80−16900
DNA conformational fluctuations, internal motion correl. times, ^{31}P NMR obs. 80−72135
DNA double helix, supercoils and torsional stiffness 79−83702
DNA double helix supercoils, linking numbers, twist, writhing number 77−12882
DNA helix-ball transition, peculiarities due to Cu^{2+} and Mn^{2+} 79−70514
DNA hydrate, stability studied by thermogravimetry 80−30650
DNA hydration characts. in H_2O/D_2O frozen solns., γ irrad. effects, PMR 78−31772
DNA in chromatin, stereochem. model for superfolding 80−35829
DNA in conc. solns. of neutral salts, conformational transitions 80−81531
DNA in water-ethanol solns., enthalpy of B-A transition 77−70412
DNA length measurement using random flight theory 77−64008
DNA of fetal globin genes, man, charact. of deletions 79−70519
DNA packing in fibrils of DNP of polytene chromosomes 80−30649
DNA secondary structure, dependence on base sequence, theoretical conformational anal. 79−53032
DNA solution, thermodynamic props., phase transition, one-dimens. Ising model study 79−16125
DNA structure of left-handed double helical DNA fragment 80−30659
DNA superhelical packing in nucleosomes *(German)* 79−53041
DNA with irreversible cross-links and low counterion conc., helix-coil transition 80−32860
DNA-adduct systems, binding geometry, determ. by induced circ. dichroism 80−55988
DNA-dependent RNA polymerase, determ. of intersubunit distances and subunit shape parameters by neutron small-angle scattering 79−53038
DNA-dye-complexes, UV excitation, energy transfer and mol. struct. 79−57578
DNA-type macromolecule, melting, low mol. wt. impurity effect 80−12050
DR antigens, human, struct. polymorphism obs. 79−66441
durene-para-dibromobenzene, binary mol. system, X-ray struct. anal. 79−55734
elastase, globule, atomic density distrib. 79−79458
electron micrograph images, determ. of structs. relative orientation 79−70714
electron microscopy, high resolution, mol. struct. determ. 80−21595
enniatin B, Rb^+ complex of LDLLDL analog, struct. and conformation anal. 79−60348
entanglement probabilities for harmonically bound macromol. 77−79716
epoxy resin, plastic deform. mechanism 80−97534
epoxy resins, struct. changes under mag. field action 80−40516
ethyl p-methoxybenzilidene aminocinnamate, dimer, mesogenic, intermol. interactions 79−46564
(ethylene-co-vinyl alcohol)-g-ethylene oxide graft copolymers, sol. behaviour 80−19682
ethylene-deuteroethylene copolymer, polymeric unit heterogeneity *(Russian)* 79−55017
ethylene-glycidylacrylate copolymer, ^{13}C-NMR microstruct. investigation, substitution increments sequence distrib. *(German)* 78−13636
ethylene-propylene copolymers, mech., photoelastic props. rel. to chain microstruct. 77−48468
F-actin conformational changes in glycerinated muscle, polarised UV fluorescence obs. 79−100567
fatty acid synthetase, from yeast, three-dimens. electron microscopy, struct. and image reconstruction 77−12883
ferredoxin, S. platensis [2Fe-2S], struct. and evolution of chloroplast-type ferredoxins 80−94165
ferricytochrome c structure, effect of different phospholipids 78−68981
fibres, natural, Brillouin scatt. shifts, comparison with synthetic polypeptide obs. 80−55991
fibrin molecule formation, thermodynamic model 79−70527
fibrinogen, adsorbed layers on polystyrene, contact angle meas. 80−61508
fibrous materials, struct., interatomic forces calcs. 79−22875
finite polycondensing system, mean chain length distrib., probabilistic theory 79−70324

macromolecular configurations continued
flexible chain collapse 78−87628
flexible chain ideal network, contraction effects 77−14625
flexible chain ideal networks, contraction effects 77−14624
Flory formula for the polymer size exponent ν 78−70985
fluorescence depolarisation, electrically-induced macromol. characteristics 77−27210
form dichroism of crystal, determ. of macromol. shape 78−60417
freely jointed polymer chain with bond vectors of fixed lengths 79−3605
Gaussian polymer molecule config., large mol. Kirchhoff matrix reduction 79−13850
Gaussian polymer molecule config., stars and random regular nets, distrib. functions 79−13849
glass fibre reinforced plastics, coupling agent/matrix interface investigation by Fourier transform IR spectroscopy 80−20884
glass transition temperature, rel. to mol. wt. 80−34176
globular proteins, bend form., conformational space, statistical mech. anal. 77−68146
globular proteins, in solutions, new method using X-ray diffuse scattering for investigation of conformation changes 79−12054
globular proteins, micro- and macro-stabilities 79−92135
glucagon, helical folding, Zimm-Bragg anal. 78−76356
glutamine synthetase macromolecular struct., electron microscopy and image anal. 80−89716
glycine, oligomer, vibr. spectra rel. to polymeric form 79−83695
glycogen phosphorylase b activity, struct. of cryst. and complexes 78−80830
GpApGpC:GpCpUpC duplex set, helix form., PMR obs. 79−22872
graft copolymers, normal vibrs., calc. method *(Russian)* 78−29871
gramicidin A channel struct., elec. meas. with lipid bilayer membranes 78−15783
gramicidin A in biomembrane channel, IR spectroscopic obs. 80−16901
gramicidin A monomer-dimer states, light scatt. studies 79−92143
haeme disorder characterisation in haeme proteins, PMR method 79−92152
haemoglobin, ^{15}N NMR determ. of residual struct. in backbone of unfolded mol. 77−90720
haemoglobin, conformational change, relation with CO binding 79−8473
haemoglobin, dynamic characts. of conformational nonequilib. states, radiolysis investig. 78−58877
haemoglobin, metal substitution effect on mol. struct. and functional props. 79−53037
haemoglobin, modulated excitation meas. of quaternary conformation struct. change rate 77−44589
haemoglobin, structure and respiratory transport 79−57576
haemoglobin Fe-N distance determ. by EXAFS 78−68989
haemoglobin-CO reaction kinetics, relax. meas. on photolytic illum. 77−70405
haemoprotein, fine structure of Fe ions 80−30661
helical molecule, extensional orientation, vibr. modes 77−23591
helical wormlike chains, statistical mechanics, approx. 78−55266
helical wormlike chains, statistical mechanics, operational method 77−560
helix-coil transitions in specific sequence biopolymers 78−35794
high moleculer weight, fibril structure induced by oriented crystallisation *(Japanese)* 79−90575
Hilhorst model, generalised, statistics of trees and branched polymers 79−3604
histidine decarboxylase quarternary struct. 79−92129
histidine-decarboxylase, molecular weight and form determ. by low angle X-ray scatter 78−76987
histidinedecarboxylase molecule, distance between heavy atom markers small angle X-ray scatt. determ. 79−55613
histone F2a solutions, effect of ionic composition of medium on struct. and effectiveness of intermol. interactions 78−48744
histones, conform. state in water, circular dichroism 77−56335
histones, H2a and H4, aggregation ionic strength effect *(Russian)* 80−55697
hydrate, struct. conversions of sugar phosphate chain and nitrogenous bases, IR spectra 80−81530
hydrocarbon chains in a lipid bilayer conformational anal. 80−81532
immunoglobulin light-chain genes, nucleotide sequences at somatic recombination sites 79−83701
interactive model building program 77−52738
intermolecular volume exclusions, config. calc. 77−58215
internal coordinates fluctuations, effect on dimensions 80−74266
isotactic polystyrene gel, anomalous X-ray diffraction effects, rel. to chain conformation and isomeric homogeneity 77−50576
Kapton H, aromatic, polyimide, conformational investig., X-ray method, pot. energy calcs. 77−3498
keratin, mammalian, organisation of polypeptide chains 77−4981
Kramers chain, mol. dynamics calc., incorrectness of random walk description confirmed 77−561
lanthanide complex, struct. and equilib. by time resolved Eu(III) spectrosc. 80−78736
lanthanide ion bound to macromol., struct. and equilib. by time resolved Eu(III) spectrosc. 80−78736
lattice chain in limited vol., behaviour *(Russian)* 78−70992
lecithin-cholesterol interaction, hydrocarbon chain length and unsaturation effects, Raman spectra 77−64012
Lennard Jones polymer, eqn. of state, collapse transition 77−19117
leucine aminopeptidase, 3D reconstruction by photosummation of projected functions 79−62183
leucine aminopeptidase crystalline aggregates, interpretation of electron microscope images 78−68988
leucine-binding protein, rat nerve, aggregation 79−62181
linear chain molecules, asymptotic form of partition functions, renewal theory appl. 77−53835
linear polymer molecules, second virial coeff., chain length effects calcs. 78−37775
linked-atom least-squares reciprocal-space refinement system, LALS, incorporating stereochemical restraints 78−26377
lipid bilayer phase transition, semiphenomenological model 77−35670
lipid membrane order, mol. theory 79−66452
lyngbyatoxin A, struct. determ. from chemical and spectral data 79−66443
lysine vasopressin, conformation in aq. soln., ^1H NMR effects 79−83692
lysozyme, adsorption kinetics, surface denaturation 79−79460
lysozyme, binding to bacterial cell wall trisaccharide NAM-NAG-NAM, X-ray cryst. struct. anal. 80−35834
lysozyme, molecular structure of adsorbed film 79−79462

macromolecular configurations continued
lysozyme, stepped character of thermal denaturing, optical density at 290 nm 78−15763
lysozyme and complex with trisaccharide inhibitor, struct. in soln. and in cryst. 77−81465
lysozyme effect of pH on dimorphic crystal growth 79−14728
lysozyme spin-labelled preps., water-protein layer microstruct. study by mag. relax. 78−76980
α-lytic protease, predicted model rel. to X-ray struct. 79−62178
macromolecular solns., associating, sedimentation equilib. distrib. anal. 77−14628
macromolecular structural studies, with synchrotron radiation, X-ray television area detectors 79−55610
macromolecules, cluster expansion 80−106408
magnetic alignment, in high mag. field 77−64163
maleic acid-styrene copolymer, aq. soln., conform. transition 78−75526
Markov chain sampling grown lattice walks, variance reduction 79−27121
medical polymers, chem. problems, conf., Prague, Czechoslovakia (Aug. 1977) 80−56996
β-melanocyte stimulating hormone and β-lipotropic hormone fraction, spectral study 77−36863
met-myoglobin, struct. determ., neutron crystallography 79−43814
metallo-proteins and model systems, susceptibility and struct., SQUID magnetometer uses 79−53036
Cd-metallothionein, test object for dark field electron microscopy of protein struct. 78−11610
metarhodopsin I-II transition obs. by absorpt. changes of eriochromblack T 77−44593
methyl methacrylate-p-chlorostyrene copolymer, side-group rot. and dielec. relax. 79−61303
methyl methacrylate-styrene copolymer, side-group rot. and dielec. relax. 79−61303
model polymer, conformation theory, correlated walk model 80−74268
molecular orientation, extensional effects, IR obs. 77−23591
molecular structure, conformation and properties 80−63874
monodisperse solutions, macromol. length rel. to anisotropic light scatt. in elec. field 77−32391
mononucleotides, conformational anal. by nuclear Overhauser effects 79−20509
mucopeptide N-acetylmuramoyl hydrolase, hen egg-white lysozyme, BC n.m.r., carboxyl group resonances 77−1878
multichain polymer system, simulating dynamic and equilib. props. 80−53179
met-myoglobin:Cu^{2+}, single cryst., EPR, conform. changes 77−73505
myoglobin, Fe-O_2 bonding and oxyhaeme struct. 78−96006
myosin, conformational changes induced by inorganic salts, Raman spectra obs. 78−96002
myosin, struct. changes in living muscle fibres, polarised UV fluoresc. microscopy 80−67037
neurotoxin, snake venom, appl. mol. graphics to struct. determ. 78−27892
neutron scattering from strained polymer networks 78−78846
NMR study of molecular conform. in soln., use of La ion probe 77−60324
nucleic acid components, pyrimidine and purine, electronic struct. 80−30654
nucleic acid-dye complexes, energy transfer obs. using laser-induced fluoresc. 80−12054
nucleic acids, double-helical, conformations 77−12880
nucleic acids, Raman spectroscopy obs. *(German)* 79−27119
nucleosomes, structs. and modes of interaction 79−62182
nucleosomes and nucleosomal DNA, electro-optical props., relax. times and chain struct. 80−85350
3′-nucleotide, calcs. to assess rigidity 80−61506
nucleotide sequences of the attachment sites of bacteriophage Mu DNA 79−79463
nylon 66, polymorphism, mol. struct. 79−14694
Nylon 6 fibre, shrinkage, influence of chain rupture during tensile deform. 79−34055
off-lattice polymer chains, Monte Carlo calcs. 78−5382
oligoesters, effect of mol. architecture on dispersion props of TiO_2 in non-aqueous liquids 80−40751
oligopeptides, conformational studies, kinetic energy problems 79−13848
optical absorption spectra and symmetry 79−55011
optical rotatory dispersion meas. method for macromol. conformation, press. effects 77−48984
organosilicon polymers, ladder-type, local conforms. *(Russian)* 77−19121
oriented polyethylene film, deformation band studies 77−52420
ovalbumin aqueous soln., macromol. gel layer formed on ultrafiltration tubular membrane, charact. 80−14260
oxyhaemoglobin, mag. props. and structure 78−48751
oxymyoglobin structure determ. by X-ray diffr. 78−56950
oxytocin, conformation in aq. soln., ^1H NMR effects 79−83692
oxytocin, H bond linking ring and tail β-turns, biofunctional evaluation 80−61511
pancreatic trypsin inhibitor, bovine, 3D protein folding model 77−90723
pancreatic trypsin inhibitor tyrosine residues in soln., laser photo-CIDNP as surface probe 78−73138
papain inactivated by OH radicals and H_2O_2, optical density, amino acid composition and fluoresc. 78−53344
path integrals with a periodic constraint: entangled strings 79−2651
PCP, oriented swollen soln., IR dichroism, short-range orient. order *(Russian)* 79−51941
pepsin crystal fusion, microcalorimetry 77−70413
peptides, α-aminoisobutyric acid containing, ^1H NMR conform. obs. 79−81311
peptides, in soln., nuclear Overhanzer effect methods for total conformational anal. 79−16136
peptides, soln. conformation by intramolecular nuclear Overhauser effect 79−16135
Pf1 filamentous bacterial virus, macromolecular structural transitions 80−3584
phosphates, cellular, heteronucl. two-dimens. NMR as conform. probe 80−3590
phosphofructokinase from Bacillus stearothermophilus, struct. and control 79−70517
phosphoglycerate kinase, sequence, struct. and activity, hingee-bending enzyme 79−74595
macromolecular configurations continued
phospholipid-d, as nonperturbing components, for Raman studies of biomembranes 78−53330
phospholipids of hydrocarbon yeasts, composition and struct. 79−53028
phytochrome subunit, evidence for symmetry 78−27890
piperylene-acrylonitrile copolymers, polymerisation, monomer composition rel. to copolymer struct. *(Russian)* 80−5651
Piv-Pro-Pro-Ala-NHMe, incipient 3_{10} helix as model for peptide folding 79−100568
plasma low-density lipoprotein, human, molecules organisation of central core 77−90722
plasma protein interaction with polyion complex studied by circular dichroism and UV spectroscopy *(Japanese)* 80−12316
plasmid DNA and DNA-histone chromatin-like complexes, conform. and soln. props. by laser light scatt. 80−55987
PMMA, atactic and syndiotactic chains, statistical mechanics, operational method 77−560
PMMA, conformational energies calc. 78−25762
PMMA, helical structure 78−66699
PMMA, isotactic, syndiotactic, ^{13}C spin-lattice relaxation times, chain config., dynamics 77−24760
PMMA, molecular alignment 78−14299
PMMA, monolayers collapse mechanism, surface press. and ellipsometric obs. 78−43214
PMMA, partial draining of low-molecular weight polymers with flexible chains 80−23592
PMMA, stereoregular, assoc. in dilute soln., PMR obs. 78−76321
poly(1,3-dioepane), dipole moments, dielectric const. meas 80−66099
poly(2-vinyl pyridine), dil. solns., translational diffusion, chain conformation influence 80−103508
poly(3,3-dimethyl oxetane), conform. energies and random-coil config. meas. 80−99590
poly(9-vinyl anthracene), struct. *(German)* 79−98256
poly(α-methylvinyl alkyl ether)s, ^1H-, ^{13}C-NMR spectra, stereoregularity 80−48112
poly(β-benzyl L-aspartate), conformational transitions 77−88613
poly(γ-benzyl)-L-glutamate, viscosity behaviour in dioxane solvent, conc. depend., aggregation 79−82371
poly(cis 1,4-isoprene), cryst. phase, elastic modulus 79−57037
poly(cis-isoprene), tagged, in untagged matrix, instantaneous shape, segmental density 78−62966
poly(diallyldimethylammonium) chloride, struct., ^{13}C NMR 77−565
poly(dimethylsiloxane) rubber, filled with modified silica, cross-linking 79−95990
poly(ethylene oxide), partial draining of low-molecular weight polymers with flexible chains 80−23592
poly(m-methylene terephthalate) polymers, IR and Raman spectra 77−52088
poly(S)-2-methylbutyl vinyl ether, conformation, IR spectra 78−1116
poly(S)-5-methyl-1-heptene, conformation, IR spectra 78−1116
poly(vinyl alcohol)-Cu(II) complex, ESR study 79−61199
poly(vinyl pyrrolidone)-Cu(II) complex, ESR study 79−61199
poly L-lysine, temp. induced conformation transition in solns., optical rotary meas. 78−46474
poly N,N-diallyldimethylammonium chloride, soln. props., struct. 79−94861
poly O-carbobenzoxyl-L-tyrosine, in soln., conformation, helix-coil transition, circular dichroism, NMR spectra 77−31037
poly-1,4-phenylene terephthalamide, in H_2SO_4, dilute soln. viscosity 78−75524
poly-1-glutamic acid, soln., u.s. absorpt., linear Ising chain kinetics 77−4980
poly-2,6-dimethyl-p-phenylene oxide solns., US and viscoelastic relax., conformational changes 77−31033
poly-4-methyl-1-hexene, optically active, ^{13}C NMR obs. of conform. 77−10801
poly-4-vinylpyridine, electro-optic study of conformational changes induced by heavy metal ions 80−84725
poly-β-benzyl-L-aspartate films, circular dichroism, IR spectra, α, β, ω conforms. 77−48197
poly-β-benzyl-L-aspartate films, conformational stability, effect of organic solvents, IR spectra 78−70988
poly-β-ethynylnaphthalene, insoluble, reson. Raman spectrum, struct. models 78−70981
poly-β-substituted vinyl ethers, cationic polymeris., stereochem. 80−21284
poly-γ-benzyl-L(D)-glutamate, soln., liq. cryst. and pretransitional regions, optical rot. 80−66145
poly-γ-benzyl-L-glutamate, lyotropic liq. cryst., trifluoroacetic acid effect on viscoelasticity, susceptibility 77−84644
poly-γ-methyl-L-glutamate, conformational props., viscosity, osmotic press. meas. 77−31032
poly-γ-methyl-L-glutamate, interfacial conformational modifications 78−2339
poly-L-glutamic acid-Na, cooperativity parameter determ. from viscometry 80−75147
poly-L-lysine, membrane phase, transport processes, helix-coil transition 78−77031
poly-L-ornithine solution, ^{15}N NMR, coil-helix transition, solvent effects and pH depend. 80−74275
poly-m-phenylene isophthalamide, soln. and cryst., conform. props. calcs. *(Russian)* 79−65009
poly-n-butyl methacrylate, θ-solns., temp. coeff. of unperturbed dimens. 78−9290
poly-n-butylisocyanate, conformation, IR spectra *(Russian)* 77−19123
poly-n-phenyleneterephthalamide, conformational and structural props. *(Russian)* 77−61889
poly-p-chlorophenyl glycidyl ether, struct., tacticity and addition isomerism, ^{13}C NMR 80−58427
poly-thio-1-N,N-diethylaminomethylethylene, optically active samples, ^{13}C NMR spectra 80−28127
polyacetylene, bond length alternation and energy gap, intermediate exciton formalism 80−29305
polyacetylene, dynamic nuclear polarisation of protons *(French)* 80−43217
polyacetylene, nascent morphology obs. 80−24379
cis-polyacetylene, static lattice calcs. for crysts. 80−10509
polyacetylene, thin film, ESR study, effects of O_2, NO and halogens 80−25186
polyacetylene films, tensile props. and partial alignment 80−104210

macromolecular configurations continued
polyacids, unsaturated carboxylic, in organic solvents, hydrogan bonding, structurisation *(Russian)* 78−71666
polyacrylamide-Cu(II) complex, ESR study 79−61199
polyacrylonitrile, copolymerisation with poly-2-hydroxyethyl methacrylate rel. to crystallinity 80−38935
polyalkane imides, crystallisability, supermol. and crystalline structures 80−84100
polyamide, aromatic, fibre, high modulus, mol. and supramol. struct. 80−79710
polyamide, aromatic, persistence length, rel. to optical anisotropy of worm-like chain 77−50577
polyamide chain, conformational freedom above MP 77−55344
polyamides, 1,3-cyclohexanebis(methylamine) based, thermal props. and glass transition temp. 80−39264
polyamides, carborane-containing, antifrictional props., chem. struct. effect *(Russian)* 79−57123
polyamidoimide film, thermomech. props. rel. to mol. struct. *(Russian)* 79−57029
polyarylate, F-2, film, rigid chain orientation in surface active medium *(Russian)* 78−88513
polyarylate-polyethylene oxide block-copolymers and mixtures, phase separation, DSC obs. *(Russian)* 79−55895
polyaspartamides, soluble, fluorescent labelling 80−58426
polybutadiene, C black filled, struct., Fourier transform IR obs. 77−50571
polybutadiene, low mol. wt., NMR study of terminal group struct. *(Russian)* 77−63912
polybutadiene networks, cis-trans, thermoelastic obs. 79−74220
polybutadiene networks, cis-trans isomerisation, γ-ray induced 79−74374
polybutadiene-polystyrene, ^{13}C NMR assignments, rel. to mol. configurations 77−54640
polybutadiene-polystyrene block copolymer, anionic prep., random coupling struct. 79−64134
polybutyl acetate-polyvinyl acetate crosslinked compositions, proton mag. relax., forced compatibility *(Russian)* 80−44950
polycaprolactam, and copolymers, optical anisotropy and rigidity 80−88959
polycapromide, fracture, interatomic bonds deform. 79−57107
polycarbonate, struct. ordering changes after annealing 79−94921
polycondensation copolymers, block length distribs. 79−31752
polycyclohexanamide, and copolymers, optical anisotropy and rigidity 80−88959
polydiacetylene-bis(toluenesulphonate), refl. spectra, 0-15 kbar, doublet press. shift 78−43891
polydiacetylenes, visual conformational transitions, absorpt. and fluoresc. spectra, pH and electrolyte effect 80−102590
polydiethylene terephthalate chains, dipole moment, config. props. 78−9288
polydimethyl siloxanes, cyclic and linear, neutron scatt. meas. of dimensions 80−18952
polydimethylsiloxane, end-cap ratio and mech. props. of block copolymer 78−91266
polyelectrolyte chain in D dimensions, conformation props. 77−31034
polyelectrolyte conformation, electrostatic interaction effects at varying conc. 77−35461
polyelectrolytes in soln., conform., small-angle neutron scatt. investigs., review 79−873
all-trans polyene, ab initio studies 80−43222
polyenes, highly branched, large networks, abnormal bond orders 79−59610
polyester resin, POLIMAL 190, influence of MgO, BeO and TiO_2 on dynamical mechanical props. *(Polish)* 79−96074
polyesters, aromatic, structural variation rel. to low temp. relax. 79−66096
polyethylene, chain conform. in solid and melt, low angle neutron scatt. 77−76329
polyethylene, chlorinated, high resolution ^{1}H and ^{13}C NMR, group fractions *(German)* 77−65551
polyethylene, chlorination reaction in soln., ^{13}C NMR for chain group sequence *(German)* 79−100366
polyethylene, conform. stability, 1-electron levels, long-range effects calcs. 80−28123
polyethylene, conformation, Monte Carlo simulation 77−10797
polyethylene, crystalline, steric struct. modelling of end defects 80−6371
polyethylene, effects of mol. rot. and crosslink on specific draw ratios *(Japanese)* 79−96099
polyethylene, epitaxial crystallisation, IR investig., macromol. struct. changes 77−35493
polyethylene, fine struct., prep., O_3 selective degradation, chromatographic obs. 78−92475
polyethylene, high molecular weight, effect of density on properties 77−90403
polyethylene, homopolymers, copolymers and model systems, ^{13}C NMR chem. shifts and relax. times 79−72449
polyethylene, linear, bulk-crystallised, morphology study 79−32918
polyethylene, linear, effect of pressure on vol. and dielec. relax. 79−61302
polyethylene, linear, in theta solvents, Mark-Houwink eqn., chain dimensions 77−38764
polyethylene, linear, irrad. crosslinking and chain scission in extended chain and bulk films 77−60095
polyethylene, linear, melt props. correl. with chain length distribs. *(Russian)* 80−37920
polyethylene, liq., very high mol. wt., pulsed NMR obs., entanglement, crosslinking, irrad. effects 78−66702
polyethylene, low-density, mol. characterisation 79−52843
polyethylene, low-temp. relax., effects of chem.- and electron irrad.-crosslinking 79−4990
polyethylene, meas. of high chain extensions by gel permeation chromatography 77−88611
polyethylene, melting, equilib. temp., confomational modifications *(Russian)* 79−51240
polyethylene, mol. conformations after recrystallisation or annealing at high press. 77−88612
polyethylene, mol. morphology determ. by NMR 78−94341
polyethylene, obtained with heterogeneous Ziegler-Natta catalysts, nascent struct. and morphology 79−96307
polyethylene, oxidised and chlorinated, dielec. ops. of mol. relax. 77−40179
macromolecular configurations continued
polyethylene, partial draining of low-molecular weight polymers with flexible chains 80−23592
polyethylene, pressure phase transition, function of pressure and temp. 79−77745
polyethylene, rapid crystn. from melt rel. to struct. 80−44152
polyethylene, short chain branching, ^{13}C NMR 79−33557
polyethylene, single crysts. chain end location, IR spectra 78−71687
polyethylene, structure formation, near and below melting point 79−65003
polyethylene, supermolecular structure, polymerisation at low pressure *(Russian)* 79−64126
polyethylene, ultra-high modulus, drawing behaviour, effect of drawing temp. 80−35232
polyethylene, ultradrawing, effects of temp. and drawing rate *(Japanese)* 79−91760
polyethylene glycol, conformation in liq. state from flow birefringence 78−76423
polyethylene glycols, ^{1}H NMR in presence of shift reagent 79−99779
polyethylene glycols, aq. solns., volumetic props. 79−20460
polyethylene imine, oligomers, solns., linear struct., props. *(Russian)* 79−50177
polyethylene oxide, dil. soln., chain dipole moment, dielec. const. meas. 77−40169
polyethylene oxide, NMR relaxation in melt, three component model 77−55723
polyethylene oxide homo and copolymers, monomer link lengths determ., IR spectral method *(Russian)* 77−32383
β-polyethylene oxybenzoate, cryst. struct. and mol. conformation 79−55674
polyethylene terephthalate, conform. statistics *(Russian)* 78−70993
polyethylene terephthalate, conformation rel. to orientation, pot. energy surfaces study 79−68338
polyethylene terephthalate, fatigue failure under cyclic loading, overstress in chem. bonds 79−57106
polyethylene terephthalate, fracture, interatomic bonds deform. 79−57107
polyethylene terephthalate film, deformation band studies 77−52420
polyglutamic acid, helix-random coil transition observed by gamma-ray ang. correlation 78−80828
polyglutamic acid molecular dynamics in soln., γ-ray perturbed angular correl. 78−94960
polyglycine, IR spectra calc. for helix and β configs. 80−45853
polyglycyl-prolyl-prolyl, triple-helical coiled-coil conform. determ. rel. to interchain interactions, collagen models 77−38762
polyheteroarylenes, linear, conform. and struct., statistical calcs. *(Russian)* 80−69284
polyhexamethylene oxide, dil. soln., chain dipole moment, dielec. const. meas. 77−40169
polyisobutylenes, dilute solns., turbulent drag reduction, influence of mol. wt. and mol. conformation 77−80189
polyisoprene, in cyclohexane soln., conform. transition *(French)* 79−7542
polyisoprene-g-styrene, dil. soln., conformation, light scatt. obs. 78−91218
polyisoprenes, partly deuterated, ^{1}H-NMR spectra, struct. 80−50202
polymer, adsorbed, conformation, excluded vol. effects 78−2372
polymer, amorphous, chain conform., small-angle neutron scatt. obs. *(Polish)* 80−10511
polymer, amorphous, conform. from simulation of filling diamond lattice with chains *(German)* 78−75595
polymer, amorphous, conform. from simulation of thermal motion *(German)* 78−75594
polymer, amorphous state struct., conf., Atlantic City, USA (Sept. 1974) 77−76327
polymer, chain molecule, excluded vol. theory based on fifth-power eqns. for unperturbed mol. dimensions 77−50578
polymer, comb-like, with amide groups in side chains, stabilisation via H bonds *(Russian)* 77−46665
polymer, conformational transitions, Brownian dynamics, simulation 79−45873
polymer, cross-linked, on basis of oligodienedihydrazides and diepoxides, characts. *(Russian)* 80−58431
polymer, crosslinked, probabilistic theory of structural and physical characteristics 80−5649
polymer, distrib. function for random walks without self-intersection 78−8350
polymer, end-to-end distribution function, for most probable molecular weight distribution 78−13635
polymer, excluded volume effect, YBG and Kirkwood hierarchies 77−46661
polymer, expansion of self-avoiding chains, studied by loop elimination 79−86100
polymer, floating chain, config. statistics, impenetrable barrier confinement 77−58216
polymer, molecular mechanism of orientation 77−69033
polymer, neutron scatt. studies of chain conform. and dynamics 78−83753
polymer, optically active stereoregular, conform. props., rel. to config. 78−33644
polymer, rot. isomeric state model, approx. anal. soln. 77−58214
polymer, rot. isomeric state model, monomer-monomer distrib. function 77−71897
polymer, semicrystalline, mol. morphology 78−38631
polymer, symmetry elements, group theory 77−19124
polymer adhesion ability enhancement by block copolymer incorporation *(Russian)* 80−61065
polymer adsorption at interface, self-avoiding random walk anal. 77−1085
polymer athermal self avoiding chains, configurational props. 80−18950
polymer attached to surface, dynamics, bead and spring model 78−75931
polymer branched chains, chain length, mol. architecture rel. to second virial coeff. 78−94964
polymer chain, adsorption on diamond lattice, span calc., self-avoiding walk model 77−15679
polymer chain, amorphous state, theor. predictions on configurations 77−80427
polymer chain, config. statistics, in impenetrable barrier confinement systems 77−562
polymer chain, direct renormalisation group procedure 80−91712

macromolecular configurations continued
polymer chain, flexible, angular correlation ranges 77−34790
polymer chain, frequency dependent energetics, Orwell-Stockmayer hopping model 80−24346
polymer chain, heuristic approach to excluded-volume problem 77−14630
polymer chain, infinite, trigonometric series evaluation 79−7041
polymer chain, long, in dilute soln., 2nd order phase transform. 79−13851
polymer chain, molecular span and end to end probability distrib. 79−64137
polymer chain, neutron scatt. obs., review 78−14245
polymer chain, renormalisation along chem. sequence 78−50669
polymer chain, renormalisation transformation 79−89816
polymer chain, self-interacting, in three-dimens. continuum 78−58876
polymer chain, virial expansion 78−5383
polymer chain, viscoelastic, local relax. props. anisotropy, internal friction influence *(Russian)* 78−37780
polymer chain conformation, determ. by neutron scatt. in amorphous polymers 77−76328
polymer chain cyclisation, lattice embedded model, discrete scatt. series representation 80−48109
polymer chain dynamics, in confined space 77−75351
polymer chain length effect on excluded volume, generalised mol. architecture 79−59607
polymer chain residing in density gradient of segments 79−13853
polymer chain statics and dynamics, Lennard-Jones interaction, calcs. 80−58425
polymer chain subjected to elongation, conformational microstruct. variation *(Russian)* 79−31756
polymer chain trapped in suddenly deformed gel, relaxation *(French)* 77−62483
polymer chains, Edwards' model, stochastic model 80−68140
polymer chains, zero component field *(French)* 80−69280
polymer chains 80−3116
polymer chains containing planar cyclic groups, flexibility, stat. mech. model *(Russian)* 77−42453
polymer chains in cubic lattice solvent, thermodynamic props., Monte Carlo method, computer simulation *(Russian)* 77−31787
polymer chains with excluded vol., molecular dynamics simulation 78−78845
polymer coatings, packing density investig. by mol. probe method *(Russian)* 77−44398
polymer coil-globule second order phase transition 77−19119
polymer coils, excluded volume parameters, light scatt. obs., graphical calcs. 80−89009
polymer configuration in amorphous and crystalline state, small-angle neutron scatt. *(German)* 77−85398
polymer conformation, correlated walk model calc. 80−78733
polymer crystal, conformational energy calcs., appl. to defect props. 80−54154
polymer film, adhesion, structure-time analogy 79−70292
polymer film, conformational transitions, activation energy determ. *(Russian)* 78−48186
polymer film, supermolecular structure and mech. stress distrib. among chem. bonds 78−75562
polymer globule formed by saturating bonds, spatial struct. *(Russian)* 77−10802
polymer linear self interacting chains, configurational props. 80−23586
polymer linear self interacting chains, internal distrib., radius of gyration 80−23587
polymer liquid, entangled, phenomenological consequences of Doi-Edwards viscoelasticity theory 80−79250
polymer macromolecules, volume interactions, coil-globule transition, statistical physics, review 80−78737
polymer melt, NMR relaxation, mol. motion, local defect component theory 77−55722
polymer melts, defect fluctuations, reptation, Monte Carlo investig., NMR autocorrel. function 77−3499
polymer microstructure morphogenesis, book contrib. 78−83757
polymer mixtures, thermodynamics, review 79−1506
polymer model equivalent to the Ising model 80−37914
polymer molecule, flexible chain shape measures, review 78−17832
polymer molecule, symmetry adapted bases and selection rules 79−55010
polymer molecules, irreducible representations of symmetry groups 79−3603
polymer network, crosslinks and trapped entanglements, two-network model 80−38962
polymer network, permanently crosslinked, topological struct. and macroscopic behaviour 80−37919
polymer network, Riemann's metric degeneration to graph metric demonstration, chain entanglement problems 80−38963
polymer network, small ang. neutron scatt. 79−90569
polymer network, small-angle neutron scatt. obs. of mol. behaviour 80−37918
polymer network formation, pre-gel intramol. reaction and gelation, shear moduli and glass transition 80−45501
polymer network formation, relaxational props. variation 80−38961
polymer network formation, struct. and mech. props., computer simulation 80−38965
polymer network in solution, free energy of deform. 80−38900
polymer networks and semi-crystalline polymers, diffusion mechanism and model, local conform. change 80−15288
polymer properties of glass transition, conformational effects anal. 79−69231
polymer quantitative analysis by pyrolysis gas chromatography 80−61180
polymer random flight chain, surface adsorbed, end-to-end mean value 78−22060
polymer rings, topological constraints and critical indices 79−81313
polymer science, conf., Pittsburgh, USA, (June, 1975) 77−38756
polymer single chain, coil-globule transition obs. 80−1098
polymer solution, concentrated, computer-aided simulation of individual chain conforms. *(Russian)* 77−42454
polymer solution, configurational props. of model lattice chains under varying solvent conditions 77−89364
polymer solution, intermolecular interpenetration and entanglement, crit. concs. 79−27900
polymer solution, light scatt. for macromol. characts. in Rayleigh-Gans-Debye region 77−42452

macromolecular configurations continued
polymer solution, second virial coeff., segment cloud model, chain length and branching study 80−24559
polymer solution and bulk state, partially labelled chains, neutron scatt. obs. 80−38899
polymer solutions, coil dimensions, Monte Carlo calc., computer simulation *(Polish)* 79−3606
polymer solutions, conformational motions, comp. of neutron and light scatt. expts. 79−41938
polymer solutions, long chain immersed in shorter chains, end-to-end dist. 79−1387
polymer solutions, moderately conc., light scatt. curves, struct. model 79−4810
polymer solutions, order, conf., Midland, USA, (Aug 1973) 79−10769
polymer solutions, solvation, preferential, effect on polymer dimensions 79−10771
polymer statistics of long chains in solns. or melts 79−31758
polymer structure and mech. props., book 78−83756
polymer structure elucidation, model construction and X-ray methods *(German)* 80−103267
polymer surface, supramol. struct. characterisation, use of C X-radiation 80−79705
polymer system, Fourier transform IR spectroscopy appl. 78−58870
polymer systems, phase dualism, gas-, liq.-like, appl. to compression effects 79−1388
polymeric chain with rigid side branches, intramol. phase transition of 1st kind *(Russian)* 80−58432
polymeric macromolecule containing mesogroups, phase diagrams *(Russian)* 80−58433
polymeric macromolecules, with structure regularity, description and design 80−23591
polymeric materials, prop. struct. concepts, review 77−7301
polymeric networks, macromol. chain conforms., computer simulation, network form. process *(Russian)* 78−70994
polymerisation chemistry, mol. wt., chain-unit struct. control, review 77−40544
polymers, adsorbed molecules, configurational behaviour, computerised dynamic display 79−874
polymers, branched, mean end to end distance 79−86097
polymers, chain folding, cross-sectional area 78−70989
polymers, confined between two adsorbing surfaces, conformational props. 77−3501
polymers, decomposition by hydrolytic mechanisms 79−55016
polymers, electrical phenomena, nature and appl., review 80−50254
polymers, ESCA investigation of struct., reactivity and bonding, O_2 (inert gas) surface modification 78−3438
polymers, gas chromatography meas. of struct. and interactions 77−90698
polymers, helical, optical activity, decorrel. approx. theory 77−63389
polymers, melt transition, theory 77−76325
polymers, mol. config. packing statistics near surface 77−35491
polymers, mol. struct. rel. to bulk props. 77−32553
polymers, small angle neutron scattering studies, deuteration effects 79−50956
polymers, specific heat, conform. effects 80−24607
polymers, stereochemical definitions, IUPAC nomenclature 80−23593
polymers, stereoregularity distortions, local oscill. freqs., eqn. *(Russian)* 80−5653
polymers, struct. determ. from elastoosmometric parameters 80−64923
polymers, synthetic, chiral, with aromatic side chains, conform. from circ. dichroism 79−55014
polymers, topological entanglements, gauge description 80−99593
polymers attached to inert interface, conformations 79−94120
polymers containing main chain heteroatoms, struct., ^{13}C NMR investigs., review 79−55013
polymethacrylamide copolymer, soluble, mobility of spin label bonded to chain end 80−63873
polymethacrylic acid, stereoregular, synthesis, ^{13}C NMR obs. 80−58422
polymethineimine, all-trans, ab initio cryst. orbital calcs. 79−77530
polymethylene, intramol. scatt. function calc. 77−38761
polymethylene, melt transition, theory 77−76325
polymethylene, short chain mean reciprocal distances, Monte Carlo calc. 77−14626
polymethylene chain, vibr. spectra, CH stretching region, struct. and assignments 78−70991
polymethylene flexible biradicals CIDNP and chain dynamics, field depend. 77−88473
polynucleotide, bihelical, secondary struct. stability 79−53030
polynucleotide, double-stranded, conform. inhomogeneity of sugar-phosphate chain rel. to compact particle optical activity 80−35839
polynucleotide hydration characts. in H_2O/D_2O frozen solns., γ irrad. effects, PMR 78−31772
polynucleotides, bihelical, conform. anal. 77−36862
polynucleotides, double helical, conformation, pairwise pot. function calcs. 80−53173
polynucleotides, double-helical, conform anal. 79−96513
polynucleotides, double-stranded conformation model 77−14631
polynucleotides, gamma-ray effects on hydration, PMR of frozen and liq. solns. 78−27900
polyolefins, isotropic semicryst., neutron scatt. obs. of struct., radius of gyration 79−94922
polyoxadiazoles, cyclochain, conform. parameters calc. 80−78732
polyoxide chains, config. partition functions, entropy, (CH_2)y-o- repeat unit 78−17829
polyoxyethylene, epitaxial crystallisation, IR investig., macromol. struct. changes 77−35493
polyoxymethylene, mol. struct., least squares refinement 79−86720
polyoxymethylene, rapid crystn. from melt rel. to struct. 80−44153
polypeptide, conformational change induced by strong elec. field 80−85336
polypeptide chain, helix-coil transition and isotope exchange reaction 79−3602
polypeptide chains, helix-coil transitions, statistical mech. calcs. 77−560
polypeptide hormones, conformations, ODMR investig. 78−76356
polypeptides, 3_1 helix-coil transition, circular dichroism obs. 78−35795
polypeptides, comparison of conformational possibilities 80−94163
polypeptides, cyclic, cryst. state conformations 79−24942
polypeptides, helical sense characterisation by IR spectra 78−17831
polypeptides, helix-coil transition dynamics, time correl. function theory 80−99591

macromolecular configurations continued
polypeptides, helix-random coil transition rates, mean relaxation rate, internal friction 77−38763
polypeptides, ionic and non-ionic, electro-optical studies of conformation 80−71379
polypeptides, mean field Ising-type model for helix-coil transition 77−70416
polypeptides, poly-L-lysine based, comb-like, struct., physicochem. props. *(Russian)* 79−55644
polypeptides, short chain conformations, long-range interactions, Monte Carlo calcs. 77−58217
polypeptides, stability of α-helix 77−61887
polypeptides, structured, nature of 4.5 Å max. on X-ray diffuse scatt. curves 78−31769
polyperfluorobutadiene, melts, solns., ^{19}F NMR, ^{13}C NMR spectra, microstruct., configurations 77−43894
polyphenylacetylene, cryst., resonant Raman scatt., opt. absorpt. 77−4630
polyphenylene oxide-polystyrene blends, spectroscope exam. of chain conform. and bonding 78−42925
polyphenylquinoxaline, soln., conform., equilib. rigidity *(Russian)* 79−55643
p-polyphenyls, band struct., mol. struct. effects calcs. *(German)* 77−47722
polyphosphazenes, new polymers with inorganic backbone atoms 77−564
polypropene-alt-1,4-butadiene and hydrogenated derivative, mol. relaxations in glassy state 80−53177
polypropylene, amorphous, ^{13}C NMR spin-lattice relaxation times of isotactic, syndiotactic sequences 77−4572
polypropylene, fracture, interatomic bonds deform. 79−57107
polypropylene, isotactic, conformational origin of peak struct. in XPS spectrum 79−89819
polypropylene, isotropic, molten and cryst., small-angle neutron scatt., chain-folding 78−63680
polypropylene, molten and cryst., mol. conformation, small angle neutron scatt. study 79−51012
polypropylene, stereochem. additions, sequence lengths, ^{13}C NMR 77−27212
polypropylene isotactic film, cryst., dynamic mech. props., influence of struct. 79−4991
polypropylene sulphide, atactic chains, dipole moments, dielec. const. meas. 80−23584
polypropylene sulphide in athermal solvent, viscosity-temp. coeffs. 80−39333
polypropylenes, iso- and syndio-tactic, Raman tacticity bands, vibr. spectrum 80−66193
polypyromelliteimide, fracture, interatomic bonds deform. 79−57107
polyquinones, ladder, partially-ladder, synthesis, struct., props., review *(Russian)* 80−7529
polyriboadenylic acid, soln., Raman spectra, struct. and conformation 77−71899
polyriboxanthylic acid, spatial struct., H bonding 80−53086
polysaccharides, vibr., conformation, IR spectra, computer anal. *(Russian)* 78−13637
polystyrene, atactic, stereoregularity study using Fourier transform IR spectroscopy 79−59612
polystyrene, atactic, structure elucidation, model construction and X-ray methods *(German)* 80−103267
polystyrene, chem. shift, conformational struct. *(Russian)* 80−5652
polystyrene, conform. and near all-trans extended-chain model relevant in gels, X-ray diffr. patterns interpret. 80−79707
polystyrene, cyclohexane soln., coil-globule transition 80−54110
polystyrene, cyclohexane soln., temp. depend. of chain dimensions, small-angle neutron scatt. 78−50671
polystyrene, depolaris. Rayleigh scatt., optical anisotropy 78−27245
polystyrene, glassy, struct., X-ray scatt. and conformational analysis 78−26449
polystyrene, in solns., intrinsic viscosity rel. to mol. wt., unperturbed dimensions 80−65268
polystyrene, isotactic, conformation in bulk crystallised state 80−43221
polystyrene, isotactic, normal vibrational anal. 78−43869
polystyrene, isotactic gel film, Fourier transform IR spectrum 80−104465
polystyrene, mol. conform., craze fracture 79−15835
polystyrene, molecular alignment 78−14299
polystyrene, partial draining of low-molecular weight polymers with flexible chains 80−23592
polystyrene, soln. ion cyclohexane, mol. dimens. near theta point 80−54105
polystyrene, solns., sedimentation behaviour, branching effects determ. 80−66887
polystyrene, stereochem. additions, sequence lengths, ^{13}C NMR 77−27212
polystyrene, sulphonated, polyelectrolyte solution, correlations and dynamics 80−104446
polystyrene and model cpds., conformational struct. influence on normal modes of benzene ring, Raman study 80−14144
polystyrene films, UV irrad., struct. changes, gel permeation chromatogram computer manipulation, substraction 79−96387
polystyrene in solns., unperturbed dimensions rel. to temp., solvent composition 79−64132
polystyrene networks, characterisation by small-angle neutron scatt. 77−38765
polystyrene-b-isoprene and hydrogenated derivative, mol. relaxations in glassy state 80−53177
polystyrene-benzene-methanol system, preferential solvation 79−10772
polystyrene-polyisoprene two-block copolymer soln., conformation, small angle neutron scattering, X-ray diffraction, review *(Rumanian)* 80−6348
polystyrenes, toluene soln., turbulent drag reduction, mol. wt. and struct. influence 79−7373
polytetramethylene terephthalate, monofilaments, chain conform. rel. to strain 77−4055
polythylene, and perdeuteropolyethylene, crysts., IR and Raman intensities, factor group splittings 79−65851
polytrimethylene terephthalate single crystals, X-ray and electron diffr. obs. of cryst. struct., packing analysis 79−94924
polyurethane, branched soln., viscous reduction props. *(Russian)* 78−87807
polyurethane elastomers, hard segment struct., model 79−64131
macromolecular configurations continued
polyurethanes, cross-linked, mol. mobility and struct., thermomechanical and NMR obs. *(Russian)* 80−69285
polyurethanes, epitaxial crystallisation, IR investig., macromol. struct. changes 77−35493
polyvinyl acetate, partial draining of low-molecular weight polymers with flexible chains 80−23592
polyvinyl carbazole, and ring chlorinated derivatives, dielectric and NMR relaxation 79−73883
polyvinylacetate solution, long-chain branching characterisation, molar masses 79−94122
polyvinylalcohol, macromol. gel layer formed on ultrafiltration tubular membrane, charact. 80−14260
polyvinylidene chloride, crystalline, preferred chain conform., mol. models 80−79709
polyvinylidene chloride, normal vibr. analysis using conform. model 80−83529
polyvinylidene chloride, vibr. spectra, amorphous and cryst. state conforms. 79−27930
polyvinylidene fluoride, elec. field induced phase changes 79−11387
polyvinylidene fluoride, piezoelec. and pyroelec. props., struct. model 79−11386
polyvinylidene fluoride, relax., influence of monomeric unit conform. and supermol. struct. *(Russian)* 79−23537
polyvinylidene fluoride, structural phase transitions, statistical mech. theory 79−82331
polyvinylpyrrolidone, conformational states investig. by atom-atom function method *(Russian)* 80−53178
polyvynyilpyridines, atactic, chem. shift, conformational struct. *(Russian)* 80−5652
poly[trityl methacrylate-co-(S)-α-methylbenzyl methacrylate], abnormal optical rot. 79−31749
prealbumin, human, struct., X-ray diffr., amino acid sequence, circular dichroism meas., comparison 77−42450
prealbumin, human plasma, secondary struct. refinement from circular dichroism data 78−27888
prealbumin, protein-DNA and protein-hormone interactions rel. to model of thyroid hormone nucl. receptor 77−66793
prealbumin-DNA-hormone interactions, X-ray studies, review 78−53322
proline, oligomer, vibr. spectra rel. to polymeric form 79−83695
protamine cDNA plasmids, coding and non-coding nucleotide sequences, sequence divergence of rainbow trout protamine mRNA 79−74596
protein, electron radiation damage on primary and secondary struct. level 80−89808
protein, metal containing, chem. characts. of conformational nonequilib. states 78−95998
protein, secondary structure determ. by laser Raman spectroscopy 77−23587
protein, structure and bonding, quantum theory, ab initio calcs. 80−61509
protein β-pleated sheet topology rel. to relatedness 77−77866
protein beta sheet structures, anal. and prediction by combinatorial approach 80−76710
protein conformation, statistical mechanical theory, appl. to homopolymers 78−64931
protein conformation, statistical mechanical theory, folding pathway 78−64932
protein conformation in nerve membrane, and energy changes, rel. to action pot. 78−44497
protein conformation in nerve membrane, interaction with elec. field, rel. to excitability 78−53377
protein conformational changes, rel. to proton transport in membranes 78−96035
protein conformational transitions, temp.-depend., using fluoresc. probes 77−70410
protein crystal dehydration, conformational changes with hydrostatic compression *(Russian)* 77−43339
protein dynamic states, role of geometry and elastic strains 78−48745
protein folding, incorporation of 1-dimens. Ising model into 3-dimens. model 77−90723
protein molecular weight and ultrastruct. determ. in STEM 80−85562
protein molecule, simulation of single mol. images combining computer and electron micrograph analysis 78−37781
protein molecules, new representation for mapping chain-folding 77−44588
protein primary structure, distrib. of identical amino acid residues 77−56334
protein secondary structure determ. by circular dichroism spectra 80−30653
protein sequencing, solid-phase techniques 77−56557
protein structural differences evaluation from electron micrographs 79−53040
protein structure, areas, vols. and packing, review 77−86441
protein structure prediction from amino acid sequence 78−24026
proteins, amide unit electron organisation, mol. orbital theory 79−2000
proteins, chain reversal regions conservation 79−83699
proteins, coiling and topology of the antiparallel β-struct. 80−40956
proteins, coiling and topology of the parallel β-struct. 80−40957
proteins, conform. anal., algorithms and data structs. for array processing 80−83530
proteins, conformations, quantitative approach 80−30652
proteins, diagmagnetic anisotropy, struct. origins 79−92136
proteins, dimensions, shape, conformational transitions, use of dielectric relaxation method 79−11888
proteins, folded, models for H exchange 78−76981
proteins, globular, intramol. relaxation 77−10798
proteins, globular, no. of turns and models of turn form. 77−77869
proteins, globular, prediction of β-turns by computer 79−83698
proteins, globular, struct. anal. in soln. by large-angle diffuse X-ray scatt. 77−86723
proteins, inductive resonance energy transfer, struct. and conform. changes 79−27120
proteins, nature of 4.5 Å max. on X-ray diffuse scatt. curves 78−31769
proteins, structure and bonding, modelling using aminoacetaldehyde 80−74273
proteins, UV fluorescence detect. of conformational rearrangements in plants 79−53031
proteins in solution, laser photo-CIDNP as surface probe 78−73138
proteins involved in active membrane transport, struct. review, book contrib. 80−108844
proteins secondary struct., IR, Raman spectral data, review 78−90330

macromolecular configurations continued
pseudoisocyanine bound by sulphated polysaccharides, dil. aq. soln., visible and circular dichroism spectra 80−45107
PTFE, γ-ray effects on 19 and 30°C phase transitions, Fourier transform IR spectroscopy 80−103387
PTFE, melt transition, theory 77−76325
PTFE grafted membranes, struct.-properties relationships, bifunctionality *(French)* 80−61137
PTFE grafted membranes, struct.-properties relationships *(French)* 80−61136
PTFE grafted membranes, struct.-properties relationships for poly-N-vinylpyrrolidone-containing membranes *(French)* 80−61138
purple membrane, orthorhombic 2D crystal form 80−85362
purple membrane, polarized IR spectroscopic struct. study 79−43809
PVC, structural studies by Raman spectroscopy 79−7044
PVC, thermally induced conformational changes, Fourier transform. IR spectroscopy 78−9287
PVC branching, origin, extent 79−7048
PVC chain branching, CH_2Cl group production mechanism, IR data evaluation 79−7047
PVC film, uniaxially stretched, mol. orientation, polarised fluoresc. investig., deform. mechanism 77−52440
PVC-THF-H_2O, precipitation fractionation, influence of stereoregularity 79−7046
Pyran copolymer containing 5-fluorouracil, synthesis and antitumor props. 79−91613
radiospectroscopy, structural energy characteristics, rotational isomerism, mol. motion *(Russian)* 79−56602
random chains, spatial configurations, review 77−38757
recent advances in polymer characterization by GPC 80−16740
replication processes, with selection, stochastic theory 77−68145
retinal chromophore, reson. Raman spectra obs. of struct. 80−94168
rhodopsin, α-helix orientation, spectroscopic study 80−89711
rhodopsin, bacterial compared with animal, H exchange 77−29096
rhodopsin, bovine, conform. in situ and solubilised with detergent 77−44587
rhodopsin, coherent states of flexible macromol., mol. basis of vision 79−79472
rhodopsin, conformeric states, spectrophotometry 77−90725
rhodopsin, presence of two closely arranged SH groups in mol. 78−53323
rhodopsin, solubilised, photoinduced conform. changes, spin-label method 77−81496
rhodopsin, transient light-induced conform. changes 78−15774
rhodopsin and bathorhodopsin, theoretical analysis of optical activity 77−52783
rhodopsin conformation, spectral studies 78−15765
ribonuclease A, thermodynamics of interaction and unfolding in transfer to aq. consolute solns. 79−24939
ribose phosphate backbone, effective partial changes calc. 80−8013
ribosomal protein S4 from Escherichia coli, circular dichroism obs. of conformation 78−96003
ribosomal RNA, conformational changes induced by ribosomal subunit proteins from E. coli 79−79466
ribosomes, E. coli, complexes of individual components, small angle X-ray scatt. study 79−11895
ribosomes, E. coli, neutron small-angle scatt., contrast variation study 79−16138
ribulose bisphosphate carboxylase, two-layered square-shaped mol. 77−56336
ribulosebisphosphate carboxylane, electron microscopy of 79−70515
rigid chain polymer solns., flow birefringence rel. to mol. wt. and chain length *(Russian)* 79−33664
$tRNA^{Phe}$, yeast, in soln., H-bonded protons in tertiary struct., PMR, assignments 77−90728
tRNA, conformation and intensity fluctuation spectroscopy, melting curves 78−35798
RNA, conformational fluctuations, internal motion correl. times, ^{31}P NMR obs. 80−72135
mRNA, H2b histone, sea urchin, sequence of 5'-end 79−74594
RNA, laser Raman spectra, cloverleaf secondary struct. 79−100569
RNA nucleotide sequence, determ using computer 79−29500
RNA solns., oriented in DC mag. field light scatt. 79−2004
RNA synthetic, duplexes in soln., struct., dynamics 79−57574
rubber, natural, crosslinked by dicumyl peroxide, modulus, swelling relations 80−59551
rubber, network, highly swollen, long time dynamics 80−38291
rubber, network entanglement contrib. to elasticity 80−39203
rubber containing entanglements, mechanical model 79−81315
rubber elasticity, molecular aspects book contrib. 78−84886
rubber mixtures in range of reversion, vulcametry, cross-linking model *(German)* 80−104113
rubber network elasticity, mol. theory 80−38290
saturated hydrocarbon polymers, conform. stability, 1-electron levels, long-range effects calcs. 80−28123
scattering methods, conf., Prague, Czechoslovakia, (July 1976) 79−1764
self-avoiding walks for chains confined on lattice strips 77−79715
self-avoiding walks of macromolecules confined to strips and capillaries 78−94345
self-avoiding walks with span limitations, cubic lattice, mean square end-to-end distance 80−62568
semicrystallised chains, small-angle neutron scatt., mean dimension evaluation 80−43220
serum albumen, bovine, adsorption kinetics, surface denaturation 79−79460
serum albumin, bovine, molecular structure of adsorbed film 79−79462
short polymer chains, end-to-end vector, distrib. function 80−87254
similarities of configurations, computer-assisted-examination of substructs. 79−81294
sodium polystyrene sulphonate, solns., infinite dilution viscoelastic props. 79−14363
solution, different-sized mols., orientation effects, surface region, lattice model 79−1540
solutions, electric field-induced optical rectification, rel. to electro-optic kerr effect 80−84726
southern bean mosaic virus, struct. at 2.8 Å resolution 80−85334
space-filling molecular models constructed by computer 77−40633
sphere radii moments, size distrib. 80−21329
spherical particle of nonuniform electron density, small-angle X-ray scatt. 77−7631
stability criteria, Lyapunov methods 79−96507

macromolecular configurations continued
statistical copolymers, normal vibrs., calc. method *(Russian)* 78−29871
structure factor calculation, by FFT 77−51268
structure factor least squares refinement procedure 77−84573
structure-forming solutions, double light refraction and viscosimetry 79−94745
styrene-α-methylstyrene copolymers, prep., charact. by pyrolysis gas chromatography *(German)* 79−29355
styrene-acrylonitrile copolymer, of azeotropic composition, Mark-Kuhn-Houwink relations *(Russian)* 79−50176
styrene-butadiene block polymers, multiphase systems, struct., props. 77−31600
styrene-isoprene block copolymers, dilute soln., conform. obs. 79−10774
styrene-isoprene triblock copolymer, mol. relax. in glassy state 80−53177
styrene-p-chlorostyrene triblock copolymers in dil. soln., conform. behaviour, temp. depend. 79−90519
subtilysin, globule, atomic density distrib. 79−79458
symmetry group construction 77−71898
syndiotactic poly(styrenesulphonic acid), conformation 77−54639
teacher resource paper on entropy an rubbery elasticity 80−17777
tetrahydrofuran-propylene oxide copolymers, prep., ^{13}C NMR, end group anal. 79−66293
thermodynamics and decoding of long molecules 79−31757
three-dimensional cubic lattice, random walk of particle, polymer chain config. approach 80−22294
tibosomal RNA interacting sequences, expt. determ., method and results 80−3586
tri-O-ethylamylose-solvent complexes, cryst. struct., chain conforms. 79−65067
triacetate-nitrocellulose, long period struct., 180-265°C, X-ray diffr. obs. *(Russian)* 79−24556
triblock copolymer, model for rheology 80−23979
triethylamylose-solvent complexes, conform. and packing analysis 78−75654
tropocollagen macromolecule form., effect of soln. pH 78−95999
α-tropomyosin, specific splitting at cysteine-190, physicochem. study of fragments 80−30647
trypsin, bovine, activation, activity and inhibition *(German)* 79−79465
trypsin crystal fusion, microcalorimetry 77−70413
trypsin inhibitor, soybean, folded, models for H exchange 78−76981
tubulin proto-filaments, three-dimensional struct. 79−70520
twisted stiff chains, theory 79−59611
twisted stiff chains theory 80−1093
unperturbed dimensions of branched cahin, star and ring polymers 78−66701
urease shear inactivation, metal ion effect, rel. to shear deform. effects in enzyme catalysis 78−76982
valinomycin in its Ba complex, novel conformation 80−94167
vinyl alcohol-vinyl acetate copolymers, mol. architecture and physiocochem. props. 80−44103
vinyl polymers with flexible side chains, configurational statistics, dipole moments 77−38760
viroid RNA, covalently closed circular mols., conform. states 80−85340
viscose, long period struct., 180-265°C, X-ray diffr. obs. *(Russian)* 79−24556
xanthane, dilute solns., viscosity rel. to temp., shear rate *(French)* 80−39332
zero-component field theories, high order behaviour without $n \to 0$ limit 79−75438
CO myoglobin struct. determ., neutron crystallography 79−43814
C_3S_2, electronic struct., optical and photoelectron spectra 78−70982
^{13}C NMR in copolymers, monomer unit distrib. *(Russian)* 77−46664
Cu complex, polyacrylic acid-polyethyleneimine-Cu(II), struct. *(Russian)* 79−55018
DNA, linear dichroism, strand separation determ. 79−62188
H^+-ATPase, soluble mitochondrial, thermal stability obs. 80−55992
$(Na^+ + K^+)$ATPase, subunit comp. 79−83704
Se, liquid, chain molecule struct. exam. by time-of-flight pulsed neutron diffr. 77−55228

macromolecular dynamics
alanine, oligomer, vibr. spectra rel. to polymeric form 79−83695
albumin, bovine serum, diffusion, hydration and soln. environment effects 77−19116
albumin, bovine serum, diffusion, hydration effects, finite conc. 77−19115
albumin, bovine serum, diffusion, hydration effects 77−19114
amino acid side chains, NMR relax. due to multiple internal rots. 78−94340
p-aromatic poly(amide hydrazide), dimethyl sulphoxide solvent, dynamic birefringence, conform., viscosity *(Russian)* 78−39525
athermal model chains, pair distrib. function, Metropolitan Monte Carlo calcs. 78−17827
ATPase, Ca^{2+}-activated, of sarcoplasmic reticulum, rot. motion and evidence for oligomeric structs. 80−72124
ATPase, Ca^{2+}-depend., struct. rearrangements during function 80−81527
Ca^{2+},Mg^{2+}-ATPase, of sarcoplasmic reticulum, transient kinetics obs. by fluoresc. 78−61156
Na^+,K^+-ATPase preparations, tryptophan fluoresc. 77−21477
bacteriorhodopsin in purple membrane, chromophore mobility 77−25366
bacteriorhodopsin reorientation due to elec. field 77−66789
bacteriorhodopsin Schiff base deprotonation dynamics using kintic reson. Raman spectroscopy 77−48981
bioenergetics, solitons, muscle contraction mechanism 79−96508
biological functions of LF phonons *(Chinese)* 78−24024
biological macromolecules, conformational dynamics subnanosecond T jump and Raman spectroscopy appl. 79−66445
biological macromolecules, relax., modified Glauber theory 77−12879
biological system, cooperative behaviour, Bose condensation, Frohlich model 78−35797
biological systems, hydrated, PMR spin-lattice relax. of water, cross-relax. effects 79−34496
biomembrane, statistical mechanics 79−66456
biomembranes, dynamic aspects, review 78−69005
biomolecules, transport in conc. systems 79−57567
biopolymer, local mode resonance enhancement in Raman spectra 77−77204
biopolymer localised modes, due to impurities, FG-matrix technique 79−34474

macromolecular dynamics continued
biopolymer molecular dynamics and structure, fluorescence spectroscopy 77−60329
biopolymer motions, nonsteady hydrodynamics, damping effects 77−36861
biopolymers, conditions of liquid crystal formation 80−30642
biopolymers, dynamics of helix-coil transition 79−29499
biopolymers, hydrophobic interactions 78−37777
biopolymers, reversible unfolding, mol. field theory 79−34479
biopolymers rotational dynamics program package 79−59609
bis(methylthio)alkanes, model compounds of polythioethers, vibr. spectra 80−58430
bose condensation, polar modes with elastic restoring forces, metastable ferroelec. state 77−81464
Brownian particles, k-dependence of long-time diffusion 80−5645
catalysis of reversible flow reaction by oligomeric enzyme 77−36859
cellulose acetate, gamma-ray effect on light absorption used as dose meas. technique 78−13345
cellulose acetate-dimethylphthalate gel, mech. props., substitution effect *(Russian)* 79−23291
chain configuration-dependent props., review 77−38758
chain conformations and local motions, Brownian motion simulation 79−86098
chain dynamics, repulsive Lennard-Jones pot. mol. dynamics calc. 79−36805
chain dynamics and Brownian motion, simulation 79−86099
chain molecule dynamics, intramolecular diffusion controlled reaction for pr. terminal reactive groups 78−9289
chain molecule in solutions, finite concentrations, different solvent conditions, simulation 79−45872
chain networks, static and dynamic entanglements, contrib. to equilib. shear modulus 80−28126
chromosome conjugation, vibratory mechanism 78−95991
chymotrypsin-like proteins, γ-irrad. rel. to UV irrad., unfolding obs. 80−35984
coil, dynamical polymer coil overlap, NMR model 80−23583
coiled linear macromolecules, effective diffusion tensor of chain mol. in shear flow 77−50579
collagen, enzyme- and alkaline-soluble, optical rot. dispersion and circular dichroism 77−70411
collagen, hydrated, PMR spin-lattice relax. of water, cross-relax. effects 79−34496
collagen, native, phasic transition, PMR 77−25363
collagen fibril, ^2H NMR of mol. motion 80−67034
computer simulation, constraint dynamics 78−9932
conference, Dublin, Eire (July 1977) 79−55012
conformational mobility, fluorescence obs. 80−63877
coordinated motion simulation, of chains 79−86721
copolymer model with alternating spins, kinetics 80−9768
copolymers, self-replicating, temporal evolution, Monte Carlo calcs. 77−83773
critical branching a statistical theory 80−3413
critical ratio in the excluded volume problem 79−64136
crystallisation, kinetic statistical theories *(Chinese)* 77−84683
crystallisation thermodynamics, various degrees of coiling 78−51445
cytochrome b_5 rotational diffusion in lipid bilayers, influence of lipid physical state 79−83693
Debye-Brinkman equation, macroscopic derivation 77−10799
deformed networks, equilibrium props. from thermomechanical anal. *(German)* 80−37917
deoxyhaemoglobin, Fe(II)-N_ϵ(His-F8) stretching freq. rel. to quaternary struct. 80−94160
dextran, aq. soln., conc., PMR *(Russian)* 80−71225
dielectric relaxation data interpret. by model for macromol. chain dynamics 77−52014
diffusion, direct and hydrodynamic forces effect 79−50172
dilute macromolecular solns., self-diffusion coeff. 78−6168
dilute solutions, self-diffusion and momentum autocorrel. functions 78−33645
dimyristoyl lecithin lipid vesicles, sonicated, ^{13}C relax. times model for gauche-trans isomerisation 78−33520
DNA, B-configuration double helix, interaction with H_2O, isoenergy contour maps 79−20504
DNA, backbone vibrational mode displacements of A-DNA and B-DNA 80−8000
DNA, double-helical model, sedimentation coeff., X-ray scatt. 77−14629
DNA, dye labelled elec. dichroism and birefringence, comparison with mol. props. from polarised fluoresc. 80−84785
DNA, fluorescence depolarisation, twisting and bending, rot. Brownian motion 79−70509
DNA, helix-coil transition, thermodynamics 79−11883
DNA, Hg (II) and Ag (I) complexes in soln., theoret. interpret. of elec. dichroism obs. 80−85347
DNA, monodisperse, rod-like mols., transient elec. dichroism 78−94344
DNA, mouse liver, time depend. correl. function, single clipped photon correl. 77−48748
DNA, mutations, quantum theory, proton transfer by dynamic interactions 77−77868
DNA, soln., phase transitions, light absorption oscills. obs. 80−26197
DNA, soln., quasielastic light scattering, in AC elec. field 79−62186
DNA, supercoiled torsional stress and local denaturation 80−72131
DNA, supercoiling, elastic model 78−15767
DNA, synthetic, duplexes in soln., struct., dynamics 79−57574
DNA, torsionally stressed, equilibrium statistical mechanics of helix coil transition 80−67032
DNA double helix supercoils, linking numbers, twist, writhing number 77−12882
DNA double helix unwinding during RNA polymerase binding 79−70512
DNA internal motions, ^{31}P NMR and PMR 80−97855
DNA secondary structure, dependence on base sequence, theoretical conformational anal. 79−53032
DNA soln., calf-thymus, time depend. correlation functions meas., three relax. components 77−40631
DNA solution, elec. birefringence, stabilised induced dipole behaviour 80−85349
DNA-type macromolecule, melting, low mol. wt. impurity effect 80−12050
drag reducing polymer solns., dynamical behaviour, mol. conformation and optical props., expt. and rheological model 79−60034

macromolecular dynamics continued
dynamic birefringence and volume effects, rigidity determ. *(Russian)* 77−42456
dynamic living polymers, thermodynamic enhancement of oligomers, end-group interactions 80−58423
dynamic viscosity of macromolecular liquids for superposition of static and oscill. vel. gradients 77−76279
E. coli, light scatt., ribosomal subunit diffusion coeffs. 80−21438
elastin, hydrated, dielectric relax. 79−5247
elastomer, relaxation processes, statistical description *(Russian)* 79−23229
enzymatic catalysis, dynamic theory, conform. rearrangements 77−36858
enzyme dynamics, statistical phys. 80−21439
epitaxial crystallisation, review 79−42409
epoxides, dielectric relax. and deform props., cross-link density effect *(Russian)* 80−60942
erythrocytes, bound water in frozen solns., proton mag. relax. 77−28472
ethylene-CO copolymer, dielec. absorpt. meas., permittivity *(French)* 80−103916
ferredoxin, pulse-radiolysis study of conformationally nonequilibrium states 79−70506
ferrocytochrome c, mol. dynamics simulation 80−87255
ferrohaemoglobin, R-T conformational change due to pseudo Jahn-Teller effect 79−70521
flexibility, detect. by time-depend. diffusion coeffs. obs. 80−23585
flexible chain molecules, mutual interpenetration, fluorescence obs. 80−63877
flexible macromolecule solutions, mol. models for mech. props. 79−59957
flexible mol. modelling, by length distrib. projection of self-avoiding random walks 77−75352
Flory formula for the polymer size exponent ν 78−70985
fluorescence depolarisation, E-type delayed, rotational motion probe techniques 80−36207
fluorescence spectroscopic investigations of the dynamic properties of proteins, membranes and nucleic acids 80−101148
force constants refinement in normal coord. calcs. 77−31035
Gaussian polymer molecule config., large mol. Kirchhoff matrix reduction 79−13850
Gaussian polymer molecule config., stars and random regular nets, distrib. functions 79−13849
Gaussian ring chain, dynamics, Langevin eqn. 78−25761
generalised polymer problems, Flory exponents 80−107039
globular protein rotatory mobility meas. by spin probe method, soln. viscosity 77−16902
glycine, oligomer, vibr. spectra rel. to polymeric form 79−83695
graft copolymers, normal vibrs., calc. method *(Russian)* 78−29871
gyration quasi-radius of ring chain, exact shape of distrib. function *(Japanese)* 77−42449
haemoglobin, allosteric effect, mathematical description 79−64125
haemoglobin, dynamic characts. of conformational nonequilib. states, radiolysis investig. 78−58877
haemoglobin, nanosec. probe of dynamics using time resolved reson. Raman scatt. 80−94162
haemoglobin reactions as interfacial phenomena, conformational changes 77−9167
haemoproteins, allosteric effect, mathematical description 79−64125
hard disc necklaces, rigid and nonrigid models, mol. dynamics 80−43219
hard-sphere suspension, viscosity, direct inter-macromolecular interactions effects 79−95199
hard-sphere system, diffusion, hydration and soln. environment effects 77−19116
hard-sphere system, diffusion, hydration effects, finite conc. 77−19115
hard-sphere system, diffusion, hydration effects 77−19114
helical to coiled relax., statistical mech. approach, appl. to DNA secondary struct. 78−3443
helical wormlike chain, dipole moment, elec. birefringence, elec. dichroism, statistical mech. calcs. 80−14262
helical wormlike chain, statistical mech., continuous limits of discrete chains 78−66697
helical wormlike chain statistical mechanics, persistence vectors, comparison rot. isomeric state model 77−50573
helical wormlike chain statistical mechanics, scatt. function 77−54637
helical wormlike chains, statistical mech., distrib. function calcs. 77−75353
helix-coil transitions in specific sequence biopolymers 78−35794
high resolution NMR investig. 80−91708
histone lysine-rich, laser scattering spectra 77−29095
homopolymer chain adsorpt. on uniform surface 78−53316
infinite polymers, long-range Coulombic interactions, LCAO-CO calcs. 79−7042
intermolecular interactions, effects of intervening medium and polar mode energy feeding 79−13857
internal motion, NMR spin-lattice relax. 79−41257
latex films, surface struct., vulcanisation, radiothermoluminesc. obs., 100-230K 78−75575
lattice model chain dynamics, simulation *(Russian)* 79−22876
lattice model polymer chain Monte Carlo study, Rouse coord. distrib. and dimens. 79−89814
lecithin, inelastic light scattering at second micellar formation 77−21492
librational motion effects on fluoresc. depolarisation and NMR relax. in macromols. and membranes 80−85324
light scattering in dynamical props. study, principles spectra derivation and applics. 80−53218
linear block copolymers, hydrodynamics 79−69273
lipid bilayer, planar, light guide effect, bilayer spectrosc. appls. 79−29509
lipid bilayer head group, orientational order and rotational diffusion, NMR obs. 80−21451
lipid bilayers, D relax. rates and mol. dynamics 80−26206
lipid monolayer, simulation using mol. dynamics 80−108838
liquids, depolarised Rayleigh scatt., review 77−40256
lysozyme macroradicals, ultraslow diffusion in an aq. matrix, EPR obs. 79−92119
macromolecular liquids, flow alignment, non-Newtonian viscosity and normal press. 77−35183
Markovian polymeric systems, Rayleigh scatt. and fluctuation correls. *(Russian)* 79−65890
N-methacryloil-ω-aminolauric acid cholesterol ester, liq. cryst. polymers, copolymers, structuring *(Russian)* 79−55665

macromolecular dynamics continued
methyl methacrylate, oligomers, dielectric relax., end-group effects 78−92019
metmyoglobin, dynamics study using Rayleigh scatt. of Mossbauer radiation 80−40963
Mossbauer spectroscopy 77−12798
multichain polymer system, simulating dynamic and equilib. props. 80−53179
multistranded complexes, macromolecules, relax., modified Glauber theory 77−12879
muscle, hydrated, PMR spin-lattice relax. of water, cross-relax. effects 79−34496
muscle proteins, rot. motions, saturation transfer EPR obs. 80−94151
myelin lattice swelling kinetics study, X-ray diffr. obs. 80−21436
myoglobin, refolding kinetics by diffusion-collision-adhesion model 80−94157
myoglobin, static and dynamic structure of biomolecules, Mossbauer effect 80−40952
myoglobins, kinetics studied by picosecond spectroscopy 79−43804
myosin conformational conversions, using acetate and acetamide spin labels 77−52733
myosin rod, and subfragments, flexibility, birefringence relax. in soln. 78−53320
myosin-auramine O system, conform. changes and excitation energy transfer 79−96512
network polymers, cured, low freq. mol. mobility, quadratic electrochromism method *(Russian)* 78−71688
nonrigid polymer chains, theory of dynamic depolarised light scattering 79−3601
nuclear acids, effective force constant corrections, in redundant mol. coords. 78−13634
nucleic acid subunits, simulation of inter- and intra-molecular interactions 80−30643
nucleic acids, H_2 exchange kinetics and internal motions 80−21440
3′-nucleotide, calcs. to assess rigidity 80−61506
nylon 6, influence of monomer and water diluents on mech. relax. 79−4993
Nylon 6 and 12 films, drawn, NMR, mol. orientation, motions *(Japanese)* 77−32268
Nylon 6 fibre, shrinkage, influence of chain rupture during tensile deform. 79−34055
oligopeptides, conformational studies, kinetic energy problems 79−13848
organosilicon polymers, ladder-type, local conformns. *(Russian)* 77−19121
PAN fibre, pre-oxidised, IR absorpt. 77−28561
pancreatic trypsin inhibitor, bovine, macromol. dynamics, high resolution NMR investig. 80−91708
pancreatic trypsin inhibitor bovine, dynamics of folded globular protein 77−64003
perylene, organic soln., picosec. fluoresc. for rot. diffusion 79−56839
phospholipid bilayers, struct. dynamics from deuterium spin-lattice relax. time meas. 79−79485
phospholipids, ^{31}p NMR, slow-motional lineshapes for very anisotropic rot. diffusion 80−5644
photon correl. spectroscopy, macromolecular soln. dynamics, review 79−59603
plasma protein interaction with polyion complex studied by circular dichroism and UV spectroscopy *(Japanese)* 80−12316
plasmid DNA and DNA-histone chromatin-like complexes, conform. and soln. props. by laser light scatt. 80−55987
PMMA, C-H stretching and bending vibs., IR spectra, selective deuteration 80−23582
PMMA, isotactic and syndiotactic, chain distrib. function calcs. 77−75353
PMMA, mol. motions in benzene soln., ^{13}C NMR and EPR 79−78551
PMMA solution in isopropylbenzene, mol. mass effect on mobility and interaction parameters *(Russian)* 79−31754
poly(3,3-dimethyl oxetane), conform. energies and random-coil config. meas. 80−99590
poly(spiro[2,4]hepta-4,6-diene) molecular characterisation, glassy state props. 80−64928
poly γ-methyl L-glutamate films, thermal motion of α-helical mols. 79−64133
poly L-lysine, temp. induced conformation transition in solns., optical rotary meas. 78−46474
poly O-carbobenzoxyl-L-tyrosine, in soln., conformation, helix-coil transition, circular dichroism, NMR spectra 77−31037
poly-1,4-phenylene terephthalamide, in H_2SO_4, dilute soln. viscosity 78−75524
poly-1,6-di-p-toluenesulphonyloxy-2,4-hexadiyne, thermal polymerisation, Raman spectra 80−35531
poly-4-vinyl-pyridine in ethanol, spin label obs. of local density of monomer units and mol. dynamics 80−44099
poly-4-vinylpyridene, protonated and deuterated vibr. spectra *(Russian)* 77−19120
poly-4-vinylpyridine, intramol. mobility and local density in soln. spin mark method obs. *(Russian)* 80−70107
poly-4-vinylpyridine, mol. dynamics and local density in conc. soln., spin mark method obs. *(Russian)* 80−70108
poly-β-benzyl-L-aspartate, soln., ^{13}C and ^{1}H NMR dynamic study 79−69737
poly-β-ethynylnaphthalene, insoluble, reson. Raman spectrum, struct. models 78−70981
poly-γ-benzyl-L-glutamate, soln., ^{13}C and ^{1}H NMR dynamic study 79−69737
poly-L-alanine, soln., ^{13}C NMR dynamical study 79−69737
poly-n-benzamide, lyotropic liq. cryst., structural orientation *(Russian)* 77−31593
poly-N-vinyl imidazole solution, light scatt., viscosity and dynamic birefringence, mol. wt. obs. *(Russian)* 79−33665
poly-N-vinylsuccinimide, dielec. and pulsed NMR relax. glass-rubber transition, mol. motions 77−48125
poly-p-phenyleneterephthalamide, diffusion in conc. H_2SO_4 *(Russian)* 79−65232
polyacrylamide, aq. solns., conform. changes, intermol. interactions, optical mixing spectroscopy 79−10770
polyacrylamide-fluorescein conjugates, fluoresc. polarisation, high press. obs. 80−20683
polyadenilic acid, semi-dil. soln., slow modes 78−53319
polyalkyleneoxide polymer, proton nuclear mag. relaxation *(Rumanian)* 78−91977

macromolecular dynamics continued
polyamino acids, macromolecules, relax., modified Glauber theory 77−12879
polyaspartamides, soluble, fluorescent labelling 80−58426
polybut-1-ene and but-1-ene-polypropylene copolymers in solution, ^{13}C spin-lattice relax. and mol. motions 79−95670
polybutadiene, mol. motion in solid and soln., ^{13}C NMR relaxation meas. *(Japanese)* 80−2666
polybutadiene, molecular mobility, influence of S cross linkage, torsion pendulum meas. *(German)* 79−13856
polybutadiene, transverse nuclear magnetisation decay rel. to slow mol. motions *(Russian)* 78−72423
polycarbonate, amorphous morphology, from NMR obs. of swelling penetrant mol. motion 79−27929
polycarbonate, magic-angle ^{13}C NMR, relax. times, motions 79−4739
polydichlorophenylsiloxane, cyclolinear, flow birefringence and orientation angles in soln. *(Russian)* 79−65835
polydimethylsiloxane proton spin-lattice relax., chain motions 78−70987
polydimethylsiloxanes, equilibrated, living oligomer distrib., end-group interactions 80−58423
polydimethylsiloxanes, liq., proton spin relax., mol. motion, network form. 79−15369
polydisperse randomly branched polymer, sedimentation coeff. 77−63966
polyelectrolyte solutions, colligative props., chain flexibility influence 78−94962
polyelectrolytes, saturation of induced dipole moment, orientation mechanism and electro-optical effects 80−84785
polyester resin, POLIMAL 190, influence of MgO, BeO and TiO_2 on dynamical mechanical props. *(Polish)* 79−96074
polyethene, small segment motion kinetics in macromolecules 79−41256
polyethylene, chain end fixing, NMR line shape calcs. *(German)* 78−76322
polyethylene, chain end fixing, spin-lattice relax. time *(German)* 78−76340
polyethylene, crystalline struct. transitions 77−51496
polyethylene, dielec. relax. mechanism, 1-80K *(German)* 78−76384
polyethylene, drawing-out effect on vibrational normal modes *(French)* 77−15527
polyethylene, elongation, conform. set change IR obs. *(Russian)* 78−37778
polyethylene, fibre, phase structure and molecular mobility, broad-line NMR spectroscopy 78−14290
polyethylene, FIR absorpt. freqs. using proved semiempirical pot. function 77−52090
polyethylene, highly oriented fibres, 2-dimens. ^{13}C NMR 77−77114
polyethylene, linear, nuclear relaxation, mol. motion *(Russian)* 80−44949
polyethylene, mol. motions, α relax, chain transport 79−15398
polyethylene, mol. ultraslow rot. obs. using D probe spin alignment tech. 80−88890
polyethylene, NMR with rotation through magic angle *(German)* 78−76341
polyethylene, perdeuterated, skeletal vibr. spectrum 78−23445
polyethylene, pulsed NMR obs., crystallinity effects 78−76342
polyethylene, single crystal texture, polarised Raman spectra 77−61888
polyethylene, vibr. data and force field consts., review 79−31750
polyethylene crystals, plastic deformation, molecular mech., TEM obs. 80−21022
polyethylene glycol, transverse nuclear magnetisation decay rel. to slow mol. motions *(Russian)* 78−72423
polyethylene melt, dynamics anal. by three components, proton relax. 79−65754
polyethylene oxide, dil. soln., neutron scatt. mol. motion obs. 77−23593
polyethylene oxide, dilute solns., mol. motion, EPR and NMR investigations 79−94863
polyethylene oxide, NMR relaxation in melt, three component model 77−55723
polyethylene single cryst., FT IR spectra, CH_2 rocking mode 78−2843
polyethylene single cryst., FT IR spectra, CH_2 wagging mode 78−2842
polyethylene terephthalate, elongation, conform. set change IR obs. *(Russian)* 78−37778
polyethylene terephthalate, IR spectra, trans-conformational band *(Russian)* 79−27122
polyethylene terephthalate, NMR relax. and mol. mobility *(Russian)* 78−88219
polyfluorostyrene, para- and meta-, dil. soln., ^{19}F magnetic resonance 78−10792
polyglutamic acid molecular dynamics in soln., γ-ray perturbed angular correl. 78−94960
polyglycidyl methacrylate, soln., mol. dynamics, by spin mark method *(Russian)* 79−60260
polyglycyl-prolyl-prolyl, triple-helical coiled-coil conform. determ. rel. to interchain interactions, collagen models 77−38762
polyheteroarylenes, linear, conform. and struct., statistical calcs. *(Russian)* 80−69284
polyimide, influence of monomer and water diluents on mech. relax. 79−4993
polyisobutene solns., X-ray scatt., Kratky cone collimation 80−19681
polyisobutylene, relax. modes of short range fluctuation, n.m.r. meas. 77−3502
polyisobutylene, transverse nuclear magnetisation decay rel. to slow mol. motions *(Russian)* 78−72423
polyisobutylene soln., NMR, chain segment motions 80−20475
polymer, amorphous, conform. from simulation of filling diamond lattice with chains *(German)* 78−75595
polymer, amorphous, conform. from simulation of thermal motion *(German)* 78−75594
polymer, branched and crosslinked molecules, mol. description of dynamics 80−9767
polymer, Brownian dynamics model for backbone chain 79−86096
polymer, chain dynamics, hydrodynamic boundary conditions 77−11155
polymer, collapse transition 77−42451
polymer, collapsing, self-interacting self-avoiding walk model, phase transition 77−38755
polymer, conformational transitions, Brownian dynamics, simulation 79−45873
polymer, crosslinked, probabilistic theory of structural and physical characteristics 80−5649
polymer, derective, freq. branch calc. of n-paraffins, fatty acids, and glymes 79−31747
polymer, excluded vol. component, physical bound 78−66698

macromolecular dynamics continued
polymer, hydrodynamic props. and Brownian motion 77−50575
polymer, linear, slow relax. processes *(Russian)* 78−46475
polymer, liq., Brillouin scatt. and segmental motion, appl. to polypropylene glycol 78−91217
polymer, mol. motion, fluctuational network of nodes *(Russian)* 79−51011
polymer, neutron scatt. studies of chain conform. and dynamics 78−83753
polymer, oriented, thermostable, relax. transitions, thermomech. and isometric heating obs. *(Russian)* 79−23538
polymer, Raman spectra, longitudinal acoustic mode 78−43858
polymer, random coil, nonzero thickness, suspension, shear viscosity conc. depend. 79−10238
polymer, relaxation times and dynamical modulus, viscoelasticity theory *(Russian)* 79−52293
polymer, soln., freely jointed chain, with excluded vol. interaction, Monte Carlo studies 80−10475
polymer, stiff, optimised Rouse-Zimm theory 78−46472
polymer, stressed, config. free energy change due to partial crystn. of chains, distrib. of cryst. orientations 79−94923
polymer, uniaxial, fluoresc. polarisation, orientation and mol. dynamics effects 78−76516
polymer, yield behaviour, interpret. w.r.t. correlated motion 78−6973
polymer adsorption/adhesion, smooth surface, mech. stress effects *(Russian)* 78−50672
polymer and fibre systems, entanglement density, statistical theory 78−5381
polymer athermal self avoiding chains, configurational props. 80−18950
polymer attached to surface, dynamics, bead and spring model 78−75931
polymer chain, θ-behaviour in solns. 77−84615
polymer chain, direct renormalisation group procedure 80−91712
polymer chain, elasticity for different vibr. modes, algorithm 78−66696
polymer chain, flexible, angular correlation ranges 77−34790
polymer chain, frequency dependent energetics, Orwell-Stockmayer hopping model 80−24346
polymer chain, linked rigid body, Brownian dynamics 80−74267
polymer chain, molecular span and end to end probability distrib. 79−64137
polymer chain, neutron scatt. obs., review 78−14245
polymer chain, of bistable oscillators, Brownian dynamics of transitions 78−86983
polymer chain, three-body intrachain collisions *(Japanese)* 77−42448
polymer chain, viscoelastic, local relax. props. anisotropy, internal friction influence *(Russian)* 78−37780
polymer chain collapse, in poor solvent, small angle neutron scatt. obs. 78−91215
polymer chain consisting of interacting chain units, mol. dynamics, relax. times *(Russian)* 79−31753
polymer chain dynamic critical index calcs. by renormalisation method 80−87256
polymer chain dynamics, ang. correl. function decay by multiple rot. pot. diffusion 80−3569
polymer chain dynamics, hydrodynamic and excluded vol. interactions, critical exponent 78−50668
polymer chain dynamics, in confined space 77−75351
polymer chain dynamics, review 77−38759
polymer chain dynamics, review of Brownian motion theory 80−23589
polymer chain in solution, mol. dynamics obs. 80−5643
polymer chain moments, charact. function, distrib. function, numerical calc. 78−78843
polymer chain motions, electron-electron double reson. obs. 79−69753
polymer chain statics and dynamics, Lennard-Jones interaction, calcs. 80−58425
polymer chains, Forsman's equations, graph theory appls. 78−55265
polymer chains, free rotating, depolarised light scatt. spectrum calcs. 80−78731
polymer chains, self-avoiding random walks, eigenvalues, Monte Carlo determ. 78−57849
polymer chains, statistics, dynamics and graph theory 77−14627
polymer chains, zero component field *(French)* 80−69280
polymer chains with excluded vol., molecular dynamics simulation 78−78845
polymer chains with rigid bonds, local relax. times, mol. dynamics study *(Russian)* 80−59373
polymer config. on interaction with interface 78−47659
polymer confined to wedge of interior ang. α, config. statistics 79−45875
polymer dynamics including side group motion, free draining limit 80−48111
polymer dynamics simulation, general theory 78−91210
polymer dynamics simulation, relax. rates and dynamic viscosity 78−91211
polymer glass, isothermal struct. relax., in high elasticity transition region, mol. model *(Russian)* 78−87629
polymer glass transition, dynamic props., mol. model *(Russian)* 78−87777
polymer lattice dynamics, relax. time Monte Carlo anal. 78−5380
polymer linear chains, excluded vol. problem 80−5650
polymer linear self interacting chains, configurational props. 80−23586
polymer linear self interacting chains, internal distrib., radius of gyration 80−23587
polymer liquid, entangled, phenomenological consequences of Doi-Edwards viscoelasticity theory 80−79250
polymer melt, NMR relaxation, mol. motion, local defect component theory 77−55722
polymer melts, defect fluctuations, reptation, Monte Carlo investig., NMR autocorrel. function 77−3499
polymer melts and solns., Brownian motion in equilib. state 79−41645
polymer melts and solns., deformation, mol. motion under flow 79−41646
polymer melts and solns., rheological constitutive eqn. 79−41647
polymer model, dynamic viscosity, simulation 78−58875
polymer molecule, in soln., end-to-end distance relax., Monte Carlo simulation, model depend. 78−22061
polymer network formation, struct. and mech. props., computer simulation 80−38965
polymer network systems, intramol. mobility, polarised luminesc. obs. *(Russian)* 77−42455
polymer off-lattice chains, Monte Carlo anal. of excluded vol. problem 80−5647
macromolecular dynamics continued
polymer relaxation kinetics, time-depend. Ising model 79−54066
polymer relaxation phenomena, conference, San Francisco, CA, USA (Aug. 1976) 79−4257
polymer science, conf., Pittsburgh, USA, (June, 1975) 77−38756
polymer single chain in soln., dynamical scaling exponent, renormalisation along the chain 79−10786
polymer soln., cross-over effects on critical indices 79−27899
polymer solns., dilute, Hartree self-consistent field analysis 80−5648
polymer solns., dynamic scaling theories at nonzero concs., tagged chain translational diffusion coeffs. 80−75143
polymer solns., entangled, relax. dynamics, viscoelastic response functions 77−31578
polymer solution, depolarised Rayleigh scatt., time correlation function 78−2862
polymer solution, diffusion of a chain, conc. effects 80−70103
polymer solution, dilute, chain mol. dynamics and transport processes 80−14989
polymer solution, dynamical scaling, neutron spin echo obs. 80−14990
polymer solution, flexible chain, entanglement effects in segmental motion, dielec. obs. 80−40050
polymer solution, flexible mols., dynamic intrinsic viscosity, hydrodynamic interaction 78−47548
polymer solution, flow singularities, polymer chain extension and hydrodynamic instabilities 78−71376
polymer solution, internal viscosity, rel. to dynamic behaviour 77−55379
polymer solution, intrinsic viscosity 78−2281
polymer solution, nematic helix-coil transtition model 79−94870
polymer solution, simulation of macromol. dynamics, Monte-Carlo method, conc. depend. *(Polish)* 78−51404
polymer solutions, diffusion of tagged interacting spherically symmetric polymers 79−81314
polymer solutions, dilute, internal viscosities, frictional coeffs. calcs. 78−6171
polymer solutions, dilute, intrachain dynamics and forward depolarised scatt. 78−68525
polymer solutions, fluctuation-dissipation relations, viscosity, mol. wt. depend. 78−14266
polymer solutions, moderately conc., light scatt. curves, struct. model 79−4810
polymer solutions, mol. dynamics, review, book contrib. 77−39268
polymer solutions, order, conf., Midland, USA, (Aug 1973) 79−10769
polymer solutions, transport coeffs. and scaling laws in dil. regime *(French)* 79−82372
polymer solutions, viscosity, intrinsic, friction coeff., porous sphere model 78−71301
polymer solutions and gels, dynamic behaviour obs. using light scatt. 80−55727
polymer system, cross-linked, influence of chem. cross-link network on spin-spin relaxation *(Russian)* 77−32284
polymeric chain with rigid side branches, intramol. phase transition of 1st kind *(Russian)* 80−58432
polymeric macromolecule containing mesogroups, phase diagrams *(Russian)* 80−58433
polymers, adsorbed molecules, configurational behaviour, computerised dynamic display 79−874
polymers, amorphous, Brillouin scatt., hypersonic relax. 79−4811
polymers, amorphous, semi-cryst., mech. motions, review 77−32616
polymers, chain folding, cross-sectional area 78−70989
polymers, electrical phenomena, nature and appl., review 80−50254
polymers, entanglement, topological theory, chain centre friction coeffs. 80−91709
polymers, glassy, amorphous, secondary loss peaks, mol. motions 79−11649
polymers, magic angle rotation ^{1}H NMR, appls. 78−43649
polymers, rectilinear on square lattice, series expansion 80−5646
polymers, self-consistent field approximation, BBGY and Kirkwood calcs. *(Russian)* 79−64981
polymers, simulation by self-avoiding nonintersecting random chains, conc. effect 78−12639
polymers, stereoregularity distortions, local oscill. freqs., eqn. *(Russian)* 80−5653
polymers, structure and molecular dynamics, neutron scatt. meas. 79−51009
polymers, synthetic, dil. solns., NMR relax., review 79−89693
polymers containing main chain heteroatoms, struct., ^{13}C NMR investigs., review 79−55013
polymethacrylamide copolymer, soluble, mobility of spin label bonded to chain end 80−63873
polymethacrylic acid network systems, intramol. mobility, polarised luminesc. obs. *(Russian)* 77−42455
polymethylene, continuous diffuse electron scatt., correl. chain motion 78−6020
polymethylene chain, vibr. spectra, CH stretching region, struct. and assignments 78−70991
polymethylene coils in solution, dimension and shape, computer simulation *(Russian)* 80−54111
polymethylene flexible biradicals CIDNP and chain dynamics, field depend. 77−88473
polynucleotide soln., order-disorder transition, Raman spectra 78−41360
polynucleotide solution, elec. birefringence, stabilised induced dipole behaviour 80−85349
polynucleotide solution, elec. field induced orientation and effects 80−85348
polyoxymethylene copolymers, solid, mol. motions, 4-315K, dynamic-mech. study 79−4258
polypeptide chain, helix-coil transition and isotope exchange reaction 79−3602
polypeptides, 3_1 helix-coil transition, circular dichroism obs. 78−35795
polypeptides, amide proton spin-lattice relax. 79−20502
polypeptides, conformational analysis, empirical pot. energy algorithm 79−50174
polypeptides, helix-coil transition dynamics, time correl. function theory 80−99591
polypeptides, helix-random coil transition rates, mean relaxation rate, internal friction 77−38763
polypeptides, in aq. poly(L-glutamic acid) soln., helix-coil transition, US relax. times 80−45849
polypeptides, short chain conformations, long-range interactions, Monte Carlo calcs. 77−58217

macromolecular dynamics continued
polyphenylacetylene, cryst., resonant Raman scatt., opt. absorpt. 77−4630
polyphenylquinoxaline, soln., conform., equilib. rigidity *(Russian)* 79−55643
polypropylene, oriented, thermooxidative degradation kinetics, durability, influence of mech. initiated processes *(Russian)* 79−24591
polypropylene glycol, depolarised Rayleigh relax. times, backbone motion 77−566
polypropylene glycol melt, mol. motion, dielectric and Kerr effect relax. obs. 80−60498
polypropylene oxide, rubber and glassy states, conformational motion, neutron scatt. study 79−41259
polypropylene oxide, solns., mol. relax., dielectric relax. and Brillouin scatt. obs. 77−23590
polysiloxane dizwitterionomers, mech., dielec. relax., effect of H_2O sorpt., thermal history 80−50261
polystyrene, amorphous, low temp. sp. ht. calcs. 77−28014
polystyrene, benzene soln., self-diffusion, test for scaling and reptation 79−77789
polystyrene, conc. soln., friction const., Rayleigh scatt. 77−35737
polystyrene, end group modified, chain dynamics studied by fluorescence depolarization 80−19724
polystyrene, glassy state, relax., free vol. fluctuations effect 80−19722
polystyrene, in mixed theta solvent, intramol. motion, photon-correlation spectra obs. 79−77480
polystyrene, in theta solvent, intramol. motion, photon correl. spectrosc. 78−90328
polystyrene, intermol. interaction, conform. *(Russian)* 79−23539
polystyrene, intramolecular, photon correlation spectroscopy 79−41255
polystyrene, isotactic crystals, plastic deformation, molecular mech., TEM obs. 80−21022
polystyrene, molecular motion obs. during thermal polymerisation of styrene, PMR 80−3342
polystyrene, monosubstituted, US relaxation, dynamics of mol. chains 80−29124
polystyrene, soln., chain motions, electron-electron double reson. obs. 79−69753
polystyrene, soln., laser light scatt. Rayleigh linewidths anal., intramol. motion 77−3500
polystyrene, soln., macromol. dynamics, us relax. 80−19882
polystyrene, soln. ion cyclohexane, mol. dimens. near theta point 80−54105
polystyrene, spin-labelled, EPR, end group mobility, temp. and solvent depend. 78−56368
polystyrene, substituted, Raman, IR and neutron spectra of LF vibs. 78−2848
polystyrene, sulphonated, polyelectrolyte solution, correlations and dynamics 80−104446
polystyrene model molecule, 2,4-di-p-bromophenyl pentane, US relax., mol. dynamics 79−73258
polystyrene model molecule, 2,4-diphenyl pentane, US relax. 77−6965
polystyrene soln., macromolecular chain dynamics, C^{13} and NMR 78−55267
polystyrene solution, conc., diffusion and NMR relax. times 77−55725
polystyrene solution, internal viscosity, model for Lamb-Matheson-Philippoff increment 77−62284
polystyrene solutions, light scatt., mol. parameters, computer anal. assessment 79−1766
polytetrahydrofuran, H bonding effects on skeletal optical and longitudinal acoustical modes 80−34914
polyurethanes, cross-linked, mol. mobility and struct., thermomechanical and NMR obs. *(Russian)* 80−69285
polyvinylidene chloride, vibr. spectra, amorphous and cryst. state conforms. 79−27930
polyvinylidene fluoride, relax., influence of monomeric unit conform. and supermol. struct. *(Russian)* 79−23537
proline, oligomer, vibr. spectra rel. to polymeric form 79−83695
protein, globular, in aqueous solutions, conformational mobility investigation 79−53033
protein, long-range interactions, approx. method 78−7317
protein, proton magnetic reson. and spin diffusion 77−28470
protein chromophores, fluoresc. props., use in macromol. equilib. struct. mobility investigs. 79−64130
protein dynamic states, role of geometry and elastic strains 78−48745
protein mobility from spin-echo determ. of about T_2 values in proton-decoupled ^{13}C NmR 78−2769
protein rotational motions, large-scale, detection by EPR and fluorescence 79−16120
protein structural dynamics, temp.-depend. X-ray diffraction 79−92133
protein-solvent systems, dynamics investigation by nucl. gamma-resonance 79−62166
protein-water system dynamic model 77−21470
proteins, conform. changes in aqueous soln. and in mixed solvents, IR absorpt. spectra 78−15762
proteins, conformational analysis, empirical pot. energy algorithm 79−50174
proteins, fluoresc., equilib. structural mobility *(Russian)* 78−76986
proteins, H_2 exchange kinetics and internal motions 80−21440
proteins, inductive resonance energy transfer, struct. and conform. changes 79−27120
proteins, methine aromatic C sites, natural abundance ^{13}C NMR at high mag. field strength 77−86443
PTFE, peroxy radical labelled, temp. dependent rots., EPR obs. 80−28125
PTFE, vib. assignment, far IR spectrum 77−48170
PVA, liq., mobilities at const. temp., vol. 78−95174
PVC, structural studies by Raman spectroscopy 79−7044
quantum many-body problem, polymer expansion 80−57181
random coil polymer chain relax., lattice model with excluded vol., head movement rules 80−5642
random coil polymer chains, asphericity relax., Monte Carlo calcs. 77−75354
random coil polymers, intramol. fluctuations by photon correl. spectroscopy 77−48184
randomly coiled polymer, in solution, models for spin relaxation 77−85607
rapid circular dichroism meas. with small gas lasers 77−37968
rhodopsin, coherent states of flexible macromol., mol. basis of vision 79−79472
rhodopsin, transient light-induced conform. changes 78−15774

macromolecular dynamics continued
rhodopsin and thermal intermediates, fast struct. fluctuations in protein component 80−72137
ribose phosphate backbone, effective partial changes calc. 80−8013
rigid macromolecule, in soln., depolarised Rayleigh spectroscopy 79−94119
rigid macromolecules, drag coeff., conc. depend., nonhydrodynamic interactions effects 78−22062
rigid symmetric top macromols., circular cylinder model, rot. dynamics 80−102591
ring chain, distrib. function of square radius of gyration 77−61885
ring polymer model with excluded volume 79−94117
ring polymers, internal viscosity, statistical theory 77−88610
t-RNA, rot. relax. time, 10^{-9}s range Fabry-Perot and photoelectron time of arrival method 80−21437
RNA solns., oriented in DC mag. field light scatt. 79−2004
RNA synthetic, duplexes in soln., struct., dynamics 79−57574
rod-like macromolecules in conc. soln., basic kinetic eqn. and appl. 78−67637
rotational diffusion, ^{13}C spin-lattice relax. data anal., computer program, appls. 79−95664
rotational diffusion props., validity of general ellipsoid model 80−95751
rotational isomeric state model, diffusion dynamics, 1-dimens. periodic pot. system 78−90315
rubber, natural, transverse nuclear magnetisation decay rel. to slow mol. motions *(Russian)* 78−72423
rubber, network, highly swollen, long time dynamics 80−38291
scattering methods, conf., Prague, Czechoslovakia, (July 1976) 79−1764
self-avoiding random walks, exact enumeration method and Monte Carlo sampling 79−67228
self-avoiding walks of macromolecules confined to strips and capillaries 78−94345
self-organizing molecular system, dynamics 80−67028
self-replicating macromolecules, Monte Carlo computer models 78−46473
self-replicating macromolecules, temporal evolution, Monte Carlo calcs. 77−83773
semirigid, dynamo-optic const. MW depend. *(Russian)* 77−20821
short chain molecule, dielectric relax. 79−95706
short polymer chains, end-to-end vector, distrib. function 80−87254
siloxane, temp. transitions, linear dilatometry and X-ray diffr. obs. *(Russian)* 80−59404
small fluid particles, dynamic props., applicability of neutron scatt. studies 79−41936
Smoluchowski eqn., one-particle generalised, perturbation solution 77−27211
sodium polystyrene sulphonate, solns., infinite dilution viscoelastic props. 79−14363
solutes, finite conc., isothermal diffusion and quasielastic light scatt. 79−82367
solution, alternating elec. field light scatt., low angle approx. 80−84721
solution, diffusion and self-diffusion phenomena, review 80−15273
solution, dynamic light scatt. by flexible macromols. in fluctuating elec. field 80−84722
solution, Rayleigh scatt., elec. reorient. rel. to spectral line rot. broadening 79−1774
solution, rigid ellipsoidal macromols. in cond. soln. at low ionic strength, specific Kerr consts. 80−84718
solution, rot. diffusion coeff. calc. method w.r.t. mol. struct., elec. birefringence relax. time data interpret. 80−85331
solution, transient elec. birefringence in reversing fields of arbitrary strength and duration 80−84719
solutions, associating, sedimentation equilib. distrib. anal., composition rel. to activity coeffs. 77−14628
solutions, light scattering, polydispersity and internal modes of motion 80−20651
solutions, orient. in laser beam elec. field, anisotropic light scatt. 79−1768
solutions and suspensions, polarised fluoresc. in elec. field, mol. props. deriv. 80−84785
spherically symmetric polymers, in soln., Faxen theorems 78−94342
spherically symmetric polymers, in soln., hydrodynamic interaction 78−94343
spheroidal macromolecules, solns., quasielastic light scatt. calcs. 78−43883
star type, characteristic function of distrib. of square radius of gyration 77−79717
statistical copolymers, normal vibrs., calc. method *(Russian)* 78−29871
stiff polymer chain dynamics, local and global mode interaction, dil. soln. viscosity, dielectric relax. 78−37776
styrene-butadiene-styrene triblock copolymer, US relax. 77−89502
styrene-methacrylic acid copolymer, intermol. interaction, conform., composition depend. *(Russian)* 79−23539
styrene-vinylpyrrolidone block copolymer soln., conform. props., light-, X-ray scatt. and viscometry obs. *(Russian)* 78−37779
Teflon, bond charge model for vib. props. *(German)* 78−75781
telechelic, chain extension, qualitative aspects 80−95752
2,4,6,8-tetraphenylnonane soln., macromol. dynamics, us relax. 80−19882
thermal rotations of mols. in soln. mol. wt. depend. 79−13847
thermodynamics and its possible relevance to physiology 80−53176
torsional oscills., HF, investig., polarised luminesc. method *(Russian)* 77−31039
tropomyosin, isotopic H exchange as function of state of ionisation of side groups 78−68979
trypsin inhibitor, mol. dynamics, computer simulation 78−9932
vinyl acetate, oligomers, dielectric relax., end-group effects 78−92019
vinyl polymer solutions, proton spin-lattice relax. and Overhauser enhancements 77−55721
^2H spin lattice relaxation, mols. with multiple internal rots., limiting behaviour 79−39356

macromolecular energy levels
biological macromolecules, intermediate states responsible for specific props. 79−96511
biomolecules, laser irradiated, selective photochemical mechanisms 79−66450
biopolymer, electronic-conformation interactions 80−3588
biopolymers, electronic struct. and possible chem. carcinogenesis mechanisms 79−22874

macromolecular energy levels continued
butadiene-acrylonitrile copolymer, electronic struct., reactivity, SCF CNDO calc. 77−50580
β-carotene, electronic struct., classical and double beam photoemission obs. 78−9285
chlorophylls a and b, photo-oxidation primary processes 79−79468
conjugated polymers, effect of long-range coulombic repulsion of electrons on ground state 77−68147
copolymer model with alternating spins, kinetics 80−9768
deoxyhaemoglobin, high mag. field Mossbauer spectra, electronic states 80−35845
deoxymyoglobin, high mag. field Mossbauer spectra, electronic states 80−35845
α,ω-diphenyl-trans-polyenes, 1st excited singlet valence states, CI and extended CNDO/S calcs. 78−74807
DNA, entropy nature of B-A transition 79−92130
DNA, molecular electrostatic pots. of complementary base pairs 78−92597
DNA, mutations, quantum theory, proton transfer by dynamic interactions 77−77868
DNA base pairs., Coulomb interaction energy calcs, electron correlation role 79−96509
electrostatic isopotential maps for large biomolecules, STO transferable bond calc. 80−3571
energy migration in one-dimensional structures with resonance interaction 80−1092
epoxy resins, correlation between valence energies and low temp. flexibility 80−25815
ESCA, polymer primary struct., extended HMO density of states and band struct., chemical shifts 78−52630
finite size polymer chain, collective excited state *(Russian)* 80−9769
fluoropolymers, linear, valence electronic struct., LCAO cryst. orbital calcs., ESCA 78−5384
heart cytosol, aspartate transaminase, electron density map interpretation 80−55990
infinite conjugated polymers, π-electron energy and energy gap, topological calcs. 80−91713
large molecule, electronic struct., photoemission and optical absorpt. spectrum, CNDO/S3 model 80−53172
nicotinamide co-enzymes, reduced, phosphorescence obs. at −196°C 79−79471
NMR estimation of equilib. consts., intermediate exchange processes effect 80−1094
oxyhaemoglobin, mag. props. and structure 78−48751
pheophytin a, photo-oxidation primary processes 79−79468
poly (4-chlorosytrene, styrene), linear copolymers ang. correls., dipole moments and dielec. consts. 77−61884
poly riboadenylic acid, time dependence of triplet-singlet excitation transfer 79−57586
poly-n-vinylcarbazole, higher-lying singlet states, CNDO/S study 79−89815
polyacetylene, soliton form. 79−76540
polyacetylene, undoped, thermally activated mobile defect, temp. EPR line broadening 80−43218
polyacrylonitrile, electronic struct., reactivity, SCF CNDO calcs. 77−50580
polybutadiene, electronic struct., reactivity, SCF CNDO calcs. 77−50580
polycaprolactam, stretched sheets, electron emission 78−88411
polydiacetylenes, excited singlet state electronic struct., band and excitonic models 78−91620
polydiacetylenes, optical props., and electronic struct., rel. to polyenes 77−23592
polyene, infinite, electronic states under local perturbation 77−57878
trans-polyenes, 1st excited singlet valence states, CI and extended CNDO/S calcs. 78−74807
polyenes, highly branched, large networks, abnormal bond orders 79−59610
polyenes, optical prop., and electronic struct., rel. to polydiacetylenes 77−23592
polyethylene, correlation between valence energies and low temp. flexibility 80−25815
polyethylene, pristine and radiation-damaged film, electron energy loss spectra 79−81312
polyethylene, stretched sheets, electron emission 78−88411
polyethylene, valence electronic struct., LCAO cryst. orbital calcs., ESCA 78−5384
polyisoprene, electronic struct., reactivity, SCF CNDO calcs. 77−50580
polymer chains, Coulombic contributions, LCAO-SCF-CO method, Fourier representations 80−32862
polymers, long-range Coulombic interaction, Fourier transform technique calcs. 79−31748
polymethine-cyanine molecular aggregate, band struct. 80−53174
polymethines, total π-electron energy bounds 77−88609
polynucleotide electron energy band studies 80−72132
polynucleotides, double-helical, conform anal. 79−96513
polyoxymethylene, electron density calc. in cylindrical coordinates, Fourier method 79−13852
polytrimethylene oxide, soln., chain dipole moment, dielec. const. meas. 77−81043
porphyrin singlet and triplet states, quenching of O_2 79−92141
protein, electron-transport type, H-bonding, ab initio MO 80−51039
protein, structure and bonding, quantum theory, ab initio calcs. 80−61509
protein model chain, aperiodic, electronic spectra, hopping cond. 80−5641
proteins, electron transfer mechanism 79−96510
PVC, extended syndiotactic, modified Urey-Bradley force field calcs. 78−25500
radiofrequency spectroscopy, structural energy characteristics, rotational isomerism, mol. motion *(Russian)* 79−56602
rhodopsin, coherent states of flexible macromol., mol. basis of vision 79−79472
TCDU, polydiacetylene cryst., elec. struct. change, stress induced 78−70990
tryptophanyls, singlet and triplet states, role in protein inactivation 79−57564

macromolecular spectra
see also spectra of organic molecules and substances
albumin, bovine serum, PMR spectra, line narrowing, convolution and pulse methods 78−78729
amino acid side chains, NMR relax. due to multiple internal rots. 78−94340
azo polyamide, solutions, spectra and viscosity 79−68340
bacteriorhodopsin, dynamics, of pH-induced spectral changes 79−57587
bacteriorhodopsin, reson. Raman evidence for secondary protein-Schiff base interactions, primary excitation mechanism 80−55981
bacteriorhodopsin, reson. Raman kinetic spectroscopy on μsec time scale 78−20320
bacteriorhodopsin, time-resolved resonance Raman spectroscopy 77−29103
bacteriorhodopsin photoconversion products, EPR and low temp. spectrophotometry 78−15769
basic pancreatic trypsin inhibitor, methyl group PMR, 360 MHz 78−27887
benzene, plasma polymerisation in glow discharge, thin film IR and free radical EPR obs. 80−2964
biological macromolecules, conformational dynamics subnanosecond T jump and Raman spectroscopy appl. 79−66445
biological macromolecules, picosec. and subpicosec. relax. and dephasing, reson. light scatt. obs. 79−45876
biological macromolecules, PMR, nuclear Overhauser enhancement difference spectroscopy 78−81091
biomolecules, dye laser spectroscopy 77−86444
biopolymer, local mode resonance enhancement in Raman spectra 77−77204
biopolymer Brownian diffusion, fluoresc. correl. spectroscopy 79−62193
biphenyl glutarate polymer, resonant Raman spectra and fluoresc. 77−24830
bis(methylthio)alkanes, model compounds of polythioethers, vibr. spectra 80−58430
butadiene elastomers, influence of intermol. interaction on durability *(Russian)* 78−76746
butadiene-nitrile elastomers, high temp., and press. chem. transformations *(Russian)* 79−52659
β-carotene, electronic struct., classical and double beam photoemission obs. 78−9285
β-carotene, solubilised in lecithin liposomes, linear dichroism, absorption statistics 78−1014
β-carotin, resonance Raman effect *(Hungarian)* 78−74666
cartenoprotein, lobster shell, photoacoustic spectroscopy obs. 79−62192
cellulose, conform. states and IR dichroism calcs. 80−55986
cellulose, UV and IR spectrum comparison with interstellar medium spectra 78−61913
chlorophyll a, fluoresc. and absorpt. spectra, resolution into components 79−57584
chlorophyll a, phosphoresc., triplet state, photochem. reacts. *(Czech)* 78−78842
chlorophyll-a, monochromatic excitation, luminesc. spectra, quasilinear struct. *(Russian)* 78−74809
chlorophylls and pheophytins, phosphorescence and fluorescence polarisation spectra 79−70522
chloroplast fragments, fine struct. of fluoresc. spectra, derivative spectroscopy method *(Russian)* 79−34502
chromophore aggregates, optical absorpt. and circular dichroism spectra, degenerate ground state model 79−70523
chymotrypsin, charge relay system, H-bond models, IR spectra 78−64935
α-chymotrypsin, e.m. mol. electronic reson.-Raman data 77−9166
circular dichroism, exciton dimer and helix-free particle absorption 79−94116
collodion, film, IR spectrum, vibr. assignments, chain config. 77−34789
conference, Dublin, Eire (July 1977) 79−55012
coupled spin systems, selective nucl. Overhauser effects calc., use in struct. chem. 80−23588
cytochrome b_5 rotational diffusion, triplet absorbance anisotropy decay obs. 79−83693
cytochrome c_3, haeme-haeme mag. interaction, Mossbauer obs. 80−108836
cytochrome c, dilute soln., reson. Raman spectra, pulsed laser excitation; optical multichannel detection 78−76999
cytochrome c, electron reactions in ethylene glycol/water glass at −196°C 79−62194
cytochrome c, ferric- and ferro-, reson. Raman excitation profile, Soret excited 79−92147
cytochrome c, low freq. modes and excitation profiles, reson. Raman spectra 80−94428
cytochrome c adsorbed on different carriers, conformation study 79−53029
cytochrome-c, complete resonance Raman polarisation spectroscopy, linear and circular, modulation techniques 77−61130
deoxyhaemoglobin high spin ferrous ion, low lying electronic states, far IR mag. reson. 80−48110
deoxymyoglobin high spin ferrous ion, low lying electronic states, far IR mag. reson. 80−48110
diene rubbers, highly filled, supermolecular struct. *(Russian)* 78−76627
dilute solution of macromols., electrically induced fluorescence polarised component change meas. 80−32863
dinucleoside monophosphates, struct. and conform. in aq. soln., Raman spectra 78−78847
DNA, dye labelled elec. dichroism and birefringence, comparison with mol. props. from polarised fluoresc. 80−84785
DNA, fluorescence depolarisation, twisting and bending, rot. Brownian motion 79−70509
DNA, Hg (II) and Ag (I) complexes in soln., theoret. interpret. of elec. dichroism obs. 80−85347
DNA, luminescence, excitation wavelength depend. in UV/VUV region 78−31768
DNA, soln., phase transitions, light absorption oscills. obs. 80−26197
DNA, soln., quasielastic light scattering, in AC elec. field 79−62186
DNA bases, polarised fluoresc. and estimated lifetimes, room temp. and in −125°C soln. 79−39352
DNA bases, selective electronic excitation using dye lasers 80−8012
DNA bases, theoretical study of electronic spectra 80−30665
DNA conformation, influence of intermol. interactions 80−16900
DNA hypochromic effect, oscillator strength, perturbation theory calc. 79−96515

macromolecular spectra continued
DNA-acridine complexes, laser-induced fluorescence decay obs. 79−66449
DNA-acridine orange complexes, energy transfer after dye laser excitation 79−2005
elastomer, segmented block, morphology, pulsed proton NMR study 80−33907
electro-optical characterisation of polarisation processes 77−24821
EPR and saturation transfer EPR spectra at high microwave field intensities 79−34488
ethenoadenosine, influence of pH and metal complexion on fluorescence parameter 79−34483
ethylcellosol, aq. soln., light scatt. rel. to conc. fluctuations *(Russian)* 78−3450
ferrocytochrome c, picosec. and subpicosec. relax. and dephasing, reson. light scatt. obs. 79−45876
fibres, natural, Brillouin scatt. shifts, comparison with synthetic polypeptide obs. 80−55991
fibrinogen, bovine, high energy-induced aggregation, time resolved spectra 80−61655
field desorption mass spectrometry, appl. to biochemistry, medicine, and environmental science 80−35592
fluorescence, apparatus for meas. electrically induced polarization changes 77−46662
fluorescence depolarisation, E-type delayed, rotational motion probe techniques 80−36207
fluorescence depolarisation, electrically-induced macromol. characteristics 77−27210
fluorescence spectroscopy in study of biochem. processes review 78−11784
fluoropolymers, linear, valence electronic struct., LCAO cryst. orbital calcs., ESCA 78−5384
glass fibre reinforced plastics, coupling agent/matrix interface investigation by Fourier transform IR spectroscopy 80−20884
gramicidin D-Na^+, NMR study 79−43805
haeme disorder characterisation in haeme proteins, PMR method 79−92152
haeme protein, resonance Raman effect *(Hungarian)* 78−74666
haeme protein solns., resonance Raman spectra at low temp. 77−23588
haemoglobin, dynamic characts. of conformational nonequilib. states, radiolysis investig. 78−58877
haemoglobin, low freq. modes and excitation profiles, reson. Raman spectra 80−94428
haemoglobin, mol. interactions, Fourier transform IR absorpt. spectra 78−96007
haemoglobin, nanosec. probe of dynamics using time resolved reson. Raman scatt. 80−94162
haemoglobin Fe-N distance determ. by EXAFS 78−68989
haemoglobin haem structure after photo-deligation, Raman spectra 80−61510
haemoglobin-haptoglobin deoxygenated complexes, Mossbauer spectroscopy 78−24020
helical wormlike chain, dipole moment, elec. birefringence, elec. dichroism, statistical mech. calcs. 80−14262
helical wormlike chain statistical mechanics, scatt. function 77−54637
hydrate, struct. conversions of sugar phosphate chain and nitrogenous bases, IR spectra 80−81530
2-hydroxy-3-crotonyloxypropyl methacrylate, polymerisation photocrosslinking *(Japanese)* 78−31376
immunoglobulin, human, high energy-induced aggregation, time resolved spectra 80−61655
interacting spherical macromols., light scatt., conc. fluctuations, transport eqn. 79−1775
intermolecular interactions, effects of intervening medium and polar mode energy feeding 79−13857
IR linear dichroism of oriented nucleic acid films 80−8013
β-lactoglobulin, absorpt. spectra for complexes formed with vitamin-A 80−30664
lanthanide complex, struct. and equilib. by time resolved Eu(III) spectrosc. 80−78736
lanthanide ion bound to macromol., struct. and equilib. by time resolved Eu(III) spectrosc. 80−78736
light scattering, quasielastic, from rigid mols., theory 79−64127
light scattering by soln. in AC electric field 79−47468
linear polyethylene melt, PMR spectrum 77−51979
lipid extract from lung surfactant, IR spectra, H-bond lengths 79−24941
lipid lamellar liquid crystalline systems, orientation studies of probe molecules by linear dichroism 77−90718
lipid peroxide oxidation fluorescing products, effect of UV on formation 79−57585
lysozyme protein solution, spectra and dye laser threshold power 79−68391
magnesium alginate, light scatt., wt.-average mol. wt., charge density 77−61882
methacrylate polymer, carbazolyl substituted, excimer and charge transfer complex trapping of excitons 80−34367
N-methacryloil-ω-aminolauric acid cholesterol ester, liq. cryst. polymers, copolymers, structuring *(Russian)* 79−55665
methaemoglobin, struct. change on addition of inositol hexaphosphate 80−72130
molecular orientation, extensional effects, IR obs. 77−23591
muscle proteins, rot. motions, saturation transfer EPR obs. 80−94151
myoglobin-Fe^{3+} compounds, Mossbauer and suscept. expts. 78−24019
myoglobins, kinetics studied by picosecond spectroscopy 79−43804
myosin, conformational changes induced by inorganic salts, Raman spectra obs. 78−96002
myosin-auramine O system, conform. changes and excitation energy transfer 79−96512
NADH coenzyme, two photon absorpt. cross section meas., reaction rate modification 80−51043
Nafion cation exchange membranes, IR spectrum assignment 79−89818
naphthylalanine polypeptides, fluoresc. quenching and energy transfer 79−34332
nicotinamide co-enzymes, reduced, phosphorescence obs. at −196°C 79−79471
NMR, internal motion determ. by relax. times 79−41257
NMR estimation of equilib. consts., intermediate exchange processes effect 80−1094
nonrigid polymer chains, theory of dynamic depolarised light scattering 79−3601

macromolecular spectra continued
nuclear Overhauser effect, truncated driven, in presence of spin diffusion 80−1095
nucleic acid components, UV resonant Raman spectra 78−48756
nucleic acid-dye complexes, energy transfer obs. using laser-induced fluoresc. 80−12054
Nylon-12 film, casting conditions effect on polymorphism 80−84903
oxyhaemoglobin, dilute soln., reson. Raman spectra, pulsed laser excitation; optical multichannel detection 78−76999
oxymetalloproteins, electronic spectroscopic data review 80−52977
oxymyoglobin, polarised electronic absorption spectrum Fe-O_2 bonding and oxyhaeme struct. 78−96006
pancreatic trypsin inhibitor, bovine, macromol. dynamics, high resolution NMR investig. 80−91708
parvalbumins, Ca-binding, lanthamide-substituted, of muscle, ^{13}C NMR obs. 79−96516
PCP, oriented swollen soln., IR dichroism, short-range orient. order *(Russian)* 79−51941
peroxidase, immobilised, spectral characts. obs. 79−57579
phosphates, cellular, heteronucl. two-dimens. NMR as conform. probe 80−3590
phospholipids, ^{31}p NMR, slow-motional lineshapes for very anisotropic rot. diffusion 80−5644
photoelectron spectroscopy, impact on biology 78−65156
photon-correlation spectrsocopy in near UV, large flexible macromol. internal modes obs. 79−75621
plasmid DNA and DNA-histone chromatin-like complexes, conform. and soln. props. by laser light scatt. 80−55987
PMMA, atactic, FT IR spectrum, ^{18}O substitution effects 80−23581
PMMA, C-H stretching and bending vibs., IR spectra, selective deuteration 80−23582
PMMA, stereoregular, assoc. in dilute soln., PMR obs. 78−76321
poly(m-methylene terephthalate) polymers, IR and Raman spectra 77−52088
poly(S)-2-methylbutyl vinyl ether, conformation, IR spectra 78−1116
poly(S)-5-methyl-1-heptene, conformation, IR spectra 78−1116
poly-1,6-di-N-carbazolyl-2,4-hexadiyne, synthesis, thermal expansion, photocond., optical transition 78−76858
poly-1,6-di-p-toluenesulphonyloxy-2,4-hexadiyne, thermal polymerisation, Raman spectra 80−35531
poly-2-vinylnaphthalene, soln., lowest triplet props., flash photolysis and radiolysis obs. 80−32861
poly-4-vinylpyridene, protonated and deuterated vibr. spectra *(Russian)* 77−19120
poly-β-benzyl-L-aspartate films, circular dichroism, IR spectra, α, β, ω conforms. 77−48197
poly-β-benzyl-L-aspartate films, conformational stability, effect of organic solvents, IR spectra 78−70988
poly-β-ethynylnaphthalene, insoluble, reson. Raman spectrum, struct. models 78−70981
poly-γ-benzyl-L-glutamate helices, optical activity 80−48113
poly-n-butylisocyanate, conformation, IR spectra *(Russian)* 77−19123
poly-N-vinyl carbazole, pulsed laser excitation, time resolved fluoresc., 80−89041
poly-n-vinylcarbazole, higher-lying singlet states, CNDO/S study 79−89815
poly-N-vinylcarbazole, soln., picosecond time-resolved fluoresc. by pulse radiolysis 80−28122
poly-p-chlorophenyl glycidyl ether, struct., tacticity and addition isomerism, ^{13}C NMR 80−58427
poly-thio-1-N,N-diethylaminomethylethylene, optically active samples, ^{13}C NMR spectra 80−28127
polyacetylene, dynamic nuclear polarisation of protons *(French)* 80−43217
polyacrylamide gel and single chain in soln., laser light scatt. obs. near phase transitions 80−93808
polyacrylic acid in aqueous systems, spin labelling using Woodward's reagent 79−96308
polyalkyleneoxide polymer, proton nuclear mag. relaxation *(Rumanian)* 78−91977
polyamidoimide film, thermomech. props. rel. to mol. struct. *(Russian)* 79−57029
polybutadiene, adsorption behaviour, surface tension exam. *(Japanese)* 78−31690
polybutadiene, C black filled, struct., Fourier transform IR obs. 77−50571
polybutadiene, mol. motion in solid and soln., ^{13}C NMR relaxation meas. *(Japanese)* 80−2666
polycapromide, fracture, interatomic bonds deform. 79−57107
polycarbonate, amorphous morphology, from NMR obs. of swelling penetrant mol. motion 79−27929
polycarbonate, colour appearance during oxidation *(Russian)* 79−24643
polycarbonate, turning yellow during oxidation, kinetic regularities *(Russian)* 79−24644
trans-1,4-polychloroprenes, prep. and struct., Raman spectra 77−66496
polydiacetylene, monocrystal, vibr. freq. stress depend., Raman obs. 77−50574
polydiacetylene, urethane substituted, conjugated polymer soln. spectral shift on planar-nonplanar conformational transition 79−64129
polydimethysiloxane, conc. soln. in benzene, polarised Raman scattering 78−9286
polyethylene, crystalline struct. transitions 77−51496
polyethylene, elongation, conform. set change IR obs. *(Russian)* 78−37778
polyethylene, FIR absorpt. freqs. using proved semiempirical pot. function 77−52090
polyethylene, H bonding effects on skeletal optical and longitudinal acoustical modes 80−34914
polyethylene, homopolymers, copolymers and model systems, ^{13}C NMR chem. shifts and relax. times 79−72449
polyethylene, irradiated, far IR spectrum rel. to crystallinity 78−27216
polyethylene, linear, bulk-crystallised, morphology study 79−32918
polyethylene, pristine and radiation-damaged film, electron energy loss spectra 79−81312
polyethylene, second order Raman scatt. 78−72504
polyethylene, single crystal texture, polarised Raman spectra 77−61888
polyethylene, single crysts. chain end location, IR spectra 78−71687
polyethylene, stretched, linear dichroism of aromatic molecules 77−88480
polyethylene, valence electronic struct., LCAO cryst. orbital calcs., ESCA 78−5384

macromolecular spectra continued
polyethylene, vinyl group reactions during γ-irrad., crystallinity effect, absorbance obs. 80−81346
polyethylene single cryst., FT IR spectra, CH_2 rocking mode 78−2843
polyethylene single cryst., FT IR spectra, CH_2 wagging mode 78−2842
polyethylene terephthalate, elongation, conform. set change IR obs. *(Russian)* 78−37778
polyethylene terephthalate, fracture, interatomic bonds deform. 79−57107
polyethylene terephthalate, IR spectra, trans-conformational band *(Russian)* 79−27122
polyethylene terephthalate, semicryst., Fourier transform IR spectra 77−23589
polyglycine, IR spectra calc. for helix and β configs. 80−45853
polyisocyanides, solns., struct. and acidification 80−19915
polymer, derective, freq. branch calc. of n-paraffins, fatty acids, and glymes 79−31747
polymer, photoradiative processes in free radical form. *(Russian)* 79−57269
polymer, uniaxial, fluoresc. polarisation, orientation and mol. dynamics effects 78−76516
polymer band structure, symposium contrib., Florida, USA (March 1979) 80−51946
polymer chain optical absorption spectra and symmetry 79−55011
polymer chains, free rotating, depolarised light scatt. spectrum calcs. 80−78731
polymer chains with rigid bonds, local relax. times, mol. dynamics study *(Russian)* 80−59373
polymer coatings, packing density investig. by mol. probe method *(Russian)* 77−44398
polymer film, stretched, interpretation of polarised absorption and emission spectra of molecules 78−1012
polymer film, stretched, orientation and transition moment directions of small planar molecules 78−1015
polymer film, supermolecular structure and mech. stress distrib. among chem. bonds 78−75562
polymer mixtures, IR spectra, ratio method anal., computer simulation 77−71387
polymer molecule, symmetry adapted bases and selection rules 79−55010
polymer network systems, intramol. mobility, polarised luminesc. obs. *(Russian)* 77−42455
polymer orientation measurement, in solid, by spectroscopic techniques, mech. anisotropy 78−75558
polymer solns. and gels dynamic behaviour by light scatt. 80−55727
polymer solution, conjugated, polymer two-photon dispersion, freq. depend., symmetry assignment and oscillator strengths 79−86094
polymer solution, light scatt. aniotropy by statistical mechs. of helical worklike chains 79−99891
polymer solution, light scatt. for macromol. characts. in Rayleigh-Gans-Debye region 77−42452
polymer system, Fourier transform IR spectroscopy appl. 78−58870
polymers, synthetic, chiral, with aromatic side chains, conform. from circ. dichroism 79−55014
polymers, synthetic, dil. solns., NMR relax., review 79−89693
polymers, vibr. spectra, theory *(Russian)* 78−13502
polymers containing main chain heteroatoms, struct., ^{13}C NMR investigs., review 79−55013
polymethacrylic acid, stereoregular, synthesis, ^{13}C NMR obs. 80−58422
polymethacrylic acid network systems, intramol. mobility, polarised luminesc. obs. *(Russian)* 77−42455
polymethylene chain, vibr. spectra, CH stretching region, struct. and assignments 78−70991
polynucleotide soln., order-disorder transition, Raman spectra 78−41360
polypeptides, poly-L-lysine based, comb-like, struct., physicochem. props. *(Russian)* 79−55644
polyperdeuteroethylene, IR and Raman spectra, 77K and room temp., vibr. anal. 78−72517
polyphenylacetylene, cryst., resonant Raman scatt., opt. absorpt. 77−4630
polypropylene, fracture, interatomic bonds deform. 79−57107
polypropylene, isotactic, conformational origin of peak struct. in XPS spectrum 79−89819
polypropylene glycol, depolarised Rayleigh relax. times, backbone motion 77−566
polypyromelliteimide, fracture, interatomic bonds deform. 79−57107
polyriboadenylic acid, soln., Raman spectra, struct. and conformation 77−71899
polyribonucleotides, dye tagged, aqueous solns., elec. induced fluoresc. changes 80−85346
polysaccharides, evidence in IR astronomical spectra 77−78857
polysaccharides, vibr., conformation, IR spectra, computer anal. *(Russian)* 78−13637
polystyrene, atactic, stereoregularity study using Fourier transform IR spectroscopy 79−59612
polystyrene, end group modified, chain dynamics studied by fluorescence depolarization 80−19724
polystyrene, epimerised isotactic, methylene C mag. resonance spectra 80−63878
polystyrene, in cyclohexane soln., mol. wt. distrib., photon correl. obs. 79−10239
polystyrene, in theta solvent, intramol. motion, photon correl. spectrosc. 78−90328
polystyrene, isotactic, normal vibrational anal. 78−43869
polystyrene, isotactic gel film, Fourier transform IR spectrum 80−104465
polystyrene, molecular motion obs. during thermal polymerisation of styrene, PMR 80−3342
polystyrene, solid, low freq. Raman scatt., vibr. density of states, 29-300K 78−72516
polystyrene, uniaxially stretched atactic thin film, mol. orientation, polarized Raman study 80−103951
polystyrene film, Fourier-transformed IR photoacoustic spectra 80−34993
polystyrene in cyclohexane, photon correlation, diffusion coeff., first mode intramolecular relaxation time determ. 79−41255
polystyrene latex spheres, characterisation using light scattering spectrom. 80−95753
polysytrene, benzene soln., characterisation using light scattering spectrom. 80−95753
polytetrahydrofuran, H bonding effects on skeletal optical and longitudinal acoustical modes 80−34914

macromolecular spectra continued
polythylene, and perdeuteropolyethylene, crysts., IR and Raman intensities, factor group splittings 79−65851
polyvinylidene chloride, vibr. spectra, amorphous and cryst. state conforms. 79−27930
porphins, reson. Raman spectra, selection rules, normal coord. treatment 80−53175
porphyrins, reduction reactions intermediate products, PMR spectra 79−53019
prealbumin, human, struct., X-ray diffr., amino acid sequence, circular dichroism meas., comparison 77−42450
protein, globular, in aqueous solutions, conformational mobility investigation 79−53033
protein, secondary structure determ. by laser Raman spectroscopy 77−23587
protein chromophores, fluoresc. props., use in macromol. equilib. struct. mobility investigs. 79−64130
protein model chain, aperiodic, electronic spectra, hopping cond. 80−5641
protein-solvent systems, dynamics investigation by nucl. gamma-resonance 79−62166
proteins, conform. changes in aqueous soln. and in mixed solvents, IR absorpt. spectra 78−15762
proteins, methine aromatic C sites, natural abundance ^{13}C NMR at high mag. field strength 77−86443
proteins, triplet state energy transfer 78−20143
proteins, UV fluorescence detect. of conformational rearrangements in plants 79−53031
PTFE, peroxy radical labelled, temp. dependent rots., EPR obs. 80−28125
PTFE, vib. assignment, far IR spectrum 77−48170
PTFE film electret, optical spectra, band theory interpretation *(Russian)* 78−88376
purple membrane, polarized IR spectroscopic struct. study 79−43809
PVC, structural studies by Raman spectroscopy 79−7044
PVC, thermally induced conformational changes, Fourier transform. IR spectroscopy 78−9287
PVC+$Br_2(I_2)$, reaction in surface-modified film subject to thermal-radiative and photochem. action *(Russian)* 77−21385
PVC branching, origin, extent 79−7048
PVC chain branching, CH_2Cl group production mechanism, IR data evaluation 79−7047
PVC-THF-H_2O, precipitation fractionation, influence of stereoregularity 79−7046
radiofrequency spectroscopy, structural energy characteristics, rotational isomerism, mol. motion *(Russian)* 79−56602
Raman spectra of assembly of partially oriented scatterers 77−16295
Raman spectroscopy, recent advances, reivew 78−41359
relaxation time spectra rel. to luminesc. depolarisation function *(Russian)* 77−31040
retinal chromophore, reson. Raman spectra obs. of struct. 80−94168
rhodopsin, α-helix orientation, spectroscopic study 80−89711
rhodopsin, isorhodopsin and bacteriorhodopsin, and photoproducts, temp. and wavelength effects on photochem. 78−11612
rhodopsin, picosecond spectroscopy obs. of primary events 80−56312
rhodopsin, primary photophys. and photochem. processes in visual excitation 78−15773
rhodopsin, resonance Raman effect *(Hungarian)* 78−74666
rhodopsin conformation, spectral studies 78−15765
ribonuclease, PMR spectra, line narrowing, convolution and pulse methods 78−78729
ribosomal protein S4 from Escherichia coli, circular dichroism obs. of conformation 78−96003
rigid macromolecule, in soln., depolarised Rayleigh spectroscopy 79−94119
t-RNA, rot. relax. time, 10^{-9}s range Fabry-Perot and photoelectron time of arrival method 80−21437
serum albumin, bovine, high energy-induced aggregation, time resolved spectra 80−61655
sodium alginate, light scatt., wt.-average mol. wt., charge density 77−61882
solution, light scattering measurements, computer processing *(Rumanian)* 79−82990
solution, Rayleigh scatt., elec. reorient. rel. to spectral line rot. broadening 79−1774
solution, spectroscopic meas. of energy barrier to electron transfer 77−38766
solutions, dilute, light scatt., Oseen's model 78−27240
solutions, light scatt., ionic charge effects calcs. 77−79714
styrene, plasma polymerisation in glow discharge, thin film IR and free radical EPR obs. 80−2964
p-substituted polystyrene, shake-up phenomena, ESCA studies 77−54638
thermal rotations of mols. in soln. mol. wt. depend. 79−13847
tripeptides, synethetic, hormone models, field desorption mass spectrometry using needleless emitters 79−34398
UPS of biological mols., ionisation energy, assignments and electron donation 78−77005
vinyl polymers quenched with electron donor (acceptor) in soln., ionic photodissoc. 79−11800
vinylidene fluoride-trifluorochloroethylene copolymers, ^{19}F NMR *(Russian)* 80−7181
visual pigment unprotonated chromophore-protein bond, ^{13}C NMR spectra 78−11607
vitamin B_{12}-^{181}Hf complex, γ-ray PAC expt., crystal and liq. 79−39341
$(CD)_x$, polymer, heavily doped, IR spectra, vibronic intensity enhancement 80−28124
$(CH)_x$, polymer, heavily doped, IR spectra, vibronic intensity enhancement 80−28124
Cu complex, polyacrylic acid-polyethyleneimine-Cu(II), struct. *(Russian)* 79−55018
H_2O, adsorbed, surface-induced NMR line splittings and augmented relax. rates 78−64288
^2H spin lattice relaxation, mols. with multiple internal rots., limiting behaviour 79−39356
Pu(IV) oxide polymer, potential pollutant from fuel reprocessing, IR spectrum 78−76456
$(SN)_n$* radicals polymerisation to $(SN)_x$ in thin films, optical spectra 80−16656

macromolecules
see also DNA; macromolecular configurations; macromolecular dynamics; macromolecular energy levels; macromolecular spectra; polymers; proteins
adsorption, onto inorganic substrate 79−69342
adsorption on charged surface, weak electrostatic attraction 77−19118
aggregates, estimation of locations of subunits from neutron interference data 79−86716
alamethicin, induced conductance in lipid bilayer membranes, pancuronium inactivation 79−39189
bacteria, photosynthesis, primary electron acceptor, EPR, ENDOR investigs. 78−77004
bead-spring-type model in nonuniform vel. gradient, dil. soln. kinetic theory results 80−64628
bioelectrets, occurrence of electret state and appl. in mol. biophysics and bioengineering 80−8007
biological, computer simulation of solvent struct. 78−40113
biological, electron microscopy obs., image analysis techniques *(Czech)* 78−31983
biological, selection models, with time varying constraints 80−67029
biological, study by scanning microcalorimeters 80−61747
biological macromolecules, conformation studied by calorimetry, review 80−97870
biological systems, hydrated, PMR spin-lattice relax. of water, cross-relax. effects 79−34496
biopolymer chains, intramol. reacts., enzyme catalysis appl., review 80−40953
biopolymer soln. heat capacity, conformational props. temp. depend. 80−8009
biopolymers, primary structure determ. algorithms 79−48209
birefringence kinetics in nonpolar mol. solns. 80−100648
burn-induced leakage of macromolecules in living tissue 79−29514
carbonic anhydrase, active site substrate binding, environmental effects, CNDO and SCF LCAO calcs. 80−8002
charged macromolecules in external elec. field, spherical case 80−75145
chemistry, macromolecules, and the needs of man 78−95907
chiral biomolecules, temp.-jump relaxation studies, transient CD meas. 78−5372
chiral substances, electro-optical responses, Jones matrix, meas. sytem for rot. anisotropy 80−84723
chloroplast-ribosomal RNA, in situ hybridisation with isolated nuclei in Euglena gracilis 79−66457
collagen, hydrated, PMR spin-lattice relax. of water, cross-relax. effects 79−34496
conference, Mainz, Germany (Sept. 1979) 80−58429
CpApUpG, self complementary oligoriboncleotide, double helix form., PMR obs. 79−22873
cytosol-ribosomal RNA, in situ hybridisation with isolated nuclei in Euglena gracilis 79−66457
diffusion, hinged long rods, exception to Einstein relation 79−2736
dimensions, mean square end-to-end distance, Monte Carlo calcs. 79−68337
dissociation rates of weak bonds, Brownian motion theory 77−36731
DNA-acridine dye complex, fluorescence studies 80−37921
double-stranded polynucleotides, exact relations for binding calculations 79−92123
drug-nucleic acid interactions, conformational flexibility at intercalation site 78−96005
dumbbell-shaped, alternating electric field light scatt. 80−1130
dumbbells, nearly-Hookean, dilute soln., rheological equation of state 80−100321
educational courses, integration with phys. chem. 78−77642
electro-optics and dielectrics, conf., Uxbridge, England (Apr. 1978) 80−82577
electron microscope contrast enhancement of negatively stained macromols. and biomembranes by single sideband phase contrast interference 77−45920
electron microscopy, high-resolution metal replication 77−25621
eukaryotic initiator tRNA, cryst. struct. from electron density map 79−43813
eukaryotic ribosomes, 2 step binding to brome mosaic virus RNA3 80−3580
ferritin, iron core particle size distrib., Mossbauer determ. 78−92696
field flow fractionation methods review, separation, characterisation studies appl. 78−90327
fluid, press. tensor symmetry 77−7496
fluid density measurement techniques, biological macromolecules appl. 78−92751
functional groups, reaction kinetics and statistics, review *(Russian)* 79−87825
graphics model building and refinement system 78−75505
haemoglobin, bovine type A, γ-induced changes obs. 79−43811
hard sphere macromolecule dil. soln. viscosity, Thorne-Enskog theory 78−91467
heart cytosol, aspartate transaminase, electron density map interpretation 80−55990
heat capacity function, of macromolecular systems, statistical thermodynamic analysis 80−61514
heat capacity of linear macromolecules, dynamic differential calorimeters comparison 78−89482
hydration kinetics, microwave obs. 79−34255
hydrocarbon chain ordering in model membrane, D quadrupole splitting 78−64947
injection into liq. cryst., interactions *(Russian)* 78−78848
interactions when introduced into liq. cryst. 80−30639
Kerr effect of charged dipolar macromolecules without condensed counterions in conducting solution 80−53171
ligand binding to macromolecules, allosteric and sequential models of cooperativity 80−12870
ligand bound to macromolecule, cross relax. effect on NMR spin-lattice relax. time 78−78723
linear, heat capacities, scanning calorimetry meas. 80−61134
linear, heat capacity, dynamic differential calorimeters comparison 78−89482
liquid, translational friction coeffs. of rigid, symm. top mols. 80−6003
macroionic solution, plus counter ions, Kirkwood theory, mean field phase transition 78−38812
macromolecules, cluster expansion 80−106408
magnetic field effects, expt. on PMMA with relevance to biological effects 77−25364
materials processing in Spacelab 78−35295
macromolecules continued
molecular structure, conformation and properties 80−63874
molecular weight measurement, light transmission meas. 78−17828
muscle, hydrated, PMR spin-lattice relax. of water, cross-relax. effects 79−34496
myosin, interaction with adenosine 5′-diphosphate, intermolecular spin diffusion study 80−18951
myosin, interactions with HDO, intermolecular spin diffusion study 80−18951
net repulsive van der Waals forces between different particles, macromolecular, or biological cells in liqs., appls. 80−34274
nonlinear laser photomodification, radiation damage 80−61120
nuclei acid phosphate group, analytical atom-pair pot., SCF-LCAO calc. 79−70516
nucleic acid bases, anal. in photographic gelatins by liquid chromatography 79−20501
nucleic acid bases, protonated, anion binding, electrostatic mol. pots. 79−1999
nucleic acid component pulse sonolysis obs. 79−53186
nucleic acid molecules, preprocessing of electron micrographs for automatic computer anal. 79−70711
nucleic acid-water interactions, review 78−44448
nucleic acids, STEM struct. anal. studies 79−16147
nucleic acids, study and theoretical physics *(Chinese)* 79−81316
nucleic acids studies, at. coords. of helices, by computer program 79−86095
nucleic-protein interactions in tobacco mosaic virus, spin label and fluoresc. obs. 80−40949
optical changes induced by macromolecules in liq. cryst. 79−64135
particle size distribution, reduced electric dipole moments, polarisabilities using electric birefringence 78−95958
permeable polymer mol. in soln., intrinsic viscosity and friction coeff. 78−30353
phase transitions, temp. and press. depend. theory, Ising model appls. 78−43105
phase transitions in semiflexible long-chain molecular crystals 78−91439
phenolic resins, average molecular weight and viscosity of acetone solns. *(Japanese)* 79−65234
physical chemistry teaching, macromol. principles 78−77643
poly-γ-benzyl-glutamate, α-helix second-order hyperpolarisability meas. 77−14623
polyethylene, diffusion of long molecules 77−27213
polymer, expansion of self-avoiding chains, studied by loop elimination 79−86100
polynucleotides, double helix, high resolution NMR, review 77−86450
polyolefins, ultra-high modulus, production by tensile drawing and hydrostatic extrusion 80−81022
polystyrene solution, binary and ternary cluster integrals, small angle neutron scattering 79−50975
porphyrins, dark transition of reduction products by disproportionation 79−53020
prebiological molecular evolution, as physico-chemical processes 77−60331
proteins, ^{13}C NMR, review 77−86449
pure and applied chemistry, conf., Tokyo, Japan (Sept. 1977) 78−95906
quantum chemical characteristics, extended Huckel calcs. 79−45874
quantum chemistry, biology, and pharmacology, conference, Kiev, USSR (Sept. 1978) 79−96499
quartz fibres, possible role as templates for biopolymers 79−39345
RNA, codon-anticodon interaction at ribosomal peptidyl-site 79−83697
RNA, low molecular weight, synthesis sensitivity to UV irradiation 79−57591
tRNA, low-resolution phase extension using matrix direct methods 77−66875
RNA in nondividing human diploid fibroblasts, effect of UV on synthesis 79−92291
RNA synthesis in root meristem cells, 2 MHz US effects, Pisum sativum 77−9218
rod-like molecules in extensional flow field, phase equilibria 78−26158
rodlike, gels, nonlinear elasticity in condensed state 80−104199
sedimentation, expt. determ., errors due to diffusion *(Russian)* 78−76934
sedimentation, rapid, under gravity, basic theory and experimental demonstrations 80−66885
self-reproducing macromolecules, selection, controlled energy fluxes constraint 80−67027
semiflexible macromolecule soln. liquid crystalline ordering 78−94963
separation method, flow field-flow fractionation 77−960
solution, birefringence kinetics 79−99847
solution, gel conc. and diffusivity at gelling determ. by ultrafiltration 80−21325
solutions, mol. orientation, time-depend. torque, rot. diffusion eqn. 78−68471
solutions, Rayleigh scatt., elec. induced variations, spectral width and intensity meas., review 78−48187
Soret-type motion of macromolecules in soln., light scatt. obs. 77−28032
spheroidal macromolecules solutions, quasielastic light scatt. 79−24325
star-shaped molecules with branched nuclei, statistics 77−89383
STEM use for two-dimensional molecular assemblies construction 78−24201
sublicons, special aspects of struct. 79−53034
thermal factor refinement procedure, restrained-parameter 80−79628
transferrin, ^{111}In labeled, perturbed angular correls. study 79−39342
US degradation in soln., simulation program 79−14148
valyl-tRNA synthetase from chick embryo brain, effect of ^{60}Co γ-radiation 79−34490
Van der Waals interaction between loose structs. 78−95996
vitamin B_{12}-^{181}Hf complex, γ-ray PAC expt., crystal and liq. 79−39341
X-ray diffraction data, numerical deconvolution procedure for partially oriented specimens 78−75497
X-ray small-angle scattering, information content and error anal., Shannon sampling 80−59340
$Li_{x+2}P_xO_{3x+1}$, polyphosphate, melting and crystallisation 80−70376

Madelung constant *see lattice energy*

magamps *see magnetic amplifiers*

Magellanic Clouds *see galaxies*

Maggi-Righi-Leduc effect *see thermomagnetic effects*

magnesium
see also nuclei with .....
$2p_{3/2}$ vacancy alignment in ion-atom collisions, electron capture role 80−83465
abundance gradient for gaseous Mg in NGC 7027 planetary nebula 80−41875
adsorption of O_2, at 100 and 300K, XPS, UPS and X-ray AES meas. 78−18901
adsorption of O_2 on polycrystalline Mg at 100 and 300K, XPS, UPS, XAES 78−18906
adsorption of S(O)(N)(C), internal and external sources of electrons 77−44097
AES, backscattering factor, Monte Carlo method calc. 80−7449
AES, KLL′ atom, solid and MgO, electronic relax., Friedel model 77−65444
AES, KLL spectra, and plasmon struct. 79−15592
AES, obtaining density of states information from self-deconvolution of Auger band-type spectra 78−92150
Allende meteorite, Mg isotope anomalies 77−78725
Allende meteorite, Mg isotopic anomalies rel. to ^{26}Al stellar nucleosynthesis 79−5809
anelastic internal stress field in easy glide region of single crystal 78−48442
anisotropic thermal expansion 79−23750
anomalous intensity ratios in H like L_α doublet in optically thick laser prod. plasmas 80−103186
atmosphere aerosols over tropica N.Atlantic Ocean, water-soluble K, Ca and Mg contents 80−72598
atom, 2p-electron excitation and ionisation by electron impact, autoionising states, electron spectra 77−14590
atom, $3s3d^3D$ and $3s4d^3D$ states, fine-struct. meas. by level crossing spectra 79−36572
atom, 4snl autoionising states ejected electron spectra, low energy impact two electron excitation 80−83494
atom, ^2P shape reson., electron scatt. calc. 79−41240
atom, and isoelectronic sequence, relativistic effects on transition probabilities 77−54532
atom, approximate relativistic Hartree-Fock eqns., soln. using Slater-type functions 80−58168
atom, Auger effect transition energies calc. 79−18168
atom, Auger spectra, CI calcs., spin-orbit interactions 77−14558
atom, beam-foil populations, charge state distribs., independent electron model 77−19035
atom, closed shell, Jastrow wave functions, var. calcs. 80−83249
atom, correlation energies, second-order, by variational-perturbation study 80−908
atom, damping const. in acetylene-air flame, Lorentz collisions, mag. field effects 80−66805
atom, direct meas. of excited state lifetimes 77−65435
atom, Doppler effects in X-ray spectra excited by accelerated ions 78−86808
atom, electron impact excitation and elastic scatt. cross sections 78−70940
atom, electron impact two-electron excitation, ejected electrons from autoionis. levels 77−88571
atom, electron scatt., effective pot. calcs. 80−53131
atom, electron scatt. cross sections, close coupling calc. with CI 80−43180
atom, forbidden Raman scatt. theory, including two-photon operators 79−54814
atom, free, electron-excited, K-Auger spectrum, including K-LM and K-MM transitions 80−5519
atom, Hanle effect and oscill. strength of $3s4p^1P_1{}^0$ level 79−72282
atom, inner-shell ionisation by H^+, He^+ impact, target atom ionic alignment, Born approx. 78−78789
atom, intercombination line oscill. strength, including core-polaris. and relativistic effects 78−25475
atom, isoelectronic sequence, excitation energies and line strengths, MC Hartree-Fock calcs. 77−83658
atom, $K\alpha^h$ hypersatellite spectra and K-shell double photoionisation cross-section 78−21874
atom, $K\alpha^h$ hypersatellite spectrum, K-shell electron double ionisation cross section, binding energy 79−36577
atom, K Auger transition rates, orbital relax. and interchannel interaction effects 78−50521
atom, K-shell ionisation by ultrarelativistic electrons, density effect 80−99576
atom, L-shell ionisation and excitation, electron spectra 77−10765
atom, low energy electron scatt., shape resonances, electron affinity 77−14581
atom, matrix isolated, ^1S-^1P transition, mag. circ. dichroism obs. 79−68248
atom, metastable, prod. in N_2O-CO flame, u.v. spectra 77−9081
atom, optical beam foil spectra, relative level populations 80−23540
atom, oscillator strengths and excitation energy, valence shell states 78−17611
atom, photoabsorpt. and photoionisation, RPA with exchange calcs. 77−54543
atom, pionic X-ray transitions, strong interaction line widths and shifts 77−23586
atom, polarisability and London coeff., ab initio variation perturbation calc. 79−13635
atom, radiative lifetimes on excitation by electron impact *(Russian)* 77−50408
atom, reson. line, Hanle effect, density depend. 79−6917
atom, SCF electron-gas local-spin-density model including correlation 80−9488
atom, single and double ionisation by electron impact, absolute cross section meas. 78−25714
atom, vertical ionis. pot. calc. from one-body Green's function 77−42440
atom, X-ray fluorescence, Kα hypersatellites 77−18830
atom, XPS, free atom core binding energy 78−74699
atom+Ar(Xe), plasma, near reson. charge exchange, spectra *(German)* 77−31425
atom+heavy ion, X-ray spectra, one-photon two-electron rearrangements 77−6712
atom+K(Ca), energy transfer and excimer form. in flowing afterglow 77−60049

magnesium continued
atom X-ray spectra, mass absorpt. coeffs. in ultrasoft region, spectral depend. 77−10622
atomic beam excited passing discharge region, new light source of forbidden lines 78−90112
atomic electron collision cross sections 77−42410
atomic fluorescence, intensity profile in acetylene-air flame 77−52680
atomic spectral line broadening, by inert gas collisions 77−79580
atomic vibr. and fermion behaviour of HCP metals 80−6474
atoms, cooling to broad band reson. light press. 80−48835
atoms, vaporised, evidence for gas-surface exchange 78−91532
Auger electron prod. by Ne^+ bombard., origin of Ne Auger peaks *(French)* 80−7461
Auger electron prod. by Ne^+ bombard. 80−7460
Auger electron production by noble gas ion bombardment 77−1778
Auger electron spectra, electron impact excited, vap. and solid state differences 78−52603
Auger line, $KL_2L_3(^1D_2)$, lineshape 78−60535
Auger spectra, KLL and KLV, screening effects and plasmon gains 80−80913
Auger spectrum, KLL, plasmon gain satellite obs. 78−76562
Auger spectrum, $L_{23}VV$, rel. to valence band density of states 78−39634
bandstruct., effect of correlation, KKR calc. 79−11060
basal slip, anal. of pairwise dislocation interactions and contrib. to flow stress 78−35440
break arc, LV, low current, electron density, temp., local thermodynamic equilib. 78−9878
burst acoustic emission during Bauschinger effect 77−48475
cathode, in Ar, spark discharge, evidence for ionic toroidal post discharge environment 77−84551
CESR linewidth and g-shift in presence of spin-orbit perturbation, spin-phonon scatt. 77−63285
CESR measurements, 4.2-300K 78−48043
characteristic energy loss, ang. depend., surface plasmon excitation 78−2962
chemisorption, charge-density maps 79−19453
chemisorption of H_2, calc. of adsorption sites and binding energy 79−46953
chemisorptive luminescence systems for surface reaction obs. 78−7236
clean annealed surface, exoelectron emission during O_2 and Cl_2 adsorption 78−39671
cluster, multibody expansions, convergence 80−23594
cold rolling texture development 80−25720
combustion, laser-initiated, time-resolved spectroscopy 77−77765
combustion of particles in air at high pressures *(Russian)* 77−70302
concentration determ. in atm. and rainwater in Vizcaya, Spain *(Spanish)* 78−57264
concentration in atmospheric sedimentable powder, in Vizcaya, Spain *(Spanish)* 78−57265
conduction-electron spin flip by phonons, expt. data anal. 79−61219
core electron expansion, kinetic energy in Compton profiles 78−72628
corrosion in aqu. NaCl soln. at room temp. *(French)* 77−59990
crustacean neuromuscular junctions, synaptic facilitation obs. 79−39412
crystals, concentrated loads, 3-D anisotropic elasticity theory 80−83734
cyclic hardening of single crystal 78−64552
Debye-Waller factor, temp. depend. study by energy dispersive X-ray method 79−51208
defect solute atom interaction investigation using channelling techniques 78−47442
defect structure of crysts., melt grown by Bridgeman method, X-ray topography 78−59770
deformed single crystals, stacking faults and dislocation dissoc. 77−31681
determination by activation anal. (α,n), (α,p) reacts. investig. 80−61206
determination by at. emission from static induction plasma, anal. curves, detection limits 79−87919
dielectric function, longitudinal, calc. 77−1383
dielectric function from APW calcs. 79−65817
diffusion in Al 77−20127
diffusion in Na_2O-Al_2O_3-SiO_2 glass, SIMS study 79−82387
diffusion in Ni-W (2%) alloy, 970-1330K, appl. of vapour collect and AES method 78−75876
discharge, hollow cathode, excitation mechanisms of triplet state atoms and decay obs. 80−44015
dislocation internal friction, orientation depend., for single crysts. 78−52882
dislocation loops induced by neutron irrad., TEM obs. 79−51113
dislocation structure, after US deform. *(Russian)* 80−29027
dissolution of H_2, resistometric study under press. 80−70417
distribution in olivine and lunar basaltic liquids 79−35158
dopant for GaP, behaviour on crystallisation from melt 77−84772
elastic constants, high press. finite strain theory *(French)* 79−1475
electric field gradient and Knight shift, temp. depend., OPW calcs. 78−56387
electric field gradient at nucleus calc. 78−39079
electric quadrupole interactions on ^{12}B and ^{12}N, obs. by depolarisation due to level mixing 77−55728
electrical resistivity; 1-1000K, data tables 79−78073
electron impact, negative ion form. and post-collision interaction *(Russian)* 79−54974
electron irrad. damage, dislocation loop growth, in situ obs. 78−87715
electron irradiation damage 77−35587
electron irradiation induced aqueous corrosion 77−81343
electron lifetime anisotropy, Dingle temp. depend. on dislocation scatt. 79−78082
electron mean free path, stopping and straggling 78−91367
electron radiation damage, determ. of threshold displacement energy 78−59837
electronic charge density, OPW-based pseudopot. calc. 78−87896
electronic surface states, (001) surface, Brillouin zone 79−24047
etch pits at dislocations in single crystal 77−72622
extruded, continuum mech. anal. of flow curve anisotropy and plastic strain *(German)* 78−84947
face, (0001), incipient oxidation, EELS and LEED studies 80−81237
failure under hydrostatic press., kinetics 78−52944
Fermi surface, stress induced changes, kinetic, pot. energy contrib. 79−60683
Fermi surface changes under uniaxial compression 78−51876
Fermi surface stress induced changes calcs., principal cross sectional areas 79−60684

magnesium continued
film, defect energy distrib., elec. resist. meas. during annealing 80−54808
film, deposited at 4.2K, elec. resist. meas. *(French)* 77−8206
film, deposition props. on specially prepared substrate, desorption energy and surface diffusion 79−90917
film, deposition using low-energy ion beam, Rutherford backscatt. and SEM anal. 77−59700
film, deposition using low-energy ion beam, Rutherford backscatt. and SEM anal. 77−70004
film, electron energy loss spectrum in excitation of volume plasmons 78−11043
film, electron inelastic scatt. mean free paths, synchrotron radiation photoelectron spectra meas. 78−76587
film, Fuchs Sondheimer theory, size effect, elec. cond., Fermi surfaces 79−99637
film, influence of isothermal and thermal cycling on porosity *(Russian)* 78−87884
film, optical cond., energy derivative spectrum 77−66551
film, polycryst., chemisorpt. of O_2, synchrotron radiation photoemission expts., 70-150 eV 78−95228
film, quench-condensed, disorder effect on optical cond. and band struct. 77−1746
film, synchrotron radiation photoemission, plasmon loss struct. 79−28897
film, vapour-quenched, unsuccessful search for supercond. above 0.3K 77−12053
film, XPS lineshapes, many body processes 78−39663
films, struct. and props., X-ray diffr. spectra anal. 80−80119
finite strain theory appl. to evaluation of compression curves *(French)* 77−69028
flame, luminesc., laser irrad. effects 77−77766
flow stress during cutting 77−59881
foil-excited ion, X-ray spectra and satellite classification 80−95567
forced-flow chromatography, detection by photometric method 80−71965
free-electrons momenta distribution, anisotropy, positron annihilation meas. 77−36309
galactic cosmic rays, Ne, Mg and Si isotopes high resolution meas. 80−51631
GK-type dwarf stars, Mg isotopic abundances 80−51757
grain boundary diffusion creep 78−11291
grain boundary struct., Kikuchi electron diffr. obs. 80−15116
graphite, spheroidal, presence of magnesium studied with electron probe microanalyser *(Ukrainian)* 80−26072
H^++Mg collisions double electron capture 78−58777
Hall effect and elec. resist., temp. depend. 78−64030
Hall resistivity, 1.7-300K, up to 2 T, cyclotron motion breakdown 77−89751
HCP, vacancy and interstitial config. 79−65071
HCP, vacancy clusters and interstitials, computer simulation study 80−64992
HCP lattice, Huang diffuse scatt. from interstitials 80−88142
HCP metals, K-emission valence bands, structure and bonding 80−7438
heat of soln. of H, electron charge distrib. calc. 78−51689
heating by shock compression, of porous material, vap. form. *(Russian)* 78−2195
hexagonal, temp. depend. anisotropy of phonon scatt. resist. 78−51967
hydriding, Kirkendall marker movement 80−75385
hydrogenation kinetics, electron microscope expts. 77−52553
ignition, critical conditions 79−100372
impurity in Al, PIXE anal., conc. profile determ. using beam energy variation 78−76965
inclusions, types and size distrib. *(German, English)* 80−97492
interface, Mg(0001)-Mg(0001), local and nonlocal contribs. to adhesive energies 77−85085
interface Mg (0001)-Mg (0001), self-consistent electronic densities and adhesive energies 78−72005
internal friction, cryst. orientation depend. *(Russian)* 77−7730
internal friction spectrum after plastic deform. *(French)* 79−15737
interstellar Mg, depletion derived from S 59 obs. of 67 stars 79−2563
interstellar Mg ionization zones around stars 77−45517
interstellar Mg lines in stellar spectra, rel. to existence of circumstellar clouds 80−94782
ion bombarded, L_{23} shell ionisation cross section, Auger spectra obs. *(French)* 77−69956
ion bombarded, L_{23} shell ionisation cross-section under H^+, heavy-ion impact, Auger spectra *(French)* 79−24406
ion bombardment, energy distrib. of positive secondary ions and sputtered atoms 77−32485
ion irradiated, Auger electron spectra struct., possible surface diagnostic methods 79−69946
ion-induced Auger electron emission, depend. on ion energy 79−78814
ions, adsorbed on porous SiO_2 glass in distilled water medium, determ. 79−24814
ions, foil-excited, EUV spectrum 80−42976
ions, He-like, satellite lines to higher-order reson. series lines in laser-prod. plasma 79−85930
ions in low density plasma, dielectronic recomb., ionization equilib. and radiative energy loss, solar corona appl. 79−68903
isoelectric series, oscill. strengths and excitation energy, RRPA calcs. 78−13471
isoelectronic sequence, electron impact excitation of reson. transitions 80−63825
isoelectronic series, atom+H^+, low-lying ^3P term excitation, cross-sections and rate consts. 79−94069
isoelectronic series, D-F transitions, Mg sequence D-F transitions 79−54809
isotope fractionation by He^+ sputtering 79−87542
isotope shifts in Mg I 77−71771
isotopic abundances in Ba star HR 774, Reticon spectra 79−25594
isotopic anomalies, role of ^{26}Al synthesis in explosive H burning 80−85929
isotopic anomalies and lack of ^{26}Al in Allende meteorite unusual inclusion 79−40142
isotopic vars. in hibonite from Murchison meteorite, ion microprobe study 79−58305
$K\alpha_1$ and $K\alpha_2$ wavelengths 80−50464
$K\alpha$ radiation, X-ray photoelectron spectroscopy resolution 80−18888
K-shell X-ray production, by 0.4 to 2.4 MeV ^4He and ^1H ions 79−47550
laser radiation absorption in craters on metal targets 80−97386
lattic dynamics and sp. ht. in extended de Launay model 79−51217
magnesium continued
lattice distortion around vacancy 79−42192
lattice dynamical props., unpaired forces, phonon dispersion relations 79−19336
lattice dynamics, phonon dispersion relations and Debye temp. 79−42171
lattice dynamics of HCP metals 78−22795
lattice phonon spectrum and thermodynamic functions, inelastic coherent cold neutron scatt. *(Russian)* 78−55917
liquid, diffusion and thermal diffusion of Fe, Si and Al, obs. using unidirectional solidification 78−30772
liquid, infiltration kinetics into porous Ti 78−60595
liquid, Percus-Yevick eqn., perturbation treatment, struct. factor 77−7641
lunar basalts and regolith, anal. of var. in Al, Mg and Si abundances 78−16320
magnetic property volume depend., Knight shifts, electron spin response 80−88729
mass balance in continental runoff 79−34859
melting temperature under shock loading 77−47553
micas and amphiboles, Mg rich, Mossbauer spectra 79−38412
molten fuel-coolant interaction studies, simulated reactor accident, wind-scale shock tube rig 78−58363
Moon, Mg/Fe large-scale var. from orbital gamma-ray data 78−12123
neuromuscular junction miniature endplate current decay, effects of extracellular Ca^{2+} and Mg^{2+} 78−24064
neutron activation anal., 14 MeV neutron cross sections 79−52838
neutron irradiation damage, TEM obs. 79−46713
nitridation in HF discharge, temp. effect 80−3399
nucleosynthesis, isotopic yields from C and Ne zones in explosion of massive star 80−90406
Orion nebula, C and Mg abundances from UV spectrum 80−41882
partial molar thermodynamic data from EMF and calorimetric meas. of Mg-In liquid solns. 80−55359
phonon density of states calc. from neutron diffr. data 77−24369
phonon density of states determ. from heat capacity *(Russian)* 80−29131
phonon spectra and eqn. of state, pseudopot. method *(Russian)* 77−24367
photoemission, influence of oxide films *(Russian)* 77−81194
photoemission theory, book contrib. 80−16159
photon emission from inert gas-surface impact 78−11059
plasma, heated by ruby laser pulses, X-ray emission spectrum 80−64781
plasma, simplified spectra obtained by electro-optic gating of radiant emission 78−22561
plasmon struct. obs. in K photoabsorpt. spectra 79−38693
plasmon-loss intensities in XPS, EELS and Auger spectra 80−10902
plastic anisotropy of extruded bars *(German)* 77−86126
plastic deform., strain rate history and temp. effects depend. 79−11684
plastic deformation mechanism, TEM appl. Mg, FCC metals *(French)* 77−1853
polycrystalline, X-ray attenuation and photoelec. coeffs. in range 0.3 to 1.3 Å 79−99979
polycrystals with axial texture, heterogeneity of props. *(Russian)* 80−29192
positron annihilation data anal. by Mijnarends' method 77−20223
powder, gas suspension, critical spark ignition conditions 79−100373
pure, Bordoni relax. behaviour after plastic deformation 80−20997
purification by vacuum distillation 79−52138
pyramidal dislocation pair interactions contrib. to flow stress during slip 78−35441
quadrupole interaction of ^{12}B and ^{12}N 78−47750
quadrupole interaction of ^{181}Ta, gamma-spectral study 80−80228
quantum interference effect in transverse magnetoresistance 77−35854
quantum interference effect in transverse magnetoresistance 77−35855
quantum interference effect in transverse magnetoresistance 77−35856
quantum oscillations of thermal EMF under mag. breakdown conditions *(Russian)* 77−69305
quenched to 4.2K, presence and mobility of H_2 77−28042
radioactive tracer for Pu nuclear fuel input accountability in reprocessing plants 80−73919
recrystallisation after cold rolling 78−72790
recrystallisation after straining by rolling, −25 to 100°C *(French)* 77−59815
reduction of $TiCl_3$ by Mg, thermodynamics and heat physics *(Russian)* 78−15331
reflectance drops and surface plasmons on deposits of different roughness 77−20392
removal from interstitial waters in reducing environments 79−66673
rolling texture formation, computer simulation in HCP and orthorhombic metals 80−3095
rutile: Ga, Mg, intersecting defect structures, TEM study 79−51123
screening of light impurities 77−85177
second Hugoniot relationship 77−35659
shock wave compression, reduced Hugoniot curve and eqn. of state *(Chinese)* 80−44259
soft X-ray emission and absorpt. edges, self-absorpt. studies 80−40183
Soft X-ray emission edge self absorption and effect of exciting voltage 77−90220
solar Mg II core absorption, wavelengths meas. and evidence for atmospheric downflow 79−12451
solubility of H_2 77−25024
spectrochemical analysis of biological solns. using wall stabilised arc source 80−41343
sputtered atoms, polarisation of emitted light 77−27008
sputtering, energy distrib. of sputtered atoms 79−91549
steel fibre reinforced Mg, fibre-matrix interfacial reactions 80−20043
superconducting transition temp., electron-phonon mass enhancement, pseudopot. calcs. 78−2604
surface, Ar^+ and e^- excited Ar Auger electron emission 79−47560
surface, mol. chemisorption, self-consistent calc. 79−95260
surface, rough, reflection loss for s and p polarised waves near surface plasmon freq. *(French)* 80−97225
surface, small angle scatt. of low energy K^+ ions 80−20752
surface nitridation, in N_2 DC glow discharge 0.3-5 torr mechanism 78−3370
surface plasmons, excitation 79−28310
surface structure autocorrelation function for rough deposits 78−26756
surface structure autocorrelation functions and Fourier transforms for rough deposits 79−69450
surfaces, Van der Waals forces computation 79−15204
thermopower calc., 1-OPW model 79−38053

magnesium continued
twin and stacking fault energies 79−38018
twin boundaries, computer simulation 80−39109
upper atmosphere, Mg and Mg^+ photochemistry 77−21954
US attenuation due to conduction electrons 79−46754
US attenuation of conduction electrons, shear waves calc. 78−91589
US attenuation of conduction electrons calc. 78−91588
US hardening kinetics rel. to dislocations 80−50644
vacancy, in single cryst., Green's function method of lattice statics 78−55865
vacancy loop behaviour on high-temp. oxidation, topography 77−76414
vaporisation from inductively stirred melt, meas. and prediction 78−51659
vapour, heavy negative ion beam prod. in range 15-90 keV by charge exchange 78−25366
vapour, tunable, coherent radiation in the Lyman-α region, 1210 to 1290 Å 79−23023
X-ray absorption and emission edges, one-electron and many-body effects 80−25484
X-ray Debye characteristic temp., powder specimens 77−84876
X-ray emission spectra, K, double plasmon high energy satellite 80−11510
X-ray excited L Auger spectra, double ionisation satellites 77−32497
X-ray spectrum, room temp. meas. using HgI_2 detector 78−78049
X-ray threshold anal. 78−31281
XPS, plasmon gains as monitor of incomplete relax., interference effects and sudden to adiabatic limits transition 80−66390
XPS, plasmon struct. of core lines 77−63530
XPS from core levels, electron energy loss spectra, intrinsic and extrinsic plasmons 77−63532
XPS investigation of density of states 78−6829
XPS theory, core level spectra, plasmon creation 78−72701
XPS theory, valence band spectra band struct. 78−72702
AgCl:Mg^{2+}, plasticity, impurity hardening effect 78−47466
Al:Mg, impurity low-field galvanomag. coeffs., 4 OPW calcs. 77−69304
Al/Mg soldered samples, UTS and fracture surface comp., 20 to 500°C 79−38941
Al-Mg, alloy, dil., electron-irradiated, impurity-interstitial interaction 77−15449
Al-Mg, alloy, surface activity of Mg, XPS and AES meas. 79−86975
Al-Mg, electron probe microanalysis, depleted zone formation in air and vacuum 79−57013
Al-Mg-Si, electron probe microanalysis, depleted zone formation in air and vacuum 79−57013
Al-oxide-Mg-Al, thin proximity effect sandwiches, spin-polarised tunnelling obs. 80−50007
Al-Zn-Mg, electron probe microanalysis, depleted zone formation in air and vacuum 79−57013
AlGaAs-GaAs:Mg heteroepitaxial wafers, surface morphology and photoluminesc. meas. laser applics. 77−3591
$Al_xGa_{1-x}As$:Mg doping characteristics, elec. props., effective hole masses 79−78117
α-Al_2O_3 fibre FP reinforced Al and Mg composites, fabrication and props. 80−81004
Al_2O_3:Mg, recombination luminesc. spectra 79−83021
β-Al_2O_3-Na_2O:Mg, ionic cond., effect of microstruct. and phase composition 78−67859
β-Al_2O_3-Na_2O:Mg, with and without Co co-doping, ionic cond. and cryst. struct. 78−26723
B fibre reinforced Mg, exam. of fatigue props. and corrosion 80−11751
B fibre reinforced Mg, fibre-matrix interfacial reactions 80−20043
C fibre-Mg matrix interaction, strength changes on heating 78−11164
CaO:Mg^+, EPR exam., hyperfine const. determ. 77−8388
CaO:Mg^+, g-shift anal. 80−29313
$CsNiF_3$:Mg, ferromag. chain system, temp. depend. of correlation length, quasi-elastic neutron scatt. meas. 77−16046
Cu-Mg catalyst, cyclohexanol dehydrogenation, kinetic model depend. of reaction rate 77−90583
GaAs:Cr, Mg, ion implanted, elec. meas. and optical activation studies 79−86806
GaAs:Mg, doped and undoped, sputtered epitaxial films, elec. props. 79−78234
GaAs:Mg, implanted, low temp. photolum. spectra 78−39583
GaAs:Mg, impurity conc. profile by glow-discharge optical spectroscopy 80−49258
GaAs:Mg, ion implanted, laser annealing, ellipsometric and Hall meas. 79−73193
GaAs:Mg, ion-implanted, capless anneal, effect of As partial press. 80−29038
GaAs:Mg, photoluminesc. temp. depend., 4.2-293K 77−69878
GaAs:Mg ion implanted, photoluminesc. and annealing characts. 77−16361
GaN:Mg, and undoped, epitaxial growth from vapour, orientation, elec. props. 77−4740
GaN:Mg, epitaxial layer, characts. from cathodoluminesc. 78−35208
Ga_2O_3:Mg single crystals, quenched, ionic and elec. props. 78−30922
GaP:Mg, excited acceptor state investig. by photoluminesc. 77−8632
GaP:Mg, ion implanted, elec. profiles 79−77628
GaP:Mg, multiple bound excitons, photoluminesc. obs. 79−95837
GaP:Mg,Te, donor-acceptor pair luminesc., excitation spectroscopy 80−25440
Ge:Mg, diffusion and p-type cond. 80−6419
Ge:Mg, energy level behaviour, Hall coeff. and elec. cond. meas. 80−34396
Ge:Mg, positron annihilation angular distrib. 80−45165
He and Ne isotopes prod. cross sections induced by 12-45 MeV protons 77−17310
He+Be^+(Mg^+) high energy, excitation cross sections, impact radiation polaris., models comparison 78−1069
He+Mg^+(Ne^+), charge exchange, Rydberg state excitations 77−58159
InAs:Mg, ion implanted, photocond., photo-EMF, and optical absorpt. spectra 80−70763
InGaAsP-InP:Mg LEDS, for high-bit-rate optical communication systems 80−5823
InP:Mg, ion implantation and PH_3 ambient annealing under VPE conditions 79−42085
KBr:Mg^{2+}, dopant aggregation and precipitation 80−107306
KCl:Mg microcrystalline powders, role of Z-centres in stabilizing coloration 80−54227
KCl:Mg^{2+}, dopant aggregation and precipitation 80−107306
KCl-Mg, thermolum. of Z-centre, optical absorpt. 80−55203
KCl-Mg, X-irrad. and F-bleached, optical and ESR spectra 77−48052
K_2MnF_4:Mg, mag. effects of impurities 80−65869
K_2MnF_4:Zn(Mg)(Ni), local magnetisation, NMR and Green's function study 80−65870
Kr:Mg_n, matrix isolated Raman spectra 78−90170
Li, one-electron calcs. of X-ray absorpt. and emission, jellium model 78−56543
LiD:Mg^{2+}, two peaks in ionic thermocurrent curves 77−31807
LiD:Mg^{2+}, X-irrad., dielec. loss 80−55024
LiF:Mg, dependence of optical absorpt. on temp. during X-ray irrad. 80−66237
LiF:Mg, effects of grain size on thermolum. and thermally stimulated exoelectron emission 79−15536
LiF:Mg, electron spin-lattice relax. of V_k-centre 78−95518
LiF:Mg, flow stress changes during precipitation 80−92594
LiF:Mg, impurity effect on elec. cond. 79−7709
LiF:Mg, light scatt., effect of electrostatic field 78−2823
LiF:Mg, Maxwell-Wagner relax. induced by impurity clouds around dislocations, ionic thermocond. meas. 80−7281
LiF:Mg, nucl. acoustic reson. 77−8445
LiF:Mg, origin of dislocations *(Russian)* 77−15425
LiF:Mg, role of impurity-vacancy pairs in thermolum. 79−8195
LiF:Mg, shock waves in ⟨111⟩ direction, elastic precursor amplitudes 80−54314
LiF:Mg, slip band struct. changes with temp. 78−47390
LiF:Mg, TLD-100, thermolum. phosphor, photolum. and absorpt. spectra, thermolum. mechanisms 80−97321
LiF:Mg, Ti, luminesc. increase by O implantation 78−64412
LiF:Mg, X-irrad., colour centres, ESR and UV asborpt. meas. 80−108069
LiF:Mg, X-irrad. induced sensitisation mechanism, optical absorpt. spectra 80−60637
LiF:Mg, X-irradiated, thermoluminesc. of Z_3-centres 78−15236
LiF:Mg, X-irradiated, Z_1-centre exam. 77−68968
LiF:Mg, X-ray irrad., trapping processes, Z-centres and dipoles, two models 80−49222
LiF:Mg, Z_2- and associated Z-centres, elec. cond., ionic thermocurrent, and optical absorpt. meas. 80−107229
LiF:Mg,Ca detectors, variation of parameters of thermally stimulated luminesc. 79−6793
LiF:Mg,Ti, defect states, ESR and ionic cond. study 80−108058
LiF:Mg,Ti, optically induced dichroism of Z_2-centres 79−28710
LiF:Mg,Ti, thermolum. related Z-centres, optical absorpt. bands 78−23540
LiF:Mg,Ti, thermoluminesc. activation energies 79−74009
LiF:Mg,Ti crystals, Z_3-centres, correlation of thermoluminescence and optical absorption 80−45154
LiF:Mg cryst., Mg electron colour centers 80−100229
LiF:Mg dosimetric cryst., light-sum storage during linear stage 79−8194
LiF:Mg,γ-irrad., phonon scatt. and interstitial clusters 80−70254
LiF:Mg^{2+}, deformed in ^{3}He and ^{4}He, dislocation struct. characteristics 79−69112
LiF:Mg^{2+}, TLD-100, precipitation reactions and ionic cond. 77−56479
LiF:Mg^{2+}, TLD-100, solution treatment temp. and ageing effects 77−56480
LiF:Mg^{2+}(CO^{2+}), X-ray induced UV absorpt., band shapes, F- and Z-centers 77−20889
LiF:MgTi, (TLD-100), optical bleaching of defect centres 79−19911
LiF:OH:Mg, γ-irrad. induced oxyhydryl complexes 80−92555
Li_2GeO_3:Si,Mg, impurity effects on elastic and piezoelec. props. 79−47388
$LiNbO_3$:Ti, Mg waveguide, diffused, Mg diffusion effects on characts. 78−66905
Li_2SO_4:Mg^{2+}, monoclinic-cubic transform., effect of impurities 79−52744
Mg ($^3P_1$) metastable atom afterglow quenching rate consts. with various mols. 77−6720
Mg (Mg^+), lifetime meas., beam foil spectra, comparison with numerical coulomb approx. calc. 80−58367
Mg I, $^3F^0$ Rydberg series, energy levels, multiconfigurational HF procedure 80−47882
Mg I, ^3p triplet system, lifetime meas. 80−47946
Mg I, $3^1P_1{}^0$ level reson. broadening and lifetime 77−57916
Mg I, extensions to the doubly excited spectra in the vacuum uv 79−6901
Mg I, fluoresc. lines polarisation and mag. depolarisation *(German)* 77−6719
Mg I, hyperfine struct., brightness distrib., form. model verification 77−57928
Mg I, isotope shift, hyperfine struct. 78−42011
Mg I, isotope shifts, extended meas. 79−72279
Mg I, Mg II, ejected electron spectrum from autoionis. levels after electron impact 77−75304
Mg I, Mg II, solar reson. lines obs. in active region 79−40163
Mg I, Mg II autoionisation state radiative decay *(Russian)* 80−5509
Mg I, Mg II lines, broadening and shift by van der Waals interactions and electron impact 77−3303
Mg I, photoabsorpt. spectrum 225-170 Å 79−72262
Mg I, press. shifts of $^1D_2$ Rydberg states 77−61711
Mg I 2852 Å line in solar spectrum, sensitivity to partial redistrib. effects 78−7951
Mg I and II in Sun, line profiles comparison with theoretical spectra, visible obs. 80−82320
Mg I b2 5175 Å index in old galaxy populations 78−41033
Mg I interstellar line structure, balloon UV obs. of ζ Orionis spectrum 79−35251
Mg I λ2852, in Sun, supergranular line profile var. 79−40164
Mg I sequences for elements Cr to Zn, $n=3\rightarrow n'=4$ transitions 79−26922
Mg I to Mg III, beam-foil excitation, Rydberg states, relative populations 80−14208
Mg, I-XII, energy levels and optical spectra 80−87065
Mg II, absorpt. lines obs. in low-redshift quasi-stellar objects spectra 79−21459
Mg II, fine struct. of ^2D and ^2F sequences by level crossing and anticrossing spectroscopy 79−6919
Mg II, Hanle effect, $^2P_{3/2}$ lifetime meas. 77−18852
Mg II, interstellar column density towards nearby stars 78−41023
Mg II, radiation press cooling of ions in Penning EM trap 78−66527
Mg II, solar reson. lines, first emission features obs. in wings 78−32429

magnesium continued
Mg II, UV line spectrum of active chromosphere star ε Eridani, models 80−77394
Mg II 2795 Å k-line, temporal var. in solar spectrum 78−93186
Mg II 280 nm line in Persei, profile, calcs. and UV obs. 80−82421
Mg II 2800 Å data for early-type stars, circumstellar clouds *(Russian, English)* 79−96992
Mg II 2934 Å emission in QSOs, possible identification 78−41073
Mg II equatorial airglow altitude distrib. 79−2418
Mg II flux profiles in cool stars, obs. rel. to chromospheric radiative loss rates 80−36611
Mg II h and k line profiles of active solar limb filament 79−44446
Mg II h and k lines in cool giant star chromospheres, mass loss determ. 80−85935
Mg II h- and k-lines in UV spectra of Cepheid β Doradus 79−40196
Mg II interstellar density along line of sight to nearby stars 78−45391
Mg II lines in quasars and Seyfert galaxies, excitation and line strength 80−67896
Mg II solar UV doublet obs. *(Japanese)* 78−61831
Mg III, autoionising transitions $ns^2np^6-nsnp^6mp$ 77−88419
Mg III, radiative lifetimes calc. 79−98037
Mg III-V, beam-foil spectra, 100-450 Å 80−83308
Mg IX, $2s2p(^3P_1{}^o)\rightarrow 2s^2(^1S_0{}^e)$ transition probabilities, CI calcs. 79−36544
Mg IX, wavefunctions and oscill. strengths, CI calcs. 80−23317
Mg isoelectronic sequence, mag. quadrupole transitions probabilities 78−37592
Mg isoelectronic sequence, static dipole quadrupole polarisabilities and shielding factors calc. using HF scheme 80−99450
Mg positron trapping and bound states 80−2367
Mg, spin susceptibility, electronic effective mass, spin density functional calcs. 78−43291
Mg V, O I like ion, solar emission lines density depend. 79−40165
Mg VII, UV lines, theoretical intensity ratios 78−90108
Mg VIII, low lying levels, excitation equilib. and line intensities 79−12401
Mg XI, He-like ion, oscillator strengths of transitions between low-lying S and P states 78−13470
Mg XI, He-like ion resonance line satellites 79−10064
Mg XI, intercomb. line obs., in laser-produced plasma 78−9106
Mg XI resonance lines, dielectronic satellite lines atomic parameters calcs. 80−78567
Mg XI-S XV ions, 2l3l-1s3l and 2l2l-1s2l radiative transitions and non-radiative decay probabilities 78−70781
Mg XII, electron temp. determ. of laser plasma from continuous recomb. radiation 79−64924
Mg XII, H-like ion, anal. of satellites to reson. lines in X-ray region 77−88421
Mg XII, resonance line, atomic parameters calc. for dielectronic satellite lines 80−42983
Mg^-, purely L^2 method for calculating resonance widths 78−46283
Mg^-, shape resonances, shift potential calcs. 80−69089
Mg^+, beam-tilted C foil interactions, charge-state distrib., photon emission, 100-400 keV 79−22814
Mg^+, electron and ion Stark effects in plasma, widths and shifts 77−46526
Mg^+ laser cooled ions bound in Penning trap, high-resolution optical spectra 80−102487
Mg^+, Penning trap, laser cooling, optical spectrum from laser freq. sweeping 80−52916
Mg^+, reson. line regularities in plasma Stark widths and shifts 80−43881
Mg^+, resonance lines electron impact excitation, polarisability 78−42225
Mg^{11+}, soft X-ray population inversion in laser plasmas, reson. photoexcitation, photon-assisted processes 80−87378
Mg^{2+}, $2p^6np-2p^5ms$ (n=3, 4; m=3,4,5) transition probabilities calc. 79−6915
Mg^{2+} atomic core states, antishielding effects calcs. 80−83299
Mg^{2+} effect on chromaffin granule electrophoretic mobility meas. by light scatt. 78−53357
Mg^{2+}, ionic size rel. to Koopmans' ionisation pot. 79−85892
Mg^{2+}, marine sediment content, western continental shelf, India 80−8289
Mg^{2+} partitioning in olivine and silicate melts 79−66683
Mg^{2+}, role in multiplication regulation of normal and transformed cells 79−2012
Mg^{2+}, second order correl. energy, Z depend. of irreducible-pair energies 80−91417
Mg^{4+}, $2s2p^5-2s2p^43s$ transition, spectroscopic investig. 79−59384
Mg^{6+}, $2s2p^3$ terms, mean lives, from beam-foil spectra 78−37601
Mg^{9+}, beam-foil excited, spin orbit-forbidden X-ray transition obs. 80−23537
Mg:^{12}B ions, decoupling of hyperfine interactions by external mag. field 77−24756
Mg:H, impurity energies and geometrics, self-consistent jellium calc. 79−99507
Mg:H, solid soln. produced by ion implantation 78−67733
Mg:H(He), interaction energy of two H(He) atoms, Hohenberg-Kohn-Sham density functional formalism 79−51519
Mg/Cr ratio in achondrites and mesosiderite silicate fraction 80−51704
Mg-AgCl seawater battery, performance and EMF at great ocean depths 80−76623
Mg-barium stearate-Mg structs., internal voltage work function meas. 79−82684
Mg-Cu_2O Schottky-barrier solar cells, surface anal. using AES 79−43759
Mg-I cycle for thermochem. decomposition of H_2O for H prod. 80−35786
Mg-inert gas, Mg reson. lines broadening, absorpt. cross sections anal. 80−32642
Mg-MgO-Ag, tunnel junction, potential barrier, equivalent rectangular shape 79−7906
Mg-MgO-Ag junction, stable room temp. light emission 78−31257
Mg-MnO_2, short-circuited cell, use as portable heater 79−61964
Mg-N_2O-CO flame, efficient chem. generation of $Mg(^3P)$ 78−63109
Mg-N_2O-CO flame, Mg catalyzed, gain meas., emission band assignment 78−66815
Mg-polymer contacts, charge transfer and contact charge spectroscopy 79−56305
Mg-Xe discharge and MgXe excimer band, emission intensities and excited-state densities meas. 80−92413

magnesium continued
Mg^{2+}-Fe^{2+} partitioning in garnet lherzolite, rel. to high-press. phase equilibria 79−66687
Mg+C (O^-), electron detachment cross-sections, 20-150 keV 78−25690
Mg+C (O^-)(F^-)(Cl^-), negative ion stripping, at. beam form. 77−6926
Mg+Ca, Ca metastable ^{1}P-state, quenching reactions, fluoresc. meas. 80−102477
Mg+F_2, crossed beam chemilum., kinetics and mechanisms 80−21264
Mg+$H_2\rightarrow MgH_2$ reaction, catalytic effect of In, kinetics 78−76851
Mg+H^+, electron capture, single and double, 1-100 keV 79−68313
Mg+H^+, electron capture and impact ionisation cross sections, CI calc. 80−23343
Mg+H^+, K-shell ionisation cross sections for 15-65 keV protons 78−90284
Mg+H^+, metastable H form. by charge exchange 79−81275
Mg+H^+(He^+) and electron impact ionis., Auger study of collisionally induced alignment 78−90279
Mg+He^+(He_2^+), inelastic collisions, 2-800 eV, excited state form. 78−94312
Mg+$O_2\rightleftharpoons MgO+O$, shock-tube study of evap. and oxidation kinetics 80−16651
Mg+O_3, matrix reaction, IR spectra, isotope shifts and blue matrix shift 78−80736
Mg^++alkali metal, effective charge exchange cross section, 20 to 1000 eV 77−42398
Mg^++H^+, Mg^{2+} form. by charge exchange and ionis., cross sections 77−83709
Mg^++He,(Ne)(Ar), 3^2P differential excitation, alignment and orientation 79−86053
Mg^++He (benzene), relative level excitation, orbital ang. momentum quantum number depend. 78−25688
Mg^++He(Ne), ns-np excitation, alignment and orientation, impact, parameter theory 80−91648
Mg^++He(Ne), slow collision, ionis. obs. 79−10194
Mg^++He(Ne)(Ar), Mg^+ collision-induced alignment, reson.-line emission polaris. obs. 80−18912
Mg^++Mg and Mg^{2+}+Mg, resonant charge transfer, phase interference effect 79−10199
Mg^++Na(K)(Rb)(Cs), charge exchange and excitation processes 78−17772
Mg^{2+}+He, relative level excitation, orbital ang. momentum quantum number depend. 78−25688
Mg^{2+}+Ne collisions, 2p-3p excitation, optical spectroscopy investig. 77−19064
Mg^{6+}+H^+, ^3P_J fine structure transitions 80−37864
Mg_2, $A^1\Sigma_u^+$-$X^1\Sigma_g^+$ system Franck-Condon factors, J-depend., fluoresc. pot. and predissoc. 77−58067
Mg_2 $A^1\Sigma_u^+$-$X^1\Sigma_g^+$ system, discrete and continuous Franck Condon factors, J-depend. 78−66811
Mg_2, Ar matrix isolated laser photoluminescence spectra, electronic absorpt., emission, vibronic and vibr. relax. 78−82744
Mg_2, empirical pot. curves, Pade approximant calcs. 80−14184
Mg_2 excimer system, laser induced fluoresc. 78−33548
Mg_2, ground state, multiple scatt. Xα calcs. 80−58149
Mg_2, low-lying states binding energy, local spin density functional formalism calcs. 79−97994
Mg_2 matrix isolated, vis. and near IR spectra 78−5214
Mg_2, Mg_2^+, electronic struct., pot. energy curves, multiconfig. SCF calcs. 78−5124
Mg_2, mol. consts. calcs., inverted perturbation approach 77−57969
Mg_2, perturbation theory calcs. 79−13644
Mg_2, pot. energy curve for $X^1\Sigma_g^+$ state, many-body perturbation calcs. 78−55216
Mg_2, $X^1\Sigma_g^+$ state, pot. curve, coupled pair many electron theory calc. 79−89621
Mg_2^++H, electron capture by slow ions, pseudo-crossing 80−43176
$Mg_{(S)}$+Ne^+, O-dependent photon emission 79−1810
MgF_2, laser window material, surface and bulk absorpt., photoacoustic meas. 78−25912
$Mg_4(Mg_4^-)$, atomic clusters, electronic struct., LCAO-MO-SCF and HF calcs. 80−63880
$MgNi_2$, four-layer, Friauf-Laves phases, stacking variants 80−96468
MgO, laser window material, surface and bulk absorpt., photoacoustic meas. 78−25912
MgO, surface reactions with H and O atoms, EPR anal. via ultrahigh vacuum/flow system 78−7232
MgO-TeO_2 glass, struct. and props. *(Japanese)* 79−32917
Mg_2SiO_4:Mg^{2+}, elec. field gradients, asymmetry parameters 80−54660
MgVII, solar emission lines, density dependence 80−21963
Mg(0001)-Mg(0001), metallic adhesion 79−73463
$^{24}Mg/^{25}Mg/^{26}Mg$ of interplanetary dust particles 80−72879
^{25}Mg, $^3P_1$ and $^1P_1$ levels, quadrupole coupling consts. 80−23434
$^{25}Mg^{2+}$, aq. ions, nucl. quadrupole relax. 78−64287
^{26}Mg excess in Allende meteorite anorthite crystal, ion microprobe obs. 78−40882
^{28}Mg carrier-free production by 50-180 MeV protons on Si, P, S, Cl, Ar and K 79−83934
^{28}Mg, intestinal absorpt. obs. in man 80−36217
Mg^*+Cl_2, collision and reaction cross section meas. 79−59537
$Mg^*+Cl_2\rightarrow MgCl^*+Cl$, chemiluminesc. studies 78−40030
Mg^*+He(Ne), model pot. curves, including CI 78−42154
$Mg^{2+}.nH_2O+PO_4H_2^-$, binding mechanisms, SCF ab initio calcs. 79−22586
Mg^{n+} (n=9,10,11,12), ionic config. via $^{24}Mg(^{32}S,^{32}S\gamma)^{24}Mg$ 67 MeV 77−67762
N_2 dissociation role in plasma positive column Mg nitridation 78−63628
N_2O-CO flame, Mg catalyzed chain reaction chemiluminesc. 77−36758
NaCl:Mg, X- and gamma-irrad., thermostimulated electrons and luminesc. 79−91505
NaCl:Mg^{2+}, Z_4-like centre, absorpt. spectra obs. 78−76498
NaCl:Mn^{++}, Mg^{++}, doubly doped, ionic thermocurrent study of linear dimer 80−79977
Ne+Be^+(Mg^+), high energy, excitation cross section, impact radiation polaris., models comparison 78−1069
Ne+Mg^+, autoionising level excitation, electron spectra 77−14554
O_2+Be(Mg)(Ca)(Sr)(Ba), reaction kinetics in diffusion flame 77−90579
RbCl:Mg, γ-irrad., thermoluminesc. 79−47528
n-Si:Mg, energy levels and degeneracy ratios determ. by Hall effect meas. 79−90993

magnesium continued
Si:Mg, Zeeman effect of excitation spectrum of neutral donors 77−63439
Si-SiO_2-Mg-Cu powder compact, nitridation to form Si_2ON_2 whiskers *(Japanese)* 80−93674
TiO_2:Mg, high-resolution reflex images of crystal defects 78−6073
YIG:Mg film, microwave losses induced by Fe^{4+} ions, ferromag. reson. study 79−1715
Zn_3P_2-Mg, diode, spectra response meas. of minority carrier diffusion length 79−78131
ZnSe:Mg, local vibrations of impurities, IR absorpt. spectra exam. 77−7815

magnesium alloys
see also magnesium compounds
Al-Mg alloy N4, irradiation with 100 and 400 keV Al ions, obs. and analysis of damage struct. 77−4133
Al-Zn-Mg (5,1 wt.%), decomp. process, TEM study 80−71660
Al-Zn-Mg (6, 3 wt.%), water vapour embrittlement and H_2 bubble form 78−15564
Br.AZhNMts 7-2.5-1.5-9 bronze, Mg-Al, type, fatigue and stress corrosion cracking, welding effects 80−3233
cryogenic, mech. props. of AMg5 and AMg6 at −196°C 77−63748
D16 extruded rod, substruct, anisotropy and decomp. at subboundaries *(Russian)* 77−25095
dilute, dynamic recrystn. during creep, dislocation substruct., quartz comparison 80−109142
dilute, electron lifetime anisotropy, Dingle temp. due to dislocation scatt. 79−78082
dilute binary alloy, residual resistivity 77−1406
Duralumin, effect of alloy purity and ageing on fracture mechanism, and resultant toughness 79−5049
fatigue, random process effect on life in type MA15 79−66160
fatigue crack generation, in air and in vacuo, structural state effect, alloy MA12 79−87728
fatigue crack growth in air and vacuum, type MA12 79−15792
fatigue endurance and cyclic fracture toughness in air and vacuum *(Russian)* 79−34188
fatigue failure in air and vacuum in type MA12 79−91800
fatigue fracture, structural state effect in air in type MA12 79−91796
fatigue of alloy MA12, low temp. effect 80−55529
hardness testing, depth of impression meas., automated 79−15892
high strength Al-Zn-Mg-Cu alloys, mechanical props. *(Japanese)* 79−91654
Laves phase alloys, long period struct. classical lattice gas model method 79−94957
Magnex AL 80, aqu. corrosion, silicate effects 77−70230
Magnox AL 80, ion beam analysis of corrosion films 77−8978
$Mg_{70}Zn_{30}$, amorphous alloy 77−27835
mischmetal-Co-Cu-Fe-Mg, mag. props. 80−35353
mischmetal-Co-Cu-Mg, mag. props. 80−35353
Mischmetal-Mg alloy, hydrogen storage materials *(French)* 79−66419
mutual alloying behaviour of the elements straddling the line Li-Mg-Cu-Au in the long periodic table 78−84769
neutron irradiation effects, on microstruct., mech. props. and swelling 79−65121
plasticity due to superimposed macrosonic and static strains 78−60719
precipitate free zones, X-ray microanal. 80−108768
quenched-in defect behaviour, effect on flow stress 79−61625
rare earth dil. alloys, anisotropic magnetoresist. 77−62905
rare earth intermetallics, RMg_2, cryst. and mag. props., ordering 78−68185
rare earth-Mg, magnetisation and neutron diffr. meas. 77−63105
residue effects on graphite spheroidization in cast Fe *(Korean)* 79−43286
reversible alloys, hydrogenation for H_2 storage *(French)* 79−74549
steel, Mg effect on precipitation of C and or N, and mech. props., during strain ageing *(German)* 78−35387
steel, Mn, effect of Mn on corrosion *(Czechoslovakian)* 77−28933
steel, stainless wire reinforced Al-Zn-Mg system, resistance to crack propagation 79−43409
steel low C, surface segregation of Mn during annealing 77−36555
strain rate effects during reverse torsional shear 77−4143
superplastic deformation mechanism, deformation model 78−31477
surface layers, cross-sectional struct., appl. of cryogenic fracturing technique 77−30219
ternary, constitution, review 77−90319
texture of cladding tubes 79−87655
trace element determ., emission spectrographic method 78−48713
YMg, exchange coulombic contrib. of cond. electrons to cryst. elec. field 79−95376
α-Ag-Mg, disordered, shaft range order diffuse scatt., electron diffr., interpretation 77−84596
Ag-Mg, low temp. internal friction, 150 to 300K *(Polish)* 79−96077
Ag-Mg (15 at.%), disordered, short-range order, X-ray diffr. obs. 79−95176
Ag-Mg (18.5 wt.%), solid soln., rheological study of crystallographic order on creep *(French)* 80−97548
Ag-MgO, laws of plasticity of dispersion strengthened materials 78−84832
AgCd-AgMg, quasibinary alloys, phase relations 79−8273
AgMg, B2 intermediate phase, slip system, ordering energy and atomic size ratio depend. 80−59471
β′-AgMg, de Haas-van Alphen effect, LMTO band struct. and Fermi surface 78−75984
AgMg, deform. at high temp., yield pts. 79−61674
AgMg single crystals, orientation and temp. depend. of slip 78−87682
AgMg two phase bicrystal growth, orientation, interface struct. 80−60773
Ag_3Mg, long-period alloy, ordered struct. 79−27949
Ag_3Mg, long-period ordered, struct., high resolution electron microscopy obs. 79−94960
Ag_3Mg, ordered, rational and irrational long period struct. 79−95175
Ag_3Mg, ordered alloy, projected pot. image of defect obs. 79−99176
Ag_3Mg, periodic antiphase boundaries, electron microscopy study *(French)* 80−59481
Ag_3Mg, structure of ordered alloy, electron diffraction, kinematical vs. dynamical diffraction calc. 80−10530
Ag_3Mg, two different types of long-period ordered alloys, characterisation by high resoln. electron microscopy 80−49181

magnesium alloys continued
AgZn-AgMg quasibinary alloy, phase relation and superlattice form. 78−3097
Al-Be-Mg (30, 5wt.%) alloy, weld solification parameters 79−24511
Al-Cu-Mg, acoustic emission power, strain rate depend. 77−4808
Al-Cu-Mg, acoustic emission during tensile testing 80−7632
Al-Cu-Mg, aged, stress corrosion cracking in NaCl soln. 80−7709
Al-Cu-Mg, alloy 2124-T351, crack tip closure assessment by electronfractography 80−16427
Al-Cu-Mg, alloy Al2048, early stages of fatigue crack propag. 77−63780
Al-Cu-Mg, alloys A-U4, A-U4G1, A-U2GN, effect of environment on fatigue crack growth 78−64677
Al-Cu-Mg, cold plastic deformation, stress/strain relations 79−56991
Al-Cu-Mg, dil. alloys, ageing response *(Korean)* 77−28832
Al-Cu-Mg, rolled plate fatigue charact. *(Russian)* 80−16437
Al-Cu-Mg, string ghost form. during solidification *(Japanese)* 79 100130
Al-Cu-Mg, tpye RR55, high strength, creep behaviour, effect rel. to anodic coatings, SEM study 80−97542
Al-Cu-Mg, tube drawing, tensile forces, plastic deformation *(French)* 79−70130
Al-Cu-Mg, type 2036, deformation at ageing temp., effect on struct. and props. 80−7605
Al-Cu-Mg, type D16 alloy, stress intensity coeff. determ. 79−87711
Al-Cu-Mg, type D16T, thin-wall cylinder cold rolling method 80−66535
Al-Cu-Mg (1.3, 1.3 at.%) alloy, natural ageing, meas. of quenching vacancy dislocation loops 79−15704
Al-Cu-Mg (2.0, 1.1 wt.%), Ostwald ripening of S′ precipitates *(Korean)* 79−38831
Al-Cu-Mg (2.6, 0.4 wt.%), Fe, Si, Mn and Ti addition effects on age-precipitation *(Japanese)* 80−20937
Al-Cu-Mg (4, 1.5 wt.%), mica dispersed, wear charact. and bearing performance 80−108591
Al-Cu-Mg (4,1 wt.%), behaviour during ductile fracture, SEM *(Rumanian)* 80−21062
Al-Cu-Mg alloy, extruded, press forming in liquid/solid coexisting state, mech. props., Mg effects 78−11151
Al-Cu-Mg alloy, influence of plastic deformation on fatigue limits, for prestrained components 78−68799
Al-Cu-Mg alloy, struct. of Guinier-Preston zones *(Russian)* 79−1870
Al-Cu-Mg alloy D16T, fatigue cracking under cyclic bending *(Russian)* 78−31506
Al-Cu-Mg alloy RR58, comparison of methods of correlating creep crack growth 78−60826
Al-Cu-Mg based, RR58, remaining creep life estimation from creep crack density meas. 78−44194
Al-Cu-Mg precipitation strengthened, Bauschinger effect 77−36585
Al-Cu-Mg/mica particulate composite mech. props. 80−100919
Al-Cu-Mg-Ag casting alloy, precipitation hardening in artificially aged condition 79−1874
Al-Cu-Mg-Fe-Ni, Hiduminium RR58, crack propag. rates in air and salt soln. 80−21063
Al-Cu-Mg-Li alloy extrusions, microstruct., embrittlement and fracture props. 80−60965
Al-Cu-Mg-Mn, shot peened, positron annihilation meas. 77−63833
Al-Cu-Mg-Mn (4.5, 1.5, 0.6 wt.%), alloy 2024-T3, exam. of residual strength of plate containing crack, fracture anal. 78−90792
Al-Cu-Mg-Mn (4.5, 1.5, 0.6, wt.%), alloy 2024-T81, plates, adhesively bonded, exam. of fatigue crack growth 78−92349
Al-Cu-Mg-Mn (4.5, 1.5, 0.6 wt.%), thin sheet, exam. of fracture toughness, and fatigue crack growth 78−92353
Al-Cu-Mg-Mn-Fe-Si, alloy D16, effect of mechanisothermal treatment on mech. props. 78−56674
Al-Cu-Mg-Mn-Si-Fe, endurance with cyclic bending, effect of loading conditions 80−50724
Al-Cu-Mg-Mn-Si-Fe, subcritical crack growth under static plane stress 80−55528
Al-Cu-Mg-Mn-Si-Fe, torsional vibrations decrement, deformed vol. effect 80−76326
Al-Cu-Mg-Mn(-Zn-Cr), low temp. deformed, ageing and mech. props. 79−1881
Al-Cu-Mg-Ni-Fe alloy RR 58, creep resistance at elevated temps., thermomechanical treatment effects 77−59836
Al-Cu-Mg-Si-Fe-Mn-Ti, Si, Fe, Mn and Ti effect on precipitation in solid soln. *(Korean)* 79−66064
Al-Cu-Mg-Si-Mn (2.5, 0.7, 0.7, 0.5 wt.%), alloy AK6, US inspection of heat treatment quality 78−76681
Al-Cu-Mg-Si-Mn alloy AK8, fatigue strength, effect of residual stresses and cold working 77−56101
Al-Cu-Mg-Zn, Mg and Zn addition effects on dendrite struct. and mech. props. *(Korean)* 77−28796
Al-Cu-Mg-(Ag), effect of addition on fatigue microstructure relationships 80−40483
Al-Cu-Mg(-Fe,Si) alloys, double-ageing, resist., hardness meas. 77−28822
Al-Cu-Mg(-Si), inclusions, oriented distrib. metallography and effects on anisotropy *(Russian)* 78−80589
Al-Cu-Mn-Mg alloy D16, sheet, corrosion fatigue strength, with anodised and painted surfaces *(Russian)* 78−35575
Al-Cu-Mn-Mg-Fe-Si, corrosive environment effect on fatigue crack growth rate 80−55584
Al-Cu-Mn-Mg-Fe-Si (4.48, 0.66, 1.55, 0.43, o.23 wt.%), alloy D16, relationship between intercrystallite corrosion depth, and elec. cond. 79−20220
Al-Cu-Mn-Mg-Fe-Si-Zn alloy D16, surface layers chem. composition rel. to fatigue resist., corrosion-fatigue resist. 79−29275
Al-Cu-Si-Mg, deform. simulation using torsional test, elastoplastic constitutive eqn. 80−93594
Al-Cu-Si-Mg (4, 0.8, 0.8 wt.%), GPB zone formation during room temp. ageing 77−44263
Al-Cu(Zn, Ag, Mg_2Si), intermediate precipitates, stability, X-ray, elec. resist. and hardness study 80−3063
Al-insulator-$In_{1-x}Mg_x$ film tunnel junction, resistance zero-bias anomalies 80−107925
Al-Li-Mg, estimation of isothermal sections of phase diagram 79−11567
Al-Li-Mg system, isothermal sections comput. 78−6896
Al-Li-Mg-Be alloys, phase composition of surface films, oxidation protection mechanism *(Russian)* 80−65417
Al-Mg, AMg6, US vibr. during superplastic deform. effect on struct. 79−38911

magnesium alloys continued
Al-Mg, AMg6 alloys, effect of chem. comp. on strength and ductility at low temps. 80−3148
Al-Mg, acoustic emission during tensile testing 80−7632
Al-Mg, acoustic emission power, strain rate depend. 77−4808
Al-Mg, acoustic emission signals in plastic deform., amplitude distrib. *(Japanese)* 78−6978
Al-Mg, age-hardenable, US cavitation erosion mechanisms, effects of comp. and heat treatment 78−53002
Al-Mg, ageing process, effects of Ag additions and pressure *(Russian)* 80−45321
Al-Mg, alloy 5083, effect of environmental factors on stress corrosion cracking 78−80684
Al-Mg, alloy A5083-O, fatigue crack propag. and crack closure behaviour under plain strain conditions *(Japanese)* 80−81160
Al-Mg, cast, chilled zone composition and thickness obs. *(Japanese)* 80−7541
Al-Mg, cold plastic deformation, stress/strain relations 79−56991
Al-Mg, cold working causing preprecipitation, thermoelec. power *(French)* 79−8306
Al-Mg, cold-worked, transport props., 1.5-8.5K 78−7059
Al-Mg, comparison of liquid impact erosion and cavitation erosion 80−104302
Al-Mg, corrosion of chill zone, solidification microstruct. effect 77−36687
Al-Mg, creep behaviour in broad stress interval at 623K 80−30044
Al-Mg, crystallization interface *(Slovak)* 79−78951
Al-Mg, deformation, tension, torsion compression test exam. *(Russian)* 78−31455
Al-Mg, determ. of distortion field, induced by substitutional defect 80−44536
Al-Mg, dil., ang. correlation of annihilation radiation from impurity trapped positrons 80−104010
Al-Mg, dil., Dingle temp. calc. 78−39005
Al-Mg, dil., electron irrad., stage I_E recovery, interstitial trapping 77−15405
Al-Mg, dil., electronic transport coeffs. for point defect scatt., 4-OPW calc. 79−42531
Al-Mg, dil., form of distortion field produced by Mg substitution, elastic neutron scatt. meas. *(German)* 79−42092
Al-Mg, dil., long-range solute-host interactions 78−95062
Al-Mg, dil., neutron irrad., 4.2K, defect prod., recovery 77−1155
Al-Mg, dil., thermal generation of vacancies involving dislocation climb 77−59808
Al-Mg, dil. alloy, ^{65}Zn diffusion 77−51540
Al-Mg, dil. alloy, residual resistivity, model pseudopot. form factors 77−8062
Al-Mg, dil. binary alloy, planar interface stability during solidification *(Slovak)* 80−108424
Al-Mg, dil. deviation from Matthiessen's rule, 4-OPW approx. calc. 79−19574
Al-Mg, discontinuous deform. under various conditions 77−63716
Al-Mg, effect of Ag addition on ageing and related props. 77−36522
Al-Mg, elastic and anelastic props. in relation to Guinier-Preston zones, US investigation *(French)* 79−38833
Al-Mg, electrical resist. and magnetoresist., 2 to 40K, Matthiessen rule deviations *(Russian)* 77−31996
Al-Mg, foil, oxidation in O_2 atm., TEM study 80−104356
Al-Mg, fracture during superplastic flow 78−60729
Al-Mg, fracture resistance at low temps. 80−104284
Al-Mg, grade 5083, superplastic, interaction effects during growth of drilled holes 79−38923
Al-Mg, grain boundary dislocation identification, TEM obs. 77−62534
Al-Mg, homogenisation process, effect of solidification rate and alloying *(Polish)* 79−78949
Al-Mg, liquid alloy energy of soln. pseudopotential calcs. *(Russian)* 79−66330
Al-Mg, liquid impact erosion 80−108598
Al-Mg, low freq. internal friction during plastic deform. *(Chinese)* 80−103420
Al-Mg, Mg effect on ductility, 25 to 250°C 79−100214
Al-Mg, new metastable phase 78−52772
Al-Mg, oxidation control study, electron opt. techniques eval. 80−85089
Al-Mg, oxidation induced stresses, dislocation network form., HVEM obs 80−14978
Al-Mg, pitting potential 78−35550
Al-Mg, plastic deform., separation of internal friction components *(Russian)* 79−52282
Al-Mg, rapidly solidified, metastable phases *(German)* 79−34011
Al-Mg, recrystallised, grain boundary dislocation identification by computer simulation of TEM image *(Japanese)* 77−47457
Al-Mg, recrystallization texture 79−91679
Al-Mg, relationship between props. and nonequilib. phase diagram 79−96000
Al-Mg, Si alloy, void form. under different precip. conditions, after Al ion irrad. 80−59529
Al-Mg, single crystal elastic consts., ultrasonic meas. during ageing 78−11263
Al-Mg, solidification, solid-liq. interface, solute conc. effects 80−59632
Al-Mg, subcritical crack growth under static plane stress 80−55528
Al-Mg, superconducting, an anomalous strain-rate sensitivity of flow stress 79−43313
Al-Mg, thermodynamic props. *(German)* 79−29027
Al-Mg, type AMg6, cryogenic welded vessels, structural strength 80−16477
Al-Mg, type AMg6, pool metal solidification kinetics in welding with electromag. stirring 80−71636
Al-Mg, type A5083P-0 effects of anisotropy in cutting mechanism *(Japanese)* 80−89232
Al-Mg, vapour press. temp. depend., 1104 to 1637K 80−24576
Al-Mg, vertically solidified, effect of fluid flow on solidification struct., and macrosegregation *(Japanese)* 78−48391
Al-Mg, work hardening under tension at 1.6-900K 79−38842
Al-Mg 80−76244
Al-Mg 0.1 at.%, neutron-irradiated, dislocation loop characterisation by TEM 79−23614
Al-Mg (0.1 at.%), neutron damage, positron annihilation 80−65056
Al-Mg (0.3 wt.%) single cryst., dislocations obs. by high voltage electron microsc. 80−79796
Al-Mg (1 to 11 wt.%), alloy A99, dissociation in solid soln., effect of treatment of liquid Al *(Russian)* 78−15353

magnesium alloys continued
Al-Mg (1 to 14 wt.%), oxidation in air, O_2, CO_2 and flue gas 77−73374
Al-Mg (1 wt.%), behaviour during ductile fracture, SEM *(Rumanian)* 80−21062
Al-Mg (1 wt.%), mechanisms of dynamic strain ageing and jerky flow 79−79024
Al-Mg (13 wt.%), aged single crysts., small angle neutron scattering 80−1961
Al-Mg (2 wt%), high temp. creep, effect of cold working on mechanism 79−43351
Al-Mg (2 wt.%), exam. of Harper-Dorn creep 79−5026
Al-Mg (2 wt.%), hardening and fracture charcts., β-phase dissolution role 80−81178
Al-Mg (2 wt.%), steady creep charcts., precip. effect 80−35189
Al-Mg (2 wt.%) subgrain formation at low stresses 78−84928
Al-Mg (2.2 at.%), creep at 573K 79−20145
Al-Mg (2.2 at.%), high temp. creep mech. determ. by stress-relaxation 77−12670
Al-Mg (2.4 wt.%) alloy, solution-treated, grain size effects on fatigue strength 77−4839
Al-Mg (2.5wt.%) sheet, surface oxide state and weldability 80−59769
Al-Mg (3 and 7 at.%) alloys, plasmon-dislocation interactions, electron microscope investig. 77−15421
Al-Mg (33 at.%), liquisol quenched, decomposition 79−61622
Al-Mg (4 wt.%), enhanced ductility at elevated temps. 77−63740
Al-Mg (4 wt.%), struct. and strengthening in hot working 80−84968
Al-Mg (4.4 and 6 wt.%), for liquefied natural gas appls., material and weld props. 79−61736
Al-Mg (4.4 and 6wt.%), liquefied natural gas appls., material and weld props. 79−61735
Al-Mg (4.6 wt.%) alloy, mech. effects during static or cyclic creep 78−39865
Al-Mg (5 wt.%), hardness-flow stress rel. during strain-controlled bending fatigue 79−74245
Al-Mg (5 wt.%), recovered dislocation substruct. during plastic flow 79−83273
Al-Mg (5 wt.%), serrated flow 79−43343
Al-Mg (5 wt.%), static strain ageing at low temp. 79−29116
Al-Mg (5 wt.%) deformed bars, cold rolled, exam. of microstruct. by thin foil TEM 78−88502
Al-Mg (5.5 at.%), applied stress change effect in creep *(Czech)* 79−70126
Al-Mg (5.5 at.%), internal stress during creep at high temp. 79−91749
Al-Mg (5.5 at.%), stress change expt. on creep 79−24584
Al-Mg (5.5 at.%), theory of internal stress for class I high temp. creep 78−19807
Al-Mg (5.5 wt.%), effect of stress changes during creep on dislocation struct., TEM study 79−74214
Al-Mg (5.5 wt.%), instantaneous plastic strain associated with stress increments during steady state creep 78−48478
Al-Mg (5.5%), creep, absence of instantaneous plastic strain upon stress changes 78−75718
Al-Mg (5.7 at.%), stress relaxation test, appl. to discerning frictional and internal stresses 77−63712
Al-Mg (5.7 wt.%) alloy, pre-precipitation, elec. resist. investig. 77−32601
Al-Mg (6 wt.%), liq., environment for Ti ductility testing at 700-900°C *(Russian)* 77−52537
Al-Mg (7 wt.%), bare surface reaction rates in aq. solns. 80−101022
Al-Mg (7 wt.%), β-phase soln. behaviour and mech. props. *(Korean)* 78−11277
Al-Mg (7 wt.%), corrosion cracking, exam. of slip dissolution and hydrogen embrittlement mechanisms 78−72852
Al-Mg (7wt.%), corrosion fatigue crack propag. 80−30145
Al-Mg alloy, AL24M, decomp. kinetics and ageing mechanism *(Russian)* 80−45269
Al-Mg alloy, charge transfer, X-ray emission spectra exam. 77−47774
Al-Mg alloy, creep rate, effect of dislocation pinning by impurity atoms *(Russian)* 78−38719
Al-Mg alloy, crystallisation front form. props., casting in EM field *(Russian)* 80−55384
Al-Mg alloy, disperse β-phase, kinetic laws of coagulation *(Russian)* 78−27518
Al-Mg alloy, nitridation process study 80−61013
Al-Mg alloy, superplastic behaviour, effects of bidirectional twisting 77−70129
Al-Mg alloy AMg5, welded structures, machine for fatigue life investigation 79−52566
Al-Mg alloy AMg6, deform. in plane stress at low temps. 78−39873
Al-Mg alloy AMg6, fatigue, random process effect on life 79−66160
Al-Mg alloy AMg6, mech. props. of welded joints, impurity effects 78−95789
Al-Mg alloy A99, intercrystalline fracture during US treatment 79−15795
Al-Mg alloy Al27-1, corrosion cracking behaviour and fine struct. *(Russian)* 79−52438
Al-Mg alloys, 3004 and 5182, oxide films, IR refl. spectra characterisation 77−77644
Al-Mg alloys, AC colour anodisation 79−20283
Al-Mg alloys, distrib. of liquid Mg at liquid-solid interface *(Slovak)* 79−91637
Al-Mg alloys, initial decomposition exam. by X-ray diffr. *(Russian)* 77−77482
Al-Mg alloys, overheating effects on microstruct. and props. 77−63698
Al-Mg cold drawn wires with FCC lattice, texture and structure 77−70067
Al-Mg foil, alloying effect on strength charcts. and weldability 80−55475
Al-Mg sheet, artificial stress raiser effect on strength and local plasticity of weld joint 80−81130
Al-Mg single crystal, fatigue deform. 79−91747
Al-Mg solid soln., AE during plastic deform. 78−64592
Al-Mg solid solns., decomposition studied by ultrasonic meas. of elastic props. 80−35184
Al-Mg spherical shell with reinforced holes, local stability 80−50686
Al-Mg supersaturated solid soln., spinodal decomposition at 20°C *(French)* 77−85987
Al-Mg surface, growth of MgO film with high secondary electron emission 78−35590
Al-Mg weldment, US testing, defect acceptance criteria, electron strength 77−70239

magnesium alloys continued
Al-Mg/Al_2O_3 composites, interface phase, Auger and electron diffr. study 80−25646
Al-Mg_2Si, ageing sequence study by electron microdiffr. 80−81068
Al-Mg_2Si, STEM microdiffr. obs. of precip. struct. 80−104167
Al-Mg_2Si (0.95 wt.%), excess Si effect on ductility 78−27580
Al-Mg_2Si (1 wt.%), precipitation reactions 80−11652
Al-Mg_2Si (1 wt.%) secondary recrystallisation by grain boundary unsewing 79−1886
Al-Mg_2Si(1.42 wt.%), aged, dislocation structs. caused by plastic deformation 80−25786
Al-Mg-Ag, age effect on age hardening *(Japanese)* 78−52831
Al-Mg-Be, solid soln. decomposition, metallographic study 77−16577
Al-Mg-Bi -Na, Bi additions to prevent Na embrittlement 77−86153
Al-Mg-Cr, tube drawing, tensile forces, plastic deformation *(French)* 79−70130
Al-Mg-Cu-Si-Cr (1,2.7,0.6,0.2wt.%), laser shock hardening of weld zones 78−39800
Al-Mg-Fe-Mg-Si-Cr, alloys, dendritic segregation with Fe, Mg, Si and Cr additions *(Polish)* 79−56980
Al-Mg-Li, subboundary brittleness due to horophilic Na *(Russian)* 77−21244
Al-Mg-Li alloy, 01420, surface layer props. *(Russian)* 78−80674
Al-Mg-Li alloy, metastable S′-phase, struct. *(Russian)* 80−103291
Al-Mg-Li alloy 01420, riveted, low-cycle fatigue strength 80−30097
Al-Mg-Li-Si system, phase diag. *(Russian)* 78−80515
Al-Mg-Li-Zr alloys, struct., mech. props. 79−24498
Al-Mg-Mn, with high Al content, resist., 1.5 to 4.2K 78−26841
Al-Mg-Mn alloy, disperse β-phase, kinetic laws of coagulation *(Russian)* 78−27519
Al-Mg-Mn alloy AMG-6M, endurance determ. by dimensionless damageability curves 79−96141
Al-Mg-Mn-Cr (4, 0.45, 0.15 wt.%), laser shock hardening of weld zones, exam. 78−39800
Al-Mg-Si, brittleness and heat treatment, statistical design of expts. 77−73349
Al-Mg-Si, cast, precip.-rich zones on grain boundaries, soln. heat treatment conditions effect on mech. props. 80−104176
Al-Mg-Si, DTA exam. after small and medium deform. 80−21002
Al-Mg-Si, deformed, orientation of recrystallisation nuclei 79−91681
Al-Mg-Si, dendritic non-homogeneity 78−56641
Al-Mg-Si, dil. alloy, Mn additions and heat treatment effect on $\beta \rightarrow \alpha$ transformation 80−7566
Al-Mg-Si, dispersoid effect on fatigue crack propag. 79−43420
Al-Mg-Si, effect of quenching on recrystn. after hot working 79−43289
Al-Mg-Si, Guinier-Preston zones, inception and effect on ageing, review *(Hungarian)* 79−11627
Al-Mg-Si, heavily rolled, electron microscope obs. of cube oriented region, rolling texture 79−29093
Al-Mg-Si, heterogeneous precipitation studies using differential scanning calorimetry 80−3062
Al-Mg-Si, Mg loss, mass spectrometry/thermogravimetry 77−16620
Al-Mg-Si, nucleation and precipitation growth on dislocations, electron microscope studies 80−3064
Al-Mg-Si, Portevin-Le Chatelier effect, effect of precipitation hardening 77−32585
Al-Mg-Si, precipitation of cube-shaped phases, electron diffr. study using TEM *(Japanese)* 79−43251
Al-Mg-Si, thermomechanically treated, age-hardening 78−11236
Al-Mg-Si, type 6010, microstruct. characts. influence on formability, heat treatment 80−81090
Al-Mg-Si, type 6061-T6, 6063-T6, effective stress range factor in fatigue 80−100924
Al-Mg-Si, under ion irradiated, modification of precipitate interface and effect of precipitates stability 79−77651
Al-Mg-Si (0.52, 0.58 wt.%), ductile fracture intergranular mechanism 79−15784
Al-Mg-Si (0.7, 0.4 at.%), effect of precipitation hardening on strain rate behaviour and yield behaviour 79−29075
Al-Mg-Si alloy, descriptive method for alloy creep tests by nonstationary loadings 78−23759
Al-Mg-Si alloy, Mg_2Si dispersion hardened US waveguides, concentrators *(Polish)* 80−89237
Al-Mg-Si alloy, Mn additions, effect on deform. 77−8876
Al-Mg-Si alloys, DTA exam. of zone form. and other solid phase conversions 77−86057
Al-Mg-Si alloys, DTA meas. of struct. changes in zones after quenching and isothermal heat treatment 79−52248
Al-Mg-Si alloys, ductile intergranular fracture mechanisms, void formation and nucleation 80−108578
Al-Mg-Si alloys, effects of dispersoids upon micromechanism of crack propagation 79−83286
Al-Mg-Si core, deformation behaviour contrib. in rod drawing *(German)* 80−11684
Al-Mg-Si liquid alloy, exam. of thermodynamic props at 780-820°C *(Czech)* 79−91626
Al-Mg-Si rod, extruded and cold drawn, annealing *(German)* 78−39804
Al-Mg-Si solid solution under stress, solute atom clustering during ageing 78−31430
Al-Mg-Si-Cu, cold plastic deformation, stress/strain relations 79−56991
Al-Mg-Si-Cu, tube drawing, tensile forces, plastic deformation *(French)* 79−70130
Al-Mg-Si-Mn, Mn addition effects on fracture 78−60791
Al-Mg-Si-Mn foil, planar defect spacing meas. by TEM 78−2135
Al-Mg-Ti-Zr alloy AL23-1, nucleating cellular dendritic crystallisation *(Russian)* 79−70055
Al-Mg-Ti(Zr), struct. and factors determining brittle intermediate compound form. 78−52817
Al-Mg-Zn, granulated, degassing atm. effect on mech. props. of semifinished products 80−7720
Al-Mg-Zn, interdiffusion 78−51751
Al-Mg-Zn, neutron small angle scatt. study 79−43255
Al-Mg-Zn, O_2^+ ion bombard., SIMS and photon emission spectra, local thermodynamic equilib. model 80−20751
Al-Mg-Zn alloy, surface Be migration, depth profiling by ion microprobe with high mass resolution 79−46894
Al-Mg-Zn alloy 7179-T651, reduced ductility under tensile after exposure to water 80−11835
Al-Mg-Zn alloys, Al-rich, weld metal comp. effect on microsegregation and eutectic phase segregation *(German)* 80−108455

magnesium alloys continued
Al-Mg-Zn alloys, evaporation effect of alloying elements Mg and Zn in in-situ EM studies 80−103388
Al-Mg-Zn alloys, liq./solid phase equilibria determ. *(German)* 80−50601
Al-Mg-Zn solid solution, thermophysical props., 0-400°C *(Russian)* 77−89548
Al-Mg-Zn-Cu, type 7050, calorimetric study of fatigue induced microstructural changes 80−85034
Al-Mg-Zr, phase diagram *(Russian)* 78−11205
Al-Mg-(Ag), effect of addition on fatigue microstructure relationships 80−40483
Al-Mg(-Cu), normal and gravity segregation in ingots, expt. study *(Japanese)* 79−24526
Al-Mg(-Cu)(Si), dimensional changes in heat treatment. 80−89271
Al-Mg(-Zn)(-Zn-Cu), exam. of precipitation struct. by neutron scattering 78−92270
Al-Mg(Cu)(Si), (5.0(4.5)(11.8) wt.%), ingots, vibr. effect during solidification on porosity formation 80−108426
Al-Mg(Mg-Cu), Al_2O_3 fibre reinforced, exam. of interface interactions during fabrication 78−76616
Al-Mg(Zn-Mg), long term strength and creep 80−60925
Al-Mg(0.1 at.%), μ^+ depolarisation 79−56697
Al-Mg(14 wt.%), macrosegregation during solidification *(Japanese)* 79−100150
Al-Mn-Mg laminated composite, fatigue fracture, fatigue strength enhancement 79−87725
Al-Ni-Mg (6, 0.3 wt.%), fine grained, Luder's band deform. 77−77527
Al-Si-Cn-Mg, alloy AL32, ageing of castings produced by pressure die castings 78−56650
Al-Si-Cu-Mg-Ni, piston, depend. between min. creep rate and time of beginning of secondary creep *(Czech)* 80−35267
Al-Si-Mg, corrosion inhibition in 0.1 N NaOH soln. 78−19924
Al-Si-Mg alloys, and Si content and Mg addition effect on mech. props., Na treatment *(Korean)* 79−38901
Al-Zn, Mg effect on transport props., GP zones 77−16588
Al-Zn-Cu-Mg (V95T1), subcritical crack growth under static plane stress 80−55528
Al-Zn-In-Mg, substitution for Mg in Mg-MnO_2 short-circuited cell, performance 79−61964
Al-Zn-Mg, acoustic emission meas. during tensile testing, reproducibility of results 80−50782
Al-Zn-Mg, age hardenable single crystal, fatigue and fatigue cracks *(German)* 77−16689
Al-Zn-Mg, age-hardenable, precipitation and dissoluton processes, positron annihilation and X-ray small-angle scattering comparison 80−89238
Al-Zn-Mg, atmosphere effect on fatigue crack propag. *(Japanese)* 80−81161
Al-Zn-Mg, cavitation during superplastic deform. *(Japanese)* 78−15464
Al-Zn-Mg, crack-arrest markings on integranular stress corrosion fracture surfaces 80−89405
Al-Zn-Mg, decomp. kinetics and ageing mechanism *(Russian)* 80−45269
Al-Zn-Mg, decomposition calorimetric study *(German)* 79−74165
Al-Zn-Mg, dil. alloy, ^{65}Zn diff. 77−51540
Al-Zn-Mg, ductile intercrystalline fracture obs. 77−77554
Al-Zn-Mg, duplex ageing effect on tensile props. 79−91721
Al-Zn-Mg, effect of microstruct. on localised shear failure 78−52996
Al-Zn-Mg, effect of microstruct. and corrosive environments on stress corrosion cracking *(Japanese)* 79−79159
Al-Zn-Mg, elec. resist. of η' precipitates 77−48441
Al-Zn-Mg, fatigue crack propag., stage I 77−36653
Al-Zn-Mg, fractographic stage I fatigue facets 77−16680
Al-Zn-Mg, grain boundary surfaces, plasmon loss satellites in Auger spectra 78−15261
Al-Zn-Mg, grain boundary segregation, AES meas. 78−72781
Al-Zn-Mg, Guinier-Preston zones, comp. and contrib. to elec. resist. 80−16316
Al-Zn-Mg, heat treatment and inversion processes, elec. resist. study *(Hungarian)* 77−25078
Al-Zn-Mg, metastable miscibility gap determ. by small angle scatt. 77−28781
Al-Zn-Mg, O transport during fatigue crack growth 78−52981
Al-Zn-Mg, oriented growth of precipitates on dislocations, model 80−108448
Al-Zn-Mg, plastic deform. influence on structural transform. and mechanical props. *(Russian)* 80−7623
Al-Zn-Mg, plastic instability rel. to grain boundary failure at low temps. 78−56702
Al-Zn-Mg, polygonized struct. in extrusions, thermal stability and mech. props. 80−50659
Al-Zn-Mg, precipitation mechanism, effect of Mg additions *(French)* 77−52330
Al-Zn-Mg, precipitation of η' phase, heat treatment, electron microscope obs. 78−68699
Al-Zn-Mg, precipitation strengthened, Bauschinger effect 77−36585
Al-Zn-Mg, role of dispersed transition metal intermetallic compounds 79−96088
Al-Zn-Mg, solid soln. decomp., 20 to 200°C 79−38830
Al-Zn-Mg, stress conversion cracking based on micromech. surface reactions 80−7716
Al-Zn-Mg, TEM and calorimetric study 80−76290
Al-Zn-Mg, TEM characteris. of precipitates 80−104166
Al-Zn-Mg, type 7075, strain rate effects on H embrittlement 80−3190
Al-Zn-Mg, type 7075-T651 plate, thickness direction inhomogeneity of mech. props. and fracture toughness 80−100892
Al-Zn-Mg, type V-95, ultimate tensile strength for brief impact 80−70309
Al-Zn-Mg, weldable, microstruct. and intercrystalline fracture 77−48550
Al-Zn-Mg, welded section stress in rolled plate edges, mechanical surface treatment and environment effects 80−21193
Al-Zn-Mg, zone composition change during ageing 79−29110
Al-Zn-Mg (2.1, 1.3 wt.%), single crysts., fatigued age-hardenable, dislocation structure *(German)* 80−54247
Al-Zn-Mg (3,1.5 wt.%), precipitation hardened and fatigued alloys, solute loss at fracture surface, EPMA exam. 78−39893
Al-Zn-Mg (3.2, 2.2 wt.%) alloy, GP zone reversion, η' of formation, quant. investig. 77−4784
Al-Zn-Mg (3.6, 1.95 wt.%), ageing and plastic deform., effect on structure, electron microsc. and X-ray diffr. study *(Russian)* 80−81108

magnesium alloys continued
Al-Zn-Mg (3.87, 1.79 wt.%) TEM exam. of early stage precipitation, on dislocation lines 79−4972
Al-Zn-Mg (3.87, 1.79 wt.%), oriented growth of precipitates on dislocations, TEM obs. 80−108447
Al-Zn-Mg (4.5, 2 to 3 at.%) solid state reactions by interrupted continuous heating 80−25737
Al-Zn-Mg (4.5, 2 wt.%), stress corrosion resist., vac. heat treatment effect 79−96203
Al-Zn-Mg (4.5, 2.5 wt.%), fatigue crack propag. 77−86171
Al-Zn-Mg (4.5, 2.5 wt.%), composition effect on stress corrosion and mech. behaviour 78−27684
Al-Zn-Mg (4.5 at.%, 2 or 3 at.%), decomposition behaviour during continuous cooling, XSAS and TEM examination 80−16264
Al-Zn-Mg (4.5 at.%, 2 to 3 at.%), decomp. behaviour during continuous heating 80−29922
Al-Zn-Mg (4.8, 1.2 wt.%), quenched, Guinier Preston zones formation 80−45273
Al-Zn-Mg (5, 1 wt.%), age hardening, conditions leading to localised plastic deform. and fracture in slip bands during fatigue 78−64670
Al-Zn-Mg (5, 1 wt.%), relation between mech. props., SCC and dislocation struct. *(German)* 77−81345
Al-Zn-Mg (5, 2 wt.%), diffusion of ^{65}Zn, 165 to 560°C 77−11743
Al-Zn-Mg (5,2 wt.%), TEM of early stages of precipitation 77−40423
Al-Zn-Mg (5,2.5 wt.%) observation of stress corrosion cracking 78−60868
Al-Zn-Mg (5.9, 2.9 wt.%), ageing effects on microstruct. 80−16306
Al-Zn-Mg (6, 2.5 wt.%), fracture toughness-transgranular fracture relation 77−52447
Al-Zn-Mg (6, 2.5 wt.%) alloy, intergranular fracture mechanism due to ledge formation 79−57089
Al-Zn-Mg (6,1.5%), influence of ageing and cold work on tensile and fracture props. *(Japanese)* 78−52842
Al-Zn-Mg (6,3 wt.%), hydrogen embrittlement and trapping 80−55490
Al-Zn-Mg (6,3 wt.%) high-strength alloy, dislocations distrib., corrosive environment influence *(Russian)* 79−52442
Al-Zn-Mg (6.0, 2.5 wt.%), aged, grain, size depend. of fracture toughness 78−48495
Al-Zn-Mg (6.27, 2.94 wt.%), single crystals, effect of environment on liquid-metal embrittlement, stress corrosion cracking and corrosion fatigue 78−64676
Al-Zn-Mg (9, 1 wt.%), superplastic flow, relative motion of grains 77−52426
Al-Zn-Mg (91, 6, 3, wt.%), H embrittlement and trapping, HVEM obs. 80−76364
Al-Zn-Mg alloy, Ag addition and pre-precipitation treatment, influence on GP zone growth 80−71658
Al-Zn-Mg alloy, microstruct. obs. by optical and electron microscopy *(German, English)* 77−52601
Al-Zn-Mg alloy, stress corrosion cracking, exam. *(Japanese)* 78−53026
Al-Zn-Mg alloy, thermomech. treatment, precipitation and strengthening 79−24527
Al-Zn-Mg alloy, welded, solute profiles at weld bead/parent metal interface 78−19942
Al-Zn-Mg alloy 1915, stress corrosion cracking, protective anodic film *(Russian)* 78−35572
Al-Zn-Mg alloy 7075, effect of thermal and mechanical pretreatments, on Guinier-Preston zone 78−39817
Al-Zn-Mg alloy 7075, unstable shear failure 77−48516
Al-Zn-Mg alloy (6, 3 wt.%), grain boundary segregation, AES exam. 78−39783
Al-Zn-Mg alloy AA-7039, stress corrosion cracking, SEM obs. 80−104323
Al-Zn-Mg alloy V95, two-stage ageing kinetics, mech. props. effects 79−83238
Al-Zn-Mg alloys, decomp. kinetics from Young's modulus obs., microprocesses *(German)* 78−64522
Al-Zn-Mg alloys, decomposition kinetics, resistivity meas., extended jump model 78−84766
Al-Zn-Mg alloys, extra-resistivity of coherent precipitates calc. using X-ray small angle scattering intensities 80−3050
Al-Zn-Mg alloys, grain boundary segregation, implications to stress corrosion cracking 80−84936
Al-Zn-Mg alloys, H_2 bubbles in embrittlement 78−19868
Al-Zn-Mg alloys, precipitation behaviour *(German)* 78−39780
Al-Zn-Mg alloys, stress corrosion cracking *(Japanese)* 77−25194
Al-Zn-Mg alloys stress corrosion 80−35395
Al-Zn-Mg granules and bands rolled from them, heat treatment 80−100862
Al-Zn-Mg plasma sputtered, mech. props. rel. to heat treatment *(Russian)* 80−40387
Al-Zn-Mg powder, selected-area electron diffr. ring patterns 80−50642
Al-Zn-Mg superplastic alloy, cavity growth under creep conditions 80−60940
Al-Zn-Mg type 7N01-T4, weld, SCC in NaCl-H_2O_2 soln. *(Japanese)* 80−108631
Al-Zn-Mg type 7017 and 7018 alloy plate, fractographic study of stress-corrosion crack propag. 79−57158
Al-Zn-Mg-Ag, detection of small amounts of Ag by energy dispersive X-ray anal. 77−60154
Al-Zn-Mg-B fibre reinforced composite, packet rolling, thermodeform. process parameters *(Russian)* 80−55433
Al-Zn-Mg-Co, crazing tendency *(Russian)* 80−30068
Al-Zn-Mg-Cu, age hardened, effect of strain rate, temp. and environment on ductility 80−45368
Al-Zn-Mg-Cu, alloy 7075, hydrostatic pressure effects on ductile fracture 78−60779
Al-Zn-Mg-Cu, alloy 7075, fatigue, loading sequence, normal and reversed sequence effect 78−68791
Al-Zn-Mg-Cu, alloy 7075, effect of purity level, dispersoid type, heat treatment, on fracture toughness 78−80636
Al-Zn-Mg-Cu, alloy 7075-T6, corrosion in halide solutions, exam. of anion dependency 78−60867
Al-Zn-Mg-Cu, alloy 7075-T6, fatigue crack closure with negative stress ratio, following single tensile overloads 78−64687
Al-Zn-Mg-Cu, flaw growth in stress corrosion environment 79−66198
Al-Zn-Mg-Cu, fracture toughness 78−7044
Al-Zn-Mg-Cu, inclusions, oriented distrib. metallography and effects on anisotropy *(Russian)* 78−80589
Al-Zn-Mg-Cu, optimum treatment combination for thermochemical processing 77−44278

magnesium alloys continued
Al-Zn-Mg-Cu, type 7075, microstruct. role in hydrogen assisted fracture 80−30091
Al-Zn-Mg-Cu 7075, extraction and phase anal. 79−15673
Al-Zn-Mg-Cu (6, 2.5, 1.5 wt.%), deform. simulation using torsional test, elastoplastic constitutive eqn. 80−93594
Al-Zn-Mg-Cu (6,2, xwt.%) type alloy, fatigue crack propag., Cu content and recryst. effect 80−60960
Al-Zn-Mg-Cu (6.76, 2.37, 1.80 wt.%), cyclic SCC in salt water *(Japanese)* 80−45435
Al-Zn-Mg-Cu age-hardened alloys, fatigue crack propagation rel. to grain size in vac. and NaCl soln. 80−16538
Al-Zn-Mg-Cu alloy, laminated, adhesively bonded alloy 7075-T6, exam. of fracture resistance 78−76754
Al-Zn-Mg-Cu alloy, stress corrosion cracking mechanisms, rel. to micrographic obs. *(French)* 77−73376
Al-Zn-Mg-Cu alloy, type 7050 and AZ 74.61, engineering props. 79−70219
Al-Zn-Mg-Cu alloy, X-ray microanalysis in scanning transmission electron microscope, limitations 78−20122
Al-Zn-Mg-Cu alloy 7075, SCC from T6 to overaged T7X 77−90487
Al-Zn-Mg-Cu alloy 7075, overaged, precracked stress corrosion specimen, incubation effects 79−91832
Al-Zn-Mg-Cu alloy 7075-T651, adiabatic shear localisation and erosion 79−96157
Al-Zn-Mg-Cu alloys, effect of alloying elements as stress corrosion failure using regression analysis 78−80669
Al-Zn-Mg-Cu foil, STEM-microanal., specimen thickness effect on X-ray count rates 77−70374
Al-Zn-Mg-Cu type 7XXX, Cu effect and recrystallisation, low cycle corrosion fatigue 79−91852
Al-Zn-Mg-Cu type 7075, heat treatment optimisation 80−60888
Al-Zn-Mg-Cu-Co (6.5, 2.5, 1.5, 0.4 wt.%), fatigue crack propag. 80−55521
Al-Zn-Mg-Cu-Co-Fe-Si, powder alloy, fatigue crack tip plasticity, from load interactions 80−21066
Al-Zn-Mg-Cu-Cr, (5.6, 2.5, 1.6, 0.3 wt.%), laminates, 8 and 22 layers, adhesively bonded exam. of fatigue crack propag. 78−92345
Al-Zn-Mg-Cu-Cr, (5.6, 2.5, 1.6, 0.3 wt.%), alloy 7075, plates, adhesively bonded, exam. of fatigue crack growths 78−92348
Al-Zn-Mg-Cu-Cr, shot peened, positron annihilation meas. 77−63833
Al-Zn-Mg-Cu-Cr-Zr, high strength Cr and Zr addition effects 77−59820
Al-Zn-Mg-Li alloys, effect of Li on thermal props. 79−24515
Al-Zn-Mg-Mn, correlation of microscopic features, with macroscopic crack propagation 78−60800
Al-Zn-Mg-Ti, Ti effect on microstructure during ageing 78−64568
Al-Zn-Mg-Zr (6.45, 2.08, 0.11 wt.%), exam. of cyclic stress strain response in corrosion fatigue 78−64788
Al-Zn-Mg-(Zr), low cycle fatigue, grain refinement effect 77−44345
Al-Zn-Mg-(Zr) alloy, microstruct. effect on fatigue crack growth 80−3164
Al-Zn-Mg(Mg-Ti), TEM exam. of early stage ageing behaviour, exam. of precip. kinetics 78−56645
Al-Zn-Mg(3.2, 2.2 wt.%), deform. strengthened by Guinier Preston zones 77−52343
Al-Zn(Ag)-Mg, metastable T′ phase 77−21151
(Al-Mg-Si)-Al_2O_3, SAP type, ageing 79−96055
AlCuMgPb, microstruct. and flow stress during deform. at 573K 77−81307
AlMg, high pressure nitriding 77−70336
Al_3Mg_2, diffusionless phase transformation 80−104150
Al_cMg_{1-c} liquid alloys, vols. and entropies of mixing, calc. 80−75363
$AlMg_2Mn$, H impurity detection by $^1H(^{15}N,\alpha\gamma)$ reaction 80−55767
AlMgSi, adhesive jointing, acoustic anal. *(German)* 78−7168
AlMg5, memory effect of plastically deformed alloy under complex loading 79−38891
AlZnMg alloy, precipitation hardened, strength 78−39786
AlZnMg, corrosion cracking *(Czech)* 79−43478
AlZnMgCuO.5, crack propag. under monotone and cyclic load 78−7006
AlZnMgCuO.5, static crack growth, stress state effect, elec. pot. meas. 78−7007
Au-Mg, charge transfer, Mossbauer effect ^{197}Au isomer shifts, XPS valence-band spectra 80−2676
β′-Au-Mg, de Haas-van Alphen effect, relativistic LMTO bandstructure, Fermi surface 79−37959
Au-Mg, high resolution electron microscope and electron diffr. investigation, obs. of $Au_{15}Mg_4$ monoclinic phase 80−1968
Au-Mg, long-period superstructures, electron diffr. obs. 79−94959
Au-Mg (18 at.%), superstruct. determ., electron microscope obs. 78−75630
Au-Mg alloy, internal oxidation, calorimetric meas. 79−43258
AuMg, B2 intermediate phase, slip system, ordering energy and atomic size ratio depend. 80−59471
B fibre reinforced Al-Mg, calc. of thermodynamic interaction potential between B fibre and matrix 80−11627
B fibre reinforced Al-Mg, heat treatment effect on struct., tensile strength 80−55487
Ba-Mg, liq. alloys, thermodynamic activities determ. 80−50604
Be-Mg, two-band alloy, electronic and optical props., multiband theory 79−37952
C fibre-Mg matrix interaction, strength changes on heating 78−11164
CC Al-Zn-Mg (4.5,1(2)(3) at.%), decomposition during ageing, preageing and cooling rate influence 80−20938
Ca-Li-Mg, isothermal section calc. 79−29034
Ca-Mg, liq. alloys, thermodynamic activities determ. using modified Ruff method *(German)* 80−11631
Ca-Mg, metallic glass, stability, microscopic calcs. 79−32914
$CaMg_2$, phonon spectra 77−20031
Cd-Mg, and Cd-Mg-Hg, magnetic susceptibility behaviour *(Russian)* 77−80912
Cd-Mg, Fermi surface press. derivatives, de Haas-van Alphen effect meas. 77−43477
Cd-Mg, mag. susceptibility near $2^1/_2$th order electron transition, non-linear magnetisation anal. *(Russian)* 80−44859
Cd-Mg, selective dissolution, static samples 80−65228
Cd-Mg, selective dissolution, rotating ring disc electrode 80−65229
Cd-Mg, solid solution hardening of Cd single crysts. with Mg 79−87647
Cd-Mg alloys, positron annihilation meas. of Fermi surface 79−56113
Cd-Mg single crystals, exam. of critical resolved shear stress from 77 to 300K *(Czech)* 79−91741

magnesium alloys continued
$Cd_{1-x}Mg_x$, energy spectrum pseudopotential calcs., mag. props., impurity scatt. *(Russian)* 80−65430
$Cd_{1-x}Mg_x$, mag. props. and electron spectrum parameters *(Russian)* 79−33453
$Cd_{1-x}Mg_x$, magnetic susceptibility anisotropy, press. effects, electronic phase transitions *(Russian)* 80−54869
Cd_xMg_{1-x}, solid-liquid transition 78−6144
Ce-Mg-Fe master-alloy innoculated cast Fe, struct. and props. 80−100843
CeMg, magnetic struct. and cryst. field, neutron diffr. exam. 78−72328
$CeMg_{12}$, reversible alloys, hydrogenation for H_2 storage *(French)* 79−74549
Ce_xMg_y, hydrogen storage materials *(French)* 79−66419
$CeMg_2Si_2$ type structure, role of elongated rhombic dodecahedron in alloy structs. 79−32946
$CeMg_{11}V(Cr)(Mn)(Fe)(Co)$, hydriding and appl. in H_2 storage 80−51009
Cu-Be-Ni-Ti-Mg (2, 0.3, 0.2, 0.02 to 0.4 wt.%), multiple step ageing *(Russian)* 78−19786
Cu-Be-Ni-Ti-Mg bronze, alloying element influence on minimum thermo EMF, cold working *(Russian)* 80−34426
Cu-Ca-Mg, exam. of phase diagrams and thermodynamics props. 79−8275
Cu-Cr-Zr-Mg (0.5, 0.1, 0.03 wt.%), exam. of low cycle fatigue props. at elevated temp. 78−64674
Cu-Mg, precipitating phase nuclei, diffuse X-ray scattering intensity determ. *(Russian)* 77−86031
Cu-Mg, study of internal oxidation using central diffusion of X-rays *(French)* 79−37839
Cu-MgO, dispersion hardened, prep. by milling Cu and Mg oxidising atmos. *(German)* 78−64509
Cu-Sn-Mg, precipitation, effect of thermomechanical treatment *(Japanese)* 79−4970
CuSnMg, crystal struct. anal. 78−91306
Cu_4SnMg, crystal struct. anal. 78−91306
DyMg, mag. props., neutron diffraction and magnetisation meas. 77−16045
DyMg, Mossbauer spectroscopy and mag. props. 77−85624
ErMg, mag. props., neutron diffraction and magnetisation meas. 77−16045
ErMg, Mossbauer spectroscopy and mag. props. 77−85624
$EuMg_5$, Mossbauer effect, effective moments, mag. ordering temp. and isomer shifts 80−34833
Eu_2Mg_{17}, Mossbauer effect, effective moments, mag. ordering temp. and isomer shifts 80−34833
$EuMg_2H_x$, Mossbauer effect exam. 78−48094
F conc. profiles determ. in Mg alloy scales using $^{19}F(p,\alpha\gamma)$ 78−88678
Fe, cast, grey, fracture surface after dynamic fracture, Mg conc. effect 80−100909
Fe, cast, mech. props., demodification influence of isothermal holding and Mg additions *(Bulgarian)* 79−15707
Fe cast, Mg, austenite isothermal transform., Sn addition effect 79−87611
Fe, cast, Mg, despheroidising effect of Bi, Sn on graphite in alloy 78−56670
Fe, cast, Mg, high strength bainitic transform. in C-shape diagram *(Russian)* 79−1860
Fe, cast, Mg, isothermal dissociation of supercooled austenite, exam. of kinetics *(Russian)* 79−29013
Fe, cast, Mg, Pb impurity effect on struct. and mech. props. 79−96089
Fe, cast, Mg effect on nodular graphite form. *(Japanese)* 77−56001
Fe, cast, Mg micro distrib., microprobe anal., electron fractography 77−70373
Fe, cast, Mg treated, fading behaviour *(Japanese)* 78−11152
Fe, cast, Mg treated, graphite modularisation by Mg gas bubbles 78−52867
Fe, cast, Mg-Sb, despheroidising composition and distribution of phases, X-ray obs. *(Russian)* 78−95732
Fe, cast, rare earth-Mg, metallurgical and technological features, appl. in China *(Chinese)* 78−84851
Fe, cast, spheroidizing effect of Mg and Ce modifiers 80−35193
Fe, cast-Mg, 78−44149
Fe-C-Mg, cast iron, graphite phase obs. *(Russian)* 77−59744
Fe-C-S-Mg melt, S and Mg effect on graphite growth shape 79−38817
Fe-C-Si-Mn (1.5-2.9, 2.4-3.4, 0.54-31.7 wt.%), discontinuous decomp. of supersaturated austenite *(Ukrainian)* 79−38788
Fe-Mg, Burgers vector determ., crystal defect observation by weak beam image *(Japanese)* 79−82130
Fe-Mg, cast ferrite-based, graphite nucleation on surface *(Russian)* 80−40360
Fe-Si-MnS-Al, Al effect on hot rolling struct., recrystallization, texture magnetic props. *(Chinese)* 78−11237
FeSe-MnSe phase relationships in presence of excess Fe 77−52291
Gd-Mg, Curie temp. and saturated mag. moment, nonmag. solute effects 78−39301
Gd-Mg, X-ray determ. of Debye temp., mean amplitude of vibr. 78−38802
Gd-Mg amorphous films, spontaneous Hall effect and elec. resist. 80−80251
GdMg, canted mag. struct. in S-ion compound, neutron diffr. obs. 78−34962
GdMg, noncollinear mag. struct., nonlinear band behaviour 80−75706
GdMg, sp. ht., magnetisation and stability of canted struct. 79−78412
$GdMg_3$, mag. props., Mg conc. depend. 78−84392
$GdMg_3$, mag. props. 78−72346
H_2 evolution during isothermal treatment in vacuum *(Russian)* 77−77625
Ho-Mg, crystal field parameters from neutron spectra, rel. to mag. props. in ordered state 77−43546
In-Mg, ordered equiatomic, lattice specific heat meas., Debye temp., superconducting transition 80−54396
LaMg, Pauli paramagnet, mag. susceptibility, nonlinear band behaviour 80−75706
La_2Mg_{17}, sorption of H_2 77−84933
La_2Mg_{27}, reversible alloys, hydrogenation for H_2 storage *(French)* 79−74549
La_xMg_y, hydrogen storage materials *(French)* 79−66419
Li-Al electrode, Mg surface additives effect on performance 80−40698
Li-Al-Mg alloy electrodes, polarisation behaviour and struct. 79−43588
Li-Mg, BCC mag. susceptibility var. with temp. *(Russian)* 77−51878

magnesium alloys continued
Li-Mg, liq., elec. transport props. and phase diagram 78−23070
Li-Mg, liq. alloy, thermoelec. power and elec. meas. 77−47788
Li-Mg, liquid alloys, thermodynamic investigation *(German)* 79−91630
Li-Mg, Mathiessen's rule, elec. and thermal deviations, impurity scatt. 80−88536
Li-Mg, positron annihilation and charge transfer 78−31274
Li-Mg, X-ray Compton scatt. 77−16421
LiMg, ordered, local density of states and local environment 79−82509
Mg alloy MA12, thermally strengthened, fatigue cracking in air and vacuum *(Russian)* 78−35481
Mg cast iron, effect of heating temp. on microstruct. and mech. props. 77−56005
Mg cast iron, microstruct. of spheroidal graphite, rel. to polishing and annealing treatments 77−56160
Mg/Mg_2Cu eutectic, hydriding and dehydriding kinetics obs. by press. sweep method 80−35765
Mg-Ag, anisotropic, dislocation interaction with tetragonal impurity, mobility 77−19953
Mg-Ag, dil., dislocation-point defect interactions in slip systems 78−47417
Mg-Ag, dil., ion irradiated, interaction between Ag and defects, channelling meas. 78−38766
Mg-Ag, ion implanted, recovery stage characterisation by electron irrad. 80 107295
Mg-Ag (0.18 at.%), channelling meas. of trapping efficiencies of solute atoms for self-interstitials 79−86829
Mg-Ag-Cd, X-ray diff. exam. of phase fields *(Russian)* 79−56957
Mg-Ag-Cu, phase comp. in Mg-rich region *(Russian)* 80−40331
Mg-Al, dil. alloy, residual resistivity, model pseudopot. form factors 77−8062
Mg-Al, thermal conductivity, data anal. and synthesis 78−95284
Mg-Al, unidirectional solidification, method for determ. of diffusion and thermal diffusion coeffs. in molten Mg 78−30772
Mg-Al (0.8 wt.%), grain-boundary sliding component in high temp. fatigue 80−50706
Mg-Al (25 wt.%) powder, reaction with high press. H_2, MgH_2 form. and decomposition *(Korean)* 78−11554
Mg-Al (5, 7, 9 and 11 at.%,) discontinuous precipitation growth kinetics 77−63677
Mg-Al (9 wt.%), ageing via cellular reaction, microanal., cell boundary vel. meas. 78−11230
Mg-Al cylindrical shells, loading history, effect on plastic buckling *(Russian)* 79−14288
Mg-Al single crystal growth, specimen for tensile testing in corrosive medium *(Russian)* 80−20774
Mg-Al-Tl(Pb) systems, phase diags., electrode pots. *(Russian)* 78−80516
Mg-Al-Zn, anelastic creep and recovery 77−63709
Mg-Al-Zn (3, 1 wt.%), alloy AZ31, mech. props. of extruded and welded pipe and sheet, optical microscopy exam. 79−34065
Mg-Al-Zn (94.3, 3.9, 1.8 wt.%), pricip. on dislocations, weak-beam TEM 80−76264
Mg-Al-Zn (9wt.%Al), sand cast, preferred orientation and mechanical props. *(Japanese)* 80−20979
Mg-Al-Zn-Mn (8, 0.5, 0.3 wt.%) casting alloy, penetration resistance 80−100901
Mg-Al(-Zn), solute-vacancy binding energies from hardness meas. 78−39789
Mg-Al(Sn)(Ni)(Cu), damping capacity 77−48474
Mg-Be, reactor fuel element cladding, corrosion resistance in $K_2Cr_2O_7$ aq. soln. 79−76074
Mg-Bi, liq., far IR reflectivity meas. 77−52105
Mg-Bi, thermodynamic study vapour pressure measurement by transpiration 78−44395
Mg-Bi (30 at.%), molten, short range order and partial struct. factor, neutron and X-ray diffr. 78−9941
Mg-Bi alloy, liq., far IR reflectivity rel. to possible transport processes 78−2827
Mg-Bi melt; X-ray and neutron diffr., conc. depend., correl. number and nearest neighbours 80−49091
Mg-Ca(Sr)(Ba), liquid, thermodynamic charact. *(German)* 77−59757
Mg-Cd, anisotropic, dislocation interaction with tetragonal impurity, mobility 77−19953
Mg-Cd, complex energy band, l-depend. pseudopot. 78−84124
Mg-Cd, dil., dislocation-point defect interactions in slip systems 78−47417
Mg-Cd, plasmon loss and plasmon gain, X-ray photoemission and AES 79−23918
Mg-Cd, single crysts., temp. depend. of crit. resolved shear stress *(Czech)* 80−29112
Mg-Cd, thermodynamic props., order-disorder transitions based on Helmholtz free energy 79−37853
Mg-Cd, variation in interatomic interaction and lattice parameters during ordering *(Russian)* 77−81255
Mg-Cd melts, atomic struct., short range order and melting *(German)* 78−14273
Mg-Cd single crysts, crit. resolved shear stress, temp. and comp. depend. 79−91659
Mg-Ce, diffusion coeff. determ. during hydriding *(German)* 79−29288
Mg-Ce, workability, aging characts. and tensile strength 80−55416
Mg-Cu, electronic struct., X-ray emission obs. 77−16428
Mg-Cu-Pb system, phase equilibria in Mg-rich corner *(French)* 78−76630
Mg-Cu(Ni), binary system, nonstoichiometry, of Laves phases, $MgCu_2$ and $MgNi_2$ *(French)* 78−52770
Mg-Er (<25%), struct. and props. 79−96001
Mg-Eu, dil. alloy, mag. suscept. meas. 77−89925
Mg-Fe, dil. alloy, single impurity Kondo behaviour in elec. resist. *(French)* 79−60815
Mg-Fe, unidirectional solidification, method for determ. of diffusion and thermal diffusion coeffs. in molten Mg 78−30772
Mg-Fe alloy film, quench-condensed, resistance meas. 79−15235
Mg-Fe film, defect energy distrib., elec. resist. meas. during annealing 80−54808
Mg-Ga, form. enthalpies and excess entropies, differential scanning calorimetry *(German)* 79−51278
Mg-Ga, metastable cryst. and glassy phases, X-ray struct. anal. and electron microscopy *(German)* 79−46601
Mg-Ga, X-ray spectra, electronic struct. *(Russian)* 77−48279

magnesium alloys continued
Mg-Ga (6 wt.%), precipitation, lattice const., ageing effects *(Chinese)* 79−43279
Mg-Ga system, thermodynamic props. of metastable and glassy phases *(German)* 79−52743
Mg-Ga-In(Tl) and Mg-In-Tl, phase diagrams and electrochem. props. *(Russian)* 80−40330
Mg-Gd(Ho), dil., magnetoresist., anomalous Hall effect 80−15502
Mg-Ge, X-ray spectra, electronic struct. *(Russian)* 77−48279
Mg-Ho, phase diagrams and transformations, Ho solubility *(Russian)* 79−52162
Mg-In, catalytic effect of In on Mg/H_2 reaction, kinetics 78−76851
Mg-In, complex energy band, l-depend. pseudopot. 78−84124
Mg-In, short-range order, temp. and conc. depend. *(Russian)* 77−43173
Mg-In dil. alloys, effect of alloying on Fermi surface, de Haas-van Alphen effect meas. 77−76732
Mg-In dil. alloys, effect of alloying on Fermi surface, pseudopot. model 77−76733
Mg-In liquid solns., EMF and calorimetric meas. 80−55359
Mg-La, workability, aging characts. and tensile strength 80−55416
Mg-La(Ce)(mischmetal) alloys, appl. to H_2 storage 80−72093
Mg-Li, complex energy band, l-depend. pseudopot. 78−84124
Mg-Li dil. alloys, effect of alloying on Fermi surface, de Haas-van Alphen effect meas. 77−76732
Mg-Li dil. alloys, effect of alloying on Fermi surface, pseudopot. model 77−76733
Mg-Li-Al, phase diag. *(Russian)* 77−59746
Mg-Li-Al (31, 1 at.%), heat treated, precipitation 80−40364
Mg-Li-Ga(Ge)(In)(Tl)(Pb), phase diagram, isothermal cross section *(Russian)* 80−20900
Mg-Li-Sn system in Mg-rich region *(Russian)* 77−52289
Mg-Li-Sn-Al, investigation in Mg rich region *(Russian)* 78−15364
Mg-$Mg_{17}Y_{13}$, high temp. hydrides for vehicular H storage 80−45793
Mg-Mg_2Ni, high temp. hydrides for vehicular H storage 80−45793
Mg-Mg_2Ni eutectic alloy and Mg_2Ni, catalytic effect in hydrogenation, surface analysis 80−30283
Mg-$MgNi_2$-Zn, diagram of state, Zn solubility, initial phase precipitation *(Russian)* 80−66478
Mg-Mn, dil., cryst. field and spin parameters, transmission ESR obs. 77−40130
Mg-Mn, dil., mag. props., EPR meas. 79−73804
Mg-Mn, dil. alloy, de Haas-van Alphen effect, exchange interaction, Kondo effect 78−88093
Mg-Mn, dil. alloy, single impurity Kondo behaviour in elec. resist. *(French)* 79−60815
Mg-Mn-Ce, MA8, dislocations at grain boundaries and grain-boundary glide 78−64605
Mg-Mn-Ce, structural changes and deformation during superplastic flow 78−15472
Mg-Mn-Ce (1.5, 0.3 wt%), superplasticity role of diffusional creep *(Russian)* 80−97528
Mg-Mn-Ce (1.5%, 0.3%), dislocation slip during superplastic deform. *(Russian)* 77−21214
Mg-Mn-Ce alloy, superplastic deform., role of grain boundaries 78−19843
Mg-Nd-Zn dilute alloy, metallography and precip. kinetics 80−71655
Mg-Nd-Zr, phase diagram, Mg rich region, microscopic anal. and elec. resistivity meas. *(Russian)* 78−56619
Mg-Ni-W-Co-Al-Cr alloy KhN56VMKYu, Al effect on excess Mg phase 80−29926
Mg-noble metal alloy, sintered, supercorroding for heat and H_2 gas generation, seawater reaction 78−15607
Mg-rare earth dilute alloy, mag. susceptibility and magnetisation 80−15689
Mg-Si, unidirectional solidification, method for determ. of diffusion and thermal diffusion coeffs. in molten Mg 78−30772
Mg-Si (5 wt.%), thermally induced strains, X-ray line broadening 77−4809
Mg-Sm, phase diagram and mech. props. *(Russian)* 80−20892
Mg-Sm, solid soln., phase diagram *(Russian)* 77−25015
Mg-Sn, melt, assoc., liquidus curve calcs. *(German)* 79−20352
Mg-Sn melt, density and free surface energy *(Russian)* 77−66074
Mg-Sr, liq. alloys, thermodynamic activities determ. 80−50604
Mg-Tb, (up to 45 wt.%), phase diagram, and mech. preps. 80−16277
Mg-Tb(Dy)(Ho)(Tm), dil., macroscopic shape effect due to quadrupole orientation, magnetostriction and thermal expansion meas. 80−60396
Mg-Tl liq. systems, thermodiffusion of Tl 77−11717
Mg-Tm, phase diagrams in Mg rich region *(Russian)* 77−52286
Mg-Y-Al alloys, phase equilib. *(Russian)* 80−20890
Mg-Y-Cd, phase equilibria and mech. props. *(Russian)* 80−20894
Mg-Y-Nd-Zn-Zr (2,2,0.3, 0.7 wt.%), heat treatment effect on casting dimensional stability, alloy mech. props. 78−44146
Mg-Y-Zn (20, 30 wt.%), phase equilibria investigation *(Russian)* 79−74131
Mg-Y-Zn alloys, phase equilib. *(Russian)* 80−16271
Mg-Y-Zn-Nd-Cd alloys, influence of Zr addition on struct. and mech. props. *(Russian)* 80−40370
Mg-Y-Zr, phase equilib. and props. *(Russian)* 77−66626
Mg-Yb, dil., Kondo scatt. from Yb, low temp. elec. resist. meas. 80−44578
Mg-Zn, amorphous sputtered film, elec. props. 78−68006
Mg-Zn, metallic glass, stability, microscopic calcs. 79−32914
Mg-Zn (5 wt.%), age hardening, X-ray diffr. anal. *(Chinese)* 80−104173
Mg-Zn alloy, aged, one dimensional transition phase β'_2, crystallographic obs. *(Chinese)* 80−60865
Mg-Zn metallic glass, hardness, elastic moduli, density, cryst. temp., mech. props., for flywheel appl. *(Dutch)* 78−52878
Mg-Zn-Zr, cast, exam. of phase composition, mech. props. 79−100217
Mg-Zn-Zr rare earth alloy, mech. props., effect of microshrinkage during solidifaction 79−43234
Mg-Zn-Zr-Cd-Nd, Lawes phase separation using acetate electrolyte, Cd and Nd effects 79−70237
Mg-Zr, cavitation during diffusion creep 77−44296
Mg_2 Ni metal hydrides, numerical physical property data for H storage 80−40929
MgAg, 4d bandwidth influence on $M_{4,5}N_{4,5}N_{4,5}$ Auger spectra 79−100017
MgAg, Auger spectra, 4d bandwidth effect 80−89093
$Mg_{1.86}Al_{1.67}Si_{2.47}O_{3.19}N_{3.81}$, 12H polytype, intergranular phases and compositional variations 80−79645

magnesium alloys continued
Mg_2Ca, reversible alloys, hydrogenation for H_2 storage *(French)* 79−74549
MgCd wire, elongation during disorder-order transform. *(Russian)* 80−104148
Mg_3Cd, disordering under electron irrad. in electron microscope 78−83849
Mg_3Cd, effect on order, of compression deformation 78−52924
Mg_3Cd, lattice imaging of B19 ordering transform. and interfacial struct. 77−36495
Mg_3Cd, order-disorder transformation kinetics 80−2138
$Mg_3Cr_2Al_{18}$, pyrochlore struct. and its relatives 79−14773
$MgCu_2$, Fermi surface investig. by de Haas-van Alphen effect 77−35857
$MgCu_2$-$MgAl_2$, Friauf-Laves phase, long-period stacking variants, electron conc. depend. 77−80444
$MgCu_2$-$MgNi_2$, electronic sp. ht. 1.5 to 4.2K, Fe impurity effects *(German)* 77−59125
$MgCu_2$-$MgZn_2$ system, heats of form. of Laves phases *(German)* 79−66337
Mg_2Cu, industrial hydride reservoir, characts., technological aspects 80−45792
Mg_2Cu polycrystals, surface study by AES, XPES and X-ray induced AES 80−65346
Mg_2Cu sorption capacity, grain size distrib., and compactness for H_2 storage appl. 79−74547
$Mg(Cu_{0.535}Al_{0.465})_2$, 2D lattice images of Friauf-Laves phase and defect type 80−24324
$Mg(Cu_{1-x}Al_x)$ with x=0.465, Friauf-Laves phase, electron microscope obs. 77−19908
$MgCu_{2-x}Ni_2$, X-ray and neutron diffr. investigation of Laves phases of $MgCu_2$-type *(German)* 80−15050
$Mg(Cu_{1-x}Zn_x)_2$, crystal struct. and lattice spacing under high press. comp. depend. 77−72581
$MgCu_{2-x}Zn_x$, X-ray and neutron diffr. investigation of Laves phases of $MgCu_2$-type *(German)* 80−15050
$Mg_{1-x}Er_x$, dil., cryst. field interactions, neutron scatt. spectra 80−50048
MgEu, dil. alloy, cold worked, valence transform. of Eu due to defect association, mag. suscept. and Mossbauer meas. 77−51404
Mg_2Ge, L, electron-phonon interaction and phonon cond. at low temp. L n-type semicond. 79−14903
Mg_2Ge, semicond., electronic band struct., reson. Raman scatt. meas. 77−12384
Mg_2Ge, three-phonon relaxation rate and phonon conductivity 78−14416
Mg_2Ge, valence band, XPS meas. 77−8018
MgHg, de Haas-van Alphen effect obs. 77−24512
β'-MgHg, energy bands and Fermi surface calc. 77−43481
MgIn, atmospheric corrosion, SEM, electron diffraction and electron probe obs. 79−24681
MgIn, X-ray diffr. exam. of compressibility 78−51610
$Mg_{0.25}In_{0.75}$ sensitising layer, effect on laser machining and ageing characts. of granular Bi film 77−62020
$Mg_2(Ni,Cu)$ cubic metal binary alloys for H energy storage 80−45787
Mg_2Ni, magnetism and H_2 storage 80−70941
Mg_2Ni sorption capacity, grain size distrib., and compactness for H_2 storage appl. 79−74547
Mg_2NiH_4, solar energy storage by metal hydride 80−61455
Mg_2NiH_x, PMR exam. of motion of H 78−56383
$MgNi_{2-x}Zn_x$, X-ray and neutron diffr. investigation of Laves phases of $MgCu_2$-type *(German)* 80−15050
$MgSi_2$, laser irrad. induced form., cryst. microstruct. 80−35011
Mg_2Si, semicond., electronic band struct., reson. Raman scatt. meas. 77−12384
Mg_2Si, stress effects on Raman spectra 77−20851
Mg_2Si, valence band, XPS meas. 77−8018
Mg_2Si, valence band density of states, pseudopot. calc. 78−72067
Mg_2Sn, L, electron-phonon interaction and phonon cond. at low temp. L n-type semicond. 79−14903
Mg_2Sn, lattice dynamics, angular force model 77−4166
Mg_2Sn, Mossbauer effect exam. under press. up to 75 kbar 79−69759
Mg_2Sn, phase transition under hydrostatic pressure, Mossbauer effect and electric resistance 78−51665
Mg_2Sn, phase transitions under high hydrostatic press., Mossbauer spectra 79−87628
Mg_2Sn, semicond., electronic band struct., reson. Raman scatt. meas. 77−12384
Mg_2Sn, stress effects on Raman spectra 77−20851
Mg_2Sn, third-order elastic constant, low temp. limit of Gruneisen parameter 79−73280
Mg_2Sn, valence band, XPS meas. 77−8018
β'-MgTl, energy bands and Fermi surface calc. 77−43481
MgTl, fermi surface exam. by de Haas-van Alphen effect 78−34752
$MgZn_2$ Laves phase, deformation-mechanism maps 79−29150
$MgZn_2$, single cryst., yield strength 77−44318
$MgZn_2$, solid soln. softening in homogeneity range, dislocation density and velocity *(German)* 77−44264
$MgZn_2$, struct. exam. using Shaw's model potential calc. 77−19906
$MgZn_2$, two-layer, Friauf-Laves phases, stacking variants 80−96468
$MgZn_2$-$MgAg_2$, Friauf-Laves phase, long-period stacking variants, electron conc. depend. 77−80444
$MgZn_2$-$MgAg_2$ system, Friauf-Laves phases, stacking variants 80−96468
$Mg_{70}Zn_{30}$ metallic glass, struct. and dynamics 79−37632
$Mg_{74}Zn_{26}$, glass, exam. of crystallisation 78−71681
$(Mn_{1-x}Cr_x(Fe_x))B$, Invar charact. 77−15602
Mo fibre reinforced AlMg, SEM study *(Slovenian)* 78−84923
Nb/Cu-Sn-Mg, superconductor, effect of Mg addition to Cu-Sn matrix 80−25028
$Nd_{0.25}La_{0.75}Mg$, cryst. field, neutron diffr. meas. 78−34810
Ni-based superalloys, hot workability, effect of S, Ca, Mg, Y and Zr minor elements 80−66552
Ni-Cr-Mg alloy, KhN70VMTYu, Mg effect on grain boundary struct., props. 79−19261
Ni-Cr-MgO system, elec. resist. variation with comp. and prep. method 78−60637
Ni-Si-Mg, thermocouple alloy, props. and thermoelec. reference data 79−26057
$Ni_2Mn_xT_{1-x}Sn$, T=Ti(V)(Cr), ferromag., magnetisation, susceptibility 77−12102
$Pr_{0.25}La_{0.75}Mg$, cryst. field, neutron diffr. meas. 78−34810
$PrMg_3$, cryst. field study, inelastic neutron scatt. and sp. ht. meas. 80−59939

magnesium alloys continued
Rh_7Mg_{44} structure types, alternative description of cryst. struct. 79−7577
Sc-Mg, low-temp. heat capacity 80−75370
SiC fibre reinforced Al-Mg, heat treatment effect on struct., tensile strength 80−55487
$SnMg_2$, ^{119}Sn temp. depend. isomer shift, pseudopot. approach 80−84675
TMg, direct coulombic contrib. of cond. electrons to cryst. elec. field 79−91005
Tb-Mg, mag. ordering temps., susceptibility meas. 80−25136
TbMg, mag. struct. and mag. props. 77−8275
$TbMg_3$, antiferromagnetic struct. 78−14930
$TbMg_3$, mag. props., Mg conc. depend. 78−84392
$TbMg_3$, mag. props. 78−72346
$ThMg_2$, cubic Laves compound, sp. ht. rel. to supercond. 79−82356
Ti-Mg-ZrC(HfC)(TiC)(TiB_2) sintered, friction and wear props. 79−70019
U/Magnox fuel element materials performance 80−47580
YMg, direct Coulomb contrib. of cond. electrons to crystalline elec. field 77−76784
YMg, Pauli paramagnet, mag. susceptibility, nonlinear band behaviour 80−75706
Zn-Al-Cu-Mg (4.1, 3.1, 0.05 at.%), thermal cond. and sp. ht. meas. below 4.2K 77−20081
Zn-Al-Cu-Mg-Pb-Sn, Cu, Mg, Pb, Sn effects on corrosion in wet steam 77−48585
Zn-Al-Cu-Mg-Pb-Sn (12, 1, 0.02, 0.01, 0.015, wt.%), combined effects of Pb and Sn additions on corrosion, in wet steam 78−39952
Zn-Al-Mg alloy, annealed, recrystallised, influence of strain and purity on orientation *(Russian)* 79−52234
Zn-Al(Mg) alloys, cold-rolled, texture formation rel. to Zn purity *(Russian)* 77−59804

magnesium compounds
see also magnesium alloys
bone china body, MgO effect on vitrification mech. props. *(Japanese)* 79−78922
carboborite, cryst. struct. *(Chinese)* 78−18615
carboborite, X-ray crystallographic investigation *(Chinese)* 78−18614
chrysotile, cryst. struct. rel. to milling, X-ray diffr. 77−55278
complex, $Mg(H_2O)_6H_2(EDTA)$, Cu^{2+} doped EPR and ground state wavefunction of Cu^{2+} 79−56605
cordierite, dense ceramic prep. with sintered condition over 300°C interval 79−33983
cordierite, thermal expansion 78−6165
cordierite glass ceramics, effect of TiO_2 and ZrO_2 content on phase sequence during heat treatment 78−48381
cordierites, synthetic end members, variation of refr. index with water content 80−80739
dichlorophosphate complexes, cryst. struct. ^{35}Cl NQR obs. 80−108108
dolomite, powders sintering, decarbonisation cycle effect 80−104102
dolomite, shock compressed, vel. of sound meas. 78−10123
enstatite-pyrope system, high press./temp. phase behaviour rel. to Earth mantle 78−11882
enstatite-type glass-ceramic, crystn. kinetics and mechanism 77−55241
eucryptite-cordierite binary system, sintering of polycrystalline bodies *(Japanese)* 77−12588
floating zone method growth, interface shapes 80−60775
fluor-richterite crystal, habit, growth in oxide-fluoride mixtures, statistical study *(German)* 78−38639
formate dihydrate, 2-D Heisenberg antiferromag., sp. ht. 78−14965
geikielite, solid soln., phase transform. during reduction *(Russian)* 78−44042
humite, real structs., mixed layer characts. 78−79567
ilmenite, cryst. struct. at various compositions 79−86769
Kikuchi pattern intensity, angular and temp. depend. 78−2349
magnesial refractory concretes, cast. props. 80−89306
magnesian-spinel materials form. using heat treatment 79−38773
magnesioferrite precipitated particles in MgO, resonance anisotropy field 77−69541
magnesite, powders sintering, decarbonisation cycle effect 80−104102
magnesite artifacts, roasted, props., filler porosity effect 80−104099
magnesite refractories, unfired, by resin phosphate binding 80−104101
magnesite-chromite powder, exam. of rheological characts., compaction 78−60628
magnesite-dolomite refractories, tar bound, fracture and wear 80−104287
magnesite-phosphate mortar, rheological props. 77−23927
magnesium formate, γ-irrad., ESR of free radicals 79−65737
magnesium hexahydrate $H_2EDTA:VO^{2+}$, single cryst., ESR spectra and spin Hamiltonian parameters 80−75845
magnesium phthalocyanine, depletion layer studies, temp. depend. of LF capacitance 80−65617
magnesium platinum oxalate, X-ray diffuse scatt., 1-D Peierls-Kohn anomaly and struct. transforms. 78−14680
$(Mg_{0.88}Fe_{0.12})_2SiO_4$, natural peridot, shock-prod. olivine glass, TEM 78−10178
$Mg_{1.34}Fe_{0.16}Al_{0.12}Ti_{0.38}OBO_3$, warwickite, cation distrib. from X-ray struct. and Mossbauer spectra anal. 79−1424
$MgAl_{2-x}Fe_xO_4$ solid solution system, solid state properties study 80−93094
micaceous-crystalline material, cast, prep. and props. 77−12591
molybdates, nonstoichiometric, IR spectra rel. to vacancy struct. *(French)* 78−43867
monticellite, solubilities of sesquioxides 79−69253
mullite-based dispersed refractory system, rheological props. at high temp. 77−16629
$Pb_3M_8Nb_2O_9$ crystals for optical radiation control 79−81554
periclase, fused, and periclase-chromite blocks, produced from beneficiated starting meterials, struct. and props. 79−87600
periclase, solubilities of sesquioxides 79−69253
periclase refractories, props. after testing at over 2000°C 80−104317
periclase-spinel refractories, phase conversions up to 1720°C 80−25670
platino-oxalate, one-dimens. conductors, prep., struct. and elec. cond. 80−24900
polyorganosiloxane-talc composites, high-temp. transitions 79−52152
serpentine minerals, milling rel. to cryst. struct., X-ray diffr. 77−55278
silicate grain formation in nova envelope 77−82254
silicate minerals, mantle related, thermodynamic props. at high press. and temp. 80−81874

magnesium compounds continued
silicates, entropy estimates at 298K from molar vols. 77−1243
sodium magnesium aluminium oxdate, elastic consts., Debye temp. 79−82275
spinel oxide, dissociation of dislocations and plastic deform., temp. effects 79−7613
steel, austenitic, type 316, in $MgCl_2$, acidity and applied potential effect on stress corrosion cracking 80−85076
symmetry anal. in neutron diffr. studies 80−25091
talc, ^{57}Fe Mossbauer analysis 80−40006
talc, lattice parameters meas. by back-reflection pseudo-Kossel technique 79−82124
talc, pulsed RF radiation produced by scratching *(Russian)* 78−19607
triple orthoarsenates, $KMgCr_2(AsO_4)_3$ and $NaMgCr_2(AsO_4)_3$, prep. by high temp. synthesis, and cryst. struct. 79−66028
vermiculite, electric field gradient, Mossbauer absorption 79−73865
vermiculite, firing temp. depend. of Mossbauer parameters 80−15837
Ag-MgF_2-Ag layered system bounding dielec., ATR ang. spectra, assoc. reson. EM oscills. 79−15541
Ag-MgO, dispersion hardened, exam. of ductile fracture 79−34144
Ag-MgO (0.1 wt.%), intergranular cavity growth at elev. temps. 79−66068
AgMgO for LV switchgear contacts, properties, prep. *(Slovak)* 78−56603
Ag_2O-Al_2O_3-MgO-Na_2O, β″-alumina, structure, X-ray determ. 80−107148
Ag_2O-MgO-Al_2O_3, ionic cond. 80−107480
Al-MgF_2, reflective multilayer coatings for far UV 77−758
Al-MgF_2 coatings for UV reflecting mirrors for space appls. *(French)* 77−67022
Al-MgF_2 layers on transparent substrates for making scales 77−798
$AlMgB_{14}$, prep. and electrothermal props. 80−20863
β-$Al_{11-y}Mg_yO_{16}$, X-ray diffuse scatt. obs. of struct. 80−107186
$Al_3Mg_2[Si_5AlO_{18}]$, cordierite cryst., effect of face symmetry on structural ordering of Al 78−22703
Al_2O_3, sintered, MgO-enhanced densification, test of second phase and impurity segregation models 78−64511
Al_2O_3:MgO, diffusion creep examined under three-point bending *(Japanese)* 79−96104
Al_2O_3:MgO, grain boundary segregation of Ca and Mg X-ray spectrosc. and STEM study 80−107269
β-Al_2O_3:MgO, strength and delayed fracture behaviour 80−35290
Al_2O_3:$MgTiO_3$, sintering temperature effect of titanate additions 80−60808
β-Al_2O_3-K_2O-MgO, cryst. struct., nonstoichiometry, ion-ion correlations 80−88129
Al_2O_3-MgO, MgO addition role in sintering 79−91608
β-Al_2O_3-MgO ceramic, formation and structure of atomic scale cracks 80−45395
Al_2O_3-MgO spinel, 9.4 GHz US wave damping, defect and phonon scatt. 77−39637
Al_2O_3-MgO/ZrO_2-CeO_2/MgF_2 triple layer antirefl. coating for crown glass in visible region 78−13777
Al_2O_3-MgO-Ag(Au)(Cr)(Cu) cermet selective surfaces for evacuated solar collectors 79−43785
Al_2O_3-MgO-Cr_2O_3, effect of Cr_2O_3 on surface grain growth 79−23815
Al_2O_3-MgO-H_2O fast proton conductor 78−91480
Al_2O_3-$MgTiO_3$, sintering *(Polish)* 79−100096
β-Al_2O_3-Na_2O, MgO stabilised sintering *(German)* 78−19696
β″-Al_2O_3-Na_2O-MgO, blocking defects observed by high resolution electron microscopy 78−55879
Al_2O_3-P_2O_5-Mg(Ca)(Sr)O glasses, Na^+, Sr^{2+} diffusion coeffs. rel. to temp. 78−30787
Al_2O_3-SiO_2-Fe_2O_3-CaO-MgO-TiO_2, refractory, corrosion and mech. behaviour correlations 80−40563
Al_2O_3-SiO_2-MgO, cordierite, powder, synthesis using silicic acid, clay and $AlCl_3$ *(German)* 79−4933
Al_2O_3-SiO_2-MgO-CaO, blast furnace slag, viscosity, MP *(Russian)* 77−25039
Al_2O_3-TiO_2-MgO.$2TiO_2$, exam. of solid solutions by X-ray phase analysis 79−95981
$(Al_2O_3)_n$MgO, spinel composition, dislocation climb, mass transport 79−32996
Au-MgO cermet film, dielectric const. and selective solar absorption 78−2937
B_2O_3.Fe_2O_3.2MgO, mag. props. up to 1200K transitions and magnetisation curves 77−36069
$BaGeO_3$-(0.25MgF_2.0.75YF_3)-Ga_2O_3 glass, synthesis and props. 80−25648
$BaGeO_3$-$CaF_2$$MgF_2$-$Ca_2Al_2GeO_7$($CaTiGeO_5$) systems, glass forming and props. 80−19717
$BaMg_2Al_{16}O_{27}:Eu^{2+}$ phosphor, for low press. fluoresc. lamp, luminesc. characts. 78−10960
$Ba_2MgCr(PO_4)_3$, cryst. data 77−39564
$Ba_2Mg_2Fe_{12}O_{22}$, hexagonal ferrite, with anisotropic g-factor, ferromag. reson. 77−69700
Ba_2MgReO_6, new seignettomagnets and ferroelectrics 78−19425
$Ba_{1-x}Mg_xSO_4:Eu^{3+}$ phosphor, thermolum. characts. 77−90203
BaO-Al_2O_3-GeO_2-MF_2 (M=0.45 CaF_2+0.55MgF_2), MgF_2 and CaF_2 effect on physicochem. props. 80−34876
BaO-PbO-GeO_2-MF_2 (M=0.45CaF_2+0.55MgF_2), MgF_2 and CaF_2 effect on physicochem. props. 80−34876
$Ba(PO_3)_2$-AlF_3-MgF_2, glass, elec. cond. and IR spectra 80−89005
$Ba(PO_3)_2$-MgF_2, IR absorption spectra exam. of hydrolytic stability 80−39291
$Ba(PO_3)_2$-MgF_2, vitrification region 77−35676
BeO_2-Al_2O_3-SiO_2-MgF_2 system glass, role of fluoride cations during crystn. 79−65176
Ca-Mg-Ni hydrides, water form. on O_2 exposure 80−97727
Ca-Mg-Zr combustion sensor, pipe-form ceramics appl. *(Japanese)* 80−55761
$CaAl_2Si_2O_8$-$CaSiO_3$-$CaMgSi_2O_6$, exam. of glass forming regions and properties of glasses 79−4958
$Ca_3Al_2Si_3O_{12}$-$Mg_3Al_2Si_3O_{12}$, synthetic garnet, soln. grown, surface features 78−2346
CaF, excited state spectroscopic consts., dissoc., chemilum. obs. 80−21264
CaF_2-MgO, melts, elec. cond., surface tension, viscosity, density *(Russian)* 80−92758
CaF_2-MgO-SiO_2, melts, elec. cond., surface tension, viscosity, density *(Russian)* 80−92758

magnesium compounds continued
- $CaF_2+SiO_2+Mg(OH)_2$ matrix, quantitative anal. of multocomponent powders, full-profile refinement of Guinier-Hagg X-ray film data 79−39249
- $CaMgB_2O_5$, crystal struct. determ. 77−15388
- $Ca_3Mg(BO_3)_2(CO_3).0.36\ H_2O$, natural sacchite, cryst. struct. determ. 79−23590
- $CaMg(CO_3)$, dolomite, kinetics and thermodynamics of decomposition to metastable solid product 78−80740
- $CaMg(CO_3)_2$, dolomite, partial dislocations and stacking faults obs. 78−3761
- $CaMg(CO_3)_2$, dolomite, reaction with ZrO_2, mineralisation during roasting 79−43180
- $CaMg_{0.95}Fe_{0.05}Si_2O_6$, pyroxene, Mossbauer line integrated intensity ang. depend. 77−90083
- $CaMgGe_2O_6$-$CaFeGe_2O_6$, solid solns., phase equilibria, cryst. optical, X-ray struct. characts. 79−11577
- $Ca_6Mg_5Mn(B_2O_5)_6$, kurchatovite, cryst. struct. 77−65967
- β-$Ca_{3-x}Mg_x(PO_4)_2$, struct. and impurity distrib., stabilising role of Mg 78−10020
- $(Ca_{1-x}Mg_x)RuO_3$, mag. props. 78−27027
- $CaMg(Si, Ge)_2O_6$, solid solns., IR spectra 77−48156
- $CaMgSiO_4$ (monticellite), high-press. phase transforms. and implications for upper mantle mineralogy 80−17255
- $CaMgSi_2O_6$, diopside, elasticity, Brillouin scatt. meas. 80−6454
- $CaMgSi_2O_6$, single cryst., IR reflection spectra, vibr. spectrum calc. 77−73142
- CaO-MgO, doloma, composition effect on creep, impurity effects 79−43318
- CaO-MgO refractory, wettability by Fe melt *(Russian)* 78−10257
- CaO-MgO-Al_2O_3-Cr_2O_3-Fe-O_2-SiO_2 system, exptl. determ. of periclase and spinel comps. 78−6906
- CaO-MgO-Al_2O_3-SiO_2, glass-ceramic prep. by hot pressing and crystallisation of powder 78−11192
- CaO-MgO-Al_2O_3-SiO_2, glass ceramic, prep. by hot pressing and crystallisation, mech. props. 78−15351
- CaO-MgO-Al_2O_3-SiO_2, shale glass, glass forming and dielec. props. 78−22660
- CaO-MgO-Al_2O_3-SiO_2, shale glass, crystn. behaviour 78−22661
- CaO-MgO-Al_2O_3-SiO_2 system, pyroxenes subsolidus phase relations rel. to geothermometry and geobarometry 79−16440
- CaO-MgO-Al_2O_3-SiO_2, quartz sand-dolomite-magnesia-clay based glasses, crystn. 80−20915
- CaO-MgO-Al_2O_3-SiO_2, glass formation, at molar ratio CaO: MgO=1 *(Russian)* 80−39269
- CaO-MgO-CeO_2, fired, phase equilibrium diagram, 1700 to 1200°C 78−92248
- CaO-MgO-Cr_2O_3-Al_2O_3-ZrO_2-SiO_2 system, subsolidus region characts. 80−97466
- CaO-MgO-$NaPO_3$ system, subsolidus struct. 79−43215
- CaO-MgO-SiO_2, diopside, exam. of synthesis by hydrothermal sintering *(German)* 79−4934
- CaO-MgO-ZrO_2-SiO_2, phase study, SiO_2 compatibility relationship 78−95734
- CaO-MgO-ZrO_2-SiO_2, phase study, ZrO_2 compatibility relationship 78−95735
- CaO-MgO-ZrO_2-SiO_2 refractories, phase diagram 80−11634
- CaO-SiO_2-Al_2O_3-MgO, phase equilibria 77−86011
- CaO-SiO_2-MgO, melt, CaO dissolution *(Japanese)* 78−6909
- CaO-SiO_2-NiO-MgO glass melt, interaction of NiO and MgO, elec. cond. and IR spectra obs. *(Japanese)* 80−24632
- Ca_2SiO_4-MgO, conditions and mechanism in cryst.-chemical stabilisation of unstable phases 80−39302
- $Ca_3(VO_4)_2$-$Mg_3(VO_4)_2$, exam. of phase composition and phase diagrams 79−1851
- $CaY_2Mg_2Ge_3O_{12}$:Nd^{3+}, optical absorpt. and fluoresc. intensities 80−29793
- $Cd_{1-x}Mg_xS$, solid soln., phase equilib. diagrams 80−108412
- $Cd_xMg_{1-x}Se$ single crystals, melt grown, struct. and microhardness anisotropy 79−86836
- $Cd_{1-x}Mg_xTe$:Al, donor-acceptor pair and self-activated luminesc. 77−52161
- $Cd_{1-x}Mg_xTe$:P, luminescence centres, photoluminesc. meas. 78−31236
- CdS-MgS, solid soln., rock salt struct., high press. phase equilibrium study 78−52777
- $(Ce_xLa_{1-x})_2Mg_3(NO_3)_{12}.24H_2O$, adiabatic demagnetisation temp., mag. entropy *(Russian)* 80−65892
- $CeMgAl_{11}O_{19}$:Tb^{3+} phosphors, for low press. fluoresc. lamps, luminesc. characts. 78−10960
- $Ce_2Mg_3(NO_3)_{12}$, AC mag. susceptibility, mag. field depend., 1-4K 79−56516
- $Ce_2Mg_3(NO_3)_{12}$, spin-lattice relax., dynamic susceptibility meas., liq. He contact effects 80−66011
- $Ce_2Mg_3(NO_3)_{12}.24H_2O$, La diluted, mag. thermometry to below 1 mK 79−30469
- $Ce_2Mg_3(NO_3)_{12}.24H_2O$, pure and dil., heat transfer with dil. ^{3}He below 50 mK 79−51413
- $Ce_2Mg_3(NO_3)_{12}.24H_2O$ demagnetization cryostats, appls. of nucl. cooling in nucl. orientation studies 79−63230
- $Ce_2Mg_3(NO_3)_{12}.24H_2O$, EPR detection at mK temps. using SQUID magnetometer 79−63290
- $Ce_2Mg_3(NO_3)_{12}.24H_2O$/He Kapitza resist., appraisal of expt. results 79−51414
- $Ce_2Mg_3(NO_3)_{12}.24H_2O$-^{3}He interface, Kapitza resist. around the mK, effect of ^{4}He impurity 79−55999
- $Ce_2Mg_3(NO_3)_{12}.24H_2O$-solid ^{3}He boundary, thermal contact below 35 mK 79−60598
- $(Co,Mg)SiF_6.6H_2O$, phase transition at low temp., IR spectra 79−24302
- Co-W alloy electrodeposition, influence of $MgSO_4$ and gum arabic additives *(Russian)* 80−80991
- Co_2GeO_4-Mg_2GeO_4, solid solubility and cation distrib., free energy 77−35700
- $Co_xMg_{1-x}Al_2O_4$, struct., catalytic activity, Co^{2+} ion distrib. 78−30595
- $Co_{1-p}Mg_pCl_2$, magnetic excitations, antiferromagnetic resonance spectra response simulation 79−99775
- $Co_{1-x}Mg_xO$ ceramics as O_2 sensors, phase stability, elec. cond. and thermoelec. power meas. 78−3420
- $Co_xMg_{1-x}O$, solid solution, EPR of Co^{2+} *(Russian)* 80−11251
- $Co_xMg_{1-x}O$ system, thermodynamic investigation, 1100 to 1300K *(German)* 80−107430
- CoO-MgO, cryst. oxide demixing in O pot. gradient 79−37849

magnesium compounds continued
- CoO-MgO-Al_2O_3-Cr_2O_3-TiO_2, form. and colour of spinel solid soln. *(Japanese)* 77−32550
- CoO-MgO-Cr_2O_3-Fe_2O_3-TiO_2, form. and colour of spinel solid soln. *(Japanese)* 80−16059
- CoO-ZnO-MgO ternary systems, solid solns., struct. charact. 80−60629
- Cr-Ti/MgO-NbC(TaC) dispersion-strengthened, high temp. wear and oxidation resist. 80−25877
- Cr_2O_3-MgO-TiO_2, phase relations in air at 1400°C *(Japanese)* 77−77465
- $CsCa_{0.95-x}Mg_xEu_{0.05}F_3$, blue luminesc. obs. 77−32428
- $CsMgBr_3(I_3)_2$ diamag. linear chain lattices, cryst. struct. 80−70172
- $CsMgCl_3$:Co^{2+}, Zeeman Raman scatt. and Zeeman IR absorpt. spectra 79−56782
- $CsMgCl_3(Br_3)$, quadrupole interaction meas. by NMR spin-echo modulation 77−85615
- Cs_2O-MgO-SiO_2 system, glasses, crystn. prods., composition, props. 79−41961
- Cu-Mg-FeO system spinel solid solns., synthesis, struct., and mag. props. 79−52142
- Cu-MgO, dispersion hardened alloys, prep. and props. 80−40291
- $CuCr_2O_4$-$MgCr_2O_4$, X-ray investig. 77−44224
- $Cu_xMg_{1-x}Al_2O_4$, spinel solid solns., solid-state and surface props. 77−66415
- CuO-MgO system, Cu ions valence states, electronic refl. spectra 78−35168
- $Eu_2Mg_3(NO_3)_{12}.24H_2O$, Zeeman effect in ahsorpt. spectrum 77−63402
- $(Fe,Mg)O_4$, magnetostriction calcs. *(Dutch)* 80−2619
- Fe/MgO composite film, optical props., rel. to solar collector appls. 78−72622
- Fe-MgO system, decomp. reactions, ferromag. reson. obs. 77−9058
- $FeMgBO_4$, and $FeMg_2MO_5$, imperfect 1D mag. systems, Mossbauer expts. 80−60466
- $FeMgBO_4$, mag. props., spin glass behaviour 79−61145
- $FeMg_2BO_5$, mag. props., spin glass behaviour 79−61145
- $Fe_{1-p}Mg_pCl_2$, magnetic excitations 78−91852
- $Fe_pMg_{1-p}Cl_2$, Ising metamagnet, dilute, tricritical point calcs. 80−50099
- $Fe_xMg_{1-x}Cl_2$, metamag. percolation, Ising model calc. 79−28542
- $Fe_xMg_{1-x}Cl_2$, metamagnetic transition, magnetooptic exam. of mag. phase diagram 77−63175
- $Fe_xMg_{1-x}Cl_2$, metamagnet, mag. phase diagram by mag. induced light scatt. 80−65883
- $(Fe_{0.19}^{2+}Mg_{0.56}^{2+}Mn_{0.25}^{2+})[Fe_{1.87}^{3+}Al_{0.13}^{3+}]O_4^{2-}$, influence of Fe^{2+} ion substitution on electron hopping, Mossbauer study 80−71247
- $(Fe_{0.35}^{2+}Mg_{0.32}^{2+}Mn_{0.03}^{2+}Cu_{0.10}^{2+})[Fe_{1.74}^{3+}Al_{0.26}^{3+}]O_4^{2-}$, influence of Fe^{2+} ion substitution on electron hopping, Mossbauer study 80−71247
- $Fe_{3-x}Mg_xO_4$, Verwey transition, Mossbauer study 80−39942
- $Fe_xMg_{1-x}SO_4.7H_2O$, EFG tensor evaluation, ^{57}Fe single crystal Mossbauer meas. 78−88237
- $Fe_{0.55}Mg_{0.47}SiO_3$, orthopyroxene, electron irrad. effects, Mossbauer study 80−40016
- $Fe_{0.2}Mg_{1.9}Ti_{0.9}O_4$, Mossbauer parameters temp. depend. 78−23381
- $Fe_{0.4}Mg_{1.8}Ti_{0.8}O_4$, Mossbauer parameters temp. depend. 78−23381
- $Fe_{1.2}Mg_{1.4}Ti_{0.4}O_4$, mag. ordering, Mossbauer effect in external mag. fields 80−71257
- $Fe_{2(1-y)}Mg_{1+y}Ti_yO_4$ spinel, incomplete mag. ordering, static magnetisation and Mossbauer meas. 77−16056
- $Fe_{2(1-y)}Mg_{(1+y)}Ti_yO_4$, Mossbauer spectra anal., model 80−20560
- $Fe_{1-x}O$-MgO, solid solns., determ. of degree of imperfection 77−80624
- Fe_2O_3-MgO-NiO, tie-lines between solid solns. of oxide and spinel at 1273K *(French)* 79−100124
- HfO_2-MgO, elec. field gradient at ^{181}Ta, TDPAC meas. 79−33577
- HfO_2-MgO system, intermediate phases existence, X-ray diffr. and IR obs. 79−38805
- $K(Fe_{1.5}Mg_{0.5}Si_4O_{10})(OH)_2$, cryst. struct. refinement 78−26545
- $KMg_3AlSi_3O_{10}F_2$, dislocations, subgrain boundaries, X-ray diffr. topography study *(Chinese)* 80−88149
- $KMgCl(ClO_4)_2.nH_2O$, IR spectra and struct. features 79−15452
- $KMgCl_3.nH_2O$, IR spectra and struct. features 79−15452
- $KMgF_3$, extreme UV spectra, 9-30 eV 78−23486
- $KMgF_3$:$Co^{2+}(Fe^{2+})(Mn^{2+})(Ni^{2+})$, high energy absorption spectra interpretation 78−6716
- $KMgF_3$:Cr^{3+}, EPR spectrum, effect of external elec. field 78−68368
- $KMgF_3$:Fe^{2+}, anomalous acoustic relax. absorpt. and APR 80−88864
- $KMgF_3$:Ni^{2+}, acoustic Faraday and Cotton-Mouton effects, theory 80−65987
- $KMgF_3$:Sm^{2+}, luminesc. spectra 4.2, 77 and 295K and Zeeman spectra, 4.2K 77−81146
- $KMgF_3$:V^{2+}, dynamical Jahn-Teller effect on spin orbit multiplets, intensity quenching 79−95374
- $KMgF_3$:Yb^{3+}, ^{19}F hyperfine interaction, anisotropic Fermi and isotropic dipolar interactions 79−78056
- $K_2Mg_4Mo_4O_{16}(OH)_2(H_2O)_2$ study of non-stoichiometry *(French)* 78−30604
- $K_2Mg_4Mo_4O_{16}.(OH)_2(H_2O)_2$, dehydration processes rel. to stoichiometry *(French)* 79−24734
- $K_2Mg_2(SO_4)_3$, langbeinites, structural phase transitions 78−83938
- $K_2Mg(S_2O_3)_2.6H_2O$, isolation, struct., decomposition *(French)* 78−52506
- $K_{1.54}Mg_{0.77}Ti_{7.23}O_{16}$, hollandite, one-dimens. superionic cond., transport model 80−107529
- $K_{1.6}Mg_{0.8}Ti_{7.2}O_{16}$, solid electrolyte, dielec. response, 5.2-77K 79−56709
- $K_xMg_{x/2}Ti_{8-x/2}O_{16}$, ionic cond., K mobility rel. to struct. and bonding *(French)* 77−76594
- $K_xMg_{x/2}Ti_{8-x/2}O_{16}$, ionic cond., rel. to struct. and chemical bonding *(French)* 78−18824
- $KMg_3[AlSi_3O_{10}].F_2$ with excess Al, synthetic fluorphlogopite, radiation-induced paramag. O$^-$ centres 80−60417
- $K_2Mn_cMg_{1-c}F_4$, EPR spectra 78−76298
- $K_2Mn_xMg_{1-x}F_4$, 2-dimens. antiferromag., sidebands on EPR lines 78−56370
- K_2O-MgO-Al_2O_3, ionic cond. 80−107480
- K_2O-MgO-B_2O_3:Cu^{2+}, micro-inhomogeneities, EPR and Raman study 80−84080
- K_2O-MgO-SiO_2 glass, crystalline phase precipitation during crystallisation early stages, DTA *(Japanese)* 78−42919
- $LaCo_{1-x}Mg_xO_3$, cryst. struct., elec. and mag. props. 79−86748
- $LaCrO_3$-MgO, LC20M electrode material in open cycle MHD systems, thermionic emission characts. 80−97394
- $La_{1-x}Mg_xCrO_3$, electronic struct. study by XPS 80−25518

magnesium compounds continued
$LaMg(NO_3):Ni^{2+}$, pressure depend. of zero-field splitting of two mag. centres *(Russian)* 77−32249
$LaMg(NO_3)_2:Cu^{2+}$, spin-lattice recovery rate 78−10760
$La_2Mg_3(NO_3)_{12}.24D_2O$, use of neutron time-of-flight technique for cryst. structs. investigation 79−19126
$La_2Mg_3(NO_3)_{12}.24D_2O$:Nd, dynamic polarisation of deuterons in individual sites 77−59484
$La_2Mg_3(NO_3)_{12}.24H_2O$, appl. in cryogenic neutron polarisation filter 77−23341
$La_2Mg_3(NO_3)_{12}.24H_2O$, neutron diffr. obs. 78−18598
$La_2Mg_3(NO_3)_{12}.24H_2O:Mn^{2+}$, linear electric field effect on ground state splitting, EPR 78−80198
$La_2Mg_3(NO_3)_{12}.24H_2O:Co^{2+}$, Ce^{3+}, relax. and ESR in magnetically cooled systems 78−88225
$La_2Mg_3(NO_3)_{12}.24H_2O$:Ce, bottlenecked Orbach relax. process, phonon lifetime 79−65151
$La_2Mg_3(NO_3)_{12}.24H_2O:Nd^{3+}$, polarised neutron diffr. from dynamically and statically polarised protons 80−44078
$La_2Mg_3(NO_3)_{12}.24H_2O:Nd^{3+}$, proton raser, self-radiating nuclear spin system *(German)* 80−53298
$LiF-MgF_2$, high-pressure phase relations rel. to mixed oxide zone of Earth mantle 77−37193
$LiF-MgF_2$, ionic conductivity increase rel. to point defect cone 77−72717
$LiF-NaPO_3-MgF_x$ glasses, IR spectroscopy study 80−16042
LiMg, $^2\Sigma^+$ and $^2\Pi$ states, mol. binding energy curves 80−58189
Li_2MgGeO_4, high temp. modif., struct. derivation *(French)* 77−47433
$LiO_2-Na_2O-MgO-TiO_2-Al_2O_3-SiO_2$, exam. of specific heat and thermal conductivity *(Russian)* 79−55898
$Li_2O-MgO-Al_2O_3$ system, subsolidus phase equilibria 80−81036
$Li_2O-MgO-Al_2O_3-SiO_2$ glass scintillator for pulsed neutron detection 80−87019
$100(Li_2O.2SiO_2).3Na_2O$, directionally solidified, thermal and mech. props. *(Japanese)* 80−16295
Li_2TiO_3-MgO (20 to 40 at.%), order-disorder transitions, DTA and X-ray anal. 79−29050
$(Mg, Fe)SiO_3$, orthopyroxenes, cation distrib., electronic and Mossbauer spectra 80−7370
$(Mg,Fe)_2SiO_4$, dislocation recovery rate affected by high-press. 80−94515
β-$(Mg, Fe)_2SiO_4$, high-press. spinel phase identification in Tenham chondritic meteorite 79−80284
$(Mg,Fe)_2SiO_4$, olivine, fayalite rich, single cryst., UV absorpt. spectra at high press. 78−85545
$Mg\ (Fe,In)_2O_4$:Pb,Pt film, LPE 77−77436
Mg complex, bis-pyridal-Mg-tetrabenz-porphyrin, disagreement with diffuse interstellar bands 80−56905
$Mg\ F_2$, vibr. anal., kinetic consts. method 80−18838
Mg ferrite, crystal lattice defectiveness and degree of inversion, effect of synthesis temp. 77−11501
Mg ferrite, sintered, cation redistribution, microstructural effects 77−55356
Mg hydroxylboracite, hydrothermal crystallisation 77−85917
Mg porphyrins, additional ligands deuteration effect on luminesc. charcts. 79−99932
$Mg\ SiO_3$ melt, instantaneous struct. simulated by mol. dynamics 80−84049
Mg, SiO_4:Th TLD phosphor, γ-ray induced sensitisation and phototransfer 79−33851
Mg vermiculite, adsorbed water mol. orientation, elec. pot. calc. 78−26763
Mg^{2+} ion complexes with HF, H_2O, and NH_3 solvent molecules, structural and electronic props. calc. 77−57873
Mg-Al spinel, hot pressed ceramic, annealing effect on transparency and microstruct. *(Japanese)* 79−74188
Mg-Al spinel, non-stoichiometric, climb dissociation of network dislocations 80−2031
Mg-Al spinel ceramics, mech. strength, non-stoichiometry and microstruct. *(Japanese)* 80−21054
Mg-Cu-Mn-Ni-Fe-O, UHF ferrites, synthesis, physicochem. state, mag. and dielec. parameters 79−11536
Mg-Fe-O ferrite system, thermodynamic stability, dissociation and phase relations *(Japanese)* 80−55378
$Mg-MgF_2$, sputtered films, opt. props. 78−80430
Mg-MgO-Ag, tunnel junction, potential barrier, equivalent rectangular shape 79−7906
Mg-MgO-Ag junction, stable room temp. light emission 78−31257
Mg-MgO-Pb tunnel junctions, aromatic ring compound adsorption, inelastic electron tunnelling 79−59521
Mg-Mn ferrite, finely divided, synthesis 77−28773
$Mg-P_3$ complexes determ. by gel chromatography with at. absorpt. flow detector 79−87890
Mg-Si-Al-O-N, grain boundary segregation, combined X-ray microanal. and lattice fringe imaging determ. 79−15681
Mg-Si-Al-O-N ceramic, phase assemblages, relationships with props. 80−60848
Mg-Si-Al-O-N system, behavioural diagrams 79−24507
Mg-Si-N-O additives to Si_3N_4 during hot pressing *(Japanese)* 77−36437
$Mg(Al,Cr,Fe)_2O_4$, spinel, elastic moduli calc. 78−6960
$Mg(AlH_4)_2$, prep., thermal decomposition, molar heat capacity, heat of form. 80−3325
$MgAlO_4:Cr^{3+}$, exchange parameters of Cr^{3+} pairs, optical and EPR meas. 77−69282
$MgAl_2O_3$, crystal growth by floating zone method using thermal imaging system 77−77373
$MgAl_2O_4$, active spinel, prep. and crystallite growth mech. 78−27465
$MgAl_2O_4$, composition rel. to ceramic microstruct. form., light transmission 79−43188
$MgAl_2O_4$, corrosion resist. in fused Li rel. to phase and microstruct. changes 77−44378
$MgAl_2O_4$ crystals, flux grown, artificial spinel twin form. by $BeAl_2O_4$ addition 80−96542
$MgAl_2O_4$, damping of elastic waves at 36.5 GHz 77−39632
$MgAl_2O_4$, dislocations, sessile dissoc. 79−46663
$MgAl_2O_4$, electrostatic lattice energy, optimisation of convergence of Ewald series 79−7569
$MgAl_2O_4$, faulted defect aggregates prod. by neutron-irrad. 80−107331
$MgAl_2O_4$ film on Al-Li-Mg-Be alloy, phase composition, oxidation protection mechanism *(Russian)* 80−65417

magnesium compounds continued
$MgAl_2O_4$, form. from amorphous substance prep. by homogeneous precipitation *(Japanese)* 79−56950
$MgAl_2O_4$, γ-irradiated crystal, TSC, thermoelec. power, thermolum. and afterglow 80−75583
$MgAl_2O_4$, IR spectrum exam. 78−76454
$MgAl_2O_4$, influence of nonstoichometry on acoustic wave attenuation 79−65146
$MgAl_2O_4$, internal strain rel. to strain tensor, group theory anal. 79−86835
$MgAl_2O_4$, irrad. stability obs. using X-ray emission meas. *(Russian)* 80−66326
$MgAl_2O_4$, lattice dynamics, rel. to space group of spinel 78−59898
$MgAl_2O_4$, microplasticity at room temp., dislocations, TEM study 80−19805
$MgAl_2O_4$, Mollwo-Ivey relation between peak-colour absorption energy and average O ion spacing 77−90179
$MgAl_2O_4$, polycrystn., strength-grain size relations 79−79081
$MgAl_2O_4$, powder effect of precursory sulphate solution anion on sintering 78−56605
$MgAl_2O_4$, pure and Fe-doped spinel, elec. cond. 80−59702
$MgAl_2O_4$, radiation damage, optical absorpt., F-centres 80−64994
$MgAl_2O_4$ spinel, anomalous thermal expansion, second order transition 80−84307
$MgAl_2O_4$ spinel, deform., stacking fault energy 77−28853
$MgAl_2O_4$, spinel, epitaxial growth by solid-state reaction of MgO with molten Al 77−8751
$MgAl_2O_4$, spinel, γ-irrad. effect on optical absorpt. and thermolum. spectra 77−85759
$MgAl_2O_4$ spinel, kinetics of form. from oxides in thin films *(Russian)* 79−52144
$MgAl_2O_4$ spinel, low energy phonon obs. by inelastic neutron scatt. 78−43084
$MgAl_2O_4$ spinel, optic frequencies, evidence for membership of F43m space group 78−48168
$MgAl_2O_4$ spinel, single cryst., fracture behaviour, temp. depend. 80−40503
$MgAl_2O_4$, spinel, space group 80−28937
$MgAl_2O_4$ spinel, surface energy calc. contribs. from Coulomb and Born-Mayer interactions 78−18890
$MgAl_2O_4$, spinel, vac. UV luminesc. spectra *(Russian)* 77−24903
$MgAl_2O_4$, spinel materials press forged, mech. props., IR appl. 78−39722
$MgAl_2O_4$ spinel material for SAW devices 79−56735
$MgAl_2O_4$ spinel refractory, enthalpy and specific heat determs. 80−88334
$MgAl_2O_4$, strength-controlling fracture energy depend. on flaw-size to grain-size ratio 80−81152
$MgAl_2O_4$, structural phase transition obs. by electron diffr. 77−66020
$MgAl_2O_4$, thermochemical coloration and annealing 79−91468
$MgAl_2O_4$ transparent ceramic, transmittance, grain size and dopant effects *(Japanese)* 80−19083
$MgAl_2O_4$, transverse elastic wave damping at 36.5 GHz 77−80583
$MgAl_2O_4:Cr^{3+}$, exchange parameters determ. from emission and luminesc. excitation spectra 77−52160
$MgAl_2O_4:Cr^{3+}$, luminesc. spectrum, N-lines *(German)* 77−16382
$MgAl_2O_4:Cr^{3+}$, luminesc. spectra, N-lines and Cr^{3+} pairs 78−2896
$MgAl_2O_4$:Dy, US attenuation 77−89500
$MgAl_2O_4-Al_2O_3$ powder prep., for plasma arc spraying, coating props. 77−66612
$MgAl_2O_4-MgFe_2O_4-FeAl_2O_4-FeFe_2O_4-FeCr_2O_4$ solid soln., thermodynamic model for natural spinel *(French)* 78−32065
$(MgAl_2O_4)_x(AMn_2O_4)_{1-x}$, A=Mn,Zn,Cd, $0<x<1$, mixed oxide spinels, chemical shifts of Mn K-absorpt. edge 80−29828
$MgAl_ySc_xFe_{2-x-y}O_4$, X-ray spectra, Mossbauer spectra, electronic struct. of Fe and Sc 77−28647
$Mg_3Al_2Si_3O_{12}$, pyrope, cryst. struct. and compressibility to 60 kbar 78−63718
$Mg_{9.10}An_{4.04}Mn_{1.89}(SO_4)_2(OH)_{26}.8H_2O$, mooreite, X-ray cryst. struct. determ. and refinement 80−92488
$MgAs_4$, cryst. struct. *(French)* 77−72583
MgB_2, band struct., LCAO calc. 79−90957
MgB_2, band struct. and density of states, metallic behaviour 77−59249
MgB_2 X-ray emission spectra and transition probability calcs. *(Russian)* 77−52203
$MgB_{12}H_{12}.10H_2O$, struct. dehydration, intermediate phases and thermooxidative degradation 80−33951
MgB_4O_7:Dy, TLD phosphor development 79−79661
$Mg_3B_7O_{13}Cl$, pyroelec. effect, spontaneous polarisation, domain struct. 77−8520.
$MgB_{12}O_{19}.5H_2O=Mg[B_3{}^5B_3{}^1O_7(OH)_5]_2$, cryst. synthesis and struct., bonding, X-ray study 80−33973
$MgB_6O_{10}.6H_2O$, cryst. struct. determ. 77−1116
$MgBSi_2O_6$, B=Mg, Fe^{3+}, Al, pyroxenes, order-disorder interpretation 80−38987
$MgBaF_4$, nonlinear optical susceptibility tensor, Maker fringes 78−13751
MgBr, adsorpt. of NO on cleavage face, triplet pt. of first monolayer 78−6227
$MgBr_2$, adsorption of NO, crit. and triple point temps. of first adsorbed layer 78−91548
$MgBr_2$, force consts., vibr. amplitude and shrinkage effects 79−22863
$MgBr_2$, polymorphic phase change of adsorbed NO 77−31900
$MgBr_2$, XPS, satellite of Br 4s line 78−56556
$MgBr_2$-ABr (A=Cs, Rb, K, Na, Tl), thermochemical and struct. investigation *(German)* 79−1423
$MgBr_2.2Et_2O$, NQR freqs. temp. depend., phase transition 79−42867
$MgBr_2.6CH_3OH$ solvates, cryst. struct. *(French)* 78−34500
$MgCO_3$, point-dipole theory and optical birefringence 79−73896
$MgCO_3$ powder, high speed method of porosity determ. 77−90543
$MgCO_3^0$, in solution, ion-pair relaxation rel. to acoustic absorpt. 79−74914
$Mg_2CO_3(OH)_2(H_2O)_3$, H bonding 78−18601
$3MgCO_3.Mg(OH)_2.3H_2O$, activation, for MgO sintering 80−89183
$Mg_5(CO_3)_4.(OH)_2(H_2O)_4$, cryst. struct., H bonding, X-ray diffr. meas. 77−47392
$MgCa(CO_3)_2$, dolomite, partial thermal decomp. into MgO and $CaCO_3$, product cryst. growth 80−108706
$MgCaH_{3.72}$, synthesis and struct. *(Japanese)* 78−84751
$Mg_{1-x}Ca_xO$, epitaxial layers by CVD *(Russian)* 79−56934
$Mg_xCd_{1-x}Te$, electroreflection spectra, comp. depend. 80−66230
$Mg_xCd_{1-x}Te$:P, vibr. modes of defects, IR absorpt. expts. 77−62601

magnesium compounds continued
MgCl, chemiluminescent spectrum obs. in Mg^*+Cl_2 crossed beams 78−90112
$MgCl_2$, aq. soln., ^{25}Mg NMR, longit. relax. rates 79−91309
$MgCl_2$ aq. soln., quasi-elastic neutron scatt. 79−37607
$MgCl_2$, aq. solns., IR spectral reflectance meas., Kramers-Kronig anal. 77−4633
$MgCl_2$, aq. solns., X-ray diffr. study 79−37608
$MgCl_2$ brine, crystallising, direct contact cooling using kerosene drops 79−1053
$MgCl_2$, conc., stress-corrosion cracking of austenitic stainless steel 78−85057
$MgCl_2$, determ. by flame spectroscopy, absorpt. and emission, analogue data processing system 77−36804
$MgCl_2$, electronic structure by intersecting spheres model 79−99482
$MgCl_2$, enthalpies of formation and of soln. 80−7844
$MgCl_2$, enthalpy calc. for solid and liq. phases 77−43349
$MgCl_2$, force consts., vibr. amplitude and shrinkage effects 79−22863
$MgCl_2$ in water+tetrabutylammonium dicarbollyl cobaltate in nitrobenzene systems, electrolyte dropping electrode investig. 77−25279
$MgCl_2$, isopiestic studies of aqueous solns., 382 to 474K 79−24815
$MgCl_2$, mol. struct. parameters, average values, geom. config., gaseous electron diffr. obs. 80−37904
$MgCl_2$, molten Raman spectrum, $MgCl_4^{2-}$ and polynuclear complexes equilib. 77−1669
$MgCl_2$, partially hydrated powder surface, electron beam effects, XPS obs. 79−33900
$MgCl_2$, photoelectron spectra, geometry 78−29816
$MgCl_2$, positron annihilation ang. correl., bonding depend. 77−20951
$MgCl_2$, sea water relaxation and sound absorption 79−68466
$MgCl_2$, solns. in methanol, conductance data anal., assoc. consts. 78−71875
$MgCl_2$ solution, Cl distrib. in oxide film on stainless steel, SIMS study *(French)* 80−108765
$MgCl_2$ solution, stainless steel (304) stress corrosion cracks initiation *(Japanese)* 80−10593
$MgCl_2$ solution, stress corrosion cracking of austenitic stainless steel, temp. effect *(Korean)* 80−93694
$MgCl_2$, sound speed as function of conc., temp., and press. 78−79668
$MgCl_2$:Co_2 spectroscopic studies of interactions 80−29769
$MgCl_2$:Co^{2+}, ground-state g-value, EPR meas. 77−16159
$MgCl_2$:Co^{2+}, Zeeman electronic Raman scatt. spectra 79−42962
$MgCl_2$:NO_2^-, aqueous solns., luminesc., absorpt. and Raman spectra *(Russian)* 77−36291
$MgCl_2$-alkali metal chloride system, solid and molten states, struct. props., Raman spectra 80−76011
$MgCl_2$-KCl, binary melt, viscosity *(Japanese)* 78−10209
$MgCl_2$-NaCl-H_2O, conc. solns., vap. press. meas. 79−23713
$MgCl_2$-NaCl-H_2O, ionic diffusion theory, use of activity coeffs. in transition-state models 78−57224
$MgCl_2$-NaCl(RbCl) binary melts, surface tensions *(Japanese)* 78−10260
$MgCl_2$-$TiCl_4$, high activity catalyst for polyethylene, struct. and mechanism investig. 80−11951
Mg_2Cl_4, equilib. config., pot. energy curves, ion model calc. 77−65540
$MgCl_2CaCl_2$, aq. soln., hydration, X-ray diffr. 77−43126
$Mg(ClO_4)_2$, solutions, preferential solvation, NMR obs. 78−95919
$Mg(ClO_4)_2.6H_2O$, dehydration, appl. analyser calibration for water determ. 77−32850
$Mg(ClO_4)_2.6H_2O$:Mn^{2+}, cryst., EPR 78−91935
$MgCl_2.6NH_3$-$MgCl_2.2NH_3$, heating and cooling of solar energy storage system 80−81484
$MgCl_2.nH_2O$, cryst. struct. *(German)* 80−1987
$MgCl_2.nH_2O$, IR spectra and struct. features 79−15452
$(Mg_{0.776}Co_{0.224})SiO_3$, synthetic orthopyroxene, cryst. struct. 78−42970
$MgCr_2O_4$, chemisorption of CO_2, surface flow of CO_2 determ. 77−47083
$MgCr_2O_4$, magneto-electric splitting of crystal field Γ_2-level of Cr^{3+} ion, neutron spectroscopic obs. 79−19562
$MgCr_2O_4$, mobility of chemisorbed CO_2, O_2 and water vapour 77−51595
$MgCr_2O_4$, reduction with graphite powder *(Japanese)* 77−56225
$MgCr_2O_4$ spinel, exam. of expansion during synthesis 79−20012
$MgCr_2O_4$, spinel refractory, enthalpy and specific heat determs. 80−88334
$MgCr_2O_4$-TiO_2, porous ceramics, humidity-sensitive electrical conduction 80−107782
$MgCr_2O_4$-TiO_2 porous ceramic humidity sensors 80−86325
$MgCr_2O_7.6H_2O$, dehydration, thermal decomposition, kinetics 79−11777
$MgCs_2(SO_4)_2.6H_2O$:Mn^{2+}, EPR, 298K, spin-Hamiltonian parameters, cryst. fields 78−27086
$MgCs_2(SeO_4)_2.6H_2O$, EPR, crystal field and hexahydrate distortion 78−91938
$MgCs_2(SeO_4)_2.6H_2O$:Mn^{2+}, EPR spectrum 78−64261
$Mg_{0.7}Cu_{0.3}Fe_2O_{4+\delta}$, disaccommodation and accommodation 77−20641
MgD, $A^2\Pi$ state radiative lifetime, pulsed dye laser excitation meas. 78−94288
MgD, emission spectra, 600 to 850 nm, rot. anal., dissoc. energies 78−62815
$MgEr_2S_4$, magnetisation and susceptibility, exchange interactions obs. 78−52242
MgF, excited state spectroscopic consts., dissoc., chemilum. obs. 80−21264
MgF, polycryst., quartz particle impacts no. effect on erosion in elastic-plastic response regime 80−81209
MgF, single crysts., neutron diffr. study, least squares refinement 79−73147
MgF+HF, V-V energy transfer collisions, 'triple beam' expt. 79−98197
MgF_2, $^4He^+$ ion scatt. spectrometry below 5 keV 80−108313
MgF_2, 0.36 μ absorptance/fluence dependence obs. 79−15506
MgF_2 (rutile), high-pressure phase transformations 79−44181
MgF_2, absolute first order Raman polarisabilities 78−64369
MgF_2, band struct., tight-binding calc. 80−24796
MgF_2, broadband dielectric mirror interference coatings, scatter losses 79−50365
MgF_2, CW CO_2 laser deposited dielect. thin film, optical and struct. props. 80−7506
MgF_2 coated Al mirrors, AES, UV irrad. effect 77−72047
MgF_2 coated blazed Al grating, complete absorpt. of P-polarised specific wavelength light 78−25957
MgF_2 coated thick Fe films, surface magnetism 80−7196

magnesium compounds continued
MgF_2, colour centre thermal stability 78−83811
MgF_2, complex dielec. const. at audio freqs., 5.5 to 380K 80−25272
MgF_2, cryst., atomic vibrs., anisotropy parameters, bonding 80−54195
MgF_2, cryst., Roentgenoluminesc., exciton emission *(Russian)* 78−95609
MgF_2, cryst. elec. field gradient determ., γ-ray anisotropy meas. after polarised neutron capture 77−12291
MgF_2 crystal, $M(D_{2h})$ centre absorption and emission spectra obs. 79−19910
MgF_2 crystal windows, transmission in vac. UV region, heat treatment effect 77−31137
MgF_2 deposited quartz resonator, restricted mass range due to film stress 78−11116
MgF_2, disordered film, optical transitions as function of prep. conditions 78−27340
MgF_2, EPR of electron irrad. induced F interstitial H- and H_A-centres 77−77099
MgF_2, elastic const. C_{44}, depend. on temp. 79−73239
MgF_2, elastic constant determ. by US pulse echo overlap 79−14874
MgF_2, electronic struct. and densities of states, tight-binding calcs. 80−15447
MgF_2, enthalpy calc. for solid and liq. phases 77−43349
MgF_2, Fabry-Perot etalon plates for vac. UV 77−5895
MgF_2 film, 1064 nm 150 ps laser pulse damage rel. to OH^- content and refr. index 79−14016
MgF_2 film, and ZnS-MgF_2 film system, Rayleigh scatt., 441.6 nm, scatt. losses correl. with deposition parameters 79−78782
MgF_2 film, contamination by 1 MeV proton bombardment, backscatt. obs. 77−11811
MgF_2 film, optical absorption meas. rel. to prep. conditions *(French)* 77−44078
MgF_2 film, refr. index and struct., deposition temp. depend. 79−4857
MgF_2 film, vac.-deposited, origin of mech. stress 79−90925
MgF_2 film, vacuum deposited, tensile stress, meas. and calc. 79−87027
MgF_2 films, electronic transitions near optical absorpt. edge, depend. on prep. conditions *(French)* 77−63429
MgF_2, force consts., mean amplitudes of vibr. 78−17647
MgF_2, force consts., vibr. amplitude and shrinkage effects 79−22863
MgF_2, gamma- or neutron irradiated, ESR meas. on hole centres 77−12201
MgF_2, grinding, polishing, mech. props. anisotropy effect 77−797
MgF_2, ground state, nonempirical LCAO SCF calcs. 78−66469
MgF_2, high temp. polymorphism and thermal props. 80−75199
MgF_2, hot pressing in vacuum, compaction kinetics, selective recryst. 77−16517
MgF_2, interatomic Auger transitions, XPS exam. 77−8692
MgF_2 laser coating, UV damage obs. 80−33056
MgF_2 layered Al, coating effects on diffraction grating efficiency 77−39064
MgF_2, layers, optical thickness monitoring using quartz cryst. monitoring 78−5592
MgF_2, localised electronic levels, thermoluminesc. and thermally stimulated current exam. 78−11001
MgF_2 long-persistence cathode-ray screen, phosphoresc. decay into second-order components 77−20907
MgF_2, long-wavelength lattice vibr. modes, symmetry coordinates 78−43081
MgF_2, M-centre, dissoc. kinetics after pulse electron irrad. 79−7601
MgF_2, mid IR laser window material, absorption props. 77−46770
MgF_2, multilayer interference film, mass production by roll coating *(Japanese)* 79−81577
MgF_2, muon Coulomb capture ratio 78−62959
MgF_2, nonactivated, X-ray luminesc., 80−2832
MgF_2, optical absortion following pulsed electron irrad., 100-500K 79−8164
MgF_2, optical ceramic, synthesis 78−52729
MgF_2, optical coating in liquid, laser damage 77−61994
MgF_2, optical film cross sections, SEM and TEM 77−19387
MgF_2, optical material, thermal expansion, 60-300K 78−33791
MgF_2 optical window, VUV light source, low-current AR arc 79−35856
MgF_2 overcoating on Al mirrors, reflective scatt. and reflectance meas. in vac. UV, moisture and oil vapour influence *(German)* 79−86227
MgF_2, point defects study, cross relaxation processes, polarised β-active nuclei 80−60431
MgF_2, polycrystalline, elastic moduli, press. and temp. depend. US meas. 77−21202
MgF_2, primary pair of radiation defects, energy of form., colour centre conversion rates *(Russian)* 78−6055
MgF_2, Raman spectra, cross section determ. 78−56471
MgF_2, reflective coatings, refr. index, UV polariser mirror coating appl. *(Russian)* 77−34928
MgF_2 refractive index and extinction coefficient meas., 115 to 400 nm 79−78640
MgF_2, rutile structure, dielectric props., neutron and Raman scatt. exam. 78−79684
MgF_2, single cryst., linear thermal resistance temp. depend. 77−66048
MgF_2, single cryst., tensile strength and yield point, temp. depend. 77−14785
MgF_2, spatial separation of components of primary radiation defect pairs 78−14376
MgF_2, stress-induced birefringence meas., 1-12 μm 77−24818
MgF_2, substrate, struct. and internal stresses in Ag ultra-thin films 78−91572
MgF_2, transient absorption and luminesc. following electron beam excitation 77−69920
MgF_2, transparent, multiphonon IR absorption spectra 80−7348
MgF_2, UV visible absorpt. by laser calorimetry, wavelength modulation spectroscopy 78−66876
MgF_2, ultra-microhardness testing for vacuum deposited film and bulk specimen 78−79910
MgF_2 underlayer for Cr film on glass substrate, thermal strength, recrystn. influence 79−87748
MgF_2, vacuum deposited, destruction props. obs., suitability for integrated optics assessment *(Slovak)* 80−33224
MgF_2, X-irradiated, radiation conductivity 79−69555
MgF_2, X-ray luminesc. polarisation 80−11462
MgF_2, XPS, core-electron peaks satellite and loss structs. 77−66571
MgF_2^-, ground state, conform., electron affinity, extended basis SCF calcs. 79−72253

magnesium compounds continued
MgF_2:Co^{2+} (Mn^{2+}), Coulomb and exchange interaction consts. optical spectra line assignment, new technique 80−45124
MgF_2:Co(Ni), laser, broadly tunable CW operation, output powers, optical pumping 80−32995
MgF_2:Co(Ni), tunable transition-metal-doped solid state lasers 80−58549
MgF_2:Fe^{2+}, γ-irrad., F-centres, Fe^{2+} ion hole traps, absorpt. and EPR meas. 79−7598
MgF_2:Li^+, atom transport, diffusion and ionic cond. meas. 80−107492
MgF_2:Li^+, defect struct., theory 77−47472
MgF_2:LiF crystal, defect struct., anelastic and dielec. relax. meas. 77−27938
MgF_2:Mn, Cd, cathodoluminophor, nature of ageing 78−10994
MgF_2:Mn, X-ray luminesc. yield temp. depend. 77−4680
MgF_2:Mn, X-ray luminesc., activator flash 79−65958
MgF_2:Mn^{2+}, MCD and linear dichroism, 3d→4s transitions 79−56768
MgF_2:Mn(Co), photoluminesc. due to X-rays, colour centre thermal breakdown 79−24359
MgF_2:Mn(Co), thermoluminesc. and TSC in activator band 79−24359
MgF_2:Ni, efficient CW optically pumped laser, 1.63 to 1.75 μm operation 79−18425
MgF_2:Ni, growth by vertical gradient freeze method, in self-sealing graphite crucibles 78−31334
MgF_2:Ni electronic transition laser, tunable IR emission 78−59030
MgF_2:Ni^{2+}, temp. depend. of luminesc. 79−83016
MgF_2:V^{2+}, MCD and linear dichroism, 3d→4s transitions 79−56768
MgF_2/In/MgF_2 struct. surface plasma wave optical excitation in In 79−91516
MgF_2-Ag (Al)(Cu)(Au) film substrate tunable external-reflector retarder, computer based anal. 80−53407
MgF_2-Ag layered system, optical excitation of surface plasma waves 78−6803
MgF_2-Al, flashlamp for I photodissoc. laser 77−79848
MgF_2-Au, cermet coatings, solar energy photothermal conversion, Bruggeman effective medium theory 79−83627
MgF_2-CeO_2, multilayer refractory oxide interf. coatings 79−7192
MgF_2-HfO_2, interference coatings perpared by electron beam evaporation, UV optical strength 79−59779
MgF_2-Na_3AlF_6 thin film deposits, quenched ageing by chopping 80−97364
MgF_2-PbF_2, multidielectric stacks as interf. filters, ageing characts. *(French)* 77−34939
MgF_2-Sb_2O_3, semitransparent wide band dielectric mirror synthesis using dispersive and absorbing materials 79−89986
MgF_2-xMgO.ySiO_2, freezing point depression meas., effect of SiO_2 compound additions 77−28798
MgF_2-ZnS, dielec. films, transparent, microscopic inhomogeneities and optical breakdown 78−10844
MgF_2-ZnS multilayers, high vacuum deposition for cold light mirror prod. *(German)* 80−53486
$MgFe_{2-x}Al_xO_4$, with added Co, effect of Na_2O admixture on props. 77−36423
$MgFe_2O_4$, epilayer, perpendicular anisotropy 80−39769
$MgFe_2O_4$, Faraday rotation in X-ray region 79−82958
$MgFe_2O_4$ ferrite form. mechanism in mixture of metallic oxide powders 77−63609
$MgFe_2O_4$, LPE growth, film quality, mag. meas. 78−11136
$MgFe_2O_4$, Mossbauer effect determ. of cation distrib. temp. depend. 77−8481
$MgFe_2O_4$, Mossbauer study 79−47375
$MgFe_2O_4$, prep. by double decomp. reaction, mag. characts. *(French)* 79−33463
$MgFe_2O_4$, sintered, cation ordering, grain size effects 78−39763
$MgFe_2O_4$, small mag. particles, anisotropy field, resonance meas. 78−64227
$MgFe_2O_4$-Co_3O_4 solid soln. spinels, domain wall formation inhibition, effect on bulk mag. props. 80−11220
$MgFe_2O_4$+ZnO, powders, cation mutual diffusion coeffs. calc. 77−15635
$Mg_{0.x}Fe_{2.x}O_4$, ferrimag. epilayer, superparamag. interface, mag. props., FMR 78−95492
$Mg_xFe_{1-x}O_{1+δ}$ cluster component method calc. of lattice params., composition, imperfection 77−25031
$Mg_xFe_{1-x}O$, diffusion of ^{59}Fe and elec. cond. 80−59700
$Mg_xFe_{3-x}O_4$, cation redistribution, effect of composition and thermal treatment 79−27966
$Mg_xFe_{3-x}O_4$, cation redistrib., lattice const. 79−60338
$Mg_xFe_{3-x}O_4$ crystals, first mag. anisotropy const., 7-295K 80−65855
$Mg_xFe_{3-x}O_4$, magnetostriction consts., 80 to 320K 78−95503
$Mg_xFe_{3-x}O_4$, polycryst., Verwey type transition, resist., magnetisation, Mossbauer effect and permeability obs. 80−75764
$Mg_xFe_{3-x}O_{4-y}$ precipitates, g-factor, ferrimag. reson. meas. 78−60337
$(MgFe_2O_4)_{1-x}(Mn_3O_4)_x$, polycrystalline, coercive forces 78−39366
$(MgFe_2O_4)_{x-1}(Mn_3O_4)_x$, soft ferrite, squareness ratio and max. induction 79−99730
$(Mg_xFe_{1-x})_2SiO_4$, olivine, Fe-rich superparamagnetic clusters, Mossbauer study 79−82831
$MgFl_2$ windows, vacuum sealing 78−94457
$MgGa_xFe_{2-x}O_4$, spinel struct., neutron diffr. exam. 77−12096
Mg_2Ge, phonon cond. 4-1000K 78−79826
Mg_2Ge, polymorphism under high press., radiographic data 77−20068
$MgGeO_3$, HP phase transform. 80−19941
$MgGeO_3$-$Ca_{0.5}Fe_{0.5}GeO_3$, solid solns., physicochem. props. 77−44223
Mg_2GeO_4, determ. of olivine-spinel transition up to 20 kbar and 1300°C 77−53044
Mg_2GeO_4, geometric flow props. 78−57198
Mg_2GeO_4, Li_4GeO_4, Li_3PO_4, structural relns. *(French)* 77−47433
Mg_2GeO_4, reduction processes by C, kinetic analysis, reaction products *(Russian)* 80−55644
Mg_2GeO_4 spinel, struct. refinement, neutron diffr. 77−72590
Mg_2GeO_4-Mg_2SiO_4 system, struct. similar solid soln. obs. and characts. 80−108403
MgH, $A^2Π$ state radiative lifetime, pulsed dye laser excitation meas. 78−94288
MgH, $A^2π−X^2Σ^+$ system, dissoc. energy 77−10686
MgH, and MgD, $B'^2Σ^+$-$X^2Σ^+$ band system, ab initio CI calcs. 79−93970
MgH, emission spectra, 600 to 850 nm, rot. anal., dissoc. energies 78−62815
MgH, Franck-Condon factors appl., rot. depend. 79−10154
magnesium compounds continued
MgH, in RF-excited heat pipe oven, efficient arc source 78−63162
MgH, mol., X and $B'^2Σ^+$ and $A^2Π$ ab initio CI calc. 79−31415
MgH, Morse and Lippincott pots., r-centroids, dissociation energy 78−13446
MgH rotational temp. and solar photospheric models 80−62099
MgH, X→A and X→B' band systems, oscill. strengths and photodissoc. cross-sections 79−94045
MgH^+, CI pot. curves and cross sections for lowest singlet states 80−23343
MgH^+, PNO-CI and CEPA calcs. of electron correl. effects 77−34561
MgH_2 formation kinetics, electron microscope obs. of H_2 reaction with Mg metal 77−52553
MgH_2, lattice energy calc. 78−83768
MgH(D), spectra in 230-235 nm region 80−48012
$Mg(H_2O)_n^{2+}$, geometric and electronic struct., CNDO calc. 79−36532
$Mg(H_2O)_6SiF_6$, Raman spectra, vibr. modes 79−61369
$Mg(H_2O)_6SiF_6$:Mn^{2+}, phase transition effects in EPR spectrum 79−42831
$Mg^{2+}(H_2O)n$ (n=1,2,4,6), FSGO-pair-pot. calcs. *(German)* 80−74278
$MgHPO_4.3H_2O$ and $MgDPO_4.3D_2O$, IR absorpt. and Raman spectra, vibr. assignments 80−97257
$MgHPO_4.3H_2O$, newberyite, struct. refinement and H bonding 80−15058
MgI_2, force consts., vibr. amplitude and shrinkage effects 79−22863
MgI_2, photoelectron spectra, geometry 78−29816
α-$Mg(IO_3)_2$, cryst. struct. using X-ray powder method *(Chinese)* 79−51059
$Mg(IO_3)_2.4H_2O$, crystal struct., unit cell, X-ray study 80−59447
$Mg(IO_3)_2.4H_2O$, struct. and phase transition using X-ray diffr. and thermal anal. *(Chinese)* 79−51059
$MgIn_xFe_{2-x}O_4$, Mossbauer spectra, elec. and mag. props. *(Russian)* 77−69737
$MgIn_2O_4$ free energy, entropy of form. 78−91433
$MgIn_2S_4$, cation distrib. and deform. parameter using Bertaut, Furuhashi and Baltzar methods 80−15041
$MgIn_2S_4$:Co(Cr), EPR powder spectra 80−25197
$MgKPO_4.6H_2O$, struvite analogue, X-ray single cryst. struct. determ. 79−19190
$MgK_2(SO_4)_2.6H_2O$:Mn^{2+}, EPR spectra spin-Hamiltonian anal. 77−77088
$MgK_2(SeO_4)_2.6H_2O$:Mn^{2+}, EPR, crystal field and hexahydrate distortion 78−91938
$MgM^{2+}{}_xFe_{2-x}O_4$, M=In,Al,Cr,Sc, comp. effects on ferrite characts. 78−52305
$Mg_{(x+2)}{}_3Mg_{(x-2)}{}_3O_x$, 145 Å superstructure 79−99143
MgMn ferrite, electrical cond., thermoelectricity, magnetoresistance meas. 78−19039
MgMn ferrite, mag. noise features at low temps. *(Russian)* 78−27060
MgMn ferrite, reaction during ferrite form. X-ray phase and mag. anal., contact volt. amperometry 77−21068
MgMn ferrite CVD epitaxial layers, bubble domains in remanence and demagnetised states 77−85516
MgMn ferrite film, magnetostriction const., mag. saturation, and internal stresses, ferromag. reson. determ. *(Russian)* 77−16126
$Mg_{0.8}Mn_{0.2}Fe_{1.8}Al_{0.2}O_4$, grade 6SChl ferrite, milling conditions effect on fine cryst. struct. and activity 79−24483
$MgMn_2O_4$, cation migration, neutron diffr. investig. 77−7896
Mg_6MnO_8, EPR in magnesium-manganese spinel *(Russian)* 78−91936
$(MgMn_2O_4)_{1-x}(MgAl_2O_4)_x$, $0<x<1$, mixed oxide spinels, chemical shifts of Mn K-absorpt. edge 80−29828
$(Mg_{0.925}Mn_{0.075})SiO_3$, synthetic orthopyroxene, cryst. struct. 78−42970
$Mg_{1-x}Mn_xTe_2$, random dil. antiferromagnet, mag. props. 80−54870
MgMnZn ferrite, ultrafine powder, prod. by cryochemical, freeze drying, spray drying or soln. techniques 80−55336
$MgMo_2O_7$, cryst. struct. 78−18596
$MgMoO_4.5H_2O$, cryst. struct. determ. by X-ray diffr. *(French)* 77−47385
$Mg(NH_3)_6(ClO_4)_2$, phase exam. by adiabatic calorimetry and X-ray diffr. methods 78−63854
$Mg(NH_3)_6(ClO_4)_2$, phase transition, group theoretical anal. 80−65218
$Mg(NH_3)_6(ClO_4)_2$, solid, mol. rot., Raman contour, quasielastic neutron scatt., and PMR obs. 79−87444
$MgNH_4PO_4.6H_2O$, struvite crysts., growth morphology and cryst. habit 79−41994
$Mg(NH_4)_2(SO_4)_2.6H_2O$:$VO(H_2O)_5^{2+}$, proton ENDOR meas. used to determine hyperfine coupling tensors 80−66075
$Mg(NH_4)(SO_4)_2.6H_2O$:$Cu(H_2O)_6^{2+}$, ^1H ENDOR 79−73854
$Mg(NH_4)_2(SO_4)_2.6H_2O$:VO^{2+}, polycryst., struct., EPR 78−15014
$Mg(NH_4)_2(SO_4)_2.6H_2O$:Cr_2O^{2-}, optical absorption study, $Cr_2O_7^{-}$ and CrO_4^{3-} centres 80−55128
$Mg(NH_4)_2(SeO_4)_2.6H_2O$:$Mn^{2+}$, EPR spectra 80−100608
$Mg(NO_3)_2$, aq. electrolyte, apparent molar heat capacity and volume, of 298.15K 79−65208
$Mg(NO_3)_2$, aq. soln., ^{25}Mg NMR, longit. relax. rates 79−91309
$Mg(NO_3)_2$, aq. soln., ionic coordination by X-ray diffr. 79−29338
$Mg(NO_3)_2$, correlation between experimental and theoretical diffusion coeffs. 77−24421
$Mg(NO_3)_2$-RNO_3 (R=Li, Na, K), thermogravimetric anal. of dehydration processes *(Japanese)* 80−66791
$Mg(NO_3)_2.6H_2O$, crystal structure changes due to substitution of Mg^{2+}, by Co^{2+} or Ni^{2+} *(German)* 80−24428
$Mg(NO_3)_2.6H_2O$-NH_4NO_3 system, molten, elec. cond. 79−51288
$Mg_{0.7}Na_{0.9}K_{2.0}Ca_{2.4}Al_{0.1}Si_{26.9}O_{72}.xH_2O$, erionite, cryst. struct. exam., stacking faults 78−2083
$MgNbF_7$, polymorphism, X-ray powder diffr. data *(French)* 80−19779
$MgNb_2O_6$, bonding characterisation 78−38680
$MgNb_2O_6$, columbite struct., normal coord. anal. 78−964
$MgNb_2O_6$, columbite struct., IR and Raman spectra *(French)* 78−19485
$MgNb_2O_6$, force fields rel. to cryst. struct. *(French)* 80−107104
$Mg_3Nb_6O_{11}$, struct. determ. and refinement from X-ray 78−91319
Mg_2NiH_4, PMR exam. of motion of H 78−56383
MgO, ^{25}Mg superhyperfine struct. of V-type defects, ENDOR 77−66439
MgO, 15-layer unrelaxed slab, lattice dynamics using breathing-shell model 79−73389
MgO, 1.7 MeV proton channelling, axial to planar transition 78−30684
MgO (:CaO) powder compacts, sintering studies, SEM obs. 79−78918
MgO (001), LEED Kikuchi pattern, surface state reson. 78−83689
MgO (001), surface relax. influence on surface vibr. modes, bulk shell model calcs. 78−71927

magnesium compounds continued
MgO (001) cleavage face, LEED Kikuchi pattern, surface reconstruction 78−84038
MgO, (001) film substrates for film growth studies by TEM, O_2 conditioning 79−82489
MgO (001) surface, AES obs. in deposited very thin Au films 79−33870
MgO, (001) surface, charge deform. and geometric relax., shell model 79−95255
MgO, (001) surface, extremal scatt. of $H_2(HD)(D_2)$ 79−95891
MgO (100), ang. depend. of Auger electron emission 79−61474
MgO (100), chain method of LEED/MEED intensity anal. 80−20018
MgO (100), surface struct., LEED study 80−39396
MgO (100) surface differential ionic relax., shell model 78−63917
MgO (111), mobility of vac. deposited Au crystallites 77−76686
MgO, a/2 ⟨110⟩ edge dislocations, lattice friction stress, atomistic calc. 78−18648
MgO, AES, obtaining density of states information from self-deconvolution of Auger band-type spectra 78−92150
MgO, a⟨100⟩ dislocation loops, TEM obs. 78−38710
MgO, additive for sintered TiO_2 ceramics, effect on props. 78−35329
MgO, adsorbed ^3He, nucl. mag. relax. props. 80−49457
MgO, adsorbed CO vibr. excitation on fracture 77−15488
MgO, adsorbed layers of S containing small paramag. ions, g-tensors, spin densities 78−46270
MgO, adsorpt. of CO, IR spectra 80−2751
MgO, adsorpt. of H_2O vapour, at high temps., IR spectra 77−47687
MgO, adsorpt. of O_2, $(O_2^-)_s$ form., thermal activation, reducing gas effects, ESR 77−9119
MgO, adsorption mechanism in selective etching 77−7727
MgO, adsorption of acetonitrile, IR and TPD study 80−70528
MgO, adsorption of CO,(N_2),(NO),(O_2), 77 to 150K, mol. motion anal. 78−84051
MgO, adsorption of Cs and Li, AES, LEED, work function, and secondary electron emission meas. 80−44407
MgO, adsorption of NO, adsorbate dimer form., heat of dissoc., EPR obs. 78−82755
MgO and MgO-dolomite, crack detection caused by thermal shock, AE technique *(Japanese)* 80−21248
MgO, anisotropy of grinding damage, chem. polishing and etching 79−47793
MgO, arc spot heat impact degradation *(Japanese)* 78−39819
MgO, at. charge densities, X-ray struct. factors, 78−79566
MgO, atomic C anal. by $^{12}C(d,p)^{13}C$ method 80−108766
MgO, atomic C anal. by laserflash induced mass spectrometry 80−108767
MgO, atomistic breathing shell model calcs. of dislocation core config. 77−35558
MgO, $B^1\Sigma^+$-$X^1\Sigma^+$ and $B^1\Sigma^+$-$A^1\Pi$ fluoresc. 78−21963
MgO bicrystal, fracture mechanism obs. 77−44339
MgO bicrystals, formed by welding single crystals with H_3PO_4, exam. 78−56796
MgO, bonding, pressure effects in lower mantle 80−72491
MgO, boundary segregation of Ca, Fe, La and Si 79−70069
MgO brick, particle-size distrib. depend. of texture and struct. *(Japanese)* 78−84753
MgO briquets, prep. by shock compaction and characteris. 79−43178
MgO, bulk and (001)-surface equal-time vibr. correlation function 78−47655
MgO, C-content determ. of single crystals grown by arc fusion 79−8456
MgO, CNDO calcs. of g-tensors and hyperfine coupling consts. of surface stabilized S_3^- radicals 77−83625
MgO, cable insulation, resistance to high-temp. and intense gamma radiation 78−25332
MgO catalyst for CO+N_2O reaction, kinetic obs. 79−29389
MgO, catalytic behaviour, rel. to XPS obs. 79−24820
MgO, cathodoluminesc. at dislocations 79−47524
MgO, chemisorption of O_2, adsorboluminescence from surface F-centres 80−20723
MgO, chemisorption on ⟨100⟩ surface, surface electronic struct. 79−11016
MgO, climb of a⟨100⟩ dislocations, TEM obs. 78−71741
MgO, clumping on substrate, effects on infrared extinction spectra, bulk absorption freq. 78−43875
MgO, coadsorpt. of CO_2 and O_2, UV irrad., ESR of radicals 78−6572
MgO coated detector for SEM backscatter to secondary electron conversion 80−68332
MgO coated moderator for slow positron beam prod. 79−17557
MgO coated moderators, slow positron form. 80−62796
MgO coated thick Fe films, surface magnetism 80−7196
MgO, coating on Fe film, Mossbauer study 80−7221
MgO, cohesive and thermophysical props., role of three-body interactions 80−92477
MgO, compressed, SCF electronic struct. calcs., necy. press. for conversion to metallic state 78−43300
MgO, compression to 8 GPa, meas. with WC-anvil X-ray apparatus and epoxy press. medium 77−89496
MgO, compressive stress-strain behaviour at high temps. 80−25774
MgO, condensates, growth from vapour, morphological comparison with, ZnO, AlN 78−34450
MgO containing Fe^{3+} and Cr^{3+}, EPR spectra obtained at room temp. and 1200°C 80−68233
MgO content of magmas rel. to tholeiitic rocks 79−88318
MgO, core struct. and energy of dislocations, breathing shell model calc. 77−39586
MgO, corrosion resist. in fused Li rel. to phase and microstruct. changes 77−44378
MgO, Cr bearing basic refractory, prod. from brine MgO 79−83158
MgO, crack propagation during in-situ deform., plastic zone formation 80−16468
MgO, crack tip dislocations and dislocation-free zones 80−96533
MgO, criteria for assessing activity 79−11820
MgO, critical voltage effect, effect of temp. *(French)* 80−10463
MgO, cryst., cumulative deform. by softer sliders 77−4154
MgO, cryst. electronic polarisability, ion size and dielectric const., hydrostatic press. effects 78−26487
MgO, cryst. preliminary processing rel. to deform. curve parameters, slip line struct. 77−52421
MgO, cryst. short-wave luminesc. V-centre electron recomb., impurity effects *(Russian)* 77−20921
MgO, cryst. surface strain and polarisation fields, breathing shell model calcs. 78−22946

magnesium compounds continued
MgO crystal, chemical etchant for old and fresh dislocations 79−65088
MgO crystal, contact damage obs. by cathodoluminesc. 80−71728
MgO crystal, diffusion of ^{51}Cr 77−35754
MgO, crystal, electron emission under uniaxial compresssion 80−7483
MgO crystal, unified approach to lattice states and dynamics 78−59878
MgO crystal, yield strength and dislocation mobility 80−93601
MgO crystal cathodoluminescence, SEM analysis 80−97349
MgO crystals, dipolar defects, thermally stimulated depolarisation 80−66101
MgO crystals, dislocation core energy from etching data 80−39100
MgO crystals, etching and polishing, inorganic or organic acids effect 80−40573
MgO crystals, etching behaviour rel. to chem. reactions 80−3229
MgO crystals, kinetics and mechanism of dissoln., etch rates in H_2SO_4 solns. 79−79136
MgO, crysts., adsorption processes in selective etching 80−39098
MgO crysts., geometrical-statistical parameters of dislocation interactions with point obstacles 80−103341
MgO crysts., plastic deform. activation parameters, rel. between macroscopic and in-situ HVEM expts. 80−103355
MgO crysts., radiation damage influence on deform. in HVEM 80−103391
MgO, defect aggregation and thermal-electric breakdown, TEM obs. 79−42069
MgO, defect centres, thermolum. examination 78−15235
MgO, defect surface, chemisorption of mol. H_2, quantum mechanical approach 77−62761
MgO, deformation induced damage, effect on optical props. 77−77258
MgO, deformed, cathodlum. obs. by STEM 80−76088
MgO, dense layer form. in pitch bearing magnesite brick, kinetics and mechanism 79−11717
MgO, determ. in glass, at. absorpt. method *(Polish)* 79−24872
MgO, dielec. band struct. calc. 79−47034
MgO, dielec. const., 5.5 to 400K 80−50249
MgO, dielectric behaviour 79−91343
MgO dielectric detector characteristics 80−27898
MgO, dielectric polarisation calcs., microscopic local fields 80−20582
MgO, dielectric properties, mean point value calc. 78−87930
MgO, direct-response UV TLD 77−13010
MgO, dislocation creep, creep deform. predictions 78−19815
MgO, dislocation motion 79−4309
MgO, displacement function calc. 80−34047
MgO, dissociation energy in range 2020 to 2160K 77−549
MgO, dissociation energy 77−550
MgO, dissociation energy from RKRV potential energy curve 78−37768
MgO, dissolution, surface roughening effects and mechanism distinction 79−47975
MgO, dissolution mechanism in acids 80−39296
MgO, doped, thermal stability of hole centres and hole recombination luminescence *(Russian)* 78−72614
MgO doped powder phosphors, photo- and thermostimulated luminesc. obs. *(Russian)* 80−66263
MgO, EPR of Mn^{2+} diffusion 78−91477
MgO, EPR spectra of Mn^{2+} along different mag. field orientations 79−47327
MgO, effect of addition on crystallisation of Na_2O-Al_2O_3-SiO_2-TiO_2 glass 78−87626
MgO, effect of B_2O_3, CaO and SiO_2 minor additives on high temp. creep 78−48450
MgO, effect of Cl^- and F^- ions on calcination and sintering *(Japanese)* 78−95719
MgO, effect of valence state on X-ray Compton line shape 77−8682
MgO, effect on carbothermic reduction of Cr_2O_3, to metallic Cr *(Japanese)* 78−48651
MgO, effect on crystallisation of Na_2O-CaO-Al_2O_3-SiO_2-F-$B_2O_3ZrO_2$ glaze 79−60279
MgO, effect on dynamical mechanical props. of polyester resin POLIMAL 190 *(Polish)* 79−96074
MgO, effect on elastic modulus temp. depend of silicate glass 79−61637
MgO, effect on microstructure of glaze 77−21083
MgO, effect on oxidation of complex (Fe, Mn)-V spinels 79−43453
MgO, effect on PbO activity in molten PbO-SiO_2 system 78−60663
MgO, effect on props. of PbO containing cryst. glass 80−24637
MgO, effect on viscosity of PbO containing crystal glasses 80−19973
MgO, elec. field effects on cond. above 1300K, elec. breakdown 79−42551
MgO, electron diffr., dynamical effects for cryst. struct. determ. 78−83679
MgO, electron irrad., V^--centres, stress-induced optical dichroism, absorpt. spectra 79−61406
MgO, electron irradiated, luminescence, radiative recombination kinetics 80−7421
MgO, electron irradiation induced mobility of substitution H 77−55390
MgO, electron irradiation damage, cryst. defects 80−107320
MgO, electronic band struct., combined tight-binding and pseudopot. approach 77−47728
MgO, electronic dielec. const. strain derivative, photoelasticity 77−4620
MgO, electronic excitations and luminescence, review *(Russian)* 78−72575
MgO, electronic struct., XPS meas. 77−73217
MgO, electronic struct., approx. SCF calcs. 79−56125
MgO, electronic struct. calc. 79−78003
MgO, electronic transition strengths, shock tube meas. 80−87183
MgO, electrophoretic deposition on stainless steel mandrel 80−11580
MgO, epitaxial layers by CVD *(Russian)* 79−56934
MgO epitaxy on alkali halides with NaCl-type struct., RHEED meas. 78−67920
MgO, etchant for revealing dislocations in (100) surface 79−19252
MgO, etching in acids, kinetics and mechanism of dissolution 78−85014
MgO, etching in acids, surface micromorphology 77−15419
MgO, etching on {100} faces by H_3PO_4 acid 78−67714
MgO, evidence for field induced trapping of defect dipole, thermally stimulated depolarisation 79−99820
MgO, exciton luminesc. spectrum, fine struct. 80−20715
MgO, exoelectron emission, mean energy, temp. depend. 80−76160
MgO, F centre luminesc., effects of uniaxial stress and ODMR 80−20690
MgO, Fe^{2+} and Fe^{3+} conc. and valency, optical density, EPR and MCD obs. 77−89462

magnesium compounds continued
MgO, Fe^{3+} and Cr^{3+} impurity ions valence conversion in single cryst. by UV irradiation *(German)* 78−84620
MgO, filamentary crysts., synthesis and props. 77−52267
MgO, filamentary crysts., mech. props. 77−52402
MgO film, delayed secondary electron emission 78−19617
MgO, film, dissoc. under heat and electron bombardment 80−7834
MgO film, graphitic C detected by surface Raman spectra 80−2297
MgO film, IR spectroscopy and RHEED analysis 77−89664
MgO film, ion induced secondary electron emission 77−44104
MgO, film, low energy electron absorpt., struct. and absorpt. centres 79−7763
MgO film, refr. index and struct., deposition temp. depend. 79−4857
MgO, film, stability, high temp. and electron irrad. effects 77−39747
MgO film, vacuum deposited on NaCl-type alkali halides, struct. characterisation 79−82490
MgO film, with high secondary electron emission, growth on Al-Mg alloy 78−35590
MgO film with ordered structure slow electrons escape depth 77−20971
MgO, fourth order elastic constants and temp. variation of second order elastic constants 79−19306
MgO, fracture and crack tip plastic zones, in situ obs. 80−108686
MgO, Franck-Condon factors rot. depend. 80−58319
MgO, free film and Au substrate, transmission spectra and photoemission characts. 77−24925
MgO, from $Mg+O_3$ matrix reaction, IR spectra, isotope shifts and blue matrix shift 78−80736
MgO, fused periclase, sintering and struct. characts. 78−23652
MgO, fusion cast compounds, crystn., microstructures rel. to conditions 80−11638
MgO, GCFR shielding material, anal. of shielding effectiveness 80−47746
MgO, granular, first-order stresses due to thermal shock 77−40409
MgO, γ-irrad. polycryst., isothermal luminesc., recomb. of electron from F_s^+ centres 80−34985
MgO, H^+ axial dechannelling temp. depend. 79−28022
MgO, hardness anisotropy obs. 79−79085
MgO, hardness increase mode, effect on dislocation mobility 79−51114
MgO, heated on W, thermal anal. using mass spectrometric, technique, vaporisation behaviour 80−79932
MgO, high temp. compatibility with BN 77−24995
MgO, high temperature interactions with Re 80−16665
MgO, high temperature prestrain effect on plastic props., dislocation struct. 80−79866
MgO, hot pressed, microstruct. influence on microhardness 79−38971
MgO, hot-pressed, elasticity props. of polycrystals and single crystals 80−54301
MgO, IR absorpt. spectra, 2300K, elec. furnace appl. *(French)* 80−27311
MgO, implanted K aggregates, TEM and optical spectra obs. 78−83838
MgO, in acetylene flame, mol. conc. meas. by laser saturation spectroscopy 79−29425
MgO, inelastic electron tunnelling spectroscopy of adsorbates, Al_2O_3 comparison 80−88686
MgO, interaction energies between vacancies and edge dislocations, shell-model calc. 78−22759
MgO, interference electron microscopy using electron holography 80−32929
MgO, interstellar, zero plasma lines rel. to origin of diffuse absorpt. bands 77−57073
MgO, interstellar grains, rel. to origin of diffuse interstellar absorpt. bands 77−9785
MgO, intrinsic defects at (001) and (011) surfaces 77−47443
MgO, intrinsic surface states at (100) and (110) surfaces 78−91740
MgO, ion irrad. induced vol. changes, optical absorpt. expts. 77−59053
MgO, ion sputter cleaning in EM 80−101895
MgO, ionic cryst., surface electronic struct., discrete variational Xα cluster method 79−4591
MgO, irrad. effects, O_3^- ion form. 79−100431
MgO irradiated with Li^+ and K^+ ions, optical props. of metal aggregates 79−65907
MgO, KLL′ Auger spectra, electronic relax., Friedel model 77−65444
MgO, Knoop microhardness anomaly on (001) planes 79−38942
MgO, laser induced photoluminesc. spectra 78−82757
MgO, lattice defects., calcination temp. effect 80−15091
MgO, lattice dynamics and vibr. sp. ht. 78−47482
MgO, lattice misorientation and displaced vol. for microhardness indentation 78−64617
MgO, Li precipitates orientation and struct. *(French)* 79−86888
MgO, light emission during adsorpt. and desorpt. of O_2 78−38949
MgO, liq., imaginary part of complex refr. index, suspension meas. *(Russian)* 79−33659
MgO, local field, microscopic electronic polarisation 80−25283
MgO, local loss of stoichiometry caused by plastic deform., cathodoluminesc. spectra 78−35209
MgO, longitudinal elastic vels. to 360 kbar 77−70642
MgO, low-energy Auger transitions 79−61476
MgO, mag. anisotropy, ionic distrib. and composition of magnesioferrite precipitates, ferrimag. reson. study 77−69699
MgO, melt-grown cryst., direct evidence for brucite precip. 77−28712
MgO, MgO-CaO (58 wt.%), comparison of high temp. creep and fracture 77−16658
MgO microcrystals, IR absorption 78−92074
MgO microcrystals, IR absorpt. 79−42963
MgO, mid IR laser window material, absorption props. 77−46770
MgO, modified electron gas theory, high press. effect 77−19899
MgO, Mollwo-Ivey relation between peak-colour absorption energy and average O ion spacing 77−90179
MgO, molten K_2SO_4 treated, phys. and chem. props. *(Japanese)* 79−57133
MgO, multiple-beam dynamic effects, in Kikuchi patterns 79−46528
MgO, muonium and positronium form. 79−56679
MgO, neutron irrad., MCD, optical absorpt. lines 77−77255
MgO, neutron irradiated, Huang diffuse scattering of neutrons 80−10544
MgO, new electronic band system in UV 77−14447
MgO, orientation relationship and struct. of Li precipitates 79−82342
MgO, oxidising properties 79−100339
MgO particles, AG dispersion strengthening appl., for electrical contacts *(Slovak)* 78−31544

magnesium compounds continued
MgO, Peierls mechanism for dislocation motion, formation of double kinks 77−68973
MgO, phonon spectra using freq. crossing techniques 78−14415
MgO, photoelastic effect anal. 77−12358
MgO, photoelasticity, exchange charge polaris. effect 77−81046
MgO, photoluminesc. during mechanical deform. 80−60665
MgO, photostimulated electron emission, manifestation of Auger processes 77−52225
MgO, planar channelling of He ions along (100), (110) and (111) directions 79−28023
MgO, plasmochemical synthesis, oxidised from metals, exam. of props. 80−2984
MgO, plastically deformed, recovery of internal friction at room temp. *(French)* 78−80577
MgO, point-obstacle distance distrib. during motion of screw dislocations 77−11744
MgO, polycrystalline, diffusion creep activation energy 78−11274
MgO, polycrystalline, ductile, porous, model 79−47653
MgO, polycrystalline, grain growth and grain boundary migration, pore effects *(Japanese)* 78−19701
MgO, polycrystalline, stress depend. of creep 79−70120
MgO polycrystals, hot-pressed, effect of annealing on props. 79−34073
MgO polycrystals, mech. props., 900-1150°C *(French)* 80−104374
MgO polycrystals, ultrafine grained, compressive creep 77−32639
MgO polycrystals, ultrafine-grained, creep microstruct. 80−35246
MgO, pore distrib. and grain size in intermediated sintering stage *(Japanese)* 79−74124
MgO porous layers, conductivity, conditions for lag and dark current 77−20476
MgO powder, active, sintering 80−20870
MgO powder, decomp. of chemisorbed ethanol, propanol and acetic acid 78−92502
MgO, powder, positronium fine struct. interval meas. by Zeeman transitions 78−95616
MgO powder, surface area determ. by adsorpt. of stearic acid and pyridine 80−107636
MgO powder, vacuum UV induced thermoluminesc. in Γ-irradiated and non-irradiated samples 77−36302
MgO, powder activation during grinding 77−90300
MgO powders, hot pressing, mechanisms 80−40300
MgO, precipitate morphology, strain energy effects 80−40358
MgO, precipitation from gas phase 78−6025
MgO, precipitation on dislocations, ultramicroscopy and chem. etching 78−67720
MgO, prereduced surfaces, room temp. activity for oxygen isotopic exchange 79−91998
MgO, produced by thermal decomposition of Mg cmpds. to periclase refractory, sinter adhesion 79−83164
MgO, pure and doped, luminesc. of free and relaxed excitons 79−74008
MgO, pure and doped crysts., X-ray stimulated luminesc. 79−28802
MgO, radiation induced O interstitials, EPR meas. 78−55866
MgO, rate of reduction by C 77−28743
MgO, reaction and bonding with Pd, below MP of starting materials, obs. in TEM 77−21419
MgO, reconstruction of the (001) surface 78−73922
MgO, recording of pulsed EM radiation in RF band during heating *(Russian)* 77−55837
MgO, red and near UV bands calc., rel. to sunspot spectra 80−12736
MgO, reduction by C, kinetics and mechanism *(Russian)* 80−93743
MgO, residual image contrast of dislocation loops 78−47382
MgO role in Al_2O_3 sintering 80−81010
MgO, room temp. Debye-Waller factors 77−62607
MgO scintillator prep. for viewing accelerator beam spots 79−6803
MgO, second-order Raman scatt. 78−10894
MgO secondary emitter, increasing of efficiency by coating with Cs or Li film 78−2960
MgO secondary emitter efficiency improvement for low primary electron energies 79−69931
MgO, segregation of aliovalent solutes adjacent {100} surfaces 79−78979
MgO, semisintered, shear strength at high press. 80−76308
MgO short time chemomechanical effects, dislocation generation and motion, drilling simulation 79−87749
MgO single cryst., γ-irrad. in presence of O_2, H_2 and H_2O adsorbates, thermostimulated surface cond. 80−34499
MgO single cryst., impact wear characts. 80−76374
MgO single cryst., impact wear damage 80−76375
MgO single cryst., internal stresses and dislocation mobility, stress relaxation method 80−6413
MgO, single cryst., order hardening by large precipitated vol. fraction of spinel particles 80−3085
MgO, single cryst., tensile creep, stress induced dislocation structs. 80−96539
MgO, single cryst., thermolum. for UV dosimetry 77−16986
MgO, single cryst., tribolum. obs. 79−52031
MgO, single cryst. grown by arc fusion, C content 77−68991
MgO, single cryst. growth using modified plasma torch furnace, doping *(Japanese)* 79−95923
MgO single crystal, absorbed fluid effect on rolling contact deform. 78−64719
MgO single crystal, corrosion by BOF slag 79−24635
MgO single crystal, dislocation struct. of slip lines, TEM 79−27990
MgO, single crystal, effect of heat treatment on mechanical props. 77−70070
MgO, single crystal, elastic consts. and internal frictions meas. by rectangular parallelepiped reson. 77−78165
MgO single crystal, grain boundaries, cathodolum. in SEM 79−1440
MgO, single crystal, thermolum. meas. *(Japanese)* 78−19577
MgO, single crystal, thermal and optical stimulation processes of V-centres *(Japanese)* 80−11485
MgO single crystal, wear and friction on sintered Al_2O_3 in vacuum 77−12710
MgO single crystal, wear charact. on low C steel disc 78−15541
MgO, single crystal, wear damage, surface cracks 78−68825
MgO single crystals, chem. polishes for {100}, {110} and {111} surfaces, spectrochem. anal. for impurity content 79−29241
MgO, single crystals, compressed, SEM exam. of cathodoluminescence 78−56525
MgO single crystals, crack formation process, micro-deformation and fracture *(Japanese)* 80−24530

magnesium compounds continued
MgO, single crystals, deform., dislocation motion and multiplication in HV electron microscope 77−84754
MgO single crystals, impurity effects on cationic cond. *(French)* 80−65286
MgO single crystals, surface atomic steps obs. by electron microscopy, dark- and bright-field techniques 80−84040
MgO single crysts., dislocation processes, obs. by HVEM in-situ deform. 80−103340
MgO, single crysts., work hardening and creep 79−43262
MgO single-layer film 2.8 μm, 3.8 μm absorpt. meas. 78−90463
MgO, sintered, refractories, props. after testing at over 2000°C 80−104317
MgO sintered-ceramic separator plate development, Li-Al/LiCl-KCl/FeS battery applications 80−61321
MgO, sintering, effect of Ca compound additions *(Japanese)* 80−55340
MgO sintering activator, effect on α-Al_2O_3 mineralisation, alumina heat treatment 80−89186
MgO, sintering by activating $3MgCo_3.Mg(OH)_2.3H_2O$ 80−89183
MgO, slip line struct. using replica electron microscope technique 79−7605
MgO, slow-electron-stimulated desorption 79−60623
MgO small cubes, surface vibr. modes, IR transmission obs. 78−22947
MgO smoke, targets, deformation process investigation 79−99995
MgO smoke crystals, growth twinning 79−60382
MgO, smoke particles, size distrib. 80−104471
MgO, solid solubility of Sc_2O_3, Al_2O_3, Cr_2O_3, SiO_2 and ZrO_2 80−15247
MgO solubility products in molten NaCl-KCl, potentiometric determ. 80−76488
MgO solution in UO_{2+x}, shell model calcs. of enthalpy, computer program for formation energies 79−42251
MgO, spherical particle impact damage, effect of crystallographic orientation 79−79135
MgO, strength under confining press. of 250 kbar, brittle-ductile transition 77−47510
MgO, stress-strain determ. by high press. X-ray diffr. 77−7792
MgO, stresses on hot pressing 77−36425
MgO, subgrain boundaries form. obs. by TEM, diffusion coeff. determ. 80−79817
MgO substrate, polycrystalline Si film deposition, using double cathode sputtering system *(Japanese)* 77−55889
MgO, substrate for ^4He film growth, vap. press. meas. 80−70499
MgO, substructure, X-ray diffraction study, rel. to preparation by thermal decomposition 77−12581
MgO supported Pt catalyst, H_2 adsorption, 300-873K *(French)* 78−38967
MgO surface, characteristics of electron-beam-cleaved surfaces by in situ Au decoration 77−51579
MgO surface, electron beam cleaved, characterisation by Au decoration 77−47657
MgO surface, $H_2+D_2 \rightleftharpoons 2HD$ catalysis, SCF UHF calc. 77−9120
MgO, surface, laser Raman fluoresc. background, OH^- excitation 78−10875
MgO surface, mobile $(CO_2\text{-}O_2)^-$ radical, ESR spectrum 80−43076
MgO surface, secondary electron emission effects on voltage breakdown curves in Penning mixture for insulated electrode discharges 78−19616
MgO, surface electron donor sites and acid-base props., adsorbed radical ESR 77−21417
MgO, surface F centre, electronic struct. 78−64091
MgO, surface layer spacing relax., electrostatic argument 79−46901
MgO, temp. depend. of int. angles for proton axial channelling 80−10586
MgO, tensile and compressive strengths of fine powder bed *(Japanese)* 80−25780
MgO, tensile creep of single crystals, substruct. effect 79−66113
MgO, thermal charact. using constant power source method 79−95222
MgO, thermal cond. up to 40 kbar 79−1533
MgO, thermal expansion, 500-1800°C, X-ray diffr. 77−35723
MgO, thermally shocked, strengthening kinetics 77−8920
MgO, thermally stimulated exoelectron emission *(German)* 80−66404
MgO, thermochemical coloration and annealing 79−91468
MgO, thermoelec. props., ionic effects with $MgCl_2$ additions 78−26895
MgO, thermoluminescence mechanism 79−15538
MgO thin film, DC conduction 78−88051
MgO, transition metal ion doped, phonon spectroscopy using freq. crossing techniques 79−42193
MgO, UV visible absorpt. by laser calorimetry, wavelength modulation spectroscopy 78−66876
MgO, ultrafine grained Fe doped, high temp. creep 79−15727
MgO, V^- centres, electronic struct., rel. to optical absorption 77−28140
MgO, vacancy-dislocation interaction energies, atomistic model calcs. 80−59513
MgO, vacuum UV luminesc., excitation by X-ray synchrotron radiation 79−8168
MgO, valence electron distrib., pseudopotential calcs. 80−2335
MgO, vaporization in O_2-H_2O atmos. *(Japanese)* 79−74279
MgO, vibrational contribution to surface thermodynamic functions 77−47659
MgO, vibrational surface modes of (001) unrelaxed face, shell model 77−43420
MgO, visible-near UV triplet-triplet transition moments and intensities 77−58085
MgO, wavelengths and relative intensities of IR bands 79−2407
MgO, wettability of single crysts. by liquid metals *(Russian)* 77−43408
MgO, with paramag. surface defects, elec. cond., 20-250°C, H_2 atm. effects 77−20313
MgO, X-ray and electron diffr. crystallite size determ. *(Polish)* 79−100153
MgO, X-ray determ. of electron density distribs., atomic scatt. factors 80−15078
MgO, XPS valence bandstruct. 80−89117
MgO:(Li), polycrystn., internal friction *(German)* 80−59577
MgO:Ag^{2+}, EPR spectrum, static, quasistatic and quasidynamic Jahn-Teller effect 77−85561
MgO:Al, and nominally pure single crystal, thermally stimulated luminesc. rel. to temp., and EPR *(Russian)* 80−84789
MgO:Al, luminescent crystals, exciton, electron hole energy transfer 78−10998
MgO:Al^{3+}, positron annihilation meas. 77−8681
MgO:$Al^{3+}(Fe^{3+})$, defect struct., shell model calcs. 79−99180

magnesium compounds continued
MgO:Al(Li)(F)(Sn), hole processes in photostimulated luminesc., electron emission, X-ray irrad., ESR relaxation 79−69889
MgO:Be epitaxial layers, vacuum UV luminescence 80−11480
MgO:$CaO(SiO_2)(B_2O_3)(Cr_2O_3)$, effective of impurities on high temp. creep 80−40455
MgO:Co ions, impurity distrib. from EPR 77−51401
MgO:Co^{2+}, ESR linewidths of Co^{2+} 80−80596
MgO:Co^{2+}, electronic and impurity-induced Raman scatt. 80−100659
MgO:Co^{2+}, strain modulated ESR, extensional and flexural modes 78−68365
MgO:Co^{2+}, strain modulated ESR, extensional and flexural modes 78−68366
MgO:Co^{2+}, weak dynamic Jahn-Teller coupling, neutron inelastic scatt. obs. 80−59934
MgO:Cr, Co, optical and ESR studies 80−50175
MgO:Cr, elec. cond. at high temp. in oxidising atmosphere 77−69323
MgO:Cr, high resolution far IR spectroscopy of lower energy levels of Cr^{2+} 80−80822
MgO:Cr^{2+}, APR spectra 79−87313
MgO:Cr^{2+}, APR under applied stress 80−88865
MgO:Cr^{2+}, critically coupled spin-phonon mode 78−67779
MgO:Cr^{2+}, dynamic Jahn-Teller effect, APR obs. 77−20693
MgO:Cr^{2+}, Jahn-Teller parameters determ. using heat pulses 77−62876
MgO:Cr^{2+}, paramag., spin-phonon coupling, inelastic neutron scatt. obs. 79−60441
MgO:Cr^{2+}, reson. scatt. of phonons by ions 78−18716
MgO:$Cr^{2+}(Fe^{2+})$, reson. relax. time for impurity electrons and localised phonons interaction, appl. to thermal cond. 80−59590
MgO:$Cr^{2+}(Fe^{2+})$, thermal magnetoresistance 79−10994
MgO:$Cr^{2+}(Mn^{2+})$, phonon spectroscopy using supercond. tunnel junctions 79−65157
MgO:$Cr^{2+}(Mn^{3+})(V^{3+})$, HF phonon spectroscopy using supercond. tunnel junctions 80−65178
MgO:$Cr^{2+}(V^{2+})$, coupling of T_{1u} and T_{2u} vibr. to $^2E_g \rightarrow {}^4A_{2g}$ transition 77−63453
MgO:Cr^{3+}, $^4T_{2g}$ excited level of Cr^{3+} 78−43920
MgO:Cr^{3+}, axial centres, EPR and fluoresc. meas. 78−2731
MgO:Cr^{3+}, broad band luminesc., relaxed level and emission processes 78−31234
MgO:Cr^{3+}, cubic centre, high resolution ESR, superhyperfine interaction 77−16162
MgO:Cr^{3+}, diffuse interstellar absorpt. bands origin 79−30101
MgO:Cr^{3+}, EPR obs., S=2 spin state D-tensor components 77−28433
MgO:Cr^{3+}, emission and excitation spectra 80−93387
MgO:Cr^{3+}, no-phonon lines associated with broad band emission *(French)* 77−52163
MgO:Cr^{3+}, ODMR, octahedral and orthorhombic site symm. 80−71243
MgO:Cr^{3+}, ODMR study, Cr^{3+} ions in tetragonal symm. sites 80−88892
MgO:Cr^{3+}, optical excitation transfer 80−97325
MgO:Cr^{3+}, single cryst., ESR linewidth 80−29605
MgO:Cr^{3+}, site symmetry of Cr^{3+}, polarised luminesc. meas. 77−12426
MgO:Cr^{3+}, strain modulated ESR 78−88175
MgO:Cr^{3+} (Mn^{2+}) spin Hamiltonian parameters, lattice expansion and vibr. effects 80−24851
MgO:Cr^{3+} crystal, radiationless relax., photoacoustic spectra 78−27264
MgO:$Cr^{3+}(V^{2+})$, $^4A_{2g} \rightarrow {}^4T_{2g}$ spectra, new expt. results 80−11441
MgO:Cr(III), radiationless relax., heat-pulse meas. technique 77−36277
MgO:Cu, dopant conc., refr. index profile rel. to integrated optics 78−5583
MgO:Er^{3+}, Γ_8 quartets, orbit-lattice interaction, e.p.r. under stress 77−1591
MgO:Er^{3+}, spin-lattice interaction in Γ_8 quartets, models tested for EPR data 78−23336
MgO:Fe, cathodolum. after plastic deform. 79−95849
MgO:Fe, Fe^{2+} oxidation and Fe^{3+} reduction kinetics, EPR obs. 79−70399
MgO:Fe crysts., oxidised and reduced, optical absorpt. spectrum at low temps. 77−63436
MgO:Fe^{2+}, $^5T_{2g} \rightarrow {}^5E_g$ adsorption, Zeeman effect meas. 77−12405
MgO:Fe^{2+}, far IR absorpt. meas. by Fourier transform, apparatus 77−177
MgO:Fe^{2+}, impurity electron-phonon reson. relax. time, thermal cond. 77−59085
MgO:Fe^{2+}, intrinsic spin-lattice relaxation rates, nonresonant US meas. 78−80203
MgO:Fe^{2+}, Jahn-Teller effect in ^5E_g state, tunnelling splitting obs. 78−19517
MgO:Fe^{2+}, lifetime of coupled spin-phonon excitations 77−69053
MgO:Fe^{2+}, microwave acoustic relaxation losses 78−43635
MgO:Fe^{2+}, phonon-induced transition interf. in EPR and IR spectra, ion-lattice coupling 77−51945
MgO:Fe^{2+}, shock compressed absorpt. spectrum, appl. to Earth mantle 80−90039
MgO:Fe^{3+}, clustering, EPR meas. 78−56372
MgO:Fe^{3+}, defect structure, and oxidation reduction behaviour of Fe 79−99181
MgO:Fe^{3+}, EPR of Fe^{3+} in orthorhombic symmetry sites 77−20689
MgO:Fe^{3+}, Mn^{2+}, X-irrad. induced anion Frenkel defects, stabilisation by Fe^{3+}, optical and ESR obs. 77−68969
MgO:Fe^{3+}, point defect complex-edge dislocation interaction energies, atomistic calc. 80−107314
MgO:Fe^{3+}, spin-lattice relax. 77−90037
MgO:Fe^{3+}, spin-lattice relax. time, meas. 80−66020
MgO:Fe^{3+} single cryst., exchange energy 80−96834
MgO:Ga, γ-irradiated, EPR and optical studies 79−73809
MgO:H(D), electron irrad. induced diffusion of interstitial impurity 77−15452
MgO:Ir^{2+}, quadrupole interactions and static Jahn-Teller effect in EPR spectra 77−72842
MgO:Ir^{2+}, superhyperfine struct. of ^{25}Mg in EPR spectra of Ir^{2+} 77−69683
MgO:Li, $[Li]^0$ defect, high temp. and ionisation induced effects 78−34509
MgO:Li, $[Li]^0$ defect, stress induced optical dichroism 78−35179
MgO:Li, $[Li]^0$ defects, magneto-optical props. 77−12365
MgO:Li, enhancement of elec. cond. by oxidation 80−44600
MgO:Li, internal friction, mech. and dielec. relax. *(German)* 80−34135
MgO:Li, mech. deformed crysts., imprinting of slip bands using Li impurities 80−59473

magnesium compounds continued
MgO:Li, oxidation and reduction up to 1700K, defect prod. 79−39013
MgO:Li, TEM studies 79−29069
MgO:Li, thermally generated $[Li]^0$ defects, valence compensation 79−77598
MgO:Li^+, quenched, elec. polarisation, thermal depolarisation and dielectric loss meas. 79−1738
MgO:$Li^+(Na^+)$, precipitation rel. to dislocations *(French)* 79−51163
MgO:LiF, accretive recrystallisation during hot pressing 77−36421
MgO:Li(Al)(F), impurity-induced UV luminesc. 79−83037
MgO:M^{2+}, M=Co, Ni, Cu, next-nearest-neighbour ion effects on impurity 2p levels 77−20987
MgO:Mn^{2+}, clustering of mag. ions, study method 80−11155
MgO:Mn^{2+}, EPR of polycrysts. with varying impurity concentration *(Russian)* 77−28438
MgO:Mn^{2+}, spin-lattice relax. time, meas. 80−66020
MgO:Mn^{2+} EPR, X-band freq., powder pattern for cubic symm. anal. *(Spanish)* 78−43636
MgO:$Mn^{2+}(Fe^{2+})(Cr^{2+})$, redox behaviour of ions, ESR and X-ray diffr. 78−52341
MgO:$Mn^{2+}(Fe^{3+})$, EPR, 94-600K, temp. depend. of cubic spin Hamiltonian parameter 78−60332
MgO:Mn^{3+}, ground state exam., thermal conductivity meas. 79−42497
MgO:Mn^{4+}, diffuse interstellar absorpt. bands origin 79−30101
MgO:Mo catalyst, adsorpt. of propylene, oxidation reactions, surface structs., IR absorpt. spectra obs. 80−66868
MgO:nAl_2O_3 spinel, plastic deformation at T<1000°C, slip systems 80−108505
MgO:Ni, heavily doped, defect characterisation, rel. to use as laser material 80−65000
MgO:Ni, optical absorpt. spectrum in mag. field, and 2p-3d charge transfer 77−52141
MgO:Ni, tunable transition-metal-doped solid state lasers 80−58549
MgO:Ni^{2+}, config. interaction and cryst. field theory 77−39811
MgO:Ni^{2+}, elastic interaction of mag. centres, EPR line width meas. 78−19315
MgO:Ni^{2+}, near IR luminesc. from isolated and exchange-coupled Ni^{2+} ion pairs, temp. depend. 80−93382
MgO:Ni^{2+}, single crystal, thin film, near IR luminescence *(Russian)* 79−28807
MgO:Ni^{2+}, temp. depend. of luminesc. 79−83016
MgO:Ni^{2+} laser system, optical parameters 80−48260
MgO:OH^-, room temp. IR spectra, heat treatment and electron irrad. effects 79−51992
MgO:Pt^{3+}, Jahn-Teller effect in EPR spectrum 80−7160
MgO:Rh^{2+}, EPR of Jahn-Teller ions, ^{17}O superhyperfine structure 77−32253
MgO:S, cathodoluminesc. spectrum *(Russian)* 80−55197
MgO:Sn, luminescent crystals, exciton, electron hole energy transfer 78−10998
MgO:V^{2+}, first and second order Jahn-Teller coupling const. calc. 79−65906
MgO:V^{2+}, Jahn-Teller system, zero-phonon line broadening due to non-radiative transitions 80−108258
MgO:V^{2+}, mag. circular dichroism in split zero-phonon line 78−56460
MgO:V^{2+}, octahedral clusters, quadratic Jahn-Teller effect and tunnelling splitting 77−72840
MgO:V^{2+}, zero-phonon line splitting in $T\times e_g$ Jahn-Teller problem 78−19006
MgO/Ni-Cr (80, 20 wt.%) cermets, sintered, elec. resist. temp. effect 80−3206
$2MgO\text{-}2Al_2O_3\text{-}5SiO_2$, cordierite, synthesis rel. to WC addition 77−8787
$MgO\text{-}(Cr_2O_3)(AP_2O_3)(Fe_2O_3)(SiO_2)$, vaporization 79−99308
MgO-Ag porous layer, secondary electron emission from ion impact, gas discharge device appl. 78−68586
MgO-Al_2O_3 spinel crysts., thermolum. spectra 79−65938
MgO-Al_2O_3 system, surface microphases investigation by X-ray electron spectral anal. 79−51269
MgO-Al_2O_3 transparent spinel ceramic, fabrication by reactive hot pressing *(Japanese)* 77−77454
$MgO\text{-}Al_2O_3\text{-}Cr_2O_3$, vacuum vaporisation, Langmuir method 78−95149
$MgO\text{-}Al_2O_3\text{-}Fe_2O_3\text{-}SiO_2$, cordierite, in ceramic, effect of heat treatment on cordierite content 79−20039
$MgO\text{-}Al_2O_3\text{-}P_2O_5$, struct. energetics and charging under irrad. *(Russian)* 77−84791
$MgO\text{-}Al_2O_3\text{-}P_2O_5$, electron beam irrad., temporal change in electric field produced 79−4760
$MgO\text{-}Al_2O_3\text{-}P_2O_5$, exam. of electron beam irrad. effects on physical props. 79−4253
$MgO\text{-}Al_2O_3\text{-}P_2O_5$ irradiated electret glasses, relax. of external field intensity on heating 80−25282
$MgO\text{-}Al_2O_3\text{-}P_2O_5$ system glass, heat treatment of aluminium metaphosphate influence on thermolum. 80−108285
$MgO\text{-}Al_2O_3\text{-}SiO_2$, exam. of microstructure and crystallisation kinetics 78−80501
$MgO\text{-}Al_2O_3\text{-}SiO_2$, glass ceramics, phase transformation processes 80−3025
$MgO\text{-}Al_2O_3\text{-}SiO_2$, glass ceramic, structure and props. *(German)* 80−38927
$MgO\text{-}Al_2O_3\text{-}SiO_2$, melt and glass crystn. with $ZrO_2\text{-}TiO_2$ nucleants 77−31599
$MgO\text{-}Al_2O_3\text{-}SiO_2$, metastable liq. phase separation region, electron microscope exam. 78−88451
$MgO\text{-}Al_2O_3\text{-}SiO_2$, sintered, cordierite, mineralogy and props. 80−60827
$MgO\text{-}Al_2O_3\text{-}SiO_2$ based cordierite glass-ceramic, strength and thermal shock, surface treatment effect 80−25884
$MgO\text{-}Al_2O_3\text{-}SiO_2$ glass ceramic, nucleation, effect of electric fields 78−83742
$MgO\text{-}Al_2O_3\text{-}SiO_2$ glass/polysulphone adhesive failure, ISS and SIMS obs. 80−55626
$MgO\text{-}Al_2O_3\text{-}SiO_2$ system glasses and glass ceramics, EPR obs. of transition elements, crystn. effects 78−23332
$MgO\text{-}Al_2O_3\text{-}SiO_2$: ZrO_2, TiO_2, glass, phase separation *(German)* 80−38932
$MgO\text{-}Al_2O_3\text{-}SiO_2$:$Ce^{3+}$ glass scintillator, energy transfer, luminesc. efficiency under UV and charged-particle excitation 79−95821
$MgO\text{-}Al_2O_3\text{-}SiO_2\text{-}NiO$ glass, gamma ray irradiated, exam. of ESR spectrum of Ni(I) 79−4719
$MgO\text{-}Al_2O_3\text{-}TiO_2\text{-}SiO_2$, glass formation, structure of cations *(Russian)* 80−38933
$MgO\text{-}Al_2O_3\text{-}ZrO_2$, wetting with liquid Fe and Al 78−22936

magnesium compounds continued
$MgO\text{-}Al_2O_3(Cr_2O_3)(Fe_xO_y)\text{-}CuO$, phase relations and microstruct. 79−74140
MgO-Au, cermet coatings, solar energy photothermal conversion, Bruggeman effective medium theory 79−83627
MgO-Au cermet film, high intensity electron bombard. effect on secondary electron yield 77−81184
MgO-Au cermet film, selective black absorbers 77−1747
MgO-Au cermet films, for selective black absorbers 79−29483
$MgO\text{-}B_2O_3$ system, glass and cryst. compd. struct. determ. by ^{11}B NMR 79−94905
$MgO\text{-}BaO\text{-}Al_2O_3\text{-}SiO_2$, glass, IR absorpt. spectra and solid struct. exam. 78−88314
MgO-C dispersion, creep, effect of C on grain size and growth 79−100213
MgO-C in melts, corrosion resist., rel to oxidation, porosity, content 80−40578
$MgO\text{-}Ca_3Mg(SiO_4)_2(CaMgSiO_4)\text{-}NaPO_3$, phase conversions 77−66641
$MgO\text{-}CaMgSiO_4$, exam. of high temp. creep behaviour 78−80601
$MgO\text{-}CaMgSiO_4\text{-}(Al_{0.5}Cr_{0.5})_2O_3(Al_2O_3)(Cr_2O_3)$, spinel phase, phase equilibrium relations and spinel bonding 80−55376
MgO-CaO, thermal expansion coefficients of refractory ceramics 79−99336
$MgO\text{-}CaO\text{-}Al_2O_3\text{-}SiO_2\text{-}Fe_{(l)}$, heterogeneous equilib. calcs. *(Russian)* 77−59093
$MgO\text{-}CaO\text{-}Al_2O_3\text{-}SiO_2(\text{-}TiO_3)$ systems, glass-ceramics, crystn. kinetics *(Russian)* 79−37626
$MgO\text{-}CaO\text{-}Fe_2O_3\text{-}Al_2O_3\text{-}SiO_2$, clinker production from dolomite and magnesite 80−55339
$MgO\text{-}CaO\text{-}FeO\text{-}Fe_2O_3\text{-}SiO_2\text{-}Cr_2O_3\text{-}Al_2O_3$ spinel refractories, physicochem. prod. conditions 80−89185
$MgO\text{-}CaO\text{-}FeO(Fe_2O_3)\text{-}Al_2O_3\text{-}SiO_2$ glass, X-ray spectra Fe ion electron config. *(Russian)* 77−8674
MgO-CaO-SiO_2, melts, mixing enthalpy, 1700-1873K 78−79785
$MgO\text{-}CaO\text{-}SiO_2\text{-}Al_2O_3\text{-}Na_2O.P_2O_5$, effect of $NaPO_3$ on phase composition rel. to basic refractories 78−80528
$MgO\text{-}CaO\text{-}SiO_2\text{-}C$, equilibrium partial press. of Mg, SiO, Ca and CO 77−36482
MgO-CdO, interface, coincidence-site-lattice relations 80−103588
MgO-CoO, high surface area, O_2 adsorpt., EPR, volumetric investigs. 80−10782
MgO-Cr_2O_3, composition obs. by thermogravimetry 79−16081
MgO-Cr_2O_3, diffusion of Cr_2O_3 and Fe_2O_3 in gas phase during firing *(French)* 78−80495
MgO-Cr_2O_3, reaction sintering *(German)* 78−11174
MgO-Cr_2O_3, vacuum vaporisation 78−91434
MgO-Cr_2O_3, vaporisation rate, O_2 partial press. effect *(Japanese)* 78−63848
MgO-Fe_2O_3, composition obs. by thermogravimetry 79−16081
$MgO\text{-}Fe_3O_4\text{-}Cr_2O_3$, isothermal sections, development of calculation data base 79−96006
$MgO\text{-}FeO\text{-}P_2O_5$ system, glass, ESR spectra, heat treatment conditions effect 79−65722
$MgO\text{-}Ga_2O_3\text{-}SiO_2$ system, subsolidus phase equilib. 78−44106
MgO-insulated Inconel-sheathed $Pt_{90}Rh_{10}$/Pt thermocouple, decalibrations during 1200°C use, ion microprobe obs. 78−57957
MgO-LiCl, solution under hydrothermal conditions, exam. of phase equilibria 79−8292
$MgO\text{-}MgAl_2O_4(FeCr_2O_4)$, thermoplastic and thermophys. props. for steel vacuuming installations 80−35281
$MgO\text{-}MgCl_2\text{-}H_2O$, cement paste, reaction products, X-ray diffr. study 78−23689
$MgO\text{-}MgF_2$ multilayer stack selective mirror with high reflectivity *(French)* 80−64131
MgO-Mn^{2+}, Q band ESR spectrum, spin Hamiltonian calcs. *(French)* 78−64262
MgO-MnO, EPR concentration dependence in magnetically diluted crystals with strong spin-spin interaction 79−42826
$MgO\text{-}NH_4F\text{-}GeO_2$:Mn phosphor, luminance. spectra due to UV irrad., 26-294°C 79−83005
$MgO\text{-}Na_2O\text{-}B_2O_3$, Raman scatt. studies of glass struct. 77−90147
MgO-NaCl refractory clinkers, Cr containing, densification, thermal treatment and phase composition effect *(French)* 80−76219
$MgO\text{-}NaMg(Ca)PO_4$, $MgO\text{-}Na_2CaMg(PO_4)_2$, partial system, phase diag. 77−86005
$MgO\text{-}NaVO_3(NaB_4O_7)(NaSi_2O_5)$ melt, transport-controlled dissolution 79−90791
$MgO\text{-}Nb_2O_5\text{-}Al_2O_3$, solid state equilibria at 1400°C phase diagram *(Italian)* 78−23671
$MgO\text{-}Nd_2O_3\text{-}Al(Cr)_2O_3$, reactions kinetics in mixtures of components and phases 77−40523
MgO-NiO, crystalline soln., microstrain rel. to lattice energy and strain energy 77−24411
MgO-NiO, STEM microanal., absorpt. effects 80−80902
MgO-NiO, solid soln. formation, initial stage obs. 77−81243
$MgO\text{-}P_2O_5$, glass, US velocity rel. to elastic props. 80−103425
$MgO\text{-}P_2O_5$ glass, diffusion of Cu^+, fluoresc. meas. 78−59980
$MgO\text{-}P_2O_5$ glass, ESR of VO^{2+} ions 80−100610
$MgO\text{-}P_2O_5\text{:}Fe_2O_3$ glass, $Fe^{2+(3)}$ impurity ions struct.-chem. state, Mossbauer data 80−40028
$MgO\text{-}P_2O_5\text{-}Al_2O_3\text{-}3P_2O_5$ glass, absorpt. shift, electron and hole traps, thermolum. meas. 79−65897
$MgO\text{-}P_2O_5\text{-}SiO_2$ glasses, photoelastic consts. and polarisability 79−65839
MgO-Pd metal-ceramic reaction, micro/macro obs. 80−66467
5 wt.% $MgO\text{-}Si_3N_4$, hot-pressed, dielec. props. 78−10822
$MgO\text{-}Si_3N_4$, hot-pressed, electrical props. 78−39136
$MgO\text{-}SiO_2$, and LiF-BeF_2 systems, complex ionic liquids, corresponding-state principle *(Japanese)* 77−56245
$MgO\text{-}SiO_2$, melt, effect of cooling rate upon glass transition, X-ray analysis 79−27920
$MgO\text{-}SiO_2$, molten, corresponding state principle with LiF-BeF_2 and appl. 79−11589
$MgO\text{-}SiO_2$, molten binary, X-ray exam. of struct. 78−38610
$MgO\text{-}SiO_2$ system, high-press. phase transistions calcs. rel. to mantle discontinuities 79−90780
$MgO\text{-}SiO_2\text{-}Si_3N_4\text{-}Mg_3N_2$, phase relations 77−63614
MgO-spinel concrete, cast, hardening by elec. heating 80−21258
MgO-Ti^{3+}, orthorhombic distortion, Jahn-Teller effect 77−66140
$MgO\text{-}TiO_2\text{-}Al_2O_3\text{-}SiO_2$ glass, γ-irrad., struct. position of Ti, EPR study 80−84644
$MgO\text{-}TiO_2\text{-}SiO_2\text{-}Al_2O_3$ glasses, internal friction during crystn. 79−52285

magnesium compounds continued
MgO-V_2O_5 system, heat treated, EPR meas. *(Russian)* 77−90025
MgO-ZnO, solid soln., surface comp., Auger and XPS investig. 78−51806
MgO-ZnO-Fe_2O_3, sintered ferrite, preparation, mag. susceptibility, DC resistivity 80−34598
MgO-ZnO-Fe_2O_3 ternary system, phase equilibria 77−21116
MgO-ZnO-Fe_2O_3-Cr_2O_3 system spinels, IR absorpt. spectra, short-range order 79−42957
MgO-ZrO_2, dispersion hardened, fracture strength and texture, rel. to temp. *(German)* 79−43378
MgO-ZrO_2 ceramic reinforced with filamentary crystals, mech. and thermal props. 80−45262
MgO-ZrO_2 ceramic sublimation at optical furnace focal spot *(Russian)* 79−95983
MgO+Si_3N_4, reaction during hot pressing 78−68658
MgO_2, from Mg+O_3 matrix reaction, IR spectra, isotope shifts and blue matrix shift 78−80736
MgO_2 powder exam. of packing behaviour *(Japanese)* 79−20016
MgO_3, from Mg+O_3 matrix reaction, IR spectra, isotope shifts and blue matrix shift 78−80736
MgO_3, visible absorpt. and reson. Raman spectra in Ar and N_2 matrices 77−65487
$(MgO)_x$-$(Al_2O_3)_y$ formation of nonstoichiometric spinel on heating hydrous $MgAl_2O_4$ 78−76672
(MgO-Fe_2O_3-Cr_2O_3-TiO_2):Na_2O, powder, prep., heat treatment, Na_2O impurity effect on props. 77−16528
$MgO(Al_2O_3)_{1.8}$, spinel, X-ray refl. topography, dislocation substructures during creep form. *(French)* 78−68737
$MgO(Al_2O_3)_n$ spinel, plastic deformation at 400°C 80−40453
MgOH (MgCl), mol. dissoc. energies calc. by high temp. mass spectrometer 80−83514
MgOH, struct. and electronic props., ab initio calcs. 80−74113
$Mg(OH)_2$, and calcination product, relations between particle size, shape and surface area 78−48355
$Mg(OH)_2$, cryst. growth from aq. soln. at 60°C, pH effects 78−23591
$Mg(OH)_2$, cryst. growth from MgCl+$Ca(OH)_2$ in brine 78−23592
$Mg(OH)_2$, decomposition to MgO, mechanism, product crystallite size rel. to reaction rate 78−85152
$Mg(OH)_2$, precip. 78−68615
$Mg(OH)_2$, sintering, IR spectra, X-ray anal. 80−66452
$Mg(OH)_2$, thermal decomposition 79−100539
$Mg(OH)_2$:Fe, crystal field properties, Mossbauer spectra, isomer shift and quadrupole splitting 79−61278
$Mg(OH)_2$-α-$Mn(OH)_2$, phase transition during ht. treatment 78−23659
$Mg_2(OH_2)CO_3$, cryst. struct. rel. to artinite topotactic thermal decomposition 77−68952
$Mg(OH_2)_6(NO_3)_2$:Mn^{2+}, EPR spectra, crystal field symm. and strength 77−69674
$Mg_3(OH)_4(NO_3)_2$, nitrate based cement binder formed from MgO powder 79−15634
$Mg_3(OH)_2SO_4[B(OH)_4]_2$, sulphoborite, cryst. struct. determ. 77−15389
$Mg(OH_2)_6(SiF_6)$, phase transitions, spectrometric exam. *(French)* 78−88291
$Mg(OH)_2.2Mg_2SiO_4$, cryst. struct. determ. 77−47410
MgO(MgO^-), electron affinity and dipole moment, ab initio calc. 78−41938
MgO(001), atomic H scatt. 77−31905
MgO.Al_2O_3 surface, crystalline, mass transport mechanisms at high temperatures *(Japanese)* 80−54479
MgO.Al_2O_3-MgO.nAl_2O_3 spinel, coordination state of atoms, charact. X-ray emission *(Japanese)* 78−6816
MgO.Al_2O_3.2SiO_2, hydrothermal synthesis, phase transitions 77−48378
2MgO.TiO_2, single cryst. and polycryst., O diffusion charcts. 77−84968
MgO.1.1 Al_2O_3 spinel, high temp. deform., cryst. orientation effect 80−107263
MgO.3B_2O_3.7.5H_2O, thermal dehydration 78−43132
MgO.3.5Al_2O_3, precipitation during creep experiments 79−47694
MgO.nAl_2O_3, nonstoichiometric spinel, DTA 77−28791
Mg_3P_2, ^{31}P multiple pulse NMR, chem. shift anisotropy 78−52369
$Mg(PO_3)_2$ glass, rate of crystallisation, SiO_2 additive effects *(Japanese)* 77−68927
$Mg(PO_3)_2$, vitreous, microhardness 80−25864
$Mg(PO_3)_2$:Mn^{2+}, EPR, computer simulation compared with expt. *(French)* 79−95635
$Mg_2P_2O_7$, α- and β-phase, vibr. spectra, Raman and IR spectra 78−19467
$Mg_2P_2O_7$-$Mg_2As_2O_7$ solid solns., formation of mixed anions $PAsO_7$, IR absorption spectra exam. 79−1508
$Mg(PO_4)_2.xH_2O$, x=8, 22, dehydration and water bonding 77−44456
$Mg(Pt(CN)_4)7H_2O$, transition energy tuning from 3.3 to 1.4 eV 79−61436
$Mg_{0.82}Pt(C_2O_4)_2\times5.3H_2O$, struct., neutron determ. 79−46640
MgR_2S_4, (R=Sc, Yb, Tm), IR and Raman spectra, force consts. 78−68503
$Mg_4R_6(SiO_4)_6F_2$, (R=Nd, Y or Yb), synthesis and characterisation 77−24992
$MgRb_2(SO_4)_2.6H_2O$:Mn^{2+}, EPR, 298K, spin-Hamiltonian parameters, cryst. fields 78−27086
$MgRb_2(SeO_4)_2.6H_2O$:Mn^{2+}, EPR spectra 80−100608
MgS:Ce^{3+} phosphors, emission and excitation spectra *(French)* 80−93380
MgS:Eu^{2+}, emission and excitation spectra obs. 80−55162
MgS:Eu^{2+} phosphors, anal. of absorption spectra $4f^N\rightarrow4f^{N+1}$5d-6s 80−7383
$MgSO_4$, aq. soln., electrolytic conduct. affected by US waves 79−23997
$MgSO_4$, negative muon capture, rel. probability meas. 77−50550
$MgSO_4$, rate constant of reaction, determ. from overall crystal growth coeff. 78−59773
$MgSO_4$, sea water relaxation and sound absorption 79−68466
$MgSO_4$, soln., electrolytic cond. dispersion, 1-6 MHz, caused by US propag. 80−44343
$MgSO_4$ soln., thermal and Fickian diffusion 78−2272
$MgSO_4$, sound speed as function of conc., temp., and press. 78−79668
$MgSO_4$, thermal decomposition, torsion-effusion cell obs. 77−77741
MgS_2O_3-$M^I_2S_2O_3$-H_2O system, M^I=Na, K, NH_4, 20°C isotherms *(French)* 78−52506
$MgSO_3.6H_2O$, thermal dissoc. *(Russian)* 79−66267
$MgSO_4.7H_2O$, cryst. regeneration and growth in contact nucleation 79−23545

magnesium compounds continued
$MgSO_4.7H_2O$, growing in aqueous solution, observation of secondary nuclei production 78−68613
$MgSO_4.7H_2O$, relation between soln. and growth rates of cryst. faces 79−14716
$MgSO_4.7H_2O$, thermo-electrochemical H_2 prod. using solar energy *(French)* 79−24918
$MgSO_4.7H_2O$:$(Cu[H_2O]_6)^{2+}$, EPR and optical spectra anal. 79−38377
$MgSO_4.xH_2O$, mag. susceptibility, polaris. paramag., water of crystallisation effect 78−31047
$MgSb_2O_6$, force fields rel. to cryst. struct. *(French)* 80−107104
$MgSc_xFe_{2-x}O_4$, Mossbauer spectra, elec. and mag. props. *(Russian)* 77−69737
$MgSeO_4.6H_2O$:Mn^{2+}, EPR obs., rel. to Mn crystallographic sites 78−79628
Mg_2Si, charact. X-ray temp. and thermal expansion coeff. 77−15599
Mg_2Si, phonon cond., 3-500K 78−79826
Mg_2Si, polymorphism under high press., radiographic data 77−20068
$MgSiF_6$, phase transform. and relax., EFG and quadrupole spectra 77−51995
$MgSiF_6.6H_2O$, orientational periodic antiphase *(French)* 80−15053
$MgSiF_6.6H_2O$:Co^{2+}, spin Hamiltonians and pair interactions 77−36119
$MgSiF_6.6H_2O$:Ni^{2+}, EPR meas., low temp. phases 77−63269
$Mg_2Si_xGe_ySn_{1-x-y}$ composite Te material with high figure of merit 77−28164
$MgSiO_2$, kinetics of dislocation etching 80−6409
$MgSiO_3$, elec. cond. under defined thermodynamic activities up to 20 kbar, 340-1100°C 80−6832
$MgSiO_3$, enstatite, high-press. phase relations, absence of oxide mixture 77−37185
$MgSiO_3$, ferroelectric-like phase transformation of pyroxene 78−61362
$MgSiO_3$, HP phase transform. 80−19941
$MgSiO_3$, Mg_2SiO_4, vapour condensed, mid IR optical props. 80−31337
$MgSiO_3$, orthorhombic perovskite, contribution to crystal chem. 80−19777
$MgSiO_3$, perovskite, synthesis and cryst. chem. charact., rel. to mantle mineralogy 78−65266
$MgSiO_3$ perovskite polymorph, high-press elastic consts. determ. 77−51428
$MgSiO_3$, perovskite struct., cryst. chem. 79−60336
$MgSiO_4$:Dy, thermolum. induced by 254 nm UV photons 80−55204
$MgSiO_4$:TB, TLD phosphor, γ-induced sensitisation and residual thermolum. 79−28844
Mg_2SiO_2:SiO_2, elec. and dielec. props. 400-900°C 80−104953
Mg_2SiO_4, ^{18}O self-diffusion expts., high-temp. creep implications 80−81870
Mg_2SiO_4, cryst. growth from PbO-SiO_2 flux 77−16484
Mg_2SiO_4 crystals, morphology and dislocation etch pits, (010) surface 80−24457
Mg_2SiO_4 crysts., dislocations configuration and cleavage steps dissoln. 80−107250
Mg_2SiO_4, determ. of electronic polarisabilities of ions 79−7570
Mg_2SiO_4, dislocations revealed by etching 79−99199
Mg_2SiO_4, forsterite, decorated dislocations 80−54245
Mg_2SiO_4, forsterite, elec. props. 78−34833
Mg_2SiO_4, forsterite, glissile splitting of dislocations, cross-slip-controlled creep and mantle rheology 78−61406
Mg_2SiO_4, forsterite, high-press. phase relations, absence of oxide mixture 77−37185
Mg_2SiO_4, forsterite, ion scatt. spectrometry, atom shielding effect of O 80−50493
Mg_2SiO_4, forsterite, O_2 self-diffusion coeffs. 80−70457
Mg_2SiO_4, forsterite, single-cryst., shock wave compression 79−84242
Mg_2SiO_4, fosterite, lattice dynamics, IR and Raman spectra meas. 79−65153
Mg_2SiO_4, gamma-irrad., ESR spectra 79−51853
Mg_2SiO_4, grown by Czochralski method, trivalent ion distrib. between melt and single crystals 78−9972
Mg_2SiO_4, ionic transport model 79−69285
Mg_2SiO_4, microhardness variation, exam. using Vicker indentor 80−25849
Mg_2SiO_4, NMR of ^{29}Si and ^{25}Mg with dynamic polarisation technique 78−56405
Mg_2SiO_4, pure forsterite, transient and steady-state creep at low stress 79−79827
Mg_2SiO_4, single cryst., (010) cleavages, etch patterns and dislocations, interferometric obs. 78−2127
Mg_2SiO_4, single cryst., preferential dissolution in molten KOH (NaOH), etching obs. 78−34513
Mg_2SiO_4, temp. in high-press. shock state 80−72490
Mg_2SiO_4:(Fe)(H), elec. cond. meas. 79−69285
Mg_2SiO_4:Fe^{3+}(Mn^{2+})(Cr^{3+})(Mg^{2+}) elec. field gradients, asymmetry parameters 80−54660
Mg_2SiO_4:Tb, sensitised TLD phosphor, photon energy dependence 80−78498
Mg_2SiO_4:Tb, TLD material, UV induced thermolum. and phosphoresc. 78−92707
Mg_2SiO_4:Tb, TLD phosphor response, heating rate effect 80−26359
Mg_2SiO_4:Tb, thermolum. phosphor, photolum. and absorpt. spectra, thermolum. mechanisms 80−97321
Mg_2SiO_4:Tb TLD, response to X-ray and electron irrad. 79−3285
Mg_2SiO_4:Tb TLD, supralinearity of response to electrons and X-rays *(Japanese)* 78−78503
Mg_2SiO_4:Tb thermoluminescence phosphor, response to high energy electrons *(Japanese)* 78−78502
Mg_2SiO_4-$Ca_3(PO_4)_2$, Mg_2SiO_4-$NaCaPO_4$ partial system, phase diag. 77−86005
Mg_2SiO_4-Fe_2SiO_4-$CaAl_2Si_2O_8$-SiO_2 system phase relations rel. to lunar basalts origin 78−65512
$Mg_2Si_2O_6$, enstite, elec. cond. var. with O_2 partial press., obs. and theory 79−1609
$Mg_4Si_4O_{12}$-$Mg_3Al_2Si_3O_{12}$ system, pyroxene-garnet solid-soln. equilibria at high press. and temps. 77−81895
$Mg_{(x+2)/3}Si_{(x-2)/3}O_x$, 145 Å superstructure 79−99143
$Mg_3Si_4O(OH)_2$, ball mill grinding, rate constant determination *(Japanese)* 78−95828
$Mg_3Si_4O_{10}(OH)_2$, ball mill grinding, wet, dry, rate constant determination *(Japanese)* 78−95827
$Mg_3Si_4O_{10}(OH)_2$, talc, for hydrothermal crystn. of fibrous amphiboles 80−20810

magnesium compounds continued
$2Mg_2SiO_4.3Mg(OH)_2$, new high-press. struct. type, cryst. struct. 80−39028
$MgSiP_2$, elec. props. and diode struct. exam. 79−51665
$MgSiP_2$, electronic struct., X-ray spectroscopic investigation 80−108300
Mg_2Si0_4, etch pits in cleaved faces, revealing low angle boundaries 79−14818
Mg_2Sn, lattice dynamics, angular force model 77−4166
Mg_2Sn, Mossbauer effect exam. under press. up to 75 kbar 79−69759
Mg_2Sn, phonon cond., 4-1000K 78−79826
Mg_2SnO_4, Gibbs' free energy of form., electrochem. determ. 78−11548
$MgTaCuO_4$, cryst. struct., synthesis 78−83790
$Mg_4Ta_{2-x}Nb_xO_9$, luminescence, model of niobate and tantalate centres 77−16373
$MgTa_2O_6$, force fields rel. to cryst. struct. *(French)* 80−107104
MgTe:Cr^+, cryst. growth and EPR 78−39393
$MgTe_2$:Mn, pyrite phase, strong axial cryst. field of Mn^{2+}, EPR meas. 78−27081
$MgTeMoO_6$, prep., cryst. struct., and catalytic props. 80−108709
$MgTiF_6.6H_2O:Ni^{2+}$, EPR meas., low temp. phases 77−63269
$MgTiO_2$, Mg_2TiO_4, $MgTi_2O_5$, formation mechanism 77−48373
$MgTiO_3$, ESR study of Fe^{3+} 80−50173
$MgTiO_3$, HP phase transform. 80−19941
$MgTiO_3:Fe^{3+}(Mn^{3+})$, EPR spectra 79−91285
$MgTi_1O_5$, formation of solid solutions, on chemical reduction, X-ray analysis of phases *(Russian)* 79−33072
$MgTi_2O_5$, grain size pseudobrookite oxide, microcracking relations 79−29194
$MgTi_2O_5$, thermal diffusivity, grain size and microcracking effects 78−10233
Mg_2TiO_4 single crystals, growth by floating zone method 79−78873
Mg_2TiO_4:Cu(Ni), ESR of Cu^{2+} and Ni^{3+} 80−97131
Mg_2TiO_4-$MgFe_2O_4$ mixed system, spinel, selective sublattice dilution, percolation problem 80−103850
$MgTl_2(SO_4)_2.6H_2O:Mn^{2+}$, EPR, 300K 79−51848
$MgUO_4$, energy transfer, cryst. struct. and chemical composition effect 80−108248
$MgUO_4$, luminesc. props. 79−83012
$MgUO_4$, standard enthalpy of formation, high-temperature thermodynamic functions 78−27811
$Mg_yU_{1-y}O_{2+x}$, thermodynamics from EMF meas., high Mg conc. 78−43143
$Mg_yU_{1-y}O_{2+x}$, thermodynamic props., EMF meas. 80−29187
MgU_8X_{17}, (X=S or Se), mag. susceptibilities 79−61073
$MgVO_3$, high-pressure modification, struct. and mag. props. 79−23727
MgV_2O_4-Mg_2VO_4 spinel solid soln., quenching and lattice const. 77−90307
$Mg_2V_2O_7$, elec. props. and EPR meas. 79−11114
$Mg_2V_2O_7$, quadrupole coupling tensor of ^{51}N nucleus 80−11290
$Mg_2V_2O_7$, V-O-V bridge stretching freq. correl. with bond angle 78−74636
$Mg_3(VO_4)_2$, determination of enthalpies of formation, from heats of solution 80−2182
$Mg_3(VO_4)_2$, luminesc. spectra in visible region, vanadate group 78−43921
$(MgV_2O_4)_c(FeFe_2O_4)_{1-c}$, struct. parameters, IR spectra, cluster-component analysis 77−47425
$MgWO_4$, luminesc. and capture centres *(Russian)* 78−52543
$MgWO_4$, luminesc. efficiency, temp. and high-press. 78−23507
$MgWO_4$ type compounds, system of polymorphic transitions 78−47268
$MgWO_4:Fe^{3+}$, effect of electric field on ESR of Fe^{3+} ions 78−88176
MgX_2 (X=F, Cl, Br, I), 2Z 80−43021
MgX_2, X=Cl, Br, valence shell electronic struct., ab initio SCF calc., photoelectron spectra 79−31383
MgX_4^{2-} (X=Cl, Br, I), pseudo-exact force consts. 77−31022
$MgX_4^{2-}(IO_4^-)$, (X=Cl,Br,I), force consts., compliance and Coriolis consts. calc. 78−42242
MgXe excimer bands, emission intensities and excited-state densities meas. 80−92413
MgZn(Cd), Ar matrix absorpt. spectra, vibronic spacing and bonding 79−3453
$Mg_{0.25}Zn_{0.75}Fe_2O_4$, ferrite, DC cond., dielec. props., lattice consts. 80−80272
$Mg_xZn_{1-x}Te$, band struct. refl. spectra meas. 80−80813
$Mg_xZn_{1-x}Te$, comp. profile, second derivative wavelength modulation 80−103967
$Mg_xZn_{1-x}Te$, high purity, luminesc. and band gap 78−68553
$Mg_xZn_{1-x}Te$, long wavelength optical phonon replica 78−60468
$Mg_xZn_{1-x}Te$, spin orbit splitting, of electron energy levels, reflectivity meas. 79−69479
$Mg_xZn_{1-x}Te$, temp. depend. of energy gap, near band gap reflectivity spectra 79−28786
MgO bicrystals, electron microscope exam. of secondary grain boundary dislocations in high angle twist boundaries 80−6415
MgO, vol. eqn. of state under static press. conditions, rel. to Earth core-mantle models 80−19904
^{24}MgH, transition probabilities, oscill. strengths, rot.-vibr. bands fine struct., stellar atm. appl. 77−18918
$^{24}MgH^+$, high resolution rot.-vibr. spectra, solar atm. appl. 77−18939
Mg(100) surface, rumpling calc. 78−14559
$Mg[Pt(CN)_4].7H_2O$, high press. tuning of optical transitions 79−28813
$Mg[Pt(CN)_4].7H_2O$, DC elec. cond. props. 79−51582
$Mg[Pt(CN)_4].7H_20$, energy band calcs. 77−39780
$(Mn,Mg)Mg(OH)_2[ZnSiO_4]$, herstmannite, comparison with $Ca[ZnSiO_4].H_2O$, clinohedrite 79−19228
Mn-MgF, cermet film, evaporated, variation of elec. resist. with prep. conditions 77−43746
Mn-MgF, cermet film, variation of resist. with deposition rate 77−43747
Mn-MgF_2 cermet, heat treated, lattice distortion, resist. meas. 79−19492
Mn-MgF_2 cermet film, resistivity-temperature variation 79−24085
Mn-Si, liq. alloys, equilibria between $MnO-SiO_2-CaO-MgO$ slags 80−10639
Mn-Zn ferrite, single crystal, electrolytic buffing studies *(Japanese)* 77−86259
Mn-Zn ferrite, single crystal, surface damaged layer study *(Japanese)* 77−86260
MnMg ferrite, products if reaction of ferrogel with $MnCl_2$ solution 77−12582
$Mn_xMg_{1-x}O$, solid solution EPR, mag. interactions *(Russian)* 80−44908
$Mn_xMg_{1-x}S$, mag. props. 77−66244
magnesium compounds continued
$Mn_xMg_{1-x}S$ solid solution, mag. props. 78−60269
$Mn_{1-x}Mg_xSe$, mag. and struct. phase transitions, mag. susceptibility and X-ray diffr. study 80−71022
$Mn_xMg_{1-x}Y_2S_4$, magnetisation and susceptibility, exchange interactions obs. 78−52242
MnO, magneto-elastic coupling by dipolar interactions and spin orientation 79−78494
$MnO-MgO-ZnO-Fe_2O_3$, grade 1.3 VT ferrite formation from hydroxides 77−90302
$MnO-SiO_2$ melt, viscosity and polymerisation *(Russian)* 78−26712
$MnO-ZnO-MgO-Fe_2O_3$ ferrites, effect of Fe^{2+} ion on initial permeability 77−8357
MnS inclusions in free-cutting steel, X-ray, light and scanning electron microscopy 77−77685
$MnSO_4$ aqueous soln. conc. depend. of third US relaxation freq. and activation energy 78−63814
$(NH_4)_2Mg(S_2O_3)_2.6H_2O$, isolation, struct., decomposition *(French)* 78−52506
Na_2-SiO_2-MgO glass, melt viscosity and IR meas. to study MgO behaviour *(Japanese)* 78−14495
$NaAl_2O_4$-$MgAl_2O_4$ spinel solid solns., activities rel. to cation distrib. 77−15377
$NaCaPO_4$-$CaMgSiO_4$ system, phase diagram 78−35370
$NaCaPO_4$-MgO, $NaCaPO_4$-$NaMgPO_4$, $NaCaPO_4$-Mg_2SiO_4, $Na_2CaMg(PO_4)_2$-MgO, partial systems, phase diag. 77−86005
NaCl:$MgCl_2$ (0.1 mol.%), thermoluminesc. glow curves, temp. distrib. and trapping centres 78−48241
NaCl-$MgCl_2$-H_2O mixed electrolyte solns., elec. transport 80−3355
NaCl-MgO mixture, high pressure uniaxial stress component effect on eqns. of state, opposed anvil X-ray determ. 80−49301
NaF-MgF_2-MgO-SiO_2, phase formation 78−27460
$NaMgF_3$, extreme UV spectra, 9-30 eV 78−23486
$NaMgF_3$, orthorhombic perovskite, contribution to crystal chem. 80−19777
$NaMgF_3:Sm^{2+}$, luminesc. spectra 4.2, 77 and 295K and Zeeman spectra, 4.2K 77−81146
$NaMgPO_4$-MgO, $NaMgPO_4$-$NaCaPO_4$, partial systems, phase diag. 77−86005
$Na_2Mg_1SiO_4$, ionic cond. meas. 80−6545
$Na_4Mg_2Si_3O_{10}$, ionic cond. meas. 80−6545
$Na_2Mg_6Si_8O_{22}F_2$, fluoramphibole, fibrous, crystn. from gas phase, mechanism 78−34451
$Na_2Mg_2Ti_6O_{14}F_2$, α and β forms, ionic conductivities *(French)* 77−43373
$(NaNO_3-Mg(NO_3)_2):Nd^{3+}$, glass, cryst., absorpt. luminesc. spectra, term struct. of Nd^{3+}, bonding 77−8624
$Na_2O-CaO-MgO-Al_2O_3-SiO_2$ glasses, ternary and quaternary, struct., Raman spectra obs. 77−36229
$Na_2O-CaO-MgO-Al_2O_3-SiO_2$, corrosion and microhardness, effect of detergents 80−16518
$Na_2O-MgO-Al_2O_3$, β''-alumina, high-resolution electron microscopy 80−75208
$Na_2O-MgO-Al_2O_3$, ionic cond. 80−107480
$Na_2O-MgO-Al_2O_3-SiO_2$, chemical durability at different pH values 78−72902
$Na_2O-MgO-B_2O_3:Cu^{2+}$, micro-inhomogeneities, EPR and Raman study 80−84080
$Na_2O-MgO-P_2O_5$, subsolidus struct. 77−63640
$Na_2O-MgO-SiO_2$ glasses, elec. cond., room temp. to 450°C 80−107473
Na_3PO_4-$Mg_3(PO_4)_2$, phase diag. and $NaMgPO_4$ and $NaMg_4(PO_4)_3$ formation 77−48412
$Nd_3Mg_3(No_3)_{12}.24H_2O:Mn^{2+}(Gd^{3+})$, EPR spectra, spin Hamiltonian anal. 79−33527
Ni-Cr/$MgSiO_3$, methanation catalysts, S resistant, XPS characterization 79−83506
$Ni_xMg_{1-x}O$, EPR in magnetoconcentrated solid solution *(Russian)* 80−39856
$Ni_pMg_{(1-p)}(OH)_2$, random magnet, AC susceptibility 79−47258
$Ni_xMg_{1-x}(OH)_2$, random magnet, magnetisation 79−24195
NiO-Cr_2O_3-$MgSiO_3$ methanation catalyst, S-resistant, IR and Raman spectra 80−93290
NiO-MgO, ESR and refl. spectra, Ni^{2+} distrib. 79−33745
NiO-MgO solid solns., surface comp. study by XPS 80−104035
NiO-MgO-ZnO, solid soln. form and colour *(Japanese)* 77−63647
$(NiV_2O_4)_c(MgFe_2O_4)_{1-c}$, struct. parameters, IR spectra, cluster-component analysis 77−47425
$Pb_3MgNb_2O_9$, photoelectretic states in real time spatial light modulators, photorefractive effect 80−80676
Pb_2MgReO_6, new seignettomagnets and ferroelectrics 78−19425
$Pb(Mg_{0.5}W_{0.5})O_3$-$BiFeO_3$, dielec. props., cryst. struct. 78−84534
PbO-B_2O_3-SiO_2-LiO_2-MgO, glass enamel, chemical durability and microstruct., MgO addition effect 79−29255
PbO-MgO-SiO_2 system, melt, viscosity meas. in temp. range 950 to 1250°C *(Japanese)* 79−77663
PbO-SiO_2-NiO-MgO glass melt, interaction of NiO and MgO, elec. cond. and IR spectra obs. *(Japanese)* 80−24632
$Pb(Z,Ti,Mg,W)O_3$, low-Q ceramics, props. and transducer appl. 80−75944
$Pr_2Mg_3(NO_3)_{12}.24H_2O:Mn^{2+}$, X-band EPR 77−66418
$Pr_2Mg_3(NO_3)_{12}.24H_2O:Gd^{3+}$, EPR X-band, fine struct., low field lines 79−15351
$RbCa_{0.95-x}Mg_xEu_{0.05}F_3$, green luminesc. obs. 77−32428
$Rb_2Co_xMg_{1-x}F_4$, neutron scatt. exam., obs. of two dimens. mag. long range order 78−56295
$RbMgF_3:Mn^{2+}$, EPR obs. and struct. interpret. *(French)* 80−50167
$RbMn_{1-x}Mg_xCl_3$, dilute pair antiferromag., mag. susceptibility and ESR meas. 79−78338
$Rb_2Mn_xMg_{1-x}F_4$, spin dynamics near percolation threshold, EPR study 80−39859
Sc_2O_3:MgO, defect struct., X-ray diffr. and pyrometric density 78−34524
Si-MgO film, dielectric constant and selective solar absorption 78−2937
Si_3N_4, MgO-fluxed, hot pressed, grain boundary phases 78−27464
Si_3N_4:$(MgO+Al_2O_3)(Y_2O_3)$, hot-pressed and sintered, microstruct. and impurity distrib. 80−49261
Si_3N_4:MgO, hot-pressed, linear thermal expansion rel. to MgO content 80−70430
Si_3N_4-Mg_2SiO_4-Si_2N_2O, compressive creep, composition effect 80−50674
Si_3N_4-MgO, (5 wt.%), hot pressed, fracture toughness as function of initial α-phase content, SEM 80−3174

magnesium compounds continued
- Si_3N_4-MgO, compressive creep, source of viscoelastic effect 80−50675
- Si_3N_4-MgO, compressive creep, oxidation induced compositional change 80−50676
- Si_3N_4-MgO, hot pressed, DC elec. props., 18-500°C, fields up to 1.1×10^4 V cm^{-1} 78−26860
- Si_3N_4-MgO, hot pressed, oxidation kinetics 79−29243
- Si_3N_4-MgO, hot pressing and α-β phase transform. 78−27461
- Si_3N_4-MgO, reaction with Fe to produce surface pitting 78−76778
- Si_3N_4-MgO (2-5 wt.%) hot pressed, tensile creep testing 80−40423
- α-Si_3N_4-MgO (5 wt.%), hot-pressed, mech. strength development 78−44195
- Si_3N_4-MgO (5 wt.%), microstructural changes during gas pressure sintering *(Japanese)* 77−12589
- Si_3N_4-Si_2N_2O-Mg_2SiO_4, melting and eutectic studies 80−45285
- Si_3N_4-SiO_2-MgO, phase relations and interrelation with mech. strength, and oxidation 78−48386
- SiO_2-Al_2O_3-B_2O_3-MgO-CaO-Na_2O, strengthened by ion exchange, exam. of internal stresses using polarising microscope 78−88549
- SiO_2-Al_2O_3-CaO-MgO-TiO_2 system glasses, phase separation and crystn. 77−24384
- SiO_2-Al_2O_3-CaO-MgO, liq. silicic and slag, struct, density, surface tension *(Polish)* 78−83711
- SiO_2-Al_2O_3-CaO-MgO-Na_2O (1.58, 7.16, 3.59, 14.9 mole.%), polished sheet, strength in commercial state and after strengthening by ion exchange 79−1904
- SiO_2-Al_2O_3-CaO-MgO-NaO-K_2O-B_2O_3-ZrO_2, glaze, exam. of zircon crystallisation 79−19155
- SiO_2-Al_2O_3-CaO-MgO-Na_2O, ion exchange and electrodiffusion of Li ions in surface layer 79−20227
- SiO_2-Al_2O_3-CaO-MgO, crystallized, prod. from inorganic waste *(Japanese)* 79−69017
- SiO_2-Al_2O_3-CaO-MgO-Na_2O-K_2O effect of partial substitution of Na_2O by K_2O, on crystallisation 80−10499
- SiO_2-Al_2O_3-CaO-MgO-FeO-Fe_2O_3 glasses, struct. transforms during heating 80−15014
- SiO_2-Al_2O_3-Fe_2O_3-CaO-MgO-Na_2O-SO_3 glass, thermophysical props. 78−18849
- SiO_2-Al_2O_3-Fe_2O_3-CaO-MgO-Na_2O-B_2O_3-SO_3, exam. of white flaky inclusions, causes and formation time 79−29237
- SiO_2-Al_2O_3-Fe_2O_3-Na_2O-K_2O-CaO-MgO glasses, Mossbauer spectra study 80−39967
- SiO_2-Al_2O_3-FeO-CaO-MgO pyroxene glasses, phase changes 80−15013
- SiO_2-Al_2O_3-MgO-CaO-Fe_2O_3, glass ceramic, crystn., microstructures rel. to conditions 80−11638
- SiO_2-Al_2O_3-MgO-TiO_2 devitrificates, microstruct. and props. *(Polish)* 80−70141
- SiO_2-Al_2O_3-MgO(-K_2O-F), glass ceramics, crystn., microstructures rel. to conditions 80−11638
- SiO_2-Al_2O_3-R_2O_3-MgO-TiO_2, T=rare earth of Ce group, glass-ceramic permittivity comp. depend. 77−43928
- SiO_2-MgO porous catalysts, EPMA quantitative anal., new correction calc. method, modified ZAF method *(Japanese)* 80−93822
- β-SiO_2-MgO reaction, diffusion controlled 78−6882
- SiO_2-MgO-BaO ceramic, steatite, glass-ceramics technology appl. 80−104097
- SiO_2-Na_2O-CaO-MgO-Al_2O_3, toughening by electrochemical treatment in Sn melt 80−11800
- SiO_2-Na_2O-CaO-MgO-Fe_2O_3-Al_2O_3-SO_3-Sn thermally polished, exam. of strength of surfaces 80−25887
- SiO_2-Na_2O-CaO-MgO float glass, surface SnO_2 distrib., ellipsometry and XPS study 80−84346
- SiO_2-Na_2O-K_2O-CaO-MgO-Al_2O_3 glass melt, anodic dissolution of Ti 80−19949
- SiO_2-NaO-K_2O-CaO-MgO-Al_2O_3 melt, anodic dissolution of Co and Ni in melt 78−88582
- SiO_3-Na_2O-CaO-MgO-Al_2O_3 charge, silicate formation during heating 80−55342
- $Sm_2Mg_3(NO_3)_{12}.24H_2O$:$Mn^{2+}$, EPR spectra, 77-298K 79−15342
- $Sn_{0.225}Fe^{3+}{}_{0.575}Fe^{2+}{}_{1.465}Mg_{0.735}BO_3O_2$, hulsite, cation distrib., X-ray determ. 79−19225
- $Sn_{2.8}Li_{1.6}Mg_{1.6}O_8$, four layer close packing, cryst. struct. determ. *(French)* 80−28999
- Sr_2MgReO_6, new seignettomagnets and ferroelectrics 78−19425
- TiB_2-MgO, thermal stability of composite materials 78−60638
- TiN-NiO, solid-phase reactions 79−11774
- Ti_2O_3-$MgTiO_3$, phase analysis 78−3103
- Ti_3O_5-$MgTi_2O_5$, solid solubility, X-ray phase and optical microscopic exam. 80−59657
- UO_2 heat-generating, molten, interaction with MgO brick 79−13468
- V/MgO composite film, optical props., rel. to solar collector appls. 78−72622
- V_2O_5-P_2O_5-MgO system glasses, phase separation, crystn. and EPR spectra 77−76321
- W-MgO cermet film, dielectric const. and selective solar absorption 78−2937
- WO_3-MgF_2, electrochromic display struct., efficiency and humidity depend. 79−81540
- $YCrO_3$-$MgCr_2O_4$ sintered ceramics, elec. cond. 80−24927
- Y_6WO_{12}:MgO, polycryst., elec. cond., 800-7400°C 80−15517
- $(Zn,Mg)_2GeO_4$:Mn^{2+} phosphor, for low press. fluoresc. lamps, luminesc. charact. 78−10960
- $(Zn,Mg)_3(PO_4)_2$:Mn^{2+}, cathodoluminescence obs. 80−71492
- $ZnFe_2O_4$+MgO powders, cation mutual diffusion coeffs. calc. 77−15635
- $Zn_{1-x}Mg_xTe$ alloys, high purity, metallurgical and analytical methods of prep. 80−40247
- $Zn_{1-x}Mg_xTe$ alloys, luminesc. and elec. props. 80−2813
- $Zn_{1-x}Mg_xTe$, growth from melt, luminesc. *(French)* 77−21019
- $Zn_{1-x}Mg_xTe$, long wavelength optical phonons, IR ref. and Raman obs. *(French)* 78−60433
- $Zn_{1-x}Mg_xTe$, variation of fundamental edge, wavelength modulated reflectivity meas. *(French)* 77−81124
- ZnS-MgF_2 alloy films, struct. and optical props. 79−90910
- ZnS-MgF_2 dielectric film, laser irrad. and microscopic inhomogeneities 78−2157
- ZnS-MgF_2 mirror, dielectric, Rayleigh scatt. at 441.6 nm 80−97367
- ZnS-MgF_2 mixtures, triple-layer broad band antireflection coatings 79−32011
- ZnS-MgF_2/MgF_2, homogeneous mixed dielecs. as antirefl. coatings effective at two visible wavelengths 79−76770

magnesium compounds continued
- ZnS-MgF_2/MgF_2 double-layer antireflection coatings, transmittance meas. 79−36967
- ZnS-MgS, exam. of piezoelectric props. and elastic compliances, as function of MgS conc. 79−95709
- ZnS-MgS, solid solution, prep. of single crystals with wurtzite structure, exam. 79−1821
- Zn_2SiO_4-Mg_2SiO_4, melt solidification behaviour 77−90337
- $(ZnV_2O_4)_c(MgFe_2O_4)_{1-c}$, struct. parameters, IR spectra, cluster-component analysis 77−47425
- ZrO_2, MgO partially stabilized, microstruct. development during ageing 79−91710
- ZrO_2-MgO, partially stabilised, growth morphology of tetragonal phase 79−4968
- ZrO_2-MgO system, intermediate phases existence, X-ray diffr. and IR obs. 79−38805

magnetic aftereffect
- Alnico, 5 and 8, spinel type permanent magnet, magnetic aftereffect 77−16118
- anelastic relaxations and magnetic aftereffects in solids, conf., Katowice, Poland (Jan. 1978) *(Polish)* 79−96072
- automatic demagnetisation and measurement system for time decreasing permeability meas. 80−62696
- disaccommodation measurement in Rayleigh range using semi-automatic equipment *(Polish)* 80−31812
- ferrites, measurement system 79−82834
- ferromagnetic materials, review 80−88830
- grains in rock, magnetic-diffusive after-effect 77−70640
- highly anisotropic material, coercive mechanism 77−69634
- isotropic media, mag. relax. phenomena and thermodynamic vectorial internal degrees of freedom 77−77145
- measurement of mag. aftereffect, high time const. relax. processes meas. 78−29129
- Permalloy-Mn film, diffusion aftereffect causing mag. state change *(Russian)* 80−103860
- rare $earth_{50}Ag_{50}$, amorphous, bulk mag. props., field, time and temp. depends. 77−89932
- rare earth metals, narrow domain walls, magnetic aftereffect obs. 77−8364
- rare earth-Ag alloy, amorphous, model calcs., of mag. props. 80−84616
- rocks, magnetic-diffusion aftereffect, Preisach-Neel diagram appl. 78−61403
- spin glasses, review 77−69578
- steel, electrotech., losses on mag. after effect *(Russian)* 77−66388
- steel 42NKhTYuA wire, hysteresis loop and differential permeab. after US and conventional drawing 79−15818
- thermofluctuation aftereffect anisotropy in Rayleigh region *(French)* 78−14989
- transition metal alloy, ferromag., H-impurity complex obs. 78−72373
- $CdCr_2Se_4$ films, mag. hysteresis, domain struct., mag. viscosity 80−25169
- $(Co,Fe)_{80}B_{20}$ glass, induced anisotropy and time changes of permeability 80−75815
- Co, electron irradiated, mag. after-effect spectrum, 20-350K 77−1570
- Co, magnetic aftereffects of H isotopes, book contrib. 79−82835
- $Co_{70.4}Fe_{4.6}Si_{15}B_{10}$, amorphous, mag. aftereffect spectra and annealing props. 80−88831
- CoO-Al_2O_3-SiO_2, spin glass, magnetic aftereffects 79−61176
- Co_5R-H(D) system, R=rare earth, mag. orientation aftereffect 80−50148
- Cu-Co, superparamagnetic, mag. aftereffects, dynamic neutron depolarisation study 80−50147
- Dy(Co,Ni)$_2$, intrinsic mag. aftereffect obs. 77−63237
- Dy(Co,Ni)$_2$, intrinsic mag. aftereffect meas., domain wall motion 80−71121
- Fe, BCC, mag. relax. due to C and N meas., 210 to 410K 77−36102
- Fe, Barkhausen effect, grain size depend. at 300K and 77K *(German)* 77−16113
- α-Fe, cold work aftereffects 80−88830
- Fe, high purity, mag. viscosity mechanism 78−19282
- α-Fe, high purity, neutron and electron-irrad., interstitial migration at 200K 79−55920
- Fe, high-purity, low-temp. mag. relax. after thermal ageing and demagnetisation 77−85502
- α-Fe, mag. aftereffect after neutron irrad. at 77K 78−2705
- Fe, mag. aftereffect meas., phenomenological description 80−88835
- α-Fe, mag. aftereffect spectrum after low temp. electron irrad. 78−2704
- α-Fe, magnetic aftereffect correlations with internal friction after low temp. neutron irradiation 78−10733
- α-Fe, magnetic aftereffect disaccommodation between 30 and 300K after low-temp. neutron-irrad. 80−29585
- Fe, magnetic aftereffect of interstitial O 78−91903
- α-Fe, magnetic aftereffect spectrum after low temp. neutron irradiation 78−10732
- Fe, magnetic aftereffects of H isotopes, book contrib. 79−82835
- Fe, magnetic disaccommodation, low temp. in neutron-irrad. sample, Bordoni relax. 77−4542
- α-Fe, neutron irradiated, low temp. mag. relax. 79−8022
- α-Fe, neutron irradiated, mobile C atom trapping, anelastic and magnetic relaxations 80−100306
- Fe, pure and doped, electron irrad., mag. aftereffect 80−88838
- Fe, study of H and D motion 78−64228
- Fe whisker, magnetic aftereffect in 180° mag. bowed Bloch walls 79−78432
- Fe, whisker domain wall interaction with mobile impurities 77−12145
- Fe:C, neutron irradiated at low temp., mag. disaccommodation 80−44881
- α-Fe:N, mag. field depend. of reverse permeability 77−80969
- Fe-Al-C alloys, C migration and mag. aftereffect, mag. permeab. disaccommodation and long-range order meas. 79−8020
- Fe-Al(Ti), O containing, mag. aftereffect and disaccommodation meas., time depend., activation energy, and ageing props. 80−88836
- Fe-Al(24.3 at.%)-C alloy, magnetic permeability disaccommodation, 260-400K 80−93144
- Fe-B, amorphous, mag. aftereffect, initial susceptibility time depend. 80−88829
- Fe-B amorphous alloys, mag. aftereffect 80−65970
- Fe-C-N, annealing in dry H_2, below 1180K, to purify to low C and N concs. 78−3072

magnetic aftereffect continued
α-Fe-C(N), containing substitutional atoms, mag. permeability disaccommodation *(Polish)* 79−95612
Fe-Co-Si-B alloy, amorphous, mag. heads appl. *(Japanese)* 80−54922
Fe-Co-Si(B), amorphous ferromagnet, mag. after effect on soft mag. props. 80−84626
Fe-Cr-Co, anisotropic, spinel type permanent magnet, magnetic aftereffect 77−16118
Fe-Ni, dil., point defect relax. after low temp. neutron irrad. 78−52316
Fe-Ni, low frequency power losses 78−95466
Fe-Ni(Al), mag. aftereffect meas., phenomenological description 80−88835
Fe-Pd, magnetic after-effect of H isotopes 80−75817
Fe-Si, irreversible Barkhausen jumps *(French)* 77−1568
Fe-Si, low frequency power losses 78−95466
Fe-Si, thermally activated motion of 180° Bloch wall 78−95457
Fe-Si (3 wt.%), power losses at extremely low freqs. 80−88815
Fe-Ti, magnetic aftereffects of H isotopes, book contrib. 79−82835
Fe-Ti:H(D), isotope effects of diatomic TiH and TiD complexes 79−47259
$(Fe\text{-}Ni\text{-}Mo)_{80}(P\text{-}B)_{20}$, amorphous, mag. aftereffects and struct. instabilities 80−88833
Fe_3Al, containing C in solid solution., mag-permeability disaccommodation *(Polish)* 79−95613
$Fe_{80}B_{20}$, amorphous, mag. permeability aftereffect during annealing 80−88834
$(Fe_{0.06}Co_{0.94})$-B, amorphous, ferromag., mag. instability rel. to struct. 79−99729
$Fe_xCo_{80-x}B_{20}$, amorphous 79−61189
$(Fe_{0.05}Co_{0.95})_{78}Si_8B_{14}$ amorphous ribbon, anomalous mag. aftereffect 80−100602
$Fe_{40}Ni_{40}B_{20}$ and $Fe_{40}Ni_{40}P_{14}B_6$, amorphous, mag. aftereffect spectra and annealing props. 80−88831
$Fe_{65}(Ni_{1-x}Cr_x)_{35}$, mag. viscosity and anomalies near Curie temp. 79−73781
$Fe_{40}Ni_{40}P_{14}B_6$, amorphous, mag. permeability aftereffect during annealing 80−88834
$Fe_{3-\Delta}O_4$, mag. aftereffects near Verwey temp. 79−87294
Fe_3O_4, magnetic after-effect by valency fluctuations assoc. with cond. transition 77−8365
Fe_3O_4, magnetite, mag. aftereffects, 4.35K 80−80571
Gd, AC susceptibility, temp. modulation studies, domain property thermal relaxation 79−61072
Gd-Co film, temp. depend. of mag. aftereffect *(Russian)* 79−8021
GdIG, thermal effect on re-entrant hysteresis loop and coercive force 78−2702
$Mg_{0.7}Cu_{0.3}Fe_2O_{4+\delta}$, disaccommodation and accommodation 77−20641
Mn ferrites, Fe^{2+} ion contrib. to induced anisotropy and mag. aftereffect 77−36101
Mn-Ni alloys, γ-phase antiferromag., lattice distortion and elastic props., ΔE effect interpret. 77−20671
$Mn_xFe_{3-x}O_{4+\gamma}$, average directional order, cation valency and repartition on A- and B-sites *(French)* 78−39369
Ni, diffusion and orientation aftereffects 80−88830
Ni, magnetic aftereffect reactivation of single crystal by plastic deform. 79−65697
Ni, magnetic aftereffects of H isotopes, book contrib. 79−82835
Ni:C, H(D), isotope effects of C-H and C-D complexes 77−20129
Ni-C, magnetic aftereffects of H isotopes, book contrib. 79−82835
Ni-Fe, magnetic aftereffects of H isotopes, book contrib. 79−82835
Ni-Fe, orientation aftereffect 80−88830
Ni-Fe, power losses at extremely low freqs. 80−88815
Ni-Fe, thermal fluctuation aftereffect meas. by pulse field method 80−88837
Ni-Fe film, relax. effects in domain boundary creep *(Russian)* 77−24723
Ni-Fe-Cu, Mu-metal, mag. aftereffects, dynamic neutron depolarisation study 80−50147
β'-NiAl B2 phase, in 15 kOe field 80−34700
Ni_3Fe, disaccommodation meas. after low temp. electron and neutron irrad. 80−88832
$Ni_xFe_{3-x-\Delta}O_4$, mag. aftereffects 79−56572
$Ni_{98}M_2$, M=impurity metal, formation of MH(D)-complexes 80−65236
NiO, antiferromag. domains exam. by magnetic neutron Laue diffr. 79−51806
NiZn ferrites, V_2O_5induced mag. aftereffects 80−60379
R_2In, R_3In, R=Gd, Tb, Dy, Ho, Nd, mag. props. 80−108009
$SmCo_5$, and $SmCo_{3.5}Cu_{1.5}$, anisotropy and coercivity, Kerr effect, magnetisation and aftereffect expts. 77−8300
$SmCo_5$, magnetic aftereffect of H and D 79−56573
$SmCo_5$, sintered, mag. after-effect, expt. and model 80−75816
$SmCo_{3.5}Cu_{1.5}$, mag. aftereffects, coercive mechanism, magnetisation reversal 77−69634
$SmCo_{2.5}Ni_{2.5}$, mag. after effect *(Russian)* 78−6544
Tb-Fe amorphous thin films, magnetic after-effect, Kerr magneto-optic effect obs. 80−97123
Tb-Fe sputtered films, amorphous, mag. aftereffect due to domain wall motion 79−73780
$Tb_{52}Ag_{48}$, amorphous, mag. after-effect meas. 79−24200
$Tb_{52}Ag_{48}$, amorphous, mag. aftereffect 80−20435
V, superconducting, microwave biased RF-SQUID system, appl. to magnetic aftereffect 79−26089
$Y_{2.5}Pr_{0.5-x}Ca_xFe_5O_{12}$, magnetic aftereffect exam. 78−23304

magnetic amplifiers
amorphous metallic materials appl. *(German)* 79−19744
linear movement transducer manufacture and static functioning 79−67279
linear movement transducers, magnetic amplifier principles 80−22341
noise reduction of second-harmonic-type magnetic modulators 78−70168
space applications of LF supercond. sensors inc. SQUID devices 80−56691

magnetic anisotropy
see also induced anisotropy (magnetic)
actinide monopnictides, anomalous mag. props., planar coupling theory 80−60245
advances in basic magnetism during past twenty-five years 80−36791
alaninium copper tetrahalides, exchange, mag. anisotropy, and spin diffusion contribs. to EPR linewidth 80−80597
p-alcoxybenzilidene butylaniline, liq. cryst., mag. anisotropy and polymorphism *(French)* 77−76532

magnetic anisotropy continued
p-alkyl-p'-cyanocyclohexylcyclohexanes, thermotropic nematics with positive dielectric and negative diamag. anisotropy 78−34435
alloys, magnetic anisotropy, influence of local symmetry *(Russian)* 80−93109
alnico, thermal magnetic hysteresis *(Russian)* 77−16119
amorphous alloys 77−16054
amorphous ferrimagnetic alloy, mag. anisotropy from dipolar interactions 79−87252
amorphous ferromagnet, metastable states in random anisotropy model 79−19710
amorphous ferromagnet, random anisotropy effects 78−68223
amorphous ferromagnet with random anisotropy, temp depend. of magnetisation 79−78442
amorphous ferromagnet with random uniaxial anisotropy, hysteresis, magnetisation 77−80963
amorphous ferromagnetic materials, deposition from vapour or liquid, uniaxial mag. anisotropy 78−10677
amorphous ferromagnets, ferromag. saturation, spatially random magnetostatic, magnetocrystalline, magnetostrictive and exchange fluctuations 78−60277
amorphous ferromagnets with random anisotropy axes, spin waves 80−7096
amorphous magnet, finite temperature calculations, random anisotropy model 78−80112
amorphous magnet, random anisotropy axis model in the infinite-range limit 80−88761
amorphous magnet with uniaxial anisotropy, dense random packing model. hysteresis 77−16108
amorphous magnetic layers, SAW device appl. 80−28389
amorphous magnetic system, microwave absorption spectra, calc. 80−50469
amorphous magnets, random anisotropy axes, high-temp. expansion for sp. ht. 80−71041
amorphous metals, mag. anisotropy, spin glass like phase 77−66295
amorphous systems, mag. props. effect of random anisotropy 79−4686
amorphous thin films, struct. and mag. props., review 80−93148
anisotropic antiferromagnet, phase transition, with external mag. field 79−11316
anisotropic ferromagnet, one-dimensional Landau-Lifshits eqn. multisoliton solutions *(Russian)* 80−71014
anisotropic Heisenberg chain, nonlinear excitations 80−70927
anisotropic materials, magnetisation reversal, 1/H law 78−84454
anisotropic pseudo one-dimensional Heisenberg systems, phase diagrams 78−52289
anisotropic spin-phonon coupling model, exact solutions *(Russian)* 80−100590
antiferrimagnet, two-sublattice, spin waves, magnetocaloric effect 78−31073
antiferromagnet, cluster approximation, Neel temp. and specific heat calc. 80−54901
antiferromagnet, easy plane, specific props. 79−1665
antiferromagnet, magnetic dislocation domains, mag. moment distribution 80−2601
antiferromagnet, magnetic phases, spin configurations in external field 80−70955
antiferromagnet, magnetoelastic coupling in nonlinear acoustic phenomena, exchange interaction effects *(Russian)* 77−90010
antiferromagnet, one-magnon light scatt., effect of anisotropy 79−33676
antiferromagnet, one-magnon light scatt. from metamagnetic phase effect of anisotropy 79−33678
antiferromagnet, one-magnon light scatt. from spin-flop and paramag. regions, effect of anisotropy 79−33677
antiferromagnet, rel. to dislocations *(Russian)* 77−51919
antiferromagnet, second-order phase transition, weakening of effect of fluctuation in order parameter near crit. point 79−15316
antiferromagnet, short range order effects on EPR frequencies 77−69669
antiferromagnet, sound damping by phonon-magnon interaction, high Neel temp. *(Russian)* 78−43626
antiferromagnet, transversely anisotropic, spin-wave theory of paramag. phase boundary 77−69552
antiferromagnet, two-dimensional, with easy-plane anisotropy, mag. excitations and two-magnon Raman scatt. 80−65839
antiferromagnet, two-magnon Raman scatt., temp. effects 77−48178
antiferromagnet, two-sublattice Neel-type, stable spin configurations, external mag. field and single-ion orthorhombic anisotropy effects 80−60249
antiferromagnet, uniaxial, influence of field direction and single-ion anisotropy on phase diagram 77−16072
antiferromagnet, uniaxial S=1, effect of cryst. field anisotropy 77−28344
antiferromagnet, with easy plane anisotropy, nonlinear self-interaction of acoustic waves *(Russian)* 78−80187
antiferromagnet mixture with different easy axes, theory 79−42717
antiferromagnetic exchange-coupled one-dimens. anisotropic chain with S=1/2, comparison with expts. 77−20530
antiferromagnetic insulator, strongly anisotropic, spin config. and magnon spectrum 77−8279
antiferromagnets, mag. anisotropy in state 77−69540
antiferromagnets, random, theory of mag. excitations, antiferromag. reson. 80−97146
austenitic stainless steel weld metal, US propag. 80−45452
basaltic bodies, mag. susceptibility anisotropy meas. rel. to flow and emplacement direction 79−29766
basalts, mag. susceptibility anisotropy meas., torque and spinner magnetometer comparison 78−21185
biaxial antiferromagnet, spin configuration in longitudinal mag. field *(Russian)* 79−7998
bicritical points, eqns. of state, cubic anisotropy and tetracriticality 77−55679
bis(triethylbenzylammonium)tetrachlorocuprate(II), mag. anisotropy, susceptibility, EPR of Cu^{2+} 78−52344
bis(trimethylbenzylammonium)tetrachlorocuprate(II), mag. anisotropy, susceptibility, EPR of Cu^{2+} 78−52344
1,3-bisdiphenylene-2-(p-chlorophenyl)-allyl, antiferromag. resonance, antiferromag. phase transition 78−6579
bubble collapse field, anisotropy field, and domain wall mobility, magneto-optic meas. 77−85534
bubble device materials, single-layer, ion-implantable small, design and development 79−82844

magnetic anisotropy continued
bubble devices, implanted disk type, domain wall energies, effective threshold anisotropy 79−78453
bubble domain film, growth induced order parameter, estimation from coercive force meas. 80−39828
bubble film, uniaxial anisotropy energy, effect of ion implantation 79−78476
bubble films, spin wave and magnetoelastic resonance meas. 78−91913
calcium copper acetate hexahydrate, $CaCu(CH_3COO)_4.6H_2O$ and $CaCu(CD_3COO)_4.6H_2O$ 78−2680
Cambrian slates of N Wales, mag. susceptibility anisotropy and correl. with strain 79−79832
canted magnetic struct. crysts., magnetoacoustic resonance, elastic vibrations 80−29599
carnauba wax thermoelectret, mag. anisotropy evidence for dipolar orientation 77−16240
Co-Ni, magnetic anisotropy induced by mag. annealing and cold rolling, calc. 80−7696
coal, mag. susceptibility anisotropy meas., coalification process indicator 79−53340
coercivity model with competing anisotropies 77−20643
coercivity with competing vol. and surface anisotropies 77−69626
composite garnet ferrite epitaxial film ferromag. resonance obs. 77−85578
compressible magnet with exchange anisotropy, crit. behaviour 78−39354
condensed ring systems, diamag. susceptibility, appl. to pregraphitic C 77−16039
conference on magnetism, Munster, Germany (Mar. 1977) 78−10626
conjugated molecule diamagnetic anisotropy, graphical anal. 79−76360
constant, determ. from torque curves 79−33474
constants from torque curves 77−69505
contiguous disc bubble patterns utilising intrinsic crystalline anisotropy 80−2611
coupled fields in one dimension: cross-over from a continuous symmetry to a discrete one 78−87758
critical field calc. of single domain particle with two types of anisotropic energy 78−61404
Cu-Co, dil., rotational hysteresis of Co fine particles 78−23301
cubic, asymptotic superparamag. time consts., negative anisotropy const. 78−10679
cubic, asymptotic superparamag. time consts., positive anisotropy 78−10678
cubic, three-dimens., scaling-field study 79−73731
cubic crystal, highly magnetostrictive, magnetoelastic surface waves on (110) plane 78−52327
cubic crystal, magnetic anisotropy constants fitting to torque curves 79−7989
current threshold sensor, struct. and operational features 80−34689
cyanobiphenyls, nematic, diaelec. consots. and diamag. anisotropies 80−7253
cyanocyclohexylcyclohexanes, nematic, diaelec. consots. and diamag. anisotropies 80−7253
cyanophenylcyclohexanes, nematic, diaelec. consots. and diamag. anisotropies 80−7253
cyclohexyl ammonium copper chloride, one dimensional spin $^1/_2$ ferromag., mag. props. 80−71000
deoxymyoglobin, single cryst., paramag. anisotropy meas. 77−21469
dialkylammonium copper chlorides nearly two dimens. Heisenberg ferromagnet, NMR study of magnetisation 77−85586
dialkylammonium copper tetrachloride, ferromagnetic layer compound, magnetostatic mode excitation 80−29538
diethylammonium copper tetrabromide, mag. struct., NMR meas. 80−71192
dimethyl ammonium copper chloride, nearly two-dimensional ferromag., nucl. transverse relax. rates meas. 77−81024
dimethylammonium copper tetrabromide, quasi two-dimensional antiferromag., mag. behaviour 80−97098
dimethylammonium copper tetrachloride, ferromag., quasi two-dimensional, ordering temp., press. depend. 80−84601
dimethylammonium copper tetrachloride-tetrabromide mixed cryst., mag. transition 80−65874
dimethylammonium manganese trichloride:Cd(Cu), impurities in quasi-one-dimens. Heisenberg systems, anisotropy effect 80−80502
dipropylammonium copper chloride, nearly 2D ferromag., spin wave theory 77−85436
dislocated ferromagnet, inhomogeneous magnetisation near dislocation effect on FMR linewidth 80−25213
disordered and amorphous mag. materials, position entropy solids, exchange and anisotropy noise 79−11295
domain lattices, parallel stripe susceptibility, uniaxial anisotropy field 80−54930
domain wall, phase transition, three-dimensional XY model 79−51805
domain wall energy, orientation depend., second anisotropy const. effect 77−12143
domain wall micromagnetic dynamics, numerical model 78−72381
egg lecithin membranes, anisotropy obs. 79−20520
electrical steel sheet, determ. method and laboratory tests *(Polish)* 80−97071
EM fields in anisotropic media, calc. *(Russian)* 79−7054
EPR line shape of magnets with strong cryst. field anisotropy 78−91926
exchange interactions, anisotropic, effect on singlet ground state system 80−65852
exciton theory in anisotropic mag. crystals *(Russian)* 79−7786
Fe-Cr-Co-Si-Mo, plastic deform. influence on structure and mag. props. *(Russian)* 79−70176
ferrimagnet, mag. torque near compensation point 79−33472
ferrimagnet, uniaxial two-sublattice, energy spectrum, magnetisation, and crit. field, Green function method 80−25060
ferrimagnetic alloy, amorphous, dipolar mechanisms for mag. anisotropy 78−64233
ferrimagnetic materials with high uniaxial anisotropy 78−43581
ferrimagnetic polycrystals, universal hysteresis loop 77−69620
ferrite, connection between limiting hysteresis loops and number of easy magnetisation axes *(Russian)* 78−72364
ferrite, epilayers for bubble appl. 80−39829
ferrite, hexagonal, with M, W and Y structures containing Fe^{2+} and Fe^{3+} mag. ions, saturation moment and anisotropy 80−71009
ferrite, hysteresis loop rectangularity rel. to anisotropy in polycryst. mat. 78−27056
ferrite, polycryst., natural gyromag. reson. and effective anisotropy *(French)* 77−1629
ferrite sphere, plane EM wave diffr. *(Russian)* 77−75373
ferrite sphere plane EM wave scatt. at arbitrary angle to mag. field *(Russian)* 79−15358
ferrite-semiconductor structure, surface magnetostatic wave instability 78−76235
ferrites, EM wave effects on mag. and optical props., lecture 78−27031
ferrites, hexagonal, mag. anisotropy 77−20581
ferrites, hexagonal, model, two-sublattice uniaxial systems with strong antisymmetric exchange 78−47971
ferrites, mag. anisotropy constant, contrib. of Fe^{2+} ion 79−33476
ferrites, unmagnetised polycrystalline, gyrotropic susceptibility and effective anisotropy 78−64224
ferro- and ferrimagnets, anisotropy energy density 80−88742
ferrogarnets, monocrystalline films, mag. anisotropy 80−2609
ferrohydrodynamics, mag. relax. models 79−94706
ferromagnet, amorphous, magnetisation, temp. depend. effect of nonrandom anisotropy 80−39773
ferromagnet, anisotropic, influence of spatially varying field on phase transitions 80−60339
ferromagnet, anisotropic, instantons 80−7066
ferromagnet, anisotropic, longitudinal correlation function 78−34948
ferromagnet, anisotropic, magnon spectrum, FMR line intensity, Curie pt. behaviour *(Russian)* 77−69694
ferromagnet, anisotropic, spin one, Callen's decoupling approx. 77−8258
ferromagnet, anisotropic Landau-Lifshitz, quasiclassical spectra *(Russian)* 80−15678
ferromagnet, critical behaviour in external field, renormalisation group approach 77−20601
ferromagnet, cubic, magnetised along ⟨110⟩ with negative first anisotropy constant, stability of lamellar domain struct. 79−15323
ferromagnet, domain wall mobility, damping, dipole-dipole interaction 80−93140
ferromagnet, domain walls, hypersound effect *(Russian)* 79−51810
ferromagnet, easy-plane, temp. and field depend., classical model 80−71008
ferromagnet, effects of biquadratic exchange and uniaxial anisotropy on T_c 80−60329
ferromagnet, exact integration of nonlinear Landau-Lifschitz equation 80−80495
ferromagnet, local variation in mag. anisotropy due to linear defects *(Russian)* 78−68214
ferromagnet, magnetic anisotropy energy, symmetrical polynomials, appl. to Ni 77−66293
ferromagnet, magnetisation at low temp., disorder induced behaviour 78−52234
ferromagnet, magnon bound state formation *(Russian)* 77−63162
ferromagnet, one-dimens., algebraic soliton in mag. field directed along anisotropy axis 80−75785
ferromagnet, one-magnon light scatt., temp. depend. 77−52063
ferromagnet, planar, with small basal plane anisotropy, crit. dynamics anal. 77−12116
ferromagnet, random anisotropy amorphous, initial magnetisation, remanence and coercivity 77−80964
ferromagnet, randomly anisotropic, long wavelength mag. excitations 78−84406
ferromagnet, S=1, variation of Curie temp. with small uniaxial anisotropy 77−85448
ferromagnet, single ion anisotropy consts. temp. depend. effect of spatial variation of mag. moment 78−91864
ferromagnet, three dimens., N-magnon coupled states *(Russian)* 77−12111
ferromagnet, two dimensional diluted, spin wave spectrum 77−66287
ferromagnet, uniaxial, coercive force associated with domain boundary pinning on plane defects *(Russian)* 78−6543
ferromagnet, uniaxial, domain struct. and elastic props. in orientation region of phase transitions *(Russian)* 78−19270
ferromagnet, uniaxial, with random exchange bonds of different signs, spin waves 78−76233
ferromagnet, uniaxial two-sublattice, anisotropic, thermodynamic and mag. props. 80−65866
ferromagnet, uniaxial with single-ion and exchange anisotropies, magnetisation in transverse mag. field 78−56277
ferromagnet, with anisotropic exchange, homogeneous relax., time const. calc. 77−16149
ferromagnet, with exchange-anisotropy and dipolar interaction, crit. dynamics 77−36086
ferromagnet with biquadratic exchange, crit. temp. 77−12124
ferromagnet with easy-plane anisotropy, HF magnon energies, kinematic consistency 80−93097
ferromagnet with random anisotropy, Curie temp., constant coupling approx. 78−76264
ferromagnet with single ion anisotropy, collective modes 77−28354
ferromagnetic, anisotropic, Green-function theory 77−16025
ferromagnetic, anisotropic, in random longitudinal field, multicrit. point, theory 80−54903
ferromagnetic crystals, uniaxial anisotropy, first order magnetisation processes theory 80−60242
ferromagnetic domain wall dynamics, soliton theory appl. 79−82813
ferromagnetic film, crit. angle of external mag. field for surface spin waves 79−47309
ferromagnetic film, ground state, effect of surface and bulk anisotropy *(Russian)* 79−11328
ferromagnetic film, mag. anisotropy and defect distrib. *(Russian)* 77−59434
ferromagnetic film, mag. props. meas. using planar magnetoresist. effect 78−21186
ferromagnetic film, spin wave parametric reson. near phase transition 79−8053
ferromagnetic film, uniaxial anisotropy, approx. determ. of anisotropy const. 78−2713
ferromagnetic film, with unidirectional anisotropy, domain struct. mag. field effect *(Russian)* 78−19289
ferromagnetic films, Bloch wall struct. and anisotropy, analytical representation 78−88151
ferromagnetic fine particles, stability of magnetisation curling mode and magnetisation helicoid struct. 80−11227
ferromagnetic Ising model, spin-one three dimensional, single-ion anisotropy, crit. behaviour 80−80540

magnetic anisotropy continued
ferromagnetic layer in perpendicular mag. field, ground state, spin wave reson. 77−85512
ferromagnetic liquid, particle anisotropy, asymmetric model *(Russian)* 77−27607
ferromagnetic magnetocrystalline anisotropy meas. in supercond. solenoid from 4 to 300K, magnetometer design 77−2673
ferromagnetic material, polycryst., magnetic texture anal. 80−108002
ferromagnetic metal, influence on spin-disorder resist. 78−56137
ferromagnetic metal, uniaxial, anisotropic spin fluctuations and anisotropic band struct. effects on resist. near T_c 80−65543
ferromagnetic nonmetallic film, stand exchange mode determ. 80−2565
ferromagnetic ordered structures, domain structure, effect of defects, electron microscopy 78−64214
ferromagnetic phase transitions, nucl. spin dynamics in anisotropic systems 80−11205
ferromagnetic polycrystals, cubic, domain structure under torsion *(Spanish)* 79−91246
ferromagnetic resonance in anisotropic Heisenberg model, magnon-magnon, phonon-magnon interactions *(Russian)* 80−11274
ferromagnetic single crystal with cubic symmetry, mag. and magnetoelastic props. 79−15332
ferromagnetic superconductor, mag. domain struct., sample thickness effects 80−39704
ferromagnetic superconductor, uniaxial, domain struct. parameters 80−39705
ferromagnetic thin films parametric oscill. with biaxial anisotropy 80−103861
ferromagnetism, band model, pseudodipolar theory of magneto crystalline anisotropy 77−36068
ferromagnetism, singlet state, theory 77−12073
ferromagnets, anisotropic, domain-wall struct. depend. on const. and oscillating mag. fields *(Russian)* 79−69691
ferromagnets, anisotropic, HF magnon energy renormalisation, kinematic consistency 80−29539
ferromagnets, Heisenberg and planar, exact results for spin-wave renormalisation 79−69660
ferromagnets, magnetic solitons propagating along anisotropy axis *(Russian)* 79−73798
ferromagnets, phase transformation theory, easy axis anisotropy, quadrupole interaction, renormalisation method calcs. *(Russian)* 79−65671
film, cylindrical, anisotropy field meas. 77−13783
film, cylindrical, critical curve meas., sense signal and magnetisation connection *(Slovak)* 77−24717
film, determ. from analysis of torque meas. 77−8368
film, magnetocryst. anisotropy, magnetostriction and micromagnetism 77−73062
film, rel. to micromagnetic dynamics in domain walls, numerical model 78−72382
film, saturation magnetisation and uniaxial anisotropy determ. using torque meas. 79−95614
film, surface pinning parameter, complex angle depend. 77−63239
film, surface spin waves and surface anisotropy effects at finite temp. 79−78452
film, vertically suspended, torque curve meas., first-order calc. anal. 80−86354
film, with perpendicular anisotropy, stripe domain struct., theory *(Russian)* 80−65973
film strip, anisotropic, wall motion meas. *(German)* 79−28573
films, ferromagnetic, perpendicularly magnetised, surface and vol. magnetoelastic waves *(Russian)* 80−93151
first-order transition induced by cubic anisotropy 79−4688
garnet, spin Hamiltonian and mag. anisotropy, appl. to $3d^4$ and $3d^6$ ions 79−99669
garnet, substituted polycryst., low FMR linewidth, relax. processes 77−20718
garnet bubble film LPE with high Pb content 79−38750
garnet bubble film with induced anisotropy, domain wall energy 79−19750
garnet bubble films, 111 orientated, mag. anisotropy predictions, model 78−68326
garnet epitaxial film, anisotropy consts. from reciprocal of susceptibility meas. 77−73057
garnet epitaxial film, damage prod. by multiple ion implantation, ferromag. reson. obs. 80−34703
garnet epitaxial film, easy magnetisation axis inclination temp. depend. 79−65699
garnet epitaxial film, stress induced magnetocrystalline anisotropy 80−71013
garnet epitaxial films, easy magnetisation axis orientation 80−60383
garnet film, bubble, anisotropy field and nonmagnetic regions in implanted layers, ferromag. reson. study 79−99774
garnet film, bubble, [111]-oriented simple method of meas. cubic anisotropy const. 78−19285
garnet film, growth rate depend. of growth-induced anisotropy 78−14992
garnet film, ion implanted bubble circuits 79−78473
garnet film, orthorhombic anisotropy, fast bubble devices 80−25168
garnet film, uniaxial, cubic anisotropy effect 77−89998
garnet films, (111)-oriented, cubic anisotropy meas. 80−54924
garnet films, LEP growth-induced anisotropy, magnetostriction theory 79−95624
garnet films with orthorhombic anisotropy, domain wall motion 80−80580
garnets, chemical site preference of rare earth ions 77−68936
garnets, large growth-induced anisotropy to preferential occupation of Fe sites 80−75754
garnets, magnetic anisotropy and magnetostriction 79−99748
garnets, superexchange operator and cryst. field interactions 80−59931
giant intrinsic magnetic hardness, review 78−48004
group velocity, four-dimensional, electromagnetic waves in electrically and magnetically anisotropic media 80−17814
guanidinium vanadium sulphate hexahydrate, singlet ground state system, low temp. mag. props. 80−44843
HBT liquid crystal, mag. susceptibility and anisotropy, smectic, nematic, isotropic phases 78−18748
HCP metals, and alloys, anisotropy of phys. props. rel. to texture 79−91700
HCP metals and alloys, calc. of elec. and mag. anisotropy *(Russian)* 77−66292
Heisenberg, ferromagnet, spin-one, uni- and biaxial anisotropy, RPA and mol. field approx. 78−34989
magnetic anisotropy continued
Heisenberg anisotropic ferromagnet, longit. correl. function, generating Green functions 78−6500
Heisenberg antiferromagnet, anisotropic, excitations at finite temp., CPA calcs. 79 95562
Heisenberg antiferromagnet, anisotropic, finite cell calcs. 80−60164
Heisenberg antiferromagnet, one dimens., spin-flop transition 79−73723
Heisenberg antiferromagnet, one-dimens., impure, mag. susceptibility 80−60168
Heisenberg chain with infinite radius of interaction, correl. functions 77−59372
Heisenberg ferromagnet, amorphisation, anisotropically distrib. exchange forces *(Russian)* 77−85408
Heisenberg ferromagnet, anisotropic, collective Green's function, dynamical RPA 80−70925
Heisenberg ferromagnet, anisotropic, with biquadratic exchange interaction and uniaxial anisotropy, Curie temp. 80−7118
Heisenberg ferromagnet, equivalence of large biquadratic exchange to small uniaxial single ion anisotropy 79−78292
Heisenberg ferromagnet, one-dimens., symm. crossover 79−87269
Heisenberg ferromagnet, spin-one, with biquadratic and uniaxial anisotropy, Curie temp. 79−61123
Heisenberg ferromagnet, strongly anisotropic with impurities, in transverse field, one-magnon states 77−69476
Heisenberg ferromagnet, two-dimens., with easy plane type anisotropy 77−16094
Heisenberg ferromagnet, with uniaxial exchange anisotropy, cumulant expansion method 77−12076
Heisenberg linear spin systems, dynamical spin correlation functions 78−31035
Heisenberg magnet, classical, with layer structure, mag. phase transitions, anisotropic lattice, theory 80−29557
Heisenberg magnets, pure and pseudo-one-dimens. temp. depend. of EPR freqs. 78−6563
Heisenberg model, anisotropic spin system, $S=^1/_2$ frustration effects 80−65763
Heisenberg model, with anisotropic biquadratic exchange interaction, two-magnon bound states 77−28356
Heisenberg model with one-ion anisotropy, closing relns. for Green's functions 78−2642
Heisenberg one-dimens. chain of classical spins with weak anisotropy, thermodynamics 77−43805
Heisenberg paramagnet, dil., uniaxial anisotropy, frequency moments of spin correlation function 78−84377
Heisenberg paramagnet with uniaxial anisotropic exchange and single-ion anisotropy, freq. moments of correlation function 79−15272
Heisenberg system, with single-ion anisotropy, longit. correl. functions 78−76214
Heisenberg thin films 79−38359
hexaferrites, $M(BaFe_{12}O_{19})$, mag. characts. correlation with substituting ions at. nos. *(Russian)* 79−91218
hexagonal material, Δs effect, anisotropic contrib. 77−90005
highly anisotropic material, mag. aftereffects, coercive mechanism 77−69634
horizontally dipped LPE film, inhomogeneities, spin wave reson. meas. 79−91298
hypercritical films, stress-induced uniaxial anisotropy influence on domain struct. *(Russian)* 79−69703
impurity uniaxial ferromagnet, thermodynamics below Curie point *(Russian)* 77−43801
insulating solid, nonmagnetic, anisotropic mag. effect 78−6509
intrinsic anisotropy constants from mag. props., book contrib. 80−11191
Invar, hysteresis loop displacement 78−52312
Invar, magnetocryst. anisotropy rel. to magnetisation 77−16070
Invar, magnetocrystalline anisotropy 77−63173
Invar, thermal expansion coefficient, origin of anisotropy, rel. to roll mag. anisotropy 77−84951
Invar neutron small angle scatt. magnetocrystalline anisotropy 77−85420
iron formate dihydrate, higher order term of uniaxial anisotropy *(Japanese)* 80−2571
Ising and Heisenberg ferromagnets with biquadratic exchange, uniaxial anisotropy, susceptibility calc. 79−99670
Ising chain, spin-1, sp. ht. in presence of impurities and mag. field 80−93128
Ising ferromagnet, high-freq. props. quantum theory, susceptibility tensor calcs. *(Russian)* 80−11143
Ising ferromagnet, S=1, single-ion type uniaxial anisotropy, cluster-variation method appl. in pair approx. 78−68281
Ising ferromagnet, spin-1, with random anisotropy, Curie temperature 77−28399
Ising ferromagnet, with transverse single-ion anisotropy, phase transitions 78−19259
Ising model, spin-one, bilinear and biquadratic interactions, phase diagram 80−75772
isopermalloy, permeability stability calc. rel. to texture *(Chinese)* 80−65959
isotropic ferromagnet, critical behaviour in random uniaxial anisotropy model 79−38349
itinerant electron ferromagnet with domain struct., spin waves 78−64182
linear electric field effects 80−65854
low temp. specific heat, elec. resistance and US absorpt. *(Russian)* 79−19734
lyotropic liquid crystals, orientation in mag. field, glass interface effects 79−1390
magmatic rocks, anisotropy var. with depth 77−9407
magnesioferrite precipitated particles in MgO, resonance anisotropy field 77−69541
magnetic anisometer based on permanent magnet torsion balance *(Bulgarian)* 79−30493
magnetic Debye crystal, with magnon-phonon coupling, crit. changes in vibr. modes 79−95094
magnetic ordering, anisotropic, via combined spin and orbital exchange scatt. of conduction electrons 80−65863
magnetic texture meas. with polarised neutrons 79−95577
magnetisation direction angle meas. with vibr. sample magnetometer, appl. to $SmFeO_3$ 77−26366
magnetometer, rotating sample, influence of eddy currents on signal spectrum 79−63278
magnetostriction in terms of hexagonal and cubic harmonics up to degree 6 80−88856

magnetic anisotropy continued
magnetostrictive ferromagnet, conditions for stress induced bulk moments 79−78493
magnons, nonlinear, multidomain ferromagnets with 180° Bloch walls 78−34967
manganese stearate, two-dimensional mag. struct. 80−108040
marble, mag. susceptibility anisotropy development through cryst. preferred orientation of calcite 78−56286
measurement of microwave freq., experimental results 80−52279
metallic glass, isotropic and anisotropic magnetoelastic effects, review 78−68352
metallic glass, micromag. calcs. and props. 80−80501
metallic glasses, atomic transport behaviour, review *(Japanese)* 79−94907
metallic glasses, mag. props., struct., and prep., book contrib. 79−65665
metallic glasses, mats. props. review 77−4043
metallic glasses quenched from melt, appl. as soft mag. materials *(German)* 78−10676
metallic magnets investigation, present state *(Polish)* 80−107987
metamagnetism, spontaneous, four-ion anisotropy as source 79−47277
metamagnetism, temperature induced, caused by mag. anisotropy 80−11195
Metglas 2605 ribbon, saturation magnetostriction meas. by small-angle magnetisation rot. 80−60391
Metglas 2826 ribbon, saturation magnetostriction meas. by small-angle magnetisation rot. 80−60391
Metglas 2826 ribbons, ferromagnetic resonance and SEM obs. 80−15804
methoxy detection by submillimetric laser spectrometer 77−40623
micromagnetic perturbation theory 78−14912
microwave freq., measurement using square resonant cavity 79−93173
model, temp. and field dependence, anisotropy constant meas., review *(Rumanian)* 80−25125
molecule, from molar Cotton-Mouton and Kerr constants 77−46652
molecules, Hartree-Fock perturbation technique, CNDO/2 *(French)* 78−37559
multidomain ferromagnetic resonance anal., appl. to stripe and bubble arrays 79−78528
multidomain magnetic disc, ferromagnetic reson. 78−68386
neopentane adsorbed on graphite, quasi two-dimens. fluid, NMR 80−102525
one dimensional magnet with easy plane, solitons and magnons 78−23260
one-dimensional magnetic compounds, orbital interaction 78−6494
one-dimensional magnetic system, spin anisotropy and exchange alternation 80−34644
one-dimensional spin system, with anisotropic interaction, high freq. props. *(Russian)* 77−80902
one-spin ferromagnet, high temp. series expansion for mag. susceptibility and sp. ht. 80−25148
orthoferrite cryst. films, local coercivity of domains boundaries *(Russian)* 80−80578
orthoferrites, weak ferromagnetism, single ion anisotropy contrib. 80−25126
paramagnet, anisotropic, spin dynamics, exchange-bond dilution effects 80−88763
paramagnet, statistical mechanics using second order Green's function theory 80−25074
paramagnetic to ferromag. transition, libron interactions, temp. depend. *(German)* 78−76237
paramagnets, anisotropic, spin dynamics 77−69481
p-pentoxybenzilidene alkylaniline, liq. cryst., mag. anisotropy and polymorphism *(French)* 77−76532
Permalloy, corrosion resist. and mag. props., effect of Cr addition 77−86219
Permalloy, FCC, mag. anisotropy induced by cold rolling 80−11188
Permalloy, high-permeability, influence of grain struct. and non-mag. particles on mag. props. *(German)* 77−16112
Permalloy, magnetisation improvement through solid state refining 78−91893
Permalloy cylindrical film, magnetisation in crossed steady/alternating fields, easy axis dispersion influence 79−8024
Permalloy film, domain wall mass and energy, wall vel. depend. calc. 80−2614
Permalloy film, domain walls streaming *(Russian)* 79−82842
Permalloy film, magnetoresistive determ. of anisotropy energy and its strain depend. 79−56575
Permalloy film, obliquely deposited, annealing and deposition parameter effects *(Russian)* 77−80971
Permalloy film, perpendicular anisotropy, structural and thermal stresses *(Russian)* 79−4708
Permalloy film, strain-dependent contrib. to uniaxial anisotropy 79−60908
Permalloy film, temp. depend. of mag. anisotropy anal. *(Russian)* 77−51901
Permalloy film, with-small surface anisotropy, ferromag. reson. 77−69701
Permalloy film demagnetising field and magnetisation curve determ. 77−73059
Permalloy film strip, wall curvature calc. with in-phase magnetisation 78−2717
Permalloy RF sputtered films, O effects in mag. and elec. props. 80−100603
Permalloy RF sputtered films, struct.-sensitive mag. props. 80−34705
Permalloy thin films, break-cross-tie wall energy 80−88842
Permalloy-Cu(Al) two-layer films, mag. anisotropy, grain boundary diffusion *(Russian)* 80−71122
Permalloy-Mn film, diffusion aftereffect causing mag. state change *(Russian)* 80−103860
Permalloy-SiO multi-layer flat ring cond., with circular anisotropy, mag. props. *(Russian)* 77−8366
permanent magnets review 79−42801
phase diagram near Lifshitz point, systems with easy plane of magnetisation 77−80936
phase diagram near Lifshitz point, uniaxial magnetisation 77−80935
phase diagrams of magnets with two sublattices *(Russian)* 78−23268
phase transitions, in systems with competing interactions 78−14963
phenyl alkyl ammonium copper chloride, quasi-two-dimens. Heisenberg ferromag., mag. props. 77−66273
phonon-induced temp. dependences of magnetocrystalline anisotropy consts. 80−65858
polycrystalline and amorphous strips, magnetostriction consts. determ. method 80−86355
polycrystalline ferrites, anisotropy const. meas. 80−97090
porous anisotropic magnets, approach to mag. saturation 80−93146
Potts model, spin anisotropy and crossover 78−56339
powdered specimen, anisotropic mag. interactions, high resolution NMR *(Russian)* 78−39418
Procopiu effect EMF in ferromag. material under torsion *(Rumanian)* 78−86986
proteins, diagmagnetic anisotropy, struct. origins 79−92136
pseudo-single domain grains, surface anisotropy rel. to stable remanence origin 78−65275
pseudospins, S=1/2, simple cubic array, with anisotropic exchange between nearest neighbours, ground state configs. 78−72340
pyridinium manganese chloride, anhydrous, quasi one-dimensional mag. behaviour, heat capacity meas. 80−80549
pyridinium nickel chloride, anhydrous, quasi one-dimensional mag. behaviour, heat capacity meas. 80−80549
quadratic antiferromagnet, with easy-plane anisotropy, spin wave theory 78−91855
quasi-two-dimensional planar spin system, mag. transition 80−65951
quenched random alloy with competing anisotropies, decoupled tetracrit. point 77−12138
random anisotropic magnetic alloys, multicrit. points 77−16091
random anisotropy model in Ising model, Monte Carlo simulation 80−80546
random quenched site model, competing exchange energies and competing anisotropy energies 80−29552
rare earth$_{50}$Ag$_{50}$, amorphous, bulk mag. props., field, time and temp. depends. 77−89932
rare earth alloy, heavy, mag. anisotropy *(Japanese)* 77−85444
rare earth alloys, amorphous, high field magnetisation and magnetoresistance 78−72136
rare earth alloys, amorphous, mag. props. rel. to struct., review 79−15298
rare earth alloys, amorphous, magnetoresistivity, exchange scatt. model 78−95287
rare earth alloys, amorphous, random anisotropy antiferromag. model 78−95428
rare earth alloys, amorphous, with random anisotropy axes, spin excitations in paramag. phase 80−80476
rare earth alloys, amorphous random anisotropy ferromagnetism in pair approx. 79−47276
rare earth alloys, Curie temperature, high press. effects *(Japanese)* 80−20444
rare earth alloys, highly magnetostrictive props. 77−12180
rare earth alloys, R_2Co_{17}, formation of mag. anisotropy role of rare earth ions *(Russian)* 78−76238
rare earth alloys, R-3d alloys (3d=Mn,Fe,Co,Ni), magnetic properties 78−52231
rare earth alloys, RFe_2, magnetostriction studies, book contrib. 80−39846
rare earth aluminium Laves phase cpds., RAl_2, anisotropic magnetostriction, temp. depend. 80−39841
rare earth amorphous alloys, antiferromagnetism, mol. field approx. 78−80142
rare earth amorphous alloys, random anisotropy antiferromag. model 80−20399
rare earth amorphous alloys, random anisotropy magnetism 80−65853
rare earth amorphous alloys, random mag. anisotropy, antiferromag., Monte Carlo calcs. 79−33471
rare earth amorphous alloys, random mag. anisotropy 80−20398
rare earth amorphous alloys, transport props. 80−20152
rare earth garnet thin films, macroscopic magn. props., magneto-optical expts. 80−46764
rare earth garnets, field depend. magnetocryst. anisotropy 77−69543
rare earth garnets, prep. and props. book contrib. 80−44193
rare earth intermetallics, magnetocryst. anisotropy 77−8299
rare earth intermetallics, magnetostriction and struct. distortion 77−63248
rare earth intermetallics, RFe_2 and $R(Co_{0.98}\ Fe_{0.02})_2$, magnetostrictive material, changes in vibr. modes near mag. phase transition 79−90736
rare earth intermetallics, $RFe_{5-x}Ni_x$, giant intrinsic mag. hardness 78−56354
rare earth iron garnet single crystal films, synthesis and props., review 78−48013
rare earth iron garnets, anisotropic, mag. props., high field and low temp. 80−75801
rare earth iron intermetallics, R_2Fe_{17} and $R_2Fe_{17-x}Ni_x(Co_x)$, mag. anisotropy and hyperfine interactions 77−8298
rare earth iron intermetallics, RFe_2, magnetostrictive, book contrib. 80−75838
rare earth Laves phase compounds, $R_xR_{1-x}Fe_2$, magnetostriction, anisotropy energy 80−25177
rare earth metal, heavy, mag. anisotropy *(Japanese)* 77−85444
rare earth metals, mag. and transport props. 79−69658
rare earth metals, two- and single-ion mag. anisotropy 77−63164
rare earth orthoferrite, $RFeO_3$, spin reorientation and magneto-optical effects *(Japanese)* 79−47414
rare earth orthoferrites, hyperfine interaction anisotropy, NMR study *(Russian)* 80−66052
rare earth orthoferrites, mag. anisotropy in cryst. field approx. 80−60241
rare earth orthoferrites, mag. dipole anisotropy and magnetostriction 79−73710
rare earth orthoferrites, Raman scatt. from magnons, anisotropy consts. determ. 80−66178
rare earth permanent magnets, physics and technology 80−20433
rare earth titanium oxides, $RTiO_3$ type, bulk mag. and struct. props., ferrimag. order 80−107993
rare earth transition metal intermetallic permanent magnets, props. and technology, book contrib. 79−65696
rare earth-$(Co_{1-x}Ni_x)_5$, single cryst., mag. props., mag. reversal 77−85489
rare earth-Ag alloy, amorphous, model calcs., of mag. props. 80−84616
rare earth-Co_{17} alloys, singular point detection 78−84414
rare earth-Co, RCo_2: ^{57}Fe, easy magnetisation directions, Mossbauer meas. and cryst. field calc. 77−63168
rare earth-Co, RCo_5, high anisotropy origin, cryst. field contrib. 77−73020

magnetic anisotropy continued
rare earth-Co, RCo_5, mag. moment orientation, anisotropic mol. field model 77−89950
rare earth-Co alloy, mag. anisotropy origin 79−38319
rare earth-Co alloy, RCo_5, mag. anisotropy, individual Co site contribution 79−78366
rare earth-Co alloys, R_2Co_{17}, substituted 77−89947
rare earth-Co-Ni alloys, $Pr(CoNi)_5$ type, mag. props. and mag. reversal phenomena *(Russian)* 77−51924
rare earth-Cu intermetallic compds. single crysts., mag. props. 80−54892
rare earth-Fe_2 Laves phase compounds, magnetostriction anisotropy 77−63250
rare earth-Fe alloys, amorphous and crystalline, small angle neutron scatt. study of mag. order and mag. microstruct. 79−15283
rare earth-Fe alloys, RFe_2, temp. depend of coercivity 79−61185
rare earth-gold amorphous alloys, R_4Au, anisotropy versus exchange 80−34624
rare earth-iron alloys, elastic vs. magnetoelastic anisotropy 78−68347
rare earth-transition metal (4f-3d) intermetallic cpds., mag. moment and mag. anisotropy 80−25107
rare earth-transition metal alloys, amorphous, anomalous low-temp. props. 78−91872
rare earth-transition metal alloys amorphous thin films, anisotropic mag. and microstruct. props. 78−95487
rare earth-transition metal amorphous film, microstruct. 77−51619
rare earth-transition metal amorphous films, radiation damage 77−66398
rare earth-transition metal film, amorphous, microstruct. and magnetism 78−64230
rare earth-transition metal intermetallics, struct. and props. review 78−10668
rare-earth alloys, amorphous study of hysteresis effects using Monte Carlo technique 79−1686
rare-earth alloys, quadrupole scatt. anisotropy, magnetically ordered material 78−64034
rare-earth orthoferrite, cubic anisotropy consts. 80−11190
residual pseudo-macrostress, X-ray meas. errors due to plastic deform. 77−68544
retinal rod external segment mag. anisotropy decrease after total photolysis 77−52838
rock strain from mag. susceptibility anisotropy 77−78170
rocks, susceptibility anisotropy meas. using inductive magnetometers 78−85541
Schiff's bases, nematic phys. props. 79−99057
screw spin ordered state through dipole-dipole interaction 78−39337
sheared crystals, magnetocrystalline anisotropy torque meas. 78−24830
single-ion anisotropy, magnetic systems, high temp. series expansion 80−34576
small magnetic particles, anisotropy field, resonance meas. 78−64227
smectic A mesophase, spin-probe longitudinal relax. 79−94871
soft ferromagnetic film, theoretical wall mobility 80−34677
spin chain with easy plane type anisotropy, coupled magnon states *(Russian)* 79−33469
spin glass materials, mag. field dependence of susceptibility peak 80−103840
spin glasses, monoionic anisotropy, influence on transform. to paramag. state *(Russian)* 79−28529
spin systems with single-ion anisotropy characts. of mag. ordering 77−69466
spin wave instability theory for cubic single cryst. mag. insulators 79−65667
spin wave resonance, surface mode magnetisation, inhomogeneities effect 77−69710
spin wave theory in strongly anisotropic magnets 77−63151
spin waves in anisotropic chain 79−33467
spin waves in randomly inhomogeneous anisotropic medium *(Russian)* 77−43828
spin waves in strongly anisotropic magnets, canonical transform theory 78−68197
spin waves in systems with weak exchange fields 79−4664
spin waves in weak antiferromagnetic exchange field system 78−43577
spin waves in weak exchange field systems 78−43576
spin-1/2 cubic lattice, with anisotropic exchange, configs. 80−65926
spin-glass and ferromagnetic behaviour induced by random uniaxial anisotropy 78−39338
steel, alloy, corrugated texture perfection, mag. anal. 80−88745
steel, C (0.01 and 0.06 wt.%), rephosphorised, mag. props. and texture 77−20634
steel, induced anisotropy influence on mag. props., thermomagnetic working *(Russian)* 80−55549
steel, mag. anisotropy, magnetostatic fields, numerical simulation 77−27220
steel, transformer, anisotropy of temp. depend. of mag. props. *(Russian)* 78−39362
steel, transformer, cold-rolled effect of uniaxial elastic stress on dynamic magnetostriction *(Russian)* 77−69651
strongly anisotropic magnets, canonical transform. method 77−85404
sublattice metamagnet, temp. dependent anisotropy, magnetisation curves, mag. transitions, classical approx. 80−39795
superconducting cable, magnetisation anisotropy meas. in hysteresis loss using Hall sensors 80−17966
superparamagnetic particles, resonance anisotropy field 77−69541
superparamagnetism, magnetisation vector diffusion coeff., anisotropy energy, vol. distrib. of particles by Mossbauer effect 78−48099
superparamagnets with cubic anisotropy, high order relax. times 77−69632
surface and interface magnetism by Mossbauer spectroscopy 80−7218
surface states, theory, in spin wave resonance, review 80−84654
TANOL, free radical, spin flopping transition, temp. depend., mag. anisotropy energy 80−54890
TCNQ alkali salt, spin-Peierls transition 80−29395
tetragonal crystals with easy plane of magnetisation, phase diagram near Lifshitz point 78−39321
tetragonal XY-like antiferromagnet, multicritical behaviour, global phase diagrams 79−42779
texture and crystallite orientation distrib. effect on anisotropy *(German)* 77−8307
thermoelectret and magnetoelectret states, diamag. anisotropy 80−97053
thermofluctuation aftereffect anisotropy in Rayleigh region *(French)* 78−14989

magnetic anisotropy continued
thin film, with uniaxial-biaxial anisotropy, low freq. ferromag. reson. 79−8055
thin films, magnetic anisotropy rel. to columnar microstruct., calc. 80−39822
ticonal, thermal magnetic hysteresis *(Russian)* 77−16119
TMMC, linear antiferromag., energy gaps in spin-wave dispersion, neutron inelastic scatt. 79−91223
TMMC, linear antiferromag., mag. phase diagram, expt. and theoretical study 80−71038
TMMC, spin dynamic exam., effect of mag. field at low temp. 79 73733
TMNB, ferromag. chains with easy-plane anisotropy, exchange const., anisotropy const. and g-value 77−80927
TMNB, linear S=1 ferromag., easy plane anisotropy, low-temp. mag. props. 78−23250
TMNC, ferromag. chains with easy-plane anisotropy, exchange const., anisotropy const. and g-value 77−80927
TMNC, linear S=1 ferromag., easy plane anisotropy, low-temp. mag. props. 78−23250
torque curve analysis, online microprocessor system 78−254
torque method, vertically suspended specimen, field intensity effect 80−86353
transition metal 3d, spin-orbital interaction effect on NMR, g-factor anisotropy *(Russian)* 77−24752
transition metal alloys, Curie temperature, high press. effects *(Japanese)* 80−20444
transition metal ferromagnetic amorphous alloys, mag. props. 77−55690
transition metal-rare earth intermetallics, two sublattice system with high competing single ion anisotropies, model 80−39767
transition metals, 3d, ferromag. props., book contrib. 80−75724
transition metals, mag. surface anisotropy 77−1553
transition metals, theory of ferromagnetism rel. to mag. anisotropy 80−2541
s-triazine, molar Cotton-Mouton const., Kerr const., 298K, 633 nm 77−16286
2,4,6-trichloro-s-triazine, molar Cotton-Mouton const., Kerr const., 298K, 633 nm 77−16286
trimethylammonium cobalt trichloride dihydrate, Ising-like system, nucl. spin-lattice relax. of ^1H and ^{35}Cl 80−29638
trimethylammonium manganese bromide, mag., anisotropy, biquadratic exchange 78−14952
TRM direction, mag. shape anisotropy effect, appl. to basalts 79−29758
twin crystals, magnetic reversals, role of magnetostatic interaction *(Russian)* 78−39361
two-sublattice magnetic system with fourth-order uniaxial anisotropy and strong antisymmetric exchange in transverse mag. field 79−56530
two-sublattice system, with strong antisymm. exchange and fourth order anisotropy, mag. configs. 78−68167
type II superconductor, equilibrium misalignment, fluxoids and appl. mag. field, anisotropy interaction 79−24112
uniaxial antiferromagnets, crystalline anisotropy energy determ. from low field torque data 78−19245
uniaxial ferromagentic with intrinsic mag. field, domain struct. 80−93141
uniaxial ferromagnet, arbitrary spin and single-ion anisotropy of second order, Green's function 78−84379
uniaxial ferromagnetic crystal, irreversible rotation processes 80−39768
uniaxial ferromagnets with single ion anisotropy in transverse field, magnetisation 77−32143
uniaxial Heisenberg antiferromagnet, phase diagrams 80−15730
uniaxial magnet, free energy of system with weak exchange interactions and high mag. anisotropy *(Russian)* 78−68213
uniaxial materials with shape anisotropy, magnetisation curves 78−60313
uniaxial weak ferromagnet, energetic spectrum *(Russian)* 79−51762
US, large magnetic anisotropy exam. 77−20585
Voigt geometry cubic crystals, odd magnetooptical effects 78−19450
weak ferromagnet, single-ion anisotropy, one-magnon Raman processes 78−27234
weak ferromagnetism, hysteretic phenomena 78−27059
X-Y ferromagnet, S=1, with uniaxial anisotropy, Curie temp. 79−78425
X-Y model with quartic anisotropy, soliton-like features 79−78429
X-Y quasi-one-dimens. system anisotropic, spin-Peierls phase transition, tricritical point 80−25142
ytterbium ethyl sulphate, crystal field effects on mag. and hyperfine props. of Yb^{3+} 80−97101
Zn-Mn(Cr), dil., mag. anisotropy below 1K, low field magnetisation meas. 80−20382
Au, resonant and nonresonant conduction-electron-spin transmission 80−75857
$AuMn_2$ mag. struct., phase transition, and magnon spectrum, random anisotropy effects 80−88722
Au_4Mn, anomalous field depend. of magnetic anisotropy const. 77−12113
Au_4Mn, magnetocrystalline anisotropy temp. depend. 77−51900
Au_4V single crystal, ordered, mag. props., domain models 80−39770
$(Ba,Sr)Fe_{12}O_{19}$, Ferroxdure, developments and research 78−84455
$Ba_2Co_{1.65}Fe_{0.35}^{2+}Fe_{28}^{3+}O_{46}$, temp.-mag. field phase diagram, torque method 80−60276
$Ba_2Co_{1.75}Zn_{0.25}Fe_{12}O_{22}$, trigonal ferrite, mag. anisotropy 79−73709
$BaFe_{12-2x}M_xTi_xO_{19}$ (M=Co, Ni, Zn), mag. props. determ. 80−75759
$BaFe_{12}O_{19}$, Ca^{2+} substitution effect on hexaferrite lattice and mag. props. 80−60243
Ba_2NiF_6, quadratic layer antiferromag., optical spectra obs. 77−16326
Ba_2NiF_6, specific heat capacity, critical amplitude, cross-over from 2-D Ising to Heisenberg behaviour 80−39791
$BaNi_2M_xFe_{16-x}O_{27}$, effect of $M=Sc^{3+}$ or In^{3+} on props. 77−47978
$BaZn_{1.38}Co_{0.62}Fe_{16}O_{27}$, W-type hexaferrite cryst., first order magnetisation processes 78−95472
$Ba_2Zn_{2-2(x+y)}Cu_{2x}Cd_{2y}Fe_{12}O_{22}$, mag. props. and Mossbauer spectrum 80−75765
$Ba_2Zn_{2-2x}Cu_{2x}Fe_{12}O_{22}$, hexagonal ferrites, prep. and mag. characterisation 79−1727
$BaZn_2Fe_{16-x}Al_xO_{27}$, saturation magnetisation, anisotropy field and Mossbauer meas. 77−69508
$BaZn_2Fe_{16-x}M_xO_{27}$ (M=Al, Ga, In, Sc), mag. props. and Mossbauer effect 80−75766
$Ba_2Zn_2Fe_{12}O_{22}$, anisotropic magnetisation and susceptibility 78−84411
$Ba_3Zn_2Fe_{24}O_{41}$, ferromag. reson., low power nonlinear effects 80−75861
Bi-MnBi directionally solidified eutectic alloys, struct. and mag. props. 79−51815

magnetic anisotropy continued
$Bi_{3-2x}Ca_{2x}Fe_{5-x-y}In_yV_xO_{12}$, single crystal by flux method ferrimag. garnet *(Chinese)* 77−40056
BiTeI, layered cryst., anisotropy and temp. depend. of mag. susceptibility 79−73673
$(BiTm)_3(FeGa)_5O_{12}$, monocrystalline films, mag. anisotropy 80−2609
CO group, NMR chem. shift, solvent's dielectric const. effect, mag. anisotropy 79−42847
Ca ferrite, composition and mag. props., anisotropy field, magnetisation 80−71109
Ca ferrite magnets, anisotropic, BaO substitution effect on mag. props. *(Japanese)* 79−99697
Ca, Ge-substituted garnet, LPE growth atm. effects on bubble props. 77−20655
$CaF_2:Tm^{3+}$, 8.2 keV excited state, mag. props., Schottky ht. capacity, nucl. quadrupole splitting 78−76037
$Ca_3Fe_2Ge_3O_{12}$, antiferromagnetic reson., anisotropy and magnetoelastic interaction effects *(Russian)* 77−69712
$Ca_3Mn_2Ge_3O_{12}$ garnet, metamagnetic transition, high anisotropy peculiarities *(Russian)* 80−60274
$Ca_3Mn_2Ge_3O_{12}$, highly anisotropic garnet, neutron diffr. obs. of mag. struct. 78−68168
$Ca_3Mn_2Ge_3O_{12}$, mag. struct. study 80−2554
Cd-Co(-Mo), amorphous films, thermal stability of mag. props. *(Japanese)* 79−47307
Cd-Mn dil. alloys, single cryst., low temp. mag. anisotropy 77−59386
$Cd_3Cr_2Ge_4O_{12}$, antiferromagnetic reson., anisotropy and magnetoelastic interaction effects *(Russian)* 77−69712
$CdCr_2Se_4$, ferromag. semicond., photoinduced mag. anisotropy 80−50086
$CdCr_2Se_4$, influence of Co ions on anisotropy and magnetostriction, ferromag. reson. meas. 77−69659
$CdCr_2Se_4$:Ag, ferromag. reson. meas. 77−8415
$CdCr_2Se_4$:Ag, ferromag. reson. field and linewidth anisotropy, Se vacancy effects 78−60338
$CdCr_2Se_4$:Ag, mag. anisotropy, effect of annealing in vacuum 77−80929
$Cd_{1-x}Mg_x$, magnetic susceptibility anisotropy, press. effects, electronic phase transitions *(Russian)* 80−54869
CdSb:Ge, anisotropy of elec., mag. props. 78−34829
Ce monopnictides, anomalous mag. props., planar coupling theory 80−60245
Ce pnictides, unusual anisotropy mechanism due to virtual valence fluctuation 80−96828
$CeAl_2$, anisotropic magnetostriction near antiferromagnetic transition 78−88157
$CeAl_2$, mag. anisotropy, transition, crystal field splitting 78−52243
CeB_6, magnetostriction, US absorpt. and thermal expansion 80−66004
CeB_6, resist. anomaly and mag. ordering obs. 79−61110
CeBi, magnetoelastic effects, anisotropic mag. behaviour 80−25176
CeBi(Sb), anisotropic mag. ordering and mag. structural transitions 79−78324
CeBi(Sb), enhanced lattice-displacement effects on cryst. field and anomalous mag. anisotropy 79−73477
$CeFe_2$, magnetostriction and magnetisation 80−39844
$Ce_x(La_{0.76}Y_{0.24})_{1-x}Bi$, mag. phase diagrams 79−56535
CeSb, magnetoelastic effects, anisotropic mag. behaviour 80−25176
Co complex, Co II high spin binuclear species, magnetic exchange and anisotropic susceptibilities 78−39308
Co complex, $Co(C_5H_5NO)_6(NO_3)_2$, simple cubic X-Y mag., specific heat, mag. exchange anisotropy meas. 78−39346
Co complex, Co(II)(1,2,4-triazole)$_2$(NCS)$_2$ quasi two-dimens. canted S=1/2 antiferromag. 80−70976
Co, electrodeposited coating, struct. and magnetic props. 79−46985
Co, electrodeposited film, saturation magnetisation and perpendicular anisotropy meas. 78−76277
Co, FCC, mag. props. of single-domain powders after plastic deform. *(Russian)* 78−6554
Co ferrite, crystalline anisotropy, FMR meas. 77−8408
Co film, evaporated, uniaxial mag. anisotropy 77−51929
Co film, ion beam sputtering prep., struct. and mag. props. 80−35085
Co film, mag. anisotropy study using NMR spin echo method 80−60384
Co, HCP, ferromag., anisotropic hyperfine interactions, NMR expt. 78−43658
Co, HCP to FCC transition, mag. domain nucleation 78−64218
Co, magnetic anisotropy induced by mag. annealing and cold rolling, expt. 80−7695
Co, magnetic anisotropy induced by mag. annealing and cold rolling, calc. 80−7696
Co, magnetic domain struct. temp. depend. 79−78436
Co, magnetocrystalline anisotropy consts. meas., 77-700K 78−43582
Co, plated film, magnetisation and mag. interface anisotropy 77−85510
Co, spin polarised photoemission, surface magnetism 79−52083
Co, uniaxial magneto-crystalline anisotropy, temp. depend. 79−42753
Co-CoO films, evaporated, exchange anisotropy 80−88841
Co-Cr recording films, perpendicular mag. anisotropy, hysteresis loop, microstruct., TEM obs. 78−95491
Co-Fe, dil., magnetocrystalline anisotropy anomalous temp. depend. 80−71007
Co-Fe, film, mag. and hyperfine field exam. of uniaxial anisotropy 77−66391
Co-Fe, soft mag. props. rel. to metallurgical aspects 80−88810
Co-Fe alloy, HCP and DHCP, magnetostriction consts. determ. 78−80184
Co-Fe alloy films, magnetostriction and orientation of easy magnetisation axes *(Russian)* 79−19756
Co-Fe alloys, mag. anisotropy induced by mag. annealing through to double h.c.p. 77−1552
Co-Fe-B films, amorphous, mag. annealing behaviour 79−73782
Co-Gd amorphous film, struct., mag. anisotropy consts., saturation magnetisation *(Russian)* 79−99735
Co-Gd-Mo films, sputtered, O effects on mag. props. during annealing 80−89374
Co-Gd-Mo-Ar film, amorphous, mag. props. 78−80182
Co-Gd(Ho) film, amorphous, stripe domains and mag. anisotropy by Lorentz microscopy 77−63243
Co-Ni, magnetic anisotropy induced by mag. annealing and cold rolling, expt. 80−7695
Co-Ni, magnetocrystalline anisotropy consts. meas., 77-700K 78−43582
Co-P, amorphous, domain struct., mag. anisotropy origin 80−80554
Co-P, amorphous, ferromag. antireson. 24 GHz microwave transmission, mag. props. 80−34778
Co-P, electrodeposited amorphous alloy, mag. permeability 78−52310
magnetic anisotropy continued
Co-P amorphous alloy, ferromagnetic reson. exam. 79−28620
Co-P amorphous alloys, electrodeposited, magnetic anisotropy 79−28568
Co-P amorphous alloys, electrodeposited, mag. anisotropy 80−15713
Co-P amorphous film, domain struct., influence of planar anisotropy 79−78472
Co-P films with various preferred orientations, mag. props. 80−100604
Co-Pt, struct. and mag. props. rel. to degree of order 78−72368
Co-Pt film, electrodeposited, saturation mag. induction, mag. anisotropy and coercive field meas. *(French)* 80−2610
Co-Pt films, mag. and magneto-optic props., appl. to holographic and bit-by-bit storage 79−33512
Co-Re, sputtered film, high coercivity and high hysteresis loop squareness 79−91259
Co-Si-B, amorphous ribbon, saturation magnetostriction meas. by small-angle magnetisation rot. 80−60391
Co-Zr, dil., mag. annealing effect, depend. of uniaxial mag. anisotropy on Zr conc. 80−39772
Co-Zr-Er alloys, mag. annealing effect, effect of Er on induced uniaxial mag. anisotropy 80−39771
$Co_{80}B_{20}$, amorphous metal ribbon, stresses, magnetoelastic anisotropy and zero-field mag. domain struct. 80−44896
$Co_{1.8}BaFe_{0.2}Fe_{16}O_{27}$, influence of spin-reorientation on magnetoelastic props. *(Russian)* 79−8028
$Co_{1.8}BaFe_{0.2}^{2+}Fe_{16}^{3+}O_{27}(Co_{1.8}W)$, magnetoelastic props. under spin-reorientation conditions 79−69709
$CoBr_2$, magnetic excitations, neutron scatt. investigation 80−39761
$CoCl_2$, antiferromag., mag. excitations, mag. neutron inelastic-scatt. meas. 77−85437
$CoCl_2.2H_2O$-$FeCl_2.2H_2O$, random mixture with competing spin anisotropies, tetracrit. transition, neutron diffr. obs. 80−2575
$CoCr_2S_4$, ferrimag. semicond., magnetocrystalline anisotropy 80−71012
$CoF_2:MnSu^{2+}$, anisotropic antiferromagnet, spin impurity approx. *(Russian)* 79−87253
$(CoFeB)_{100-x}Cr_x$ thin films, magnetic props. and corrosion resist. 80−34709
$Co_{1-x}Fe_{2+x}O_4$, prep. by wet and ceramic methods, struct., mag. and surface props. 78−52307
$Co_xFe_{3-x}O_4$ film, magnetooptic recording material, mag. and magnetooptic props. 77−20832
Co_xGa_{1-x} alloys, cluster spin glass, host and impurity NMR and AC susceptibility 80−71194
CoGd, H_2 and N_2 contaminated amorphous films, mag. props. 79−1690
$(Co_{1-x}Mn_x)_2B$, magnetocrystalline anisotropy meas., 4.2-300K 80−71006
$Co_{0.25}Mn_{0.75}Fe_2O_4$, ferromag. reson. in frozen lattice model, anisotropy consts. 79−51859
$Co_{40}Ni_{40}B_{20}$, magnetostriction, temp. depend. 78−91921
$Co_x(Ni_{0.5}Cu_{0.5})_{1-x}Fe_2O_4$ ferrite, relation between elec. cond. and mag. anisotropy 80−75548
$CoO:Ni^{2+}$, far IR absorpt. by impurities and collective antiferromag. reson. mode 77−8576
CoP, and CoNiP, cylindrical amorphous electrodeposited layers, mag. props., torsion influence 80−88848
$Co_{35}P_{15}$, amorphous, strip domains, anisotropy const. effects 80−29571
$CoSiF_6.6D_2O$, phase transition, mag. anisotropy and IR absorption spectra 77−89537
$CoSiF_6.6H_2O$, effect of press. on struct. phase transition, 100 to 300K 77−80616
$Co_{1-x}Ti_x$, ferromag. props., Ti conc. effect 80−54872
$CoTiO_3$, antiferromag., mag. anisotropy, magnetisation meas. 80−65856
$CoZrF_6.6H_2O$, effect of press. on struct. phase transition, 100 to 300K 77−80616
Cr, antiferromag., muon depolarisation, mag. anisotropy determ. *(Russian)* 79−61290
Cr, mag. struct., phase transition, and magnon spectrum, random anisotropy effects 80−88722
Cr, magnetic phase diagram in external mag. field, spin reorientation curve, critical point coordinates *(Russian)* 80−29548
Cr, spin-density-wave antiferromagnet, uniaxial anisotropy 78−10640
Cr-Co-Fe permanent magnet anisotropic alloys, plastic deform., ageing, particle alignment temp. 80−35254
Cr-Fe, dil., spin correlations and neutron scatt. near crit. conc., theory 80−60327
$CsFeCl_3$, single cryst. mag. susceptibility meas. 77−20560
$CsMnBr_3.2D_2O$, extended scaling in spin flop system 79−73737
$CsMnCl_3$, anisotropy constants at 4.2K 79−11310
$CsMnCl_3.2H_2O$, linear antiferromagnet, specific heat, exchange interactions and anisotropy effects 77−1556
$CsMnCl_3.2H_2O$, spin wave anal. 77−8292
$CsMn_{1-x}Cu_xCl_3.2H_2O$, impurities in quasi-one-dimens. Heisenberg systems, anisotropy effect 80−80502
$CsMnF_3$, mag. struct., phase transition, and magnon spectrum, random anisotropy effects 80−88722
$CsMnF_3$, optical investig. of spontaneous tilt of mag. sublattices *(Russian)* 77−40215
$CsMnF_3$, spin-wave dispersion relations, neutron inelastic scatt. obs. 77−51895
$CsNiCl_3$, nearly one-dimensional antiferromag., spin-flop transition 78−6527
$CsNiCl_3$, nuclear spin-lattice relax., temp. depend., anisotropic effects 78−64293
$CsNiCl_3(F_3)$, one-dimensional anisotropic paramag., nucl. relax. rate and spin dynamics 77−69723
$CsNiF_3$, anisotropic Heisenberg chain, nonlinear excitations 80−70927
$CsNiF_3$, demagnetising effects on antiferromag. reson. 80−15803
$CsNiF_3$, in mag. field, spin wave dispersion, inelastic neutron scatt. 77−77046
$CsNiF_3$, linear S=1 ferromag., easy plane anisotropy, low-temp. mag. props. 78−23250
$CsNiF_3$, one dimens. ferromag., spin wave dynamics, inelastic neutron scatt. study 79−47270
$CsNiF_3$, one dimensional ferromag., magnetisation, FMR, 2.61-20K 77−20719
$CsNiF_3$, one-dimensional mag., Young's modulus softening along linear-chain direction 77−62578
$CsNiF_3$, quasi-one-dimensional ferromagnet, subthreshold parallel pumping of magnons 80−75745
$CsNiF_3$, single cryst. mag. susceptibility meas. 77−20560
$CsTmO_2$, mag. props. of normal-temp. form, 2.9-251.3K *(German)* 79−91205

magnetic anisotropy continued
Cu compounds, layered, anisotropic and dipolar interaction terms effect on mag. phase transition 77−63210
Cu ferrite films, Mn-, Ni- and Al-substituted, LPE growth 80−96752
Cu, resonant and nonresonant conduction-electron-spin transmission 80−75857
Cu:Co precipitates, mag. anisotropy, precipitate shape, coercive force 80−80500
Cu-Mn alloy spin glass, macroscopic mag. anisotropy, transverse susceptibility and zero field NMR enhancement 80−80525
Cu-Ni films, compositionally modulated, magnetic anisotropy, magnetisation curves 80−88840
$CuCl_2$, anhydrous, single crysts., prep. 77−85932
$CuCl_2$, anhydrous, single cryst., mag. behaviour in low temp. ordered phase 79−7974
$CuCl_2$, anhydrous paramagnetic phase, mag. susceptibility depend. on temp. 79−7965
$CuCl_2.2H_2O$, antiferromag. reson., HF, press. depend. *(Russian)* 77−36137
$CuCl_2.2H_2O$, influence of high hydrostatic press. on intermediate state associated with spin flopping 78−35020
CuCr(Fe)(Mn), dil., anisotropic hyperfine coupling, NMR study 80−65784
$CuCr_2Se_4$, experimental obs. 78−76227
$CuCr_2Se_4$ single crystal, magnetic props. *(Japanese)* 78−6520
$CuK_2Cl_4.2H_2O$, Heisenberg ferromagnet, spontaneous magnetisation under press. *(Russian)* 77−36058
CuMn, hysteresis, spin orbit scattering effect on anisotropy in spin glass state 80−71095
CuMn, magnetisation processes below freezing temp. 80−15748
CuMn, spin glass, mag. hysteresis meas. 80−34691
CuMn, spin glass, remanence, new approach from zero field NMR 80−34785
CuMn-like alloys, model calcs. on magnetisation processes in moderate fields below freezing temp. 79−24188
$Cu_{0.86}Mn_{0.14}$, hysteresis loop development 80−65922
Cu_2MnAl, Heusler alloy, magnetisation mag. anisotropy, magnetostriction and elastic consts. 78−23318
dimethylammonium manganese tetrachloride, 2D Heisenberg antiferromag., spin wave anal. 80−54879
Dy and dilute alloys of Dy, fan phase, hexagonal anisotropy 77−77051
Dy, basal plane mag. anisotropy constant, field depend. meas., 4.2-120K 77−63165
Dy, change in easy axis during magnetisation 77−8306
Dy, domain wall dynamics, NMR 77−69614
Dy, ferromag., rel. to magnetoresist., fields up to 75 kOe, 1-70K 77−20297
Dy film, helimag. order, surface deform., exchange and single-ion magnetocrystalline anisotropy energy 77−66390
Dy, helical antiferromagnetic phase, basal plane anisotropy 78−84412
Dy, mag. anisotropy and susceptibility 77−69539
Dy, mag. characts. in strong mag. field 77−89936
Dy, magnetic anisotropy and ^{161}Dy Mossbauer effect 78−92001
Dy, magnetocrystalline anisotropy, perturbation theory 78−2675
Dy, single crystal, plastic and magnetoplastic deform. 77−63713
Dy, spin wave exam. 78−56306
Dy-Co amorphous film, prep. by dual-source evaporation, mag. props. 77−89988
Dy-Sn alloy, hyperfine fields acting on diamag. impurities and anisotropic exchange, Mossbauer spectra 77−1625
Dy-Th, single cryst., mag. susceptibility, transitions, anisotropy 80−54873
Dy-Y, paramag. susceptibility in basal plane and hexagonal axis 77−20548
$DyCo_2$, magnetocryst. anisotropy props. by ^{57}Fe Mossbauer spectroscopy 77−63328
$DyCo_{3.4}$, amorphous, mag. props. 77−32177
$DyCo_{5.3}$ noncollinear mag. struct. appearance in mag. fields, magnetostriction meas. *(Russian)* 80−100607
Dy_2Co_{17}, and $Y_{2x}Dy_{2(1-x)}Co_{17}$, 77-383K 77−89949
Dy_xCu_{1-x}, amorphous film, magnetisation meas., local anisotropy effects 78−68309
$Dy_2(Fe,Co)_{17}$, mag. anisotropy fields by singular pt. detection 79−24156
$Dy_2(Fe,Co)_{17}$, magnetic anisotropy meas. by singular point detection method 77−63170
DyFe amorphous film, Mossbauer and mag. meas. 80−15844
$DyFe_2$, magnetisation and magnetic anisotropy 78−91862
$DyFe_3$, Mossbauer spectra, easy magnetisation axis temp. rot. 80−15859
Dy_2Fe_{17}, domain structures and anisotropy constant. 80−93136
$DyFeO_3:Al^{3+}$, Morin transition, mag. vacancies effect *(Russian)* 78−27039
Dy_xGd_{1-x}, mag. anisotropy energy, composition depend. 77−16071
$Dy_{1-x}Gd_xAl_2$, ferromag, easy axis rot., ^{163}Dy NMR obs. 79−78562
DyIG, mag. and magnetooptical props., temp. and field depends. 77−89927
DyM_3, M=Fe, Co, Ni, amorphous, mag. struct. and moments 77−66260
$DyNi_2$, single cryst. mag. props. 77−24684
$DyNi_5$ crystal, basal plane anisotropy, torque meas. 80−65857
DySb, quadrupole scatt. anisotropy, magnetically ordered material 78−64034
$Dy_xTb_{1-x}Fe_2$, and $Ho_xTb_yDy_{1-x-y}Fe_2$, high magnetostriction cpd., mag. anisotropy origins 78−68217
$Dy_xTb_{1-x}Fe_2$, single cryst., torque meas. 80−65877
$Dy_xTb_{1-x}FeO_3$ orthoferrites, Dy^{3+} and Tb^{3+} contribs. to anisotropy const. *(Russian)* 77−89946
$DyVO_4$, basal plane magnetisation anisotropy under Jahn-Teller distortion 78−68222
$Dy_xY_{1-x}Al_2$, domain wall dynamics, NMR 77−69614
Er, magnetisation and susceptibility in basal plane in strong mag. field *(Russian)* 80−50145
Er, spin wave exam. 78−56306
ErB_4, mag. and elec. props., metallic character 80−20386
$ErCo_2$, magnetocryst. anisotropy props. by ^{57}Fe Mossbauer spectroscopy 77−63328
$ErCo_{5.6}$, easy magnetisation direction 78−84415
Er_2Co_{17}, magnetisation, magnetocryst. anisotropy and magnetostriction 77−8303
$Er_{65}Co_{35}$, amorphous, amg. ordering, susceptibility, magnetisation and hysteresis meas. 78−68190

magnetic anisotropy continued
$Er_2(Co_{1-x}Fe_x)_{17}$, mag. anisotropy and intersublattice exchange interactions 78−31066
$Er_2Co_{17-x}Fe_x(Mn_x)(Ni_x)$, saturation magnetisation, Curie temp., easy direction, and anisotropy field 77−8304
$Er_2Co_{17-x}M_x$, M=Cr, Ni, effect of substitution on mag. props. 79−78363
$Er_2(Co_{1-x}Ni_x)_{17}$, mag. anisotropy and intersublattice exchange interactions 78−31066
$Er_2EuFe_{5-x}Ga_xO_{12}$, rag-domain garnet film, controlled variation of props. under O_2 annealing 79−15328
$ErFe_3$, 47K magnetic anomaly, point charge crystal field model 77−20517
$ErFe_3$, Mossbauer and magnetisation investig. of 47K mag. anomaly, atomic rearrangement 77−20766
Er_6Fe_{23}, lower critical field 80−20414
$ErFeO_3$, sound velocity meas. at high press., spin-reorientation transition 78−76254
ErGa garnet, crystal field theory calcs. 77−8259
ErIG, high-field magnetisation, low temp. mag. anisotropy 80−75802
$Er_xY_{3-x}Fe_5O_{12}$, garnet, mag. anisotropy and magnetostriction 80−11189
$Er_xY_{3-x}Fe_5O_{12}$, spin reorientation transitions 78−2686
ErZn, magnetoelastic and quadrupolar couplings 78−52328
ErZn, preferred mag. domain orientation, and microstructural defects, magnetostriction meas. 79−73769
$(Eu,La,Ca)_3(Fe,Ga,Al)_5O_{12}$ film, LPE growth and induced orthorhombic anisotropy 77−20652
$(Eu,Lu)_3(Fe,Al)_5O_{12}$ film, epitaxial, increased domain wall velocities, due to orthorhombic anisotropy 77−20653
$(Eu,Lu)_3Fe_5O_{12}$, epitaxial film, orthorhombic mag. anisotropy 78−19290
$(Eu,Lu)_3Fe_5O_{12}$, submicron bubble films on rare earth-Ga garnet substrates, prep. and mag. props. 78−91909
Eu, mag. anisotropy of helicoidal struct., magnetisation, 4.2-300K *(Russian)* 79−56499
$Eu_{3-x}Ca_xSi_xFe_{5-x}O_{12}$, bubble film, LPE growth induced anisotropy 77−20659
EuGaYIG film, bubble dynamics, anisotropy depend., ferromag. reson. expts. 77−63240
EuIG:Ga(Al), pure and doped, mag. anisotropy, magnetisation meas. 80−60240
EuIG:Pb film saturation magnetisation improved by Sb^{5+} substitution 80−54926
EuIG:Sb(Ca)(Ti), growth from PbO-B_2O_3 based flux, prop. depend. on Pb content 80−39824
EuIG+Pb, (100) LPE film, magnetocryst. anisotropy and lattice mismatch 77−20647
$(EuLu)_3(FeAl)_5O_{12}$, film epitaxial growth on Gd_3GaO_{12} substrate, mag. props. 80−65402
$(EuLu)_3Fe_5O_{12}$, Ga, Al or (Ca,Ge) substituted, mag. props. and growth of 2 μm bubbles 78−91910
$Eu_2(SO_4)_3.8H_2O$, mag. props., thermal var., cryst. field reduced matrix elements 77−51875
$EuSb_2$, cryst. struct. and antiferromag. props. 79−32973
$Eu_zY_{3-z}Ga_tFe_{5-t}O_{12}$, epitaxial garnet films, props. at compensation points 80−39823
EuYIG:Sb, growth from PbO-B_2O_3 based flux, prop. depend. on Pb content 80−39824
Fe complex, $Fe(Br)[S_2CN(C_2H_5)_2]_2$, 3-D Ising ferromag., cryst. susceptibility, 1.5-20K 80−20390
Fe complex, $Fe(Cl)[S_2CN(C_2H_5)_2]_2$, 3-D Ising ferromag., cryst. susceptibility, 1.5-20K 80−20390
Fe complex, tetraphenylporphynate iron III bromide, mag. props., zero-field splitting 80−34584
Fe, energy of mag. anisotropy, band calcs. *(Russian)* 77−20583
Fe film, evaporated at oblique incidence, columnar grain struct. using anisotropy field meas. 77−59231
Fe film, evaporated at oblique incidence, optical and mag. anisotropies 80−7134
Fe film, ferromag. reson., thermodynamical anal., effect of mech. stress 79−42840
Fe, film, ion beam sputtering prep., struct. and mag. props. 80−35085
Fe film, on Cu and Ag substrates, mag. props., Mossbauer spectra meas. 80−11233
Fe film coated by MgO, Mossbauer spectra, mag. hyperfine field 80−7221
γ-Fe film on Cu (111) mag. props. 78−31098
Fe, fine particle dispersions, shock induced mag. effects 79−82832
Fe foil, ferromag. domain-wall width, anisotropy depend. 78−19269
Fe garnets, thin film, low freq. excitation spectra, mobility of domain boundaries 79−42815
Fe group, mol. Jahn-Teller reson. states as possible antecedents to magnetism 80−75701
Fe group ions in singlet ground state, magnetocryst. anisotropy and magnetostriction 77−73021
α-Fe particles, in fused SiO_2, g-values and anisotropy consts., FMR study 79−82876
Fe, plastically deformed, high field suscept. anisotropy and domain struct. 78−15002
Fe pole pieces, in electromagnets, mag. anisotropy effect on mag. field homogeneity *(Japanese)* 80−93111
Fe, spin polarised photoemission, surface magnetism 79−52083
Fe, whisker single crystals, ferromag. reson. and surface anisotropy 80−71187
Fe whiskers, magnetisation and temp. depend. near T_c 80−39766
α-Fe:N, mag. field depend. of reverse permeability 77−80969
Fe-Al (25 at.%), long-range ordered, compression induced mag. anisotropy 77−69546
Fe-B, sputtered amorphous film, strong stripe domains, Kerr effect obs. and theory 79−91265
Fe-B amorphous alloy, mag. anisotropy temp. depend. 80−15846
Fe-B ferromag. film, props. 79−4709
Fe-B films, amorphous, mag. annealing behaviour 79−73782
Fe-B-Si amorphous ribbons, effect of annealing conditions on magneto-mechanical props. 80−34740
Fe-Co (46%) film, evaporated, uniaxial mag. anisotropy 77−51929
Fe-Co film, magnetisation induced uniaxial anisotropy 77−48016
Fe-Co-Cr-Si, structural transform. and mag. props. following heat treatment *(Russian)* 77−81274
Fe-Co-Ni Perminvar, mag. props. singularities in region of mag. anisotropy *(Russian)* 80−84614

magnetic anisotropy continued
Fe-Co-Si-B sputtered amorphous thin film, coercivity, galvanomagnetic props., resistivity 80−29578
Fe-Cr, Invar alloy, explanation of phys. anomalies *(Russian)* 78−88112
Fe-Cr (10 to 70 at.%), ferromag. reson., anisotropy const., and saturation magnetisation *(Russian)* 77−81013
Fe-Cr (70-92 at.%), coexistence of ferro- and antiferromagnetism *(Russian)* 78−47955
Fe-Cr-Co, mechanism of coercive force 80−34674
Fe-Cr-Co alloy, coercive force mechanism 80−71103
Fe-Cr-Co-V alloy, microstruct. and mag. props. 78−68221
Fe-Gd film, amorphous, mag. props., mean field analysis 78−64236
Fe-Gd film, amorphous, O_2 contamination effects on mag. props. 78−64231
β-Fe-Ge, mag. props. from X-ray, magnetisation and Mossbauer meas. 79−42755
Fe-meteorites, mag. anisotropy rel. to origin of magnetisation 78−65564
Fe-Mn-P-B-Al metallic glass, exchange anisotropy 77−16068
Fe-Mn-Ti-Al, magnetic texture rel. to annealing temp., Mossbauer investig. 77−28499
Fe-Ni, Invar alloy, explanation of phys. anomalies *(Russian)* 78−88112
Fe-Ni, secondary recrystn. and mag. props. 80−89247
Fe-Ni (23-35 at.%), cooled below 70K in mag. field, uniaxial anisotropy *(Russian)* 78−19244
Fe-Ni (308-44.1 at.%) Invar alloys, anomalous mag. anisotropy and thermal expansion 80−75755
Fe-Ni (47 to 65 wt.%), soft magnetic alloy with crystallographic texture and field induced anisotropy, pulse permeability and excursion rate *(German)* 79−73779
Fe-Ni (50 to 94 wt.%), FCC, form. and migration energy of vacancies, induced magnetic anisotropy *(French)* 78−2110
Fe-Ni alloy, low-noise, for cores of ferromag. probes and mag. modulators 79−8017
Fe-Ni alloy type YuNDK25B, anomalous magnetocaloric effect 80−60278
Fe-Ni evaporated films with perpendicular anisotropy, magnetoresistance obs. 78−2585
Fe-Ni/pure Fe exchange coupled films, mag. reversals, hard layer thickness effects *(Russian)* 78−56359
Fe-Ni-Al, magnetic anisotropy form. and struct. changes by annealing, Mossbauer obs. 80−39994
Fe-Ni-Al-Cu (25, 14, 4 wt.%), alloy YuND24, effect of Ti addition on structure, mag. props. 80−15714
Fe-Ni-Co-B-P soft magnetic metallic glasses, status report 78−64226
Fe-P amorphous alloys, electrodeposited, mag. anisotropy 80−15713
Fe-P-C alloys, amorphous, mag. anisotropy, Mossbauer obs., prior cooling effects *(Russian)* 77−32300
Fe-Pd alloy, uniaxial ferromag., anisotropic component of localised mag. field, Mossbauer meas. *(Russian)* 79−15382
Fe-Pt alloy, ordered, anisotropy of mag. props. *(Russian)* 78−60280
Fe-Pt films, mag. and magneto-optic props., appl. to holographic and bit-by-bit storage 79−33512
Fe-Pt Invar alloy, magnetocryst. anisotropy energy, itinerant electron model 80−54884
Fe-Pt Invar alloys, magnetocrystalline anisotropy const. determ. 80−65861
Fe-R alloys, mag. elastic properties 78−52331
Fe-Si, amorphous film, comp. depend. 77−1575
Fe-Si (3 wt.%), directional, power loss anomalies temp. depend., effect of intrinsic parameters 77−12156
Fe-Si (3 wt.%) grain-oriented transformer sheet, effect of phosphate coating containing Cr_2O_3 and CaO 77−16135
Fe-Si (3 wt.%) single crysts., rolling-induced mag. anisotropy *(Russian)* 78−19243
Fe-Si (6.5 wt.%), effect of ordering on mag. props. 79−51833
Fe-Si ferromag. film, props. 79−4709
Fe-Si-Al-Ni alloy, Super Sendust, Ni content and thermomag. treatment effects 77−4861
Fe-SiO_2, granular compound, superpara- to ferromag. transition temp. meas. 77−69633
Fe-W-Cr-Mo system, mag. and mech. props. rel. to production methods *(Japanese)* 80−71107
Fe-Zn alloys, coercive force anisotropy after cold plastic deform. *(Bulgarian)* 80−75809
Fe_3Al, roll magnetic anisotropy and dislocations *(Japanese)* 77−80930
Fe_cAu_{1-c}, amorphous ferromagnetic, resistivity, anisotropic, field dependence 78−87960
$Fe_{1-x}B_x$ amorphous films, mag. props. and thermal stability 79−78446
$Fe_{80}B_{20}$ amorphous alloy, low field magnetic props. 77−55690
$Fe_{80}B_{20}$ glass, low-field mag. props. 77−8380
$Fe_{80}B_{20}$, glassy, ferromag. anisotropy of resistivity 79−23939
$Fe_{80}B_{20}$, METGLAS 2605, mag. anisotropy and electronic struct., Mossbauer meas. 77−28384
$Fe_{80}B_{20}$, magnetostriction, temp. depend. 78−91921
$Fe_{80}B_{20}$, metallic glass, ferromag. props. 77−16107
$Fe_{80}B_{20}$, sputter deposited amorphous, low field mag. props. 78−68335
$Fe_{81}B_{19}$ amorphous alloy, mag. anisotropy temp. depend. 78−14953
$Fe(BF_4)_2.6H_2O(6D_2O)$, phase transition, mag. susceptibility and anisotropy and permittivity meas. 79−23718
$FeBO_3$, basal mag. anisotropy, antiferromag. reson. *(Russian)* 79−47338
$FeBO_3$, magnon dispersion by light scatt. and ferromag. reson. 77−55668
$Fe_{78}B_{12}Si_{10}$, amorphous, Mossbauer study of hyperfine interaction and mag. anisotropy 80−40027
$Fe_{80}B_{15}Si_5$ metallic glass, large uniaxial magnetostrictive anisotropy, magnetisation reversal 80−34736
$Fe_{81.5}B_{14.5}Si_4$, amorphous metal ribbon, stresses, magnetoelastic anisotropy and zero-field mag. domain struct. 80−44896
$FeBr_2(Cl_2)(I_2)$, far IR antiferromag. reson. 77−36138
Fe_xC_{1-x} amorphous sputtered film, mag. props. 78−68311
$FeCl_2$, magnetic excitation in presence of transverse field, ferromag. reson. 78−19335
$(Fe_{0.06}Co_{0.94})$-B, amorphous, ferromag., mag. instability rel. to struct. 79−99729
$Fe_{(1-x)}Co_xCl_2.2H_2O$, random mixture of anisotropic antiferromags., isotropic state obs. 78−84396
$Fe_{(1-x)}Co_xCl_2.2H_2O$, antiferromag. random mixture, sp. ht. meas. 79−65678
$Fe_{0.5}Co_{0.5-x}Cr_x$ films, vacuum-deposited cryst. and mag. struct. *(Russian)* 80−93081

magnetic anisotropy continued
$(Fe_{1-x}Co_x)_{78}Si_{10}B_{12}$, amorphous alloys, magnetic anisotropy meas. 80−2570
$(Fe_{1-x}Co_x)_{78}Si_{10}B_{12}$, amorphous, roll mag. anisotropy 80−75757
$Fe_{4.7}Co_{70.3}Si_{15}B_{10}$, amorphous ferromag., roll mag. anisotropy 79−51773
$(Fe_xCo_{1-x})_{78}Si_8B_{14}$, amorphous, saturation magnetostriction, strain modulated FMR obs. 80−75863
FeF_2, antiferromag. spin flop boundary 78−84419
FeF_2, antiferromagnet, fourth-order spin Hamiltonian terms for Fe^{2+} 78−10628
FeGd, H_2 and N_2 contaminated amorphous films, mag. props. 79−1690
$FeGe_2$ canted antiferromagnet, mag. susceptibility anisotropy and temp. dependence 80−25112
Fe_3Ge, mag. props. of cubic and hexagonal phases 77−8475
Fe_5LiO_8, magneto-crystalline anisotropy, magnetoelectric effect interpretation *(French)* 79−47316
Fe_5LiO_8, magnetoelec. effect interpretation by magneto-cryst. anisotropy *(French)* 79−33515
$Fe_{78}Mo_2B_{20}$, glassy, ferromag. anisotropy of resistivity 79−23939
FeN alloy, coercive force, effect of $Fe_{16}N_2$, anisotropic model 77−85501
$Fe_{40}Ni_{40}B_{20}$, amorphous, induced mag. anisotropy, reorientation kinetics 77−43829
$(Fe_xNi_{1-x})_{80}B_{20}$, $(Fe_xNi_{1-x})_{80}P_{14}B_6$, new soft amorphous ferromagnetic glasses *(Croatian)* 79−11298
$Fe_{32}Ni_{36}Cr_{14}P_{12}B_6$, metallic glass, changes in Curie temp., physical dimensions and mag. anisotropy during annealing 77−85446
$Fe_{40}Ni_{38}Mo_4B_{18}$, amorphous, mag. anisotropy, Mossbauer study 80−65864
$Fe_{40}Ni_{38}Mo_4B_{18}$, amorphous, reversible enhancement of mag. directional ordering rate 80−103829
$Fe_{40}Ni_{38}Mo_4B_{18}$ metallic glass, reorientation kinetics of magnetization 79−24155
$Fe_{40}Ni_{38}Mo_4B_{18}$, metallic glass, mag. and transport props. 80−39752
$Fe_{40}Ni_{38}Mo_4B_{18}$ ribbon, magnetic characterisation 80−34680
$(Fe_{1-x}Ni_x)_2P$, mag. props. 78−23248
$(Fe_{1-x}Ni_x)_{80}P_{10}B_{10}$, amorphous microwires, magnetisation reversal and anisotropy 78−91885
$Fe_{27}Ni_{53}P_{14}B_6$, metallic glass, changes in Curie temp., physical dimensions and mag. anisotropy during annealing 77−85446
$Fe_{40}Ni_{40}P_{14}B_{06}$, amorphous, strip domains, anisotropy const. effects 80−29571
$Fe_{40}Ni_{40}P_{14}B_6$, amorhpous ribbon, influence of torsion on mag. props. 80−7138
$Fe_{40}Ni_{40}P_{14}B_6$, amorphous, thermal stress effect on mag. easy axis 77−80928
$Fe_{40}Ni_{40}P_{14}B_6$, amorphous, domain struct. 78−10719
$Fe_{40}Ni_{40}P_{14}B_6$ amorphous ribbon, mag. anisotropy distrib. near surface 78−95430
$Fe_{40}Ni_{40}P_{14}B_6$ amorphous ribbon, mag. domains and anisotropy distrib. 80−108029
$Fe_{40}Ni_{40}P_{14}B_6$, and $Fe_{32}Ni_{36}Cr_{14}P_{12}B_6$, glassy, ferromag. anisotropy of resistivity 79−23939
$Fe_{40}Ni_{40}P_{14}B_6$, induced anisotropy energy and saturation magnetisation temp. depend., torque magnetometer meas. 78−10680
$Fe_{40}Ni_{40}P_{14}B_6$ metallic glass, ferromag. reson., spin waves, thermal ageing and long-range order effects 80−25214
$Fe_{40}Ni_{40}P_{14}B_6$, Metglas 2826, ferromag. antireson. transmission at 24 GHz, anisotropy effects 77−69696
$Fe_{40}Ni_{40}P_{16}B_6$, amorphous, kinetics of induced mag. directional order 80−44824
$Fe_{29}Ni_{49}P_{14}B_6Si_2$, metallic glass, changes in Curie temp., physical dimensions and mag. anisotropy during annealing 77−85446
$(Fe_{1-x}Ni_x)_{78}Si_{10}B_{12}$ amorphous alloys, cold rolled and as-quenched, mag. anisotropy 80−97089
$Fe_{1.985}Ni_{0.975-x}Zn_xCo_{0.04}O_{4+\gamma}$, elementary coupling energy of Co^{2+} to lattice 77−1549
$Fe_{1-x}O$, cryst. field anisotropy parameter calc. 79−4665
α-Fe_2O_3, antiferromag. reson. in absence of external field, 150 and 320K *(Russian)* 79−4730
α-Fe_2O_3, Morin transition, Mossbauer spectra meas. 78−31071
γ-Fe_2O_3, particle interactions, in inhomogeneous anisotropic magnetic materials, average field effect 77−32217
γ- Fe_2O_3:Co powder, increased coercivity by epitaxial doping 79−82833
α-Fe_2O_3:Sn^{4+}, antiferromag. reson. *(Russian)* 80−7175
Fe_3O_4 ferrofluid suspension, mag. props., stability 79−87293
Fe_3O_4 ferrofluids, spin glass behaviour 80−71120
Fe_3O_4, magnetically biased rel. to linear and bilinear magnetoelec. susceptibility, 4.2K 77−40106
Fe_3O_4, magnetite, low temp. phase 77−20584
Fe_3O_4, magnetite, magnetoelec. effect at 77K, elec. field depend. of mag. anisotropy 80−29594
Fe_3O_4, magnetocrystalline anisotropy, anomolies in magnetostriction and elastic constants 80−60244
Fe_3O_4, magnetoelastic coupling effect on anisotropy below transition temp. 77−69657
Fe_3O_4, magnetoelectric effects from electric field depend. macroscopic mag. anisotropy energy 77−69656
Fe_3O_4, monoclinic phase, saturation magnetisation near Verwey temp. 77−77038
Fe_3O_4, single cryst., surface magnetism, spin polarized photoemission 78−52622
Fe_3O_4, spin polarised photoemission, surface magnetism 79−52083
Fe_xO_y powder coated with $NaPO_3$, anomalous coercivity increase 77−89980
Fe_2P, magnetisation, susceptibility, thermal expansion and elec. resist. meas. 77−77037
$Fe_{2-x}P$, first order ferro- to paramag. transition, 216K, susceptibility obs. 78−39322
$Fe_{82}P_{18}$, amorphous, uniaxial mag. anisotropy 78−19246
$Fe_{80}P_{13}C_7$, amorphous, mag. anisotropy 79−65670
$Fe_{75}P_{15}O_{10}$, amorphous, ferromag. domain-wall width, anisotropy depend. 78−19269
FePd epitaxial film, vacuum-deposited, for thermomag. recording, mag. and magneto-optical props. *(Russian)* 78−60319
$FePd_{1-x}Pt_x$, permanent magnet, coercive force increased by Pt 79−24157
$Fe_{1-x}Pd_x$ films, vacuum deposited, mag. and corrosion props. 79−56574
FePt epitaxial film, vacuum-deposited, for thermomag. recording, mag. and magneto-optical props. *(Russian)* 78−60319
Fe_3Pt Invar alloy, mag. props., martensitic transform. 79−78365

magnetic anisotropy continued
$Fe_{0.9}S$, ferrimag. transition, mag., thermodynamic props., kinetics 79−47280
Fe_7Se_8, 3c struct., spin axis transition 78−14967
$Fe_{75}Si_{15}B_{10}$, mag. behaviour rel. to magnetostatic interactions 80−11224
Fe_3Sn_2, Mossbauer effect and magnetisation meas. 78−31132
Fe_xSn_{1-x} amorphous alloy films, magnetisation meas. and Mossbauer spectra 78−95489
$Fe_{1-x}Ti_x$, ferromag. props., Ti conc. effect 80−54872
$FeTiO_3$, ilmenite, lunar and terrestrial, cell dimensions and antiferromagnetism 77−21764
Fe_2TiO_5, anisotropic spin glass behaviour 79−99707
Fe_2TiO_5, anisotropic spin glass type behaviour 80−60296
$Fe_{3-x}Ti_xO_4$, spin glass behaviour, susceptibility and hysteresis meas. 80−65917
$Fe_{1-x}Zn_xF_2$, dil. antiferromag., electronic and mag. props., Raman scatt. and optical absorpt. study 80−108207
$Fe_{1-x}Zn_xF_2$, electronic Raman scatt., mag. anisotropy 80−66184
$Fe_xZn_{1-x}F_2$, Neel temp., CPA calc. 78−68233
$Fe_xZn_{1-x}F_2$, Neel temp. mag. cone depend., CPA calcs. 78−88122
$Ga_{1-x}In_xSe$, magnetic susceptibility anisotropy, chemical bonds, electron density distribution *(Russian)* 80−50073
$GaSe_{1-x}S_x$, magnetic susceptibility anisotropy, chemical bonds, electron density distribution *(Russian)* 80−50073
$(Gd,Dy)Al_2$, spin adjustment, NMR spin echo obs. 78−15058
$(Gd,Lu)_3(Fe,Mn,Al)_5O_{12}$ epilayer with orthorhombic anisotropy, domain wall vel. 78−52322
$(Gd,Tm,Y)_3(Fe,Ga)_5O_{12}$ film, magnetocrystalline anisotropy 79−78450
$(Gd,Tm,Y)_3(Fe,Ga)_5O_{12}$ LPE garnet thin films, magnetocrystalline anisotropy 80−93147
Gd alloys, amorphous, mag. props. and ferromag. reson. 80−54952
Gd, high quality single cryst. 78−84413
Gd, mag. domain struct., 77K 78−84447
Gd, magnetic crystalline anisotropy, Fermi level, electronic density of states 80−84596
Gd, magnetisation and magnetocaloric effects *(Russian)* 78−34985
Gd, magnetocrystalline anisotropy, temp. and press. depend. 77−20586
Gd, nonmagnetic inclusions, effect on easy direction 77−77052
Gd, spin wave exam. 78−56306
^{160}Gd, ferromagnetic, isotopically enriched single crystals short-range order 79−4653
Gd-Al, amorphous film, microwave mag. reson. 78−91948
Gd-Al, amorphous film, microwave mag. reson. 78−92060
Gd-Al(C)(Cu)(Ga)(Ni)(Pd)(Rh) alloys, amorphous, mag. and elec. props. 80−80499
Gd-Ce(Eu)(Yb), magnetocrystalline anisotropy, magnetisation and torque curve meas. 80−65859
Gd-Co, amorphous film, with cylindrical mag. domains, sputtering prep. *(Russian)* 77−12176
Gd-Co, amorphous films, mag. props. ferromag. reson. meas., 20-520°C *(Russian)* 80−97144
Gd-Co, and Gd-Co-Mo films, amorphous, mag. props., annealing effects 78−64235
Gd-Co, and Gd-Co-X (X=Mo, Cu, Au), sputter deposited amorphous alloy, substrate bias, magnetic anisotropy, annealing 78−48006
Gd-Co, evap. amorphous films, anisotropy, magnetisation and FMR meas. 77−66392
Gd-Co, film, evaporated and sputtered, struct. and mag. anistoropy, electron microscopy 79−56578
Gd-Co, LV multitarget sputtered film, substrate bias effect on anisotropy 77−16125
Gd-Co, sputtered film, growth induced anisotropy 77−16123
Gd-Co, thermally evap. amorphous film 77−16122
Gd-Co alloy, sputtered film, mag. props. determ. *(Chinese)* 78−2714
Gd-Co amorphous film, DC or RF sputtered, mag. props., He^+-backscatt. investig. 77−20650
Gd-Co amorphous film, mag. anisotropy 77−20649
Gd-Co amorphous film, sputtered, perpendicular anisotropy exam. 79−73707
Gd-Co amorphous films, annealed, short-range order and perpendicular mag. anisotropy 80−15765
Gd-Co amorphous films, correlation between struct. and mag. props. *(Chinese)* 80−54532
Gd-Co amorphous films, mag. anisotropy, static and ferromag. reson. expts. 79−33477
Gd-Co amorphous films, mag. struct., mag. bubbles, electron diffr. study *(Chinese)* 80−71126
Gd-Co amorphous films, model calculations for anisotropy formation induced by resputtering processes 78−64242
Gd-Co amorphous films, RF sputtered, magnetisation ripple effects 80−11232
Gd-Co amorphous films, struct. and mag. anisotropy 80−20438
Gd-Co amorphous sputtered films, magnetoelastic contrib. to perpendicular anisotropy, internal stress meas. 78−95490
Gd-Co amorphous sputtered film, magnetostriction and anisotropy 80−39821
Gd-Co amorphous thin film, mag. and optical props., conc. depend 79−19748
Gd-Co based amorphous sputtered films, microstruct. variability and mag. anisotropy, implanted ion effects 80−88459
Gd-Co film, amorphous, for bubble device appl., prep. and perpendicular anisotropy 77−69641
Gd-Co film, amorphous, magnetisation and anisotropy meas. 77−8370
Gd-Co film, amorphous, perpendicular uniaxial anisotropy, dominant contrib. of preferential resputtering effect 77−36103
Gd-Co film, amorphous, phase separation as source of perpendicular anisotropy 78−64244
Gd-Co film, amorphous ferrimagnet, anisotropic short range order effects on mag. props. 79−1691
Gd-Co film, amorphous ferrimagnet, mag. anisotropy, effect of ion bombard. during prep. 79−1692
Gd-Co film, bias-sputtered, dipolar mechanisms for mag. anisotropy 78−64233
Gd-Co film, sputtered, inert gas incorporation effect on uniaxial anisotropy 78−64232
Gd-Co film, sputtered from segment target, composition and mag. props. 78−27062
Gd-Co film, temp. depend. of mag. aftereffect *(Russian)* 79−8021
Gd-Co film, with layer struct., mag. torque and anisotropy 77−63246
Gd-Co films, amorphous, mag. anisotropy from torque meas. 77−47987

magnetic anisotropy continued
Gd-Co intermetallic compounds, magnetocrystalline anisotropy obs. *(Japanese)* 77−80926
Gd-Co-Cu film, amorphous, influence of biased magnetron deposition parameters on props. 77−43856
Gd-Co-Fe film, amorphous, bias-sputtered, uniaxial perpendicular anisotropy 78−64234
Gd-Co-Mo alloy film, amorphous ion implantation damage effects 77−89991
Gd-Co-Mo film, amorphous, in-plane susceptibility near compensation point 78−64238
Gd-Co(-Mo) films, amorphous, inhomogeneities of mangetization and anisotropy 79−65698
Gd-Co(Fe) amorphous films, microstruct. and mag. anisotropy 79−82838
Gd-Co(Ni)(Cu)(Rh)(Ru)(Pd)(Ga), amorphous, mag. props. and ferromag. reson. 80−75862
Gd-Dy, magnetostriction contrib. to thermal expansion *(Russian)* 77−12184
Gd-Dy alloy, mag. anisotropy, magnetisation meas. 77−12115
Gd-Er alloy, mag. anisotropy, magnetisation meas. 77−12115
Gd-Fe, amorphous sputtered film, magnetostriction 79−47320
Gd-Fe, DC bias RF sputtered film, mag. props. 77−16124
Gd-Fe, LV multitarget sputtered film, substrate bias effect on anisotropy 77−16125
Gd-Fe, sputter deposited amorphous alloy, substrate bias, magnetic anisotropy, annealing 78−48006
Gd-Fe amorphous film, atomic diffusion of deposited Co 79−73346
Gd-Fe amorphous film, prep. by dual-source evaporation, mag. props. 77−89988
Gd-Fe amorphous films, anisotropy dispersion, FMR meas. 79−73824
Gd-Fe amorphous films, stress contrib. to perpendicular anisotropy 80−75819
Gd-Fe amorphous sputtered films, magnetoelastic contrib. to perpendicular anisotropy, internal stress meas. 78−95490
Gd-Fe film, amorphous, mag. props., annealing effects 78−64235
Gd-Fe(Co) amorphous films, O_2 adsorption, effect on perpendicular anisotropy 80−34713
Gd-Ho alloy, mag. anisotropy, magnetisation meas. 77−12115
Gd-Tm alloy, from magnetisation meas. at 4.2K 78−68216
$GdAl_2$, anisotropy and magnetostriction 78−10741
$GdAl_2$, spin reorientation, NMR features rel. to preferred magnetisation direction change 77−63213
$Gd_{37}Al_{63}$ amorphous film, spin glass, microwave mag. resonance, freq. dependence 80−39798
$GdAlO_3$, bicrit. and tetracrit. behaviour, susceptibility obs. 77−47992
$GdCl_3$, crystn. field parameter of Gd^{3+} 80−10930
GdCo amorphous film, O_2 contaminated, TEM obs. of source of perpendicular anisotropy 78−14993
GdCo films, deposited on simple-crystal substrates *(Russian)* 80−24747
GdCo sputtered amorphous film, third elements effect on mag. anisotropy 79−91260
$Gd_{2+x}Co_{17-x}$, magnetocryst. anisotropy, stoichiometry and temp. effects 77−8296
Gd_xCo_{1-x} annealing amorphous film, ferromag. reson. 77−85580
$(Gd_xCo_{1-x})_{1-y}Ar_y$ amorphous films, effective anisotropy field, ferromag. reson. obs. 80−71123
a-GdCoAu(Mo) films, perpendicular anisotropy temp. depend., Lorentz microscopy 77−28419
$Gd_{0.12}Co_{0.59}Cu_{0.29}$, sputtered film prep. for bubble device 77−16493
GdCoMo film, amorphous, sputtered, ferrimag., in-plane susceptibility near compensation point 78−64240
$GdCo_{5c}Ni_{5-5c}$, intrinsic coercivity, anisotropy, exchange and cryst. field interactions 80−75806
$GdCrO_3$, magnetisation, appl. of molecular field theory 79−4637
$Gd_2(Fe,Co)_{17}$, mag. anisotropy fields by singular pt. detection 79−24156
$Gd_2(Fe,Co)_{17}$, magnetic anisotropy meas. by singular point detection method 77−63170
GdFe amorphous film, Mossbauer and mag. meas. 80−15844
GdFe, amorphous films, thermal stability of mag. props. *(Japanese)* 79−47307
GdFe films, deposited on single-crystal substrates *(Russian)* 80−24747
$GdFe_2$, easy direction of magnetisation 80−20535
$Gd_x(Fe_{1-y}Co_y)_{1-x}$, evap. amorphous film, pair ordering 77−32219
GdIG, local mag. anisotropy in stress field of single dislocation 80−88744
GdNi, single cryst., magnetocrystn. anisotropy 80−88746
$Gd_{70}Tb_{30}$, magnetisation, AC susceptibility and microwave absorption meas. 80−60221
$Gd_{0.9}YTm_{1.1}Ga_{0.44}Fe_{4.56}O_{12}$, ion implanted, ferromag. reson. meas. 78−68385
Ge-Fe amorphous film, sputtered, stress induced anisotropy 79−73706
$HgCr_2Se_4$, influence of Co ions on anisotropy and magnetostriction, ferromag. reson. meas. 77−69659
Ho, low field susceptibility and helical-ferromag. field induced phase transition 78−47975
Ho-Ag(Cu)(Mg)(Zn), crystal field parameters from neutron spectra, ordered state mag. props. 77−43546
Ho-Co amorphous film, prep. by dual-source evaporation, mag. props. 77−89988
Ho-Co film, evaporated, struct. and mag. anistoropy, electron microscopy 79−56578
$HoAl_2$, biquadratic pair coupling from mag. anisotropy 77−28383
$HoAl_2$, heat capacity, 1.5-12K, magnetocryst. anisotropy effects 78−68236
$HoAl_2$, spin reorientation, sp. ht. meas. 79−73724
$HoCo_2$, cryst. field induced spin rot., Mossbauer meas. 77−16227
$HoCo_2$, easy direction of magnetisation, Mossbauer data, 4.2K 78−43584
Ho_2Co_{17}, magnetisation, magnetocryst. anisotropy and magnetostriction 77−8303
Ho_xCo_{1-x} amorphous films, microstruct. and mag. anisotropy 79−82838
Ho_xCu_{1-x}, amorphous film, magnetisation meas., local anisotropy effects 78−68309
$Ho_{0.5}Dy_{0.5}FeO_3$ orthoferrite, domain wall struct., stability conditions, Morin transition, anisotropy const. 80−34684
$Ho_xDy_yTb_{1-x-y}Fe_2$, Laves phase cpds., anisotropy and magnetostriction 77−63167
$HoFe_2$, magnetostriction and magnetisation temp. depend. 79−73795
$Ho_{0.01}Gd_{1-x}Y_xNi_2$, spin echo meas. on ^{165}Ho, limited quenching of Ho moment by cryst. field 79−73851

magnetic anisotropy continued
HoSb, quadrupole scatt. anisotropy, magnetically ordered material 78−64034
$Ho_xTb_{1-x}Co_2$ lave phase compounds, elastic props., temp. and magnetic field dependence 80−60393
$Ho_{0.58}Tb_{0.2}Dy_{0.22}Fe_2$ magnetoelastic surface wave dispersion obs. 79−47321
$(Ho_{0.58}Tb_{0.2}Dy_{0.22})Fe_2$, microwave mag. props. 80−65860
$Ho_xTb_{1-x}Fe_2$, and $Ho_xTb_yDy_{1-x-y}Fe_2$, high magnetostriction cpd., mag. anisotropy origins 78−68217
$Ho_xTb_{1-x}Fe_2$, Laves phase, mag. anisotropy meas., cubic harmonic anal. 78−84410
$Ho_xTb_{1-x}Fe_2$, single cryst., spin orientations 78−84425
HoZn, magnetoelastic and quadrupolar couplings 78−52328
$KCoF_3$, antiferromag., obs. of domains by X-ray topography 78−14981
K_2CoF_4, obs. of short range order by optical birefringence 79−11318
K_2CoF_4, specific heat capacity, critical amplitude, cross-over from 2-D Ising to Heisenberg behaviour 80−39791
$K_2CuCl_4.2H_2O$ structure compounds, 3-dimens. ferromag., exchange anisotropy by NMR 77−55714
K_2CuF_4, 2-D ferromagnet, optical and magneto-optical props. 77−52062
K_2CuF_4, Curie temp. XY-like anisotropy effect, inter-layer exchange 77−59406
K_2CuF_4, layered spin system, planar rotator symmetry, phase transition 80−65951
K_2CuF_4, nearly two-dimensional ferromag. nucl. transverse relax. rates meas. 77−81024
$K_2FeCl_5(H_2O)$, phase diagram, antiferromag., paramag. and spin flop phases 80−44831
K_2FeF_4, antiferromagnet, two-dimensional, mag. excitations 80−80492
K_2FeF_4, Raman scatt. in two dimens. antiferromagnet 78−19488
K_2FeF_5, one-dimens. antiferromag., single cryst. Mossbauer spectra 78−23376
KH_2PO_4, low impurity content, magnetic anisotropy *(Russian)* 78−6506
$K_3Mn(CN)_6$, low-spin mag. studies 79−95582
K_3MnF_4, specific heat capacity, critical amplitude, cross-over from 2-D Ising to Heisenberg behaviour 80−39791
K_2MnF_4, two-dimensional antiferromag., NMR, magnetisation field-depend., spin-wave theory 77−63294
K_2MnF_4-Ni^{2+}, and undoped, magnon spectra, Raman, far IR and fluorescence meas. 77−20573
$K_3Mn_2F_7$, double-layer antiferromag., mag. prop. meas. and calc. 77−55666
$K_3Mn_2F_7$, two magnon Raman scatt., magnon dispersion, susceptibility, Green's function methods 80−50340
$K_2Mn_{1-x}Fe_xF_4$, anisotropy on two and three dimens. mag. order 77−66259
$K_2Mn_{1-x}Fe_xF_4$, layered antiferromag., anisotropy effects on mag. ordering, neutron diffr. study 79−47254
$K_2Mn_{1-x}Fe_xF_4$, vs. transition temperature, phase diagram, critical lines crossing tetracritical point, discussion 78−39326
$KNiF_3$, antiferromag., obs. of domains by X-ray topography 78−14981
$KNiF_3$, antiferromag. domain behaviour 77−69607
$KNiF_3$, low anisotropy antiferromag., phase boundary crossover behaviour 79−38324
K_2NiF_4, quadratic layer antiferromag., optical spectra obs. 77−16326
K_2NiF_4, specific heat capacity, critical amplitude, cross-over from 2-D Ising to Heisenberg behaviour 80−39791
$K_5V_3F_{14}$, ferrimagnetic props., ordering temp. and anisotropy *(French)* 77−47990
La ferrite, composition and mag. props., anisotropy field, magnetisation 80−71109
La-Gd-Au, amorphous spin glasses, mag.-cluster description 79−42776
La-Sm-Lu iron garnet film grown as NdGaG substrates, mag. props. 80−44888
La_2Co_7, mag. saturation and anisotropy, density, lattice parameters 77−85426
$La_{1-x}Tb_xAg(Sn_3)(Al_2)$, paramag. anisotropy of Tb^{3+} in cubic cryst. field 80−15687
Li ferrites, porous, porosity effect on saturation of magnetisation 80−108036
$Li_{0.5}Fe_{2.5}O_4$, microwave material, mag. props., review 79−33504
$Li_{0.5}Fe_{2.5-x}Cr_xO_4$, ferromag. reson. meas. 77−69542
$Li_{0.5}Fe_{2.5-x}Cr_xO_4$ press. depend. of anisotropy consts. 80−65865
$Li_{0.5}Fe_{2.5}O_4$, uniaxial anisotropy energy, elec. field depend. 78−68346
LiH, mag. domains and nucl. mag. ordered phases, antiferromag. and ferromag. neutron diffr. obs. 80−50051
$LiRF_4$, (R=Tb, Dy, Ho, Er, Yb), paramag. phase props., basal plane anisotropy and cryst. field parameters 77−69486
$LiTmF_4$, van-Vleck paramagnet, giant magnetostriction *(Russian)* 80−103872
$LiYF_4:Tm^{3+}$, cryst. field parameters, appls. 77−20277
$LuCrO_3:Er^{3+}$, doping effect on ^{53}Cr NMR in domain walls 80−71219
Mg $(Fe,In)_2O_4$:Pb,Pt film, LPE 77−77436
$MgFe_2O_4$, epilayer, perpendicular anisotropy 80−39769
$Mg_xFe_{3-x}O_4$ crystals, first mag. anisotropy const., 7-295K 80−65855
$(MgFe_2O_4)_{1-\gamma}(Mn_3O_4)_\gamma$, polycrystalline, coercive forces 78−39366
MgO, mag. anisotropy, ionic distrib. and composition of magnesioferrite precipitates, ferrimag. reson. study 77−69699
Mn ferrites, Fe^{2+} ion contrib. to induced anisotropy and mag. after-effect 77−36101
Mn-Al-C, permanent magnet, mag. props., machinability 77−85505
Mn-Al-C anisotropic permanent mag., cryst. orientation and form., X-ray diffr. anal. 79−82778
Mn-Bi, magnetically uniaxial, strongly anisotropic, discontinuous mag. reversal singularities *(Russian)* 77−48010
Mn-Bi alloys, mag. props. improvement study *(Japanese)* 78−43617
Mn-Ga, DO_{22} type alloys, magnetic props., crystal struct. *(Japanese)* 78−59784
Mn-substituted garnet film, growth characts. and mag. props. 80−39826
Mn-Zn ferrite, domain struct. and initial permeability, effect of O nonstoichiometry 78−35001
Mn-Zn ferrite single crystals, mech. polishing effect on mag. props. *(Japanese)* 80−16569
MnAs pseudocrystals, ferromag. and ferro-paramag. transition region 77−4537
$MnAs_{0.97}P_{0.03}$, orthorhombic, mag. anisotropy 77−43832
$MnAs_{1-x}P_x$, mag. and crystallographic anal. 79−47257
$MnAs_{1-x}Sb_x$, mag. and crystallographic anal. 79−47257

magnetic anisotropy continued
MnBi film anisotropy field intensity meas. by Faraday rotation *(Russian)* 77−12162
MnBi, Kerr effect and TEM obs. of mag. domains 77−89974
$Mn(Br_{1-x}Cl_x)_24H_2O$, antiferromagnetism, controllable anisotropy 80−93116
$MnCl_2.2H_2O$, magnetisation and mag. resonance 79−11349
$MnCl_2.4H_2O$, single cryst., mag. phases, obs. by ^{54}Mn nucl. polarisation 77−81031
$Mn_{2-x}Cr_xSb$, sintered, intrinsic coercivity 77−89983
MnF_2, antiferromag., magnetocryst. anisotropy, susceptibility, static torque meas. 77−69545
MnF_2, mag. anisotropy at OK 79−33473
MnF_2, specific heat, Heisenberg to Ising crossover near Neel temp. 78−47980
MnF_2, uniaxial antiferromag. anisotropy in paramag. susceptibility, cluster variation theory 78−52200
$Mn_{1-x}Fe_xAs$, mag. props. in ground state *(Russian)* 78−56294
$Mn_xFe_{3-x}O_4$ epitaxial films, mag. and reson. props. 80−50149
$Mn_xFe_{3-x}O_{4+\gamma}$, average directional order, cation valency and repartition on A- and B-sites *(French)* 78−39369
Mn_3Ge, triangular spin ordering, weak ferromagnetism 79−47237
Mn_4N, mag. struct. non-collinearity, neutron diffr. obs. 80−65796
$Mn(Nb_{0.5}Ta_{0.5})_2O_6$, nonuniaxial spin-flop magnet, bicrit. lines, crossover 78−14973
$Mn_{3-x}Ni_xB_4$, mag. props. *(Russian)* 77−51923
MnO, magneto-elastic coupling by dipolar interactions and spin orientation 79−78494
$MnO:Mn_3O_4$, mag. props., susceptibility and magnetisation meas. 80−65824
MnP, anisotropic, ferromagnetic microwave resonance relations 80−15805
MnSb, magnetic losses, ferromagnetic resonance and antiresonance 80−100618
$Mn_{1.15}Sb$, Kerr effect and TEM obs. of mag. domains 77−89974
MnSi, mag. anisotropy exam., ferromag. to antiferromag. transition 79−73708
Mn_3Sn, triangular spin ordering, weak ferromagnetism 79−47237
MnZn ferrite, appreciable SiO_2 content, origin of core losses, microstructure and mag. props. 78−64225
MnZn ferrite, initial mag. permeability rel. to mag. anisotropy 80−80557
MnZn ferrite, mag. anisotropy, effect on recording head characts. 80−39765
MnZn ferrite, thermal cond. of single crystals 77−36079
MnZn ferrites, Ti substituted, mag. permeab. meas., grain boundary comp. AES obs. 78−95473
MnZn ferrous ferrite, initial mag. permeability second-order magnetocrystalline anisotropy influence 80−88820
MnZn ferrous ferrites, mag. permeability stress depend. 80−88822
$Mn_{1-x}Zn_xF_2$, randomly diluted uniaxial antiferromagnet, CPA theory 79−78388
$Mn_cZn_{1-c}F_2$, rel. to crit. neutron scatt. near percolation threshold 78−2693
$Mn_xZn_{1-x}F_2$, antiferromag. spin flop crit. field 79−24218
MoS_2, prep. and mag. props. *(French)* 80−93072
$(NH_4)_6MnMo_9O_{32}.8H_2O$, mag. susceptibility, rel. to EPR, zero field splitting parameter 77−36122
NI, $X_{2spin\ down}$ hole pocket in Fermi surface 78−39314
Nb, type II superconductor, equilibrium misalignment, fluxoids and appl. mag. field, anisotropy interaction 79−24112
$Nb_{50}Ni_{50-x}Fe_x$, amorphous, mag. ordering and local random anisotropy 78−68273
$Nb_xY_{3-x}Fe_5O_{12}$, low-temp. magnetocrystalline anisotropy study 79−95586
Nd, elastic constants, low-temp., mag. field depend. 78−76290
$NdCo_2$, cryst. field induced spin rot., Mossbauer meas. 77−16227
$NdCo_2$, magnetocrystalline anisotropic props., torque meas. 80−108003
$NdCo_5$, single ion anisotropy consts. temp. depend. effect of spatial variation of mag. moment 78−91864
$NdCo_5$, spin reorientation, magnetisation and torque curves, 77-925K 77−4532
Nd_2Co_7, mag. saturation and anisotropy, density, lattice parameters 77−85426
$Nd_{64}Co_{36}$, amorphous, amg. ordering, susceptibility, magnetisation and hysteresis meas. 78−68190
Nd_xCo_{1-x} film, amorphous, mag. props. meas. 78−68312
$Nd(Co_{1-x}Cu_x)_5$, coercive force temp. depend. 79−82823
$Nd_{1-x}Dy_xCo_5$, rotational type spin reorientation, appl. to thermomagnetic generator 77−85451
Nd_xFe_{1-x} film, amorphous, mag. props. meas. 78−68312
$(Nd_xSm_{(1-x)})_2(Co_{0.7}Fe_{0.3})_{17}$, mag. anisotropy 80−34622
$Nd_{1-x}U_xCo_5$, mag. props. and spin-reorientation phase transitions *(Russian)* 78−60284
$Nd_2Y_{1-x}Co_5$, saturation magnetisation and anisotropy, 4.2K-T_c 77−85427
Ni, (110) film, strain effects, substrate temp. depend. 77−80972
Ni, anisotropic magnetisation meas., 4-250K 80−65862
Ni, anisotropy consts., K_3 and K_1, determ. 77−4512
Ni, anisotropy energy in (100) plane, temp. dependence 78−2674
Ni, deformed, coercivity and remanence anisotropy 78−31093
Ni, effective mag. anisotropy const., magnetoelastic contrib. 78−14951
Ni, electrodeposited film, saturation magnetisation and perpendicular anisotropy meas. 78−76277
Ni electrodeposits on (001)Cu films, growth and mag. anisotropy 79−42810
Ni epitaxial films (110), uniaxial anisotropy, expt. 77−20648
Ni, ferromagnetic reson. determ. of first three anisotropy consts. 77−8414
Ni film, effect of He ion implantation on domain struct., Lorentz electron microscopy 77−20654
Ni film, evaporated, uniaxial mag. anisotropy 77−51929
Ni film, evaporated at oblique incidence, residual stress, mag. anisotropy meas. 78−22992
Ni film, ferromag. reson., thermodynamical anal., effect of mech. stress 79−42840
Ni film, ion beam sputtering prep., struct. and mag. props. 80−35085
Ni film, microstructure of charged boundary between ferromag. domains 79−69705
Ni film, thickness dependence of perpendicular mag. anisotropy 77−80974

magnetic anisotropy continued
Ni films, electronic struct. calc., effects of chemisorption; contact pot. and surface magnetisation 80−103734
Ni films, oriented, hypersound excitation at 8.9 GHz by exploiting mag. anisotropy 77−85541
Ni, mag. anisotropy energy, symmetrical polynomials 77−66293
Ni, mag. props. of single-domain powders after plastic deform. *(Russian)* 78−6554
Ni, magnetic anisotropy energy 77−28382
Ni, magnetic surface anisotropy of transition metals, model calc. 80−34625
Ni, magnetocryst. anisotropy consts., determ. from magnetisation perpendicular to applied field 78−68219
Ni, magnetocrystalline anisotropy energy in (100) plane, 13.8 to 258K 77−63171
Ni, magnetocrystalline anisotropy energy, temp. and magnetisation depend. 78−6525
Ni microcrystals, H_2 chemisorption effect on superparamagnetic relax. time, Mossbauer meas. 79−61284
Ni, plated film, magnetisation and mag. interface anisotropy 77−85510
Ni, spin polarised photoemission, surface magnetism 79−52083
Ni, stress induced crossover effect near Curie point *(German)* 80−103874
Ni-Co, ferromagnetic resonance, surface anisotropy 78−95526
Ni-Co, mag. props. of single-domain powders after plastic deform. *(Russian)* 78−6554
Ni-Co film, magnetisation induced uniaxial anisotropy 77−48016
Ni-Co plate, surface anisotropy from ferromagnetic reson. 78−48049
Ni-Cu, mag. anisotropy, temp. and conc. depend. 77−63172
Ni-Cu alloy, nearly ferromag., spin-glass-like distrib. of interaction fields 79−91243
Ni-Fe, electronic struct. calc., effects of chemisorption; contact pot. and surface magnetisation 80−103734
Ni-Fe, magnetisation curling in superparamagnetic spheres 77−8363
Ni-Fe, soft mag. props. rel. to metallurgical aspects 80−88810
Ni-Fe (15%) film, evaporated, uniaxial mag. anisotropy 77−51929
Ni-Fe alloy, extraordinary viscous magnetic wall motion 78−84465
Ni-Fe epitaxial films (110), uniaxial anisotropy, expt. 77−20648
Ni-Fe film, mag. and hyperfine field exam. of uniaxial anisotropy 77−66391
Ni-Fe film, oligatomic, ferromag. reson. and torsion magnetometry, 123-373K 77−59461
Ni-Fe film, unidirectional anisotropy by exchange coupling, appl. to biasing of magnetoresist. read head 78−91907
Ni-Fe-Co, alloy with step hysteresis loops *(German)* 79−42806
Ni-Fe-Co alloy films for logic devices, mag. switching vel., anisotropy field and coercive force *(Korean)* 77−51930
Ni-Fe-Co film, nonmagnetostrictive, effect of deposition parameters of Al underlayer 77−77078
Ni-Fe-Nb, Hardperm, origin of high magnetic permeability 77−8362
Ni-Mn alloy, disordered, exchange-anisotropy field, magnetisation curves 78−72365
Ni-Pd alloy, magnetostriction and mag. anisotropy meas. 79−4713
Ni-Pd(Cu)(Cr), directional order anisotropy energy induced by neutron irradiation, temp. depend. 77−66294
Ni-Pt alloys, mag. props. under hydrostatic press. 78−6556
Ni-Ru (3.3 at%), magnetisation, magnetocrystalline anisotropy, magnetostriction and elastic consts., thermal variations 79−28563
Ni-Ru ($\leq$4 at.%), influence of alloying on mag. anisotropy 80−71010
Ni-SiO_2 supported catalysts, particle size, H_2 chemisorption, Mossbauer study 80−7219
Ni-V, del. alloy, anisotropy consts., K_3 and K_1, determ. 77−4512
Ni-V, ferromag. reson. meas., anisotropy consts. determ. 78−39410
Ni-V alloys, temp. and conc. depends., rel. to resistivity 77−40052
$Ni_{0.95}$ S Fe, spin glass, spin flop in exchange field 80−34640
$NiBr_2.6H_2O$, antiferromag. ordering and paramag. behaviour 78−14941
$NiBr_2.6H_2O$, small anisotropy, spin Hamiltonian fit of susceptibility 77−69587
$Ni_{1-x}Cd_xFe_2O_4$, mag. props. rel. to ionic struct. 80−75756
$NiCl_2.2H_2O$, mag. phase diagram and exchange parameters 77−77054
$NiCl_2.6H_2O$, antiferromag., phase diagram, low temp. canted paramag. boundary, bicritical point 79−47282
$Ni_{2-x}Co_xBaFe_{16}O_{27}$, ferromagnetic reson., anisotropy and g-factor, spin-orbit interactions 77−24749
$Ni_xCo_{1-x}Cl_2.6H_2O$, mixed uniaxial planar antiferromag., magnetisation process 80−88788
$Ni_{1-x}Co_xO$, LF magnons, inelastic neutron scatt. exam. 77−66288
NiFe film, ferromag. reson., thermodynamical anal., effect of mech. stress 79−42840
NiFe, magnetic surface anisotropy of transition metals, model calc. 80−34625
NiFe, magnetising energy, anisotropic effects 80−88743
NiFe soft magnetic alloys, magnetic props., effect of annealing and fabrication *(German)* 78−53004
NiFe thin films, magnetoresistance, quasi-static characts. 80−107766
$Ni_{1-x}Fe_x$, short range order exam. allowing for formation of structural domains *(Russian)* 78−6888
Ni_3Fe, compression induced mag. anisotropy and superlattice dislocations, annealing effect 78−31067
Ni_3Fe, magnetocryst. anisotropy, annealing temp. depend. 80−103828
Ni_3Fe, roll magnetic anisotropy and dislocations *(Japanese)* 77−80930
Ni_3Fe:C, mag. anisotropy depend. on C content, magnetometric study *(Russian)* 80−54887
$NiFe_{2-x}Al_xO_4$, stress-induced anisotropy in LPE grown single cryst. films, domain struct. 79−28238
$Ni_{50}Fe_{30}B_{20}$, magnetostriction, temp. depend. 78−91921
$NiFe_2O_4$, domain wall size and mag. losses in freq. spectra 77−85481
$NiFe_2O_4$, ferrite, mag. anisotropy compensation under neutron irrad. 80−75807
$NiFe_2O_4$:Ir^{4+}, single ion contrib., octahedral sites 77−4511
$Ni_{1-x}Fe_{2+x}O_4$, mag. anisotropy constant, contrib. of Fe^{2+} ion 79−33476
$(Ni_{1-x}Fe_x)_{1-\delta}S$, anisotropic spin glass, mag. props. 80−39793
Ni_3Mn, partially ordered, field induced uniaxial anisotropy at low temp. 77−40053
$NiNb_2O_6$, magnetisation and susceptibility, antiferro-paramag. transition, expt. and theory 77−43822
NiO (111) platelets, antiferromag. S domains, optical obs., spin flop 80−54915
NiO (111) platelets, magnetic torque and susceptibility meas. 80−54885
NiO, thin films with spinel-type defect structure, FMR study 80−39877

magnetic anisotropy continued
NiO, with spinel-type defect struct., ferromagnetic reson. meas. 78−43647
NiO:Fe, exchange anisotropy of Ni-ferrite precipitates 79−28520
$Ni_{1-x}Ti_x$, ferromag. props., Ti conc. effect 80−54872
$NiTiO_3$, antiferromag., mag. anisotropy, magnetisation meas. 80−65856
$NiWO_4$, antiferromag., low symmetry exhibited during spin-flop phase transition 80−60263
$NiWO_4$ monoclinic antiferromagnet, orientational phase transition and intermediate state *(Russian)* 80−15725
$Ni_{0.85}Zn_{0.15}Fe_2O_4$, ferrite, mag. anisotropy compensation under neutron irrad. 80−75807
$Ni_{1-x}Zn_xFe_2O_4$, polycryst., domain wall energy rel. to anisotropy 80−71090
O_2 solid, magnetic props. theory for Heisenberg system *(Russian)* 80−54900
α-O_2, elementary excitations, effect of mag. anisotropy *(Russian)* 78−76317
Os-Re alloy, mag. suscept. of HCP transition metal alloys *(Russian)* 78−80138
$PbFe_{12-x}Ga_xO_{19}$ ferrite, single cryst., ferromag. reson. 80−50193
Pd, magnetic properties in para-process region *(Russian)* 78−2672
Pd-Fe, magnetic anisotropy near Curie point, quasi domain struct. *(Russian)* 80−65867
Permalloy, domain struct., influence of planar anisotropy 79−78472
Pr compounds, Van Vleck paramagnets, mag. props., anisotropy from NMR anal. 80−54862
Pr, magnetic excitations, exchange, crystal field and magnetoelastic interactions 80−2563
PrB_4, ferromag. props. *(French)* 77−20566
PrB_4, mag. and elec. props. 80−20386
$PrCo_2$, magnetocryst. anisotropy props. by ^{57}Fe Mossbauer spectroscopy 77−63328
$PrCo_5$, uniaxial ferromag. cryst., irreversible rotation processes 80−39768
$PrCo_{5\pm x}$, high field first order transitions, role of K_3 anisotropy const. 80−65879
Pr_2Co_7, mag. saturation and anisotropy, density, lattice parameters 77−85426
$Pr(Co_{1-x}Cu_x)_5$, coercive force temp. depend. 79−82823
$Pr(Co_{1-x}Cu_x)_5$, saturation magnetisation anisotropy 78−47960
$Pr_2(Co_{1-x}Fe_x)_{17}$, hard direction magnetisation, 5-300K, and anisotropy field 77−12114
$PrFe_2$, Laves phase, mag. props., Mossbauer spectra, crystalline field mag. anisotropy 80−65851
$Pr_xSm_{1-x}Co_5$, magnetisation and magnetocryst. anisotropy 78−68215
Pt-Co, magnetically hard, struct. and morphology, electron microscope study 79−82171
Pt-Fe alloy, ordered, T-c phase diagram, antiferro- and ferromagnetism *(Russian)* 80−65871
Pt-Fe(Co)(Mn), dil., skew scatt. Hall effect, magnetoresist. and mag. anisotropy, orbital magnetism of impurity 80−70678
Pt-Mn dilute alloy, cubic foil, Mn spin behaviour, nuclear orientation technique 78−27044
$RbCoF_3$, antiferromag., anisotropic exchange, dispersion relations of mag. excitations 77−69532
Rb_2CrCl_4, planar ferromag., spin waves 80−65835
Rb_2FeF_4, antiferromagnet, two-dimensional, mag. excitations 80−80492
Rb_2MnCl_4, 2D Heisenberg antiferromag. spin wave analysis 80−54879
$RbMnF_3$, antiferromag. domain struct. in fields exceeding spin-flop value 79−69693
$Rb_3Mn_2F_7$, double-layer antiferromag., mag. prop. meas. and calc. 77−55666
$RbNiCl_3$, nearly one-dimensional antiferromag., spin-flop transition 78−6527
Rb_2NiF_4, quadratic layer antiferromag., optical spectra obs. 77−16326
Rb_2NiF_4, specific heat capacity, critical amplitude, cross-over from 2-D Ising to Heisenberg behaviour 80−39791
Re-W alloy, mag. suscept. of HCP transition metal alloys *(Russian)* 78−80138
Rh based ferromag. Heusler alloys, peaks in low field AC susceptibility 80−50071
Ru based ferromag. Heusler alloys, peaks in low field AC susceptibility 80−50071
Ru-Nb alloy, mag. suscept. of HCP transition metal alloys *(Russian)* 78−80138
$(SN)_x$, supercond. polymer, mag. props. meas. 80−107953
Sc-Gd(Tb), spin glasses, low-field susceptibility, role of single-ion anisotropy 77−48000
$ScFe_{2-2x}Al_{2x}$, mag. props., composition depend. 77−20593
$(Sm,Lu)_3Fe_5O_{12}$, submicron bubble films on rare earth-Ga garnet substrates, prep. and mag. props. 78−91909
$Sm_2(Co,M)_{17}$, (M=Fe, Mn, Cr), exchange and crystal field parameters, anisotropy meas. 77−69535
$Sm_2(Co_{1-x}M_x)_{17}$ 77−40054
Sm intermetallics temp. depend. of Sm^{3+} magnetisation, exchange and cryst. field effects 77−8302
$SmCo_5$, and $SmCo_{3.5}Cu_{1.5}$, anisotropy and coercivity, Kerr effect, magnetisation and aftereffect expts. 77−8300
$SmCo_5$ based ternary and quaternary permanent mag. materials with low reversible temp. coeffs. 79−82822
$SmCo_5$ hydride films, mag. props. 78−68306
$SmCo_5$, intrinsic magnetic props. 79−82779
$SmCo_5$, mag. domains structure rel. to crystal defects, electron microscopy 80−103856
$SmCo_5$, magnetic anisotropy, Co contrib., ^{59}Co NMR Obs. 78−43583
$SmCo_5$ permanent magnets, crystal texture effects on props. 80−100600
$SmCo_5$, single cryst. and liq. phase sintered, rel. to field depend. of magnetostriction 77−63245
$SmCo_5$, single crysts., mag. props. study and role of anisotropy *(French)* 79−38356
$SmCo_5$, sintered, mag. props. *(German)* 77−43852
$SmCo_5$, sintered, orientation of particle easy axes, statistical model 77−8305
$SmCo_5$, sintered permanent magnet, 4.2-300K, fields up to 100 kOe 77−8341
$SmCo_5$, temp. depend. of Sm^{3+} magnetisation, exchange and cryst. field effects 77−8302
$SmCo_x$-Fe composite permanent magnet material, mag. props. 77−40089
Sm_xCo_y, mag. props. 78−43568
$Sm_2(Co_{1-x}Al_x)_{17}$ *(Russian)* 78−64202

magnetic anisotropy continued
$SmCo_{3.5}Cu_{1.5}$, mag. aftereffects, coercive mechanism, magnetisation reversal 77−69634
$SmCo_{3.5}Cu_{1.5}$, single crysts., mag. props. study and role of anisotropy *(French)* 79−38356
$SmCo_{4.3}Cu_{0.7}$, highly anisotropic ferromag., mag. state after large Barkhausen jump *(Russian)* 79−4699
$Sm_2(Co_{1-x}Fe_x)_{17}$, anisotropy consts., conc. and temp. depend. *(Russian)* 78−64202
$Sm_2(Co_{1-x}Fe_x)_{17}$, Th; Mn or Cr substituent effects 77−8297
$Sm(CoFeCuMn)_7$, coercive force and anisotropy temp. depend. 78−68297
$Sm_2(Co_{1-x}M_x)_{17}$, bulk magnetisation and magnetocryst. anisotropy, interpretation 77−40055
$Sm_2Co_{17-x}M_x$, M=Cr, Ni, effect of substitution on mag. props. 79−78363
$SmCo_{5-x}Ni_x$, giant intrinsic magnetic hardness analysis 78−88146
$Sm_2Co_{17-x}Ni_x$, effect of Ni on mag. props. 78−68296
$Sm_2Cu_{1.6}Zr_{0.16}Fe_{3.3}Co_{12}$, enhancement of mag. props. 79−82825
$SmFeO_3$, magnetisation direction angle meas. in spin reorientation region 77−26366
$Sm_{2-x}Gd_xCo_{17-y}Mn_y$, saturation magnetisation and anisotropy field temp. depend., suitability for microwave/millimetre wave TWT 79−82824
$(SmLu)_3(FeAl)_5O_{12}$, film epitaxial growth on $Gd_3Ga_5O_{12}$ substrate, mag. props. lattice mismatch 80−65402
$Sm_{1-x}Nd_xCo_5$ alloys, magnetisation, magnetocrystalline anisotropy, 4.2 to 280K 78−91863
$SmNi_{5-x}Cu_x$, giant intrinsic mag. hardness due to randomised cryst. field interactions 78−68208
$Sm_{1-x}Pr_xCo_5$ single crystals, magnetocryst. anisotropy and stepwise mag. reversals *(Russian)* 77−66291
$Sm_{0.05}Tb_{0.45}FeO_3$, singularities of domain struct. in spin-flip region 78−19272
$(SmTm)_3(FeGa)_5O_{12}$, small-bubble appl. 79−82845
SmTmIG, epitaxial layer with submicron bubbles, mag. props. 77−12172
$Sm_{0.4}Y_{2.6}Fe_{3.8}Ga_{1.2}O_{12}$ epitaxial films, uniaxial mag. anisotropy, ferrimag. reson. study 80−80577
$Sm_xY_{3-x}Fe_5O_{12}$, mag. anisotropy, meas. temp., depend. 78−19247
$Sm_xY_{3-x}Fe_5O_{12}$, spin reorientation transitons 78−2686
$Sm_{0.4}Y_{2.6}Ga_{1.2}Fe_{2.8}O_{12}$, H^+ implanted film, epitaxial, mag. bubbles, walls and fine struct. 77−63241
$(SnBr_{0.4})_x$ 80−107953
$Sr_2(Co_{1-x}M_x)_{17}$, M=Mn, Ti, Zr, powders, influence of substitutes on mag. props. 80−100601
$SrCoO_{3-x}$, mag. and neutron diffr. study 80−65805
$Sr_{1-x}Eu_xS$, dilute spin glass, mag. props. 79−78386
$SrFe_{12}O_{19}$, Ca^{2+} additives effect on hexaferrite lattice and mag. props. 80−60243
$SrR_2Fe_2O_7$ series, mag. struct. and spin reorientation, neutron diffr. and Mossbauer meas. 77−69503
$SrRuO_3$, mag. props., mag. torque meas. 78−23295
$SrRuO_3$ single cryst., reduced ferromag. moment obs. 77−20564
$SrRuO_3$ single cryst., magnetocryst. anisotropy and reduced ferromag. moment 77−24691
TMMC, antiferromagneric chain, 3-D ordering temp. controlled by solitons and defects, mag. field depend. 80−60275
Tb, anisotropy energy in basal plane, temp. dependence 78−2673
Tb, basal plane mag. anisotropy energy meas. at low temps. 77−63166
Tb compounds with garnet and zircon structure, anisotropic magnetoelastic props. 77−69660
Tb, mag. characts. in strong mag. field 77−89936
Tb, magnetisation, AC susceptibility and microwave absorption meas. 80−60221
Tb, magnetocrystalline anisotropy, perturbation theory 78−2675
Tb, spin wave exam. 78−56306
Tb-Fe, amorphous sputtered film, magnetostriction 79−47320
Tb-Fe amorphous film, sputtered, stress induced anisotropy 79−73706
Tb-Gd alloy, single cryst., mag., magnetoelastic and elec. props. *(Russian)* 78−2677
Tb-Ho (50%), antiferromag., hexagonal anisotropy effect on thermal expansion 79−51283
Tb-Ho film, helimag. order, surface deform., exchange and single-ion magnetocrystalline anisotropy energy 77−66390
Tb-Y(Gd) alloys, contrib. from single-ion cryst. anisotropy and anisotropic exchange *(Russian)* 80−29546
$Tb_{52}Ag_{48}$, amorphous, bulk magnetic props., evidence of strong local anisotropy 77−43830
$Tb_{52}Ag_{48}$, amorphous, model for anisotropy 79−24200
$TbAl_2$, origin of magnetostriction 79−78499
TbB_2, mag. struct., ferromag. ordering, neutron diffr. study 80−15692
$TbBe_{13}$, magnetic structure at low temps., antiferromagnetic, neutron diffraction study *(French)* 80−39743
$TbCo_2$, magnetocryst. anisotropy props. by ^{57}Fe Mossbauer spectroscopy 77−63328
$TbCo_2$, magnetocrystalline anisotropy and spontaneous magnetostriction 80−75831
$TbCo_2$, origin of magnetostriction 79−78499
$TbCo_2$, spontaneous distortion, mag. props. due to cryst. field, exchange field, magnetoelastic energy 79−61096
$TbCo_{5.1}$, sublattice magnetisation, temp. depend., neutron diffr. anal. *(Russian)* 80−103815
Tb_2Co_{17}, magnetisation, magnetocryst. anisotropy and magnetostriction 77−8303
Tb_xCu_{1-x}, amorphous film, magnetisation meas., local anisotropy effects 78−68309
$Tb_{0.27}Dy_{0.73}Fe_2$, anomalous thermal expansion and magnetostriction 77−90003
$Tb_{0.27}Dy_{0.73}Fe_2$, magnetisation and magnetic anisotropy 78−91862
$Tb_{0.3}Dy_{0.7}Fe_2$, elastic vs. magnetoelastic anisotropy 78−68347
$Tb_{1-x}Dy_xFe_2$, pseudobinary Laves cpds., spin-orientation diagram, Mossbauer effect meas. 77−55739
$TbFe_2$, magnetisation and magnetic anisotropy 78−91862
$Tb_xGd_{1-x}Al_2$, magnetic anisotropy, magnetostriction 78−56364
$(Tb_{1-x}Gd_x)_3Co$, intermetallic cpd. mag. props., phase transform, and mag. hystersis *(Russian)* 80−93113
TbIG, anisotropic forced magnetostriction meas. 78−64251
TbIG, anisotropic garnet, mag. struct., magnetisation and Faraday rotation obs. 78−68169
TbIG, mag. linear double refr., two-sublattice model *(Russian)* 79−28728

magnetic anisotropy continued
TbIG, refr. index, higher-order anisotropic mag. contrib. 77−69808
$Tb_2Lu_1Fe_5O_{12}$ film, magnetostriction meas. using double cryst. X-ray diffractometry 78−84468
$Tb(OH)_3$, powder and single crystal, mag. props. 80−2558
Tb_2O_2S, tunnelling effect and mag.-cryst. transition, neutron diffr. expts. 77−63180
TbSc, basal plane magnetocrystalline anisotropy and ferromag. ordering 79−1667
$Tb_{1-x}Y_x$ alloy, helicoidal antiferromag. to ferromag. transition 78−10687
$(Tb_{1-x}Y_x)_3Co$, mag. props. and transitions, conc. depend. *(Russian)* 78−10671
$Tb_xY_{1-x}Co_{5+0.1x}$, exchange interactions and magnetocrystalline anisotropy 80−34618
$ThCo_5$, lattice consts., magnetisation, and anisotropy fields 79−78364
$ThFe_5$, mag. props., ferrimag. moment arrangement 79−33475
$Th_{1-x}Y_xCo_{5-y}Fe_y$, lattice consts., magnetisation, and anisotropy fields 79−78364
α-Ti, anisotropy of susceptibility and elec. resist. *(Russian)* 77−66292
Ti-Permalloy thin film diffusion couples, low temp. interdiffusion interdiffusion 78−71889
$(Ti_{1-x}V_x)_2O_3$, single crystal, anisotropic susceptibility 79−87228
$(Ti_{1-x}V_x)_2O_3$, spin glass props. and anisotropy, comp. depend. 77−66368
$(Ti_{1-x}V_x)_2O_3$, spin-glass props., 0.05-300K 80−25149
Tm, para-, ferro- and ferrimag. and c-axis modulated phases 78−2660
$Tm_{2.2}Bi_{0.8}Fe_{3.5}Ga_{1.5}O_{12}$ epitaxial film, Faraday effect and domain struct. near compensation point 77−20838
$TmCo_5$, easy magnetisation direction 78−84415
$TmFe_2$, low temp. magnetisation and magnetostriction 78−64249
$TmFe_2$, magnetisation and magnetic anisotropy 78−91862
$Tm_2Fe_{17-x}Co_x$, and related cpds., easy magnetisation direction, Mossbauer spectra 77−63169
TmSe, mixed valency, field depend. mag. field transition 78−10657
U chalcogenides and pnictides 79−42754
UAs, anisotropic susceptibility 79−42754
UAs, anisotropic susceptibility 80−7087
U_3As_4, high-field magnetisation, field-induced phase transition near hard (100) directions 77−28413
U_3As_4, mag. anisotropy, magnetisation meas. 80−50085
U_3As_4, magnetisation in strong fields, 4.2 to 200K anisotropy and exchange forces 80−54886
UAs(Sb), anisotropic mag. ordering and mag. structural transitions 79−78324
$UCo_{5.3}$, mag. props., cryst. and domain struct. *(Russian)* 77−4529
$UCo_{5.3}$, mag. props. and cryst. struct. *(Russian)* 77−51925
UFe_2, giant magnetoelastic deform. of cryst. struct. mag. props. *(Russian)* 80−93159
UFe_2, single cryst. 79−56527
UGa_2, mag. and magnetoelastic props. 80−15775
UN, cubic antiferromag., anisotropic critical neutron scatt. behaviour 79−61112
UN, single crystal, mag. props. 77−77042
UP, anisotropic susceptibility 80−7087
U_3P_4, magnetocryst. anisotropy, torque meas. at 0.34, 0.65 and 0.91 T, 118K 78−47969
U_3P_4, single cryst., Barkhausen effect 77−28410
US, magnetisation temp. and field depend. 77−20565
USb, anisotropic susceptibility 80−7087
USb, antiferromag., neutron diffr. exam. of ordered state 77−20557
USb, neutron inelastic scatt. meas., phonon spectra, mag. response, anisotropy 80−50065
USe, anisotropic mag. moments 79−42754
$(U_xTh_{1-x})Sb$, magnetisation, U valence change 80−7089
U_3X_4, (X=P, As, Sb, Bi), molecular field approx. study of mag. ordering, Curie temp., paramagnetic susceptibility 79−78410
V_2O_{3+x}, $0 \leq x \leq 0.08$, mag. and elec. props. 80−49833
V_3O_5, mag. anisotropy 77−85441
$(Y,Eu,Tm)_3(Ga,Fe)_5O_{12}$ film, domain boundary mobility, effect of easy magnetization axis inclination 78−19293
$(Y,Sm,Ca)_3(Fe,Ge)_4O_{12}$, garnet thin film, mag. anisotropy, Faraday effect meas. 79−42812
$(Y,Sm,Lu,Ca)_3(Fe,Ge)_5O_{12}$ bubble magnetic garnet film, LPE grown, props., $CaCO_3/GeO_2$ molar ratio influence 80−50152
$(Y,Sm,Lu)_3(Fe,Ga)_5O_{12}$, LPE mag. film, suitability for 1 to 3 micron bubble devices 78−68323
$(Y,Sm)_3(Ga,Fe)_5O_{12}$ epitaxial layers, annealing effect on mag. props. 79−61191
$(Y,Sm)_3(Ga,Fe)_5O_{12}$ film, domain boundary mobility, effect of easy magnetization axis inclination 78−19293
Y ferrite-garnet, porous polycrystal, law of approach to saturation *(Russian)* 78−47956
YAG:Er^{3+}, crystal field theory calcs. 77−8259
$Y_{3-x}Ca_{2x}Fe_{2-y}In_yFe_{3-x}V_xO_{12}$, first magnetocryst. anisotropy const., ferrimag. reson obs. 78−68218
$Y_{3-y}Ca_yFe_{2-y}Zr_yFe_3O_{12}$, first magnetocryst. anisotropy const., ferrimag. reson obs. 78−68218
YCaSmTmGeIG, epitaxial layer with submicron bubbles, mag. props. 77−12172
$(YCdYbBi)_3(FeAl)_5O_{12}$, cylindrical domain wall vel. anisotropy *(Russian)* 77−59440
YCo_3 amorphous film, domain struct., influence of planar anisotropy 79−78472
YCo_3 amorphous films, ^{59}Co spin echo study 80−80636
YCo_3 film, amorphous, DC sputtered, easy axis and easy plane magnetisation 78−64237
YCo_3 film, amorphous, induced and surface anisotropies, ferromag. reson. and static meas. 77−85507
YCo_5, substituted, magnetocryst. anisotropy, different contribs. of two Co sites 77−8301
YCo_5, uniaxial intermetallic, large magnetisation anisotropy 80−71011
$Y_{2+x}Co_{17-2x}$ single crystal, magnetocrystalline anisotropy 79−38320
Y_2Co_{17}, and $Y_{2x}Dy_{2(1-x)}Co_{17}$, 77-383K 77−89949
$Y_2(Co_{0.31}Fe_{0.69})_{19.2}$, statistical site occupancy deviations, effect on mag. anisotropy 77−7717
$Y_2(Co_xFe_{1-x})_{17}$, mag. anisotropy assoc. with Fe substitution 78−76240
$Y_2(Co_{1-x}M_x)_{17}$ 77−40054
$Y_2(Co_{1-x}M_x)_{17}$, bulk magnetisation and magnetocryst. anisotropy interpretation 77−40055
$Y_2(Co_{1-x}M_x)_{17}$, M=Al, Cu, single crystal, mag. props. 77−47993

magnetic anisotropy continued
$Y(Co_{1-x}Ni_x)_5$, spontaneous magnetisation mag. anisotropy, spin reorientation transformation *(Russian)* 80−7082
$Y_2Co_{17-x}Ni_x$, effect of Ni or mag. props. 78−68296
$YCrO_3$, bubble domain struct. temp. depend. 80−71137
$Y_xEr_{1-x}Al_2$, paramag. anisotropy 80−39737
$(YEu)_3(FeGa)_5O_{13}$, LPE growth, uniaxial magnetocryst. anisotropy 77−8766
$(YEuYbCa)_3(GeFe)_5O_{12}$ bubble film with ion-implanted layer, FMR study 80−2643
$Y_2(Fe,Co)_{17}$, mag. anisotropy fields by singular pt. detection 79−24156
$Y_2(Fe,Co)_{17}$, magnetic anisotropy meas. by singular point detection method 77−63170
Y_xFe_{1-x} amorphous films, microstruct. and mag. anisotropy 79−82838
$Y(Fe_{0.022}Co_{0.978})_2$ mag. props., Mossbauer expts., 0.15-4.2K 78−43712
$Y_3Fe_{5-x-y}Co_xGe_yO_{12}$, anisotropy and magnetostriction, ferromag. reson. expts., 4.2-500K 78−27030
$YFe_{1-x}Co_xO_3$, reorientation transitions, neutron diffr., mag. behaviour *(Russian)* 77−24678
$Y_3Fe_{5-x}Co_{x/2}Si_{x/2}O_{12}$, spin reorientation, NMR and ferromag. reson. meas. 80−65890
$Y_3Fe_{4.2}Ga_{0.8}O_{12}$, LPE grown thin film, ferromag. reson. 78−35041
$Y_3Fe_{5-t}Ga_tO_{12}$ garnet, spin wave parametric excitation threshold anisotropy in second region 80−29542
$YFeO_3$, Co^{2+} substituted, reorientational transitions 77−59419
$YFeO_3$, mag. anisotropy in cryst. field approx. 80−60241
$YFeO_3$ plate, anisotropy of domain wall velocity, magneto-optical obs. 79−99725
$YFeO_3$:Co_3 NMR of ^{57}Fe, spin echo 78−91987
$YFeO_3$:Co^{2+}, weak ferromagnetism, single ion anisotropy contrib. 80−25126
$Y_{3-3x-2z}Gd_{3x}Ca_{2z}Fe_{5-z-u}V_zSi_uCo_uO_{12}$, mag. props., effect of V substitution 77−20582
$Y_{1-x}GdCo_5$, exchange interactions and magnetocrystalline anisotropy 80−34618
YGdIG, with various domain wall orientations, natural spin reson. 80−66040
YIG bubble films, light scatt. from spin waves, hysteresis meas. by Voigt effect 80−15770
YIG, cation sites distrib. and valence states 79−99167
YIG, determ. from high press. ferromag. reson. expts. up to 6.5 kbar 77−51956
YIG, domain wall size and mag. losses in freq. spectra 77−85481
YIG, epitaxial, temp. stabilisation of ferrimag. reson. field by Ga, La substitution 77−77104
YIG film, domain struct., influence of planar anisotropy 79−78472
YIG, film, spin wave reson., complex mag. surface energies 77−4561
YIG, film, spin-wave spectra in terms of mag. boundary conditions 79−78532
YIG, mag. linear double refr., two-sublattice model *(Russian)* 79−28728
YIG, magnetocrystalline surface anisotropy energy, one-ion mechanism 79−42756
YIG, magnetocrystalline surface anisotropy energy, one-ion mechanism 79−78362
YIG, magnetostatic volume waves, magnetocrystalline anisotropy effects, group delay 79−78355
YIG, refr. index, isotropic exchange and higher-order anisotropic mag. contribs. 77−69808
YIG, single cryst., spin wave propagation direction, parallel pumping, effect of crystalline anisotropy 79−1660
YIG substrates, magnetoelastic surface waves, magnetostatic reson. anal. 80−20441
YIG: Si single crysts., mag. props. 80−107981
YIG:Co LPE films, with rectangular bubble domains, prep. and props. 79−82848
YIG:Eu,Pb, bubble domain film, magnetocrystalline anisotropy coeff. reduction, by Pb addition 79−11329
YIG:Fe^{2+}, magnetocrystalline anisotropy, effect of high hydrostatic press. 77−43831
YIG:Ir, Ir on tetrahedral sites, contrib. to mag. anisotropy, optical absorpt. meas. 77−69867
YIG:La,Ga film, uniaxial anisotropy, variation along growth direction 77−28416
YIG:La(Ga) films, ferromagnetic resonance, ion implantation effect 80−97145
YIG:Nb, tetrahedral Fe^{2+} detect. by induced anisotropy ang. variation 79−11311
YIG:Pb(Si) film, (111) LPE, in-plane mag. anisotropy and ferromag. reson. meas. 78−2706
YIG:Ru(Ru,Zn), single ion contribs. 77−69544
YIG:Si, thermomagnetic processing and illum. effects on mag. props. *(Russian)* 77−8410
YIG:Sm^{3+}, mag. anisotropy, effect of Sm^{3+} ferromag. reson. study 80−80615
YIG:V, mag. anisotropy and magnetostriction, effect of V 78−27029
YIG-Ge layered struct., anisotropy of EMF under nonlinear ferromag. reson. conditions 77−8417
$Y_{2.85}La_{0.15}Fe_{3.75}Ga_{1.25}O_{12}$, inhomogeneous bubble film, spin wave reson. 77−32265
$Y_{3-x}La_xFe_{5-y}Ga_yO_{12}$, mag. bubble film, low freq. ferrimag. reson. 78−31110
$Y_{3-x}La_xFe_{5-y}Ga_yO_{12}$ film, horizontally dipped LPE grown, FMR, anisotropy field obs. 79−78449
$Y_{3-x}La_xFe_5O_{12}$, mag. props. rel. to ionic struct. 80−75756
$Y_6(Mn_{0.75}Fe_{0.25})_{23}$, mag. scatter state, hysteresis loops 78−56350
$Y_{0.25}Nd_{0.75}Co_5$, basal plane anisotropy 77−8295
$Y_{1-x}Nd_xCo_5$, exchange interactions and magnetocrystalline anisotropy 80−34618
$Y_{1-x}R_xCo_5$, R=Gd,Tb,Nd, ferrimag., magnetisation, exchange interactions, mag. anisotropy 80−80565
$(Y_{1-x}R_x)_3Fe_5O_{12}$, rel. to photoinduced decrease in permeability, 77K 77−85497
$Y_{1.62}Sm_{0.21}Lu_{0.27}Cu_{0.9}Ge_{0.9}Fe_{4.1}O_{12}$, implanted bubble garnet, anisotropy profile, FMR study 80−7103
$Y_{2.6}Sm_{0.4}Fe_{3.8}Ga_{1.2}O_{12}$, garnet films, LPE growth, mag. anisotropy field control 77−69642
$Y_{3-y}Sm_yFe_{5-x}Ga_xO_{12}$ film, LPE growth induced mag. anisotropy 78−2709
$Y_{2.6}Sm_{0.4}Fe_{5-x}Ga_xO1_2$, epitaxial, domain wall crit. vel., effect of material parameters 79−99740

magnetic anisotropy continued
$Y_{3-x}Sm_xFe_5O_{12}$, cubic and induced anisotropy, temp. depend., 100-300K, ferromag. reson. obs. *(Russian)* 78−39313
YSmLuCaFeGe garnets, growth and temp. characts. of small bubbles 78−80183
$(YSmLuCa)_3(FeGe)_5O_{12}$, mag. props. and growth of 2 μm bubbles 78−91910
$(YSmLuCa)_3(FeGe)_5O_{12}$, epitaxial films, LPE grown, annealing effects on mag. anisotropy 80−66548
$(YSmTm)_3(FeGa)_5O_{12}$, small-bubble appl. 79−82845
$Y_{1-x}Tb_xCo_5$, spontaneous magnetisation anisotropy, spin reorientation transforms. *(Russian)* 80−7082
YVO_4:Tm^{3+}, cryst. field parameters, appls. 77−20277
$(Y_{1-x}2Co_x)Co_5$, anisotropy fields, coercivities, annealing effects 78−91898
Zn-Cr, dil., mag. anisotropy, 0.001 to 2K 78−68157
Zn-Mn(Cr), dil, mag. anisotropy, Hartree-Fock calcs. 80−11162
$Zn_xCn_{0.1}Fe_{2.9}O_4$, Cu, Zn substituted magnetite, domain wall resonance, mag. props. 80−15756
$ZnCr_2Se_4$:Mn, paramagnetic, giant cubic anisotropy 80−7073
$ZnGa_2O_4$:Fe^{3+}(Mn^{2+}), EPR, spin Hamiltonian parameters 80−25195
Zn_2Y, magnetostatic volume waves, magnetocrystalline anisotropy effects, group delay 79−78355
$Zr_{40}Cu_{60-x}M_x$ (M=Fe,Mn,Gd,Tb), amorphous, mag. ordering and local random anisotropy 78−68273
$Zr(Fe,Al)_2$, weak itinerant ferromag., mag. anisotropy effects on mag. isotherms 80−11187
$Zr(Fe_{1-x}Al_x)_2$, Curie temp., magnetisation, and cryst. struct., conc. depend. 80−75730
$ZrSiO_4$:Er(Yb), anisotropic mag. susceptibility meas. 77−43806

magnetic annealing
see also induced anisotropy (magnetic)
Alnico 5, thermal treatment in mag. field, mag. props. 78−91905
ferromagnetic amorphous system, directional order and induced anisotropy energy, theory 78−95431
ferromagnetic single crystal, mag. anisotropy induced by cold rolling *(Russian)* 80−84595
garnet film preparation, single-crystal, for magnetic bubble domain appl. 78−60588
neutron-irrad., void annealing, positron annihilation obs. 77−76469
Permalloy, high permeability, effect of hardening additions on mag. props. *(German)* 79−28566
Permalloy-Cu(Al) two-layer films, mag. anisotropy, grain boundary diffusion *(Russian)* 80−71122
Co, magnetic anisotropy induced by magnetic and stress annealing 78−35010
Co, magnetic anisotropy induced by mag. annealing and cold rolling, expt. 80−7695
Co, magnetic anisotropy induced by mag. annealing and cold rolling, calc. 80−7696
Co-Cu-Fe-Ce, mag. characteristics of sintered permanent magnets 78−60312
Co-Fe-B films, amorphous, mag. annealing behaviour 79−73782
Co-Fe(Ni), magnetic anisotropy induced by magnetic and stress annealing 78−35010
Co-Gd(Nd)(Pr)(Sm), dilute, magnetic annealing effect, induced anisotropy 77−73054
Co-Ni, magnetic anisotropy induced by mag. annealing and cold rolling, expt. 80−7695
Co-Ni, magnetic anisotropy induced by mag. annealing and cold rolling, calc. 80−7696
Co-P, electrodeposited amorphous alloys with high permeability, thermal treatment with and without field 80−89372
Co-P amorphous alloys, electrodeposited, magnetic anisotropy 79−28568
Co-Pt, ordering, study using X-ray scatt. *(Russian)* 80−81052
Co-rare earth dilute alloys, mag. annealing, conc. depend. 78−35011
Co-Zr, dil., mag. annealing effect, depend. of uniaxial mag. anisotropy on Zr conc. 80−39772
Co-Zr-Er alloys, mag. annealing effect, effect of Er on induced uniaxial mag. anisotropy 80−39771
$Co_{79}Fe_{6.5}B_{14.5}$ amorphous thin films, zero magnetostriction, high magnetisation 80−34708
$(Co_{0.89}Fe_{0.11})_{72}Mo_3Si_{15}B_{10}$, metallic glass, strain- and field-induced mag. anisotropy 80−108004
$Co_{73}Mo_2Si_{15}B_{10}$, metallic glass, strain- and field-induced mag. anisotropy 80−108004
Cr-Co-Fe, chromindur alloy, field heat treatment, and mag. props. 80−35354
CrO_2 powder, thermal-magnetic props. 79−51821
$(Fe,Ni)_{83}B_{15}C_2$, amorphous alloy, mag. props., possible appl. to power transformers 79−28558
$(Fe,Ni)_{80}P_{14}B_6$ amorphous alloy, mag. props., possible appl. to power transformers 79−28558
Fe-Al(4 wt.%), ferromag. alloy, mag. anisotropy induced by cold rolling 80−30114
Fe-B, amorphous, induced anisotropy, development by mag. annealing and under applied mech. stress 80−65868
Fe-B films, amorphous, mag. annealing behaviour 79−73782
Fe-B-C amorphous alloys, effect of Si addition on mag. props. 80−34694
Fe-Co-Ni Perminvar, mag. props. singularities in region of mag. anisotropy *(Russian)* 80−84614
Fe-Co-Si-B, zero magnetostrictive amorphous alloy with high saturation induction, mag. annealing 80−60362
Fe-Co-Si-B alloy, amorphous, rapidly quenched, mag. heads appl. *(Japanese)* 80−54922
Fe-Cr-Co-Mo high energy permanent magnets, mag. props. 80−97119
Fe-Cr-Co(-Mo), mag. props. after isothermal thermomag. treatment *(Russian)* 80−25159
Fe-Ni, secondary recrystn. and mag. props. 80−89247
Fe-Ni metallic glass wide strips, low-field mag. props. 79−51822
Fe-Ni-B(-P) amorphous alloys, mag. annealing mechanism, induced anisotropy 78−95484
Fe-Ni-P-B alloy, magnetically induced anisotropy 77−89948
Fe-Si, grain-oriented, AC magnetostriction at high temp., mag. annealing effects 77−20672
Fe-Si, grain-oriented, surface coating effect on transverse magnetostriction 77−66402
Fe-Si-B ferromagnetic amorphous alloys, Young's modulus and delay time characts. *(Japanese)* 77−85543

magnetic annealing continued
Fe-Si(3 wt.%), ferromag. alloy, mag. anisotropy induced by cold rolling 80−30114
$Fe_{80}B_{20}$ amorphous ribbons, magnetomechanical coupling constant and Young's modulus, mag. annealing 79−15333
$Fe_{80}B_{20}$, metallic glass, ferromag. props. 77−16107
$(Fe_{1-x}Co_x)_{77}Si_{10}B_{13}$ alloys, amorphous, induced mag. anisotropy by mag. annealing 79−4671
$Fe_5Co_{70}Si_{10}B_{15}$ amorphous magnetic alloy, decrease of permeability after demagnetisation, disaccommodation 80−39814
$Fe_{40}Ni_{40}B_{20}$, amorphous, RF annealing effects 80−108037
$(Fe_yNi_{1-y})_{80}B_{20}$, mag. anneal anisotropy in amorphous alloys 77−16069
$Fe_{40}Ni_{40}P_{14}B_6$, amorphous ferromagnet, domain struct., Rayleigh region and coercive field 79−28559
$Fe_{40}Ni_{40}P_{16}B_6$, amorphous, kinetics of induced mag. directional order 80−44824
$Fe_{80}P_{13}C_7$, amorphous ribbon, giant ΔE effect, magnetomech. coupling factor 77−8379
$Fe_{78}Si_{10}B_{12}$ amorphous ribbons, magnetomechanical coupling constant and Young's modulus, mag. annealing 79−15333
Gd, thermal modulation, annealed and unannealed sample comparison 79−61072
Gd-Co, and Gd-Co-X (X=Mo, Cu, Au), sputter deposited amorphous alloy, substrate bias, magnetic anisotropy, annealing 78−48006
Gd-Fe, sputter deposited amorphous alloy, substrate bias, magnetic anisotropy, annealing 78−48006
Ni-Co (25 wt.%), single crysts., mag. annealing effect on magnetostriction and magnetisation *(Japanese)* 80−34744
Ni-Co (25 wt.%), single crysts., mag. annealing effect on magnetostriction and magnetisation at high temps. 80−108047
Ni-Fe-Co, alloy with step hysteresis loops *(German)* 79−42806
Ni_3Mn, at. ordering during annealing, mag. field effect 78−15394

magnetic bays *see geomagnetic variations*

magnetic bottles
see also magnetic mirrors
field-reversing electron ring generation in RECE Christa, millisec. lifetime, mag. probe meas. 77−24173
neutrons storage using superconducting mag. storage ring 79−59293
ohmic heating, mag. field aligned currents, internal ring config. 78−18426
ring cusp, plasma width meas. 80−87927

magnetic breakdown
diamagnetic band structure, second order calc. using Landau functions, mag. breakdown determ. 80−24784
hexagonal compensated metal, chemical pot. shift due to coupled orbit conduction 79−28273
metal, acoustic breakdown, electron energy spectrum and interaction with mag. breakdown *(Russian)* 78−18948
metal, electric domains at low temp. 79−65368
metal, low temp. static cond., nonlinear effects due to mag. breakdown *(Russian)* 78−76062
metal, transport coeffs. in strong mag. field, Wiedemann-Franz law and Mott rule 77−69303
metal, transport kinetic coeffs. quantum oscills. in mag. breakdown regime *(Russian)* 79−91035
nonlinear magnetisation of metals *(Russian)* 80−44859
A, magnetoresistance, field strength function, electrodeless methods 79−91026
Al, cryst. and polycryst., inhomogeneity effects on galvanomagnetic props. 78−60109
Al, high-purity, anomalous longit. magnetoresist. anisotropy 77−76793
Al, linear resist. growth in strong mag. field, mag. breakdown and grazing electron scatt. effects *(Russian)* 78−51972
Al, quantum oscills. of thermal EMF under mag. breakdown conditions *(Russian)* 77−69305
Al, quantum phenomena on mag. breakdown *(Russian)* 78−43290
Al, single crystals, high purity, anisotropy of apparent resist. in longit. mag. fields 80−75550
Al, thermoelectric power and Nernst-Ettingshausen effect 78−56134
Al-Ag alloys, dilute, electrical magnetoresist., temp. depend., mag. breakdown 79−99532
Be, quantum oscills. of thermal EMF under mag. breakdown conditions *(Russian)* 77−69305
Cd, de Haas-van Alphen effect and mag. breakdown *(Russian)* 77−80722
Cd, thermo EMF oscills. on mag. breakdown *(Russian)* 79−60801
Cr, antiferromag., electron interference oscills. and spin-density-wave energy gaps at Fermi surface 80−49574
Cr, antiferromag., transverse magnetoresist., electron interference oscills. 80−65534
Fe, whisker, magnetoresistance, deviations from Kohler's rule 80−70673
Ga, Femi surface, de Haas-van Alphen effect study, mag. breakdown obs. 78−84132
$Hg_{3-x}AsF_6$, linear chain cpd., open orbits, induced torque meas. 80−29309
LaB_6, de Haas-van Alphen effect, low-field 80−75497
Mg, Hall resist., 1.7-300K, up to 2T, cyclotron motion breakdown 77−89751
Mg, quantum oscills. of thermal EMF and mag. breakdown conditions *(Russian)* 77−69305
Mg-In(Li), dil., alloying effect on Fermi surface, de Haas-van Alphen effect meas. 77−76732
Nb, Fermi surface, cycloton effective masses and mag. breakdown effects, de Haas-van Alphen study 78−43288
Nb, mag. breakdown and thermo-EMF *(Russian)* 77−80884
Re, Hall effect, 4.2K, under 12 kbar press. *(Russian)* 77−80762
ReO_3, mag. breakdown above compressibility collapse transition 80−103617
Ru, electronic structure and mag. breakdown, galvanomag. props. obs., 1.3-20.4K 78−91600
Ru, giant thermopower oscillations due to magnetic breakdown trajectories 79−60688
Ru, magnetoresistance and Hall effect under mag. breakdown conditions *(Russian)* 79−95389
Ru, quantum oscillations, of thermo EMF and Nernst effect *(Russian)* 78−95290
Ru, thermo-EMF and Nernst effect under mag. breakdown conditions *(Russian)* 80−24878
Ru, thermopower and mag. breakdown meas., 2-17K 78−51972

magnetic breakdown continued
Sn, white, Fermi surface, US quantum oscills., orbits attributable to mag. breakdown obs. 78−47694
$TaSe_2$, TaS_2, layer compounds, oscillatory magnetoresist. 77−85241
Tl, HCP, mag. breakdown matrix at Brillouin zone R point 78−10335
V, magnetoresistance and thermopower behaviour 79−33222
Zn based Kondo alloys, with mag. breakdown, anal. of de Haas-van Alphen effect data 78−34751
Zn, quantum oscills. of thermal EMF under mag. breakdown conditions *(Russian)* 77−69305

magnetic bubble devices
amorphous film sputtering, multiple target method 77−16493
bistable bubble domains in annular plates, appl. to bubble RAM 77−85532
bubble chip planar fabrication techniques 79−78485
bubble moving schemes and cylindrical bubble movement, theory 79−1698
contiguous disc structs., bubble propag. dynamics 80−34718
current access device, bubble wall state coding 79−73785
domain structure observation technique, bubble propagation circuits 78−84464
epitaxial garnet films for magnetic bubble memories *(Czech)* 78−88147
fabrication, appl. of sputtter etching in Ar-O plasma 79−83347
ferrite, microstruct. depend. of props. and applics., review 78−88548
garnet bubble film LPE with high Pb content 79−38750
garnet ferrite epitaxial layer, flaw detection method 78−2719
garnet film, 1 μm bubble contiguous-disk device, orientation depend. of propagation margin 79−82846
garnet film, Ga and Ge substituted, mag. prop. control during LPE growth and processing 78−68638
garnet film, ion implanted bubble circuits 79−78473
garnet film, mag. bubble domain, annealing by laser pulse 80−15769
garnet film LPE growth, for bubble memory appl., review, book contrib. 79−70009
garnet films appl., single-crystal, magnetic properties control during processing 78−60588
garnet LPE film, props., prep. and technology *(Polish)* 77−77076
garnet thin films for fast bubble devices 80−25168
garnets, bubble domain memory appls., growth requirements 77−20660
generator modelling and optimisation 78−6547
high speed magneto-optic camera system, for obs. of mag. bubble domain devices 77−79186
implanted disk type, domain wall energies, effective threshold anisotropy 79−78453
ion implantation appls. to bubble technology 79−15329
ion milling fabrication process, string segment motion algorithm 80−71779
ion-implanted propag. patterns, cryst. symm. effects, roof-top designs 80−15768
large-area ion milling from small sources 79−75510
LPE garnet bubble films, capping layer upper cap-switch field, model 78−95498
magneto-optic bubble spatial light modulators, appl. in optical processing systems 78−79139
manipulation of 1 μm bubbles with coarse overlay patterns 78−39377
memories, amorphous thin film materials, review *(Polish)* 80−34715
memories, rotational field coils winding turns counting, using moire system 80−73428
memory chip fabrication, single level masking approach 79−78486
memory device, magnetisation distrib., in Permalloy strip *(Russian)* 77−48021
memory device prod., ion beam etching 79−78487
memory technology, developments 78−52325
metallic amorphous film, bubble technology *(Polish)* 77−77076
multilayer self-structured bubble memories 79−78483
performance, influence of Ni-Fe overlayer quality 79−78466
Permalloy, conductor crossing effect on bubble propagation margins 80−29588
Permalloy film preparation by RF sputtering 78−3044
Permalloy I-bars, Kerr magneto-optical effect meas., domain wall location determ., Kerr effect probe 78−68328
Permalloy overlay bars, calc. of forces on ferrofluid particles on surface 78−68329
Permalloy-SiO_2-Schott glass, bubble propagation struct. 80−34719
production, heavy ion beams application 77−55310
propagation, recurrence and synchronism *(Japanese)* 79−56579
propagation circuits, optimum design 79−78481
propagation modelling, domain struct. effects 79−78488
propagation pattern anal. 79−78482
review of bubble material props. and prep. methods *(Rumanian)* 80−93149
single level masking NiFe sputter deposition 77−12532
single-layer ion-implantable small bubble device materials, design and development 79−82844
small-bubble-diameter mag. memory materials, past, present and future requirements 79−78458
solid-state device conference, Tokyo, Japan (Sept. 1976) 77−76901
storage appls., status and prospects 77−77079
stretch propagation dependence on chevron patterns 78−84462
X-ray lithography using synchrotron radiation 77−22628
$(Fe_{1-x}Ni_x)_{80}B_{20}$ amorphous soft magnetic films 79−82836
Gd-Co influence of gaseous phase on mag. props. *(Polish)* 80−39820
Gd-Co-Mo amorphous film devices, bubble dynamics 77−89997
Gd-Fe influence of gaseous phase on mag. props. *(Polish)* 80−39820
$Gd_3Ga_5O_{12}$ single crystals, polishing charact., chemical, mechanical methods comparison, bubble device appl. *(Japanese)* 79−5067
Ni-Fe films, coercivity control for single-level masking bubble devices using surface modification and intermediate layers 79−51816
$(Sr/Ba)(Fe/Al/Ga)_{12}O_{19}$ solid soln. crystal for hexaferrite layer substrate *(German)* 78−23672
$(Y,Eu,Lu,Ca)_3(Fe,Ge)_5O_{12}$, bubble memory chip, dynamic conversion comparison with $(Y,Sm,Lu,Ca)_3(Fe,Ge)_5O_{12}$ 78−68319
$(Y,Re)_{3-x}Ca_xGe_{5-x}Ge_xO_{12}$, garnet films, LPE growth for bubble memory appls. 77−11813
$(Y,Sm,Lu,Ca)_3(Fe,Ge)_5O_{12}$, bubble memory chip, dynamic conversion comparison with $(Y,Eu,Lu,Ca)_3(Fe,Ge)_5O_{12}$ 78−68319
$(Y,Sm,Lu)_3(Fe,Ga)_5O_{12}$, LPE mag. film, suitability for 1 to 3 micron bubble devices 78−68323
YEuLuCaGe garnets, 7 μm-period bubble devices 80−44887
YEuLuGa garnets, 7 μm-period bubble devices 80−44887

magnetic bubble devices continued
YEuTmCaGe garnets, 7 μm-period bubble devices 80−44887
YEuTmGa garnets, 7 μm-period bubble devices 80−44887
$Y_3Ga_xFe_{1-x}O_{12}$, film growth conditions rel. to memory element props. 77−66399
YIG:Eu, anisotropy energy coeff. reduction, by Pb addition 79−11329
YSmLuCaGe garnets, 7 μm-period bubble devices 80−44887
$(YSmLuCa)_3(GeFe)_5O_{12}$, LPE low defect density films, prep. for mag. bubble device fabrication 79−87590
YSmLuGa garnets, 7 μm-period bubble devices 80−44887
YSmTmCaGe garnets, 7 μm-period bubble devices 80−44887
$(YSmTmCa)_3(GeFe)_5O_{12}$ film, YY pattern racetrack discrimination and state stability of S=1 and 0 bubbles 78−91908
$(YSmTm)_3(FeGa)_5O_{12}$, small-bubble appl. 79−82845
YSmTmGa garnets, 7 μm-period bubble devices 80−44887

magnetic bubbles
see also magnetic bubble devices
amorphous bubble-domain materials, Hall effect hysteresigraph for coercivity measurement 79−73786
in axially symmetric fields 77−85523
azimuthal angular rotation in domain walls during radial motion of bubble domains 79−56583
ballistic overshoot, elliptical distortion mechanism 78−68315
bistable bubble domains in annular plates 77−85532
Bloch wall structure, horizontal, mag. bubble domains in implanted films 80−71131
Bloch-line rotation instability during gradient propagation of S=0 bubble in an in-plane field 77−40095
bubble garnet, domain-wall dynamics in in-plane field 79−87296
bubble garnet film, saturation velocity, in-plane field effects 80−108041
bubble moving schemes and cylindrical bubble movement, theory 79−1698
bubbly dynamics and jump probability 80−65977
characterisation of bubble materials, using spatial filtering 77−12175
charged domain walls in implanted layers, theory 80−71130
charged magnetic domains, formation, existence, dynamics, collective props., review 78−23310
charged wall behavior in 1-μm bubble implanted structures 78−91892
circular bubble translation motion analysis 78−14999
collapse and stripout field, microwave meas. technique using mag. reson. apparatus 77−20661
collapse field, anisotropy field, and domain wall mobility, magneto-optic meas. 77−85534
complementary σ-bubbles in bubble automation 79−78465
computer program, BUBMAT, for parameters of strip and cylindrical domains 77−12173
contiguous disc bubble patterns utilising intrinsic crystalline anisotropy 80−2611
crystals of magnetic flux, review 79−99664
cylindrical magnetic bubble domain memory materials 79−61194
cylindrically symmetric bubbles, static and dynamic props. 80−39835
diameter, collapse field and runout field intensity meas. 79−78490
domain film, growth induced order parameter, estimation from coercive force meas. 80−39828
domain transfer using homogeneous mag. fields *(German)* 77−63244
domain transient shapes, during gradient propagation and overshoot 77−85524
domain wall states, discrimination by bubble collapse time 80−39830
domain walls in uniaxial crystals, static and dynamics behaviour *(Polish)* 77−69650
dynamic collapse expt., in presence of inplane field 77−85479
dynamic measurements by rocking technique *(Chinese)* 80−65981
dynamic measurements of magnetic bubbles *(Chinese)* 79−99741
dynamic properties of magnetic domain walls and magnetic bubbles, review 80−88784
dynamic props. rel. to bias-field-determined bubble size 78−91915
dynamics by rotating gradient meas. 79−51827
dynamics of bubble domains at low drive field 79−51828
dynamics of mag. domain walls and bubbles 78−14995
effective mass of domain walls 79−24205
epitaxial film device appl. 77−32223
epitaxial garnet film, mag. domain wall damping, vel. depend. 77−85517
exchange vortexes of magnetisation, micromagnetic bubble domains 80−71138
existence in absence of mag. field, near phase transition 78−48012
ferrimagnetic single crystal layer, light diffr. by mag. bubbles *(German)* 79−56769
ferrite, epilayers for bubble appl. 80−39829
ferrite bubble film struct., EM and RHEED, Mn and Mn-Cu ferrites 77−11801
ferrite garnet film, ion-implanted, hard mag. bubble suppression mechanism 80−44890
ferrite plate, stable bubbles near compensation point 77−40099
ferromagnet, bubble lattice existence near compensation point *(Russian)* 77−80977
ferromagnet, limiting velocity of domain wall motion *(Russian)* 78−56342
ferromagnetic film, effect of propag. on shape 77−16134
ferromagnetic film, heterogeneity influence on static and dynamic props. of domain walls *(Russian)* 80−65974
field distribution meas. by InSb ultramicro Hall element 79−56585
film, domain wall mass, under large in-plane fields 79−95618
film, domain wall oscillations and dynamic collapse, saturation velocity and ballistic overshoot theory 77−8372
film, ellipsometric meas. of thickness and refr. index 79−78463
film, ferromagnetic, bubble domain lattice, parametric excitation of oscillations 77−8374
film, mag. characterisation procedures 79−78462
film, mag. hysteresis curve, multiple particle model *(German)* 78−80178
film, quenching of coercive force by domain wall restoring forces, theory and expt. test 79−78460
film, uniaxial anisotropy energy, effect of ion implantation 79−78476
film, validity of one-dimens. wall theory for bubble materials 78−56361
film disc containing bubble, two-dimens. magnetostatic reson. 79−78469
films, spin wave and magnetoelastic resonance meas. 78−91913
formation and computer storage elements appls. 77−20662
full wafer magnetic bubble films, devices for characterisation 79−78461
garnet, bubble conversion to anomalous behaviour 78−23309
garnet, bubble film, LPE growth reproducibility 79−1830

magnetic bubbles continued
garnet, bubble-collapse and stripe-chop mechanism 77−80975
garnet, domain-wall dynamics in in-plane field 79−87296
garnet, epitaxial film, mag. bubble props., permanent local modification by laser annealing 80−2612
garnet, film, bubble domain, saturation velocity, empirical relation 78−95496
garnet, ion-implanted, gradientless propulsion for S=1 bubble 79−78470
garnet, ion-implanted film, large automotion of $S=^1/_2$ bubble 79−24203
garnet, low loss bubble material, wall struct. changes 77−89994
garnet, LPE film, domain dynamics in microwave field 77−20663
garnet, Permalloy-coated film, bubble vel. and stability, influence of planar domains 80−39831
garnet and under permalloy bars, bubble state stability in rot. field 78−68317
garnet bubble film with induced anisotropy, domain wall energy 79−19750
garnet bubble films, 111 orientated, mag. anisotropy predictions, model 78−68326
garnet bubble materials, low loss, mag. domain wall dynamics 78−10738
garnet epitaxial film multilayer structures, interphase boundary rearrangement obs. 79−78489
garnet film, 180° capped double layer LPE film, bubble wall states coding 80−34716
garnet film, bubble, anisotropy field and nonmagnetic regions in implanted layers, ferromag. reson. study 79−99774
garnet film, bubble, [111]-oriented simple method of meas. cubic anisotropy const. 78−19285
garnet film, domain wall, dynamics, time depend. effects 77−12168
garnet film, domain wall displacement in pulsed field 77−16129
garnet film, dynamic behaviour of domain walls and bubbles 78−52321
garnet film, dynamic charges in bubble domain lattice 78−60325
garnet film, fuzzy walls obs. 79−99738
garnet film, gradient propag., ballistic overshoot, in-plane field effect 77−12170
garnet film, gradientless propulsion of bubbles 77−4535
garnet film, high g, two resonant peaks 78−68388
garnet film, ion implanted bubble propag., wall states 77−16128
garnet film, ion-implanted, bubble collapse field, in-plane mag. field effect 77−73060
garnet film, ion-implanted, controlled generation and discrimination of χ_+ and χ_- bubbles by single bias pulse 79−51826
garnet film, ion-implanted, discrimination of S=1 and S=0 bubbles by dynamic bubble collapse 79−51825
garnet film, mag. bubble domain, annealing by laser pulse 80−15769
garnet film, magnetoelastic energy of stripe domain patterns 78−68334
garnet film, minimum bubble drive field, ion implantation effect 77−24721
garnet film, motion of mag. bubble domains near point defect 79−28575
garnet film, non-implanted, surface mag. struct. 80−84628
garnet film, numerical display element exploiting rag domains 78−68339
garnet film, physics of domain walls 79−99727
garnet film bubble material, high peak velocity 77−85513
garnet film for fast bubble devices 80−25168
garnet film ion implanted contiguous disk structure dynamics of 1 μm bubbles 79−78474
garnet films, bubble statics, dynamics *(Japanese)* 78−52326
garnet films with orthorhombic anisotropy, domain wall motion 80−80580
garnet layers, ion-implanted, domain-wall behaviour for 1-μm bubble devices 80−2613
garnet LPE bubble film, growth-induced anisotropy, effect of La 77−85514
garnet LPE film, props., prep. and technology *(Polish)* 77−77076
garnet LPE film containing Lu bubble collapse field temp. depend., flux effect 77−85515
garnet LPE layers, bubble collapse field meas., new method 78−56356
garnet thin film, bubble domain lattice collapse characts. in alternating mag. field 80−54932
garnets, domain wall oscillations, bubble domain wall motion 80−108042
garnets, dynamics of mag. domain walls and bubbles 77−69599
garnets, film, ion-implanted, domain wall mobility 78−95495
garnets, skew cylindrical mag. domains, light modulator appl. anal. 79−38360
garnets, wall oscill. and overdamped motion, in mag. bubble domains 78−6550
gradientless propulsion, state switching 77−12167
half-bubble stability in platelets with domain wall energy density gradients 77−1576
hard, lattice dynamics, effect of Bloch lines in domain walls 77−32228
hard bubble formation due to bias pulse field *(Chinese)* 80−71127
hard bubbles, static and dynamic props., micromagnetic struct. 80−11236
high magnetic field props., review *(Japanese)* 78−52303
high speed bubble domain motion, high resolved obs. system 77−40096
high-Q bubble materials, wall twist computation method 79−69704
hollow half bubbles, static forces, bubble nucleation 77−85522
horizontal Bloch line motion 80−11237
infinite film, bubble domains with twisted walls, calc. 78−64245
interacting bubble domains, dynamics, theory 80−71132
interaction with concentric hard overlay 79−8025
ion implanted channels, mag. bubble stability, model 78−68320
ion-implanted bubble garnet film, vel. asymmetry during stripe head propag. 80−39834
ion-implanted garnet films in rotating magnetic field, threefold bubble symmetry 78−64243
ion-implanted propag. patterns, cryst. symm. effects, roof-top designs 80−15768
lattice propagation control by standing acoustic waves 79−82841
light diffraction by domain gratings, and appl. 80−88970
light diffraction in mag. bubble fields 79−73904
LPE double layer films, wall state stability of bubbles 78−95497
LPE garnet bubble films, capping layer upper cap-switch field, model 78−95498
magnetic bubbles, electron microscope obs., review 77−28417
magnetic film, bubble domains, magnetoelastic interactions 80−103865
magnetoacoustic resonance in a magnetic bubble domain lattice 78−88161
magnetoelastic interactions 80−65976
magnetostatic field approximation formula 77−77080
materials, prep. of memory element, review 80−50153

magnetic bubbles continued
materials characterisation using spatial filtering techniques 77−85528
memory research material, Czochralski-type cryst. growth system 79−91581
memory technology, new developments in technologically important materials, review 79−33509
metallic amorphous film, bubble technology *(Polish)* 77−77076
micromagnetic analysis of S=1 magnetic bubbles with curvature effects 79−73784
micromagnetic method, bubble domain statics and dynamics 80−71081
motion, 'ballistic', multiple high-speed photography study 78−72383
motion, computer simulation 77−85526
motion at small drive fields 77−89993
motion due to closure domain interaction with loop current 77−85525
motion in inhomogeneous pulsed mag. field 78−27064
motion of bubble domain Bloch lines, computer simulation 80−54916
moving magnetic domain, force, momentum and topology 79−91264
multidomain ferromagnetic resonance anal., appl. to stripe and bubble arrays 79−78528
nucleation of 1 μm bubbles via charged walls 79−78479
one-dimensional domain wall motion under biased in-plane field, numerical anal. 79−15321
orthoferrite garnet, mag. bubble lattice nucleation obs. 78−76283
orthoferrites, skew cylindrical mag. domains, light modulator appl. anal. 79−38360
peak velocity, analytical method of determ. from overshoot data 79−33513
peak velocity of domain wall in mag. bubble film under large in-plane field 79−19751
Permalloy, conductor crossing effect on bubble propagation margins 80−29588
Permalloy overlay bars, bubble stray field effect on domain wall struct., interference contrast technique 79−78457
Permalloy sheet, infinite, unsaturated, statics of mag. bubble domain interaction 77−66397
Permalloy-coated garnet films, bubble properties 78−2715
Permalloy-SiO_2-Schott glass, bubble propagation struct. 80−34719
propagation, turn around effect 77−12169
propagation by domain drag in amorphous films 79−42814
pure chirality, discrimination between right and left handed bubbles 80−34723
rare earth garnet thin films, macroscopic magn. props., magneto-optical expts. 80−46764
rare earth iron garnet single crystal films, synthesis and props., review 78−48013
rare earth iron garnets, Ca-Ge substituted, mag. loss and domain wall mobility 80−65980
review of bubble material props. and prep. methods *(Rumanian)* 80−93149
SEM, mag. contrast, with reference to bubble domain struct. 78−18511
shape, eqn. of motion of domain wall 79−78467
skew bubble domains, theory 77−85531
spin precession effects on bubble stability 77−32226
stability functions, efficient calc. 78−52323
state identification and stability 79−56581
static and dynamic props. of lattice of mag. bubbles *(Russian)* 77−59439
static and kinetic parameters of bubble walls having horizontal Bloch line pair 80−39836
static bubble collapse analysis, in inhomogeneous external magnetic field *(German)* 79−95621
static spin config. in cylindrical coordinates 80−54928
static wall structure, under large in plane fields 78−76282
statics, in axially symm. total mag. field, energy expressions 78−6551
stationary circular motion 80−84629
susceptibility measurements as characterisation method 78−68325
T bar, domain wall study employing ferrofluid, rel. to magneto-optical Kerr effect meas. 80−60360
thick wall elliptical bubbles, magnetisation distrib. 77−69649
tilted cylindrical magnetic domains, parameters and stability 78−64246
translational motion, mechanism for inertial effects 80−100606
translational motion anal. for normal bubble 77−48019
transverse mass in rotating gradient 80−39832
twisted domain wall energy, thickness depend., simplified calc. *(Slovak)* 80−103862
two dimensional mag. domain wall, uniform magnetisation, effective force density of magnetostatic origin, mag. bubble motion anal. 80−100595
unichiral magnetic bubbles, radial motion in in-plane field 80−34724
velocity, acoustic wave effect 77−12171
wall dynamics, review 80−75823
wall motion, coherent precession mode of twisted wall 79−78468
wall motion, one-dimens., static in-plane field-biased, dynamic characts *(Japanese)* 79−73767
wall oscillations in presence of in-plane fields in mag. bubble material 79−56582
wall oscillations in presence of in-plane fields in magnetic bubble material 79−99737
wall velocity depend. on bubble radial motion momentum 80−71136
waves, displacement and pulsation-type, coupled oscills. in low density lattice 77−32227
$(YSmEuCa)_3(FeGe)_5O_{12}$, garnet film, ion implanted, bubble domain props. 78−88152
$(Ba,Sr)Fe_{12}O_{19}$, Ferroxdure, developments and research 78−84455
Ba ferrite, FMR in uniaxial crystal plate with bubble domain lattice 80−93182
$BaFe_{12}O_{19}$, bubble and stripe lattice domain wall oscills. 80−97115
$(BiTm)_3(FeGa)_5O_{12}$ ion implanted epitaxial garnet film, bubble domains, cryst. struct. disorder 80−93150
Ca, Ge-substituted garnet, LPE growth atm. effects on bubble props. 77−20655
$Ca_3Ga_2Ge_3O_{12}$, substrate, electron examination of microstruct. and microsegregation 78−67919
Co, foil, wall struct., bubble, plate domains, 1 MeV electron microscope study 78−84463
Co-Gd-Mo, amorphous film, mag. props., temp. depend. 78−10734
$DyFe_{0.998}Co_{0.002}O_3$, orthoferrite, domain struct. near mag. transitions 80−2599
$DyFeO_3$, bubble domain struct. temp. depend. 77−69647
$(Eu,La,Ca)_3(Fe,Ga,Al)_5O_{12}$ film, LPE growth and induced orthorhombic anisotropy 77−20652

magnetic bubbles continued
$(Eu,Lu)_3Fe_5O_{12}$, submicron bubble films on rare earth-Ga garnet substrates, prep. and mag. props. 78−91909
$(Eu,Lu)_3Fe_5O_{12}$:Ga(Al)(Ca,Ge), bubble material, dynamic characterisation, comparison between transport and FMR methods 80−39833
$Eu_{3-x}Ca_xSi_xFe_{5-x}O_{12}$, bubble film, LPE growth induced anisotropy 77−20659
EuGaYIG film, bubble dynamics, anisotropy depend., ferromag. reson. expts. 77−63240
EuGaYIG:Cr, epitaxial garnet film, interaction pot. of domain walls with localised stress fields 80−44889
EuIG:Pb film saturation magnetisation improved by Sb^{5+} substitution 80−54926
$(EuLu)_3(FeAl)_5O_{12}$, film epitaxial growth on Gd_3GaO_{12} substrate, mag. props. 80−65402
$(EuLu)_3Fe_5O_{12}$, Ga, Al or (Ca,Ge) substituted, mag. props. and growth of 2 μm bubbles 78−91910
$(EuY)_3(FeGa)_5O_{11}$, ferrite garnet film, mag. bubble motion delay 79−91269
$Eu_{0.6}Y_{2.4}Ga_{1.26}Fe_{3.74}O_{12}$ garnet film, Walker oscills., detection by mag. bubble collapse 78−68318
$Eu_{0.6}Y_{2.4}Ga_{1.26}Fe_{3.74}O_{12}$ garnet film, dynamic bubble-collapse determ. of domain wall motion oscillation 79−78454
$Eu_zY_{3-z}Ga_1Fe_{5-1}O_{12}$, epitaxial garnet films, props. at compensation points 80−39823
$Fe_{75}P_{15}C_{10}$ amorphous foil, ferromag. domain orientation, Mossbauer exam. 78−52402
$Fe_{75}P_{15}C_{10}$ foils, amorphous, ferromag. domain orientation, Mossbauer study 78−15000
$(Gd,Tm,Y)_3(Ga,Fe)_5O_{12}$, bubble domain gradient propag., elliptical distortion and bias compensation 78−19292
Gd-Co alloy, sputtered film, mag. props. determ. *(Chinese)* 78−2714
Gd-Co amorphous films, mag. struct., mag. bubbles, electron diffr. study *(Chinese)* 80−71126
Gd-Co film, amorphous, for bubble device appl., prep. and perpendicular anisotropy 77−69641
Gd-Co film, sputtered from segment target, composition and mag. props. 78−27062
Gd-Co sputtered films, preparation process, props. 77−59688
Gd-Co-Mo film, amorphous, bubble and stripe domain wall vel. meas. 77−40094
Gd-Mo-Mo amorphous film, domain drag effect obs. 78−91911
GdCoAu amorphous film, bias field depend. of domain drag propagated bubble domains 79−78471
a-GdCoAu(Mo) films, perpendicular anisotropy temp. depend., Lorentz microscopy 77−28419
$Gd_{0.12}Co_{0.59}Cu_{0.29}$, sputtered film prep. for bubble device 77−16493
$Gd_3Ga_5O_{12}$, substrate, electron examination of microstruct. and microsegregation 78−67919
$(Gd_{1-y}Nd_y)_{1-x}Fe_x$ amorphous bubble films with good temp. characts. 79−95616
GdTmGa garnet bubble film, ion implanted, pot. wells under charged wells 80−34717
$Gd_{0.9}YTm_{1.11}Ga_{0.44}Fe_{4.56}O_{12}$, ion implanted, ferromag. reson. meas. 78−68385
La-Sm-Lu iron garnet film grown as NdGaG substrates, mag. props. 80−44888
$(LaLuSm)_3(GaFe)_5O_{12}$ bubble garnet film, coercivity 79−78459
$(LaTmCa)_3(Fe_{5-x}Ge_x)O_{12}$ film, high g, for mag. bubble applics. 77−85529
$(Lu,Bi)Fe_5O_{12}$, magneto-optic colour effects 78−23308
$(Lu, La, Y, Ca)_3(Ge, Fe)_5O_{12}$, temperature compensated high mobility bubble garnet, LPE and props. 77−20656
$Lu_{3-x}Ca_xFe_{5-x}Si_xO_{12}$ film on $Ca_3Ga_2Ge_3O_{12}$, mag. bubble props. 77−28418
MgMn ferrite CVD epitaxial layers, bubble domains in remanence and demagnetised states 77−85516
Mn-substituted garnet film, growth characts. and mag. props. 80−39826
NiFe stripes, mag. props. and domain struct. 80−44886
$NiFe_{2-x}Al_xO_4$, stress-induced anisotropy in LPE grown single cryst. films, stripe domains and mag. bubbles struct. 79−28238
$PbFe_{12}O_{19}$, bubble and stripe lattice domain wall oscills. 80−97115
$PbFe_{12}O_{19}$ platelets, ferromag. reson. absorpt. of close-packed bubble lattice 77−69709
$(Sm,Lu)_3Fe_5O_{12}$, submicron bubble films on rare earth-Ga garnet substrates, prep. and mag. props. 78−91909
Sm-YIG garnets, implanted and Permalloy coated, comparison between planar domain walls in bubbles 77−85520
SmCaGe garnet LPE bubble film, coercivity, thickness depend. 78−68324
$(SmLu)_3(FeAl)_5O_{12}$, film epitaxial growth on $Gd_3Ga_5O_{12}$ substrate, mag. props. lattice mismatch 80−65402
$Sm_{0.3}Lu_{0.2}Tm_{0.2}Y_{1.45}Ca_{0.85}Fe_{4.15}Ge_{0.85}O_{12}$, LPE growth, saturation magnetisation, collapse field, bubble diameter 78−95703
$(SmLuYCa)_3(FeGe)_5O_{12}$ film, ion implant profile 79−78477
$Sm_{0.55}Tb_{0.45}FeO_3$, orthoferrite cryst., domain memory effect *(Russian)* 77−55693
SmTmIG, epitaxial layer with submicron bubbles, mag. props. 77−12172
$Sm_{0.1}Y_{1.9}CaFe_4GeO_{12}$, LPE growth, saturation magnetisation, collapse field, bubble diameter 78−95703
SmYGa garnet, bubble motion depend. on wall pinning 79−78455
$Sm_{0.4}Y_{2.6}Ga_{1.2}Fe_{2.8}O_{12}$, H^+ implanted film, epitaxial, mag. bubbles, walls and fine struct. 77−63241
$(Y,Eu,Sm)_3(Ga,Fe)_5O_{12}$ film, mag. loss and bubble dynamics 77−8371
$(Y, Eu, Yb, Ca)_3(Ge, Fe)_5O_{12}$, bubble film, LPE on $Gd_3Ga_5O_{12}$, mismatch and faceting 77−20657
$(Y,Eu)_3(Fe,Ga)_5O_{12}$, LPE growth from molybdate fluxes, bubble props. 78−68322
$(Y,Eu)_3(Ga,Fe)_5O_{12}$ film, bubble wall state stability obs. 77−20651
$(Y,Gd,Tm)(Fe,Ga)_5O_{12}$, cylindrical mag. domain behaviour in external mag. field *(Russian)* 78−6553
$(Y,Gd,Yb,Bi)_3(Fe,Al,Ga)_5O_{12}$ films, magnetic bubble domains, domain wall motion examined 78−19294
$(Y,Sm,Ca)_3(Fe,Ge,Si)_5O_{12}$ single-crystal films, props. 78−64247
$(Y,Sm,Ca)_3(Fe,Ge)_5O_{12}$, domain wall, radial motion, method of dynamic collapse of mag. bubbles 79−8026
$(Y,Sm,Ca)_3(Fe,Ge)_5O_{12}$ epitaxial films, mag. props., growth condition effects 80−97124
$(Y,Sm,Ca)_3(Ge,Fe)_5O_{12}$ film, bubble wall state stability obs. 77−20651

magnetic bubbles continued
$(Y,Sm,Ga)_3(Fe,Ge,Si)_5O_{12}$ film, bubble domain collapse field, 20-160°C 77−24725
(Y, Sm, Lu, Ca)$_3$(Fe, Ge)$_5$O$_{12}$:Ne$^+$, film, S=1 bubbles dynamic props., temp. depend. 77−20658
$(Y,Sm,Lu,Ca)_3(Fe,Ge)_5O_{12}$ bubble magnetic garnet film, LPE grown, props., $CaCO_3/GeO_2$ molar ratio influence 80−50152
$(Y,Sm,Lu,Ca)_3(Ga,Ge,Fe)_5O_{12}$, film growth and mag. props. for bubble-memory appl. 79−87297
$(Y,Sm,Lu,Cu)_3(Fe,Ge)_5O_{12}$, ion implanted, hard bubble suppression 80−11238
$(Y,Sm,Lu,Tm,Ca)_3(Fe,Ge)_5O_{12}$, epitaxial garnet film, temp. depend. mag. props. 80−39825
$(Y,Sm)_3(Fe,Ga)_5O_{12}$ film, bubble domain collapse field, 20-160°C 77−24725
$(Y,Sm)_3(Ga,Fe)_5O_{12}$ films, growth from melt, growth property control 78−27395
$(Y,Sm)_3(Ga,Fe)_5O_{12}/(Eu,Er)_3(Ga,Fe)_5O_{12}$ double-layer self-biasing garnet films, dynamic behaviour of domain walls 80−34722
$Y_{1-4}BiFe_{3.8}Ga_{1.2}O_{12}$ garnet films, bistable bubble domain 79−15331
$Y_2BiFe_{3.8}Ga_{1.2}O_{12}$, film, dynamics of domain walls 78−27065
$Y_{2.7}Bi_{0.3}Fe_{3.8}Ga_{1.2}O_{12}$ epitaxial film, mag. domains in microwave mag. field, Faraday obs. 78−19295
YCaSmTmGeIG, epitaxial layer with submicron bubbles, mag. props. 77−12172
$(YCdYbBi)_3(FeAl)_5O_{12}$, cylindrical domain wall vel. anisotropy *(Russian)* 77−59440
$YCrO_3$, bubble domain struct. temp. depend. 80−71137
$(YErCa)_3(Fe_{5-x}Ge_x)O_{12}$ film, high g, for mag. bubble applics. 77−85529
$(YEu)_3(FeGa)_5O_{12}$ rigid magnetic bubble transition to normal behaviour 78−95501
$Y_{2.45}Eu_{0.55}Fe_{3.8}Ga_{1.2}O_{12}$, hard bubble conversion in in-plane field 78−14998
$Y_{2.35}Eu_{0.65}Ga_{1.2}Fe_{3.8}O_{12}$, bubble translation vel., ion-implantation effects 78−68327
$(YEuLuCa)_3(FeGe)_5O_{12}$ film, stable state of bubbles containing Bloch lines 78−76281
YEuTmCa garnet bubble films, domain wall transition 79−56584
$(YEuTmCa)_3(FeGe)_5$ bubble garnet films, ion-implanted, mag. susceptibility meas. 79−47311
$(YEuTmCa)_3(GeFe)_5O_{12}$ film, Bloch loop punch-through in mag. bubbles 77−59437
$Y_{1.52}Eu_{0.3}Tm_{0.3}Ca_{0.88}Ge_{0.88}Fe_{4.12}O_{12}$, bubble translation vel., ion-implantation effects 78−68327
$(YEuTm)_3(FeGa)_5O_{12}$ film, dynamic props. of bubble domains by high speed photography 80−15771
$(YEuTm)_3(FeGa)_5O_{12}$ garnet film, bubble domain steady state motion on a circle 80−29589
YEuTmGa garnet bubble film, dynamic diffuse wall deform. 80−54927
$(YEuTm)_3(GaFe_5)O_{12}$ ferrite garnet films, mag. bubbles, translational motion, mechanism for inertial effects 80−100606
$Y_{1.57}Eu_{0.78}Tm_{0.65}Ga_{1.05}Fe_{3.95}O_{12}$, bubble garnet, low drive stripe head vel. 77−32225
$Y_{1.57}Eu_{0.78}Tm_{0.65}Ga_{1.05}Fe_{3.95}O_{12}$ film, gradient propagation, overshoot and creep 78−19291
$(YEuYbCa)_3(FeGe)_5O_{12}$, ion-implanted, in-plane mag. field effects on bubble props. 77−85521
$(YEuYbCa)_3(FeGe)_5O_{12}$ film, mag. σ-bubbles, automation props. 78−88150
$(YEuYbCa)_3(FeGe)_5O_{12}$ bubble films, Ne$^+$-implanted, cryst. and mag. props., X-ray diffr. obs. 79−38362
$(YEuYbCa)_3(FeGe)_5O_{12}$ film, isolated straight stripe domain dynamic props. 79−33514
$(YEuYbCa)_3(GeFe)_5O_{12}$ bubble film with ion-implanted layer, FMR study 80−2643
$YFeO_3$, bubble domain struct. temp. depend. 77−69647
$YFeO_3$, direct meas. of stray mag. field distrib. using micro Hall element, expt. 77−40097
$YFeO_3$ monocrystalline, mag. field depend. of magnetic domain *(Korean)* 78−68337
$YFeO_3$ orthoferrite, weak ferromagnet domain struct. near Neel temp. 79−99739
$YFeO_3$, skew bubble domains, stripe domains 77−89999
$Y_{1.4}Gd_{0.6}BiFe_{3.8}Ga_{1.2}O_{12}$ film, bistable bubble domains, static, dynamic and optical props. 79−28574
Y_2GdIG film, amorphous, mag. bubbles obs. and structural transformation 80−75824
$YGdTmFe_{4.3}Ga_{0.7}O_{12}$ epitaxial films, bubble-domain lattices with specified parameters 80−60386
$(YGdTm)_3(FeGa)_5O_{12}$ epitaxial film, formation of lattice of cylindrical mag. domains from stripe domains *(Russian)* 80−80579
$(YGdYbBi)_3$ $(FeAl)_5O_{12}$ epitaxial film, diffuse domain wall, bubble domain expansion 80−25170
$Y_{0.9}Gd_{1.1}Yb_{0.7}Bi_{0.3}Al_{0.9}Ga_{0.2}Fe_{3.9}O_{12}$ films, cylindrical mag. domain form. *(Russian)* 77−40098
$(YGdYbBi)_3.(FeAl)_5O_{12}$ films, substrate orientation influence on max. vel. of domain boundaries 79−15330
YIG bubble films, light scatt. from spin waves, hysteresis meas. by Voigt effect 80−15770
YIG, cylindrical mag. domains, translational motion 80−108043
YIG, double layer struct., LPE growth from molybdate and Pb borate fluxes 80−39827
YIG epitaxial films, substituted, floating bubble domains, effect of structural stratification 80−2615
YIG film, Ca, Ge-substituted, having mag. bubbles, LPE growth 78−31350
YIG film, microwave generation and manipulation 78−39378
YIG magnetic bubble domain grating, light diffr. *(German)* 79−95737
YIG:Ca films, rapid O diffusion at 25 to 250°C 77−85120
YIG:Co LPE films, with rectangular bubble domains, prep. and props. 79−82848
$Y_{2.85}La_{0.15}Fe_{3.75}Ga_{1.25}O_{12}$, inhomogeneous bubble film, spin wave reson. 77−32265
$Y_{2.85}La_{0.15}Fe_{3.75}Ga_{1.25}O_{12}$ epitaxial film, spin wave reson. spectrum 77−69703
$Y_{3-x}La_xFe_{5-y}Ga_yO_{12}$, mag. bubble film, low freq. ferrimag. reson. 78−31110
$Y_{3-y}La_yFe_{5-x}Ga_xO_{12}$, garnet film, radial oscillation of bubble lattice 79−73787
magnetic bubbles continued
$(YLuSmCa)_3(FeGe)_5O_{12}$ garnet film, bubble domain expansion, fuzzy wall struct. 80−71128
$(YLuSmCa)_3(GeFe)_5O_{12}$ bubble garnet film, coercivity 79−78459
$(YLuSmCa)_3(GeFe)_5O_{12}$ garnet films, bubble expansion saturation vel., sampling optical photography 80−75820
$Y_{1.62}Sm_{0.21}Lu_{0.27}Cu_{0.9}Ge_{0.9}Fe_{4.1}O_{12}$, implanted bubble garnet, anisotropy profile, FMR study 80−7103
$(YSmCa)_3$ $(FeGe)_5O_{12}$ mag. bubble garnets, ion implantation induced stress influence on props. 79−91274
$(YSmCa)_3(FeGe)_5O_{12}$ LPE films, optimum growth conditions for low coercivity 78−95499
$(YSmCa)_3(FeGe)_5O_{12}$ films, cc $(YSmLuCa)_3(FeGe)_5O_{12}$ films, mag. bubble props. mag. bubble props. and LPE conditions 79−74107
$(YSmCaLu)_3(FeGe)_5O_{12}$, bubble film inhomogeneity, spin wave reson. meas. 80−44439
$Y_{2.6}Sm_{0.4}Fe_{3.8}Ga_{1.2}O_{12}$, garnet films, LPE growth, mag. anisotropy field control 77−69642
$Y_{3-y}Sm_yFe_{5-x}Ga_xO_{12}$ film, LPE process exam. by induced striation 77−69643
$Y_{2.6}Sm_{0.4}Fe_{5-x}Ga_xO_{12}$, epitaxial, domain wall crit. vel., effect of material parameters 79−99740
$Y_{2.6}Sm_{0.4}Ga_{1.2}Fe_{3.8}O_{12}$ film, ion-implanted, bubble domain behaviour 77−12177
$(Y_{1.5}Sm_{0.3}Lu_{0.3}Ca_{0.9})(Fe_{4.1}Ge_{0.9})O_{12}$, growth reproducibility, static bubble props. 77−16130
$(YSmLuCa)_3(FeGaGe)_5O_{12}$, reproductibility in bubble garnet LPE growth 78−92204
YSmLuCaFeGe garnets, growth and temp. characts. of small bubbles 78−80183
$(YSmLuCa)_3(FeGe)_5O_{12}$, mag. props. and growth of 2 μm bubbles 78−91910
$(YSmLuCa)_3(FeGe)_5O_{12}$, LPE growth, growth reproducibility of bubble props. 78−92208
$(YSmLuCa)_3(FeGe)_5O_{12}$ films, mag. bubble props. and LPE conditions 79−74107
$(YSmLuCa)_3(FeGe)_5O_{12}$ film, bubble propagation direction effects on high frequency bias margin 79−78480
$(YSmLuCa)_3(FeGe)_5O_{12}$, double layer struct., LPE growth from molybdate and Pb borate fluxes 80−39827
$(YSmLuCa)_3(FeGe)_5O_{12}$, bubble material, dynamic characterisation, comparison between transport and FMR methods 80−39833
$YSm_{0.5}Lu_{0.7}Ca_{0.8}Ge_{0.8}Fe_{4.2}O_{12}$ film, magnetic bubble propagation with 8 μm period ion implanted propagation patterns 79−78475
YSmLuCaGeIG, mag. props. and defects, depend. on B_2O_3 conc. on growth in PbO-B_2O_3 solvents 78−68321
YSmLuCaGeIG films, epitaxial growth with 3 μm magnetic bubbles 79−61518
$(YSmLu)_3(FeGaSc)_5O_{12}$, submicron mag. bubble garnet 80−54929

magnetic circuits
see also transformer magnetic circuits
air gap field configuration rel. to pole piece geometry and material inhomogeneity 79−30500
current transformer, zero-flux, for AC/DC current meas. up to 25 kA 77−30177
direct-reading displacement digitiser construction and coding *(Russian)* 77−9983
electromagnet pole-piece design, air gap field computation 79−41295
electron optical element computation by finite element method 79−31785
electrotechnical steel, quality significance on energy and materials savings in magnetic circuits *(Czech)* 80−20947
induction motor, polyphase, at no-load, nonlinear magnetostatic field determ. 78−33647
linear induction MHD machine, elec. cond. body motion in mag. field *(Russian)* 77−7468
loss meas. by warming/cooling method 77−57368
low permeability or saturated parts with permanent magnet, analytical calc. *(German)* 80−23596
MHD magnetic circuit, field calcs. *(Russian)* 77−3883
NMR radiospectrometer electromagnet field uniformity rel. to pole piece shape and material 78−86309
nuclear fusion expt., switch for mag. cct. supply *(German)* 78−37441
permanent magnets in instruments with partially closed mag. ccts., meas. errors *(Russian)* 77−67480
photocardiogram contact microphone 77−21634
pulsed gap field geometry, skin effect, numerical calc. 77−573
slotted boundary machine field soln., conformal transformation and integral methods 79−41272
theory by analogy with electric ccts. 79−27123
transducer, matrix eddy-current, with magnetic circuit, design and construction 80−68228
transducer for force meas. *(Russian)* 77−65021
Co permanent magnet material savings *(German)* 80−103851

magnetic circular dichroism
activated crystals, Jahn-Teller effect in optical bands of impurity centres 78−6706
alkali halide, Tl$^+$-type centres, struct. of Jahn-Teller induced B absorption band 77−12410
alkali halides, doped, optical absorption and MCD spectra, Gaussian quadrature calc. 80−7367
alkali halides, F-centres, optical pumping, spin-orbit and hyperfine coupling 77−16360
alkylammonium iodides, solns., MCD spectra of iodide ions 78−94268
allene, gas and soln., UV absorpt. and MCD spectra 79−50056
amphotericin B in H_2O and hydroalcoholic solns., circular dichroism, Rayleigh scatt., absorpt. spectra, temp. depend. *(French)* 78−62807
aniline, IR absorpt. and MCD spectra, Rydberg transitions 77−27068
[4N+2]annulenes, MCD spectra, B terms, semiempirical models 77−6814
(2,2) (2,6) azulenophanes, mag. circular dichroism and anomalous fluoresc. spectra 80−83398
benzene, $^1B_{1u}$ state, vibronic mag. rot. strengths and oscill. strengths, CNDO/S calcs. 77−34670
benzene, and methyl derivatives, $^1E_{1u}$ N-V state mag. moments, MCD obs. 80−23575
benzene, mono-substituted, MCD, CNDO/S calcs. using capable ang. momentum operator 77−46587
benzene, p-disubstituted, MCD and absorpt. spectra, PPP calcs. 78−66574

magnetic circular dichroism continued
benzene, symmetry forbidden transitions in MCD and electronic spectra 77−65494
bromomethane, mol. Rydberg transitions mag. circular dichroism 80−43081
carbonyl group, mag. rot. strength of spin-forbidden transitions 77−14468
chlorides, I^- or Br^- doped, optical investigation of atomic hydrogen centres 78−88351
chlorophyll a and protochlorophyll a, optical transitions anisotropy 79−43825
chromophores, semiempirical rules in circular dichroism, Cotton effect sign correl. with stereochem. 80−1006
commercial circular dichroism instruments, magnetic shielding problems 77−87807
conjugated molecules, linear and mag. cir. dichroism interpretation 78−62835
coronene, excited state Faraday values mag. circular dichroism spectra and MO CI calcs. 80−18877
cubic crystal Zeeman anisotropy in absorpt., emission and MCD, eigenfunctions 77−55773
cubic crystals, isotropy of MCD 78−10872
cyclic π-electron systems 77−88481
cyclopentadienyl Ho(III), cyclooctadienyl sandwich compound, mag. circular dichroism and absorption spectra, anal. 80−23449
decacyclene, MCD and absorpt. spectra 79−54875
deoxyhaemoglobin, ferrous heme of high-spin type, MCD spectra in Soret, visible and near IR regions 80−94156
dialkylammonium copper chlorides, mag. and struct. transitions, IR absorption 77−52097
diamond, irradiated, MCD spectrum of GR1 line, neutral vacancy model 77−69850
dichrograph for measuring dichroism in 200 to 850 nm region 80−101806
N,N-diethylaniline, IR absorpt. and MCD spectra, Rydberg transitions 77−27068
ditetraethylammonium manganese bromide $^4T_1$ excited state, absorpt., MCD, Jahn-Teller model 78−43907
electric dipole allowed transitions, long-range dispersion-induced circular dichroism 79−81196
electronic spectra of molecules, pure elec. quadrupole transition polaris. 80−63691
ethylene, near vac. UV MCD obs., assignments, new transition 77−38684
europium ethylsulphate nonahydrate, MCD due to mag. dipole transitions 77−24825
ferrimagnetic single crystal layer, light diffr. by mag. bubbles *(German)* 79−56769
ferromagnetic sol, relaxation of mag. birefr. and dichroism 79−57301
group theoretical techniques, one-electron reduced matrix elements 80−45048
haemoglobin, ferrous high-spin derivatives, MCD at room and liq. N_2 temps. 78−76997
heavy atom, parity violation in forbidden mag. transitions, chiral absorpt. of polarized light and circular dichroism in crossed DC fields 80−23370
heterocycles, five membered ring, MCD spectra dnd π-electron approx. calcs. 79−812
hexabenzocoronene, MCD and absorpt. spectra 79−54875
inorganic materials, spectroscopic appls. of magneto-optics, review 77−52050
iodoform, soln., MCD spectra, assignments 79−31567
ketones, saturated, MCD spectra, forbidden transitions generated by struct.-vibr. perturbations 77−50460
Kramers-Kronig transforms, Fourier method numerical soln. by computer 78−2825
light diffraction in mag. bubble fields 79−73904
magnesium porphin soln., mag. circular dichroism spectra, Jahn-Teller coupling 77−3391
magnetic liq. birefringence and dichroism kinetics, Brownian diffusion *(Russian)* 78−5806
magnetic materials, transparent, optical studies of phase transitions 77−66481
matrix isolated species, mag. circ. dichroism and mag. circularly polarised luminesc. 78−46379
matrix-isolated high-temp. molecules, apparatus for meas. of spectra 80−86356
metallophthalocyanines, α-phase solid, absorpt. and MCD spectra 79−73964
methyl iodide, mag. circular dichroism, mol. Rydberg transitions 78−66573
methylene iodide, soln., MCD spectra, assignments 79−31567
molecular forbidden transitions, generated by struct.-vibr. perturbations 77−50459
molecule, moment summation method 77−27102
myoglobin, ferrous high-spin derivatives, MCD at room and liq. N_2 temps. 78−76997
nematic-chiral-dye mixture, circular dichroism, selective light scatt. *(Russian)* 80−103944
optical instrumentation, atomic and mol. structure determ. 78−54466
oxy- and deoxyhaemoglobin, optical spectra, dichroism 79−20514
paramagnetic matrix isolated species, MCD spectrosc. appls. 78−46378
paramagnetic system with quadrupole splitting, magneto-optical effects, magnetic resonance saturation 80−60404
peroxidase, ferrous high-spin derivatives, MCD at room and liq. N_2 temps. 78−76997
peroxidase, low-temperature radioreduction, MCD and absorpt. spectra 78−31763
phenylalanine, and derivatives, circ. dichroism and mag. circ. dichroism 79−87418
photoacoustic spectroscopy, dichroism meas. 78−62227
polarisation ellipse, rel. to MCD and Faraday rot. meas. 77−43975
polyacenes, MCD, CNDO/S calcs. 77−79637
polymer, magneto-optical props., MCD, Frenkel exciton model 78−10873
porphin, MCD, LCAO MO SCR π-electron calcs., PPP approx. 78−9178
porphyrin a, MCD, LCAO MO SCR π-electron calcs., PPP approx. 78−9178
potassium halides, F-centres, optical pumping, spin-orbit and hyperfine coupling 77−16359
protoporphyrin, MCD, LCAO MO SCR π-electron calcs., PPP approx. 78−9178
recorder calibration at 10.6 μm 80−90876
ring laser props., optical elements with mag. circular dichroism 79−31951
Rydberg transitions, field effects in vacuum UV region 78−66561
saturation of MCD/MCPL, appl. to $D_{\infty h}$ mols. and subgps. 78−74687
semiconductor, dichroism at E_1 edges 78−92051
semiconductor, MCD due to free carriers 78−56462
signal controller for photomultiplier output in magnetic circular dichroism 77−67511
sodium uranyl acetate, absorpt. spectra, MCD and natural dichroism, UV and visible 79−69853
spectroscopic apparatus, permanent mag. interface, rot. system 78−62232
spectroscopy, variable-temp. cryostat design and construction 77−22554
di-(tetraethylammonium)tetrahalomanganate, mag. circular and linear dichroism obs. 80−29725
theory rel. to impurity absorpt. in crystals 77−8556
thiophene, mag. circ. dichroism, vis. transitions 77−83628
TiO in Ar matrix, meas. of MCD spectra 80−86356
transition metal complexes, ligand field spectroscopy, selection rules, intensity enhancement of forbidden transitions 80−45049
transition metal trinuclear carbonyl complexes, electronic structures. and spectra 79−59480
tribenzo [12] annulene, monovalent anion, MCD and absorpt. spectra 78−70859
triphenylene, excited state Faraday values mag. circular dichroism spectra and MO CI calcs. 80−18877
triphenylene positive ion, MCD spectra, test of pairing theorem 79−31565
two-photon magnetooptic effects, theory 77−83629
two-photon MCD 79−76457
uranyl complexes, MCD spectra, electronic struct. of lowest excited states *(Japanese)* 79−27014
zinc porphin soln., mag. circular dichroism spectra, Jahn-Teller coupling 77−3391
Bi, Faraday effect and magnetic circular dichroism 80−83399
CS_2, $^3A_2$ state, triplet bands, MCD spectrum, near UV absorpt. spectrum 80−48010
CS_2, $^3A_2$-state, MCD and UV spectrum, theoretical anal. 80−48011
CaF_2:Co^{2+}, MCD spectra 77−28603
CaF_2:Dy, colour centres, antiresonance-type phenomenon in external fields 78−68529
CaF_2:Dy crystal with M centre, antiresonance line, mag. field effect 80−55138
CaF_2:Sm^{2+}(Eu^{2+}), cubic crysts., MCD absorpt. curves 77−81131
CaF_2:U^{3+}, anomalous magnetooptic props., optical detection of ESR and cross-relax. resonances 80−93287
CaF_2:Yb^{2+}, divalent ion radiative state, magneto-optical obs. 77−69893
CaO, neutron irrad., optical absorpt. lines 77−77255
CaS, phosphor, capture centre investigation 78−10951
$CdBr_2$:Fe^{2+}(Co^{2+})(Ni^{2+}), charge transfer near UV spectra, 4.2K, mag. circular dichroism 78−80378
$CdCl_2$:Fe^{2+}, magneto optical study, ferromagnetically coupled Fe(II) pairs 78−6711
$CdCr_2Se_4$ film, mag. linear and circular dichroism and Faraday rot. 79−99966
$CdCr_2Se_4$, reflectance magneto-circular dichroism 77−81120
$CdCr_2Se_4$:Ag, magneto-optical effects in impurity spectral region 80−97313
CdF_2:Co^{2+}, MCD spectra 77−28603
CdI_2-Ni^{2+}, absorption and mag. circular dichroism, spectra, phonon density of states of CdI_2 deduced 79−19913
CdTe:Mn^{2+}, magneto-optical and microwave-optical double reson. meas. of exciton band *(Russian)* 77−81087
Cl_2 in Ar matrix, MCD, emission spectrum at 13600 cm^{-1}, Zeeman anisotropy 78−82057
$Co_xFe_{3-x-y}Cr_yO_4$, epitaxial, magneto-optical props., effect of Cr^{3+} 78−52590
$CrBr_3(Cl_3)$, two-dimensional mag. insulators, cryst. field spectra, mag. circular dichroism 79−47058
$CrBr_3(Cl_3)$, two-dimensional mag. insulator, cryst. field splitting, spectroscopic g-factors 79−47059
$Cr(CO)_6$, MCD spectra, charge transfer transitions 80−95658
CsBr(Cl), spin-lattice relax. of F-centres, magneto-optical meas. 77−43884
$Cs_3Cr_2Br_9$, Cr (III) trigonal pair, exchange interactions, absorpt., MCD and Zeeman spectra 78−19009
$Cs_3Cr_2Cl_9$, optical absorpt., MCD, exchange interactions 78−10917
CsF, EPR of self trapped exciton and MCd meas. 77−48091
Cs_2GeF_6:Mn^{4+}, magnetically circularly polarised emission and MCD of vibronic lines 77−16377
CsI:Na, X-ray irradiated, optical and ESR studies in IR absorption band 80−80828
$Cs_2NaTbCl_6$, mag. circ. polarised emission, MCD, $^7F_J \rightleftarrows {}^5D_4$ transitions 77−77242
$Cs_2NaTmCl_6$, UV absorpt. spectra, mag. circular dichroism spectra, vibr. obs. 80−29758
Cs_2TiF_6:MnF_6^{2-}, $^4A_g \rightleftarrows {}^2E_g$ transition of Mn^{4+}, absorpt., emission, linear and MCD, MCE 78−10929
$CsUO_2(NO_3)_3$, absorpt. spectra, MCD and natural dichroism, UV and visible 79−69853
Cs_2ZrBr_6:Os^{4+}, intraconfig. absorpt. and MCD spectra 80−80776
Cs_2ZrCl_6:Os^{4+}, intraconfig. absorpt. and MCD spectra 80−80776
CuBr, evaporated film, magneto-optical effects on exciton bands 78−72624
CuCl, evaporated film, magneto-optical effects on exciton bands 78−72624
DyIG, mag. and magnetooptical props., temp. and field depends. 77−89927
$DyPO_4$, mag. phase diagram and crit. exponents 77−66307
Eu^{3+} in aq. soln. MCD spectrum, sign inversion 77−34669
Eu-Fe garnet, light mag. linear birefringence and dichroism near absorption band *(Russian)* 80−55063
$EuCl_3$, solns., $^7F_0 \rightarrow {}^5D_1$ and $^7F_1 \rightarrow {}^5D_0$ transitions, MCD 79−31566
$Eu(ClO_4)_3$, aq. soln., Eu^{3+} $^5D_{0,1,2} \leftarrow {}^7F_{0,1,2}$ transitions, MCD and absorpt. spectra 78−19446
$Fe(CO)_5$, matrix isolated species, MCD spectrosc. appls. 78−46378
$FeCl_2$, light scatt., metamagnetic transition effects 77−4513

magnetic circular dichroism continued
n-GaAs, heavily doped, test of cond. band edge random fluctuations 77−63438
GaP, ground state of indirect free exciton 77−51670
GaP, MCD of phonon-assisted exciton transitions 78−92053
GaSe, triplet indirect bound exciton, level anticrossing effect on magnetolum. 79−47513
Gd-Co-Mo amorphous film, MCD, oxide surface layer effect 77−90132
GdCo, amorphous film, MCD *(Japanese)* 78−39530
HgI_2, phonon struct. in wavelength modulated refl. spectra and mag. circular dichroism 79−8125
I_2, N_2 and Ar matrix isolated, magnetic circular dichroism spectrum 80−5567
I_2-benzene mixture, N_2 and Ar matrix isolated, magnetic circular dichroism spectrum 80−5567
KBr, F-centre luminesc., MCD effects 78−39598
KBr, F-centre spin-lattice relax., theory and MCD meas., phonon-modulated HFS 77−43883
KBr, spin-lattice relaxation time of relaxed excited state of F-centre, MCD meas. 79−61350
KBr:Au^-, optical absorpt. bands and MCD, electron-lattice interaction 80−108236
KBr:In^+, B-band, optical absorpt. and mag. circular dichroism calcs. 80−29765
KBr:In^+, mag. circular dichroism spectra line shape, lattice mode calcs. 79−82957
KBr:In^+, optical absorption and MCD spectra, Gaussian quadrature calc. 80−7367
KBr:$In^+(Ga^+)$, mag. circular dichroism meas. 79−42988
KBr(Cl)(I), electron-spin memory and magnetic-circular-dichroic effects in F-centre luminesc. 80−29794
KBr(F), orbital g-factor and spin-orbit splitting of F-centre excited state, magnetoabsorpt. and MCD 78−2886
KCl, F_2-centre triplet-triplet transition at 685 nm, MCD obs. *(French)* 77−63433
KCl, F-centre luminesc., MCD effects 78−39598
KCl, MCD of R_1 band 77−8551
KCl, mag. circular dichroism of R-center, point-ion lattice model 79−69814
KCl, magneto-optical parameters of R-centre in H_3-mol. model 77−77253
KCl:Au^-, absorption bands and MCD, electron-lattice interaction 77−55808
KCl:Au^-, absorption band shape in D-mode model 79−47485
KCl:Cu^+, exciton bands, optical absorpt. and MCD spectra 80−80821
KCl:Pb^{2+}, X-ray irrad., electron-trapped centres, Pb^+ and Pb^0, optical absorpt. spectra 80−71461
KCl:Tl^+ cryst., A band, mag. field effect 80−34897
K_2CuF_4, 2-D ferromagnet, optical and magneto-optical props. 77−52062
K_2CuF_4, two-dimens. ferromag., magneto-optical props., absorpt., MCD and MLD 79−87419
KI, F-centre luminesc., MCD effects 78−39598
KI, MCD of α and β bands 78−27192
KI, mag. circular dichroism in luminesc. of F-centres 77−20919
KI, spin-lattice relaxation time of relaxed excited state of F-centre, MCD meas. 79−61350
KI:Cu^+, exciton bands, optical absorpt. and MCD spectra 80−80821
KI:$Ga^+(In^+)(Sn^+)$, magnetic circular dichroism of A- and B-absorption band region 77−12412
KI:$In^+(Tl^+)(Ga^+)$, mag. circular dichroism meas. 79−42988
KI:Pb^{2+}, UV absorpt. and mag. circular dichroism spectra 80−25418
$KMgF_3:Co^{2+}$, γ-irrad. single cryst., visible and IR absorption, MCD, annealing data 78−10926
$KMgF_3:Co^{2+}$, MCD and linear dichroism, 3d→4s transitions 79−56768
$KMgF_3:Mn^{2+}$, MCD and linear dichroism, 3d→4s transitions 79−56768
$KMgF_3:Ni^{2+}$, absorpt., MCD and emission spectra 79−51953
$KMgF_3:V^{2+}$, MCD and linear dichroism, 3d→4s transitions 79−56768
$K_2NaGaF_6:Cr^{3+}$, mag. circular dichroism and absorption spectra 77−77254
$K_2NaGaF_6:Cr^{3+}$, magneto-optical study of $^2T_{1g}$, $^4T_{2g}$, ^2E_g-$^4A_{2g}$ transitions 80−71384
$KNiF_3$ and K_2NiF_4, MCD and stress linear dichroism on double excitonic transitions 77−52051
$KZnF_3:Ni^{2+}$, absorpt., MCD and emission spectra 79−51953
$KZnF_3:Ni^{2+}$, Mn^{2+}, interference transition electric dipole mechanism 80−34896
KrF, matrix isolated, mag. circ. dichroism, UV and vis. absorpt. and saturation 78−46379
$La_2Mg_3(NO_3)_{12}.24H_2O:Ce^{3+}$, mag. circular dichroism of Ce^{3+} 77−69869
Li ferrite film, magnetic circular and linear dichroism, temp. depend. 79−69815
Mg, matrix isolated, ^1S-^1P transition, mag. circ. dichroism obs. 79−68248
$MgF_2:Co^{2+}$, MCD and linear dichroism, 3d→4s transitions 79−56768
$MgF_2:Mn^{2+}$, MCD and linear dichroism, 3d→4s transitions 79−56768
$MgF_2:V^{2+}$, MCD and linear dichroism, 3d→4s transitions 79−56768
MgO, Fe^{2+} and Fe^{3+} conc. and valency, optical density, EPR and MCD obs. 77−89462
MgO, neutron irrad., optical absorpt. lines 77−77255
MgO:Li, $[Li]^0$ defects, magneto-optical props. 77−12365
MgO:V^{2+}, mag. circular dichroism in split zero-phonon line 78−56460
$MnCl_2$, $MnBr_2$, mag. phase diagram, optical absorption meas. 77−4514
MnF_2, MCD spectrum, Zeeman splitting of purely excitonic lines 77−40262
MnO_3Cl, matrix isolated species, MCD spectrosc. appls. 78−46378
$Mo(CO)_6$, MCD spectra, charge transfer transitions 80−95658
MoS_2, excitons 79−23900
$MoSe_2$, excitons 79−23900
NaBr(Cl), spin-lattice relax. of F-centres, magneto-optical meas. 77−43884
NaCl(Br), orbital g-factor and spin-orbit splitting of F-centre excited state, magnetoabsorpt. and MCD 78−2886
NaI:F, electron-lattice coupling of F-centres, optical props. 80−60641
Na_2O-SiO_2 glass, magnetooptical props. 78−80318
Na_2O-SiO_2-$Pr_2O_3(Ho_2O_3)$ glass, magneto-optical props. 79−65894
$Na_3Pr(C_4H_4O_5)_3.2NaClO_4.6H_2O$, absorpt., circular dichroism, and mag. circular dichroism spectra 80−97243
$NdMoO_4$, photoacoustic spectroscopy, dichroism meas. 78−62227
Ni film, temp. depend. of magneto-optical effects 77−81167
Pr^{3+} aquo ion spectra, MCD of $^3P_0$←$^3H_4$ transition 80−7331

magnetic circular dichroism continued
RbCl:Au^-, optical absorpt. bands and MCD, electron-lattice interaction 80−108236
$RbNiF_3$ and Rb_2NiF_4, MCD and stress linear dichroism on double excitonic transitions 77−52051
Si, ground state of indirect free exciton 77−51670
SiO_2-Na_2O-Nd_2O_3 glass, magneto-optical props., absorpt. spectrum 80−88969
$SrCl_2:Cu^+$, exciton bands, optical absorpt. and MCD spectra 80−80821
SrO:Co^{2+}, EPR, optical, MCD absorpt. spectra 78−43692
$U(BH_4)_4$, in $Hf(BH_4)_4$, excited state assignments and E-symmetry ground state, near IR MCD obs. 80−66153
$V(CO)_6$, paramag. matrix isolated species, MCD spectrosc. appls. 78−46378
VI_2, MCD spectra, interpretation rel. to mag. struct. 80−66222
$W(CO)_6$, MCD spectra, charge transfer transitions 80−95658
WS_2, excitons 79−23900
WSe_2, excitons 79−23900
XeX, (X=F,Cl,Br,I), Ar matrix isolated, MCD, low temp. depend., spectroscopic parameters calc. 77−38682
$YCrO_3$, mag. circular dichroism and Faraday rotation in R-lines region 79−28725
$Y_3Fe_{5-x}Sc_xO_{12}$, garnets, magnetooptical spectra, 15000-21000 cm^{-1} 77−90131
YIG films, MCD spectrum 79−28722
YIG, MCD meas. by retardation modulation technique 80−16014
YIG: Ca^{2+} epitaxial films, Fe^{4+} centres, MCD, optical absorpt., and thermoelectric power meas. 78−95595
YIG:Nb, tetrahedral Fe^{2+} detect. by induced anisotropy ang. variation 79−11311
YIG:Ru, optical absorpt. and MCD obs. of Ru^{4+} site occupancy 80−71456
YIG:Si, enhanced photoinduced mag. circular and linear dichroism 77−52053
YIG:Si, relative Fe^{2+} ion conc. depend. 77−48150
YIG:Sn, IR absorpt. and MCD 78−19447
YIG:Sn, mag. circular dichroism orientation depend., optical absorpt. 79−99914
YIG:Zr, near IR absorpt. and magnetic circular dichroism 80−60580
ZnS, phosphor, capture centre investigation 78−10951
ZnS:Mn^{2+}, $^4T_1$ excited state, absorpt., MCD, Jahn-Teller model 78−43907
ZnSe, magnetoreflectance of exciton-polaritons, semiclassical treatment 79−99857

magnetic clutches *see clutches*

magnetic cooling
adiabatic demagnetisation, calc. of lowest temps. obtainable *(Dutch)* 77−61072
adiabatic demagnetisation of nucl. spins, refrigeration 78−49844
adiabatic demagnetisation using near nπ RF pulse strings 77−90050
hyperfine enhanced nuclear magnetic cooling 79−1674
magnetic refrigerator for operation near 2K 78−37012
magnetic refrigerators for use at room temp. and below 79−67314
neodymium ethyl sulphate, cryst. c-axis demag. from 25000G, magneto-hydrodynamic props. to 0.01K 77−20599
nuclear demagnetisation refrigerator, double range, microkelvin range 80−31769
nuclear demagnetisation refrigerator, two stage *(Japanese)* 80−47063
nuclear demagnetisation refrigerator, two-stage 80−52244
nuclear demagnetization refrigerator, sintered Cu heat exchangers 79−58696
nuclear spin system, ultra low temp., nuclear adiabatic demagnetisation *(Japanese)* 79−12807
one-dimensional system obeying third law of thermodynamics, exact theory of mag. cooling 77−66321
paramagnets with antiferromag. Ising interactions, mean-field formalism 77−36076
reciprocating magnetic refrigerator for 2-4K operation 80−2577
rotating Carnot-cycle magnetic refrigerators for use near 2K 78−57965
S=1, singlet ground state systems, mag. props. 80−11157
spin refrigeration of $(Yb,Y)(C_2H_5SO_4)_3.9H_2O$ cryst. in nonuniform mag. field 77−83435
Stirling cycle wheel, refrigerator and heat engine modes of operation 78−57964
TCNQ salt, $Qn(TCNQ)_2$, Heisenberg antiferromag. chain for low temp. thermometry and cooling, EPR expts. 79−63217
$AuIn_2$, pulsed NMR expts, rel. to performance as nuclear refrigerant 79−61259
$CaF_2:Tm^{2+}$, single cryst., ^{19}F nucl. spin cooling of Tm^{2+} electronic spin *(French)* 77−66440
$(Ce_xLa_{1-x})_2Mg_3(NO_3)_{12}.24H_2O$, adiabatic demagnetisation temp., mag. entropy *(Russian)* 80−65892
Cu adiabatic demagnetisation for nucl. refrigeration of ^3He 79−67315
$Cu(NO_3)_2.2.5H_2O$, spin-pair system, spin ordering, XY-model in external field 77−73033
$Cu(NO_3)_2.2.5H_2O$, adiabatic magnetisation cooling by pulsed mag. field 77−20600
Fe-Cr-Co alloys, (5-9 wt.% Co), obtained by slow cooling under mag. field, permanent magnet props. 80−75797
Fe_3O_4, NMR exam. of low temp. phase 78−56401
n-Ge EM wave interaction with hot electrons, in strong mag. field with Voigt config. 77−69367
H_2, solid, adiabatic demagnetisation of stabilised H atoms *(Russian)* 79−82412
^3He, by double bundle nuclear demagnetisation refrigerator, design and construction 78−93692
^3He, cooling by double bundle nucl. demagnetisation refrigerator atom to 0.4 mK 79−49236
^3He, demagnetisation expt. using hyperfine nuclear cooling capability of $PrNi_5$ powder 79−44909
^3He melting curve obs. by Pomeranchuk cooling 79−7731
^3He, solid, production and obs. of ordered state, adiabatic demagnetisation *(French)* 77−59173
^3He, solid, strongly magnetised, low-temp. melting props. possible adiabatic demagnetisation 77−11765
$HgCr_2S_4$, cooling efficiency near 60Kas mag. refrigerant 80−71034
$HoVO_4$, enhanced nuclear cooling and antiferromagnetism 79−61070
$La_2Mg_3(NO_3)_{12}.24H_2O:Co^{2+}$, Ce^{3+}, relax. and ESR in magnetically cooled systems 78−88225

magnetic cooling continued
LiH, mag. domains and nucl. mag. ordered phases, antiferromag. and ferromag. neutron diffr. obs. 80−50051
LiH, nuclear antiferromagnetism, dynamic nuclear polaris., NMR 79−1724
LiH, nuclear ordered ferromag. and antiferromag. phases, neutron diffr. study 80−50052
N_2, solid, adiabatic demagnetisation of stabilised N atoms *(Russian)* 79−82412
Ne solid, ultraslow diffusion of ^{21}Ne, adiabatic demagnetisation in rotating reference frame 77−73095
^{17}O, NQR at natural isotope abundance, double reson. new techniques using adiabatic demagnetisation, review 80−53013
Pr intermetallic compounds, singlet ground state magnetism, hyperfine enhnaced nuclear cooling *(Japanese)* 79−51744
$PrBe_{13}$, hyperfine enhanced nuclear mag. cooling 79−63216
$PrNi_5$, nucl. demagnetization, end temps., nucl. entropy 79−19718
$PrNi_5$, nuclear demagnetisation, cooling of ^3He to 1 mK 77−65037
PrS, nucl. demagnetization, end temps., nucl. entropy 79−19718
$TmVO_4$, enhanced nuclear cooling and spin-lattice relax. time 80−80632

magnetic cores
amorphous magnetic alloys, review, engineering magnetic props. and potential applications 80−71078
amorphous toroidal core, switching characts. and domain structs. 78−95477
complex mutual inductance concept for bioelectric impedance transformer bridge 80−63886
DC permeameter for ring specimens 80−98954
ferrite, appl. to reluctance transducers *(Polish)* 78−29100
ferrite, strength improvement method, SiO_2 and Bi_2O_3 additions, mag. characts. 79−24484
ferrite pot core pressure transducer development and compensation 79−75519
ferromagnetic materials, grain-oriented demagnetisability 78−84449
ferromagnets, cyclically remagnetised, discrete spectra of induction calcs., demagnetising factor 80−103859
ferroprobes characteristics alteration, by using composite cores 77−87796
floating-core flux-gate compass design and operation 77−71354
gapped pot core and Permalloy foil pressure transducer 79−75520
hysteresis loop rectangularity rel. to anisotropy in polycryst. mat. 78−27056
iron core inductor time invarying inductance meas. method 78−62207
magnetic field of current ring 77−569
magnetic particle crack detection, remanent magnetism 77−63841
magnetostrictive core dimens., influence on internal friction and shear modulus 'defect' 78−95506
multivibrators, tensile stress measurement appl. 78−9615
Permalloy thin film cores, domain wall motion and flux patterns, Kerr magneto-optic effect obs. 80−34721
production method, ferromag. probe appl. 78−44334
'Pulsed ferrite core tests for 50-ns linear induction accelerator' 79−690
ring core flux-gate thickness transducer with permanent magnet 79−67280
Rogowskii loop with ferrite core, precision meas. of high-power current pulse 78−4639
saturated flux density measurement using compensation technique, for cores with square hysteresis loop *(Russian)* 79−54158
tape cores carrying current, torsional stress effects 80−34742
temperature sensitive, appl. to new temperature telemeter 79−199
toroidal core with invertor circuit, for mag. field meas. 77−82577
transformer, 1000 kVA, vibration calc. method 77−74219
transformer, use of high permeability Fe-Si materials 80−88793
transient skin effect in laminated cores with sectionally different material props. *(German)* 79−41280
$(Fe,Ni)_{83}B_{15}C_2$ amorphous alloy core, mag. props. 79−28558
$(Fe,Ni)_{80}P_{14}B_6$ amorphous alloy core, mag. props. 79−28558
Fe, atomised powder compacts for mag. cores, oxidation, compressibility, heat treatment *(Japanese)* 78−72752
Fe, atomized powder compacts for mag. cores, mag. props., green densities *(Japanese)* 78−72751
Fe core coils, mag. field dispersion 79−64139
Fe laminated cores, eddy currents calc. in arbitrarily shaped three-dimens. cores, appls. *(German)* 79−45886
Fe, three dimensional arbitrarily shaped cores, eddy currents calc. *(German)* 80−18956
Fe-Ci, high permeability, mag. props., applied stress effects 80−34726
Fe-Ci (3 wt.%), commercially produced, grain-oriented, mag. props., stress coating effects 80−34727
Fe-Co-Si (4,1.5 wt.%), textured, mag. props. 80−35200
Fe-Ni alloy, low-noise, for cores of ferromag. probes and mag. modulators 79−8017
Fe-Ni alloy toroidal core, magnetic noise *(Russian)* 78−60308
Fe-Ni-Co-Mo-Ge alloy 40NKM, excess mag. noise after various thermomag. treatments *(Russian)* 80−29575
Fe-Si, grain oriented transformer sheets, permeability and magnetostriction, tensile stress effects 80−88843
Fe-Si, influence of stress on rotational loss, lamination appl. 78−35384
Fe-Si, mag. props., stress and reannealing effects 80−88844
Fe-Si, stator core, grain-oriented and non-oriented, magnetic flux and loss distrib. 80−88798
Fe-Si, steel sheet static mag. props., elastic tensile stress effect 78−47999
Fe-Si (3 wt.%), grain oriented tape-wound core, dynamic domain size var. and Fe losses 77−12146
Fe-Si (3 wt.%), mag. props., stress coating effects 80−34728
Fe-Si (3 wt.%), transformer steel, grain-oriented, magneto-optical domain obs., magnetisation mechanism 77−12364
Fe-Si (3 wt.%), transformer laminations, processing and props. 78−52325
Fe-Si (3 wt.%) cores with insulative coatings, morphological and struct. SEM characteris. 78−23881
Fe-Si (3 wt.%) steel, oriented, stress depend. mag. props., coating effects 80−34729
Fe-Si(6.5 wt.%) steel, core mat. development *(Korean)* 78−60852
$Li_{0.5}Mn_{0.15}Fe_{2.35}O_4$ ferrite cores with rectangular hysteresis loops, pulse parameters, effect of Fe_2O_3 heat treatment 80−60370
MnZn ferrite, mag. permeability spectra, 0.001-100 MHz range *(Russian)* 77−8355

magnetic cores continued
Ni-Fe alloys, pulse permeability and loss in toroidal core pulse current transformers 78−43615
NiZnCo ferrites, voltage response under sinusoidal and pulse magnetisation effected by hydrostatic press. 80−88846

magnetic devices
see also clutches; ferrite devices; magnetic amplifiers; magnetic lenses; magnetic storage devices; magnetic thin film devices; magnetostrictive devices
AC demagnetisation apparatus, palaeomagnetic research appl. 78−85733
active permanent magnet suspensions, scientific instruments appls. 78−24829
alternating magnetic field, 2.5-5.8 Hz, for psychosomatic complaint treatment 78−15878
amorphous magnetic alloys, review, engineering magnetic props. and potential applications 80−71078
angle convertor accuracy test method 78−77948
brush development characteristics for xerography 80−4798
ceramic suspension, ferromagnetic filtration apparatus improvement 78−11561
coercivity meter with portable display system 78−53135
cold rolling rolls, magnetic inspection at heat treatment quality 78−88613
compact cyclotron, magnetic analyser 78−66439
conference, Florence, Italy (May 1978) 78−91833
conference, Los Angeles, Calif., USA (June 1977) 77−85400
conference on magnetism and mag. materials Cleveland, USA (Nov. 1978) 79−73651
constant magnetomotive force, testing and anal. using mag. potentiometer 78−62210
damper for satellite stability, asymptotic theory *(Russian)* 79−30496
defectoscopes, nonsinusoidal periodic currents meas. 80−104386
discharge manometric convertor 80−31779
displacement sensor *(Japanese)* 79−12761
dual-spin satellite magnetic attitude control system, geomag. field effects 78−65484
dynamic quantities sensing devices *(Japanese)* 79−12776
eddy-current flaw detection of long ferromag. products, magnetizing device parameters 80−89447
electromagnetic probe, of thickness gauges, linearisation of output signal 78−56862
electron spectrometer for TEM energy analysis 79−26190
EM flowmeter, for industrial appl. 80−1701
energy conversion devices using mag. liqs., long term stability 77−29051
explosive mag. generator, magnetic accumulation in plane liner, flux loss and equiv. cct. 79−14571
ferromagnetic material, NDT stress determ. by portable magnetic equipment 78−53172
ferromagnetic material NDT, magnetising device, stabilization of Barkhausen discontinuities 80−89457
ferromagnetic plate, surface magnetostatic wave excitation 80−25119
ferromagnetic probe, with square cross section, numerical computation of eddy current phenomena *(German)* 78−77951
ferromagnetic probe inspection unit for automatic inspection of welded tubing 78−56860
ferromagnetic probe unit, MD-10F, automatic 78−56861
flaw detection system for underground pipeline insepction 78−53103
flaw detector, using magnetic powder method 77−90571
flowmeter, EM type, optimal mag. system design *(Russian)* 79−1275
flowmeter construction and reliability 79−23386
flowmeters, bubble noise effects on output signal, Na loop test 78−91038
galvanomagnetic transducers, steady pressure effects 77−79129
HF magnetic chopper for polarised neutrons 77−14293
high resolution sensor advances *(Japanese)* 79−12826
homogeneous magnetic field sources, for studying NQR devices characts. 77−61102
hysteresis-free magnetic transducer, features *(Russian)* 78−86305
imaging magnetic energy filters free of second-order aberrations, optimization 80−4816
impedance type ferromagnetic probe sensors for magnetic inspection 78−48599
induction defectoscope with adjustment 78−53105
ion source, magnetic-discharge pump for pulsed H injection 77−23318
magnetic soft and hard materials, garnets, magnetic properties and applications, structural props. 80−65760
magnetism and magnetic materials conf., Pittsburgh, USA (June 1976) 77−12071
magnetodynamic method of part inspection 79−96272
magnetoferroprobe rail defectoscope, MRD-72, electronic circuit 78−53128
magnetographic flaw detector for monitoring cylindrical articles 80−35478
magnetohydrostatic laboratory systems, design and appl. 78−74812
magnetostatic separator, ferrofluid free surface shape, suspended in mag. gap *(Russian)* 79−876
magnetostrictometer, rotating field, YIG, magnetostriction meas. 78−12733
magnetovibration analyser for magnetite suspension 78−4668
mass separator with low stray fields 77−10133
micromagnetic susceptometer with variable temp. 4.2K to 300K for small sample meas. 80−73395
modulator operating near Curie point temp., equivalent input noise study 77−74462
momentum filter for separation of electrons and negative ions 78−78034
Mossbauer ferritometer 79−17453
noise reduction of second-harmonic-type magnetic modulators 78−70168
nuclear demagnetisation refrigerator, double bundle, for ^3He cooling, design and construction 78−93692
particle separator for aerosols in airflows 77−4945
pickup for shock wave meas. 78−5707
plating thickness meas. with MIP-10 78−53144
position sensor, differential, built with magnetic resistances *(Italian)* 79−85155
proton storage ring, NAP-M, mag. and vacuum system 77−65362
rectangular field coil with split winding, uniformity condition 78−41335
resistance strip electron multiplier, protons and H atoms detect. efficiency 77−10552
resonant bending fatigue apparatus for approx. determ. of dislocation density 77−86279

magnetic devices continued
rolled sheet thickness effect in magnetic inspection of mech. props. 79−91894
seals, mag. liquid, using ferrofluids 79−43637
sector mag. analyzer, compact notation of second-order ion-optical coeffs. 80−63911
separation, dynamics of particle attracted by magnetised wire, theory 77−84307
separator, high gradient, mag. traction force in ordered matrix 78−50674
separator equations, approx. solns. 78−74811
shield, particle scatt. props. 79−21791
steel, crankshaft forgings, by type NChG instrument 78−53133
steel 40 G, coercimeters with attached electromagnets used for quality control 80−108672
suspension densimeter, simplified, for absolute density meas. 77−30132
theory of attachment having magnetic circuit 79−30498
thermo-sensors utilizing temperature-sensitive magnetic characteristics *(Japanese)* 79−12790
thermomagnetic gas analysers, for use in power stations *(Russian)* 80−3445
thermometer, for 2K to 30K range 77−5850
thickness gauge, stressed condition effect on reading for Ni galvanic plating 78−88611
thin rolled sheet, IMA-4 impulse magnetic analyser 80−35470
weld joint, furnace welded pipe inspection unit for above 1000°C 78−53134
$Ce_xLa_{2-x}Mg_3(NO_3)_{12}.24H_2O$, magnetically diluted thermometer 79−17420
Ni-Fe soft magnetic alloys, developments and components *(Hungarian)* 78−48000

magnetic dipoles *see magnetic moments*

magnetic disc and drum storage
flexible disc/head interaction analysis 80−92093
intraoperative X-ray diagnosis, exposure reduction by magnetic disc store 79−92345
IR spectrophotometer, digital data acquisition/analysis system 80−73482
signature analysis systems with Fourier analyzer 78−87195

magnetic disc storage *see magnetic disc and drum storage*

magnetic domain walls
activation energy of thick domain walls 79−56751
Alnico, domain struct., variation under influence of heat treatment *(Russian)* 78−23292
amorphous ferromagnet with random uniaxial anisotropy, hysteresis, magnetisation 77−80963
amorphous ferromagnetic alloys, domain struct. and mag. microstruct., review 80−15751
amorphous magnetic materials, review 79−82839
amorphous ribbons, twisted, magnetisation process, domain theory 80−71101
anisotropic materials, magnetisation reversal, 1/H law 78−84454
antiferromagnet, domain boundary movement, thickness depend. *(Russian)* 78−43611
antiferromagnet, domain wall eqns. of motion *(Russian)* 78−27054
antiferromagnet, first-order orientational phase transition, second acoustic-harmonic generation 78−27067
antiferromagnet, interphase boundary dynamics, domain wall motion and scatt. *(Russian)* 80−108032
antiferromagnet, nonlinear magnetisation waves *(Russian)* 79−91251
antiferromagnet, rel. to dislocations *(Russian)* 77−51919
antiferromagnet, with weak ferromagnetism, domain struct. theory 78−47997
antiferromagnets, magnetoacoustic resonance of domain boundaries *(Russian)* 80−65636
antiferromagnets, nonlinear waves 80−84612
antiferromagnets in high-freq. mag. field, domain struct. 79−65694
asymmetric, width meas., extrapolation technique 77−80959
azimuthal angular rotation in domain walls during radial motion of bubble domains 79−56583
band model of ferromagnetism approach to domain struct. theory 77−80954
bitter technique, model calc. for colloid accumulation on surface in mag. field *(German)* 77−9139
Bloch wall, irreversible motion *(French)* 78−95465
Bloch wall, narrow, magnetic excitations, pole field effect 78−91853
Bloch wall bound spin waves, equations of motion 80−34612
Bloch wall containing Bloch lines, excitation spectrum 77−4527
Bloch wall displacement, rel. to rotational hysteresis in weak magnetic fields 80−75804
Bloch wall of finite size, distrib. of Neel segments *(Russian)* 78−56348
Bloch wall steady-state motion in ferromag. 78−68291
Bloch wall structure, horizontal, mag. bubble domains in implanted films 80−71131
Bloch walls, history 80−86065
Bloch walls, irreversible movements, loss contribs. from correlations 77−85483
Bloch-Neel domain wall transition, discontinuity of limiting velocities *(Russian)* 80−75788
bowing and stability 78−43609
bubble, static spin config. in cylindrical coordinates 80−54928
bubble, transverse mass in rotating gradient 80−39832
bubble collapse field, anisotropy field, and domain wall mobility, magneto-optic meas. 77−85534
bubble devices, implanted disk type, domain wall energies, effective threshold anisotropy 79−78453
bubble domains with twisted walls, calc. 78−64245
bubble film, domain wall mass, under large in-plane fields 79−95618
bubble film, domain wall oscillations and dynamic collapse, saturation velocity and ballistic overshoot theory 77−8372
bubble film, peak vel. of domain wall large in-plane field 79−19751
bubble film, quenching of coercive force by domain wall restoring forces, theory and expt. test 79−78460
bubble formation and computer storage element appls. 77−20662
bubble garnet, domain-wall dynamics in in-plane field 79−87296
bubble garnet film, fuzzy walls obs. 79−99738
bubble garnet film, saturation velocity, in-plane field effects 80−108041
bubble material, coherent precession mode of twisted wall 79−78468
bubble material, wall oscillations in presence of in-plane fields 79−56582
bubble material, wall oscillations in presence of in-plane fields 79−99737

magnetic domain walls continued
bubble peak vel., analytical method of determ. from overshoot data 79−33513
bubble propagation, turn around effect 77−12169
bubble propagation modelling, domain struct. effects 79−78488
bubble shape, eqn. of motion of domain wall 79−78467
bubble wall dynamics, review 80−75823
bubbles, hard, lattice dynamics, effect of Bloch lines in domain walls 77−32228
bubbles, horizontal Bloch line motion 80−11237
bubbles, in uniaxial crystals, static and dynamics behaviour *(Polish)* 77−69650
bubbles, stationary circular motion 80−84629
charged, zigzag form 80−44852
charged domain walls in implanted layers, theory 80−71130
charged wall behavior in 1-μm bubble implanted structures 78−91892
charged walls in mag. domain structures, energy determ. 79−47296
chevron stacks, stroboscopic meas. of strip domain expansion 80−39810
chromindur, origin of coercivity, Lorentz microscopy, magnetisation and Mossbauer effect 78−64219
chromindur, phase separation, Mossbauer obs. 78−88116
circular bubble translation motion analysis 78−14999
complementary σ-bubbles in bubble automation 79−78465
coupled fields in one dimension: cross-over from a continuous symmetry to a discrete one 78−87758
crystals, description of Bloch, Neel and periodic walls 77−59424
cubic ferromagnet, localised magnon modes in narrow domain walls 77−69523
current access device, bubble wall state coding 79−73785
cylindrical magnetic domain material coercive force meas. 77−79130
cylindrically symmetric bubbles, static and dynamic props. 80−39835
dipolar conducting liquids, rel. to mag. transport props. at ambient temp. 79−91258
dislocation interaction, flexibility, rel. to hysteresis 77−4525
domain wall states, discrimination by bubble collapse time 80−39830
drag effect in presence of variable mag. field or variable transport current 79−78433
dynamic collapse expt., in presence of inplane field 77−85479
dynamic properties of magnetic domain walls and magnetic bubbles, review 80−88784
dynamic shift of NMR freq. of nuclei located in domain walls 80−15823
dynamics of mag. domain walls and bubbles 78−14995
eddy current contrib. to effective mass 80−29570
eddy current dominated domain wall dynamics and magnetisation losses 80−88778
effective mass in magnetic-bubble material 79−24205
electron microholography obs., off-axis 78−82080
energy, orientation depend., second anisotropy const. effect 77−12143
epitaxial garnet film, mag. domain wall damping, vel. depend. 77−85517
exchange energy near singular points or lines 80−93106
ferrimagnetic Bloch wall oscills., viscosity coeffs. freq. depend., permeability and mag. losses 80−71094
ferrimagnetic film, uniaxial epitaxial, induced canted mag. struct., problem of domain wall broadening 78−35016
ferrite, domain boundary movement, thickness depend. *(Russian)* 78−43611
ferrite-garnet film, local conc. of effective mass of domain boundaries *(Russian)* 77−12179
ferro-fluid particle formation on permalloy overlay bar surface, calc. and anal. 78−68329
ferroics, secondary, polycryst., poling effects 77−16102
ferromagnet, acoustic wave scatt. and reemission by moving domain walls 77−24713
ferromagnet, anisotropic, solitary-wave solns. 79−58553
ferromagnet, Barkhausen discontinuities in model of rigid domain boundaries *(Russian)* 77−51922
ferromagnet, Bloch wall-Neel wall transformation in a mag. field *(Russian)* 79−1682
ferromagnet, Bloch walls correlation and magnetic loss 78−95456
ferromagnet, cubic, domain wall dynamics 79−73770
ferromagnet, domain wall dynamic slowing down *(Russian)* 79−78438
ferromagnet, domain wall mobility, damping, dipole-dipole interaction 80−93140
ferromagnet, domain wall motion, effect of transverse mag. field 78−68292
ferromagnet, domain wall motion, exact soln. 79−87283
ferromagnet, domain wall motion, pinning by lattice defects, magnetisation 80−71079
ferromagnet, domain wall retardation by spin waves *(Russian)* 80−25154
ferromagnet, domain walls, hypersound effect *(Russian)* 79−51810
ferromagnet, freq. const. for thermal activation 77−89976
ferromagnet, lattice coercivity of narrow domain walls 79−28552
ferromagnet, limiting velocity of domain wall motion *(Russian)* 78−56342
ferromagnet, localised nonlinear oscillations, unidimensional magnetisation soliton, analytic soln. *(Russian)* 79−78437
ferromagnet, low-field magnetoresistance and domain drag 78−68014
ferromagnet, multidomain, with 180° Bloch walls, sound generation by RF field *(Russian)* 77−32235
ferromagnet, narrow domain wall, localised modes 80−34681
ferromagnet, pinned domain wall motion, magnetic damping studies 80−65956
ferromagnet, polycrystal, magnetisation law, Bloch wall motion *(French)* 79−95606
ferromagnet, rigid boundary model, magnetisation distrib. function *(Russian)* 77−80955
ferromagnet, spin wave excitation, with moving domain wall *(Russian)* 78−88103
ferromagnet, spin waves with moving domain wall 80−39764
ferromagnet, uniaxial, coercive force associated with domain boundary pinning on plane defects *(Russian)* 78−6543
ferromagnet, uniaxial, in weak mag. field, domain wall struct. transform. 77−59425
ferromagnet, uniaxial one-dimens., role of Bloch walls in statistical mechanics 77−40079
ferromagnet in external mag. field, domain wall crit. vel. 79−38354
ferromagnet with narrow domain boundaries, magnetic reversal processes 79−87287
ferromagnet with random anisotropy, spin correlation 79−73722

magnetic domain walls continued
ferromagnetic crystal, domain wall pinning effect and intrinsic coercivity, computer simulation 78−64217
ferromagnetic crystal, magnetic damping due to pinned domain wall motion 79−56598
ferromagnetic crystal, pinning and nucleation of mag. domain walls at antiphase boundaries 80−11216
ferromagnetic crystal with defects, domain boundary displacement and magnetisation discontinuities, statistical theory *(Russian)* 79−51800
ferromagnetic domain wall, soliton theory and dynamics 80−29569
ferromagnetic domain wall dynamics, soliton theory appl. 79−82813
ferromagnetic domain wall dynamics and soliton theory, coercive force determ. 79−42796
ferromagnetic domain wall pinning, planar defects, coercive force and correl. length, soliton theory 78−31092
ferromagnetic domain wall pinning rel. to coercive force 77−1561
ferromagnetic domain wall width, comments on definition 79−24193
ferromagnetic film, ϕ^4 domain walls, magnetisation, occurrence of crit. point 78−95500
ferromagnetic film, band model of domain struct. 77−36105
ferromagnetic film, cross tie domain wall struct. and energy 77−59438
ferromagnetic film, domain wall width meas. with electron microscope, astigmatism effects 79−19753
ferromagnetic film, heterogeneity influence on static and dynamic props. of domain walls *(Russian)* 80−65974
ferromagnetic film, phenomenology of domain walls, review *(Rumanian)* 78−60324
ferromagnetic film, unipolar simple domain walls *(Rumanian)* 79−19752
ferromagnetic film domain wall profile determ. by differential phase contrast electron microscopy 79−61195
ferromagnetic film thickness meas. by diffraction electron microscopy 78−86392
ferromagnetic films, Bloch wall struct. and anisotropy, analytical representation 78−88151
ferromagnetic irreversible Bloch wall jumps and static losses 78−19276
ferromagnetic metal, transient enhancement of AC susceptibility, domain wall pinning centre diffusion 77−20633
ferromagnetic metals, domain wall motion, voltage generation 80−34679
ferromagnetic metals, with domain struct., low-temp. resist. 77−47791
ferromagnetic ordered structures, domain structure, effect of defects, electron microscopy 78−64214
ferromagnetic plate, EM wave diffr. by domain walls 79−99724
ferromagnetic plate, twisted domain wall dynamics 78−68340
ferromagnetic scalar spin systems, wall and boundary free energies 78−155
ferromagnetic superconductor, mag. domain struct., sample thickness effects 80−39704
ferromagnetic superconductor, uniaxial, domain struct. parameters 80−39705
ferromagnetic thin film, direct determ. of mag. domain wall profiles, using split detector STEM 80−103867
ferromagnetic thin film, mag. domain wall energy determ. 79−95620
ferromagnetic thin film edge domain structures, Bitter pattern. obs. 77−73063
ferromagnetic twin crystals, Bloch mag. struct., depend. on crystallite thickness and mag. field *(Russian)* 79−42792
ferromagnetics, uniaxial, domain structure, influence of rapidly oscillating mag. field *(Russian)* 77−43847
ferromagnets, anisotropic, domain-wall struct. depend. on const. and oscillating mag. fields *(Russian)* 79−69691
ferromagnets, domain boundary interaction with solute atoms, review *(Russian)* 79−42098
ferromagnets, domain struct. effects on dynamic props., review 80−34678
ferromagnets, solitary domains, Bloch and Neel stability, calcs. 80−25157
ferromagnets, spin waves in domain struct. 80−70993
ferromagnets and antiferromagnets, EM and acoustic energy attenuation in many-domain magnets 80−7140
film, Barkhausen effect, general behaviour and stationarity along hysteresis loop 78−56357
film, charged domain walls, variational method calc. 80−11235
film, domain wall discontinuities during pulsed mag. reversals *(Russian)* 78−48008
film, domain wall struct. by Faraday effect 79−65702
film, micromagnetic dynamics, numerical integration of Landau-Lifshitz-Gilbert eqn. 79−56580
film, micromagnetic dynamics, numerical model 78−72382
film, validity of one-dimens. wall theory for bubble materials 78−56361
film strip, anisotropic, wall motion meas. *(German)* 79−28573
films, domain wall energy analysis 79−99721
films and plates, nonlinear oscills. of domain boundaries *(Russian)* 78−56358
frustration network, phase transitions 80−2596
garnet, bubble conversion to anomalous behaviour 78−23309
garnet, film, bubble domain, saturation velocity, empirical relation 78−95496
garnet, ion-implanted film, crit. curves for determining magnetisation directions 79−91263
garnet, low loss bubble material, wall struct. changes 77−89994
garnet, uniaxial, phase diagram, domain wall struct., near compensation point *(Russian)* 77−12149
garnet bubble film with induced anisotropy, domain wall energy 79−19750
garnet bubble materials, low loss, mag. domain wall dynamics 78−10738
garnet crystal, planar wall mobility, computer simulation and meas. 77−12148
garnet film, domain wall, dynamics, time depend. effects 77−12168
garnet film, domain wall displacement in pulsed field 77−16129
garnet film, dynamic behaviour of domain walls and bubbles 78−52321
garnet film, ion implanted bubble propag., wall states 77−16128
garnet film, LPE, stripe domain, time resolved obs. of contracting motion 77−85519
garnet film, physics of domain walls 79−99727
garnet film, wall velocity at high drive fields 77−85518
garnet film bubble material, domain wall mobilities 77−85513
garnet film in mag. field, domain dynamics *(Russian)* 79−4711
garnet films with orthorhombic anisotropy, domain wall motion 80−80580

magnetic domain walls continued
garnet layers, ion-implanted, domain-wall behaviour for 1-μm bubble devices 80−2613
garnets, domain wall oscillations, bubble domain wall motion 80−108042
garnets, dynamics of mag. domain walls and bubbles 77−69599
garnets, epilayers, domain structure, technique for observation 78−91914
garnets, film, ion-implanted, domain wall mobility 78−95495
garnets, magnetic relaxation phenomena 79−99776
garnets, photomagnetic effects, irreversible 79−99719
garnets magnetic excitations 79−99695
GdCo amorphous film, magnetic compensation walls 77−8375
half-bubble stability in platelets with domain wall energy density gradients 77−1576
hard magnetic material, coercive field, planar defect influence 77−24710
hard magnetic material, micromagnetism, theory 78−52301
Heisenberg ferromagnet, classical one-dimensional, transfer integral and collective coordinate results for free energy 80−93067
Heisenberg ferromagnet, nuclear spin quantum mechanical behaviour 77−51872
Heisenberg ferromagnet, spin configurations near singularities in micromagnetism 80−54908
Heisenberg ferromagnet, with 180° domain walls, quantum mech. treatment 77−48007
Heisenberg Hamiltonian with local and exchange anisotropy 78−14917
Heisenberg one-dimens. chain of classical spins with weak anisotropy, thermodynamics 77−43805
helical magnetic structure, Bloch wall effects on small angle neutron scatt. 79−47297
high-Q bubble materials, wall twist computation method 79−69704
image formation in reflection mode of SEM *(Japanese)* 77−32212
interaction energy with spherical cavity 77−8335
interaction with strongly localised pinning centres, influence on hysteresis *(Russian)* 80−65961
intrinsic coercivity in narrow magnetic domain wall material 80−2597
ion-implanted bubble garnet film, vel. asymmetry during stripe head propag. 80−39834
Ising ferromagnetic half-plane, surface, pinned domain wall, free energy and magnetisation profile 80−60361
Ising model, classical, in transverse field, molecular dynamics 78−80115
Ising model, nonlinear excitations and coherent states in transverse field 80−68143
Ising model, transverse field 78−14917
Ising model with competing interactions, solitons and phasons 80−34653
itinerant ferromagnet, effect of planar defects on electronic struct. and mag. ordering 79−99672
kinking, Aleonard-Brissonneau-Neel expt. 79−56564
light propagation along domain boundary 77−8554
localised defect interactions, unidimensional flow of configs. *(Russian)* 80−65954
Lorentz microscopy, mag. domain images resolution, computer calcs. 78−35004
Lorentz microscopy, thin film and bulk specimen, recent advances 78−35002
Lorentz microscopy using STEM for domain wall profiles determ. 78−35003
LPE double layer films, wall state stability of bubbles 78−95497
magnetic bubble nucleation via charged walls 79−78479
magnetic bubbles, translational motion, mechanism for inertial effects 80−100606
magnetic moment waves, nonlinear, limiting vel. and types *(Russian)* 78−60276
magnetic neutron small angle scattering, using dynamical theory of diffr., determ. of scatt. angle 79−11325
magnetic neutron small-angle scattering, using dynamical theory of diffr., behaviour of neutron intensity after transition through a helical mag. struct. 79−11326
magnetic sheet with simple bar-like 180° domain structs., eddy current losses 80−39808
magnetic soft and hard materials, garnets, magnetic properties and applications, structural props. 80−65760
magnetic structures, non-periodic, ferromagnetic spin wave propagation, interaction with domain walls 79−99692
magnetisation jumps assoc. with irreversible displacement of domain boundaries, statistical theory *(Russian)* 77−8346
magnetostrictive displacement at surface due to mag. domain wall junctions 78−48014
magnons, nonlinear, multidomain ferromagnets with 180° Bloch walls 78−34967
mass at high vel., numerical anal. 80−11217
metal, wall mass, press. due to eddy currents 77−12144
metallic crystal, perfect, mag. domain wall bowing 77−1566
metallic crystal, perfect, wall bowing 78−43608
metallic glasses, mag. props., effect of mech. deform. 80−39840
metallic lamination, domain wall bowing, simulation using new spline model 79−51807
metamagnetic transition, nucleation of new phase, role of planar, linear and point defects 77−24695
metamagnetic transition in magnets with multi-sublattices *(Russian)* 78−23267
micromagnetic analysis of S=1 magnetic bubbles with curvature effects 79−73784
micromagnetic dynamics, numerical model 78−72381
micromagnetic struct. of planar charged walls 79−78478
mischmetal-cobalt alloy, $MMCo_5$, polished, domain wall grooving, optical microscopy and SEM obs. 77−8334
motion, magneto-dipole EM wave radiation generation *(Russian)* 80−80555
motion, one dimens., static in-plane field-biased, dynamic characts. *(Japanese)* 79−73767
motion, self-oscillating mode in const. mag. field *(Russian)* 79−28549
motion, thermally activated, 77-423K 79−51804
motion, thermally activated, and Stacey's theory 77−85486
motion, uniform and nonuniform, crit. mag. field intensities determ., spin wave approx. treatment 77−69596
motion in external mag. field *(Russian)* 79−51811
motion of Bloch wall in imperfect cryst., model pot. function 79−42798
motion of bubble domain Bloch lines, computer simulation 80−54916
motion under static mag. field, energy dissipation 79−95605
neutron birefringence measurements in mag. struct. 79−47298
neutron refraction on rough Bloch walls 77−26815
neutron small-angle scatt. from dynamical theory of diffr. 79−24189

magnetic domain walls continued
observation device for use with 1 MeV electron microscope 80−101882
one dimensional, effect of inplane field on wall motion 77−85480
one-dimensional Bloch wall, instability threshold 78−52302
one-dimensional domain wall motion under biased in-plane field, numerical anal. 79−15321
orthoferrite cryst. films, local coercivity of domains boundaries *(Russian)* 80−80578
orthoferrites, struct. of domain walls 80−34684
orthorhombic ferrimagnets, domain wall motion at near sonic velocity, magnetoelastic interactions 80−34683
oxide, polycryst., dynamic susceptibility of bulging domain wall model 78−23296
parade motion, low freq. *(Russian)* 80−103852
parade motion *(Russian)* 77−80956
particle capture 80−71093
Permalloy, magnetisation improvement through solid state refining 78−91893
Permalloy barrier film, worm-like motion of domain boundaries *(Russian)* 78−39375
Permalloy film, Bloch wall motion obs. *(German)* 77−16133
Permalloy film, break-cross-tie domain walls, thickness depend. 78−43619
Permalloy film, coercive force associated with domain boundary displacement *(Russian)* 80−50151
Permalloy film, domain wall mass and energy, wall vel. depend. calc. 80−2614
Permalloy film, domain walls, magnetisation components distrib. 79−87298
Permalloy film, domain walls streaming *(Russian)* 79−82842
Permalloy film, double layer, wall splitting effect 77−85530
Permalloy film, in weak field, pulse mag. reversal mechanism *(Russian)* 77−80976
Permalloy film, mobility of Bloch lines 77−28421
Permalloy film, movement of circular Bloch line in cross-tie wall 78−31099
Permalloy film, quasistatic and pulsed mag. reversals of Neel domain walls *(Russian)* 78−39374
Permalloy film, streaming of domain walls *(Russian)* 78−72380
Permalloy film, two-layer, with magnetostatic coupling, creep of domain boundaries *(Russian)* 77−43857
Permalloy film, velocity of motion of nonequilibrium walls of edge domains *(Russian)* 79−1694
Permalloy film strip, unidirectional domain wall propag. with in-plane magnetisation 80−71134
Permalloy film strip, wall curvature calc. with in-phase magnetisation 78−2717
Permalloy films, domain propelling tunnel, domain struct. displacement *(Russian)* 79−99736
Permalloy films, thickness depend. of Bloch line mobility 79−24204
Permalloy I bars, hysteretic props., Bitter soln. obs. and Kerr effect meas. 79−78439
Permalloy I-bar elements, magnetostatic effects, unifying overview of domain and continuum results 80−44853
Permalloy I-bars, Kerr magneto-optical effect meas., domain wall location determ., Kerr effect probe 78−68328
Permalloy overlay bars, bubble stray field effect on domain wall struct., interference contrast technique 79−78457
Permalloy thin film cores, domain wall motion and flux patterns, Kerr magneto-optic effect obs. 80−34721
Permalloy thin films, break-cross-tie wall energy 80−88842
Permalloy thin films, Neel wall transitions into cross-tie walls 79−95619
Permalloy-Co film, domain walls, magnetisation ripple *(Russian)* 79−47314
Permalloy-Mn film, diffusion aftereffect causing mag. state change *(Russian)* 80−103860
phase transition, three-dimensional XY model 79−51805
pinning of curved domain walls by randomly distributed lattice defects 77−69611
pinning on defects with finite radius of interaction, random pot. form effect on mag. hysteresis *(Russian)* 80−84611
pinning simulation, coercive force, susceptibility, defect depend. 77−16103
porous ferromagnet, with Bloch walls and self-consistent magnetisation, energy and coercive field 80−15760
porous ferromagnet with Bloch walls, energy and coercive field 79−51818
psarks, identification with domain walls moments 78−65274
pseudo-single domain grains, stable remanence origin 78−65275
rare earth alloy, $R(Co,M)_5$, magnetisation reversal and high coercive force, domain boundary pinning *(Russian)* 77−8345
rare earth cobalt intermetallics, Cu or Ni-substituted, narrow Bloch walls, magnetisation, 4.2K 77−8333
rare earth iron garnet single crystal films, synthesis and props., review 78−48013
rare earth iron garnets, Ca-Ge substituted, mag. loss and domain wall mobility 80−65980
rare earth metals, narrow domain walls, magnetic aftereffect obs. 77−8364
rare earth orthoferrite, phonon slowing down of domain wall *(Russian)* 79−33503
rare earth orthoferrites, domain wall dynamics 80−65957
rare earth orthoferrites, slow neutron elastic scattering, domain boundary observation *(Russian)* 79−82811
rare earth-Co-Ni alloys, $Pr(CoNi)_5$ type, mag. props. and mag. reversal phenomena *(Russian)* 77−51924
rare earth-transition metal amorphous thin films, mag. potential distribution and wall velocity meas. 80−34725
rare-earth orthoferrite, domain wall crit. vel. 79−38354
rare-earth-transition metal amorphous films, domain structure, technique for observation 78−91914
rigid, displacement theory including demagnetising field random perturbations *(Russian)* 77−8344
scaling relations in mag., mechanical and superconducting pinning theory 77−76403
SEM, emission area of back scattered electrons 77−27795
SEM, magnetic contrast, type-2, isolation by lock-in technique, domain wall movement 80−13184
SEM image contrast 77−4528
severely bowed, steady-state motion, simple approx. analytic treatment 77−32211
magnetic domain walls continued
sine-Gordon Hamiltonian, general soln., domain walls appl. 78−19198
single-axis magnetic material, domain wall movements, high speed photography *(Hungarian)* 77−51918
$Sm_{1-x}R_xCo_5$ (R=Y, La, Ce, Nd), mag. props., domain boundary pinning on statistical conc. heterogeneities *(Russian)* 79−99728
soft ferromagnetic film, theoretical wall mobility 80−34677
soft magnetic materials, Barkhausen jumps effect on static losses *(Slovak)* 79−4695
spinels, domain wall formation inhibition, effect on bulk mag. props. 80−11220
spontaneous symmetry breaking and magnon-phonon spectra 80−65991
static and kinetic parameters of bubble walls having horizontal Bloch line pair 80−39836
static props. of lattice of cylindrical domains with complex wall struct. *(Russian)* 77−66381
steady-state eddy-current dominated magnetic domain wall motion with severe bowing and necking 79−91248
steel, C, rotational hysteresis 78−91889
steel, high-speed, low temp. mag. cycling effects, dislocation interactions with mag. domain walls. 80−100928
steel, mild, rotational hysteresis 78−91889
steel struct. testing from anal. of Barkhausen noise statistics 77−77647
STEM, magnetic contrast 79−21854
structure and movement, study using Faraday effect *(Dutch)* 77−63242
superdiamagnetic and ferromagnetic state struct., gradient invariant free energy functional *(Russian)* 80−7143
susceptibility of materials having spherical grains with statistical distribution of diameters 78−95454
T bar, domain wall study employing ferrofluid, rel. to magneto-optical Kerr effect meas. 80−60360
theory, rel. to X-ray topography data 78−64254
thermal activation of walls from planar pinning sites 79−87285
thermally activated domain wall motion and coercive field in materials with extremely narrow domain walls 80−25156
thickness, neutron small-angle scatt. meas. 80−71092
three-dimensional crystal, with strong spin-phonon interaction, domain wall quantum mechanics 78−51622
Ticonal, domain struct., variation under influence of heat treatment *(Russian)* 78−23292
transparent magnetic material, wave props. of domain wall 78−48011
twisted domain wall energy, thickness depend., simplified calc. *(Slovak)* 80−103862
two dimensional mag. domain wall, uniform magnetisation, effective force density of magnetostatic origin, mag. bubble motion anal. 80−100595
type II magnetism in mixed magnets and spin glasses 78−23281
uniaxial crystal, with narrow domain boundaries, coercive force *(Russian)* 80−50140
uniaxial ferromagentic with intrinsic mag. field, domain struct. 80−93141
uniaxial ferromagnet, nonlinear resonance 77−43848
unichiral magnetic bubbles, radial motion in in-plane field 80−34724
velocity, acoustic wave effect 77−12171
velocity, damping parameter meas. from low field microwave excitations 80−34676
velocity and starting field, mag. field pulse duration influence *(Russian)* 79−65701
velocity dependence on bubble radial motion momentum 80−71136
velocity of propagation of simple magnetic moment waves 77−16105
weak ferromagnet, domain wall dynamics, nonlinear waves, mag. solitons *(Russian)* 80−75793
weak ferromagnets, Landau-Lifshitz eqn. solutions, moving domain walls, struct. *(Russian)* 80−100596
Wehrls entropy conjecture proof, Bloch coherent spin states analogous problem 78−89418
Ag-Ni, composite, fibre and layer structs., anomalous props. caused by internal phase boundaries 78−72754
$BaFe_{12}O_{19}$, bubble and stripe lattice domain wall oscills. 80−97115
$BaFe_{12}O_{19}$, nucl. spin-lattice and spin-spin relax. in domain walls 77−69610
$Ca_3Mn_2Ge_3O_{12}$, antiferromagnetic garnet, neutron diffr. study in mag. field 80−50060
$CdCr_2Se_4$, ferromag. semicond., photoinduced mag. anisotropy 80−50086
$CdCr_2Se_4$, mag. semicond., photoinduced binding of domain walls *(Russian)* 78−80174
$CdCr_2Se_4$ magnetic semiconductor, photoinduced centre kinetics 80−71110
$(Co,Fe)_{80}B_{20}$ glass, induced anisotropy and time changes of permeability 80−75815
Co, electrical resistivity, effect of domain wall orientation at 4K 78−91662
Co film, mag. domain wall obs. by electron holography 80−80582
Co film, magnetic domain wall width, shadow and interf. electron microscope exam. 79−11330
Co, foil, wall struct., bubble, plate domains, 1 MeV electron microscope study 78−84463
Co, HCP, NMR and nucl. relax. meas. in domain walls 77−36146
Co, magnetic permeability, effect of ion implantation 77−28414
Co, NMR enhancement of modulating field due to anisotropic component of hyperfine field 77−55729
Co, NMR spectra temp. depend. 78−52364
Co-Fe-Nb alloy, mag. precipitation-hardening and Bloch wall pinning 78−80173
Co-Fe-Nb semihard mag. alloy, mag. precip. hardening 77−8960
Co-Fe-Ti alloy, precipitation hardened, rel. between struct. and mag. props. 78−95470
Co-Pt, struct. and mag. props. rel. to degree of order 78−72368
$Co_{1.8}BaFe_{0.2}{}^{2+}Fe_{16}{}^{3+}O_{22}(Co_{1.8}W)$, magnetoelastic props. under spin-reorientation conditions 79−69709
CoNiZn ferrites, Fe excess, complex permeab. var. with annealing temp. 77−89979
Co_5Sm, magnetic domains, nucleation and pinning, magneto-optical Kerr effect 80−39811
$Co_{90}Zr_{10}$, ferromag. amorphous alloy, crystn. and domain struct. study 80−107056
Cr, single cryst., mag. hysteresis, neutron diffr. obs. inertia of domain wall motion 79−15327
$CrBr_3$, HF spectra, susceptibility, spin waves in domain walls *(Russian)* 80−80909
$CsCoCl_3$ spin dynamics, neutron scatt. study 80−80493

magnetic domain walls continued
$Cs_2CuCl_4.2H_2O$, Bloch-wall NMR, anisotropic hyperfine interaction 79−51864
$CsMnCl_3$, antiferromagnetic resonance, parametric spin wave excitation *(Russian)* 80−93183
Cu crysts., thick imperfect, dynamical X-ray diffr., topographic effects 77−68898
Cu HCP film, uniaxial, mag. domain struct. 80−60385
Cu-Fe, composite, fibre and layer structs., anomalous props. caused by internal phase boundaries 78−72754
Dy, domain wall dynamics, NMR 77−69614
$Dy(Co,Ni)_2$, intrinsic mag. aftereffect meas., domain wall motion 80−71121
Dy_2Co_{17}, domain wall behaviour, TEM expts. 77−4524
$Dy(Fe,Al)_2$, magnetostriction meas., domain wall pinning 77−63256
Dy_2Fe_{17}, domain structures and anisotropy constant. 80−93136
$DyFe_{0.998}Co_{0.002}O_3$, orthoferrite, domain struct. near mag. transitions, domain wall bending 80−2599
$Dy_{1-x}Gd_xAl_2$, ferromag, easy axis rot., ^{163}Dy NMR obs. 79−78562
$Dy_xY_{1-x}Al_2$, domain wall dynamics, NMR 77−69614
$ErCo_3$, $ErCo_6$ and Er_2Co_{17}, Kerr effect determ. of domain structure, Bloch wall energy 80−39805
$ErCo_{5-x}Ni_x$ ferrimagnetic series, magnetisation, coercive field meas. 78−91896
$ErCrO_3$, field-induced spin reorientation relax. 79−78402
$Er_2Fe_3Co_{14}$, Kerr effect determ. of domain structure, Bloch wall energy 80−39805
$(Eu,Lu)_3(Fe,Al)_5O_{12}$ film, epitaxial, increased domain wall velocities, due to orthorhombic anisotropy 77−20653
$(Eu,Lu)_3Fe_5O_{12}$, epitaxial film, orthorhombic mag. anisotropy, high domain wall velocity 78−19290
$EuFeO_3$, cryst. domain wall energy density determ. 77−1567
EuGaYIG film, bubble dynamics, anisotropy depend., ferromag. reson. expts. 77−63240
EuGaYIG:Cr, epitaxial garnet film, interaction pot. of domain walls with localised stress fields 80−44889
EuS films, mag. and elec. props. rel. to stoichiometry and defects 80−97122
EuTe, mag. semicond., antiferromag. reson. meas. 80−44926
$Eu_{0.6}Y_{2.4}Ga_{1.26}Fe_{3.74}O_{12}$ garnet film, dynamic bubble-collapse determ. of domain wall motion oscillation 79−78454
$(Fe,Ni)_{83}B_{15}C_2$, amorphous alloy, mag. props., possible appl. to power transformers 79−28558
$(Fe,Ni)_{80}P_{14}B_6$ amorphous alloy, mag. props., possible appl. to power transformers 79−28558
Fe, 90° walls, stable orientations, theory and X-ray observations *(Japanese)* 80−60359
Fe alloy wire, glassy, shape, energy, eddy current loss and relax. damping of mag. domain walls 77−89975
Fe, Barkhausen effect, grain size depend. at 300K and 77K *(German)* 77−16113
Fe, domain wall-dislocation interaction, magnetoelastic damping 78−14980
Fe, film, asymmetric 180° Bloch walls, Lorentz electron microscopy obs. 78−27063
Fe film, domain wall struct. obs. by Lorentz electron microscopy 77−85527
Fe film, effect of tensile stress on mag. domain struct. 78−68332
Fe film, enriched, NMR obs. 78−39443
Fe film, single crystal, less than 1000 Å thick, inclined 90° walls 78−72384
Fe foil, ferromag. domain-wall width, anisotropy depend. 78−19269
Fe garnet, Bi-substituted, film, domain boundary transform. into canted phase at compensation point 77−24724
Fe garnets, thin film, low freq. excitation spectra, mobility of domain boundaries 79−42815
Fe, high purity, dislocation-magnetic domain wall interaction, magnetomechanical damping expts. 78−39360
Fe, high purity, magnetomechanical sampling, magnetic field variations 80−93156
Fe, high-purity, magnetic 90° domain wall-dislocation tangle interaction, magnetomechanical damping expts. 79−78496
Fe, polycryst., rel. to magnetostriction sign change under compressive stress 80−29596
Fe, pure, magnetoelastic damping at low shear stress amplitudes *(French)* 77−59441
Fe, rotational hysteresis 78−91889
Fe sheet, surface magnetisation, ferromag. nucl. reson. meas. 78−60348
Fe thin layers, vacuum coated on PMMA, mag. behaviour during mech. stress cycles *(German)* 80−80581
Fe, whisker, interaction with mobile impurities 77−12145
Fe whisker, magnetic aftereffect in 180° mag. bowed Bloch walls 79−78432
Fe whisker crystals, domain walls, interaction with dislocation bundle, X-ray topography obs. 79−87282
Fe, zig-zag 90° Bloch wall, magnetoelastic problem 77−4526
Fe-Cr-Co, magnetic domain walls, Lorentz microscopy 80−103854
Fe-Cr-Co-V-(Ti) hard magnets, V and V-Ti effects on mag. and mech. props. 79−91810
Fe-Ni, ferromagnetic films, domain boundary creep relaxation effects *(Russian)* 79−82840
Fe-Ni alloy, rel. to effect of thermomag. treatment in rotating field *(Russian)* 77−21294
Fe-Ni-Co, magnetic permeability, effect of ion implantation 77−28414
Fe-Ni-Co, rel. between induced uniaxial anisotropy and coercive force 78−91904
Fe-Si, 180° Bloch wall motion, Barkhausen jumps *(French)* 78−23294
Fe-Si, Bloch wall motion, irreversible processes 79−78431
Fe-Si, Bloch wall motion self-similarity *(French)* 79−82810
Fe-Si, hysteresis loops described by 180° Bloch wall *(French)* 79−15322
Fe-Si, internal friction, domain boundary area *(Russian)* 79−24562
Fe-Si, magnetostatic couplings between 180° Bloch walls 77−69613
Fe-Si, single cryst., mag. domain wall motion, X-ray topography study 80−65953
Fe-Si, stress and plastic deform. effect on Barkhausen effect, instrumentation 78−52313
Fe-Si, thermally activated motion of 180° Bloch wall 78−95457
Fe-Si (2.5%), Bloch wall zig-zag struct., neutron small angle scatt. 77−16099
Fe-Si (3 wt.%), Barkhausen effect meas. 77−85492

magnetic domain walls continued
Fe-Si (3 wt.%), domain struct. rel. to cryst. size *(Russian)* 80−29568
Fe-Si (3 wt.%), domain wall spacing and losses, orientation depend. 78−56343
Fe-Si (3 wt.%), domain wall drift due to nucleation during cyclic magnetisation 78−95461
Fe-Si (3 wt.%), domain wall spacing and core loss, forsterite and stress coatings effect 80−88780
Fe-Si (3 wt.%), EM losses, effect of bending of 180° domain boundaries *(Russian)* 78−39357
Fe-Si (3 wt.%), grain oriented, domain wall variation throughout magnetisation cycle 78−95459
Fe-Si (3 wt.%), grain oriented, power loss depend. on domain wall bowing 78−95460
Fe-Si (3 wt.%), grain-oriented, effect of forsterite coatings in domain struct. 78−23293
Fe-Si (3 wt.%), grain-oriented, domain wall profiles throughout magnetisation cycle 80−88781
Fe-Si (3 wt.%), grain-oriented, power loss and domain wall variation with lamination thickness 80−88814
Fe-Si (3 wt.%), mag. domain wall contrast in synchrotron X-ray topographs 80−75792
Fe-Si (3 wt.%), scratching effects on mag. losses in single crysts. with orientation near (110)[001] 79−51802
Fe-Si (3 wt.%) (110), domain size depend. on crystal thickness *(Russian)* 79−69692
Fe-Si (3 wt.%) alloy, domain structure influence on eddy current losses *(Slovak)* 79−4693
Fe-Si (3%), power loss, domain wall motion depend. 77−16100
Fe-Si (3%), spikn related contrast effect, visibility of 180° ferromag. domain walls 78−43612
Fe-Si (3%wt.), dynamics of 180° domain boundaries and electromag. losses *(Russian)* 79−51801
Fe-Si (3.25 wt.%) alloy, single cryst. with (007) planes, domain struct. influence on mag. torque 80−108034
Fe-Si (3.5 wt.%), Barkhausen noise, strain depend., interaction of dislocations and domain walls 77−12155
Fe-Si (3.5 wt.%), dynamic neutron depolarisation meas. of ferromag. domain struct. 79−82812
Fe-Si (3.5 wt.%), magnetisation reversal and domain walls 78−84451
Fe-Si (3.5 wt.%), static neutron depolarisation meas. of ferromag. domain struct. 78−14978
Fe-Si (3.5 wt.%) picture frame cryst. , domain wall bowing dynamic neutron depolarisation 78−56344
Fe-Si (3.5 wt.%) picture frame, domain wall bowing, time-depend. neutron depolarisation 78−95458
Fe-Si (4 at.%), Bloch wall thickness determ. by neutron small-angle scatt. 80−15754
Fe-Si (4 wt.%), freq. depend. of Fe losses in single crysts. with (100)[001] 79−51803
Fe-Si (4%), (110)[001] and (100)[001], dynamic domain struct., AC excitation 77−16097
Fe-Si single crysts., interaction of {110} 90° walls with lattice imperfections 80−39807
Fe-Si(4 wt.%), (110) and (100)[001] oriented, simulation of domain wall bowing 80−44854
$Fe_{80}B_{20}$, elastic, magnetoelastic and thermal props. 79−19759
$Fe_{80}B_{15}Si_5$ metallic glass, large uniaxial magnetostrictive anisotropy, magnetisation reversal 80−34736
$FeCl_2$, metamagnetic hysteresis, magnetooptical rot. meas. 77−40057
$Fe_5Co_{75}B_{20}$, amorphous, magnetisation reversal and domain boundary configs. 80−88809
$Fe_5Co_{70}Si_{10}B_{15}$ amorphous magnetic alloy, decrease of permeability after demagnetisation, disaccommodation 80−39814
Fe_5LiO_8, magnetoelectric-effect and magnetisation process 79−1688
FeN alloy, coercive force, effect of $Fe_{16}N_2$, anisotropic model 77−85501
FeNi-Cu, composite fibre and layer structs., anomalous props. caused by internal phase boundaries 78−72754
$Fe_{80-x}Ni_xB_{20-y}P_y$, amorphous, Rayleigh region and coercive force 80−88806
$Fe_{32}Ni_{36}Cr_{14}P_{12}B_6$, elastic, magnetoelastic and thermal props. 79−19759
$Fe_{40}Ni_{40}P_{14}B_6$, amorphous, domain struct. 78−10719
$Fe_{40}Ni_{40}P_{14}B_6$, elastic, magnetoelastic and thermal props. 79−19759
$Fe_{40}Ni_{40}P_{14}B_6$, $Fe_{35}Ni_{32}Cr_{15}P_{12}B_6$, amorphous ferromagnets, Barkhausen noise, clustering of Bloch wall jumps 77−69618
$Fe_{40}Ni_{40}P_{14}B_6$, Metglas 2826, amorphous ribbon under tension, mag. domain walls and pulsed magnetisation reversal 80−88825
$(Fe_xNi_{1-x})_{80}P_{10}B_{10}$, amorphous, magnetisation reversal and domain boundary configs. 80−88809
Fe_3O_4 (magnetite), multidomain particles 180° domain walls rel. to magnetisation 79−66686
Fe_3O_4, magnetic after-effect by valency fluctuations assoc. with cond. transition 77−8365
Fe_3O_4, magnetite, coercive force spectrum at high temps. rel. to thermal activation below blocking temp. 77−91111
$Fe_{75}P_{15}O_{10}$, amorphous, ferromag. domain-wall width, anisotropy depend. 78−19269
FeSi, (110), Neel cryst., refr. of neutrons in Bloch walls using double cryst. arrangement 79−24191
FeSi picture frame single cryst., domain wall motion and magnetisation reversal, time-depend. neutron depolarisation study 80−88782
FeSi, single cryst., orientation of pieces of zigzag Block walls, neutron small-angle scatt. determ. 79−24190
FeV (2 at.%), NMR spin echoes, domain wall effects 80−75883
^{57}Fe powder, NMR excitation function, drumhead model of Bloch walls 80−15810
Fo-Fe-Nb, cold-worked and aged, mag. props. and microstruct. 80−34690
$(Gd,Bi)_3(Fe,Al,Ga)_5O_{12}$ LPE film, 180° Bloch wall pinning at etched nucl. tracks 78−39376
$(Gd,Bi)_3(Fe,Ga)_5O_{12}$, LPE film, coercivity, influence of nuclear tracks 79−51829
$(Gd,Lu)_3(Fe,Mn,Al)_5O_{12}$ epilayer with orthorhombic anisotropy, domain wall vel. 78−52322
Gd, mag. domain struct., 230-293K 80−88783
Gd, transient enhancement of AC susceptibility, domain wall pinning 77−20633
Gd-Co amorphous film, magnetisation processes near compensation point 77−69644
Gd-Co amorphous film 80−34725

magnetic domain walls continued
Gd-Co film, amorphous, magnetisation processes near compensation point 77−40101
Gd-Co film, amorphous, rel. to inverted and biased loops 77−89996
Gd-Co-Au amorphous magnetic films, domain wall obs. by Lorentz electron microscopy 77−80979
Gd-Co-Mo film, amorphous, bubble and stripe domain wall vel. meas. 77−40094
Gd-Co(-Au) amorphous film, domain wall dynamics near compensation point 79−1696
Gd-Fe, DC bias RF sputtered film, mag. props. 77−16124
Gd-Fe film, amorphous, in-situ ion beam sputtered, microstruct. and Lorentz mag. struct. 78−63947
GdIG, thermal effect on re-entrant hysteresis loop and coercive force 78−2702
$Gd_2(MoO_4)_3$, domain wall motion dynamics 80−108030
$HgCr_2Se_4$, initial mag. permeab., 77 to 300K, domain wall motion and damped ferromag. reson. 79−28562
Ho, low field susceptibility and helical-ferromag. field induced phase transition 78−47975
$HoCo_3$, Ho_2Co_7, $HoCo_{5.5}$ and Ho_2Co_{17}, Kerr effect determ. of domain structure, Bloch wall energy 80−39806
$Ho_{0.5}Dy_{0.5}FeO_3$ orthoferrite, domain wall struct., stability conditions, Morin transition, anisotropy const. 80−34684
$Ho_2Fe_3Co_{14}$, Kerr effect determ. of domain structure, Bloch wall energy 80−39806
$KCoF_3$, antiferromag., obs. of domains by X-ray topography 78−14981
$KCoF_3$, antiferromag. domain wall motion under external stress 80−80583
$K_2CuCl_4.2H_2O$, Bloch-wall NMR, anisotropic hyperfine interaction 79−51864
$KNiF_3$, antiferromag., obs. of domains by X-ray topography 78−14981
$KNiF_3$, antiferromag. domain wall motion obs. by X-ray synchrotron topography 78−88139
La-Sm-Lu iron garnet film grown as NdGaG substrates, mag. props. 80−44888
$Li_{0.5}Fe_{2.5}O_4$, magnetic domain walls, mobility 80−2600
$Li_{0.5}Ga_{0.095}Fe_{1.55}O_4$ ferrites, linear magnetostriction in weak field, 150 to 300K *(Russian)* 77−80983
$LuCrO_3:Er^{3+}$, doping effect on ^{53}Cr NMR in domain walls 80−71219
Mn-Bi, magnetically uniaxial, strongly anisotropic, discontinuous mag. reversal singularities *(Russian)* 77−48010
Mn-Bi film, negative transverse magnetoresist. in c-plane, domain wall effects 77−20465
MnBi, domain boundaries shift, mag. reversal processes 79−87286
MnBi, domain boundary inertia during mag. reversals *(Russian)* 80−88776
MnBi, thin film, fine mag. domains, SEM obs. 79−24202
MnBi, two-phase coercive force for domain wall motion, mag. reversal nucleation mechanism *(Russian)* 77−48009
$MnFeO_2$: ^{55}Mn, NMR freq. dynamical shift for nuclei in domain walls *(Russian)* 77−40148
$MnFe_2O_4$, ferrite, dynamic shift of NMR freq. of nuclei located in domain walls 80−15823
$MnFe_2O_4$, nuclear reson. and relax. from domains and domain walls 77−8448
MnP, noncubic ferromag., relax. times for domain and wall resonances 77−77119
Mn_2Sb, domain and domain wall resons. in ^{55}Mn NMR spectrum 80−25219
$MnSb_{1-x}Sn_x$, zero-field NMR investig. of domains and domain walls 77−32271
MnZn ferrite, initial mag. permeability rel. to mag. anisotropy 80−80557
MnZn ferrite, wall topography change induced by external press. 80−34734
$Mn_{0.4}Zn_{0.42}Fe_{2.16}O_{4+x}$, permeability, rel. to intrinsic mag. props. 79−4702
$(NH_4)_2CuCl_4.2H_2O$, Bloch-wall NMR, anisotropic hyperfine interaction 79−51864
$Nd(Co_{1-x}Cu_x)_5$, coercive force temp. depend., domain wall spin struct. and energy 79−82823
Ni, 109° and 71° walls, stable orientations, theory and X-ray observations *(Japanese)* 80−60359
Ni (100), Bloch wall meas. by enutron small-angle meas. 80−15753
Ni alloy, PE 16, Bloch wall motion, thermally activated 78−43610
Ni, creep, effect of AC mag. field, 1.5-4.2K *(Russian)* 79−11657
Ni, crysts., thick, imperfect, dynamical X-ray diffr., topographic effects 77−68898
Ni, Czochralski growth conditions rel. to cryst. imperfections, mag. domain walls 77−68937
Ni, Czochralski-grown single crysts. X-ray topography 77−20630
Ni, electroplated layers, internal friction and ΔG effect, rel. to bath comp. and annealing 78−19296
Ni, ferromagnetic domain struct., static neutron depolarisation meas. 79−82812
Ni film, two-dimens. ⟨110⟩ domain wall 77−69648
Ni, intermodulation generation in RF mag. field, field interaction with domain walls 79−56600
Ni, magnetic aftereffect reactivation of single crystal by plastic deform. 79−65697
Ni, magnetic permeability, effect of ion implantation 77−28414
Ni, magnetic permeability, reversible, deform. and ion implantation effects 77−48013
Ni, oblique mag. domain walls, obs. by X-ray topography 78−6540
Ni, rel. to mag. field effect on creep 77−16141
Ni-Fe, film, magnetisation reversal, magnetoresistance meas. 77−16132
Ni-Fe (50%), slow mag. domain wall motion 77−69597
Ni-Fe alloy, extraordinary viscous magnetic wall motion 78−84465
Ni-Fe film, Barkhausen noise spectra meas. 77−16131
Ni-Fe film, differential susceptibility, struct. const. and losses 79−91271
Ni-Fe film, effect of tensile stress on mag. domain struct. 78−68332
Ni-Fe film, low field domain wall mobility 80−25167
Ni-Fe film, relax. effects in domain boundary creep *(Russian)* 77−24723
Ni-Fe film, thermally activated domain wall motion 80−88777
Ni-Fe films, energy change of Bloch wall with angle to easy axis, calc. *(Slovak)* 80−103863
Ni-Fe films, viscous magnetic domain wall motion anal. 79−95617
Ni-Fe multilayered films, mag. domain structures 79−82847

magnetic domain walls continued
Ni-Fe oxidised film, extraordinary viscous wall motion at extreme vel. 78−14997
Ni-Fe wire, hard-drawn, increased Barkhausen noise at low temps. 77−16114
Ni-Fe-Co film, domain wall energy meas., by domain tip propag. method 77−55692
Ni-Fe-Co films, saw tooth domains investigated 78−14994
Ni-Fe-Cr alloy, PE 16, coercivity of picture frame cryst. 78−14988
Ni-Fe-Cr alloy, PE 16, thermally activated domain wall motion 79−95603
Ni-Fe-Cr-Mo-Ti-Al, PE 16, thermally activated domain wall motion 80−88777
Ni-Zn ferrite, neutron irrad., mag. spectra, domain wall behaviour 77−48006
NiFe film, domain wall mass and relax. time from forced oscills. 80−71133
NiFe, grain oriented, slow motion, tunnelling mechanism 77−32210
NiFe tape, rapid surface and vol. magnetisation, eddy-current-limited domain wall motion 77−12159
$Ni_{0.83}Fe_{0.17}$ films, reson. oscills. of mag. domain walls and Bloch lines, stroboscopic electron microscopy 80−54931
$NiFe_2O_4$, domain wall size and mag. losses in freq. spectra 77−85481
NiFr, mag. film, pulse switching at low temp. 80−103868
NiO (111) platelets, antiferromag. S domains, optical obs., spin flop 80−54915
NiO, transport props., temp. and stoichiometry depend., antiferromag. T-domain influence 77−8332
NiS_2, mag. torque curve 79−47305
NiZn ferrite, magnetic props., porosity and grain size effects 77−36095
NiZn ferrite, wall topography change induced by external press. 80−34734
$Ni_{1-x}Zn_xFe_2O_4$, polycryst., domain wall energy rel. to anisotropy 80−71090
$PbFe_{12}O_{19}$, bubble and stripe lattice domain wall oscills. 80−97115
$PrCo_5$, heat treated, coercive force exam. 78−68298
$Pr(Co_{1-x}Cu_x)_5$, coercive force temp. depend., domain wall spin struct. and energy 79−82823
$Pt_{0.7}Ni_{0.3}Fe$, magnetically hard, cryst. morphology and mag. domain struct. 77−69615
$Rb_2CuCl_4.2H_2O$, Bloch-wall NMR, anisotropic hyperfine interaction 79−51864
Si-Fe, ferromagnetic domains and their junctions, simulation of X-ray topographs 79−78434
Si-Fe, freq. spectrum of Barkhausen noise of moving 180° domain wall 77−16115
Sm-Co-Cu-Fe, single phase 2-17 sample, hard mag. props. 77−8349
Sm-Co-Cu-Fe-Te magnets, domain-wall pinning model for coercivity 79−15326
Sm-YIG garnets, implanted and Permalloy coated, comparison between planar domain walls in bubbles 77−85520
$SmCO_5$, etched microparticles, Barkhausen discontinuity, nucleation, and domain wall pinning 79−87288
Sm(Co, Cu) alloys, coercivity mech. 80−44862
$SmCo_5$, and related alloys, nucleation and pinning at 360° domain walls 77−73042
$SmCo_5$, and $SmCo_{3.5}Cu_{1.5}$, anisotropy and coercivity, Kerr effect, magnetisation and aftereffect expts. 77−8300
$SmCo_5$, Bloch wall energy determ. *(German)* 78−19271
$SmCo_5$, Cu-modified, magnetisation reversal mechanism 77−8350
$SmCo_5$, domain wall nucleation sites and magnetization reversal 79−56563
$SmCo_5$, heat treated, coercive force exam. 78−68298
$SmCo_5$, polished, domain wall grooving, optical microscopy and SEM obs. 77−8334
$SmCo_5$ single crystals subjected to shock waves, magnetisation, creation of high-coercivity state *(Russian)* 77−66384
$SmCo_5$, sintered, high coercivity, microstruct. and mag. props. 77−69629
$SmCo_5$, sintered, mag. after-effect, expt. and model 80−75816
$SmCo_5$, sintered, mag. props. *(German)* 77−43852
$Sm(Co_{0.87}Cu_{0.13})_{7.8}$, coercivity and microstruct. 79−56569
$Sm(Co_{1-x}Cu_x)_{7.8}$ alloys, coercive fields, domain wall energies, mag. and metallographic exam. 78−91897
$SmCo_{3.5}Cu_{1.5}$, single cryst., domain wall motion and domain form. 78−39359
$SmCo_{3.5}Cu_{1.5}$, time dependent magnetisation 78−80176
$SmCo_4Cu$, domain boundaries shift, mag. reversal processes 79−87286
$SmCo_{5-y}Cu_y$, giant intrinsic magnetic hardness, high field meas. 78−68289
$SmCo_{2.5}Ni_{2.5}$, mag. after effect *(Russian)* 78−6544
$SmCo_{5-x}Ni_x$, giant intrinsic magnetic hardness, high field meas. 78−68289
$Sm_{1-x}Pr_xCo_5$ single crystals, magnetocryst. anisotropy and stepwise mag. reversals *(Russian)* 77−66291
SmYGa garnet, bubble motion depend. on wall pinning 79−78455
$Sm_{0.4}Y_{2.6}Ga_{1.2}Fe_{2.8}O_{12}$, H^+ implanted film, epitaxial, mag. bubbles, walls and fine struct. 77−63241
$Sr(Fe_xAl_{12-x})O_{19}$, cryst. domain wall energy density determ. 77−1567
Tb-Fe amorphous magnetic films, domain wall obs. by Lorentz electron microscopy 77−80979
Tb-Fe amorphous thin films, magnetic after-effect, Kerr magneto-optic effect obs. 80−97123
Tb-Fe sputtered films, amorphous, mag. aftereffect due to domain wall motion 79−73780
$Tb_{0.27}Dy_{0.73}Fe_2$, domain configurations, obs. by Kerr effect and synchrotron radiation topographs 78−64215
$TbFe_2$, domain configurations, obs. by Kerr effect and synchrotron radiation topographs 78−64215
$TbFe_2$ monocrystalline (111), under elastic compressive stresses, domain structure *(Russian)* 79−91247
Tm ferrogarnet film, cylindrical mag. domain motions, domain boundary oscills. *(Russian)* 80−71140
$TmFeO_3$, orthoferrite, vel. of planar domain wall 78−72363
$UCo_{5.3}$, mag. props., cryst. and domain struct. *(Russian)* 77−4529
VI_2, antiferromag., zone-boundary phonon Raman scattering, modulation of exchange interaction 80−11386
$(Y,Eu,Sm)_3(Ga,Fe)_5O_{12}$ film, mag. loss and bubble dynamics 77−8371
$(Y,Eu,Tm)_3(Ga,Fe)_5O_{12}$ film, domain boundary mobility, effect of easy magnetization axis inclination 78−19293
$(Y,Eu)_3(Fe,Ga)_5O_{12}$, epitaxial, cylindrical mag. domain struct., radial wall motion effect *(Russian)* 77−8373

magnetic domain walls continued
$(Y,Gd,Yb,Bi)_3(Fe,Al,Ga)_5O_{12}$ films, magnetic bubble domains, domain wall motion examined 78−19294
$(Y,Gd,Yb,Bi)_3(Fe,Al)_5O_{12}$ film, nonreciprocal effects in domain boundary motion in inhomogeneous field 77−24726
$(Y, Gd, Yb, Bi)_3(Fe, Al)_5O_{12}$ epitaxial film, domain wall motion and oscill. 80−2616
$(Y,Sm,Ca)_3(Fe,Ge)_5O_{12}$, domain wall, radial motion, method of dynamic collapse of mag. bubbles 79−8026
$(Y,Sm,Ga)_3(Fe,Ge,Si)_5O_{12}$ film, domain wall energy and vel., 20-160°C 77−24725
$(Y,Sm)_3(Fe,Ga)_5O_{12}$ film, domain wall energy and vel., 20-160°C 77−24725
$(Y,Sm)_3(Ga,Fe)_5O_{12}$ film, domain boundary mobility, effect of easy magnetization axis inclination 78−19293
$(Y,Sm)_3(Ga,Fe)_5O_{12}/(Eu,Er)_3(Ga,Fe)_5O_{12}$ double-layer self-biasing garnet films, dynamic behaviour of domain walls 80−34722
Y-Sm ferrogarnet *(Russian)* 80−71140
$Y_2BiFe_{3.8}Ga_{1.2}O_{12}$, film, dynamics of domain walls 78−27065
$Y_{3-x}Bi_xFe_{5-y}Ga_yO_{12}$, epitaxial film, domain wall dynamics *(Russian)* 78−2718
$(YBi)_3.(FeGa)_5O_{12}$ film, interaction between Bloch walls and dislocations *(Russian)* 79−61196
$(YCdYbBi)_3(FeAl)_5O_{12}$, cylindrical domain wall vel. anisotropy *(Russian)* 77−59440
YCo_5, NMR enhancement of modulating field due to anisotropic component of hyperfine field 77−55729
$YCrO_3$, antiferromag., mag. domain walls, ^{53}Cr NMR study 79−11327
$Y_{2.45}Eu_{0.55}Fe_{3.8}Ga_{1.2}O_{12}$, hard bubble conversion in in-plane field 78−14998
$(YEuLuCa)_3(FeGe)_5O_{12}$ film, stable state of bubbles containing Bloch lines 78−76281
YEuTmCa garnet bubble films, domain wall transition 79−56584
YEuTmGa garnet bubble film, dynamic diffuse wall deform. 80−54927
$(YEuTm)_3(GaFe_5)O_{12}$ ferrite garnet films, mag. bubbles, translational motion, mechanism for inertial effects 80−100606
$(YEuYbCa)_3(FeGe)_5O_{12}$, ion-implanted, in-plane mag. field effects on bubble props. 77−85521
$(YEuYbCa)_3(FeGe)_5O_{12}$, garnet film, isolated straight stripe domain, dynamic behaviour 80−39809
$Y_3Fe_{5-x}Ga_xO_{12}$, mag. domains and cryst. defects 80−75789
$YFeO_3$, Bloch, Neel and head to head domain wall mobilities 77−1562
$YFeO_3$, Bloch, Neel and head to head wall vels. 78−68287
$YFeO_3$, domain boundary inertia during mag. reversals *(Russian)* 80−88776
$YFeO_3$, domain wall motion, magnetoelastic coupling 79−78435
$YFeO_3$, domain walls vel. *(Russian)* 79−28553
$YFeO_3$, influence of photomagnetic effects on ^{57}Fe NMR 78−52365
$YFeO_3$ monocrystalline, mag. field depend. of magnetic domain *(Korean)* 78−68337
$YFeO_3$, orthoferrite, vel. of planar domain wall 78−72363
$YFeO_3$, orthoferrite, domain boundary vel. exceeding limiting vel. *(Russian)* 79−24192
$YFeO_3$, orthoferrite, crit. domain wall vel. 80−71135
$YFeO_3$, photomagnetic effects, ^{57}Fe NMR obs. 78−95464
$YFeO_3$ plate, anisotropy of domain wall velocity, magneto-optical obs. 79−99725
$YFeO_3$ platelets, domain wall mobility, dynamic coercivity 78−91884
$YFeO_3$, spin-wave damping of domain walls 79−42795
$YFeO_3$, transit time meas. of domain-wall mobilities, magnetostatic and magnetoacoustic effects 79−42794
$YFeO_3$, weak ferromagnet, domain wall motion and velocity *(Russian)* 80−54917
$Y_3Fe_{5-x}Si_xO_{12}$, photoinduced change of mag. permeability *(Russian)* 77−1560
YGdIG, with various domain wall orientations, natural spin reson. 80−66040
$(YGdYbBi)_3$ $(FeAl)_5O_{12}$ epitaxial film, diffuse domain wall, bubble domain expansion 80−25170
$(YGdYbBi)_3(FeAl)_5O_{12}$, epitaxial film, 360° domain walls with periodically distrib. Bloch lines 80−7127
$(YGdYbBi)_3(FeAl)_5O_{12}$ ferrite-garnet films, effect of in-plane field on dynamics of domain walls 80−65979
$(YGdYbBi)_3.(FeAl)_5O_{12}$ films, substrate orientation influence on max. vel. of domain boundaries 79−15330
YIG, Barkhausen effect *(German)* 78−14986
YIG, Bi-substituted, LPE, domain wall reson. 80−60387
YIG, Bloch line mass and mobility in a domain boundary *(Russian)* 80−93138
YIG, Bloch wall mobility, effect of dynamic change in wall struct. *(Russian)* 78−2698
YIG, bulk, low mag. domain wall mobility 78−95463
YIG, cylindrical mag. domains, translational motion 80−108043
YIG, dilute, magnetoacoustic surface wave excitation by RF field on Bloch walls 80−25178
YIG, domain boundary nuclear spin echo excitation, NMR domain freq. capture effect *(Russian)* 80−44955
YIG, domain wall mobility and mass meas. method *(Russian)* 80−108033
YIG, domain wall size and mag. losses in freq. spectra 77−85481
YIG, dynamic characts. of domain walls, low temp. behaviour 77−69598
YIG film, low field microwave excitations of mag. domain walls 79−78456
YIG, influence of X-ray radiation on mag. props. 77−8337
YIG, interaction force between 180° domain wall and edge dislocation 77−28408
YIG, mag. domain walls, Lorentz microscopy 79−91249
YIG, magnetic domain wall motion in high drive fields 80−65955
YIG, permeability, domain rot. and wall displacement contrib. 80−80564
YIG, polycryst., initial and reversible parallel susceptibilities, hydrostatic press. effects 80−75835
YIG, single cryst., Neel lines, Faraday effect obs. 78−64216
YIG, single crystal., domain wall struct. and cryst. orientation 77−16104
YIG:Co film, influence of stress induced anisotropy on domain struct. 80−100605
$(YLuSmCa)_3(GeFe)_5O_{12}$ garnet films, bubble expansion saturation vel., sampling optical photography 80−75820
$(YSmCa)_3(FeGe)_5O_{12}$ LPE film, growth and coercivity 79−4707
$Y_{2.6}Sm_{0.4}Fe_{5-x}Ga_xO1_2$, epitaxial, domain wall crit. vel., effect of material parameters 79−99740

magnetic domain walls continued
$(YSmLuCa)_3(GeFe)_5O_{12}$, stripe domain wall, form. and punch-through of horizontal Bloch line 79−99723
$Zn_xCn_{0.1}Fe_{2.9}O_4$, Cu, Zn substituted magnetite, domain wall resonance, mag. props. 80−15756
$Zn_xCu_{1-x}Fe_2O_4$, mag. props., Mossbauer spectra 79−87344
$Zn_xFe_{3-x}O_4$, mag. ordering and domain wall relax. 77−8336
$Zn_xFe_{3-x}O_4$, Mossbauer exam. of relax. phenomena 77−8479

magnetic domains
see also magnetic bubbles; magnetic domain walls
Alnico, interaction domains after heat treatment in mag. field *(Russian)* 78−68286
amorphous ferromagnetic alloys, domain struct. and mag. microstruct., review 80−15751
amorphous magnetic materials, props. *(Japanese)* 79−28561
amorphous toroidal core, switching characts. and domain structs. 78−95477
antiferromagnet, cylindrical magnetic domains, statistical props. 77−40080
antiferromagnet, dislocations producing domains and disclinations *(Russian)* 77−32213
antiferromagnet, first order orientational transition, sound propag. anomalies 77−1580
antiferromagnet, magnetic dislocation domains, mag. moment distribution 80−2601
antiferromagnet, rel. to dislocations *(Russian)* 77−51919
antiferromagnet, rel. to NMR under magnon bottleneck conditions, eqns. of motion 77−66429
antiferromagnet, sound generation by EM wave near orientational phase transform. of first kind *(Russian)* 78−39329
antiferromagnet, with weak ferromagnetism, domain struct. theory 78−47997
antiferromagnetic, indirect evidence, direct obs. methods, wall motion, review 79−51799
antiferromagnets in high-freq. mag. field, domain struct. 79−65694
band model of domain struct. 77−69608
banded domain structure, magnetostatically coupled with uniaxial substrate, mag. reversals *(Russian)* 78−48016
boundary conditions and surface tension for inclined boundaries *(Russian)* 77−69616
bubble domain film, growth induced order parameter, estimation from coercive force meas. 80−39828
cluster size distribution, perimeter for two-dimensional percolation 77−9967
cobalt formate dihydrate, mag. relax. phenomena near T_N 79−65656
colloid patterns interference colours associated with mag. domains 80−2598
colloid-SEM method, fine magnetic domain observation *(Japanese)* 78−37105
conference on magnetism, Munster, Germany (Mar. 1977) 78−10626
critical field calc. of single domain particle with two types of anisotropic energy 78−61404
cubic ferromagnet, magnetised along ⟨110⟩, stability of lamellar domain struct. 79−15323
curling-type magnetic domains in narrow film strips 77−48020
cylindrical, possibility of thermomagnetic generation *(Russian)* 78−6539
cylindrical, stationary motion in field of point defect *(Russian)* 77−51916
cylindrical magnetic domains, light diffr. 79−73908
cylindrical magnetic domains, static and dynamic props. of isolated domain *(Russian)* 77−51915
demonstration experiment for teachers, using Kerr magneto-optical effect 78−69949
dialkylammonium copper tetrachlride, ferromag., static and dynamic mag. props. 80−50074
diffraction gratings with alterable magnetic domains for optoelectronics 78−63197
dipropylammonium coppertetrabromide, Faraday effect obs. of mag. struct., and domains 77−63399
domain structure dynamics, EM losses 79−87281
dry colloid observation apparatus, 90K to 290K 80−73394
dynamic behaviour, struct., rel. to ferromag., teaching appls. 78−86080
ellipsoid with domain struct., magnetostatic oscills., theory 80−93102
epitaxial ferrite-garnet films with inversion layers, behaviour of cylindrical mag. domains, visual tracking method 80−71139
ferric solution ferromagnetic liquid insulation in redox flow battery, quantum parameters separation 80−61338
ferrimagnet, cubic, mag. phase diagram, domain struct. analysis *(Russian)* 78−19249
ferrimagnetic materials, RF, dispersion props. 79−73772
ferrite, hysteresis loop rectangularity, inverse domain vol. depend. *(Russian)* 78−76270
ferrite, microstruct. depend. of props. and applics., review 78−88548
ferrite rod with domain structure, magnetostatic waves and internal field *(Russian)* 78−76236
ferrite with platelike domain struct., FMR absorpt. line intensity and shape 77−90041
ferrite-garnet film, local conc. of effective mass of domain boundaries *(Russian)* 77−12179
ferrites, unmagnetised polycrystalline, gyrotropic susceptibility and effective anisotropy 78−64224
ferrofluid decorated mag. domain patterns, Fraunhofer diffr., domain struct. determ. 78−6541
ferromag. domain obs. by TEM *(Hungarian)* 79−56565
ferromagnet, acoustic wave scatt. and reemission by moving domain walls 77−24713
ferromagnet, domain struct. study by time depend. neutron depolarisation 80−50138
ferromagnet, domain structure anal. by neutron depolarisation 77−40081
ferromagnet, dynamical props. of flat parallel domain struct. *(Russian)* 78−6499
ferromagnet, dynamics of domain struct. and microeddy currents in HF fields *(Russian)* 77−80957
ferromagnet, effect on domain neighbourhood *(Russian)* 78−39356
ferromagnet, elec. resist., just below crit. temp., effect of mag.-domains 80−39557
ferromagnet, interaction with mag. monopole 77−40078
ferromagnet, many-domain, indirect interaction of electrons via spin waves 77−85382

magnetic domains continued
ferromagnet, multiaxial, domain struct., applied stress effect *(Russian)* 78−76267
ferromagnet, neutron scattering, vector polarisation techniques 77−63117
ferromagnet, polydomain magnetic struct., excitation of sound 78−88162
ferromagnet, rel. to NMR under magnon bottleneck conditions, eqns. of motion 77−66429
ferromagnet, uniaxial, domain struct. and elastic props. in orientation region of phase transitions *(Russian)* 78−19270
ferromagnet, uniaxial, with flat-parallel domain struct., classical phenomenological description 78−56316
ferromagnet, with periodic domain struct., magnetoacoustic singularities of sound propag. *(Russian)* 77−24727
ferromagnet. with itinerant electrons, domain struct. stability 77−20629
ferromagnetic (111) films, macrostripe and microstripe domain structs. *(Russian)* 79−28572
ferromagnetic and antiferromagnetic domains, neutron techniques for obs., review 78−64213
ferromagnetic conductor, microscopic analysis of eddy current losses 77−85484
ferromagnetic domain structure, Landau-Lifshiftz, in appl. mag. field *(Russian)* 78−60305
ferromagnetic domain theory, quasi-dislocation theory appl. *(Japanese)* 80−60358
ferromagnetic film, mag. props., rel. to struct. 79−91270
ferromagnetic film, spin wave parametric reson. near phase transition 79−8053
ferromagnetic film, uniaxial anisotropy, approx. determ. of anisotropy const. 78−2713
ferromagnetic film, with domain struct., magnetostatic oscills. 78−48010
ferromagnetic film, with unidirectional anisotropy, domain struct. mag. field effect *(Russian)* 78−19289
ferromagnetic film with domain structure, transient state, mag. field calc. 77−4536
ferromagnetic materials, phase transition, mathematical bifurcation process 80−29572
ferromagnetic materials, TEM lens system with eucentric goniometer 77−72530
ferromagnetic medium, infinite, energy and mobility of Bloch point singularities 78−68331
ferromagnetic metal, dragging of domains by temp. gradient 80−34425
ferromagnetic metal, transient enhancement of AC susceptibility, domain nucleation, crit. effects 77−20633
ferromagnetic metal, with domain struct., resistivity 78−95285
ferromagnetic metals, transport props., crit. behaviour 80−65522
ferromagnetic particle system, micromagnetism and mag. reversal 79−82830
ferromagnetic plate, domain struct. during spin reorientation, phase diagram *(Russian)* 78−52320
ferromagnetic plate, domain struct. near first-order phase transition resembling second-order transition 80−93139
ferromagnetic plate, magnetic hysteresis theory, singularities of magnetic reversals on industrial freq. *(Russian)* 78−39373
ferromagnetic plate, monocrystalline, EM losses, influence of 90° domain wall motion *(Russian)* 78−27052
ferromagnetic plate, phase diagram in magnetic field *(Russian)* 77−48018
ferromagnetic plates, domain struct. and magnetisation curves *(Russian)* 79−19743
ferromagnetic polycrystals, cubic, domain structure under torsion *(Spanish)* 79−91246
ferromagnetic superconductor, mag. domain struct., sample thickness effects 80−39704
ferromagnetic superconductor, supercond. Bloch wall 80−20349
ferromagnetic superconductor, uniaxial, domain struct. parameters 80−39705
ferromagnetic superconductor, with domain struct. mag. induction vector 79−65585
ferromagnetic thin film, mag. domain wall energy determ. 79−95620
ferromagnetic uniaxial particles, domain struct, and crit. size *(Russian)* 80−25153
ferromagnets, domain struct. effects on dynamic props., review 80−34678
ferromagnets, domain structure image obtained by SEM *(Polish)* 80−34682
ferromagnets, solitary domains, Bloch and Neel stability, calcs. 80−25157
film, domain width in in-plane field, Faraday rot. meas. 77−4534
film, ferromag., dynamics near transition pt. from homogeneous to inhomogeneous magnetis. state 80−108038
film, ferromagnetic resonance in cylindrical mag. domains *(Russian)* 78−10780
film, honeycomb domain struct. *(Russian)* 78−56360
film, mag. moment, coupled oscills. in elec. circuit during HF mag. reversals *(Russian)* 78−23307
film, mag. phase states when easy magnetisation axis is inclined rel. to film surface *(Russian)* 80−103864
film, magnetisation changes during main stage of nonuniform rot. *(Russian)* 77−32224
film, magnetization amplitude and direction var., electron-microscope obs. procedure 78−6548
film, magnetocryst. anisotropy, magnetostriction and micromagnetism 77−73062
film, resonance props. in network of cylindrical mag. domains *(Russian)* 80−50194
film, striped domain struct., 2D model of distrib. of magnetisation *(Russian)* 78−88149
film, with perpendicular anisotropy, stripe domain struct., theory *(Russian)* 80−65973
film, with stripe domain structure, mechanism of mag. reversals *(Russian)* 77−80978
film for optical image recording, banded domain structure, effect of recording field strength on energy characts. *(Russian)* 78−19297
fine structure determ., high resolution colloid-SEM method 77−43846
garnet, LPE film, domain dynamics in microwave field 77−20663
garnet, Permalloy-coated film, bubble vel. and stability, influence of planar domains 80−39831
garnet, structure obs. by birefringence of mag. colloid 79−51809
garnet epitaxial film, elastic surface wave propag., stripe domain motion 77−20669
garnet film, domain obs. by SEM 77−69646
magnetic domains continued
garnet film, LPE, time resolved obs. system for domain dynamics, appl. to contracting motion of stripe domains *(Japanese)* 79−47312
garnet film, magnetic rag-domains, appl. to magneto-optical displays 78−91912
garnet film, uniaxial, cubic anisotropy effect 77−89998
garnet LPE film, laser beam deflector 77−54803
garnets, magnetic anisotropy and magnetostriction 79−99748
HOAB, smectic C liquid crystal, spin label probe obs. 77−19867
hypercritical films, stress-induced uniaxial anisotropy influence on domain struct. *(Russian)* 79−69703
hysteresis, local microscopic magnetisation intensity in presence of Shirobokov's domain struct. *(Russian)* 77−43851
image formation in reflection mode of SEM *(Japanese)* 77−32212
image profiles and resolution in SEM 78−47996
imaging by magneto-optics, domain struct. obs. 77−48151
imaging by SEM, computer simulation 80−71091
inhomogeneous ferromagnetic conductors, skin effect *(Russian)* 77−47847
itinerant electron ferromagnet with domain struct., spin waves 78−64182
lattice of transparent crystal regular birefr. regions, optical wave diffr. divergence 80−102616
lattices, parallel stripe susceptibility, uniaxial anisotropy field 80−54930
light diffraction, by cylindrical and elliptical domains *(Russian)* 79−1753
light diffraction by domain gratings, and appl. 80−88970
Lorentz electron microscope obs. with field emission gun 77−63228
LPE garnet bubble films, capping layer upper cap-switch field, model 78−95498
magnetic domain, SEM obs., method of removing fine magnetite particles from surface *(Japanese)* 80−108655
magnetic sheet with simple bar-like 180° domain structs., eddy current losses 80−39808
magnetically uniaxial ferromagnetic particles, high-anisotropy many domain, magnetisation, hysteresis *(Russian)* 79−91256
magnetisation distribution in magnetostatic oscillations 78−68293
magneto-optical concentration of light, by regular domain structures *(Russian)* 79−24297
magneto-optical controlled transparencies, page composers 78−50932
magneto-optical imaging of domain struct. in thick cryst., multiple diffr. effects 77−8552
magnetostatic waves in long rectangular bars, with domain struct. *(Russian)* 77−66383
metal, diamag. domain, helicon attenuation *(Russian)* 78−10721
metallic glasses, mats. props. review 77−4043
metallic glasses quenched from melt, appl. as soft mag. materials *(German)* 78−10676
metamagnets, intermediate state, theory 78−72360
microbeam analysis developments, mag. contrast obs. with HV SEM, quantitative analysis by ion microprobe with quadrupole mass filter *(Japanese)* 78−3432
micromagnetic perturbation theory 78−14912
micromagnetics and domain theory, developments from 1930 78−68288
motion in field of point defect *(Russian)* 78−39358
moving magnetic domain, force, momentum and topology 79−91264
multidomain ferromagnetic resonance anal., appl. to stripe and bubble arrays 79−78528
multidomain grains demagnetisation field, effect of domain walls displacements 78−65273
multidomain magnetic disc, ferromagnetic reson. 78−68386
Neel ferrimagnets, phase transitions, field-induced spin-orientational 80−75767
neutron beam channelling and focusing in ferromagnets *(Russian)* 80−107351
neutron depolarisation studies of ferromagnetic domain structures 80−25155
neutron diffr. study, symm. anal., polarisation effects 80−93083
neutron diffraction topography, domain and cryst. defect studies, results 79−46520
neutron Laue diffraction method, appl. to domain struct. in NiO and Fe_2O_3 78−95455
nuclear magnetic ordering, domains, neutron diffr. patterns, theory 80−100577
observation, simple method for magnetite fine particle removal from sample surface *(Japanese)* 79−61181
one-dimensional conductor, Curie const. discontinuity explained as paramag. domain tip alignment 77−16035
optical anisotropy in magnetic multidomain mats. 77−16279
orthoferrite crystals, band domains *(Russian)* 77−12178
orthoferrite plate, domain boundary crit. velocity *(Russian)* 78−35015
oxide particles, single domain, as source of rocks TRM 78−65271
periodic domain structures, micromagnetic theory, stability problem 77−69612
permalloy, cylindrical domain static performance in inhomogeneous external field *(German)* 77−63226
Permalloy, T- and I-shaped elements with cylindrical mag. domains, magnetisation distrib. 77−77074
Permalloy film, domain nucleation using low intensity US 80−34731
Permalloy film, in weak field, pulse mag. reversal mechanism *(Russian)* 77−80976
Permalloy film, magnetic leakage fields above stripe domains 77−77077
Permalloy film, stray fields arising during pulse reversal 77−80980
Permalloy film, stripe domain struct., distrib. of magnetisation *(Russian)* 77−66396
Permalloy film, submicroscopical magnetisation structs. induced by fields normal to film plane 79−1697
Permalloy film, with band domain struct., pulse mag. reversals *(Russian)* 79−38361
Permalloy films, domain propelling tunnel, domain struct. displacement *(Russian)* 79−99736
Permalloy films, domain struct., nonuniform rotation of magnetisation *(Russian)* 79−47313
Permalloy films with band domain struct., thermomag. recording, resolving power *(Russian)* 80−75769
Permalloy I bars, hysteretic props., Bitter soln. obs. and Kerr effect meas. 79−78439
Permalloy thin-film head pole struct., domain configurations, SEM obs. 80−65975
permanent magnets review 79−42801
plate, magnetoelastic energy and temp. depend. of mag. domain width *(Russian)* 79−47317

magnetic domains continued
plate of layered media, band domains *(Russian)* 77−12178
polycrystal subjected to successive asymmetrical hysteresis cycles, mag. props. evolution, reptation phenomenon *(French)* 78−10730
polycrystalline ferromagnets, demagnetisation and reptation (creep) anisotropy *(French)* 78−43616
pyrrhotite, pseudosingle-domain effects and single-domain multidomain transition 77−64274
rare earth compounds and alloys, spin-reorientation transitions, review 77−36073
rare earth intermetallic, $R(Fe_{1-x}Mn_x)_2$, phase struct., mag. and Mossbauer meas. 77−20563
rare earth iron alloy, amorphous film, cosputtered, struct. and mag. props. 78−60323
rare earth metals, mag. structs., nonspherical Fermi surface in RKKY theory 77−63227
rare earth orthoferrite, stripe domain struct. near spin-reorientation points 77−24707
rare earth-transition metal amorphous films, radiation damage 77−66398
regular domain structs., magneto-optical characts., optoelectronics appls. 80−40098
rock, reversible effect of small uniaxial stress on remanent mag., single-domain theory 78−20393
rock magnetism, domain structure obs. by Lorentz electron microscopy 80−72502
rocks, domain state depend. of uniaxial stress effect upon remanent magnetisation 80−26505
Rossville-type diabase, Pennsylvania, probably pseudo single domain behaviour 77−56621
screw spin structure, method of controlling the sense 80−70944
SEM, mag. contrast, type-2, effect of collector position 79−12909
SEM, magnetic contrast, techniques and appls. 79−6236
SEM, signal-to-noise ratio, in recorded images, by random variations in angle of incidence of electron beam 79−12910
SEM image contrast 77−4528
SEM observation magnetic domain obs. 77−69606
single domain grain assembly, theory for magnetisation processes 80−88828
soft ferromagnetic cylinders and spheres, micromagnetics 77−12150
soft magnetic materials, meas. methods, review 80−86345
spin glass, rel. to behaviour near T=0 77−4479
spin glass, transitions, field-induced, masking effects 80−65943
spin-reorientation phase transition *(Russian)* 80−93122
steel, alloy, YuNDK24, magnetisation direction in interaction domains *(Russian)* 79−99720
steel, C, magnetomechanical acoustic emission for residual stress NDT 80−71149
steel, ferritic, magnetomechanical acoustic emission for residual stress NDT 80−71149
steel, induced anisotropy influence on mag. props., thermomagnetic working *(Russian)* 80−55549
steel, magnetisation transitions, Barkhausen noise 78−91894
steel, Si, highly-oriented domain and grain obs. methods, using ferromagnetic colloid technique 80−11856
steel, Si, with coating, grain-oriented, domain pattern measurements *(Japanese)* 79−38353
steel, stainless, plastic working of wires, high-density current appl. 79−57002
steel, transformer, domain struct., triaxial ferromagnets, spontaneous magnetisation distrib., plane stress state influence *(Russian)* 79−61071
strip films, bulk and surface spin oscills., mag. reson. 80−97149
stripe domain structure, magnetostatic modes 78−68333
stripe head vel. meas. using magnetoresist. signal 78−68316
structure obs. by Kerr-magneto-optical effect, laser speckle suppression 80−85093
structure studies by neutron depolarisation 79−47299
superconducting plate, intermediate state, Landau's laminar model 78−26987
Tertiary basalts with low Curie temps., palaeomag. data reliability 78−28166
texture analysis, generalisation of dispersion theory 80−80556
thermofluctuation aftereffect anisotropy in Rayleigh region *(French)* 78−14989
thermomagnetic recording singularities at Curie point, cylindrical domain form. *(Russian)* 77−8318
thick layers with regular domain structure, magnetooptical diffr. of light 80−108188
thin uniaxial platelet with stripe domain struct. magnetised along easy axis, FMR absorpt. 79−42841
Ticonal, interaction domains after heat treatment in mag. field *(Russian)* 78−68286
titanomagnetite, monodomain behaviour in multiphase oxidised material 77−60366
titanomagnetite, single-domain particles identification by TEM 79−88342
titanomagnetites, domain struct. var. with temp. 78−65272
transversely heterogeneous magnetically uniaxial plates, non-through mag. domains *(Russian)* 80−93135
triaxial crystals, domain struct. and magnetisation phenomena *(Russian)* 79−47295
twisted uniaxial polycrystals, magnetisation process, model 79−91254
two-layer mag. structures, thermomag. recording 80−100588
uniaxial ferromagnet, domain struct. in mag. field 80−103853
uniaxial ferromagnet, neutron depolarisation calc. 78−64192
uniaxial ferromagnet domain struct., phase transition *(Russian)* 80−108044
US spectrum, RF field in multidomain struct. 78−68056
wall flexibility, implications on interaction with dislocations and hysteresis existence 77−4525
$Ag_{1/2}In_{1/2}Cr_2S_4$, first order macro to microdomain transition 77−69562
Al, with diamag. domains, helicon attenuation below 1K *(Russian)* 77−85254
AuMn, mag. struct., phase transition, and magnon spectrum, random anisotropy effects 80−88722
Au_4V single crystal, ordered, mag, props., domain models 80−39770
$BaFe_{12}O_{19}$ particles, magnetic domain study by colloid-SEM method 80−97120
$BaFe_{12}O_{19}$ plate, with cylindrical domain struct., ferromag. reson. at arbitrary magnetisation 77−81017

magnetic domains continued
$BaO\text{-}Fe_2O_3$, chemically coprecipitated, mag. props., orientation 80−15763
$BaO.6Fe_2O_3$, ferrite polycryst., depend. of domain width on sample thickness 80−108031
BiIG, transparent, domain struct. realignment in external mag. field 78−10739
$(BiTm)_3(FeGaTm)_3O_{12}$, layer separation of domain struct. 80−44857
$CdCr_2Se_4$ films, mag. hysteresis, domain struct., mag. viscosity 80−25169
$CdCr_2Se_4$, mag. semicond., domain struct. by IR Faraday effect 79−95604
$CdCr_2Se_4$, mag. semicond. effect of illum. on domain struct. 79−99726
Co, FCC, ferromag. domains of fine particles, Lorentz electron microscopy obs. 78−27053
Co, ferromag., domain struct., small-angle neutron scatt. 77−66382
Co, HCP to FCC transition, mag. domain nucleation 78−64218
Co, HCP-FCC transition, mag. domain behaviour, Lorentz electron microscopy 77−80958
Co, magnetic domain struct. temp. depend. 79−78436
Co-CoO films, evaporated, exchange anisotropy 80−88841
Co-Cr films, mag. props. in range of transition from thin-film to hypercritical state *(Russian)* 79−51824
Co-Gd(Ho) film, amorphous, stripe domains and mag. anisotropy by Lorentz microscopy 77−63243
Co-Ni alloys, electrodeposited, struct., internal stress, and mag. props. 78−95471
Co-P, amorphous, domain struct., mag. anisotropy origin 80−80554
Co-P, amorphous alloy, domain struct., effect of annealing 78−60304
Co-P, amorphous electrodeposited films, domain wall motion, Kerr effect 78−60322
Co-P amorphous alloy, domain struct. 78−10720
Co-P amorphous alloy film, mag. domain struct. 77−69604
Co-P amorphous film, domain struct., influence of planar anisotropy 79−78472
Co-Pt, atomic ordering props. and domain growth in strong pulsed mag. field *(Russian)* 80−54918
$Co_{80}B_{20}$, amorphous metal ribbon, stresses, magnetoelastic anisotropy and zero-field mag. domain struct. 80−44896
$CoBr_2$, lamellar, field depend. of uniform magnon. energies, antiferromag. reson. meas. 77−73086
$CoCl_2$, lamellar, field depend. of uniform magnon. energies, antiferromag. reson. meas. 77−73086
CoF_2, 180-degree antiferromag. domain obs. by new magnetooptical effect 80−44855
CoF_2, deformed, magnetoelastic interactions and single-domain antiferromag. state 77−43849
CoF_2, domain formation in staggered field induced by uniaxial stress, neutron diffr. exam. 78−76289
CoF_2, visual obs. of 180° antiferromag. domains, mag.-optical effect *(Russian)* 79−61349
$Co_{35}P_{15}$, amorphous, strip domains, anisotropy const. effects 80−29571
CoPd, single crysts., domain struct., temp. and field depend. 80−71085
Co_5Sm, coercive field temp. depend. 77−8358
Cr, antiferromagnetic, polarisation domain effects on US velocity 78−52329
Cr, antiferromagnetic, US attenuation and phase diagram 80−103831
Cr, antiferromagnetic spin-density-wave domain and size and behaviour, X-ray and neutron topography 79−42793
Cr, mag. struct., phase transition, and magnon spectrum, random anisotropy effects 80−88722
Cr, magnetic torque anal. in thermally activated domain model, near spin-flip temp. 77−63229
Cr, temp. limits of cryomagnetic method of obtaining single-modulation state 78−72374
Cr, transverse magnetoresist. meas. in multi-Q and single-Q domains, 15 to 80°C 77−85197
Cr, transverse spin-density-wave phase, absence of neutron diffr. line broadening due to polarisation domains 77−24677
$CrBr_2$, ferromag. domains, using liq. He mag. specimen stage 80−103855
$CrBr_3$, HF spectra, susceptibility, spin waves in domain walls *(Russian)* 80−80909
Cr_2O_3, dielec. const. in mag. field, nonlinear magnetoelec. effect in Neel pt. region 80−66006
$CsMnCl_3$, mag. anisotropy measurement 79−11310
$CsMnF_3$, mag. struct., phase transition, and magnon spectrum, random anisotropy effects 80−88722
$CsNiF_3$, one-dimens. ferromag., solitons in external mag. field 79−19724
$CsNiF_3$, quasielastic neutron scatt. around Neel-point 80−75768
Cu ferrite films, Mn-, Ni- and Al-substituted, LPE growth 80−96752
Cu, with diamag. domains, helicon attenuation below 1K *(Russian)* 77−85254
Cu:Co precipitates, mag. anisotropy, precipitate shape, coercive force 80−80500
Cu-Mn spin glass, magnetisation reversal and macroscopic mag. domain obs. 79−61168
Cu-Mn(1%) spin glass, remanent mag., zero-field NMR obs. 79−33492
$CuCr_2S_4$, ferromag., spin wave contrib. to nucl. spin-lattice relax. time meas. 77−36147
$CuFe_2O_4$, LPE grown, domain struct. rel. to tetragonal distortion 78−92205
Dy, antiferromagnetic, thermal expansion, US attenuation anomalies 79−47319
Dy, change in easy axis 77−8306
Dy, domain effects near order-disorder and order-order ferromagnetic transitions 80−65886
Dy, ferromag., rel. to magnetoresist., fields up to 75 kOe, 1-70K 77−20297
Dy, magnetic domain structure, hysteresis, thermal modulation study 80−71082
Dy, magnetostriction meas. re-analysis, domain effects corrected by phase theory 78−6555
Dy-Co amorphous film, prep. by dual-source evaporation, mag. props. 77−89988
DyAG, light scatt. from metamag. domains, crit. exponent determ. 77−66482
$Dy_xCe_{1-x}Ru_2$, supercond., domain struct. model 79−11267
DyCu film, amorphous, asperomagnetic domains, Barkhausen jumps in hysteresis loop 80−75822
Dy_2Fe_{17}, domain structures and anisotropy constant. 80−93136

magnetic domains continued
$DyFe_{0.998}Co_{0.002}O_3$, orthoferrite, domain struct. near mag. transitions 80−2599
$DyFeO_3$, magnetic intermediate state at antiferromag. to weakly ferromag. transition *(Russian)* 77−40059
$DyFeO_3$, orthoferrite, domain struct. 77−77071
$DyFeO_3$, phase domains, polarisation microscope obs. 77−28407
$DyFeO_3$ single crystal, mag. domain width, temp. depend. 4.2 to 293K 77−40100
$DyFeO_3$, spin reorientation near Morin temp., magnetooptical exam. 78−68284
$Dy_{0.5}Ho_{0.5}FeO_3$ orthoferrite, domain struct., temp. depend. 80−71086
$DyPO_4$, mag. transitions under hydrostatic press., neutron diffr. study 80−71030
$(Er,Tb,Gd_3)Fe_5O_{12}$ plate, pseudouniaxial, domain struct., magneto-optical obs. 80−11221
$(ErBi)_3Fe_{5-x}Ga_xO_{12}$ film, ferrimag., splitting of domains into layers 77−28420
$ErCo_3$, $ErCo_6$ and Er_2Co_{17}, Kerr effect determ. of domain structure, Bloch wall energy 80−39805
$(ErEu)_3(FeGa)_5O_{12}$ film, for mag. writing and magneto-optical displays 78−6549
$Er_2EuFe_{5-x}Ga_xO_{12}$, rag-domain garnet film, controlled variation of props. under O_2 annealing 79−15328
$Er_2Fe_3Co_{14}$, Kerr effect determ. of domain structure, Bloch wall energy 80−39805
$ErFeO_3$, spin flip, Faraday effect and absorption spectrum meas. 77−43842
$Er_3Fe_5O_{12}$, low temp. CVD epitaxial film growth and mag. props. 79−42406
ErZn, preferred mag. domain orientation, and microstructural defects, magnetostriction meas. 79−73769
$(Eu,Y)_3Fe_5O_{12}$, low temp. CVD epitaxial film growth and mag. props. 79−42406
$(Eu,Yb)_3Fe_5O_{12}$, low temp. CVD epitaxial film growth and mag. props. 79−42406
Eu, magnetoresist., irreversible component rel. to antiferromag. struct. *(Russian)* 77−35920
Eu, negative magnetoresist. obs., rel. to antiferromag. domain struct. 77−8073
$EuFeO_3$, minute single crystal domain struct. 77−20646
EuS, ferromag. semicond. film, Hanle effect, optical orientation time consts. meas. 77−40214
$Eu_xSr_{1-x}S$, onset of ferromagnetism for x near 0.5 neutron diffr. obs. 79−24181
Fe, [111] oriented whisker, mag. domain struct. and approach to saturation 79−82814
Fe alloy, low, (110)[001] oriented, mag. charact. 77−1879
Fe, ferromag., domain struct., small-angle neutron scatt. 77−66382
Fe foil, electrodeposited, phys. and mag. props. 79−91275
Fe, magnetomechanical acoustic emission for residual stress NDT 80−71149
Fe, Mossbauer absorpt. spectrum, domain struct. effect 79−69758
Fe, plastically deformed, dislocation arrangement exam. by ferromag. techniques 78−63774
Fe, plastically deformed, high field suscept. anisotropy and domain struct. 78−15002
Fe, pure, tensile deform., sources of acoustic emission 78−19814
Fe, stray mag. fields above stripe domains, electron microscope and μ^*-tensor determ. 80−71089
Fe, stress fields and strains energies associated with closure domains 77−1563
Fe thin layers, vacuum coated on PMMA, mag. behaviour during mech. stress cycles *(German)* 80−80581
Fe whisker, optimisation of magnification of magneto-optic Kerr effect by interference layers 79−51808
Fe whiskers, elastically and plastically deformed, mag. domain structs. 80−15752
Fe whiskers, struct., dislocations, mag. domains *(Polish)* 79−33210
Fe-Al, domain struct. and magnetostriction, heat treatment effect 80−60398
Fe-Al-C alloys, C migration and mag. aftereffect, mag. permeab. disaccommodation and long-range order meas. 79−8020
Fe-B, sputtered amorphous film, strong stripe domains, Kerr effect obs. and theory 79−91265
Fe-B amorphous alloy, annealed, microstruct. and mag. domain changes 80−75790
Fe-B amorphous alloy, mag. anisotropy temp. depend. 80−15846
Fe-Co, amorphous alloy, stress effect on mag. domain struct. 79−33502
Fe-Co-V, Vicalloy, magnetisation reversal by stretching and twisting 80−34733
Fe-Cr-Co-Si alloy, interaction domains after heat treatment in mag. fields *(Russian)* 78−68286
Fe-Cr-Co-V alloy, microstruct. and mag. props. 78−68221
Fe-Ni films, dynamic domains and pulse mag. reversals *(Russian)* 79−28571
Fe-Ni-Co foils, mag. reversals of mag. domains in low-coercivity channels *(Russian)* 79−42813
Fe-P electrodeposited foil, amorphous, mag. domains 80−75821
Fe-P film, amorphous, ion implanted, struct. and domain struct. obs. 79−91272
Fe-Si, coated, effective domain and grain obs. methods and Fe losses 80−34675
Fe-Si, domain struct., influence of insulating coating, high voltage SEM obs. 77−1565
Fe-Si, domain struct. obs. by high voltage SEM 77−1564
Fe-Si, domain structure of Neel oriented samples 77−69601
Fe-Si, grain oriented, effect of tensile stress on domain struct. 78−95462
Fe-Si, grain-oriented, magnetostriction, and domain struct. 79−1703
Fe-Si, maze domains upon appl. of horizontal mag. field or mech. tension 80−11218
Fe-Si, simple domain structs., magnetisation jumps 77−69624
Fe-Si, thin cryst., domain struct. behaviour during magnetisation *(Russian)* 78−2697
Fe-Si, type B_1 domain struct., Mossbauer exam. 77−51931
Fe-Si (110)[001] sheet, normal stress effect on magnetostriction 77−40102
Fe-Si (2.4 wt.%), simulation of X-ray topographies of ferromag. domains *(French)* 77−77070
Fe-Si (2.5%), mag. stray fields above stripe domains, electron optic meas. 80−15755
magnetic domains continued
Fe-Si (3 wt.%), domain struct. rel. to cryst. size *(Russian)* 80−29568
Fe-Si (3 wt.%), eddy current and hysteresis losses, role of domain struct. *(Russian)* 77−80961
Fe-Si (3 wt.%), ferromag. domains, imaging by neutron interferometry 80−71087
Fe-Si (3 wt.%), grain oriented tape-wound core, dynamic domain size var. and Fe losses 77−12146
Fe-Si (3 wt.%), grain oriented, mag. domain movements 79−82815
Fe-Si (3 wt.%), grain-oriented, domain struct. regulation and power loss reduction 80−88779
Fe-Si (3 wt.%), hysteretic losses, domain struct. and cryst. defects 79−19747
Fe-Si (3 wt.%), Mossbauer spectra, domain magnetisation vector rotations, domain struct. 79−69761
Fe-Si (3 wt.%), oriented, losses and domains, mech. stress effects 80−88852
Fe-Si (3 wt.%), polycryst. (110), synchrotron radiation topographs and mag. domain obs. 78−67620
Fe-Si (3 wt.%), polycrystal in mag. field, stress induced magnetisation, synchrotron Bragg refl. topography obs. 80−50139
Fe-Si (3 wt.%), square etch pit characts., subgrain misorientation and mag. domain patterns 77−25199
Fe-Si (3 wt.%), stripe domain structure, dynamic behaviour at high max. induction values *(Russian)* 80−80553
Fe-Si (3 wt.%), total losses under tensile stress, rel. to orientation near (110)[001] 78−76272
Fe-Si (3 wt.%), transformer steel, grain-oriented, magneto-optical domain obs., magnetisation mechanism 77−12364
Fe-Si (3 wt.%) alloy, mag. domain movements prod. by mech. stress 79−87284
Fe-Si (3 wt.%) domain struct., tensile load effects *(Russian)* 78−47995
Fe-Si (3 wt.%) laminations, isotropic and cube-on-face, magnetostriction behaviour 80−39843
Fe-Si (3 wt.%) laminations, magnetostriction behaviour associated with closure domain spikes 80−75834
Fe-Si (3 wt.%) locally deformed, EM loss depend. on cryst. struct. and orientation *(Russian)* 80−7694
Fe-Si (3 wt.%) mag. domain motion quasi-lifetime topography using white synchrotron radiation, mag. field effects 79−42797
Fe-Si (3 wt.%) sheet, obs. through surface coating of domain struct., SEM 77−85482
Fe-Si (3.2 wt.%), single cryst., prism-shaped closure domains on (110) surface 79−69690
Fe-Si (3.22 wt.%), topographic and type-2 magnetic contrast, effect of collector position in SEM 79−12909
Fe-Si (3.5 wt.%), dynamic neutron depolarisation meas. of ferromag. domain struct. 79−82812
Fe-Si (3.5 wt.%), static neutron depolarisation meas. of ferromag. domain struct. 78−14978
Fe-Si (4 wt.%) alloy, coercive force, influence of stabilisation of domain struct. on temp. depend. *(Russian)* 77−52513
Fe-Si alloys, polycrystalline, domain struct. at grain boundaries *(Russian)* 77−51917
Fe-Si plate, ferromag. domain structure obs. by neutron diffr. topography 77−69645
Fe-Si transformer steel, supplementary domain struct. of misoriented grains *(German)* 78−14979
Fe-Si-B metallic glasses, mag. props., depend. on metalloid content 77−85485
$Fe_{80}B_{20}$ amorphous alloys, domain struct. exam., magneto-optic Kerr effect 79−28550
$Fe_{80}B_{20}$, METGLAS 2605, mag. anisotropy and electronic struct., Mossbauer meas. 77−28384
$Fe_{80}B_{20}$, metallic glass, ferromag. props. 77−16107
Fe_3BO_6, canted mag. struct. near Neel point, Mossbauer meas. 78−35073
$Fe_{81.5}B_{14.5}Si_4$, amorphous metal ribbon, stresses, magnetoelastic anisotropy and zero-field mag. domain struct. 80−44896
$FeCO_3$, mag. neutron scatt., spin orbit coupling effects 77−85419
$Fe_{0.5}Co_{0.5-x}Cr_x$ films, vacuum-deposited cryst. and mag. struct. *(Russian)* 80−93081
$FeGe_2$ canted antiferromagnet, mag. susceptibility anisotropy and temp. dependence 80−25112
FeI_2, neutron inelastic scatt. from mag. excitations 80−50078
$Fe_{40}Ni_{38}Mo_4B_{18}$ ribbon, magnetic characterisation 80−34680
$Fe_{40}Ni_{40}P_{14}B_{06}$, amorphous, strip domains, anisotropy const. effects 80−29571
$Fe_{40}Ni_{40}P_{14}B_6$, amorphous, domain struct. 78−10719
$Fe_{40}Ni_{40}P_{14}B_6$ amorphous ribbon, mag. anisotropy distrib. near surface 78−95430
$Fe_{40}Ni_{40}P_{14}B_6$, amorphous ferromagnet, domain struct., Rayleigh region and coercive field 79−28559
$Fe_{40}Ni_{40}P_{14}B_6$ amorphous ribbon, mag. domains and anisotropy distrib. 80−108029
$Fe_{40}Ni_{40}P_{14}B_6$, Metglas 2826, magnetising processes 78−10725
α-Fe_2O_3, haematite, birefr. under uniaxial stress in mag. field *(Russian)* 78−88285
Fe_2O_3, haematite, mag. domain distrib., appl. of mag. Laue neutron diffr. method 78−95455
Fe_2O_3, haematite, single domain, defect moment components coercivities 79−16438
α-Fe_2O_3, hematite, field-induced domain struct., neutron diffr. meas. *(German)* 77−16101
α-Fe_2O_3, hematite, weakly ferromag. domain struct., X-ray topography obs. 79−28551
α-Fe_2O_3, neutron Laue diffr. investig. of domain distrib. 77−24712
α-Fe_2O_3, single cryst., hematite, X-ray topographic obs. of domain struct. changes in external mag. field 80−88785
Fe_3O_4 (magnetite), multidomain particles magnetisation 79−66686
Fe_3O_4, magnetite, grain size limits for pseudosingle domain behaviour, rel. to palaeomagnetism 80−11215
Fe_3O_4, magnetite, TRM props. of single-domain, pseudo-single-domain and multidomain particles 78−40544
Fe_3O_4-$FeTiO_3$ intergrowth, thermal magnetization of granules 79−44182
$Fe_{75}P_{15}C_{10}$ amorphous foil, ferromag. domain orientation, Mossbauer exam. 78−52402
$Fe_{80}P_{13}C_7$, amorphous, mag. domain struct. obs. 77−36091
$Fe_{80}P_{13}C_7$, amorphous, rapidly quenched, magnetic props., effect of annealing 77−16701

magnetic domains continued
$Fe_{25}Pd_{50}Au_{25}$, atomic ordering influence on mag. props. and elec. resistance *(Russian)* 80−7551
FeSi, domain struct. and magnetisation reversal, time depend. neutron depolarisation 80−50138
FeSi, single crysts., domain struct., temp. and field depend. 80−71085
$Fe_{2.6-x}Ti_{0.4}Al_xO_4$, $Fe_{2.4-x}Ti_{0.6}Al_xO_4$, titanomagnetite, monodomain, mag. props. 78−56346
$Fe_{2.4}Ti_{0.6}O_4$, TRM acquired by multi-domain single cryst. 80−36293
$Fe_{2.4}Ti_{0.6}O_4$, titanomagnetite, single-crystal, mag. props. of multidomain TRM 78−56345
Gd, AC susceptibility, temp. modulation studies, domain property thermal relaxation 79−61072
Gd, AC susceptibility near Curie point, domain nucleation 77−4515
Gd, domain effects near order-disorder and order-order ferromagnetic transitions 80−65886
Gd, domain struct., 77K 78−84447
Gd, ferromag., domain struct., small-angle neutron scatt. 77−66382
Gd foil, domain and domain wall structure 77−69603
Gd, Lorentz microscopy obs. 78−84448
Gd, mag. domain obs. at 77K 77−69602
Gd, mag. domain struct. obs. by wet and dry colloid techniques 78−6542
Gd-Co, amorphous film, with cylindrical mag. domains, sputtering prep. *(Russian)* 77−12176
Gd-Co, and Gd-Co-Mo films, amorphous, mag. props., annealing effects 78−64235
Gd-Co alloy, sputtered film, mag. props. determ. *(Chinese)* 78−2714
Gd-Co amorphous film, sputtered, perpendicular anisotropy exam. 79−73707
Gd-Co amorphous films, struct. and mag. anisotropy 80−20438
Gd-Co amorphous thin films, crystn. process and domain struct. *(Chinese)* 80−54533
Gd-Co film, sputtered from segment target, composition and mag. props. 78−27062
Gd-Co(-Au) film, ferrimag. amorphous, coated with Permalloy films, mag. props. 79−1695
Gd-Co(Fe) amorphous films, microstruct. and mag. anisotropy 79−82838
Gd-Fe, co-evap. amorphous film, anomalous hysteresis loop, domains obs. 77−89995
Gd-Fe amorphous film, prep. by dual-source evaporation, mag. props. 77−89988
Gd-Fe film, amorphous, mag. props., annealing effects 78−64235
Gd-Mo-Mo amorphous film, domain drag effect obs. 78−91911
GdB_6 single crystals, mag. behaviour and structure change at low temp. 80−71018
$Gd_{1-x}Co_x$, film, resistivity, Hall effect, domain wall density 78−76169
^3He, vacancy struct., neighbouring ferromag. domains *(Russian)* 77−20161
Ho, single cryst., transverse magnetoresist. 77−66154
Ho-Co amorphous film, prep. by dual-source evaporation, mag. props. 77−89988
$HoCo_3$, Ho_2Co_7, $HoCo_{5.5}$ and Ho_2Co_{17}, Kerr effect determ. of domain structure, Bloch wall energy 80−39806
Ho_xCo_{1-x} amorphous films, microstruct. and mag. anisotropy 79−82838
$Ho_2Fe_3Co_{14}$, Kerr effect determ. of domain structure, Bloch wall energy 80−39806
$KCoF_3$, antiferromag. domains obs. by cryogenic X-ray topography 77−39507
$KCoF_3$, strain sensitive props., Mossbauer spectra obs. 77−20765
$KFeF_3$, strain sensitive props., Mossbauer spectra obs. 77−20765
$KMnF_3$, mag. props. and struct. transitions, antiferromag. reson. meas. 79−8052
$K_2Mn_{0.987}Fe_{0.022}F_4$, antiferromag., mag. field induced transitions, neutron scatt. meas. 79−82782
$KNiF_3$, ^{19}F spin-lattice relaxation 80−93211
$KNiF_3$, antiferromag. domains obs. by cryogenic X-ray topography 77−39507
$KNiF_3$, antiferromag. domain behaviour 77−69607
$KNiF_3$, antiferromagnetic, field-induced domain reorientation, NMR obs. 79−82816
$Li_{0.5}Fe_{2.17}Al_{0.33}O_4$:Co, single cryst., domain struct., mag. annealing effect depend. on induced anisotropy 78−68290
$Li_{0.5}Fe_{2.5}O_4$, domain struct. in (110) and (111) plates, Faraday effect meas. 79−61180
$Li_{1-x}Fe_{5-x}O_8$:Co, single cryst., domain struct., mag. annealing effect depend. on induced anisotropy 78−68290
LiH, mag. domains and nucl. mag. ordered phases, antiferromag. and ferromag. neutron diffr. obs. 80−50051
LiH, nuclear ordered ferromag. and antiferromag. phases, neutron diffr. study 80−50052
$(Lu,Bi)Fe_5O_{12}$, magneto-optic colour effects 78−23308
LuTb garnet film, scratch-modified mag. domain patterns 78−48007
Mn intermetallic compounds, energy of veriform struct. 78−91882
Mn-Al alloy, domain struct., cryst. defect effects 77−69609
Mn-Zn ferrite, domain struct. and initial permeability, effect of O nonstoichiometry 78−35001
MnAlGe film, mag. domains and amorphous to cryst. phase transition, electron microscopy obs. 80−71129
$MnAu_4$, domain struct. exam. by powder method *(German)* 78−91883
MnBi, Kerr effect and TEM obs. 77−89974
MnBi particles, effect of grinding on coercivity 77−36098
MnBi, thin film, struct. and mag. props. 79−47315
$MnCl_2.4H_2O$, single cryst., mag. phases, obs. by ^{54}Mn nucl. polarisation 77−81031
MnF_2, antiferromag. and piezomag. domain struct., neutron topography study 80−71088
MnF_2, antiferromag. domains, obs. using neutron technique 78−64213
$MnFe_2O_4$, nuclear reson. and relax. from domains and domain walls 77−8448
MnGaGe film, mag. domains and amorphous to cryst. phase transition, electron microscopy obs. 80−71129
MnO, antiferromag. reson. lines due to domain groups 77−40134
$MnO-Al_2O_3-SiO_2$ glass, spin freezing, muon spin depolarisation, superparamag. domain model 78−68272
$MnO-Al_2O_3-SiO_2$ glass, optical spectra 78−68528
MnP, noncubic ferromag., relax. times for domain and wall resonances 77−77119
$Mn_{1.15}Sb$, Kerr effect and TEM obs. 77−89974

magnetic domains continued
Mn_2Sb, domain and domain wall resons. in ^{55}Mn NMR spectrum 80−25219
$MnSb_{1-x}Sn_x$, zero-field NMR investig. of domains and domain walls 77−32271
MnZn ferrite, mag. permeability accommodation depend. on mag. field *(Russian)* 80−34685
MnZn ferrite, surface damaged layer, mag. domain obs. by taper section SEM 77−59423
MnZn ferrites, mag. domains on worked surfaces 79−99722
β_1-MnZn, ferromag., spin wave contrib. to nucl. spin-lattice relax. time meas. 77−36147
$(NH_4)_2CuBr_4.2H_2O$, ferromag., static and dynamic mag. props. 80−50074
Nd-Co film, amorphous, exam. of domain struct. 78−68336
Ni, Czochralski grown single cryst., X-ray topography 77−12147
Ni electrodeposit, mag. domain struct., neutron depolarisation 78−2716
Ni, electrodeposited sheet, mag. domain struct. obs. by neutron depolarisation 77−69605
Ni ferrite with domain struct., FMR absorpt. line intensity and shape 77−90041
Ni, ferromag., domain struct., small-angle neutron scatt. 77−66382
Ni, ferromagnetic domain struct., static neutron depolarisation meas. 79−82812
Ni film, effect of He ion implantation on domain struct., Lorentz electron microscopy 77−20654
Ni film, microstructure of charged boundary between ferromag. domains 79−69705
Ni film, single cryst., domain width from ferromag. reson. 80−39879
Ni, formed in decomposing β-NiH α-phase precipitate detection by Bitter powder pattern 79−28104
Ni, mag. layer, domain struct., neutron depolarisation study 79−47299
Ni, magnetised mono- and polycryst., activation vol. var. during low temp. deform. *(Russian)* 78−3178
Ni, μ^*-tensor method, temp. and surface orientation depend. 77−16098
Ni, neutron depolarisation near Curie point *(German)* 78−14934
Ni, single cryst., rel. to magnetisation and US attenuation, mag. field depend. *(Russian)* 78−6559
Ni, single crystal, structure of mag. domains 79−65695
Ni single crystals, cyclically deformed, behaviour during annealing 78−71740
Ni, stray mag. fields above stripe domains, electron microscope and μ^*-tensor determ. 80−71089
Ni, thermal softening, influence of alternating mag. field *(Russian)* 78−23312
Ni, US attenuation, mag. field and temp. depend. 77−90008
Ni, US induced mag. reversals, stroboscopic electron microscope obs. 77−48026
Ni-Co-P, amorphous electrodeposited films, domain wall motion, Kerr effect 78−60322
Ni-Fe, film, domain struct., effect of biaxial stresses 78−88153
Ni-Fe (20 wt.%), thin film ferromagnetic band, magnetisation under domain creep conditions *(Russian)* 79−91262
Ni-Fe (36 to 50 wt.%), initial permeability, domain struct. model 80−88811
Ni-Fe film, domain struct., uniaxial stress effects 78−10740
Ni-Fe films, magnetisation reversal in narrow strips, TEM study 80−34720
Ni-Fe narrow stripes, mag. props. and domain struct. 79−82843
Ni-Fe-Co (17,3 wt.%), thin film ferromagnetic band, magnetisation under domain creep conditions *(Russian)* 79−91262
Ni-Fe-Ho film strips, domain struct. and new rot. processes 77−85533
Ni-P electrodeposit, magnetisation coercivity and magnetostriction 78−68338
Ni-P film, amorphous, ion implanted, struct. and domain struct. obs. 79−91272
$Ni_{1-x}Co_xO$, LF magnons, inelastic neutron scatt. exam. 77−66288
NiFe, single and multilayer thin films, strip domains, inplane magnetisation 80−103866
NiFe, US induced mag. reversals, stroboscopic electron microscope obs. 77−48026
NiFe-Ho film strips, curling-type mag. domains 77−48020
Ni_3Fe, domain struct. after tensile deform., dislocation effects 80−71083
$NiFe_{2-x}Al_xO_4$, stress-induced anisotropy in LPE grown single cryst. films, stripe domains and mag. bubbles struct. 79−28238
$NiFe_2O_4$, parametric excitation of spin waves in samples with regular domain struct. *(Russian)* 77−32183
Ni_3Mn, mag. domains perpendicular to AC demagnetising field 77−20632
Ni_3Mn, magnetic phase exam. 77−20631
NiO, antiferromag. domains, obs. using neutron technique 78−64213
NiO, antiferromag. domains exam. by magnetic neutron Laue diffr. 79−51806
NiO, linear birefringence in S-domains near antiferromag. phase transition 80−60261
NiO, mag. struct., neutron Laue diffr. method 80−70951
NiO, magnetic neutron Laue diffr. study of domain struct. and distrib. 78−95455
NiO, multidomain mat., opt. anisotropy meas. at T_N 77−16279
NiO, thermal expansion, birefringence, AC susceptibility, temp. depend. 78−10664
NiO, thin plate, antiferromag. domain obs. by neutron diffr. topography 77−32209
NiO, transport props., temp. and stoichiometry depend., antiferromag. T-domain influence 77−8332
NiS_2, weak ferromagnet, galvanomagnetic effect 79−11148
$NiWO_4$ monoclinic antiferromagnet, orientational phase transition and intermediate state *(Russian)* 80−15725
$NiWO_4$, monoclinic antiferromag., domain struct. induced by strong mag. field 80−44856
$PbFe_{12}O_{19}$, Mossbauer spectra, domain magnetisation vector rotations, domain struct. 79−69761
$Pb_5Ge_3O_{11}$, multidomain mat., opt. anisotropy meas. at mag. crit. temps. 77−16279
Pd-Fe, magnetic anisotropy near Curie point, quasi domain struct. *(Russian)* 80−65867
Permalloy, domain struct., influence of planar anisotropy 79−78472
$RbCoF_3$, single oriented antiferromag. domain, polarised Raman scatt. under uniaxial stress 78−23463
$Rb_2CuBr_4.2H_2O$, ferromag., static and dynamic mag. props. 80−50074
$RbMnCl_3$, antiferromag. static mag. props. *(Russian)* 78−60270

magnetic domains continued
$RbMnF_3$, antiferromag. domain struct. in fields exceeding spin-flop value 79−69693
Si-Fe, domain and grain obs. using ferromag. colloid technique 80−11219
Sm-Co-Cu-Fe-Zr alloy, reversible changes in coercive force and struct. state during heat treatment 400-800°C *(Russian)* 80−29574
$SmCo_5$, improvement of mag. domain contrast in SE-mode of SEM *(German)* 77−51920
$SmCo_5$, nucleation of reversed domains at Co_7Sm_2 precips. 80−75791
$SmCo_5$, rel. to crystal defects, electron microscopy 80−103856
$SmCo_5$, sintered, high coercivity, microstruct. and mag. props. 77−69629
$SmCo_5$, sintered alloy permanent magnets, temp. depend. of domain struct. *(Russian)* 77−66380
$Sm(Co_{0.84}Cu_{0.16})_{6.9}$, microstruct. and domain struct., mag. reversal *(Russian)* 80−20429
$SmCo_{3.5}Cu_{1.5}$, single cryst., domain wall motion and domain form. 78−39359
$SmCo_4Cu$, nonuniform comp., domain struct. and mag. reversals process *(Russian)* 79−1681
$SmCo_{4.3}Cu_{0.7}$, highly anisotropic ferromag., mag. state after large Barkhausen jump *(Russian)* 79−4699
SmGa garnet film, scratch-modified mag. domain patterns 78−48007
$Sm_{0.5}Pr_{0.5}Co_5$, sintered alloy permanent magnets, temp. depend. of domain struct. *(Russian)* 77−66380
$Sm_{0.05}Tb_{0.45}FeO_3$, singularities of domain struct. in spin-flip region 78−19272
$Sr(Fe_{7.2}Al_{4.8})O_{19}$, minute single crystal domain struct. 77−20646
$SrRuO_3$, mag. props., mag. torque meas. 78−23295
Tb, ferromag. domains obs. by cryogenic X-ray topography 77−39507
Tb, ferromagnetic domain structures down to 95K 80−71080
Tb, Lorentz microscopy obs. 78−84448
Tb, single cryst., transverse magnetoresist. 77−66154
Tb-Fe film, undoped and O-doped, amorphous, microstruct. and mag. props. 79−91273
Tb-Ho (50%), antiferromagnetic, thermal expansion, US attenuation anomalies 79−47319
$(Tb_{0.27}Dy_{0.73})Fe_2$, magnetisation, ferromag. domains 80−25162
$Tb_{0.7}Er_{1.3}Gd_{1.0}Al_{0.2}Fe_{4.8}O_{12}$, garnet plate, domain struct. 80−2602
$TbFe_2$, magnetisation, ferromag. domains 80−25162
$TbFe_2$ monocrystalline (111), under elastic compressive stresses, domain structure *(Russian)* 79−91247
TbIG, X-ray topographic obs. of domain evolution in mag. field 77−69600
Tm ferrogarnet film, cylindrical mag. domain motions, domain boundary oscills. *(Russian)* 80−71140
$Tm_{2.2}Bi_{0.8}Fe_{3.5}Ga_{1.5}O_{12}$ epitaxial film, Faraday effect and domain struct. near compensation point 77−20838
$Tm_{2.7}Bi_{0.3}Ga_{0.3}Co_xFe_{4.7-x}O_{12}$, Co ion concentration effect on mag. props. close to mag. compensation point *(Russian)* 79−73788
$TmFeO_3$, domain struct. in spin reorientation region, Faraday effect obs. 77−20835
TmSe, intermediate valence state, resistivity of magnetically ordered ground state 79−1683
TmSe, mixed valency, field depend. mag. field transition 78−10657
U_3As_4 (110), (211) single crystal, Bitter figure obs. 79−65693
U_3As_4, elec. resist. in vicinity of Curie point, influence of mag. field 77−69314
$UCo_{5.3}$, mag. props., cryst. and domain struct. *(Russian)* 77−4529
UN, single crystal, mag. props. 77−77042
UO_2, antiferromag., new type of mag. domains *(Russian)* 77−59430
US, low field mag. props. 77−73047
WC-Co hardmetals, heat-treated, single domain obs. 79−73771
$(Y,Gd,Yb,Bi)_3(Fe,Al)_5O_{12}$ film, orientation of stripe domains in inhomogeneous mag. field 77−24726
$(Y,Gd,Yb)_{3-x}Bi_x(Fe,Al)_5O_{12}$, LPE, for magneto-optical appls. 78−48341
$(Y,Gd,Yb)_3(Fe,Ga)_5O_{12}$ film, magnetisation processes and domain struct. near compensation temp. 78−14996
$(Y,Sm,Ga)_3(Fe,Ge,Si)_5O_{12}$ film, period of stripe domains, 20-160°C 77−24725
$(Y,Sm)_3(Fe,Ga)_5O_{12}$ film, period of stripe domains, 20-160°C 77−24725
Y-Fe, evap. amorphous alloys, thermomag. history effects 77−66389
Y-Sm ferrogarnet *(Russian)* 80−71140
$(YBiEr)_3(FeGa)_5O_{12}$ ferrite-garnet film, micron cylindrical mag. domains, high recording density 80−65978
$(YBi)_3Fe_{5-x}Ga_xO_{12}$ film, ferrimag., splitting of domains into layers 77−28420
$Y_2BiFe_{3.8}Ga_{1.2}O_{12}$ film, colour contrast between different domains 77−12166
$Y_{2.7}Bi_{0.3}Fe_{3.8}Ga_{1.2}O_{12}$ epitaxial film, mag. domains in microwave mag. field, Faraday obs. 78−19295
$(YCaEuYb)_3(FeGe)_5O_{12}$, LPE, stripe end motion, effect of in-plane field 78−68330
YCo_3 amorphous film, domain struct., influence of planar anisotropy 79−78472
$(YEuYbCa)_3(FeGe)_5O_{12}$ film, isolated straight stripe domain dynamic props. 79−33514
$(YEuYb)_3(FeGa)_5O_{12}$, LPE, stripe end motion, effect of in-plane field 78−68330
$Y(Fe,Ga)_5O_{12}$, garnet film, strip domain struct. behaviour in applied field 78−68341
Y_xFe_{1-x} amorphous films, microstruct. and mag. anisotropy 79−82838
$Y_3Fe_{5-x}Al_xO_{12}$, permeability spectra rel. to microstruct. 80−71100
$YFe_{1-x}Ga_xO_3$, zone refined, exam. of Curie point and magnetisation 79−4673
$YFe_{4.5}Ga_{0.5}O_{12}$ domains, neutron dpolarisation and Faraday rotation study 80−93137
$Y_3Fe_{4.5}Ga_{0.5}O_{12}$, domain struct., neutron depolarisation and Faraday rot. 80−71084
$Y_3Fe_{5-x}Gd_xO_{12}$, permeability spectra rel. to microstruct. 80−71100
$YFeO_3$, skew bubble domains, stripe domains 77−89999
$YFeO_3$, thermomag. recording in surface layer of orthoferrite 79−24165
$YFeO_3$, weak-ferromagnet, domain boundary dynamics *(Russian)* 79−73768
$Y_3Ga_xFe_{5-x}O_{12}$ film, growth kinetics of film with cylindrical mag. domains 77−1577
$Y_{2.6}Gd_{0.4}Fe_{3.9}Ga_{1.1}O_{12}$, epitaxial uniaxial film, mag. phase diagram, optical expts. *(Russian)* 77−48022
$(YGdTm)_3(FeGa)_5O_{12}$ epitaxial film, formation of lattice of cylindrical mag. domains from stripe domains *(Russian)* 80−80579

magnetic domains continued
$Y_{0.9}Gd_{1.1}Yb_{0.7}Bi_{0.3}Al_{0.9}Ga_{0.2}Fe_{3.9}O_{12}$ films, cylindrical mag. domain form. *(Russian)* 77−40098
$(YGdYbBi)_3(FeAl)_5O_{12}$, garnet, epitaxial film, interior domains 79−91268
$(YGdYbBi)_3(FeAl)_5O_{12}$ epitaxial garnet film, uniaxial ferromagnet domain struct., phase transition *(Russian)* 80−108044
YIG film, domain struct., influence of planar anisotropy 79−78472
YIG film, stripe domain struct. with two periods 79−69706
YIG LPE film, optical waveguide in mag. strip domains *(French)* 77−83979
YIG, light diffr. by banded domain struct. *(Russian)* 78−15150
YIG, permeability spectra rel. to microstruct. 80−71100
YIG, plastic deform. and mag. props 77−40087
YIG substrates, magnetoelastic surface waves, magnetostatic reson. anal. 80−20441
YIG, transparent, domain struct. realignment in external mag. field 78−10739
$Y_{2.2}Sm_{0.4}(Fe,Ga)_5O_{12}$, garnet film, strip domain struct. behaviour in applied field 78−68341
$ZnCr_2Se_4$, screw spin structure, method of controlling the sense, polarised neutron diffr. study 80−70944

magnetic double refraction *see magneto-optical effects*

magnetic double resonance
see also CIDEP; double nuclear magnetic resonance; dynamic nuclear polarisation; ELDOR; ENDOR; microwave-optical double resonance; nuclear polarisation
acoustic magnetic resonance in crystals, review 77−32291
alkali metal vapour, optically pumped, longit. relax. in hyperfine states 77−57908
antiferromagnets, nonlinear dynamics of electron-nuclear spin system 77−66438
benzophenone $^3(n,\pi^*)$, and isotopic forms, in 4,4′-dibromodiphenylether, level anticrossings, ODMR obs. 78−2772
chlorophyll b derivatives, metal substitution effect on triplet state, intersystem crossing 77−88476
condensed matter, Summer School, Pula, Yugoslavia (Sept., 1976) 78−76293
cyclopropylamine struct., microwave spectrum 79−10096
p-dichlorobenzene, ^{35}Cl NQR line narrowing by nonreson. RF photon dressing 80−63662
p-dichlorobenzene, in p-dibromobenzene, optical detection of Cl NQR in mag. field 80−50228
external magnetic double resonance, principles and sensitivity 77−85616
ferromagnetic film, magnon avalanche under NMR saturation 78−10783
gamma-ray scattering under double γ-reson. conditions 79−73873
ice II, NQR of ^2D and ^{17}O 77−1617
molecular crystals, triply-excited impurity centres, effect of acoustic wave on phosphorescence 78−27115
NMR, resonant, near mag. transition 78−76265
NMR under optical pumping conditions 80−25253
optically oriented atoms, relaxation induced by random RF fields, non-Born contribution *(Russian)* 77−40149
pyridinium(-d_5) ion, triplet state obs. by ODMR, rel. to CNDO/2 STO calcs. 77−18951
quartz, muonium EPR transitions by muon-spin rot. 80−29668
quinoxaline, in p-dibromobenzene, ^{81}Br, elec. field grad. distortion near defect sites, optically NQR 79−38409
semiconductor, optical orientation and spin system cooling *(Russian)* 78−88229
semiconductors, spin orientation by optical pumping, review 79−38410
spin polarisation torsional spectroscopy, four time domains 80−20510
1,2,4,5-tetrachlorobenzene, multiple-quantum spin-phonon interactions, acoustically-induced phosphoresc. obs. 77−40150
1,2,5-thiadiazole, substitution struct., mag. double reson. 79−27105
Fe-Ni-Co film, electron-nucl. mag. reson. 78−35063
GaAs:Al, optical detection of NQR 79−69752
KCl, distant F-centre pairs, ODNMR 78−68414
KCl, F centre pairs, ODMR, close and distant pairs 78−43691
$LaF_3:Pr^{3+}$, 2K, optically detected coherent transients in nuclear hyperfine levels 79−19806
α-$LiIO_3:Fe^{3+}$, local environment and superhyperfine interactions by RF discrete saturation 77−85554
$LiYF_4$:Pr, NMR meas. of hyperfine const. of Pr^{3+} excited state 80−88895
^8Li, in $LiTaO_3$, multiple quantum NMR transitions obs., quadrupole moment determ. 77−73090
MnF_2, reson. NMR near phase transition 78−76265
NO_2, optical RF double reson. for $^2B_2$ state g values 79−64022
NSF_3, RF-mm wave double reson. of vibr. excited state 79−50054
SiH_4, second-order stark effects, RF-IR double reson. 78−58739
Ta, NMR-Mossbauer double reson. 80−40019
Tl atomic beam tubes, freq. pulling effect with mag. double reson. 80−37802
YIG, magnon high amplitude collective oscills., double parametric reson. *(Russian)* 77−28451
YIG, parallel microwave pumping threshold, RF modulation of mag. field 78−88195
Zn etioporphyrin, excited triplet states absolute rate consts., ODMR meas. 78−33533

magnetic drum storage *see magnetic disc and drum storage*

magnetic epitaxial layers
bubble collapse field meas., new method 78−56356
bubble domain stability, spin precession effects 77−32226
bubble dynamic props. rel. to bias-field-determined bubble size 78−91915
bubble garnet epitaxial film multilayer structures, interphase boundary rearrangement obs. 79−78489
bubble stretch propagation dependence on chevron patterns 78−84462
composite garnet ferrite epitaxial film ferromag. resonance obs. 77−85578
device applications 77−32223
epitaxial garnet film, mag. domain wall damping, vel. depend. 77−85517
epitaxial garnet films for magnetic bubble memories *(Czech)* 78−88147
ferrimagnet, uniaxial, induced canted mag. struct., problem of domain wall broadening 78−35016
ferrimagnetic light diffr. by mag. bubbles *(German)* 79−56769
ferrite, epilayers for bubble appl. 80−39829
ferrite bubble film struct., EM and RHEED, Mn and Mn-Cu ferrites 77−11801

magnetic epitaxial layers continued
ferrite films, hexagonal, growth by LPE 78−3062
ferrite garnet film growth, automatic machine 78−27418
ferrite spinel films, LPE growth and props., SIMS, X-ray diffr., and spin wave reson. obs. 80−34323
ferrite-garnet films with inversion layers, behaviour of cylindrical mag. domains, visual tracking method 80−71139
ferrites, hexagonal and spinel, growth on nonmag. spinel substrate by isothermal dipping LPE 77−12552
ferrites, LPE growth and characterisation 78−68640
ferrogarnets, monocrystalline films, mag. anisotropy 80−2609
garnet, 180° capped double layer LPE film, bubble wall states coding 80−34716
garnet, anisotropy consts. from reciprocal of susceptibility meas. 77−73057
garnet, bubble film, LPE growth reproducibility 79−1830
garnet, complementary σ-bubbles in bubble automation 79−78465
garnet, decomp. caused by annealing 78−18918
garnet, dynamic behaviour of domain walls and bubbles 78−52321
garnet, elastic surface wave propag., magnetoelastic effect 77−20669
garnet, Faraday effect and magnetometrical meas. 78−52317
garnet, growth rate depend. of growth-induced anisotropy 78−14992
garnet, high speed bubble domain motion, time resolved obs. system 77−40096
garnet, ion-implanted, threefold symmetrical bubble properties 78−64243
garnet, LPE film, domain dynamics in microwave field 77−20663
garnet, mag. bubble props., permanent local modification by laser annealing 80−2612
garnet, magnetic bubble materials, review 80−50153
garnet, physical thickness and refr. index meas. 77−77309
garnet, technique for magnetostriction coeff. meas. 80−243
garnet bubble film LPE with high Pb content 79−38750
garnet bubble films, 111 orientated, mag. anisotropy predictions, model 78−68326
garnet bubble materials, low loss, mag. domain wall dynamics 78−10738
garnet epitaxial film, easy magnetisation axis inclination temp. depend. 79−65699
garnet epitaxial film, stress induced magnetocrystalline anisotropy 80−71013
garnet ferrite epitaxial layer, flaw detection method 78−2719
garnet film, domain obs. by SEM 77−69646
garnet film, domain wall, dynamics, time depend. effects 77−12168
garnet film, domain wall displacement in pulsed field 77−16129
garnet film, double heteroepitaxy, magneto-optical devices for phase matching *(French)* 77−3675
garnet film, Ga and Ge substituted, mag. prop. control during LPE growth and processing 78−68638
garnet film, LPE, stripe domain, time resolved obs. of contracting motion 77−85519
garnet film, LPE, time resolved obs. system for domain dynamics, appl. to contracting motion of stripe domains *(Japanese)* 79−47312
garnet film, LPE technique, difficulties and advantages 79−28958
garnet film, magnetoelastic energy of stripe domain patterns 78−68334
garnet film bubble material, high peak velocity 77−85513
garnet film in mag. field, domain dynamics *(Russian)* 79−4711
garnet film preparation, single-crystal, for magnetic bubble domain appl. 78−60588
garnet film waveguide, magnetooptical effects 77−3650
garnet films, damage prod. by multiple ion implantation, ferromag. reson. obs. 80−34703
garnet films, easy magnetisation axis orientation 80−60383
garnet films, for magneto-optic appls., substituted rare earth garnet substrate crystals 78−31351
garnet films, isolated steps, rate analysis of growth parameters 80−10805
garnet films, layer/substrate lattice mismatch meas. using X-ray double-crystal method 79−28235
garnet films, LEP growth-induced anisotropy, magnetostriction theory 79−95624
garnet films, LPE, thermally induced substrate fracture 78−68639
garnet films with orthorhombic anisotropy, domain wall motion 80−80580
garnet LPE bubble film, growth-induced anisotropy, effect of La 77−85514
garnet LPE film, bubble technology *(Polish)* 77−77076
garnet LPE film, laser beam deflector 77−54803
garnet LPE film containing Lu, Curie temp. and flux spin-off, melt comp. effect 77−85515
garnet LPE layers, growth rate depend. on supercooling, induced striation expt. 79−24453
garnet LPE layers, SIMS in-depth conc. profiling 77−24489
garnet optical waveguide, with high Faraday rotation, mode degeneracy 78−94454
garnets, bubble domain memory appls., growth requirements 77−20660
garnets, domain struct., obs. technique 78−91914
horizontally dipped LPE film, inhomogeneities, spin wave reson. meas. 79−91298
lattice plane, X-ray topographic measurement, local variations in spacing and orientation of lattice plane *(Japanese)* 78−38585
LPE double layer films, wall state stability of bubbles 78−95497
LPE garnet bubble films, capping layer upper cap-switch field, model 78−95498
Neel ferrimagnets, phase transitions, field-induced spin-orientational 80−75767
rare earth garnet prep., novel Li_2MoO_4-$R_2(MoO_4)_3$ flux system 77−48359
rare earth garnets, prep. and props. book contrib. 80−44193
rare earth garnets, preparation, substrate and epitaxial layer surface quality control, X-ray topography *(German)* 77−55432
rare earth iron garnet single crystal films, synthesis and props., reviews 78−48013
spin wave resonance spectrum, internal isotropically coupled impurity layer 78−80223
sputter deposition, review 77−32521
transparent magnetic material, wave props. of domain wall 78−48011
$(BiTm)_3(FeGa)_5O_{12}$, monocrystalline films, mag. anisotropy 80−2609
$Bi_xYb_{3-x}Fe_5O_{12}$ LPE film, phase grating integrated optic coupler-modulator 77−11048
Ca, Ge-substituted garnet, LPE growth atm. effects on bubble props. 77−20655
magnetic epitaxial layers continued
$Ca_3Ga_2Ge_3O_{12}$, substrate, electron examination of microstruct. and microsegregation 78−67919
$CdCr_2Se_4$, spinel film, struct. SEM study, props. 78−79905
Co, even magneto-optical effects 80−76007
Co-Fe, dil., effective mag. field at ^{59}Co, impurity conc. depend., spin echo expts. 78−48080
Co-Ni, dil., effective mag. field at ^{59}Co, impurity conc. depend., spin echo expts. 78−48080
Co-Pt films, mag. and magneto-optic props., appl. to holographic and bit-by-bit storage 79−33512
$Co_xFe_{3-x-y}Cr_yO_4$, magneto-optical props., effect of Cr^{3+} 78−52590
$CoFe_2O_4$, epitaxial layer prod. by chem. transport 77−81224
$Co_xFe_{3-x}O_4$, single cryst. mag. films, holograms recording and thermomagnetic writing 78−55324
CrO_2, epitaxial growth on rutile, possible appl. as bit oriented mag. material 77−16127
CrO_2, ferromag. films, epitaxial growth in air, electron diffr. and SEM obs. 79−42410
Cu ferrite films, Mn-, Ni- and Al-substituted, LPE growth 80−96752
$CuFe_2O_4$, LPE grown, domain struct. rel. to tetragonal distortion 78−92205
$(ErEu)_3(FeGa)_5O_{12}$ film, for mag. writing and magneto-optical displays 78−6549
$(Eu,Lu)_3Fe_5O_{12}$, induced orthorhombic anisotropy 77−69640
$(Eu,Lu)_3Fe_5O_{12}$, orthorhombic mag. anisotropy 78−19290
$(Eu,Lu)_3Fe_5O_{12}$, submicron bubble films on rare earth-Ga garnet substrates, prep. and mag. props. 78−91909
$Eu_{3-x}Ca_xSi_xFe_{5-x}O_{12}$, bubble film, LPE growth induced anisotropy 77−20659
EuGaYIG:Cr, epitaxial garnet film, interaction pot. of domain walls with localised stress fields 80−44889
EuIG:Si, magnetoresistance meas. 79−78120
EuIG+Pb, (100) LPE film, magnetocryst. anisotropy and lattice mismatch 77−20647
$(EuLu)_3(FeAl)_5O_{12}$, film epitaxial growth on Gd_3GaO_{12} substrate, mag. props. 80−65402
$(EuLu)_3Fe_5O_{12}$, Ga, Al or (Ca,Ge) substituted, mag. props. and growth of 2 μm bubbles 78−91910
$Eu_{2.9}Lu_{0.1}Fe_5O_{12}$:Si magnetoresistance meas. 79−78120
EuTm-CaGe, magnetic FE garnet film, LPE growth and composition 78−23634
$Eu_{0.6}Y_{2.4}Ga_{1.26}Fe_{3.74}O_{12}$ garnet film, Walker oscills., detection by mag. bubble collapse 78−68318
$Eu_zY_{3-z}Ga_tFe_{5-t}O_{12}$, epitaxial garnet films, props. at compensation points 80−39823
Fe epitaxial film, Mossbauer effect, depth profiling of mag. hyperfine field 80−11295
Fe epitaxial film, Mossbauer effect, interface magnetism 80−11297
Fe, even magneto-optical effects 80−76007
γ-Fe, FCC film, epitaxial growth on CuAu (111) surfaces, strong ferromagnetism 80−70557
γ-Fe, ferromagnetism, spontaneous magnetisation and Curie temp. determ. 78−2711
γ-Fe film on Cu (111) mag. props. 78−31098
Fe garnet, Bi-substituted, domain boundary transform. into canted phase at compensation point 77−24724
Fe garnet, thermomag. data recording by electron beam heating 78−27066
Fe garnets, low freq. excitation spectra, mobility of domain boundaries 79−42815
Fe-Pt films, mag. and magneto-optic props., appl. to holographic and bit-by-bit storage 79−33512
γ-Fe_2O_3:Co acicular powder epitaxially doped, coercivity increase, surface anisotropy *(Chinese)* 80−7130
Fe_3O_4 single cryst., Mossbauer γ-ray diffr. 77−84600
Fe_xO_y epitaxial film, ferromag. reson. 77−51964
FePd, vacuum-deposited, for thermomag. recording, mag. and magneto-optical props. *(Russian)* 78−60319
FePt, vacuum-deposited, for thermomag. recording, mag. and magneto-optical props. *(Russian)* 78−60319
$(Gd, Bi)_2$ $(Fe, Ga)_5O_{12}$ magneto-optic LPE garnet films, high-energy heavy ion irrad., props. 80−71390
$(Gd,Bi)_3(Fe,Al,Ga)_5O_{12}$ LPE film, 180° Bloch wall pinning at etched nucl. tracks 78−39376
$(Gd,Bi)_3(Fe,Ga)_5O_{12}$ magneto-optic film, ion irrad. effect on storage props. 78−52324
$(Gd,Bi)_3(Fe,Ga)_5O_{12}$, LPE film, coercivity, influence of nuclear tracks 79−51829
$(Gd,Bi)_3(Fe,Ga)_5O_{12}$ epitaxial garnet film, nucl. tracks effect on mag. props. 80−11234
$(Gd,Lu)_3(Fe,Mn,Al)_5O_{12}$ epilayer with orthorhombic anisotropy, domain wall vel. 78−52322
$(Gd,Tm,Y)_3(Fe,Ga)_5O_{12}$ film, magnetocrystalline anisotropy 79−78450
$(Gd,Tm,Y)_3(Fe,Ga)_5O_{12}$ LPE garnet thin films, magnetocrystalline anisotropy 80−93147
$(Gd,Tm,Y)_3(Ga,Fe)_5O_{12}$, bubble domain gradient propag., elliptical distortion and bias compensation 78−19292
$Gd_3Ga_5O_{12}$, substrate, electron examination of microstruct. and microsegregation 78−67919
$Ho_{0.7}Er_{0.3}FeO_3$, crystn. on seeds, layer morphology 78−72041
$Ho_3Fe_5O_{12}$:Pb film, grown from fluxed metals by LPE 77−24972
La-Sm-Lu iron garnet film grown as NdGaG substrates, mag. props. 80−44888
$(LaLuSm)_3(GaFe)_5O_{12}$ bubble garnet film, coercivity 79−78459
$(Lu,Bi)Fe_5O_{12}$, magneto-optic colour effects 78−23308
$(Lu, La, Y, Ca)_3(Ge, Fe)_5O_{12}$, temperature compensated high mobility bubble garnet, LPE and props. 77−20656
$Mg_x(Fe,In)_2O_4$:Pb,Pt film, LPE 77−77436
$MgFe_2O_4$, epilayer, perpendicular anisotropy 80−39769
$MgFe_2O_4$, LPE growth, film quality, mag. meas. 78−11136
$Mg_{0.5}Fe_{2.5}O_4$, ferrimag. epilayer, superparamag. interface, mag. props., FMR 78−95492
MgMn ferrite CVD epitaxial layers, bubble domains in remanence and demagnetised states 77−85516
Mn ferrite, monocrystalline epitaxial layers, surface spin-wave modes in ferromag. reson. 78−2743
Mn-substituted garnet film, growth characts. and mag. props. 80−39826
$Mn_xFe_{3-x}O_4$ epitaxial films, mag. and reson. props. 80−50149
Ni, (110) film, strain effects on mag. anisotropy 77−80972
Ni epitaxial (110) layer, uniaxial anisotropy, expt. 77−20648

magnetic epitaxial layers continued
Ni, even magneto-optical effects 80−76007
Ni, mag. layer, domain struct., neutron depolarisation study 79−47299
Ni-Fe, mag. structures and stresses, ferromag. resonance 78−72375
Ni-Fe (40%), Mn coating, mag. interface effects 77−69638
Ni-Fe (40%) (111) film with C coating, surface magnetism 77−73056
Ni-Fe epitaxial (110) layer, uniaxial anisotropy, expt. 77−20648
$NiFe_{2-x}Al_xO_4$, stress-induced anisotropy in LPE grown single cryst. films, domain struct. 79−28238
$NiFe_2O_4$, LPE growth, film quality, mag. meas. 78−11136
$NiFe_2O_4$, on NdGG, structural and ferromagnetic reson. meas. 77−1574
$Ni_{1-x}Zn_xFe_2O_4$, LPE growth, film quality, mag. meas. 78−11136
$Pr_xY_{3-x}Fe_{5-y}Ga_yO_{12}$, IR absorpt. and Faraday rot. spectra 77−52093
$(Sm,Er)(Ga,Fe)_5O_{12}$, LPE, non-grooved film, thermomag. writing 78−76278
$(Sm,Lu)_3Fe_5O_{12}$, submicron bubble films on rare earth-Ga garnet substrates, prep. and mag. props. 78−91909
$(Sm,Y)_3(Fe,Ga)_5O_{12}$, epitaxial mag. layer, LPE, growth rotation rate, effect on props. 78−56053
SmCaGe garnet LPE bubble film, coercivity, thickness depend. 78−68324
$(SmLu)_3(FeAl)_5O_{12}$, film epitaxial growth on $Gd_3Ga_5O_{12}$ substrate, mag. props. lattice mismatch 80−65402
$Sm_{0.3}Lu_{0.2}Tm_{0.2}Y_{1.45}Ca_{0.85}Fe_{4.15}Ge_{0.85}O_{12}$, LPE growth, saturation magnetisation, collapse field, bubble diameter 78−95703
$(SmLuYCa)_3(FeGe)_5O_{12}$ film, ion implant profile 79−78477
SmTmIG, epitaxial layer with submicron bubbles, mag. props. 77−12172
$Sm_{0.1}Y_{1.9}CaFe_4GeO_{12}$, LPE growth, saturation magnetisation, collapse field, bubble diameter 78−95703
$(SmY)_3(FeGa)_5O_{12}$, LPE on $Gd_3Ga_5O_{12}$, growth kinetics, 920-980°C 78−3064
$Sm_{0.4}Y_{2.6}Fe_{3.8}Ga_{1.2}O_{12}$ epitaxial films, uniaxial mag. anisotropy, ferrimag. reson. study 80−80577
$Sm_{0.4}Y_{2.6}Ga_{1.1}Fe_{3.9}O_{12}$, LPE, growth rate anisotropy and kinetic coeffs. of vicinal faces 78−51846
$Sm_{0.4}Y_{2.6}Ga_{1.2}Fe_{2.8}O_{12}$, H^+ implanted, mag. bubbles, walls and fine struct. 77−63241
TbIG:Si magnetoresistance meas. 79−78120
$Tm_{2.2}Bi_{0.8}Fe_{3.5}Ga_{1.5}O_{12}$ epitaxial film, Faraday effect and domain struct. near compensation point 77−20838
$Tm_{2.7}Bi_{0.3}Ga_{0.3}Co_xFe_{4.7-x}O_{12}$, Co ion concentration effect on mag. props. close to mag. compensation point *(Russian)* 79−73788
$(Y,Ca)_3(Fe,Ge)_5O_{12}$ LPE layer, exchange stiffness coeffs., 30-300K 79−78464
$(Y,Eu,Tm,Ca)_3(Fe,Ge)_5O_{12}$, Ca, Ge substituted garnet LPE films, elec. props., charge imbalance, Seebeck effect 78−68101
$(Y,Eu,Tm,Ca)_3(Fe,Ge)_5O_{12}$ garnet film coercivity, new annealing method 78−84459
$(Y,Eu,Tm)_3(Ga,Fe)_5O_{12}$, domain boundary mobility, effect of easy magnetization axis inclination 78−19293
(Y, Eu, Yb, Ca)$_3$(Ge, Fe)$_5$O$_{12}$, bubble film, LPE on $Gd_3Ga_5O_{12}$, mismatch and faceting 77−20657
$(Y,Eu)_3(Fe,Ga)_5O_{12}$, epitaxial, cylindrical mag. domain struct., radial wall motion effect *(Russian)* 77−8373
$(Y,Eu)_3(Fe,Ga)_5O_{12}$, LPE growth from molybdate fluxes, bubble props. 78−68322
$(Y,Gd,Yb,Bi)_3(Fe,Al,Ga)_5O_{12}$, stripe domain and bubble domain wall motion 78−19294
$(Y,Gd,Yb,Bi)_3(Fe,Al)_5O_{12}$, nonreciprocal effects in domain boundary motion in inhomogeneous field 77−24726
(Y, Gd, Yb, Bi)$_3$(Fe, Al)$_5$O$_{12}$ epitaxial film, domain wall motion and oscill. 80−2616
$(Y,Gd,Yb)_{3-x}Bi_x(Fe,Al)_5O_{12}$, garnet single cryst. film, possible bubble appl. 78−6552
$(Y,Gd,Yb)_{3-x}Bi_x(Fe,Al)_5O_{12}$, LPE, for magneto-optical appls. 78−48341
$(Y,Gd)_3(Fe,Ga)_5O_{12}$, thin film lightguide, noninteracting mode conversion *(Russian)* 78−1347
$(Y,Lu)_3(Fe,Sc)_5O_{12}$ LPE layer, exchange stiffness coeffs., 30-300K 79−78464
$(Y,Re)_{3-x}Ca_xGe_{5-x}Ge_xO_{12}$, garnet films, LPE growth for bubble memory appls. 77−11813
$(Y,Sm,Ca)_3(Fe,Ge,Si)_5O_{12}$ single-crystal films, props. 78−64247
$(Y,Sm,Ca)_3(Fe,Ge)_4O_{12}$, garnet thin film, mag. anisotropy, Faraday effect meas. 79−42812
$(Y,Sm,Ca)_3(Fe,Ge)_5O_{12}$, domain wall, radial motion, method of dynamic collapse of mag. bubbles 79−8026
$(Y,Sm,Ca)_3(Fe,Ge)_5O_{12}$ epitaxial films, mag. props., growth condition effects 80−97124
$(Y,Sm,Ga)_3(Fe,Ge,Si)_5O_{12}$, static and dynamic mag. props., 20-160°C 77−24725
$(Y,Sm,Lu,Ca)_3(Fe,Ge)_5O_{12}$ garnet film coercivity, new annealing method 78−84459
$(Y,Sm,Lu,Ca)_3(Fe,Ge)_5O_{12}$ bubble magnetic garnet film, LPE grown, props., $CaCO_3/GeO_2$ molar ratio influence 80−50152
(Y, Sm, Lu, Ca)$_3$(FeGe)$_5$O$_{12}$ LPE films, factors affecting coercivity 79−91267
$(Y,Sm,Lu,Cu)_3(Fe,Ge)_5O_{12}$, ion implanted, hard bubble suppression 80−11238
$(Y,Sm,Lu,Tm,Ca)_3(Fe,Ge)_5O_{12}$, epitaxial garnet film, temp. depend. mag. props. 80−39825
$(Y,Sm,Lu)_3(Fe,Ga)_5O_{12}$, LPE mag. film, suitability for 1 to 3 micron bubble devices 78−68323
(Y, Sm, Tm)$_3$(FeGa)$_5$ O$_{12}$ LPE films, factors affecting coercivity 79−91267
$(Y,Sm)_3(Fe,Ga)_5O_{12}$, static and dynamic mag. props., 20-160°C 77−24725
$(Y,Sm)_3(Fe,Ge)_5O_{12}$, Ca, Ge substituted garnet LPE films, elec. props., charge imbalance, Seebeck effect 78−68101
$(Y,Sm)_3(Ga,Fe)_5O_{12}$, domain boundary mobility, effect of easy magnetization axis inclination 78−19293
$(Y,Sm)_3(Ga,Fe)_5O_{12}$ epitaxial layers, annealing effect on mag. props. 79−61191
$(YBiEr)_3(FeGa)_5O_{12}$ ferrite-garnet film, micron cylindrical mag. domains, high recording density 80−65978
$Y_{1-4}BiFe_{3.8}Ga_{1.2}O_{12}$ garnet films, bistable bubble domain 79−15331
$Y_2BiFe_{3.8}Ga_{1.2}O_{12}$, colour contrast between different domains 77−12166
$Y_{2.7}Bi_{0.3}Fe_{3.8}Ga_{1.2}O_{12}$, mag. domains in microwave mag. field, Faraday obs. 78−19295
$Y_{3-x}Bi_xFe_{5-y}Ga_yO_{12}$, epitaxial film, domain wall dynamics *(Russian)* 78−2718
magnetic epitaxial layers continued
$(YCaEuYb)_3(FeGe)_5O_{12}$, LPE, stripe end motion, effect of in-plane field 78−68330
YCaSmTmGeIG, epitaxial layer with submicron bubbles, mag. props. 77−12172
$(YEu)_3(FeGa)_5O_{12}$ rigid magnetic bubble transition to normal behaviour 78−95501
$(YEu)_3(FeGa)_5O_{13}$, LPE growth, uniaxial magnetocryst. anisotropy 77−8766
$Y_{2.45}Eu_{0.55}Fe_{3.8}Ga_{1.2}O_{12}$, hard bubble conversion in in-plane field 78−14998
$Y_{2.35}Eu_{0.65}Ga_{1.2}Fe_{3.8}O_{12}$, bubble translation vel., ion-implantation effects 78−68327
$(YEuLuCa)_3(FeGe)_5O_{12}$, stable state of bubbles containing Bloch lines 78−76281
$Y_{1.52}Eu_{0.3}Tm_{0.3}Ca_{0.88}Ge_{0.88}Fe_{4.12}O_{12}$, bubble translation vel., ion-implantation effects 78−68327
$(YEuYbCa)_3(FeGe)_5O_{12}$, ion-implanted, in-plane mag. field effects on bubble props. 77−85521
$(YEuYbCa)_3(FeGe)_5O_{12}$ bubble films, Ne^+-implanted, cryst. and mag. props., X-ray diffr. obs. 79−38362
$(YEuYb)_3(FeGa)_5O_{12}$, LPE, stripe end motion, effect of in-plane field 78−68330
$Y(Fe,Ga)_5O_{12}$, garnet film, strip domain struct. behaviour in applied field 78−68341
$Y_3Fe_{4.2}Ga_{0.8}O_{12}$, LPE grown thin film, ferromag. reson. 78−35041
$Y_3Fe_{4.6}Ga_{0.4}O_{12}$, surface spin wave reson. 77−85576
$Y_3Fe_{5-x}Ga_xO_{11}$ current-induced soln. growth 77−48358
$Y_3Fe_{5-x}Ga_xO_{12}$ epitaxial layers grown from soln., prep. and props. *(German)* 78−52691
$Y_3Fe_{5-x}Sc_xO_{12}$, garnets, magnetooptical spectra, 15000-21000 cm^{-1} 77−90131
$Y_3Ga_xFe_{1-x}O_{12}$, film growth conditions rel. to memory element props. 77−66399
$Y_3Ga_xFe_{5-x}O_{12}$ film, growth kinetics of film with cylindrical mag. domains 77−1577
$Y_3Gd_3Bi_3(FeAlGa)_5O_{12}$, epitaxial film, thermomag. recording *(Russian)* 77−1571
$Y_{2.6}Gd_{0.4}Fe_{3.9}Ga_{1.1}O_{12}$, mag. phase diagram, optical expts. *(Russian)* 77−48022
$(YGd)_3(GaFe)_5O_{12}$, nonlinear magnetoelastic effects *(French)* 80−34745
$YGdTmFe_{4.3}Ga_{0.7}O_{12}$ epitaxial films, bubble-domain lattices with specified parameters 80−60386
$(YGdTm)_3(FeGa)_5O_{12}$ epitaxial film, formation of lattice of cylindrical mag. domains from stripe domains *(Russian)* 80−80579
$(YGdYbBi)_3$ (FeAl)$_5$O$_{12}$ epitaxial film, diffuse domain wall, bubble domain expansion 80−25170
$Y_{0.9}Gd_{1.1}Yb_{0.7}Bi_{0.3}Al_{0.9}Ga_{0.2}Fe_{3.9}O_{12}$ films, cylindrical mag. domain form. *(Russian)* 77−40098
$(YGdYbBi)_3(FeAlGa)_5O_{12}$ film, motion of mag. bubble domains in inhomogeneous pulsed mag. field 78−27064
$(YGdYbBi)_3(FeAl)_5O_{12}$, epitaxial garnet film, with mag. compensation point, behaviour of 'compromise' phase boundary 78−60321
$(YGdYbBi)_3(FeAl)_5O_{12}$, garnet, epitaxial film, interior domains 79−91268
$(YGdYbBi)_3(FeAl)_5O_{12}$, epitaxial film, 360° domain walls with periodically distrib. Bloch lines 80−7127
$(YGdYbBi)_3(FeAl)_5O_{12}$ epitaxial garnet film, uniaxial ferromagnet domain struct., phase transition *(Russian)* 80−108044
$(YGdYbBi)_3(FeAl)_5O_{12}$ films, substrate orientation influence on max. vel. of domain boundaries 79−15330
$Y_{1.3}GdYb_{0.7}GaO_{12}$, epitaxial film, ferromagnetic reson. exam. 77−85579
YIG, Bi-substituted, LPE film, optical absorpt. changes due to impurity incorporation 77−1702
YIG, Bi-substituted, LPE, domain wall reson. 80−60387
YIG bubble films, light scatt. from spin waves, hysteresis meas. by Voigt effect 80−15770
YIG, CVD defect free epitaxial growth, conditions depend. 77−16502
YIG, double layer struct., LPE growth from molybdate and Pb borate fluxes 80−39827
YIG, epitaxial, temp. stabilisation of ferrimag. reson. field by Ga, La substitution 77−77104
YIG epitaxial film, strong in-plane ang. depend. of spin-wave intensities 77−69521
YIG epitaxial film and cryst., bound magnetostatic waves controlled by field gradients 78−95425
YIG epitaxial films, substituted, floating bubble domains, effect of structural stratification 80−2615
YIG epitaxial layers grown from soln., prep. and props. *(German)* 78−52691
YIG ferromagnetic film, quasi surface spin wave giant oscills. *(Russian)* 80−15767
YIG film, Ca, Ge-substituted, having mag. bubbles, LPE growth 78−31350
YIG, film, magnetostatic surface wave refl. at shallow groove 78−19283
YIG film, shallow groove, magnetostatic surface wave reflectivity 77−73055
YIG film, shallow groove effect on magnetostatic forward volume wave reflection 78−84473
YIG, film, spin wave reson., complex mag. surface energies 77−4561
YIG film, stripe domain struct. with two periods 79−69706
YIG, high energy heavy ion irrad., lattice strain 80−49278
YIG, in multilayer planar structure, magnetostatic propag. 77−16120
YIG, LPE, annealing-induced relief of compressive misfit strain 78−2386
YIG, LPE film, boundary effects, spin wave reson. meas. 79−78447
YIG, LPE film, magnetostatic wave to exchange resonance coupling 79−82774
YIG, LPE film, non-Ohmic currents 78−68099
YIG LPE film, optical waveguide in mag. strip domains *(French)* 77−83979
YIG, LPE grown, FMR linewidth, Pb incorporation effects 77−8407
YIG, La- and Ga-substituted, inhomogeneous epitaxial films, spin wave reson. 79−99773
YIG, magnetoresistance of bulk and epitaxial films 78−91706
YIG, magnetostatic volume wave propag. 78−10736
YIG, monocrystal film growth by chem. transport in closed system 77−77392
YIG multilayered film, magnetostatic spectrum 78−23350
YIG, n and p-type, UPS, elec. struct. 77−4710

magnetic epitaxial layers continued
YIG, on GdGaG, mag. excitations, diffusion layer effects 78−31112
YIG, photoinduced mag. surface anisotropy spin wave reson. 77−4560
YIG, pinning effects on magnetostatic modes 78−31111
YIG, prep. and imperfections, rel. to props. 79−100031
YIG, thick epilayer, unpinned magnetostatic modes 77−63290
YIG: Ca,(Mg), films, microwave losses induced by Fe^{4+} ions, ferromag. reson. study 79−1715
YIG: Ca^{2+} epitaxial films, Fe^{4+} centres, MCD, optical absorpt., and thermoelectric power meas. 78−95595
YIG:Be^{2+} LPE film, microwave relaxation props. 79−65741
YIG:Ca, epilayer, reversible oxidation, ferromag. reson. 78−76781
YIG:Ca, O diffusion depend. on defect conc. 78−67857
YIG:Ca film, strong mag. reson. of Fe^{4+} 78−48047
YIG:Co LPE films, with rectangular bubble domains, prep. and props. 79−82848
YIG:Gd, Ga, optical probing of magnetoelastic Rayleigh waves 79−78495
YIG:Pb(Si) film, (111) LPE, in-plane mag. anisotropy and ferromag. reson. meas. 78−2706
YIG-semiconductor coupled system, magnetostatic surface wave amplification, ferromag. loss 77−85434
$Y_{2.85}La_{0.15}Fe_{3.75}Ga_{1.25}O_{12}$, magnetostriction consts., microwave reson. meas. 77−24716
$Y_{2.85}La_{0.15}Fe_{3.75}Ga_{1.25}O_{12}$, inhomogeneous bubble film, spin wave reson. 77−32265
$Y_{2.85}La_{0.15}Fe_{3.75}Ga_{1.25}O_{12}$ epitaxial film, spin wave reson. spectrum 77−69703
$Y_{2.85}La_{0.15}Fe_{3.75}Ga_{1.25}O_{12}$ LPE films, ion implantation effect on spin waves 80−71124
$Y_{3-x}La_xFe_{5-y}Ga_yO_{12}$, mag. bubble film, low freq. ferrimag. reson. 78−31110
$Y_{3-x}La_xFe_{5-y}Ga_yO_{12}$ film, horizontally dipped LPE grown, FMR, anisotropy field obs. 79−78449
$Y_{3-y}La_yFe_{5-x}Ga_xO_{12}$, garnet radial oscillation of bubble lattice 79−73787
$(YLuSmCa)_3(GeFe)_5O_{12}$ bubble garnet film, coercivity 79−78459
YRBiFe garnets, epitaxial films, R=Gd+Yb, Faraday effect and phys. props. 77−69928
$(YRBi)_3(FeAl)_5O_{12}$ films, R=Gd, Yb, Faraday effect in transverse mag. field, orientation depend. 80−88971
YScIG, expitaxial film, magneto-spatial interaction, conversion coeffs. 77−55774
$(YSmCa)_3$ $(FeGe)_5O_{12}$ mag. bubble garnets, ion implantation induced stress influence on props. 79−91274
YSmCaFeGe, mag. garnet films, segregation of Ca and Ge in LPE growth 80−29959
$(YSmCa)_3(FeGe)_5$ O_{12} film, mag. bubble props. and LPE conditions 79−74107
$(YSmCa)_3(FeGe)_5O_{12}$ LPE films, optimum growth conditions for low coercivity 78−95499
$(YSmCa)_3(FeGe)_5O_{12}$ LPE film, growth and coercivity 79−4707
$(YSmCaLu)_3(FeGe)_5O_{12}$, bubble film inhomogeneity, spin wave reson. meas. 80−44439
$Y_{2.2}Sm_{0.4}(Fe,Ga)_5O_{12}$, garnet film, strip domain struct. behaviour in applied field 78−68341
$(YSm)_3(FeGa)_5O_{12}$ film, LPE on $Gd_3Ga_5O_{12}$, interface processes, horizontal dipping obs. 80−49552
$(YSm)_3(FeGa)_5O_{12}$, growth rate anisotropy and kinetic coefficients of vicinal faces 78−63954
$Y_{2.6}Sm_{0.4}Fe_{3.8}Ga_{1.2}O_{12}$, garnet films, LPE growth, mag. anisotropy field control 77−69642
$Y_{3-y}Sm_yFe_{5-x}Ga_xO_{12}$ film, LPE process exam. by induced striation 77−69643
$Y_{3-y}Sm_yFe_{5-x}Ga_xO_{12}$ film, LPE growth induced mag. anisotropy 78−2709
$Y_{3-y}Sm_yFe_{5-x}Ga_xO_{12}$ epitaxial layers grown from soln., prep. and props. *(German)* 78−52691
$Y_{2.6}Sm_{0.4}Fe_{5-x}Ga_xO_{12}$, epitaxial, domain wall crit. vel., effect of material parameters 79−99740
$(Y_{1.5}Sm_{0.3}Lu_{0.3}Ca_{0.9})(Fe_{4.1}Ge_{0.9})O_{12}$, growth reproducibility, static bubble props. 77−16130
$(YSmLuCa)_3(FeGaGe)_5O_{12}$, reproductibility in bubble garnet LPE growth 78−92204
YSmLuCaFeGe garnets, growth and temp. characts. of small bubbles 78−80183
$(YSmLuCa)_3(FeGe)_5O_{12}$, mag. props. and growth of 2 μm bubbles 78−91910
$(YSmLuCa)_3(FeGe)_5O_{12}$, LPE growth, growth reproducibility of bubble props. 78−92208
$(YSmLuCa)_3(FeGe)_5O_{12}$ films, mag. bubble props. and LPE conditions 79−74107
$(YSmLuCa)_3(FeGe)_5O_{12}$ film, bubble propagation direction effects on high frequency bias margin 79−78480
$(YSmLuCa)_3(FeGe)_5O_{12}$, double layer struct., LPE growth from molybdate and Pb borate fluxes 80−39827
$(YSmLuCa)_3(GeFe)_5O_{12}$, LPE low defect density films, prep. for mag. bubble device fabrication 79−87590
YSmLuCaGeIG, mag. props. and defects, depend. on B_2O_3 conc. on growth in PbO-B_2O_3 solvents 78−68321
$ZnFe_2O_4$, LPE growth, film quality, mag. meas. 78−11136
$Zn_{0.7}Ni_{0.3}Fe_2O_4$, epitaxial deposition, comp. and mag. prop. obs. using Mossbauer effect 79−38748

magnetic field effects
see also biomagnetism; galvanomagnetic effects; magnetic levitation; magnetic properties of substances; magnetic separation; magneto-optical effects; magnetoacoustic effects; magnetocaloric effects; magnetoelectric effects; magnetohydrodynamics; magnetomechanical effects; particle optics; Scott effect; Senftleben-Beenakker effect; thermal magnetoresistance; thermomagnetic treatment
acetylene-air flame, Li(Na)(K)(Mg)(Ca) damping consts., Lorentz collisions, mag. field effect 80−66805
APAPA, nematic liq. cryst., effect of mag. field on US attenuation *(Japanese)* 79−19144
arc, low-press., motion in strong mag. field 78−83637
arc (electric) in transverse aerodynamic and mag. fields, approx. model 80−24285
aromatic radical ion recomb., mag. field modulation, Liouville eqn. soln. 77−28995
atomic collisions in intense mag. field, quasi-resonant *(French)* 77−527
atomic nonresonant collisions in intense mag. field, van der Waals pot. 77−3440
atomic photoionisation, in intense radiation and magnetic fields, quasienergy formalism 79−72284
bacteria, effect of mag. field on recomb. fluoresc. 80−35856
barley growth in very weak magnetic field *(Russian)* 78−20200
bean and corn seed growth effects of constant mag. field *(Russian)* 79−83811
behavioural sensitivity of a domestic bird to 60-Hz AC and to DC mag. fields 80−61622
benzophenone ketyl radical, in micelle, decay rate in mag. field, photolysis meas. 80−85154
biexciton, change of binding type and dissoc. in strong mag. field 78−62744
biomolecular effects of 50 Hz EM fields, mechanism of effect *(Russian)* 80−51158
biradical, triplet state, S-T_0 CIDNP, biradical scavenging rate const. from mag. field depend. CIDNP 79−3461
biradical magnetic field dependent ^{13}C and ^1H CIDNP, hyperfine coupling 79−3460
bituminous pitch oils, flow curves, mag. field effect 80−33553
black hole, rotating, in mag. field, particle creation 77−2452
black hole, rotating, interaction with weak mag. field, ang. momentum changes 77−74080
black hole in external mag. field, relativistic particle radiation 80−22035
blood microcirculatory phenomena occurrence mechanism 77−32935
bone healing in humans, appl. of pulsed mag. field to stimulation 78−28029
bone stimulation devices, anal. of sinusoidal EM fields 80−108990
boundaries, effect on cylindrical defect field 78−53093
brass, sliding contact in magnetic field, model for cross diffusion 79−79121
bremsstrahlung from electron high-energy collisions, mag. field effects *(Russian)* 77−61906
cancer cause, nature and cure, possible effects of static mag. fields 77−32914
capillary-porous bodies, internal mass transfer, influence of inhomogeneous elec. and mag. fields 80−6138
catalyst surface mag. field effect on mol. dissoc. rate 80−16721
charged particle potential scattering, in presence of mag. and laser field 79−81248
charged particle scattering in homogeneous mag. field, transition amplitude 79−10218
chemical reactions, 1- and 3-dimens. models 78−19992
Chevrel phase materials, indirect meas. of Fermi surface parameters 79−60686
chlorodifluoromethane, IR multiphoton dissoc., mag. field effect 80−93772
cholesteric liquid crystal mixture, with positive dielectric anisotropy influence of external fields *(Rumanian)* 78−59751
conduction flow meter, effect on weighting function *(Russian)* 77−47121
conference, Munster, Germany (March 1979) 80−12843
cosmic radiation intensity on Earth and in Galaxy, diffusion restriction by mag. fields 77−13191
crack polarisation when magnetised in a longitudinal alternating field, detection method 78−53094
crystallisation, comp. control of crysts. grown in elec. and mag. fields 79−33920
crystallization, effect of constant field *(Russian)* 79−37641
cylindrical defect detection, boundary effect calc. during magnetic study 78−53150
DC arc as spectroscopic light source, mag. field effect on line intensities 78−87550
diamagnetic solids cyrstallised from melt, mag. fluid effect on props. 79−37815
diamond, electrolytic grinding, magnetic field effect 80−11790
disordered anisotropic antiferromagnet. random field effects 80−2580
drift instability, current-driven, sheared mag. field, finite-beta effect on transport 80−28617
E-region drift speeds, magnetic activity effects 79−88541
EBBA, liq. cryst., rapid cooling and mag. field effects on NMR relax. and thermal behaviour 79−82321
EBBA, nematic, mol. alignment, elec. and mag. field effects, dielec. const. obs. 77−11472
EBBA, nematic liq. cryst., effect of mag. field on US attenuation *(Japanese)* 79−19144
elastic medium, diffusion *(Rumanian)* 78−47558
electric breakdown in long tube 80−24120
electrochemical reactions occurring at metal-flow electrolyte interface 77−73369
electrolysis, annulus flow, solenoidal mag. field effect on ionic mass transport 80−26021
electron beam, relativistic, propag. in strong mag. field *(Japanese)* 80−91737
electron beam dose distrib. modification by transverse mag. fields 78−65132
electron cloud in equilib., mag. field effect, pot. and space charge distrib. 80−92410
electron dose distrib. in radiation therapy, magnetic enhancement 77−81570
electron dose distribution in phantom, mag. enhancement 77−48872
electron gas, dielectric response and Kohn effect in strong mag. field 77−4279
electron gas, dielectric transition temp. in strong mag. field 80−24813
electron gas, two-dimensional, in mag. field, polarisability 80−107888
electron gas, two-dimensional, study in intermediate mag. field 79−60743
electron gas, two-dimensional, study in weak mag. field 79−60742
electron solid in superstrong mag. field, bifurcation theory approach 80−4640
ELF magnetic field effect on personal vegetative status meas. by elec. resist. between hands 77−81533
EM wave, homogeneous, energy flux under conical refraction and induced gyrotropy 78−17861
epoxide compound, polymerisation in non-uniform magnetic field, exam. of structural changes 80−7791
epoxy resins, struct. changes under mag. field action 80−40516
excited nuclei moving through ferromag. media, transient mag. field effect, mag. moment meas. 80−37325

magnetic field effects continued
fatigue testing, magnetic field of test machine, effect on results 79−91890
ferroelectric, band struct. changes rel. to vibronic theory of ferroelectricity 79−19854
ferroelectric semiconductor, magnetic field influence, ferroelectric transitions 80−55049
ferromagnetic film with domain structure, transient state, mag. field calc. 77−4536
field emitter vacuum breakdown, external mag. field effects, transition period 80−38824
flexible tie, problems connected with body blow *(Russian)* 78−42541
fluids, conducting, dynamics under rotational mag. forces 80−48820
fluorenone photoreduction by DABCO, ion-radical yield enhanced by mag. field, cage recomb. region 79−79268
fusion switch vacuum arc development 78−13341
gaseous electrical breakdown characts. in crossed mag. field, prediction 79−32839
gauge variance for particles in an external magnetic field 80−47167
glow discharge tube, EM MM-wave detection properties 80−70059
glyoxal, intersystem crossing in weak mag. field 78−78743
graphite, pure, sp. ht. anomalies around 1.45K in 13.7 T mag. fields 79−42270
Gribble Limnoria tripinctata, reaction to intensity gradient of mag. fields *(German)* 80−56074
heavy particle beam cooling in an electron flux, mag. field effects 78−82557
HF combined mag. treatment, device and expt. *(Russian)* 79−15682
human beings, effects of elec. and mag. fields, HV lines to 800 kV *(French, English)* 80−72209
HV transmission line elec. and mag. field exposure effects and hazards 78−77083
hyperthermia by magnetically induced currents, freq.-depth-penetration, comments and reply 80−108991
interplanetary magnetic field polarity effects on equatorial geomagnetic field and ionosphere 78−36416
interplanetary magnetic field Z-components, variations causing magnetic storm main phase 80−4200
ionisation and breakdown of gases in crossed magnetic field 80−64805
isotropic medium, elastic waves, mag. field effects 80−58955
IV-VI compounds, mag.-field-induced displacive phase transition 80−50278
liquid metal boiling, mag. field effect on bubble growth 79−32217
liquids, potential and flux conserving static equilibria in elec. or mag. fields, determ. 80−88399
living organisms, static field perception and teratogenic effects of microwaves 77−81532
low melting, metals, on Cu surface, spreading kinetics 80−10742
low temperature measurement in high mag. fields, instrumentation and methods, review 78−37003
low-temperature measurement, mag. field effects on Krion 1-2 instrument errors 78−222
low-temperature thermometer characteristics in strong mag. fields 78−37005
lubricating oil treatment, HF combined mag. treatment *(Russian)* 79−15682
lymphocytes, living and dead, mag. props. and mag. sedimentation 80−35925
lysozyme, 0.01% soln., mag. and radiofreq. effects on activity 78−61136
magnetic quenching, enhancement of radiationless decay, direct and indirect mechanisms 77−42345
magnetic separation, review of current activity 77−63961
magnetisable conducting sphere, mag. levitation conditions, mag. dipole response to nonuniform mag. fields 79−98260
magneto-rheological suspensions, elec. cond. 80−11960
magnetophosphenes, quantitative anal. of thresholds 80−72184
magnetophosphenes, quantitative determ. of thresholds 80−61620
magnetosolid mechanics, semi-infinite cylindrical shell with strain depend. permeability, torsional response 79−94483
magnetotherapeutic apparatus and application statistics *(German)* 79−16340
mammalian cells, morphological and physiological transform., 5000 Oe 77−21500
α-martensite, quenching in const. magnetic field, struct. peculiarities *(Russian)* 79−52204
mass centre separation in homogeneous mag. fields 79−80
MBBA, anisotropic interactions with surface-treated substrates, wall effects on Freedericksz transition 79−99070
MBBA, mol. alignment in elec. and mag. fields 77−58956
MBBA-cholesteryl chloride mixture, mol. orientation during mag. field induced cholesteric-nematic transition 79−28086
medical treatment of rheumatic and psychosomatic complaints, magnetiser device construction 78−15878
metal, single crystal, dislocation loop formation, during deformation in quantising mag. fields *(Russian)* 80−103354
metal-insulator-metal junction, hopping model of zero-bias tunnelling anomalies, mag. field effect 79−60936
MHD channel, anisotropically conducting plasma in inhomogeneous elec. and mag. fields, current calc. *(Russian)* 80−74995
mice activity levels, effects of 60 Hz magnetic fields 78−40266
molecular cryst., triplet exciton annihilation and triplet exciton quenching by free radicals, analytical form of mag. field depend. of rate consts. 79−15094
monochrome cinefilm development process *(Russian)* 79−17534
multi-spiral electron current, interaction with EM wave, nonlinear anal. *(Russian)* 79−22886
multiple scatt. of particle beams, axial mag. field effect 78−70712
nematic cells, pretilted, Freedericksz transition in mag. field normal to director 79−99071
nematic liquid crystal, capacitance response to elec. and mag. fields, appl. to elastic const. determ. 79−90545
neutron dynamical diffraction, gravitational and mag. field effects 80−59345
neutron optical activity in helicoidal antiferromagnetic materials 78−74419
nuclear electron capture probability, strong mag. field effect *(Russian)* 77−34266
pair production in intense mag. fields 77−13505
particles suspended in electrolytes, in crossed elec. and mag. fields, trajectories, rel. to organisms' sensitivity to fields 78−48657
Peierls transition in quantizing mag. field, possibility 80−103441
perfectly conducting elastic sphere, in vacuum, radial vibr. freq., mag. field effects 80−58955
photoinduced radical pair recombination in high mag. field, Monte Carlo method 79−87861
plasma simulation, heat transport 80−28817
plasma transverse Cherenkov mode nonlinear stabilisation by external mag. field 80−38642
plasma with strongly inhomogeneous magnetic field, linear echo 80−106919
plasma-deposited thin film stoichiometry adjustment by mag. field 79−78900
plasmas, magnetically confined, modes and ballooning 80−28650
plastic:Eu^{3+}, Faraday rotation sign oscill. in very strong mag. fields *(Russian)* 80−88973
PMMA, effects of permanent mag. field on macromolecules 77−25364
polar gases, viscomagnetic effect 77−84384
poly(γ-benyl-D-glutamate) liquid crystal, orientation in magnetic field, NMR study *(Japanese)* 77−72550
poly-γ-benzyl-L-glutamate, lyotropic liq. cryst., crosslinking in mag. fields, aligned orientation form. 77−43137
polyatomic gas, Dufour effect, mag. field influence, Onsager relation 78−18369
polyatomic gas, thermomagnetic phenomena at intermediate press. *(Russian)* 79−77329
polymer, magnetic field, nonuniform const., effect on props. during hardening 78−11235
porous solid layer form. on viscose fibre, EM field effect *(Russian)* 77−66595
positive column, deflection of radiation intensity by transverse mag. field 80−28866
powder consolidation by pulsed magnetic fields *(German)* 77−8783
pyrene+N,N-dimethylaniline (deuterate)(3,5 dimethoxy-N,N-dimethylaniline), geminate recomb., solvent, isotope, mag. field effects 78−56888
quantum magnetometers, effect of external sinusoidal magnetic fields on sensitivity *(Russian)* 80−90870
quartz crystal, oscill. props., mag. field effects 77−59516
rarefied flow, visco-magnetic heat flux 79−98844
relativistic electron beam on air, He and H_2, charge neutralisation press. depend. *(Russian)* 77−19668
relativistic electrons in strong mag. field, Raman scatt., pulsar radiation *(Chinese)* 77−53418
relativistic theory of H atom in superstrong magnetic field 80−23320
resistance thermometer, Speer C, low-temp. magnetoresistance props. 78−49835
retardation of electrolytic mass transport in collinear electric-magnetic fields 80−104443
RF discharge plasmas, mag. field effects, probe and microwave meas. 77−7594
semiconductor surface plasma, van der Waals interaction with neutral atom, mag. field effects 77−59316
semimetal, excitonic phase and gas-liquid transition in strong mag. field 79−4514
shock waves, cylindrical relativistic propag. in presence of mag. field 79−53708
sparking potential in longit. mag. fields 80−106996
spatially modulated electron beam, parametric instability, periodic mag. field effect 80−87285
spherical cavity in infinite medium, radial vibr. freq., mag. field effects 80−58955
stability of conductor suspended in alternating mag. field, theory and expt. 80−32869
static bubble collapse analysis, in inhomogeneous external magnetic field *(German)* 79−95621
steel, high speed tool, sliding contact in magnetic field, model for cross diffusion 79−79121
steel, magnetic field effect on retained austenite transformation 77−16580
steel, martensitic transformation kinetics 79−87630
steel, mild, sliding contact in magnetic field, model for cross diffusion 79−79121
steel, Mn-Ni-Cr-C, supercooled austenite, influence of constant mag. field on diffusional decomp. *(Russian)* 79−4964
steel, quenched, verification of change of props. in mag. field 78−52985
steel Ni, type 52X2H23, martensitic transform. induced by pulsed mag. field 79−15667
stellar atmospheres, transverse mag. field effects on linear waves in radiating scatt. medium 77−56911
structural transition, magnetic field effect on critical temp. *(Russian)* 77−11667
superdense glow discharge, effect of transverse magnetic field on ion concentration 80−87972
temperature error of some low-temp. thermometers 79−12802
temperature measurement, error due to time varying mag. fields, effects on thermocouples 78−4617
thermionic emission between parallel cathodes, mag. modulation 78−52615
thermomagnetophoresis of particles in magnetic suspensions 80−35581
triode and diode guns, electron optics numerical determ. of beam profile 80−106435
triplet exciplexes, rapid rot., spin-selective depopulation of sublevels, heavy atom-induced mag. field effect 80−95552
triplet exciton annihilation rate, magnetic field depend. effect of spin-lattice relaxation 80−65459
tumour cell in vitro radiosensitivity and recovery, effect of 1400 gauss mag. field 77−44723
turbomolecular pump in pulsed mag. field, operational effects 78−50402
unsaturated fatty acids, free radical oxidation, mag. field effects 79−15992
vacuum breakdown voltage in weak mag. field 77−19781
vacuum polarisation by ambient mag. field, effects on Compton scatt. by unmagnetised electrons 80−86631
vacuum polarisation by strong mag. field, effects of Thomson scatt. 80−86632
water, crystn., crystal size reduction *(Russian)* 77−11670
water, mag. treatment affecting props., proposed mechanism 78−84827
Al plastic deformation depend. on mag. field at 4.2K *(Russian)* 79−91754
Al superconducting surface, layer struct. and dynamics on switching off mag. field 79−60998

magnetic field effects continued
Al-Ni, solidification in mag. field, crystallite obs. *(Russian)* 77−4770
Ar, effect of high mag. fields on vapour pressure 78−38825
Ar gas, primary ionisation coeffs. in cross mag. field 80−83879
Ar+CO_2, drift properties of tubular drift chambers in high magnetic fields 80−53917
Ar+isobutane+methylal, drift properties of tubular drift chambers in high magnetic fields 80−53917
Be, low temp. elec. and thermal cond. in mag. field, use as heat switch 77−35923
Bi, amorphous metal films, crystallisation with and without mag. field 80−70570
Bi-Cd, solidification in mag. field, crystallite obs. *(Russian)* 77−4770
Ca ions activity change due to magnetisation as possible mechanism of biological effect *(Russian)* 79−39423
$CaCO_3$, acceleration of growth of particles, Lorentz forces, electric and mag. field effects 78−51455
$CaCO_3$ polydisperse particles, in $Ca(HCO_3)_2$ soln., growth, soln. in mag. field 78−53260
$CaSO_4.2H_2O$, gypsum, cryst. growth from supersaturated soln., at 298 and 313K *(Russian)* 78−9973
Cd-Zn, solidification in mag. field, crystallite obs. *(Russian)* 77−4770
$Cd_xHg_{1-x}Te$, thermal cond. in mag. field, thermopower, and Nernst-Ettingshausen effect 77−31814
CdMnTe, exciton ground state, magnetic field influence 80−54616
CoO, reduction, magnetic field effects 79−52764
Co_3O_4, reduction, magnetic field effects 79−52764
Cu complex, (acetylacetonate), liq. cryst. matrix, EPR ang. depend., mag. field effect 78−9175
Cu/Cu+Fe low-temp. thermocouples thermo EMF, strong magnetic field effects 78−220
Fe alloys, anisotropic precipitation struct. in external mag. field *(German)* 78−72785
Fe-Cr-(Co), decomposition of solid soln. in mag. field, neutron and X-ray diffr. study *(Russian)* 78−68694
Fe-N crystal, orienting $Fe_{16}N_2$ particles by external magnetic field *(German)* 77−25058
$FeCl_2.4H_2O$, pressure effects on hyperfine interaction in single crysts. in mag. field 77−16211
α-Fe_2O_3, haematite, reduction by H_2, mag. field effect 77−12827
Fe_3O_4, FeO reduction rates, effects of mag. field 77−44461
Ga, amorphous metal films, crystallisation with and without mag. field 80−70570
n- GaAs, hybrid-hybrid mode interaction in crossed elec. and mag. fields 78−51997
Ge, deform. of laser induced electron-hole drops under high magnetic fields *(German)* 78−23027
Ge resistive sensing devices, temp. calibration and reproducibility, high mag. field effect *(Czech)* 80−37029
Ge:As(Sb), phonon-bound donor resonance scatt., donor-electron radius mag. field depend. 79−77847
H atom, proton spreading in strong mag. field 78−70769
H atom in mag. field, Schrodinger eqn., Monte Carlo soln. 80−31545
H, beam, $2^2S_{1/2}$ metastabld ats., nonadiabatic transition in mag. field 78−55157
H bound states in strong mag. field 80−99438
H, effect of infinite magnetisation on spectrum and energy levels 80−77282
H, longit. excited states in intense mag. fields, rel. to pulsars 80−91469
H maser, frequency changes due to nonuniform magnetic field 80−99687
H, relativistic, in strong mag. field 80−9518
H, relativistic energy levels in strong mag. fields 80−102454
H_2, ortho-para conversion, magneto-catalytic reaction, quantum formulation 80−108750
H_2, ortho⇌para conversion, on CoO, MnO mag. surfaces 79−47969
H_2^+, bound states in strong mag. field 80−99438
H_2^+, high (10^9 G) mag. fields, dissoc. energy, electron binding energy and equilib. separation 80−52910
H_2^+, mol. props. in intense mag. fields 79−81169
H_2-like molecules, change of binding type and dissoc. in strong mag. field 78−62744
H_2O, band spectra after HF combined mag. treatment *(Russian)* 79−15682
H_2O, neutron irradiation and mag. field effects on cavitation and nuclei spectra 77−62568
H_2O_2, rate of decomposition by catalase and $[Fe^{3+}(EDTA)]_2$ 79−52631
He II-^{3}He solns., in strong mag. field *(Russian)* 78−18866
He, liq., surface with trapped electron, parallel mag. field effect on interband transition 78−87835
He liquid surface, parametric excitation of electrons in mag. field 79−51389
He^-, existence in strong mag. field, binding energy, isoelectronic semicond. impurity trapping 78−9097
^{3}He, solid, possible explanation for recently obs. phase transition in high mag. fields 80−20006
^{3}He, superfluid, creation of mag. solitons 77−15653
^{3}He, superfluid, distortion in elec. and mag. fields, NMR shifts 77−35780
^{3}He, superfluid A-phase, orbital dynamics in presence of heat flow and mag. field 79−51337
^{3}He-^{4}He solution, periodic inhomogeneities, excitation in external mag. field parallel to temp. gradient 80−88392
K, high-field thermal magnetoresist., 2.5-8K 78−23072
N^+, acceleration by intense relativistic electron beam in spatially periodic mag. field *(Russian)* 79−10255
N_2, effect of high mag. fields on vapour pressure 78−38825
N_2-O_2, vap.-low. equilib., mag. field effect 78−91429
NO_2, mag. fluoresc. quenching mechanism, up to 18 kG, press. and λ depends. 77−65498
NaK, liquid metal natural convection under transverse magnetic field 80−69827
Ne discharge in high press. narrow tube, Kadomtsev-Nedospasov instability 80−107004
Ni, chemisorption of CO, carbonylation rate mag. field depend. 79−24828
Ni, intermodulation generation in RF mag. field, field interaction with domain walls 79−56600
Ni-Cr foldfoil strain gauge, for cryogenic anal. of supercond. structs. in high mag. fields, fusion reactors 78−54947
NiO, strong mag. field effect on reduction 77−4868

magnetic field effects continued
O_2, effect of high mag. fields on vapour pressure 78−38825
O_2, liquid, pool boiling in inhomogeneous mag. field 77−31766
$Pb_{1-x}Ge_xTe$, degenerate semiconducting ferroelectric, structural phase transition temp., mag. field effects 80−45017
$Pb_{1-x}Sn_xTe$, effect of mag. field on thermal cond. 79−65263
S^-, photodetachment cross section mag. field depend. struct., obs. 78−55148
Si, amorphous film, glow discharge deposition, rate enhancement by mag. field 80−65412
Si, neutron diffraction by perfect cryst., mag. field effects 79−73071
Si, stressed, at high mag. field, submillimeter cyclotron res. of electrons 77−81012
$Sm_{1-x}Gd_xS$, phase transition temp. depression by mag. field, hybridisation 77−62828
V_xO_y, metal-insulator transition, external mag. field effects 80−92819
W, field emission, mag. field effects 80−93463
Yb, amorphous metal films, crystallisation with and without mag. field 80−70570
Zn, twinning, influence of dislocation drag. mag. field effects 80−59472

magnetic field measurement
see also field plotting; fluxmeters; magnetometers
absolute intensity of weak mag. field, use of RF biases SQUID 80−82794
alternating magnetic field amplitude meas. *(French)* 80−73332
amplitude of alternating magnetic fields, EPR method 80−52277
anisotropy of cylindrical thin films 77−13783
archaeomagnetic intensity meas. using SQUID magnetometer 78−352
Aryabhata, Indian scientific satellite, magnetic testing 78−40793
automatic tracking nuclear mag. reson. gaussmeter 78−16825
biomagnetism, mag. fields of dipole in volume conductor shapes 77−81514
bipolar semiconductor sensor using carrier domain rotation, proposed device design 77−2670
bipolar semiconductor sensor using carrier domain rotation, operation and performance 77−2671
brain, human, neural generator localisation underlying auditory evoked mag. fields 80−104703
bubble chamber, SKAT, main parameters and magnetic field meas. 80−69022
bubble collapse field, anisotropy field, and domain wall mobility, magneto-optic meas. 77−85534
bubble diameter, collapse field and runout field intensity meas. 79−78490
bubble field distribution meas. by InSb ultramicro Hall element 79−56585
cardiac electrical activity, mag. detect. *(Japanese)* 77−81515
carrier-domain magnetometer, novel Si mag. field sensor 79−9224
cerebral magnetic field meas. and personnel selection 79−2026
CERN muon storage ring, calib. of NMR magnetometers and mag. field meas. system 77−57780
CERN muon storage ring, NMR mag. field meas./stabilisation system 77−57779
CERN Super Proton Synchrotron beam-splitting steel septum magnets 79−31295
circular discs and rectangular plates, shadow-side field meas. 77−79731
collective accelerator magnetic field meas. apparatus 79−31354
compact preset SQUID for total field measurement 80−22392
constant magnetic fields, investigation via improved F4354/1 Tesla-ammeter 77−26364
cores with square hysteresis loop, measurement of saturated flux density using compensation technique *(Russian)* 79−54158
cylindrical ferromagnetic bars, meas. of two-dimens. mag. field of array in uniform mag. field 79−12825
Daresbury Laboratory automated magnet field meas. facility 79−30509
detector using second harmonic oscillation 79−54161
development review, 1980 status *(French)* 80−95114
development trends *(Italian)* 79−80650
digital calibration device for mag. field, appl. to EPR spectroscopy *(French)* 77−152
digital NMR gaussmeter using hybrid IC 79−71501
digital teslameter, circuitry and calibration 79−63287
distribution rapid meas. using NMR 80−27322
dual magnetometer method, extension for use on dual spinning spacecraft 78−77459
electro-dynamic vibration exciter, used in resonance testing of structures 79−81779
electrodynamic earphone, mag. field probe 79−34690
electron beam deflection tube, for induction meas. 78−54393
electronic fluxmeters, construction, appls. *(German)* 77−74467
electrostrictive magnetic-field transducer design 77−57371
electrotechnical steel, hysteresis curves, plotting *(Russian)* 78−76269
eye, retina injuries, magnetoretinographic meas. using SQUID magnetometer 80−104702
Fermilab energy doubler, supercond. magnets, mag. field meas. 79−31258
ferrofluids, magnetic material conc. distrib. meas. device 78−16821
ferromagnetic film, sinusoidal voltage prod., mag. field meas. 78−26972
ferromodulated transducer local excitation *(Russian)* 78−86306
flaw detector magnetizing units with semiconductor rectifiers, magnetic field meas. 78−53076
flux compression by explosives, intense transient mag. field prod. and meas. *(French)* 77−149
fluxgate magnetometer, remote geophysical operations appl. 77−53246
fluxgate magnetometer using sensor with direct time-coded output signal 78−89510
Fresnel region mag. field intensity meas. accuracy 77−79132
gaussmeter, Hall-probe adapter cct. for use with digital multimeter, leakage detect. 80−37014
geomagnetic pulsations, detect. using solenoid with ferrite core 78−24384
geomagnetic surveys, field difference method with noise reduction 80−21850
gradiometer, balancing, system of adjustable superconducting plates, biomag. signal meas. 79−25162
gradiometer, thin film DC SQUID 77−30187
gradiometer for human heat magnetic field study 78−48914
gradiometers, unidirectional 80−68220
Hall device for grain detection in Fe-Si sheets 78−11470
Hall effect device method 78−41336

magnetic field measurement continued
Hall effect magnetic field monitor 77−67477
Hall effect monitor operational principles *(Polish)* 79−85130
Hall effect probes, linearity improvement of type TLMK Hall probes *(Slovak)* 80−82795
Hall effect transducer, for weak magnetic field meas., features 77−57370
Hall generator appl. *(German)* 78−253
Hall probes appl. to small mag. field detection, temp. matching 79−40592
Hall-effect magnetic field detection, for fields down to 10^{-3} T 80−244
HF, hazards to living organisms, sensors *(Polish)* 77−87797
HF magnetic field standards, calibration field strength meters, biologically active, RF interference fields appl. *(Polish)* 80−51311
high field (up to 23 T), low temp. (1.5-300K) methods and instrumentation 77−30171
high field production and meas. 78−8425
high-energy physics magnet meas. 79−31353
high-fields, strength and inhomogeneity measurements using Be single-crystal indicator 79−63280
holographic processing of mag. field distribs. of thin foils 79−89868
IC Hall generator appl. *(German)* 80−52276
induction, in cylindrical geometry, Fourier components, rel. to plasma problem 77−65907
induction accelerator charact. meas. instrument 78−5073
induction meters, constants determ. using nutation teslameter 80−98946
intensity changes detected by an oscillator employing a saturable-core reactor 78−12729
intensity measurement methods, ranges and sensitivities *(Chinese)* 79−44922
International Sun-Earth Explorer 1 and 2, plasma wave investigation 78−85802
interstellar dense cloud complexes, mag. fields determ. via Zeeman splitting obs. 79−5757
invertor circuit with toroidal core, mag. field meas. 0.01 to 1.0 KOe range 77−82577
ISABELLE storage ring magnets, mag. field meas. 79−68089
isochronous cyclotron mag. field automatic meas. system 78−82547
isotropic RF electric/magnetic field strength meter, design 80−82751
Josephson element principles, applications to precision meas. of electric potential and magnetic flux at high freq. *(Norwegian)* 80−80447
KEK main ring, dipole magnets field meas., B-clock system 77−83308
laser sensing system for elec. and mag. fields in power transmission 77−45870
LF stray fields, search-coil magnetometer *(German)* 77−41657
low temperature, probe characts. 78−37003
lung, calc. of effect of changing parameters on two methods of meas. 80−104712
magnet technology, conference, Bratislava (1977) 79−30499
magnetic bubble stray field distribution using micro Hall element, expt. 77−40097
magnetic field diffr. meas. on axes of disks and apertures, Babinet principle, complex spirals 80−102599
magnetic heart vector components, simultaneous meas. with unipositional lead system 80−104697
magnetic induction Hall probe, for remote meas. of axial/radial field components in conducting coils 78−93659
magnetic pickup for spontaneous magnetic fields meas. near laser plasma 80−24246
magnetic traces, observation technique 77−87616
magnetisation evaluation of magnetised structure via virtual magnetic charges 80−57341
magnetocardiography, field meas. techniques *(French)* 77−37073
magnetocardiography in weak DC ambient magnetic fields 79−79567
magnetometer, rotating sample, role of eddy currents in studies of magnetic anisotropy 79−63278
magnetometer system, automatic field-tracking, 0.1 to 3.2 T, for use with ESR/NMR spectrometers 79−63279
magnetoresistive transducers for strong field meas. at 4.2-300K temp. range 78−45660
magnetotelluric sounding technique using SQUID devices 78−96322
mapping system for particle spectrometers at Fermilab 77−10513
mass spectrometers, meas. of mag. field applied to traversing ions using improved Hall probe 79−88987
measuring loop antenna characteristic improvement 78−49174
megagauss field, meas. of field intensity, magnetisation, susceptibility 78−93739
microfields, quantitative registration on solid surface, using raster electron microscope 80−31790
microwave magnetic-field distribution meas. using new resonant scatterer 79−49211
Milan superconducting 1:6 model magnet, mag. field meas. 79−54669
MIS-3M magnetic measuring system (USSR), testing small permanent magnets 80−62699
MSU 500 MeV superconducting cyclotron, mag. field meas. 79−54668
multi-coil mag. probe in plasma diagnostics, reliability assessment 79−55544
multihole SQUID, miniature, with preset point contact, sensitivity 77−37952
NMR device for high induction meas. *(German)* 79−21789
nMR gaussmeter for measuring field distributions of electromagnets 79−2797
NMR magnetometer, precision field averaging, for low and high fields, using flowing water 79−67359
NMR magnetometer, type 9298, homogeneous mag. field meas. 78−32839
NMR magnetometer display using freq. to magnetic field convertor 79−71490
NMR probe using single IC for HF head 80−62697
NMR radio spectrometers, meas. of field uniformities in gap of precision magnets 80−105683
NMR technique, influence of apparatus parameters on meas. accuracy 78−249
nonsteady mag. field induction meas. by prerecorded tape signal attenuation 79−67355
ocean bottom magnetic field meas. with superconducting magnetometer 77−87102
using operational amplifier and voltmeter *(French)* 79−63277
optical and magnetic resonance studies, 3-axis computer controlled low field magnet 80−95113
optical fibre magnetic field sensors 80−69510

magnetic field measurement continued
optical fibre magnetostrictive perturbation for possible mag. field detect. 80−53450
ORIC, remapping of mag. field, meas. system 77−83221
ORIC mag. field meas. study implementation 79−68036
Permalloy magnetoresistive mag. field sensor, performance calc. 80−57342
plasma, hot, mag. field determ. using Faraday rot. *(Rumanian)* 80−87950
plasma, self-generated mag. fields, two-dimens. distrib., laser-plasma reson., mag. tape irradiation 79−41877
plasma magnetic field determ. from charged particle beam defl. 80−28825
precision, using Ampere's law 78−93660
precision, using Ampere's law 79−21720
precision magnetic measurements by the floating wire analog technique 79−67354
probe, magnetometric, calib. by supercond. solenoid using NMR *(Czech)* 78−29130
Proton-Electron Tandem Ring Accelerator magnet field meas. 79−31271
pulsed intensive field meas. by inductive method *(Chinese)* 79−75506
pulsed magnetic fields, measurement of magnetisation and susceptibility using Cu-Be search coils 79−63281
quadrupole gradient-length product meas. device 79−76232
quantum devices appl., Rb maser, threshold sensitivity and short-term fluctuations determ. 80−22394
RF industrial heaters, elec. and mag. field strengths meas. 80−52175
RF standard magnetic field generator, with loop antenna, freq. charact. improvement 77−26348
SATURNE II proton synchrotron, magnet design and meas. 77−83241
scanning electron microscope, two-dimensional stray microfields 80−86514
scanning mirror electron microscopy, quantitative evaluation of elec. microfields 78−74110
SEM, shadow scanning method for studying magnetic fringing fields 79−6233
separated-sector cyclotron, mag. field meas. processing methods 79−68037
shallow-water mineral exploration by controlled-source audiomagnetotellurics and resistivity profiling 77−5356
shielding case for terrestrial mag. field screening, rel. to Cs primary freq. standard meas. *(Japanese)* 77−22582
soft magnetic materials meas., in yoke, Br and Hc parameters estimation *(Czech)* 78−65944
solenoid, superconducting, magnetic field inhomogenity measurement method, Hall probe appl. *(Czech)* 80−13107
spinning-plate magnetometer, for meas. 10^{-8}-10^{-2} T fields 78−37039
SQUID (DC) as mag. flux detector 77−26358
SQUID appl. 77−26369
SQUID arrays, for mag. field meas., geophysical, biomedical appls. 78−32830
SQUID detector appl. in biomagnetism, techniques 78−96061
standard field measurement methods, formulae, EM effect on living organisms appl. *(Polish)* 79−39450
stray field due to defects in ferromag., optical detection 78−31602
strong inhomogeneous magnetic field meas. using n-type Si photoconductance 78−45661
strong magnetic field induction metrology 78−37040
superconducting mag. field meas. using signal ave. 77−83231
superconducting magnet, for energy saver doubler project, testing and field meas. 77−26899
superconducting magnetic gradiometer, LF noise spectra 77−33203
superconducting solenoids, automatic meas. using NMR 80−57344
superconducting thin-film gradiometer 78−77947
superconductive magnetic gradiometer for meas. of mag. gradients from ocean waves 79−29867
tectonomagnetism, improved signal discrimination and volcanomag. effect at Kilauea, Hawaii 79−92629
terms and concepts in magnetic meas. 79−97334
Tokamak, poloidal field meas. by far IR polarimetry 79−32794
Tokamak plasma meas. using laser light scattering 78−34370
toroidal controlled fusion poloidal mag. field meas. by far IR Faraday rotation 80−59303
two-dimensional mag. microfield electron microscopy 79−6239
ultra-high, using image convertor camera *(Japanese)* 77−67505
visualisation based on narrow light beam reflection at inclined liquid surfaces *(German)* 80−31817
weak, SQUIDS, review 80−86267
weak field methods, max. sensitivity 79−17455
Wheatstone bridge, unbalanced with magnetodiodes, for measuring magnetic induction 79−80644
Wiegand module, magnetic field sensor *(German)* 80−62694
Al, thick-walled conducting shield in biomag. expts. 80−104845
Al thick-walled enclosure for LF biomag. meas. 80−62698
$Cd_xHg_{1-x}Te$ thin film Hall probes for high mag. fields 79−30452
Ge microconductor mag. field transducer, cast, galvanomag. recomb. effect 79−19609
^{3}He, optically oriented nuclei, maser excitation and characts., appls. 78−17891
^{3}He, optically oriented nuclei, in two-chamber cell, spin maser appls. 78−17892
InSb, micron size Hall probe for precision mag. field mapping 79−75558

magnetic field variations, earth *see geomagnetic variations*

magnetic fields
see also electromagnetic fields; geomagnetism; interplanetary magnetic fields; interstellar magnetic fields; magnetic field effects; magnetic field measurement; solar magnetism; superconducting critical field
AC, three-dimensional, finite element analysis, Tokamak device appl. 79−50191
AC distribution in solid turns with skin effect, calc. *(German)* 80−69319
AC field incident on surfaces of conducting bodies *(French)* 79−68350
AC fields, human response 77−77923
accelerator, magnetic field configuration recovery, in interpolar gap 78−5070
accelerator magnetic field azimuthal variations, two-dimens. approx. calcs. 77−26908
accelerator PEP, mag. field quality requirements 77−83205
Adone storage ring transverse wiggler magnet design 79−41054

magnetic fields continued
air coils, magnetostatic field FFT calcs., linear system theory 80−32868
Allende meteorite chondrules, primordial mag. field meas. 78−49399
Ampere's theorem appl. to magnetic effect of finite length line current 77−71905
amplification in early Universe during radiation era 78−96577
analysis and computation, computer appl. book 78−37787
analysis by separation of variables *(Polish)* 78−90338
astronomical compact thermal sources, mag. fields determ. via linear polarisation spectrum *(Russian)* 80−90344
astrophysical, root mean square mag. field in turbulent diffusion 78−36449
astrophysical magnetic fields, generation at high mag. Reynolds number 78−36448
astrophysical plasmas in mag. and gravitational fields, MHD separation of high energy plasma 80−67547
astrophysics, existence of mag. fields $>10^{20}$ gauss 78−4094
auroral zone magnetic field lines, electrostatic wave measurements 79−88555
axisymmetric bodies, mutual interaction between rot. and mag. fields 79−94130
axisymmetric stationary mag. field calc. on nonlinear ferromag. media by iterative method *(Ukrainian)* 79−94127
bar magnet field, analogue simulation by electrostatic field, boundary conditions 77−61892
bifilar electric line, cranked symmetry, mag. field lines *(French)* 78−42255
biological cells, moving, magnetic force 77−70486
Biot Savar law, quantum mechanical generalisation, mag. field from current of assigned geometry 78−70997
boundary-value problems, finite element and finite difference anal. 78−94353
brain, mag. evoked field mapping 80−104705
bubble magnetostatic field approximation formula 77−77080
3C 105, struct., polarisation and mag. field direction 79−35413
4C 32.69, quasar, discovery of ordered mag. field assoc. with radio jet 80−105375
3C 382, 3C 386, radio galaxies, radio polarisation obs. rel. to mag. fields directions 78−86031
calculation of magnetic field and force eqns., solns. using programmable calculator 80−91721
Cassiopeiae A, supernova remnant, mag. field origin 80−85989
Centaurus A giant radio lobes, mag. field strength from X-ray emission obs. 78−41055
charged extended body interaction with mag. field 79−13879
charged particle acceleration in nonadiabatically varying uniform mag. field 77−27236
charged particle diffusion in turbulent mag. field 77−70989
charged particle interaction, mag. field energy, spatial distrib. of interaction contrib. 80−73625
charged particle motion in mag. field of ferromag. filaments 77−46675
charged particles in single wave fields, adiabatic and stochastic motion 80−9795
circuits with low permeability or saturated parts with permanent magnet, analytical calc. *(German)* 80−23596
circular cylinder between infinite pole pieces, mag. field and demagnetising factor *(German)* 77−6972
coaxial loops, field config. at median surface, current ratio depend. 77−19127
coil, mag. potential difference between to points on revolution axis *(French)* 77−568
Coma galaxy cluster, intracluster mag. field from halo radio source meas. 78−86027
cometary, tail magnetic field, size 79−88626
comets, magnetic tail, laboratory simulation 79−62793
comets type I tails, large-scale mag. fields rel. to ray struct. and electrodynamical forces *(Russian)* 79−101119
compressed magnetic field power supplies, charact. of helically wound generators, using a 2-d MHD computational model 78−17838
computation, conference, Grenoble (1978) 79−41262
computation principles 79−31771
computer drawn fields for diverse configurations, program 77−22401
computer methods, MHD and finite elements method 80−32879
conducting continua containing inhomogeneous inclusions, fields in presence of Hall effect *(Ukrainian)* 77−31986
conducting cylinders in field of conductors perpendicular to side surfaces *(German)* 80−106415
conducting fluid, two dimens. motion, mag. field evolution, anti-dynamo theorem extension *(Russian)* 80−59127
conductor gap, geometry effect, skin effect 77−573
construction by ferrofluid birefringence *(Russian)* 77−65553
contactless suspension of objects, oscill. field stabilising effect 77−68150
corners, elec. and mag. fields external to series of corners 77−75360
correction, using Anderson-type elec. current shims role of image currents 77−49745
cosmic magnetic fields dynamics, effects of photon rest mass 77−45708
cosmological magnetic fields and the Faraday rotation from QSOs 80−22087
crack length meas., inductive and videoelectronic methods *(German)* 77−63866
crossed field plasma discharges charact. 80−100116
current dipole models of biological sources, mag. field distribs. 78−7375
current ring, appl. to cores 77−569
curved rectangular conductor magnetic field calc. 77−61895
cyclotron, one prameter function representation 80−18725
cyclotron, heavy ion, proposed for Chalk River, mag. field related mech. tolerances 78−58511
cylinder solenoid, method of the magnetic field synthesis 78−74814
cylindrically symmetric fields, interpolation scheme 78−25769
defect in medium, technical-saturation approx. 80−87262
deflection yokes, mag., integral eqn. method for anal. 79−50183
detection by invertebrates Tenebrio and Talitrus, distinct from light detect. 78−77073
diffusion processes in rectangular conductor, equiv. time constant *(Polish)* 77−65008
dipole, charged particle beam linear transformation coeffs. 80−5681
dipole field, charged particle motion, forbidden zone 78−46501
dipole fields, particle periodic motions in meridian plane 78−85841
dipole fields, particle periodic motions in meridian plane 78−89053
dipole moment of nuclear state using transient mag. field from ion passing through ferromag. *(Dutch)* 78−29386
magnetic fields continued
discontinuous metal films, elec. and mag. field distrib., TEM obs. 79−95518
distributed computing system THESEUS for mag. field analysis 79−41293
dynamic regime of current-carrying bars *(Rumanian)* 79−72455
eddy current induced, in conducting plate, computer soln. *(Polish)* 78−29878
eddy current induced in plate fixed in air-gap between salient poles *(German)* 79−86106
eddy current losses in thin conducting coatings *(Polish)* 79−98263
eddy current losses in thin conducting sheets, variational estimation 79−41296
eddy current magnetic field time constant calc *(Polish)* 77−83779
eddy currents force effects calc., induced in thin plate by cylindrical magnetic field 80−14269
eddy currents induced in solid cylinder fixed in air gap *(German)* 79−89827
eddy field sources determination using magnetic scalar potential method 79−81326
eddy-current feed-through transducer, approx. calc. of mag. field, nonferromag. media 80−78746
education, Dirac monopole, calc. of strength 77−33764
einzel lenses, magnetic, general theory based on axial field distrib. model 79−55045
electric machine end zone magnetic field calc. using approx. analytic method 80−106416
electrode fields calc., blade-type *(Czech)* 78−55273
electromagnet, analysis of inhomogeneities of mag. field 78−29881
electromagnet, mag. field inhomogeneity prod. by deviation from pole parallelism 77−27217
electromagnet, normal and stray flux flow dividing line definition *(Bulgarian)* 77−61094
electromagnet, sectorial, mag. field in inhomogeneities along central ray 79−31768
electromagnet, shell-type, with supersaturated polepieces, field topography 78−74033
electromagnet field control system 77−37950
electromagnet windings with constant current density, maximum permissible mag. field 78−57990
electromagnet with inclined pole faces, mag. field distrib. 77−71352
electromagnetics, use of total scalar pot. in numerical soln. 79−31764
electron beam, magnetized, flowing through cavity, self-consistent potential calculation 80−91743
electron optics, mag. field with min. spherical aberration 78−9313
energy relation to forces acting on magnetic cct. moving part 77−19128
ether, generation of magnetic field by electric current, Einstein early paper *(Russian)* 79−84925
external, analytical extrapolation into two-dimens. magnetised body *(German)* 79−48393
external physical fields of sources investigation, modelling devices construction 80−17817
extragalactic compact radio sources, ripple radiation rel. to low-freq. variability 79−21450
extragalactic radiosources, inhomogeneous magnetic fields 79−40285
fast magnetic field line reconnection in elec. cond. incompressible fluid 77−55097
fast reconnection in astrophysics 77−53424
fast rising mag. field with long pulse duration for plasma expts. 77−2672
ferromagnetic particle anisotropy, asymmetric model *(Russian)* 77−27607
ferrosuspension, motion induced by travelling mag. field *(Russian)* 77−27606
field of a strongly elongated elliptical cylinder in a nonlinear medium 79−91895
field weakening effect of rect. cond. cylinders in air gap *(German)* 79−86105
fields generated near rapidly rotating gravitating bodies 78−46487
finite element calculation from current distrib. 78−94358
finite elements in electrical and magnetic field problems, book 80−62399
finite-element magnetic field calc. allowing for saturation and hysteresis 79−41278
flow redistribution using const. mag. fields, liq. metals *(Russian)* 79−1261
flowmeter, MHD type, with circ. cross section, inhomogeneous mag. field effect on signal 80−33709
focusing field generation, geometric and analytic solns. *(Russian)* 79−64164
force free fields equilib. and stability 77−17357
force-free field, new aproach and appl. to solar active regions mag. field 80−62011
force-free fields, time evolution 78−85843
Fourier anal. within finite elements 77−71903
frequency/depth-penetration considerations in hyperthermia by magnetically induced currents 80−63887
frozen force-free mag. field *(Chinese)* 77−71902
fusion reactor, toroidal device with nonplanar mag. axis, magnet and coil engineering 78−55009
fusion reactor RFC-XX, coil system, design, fabrication, testing 78−55007
fusion reactor vacuum vessel, magnetic stress induced by plasma motion, 3-dimens. anal. 78−66370
galactic magnetic field interaction with hot intergalactic gas, magnetosphere existence 80−67876
galaxies, new mag. theory for Hubble sequence 77−71142
Galilean satellites, dynamo mag. fields possible strengths 79−16873
generalised finite element method for magnetostatics 79−41270
geomagnetic field interpretation, optimal computing scheme construction 77−33201
geometric distortion by eddy currents in cylindrical conductors 77−50584
gradient septum magnet, effect of pole gradient 78−25369
grid and metric optimisation, finite difference and finite element methods 78−94352
Hall cross in perpendicular inhomogeneous mag. field 79−81323
Hermaean magnetosphere, compression by solar wind 79−96936
Hertz Quincke effect 79−36808
high energy accelerators, superconducting dipole magnets with high field uniformity, development and investigation *(Russian)* 80−5416
high field production and meas. 78−8425

magnetic fields continued
high pulsed mag. fields for nuclear fuel rod sealing 78−8910
hole in conducting wall near oscillating mag. field, perturbations 77−47246
hollow cone, mag. field strengthening in confocal motion subjected to plastic deform. 77−83787
homing pigeon sensitivity to Earth-strength mag. field, 0.5 gauss 77−52812
homogeneous magnetic field generation, using thin circular current carrying coils *(Polish)* 79−98262
homogeneous magnetic field sources, for studying NQR devices characts. 77−61102
homogeneous magnetic field synthesis in internal region of cylindrical solenoid *(German)* 80−37923
homopolar machine for fusion experiments, calc. of steady state mag. fields 77−23288
human heart consistent rectangular/spherical coordinate system for EEG and magnetocardiography 77−86679
hybrid magnets for high mag. field generation, polyhelix coils, optimization calcs. 80−240
imploding wire array, mag. field study 79−55021
induction motor, polyphase, at no-load, nonlinear magnetostatic field determ. 78−33647
infinite cylinder with eccentric cylindrical inclusion, determ. of transverse magnetostatic field 78−82882
of infinitely long conductor, DC current supplied, calc. *(Czech)* 77−19125
inhomogeneous field visible display using optically pumped cell 77−65027
inhomogeneous magnetic field from electromagnet produced by parallel shift of central axis of one pole 78−55276
inhomogeneous medium, numerical calc. 79−72454
inside long rod of magnetised material, calcs. 78−73795
integral equations 79−72453
intense, prep. and appl. 78−41337
interaction force calc. between permanent and ferromagnetic material *(Russian)* 77−26347
interfacial entropy, elec. and mag. interfacial polarisation *(French)* 79−7050
intergalactic magnetic field, rel. to galactic spiral structs. origin 79−25714
intergalactic magnetic fields, suprathermal grains prod. 79−48911
intergalactic magnetic fields and Faraday rotation of extragalactic radio sources 80−22086
inverse problems, soln. *(Russian)* 80−1102
ion mass-energy spectrograph for space plasmas anal., double-focusing field geometry 77−53401
isochronous cyclotron sector magnet field calc., integral eqn. method 79−41053
Jupiter, bow shock and magnetosphere, Voyager 2 magnetometer obs. 80−77339
Jupiter, charged particles accel. in Io flux tube rel. to decametric radiation modulation 78−89110
Jupiter, effect of rot. on inflated magnetosphere, similarity model 78−57492
Jupiter, effect on charged dust particles in ring, orbit changes 80−82273
Jupiter, electrodynamic interaction with Io 78−81583
Jupiter, linear polarisation obs. at 6, 11 and 21 cm rel. to field configuration 77−87313
Jupiter, mag. field from 21 cm obs. of radiation belts 80−105195
Jupiter, mag. field meas. rel. to magnetodisc 79−58297
Jupiter, mag. field rel. to Io Na emission region morphology 77−49329
Jupiter, mag. field rel. to plasma sheet self-consistent model 78−57494
Jupiter, mag. fields in dynamic current sheet high β plasma 79−16872
Jupiter, mag. reconnection as magnetosphere energy source, comparison with Earth 79−58201
Jupiter, magnetic field similarities with pulsars, explanation for radio similarities *(Russian)* 80−77333
Jupiter, Pioneer 11 mag. field model rel. to decametric radiation sources locations 79−75148
Jupiter corotating magnetosphere, self-consistent model 78−89109
Jupiter Galilean satellites, intrinsic mag. fields and magnetospheres props. 80−46465
Jupiter magnetic field, implications of radio emission polarisation obs. at 11 and 18 cm wavelength 80−67637
Jupiter magnetic field, influence on Galilean satellites volcanism and rot. 80−31247
Jupiter magnetic field studies by Voyager 1, preliminary results 80−26793
BL Lacertae type objects, linear optical polarisation study rel. to mag. fields *(Russian)* 78−57640
Laplacian mag. field component computation from boundary obs. only 77−3513
large algebraic eqn. systems, direct and iterative solns. 79−41274
LF and MF ground waves in realistic terrain, field strength meas. at LF and MF 78−88795
lightning intracloud discharges, mag. fields rel. to dipole axis inclination 78−73440
lightning return stroke elec. and mag. fields, obs. in Florida 80−31096
linear accelerator ring compressor, magnetic field distortion by disconnected multiturn coils 78−66436
linear system solution by modified Stone finite element method *(French)* 79−41279
lines of force reconnection in plasma, astrophys., geophys. and lab. appl. *(Russian)* 78−91083
loop diagrams calculation in strong mag. field *(Russian)* 78−25786
loop induced magnetic fields in classrooms for the hard of hearing, using heuristic development 77−61893
LPE garnet bubble films, capping layer upper cap-switch field, model 78−95498
lunar far-side magnetised regions, correl. with ringed impact basins 80−36521
lunar magnetic fields, magnetometer data errors and EM induction studies 79−96932
lunar palaeomagnetism, origin 78−93132
magnet, rot. near Cu disc, field lines, lecture room demonstration 78−54131
magnetic Faraday's law analogue, appl. to slow charge convection, for teaching 78−49607
magnetic induction stabilised source 78−94360
magnetic multipole expansion, education 80−105456

magnetic fields continued
magnetic separator, drum-type with alternating polarity, analytical description of magnetic field *(Russian)* 80−99602
magnetisation curve analytic functions, numerical parameter calc., variational methods appl. *(Russian)* 80−14267
magnetised ferromagnetic object induced signal characts. *(Japanese)* 77−53963
magnetofluid flows, intrinsic eqns. 79−37409
magnetosphere, GEOS-1 meas. of electric and magnetic wave fields and cold plasma parameters 79−48620
magnetosphere, magnetic flux transfer, correlative study 79−101024
magnetosphere model, particle (electric current) approach 80−17442
magnetosphere reconnection, substorms and energetic particle acceleration 80−31169
magnetostatic axisymmetric poloidal problem in circular torus, generalised axisymmetric Poisson eqn. 77−22383
magnetostatic computer program GFUN3D, user guide 77−31044
magnetostatic equations, axially symmetrical, solution by difference methods 77−50585
magnetostatic field, rotational-symmetrical, modelling, variational method, difference equations *(Polish)* 79−81319
magnetostatic monopoles in Cartesian coordinates 79−5932
magnetostatic problems, 3-dimens., soln. using scalar potentials 79−22879
magnetostatic problems, soln. by MAGGY2 problem package 80−28134
magnetostatic two-dimensional problems, numerical soln. by augmented Lagrangian methods 78−1119
magnetostatics, three dimens. external mag. field calc., pot. theory *(Russian)* 78−1120
magnetotail, substorm magnetic fields, 3-dimens. analysis 78−61666
Mars, magnetospheric interaction with solar wind 80−72835
Mars magnetic field, Mars 2 and 3 evidence 78−49361
Mars magnetic field, Mars 3 evidence re-examined 78−49359
Mars magnetic field, Mars 5 evidence 78−49362
Mars magnetic field, Mars 5 evidence re-examined 78−49360
matter-antimatter boundary layers, mag. field effects on ambiplasma balance 77−49284
matter-antimatter boundary layers with mag. neutral sheet, model 78−53807
Maxwell's equations as one quaternion eqn., appl. to wave propag., for teaching 78−54133
megagauss fields, macroparticle acceleration 80−47789
Mercury, dipole displacement 79−80252
Mercury, dynamo origin 77−29675
Mercury, mag. field characts. and origin 78−12131
Mercury magnetospheric mag. field model 77−45336
meteorites, characts. of first order shock induced mag. transitions in Fe, discrimination from TRM 78−64205
meteorites, evidence for primordial mag. field in parent body era 78−45293
MG field generation by EM flux-compression, computer simulation 79−50189
MHD convertor channel and regions, eddy current losses due to magnetic field variations 80−40874
MHD generators, coaxial, magnetic field distrib. *(French)* 78−55758
MHD machine, EM field eqns. averaging at finite mag. Reynolds nos. *(Russian)* 79−1351
MHD magnetic circuit, field calcs. *(Russian)* 77−3883
microtron electromagnet, mag. field distrib. using mag. scalar pot. 80−102597
modulation, using superconductive coil 77−18056
Moon, ancient mag. fields rel. to cosmic ray irradiation of lunar rocks and grains 77−60562
Moon, ancient magnetic field inferred from palaeomagnetism 77−60686
Moon, anisotropic mag. fluctuations rel. to elec. cond. anomaly beneath Mare Serenitatis 80−56730
Moon, characts. of first order shock induced mag. transitions in Fe, discrimination from TRM 78−64205
Moon, intensity and origin of ancient mag. field 77−60656
Moon, mag. field at Apollo 14 site rel. to surface interaction with plasma sheet 77−2354
Moon, origin of primaeval melting and internal mag. field 78−24478
Moon, Rima Sirsalis, linear magnetisation feature 77−29668
multipole DC electromagnet, working gap field analysis *(Russian)* 80−28142
multipole expansion for magnetostatic field using scalar potential, teaching 79−58493
multiterminal representations 79−68345
NGC 315, NGC 6251, very large radio galaxies intergalactic mag. fields from 11.1 cm obs. 78−86014
NMR linear field correction, optimum size of rectangular current shim off mag. pole face 78−86314
non-stationary, calc. for current filament over conducting layer *(Czech)* 80−52283
nonlinear field eqns., time discretisation and mixed finite element methods 79−40384
nonlinear field problems, finite element method *(Russian)* 78−46485
nonlinear magnetic field simulator for electromagnetic fields anal. *(Japanese)* 80−95756
nonlinear magnetostatic fields, three-dimens. anal. in saturable reactor 79−13860
nonmagnetic strip in transverse uniform alternating magnetic field 78−94362
nucleus, Cabibbo angle, and CP violation 77−41918
numerical analysis, fundamental equations and historical evolution *(Portuguese)* 80−78739
numerical computation, using ELMAG program system *(German)* 77−3516
numerical techniques in field calcs. 80−32878
off-axis Helmholtz field 79−2587
one-dimensional force-free magnetic field, singular lines *(Russian)* 79−48670
oscillating conducting sphere in mag. field, forces calc. 78−25771
pair of square section thick circular coils, optimum spacing 78−71001
parallel computation array-processor structure 79−41277
particle acceleration near singular line of mag. field, energy spectrum *(Russian)* 80−90332
penetration, through cond. ellipsoidal shield with slits and holes 77−50587
penetration into half-space with nonlinear permeability in quasi-stationary state *(Czech)* 77−46667

magnetic fields continued
permanent magnet and current-carrying conductor fields, Fe filing pictures, theory *(German)* 80−28145
permanent magnet gap field with conical poles clad with soft mag. materials, anal. *(Russian)* 79−41266
permanent magnet plane periodic system, mag. field, energy and interaction force distrib. 78−46483
permanent multipole magnets of oriented rare earth cobalt materials 80−37925
PETRA magnets, results of field meas. 79−68040
plane permanent magnet system field distrib. model *(Russian)* 80−28133
planetary, effect of photon mass 77−33477
planetary magnetic fields, apparent source depths 78−57478
planetary magnetic fields, survey of expt. data 78−73664
planetary magnetism, and interiors of Moon and Mercury 78−12115
planets terrestrial *(Hungarian)* 77−73987
plasma, infinitely conducting, pinch effect, dynamical accumulation towards neutral line of magnetic field 80−83977
plasma, laser-induced, spontaneous mag. fields 79−32793
plasma, laser-produced, magnetic field generation 80−77818
plasma, magnetic field parametric generation under intense irrad. *(Russian)* 79−77412
plasma, magnetic tape method obs. of self generated mag. fields 80−64775
plasma, Rayleigh-Taylor instability generation of mag. fields, effects on laser fusion 79−19025
plasma field line integration for MHD equilibria near a closed magnetic field line 78−59651
plasma magnetic field generation, laser light reson. absorpt., stress tensor anal. 78−18419
plasma trap for magnetic flux, loop probe meas. 79−14621
pole pieces with cavities, correction effect modelling by computers *(Czech)* 79−45879
potential problems in systems including mag. material, harmonic analysis 77−6971
powers determination using direct analogue method *(Czech)* 80−69290
principles and appls., book 80−32866
production and usage of megagauss fields for solid state physics 79−71491
production of transient 400 tesla field by explosive compression *(French)* 77−149
protostellar cloud ang. momentum problem, mag. breaking 80−82342
pulsed intense magnetic field prod. by mag. flux compression device *(French)* 77−61095
quadrupole lens spatial field determ. 78−55292
quasi-stationary, finite element anal. 78−94356
radio double sources (astronomical), beam and cloud stability, shear layers, two dimens. computations 80−67893
radio sources, compact, extragalactic, mag. fields rel. to radio spectra interpretation 80−62299
radio sources, compact, strong mag. dipole model 79−17115
reciprocity theorem for corrugated surfaces used in conical diffraction mountings 80−1333
recording heads scattered fields anal. using SEM 79−89045
relativistic vector formulation *(Italian)* 78−12448
representation of internal and external fields of two dimensional magnetised bodies *(German)* 78−78849
rotating body magnetic field effects and properties 78−17837
rotationally symmetric mag. field expansions into zonal harmonic functions 79−31772
saturable, finite element method appl., using scalar magnetic potential 77−38773
saturable medium, uniqueness theorem of quasistatic mag. field 78−5388
Saturn, cosmic ray cutoff rigidities in dipole mag. field 80−72873
Saturn, dynamo precession model *(Russian)* 80−94752
Saturn, Pioneer 11 obs. 80−82292
Saturn magnetosphere, bowshock and magnetopause detect. by Pioneer 11, mag. field determ. 80−82283
separator, magnetostatic energy of paramag. particles 77−38768
single-polepiece magnetic lens axial field distrib. 80−69317
slot permeance ratio evaluation by numerical methods *(Italian)* 78−86987
slotted boundary machine field soln., conformal transformation and integral methods 79−41272
small apertures in perfectly conducting wall, polarisability 77−19136
solenoid, semiinfinite, thin, mag. field and current density distribs. near edge Wiener-Hopf calc. 78−70999
solenoid, supercond., mag. field stability in persistent mode *(Czech)* 78−29131
solenoid, synthesis on axis, Tichinov's regularisation method *(German)* 77−42458
solenoid, thin-walled, end effect for mag. field max. 77−83784
solenoid generating homogeneous field, ampere turn deposition determ. 78−42253
solid state physics, high mag. fields, generation and application 80−27321
spectrometer magnets, field parametrisation 79−880
sphere, $\mu \neq 1$, in arbitrary freq. mag. field, mech. pot. energy calc. 77−50586
sphere between pole pieces of electromagnet, demagnetizing factor 78−13643
spheres and current carrying coils, integral representation of inductance 80−80469
spherical magnets, analytic soln. of magnetostatic field *(Ukrainian)* 79−50181
spinning magnetic field inducing elec. field, moving and non-moving force line hypotheses 78−9296
stabilisation using directly coupled IC op. amps, for EPR spectrometer *(Czech)* 79−26095
static field and eddy current problems, computational methods for soln. via Fredholm eqns. 79−68344
static field problems, numerical soln. algorithms 80−95757
stationary config. production in magnetic reversal apparatus, time required 78−21182
stationary field iterative modelling with hybrid analyser 77−42463
stationary magnetic field calc. in nonlinear ferromag. medium *(Russian)* 79−13861
stationary magnetic fields calc., in nonlinear ferromagnetic medium *(Russian)* 79−59613
magnetic fields continued
steady field penetration into ferromagnetic halfspace *(German)* 79−45878
steady magnetic field from charges in arbitary motion, education 80−105460
steel, electrical, mag. hysteresis representation in numerical modelling of mag. fields 80−88813
steel, mag. anisotropy, magnetostatic fields, numerical simulation 77−27220
stellarator toroidal field production by modular systems 80−10441
stochastic mag. field fluctuations, self-consistent model 80−100074
straight-line current element, vector expression for mag. field 80−58440
strong, generation and control *(Japanese)* 78−45659
superconducting accelerator magnets, magnetization effects on field shape 79−31253
superconducting magnet, calc. by harmonic current layer method *(Croatian)* 77−28341
superconducting magnets, influence of magnetization in multifilamentary composites on central field 79−65599
superconducting systems, calculation method from boundary conditions *(Ukrainian)* 80−34545
superconductor tube, thick-walled, mag. field distrib. in axial region *(French)* 77−51856
supernova remnant prod. 80−77474
superstrong field production using implosion generator, solenoid for generation of initial mag. flux 80−105681
surface field calc., floating random walk method 79−41273
suspension of torus in field of coax. coil and conductor *(Russian)* 77−23596
synchronous machines, slot-less, armature and excitation field, analytical calc. method using polar coordinates *(German)* 80−32870
synchronous machines, slot-less, winding reactances and inductances determ. under stationary conditions *(German)* 80−32871
synthesis at mid-plane of solenoid *(Polish)* 79−94123
teaching demonstration, casting to obtain permanent 3-dimens. patterns of Fe filings 78−8193
teaching w.r.t. chemistry, guide to units 80−12871
terrestrial planets, mag. fields 78−12125
thick ellipsoidal coil and ferromagnetic ellipsoid system, vector potential 79−41269
three dielectric media image method for potential eqn., discussion and reply 79−3610
three dimensional finite element program 77−38769
three magnets problem, collinear case *(Ukrainian)* 79−36807
three phase induction motor heat flow model, locked rotor and running-up temp. rise calcs. *(German)* 79−90115
three-dimensional, determ. using scalar potential, finite element soln. 77−88616
three-dimensional field modelling, finite-element interactive computer methods *(French)* 79−41294
three-dimensional magnetostatic problem soln. using scalar potentials 79−41271
time dependent vector field effects on mag. multipoles 80−99597
time-varying magnetic field problems, finite element formulations 79−41265
tissue, RF mag. field penetration, phase shift and power dissipation, rel. to NMR imaging 78−73189
Titan, dynamo mag. fields possible strengths 79−16873
Tokamak, TNS, equilib. field coils and free boundary equilib. considerations 78−58420
Tokamak fusion, Impurity Study Experiment, mag. field calcs. using GFUN-3D programme 78−66368
Tokamak reactors, supercond. toroidal magnets, max. mag. fields, mech. stress calcs. 79−36405
Tokamak reactors, toroidal magnetic field strength requirements, physical parameters, cost 77−19777
topology of magnetic field in toroidal systems 77−19757
toroidal field coils, EM parameters calcs. of current paths in homogeneous media *(Japanese)* 80−106155
toroidal ring in field of moving coil with currents, calc. 79−64149
toroidal shells, conducting, vector pot. calc. 77−3514
toroidal solenoid, Aharonov-Bohm effect *(Russian)* 78−77770
toroidal thick coil, mag. field calc. 78−17839
torus carrying DC current, anal. *(German)* 77−6969
transient field buildup phenomenon is confined conducting medium at quasisinusoidal excitation *(Russian)* 77−31041
transient loss analysis and measurements on normal conductors and composite superconductors using equivalent circuit technique 79−60978
transverse mag. dipole field diffraction on sphere with circular hole *(Ukrainian)* 79−31761
transverse magnetic field penetration through slits in ideal shield 80−78745
tridimensional numerical calc. of magnetic fields using summation method *(German)* 80−106414
turbulence, intermittency and magnetic fields 78−89059
turbulent dynamo, dynamic eqn. of magnetic field 80−32880
twisted magnetic fields, stability 78−45217
two dimensional H/r mag. field, ion optical characts. of two-sector system 78−66744
two dimensional magnetic field computation, by Schwarz-Christoffel mapping function numerical integration *(German)* 79−89826
two- and three-dimensional in moving electromotive media, calc. methods *(Russian)* 77−53745
two- and three-dimensional magnetostatic problem program packages 79−41276
two-dimensional boundary integral eqn. method 78−94355
two-dimensional field with open boundaries, anal., exterior finite elements 78−22064
two-dimensional graph-theoretic model 80−87260
two-dimensional nonlinear magnetostatic fields, isoparametric Hermite finite element program 79−41275
two-dimensional open boundary problems, finite element anal. 78−94354
two-domain analysis of field producing bodies using fictitious poles 78−33649
unbounded two-dimensional linear eddy current algorithm 79−41300
uniformly magnetised body, mag. field strength invariance 80−58441
Uranus, struct. and mag. field theory using two-layer model 80−4298
Uranus magnetosphere, mag. field and plasma dynamics laboratory simulation 79−16757
vector potential of parallel conductors in rectangular metallic tunnel *(Polish)* 77−83778

magnetic fields continued
Venus, intended mag. field meas. by Pioneer Venus Orbiter 77−73996
Venus, measured mag. field rel. to solar wind interaction 79−58288
Venus ionosphere, mag. flux ropes nature *(Russian)* 80−77313
Venus magnetic tail field structure, role of unipolar induction effects 80−62060
zoom lens quadrupole magnets for Colorado Univ. energy-loss spectrograph 77−83410
F+Co(Fe) recoil, transient mag. field 78−29838
Fe analysing magnet, fast precise field control 79−45883
Fe core coils, mag. field dispersion 79−64139
Fe, in magnetostatic field prod. by toroidal conductor 80−1104
Fe, nonlinear magnetostatic problem soln. *(Russian)* 79−64138
Fe_3B, distinctness of magnetic hyperfine fields associated with structurally unique Fe sites 77−63330
Fe_3O_4 ferrofluid, mag. birefringence, estimation of particle size 79−33511
H_2 atoms trapping and thermal detection using superconducting magnet of low temp. 80−73396
He, self-oscillating props. of discharge in mag. field 80−64814
Nb_3Sn multifilamentary dipole magnets, supercond. props., 4.2 to 15K 79−31275
Si+Co(Fe) recoil, transient mag. field 78−29838
SiFe sheets, grain-oriented, stray field meas. 80−88775

magnetic film stores
see also magnetic bubble devices
bubble lattice propagation control by standing acoustic waves 79−82841
bubble materials, review 80−50153
bubble memories, status and prospects 77−77079
bubble memory chip fabrication, single level masking approach 79−78486
bubble memory device prod., ion beam etching 79−78487
cross-tie shift register memory device 79−78484
cylindrical magnetic bubble domain memory materials 79−61194
epitaxial garnet films for magnetic bubble memories *(Czech)* 78−88147
garnet film, Ga and Ge substituted, mag. prop. control during LPE growth and processing 78−68638
garnets, bubble domain memory appls., growth requirements 77−20660
multilayer self-structured bubble memories 79−78483
optical image recording, banded domain structure, effect of recording field strength on energy characts. *(Russian)* 78−19297
$Co_xFe_{3-x}O_4$, single cryst. mag. films, holograms recording and thermomagnetic writing 78−55324
Cr_7Te_8 film, optical and magneto-optical props., appl. as storage medium 78−23545
Fe garnet epitaxial film, thermomag. data recording by electron beam heating 78−27066
Gd-Co, amorphous film, with cylindrical mag. domains, sputtering prep. *(Russian)* 77−12176
GdFe garnet, thermomagnetic recording on magnetised single cryst. plate 79−47285
Mn-Cu-Bi ternary cpd. thin films for magneto-optic memory applic. *(Japanese)* 77−63238
Mn-Cu-Ni-Bi, magneto-optic film for storage appl. 77−12165
$Mn_{0.75}Ti_{0.25}Bi$ films as magnetooptic storage medium, mag. interferogram recording 78−19288
Ni-Fe polycrystalline film cross-tie memory for shipborne radar/sonar 80−42204
$(Y,Eu,Lu,Ca)_3(Fe,Ge)_5O_{12}$, bubble memory chip, dynamic conversion comparison with $(Y,Sm,Lu,Ca)_3(Fe,Ge)_5O_{12}$ 78−68319
$(Y,Sm,Lu,Ca)_3(Fe,Ge)_5O_{12}$, bubble memory chip, dynamic conversion comparison with $(Y,Eu,Lu,Ca)_3(Fe,Ge)_5O_{12}$ 78−68319
$Y_3Ga_xFe_{1-x}O_{12}$, film growth conditions rel. to memory element props. 77−66399

magnetic films *see magnetic thin films*

magnetic fluids
active permanent magnet suspensions, scientific instruments appls. 78−24829
agglomeration, reversible, field-induced 78−3380
application in mineral microcrystal density determ. technique 80−85751
applications *(Chinese)* 79−83518
aqueous colloid distrib. by method of polyvinyl alcohol substitution, electron micrography 77−73477
aqueous magnetic fluid prep. by peptisation with anionic surfactant 78−44408
barbotage and sedimentation, multivelocity model 80−61161
behavioural props. *(German)* 80−61159
bibliography 80−57021
birefringence and dichroism, magnetically-induced, sign inversion 80−60548
boundary layer, flow stability 79−64782
cavitation bubble, in magnetisable fluid, mag. field and press. effects on shape *(Russian)* 77−27608
charged wall behavior in 1-μm bubble implanted structures 78−91892
classification of solutions magnetic phenomena *(Russian)* 77−8384
colloid, birefringent effects, appl. in obs. of mag. domain structs. 79−51809
colloids, magnetic, theoretical estimates fo equilibrium chain lengths 79−79309
colloids, magnetic, theory of large agglomerates 79−79310
conducting, low intensity jump struct. *(Russian)* 78−75214
conductive, nonlinear magnetosonic waves 80−59121
conference, Orlando, USA (Mar. 1980) 80−56995
continuum mechanics, global balance law approach 80−60388
convection, natural, heat transfer of cable coolant 78−94846
convection in vertical layer in current-carrying plate mag. field *(Russian)* 77−65806
convective stability depend. on mag. field in magnetizable liq. *(Russian)* 78−47051
cylindrical column, motion in rot. mag. field *(Russian)* 78−75212
dielectric, magnetohydroelectric waves 79−27703
dipolar conducting liquids, mag. transport props. at ambient temp. 79−91258
dispersive magnetisable media, hydrodynamics including Brownian motion 80−59120
drop, magnetised, shape in homogeneous mag. field 79−76544
drops in homogeneous magnetic field, shape *(Russian)* 79−877
dynamics of cylinder, partially full of mag. liquid rolling in mag. field 77−19515
ejecting force on nonuniform mag. bodies in ferromag. liq. 80−83855

magnetic fluids continued
electrophysical effect control by susceptibility variation *(Russian)* 79−95628
experimental study of mag., optical, and hydrodynamic props.,, review 80−60376
ferric solution ferromagnetic liquid insulation in redox flow battery, quantum parameters separation 80−61338
ferrimagnetic suspension, behaviour in mag. field rel. to magnetochem. separation 77−20628
ferrite F-600, suspension in caster oil, residual magnetisation *(Russian)* 79−1689
ferro-fluid particle formation on permalloy overlay bar surface, calc. and anal. 78−68329
ferrofluid, convective stability of horizontal layer in mag. field *(Russian)* 77−3885
ferrofluid, dielec. behaviour in uniform mag. field 80−60390
ferrofluid, dynamic magnetisation obs. 78−72370
ferrofluid, force on immersed magnet, surface integral calc. 78−94350
ferrofluid, heavy, suspended in magnetostatic separator electromagnet gap, free surface shape 79−76543
ferrofluid, heavy, suspended in magnetostatic separator mag. gap, free surface shape calc. *(Russian)* 79−876
ferrofluid, helical flow with heat cond. between coaxial porous tubes 79−23371
ferrofluid, mag. birefringence pulsed field meas. 79−82943
ferrofluid, nonlinear surface waves, bifurcation theory approach 80−58439
ferrofluid, particle size distrib. parameters 79−1687
ferrofluid, Procopiu effect 79−33519
ferrofluid, relativistic conducting, wave propagation, velocities *(French)* 77−15138
ferrofluid, relax. in external mag. field, cubic cryst. case 80−71113
ferrofluid, suspension, magnetodiffusion, interferometric obs. *(Russian)* 77−4946
ferrofluid, transverse heat transport in mag. field 80−59031
ferrofluid, US response time, mag. field depend. 79−1702
ferrofluid behaviour in the presence of a rotating nonhomogeneous mag. field *(French)* 80−96313
ferrofluid birefringence, construction of mag. fields *(Russian)* 77−65553
ferrofluid constitution examination by rotating test tube method 80−33693
ferrofluid decorated mag. domain patterns, Fraunhofer diffr., domain struct. determ. 78−6541
ferrofluid devices, magnetostatic and centrifugal, nonmagnetic body motion 80−33700
ferrofluid droplet, interphase boundary hydrostatic characts. in uniform mag. field 80−33692
ferrofluid droplet dynamics in magnetographic printing 79−50772
ferrofluid flow in circular pipe, uniform mag. field effects 80−43782
ferrofluid flow under influence of rotating mag. fields 80−59118
ferrofluid hydrostatics, stress theories 78−6116
ferrofluid motion, rot. mag. field effects 77−950
ferrofluid patterns on thin film materials, zigzag form of charged domain wall 80−44852
ferrofluid seal, for blood flow statis during surgery, hydrostatic loading 77−13031
ferrofluid seal against liq. 80−57270
ferrofluid susceptibility meas. device and method *(Czech)* 77−26345
ferrofluid US attenuation anomalies 79−55830
ferrofluid/lyotropic liq. cryst. combination, ferronematics and ferrocholesterics 80−59378
ferrofluids, agglomeration, review 80−61162
ferrofluids, appl. as acoustic transducer material 80−58877
ferrofluids, conc. depend. mag. grain correls., small angle X-ray scatt. study 80−61160
ferrofluids, coupling with nematic lyomesophases 79−90526
ferrofluids, dissipative process in non-homogeneous mag. field 80−59119
ferrofluids, exptl. obs. of agglomeration in presence of mag. field *(French)* 78−92514
ferrofluids, Landau and Lifshitz hydrostatic press., thought expts. 80−59111
ferrofluids, magnetic liquid vacuum seals 79−63244
ferrofluids, magnetic material conc. distrib. meas. device 78−16821
ferrofluids, phase diagrams and eqn. of state 80−60280
ferrofluids, Procopiu effect with different vol. conc. *(French)* 77−43845
ferrohydrodynamics, mag. relax. models 79−94706
ferroliquid, deviation of free flow by inhomogeneous mag. field 77−65800
ferroliquid, magnetoelastic oscills. 79−94639
ferroliquid in annular channel, hydromag. stability, thermomagnetic effect 79−94593
ferroliquids, colloidal, magnetic and hydrodynamic properties *(Czech)* 77−16109
ferroliquids, phenomenological theory 79−16042
ferromagnetic colloid, field depend. chain formation 79−100451
ferromagnetic colloid, natural convection, mag. field effects *(Russian)* 77−62307
ferromagnetic colloids, domain and grain obs. of highly-oriented Si steel 80−11856
ferromagnetic colloids, ferrohydrodynamics and magnetic viscosity 78−15715
ferromagnetic colloids, helical flow in mag. field *(Russian)* 78−75213
ferromagnetic fluid, 1D Ising and 3D Heisenberg solns. 77−85478
ferromagnetic fluid, in appl. mag. field equilib. surface patterns 77−84332
ferromagnetic fluid, magneto-optical activity in polarised reflected light *(Russian)* 78−76438
ferromagnetic fluid, molecule system eqn. of state, exchange interactions, spin independent forces 77−59412
ferromagnetic fluid rotating about vertical axis, convective instability of layer 79−27698
ferromagnetic fluids, convective heat transfer 79−98725
ferromagnetic layer boiling, mag. characteristics meas. 78−59499
ferromagnetic liquid, US vibr., reson. excitation by mag. field *(Russian)* 78−48020
ferromagnetic liquids, long term stability for energy conversion devices 77−29051
ferromagnetic particle suspensions in non-conducting and metallic liqs., review 80−60372

magnetic fluids continued
ferromagnetic particles, mag. flocculation effects during mag. beneficiation 77−77809
ferromagnetic sol, relaxation of mag. birefr. and dichroism 79−57301
ferromagnetic suspension, bulk viscosity calc. *(Russian)* 77−81429
ferromagnetic suspension, mag. field effect on heat transfer, thermal cond. 78−59500
ferromagnetic suspension, magnetorheological characts. meas., errors 80−33550
ferromagnetic suspension, residual magnetisation 80−84623
ferromagnetic suspension serving as a liquid magnet 80−84622
ferromagnetism, mean-field criterion 79−42791
ferrosuspension, magnetorheologic characts. *(Russian)* 77−65786
ferrosuspension, MHD flow, heat transfer *(Russian)* 78−26203
ferrosuspension, motion in rot. homogeneous mag. field *(Russian)* 77−27604
ferrosuspension, residual magnetisation effect in nonuniform mag. field 79−78443
ferrosuspensions, internal rotations and the other transport phenomena 80−28573
ferrosuspensions, mag. field effects on mech. props. 78−87321
film flow in mag. field, laminar regime 78−34203
flow in rotating vessel, homogeneous mag. field effect 80−33691
flow stability of thin layer *(Russian)* 78−9721
flow through porous medium with uniform mag. field oblique to interface 80−59107
heat and mass transfer 80−59123
heat transfer, in coaxial cylinder system, numerical calcs. *(Russian)* 77−47015
hydrodynamic suspensions, physical property variations *(Russian)* 78−47022
hydrodynamics and torques in rot. mag. field 79−94632
hydrosols, mag., struct. and stability *(Russian)* 78−80794
ink, water based colloid with Fe_3O_4 or Fe, prep. 77−9128
instabilities, leading to rupture of continuity 80−59003
instability of plane layer in mag. field *(Russian)* 78−26210
interpenetrating EM structured continua, thermodynamic and mech. props. calcs. *(Russian)* 77−47580
kerosene-base mag. fluid, sound vel. meas. 77−63969
layer, thermocapillary instability with thermally insulated boundary 80−33595
light polarisation, magnetically-induced 77−73130
light scattering and polarisation 80−60616
liquid crystal, ferronematic with magnetic platelets, equil. positrons w.r.t. applied field 77−11476
liquid shaft seal, using ferrofluids 79−43637
loudspeaker design parameter dependence on props. 80−38206
magnetic liq. birefringence and dichroism kinetics, Brownian diffusion *(Russian)* 78−5806
magnetisable liquid, thin layer instability 79−41762
magnetisable liquid layer, with solid boundaries, convective stability 79−94592
magnetisation, absence of anisotropy effects 80−50146
magnetofluid flows, intrinsic eqns. 79−37409
magnetorheological systems, heat transfer 79−81988
motion in rotating homogeneous mag. field 80−28572
Newtonian eqns. and exact unidimensional nonstationary solns. *(Russian)* 78−47048
optical birefr. and dichroism in mag. field 80−60547
paramagnetic fluid, non-conducting sphere steady rotation 79−72900
particle cluster configuration, Monte Carlo study 80−88827
particle coagulation, rel. to NDT by magnetic powder method 78−60942
permanent magnet immersed in mag. liq., buoyancy forces obs. *(Russian)* 78−47050
polariser for magnetising liquid, in NMR devices 80−57351
power-law liquid, shear flow, general soln. for mag. rheology *(Russian)* 78−47003
pressure measurement using nonmag. manometer *(Russian)* 78−24785
properties and applications *(Czech)* 79−47984
relativistic magnetofluids and symmetry mappings 79−27700
relativistic magnetofluids and symmetry mappings. II 79−27701
resonance excitation of ultrasound in ferromagnetic fluids 78−95112
response to mechanical, mag. and thermal forces 80−59122
seal, dynamic loading 78−62186
seals, application of mag. fluids 79−95609
seals, high-speed cryogenic mag. fluid, for high-vacuum chambers 80−57314
shaft seal, high-speed mag. fluid, heat dissipation 80−59032
slurry, effect on performance of EM flowmeter 78−26219
spherical drop, motion in rot. mag. field *(Russian)* 78−75212
superparamagnetic particles, mutual attraction 80−29581
surface equilibrium forms *(Russian)* 77−27605
surface instability in nonisothermal layer *(Russian)* 78−94834
surface monolayer motion of magnetised fluid 79−76545
surface stability of magnetised liqs. separated by thin elastic film 79−94727
surface vibration mode obs., steady-state, for teaching lab. 78−41111
surface wave excitation, by travelling mag. field *(Russian)* 77−47099
surfactant monolayer, motion in mag. field *(Russian)* 79−1260
suspension, appl. to contact recoring of flaw patterns 78−53102
suspensions, influence of dispersion factor *(Russian)* 79−52788
suspensions, magnetic and rheological props. *(Russian)* 79−55350
T bar, domain wall study employing ferrofluid, rel. to magneto-optical Kerr effect meas. 80−60360
temperature-sensitive magnetic fluid, use in instrument for temp. meas. 80−31745
thermoconvective instability, with mag. field perturbations 78−94847
thermomagnetic convection between coaxial cylinders with distributed heat source 79−94622
thermomagnetophoresis of particles in magnetic suspensions 80−35581
thermomechanics, mag. fluid as continuum with internal degrees of freedom 80−60377
thin layer with two free boundaries, instability conditions, surface wave dispersion eqn. *(Russian)* 78−1752
US attenuation, MHD approach 80−60389
US attenuation anomaly in mag. field 78−68345
US vel. anisotropy in mag. field 78−68344
viscoplastic conducting liq., finite perturbations, Hartman flow instability *(Russian)* 78−47049
viscous, motion in external mag. field, Couette and Poiseuille flow 79−14491

magnetic fluids continued
waves, nonstationary, one-dimens., in fluid with intrinsic ang. momentum 80−33690
Al_2O_3-martensitic steel, mag. and dielec. emulsion, prep. by abrasion of steel surface 78−27826
Co particles, ferromagnetic colloids in toluene, small-angle X-ray scatt., interparticle correlations 79−11831
$CoFe_2O_4$ mag. fluid particles, comp., struct., and mag. props. 80−60374
CrO_2 acicular particle suspensions, mag. props., optical meas. 80−44874
Fe colloidal dispersion, mag. props., struct. and oxidation 80−34699
Fe particles, dispersed in Hg, mag. props., aggregate form. 80−60375
Fe particles in Hg, ferromag. liquid, mag. props., ageing effects 77−12154
Fe particles in Hg, ferromagnetic liquid, resistivity 79−1591
Fe_2O_3, flocculated suspension in ethylene glycol, intrinsic viscosity rel. to shear rate 80−1502
γ-Fe_2O_3:Cr, pure and doped, acicular particle suspensions, mag. props., optical meas. 80−44874
Fe_2O_4, suspension in oil, motion in rotating mag. field *(German)* 77−75983
Fe_3O_4 aqueous mag. fluids, dilution-stable, prep. by extended peptization techniques 80−60373
Fe_3O_4 ferrofluid suspension, mag. props., stability 79−87293
Fe_3O_4 ferrofluids, spin glass behaviour 80−71120
Fe_3O_4 in kerosene, thermal and electrical cond. in mag. field *(Russian)* 78−6188
Fe_3O_4 in suspension, ferromagnetic colloid, optical meas. 78−10906
Fe_3O_4 mag. fluid particles, comp., struct., and mag. props. 80−60374
Fe_3O_4 particle suspensions in non-conducting and metallic liqs., review 80−60372
Fe_3O_4, suspensions, ferrofluid motion, rot. mag. field effects 77−950
Fe_3O_4, ultrafine particles in ferrofluid, superparamag. and ferromag. reson. 78−15026
$Fe(OH)_3$-$Fe(OH)_2$ suspension system, potential-pH diagram 80−55728
Fe_2O_3martensitic steel, mag. and dielec. emulsion, prep. by abrasion of steel surface 78−27826
MnAs in suspension, ferromagnetic colloid, optical meas. 78−10906
$MnCl_2$, aq. soln., thermomagnetic convection, in transverse flow round cylinder *(Russian)* 77−47100
$NiFe_2O_4$ mag. fluid particles, comp., struct., and mag. props. 80−60374
Si-Fe, domain and grain obs. using ferromag. colloid technique 80−11219

magnetic flux
see also flux creep; flux flow; flux-line lattice; flux pinning; fluxmeters; skin effect
absolute standard *(Polish)* 77−67482
Alnico 5 and 8, spinodally decomposed magnetic alloy, magnetic flux temp. coeff. *(Japanese)* 78−35006
Alnico alloys, effect of Ce addition on mag. props. 78−2699
Alumel, thermocouple alloy, heat treatment effects on thermoEMF and mag. flux 77−63235
ballistic galvanometer, error due to non-transient impulses, integral expression 80−86349
bar magnet, rel. between magnetometric and ballistic moments *(German)* 79−28511
Chromel, thermocouple alloy, heat treatment effects on thermo EMF and mag. flux 77−63235
compression by explosives, intense transient mag. field prod. and meas. *(French)* 77−149
conservation, test using radially resolving diamag. loop 78−12734
cores with square hysteresis loop, measurement of saturated flux density using compensation technique *(Russian)* 79−54158
cryogenics, magnetic flux-free environment creation 80−101797
crystals of magnetic flux, review 79−99664
DC electromagnetic pump using supercond. magnet, performance characts. 77−82994
diagonal-type nonequilibrium plasma MHD generator, resistive electrode and mag. flux distrib. effects 79−41884
explosive mag. generator, magnetic accumulation in plane liner, flux loss and equiv. cct. 79−14571
fast magnetic field line reconnection in elec. cond. incompressible fluid 77−55097
ferromagnet, flux density curve anal., transverse magnetisation by variable mag. field *(Russian)* 79−69696
ferromagnet, vortex lines, Heisenberg model calc. 80−50026
ferromagnetic cylinders, sinusoidally varying end fields, eddy current phenomena numerical calcs. *(German)* 79−94131
ferromagnetic substances, flux quantisation 78−80136
field measurement in toroidal plasma systems 80−49004
gyromagnetic ratio of proton in strong mag. field, meas. 79−40527
high-coercivity, magnetisation characteristic linearity determ. using flux controlling technique *(Russian)* 80−100597
Josephson effect, appl. of elliptic sine equations in two space dimens. 77−55640
Josephson junction with mag. impurities, possibility of spontaneous mag. flux 78−47915
magnetocardiogram enhancement by applied mag. field 80−104701
megagauss field production by electromag. compression of flux 78−93739
NK, thermocouple alloy, heat treatment effects on thermoEMF and mag. flux 77−63235
permanent magnets flux stability enhancement, by thermomechanical treatment, gyroscope-based guidance systems performance improvement 80−50144
planar explosion mag. generator with resistive load, work performance optimisation 79−6156
plasma loop, 'mag. projectile' as mag. flux carrier for longitudinal current excitation 79−19079
plasma-β measurements in high-β fusion experiments from magnetic flux and luminosity profiles 80−49007
pulsed intense magnetic field prod. by mag. flux compression device *(French)* 77−61095
quantisation, topology theory appl. *(Russian)* 80−8770
RF-SQUID magnetometer, biased by harmonic magnetic flux meas. stability 79−93175
SA, thermocouple alloy, heat treatment effects on thermoEMF and mag. flux 77−63235
skin effect transients on hollow sphere in plane field of system of conductors *(German)* 80−37927
solenoid, supercond., mag. flux conc. using Tb cryst. 78−49869

magnetic flux continued
solenoid magnetic flux density calc. formula *(Norwegian)* 79−31762
SQUID (DC) as mag. flux detector 77−26358
SQUIDs, multiple mag. flux entry, cosϕ conductance exam. 79−4623
steady field penetration into ferromagnetic halfspace *(German)* 79−45878
steel, electrical, mag. hysteresis representation in numerical modelling of mag. fields 80−88813
steel plate, fundamental and harmonic flux, sinusoidal applied mag. field 78−2708
steel sheets, apparatus for mag. props. meas. in freq. range 50 to 10000 Hz 79−30497
superconducting intermediate state, mag. props. and N-S surface energy 78−2633
superconducting loop, bimetallic, acoustically generated mag. flux 77−16010
superconducting round wire, flux distribution and hysteresis loss 80−34570
superconductivity, definition of terms for fundamental states, flux phenomena, meas. practices 78−34916
thermomagnetic motor, dynamic characts. and stable operation *(Japanese)* 80−16840
thin laminations, minor loop hysteresis loss calc. 78−90342
Tokamak machine with iron cct., flux mapping and current distrib. 79−41866
two-domain analysis of field producing bodies using fictitious poles 78−33649
type I superconductor, local mag. field, penetration through large sheets 78−23211
weak magnetic samples, conduction of flux 79−28560
Al superconducting film, order-parameter variations meas. 80−103797
Fe-Cr-Co, spinodally decomposed magnetic alloy, magnetic flux temp. coeff. *(Japanese)* 78−35006
Fe-Si, loss meas. at high flux densities 80−88799
Fe-Si, stator core, grain-oriented and non-oriented, magnetic flux and loss distrib. 80−88798
Fe-Si, strips and rods, spatial extent of flux due to irreversible changes of mag. polarisation 79−33506
Fe-Si sheets surface flux meas., nondestructive testing appl. *(Slovak)* 79−5090
^{3}He, superfluid, meas. using RF-biased SQUID 77−31827
In, superconducting, thermoelec. transport effect 78−39257
$Li_{0.45}Ni_{0.1}$, $Fe_{2.45}O_4$, sintering, mag. props., rare earth oxide additive effects *(Japanese)* 77−66602
Nb superconducting cylinder, hollow, flux-flow voltages during guided flux collapse 77−16012
Nb-NbO_x-Sn long Josephson junctions, flux-flow voltage, dynamic vortex motion 79−4620
Nb-Ti (50%), supercond., cryostat design for magnetisation study *(Spanish)* 80−75673
NiZn ferrite, magnetic props., porosity and grain size effects 77−36095
Pb film, supercond., flux dynamics during current-induced breakdown, magneto-optical flux detection 77−24646
Pb film, supercond., flux nucleation in current-induced resistive state 78−23210
Sn, single crystal cylinder, threshold current of paramagnetic effect *(Russian)* 79−87194
Sn, superconducting loops, thermally generated mag. flux 79−56452
Sn, type I supercond., temp. depend. of energy dissipation 78−76198
Sn-SnO_x-Sn long Josephson junctions, flux-flow voltage, dynamic vortex motion 79−4620
Tb single crystal flux concentrator for supercond. solenoids 78−57991

magnetic flux jumping *see Meissner effect*

magnetic glasses *see spin glasses*

magnetic hardness *see ferromagnetic properties of substances*

magnetic heads
coercivity meter, ferromagnetic cores, probe core, component 78−57996
ferrite, coprecipitated, hot pressed, for appl. to mag. heads 77−85968
magnetoresistive head Barkhausen noise voltage meas. 79−82821
Permalloy, magnetic head wear resistance and surface charact. against magnetic tape *(Japanese)* 80−35335
Permalloy, solid boriding for mag. head appl., wear resist. and microhardness 80−21172
Permalloy sputtered film, bevelling by chemical etching, for this film mag. header 78−92375
Permalloy thin-film head pole struct., domain configurations, SEM obs. 80−65975
recording head wear by magnetic tape, wear meas. using Knoop diamond indentations 77−70192
scattered fields anal. using moire and shadowgraph electron microscope patterns 79−89045
Sendust alloy, magnetic head wear resistance and surface charact. against mag. tape *(Japanese)* 80−35335
thin layer read heads, appl. of magnetoresistance effect *(German)* 78−68013
vacuum-deposited layers formation, use of borosilicate glass intermediate layer 80−80979
CoNiB, corrosion-resistant amorphous mag. thin films 80−54923
Fe-Co-Si-B alloy appl., amorphous, rapidly quenched *(Japanese)* 80−54922
Fe-Si-Al, Sendust, 12 μ thick film prep. by sputtering, for recording head core 77−55888
Fe-Si-Al ribbon-form Sendust alloy made by rapid roll quenching, mag. props., recording head appls. 80−81001
FeAl-Pr (16 wt.%), resist. depend. on rolling process, thermal treatment, tape recording appl. *(Polish)* 80−39555
FeCoB, corrosion-resistant amorphous mag. thin films 80−54923
$(Fe_{1-x}Ni_x)_{80}B_{20}$ amorphous soft magnetic films 79−82836
FeTiB, corrosion-resistant amorphous mag. thin films 80−54923
MnZn ferrite, mag. anisotropy, effect on recording head characts. 80−39765
MnZn ferrite fabricated by hot isostatic pressing, recording head appl. 80−35139
Ni-Fe film, unidirectional anisotropy by exchange coupling, appl. to biasing of magnetoresist. read head 78−91907
Ni-Fe-Nb-Al(-Mo), wear resisting mag. head material, mag. props. and struct. 80−35350
Ni-Fe-Nb-Mo-Al, head material for mag. recording, DC and AC mag. props. 80−88812

magnetic heads continued
Ni-Zn ferrite:Co^{2+}, synthesis of optimal quality recording head mat. 77−52272
Ni-Zn ferrites, mag. recording head props. rel. to manuf. from schoenite-type solid solns. 77−85496
NiZn ferrites, mag. head props., technical possibilities and limitations 80−88803
$(Ni_{0.47}Zn_{0.53})_{1-x}Fe_{2+x}O_4$, recording head medium 77−86187

magnetic hysteresis
alnico, thermal magnetic hysteresis *(Russian)* 77−16119
Alnico type YuNDK25DA alloy permanent magnets, thermal mag. hysteresis 80−75818
amorphous ferromagnet with random uniaxial anisotropy, hysteresis, magnetisation 77−80963
amorphous ferromagnets, mag. fundamentals, props. and appl. *(German)* 79−28557
amorphous magnet with uniaxial anisotropy, dense random packing model 77−16108
amorphous magnetic materials, props. *(Japanese)* 79−28561
amorphous systems, mag. props. effect of random anisotropy 79−4686
basalts, mag. grains nature and implications for palaeomag. 79−84243
Bi, current states, symmetry and self-oscills., macroscopic mag. moment by RF irradiation *(Russian)* 79−19749
bubble-domain materials, amorphous, Hall-effect hysteresigraph for coercivity measurement 79−73786
Clarke solder-blob junctions, hysteresis studies 79−28478
Cu-Co, dil., rotational hysteresis of Co fine particles 78−23301
curves, computer-aided approximation *(German)* 77−8338
DC permeameter for ring specimens 80−98954
demagnetised cubic magnetic crystals, hysteresis in spin-orientation phase transitions 79−73761
domain boundaries, pinning on defects with finite radius of interaction, random pot. form effect on mag. hysteresis *(Russian)* 80−84611
domain boundary with strongly localised pinning centres, influence on hysteresis *(Russian)* 80−65961
domain drag effect in presence of variable mag. field or variable transport current 79−78433
domain wall flexibility, implications on interaction with dislocations and hysteresis existence 77−4525
dynamic magnetization curves, apparatus for display on CRO 79−17451
electromagnet, sectorial, mag. field inhomogeneities along central ray 79−31768
electromechanical actuator, vibr. linearisation of mag. hysteresis charact. *(Russian)* 79−12789
$Fe_{40}Ni_{40}P_{14}B_6$, amorphous, tape wound core, fluctuations of driving field 78−10726
ferrimagnetic polycrystals, universal hysteresis loop 77−69620
ferrite, connection between limiting hysteresis loops and number of easy magnetisation axes *(Russian)* 78−72364
ferrite, hysteresis loop rectangularity, inverse domain vol. depend. *(Russian)* 78−76270
ferrite, hysteresis loop rectangularity rel. to anisotropy in polycryst. mat. 78−27056
ferrite, microstruct. depend. of props. and applics., review 78−88548
ferrite F-600, suspension in caster oil, residual magnetisation *(Russian)* 79−1689
ferrites, hysteresis loops, formation processes 80−39813
ferrites, soft and microwave, grain-size effects on mag. props., review 78−64222
ferrites, square hysteresis loop magnetisation mechanism and conditions 80−29577
ferromagnet, polycrystal, magnetisation law, Bloch wall motion *(French)* 79−95606
ferromagnet, soft, hysteresis rel. to irreversible phase transition 80−34693
ferromagnet, symmetric hysteresis loops, polynomial expression *(Spanish)* 77−73044
ferromagnetic, swallow tail catastrophe anal. 78−56349
ferromagnetic alloy, transition to spin glass ordering 80−34628
ferromagnetic alloys, amorphous, sputter-deposited, soft mag. props., magnetostriction 80−34696
ferromagnetic amorphous alloys, temp. depend. of mag. hystersis props. 79−61186
ferromagnetic crystal with defects, branches of hysteresis loop *(Russian)* 79−51800
ferromagnetic film, with unidirectional anisotropy, domain struct. mag. field effect *(Russian)* 78−19289
ferromagnetic fine particles, stability of magnetisation curling mode and magnetisation helicoid struct. 80−11227
ferromagnetic fluid, in appl. mag. field equilib. surface patterns 77−84332
ferromagnetic material magnetisation curve determ. by plane surface attachment *(Russian)* 79−63282
ferromagnetic materials, orthogonally magnetised, study of mechanism using digital computer *(Rumanian)* 77−55687
ferromagnetic materials in strong fields, determination using equipment with Hall transducer 80−4745
ferromagnetic medium with variable permeability and hysteresis loss, plane EM wave *(Polish)* 77−79722
ferromagnetic object inspection, method of higher harmonics, difference schemes 80−89444
ferromagnetic plate, magnetic hysteresis theory, singularities of magnetic reversals on industrial freq. *(Russian)* 78−39373
ferromagnetic solids, magnetomechanical effects, magnetostriction, hysteresis; stress, yielding, fatigue damage, crack growth *(Polish)* 80−71150
ferromagnetic thin film magnetometer, development and performance 80−31808
ferromagnetic wire, circular magnetisation meas. 78−70167
ferromagnetics, magnetisation in unidirectional field *(Russian)* 77−24660
ferromagnetics in unidirectional field, magnetisation, math. model *(Russian)* 78−88140
ferromagnets, cyclically remagnetised, discrete spectra of induction calcs., demagnetising factor 80−103859
ferromagnets, polycryst., static models 77−85490
ferromagnets and antiferromagnets, EM and acoustic energy attenuation in many-domain magnets 80−7140
film, Barkhausen effect, general behaviour and stationarity along hysteresis loop 78−56357

magnetic hysteresis continued
film, noise due to amplitude and phase fluctuations *(Russian)* 77−77075
film, two-layer, exchange-coupled, switching, differential permeability *(Russian)* 78−27061
finite-element magnetic field calc. allowing for saturation and hysteresis 79−41278
full wafer magnetic bubble films, devices for characterisation 79−78461
garnet epitaxial film, Faraday effect and magnetometrical meas. 78−52317
hardness, elec. cond., photo emission, and mag. props. *(Norwegian)* 79−32909
hydrostatic pressure effect on ferrite props. of pressure sensors *(Polish)* 80−31707
hysteresigraph with data printout 79−58760
hysteresisgraph with discontinuous sweep mode 80−86351
igneous rock bodies, in situ mag. meas. 79−84521
induction meter testing, electromagnet reference measure from hysteresis effects 80−77817
Invar, ferromagnetism and antiferromagnetism coexistance at low temp. 77−66320
Invar, hysteresis loop displacement 78−52312
isomorphic transformation, characterisation of hysteresis processes *(Russian)* 80−80562
local microscopic magnetisation intensity in presence of Shirobokov's domain struct. *(Russian)* 77−43851
loop tracer for mag. phase detection 80−22393
losses from field eqns., determ. *(German)* 78−60306
magnetic tape, demagnetisation curve, hysteresis model represent. *(German)* 77−36096
magnetically uniaxial ferromagnetic particles, high-anisotropy many domain, magnetisation, hysteresis *(Russian)* 79−91256
magnetostriction hysteresis loop meas. by induction method *(Russian)* 77−56171
metallic, glasses, soft-magnetic properties *(German)* 80−71108
metallic glasses, mag. props., struct., and prep., book contrib. 79−65665
metallic glasses and amorphous magnetism, review 79−82818
model magnet, for reson. spectrometer, reproducibility of fields, field heights and magnetisation props. of materials *(German)* 78−24832
modelling and simulation of dipole element, using cubic spline functions *(German)* 79−4706
multiple-particle problem, four-parameter formula *(German)* 78−80178
nonlinear dynamics of first order phase transitions 79−11322
oriented Si steel, magnetisation hysteresis loops prediction 78−64221
orthogonal lattice, interacting hysteresis dipoles, lattice sums and switching, chain breakdown 77−51860
oscillography of hysteresis loops using ferroprobe transducer 79−87785
particles, interacting, switching behaviour, dipole and Stoner-Wohlfarth models 80−44870
Permalloy, conductor crossing effect on bubble propagation margins 80−29588
Permalloy, reference materials charact. obs., temperature effect 80−80563
Permalloy film, hysteresis loop meas. using magnetooptical system 79−69707
Permalloy film, M-H curve meas., magneto-optical instrument *(Japanese)* 77−37953
Permalloy I bars, hysteretic props., Bitter soln. obs. and Kerr effect meas. 79−78439
Permalloy RF sputtered films, struct.-sensitive mag. props. 80−34705
permanent magnets review 79−42801
polycrystal subjected to successive asymmetrical hysteresis cycles, mag. props. evolution, reptation phenomenon *(French)* 78−10730
polycrystalline ferromagnets, demagnetisation and reptation (creep) anisotropy *(French)* 78−43616
Preisach's theory used for representation of mag. charact. 78−80179
probabilistic mathematical models *(Polish)* 77−80960
pulse magnetic reversal in magnets with rectangular loops, nuclei formation *(Russian)* 77−32214
rare earth alloys, amorphous, mag. props. rel. to struct., review 79−15298
rare earth amorphous alloys, random mag. anisotropy, antiferromag., Monte Carlo calcs. 79−33471
rare earth garnet thin films, macroscopic magn. props., magneto-optical expts. 80−46764
rare earth-$(Co_{1-x}Ni_x)_5$, single cryst., mag. props., mag. reversal 77−85489
rare earth-Ag alloy, amorphous, model calcs., of mag. props. 80−84616
rare earth-transition metal alloys, amorphous, electronic and mag. props. 80−93093
rare earth-transition metal amorphous film, Kerr and Hall effect meas. 77−24722
rare-earth alloys, amorphous study of hysteresis effects using Monte Carlo technique 79−1686
Rayleigh hysteresis, reexam. 78−48002
Rayleigh hysteresis loops, visualisation, geometrical method 77−77072
Rayleigh law, failure in low mag. fields, expts. on Gd and NiFe 77−40086
relays inductance measurement to TGL 24961 specification methods for Fe-cored coils *(German)* 80−4736
ring ferromagnetic samples, remagnetisation dynamics *(Russian)* 78−19275
rocks, ferromagnetic component indication by magnetic hysteresis 77−64271
rocks, magnetic-diffusion aftereffect, Preisach-Neel diagram appl. 78−61403
rocks, stress wave attenuation, linear magnetic hysteresis model *(Chinese)* 79−39702
rotational hysteresis in weak magnetic fields 80−75804
rotatory hysteresis in alternating magnetic fields *(Russian)* 78−68294
saturation, reactive power, and harmonics anal. *(Slovene)* 77−85488
simulation, mathematical model 77−85500
single domain particles, partial hysteresis cycles, asymmetry *(Russian)* 78−76268
soft mag. material representation 80−88787
soft magnetic materials, hysteresis model 80−2606
soft magnetic materials, meas. methods, review 80−86345
spin glass, metastability, Onsager theory 79−82796
spin glass systems, experimental props. and theories 79−65688
spin glasses, review 77−69578
magnetic hysteresis continued
spinels, domain wall formation inhibition, effect on bulk mag. props. 80−11220
square loop characteristics, modelling using Preisach's theory 78−2701
SQUID, with V-VO_x-Pb Josephson tunnel junctions, quantum interference, critical currents 78−91821
steel, austenitic stainless, neutron irrad., mag. props. 80−29067
steel, C, rotational hysteresis 78−91889
steel, cold-rolled, isotropic, specific magnetic loss meas. at high frequency 80−101808
steel, elect., mag. props. determ. with Epstein hysteresis tester 80−60364
steel, electrical, mag. hysteresis representation in numerical modelling of mag. fields 80−88813
steel, high-speed, low temp. mag. cycling effects on ferromag. struct. 80−100928
steel, low alloy and C, hardened and tempered parts, nondestructive magnetic inspection 78−95889
steel, low alloy and C, hardened and tempered parts, nondestructive magnetic inspection 79−1929
steel, mech. strength determ. from dynamic hysteresis loop EMF spectral content of coil, expt. 77−73414
steel, mild, rotational hysteresis 78−91889
steel, structural, nondestructive method of struct. damage investig. using cyclic loading effects and mag. charact. 78−3275
steel, transformer, cold-rolled effect of uniaxial elastic stress on dynamic magnetostriction *(Russian)* 77−69651
steel 42NKhTYuA wire, hysteresis loop and differential permeab. after US and conventional drawing 79−15818
steel plate, fundamental and harmonic flux, sinusoidal applied mag. field 78−2708
steel strips, electrotechnical, mag. props. meas. using AC compensated permeameter 80−86352
Stoner-Wohlforth particle, two-component, hysteretic props. 80−11228
stroboscopic instrument for plotting hysteresis loops, 400 Hz-50 kHz 77−71350
superconducting cable, magnetisation anisotropy meas. in hysteresis loss using Hall sensors 80−17966
superconducting composite, multifilamentary, AC losses in transverse AC mag. field 80−34568
superconducting magnets, pulsed, hysteretic and mechanical loss calcs. 79−80649
superconducting plate, hysteresis losses 78−84345
superconducting round wire, flux distribution and hysteresis loss 80−34570
superconductor, type II, hysteresis losses for round cross section with collective interaction 78−43513
thin laminations, minor loop hysteresis loss calc. 78−90342
ticonal, thermal magnetic hysteresis *(Russian)* 77−16119
titanomagnetite, monodomain behaviour in multiphase oxidised material 77−60366
titanomagnetites, hysteresis props., grain size and comp. depend. 77−37187
transient and steady-state magnetisation charact. with hysteresis 77−66385
TTF-$CuS_4C_4(CF_3)_4$, spin-Peierls system, high-field phase 80−39816
twisted uniaxial polycrystals, magnetisation process, model 79−91254
two-dimensional nonlinear magnetostatic fields, isoparametric Hermite finite element program 79−41275
type II superconductor, direct obs. of flux creep in minor hysteresis loops 78−6487
type II superconductors, magnetic hysteresis and flux profiles, review 79−1651
US, large magnetic anisotropy exam. 77−20585
vector model, based on interacting dipoles 78−76271
weak ferromagnetism, hysteretic phenomena 78−27059
$Al_2Mn_3Si_3O_{12}$, amorphous insulating spin glass, susceptibility and magnetisation meas. 80−88765
$Au_{85}Fe_{15}$, and $Au_{82}Fe_{18}$, mag. props. 80−84592
Ba hexaferrite, irradiated by fast neutrons, mag. props. 80−97116
$BaFe_{12}O_{19}$, effect of impurity concentrations, and sintering conditions on grain size *(German)* 79−23630
$BaFe_{12}O_{19}$ microparticles, magnetisation reversal, hysteresis loop obs. 80−75813
$BaFe_{12}O_{19}$ powder, hysteresis of microwave absorpt. and magnetisation reversal 80−75814
$Ba_xLa_{1-x}CoO_3$, x=0 to 0.5, structural, elec. and mag. props., Zener double exchange and Goodenough's model 79−65663
BaO-Mn_2O_3-B_2O_3, amorphous mag. oxide, field-cooling effect *(Japanese)* 80−84615
Bi-MnBi directionally solidified eutectic alloys, struct. and mag. props. 79−51815
Bi-MnBi eutectic composites, microstructure and mag. props., annealing effect 79−82827
$CdCr_2S_4$ ferromag. semicond. film, props. 78−76175
$CdCr_2Se_4$, ferromag. semicond., photoinduced mag. anisotropy 80−50086
$CdCr_2Se_4$ films, mag. hysteresis, domain struct., mag. viscosity 80−25169
$CdCr_2Se_4$:Cu(In), ferromag. semicond., mag. and elec. props. 77−20588
$CdCr_2Se_4$:Ir(Cu), mag. props. near Curie temp. *(Russian)* 77−63234
Ce-Co-Cu-Fe-Ti, sintered magnet, prep. and mag. props. 77−73043
$Ce_x(La_{0.76}Y_{0.24})_{1-x}Bi$, mag. phase diagrams 79−56535
CeSb, press. effect. on mag. props. 78−23315
Co, FCC, mag. props. of single-domain powders after plastic deform. *(Russian)* 78−6554
Co film, ion beam sputtering prep., struct. and mag. props. 80−35085
Co, sputtered film, high coercivity and high hysteresis loop squareness 79−91259
Co-CoO films, evaporated, exchange anisotropy 80−88841
Co-Cr recording films, perpendicular mag. anisotropy, hysteresis loop, microstruct., TEM obs. 78−95491
Co-Fe alloys, effects of annealing 78−6558
Co-Fe amorphous alloys, high permeability props. *(Japanese)* 77−51927
Co-Fe amorphous alloys, worked, perminvar type mag. hysteresis loop, longit. Kerr effect obs. 80−65958
Co-Fe-Nb, heavily cold worked, magnetic hardening 79−20073
Co-Fe-Nb alloy, mag. precipitation-hardening and Bloch wall pinning 78−80173
Co-Fe-Nb alloys, effect of cold working on mag. props., and precipitation morphology 78−39803
Co-Fe-Ti alloy, precipitation hardened, rel. between struct. and mag. props. 78−95470

magnetic hysteresis continued
Co-Ni fine particles, anhysteretic growth of exchange fixed remanent states 77−16116
Co-Ni-P, film, props. independent of mag. hysteretic and anhysteretic remanences *(French)* 80−2604
Co-P, electrodeposited amorphous alloy, mag. permeability 78−52310
Co-P, electrodeposited amorphous alloys with high permeability, thermal treatment with and without field 80−89372
Co-P electroless film on Al base disc substrate, microstruct. rel. to mag. props. 78−68304
Co-P films, electrodeposited, magnetic recording media *(Japanese)* 80−29587
Co-Pt, struct. and mag. props. rel. to degree of order 78−72368
Co-Re, sputtered film, high coercivity and high hysteresis loop squareness 79−91259
Co-Sm-Gd(Ho) magnets, prep. and characterisation 77−8351
Co-W alloy electrodeposition, influence of $MgSO_4$ and gum arabic additives *(Russian)* 80−80991
Co-W alloy electrolytic coatings, heat treatment effects on coercivity, hysteresis and structure *(Russian)* 80−60381
Co(-Re) sputtered films, mag. props. and microstructures 79−82837
Co_4CuCe, cryst. struct., mag. charact., ageing and decomposition *(Russian)* 79−4272
$(Co_{1-x}Fe_xNi_y)_{80}(Si_{1-z}B_z)_{20}$, amorphous films, spin wave spectra 80−34777
$CoFe_2O_4$ mag. fluid particles, comp., struct., and mag. props. 80−60374
$Co_{0.08}(Ni,Cu)_{0.92}Fe_2O_4$ sphere, rotational hysteresis, mag. field strength and orientation depend. *(Russian)* 77−16110
CoP, amorphous film, Kerr effect, hysteresis loop 78−60322
$CoS_{2-x}Se$, magnetism and metamagnetic transition, neutron diffr. and NMR meas. 80−15717
Cr, single cryst., mag. hysteresis, neutron diffr. obs. 79−15327
Cu-Mn alloy spin glass, macroscopic mag. anisotropy, transverse susceptibility and zero field NMR enhancement 80−80525
Cu-Mn spin glass, hysteresis loops, temp. and field depend. 80−15742
Cu-Mn spin glass, magnetisation reversal and macroscopic mag. domain obs. 79−61168
Cu-Mn-Al, constricted hysteresis loop rel. to microstruct. 78−19273
Cu-Mn-Al alloys, displaced hysteresis loop and microstructure obs. 80−84613
$Cu_{0.67}Cr_{1.78}Se_{2.67}Br_{1.34}$, polycrystalline mag. semicond., mag. and elec. props. 79−7846
CuMn, hysteresis, spin orbit scattering effect on anisotropy in spin glass state 80−71095
CuMn, spin glass, mag. hysteresis meas. 80−34691
CuMn, spin glass, remanence, new approach from zero field NMR 80−34785
$Cu_{0.86}Mn_{0.14}$, hysteresis loop development 80−65922
$D\text{-}_{12}Fe_{32}O_2$, anomalous magnetisation, compensated to uncompensated mag. arrangement transition 78−52254
Dy, magnetic domain structure, hysteresis, thermal modulation study 80−71082
Dy-Cu, amorphous, mag. phase diagram, magnetisation and sp. ht. meas. 80−80532
Dy-Y, magnetisation and hysteresis, temp. depend. 79−69673
DyAG, light scatt. from metamag. domains, crit. exponent determ. 77−66482
$DyAl_2$, first order transition and tricrit. points, three-state Potts model 78−43589
$Dy_xCe_{1-x}Ru_2$, supercond., mag. props. 79−11267
DyCu film, amorphous, asperomagnetic domains, Barkhausen jumps in hysteresis loop 80−75822
$DyFe_2$ powders, mag. and hysteresis props. *(Russian)* 79−42800
$DyFeO_3$, orthoferrite, magneto-optical obs. 77−77071
$DyPO_4$, mag. transitions under hydrostatic press., neutron diffr. study 80−71030
$DyVO_4$, basal plane magnetisation anisotropy under Jahn-Teller distortion 78−68222
$Er_{65}Co_{35}$, amorphous, amg. ordering, susceptibility, magnetisation and hysteresis meas. 78−68190
$ErCo_{5-x}Ni_x$ ferrimagnetic series, magnetisation, coercive field meas. 78−91896
$ErFe_2$ powders, mag. and hysteresis props. *(Russian)* 79−42800
$(Er_{65}Fe_{35})_{100-x}B_x$ glasses, mag. props. 79−73693
$Eu_{1-x}Gd_xS$ films, mag. and elec. props. 80−15766
(Fe,Co,Ni)-Si(B), amorphous mag. alloy, magnetostriction rel. to soft mag. props. 80−84633
Fe, carbonyl powder, mangetic material 77−12160
Fe colloidal dispersion, mag. props., struct. and oxidation 80−34699
Fe, ferromagnetics, conductive, loss anal. by saturation/hysteresis simulation 77−12153
Fe, film, ion beam sputtering prep., struct. and mag. props. 80−35085
Fe, high purity, mag. viscosity mechanism 78−19282
Fe, rotational hysteresis 78−91889
Fe-Al alloys, rapidly quenched, mag. props. 80−29579
Fe-Co based amorphous alloys, mag. props. *(Japanese)* 79−95971
Fe-Co-B powders, synthesis and mag. props., appl. to mag. recording 80−20432
Fe-Co-Ni Perminvar, mag. props. singularities in region of mag. anisotropy *(Russian)* 80−84614
Fe-Co-Si-B, amorphous soft ferromagnet with high mag. induction 80−84619
Fe-Co-Si-B sputtered amorphous thin film, coercivity, galvanomagnetic props., resistivity 80−29578
Fe-Co-Si(B), amorphous ferromagnet, mag. after effect on soft mag. props. 80−84626
Fe-Cr (70-92 at.%), coexistence of ferro- and antiferromagnetism *(Russian)* 78−47955
Fe-Cr alloys, mixed ferro-/antiferromag. interactions *(Russian)* 77−32173
Fe-Cr-Co alloys, (5-9 wt.% Co), obtained by slow cooling under-mag. field, permanent magnet props. 80−75797
Fe-Cr-Co ductile magnet, with high $(BH)_{max}$, processing, mag. props., and microstruct. 77−8957
Fe-Cr-Co-Al (27.5, 17.5, 0.5) alloy, mag. props. and microstruct. obs. 78−72367
Fe-Gd amorphous films with comp. gradient, volume and surface hysteresis *(Russian)* 78−88148
Fe-Mn-P-B-Al metallic glass, exchange anisotropy 77−16068
Fe-Mo(W), semihard magnetic alloys, magnetic, elec. mech. props. *(Japanese)* 79−70078
magnetic hysteresis continued
Fe-Nb(Ta)-Co, Recalloys, semihard mag. alloys, mag. and elec. props., hardness, thermal expansion *(Japanese)* 79−5066
Fe-Ni (23-35 at.%), cooled below 70K in mag. field, uniaxial anisotropy *(Russian)* 78−19244
Fe-Ni based metallic glasses, hydrostatic press. effect on mag. props. 78−19300
Fe-Ni metallic glass wide strips, low-field mag. props. 79−51822
Fe-Ni/Fe, bimetal film, exchange const. determ. from hysteresis loops *(Russian)* 77−48015
Fe-Ni/pure Fe exchange coupled films, mag. reversals, hard layer thickness effects *(Russian)* 78−56359
Fe-Si, (110) [001] oriented, mag. props., compressive stress effects 80−60392
Fe-Si, grain oriented sheet, AC hysteresis, surface struct. and elastic stress effects 80−88791
Fe-Si, hysteresis loops described by 180° Bloch wall *(French)* 79−15322
Fe-Si, irreversible Barkhausen jumps *(French)* 77−1568
Fe-Si, magnetostatic couplings between 180° Bloch walls 77−69613
Fe-Si, thermally activated motion of 180° Bloch wall 78−95457
Fe-Si (3 wt.%), eddy current and hysteresis losses, role of domain struct. *(Russian)* 77−80961
Fe-Si (3 wt.%), grain-oriented, stacking effect on power loss, mag. props. 80−88795
Fe-Si (3 wt.%), hysteretic losses, domain struct. and cryst. defects 79−19747
Fe-Si (3 wt.%), prediction of magnetisation hysteresis loops for distorted waveforms 79−47303
Fe-Si (3 wt.%), scratching effects on mag. losses in single crysts. with orientation near (110)[001] 79−51802
Fe-Si (3 wt.%), total losses under tensile stress, rel. to orientation near (110)[001] 78−76272
Fe-Si (3 wt.%) alloy, domain structure influence on eddy current losses *(Slovak)* 79−4693
Fe-Si (6.5 wt%) filament, formation by modified Taylor technique, and mag. props. 80−75795
Fe-Si-Al Sendust alloy ribbon form, rapid quench prepared, elec. cond., coercive field, permeability 79−83151
Fe-Si-B, magnetic metallic glasses, mag. props. 80−84620
Fe-Tb, magnetoelastic hysteresis, elastic stress and mag. field depend. *(Russian)* 80−65982
Fe-W-Cr-Mo system, mag. and mech. props. rel. to production methods *(Japanese)* 80−71107
$Fe_{80}B_{20}$, hardness, elec. cond., photo emission, and mag. props. *(Norwegian)* 79−32909
$Fe_{80}B_{20}$, sputter deposited amorphous, low field mag. props. 78−68335
$FeCl_2$, metamagnetic hysteresis, magnetooptical rot. meas. 77−40057
$FeCl_2.2H_2O$, and $FeCl_2.2D_2O$, Raman scatt. at metamagnetic phase transitions, mag. hysteresis 78−14958
$(Fe_{0.06}Co_{0.94})$-B, amorphous, ferromag., mag. instability rel. to struct. 79−99729
$Fe_5Co_{75}B_{20}$, amorphous, magnetisation reversal and domain boundary configs. 80−88809
$Fe_{35}Co_{32}B_{20}Si_{10}Al_3$, stress-induced variation in magnetisation and dynamic magnetostrictive charact. 80−88855
$(Fe_{1-x}Co_x)_{80}P_{13}C_7$ amorphous alloy, soft mag. material, props. 77−4533
$(Fe_{0.05}Co_{0.95})_{78}Si_8B_{14}$ amorphous ribbon, anomalous mag. aftereffect 80−100602
$(Fe_{1-x}Co_x)_{75}Si_{15}B_{10}$ amorphous alloy, soft mag. material, props. 77−4533
$Fe_5Co_{70}Si_{15}B_{10}$, amorphous ribbon, zero magnetostriction, low residual mag. loss 77−12157
$Fe_5Co_{70}Si_{15}B_{10}$, amorphous, change of mag. props. by low temp. annealing 78−27058
$Fe_xCu_{1-x}Rh_2S_4$, mag. tetrahedral intrasublattice interaction, X-ray, magnetisation and Mossbauer expts. 78−52241
$FeGa_2O_4$, magnetic props. by Mossbauer effect, neutron diffr. and magnetisation meas. 77−43918
$Fe_{40}Ni_{38}\text{-}Mo_4B_{18}$ amorphous alloys, compatibility of DC and AC mag. props. 80−34695
$(FeNi)_{80}Bi_{17.5}Al_2Si_{0.5}$, stress-induced variation in magnetisation and dynamic magnetostrictive charact. 80−88855
$Fe_{40}Ni_{40}P_{14}B_6$, amorphous tape wound cores, mag. props. *(German)* 78−10727
$Fe_{40}Ni_{40}P_{14}B_6$, glassy metal fabric for mag. shield 77−8347
$Fe_{40}Ni_{40}P_{14}B_6$, hardness, elec. cond., photo emission, and mag. props. *(Norwegian)* 79−32909
$(Fe_xNi_{1-x})_{80}P_{10}B_{10}$, amorphous, magnetisation reversal and domain boundary configs. 80−88809
$\alpha\text{-}Fe_2O_3$, haematite, temp. mag. hysteresis near Morin temp. 79−56566
$\alpha\text{-}Fe_2O_3$, neutron Laue diffr. investig. of domain distrib. 77−24712
$\gamma\text{-}Fe_2O_3$, particle interactions, in inhomogeneous anisotropic magnetic materials, average field effect 77−32217
$\alpha\text{-}Fe_2O_3\text{-}Li_2O$, structural and thermal phase behaviour from mag., spectral and thermal studies 80−2673
$Fe_2O_3\text{-}Na_2O\text{-}BaO$ glass, mag. props. 4.2-295K, mictomagnetism *(French)* 80−39782
Fe_3O_4 (magnetite), multidomain particles magnetisation 79−66686
Fe_3O_4 mag. fluid particles, comp., struct., and mag. props. 80−60374
Fe_3O_4, magnetite particles, interaction fields effect on hysteretic props. 80−54921
Fe_3O_4, metallic phase, photocond. and mag. permeab., photoinduced changes 80−15566
Fe_xO_y powder coated with $NaPO_3$, anomalous coercivity increase 77−89980
$Fe_{80}P_{13}C_7$, amorphous, rapidly quenched, magnetic props., effect of annealing 77−16701
$Fe_{1-x}Pd_x$ film, UHV deposited, effects of applied stress on B-H loops 78−64239
$Fe_{80}Si_5B_{15}$, amorphous, soft mag. props. and potential uses 80−88807
$Fe_{2.6-x}Ti_{0.4}Al_xO_4$, $Fe_{2.4-x}Ti_{0.6}Al_xO_4$, titanomagnetite, monodomain, mag. props. 78−56346
Fe_2TiO_4, ulvospinel, mag. props. weak ferromag. in 4-200K temp. range 78−56351
$Fe_2TiO_4\text{-}Fe_3O_4$, titanomagnetite, prepared at different oxidation conditions, hysteresis props. 78−56352
$Fe_{2.4}Ti_{0.6}O_4$, titanomagnetite, single-crystal, mag. props. of multidomain TRM 78−56345
$Fe_{3-x}Ti_xO_4$, $0.5 \leq x \leq 1$, mag. props. of antiferromag. phase 80−70960

magnetic hysteresis continued
$Fe_{3-x}Ti_xO_4$, spin glass behaviour, susceptibility and hysteresis meas. 80−65917
Fo-Fe-Nb, cold-worked and aged, mag. props. and microstruct. 80−34690
$(Gd,Tm,Y)_3(Fe,Ga)_5O_{12}$ LPE garnet thin films, magnetocrystalline anisotropy 80−93147
Gd alloys, amorphous, mag. props. and ferromag. reson. 80−54952
Gd, departure from Rayleigh law in low mag. fields 77−40086
Gd-Co alloy, sputtered film, mag. props. determ. *(Chinese)* 78−2714
Gd-Co amorphous film, DC or RF sputtered, mag. props., He^+-backscatt. investig. 77−20650
Gd-Co amorphous films, struct. and mag. anisotropy 80−20438
Gd-Co film, amorphous, inverted and biased loops 77−89996
Gd-Co film, amorphous, stability of small bits to temp. and mag. field changes 78−68314
Gd-Co film, temp. depend. of mag. aftereffect *(Russian)* 79−8021
Gd-Co films, anomalous magneto-optical hysteresis loops obs. 77−12174
Gd-Co(-Au) film, ferrimag. amorphous, coated with Permalloy films, mag. props. 79−1695
Gd-Fe, co-evap. amorphous film, anomalous hysteresis loop, domains obs. 77−89995
GdB_6 single crystals, mag. behaviour and structure change at low temp. 80−71018
$Gd_{65}Co_{35}$, amorphous, amg. ordering, susceptibility, magnetisation and hysteresis meas. 78−68190
$(Gd_{65}Fe_{35})_{100-x}B_x$ glasses, mag. props. 79−73693
GdIG, thermal effect on re-entrant hysteresis loop and coercive force 78−2702
Ho:^{119}Sn, mag. hysteresis of hyperfine field, compensation in mag. field *(Russian)* 77−81039
Ho-Co amorphous film, anomalous Hall hysteresis loops near compensation point 78−19286
$HoAl_2$, magnetisation reorientation 79−87291
Li-Zn ferrite, mag. and microstruct. props., effect of V_2O_5 addition *(Japanese)* 77−28415
$LiFe_5O_8$, hysteresis and other mag. props. rel. to microstruct., TEM investig. 77−20636
$LiFe_5O_8$, microstruct. and magnetic props., electron microscope obs. 79−87290
$Li_{0.5}Fe_{2.5}O_4$, effects of low-melting additive on struct. and dielec. props. 77−85494
$(Li_{0.5}Fe_{2.5}O_4)_{0.8}(CuFe_2O_4)_{0.2}$, struct., magnetic props., rectangular hysteresis loop 77−20645
$Li_{0.5(1-x)}Mn_x\ Fe_{2.5-0.5}O_4$, rectangular hysteresis loop, microstruct. form. 77−12718
$Li_{0.5}Mn_{0.15}Fe_{2.35}O_4$ ferrite cores with rectangular hysteresis loops, pulse parameters, effect of Fe_2O_3 heat treatment 80−60370
$Li_{0.45}Ni_{0.1}$, $Fe_{2.45}O_4$, sintering, mag. props., rare earth oxide additive effects *(Japanese)* 77−66602
$(MgFe_2O_4)_{x-1}(Mn_3O_4)_x$, soft ferrite, squareness ratio and max. induction 79−99730
Mn-Bi, magnetically uniaxial, strongly anisotropic, discontinuous mag. reversal singularities *(Russian)* 77−48010
Mn-Bi eutectic alloy, mag. anisotropy 78−68220
Mn-Bi film, with perpendicular anisotropy, galvanomag. props., hysteresis loops 77−20464
Mn-Cu-Ni-Bi, magneto-optic film for storage appl. 77−12165
Mn-Zn ferrite single crystals, mech. polishing effect on mag. props. *(Japanese)* 80−16569
MnAs, formation of nuclei in ferromag. paramag. transition, thermal hysteresis 79−73720
$MnAs_{1-x}P_x$, low temp. resistivity minimum 77−8122
MnBi film, magnetic reversal mechanism, hysteresis loops for polycryst. and single cryst. specimens *(Russian)* 78−60318
MnBi, thin film, struct. and mag. props. 79−47315
$Mn_{2-x}Cr_xSb$ film, prep. and mag. props. 78−48009
$Mn_xFe_{3-x}O_{4+y}$, prep., resist., hysteresis loop and mag. disaccommodation *(Spanish)* 77−73045
$Mn_{3-x}Ni_xB_4$, mag. props. *(Russian)* 77−51923
MnO:Mn_3O_4, mag. props., susceptibility and magnetisation meas. 80−65824
MnS_2, first order antiferromag. phase transition 77−8317
MnSe, thermal hysteresis, ESR spectra 79−99758
MnSi, low field mag. studies 78−23255
MnZn ferrite, appreciable SiO_2 content, origin of core losses, microstructure and mag. props. 78−64225
MnZn ferrite, mag. loss accommodation depend. on freq. and amplitude of mag. field *(Russian)* 80−34686
MnZn ferrite, mag. permeability accommodation depend. on mag. field *(Russian)* 80−34685
$(Mn_{0.7}Zn_{0.3})_xFe_yO_4$, electromag. props. rel. to Fe content 78−43613
Nb, high crit. flux density gradient near surface 79−87221
Nb, superconducting, hysteresis in time depend. fields up to 3 kOe 77−24637
Nb-Ti, multi-filamentary superconducting wires, mag. field dependence of AC losses 78−60256
Nb-Ti, single core conductor, carrying DC transport current, alternating field losses 80−34550
Nb_3Ge, hysteretic losses in parallel AC and DC mag. fields 79−87217
Nb_3Sn multifilamentary superconductor AC hysteresis losses 79−33437
$Nd_{64}Co_{36}$, amorphous, amg. ordering, susceptibility, magnetisation and hysteresis meas. 78−68190
$Nd(Mn_{1-x}Cr_x)_2Si_2$, mag. and structural props. 79−78342
Ni film, 618 MHz SAW attenuation rel. to mag. field 77−40110
Ni film, ion beam sputtering prep., struct. and mag. props. 80−35085
Ni, hydrostatic press. effect on magnetisation Procopiu effect and hysteresis meas. 77−48023
Ni, mag. props. of single-domain powders after plastic deform. *(Russian)* 78−6554
Ni, temperature magnetic hysteresis near Curie temp. 79−56567
Ni wire, polycryst., inverse Wiedemann effect for low torsional stress 79−11332
Ni wire, polycryst., magnetoelastic hysteresis with torsion, inverse Wiedemann effect *(Spanish)* 77−73064
Ni-Co, mag. props. of single-domain powders after plastic deform. *(Russian)* 78−6554
Ni-Co-P, amorphous film, Kerr effect, hysteresis loop 78−60322
Ni-Co-Zn ferrite, exam. of electromag. characteristics 79−1409
Ni-Fe, new soft magnetic material for pulse transfer and choking in power electronics *(German)* 79−28555
Ni-Fe (40%), Mn coating, mag. interface effects 77−69638
Ni-Fe-Co, alloy with step hysteresis loops *(German)* 79−42806
Ni-Fe-Co alloy films, for logic devices, mag. switching vel., anisotropy field and coercive force *(Korean)* 77−51930
Ni-Fe-Cr film, hysteresis loop meas. using magnetooptical system 79−69707
Ni-Mn alloy, disordered, exchange-anisotropy field, magnetisation curves 78−72365
Ni-Mn base polynary alloys, magnetic and elect. props. *(Japanese)* 78−15551
Ni-Mn base polynary alloys, magnetic, and elec. props., composition and heat treatment effects 79−11710
Ni-Mn-H, hydride phase form. and decomposition in hygh-press. gaseous H_2, magnetisation meas. 79−56953
Ni-P electrodeposit, magnetisation coercivity and magnetostriction 78−68338
Ni-Zn ferrites, mag. recording head props. rel. to manuf. from schoenite-type solid solns. 77−85496
NiCo ferrite, induced mag. anisotropy, hysteresis loops, Barkhausen effect *(Russian)* 78−64203
NiFe, departure from Rayleigh law in low mag. fields 77−40086
$NiFe_2O_4$, hysteresis and other mag. props. rel. to microstruct., TEM investig. 77−20636
$NiFe_2O_4$ mag. fluid particles, comp., struct., and mag. props. 80−60374
$NiFe_2O_4$, microstruct. and magnetic props., electron microscope obs. 79−87290
$NiFe_2O_4$, soft ferrite, squareness ratio and max. induction 79−99730
$Ni_{1-x}Fe_xS_2$ (x=0 to 0.075), weak ferromag. exam. 79−51755
Ni_3Mn, partially ordered, field induced uniaxial anisotropy at low temp. 77−40053
$(Ni_{0.75}Mn_{0.25})_{82}Si_{10}B_8$, amorphous, exchange anisotropy, mag. susceptibility meas., 4.2K to room temp. 80−11186
NiS_2, weak ferromagnetic semiconductor single crystal, elec. and magnetic props. 77−85226
NiZn ferrite, effect of reactor radiation on mag. props. 77−32215
NiZn ferrite, magnetic props., porosity and grain size effects 77−36095
Ni(110), ferromag., surface magnetisation, polarised LEED expt. 80−97118
Pb, supercond., mag. hysteresis meas. *(French)* 77−4463
$Pb_{0.87}Sn_{0.129}$, supercond., hysteresis in flux flow characts., normal metal precipitates 78−80107
$(Pd_{0.9965}Fe_{0.0035})Mn_{0.05}$, ferromag. and spin-glass props. 80−2590
Pt-Fe alloy, ordered, T-c phase diagram, antiferro- and ferromagnetism *(Russian)* 80−65871
R_2In, R_3In, R=Gd, Tb, Dy, Ho, Nd, mag. props. 80−108009
Sm-Co-Cu-Fe, single phase 2-17 sample, hard mag. props. 77−8349
Sm-Co-Cu-Fe-Zr magnet, production and mag. props. 77−40085
$SmCO_5$, etched microparticles, Barkhausen discontinuity, nucleation, and domain wall pinning 79−87288
$Sm(Co,Cu)_z$, precip.-hardened, mag. and metallographic props. 77−8339
$SmCo_5$, Cu-modified, magnetisation reversal mechanism 77−8350
$SmCo_5$ permanent magnet, liq. phase sintered, hysteresis loops, ageing, temp. depend. *(Chinese)* 77−51921
$SmCo_5$, permanent magnet stability, during long-term ageing *(Chinese)* 80−55428
$SmCo_5$ powder alloy, densification by cold working 77−4753
$SmCo_5$, single crysts., mag. props. study and role of anisotropy *(French)* 79−38356
$SmCo_5$, sintered, hard mag. material, magnetisation behaviour 80−75805
$SmCo_5$, sintered permanent magnet, 4.2-300K, fields up to 100 kOe 77−8341
$SmCo_5$, sprayed magnet, microstruct. and mag. props. between 650°c and 800°C 79−82829
$SmCo_5$, substituted alloy, low reversible temp. coeff. 78−68178
$SmCo_x$-Fe composite permanent magnet material, mag. props. 77−40089
Sm_2Co_{17}, coercive force depend. on annealing temp. 80−65964
$SmCo_{3.5}Cu_{1.5}$, single crysts., mag. props. study and role of anisotropy, effects of cryst. field *(French)* 79−38356
$Sm_2Co_{17-x}Ni_x$, effect of Ni on mag. props. 78−68296
$SmFe_2$ powders, mag. and hysteresis props. *(Russian)* 79−42800
$Sm_{1-w}MM_w(Co_{1-x-y}Cu_xFe)_z$, (MM-mischmetal), mag. meas. and metallographic exam. 77−56119
Sn, supercond., mag. hysteresis meas. *(French)* 77−4463
$SrFe_{12}O_{19}$, hysteresis loops, formation processes 80−39813
$SrFe_{12}O_{19}$, microstruct. and magnetic props., electron microscope obs. 79−87290
Tb-Y alloy, mag. hysteresis in antiferromag.-ferromag. transition *(Russian)* 79−33508
$Tb_{52}Ag_{48}$, amorphous, bulk magnetic props., evidence of strong local anisotropy 77−43830
$Tb_{52}Ag_{48}$, amorphous, mag. after-effect meas. 79−24200
TbAu, amorphous, magnetisation characts., 5 to 300K, hysteresis cycle *(French)* 77−80965
$TbFe_2$, amorphous, temp. depend. of mag. hystersis props. 79−61186
$TbFe_2$, magnetoelastic props., magnetostriction hysteresis *(Russian)* 80−29590
$TbFe_2$ powders, mag. and hysteresis props. *(Russian)* 79−42800
$(Tb_{1-x}Gd_x)_3Co$, intermetallic cpd. mag. props., phase transform, and mag. hystersis *(Russian)* 80−93113
TbMg, mag. struct. and mag. props. 77−8275
$(Tb_{1-x}Y_x)_3Co$, mag. props. and transitions, conc. depend. *(Russian)* 78−10671
$Tb_xY_{3-x}Fe_5O_{12}$, anomalies of magnetisation and magnetostriction obs. in strong fields, 4.2K 77−1581
UAs, magnetisation, in fields up to 40 T 79−33505
UP, magnetisation, in fields up to 40 T 79−33505
US, magnetisation, temp., mag. field and orientation depend. 77−63232
USb, magnetisation, in fields up to 40 T 79−33505
V (-Ti), supercond., rotating discs, hysteresis losses and mag. phenomena 80−75695
V, supercond., creep effect in periodically swept minor hysteresis loops 79−60964
V, superconducting, microwave biased RF-SQUID system, appl. to magnetic aftereffect 79−26089
$(Y,Gd,Yb)_3(Fe,Ga)_5O_{12}$ film, magnetisation processes and domain struct. near compensation temp. 78−14996
$Y_2Co_{17-x}Ni_x$, effect of Ni or mag. props. 78−68296
$(Y_{65}Fe_{35})_{100-x}B_x$ glasses, mag. props. 79−73693
$Y(Fe_xCo_{1-x})_2$, x≤0.2, mag. props. and Mossbauer meas. 80−75798

magnetic hysteresis continued
YIG bubble films, light scatt. from spin waves, hysteresis meas. by Voigt effect 80−15770
$Y_6(Mn_{0.75}Fe_{0.25})_{23}$, mag. scatter state, hysteresis loops 78−56350
$Zr_{40}Cu_{60-x}Fe_x$, electronic and mag. props. 77−8271
$Zr_{40}Cu_{60-x}Gd_x$, magnetically dil. glass, 4f moments, mag. susceptibility and magnetisation meas. 79−95575
$Zr_{40}Cu_{60-x}Tb_x$, magnetically dil. glass, 4f moments, mag. susceptibility and magnetisation meas. 79−95575

magnetic impurity interactions
alloys, dil. mag., transport props. in mag. field, impurity-electron scatt. 80−65541
alloys, magnetic localisation and charge oscillations 80−75781
aluminoborate glass, Fe and Cr ion interaction, mag. and spectral props. 80−103883
Anderson impurities, interacting, pair, Fermi-liq. theory 80−44803
Anderson model, direct interaction between impurities 80−54681
Anderson model, exactly soluble local moment problem 78−52194
Anderson model, perturbation expansion in infinite conduction bandwidth limit, Kondo temp. 79−28506
anthracene-TCNB, 1:1 charge transfer complex, proton-paramagnetic impurity interaction 79−7690
antiferromagnet, Heisenberg or X-Y model, one-dimens., Friedel type oscills. 78−60296
antiferromagnet, impure, Heisenberg model, impurity banding and mag. reson., theory 80−93181
antiferromagnet, itinerant model, spin density wave transition, impurities effect 77−72986
antiferromagnet, randomly dil., spin wave excitation exam. 77−24665
antiferromagnetic, impurity-induced mag. susceptibility *(Russian)* 77−32172
antiferromagnets, magnon damping due to impurity scatt. 78−68206
Baxter-Wu model, site impure modified crit. behaviour and crossover 80−60322
BCC magnetically ordered alloys, effects on at. ordering-spontaneous magnetisation reln. *(Russian)* 78−19261
BCS-superconductor with mag. impurities, transition temp. in spin fluctuation limit 77−32104
binary magnetic alloys, Monte Carlo calc. beyond homogeneous mol. field approx., anomalous Kondo effect 77−8308
borosilicate glass, Fe and Cr ion interaction, mag. and spectral props. 80−103883
bottlenecked EPR, singly, doubly, multiply bottlenecked systems 78−27078
α-Ce, ESR of Gd, Dy and Er impurities 78−39398
classical Heisenberg chain with mag. impurities, susceptibility 77−4490
conduction electron polarisation and mag. hyperfine fields at nonmag. impurities in mag. materials 77−63174
conduction electron-magnetic ion Coulomb interactions, unitary transform., spin angular momentum operators 80−84451
Cr-Au alloys, dil., elec. resist., 77-700K 78−64035
critical temperature for Ising systems with regularly arranged impurities 80−44785
demagnetisation through level crossing, effect of charge fluctuations 78−52193
dilute alloy, appl. of low temp. nucl. orientation 80−15825
dilute alloy, interaction of cond. electrons with ordered impurity system 77−20550
dilute alloy, localised magnon mode in extended Wolff-Clogston 79−61097
dilute ferromagnet, slow neutron inelastic scatt. by spin excitations, cluster approx. 80−11168
dilute magnetic alloys, electron sound absorpt., disordered mag. impurities, spin glasses *(Russian)* 80−80503
dilute rare earth in metal, effective exchange interaction model 80−25127
dimethyl ammonium manganese chloride, quasi one-dimensional mag. systems, impurity effects 80−71015
dimethylammonium manganese trichloride:Cd(Cu), impurities in quasi-one-dimens. Heisenberg systems, anisotropy effect 80−80502
electron gas, spin-polarised, self-consistent screening of positive muon 78−47714
ferromagnet, chain type, with uniaxial exchange, localised one-magnon states in presence of impurity *(Russian)* 77−63143
ferromagnet, impurity spin critical dynamics 80−2593
ferromagnet, metallic, correl. of temp. anomalies of hyperfine field and thermal expansion of lattice 80−20400
ferromagnet, one-dimensional localised nuclear magnon modes 80−93098
ferromagnet, randomly dil., spin wave excitation exam. 77−24665
ferromagnet, unaxial, random with dipolar interactions, crit. amplitude ratio change 78−31083
ferromagnet, with weakly bound ferromag. impurity, thermodynamic and dynamic props. *(Russian)* 78−27032
ferromagnet with resonant impurities, Heisenberg model *(Russian)* 79−87280
ferromagnetic alloys, hyperfine field systematics of nonmag. ions 78−60093
ferromagnetic Fermi-liquid model, electron-impurity system hydrodynamics, elec. cond. 80−103835
ferromagnetic metal, temp. depend. of hyperfine fields at impurities 79−15300
ferromagnetic nondegenerate semiconductor, magnetoresistance 80−11019
ferromagnetic system with quenched random impurities, random spherical model in nonzero mag. field 77−55677
ferromagnetic transition metal, Fano effect and hyperfine field of non-transition impurity 80−25128
ferromagnetic with impurity atoms, Mossbauer effect *(Russian)* 77−48098
ferromagnets, spin wave excitation due to parallel pumping, mag. impurity interactions *(Russian)* 80−80497
ferromagnets and antiferromagnets, mag. impurity levels, standard basis operator method *(Russian)* 80−11192
fluorite type crystal; $Tm^{2+}(Yb^{3+})$, axial g-values of $4f^{13}$ ions with trigonal symmetry *(Korean)* 79−24135
graphite, neutron-irrad., sp.ht., 0.4-4.5K, rel. to localised spin transition 77−28389
Heisenberg, impure classical chain, dynamic props. using local-moment pair correl. functions 80−15728

magnetic impurity interactions continued
Heisenberg antiferromagnet, disordered, magnetic atom-conc. near percolation threshold, mag. props. *(Russian)* 78−80171
Heisenberg antiferromagnet, one-dimens., impure, mag. susceptibility 80−60168
Heisenberg antiferromagnet, randomly diluted, field-induced phase transitions 77−36089
Heisenberg crystal, effect of impurity on local density of states 79−33263
Heisenberg dilute magnet excitations near percolation threshold 79−87270
Heisenberg ferromagnet, localised magnons around impurity 78−39305
Heisenberg ferromagnet, localized magnons in a spin chain with two 'surface' impurities 79−38310
Heisenberg ferromagnet, strongly anisotropic with impurities, in transverse field, one-magnon states 77−69476
Heisenberg magnet, impurity band resonance at 0K, theory 80−66041
Heisenberg model, randomly dilute, renormalisation group calcs. 80−60321
Heisenberg model, spin glass state, magnetisation of dil. mag. impurities, molecular field approx. 77−20623
Heisenberg paramagnet, dil. isotropic, freq. moments of spin-correlation function 78−31037
impurity spin-unpolarised lattice nuclei interaction, dynamic susceptibility 79−69648
insulating systems, magnetic, review of expts. 78−68240
insulator, localised surface impurity modes 77−1545
Ising chain, spin-1, sp. ht. in presence of impurities and mag. field 80−93128
Ising ferromagnet, randomly dilute, conc. expansion study 80−60315
Ising lattice, two-dimensional, interstitial impurity effect on sp. ht. 77−89957
Ising model, bond-dil. two-dimens., phase transition 80−60320
Ising model, spin glass state, magnetisation of dil. mag. impurites, molecular field approx. 77−20623
Ising model, with regularly spaced blocks of impurities, crit. temp. and sp. ht. 77−69576
Ising system, local crit. behaviour at impurities 77−48001
itinerant electron antiferromagnet, effects of paramagnetic impurities on Neel temperature 79−4678
itinerant electron antiferromagnet, localised spin coupling 78−68142
Kondo alloy, low temp. props. 80−2569
Kondo effect in supercond., transition temp. and upper crit. field 77−55634
Kondo resistivity, impurity-impurity interaction effects 78−51981
Kondon lattice, impurity interactions, ground state calc., impurity conc. effect 80−65782
linear conductor, localized mag. moment formation and one and two impurity sites 80−50087
local paramagnon model, second-order phase transition, impurity effects calcs. 77−77067
magnetic alloys, dil., transition metal hosts, props. review 78−84417
magnetic ordered cryst., with degenerate orbital impurities, one- and two-magnon light absorption 77−63444
manganese formate dihydrate, Zn- and Mg-substituted, anomalous crit. phenomena 80−60316
metal, mag. susceptibility, effects of impurities and temp. *(Russian)* 78−84429
metal, magnetic impurity, model of resonance level in Kondo problem *(Russian)* 78−80129
metal, quasimagnetic impurity, exact solution of Wolff's model 78−56105
metal, quasionedimensional, effect of small mag. impurities on conductivity *(Russian)* 77−4328
metal with magnetic impurities, variational method, Wolff model 78−80110
metal with magnetic impurity, appl. of low temp. nucl. orientation, book 80−3
metal-insulator-metal junction, hopping model of zero-bias tunnelling anomalies, mag. field effect 79−60936
metals, hyperfine mag. fields at ^{119}Sn nuclei 80−60248
metals, Kondo effect, Anderson hamiltonian 80−60187
metals, localised moment interaction, Alexander-Anderson model, perturbation expansion 80−29524
metals, magnetic impurity-conduction electron interaction, g factor renormalisation 79−69652
metals, magnetic suscept., optical data determ. of individual contributions 77−12088
metals, with mag. impurities, kinetic exchange interaction, Curie-Weiss high temp. susceptibility 79−33457
MIM tunnel junction, magnetically doped, hopping model of zero-bias tunnelling anomalies, comparison with expt. 80−65703
noble metal-rare earth alloy, dil., magnetotransport props., theory 78−39097
nondegenerate Wolff model, variational method extension to include orbital degeneracy 79−38302
nonequilibrium superconductor, effect of pair breaking on branch relax. 79−78257
nonmagnetic metal, s-d exchange model exact solution, mag. susceptibility, mag. impurity interactions *(Russian)* 80−70943
one dimensional randomly dilute Ising ferromagnet, dynamics 80−70922
one-dimensional Hubbard model, Friedel oscills. around a nonmagnetic impurity 80−25073
one-dimensional systems, impurity effects on ordered phases 80−24905
optical absorption of mag. impurity ion in mag. ordered cryst. 77−16355
paramagnetic impurities in conductors, relaxation and indirect exchange interaction 78−2728
Permalloy, magnetisation improvement through solid state refining 78−91893
proximity systems with magnetic impurities, DC Josephson effect 80−100554
quantum chain, mag. impurity reson., Fresnel diffr. pattern 77−63051
quasi-low dimensional spin system, 3-D mag. ordering, randomness effects 78−10710
random site Ising model near percolation threshold 78−23282
random uniaxial systems with dipolar interactions, crit. dynamics 77−73034
randomly diluted lattice, phase transitions, near percolation threshold, scaling theory 77−40066
rare earth alloys, cryst. field effect on EPR and NMR 78−56391

magnetic impurity interactions continued
rare earth systems, Anderson model susceptibility for high mag. impurity conc. 77−63069
rare earth-Co_2-Al, dil., nonmag. impurities effect on ordering temp. 78−84427
rare-earth impurities in s-p hosts, self-polarization hyperfine fields 79−33456
scalar interactions, microscopic, histogram collection by FORTRAN program 78−34958
semiconductor, doped, indirect interactions between localised mag. moments 77−66296
semiconductor, doped with mag. impurity, ordering mechanism 80−2572
semiconductor, ferromagnetic, with mag. impurities, low-energy localised states, direct and s-d exchange interactions *(Russian)* 79−19543
solid solution, crit. phenomena of random spin systems, renormalisation group approach 78−52263
spherical model with layered impurities, critical behaviour 80−93124
spin dynamics in rapid spin relax. ferromagnet *(Russian)* 77−51960
spin systems with quenched random impurities, dynamics, replicas and frustration approaches 80−34673
spin XY one dimensional system containing impurities, static mag. props. *(Russian)* 80−65826
superconducting alloys with ordered magnetic moment distribution, thermoelec. effect 78−91811
superconducting amorphous metals, mag. impurity interactions 80−44777
superconducting virtual bound state alloys with resonant impurity scatt. centres theory 79−99654
superconductive system with weak coupling, current in ground state *(Russian)* 77−47944
superconductor, paraconductivity, mag. impurities effect *(Japanese)* 77−43785
superconductor, theory 77−39997
superconductor, with magnetic impurities, electric charge density oscillation *(Russian)* 78−56255
superconductor with mag. impurities, elec. field distrib. 78−88070
superconductor with mag. impurities, longit. elec. field penetration *(Russian)* 79−19694
superconductor with mag. impurities, Shiba theory consequences beyond s-wave scatt., sp. ht. discontinuity 80−2516
superconductor with magnetic impurities, EM penetration depth 77−66225
superconductors with transition metal impurities, kinetic coeffs. *(Russian)* 77−32111
symmetric Wolff model, weak-coupling−long-time−zero-temp limit 77−80907
TMMC:Cu, dynamic props. using local-moment pair correl. functions 80−15728
TMMC:Cu, EPR linewidth freq. depend., spin dynamics 80−15794
TMMC:Cu(Ni), effects on suscept. and Neel temp. 77−66312
TMMC:M, impurity (M) effects on Neel temp. and low temp. mag. susceptibility 78−88113
TMMC, effect of impurity spins on three-dimensional ordering 79−24159
TMMC, one dimens. antiferromag., neutron scatt. exam. of impurity effects 78−43598
TMMC, one-dimens. magnet, local magnon modes 80−65829
transition at T=0, crit. oscills. in scaling laws corrections 78−76259
transition metal diiodides, (V, Cr, Mn, Fe, Co, Ni, Cd), Mossbauer spectrum, electronic and mag. props. 77−32302
transition metal-rate earth alloy, dil., hyperfine fields, theory 78−68226
transition metals, surface- or defect-induced magnetism, nearly half-filled bands 79−1671
trimethylammonium cobalt trichloride:CU, bound impurity effect, heat capacity meas. 79−61146
weakly disordered uniaxial ferromagnet, phase transition *(Russian)* 78−23291
Wolff model, effective mag. interactions between impurity and conduction electrons 78−68143
Wolff model of magnetic impurity in metal 79−61052
Wolff-Clogston model, effective exchange interactions calcs. 78−34812
Ag-Mn, dil., nuclear orientation expts. 78−43713
Al-Mn(Cr), dil. alloys, single impurity and interaction effects in susceptibility 77−8269
Au alloys, dil., conduction electron-local moment interactions using dHvA waveshape anal. 79−77981
Au-Co, dil. alloy, de Haas-van Alphen obs. of spin dependent scatt. by mag. pairs 77−32007
Au-rare earth alloy, dil., magnetoresist., quadrupole scatt. effects 78−39096
BaF_2:Tm^{2+}, EPR meas. of Tm^{2+} ion pair interactions 79−95641
C, soft, sp. ht., 0.4-4.5K, rel. to localised spin transition 77−28389
$CD_{1-x}In_xCr_2S_{4-x}P_x$, ferromagnetic spinel, Cr^{3+} exchange interaction mechanism, Cr^{2+} relaxation, EPR line width depend. 79−69715
CaF_2:Tm^{2+}, EPR meas. of Tm^{2+} ion pair interactions 79−95641
CaF_2+Yb^{3+}, Stark level Zeeman energies, mag. susceptibiltiy, Schottky specific heat, crystal field splitting 78−26831
$CdCr_2S_4$:In(Ga), resist. and magnetoresist. meas., effect of donor impurities 79−19608
$CdCr_2S_{4-\gamma}$, spinel, anomalies in paramag. susceptibility, Curie pt. *(Russian)* 77−80910
$CdCr_2Si_4$:Ga, negative magnetoresist. effects near Curie temp. 79−11152
$Cd_{1-x}Ga_xCr_2S_3$, spinel, anomalies in paramag. susceptibility, Curie pt. *(Russian)* 77−80910
$Cd_{1-x}In_xCr_2S_4$, ferromagnetic spinel, Cr^{3+} exchange interaction mechanism, Cr^{2+} relaxation, EPR line width depend. 79−69715
$Cd_{1-x}Mg_x$, energy spectrum pseudopotential calcs., mag. props., impurity scatt. *(Russian)* 80−65430
$Cd_{1-x}Mg_x$, magnetic susceptibility anisotropy, press. effects, electronic phase transitions *(Russian)* 80−54869
CdS, amorphous antiferromag., mag. props. of dilute neutral donors 79−78367
CdTe:Fe, annealed, magnetically ordered, Hall effect and photocond. 78−19060
$CePd_3$-Gd, ultralow interaction temp. and cryst. field effects for Gd impurities 79−61100
Co host, dil. impurity hyperfine fields, comparison with models 78−14954
Co, local magnetic fields probed by μ^+ 78−48103
Co:Ga(Ge)(As), temp. anomalies of hyperfine fields 78−23265
magnetic impurity interactions continued
Co-3d transition metal alloys, hyperfine field and mag. perturbation distrib., NMR spectra meas. 79−61263
Co-Cd, dil. alloy, impurity hyperfine interactions 78−84416
Co-Fe, dil., effective mag. field at ^{59}Co, impurity conc. depend., spin echo expts. 78−48080
Co-Fe, dil., hyperfine mag. fields, press. effect, Mossbauer meas. 80−71277
Co-Ni, dil., effective mag. field at ^{59}Co, impurity conc. depend., spin echo expts. 78−48080
Co-Ru, dil., mag. hyperfine fields, TDPAC meas. 78−43702
$CoCl_2$, spin orientation of mag. impurity atom 77−59403
CoF_2:$MnSu^{2+}$, anisotropic antiferromagnet, spin impurity approx. *(Russian)* 79−87253
Co_2HfSn-Fe, dil., Heusler alloy, Fe hyperfine fields, Mossbauer obs. 78−68424
$Co_{1-c}Mn_cF_2$, antiferromagnet mag. impurities, spin excitation spectrum collective rearrangement in external mag. field 80−50199
Co_2TiSn-Fe, dil., Heusler alloy, Fe hyperfine fields, Mossbauer obs. 78−68424
Co_2ZrSn-Fe, dil., Heusler alloy, Fe hyperfine fields, Mossbauer obs. 78−68424
Cr alloys, localised magnetic moments in band antiferromagnets, impurity interactions *(Russian)* 80−54888
Cr, and alloys, surface- or defect-induced magnetism, nearly half-filled bands 79−1671
Cr, antiferromag., mag. and non-mag. impurities, hyperfine interactions, ^{181}Ta and ^{100}Rh TDPAC meas. 78−43704
Cr, spin density wave, stress and impurity conc. depend. 77−73029
Cr-Fe, dil., magnetisation, Fe local moments 80−60215
Cr-Fe, dilute, localised moment cluster model, ferromagnetic exchange coupling 80−39774
Cr-Fe (6.5 wt.%), atomic clustering and mag. defects, mag. moments 80−60246
Cr-Fe alloys, itinerant antiferromag. effect of mag. impurities 77−32186
Cr-Fe_x (x=0.5, 1.5 and 3.5 at.%), antiferromag., Kondo anomaly 80−11163
Cr-Mo, behaviour of mag. impurities 79−4672
Cr-Pt, dil., effect of Pt on itinerant antiferromagnetism 78−64191
Cr-Rh, dil., hyperfine fields meas. 79−47056
Cr-Ru, dil. absence of mag. hyperfine field, TDPAC meas. 80−50237
Cr-Si, dilute alloy, mag. susceptibility and Neel temp. meas. 80−71017
$(Cr_{1-x}Ti_x)_5S_6$, mag. props. 77−69548
$(Cr_{1-x}V_x)_5S_6$, mag. props. 77−69548
$CsCdF_3$:Cr^{3+} (Fe^{3+}), ligand polarisation and transferred hyperfine interactions 79−51535
$CsMnCl_3.2H_2O$, quasi one-dimensional mag. systems, impurity effects 80−71015
$CsMnCl_3.2H_2O$:Cu(Co), quasi one-dimens. antiferromag., mag. impurity effect on Neel temp. and spin-flop field 79−61099
$CsMn_{1-x}Cu_xCl_3.2H_2O$, impurities in quasi-one-dimens. Heisenberg systems, anisotropy effect 80−80502
Cs_2NaYCl_6:^{249}Cf, mag. susceptibility of Cf^{3+} in octahedral site 77−12089
$CsNiF_3$, one-dimens. magnet, local magnon modes 80−65829
$CsNiF_3$:Mg, ferromag. chain system, temp. depend. of correlation length, quasi-elastic neutron scatt. meas. 77−16046
Cu:Cr(Mn)(Fe), NMR satellite data rel. to impurity struct. 78−35052
Cu-Al-Fe, dil. liq. alloy, localised mag. state interactions *(German)* 77−1539
α-Cu-Al(Fe) dil. alloys, Al ion charge screening, elec. resist. obs. 77−4500
Cu-Cr, dil. alloys, Frenkel defects, effects on anomalous resistivity and thermopower 77−8084
Cu-Fe group, dil., NMR satellite data calc., struct. of mag. impurities 80−103894
Cu-Mn alloy, dil., evidence for Mn clustering from high field magnetisation curves 79−78426
Cu-Mn-Au(Pt) spin glasses, anisotropic exchange interactions, effect of nonmag. impurities 80−80534
$CuAl_{1-x}Fe_xS_2$ system, delocalisation of d-electrons, mag., elec. and optical obs. 78−34804
CuCr(Fe)(Mn), dil., anisotropic hyperfine coupling, NMR study 80−65784
$CuCr_2S_{4-\gamma}$, spinel, anomalies in paramag. susceptibility, Curie pt. *(Russian)* 77−80910
CuMn, hysteresis, spin orbit scattering effect on anisotropy in spin glass state 80−71095
Dy-Sn alloy, hyperfine fields acting on diamag. impurities and anisotropic exchange, Mossbauer spectra 77−1625
$DyFeO_3$:Al^{3+}, Morin transition, mag. vacancies effect *(Russian)* 78−27039
$EuB_{6-x}C_x$, magnetisation, effects of C 80−25163
EuO, Curie temp. raising by impurity addition *(Russian)* 77−47994
EuO, nonstoichiometric film with excess EU, effect on resist. and Curie temp. 79−8204
$Eu_{1-x}Sm_xO$, mag. semicond., thermodynamics of mag. quasimols. 78−19266
Fe alloys, dilute, residual resist. in two-current model, impurity mag. moments 77−15818
Fe, electronic structure of nontransition element impurity atoms 77−73023
Fe host, dil. impurity hyperfine fields, comparison with models 78−14954
Fe, hyperfine field at nonmagnetic impurities 80−25129
Fe, hyperfine fields at impurity sites 77−66297
Fe, hyperfine fields at impurities in ferromag. metal 78−52244
Fe, non-mag. impurities, size effects on mag. hyperfine fields 78−43586
Fe: ^{119}Sn, pressure dependence of effective magnetic fields 78−52382
Fe-Al, dil. alloy, temp. depend. of ^{27}Al hyperfine field 78−47972
Fe-based alloys, volume interactions between substitutional sp and 3d solutes 79−78069
Fe-Cr, mag. props. of Fe, local coupling with spin modulation of matrix 79−15299
Fe-Cu, dilute, coercive field, initial permeability and relax. loss, non-mag. impurity effect 77−69628
Fe-Cu alloys, mag. moment distrib., elastic neutron scatt. obs. 79−78340
Fe-Cu metastable dil. alloy film, hyperfine interactions 78−52398
Fe-Mn, dil. alloy, mag. moment distrib., temp. depend., diffuse polarised neutron scatt. study 79−47250
Fe-P(Ga)(As)(Sb), dil., short range order, NMR study 80−71237

magnetic impurity interactions continued
Fe-Pu, dil., effective mag. fields, temp. depend. *(Russian)* 78−43587
Fe-rare earth, dil., contact contribution to mag. hyperfine interaction of rare earth impurities 77−80932
Fe-Sb-Ni(Cr), dil., short range order, NMR study 80−71237
Fe-Ti, mag. moment distrib. and environmental effects around Ti impurity 80−7092
Fe-Ti:H(D), isotope effects of diatomic TiH and TiD complexes 79−47259
γ-Fe-transition metal alloy, mag. moment in FCC d-metal lattices *(Russian)* 78−72337
Fe-V(Cr)(Mn), dil., local mag. moments, polarised neutron elastic diffuse scatt. 80−50088
$FeBr_2$:Mn^{2+}, antiferromag., impurity spin reson. 77−43876
$FeCl_2$, spin orientation of mag. impurity atom 77−59403
$Fe_xCo_{1-x}S_2$, ferromagnetic solid soln., electronic props. 79−7990
FeF_2:Mn, antiferromag., NMR relax., impurity bonding 80−66061
FeF_2:Mn, antiferromag. reson. and local magnon mode, FIR laser study 80−66042
FeF_2:Mn, Heisenberg antiferromagnet, impurity thermodynamics, NMR meas. 79−61098
FeF_2:Mn, Heisenberg model, impurity band resonance at 0K, theory 80−66041
$(Fe_{1-x}Mn_x)_2Y(B)$, Mn effect on Fe mag. moments, Mossbauer and mag. meas. 80−71016
$Fe_{65}Ni_{35}$, H-infused, internal mag. field determ., Mossbauer effect 78−23382
$Fe_{66}Ni_{31}Mn_3$, H-infused, internal mag. field determ., Mossbauer effect 78−23382
$(Fe_{0.2}Ni_{0.8})_{1-y}(SiO)_y$, Permalloy material, magnetisation, temp. and impurity atom conc. depend., band model calcs. *(Russian)* 80−93088
Fe_3O_4:^{119}Sn, magnetic interactions, Mossbauer spectra 79−15301
Fe_2P:Cu, Mossbauer spectra, mag. transition 80−50240
$Fe_{79}P_{13}B_8$ amorphous alloys, splat cooled, Mn, Cr and V substituted, mag. and transport props. 80−84593
FeS_2 (marcasite), temp. depend. mag. susceptibility 80−20391
FeS_2, natural single cryst., mag. susceptibility, 4.2-620K 77−40031
Fe_3Si-based dil. alloys, conduction electron polarisation, moment perturbations 78−68225
GaAs:Fe, ordering of Fe impurity, NMR anomalous line shift obs. 78−27102
GaSe:Mn, ESR spectra, influence of temp. and antiferromag. inclusions 79−99763
Gd host, dil. impurity hyperfine fields, comparison with models 78−14954
Gd, local magnetic fields probed by μ^+ 78−48103
Gd-Sc, dil. alloy, ferromag. hyperfine field determ. 77−43919
Gd-Yb(Ir), dil., ferromag., mag. hyperfine fields of ^{170}Yb and ^{193}Ir, Mossbauer effect meas. 79−24242
In-Mn, dil., supercond. film, H_{c2} meas., mag. impurity effects, pair breaking theory 79−42708
InSb:Mn^{2+} nondegenerate semicond., mag. impurity indirect interaction *(Russian)* 80−34591
K_2CoF_4:Mn^{2+}, impurity induced mag. excitations, magnon gap mode, far IR spectra obs. 80−44821
$KMgF_3$:Fe, EPR temp. depend. 78−80202
K_2MnF_4:Zn(Mg)(Ni), mag. effects of impurities 80−65869
K_2MnF_4:Zn(Mg)(Ni), local magnetisation, NMR and Green's function study 80−65870
$KMn_{0.1}Zn_{0.9}F_3$, exchange interaction determ. by neutron scatt. 79−47274
$LaAl_2$:Gd(Ce), supercond., electronic thermal cond. 77−12063
$(La_{1-x}Gd_x)Al_2$, dil., reverse resistance anomaly 78−76054
$La_{3-x}Gd_xIn$, mag. impurity ordering and superconductivity, EPR exam. *(Russian)* 77−8400
$(La_{.993}Lu_{.007})_{1-x}Gd_xRu_2$, exchange enhanced supercond., compensation effect on H_{c2} 77−4474
$La_{3-x}V_xS_4$:Gd^{3+} localised moment-conduction electron interact., ESR obs. 78−88183
$Li_{0.5}Fe_{2.5}O_4$, microwave material, mag. props., review 79−33504
Li_5AlO_4, NMR relaxation by paramag. impurities 79−42866
Lu-Gd, positive exchange const. Kondo system, resistivity meas. 78−47775
MgO, ^{25}Mg superhyperfine struct. of V-type defects, ENDOR 77−66439
γ-Mn-Cu, antiferromag. defect neutron scatt. study 79−47252
γ-Mn-Pd, antiferromag. defect neutron scatt. study 79−47252
$Mn_{1-x}Co_xSb$, ferromagnetic, NMR exam. 79−24228
MnO:Mn_3O_4, mag. props., susceptibility and magnetisation meas. 80−65824
$(Mo_{0.6}Ru_{0.4})_{0.8}G_{0.2}$-Fe (G=P,B), amorphous supercond., upper crit. field as function of temp. 79−73646
$Na_2O.2Al_2O_3.5SiO_2$:Fe^{3+}, Mossbauer effect and magnetometric exam. 78−6613
$Nb_{78}Ga_{22-x}Mn_x$, supercond. props., influence of Mn mag. impurities 80−54825
$Nb_{80}Ga_{20-x}Mn_x$, supercond. props., influence of Mn mag. impurities 80−54825
$Nb_{50}Ni_{50-x}Fe_x$, amorphous alloy, mag. interactions 78−95432
$NbSe_2$(2H) layered supercond., effect of Fe impurities on sp. ht. 79−60972
Ni, electronic structure of nontransition element impurity atoms 77−73023
Ni host, dil. impurity hyperfine fields, comparison with models 78−14954
Ni, paramag. region, Fe and Co impurity effects on susceptibility, Faraday obs. *(Russian)* 80−88731
Ni:^{119}Sn, 78−52382
Ni-Al-Fe(Co), electrical and mag. anomalies due to substitutional atoms 77−15839
Ni-Fe, dil., hyperfine mag. fields, press. effect, Mossbauer meas. 80−71277
Ni-Fe-Mn ferromagnetic alloy, magnetic state of Mn atom, local environment effect 77−66298
Ni-M, dil., high field susceptibility 78−52230
Ni-Mn ferromagnetic alloy, magnetic state of Mn atom, local environment effect 77−66298
Ni-Pu, dil., effective mag. fields, temp. depend. *(Russian)* 78−43587
Ni-Ti, mag. moment distrib. and environmental effects around Ti impurity 80−7092
$Ni_{0.95}$ S Fe, spin glass, spin flop in exchange field 80−34640

magnetic impurity interactions continued
β′-NiAl, self consistent embedded cluster model for Fe, Co, Ni mag. impurities 80−2549
β′-NiAl, self-consistent embedded-cluster model for mag. impurities 78−67973
$Ni_{1-x}Au_x$-Co, dil., Mossbauer effect, mag. hyperfine field 80−20528
$NiCl_2$, spin orientation of mag. impurity atom 77−59403
$NiFe_2O_4$:Ir^{4+}, mag. anisotropy, single ion contrib., octahedral sites 77−4511
$(Ni_{1-x}Fe_x)_{1-\delta}S$, anisotropic spin glass, mag. props. 80−39793
$Ni_{98}M_2$, M=impurity metal, formation of MH(D)-complexes 80−65236
$Ni_2Mn_xTi_{1-x}Sn$, Mossbauer spectra, mag. hyperfine field 80−15857
$Ni_{1-x}Rh_xS$, nonvolume effect of Rh substitution on paramag. metal-antiferromag. nonmetal transition 79−28277
Pb:Ni, paramag. impurity effect on work hardening at superconducting transition *(Russian)* 77−47915
Pb-Mn, dil., supercond. film, H_{c2} meas., mag. impurity effects, pair breaking theory 79−42708
PbF_2:Mn, NMR relaxation by paramag. impurities 79−42866
$Pb_{1-x}Sn_xTe$: Mn, Mn mag. and elec. active states, mag. impurity behaviour 80−44627
Pd-Fe, dil., transport props. at low temp. 0.05 to 5K 79−38046
Pd-Fe, highly dil., mag. behaviour, 0.06-300K, Mossbauer expt. 78−43711
PdAgFe, ferromag., Curie temp. depend. on susceptibility, non-mean field theory 80−44829
PdFeRh, ferromag., Curie temp. depend. on susceptibility, non-mean field theory 80−44829
$(Pd_{95}Rh_5)$Co, exchange enhanced system, AC susceptibility meas. 77−16096
Pr-Nd (5%), impurity modes and mag. ordering 78−84422
PrEu(Gd), magnetic interactions, Mossbauer spectra quadrupole splitting, crystal field parameters 80−39907
$PrIn_3$, nucl. orientation of ^{144}Pm in singlet ground state, exchange interaction and cryst. field splitting obs. 80−71275
Pt-Co, dil, magnetopower, magnetoresistivity 78−68016
Pt-Mn dilute alloy, cubic foil, Mn spin behaviour, nuclear orientation technique 78−27044
$RbMnF_3$, pure and Fe, Co or Ni doped, thermal cond., spin wave and mag. impurity contribs. 77−40046
$(SN)_x$, thermopower from 0.15 to 4.2K 80−34427
Si:Gd, magnetic props. and interaction of impurities 79−11286
Si:Gd(Pr), photoconductivity anomalies due to mag. impurities *(Russian)* 80−103722
Sm, polycrystalline with ferromag. impurities, mag. props., 1.5-300K 77−69547
SrF_2:Tm^{2+}, EPR meas. of Tm^{2+} ion pair interactions 79−95641
SrF_2:Yb^{3+}, trigonal centres, superhyperfine interaction, model 78−88114
$TaSe_2$:Fe, competition between charge and spin density waves, Landau-Ginzburg theory 79−95352
Tb-Sc(Y)(La)(Lu)(Yb)(Mg)(Th), mag. ordering temps., susceptibility meas. 80−25136
Tb-Sn, effective field at diamag. Sn impurities, 4.2 to 235K *(Russian)* 77−69549
$Tb(OH)_3$:Er^{3+}, ferromag., anisotropic exchange effects in optical spectra 78−80141
Tc-Fe alloy, Mossbauer spectra, hyperfine field 80−20526
$Y(Fe_{1-c}Al_c)_2$, mag. and Mossbauer study, local environment effects 78−27033
$Y(Fe_{1-x}Ir_x)_2$, magnetisation, mag. hyperfine field 80−20531
YIG, diamagnetically substituted, annealing effects on cation distrib. 79−1455
YIG, LPE grown, FMR linewidth, Pb incorporation effects 77−8407
YPd_3-Gd, ultralow interaction temp. and cryst. field effects for Gd impurities 79−61100
Zn-Cr, dil., mag. anisotropy, 0.001 to 2K 78−68157
Zn-Mn, supercond., thermal cond. compared with Shiba's theory 77−8228
ZnMn, dil., magnetoresist. meas., temp. depend. anisotropy 80−65532
ZnS:Mn^{2+}, heavily doped, anomalies in reflectivity 77−20891
ZnTe:Mn, ordering mechanism 80−2572
$Zr_{40}Cu_{60-x}M_x$, (M=Gd, Tb, Fe or Mn), amorphous alloy, mag. interactions 78−95432

magnetic inks *see magnetic fluids*

magnetic leakage
amorphous alloys, mag. loss meas. 79−73776
amorphous alloys, mag. props. and appls. 79−8016
amorphous alloys, mag. props. rel to device appl. 80−88804
amorphous ferromagnetic ribbon, HF mag. characts., magnetostriction role 77−66408
amorphous magnetic alloys, ferromagnetic props. and appl. 80−50143
Bloch walls, irreversible movements, loss contribs. from correlations 77−85483
charged particles, multiple times for nonadiabatic leakage from mag. mirror traps 80−33806
composite multifilamentary superconductor carrying DC transport currents, transient field losses 80−84551
composite superconductor, effect on losses in variable mag. field of mag. props. 80−34549
composite superconductor, losses under high rate pulsed transverse field 79−33385
composite superconductor, transport current, interaction with transient external field 79−33393
composite superconductors for fusion magnets, current distrib. and losses 77−28331
defect characterisation from magnetic leakage fields 77−12750
detection methods 78−3296
electrical steel sheets, specific core loss meas. using analogue wattmeter *(German)* 80−13099
electrotechnical steel, quality significance on energy and materials savings in magnetic circuits *(Czech)* 80−20947
energy doubler magnets, AC loss meas. 79−31277
energy doubler magnets, production characts. 79−31276
equipotential and mag. intensity contour line visualisation by SEM 79−6149
errors, systematic and random, in wattmeter apparatus for measuring unit losses in electrical steel sheet 80−71858
explosive mag. generator, magnetic accumulation in plane liner, flux loss and equiv. cct. 79−14571

magnetic leakage continued
ferrimagnetic Bloch wall oscills., viscosity coeffs. freq. depend., permeability and mag. losses 80−71094
ferrites, soft, production and props. 80−88801
ferromagnet, Bloch walls correlation and magnetic loss 78−95456
ferromagnet, magnetisation noise and power loss 79−24197
ferromagnetic medium with variable permeability and hysteresis loss, plane EM wave *(Polish)* 77−79722
ferromagnetic plate, monocrystalline, EM losses, influence of 90° domain wall motion *(Russian)* 78−27052
ferromagnetic plates eddy current phenomena numerical computation method *(German)* 80−65952
ferromagnetics in unidirectional field, magnetisation, math. model *(Russian)* 78−88140
form factor influence on measurement of losses in sheets *(Rumanian)* 80−68226
gaussmeter, Hall-probe adapter cct. for use with digital multimeter, leakage detect. 80−37014
hot-rolled rods, surface defect detection without scale removal by NDT 78−95890
losses in general cylindrical body, determ. from field quantities *(German)* 78−60306
multifilamentary superconductor with alternating twist, losses in transverse pulsed field 78−10602
NDT inspection of tubing and round billets, leakage flux probe 77−12753
non-oriented elec., internal oxidation and nitridation effects on mag. props. 79−83336
Permalloy film, magnetic leakage fields above stripe domains 77−77077
power loss meas. under sinusoidal flux conditions 80−86348
'Pulsed ferrite core tests for 50-ns linear induction accelerator' 79−690
residual pseudo-macrostress, X-ray meas. errors due to plastic deform. 77−68544
soft magnetic materials, Barkhausen jumps effect on static losses *(Slovak)* 79−4695
soft magnetic materials, meas. methods, review 80−86345
standards for practical superconductors, development 79−33442
steel, B-Si, grain-oriented, high induction, Cu impurity effects 80−89366
steel, C (0.01 and 0.06 wt.%), rephosphorised, mag. props. and texture 77−20634
steel, cold-rolled, isotropic, specific magnetic loss meas. at high frequency 80−101808
steel, crystallographic texture perfection in sheet with S,Mn inhibitors *(Russian)* 79−91709
steel, electrotech., losses on mag. after effect *(Russian)* 77−66388
steel, low C, Al-killed, effect of V on mag. props. 79−83339
steel, nonoriented, mag. props. texture, Cr addition effect 77−1880
steel, transformer, EM losses, influence of charact. of substruct. distrib. *(Russian)* 78−7058
steel, transformer, magnetic loss variation due to nonuniform normal press. *(Russian)* 79−91250
steel, transforms CC types M6 and M3N, elastoplastic bending, insulating coating influence on magnetic losses *(Russian)* 79−100284
steel plate, fundamental and harmonic flux, sinusoidal applied mag. field 78−2708
steel sheets, apparatus for mag. props. meas. in freq. range 50 to 10000 Hz 79−30497
superconducting coil, electronic apparatus, for loss meas. 77−26361
superconducting multifilamentary coil, hysteresis losses 77−26363
superconducting pulsed solenoid ORPUS-1, poloidal field coil performance 77−26352
superconducting solenoid, 60 Hz AC loss meas. 77−26362
superconducting threads of mixed materials containing many filaments, stability and transverse conductivity meas. *(French)* 79−73629
superconductor, AC losses from combined action of transport current and applied field 79−33383
superconductor, multifilament type, AC losses reduced below level of filament hysteresis losses by field screening 78−27000
superconductor, multifilament type, scaling law for AC losses 78−27001
superconductor, multifilamentary, mag. props. effect on losses in variable mag. field 80−60136
superconductors, high-current, low-freq. losses, phenomenological model 78−6486
Tokamak superconducting toroidal field coils, pulsed field losses, expt. simulation 77−26871
type II superconductor, nonideal slab, AC losses in small AC mag. field of trapezoidal wave form 78−39272
Co-Fe-V-Ni, mag. and mech. props., heat treatment and stress effects 80−60363
$Co_{57}Fe_5Ni_{10}(Si,B)_{28}$, amorphous, soft mag. props., switched-mode power supply appls. 80−88850
Fe, carbonyl powder, mangetic material 77−12160
Fe powder-plastic composite, soft mag. material, mag. and mech. props. 80−75812
Fe whisker, mag. memory function at crit. temp. 77−24714
Fe-B-C amorphous alloys, room-temp. saturation induction over 17.5 kG 79−47300
Fe-B-C amorphous alloys with high saturation induction 80−84617
Fe-Ci, high permeability, mag. props., applied stress effects 80−34726
Fe-Ci (3 wt.%), commercially produced, grain-oriented, mag. props., stress coating effects 80−34727
Fe-Ci (3 wt.%), local magnetisation losses, grain orientation effect 80−88817
Fe-Co alloy ring samples, force fitting effect on mag. props. 77−40083
Fe-Co amorphous ribbon, mag. props. in low fields 79−73777
Fe-Co-Ni Perminvar, mag. props. singularities in region of mag. anisotropy *(Russian)* 80−84614
Fe-Co-Si (4,1.5 wt.%), textured, mag. props. 80−35200
Fe-Co-Si-B, amorphous soft ferromagnet with high mag. induction 80−84619
Fe-Ni, low frequency power losses 78−95466
Fe-Ni-Co-B-P soft magnetic metallic glasses, status report 78−64226
Fe-Ni-Mn, Invar, RF collapse and thermal effects, Mossbauer study 80−100624
Fe-Si, (110) [001] oriented, mag. props., compressive stress effects 80−60392
Fe-Si, coated, effective domain and grain obs. methods and Fe losses 80−34675
Fe-Si, grain oriented, core losses *(Japanese)* 78−60303
Fe-Si, grain oriented, misorientation effects on mag. props 80−88792

magnetic leakage continued
Fe-Si, grain-oriented sheets, high permeability, low losses, review 80−88790
Fe-Si, influence of stress on rotational loss, lamination appl. 78−35384
Fe-Si, loss meas. at high flux densities 80−88799
Fe-Si, low frequency power losses 78−95466
Fe-Si, mag. losses, depend. on stress and orientation 77−1882
Fe-Si, mag. props., stress and reannealing effects 80−88844
Fe-Si, magnetic props., material for electrical engineering *(German)* 77−21293
Fe-Si, power loss and permeability meas. by means of Hall probes and stochastic ergodic correl. 80−86350
Fe-Si, stator core, grain-oriented and non-oriented, magnetic flux and loss distrib. 80−88798
Fe-Si (3 to 5 wt.%) sinters, mag. props., Si and Fe-Si additions effect 80−71104
Fe-Si (3 wt.%), directional, power loss anomalies temp. depend., effect of intrinsic parameters 77−12156
Fe-Si (3 wt.%), domain wall spacing and losses, orientation depend. 78−56343
Fe-Si (3 wt.%), domain wall spacing and core loss, forsterite and stress coatings effect 80−88780
Fe-Si (3 wt.%), effect of heating rate during primary recrystn. on props. after secondary recrystn. 78−84837
Fe-Si (3 wt.%), grain oriented tape-wound core, dynamic domain size var. and Fe losses 77−12146
Fe-Si (3 wt.%), grain oriented, lowest core loss 78−91887
Fe-Si (3 wt.%), grain oriented, power loss depend. on domain wall bowing 78−95460
Fe-Si (3 wt.%), grain-oriented, effect of forsterite coatings in domain struct. 78−23293
Fe-Si (3 wt.%), grain-oriented, stacking effect on power loss, mag. props. 80−88795
Fe-Si (3 wt.%), grain-oriented, power loss and domain wall variation with lamination thickness 80−88814
Fe-Si (3 wt.%), high permeability, use in transformer cores 80−88793
Fe-Si (3 wt.%), hysteretic losses, domain struct. and cryst. defects 79−19747
Fe-Si (3 wt.%), loss prediction, from distorted waveforms 78−76273
Fe-Si (3 wt.%), losses, demagnetisation freq. and grain orientation depend. 80−88796
Fe-Si (3 wt.%), mag. loss and magnetostriction, DC flux alternation effects 80−88794
Fe-Si (3 wt.%), mag. props., stress coating effects 80−34728
Fe-Si (3 wt.%), oriented, losses and domains, mech. stress effects 80−88852
Fe-Si (3 wt.%), power losses at extremely low freqs. 80−88815
Fe-Si (3 wt.%), rotational power losses, freq. depend. 78−91888
Fe-Si (3 wt.%), scratching effects on mag. losses in single crysts. with orientation near (110)[001] 79−51802
Fe-Si (3 wt.%), stripe domain structure, dynamic behaviour at high max. induction values *(Russian)* 80−80553
Fe-Si (3 wt.%), total losses under tensile stress, rel. to orientation near (110)[001] 78−76272
Fe-Si (3 wt.%), transformer steel, grain-oriented, magneto-optical domain obs., magnetisation mechanism 77−12364
Fe-Si (3 wt.%) grain-oriented transformer sheet, effect of phosphate coating containing Cr_2O_3 and CaO 77−16135
Fe-Si (3 wt.%) laminations, orientation and stacking influence on losses obs. *(Slovak)* 79−4696
Fe-Si (3 wt.%) laminations, grain oriented, plastically deformed, anomalous losses 80−88853
Fe-Si (3 wt.%) locally deformed, EM loss depend. on cryst. struct. and orientation *(Russian)* 80−7694
Fe-Si (3 wt.%) steel, high permeability, grain oriented 78−91886
Fe-Si (3 wt.%) steel, oriented, stress depend. mag. props., coating effects 80−34729
Fe-Si (3%), power loss, domain wall motion depend. 77−16100
Fe-Si (3%wt.), dynamics of 180° domain boundaries and electromag. losses *(Russian)* 79−51801
Fe-Si (4 wt.%), freq. depend. of Fe losses in single crysts. with (100) [001] 79−51803
Fe-Si (6.5 wt.%) ribbon, splat-cooled, mag. props. 80−88805
Fe-Si(6.5 wt.%) steel, core mat. development *(Korean)* 78−60852
$Fe_{80}B_{20}$ glass, low-field mag. props. 77−8380
$Fe_{40}B_{40}P_{14}B_6$ and $Fe_{80}B_{20}$, Metglas 2826 and 2605, amorphous ribbon, power loss variation with freq. and applied stress 80−88849
$Fe_5Co_{70}Si_{15}B_{10}$, amorphous ribbon, zero magnetostriction, low residual mag. loss 77−12157
$Fe_5Co_{70}Si_{15}B_{10}$ amorphous ferromag. ribbons, change of permeability by heat treatment 77−85493
$Fe_{40}Ni_{40}B_{20}$, amorphous, mag. loss meas. 79−73776
$Fe_{40}Ni_{40}B_{20}$, amorphous ribbon, power loss variation with freq. and applied stress 80−88849
$(Fe_xNi_{1-x})_{80}B_{20}$, amorphous alloys, engineering mag. props. 79−51832
$Fe_{40}Ni_{40}(Mo,Si,B)_{20}$, amorphous, soft mag. props., switched-mode power supply appls. 80−88850
$Fe_{40}Ni_{40}P_{14}B_6$, $Fe_{35}Ni_{32}Cr_{15}P_{12}B_6$, amorphous ferromagnets, Barkhausen noise and core losses 77−69618
$Fe_{80}P_{13}C_7$ amorphous ferromag. ribbons, change of permeability by heat treatment 77−85493
$Fe_{78}Si_{10}B_{12}$ amorphous ferromag. ribbons, change of permeability by heat treatment 77−85493
$Fe_{80}Si_5B_{15}$, amorphous, soft mag. props. and potential uses 80−88807
GdGa garnet, microwave losses 77−4531
MnSb, magnetic losses, ferromagnetic resonance and antiresonance 80−100618
MnZn ferrite, appreciable SiO_2 content, origin of core losses, microstructure and mag. props. 78−64225
MnZn ferrite, combined Sn-Ti substitutions, improved props. *(German)* 77−20644
MnZn ferrite, mag. loss accommodation depend. on freq. and amplitude of mag. field *(Russian)* 80−34686
MnZn ferrite, props. rel. to raw materials *(German)* 77−21074
MnZn ferrite, weak mag. losses, microcalorimetric meas. 77−51926
MnZn soft ferrites, commercial grade, microstruct. rel. to mag. props. 80−34009
Nb, supercond., surface effect on crit. current density 79−61014
Nb-Ti, single core conductor, carrying DC transport current, alternating field losses 80−34550

magnetic leakage continued
Nb-Ti multifilamentary superconducting composite, subjected to rotating mag. induction, losses 79−33386
Nb-Ti-Zr, supercond. wire, anomalous increments of AC losses due to flux jumps 77−28289
Nb-Ti-Zr, superconducting wire, coil simulation meas. of losses and instabilities 80−37050
Nb_3Ge, CVD, AC losses, temp. depend., 4-20K 77−28311
Nb_3Ge, CVD, hysteretic losses, precipitates and deposition temp. effects 77−28319
Nb_3Ge film, CVD on inside of Cu tube, AC losses 77−28312
Nb_3Sn multifilament superconductors, designed for high B appl., losses 79−33414
Nb_3Sn, multifilament superconductor, pulsed mag. field losses and critical current densities 80−54853
Nb_3Sn, supercond., effect of trapped mag. flux on AC losses 79−33420
Nb_3Sn superconducting multifilamentary conductors, AC losses 79−33394
NbTi cabled and soldered superconds. with low losses, for fusion research magnets, development 79−35796
Ni-Fe, power losses at extremely low freqs. 80−88815
Ni-Fe alloys, pulse permeability and loss in toroidal core pulse current transformers 78−43615
Ni-Fe film, differential susceptibility, struct. const. and losses 79−91271
$NiFe_2O_4$, domain wall size and mag. losses in freq. spectra 77−85481
Pb-In alloys, supercond., AC losses of EM energy, critical current densities 79−33423
$SmCo_5$, intrinsic coercivity losses, temp. depend. 78−95468
V_3Ga, multifilament superconductor, pulsed mag. field losses and critical current densities 80−54853
$(Y,Eu,Sm)_3(Ga,Fe)_5O_{12}$ film, mag. loss and bubble dynamics 77−8371
YIG, domain wall size and mag. losses in freq. spectra 77−85481
YIG: Ca,(Mg), films, microwave losses induced by Fe^{4+} ions, ferromag. reson. study 79−1715

magnetic lenses
see also aberrations
aberration correction, mag. deflection systs. 78−66740
aberration formulae, approximate 80−95781
aberrations, reduction by optimisation techniques 80−87290
aberrations and electron optic props. for lens and deflection system *(Chinese)* 77−58244
anastigmatic electron deflection system between beam-shaping lens and probe target 79−27155
beam matching problems, improved analytic starting points 79−72163
beta-ray coinc. spectrom. with reduced spherical aberration 77−10529
cathode lenses, with combined elec. and mag. fields, third order aberration theory 79−41317
chromatically corrected objective lens, of electron microscope, test *(German)* 79−892
circuit reduction, saturation onset delay, superconducting coil appl. *(French)* 77−82650
combination intermediate-image magnetic plus Si(Li) electron spectrometer for in-beam experiments 79−31308
combined system of electrostatic round lens and mag. deflector, electron-optical characteristics *(Chinese)* 78−82897
cryogenic booster linac, heavy ion beam dynamics in chopper, buncher, mag. lenses 77−67919
cylindrical magnetic lens, 100-300 kOe, use of Li 79−9257
deflection systems combined with mag. lenses, optical props. 80−31938
design, finite element program improvement 80−69316
developments at the Cavendish Laboratory 80−37948
double focusing bending magnet, meas. of optical props. with thin alpha source 78−55073
einzel, general theory based on axial field distrib. model 79−55045
einzel lens, satisfying anastigmatic and achromatic conditions 80−87288
electron, min. spherical aberration 80−87287
electron deflection and focusing system *(French)* 79−41319
electron gun, with electrostatic and electromagnetic lenses 80−99007
electron microscope lenses, comparison of conventional mag. lens, and high power superconducting lens 78−32928
electron microscope objective lens focus and spherical aberration meas. 77−54024
electron microscope spiral distortion correction double-lens system 80−68327
electron-beam focusing optimisation with specified image parameters 78−86385
explosion parabolic lenses, mag. fields of 0.3 to 1 MOe 78−66739
focus-deflection practical system for shaped electron beams 79−76572
foil lens characts. for spherical aberration correction 79−71567
hexapole magnetic lens, for ultracold neutrons *(Russian)* 78−21273
ion beam, intense, lens system using toroidal mag. field 77−34053
ion beam image transformation using magnetic quadrupole lenses 78−55071
ion linacs, permanent magnet quadrupoles, development 77−38494
LAMPF, quadrupole field aberrations, source of emittance growth 77−38508
low aberration, use in field emission guns 77−54023
low gradient thin yoke quadrupole with rectangular aperture 77−10134
magnetic focusing of proton beams by single dipole coil 79−40642
magnetic optical achromat, second order, design 79−72161
magnetic vector man analyser, stigmatic focusing condition 78−70215
Mollenstedt filter images, correction by auxiliary lenses, appl. to bend contour obs. for Al 77−39520
monitoring, by multichannel analogue device 77−23604
optical parameter formulae, of mag. electron lenses *(Chinese)* 77−88633
optical properties and aberrations, lenses with electron-transparent foils 77−10828
parabolic lens, mag. field limited, mech. strength and dynamic loading 79−18341
permanent-magnet focusing systems, complex shaped pole pieces, induction distrib. anal. *(Russian)* 77−83786
photoelectronic streak camera tube, magnetically focused 78−33907
pulsed multipole mag. field with zero skin depth, anal. method, nonstandard electrode optimization 79−13863
quadrupole, detection system for charged particles prod. by neutrons 78−29712
quadrupole, spin precession of polarised proton beam, analytic soln. 77−30692

magnetic lenses continued
quadrupole doublet, field coupling and higher order aberrations 77−38534
quadrupole lens, aberration coeff. from rectangular model *(French)* 77−68161
quadrupole lens for proton beam focusing to micrometer dimensions 77−46444
quadrupole lens spatial field determ. 78−55292
quadrupole lenses, electrostatic and mag., ion orbit 5th order solns. 77−19159
quadrupole lenses, magnetically hard, for ion drift tubes in linear accelerators 79−3261
quadrupole lenses, symmetric system, beam identity transformations 77−31057
quadrupole lenses with sector magnets, nonzero emittance beam focusing conditions 80−23612
relativistic electron storage device, phase-free cavity resonator with two mag. mirrors 77−10504
RILAC, variable freq. heavy ion linac 77−38454
rotation-free mag. lens for transmission electron microscope 78−78042
saturated symmetrical condenser-objective lens, optical characts. 78−25788
sextupole corrector limitations 80−102604
sextupole system for spherical aberration correction 80−43246
single-pole, for field emission electron gun systems 79−31784
single-pole magnetic lens as condenser for field emission electron gun 80−68325
single-polepiece lenses, magnetised iron sphere model 78−32940
single-polepiece magnetic lens axial field distrib. 80−69317
single-polepiece objective and projector lenses for electron microscope 80−68326
sperical aberration, correction by foil lens, appl. to STEM 80−87294
spherical aberration correction with foil lens 77−67537
stabilized current supply, drift reduction 77−45867
stressed parabolic magnetic lens, thermal effects 79−27151
superconducting, bright-field imaging of single heavy atoms in an electron microscope with superconducting lens system 80−10472
superconducting electron lenses, direct meas. of dynamic mag. induction coeffs. *(French)* 77−61096
superconducting electron microscope lenses, construction of cryostat for testing 77−22627
superconducting lens, electron microscope appl. 80−86530
superconducting lens system for 500 kV electron microscope 80−68321
superconducting lenses applic. to electron microscopy 77−71408
superconducting microwave, in HV electron microscopes, development prospects w.r.t. mol. imaging 77−10147
superconducting solenoid as focusing element for heavy ion linac 77−38460
surface coils to improve magnet homogeneity 77−10829
TEM, magnetic energy filter optics 78−32944
TEM, spiral distortion correction 78−32942
TEM, universal magnification curve 79−49340
TEM, viewing arrangement improvements 78−32941
third-order field geometrical aberration of single slot lenses forming electron probe 79−3619
toroidal field, for intense ion beam production, appl. to fusion ignition, X-ray laser 77−67535
two-lens projection systems, reduction of third-order distortion 80−48134
wide-angle focusing device for low energy π collection 78−70664
X-ray tube, microfocus, electron source with single pole mag. lens and novel focusing system 78−32964
ZGS beam transport for transverse and longitudinally polarised protons 78−55074
zoom lens quadrupole magnets for Colorado Univ. energy-loss spectrograph 77−83410
Fe lenses for muon beam transport 77−30685
Fe-free ribbon type multipole magnetic lens 80−42300
Li cylindrical lens for high energy particle focusing, aberrations 77−14649

magnetic levitation
conducting mag. top, fast rot. in inhomogeneous alternating mag. field 79−41264
diamagnetic bodies, mag. systems for free suspension 79−2794
diamagnetic sphere supported by field from annular current 78−66714
education, eddy currents, levitation, metal detectors and induction heating 78−61967
electrodynamic suspension system, current coil interaction with semiinfinite superconducting sheet *(Russian)* 80−83539
exterior regions containing moving conductors, finite element models 79−41291
fusion reactor, multipole fusion confinement with 2 MA levitated superconducting coil 80−106191
graphite particles, diamag. levitation, Brownian-motion press. gauge appl. 78−24807
laminar near wake, of magnetically suspended cones, meas. probe interference 77−84257
magnetisable conducting sphere, mag. levitation conditions, mag. dipole response to nonuniform mag. fields 79−98260
melting process control *(Russian)* 78−80531
metal melting in suspended state, large vol. and mass samples *(Russian)* 78−44036
metal spheres, stability criteria for centre of mass 78−66713
metals prep. by electromagnetic levitation in ultrahigh vac. 80−29899
multifilamentary composite superconductor power losses 79−30507
particulate materials in paramag. solns., meas. of specific gravity and mag. susceptibility 77−10070
prototype Nb gravitational radiation antenna 79−44841
solid sphere dynamics in alternating EM field *(Russian)* 77−88618
splat-quenching device, refractory metals and alloys *(Croatian)* 79−11639
torus, free suspension in field of coax. coil and conductor *(Russian)* 77−23596
tracked high speed traffic, levitation methods 79−49011
ultracentrifuge with magnetic suspension, contactless meas. of adhesivity and cond. appl. 77−16776
Fe body, stable levitation using superconductors 77−38799
Nb-Ti, sheet, flux trapping, appl. to mag. shielding and levitation 80−31806

magnetic lines of force *see magnetic flux*
magnetic liquids *see magnetic fluids*
magnetic logic
Ni-Fe-Co alloy films for logic devices, mag. switching vel., anisotropy field and coercive force *(Korean)* 77−51930
magnetic losses *see magnetic leakage*
magnetic materials
see also ferrites; garnets; magnetic fluids; magnetic thin films; permalloy; permanent magnets
bibliography of William Fuller Brown, Jr 80−8751
book, magnetism and metallurgy of soft magnetic materials 78−31029
conference, 2nd joint INTERMAG-MMM, New York, USA (July 1979) 80−27031
conference, Cleveland, USA (Nov. 1978) 79−73651
Conference, Freudenstadt and Bad Nauheim, Germany (March and April 1978) 79−24121
conference, Los Angeles, Calif., USA (June 1977) 77−85400
conference, Minneapolis, USA (Nov. 1977) 78−64176
conference, Munich, Germany (Sep. 1979) 80−56997
conference, Munster, Germany (March 1979) 80−12843
conference, Pittsburgh, USA (June 1976) 77−12071
development, properties, manufacture and appl. 77−8331
emulsion, magnetic and dielectric, prep. *(German)* 78−3376
energy losses in magnetically soft materials, determ. *(Russian)* 79−8014
energy relations in hard and soft mag. materials 77−8353
experimental magnetism, book 80−8747
halide, crystals, method of growing low-dimensional single crystal *(Japanese)* 80−50539
hard, normalised characts. derivation using statistical anal. *(Russian)* 77−18054
hard material demagnetisation curve evaluation 80−90869
high-energy, props., treatment procedures and testing *(Italian)* 80−54914
homogeneous, with constant mag. permeability, EM field calc. *(Russian)* 77−68151
intermetallic compounds development, 20-years research results 77−7843
layer magnetic properties meas. on saturated substrate 80−13108
magnet technology, conference, Bratislava (1977) 79−30499
magnetic anisotropy of electrical steel sheet, determ. method and laboratory tests *(Polish)* 80−97071
magnetics research, materials development and appl. during past 25 years 80−36792
magnetostriction hysteresis loop meas. by induction method *(Russian)* 77−56171
manufacturing errors analysis, affecting reversible permeability, restoration factor spread calc. *(Russian)* 77−12152
metalloceramic materials, NDT of microstructure and porosity using mag. props. 77−73416
nonferromagnetic media, triple-layer, approx. calc. of mag. field of feed-through transducer 80−78746
permanent, characteristics and appl. *(German)* 77−80966
permanent, technology, development *(Polish)* 77−89973
prediction of existence using cybernetic computer learning methods 80−108048
rare earth magnetically hard materials, review 77−73051
rare earth metals, alloys, and cpds., book 80−36785
rare earths, physics and chemistry (book) 79−69384
recording on particulate media, conference, Gardone Riviera, Italy (Sep. 1979) 80−41930
reinforced magnetically hard material, fibre-reinforced, porosity and impact strength 77−55916
sintering, structure and props., external mag. and elec. field influence 80−50570
soft, conf., Munster, Germany (Sept. 19 79) 80−86032
soft magnetic materials, hysteresis model 80−2606
soft magnetic materials, powder-based, phase comp., thermal analysis 77−51928
B and borides, conference, Varna, Bulgaria (Oct. 1978) 80−12842
Co permanent magnet material savings *(German)* 80−103851
magnetic materials, amorphous *see magnetic properties of amorphous substances*
magnetic memories *see magnetic storage systems*
magnetic mirrors
2XIIB, liq. N_2 cooled liners 78−50406
2XIIB, quasilinear model, stability of larger scaled machines 77−76165
2XIIB mirror machine, neutral-beam-injected, field reversal expts. 79−86589
2XIIB neutral beam injection confinement expts., stream stabilization 77−76164
2XIIB plasma, evidence for neutral-beam-injected O impurities 79−37547
ω_{ci} instability, suppression by electron beam injection in mirror confined plasma 78−47114
adiabatic compression of ion rings and associated plasma, kinetic theory 79−46469
adiabatic trap, charged particles motion, mag. field inhomogeneity effect, drift instability *(Japanese)* 77−43054
ambipolar plasma traps, resonance particle diffusion 79−86601
astron E-layers, mag. field distrib. and image field index 79−27817
axisymmetric mirror machine, MHD stable confinement possibilities 80−83988
beam-plasma interaction, high current electron beam trapping and ion heating 78−9795
Beta II, field reversed expt., device description 80−91274
Beta-II, magnetised coaxial plasma gun mechanical design and construction 80−91271
bumpy torus, NBT-I, effective toroidal curvature, error field, electron beam diagnostics 80−24237
bumpy torus plasma, weak vertical mag. field effect on fluctuation induced transport 80−48946
bumpy torus reactor, beam driven 80−42859
charged particles, multiple times for nonadiabatic leakage from mag. mirror traps 80−33806
collimator mirrors, grinding and polishing processes *(German)* 79−71433
collisional loss of electrostatically confined species in a magnetic mirror 78−79455
cone instability suppression in mag. mirror by profiled mag. field *(Russian)* 77−51167
magnetic mirrors continued
confinement of LiH plasmas, decay, density measurement 79−46470
confinement times for quasi-trapped particles 79−1327
convective loss-cone instability is absolute 79−64900
cyclotron and betatron oscills. in mag. mirror with RF field, cyclic accelerator theory 79−41051
drift cone mode, stabilisation at finite beta by warm plasma 77−7533
drift cone mode stabilisation with warm plasma, radial normal mode calcs. 78−51294
drift cone modes, electron stabilisation in mirror plasmas 77−72430
drift cyclotron instabilities driven by ion temp. gradient 79−10654
drift cyclotron loss cone instability, localised cold plasma effect 79−32797
drift cyclotron loss cone instability, stabilisation by addition of cool plasma 77−7526
drift cyclotron loss cone mode stabilisation in mirror machines 79−27814
drift loss cone instability in inhomogeneous mag. field 80−48934
drift-cone instabilities in mirror-confined plasma 80−28630
drift-cone instability, nonlocal hybrid-kinetic stability anal. 80−24230
drift-cone mode stabilisation in PR-6 mirror by RF power injection 79−90399
driven magnetic fusion reactors, conf., Erice-Trapani, Italy (Sept. 1978) 80−41948
EBT expts., simple annulus power balance 80−48947
electron and ion escape over pot. barrier in mirror field 79−4173
electron and plasma stream reflection at a nonadiabatic mirror 80−87929
electron beam, relativistic, electrostatic trapping in mag. mirror 77−24120
electron beam production, μs, high-current, device design and characts. 77−82642
electron beam stabilised mirror confined gas, hot electron population study 80−100089
electron cloud confinement, radial and longitudinal distrib. determ. 80−14928
electron cloud injection, confinement, and ejection in a mag. mirror 79−4170
electron clouds, neutral and nonneutral, mag. mirror confinement, radial distrib. 79−23445
electron density fluctuation amplitudes in mag. mirror device, microwave meas. 77−3985
electron dynamics, Q-factor enhancement 77−76175
electron energy distrib. of relativistic plasma in mag. mirror, synchrotron radn. meas. 79−10717
electron heating, ion cyclotron influence in min-B mirror trap 80−79521
electrostatic ion stoppering in mag. mirror field 78−1871
electrostatic ion stopping in mag. mirror field 77−39452
electrostatic ion-cyclotron wave spectrum in neutral beam injected 2XIIB device 78−9775
electrostatic modes in non-neutral electron clouds in mag. mirror, probe diagnostics 79−46466
electrostatic trapping of intense relativistic electron beam in magnetic mirror 77−24172
electrostatic well accumulation of multicharged ions in mag. mirror plasma by electron cyclotron reson. 79−32804
ELMO Bumpy Torus Reactor toroidal magnet system design 79−31196
end plugs, energy confinement increase 78−51336
end stoppering by the reversed field multiple-mirror concept 79−10687
end-stoppered, ion losses, linearised Fokker-Planck eqn. 78−34357
enhanced plasma confinement by MHD oscillation 80−24205
feedback controlled particle suspension system for laser initiated target expt. mag. mirror fusion facility 78−1864
feedback stabilised and stable, transfer function meas. 77−51215
field compression method, in which mirror field is propagating macroscopic wave 79−98957
field reversal, in mirror machine, computer simulation 78−26316
field reversal studies 80−27802
field reversed mirror configuration, sustaining a toroidal current 80−28804
field reversed mirror confinement, finite gyro-radius effects 80−83989
field reversed mirror neutral beam startup, hybrid plasma code simulation 80−99313
field reversed mirror reactor, 2nd generation design calcs. 78−58465
field reversed mirrors, fusion product energy distribs. 80−37595
field-reversed mirror, reactor parameters 78−8983
field-reversed mirror startup by neutral beam injection 79−86605
field-reversed mirrors, stability of low-frequency modes 79−86606
field-reversed mirrors as fusion power reactors 78−8979
first wall surface conditions control in 2XIIB device 77−31501
flute mode stabilisation by axial feedback in multiple mirror 78−75408
flute oscillation suppression by automatic EM control *(Russian)* 78−30464
fusion and hybrid reactors, plasma models 80−6273
fusion central power station, 1 GW, tritium containment and blanket design problems 77−38414
fusion device, plasma buildup, model 78−8981
fusion energy program, mirror approach 80−42855
fusion mirror reactor, efficient high-energy high-power neutral beams 79−49836
fusion plasma, electron heating using external power 78−87482
fusion reactions, measuring MeV ions in magnetic mirror experiments 80−6281
fusion reactor, direct energy conversion 78−5018
fusion reactor, field-reversed mirror 80−42857
fusion reactor, flute mode axial feedback stabilisation 77−80344
fusion reactor, mirror type, MHD gas turbine energy conversion 79−41885
fusion reactor, tandem mirror device, operation, Q-factor calcs. *(Russian)* 78−74466
fusion reactor. time-dependent tandem mirror confinement, start-up and alpha particle build-up 80−10419
fusion reactor, TMX, magnets, mech. design 78−58494
fusion reactor, using toroidally-linked mirrors 80−42858
fusion reactor and plasma physics magnets, USA development 79−31193
fusion reactor appls. 78−50343
fusion reactor mirror machines, nonaxisymm., quadrupole field and orbital reson. 79−59250
fusion reactor studies 77−74980
fusion reactors, confinement of advanced fuels 79−13516

magnetic mirrors continued
fusion reactors, differences between mirror and toroidal fusion systems, superconducting magnets 80−32429
fusion reactors, field reversed mirrors 80−43961
fusion reactors, theoretical status of mirror machine confinement, review 77−38398
fusion reactors, Tokamak and tandem mirror reactors, neutral beam injection and superconducting magnets 80−63391
fusion reactors conceptual designs, with standard, tandem and field-reversed mirrors 79−49857
fusion research, philosophy 80−42854
fusion test facility, reactor-like devices technology development 79−49856
fusion-fission hybrid reactor, mirror confinement, fuel design consideration 79−22472
fusion-fission hybrids, mag. mirror blankets and drivers 79−13517
GAMMA 6, tandem mirror confinement expt. 80−28786
gas lasers with non-self-sustaining discharge, mag. mirrors *(Russian)* 80−106530
geometric higher order adiabatic invariants, nonadiabatic diffusion 77−68846
GOL-1 device, homogeneous mag. field prod. 78−67402
Hamiltonians of particle motion, canonical transforms. 80−33748
HF convective loss cone instability in short mirror machines 79−90401
high β, gas-stabilised, plasma in 2×IIB mirror machine 77−7582
high beta mirror machine, kinetic and guiding centre fluid theory 77−76166
high beta reactor, simple binary collision theory 79−86603
high density machines, critical lengths 80−64768
high density plasma in multiple mirror, low freq. instability 80−48870
high voltage Penning discharge reflex system, confinement in mag. mirror field 79−86600
high-beta three-dimens. mirror equilibria 77−15235
HIP-1 hot ion plasma, effect of anode-cathode geometry on performance characts. 77−24112
hollow axisymmetric mirror, MHD stable, multipole field stabilization *(Russian)* 80−33801
hot electron ring, conducting wall stabilisation 78−1881
hot-electron plasma in simple mirror, stability, X-ray diagnostics 77−24176
hybrid tandem mirror reactors, design, fissile fuel production 80−27811
impurity seeded multiple-mirror end plug, linear fusion reactor 78−63580
inertial fusion by oscillating relativistic electron beams in magnetic mirror *(French)* 79−54595
injected plasma particle refl. (trapping), quiescent (turbulent) plasma 80−48955
instabilities, feedback suppression of spatial channelling modes *(Russian)* 77−47243
ion beam, charge-neutralized, mag. compression in mag. mirror field 77−76182
ion beam creation of rot. ion layer 78−5889
ion confinement increases, Joule heating 80−83985
ion motion, superadiabatic and stochastic, in mirror-machine plasma, in presence of electrostatic wave 80−53933
ion ring, precessional mode stabilisation using general mag. multipole field 77−24174
ion ring compressor, power generation in combination with subcritical fission blanket 77−23276
ion velocity space diffusion and ion-cyclotron oscill. enhancement in mirror confined plasma 77−24059
ion-cyclotron instability meas. in mirror-confined plasma 77−3991
Langmuir waves in spatially periodic mag. field 79−10655
laser start-up system for mag. mirror fusion 77−62383
linear gasdynamic confinement system 80−48957
linear multimirror expt., dissipative and reactive modes 78−63558
linear reactor system with impurity-seeded multiple-mirror end plug 78−78493
linked mag. mirror fields, minimum-average-B wells 79−19066
loss suppression from mirror ends 80−83987
lower hybrid reson. heating, canted mag. mirror electron cyclotron reson. plasma 77−19727
lower hybrid wave excitation, of mirror mag. field plasma 79−19054
magnetic compression of relativistic electron beams, transmission through mag. mirror 77−1012
magnetic-curvature-driven interchange instability, surface line tying stabilisation 79−41865
MFTF, BBC CQK 200-4 modulator tube for sustaining neutral beam power supply 80−99290
MFTF, cryogenic system 80−106163
MFTF, electrical systems, overview 80−91278
MFTF, end loss region high energy plasma gettering 80−102343
MFTF, exception handling control system 80−99325
MFTF, intense neutron environment, test cell side wall design, shielding materials 80−102318
MFTF, ion and neutral beams dumps, design 80−102317
MFTF, mag. cryostability 80−106198
MFTF, neutral beam accel power supply protection 80−102380
MFTF, neutral beam module component design and development 80−91270
MFTF, neutral beam source development 80−102368
MFTF, plasma buildup, contaminant control 80−95461
MFTF, plasma diagnostics system 80−95444
MFTF, plasma streaming system, description 80−91280
MFTF, power supply system, digital simulation using EMTP code 80−91286
MFTF, start up neutral beam power supply system 80−91281
MFTF, superconducting mag. quench vent rate 80−106197
MFTF, supervisory control and diagnostics system, database management system 80−99326
MFTF, supervisory control and diagnostics system, database management system, data structs. 80−99327
MFTF, supervisory control and diagnostics system software 80−99324
MFTF, sustaining neutral beam power supply, cct. anal. using ASTAP and EMTP codes 80−91284
MFTF, sustaining neutral beam power supply, shunt preconditioner, IBM-ASTAP anal. 80−102332
MFTF, sustaining neutral beam power supply system, modelling with ASTAP code 80−91285
mFTF plasma diagnostics Data Acquisition System 80−99319
MFTF superconducting mag. design and construction 80−101008
magnetic mirrors continued
MFTF-B, full tandem extension, description 80−99294
microwave generation during strong electron beam-plasma interaction in mag. mirror field *(Russian)* 77−11355
Migmacell, diamag. limitations to fusion rate 78−42791
Mirror Fusion Test Facility, superconductor core manufacturing and quality 80−93521
mirror fusion test facility 80−43962
Mirror Fusion Test Facility supercond. coil development 79−31202
mirror hybrid reactors 80−42860
mirror machine, fusion reactors, survey 80−47721
mirror machine diagnostics 80−48958
mirror machines, nonadiabaticity 78−55740
mirror reactors, economic significance of Q 80−47722
Mirror-Torus-System-1 with divertor mag. field, plasma density and depolarisation current 80−70022
multimirror experiment, linear, trapped electron instability 79−60181
multiple mirror, coil design and economic optimisation 80−99284
multiple mirror mag. trap ion distrib. function, high energy tail 78−83596
multiple mirror reactor with depressed ion temp., power balance 78−67393
multiple mirror system, for high density confinement 80−92364
multiple-mirror confined plasma, interchange modes stabilisation 78−42790
multiple-mirror field config., transient plasma confinement 78−5911
multiple-mirror plasmas, MHD stabilisation 80−6244
neutral beam-injected mirror-confined plasma transport 78−22461
nonadiabatic leakage of particles from mag. mirror trap, multiple lifetimes 80−106968
nonlinear converging resonance cones in Princeton L-3 device 80−59262
nonlinear Landau damping in mirror plasmas 79−27766
OGRA-3 installation, large plasma density during feedback stabilisation, unstable oscills. characts. *(Russian)* 77−47245
Ogra-3 mirror device, loss mechanism due to cyclotron instabilities 80−28788
Ogra-3B, ECR as a diagnostic for mirror trap plasma 80−38709
Ogra-3B, open mag. mirror trap, with min. B, LF oscills. 80−38708
open trap with ambipolar mirrors, thermonuclear plasma behaviour 77−76167
particle motion and diffusion in mag. mirrors 77−15234
particle orbits in field reversed mirrors 79−19067
particle stochastic motion in mirror machines 80−59264
Penning discharge, in mag. mirror field, characts. 77−72520
Penning discharge plasma, residual gas density and elec. potential profile meas. 78−67485
PHAEDRUS RH heated tandem mirror, single particle orbits 78−79456
picket-fence surface magnetic fields at end of magnetised plasma 80−87922
pitch angle diffusion eqn. of trapped particles in presence of loss. cone, finite difference integration 79−70931
plasma confinement in mirror and cusp fields, Monte Carlo simulation 80−96379
plasma confinement time investigation using Monte Carlo simulation 80−64770
plasma density, increase due to transverse energy increase 79−64889
plasma diffusion rate, meas. by trapped particle echoes in mirror machine 77−35324
plasma loss suppression at mirror end by ponderomotive force 79−14593
plasma production modified magnetron discharge facility 78−75380
plasma resonant behaviour, near lower hybrid freq., mirror config. effects 77−15202
PR-6 mirror trap, drift loss-cone instability stabilisation by cold ions addition 79−32800
pressure anisotropy stabilisation of axisymmetric mirror machines 79−4169
production of large-radius, high-beta, confined mirror plasma 80−87907
proton beam, intense, space charge neutral, trapping in mag. mirror, simulation 78−9825
proton ring, static compression and trapping, simulation 77−84491
proton rings in mag. mirrors, computer simulation 78−67405
Q-enhanced mirror fusion system, plasma-surface interaction 78−94130
quasi steady high beta plasma in multiple mirror machine, density oscill., stability obs. 80−28663
quasi-linear equation of plasma in mag. field, appl. to mirror confinement 79−1297
quasilinear transport model 77−76181
RECE-Christa device, axial translation of field-reversing E layers 79−19065
RECE-Christa device, field-reversing electron ring production, by ring stacking 77−84482
reflex discharge, device for generation, confinement and plasma heating *(Rumanian)* 78−47151
relativistic electron beam, magnetic compression of high current beams 77−87876
relativistic electron storage device, phase free cavity resonator+mag. mirrors 77−83172
relativistic electron storage device, phase-free cavity resonator with two mag. mirrors 77−10504
research and compact fusion power plants 78−744
reversal field mirror, alpha-particle effects 78−58468
reversed field config. generation without toroidal field 79−86599
reversed field mirror reactors, startup using coaxial plasma guns, scaling laws 80−99279
RF cavity with magnetic mirrors, computer simulation of confine 78−59648
RF plugging, appl. thermonucl. plasma 77−76169
RF plugging, confinement times 78−1872
RF plugging of high density plasma 79−10694
RF plugging of high-density plasma 78−83604
RF produced mag. confined nonneutral electron plasma 79−10677
SAFFIRE, Cat-D fueled, synthetic and fissile fuel prod. 80−99280
spheroimak devices, magnetohydrostatic equilibrium config. 80−83965
stream density through mag. mirror, reduction by HF rot. dipole mag. field *(Russian)* 77−47244
strong ion ring, production in long pulse ion accelerator, effect of mirror rise time 77−24113
superconducting magnet system for mirror fusion expt. 77−27743
superconducting magnet systems, USSR designs 79−31192
superconducting magnets, mirror fusion test facility 80−42862
tandem mirror, passive generation of ambipolar pot. barriers 80−24203

magnetic mirrors continued
tandem mirror confinement studies 80−28785
tandem mirror end plugs, ICRF fuelling 79−19070
tandem mirror hybrid; ^{233}U prod. 80−47708
tandem mirror physics, fusion plasma confinement 80−43960
tandem mirror plasmas, alpha particle dynamics 80−83986
Tandem Mirror Reactor, end plug mag. system design 80−102347
tandem mirror reactor, new plasma confinement scheme with high system Q 77−42183
tandem mirror reactor, plasma parametric studies and appl. 80−42865
Tandem Mirror Reactor power plant, maintenance and handling economics 80−102311
Tandem Mirror Reactor startup and shutdown, simulation and control 80−99277
Tandem Mirror Reactor steady state, simulation and control 80−99278
Tandem mirror reactors, anomalous and classical transport effect 80−13862
tandem mirror reactors, DT and DD operation 78−8982
tandem mirror reactors, fusion power reactor and fusion-fission hybrid reactor 80−42856
tandem mirrors, ambipolar pot-enhancement by neutral beam injection 79−94806
tandem mirrors, analytic approx. to resonant plateau transport coeff. 80−32486
thermonuclear open mag. trap geometry, double mirrors *(Russian)* 77−3970
theta-pinch, end plugging by pulsed mirrors 79−14602
theta-pinch, linear, end loss reduction by solid and plug 77−89293
theta-pinch, linear, end losses simulated by numerical technique 77−89295
theta-pinch, linear, RF oscill. multiple mirror stabilisation and heating 77−89290
theta-pinch, linear, solid end plugs and mag. mirrors, fusion reactor 77−89294
theta-pinch, toroidal multiple mirror field, high-beta, opt. obs. 77−24136
TMX, config., liq. N_2 supply and operation of vacuum system 80−95448
TMX, injector system mech. design and installation 80−99393
TMX, installation and operation of cryoliners in vacuum system 80−95449
TMX, mag. control system 80−95442
TMX, magnet construction and alignment 80−91266
TMX, neutral beam control systems 80−99323
TMX, neutral beam system startup 80−99306
Tormac DT fusion reactor, power gain and net output 78−58402
toroidal collective focusing accelerator for heavy ion acceleration 80−14015
toroidally linked mirror reactors, Q calcs. 77−34439
transverse confinement of high press. plasma in corrugated mag. field 80−48944
turbulent diffusion regimes along the pitch angle in a geomagnetic trap *(Russian)* 79−55534
turbulent heating of magnetic mirror confined plasma, rel. to Buneman instability 77−24106
Twin Beam Mirror, effect of hot beam injection angle 80−48939
twin beam mirrors, effect of hot beam injection angle 78−58466
two-temp. electron-ion plasma with mirror reflection, EM fluctuations, space charge correl. *(Russian)* 78−59548
unneutralized electron cloud injection and containment in bumpy toroidal mag. field 80−64761
USA, mirror machine research progress 80−74016
variations of magnetic mirrors, classical surface of section determ. 77−13231
μ^+ polarisation dynamics in mag. mirror field, neutrino emission asymmetry 77−61645
D-^{3}He field reversed mirror 79−13516
D-^{3}He satellite fusion reactor, field-reversed mirror confinement 78−70643
DT multiple mirror reactor, power balance, impurities 77−74998

magnetic moments
see also atomic magnetic moment; hyperon magnetic moment; local moments in dilute systems; meson magnetic moment; molecular moments; nuclear magnetic moment; proton magnetic moment
20-plet baryons, charm quantum numbers, SU(4) symm. model 77−61257
actinide elements and compounds, mag. props., book contrib. 80−75727
actinide intermetallic cpds., cubic, var. from localised to itinerant magnetism 77−20534
actinide intermetallics, $AnFe_2$, (An=U, Np, Pu, Am), magnetisation, neutron diffr. and Mossbauer expts. 77−63137
actinide metallic systems, magnetism 80−7076
alkali metal-transition metal double molybdates, paramag. behaviour *(French)* 80−39734
alkaline-earth-Os ternary oxide system, solid state prep. and reactions, cryst. struct., mag. and elec. props. 79−24739
alloy, binary, magnetic moment determ. from neutron scatt. 77−73011
alloy, binary, with mixed ferro- and antiferromag. exchange, magnetisation, phenomenological theory *(German)* 78−56297
alloy with two ferromagnetic components, surface excitations 80−25179
alloys, amorphous, mag. props., review *(Japanese)* 78−52259
alloys, crystalline and amorphous mag. props. from Rhodes-Wohlfarth plot 78−52190
amorphous alloys, at. order effects 77−73006
amorphous alloys 77−16054
amorphous ferrimagnetic alloy, mag. anisotropy from dipolar interactions 79−87252
amorphous ferromagnet, excitations, calc. using hard sphere models 77−66289
amorphous ferromagnets, book contrib. 80−75743
amorphous magnet, magnetisation, mag. moment temp. distrib. 80−15848
amorphous magnetic layers, SAW device appl. 80−28389
anisotropic paramagnet with exchange-bond dilution, sixth freq. moments 80−44789
anomalous magnetic moment, perturbative expansion divergence 80−78063
anomalous magnetic moment calcs., spin induced mass 77−61228
antiferromagnet, mag. moment and sp. ht. fluctuations near critical temp. 78−91867
antiferromagnet, magnetic and thermal props. 78−14937
antiferromagnet, magnetic dislocation domains, mag. moment distribution 80−2601
antiferromagnet, phase transformations in strong mag. fields, mag. moments collapse, strengthened magnetoelastic links *(German)* 78−68227
arbitrary moving magnetic dipole, EM field calc. *(Russian)* 80−9772
bar magnet, rel. between magnetometric and ballistic moments *(German)* 79−28511
baryon, calc. using quark confinement ideas 77−57539
baryon, incorrect value from static compound quark models 80−9169
baryon, magnetic moments, ground-state, SU(6) symmetry 80−78064
baryon magnetic moments, implications for quark model 80−13290
baryon sum rules in SU_4 charm symmetry scheme 77−30380
baryons, b-quark, magnetic moments, broken SU(5) symmetry 80−95257
baryons, charmed, mag. dipole moments and mag. quarks 79−97573
baryons, current status, additional symmetry breaking assumptions 80−4995
baryons, EM characteristics, bag model *(Russian)* 79−93380
baryons, five quark models and mag. moments 79−26297
baryons, leptonic decays and mag. moments in nonlocal quark model *(Russian)* 80−86711
baryons, mag. moment calcs. in quark models 80−27505
baryons, ordinary and charmed, magnetic moments in broken SU(4) 80−18136
baryons, resonances in higher symmetry schemes, charm particles 77−57538
baryons, spin $1/2^+$, mag. moment sum rule, in SU_3 for u-, d- and c-quark sector 78−21428
Bi, current states, symmetry and self-oscills., macroscopic mag. moment by RF irradiation *(Russian)* 79−19749
bisgalvinoxyl biradical, cryst., spin-spin dipolar and exchange interactions 78−52356
borate glass: Ni, absorption spectra, mag. props., coordination behaviour *(German)* 80−40147
borides, transition metal, rare earth, and actinide, mag. props., book contrib. 78−47978
bound triquark nucleon model, mag. moment and weak interaction coupling constant ratios 79−67517
broken SU(3) gauge model of strong and EM interactions, scatt. lengths, baryon mag. moments 78−74133
bubble device materials, single-layer, ion-implantable small, design and development 79−82844
charged particle, mag. moment vac. on nonadiabatic motion in dipole field *(Russian)* 77−42476
charged particle interaction with linearly polarised MHD plane wave, mag. moment invariance 77−78580
charmed baryons, dipole mag. moments, new U_3 scheme using u, d, c quarks 78−58165
charmed baryons, mag. moments in quark model 77−30332
charmed baryons, magnetic moments, broken SU_3 subsymmetries of SU_4 79−63382
charmed baryons, magnetic moments by SU_3 and SU_4 symmetry 78−82209
charmed baryons, semileptonic decays, SU(4) breaking, mag. moments, suppression factors 79−387
charmed baryons, static and transition magnetic moments in quark model 77−46050
charmed hadrons, mag. moments, additive-quark-model 77−82707
chromocene, mag. props., complete ligand field theory 78−31048
chromocene, mag. suscept., zero-field splitting, ligand field, 1-303K 77−89924
classical mag. moment system, antiferromag. phase transition, secular dipole interactions 80−80551
classical Yang-Mills theory, mag. dipole soln. 78−62302
cobaltocene, mag. props., complete ligand field theory 78−31048
composite leptons and quarks, anomalous mag. moment, flavour as dynamical quantum number 80−105854
composite leptons and quarks, mag. moment 80−105896
composite models, mag. moments of quarks, leptons and hadrons 80−32081
composite quarks and leptons, mag. moments 80−91056
conducting body in uniform electric field, computations *(Polish)* 79−76546
copper formate tetrahydrate, antiferromag. phase, neutron diffr. study 80−93085
coupled Einstein-Higgs field, mag. monopole and dipole soln. *(Chinese)* 78−82112
coupling constant singularities in QED 79−21991
covariant wave equations, Galilei group and mag. moment of electron 77−64955
current density and electric and magnetic multipole-moment operators in quantum mechanics 80−27433
cyclohexyl ammonium copper chloride, one dimensional spin $^1/_2$ ferromag., mag. props. 80−71000
deuteron magnetic structure function meas. in ed elastic scatt. at 1.0 $(GeV/c)^2$ 77−57537
dimethylammonium copper chloride bromide, mag. props., pulsed NMR expts. 80−11292
disordered Heisenberg binary magnetic alloy with mixed exchange interaction, compensation point *(Russian)* 77−51898
domain wall velocity, simple mag. moment wave propag. 77−16105
dual-spin satellite magnetic attitude control system, geomag. field effects 78−65484
education, Dirac delta function, appl. elec. current and mag. multipole distribs. 80−17740
electron, anomalous magnetic moments, eighth order contrib. calcs., QED tests 78−45821
electron, in mag. field, intrinsic mag. moment, measurement possibilities *(Russian)* 78−86430
electron anomalous mag. moment, dispersive approach, 6th order contrib. in QED 79−9316
electron anomalous magnetic moment, muon effects in QED 80−62899
electron anomalous magnetic moment, Pauli eqn. in crossed mag. electrostatic fields *(Russian)* 78−16962
electron gas, magnetised, confinement effects 79−28494
electron gas in ultraquantum limit of strong mag. field *(Russian)* 77−28361
electron magnetic moment anomaly determ. using two level dual vac. polarisation model 78−54632

magnetic moments continued
electron moving in strong EM field, radiational corrections to mass and mag. moment *(Russian)* 77−61226
electron pair, in one-dimens. pot. box, possible ferromagnetism 79−61020
EM field radiation on smooth convex surfaces 78−62977
europium ethylsulphate nonahydrate, MCD due to mag. dipole transitions 77−24825
f-quark, five quark models and baryon magnetic moments 79−13020
fermi crystal, mag. props. of vacancies *(Russian)* 79−46881
ferrimagnet, mag. torque near compensation point 79−33472
ferrite, hexagonal, with M, W and Y structures containing Fe^{2+} and Fe^{3+} mag. ions, saturation moment and anisotropy 80−71009
ferrites, hexagonal, model, two-sublattice uniaxial systems with strong antisymmetric exchange 78−47971
ferrites of divalent metals, prep. by double decomp. reaction, mag. charcts. *(French)* 79−33463
ferrofluid, magnetically induced polarisation, particle size determ. 77−73130
ferrofluids, magnetisation, absence of anisotropy effects 80−50146
ferromagnet, Barkhausen discontinuities in model of rigid domain boundaries *(Russian)* 77−51922
ferromagnet, dislocation motion, mag. moments around screw dislocations, spin waves retarding dislocations 78−87670
ferromagnet, Heisenberg, spin wave relaxation due to dipole interactions, damping temp. depend. 79−69664
ferromagnet, itinerant, mag. props., temp. depend., functional integral approach 80−60170
ferromagnet, magnetic moment fluctuations and sp. ht. near crit. point 77−28388
ferromagnet, tight binding model, surface magnetisation 80−103807
ferromagnet, two-dimensional, dipole forces and phase transition *(Russian)* 79−51782
ferromagnet in strong alternating mag. field, eqn. of motion of total mag. moment *(Russian)* 78−88097
ferromagnet magnetisation, influence of high intensity longitudinal sound waves 80−103875
ferromagnetic alloys, amorphous, sputter-deposited, soft mag. props., magnetostriction 80−34696
ferromagnetic alloys, disordered crystalline and amorphous, dipole field distribution 80−25101
ferromagnetic BCC and HCP crystals, anisotropy of dipole fields, at interstitial sites 79−33584
ferromagnetic film, electric-charge-induced magnetisation, mag. balance and Mossbauer effect meas. 79−69700
ferromagnetic helical structures, magnetooptic light interaction 79−65843
ferromagnetic material thickness determ., NDT technique 79−79187
ferromagnetic medium, Landau-Lifshitz nonlinear equation, N-soliton solutions *(Russian)* 79−24184
ferromagnetic metal surface, Fermi level shift by charging, mag. moment and hyperfine splitting 77−20677
ferromagnetic nondegenerate semiconductor, magnetoresistance 80−11019
ferromagnetic random binary alloys, elastic neutron scatt. cross section 78−91845
ferromagnetic semiconductor, degenerate, surface magnetisation 77−8385
ferromagnetic semiconductor, homogeneous state, phase transition and stability 78−6528
ferromagnetic transition metal alloys, mag. props. review 80−44823
ferromagnetic twin crystals, Bloch mag. struct., depend. on crystallite thickness and mag. field *(Russian)* 79−42792
ferromagnetism and ferroelectricity, coexistence in systems with electron-hole pairing 80−7310
ferromagnets, easy plane, containing dislocations, static props. 79−95626
ferromagnets, solitary domains, Bloch and Neel stability, calcs. 80−25157
fluctuations, excitations and induced moments in system with two singlet levels 79−61022
fluctuations and mag. eqn. of state 78−64194
free magnetic dipole in field of ellipsoid, stability of orbital motion 77−88630
frequency-dependent electric and magnetic multipole moments and Siegert's theorem 80−27432
fundamental constants, self-consistent values *(German)* 79−12758
giant moments and spin glasses, order out of disorder *(Dutch)* 80−97107
hadron magnetic dipole transition, quark anomalous mag. moments *(Russian)* 80−82975
haemoglobin, deoxygenated, vibronic coupling effect on paramagnetisms 77−57899
hamiltonian for the nonrelativistic two-fermion bound state 80−13273
Heisenberg, paramagnetic with bond dilution, freq. moments of spin correlation function 79−15272
Heisenberg ferromagnet, two-dimens. second order phase transition 77−16094
Heisenberg model, two-dimensional, thermodynamics taking into account mag. dipole interaction *(Russian)* 77−32144
Heisenberg open finite chains, effective mag. moments as functions of reduced temp. calc. 77−51868
Heisenberg paramagnet, exchange bond dilution, freq. moments of spin correl. function 80−50030
Heisenberg system, ordered phase, reaction field approx., anisotropy presence 79−61030
hexagonal antiferromags., ground states antiferromag. vectors, ferromag. moments *(Russian)* 78−27040
high-field solenoid field gradient appl. 80−31813
hindered rotator in mag. field, mag. moment due to orientational tunnelling 77−68931
Hubbard model, arbitrary electron density case, functional integral approach 78−76219
Hubbard model, half-filled, charge ordered solution local mag. moments, repulsion energy renormalisation 79−61034
Hubbard model, neutral, strong-coupling props. 77−24667
hyperon mag. moments, transition moments, SU(3) calcs. 79−13128
induced moment systems, effect of spin fluctuations 80−2585
induced-moment singlet-triplet model, rel. between ground-state moment and crit. temp. 79−78282
insulating solid, nonmagnetic, anisotropic mag. effect 78−6509
intermediate valence compounds, dynamic susceptibilities 80−70653

magnetic moments continued
intrinsic dipole moments, discussion as to their nature 78−28969
intrinsic semiconductors, indirect exchange interaction, finite temp., valence bands and energy gaps effect 80−59943
Invar, magnetic and thermal anomalies 80−34603
Invar alloys, mag. struct. small angle neutron scatt. study 79−47249
Invar film, mag. props. and elec. resist. 77−32221
Invar films, exchange interaction depend. on lattice parameter, spin-wave reson. and magnetisation meas. *(Russian)* 79−42751
Ising model, disordered, thermodynamic pot., ferro-and antiferromagnetic bonds, mag. moment and entropy *(Russian)* 79−19714
itinerant electron antiferromag., localised mag. states 79−28500
itinerant electron ferromagnetism, single-site functional integral approach 79−65637
itinerant ferromagnet, effect of planar defects on electronic struct. and mag. ordering 79−99672
itinerant-electron ferromagnetic film on nonmagnetic metallic substrate, mag. props. 80−20371
kaolinite, aq. suspension, mag. and optical props., Fe_2O_3 impure particles 78−76933
Kondon lattice, impurity interactions, ground state calc., impurity conc. effect 80−65782
laser plasma, spontaneous mag. fields of dipole configuration *(Russian)* 79−77411
lattice nuclear mag. system simulation by classical mag. moments 77−69713
Lee model in EM field, mag. moment calc. using Schwinger source theory 80−42350
light emission by mag. and elec. dipoles, radiation patterns 80−32886
linear gyrotropic media, E2, M1 moment contribs. to linear polarisation *(Russian)* 77−8540
liquid metals and alloys, mag. model 80−88719
low lying baryons, anomalous mag. moment contrib. from quarks 80 42462
Lu-tinger-Tisza method generalisation, appl. to highly anisotropic dipole-dipole interactions 77−20514
magnetic electron gas induced by van Vleck ion, spin polarisation, ion mag. moment 79−56176
magnetic multipole expansion, education 80−105456
magnetic structure elastic polarised neutron scatt. atomic mag. moments 80−29531
magnetisable conducting sphere, mag. levitation conditions, mag. dipole response to nonuniform mag. fields 79−98260
magneto-gravitational effect *(Russian)* 77−9935
magnetostrictive ferromagnet, conditions for stress induced bulk moments 79−78493
manganese carboxylate, dodecanuclear mixed-valence, prep., struct., and mag. props. 80−107196
massive neutrinos, mag. moment and spin rotation 80−105895
metal, conduction electrons spin magnetisation kinetics, role of surface scatt. *(Russian)* 77−80989
metal hydrides, rare earth and intermetallic, electronic and mag. props., Mossbauer study 80−34830
metal whiskers, quantum oscills. of mag. moment 79−15280
metal-H systems at high H press., physicochemical props., book contrib. 80−24535
metallic glasses, mats. props. review 77−4043
metallic whisker single crystals, low temp. magnetometer 79−88986
metallo-proteins and model systems, susceptibility and struct., SQUID magnetometer uses 79−53036
metals, ferromagnetic, point contact spectroscopy, electron-magnon interactions *(Russian)* 80−54766
metals, ground state of solids, spin density functional method, binding energy, compressibility 80−65477
metals, neutron mag. form factors, magnetisation densities, APW wavefunction calcs. 79−47243
metals, polar states and free electron gas, mag. moments *(Russian)* 80−84415
metastable polarised crystals, decay kinetics, exchange magnon-phonon interactions *(Russian)* 80−7060
MIT bag model, charmed and b-flavoured hadron mag. moments 80−95271
muon, corrections of the sixth-order anomalous magnetic moment of the muon 79−54371
muon anomalous mag. moment in lepton struct. model 77−61250
muon mag. moment, pionic contrib. lower bound 77−26527
N-alkylated phenazine type radicals, mag. props. 79−73671
naive quark model predictions for meson mass and baryon mass and mag. moment 80−78036
neodymium ethyl sulphate, cryst. c-axis demag. from 25000G, magneto-hydrodynamic props. to 0.01K 77−20599
neodymium ethyl sulphate, magnetothermodynamics, absolute temp. scale, mag. moment and magnetization , below 0.5K 78−34984
neodymium ethyl sulphate hydrate, spherical single crystal, magnetothermodynamic props. 77−55365
neutron, Bloch-Siegert effect in Ramsey separated oscill. field technique 79−3063
neutron, dipole moments and spin rot. meas. 79−36080
neutron, electric and magnetic dipole moments 80−4993
neutron, expt. determ. and degree of precision, review 79−58961
neutron, expt. determ. using meas. of ratio of p/n Larmour frequency 79−58962
neutron, fundamental phys. expts. with reactor neutrons and neutrinos, summary 79−67543
neutron, fundamental physics with reactor neutrons and neutrinos [conf. ILL, Grenoble, France (Oct. 1977)] 79−59112
neutron magnetic moment meas., separated oscillatory-field magnetic resonance technique 80−22613
neutron magnetic moment meas. 78−8719
neutron resonances, polarised neutron expts., spin depend. of neutron cross-sections, mag. moments, radiation capture of neutrons *(Russian)* 80−52654
neutron spinor rotation, search using Fresnel interferometer *(German)* 79−9376
$(Ni_{1-x}Co_x)_{0.98}Mn_{0.02}$, average mag. moment of Mn atoms 79−28509
non-stoichiometric phase, physico-chemical props. 80−29532
nonequilibrium semiconductor with electron-hole pairing, mag. moment quantum oscills. *(Russian)* 77−28131
nonlinear waves, mag. moments, limiting rel. and types *(Russian)* 78−60276

magnetic moments continued
nuclear magnetism and ultralow temperature, review *(Japanese)* 80−86806
nucleon, gluon exchange corrections in MIT bag model 77−26528
nucleon, upper bounds in terms of Compton scattering cross sections 77−2836
nucleon isoscalar anomalous mag. mom. calc. 78−82212
one-spin ferromagnet, high temp. series expansion for mag. susceptibility and sp. ht. 80−25148
orthoferrites, weak ferromagnetism, single ion anisotropy contrib. 80−25126
oxovanadium carboxylates, near one-dimensional antiferromagnetism, thermal and mag. props. calc. 77−20602
oxyhaemoglobin, mag. props. and structure 78−48751
paramagnet with noninteracting mag. moments, magnetisation *(Russian)* 78−47938
paramagnetic metal, narrow band electron system, temp.-induced local mag. moment 78−76221
particles with anomalous moments, motion in external EM field *(Russian)* 79−9321
periodic lattice, theory of coexistence of supercond. and magnetism, supercond. transition temp. 80−34543
Permalloy-Rh, film, influence of Rh on corrosion resist. and mag. props. 80−3235
phosphate glass: Ni, absorption spectra, mag. props., coordination behaviour *(German)* 80−40147
planetary magnetic moments, two predictions from scaling law test 80−21934
polarisation and magnetisation of electronic matter 80−75929
polyarylenealkyls, colour, EPR, electron density delocalisation degree determ. *(Russian)* 80−7152
quark anomalous magnetic moments and meson radiative decays in naive quark model 79−17693
quark colour magnetic moment 80−42400
quark magnetic moment, rel. to quark mass and hadron mass in SU(3) breaking 79−13050
rare earth alloys, CPA calc. of mag. moments and transition temps. 78−84423
rare earth alloys, R_3Pt_4, R=Nd, Gd, Tb, Dy, Ho, Er, Tm, mag. props., 4.2 to 160K 79−78343
rare earth alloys, RCoAl, mag. props. 78−2659
rare earth alloys, RCu_x, mag. props., 4.2 to 200K 79−87233
rare earth and rare earth intermetallic hydrides, magnetic properties, effect of hydrogenation 78−68210
rare earth cobaltides, R_2Co_{17}, ^{59}Co NMR obs. of hyperfine fields and mag. moments 77−20726
rare earth compounds, binary, regression eqns., for calc. props. from electron struct. 80−39498
rare earth compounds, connection between exchange field and Fe and Co moments 77−1551
rare earth compounds, mag. moment and valence fluctuations 78−23244
rare earth dihydrides and dideuterides, electronic and mag. props. 80−25260
rare earth ferrite-garnets, compensation temp., rare earth ion influence 79−51775
rare earth ferromagnets, spin polarised electron tunnelling 78−68094
rare earth intermetallic, $R(Fe_{1-x}Mn_x)_2$, phase struct., mag. and Mossbauer meas. 77−20563
rare earth intermetallic cpds., mag. props., book contrib. 80−39759
rare earth intermetallics, mag. props. 78−84380
rare earth intermetallics, R_2Al and R_2Au, mag. characts. 78−68183
rare earth intermetallics, $RAu_{3.6}$, ordering temps. and effective moments 78−60283
rare earth intermetallics, RAu_3 (R=Gd, Tb, Dy, Ho, Er, Tm), mag. props. *(German)* 79−51761
rare earth intermetallics, $RNiSi_3$, susceptibility, 80-1200K *(Russian)* 77−66281
rare earth iron garnets, mol. field coeffs. 77−1544
rare earth metal, ferromagnet-simple helix transition, cond. electron spin polarisation *(Russian)* 79−7995
rare earth metasilicates, $R_2(SiO_3)_3$, mag. susceptibility, temp. depend., 77-800K 80−20372
rare earth mixed ferrite-chromites, mechanism of polarisation of rare earth ions 79−42740
rare earth mixed valence compounds, charge dominated fluctuation props. comparison, mag. moments and ordering 80−54659
rare earth orthotitanites, unusual mag. props., role of mag. moments 78−84400
rare earth oxyfluorides, mag. susceptibility, 2-1000K *(Russian)* 79−82750
rare earth palladinides, R_3Pd_4, mag. props. 77−47980
rare earth perovskites, prep. and props. book contrib. 80−44193
rare earth selenides of yttrium subgroup, paramag. props. *(Ukrainian)* 77−32153
rare earth ternary compounds, coexistence of superconductivity and long-range magnetic order 79−11264
rare earth-$(Co_{1-x}Ni_x)_5$, single cryst., mag. props., mag. reversal 77−85489
rare earth-Ag alloy, amorphous, model calcs., of mag. props. 80−84616
rare earth-Au(Cu), amorphous, mag. and transport props. 80−34605
rare earth-Co, RCo_3 (R=Gd, Dy and Ho), effect of absorbed H_2 on mag. behaviour 79−33483
rare earth-Co, RCo_5, mag. moment orientation, anisotropic mol. field model 77−89950
rare earth-Co-Ni alloys, $Pr(CoNi)_5$ type, mag. props. and mag. reversal phenomena *(Russian)* 77−51924
rare earth-cobalt intermetallic RCo_2, sublattice magnetisation, powder neutron diffr. meas. 79−19725
rare earth-Cu intermetallic compds. single crysts., mag. props. 80−54892
rare earth-Fe_2, mag. props. changes due to H_2 absorption, unit cell vol. 77−63178
rare earth-gold intermetallics, RAu_2, mag. props., 4.2-300K 79−7972
rare earth-transition metal (4f-3d) intermetallic cpds., mag. moment and mag. anisotropy 80−25107
rare earth-transition metal alloy, disordered, saturation mag. moment using CPA 77−20515
rare earth-transition metal alloys, CPA calcs., moments and transition temps. 78−52252
rare earth-transition metal alloys, cryst. and amorphous, mag. props. 77−73008
rare earth-transition metal alloys, $RM_2Si_{2-x}Ge_x$ and $RM_{4+x}Al_{8-x}$, magnetism and hyperfine interactions, magnetisation and Mossbauer effect studies 80−75892
rare earth-transition metal hydrides, magnetic props., book contrib. 79−82754
rare earth-transition metal Laves phase, thermodynamic exam. of formation 77−1241
rare earth-Zn_{12}, mag. props. and structs. 78−84393
rare earths in metallic environment 78−6515
rare-earth-Cu double oxides, catalytic props., mag. props., elec. conductivity 79−66350
rotating coordinate system with quadrupole splitting, paramag. susceptibility 80−11178
rotation operators, time-depend. aspects, teaching 80−90634
ruby, magnetic dipole moment, phase meas. 78−72394
self-channelled states of mag. moment in rotating mag. field *(Russian)* 78−88102
semiconductor, intrinsic, indirect interactions between localised mag. moments 78−43578
semiconductor, metamagnetic, magnetostriction ferrons 78−88160
semiconductor, narrow band gap, ferromagnetism of electrons in filled band *(Russian)* 79−78300
semiconductor, paramagnetism switching off in strong electric field *(Russian)* 78−80124
semiconductors, spin splitting in strong electric fields 79−56175
single particle theory, g-2 calc., charged spin-one Yang-Mills particle appl. 77−13872
spatial distribution in single ground state systems with impurities 80−97074
sphere, elec. cond., uniformly rotating in temporally periodic homogeneous external mag. field, EM field calc. *(German)* 79−86107
spin glass, molecular field approx. *(Russian)* 77−80940
spin glasses dipolar anisotropy and crit. behaviour in small AC fields 77−32199
spin system, absorpt. of energy under parallel pumping conditions 80−2592
spin wave damping, magnetic materials with canted mag. struct., thermodynamic and high freq. props. 80−11184
spin XY one dimensional system containing impurities, static mag. props. *(Russian)* 80−65826
spin-1 particle, quantum gravity corrections to anomalous mag. and quadrupole moments 77−65130
spinels, MCr_2O_4 and MV_2O_4, valency and ionicity rel. to magnetism 78−52229
spinning charge, torsion contrib. to magnetic field 80−77676
SQUID magnetometer for meas. of macroscopic quadrupole field for antiferromagnetic order determ. 79−24140
steel, Cr-Ni-Mo-V, Mossbauer austenitometry and mag. props. 80−40003
SU(2)×U(1) gauge model, muon anomalous mag. moment, charged Higgs boson contrib. 80−78011
superconducting alloys with ordered magnetic moment distribution, thermoelec. effect 78−91811
superconductor, critical temperature mag. field depend., strong diamagnetism *(Russian)* 80−7022
superconductor, mag. scatt. of neutrons 80−103819
superconductor, magnetic, spin fluctuation and US attenuation 80−80445
superconductors with paramag. impurities, NMR theory in singlet state 79−28445
superparamagnetic particles, magnetic moment time development and discrete orientation model 80−60378
superparamagnetic particles, Mossbauer spectra, magnetisation vector precession 80−15872
surface and interface magnetism by Mossbauer spectroscopy 80−7218
surface structure, ferromag. or antiferromag., behaviour of localised mag. moments 79−28400
TCNQ salts, $Mn(TCNQ)_2$ and hydrates, mag. and elec. props. 79−82767
ternary superconductor, mag. interactions 79−73613
texture analysis, generalisation of dispersion theory 80−80556
transition metal, 3d and 4d, local density theory, mech. and mag. props. evaluation 78−91630
transition metal, magnetic ground state props., simple one-electron theory 77−63063
transition metal, magnetic moment near surface, one-electron band model 79−82747
transition metal 3d monoxides, specific vol. and mag. moment calcs. 80−65822
transition metal alloy, ferromag., local environment effect on atomic moments, itinerant model 78−68188
transition metal alloys, amorphous, mag. props., chem. short-range order 80−75739
transition metal alloys, amorphous, mag. props., structure and preparation 80−75737
transition metal alloys, ferromag., high-field susceptibility 80−7083
transition metal alloys, surface magnetism 78−48025
transition metal alloys, temp. depend. of asphericity of mag. moment distrib. 77−20538
transition metal alloys, Wolff model of origin of localised mag. moments 79−61049
transition metal amorphous alloys, mag. props. 80−29576
3d-transition metal complexes, low spin-high spin paramag. transition, Ising model calc. 80−93073
transition metal compounds, Jahn-Teller induced high spin-low spin transitions 79−69676
transition metal intermetallic cpds., H absorption and mag. props. 80−60224
transition metal itinerant magnets, neutron scatt. expts. 77−73002
transition metal surfaces, mag. props. 80−44861
transition metal-metalloid amorphous alloys, mag. props. review 78−52300
3d-transition metal-metalloid cryst. and glassy alloys, electronic struct. from magnetisation and Mossbauer meas. 80−29363
transition metal-metalloid glass, mag. props., charge transfer model 78−39324
transition metals, paramagnetic state, itinerant electron model 80−65769
transverse mag. dipole field diffraction on sphere with circular hole *(Ukrainian)* 79−31761

magnetic moments continued
two-sublattice magnetic system with fourth-order uniaxial anisotropy and strong antisymmetric exchange in transverse mag. field 79−56530
type I superconductor, mag. dipole effect on order parameter *(French)* 77−89899
uniaxial antiferromagnetic, phase diagram, spin flop transition *(Russian)* 80−100587
uniaxial ferromagnet, Landau-Lifshitz eqns., self-localised solns., accidental degeneracy *(Russian)* 79−33444
unit mag. moment primary USSR state standard 79−2753
US, large magnetic anisotropy exam. 77−20585
weak ferromagnetism, associated with third-order invariants *(Russian)* 78−95435
Wigner crystal, lattice quantum oscills. in mag. field, specific heat, mag. moments *(Russian)* 80−49636
Yang heavy axion, contradiction of muon anomalous mag. moment data *(Russian)* 79−49484
bb baryons, mag. moment sum rules, in Su(S) 80−78065
$\chi \rightarrow \psi\gamma$, charmonium E1 radiative transitions and quark mag. moments 80−86721
D and F meson spectra, electromagnetic interactions effect 80−47293
Δ(1236) M1 and E2 photoexcitation $N \rightarrow \Delta$ in $\gamma N \rightarrow \pi N$ 78−70377
Δ^{++}, bremsstrahlung peak in resonance region of $\pi^+ p$ radiative scatt., mag. moment 78−45944
$\Delta^{++}(1232)$, mag. dipole moment calc., from πp data 79−22133
e, anomalous magnetic moment, QED test 80−77996
e, anomalous moment near conducting plane, non-relativistic calc. 77−61229
e anomalous mag. moment, γ-γ scatt. contrib. 79−433
e moving in polarized EM wave, anomalous mag. moment determ. *(Russian)* 78−49998
e^- and e^+ anomalous mag. moments compared 77−18365
e^- anomalous mag. moment calc. 78−37254
μ, anomalous mag. moment, eighth-order contribution calc. 78−29261
μ, anomalous mag. moment, finite QED 80−47222
μ, anomalous mag. moment, sixth order, photon-photon contrib. 78−16958
μ, anomalous mag. moment, two-pion contrib. 78−66181
μ, anomalous mag. moment meas. 77−46094
μ, anomalous magnetic moment, QED test 80−77996
μ, sixth-order anomalous mag. moment 78−74190
μ anomalous mag. moment, weak correction in gauge models 78−16965
μ anomalous mag. moment in SU(3)×U(1) gauge model 79−3026
μ anomalous mag. moment meas. 77−61235
μ anomalous magnetic moment, free gluon mass, lower bound in integer-quark-charge model 80−78042
μ magnetic moment, pionic contrib., using exact soln. of Meiman problem concerning form factors 78−78182
μ magnetic moment, weak coupling contribution, Weinberg-Salam model 80−22607
μ magnetic moment form factor 80−18138
μ:p magnetic moment ratio, discrepancy between direct and indirect determinations 77−18287
μ^+, magnetic moment determ. from Larmor precession meas. in liq. Br 78−82259
$\mu^\pm$, anomalous mag. moment, elec. dipole moment, and test of relativistic time dilation 79−45088
n, anomalous magnetic moment in struct. model using phions 80−18134
ν, EM form factors and mag. moments, Weinberg-Salam model and extensions *(German)* 80−62904
ν_μ, transition magnetic moment 78−78168
$\psi' \rightarrow \chi\gamma$, charmonium E1 radiative transitions and quark mag. moments 80−86721
ρ-meson, EM form factor, elec. quadrupole and mag. dipole moments 78−12913
τ(1.8), charged lepton anomalous mag. moment, Weinberg-Salam model effects 79−13126
W boson, Weinberg model 77−30383
W bosons produced in pp and $\bar{p}$ collisions 79−97640
β-Al_2O_3:Mn(Co)(Ni), absorpt. and emission spectra, mag. susceptibility 79−87471
Au-Co solid solution, mag. props., freq. depend. suscept. maximum 79−69655
Au-Fe, spin glass, mag. moment dynamics, neutron diffuse scatt. meas. 77−69584
Au-Fe (22 at.%), ferromag. phase, AC susceptibility near T_c 78−43575
AuFe alloy films, mag. susceptibility, Fe concentration and annealing depend. 79−61119
$Au_{85}Fe_{15}$, and $Au_{82}Fe_{18}$, mag. props. 80−84592
Au_4V, partially disordered, magnetisation distrib., polarised neutron diffr. study 79−47244
$Ba_x(Ba_{1-x}Al_x)Fe_2S_6[S_{1-y}(S_2)_y]$, cryst. struct., Mossbauer and mag. behaviour 77−55273
$BaCuO_2$, prep. and props. *(French)* 77−43201
$BaCuO_{2+x}$ ($0 \leq x \leq 0.12$), study of mag. and elec. props. rel. to the non-stoichiometry *(French)* 78−95051
$Ba_3(PO_4)_2$ transition metal ion, optical and magnetic props. 78−64196
$BaVS_3$, magnetisation and neutron study 80−84588
$BaVSe_3$, one-dimensional, struct. and mag. props. 80−28993
$Ba_2Zn_2Fe_{12}O_{22}$, model for low mag. moment, magnetisation meas., 5-1375K 78−2655
BamSrmPb hexaferrites, prep. by cernet procedure, mag. props. 77−32174
$Be_2Mn_{1-x}Fe_x$, mag. props., giant moment clusters 79−28508
$BiFeO_3$, pyroelectric-antiferromag., magnetoelectric effect *(Russian)* 78−43625
$Bi_2Fe_4O_9$, mag. struct., neutron diffr., transition 78−52217
$CD_{1-x}In_xCr_2S_4$, ferromagnetic spinel, Cr^{3+} exchange interaction mechanism, Cr^{2+} relaxation, EPR line width depend. 79−69715
$CD_{1-x}In_xCr_2S_{4-y}P_x$, ferromagnetic spinel, Cr^{3+} exchange interaction mechanism, Cr^{2+} relaxation, EPR line width depend. 79−69715
CaB_6-SmB_6, mag. props., comp. depend. 80−50034
$CaCu_3Ti_4O_{12}$, mag. struct. and props. *(French)* 77−69495
$CaIr_xRe_{1-x}O_3$, ($0<x<1$), sintered, exam. of mag. and electrical props. 78−80135
$CaIr_xTi_{1-x}O_3$, semiconductor, struct., mag. and elec. props. 79−91046
$Ca_2Mn_3O_8$, mag. props. and EPR 79−91215
$Ca_3Ti_{2x}V_{1.5-x}Fe_{3.5-x}O_{12}$, garnet, mag. and neutron diffraction investigation 77−16044
$CaWO_4:Er^{3+}$, magnetocaloric behaviour, cryst. field theory 77−4520
magnetic moments continued
n-$CdCr_2Se_4$, single crystal, transport props. near Curie temp. *(Japanese)* 78−6406
$CdCr_2Se_4$-$ZnCr_2Se_4$, single cryst., mag. props. 79−28526
$Cd_2Mn_3O_8$, mag. props. and EPR 79−91215
$Cd_{1-x}Mn_xTe$, magneto-optical props. of free excitons rel. Mn^{2+} ions spin alignment 79−47419
$Cd_{1-x}Ni_xFe_2O_4$, solid soln., mag. and structural characterisation 80−103906
CdS, press. quenched, mag. moment, semicond.-conducting transition 80−15683
Ce-Th, mag. suscept. and sp. ht. 79−78411
$CeAl_2$, Anderson lattice system, mag. moment reduction, press. effects 80−7093
$CeAl_2$, mag. ordering, neutron diffr. meas. 78−6518
$CeFe_2$, ferromagnetic cpds., mean field exchange consts., Stoner itinerant model calcs. 80−50084
$CeFe_2$, H_2 absorption effect on mag. props. and struct. 77−40045
$CeIn_3$, mag. struct., neutron diffr. study 80−80481
$Ce_xLa_{1-x}B_6$ solid solutions, Weiss const. antiferromagnetic ordering calcs., mag. props. *(Russian)* 79−91212
$Ce_2Mg_3(NO_3)_{12}$·$24H_2O$, ground state with dipole-dipole and exchange interactions in external mag. field 80−84582
$CeNi_3$, and ternary hydride, mag. props. 80−108007
$CePd_3$, neutron scatt., spontaneous relax. of 4f magnetisation, interconfig. fluctuations 77−77025
CeSb, press. effect. on mag. props. 78−23315
CeX (X=P, As, Sb, Bi), neutron inelastic scatt. expts. 80−19674
$(Ce_xY_{1-x})Fe_2$, mag. susceptibility and Mossbauer meas., lattice parameters 80−97068
Co, atomic magnetic moments comparison to values of ferromagnetic metal 78−52244
Co based alloys, mag. interactions, effects on moments *(Rumanian)* 79−15296
Co complex, Co(III) five coordinate, paramagnetic behaviour 79−15276
Co complex, dipyridine chloride, single crystal metamagnetism 78−72345
Co, dipole field anisotropy, at interstitial sites, lattice-deformation effects 79−33584
Co, ferromag., spin subband level position determ. by de Haas-van Alphen meas. under press. *(Russian)* 79−90947
Co fine particles in Cu, interface magnetisation 80−88858
Co, spin polarised photoemission, surface magnetism 79−52083
Co-B alloys, amorphous, mag. moment and exchange stiffness constant 79−1662
Co-B alloys, amorphous, saturation magnetisation, mag. moments, X-ray diffr. obs. 79−4704
Co-Fe alloys, FCC structure, average mag. moment, conc. depend. 78−88099
Co-Fe-Mn, dil. ferromag. alloy, mag. moment, saturation magnetisation meas. 78−64195
Co-Ga alloys, ferromag., local configuration studies, neutron scatt. and spin echo NMR 77−63114
Co-Mn alloys, FCC, mag. moments of Mn atoms 78−76226
Co-Mn alloys, ferromagnetic, high field mag. susceptibility meas. 80−75729
Co-Ni (5 to 95 at.%), paramag. props., 800-1800°C *(Russian)* 77−55660
Co-V, Co rich, ferromag. behaviour, mag. moments, Curie temp., and NMR spectrum 80−70964
Co-V (12.4-18.7 at.%), ferromag. behaviour 79−24163
$Co_{100-x}B_x$ glassy alloys, mag. props. 79−73689
$(Co_{1-x}Fe_x)$-B-Si, amorphous props. *(Japanese)* 77−85433
Co_xGa_{1-x}, NMR expts. interpretation 80−75870
$Co_2Ga_{2-x}Cr_x$, ferromag., local configurational studies, neutron scatt. and spin echo NMR 77−63114
$Co_2Ga_{2-x}Cr_x$, ferromag., site selecting and moment distrib. 77−77031
$Co_2Ga_{2-x}V_x$, ferromag., local configuration studies, neutron scatt. and spin echo NMR 77−63114
$Co_2Ga_{2-x}V_x$, ferromag., site selectivity and moment distrib. 77−77031
$(Co_{1-x}M_x)B$, M=Mn or Fe, ferromag., internal fields meas. by NMR spin echo 80−29646
CoMnP, ferromagnetism and metamagnetism, polarized neutron diffr. study 80−44809
$CoMnSi$, $CoMnSi_{0.85}Ge_{0.15}$, mag. props. 79−42758
$Co_3Mn_3Si_2$, Curie-Weiss law depend. of susceptibility, mag. props. *(Russian)* 79−65655
$CoMnSi_{1-x}Ge_x$, amg. props. 80−60270
$CoMoO_4$, mag. susceptibility and electrical transport props. 79−56511
$Co_{2-x}(Ni,Fe)_xTiSn$, Heusler alloy, positive contribs. to hyperfine fields, magnetisation and NMR meas. 78−43654
$Co_{80}P_{20}$ glass, saturation moments, 4.2K 77−63125
$CoS_{2-x}Se$, magnetism and metamagnetic transition, neutron diffr. and NMR meas. 80−15717
$CoS_{2-x}Se_x$, conc. and temp. effects on metamagnetic transition 80−15716
$Co(S_xSe_{1-x})_2$, ($0 \leq x \leq 1$), mag. props. and elec. resist. 79−65657
$Co(S_xSe_{1-x})_2$, high field magnetisation, metamag. 79−91253
$CoSe_2$, temp. induced local mag. moments, ^{59}Co NMR 79−65747
$Co_{75}Si_{25-x}B_x$ glass, metalloid comp. depend. 77−55665
Co_2SnO_4, $CoMg(Zn)SnO_4$ and $Co_{2-x}Mg_2TiO_4$, magnetic props., short-range ordering 77−32155
$Co_{1-x}Te$, fluctuating localised mag. moments, d band motion, Mossbauer study 80−65768
$Co_{1-x}Ti_x$, ferromag. props., Ti conc. effect 80−54872
$CoTi_{1-x}Al_x$, form. of mag. moment of Co atom, X-ray diffr., mag. meas. and NMR 77−43819
Co_2TiAl, ferromag., rel. to ^{59}Co NMR 78−2760
Co_2TiSn, Heusler alloy, positive contribs. to hyperfine fields, magnetisation and NMR meas. 78−43654
CoU_2S_5, mag. struct. and props. 80−11166
CoV alloys, phase dependent MNR spectra 80−108114
$CoWO_4$, mag. struct. refinement, neutron diffr. meas. *(German)* 77−16049
Cr alloys, localised magnetic moments in band antiferromagnets, impurity interactions *(Russian)* 80−54888
Cr, electronic struct., spin-density functional calcs. 80−88476
Cr, electronic structure model, Invar effect, antiferromagnetic-non mag. transitions 80−20370
Cr-Al alloys, antiferromag., charge and spin density, neutron and X-ray diffr. 77−31971

magnetic moments continued
Cr-Fe, antiferromagnetic, effect of press. on hyperfine mag. fields at Fe nuclei *(Russian)* 80−15936
Cr-Fe, disordered, polarised neutron diffuse scatt. meas., 4.6-110K 80−34592
Cr-Fe, mag. moment of Fe, mag. suscept. meas. 79−61079
Cr-Fe (6.5 wt.%), atomic clustering and mag. defects, mag. moments 80−60246
Cr-Fe(2.8 at%), antiferromag., meas. of incoherent elastic neutron scatt. cross section 79−19723
Cr-Ge system, XPS, X-ray and neutron diffr. and mag. meas. to study chem. bonding and electronic struct. 80−60749
Cr-Mo, behaviour of mag. impurities 79−4672
Cr-Pd dilute alloys, itinerant antiferromag., neutron diffr. meas. 77−77032
Cr-Pt alloy, mag. props., effect of atomic environment 78−23247
Cr-Si-Fe, mag. moment of Fe, mag. suscept. meas. 79−61079
Cr-V-Fe, mag. moment of Fe, mag. suscept. meas. 79−61079
CrB_2, CrB, and Cr_5B_3, mag. and thermal props. at low temps. 80−20385
CrB_2, helical mag. struct., neutron diffr. meas. 77−85425
$Cr_{0.6}Mn_{0.4}$, mag. moment, neutron diffr. study 79−33459
$Cr_xMn_{1-x}As$, antiferromagnetic-ferromagnetic transition, mag. moment and elec. resist. meas. 80−15718
$Cr_xMn_{1-x}As$, antiferromag. to ferromag. transitions, superexchange-double exchange mag. coupling, susceptibility and resist. obs. 80−50070
$Cr_xMo_{1-x}O_2$ ($x \leq 0.5$), mag. moment rel. to Cr content 80−70177
CrO_2, particulate, proton donor adsorption effect on mag. moment, XPS anal. 80−71117
β-CrOOH, neutron diffr. exam., cryst. and magnetic struct. *(French)* 78−2654
$CrPS_4$-Li intercalation cpd., phys. props. 79−19788
$Cr_{1-x}Ti_xN$, cryst. and mag. struct., at low temps. *(French)* 80−29005
$CrUSe_3$, mag. struct. and delocalized moments, powder neutron diffr. obs. 77−69496
$Cr_{1-x}V_xN$, solid soln., mag. struct. *(French)* 78−6519
$Cs_2KTmBr_6(Cl_6)(F_6)$, Cs_2NaTmF_6 and Cs_2RbTmF_6, mag. behaviour 2.9 to 251.3K, cryst. field levels, ang. overlap model *(German)* 80−29520
$CsMn_{1-x}Co_xF_3$, ferrimag., mag. props. and cryst. struct. 77−77056
$CsMnF_4$, planar ferromag., cryst. and mag. struct., Jahn-Teller effect 80−75715
$CsMn_{1-x}Ni_xF_3$, ferrimag., mag. props. and cryst. struct. 77−77056
$Cs_2NaTmCl_6$, UV absorpt. spectra, mag. circular dichroism spectra, vibr. obs. 80−29758
$CsNiBr_3$, nearly one-dimensional antiferromag., thermal and mag. props. meas. 77−77041
$CsNiCl_3$, linear chain antiferromag., mag. props., 1.1 to 7K 79−61076
$CsNiCl_3$, mag. props. 79−73736
$CsNiF_3$, demagnetising effects on antiferromag. reson. 80−15803
$CsNiF_3$, one-dimensional ferromagnet, optical absorpt. and static spin correlation functions 80−71415
$CsYbO_2$, normal-temp. form, mag. props. *(German)* 80−54864
Cu complex, tetrameric Cu(II) complex, higher-order spin coupling 79−99690
Cu complexes, paramag., XPS, temp. depend. 79−15582
Cu complexes with amino acids, static mag. susceptibility and effective mag. moment 77−12082
Cu-Mg-FeO system spinel solid solns., synthesis, struct., and mag. props. 79−52142
Cu-Mn, spin glass alloy, magnetic excitations, neutron scatt. 78−10695
Cu-Mn (10 at.%), meas. of mag. viscosity below freezing temp. 79−24171
Cu-Mn mictomagnet, effect of ageing on mag. moment 77−43841
Cu-Mn-Al effect of Mn atoms on formation of mag. moments and mag. order 79−24139
Cu-Ni, disordered ferromag., spin density asphericity, neutron diffr. study 79−47251
Cu-Ni, random ferromag. alloy, local mag. moment calc. 80−70974
Cu-Ni alloys, distrib., chemical clustering influence 78−14931
$CuCl_2.CuCl_2.2D_2O$, neutron scatt. aspherical effects, mag. form factor 78−27017
$CuCr_2Se_4$, electronic state, polarized neutron diffr. obs. 79−56501
$CuCr_2Se_4$, experimental obs. 78−76227
$CuCr_2Se_4$, mag. moment distrib. by neutron diffr., Goodenough model 80−70945
$CuCr_2Se_4$ single crystal, magnetic props. *(Japanese)* 78−6520
$Cu_{1-x}Cr_2Se_4$, influence of excess Cu on physical props. 80−103836
$CuCr_2Se_4(S_4)(Te_4)$, binary and ternary solid solns., mag. and elec. props. 80−2407
$Cu_{0.5}Fe_{2.5}O_4$-$ZnFe_2O_4$, cation distrib., mag. moment, Mossbauer spectra, chem. anal. 80−75210
$CuFe_2S_3$, cubanite, spontaneous magnetisation, polarised neutron obs. *(French)* 78−23245
CuMn, spin glass, random moments time correl., zero field muon spin relax. meas. 80−60335
CuMn-like alloys, model calcs. on magnetisation processes in moderate fields below freezing temp. 79−24188
Cu_3Mn, interaction between local mag. moments 77−1540
Cu_2MnAl, alloy, magnetic moment calc. 79−4507
Cu_2MnAl, ferromag. Heusler alloy, polarised neutron study of mag. moment density 78−84391
Cu_2MnAl superparamagnetic particles in Cu_3Al lattice, magnetic moment ferromagnetic ordering *(Russian)* 79−78444
$Cu_2Mn_{0.863}Al_{1.057}$, Heusler alloy, mag. moment distrib., polarised neutron study 79−47247
$Cu(NO_3)_2.2^1/_2H_2O$, long-range ordered state, mag. props. 78−39417
$Cu_4NiSi_2S_7$, X-ray cryst. struct. determ., mag. props. 80−107172
α-$Cu_xV_2O_5$, EPR and mag. susceptibility meas., mag. moment calc. 80−2627
Dy film, helimag. order, surface deform., exchange and single-ion magnetocrystalline anisotropy energy 77−66390
Dy, liq., mag. susceptibility, elec. resistivity 80−20377
Dy, visible spectra obs., hyperfine struct., mag. dipole and electric quadrupole interaction const. anal. 80−91698
Dy-Co amorphous film, prep. by dual-source evaporation, mag. props. 77−89988
Dy-Pr(Nd) alloys, mag. struct. and ordered moments, neutrons diffr. data 77−66252
Dy-Sm, magnetic moment growth due to Sm addition *(Russian)* 80−34608
Dy-Sm(Eu), mag. props. at low temp. in high mag. fields 79−56570

magnetic moments continued
Dy-Y, paramag. susceptibility, effective mag. moments 77−20548
Dy_2C_3, cryst. struct., mag. struct. and props., 1.6 to 300K 79−11296
$DyCo_2$-$DyAl_2$ system, mag. and structural studies 80−108006
Dy_4Co_3, cryst. field effect on mag. moment direction, neutron diffr. meas. 78−80132
$DyCrO_4$, determ. of mag. struct. by neutron diffr. 79−51753
$Dy_{1-x}Fe_x$, mean mag. moment calc. 79−82761
$DyFe_2H_2$, mag. props., ^{57}Fe and ^{161}Dy Mossbauer spectra and magnetisation meas. 79−78579
$Dy(Fe_xNi_{1-x})$, mag. interactions, mol. field model 77−73010
$Dy_{1-x}Ho_xNi_2$, cryst. field quenching of Dy^{3+} 4f shell, Mossbauer effect meas. 78−39480
DyM_3, M=Fe, Co, Ni, amorphous, mag. struct. and moments 77−66260
Dy_6Mn_{23}, magnetic moments, magnetisation 80−25094
Dy_2Se_3, mag. susceptibility 77−40032
$Dy_{1-x}Y_xAl_2$, cryst. field quenching of Dy^{3+} 4f shell, Mossbauer effect meas. 78−39480
$ErCo_{5.6}$, easy magnetisation direction 78−84415
Er_4Co_3, cryst. field effect on mag. moment direction, neutron diffr. meas. 78−80132
$ErCo_3B_2$, ferromag. ordering and saturation moments 77−24711
$ErFe_2$, effect of H on sublattice magnetization, elastic neutron scatt. obs. 79−78327
$(Er_{65}Fe_{35})_{100-x}B_x$ glasses, mag. props. 79−73693
$ErFe_2H_{3.9}$, mag. props. and lattice consts., effect of hydrogen absorpt. 77−20561
$ErFe_2H_x$, mag. props. 80−25095
ErH_3, cryst. fields and mag. props. 78−68181
Er_6Mn_{23}, magnetic moments, magnetisation 80−25094
$ErRh_4B_4$, superconducting, magnetic dilemma 80−75680
Er_2Se_3, mag. susceptibility 77−40032
$ErTiO_3$, magnetic structure determination, neutron scatt. study 80−65809
$ErVO_3$, produced by $Er_2O_3+VO_2$ high-press. reaction, cryst. struct. and mag. props. meas. 80−19773
$EuCrO_3$, long term mag. ordering, antiferromagnetic resonance study *(Russian)* 80−54953
Eu_2IrH_5, prep., cryst. struct., mag. and elec. props. 80−88117
$EuMg_5$, Mossbauer effect, effective moments, mag. ordering temp. and isomer shifts 80−34833
Eu_2Mg_{17}, Mossbauer effect, effective moments, mag. ordering temp. and isomer shifts 80−34833
EuO(S)(Se)(Te), cryst. and electronic struct., mag., elec., and optical props., book contrib. 80−39760
EuO(s), mag. semicond., s-f model, intermediate coupling theory 79−95326
EuS-Ga_2S_3-GeS_2, chalcogenide glasses, conditions of form. of glassy prod. *(French)* 80−100325
$Eu_xSr_{1-x}M_4O_{11}$, M=Nb, Ta, electrophys. and mag. props. 77−89760
$Eu_xSr_{1-x}S$, dil. insulator spin-glass versus blocking 80−34641
EuX_5, X=Cu, Zn, Ag, Au, cond. electron spin polarisation effects 77−63136
$Eu_{1-x}Yb_xTe$, ($0<x<1$), mag. semicond., elec., mag. and optical props. 80−97070
$(Fe,Ni)_{80}(P,B)_{20}$, quenched alloy ribbon, mag. moments, Curie temp. 77−40041
Fe alloys, BCC, Mossbauer spectra, local mag. moments 80−15861
Fe alloys, FCC, Invar effect, model 80−25105
γ-Fe, atomic mag. moment in FCC lattice of transition d-metals *(Russian)* 78−72337
Fe, atomic magnetic moments comparison to values of ferromagnetic metal 78−52244
Fe base amorphous alloys, Invar and Elinvar characts. 80−29592
Fe, cold work stored energy effects on mag. moment vs. temp. curve 78−95419
Fe colloidal dispersion, mag. props., struct. and oxidation 80−34699
Fe complex, dithiocyanato bis(4-methyl-1, 10-phenanthroline) iron, Mossbauer effect and magnetism down to 0.98K 77−28490
Fe complex, tris(1-pyrrolidinecarbodithioato)iron(III), and related cpds. mag. props., struct. 77−89933
Fe complexes, 2- or 3-pyridyl imine complexes of $FeCl_2$, Mossbauer and mag. props. 80−15896
Fe complexes, paramag., XPS, temp. depend. 79−15582
Fe complexes with dimethylformamide, dimethylthioformamide, Mossbauer and mag. props. 80−39974
Fe epitaxial film, Mossbauer effect, interface magnetism 80−11297
γ-Fe, FCC film, epitaxial growth on CuAu (111) surfaces, strong ferromagnetism 80−70557
Fe, ferromagnetic, cluster method, environmental effects 78−95405
Fe ferromagnetism, transition metal valence electron struct. explanation 78−47932
Fe film, amorphous and polycrystalline, Hall effect, resistivity and mag. moment 78−91786
α-Fe film, mag. mechanism, at. mag. moment *(Korean)* 79−7973
Fe film, nuclear spin system dynamics Mossbauer study in FMR conditions *(Russian)* 80−80651
Fe garnet, ferrimagnetic, sublattice magnetisation calc. 77−16063
Fe group, mol. Jahn-Teller reson. states as possible antecedents to magnetism 80−75701
Fe, mag. surface props., Mossbauer effect 77−69757
Fe, magnetic moments, local short range order, high temp. effects 80−65902
Fe, nitrided wire, magnetic charact. and microstruct. *(Korean)* 78−19277
Fe powder, BH_4 reduced, coercive force and remanence ang. variation 80−44879
Fe powders, prep. by BH_4 process, comp. and stability 80−44878
Fe pyrophoric powders, stabilising layer form. during passivation, saturation moment meas. 80−44865
Fe, rel. to lattice vibrations, temp. depend. 78−95124
Fe, spin polarised photoemission, surface magnetism 79−52083
Fe, var. in mag. moment of ferromags. during plastic deform. *(Russian)* 77−66401
Fe-Al, local ordering, neutron scatt. study 78−64193
Fe-Al, magnetic moment determ. from neutron scatt. 77−73011
Fe-Al, Mossbauer spectra, local mag. moments 80−15861
Fe-Al, paramag. props., T_c to 1500K 78−68153
Fe-Al-Fe, phase diagram, microscopic model 80−34630

magnetic moments continued
Fe-B, amorphous, Invar-type alloy, mag. moment and high field susceptibility 78−34965
Fe-B, amorphous alloy, mag. props. 80−84618
Fe-B, amorphous ferromag., Invar type, magnetisation, elec. resist. and thermal expansion meas. 78−2663
Fe-B alloys, rapidly quenched metastable solid solns., prop. and mag. props. 78−92218
Fe-B amorphous alloys, Mossbauer spectra, mag. moment conc. depend. 80−15847
Fe-B-C, amorphous, effects of replacement of B by C on mag. props. 80−84621
Fe-B-C alloys, amorphous, temp. depend. of magnetisation 79−73690
Fe-B(P) amorphous alloy, Invar effects, mag. props. meas. 79−56594
Fe-Co, local environment effect on at. mag. moment 79−82763
Fe-Co, mag. moment of Cr and Mn atoms, polarised neutron scattering 79−11290
Fe-Co alloys, at. valence states *(Ukrainian)* 78−2656
Fe-Co based Laves phases, Co conc. depend., NMR exam. 78−15037
Fe-Co-Cr alloys, atomic mag. moment, magnetisation, Mossbauer spectra and NMR spin echo spectra 77−63127
Fe-Co-Mn, BCC, mag. state of Mn, NMR and saturation magnetisation meas. 78−39442
Fe-Co-Mn alloys, BCC, atomic mag. moment, magnetisation, Mossbauer spectra and NMR spin echo spectra 77−63127
Fe-Co-Ni, at. mag. moments, neutron scatt. and Mossbauer meas. 79−42744
Fe-Cr, BCC, local moments in Mossbauer study 80−108125
Fe-Cr, Invar alloy, explanation of phys. anomalies *(Russian)* 78−88112
Fe-Cr, mag. props. of Fe, local coupling with spin modulation of matrix 79−15299
Fe-Cr, random ferromag. alloys, local mag. moment calc. 80−70974
Fe-Cr alloy, magnetis. obs. 78−76276
Fe-Cr alloys, mixed ferro-/antiferromag. interactions *(Russian)* 77−32173
Fe-Cr-Al alloys, localised mag. moment determ. and electron struct. 77−66268
Fe-Cr-B, amorphous, Elinvar and Invar charact. *(Japanese)* 80−11832
Fe-Cr-Ni, Fe-Co-Mn, Fe-Cr-Co and Fe-Ni-Mn alloys, BCC, atomic mag. moments determ. 77−59396
Fe-Cu alloys, mag. moment distrib., elastic neutron scatt. obs. 79−78340
Fe-Fe_2O_3-$NaFeO_2$, study of Na-containing wustite region *(French)* 77−73264
β-Fe-Ge, mag. props. from X-ray, magnetisation and Mossbauer meas. 79−42755
Fe-Mn, dil. alloy, mag. moment distrib., temp. depend., diffuse polarised neutron scatt. study 79−47250
Fe-Ni, local environment effect on at. mag. moment 79−82763
Fe-Ni, local ordering, neutron scatt. study 78−64193
Fe-Ni, magnetisation calc. method based on moments of density of states 80−65770
Fe-Ni alloy, cold work stored energy effect on mag. moment vs. temp. curve 78−95419
Fe-Ni alloys, at. valence states *(Ukrainian)* 78−2656
Fe-Ni alloys, FCC, mag. props. calc. 79−65659
Fe-Ni based alloy, amorphous rapidly quenched, mag. props. 77−66269
Fe-Ni films, lattice constants rel. to mag. moments *(Russian)* 77−32218
Fe-Ni system, ferro-antiferromag. transition, γ phase mag. struct. 79−91231
Fe-Ni-Mn, BCC, mag. state of Mn, NMR and saturation magnetisation meas. 78−39442
Fe-Ni-Mn alloy, rel. to temp. coeff. of linear expansion *(Russian)* 77−80634
Fe-Ni(Cr), Invar, exchange interactions between ferromag. and antiferromag. components 80−29545
Fe-P-B, amorphous alloy, Mossbauer effect and short-range order 80−2675
Fe-P-B, amorphous alloys, mag. props., conc. depend. 77−8314
Fe-P-C, amorphous alloy, Mossbauer effect and short-range order 80−2675
Fe-Pd, mag. moment, comp. depend. *(Russian)* 78−47280
Fe-Pd alloy, uniaxial ferromag., anisotropic component of localised mag. field, Mossbauer meas. *(Russian)* 79−15382
Fe-Pd Invar alloys, elec. and mag. props. and thermal expansion 80−75732
Fe-Pt, Invar alloy, strong ferromagnetism, magnetostriction and thermal expansion 79−8037
Fe-Pt-Ir, Mossbauer effect of ^{193}Ir and ^{57}Fe, hyperfine field, isomer shift 78−15072
Fe-Si (7.5, 14.3 at.%), mag. moments and form factors, neutron diffr. obs., d-band electron redistrib. 79−51751
Fe-Si-Al (6,4 wt.%), Sendust alloy, effect of Ni content on mag. props. 78−72897
Fe-Si-Al-Ni alloy, Super Sendust, Ni content and thermomag. treatment effects 77−4861
Fe-Si-B amorphous alloys, metalloid content effects on Curie temp. and mag. moments 78−14956
Fe-SiO multilayer film, interface magnetisation 80−7135
Fe-SiO multilayer films, interface magnetisation 80−88858
Fe-Si(Ge)(Al), solid and liq. paramag. props. *(Russian)* 77−66247
Fe-Ti, BCC, mag. moment distrib. 79−47240
Fe-Ti, mag. moment distrib. and environmental effects around Ti impurity 80−7092
Fe-V, conc. depend. of mag. moment distrib., polarised neutron diffr. meas. 78−19218
Fe-V alloys, BCC, ferromag., polarised neutron diffr., appl. of multiband CPA theory 77−77033
Fe-V alloys, hyperfine fields at solute and solvent sites rel. to mag. moments 77−8461
Fe-V alloys, Mossbauer study, hyperfine field effect on formation of local moments 78−27134
Fe_2Al, mag. moment determ., role of local environment, self consistent calcs. 80−44815
Fe_3Al, super-lattice, band theory 77−15758
$Fe_{3-x}Al_xO_4$, cation distrib., mag. and other phys. props. 77−43818
$Fe_3Al(Si)$, electronic structure, magnetic moments 80−107695
Fe_cAu_{1-c}, amorphous ferromagnetic, resistivity, anisotropic, field dependence 78−87960
$Fe_{1-x}B_x$, amorphous, hyperfine fields and local mag. moments, Mossbauer study 80−75895
magnetic moments continued
$Fe_{80}B_{20}$, amorphous ferromag., temp. depend. of hyperfine field distrib. 78−43756
$Fe_{80}B_{20}$, amorphous ferromag., hyperfine field distrib., Mossbauer effect 78−60371
$Fe(BF_4)_2.6H_2O(6D_2O)$, phase transition, mag. susceptibility and anisotropy and permittivity meas. 79−23718
$Fe_{80}B_{20-x}Si_x$, metallic glass, mech. and mag. props., depend. on metalloid content 79−91213
Fe_xC_{1-x} amorphous sputtered film, mag. props. 78−68311
$FeCl_2$, in transverse mag. field, magnetoelastic coupling effect on mag. props. 79−28582
$FeCl_2$, magnetic transition and sublattice mag. moment rotation nonequivalence *(Russian)* 80−100586
$FeCl_2$, reorientation of mag. moments under mech. stresses at 0K 80−93153
$(FeCo)_{80}B_{20}$, metallic glass, saturation moments and Curie temp. 77−1542
$(Fe_{0.5}Co_{0.5})_{1-x}B_x$, amorphous, hyperfine fields and local mag. moments, Mossbauer study 80−75895
$Fe_{1-x}Co_xGe_2$ solid solns., mag. susceptibilities, multiple stages in mag. transitions, effective mag. moment 77−8286
$(Fe_{1-x}Co_x)_3P$, cryst. struct. and mag. props. 78−19222
$Fe_{3-x}Co_xSi$, structural, mag. moment, and hyperfine field behaviour, local environment model 79−65762
$(Fe_{1-x}Co_x)_{77}Si_{10}B_{13}$, amorphous, mag. moments at 0K, Curie temp., mag. interactions 79−4670
$(Fe_xCo_{100-x})_{100-(y+z)}Si_yB_z$ amorphous ribbon, mag. moment and Curie temp., comp. depend. 78−95421
$(Fe_{1-x}Cr_x)$-P-C amorphous, mag. props. *(Japanese)* 77−85433
$FeCr_{2-x}In_xSe_4$, struct. and mag. props., comp. depend. 77−66262
$(Fe_{98}Cr_2)_{79}P_{13}B_8$ and $(Fe_{96}Cr_4)_{79}P_{13}B_8$, amorphous, low temp. sp. ht., mag. contribs. 80−80552
FeGe, hexagonal, low-temp. mag. struct., neutron diffr. meas. 78−95418
$FeGe_2$ canted antiferromagnet, mag. susceptibility anisotropy and temp. dependence 80−25112
Fe_3Ge, mag. props. of cubic and hexagonal phases 77−8475
Fe_xGe_{1-x} amorphous alloys, high field mag. meas. 79−82765
Fe_xGe_{1-x} amorphous film, low temp. conversion electron Mossbauer spectroscopy 78−48101
Fe_xI_y cyclodextrin, quasi-one-dimens. cpd., synthesis, elec. and mag. props. 80−2380
$Fe_{3-x}In_xO_4$, ferrospinels, cation distrib., Curie point and magnetisation meas. 79−42095
$(Fe_{1-x}M_x)_2P$, (M=Co,Ni), magnetisation, susceptibility, thermal expsn. 79−11302
$(Fe_{1-x}M_x)_3P$, cryst. struct. and mag. props. 78−19222
FeMn, dil., diffuse scatt. cross sections, polarized neutrons 78−43567
$(Fe_{1-x}Mn_x)_3Al$ alloys, disordered, mag. moments and distrib. on lattice sites 77−63112
$(Fe_{1-x}Mn_x)_3Al$, mag. moments determ. from magnetisation and neutron and electron diffr. expts. 79−56520
$(Fe_{1-x}Mn_x)_3P$, cryst. struct. and mag. props. 78−19222
$Fe_xMn_{1-x}Pt_3$, ferro-antiferromag. transform. at 4.2K *(Russian)* 78−88117
$(FeMn)_3Si$ alloys, mag. and crystallographic props. 77−59393
$Fe_{3-x}Mn_xSi$, evidence for the ang. depend. of the hyperfine interactions 78−76241
$(Fe_{1-x}Mn_x)_2Y(B)$, Mn effect on Fe mag. moments, Mossbauer and mag. meas. 80−71016
Fe_2MoO_4, electron exchange between $Fe^{2+}-Fe^{3+}$ ions on tetrahedral and octahedral sites, Mossbauer spectra 79−78585
$Fe(N_3)_5^{2-}$, paramag. relax. in trigonal bipyramidal environment, Mossbauer spectra 80−15871
$(FeNi)_{80}B_{20}$, metallic glass, saturation moments and Curie temp. 77−1542
$(Fe_{1-y}Ni_y)_{0.8}B_{0.2-x}P_x$, amorphous, hyperfine fields and local mag. moments, Mossbauer study 80−75895
$Fe_{1.6}Ni_{78.4}B_{10}P_{10}$ metallic glass, superparamag. behaviour, chem. inhomogeneities role 80−84625
$(Fe_{1-x}Ni_x)_3P$, cryst. struct. and mag. props. 78−19222
$(Fe_{1-x}Ni_x)_{80}P_{20}$, amorphous, ferromagnetic alloys, mag. anomalies of Invar type *(Russian)* 80−93089
$(Fe_{1-x}Ni_x)_{77}Si_{10}B_{13}$ amorphous alloy system, saturation mag. moment, Curie temp., mag. susceptibility 80−39753
FeO-FeS, mag. susceptibility, eutectic phase diagram *(Russian)* 80−15682
Fe_2O_3, haematite, single domain, defect moment origin and props. 79−16438
α-Fe_2O_3, haematite, substituted, Morin transition, neutron diffr. study 80−54897
γ-Fe_2O_3, sat. moment *(French)* 77−85431
Fe_3O_4 in suspension, ferromagnetic colloid, optical meas. 78−10906
Fe_3O_4, magnetite, reduced A-site moments, polarised neutron study 79−47253
Fe_3O_4, spin polarised photoemission, surface magnetism 79−52083
Fe_3O_4, tetrahedral-site Fe^{3+} ion, moment density, transfer to O ion 79−15285
$FeOHSO_4$, mag. structure, modulation of moments, neutron diffr. meas. 77−69499
$Fe_{100-x}P_x$, amorphous, effect of metalloids on mag. props. 79−11304
Fe_2P, grown in liq. Cu medium, composition and mag. props. 79−11313
Fe_2P, mag. moments and form factors, polarised neutron diffr. study 79−65650
Fe_2P, mag. struct., neutron diffr. study 78−23246
Fe_2P, Mossbauer spectra and mag. props., Curie temp. dispersion 77−36162
$Fe_{80}P_{20}$ glass, saturation moments, 4.2K 77−63125
$Fe_{79}P_{13}B_8$ amorphous alloys, splat cooled, Mn, Cr and V substituted, mag. and transport props. 80−84593
$Fe_{80}P_{14}B_6$, average hyperfine field to mag. moment ratio 79−11367
$Fe_{80}P_{20-x}C_x(Si_x)(Ge_x)$, amorphous, size effect of metalloids on mag. props. 80−84594
$Fe(Pd_{1-x}Au_x)_3$, mag. struct. ferro-antiferromagnetism coexistence *(Russian)* 79−82759
Fe_3Pt, Invar alloy, theory of elastic-anomalies 78−95505
Fe_3Pt, non-linear local environment effect, Mossbauer effect of ^{57}Fe and ^{195}Pt 80−39910
$Fe_{3-x}Pt_{1+x}$, ordered and disordered, mag. props. at low temp. 79−56517
FeRh, antiferromag., band structure and effect of Fe impurity on mag. props. 77−28377

magnetic moments continued
FeRh, antiferromag., band struc., off-stoichiometry effects 78−10341
FeS_2, Mossbauer effect in mag. field, absence of mag. moment 77−12288
$Fe_{0.9}S$, ferrimag. transition, mag., thermodynamic props., kinetics 79−47280
β-$FeSO_4$, high-temp. polymorph, stability, mag. struct., mag. props. 77−43815
Fe_3Se_4, mag. props., 4.2-600K 78−43570
Fe_3Se_4, thermal expansion, compressibility, magnetisation, susceptibility and magnetostriction 77−66318
Fe_3Si, 3d transition metal substituted, limits of solubility, mag. props. and electron conc. 78−10670
Fe_3Si-based alloy, dil., cond. electron polarisation and moment perturbations 78−68224
Fe_xSi_{1-x}, amorphous, struct. and mag. props., giant moment form. at mag. ordering 78−68192
$Fe_6Si_4O_{10}(OH)_8$, greenalite, metamag. clay mineral, mag. props. *(French)* 78−88817
Fe_3Sn_2, Mossbauer effect and magnetisation meas. 78−31132
$Fe_{1-x}Te$, fluctuating localised mag. moments, d band motion, Mossbauer study 80−65768
FeTi alloy, elec. and mag. props. near order-disorder transition 79−82576
$Fe_{1-x}Ti_x$, ferromag. props., Ti conc. effect 80−54872
Fe_2TiO_4 magnetisation, Mossbauer spectra 79−87244
$Fe_{1-y}Zn_{3y/2}O_3$, solid soln. prep., struct. and mag. moment 78−52228
$Fe_{80}b_{20-x}C_x(Si_x)(Ge_x)$, amorphous, size effect of metalloids on mag. props. 80−84594
$(Gd,Dy)Al_2$, spin adjustment, NMR spin echo obs. 78−15058
Gd alloys, Curie temp. and saturated mag. moment, nonmag. solute effects 78−39301
Gd, dipole field anisotropy, at interstitial sites, lattice-deformation effects 79−33584
Gd, liq., mag. susceptibility, elec. resistivity 80−20377
Gd, rel. to longitudinal galvanomag. effect in single crysts. *(Russian)* 78−56132
Gd-Al(C)(Cu)(Ga)(Ni)(Pd)(Rh) alloys, amorphous, mag. and elec. props. 80−80499
Gd-Au(Ni)(Co), amorphous ferromag., mag. and transport meas. 77−89930
Gd-Co, CPA calcs., moments and transition temps. 78−52252
Gd-Co-Ni series intermetallics, induced moments, magnetisation meas. 77−63138
Gd-Fe, CPA calcs., moments and transition temps. 78−52252
Gd-Fe, mag. moment of Fe, multiplet splitting in photoemission 79−78846
Gd-Fe amorphous film, prep. by dual-source evaporation, mag. props. 77−89988
Gd-Fe(Co), mol. field model 77−4498
Gd-Mn(-Co) alloys, amorphous, ferrimag. props. and Hall effect 79−73692
Gd-Ni, CPA calcs., moments and transition temps. 78−52252
Gd-Sm(Eu), mag. props. at low temp. in high mag. fields 79−56570
Gd-Yb(Ir), dil., ferromag., mag. hyperfine fields of ^{170}Yb and ^{193}Ir, Mossbauer effect meas. 79−24242
$GdAl_2$-$GdCo_2$ system, EPR and mag. props. 79−33478
Gd_2Al, magnetic properties, 4.2 to 400K, metamagnetism 77−32193
$Gd_{80}Au_{20}$, amorphous ferromag., critical phenomena and mag. props. 77−85469
GdCa garnets, solid soln., mag. and cryst. chem. props. 77−16057
$GdCo_5$, spin polarised energy band struct., APW calc. 78−10342
$GdCo_3B_2$, ferromag. ordering and saturation moments 77−24711
$Gd(Co_xIr_{1-x})_2$, C15 Laves phase struct., g shift, linewidth EPR meas., Fermi level movement interpretation 79−61210
$Gd(Co_xIr_{1-x})_2$, struct. and mag. moments, comp. depend. 79−86743
$Gd(Co_xNi_{1-x})_2$, Mossbauer spectra, mag. props. 80−20563
Gd_xCu_{1-x}, amorphous film, magnetisation meas., fully aligned moment 78−68309
GdCuGe, $Gd_6Cu_8Ge_8$ and $GdCu_2Ge_2$, magnetic props. 77−32180
$Gd_xEu_{1-x}B_6$, solid solns., mag. susceptibility, 80 to 1000K *(Russian)* 80−88713
$GdFe_2$ films, electron beam deposited, amorphous and cryst., mag. and struct. props. 79−4710
$Gd(Fe_{1-x}Al_x)_2$, magnetisation, Curie temps., and mean mag. moments 79−51817
$(Gd_{65}Fe_{35})_{100-x}B_x$ glasses, mag. props. 79−73693
$Gd(Fe_xCo_{1-x})_2$, paramag. behaviour, itineracy 78−39289
$Gd(Fe_xT_{1-x})_2$, Mossbauer spectra, mag. props. 80−20563
GdIG, local mag. anisotropy in stress field of single dislocation 80−88744
$Gd_xLa_{1-x}B_6$, solid solns., mag. susceptibility, 80 to 1000K *(Russian)* 80−88713
$Gd_{0.9}La_{0.1}Ni_2$, Ni contrib. to ordering, ^{139}La NMR spin echo 77−63317
$Gd_{1-x}M_x$, M=Co, Ni, Fe, temp. depend. of magnetisation 77−77043
$Gd_{1-x}M_x$, M=Ni, Fe, Co, CPA calcs. 77−72997
$GdMn_2$-$GdAl_2$ intermetallics, mag. props., 80-650K 78−60282
$GdMn_2$-$GdAl_2$ system, mag. and structural studies 80−108006
Gd_6Mn_{23}, magnetic moments, magnetisation 80−25094
$Gd_2Ni_{17-x}Al_x$, mag. behaviour in paramagnetic region 79−73675
$GdRh_4B_4$, magnetic and electrostatic props., NMR study 80−93195
$Gd(Rh_{1-x}Fe_x)_2$, $x \leq 0.15$, magnetisation and EPR studies 80−34767
GdS, low temp. phase transitions, mag. moment orientation, spin flip 79−99700
Gd_xS_y, nonuniform ferro-antiferromag. ordering, 1.6 to 300K range obs. *(Russian)* 77−69504
GdSe, low temp. phase transitions, mag. moment orientation, spin flip 79−99700
Gd_2Se_3, mag. susceptibility 77−40032
GdTe, low temp. phase transitions, mag. moment orientation, spin flip 79−99700
$(Gd_xY_{1-x})_4Co_3$, Curie temp. and resist.-temp. curves, comp. depend. 80−71020
$(Gd_xY_{1-x})Fe_2$, Fe mag. behaviour, FMR measurements, mag. props., Vangsness relation anal. 79−78336
$^{72}Ge^{32}S$, $^{74}Ge^{80}Se$, $^{74}Ge^{130}Te$, rot. g_J-factor meas., $^1\Sigma$ ground state *(German)* 77−30865
GeSe, antiferromagnetic behaviour, res. to negative magnetoresistance effect 79−73719
$Ge_xZn_{1-x}Fe_2O_4$, ferrimagnetism and ion distrib. 77−12103

magnetic moments continued
^3He, liquid-ordered ferromagnet interface magnetic Kapitza conductance, surface spin wave effects 79−99406
^3He, solid, melting, formal treatment of low temp. props. 79−69315
$HfCo_6$, saturation magnetisation, Co mag. moment and electron transfer 77−73005
Hf_2Fe, moment form. on H_2 absorpt. 79−87343
$Hf(Fe_{1-x}Co_x)_2$, mag. props., Mossbauer spectra and magnetisation meas. 80−39948
$HfMn_2$, Curie-Weiss law depend. of susceptibility, mag. props. *(Russian)* 79−65655
$HgCr_2S_4$, cooling efficiency near 60Kas mag. refrigerant 80−71034
$(Ho,Y)Co_2$, first order phase transitions 78−84426
$(Ho,Y)Co_2$, mag. props., elec. resist. and thermal expansion 78−76246
Ho, liq., mag. susceptibility, elec. resistivity 80−20377
Ho-Co amorphous film, prep. by dual-source evaporation, mag. props. 77−89988
Ho-Dy-Sm, magnetic moment growth due to Sm addition *(Russian)* 80−34608
Ho-Pr(Nd) alloys, mag. struct. and ordered moments, neutron diffr. data 77−66252
Ho-Sm, magnetic moment growth due to Sm addition *(Russian)* 80−34608
Ho-Sm(Eu), mag. props. at low temp. in high mag. fields 79−56570
$HoAl_2$, Ho moment reorientation, polarized neutron diffr. study 79−42761
$HoAl_2$, magnetisation and neutron diffr. meas., cryst. field and exchange 77−63163
$HoCo_2$, paramag. and ordered phases, Pauli type Co susceptibility, polarised neutron diffr. obs. 77−63077
Ho_4Co_3, cryst. field effect on mag. moment direction, neutron diffr. meas. 78−80132
$HoCo_2Ge_2$, crystal and magnetic structure obs. 80−64976
$HoFe_2$, effect of H on sublattice magnetization, elastic neutron scatt. obs. 79−78327
$HoFe_2$, magnetostriction and magnetisation temp. depend. 79−73795
$HoFe_2H_{4.5}$, mag. props. and lattice consts., effect of hydrogen absorpt. 77−20561
$HoFe_2H_x$, mag. props. 80−25095
HoFeMn, Laves phase, mag. moment on Ho, neutron diffr. obs. 77−63107
$Ho(Fe_xNi_{1-x})$, mag. interactions, mol. field model 77−73010
$Ho_{12}Fe_{32}O_2$, struct. and ferrimag. props., neutron diffr. obs. 79−78319
$Ho_{0.01}Gd_{1-x}Y_xNi_2$, spin echo meas. on ^{165}Ho, limited quenching of Ho moment by cryst. field 79−73851
Ho_5Ge_4, mag. struct., neutron diffr. study 80−25093
$HoMn_2$, Laves phase, mag. moment on Ho, neutron diffr. obs. 77−63107
$HoMo_6S_8$, reentrant supercond., direct. obs. of long range ferromag. order 78−76190
Ho_2Ni_{17}, ferrimag. struct., neutron diffr. expt., cryst. field calcs. 77−73001
Ho_2Se_3, mag. susceptibility 77−40032
Ho_xTe, mag. ordering, neutron diffr. meas. 78−2649
$HoTiO_3$, magnetic structure determination, neutron scatt. study 80−65809
InR_2 (R-Y, Nd, Sm, Gd, Tb, Dy, Ho, Er, Tm), mag. props., 4.2 to 270K 79−56512
InSb:Mn^{2+} nondegenerate semicond., mag. impurity indirect interaction *(Russian)* 80−34591
$IrMn_{1+x}Sb$ alloys, crystal struct., and mag. props. 78−34466
$K_2Co_2(SO_4)_3$, cubic langbeinite struct., low temp. mag. susceptibility 78−56299
K_2CuF_4, magnon condensation obs. in quasi-2D planar ferromag. phase 80−60232
K_2FeF_5, one-dimensional antiferromag., neutron diffr. and mag. meas. *(French)* 79−47241
$KFeO_2$, cryst. and mag. struct., neutron and X-ray powder diffr., and Mossbauer effect meas. 77−84722
$KMgF_3:Ni^{2+}$, EPR meas., g-factor, spin-orbit coupling const. and mag. moment determ. 77−80999
$K_2Mn_2(SO_4)_3$, cubic langbeinite struct., low temp. mag. susceptibility 78−56299
$K_2Ni_2(SO_4)_3$, cubic langbeinite struct., low temp. mag. susceptibility 78−56299
La-Fe alloy, amorphous, sputtered at high rate, mag. props. 80−75753
La-Fe bulk amorphous alloys, mag. props. *(Japanese)* 79−95588
$LaCO_{1-x}M_xO_3$, M=Mg, Ti, cryst. struct., elec. and mag. props. 79−86748
$(La_{0.8}Ca_{0.2})MnO_{3+y}$, mag. props., Faraday method meas. 80−103832
$(La_{1-x}Ce_x)Al_2$, Kondo system, antiferromag., specific heat 79−24179
$La_{1-x}Co_x$, amorphous, conc. depend. of Co moment 78−56300
$LaCoO_3$, Mott isolator, paramag. props., calc. 80−93071
$LaLi_{0.5}Ir_{0.5}O_3$, perovskite, prep. and mag. study 80−80486
$LaMnO_3$, phase diagram, mag. moments, neutron diffr. study 80−108414
La_3NbO_7, weberite-type, elec., mag. and opt. props. 77−85212
$LaNi_{1-x}Fe_xO_3$, Mossbauer spectra, mag. hyperfine field 80−20537
$LaRu_xFe_{1-x}O_3$ perovskites, cryst. struct., elec., mag. and Mossbauer behaviour 77−55274
$La_{1-x}Sr_xCoO_3$ ($0.5 \leq x \leq 1.0$), effective mag. moments as function of composition 79−24154
Li ferrite, fine particle, for arc plasma spraying mm-wave phase shifter 78−64469
Li-transition metal dioxide intercalation compounds, mag. props., decomposition effects 80−25075
$LiCrO_2$, EPR of Cr^{3+} ion, g-factor and effective mag. moment 77−73073
$Li_xCr_yV_{1-y}S_2$, Mossbauer and mag. studies 79−73869
$Li_{0.5}Fe_{2.5}O_4$, temp. depend. of mag. moments, neutron diffr. data *(Russian)* 77−28371
$Li_{0.5}Fe_{2.5}O_4$-$CuFe_2O_4$-$MnFe_2O_4$, structural characteristics and mag. props. of solid solutions 77−35696
$Li_{0.5}Fe_{2.5}O_4$-$CuFe_2O_4$-$ZnFe_2O_4$, order-disorder transition, quadratic transformation *(French)* 78−76447
$Li_xFe_yV_{1-y}S_2$, Mossbauer and mag. studies 79−73869
Li_2O-NiO-O_2, phase diagram and mag. props. of $Li_xNi_{1-x}O_{1\pm y}$ 78−48380
$LiYF_4:Er^{3+}$, magnetocaloric behaviour, cryst. field theory 77−4520
$LuFe_2$, ferromagnetic cpds., mean field exchange consts., Stoner itinerant model calcs. 80−50084

magnetic moments continued
$LuRh_4B_4$, magnetic and electrostatic props., NMR study 80−93195
$Lu_2V_2O_7$, pyrochlore struct., mag. props. 78−72335
Ma-Cu (10 at.%), antiferromag. defect scatt., neutron polarisation anal. 78−2652
$MgCr_2O_4$, magneto-electric splitting of crystal field Γ_2-level of Cr^{3+} ion, neutron spectroscopic obs. 79−19562
α-Mn, electronic structure model, Invar effect, antiferromagnetic-non mag. transitions 80−20370
α-Mn film, rel. to effect of deposition conditions on low temp. resist. 79−78223
α-Mn, localised spin fluctuations, Knight shift obs. 80−60181
δ-Mn, paramag., antiferromag. and ferromag., magnetic moment calcs. 80−60223
γ-Mn-Cu, antiferromag. defect neutron scatt. study 79−47252
Mn-Cu, mag. and cryst. struct., neutron and X-ray diffr. meas. *(Russian)* 78−22694
Mn-Cu, mictomagnetic props., neutron diffr. obs. 80−65906
Mn-Ni(Pd), atomic and mag. order, neutron diffr. exam. 79−73697
γ-Mn-Pd, antiferromag. defect neutron scatt. study 79−47252
Mn-Pd (10 at.%), antiferromag. defect scatt., neutron polarisation anal. 78−2652
Mn-Pt alloys, mag. struct., neutron diffr. study 79−91210
τ-MnAl, estimated theoretical limit of mag. moment 80−97072
MnAs in suspension, ferromagnetic colloid, optical meas. 78−10906
$MnAs_{0.925}P_{0.075}$, low spin state electron config. *(Japanese)* 77−43813
$MnAs_{1-x}P_x$, mag. and crystallographic anal. 79−47257
$MnAs_{1-x}Sb_x$, mag. and crystallographic anal. 79−47257
$Mn_{2.5}Cr_{0.5}O_4$, mag. struct., neutron diffr. obs. 79−33460
γ-MnCu, Mn-rich, inclined spin axis, neutron diffr. study 80−75723
$MnFe_2O_4$, noncollinear spin model 77−28376
$Mn_3N_{0.86}$, cryst. and mag. struct. at low temps. *(French)* 77−73003
x.MnO.(1−x)[19TeO$_2$.PbO], glass, antiferromag. behaviour, mag. props. 80−50072
$Mn_{1+\delta}Sb$, Mn electronic state, neutron diffr. study 80−65806
Mn_2Sb, large anisotropy in mag. hyperfine field at ^{121}Sb, Mossbauer spectra meas. 77−73101
MnSi-CoSi solid solution, mag. props. 78−56403
MnZn ferrites, neutron diffr. exam. of influence of technology on mag. and cryst. parameters 79−42741
Mo complex, [triply bridged binuclear Mo (V) cation][$MoOCl_4(H_2O)$] $^-$, struct. 77−76371
Mo complexes with poly(iminoethylene)-dithiocarbamate polymer, synthesis and spectra 77−77189
NO+N_2(Ar), $^2\Pi_{3/2}$, $^2\Pi_{1/2}$ states, line broadening, mag. moment effect 79−72391
$NaCrX_2$, X=S, Se, EPR meas., g-factors, effective mag. moments, and dipolar shifts 79−8043
$Na_2(Fe,Mg)_5Si_8O_{22}(OH)_2$, riebeckite, low temp. Mossbauer obs. of oriented single cryst., behaviour and mag. props. 80−84674
α-$NaFe_2O_3$:Mg^{2+}(Co^{2+})(Zn^{2+}), substitution of Fe^{2+} *(French)* 78−95034
Na_2O-CaO-P_2O_5:Co glass, bonding, symmetry meas. 79−46572
$Na_xVS_2(Se_2)$, mag. and elec. props. rel. to struct. transitions 78−91848
$NdAg_x$, low temp. mag. meas. 80−107989
$NdAl_2$, mag. form factor, diffuse moment density, polarised neutron meas. 77−63108
$Nd_xEu_{1-x}B_6$ solid solution, mag. susceptibility, lattice parameters, Weiss temp. 80−29535
NdF_3, mag. props. between 2 and 4.2K *(French)* 79−61039
$NdFe_2$, amorphous, magnetization and neutron scatt. meas. 79−78314
Nd_3NbO_7, weberite-type, elec., mag. and opt. props. 77−85212
$NdRh_4B_4$, possible obs. of coexistence of supercond. and long-range mag. order 79−82730
NdSi mag. struct. and mag. moments, neutron diffr. meas. 77−85424
$Nd_{1-x}U_xCo_5$, mag. props. and spin-reorientation phase transitions *(Russian)* 78−60284
$Nd_xY_{1-x}Zn$ system, solid soln., mag. susceptibility, 77 to 600K *(Russian)* 80−65776
Ni (100) films, spin density by self-consistent linear APW method 80−65710
Ni alloys, mag. moment distrib. 77−32178
Ni, atomic magnetic moments comparison to values of ferromagnetic metal 78−52244
Ni crystals, at mag. crit. temp., sp. ht. rounding 79−95595
Ni, ferromagnetic, electronic struct. by real space approach 80−65432
Ni film, few atomic layers thick, transition from Pauli paramag. to band ferromag. 80−44885
Ni, mag. densities, spin and orbital contrib., neutron diffr. meas. 79−78316
Ni, paramag. region, Fe and Co impurity effects on susceptibility, Faraday obs. *(Russian)* 80−88731
Ni, rectilinear screw dislocation, magnetisation distrib., mag. moment anal. 80−44897
Ni, spin polarised photoemission, surface magnetism 79−52083
Ni, surface electronic structure, rigid exchange splitting model 77−11977
Ni-Au, local environment effects, magnetisation decrease 79−65664
Ni-Co-Mn, dil. ferromag. alloy, mag. moment, saturation magnetisation meas. 78−64195
Ni-Cr(V)(Co)(Mn)(Mo)(Ru)(Fe), spin wave stiffness consts., RPA CPA band model 79−61088
Ni-Cu, ferromag., mag. moment, local environment effects, HF CPA cluster calc. 80−65817
Ni-Cu, local environment effects, magnetisation decrease 79−65664
Ni-Cu alloy, ferromag. polarised neutron scatt., evidence for mag. environment effect 77−40039
Ni-Fe (40%), Mn coating, mag. interface effects 77−69638
Ni-Fe film, oligatomic, ferromag. reson. and torsion magnetometry, 123-373K 77−59461
Ni-Fe/Mn interface, mag. surface effects, dead layers and exchange anisotropy 77−24718
Ni-Fe-Mn alloy, NMR signals due to Mn atoms with antiparallel moments 78−27113
Ni-Fe-Pd thin films, mag., surface and corrosion props. 80−34707
Ni-Mn, mag. moment and asphericity of spin density distrib., polarised neutron scatt. obs. 80−44813
Ni-Mn, temp.-resist. graph deflection points, mag. moment orientation rel. to magnetisation matrix *(Russian)* 79−60788
Ni-Mn alloy, NMR signals due to Mn atoms with antiparallel moments 78−27113

magnetic moments continued
Ni-Mn alloys, ferromagnetism-to-spin glass phase transition and strong mag. field effect 80−75773
Ni-Mn disordered alloys, mag. moment and Curie point 78−76243
Ni-P-B alloy, amorphous, giant moments and short-range orders 77−4499
Ni-Pd, mag. moment distrib., one-mag.-species model calc. 80−65788
Ni-Pd alloy, disordered, local environment effects, neutron scatt. expts. 78−68172
Ni-Pd-Mn ternary alloys, mag. characts., use for thermoseed 80−107995
Ni-Pt, magnetic moment distrib., diffuse neutron scatt. meas. 80−34593
Ni-Pt alloys, magnetic-moment distrib. neutron study 80−97066
Ni-Rh, mag. moment distrib., one-mag.-species model calc. 80−65788
Ni-Rh alloy, disordered, local environment effects, neutron scatt. expts. 78−68172
Ni-Rh alloys, ferromag., local-environment effects, mag. diffuse neutron scatt. cross-section meas. 77−55664
Ni-Rh alloys, thermal EMF, elec. resist., mag. susceptibility, mag. moment and Curie temps., 18-500°C *(Russian)* 77−20288
Ni-Rh ferromagnetic alloy, mag. moment spatial distrib. 77−66275
Ni-Ru, environmental effects and mag. moment distrib., magnetisation and neutron scatt. meas. 79−91211
Ni-SiO multilayer film, interface magnetisation 80−7135
Ni-SiO multilayer films, interface magnetisation 80−88858
Ni-SiO_2 supported catalysts, particle size, H_2 chemisorption, Mossbauer study 80−7219
Ni-Ti, mag. moment distrib. and environmental effects around Ti impurity 80−7092
Ni-Ti(Mn)(Cu), tunnelling electron spin polarisation 77−73058
Ni_3Al, electronic, mag., and cohesive props. 80−44491
Ni_3Al, unpaired spin density distrib., polarised neutron diffr. 78−10659
$Ni_{100-x}B_x$, rapidly quenched, mag. moment, temp. and comp. depend. 78−47957
$NiBr_2$, commensurate and incommensurate mag. struct., neutron diffr. study 80−97067
$(Ni_xCu_{1-x})_2MnSn$, mag. props. and lattice parameter, composition depend. 77−80916
$Ni_{0.7}Cu_{0.3-x}Si_x$, magnetic props., 4.2 to 800K 77−8290
Ni(Fe,Cr) and Ni_3(Fe,Cr), electron states density model and mag. characts. calcs. *(Russian)* 80−92804
Ni_3(Fe,M), M=Cu, Cr, Mo, W, kinetic phenomena rel. to ordering and electron struct. *(Russian)* 78−76043
Ni_3Fe, non-linear local environment effect, Mossbauer effect of ^{57}Fe 80−39909
$NiFe_{2-t}Al_tO_4$, cryst. and mag. props. 78−14940
$NiFe_2O_4$ ferrite, mag. props., neutron irrad. 80−103858
NiH_x, magnetization, elec. resist., and non-occurrence of supercond. 79−56195
$Ni_2Mn_{0.9}Fe_{0.1}Sn$, Fe site hyperfine field and mag. moment, Mossbauer effect meas. 78−76365
NiMnGe, crystal and spiral mag. struct., Neel temp., X-ray and neutron diffr. 77−16052
Ni_2MnSn, Heusler alloy, mag. interactions and cond. electron polarisation, spin echo NMR meas. 77−77125
$Ni_2Mn_xT_{1-x}Sn$, (T=Ti, V or Cr), Heusler alloy, mag. moment exam. 77−24682
$Ni_2Mn_xT_{1-x}Sn$, T=Ti(V)(Cr), ferromag., magnetisation, susceptibility 77−12102
$Ni_{80}P_{20}$ glass, saturation moments, 4.2K 77−63125
NiS, antiferromag., press. effect on metal-nonmetal transition 77−69229
NiS_2, mag. torque curve 79−47305
NiS_2, neutron diffr. anomaly at Curie temp., antiferromag. refl. 78−76260
$Ni_{1-x}S$, and $Ni_{1-x}S_{1-y}O_y(Se_y)$, mag. state in metal-semicond. transition region, neutrnon diffr. obs. *(Russian)* 77−89926
$Ni_{1-x}Te$, fluctuating localised mag. moments, d band motion, Mossbauer study 80−65768
$Ni_{1-x}Ti_x$, ferromag. props., Ti conc. effect 80−54872
$NiWO_4$, mag. struct. refinement, neutron diffr. meas. *(German)* 77−16049
NiZn ferrites, comp., X-ray diffr. and saturation magnetisation obs. 78−18617
Ni(001) surface states, surface magnetisation, electron spin polarisation 80−88612
$NpFe_{2-x}Co_xSi_2$, mag. and hyperfine props. 80−7247
NpO_2, mag. transition at 25K, Kramers doublet as cryst. field ground state 80−59936
Pb superconducting slabs, magnetisation and migration field, reversible stage 80−65737
$PbMo_6S_8$, influence of Fe on superconduction transition temp., and mag. props. *(Russian)* 79−42686
$PbMo_6S_8$:Fe, elec. cond. anomalous temp. depend., mag. moments *(Russian)* 80−92878
$^{208}Pb^{32}S$, $^{203}Pb^{80}Se$, rot. g_J-factor meas., $^1\Sigma$ ground state *(German)* 77−30865
Pd, hydride and alloys, electronic band struct., comparative study of electric and mag. props. 78−95259
Pd, magnetic properties in para-process region *(Russian)* 78−2672
Pd, sd hybridisation, paramagnetic Curie temp. and susceptibility *(Russian)* 80−103808
Pd-Fe (25-55 at.%) ^{57}Fe effective field and mag. struct., Mossbauer and magnetisation expts. *(Russian)* 77−90085
Pd-Fe alloys, dil., spin polarisation effect on hyperfine interactions, anal. of Mossbauer meas. *(Russian)* 79−47055
Pd-Mn, dil. alloy, very temp. magnetisation 80−34692
Pd-Mn dilute alloys, mag. moment distrib., polarised neutron diffuse scatt. meas. 77−80914
$Pd_{0.98}Fe_{0.01}$ $Gd_{0.01}$, Pd-Gd exchange const., neutron diffuse scatt. meas. 80−71002
$PdH_x(\alpha')Fe_{0.003}$, depend. of mag. moment on H content 79−61054
β′-PdIn, electrical resistance, mag. susceptibility and IR freq. dispersion *(Russian)* 80−107759
$(Pd_{1-y}M_y)_{100-x}Fe_x$, M=Ag, Rh, exchange-enhanced alloys, mag. ordering 79−61050
PdMn, giant moment-spin glass high field magnetisation, exchange parameter, saturation moment estimation 79−61143
$Pd_{1+x}MnSb$ Heusler alloys, magnetic hyperfine fields on ^{111}Cd, TDPAC and magnetisation meas. 80−93219
Pd_2MnSn, Heusler alloy, interaction between local mag. moments 77−1540

magnetic moments continued
Pd_2MnSn, Heusler alloy, mag. interactions and cond. electron polarisation, spin echo NMR meas. 77−77125
$PrAg_x$, low temp. mag. meas. 80−107989
$PrCo_2Ge_2$, crystal and magnetic structure obs. 80−64976
$PrCu_2Ge_2$, magnetic props. 77−32180
PrEu(Gd), magnetic interactions, Mossbauer spectra quadrupole splitting, crystal field parameters 80−39907
$Pr_{1-c}La_cAl_2$, mag. props. 79−65658
PrSb, pressure-induced antiferromag., neutron scatt. study 80−39750
PrSi, mag. struct. and mag. moments, neutron diffr. meas. 77−85424
Pt-Fe alloy, ordered, T-c phase diagram, antiferro- and ferromagnetism *(Russian)* 80−65871
Pt_3Cr, ferrimag., magnetisation density, polarised neutron diffr. meas. 80−60204
$Pt_3Mn_xCr_{1-x}$ alloys, mag. props. 80−2562
$PuFe_2$, ferromag. mag. cross section, form factors, saturation magnetisation values, polarized neutron study 79−47245
PuP, ferromag. mag. cross section, form factors, saturation magnetisation values, polarized neutron study 79−47245
RFeAl, scatter order cpds., mag. props. 77−51891
$RbCoCl_3.2D_2O$, metamagnetic phase transition, crystallographic and mag. struct., neutron diffr. meas. 80−44174
Rb_2CrCl_4, two-dimens. easy-plane ferromag., cryst. and mag. struct., temp. variation of moment 77−66255
$RbFeCl_3.2H_2O$, pseudo-one-dimensional canted Ising antiferromag., spin-cluster excitations 80−70989
$RbMnCl_3$, antiferromag. static mag. props. *(Russian)* 78−60270
Rb_2MnCl_4 antiferromagnet, spin flopping in mag. fields 79−69687
$RbNiCl_3$, mag. props. 79−73736
Rh_2CoSn, ferromag., mag. hyperfine fields of ^{119}Sn, Mossbauer meas. 78−10816
Rh_2FeSn, ferromag., mag. hyperfine fields of ^{119}Sn, Mossbauer meas. 78−10816
Rh_2MnSn, and related cpds., with Heusler and Heusler-related struct., mag. props. 77−8311
$ScFe_2$, Mossbauer effect of ^{57}Fe 80−75903
$ScFe_2H_2$, Mossbauer effect of ^{57}Fe 80−75903
α-Sm, low temp. phase transition *(Russian)* 79−32937
Sm, polycrystalline with ferromag. impurities, mag. props., 1.5-300K 77−69547
Sm^{3+} in magnetically ordered Sm compounds, crystal-field effects on cross-over temp. of magnetisation 79−69656
Sm-Hf-Co alloy, rare-earth electron transfer 77−40028
$SmCo_5$, spin polarised energy band struct., APW calc. 78−10342
$Sm_2(Co_{1-x}Al_x)_{17}$ *(Russian)* 78−64202
$SmCo_3B_2$, high coercive forces, ferromag. ordering and saturation moments 77−24711
$SmCo_{5-x}Cu_x$, giant intrinsic mag. hardness 79−91255
$Sm_2(Co_{1-x}Fe_x)_{17}$, anisotropy consts., conc. and temp. depend. *(Russian)* 78−64202
$SmCo_{5-x}Ni_x$, giant intrinsic magnetic hardness analysis 78−88146
$SmFe_2$, ferromagnetic-ferrimag. cpds., mean field exchange consts., Stoner itinerant model calcs. 80−50084
$Sm_{1-x}La_xS$, mag. suscept., moment, impurity effects, indirect exchange interaction 78−68147
$Sm_6Mn_{23-x}Fe_x$, magnetic behaviour, temp. and comp. depend. 80−93090
SmN, magnetic props., neutron diffr. and mag. susceptibility meas. 80−50036
SmZn, ferromag., cond. band antiparallel polarisation exceeding 4f moment 80−60207
$^{120}Sn^{32}S$, $^{120}Sn^{80}Se$, $^{120}Sn^{130}Te$, rot. g_J-factor meas., $^1\Sigma$ ground state *(German)* 77−30865
$SrF_2:Tb^{3+}$, mag., thermal and hyperfine props. 80−29368
$SrFe_{12}O_{19}$, hysteresis loops, formation processes 80−39813
$SrFe_{12}O_{19}$, mag. props., effect of Sr dissolution by milling in water 77−25000
$SrMCrO_4$, M=La, Nd, mag. struct. determ. by neutron diffr. *(French)* 79−28507
$SrRuO_3$ single cryst., reduced ferromag. moment obs. 77−20564
$SrRuO_3$ single cryst., magnetocryst. anisotropy and reduced ferromag. moment 77−24691
$Sr_xZn_2Y(Y=Ba_{2-x}Fe_{12}O_{22})$, x=0, 1, 1.6, mag. moments reorientation 80−44851
Tb, liq., mag. susceptibility, elec. resistivity 80−20377
Tb, neutron elastic scattering, high-angle, anal. 80−80480
Tb-Fe, amorphous magnetism in bulk samples 77−66278
Tb-Ho film, helimag. order, surface deform., exchange and single-ion magnetocrystalline anisotropy energy 77−66390
Tb-Pr(Nd) alloys, mag. struct. and ordered moments, neutrons diffr. data 77−66252
Tb-Sm *(Russian)* 80−34608
$TbAsO_4$, mag. ordered, neutron diffr. study 79−47238
TbB_2, mag. props. and neutron diffr. 78−84401
TbBi, type II antiferromag., trigonal lattice distortion, temp. depend. 79−23732
$TbCo_2$, magnetocrystalline anisotropy and spontaneous magnetostriction 80−75831
$TbCo_5$, mag. state of Tb sublattice neutron diffr. meas. *(Russian)* 77−80915
Tb_4Co_3, cryst. field effect on mag. moment direction, neutron diffr. meas. 78−80132
TbD_2, mag. struct., neutron diffr. study 77−85421
$Tb_{0.27}Dy_{0.73}Fe_2$, anomalous thermal expansion and magnetostriction 77−90003
$Tb(Fe_{1-x}Rh_x)_2$, Fe sublattice spin reorientation possibility, Mossbauer spectra *(Russian)* 79−78335
$TbGa_2$, mag. props. and struct., neutron diffr. patterns at 4.2, 300K 77−63109
$(Tb_{1-x}Gd_x)_3Co$, intermetallic cpd. mag. props., phase transform, and mag. hystersis *(Russian)* 80−93113
$TbMnO_3$, mag. struct., ordering of Mn^{3+}, Tb^{3+} moments, neutron diffr. expt. 77−69500
TbP (As)(Sb)(Bi), mag. transitions, quadrupolar interaction effects 80−80512
TbP, singlet-groundstate magnetism, static mag. props. 80−7109
TbS, type II antiferromag., trigonal lattice distortion, temp. depend. 79−23732
Tb_xS, mag. ordering, neutron diffr. meas. 78−2649
TbSe, type II antiferromag., trigonal lattice distortion, temp. depend. 79−23732
magnetic moments continued
TbTe, type II antiferromag., trigonal lattice distortion, temp. depend. 79−23732
Tb_xTe, mag. ordering, neutron diffr. meas. 78−2649
$(Tb_{1-x}Y_x)_3Co$, mag. props. and transitions, conc. depend. *(Russian)* 78−10671
$Tb_xY_{1-x}Co_{5+0.1x}$, exchange interactions and magnetocrystalline anisotropy 80−34618
Th-Dy, dil., type I superconductor, paramag. Dy moment relax., Mossbauer spectra study 80−65755
$ThCo_5$, mag. transition due to Co moment change, metamagnetism of 3d-band 77−63184
$ThFe_3$, H_2 absorption effect on mag. props. and struct. 77−40045
$ThFe_5$, mag. props., ferrimag. moment arrangement 79−33475
$Th_{1-x}Fe_x$ amorphous alloys, mag. props. and Mossbauer spectra 79−91326
Th_7Fe_3, H induced change from supercond. to mag. ordered state 79−28525
$Th_6Mn_{23}H_x$, H induced mag. ordering obs. 77−85423
Ti-Cu alloys, mag. susceptibility meas., paramagnetic susceptibility meas. Curie temp. and mag. moments calc. *(Russian)* 78−34956
Ti-Fe, H storage material, Mossbauer surface studies, Fe clusters 80−97167
$TiBe_2$, itinerant antiferromagnetism, mag. susceptibility obs. 79−15288
$TiBe_2$, neturon diffr. study of mag. ordering 80−44811
$TiFe_{1-x}Co_x$, electronic struct. and mag. moment calcs. 80−65821
$TiMn_2$, Curie-Weiss law depend. of susceptibility, mag. props. *(Russian)* 79−65655
Ti_4O_7 and $(Ti_{1-x}V_x)_4O_7$, metal-insulator transitions, EPR, elec. and mag. props. 80−2336
$(Ti_{1-x}V_x)_2O_3$, O<x<0.1, magnetisation and mag. moments 80−65772
$(Ti_{1-x}V_x)_2O_3$, spin-glass props., 0.05-300K 80−25149
$Tm_{2.7}Bi_{0.3}Ga_{0.3}Co_xFe_{4.7-x}O_{12}$, Co ion concentration effect on mag. props. close to mag. compensation point *(Russian)* 79−73788
$TmCo_2$, paramag. and ordered phases, Pauli type, Co susceptibility, polarised neutron diffr. obs. 77−63077
$TmCo_5$, easy magnetisation direction 78−84415
Tm_4Co_3, cryst. field effect on mag. moment direction, neutron diffr. meas. 78−80132
$TmFe_2$, low temp. magnetisation and magnetostriction 78−64249
$TmFe_2H_{4.3}$, mag. props. and lattice consts., effect of hydrogen absorpt. 77−20561
$TmFe_2H_x$, mag. props. 80−25095
$Tm_3Fe_5O_{12}$, mol. field coeffs., mag. moment/temp. relations 80−50067
TmSe, mag. ordering under press., neutron diffr. obs. 80−70947
TmSe, mag. props. and struct. 80−25109
TmSe, mixed valency, field depend. mag. field transition 78−10657
Tm_3Se_4, mag. susceptibility 77−40032
$TmSe_{0.83}Te_{0.17}$, spontaneous magnetisation, mag. susceptibility, magnetostriction, elec. cond. 79−24146
$Tm_2V_2O_7$, pyrochlore struct., mag. props. 78−72335
U monopnictides, mag. props. 78−43554
U_3As_4, high-field suscept. at He temp. 77−89935
UFe_2, giant magnetoelastic deform. of cryst. struct. mag. props. *(Russian)* 80−93159
UFe_2, magnetisation meas. 79−51756
$U(Fe_{1-x}Mn_x)_2$, Curie temp. and saturation moment at 4.2K 80−70966
UGa_2, cryst. struct., mag. and magnetoelastic props. *(Russian)* 79−38364
UGa_2, mag. and magnetoelastic props. 80−15775
UGeY, (Y=S, Se, Te), mag. struct. and ordered moments, powder diffr. data 78−72329
UH_3, magnetic props., book contrib. 79−82754
UN, system with two singlet levels, fluctuations, excitations and induced moments 79−61022
U_2N_2Te, mag. struct. 77−63119
US(Se)(Te), photoelectron energy distrib. and spin polarisation, electronic and mag. props. 80−16146
USb, neutron inelastic scatt. meas., phonon spectra, mag. response, anisotropy 80−50065
$USb_{0.8}Te_{0.2}$, magnetisation and polarised neutron studies 79−56515
$USb_{0.8}Te_{0.2}$, magnetisation and neutron meas., mag. moments 80−15703
USe, anisotropic mag. moments 79−42754
USe, ferromag., spin polarisation of photoelectrons 79−78831
UTe, magnetisation and neutron meas., mag. moments 80−15703
$U_xZr_{1-x}Fe_2$, Curie temp. and saturation moment at 4.2K 80−70966
V fine particles, appearance of mag. moment 78−68152
V hyperfine particles, appearance of mag. moments, mag. susceptibility meas. 77−36097
V, magnetic moment near surface, one-electron band model 79−82747
V surface, spin fluctuations, finite temp. mag. props. study 80−107994
^{51}V, nucl. acoustic reson. absorpt. and dispersion via coupling to mag. dipole moment 77−48065
V_3 single cryst., supercond., Ginzburg-Landau parameters, magnetisation meas. 78−2620
$V_xCr_{3-x}S_4$, elec. and mag. props. 79−28523
$V(Ir_{1-x}Pt_x)_3$, NMR study of ferromag. 79−65760
V_2O_3, high-temp. transition domain, small angle diffuse neutron-scatt., 400-600K 77−69231
V_5S_8, paramag. cryst., struct. factors using polarised neutron diffr. 80−15691
V_3Se_4, itinerant antiferromag., spin fluctuations, NMR study 80−75874
V_5Se_8, itinerant antiferromag., spin fluctuations, NMR study 80−75874
VUS_3, mag. struct. and delocalised moments, powder neutron diffr. obs. 77−69496
Y-Co, CPA calcs., moments and transition temps. 78−52252
Y-Fe alloys, mag. interactions, effects on moments *(Rumanian)* 79−15296
Y-Fe(Co), mol. field model 77−4498
Y-Mn(-Co) alloys, amorphous, paramag. props. and Hall effect 79−73692
YCa garents, solid soln., mag. and cryst. chem. props. 77−16057
YCo_5, spin polarised energy band struct., APW calc. 78−10342
$Y_{1-x}Co_x$, amorphous, conc. depend. of Co moment 78−56300
$Y_{1-x}Co_x$, CPA calcs. 77−72997
$Y_{1-x}Co_x$, temp. depend. of magnetisation 77−77043
$Y_2(Co_{1-x}M_x)_{17}$, M=Al, Cu, single crystal, mag. props. 77−47993
YFe_2, ferromagnetic cpds., mean field exchange consts., Stoner itinerant model calcs. 80−50084
$Y_{1-x}Fe_x$, amorphous, Mossbauer spectra, appearance of magnetism 78−52401

magnetic moments continued
$Y_{1-x}Fe_x$, mean mag. moment calc. 79−82761
$Y(Fe_{1-c}Al_c)_2$, local model for mag. behaviour 77−63135
$Y(Fe_{1-c}Al_c)_2$, mag. and Mossbauer study, local environment effects 78−27033
$YFe_{2-x}Al_x$, magnetisation behaviour, mag. scatter order 77−28373
$Y(Fe_xAl_{1-x})_2$, Mossbauer spectra and mag. props. 80−39950
$Y_6(Fe_{1-x}Al_x)_{23}$, cryst. struct. and mag. props. 79−82180
$(Y_{65}Fe_{35})_{100-x}B_x$ glasses, mag. props. 79−73693
$Y(Fe_xCO_{1-x})_2$ model, Co, mean mag. moment composition depend.; reciprocal susceptibility, thermal var. 78−47945
$YFe_{0.62}Cr_{0.38}O_3$, compensation of weakly ferrimag. moment 79−8035
$YFe_{1-x}Cr_xO_3$, weak ferrimagnet, anomalous mag. props. explained by exchange interactions *(Russian)* 77−69538
$Y(Fe_{1-x}Mn_x)_2$, Mossbauer spectra and mag. props. 80−39952
$YFe_{2x}Mn_{2-2x}$, mag. props. and FMR 79−95581
$Y_6(Fe_{1-x}Mn_x)_{23}$, Mn-rich compounds, Mossbauer effect study 80−71276
$YFeO_3:Co^{2+}$, weak ferromagnetism, single ion anisotropy contrib. 80−25126
$Y_3Fe_5O_{12}$, amorphous, mag. moments, susceptibility, Mossbauer studies 79−78345
$Y(Fe_xT_{1-x})_2$, Mossbauer spectra, mag. props. 80−20563
$Y_{1-x}GdCo_5$, exchange interactions and magnetocrystalline anisotropy 80−34618
$(Y_{1-x}Gd_x)Co_2$, spin echo NMR of mag. states 80−7190
YIG, polariser neutron study of covalency effects 80−2552
YIG:Tb garnet, Faraday effect in strong mag. field *(Russian)* 80−100651
Y_6Mn_{23}, magnetic moments, magnetisation 80−25094
$YMn_{2-x}Co_x$, mag. order in pseudobinary region 79−99689
$Y_6(Mn_{1-x}Fe_x)_{23}$, hydriding characts. and mag. props. 77−69527
$Y_6Mn_{23}H_x$, influence of absorbed H on mag. behaviour 77−85423
$Y_{1-x}Nd_xCo_5$, exchange interactions and magnetocrystalline anisotropy 80−34618
Y_2Ni_{17}, ferromag. struct., neutron diffr. expt., cryst. field calcs. 77−73001
YPd_3, rare earth impurities, magnetostriction 79−4714
Yb-Eu alloys, mag. ordering, magnetisation meas. 80−7081
YbCuAl, mixed valence behaviour, mag. props. 78−68150
$YbFeO_3$:Co, mag. struct. factors, neutron diffr. study 79−47248
Yb_xSy, synthesis and mag. props. 78−23242
$Yb_2V_2O_7$, pyrochlore struct., mag. props. 78−72335
Zn whiskers, quantum oscills. of mag. moment 79−15280
Zn-Mn(Cr), dil, mag. anisotropy, Hartree-Fock calcs. 80−11162
$Zn_xMn_{2-x}Sb$, anti-PbFCl type, cryst. struct. and ferromag. ordering 77−84723
$Zn_{1-x}Ni_xCr_2S_4$, spin struct., mag. props. meas. 77−85428
ZnO surface, quantised accumulation layer magnetoresistance, spin scattering model 79−69529
Zr-3d Laves phase binary and pseudobinary intermetallics, mag. props. H absorpt. effect 80−88821
$Zr_{1-x}Co_x$, amorphous, conc. depend. of Co moment 78−56300
$Zr(Fe_{1-x}Al_x)_2$, Curie temp., magnetisation, and cryst. struct., conc. depend. 80−75730
$Zr_{0.9}Fe_{0.1}V_2$, NMR and mag. susceptibility 78−95527
$ZrMn_2$, Curie-Weiss law depend. of susceptibility, mag. props. *(Russian)* 79−65655
$Zr_{1-x}Nb_xZn_2$, microscopic mag. props., NMR investigation 80−15807
$Zr_{0.99}Pt_{0.99}V_2$, NMR and mag. susceptibility 78−95527
ZrV_2, NMR and mag. susceptibility 78−95527

magnetic monopoles
(2+1) dimensional Georgi-Glashow model, critical Higgs mass, clustering, monopoles 80−52441
't Hooft's mag. monopole unicity 78−16908
't Hooft magnetic monopole, energy levels in the Prasad-Sommerfield limit 79−54268
't Hooft monopoles, interaction energy in Prasad-Sommerfield limit 79−12950
't Hooft Polyakov monopoles, force between widely separated interacting monopoles 77−87895
't Hooft type monopoles, time depend. generalizations, gauge theory solns. 77−6023
't Hooft-Polyakov mag. monopole electric charge in CP nonconserving theories, $e\theta/2\pi$ charge dyon 79−97534
't Hooft-Polyakov magnetic monopole soln., uniqueness in 0(3) gauge theory 77−2747
't Hooft-Polyakov monopole, fermion binding *(Russian)* 77−2548
't Hooft-Polyakov monopole, zero energy eigenvalues for quantum fluctuations, quantisation 79−9318
't Hooft-Polyakov monopole interactions, Prasad-Sommerfield limit, Yang-Mills-Higgs system 79−251
Abelian magnetic monopoles in Euclidean lattice model, improved Schwinger-Zwanziger Lagrangian 79−97515
Abelian self-dual multimonopoles, covariant Laplace operator Green function 80−77969
action-at-a-distance theory of electrodynamics with Dirac's monopoles 79−63059
angular momentum of scalar isodoublet in magnetic monopole field 78−41428
asymptotic behaviour of 't Hoofts mag. monopole 78−32974
Backlund transformations describing SU(2) mag. monopoles 79−2915
Backlund transforms. for mag. monopoles in SU(2) gauge theory 79−2916
baryons, charmed, mag. dipole moments and mag. quarks 79−97573
Bogomolny-Prasad-Sommerfield monopole, multiinstanton ADHM generalisation 80−52407
Bogomolny-Prasad-Sommerfield one-monopole soln. by Backlund transformation 80−99059
bound monopole states, SU(4) spontaneously broken 77−82679
bound states composed of the baryon and the monopole *(Chinese)* 79−63340
BPS one monopole generation by Backlund transform 80−77980
in Cabibbo-Ferrari two-pot. theory, comments 77−67304
charge particle-magnetic monopole scattering, zeroth order eikonal approx. 79−12990
charge quantisation, theorem *(Russian)* 79−63390
charge quantisation condition with N strings, charge monopole systems 77−65121
charge-monopole composites, Poincare invariance and parity violation 77−2762
charge-monopole composites, system of identical particles, statistics 78−93796
charge-monopole duality and nonAbelian gauge theory phases 79−71625
charge-monopole duality in spontaneously broken gauge theories 79−267
charge-monopole system, mech. model 78−62343
charged particle motion in fixed mag. monopole field, quantum mech. treatment 78−66062
charged particle scattering by mag. monopoles, SO(3), gauge theory 77−13907
charmed baryons, elec. and mag. quarks rel. to Dirac mag. monopoles 80−402
classical angular momentum of an electron-magnetic monopole *(Chinese)* 78−86460
classical field eqns. with a mag. charge 80−4872
classical gauge field theory solns., stability, absolute minima of energy 77−30261
classical interactions of 't Hooft monopoles 78−78233
classical Lagrangian theory with radiative reaction, monopoles and positrons in Rohrlich formalism 79−72
classical Lagrangian theory with radiative reaction, Rohrlich two field formalism extension to include monopoles 78−45488
classical string like solns., masses for monopole and dion *(Russian)* 77−5677
classification in terms of Yang-Mills fibre bundles topology 77−22635
classification of SU(3) mag. monopole 78−364
Clebsch-Gordan coefficient summing, appl. to mag. monopole theory 77−41505
complex structure of monopoles, instanton techniques, classical monopole eqns. 78−54537
condensed monopoles and Abelian confinement 78−78140
conference on hadron struct. and lepton-hadron interactions, Cargese, France (July 1977) 80−4473
confinement, spin depend. forces, semiclassical model 79−67500
conserved opposite parity currents, coupling to single vector field 79−21990
cosmic, behaviour in geomagnetic field *(Chinese)* 80−46358
cosmic OH molecules, detection of monopoles by nonlinear effects in interstellar masers 77−91609
cosmic ray, magnetic monopole candidate, reassessment of 1975 Lexan and emulsion meas. 79−3333
cosmic ray flux, upper limit from fossil tracks in pallasites 77−9641
cosmic ray study, new interpretation of event attributed to mag. monopole 78−69635
cosmic ray tachyon monopole search 79−16770
coupled Einstein-Higgs field, mag. monopole and dipole soln. *(Chinese)* 78−82112
covariant field equations for an electromagnetic string with mass points at the ends 79−309
De Rham currents, field and mag. monopoles extended singularities 78−4810
detection in balloon borne track detectors 77−22822
Dirac, stringless, global U(1) gauge theory commutational relation *(Chinese)* 79−35919
Dirac's monopole, generalisation to SU(2) gauge field theory 78−32975
Dirac's monopole and the Hopf map 80−27402
Dirac's monopoles and action-at-a-distance theory: classical dynamics 80−95210
Dirac's veto, classical Lagrangian theory of Dirac's monopole 79−40383
Dirac's veto in monopole theory 77−46096
Dirac charge Ze particle scatt. by mag. monopole, helicity amplitudes 77−65123
Dirac charged particle with extra mag. moment in mag. monopole field, bound states 77−67604
Dirac equation, normalisable solutions in the presence of magnetic monopole 79−67488
Dirac magnetic monopole, gauge independ. formulation 78−41427
Dirac monopole, relativistic theory, canonical quantisation 78−45517
Dirac monopole, search with Cherenkov photographic detector 78−70700
Dirac monopoles and the Hopf map $S^3 \to S^2$ 80−32042
Dirac particle+fixed magnetic monopole bound system, elec. and mag. dipole moments 78−24966
Dirac particle in mag. field, symmetry breaking by monopole singularities 78−16977
Dirac quantum conditions, mag. charges and monopoles *(Norwegian)* 77−34109
Dirac string Lagrangian in A^0-0 gauge, path integral quantisation 80−32007
Dirac strings, monopoles, duality, triality 78−12864
Dirac strings, theory 77−22634
Dirac theory with and without strings 77−41794
direct action, interaction of charges and monopoles 77−13619
direct action theory 78−28963
dual charge of nonAbelian gauge groups, mag. monopoles *(Chinese)* 77−34076
duality invariance, simple gauge theories including EM-type fields with sources 80−27440
duality rotations in EM charge space, secondary symmetry, magnetic current conservation 80−27431
dynamical groups, symmetries and constants of motion for electric and mag. charges 80−101945
dyon solution of non-Abelian gauge theory with surface terms 77−74592
dyon-dyon nonrelativistic scatt., classical and quantum anal. 77−5985
dyonium model, space reflection operator and boson fermion puzzle 79−36118
dyons, spin statistics connection 79−54248
education, Dirac monopole, calc. of strength 77−33764
education, magnetic charge quasiclassical quantisation 77−87595
education, topological solitons in physics, vortices and mag. monopoles as examples 79−25793
Einstein-Maxwell generalised eqns., Birkhoff's theorem and mag. monopole solns. 78−45535
electric and magnetic charges as extra components of four momentum 79−71603
electrodynamics, classical, gauge-invariant Hamiltonian formulation including mag. monopoles 78−45489
electrodynamics, formulations with magnetic monopoles, book contrib. 79−58915
electrodynamics with strings and monopoles, book contrib. 79−58916
electron, photon and mag. monopole interactions, quantized theory 79−13004

magnetic monopoles continued
electron+monopole, scatt. through small angles, Dirac-Schwinger monopole 80−68398
electron-mag. monopole interactions, without Dirac strings, quantum-mech. formulation 79−21994
electron-monopole system dynamics in U(1) gauge theory 79−54247
elementary particle energy level calcs., Coulombian field approx. 79−26311
elementary particle mass, mag. quark models 79−26312
EM pot. representation in broken SO_3 and SU_2 gauge theories *(Chinese)* 78−86459
energy tension and gravitational field *(French)* 80−52075
Euclidean manifolds, N-dimensional instantons and monopoles 80−42321
Euclidean Yang-Mills fields, instantons and monopoles 78−4760
existence in unified field theories 79−25957
existence of quarks, monopoles, tachyons, etc., review of expts. 78−12872
exotic atoms containing monopoles, energy levels and stationary states *(Chinese)* 78−86982
fermion-boson puzzle, coupled Yang-Mills isovector Higgs system, canonical formalism 78−41415
fiber bundle analysis of global feature of gauge field theory 79−71616
fibre bundles, mag. monopoles and gauge fields *(Chinese)* 79−80741
field strenghts of accelerated monopole *(Chinese)* 78−77740
field theory of electric and magnetic charge 79−6306
fractional electric charges and mag. monopoles, existence in matter, model 79−13238
fundamental monopoles and multimonopole solutions for arbitrary simple gauge groups 80−77952
gauge field of mag. monopoles 77−64950
gauge field theory, magnetic charges in SU_2 and U_1 theories *(Chinese)* 77−71437
gauge theories, canonical formalism, appl. to monopole solns. 77−206
gauge theories, exact gauge symm. group, ang. momentum operator, mag. monopole props. 77−2764
gauge theories and magnetic charge 77−79215
gauge theory monopole solns. Poincare group algebra representation 78−16925
gauge transformation and vector pot. 78−4494
Gaussian fluctuations: 't Hooft's method and an approximate method 79−85236
generalised 't Hooft monopole solns. in gauge theories 77−13854
geometric aspects of monopole theories 77−74591
geometric configuration of mag. flux string and monopoles, compared to O(3) nonlinear σ-model 80−57527
grand unified theories, compatibility with big bang cosmology, superheavy monopoles 80−86647
grand unified theories, mag. monopoles and cosmological implications 80−86643
gravitational analogue of mag. monopole, Mandelstam path-dependent formalism 78−81898
group theoretical approach 77−71434
harmonics of monopoles anal. 78−8720
heuristic potential theory, for monopoles without strings, teaching approach 79−5931
Higgs field and mag. monopoles *(Chinese)* 77−10174
Higgs field zeros for axially symmetric multi-monopole configurations 80−82887
Higgs-Kibble-Yang-Mills field eqns., axially symm. solns. 78−368
high-spin meson possibility with mag. monopole and antimonopole *(Chinese)* 78−17068
holistic physics in the theory of magnetic monopoles 79−49369
index theorem, axial-vector anomalies, in Schwarzschild and Taub-NUT spaces 78−93832
instantaneous Coulomb interaction in SU(2) Yang-Mills QCD 80−22574
instanton interactions and Riemannian geometry 77−71447
instantons and monopoles in Yang-Mills gauge field theories 80−91003
interaction with ferromag. domain, calc. 77−40078
invariance props. of Dirac monopole 77−61208
ionisation cross section as means of distinguishing from charged particles (student level) 77−23594
isofermion Dirac particles, energy spectra in 't Hooft Polyakov monopole field 78−24965
linear deformations of the Prasad-Sommerfield monopole 80−52419
long range interactions in non-Abelian gauge fields 80−22520
Lorentz invariance of quantum field theory of electric and mag. charge 78−33010
magnetic monopole mobility spectrometer for teachers 78−62000
magnetic quark confinement, flux tube in gauge field model 77−6084
magnetically bound monopole pair, possible fermion struct. 80−86661
magnetically extended Lagrangian theory, 0(3) gauge theories with spontaneous symm. breaking, shared photon sector 78−62306
mass spectrum for integral isospin monopoles, bag model as high isospin limit 78−24935
massive electrodynamics with magnetic charges, duality covariant form of Maxwell's eqns. 78−4495
Maxwellian electrodynamic theory, history from eqn. discovery to mag. monopoles *(German)* 78−65791
ME-EM field model of free electron state 78−49988
monopole concept and elementary theory 79−49366
monopole soln. uniqueness 77−41760
monopole-dyon system in nonAbelian gauge theories, Georgi-Glashow model 77−79213
monopoles, topology and symmetry 79−49370
monopoles with no strings, action principle and canonical quantisation 80−31990
multiply charged monopoles in higher rank gauge theories 77−45960
Nambu mechanics, particle-SU(2) monopole interaction 78−4478
'new particle' searches and discoveries, 'Review of Particle Properties' 1976 supplement 77−57515
non conventional monopoles in field theory, book contrib. 79−58919
non-Abelian gauge theories and mag. monopoles, strong interaction models and quark confinement 79−49367
non-Abelian gauge theory, mag. charges, quark confinement 77−49849
non-Abelian symmetry, Dirac strings and monopoles 77−41773
nonAbelian gauge field monopole, ang. momentum operator *(Chinese)* 79−58865
nonAbelian gauge groups, dual charge (mag. monopole) problem 79−63376
nonAbelian gauge model, radially separated monopole solns. 77−74593
nonAbelian gauge theories, topological configurations, magnetic poles on flux strings 79−49368
nonAbelian gauge theory, spherically symm. monopoles 77−61191
observable phase factors and symmetry of electric and magnetic charges 78−86428
parity conservation in EM interactions, connection with absence of magnetic monopoles 77−6044
path group appl. to gauge theory and quarks 80−31985
path-depend. approach to coloured mag. monopoles 78−37127
plasma-wave dispersion rels., modification due to magnetic monopoles, pulsar emission 79−75704
Polyakov-'t Hooft monopole and dyon, quantum theory *(Russian)* 78−392
Prasad-Sommerfield dyon (monopole) soln. of SU(2) Yang-Mills field with Higgs multiplet 80−339
Prasad-Sommerfield monopole, time depend. soln. of SU(2) Yang-Mills-Higgs system 79−273
Prasad-Sommerfield soliton mag. monopole, excited states and SU(3) generalisation 79−40665
primordial magnetic monopoles in unified gauge theories 80−91035
prod. in atmospheric high-energy collisions 78−49262
proton magnetic monopole struct., observational limits, from 42 cm neutral galactic H absorpt. 79−53717
PT-invariant theory of massive dually charged particles, Dirac-like eqn. 80−52429
pulsars, mag. monopoles creation 79−35287
pulsars, mag. monopoles creation 79−44516
pure gauge fields on coset space 79−40673
QFT of mag. charges, one pot. formulation 80−22512
quantisation condition for t'Hooft monopoles in compact simple Lie groups 77−13869
quantisation of systems with no singularity-free Lagrangian 77−49625
quantum field theory, review 79−26234
quantum soliton operators for monopoles and Fermionization mechanism of dyons 79−35940
quantum strings and gauge invariance 78−33009
quark confinement, Dirac's magnetic monopole string theory 77−13927
regular N-instanton fields and singular gauge transformations 78−4772
relativistic classical eqns. of motion, electric dipole moment case 80−37195
relativistic mechanics of mag. monopoles and electric charges 78−28967
relativistic strings, Dirac monopoles at end points 77−34135
relic 't Hooft Polyakov mag. monopoles in the Universe 79−9317
relic monopoles from big bang, cosmological problem for standard unified theories 80−77532
rotationally invariant solutions of Yang-Mills-Higgs system for general gauge group, mag. monopoles 78−29235
scattering with electric charge, analytic struct. of quantum amplitude 78−54226
scattering with electric charge, rotationally invariant approx. 78−54225
search, CERN ISR 78−66176
search in 70 GeV proton synchrotron 77−14011
self-coupled vector fields, calcs. using Dirac quantisation procedure 78−89610
sine-Gordon equation, classical solns. of field eqns., moving t'Hooft-Polyakov monopole *(Russian)* 78−16935
singular gauge transformations, monopole vortex line systems, Nielsen Olsen SU(2) Higgs model, Nambu model 78−66034
singular state problems, monopole pair energy levels, charged monopole-electron system *(Chinese)* 80−101733
six dimensional space time formalism of electromagnetism, mag. monopole behaviour of electrically charged tachyons 78−54182
SO_3 monopoles, spherical symm. limits on mag. charge, gauge independent proof of Guth-Weinberg theorem 77−30231
SO(3) gauge group, monopoles, spontaneously broken gauge theory 77−2753
SO(3) non-Abelian gauge theory, configurations of monopoles with multiple magnetic charge 77−2745
soliton solns., mag. monopoles as gauge particles 78−16920
spherically symm. monopole soln. 78−8539
spherically symm. monopoles anal. 77−71417
spherically symmetric fields in gauge theories, Yang Mills eqns., mag. monopoles 78−16914
spin 1/2 particle, motion in field on mag. monopole 80−18097
spin (10) grand unified theory, monopole mass 80−99080
spin-1 particles, elec. and mag. fields and charges 77−60948
spin-1/2 particle in monopole field 78−4766
spinor monopole soln. *(Chinese)* 78−78097
spontaneous compactification, mag. monopoles in higher dimens., Wu Yang global gauge descript. 79−2920
spontaneous compactification of arbitrary space-time dimens., mag. monopole soln. of gauge field 77−22458
spontaneously broken SU(2) gauge theory, nonexistence of spherically symmetric monopoles with multiple mag. charge 77−6010
stability analysis, Yang-Mills equations 80−31987
static magnetic SU(2) Yang-Mills-Higgs system, static axial and mirror symmetric monopoles 80−90992
static monopole fields, propagation functions, Yang-Mills instanton equivalence 79−35928
stationary charged C-metric 80−17849
stopping-power formula for mag. monopoles 78−46242
string-like topological excitations of the electromagnetic field 78−93835
$SU_2 \times U_1$ invariance, magnetic monopole principal bundles, physical implications 79−6296
SU_2 monopole harmonics 79−17646
SU(2) and SU(3) gauge field theories, classification of monopoles 77−38082
SU(2) gauge fields, sourceless solns. of static monopole systems *(Chinese)* 78−86418
SU(2) gauge group, magnetic monopole as finite energy smooth soliton soln., review 78−89625
SU(2) gauge mag. monopole, non-Abelian group *(Chinese)* 78−78096
SU(2) gauge theory, exact monopole and dyon solns. for arbitrary semi-simple compact group 79−71599
SU(2) magnetic monopole solns., parameter counting in Prasad Sommerfield limit 80−352
SU(2) monopoles in non-Abelian gauge theory, Bogomolny eqn. for interacting monopoles 79−85225
SU(2) Yang's monopole, quaternionic gauge fields on S^7 80−57473

magnetic monopoles continued
SU(2) Yang-Mills field, 't Hooft monopole, Julia-Zee dyon, stable solns. 79−26229
SU(2) Yang-Mills-Higgs system, classical finite energy solns. embedding in supersymmetric extension 79−2950
SU(3) colour gauge group, coloured monopoles 80−68360
SU(3) gauge model, monopole solns. 77−6047
SU(3) gauge theories without scalars, mag. monopoles, dyons, other topologically stable solns. 77−49819
SU(3) theory of Yang-Mills-Higgs fermion-monopole system, topologically stable soln. 77−13888
SU(4) gauge theories 78−24918
SU(4) monopole and dyon solns. *(Chinese)* 79−9307
SU(5) grand unification, spin from isospin, half integer spin charge monopoles 80−68406
SU(5) model, dyons and monopoles 80−82931
SU(5) monopoles, magnetic symmetry and confinement 80−99078
SU(N+1) gauge theory, exact monopole solns. with spherical symmetry 79−71626
SU(N) gauge theory, current synchrospherical symmetrical monopole in multisynchrospherical symmetrical case *(Chinese)* 80−22527
SU(n) gauge theory, spontaneously broken, monopole solns. 78−82103
SU(N) lattice gauge model, weak coupling, monopole condensation and quark confinement 79−75683
SU(N) spontaneously broken to U(1), composite magnetic monopoles 77−2765
SU(S) based grand unified theory, monopoles and vector bosons, symmetry breaking 80−99079
superfluid flow analogy to Dirac's monopole 80−6575
superheavy magnetic monopoles, cosmological prod. in grand unified models 80−8884
supersymmetric mag. monopoles and dyons, quantum corrections 78−62334
supersymmetric point particles and monopoles with no strings 80−52432
supersymmetric solitons in four space-time dimens., the mag. monopole 79−21896
tachyon + bradyon interactions, superluminal and subluminal EM fields 80−12902
tachyon magnetic monopoles, existence in 6 dimens. space, superluminal transforms. in Dirac theory 78−54183
tachyons, monopoles and related topics, book 79−44718
tachyons and magnetic monopoles in the de Sitter universe, book contrib. 79−44726
time-independent Yang-Mills statics 79−12957
topological charges for N=4 supersymmetric gauge theories and monopoles of spin 1 79−63364
topological lines and collinear monopoles 78−16907
track characteristics in plastic detectors 77−18759
transitional radiation for magnetic charge *(Russian)* 79−22888
two-potential formulation of electrodynamics with magnetic monopoles *(Russian)* 80−62893
unified gauge theory of gravit., e.m., mag. monopole fields 77−57263
unitarity and renormalized 't Hooft identities 80−13205
van der Waals force in pp scatt., monopole model of hadrons 78−41563
very early Universe, phase transitions and mag. monopole prod., grand unification 80−51934
vortex strings, mag. monopoles in gauge field theory 78−70283
wave function for electron motion in monopole pot. *(Chinese)* 78−77768
wave function of charged particles near mag. monopole *(Chinese)* 77−67600
Yang-Mills and unified gauge theories, mag. monopole solns. 78−21320
Yang-Mills coloured theory, string like phase 78−32990
Yang-Mills eqns., monopole solns. 77−67566
Yang-Mills fields, equivalence with equation of motion of monopole system, 't Hooft monopolar solution 80−9084
Yang-Mills fields, mag. charge in terms of Higgs fields, SO(4), SU(4) 77−45935
Yang-Mills monopole, rotational covariance 77−13870
Yang-Mills theory, conversion of isospin degree of freedom into spin degree of freedom 78−89617
Yang-Mills theory, magnetic monopoles in the presence of quark sources 80−13213
Yang-Mills-Higgs model, axially symm. monopole-type soln. 78−54561
Yang-Mills-Higgs SO(3,1) gauge theory, mag. and electric charge 78−54550
Z(N) gauge theories, phase transitions 80−73609
zero energy fermions in U(1) pointwise monopole field *(Chinese)* 80−42345
Zwanzigers local Lagrangian quantum field theory, electric and mag. charge, Lorentz invariance 79−6286
pp→ppGG, mag. monopole search with plastic detectors 79−6351

magnetic permeability
alkaline earth-ReO_6, ordered or perovskite type struct., magnetic and elec. props. 79−65053
Alnico 5 and 8, spinodally decomposed magnetic alloy, magnetic flux temp. coeff. *(Japanese)* 78−35006
amorphous alloy, mag. props. and appls. 78−95475
amorphous alloys, mag. props. and appls. 79−8016
amorphous alloys, mag. props. rel to device appl. 80−88804
amorphous ferromagnetic ribbon, HF mag. characts., magnetostriction role 77−66408
amorphous ferromagnets, structural instabilities and mag. permeability relax., 77 to 400K 80−80559
anelastic relaxations and magnetic aftereffects in solids, conf., Katowice, Poland (Jan. 1978) *(Polish)* 79−96072
Clausius-Mossotti problem for cubic arrays of spheres 78−52422
composite superconductor, effect on losses in variable mag. field of mag. props. 80−34549
cylindrical magnetic film, calc. of impedance and susceptibility *(Russian)* 77−89992
cylindrical shell with strain depend. permeability, torsional response in radial and axial mag. fields 79−19754
DBTTF$(BF_4)_{0.8}$, new conducting compound, synthesis, elec. and mag. props. 79−28341
dialkylammonium copper tetrachloride, ferromagnetic layer compound, magnetostatic mode excitation 80−29538
dispersive medium, energy density of arbitrary EM field and dissipation 77−27226

magnetic permeability continued
electric steel, induction above magnetisation curve knee from pole density texture 77−12151
electrotechnical steel, quality significance on energy and materials savings in magnetic circuits *(Czech)* 80−20947
EM wave propagation in ferromag. material, nonlinear waves and strong discontinuities *(Russian)* 78−74819
EMF in ferromag. material under torsion *(Rumanian)* 78−86986
ferrimagnetic Bloch wall oscills., viscosity coeffs. freq. depend., permeability and mag. losses 80−71094
ferrimagnetic magnetisation theoretical models, for uniparametric materials 80−65960
ferrimagnetic materials, RF, dispersion props. 79−73772
ferrite, coprecipitated, hot pressed, for appl. to mag. heads 77−85968
ferrite, frequency dispersion determination using Kramers-Kronig relation 78−39355
ferrite, grade 2000NM1, effect of CaO, MgO and SiO_2 impurities on props. 77−40412
ferrite, magnetisation effect on RF dispersion of permeability *(Russian)* 79−4700
ferrite, microstruct. depend. of props. and applics., review 78−88548
ferrite, microwave mag. props., grain size effect 78−10722
ferrite, partially magnetised, tensor permeability 77−89981
ferrite powders, mag. props., explosive shock treatment effects 79−52395
ferrite sphere plane EM wave scatt. at arbitrary angle to mag. field *(Russian)* 79−15358
ferrites, anomalous permeability in Polder-Smit region 78−19278
ferrites, partially magnetised, diagonal components of permeability tensor and resonance 79−47306
ferrites, partially magnetised, modified expression for permeability tensor 77−73048
ferrites, permeability tensor element in Polder-Smit region 77−36090
ferrites, soft, production and props. 80−88801
ferrites, soft and microwave, grain-size effects on mag. props., review 78−64222
ferromagnet, symmetric hysteresis loops, polynomial expression *(Spanish)* 77−73044
ferromagnetic cylinders with field intensity-dependent permeability, eddy current anal. *(German)* 77−40088
ferromagnetic layer boiling, mag. characteristics meas. 78−59499
ferromagnetic medium with variable permeability and hysteresis loss, plane EM wave *(Polish)* 77−79722
field penetration into half-space with nonlinear permeability in quasi-stationary state *(Czech)* 77−46667
film, two-layer, exchange-coupled, switching, differential permeability *(Russian)* 78−27061
garnets, photoinduced phenomena 79−99718
garnets, photomagnetic effects, irreversible 79−99719
heterogeneous matrix system, generalised conductivity and loss, tangent 80−7289
heterogeneous systems with disordered structure, generalised cond. coeffs. 79−87075
homogeneous mag. materials, with constant mag. permeability, EM field calc. *(Russian)* 77−68151
isopermalloy, permeability stability calc. rel. to texture *(Chinese)* 80−65959
magnetisable conducting sphere, mag. levitation conditions, mag. dipole response to nonuniform mag. fields 79−98260
magnetisation curves representation by cubic spline functions *(German)* 80−71112
magnetization curve and Gaussian error function *(German)* 80−50137
magnetosolid mechanics, semi-infinite cylindrical shell with strain depend. permeability, torsional response 79−94483
metal powders, packed, complex mag. permeability calcs. 80−29583
metallic, glasses, soft-magnetic properties *(German)* 80−71108
metallic glasses, characts. and appls. *(French)* 80−39815
metallic glasses, mag. props. and development *(German)* 79−51813
metallic glasses, soft mag. props. 79−73774
microwave absorbing ferrite-dielectric composite 77−7880
Moon, magnetometers data errors and lunar induction studies 79−96932
multiphase material, average bulk props. calc., bounds 77−16237
non-magnetic material wear in presence of magnetic field 80−60982
nonlinear media classification for nonstationary electrodynamics 79−21567
nonoptically active media, susceptibilities, elec. and mag. polarisation fluctuation 77−77140
nonuniform systems, effective conductivity from percolation and conduction theory 80−62597
parallel conductors, with one-sided Fe shield, EM field calc. *(Polish)* 77−31046
Permalloy, 50NP, and 79NM, magnetic properties and structure, environment effect during annealing 80−60366
Permalloy, corrosion resist. and mag. props., effect of Cr addition 77−86219
Permalloy, magnetisation improvement through solid state refining 78−91893
Permalloy narrow stripes, permeability 77−89987
rare earth-Al_2, cubic Laves phases, prep. and phys. props. *(German)* 78−23075
relativistic EM fluid flows, geometry 79−58601
reversible, restoration factor spread calc., use in manufacturing errors determination *(Russian)* 77−12152
ring specimens, computer controlled mag. meas. system 80−86346
screens, high permeability, high mag. fields, large vol., appls. *(German)* 77−38772
semiconductor and semimetal powders, EPR, effect of mag. field depend. of elec. parameters 79−99749
steel, austenitic, crack determ. using mag. permeability probe *(German)* 79−52549
steel, austenitic, Mn-Al-V-F2, EM characts. after nitriding, aging, austenitizing, NDT of nitrided layer depth 79−11750
steel, austenitic stainless, neutron irrad., mag. props. 80−29067
steel, austenitic stainless, stress corrosion cracking in H_2SO_4-NaCl soln., Ni and N_2 effects *(Japanese)* 79−100289
steel, B-Si, grain-oriented, high induction, Cu impurity effects 80−89366
steel, C, cold rolled St3Kp, annealed, mag. nondestructive inspection of strip and ribbon 78−60913
steel, C (0.01 and 0.06 wt.%), rephosphorised, mag. props. and texture 77−20634
steel, low C, Al-killed, effect of V on mag. props. 79−83339

magnetic permeability continued
steel, non-oriented, texture and mag. props., effect of Mn and S content 77−86047
steel, nonoriented, mag. props. texture, Cr addition effect 77−1880
steel, saturated, equivalent permeability calc., Stefan's equation with small parameter *(French)* 77−28409
steel, Si, grain-oriented, high permeability, dissoln. and precip. of AlN and MnS 80−89223
steel, Si, nonoriented elec. sheet, solute oxidation effect on mag. props. 79−83335
steel, Si, permeability change due to stress variation after demagnetization in Rayleigh region 80−88854
steel, Si(3 wt.%) grain oriented, high permeability obs. 77−1881
steel, Si-Al, non-oriented elec., internal oxidation and nitridation effects on mag. props. 79−83336
steel, Zi, high permeability grain-oriented, AlN precip. study 79−83337
steel 42NKhTYuA wire, hysteresis loop and differential permeab. after US and conventional drawing 79−15818
steel plate, fundamental and harmonic flux, sinusoidal applied mag. field 78−2708
steel sheets, apparatus for mag. props. meas. in freq. range 50 to 10000 Hz 79−30497
steel strips, elec., grain-oriented, effect on stress-relief annealing treatments on permeability and ageing 78−23832
steel strips, elec., grain-oriented, effects of ageing on mag. AC permeability 78−23833
steels, ferritic and martensitic, C and N migration at low temps., monograph 80−22149
steels, high permeability grain oriented elec., and instrument current transformers 80−88824
superconductors, type II, defect-free, AC permeab. 77−8250
three-dimensional permeable solid, magnetisation distrib., computer calc. 78−72366
transition metal amorphous alloys, mag. props. 80−29576
type superconductor with field-dependent surface barrier, AC losses 79−87216
undirectional fibre composites, anisotropic constituents, effect elastic moduli and other props. 80−58911
van der Waals force in cond. media, fluctuating electrodynamics, nonlocal mag. permeability 78−30876
water, Earth surface forms, at frequencies below 1000 GHz 78−24310
Au ultrafine particles, optical props. 78−19481
$Ba_3Co_{2+x}Ti_xFe_{24-2x}O_{41}$, z-type ferroxplan, effect of Co^{2+} ions 77−36094
$Ca_xNi_{1-x}Fe_2O_4$, initial permeability and Curie temp. 80−25130
$CdCr_2Se_4$, ferromagnetic low anisotropy semicond., spontaneous magnetisation RF determ. 80−22396
$CdCr_2Se_4$ magnetic semiconductor, photoinduced centre kinetics 80−71110
$CdCr_2Se_4$, spin system heating by drifting current carriers, magnon-phonon system energy transfer *(Russian)* 80−29541
$CdCr_2Se_4$-$ZnCr_2Se_4$, single cryst., mag. props. 79−28526
$Cd_{1-x}Hg_xCr_2Se_4$, photoferromag. effect and photocond. obs. 79−28376
Cd_2X_2, X=P,As,Sb, phys. props. 78−26527
$(Co,Fe,M)_{78}Si_8B_{14}$ amorphous alloys (M=V,Nb,Ta,Cr,Mo,W,Mn or Ni), zero magnetostriction and low field mag. props. 80−34741
$(Co,Fe)_{80}B_{20}$ glass, induced anisotropy and time changes of permeability 80−75815
Co, magnetic permeability, effect of ion implantation 77−28414
Co-Cu-Fe-Ce alloys, sintered permanent magnets, mag. charcts. 77−43855
Co-Fe, soft mag. props. rel. to metallurgical aspects 80−88810
Co-Fe amorphous alloys, high permeability props. *(Japanese)* 77−51927
Co-Fe-Ni-Si-B glasses, soft mag. props. 79−73774
Co-Fe-Si-B, amorphous alloys, substitution effect on mag. props. 79−69695
Co-Mn-Ni-Fe-Si-B amorphous alloys, mag. props., low magnetostriction 80−75832
Co-Ni(Ti)(Cu)(Mn), cryst. struct. and stacking fault influence on mag. props. *(Russian)* 80−25164
Co-P, amorphous foil, complex permeability and eddy currents, annealing induced short-range order 77−8360
Co-P, electrodeposited amorphous alloy, mag. permeability 78−52310
Co-P, electrodeposited amorphous alloys with high permeability, thermal treatment with and without field 80−89372
Co-P amorphous alloy, mag. props. 78−10724
Co-Si-B-Fe alloy magnet, Al_2O_3 particle embedded surface, amorphous mag. anal. using electron diffr. 79−56568
$Co_{74}Fe_6B_{20}$, metallic glass, zero magnetostriction, magnetisation characts. 77−12158
$Co_{79}Fe_{6.5}B_{14.5}$ amorphous thin films, zero magnetostriction, high magnetisation 80−34708
CoNiZn ferrites, Fe excess, complex permeab. var. with annealing temp. 77−89979
Co_2Z ferroxplana form. process peculiarities 80−89368
$CuCr_2Se_4$, crystal growth from melt, exam. of props. 80−55283
EuO, spin system heating by drifting current carriers, magnon-phonon system energy transfer *(Russian)* 80−29541
Fe, carbonyl powder, mangetic material 77−12160
Fe, carbonyl powder, particle size distrib. anal. by microscopy with statistical anal. of results 78−19691
Fe, cast, grey, pearlitic relationship of magnetic props. to condition of C 78−56353
Fe, high-purity, low-temp. mag. relax. after thermal ageing and demagnetisation 77−85502
Fe, motion of H and D, mag. relax. meas. 78−64228
Fe powder, carbonyl, R10 and R20, manufacturing effects on magnetic permeability 78−35009
Fe powder, sintered and hot pressed, effect of porosity, grain size on magnetic props. 79−96159
Fe powder-plastic composite, soft mag. material, mag. and mech. props. 80−75812
α-Fe, quenching, C atom pair form., isothermal mag. permeability disaccommodation meas. 77−36540
α-Fe:N, mag. field depend. of reverse permeability 77−80969
α-Fe-Al, migration of C, mag. permeability disaccommodation meas. 77−36100
Fe-Al (12 wt.%) alloy 23 kHz US transducer piezomagnetic props. 78−59240
Fe-Al alloys, rapidly quenched, mag. props. 80−29579
Fe-Al-C, mag. permeability disaccommodation 78−88141
magnetic permeability continued
Fe-Al-C alloys, C migration and mag. aftereffect, mag. permeab. disaccommodation and long-range order meas. 79−8020
Fe-Al(24.3 at.%)-C alloy, magnetic permeability disaccommodation, 260-400K 80−93144
Fe-B-Si amorphous ribbons, effect of annealing conditions on magneto-mechanical props. 80−34740
α-Fe-C(N), containing substitutional atoms, mag. permeability disaccommodation *(Polish)* 79−95612
Fe-Ci, high permeability, mag. props., applied stress effects 80−34726
Fe-Ci (3 wt.%), commercially produced, grain-oriented, mag. props., stress coating effects 80−34727
Fe-Co amorphous ribbon, mag. props. in low fields 79−73777
Fe-Co-Ni-Si-B amorphous alloy, magnetostriction and permeability, effect of annealing 79−1701
Fe-Co-Si-B, zero magnetostrictive amorphous alloy with high saturation induction, mag. annealing 80−60362
Fe-Co-Si-B alloy, amorphous, rapidly quenched, mag. heads appl. *(Japanese)* 80−54922
Fe-Cr-Co, spinodally decomposed magnetic alloy, magnetic flux temp. coeff. *(Japanese)* 78−35006
Fe-Cu, dilute, coercive field, initial permeability and relax. loss, non-mag. impurity effect 77−69628
Fe-Fe_3O_4, sintered two-phase soft mag. material, prep. and props. 77−63813
Fe-Ni, coercive force depend. on grain struct. and inclusions 77−20635
Fe-Ni, Invar, Curie point, annealing effects and time depend. 80−80508
Fe-Ni, secondary recrystn. and mag. props. 80−89247
Fe-Ni (47 to 65 wt.%), soft magnetic alloy with crystallographic texture and field induced anisotropy, pulse permeability and excursion rate *(German)* 79−73779
Fe-Ni alloy, effect of thermomag. treatment in rotating field *(Russian)* 77−21294
Fe-Ni alloy toroidal core, magnetic noise *(Russian)* 78−60308
Fe-Ni-Co, magnetic permeability, effect of ion implantation 77−28414
Fe-Ni-Si-Mn-Cr(Co-Mo), effect of prolonged aging on mag. props. 80−16513
Fe-P amorphous alloys, initial permeability, time depend. 80−15759
Fe-Rh, mag. phase transitions, triple point 79−1672
Fe-Si, grain oriented transformer sheets, permeability and magnetostriction, tensile stress effects 80−88843
Fe-Si, grain-oriented sheets, high permeability, low losses, review 80−88790
Fe-Si (1-5 wt.%), optimum sintering conditions and mag. props. 77−85958
Fe-Si (3 wt.%), Al-bearing, grain-oriented, N_2-H_2 annealing effect on texture, mag. props. 77−12714
Fe-Si (3 wt.%), AlN-inhibited, Se effect on primary grain recrystallisation 77−12715
Fe-Si (3 wt.%), containing B, grain boundary segregation, AES evidence 77−86046
Fe-Si (3 wt.%), cube-on-edge oriented, high permeability, mill processing and mag. props. 77−86045
Fe-Si (3 wt.%), grain oriented tape-wound core, dynamic domain size var. and Fe losses 77−12146
Fe-Si (3 wt.%), grain oriented, MnS-AlN-inhibited, precipitate morphology 77−12648
Fe-Si (3 wt.%), grain oriented, lowest core loss 78−91887
Fe-Si (3 wt.%), grain-oriented, stacking effect on power loss, mag. props. 80−88795
Fe-Si (3 wt.%), high induction grain oriented, metallurgical treatment and mag. props. 77−86044
Fe-Si (3 wt.%), high permeability, use in transformer cores 80−88793
Fe-Si (3 wt.%), mag. props., stress coating effects 80−34728
Fe-Si (3 wt.%), orientation distrib. in primary recrystallised textures, mag. permeability 77−12712
Fe-Si (3 wt.%), secondary recrystn., struct. inhibition, permeability improvement 77−12713
Fe-Si (3 wt.%) steel, high permeability, grain oriented 78−91886
Fe-Si (3 wt.%) steel, high permeability, magnetostriction, stress inducing coating effects 80−34730
Fe-Si (6.5 wt%) filament, formation by modified Taylor technique, and mag. props. 80−75795
Fe-Si (6.5 wt.%), ductility and mag. props., Ni and Mn addition effects 78−76704
Fe-Si (6.5 wt.%), effect of ordering on mag. props. 79−51833
Fe-Si (6.5 wt.%), Ni, Al and Mn additions effect on mech. and mag. props. 77−12667
Fe-Si steel, high permeability, processing effect on recrystn. and deform. 77−12716
Fe-Si-Al, Sendust, 12 μ thick film prep. by sputtering, mag. and other props. 77−55888
Fe-Si-Al, Sendust, ribbon-form, prep. by rapid quenching, mech. and mag. props. 80−71611
Fe-Si-Al (6,4 wt.%), Sendust alloy, effect of Ni content on mag. props. 78−72897
Fe-Si-Al (9.6, 5.4 wt.%), ribbon-form Sendust alloy, mag. props., annealing effects 80−88800
Fe-Si-Al Sendust alloy ribbon form, rapid quench prepared, elec. cond., coercive field 79−83151
Fe-Si-Al-Ni alloy, Super Sendust, Ni content and thermomag. treatment effects 77−4861
Fe-Si-B, high induction, hot rolling treatment 80−89266
Fe-Si-B, melt C content effect on grain growth and induction 80−35351
Fe-Si-B amorphous films, mag. props. 80−34710
Fe-Si-B glassy alloys, mag. props., comp. effects 80−88752
Fe-Si-B-S, grain-oriented, high induction, B and S addition effect on magnetic props. *(Slovak)* 79−4697
Fe-Si-Mn, effect of Mn addition on mag. props. and elec. resist. 78−91890
Fe-Ti, mag. permeability disaccommodation rel. to dissolved N migration *(Polish)* 79−95611
α-Fe-Ti-N, mag. migrational relax., −60 to +200 degrees C 77−36099
Fe_3Al, containing C in solid solution., mag-permeability disaccommodation *(Polish)* 79−95613
$Fe_{100-x}B_x$ ribbon, magnetostriction exam. 79−73794
$Fe_{80}B_{20}$ glass, low-field mag. props. 77−8380
$Fe_{80}B_{20-x}M_x$ (X=Al, Si, Ge, C, P) and $(FeCo)_{80}B_{20}$ glass, magnetisation, Curie and crystn. temps. 79−87289
$Fe_{82}B_{18-x}Si_x$ glasses, soft mag. props. 79−73774
$Fe_xCo_{80-x}B_{20}$, amorphous, mag. after-effect 79−61189

magnetic permeability continued
$(Fe_{0.07}Co_{0.93})_{75-x}Cr_xSi_{15}B_{10}$, amorphous, disaccommodation of mag. permeability and induced anisotropy 80−88741
$(Fe_{1-x}Co_x)_{80}P_{13}C_7$ amorphous alloy, soft mag. material, props. 77−4533
$(Fe_{1-x}Co_x)_{75}Si_{15}B_{10}$ amorphous alloy, soft mag. material, props. 77−4533
$(Fe_{1-x}Co_x)_{78}Si_8B_{14}$ ribbon, magnetostriction exam. 79−73794
$Fe_5Co_{70}Si_{10}B_{15}$ amorphous magnetic alloy, decrease of permeability after demagnetisation, disaccommodation 80−39814
$Fe_5Co_{70}Si_{15}B_{10}$, amorphous ribbon, zero magnetostriction, low residual mag. loss 77−12157
$Fe_5Co_{70}Si_{15}B_{10}$ amorphous ferromag. ribbons, change of permeability by heat treatment 77−85493
$(Fe_xCo_{1-x})_{100-y}(Si_{0.4}B_{0.6})_y$ amorphous alloy zero magnetostrictive, mag. props. 79−99743
$Fe_{40}Ni_{38}$-Mo_4B_{18} amorphous alloys, compatibility of DC and AC mag. props. 80−34695
$(Fe_xNi_{1-x})_{80}B_{20}$, amorphous alloys, engineering mag. props. 79−51832
$Fe_{40}Ni_{38}Mo_4B_{18}$ glassy alloy, high permeability, low field mag. charact. 78−68301
$Fe_{40}Ni_{40}P_{14}B_6$, amorphous, mag. props. 78−10728
Fe_3O_4, mag. relax., permeability and loss tangent determ. at 4.2 to 300K 77−32263
Fe_3O_4, metallic phase, photocond. and mag. permeab., photoinduced changes 80−15566
$Fe(OH)_3$-$Fe(OH)_2$ suspension system, potential-pH diagram 80−55728
$Fe_{80}P_{13}C_7$ amorphous ferromag. ribbons, change of permeability by heat treatment 77−85493
$Fe_{100-x}Si_x$ ribbon, magnetostriction exam. 79−73794
$Fe_xSi_yAl_z$ ribbon, magnetostriction exam. 79−73794
$Fe_{78}Si_{10}B_{12}$ amorphous ferromag. ribbons, change of permeability by heat treatment 77−85493
$Fe_{80}Si_5B_{15}$, amorphous, soft mag. props. and potential uses 80−88807
Fe_2TiO_4, ulvospinel, containing magnetized inclusions, mag. behaviour, cooling through Curie point 78−56314
Gd, coil noise due to permeability fluctuations at phase transition temp. 80−84598
Gd, ferromag., activation energies using transient enhancement of AC permeability 77−59431
$GdNi_5$, anomalous behaviour near Curie point 78−91880
$HgCr_2Se_4$, initial mag. permeability freq. depend. near Curie temp. 78−10729
$HgCr_2Se_4$, initial mag. permeab., 77 to 300K, domain wall motion and damped ferromag. reson. 79−28562
HoIG, Faraday rotation expts. 77−16287
LiTiZn ferrites, effects of Mn and Bi additives, expt. *(German)* 77−28411
LiTiZn ferrites, elec. resist., mag. props., effect of Bi addition 78−95474
$Mg_{0.7}Cu_{0.3}Fe_2O_{4+\delta}$, disaccommodation and accommodation 77−20641
$Mg_xFe_{3-x}O_4$, polycryst., Verwey type transition, resist., magnetisation, Mossbauer effect and permeability obs. 80−75764
$MgM^{3+}{}_xFe_{2-x}O_4$, M=In,Al,Cr,Sc, comp. effects on ferrite charact. 78−52305
Mn ferrite, magnetic permeability, photoinduced reduction *(Rumanian)* 80−75794
Mn ferrites, Fe^{2+} ion contrib. to induced anisotropy and mag. after-effect 77−36101
MnFe ferrite, mechanically induced anisotropy, effect on mag. permeability 78−47970
MnO-ZnO-MgO-Fe_2O_3 ferrites, effect of Fe^{2+} ion on initial permeability 77−8357
MnZn ferrite, anomalous thermal change of permeability near Curie point 77−20638
MnZn ferrite, appreciable SiO_2 content, origin of core losses, microstructure and mag. props. 78−64225
MnZn ferrite, combined Sn-Ti substitutions, improved props. *(German)* 77−20644
MnZn ferrite, gas phase fluorination for improved props. 78−52306
MnZn ferrite, initial mag. permeability rel. to mag. anisotropy 80−80557
MnZn ferrite, mag. permeability spectra, 0.001-100 MHz range *(Russian)* 77−8355
MnZn ferrite, mag. permeability accommodation depend. on mag. field *(Russian)* 80−34685
MnZn ferrite, mag. relax., permeability and loss tangent determ. at 4.2 to 300K 77−32263
MnZn ferrite, mag.-mechanical-microstruct. interaction 77−1578
MnZn ferrite, mechanically induced anisotropy, effect on mag. permeability 78−47970
MnZn ferrite, microstructure and initial permeability, presintering process effect 80−89367
MnZn ferrite, props. rel. to raw materials *(German)* 77−21074
MnZn ferrite fabricated by hot isostatic pressing, recording head appl. 80−35139
MnZn ferrites, field depend. of mag. permeability accommodation *(Russian)* 79−69694
MnZn ferrites, initial mag. permeabilities under low temp. reactor irrad. 77−36093
MnZn ferrites, internal friction and ΔE effect depend. on demagnetisation method 80−80584
MnZn ferrites, low loss, highly stable, study *(Slovene)* 78−27055
MnZn ferrites, post sinter-cooling rates effects 80−89369
MnZn ferrites, Ti substituted, mag. permeab. meas., grain boundary comp. AES obs. 78−95473
MnZn ferrous ferrite, initial mag. permeability second-order magnetocrystalline anisotropy influence 80−88820
MnZn ferrous ferrites, mag. permeability stress depend. 80−88822
MnZn polished ferrite, electron diffraction meas. method appl. *(Japanese)* 78−10742
MnZn soft ferrites, commercial grade, microstruct. rel. to mag. props. 80−34009
$Mn_{0.4}Zn_{0.42}Fe_{2.16}O_{4+x}$, permeability, rel. to intrinsic mag. props. 79−4702
$Mn_{0.510}Zn_{0.417}Fe_{2.073}O_{4+\delta}$ relationship between magnetic permeability and stoichiometry 79−42799
$(Mn_{0.7}Zn_{0.3})_xFe_yO_4$, electromag. props. rel. to Fe content 78−43613
Mo-permalloy, magnetic permeability and order form. kinetics under annealing, conc. depend. 77−8356
Mo_5GaS_6, struct. transform. below 50K, mag. permeability and elec. cond. meas. *(Russian)* 77−7864
magnetic permeability continued
Nb, magnetic surface barrier breakdown by O diffusion, permeability meas. 79−56601
Nb-Ta type II supercond., defect-free, AC permeab. 77−8250
Ni alloys, magnetic props. at freq. up to 1 MHz *(Russian)* 77−8330
Ni ferrite, gas phase fluorination for improved props. 78−52306
Ni, ferromag. props., teaching expt. 80−82608
Ni, magnetic permeability, effect of ion implantation 77−28414
Ni, magnetic permeability, reversible, deform. and ion implantation effects 77−48013
Ni, magnetoelastic effect on longitudinal compression, weak field spin rotation model 79−82851
Ni-Al-Ti ferromagnetic non-homogeneous alloy, composition determination by Curie temp. meas. 80−11196
Ni-Fe, soft mag. props. rel. to metallurgical aspects 80−88810
Ni-Fe (36 to 50 wt.%), initial permeability, domain struct. model 80−88811
Ni-Fe alloys, high-permeability, development trends *(Slovak)* 79−4694
Ni-Fe alloys, pulse permeability and loss in toroidal core pulse current transformers 78−43615
Ni-Fe overlay, influence on bubble device performance 79−78466
Ni-Fe-Co, alloy with step hysteresis loops *(German)* 79−42806
Ni-Fe-Nb, Hardperm, origin of high magnetic permeability 77−8362
Ni-Fe-Nb, hardperm alloy, effect of sheet thickness and heat treatment on magnetic props. *(Japanese)* 78−31095
Ni-Fe-Nb, Hardperm alloy, sheets, effect of sheet thickness, and annealing, on mag. props. 78−76772
Ni-Fe-Nb (Mo), magnetic alloy, TEM and X-ray obs. *(Chinese)* 80−24401
Ni-Fe-Nb alloys, mag. permeability and struct. *(Chinese)* 78−84450
Ni-Fe-Nb-Al alloys, mag. permeability and struct. *(Chinese)* 78−84450
Ni-Fe-Nb-Al(-Mo), wear resisting mag. head material, mag. props. and struct. 80−35350
Ni-Fe-Nb-Mo (11.42, 6.92, 1.54 wt.%), Hardperm, high magnetic permeability alloys 77−8361
Ni-Fe-Nb-Mo-Al, head material for mag. recording, DC and AC mag. props. 80−88812
Ni-Fe-Nb(Ta)-W, high magnetic permeability alloys, Hardperm 77−48012
Ni-Mn base polynary alloys, magnetic and elect. props. *(Japanese)* 78−15551
Ni-Mn base polynary alloys, magnetic, and elec. props., composition and heat treatment effects 79−11710
Ni-Zn ferrite, neutron irrad., mag. spectra, domain wall behaviour 77−48006
Ni-Zn ferrite:Co^{2+}, synthesis of optimal quality recording head mat. 77−52272
Ni-Zn ferrites, hot-pressed, key props. 78−15348
Ni-Zn ferrites 600 NN and M450 NNI, Curie point radiative shift due to neutron irrad. *(Russian)* 80−39775
$Ni_{0.5-x}Co_xZn_{0.5}Fe_2O_4$ ferrospinal solid solutions, cryst. lattice defects and props. 80−19796
NiFe soft magnetic alloys, magnetic props., effect of annealing and fabrication *(German)* 78−53004
$NiFe_2O_4$, ferrite, mag. anisotropy compensation under neutron irrad. 80−75807
$NiFe_2O_4$-Fe_2O_3, effects of excess Fe_2O_3 on mag. props. 77−85495
$Ni_{65}Mo_2Fe$, O_2 effect on secondary recrystallisation and mag. props. 80−35201
NiZn ferrite, effect of reactor radiation on mag. props. 77−32215
NiZn ferrite, mag.-mechanical-microstruct. interactions 77−1578
NiZn ferrite, magnetic props., porosity and grain size effects 77−36095
NiZn ferrite, ZrO_2 additions influence on sintering and physicochem. props. 80−108369
NiZn ferrites, density and mag. props., isostatic pressure effect 80−60816
NiZn ferrites, internal friction and ΔE effect depend. on demagnetisation method 80−80584
NiZn ferrites, mag. head props., technical possibilities and limitations 80−88803
NiZnCo ferrite, model of photomagnetic effect 77−43853
$Ni_{0.32}Zn_{0.68}Fe_2O_4$ ferrite, effects of silica content, sintering temp. and sintering time obs. 79−87746
$Ni_{0.85}Zn_{0.15}Fe_2O_4$, ferrite, mag. anisotropy compensation under neutron irrad. 80−75807
$Ni_{1-x}Zn_xFe_2O_4$, polycryst., domain wall energy rel. to anisotropy 80−71090
$(Sc_xLu_{1-x})_2V_2O_7$ 80−29547
Sn, superconductor, paramagnetic effect fine struct. apparent mag. permeability *(Russian)* 79−95550
Ta_5Si_3, supercond. transition temp. meas. *(Russian)* 77−20485
$Tb_{0.26}Dy_{0.74}Fe_2$, temp. depend. of magnetomechanical coupling factor 77−90002
$Tb_{0.27}Dy_{0.13}Fe_{1.98}$, grain-oriented, permeability, magnetomechanical coupling and magnetostriction 79−78491
$Tb_{0.20}Dy_{0.22}Ho_{0.58}Fe_{1.95}$, grain-oriented, permeability, magnetomechanical coupling and magnetostriction 79−78491
$Tb_xDy_xHo_xFe_2$, temp. depend. of magnetomechanical coupling factor 77−90002
$Y_3Fe_{5-x}Al_xO_{12}$, permeability spectra rel. to microstruct. 80−71100
$Y_3Fe_{5-x}Gd_xO_{12}$, permeability spectra rel. to microstruct. 80−71100
$Y_3Fe_{5-x}Si_xO_{12}$, charact. of photoinduced mag. effects in weak magnetising field 78−27071
$Y_3Fe_{5-x}Si_xO_{12}$, photoinduced change of mag. permeability *(Russian)* 77−1560
$Y_3Fe_{5-x}Si_xO_{12}$, photoinduced jumps of permeability 79−28564
$Y_{3-3x-2z}Gd_{3x}Ca_{2z}Fe_{5-z-u}V_zSi_uCo_uO_{12}$, mag. props., effect of V substitution 77−20582
YIG ceramic, transient flash effect on permeability 78−27024
YIG, influence of X-ray radiation on mag. props. 77−8337
YIG, permeability, domain rot. and wall displacement contrib. 80−80564
YIG, permeability spectra rel. to microstruct. 80−71100
YIG, plastic deform. and mag. props 77−40087
YIG:Co^{2+}, mag. permeability, illumination and impurity depend. *(Russian)* 78−64220
YIG:Si, photo-induced low freq. mag. permeab. *(Russian)* 78−39368
YIG:Si^{4+}, mag. permeability, illumination and impurity depend. *(Russian)* 78−64220
YIG:$Si^{4+}(Ti^{4+})(Zr^{4+})$, X-ray induced change in initial permeability 78−19280

magnetic permeability continued
$(Y_xLu_{1-x})_2V_2O_7$ semiconducting ferromag. pyrochlore, mag. props. 80−29547
$(Y_{1-x}R_x)_3Fe_5O_{12}$, photoinduced decrease in permeability, 77K 77−85497
YbIG, Faraday rotation expts. 77−16287
$Zn_xCn_{0.1}Fe_{2.9}O_4$, Cu, Zn substituted magnetite, domain wall resonance, mag. props. 80−15756
$Zn_xFe_{3-x}O_4$, mag. ordering and domain wall relax. 77−8336
ZnMn ferrites, prepared by wet chemical and ceramic methods, comparison of struct. and mag. props. *(German)* 79−24470
Zn_3X_2, X=P,As,Sb, phys. props. 78−26527

magnetic permeability measurement
anelastic relaxations and magnetic aftereffects in solids, conf., Katowice, Poland (Jan. 1978) *(Polish)* 79−96072
automatic demagnetisation and measurement system for time decreasing permeability meas. 80−62696
Burrows permeameter, improved design 77−10067
calibration of permeability meters, short cct. coaxial lines as inductance standards 80−77816
cavity perturbation measurements, elimination of influence of non-ideal microwave circuit 79−88979
DC permeameter for ring specimens 80−98954
dielectric material, time-domain spectroscopy 77−18015
Epstein permeameter, 25 cm, parallel stray mangetic flux compensation *(Polish)* 79−2798
ferrites, at 9.5 GHz, precision test unit 77−74465
ferrites, disaccommodation meas., errors analysis *(Bulgarian)* 78−21181
ferrites, mag. permeability meas. method, UHF wave total internal reflect. 78−57994
ferrites, toroidal samples, apparatus for measurement of initial permeability as function of temp. 80−57346
HF standard samples, ferrites and carbonyl Fe 79−35801
homogeneity and wear resistance estimation 77−90558
low permeability meas. at cryogenic temperatures 79−30514
magnetic disaccommodation measurement, device, graphical or digital registration *(Polish)* 79−93180
magnetically-soft materials, mag. characts. determ. methods, review 79−40593
magnetodielectric materials in waveguide, resonance method 79−17449
permeameter, electronic, for routine and standards use 77−5875
permeameter for testing magnetically hard materials *(Polish)* 79−5099
RF method of determining spontaneous magnetisation of ferromag. with low anisotropy 80−22396
sensors, shrinking and thermal tension estimations in epoxy resins appl. *(Polish)* 80−35456
steel, austenitic, heat resistant, mag. permeability increase, measurement method 78−53039
steel, austenitic stainless, magnetic phase content determ. via permeability meas. using MF-10F probe 77−77648
weakly magnetic materials, magnetising field polarity reversal method 78−32838
Fe-Si, power loss and permeability meas. by means of Hall probes and stochastic ergodic correl. 80−86350

magnetic pinch *see pinch effect*

magnetic properties of amorphous substances
alloy, amorphous, magnetic, transport props. 79−73485
alloy, indirect exchange interaction and paramag. Curie temp. 80−75752
alloy, struct. relax., compositional SRO 78−79538
alloy resistivity, contrib. of mag. ordering *(French)* 77−89746
alloys, amorphous, mag. props., review *(Japanese)* 78−52259
alloys, bulk amorphous, prep. by high rate sputter deposition *(Japanese)* 80−29906
alloys, crystalline and amorphous mag. props. from Rhodes-Wohlfarth plot 78−52190
alloys, Curie temp. comp. depend. 80−84597
alloys, for magnetic amplifiers and thermal recording appl. *(German)* 79−19744
alloys, mag. and nonmag., thermoelec. power, 15 to 580K 80−80255
alloys, mag. props. and appls. 78−95475
alloys, mag. props. rel to device appl. 80−88804
alloys, manufactured by special quenching, magnetic strip appl. *(German)* 77−16700
alloys, props. and appls. 79−8016
alloys and semiconductors, Mossbauer spectrometry *(French)* 80−80660
amorphous films of rare earth transition metal system, preparation by co-sputtering 79−56928
amorphous magnetic alloys, review, engineering magnetic props. and potential applications 80−71078
amorphous ribbon, saturation magnetostriction, and electronically controllable delay line 79−1700
amorphous systems, mag. props. effect of random a nisotropy 79−4686
anisotropy due to spin-orbit interaction, spin glass like phase 77−66295
antiferromagnet, amorphous, spin waves, exchange fluctuations, calc. 80−65847
antiferromagnet, spin waves, semiclassical theory 77−36064
antiferromagnetism in amorphous Heisenberg magnet, ground state and frustration, theory 80−65766
asperomagnetic alloy, amorphous, spin-wave theory including short range order 79−38313
atomic order effects 77−73006
atomic structure, energy dispersive X-ray diffr. obs. 79−73100
Bethe-Peierls-Weiss approx. for amorphous magnets 78−76263
bibliography, 1950-1976 77−80894
binary alloy, annealed Ising ferromagnet 78−47927
binary magnetic alloys, Monte Carlo calc. beyond homogeneous mol. field approx., anomalous Kondo effect 77−8308
bubble film, magnetoelastic interactions 80−65976
bubble materials, props. and prep. methods, review *(Rumanian)* 80−93149
bubble propagation by domain drag in amorphous films 79−42814
bubble-domain materials, amorphous, Hall-effect hysteresigraph for coercivity measurement 79−73786
cluster effective lattice method, mag. and electron props. 77−66242
collinear and random mag. structures, review 78−68173
compensation-point Hall effect temperature sensor 78−93679
critical dynamics, renormalisation group 77−77069
critical dynamics, renormalisation group methods 77−43844
critical dynamics of disordered spin systems 79−40516
Curie temperature and mag. excitation spectrum 78−10693

magnetic properties of amorphous substances continued
dense random packing model, uniaxial anisotropy, hysteresis curves 77−16108
density of states and itinerant ferromagnetism, dense random packed hard sphere struct. 78−34950
disordered and amorphous mag. materials, position entropy solids, exchange and anisotropy noise 79−11295
disordered anisotropic antiferromagnet. random field effects 80−2580
disordered Heisenberg binary magnetic alloy with mixed exchange interaction, compensation point *(Russian)* 77−51898
easy plane amorphous wire, magnetisation, variational calc. 80−71098
education, metallic glasses, phase transition and mech., elec. and mag. props. 78−36765
excitations and critical phenomena within framework of phenomenological models 78−52267
$Fe_{40}Ni_{40}P_{14}B_6$, amorphous, tape wound core, fluctuations of driving field 78−10726
$Fe_{40}Ni_{40}P_{14}B_6$, $Fe_{32}Ni_{36}Cr_{14}P_{12}B_6$, amorphous Hall effect, press. and temp. depends. 77−66155
ferrimagnet, molecular field theory, struct. fluctuations 77−40018
ferrimagnetic alloy, dipolar mechanisms for mag. anisotropy 78−64233
ferrimagnetic alloy, mag. anisotropy from dipolar interactions 79−87252
ferromaget with random anisotropy, temp depend. of magnetisation 79−78442
ferromagnet, amorphous, dispersion rels. and spin-wave spectroscopy *(Russian)* 79−7983
ferromagnet, amorphous, magnetisation, temp. depend. effect of nonrandom anisotropy 80−39773
ferromagnet, amorphous, resist. 78−64021
ferromagnet, amorphous and fine-crystalline, with dipole-dipole interaction, spin waves *(Russian)* 78−56308
ferromagnet, apparent spin wave stiffness, low temps. 79−82776
ferromagnet, disordered, phase transitions, mol. field and Landau-Ginzburg theories 80−93118
ferromagnet, effective-field distrib. and resistivity minima 79−73501
ferromagnet, excitations, calc. using hard sphere models 77−66289
ferromagnet, ferromag. saturation, spatially random magnetostatic, magnetocrystalline, magnetostrictive and exchange fluctuations 78−60277
ferromagnet, Ising amorphous, crit. temp. 80−11207
ferromagnet, Ising model, Curie temp., exchange integral fluctuation effects 80−50121
ferromagnet, Landau-Ginzburg theory, magnetisation and Curie temp. 80−75700
ferromagnet, law of approach to magnetic saturation, effect of precipitates 78−72334
ferromagnet, localised spin and phonon excitations, theory 79−7979
ferromagnet, mag. excitations 78−68204
ferromagnet, magnetisation at low temp., disorder induced behaviour 78−52234
ferromagnet, metastable states in random anisotropy model 79−19710
ferromagnet, random anisotropy amorphous, initial magnetisation, remanence and coercivity 77−80964
ferromagnet, random anisotropy effects 78−68223
ferromagnet, random model, spin wave spectrum 77−89918
ferromagnet, randomly anisotropic, long wavelength mag. excitations 78−84406
ferromagnet, spin wave excitations, similarity to liquid metal electronic struct. 77−12109
ferromagnet, spin wave spectra *(Chinese)* 79−91219
ferromagnet, spin wave spectrum 79−24148
ferromagnet, spin wave spectrum rel. to struct. 77−66290
ferromagnet, thermal cycling and annealing, critical behaviour 79−42790
ferromagnet, with random uniaxial anisotropy, hysteresis, magnetisation 77−80963
ferromagnetic, deposition from vapour or liquid, uniaxial mag. anisotropy 78−10677
ferromagnetic, developments and appl. 80−50143
ferromagnetic, mag. fundamentals, props. and appl. *(German)* 79−28557
ferromagnetic alloys, amorphous, sputter-deposited, soft mag. props., magnetostriction 80−34696
ferromagnetic alloys, disordered cryst. and amorphous, mag. dipolar field distrib., computer simulation 80−65790
ferromagnetic alloys, disordered crystalline and amorphous, dipole field distribution 80−25101
ferromagnetic alloys, domain struct. and mag. microstruct., review 80−15751
ferromagnetic alloys, form. and stability 77−16515
ferromagnetic alloys, micromagnetic eqns. for case of dipolar and magnetocryst. fluctuations 80−11171
ferromagnetic alloys, temp. depend. of mag. hystersis props. 79−61186
ferromagnetic amorphous alloys, thermal expansion anomaly near Curie temp. *(Japanese)* 77−85542
ferromagnetic amorphous system, directional order and induced anisotropy energy, theory 78−95431
ferromagnetic materials status and appls. *(Japanese)* 79−15325
ferromagnetic ribbon, HF mag. characts., magnetostriction role 77−66408
ferromagnetic systems, inhomogeneous, Ginzburg-Landau theory, free energy and Curie temp. 79−51789
ferromagnetic thin films, mag. props. 78−91881
ferromagnetic transitions model 78−2690
ferromagnets, book contrib. 80−75743
ferromagnets, classical-spin model 79−33446
ferromagnets, Curie temp. depend. on nearest neighbour fluctuations 80−50120
ferromagnets, hidden excitations, theory 80−75748
ferromagnets, itinerant electron model, Invar anomalies, review 78−95413
ferromagnets, itinerant electron model 79−73664
ferromagnets, localised spin excitations 80−15708
ferromagnets, magnetic and phonon rotons 79−61087
ferromagnets, micromagnetic theory 78−10661
ferromagnets, possibility of low temp. phase below ferromag. phase 79−4674
ferromagnets, resist. and magnetoresist. 77−66148
ferromagnets, structural instabilities and mag. permeability relax., 77 to 400K 80−80559
ferromagnets with random anisotropy axes, spin waves 80−7096
film, SAW device appls. 80−28389
film sputtering for bubble devices, multiple target method 77−16493

magnetic properties of amorphous substances continued
finite temperature calculations, random anisotropy model 78−80112
GdCo amorphous film, magnetic compensation walls 77−8375
glass, magnetic susceptibility measurement, torsional reson. technique 80−82796
glasses, soft-magnetic properties *(German)* 80−71108
hardness, elec. cond., photo emission, and mag. props. *(Norwegian)* 79−32909
Heisenberg amorphous ferromagnet, magnetisation and Curie temp., CPA calc. 80−75703
Heisenberg and Ising chains, thermodynamics 80−108022
Heisenberg ferromagnet, amorphisation, anisotropically distrib. exchange forces *(Russian)* 77−85408
Heisenberg ferromagnet, spin disorder resist., force-force correl. function method 80−24918
Heisenberg ferromagnet, spin wave excitations and magnetization curve 79−15292
Heisenberg ferromagnet, spin waves, effective medium approx. 78−68203
Heisenberg ferromagnet, structural disorder effects on Curie temp. 79−78417
Heisenberg ferromagnet, structurally and chemically disordered, critical behaviour 77−43838
Heisenberg ferromagnet, variational cluster method 80−39728
Heisenberg model, amorphisation *(Russian)* 78−80118
Heisenberg model, commutator and anticommutator Green's functions 79−51792
indirect exchange interaction in amorphous magnet 79−65669
Invar alloys elastic and magnetoelastic effects 79−56589
Invar behaviour in crystalline and amorphous alloys 79−56489
Invar problem, conf., Nagoya, Japan (Sept. 78) 79−56481
ionic compounds, amorphous, exhibiting Mossbauer spectra, magnetic props. *(French)* 80−80490
ionic compounds, amorphous, Mossbauer study, frozen mag. state and hyperfine interaction *(French)* 80−80661
Ising antiferromagnetic model, frustration effects 80−103838
Ising chain, finite, thermodynamic behaviour 79−61028
Ising model, bond-diluted, percolation-thermal crossover index calc. 80−11145
Ising model, computer simulation 80−60299
itinerant ferromagnetism and density of states, off-diagonal disorder effects 77−28360
magnetic excitations in amorphous ferromagnets 79−78356
magnetic loss measurement 79−73776
magnetic materials, review 79−82839
magnetic thin films, substructural defect anal. by coherent methods *(Russian)* 79−61190
magnetisation, mag. moment temp. distrib. 80−15848
mathematical models of disordered systems, book 80−1878
metal, amorphous ferromagnetic, paramagnetic Curie temp. determ. 78−76242
metal-metalloid systems, review 77−16054
metallic amorphous films for mag. bubble memories, materials review *(Polish)* 80−34715
metallic film, bubble technology *(Polish)* 77−77076
metallic glass, annealing, struct. relax. and crossover effect 79−86715
metallic glass, bulk and surface properties, review 80−44147
metallic glass, isotropic and anisotropic magnetoelastic effects, review 78−68352
metallic glass, magnetostrictive film, overlay for variable SAW delay line 78−63240
metallic glass, micromag. calcs. and props. 80−80501
metallic glass, prep. and phys. props. development 80−81003
metallic glass, splat cooled, mag. props. 80−80491
metallic glass ribbon, magnetostrictive stress depend. of longitudinal wave rel. 80−75825
metallic glasses, anal. *(German)* 77−89977
metallic glasses, Brillouin-Mandelstam scattering from thermal and excited magnons 80−70980
metallic glasses, characts. and appls. *(French)* 80−39815
metallic glasses, electronic structure, neutron scatt., elec. resist., Hall coeff., mag. susceptibility and XPS 78−23013
metallic glasses, electronic structure rel. to elec. cond., supercond. and mag. props. 80−65429
metallic glasses, mag. props., struct., and prep., book contrib. 79−65665
metallic glasses, mats. props. review 77−4043
metallic glasses, physical principles, manufacture, mech. and mag. props. *(French)* 78−83744
metallic glasses, review *(German)* 79−41962
metallic glasses, soft mag. props. 79−73774
metallic glasses, structure, stability and prod., elec., mag. and mech. props., review 80−44134
metallic glasses, structure and properties, review 78−47245
metallic glasses, Vitrovac materials, mag. props. *(German)* 79−51813
metallic glasses and amorphous magnetism, review 79−82818
metallic glasses manufacture, struct. and stability *(Norwegian)* 79−14687
metallic glasses props., development and appl. 80−19710
metallic glasses quenched from melt, appl. as soft mag. materials *(German)* 78−10676
metals, glassy, structure, transport props., magnetic behaviour, review 80−70138
metals, rapidly quenched, conf., Brighton, England (July 1978) 80−67934
metals and alloys, amorphous, exhibiting Mossbauer spectra, mean magnetic props. *(French)* 80−80489
Metglas 2605 ribbon, saturation magnetostriction meas. by small-angle magnetisation rot. 80−60391
Metglas 2826 ribbon, saturation magnetostriction meas. by small-angle magnetisation rot. 80−60391
Metglas 2826 ribbons, ferromagnetic resonance and SEM obs. 80−15804
Metglas 2826-A, anomalous magnetisation, critical effects, superparamagnetism 77−8328
Metglas 2826A, Invar related system, high press. Mossbauer spectra 79−56642
microwave absorption spectra of amorphous magnetic system 80−50469
phase diagram and statistical mechanics 78−52268
phase transition theory for new spin structure *(Chinese)* 79−24166
polymetal phosphinates, linear chain magnet, ^{31}P NMR, spin density 77−77108

magnetic properties of amorphous substances continued
polystyrene, γ-Fe_2O_3 powder filled, mag. films, packing and particle orientation *(Japanese)* 80−104115
polyvinyl acetate, γ-Fe_2O_3 powder filled, mag. films, packing and particle orientation *(Japanese)* 80−104115
polyvinyl butyral, γ-Fe_2O_3 powder filled, mag. films, packing and particle orientation *(Japanese)* 80−104115
preparation and appraisal of amorphous mag. materials *(Japanese)* 77−36420
pyrite structured 3d-transition metal chalcogenide mag. props. from Mossbauer effect obs. *(Japanese)* 80−15933
quenched free energy of mag. systems with random interactions, upper bounds 80−103845
random anisotropy axes, high-temp. expansion for sp. ht. 80−71041
random anisotropy axes, low temp. specific heat, elec. resistance and US absorpt. *(Russian)* 79−19734
random anisotropy axis model in the infinite-range limit 80−88761
random ferromagnets, crit. exponents 78−10694
random-axis model, low temp. renormalisation group anal. 79−61137
rare $earth_{50}Ag_{50}$ alloys, bulk mag. props., field, time and temp. depends. 77−89932
rare earth alloy, amorphous, ferromag. state, non-axial elec. field gradient effect 80−75728
rare earth alloys, amorphous, magnetoresistivity, exchange scatt. model 78−95287
rare earth alloys, amorphous, random anisotropy ferromagnetism in pair approx. 79−47276
rare earth alloys, mag. props., Mossbauer spectra 80−7225
rare earth alloys, mag. props. rel. to struct., review 79−15298
rare earth alloys, magnetic amorphous, nonaxial elec. field gradients 78 39285
rare earth alloys, $R_{69}Ni_{31}$, amorphous, Curie temp., mag. susceptibility and coercive force, 4.2 to 300K 80 93092
rare earth alloys, random anisotropy antiferromag. model 78−95428
rare earth alloys, random anisotropy antiferromag. model 80−20399
rare earth alloys, spin glasses, bulk mag. props. in amorphous and cryst. systems 80−20415
rare earth alloys, transport props. 80−20152
rare earth alloys, with random anisotropy axes, spin excitations in paramag. phase 80−80476
rare earth amorphous alloys, antiferromagnetism, mol. field approx. 78−80142
rare earth amorphous alloys, random anisotropy magnetism 80−65853
rare earth amorphous alloys, random mag. anisotropy, antiferromag., Monte Carlo calcs. 79−33471
rare earth amorphous alloys, random mag. anisotropy 80−20398
rare earth compounds, $RFeO_3$, amorphous films for mag. bubble memories, materials review *(Polish)* 80−34715
rare earth iron alloy films, cosputtered, struct. and mag. props. 78−60323
rare earth-Ag alloy, model calcs. of mag. props. 80−84616
rare earth-Au(Cu), amorphous, mag. and transport props. 80−34605
rare earth-Co, $R_{69}Co_{31}$, amorphous, mag. props. 80−84590
rare earth-Co amorphous alloys, mag. compensation temp. 77−66277
rare earth-Co systems, anomalous Hall effect and Kerr rotation obs. 77−11897
rare earth-Fe alloy, amorphous, random anisotropy model, generalised mol. field calcs. 77−28345
rare earth-Fe alloys, amorphous and crystalline, small angle neutron scatt. study of mag. order and mag. microstruct. 79−15283
rare earth-Fe alloys, magnetostrictive, elastic props. 78−84469
rare earth-gold amorphous alloys, R_4Au, anisotropy versus exchange 80−34624
rare earth-transition metal alloy, disordered, saturation mag. moment using CPA 77−20515
rare earth-transition metal alloy amorphous film, magnetostriction, dipolar mechanism 78−95502
rare earth-transition metal alloys, amorphous, anomalous low-temp. props. 78−91872
rare earth-transition metal alloys, amorphous, electronic and mag. props. 80−93093
rare earth-transition metal alloys, amorphous, ferrimag., spin arrangements in large fields 80−75718
rare earth-transition metal alloys, amorphous, Hubbard hamiltonian 77−72985
rare earth-transition metal alloys, amorphous, struct. and mag. props., book contrib. 80−39818
rare earth-transition metal alloys, cryst. and amorphous, mag. props. 77−73008
rare earth-transition metal alloys, review 77−16054
rare earth-transition metal alloys amorphous thin films, anisotropic mag. and microstruct. props. 78−95487
rare earth-transition metal amorphous alloy films with single mag. species 77−16121
rare earth-transition metal amorphous alloys, atomic order, mag. behaviour 78−19221
rare earth-transition metal amorphous film, Kerr and Hall effect meas. 77−24722
rare earth-transition metal amorphous film, microstruct. 77−51619
rare earth-transition metal amorphous films, radiation damage 77−66398
rare earth-transition metal amorphous thin films, mag. potential distribution and wall velocity meas. 80−34725
rare earth-transition metal amorphous thin films for thermomag. recording 80−20403
rare earth-transition metal film, microstruct., TEM obs. 78−72018
rare earth-transition metal film, microstruct. and magnetism 78−64230
rare earth-transition metal garnets, $R_3M_5O_{12}$, amorphous films for mag. bubble memories, materials review *(Polish)* 80−34715
rare-earth alloys, amorphous study of hysteresis effects using Monte Carlo technique 79−1686
review *(Chinese)* 79−56508
review of props. *(Japanese)* 79−28561
review of struct. characts., appl. and prod. methods *(Chinese)* 79−33521
ribbon materials manufacture, props. improvement and appl. 80−7693
ribbons, magnetostrictive, theory of giant ΔE effect 77−85537
ribbons, twisted, magnetisation process, domain theory 80−71101
RKKY interaction range 79−15295
semiconductor, localised gap states, hopping cond., mag. susceptibility and EPR 77−72866

magnetic properties of amorphous substances continued
Sendust ribbon, mag. props. 80−15761
soft magnetic material, new developments in technologically important materials, review 79−33509
spectral density functions for amorphous solids 79−47269
spin glass phase possibility *(Russian)* 78−72362
spin glass transitions, model 78−2690
spin glass-ferromagnetic phase, mean field theory 80−103841
spin waves in amorphous ferromagnets, asperomagnets and spin-glasses 80−75747
spin-glass and ferromagnetic behaviour induced by random uniaxial anisotropy 78−39338
spin-wave excitations 78−80139
steels Kh18N(10-25), mag. susceptibility, 4.2 to 300K, and magnetoelasticity *(Russian)* 80−65812
superconducting amorphous metals, mag. impurity interactions 80−44777
tape cores carrying current, torsional stress effects 80−34742
thermodynamic properties at high temp. 77−16078
thin films, struct. and mag. props., review 80−93148
transition metal alloys, amorphous, mag. props., chem. short-range order 80−75739
transition metal alloys, amorphous, mag. props., structure and preparation 80−75737
transition metal amorphous alloys 80−29576
transition metal based amorphous alloys, elec. resist., 20 mK to 300K 79−73483
transition metal based amorphous mag. alloys, elec. field gradient 78−39475
transition metal ferromagnetic amorphous alloys, mag. props. 77−55690
transition metal ions in amorphous compounds, crystal field theory and mag. props. 78−72318
transition metal-metalloid amorphous alloys, mag. props. review 78−52300
3d-transition metal-metalloid cryst. and glassy alloys, electronic struct. from magnetisation and Mossbauer meas. 80−29363
transition metal-rare earth alloys, amorphous, mag. props., mean field anal. 79−4701
transition metals and alloys, elec. resistivity, Hall coeff., mag susceptibility 78−95280
vibrating reed, influence of magnetomechanical pole-effect 79−73791
AL_2O_3-CoO-SiO_2 glasses, spin correls., neutron diffr. meas. 80−15694
$Al_2Mn_3Si_3O_{12}$, amorphous insulating spin glass, susceptibility and magnetisation meas. 80−88765
$Al_2Mn_3Si_3O_{12}$, spin correlations and phase transitions, neturon diffr. exam. 78−84390
$Al_2Mn_3Si_3O_{12}$ spin glass, spin dynamics, neutron scatt. meas. 80−15741
Al_2O_3-MnO-SiO_2 glasses, spin correls., neutron diffr. meas. 80−15694
As, amorphous, thermally generated paramagnetism 79−19720
As-Se glass, magnetic susceptibility meas. at room temp. *(Japanese)* 79−82748
Au-Si-Mn, amorphous spin glass film, mag. susceptibility 79−42775
B-Fe (16 at.%), magnetisation in high mag. field, Arrott-Noakes plot 80−54919
B_2O_3-PbO-GeO_2-Fe_2O_3 glasses, mag. props. and Mossbauer spectra, speromag. order at low temps. 80−80530
BaO-Fe_2O_3, splat quenching struct. and crystn. mechanism *(French)* 78−51426
BaO-Fe_2O_3 system, splat cooled phases struct., magnetisation and susceptibility 300-1100K *(French)* 77−48017
BaO-Fe_2O_3-B_2O_3 glass system, mag. struct., Mossbauer study 78−39485
BaO-Fe_2O_3-B_2O_3 glass, Mossbauer study of struct. and mag. props. 79−47369
BaO-Fe_2O_3-B_2O_3 glass, struct. and mag. props., Mossbauer spectra 80−7226
BaO-Fe_2O_3-B_2O_3 glass, splat cooled, low temp. micromagnetism 80−34660
BaO-Fe_2O_3-B_2O_3(Na_2O) glasses, high Fe_2O_3 content, mictomagnetic props. 80−65916
BaO-Fe_2O_3-Na_2O glass, mag. props. 78−88123
BaO-Fe_2O_3-(Na_2O) glass, rapidly quenched, mag. and ferrimag. props. 80−75744
BaO-Mn_2O_3-B_2O_3, amorphous mag. oxide, field-cooling effect *(Japanese)* 80−84615
$Bi_2Fe_4O_9$, antiferromag., mag. glass props. *(Russian)* 77−4519
C, amorphous, anomalous low temp. mag. and thermal props. 78−10647
C, char, amorphous, mag. interactions between localised spins 80−34587
C, evaporated, paramag. and diamag. susceptibility meas., 77 to 1400K 77−28362
CaO-Al_2O_3-SiO_2 glass, remanent magnetisation, log t low 78−68300
Cd-Co(-Mo), amorphous films, thermal stability of mag. props. *(Japanese)* 79−47307
$CdGe_{1-x}Sm_xAs_2$, radial distrib. anal. and mag. susceptibility meas. 77−43152
CdS, amorphous antiferromag., mag. props. of dilute neutral donors 79−78367
$Ce_{30}Au_{20}$, amorphous, cryst. field effects and mag. interactions, magnetisation and transport props. meas. 78−68191
$Ce_{80}Au_{20}$, mag. ordering and cryst. field effects, speromagnetism 80−80531
$(Co,Fe,M)_{78}Si_8B_{14}$ amorphous alloys (M=V,Nb,Ta,Cr,Mo,W,Mn or Ni), zero magnetostriction and low field mag. props. 80−34741
$(Co,Fe)_{80}B_{20}$ glass, induced anisotropy and time changes of permeability 80−75815
Co alloys, amorphous, effects of metalloids on mag. props. 80−75738
Co amorphous ferromag. film, resist. anisotropy rel. to struct. 77−72926
Co based amorphous alloy, mag. ordered, hyperfine field distribs., NMR meas. 78−68409
Co based amorphous alloys, struct. and thermomag. meas. 77−16055
Co film magnetoresist. in fields up to 80 kG 77−39823
Co-B alloys, amorphous, mag. moment and exchange stiffness constant 79−1662
Co-B alloys, saturation magnetisation, mag. moments, X-ray diffr. obs. 79−4704
Co-B-Si, mag. props. different in amorphous and cryst. phases 77−69617
Co-B(-Cr) thin film glasses, mag. props. and corrosion resist. 80−80576
Co-Fe amorphous alloys, worked, perminvar type mag. hysteresis loop, longit. Kerr effect obs. 80−65958
Co-Fe-B and Co-Fe-Cr-P-B sputtered amorphous films, mag. props. and corrosion resist. 79−28567

magnetic properties of amorphous substances continued
Co-Fe-B films, mag. annealing behaviour 79−73782
Co-Fe-Ni-Si-B glasses, soft mag. props. 79−73774
Co-Fe-Si-B, amorphous alloys, substitution effect on mag. props. 79−69695
Co-Fe-Si-B, ferromag., magneto-optical spectra in amorphous and cryst. states *(Russian)* 80−84749
Co-Gd amorphous film, struct., mag. anisotropy consts., saturation magnetisation *(Russian)* 79−99735
Co-Gd-Mo, amorphous film, mag. props., temp. depend. 78−10734
Co-Gd-Mo-Ar film, amorphous, mag. props. 78−80182
Co-Gd-Mo(Au) alloy film, Hall effect 77−85347
Co-Gd(Ho) film, amorphous, stripe domains and mag. anisotropy by Lorentz microscopy 77−63243
Co-Mn-Ni-Fe-Si-B amorphous alloys, mag. props., low magnetostriction 80−75832
Co-Ni-Fe-Si(B), amorphous ribbon, magnetostriction meas. 80−15778
Co-P, amorphous, ferromag. antireson. 24 GHz microwave transmission, mag. props. 80−34778
Co-P, amorphous, sound propagation 77−62586
Co-P, amorphous alloy, domain struct., effect of annealing 78−60304
Co-P, amorphous electrodeposited films, domain wall motion, Kerr effect 78−60322
Co-P, cryst. and amorphous mag. films, ferromag. resonance line width *(Russian)* 78−88192
Co-P, domain struct., mag. anisotropy origin 80−80554
Co-P, electrodeposited amorphous alloy, mag. permeability 78−52310
Co-P, electrodeposited amorphous alloys with high permeability, thermal treatment with and without field 80−89372
Co-P alloys, electrodeposited, mag. anisotropy 80−15713
Co-P amorphous alloy, domain struct. 78−10720
Co-P amorphous alloy, ferromagnetic reson. exam. 79−28620
Co-P amorphous alloy, mag. props. 78−10724
Co-P amorphous alloy film, mag. domain struct. 77−69604
Co-P amorphous alloys, electrodeposited, magnetic anisotropy 79−28568
Co-P amorphous film, domain struct., influence of planar anisotropy 79−78472
Co-P foil, complex permeability and eddy currents, annealing induced short-range order 77−8360
Co-Si-B, amorphous ribbon, saturation magnetostriction meas. by small-angle magnetisation rot. 80−60391
Co-Si-B-Fe alloy magnet, Al_2O_3 particle embedded surface, amorphous mag. anal. using electron diffr. 79−56568
Co-Si-B-Fe amorphous alloy, electron diffr., mag. anal. *(German)* 79−61182
$Co_{1-x}Au_x$, elec. resist., temp. depend., spin wave contrib. and resist. minimum 78−51961
$Co_{1-x}B_x$, polycrystalline and amorphous sputtered films, Brillouin spectra 80−2775
$Co_{100-x}B_x$, amorphous, mag. struct., mag. susceptibility meas. 80−80485
$Co_{100-x}B_x$ glassy alloys, mag. props. 79−73689
Co_3B, hyperfine field distrib., ^{59}Co spin echo spectra 80−80635
$Co_{80}B_{20}$, amorphous metal ribbon, stresses, magnetoelastic anisotropy and zero-field mag. domain struct. 80−44896
$(Co_{1-x}Fe_x)$-B-Si, amorphous mag. props. *(Japanese)* 77−85433
$Co_{74}Fe_6B_{20}$, metallic glass, zero magnetostriction, magnetisation characts. 77−12158
$(CoFeB)_{100-x}Cr_x$ thin films, magnetic props. and corrosion resist. 80−34709
$(Co_{0.93}Fe_{0.07})_{75-x}Cr_xSi_{15}B_{10}$ amorphous alloy, thermal stability, Cr conc. effects, DTA expts. 80−59395
$(Co_{0.89}Fe_{0.11})_{72}Mo_3Si_{15}B_{10}$, metallic glass, strain- and field-induced mag. anisotropy 80−108004
$Co_{57}Fe_5Ni_{10}(Si,B)_{28}$, amorphous, soft mag. props., switched-mode power supply appls. 80−88850
$(Co_{1-x}Fe_xNi_y)_{80}(Si_{1-z}B_z)_{20}$, amorphous films, spin wave spectra 80−34777
$Co_{70.4}Fe_{4.6}Si_{15}B_{10}$, amorphous, mag. aftereffect spectra and annealing props. 80−88831
CoGd, H_2 and N_2 contaminated amorphous films, mag. props. 79−1690
$Co_{73}Mo_2Si_{15}B_{10}$, metallic glass, strain- and field-induced mag. anisotropy 80−108004
CoNiB, corrosion-resistant amorphous mag. thin films 80−54923
$Co_{50}Ni_{20}Fe_6Si_{12}B_{12}$, amorphous, mag. props., effects mech. deform. 80−39840
CoNiP film, amorphous, electrolytic, prep. and props. *(Slovak)* 79−51823
CoO-Al_2O_3-SiO_2, spin glasses, low-field susceptibility, freq. depend. 78−47981
CoO-Al_2O_3-SiO_2, spin glass, magnetic aftereffects 79−61176
CoO-Al_2O_3-SiO_2 spin glass, new state in very weak mag. field 79−78416
CoP, and CoNiP, cylindrical amorphous electrodeposited layers, mag. props., torsion influence 80−88848
$Co_{0.9}P_{0.1}$ noncrystalline ferromagnet, electroless deposited, struct. and microscopic mag. props. 80−88063
$Co_{1-x}P_x$ glass, crystn., spin wave reson. 79−73104
Co_4P, amorphous ferromag., mag. excitations calc. in Heisenberg model 77−1546
Co_4P, mag. excitations and static struct., neutron scatt. obs. 78−68204
$Co_{80}P_{20}$, amorphous, sign and magnitude of ^{60}Co hyperfine field, nucl. orientation 78−48100
$Co_{80}P_{20}$ glass, saturation moments, magnetisation and T_c 77−63125
$Co_{85}P_{15}$, strip domains, anisotropy const. effects 80−29571
$Co_xPd_{80-x}Si_{20}$ low field susceptibility near transition temp. 77−66359
$Co_xPd_{80-x}Si_{20}$, structural and mag. heterogeneities 80−80484
CoPr, coercive force variation as function of annealing temp. *(Japanese)* 79−47787
$Co_{74}Si_{10}B_{16}$ amorphous toroidal core, switching characts. and domain structs. 78−95477
$Co_{74}Si_{10}B_{16}$, amorphous ferromagnetic alloy, isothermal annealing effect on static magnetic props. *(Japanese)* 79−52398
$Co_{75}Si_{25-x}B_x$ glass, mag. moment, Curie temp., and microhardness, metalloid comp. depend. 77−55665
Co_5Sm, coercive force variation as function of annealing temp. *(Japanese)* 79−47787
$Co_{90}Zr_{10}$, ferromag. amorphous alloy, crystn. and domain struct. study 80−107056
CrO_2 amorphous thin films, Mossbauer and magnetisation data 80−34712
$Cr_xPd_{82-x}Ge_{18}$ amorphous alloys, magnetoresist., mag. susceptibility, magnetisation 78−80148

magnetic properties of amorphous substances continued
CuCl, disordered, diamag. transition 80−34636
Dy-Co amorphous film, prep. by dual-source evaporation, mag. props. 77−89988
Dy-Cu, mag. phase diagram, magnetisation and sp. ht. meas. 80−80532
Dy-Cu amorphous mag. alloy, linear sp. ht. due to single-ion excitation 78−91874
Dy-Fe, amorphous ferrimag. film, mag. props. and Curie point writing 77−12164
Dy-Fe, amorphous film, Kerr readout charact. 79−15439
Dy-Fe, random anisotropy effects 78−68223
Dy-Fe alloy film, contact printing 77−73061
$Dy_{0.25}$ $Co_{0.75}$ film, displacement of mag. compensation temp. by elastic stress *(Russian)* 78−19284
DyCu film, asperomagnetic domains, Barkhausen jumps in hysteresis loop 80−75822
Dy_xCu_{1-x}, amorphous film, magnetisation meas., local anisotropy effects 78−68309
DyFe amorphous film, Mossbauer and mag. meas. 80−15844
$DyFe_2$, amorphous, mag. struct., US meas. 79−99683
$DyFe_2$, amorphous, struct. determ. EXAFS exam. 78−51421
$DyFe_2$, amorphous, ultrasonic exam. below T_c 79−73793
DyM_3, M=Fe, Co, Ni, amorphous, mag. struct. and moments 77−66260
Er-Fe amorphous alloys, mag. props. 79−90557
$ErCo_2$, amorphous, mag. correlations, neutron exam. 79−73682
$ErCo_2$, amorphous, mag. correlations, neutron exam. 79−73683
$Er_{65}Co_{35}$, amorphous, amg. ordering, susceptibility, magnetisation and hysteresis meas. 78−68190
$(Er_{65}Fe_{35})_{100-x}B_x$ glasses, mag. props. 79−73693
Eu-Ag alloy, formation and mag. props. 79−91216
$Eu_{0.14}Si_{0.31}O_{0.55}$ glass, optical, magnetic, and magneto-optical props., chemical clustering 79−42951
$Eu_{0.14}Si_{0.31}O_{0.55}$, insulating amorphous mag., optical, mag., and magneto-optical props. 79−61344
(Fe,Co,Ni)-Si(B), amorphous mag. alloy, magnetostriction rel. to soft mag. props. 80−84633
$(Fe,Mo)_{80}B_{20}$, glassy alloy, Curie temp. and crystn. temp., Mo additions effect, Mossbauer spectra 78−68428
$(Fe,Ni)_{83}B_{15}C_2$, amorphous alloy, mag. props., possible appl. to power transformers 79−28558
$(Fe,Ni)_{80}(P,B)_{20}$, quenched alloy ribbon, mag. moments, Curie temp. 77−40041
$(Fe,Ni)_{80}P_{14}B_6$ amorphous alloy, mag. props., possible appl. to power transformers 79−28558
Fe alloy wire, glassy, shape, energy, eddy current loss and relax. damping of mag. domain walls 77−89975
Fe alloys, amorphous, effects of metalloids on mag. props. 80−75738
Fe alloys, amorphous, mag. saturation, spin wave stiffness, temp. depend. 80−75741
Fe alloys, amorphous, saturation magnetisation, Curie temp. and size effect 80−65815
Fe, amorphous film, Hall effect and magnetisation *(Russian)* 77−35922
Fe and Fe-Ni Metglas alloys, ohmic and Hall resist. 100-700K, mag. behaviour 80−80254
Fe base amorphous alloys, magnetoelastic props. *(Japanese)* 78−23316
Fe base amorphous alloys, Invar and Elinvar charact. 80−29592
Fe based alloys amorphous toroidal core, switching charact. and domain structs. 78−95477
Fe based amorphous alloy, mag. ordered, hyperfine field distribs., NMR meas. 78−68409
Fe based amorphous alloys, struct. and thermomag. meas. 77−16055
Fe based amorphous alloys, Invar effects, mag. and elastic props. *(Japanese)* 79−20100
Fe based metallic glasses, Curie temp., struct. relax. effects 77−8313
Fe, noncrystalline, mag. hyperfine data from Mossbauer spectra 78−39477
Fe sputtered film, amorphous, Mossbauer study and electron diffr. obs. 80−75897
Fe-Al alloys, rapidly quenched, mag. props. 80−29579
Fe-B, (16.3 at.%) amorphous, coercive force temp. depend. 80−25158
Fe-B, amorphous, induced anisotropy, development by mag. annealing and under applied mech. stress 80−65868
Fe-B, amorphous, induced anisotropy by heat treatment in mag. field and under applied mech. stress 80−75758
Fe-B, amorphous, Invar-type alloy, mag. moment and high field susceptibility 78−34965
Fe-B, amorphous, mag. aftereffect, initial susceptibility time depend. 80−88829
Fe-B, amorphous ferromag., temp. depend. of resist., appl. of extended Ziman theory 80−59950
Fe-B, amorphous metallic glasses, high-temp. mag. anal. 78−91258
Fe-B, rapidly quenched, Curie temp., saturation magnetisation 80−84618
Fe-B, sputtered amorphous film, strong stripe domains, Kerr effect obs. and theory 79−91265
Fe-B (14-25 at.%), saturation magnetisation, temp. and comp. depend. 77−85430
Fe-B (15-25 at.%) glass, quasicryst. struct. Mossbauer expts. 79−4255
Fe-B amorphous alloy, annealed, microstruct. and mag. domain changes 80−75790
Fe-B amorphous alloy, mag. anisotropy temp. depend. 80−15846
Fe-B amorphous alloys, mag. aftereffect 80−65970
Fe-B amorphous alloys, Mossbauer spectra, soft ferromag. props. 80−11302
Fe-B amorphous alloys, Mossbauer spectra, mag. moment conc. depend. 80−15847
Fe-B amorphous Invar alloy, elastic props., Elinvar charact. and ΔE effect 79−56595
Fe-B ferromag. film, props. 79−4709
Fe-B films, mag. annealing behaviour 79−73782
Fe-B metallic glass, role of Fe_3B in crystn., mag. and Mossbauer expts. 78−94997
Fe-B metallic glasses, struct., stability and crystn. 80−75173
Fe-B metallic ribbons, correl. between quenching temp. and mech. and mag. props. 80−89373
Fe-B metastable alloys, Mossbauer spectroscopy and electron microscopy 79−28653
Fe-B ribbon, microhardness, and static coercive force, melt overheating effect 80−84978
Fe-B-C, effects of replacement of B by C on mag. props. 80−84621
Fe-B-C, formation, mag. props., thermal stability and density 80−75796

magnetic properties of amorphous substances continued
Fe-B-C alloys, temp. depend. of magnetisation 79−73690
Fe-B-C amorphous alloys, room-temp. saturation induction over 17.5 kG 79−47300
Fe-B-C amorphous alloys, atomic struct., energy dispersive X-ray diffr. meas. 79−73100
Fe-B-C amorphous alloys, effect of Si addition on mag. props. 80−34694
Fe-B-C amorphous alloys for use in power transformers 80−88808
Fe-B-C amorphous alloys with high saturation induction 80−84617
Fe-B-Cr(Mo), metallic glasses, mag., struct., and elec. props. 80−88751
Fe-B-Cr(Si) thin film glasses, mag. props. and corrosion resist. 80−80576
Fe-B-Si, amorphous ferromag. alloys, mag. struct., Mossbauer study 80−39746
Fe-B-Si amorphous alloys, crystallisation temp., Curie temps., saturation magnetisation 79−82820
Fe-B-Si ribbon, strain induced anisotropy, and toroid diam. effect on mag. props. 80−34623
Fe-B-Si-C amorphous alloys, prep. and props. 80−88748
Fe-B(-Si), glassy, field-induced mag. anisotropy near eutectic comp. 80−93110
Fe-B(B) alloys, anomalous thermal expansion, ΔE effect, Invar and Elinvar charact., delay time 80−80589
Fe-B(P) amorphous alloy, Invar effects, mag. props. meas. 79−56594
Fe-c, Fe-Si-B, and Fe-Cr-P-C sputtered amorphous films, mag. props. and corrosion resist. 79−28567
Fe-C-B alloy, room-temp. saturation induction 78−95476
Fe-Co, stress effect on mag. domain struct. 79−33502
Fe-Co amorphous ribbon, mag. props. in low fields 79−73777
Fe-Co based amorphous alloys, mag. props. *(Japanese)* 79−95971
Fe-Co-B powders, synthesis and mag. props., appl. to mag. recording 80−20432
Fe-Co-C-B alloy, room-temp. saturation induction 78−95476
Fe-Co-Ni-Si-B amorphous alloy, magnetostriction and permeability, effect of annealing 79−1701
Fe-Co-Si-B, amorphous soft ferromagnet with high mag. induction 80−84619
Fe-Co-Si-B, zero magnetostrictive amorphous alloy with high saturation induction, mag. annealing 80−60362
Fe-Co-Si-B alloy, rapidly quenched, mag. heads appl. *(Japanese)* 80−54922
Fe-Co-Si-B sputtered amorphous thin film, coercivity, galvanomagnetic props., resistivity 80−29578
Fe-Co-Si(B), mag. aftereffect on soft mag. props. 80−84626
Fe-Cr-B, amorphous, Elinvar and Invar charact. *(Japanese)* 80−11832
Fe-Cr-b amorphous Invar alloy, elastic props., Elinvar charact. and ΔE effect 79−56595
Fe-Gd amorphous film, struct. and mag. props. 80−20439
Fe-Gd amorphous films with comp. gradient, volume and surface hysteresis *(Russian)* 78−88148
Fe-Gd film, mag. props., mean field analysis 78−64236
Fe-Gd film, O_2 contamination effects on mag. props. 78−64231
Fe-Ge amorphous films, conversion electron Mossbauer spectra, mag. moments 77−16231
Fe-La, Fe-rich alloys, mag. props. for bulk amorphous deposits *(Japanese)* 79−95971
Fe-La(Zr) amorphous films, mag. props., Mossbauer effect and magnetisation meas. 79−69701
Fe-Mn-P-B-Al metallic glass, exchange anisotropy 77−16068
Fe-Ni base amorphous alloys, effect of annealing on Curie temp. 80−34632
Fe-Ni based alloy, amorphous rapidly quenched, mag. props. 77−66269
Fe-Ni based amorphous alloys, Hall and ohmic resistivities 79−91013
Fe-Ni based metallic glasses, hydrostatic press. effect on mag. props. 78−19300
Fe-Ni based metallic glasses, search for Invar-like magnetoelastic behaviour 79−56596
Fe-Ni based metallic glass, Metglas 2826 MB, Mossbauer study 80−75897
Fe-Ni metallic glass wide strips, low-field mag. props. 79−51822
Fe-Ni-B-Si, amorphous, mag. props., heat treatment effects 80−89370
Fe-Ni-B(-P), ferromag., magneto-optical spectra in amorphous and cryst. states *(Russian)* 80−84749
Fe-Ni-B(-P) amorphous alloys, mag. annealing mechanism, induced anisotropy 78−95484
Fe-Ni-C-B alloy, room-temp. saturation induction 78−95476
Fe-Ni-Co-B-C-Si alloy, room-temp. saturation induction 78−95476
Fe-Ni-Co-B-P soft magnetic metallic glasses, status report 78−64226
Fe-Ni-P-B, amorphous ferromag. alloys, mag. struct., Mossbauer study 80−39746
Fe-Ni-P-B, metallic glasses, struct. relax., annealing effects on mag. props. 80−89261
Fe-Ni-P-B alloy, magnetically induced anisotropy 77−89948
Fe-P, amorphous, temp. depend. of saturation magnetisation 78−19223
Fe-P alloys, amorphous, Mossbauer spectra 79−51886
Fe-P alloys, electrodeposited, mag. anisotropy 80−15713
Fe-P alloys, initial permeability, time depend. 80−15759
Fe-P electrodeposited foil, amorphous, mag. domains 80−75821
Fe-P film, amorphous, ion implanted, struct. and domain struct. obs. 79−91272
Fe-P-B alloys, conc. depend. 77−8314
Fe-P-B-Al, magnetostriction as function of glass formers 78−19299
Fe-P-C, amorphous, struct. and mag. props., Mossbauer, X-ray diffr. and elec. resist. meas. 78−2009
Fe-P-C alloys, amorphous, mag. anisotropy, Mossbauer obs., prior cooling effects *(Russian)* 77−32300
Fe-R alloys, mag. elastic properties 78−52331
Fe-rare earth alloys, magnetoelasticity and moment rot., US vel. calc. and neutron scatt. meas. 80−65992
Fe-Sb amorphous films, Mossbauer effect study 80−75896
Fe-Si, film, mag. props. 77−1575
Fe-Si amorphous film, struct. and crystallisation, Mossbauer study 80−11300
Fe-Si amorphous films, mag. and magnetoelastic props. 79−99746
Fe-Si ferromag. film, props. 79−4709
Fe-Si-B, magnetic metallic glasses, mag. props. 80−84620
Fe-Si-B amorphous alloys, metalloid content effects on Curie temp. and mag. moments 78−14956
Fe-Si-B amorphous films, mag. props. 80−34710

magnetic properties of amorphous substances continued
Fe-Si-B ferromagnetic amorphous alloys, Young's modulus and delay time characts. *(Japanese)* 77−85543
Fe-Si-B glassy alloys, mag. props., comp. effects 80−88752
Fe-Si-B magnetic powder, amorphous, prep. by atomisation technique 78−92213
Fe-Si-B metallic glasses, mag. props., depend. on metalloid content 77−85485
Fe-Si-B powder, production by spark erosion, and mag. props. 77−90290
Fe-Tb dilute alloy, amorphous, small angle mag. scatt. 78−27021
Fe-Y, amorphous, resist. and magnetoresist. meas., local moment system 78−68018
Fe-Y(Lu) amorphous films, mag. props., Mossbauer effect and magnetisation meas. 79−69701
$(Fe\text{-}Co\text{-}Ni)_{78}Si_8B_{14}$, low coercivity and zero magnetostriction 78−23299
$(Fe\text{-}Ni\text{-}Mo)_{80}(P\text{-}B)_{20}$, amorphous, mag. aftereffects and struct. instabilities 80−88833
$Fe_{1-x}Au_x$, elec. resist., temp. depend., spin wave contrib. and resist. minimum 78−51961
Fe_cAu_{1-c}, amorphous ferromagnetic, resistivity, anisotropic, field dependence 78−87960
$Fe_{1-x}B_x$, amorphous, hyperfine fields and local mag. moments, Mossbauer study 80−75895
$Fe_{1-x}B_x$, amorphous films, mag. props. and thermal stability 79−78446
$Fe_{1-x}B_x$ metallic glasses, struct. and cryst., Mossbauer spectra, DSC, and magnetisation meas. 79−94906
$Fe_{1-x}B_x$, polycrystalline and amorphous sputtered films, Brillouin spectra 80−2775
$Fe_{100-x}B_x$ $(11.5 \leq x \leq 22)$, magneto-volume effect 78−91922
$Fe_{100-x}B_x$, amorphous, effect of metalloids on mag. props. 79−11304
$Fe_{100-x}B_x$, amorphous, mag. struct., mag. susceptibility meas. 80−80485
$Fe_{100-x}B_x$ amorphous alloys, magnetostriction meas. 79−19760
$Fe_{100-x}B_x$, crystalline and glassy, low temp. magnetisation study 79−95608
$Fe_{100-x}B_x$ glass, magnetostriction meas., temp. depend. 79−73792
$Fe_{100-x}B_x$, mag. and struct. props., comp. depend. 78−60314
$Fe_{100-x}B_x$ metallic glass, magnetisation meas. 78−80134
$Fe_{100-x}B_x$ ribbon, magnetostriction exam. 79−73794
$Fe_{80}B_{20}$, amorphous, Brillouin scatt. from magnons, ferromag. reson. 80−65844
$Fe_{80}B_{20}$, amorphous, deform. and annealing effects on mag. and mech. props. 77−12717
$Fe_{80}B_{20}$, amorphous, mag. permeability aftereffect during annealing 80−88834
$Fe_{80}B_{20}$, amorphous, transverse magnetoresist., stress effect 80−15501
$Fe_{80}B_{20}$ amorphous alloy, low field magnetic props. 77−55690
$Fe_{80}B_{20}$ amorphous alloys, domain struct. exam., magneto-optic Kerr effect 79−28550
$Fe_{80}B_{20}$, amorphous ferromag., temp. depend. of hyperfine field distrib. 78−43756
$Fe_{80}B_{20}$, amorphous ferromag., hyperfine field distrib., Mossbauer effect 78−60371
$Fe_{80}B_{20}$, amorphous ferromag. metallic glass, stress-induced rot. of magnetisation, Mossbauer study 80−20445
$Fe_{80}B_{20}$, amorphous ferromagnet, Mossbauer hyperfine fields, mag. struct. 80−75894
$Fe_{80}B_{20}$ amorphous ribbons, magnetomechanical coupling constant and Young's modulus, mag. annealing 79−15333
$Fe_{80}B_{20}$ amorphous ribbon, initial susceptibility time lag 80−100579
$Fe_{80}B_{20}$, ferromagnetic metallic glasses, Brillouin scattering 78−92085
$Fe_{80}B_{20}$ film, amorphous metallic, standing spin waves, Brillouin scatt. obs. 80−97291
$Fe_{80}B_{20}$ glass, magnetisation reorientation, Mossbauer effect 80−66092
$Fe_{80}B_{20}$, glassy, ferromag. anisotropy of resistivity 79−23939
$Fe_{80}B_{20}$, hardness, elec. cond., photo emission, and mag. props. *(Norwegian)* 79−32909
$Fe_{80}B_{20}$, METGLAS 2605, mag. anisotropy and electronic struct., Mossbauer meas. 77−28384
$Fe_{80}B_{20}$, metallic glass, ferromag. props. 77−16107
$Fe_{80}B_{20}$, metallic glass, low temp. specific heat, metalloid effects 80−34654
$Fe_{80}B_{20}$ metallic glass, crystn. and struct. relax., Mossbauer effect study 80−75182
$Fe_{80}B_{20}$ metallic glasses, stability and transforms. 80−75174
$Fe_{80}B_{20}$ Metglass, Mossbauer spectra line broadening 78−52400
$Fe_{80}B_{20}$, sputter deposited amorphous, low field mag. props. 78−68335
$Fe_{81}B_{19}$ amorphous alloy, mag. anisotropy temp. depend. 78−14953
$Fe_{83.4}B_{16.6}$, amorphous, mag. props. and microstruct., cooling rate and melt overheating effects 80−65965
$Fe_{83.4}B_{16.6}$ amorphous, mag. props., melt overheating and cooling rate effects 80−89371
Fe_xB_{100-x}, amorphous, mag. props., ^{57}Fe Mossbauer spectra and magnetisation meas. 79−95693
$Fe_{80}(B_yC_{1-y})_{20}$, saturation magnetostriction, comp. effects 80−34735
$Fe_{84}B_{16-x}C_x$, hyperfine interaction and Curie temps., Mossbauer meas. 79−73858
$Fe_{80}B_{20-x}M_x$ (X=Al, Si, Ge, C, P) and $(FeCo)_{80}B_{20}$ glass, magnetisation, Curie and crystn. temps. 79−87289
$Fe_{80}(B_{1-x}P_x)_{20}$ amorphous alloys, isothermal crystallisation kinetics 80−33895
$Fe_{40}B_{40}P_{14}B_6$ and $Fe_{80}B_{20}$, Metglas 2826 and 2605, amorphous ribbon, power loss variation with freq. and applied stress 80−88849
$Fe_{78}B_{12}Si_{10}$, amorphous, Mossbauer study of hyperfine interaction and mag. anisotropy 80−40027
$Fe_{78}B_{12}Si_{10}$, amorphous ferromagnet, long and short range exchange interactions, Mossbauer spectra and interpretation 79−56526
$Fe_{80}B_{15}Si_5$ metallic glass, large uniaxial magnetostrictive anisotropy, magnetisation reversal 80−34736
$Fe_{80}B_{20-x}Si_x$, metallic glass, mech. and mag. props., depend. on metalloid content 79−91213
$Fe_{80}(B_ySi_{1-y})_{20}$, saturation magnetostriction, comp. effects 80−34735
$Fe_{81.5}B_{14.5}Si_4$, amorphous metal ribbon, stresses, magnetoelastic anisotropy and zero-field mag. domain struct. 80−44896
$Fe_{82}B_{15}Si_3$, metallic glass, low temp. specific heat, metalloid effects 80−34654
$Fe_{82}B_{18-x}Si_x$ glasses, soft mag. props. 79−73774
$Fe_{83}B_{16.5}Si_{0.5}$, spin waves, inelastic neutron scatt. meas. 79−73701
$Fe_{100-x}Be_x$, amorphous ribbon, saturation magnetostriction, and electronically controllable delay line 79−1700
Fe_yC_{1-y} amorphous sputtered film, mag. props. 78−68311
$(Fe_{0.06}Co_{0.94})$-B, ferromagnetic, mag. instability rel. to struct. 79−99729

magnetic properties of amorphous substances continued
FeCoB, corrosion-resistant amorphous mag. thin films 80−54923
$(Fe_{0.5}Co_{0.5})_{1-x}B_x$, amorphous, hyperfine fields and local mag. moments, Mossbauer study 80−75895
$Fe_5Co_{75}B_{20}$, amorphous, magnetisation reversal and domain boundary configs. 80−88809
$Fe_{71}Co_9B_{20}$, glassy ribbon, magnetostatic effects 79−73790
$Fe_{80-x}Co_xB_{20}$, ferromag. metallic glass saturation magnetostriction meas. 77−36108
$Fe_xCo_{80-x}B_{20}$, mag. after-effect 79−61189
$Fe_{35}Co_{32}B_{20}Si_{10}Al_3$, stress-induced variation in magnetisation and dynamic magnetostrictive charact. 80−88855
$(FeCoNi)_8B_{20}$, glass, evidence supporting split-band model from magnetostriction 78−95509
$(Fe_xCo_yNi_{1-x-y})_{78}Si_8Bi_{14}$ amorphous ribbons, saturation magnetostriction and vol. magnetostriction 77−85538
$(Fe_{0.2}Co_{0.8})_{80}P_{17}Al_3$, Mossbauer spectra, isomer shift, mag. hyperfine field 80−11301
$(Fe_{100-x}Co_x)_{79}P_{13}B_8$, amorphous, hyperfine field distrib., ^{59}Co NMR spin-echo meas. 80−34818
$(Fe_{1-x}Co_x)_yPBAl$ metallic glasses, influence of composition and ageing on Curie temps. 77−85445
$(Fe_{0.05}Co_{0.95})_{78}Si_8B_{14}$ amorphous ribbon, anomalous mag. aftereffect 80−100602
$(Fe_{0.9}Co_{0.1})_xSi_yB_2$, $(Fe_{1-x}Co_x)_{78}Si_8B_{14}$ amorphous ribbons, magnetomech. coupling and saturation magnetostriction 78−68353
$(Fe_{1-x}Co_x)_{77}Si_{10}B_{13}$ alloys, amorphous, induced mag. anisotropy by mag. annealing 79−4671
$(Fe_{1-x}Co_x)_{77}Si_{10}B_{13}$, amorphous, mag. moments at 0K, Curie temp., mag. interactions 79−4670
$(Fe_{1-x}Co_x)_{78}Si_{10}B_{12}$, amorphous, Hall effect and magnetoresist. *(Japanese)* 77−85199
$(Fe_{1-x}Co_x)_{78}Si_{10}B_{12}$, amorphous alloys, magnetic anisotropy meas. 80−2570
$(Fe_{1-x}Co_x)_{78}Si_{10}B_{12}$, amorphous, roll mag. anisotropy 80−75757
$(Fe_{1-x}Co_x)_{78}Si_8B_{14}$ ribbon, magnetostriction exam. 79−73794
$Fe_{4.7}Co_{70.3}Si_{15}B_{10}$, amorphous ferromag., roll mag. anisotropy 79−51773
$Fe_5Co_{70}Si_{10}B_{15}$ amorphous magnetic alloy, decrease of permeability after demagnetisation, disaccommodation 80−39814
$Fe_5Co_{70}Si_{15}B_{10}$, amorphous ribbon, zero magnetostriction, low residual mag. loss 77−12157
$Fe_5Co_{70}Si_{15}B_{10}$ amorphous ferromag. ribbons, change of permeability by heat treatment 77−85493
$Fe_5Co_{70}Si_{15}B_{10}$, amorphous, change of mag. props. by low temp. annealing 78−27058
$Fe_5Co_{70}Si_{15}B_{10}$, amorphous ferromagnetic alloy, isothermal annealing effect on static magnetic props. *(Japanese)* 79−52398
$Fe_5Co_{70}Si_{15}B_{10}$, amorphous, crystn. effect on mag. props. *(Russian)* 80−44858
$(Fe_xCo_{1-x})_{100-y}(Si_{0.4}B_{0.6})_y$ amorphous alloy zero magnetostrictive, mag. props. 79−99743
$(Fe_xCo_{1-x})_{78}Si_8B_{14}$, amorphous, saturation magnetostriction, strain modulated FMR obs. 80−75863
$(Fe_xCo_{100-x})_{100-(y+z)}Si_yB_z$ amorphous ribbon, mag. moment and Curie temp., comp. depend. 78−95421
$(Fe_{1-x}Cr_x)$-P-C, amorphous mag. props. *(Japanese)* 77−85433
$Fe_{85-x}Cr_xB_{15}$ metallic glass, Curie temp., crystn. temp. and room temp. elec. resist., Cr content effect 79−91229
$(Fe_{98}Cr_2)_{79}P_{13}B_8$ and $(Fe_{96}Cr_4)_{79}P_{13}B_8$, amorphous, low temp. sp. ht., mag. contribs. 80−80552
FeF_2, types of magnetism and methods of study *(French)* 80−80490
FeF_3, amorphous, characterisation by thermal, mag. and Mossbauer study 79−42782
FeF_3, amorphous, mag. props. and Mossbauer spectra, speromagnetism and mictomagnetism 80−75778
FeF_3, amorphous, struct. and mag. props., computer model 80−96446
FeF_3, noncryst. magnet with antiferromag. interactions 79−91228
FeGd, H_2 and N_2 contaminated amorphous films, mag. props. 79−1690
Fe_xGd_{1-x}, $0.5>x>0.65$, amorphous film, FMR, spin wave spectra 77−16181
Fe_xGe_{1-x} amorphous alloys, high field mag. meas. 79−82765
Fe_xGe_{1-x}, amorphous film, FMR meas. of mag. props., temp. and comp. depend. 77−69636
Fe_xGe_{1-x} amorphous film, low temp. conversion electron Mossbauer spectroscopy 78−48101
Fe_xGe_{1-x} amorphous film, XPS and Mossbauer exam. 79−56577
FeMn hydrated oxides, ferromanganese freshwater nodules, antiferro- to speromag. order 77−70649
$(Fe_{1-x}Mn_x)_{75}P_{16}B_6Al_3$, amorphous, spin-glass-ferromag. multicritical point, AC susceptibility meas. 80−50117
$(Fe_xMn_{1-x})_{75}P_{16}B_6Al_3$, amorphous, mag. ordering temp., hyperfine field distrib., elec. resist. 80−34633
$(Fe_{1-x}Mn_x)_{75}P_{15}C_{10}$, amorphous, mag. ordering, Mossbauer study 80−39747
$(Fe_{1-x}Mn_x)_{75}P_{15}C_{10}$, amorphous pair radial distrib. functions, neutron scatt. study 80−49128
$Fe_{78}Mo_2B_{20}$, amorphous, transverse magnetoresist., stress effect 80−15501
$Fe_{78}Mo_2B_{20}$, amorphous ferromag., $T^{3/2}$ depend. of hyperfine field 78−39474
$Fe_{78}Mo_2B_{20}$, amorphous ferromag., mag. props. 79−38309
$Fe_{78}Mo_2B_{20}$, glassy, ferromag. anisotropy of resistivity 79−23939
$(Fe_{93}Mo_7)_{80}B_{10}P_{10}$, neutron scatt. investig. of spin waves, magnetisation 77−47984
$(Fe_xMo_{1-x})_{75}P_{16}B_6Al_3$, effects of Mo on mag. props., Mossbauer meas. 79−73859
$Fe_{40}Ni_{38}$-Mo_4B_{18} amorphous alloys, compatibility of DC and AC mag. props. 80−34695
$(Fe_{1-x}Ni_x)_{83}B_{17}$, amorphous alloys ferromagnetic resonance 80−108080
$Fe_{38}Ni_{38}B_{24}$, magnetisation and FMR expts. 79−95607
$Fe_{40}Ni_{40}B_{20}$, amorphous, induced mag. anisotropy, reorientation kinetics 77−43829
$Fe_{40}Ni_{40}B_{20}$, amorphous, casting conditions effect on mag. props. *(Japanese)* 80−34698
$Fe_{40}Ni_{40}B_{20}$, amorphous, mag. props., effects mech. deform. 80−39840
$Fe_{40}Ni_{40}B_{20}$, amorphous, RF annealing effects 80−108037
$Fe_{40}Ni_{40}B_{20}$, amorphous ribbon prod., apparatus parameters effect on dimens. 77−12570
$Fe_{40}Ni_{40}B_{20}$, amorphous ferromag., resist. and galvanomagnetic props., rel. to magnetisation 78−14712

magnetic properties of amorphous substances continued
$Fe_{40}Ni_{40}B_{20}$, amorphous ribbon, power loss variation with freq. and applied stress 80−88849
$Fe_{40}Ni_{40}B_{20}$ and $Fe_{40}Ni_{40}P_{14}B_6$, amorphous, mag. aftereffect spectra and annealing props. 80−88831
$Fe_{40}Ni_{40}B_{20}$, high-field magnetisation curve, spin wave spectrum and microstructural inhomogeneities 80−15702
$Fe_{40}Ni_{40}B_{20}$, mag. loss meas. 79−73776
$Fe_{40}Ni_{40}B_{20}$, metallic glass, low temp. specific heat, metalloid effects 80−34654
$Fe_{40}Ni_{40}B_{20}$, processing conditions effect on mag. props. 79−73775
$Fe_{80-x}Ni_xB_{20}$ and $Fe_{80-x}Ni_xP_{14}B_6$ amorphous alloys, microhardness correl. with mag. props. 80−88826
$Fe_{80-x}Ni_xB_{20}$, $Fe_{80-x}Ni_xP_{14}B_6$, amorphous, microhardness meas., dependence on mag. props. *(Croatian)* 79−11688
$Fe_{80-x}Ni_xB_{20}$, ferromag. metallic glass, saturation magnetostriction meas. 77−36108
$(Fe_{1-x}Ni_x)_{80}B_{20}$ amorphous soft magnetic films 79−82836
$(Fe_xNi_{1-x})_{80}B_{20}$, $(Fe_xNi_{1-x})_{80}P_{14}B_6$, new soft amorphous ferromagnetic glasses *(Croatian)* 79−11298
$(Fe_xNi_{1-x})_{80}B_{20}$, amorphous alloys, engineering mag. props. 79−51832
$(Fe_xNi_{1-x})_{80}B_{20}$, amorphous, Mossbauer spectra, mag. props. 80−15843
$(Fe_xNi_{100-x})_{80}B_{20}$, glassy, elec. resist. at elevated temp. 79−73484
$Fe_xNi_{80-x}B_{20}$ and $Fe_xNi_{80-x}P_{14}B_6$ metallic glasses, low temp. resist. and galvanomag. effects, mag. state influence 80−84461
$Fe_xNi_{80-x}B_{20}$, $Fe_xNi_{80-x}P_{14}B_4$, amorphous Hall effect voltage meas. *(Croatian)* 79−11102
$Fe_xNi_{80-x}B_{20}$, $Fe_xNi_{80-x}P_{14}B_6$, amorphous ferromag., galvanomag. props. 79−56196
$Fe_xNi_{80-x}B_{20}$ glass, resist., magnetoresist., and thermoelec. power 80−70681
$(Fe_yNi_{1-y})_{80}B_{20}$, mag. anneal anisotropy in amorphous alloys 77−16069
$(Fe_{1-y}Ni_y)_{0.8}B_{0.2-x}P_x$, amorphous, hyperfine fields and local mag. moments, Mossbauer study 80−75895
$Fe_{1.6}Ni_{78.4}B_{10}P_{10}$ metallic glass, superparamag. behaviour, chem. inhomogeneities role 80−84625
$Fe_{20}Ni_{60}B_{19}P_1$, spin waves, inelastic neutron scatt. meas. 79−73701
$Fe_{80-x}Ni_xB_{20-y}P_y$, amorphous, Rayleigh region and coercive force 80−88806
$(FeNi)_{80}Bi_{17.5}Al_2Si_{0.5}$, stress-induced variation in magnetisation and dynamic magnetostrictive charact. 80−88855
$Fe_{40}Ni_{40}C_{14}P_6$ amorphous film, dislocation and mag. struct., neutron diffr. study 80−70956
$Fe_{32}Ni_{36}Cr_{14}P_{12}B_6$, Metglas 2826 A, ferromag. reson. for g-values and relax. parameters, 77 to 430K 77−63289
$Fe_{32}Ni_{36}Cr_{14}P_{12}B_6$, metallic glass, changes in Curie temp., physical dimensions and mag. anisotropy during annealing 77−85446
$Fe_{32}Ni_{36}Cr_{14}P_{12}B_6$, Metglas 2826A, Hall resistivity, effect of thermal cycling and annealing 78−56125
$Fe_{32}Ni_{36}Cr_{14}P_{12}B_6$, amorphous ferromagnet, long and short range exchange interactions, Mossbauer spectra and interpretation 79−56526
$Fe_{32}Ni_{36}Cr_{14}P_{12}B_6$, amorphous mag. solids, Mossbauer exam. 79−61281
$Fe_{32}Ni_{36}Cr_{14}P_{12}B_6$, Metglass 2826A, mag. props. under high press., Mossbauer meas. 79−73860
$Fe_{32}Ni_{36}Cr_{14}P_{12}B_6$, Metglas 2826A, EPR at 20 GHz 80−75848
$Fe_{40}Ni_{40}(Mo,Si,B)_{20}$, amorphous, soft mag. props., switched-mode power supply appls. 80−88850
$Fe_{40}Ni_{38}Mo_4B_{18}$, amorphous, mag. anisotropy, Mossbauer study 80−65864
$Fe_{40}Ni_{38}Mo_4B_{18}$, amorphous, reversible enhancement of mag. directional ordering rate 80−103829
$Fe_{40}Ni_{38}Mo_4B_{18}$ and $Fe_{78}Mo_2B_{20}$ amorphous ribbons, magnetoelastic effects in as-quenched and stress-relieved states 80−80588
$Fe_{40}Ni_{38}Mo_4B_{18}$ glassy alloy, high permeability, low field mag. characts. 78−68301
$Fe_{40}Ni_{38}Mo_4B_{18}$ metallic glass, reorientation kinetics of magnetization 79−24155
$Fe_{40}Ni_{38}Mo_4B_{18}$, metallic glass, mag. and transport props. 80−39752
$(Fe_{1-x}Ni_x)_{80}P_{20}$, amorphous, ferromagnetic alloys, mag. anomalies of Invar type *(Russian)* 80−93089
$(Fe_{0.04}Ni_{0.96})_{80}P_{10}B_{10}$, amorphous, mictomagnetic to ferromag. transition 78−34981
$(Fe_{0.04}Ni_{0.96})_{80}P_{10}B_{10}$, amorphous magnetisation, field and temp. depend. 80−39755
$(Fe_{1-x}Ni_x)_{80}P_{10}B_{10}$, amorphous, magnetostriction meas. by ferromag. reson., induced anisotropy 77−32232
$(Fe_{1-x}Ni_x)_{80}P_{10}B_{10}$, amorphous microwires, magnetisation reversal and anisotropy 78−91885
$Fe_{20}Ni_{60}P_{14}B_6$, $Fe_{30}Ni_{50}P_{14}B_6$, amorphous ferromags., thermoelec. power and resistivity near Curie temp. 79−56200
$Fe_{27}Ni_{53}P_{14}B_6$, amorphous, Hall resist. and mag. props., short range order effects 80−34422
$Fe_{27}Ni_{53}P_{14}B_6$, metallic glass, changes in Curie temp., physical dimensions and mag. anisotropy during annealing 77−85446
$Fe_{40}Ni_{40}P_{14}B_{06}$, strip domains, anisotropy const. effects 80−29571
$Fe_{40}Ni_{40}P_{14}B_6$, (Metglas 2826), ferromag. Curie temp. determ. 78−64206
$Fe_{40}Ni_{40}P_{14}B_6$, amorphous ribbon, cold rolling, annealing mag. props. 77−8958
$Fe_{40}Ni_{40}P_{14}B_6$, amorphous, deform. and annealing effects on mag. and mech. props. 77−12717
$Fe_{40}Ni_{40}P_{14}B_6$, amorphous, domain struct. 78−10719
$Fe_{40}Ni_{40}P_{14}B_6$, amorphous tape wound cores, mag. props. *(German)* 78−10727
$Fe_{40}Ni_{40}P_{14}B_6$, amorphous, mag. props. 78−10728
$Fe_{40}Ni_{40}P_{14}B_6$ amorphous ribbon, mag. anisotropy distrib. near surface 78−95430
$Fe_{40}Ni_{40}P_{14}B_6$, amorphous ferromagnet, domain struct., Rayleigh region and coercive field 79−28559
$Fe_{40}Ni_{40}P_{14}B_6$, amorphous, transverse magnetoresist., stress effect 80−15501
$Fe_{40}Ni_{40}P_{14}B_6$, amorphous, mag. props., effects mech. deform. 80−39840
$Fe_{40}Ni_{40}P_{14}B_6$, amorphous ferromagnet, Mossbauer hyperfine fields, mag. struct. 80−75894
$Fe_{40}Ni_{40}P_{14}B_6$, amorphous, mag. permeability aftereffect during annealing 80−88834
$Fe_{40}Ni_{40}P_{14}B_6$, amorphous ferromag., spin wave excitations 80−97079
$Fe_{40}Ni_{40}P_{14}B_6$ amorphous ribbon, mag. domains and anisotropy distrib. 80−108029
$Fe_{40}Ni_{40}P_{14}B_6$, and $Fe_{32}Ni_{36}Cr_{14}P_{12}B_6$, glassy, ferromag. anisotropy of resistivity 79−23939

magnetic properties of amorphous substances continued
$Fe_{40}Ni_{40}P_{14}B_6$, $Fe_{35}Ni_{32}Cr_{15}P_{12}B_6$, amorphous ferromagnets, Barkhausen noise and core losses 77−69618
$Fe_{40}Ni_{40}P_{14}B_6$, ferromagnetic metallic glasses, Brillouin scattering 78−92085
$Fe_{40}Ni_{40}P_{14}B_6$ glass, ferromag., low temp. heat capacity meas., electronic, phonon contributions exam. 78−10689
$Fe_{40}Ni_{40}P_{14}B_6$ glass, crystn. kinetics, DSC expts. 78−26444
$Fe_{40}Ni_{40}P_{14}B_6$, glassy metal fabric for mag. shield 77−8347
$Fe_{40}Ni_{40}P_{14}B_6$, glassy, mag. props. and hyperfine interactions, Mossbauer obs., 4.2-1000K 78−10812
$Fe_{40}Ni_{40}P_{14}B_6$, hardness, elec. cond., photo emission, and mag. props. *(Norwegian)* 79−32909
$Fe_{40}Ni_{40}P_{14}B_6$, high-field suscept. and spin wave spectrum 78−10662
$Fe_{40}Ni_{40}P_{14}B_6$, mag. polarisation in approach to ferromag. saturation 80−80560
$Fe_{40}Ni_{40}P_{14}B_6$, magnetoelastic props. 77−16136
$Fe_{40}Ni_{40}P_{14}B_6$ metallic glass, ferromag. reson., spin waves, thermal ageing and long-range order effects 80−25214
$Fe_{40}Ni_{40}P_{14}B_6$, Metglas 2826, ferromag. reson. for g-values and relax. parameters, 77 to 430K 77−63289
$Fe_{40}Ni_{40}P_{14}B_6$, Metglas 2826, ferromag. antireson. transmission at 24 GHz, 26 to 270°C 77−69696
$Fe_{40}Ni_{40}P_{14}B_6$, Metglas 2826, magnetising processes 78−10725
$Fe_{40}Ni_{40}P_{14}B_6$, Metglas 2826, amorphous ribbon core, appl. in force transducer 78−93669
$Fe_{40}Ni_{40}P_{14}B_6$ Metglass, spontaneous vibr. modes excited by reversible magnetostriction 79−56587
$Fe_{40}Ni_{40}P_{14}B_6$, Metglas 2826, amorphous ribbon under tension, mag. domain walls and pulsed magnetisation reversal 80−88825
$Fe_{40}Ni_{40}P_{14}B_6$, quenched amorphous, high field susceptibility and microstructure 77−69506
$Fe_{40}Ni_{40}P_{14}B_6$, stress-induced mag. easy axis 79−33516
$Fe_{40}Ni_{40}P_{14}B_6$, thermal stress effect on mag. easy axis 77−80928
$Fe_{40}Ni_{40}P_{16}B_6$, amorphous, kinetics of induced mag. directional order 80−44824
$Fe_{40}Ni_{40}P_xB_{20-y}$, amorphous, mag. props. effect of metalloid elements 79−28658
$Fe_{46}Ni_{40}P_{16}B_6$, ferromagnetic amorphous alloy, even magneto-optic effects 77−55776
$Fe_cNi_{80-c}P_{14}B_6$, amorphous, annealing effects on mag. props. 79−78383
$Fe_xNi_{1-x}P_{14}B_6$, amorphous, spin-glass regime, magnetoresist. meas. 80−34418
$(Fe_xNi_{1-x})_{80}P_{10}B_{10}$, amorphous, magnetisation reversal and domain boundary configs. 80−88809
$(Fe_xNi_{1-x})_{80}P_{10}B_{10}$, weak itinerant ferromag., Arrott plots 77−73007
$(Fe_xNi_{1-x})_{80}P_{14}B_6$, amorphous, hyperfine field distrib., ^{57}Fe Mossbauer spectra 79−11367
$Fe_xNi_{80-x}P_{14}B_6$, amorphous, sp. ht. and susceptibility meas., spin glass and mictomag. props. 78−68274
$Fe_xNi_{80-x}P_{14}B_6$, amorphous ferromag., resistivity, mag. contrib., 1.5-50K 79−56182
$Fe_xNi_{80-x}P_{14}B_6$, and $Fe_xNi_{80-x}B_{20}$ glass, microhardness, correl. with mag. props. 79−57085
$Fe_xNi_{80-x}P_{14}B_6$ glass, resist., magnetoresist., and thermoelec. power 80−70681
$(Fe_{0.3}Ni_{0.7})_{0.75}P_{0.16}B_{0.06}Al_{0.03}$, amorphous, spin wave spectrum, neutron scatt. 77−16064
$(Fe_{0.5}Ni_{0.5})_{75}P_{16}B_6Al_3$ glass, struct. relax. as origin of Curie temp. ageing 78−84418
$(Fe_{1-x}Ni_x)_{75}P_{16}B_6Al_3$, amorphous alloy, low temp. elec. resist. saturation 78−68005
$(Fe_{1-x}Ni_x)_{75}P_{16}B_6Al_3$, saturation magnetisation, temp. depend., ferromag. reson. meas. 79−73818
$(Fe_{65}Ni_{35})_{75}P_{16}B_6Al_3$, amorphous ferromag., high temp. spin dynamics 78−47965
$(Fe_{65}Ni_{35})_{75}P_{16}B_6Al_3$, mag. excitations 79−7984
$(Fe_xNi_{1-x})_{75}P_{16}B_6Al_3$, spin wave excitations and low temp. magnetisation 79−33468
$(Fe_xNi_{1-x})_{75}P_{16}B_6Al_3$, magnetisation temp. depend., spin wave theory 80−44927
$Fe_{29}Ni_{49}P_{14}B_6Si_2$ glass, crystn. kinetics, DSC expts. 78−26444
$Fe_{29}Ni_{49}P_{14}B_6Si_2$, Metglas 2826 B, paramag. reson. for g-values and relax. parameters, 77 to 430K 77−63289
$Fe_{29}Ni_{49}P_{14}B_6Si_2$, metallic glass, changes in Curie temp., physical dimensions and mag. anisotropy during annealing 77−85446
$Fe_{29}Ni_{49}P_{14}B_6Si_2$, Metglas 2826B, Hall, elec. resist., magnetisation and heat capacity meas. 78−68019
$Fe_{29}Ni_{49}P_{14}B_6Si_2$, Metglass 2826B, saturation magnetisation, temp. depend., ferromag. reson. meas. 79−73818
$(Fe_{1-x}Ni_x)_{77}Si_{10}B_{13}$ amorphous alloy system, saturation mag. moment, Curie temp., mag. susceptibility 80−39753
$(Fe_{1-x}Ni_x)_{77}Si_{10}B_{13}$, amorphous, Landau-Ginzburg theory, magnetisation and Curie temp. 80−75700
$(Fe_{1-x}Ni_x)_{78}Si_{10}B_{12}$, amorphous, Hall effect and magnetoresist. *(Japanese)* 77−85199
$(Fe_{1-x}Ni_x)_{78}Si_{10}B_{12}$ amorphous alloys, cold rolled and as-quenched, mag. anisotropy 80−97089
$Fe_{62.4}Ni_{15.6}Si_7B_{15}$ amorphous ferromagnetic alloy, anomalous magnetisation possible reasons, Mossbauer spectra *(Russian)* 79−78441
Fe_2O_3, amorphous, temp. depend. of hyperfine field, Mossbauer spectroscopy 78−84508
Fe_2O_3 amorphous film, Mossbauer spectra, mag. props. 80−15851
Fe_2O_3 amorphous layer on graphite, Mossbauer spectra, superparamag. props. 80−60474
Fe_2O_3 amorphous RF sputtered thin films, Mossbauer and mag. study 80−34711
Fe_2O_3 amorphous thin films, Mossbauer and magnetisation data 80−34712
Fe_2O_3, types of magnetism and methods of study *(French)* 80−80490
Fe_2O_3-BaO-B_2O_3, magnetic props. of Fe-rich amorphous oxide *(French)* 80−80511
Fe_2O_3-Dy_2O_3-Na_2O-B_2O_3 glass, AC mag. susceptibility, antiferromag. interactions 77−32179
Fe_2O_3-Na_2O-BaO glass, mag. props. 4.2-295K, mictomagnetism *(French)* 80−39782
Fe_2O_3-PbO-B_2O_3 glass, X-ray and electron microscope studies, mag. and Mossbauer effect meas. 80−28919
FeOOH gels, Mossbauer spectra, mag. props. 80−11303
$xFe_2O_3(1-x)[PbO.3B_2O_3]$ glasses, mag. props. 77−73012

magnetic properties of amorphous substances continued
$Fe_{100-x}P_x$, structural analysis of models for amorphous metallic alloys 80−103249
$Fe_{80}P_{20}$, binary amorphous ferromagnet, Mossbauer study 80−34829
$Fe_{80}P_{20}$ glass, saturation moments, magnetisation and T_c 77−63125
$Fe_{82}P_{18}$, amorphous, uniaxial mag. anisotropy 78−19246
$Fe_{79}P_{13}B_8$ amorphous alloys, splat cooled, Mn, Cr and V substituted, mag. and transport props. 80−84593
$Fe_{80}P_{14}B_6$ glass, ferromag., low temp. heat capacity meas., electronic, phonon contributions exam. 78−10689
$Fe_{80}P_{16}B_1C_3$, ferromag. metallic glass, Mossbauer spectra, crystn. 77−12276
$Fe_{0.75}P_{0.15}C_{0.10}$, mag. excitations and static struct., neutron scatt. obs. 78−68204
$Fe_{75}P_{15}C_{10}$ amorphous foil, ferromag. domain orientation, Mossbauer exam. 78−52402
$Fe_{75}P_{15}C_{10}$ foils, amorphous, ferromag. domain orientation, Mossbauer study 78−15000
$Fe_{75}P_{15}C_{10}$, glassy ferromag., crit. sp. ht. meas. 78−10716
$Fe_{75}P_{15}C_{10}$, magnetoelastic props. 77−16136
$Fe_{75}P_{15}C_{10}$, spin echo NMR of ^{31}P 78−2770
$Fe_{75}P_{15}C_{10}$, temp. depend. of the ΔE-effect 78−80188
$Fe_{80}P_{13}C_7$, amorphous, mag. domain struct. obs. 77−36091
$Fe_{80}P_{13}C_7$, amorphous, rapidly quenched, magnetic props., effect of annealing 77−16701
$Fe_{80}P_{13}C_7$, amorphous ferromag. ribbons, US rel. meas. 77−80582
$Fe_{80}P_{13}C_7$ amorphous ferromag. ribbons, change of permeability by heat treatment 77−85493
$Fe_{80}P_{13}C_7$, amorphous ferromagnetic alloy, isothermal annealing effect on static magnetic props. *(Japanese)* 79−52398
$Fe_{80}P_{13}C_7$, amorphous ribbon, giant ΔE effect, magnetomech. coupling factor 77−8379
$Fe_{80}P_{13}C_7$, mag. anisotropy 79−65670
$Fe_{80}P_{20-x}C_x(Si_x)(Ge_x)$, amorphous, size effect of metalloids on mag. props. 80−84594
$Fe_{75}P_{15}O_{10}$, amorphous, ferromag. domain-wall width, anisotropy depend. 78−19269
$Fe_{34}Pd_{46}P_{20}$, amorphous, sp. ht. and resist. near ferromag. phase transition 78−56333
$Fe_xPd_{80-x}Si_{20}$, low field susceptibility near transition temp. 77−66359
$Fe_xPd_{80-x}Si_{20}$, structural and mag. heterogeneities 80−80484
$Fe_xPd_{82-x}Si_{18}$, amorphous, magnetisation, magnetoresist., spin glass and ferromag. phases 80−34697
$Fe_xPd_{82-x}Si_{18}$ metallic glass, mag. phase diagram, weak ferromagnet-spin glass transition 80−54893
$Fe_xPd_{82-x}Si_{18}$ metallic glass, long range interaction and spin wave interactions 80−65949
Fe_xSi_{1-x} alloys, magnetisation meas. showing crit. conc. at x=0.4 77−59429
Fe_xSi_{1-x}, amorphous, high field magnetisation meas. 78−39367
Fe_xSi_{1-x}, amorphous, struct. and mag. props., giant moment form. at mag. ordering 78−68192
Fe_xSi_{1-x}, amorphous film, magneto-optic Kerr effect 80−66158
$Fe_{75}(Si_{0.5}B_{0.5})_{25}$ film, amorphous, sputtered, ferromag., thermal stability 78−76280
$Fe_{75}Si_{15}B_{10}$, amorphous ferromag. ribbons, US rel. meas. 77−80582
$Fe_{75}Si_{15}B_{10}$, amorphous ferromagnetic alloy, isothermal annealing effect on static magnetic props. *(Japanese)* 79−52398
$Fe_{78}Si_{10}B_{12}$ amorphous ferromag. ribbons, change of permeability by heat treatment 77−85493
$Fe_{78}Si_{10}B_{12}$ amorphous ribbons, magnetomechanical coupling constant and Young's modulus, mag. annealing 79−15333
$Fe_{80}Si_5B_{15}$, amorphous, soft mag. props. and potential uses 80−88807
$(Fe_{1-x}Si_x)_{1-y}By$, metallic glass, mag. props., crystallisation 80−65885
Fe_xSn_{1-x} amorphous alloy films, magnetisation meas. and Mossbauer spectra 78−95489
Fe_xSn_{1-x}, amorphous alloy, Mossbauer spectra, charge transfer and atomic vol. effects 80−39959
Fe_xSn_{1-x}, amorphous film, struct. and mag. props. 80−65972
FeTiB, corrosion-resistant amorphous mag. thin films 80−54923
$Fe_{80}b_{20-x}C_x(Si_x)(Ge_x)$, amorphous, size effect of metalloids on mag. props. 80−84594
Gd alloys, mag. props. and ferromag. reson. 80−54952
Gd-Ag, vap. quenched alloys, struct. and mag. props. 78−84461
Gd-Ag (0-16 at.%), vapour-quenched, struct. and mag. props. 78−38980
Gd-Ag(Cu) alloy film, amorphous, struct. and mag. props. 78−52318
Gd-Al sputtered amorphous films, spin glass state 77−66393
Gd-Al(C)(Cu)(Ga)(Ni)(Pd)(Rh) alloys, mag. and elec. props. 80−80499
Gd-Al(Cu), amorphous alloy films, mag. phase diagram, spin glass and ferromag. regions 78−68234
Gd-Al(Cu)(Ga)(Rh)(Pd), amorphous alloys, mag. coupling of rare earth moments 78−88108
Gd-Co, amorphous film, anisotropy due to resputtering effect 77−89989
Gd-Co, amorphous film, RF sputtering, DC bias role 77−16494
Gd-Co, amorphous film, with cylindrical mag. domains, sputtering prep. *(Russian)* 77−12176
Gd-Co, amorphous films, mag. props. ferromag. reson. meas., 20-520°C *(Russian)* 80−97144
Gd-Co, and Gd-Co-Mo films, mag. props., annealing effects 78−64235
Gd-Co, and Gd-Co-X (X=Mo, Cu, Au), sputter deposited amorphous alloy, substrate bias, magnetic anisotropy, annealing 78−48006
Gd-Co, disordered, saturation mag. moment calc., CPA 77−20515
Gd-Co, evap. amorphous film, mag. props. 77−24720
Gd-Co, evap. amorphous films, anisotropy, magnetisation and FMR meas. 77−66392
Gd-Co, evaporated amorphous film, perpendicular anisotropy by controlled O_2 contamination 77−89990
Gd-Co, film, evaporated and sputtered, struct. and mag. anistoropy, electron microscopy 79−56578
Gd-Co, LV multitarget sputtered film, substrate bias effect on anisotropy 77−16125
Gd-Co, sputtered film, growth induced anisotropy 77−16123
Gd-Co, sputtered very thin film struct. 77−15707
Gd-Co, thermally evap. amorphous film, mag. anisotropy 77−16122
Gd-Co alloy, sputtered film, mag. props. determ. *(Chinese)* 78−2714
Gd-Co amorphous film, DC or RF sputtered, mag. props., He^+-backscatt. investig. 77−20650
Gd-Co amorphous film, mag. anisotropy 77−20649
Gd-Co amorphous film, magnetisation processes near compensation point 77−69644

magnetic properties of amorphous substances continued
Gd-Co amorphous film, sputtered perpendicular mag. anisotropy 79−56576
Gd-Co amorphous film, sputtered, perpendicular anisotropy exam. 79−73707
Gd-Co amorphous film, sputtered, FMR spectra 79−73822
Gd-Co amorphous films, correlation between struct. and mag. props. *(Chinese)* 80−54532
Gd-Co amorphous films, mag. anisotropy, static and ferromag. reson. expts. 79−33477
Gd-Co amorphous films, mag. struct., mag. bubbles, electron diffr. study *(Chinese)* 80−71126
Gd-Co amorphous films, RF sputtered, magnetisation ripple effects 80−11232
Gd-Co amorphous films, struct. and mag. anisotropy 80−20438
Gd-Co amorphous ribbons, mag. props. and Invar effects 80−2574
Gd-Co amorphous sputtered films, magnetoelastic contrib. to perpendicular anisotropy, internal stress meas. 78−95490
Gd-Co amorphous sputtered film, magnetostriction and anisotropy 80−39821
Gd-Co amorphous thin film, mag. and optical props., conc. depend 79−19748
Gd-Co based amorphous sputtered films, microstruct. variability and mag. anisotropy, implanted ion effects 80−88459
Gd-Co film, amorphous, magnetisation processes near compensation point 77−40101
Gd-Co film, amorphous, perpendicular uniaxial anisotropy, dominant contrib. of preferential resputtering effect 77−36103
Gd-Co film, Ar sputtered, struct. 78−63946
Gd-Co film, bias-sputtered, dipolar mechanisms for mag. anisotropy 78−64233
Gd-Co film, ferrimagnet, anisotropic short range order effects on mag. props. 79−1691
Gd-Co film, ferrimagnet, mag. anisotropy, effect of ion bombard. during prep. 79−1692
Gd-Co film, for bubble device appl., prep. and perpendicular anisotropy 77−69641
Gd-Co film, inverted and biased loops 77−89996
Gd-Co film, phase separation as source of perpendicular anisotropy 78−64244
Gd-Co film, RF sputtered, prep. and props. 79−1693
Gd-Co film, selective resputtering-induced anisotropy 78−72376
Gd-Co film, sputtered, inert gas incorporation effect on uniaxial anisotropy 78−64232
Gd-Co film, stability of small bits to temp. and mag. field changes 78−68314
Gd-Co films, amorphous, mag. anisotropy from torque meas. 77−47987
Gd-Co films, annealed, short-range order and perpendicular mag. anisotropy 80−15765
Gd-Co sputtered amorphous films, resistivity anomalies, 42 to 300K *(Chinese)* 80−7001
Gd-Co-Au amorphous magnetic films, domain wall obs. by Lorentz electron microscopy 77−80979
Gd-Co-Cu film, amorphous, influence of biased magnetron deposition parameters on props. 77−43856
Gd-Co-Fe film, bias-sputtered, uniaxial perpendicular anisotropy 78−64234
Gd-Co-Mo, sputtered very thin film struct. 77−15707
Gd-Co-Mo alloy film, ion implantation damage effects 77−89991
Gd-Co-Mo amorphous film, MCD, oxide surface layer effect 77−90132
Gd-Co-Mo film, amorphous, bubble and stripe domain wall vel. meas. 77−40094
Gd-Co-Mo film, Ar sputtered, struct. 78−63946
Gd-Co-Mo film, bubble dynamics 77−89997
Gd-Co-Mo film, in-plane susceptibility near compensation point 78−64238
Gd-Co(-Au) amorphous film, domain wall dynamics near compensation point 79−1696
Gd-Co(-Au) film, ferrimag. amorphous, coated with Permalloy films, mag. props. 79−1695
Gd-Co(-Mo) films, inhomogeneities of mangetization and anisotropy 79−65698
Gd-Co(Fe) amorphous films, microstruct. and mag. anisotropy 79−82838
Gd-Co(Ni)(Cu)(Rh)(Ru)(Pd)(Ga), mag. props. and ferromag. reson. 80−75862
Gd-Cu sputtered amorphous films, ferromag. props. 77−66393
Gd-Fe, amorphous film, Kerr readout charcts. 79−15439
Gd-Fe, amorphous film, stress induced anisotropy 77−89989
Gd-Fe, amorphous film, thermomagnetic writing 78−84428
Gd-Fe, co-evap. amorphous film, anomalous hysteresis loop, domains obs. 77−89995
Gd-Fe, DC bias RF sputtered film, mag. props. 77−16124
Gd-Fe, disordered, saturation mag. moment calc., CPA 77−20515
Gd-Fe, LV multitarget sputtered film, substrate bias effect on anisotropy 77−16125
Gd-Fe, sputter deposited amorphous alloy, substrate bias, magnetic anisotropy, annealing 78−48006
Gd-Fe, sputtered film, magnetostriction 79−47320
Gd-Fe alloy film, contact printing 77−73061
Gd-Fe amorphous alloys, mag. props. and crystn. 79−90557
Gd-Fe amorphous film, atomic diffusion of deposited Co 79−73346
Gd-Fe amorphous film, prep. by dual-source evaporation, mag. props. 77−89988
Gd-Fe amorphous films, anisotropy dispersion, FMR meas. 79−73824
Gd-Fe amorphous films, stress contrib. to perpendicular anisotropy 80−75819
Gd-Fe amorphous films with CeO_2 coatings, Kerr magneto-optical effect enhancement 79−19866
Gd-Fe amorphous sputtered films, magnetoelastic contrib. to perpendicular anisotropy, internal stress meas. 78−95490
Gd-Fe film, in-situ ion beam sputtered, microstruct. and Lorentz mag. struct. 78−63947
Gd-Fe film, mag. props., annealing effects 78−64235
Gd-Fe-Y, amorphous film, thermomagnetic writing 78−84428
Gd-Fe(Co) amorphous films, O_2 adsorption, effect on perpendicular anisotropy 80−34713
Gd-Fe(Co) film, amorphous, preferential resputtering effect induced anisotropic distrib. of atomic pairs 78−63950
Gd-Mn(-Co) alloys, ferrimag. props. and Hall effect 79−73692
Gd-Mo-Mo amorphous film, domain drag effect obs. 78−91911

magnetic properties of amorphous substances continued
Gd-Ni, amorphous, Mossbauer spectra 80−25262
Gd-Ti(V)(Cr)(Mg)(Nb)(Ge)(Si)(Au) amorphous films, spontaneous Hall effect and elec. resist. 80−80251
Gd-transition metal, amorphous film, galvanomag. effects, Hall detector 77−89882
$Gd_{54}Ag_{46}$, susceptibility and magnetisation, 6-300K *(French)* 77−36060
$GdAl_2$, mag. heat capacity 77−89969
$Gd_{0.37}Al_{0.63}$, amorphous film, anomalous resonance field shift 79−73821
$Gd_{0.37}Al_{0.63}$ sputtered film, amorphous, conc. spin glass, microwave reson. spectrum obs. 78−15018
$Gd_{37}Al_{63}$ amorphous film, spin glass, microwave mag. resonance, freq. dependence 80−39798
$Gd_{80}Au_{20}$, amorphous ferromag., critical phenomena and mag. props. 77−85469
$Gd_{80}Au_{20}$, amorphous ferromag., mag. and transport meas. 77−89930
GdCo, amorphous film, MCD *(Japanese)* 78−39530
GdCo amorphous film, O_2 contaminated, TEM obs. of source of perpendicular anisotropy 78−14993
GdCo amorphous sputtered film mag. props. from Mossbauer effect obs. *(Japanese)* 80−15933
GdCo film, sputtered, in-plane anisotropy induced by rare gas annealing 78−84458
GdCo film structure, dependent on substrate type *(Russian)* 80−24747
GdCo sputtered amorphous film, third elements effect on mag. anisotropy 79−91260
GdCo, thin film, for thermomagnetic recording *(Japanese)* 80−11562
$Gd_{1-x}Co_x$ amorphous thin film, magnetostriction 79−91281
$Gd_{1-x}Co_x$ film, Curie and compensation temps., effect of O or Ar impurity 77−40093
$Gd_{1-x}Co_x$, film, resistivity, Hall effect, domain wall density 78−76169
Gd_2Co, amorphous ferromag. obtained by splat cooling, local and bulk mag. props. 79−1685
$Gd_{65}Co_{35}$, amorphous, amg. ordering, susceptibility, magnetisation and hysteresis meas. 78−68190
$Gd_{67}Co_{33}$, amorphous ferromag., mag. and transport meas. 77−89930
Gd_xCo_{1-x} annealing amorphous film, ferromag. reson. 77−85580
$(Gd_xCo_{1-x})_{1-y}Ar_y$ amorphous films, effective anisotropy field, ferromag. reson. obs. 80−71123
GdCoAu amorphous film, bias field depend. of domain drag propagated bubble domains 79−78471
GdCoAu(Mo), film, perpendicular anisotropy temp. depend., Lorentz microscopy 77−28419
$GdCo_2(Fe_2)$, amorphous alloys, atomic order, mag. behaviour 78−19221
GdCoMo amorphous alloy films, mag. cobalt alloys susceptibility, uniaxial anisotropy field 80−54930
GdCoMo film, amorphous, sputtered, ferrimag., in-plane susceptibility near compensation point 78−64240
$Gd_{6.9}Co_{74.0}Mo_{12.8}Ar_{6.3}$, amorphous film, spin wave reson. 79−73823
Gd_xCu_{1-x}, amorphous film, magnetisation meas., fully aligned moment 78−68309
GdFe amorphous film, Mossbauer and mag. meas. 80−15844
GdFe, amorphous films, thermal stability of mag. props. *(Japanese)* 79−47307
GdFe film structure, dependent on substrate type *(Russian)* 80−24747
GdFe homogeneous amorphous films, compensation point switching, magneto-optical Kerr signal anal. 80−15726
$GdFe_2$ films, electron beam deposited, amorphous and cryst., mag. and struct. props. 79−4710
$(Gd_{65}Fe_{35})_{100-x}B_x$ glasses, mag. props. 79−73693
$(Gd_{65}Fe_{35})_{90}B_{10}$, amorphous, mag. props., Mossbauer study 80−93093
GdFeBi, amorphous ferrimag. films, magneto-optical props., optical spectra 80−76008
$(Gd_{1-x}Fe_x)_{1-y}Bi_y$ amorphous films, saturation magnetisation, Kerr and Faraday rotation 80−40093
GdFe(Co), amorphous film, XPS meas. 79−87295
$Gd_x(Fe_{1-y}Co_y)_{1-x}$, evap. amorphous film, mag. anisotropy due to pair ordering 77−32219
$Gd_{18}Fe_{82-x}Ni_x$, amorphous film, mag. and galvanomag. props. 77−24715
GdIG, amorphous, Mossbauer specfra, mag. props. 80−15849
$(Gd_{1-y}Nd_y)_{1-x}Fe_x$ amorphous bubble films with good temp. characts. 79−95616
$Gd_{68}Ni_{32}$, amorphous ferromag., mag. and transport meas. 77−89930
Gd_xNi_{1-x} sputtered amorphous films, mag. props. and Hall meas. 78−95488
$GdNi_2H_4$, effect of absorbed H_2 on struct. and mag. behaviour 78−2682
$Gd_xPd_{82-x}Si_{18}$, mag. susceptibility, 4.2-300K 77−66248
Ge powder, diamag., strong mag. particle form., mag. props., EPR *(Russian)* 80−54863
Ge-Fe amorphous film, sputtered, stress induced anisotropy 79−73706
Ge-Se-Fe films, metallic and semicond., amorphous, mag. and elec. props. 78−52319
Ge-Si amorphous film, ferromagnetic interaction between spins 78−2710
Go-P film, spin wave dispersion law, spin wave reson. obs. *(Russian)* 78−88196
Ho-Co amorphous film, prep. by dual-source evaporation, mag. props. 77−89988
Ho-Co film, anomalous Hall hysteresis loops near compensation point 78−19286
Ho-Co film, evaporated, struct. and mag. anistoropy, electron microscopy 79−56578
HoCo film, sputtered, in-plane anisotropy induced by rare gas annealing 78−84458
Ho_xCo_{1-x} amorphous films, microstruct. and mag. anisotropy 79−82838
Ho_xCu_{1-x}, amorphous film, magnetisation meas., local anisotropy effects 78−68309
$HoFe_2$, amorphous, struct. determ., EXAFS exam. 78−51421
$HoFe_2$, amorphous, ultrasonic exam. below T_c 79−73793
$(Ho_2O_3)_{0.194}(Al_2O_3)_{0.227}(SiO_2)_{0.579}$, amorphous, low temp. spin glass behaviour 80−60297
$KFeF_4$, amorphous, mag. props. and Mossbauer spectra, speromagnetism and mictomagnetism 80−75778
K_2O-Al_2O_3-B_2O_3:Fe_2O_3, glasses, liq.-liq. phase separation, Fe^{3+} ions rel. to mag., optical props. 77−15322
La-Fe, amorphous alloy film, spin reson. meas. 78−68389
La-Fe alloy, amorphous, sputtered at high rate, mag. props. 80−75753
La-Fe bulk amorphous alloys, mag. props. *(Japanese)* 79−95588
La-Gd-Au, amorphous spin glasses, mag.-cluster description 79−42776
La-Gd-Au alloys, amorphous, high Gd content, bulk mag. props. 77−59426
$La_{1-x}Co_x$, amorphous, conc. depend. of Co moment 78−56300

magnetic properties of amorphous substances continued
$La_{80-x}Gd_xAu_{20}$, amorphous dil. alloy, RKKY interaction, magnetisation meas. 77−32207
$La_{80-x}Gd_xAu_{20}$, amorphous, supercond. and spin-glass regime, magnetisation and resist. meas. 77−36011
$La_{80-x}Pr_xAu_{20}$, mag. and supercond. props. 80−75713
$Li_2B_2O_4$-$LiFe_5O_8$, borate glass, mag. props. of Fe^{3+} cations 80−100599
$Li_2B_2O_4$-$LiFe_5O_8$ glass, rapidly quenched, mag. and ferrimag. props. 80−75744
$(Li_2O$-Al_2O_3-$SiO_2)$:Fe_2O_3, glass, pyroceramic form., colour centres, magnetochem. investig. 77−16537
Lu-Fe, amorphous alloy film, spin reson. meas. 78−68389
Mn-Bi film, amorphous, form. and crystn. 79−28923
Mn-Nd, mag. props. for bulk amorphous deposits *(Japanese)* 79−95971
MnAlGe film, mag. domains and amorphous to cryst. phase transition, electron microscopy obs. 80−71129
MnGaGe film, mag. domains and amorphous to cryst. phase transition, electron microscopy obs. 80−71129
MnO-Al_2O_3-SiO_2, amorphous, spin glass like behaviour at low temp. 79−61177
MnO-Al_2O_3-SiO_2, amorphous spin glass, AC susceptibility 80−80520
MnO-Al_2O_3-SiO_2, spin glasses, low-field susceptibility, freq. depend. 78−47981
MnO-Al_2O_3-SiO_2 glass, spin freezing, muon spin depolarisation, superparamag. domain model 78−68272
MnO-Al_2O_3-SiO_2 glass, optical spectra 78−68528
$x.MnO.(1-x)[19TeO_2.PbO]$, glass, antiferromag. behaviour, mag. props. 80−50072
$Mn_xPd_{82-x}Ge_{18}$, amorphous alloys, mag. props. 78−91906
MnPt, disordered film produced by RF sputtering, ferromag. behaviour 78−68310
MnSi amorphous, conc. spin glass system, temp. effect on susceptibility 79−61142
MnSi, amorphous magnetisation meas. 80−34599
MnSi, sputtered, mag., elec., struct. and thermal props., spin glass behaviour 80−50124
MnSi(Ge), spin glass transition, AC susceptibility meas. 80−75779
$NaFeF_4$, amorphous, mag. props. and Mossbauer spectra, speromagnetism and mictomagnetism 80−75778
α-$Na_3Fe_2(PO_4)_3$ orthophosphate, cryst. and vitreous, Mossbauer spectroscopy and mag. susceptibility *(French)* 80−80657
$Nb_{50}Ni_{50-x}Fe_x$, amorphous, mag. ordering and local random anisotropy 78−68273
$Nb_{50}Ni_{50-x}Fe_x$, mag. interactions 78−95432
$Nb_{50}Ni_{50-x}Fe_x$, magnetically dil. glass, 3d moments, mag. susceptibility and magnetisation meas. 79−95574
Nd-Co film, amorphous, exam. of domain struct. 78−68336
$Nd_{21}Ag_{79}$, and $Nd_{50}Ag_{50}$, susceptibility and magnetisation 80−60182
$Nd_{64}Co_{36}$, amorphous, amg. ordering, susceptibility, magnetisation and hysteresis meas. 78−68190
Nd_xCo_{1-x} film, amorphous, mag. props. meas. 78−68312
$NdFe_2$, magnetization and neutron scatt. meas. 79−78314
Nd_xFe_{1-x} film, amorphous, mag. props. meas. 78−68312
Ni, amorphous film, getter sputtered at 25K, resistivity, Curie temp. 78−52673
Ni dispersions, semi-amorphous, on Al_2O_3-graphite, mag. characterisation 80−44876
Ni, electrodeposited film, thermal anal., occlusion of gases rel. to mag. props. 80−59823
Ni-Au film, magnetoresist. in fields up to 80 kG 77−39823
Ni-B alloy film, magnetisation-temp. characts., order-disorder transform. *(Japanese)* 78−76279
Ni-B thin film glasses, mag. props. and corrosion resist. 80−80576
Ni-Co amorphous alloys, magnetostriction 80−34738
Ni-Co-P, amorphous alloy, electrical and mag. props. 78−95281
Ni-Co-P, amorphous electrodeposited films, domain wall motion, Kerr effect 78−60322
Ni-Co-P, ferromag. film, amorphous to cryst. transition, diffr. and resistivity meas. 78−60587
Ni-Fe based metallic glasses, Curie pt. anomalies 80−60256
Ni-Mn disordered alloys, mag. moment and Curie point 78−76243
Ni-P, amorphous electrodeposited alloys, phase-separation *(Japanese)* 80−54140
Ni-P, amorphous magnetisation, NMR and coercive force meas. 77−32187
Ni-P, electrodeposited film, thermal anal., occlusion of gases rel. to mag. props. 80−59823
Ni-P, NMR expts. and interpretation 79−8060
Ni-P film, amorphous, ion implanted, struct. and domain struct. obs. 79−91272
Ni-P-B, giant moments and SRO 77−4499
Ni-Pd-P, Ni-Pt-P, amorphous and electronic structs., NMR Knight shifts and linewidths meas. 78−68400
Ni-Pd-Si, amorphous, low-field mag. susceptibility meas., 4.2-580K 79−61057
Ni-S, electrodeposited film, thermal anal., occlusion of gases rel. to mag. props. 80−59823
Ni-Y, amorphous, resist. and magnetoresist. meas., weak itinerant ferromagnet 78−68018
$Ni_{1-x}Au_x$, elec. resist., temp. depend., spin wave contrib. and resist. minimum 78−51961
$Ni_{100-x}B_x$, amorphous, mag. struct., mag. susceptibility meas. 80−80485
$Ni_{100-x}B_x$, rapidly quenched, mag. moment, temp. and comp. depend. 78−47957
$(Ni_{1-c}Co_c)_{0.78}P_{0.14}B_{0.08}$, mag. props., local environment model 77−12119
$Ni_{36}Fe_{32}Cr_{14}P_{12}B_6$ metallic glass, mech. props. and thermal stability 80−76362
$(Ni_{100-x}Fe_x)_{79}P_{13}B_8$, amorphous dil. alloys, spin glasses, magnetisation meas. 79−61178
$Ni_{80-x}Fe_xP_{14}B_6$, amorphous alloy, resistivity variations near critical temp. 79−73488
$(Ni_{99}Fe_1)_{79}P_{13}B_8$, amorphous, low temp. sp. ht., mag. contribs. 80−80552
$(Ni_xFe_{1-x})_{80}P_{10}B_{10}$, Curie temp., press. effect 80−75833
$(Ni_{0.75}Mn_{0.25})_{82}Si_{10}B_8$, exchange anisotropy, mag. susceptibility meas., 4.2K to room temp. 80−11186
$Ni_{1-x}P_x$, electrodeposited, amorphous, mag. and transport props. 78−52106
$Ni_{80}P_{20}$ glass, saturation moments, magnetisation and T_c 77−63125
$Ni_{78}P_{14}B_8$, $Ni_{80}P_{12}B_8$, amorphous mag. clusters, sp. ht. meas. 78−68274

magnetic properties of amorphous substances continued
$Ni_{80}P_{14}B_6$ glass, ferromag., low temp. heat capacity meas., electronic, phonon contributions exam. 78−10689
Ni_xZr_{1-x} metallic glass, crystallisation kinetics, elec. resist. and mag. susceptibility meas. 80−103659
O_2 adsorbed layer porous Vycor glass, props. characteristic of amorphous antiferromag. obs. 78−10665
$PbFe_{12}O_{19}$ hexagonal ferrite amorphous films for mag. bubble memories, materials review *(Polish)* 80−34715
$PbMnFeF_7$ and Pb_2MnFeF_9, vitreous, insulating, evidence of spin-glass transition 80−97112
Pd-Co-P amorphous alloy, mag. an elec. props. 77−40043
Pd-Si(−Cu), glassy, liq. and cryst., mag. and elec. props. 77−66249
$Pd_{80-x}Si_{20}Fe_x$, amorphous, low x, hyperfine interactions and mag. ordering temp. 79−15303
$Pd_{35}Zr_{65}$, mag. susceptibility meas. 80−75740
$Pr_{21}Ag_{79}$, amorphous, sp. ht. at low temp. 80−75780
$Pr_{21}Ag_{79}$, $Pr_{50}Ag_{50}$, $Pr_{10}Lu_{40}Ag_{50}$, susceptibility and magnetisation 80−60182
RuS_2 amorphous, preparation at ambient temp., magnetic susceptibility meas. 80−35119
Si, amorphised by ion implantation, EPR obs. of mag. ordering 79−24186
$((SiO_2)_{45}(CaO)_{55})_{65}$ $(Fe_2O_3)_{35}$ glass, effect of melt atmosphere on mag. props. 78−68299
Sm-Co, plasma-sprayed, role of Ar or H_2 atm. in mag. props. and crystn., rel. to H_2 storage 80−64898
$Sm_{21}Ag_{79}$, amorphous, sp. ht. at low temp. 80−75780
$SmCo_5$, amorphous, supermag.-ferromag. transition and directional crystallisation 80−65891
$SrO\text{-}Fe_2O_3$, splat quenching struct. and crystn. mechanism *(French)* 78−51426
Tb-Fe, amorphous ferrimag. film, thermomag. writing using He-Ne laser 77−12163
Tb-Fe, amorphous ferrimag. film, mag. props. and Curie point writing 77−12164
Tb-Fe, amorphous film, Kerr readout characts. 79−15439
Tb-Fe, bulk samples, magnetistion meas. 77−66278
Tb-Fe, random anisotropy effects 78−68223
Tb-Fe, sputtered film, magnetostriction 79−47320
Tb-Fe alloy film, contact printing 77−73061
Tb-Fe amorphous film, sputtered, stress induced anisotropy 79−73706
Tb-Fe amorphous magnetic films, domain wall obs. by Lorentz electron microscopy 77−80979
Tb-Fe amorphous thin films, magnetic after-effect, Kerr magneto-optic effect obs. 80−97123
Tb-Fe film, thermomag. contact printing 77−89986
Tb-Fe film, undoped and O-doped, amorphous, microstruct. and mag. props. 79−91273
Tb-Fe sputtered films, mag. aftereffect due to domain well motion 79−73780
$Tb_{52}Ag_{48}$, amorphous, mag. after-effect meas. 79−24200
$Tb_{52}Ag_{48}$, amorphous, mag. aftereffect 80−20435
$Tb_{52}Ag_{48}$, bulk magnetic props., evidence of strong local anisotropy 77−43830
TbAu, magnetisation characts., 5 to 300K, hysteresis cycle *(French)* 77−80965
Tb_xCu_{1-x}, amorphous film, magnetisation meas., local anisotropy effects 78−68309
$TbFe_2$, amorphous, mag. struct., US meas. 79−99683
$TbFe_2$, amorphous, Mossbauer spectra *(French)* 80−25261
$TbFe_2$, amorphous, struct. determ., EXAFS exam. 78−51421
$TbFe_2$, temp. depend. of mag. hystersis props. 79−61186
Tb_xFe_{1-x} film, magnetostriction and magnetisation 78−68305
$Th_{1-x}Fe_x$ amorphous alloys, mag. props. and Mossbauer spectra 79−91326
$TiO_2\text{-}P_2O_5$ glasses, reduced, mag. susceptibility, 1 to 400K, mag. exchange between Ti^{3+} ions 79−73691
$TmFe_2$, amorphous, neutron scatt. at transition, spin diffusion, magnetisation meas. 78−68174
Y-Co, amorphous alloy film, spin reson. meas., exchange stiffness 78−68389
Y-Fe, evap. amorphous alloys, thermomag. history effects 77−66389
Y-Mn(-Co) alloys, paramag. props. and Hall effect 79−73692
Y-Ni amorphous alloy, spontaneous magnetisation, Curie temp. and paramag. susceptibility 78−68189
YCo_3, amorphous ferromagnet, exchange dominated surface modes 78−52359
YCo_3 amorphous film, domain struct., influence of planar anisotropy 79−78472
YCo_3 amorphous films, ^{59}Co spin echo study 80−80636
YCo_3 film, amorphous, induced and surface anisotropies, ferromag. reson. and static meas. 77−85507
YCo_3 film, amorphous, impurity like relaxation mechanism 79−73820
YCo_3 film, DC sputtered, easy axis and easy plane magnetisation 78−64237
YCo_3 film, sputtered, in-plane anisotropy induced by rare gas annealing 78−84458
$Y_{1-x}Co_x$, amorphous, conc. depend. of Co moment 78−56300
$Y_{1-x}Co_x$, amorphous, mag. props. 80−84590
$Y_3Fe_5O_{12}$, types of magnetism and methods of study *(French)* 80−80490
YFe_2, amorphous, mag. order, cluster phenomena, hyperfine struct. 77−16079
YFe_2 amorphous, spin-glass and mag. blocking transitions, low field DC susceptibility meas. 79−61141
YFe_2, amorphous concentrated spin glass, susceptibility, Mossbauer and neutron scatt. meas. 80−39783
YFe_2, surface ferromag. layer, spin wave reson. Rutherford backscatt., and magnetisation meas. 79−73819
$Y_{1-x}Fe_x$, amorphous, Mossbauer spectra, appearance of magnetism 78−52401
$Y_{1-x}Fe_x$, amorphous, spin resonance exam. 79−51860
Y_xFe_{1-x} amorphous films, microstruct. and mag. anisotropy 79−82838
$(Y_{65}Fe_{35})_{100-x}B_x$ glasses, mag. props. 79−73693
$Y_3Fe_5O_{12}$, mag. moments, susceptibility, Mossbauer studies 79−78345
Y_2GdIG film, amorphous, mag. bubbles obs. and structural transformation 80−75824
YIG, amorphous, ionic glass, hard-sphere random-packing model 80−24369
$Y_{0.22}Ni_{0.78}$ amorphous alloy, low temp. sp. ht. 79−65680

magnetic properties of amorphous substances continued
Y_xNi_{1-x}, amorphous, high press. magnetisation and Curie temp. 80−20442
Zr-Co(Fe), amorphous alloy film, spin reson. meas. 78−68389
Zr-Pd, metallic glasses, electronic props. and supercond. 79−73486
$Zr_{1-x}Co_x$, amorphous, conc. depend. of Co moment 78−56300
$Zr_{40}Cu_{50}Fe_{10}$, magnetically dil. glass, 3d moments, mag. susceptibility and magnetisation meas. 79−95574
$Zr_{40}Cu_{60-x}Gd_x$, magnetically dil. glass, 4f moments, mag. susceptibility and magnetisation meas. 79−95575
$Zr_{40}Cu_{60-x}M_x$ (M=Fe,Mn,Gd,Tb), amorphous, mag. ordering and local random anisotropy 78−68273
$Zr_{40}Cu_{60-x}M_x$, (M=Gd, Tb, Fe or Mn), mag. interactions 78−95432
$Zr_{40}Cu_{50}Mn_{10}$, magnetically dil. glass, 3d moments, mag. susceptibility and magnetisation meas. 79−95574
$Zr_{40}Cu_{60-x}Tb_x$, magnetically dil. glass, 4f moments, mag. susceptibility and magnetisation meas. 79−95575
$(Zr_{1-x}Er_x)_3Rh$, amorphous, influence of mag. ordering on supercond. props. 80−29511

magnetic properties of dilute alloys *see magnetic properties of dilute systems*

magnetic properties of dilute systems
see also local moments in dilute systems; magnetic impurity interactions
alloy, density of energy states from sp. ht. as function of temp. 79−19741
alloy, electrical resistivity, Kondo effect vs. spin glass behaviour 78−68269
alloy, Freidel, Anderson and Wolff alloys *(Rumanian)* 78−91843
alloy systems, conc., Kondo type effects, phenomenological dilution model 77−72858
alloy with mixed types of order, uniform mag. phase diagram 79−78368
alloys, dil., long-range interaction of mag. impurities 78−19216
alloys, dilute, mag., press. effects 79−99676
alloys, mag. impurity ordering 77−28370
Anderson model, spin polarisation and spin correl. densities, local singlet. state 77−63068
Anderson model coupled to boson field, HF approx. and RPA 77−40033
anisotropic magnet, dil., crit. behaviour near percolation threshold 80−88767
anisotropic magnets, dil., scaling representation meas. percolation threshold 80−88766
antiferromagnet, itinerant, paramag. impurity effects on Neel temp., calc. 80−60257
antiferromagnetic metal, with paramag. impurities, Neel temp., impurity conc. depend calc. 78−68232
classical Heisenberg ferromagnet, position space treatment 79−87268
coupled fields in one dimension: cross-over from a continuous symmetry to a discrete one 78−87758
Cu-Co, dil., rotational hysteresis of Co fine particles 78−23301
CuCr, dil., specific heat, impurity contrib. Kondo temp. 80−65903
diamagnetic crystal, with non-Kramers mag. impurity, relax. of lattice nucleus 77−32282
dilute Heisenberg magnet, cluster expansion 80−15734
dilute magnetic alloys, electron sound absorpt., disordered mag. impurities, spin glasses *(Russian)* 80−80503
diluted ferromagnetic systems, cluster theory, second-neighbour interaction 77−89965
disordered binary alloys of ferromag. crystals, mag. dipole fields at interstitial sites 80−97176
disordered substitutional alloy, mag. props., Heisenberg model 79−38342
dynamics of spins interacting with quenched random impurities 77−40065
elastic properties of magnetic materials, review 80−7142
EPR concentration dependence in magnetically diluted crystals with strong spin-spin interaction 79−42826
exchange field, paramag. impurity conc. depend. 77−47970
ferrimagnet, dil., sequence of mag. transforms. *(Russian)* 78−19252
ferromagnet, Curie temp. 79−11312
ferromagnet, diluted, two-dimens., with anisotropic exchange interaction, excitation spectra 77−43826
ferromagnet, slow neutron inelastic scatt. by spin excitations, cluster approx. 80−11168
ferromagnet, spin wave excitations, multicomponent CPA theory 78−68135
ferromagnet two-dimensional, magnetically dilute, concentration expansion, series anal. *(Japanese)* 77−20587
ferromagnet with antiferromag. impurity with arbitrary spin, ground state calc. *(Russian)* 78−43585
ferromagnetic Curie temperature *(Japanese)* 79−33484
ferromagnetism of disordered systems, review 80−29513
ferromagnets, dilute, spin waves at surface 79−61089
frustrated lattice, spin-glass ordering, triangle and FCC lattices, Monte Carlo simulation 80−15746
Heisenberg, paramagnetic with bond dilution, freq. moments of spin correlation function 79−15272
Heisenberg, spin $^1/_2$ dil. magnet, crit. props. 80−15733
Heisenberg antiferromagnet, mean spin on finite clusters 78−68139
Heisenberg antiferromagnetic alloy, critical behaviour *(Russian)* 78−88128
Heisenberg dilute systems, computer simulation, mag. conc. of clusters, linearised eqns. of motion 79−78409
Heisenberg ferromagnet, dil., CPA theory, spin-wave stiffness and Curie temp. 78−31080
Heisenberg ferromagnet, dil., spin wave localisation near percolation threshold 80−25120
Heisenberg ferromagnet, structurally and chemically disordered, critical behaviour 77−43838
Heisenberg ferromagnetic alloy, critical behaviour *(Russian)* 78−88127
Heisenberg magnet, dil., renormalisation group calcs. 79−56550
Heusler alloy with nonmagnetic impurity, transferred hyperfine field using volume overlap model 79−78054
impurity ion clusters in a two-dimensional lattice 78−23047
Ising, internally dil. film, surface enrichment as possible source of surface magnetism 80−15731
Ising, spin $^1/_2$ dil. magnet, crit. props. 80−15733
Ising and Heisenberg, systems with competing interactions, mag. ordering, appl. to $Eu_xSr_{1-x}S$ 80−65914
Ising and Heisenberg magnets with competing interactions, phase diagrams and mag. props. 80−34672
Ising chain, disordered, linear renormalisation transformations, appl. to dil. soln. model 78−34941

magnetic properties of dilute systems continued
Ising ferromagnet, crit. props. in percolation limit 79−1677
Ising film, diluted, surface and bulk magnetic phases 79−82797
Ising metamagnet, dilute tricritical point calcs. 80−50099
Ising model lattice, impurities and probe independence of hyperfine crit. exponents 79−87267
kinetics, generating functional method appl. *(Russian)* 77−43579
Kondo system, magnetoresist calc. 77−62918
long-range correlation of localised spins in s-d exchange model 77−16043
mag. props. from Mossbauer effect obs. *(Japanese)* 80−15933
magnetic 3d impurity in non-magnetic metal, effective ion Hamiltonian 78−64016
magnetic alloys, dil., transition metal hosts, props. review 78−84417
magnetic ions in metals, Friedel-Anderson VBS and ionic approaches, compatibility 79−61051
magnetic ordering of impurities in dilute alloys, random phase approx. and conc. limits 79−24187
manganese zinc formate dihydrate, two-dimens. antiferromag., anomalous crit. phenomena, neutron scatt. and PMR obs. 80−50104
metals, ferromagnetic, nonmagnetic impurity hyperfine field temp. depend. 80−34402
one-dimensional dilute Heisenberg system, mag. props. 78−64179
one-dimensional dilute random magnet, low temp. behaviour of susceptibility, sp. ht. and correl. length 79−69682
paramagnet, dilute, under bottleneck conditions, kinetics 77−77029
percolation clusters, one dimens., crit. exponents 78−31082
rare earth alloys, magnetic properties, impurity effects, CPA calc. 80−44784
rare earth compounds, mag. susceptibility in intermediate valence state 78−14928
rare earth intermetallics, RAl_2-Gd(Er)(Dy)(Nd), dil., (R=La, Yb, Lu), EPR and mag. susceptibility 80−15797
rare earths in metallic environment, mag. moments 78−6515
reverse Kondo effect, magneto-transport theory 80−15509
specific heat at and above spin glass transition, role of fluctuations 77−69580
spin correlation in dil. mag. alloys 78−84385
spin glasses, mean field theory, replica method 80−34658
transition metal alloy, spin fluctuation contribution to elec. resist., field depend. 77−1413
transition metal alloys, dilute ferromagnetic, itinerant d-electron(hole) degenerate, spin stiffness constant 80−70930
transition metal alloys, spin glasses, mag. ordering, book contrib. 80−75787
transition metal compounds and dil. alloys, mag. ordering phenomena in high mag. fields 80−50075
transition metal magnetic alloys, dilute, props., review of theory 79−15282
transition metals, ferromag., dil. H electronic struct. 80−70638
transport props. from Suhl's dispersion relations in mag. field 77−62891
two-impurity spin correl., self-consistent treatment 77−24672
Ag-Mn, dil., thin-film spin glass, mag. susceptibility and T_G meas., 1.2-60K 79−38346
Ag-Tb(Ho)(Dy)(Er)(Tm) dil., single and polycrystals, low temp. magnetostriction meas. 79−78501
AgCr, dil., specific heat, impurity contrib. Kondo temp. 80−65903
AgNi, dil., mag. susceptibility of isolated Ni atoms 80−65777
Al-Ag alloys, dilute, electrical magnetoresist., temp. depend., mag. breakdown 79−99532
Al-Fe, alloy with mixed types of order, uniform mag. phase diagram 79−78368
Al_2O_3-Fe_2O_3:Cr^{3+}, dil. paramag. system, Cr^{3+} conc., effect on cross relax. 79−15387
Al_2O_3-Fe_2O_3(:Cr^{3+}) paramag. system, cross relax. temp. and mag. field effects on Mossbauer spectra 79−33576
Au-Er, cold-worked, EPR expts. 80−39864
Au-Fe, alloy with mixed types of order, uniform mag. phase diagram 79−78368
Au-Fe, dil., approach to saturation of magnetisation 78−56293
Au-Fe, dil., crit. dynamics 80−60325
Au-Fe, dil. alloys, spin glasses, modified bond model calcs. 79−33489
Au-Fe (1 at.%), spin glass, specific heat 80−60355
Au-Fe (1-7 at.%), extraordinary Hall effect, near ferromag. percolation limit 79−19575
Au-Fe (3.1-10.4 at.%) spin glass alloys, high field magnetisation curves 80−11213
Cd-Cr(Mn)(Ni), dil., mag. and supercond. props. 79−38237
$Cd_{1-x}Ag_xCr_2Se_4$, Ag acceptor states effect on exchange interaction 80−20397
Ce dilute alloys, cryst. field and Kondo effect 77−43809
$Ce_xLa_{1-x}Al_3$, Kondo system, mag. susceptibility, 1.5 to 20K 79−78310
$CePd_3$-Er, dil., low field mag. susceptibility, electro-nuclear effects 80−60189
$CePd_3$-Gd, EPR of Gd^{3+} impurities in host with interconfig. fluctuations 78−56377
$Ce_{0.08}Y_{0.92}Sb$, dilute f-electron system in cluster regime, crystal field and exchange splittings 80−97062
Co-Fe, dil., magnetocrystalline anisotropy anomalous temp. depend. 80−71007
Co-Gd(Nd)(Pr)(Sm), dilute, magnetic annealing effect, induced anisotropy 77−73054
Co-rare earth dilute alloys, mag. annealing, conc. depend. 78−35011
Co-W alloy electrodeposition, influence of $MgSO_4$ and gum arabic additives *(Russian)* 80−80991
CoMn(Cr)(V)(Ti), dil., low temp. specific heat and magnetisation 80−65925
Cr antiferromagnetic with nonmagnetic impurities, mag. susceptibility using two band model 80−2559
Cr-Co, dil., antiferromag., elec. resist. min., press. and impurity effects 80−59970
Cr-Co (4.0 at.%) alloy, antiferromag., disappearance of resist. min. under press., and press. coeff. of T_N 80−10960
Cr-Co-V alloys, dil., elec. resist. min. 80−54680
Cr-Fe, alloy with mixed types of order, uniform mag. phase diagram 79−78368
Cr-Fe, antiferromag., mag. incoherent elastic neutron scatt. 79−73678
Cr-Fe, dil., antiferromag., elec. resist. min., press. and impurity effects 80−59970
Cr-Fe, dil., spin correlations and neutron scatt. near crit. conc., theory 80−60327

magnetic properties of dilute systems continued
Cr-Fe-Co dilute alloys, Neel temp., thermal expansion rel. to Co content 79−47281
Cr-Ga alloys, dil., Neel temp., elec. resist. and thermal expansion meas. 79−51778
Cr-Ni(V), dil., mag. susceptibility, 77 to 400K *(Russian)* 80−50066
Cr-Re (0.18 wt.%), mag. excitations in longitudinal and transverse SDW phases 80−70946
Cr-Sb alloy, dil., mag. phase diagram, elec. resist. and thermal expansion obs. 79−1669
Cr-Si-V, (2, 0.1 at.%), paramag. to commensurate spin density wave transition 80−65875
$Cr_{1-x}Fe_x$, Mossbauer spectra, mag. behaviour 80−20532
Cu-Cr, mag. susceptibility 77−63092
Cu-Fe, dil., local susceptibility, Mossbauer meas. 78−19400
Cu-Fe, dilute, low temp. heat capacity in mag. field, superparamagnetism 80−39804
Cu-Mn (4.7 at.%), spin glass, spin correlations, neutron scatt. cross section meas. 79−51790
Cu-Mn(1%) spin glass, remanent mag., zero-field NMR obs. 79−33492
Cu-V, dilute, Knight shift of ^{51}V reson., and host satellite resonances 77−85594
$Er_cCe_{1-c}Pd_3$, cryst. field spectra, neutron scatt. study 80−50047
$Eu_xSr_{1-x}S$, blocking of pairs and spin glass freezing 79−61174
$Eu_xSr_{1-x}S$, dilute Heisenberg magnet, complex susceptibility of blocked spins 80−15740
$Eu_xSr_{1-x}S$, ferromagnet-spin glass transition, mag. ordering, mag. susceptibility and neutron scatt. meas. 80−50135
$(Eu_xSr_{1-x})S$, very dil., magnetisation dynamics 80−65915
Fe-Cr, dil., spin density wave under high press., neutron diffr. study 80−65798
Fe-Ni, point defect relax. after low temp. neutron irrad. 78−52316
Fe-nonmagnetic impurity, transferred hyperfine field using volume overlap model 79−78054
$(Fe_{100-x}Co_x)_{79}P_{13}B_8$, amorphous, hyperfine field distrib., ^{59}Co NMR spin-echo meas. 80−34818
$Fe(H_2O)_6^{3+}$, in frozen aqueous soln., Mossbauer spectrum, hyperfine struct. 77−77130
$Fe_{1-p}Mg_pCl_2$, magnetic excitations 78−91852
FeMn, dil., diffuse scatt. cross sections, polarized neutrons 78−43567
Fe_xNbSe_2 (2H), mag. susceptibility meas., 1.3-300K 80−39740
FeP(Ga)(As)(Sb), short-range order, neutron diffuse scatt. and spin echo NMR 80−50106
$Fe_xV_{1-x}O_2$, mag. props. and Mossbauer spectra meas., exchange-coupled Fe^{3+} clusters at lower temp. 78−31136
$Fe_{3-x}V_xSi$, Fe hyperfine fields 79−78055
$Fe_{3-x}V_xSi$, selective site substitution and spin polarisation 79−78583
$Fe_{1-x}Zn_xF_2$, dil. antiferromag., electronic and mag. props., Raman scatt. and optical absorpt. study 80−108207
Gd-Au, hyperfine interaction of ^{197}Au, Mossbauer obs. 77−20773
$Gd_{1-x}Co_x$ film, amorphous, Curie and compensation temps., effect of O or Ar impurity 77−40093
$Gd(Rh_{1-x}Fe_x)_2$, $x \leq 0.15$, magnetisation and EPR studies 80−34767
$K_2Cu_xZn_{1-x}F_4$, two-dimens. ferromag., spin correls. near percolation limit 80−44840
(La,Y)Ce, dil., Kondo supercond., transition temp., susceptibility and resist. 80−65733
$(La_{1-n}Ce_n)_3Al$, mag. impurity effects in normal and supercond. state, NMR 78−2622
$La_{1-x}Gd_xAg$, ^{139}La NMR 78−15038
$(La_{1-n}Gd_n)_3Al$, mag. impurity effects in normal and supercond. state, NMR 78−2622
$La_{1-x}Gd_xZn$, ^{139}La NMR 78−15038
$LaNi_5$-Gd, dil., ESR spectra, fine struct. and random stresses 80−25203
$La_{80-x}Pr_xAu_{20}$, amorphous, mag. and supercond. props. 80−75713
Mg-Mn, mag. props., EPR meas. 79−73804
Mg-rare earth dilute alloy, mag. susceptibility and magnetisation 80−15689
$Mg_{1-x}Mn_xTe_2$, random dil. antiferromagnet, mag. props. 80−54870
MgO:Cr^{2+}, paramag., spin-phonon coupling, inelastic neutron scatt. obs. 79−60441
$Mn_xMg_{1-x}Y_2S_4$, magnetisation and susceptibility, exchange interactions obs. 78−52242
Mo-Fe, Kondo effect of RKKY interaction 78−31052
Ni-Fe, dil., temp. depend. of Mossbauer absorpt. near Curie point *(French)* 80−11305
Ni-Ta, crit. behaviour, ^{181}Ta PAC expt. 78−43723
Ni-V, del. alloy, anisotropy consts., K_3 and K_1, determ. 77−4512
$Ni_{1-x}Au_x$-Co, dil., hyperfine field and isomer shift, precip. process, Mossbauer expts. 80−25267
Ni_3Fe-Sn, dil., atomic order detection by ^{119}Sn spectroscopy 80−39993
$(Ni_{100-x}Fe_x)_{79}P_{13}B_8$, amorphous dil. alloys, spin glasses, magnetisation meas. 79−61178
$Ni_2Mn_xM_{1-x}Sn$ (M=Ti,V) mag. hyperfine fields, ^{119}Sn Mossbauer spectra study 80−55003
$(Ni_{1-x}X_x)_{99}Mn$, X=Rh, Fe, Mn, ferromagnetic, NMR study of local environment effect, relaxation mechanism 80−7193
Pd-Ag(Mo)(Nb)(Rh)(Ru), low temp. sp. ht. and mag. susceptibility 77−62650
Pd-Co, breakdown of ferromag. order, magnetoresist. obs. 80−71046
Pd-Co, dilute alloy, ferromag. ordering, depend. on Co impurity at low temp. 79−61055
Pd-Co, very dil., Mossbauer emission spectra of ^{57}Co, relax. effects 80−29656
Pd-Cr, dil., appearance of mag. order for Cr impurities in exchange enhanced hosts 79−4690
Pd-Fe, del. alloy, Mossbauer obs., 0.018-300K 77−69740
Pd-Fe, very dilute, very low temp., spin glass-like behaviour 79−99708
Pd-Fe alloys, dil., spin polarisation effect on hyperfine interactions, anal. of Mossbauer meas. *(Russian)* 79−47055
Pd-Fe resist. min. 80−11050
Pd-Fe type dil. ferromag. alloys, spin wave propag. *(Russian)* 77−12110
Pd-Fe-Mn, dil. alloy, high press. study 80−34600
Pd-Mn, dil. alloy, very temp. magnetisation 80−34692
Pd-Mn(Fe), mag. ordering phenomena, neutron scatt. obs. 80−44812
Pd-Ni, resist. min. 80−11050
PdAgFe, ferromag., Curie temp. depend. on susceptibility, non-mean field theory 80−44829
$(Pd_{0.67}Fe_{0.33})_{1-x}Au_x$, ordering effects on mag. props. *(Russian)* 78−47942

magnetic properties of dilute systems continued
PdFeRh, ferromag., Curie temp. depend. on susceptibility, non-mean field theory 80−44829
$Pd_{0.95}Gd_{0.05}$, mag. transition temp. determ., magnetisation data 77−12123
$Pd_2MnSn_{1-y}Sb_y$-Cd, Heusler alloy, hyperfine mag. field on Cd, TDPAC obs. 79−8075
Pr-Eu, dil., magnetisation, Mossbauer spectra 80−15928
Pr-rare earth dilute alloy, low field magnetic props. 78−84443
Pt-Cr, dil., appearance of mag. order for Cr impurities in exchange enhanced hosts 79−4690
Pt-Fe, breakdown of ferromag. order, magnetoresist. obs. 80−71046
Pt-Fe(Co)(Mn), skew scatt. Hall effect, magnetoresist. and mag. anisotropy, orbital magnetism of impurity 80−70678
$Rb_2Co_cMg_{1-c}F_4$, magnetic specific heat, dilution on a two-dimensional Ising-like antiferromagnet 78−91871
$Rb_2Co_pMg_{1-p}F_4$, dilute antiferromag. two dimens. Ising system, phase boundary effective medium theory 80−50130
$ScAl_2$-Er(Dy)(Nd), dil., EPR and mag. susceptibility 80−15797
Si-Cr, dil., spin density wave under high press., neutron diffr. study 80−65798
Sm-Eu alloy, mag. and elec. hyperfine interac., TDPAD obs., paramag. behaviour, exchange integral 80−103908
$Sm_{1-x}La_xS$, mag. suscept., moment, impurity effects, indirect exchange interaction 78−68147
Tc:^{51}Fe, dilute, quadrupole splitting and isomer shift 78−48096
Ti-U(Cr)(Mo)(W), dilute, superconducting transition temp. and mag. suscept. 78−47899
(Tm,La)Al_2 disordered alloys, cryst. field transitions, inelastic neutron scatt. obs. 80−50055
$(U_xTh_{1-x})S$, metallic, 5f virtual bound states, elec. resist. and mag. susceptibility meas. 77−28363
$(U_xTh_{1-x})Se$, metallic, 5f virtual bound states, elec. resist. and mag. susceptibility meas. 77−28363
YAl_2-Er(Dy)(Nd), dil., EPR and mag. susceptibility 80−15797
$Y(Fe_{0.022}Co_{0.978})_2$ mag. props., Mossbauer expts., 0.15-4.2K 78−43712
Zn-Mn_2, Kondo-system, ion implantation as method for study 80−70241
$ZrZn_2$:^{57}Fe mag. props. from Mossbauer effect obs. *(Japanese)* 80−15933

magnetic properties of fine particles
see also superparamagnetism
anisotropy field, resonance meas. 78−64227
asymptotic superparamag. time consts., negative anisotropy const. 78−10679
asymptotic superparamag. time consts., positive anisotropy 78−10678
basalts, mag. grains effect on remanent magnetisation 77−37191
bronze, spherical powder, negative magnetic resistance changes 77−1410
catalyst, mag. characterisation, review 78−64881
coercivity and remanence, particle size distrib. effect 77−73053
Cu-Co, dil., rotational hysteresis of Co fine particles 78−23301
Fe particles in glass-like C matrix, identification and props. 80−11229
ferrimagnet, conc. characts. of magnetic props. 77−73052
ferrite F-600, suspension in caster oil, residual magnetisation *(Russian)* 79−1689
ferrite powders, mag. props., explosive shock treatment effects 79−52395
ferrofluid, dynamic magnetisation obs. 78−72370
ferromagnet, conc. characts. of magnetic props. 77−73052
ferromagnetic particle system, micromagnetism and mag. reversal 79−82830
ferromagnetic particles, quantum effects *(Russian)* 80−29584
ferromagnetic particles, stability of magnetisation curling mode and magnetisation helicoid struct. 80−11227
ferromagnetic particles, thermal fluctuations, Brownian motion theory 80−11226
ferromagnetic particles in metallic carrier fluid, long term mag. stability 77−29051
ferromagnetic suspension, birefringence in mag. field *(Russian)* 77−43979
ferromagnetic uniaxial particles, domain struct, and crit. size *(Russian)* 80−25153
fine particle systems, physical basis and applications 78−84457
haematite, grain size and coercive force from high temp. AF demag. 77−37189
hysteresis, vector model, based on interacting dipoles, with appl. to recording 78−76271
igneous rocks, TRM and var. with grain size 78−65270
inhomogeneous anisotropic magnetic materials, average field effect 77−32217
interacting, switching behaviour, dipole and Stoner-Wohlfarth models 80−44870
interacting single-domain grains, thermoremanence and ideal magnetization calc. 79−25232
magnesioferrite precipitated particles in MgO, resonance anisotropy field 77−69541
magnetically uniaxial ferromagnetic particles, high-anisotropy many domain, magnetisation, hysteresis *(Russian)* 79−91256
magneto-volume resonance in small particles *(Russian)* 77−73085
metal clusters, electronic states and mag. props., MO calc. 77−20219
metal powders, packed, complex mag. permeability calcs. 80−29583
metallic particles, effect of spin-orbit interaction on susceptibility 77−59433
metallic very small particles, mag. ordering temps., ferro- and antiferromag. spin structures 77−73027
microcrystals, magnetically ordered, high temp. behaviour 78−84456
multidomain grains, demagnetisation field 78−65273
multidomain grains, psarks, rel. to pseudo-single-domain behaviour 78−65274
oxide particles, single domain, as source of rocks TRM 78−65271
powder, torsional vibr. and stimulated echo with long memory, two and three pulse echo *(Russian)* 77−63258
pseudo-single domain grains, stable remanence origin 78−65275
quantum size effects, CESR and NMR obs. 77−20700
recording medium, packing density rel. to chain assembly 78−10731
recording on particulate media, conference, Gardone Riviera, Italy (Sep. 1979) 80−41930
remanent loop measurement, single magnetic particles 80−17967
single domain particles, partial hysteresis cycles, asymmetry *(Russian)* 78−76268
single particle material for tape and disc manufacture, prep., props., and appls. 78−52308

magnetic properties of fine particles continued
Stoner-Wohlforth particle, two-component, hysteretic props. 80−11228
superparamagnetic, dipole interactions and mag. props. *(Russian)* 78−60316
superparamagnetic particles, magnetic moment time development and discrete orientation model 80−60378
superparamagnetic particles, magnetis. vector movement, relax. freqs. *(Russian)* 79−95610
superparamagnetic particles, resonance anisotropy field 77−69541
superparamagnetic spheres, magnetisation curling 77−8363
superparamagnetism, Mossbauer effect study of relaxation of magnetisation vector 78−19402
superparamagnets with cubic anisotropy, high order relax. times 77−69632
tapes, static and antihysteretic mag. props. 80−44868
TCNQ salts, Qn(TCNQ)$_2$ and Cs(TCNQ)$_3$, surface magnetism 78−2703
time constants of superparamag. particles 77−69631
titanomagnetites, hysteresis props., grain size and comp. depend. 77−37187
TTF-TCNQ, surface magnetism 78−2703
ultrafine particles, VEROS prep. method and superparamag. props. *(Japanese)* 77−85954
US pulse echoes and suppression 77−28520
Al_2O_3-martensitic steel, mag. and dielec. emulsion, prep. by abrasion of steel surface 78−27826
Au-Fe, finite mag. clusters near percolation conc. 78−72371
$BaFe_{12}O_{19}$ microparticles, magnetisation reversal, hysteresis loop obs. 80−75813
$BaFe_{12}O_{19}$ particles, magnetic domain study by colloid-SEM method 80−97120
$BaFe_{12}O_{19}$ powder, hysteresis of microwave absorpt. and magnetisation reversal 80−75814
BaO-Fe_2O_3, chemically coprecipitated, mag. props., orientation 80−15763
$Bi_{0.96}Mn_{0.04}$, powder particles, magnetisation 77−48014
Co, amorphous ferromag. film, resist. anisotropy rel. to struct. 77−72926
Co, anisotropy field, resonance meas. 78−64227
Co catalyst, magnetooptical investigation of mag. props. 79−69858
Co, FCC, ferromag. domains of fine particles, Lorentz electron microscopy obs. 78−27053
Co, FCC, mag. props. of single-domain powders after plastic deform. *(Russian)* 78−6554
Co fine particles in Cu, interface magnetisation 80−88858
Co, fine powder, magnetic props., effects of electrolysis conditions in prep. 77−40091
Co single domain particles, randomly oriented easy axes and particle size distrib., coercivity 80−71119
Co, ultrafine particles prepared by vacuum evap. on running oil substrate, mag. behaviour 79−28565
Co-Ni fine particles, anhysteretic growth of exchange fixed remanent states 77−16116
Co-P grains, mag. props. *(French)* 79−33510
$CoFe_2O_4$ mag. fluid particles, comp., struct., and mag. props. 80−60374
$CoFe_2O_4$, surface effects on saturation magnetisation 77−69630
Cr, δ- and BCC, fine particles, mag. props. 78−52314
Cr, surface magnetisation, explanation of expt. work 78−23303
CrO_2 and CrO(OH), fine particle obs. of cryst. morphology and topotaxy 80−65969
CrO_2, oxidative prep. method, mag. props. 80−44863
CrO_2, particulate, proton donor adsorption effect on mag. moment, XPS anal. 80−71117
CrO_2 powder, thermal-magnetic props. 79−51821
CrO_2 powders, print through values and mag. characts. 80−44871
CrO_2, single mag. particle, remanent coercive force and remanent loop meas. 78−95480
CrO_2, single particle material for tape and disc manufacture, prep., props., and appls. 78−52308
CrO_2, synthesis and morphology 79−24481
$Cr_{1-x}Rh_xO_2$, oxidative prep. method, mag. props. 80−44863
Cu-Mn-Al, Heusler alloys, ferromag. inclusions, mag. props. and struct. study *(Russian)* 80−80570
Cu-Ni-Co, mag. props. of system of disperse ferromag. particles, 73 to 673K *(Russian)* 80−65968
Cu-Ni-Fe (14, 7 wt.%), solid soln., decomposed, magnetostatic interaction between ferromag. particles *(Russian)* 77−80967
Cu-Ni-Fe solid solution, after precip., susceptibility of interacting superparamag. grains 79−99733
Cu_2MnAl superparamagnetic particles in Cu_3Al lattice, magnetic moment ferromagnetic ordering *(Russian)* 79−78444
$DyFe_2$ powders, mag. and hysteresis props. *(Russian)* 79−42800
$ErFe_2$ powders, mag. and hysteresis props. *(Russian)* 79−42800
$EuFeO_3$, minute single crystal domain struct. 77−20646
Fe aerosol powders, oxidised, nucl. gamma reson. study *(Russian)* 79−1725
Fe aerosoled fine particles, Mossbauer spectra 80−7223
Fe, atomized powder compacts for mag. cores, mag. props., green densities *(Japanese)* 78−72751
Fe, carbonyl powder, particle size distrib. anal. by microscopy with statistical anal. of results 78−19691
Fe clusters, supported, Mossbauer spectra 80−7220
Fe, fine particle dispersions, shock induced mag. effects 79−82832
Fe, fine particles, chemisorption of CO, H_2, Mossbauer study 80−39415
Fe, finely dispersed, superparamagnetism, Mossbauer meas. 78−68303
Fe, first order shock induced mag. transitions characts. and discrimination from TRM 78−64205
Fe, magnetic powder, particle deformation effects on mag. props. 77−63236
Fe, Mossbauer spectra, demagnetising field effect on magnetic splitting 80−39932
α-Fe particles, in fused SiO_2, g-values and anisotropy consts., FMR study 79−82876
Fe particles, lunar matter, FMR study, effective linewidth method 78−95523
Fe powder, prep. by reducing iron phthalate in mag. field, mag. props. 77−40090
Fe powder-plastic composite, soft mag. material, mag. and mech. props. 80−75812
Fe powders, Co- or Cu-plated, prep. by rad. and chem. plating, mag. props. 80−44867
Fe powders, prep. by BH_4 process, comp. and stability 80−44878

magnetic properties of fine particles continued
γ-Fe precipitates, antiferromag. ordering, press. depend., Mossbauer meas. 79−73861
Fe pyrophoric powders, stabilising layer form. during passivation, saturation moment meas. 80−44865
Fe, small particles, magnetisation-pressure isotherms for H_2 and SO_2 78−39949
Fe, spin collinearity, Mossbauer spectra study 80−71114
Fe ultrafine particles, Fe_3O_4/γ-Fe_2O_3 surface layers, Mossbauer expts. 79−8081
Fe ultrafine particles prepared by vacuum evaporation, mag. props. 78−35007
Fe, ultrafine particles prepared by vacuum evap. on running oil substrate, mag. behaviour 79−28565
Fe-Al_2O_3 granular film, interface props., Mossbauer spectroscopy 80−34336
Fe-Co alloy particles for mag. tapes, mag. props. 78−95479
Fe-Co-B powders, synthesis and mag. props., appl. to mag. recording 80−20432
Fe-Co-Ni-O, mag. powder prod. by reduction of oxalates 77−63582
Fe-Pd-Pt alloy powders, coercive force and specific remanence *(Russian)* 79−47302
Fe-Si-B amorphous powder, production by spark erosion, and mag. props. 77−90290
Fe-SiO_2, granular compund, superpara- to ferromag. transition temp. meas. 77−69633
Fe-SiO_2 granular film, interface props., Mossbauer spectroscopy 80−34336
Fe-ZrO_2 granular film, interface props., Mossbauer spectroscopy 80−34336
$Fe(CO)_5$, R-10, R-20, optimum process parameters for mag. permeability temp. depend. 78−35009
$Fe_{3-x}Co_xO_4$, effect of Fe^{2+} content on coercivity instability 79−51820
γ-Fe_2O_3 acicular particles, coercivity, magnetic recording tape appls. 78−14983
γ-Fe_2O_3 acicular particles, coercivity increase by Co ferrite surface crystn. 80−44866
γ-Fe_2O_3, clean and SiO_2 coated, reduction temp. influence on coercivities, coercivity factors and rheological props. 79−69698
γ-Fe_2O_3, densified, rheological and mag. props. 80−44873
Fe_2O_3, haematite, single domain, defect moment origin and props. 79−16438
γ-Fe_2O_3, magnetisation distribution in isolated transitions 80−29580
γ-Fe_2O_3, microstruct. and magnetisation 80−44875
γ-Fe_2O_3, particle interactions, in inhomogeneous anisotropic magnetic materials, average field effect 77−32217
γ-Fe_2O_3 particles, growing Fe-Co ferrite, coercivity increase 79−56571
γ-Fe_2O_3 particles, mag. props. rel. to mag. tape appl. 80−15762
γ-Fe_2O_3 powders, influence of densification on mag. props. 78−95481
γ-Fe_2O_3 powders, mag. props., effect of Co plating 79−69699
γ-Fe_2O_3, single mag. particle, remanent coercive force and remanent loop meas. 78−95480
α-Fe_2O_3, single particle material for tape and disc manufacture, prep., props., and appls. 78−52308
γ-Fe_2O_3, small particle composite, preparation methods, superparamagnetism, optical transparency 78−60315
γ-Fe_2O_3 small particles, hyperfine field below superparamag. blocking temp., Mossbauer obs. 78−19392
γ-Fe_2O_3 small particles, noncollinearity as crystallite-size effect, Mossbauer study 80−39939
γ-Fe_2O_3, surface effects on saturation magnetisation 77−69630
γ-Fe_2O_3:Co acicular powder epitaxially doped, coercivity increase, surface anisotropy *(Chinese)* 80−7130
γ-Fe_2O_3:Co powder, increased coercivity by epitaxial doping 79−82833
Fe_2O_3-martensitic steel, mag. and dielec. emulsion, prep. by abrasion of steel surface 78−27826
γ-Fe_2O_3-organic interfaces, mag. struct., Mossbauer effect, IR absorpt., and magnetisation meas. 80−44869
Fe_3O_4 (magnetite), multidomain particles magnetisation 79−66686
Fe_3O_4 entrapped in drug carrying microsphere, intravascular mag. guidance method 78−73188
Fe_3O_4 ferrofluid, mag. birefringence, estimation of particle size 79−33511
Fe_3O_4 mag. fluid particles, comp., struct., and mag. props. 80−60374
Fe_3O_4, magnetite, ARM, TRM and magnetic interactions: concentration dependence 79−44177
Fe_3O_4, magnetite, anhysteretic remanence and thermoremanence in submicron particles 77−5191
Fe_3O_4, magnetite, coercive force spectrum at high temps. rel. to thermal activation below blocking temp. 77−91111
Fe_3O_4, magnetite particles, interaction fields effect on hysteretic props. 80−54921
Fe_3O_4 particles, nonstoichiometric, morphology and enhanced coercivity, Mossbauer meas. 80−7132
Fe_3O_4 powder, oxidation to γ-Fe_2O_3, coercivity changes 80−44864
Fe_3O_4, ultrafine particles in ferrofluid, superparamag. and ferromag. reson. 78−15026
Fe_xO_y powder coated with $NaPO_3$, anomalous coercivity increase 77−89980
$Fe(OH)_3$-$Fe(OH)_2$ suspension system, potential-pH diagram 80−55728
β-FeOOH, colloidal suspension, ionic spin relax. theory for Mossbauer spectra 78−19384
FeOOH gels, Mossbauer spectra, mag. props. 80−11303
α-FeOOH, goethite small particles, mag. hyperfine field, bulk and surface contribs. 77−69758
β-FeOOH, ultrafine particles, mag. struct., Mossbauer spectroscopy 78−72372
α-FeOOH ultrafine particle NGR spectra, size distrib. and surface effects 80−11299
FeS_2, pyrite, magnetokinetics of oxidation, appl. to mag. separation from coal 77−12161
^{57}Fe powder, NMR excitation function, drumhead model of Bloch walls 80−15810
Gd clusters in faujasite type zeolites, mag. suscept. temp. depend. 78−14925
Ge powder, diamag., strong mag. particle form., mag. props., EPR *(Russian)* 80−54863
Ho particles, effect of size on paramag. Curie temp. 78−60317
$MgFe_2O_4$, small mag. particles, anisotropy field, resonance meas. 78−64227
Mn, surface magnetisation, explanation of expt. work 78−23303

magnetic properties of fine particles continued
MnBi particles, demagnetised, coercivity, remanence and magnetisation reversal 78−19281
MnBi particles, effect of grinding on coercivity 77−36098
MnZn ferrite particles, mag. filtration from air streams 77−4945
Na_2O-Fe_2O_3-SiO_2 glass, partially crystallised 78−23302
Ni catalyst, magnetooptical investigation of mag. props. 79−69858
Ni, mag. props. of single-domain powders after plastic deform. *(Russian)* 78−6554
Ni, powder, magnetic resistance changes 77−1411
Ni, single-domain particles, LF mag. susceptibility, 2K up to Curie point 80−29582
Ni, ultrafine particles prepared by vacuum evap. on running oil substrate, mag. behaviour 79−28565
Ni-Co, mag. props. of single-domain powders after plastic deform. *(Russian)* 78−6554
Ni-SiO_2 supported catalysts, particle size, H_2 chemisorption, Mossbauer study 80−7219
$NiFe_2O_4$ mag. fluid particles, comp., struct., and mag. props. 80−60374
$Ni_xFe_{3-x}O_4$, spinels, fine particles, magnetic properties obs. 80−71031
NiO, mag. props. rel. to physicochem. props. 78−52315
Pd, confined geometry, p-wave supercond. or itinerant ferromag. 80−11129
Pt-Fe alloys, supported, mag. prop. meas. in H_2 and O_2, 77 to 700K 79−91257
Sm-Co base ternary alloy, mag. props. and cryst. struct. 77−8352
$SmCO_5$, etched microparticles, Barkhausen discontinuity, nucleation, and domain wall pinning 79−87288
$SmCo_5$, powder, comminution temp. effect on mag. props. 80−39819
$SmCo_5$, powder, exam. of protective preps. of organic media against oxidation 79−96220
$SmCo_5$ powder alloy, densification by cold working 77−4753
$SmCo_5$, powder prod. by electroerosion mag. props. 77−59718
$Sm(Co_{0.81}Cu_{0.15}Fe_{0.04})_{6.9}$ and $Sm(Co_{0.84}Cu_{0.16})_{6.9}$ powders, mag. props. *(Russian)* 80−20434
$SmFe_2$ powders, mag. and hysteresis props. *(Russian)* 79−42800
$Sm_xNd_{1-x}Co_5$ powders, mag. props. *(Russian)* 79−51812
$Sr(Fe_{7.2}Al_{4.8})O_{19}$, minute single crystal domain struct. 77−20646
Tb, small particles, disappearance of mag. order., mag. susceptibility and magnetisation meas. 77−16117
$Tb_xDy_{1-x}Fe_2$, Laves phase alloy, magnetostriction depend. on powder orientation before sintering 78−76284
$TbFe_2$ powders, mag. and hysteresis props. *(Russian)* 79−42800
U_2N_2Te, powdered, high field magnetisation 78−35008
V, appearance of mag. moment 78−68152
V hyperfine particles, appearance of mag. moments, mag. susceptibility meas. 77−36097
V, surface magnetisation, explanation of expt. work 78−23303

magnetic properties of substances
see also antiferromagnetic properties of substances; demagnetisation; diamagnetic properties of substances; ferrimagnetic properties of substances; ferromagnetic properties of substances; magnetic permeability; magnetic properties of amorphous substances; magnetic properties of dilute systems; magnetic properties of fine particles; magnetic structure; magnetic surface phenomena; magnetic susceptibility; magnetic transitions; magnetisation; magnetocaloric effects; paramagnetic properties of substances
actinide compounds, structure, mag. and related props., review 80−6389
actinide systems, review 78−84383
ceramics, engineering materials, nature and props., book 78−72707
charge ordered crystals, mag. props., energy spectrum, triplet excitations 78−18979
composite materials, phys. props. review 77−4720
conference, Cleveland, USA (Nov. 1978) 79−73651
conference, Donetsk, USSR (Sept. 1977). 79−82733
conference, Florence, Italy (May 1978) 78−91833
conference, Munich, Germany (Sep. 1979) 80−56997
conference, Pittsburgh, USA (June 1976) 77−12071
EM NDT phenomena, fissile element modelling 80−40633
glass, engineering materials, nature and props., book 78−72707
glasses, elec., mag., and optical props., conference, Troy, NY, USA (Aug. 1979) 80−105417
haemoilmenites, magnetic characts. of low-Curie point specimens 77−41022
lanthanum diluted cerium magnesium nitrate at milli Kelvin region *(Japanese)* 77−71331
magnetism, conf., Bad Nauheim, Germany (Mar. 1976) 77−8255
magnetites, superleak behaviour in superfluid ^4He 77−43399
materials, electronic, optical, magnetic and thermal props., rel. to energy technology 78−88412
metallic glasses, atomic struct., mech. and mag. props., prod. methods, uses 77−1081
metals, engineering materials, nature and props., book 78−72707
muon spin rotation techniques, appl. to study of mag. systems 79−65782
neutron scattering and magnetism, conference, Julich, Germany (Aug. 79) 80−41934
polymers, engineering materials, nature and props., book 78−72707
random heterogeneous materials, statistical theory of effective elec. thermal and mag. props. 77−48118
rare earth alloys and compounds, book 80−36785
rare earth metals magnetism, review 77−63123
rare earth-Sn-X, X=Rh, Ir, Ru, Co, cryst. growth and cryst.-chem. invest, supercond./mag. ternary cpds. 80−100777
rare earths, light, stacking faults and magnetism, transform. effects 80−75840
solid state physics, book 80−101676
solid state physics, historical aspects, symposium, London, England (Apr.-May 1979) 80−56999
Swiss Physical Society, autumn sessions 78−72053
texture, influence on mech. and phys. props. 79−83224
titanomagnetite sand from New Zealand, density, elec. and mag. prop 80−98311
transuranic compounds, 5f electrons delocalisation *(French)* 77−27857
wustite solid solns., props. connected with localised electron state 80−107734
$CeSn_3$, valence instabilities 79−78546
$Fe_{2-x}Co_xP_{1-y}As$, mag. props., Mossbauer effect 77−40156
^3He, BCC solid, mag. props. near phase transition 79−65291
Pt-Ni (42 wt.%) relationship between mag. saturation flux and tensile strength 79−15819

magnetic properties of substances continued
Pu and other actinides, conf., Baden-Baden, Germany (Sept. 1975) 77−19807
Sn ternary intermetallic systems, new supercond./mag. cpds., X-ray powder diffr. data 80−100215
$Tb^{57}Fe_{1-x}Cr_xO_3$ mag. props. from Mossbauer effect obs. *(Japanese)* 80−15933
$YbAl_3$, valence instabilities 79−78546

magnetic read/write heads *see magnetic heads*

magnetic recording
see also tape recorders; thermomagnetic recording
bioelectric process, FM freq. convertor 78−7469
body surface potential distribution map recording and processing 78−57116
chemical reaction residence time measurement appl. 78−81953
cinematography, magnetic sound records release print KMP-23 *(Russian)* 80−90918
conference on magnetism and mag. materials Cleveland, USA (Nov. 1978) 79−73651
$Cr_{1-x}Rh_xO_2$, ferromag., new prep. method by high-pressure oxidation, SEM characterisation, video appls. 79−43164
data recording and reproduction using magnetic tape 79−88934
digital, comparison with natural storage of information in DNA 79−2009
digital, magnetisation distribution in isolated transition 80−29580
ECG, long-term recording on mag. tape 80−56243
ECG slew rates, adults and infants 78−53544
ferrite film, reactive RF sputtering prep., high mag. recording density 77−12528
fine particle magnetization process, packing density rel. to chain assembly 78−10731
magnetographic fault location, local field representation using biased magnetic tape 78−72965
magnetographic fault location, local field representation using biased magnetic tape 78−72966
NDT, local field image recording on magnetic tape without bias 78−53130
NDT, local magnetic field image recording on magnetic tape without bias 78−53129
output characteristics rel. to carrier velocity fluctuations 77−26279
on particulate media, conference, Gardone Riviera, Italy (Sep. 1979) 80−41930
particulate media, hysteresis, appl. of vector model, based on interacting dipoles 78−76271
recording heads, thin layer, magnetoresistance effect *(German)* 78−68013
synchronisation unit, direct and reversible, for one-channel recording 78−3620
tape material, gyroremanent magnetisation in anisotropic mag. material 80−50142
tape recorders, portable, FM- and direct-recording types comparison 79−1028
thermal diffusivity meas. by laser-pulse technique, instrumental recording and data processing 77−45846
time reference singal for tape recording, IRIG and NASA code formats 80−57262
Co films layered over Cr by DC sputtering for digital mag. recording 79−83118
Co-Cr recording films, perpendicular mag. anisotropy, hysteresis loop, microstruct., TEM obs. 78−95491
Co-Ni fine particles, anhysteretic growth of exchange fixed remanent states, appl. in mag. recording 77−16116
Co-P films, electrodeposited, magnetic recording media *(Japanese)* 80−29587
$Co_xFe_{3-x}O_4$ film, magnetooptic recording material, mag. and magnetooptic props. 77−20832
Cr-Co-Ni hard film on Mo substrate 80−2608
Fe-Co alloy particles for mag. tapes, mag. props. 78−95479
Fe-Co-Cr film RF sputtering 80−2947
Fe_3O_4, Co modified, synthesis with autoclave in H_2 atm. 80−35117
MnBi magnetic film, method for recording holograms of diffusely scattering objects 78−74862
Ni-Fe-Nb-Mo-Al, head material for mag. recording, DC and AC mag. props. 80−88812

magnetic relaxation
see also ferromagnetic relaxation; magnetic resonance; spin-lattice relaxation; spin-spin relaxation
A_3 spin system, NMR relax. kinetics 78−80238
alkali metal vapour, optically pumped, longit. relax. in hyperfine states 77−57908
amorphous ferromagnets, structural instabilities and mag. permeability relax., 77 to 400K 80−80559
antiferromagnet, easy-plane, antiferromag. reson. linewidth and relax., theory 80−71189
antiferromagnet, sound attenuation, rel. to spin wave damping 77−24750
antiferromagnetic resonance relaxation, multimagnon processes 77−4564
cross relaxation under action of 90° pulse trains, characts. 80−60402
cross-relaxation between Zeeman and spin-spin degrees of freedom *(Russian)* 77−32237
diamine oxidase solutions, proton mag. relax. dispersion obs. 80−51136
electrolyte solutions, preferential solvation, NMR obs. 78−95919
electrolyte solutions, preferential solvation and mol. motion, NMR obs. 78−95920
electron-nuclear spin system in solids, nucl. spin-spin flips *(Russian)* 77−24763
exciton insulator, coherence factors and transport props. 79−28291
ferromagnetic with impurity atoms, Mossbauer effect *(Russian)* 77−48098
gapless semiconductor, nucl. spin relax. due to interaction with electrons 78−56398
Heisenberg exchange interaction between unlike free radicals, spin relax. 78−84490
intermolecular relaxation operator, dipole coupling 77−68057
intermolecular spin relaxation by reorientation of off-center spins 79−42821
Ising magnet, kinetic processes, 1-D chain, magnetic relaxation, quantum stat. mechs. 80−80471
Ising magnet, kinetic processes, reduction of statistical description of system during evolution 80−80470

magnetic relaxation continued
CW Leonis (IRC+10216), IR C star, circumstellar dust orientation by paramag. relaxation rel. to intrinsic polarisation 80−67730
linear irreversible processes, spin relax., role of entropy prod. 77−20678
liquid alloys, concentration fluctuations, nucl. quadrupole spin relax. 78−91975
liquid metals, nucl. quadrupole relaxation, Sternheimer antishielding and fluctuating elec. field gradients 77−55726
longitudinal magnetisation initial relax., absence of cross-correls. 77−59445
magnetic resonance line, exchange narrowing at low temp. *(Russian)* 78−56366
Mattis model, modified, mag. relax. 80−65947
measurement of mag. aftereffect, high time const. relax. processes meas. 78−29129
methacryloyloxyethyleneoxycarbonyloxypropylene, NMR relaxation mechanism *(German)* 78−33527
3- methylhexane, glass, γ-irradiated, trapped electron-radical mag. energy transfer, ELDOR, cross relax. 77−16209
2-methyltetrahydrofuran, glass, γ-irradiated, trapped electron-radical mag. energy transfer, ELDOR, cross relax. 77−16209
microwave spectrometer control pulse shaper for two-pulse relaxation time meas. 79−67363
molecule adsorbed on solid, NMR, paramag. relax. times *(Russian)* 77 39737
Mossbauer lineshape, in presence of electronic relaxation *(Rumanian)* 78−60368
nematic liquid crystals, nucl. spin relax. and slow solute motion 79−95662
NMR relaxation parameters, use of superoperators *(Russian)* 77−14458
NMR relaxation processes, macroscopic evolution eqns. and virtual spins importance *(French)* 80−32739
NMR relaxation times, computer-assisted meas. method 77−22586
NMR saturated bandshapes of coupled multispin systems, simple line approx. anal. 79−75561
noisy exponential decays, algebraic anal. for on-line computer anal. 77−67415
nonlinear dynamics of first order phase transitions 79−11322
nuclear dipolar energy relaxation time 77−24755
nuclear quadrupole relax rate in unmixed complexes with ligands, temp. depend. 77−16203
nuclear relaxation under ESR saturation conditions 77−8451
nuclear spin longit. relax., theory of nonequilib. statistical operators 77−13696
nuclear spin relaxation via contact hyperfine interaction with excitons 77−51983
one-dimensional semi-infinite chain, enhanced surface exchange interaction, mag. relax. 80−29558
optically oriented atoms, relaxation induced by random RF fields, non-Born contribution *(Russian)* 77−40149
optically polarized spin system, long relaxation time meas. *(Russian)* 78−12737
optically pumped vapour, atomic collisions, transverse relaxation *(Polish)* 78−55229
paramagnetic crystal, magnetisation change by light pulse 80−70932
paramagnetic impurities in conductors, relaxation and indirect exchange interaction 78−2728
paramagnetic impurities metal, contrib. of collective excitations to mag. relax. 77−12190
paramagnetic relaxation *(Chinese)* 79−87307
pnictides, cubic Van Vleck compounds, paramag. fluctuations, ESR or NMR relax. 77−66420
polyethylene, NMR relaxation times, computer-assisted meas. method 77−22586
polyvinyl carbazole, and ring chlorinated derivatives, dielectric and NMR relaxation 79−73883
rare earth metals, narrow domain walls, magnetic aftereffect obs. 77−8364
ruby, ^{27}Al NQR relax. times at very low temps. 79−65757
self-diffusion NMR pulsed-gradient meas. noise pulse generator 77−53965
semiconductor, nucl. relax. interaction with excitons 78−56399
semiconductor, spin relax., in quantising mag. field, effect of carriers 78−72388
semiconductor, spin relax. of deep impurity centres, exchange scatt. 77−43870
spin glass, order parameter relaxation 78−80161
spin glasses, magnetisation relaxation time near freezing temp., HF calc. 80−34665
spin system, paramagnetic, two-level open system, kinetic theory of resonance and relaxation 80−88859
spins in fluids, magnetic relaxation in Bogolyubov hierarchy of relaxation times 78−39383
superconducting fine particles, nucl. spin relax. *(Russian)* 77−80875
superconductors, type I, spectroscopy using mag. impurity relax. of Josephson junction-Fiske modes 77−80880
superparamagnetic FCC particles, relaxation times in external mag. fields 78−95482
thermodynamic vectorial internal degrees of freedom, dielec. and mag. relax. phenomena 77−77145
tunnelling, relaxation, competing models, paramagnetic defects 79−37787
two spin cross relaxations, temp. depend. statistical theory 78−80190
type II superconductor, spin diffusion in inhomogeneous mag. fields 78−2618
X-Y model, 3-dimensional, relax. function 77−69666
Al:^{12}B, relax. mechanism for polarised implant 78−87693
$(Al_2O_3\text{-}Fe_2O_3):Cr^{3+}$, (0.04 mol.% Fe_2O_3), paramag., cross relax., annealing temp. effect from Mossbauer meas. 80−44983
^{27}Al, in aqueous soln., quadrupolar relax., formulation of relax. rate 77−85600
^{27}Al in aqueous soln., quadrupolar relax., reorientational motion of hydration water mols. 77−85601
^{27}Al in aqueous soln., quadrupolar relax., motions of hydration water mols. 78−64291
Au-Fe, spin glasses, alternating susceptibility 80−65912
Au-Fe (4 at.%), spin glass, magnetisation and energy relax. below T_g 80−65921
Au-Fe spin glass, energy flux associated with remanent magnetization relaxation *(French)* 80−7110

magnetic relaxation continued
Au-Fe spin glass, long-time relax. processes, heat capacity expts. 77−66374
B_4H_{10}, ^{11}B NMR line broadening, B-B coupling 78−62826
B_5H_9, ^{11}B NMR line broadening, B-B coupling 78−62826
Bi, μ^+ diffusion, spin relax. temp. depend. *(Russian)* 77−48115
Bi-Sn(Pb), liq., conc. and temp. depend. nucl. relax. rates meas. 78−19357
CaH, spin doubling, SCF calcs. 80−95649
Cu-Mn, mag. viscosity below freezing temp. 80−65910
Cu-Mn, spin glasses, alternating susceptibility 80−65912
Cu-Mn (10 at.%), meas. of mag. viscosity below freezing temp. 79−24171
EuO, dynamic dipolar cross over 78−76339
Fe, BCC, mag. relax. due to C and N meas., 210 to 410K 77−36102
Fe complex, Fe(III) Schiff-base complexes, mag. relax., Mossbauer spectra 80−15897
Fe complex, halobis(morpholydithiocarbamato)Fe(III), Mossbauer HFS spectra, mag. relax. and cooperative transitions 78−27130
Fe, high-purity, low-temp. mag. relax. after thermal ageing and demagnetisation 77−85502
α-Fe, neutron irradiated, low temp. mag. relax. 79−8022
Fe_3O_4, mag. relax., permeability and loss tangent determ. at 4.2 to 300K 77−32263
Fe_3O_4, magnetite, mag. aftereffects, 4.35K 80−80571
n-Ge, μ^+ depolarisation, post muonic stage *(Russian)* 77−48116
^{3}He, HCP solid, with ^{4}He impurities, ^{3}He nucl. mag. relax. behaviours 79−56027
^{3}He, liq., highly mag. polarised, prep. and obs. 79−46870
^{3}He, superfluid, anomalous magnetic relaxation *(Russian)* 79−23801
^{3}He, superfluid, longit. mag. relax. near crit. temp. 78−18862
^{3}He, superfluid, longitudinal magnetic relaxation 78−79840
^{3}He, superfluid, spin relaxation effects in nonlinear parallel ringing of magnetisation 78−6193
^{3}He, superfluid A-phase, longitudinal mag. relax. 80−59751
^{3}He, superfluid B-phase, low-temp. spin relax. 79−55989
^{3}He-^{4}He liquid mixture, anomalous nuclear spin relaxation 78−79849
Hg, liq., nucl. spin relax. and quadrupolar relax. mech. 78−64292
In-Sn(Pb), liq., conc. and temp. depend. nucl. relax. rates meas. 78−19357
$KM_{0x}Mg_{1-x}F_3$, randomly diluted Heisenberg paramag. nucl. relax. 80−60444
Li-Zn ferrites, (Li, Zn, Ti, Cr substituted), Mossbauer spectrometry, effect of supertransferred hyperfine fields and relaxation *(French)* 80−80654
MnP, noncubic ferromag., relax. times for domain and wall resonances 77−77119
MnZn ferrite, mag. relax., permeability and loss tangent determ. at 4.2 to 300K 77−32263
Na_3RuO_4, ^{99}Ru Mossbauer spectra, antiferromag. order, mag. relax. 80−50234
Ni microcrystals, H_2 chemisorption effect on superparamagnetic relax. time, Mossbauer meas. 79−61284
Ni-Co (25 wt.%), single crysts., mag. annealing effect on magnetostriction and magnetisation at high temps. 80−108047
$Ni_{98}M_2$, M=impurity metal, formation of MH(D)-complexes 80−65236
Pd-Co, very dil., Mossbauer emission spectra of ^{57}Co, relax. effects 80−29656
$SmCo_5$, magnetic aftereffect of H and D 79−56573
$(Ti_{0.9}V_{0.1})_2O_3$, spin glass, dynamic mag. susceptibility meas. 80−39792
YIG, homogeneous crit. relax. in dipole region *(Russian)* 78−10782
YIG, magnetostatic wave linewidth, wave no. depend., mag. relax., rods and films *(Russian)* 78−2667

magnetic resonance
see also acoustic magnetic resonance; antiferromagnetic resonance; atomic beam magnetic resonance; ferrimagnetic resonance; ferromagnetic resonance; laser magnetic resonance; magnetic double resonance; magnetic relaxation; molecular beam magnetic resonance; nuclear magnetic resonance; paramagnetic resonance
alkali metal atom, Bloch theory appl. to optical pumping and mag. reson. 79−59403
alkali metal mag. reson. spectrum, rapid spin exchange effects 78−25460
angular velocity nonuniformity meas. *(Russian)* 80−62637
atom spin transition, nonadiabatic, in time-depend. mag. field 80−9576
atomic and laser spectroscopy, book 77−79554
atomic RF spectroscopy, nonlinear and parametric effects, review 80−18816
Bloch equation, general solution, for broadband modulation of resonance conditions 79−65708
broadband modulation of resonance conditions, general solution of Bloch equations 79−65706
chlorophylls, mag. reson., site selected fluoresc. detection 80−69164
conference, Banff, Canada (May 1977) 78−68357
conference on magnetism, Munster, Germany (Mar. 1977) 78−10626
conference on magnetism, Munster, Germany (March 1979) 80−12843
crystal, mag. ordered, mag. reson. symmetry and freqs. *(Russian)* 79−61197
deoxyhaemoglobin high spin ferrous ion, low lying electronic states, far IR mag. reson. 80−48110
deoxymyoglobin high spin ferrous ion, low lying electronic states, far IR mag. reson. 80−48110
dielectric thin slab. magneto-exchange modes with arbitrary pinning 77−63261
dipole-dipole reservoir manifestations in discrete saturation conditions 78−35022
domain wall in uniaxial ferromagnet, nonlinear resonance 77−43848
exchange narrowing, of mag. resonance line at low temp. *(Russian)* 78−56366
ferrite, polycryst., natural gyromag. reson. and effective anisotropy *(French)* 77−1629
film disc containing bubble, two-dimens. magnetostatic reson. 79−78469
fluoromethane, rot. mag. moment spectra, mol. beam mag. reson. obs. 77−14509
gamma-magnetic resonance, review of γ-reson. spectroscopy under HF excitation 77−48113
gamma-ray, possibility of obs. by conversion electron Mossbauer spectroscopy 77−51997
inhomogeneous resonance lines with rapid spectral diffusion, slow-passage absorpt. *(French)* 77−59444
integrated line intensities from first-derivs. by AW^2 method 77−48062

magnetic resonance continued
ion beam mag. reson. technique using laser-induced fluoresc. 78−41986
Ising model, 2-D, appl. to $FeCl_2$ 79−47323
line broadening and narrowing, trigonometric functions 78−91925
line shape for inhomogeneous mag. field 79−38365
line width, theory of exchange narrowing 77−66411
lineshape, with slow mol. motion, asymptotic method, strong collision limit 77−48063
Lorentzian lines, calculation modulation broadened line widths 77−48029
magnet power supply, current-regulated, for mag. reson. and susceptibility meas. 77 22587
Magnetic dipolar Hamiltonian 80−25181
magnetic semiconductor, helicon wave propag., hyperfine interaction effect 80−80307
magnetism, conference, Munich, Germany (Sep. 1979) 80−56997
magneto-volume resonance in small particles *(Russian)* 77−73085
many-spin system, dynamics, group approach *(Russian)* 79−11324
many-spin system, group approach in dynamics *(Russian)* 80−44900
methane, rot. mag. moment spectra, mol. beam mag. reson. obs. 77−14509
modulation-induced sidebands 77−48028
muonic radicals, muon spin resonance frequency spectra, theory 80−1088
muonium, ground state, muon mag. moment and HFS, Zeeman transition obs. 77−75345
octupole and hexadecapole dynamics in solid state physics, algebraic struct. 77−88682
optically oriented atoms in inhomogeneous RF fields *(Russian)* 77−27004
paramagnets, low-dimensional dense, mag. reson. spectra 79−47322
protochlorophyl, mag. reson., site selected fluoresc. detection 80−69164
radiation problems, semiclassical theory 78−74684
rare earth metals, alloys, and cpds., book 80−36785
refractory elements, atomic-beam mag. reson. nuclear spin and hyperfine structure meas. 79−776
rotating coordinate system with quadrupole splitting, paramag. susceptibility 80−11178
ruby, spin level population inversion, coherent phonon amplification and generation *(Russian)* 77−24364
semiconductor, multiphoton absorption of intense EM waves 77−1648
shift and width of reson. line at low temps. 78−27073
single differential equation solution *(Russian)* 77−28424
small magnetic particles, anisotropy field, resonance meas. 78−64227
solid, in rotating coord. system, nonequilib. statoperator technique *(Russian)* 77−80991
spectral diffusion at low temp. 77−43861
spin generator, determ. of oscillation amplitude, at side frequency 79−65707
spin oscillator action of transverse fields 78−49873
spin resonance phenomena, classical calcs. 77−69665
spin system, paramagnetic, two-level open system, kinetic theory of resonance and relaxation 80−88859
spin-1/2 system, mag. resonance in arbitrarily oriented fields 77−42263
spin-Hamiltonian perturbation energies and state vectors calc., diagrammatic technique 78−65810
submillimetre spectroscopy, applic. to magnetic excitations 77−37955
symmetry adaptation and operator equivalents *(French)* 78−91924
two spin cross relaxations, temp. depend. statistical theory 78−80190
weak field absolute induction meas. HFS magnetometer 78−77949
Al, nonlinear helicon resonance *(Russian)* 77−28208
As, neutron-deficient isotopes, nuclear spin meas. by at. beam mag. resonance 77−18386
$Bi_{1-x}Sb_x$, semicond. alloy, EM wave propag. in direction perpendicular to mag. field 79−60687
Cs, HFS of optically inaccesible excited states 78−37582
Gd-Al, amorphous film, microwave mag. reson. 78−91948
Gd-Al, amorphous film, microwave mag. reson. 78−92060
Ge, electron-hole drop magnetoplasmas, radius-independent elec. and mag. reson. 79−73446
$GeH_4(F_4)$, rot. mag. moment spectra, mol. beam mag. reson. obs. 77−14509
He, subDoppler lineshape obs., of IR mag. reson. Rydberg transitions, using motional Stark effect 78−947
He_2, $a^3\Sigma_u^+$ metastable state, fine struct., mol. beam mag. reson. obs. 78−78720
^{3}He, superfluid A-phase, composite solitons and mag. reson. 77−80674
^{3}He, superfluid A-phase, dynamic spin behaviour in presence of textures 79−1536
^{3}He, superfluid A-phase, linear texture and mag. reson. 79−4451
^{3}He, superfluid A-phase, mag. resons. associated with linear textures 79−60585
^{3}He, superfluid A-phase, planar $\hat{l}$ textures and mag. reson. 77−80673
^{3}He-^{4}He isotope mixtures, mag. resonance line widths of 2^3S_1 states, metastability exchange cross sections *(Russian)* 77−10614
^{4}He, electronic g_J-value of 2^3S_1 state, by atomic beam mag. reson. method 77−23446
^{179}Hf, hyperfine struct. in ground multiplet ^{3}F and nucl. quadrupole moments of ^{177}Hf and ^{179}Hf 77−83520
Hg, atoms, detection by forward scatt. of reson. radiation in mag. field and Voigt effect *(Japanese)* 77−60155
Hg, odd isotopes, Lande factor of 6^3P_0 metastable level *(French)* 78−5162
InSb, charact. and phys. props., review *(Japanese)* 80−39576
^{191}Ir, magnetic hyperfine struct. 78−934
Kr*+Kr, $^3P_2$ state, metastability-exchange and depolarisation, press. broadening of mag. reson. curves 77−71853
Li, atomic beam mag. reson., Ramsey patterns of field depend. transitions 77−71767
$ND_2(NH_2)$, ν_2 band, laser mag. reson., 9-10 micron 80−9601
Na, spin polarisation in flames by optical pumping, mag. reson. transitions 78−29762
Na-He-N_2 dense vapour system, optical pumping, RF spectrum analyser appl. 79−76393
Ne, $2p^53s^3P_0$ state, optical pumping, g-factor, metastability exchange cross section 80−947
Ne, Lamb-dip structure anal., linear and helicoidal polaris. 78−25852
Ne*+Ne, metastability exchange by optical pumping *(French)* 77−61845
Rb, HFS of optically inaccesible excited states 78−37582
Rb, optical pumping of vap. in mag. field, at. alignment 79−31476

magnetic resonance continued
SF_6, mol. beam mag. resonance, rot. mag. moment spectrum 77−34661
SO, and isotopic forms, $X^3\Sigma^-$ state, CO_2 laser mag. reson. spectroscopy 80−9602
SeH($X^2\Pi$), IR LMR spectrum, spin-orbit coupling const. direct determ. 79−76429
$SiH_4(F_4)$, rot. mag. moment spectra, mol. beam mag. reson. obs. 77−14509
^{181}Ta, magnetic hyperfine struct. 78−934
Tl, ground-state hyperfine struct. tensor polarisability 77−6708
^{183}W, magnetic hyperfine struct. 78−934
$^{129}Xe^+$, hyperfine struct., ion-beam mag reson., laser induced fluoresc. for signal detect and state selection 78−41986
$^{131}Xe^*$, hyperfine struct., ion-beam mag reson., laser induced fluoresc. for signal detect and state selection 78−41986
$Xe^* + Xe$, $^3P_2$ state, metastability-exchange and depolarisation, press. broadening of mag. reson. curves 77−71853
YGdIG, with various domain wall orientations, natural spin reson. 80−66040
YIG, Bi-substituted, LPE, domain wall reson. 80−60387
^{91}Zr, magnetic hyperfine struct. 78−934

magnetic resonance spectrometers
amplifier-generator for nuclear acoustic resonance spectrometer 80−27324
APR investigation by low-temp. spectrometer using Bragg diffraction of laser light 80−27326
atomic beam magnetic resonance system for on-line hyperfine struct. meas. in short lived nuclides 78−25379
atomic-beam mag. reson. spectrom. 78−16824
auto-increment circuit, for digital pulse programmer 77−79134
autodyne detector of acoustic nuclear magnetic resonance 79−17457
automatic calibration by EPR spectroscopic magnetometer 78−89513
automatic magnetic field control, 0.1 to 2 T *(French)* 79−30450
automatic magnetic induction meter phase detectors anal. *(Polish)* 78−70171
automatic NMR field-freq. lock, pulsed phase locked loop approach 78−74041
automatic NMR gaussmeter *(Polish)* 77−79133
auxiliary system for broadband NMR on strongly magnetic systems 78−70172
balanced resonator for ESR research 77−53966
benzil crystals, triplet state spin-lattice relaxation, zero field magnetic resonance spectrometer analysis 79−97409
bridge RF spectrometer, high freq. preamplifier 80−22380
broadband transmit/receive circuit for NMR 78−89520
coherent spectrometer, for ^{14}N NQR of hexamethylenetetramine complexes 77−10075
computer controlled wide line CW double NMR spectrometer 78−45667
cross-polarisation ^{13}C NMR with magic angle spinning, appl. to fossil fuels and polymers 80−77819
cryopump system, for QQDDQ Big Karl magnet spectrometer 79−63257
CW NMR spectrometer, appl. short spin-lattice relax. time meas. 77−57374
design and circuitry for 100-1200 MHz use 77−30189
diaphragmed, analysis and definitions for momentum transmission 79−67366
diaphragmed, first-order calcs. of momentum transmission 79−67367
differential EPR susceptance unit, USSR primary standard 77−30190
digital lock-in amplifier simulation 77−151
dispersion-absorption plots, for spectral line shape anal. 78−89511
ELDOR spectrometer with computer-controlled scanning 77−1619
electron-nuclear-nuclear triple-reson. spectrometer 77−41662
ENDOR, low impedance design 80−246
ENDOR cavity for electron spin echo experiments 78−82013
ENDOR cell operating in 120-350 G field 78−4671
ENDOR resonant helix cell with high RF fields for steady-state experiments 79−49264
ENDOR spectrometer, computer-controlled 79−80654
EPR, block for electronic digital sweep of mag. field 77−26371
EPR, Hall effect generator for magnetic field regulator *(Polish)* 78−41340
EPR, magnetic field stabiliser using directly coupled IC op. amps *(Czech)* 79−26095
EPR, microwave cavity for high hydrostatic pressures 78−89518
EPR, microwave cavity variable coupling with solid construction 77−13790
EPR, resonant cavity microwave polarimeter, meas. of Cotton-Mouton-Voigt effect *(French)* 78−89514
EPR cavity matching device for use at low temperatures 78−54420
EPR cavity sensitivity improvement 78−54419
EPR high-temperature cavity for easily oxidised fluorides 80−77831
EPR method of appl. strong electric fields at low temp. 79−21792
EPR multipurpose cavities, 1.6-1300K appl. 78−8430
EPR signal recording unit at modulation freq. of mag. field 79−21795
EPR spectrometer, 2 mm band, with re-entrant resonator 78−86311
EPR spectrometer, 34-370 GHz, 77-550K, zero field splitting of Fe^{3+} in rutile and andalusite *(Russian)* 77−57372
EPR spectrometer, conversion to 1 MHz field modulation 77−49759
EPR spectrometer, second harmonic extsn. for saturation transfer meas. 79−40599
EPR spectrometer, simple temp. controller, 85-400K *(German)* 78−45663
EPR spectrometer attachment for studying materials in 120 to 350K. 1-10^4 atm. range 80−105686
EPR spectrometer with klystron freq. control and ICs 79−21796
EPR spectrometer with mag. field modulation in 10 Hz to 1 MHz range, 30 MHz IF amplifier 80−98955
EPR spectroscopy in strong elec. fields at 77 and 4.2K 78−86310
EPR superheterodyne spectrometer for Si defects detect. 77−43885
EPR techniques, developments 78−74045
EPR tensile testing apparatus 78−85086
EPR X-band and Q-band spectrometers, liquid He cooling units 77−2675
EPR/ENDOR, modified Ka-band spectrometer, obs. of electron spin echoes at 35 GHz 80−13113
ESR, superheterodyne, for UHF in temp. range 0.04-4.2K 78−257
ESR dual sample cavities for Q-band and spectrometers with small magnets 79−58761
ESR pressure cell for meas. at hydrostatic pressures to 60 kilobars 78−54418

magnetic resonance spectrometers continued
ESR spectrometer, synchronous detector 79−35802
ESR spectrometer with wideband resonator for aqueous samples 77−10081
ESR spectrometers with crossed resonators in K-X range 77−87798
ESR/ENDOR spectrometer sensitivity enhancement using microwave amplifiers 78−82014
ferromagnetic resonance absorpt. lineshape 24 GHz microwave transmission apparatus 77−49755
field-frequency lock, for a superconducting spectrometer 78−86312
Fourier NMR spectrometer, TESLA BS 497 adaption *(Czech)* 79−6157
Fourier transform, NMR spectrometer, magic-angle rot. 80−105688
Fourier transform NMR spectrometer, pulsed field gradient system 80−57353
FT NMR sensitivity improvement for spectrometer using double-tuned receiver coil 80−31824
FT NMR spectral phase and intensity anomalies reduction for Varian XL-100 spectrometer 77−45873
glass capillary for high resolution NMR measurements at pressures up to 400 MPa 78−65950
high resolution, high pressure, commercial NMR spectrometer modifications, vol. of activation meas. 78−45664
high-pressure chamber for pulsed NQR spectrometer 78−86308
high-resolution multipulse NMR spectrometer 78−58000
high-resolution NMR spectrometer field homogeneity rel. to pole tip edge saturation 79−30522
high-temp. EPR spectrometer with CO_2 laser-heated sample holder 80−68233
instrumental techniques and design improvements 79−30519
laser magnetic resonance spectrometers, sensitivity improvement using laser properties 80−13115
low-temperature UHF detector, with low noise preamplifier based on n-type InSb 80−68230
magnetic field modulator, EPR radiospectrometer having discrete set of modulation frequencies 80−52285
magnetic flux stabiliser, resonance conditions stabilisation 80−52286
magnetometer system, automatic field-tracking, 0.1 to 3.2 T, for use with ESR/NMR spectrometers 79−63279
metallic magnetic resonance meas. using limiting oscillator circuit with improved S/N ratio 79−26096
microcomputer-based data acquisition system for NMR spectrometer interfacing 78−74042
microwave, for ferromagnetic resonance of wide resonant lines *(Slovak)* 79−12829
microwave cavity Q-factor meas. appl. *(Polish)* 78−93728
microwave spin resonance spectrometer, influence of nonlinearity of microwave network characteristics 80−62707
model magnet, reproducibility of fields, field heights and magnetisation props. of materials *(German)* 78−24832
moderate-pressure low-temperature spectrometer for paramag. reson. appl. 78−266
multichannel synchronous detector for NQR signals 77−61098
NMR, automatic system, for recording, processing and summation 80−27327
NMR, commercial spectrometer modification for rot. frame spin-lattice relax. meas. 80−22407
NMR, current shim calcs. in form of flat conductors 79−80652
NMR, CW, signal intensity, effect of coil design parameters 77−49756
NMR, Faraday screen for crossed coil instrument 78−4670
NMR, for quantitative analysis, microprocessor-controlled digital integrator 80−11971
NMR, for simultaneous multinucl. NMR by alternate scan recording of ^{31}P and ^{13}C spectra 80−26426
NMR, Fourier transform, resolution enhancement, digital filtering by sinusoidal window 79−93195
NMR, Fourier transform, small signals meas. in presence of intense peaks 79−93196
NMR, Fourier transform, standard spectrometers use for multicomponent self-diffusion meas. by spin echo 80−22401
NMR, high resolution by susceptibility compensation of detection coil 78−12736
NMR, line-broadening mechanisms, dispersion-absorption plots 78−89512
NMR, lock-type cell for high pressures and low temps. 78−54416
NMR, magic angle spinner, high-speed 78−89516
NMR, magnetic field in superconducting solenoid meas. method *(Czech)* 80−13107
NMR, multipurpose 7T, with superconducting magnet 79−97411
NMR, noninvasive meas. of biological information, magnetic focus generation *(Japanese)* 78−85355
NMR, probe design 77−53967
NMR, programming device for control of frequency synthesizers 80−22400
NMR, proton-enhanced ^{13}C, programmable digital pulse generator 79−58762
NMR, pulse type, programmable pulse sequence generator 80−17979
NMR, pulsed, two channel boxcar integrator appls. 79−80657
NMR, signal to noise ratio, reciprocity principle calcs. 77−13792
NMR, slotted tube resonator as probe head at high freqs. 77−30192
NMR, thermostatically controlled resonant cell 79−93181
NMR, time-sharing control by minicomputer 79−93192
NMR, widebore supercond. magnet systems, sideways-spinning 20 mm tube probe 79−30518
NMR apparatus for meas. of self-diffusion coeffs. in solids 79−217
NMR detection, appl. of integrated cct. Robinson oscillator 77−74475
NMR double resonance, rotating frame, experimental set-up *(Rumanian)* 79−58763
NMR electromagnet current stabiliser 77−87800
nMR gaussmeter for measuring field distributions of electromagnets 79−2797
NMR high-pressure probe, high-resolution proton NMR 78−89517
NMR imaging, thin-section 78−78728
NMR in internal fields of ferromagnets for freq. range 10 to 230 MHz 80−27325
NMR in undergrad. instruction, general purpose microcomputers use for hypothetical spectra synthesis 80−42009
NMR linear field correction, optimum size of rectangular current shim off mag. pole face 78−86314
NMR meas. of transient species and effects in flowing systems 77−150

magnetic resonance spectrometers continued
NMR measuring head for expts. in supercond. mag., characts., appls. *(German)* 77−41661
NMR of biological systems 78−28148
NMR probe, for combined homonuclear multiple pulse decoupling and magic angle spinning 78−12735
NMR probe and preamplifier for low freqs., fast recovery and high sensitivity 79−35806
NMR probe assembly, He-cooled, for proton-enhanced ^{13}C reson. 80−17978
NMR probe double-tuned matching boxes for experiments at 94 and 100 MHz 77−45874
NMR probe for high-pressure and high-temp. expts. 80−22403
NMR probes, acoustic ringing effects 78−86313
NMR pulse frequency-ratio spectrometer for investigating isotopic effects of light nuclei 79−21793
NMR pulsed broadband spectrometer 79−49265
NMR pulsed spectrometer wideband preamplifier 79−71502
NMR Q-meter spectrometer modification, servomechanism for automatic tuning *(French)* 77−18061
NMR radio spectrometers, meas. of field uniformities in gap of precision magnets 80−105683
NMR radiospectrometer electromagnet field uniformity rel. to pole piece shape and material 78−86309
NMR radiospectrometers, calc. of optimal configuration of shims 80−73398
NMR receiver, description and design 78−21193
NMR relaxation times, computer-assisted meas. method 77−22586
NMR signal enhancement by rod-induced convection 80−77823
NMR spectrom., pulsed, 10 MHz, using solid state devices 80−86361
NMR spectrometer, FT, multipurpose, design and computer interfaces 80−86362
NMR spectrometer, low-temp., low-noise circuitry 78−4672
NMR spectrometer, pulse, controlled by programmable digital unit *(Czech)* 78−77952
NMR spectrometer, transverse AC component of magnetisation detected by transverse SQUID 80−37064
NMR spectrometer interfacing 79−12828
NMR spectrometer-computer interface, demonstration expt., signal averaging influences on S/N ratio 80−36813
NMR spectrometers, SQUID-based sensitivity limit 80−98961
NMR spectroscopy, digital pulse programmer cct. 77−74474
NMR thermometry at ultra-low temperatures, appl. 77−17985
NMR Varian CFT-20 spectrometer/computer system, data retrieval technique 78−77954
NMR Varian XL-100-15 spectrometer, 22 mm probe construction 78−77955
NMR Varian XL-100-15 spectrometer, multinucl. 18 mm probe construction 77−57376
NMR weak signal recording by second-harmonic oscillogram 77−10080
NMR wideband detectors, R-LC and autodyne types, performance comparison 77−74473
NMR/ESR wide-line spectroscopy, inexpensive phase sensitive detector system 77−13791
nonexponential nuclear relaxation data acquisition and processing system using Nairi-2 computer 78−32800
NQR, continuous-wave scanning, signal recovery system 78−74039
NQR, CW, signal intensity, effect of coil design parameters 77−49756
NQR, programming device for a spin-echo installation 80−17972
NQR, pulsed spectrometer for metre and decimetre ranges 77−10076
NQR, small sample enhanced coupling using ferrite coils 80−52287
NQR, weak signal relax. meas. with Sigma type digital storage device, pulse-train program blocks 80−17970
NQR absorption precision thermometer 77−5841
NQR and NMR CW spectrometers, RF coil and signal intensity 78−89515
NQR injection and phase locked spectrometer for Zeeman NQR studies 80−54979
NQR pulse spectrometer modulator 80−17971
NQR scanning spectrometer, improved super-regenerative oscillator and quench generator 78−8429
NQR short range remote spectrometer for anal. 80−55742
NQR signals, detection method 77−13786
NQR spectrometer, digital freq. modulation 78−21189
NQR spectrometer, fast pocket computer frequency-controlled 79−80655
NQR spectrometer, super-regenerative, continuous freq. monitoring 79−63190
NQR spectrometers for precision measurement of temp., optimisation *(Russian)* 80−22412
NQR temperature meas. and regulation system 77−10020
NQR thermometer, capture effect 77−10018
NQR thermometer, pulsed, for temps. up to 870K 77−13749
NQR thermometer circuit 77−10019
NQR thermometer with high precision 77−10017
nuclear quadrupole double resonance spectrometer with programmable calculator control 79−12830
nuclear quadrupole type for Cl compounds, superregenerative oscillator scheme *(Slovak)* 77−18059
null line stabiliser of NMR spectrometer with time division 79−2800
ODMR spectrometer system, use of signal averager with minicomputer facilities for control, data recording and evaluation 80−31825
off-resonance nuclear spin-lattice relaxation time, pulsed NMR method for mol. motion in condensed phases 79−78554
panoramic pulsed NQR spectrometer programmer, design, basic functions 77−61100
PMR, 90 MHz multiple pulse spectrometer 77−48060
polarimeter, for 8 mm (35 GHz) band, MnF_2 Cotton-Mouton-Voigt effect *(French)* 78−74040
probe cct. with transmission line tuning for double nucl. mag. reson. 77−26375
probe for double NMR 78−264
probehead for double NMR based on crossed slotted tube resonator 78−265
programmable timer for pulsed NMR spectrometers 79−40598
pulse generator, HF oscillator with single coil transducer, for NMR spectrometer 79−2802
pulse programmer for high power nuclear resonance equipment 77−10079
pulse programmer for high resolution multiple pulse NMR in solids *(German)* 77−41660

magnetic resonance spectrometers continued
pulsed FT NQR spectrometer, automation for single crystal Zeeman studies 80−66066
pulsed NMR, anal. of homogeneous RF field delay line probe 77−49758
pulsed NMR, digital integrator 77−26372
pulsed NMR spectrometer, high-isolation duplexing switch 80−86363
pulsed NMR spectrometer, thyristor temp. regulator 80−105687
pulsed NMR spectrometer incorporating microprocessor, operational, software and hardware details 78−45666
pulsed NMR spectrometer incorporating phase-splitting circuit 80−62704
pulsed NMR thermometry below 0.1K 77−5852
pulsed NMR transmitter, for relaxation time meas. in biological samples, construction and operational details 78−93745
pulsed NQR-FFT radiofrequency spectrometer for ^{14}N, description and operation 80−17982
pulsed panoramic RF spectrometer for NQR 77−10074
RE-1306 radiospectrometer for crystals obs., using LF modulation of magnetic field 80−57350
RF switch, linear, MOS transistors, analogue signals, NMR and nuclear quadrupole resonance pulse spectrometer appl. 77−10078
RYa-2308 radiospectrometer, attachment for obs. of DNMR in ^{31}P 80−98957
scanning NQR spectrometer freq. marker system 78−21191
signal register, IC, for pulsed two-freq. NQR spectrometer 77−61099
single channel two freq. ^{14}N NQR pulse spectrometer, multiplet spectra 80−17968
single crystal NMR probe and circuitry *(Chinese)* 79−35807
single-channel quadrature detection, improvement of technique, Fourier transform NMR spectrometers 77−45875
single-coil triple-tuned NMR probe for simultaneous stimulation of ^{1}H, ^{2}H and ^{13}C resonances 80−86364
SQUID NMR meas. at low-temp., improved technique 78−54417
stroboscopic integrator for studying NQR relax. processes 80−17969
submillimetre laser sources for magnetic resonance spectroscopy, standard frequencies 77−13788
superconducting NMR, efficient decoupler coil design to reduce heating in conductive samples 80−31828
teaching, mobile spectroscopy, chem. anal. laboratory 78−93502
temperature controller for ESR and NMR spectrometers 79−35803
temperature variator coupling to EPR radiospectrometer 78−58003
time resolved ESR, time profile meas. and anal. 77−5878
time sharing method in high modulation NMR of fluids *(German)* 78−16822
transmission EPR spectrometer, appl. of tunable waveguide refl. maser. 78−5443
transmission oscillator US spectrometer with new calibration technique 77−67486
transmitter for low-frequency pulsed NQR spectrometer 77−61101
triple NMR technique for N-containing molecules, ^{13}C-{^{1}H,^{14}N} triple reson. 79−81219
tuned limiter for receiver amplifier in a fast-recovery pulsed NMR spectrometer 78−70173
two radiation source spectrometer, signal decrease, beat phenomena *(French)* 78−41338
two-mode hybrid resonator for nonlinear magnetisation expts. 78−58001
two-way EPR cavity, for Stark effect meas. on NO_x 80−90872
two-way ESR cavity for magnetic- and electric-dipole transitions 79−17459
UHF spectrometer for NQR studies at liquid N_2 temp. 80−13114
variable temperature probe, magic angle rot. H NMR spectra meas., polymer gel appl. 80−31830
Varian EM-360 NMR spectrometer interface with Altair 8800B microcomputer 78−89519
Varian HA-100D NMR spectrometer improvements for double NMR and ENDOR expts. 79−80651
Varytemp NMR for pulse spectrometers, applic. to lineshape determ. 77−2674
X-band cavity for electron spin resonance experiments 80−248
X-band ESR spectrometer, microwave kit for conversion to K-band operation 78−21192
XL-100 spectrometer, design of voltage-controlled oscillator 80−71211
Ag beam mag. resonance apparatus as freq. standard, features 78−89458
CO laser, quantitative detection of NO_2 in ppm of N_2 77−12855
^{13}C NMR probe for high resolution Fourier spectroscopy, cw time sharing appl. *(German)* 78−16823
Cl NQR spectrometer with exact reading of resonant freq. 80−42247
^{14}N NQR, observation equipment and techniques 80−22399

magnetic resonance spectroscopy
acoustic ringing effects in pulsed nuclear magnetic resonance probes 78−86313
l-alanine powder, short dipolar relaxation time meas. by saturation method 80−60441
Anderson localisation of mol. excitons, substitutionally disordered systems 77−89733
anisotropic motion, and reson. line shape 80−7144
autotype detector, spin resonance detection 80−22397
composite transducer for longitudinal strain modulation for ESR and optical spectroscopy 79−12791
computer programmable digital pulse generator for Fourier NMR spectroscopy 80−98959
cryostat for low-temp. EPR studies 80−86321
current filament over conducting layer, non-stationary magnetic field calc. *(Czech)* 80−52283
digitised EPR system, appln. to saturation transfer 80−77825
2,6-dimethylbenzoic acid, ^{1}H chem. shift recovery from combined multiple pulse NMR and sample spinning 80−32738
discharge-flow systems, noise reduction in EPR studies 79−39256
dynamic NMR spectroscopy, mechanistic obs. of rearrangements and exchange reactions, review, book contrib. 79−30521
eigenvectors and eigenvalues from mag. reson. results, error estimation by linear data-fitting techniques 80−68018
electron spin echo modulation spectroscopy, envelopes ratio anal. in disordered matrix 79−88991
EPR, elec. field modulated, appl. to study of ferroelectrics 80−75841
EPR, instrument cavities, TE_{011} and TE_{102}, inhomogeneous static fields, spurious line feature obs. 80−31833
EPR, ns time-resolved, in pulse radiolysis, via spin echo method 80−43075

magnetic resonance spectroscopy continued
EPR analysis, accuracy improvement 79−52827
EPR Dewars containing liq. N_2, bumping elimination 79−40600
EPR intensity standard, description and use 79−54164
EPR standard, Picein 80 cement, for g-factor and spin conc. determination 79−80658
ESR, appl. in photosynthesis, review 79−92450
ESR meas. at hydrostatic pressures to 60 kilobars 78−54418
ferromagnetic-resonance linewidth meas. method and apparatus 80−22411
flint artefacts, ancient heat treatment identification by ESR spectroscopy 79−12831
fluorite lattices, $^{19}F^-$, self-diffusion, spin lattice relax., NMR techniques 80−34801
Fourier transform multiple quantum NMR 80−31819
free radicals, high resolution spectroscopy *(Japanese)* 79−79355
FTNMR, effect of inhomogeneous mag. field on line shape and resolution enhancement 79−63289
heteronuclear cross-correlation spectroscopy, rot. frame coherence transfer theory 79−97412
high power pulsed NMR, automation and control 80−86359
high pressure, using 20 kbar pressure system employing reciprocating hand pump 79−67335
INDOR, pseudo, heteronuclear selective decoupling, automatic, using Fourier transform NMR spectrometer appl. 79−93185
laser magnetic resonance using optically pumped far IR laser 77−54725
liquid, electron spin echo phase memory decay, generalised cumulant expansions appl. 79−11334
liquid crystals, dipole coupled ^{13}C NMR technique 79−99073
Lorentzian lineshapes and isotropic distrib. of molecules, analytical expressions derived for powder samples 80−60401
low field magnet, computer controlled, for optical and magnetic resonance studies 80−95113
macromolecular spin-labelling using Woodward's reagent, appl. to polyacrylic acid 79−96308
magnetic bubble films, spin wave and magnetoelastic resonance meas. 78−91913
microprocessor-controlled target polarization monitor using NMR 79−88990
microwave network characteristics, influence of nonlinearity on shape of mag. resonance spectra 80−62707
modified pulsed gradient technique for measuring diffusion in the presence of large background gradients 80−31831
molecular spectroscopic laboratory strategies, queueing theory and digital simulation use 80−30299
multinuclear magnetic resonance spectroscopy, universal referencing, solvent effects 80−73402
multiple pulse NMR cycle technique, appl. to homonuclear dipolar decoupling in solids 79−67365
multiple pulse zero-crossing NMR technique, rel. to ^{19}F chem. shift in solids 79−9230
nematic liquid cryst., one-deuteron system, multiple quantum spin-echo spectroscopy 80−31832
neutron spin-echo integral transform spectroscopy 80−4748
NMR, broad-line, reduction of spurious baseline effects 79−75562
NMR, double sample cell technique for mag. susceptibility meas. in solid ^3He 79−63225
NMR, Fourier, S/N ratio optimisation, influence of receiver circuit and digital processing *(Czech)* 79−17461
NMR, Fourier transform, resolution enhancement using double exponential function 79−35804
NMR, Fourier transform, standard spectrometers use for multicomponent self-diffusion meas. by spin echo 80−22401
NMR, group theory, independent-particle Hamiltonian 80−43074
NMR, high-resolution, broadband decoupling and scaling of heteronucl. spin-spin interactions 80−17980
NMR, homonuclear selective population inversion in AB system 80−75865
NMR, J-resolved, two-dimensional, spin decoupling, appl. to 2,3,4-trichlorphenol 80−31823
NMR, measurement of nuclear spin-lattice relaxation times based on null method 80−22402
NMR, multiple-quantum coherence, selective excitation, appl. to benzene 80−23439
NMR, phase-modulated spin echoes, derivation of pure absorpt. spectra 80−22410
NMR, population distribution to enhance sensitivity and allow decoupling of low gyromagnetic ratio nuclei 80−73399
NMR, pulse Fourier transform, commercial waveform analyser use 80−17977
NMR, rot. frame, ^{13}C spin-lattice relax. using proton decoupled Fourier transform spectra, errors origin 80−18945
NMR, selective excitation with single-freq. off-reson. decoupling 80−17981
NMR, simultaneous multinucl., by alternate scan recording of ^{31}P and ^{13}C spectra 80−26426
NMR, solid, 'magic angle' spinning apparatus 80−17983
NMR, two-dimens. spin-echo spectra, anomalous spinning sidebands 80−17976
NMR, zeugmatography, rotating frame 79−93186
NMR bandshape, complex exchange-broadened, iterative computer anal. 79−35805
NMR data bank, ^{13}C, DARC PLURIDATA system 80−30298
NMR detector, transistorised marginal oscillator, for student lab. 80−27078
NMR Fourier transform spectroscopy, free induction decay, resolution enhancement function 79−80656
NMR Fourier transform spectroscopy, high-field, of biological systems 79−39457
NMR image resolution from sensitive line method, magnetisation vector 79−93182
NMR imaging of biological objects, sensitivity, performance time 79−96718
NMR imaging rotating frame selective pulses 80−68232
NMR in undergrad. instruction, general purpose microcomputers use for hypothetical spectra synthesis 80−42009
NMR J cross-polarisation in liquids, refocusing method 80−22406
NMR limb blood flowmeter, clinical appls. 80−17178
NMR meas. at ultra-low tapes, S/N ratio, appl. to thermometry 80−73400
NMR medical imaging, resolution and S/N ratios 80−26406
magnetic resonance spectroscopy continued
NMR probe assembly, He-cooled, for proton-enhanced ^{13}C reson. 80−17978
NMR probe heating furnace for high mag. field use 80−247
NMR pulsed, automatic trigger pulse logic for pulse programmer 80−47084
NMR spectra recording processing and accumulation, using mag. tape system *(Russian)* 79−26097
NMR spectrometers, high freq. effects 80−77829
NMR spectroscopy, appl. to organic compounds anal. 80−16756
NMR spectroscopy, high resolution, using nematic liq. crysts. with negative anisotropy 79−40596
NMR spectroscopy, resolution enhancement, effective sample volume restriction effects 80−31836
NMR spin echo, rotating solid sample, Fourier transform anal. 79−65759
NMR spin imaging by mag. field modulation 80−90873
NMR spin-lattice relax. time meas., fast inversion-recovery technique 80−77826
NMR-ESR spectroscopy, miniature magnetic assembly, teaching 80−105467
NMR-NQR double resonance, two-freq. methods, resonance spectrometers 80−20512
NNR, multiple pulse, of solids, accurate phase adjustment 80−22404
nonlinear absorption method in magnetic field for spectral line width and shift meas. 80−37066
NQR, bisymmetric Zeeman modulator 80−98960
NQR, electronics appls. 80−63668
NQR, pulsed spin locking technique, theory 80−98958
NQR, quantum kinetic theory 80−52288
NQR T_1 relax. time meas., steady state pulse method, master eqn. 80−54975
NRM, error theory, target factor, appls. 79−49263
nuclear magnetism of liquid systems in the Earth field range, review 80−50206
nuclear spin-lattice relaxation measurement, variable perturbation method 80−22408
ODMR, modulation technique, discrimination between homogeneous and inhomogeneous lines 79−44923
optogalvanic double-resonance spectroscopy 80−57385
paramagnetic centre inhomogeneous distrib. meas. by EPR 79−93184
phase diagrams, construction, use of NMR, Mossbauer effect, and gamma ray perturbed angular correlation 79−8417
photographic emulsion supersensitization by Dember effect, ESR meas. 79−20423
photon counter, microprocessor-controlled, for pulsed ODMR 79−88992
PMR, tunable notch filter for solvent elmination 80−22405
polyethylene tube insert, for tritiated NMR sample handling 79−40546
propylene copolymers, ethylene incorporation meas. by ^{13}C NMR and IR spectrosc. 79−39225
proton 2D J spectra, phase-sensitive displays 80−77830
pulse NMR, spurious ringing 79−93187
pulse radiolysis, applic. of NMR and CIDNP 77−32814
pulsed Fourier transform NMR spectroscopy resolution enhancement, multiple pulse technique 79−40595
pulsed magnetic field gradient programme, meas. of water diffusion adsorbed on protein mols. 79−21794
pulsed NMR, high resolution, adjusting conditions of pulse sequences 80−93184
pulsed NMR, microcomputer system, appl. *(Japanese)* 79−75564
pulsed NMR in solids, survey 80−34782
quick access sample system for low temp. K-band ESR and ENDOR 80−57352
RF preamplifier, tunable, low-dissipation, for low temp. NMR appls. 79−17458
saturated bandshapes of coupled multispin systems, simple line approx. anal. 79−75561
saturation transfer EPR spectroscopy detection system by Fourier transformation 80−86357
scaling of heteronuclear spin interactions by multipulse sequences 80−73405
semiconductors, optical orientation of electronic and nuclear spins 78−79928
solid materials, high resolution ^{13}C NMR spectroscopy 80−97150
solid state ^2H NMR, magic angle sample spinning to remove quadrupole broadening 79−97410
solid state NMR, selection of nonprotonated ^{13}C resons. 80−50201
solid torsional oscillators, rotating frame, nucl. spin polarisation losses, torsional spectroscopy 80−31821
solution NMR, enhanced selection of non protonated C resonances, ^{13}C spin echo obs. 80−31835
spectral simulation via finite elements, variational method and stochastic-Liouville eqn. 79−85157
spin-lattice relaxation time meas. using saturation, inversion and fast inversion expts. 80−57356
spin-lattice relaxation times meas., mathematical formulation 80−62703
SQUID detection of high sensitivity mag. reson. 79−75560
SQUID detection of NMR, appl. to liq. ^3He 79−67368
stationary NMR signals, theory, dynamic freq. shift effects *(Russian)* 79−22734
successive oscillatory fields, molecular beam resonance method 80−91706
super-regenerative NQR spectrometric obs. of apparent spin-spin time 80−54963
TGS, proton and deutron NMR anal. of temp. depend. 80−33919
thymopoietin active fragment in H_2O, soln. conformation by DNMR spectroscopy 80−89710
transmission electron spin resonance, experimental methods *(Japanese)* 79−75563
transversely polarised deuteron target for kaon-nucleon interaction studies 80−37669
two dimensional ^{13}C NMR spectroscopy, high sensitivity 80−31826
two radiation source spectrometer, signal decrease, beat phenomena *(French)* 78−41338
two-centre integrals involving one-electron dipolar coupling and Slater AOs, computational procedure 80−23291
Voigt lineshape, evaluation and characterisation 80−73401
yaRV-2 compact automatic nuclear resonance hygrometer 80−105657
zeugmatographic imaging, gradient control device using microprocessor 80−89822

magnetic resonance spectroscopy continued
BO_2, gas, optically detected mag. reson. spectrum, $X^2\Pi$ rovibronic sublevels 78−82756
Ba, atomic beam and resonance spectroscopy 80−58180
$^{13}CO^+ + CO$, charge-exchange detection of $^{13}CO^+$ electronic absorption spectrum, hyperfine consts. calc. 78−70822
^{13}C Fourier transform NMR, method for tailored detection of signals 79−40597
^{13}C NMR spectroscopy, 270 and 90 MHz, ^1H noise decoupling field heating effects 79−38389
^{43}Ca, atomic beam and resonance spectroscopy 80−58180
CdS crystal, magnetic field intensity meas. by obs. of Faraday effect 78−93739
Cl NQR spectroscopy, parametric superrogenerator with phase quantisation application 80−22398
ClO_2 radical, ν, band, tuning by avoidance of Zeeman level crossing 78−94263
DO_2, ν_2 fundamental band, 9.8 micron, laser mag. reson. spectroscopy 79−85961
HO_2 radical, ν_3 fundamental band, laser mag. reson. 78−66566
^1H, hydrostatic liquids for obs. of NMR at high press. and low temp. 79−2801
^{15}N NMR, J cross-polarisation for signal enhancement for liquids 79−78537
^{14}N NMR, single cryst., separation of dipolar and quadrupolar splittings, new technique 80−25217
^{14}N NQR, observation equipment and techniques 80−22399
^{15}N NMR heteronuclear spectroscopy, two dimensional Fourier transform technique 80−31818
^{17}O, NQR at natural isotope abundance, double reson. new techniques 80−53013
SO, $a^1\Delta$ state, laser mag. reson. spectrosc. 78−94265
$SeH(X^2\pi_{3/2})$, far IR LMR spectrum 78−66564
YCo_3, amorphous ferromagnet, exchange dominated surface modes 78−52359

magnetic screening *see magnetic shielding*

magnetic semiconductor materials *see magnetic semiconductors*

magnetic semiconductors
antiferromagnet, spin-magnetomagnon resonance 80−2566
antiferromagnetic, ferron-polaron states of carriers 77−69257
antiferromagnetic, heavily-doped, stability of canted order 77−12095
antiferromagnetic, magnetostriction ferrons 78−88160
antiferromagnetic, magnon-plasmon interaction and its effect on Raman scatt., theory 78−56302
antiferromagnetic, sound propagation 78−72211
antiferromagnetic degenerate semiconductor, thermal and mag. props. 78−19224
antiferromagnetic Faraday light depolarisation in mixed mag. states 80−29726
antiferromagnetic resonance rel. to surface impedance, magnetoelastic contrib. 80−50200
antiferromagnetic semiconductor, magnon-spin flip excitations in Raman scatt., g-factors 77−66494
antiferromagnetic semiconductor, spin-wave amplification 80−7099
antiferromagnetic semiconductor, theory of Raman scatt. due to magnon-spin flip excitation 77−36209
antiferromagnetic semiconductors, magnetoelec. effect, magnetization and ferroelec. props. 80−25180
chalcogenide spinel-type, crystal growth using closed tube vapour transport method *(Japanese)* 80−25539
chalcogenide spinels, Faraday effect optical isolators for CO_2 laser system 78−50816
chalcogenide spinels, specific heats 79−11315
chalcogenide spinels, thermal stability, thermochemical, thermodynamic and crystallochemical props. 77−51519
conduction electron spectrum, influence of nonlinear spin waves 79−28270
conductivity electrons, energy depend. on wave vector *(Russian)* 78−43580
conference, Montpellier, France (Sept. 79) 80−94916
coupled LO phonon-plasmon modes 79−73459
degenerate, mag. excitations, light scatt. 77−63161
dichalcogenides, pyrite-type, ^{57}Fe isomer shift, quadrupole splitting, Mossbauer study 80−15832
doped semiconductors, local spin-density-functional method, appl. to metal-insulator transition 80−96789
double exchange and small-polaron hopping 79−19591
electron density dependent ordering parameter and role in elec. prop. anomalies *(Russian)* 77−43582
electron propagation, s-d model, red shift theory 77−51736
electron spectrum, light absorpt. spectrum, calcs. 80−2793
electron spin-lattice relaxation in ferromag. metals and semiconds. *(Russian)* 80−103823
electron struct. and indirect exchange mechanisms 80−25123
electronic properties, critical behaviour, theory 80−96861
EuSe, photocond. and photodiffusive voltage spectra 80−96940
exchange interaction, indirect, between localised moments 80−93079
exchange interaction mechanism, effect of doping 78−31064
exchange interaction mechanisms, theory *(Russian)* 78−39312
exchange interactions, long-range 77−69531
exciton ferromagnetism 79−28293
ferrimagnetic, cyclotron-magnon reson. 79−69725
ferrimagnetic, magnetomagnon reson. 79−69663
ferromagnet, anomalous Hall effect, s-f model 78−10478
ferromagnet, autolocalised electron states 78−51924
ferromagnet, CESR in strong alternating electric field 78−35038
ferromagnet, CESR line width, two-magnon exchange splitting 80−29621
ferromagnet, light scatt. from magnons under strong fields, appl. to $CdCr_2Se_4$ 78−84554
ferromagnet, magnon coupling to plasmons and LA phonons, s-d model 80−29536
ferromagnet, magnon instability, under intense EM field 77−40048
ferromagnet, refr. index variation in strong alternating mag. field 80−23741
ferromagnet in quantizing mag. field, spin wave spectrum 78−19236
ferromagnet s-d model, electronic struct. from lowest six momenta 80−39732
ferromagnetic, absorpt. edge and cond. band width, temp. and mag. field depend. 77−36267

magnetic semiconductors continued
ferromagnetic, acoustic plasmons 80−7098
ferromagnetic, anomalous carrier density mag. field depend., EuSe appl. 80−49774
ferromagnetic, bound mag. polaron 79−90976
ferromagnetic, carrier mobility, electron-two magnon scatt., Hall effect 78−51992
ferromagnetic, carrier-assisted magnon contrib. to phonon damping 77−20018
ferromagnetic, dielectric function depend. on magnetisation, light absorpt. coeff. *(Russian)* 80−15467
ferromagnetic, doped, electron spin polarisation and conduction band struct. 80−65449
ferromagnetic, electric field response and electrofluctuation instability *(Russian)* 78−56083
ferromagnetic, electronic props., effect of electron-ion spin coupling 77−28359
ferromagnetic, electronic quasiparticle spectrum in sf-model 78−52188
ferromagnetic, electronic spectra, s-d model, method of moments 80−7070
ferromagnetic, energy and mobility of spin polarons 80−70982
ferromagnetic, heavily-doped, surface magnetisation 77−8385
ferromagnetic, HF magnon generation by pumping *(Russian)* 77−24686
ferromagnetic, localised states on imperfections and red shift of absorpt. edge 77−66527
ferromagnetic, longitudinal response function 77−72831
ferromagnetic, magnon damping under intense radiation 77−63150
ferromagnetic, magnon-plasmon system 79−69659
ferromagnetic, nonlinear magnetoelec. effect 77−20676
ferromagnetic, paramag. waves travelling near the paramag. resonance freq. 78−88168
ferromagnetic, phase transition and instability of homogeneous state 77−28398
ferromagnetic, Raman scatt. due to magnon-spin flip of cond. electrons 77−20839
ferromagnetic, red shift effect, optical absorpt. edge calc. 80−66140
ferromagnetic, s-f interaction on conduction band, red shift effect theory 80−59872
ferromagnetic, spectrum of quantum spin waves in field of strong EM wave 78−91857
ferromagnetic, spin-helicon wave parametric amplification 79−69665
ferromagnetic, surface localised low energy electron-magnon states *(Russian)* 80−88734
ferromagnetic, theory review 80−20369
ferromagnetic, wide-gap, nonlinear galvanomag. effects 77−39862
ferromagnetic, with defects, exchange Hamiltonian 79−82777
ferromagnetic degenerate semiconductor, homogeneous state, phase transition and stability 78−6528
ferromagnetic degenerate semiconductor, magnon spectrum near instability of homogeneous state 79−28516
ferromagnetic degenerate semiconductors, Curie temp. 78−6529
ferromagnetic multivalley anisotropic, electron autolocalisation *(Russian)* 80−92848
ferromagnetic nondegenerate semiconductor, magnetoresistance 80−11019
ferromagnetic nondegenerate semiconductors, magnon drag thermoelec. power calcs. 78−80012
ferromagnetic semiconductor, carrier-assisted radiation pumping of spin waves under strong mag. field 77−55667
ferromagnetic semiconductor, electronic excitation spectrum 80−11149
ferromagnetic semiconductor, electronic spectrum, influence of finite carrier conc. 78−76220
ferromagnetic semiconductor, hot electron relax. *(Russian)* 79−51593
ferromagnetic semiconductor, LF magnetostatic waves with discrete spectrum 77−89792
ferromagnetic semiconductor, localised magnon mode relax. theory 80−70986
ferromagnetic semiconductor, mag. polaron stability 80−96803
ferromagnetic semiconductor, optical transparency, photoferromag. effect, Curie temp. shift *(Russian)* 78−72387
ferromagnetic semiconductor, polaron solitary waves 80−70625
ferromagnetic semiconductor, spectral density approach for s-f model quasiparticle concept 80−80173
ferromagnetic semiconductor, spin polaron props., effect on carrier scatt. 80−60233
ferromagnetic semiconductor, thermoelec. amplification of magnons 78−14748
ferromagnetic semiconductor, two-band s-d model hybridization 80−65446
ferromagnetic semiconductor with mag. impurities, low-energy localised states *(Russian)* 79−19543
ferromagnetic semiconductors, conduction electron heating, critical scatt. effects 79−91040
ferromagnetic semiconductors, cryst. growth, review 77−85923
ferromagnetic semiconductors, electronic quasiparticle spectrum 80−97051
ferromagnetic semiconductors, free carrier absorpt. of radiation 80−97227
ferromagnetic semiconductors, giant blue shift of absorption edge *(Russian)* 77−32401
ferromagnetic semiconductors, hot electron relax. time 80−59996
ferromagnetic semiconductors, parametric amplification of coupled spin, helical and acoustic waves *(Russian)* 80−2621
ferromagnetic semiconductors, parametric excitation of magnetoplasma reson. 79−28623
ferromagnetic semiconductors, short wavelength magnon generation 80−70987
ferromagnetic semiconductors with doubly charged donors, quasiphase transition 79−65684
ferromagnetic semiconductors with hot electrons, instability of coupled spin-helical waves 80−107841
ferromagnets with double exchange, quantum theory 78−19204
free carrier absorption below Curie temp. 79−47440
galvanomagnetic semiconductor voltage and current transducers, Gauss effect compensation 78−77892
heavily doped paramagnetic, linear response functions and magnetoresist. 77−51770
helicon wave propag., hyperfine interaction effect 80−80307
Hubbard antiferromag. semiconductor, electron correlations, weak coupling 78−67969

magnetic semiconductors continued
Hubbard antiferromagnetic semiconductor, collective excitations, weak coupling limit 78−19210
impure, semicond.-metal transition and instability phenomena 77−59257
indirect exchange interaction, mean free path effects 80−97088
intrinsic, indirect exchange interaction, finite temp., valence bands and energy gaps effect 80−59943
intrinsic semiconductor, indirect interactions between localised mag. moments 78−43578
magnetic colour centre, continuum model 79−28321
magnetic semiconductor, light scatt. by magnons, appl. to $CdCr_2Se_4$ and EuTe 77−69805
magnetoelectric effect, classical and quantum theory, magnon drag effect 80−34746
magnon-acoustic phonon interaction 77−72893
many-valley, electron fluctuon states spin direct interactions 80−29364
Mott type, freq. depend. elec. cond. 77−11907
multispin indirect exchange *(Russian)* 78−56311
narrow band gap, ferromagnetism of electrons in filled band *(Russian)* 79−78300
nearly ferromagnetic, spin fluctuation theory 79−65636
ordering in systems with low carrier densities 78−2684
paramagnetism switching off in strong electric field *(Russian)* 78−80124
parametric down-conversion of laser beam 79−64287
photomagnetisation, photoinduced heterojunctions 77−63259
physics of semiconductors, conf., Edinburgh, Scotland (Sept. 1978) 79−95303
Raman scattering of light on plasmon excitations 80−2738
rare earth compounds, $R_2V_2O_7$, (R=Tm, Yb, Lu), physical props. 78−39320
rare earth compounds, Raman light scatt., phonons and valence fluctuations, review 77−63415
rare earth cpds., studies in Soviet Union, review 80−96875
rare earth orthotitanites, unusual mag. props., role of mag. moments 78−84400
resist. and magnetoresist. meas., effect of donor impurities 79−19608
resistivity of magnetic systems, critical behaviour 78−87955
s-f system, excitation spectrum, temp. and band occupation depend. 80−49588
self-trapped electrons 77−59262
semimagnetic semiconductors, mixed crystal, review 80−49702
small polaron form. and motion 80−96882
small-polaron hopping, many-electron approach 79−95409
small-sample mag. semiconductor thermoelectric power meas. installation 80−31795
sound-like plasma oscillations in electron gas *(Russian)* 78−23125
spin polarons in s-d model with off-diagonal exchange 78−34784
spin wave electron amplification theory 80−97083
spinel ferrites, thermoelectric power, effect of exchange interactions 78−43422
static magnetic properties, mean field approach 80−7090
TCNQ salt, dibenzo-TTF-$TCNQCl_2$, one-dimens. mag. semicond., mag. and elec. props. 80−88601
Ba-ferrite, Hall effect 79−38109
Ba-ferrite, Hall effect and electrical conductivity 79−42564
$BaFe_{12}O_{19}$, Hall effect, magnetisation and elec. resist., 30 to 80°C 77−51766
$CaFeO_3$, preparation, cryst. struct., mag. and elec. props. 78−44066
$Cd_{1-x}Ag_xCr_2Se_4$, Ag acceptor states effect on exchange interaction 80−20397
$Cd_{1-x}Ag_xCr_2Se_4$, ferromag. semicond., influence of strong elec. field on microwave absorption 77−28207
$Cd_{1-x}Ag_xCr_2Se_4$, ferromag., magneto-resistance exam. *(Russian)* 78−84238
$CdCr_2O_4(S_4)(Se_4)$, magnetic exchange interactions 77−24690
$CdCr_2S_4$, $Cd_{1-x}X_xCr_2Se_4$, (X=Zn, Hg), optical and magneto-optical surface effects 79−82953
$CdCr_2S_4$ crystal growth, structural defects, physical properties 80−60759
$CdCr_2S_4$, EPR line profiles in paramag. and ferromag. phases 79−28602
$CdCr_2S_4$ Faraday effect isolator, laser damage tests 77−46750
$CdCr_2S_4$ ferromag. semicond. film, props. 78−76175
$CdCr_2S_4$, ferromag. semicond., IR refl. spectra, phonon props. and dielec. function 80−66191
$CdCr_2S_4$, Heisenberg ferromag., obs. of dynamic dipolar crossover, ESR linewidths meas. 79−24209
$CdCr_2S_4$, hot-pressed, optical isolation appl. at 10.6 μm, intrinsic absorpt. props. 78−42368
$CdCr_2S_4$, magnetic semicond., resonance Raman scatt., mag. circular polarisation props. 80−50341
$CdCr_2S_4$, phonon Raman scatt., mag. circular polarization effects 79−8134
$CdCr_2S_4$, photothreshold changes below mag. ordering temp. 80−97406
$CdCr_2S_4$, polycrystalline films, mag. semicond., spinel-type, magneto-optical effects *(Japanese)* 79−47415
p-$CdCr_2S_4$, single cryst., elec. cond. 79−15148
$CdCr_2S_4$, single cryst. prep. and elec. props. 79−38727
$CdCr_2S_4$, single crystal ferromagnetic semiconductor, vapour-liquid transport growth method 77−21013
$CdCr_2S_4$, single crysts., EPR linewidth near Curie point, temp. and susceptibility depend. 77−63272
$CdCr_2S_4$, spin dependent phonon Raman scatt., resonance effects 77−73145
$CdCr_2S_4$, thermodyn. props. 78−51703
$CdCr_2S_4$, thermoreflectance near Curie point 79−78659
$CdCr_2S_4$:Ag, ferromagnetic resonance angular and temp. depend. 79−69730
$CdCr_2S_4$:Cu, magnetic microregions caused by s-d exchange 77−77050
$CdCr_2S_4$:Gd, ferromag. reson. and electrical cond. 79−28626
$CdCr_2S_{4-\gamma}$, spinel, anomalies in paramag. susceptibility, Curie pt. *(Russian)* 77−80910
$CdCr_2S_4(Se_4)$, electron spectrum, light absorpt. spectrum, calcs. 80−2793
$CdCr_2S_4(Se_4)$, ferromagnetic semiconductors, spinel-type, resonance Raman scattering and electronic structure *(Japanese)* 79−47421
$CdCr_2S_4(Se_4)$, spin depend. phonon Raman scatt., band struct. 78−68491
$CdCr_2S_4(Se_4)$, thermoreflectance, photoconductance, Raman scatt. near mag. phase transition 80−97298
$CdCr_2(S_xSe_{1-x})_4$, mag. transition obs. *(Russian)* 77−4517

magnetic semiconductors continued
$CdCr_2S_{4-x}Se_x(O_x)$ X=0, 4, and solid solns., imperfect struct. model from cryst.-chem. investigs. 79−42053
$CdCrSe_4$, ferromag. semiconductor, mag. props. near Curie pt., doping effects 79−1670
$CdCr_2Se$, ferromag. semicond., high field effects, magnon carrier scatt. 78−87981
$CdCr_2Se_3$:Ga, synthesis and photoferromag. effect 77−51936
$CdCr_2Se_4$, crit. behaviour of optical absorption edge 78−35143
$CdCr_2Se_4$, Crit. relax. processes, mag. reson. expts. 80−60425
$CdCr_2Se_4$, crystn. from high temp. soln., $CdCr_2Se_4$-$CdCl_2$ phase diagram 78−3009
n-$CdCr_2Se_4$, current- and voltage-controlled negative resist. obs. 78−19041
$CdCr_2Se_4$, deviation from Kittel's mag. resonance formula near T_c 79−87322
$CdCr_2Se_4$, domain struct. by IR Faraday effect 79−95604
$CdCr_2Se_4$, energy band struct calc. by augmented plane wave method 80−103621
$CdCr_2Se_4$, energy structure, magnetooptic effects 80−71394
$CdCr_2Se_4$, ferromag., localised states on imperfections and red shift of absorpt. edge 77−66527
$CdCr_2Se_4$, ferromag. semicond., P-T phase diagram by annealing expts. between 600 and 964°C 77−63636
$CdCr_2Se_4$, ferromag. semiconductor, light scatt. from magnons under strong fields 78−84554
$CdCr_2Se_4$, ferromag. semicond., photoinduced mag. anisotropy 80−50086
$CdCr_2Se_4$, ferromag. semicond., conc. anomalies rel. to red shift of absorpt. edge 80−70732
$CdCr_2Se_4$, ferromagnetic semiconductor, P_{Se}-T phase diagram, where $Se=Se_2$, near peritectoid reaction temps. *(Japanese)* 77−52290
$CdCr_2Se_4$, ferromagnetic low anisotropy semicond., spontaneous magnetisation RF determ. 80−22396
$CdCr_2Se_4$ film, absorpt. and Faraday effect 78−2936
$CdCr_2Se_4$ film, electron irradiated, struct. 79−15032
$CdCr_2Se_4$ film, ferromag. semicond., prep. by vacuum condensation 77−28724
$CdCr_2Se_4$ film, mag. linear and circular dichroism and Faraday rot. 79−99966
$CdCr_2Se_4$ films, mag. hysteresis, domain struct., mag. viscosity 80−25169
$CdCr_2Se_4$, influence of Co ions on anisotropy and magnetostriction, ferromag. reson. meas. 77−69659
$CdCr_2Se_4$, influence of ferromag. ordering on phonon Raman scatt. 78−2853
$CdCr_2Se_4$, light scatt. by magnons 77−69805
$CdCr_2Se_4$, mag. semicond., threshold and mag. memory switching in single crysts. 77−43672
$CdCr_2Se_4$, mag. semicond., photoinduced binding of domain walls *(Russian)* 78−80174
$CdCr_2Se_4$, mag. semicond. effect of illum. on domain struct. 79−99726
$CdCr_2Se_4$, magnetic red shift origin, specular reflectivity, band struct. 80−40127
$CdCr_2Se_4$ magnetic semiconductor, photoinduced centre kinetics 80−71110
$CdCr_2Se_4$, magnetisation, study of photoindduced charges 80−80567
$CdCr_2Se_4$, magnon instability, under intense EM field 77−40048
$CdCr_2Se_4$, modulated piezoreflection spectra 80−97237
$CdCr_2Se_4$, Mott ferromagnetic semiconductor, optical absorption edge, critical behaviour 80−97226
$CdCr_2Se_4$, narrow conduction band, crit. behaviour of resistivity 79−78096
$CdCr_2Se_4$, optical absorption due to transitions between bands and local levels 79−38537
$CdCr_2Se_4$, optical reflectivity, dielectric const. by expt. data Kramers-Kronig anal., spinel struct. 79−99903
$CdCr_2Se_4$, photoferromag. effect quenching, photocond. 78−68488
$CdCr_2Se_4$, photoinduced infra-red optical absorption 78−23455
$CdCr_2Se_4$, reflectance magneto-circular dichroism 77−81120
$CdCr_2Se_4$, refr. index variation in strong alternating mag. field 80−23741
p-$CdCr_2Se_4$, resistivity anomalies at mag. transitions, sp.ht. 80−39785
$CdCr_2Se_4$, resonant Raman scatt. 79−4802
n-$CdCr_2Se_4$ single crystal near Curie temp., anomalous transport props. *(Japanese)* 78−6406
$CdCr_2Se_4$, single crysts., mag. semicond., spinel-type, magneto-optical effects *(Japanese)* 79−47415
$CdCr_2Se_4$, single cryst. growth by chem. transport reactions 80−16163
$CdCr_2Se_4$, spin dependent phonon Raman scat., resonance effects 77−73145
$CdCr_2Se_4$, spin system heating by drifting current carriers, magnon-phonon system energy transfer *(Russian)* 80−29541
$CdCr_2Se_4$, spinel film, struct. SEM study, props. 78−79905
$CdCr_2Se_4$, velocity-field characts., above T_c 78−64049
$CdCr_2Se_4$:Ag, ferromag. reson. meas. 77−8415
$CdCr_2Se_4$:Ag, ferromag. reson. field and linewidth anisotropy, Se vacancy effects 78−60338
$CdCr_2Se_4$:Ag, ferromag. linewidth and eddy current losses 79−33541
$CdCr_2Se_4$:Ag, impurity contrib. to low temp. ferromag. reson. linewidth 79−65743
$CdCr_2Se_4$:Ag, mag. anisotropy, effect of annealing in vacuum 77−80929
$CdCr_2Se_4$:Ag, magneto-electrical props. temp. behaviour depend. on dopant conc. *(Russian)* 80−11006
$CdCr_2Se_4$:Ag, magneto-optical effects in impurity spectral region 80−97313
p-$CdCr_2Se_4$:Ag, oscillatory magnetoresist., temp. and mag. field depend. 78−52011
$CdCr_2Se_4$:Ag(Gd), doping effects on exchange interaction 78−43579
$CdCr_2Se_4$:Cu(In), ferromag. semicond., mag. and elec. props. 77−20588
$CdCr_2Se_4$:Ga, sp. elec. resist., temp. and mag. field depends. *(Russian)* 78−26893
$CdCr_2Se_4$:Ga(Ag), and pure, photocond. and photomagnetoresist. spectra 77−80809
$CdCr_2Se_4$:Ga(In), photoconductivity, photomagnetoresistance near Curie point *(Russian)* 80−100485
$CdCr_2Se_4$:In, elec. cond., annealing effect 79−87102
$CdCr_2Se_4$:In, ferromag. semicond., carrier mobility, electron-two magnon scatt. Hall effect 78−51992
$CdCr_2Se_4$:In, influence of Se-deficiency on props. 78−30921
$CdCr_2Se_4$:In, nondegenerate ferromagnetic semiconductor, positive magnetoresistance 78−2505

magnetic semiconductors continued
$CdCr_2Se_4$:In , impurity band, photocond. spectral depend. 78−19088
$CdCr_2Se_4$:In(Ga), elec. resist. and magnetoresist., 2 to 200K 80−96876
$CdCr_2Se_4$:In(Ga)(Cu), magnetic microregions caused by s-d exchange 77−77050
$CdCr_2Se_4$-$ZnCr_2Se_4$, single cryst., mag. props. 79−28526
$CdCr_2Se_{4-x}S_x$, influence of anion substitution on red shift of optical absorption band edge 77−32399
$CdCr_2Se_4(S_4)$, ESR line intensity near Curie point 78−64269
$CdCr_2Se_4(S_4)$, ferromag. properties and use for making devices, review 78−60131
$CdCr_2Si_4$:Ga, negative magnetoresist. effects near Curie temp. 79−11152
$CdCr_2Sr_4$, press. depend. optical aborption edge shift and compressibility 79−28714
$CdCr_2S_4(se_4)$, ferromag. semicond., band struct., EHT calc. 80−54608
$Cd_{1-x}Cu_xCr_2S_4$, elec. resist., temp. depend., behaviour at Curie point 77−62929
$Cd_{0.93}Cu_{0.07}Cr_2Se_4$, single cryst., galvanomagnetic props. 79−7848
$Cd_{1-x}Fe_xCr_2S_4$ series, magneto-optical effects, expt. *(Japanese)* 77−40212
$Cd_{1-x}Fe_xCr_2S_4$, single cryst., mag. semicond., spinel-type, magneto-optical effects *(Japanese)* 79−47415
$Cd_{1-x}Fe_xCr_2S_4$:Cu, effect of doping on elec. props. and Curie temp. 78−84214
$Cd_{1-x}Ga_xCr_2S_3$, spinel, anomalies in paramag. susceptibility, Curie pt. *(Russian)* 77−80910
$Cd_{1-x}Hg_xCr_2Se_4$, ferromag. semicond. surface magnetism, magneto-optical meas. 77−20831
$Cd_{1-x}Hg_xCr_2Se_4$, photoferromag. effect and photocond. obs. 79−28376
$Cd_{1-x}In_xCr_2Se_4$, electric, photoelectric and mag. props., metal-semicond. transition *(Russian)* 80−54738
$CdIn_2S_4$:Cr, ligand field induced photocond. and photoluminesc. 77−28214
CdMnTe, semimagnetic semiconductor, band structure, optical properties 79−95331
$Cd_{1-x}Mn_xTe$, EPR, mag. crit. point 80−39851
$Cd_{1-x}Mn_xTe$, exchange induced ionization of bound excitons, luminesc. meas. 80−97328
$Cd_{1-x}Mn_xTe$, indirect exchange interaction 80−97087
$Cd_{1-x}Mn_xTe$, magnetic behaviour of Mn 78−14938
$Cd_{1-x}Mn_xTe$ mixed crystals, excitonic magnetoabsorption 80−40095
$Cd_{1-x}Mn_xTe$, semimagnetic, exchange interactions between localised and delocalised electrons 80−97245
$Cd_{1-x}Mn_xTe$, spin-orbit coupled bands, indirect exchange interaction via electrons 80−34407
CdS, amorphous antiferromag., mag. props. of dilute neutral donors 79−78367
$Cd_{1-x}Zn_xCr_2Se_4$, ferromag. semicond., surface magnetism, magneto-optical meas. 77−20831
$Cd_{1-x}Zn_xCr_2Se_4$, mag. semicond., neutronographic obs. *(Russian)* 79−11297
$Cd_{1-x}Zn_xCr_2Se_4$, synthesis Curie pt., photomag. effect 77−51937
$CoCr_2S_4$, CVD grown, surface microstruct. 79−4905
$CoCr_2S_4$, ferrimag. semicond., magnetocrystalline anisotropy 80−71012
$CoCr_2S_4$ films, galvanomagnetic and thermoelec. props. 80−54717
$Co_{1-x}Cu_xCr_2S_4$, paramag. susceptibility 80−20373
$Co_{0.7}Cu_{0.3}Cr_2S_{4-x}Se_x$, ferrimag. chalcospinel, paramag. susceptibility 80−15681
$Co_{1-x}Fe_xCr_2S_4$, ferrimag. spinel semicond., Curie temp. variation with composition and elec. props. 77−15849
Co_2RhS_4, mag. semicond., mag. and elec. props. 80−93121
CoS_2, narrow-band ferromag., high press. effect on anomalous elec. resist. 80−70698
$Co(S_xSe_{1-x})_2$, galvanomag. effects, obs. and interpretation 80−70726
Cr_2AX_4 type, physical props. and possible applications 78−2474
Cr_2O_3, electron structures calc. using models, ESCA and X-ray spectral data 77−35863
$CrPr_2S_4$, synthesis, single crystal growth, mag. and elec. props. 79−78857
CrTe, effect of high pressures on magnetic properties 78−52238
$CuCr_2S_{4-\gamma}$, spinel, anomalies in paramag. susceptibility, Curie pt. *(Russian)* 77−80910
$CuCrSe_2$, influence of excess Cu on physical props. 80−103836
$CuCr_2Se_{4-x}Br_x$, elec. resistance, Hall const., magnetoresistance singularities *(Russian)* 79−91078
$Cu_{0.67}Cr_{1.78}Se_{2.67}Br_{1.34}$, polycrystalline mag. semicond., mag. and elec. props. 79−7846
$Cu_yCr_2Se_{4-x}Br_x$, ferromag. magneto-resistance exam. *(Russian)* 78−84238
$Cu_yCr_2Se_{4-x}Br_x$, ferromagnetic, Hall effect 80−60012
$Cu_yCr_2Se_{4-z}Br_x$, degenerate ferromag. semicond., resist. minimum 79−73517
$CuCr_2Se_4(S_4)(Te_4)$, binary and ternary solid solns., mag. and elec. props. 80−2407
$Cu_{1-x}Fe_{2+x}O_4$, elec. resist., Seebeck coeffs., 20 to 900°C, cation distrib. 79−4575
$CuFeS_2$, electronic struct., Mossbauer expt. 78−27150
$CuFeS_2$ single crystal, optical reflectivity spectrum 80−40129
Cu_5FeS_4, mag. ordering and vacancy clustering, mag. susceptibility and Mossbauer spectra meas. 77−85625
$Cu_{1-x}In_xCr_2S_4$, light induced magnetisation 78−76275
$Dy_2(MoO_4)_3$, mag. susceptibility, ferromagnetism, mol. field theory 78−34966
$Er_2(MoO_4)_3$, mag. susceptibility, ferromagnetism, mol. field theory 78−34966
Eu chalcogenide mag. semiconductors, modulation spectroscopy *(Japanese)* 77−24862
Eu chalcogenides, anomalous Hall effect, analysis 77−20344
Eu chalcogenides, anomalous Hall effect, impurity scatt. 78−39131
Eu chalcogenides, heavily doped mag. semiconductors, effect of carriers statistics on indirect exchange 77−69280
Eu chalcogenides, mag. polaron stability 80−96803
Eu chalcogenides, magnetic semiconductor, light scatt. exam. 79−61372
Eu chalcogenides, multiphonon inelastic light scatt., hot recomb. 77−8559
Eu chalcogenides, paramagnetic, optical orientation of 4f electrons 77−69799
Eu chalcogenides, resonant Raman scattering model via magnetic exciton in ferromagnetic phase 80−93326
Eu chalcogenides, spin-dependent Raman scatt. from phonons 80−97274

magnetic semiconductors continued
Eu solid solutions with lanthanides, monosulfides, and oxides, vacant d states, X-ray absorpt. 80−103623
$EuAl_2S_4$, mag. susceptibility and EPR meas. 80−71173
EuB_6, electronic struct., transport and mag. props. 80−96782
EuB_6, ferromag., spin-polarised energy band struct., APW calc. 80−96779
EuB_6, Hall effect and resistivity data, ferromagnetic ordering temp., pressure depend. 80−60010
EuB_6, mag. and transport props. 80−54689
EuB_6, resist., Hall effect, and magnetoresist. under hydrostatic press., 4.2 to 300K 80−96879
$EuB_{6-x}C_x$, Mossbauer spectra, cond. electrons effect 80−20545
$EuGa_2S_4(Se_4)$, mag. susceptibility and EPR meas. 80−71173
$Eu_{1-x}Gd_xO$, specific heat, magnetocaloric effect 79−69688
$Eu_{1-x}Gd_xO_{1-x}N_x$, ferromag. semicond., prep., ferromag. props. *(French)* 77−69550
Eu_2IrH_5, prep., cryst. struct., mag. and elec. props. 80−88117
EuO (100), disordered, LEED and electron spectroscopy 79−28178
EuO, anti-Stokes luminesc., magnon assisted 78−31252
EuO, crit. behaviour of opt. absorpt. edge 77−59418
EuO; Curie temp. raising by impurity addition *(Russian)* 77−47994
EuO, degenerate ferromag. semiconductor, mechanism of transition to insulating state *(Russian)* 77−8024
EuO, electronic struct. and props., mol. cluster approx. 77−11852
EuO, electronic struct. investigation by electron spectroscopy method 80−92812
EuO, electronic structure, octahedral clusters, determ. by X_α method 78−10350
EuO, Eu doped, temp. depend. of carrier conc. and mag. susceptibility 77−69483
EuO, excitation of spin waves by current carriers, magnetisation and elec. cond. reduction *(Russian)* 79−7981
EuO, ferromag., absorpt. edge and cond. band width, temp. and mag. field depend. 77−36267
EuO, ferromag., light scatt. from bulk and surface spin waves 79−28778
EuO, ferromag. semicond., electronic spectrum, influence of finite carrier conc. 78−76220
EuO, ferromagnetic, mag. field effect on optical absorpt. edge, piezotransmission spectra 78−95578
EuO, ferromagnetic piezotransmission behaviour in magnetic field 80−97272
EuO, ferromagnetic resonance and dielectric losses 78−2748
EuO film for thermomagnetic recording, anisotropy of resolving power 80−20404
EuO, HF conductivity meas. 79−33304
EuO, light absorpt. during ferromag. reson. *(Russian)* 79−28618
EuO, light scatt. from spin waves and magneto-optic hysteresis meas. 80−97244
EuO, light-induced metal-insulator transition, mol. mag. polarons 77−4396
EuO, mag. semicond., dielec. and optical props. meas. 78−10824
EuO magnetic semiconductor, quasiparticle lifetimes, CPA study 80−65443
EuO, magnetic susceptibility, quasiphase transition 79−65684
EuO, microwave and DC cond., dielec. const., 1.7 to 300K 77−20347
EuO, microwave cond., influence of mag. ordering 79−69544
EuO, nonstoichiometric film with excess EU, optical magneto-optical and elec. props. 79−8204
EuO nonstoichiometric film, ESR spectra and exchange interaction 80−93176
EuO, optical orientation of f-electrons, Curie temp. variation due to exchange interactions *(Russian)* 79−15431
EuO, origin of exchange interaction 78−10675
EuO, photoelectron anomalous transport phenomena 78−23114
EuO, physical and physicochem. props., review 80−96875
EuO, piezoresistance effect, 4.2 to 300K 80−34450
EuO, rotation of polarisation plane in very high mag. field 78−92054
EuO, spin system heating by drifting current carriers, magnon-phonon system energy transfer *(Russian)* 80−29541
EuO, spin-dependent Raman scattering 79−95782
EuO, stoichiometric, crit. behaviour of piezotransmission at Curie temp. 77−85688
EuO, transmission and resistivity, stress modulation effect near Curie temperature 80−96874
EuO, transport properties at ferromag. reson. 78−68387
EuO, zero-wave vector kinetic coefficient near T_c 79−73714
EuO:Eu, doped ferromag. semicond., carrier density and mag. susceptibility rel. to M-S transition 77−72820
EuO:Gd, 4f-photoelectron spin polarization, temp. depend. 79−78842
EuO:Gd, critical specific heat depend. on doping, microwave cond. 79−95602
EuO:Gd, elec. cond. under hydrostatic press., Curie temp. 80−96881
EuO:Gd, electron mobility below Curie temp. 78−91696
EuO:Gd, ferromag. semicond., electron spin polarisation and conduction band struct. 80−65449
EuO:Gd, mag. props. and instability phenomena 79−1666
EuO:Gd, pure and doped, elec., mag., and optical props. rel. to electronic conc. 80−96880
EuO:Gd, surface depolarisation of photoelectrons 78−15286
EuO:Gd, surface mag. props. 80−71566
EuO:La, photothreshold reduction by mag. induced space charge layer 78−72692
EuO:La(Gd), photoelectron spin polarisation, temp. depend. 77−69966
EuO:La(Gd), photothreshold changes below mag. ordering temp. 80−97406
EuO:Yb(Sm), electron transition and valence state of impurities, X-ray spectroscopy and structural anal. 78−39064
EuO-RN solid soln., (R=Nd,Eu,Gd), ^{151} Mossbauer spectroscopy 78−6610
$Eu_{1-x}O$, optical absorpt. spectra at metal insulator transition 78−10928
$EuO_{1-x}N_x$, ferromag. semicond., elec. and mag. props. *(French)* 78−79993
EuO(S), effect of pressure on energy gaps 78−19239
EuO(S), ferromagnetic electronic structure, absorption, thermoreflection and thermotransmission spectra *(French)* 80−97300
EuO(S):Gd, indirect exchange 78−23264
EuO(S)(Se) electronic props., effect of electron-ion spin coupling 77−28359
EuO(S)(Se), spin assisted Raman scatt. theory 78−43866

magnetic semiconductors continued
EuO(S)(Se)(Te), cryst. and electronic struct., mag., elec., and optical props., book contrib. 80−39760
EuO(S)(Se)(Te), exchange interaction mechanisms, theory compared with expt. *(Russian)* 78−39312
EuO(S)(Se)(Te), Heisenberg ferromag. semicond., hyperfine and exchange interactions 77−69530
EuO(S)(Se)(Te), mag. struct. and transition temp., indirect exchange 78−91860
EuO(S)(Se)(Te), phase transition spectroscopy 77−63426
EuO(S)(Se)(Te), spin order and fluctuations, Raman scatt. study 80−97273
EuO(Se), complex elec. cond. anomalies 80−107812
EuO(s), s-f model, intermediate coupling theory 79−95326
$Eu_{1-x}^{2}R_x^{+}O_{1-x}$ (R=Nd, Eu, Gd), lattice parameters, mag. and elec. props. 80−100578
EuS, conduction band density of states, redistrib. near ferromag. saturation 78−67939
EuS, defect struct., etch pitting and electron microscopic obs. 79−27989
EuS, electronic struct. and props., mol. cluster approx. 77−11852
EuS, exchange magnetostriction in paramagnetic phase 79−78492
EuS, ferromag., absorpt. edge and cond. band width, temp. and mag. field depend. 77−36267
EuS, ferromag., on W, electron field emission 79−8230
EuS, ferromag., optical spin orientation, Curie temp. increase 77−20627
EuS, ferromag. semicond. film, Hanle effect, optical orientation time consts. meas. 77−40214
EuS, ferromag. semicond., high field susceptibility, spin waves 80−75735
EuS, ferromagnetic film, optically induced magnetisation amplification, Curie temp. increase *(Russian)* 77−24719
EuS film, influence of prep. on mag. props. 79−24201
EuS, film, intrinsic demagnetising fields 78−10735
EuS, film, mag. surface reconstruction, ferromag. reson. 78−10781
EuS film, struct., elec. and opt. prop. changes during annealing in air 77−7983
EuS films, ferromag., optical spectra and light scatt. from spin waves 80−16116
EuS films, mag. and elec. props. rel. to stoichiometry and defects 80−97122
EuS films, thermoreflectance spectra below Curie temp. 77−66550
EuS, light scatt. from spin waves and magneto-optic hysteresis meas. 80−97244
EuS, mag. phase depend. Raman scatt. 78−10886
EuS, origin of exchange interaction 78−10675
EuS, pure and Gd doped, electronic struct., mag. exchange and elec. transport props. 78−87974
EuS, spin polarised tunnelling and mixed spin states in conduction band 79−52085
EuS, spin relaxation crit. behaviour 78−76251
EuS, thermo- and magnetorefl. spectra, dynamical spin fluctuation effect on exciton state 77−52126
EuS, thin film, Brillouin scattering from spin waves 80−65843
EuS:Yb(Sm), electron transition and valence state of impurities, X-ray spectroscopy and structural anal. 78−39064
EuS-W interface, electron spin polarisation in field emission 78−35265
EuS(Se)(Te), spin-assisted phonon Raman scatt., mag. phase depend. 80−71413
EuS(Se)(Te)(O), Raman scatt. near mag. phase transitions 79−47458
EuSe, annealed, AC conductivity and dielectric anomaly 80−34445
EuSe, bound mag. polaron, temp. and field depend. of resist. 79−90976
EuSe, dynamical conductivity in high mag. fields 79−78118
EuSe, first- and second-order Raman scatt. near T_N 79−61374
EuSe, HF conductivity meas. 79−33304
EuSe, Hall effect, elec. cond. and magnetoresistance temp. depend. 79−33296
EuSe, high field Faraday rot., 1.7-3 eV 77−52131
EuSe, mag. phase depend. Raman scatt. 78−10886
EuSe, mag. semicond., dielec. and optical props. meas. 78−10824
EuSe, microwave and DC cond., dielec. const., 1.7 to 300K 77−20347
EuSe, optical absorption exam., electron phonon interactions 78−10923
EuSe, polarisability of shallow donors, permittivity meas. 80−24833
EuSe, Raman scatt. near mag. phase transitions 79−61373
EuSe, VPE by hot-wall technique 80−80958
EuSe:Gd, mag. props. explained by band struct. 78−43324
EuSe(Te), magnetic phase transitions, thermal modulation spectroscopy study *(French)* 80−97301
$Eu_{0.98}Sm_{0.02}O$, ferromag. semicond., elec. cond. meas. 80 to 370K, press. effect to 20 kbar 77−51751
$Eu_{1-x}Sm_xO$, ferromag. semiconductor with elevated Curie temp. 77−51903
$Eu_{1-x}Sm_xO$, thermodynamics of mag. quasimols. 78−19266
$Eu_{1-x}Sm_xS$, electronic transition in Sm impurity ions, rel. to exchange interactions, L absorpt. spectra 77−59644
$Eu_xSr_{1-x}S$, magneto-optical redshift in absorpt. and photoluminesc., mag. short-range order 80−71388
EuTe 79−61373
EuTe, antiferromag. semicond., Raman scatt., spin-phonon interactions 80−66185
EuTe, field depend. correl. function theory of Raman scatt. near antiferromag.-paramag. transition 78−68490
EuTe, high field Faraday rot., 1.7-3 eV 77−52131
EuTe, light scatt. by magnons 77−69805
EuTe, mag. semicond., antiferromag. reson. meas. 80−44926
EuTe, magnetic impurity states, mag. and transport props. 80−96913
EuTe, optical absorpt. in high mag. field 79−28726
EuTe, Raman scatt. exam. 79−61375
EuTe, spin-dependent Raman scattering 79−95782
EuX type, physical props. and possible applications 78−2474
$Eu_{1-y}X_yS$ (X=Sr,Gd), spin-disorder-induced Raman scatt. from phonons, expt. investigation 80−20635
$Eu_{1-y}X_yS$ (X=Sr,Gd), spin-disorder-induced Raman scatt. from phonons, theory 80−20636
EuX(X=0,S,Se) 80−20635
EuX(X=0,S,Se), spin-disorder-induced Raman scatt. from phonons, theory 80−20636
$Eu_{1-x}Yb_xO$, solid soln., ferromag. semicond., increase of exchange interaction 78−88109
$Eu_{1-x}Yb_xS$, solid soln., ferromag. semicond., increase of exchange interaction 78−88109
$Eu_{1-x}Yb_xTe$, ($0<x<1$), mag. semicond., elec., mag. and optical props. 80−97070

magnetic semiconductors continued
$FeAl_{2-x}Cr_xO_4$, spinel, elec. cond. behaviour during oxidation 79−19593
γ-$(Fe_{1/3}Al_{2/3-y}Cr_y)_2O_3$, lacunar spinels, elec. cond. behaviour during oxidation 79−19593
$Fe_{0.2}Co_{0.8}S_2$, narrow-band ferromag., high press. effect on anomalous elec. resist. 80−70698
$Fe_{1-x}Co_xSi$ solid solution, semiconductor-metal transition 80−103627
$FeCr_2S_4$, elec. and galvanomag. props. 78−23111
$FeCr_2S_4$, ferrimag. semicond., elementary step growth on surface of vapour grown cryst. 77−76649
$FeCr_2S_4$, pure and doped, CVD grown, surface struct., elec. props. and band struct. 79−4905
$FeCr_2S_4$, single crysts., vapour grown, growth of triple unit cell steps on surface 79−19984
$FeCr_2S_4$, vapour grown, struct. and stoichiometry, X-ray fluoresc. anal. 79−4263
$FeCr_2S_{4-x}Se_x$ chalcospinels, ESR spectrum and paramag. susceptibility 80−15789
$FeCr_2S_{4-x}Se_x$, elec. props. 78−23083
$Fe_{0.5}Cu_{0.5}Cr_2S_4$, ESR spectra, elec. and mag. props., Curie temp. 80−97137
$Fe_{1-x}Cu_xCr_2S_4$, mag. semicond., mag. props. and elec. cond. *(Japanese)* 79−47111
$Fe_{0.91}O$, photothreshold changes below mag. ordering temp. 80−97406
α-Fe_2O_3, photochem. props. of sintered and doped samples for solar photoelectrochem. cell appls. 80−89651
Fe_3O_4, magnetites, cond. mechanisms *(Russian)* 79−42539
Fe_3O_4, nuclear gamma reson. investig. of high temp. electronic struct. 77−20751
$FePS_3$ and $FePSe_3$, antiferromag., mag. props., NMR meas. 79−24223
$FeRh_2S_4$, mag. semicond., mag. and elec. props. 80−93121
$FeSb_2$, quasi-magnetic semicond., mag. susceptibility 80−39757
FeSi, nearly ferromag. semicond. mag. and thermal props., spin fluctuation theory 79−65687
$FeTiO_3$, electronic struct., Mossbauer expt. 78−27150
n-GaAs, coupled LO phonon-plasmon modes 79−73459
$Ga_{1-x}Mn_xSb$ alloys, mag. phase transition obs. 78−52248
$Ga_{1-x}Mn_xSb$, elec. cond., mag. susceptibility, Hall const., and thermo-EMF, 80 to 1000K *(Russian)* 80−88549
GdP, electronic struct., mag. exchange and elec. transport props. 78−87974
GdS, electronic struct., mag. exchange and elec. transport props. 78−87974
Gd_2S_3, antiferromag. to ferromag. and semiconductor to metal transitions *(Russian)* 79−33485
Gd_2S_3 with excess Gd, magnetoresist. meas. 80−49777
Gd_xS_y, nonuniform ferro-antiferromag. ordering, 1.6 to 300K range obs. *(Russian)* 77−69504
$Gd_{3-x}\square_xS_4$, transport and mag. props., mag. Wigner localisation 80−97069
$GeFe_2O_4$, single crysts., elec. and mag. props, optical absorpt. spectra 80−54719
$Ge_{1-x}Mn_xTe$, magnetic behaviour of Mn 78−14938
GeTe:Mn, thermoelec. power, 2.5-25K, magnon drag effect 78−56169
^{3}He, solid, as mag. semicond., analogy to Mott insulator 80−96720
$HgCr_{2-x}Al_xSe_4$ and $HgCr_{2-x}Ga_xSe_4$, temp. depend. of ESR linewidth, 105-300K 80−71161
$HgCr_2O_4(S_4)(Se_4)$, magnetic exchange interactions 77−24690
$HgCr_2Sd_{4-x}Te_x$, ferromag. semicond., zero bandgap transition 80−96783
$HgCr_2Se_4$, ESR line intensity near Curie point 78−64269
$HgCr_2Se_4$, electronic props. rel. to departure from stoichiometry 80−100472
$HgCr_2Se_4$, ferromag. semicond., surface magnetism, magneto-optical meas. 77−20831
$HgCr_2Se_4$, ferromag. semicond., Raman spectra 78−52496
$HgCr_2Se_4$, ferromag. semicond., transport props. 78−68039
$HgCr_2Se_4$, influence of Co ions on anisotropy and magnetostriction, ferromag. reson. meas. 77−69659
$HgCr_2Se_4$, initial mag. permeability freq. depend. near Curie temp. 78−10729
$HgCr_2Se_4$, initial mag. permeab., 77 to 300K, domain wall motion and damped ferromag. reson. 79−28562
$HgCr_2Se_4$, n-type ferromag. semicond., galvanomagnetic props. 80−70727
$HgCr_2Se_4$, optical and magneto-optical surface effects 79−82953
n-$HgCr_2Se_4$, plasmon refl., 86 to 320K 80−50346
$HgCr_2Se_4$, Raman scattering, as function of temp. and incident photon energy 79−95781
$HgCr_2Se_4$, thermorefl. near ferro- to paramagnetic transition 79−78660
$HgCr_2Se_4$, thermoreflectance, photoconductance, Raman scatt. near mag. phase transition 80−97298
$HgCr_2Se_4$, vapour growth using $AlCl_3+Cl_2$ as transport components 78−35282
$HgCr_2Se_4$-$CdIn_2S_4$ heterojunctions, prep. and photovoltaic prop. 78−34892
$HgCr_2Se_{4-x}S_x$, temp. depend. of EPR line intensity 78−27074
$Hg_{1-x}Mn_xS(Se)$ solid solution, magnetic props. 79−51758
$Hg_{1-x}Mn_xSe$, band struct. from anomalous Shubnikov-de Haas effect 80−20080
$Hg_{1-x}Mn_xSe$, spin-orbit coupled bands, indirect exchange interaction via electrons 80−34407
HgMnTe, semimagnetic semiconductor, band structure, transport phenomena 79−95331
$Hg_{1-x}Mn_xTe$, EPR investigation of ordering effects 79−47330
$Hg_{1-x}Mn_xTe$, indirect exchange interaction 80−97087
$Hg_{1-x}Mn_xTe$, mag. props., self-consistent two spin cluster model 80−54874
$Hg_{1-x}Mn_xTe$, mag. susceptibility, 2.3-300K 77−63074
$Hg_{1-x}Mn_xTe$, mag. susceptibility, 2.4 to 300K 80−20379
$Hg_{1-x}Mn_xTe$, magnetic behaviour of Mn 78−14938
$Hg_{1-x}Mn_xTe$, non-parabolic zero-gap semicond., indirect exchange interaction 80−80498
$Hg_{1-x}Mn_xTe$, semimagnetic, exchange interactions between localised and delocalised electrons 80−97245
$Hg_{1-x}Mn_xTe$, spin-orbit coupled bands, indirect exchange interaction via electrons 80−34407
$Hg_{1-x}Mn_xTe$, transverse magnetoresistance in quantised mag. fields 80−96922
HgTe, Γ_8 symm. acceptor centre hole mag. props. *(Russian)* 80−88733
$Hg_{1-x}Zn_xCr_2Se_4$, magnetic struct., neutrongraphic and mag. investigation *(Russian)* 80−88726

magnetic semiconductors continued
$Ho_2(MoO_4)_3$, mag. susceptibility, ferromagnetism, mol. field theory 78−34966
p-InSb, negative piezomagnetoresist. and Hall effect meas., antiferromag. order form. 78−19061
p-InSb, uniaxially deformed, mag. field induced semicond.-metal transition 79−95457
IrP_2, prep. and characterisation 78−39679
LaB_6, elec. cond. under hydrostatic press. 79−7832
$La_{1-x}Sr_xCoO_3$, $(0.5 \leq x \leq 0.9)$, ferromag., elec. props., itinerant electron model 80−107785
$Li_xMn_{1-x}Se$, anomalies obs. in mag. and elec. props. 77−69509
$Mg_{1-x}Mn_xTe_2$, random dil. antiferromagnet, mag. props. 80−54870
$Mn_xCd_{1-x}Te$, phonons, Raman scatt. and IR absorpt. meas. *(French)* 80−97275
$Mn_{1-x}Cu_xCr_2S_4$, phase relationships and mag. phase diagram 79−78374
$Mn_xFe_{3-x}O_4$ ferrite film, exchange interaction depend. on conduction electrons *(Russian)* 80−34621
MnO, Hall mobility of photoelectrons 77−69352
MnP, elec. resist. of different mag. phases, temp. depend. 80−54691
$MnPS_3$ and $MnPSe_3$, antiferromag., mag. props., NMR meas. 79−24223
MnS, thermal cond., temp. depend., paramag.-antiferromag. transition effects 80−65321
$MnSe_2$, IR lattice vibrs., dielectric dispersion 79−28735
MnTe, magnetic resonance at high hydrostatic pressure 78−76247
MnTe, resistivity anomalies at mag. transitions, sp.ht. 80−39785
$MnTe_2$, pyrite struct., susceptibility, 4.2-450K, exchange consts. 77−77040
MnZn ferrites, elec. cond. mechanism in paramag. and ferrimag. phases 80−15524
$NaCrS_2$, antiferromag. semicond., Raman and far-IR spectra 79−47454
Ni-Zn ferrite, electrical cond., Seebeck coeff. and saturation magnetisation 77−20315
$Ni_{1-x}Cr_xS$, elec. transport, mag. susceptibility and DTA meas. 80−96954
$NiPS_3$, antiferromag., mag. props., NMR meas. 79−24223
NiS_2, weak ferromagnetic semiconductor single crystal, elec. and magnetic props. 77−85226
$NiS_{2-x}Se_x$, mag. struct., ^{57}Fe Mossbauer study 78−56409
$Ni_{0.5}Zn_{0.5}Fe_2O_4$, Hall mobility, elec. cond. and carrier conc., 30 to 180°C 77−51765
$Pb_{0.82}Sn_{0.18}Te$, narrow gap semicond., mag. susceptibility meas. *(Russian)* 78−84397
$Ru_2Ge_{3-x}Sn_x$, and $Ru_2Ge_{3-y}Si_y$, diffusionless phase transitions, elec. and mag. props. 80−96871
RuP_2, prep. and characterisation 78−39679
$(Sc_xLu_{1-x})_2V_2O_7$ 80−29547
SmB_6, mixed valent semicond., transport props. and electonic struct., review 80−96877
$Sm_{1-x}La_xS$, mag. suscept., moment, impurity effects, indirect exchange interaction 78−68147
$Sm_{1-x}La_xS$, magnetoresist. in semicond. and metallic phases 80−96914
SmS, electron-phonon interaction, lattice dynamical model 80−96610
SmS, high-pressure mixed-valence phase, diagram and electronic entropy, neutron diffr. obs. 79−33267
$SmS_{1-x}As_x$, magnetoresist. in semicond. and metallic phases 80−96914
$Sm_{1-x}Y_xS$, magnetoresist. in semicond. and metallic phases 80−96914
$Sn_{1-x}Mn_xTe$, $0.02<x<0.08$, transport and magnetic properties, low magnetic field 79−99569
$Sn_{1-x}Mn_xTe$, degenerate mag. semicond., thermoelec. power meas. 80−29392
$Sn_{1-x}Mn_xTe$, electronic struct., transport props., mag. ordering effects 80−65441
$Sn_{1-x}Mn_xTe$, IR reflectivity, elec. susceptibility mag. order effects 79−47433
$Sn_{1-x}Mn_xTe$, magnetic behaviour of Mn 78−14938
SnTe:Mn, ferromag.-ordering, transverse magnetoresist. and Hall effect meas. 77−85240
SnTe-MnTe, degenerate semicond., anomalous Hall effect 80−29420
Ti_2O_3, electron structures calc. using models, ESCA and X-ray spectral data 77−35863
$Tl_2Mn_2O_7$, synthesis, mag. and elec. props. and cryst. struct. 80−33963
TmSe, Anderson lattice resist. for antiferromag. ordering 80−65556
TmSe, elec. resist. under press. at very low temp. 80−96878
TmSe-TmTe(EuSe), semiconductor-metal transitions 80−96953
UAsSe, strongly anisotropic ferromag., negative magnetoresist. meas., 77-135K 77−89774
UO_2, 5f-magnetic semiconductor, spectroscopic data, review 80−97299
UO_2, electronic transitions, crystal field effects and phonons, phase transition 80−97303
UO_2, optical props. and electronic struct. 78−68527
UO_2, temp. depend. of 5f to $6de_g$ absorption edge and intra-5f transitions 79−24314
V_2O_3, electron structures calc. using models, ESCA and X-ray spectral data 77−35863
YIG, elec. props. meas., 600-1500K 77−8098
$(Y_xLu_{1-x})_2V_2O_7$ semiconducting ferromag. pyrochlore, mag. props. 80−29547
$ZnCr_2O_4(S_4)(Se_4)$, magnetic exchange interactions 77−24690
$ZnCr_2Se_4$, electroconductivity, thermoelectromotive force, Hall effect *(Russian)* 80−70694
$ZnCr_2Se_4$, screw spin struct., neutron diffr. exam. 78−27019
$ZnCr_2Se_4$, screw spin structure, method of controlling the sense, polarised neutron diffr. study 80−70944
$ZnCr_2Se_4$, screw spin structure, magnetoelectric effect 80−75827
$ZnCr_2Se_4$:In, magnetoresist. and elec. resist. above and below Neel temp. *(Russian)* 80−88576
$Zn_xFe_{0.85-x}O$, prep. and struct., mag. and semicond. props. *(French)* 78−51506

magnetic separation
coal, mag. and Mossbauer characterisation 78−64903
coal liquefaction residues, Mag. separability enhancement, thermomagnetic anal. and Mossbauer study 79−83544
conference, Florence, Italy (May 1978) 78−91833
cylindrical ferromagnetic bars, meas. of two-dimens. mag. field of array in uniform mag. field 79−12825
direct energy conversion from fusion plasma exhaust of divertor 78−54898
domain wall capture of mag. particles 80−71093
erythrocyte high gradient magnetic separation 78−53585

magnetic separation continued
ferrofluid, heavy, suspended in magnetostatic separator electromagnet gap, free surface shape 79−76543
ferrofluid devices, magnetostatic and centrifugal, nonmagnetic body motion 80−33700
high gradient magnetic separation at moderate Reynolds number 80−38500
high-gradient magnetic separation, axial particle trajectory meas. using human red blood cells 79−53165
high-gradient magnetic separation in region of high aerodynamic loading 79−86108
high-gradient magnetic separator, flow characterisation 79−41740
magnetic separator, drum-type with alternating polarity, analytical description of magnetic field *(Russian)* 80−99602
magnetic separator, high gradient mag. traction force in ordered matrix 78−50674
magnetic separator equations, approx. solns. 78−74811
magnetostatic energy of paramag. particles 77−38768
mineral microcrystals, mag. fluid technique for density determ. 80−85751
minerals, mag. separation using supercond. mags. *(Czech)* 78−88923
paramagnetic particle stream trajectories near ferromag. fibre 79−86128
paramagnetic particle trajectories in a lattice of parallel magnetized fibers 80−53204
paramagnetic particles in mag. separators, magnetostatic energy 79−50182
particle capture and axial filters, theory 78−92516
particle capture in axial filters, theory and performance 78−92515
particle separator for aerosols in airflows 77−4945
quartz, magnetic separation for thermolum. dating of ancient kiln 77−34070
synovial fluid analysis by ferrography 80−101242
uniformly magnetised body, mag. field strength invariance 80−58441
Cu-Fe-O system, ternary phases, activities in spinel solid soln., phase equilibria and thermodynamic props. 78−6910
Fe analysing magnet, fast precise field control 79−45883
Fe-containing minerals, in coals, mag. hyperfine fields meas. 78−88234
Fe-containing minerals in coals, magnetic hyperfine fields meas. 78−68427
FeS_2, pyrite, magnetokinetics of oxidation, appl. to mag. separation from coal 77−12161
MnZn ferrite particles, mag. filtration from air streams 77−4945
Ni, recovery from nickeliferous pyrrhotite, by thermal upgrading 77−60034
WC-Co hard metal, binder phase charact. by magnetic props. 79−29439

magnetic shielding
alkanes, H^+ chemical shifts, extended Huckel calcs. with gauge in variant atomic orbitals 80−102449
barrier LF field penetration 78−82886
benzene, H^+ chemical shifts, extended Huckel calcs. with gauge in variant atomic orbitals 80−102449
biomagnetic measurement facility installation in hospital environment, design criteria and procedure 80−104707
case, for terrestrial mag. field screening, rel. to Cs primary freq. standard meas. *(Japanese)* 77−22582
closed cylindrical vol., charact. of shield 80−43244
commercial circular dichroism instruments, magnetic shielding problems 77−87807
conducting liquid, in cylindrical induction furnace, velocity and EM field distrib. calcs. *(Russian)* 77−47106
eddy current losses, estimation method, in large steel plate having one-phase excitation *(Polish)* 80−93145
eddy current losses in semi-infinite shielded/unshielded mag. solid due to AC in parallel conductors *(Polish)* 80−37929
eddy-current losses in shielded magnetic solid, due to AC in parallel conductors *(Polish)* 80−32873
electron microscope corrector shielding *(German)* 78−24895
electron ring accelerators, shielding effect on ring motion 80−13991
EM pulse shielding of soft mag. materials 80−28143
ethylenic compounds, H^+ chemical shifts, extended Huckel calcs. with gauge in variant atomic orbitals 80−102449
ferromagnetic shield walls, in varying mag. field, AC magnetisation effects 77−26368
field penetration, through cond. ellipsoidal shield with slits and holes 77−50587
high permeability magnetic screens, high mag. fields, large vol., appls. *(German)* 77−38772
insulation loss-angle and capacitance test trolley *(Russian)* 77−10041
longitudinal magnetic field shielding with concentric cylinders of high permeability material 79−71499
low temp. torsion pendulum, magnetic shielding for ether drift expt. 79−88988
magnet technology, conference, Bratislava (1977) 79−30499
MHD screened duct, conducting liq. layer mag. field interaction, screening effects. *(Russian)* 78−5819
neutral beam source, cryopumping and mag. shielding, fabrication and operating cost 80−106229
neutral-beam divergence due to imperfect magnetic shielding 78−78489
parallel conductors, with one-sided Fe shield, EM field calc. *(Polish)* 77−31046
particle scattering properties 79−21791
photomultiplier array in strong external field 80−32573
quantum magnetometer with Hanle effect, three layer superconducting shield 77−53962
sampling probe for medium-press. magnetoplasma diagnostics, magnetic shielding 78−22560
scintillation counter, permalloy magnetostatic shield 78−5053
SQUID instruments and shielding for low level mag. meas. 77−40840
SQUID magnetometers, geophysical dewar systems design 80−101462
superconducting shell, closed axisymmetric, for weak mag. fields 77−74470
superconducting shell, shielding weak mag. field, theory 79−68351
superconductive helmet with SQUID for magnetoencephalography 80−104708
theory, shielding against direct lightning strokes 78−88899
Tokamak divertor slot design to enhance mag. shielding 78−5028
Tokamak toroidal field coil shielding calc. 79−31212
vacuum power transmission lines, pulse propag. 79−85765
Al shielded room for biomag. meas. 80−104846
Al, thick-walled conducting shield in biomag. expts. 80−104845

magnetic shielding continued
Al thick-walled enclosure for LF biomag. meas. 80−62698
$Fe_{40}Ni_{40}P_{14}B_6$, glassy metal fabric for mag. shield 77−8347
H maser, field-operable design improvements 79−55099
$NH_4H_3(SeO_3)_2$, single crystal, ^{77}Se magnetic shielding, chemical shift tensors 80−71207
Nb-Sn sintered material tubes for magnetic shielding 79−67446
Nb-Ti, sheet, flux trapping, appl. to mag. shielding and levitation 80−31806
Nb-Ti/Cu sheet composite, flux trapping and shielding capabilities in transverse fields 80−15667
Nb_3Sn, flux trapping and shielding capabilities in transverse fields 80−15667

magnetic shielding, nuclear *see nuclear screening*

magnetic stars
A_p stars, Fe I photoionisation spectrum causing UV absorpt. 80−109437
A-type, mag. field generation by Coriolis EMF 78−8027
early A-type, V/H abundance ratio 79−21314
A-type stars, normal and metallic-line, models pulsational stability 78−16414
abnormal stars in open clusters, freq. of occurrence 79−71038
adiabatic stability, of stars containing mixed poloidal and toroidal mag. fields 80−67706
Am and Ap stars, photometric parameters 78−96483
Am and Ap-stars and high southern galactic latitude, four colour and Hβ obs. 80−82357
Am stars, τ Ursae Majoris and 15 Vulpeculae, energy distrib. from spectral obs. 80−85949
Am stars, evolved, search for photometric variability on lower part of Cepheid instability strip 80−62145
Am stars, multicolour photometry Hα and O I obs. 77−67101
Am stars, photoelec. K-line indices 79−16953
Am stars, photometric stability 77−56953
Am stars, UBVRI photometry of 225 objects 78−69799
Am stars in main sequence, rotational vel. effect on metallicity 79−48814
Am stars in spectroscopic binary systems, evolutionary status, statistical anal. 78−93262
Am-stars, α,λ photometry 78−81638
Am-stars, photometric study of three objects 79−40204
Am-type, binary stars, tidal interaction producing stable atm., evolution 80−67752
Am-type stars, envelope transport processes, implications of Li, Be and B obs. 78−93202
Am-type stars, envelopes circulation 80−4370
Am-type stars with known spectral types, second catalogue 80−36514
α Andromedae, HgMn star, evidence for Hg in thin atmospheric layer rel. to diffusion model 80−105243
AN Andromedae, light curve of Am binary systems, possible third body 79−58374
ET Andromedae (HR 8861), Ap star, light vars. and period 80−46571
Ap, Am and A stars, radii from observed energy curves 77−87403
Ap, Am stars, among composite spectrum stars of Hynek's (1938) list *(French)* 80−56876
Ap, Am stars, chemical differentiation and abundance spots prod. by diffusion 80−77381
Ap, Am stars in α Persei cluster, spectral types 79−58385
Ap, Bp stars catalogue of photometric data rel. to surface mag. fields 80−85873
Ap and Am stars, numerical taxonomy 80−22015
Ap and Am stars, possible nuclear origin of comp. anomalies 79−35277
Ap and Am stars, space distrib. 77−71117
Ap and Am stars in open cluster M34 78−12311
Ap and Bp stars, radiation forces and B abundance diffusion theory 79−88664
Ap and Bp stars, surface mag. field intensity rel. to Geneva photometry 80−105248
Ap and Hg-Mn stars, spectrophotometric scans, search for broad continuum features 78−12247
Ap Si stars, UV spectral vars. 79−8927
Ap star, spectral line profiles *(Russian)* 77−87421
Ap stars, angular diameters, radii, and effective temps. 80−26870
Ap stars, Barnes-Evans relation appl. as clue to atmospheric struct. and evolutionary status 79−67011
Ap stars, CN lines identification 77−91551
Ap stars, decentred dipole and dipole quadrupole magnetic field models, anharmonic analysis 79−101154
Ap stars, flows and mag. fields in surface layers 79−62854
Ap stars, heavy element abundances from Copernicus UV data, reference stars α Lyrae and α Canis Majoris A 78−28688
Ap stars, line blanketed model atmospheres 79−44495
Ap stars, line blanketed model atms. 79−21304
Ap stars, line identifications, new wavelength lists 79−16967
Ap stars, mag. fields meas. techniques and field geometries 80−82213
Ap stars, mag. latit. of metals 79−58341
Ap stars, model atmospheres 79−16973
Ap stars, narrow band photometry of broad absorpts. 77−67095
Ap stars, new Δa-photometry and evidence for two-component struct. of 5200 Å feature 80−67734
Ap stars, obs. evidence for pulsational stability 79−21303
Ap stars, photoelec. obs. of light vars. *(German)* 78−20841
Ap stars, photometric peculiarity index 77−91550
Ap stars, recognition in Vilnius photometric system 78−65635
Ap stars, review of obs. and possible nucl. reactions *(Russian)* 78−20843
Ap stars, spectral variations, abundance peculiarities 79−62821
Ap stars, spectroscopic search of open clusters 78−45367
Ap stars, steady dynamos bifurcation from oscillating dynamos in nonlinear dynamo theory 78−49306
Ap stars, summary of physical and chemical props. from UV obs. *(Italian)* 78−32479
Ap stars, surface heterogeneities 78−12254
Ap stars, thickness estimation of anomalous chem. comp. layer in atm. *(Russian)* 78−93279
Ap stars abundance anomalies, correl. with fission mass distribs. in astrophysical r-process 78−93204
Ap stars broad flux depressions, comparison between synthetic spectra and spectrophotometry 80−67735
Ap stars in close detached binaries chem. anomalies surface distrib. 80−109475

magnetic stars continued
Ap stars in NGC 2516, thirty identifications 79−16972
Ap stars in spectroscopic binary systems, chemical anomalies surface distrib. 80−62140
$δ_{1400}$-Ap type stars, excess UV index, photometry obs. 80−72963
Ap- and Bp-stars, 206-287 nm UV spectra 80−51776
Ap-stars, decentred magnetic dipole models for 17 objects 79−67013
Ap-stars, detection of 4200 and 5200 Å, continuum features 79−75215
Ap-stars, Hα and O I photometry of 23 objects 78−81640
Ap-stars, mag. field obs. using photoelec. method, visible spectra obs. 80−82373
Ap-stars, oblique rotator model, Deutsch and Khoklova methods 79−35271
Ap-stars, photometry and surface magnetic fields 80−56847
Ap-stars, spectral energy distrib., spectrophotometry in 3300 to 7100 Å region 80−85953
Ap-stars, Stromgren photometry of 341 objects 79−71047
σ Aquarii (A0 IVs), hot metallic-line star, abundance anal. from model atmosphere 80−90415
SX Arietis, He spectrum variable, UV photometry with ANS 78−36585
56 Arietis, spectrophotometry of Ap star, continuum features vars. 80−36638
γ Arietis, visual binary Ap-system, photometry 78−85950
AR Aurigae, eclipsing binary Hg star, peculiar spectral var. during eclipse 80−98679
late B-type stars small v sin i values, Ap star determ., visible spectra 80−77409
binaries, charged particle motion in magnetic dipole field 78−69828
Bp-star (No.7) in cluster near IC 1805, photometry 80−62214
53 Camelopardalis, Ap star, Ca II K and Hδ lines rapid vars. *(Russian)* 80−90458
53 Camelopardalis, Ap star, radial vels. and binary nature 79−80320
53 Camelopardalis, photometric vars. 80−4367
53 Camelopardalis (AX Camelopardalis), Ap star, UBV photoelectric photometry and period of var. *(Italian)* 80−90448
κ Cancri, Hg-Mn star, diffusion processes and abundance amometers 77−87407
49 Cancri, spectrophotometry of Ap star, continuum features vars. 80−36638
$α^2$ CAnum Venaticorum, line blanketed model atmospheres of Ap-star 80−90440
$α^2$ Canum Venaticorum, mag. Ap star high-resolution polarisation obs. inside spectral line 78−40951
$α^2$ Canum Venaticorum, magnetic field gradient in Ap-star atmosphere, Zeeman spectra 78−85953.
$α^2$v Canum Venaticorum, magnetic variable, H I lines and atmospheric parameters 79−97011
$α^2$ Canum Venaticorum, UV flux distrib. 79−80313
$α^2$ Canum Venaticorum type stars, dynamical parallax, absolute magnitudes and masses *(Russian)* 79−88690
XY Ceti, light vars. of eclipsing binary with Am spectra 78−93310
XY Ceti, metallic line eclipsing binary, masses, radii and luminosities from revised photometric elements 80−109458
chemically peculiar A-type stars, accretion of grains 79−67017
17 Comae A, Ap star, mag. field meas. and rot. period *(Russian)* 80−90457
convective stability in magnetic stars, theory 80−94781
β Coronae Borealis, Ap star, Ca II K and Hδ lines rapid vars. *(Russian)* 80−90458
β Coronae Borealis, Ap star, high resolution polarization obs. 78−8011
β Coronae Borealis, Hα line variability *(Russian)* 78−69815
β Coronae Borealis, H I Paschen lines and Ca II triplet study 80−26869
ιCoronae Borealis, Hg-Mn star, spectroscopic binary, visible spectra obs. 80−72983
β Coronae Borealis, mag. deform. ot evolved stellar model, hypothesis 79−30076
β Coronae Borealis, mag. star, spectral peculiarities *(Russian)* 77−64773
β Coronae Borealis, magnetic field gradient in Ap-star atmosphere, Zeeman spectra 78−85953
β Coronae Borealis, magnetic field of Ap-star 79−5822
β Coronae Borealis, obs. with Zeeman analyzer system on McDonald 2.7 m telescope 80−62021
V389 Cygni, peculiar (Ap-type) binary, spectroscopic obs. 78−85975
δ Delphini stars in Michigan Spectral Catalogue, uvbyβ photometry rel. to spectral types 80−4377
73 Draconis, spectral variability of Ap star *(Russian)* 78−65624
early type peculiar stars, Cr, Mn and Fe abundances 77−78803
effective temperatures, radii and bolometric magnitudes of Ap and Am stars 79−16970
equatorially symmetric rotator model, inhomogeneous element distrib. 80−4371
equilibrium struct. of uniformly rot. polytrope with large toroidal field 77−87367
γ Equulei, magnetic field obs. of Ap-star 80−51782
γ Equulei, peculiar A-type star, line identification study, 3086 to 3807 Å 79−88659
Feige 86, $^3He/^4He$ from He I 6678 Å obs. of He deficient blue horizontal-branch star 79−92774
Feige 86, UV high-resolution spectrum 80−41834
Feige 86, UV spectrum of peculiar hot halo stars 79−48811
GC 17353, Ap star with large photometric var., period *(French)* 79−2545
HD 101065, Przybylski's star, light variability freq. anal. 80−62152
HD 101065, search for light vars. 78−69812
HD 101065 (Przybylski's star), Ap-star model rel. to light vars. and temp. 79−101151
HD 10783, Ap star, spectrophotometric obs. 80−98663
HD 111133, Ap star, 5200 Å flux depression variability *(German)* 79−44496
HD 116890, Si Ap star, UBV photometry, periodicity 79−80318
HD 124224, He Si variable, spectroscopic obs., starspots, oblique rotator model 78−12239
HD 125248, Ap star, UBV photometry, light curve, period 78−32472
HD 129494, new pulsating δ Delphini star, photometric obs. and luminosity 80−67750
HD 129708, bright short-period Cepheid with δ Delphini tube spectrum, photometric obs. 80−67751
HD 134793, Ap star, UBV photometry, light curve, period 78−32472
HD 153882, obs. with Zeeman analyzer system on McDonald 2.7 m telescope 80−62021

magnetic stars continued
HD 161698, Hg-Mn star, chemical elements identification in spectrum 79−58354
HD 161698, Hg-Mn star, curve of growth anal. 79−30070
HD 184905, Ap star, UBV photometry, light curve, period 78−32472
HD 184905, H I line strength var. in Ap-star 79−16987
HD 184905, magnetic variable, H I lines and atmospheric parameters 79−97011
HD 184927, He variable star, spectroscopic props. 80−51790
HD 186205, He star, fine abundance anal. 77−87408
HD 187473, rare earths in Si star 80−98671
HD 193857, metallic-line binary star, orbital elements 79−75250
HD 215038, Ap star, line identification list 78−32484
HD 215441, mag. field geometry 78−53950
HD 215441 (Babcock's star), magnetic vars., non-axisymmetric eccentric dipole model 80−51779
HD 216533, Ap star, spectroscopic binary oblique rotator model, spectral var. study 79−101153
HD 21699, Si star in α Persei cluster, OAO 2 UV photometry 78−93331
HD 221568, Ap star, light var. period 80−56856
HD 30849 periodic variability photometric obs. *(French)* 79−101157
HD 34452, Si Ap star, spectroscopic study 78−65634
HD 3473, A2p star, spectrograms, Si and rare earth elements overabundance 77−74071
HD 3580, 187473, 212432, Si stars, uvby photometry and periods 78−96487
HD 36619, Am-type star previously misclassified as O7 type 79−84805
HD 3980, late Ap star, photometric and mag. variability obs. 80−56845
HD 64740, He rich star, UV spectral vars. 80−22016
HD 72968, low amplitude photometric double wave Ap star, light curve 78−28697
HD 92664, Ap star, photometric variability and period 79−40199
HD 9996, Ap star, spectrsocopic obs. 78−77558
ϕ Herculis, Ap star, X-ray emission obs. 79−101160
ϕ Herculis, Hg-Mn star, corona search, UV obs. 80−72986
52 Herculis, magnetic, spectral and photometric vars. of Ap-star 78−85952
HR 1217, Ap star, spectrum and light vars. relationship 80−26878
HR 3413, Ap star, photometric vars. and period *(French)* 78−32471
HR 3448, He weak variable, discovery during photometric search for β Cephei stars 79−71040
HR 4594, pulsating marginal metallic line (Am) star, obs. 78−49448
HR 5049, Co II in spectrum of southern magnetic Ap-star 80−82384
HR 6127, chemically peculiar star, spectral lines and equivalent width lists, visible obs. 80−82387
HR 7129, He variable, oblique rotator model 79−62838
HR 8210, pulsating marginal metallic line (Am) star, obs. 78−49448
HR 96, Ap-type star, atm. parameters and stellar comp., visible obs. 80−67740
HR 976, Am-type star, soft X-ray source obs. 78−81634
intrinsic rotation of magnetic variables, correl. with colour index and masses 78−40967
Jeans spheroids with toroidal mag. fields, equilib. and stability 78−45319
late B-type peculiar stars, Ca II K-line profiles 78−73722
60 Leonis, scanner obs. of metallic-line star 79−5827
20 Leonis, triple system with two Am stars and δ Scuti variable 77−49440
μ Leporis, HgMn star, evidence for Hg in thin atmospheric layer rel. to diffusion model 80−105243
χ Lupi, HgMn star, evidence for Hg in thin atmospheric layer rel. to diffusion model 80−105243
magnetic buoyancy in rotating gas, effect of fine electrical and thermal conductivities 78−57436
magnetodynamic mechanism 77−87404
marginal metallic line (Am) stars, metallicism and pulsation 78−49448
metallic line stars, spectral energy distrib. *(Russian)* 80−72975
metallic-line stars, theoretical pulsation models 79−97004
model, circulation within nuclear burning shell rel. to latit. depend. chem. comp. *(Russian)* 79−16940
NGC 2287, open cluster, spectral classification of brightest stars 80−26919
oblique rotator model and Si overabundance by diffusion 79−30067
oblique rotator production of EM field, lowest order solns. 79−21176
oblique rotator with irrotational axisymmetric mag. field surface distrib., effective mag. field 80−26872
ω Ophiuchi, UBV photometry of Ap star, periodicity in luminosity vars. *(French)* 78−57559
σ Orionis E, mag. field discovery 78−93268
oscillations, nonradial mode splitting 80−77414
peculiar bright southern stars, identification and spectral types 77−82225
perpendicular rotator model, with meridional circulation 78−16438
IW Persei, metallic-line close binary star, photometric and spectroscopic obs. 80−62186
21 Persei, spectrophotometry of Ap star, continuum features vars. 80−36638
ξ Phoenicis, periodic variability photometric obs. *(French)* 79−101157
Pleiades, spectral classification of brightest stars, Ap, Am and shell stars 78−57601
polarity changes, skin effect of electrically conducting spherical shell 80−46389
polarity reversals, appl. of skin effect approx. 80−62010
Przybylski's star (HD 101065), β photometry and period determ. 80−41835
rotating stars, exact MHD solns. 78−69800
3 Scorpii, He weak star, mag. field discovery 79−88676
δ Scuti type pulsation in Ap and Am stars 79−62847
southern Ap stars, photometric vars. *(French)* 79−16981
southern peculiar A-type stars, spectra and atmospheric anals. 78−24517
spectral classification from UV line features, Am and Ap stars appl. 79−21272
spectral types of stars with unusual photometric indices 79−71033
strong internal mag. field diffusion through radiative envelope of 2.25 M⊙ star 78−85931
structure and oscill. of uniformly rotating polytrope 77−87366
41 Tauri, Ap star, Ca II K and Hδ lines rapid vars. *(Russian)* 80−90458
thermal emission of an optically thick plasma containing a strong magnetic field 79−25469
upper main-sequence peculiar stars, chemical and physical props. rel. to radiatively driven diffusion theory 80−82374
in Ursa Major stream, spectral types 78−85984
τ Ursae Majoris, Am star, energy distrib. from spectral obs. 80−85949
τ Ursae Majoris, Am star, microturbulence and metal content determ. 80−82377
CQ Ursae Majoris, Ap star, UBV photometry, light curves, colour indices 78−49454
CQ Ursae Majoris, Ap star, UBV photometry, light vars., period determ. 79−88667
CQ Ursae Majoris, line identification list and radial vel. 80−41841
τ Ursae Majoris, scanner obs. of metallic-line star 79−5827
32 Virginis, A-type main-sequence and Am-type star components 79−30091
78 Virginis, Ap star, mag. field geometry, oblique rotator model 80−51773
CU Virginis, He I 4026 Å line var., photoelectric meas. 78−77555
CU Virginis, He spectrum variable, UV photometry with ANS 78−36585
78 Virginis, magnetic Ap star, high resolution polarisation obs. inside spectral lines 80−51772
78 Virginis, magnetic field gradient in Ap-star atmosphere, Zeeman spectra 78−85953
CU Virginis (HD 124224), Ap star, spectrophotometric obs. 80−98663
15 Vulpeculae, Am star, energy distrib. from spectral obs. 80−85949
15 Vulpeculae, scanner obs. of metallic-line star 79−5827
Cr stars, classification criteria, Cr II lines with blending 78−85951
Dy III lines in spectra of Ap and Bp stars 80−12764
H deficient and He weak stars, uvby photometry, variability 80−46579
He abundance anomalies, radiative forces calcs. in stellar envelopes 80−31291
He rich stars, elec. fields influence on accretion and stellar winds 79 48772
He rich stars, intermediate and extreme, spectral atlas in 3700 to 4600 Å range 80−94806
He strong stars, mag. fields meas. 79−44486
He variable stars, IR excesses obs. 80−67733
He weak and He strong stars, spectrum variability 79−40201
He-proton diffusion coeff. in stars 79−16811
^{3}He stars, spectroscopic search, diffusion hypothesis 79−35264
Hg-Mn binary stars, inhibition of atmos. diffusion 80−62153
Hg-Mn stars, absolute magnitude 80−46564
Hg-Mn stars, chemical abundances 80−56838
HgMn stars, diffusion and line asymmetries 78−40948
HgMn stars, rot. and incidence among late B-type stars 78−89199
HgMn stars, spectrophotometry 80−26867
Mn stars, Hg II line oscillator strength determ., diffusion models implication 80−72966
Mn-Hg stars, surface gravity and stellar temp. derivation from uvbyβ data, statistical anal. 80−82397
U stars and related objects, spectroscopic study 78−49465

magnetic storage devices
bubble formation and computer storage element appls. 77−20662
bubble memory technology, developments 78−52325
conference, Florence, Italy (May 1978) 78−91833
disc memory recording heads, investigation of dynamic mechanical props. that appear as stresses during small motions 80−22422
magnetism and magnetic materials conf., Pittsburgh, USA (June 1976) 77−12071
magneto-optical photoconductor sandwich 77−40213
surface flatness meas., moire angular readout device 79−93209

magnetic storage systems
see also magnetic disc and drum storage; magnetic film stores; magnetic tape storage
magneto-optic memories, state of the art 77−42494
recording on particulate media, conference, Gardone Riviera, Italy (Sep. 1979) 80−41930

magnetic stores *see magnetic storage systems*

magnetic storms
see also micropulsations
440 keV proton precipitation at middle latitudes during the recovery phase of magnetic storms 78−20579
1880 to 1974, mag. storms. rel to solar activity and connected tropospheric instability 79−92580
1967 September 13 storm, ion composition changes in low latitude topside ionosphere 78−16232
1968, October-November, obs. of high-latit. NO in lower thermosphere 77−37467
1969, February 2, Pc 1 pulsations rel. to interplanetary plasma flow struct., 78−45142
1969 November 8-9, thermospheric response 80−12574
1970, December 14, electron density obs. at 1000 km by (Kosmos 381) 77−64513
1970, December 29-30, correlated changes in equatorial electrojet and interplanetary mag. field 78−85766
1970, March 6, substorms rel. to interplanetary mag. field polarity and plasma sheet thinning 77−25874
1970, March 8, global exospheric temps. and densities 77−33234
1970, March 8, midlatit. ionospheric disturbances caused by high energy particles 77−60517
1970, November 21, positive disturbance, ionospheric elec. fields and particle fluxes 77−21970
1970 December 10 to 20, electron temp. behaviour meas. in main ionosphere valley 80−4170
1970 to 1975, effect on dispersion characts. of whistlers observed at Sofia 79−8779
1971, December 12 to 21, mid-latit. trough obs. by Ariel 4 78−85765
1971, December 16, energetic electron precip. and VLF phase disturbances at midlatit. 77−53284
1971, December 16, high-energy electron and ELF radiation fluxes 78−69564
1971, December 17 storm, Kosmos 426 obs. of outer radiation belt dynamics 77−33281
1971, December 17-18, search for the ions in recovery phase 77−70947
1971 December 14 to 21 event, pattern of 6300 Å emission over polar cap 79−75012
1971 December 17, outer radiation belt behaviour 78−16248
1972, April 15 to 26, struct. of solar proton fluxes in high-latit. magnetosphere 77−64532

magnetic storms continued
1972, August, ionospheric and thermospheric responses 77−25858
1972, August, magnetosphere response 77−25888
1972, August, substorm effects in polar cap absorpt. and auroral events 77−29567
1972, August 4, 'low' E_s-layer studies and latit. regularities *(Russian)* 79−8749
1972, August 4, sudden commencements, incoherent scatt. radar obs. of ionospheric response 77−33264
1972, August 4 to 5, extra-storm rel. to flare interplanetary plasma flow hydromagnetic struct. 79−53653
1972, August 4-5, ionospheric storm in Asia-Australia-Pacific sector 77−33269
1972, August 4-5, plasma wave obs. in magnetosphere 77−29594
1972, August 4-7, incoherent scatt. radar obs. of ionosphere 77−45248
1972, August 8-9, solar protons auroral zone precip. assoc. with storm sudden commencements 77−82081
1972, February 13, equatorial electrojet obs. 77−33276
1972, February 24, positive disturbance, ionospheric elec. fields and particle fluxes 77−21970
1972, February to April, correl. with solar disc central features 79−40040
1972 August, geomag. activity correl. with microearthquakes 79−66638
1972 December 12, outer belt 77−9619
1973, April 1 to 2, neutral atmosphere response, two-satellite study 77−9582
1974, April 18, F-region scintillations and aurora 77−87158
1974, February 9-15, neutral comp. and ionospheric vars. 77−87142
1974, January 25, ring current protons dynamics 79−80083
1974, July 4-6, form. and decay of energetic electron belt injected into magnetosphere 78−69617
1974, November 14, electron precip. event obs. at Sanae, Antarctica 77−87182
1974 August to November, effects on nighttime electron content of mid-latit. plasmasphere 80−94642
1974 July 6, ring current protons asymmetric injection 78−45144
1974 June 30, polar substorms rel. to midlatit. thermosphere neutral wind meas. 80−31153
1974 October effect on plasmasphere electron content, radio beacon obs. 77−45229
1975, April 11, strong partial refl. in auroral D-region during absorpt. event 78−36388
1975, January 6-7, effect on Tordo 1 polar cusp Ba plasma injection expt. 78−77402
1975, May 16, ionosphere temps. and low-energy particles obs. in turbulent polar cusp 78−96343
1976, December 8 substorm, magnetic and ionospheric disturbances features, morphology study 80−4201
1976, March 26, onset, high resolution electron energy spectra in active aurora 77−33257
1976 March 26, midlatitude thermospheric neutral winds and temps. 79−53594
1976 March 26-27, meas. of precipitating protons, α particles and heavy ions 79−53667
1976 October 7, ground-based obs. of auroral zone elec. currents using two-dimensional magnetometer array 80−90245
1977, August to October, geomag. activity assoc. with solar McMath region 14943 79−48625
1977, December 11, ring current comp. and dynamics, ISEE-1 obs. 79−84589
1977, December 2, magnetosphere thermal/suprathermal plasmas obs. by GEOS-1 S-302 expt. 79−35070
1977, July 29, substorm-assoc. energetic ions injections obs. around synchronous altitude 79−35075
1977, September 19 to 21 event, cusplike electron precip. regions DMSP-F2 obs. 79−35056
1977, September 21, low energy electrons obs. by AE-C in S polar cusp 79−35076
1978 December 11, mini-substorm and long-period Pi 2 event obs. by Jikiken satellite *(Japanese)* 80−94653
1978 February, substorm activity rel. to proton flux obs. by Geostationary Meteorological Satellite (GMS) 79−75056
1978 July 15, severe scintillation of VHF and GHz waves from geostationary satellites 80−109302
1978 September 29, unusual VLF noise event obs. at Sakushima 79−101031
A_p-index, 1964-1976, rel. to geomag. field and interplanetary field states 80−104866
adiabatic evolution of trapped particle pitch angle distribs. during storm main phase 77−70949
airglow during magnetic storm, O I 7774 Å multiplet obs. 80−72663
Akasofu substorm parameter, interpretation 79−75053
annual variation in disturbed intervals, rel. to interplanetary mag. field sector polarity 77−86767
associated sporadic-E enhancements over Brazilian Geomagnetic Anomaly 78−28431
atmospheric pressure during geomagnetic disturbances, geographical dependence of solar-atmospheric connections 79−25315
atmospheric useful potential energies rel. to geomagnetic disturbances 77−70791
auroral absorption substorm, onset obs. 78−96362
auroral and magnetic substorm development at mag. midnight 79−66888
auroral arcs location near substorm onsets 78−88968
auroral bulge expansion features during substorms 80−41597
auroral E-region fine structure obs. in substorm 80−36452
auroral infrasonic substorm obs. with Chatanika radar 77−17269
auroral infrasonic waves in substorm area, source regions *(Japanese)* 80−85788
auroral ionosphere, electric field and conductivity meas. during substorms 79−80073
auroral magnetic disturbances indicated by kilometric radiation 77−70909
auroral processes, IAGA/IAMAP symposium (Seattle, August 1977) 79−88521
auroral proton bursts struct. during mag. quiet times and substorms 77−29531
auroral substorm, assoc. mag. variation and auroral motion 80−51593
auroral substorm, expansive phase, ions and electrons, rocket obs. 78−45115
auroral substorm, ionospheric irregularities simultaneous rocket probe, scintillation and incoherent scatter radar obs. 80−94640

magnetic storms continued
auroral substorm, mag. reconnection rel. to plasma accel., heating and shock form. 78−40773
auroral substorm absorption events, at low auroral latits , apparent equatorward propag. 79−8769
auroral substorm expansion phase, ionospheric currents and elec. field vars. assoc. with absorpt. spikes 79−35039
auroral substorms, HF signals statistical charact. 78−69583
auroral substorms, high-latit. ionospheric currents prod. by vars. of asymmetric ring current 77−21971
auroral substorms, small scale ionospheric absorpt. events 77−56791
auroral zone E-region, atmospheric motions during disturbed conditions, spaced receiver obs. 77−87172
BDI position and plasmapause position during Feb. 1972 mag. storm 80−56666
chorus VLF and ELF emission, plasmapause origin model 80−41608
cleft region dynamics 80−101483
cosmic radio noise absorpt. rel. to mag. storms at Delhi 78−69589
cosmic ray intensity daily variation, mag. storms depend 79−35082
current interruption mechanism in collisionless plasma 78−42721
currents generated, delineation of cosmic ray flux, Earth mag. field *(German)* 80−51609
D_{st}, contrib. to aurora equatorward shift 79−75013
D_{st} index, annual and daily vars. 78−96351
D_{st} index, correl. with ring current growth and interplanetary quantity ε 79−75057
D_{st} index, negative change assoc. with whistler ducts formation 80−94659
D_{st} index, rel. to current fields at magnetopause and in radiation zone 79−53658
D_{st} index, standard reference level 77−29246
D_{st} variation asymmetry, as function of local time 80−41643
D_{st} variations, influence of solar wind parameters 79−40054
D_{st} variations analyses, comparison using distortion free filter 80−17419
D-region, diurnal vars. during storm after-effect 78−65451
D-region, mid-latit., energetic particles precip. during baylike absorpt. disturbance 79−12333
D-region, NO prod. rel. to winds and electron densities time vars. correl. 79−25389
development rel. to interplanetary energy flux 78−85771
disruption effects in power and communications, research progress report 79−101021
disturbance index, K_p rel. to O I 6300 Å airglow emission rate 77−45215
DS latitudinal variation abnormalities 79−84591
Dst space-time patterns during individual mag. storms 77−13184
Dst variations and interplanetary B_z component vars., time displacement 79−101032
E_s-layer, props. at Sodankyla, Finland rel. to auroral substorms 77−87183
E-region, disturbance effects on daytime critical freq. 77−64527
E-region, elec. fields meas. in aurora during mag. storm 77−82077
E-region, low-latitude, ionisation by energetic ring current particles 78−77415
effect on low latitude whistler activity *(Japanese)* 79−16769
effect on mesopause wind, meas. by ionospheric drift obs. 79−35025
effect on plasmasphere electron content 78−36403
electric currents in cosmic plasmas 78−12094
electric field variation during low solar activity *(Japanese)* 79−40032
electrojet intensification by substorm 80−85796
electron fluxes >0.7 MeV near belt boundary during substorm 78−96349
electron precipitation during substorm, modulation by hydromagnetic waves 80−105113
electron spectra in Earth's radiation belts during mag. storms 77−53314
EM cyclotron instability, effect of plasma drift 79−60150
energetic neutral atom precipitation, optical emission, ionization and energy deposition 79−75047
energetic particle meas. at 6.6 R_E, low-energy electron anisotropies and short-term substorm predictions 79−16766
energy flow at magnetopause rel. to geomagnetic activity 78−28428
energy transfer of injected particles to lower atm. by IR emission 79−53425
equatorial ionosphere, elec. fields. rel. to geomag. vars. 77−78578
equatorial spread-F, geomag. disturbance effects 79−35044
evening magnetic pulsations in auroral zone during substorm 77−25884
exosphere, geomagnetic density and temp. effect propag. 79−48593
expansion phase of substorm and energetic protons in plasma sheet boundary 79−35062
f0E, storm time var. at low latit. station 79−44295
F_2-layer, low-latit., vertical motions during prolonged and isolated mag. storms 77−37479
F_2-layer, midlatitude storms in daytime and nighttime 79−8757
F_2-layer electron density, mag. storm effects 80−61970
F-layer, anomalous decrease in equatorial f_0 during strong storms 80−77197
F-region, equatorial, mag. storm effects on topside and bottomside struct. 78−36373
F-region, total electron density content and peak electron vars., 140 MHz obs. 80−101471
F-region effects at magnetic field line L=4, electron data anal. 80−8472
F-region height and electron content changes at midlatit. during mag. storms 77−21984
F-region response to storm of June 1972, thermosphere-ionosphere coupling 80−41617
field changes, ionospheric-magnetospheric contribs. 80−12612
Forbush decreases and geomagnetic storms rel. to interplanetary parameters 77−70956
Geomagnetic Meridian Project, magnetic var. of auroral electrojets 79−29936
gradual commencements, rel. to interplanetary mag. field intensity vars. *(Russian)* 80−105127
gravity wave assoc. with sudden commencement, ionospheric effects 78−57385
HF radio noise study during auroral substorms, freq. range 8 to 25.5 MHz 80−41670
high-energy protons produced by substorms, interplanetary conditions 80−51615
high-latitude substorms, charact. 80−109315

magnetic storms continued
horizontal field variations in Indian peninsula, induction at short periods 77−86773
India equatorial region, mag. activity rel. to PC 1 pearl pulsations occurrence 79−25405
induced geomagnetic vars. in India, regional charact. 79−39639
influences on man-made technologies 80−12887
initiation and propag. from solar flares *(Korean)* 77−53335
inner magnetosphere penetration by energetic particles 80−72716
interplanetary disturbances rel. to mag. and comsic ray storms 77−33313
interplanetary magnetic field changes correl. to geomag. storms 80−41642
interplanetary magnetic field Z-components, variations causing magnetic storm main phase 80−4200
interplanetary shock and substorm activity, with increased solar wind energy deposition 80−77237
ion composition and origin, of high-altitude region during mag. storm 80−82144
ionosphere, daytime positive storm effects at middle latits., prod. by travelling atmospheric disturbances 79−25394
ionosphere, daytime scintillation assoc. with geomagnetic storm 77−78563
ionosphere, elec. fields induced by ion drag and substorms 80−77199
ionosphere, electric fields and currents in substorms, simulation 80−12601
ionosphere, equatorial irregularity belt movement 78−40757
ionosphere, geomag. disturbances rel. to transitional electrodynamic processes 77−60515
ionosphere, geomag. field dependence of global absorpt. meas. on board ships 80−98500
ionosphere, Injun 5 low-energy plasma obs. during major mag. storm 78−88987
ionosphere, ionization vertical lifting during mag. storms, satellite meas. of ion comp. 78−36395
ionosphere, lower, storm-produced disturbances in long-distance mid-latit. VLF transmission 80−8485
ionosphere, mag. storm effect on struct. at low latitude, 406 kHz impedance obs. 80−67468
ionosphere, mag. storms rel. to radio waves winter absorpt. anomaly at middle latits. 80−67459
ionosphere, press. oscills. rel. to atmosphere acoustic-gravity waves oscills. 78−77296
ionosphere, substorm development in postmidnight sector, electron density vars. 77−60525
ionosphere, total electron content, equatorial electrojet control 79−88539
ionosphere, total electron content obs. at low and mid latitude 78−77396
ionosphere, unusual mid-latitude disturbance of corpuscular origin 78−28374
ionosphere and thermosphere, response to mag. storm, OGO 6 in situ meas. 77−9588
ionosphere disturbance assoc. with storm, electron density vars. with latitude 80−101474
ionosphere during auroral substorm expansion, riometer absorpt. spikes obs. 80−85799
ionosphere E-region, latit., geomag. storms effect on electron density 79−44294
ionosphere polar electric field, horizontal transmission to equator 80−8478
ionosphere radiowave propagation, disturbance effects and their predictability 79−58171
ionosphere storms, behaviour of electron content during positive phase 77−37480
ionosphere total electron content, storm-time changes at nearby mid-latit. locations 80−31164
ionosphere total electron content during magnetic storms over Hawaii 78−16238
ionospheric absorption and Pc 1 pulsations following enhanced geomag. activity 77−53332
ionospheric and magnetospheric current systems during mag. storms 79−12349
ionospheric daytime slab thickness depend. on geomag. activity 77−21992
ionospheric ions in storm-time ring current 78−28430
ionospheric projection of plasmapause, intense poleward-directed elec. fields during mag. storm 78−20574
ionospheric recurrent storms, effects on HF radio communication 78−4028
ionospheric slab thickness during storms 79−88538
ionospheric total electron content, mag. storm effects, Indian region 79−84576
isolated substorm, incoherent scatter radar meas. of F-region electron density and ion vel. 78−65452
isolated substorm over Scandinavia, 1st March 1977, ground-based obs. 80−105132
kilometric radiation, theory 79−70900
large-scale circulation influence on neutral composition 77−49206
largest geomagnetic storms per solar cycle, statistics 77−2306
LF signals knife-edge type field strength depression during mag. storms 78−40740
magnetic field low-freq. oscills., prod. by Alfven and compressional waves coupling 78−89001
magnetic merging during substorms and solar flares, role of O-type neutral lines 79−53665
magnetic ULF waves over auroral arc during substorm event 80−72722
magnetosphere, charged particle fluxes obs. by JIKIKEN satellite rel. to mag. storms *(Japanese)* 80−94654
magnetosphere, connection with solar flare activity 80−72919
magnetosphere, disturbances, rel. to troposphere pot. gradient slow vars. and short-period pulsations 79−12188
magnetosphere, elec. field in VLF to HF range, EXOS-B obs. 80−67478
magnetosphere, geomag. activity correl. with energetic electrons bursts in magnetosheath and solar wind 79−80095
magnetosphere, increasing freq. MHD wave generation in evening sector during substorms 79−62680
magnetosphere, ion comp. dynamics during mag. storms, GEOS mass spectrometer obs. 79−35069
magnetosphere, large transient elec. fields obs. 78−28440
magnetosphere, magnetic energy conversion in substorms 80−56682
magnetosphere, magnetic field models 80−41640

magnetic storms continued
magnetosphere, particle streaming obs. by GEOS-1 keV plasma expt. 79−35068
magnetosphere, substorms and solar flares, similar plasma processes 80−41671
magnetosphere, substorms assoc. with interplanetary energy flux 79−48636
magnetosphere, VLF emissions and electron enhancements assoc. with geomag. disturbances 77−33285
magnetosphere disturbances, effects on high-latit. ionospheric absorpt., riometer meas. 80−8488
magnetosphere evening sector, proton cyclotron instability during substorms *(Russian)* 77−91378
magnetosphere long-period hydromagnetic waves assoc. with substorms, longit. extent 78−40772
magnetosphere midnight sector, coexistence of two substorms 77−53330
magnetosphere reconnection, substorms and energetic particle acceleration 80−31169
magnetosphere response to interplanetary mag. field changes, substorms 78−4038
magnetosphere ring current plasma injection, correl. with solar wind parameters 78−96363
magnetosphere substorm, energy transfer 79−12343
magnetosphere substorm, source movements assoc. with IPDP pulsations 79−25404
magnetosphere substorm activity, local time var. of ELF emissions 77−53328
magnetosphere substorm and simultaneous thunderstorm, elec. fields, electron precip. and VLF radiation 80−67392
magnetosphere substorm onset, coincidence with kilometric radiation enhancement, JIKIKEN (EXOS-B) satellite obs. *(Japanese)* 80−94648
magnetosphere substorms, assoc. with relativistic electron precip. events 77−25827
magnetosphere substorms, cause of plasma sheet thinning 80−72705
magnetosphere substorms, dayside aurora response 77−87148
magnetosphere substorms, dusk-dawn asymmetry in response to interplanetary mag. field B_y-component 78−89006
magnetosphere substorms, effects of magnetotail localised induced elec. field 77−53329
magnetosphere substorms, inductive elec. fields 79−80093
magnetosphere substorms, ionosphere elec. fields determ. from Doppler sounding 80−4169
magnetosphere substorms, multiple satellite studies of plasma sheet radial dynamics 77−25871
magnetosphere substorms, onset identification via Pi 2 mag. pulsation 77−9626
magnetosphere substorms, particle-flux vars. obs. at L=6 to 8 by (GEOS-1) 79−35067
magnetosphere substorms, prediction of occurrence by solar wind and IMF obs. 80−41648
magnetosphere substorms, similarities and differences with solar flares 77−17477
magnetosphere substorms, statistical mag. signature 78−49237
magnetosphere substorms, trapped particle outer boundary motion, obs. at synchronous orbit 77−29586
magnetospheric plasma discontinuity obs. using geostationary differential phase method during storms 78−20584
magnetospheric substorm, onset model 79−29938
magnetospheric substorm development and Pi 2 pulsations parameters var. 77−25864
magnetospheric substorm physics, book 77−33298
magnetospheric substorms, assoc. three-dimens. current system modelling 77−56793
magnetospheric substorms, charged particles trajectory traces 79−16761
magnetospheric substorms, energetic particle accel., lab. and space expts. 77−5400
magnetospheric substorms, Imp 6 meas. of particle entry in distant polar cusp 79−2439
magnetospheric substorms, impulsive flux transfer events, theory 77−17495
magnetospheric substorms, multiple-satellite studies of polar mag. substorms and convection bays 78−45159
magnetospheric substorms, onset and intensification, Pi 2 micropulsations as indicators 79−88552
magnetospheric substorms, Pi3 long-period irregular mag. pulsations 78−45164
magnetospheric substorms, plasma sheet recovery and auroral zone leaps 79−25401
magnetospheric substorms 78−69613
magnetospheric substorms and Pi 2 pulsations assoc. mechanism 77−22018
magnetospheric substorms at night, ionospheric effects 79−62656
magnetospheric substorms correl. with terrestrial kilometric radiation 78−28450
magnetospheric substorms effect on plasma sheet oscills. 77−17296
magnetospheric substorms rel. to interplanetary magnetic field orientation changes 78−28478
magnetospheric substorms rel. to solar plasma clouds and streams 77−87207
magnetospheric VLF emissions during mag. storms, Ariel 3 and ground-based obs. 77−56794
magnetotail, particle accel. by induced substorm electric field 77−73909
magnetotail, plasma flow during substorm 80−51616
magnetotail, substorm assoc. current changes 79−12347
magnetotail, substorm electric field effects on charged particles 78−77425
magnetotail, substorm magnetic fields, 3-dimens. analysis 78−61666
magnetotail boundary large amplitude substorm motion 79−62684
magnetotail lobe plasma, double-peaked ion spectra during geomagnetically active period 78−32299
magnetotail neutral sheet southward mag. field rel. to energetic electrons distrib. and substorms 80−26695
magnetotail plasma at lunar distance response to changes in interplanetary mag. field, solar wind and substorms 79−70932
magnetotail reconnection, expected signatures 78−96361
magnetotail substorm processes, hot tenuous plasmas, fireballs and boundary layers 78−32300
magnetotail transient phenomena rel. to substorms 79−80101
mesosphere, day-night depend. of geomag. activity effects on temp. 77−21835

magnetic storms continued
mid-latitude substorm data, Earth induction effects simulation 78−15960
midlatitude disturbances, assoc. VLF radio wave phase anomalies 80−56671
morning sector, eastward movement of auroral radio absorption events 77−56792
morphological scheme of post-storm event in D-region 79−88523
multiple onset substorms, ground signatures of expansion phase 77−17299
negative ionosphere storms, numerical simulation using observed neutral comp. data 79−25393
negative storm effects in ionosphere and upper atmosphere, seasonal vars. 77−53289
neutral atm. disturbances, reaction of midlatit. ionosphere 77−25805
nightglow from N_2^+, correl. to geomagnetic activity 80−72665
outer radiation belt dynamics during strong mag. storm 79−62678
particle density effects of geomagnetic storms, in thermosphere and ionosphere, OGO 6 obs. *(Japanese)* 78−85754
particle trajectories at mag. neutral point 79−66886
Pc 1 pulsations, statistical study at synchronous orbit rel. to assoc. with mag. storms 77−25875
Pc 4,5 geomagnetic pulsations generation, influence of bounce effects 80−4197
Pc 5 pulsation substorms morphological features at high latits. 78−49232
Pc 5 pulsations, stormtime, obs. at synchronous orbit, correl. with partial ring current 78−45163
Pi 1-2 on dayside cleft field lines 77−87206
PiB magnetic pulsation during substorm 80−72723
pigeon homing performance, correlation with magnetic storm due to sunspots 79−2087
plasma dynamics, vertical displacement during substorms 80−4184
plasma sheet, near-Earth, search for mag. neutral line from Imp 6 mag. field obs. 78−89007
plasma sheet dynamics and mag. storms, conceptual model 80−77236
plasma sheet outer boundary, satellite meas. and field-line mapping during substorms 78−88990
plasma sheet thinning, one-dimensional model 77−78579
plasma sheet thinning during substorms 80−105131
plasma stability during storm conditions, Alfven waves and drift modes 80−82150
plasmapause, 1-30 Hz waves generation by reson. electron instability 78−49235
plasmapause electric field variation from pulsation-pearl method, effect of substorm phases 77−25848
plasmasphere, electron precip. and LF noise emissions during mag. storm. 79−80069
plasmasphere, slant total electron content temporal var. with geomag. activity 78−28404
plasmasphere electron content, solar wind influences during magnetic storms 79−16767
plasmasphere electron density, storm assoc. vars. from whistler data 78−88985
plasmasphere response to quiet mag. conditions onset, plasma convection patterns 77−45244
polar cap, mag. field perturbations compared to solar electron profile 80−72718
polar cap and low latitude bays during substorms, ionospheric current systems 77−17300
polar cap magnetic activity as a signature of substorm development 79−40026
polar cap riometer absorpt. and solar protons, night and day relationships 78−28413
polar magnetic substorm development, two-dimensional magnetometer array study 77−91368
polar magnetic substorm observed in the evening sector with a two-dimensional magnetometer array 79−8776
polar magnetic substorms, relationship with ionospheric height rises and spread-F occurrence 78−81494
polar substorm, effect of induced currents in sea on mag. bays observed at coastal observatory 78−65462
polar substorm, F_2-layer vertical drift 79−53618
polar substorms, equatorial-auroral ionosphere coupling 78−32291
polar substorms, obs. with two-dimens. magnetometer array 78−40766
polar substorms, rel. to ring current development and midlatit. convection elec. fields 78−57395
polar substorms, temporal and spatial changes rel. to auroral infrasonic wave emissions 79−100996
polar substorms modelling, Earth induction effects problem 77−9628
positive ionospheric storms, worldwide distrib. 79−44290
poststorm quieting period, intense keV electron fluxes obs. over polar cap 77−25835
prediction by multivariate statistical anal. *(Chinese)* 80−12614
presubstorm field changes and plasma sheet thinning 78−96352
proton ring current during storms, magnetic effect 78−96348
protonosphere depletion assoc. with mag. storm, and recovery 80−85784
protonospheric replenishment after geomagnetic storm 78−28452
Ps 6 magnetic disturbances, seasonal and diurnal var. 80−67477
Ps 6 pulsation assoc. with magnetospheric substorm, obs. polarization, two-snake model 79−66887
Psc 6 rel. to SSC and dayside polar region obs. 77−73908
pulsations of decreasing period, relation to D_{st} vars. field 79−53655
radar auroral substorms, signatures of auroral east-west motions 77−29535
radar auroral substorms, signatures of expansive and recovery phases 77−25812
radiation belt energetic electron precip., natural depletion mechanism for stratospheric O_3 77−41134
radiation belt particles equatorial pitch angle distrib., transient localised sources effects 77−64538
radiowave propag. errors due to troposphere and ionosphere during mag. storms 80−4077
recovery phase, evidence for ring current consisting of He ions 77−22014
recovery phase, low and high altitude obs. of ring current ions 77−70948
recurrent disturbances, assoc. with solar coronal holes, obs. in Fe XIV 5303 Å line 79−16762
recurrent geomag. disturbances and assoc. solar wind streams rel. to coronal holes 77−17522
recurrent storms, interplanetary magnetic field and plasma data 78−20585
magnetic storms continued
ring current electron trajectories associated with VLF emissions 79−2444
ring current growth, axially symmetric model 79−40030
ring current growth during mag. storm main phase, time-dependent soln. 77−60545
ring current magnetic field characts., spherical harmonic analysis 80−101493
ring current particle origin, by inward displacement of trapped particles 80−72708
ring current radii determ. from cosmic ray data during mag. storm 79−62685
satellite geomagnetic substorm charging simulation 79−96886
search for interplanetary quantity controlling development of magnetospheric storms, review 80−17447
short wave radio cct., field strength var. at Hiraiso, Japan, rel. to mag. storms 79−53650
solar 146 MHz C-type bursts correl. with mag. storms *(Chinese)* 80−4321
solar and geomag. activity universal connection 79−40039
solar cosmic-ray fluxes in high-latit. magnetosphere, isotropic diffusion model calc. 77−64531
solar current sheet, radial deformation rel. to geomagnetic storms 79−84623
solar wind, effect on mag. storms and weather *(Swedish)* 79−79910
solar wind parameters depend. of geomag. activity, statistical anal. 79−48402
solar wind-magnetosphere dynamo, energy coupling function and substorms 80−105134
solar wind-magnetosphere energy coupling, geomag. disturbances 80−85821
spherical harmonic analysis appl. 78−49164
sporadic storm, approx. expression for aperiodic var. of geomag. field 77−67012
sporadic-E, nighttime occurrence rel. to geomag. storms 79−35032
spread-F, midlatitude, occurrence during mag. storms 79−29924
spread-F and magnetic activity at Kodaikanal, India 79−88542
spread-F intensity, at Halley Bay high latitude station, India 79−75034
Sq vars. at low latitudes during storms 79−25402
SSC, shock wave form. in magnetosheath 78−45147
SSC at Hyderabad, diurnal var. 77−70922
SSC magnitudes, equatorial enhancement 80−31174
SSC triggering poleward expansion of auroral absorption regions 78−57403
stable auroral red arc formation, proton obs. supporting ion cyclotron wave heating theory 78−49197
stratosphere, electric field in mag. storm negative phase, 1975 March 20-21, balloon obs. 79−79921
substorm, 1973, July 31, microburst electron precip. obs. at L∼4 77−33260
substorm, auroral activity in midnight sector, electrojet and precip. particle characts. 78−12039
substorm, definition of phenomena 80−82145
substorm, DP_{11} and DP_{12} current systems at midlatit. conjugate points 77−29582
substorm, dynamics of high latit. trapping boundary of energetic electrons 77−91374
substorm, effect on stratospheric elec. fields and currents at Syowa Station, Antarctica 77−53142
substorm, ionospheric elec. field wavelike fluctuations obs. at Ft. Churchill, Canada 77−21982
substorm, trapped electrons dynamics in auroral zone 78−40767
substorm activity, dusk-dawn asymmetry in magnetosphere response to interplanetary mag. field B_z component 77−2310
substorm activity, rel. to equatorward boundary of instantaneous nightside auroral oval 78−32289
substorm activity, rel. to rapid subauroral ion drifts obs. by Atmosphere Explorer C 80−4188
substorm activity and assoc. VLF emissions near plasmapause 77−45258
substorm activity rel. to evening sector auroral oval dynamics, DMSP photographs 79−96853
substorm and auroral activity, development after southward turning of interplanetary mag. field 78−28435
substorm associated electrons, satellites simultaneous obs., dawn-dusk elec. field calc. 77−33292
substorm associated field-aligned currents large-scale characts. 78−45156
substorm associated long period MHD waves 77−87195
substorm auroras, pot. and inductive elec. fields on magnetosphere 80−21878
substorm current systems, rel. to dayside aurora and mag. field merging 79−96852
substorm development and auroral oval motions 77−2295
substorm electric fields in nightside plasmasphere, whistler obs. 79−40009
substorm electric fields in plasmasphere, model based on whistler data 80−41661
substorm electron beams, temp. characts. 79−101027
substorm expansion, intense electron and proton fluxes poleward of trapping boundary 77−87164
substorm expansion rel. to auroral fading before breakup 79−2420
substorm inhomogeneities affected by ionosphere, experimental verification proposed 80−4199
substorm mode saturation by mag. trapping EM instability 78−24412
substorm occurrence probability, depend. on interplanetary mag. field and auroral oval size 78−32298
substorm related electron and proton bursts over polar cap 77−91380
substorm sequences, unified phenomenological model 78−77432
substorm variation field modeling, current system anal. 80−105130
substorm-associated height changes in low latitude ionosphere 78−36377
substorms, 1974 August 18, magnetospheric particle injection 78−28444
substorms, Alfven waves excitation by bouncing electron beams rel. to nightside mag. pulsations 80−4203
substorms, assoc. variability of plasma sheet dynamics 80−98518
substorms, chorus generation by energetic electrons 78−96356
substorms, classical equiv. stream systems *(Russian)* 80−85806
substorms, comprehensive model current system for high-latit. mag. activity 79−92640
substorms, contrib. to geomag. field fluctuations at synchronous orbit 78−96358
substorms, effects on ionosphere large-scale elec. field 77−87159

magnetic storms continued
substorms, electron flux intensity rel. to form of auroral absorpt. bays 78−69619
substorms, electron flux vars. in inner radiation belt during substorms 80−67470
substorms, EM and electrostatic emissions at cusp-magnetosphere interface 79−66880
substorms, EM radiation bursts assoc. with auroral electron beam 79−88557
substorms, energy rel. to auroral oval size, DMSP photographs results 77−13146
substorms, field-aligned currents and auroral electrojet obs. in morning sector 77−29573
substorms, fluctuations of auroral zone current system and geomag. pulsations 77−87188
substorms, geomag. induction effects in central Australia 80−72424
substorms, ground magnetogram timing of onset 79−88553
substorms, ionosphere press. oscills. transfer to neutral atmosphere 79−58158
substorms, latit. morphology of >100 keV protons precip. 79−80080
substorms, mag. merging obs. in magnetotail, appl. to solar flares 77−17301
substorms, magnetic vars. rel. to auroral electrojet model 77−13163
substorms, magnetosphere global fine structural forms. development 79−58190
substorms, onset in magnetotail 79−88554
substorms, phase rel. to daytime ionospheric absorpt. surges occurrence 78−73575
substorms, plasma flows and mag. field vectors in plasma sheet 78−96357
substorms, plasma sheet mag. field obs. rel. to mag. neutral line form. 77−25872
substorms, precursory polar cap mag. activity 77−33295
substorms, relation to interplanetary mag. field, model 77−29587
substorms, relation to two types of magnetospheric ELF chorus 78−28437
substorms, review 77−91381
substorms, role of ionosphere, field-aligned currents generation 78−88998
substorms, role of solar wind EM field in Earth magnetosphere 78−28419
substorms, satellite obs. of impulsive bremsstrahlung X-ray events, electron precip. 79−2438
substorms, significance of plasma flow pulsations in mag. tail 78−77436
substorms, ULF mag. vars. assoc. with ionospheric cond. changes 78−88994
substorms appearing north of Cambridge Bay, influence on AE index 79−75054
substorms in subauroral ionosphere 77−49217
substorms triggering by solar wind discontinuities 77−29596
sudden commencement, negative impulse at equatorial stations 79−16768
sudden commencement, power harmonic radiation enhancement 79−2184
sudden commencement, uniform ionosphere transient response rel. to preliminary reverse impulse 80−8477
sudden commencement absorpt. events at polar cap edge 77−70935
sudden commencement absorption events at S. pole, rel. to lower cleft boundary 78−77437
sudden commencement amplitudes, equatorial enhancement, solar activity, depend. and elec. field effect 77−78575
sudden commencement in equatorial region, 1958 to 1972 period *(French)* 80−51606
sudden commencements, assoc. proton flux increases 77−9637
sudden commencements, global struct. 77−56795
sudden commencements, H amplitude at Sabhawala, India, rel. to subsurface elec. cond. 79−66889
sudden storm commencements, analytical study of ionospheric response *(Japanese)* 80−101490
synchronous orbit magnetosphere behaviour during nighttime substorm 80−85811
telluric currents, induced, in Alaska oil pipeline, meas. by gradient fluxgate and SQUID magnetometers 80−98231
thermosphere, comp. changes during mag. storms, spherical asymm. 77−64501
thermosphere, large-scale waves, obs. during mag. storms 79−35021
thermosphere, midlatitude winds rel. to storm time disturbance change rate 79−12323
thermosphere, nighttime wind and temp. meas. during mag. storms 77−9585
thermosphere density enhancement and perturbations form. during geomag. storm, obs. in equatorial zone *(French)* 79−96846
thermosphere heating during magnetic storm, dynamic energy transport from high to low latits. 80−26657
thermosphere neutral wave obs. during mag. storm 77−9581
thermospheric storms and related ionospheric effects during mag. storms 77−9583
topside ionosphere, effects of magnetic and sunspot activities 77−70918
tropical UV airglow, mag. storm effects 77−45214
upper atmosphere, storm induced winds rel. to vars. in disturbances latit. struct. 78−32264
upper atmosphere emissions during 1974, March 16 magnetic storm 77−49209
upper atmosphere perturbations assoc. with mag. storms, review 80−98495
VLF wave activity during mag. storm, stimulated by power line radiation 77−87199
whistlers, meas. of occurrence rate during geomagnetic magnetosphere storms 80−12621
whistlers at low-latitude during mag. storm, equatorial elec. field 80−85817
O^+ energetic ions precip. during mag. storms and magnetosphere-thermosphere coupling 80−26665

magnetic structure
see also canted spin arrangements
actinide compounds, neutron scatt. studies 80−75716
actinide monopnictides, anomalous mag. props., planar coupling theory 80−60245
alkali metal metastable magnetic crystal, aligned electronic spins, mag. props. 77−77035
alloy, binary, simultaneous mag. and spatial long-range order 77−69491

magnetic structure continued
amorphous alloys and semiconductors, Mossbauer spectrometry *(French)* 80−80660
amorphous magnetic order, review 78−68173
amorphous materials, phase transition theory for new spin structure *(Chinese)* 79−24166
anti ferromagnet, spin arrangement of field-induced phases, mag. space aroups 77−32166
antiferrimagnet, vivianite type spin structure model, mol. field approx. 77−66232
antiferromagnet, appl. stress effects on equilib. config. 78−56365
antiferromagnet, effects of four spin interactions 77−51885
antiferromagnet FCC lattice of second kind, surface magnons and mag. structs. 78−23261
antiferromagnetic insulator, strongly anisotropic, spin config. and magnon spectrum 77−8279
bubble garnet film, non-implanted, surface mag. struct. 80−84628
cobalt formate dihydrate, mag. struct., antiferromag. mode 79−99678
coloured lattices, rot. symmetry effect, appl. to mag. structs. 79−90587
cone helix structured magnet, elastic wave spectrum *(Russian)* 78−68342
conference on neutron inelastic scattering, Vienna, Austria (Oct. 77) 79−41912
copper formate anhydrate, cryst. struct. and mag. props. 80−79768
copper formate tetrahydrate, antiferromag. phase, neutron diffr. study 80−93085
copper oxalate, two dimens. antiferromag., proton reson. exam. 77−28453
crystals, mag. struct., exchange multiplets 80−60202
cubic spinels, appl. of determinant method *(French)* 80−54854
di-(2,2,6,6-tetramethyl-4-piperidinyl-1-oxyl)-suberate, spin densities, polarised neutron diffr. meas. 80−50037
diethylammonium copper tetrabromide, mag. struct., NMR meas. 80−71192
dimethyl ammonium manganese trichloride, NMR for mag. ordered state at 3.6K 79−47340
dimethylammonium copper tetrachloride-tetrabromide mixed cryst., mag. transition 80−65874
1,5-dinitronaphthalene, diamag. cryst., mag. axis, struct. interpretation 80−50039
dipropylammonium coppertetrabromide, Faraday effect obs. of mag. struct., and domains 77−63399
disordered and amorphous mag. materials, position entropy solids, exchange and anisotropy noise 79−11295
disordered system, neutron diffr., book contrib. 79−60228
DPPH-benzene, organic radical, pressure induced mag. ordering *(Russian)* 78−88120
dynamical neutron diffraction and its application, book contrib. 79−60231
elastic polarised neutron scatt. atomic mag. moments 80−29531
electron and magnetisation densities in molecules and crystals, Arles, France (Aug. 1978) 80−105428
electron-hole paired systems, ferromagnetic ordering phase diagram 80−97097
exciton ferromagnet, incommensurate mag. structs., inhomogeneous magnetisation *(Russian)* 80−29566
FCC alloys, atomic ordering and antiferromagnetism 78−72330
ferrimagnet, dil., sequence of mag. transforms. *(Russian)* 78−19252
ferromagnet, dislocation effects on phys. props. at $T \neq 0K$ *(Russian)* 77−8378
ferromagnet, electron capture spectroscopy, technique for surface science and ferromagnetism 80−92766
ferromagnetic alloys, disordered cryst. and amorphous, mag. dipolar field distrib., computer simulation 80−65790
ferromagnetic and nonferromagnetic conductor, scattering by associated helical-sonic and spin-helical-sonic waves *(Russian)* 79−24136
ferromagnetic film, Fourier optics, mag. struct. determ. *(Russian)* 78−39371
ferromagnetic metal, inhomogeneously magnetised, muon (μ^+) method, mag. struct. study 79−42739
ferromagnets and antiferromagnets, one-dimens., thermodynamically stable long-range order *(Russian)* 79−27946
field dependent tensors, solid state physics appl. 78−31055
finite sample, mag. rearrangements near surface 80−11240
garnet, magnetic ordering of S-ions *(Russian)* 79−95579
garnet, specific heat meas., elastic type of antiferromag. ordering *(Russian)* 77−55686
garnets, neutron diffraction patterns, group theoretical, exchange Hamiltonian symm. anal. *(Russian)* 79−65648
garnets with Fe^{3+} ions in tetrahedral sublattice, mag. ordering and bond geometry 77−32163
GdH_3, mag.-ordering at 1.8K 80−50062
group theoretical anal. of second order phase transitions 79−91239
group theory description, single irreducible group representation *(Russian)* 80−44804
harmonic rotor model, interactions, spirals and phase transitions with and without long range order 80−60350
Heesch group struct., rel. to mag. prop. tensors 77−8274
Heisenberg ferromagnet, randomly noncollinear mag. struct. and spin waves *(Russian)* 79−42764
Heisenberg thin films 79−38359
Heisenberg-Mattis model, long-wavelength dynamic response 80−20409
helical magnet, surface spin waves and spin arrangements 78−68198
helical magnetic structure, Bloch wall effects on small angle neutron scatt. 79−47297
hexagonal lattice, mag. subband struct. of electrons 79−95307
Invar, local moment model 79−56505
Invar, magnetic structure, absorbed H_2 effect 80−20534
Invar, magnetic structure, depend. on absorbed H, Stoner's band model calcs., Mossbauer spectra 80−65787
Invar, stainless, thermal expansion, elastic props. and Mossbauer effect 79−56502
Invar alloys, mag. struct. small angle neutron scatt. study 79−47249
Invar film, superfine mag. struct. *(Russian)* 80−80572
ionic compounds, amorphous, exhibiting Mossbauer spectra, mag. props. *(French)* 80−80490
ionic compounds, amorphous, Mossbauer study, frozen mag. state and hyperfine interaction *(French)* 80−80661
Ising ferromagnet and antiferromagnet, two-dimens. square, ground state, apparent 3-spin interactions 80−88709
Ising film, diluted, surface and bulk magnetic phases 79−82797

magnetic structure continued
isotropic three-sublattice ferrimagnet, magnetisation 80−2605
itinerant ferromagnet, effect of planar defects on electronic struct. and mag. ordering 79−99672
itinerant ferromagnet, spin-wave dispersion and linewidth 79−4668
lattice internal rearrangement modes, correlation betwen lattice structural and magnetic structural transitions 78−47987
liquid ferromagnet, model calculation 78−88088
longitudinal static spin wave struct., magnetotropic interaction of light *(Russian)* 80−93285
macroscopic quadrupole field meas. with SQUID magnetometer, order determ. 79−24140
magnetic materials, μSR meas. 79−56660
magnetic neutron small angle scattering, using dynamical theory of diffr., determ. of scatt. angle 79−11325
magnetic neutron small-angle scattering, using dynamical theory of diffr., behaviour of neutron intensity after transition through a helical mag. struct. 79−11326
magnetic resonance symmetry and frequencies in mag. ordered crystals *(Russian)* 79−61197
magnetic symmetry and representational anal. methods 79−82757
magnetically ordered crystals, exchange symm., mag. struct. *(Russian)* 80−65785
magnetisation density distrib. determ. by polarised neutron beam technique 79−77456
Magnico alloy, with Si, Nb, Ti and La, low-temp. thermomag. treatment 77−63812
manganese aluminosilicate glass, insulating spin glass, exchange dipole optical transition 80−40136
metal, cond. electron polarisation, magnetisation densities, neutron mag. form factors 77−72981
metallic very small particles, mag. ordering temps., ferro- and antiferromag. spin structures 77−73027
metals, neutron mag. form factors, magnetisation densities, APW wavefunction calcs. 79−47243
mixed crystal, coexistence of different spin structures, computer simulation 77−8276
Mo Co_2, single crystal, polarised neutron diffraction, various temp. and applied fields 78−2650
Mossbauer effect, crystallographic and spin texture determ. 77−69735
Mossbauer spectra, struct., electronic and mag. props. 79−91320
neutron anal. techniques at Grenoble high flux reactor *(Italian)* 77−15289
neutron birefringence measurements in mag. struct. 79−47298
neutron diffr., integrated intensity heats, crystal and mag. struct. determ. 80−44079
neutron diffr. study, symm. anal., polarisation effects 80−93083
neutron diffraction, book, with emphasis on technical aspects 79−60225
neutron diffraction, symmetry anal., group theoretical group anal. of exchange Hamiltonian 80−29527
neutron diffraction anal., group theory approach, mag. lattice determ. *(Russian)* 79−47236
neutron diffraction dynamical theory in mag. crystals 77−40040
neutron diffraction magnetisation density distrib. expt. determs., review 77−77034
neutron diffraction patterns, group theoretical, exchange Hamiltonian symm. anal. *(Russian)* 79−65648
neutron diffraction studies of mag. materials, book contrib. 80−11169
neutron probing 77−43102
neutron scatt. techniques in applied research, medium-flux research reactors 79−13514
neutron scattering as probe of magnetism on microscopic scale 77−24676
neutron scattering conference, Gatlinburg, TN, USA (June 1976) 79−41910
neutron scattering determ., book contrib. 79−61064
neutron scattering investigation, review *(Japanese)* 78−52227
neutron scattering studies of one- and two-dimens. mag. systems, review 77−66254
nuclear dipolar magnetic ordering, dipole-dipole interactions review 77−85475
nuclear magnetic ordering 79−65654
nuclear orientation and NMR of oriented nuclei, appl. to solid state magnetism 80−44928
one dimensional magnet with easy plane, solitons and magnons 78−23260
one dimensional magnetic behaviour 79−28495
oxides, $RCu_3Mn_4O_{12}$, R=La to Lu, Y, synthesis and mag. props. 80−75717
oxides with perovskite struct., neutron diffr., ferri- and ferromag. props. 78−52214
paramagnetic metal, polarised neutron inelastic and quasi-elastic scattering 80−50045
paramagnetic metals, polarised neutron studies of field induced magnetisation 80−25084
partly disordered magnetic structures 77−51908
Permalloy, order-disorder transform. and magnetic props. obs., by neutron diffraction method *(Slovak)* 79−4963
photoemission technique for meas. of magnetic order and spin depend. of electron scatt. 80−60748
point groups, corepresentations *(French)* 77−51884
polarisation analysis of diffuse neutron scattering 80−25098
polarised neutron diffraction, determ. of magnetic form factors, pioneering work 80−24321
polarised neutrons in condensed matter [conference, Zaborow, Poland (Sept. 1979)] 80−22136
polytwin ferromagnetic cryst., crystallite thickness effects on mag. struct. *(Russian)* 77−80913
powder least-squares program, POWLS 80−1892
pyridinium manganese chloride, anhydrous, quasi one-dimensional mag. behaviour, heat capacity meas. 80−80549
pyridinium nickel chloride, anhydrous, quasi one-dimensional mag. behaviour, heat capacity meas. 80−80549
quasi one-dimensional system, helicoidal and sinusoidal ordering *(Russian)* 78−10717
random chain, low-energy density of states and long-time behaviour, scaling approach 79−25994
rare earth alloys, $CaZn_5$ type struct., mag. symmetry 79−24143
rare earth alloys, phase transitions in complex mag. struct. *(Russian)* 78−72361
rare earth alloys, R-3d alloys (3d=Mn,Fe,Co,Ni), magnetic properties 78−52231
rare earth alloys, RCo_2 and R_2Fe_{17}, Invar props. 79−56593
rare earth amorphous alloys, mag. props., Mossbauer spectra 80−7225
rare earth cpds., RRh_4B_4 and RMo_6X_8 (X=S, Se), mag. order and supercond., neutron scatt. studies 80−44807
rare earth intermediate valence systems, neutron scatt., review 80−49674
rare earth intermetallic compounds, ferromag. props., book contrib. 80−75726
rare earth intermetallic cpds., mag. props., book contrib. 80−39759
rare earth intermetallics, cubic, magnetic order effects on cryst. field parameters 77−40019
rare earth intermetallics, mag. struct. 80−15698
rare earth intermetallics, neutron scatt., induced moment magnetism, high press. 80−15699
rare earth intermetallics, RAl_2, orbital and spin polarisations of cond. electrons 80−65791
rare earth intermetallics, RM_{12}, mag. interactions, mag. meas. and neutron diffr. 77−63103
rare earth ion, R^{3+}, relativistic mag. form factors, Dirac-Fock calc. 77−40037
rare earth iron garnets, anisotropic, mag. props., high field and low temp. 80−75801
rare earth iron garnets, level intersection and instability of mag. struct. *(Russian)* 77−43816
rare earth metals, EFG produced by conduction electrons, mag. ordering effects 77−40020
rare earth metals, electronic sound attenuation anomalies at transition to helical phase, Fermi surface topology *(Russian)* 80−92807
rare earth metals, nonspherical Fermi surface in RKKY theory 77−63227
rare earth metals and alloys, ferromag. props., book contrib. 80−75725
rare earth mixed valence compounds, spin dynamics, mag. neutron scatt., Mossbauer effect, XPS studies 80−39786
rare earth orthochromites, mag. interactions and weak ferromagnetism 78−52220
rare earth orthovanadites, RVO_3, magnetic and cryst. struct., Jahn-Teller effect 77−32169
rare earth perovskites, prep. and props. book contrib. 80−44193
rare earth pnictides, prep. and props., book contrib. 80−54212
rare earth systems, magnetic structures and inelastic neutron scattering, review 79−69654
rare earth ternary compounds, coexistence of superconductivity and long-range magnetic order 79−11264
rare earth titanium oxides, $RTiO_3$ type, bulk mag. and struct. props., ferrimag. order 80−107993
rare earth-Al_2, cubic Laves phases, prep. and phys. props. *(German)* 78−23075
rare earth-Cu intermetallic compds. single crysts., mag. props. 80−54892
rare earth-Fe alloys, amorphous and crystalline, small angle neutron scatt. study of mag. order and mag. microstruct. 79−15283
rare earth-Ga_2 intermetallics, mag. structs. 78−84394
rare earth-Mg, magnetisation and neutron diffr. meas. 77−63105
rare earth-transition metal alloys, amorphous, ferrimag., spin arrangements in large fields 80−75718
rare earth-transition metal alloys, amorphous, struct. and mag. props., book contrib. 80−39818
rare earth-transition metal alloys, $RM_2Si_{2-x}Ge_x$ and $RM_{4+x}Al_{8-x}$, magnetism and hyperfine interactions, magnetisation and Mossbauer effect studies 80−75892
rare earth-Zn_{12}, mag. props. and structs. 78−84393
rare-earth metal, semi-infinite surfaces with mag. struct., density of states calc. 80−10851
scaling and multiplicative renormalising in solid state physics *(Hungarian)* 79−11289
screw spin structure, method of controlling the sense 80−70944
semiconductor, doped with mag. impurity, ordering mechanism 80−2572
semiconductors, many-valley, magnetic electron fluctuon states spin direct interactions 80−29364
singlet ground state system, mag. props. 80−44850
small-angle scattering, of X-rays and neutrons, (fourth international conf., Gatlinburg, USA (Oct. 77)) 79−10745
solitons, mag., obs. in one-dimensional mag systems *(Japanese)* 80−2555
space groups, assignment 77−59387
space groups, assignment 77−59388
space groups, minimal supergroups 77−85417
speromagnetism phase transition, random distrib. mol. field model 79−73730
spin arrangement determ. by ^{57}Fe Mossbauer spectroscopy with polarised γ-rays 79−33568
spin glass, spin-wave spectrum, of systems without long-range mag. order 79−33450
spin systems with single-ion anisotropy charact. of mag. ordering 77−69466
spinels, diluted, percolation and mag. order 78−68165
spinels, symmetry anal. in neutron diffr. studies 80−25091
static properties of spin systems with truncated secular dipolar coupling 78−88130
submicron magnetic objects, mag. struct. study using magnetooptic micromagnetometer 80−57349
superconductor, helical ordering of spins 80−88669
superconductor, magnetic, spin-spiral ordering 80−2517
symm. anal. in neutron studies periodicity changes at mag. phase transitions 79−99680
symmetry, wreath groups 80−88724
symmetry anal. in neutron studies, phase transition concept 79−99679
symmetry restrictions on constitutive eqns. for mag. materials, group theoretical procedure 77−55255
TCNQ salt, quinolinium, electron spin location, elec., mag., and thermal props. 80−25189
tetrabutylammonium iron tetraiodide, structural and mag. props., ^{57}Fe and ^{129}I Mossbauer spectra 79−61282
tetraethylammonium iron tetraiodide, structural and mag. props., ^{57}Fe and ^{129}I Mossbauer spectra 79−61282
thermal neutron scatt. of condensed matter under high press. 79−37592
TMMC, antiferromag. reson. below 1K 78−39408
5d-transition metal antifluorite crystal, struct. props. and lattice dynamics, mag. struct. 80−44268

magnetic structure continued
transition metal complexes, electron densities, local orbital populations, polarised neutron diffraction 80−88725
transition metal compounds, 3d-cation solids, mag. ordering at low temps., exchange perturbation theory 77−69529
transition metal diiodides, (V, Cr, Mn, Fe, Co, Ni, Cd), Mossbauer spectrum, electronic and mag. props. 77−32302
transition metal elements and alloys, spin distribution, neutron diffraction expts. 80−25097
transition metal itinerant magnets, neutron scatt. expts. 77−73002
transition metal magnetic clusters, neutron inelastic scatt., review 80−50083
transition metals, polarized neutron diffractoin in high magnetic fields 79−73684
TTF-bis-dithiolene metal complex compounds, donor-acceptor type, one-dimens. mag. variety and props. 77−66271
two-sublattice system, with strong antisymm. exchange and fourth order anisotropy, mag. configs. 78−68167
uniaxial antiferromagnets in transverse mag. field, quantum theory, spin configuration 79−69647
VI_2, mag. structs. and props. 79−61063
weak ferromagnets, Landau-Lifshitz eqn. solutions, moving domain walls, struct. *(Russian)* 80−100596
AL_2O_3-CoO-SiO_2 glasses, spin correls., neutron diffr. meas. 80−15694
Ag-Mn, dil. alloy, transverse magnetoresist. in spin glass regime 80−34417
$Ag_{1/2}In_{1/2}Cr_2S_4$, first order macro to microdomain transition 77−69562
Al_3Ce and $Al_{11}Ce_3$, Kondo cpds., mag. behaviour obs. by neutron diffr. 80−50049
$Al_2Mn_3Si_3O_{12}$ glass, mag. ordering effects at low temps., Mossbauer and neutron diffr. meas. 77−16047
Al_2O_3-MnO-SiO_2 glasses, spin correls., neutron diffr. meas. 80−15694
$^{243}AmO_2$, neutron diffraction study, possible occurrence of antiferromagnetism 79−78332
Au-Fe, dil. alloy, transverse magnetoresist. in spin glass regime 80−34417
Au-Mn-Cr(Pd) alloy, ferro- to non-mag. transform. 77−12117
$Au_2(Mn,Z)_2$, Heusler alloy, (Z=Al, Cu, Ga, In or Zn), magnetic order and coupling 79−38303
AuMn, mag. struct., phase transition, and magnon spectrum, random anisotropy effects 80−88722
Au_4V, partially disordered, magnetisation distrib., polarised neutron diffr. study 79−47244
$BaCo_2(AsO_4)_2$, magnetic field effect on mag. ordering neutron diffr. obs. 80−50053
$BaCo_2(AsO_4)_2$, planar X-Y model, mag. ordering 77−66256
$BaCo_2(AsO_4)_2$, quasi 2D XY helimag., sp. ht. meas. 79−61151
$BaCo_2(PO_4)_2$, quasi 2D XY helimag., sp. ht. meas. 79−61151
$BaFe_{12-x}M_xO_{19}$ (M=Al, Ga, Sc, In) ferrites, mag. props. and struct. 80−15690
$BaFe_4Ti_2O_{11}$, R-type hexaferrite, spin struct. and mag. props. 78−52216
$BaLa_2Fe_2O_7$, Mossbauer exam. of mag. struct. 77−40157
$BaMnF_4$, mag. and structural phase transitions, neutron scatt. obs. 79−87259
$BaMnF_4$, magnetic neutron scatt. from structurally distorted cryst. 80−93086
$BaNi_2(PO_4)_2$ and $BaNi_2(AsO_4)_2$, mag. props., neutron diffr. and sp. ht. meas. 80−70948
Ba_2NiReO_6, mag. and cryst. struct. 77−20554
BaO-Fe_2O_3-B_2O_3 glass system, mag. struct., Mossbauer study 78−39485
$BiFeO_3$, ferroelec., antiferromag., cryst. and mag. struct., neutron diffr. study 80−65786
$Bi_2Fe_4O_9$, mag. struct., neutron diffr., transition 78−52217
$Bi_2Fe_4O_9$, mag. struct., neutron diffr. meas. 78−91844
$Ca(Cu_{0.78}Mn_{0.22})_3Mn_4O_{12}$, perovskite-like struct., neutron diffr. powder data, 350K ferromag. T_c 77−69502
$CaCu_3Ti_4O_{12}$, mag. struct. and props. *(French)* 77−69495
$CaCu_3Ti_4O_{12}$, perovskite-like struct., neutron diffr. powder data, 27K T_N 77−69502
$Ca_3Fe_xCr_{2-x}Ge_3O_{12}$, antiferromagnetic order below 12K, Mossbauer study 80−39945
$CaLaFeO_4$, two-dimens. mag. props. rel. to cryst. struct. 80−75776
$Ca_3Mn_2Ge_3O_{12}$, antiferromagnetic garnet, neutron diffr. study in mag. field 80−50060
$Ca_3Mn_2Ge_3O_{12}$, highly anisotropic garnet, neutron diffr. obs. of mag. struct. 78−68168
$Ca_3Mn_2Ge_3O_{12}$, mag. struct. study 80−2554
$Ca_3SbSnFe_3O_{12}$, mag. ordering and bond geometry rel. to tetrahedral Fe^{3+} 77−32163
$Ca_3Ti_{2x}V_{1.5-x}Fe_{3.5-x}O_{12}$, garnet, mag. and neutron diffraction investigation 77−16044
$Ca_3ZrSbFe_3O_{12}$, mag. ordering and bond geometry rel. to tetrahedral Fe^{3+} 77−32163
$CdCr_2S_4$, thermoreflectance near Curie point 79−78659
$Cd_xMn_{1-x}Fe_2O_4$, substitution effect on mag. struct. and exchange interaction *(Russian)* 78−47949
Ce monopnictides, anomalous mag. props., planar coupling theory 80−60245
CeAg(Mg)(Zn), magnetic struct. and cryst. field, neutron diffr. exam. 78−72328
CeAl, mag. props. and mag. struct. 78−6517
$CeAl_2$, low temp. mag. behaviour, neutron diffr. 78−84395
$CeAl_2$, mag. ordering, neutron diffr. meas. 78−6518
$CeAl_2$, mag. ordering and anomalous ground state, neutron diffr. obs. 79−78331
$CeAl_2$, multiple q mag. struct. 79−78330
$CeAl_2$, multiple-q mag. struct. 80−25100
$CeAl_2$, multiple-*q* structure or coexistence of different mag. phases, neutron diffr. study 80−107985
$CeAl_2$, neutron diffr. at low temp., magnetism 80−20383
$CeAl_2$, specific heat between 0.02 and 1K 79−1680
CeBi, lattice distortion modes and mag. structural transitions 79−78325
CeBi(Sb), anisotropic mag. ordering and mag. structural transitions 79−78324
$(Ce_{1-c}Ho_c)Ru_2$, superconducting, mag. props., neutron scatt. study 80−44808
$CeIn_3$, mag. struct., neutron diffr. study 80−80481
$Ce_x(La,Y)_{1-x}Sb$, and $Ce_x(La,Y)_{1-x}Bi$, antiferromag. spin arrangement, neutron diffr. obs. 77−63106
$CeMn_2Si_2$, cryst. and mag. struct. determ. 78−52225
magnetic structure continued
$Ce_{1-x}Pr_xAl_2$, mag. struct., comp. depend., neutron diffr. and mag. susceptibility meas. 80−50054
CeSb, antiferromag., first-order transitions, mag. phase diagram 80−60252
CeSb, commensurate-commensurate transitions and devil's staircase 79−78317
CeSb, mag. phase diagram and mag. struct., neutron diffr. determ. 77−63182
CeSb, mag. phase diagram for mag. field applied along ⟨111⟩ direction 79−33458
CeSb, mag. phase transitions, zero applied mag. field 78−31070
CeSb, mag. transition, effect of applied mag. field 78−43590
CeSb, phase diagram and mag. struct. 77−85422
$CeSn_3$, field induced form factor, temp. depend. 79−78308
$CeSn_3$, mixed valence cpd., electronic struct. and mag. props. 80−70649
$Ce_{0.736}Th_{0.264}$, induced mag. form factor 79−78307
$Ce_{1-x}Th_x$, mixed valence systems, spin dynamics and mag. ordering 78−68162
CeZn, mag. struct. and cryst. field effects 78−52223
Co complex, Co(II)(1,2,4-triazole)$_2$(NCS)$_2$ quasi two-dimens. canted S=1/2 antiferromag. 80−70976
Co complex, dipyridyl chloride, metamag., mag. struct., NMR 77−85418
Co^{2+}, mag. form factors, spherical and aspherical parts 79−78315
Co-Al, mag. struct. of Co rich intermetallic cpd., neutron scatt., cluster model 78−80130
Co-Ga-Mn(Fe), small-angle mag. neutron scatt., states of mag. order study rel. to Mn and Fe substitution 79−11292
$Co_{100-x}B_x$, amorphous, mag. struct., mag. susceptibility meas. 80−80485
$Co_3B_7O_{13}I$, neutron diffr. investig. of mag. and cryst. struct., ferro- and paraelec. phases 77−32170
$CoBr_2.6D_2O$, crystallographic and mag. struct. determ. 77−8278
$CoBr_2.6[(D_2O)_{0.48}(H_2O)_{0.52}]$, antiferromag. ordering, quasi-elastic neutron scatt. study 79−61068
$CoCO_3$, weak ferromagnet, light absorpt. dichroism and mag. config. *(Russian)* 79−87457
$CoCO_3$, weakly ferromag., light absorpt. dichroism and mag. config. 80−66223
$CoCl_2.6D_2O$, crystallographic and mag. struct. determ. 77−8278
$CoCl_2.6D_2O$, neutron diffr. study, cryst. and mag. struct. *(French)* 78−42946
$Co_2Ga_{2-x}Cu_x$, mag. and struct. phases from magnetisation, neutron, X-ray diffr. techniques 78−52253
$Co_2Ga_{2-x}Ni_x$, mag. and struct. phases from magnetisation, neutron, X-ray diffr. techniques 78−52253
CoMnP, cryst. mag. struct., neutron diffr. study *(French)* 80−59439
CoMnP, ferromagnetism and metamagnetism, polarized neutron diffr. study 80−44809
$CoNb_2O_6$, magnetic struct., neutron diffr. and mag. susceptibility meas. 80−15693
$Co_xNi_{1-x}O$, antiferromagnet, neutron diffr. study of mag. struct. 80−34595
$Co_{2-x}Ni_xTiSn$, mag. ordering, ^{119}Sn Mossbauer spectroscopy and magnetisation meas. 78−43753
CoO, collinear antiferromag., equiv. type-II mag. struct. 78−56296
Co_4P, amorphous, mag. excitations and static struct., neutron scatt. obs. 78−68204
CoU_2S_5, mag. struct., exchange energy, magnetisation and neutron diffr. expts. 78−68170
CoU_2S_5, mag. struct. and props. 80−11166
$CoWO_4$, mag. struct. refinement, neutron diffr. meas. *(German)* 77−16049
$Co_xZn_{1-x}Rh_2O_4$ spinel, crit. conc. for long range mag. order, expt. evidence 79−47239
$Co_{2-y}Zn_yTiO_4$, spinel series, exchange integrals, mag. struct. and coercive force, magnetisation meas. 77−69507
$(Cr, Mn)_2As$, mag. props. and struct. 78−64190
Cr, antiferromagnetic structure, mag. field effect, spin density wave model *(Russian)* 80−70953
Cr, incommensurate antiferromag., inelastic neutron scatt. meas. 80−25088
Cr, mag. struct., effect of mag. field direction, neutron diffr. obs. 77−63121
Cr, mag. struct., phase transition, and magnon spectrum, random anisotropy effects 80−88722
Cr, paramag., mag. form factors, neutron diffr. study 79−47234
Cr, spin density wave Q vector, vel. depend. 79−4669
Cr-Fe alloy, dil., antiferromag., mag. incoherent elastic neutron scatt. 79−73678
Cr-Fe(2.8 at%), antiferromag., meas. of incoherent elastic neutron scatt. cross section 79−19723
Cr-Mn, order of mag. transitions in antiferromag. alloys 79−4677
Cr-Pt alloys, neutron diffraction study, (100) magnetic peak, magnetic structure transitions 79−56506
Cr-Si alloys, antiferromag.-ordering, neutton diffr. 77−69492
CrB_2, helical mag. struct., neutron diffr. meas. 77−85425
$(CrF_6)^{3-}$ 6a AR→AT complexes, electron densities, local orbital populations, polarised neutron diffraction 80−88725
$(Cr_{1-x}Fe_x)_{1+\delta}Sb$, interstitial occupancy, Cr:Fe distrib., X-ray and neutron diffr. study 79−42012
$Cr_{995}Mn_{005}$, spin density wave Q vector, vel. depend. 79−4669
CrN, mag. struct. and first-order antiferromag. transition 79−61132
β-CrOOH, neutron diffr. exam., cryst. and magnetic struct. *(French)* 78−2654
$Cr_{0.995}Pt_{0.005}$ alloy, mag. struct., neutron diffr. study 80−60198
CrS, magnetic struct. from neutron diffr. meas., Neel point 77−32164
CrS_xTe_{1-x} (x=0 to 0.2), magnetic props. study 80−11194
$Cr_2Se_{3-x}Te_x$, mag. props. and lattice parameters, comp. depend. 77−66263
$Cr_3Se_{4-x}Te_x$, mag. props. and lattice parameters, comp. depend. 77−66263
CrTe, effect of high pressures on magnetic properties 78−52238
CrTe, mag. ordering under high-press., ferromag. transition, ESR and neutron diffr. *(French)* 78−31053
Cr_5Te_6, magnetoresist. in region of mag. phase transforms. *(Russian)* 77−66299
$Cr_{1-x}Ti_xN$, cryst. and mag. struct., at low temps. *(French)* 80−29005
CrUSe$_3$, mag. struct. and delocalized moments, powder neutron diffr. obs. 77−69496
$Cr_{1-x}V_xN$, solid soln., mag. struct. *(French)* 78−6519

magnetic structure continued
$CsCoCl_3$, mag. struct., neutron diffr. meas. 78−43563
$CsCrCl_3$, mag. structure and excitations, neutron diffr. and susceptibility meas. 80−44806
$CsCrI_3$, Mossbauer spectra, struct., electronic and mag. props. 79−91320
$CsCrI_3$, neutron diffr. expts. at 300, 77 and 1.2K 80−107163
$CsCuCl_3$, helical mag. struct., neutron diffraction study 80−107983
Cs_2FeF_5, mag. struct. and one-dimens. antiferromagnetism 80−60209
$CsMnBr_3.2D_2O$, spin-flop systems, neutron scatt. expts. 79−61109
$CsMnBr_3.2D_2O$, spin-flop system, extended scaling near bicrit. pt. 79−51752
$CsMnCl_3.2H_2O$, quasi-onedimens., effect on microwave absorpt. spectrum *(Russian)* 77−51962
$CsMnCl_3.2H_2O$, spin wave anal. 77−8292
$CsMnF_3$, antiferromagnet, struct. with compensated magnetisation in non-collinear phase *(Russian)* 78−88095
$CsMnF_3$, light absorpt. spectrum in mag. fields up to 300 kOe *(Russian)* 77−52115
$CsMnF_3$, mag. props. above T_n, NMR obs. of induced ferrimagnetism 79−99780
$CsMnF_3$, mag. struct., phase transition, and magnon spectrum, random anisotropy effects 80−88722
$CsMnF_4$, planar ferromag., cryst. and mag. struct., Jahn-Teller effect 80−75715
$CsMnFeF_6$, mag. short-range ordered, neutron scatt. meas. 77−16048
Cs_2MnNiF_6, cation distrib. and mag. struct. *(French)* 78−14935
$CsNiF_3$, one-dimens. ferromag., solitons as gas of quasiparticles, inelastic neutron scatt. obs. 79−73679
$CsNiF_3$, quasielastic neutron scatt. around Neel-point 80−75768
CsO_2, low temp. phases, mag. order, EPR and antiferromag. reson. 79−95630
$CsVI_3$, Mossbauer spectra, struct., electronic and mag. props. 79−91320
Cu complex, $Cu(ONC_5H_5)_6X_2$, X=ClO_4, BF_4, cooperative Jahn-Teller ordering and mag. struct., EPR meas. 79−60505
Cu complex, hexa(pyridine-N-oxide)$(BF_4)_2$, Heisenberg antiferromag., mag. props. and sp. ht. 78−23287
Cu, nuclei, antiferromag. ordering, mean field theory 79−78333
Cu-Mn (8 to 75 at.%), spin correl., neutron polarisation anal. study 80−65905
Cu-Mn-Al, mag. props. and atomic ordering 79−24139
$CuCl_2$, anhydrous, single cryst., mag. behaviour in low temp. ordered phase 79−7974
$CuCl_2.CuCl_2.2D_2O$, neutron scatt. aspherical effects, mag. form factor 78−27017
$CuCr_2S_4$, neutron diffr. study of mag. struct. *(Russian)* 79−95580
$CuCr_2Se_4$, electronic state, polarized neutron diffr. obs. 79−56501
CuFeCrMn spinel oxides, struct. determ., mag. states of Mn^{3+} ions *(Russian)* 78−19227
Cu_2FeGeS_4, crystallographic and magnetic structure *(French)* 80−28998
$Cu_{0.5}Ga_{0.5}Cr_2S_4$, mag. struct. determ. 77−8272
$Cu_{1/2}In_{1/2}Cr_2S_4$, transition from long-range to short-range mag. ordering 77−36087
Cu_2MnAl, ferromag. Heusler alloy, polarised neutron study of mag. moment density 78−84391
$Cu_2Mn_{0.863}Al_{1.057}$, Heusler alloy, mag. moment distrib., polarised neutron study 79−47247
Cu_2MnSnS_4, mag. struct. discussed rel. to Cu_2FeGeS_4 *(French)* 80−28998
$Cu(NO_3)_2.2^1/_2H_2O$, singlet ground state system, mag. props. 80−44850
$Cu(NO_3)_2.2.5\ D_2O$, magnetic ordering, neutron diffr. meas., 0.08-0.25K 80−39749
$Cu(NO_3)_2$(pyrazine), single cryst. PMR 78−2761
Dy, elec. resist. and mag. struct. near Neel point *(Russian)* 79−47074
Dy, helical antiferromagnetic phase, basal plane anisotropy 78−84412
Dy, magnetic phases, US study 78−31101
Dy-Pr(Nd) alloys, mag. struct. and ordered moments, neutrons diffr. data 77−66252
DyAG, induced staggered mag. fields and order parameters 77−63099
DyAg, neutron diffr. expts. in external mag. field, temps. below 1.2K 79−61067
DyB_4, cryst. and mag. struct., neutron diffr. meas. 80−15692
Dy_2C_3, cryst. struct., mag. struct. and props., 1.6 to 300K 79−11296
$DyCo_{5.3}$ noncollinear mag. struct. appearance in mag. fields, magnetostriction meas. *(Russian)* 80−100607
$DyCrO_4$, determ. of mag. struct. by neutron diffr. 79−51753
$DyFe_2$, amorphous, mag. struct., US meas. 79−99683
DyH_2, mag. and electronic props., ^{161}Dy Mossbauer spectroscopy 78−80262
DyM_3, M=Fe, Co, Ni, amorphous, mag. struct. and moments 77−66260
DyMg, mag. props., neutron diffraction and magnetisation meas. 77−16045
Dy_6Mn_{23}, noncollinear mag. struct., magnetization meas. 79−78322
$DyMo_6S_8$, long range mag. order in supercond. state 79−65653
$DyMo_6S_8$, supercond. and antiferromag. coexistence, neutron study 78−95401
$DyMo_6S_8$, superconductor, neutron scatt. exam. of mag. phase 79−73680
$Dy_{1.2}Mo_6S_8$, long-range mag. order and supercond., neutron diffr. obs. 79−78320
$Dy_{1.2}Mo_6S_8$, mag. ordering in supercond. state, resist. and AC susceptibility meas. 78−19194
Dy_2Ni_{17}, magnetic struct. by neutron diffr. and Mossbauer spectra *(French)* 77−32165
$Dy_2O_2SO_4$, mag. ordering, magnetisation, AC susceptibility and Zeeman effect meas. 80−60205
$Dy_2O_2SO_4$, magnetic struct. in antiferromag. and ferrimag. states 80−15695
$DyPO_4$, metamagnet, mag. phase transitions, elastic neutron scatt. study 79−78371
Er-La, HCP, mag. phase diagram, neutron diffr. meas. 80−70950
$ErAl_3$, 15 layer rhombohedral struct., Mossbauer meas. 77−63104
ErB_4, cryst. and mag. struct., neutron diffr. meas. 80−15692
$ErFe_2$, effect of H on sublattice magnetization, elastic neutron scatt. obs. 79−78327
$ErFe_3$, powder neutron diffr. meas. 78−2651
$ErFe_4Al_8$, neutron diffr. exam., mag. struct. 78−10656
ErMg, mag. props., neutron diffraction and magnetisation meas. 77−16045
Er_6Mn_{23}, noncollinear mag. struct., magnetization meas. 79−78322
$ErMo_6S_8$, long range mag. order in supercond. state 79−65653

magnetic structure continued
$Er_{1.2}Mo_6S_8$, mag. ordering in supercond. state, resist. and AC susceptibility meas. 78−19194
$ErMo_6Se_8$, crystal field excitations, inelastic neutron scatt. obs. 79−78321
$ErMo_6Se_8$, mag. ordering and supercond., neutron diffr. 78−68125
Er_2Ni_{17}, magnetic structure by neutron diffr. 77−73000
$ErNi_{0.6}Cu_{0.4}$, sp. ht. and modulated mag. struct. 77−32167
$ErRh_4B_4$, reentrant supercond., mag ordering, neutron diffr. obs. 78−14879
$ErRh_4B_4$, superconducting, magnetic dilemma 80−75680
$ErRh_4B_4$, superconductor, neutron scatt. exam. of mag. phase 79−73680
$ErTiO_3$, magnetic structure determination, neutron scatt. study 80−65809
Eu, exchange integral, spiral spin configuration, ab initio calcs. 79−47275
Eu, mag. anisotropy of helicoidal struct., magnetisation, 4.2-300K *(Russian)* 79−56499
EuB_6, correlation between mag. struct. and elec. props. 77−63192
EuO, mag. form factor of Eu^{2+}, solid state effects 78−2653
EuO, mag. struct. and transition temp., indirect exchange 78−91860
EuO, magnetic semiconductor, piezoresistance effect, 4.2 to 300K 80−34450
EuO, spin-dependent Raman scattering 79−95782
EuO(S)(Se), surface magnons and surface mag. struct. 77−36066
EuS, film, mag. surface reconstruction, ferromag. reson. 78−10781
EuS, mag. struct. and transition temp., indirect exchange 78−91860
EuSe, mag. phase stability, theory 77−63183
EuSe, mag. struct. and transition temp., indirect exchange 78−91860
EuSe, MnO-type antiferromag. spin order, Faraday rotation obs. 77−47974
EuSe, spin structs., mol. field theory 78−31054
EuTe, antiferromag. FCC lattice of second kind, surface magnons and mag. structs. 78−23261
EuTe, mag. struct. and transition temp., indirect exchange 78−91860
EuTe, spin alignment, high field Faraday rotation expt. 77−63401
EuTe, spin-dependent Raman scattering 79−95782
(Fe,Mn)WO_4, mixed cryst., magnetically disordered system, Mossbauer and neutron diffr. meas. 77−16225
Fe (III)M (II)$F_5.7H_2O$, M=Fe, Co, Ni, Zn, antiferromagnetism 77−59395
Fe complex, Fe(II) oxalato-bridged chain compounds, Mossbauer spectra 80−15890
Fe complexes, Fe (III) bis(dithiocarbamato) iodides, transferred hyperfine interactions and mag. ordering 77−20759
Fe, film, FCC, antiferromag. ordering, Mossbauer expts. 77−85508
Fe garnets, thin film, low freq. excitation spectra, mobility of domain boundaries 79−42815
γ-Fe, mag. struct. Mossbauer studies 80−39917
Fe, magnetism at high temps. 80−75721
Fe, molten, mag. neutron scatt. at small momentum transfer caused by spin fluctuations 77−47968
Fe particles, spin collinearity, Mossbauer spectra study 80−71114
Fe powder, Debye-Waller factor by neutron diffraction 79−95113
Fe, spin correlation function 79−78334
Fe^{2+}, mag. form factors, spherical and aspherical parts 79−78315
Fe-B-Si, amorphous ferromag. alloys, mag. struct., Mossbauer study 80−39746
Fe-Co-Ni-Al, Si alloying of mag. hard alloys *(Russian)* 79−73765
Fe-Cr-Ni, spin system, relaxation props. at low temp. 79−82758
Fe-Cr-Ni alloys, linear expansion, 4.2-300K rel. to antiferromag. rearrangement 78−43146
Fe-Mn, electron redistrib. and BCC struct. stability, Mossbauer meas. *(Russian)* 79−42873
Fe-Ni, hardening by plastic deform. during polymorphic transform., struct. mechanics for γ-phase form. *(Russian)* 77−90344
Fe-Ni (32.3 at.%), mag. struct. in commensurable approx., neutron diffr. study 80−60212
Fe-Ni (33-38 at.%), low-angle neutron diffr., anomalous crit. scatt. *(Russian)* 80−60193
Fe-Ni alloys, mag. state of austenite and γ→α transform. *(Russian)* 80−40350
Fe-Ni Invar alloy magnetic inhomogeneous struct. model 79−56503
Fe-Ni-Cr, mag. props. in weak mag. fields *(Russian)* 80−75771
γ-Fe-Ni-Cr, mag. struct., neutron scatt. study *(Russian)* 78−68160
Fe-Ni-Mn(Mo) alloys, two-stage martensitic transformation kinetics, depend. on austenite initial state, mag. order clusters *(Russian)* 79−74151
Fe-Ni-P-B, amorphous ferromag. alloys, mag. struct., Mossbauer study 80−39746
Fe-Ni(-Al)(Mn) Invar alloys, mag. heterogeneities *(Russian)* 77−66251
Fe-P-C alloys, amorphous, mag. anisotropy, Mossbauer obs., prior cooling effects *(Russian)* 77−32300
Fe-Pd alloy, mag. struct. determ., neutron scatt., Mossbauer and mag. meas. *(Russian)* 78−2648
Fe-Pd alloys, spin density radial distrib. determ. 79−73685
Fe-Pd(Pt), magnetic struct. changes assoc. with crystallite thickness increase *(Russian)* 77−80913
Fe-Pt, high mag. field phase transition 77−66301
Fe-Rh alloy, nonmag. and mag., band theory 79−37973
Fe-Si, Mossbauer study of mag. ordering 79−24245
Fe-Si (7.5, 14.3 at.%), mag. moments and form factors, neutron diffr. obs., d-band electron redistrib. 79−51751
Fe-Tb dilute alloy, amorphous, small angle mag. scatt. 78−27021
Fe_3Al, magnetic form factor 78−76222
$Fe_{100-x}B_x$, amorphous, mag. struct., mag. susceptibility meas. 80−80485
$Fe_{80}B_{20}$, amorphous ferromagnet, Mossbauer hyperfine fields, mag. struct. 80−75894
$Fe_{80}B_{20}$ metallic glass, spin texture determ. 80−15842
$FeBO_3$, Mossbauer coherent scatt. polaris., rel. to cryst. mag. struct. *(Russian)* 79−11368
Fe_3BO_6, canted mag. struct. near Neel point, Mossbauer meas. 78−35073
Fe_3BO_6, weak ferromag. state, Mossbauer determ. of mag. struct. 77−40164
$Fe_3B_7O_{13}I$, ferroelec., mag. ordering, neutron diffr. meas. 78−72331
$FeCO_3$, mag. field drawn destruction of antiferromag. destruction, light depolarisation at mag. transform. *(Russian)* 78−23432
$FeCO_3$, mag. neutron scatt., spin orbit coupling effects 77−85419
$Fe_2Ca_3Si_3O_{12}$ glass, mag. ordering effects at low temps., Mossbauer and neutron diffr. meas. 77−16047

magnetic structure continued
$FeCl_2.2D_2O$, metamagnetic, excitonic Davydov splitting in Raman spectrum 79−33704
$Fe_{1-x}Co_xCl_2.2H_2O$, random mixture with competing spin anisotropies, tetracrit. behaviour 80−60324
$Fe_{0.5}Co_{0.5-x}Cr_x$ films, vacuum-deposited cryst. and mag. struct. *(Russian)* 80−93081
$FeCr_{2-x}In_xSe_4$, struct. and mag. props., comp. depend. 77−66262
$(Fe_{1-x}Cr_x)_2O_3$, Mossbauer exam. of mag. struct. 77−24694
$Fe_{3-x}Cr_xO_4$, electron transfer and spin density distribs., Mossbauer spectra 79−24243
$FeGa_2O_4$, magnetic props. by Mossbauer effect, neutron diffr. and magnetisation meas. 77−43918
FeGe, hexagonal, low-temp. mag. struct., neutron diffr. meas. 78−95418
$FeGe_2$, collinear and canted antiferromag. structures 77−51887
$FeGe_2$, mag. struct., Mossbauer method 78−60268
Fe_5Ge_3, collinear mag. struct. from Mossbauer effect meas. 77−63343
FeI_2, antiferromag. struct., four spin exchange interaction 78−14948
FeI_2, eight sublattices model, antiferromag. reson. uniform modes and metamag. behaviour 77−69498
FeI_2, first order mag. phase transition, neutron scatt. study 80−50090
$FeMO_2S_4$, Mossbauer investigation, Neel point, superparamag. effects 80−97170
$Fe_{1.2}Mg_{1.4}Ti_{0.4}O_4$, mag. ordering, Mossbauer effect in external mag. fields 80−71257
$Fe_{2(1-y)}Mg_{1+y}Ti_yO_4$ spinel, incomplete mag. ordering, static magnetisation and Mossbauer meas. 77−16056
$(Fe_{1-x}Mn_x)_{75}P_{15}C_{10}$, amorphous, mag. ordering, Mossbauer study 80−39747
$(Fe_{1-x}Mn_x)_{75}P_{15}C_{10}$, amorphous pair radial distrib. functions, neutron scatt. study 80−49128
$Fe_xMn_{1-x}Pt_3$, ferro-antiferromag. transform. at 4.2K *(Russian)* 78−88117
$(Fe_{1-x}Mn_x)Si$, US vel. rel. to mag. struct. and phase transforms *(Russian)* 77−47976
Fe_2MnSi, antiferro- and ferromag. props. 77−12104
$Fe_{3-x}Mn_xSi$, Mossbauer and NMR exam. of site substitution and mag. struct. 77−12092
Fe_2MoO_4, magnetic struct. of low and room temp. by neutron diffr. 77−63100
$FeMo_2S_4$, cryst. struct., mag. struct. and props., neutron diffr. meas. *(French)* 77−47971
$FeNb_2O_6$, magnetisation, 1.4-80K, antiferromag. ordering 78−10666
$(Fe_{0.45}Nb_{0.53})O_2$, rutile, cation distrib. and mag. ordering *(German)* 80−107116
$Fe_{0.66}Ni_{0.34}$ Invar alloy, magnetic form factor 79−56504
$Fe_{65}Ni_{35}$, mag. cluster structs., 25-422°C 77−69493
$Fe_{70}Ni_{30}$, short range order, diffuse elastic neutron scatt. study 78−52219
$Fe_{40}Ni_{40}C_{14}P_6$ amorphous film, dislocation and mag. struct., neutron diffr. study 80−70956
$Fe_{65}(Ni_{1-x}Mn_x)_{35}$, magnetic struct. and inhomogeneities by neutron scatt. and Mossbauer effect *(Russian)* 77−63122
$Fe_{65}Ni_{28}Mn_1$, disordered, mag. struct. near ferro-antiferromagnetic transition 80−60211
$Fe_{40}Ni_{40}P_{14}B_6$, amorphous, stress-induced mag. easy axis 79−33516
$Fe_{40}Ni_{40}P_{14}B_6$, amorphous ferromagnet, Mossbauer hyperfine fields, mag. struct. 80−75894
γ-Fe_2O_3, elongated particles, mag. struct. 78−88096
α-Fe_2O_3:$Al^{3+}(Ga^{3+})(Cr^{3+})(In^{3+})$, substitution effect on Morin transition, neutron diffr. study 80−44827
γ-Fe_2O_3-organic interfaces, mag. struct., Mossbauer effect, IR absorpt., and magnetisation meas. 80−44869
Fe_3O_4, crit. exponents meas. by polarized neutron scatt. 80−44828
Fe_3O_4, low temp. phase ionic ordering, NMR *(Russian)* 78−23354
Fe_3O_4, magnetite, reduced A-site moments, polarised neutron study 79−47253
Fe_3O_6, O_2 annealed, optical absorpt., spin struct., polaronic absorpt., cryst. field transitions 78−68493
Fe_xO, non-stoichiometric, mag. struct., neutron diffr. exam. 79−42737
$FeOHSO_4$, neutron diffr. meas., modulation of moments 77−69499
FeOOH, high-pressure phase, neutron diffraction study 78−52212
ε-FeOOH, synthesis, mag. struct. 78−34961
β-FeOOH, ultrafine particles, mag. struct., Mossbauer spectroscopy 78−72372
FeP, mag. suscept., resistivity and thermal expansion meas. 78−2661
Fe_2P, mag. moments and form factors, polarised neutron diffr. study 79−65650
Fe_2P, mag. struct., neutron diffr. study 78−23246
$Fe_{0.75}P_{0.15}C_{0.10}$, amorphous, mag. excitations and static struct., neutron scatt. obs. 78−68204
$Fe_2(PO_4)Cl$, Mossbauer study of mag. ordering and local co-ordination 80−39972
$Fe(Pd_{1-x}Au_x)_3$, mag. struct. ferro-antiferromagnetism coexistence *(Russian)* 79−82759
FeS, zinc blende type, mag. struct. *(French)* 78−91846
$Fe_{0.9}S$, ferrimag. transition, mag., thermodynamic props., kinetics 79−47280
β-$FeSO_4$, high-temp. polymorph, stability, mag. struct., mag. props. 77−43815
Fe_5SiB_2, Mossbauer spectra, 140-784K, spin rotation 78−52409
Fe_2SiS_4, Mossbauer effect and magnetisation meas. of mag. struct. *(French)* 77−12282
Fe_3Sn_2, spin direction, variation with temp. 79−11294
$(Fe_{0.5}Ta_{0.5})O_2$, rutile, cation distrib. and mag. ordering *(German)* 80−107116
Fe_2TeO_5, mag. struct. 78−27020
$FeTh_2S_5$, mag. struct. and props., neutron diffr. and mag. meas. 80−60201
FeU_2S_5, mag. struct., exchange energy, magnetisation and neutron diffr. expts. 78−68170
$Fe_{3-x}V_xSi$, Fe hyperfine fields 79−78055
Fe_2WO_6, neutron diffr. patterns and mag. struct. 77−66250
$GaMn_3(C_{1-x}N_x)$ phase transition, rel. to valence instabilities in rare earth compounds *(French)* 80−34596
Gd, mag. short range order, 80 to 425K 79−42784
Gd-Co amorphous films, mag. struct., mag. bubbles, electron diffr. study *(Chinese)* 80−71126
Gd-Fe film, amorphous, in-situ ion beam sputtered, microstruct. and Lorentz mag. struct. 78−63947
Gd-La, magneto-optic reson. *(Russian)* 79−47426

magnetic structure continued
$GdAl_2$, hyperfine fields, ferromagnetic coupling between rare earth spins, NMR study 80−39880
$GdAlO_3$, magnetoelec. susceptibility, mag. struct., mag. phase diagram and crit. coeffs. 77−66303
$Gd_xCe_{1-x}Ru_2$, magnetic ordering by ^{155}Gd Mossbauer spectroscopy 78−27139
$Gd_{65}Co_{35}$, amorphous, amg. ordering, susceptibility, magnetisation and hysteresis meas. 78−68190
$GdCu_{1-x}Zn_x$, mag. struct. determ. 79−87238
GdIG, spin struct. by Faraday rotation expts. in fields up to 200 T 77−69809
GdIG, spin-orientation phase transitions, magneto-optic and visual exam. 77−24675
GdMg, noncollinear mag. struct., nonlinear band behaviour 80−75706
$GdMg_3$, mag. props., Mg conc. depend. 78−84392
$GdMg_3$, mag. props. 78−72346
Gd_6Mn_{23}, noncollinear mag. struct., magnetization meas. 79−78322
$GdMo_6S_8$, long range mag. order in supercond. state 79−65653
GdN, and $GdN_{1-x}O_x$, mag. interactions 80−60218
$GdVO_4$, antiferromag., US attenuation at 9 GHz 77−24728
$(Gd_{0.5}Y_{0.5})Ni$, FeB struct., cryst. field effects on mag. struct. 78−52226
^3He, solid mag., review 78−38906
^3He, solid mag. ordering, lattice dynamical approach 78−56020
$HgCr_2S_4$, spinel, symmetry anal. in neutron diffr. studies 80−25091
$Hg_{1-x}Zn_xCr_2Se_4$, magnetic struct., neutrongraphic and mag. investigation *(Russian)* 80−88726
$Hg_xZn_{1-x}Cr_2Se_4$, absorption spectra near the absorption edge 78−80340
Ho, Hall effect, field and temp. depend., 4.2-150K, singularities *(Russian)* 80−29387
Ho, phase transition along mag. field, X-ray obs., 77-292K *(Russian)* 77−4504
Ho:^{119}Sn, mag. hysteresis of hyperfine field, mag. struct. freezing and rearrangement *(Russian)* 77−81039
Ho-La, HCP, mag. phase diagram, neutron diffr. meas. 80−70950
Ho-Pr(Nd) alloys, mag. struct. and ordered moments, neutron diffr. data 77−66252
Ho-Sm alloy, Hall effect, field and temp. depend., 4.2-150K, singularities *(Russian)* 80−29387
$HoAl_2$, Ho moment reorientation, polarized neutron diffr. study 79−42761
HoAlGa, mag. props. and struct. 78−39302
$HoCo_2Ge_2$, crystal and magnetic structure obs. 80−64976
$HoCrO_3$, Ho^{3+} mag. form factor meas. by inelastic neutron scatt. 78−52221
$HoCrO_3$, mag. form factor of Ho^{3+}, inelastic neutron scatt. meas. 77−16050
$HoCu_2$, mag. struct. and elec. resist., neutron diffr. obs. 80−60206
$HoFe_2$, effect of H on sublattice magnetization, elastic neutron scatt. obs. 79−78327
$HoFe_2$, mag. struct., polarized neutron diffr. study 79−78326
$Ho_{12}Fe_{32}O_2$, struct. and ferrimag. props., neutron diffr. obs. 79−78319
$Ho_3Ga_5O_{12}$, hyperfine interac. induced antiferromag. order *(French)* 77−59392
$Ho_{1.15}Lu_{0.05}Mo_6S_8$, long range mag. order in supercond. state 79−65653
$HoMo_6S_8$, long range mag. order in supercond. state 79−65653
$HoMo_6S_8$, superconductor, neutron scatt. exam. of mag. phase 79−73680
$Ho_{1.2}Mo_6Se_8$, crystal field excitations, inelastic neutron scatt. obs. 79−78321
Ho_2Ni_{17}, ferrimag. struct., neutron diffr. expt., cryst. field calcs. 77−73001
$HoNi_{0.5}Cu_{0.5}$, sp. ht. and modulated mag. struct. 77−32167
$HoNi_{0.7}Cu_{0.3}$, mag. behaviour 79−99688
$Ho_2O_2SO_4$, mag. ordering, magnetisation, AC susceptibility and Zeeman effect meas. 80−60205
$Ho_2O_2SO_4$, magnetic struct. in antiferromag. and ferrimag. states 80−15695
HoP, flopside mag. struct. to ferromag. transition, elastic neutron scatt. obs. 80−50058
$HoPO_4$, metamagnet, mag. phase transitions, elastic neutron scatt. study 79−78371
$HoRh_4B_4$, ferromag., mag. struct., neutron diffr. obs. 79−78323
Ho_xTe, mag. ordering, neutron diffr. meas. 78−2649
$HoTiO_3$, magnetic structure determination, neutron scatt. study 80−65809
$HoVO_3$, antiferromag., at. and mag. struct., neutron diffr. meas. 79−24142
$Ho_{1-x}Y_xNi$, ferromag. behaviour, struct., Curie temp. 79−99677
$KCoF_3$, mag. form factor calc. for Co^{2+} 77−20555
$KCrF_3$, mag. struct. and cooperative ordering or orbitals 79−99687
$KCrO_2$, two-dimens. mag. order, neutron powder diffr. obs. 80−44805
$KCrO_2$, two-dimens. mag. props. rel. to cryst. struct. 80−75776
$KCuF_3$, mag. struct. and cooperative ordering or orbitals 79−99687
K_2CuF_4, 2-dimens. ferromagnet, low-temp. mag. struct. *(Japanese)* 79−33461
K_2CuF_4, ferromag., orbital ordering, review *(Japanese)* 78−76224
$K_3Fe(CN)_6$, mag. ordering and spin struct., Mossbauer obs. 77−40038
$KFeF_3$, magnetisation density of Fe^{2+} 79−78313
K_2FeF_5, mag. struct. and one-dimens. antiferromagnetism 80−60209
K_2FeF_5, one dimensional antiferromagnet, Mossbauer effect, mag. and electric field gradient axes 79−78587
K_2FeF_5, one-dimensional antiferromag., neutron diffr. and mag. meas. *(French)* 79−47241
$KFeO_2$, cryst. and mag. struct., neutron and X-ray powder diffr., and Mossbauer effect meas. 77−84722
$KFeS_2$, cryst. struct. and mag. ordering, neutron diffr. and mag. susceptibility meas. 80−54867
$KFeS_2$, spin analogue of active sites of ferrodoxins, mag. struct., neutron diffr. exam. 79−73688
$KMnCl_3$, magnetic spiral struct., neutron diffr. study 80−39748
$K_3Mn_2F_7$, double layer antiferromagnet, susceptibility 77−16061
$K_3Mn_2F_7$, double-layer antiferromag., mag. ordering, neutron scatt. meas. 79−61062
$K_3Mn_3F_7$, Heisenberg double-layer antiferromag., neutron scatt. 79−61065
$K_2Mn_{1-x}Fe_xF_4$, layered antiferromag., anisotropy effects on mag. ordering, neutron diffr. study 79−47254
$KNiF_3$, mag. form factor calc. for Ni^{2+} 77−20555
KO_2, low temp. phases, mag. order, EPR and antiferromag. reson. 79−95630

magnetic structure continued
KTb_3F_{10}, mag., optical, magneto-optical behaviour 78−68484
$(La_{0.8}Ca_{0.2})MnO_{3+y}$, mag. props., Faraday method meas. 80−103832
LaEu, mag. supercond., phase diagram, bulk susceptibility meas. 77−59353
$La_{1-x}Gd_xAg$, antiferromagnet, spin echo NMR anal. 80−15821
$(La_{1-x}Gd_x)_{1.0}Mo_6Se_8$, Gd-rich, supercond. state, phase transition, sp. ht. anomaly and mag. susceptibility 78−6480
La_2MnFeS_5, antiferromag., mag. props. and mag. struct., neutron diffr. and magnetisation meas. 80−65801
$LaMnO_3$, monoclinic and cubic perovskite struct., mag. props., neutron diffr. meas. 78−27022
$La_2(MnO_3)_3$, hydrostatic press. effect on mag. struct., neutron diffr. 77−51886
La_2MnZnS_5, antiferromag., neutron diffr. study 80−25099
$La_{1-x}Na_xFeO_{3-x}$, defect perovskite system, Mossbauer effect 77−36159
LiAl ferrite, substituted ferrospinel, spin configuration determ. *(Russian)* 77−32162
$LiCrO_2$, two-dimens. mag. order, neutron powder diffr. obs. 80−44805
$LiCrO_2$, two-dimens. mag. props. rel. to cryst. struct. 80−75776
LiGa ferrite, substituted ferrospinel, spin configuration determ. *(Russian)* 77−32162
LiH, mag. ordering in nucl. antiferromag. state, neutron diffr. obs. 79−65654
LiH, neutron diffr. evidence of nuclear antiferromagnetism 79−61066
LiH, nuclear ordered ferromag. and antiferromag. phases, neutron diffr. study 80−50052
$Li_2Mn_xTi_{1-x}O_3$, EPR exam. of antiferromag. props. 78−15015
$LiRF_4$, R=rare earth, low-temp. magnetically ordered states 77−63098
$LiTbF_4$, mag., optical, magneto-optical behaviour 78−68484
LiTi, substituted ferrite, cation distribution, Mossbauer, X-ray, neutron diffr. study 80−28975
LiZn ferrospinel, sequence of mag. transforms. *(Russian)* 78−19252
LiZn, substituted ferrite, cation distribution, Mossbauer, X-ray, neutron diffr. study 80−28975
$Li_{0.2}Zn_{0.6}Fe_{2.2}O_4$, ferrite, mag. ordering at low temp. *(Russian)* 77−32171
Lu, mag. form factor, field-induced, polarised neutron technique meas. 77−72998
Ma-Cu (10 at.%), antiferromag. defect scatt., neutron polarisation anal. 78−2652
$MgCr_2O_4$, magneto-electric splitting of crystal field Γ_2-level of Cr^{3+} ion, neutron spectroscopic obs. 79−19562
$MgFe_2O_4$, Mossbauer study 79−47375
$Mg_{1-x}Mn_xTe_2$, random dil. antiferromagnet, mag. props. 80−54870
MgV_2O_4, spinel, symmetry anal. in neutron diffr. studies 80−25091
γ-Mn, antiferromagnetic, self-consistent bandstructure calcs. 80−88475
γ-Mn, collinear spin structure stability 80−107984
Mn complex, manganese (II)(1,2,4-triazole)$_2$(NCS)$_2$, 2-dimens. Heisenberg antiferromag., mag. props. 78−72336
γ-Mn-Au(Pd), magnetic struct. for compositions near onset of antiferromag. ordering 77−63111
Mn-Bi alloy, melting and solidification under microgravity, mag. props. *(German)* 80−45296
Mn-Cu alloy, plastic deform. mechanism and shape-memory effect, mag. struct. obs. *(Russian)* 78−60705
Mn-Cu alloys, stressed, diffuse neutron scatt. exam. 78−47950
γ-Mn-Fe, FCC→FCT transform. temp. and Neel temp., X-ray and neutron diffr. expts. *(Russian)* 78−84797
Mn-Ga, mag. and cryst. struct. in conc. region of gamma phase, temp. depend. *(Russian)* 79−65649
γ-Mn-Ni (15 at.%), antiferromag. defect scatt., neutron polarisation anal. 80−50056
Mn-Pd (10 at.%), antiferromag. defect scatt., neutron polarisation anal. 78−2652
Mn-Pt alloys, mag. struct., neutron diffr. study 79−91210
β-Mn-Sn, Mossbauer and neutron diffr. exam. 77−66253
$Mn_{1.11}Al_{0.89}$, neutron diffr. investig. of mag. struct., degree of order 77−55662
$Mn_3Al_2Ge_3O_{12}$, garnet, mag. ordering, neutron diffr. patterns 78−19220
MnAs, estimation of ionic states through neutron form factor meas. 77−63115
MnAs, high spin state electron config. *(Japanese)* 77−43812
MnAs, struct. and mag. props., temp. depend., neutron study 79−47246
Mn_2As-Mn_2Sb, structural and magnetic props. determ. 78−76248
$MnAs_{0.925}P_{0.075}$, estimation of ionic states through neutron form factor meas. 77−63115
$MnAs_{0.925}P_{0.075}$, low spin state electron config. *(Japanese)* 77−43813
$MnAs_{0.97}P_{0.03}$, orthorhombic, mag. anisotropy 77−43832
Mn_3B_4, Hall effect temp. depend. mag. struct. effects *(Russian)* 77−51764
MnCoSi, mag. struct. *(French)* 78−39323
$MnCrF_5$, antiferromag., mag. struct. *(French)* 78−52211
$Mn_3Cr_2Ge_3O_{12}$, magnetically ordered Mn^{2+} and Cr^{3+} ions *(Russian)* 77−8281
$Mn_{2.5}Cr_{0.5}O_4$, mag. struct., neutron diffr. obs. 79−33460
$Mn_xCr_{3-x}O_4$, mag. struct. determ. by neutron diffr. 77−40035
$MnCr_2S_4$, mag. struct. under applied mag. field 80−97065
$MnCr_2S_4$, substituted, mag. struct. and transitions 80−65795
$MnCr_{2-x}V_xS_4$ Yafet-Kittel to Neel ferrimagnet transition temp. 77−66264
γ-MnCu, Mn-rich, inclined spin axis, neutron diffr. study 80−75723
MnF_2 antiferromag., mag. space groups, Clebsch-Gordan coeff. calcs. 80−79731
MnF_2, spin-flop transition obs. by neutron diffr. 79−73734
Mn_4Fe non-collinear component in mag. struct. 80−25089
$Mn_{1-x}Fe_xAs$, mag. props. in ground state *(Russian)* 78−56294
$MnFe_2O_4$ magnetic moments and high field susceptibilities, spin model 77−28376
$MnFe_2O_4$:Sn, hyperfine mag. fields at ^{119}Sn and ^{57}Fe nuclei, influence of press. 79−99811
$Mn_{1-c}Fe_cPt_3$, noncollinear mag. structs., neutron diffr. anal. *(Russian)* 80−25087
$Mn_{2-x}Fe_xSb$, mag. struct. and spin flop transition, ^{57}Fe Mossbauer expts. 77−66261
Mn_3GaC, mag. symmetry of ordered phases 78−71698
$Mn_3Ga_{1-x}Mn_xN$, perovskite struct., phase transformations *(French)* 80−81048
$Mn_3GaN_{1-x}C_x$, perovskite struct., phase transformations *(French)* 80−81048
$Mn_xMg_{1-x}S$ solid solution, mag. props. 78−60269
$Mn_2N_{0.86}$, cryst. and mag. struct. at low temps. *(French)* 77−73003
Mn_4N, mag. struct. non-collinearity, neutron diffr. obs. 80−65796
MnO, magneto-elastic coupling by dipolar interactions and spin orientation 79−78494
MnO, neutron diffr. meas., 100 to 700K, spin correls, above and below T_N 77−59390
MnO:Mn^{2+}, EPR, antiparallel spin coupling above Neel point, antiferromagnetic clusters *(German)* 77−16168
MnOOH, mag. ordering, fine struct. and crit. behaviour, neutron diffr. meas. 80−65800
MnP, appl. of method for study of mag. structs. *(Russian)* 80−39741
MnS, crit. behaviour, neutron diffr. exam. 78−80169
$MnSO_4$, mag. struct. and phase transitions, neutron diff. study 80−60208
$MnS_2(Se_2)(Te_2)$, antiferromagnetic ordering, effective electron model 77−47975
$MnS_2(Se_2)(Te_2)$, mag. ordering, 2 cation, 2-anion indirect exchange interactions *(French)* 78−43566
MnSb, electronic state, neutron diffr. study 78−87906
MnSb-CrSb, NiAs-type system, single crystals, neutron diffr. studies 80−60200
MnSi, helically ordered state, ^{55}Mn and ^{28}Si NMR 78−43655
Mn_5Si_3, polycrst., mag. struct., 66-100K *(Russian)* 78−68161
$Mn_5(Si_{1-x}Ge_x)_3$, magnetic and cryst. struct., ferromag. props. 77−59391
$Mn_5(Si_xGe_{1-x})_3$ solid solution, mag. ordering, magnetisation and neutron scatt. meas. 78−27023
$MnSiN_2$, 180°C Neel temp., mag. struct. and atomic coords., neutron diffr. meas. *(French)* 77−32168
Mn_2SnS_4, cryst. struct. refinement and mag. struct. determ. *(French)* 80−107131
Mn_2TeO_6, magnetic structure, stability of mag. modes, neutron diffraction study *(French)* 80−39744
$Mn_{1-x}Zn_xFe_2O_4$, noncollinear mag. structure, Mossbauer spectrum 77−69501
$Mn_{1-x}Zn_xFe_2O_4$, prepared by wet method, neutron diffr. and high field Mossbauer expts. 80−75719
$NaCa_2Sb_2Fe_3O_{12}$, mag. ordering and bond geometty rel. to tetrahedral Fe^{3+} 77−32163
$NaCrO_2$, two-dimens. mag. order, neutron powder diffr. obs. 80−44805
$NaCrO_2$, two-dimens. mag. props. rel. to cryst. struct. 80−75776
α-$Na_3Fe_2(PO_4)_3$ orthophosphate, cryst. and vitreous, Mossbauer spectroscopy and mag. susceptibility *(French)* 80−80657
$NaFeS_2$, mag. hyperfine fields and covalency, Mossbauer effect meas. 77−90077
$NaMnCl_3$, antiferromagnet, exciton self-localisation luminesc. and excitation spectra *(Russian)* 80−11456
$NaMnCl_3$, mag. struct. and spin-flip transition, powder neutron diffr. exam. 80−60210
$NaMnCrF_6$, mag. struct., neutron Laue diffr. method 80−70951
$NaMnCrF_6$, magnetic struct., neutron Laue diffr. study *(French)* 79−99682
$Na_3Te_2Fe_3O_{12}$, mag. ordering and bond geometry rel. to tetrahedral Fe^{3+} 77−32163
Na_xVSe_2, mag. and elec. props. rel. to struct. transitions 78−91848
Nb, paramag., mag. form factors, neutron diffr. study 79−47234
Nd, mag. ordered, single cryst. elastic consts. meas., 4-50K 77−63249
Nd, mag. struct., 18.6K mag. phase transition 80−65799
Nd, mag. struct., heat capacity meas., 2 to 10K 79−51788
Nd, magnetic form factors, polarised neutron diffr. meas. 80−50057
Nd, magnetic structure, 2D modulated 80−15697
Nd, magnetic structure and crit. behaviour 78−47951
Nd, magnetic-structure, neutron and X-ray diffr. study 80−60197
Nd, magnetoresistance, mag. struct., elec. resistance at low temps. *(Russian)* 80−54936
Nd, triple-q magnetic structure, neutron polarisation and diffr. investig. 79−73686
Nd, triple-q magnetic structure, neutron and X-ray diffr. investig. 79−73687
Nd, two-dimensionally modulated mag. struct. 79−78317
$NdAl_2$, mag. form factor, diffuse moment density, polarised neutron meas. 77−63108
Nd_xCo_{1-x} film, amorphous, mag. props. meas. 78−68312
$Nd(Co_{1-x}Cu_x)_5$, coercive force temp. depend. 79−82823
$NdFe_2$, amorphous, magnetization and neutron scatt. meas. 79−78314
Nd_xFe_{1-x} film, amorphous, mag. props. meas. 78−68312
$NdFeO_3$, magnetic struct., time of flight neutron diffr. method 77−8280
$NdRh_4B_4$, possible obs. of coexistence of supercond. and long-range mag. order 79−82730
Nd_3S_4 chem. and mag. structures, neutron diffr. obs., ferromag. long-range order *(German)* 78−10654
NdSi mag. struct. and mag. moments, neutron diffr. meas. 77−85424
Ni (110) surface, electron spin polarisation, effect of H_2 adsorption, electron capture spectroscopy 78−14933
Ni, itinerant ferromagnet, spin-wave dispersion and linewidth 79−4668
Ni, mag. densities, spin and orbital contrib., neutron diffr. meas. 79−78316
Ni, neutron depolarisation near Curie point *(German)* 78−14934
Ni, paramagnetic, mag. form factors in Stoner-like model 80−97061
Ni surface, spin distribution of electrons, electron capture spectroscopy 78−14932
Ni^{2+}, mag. form factors, spherical and aspherical parts 79−78315
Ni/Al_2O_3, sintered catalysts, mag. and catalytic props. for methanation reaction 79−79296
Ni-Al, ferromag. solid sol., electronic struct., X-ray absorpt. spectra meas. 79−69653
Ni-Cu, ferromag., mag. moment, local environment effects, HF CPA cluster calc. 80−65817
Ni-Fe alloy, atomic and mag. ordering, cluster variation calc. *(Russian)* 78−15391
Ni-Fe films, in state of undersaturation in perpendicular fields, micromagnetic struct. *(Russian)* 79−61193
Ni-Mn, mag. moment and asphericity of spin density distrib., polarised neutron scatt. obs. 80−44813
Ni-Mn (17-27 at.%), low-angle neutron diffr., anomalous crit. scatt. *(Russian)* 80−60193
Ni-Pd, mag. form. factor, polarised neutron diffr. meas. 80−29525
Ni-Pt alloys, magnetic-moment distrib. neutron study 80−97066
Ni-Ti (2wt.%) alloy, polarised neutron diffuse scatt. 77−36057
Ni_3Al, unpaired spin density distrib., polarised neutron diffr. 78−10659
$Ni_{100-x}B_x$, amorphous, mag. struct., mag. susceptibility meas. 80−80485

magnetic structure continued
$NiBr_2$, commensurate and incommensurate mag. struct., neutron diffr. study 80−97067
$NiBr_2$, low-temperature magnetic phase, incommensurate spin structure 80−93082
$NiCl_2$, mag. struct. at 4.2K, neutron diffr. *(French)* 77−63097
$NiCl_26NH_3$, low temp. sp. ht. and mag. ordering 80−75784
$NiCo_2O_4$, ferrimagnetic spinel, neutron diffr. study 79−99681
NiF_2, magnetisation and antiferromagnetic resonance freq. in mag. field *(Russian)* 80−34781
$NiFe_2O_4$ ferrite, mag. props., neutron irrad. 80−103858
NiI_2 anhydrous, magnetic phase transition, neutron diffr. study 80−71033
NiI_2, antiferromagnetic, neutron diffr. and sp. ht. meas. 77−55663
Ni_3Mn, fission neutron disordering at 5K, exam. 78−47434
NiMnGe, crystal and spiral mag. struct., Neel temp., X-ray and neutron diffr. 77−16052
$NiMnGe_{1-x}Si_x$, mag. props., neutron diffr. and magnetometric meas., 80-600K 80−65793
$Ni_2Mn_xM_{1-x}Sn$ (M=Ti,V) mag. hyperfine fields, ^{119}Sn Mossbauer spectra study 80−55003
$Ni_2Mn(Mn_xSn_{1-x})$, Heusler alloy, antiferromagnetic order, X-ray and neutron diff. 78−64189
$Ni(NH_3)_2Ni(CN)_4.2C_{12}H_{10}$, mag. susceptibility, sp. ht., spin arrangements and transition obs. 77−20590
NiO (001), surface layers, sublattice magnetisation temp. depend., LEED exam. 78−27018
NiO (100), LEED calcs. of exchange refls. 78−14949
NiO, mag. struct., neutron Laue diffr. method 80−70951
$Ni_{0.97}Ru_{0.03}$, mag. form factor and moment distrib., obs. using polarised neutrons 78−68171
$Ni_{0.97}Ru_{0.03}$, mag. moment distrib. polarised neutron study 79−42738
NiS_2, antiferromag. struct., effects of four spin interactions 77−51885
NiS_2, mag. struct. at 5K, polarised neutron study 78−80131
NiS_2, neutron diffr. anomaly at Curie temp., antiferromag. refl. 78−76260
NiS_2, pyrite type, mag. struct., antiferromag. refl. of neutron diffr., susceptibility meas. 77−69497
NiS_2, spin struct. and mag. props. 78−39300
$Ni_{1-x}S$, and $Ni_{1-y}S_{1-y}O_y(Se_y)$, mag. state in metal-semicond. transition region, neutrnon diffr. obs. *(Russian)* 77−89926
$NiS_{2-x}Se_x$, mag. struct., ^{57}Fe Mossbauer study 78−56409
Ni_2Sc_2W, mag. order 77−63120
$NiWO_4$, mag. struct. refinement, neutron diffr. meas. *(German)* 77−16049
NiZn ferrites, substituted ferrospinel, spin configuration determ. *(Russian)* 77−32162
$Ni_{0.32}Zn_{0.68}Fe_2O_4$, mag. props. and neutron damage 77−47973
$Ni_{1-x}Zn_xFe_2O_4$ spinel, low-temp. transitions and spin configurations, Mossbauer study 78−27144
$NpCo_2Si_2$, mag. struct., neutron diffr. determ. 80−93084
$NpCu_2Si_2$, mag. struct., neutron diffr. determ. 80−93084
$NpFe_{2-x}Co_xSi_2$, mag. and hyperfine props. 80−7247
O_2 adsorbed monolayers, antiferromag. struct. obs. by neutron diffr. 77−66257
O_2 monolayer, adsorbed on graphite, mag. order through magnetostrictive distortion 79−73401
β-O_2, solid, possible mag. struct. *(Russian)* 79−56500
Pd, electronic struct., field-induced magnetisation density and mag. form factor 77−4496
Pd, paramag., mag. form factors, neutron diffr. study 79−47234
Pd-Cr, dil., appearance of mag. order for Cr impurities in exchange enhanced hosts 79−4690
Pd-Fe (25-55 at.%) ^{57}Fe effective field and mag. struct., Mossbauer and magnetisation expts. *(Russian)* 77−90085
Pd-Mn dilute alloys, mag. ordering, sp. ht. calc. by Monte Carlo method 77−77030
Pd-Mn(Fe), mag. ordering phenomena, neutron scatt. obs. 80−44812
$Pd_2MnIn_{1-y}Sb_y$, Heusler alloy, mag. order obs. 80−29528
$Pd_{2-x}MnSb$, struct., appl. as improved neutron polariser 80−60199
$Pd_2MnSb_{1-x}Sn_x$, Mossbauer meas. of ^{119}Sn mag. hyperfine struct. 77−12258
Pr, antiferromagnetic ordering 80−15709
Pr, magnetic form factors, polarised neutron diffr. meas. 80−50057
Pr, magnetic ordering, stress induced 80−15776
Pr, quasielastic mode damping, dynamic susceptibility 80−15705
PrAl, annealed, mag. props. and mag. struct. 78−6517
$Pr_{0.9}Ca_{0.1}MnO_3$, neutron diffr. and magnetisation study 79−61061
$Pr_{1-x}Ca_xMnO_3$, struct. and magnetisation study 80−65804
$Pr(Co_{1-x}Cu_x)_5$, coercive force temp. depend. 79−82823
$PrCo_2Ge_2$, cryst. and mag. struct., neutron diffr. study 79−69059
$PrCo_2Ge_2$, crystal and magnetic structure obs. 80−64976
PrF_3, Pr^{3+} mag. form factor meas. by inelastic neutron scatt. 78−52221
$PrFeO_3$, magnetic struct., time of flight neutron diffr. method 77−8280
$PrPd_3$, heat capacity at low temps. 79−28547
PrSb, neutron scatt., press. induced antiferromag. 80−15699
PrSb, pressure-induced antiferromag., neutron scatt. study 80−39750
PrSi, mag. struct. and mag. moments, neutron diffr. meas. 77−85424
Pt, paramagnetic, induced magnetic form factor, 73 kOe at 78K 79−33454
Pt-Cr, dil., appearance of mag. order for Cr impurities in exchange enhanced hosts 79−4690
$PuFe_2$, ferromag. mag. cross section, form factors, saturation magnetisation values, polarized neutron study 79−47245
PuP, ferromag. mag. cross section, form factors, saturation magnetisation values, polarized neutron study 79−47245
$RbCoCl_3.2D_2O$, metamagnetic phase transition, crystallographic and mag. struct., neutron diffr. meas. 80−44174
$RbCoF_3$, mag. space group and Raman tensors in antiferromag. phase 79−82760
$Rb_2Co_xMg_{1-x}F_4$, neutron scatt. exam., obs. of two dimens. mag. long range order 78−56295
Rb_2CrCl_4, two-dimens. easy-plane ferromag., cryst. and mag. struct., temp. variation of moment 77−66255
$RbFeCl_3.2D_2O$, cryst. and mag. struct., neutron scatt. and NMR expts. 79−7969
$RbFeF_3$, magnetisation density of Fe^{2+} 79−78313
Rb_2FeF_5, mag. struct. and one-dimens. antiferromagnetism 80−60209
$Rb_3Mn_2Cl_7$, two dimens. double layer antiferromag., neutron diffr. exam. 77−8277

magnetic structure continued
RbO_2, low temp. phases, mag. order, EPR and antiferromag. reson. 79−95630
Rh_2MnX, (X=Al, Ga, In, Tl, Sn, Pb, Sb), Heusler and Heusler-related cpds., mag. and cryst. props. 77−20568
RuF_5, mag. props. 80−15707
Sc, paramag., mag. form factors, neutron diffr. study 79−47234
$SmAl_2$, hyperfine fields, ferromagnetic coupling between rare earth spins, NMR study 80−39880
$SmCo_5$ sintered magnets, periodic struct. and coercive force *(Russian)* 79−28554
$SmCo_5$, temp. depend. of Sm mag. form factor, polarized neutron expts. 79−78329
$Sm_{1-x}Gd_xAl_2$, hyperfine fields, ferromagnetic coupling between rare earth spins, NMR study 80−39880
SmN, magnetic props., neutron diffr. and mag. susceptibility meas. 80−50036
$Sm_{0.5}Pr_{0.5}Co_5$ sintered magnets, periodic struct. and coercive force *(Russian)* 79−28554
SmS, mixed valence, induced mag. form factor 78−68163
$Sm_{0.76}Y_{0.24}S$, mixed valence, induced mag. form factor 78−68163
SmZn, ferromag., cond. band antiparallel polarisation exceeding 4f moment 80−60207
SmZn, unusual form factor, polarised neutron scatt. 79−99684
$SrCoO_3$:Fe^{4+}, ferromag., sign of Fe^{4+} hyperfine field, spin struct., Mossbauer study 80−39933
$SrCoO_{3-x}$, mag. and neutron diffr. study 80−65805
$SrFe_6Ga_6O_{19}$ ferrite, mag. struct., Mossbauer study 80−93087
$SrFeO_{3-x}$, neutron diffr. exam. of mag. struct. 77−20553
$SrLaCoO_4$, struct. and mag. props., electronic struct. of trivalent Co *(French)* 79−86760
$SrLaFeO_4$, mag. and cryst. struct. determ. *(French)* 80−54866
$SrLaFeO_4$, two-dimens. mag. props. rel. to cryst. struct. 80−75776
$SrMCrO_4$, M=La, Nd, mag. struct. determ. by neutron diffr. *(French)* 79−28507
$SrNd_2Fe_2O_7$, mag. struct., neutron diffr. determ. *(French)* 78−52224
$SrR_2Fe_2O_7$, (R=Pr,Nd,Sm,Eu,Gd or Tb), Mossbauer exam. of mag. struct. 77−40157
$SrR_2Fe_2O_7$ series, mag. struct. and spin reorientation, neutron diffr. and Mossbauer meas. 77−69503
$Sr_xZn_2Y(Y=Ba_{2-x}Fe_{12}O_{22})$, x=0, 1, 1.6, mag. moments reorientation 80−44851
steel, Cr-Ni, ferrite precip. *(Japanese)* 80−35187
Tb alloy, antiferromag. state, decrease in stability 77−20556
Tb-Er alloy, magnetisation process of helical spin struct., neutron diffr. and magnetisation meas. 77−43850
Tb-Pr(Nd) alloys, mag. struct. and ordered moments, neutrons diffr. data 77−66252
Tb-Tm alloys, mag. struct., neutron diffr. 77−8273
TbAlGa, mag. props. and struct. 78−39302
$TbAsO_4$, mag. ordered, neutron diffr. study 79−47238
TbB_2, mag. struct., ferromag. ordering, neutron diffr. study 80−15692
TbB_4, ferromag. ordering, neutron scatt. meas. 78−10655
$TbBe_{13}$, mag. struct., neutron diffr. meas., 4.2K 78−47953
$TbBe_{13}$, magnetic structure at low temps., antiferromagnetic, neutron diffraction study *(French)* 80−39743
$TbCo_5$, mag. state of Tb sublattice neutron diffr. meas. *(Russian)* 77−80915
$TbCu_2$, collinear mag. struct., neutron diffr. meas. 79−87242
TbD_2, mag. struct., neutron diffr. study 77−85421
TbD_x, non-stoichiometric, complex antiferromag. struct., neutron diffr. study 80−50061
$Tb_{1-x}Dy_xFe_2$, pseudobinary Laves cpds., spin-orientation diagram, Mossbauer effect meas. 77−55739
$TbFe_2$, amorphous, mag. struct., US meas. 79−99683
$TbFe_3$, ferrimag., mag. struct., powder neutron diffr. determ. 79−78328
$TbFe_4Al_8$, commensurate-incommensurate modulated mag. struct., neutron diffr. obs. 79−95576
$TbFe_4Al_8$, neutron diffr. exam., mag. struct. 78−10656
$Tb(Fe_{1-x}Rh_x)_2$, Fe sublattice spin reorientation possibility, Mossbauer spectra *(Russian)* 79−78335
$TbGa_2$, mag. props. and struct., neutron diffr. patterns at 4.2, 300K 77−63109
$Tb_3Ga_5O_{12}$, hyperfine interac. induced antiferromag. order *(French)* 77−59392
TbIG, anisotropic garnet, mag. struct., magnetisation and Faraday rotation obs. 78−68169
$(Tb_cLa_{1-c})Be_{13}$, mag. struct., cryst. field effects, neutron diffr. study 80−65789
TbMg, mag. struct. and mag. props. 77−8275
$TbMg_3$, antiferromagnetic struct. 78−14930
$TbMg_3$, mag. props., Mg conc. depend. 78−84392
$TbMg_{3+x}$ mag. props. 78−72346
$TbMnO_3$, ordering of Mn^{3+}, Tb^{3+} moments, neutron diffr. expt. 77−69500
$TbMo_6S_8$, long range mag. order in supercond. state 79−65653
$TbMo_6S_8$, superconductor, neutron scatt. exam. of mag. phase 79−73680
$Tb_{1.2}Mo_6S_8$, long-range mag. order and supercond., neutron diffr. obs. 79−78320
$Tb_{1.2}Mo_6S_8$, mag. ordering in supercond. state, resist. and AC susceptibility meas. 78−19194
$Tb_{1.2}Mo_6Se_8$, crystal field excitations, inelastic neutron scatt. obs. 79−78321
Tb_2Ni_{17}, magnetic structure by neutron diffr. 77−73000
Tb_2O_2S, tunnelling effect and mag.-cryst. transition, neutron diffr. expts. 77−63180
Tb_xS, mag. ordering, neutron diffr. meas. 78−2649
Tb_xTe, mag. ordering, neutron diffr. meas. 78−2649
$Tb_{0.76}Y_{0.24}$, spin waves rel. to cond. electron susceptibility 78−68195
$Tb_{0.26}Y_{2.74}Fe_5O_{12}$ garnet, mag. transition, mag. props. anomaly 80−93120
Tc, paramagnetic form factor, polarised neutron diffr. study 80−39745
$ThCo_5$ itinerant electron metamagnetism, polarised neutron study 80−39742
$ThCu_3Mn_4O_{12}$, mag. struct. of new perovskite-type ferrimag. 78−52222
$ThCu_3Mn_4O_{12}$, perovskite-like struct., neutron diffr. powder data, 430K ferrimag. T_c 77−69502
$ThFe_5$, mag. props., ferrimag. moment arrangement 79−33475
Ti, paramag., mag. form factors, neutron diffr. study 79−47234
$TiBe_2$, neturon diffr. study of mag. ordering 80−44811
$(Ti_{1-x}V_x)_2O_3$, metallic antiferromag. struct., neutron studies 80−65797

magnetic structure continued
$TlMnCl_3$, weak ferromag. and mag. struct., temp. depend. 78−19219
Tm magnetic transitions, effect of H_2 in solid solns., elec. resist. meas. 80−100585
$TmAl_2$, ferromagnetic structs., elastic neutron scatt. obs. 80−50055
TmS, antiferromag. struct. below 8.9K, neutron diffr. obs. 79−78318
TmSe, intermediate valence compound, mag. neutron scatt. 78−68164
TmSe, intermediate valence state, resistivity of magnetically ordered ground state 79−1683
TmSe, mag. neutron scatt. 80−25096
TmSe, mag. props. and struct. 80−25109
TmSe, mixed valence systems, spin dynamics and mag. ordering 78−68162
U dipnictides, elec. and mag. props. 78−84399
α-U, electronic band struct. and props. 80−10861
α-U, induced magnetisation density 78−47952
U sesquichalcogenides, mag. props. temp. depend. 77−8287
α-U, spin density determ. by polarised slow neutron scatt. 77−28375
U-Ga system cpds., neutron diffr. obs. 77−20559
UAs, magnetic struct. in high mag. fields, neutron diffr. study 80−34597
UAs, magnetisation, ferrimag. spin struct. 80−7088
U_3As_4, magnetisation in strong fields, 4.2 to 200K anisotropy and exchange forces 80−54886
U_3As_4, neutron diffr. and magnetis. obs. 77−20559
$U_3As_4(Bi_4)(P_4)(Sb_4)(Se_4)(Te_4)$, symmetry changes in mag. phase transitions 77−20597
UAs(Sb), anisotropic mag. ordering and mag. structural transitions 79−78324
$UCo_{5.3}$, mag. props. and cryst. struct. *(Russian)* 77−51925
UGe_3, induced magnetisation density and f-d bonding, polarised neutron diffr. study 80−50063
UGe_3, magnetisation density, neutron scatt. meas. 80−50038
UGeY, (Y=S, Se, Te), mag. struct. and ordered moments, powder neutron diffr. data 78−72329
UH_3, hyperfine splitting of proton determ. by inelastic neutron scatt. 77−43814
UN, mag. inelastic scatt. 80−7079
$U_2N_2As(P)(S)(Se)$, struct. types 77−20569
U_2N_2Te, mag. struct. 77−63119
UO_2, mag. struct. 77−59389
UO_2, phase transition crossover from first- to second-order in symmetry-breaking field 79−82805
UO_2, single crysts., nucl. neutron diffr. intensity meas. analysis, extinction 79−27957
UO_2, symmetry changes in mag. phase transitions 77−20597
UP-PrP (NdP) systems, mag. phase diagrams 78−84424
UPb_3, crystal field energy levels, magnetisation and susceptibility, neutron spectra obs. 80−50064
UPd_3, crystalline electric field levels of U, neutron scatt. exam. 78−60267
UPd_3, U^{4+}, mag. form factor meas. by inelastic neutron scatt. 78−52221
URh_3, magnetisation density 78−52203
USb, neutron inelastic scatt. from collective excitation 80−7080
USb, short-range spin correlations, neutron study 78−39293
$USb_{0.9}Te_{0.1}$, multiaxial mag. ordering, magnetisation and neutron scatt. meas. 79−51750
$USb_{0.9}Te_{0.1}$, multiaxial mag. structure 80−15696
$USb_{1-x}Te_x$, mag. struct. and mag. phase diagram, neutron diffr. study 80−50059
V, paramag., mag. form factors, neutron diffr. study 79−47234
V, search for antiferromagnetism, neutron diffr. meas. *(Russian)* 78−6516
$V_{3-x}Cr_xSi$, x=0 to 3, struct., supercond. and mag. props. 80−1962
VI_2, MCD spectra, interpretation rel. to mag. struct. 80−66222
VI_2, mag. struct., long- and short-range order and Mossbauer spectroscopy 80−65803
VI_2, mag. superlattice, neutron oscill. and Weissenberg photography 80−65802
VO_2, metallic, magnetisation distribution and band structure 78−76223
V_2O_3, insulating phase, mag. struct. 79−38305
V_2O_3 insulating phase, realistic Hartree-Fock calc. 79−38306
V_2O_3, low temp. antiferromag. phase 78−52213
V_2O_3-M_2O_3, M=Ti, Cr, struct. and mag. props. 78−27041
V_5S_8, paramag. cryst., struct. factors using polarised neutron diffr. 80−15691
VUS_3, mag. struct. and delocalised moments, powder neutron diffr. obs. 77−69496
V_2WO_6, magnetic structure, stability of mag. modes, neutron diffraction study *(French)* 80−39744
Y, paramag., mag. form factors, neutron diffr. study 79−47234
$(Y_{3-x}Ca_x)(Fe_{2-x}Sn_x)(Fe_3)O_{12}$, long and short range magnetic order 79−38419
$YCa_3Zr_2Fe_{2.75}Ga_{0.25}O_{12}$, mag. ordering and bond geometry rel. to tetrahedral Fe^{3+} 77−32163
$(Y_{3-x}Ca_x)[Fe_{2-x}Sn_x](Fe_3)O_{12}$, Mossbauer spectra of Fe^{27} and Sn^{119} nuclei 79−95578
$Y(Co_{1-x}Ni_x)_5$, mag. heterogeneities and coercive force, neutron scatt. study 80−2553
YFe_2, amorphous, mag. order, cluster phenomena, hyperfine struct. 77−16079
YFe_2, amorphous concentrated spin glass, susceptibility, Mossbauer and neutron scatt. meas. 80−39783
$YFe_{2-x}Al_x$, magnetisation behaviour, mag. scatter order 77−28373
$Y(Fe_xAl_{1-x})_2$, mag. order in pseudobinary systems down to millikelvin temps. 78−19251
$YFe_{1-x}Co_xO_3$, reorientation transitions, neutron diffr., mag. behaviour *(Russian)* 77−24678
$Y_3Fe_{5-x}Ga_xO_{12}$, garnet, magnetically inequivalent positions of cations in external mag. field 80−11307
$Y_6(Fe_xMn_{1-x})_{23}$, mag. order in pseudobinary systems down to millikelvin temps. 78−19251
$YFeO_3$, hydrothermal synthesis, mag. struct. 77−47972
YFe_2O_4, two-dimensional spin ordering, neutron diffr. study 80−29530
$Y_3Fe_{5-x}Sc_xO_{12}$, local spin struct., Mossbauer obs. 77−32305
$Y_3Ga_xFe_{5-x}O_{12}$, spin struct. obs. by Faraday rotation expts. in fields up to 200 T 77−69809
$Y_{1-x}Gd_xRh_4B_4$, mag. supercond., anomalous temp. depend. of upper crit. fields 80−29510
YIG film, surface pinning parameter, symm. props. 79−28570
YIG, magnetisation density, polarized neutron expts. 78−52215
YIG, polariser neutron study of covalency effects 80−2552
YIG, spin struct. obs. by Faraday rotation expts. in fields up to 200 T 77−69809
YIG:Ho(Er), magnetisation anomalies in strong mag. fields, noncollinear mag. struct. *(Russian)* 77−43854
Y_6Mn_{23}, ferrimag., mag. interactions, polarized neutron diffr. meas. 79−78322
Y_2Ni_{17}, ferromag. struct., neutron diffr. expt., cryst. field calcs. 77−73001
Yb-Eu alloys, mag. ordering, magnetisation meas. 80−7081
YbB_4, mag. props. *(French)* 77−20566
$YbFeO_3$:Co, mag. struct. factors, neutron diffr. study 79−47248
$ZnCr_2O_4$, mag. phase with short range order *(French)* 77−63203
$ZnCr_2Se_4$, screw spin struct., neutron diffr. exam. 78−27019
$ZnCr_2Se_4$, screw spin structure, method of controlling the sense, polarised neutron diffr. study 80−70944
$ZnCr_2Se_4$, screw spin structure, magnetoelectric effect 80−75827
$Zn_xMn_{1-x}Fe_2O_4$, substitution effect on mag. struct. and exchange interaction *(Russian)* 78−47949
$Zn_{0.75}Ni_{0.25}Fe_2O_4$, mixed ferrite-spinel, helicoidal struct. 79−47242
Zr, magnetic form factor, field-induced, polarised neutron scatt. meas. 80−50044
$Zr(Fe_{1-x}Al_x)_x$, transition region, spin glass or long range mag. order 80−44841
$Zr(Fe_{1-x}Co_x)_y$, transition region, spin glass or long range mag. order 80−44841
$Zr(Fe_xCo_{1-x})_2$, mag. order in pseudobinary systems down to millikelvin temps. 78−19251
$(Zr_{1-x}Nb_x)Fe_2$, antiferromag. spin struct., Mossbauer effect study 80−66086

magnetic surface phenomena
adsorbed layers near λ-transition, thermodynamic relns. of Pippards type for dielectric and mag. props. 78−79881
alloy, surface disorder, source of magnetism 79−56487
alloy with two ferromagnetic components, surface excitations 80−25179
antiferromagnet, long-wavelength, surface spin-waves 80−88737
antiferromagnetic and paramagnetic surfaces, ortho to para H_2 conversion 79−34362
atomically rough surfaces, mag. excitations 77−69664
binary alloys, magnetic interface struct. 80−29564
bitter technique, model calc. for colloid accumulation on surface in mag. field *(German)* 77−9139
bubble garnet film, non-implanted, surface mag. struct. 80−84628
CESR transmission, surface relax. effects 79−61218
chemisorption and magnetisation, book 77−25311
coating stresses in oriented transformer steel determ. by bending expts. *(German)* 79−28569
coercivity with competing vol. and surface anisotropies 77−69626
Cu_xNi_{1-x}, magnetism of surface 78−95511
cubic crystal, highly magnetostrictive, magnetoelastic surface waves on (110) plane 78−52327
dipolar magnet, surface effects on phase transitions, local spontaneous polarisation 80−2708
domain wall, severely bowed, steady-state motion, simple approx. analytic treatment 77−32211
elastic ferromagnets, higher order surface couplings 78−79212
electron gas, Bloch, in opposing elec. and mag. fields at 0K 78−63992
electron scatt. from ferromagnet in presence of mag. surface reconstruction 79−1705
epitaxial ferrite-garnet films with inversion layers, behaviour of cylindrical mag. domains, visual tracking method 80−71139
exchange and dipoles coupled ferromags., light scatt. from mag. surfaces, response theory 79−42820
FCC lattice, second-neighbour surface magnons 77−28378
ferrite rods, magnetised longitudinally, surface mode propag. 80−54878
ferrite sheet, magnetised, excitation of surface EM waves 78−10747
ferrite slab, transversely magnetised, adjacent to semicond., mag. surface wave amplification 78−72339
ferrite-n-GaAs layer struct., boundary spin wave amplification *(Russian)* 77−73016
ferrite-semiconductor structure, surface magnetostatic wave instability 78−76235
ferrofluid, nonlinear surface waves, bifurcation theory approach 80−58439
ferromagnet, Brillouin light scatt. by spin waves 80−93359
ferromagnet, itinerant electron, surface spin waves, tight-binding Hubbard model 80−39763
ferromagnet, spin wave resonance temp. depend., surface mode threshold conditions 77−28450
ferromagnet, surface and bulk nucl. spin waves, Green function formalism 80−70984
ferromagnet, surface magnetoelastic waves in the presence of exchange interactions and pinning of surface spins 78−80186
ferromagnet, surface spin waves and surface spin correlations in presence of mag. surface reconstruction 78−6522
ferromagnet, tight binding model, surface magnetisation 80−103807
ferromagnet film, spin wave propagation near surface 78−68308
ferromagnet-semiconductor structure, periodic, surface magnetostatic waves 78−27070
ferromagnet-semiconductor structure, surface wave gain, ang. depend. 77−51938
ferromagnetic (111) films, macrostripe and microstripe domain structs. *(Russian)* 79−28572
ferromagnetic alloys, surface spin waves, cluster Bethe lattice approach 80−70983
ferromagnetic bodies calc., rectangular, surface charge distribution, using iterative methods *(Slovak)* 79−4656
ferromagnetic conductor magnetoelastic surface wave attenuation 77−20667
ferromagnetic film, crit. angle of external mag. field for surface spin waves 79−47309
ferromagnetic film, electric-charge-induced magnetisation 79−69700
ferromagnetic film, magnetostatic surface wave propag. 79−4661
ferromagnetic films, spin correl. functions, crit. indices 80−7133
ferromagnetic metal, Fermi level shift by charging, mag. moment and hyperfine splitting 77−20677
ferromagnetic metal, RKKY oscills. in surface spin density, density functional formalism 77−20512

magnetic surface phenomena continued
ferromagnetic plate, surface magnetostatic wave excitation 80−25119
ferromagnetic plate, with anisotropic surface discontinuities, spectrum and damping of quasi-surface spin waves 80−11185
ferromagnetic resonance freq. in semi-infinite cryst., theory 79−65742
ferromagnetic semiconductor, degenerate, surface magnetisation 77−8385
ferromagnetic slab, finite thickness, spin correl. functions 80−80522
ferromagnetic slab, light scattering from bulk and surface spin waves, theory 80−71389
ferromagnetic substrates, propag. of surface magnetoelastic waves 77−55698
ferromagnetic surface spin waves, microscopic theory, mag. field effects 78−35044
ferromagnetic-paramagnetic transition, surface energy effect *(Russian)* 79−87260
ferromagnetic-semiconductor-dielectric multilayer struct., convective surface wave instability 77−24732
ferromagnetism in 2-D electron system 78−60258
ferromagnets, dilute, spin waves at surface 79−61089
ferromagnets, exchange and dipolar coupled, spin wave renormalisation, Damon-Eshbach surface spin waves 80−2564
film, complex surface pinning parameter and quasi-localised surface spin wave modes 80−50150
film, electron states in longitudinal mag. field 78−91784
film, neutron depolarisation in refl. and refraction at mag. film surface *(Russian)* 78−95493
film, spin pinning and mag. surface reconstruction, effect on standing spin waves 77−1600
film, surface pinning parameter, complex angle depend. 77−63239
film, surface spin waves and surface anisotropy effects at finite temp. 79−78452
films, ferromagnetic, perpendicularly magnetised, surface and vol. magnetoelastic waves *(Russian)* 80−93151
finite sample, mag. rearrangements near surface 80−11240
garnet epitaxial film, elastic surface wave propag., magnetoelastic effect 77−20669
gyromagnetic slab magnetised in arbitrary direction, magnetostatic mode characteristics 78−2670
Heisenberg antiferromagnet, light scatt. off surface 78−23475
Heisenberg FCC ferromagnet, surface spin instabilities 77−69475
Heisenberg ferromag. localised magnons around surface impurity *(Russian)* 78−84376
Heisenberg ferromagnet, surface magnetisation profile and localised magnons 80−70985
Heisenberg ferromagnet, surface spin instabilities 77−20533
Heisenberg ferromagnet, surface spin waves theory *(Russian)* 77−89939
Heisenberg ferromagnet interface, low temp. sp. ht. *(French)* 77−72767
Heisenberg ferromagnet surface, spin behaviour, review 77−20527
Heisenberg ferromagnets, surface effect on thermodynamic props. and excitation spectra 79−11282
Heisenberg magnets, with two kinds of exchange interactions, surface magnons and surface spin arrangements 77−36043
Heisenberg model, magnetic excitations on ideas and atomically rough surfaces 78−14944
Heisenberg thin films 79−38359
helical magnet, surface spin waves and spin arrangements 78−68198
hexagonal planar ferrite slab, magnetostatic modes 77−24731
induced moment effect on spin wave spectrum 78−19234
insulator, localised surface impurity modes 77−1545
Invar, Fe-Ni-C, spin pinning effect in RF collapse studies, Mossbauer spectroscopy 80−44971
Ising, internally dil. film, surface enrichment as possible source of surface magnetism 80−15731
Ising ferromagnetic half-plane, surface, pinned domain wall, free energy and magnetisation profile 80−60361
Ising film, diluted, surface and bulk magnetic phases 79−82797
Ising model, renormalisation group calc. of crit. props. of free mag. surface 77−40068
Ising model, surface crit. behaviour, layer and local susceptibility 80−71058
Ising model, surface critical behaviour, renormalisation group theory 78−47988
Ising model, surface magnetic order, Cayley tree approx. 77−72964
Ising model strips, scaling theory, wall effects in crit. systems 80−80539
itinerant ferromagnet, surface spin waves 77−69480
LEED study of surface magnetism *(Japanese)* 78−43627
mag. excitations, atomically rough surfaces, isolated cluster of overlayer spin 78−31102
magnetic wave interaction with drifting charges 78−95485
magnetically soft cylinders, micromagnetics of curling configurations 79−82826
magnetisation, size effect 78−15008
magnetisation profile, in crit. region by ε-expansion, Wilson perturbation theory calc. 80−50100
magnetite, spin polarisation, effect of temp. and photon energy 80−45221
magneto-optical relax., refl. rad. polarisation plane, monopolar mag. field pulses on solid surface 77−81086
magnetoelastic surface wave convolution, approx. theory 78−68354
magnetostatic surface waves, dispersion relation, effect of metal 78−19232
magnetostrictive displacement at surface due to mag. domain wall junctions 78−48014
metal, conduction electrons spin magnetisation kinetics, role of surface scatt. *(Russian)* 77−80989
metal, magnetic surface states induced linear magnetoresistance 79−60798
metal film, CESR line width and shape, surface relax. contrib. *(Russian)* 77−32260
metal surface, spin susceptibility, density-functional approach 77−90011
Monte Carlo studies, surface physics appl., book contrib. 79−82426
Mossbauer spectroscopy and surface phenomena study 80−39916
Mossbauer spectroscopy of surface and interface magnetism 80−7218
multicritical phenomena 77−32208
nonellipsoidal sample, demagnetising factor meas., magnetoelastic Rayleigh wave convolution 77−10072
nonexchange surface spin waves at interface between two ferromagnets 80−29544
one-dimensional semi-infinite chain, enhanced surface exchange interaction, mag. relax. 80−29558

magnetic surface phenomena continued
one-magnon states in BCC Heisenberg antiferromag., spectral density near stepped surfaces 80−20396
ordered Heisenberg ferromagnet/liq. ^{3}He system, mag. Kapitza cond. calc. 79−51415
ordering temps. determ. by Bethe-Peierls-Weiss (BPW) method 80−54912
Permalloy platelets, FMR mode positions, spin pinning 77−4562
photoemission, spin energy analysed, feasibility anal. 80−55271
polarised electron scatt. study 80−93160
Rayleigh wave propagation in strongly magnetostrictive materials 77−40111
Schottky barrier, mag. surface levels in presence of depletion-type band bending 80−20285
semiconductor-ferrite structure, spin wave amplification 79−65668
semiconductor-ferrite structure, surface spin waves, current-induced amplification, effect of static state inhomogeneity 79−28519
semiconductor-ferrite-semiconductor structure, absolute instability of magnetostatic surface waves interacting with drifting carriers 78−95486
short rectangular prism, field-depend. local surface magnetisation, numerical calc. 77−36110
singlet-doublet model of induced moment system, surface magnetism near Curie point 77−1530
spin wave resonance, surface mode magnetisation, inhomogeneities effect 77−69710
spin wave resonance, theory of magnetic surface states, review 80−84654
strip films, bulk and surface spin oscills., mag. reson. 80−97149
sublimation current and vapour press. of mag. solids 80−34182
surface, itinerant antiferromagnetism and density waves 79−82743
TCNQ salts, $Qn(TCNQ)_2$ and $Cs_2(TCNQ)_3$, surface magnetism obs. 78−6561
TCNQ salts, $Qn(TCNQ)_2$ and $Cs(TCNQ)_3$, surface magnetism 78−2703
TCNQ salts, surface magnetism, magnetisation field curves meas. 77−59428
thin film alloys, surface magnetism props., Curie temp., Ising model 80−108039
thin surface layer, interactions between nondegenerate electrons, effect on cyclotron resonance, mag. cond. *(Russian)* 80−15802
transition metal, chemisorption of H, effect of surface spin fluctuations 80−75613
transition metal, FCC, semi-infinite, susceptibilities near (001) surface 80−15701
transition metal, magnetic moment near surface, one-electron band model 79−82747
transition metal, magnetic order 78−95439
transition metal, nonmag., possibility of mag. monolayer formation 78−15009
transition metal, spin fluctuations 78−95451
transition metal alloys, surface magnetism 78−48025
transition metals, mag. surface anisotropy 77−1553
transition metals, review 77−73071
transition metals, review 80−44861
transition metals, surface- or defect-induced magnetism, nearly half-filled bands 79−1671
TTF-TCNQ, surface magnetism 78−2703
TTF-TCNQ, surface magnetism obs. 78−6561
CO, chemisorbed layer on Au(Pt), mag. phase transition obs. *(Russian)* 77−77083
$Cd_{1-x}Hg_xCr_2Se_4$, ferromag. semicond. surface magnetism, magneto-optical meas. 77−20831
$Cd_{1-x}Zn_xCr_2Se_4$, ferromag. semicond., surface magnetism, magneto-optical meas. 77−20831
Co fine particles in Cu, interface magnetisation 80−88858
Co, magnetic order 78−95439
Co, spin polarised photoemission, surface magnetism 79−52083
Co surface, electron spin polarisation, electron capture spectroscopy 78−95645
Co_5Sm sintered magnet, effect of surface conditions on mag. props. 79−28556
Cr and alloys, itinerant antiferromagnetism and density waves at surface 79−82743
Cr, and alloys, surface- or defect-induced magnetism, nearly half-filled bands 79−1671
Cr, δ- and BCC, fine particles, mag. props. 78−52314
Cr, ferromagnetic surface layer on antiferromag. bulk, determ. by surface magnetoplasma wave detect. 78−68356
Cr hyperfine particles, surface magnetisation, explanation of expt. work 78−23303
Cr-Re, surface spin-density wave near T_N 79−91238
Dy film, helimag. order, surface deform., exchange and single-ion magnetocrystalline anisotropy energy 77−66390
$DyFe_3$, effect of adsorbed H on mag. props. 77−63129
EuO (100), disordered, LEED and electron spectroscopy 79−28178
EuO, ferromag. light scatt. from bulk and surface spin waves 79−28778
EuO, light scatt. from bulk and surface spin waves 78−19497
EuO:Gd, surface depolarisation of photoelectrons 78−15286
EuO:Gd, surface mag. props. 80−71566
EuO:La, photothreshold reduction by mag. induced space charge layer 78−72692
EuO(S)(Se), surface magnons and surface mag. struct. 77−36066
EuS, film, mag. surface reconstruction, ferromag. reson. 78−10781
Fe epitaxial film, Mossbauer effect, interface magnetism 80−11297
Fe, ferromagnetic, chemisorption of H, spin-spin interactions, UPS spectra calc. 80−6630
Fe film, chemisorption induced mag. dead layers, ferromag. reson. obs. 79−91261
Fe film, coated, interface magnetism by Mossbauer spectroscopy 80−75890
Fe film coated by MgO, MgF_2 and Sb, surface mag. 80−7196
Fe film coated by MgO, Mossbauer spectra, mag. hyperfine field 80−7221
Fe, itinerant model of spin polarised field emission 78−95685
Fe, magnetic order 78−95439
Fe, Mossbauer effect, local moment, ferromag. order 77−69757
Fe sheet, surface magnetisation, ferromag. nucl. reson. meas. 78−60348
Fe single crystal frames, use in transient field meas., surface magnetisation meas. 79−59324
Fe, spin polarisation in electron field emission, surface magnetism 78−68607
Fe, spin polarised photoemission, surface magnetism 79−52083

magnetic surface phenomena continued
Fe, whisker single crystals, ferromag. reson. and surface anisotropy 80−71187
Fe-SiO multilayer film, interface magnetisation, neutron Bragg refl. 78−56355
Fe-SiO multilayer films, interface magnetisation 80−88858
Fe_3, effect of adsorbed H on mag. props. 77−63129
$Fe_{40}Ni_{40}P_{14}B_6$ amorphous ribbon, mag. anisotropy distrib. near surface 78−95430
α-Fe_2O_3, hematite, surface magnetism, magneto-optical meas. 77−20831
γ-Fe_2O_3:Co acicular powder epitaxially doped, coercivity increase, surface anisotropy *(Chinese)* 80−7130
γ- Fe_2O_3:Co powder, increased coercivity by epitaxial doping 79−82833
γ-Fe_2O_3-organic interfaces, mag. struct., Mossbauer effect, IR absorpt., and magnetisation meas. 80−44869
Fe_3O_4, single cryst., surface magnetism, spin polarized photoemission 78−52622
Fe_3O_4, spin polarised photoemission, surface magnetism 79−52083
$Fe_3O_4/\gamma Fe_2O_3$ surface layers formed on small Fe particles, Mossbauer expts. 79−8081
Fe_xO, antiferromag., surface magnetism probe by photoelec. currents 77−73214
α-FeOOH, goethite small particles, mag. hyperfine field, bulk and surface contribs. 77−69758
α-FeOOH ultrafine particle NGR spectra, size distrib. and surface effects 80−11299
FeTi, hydrogenation, effect of surface segregation on mag. props. 78−84819
n-GaAs-YIG layered structure, magnetostatic surface wave amplification 78−88107
GaYIG, magnetoelastic surface wave attenuation 77−20667
Gd, ferromag., spin polarised electron gas model 77−8034
^{3}He admixed with C particles, surface induced ferromagnetism, pulsed NMR expts. 79−51362
^{3}He, in Grafoil, NMR obs. of magnetisation 79−51370
^{3}He in Grafoil, ultralow temp. NMR mag. susceptibility, surface magnetisation and transition 78−79843
^{3}He, liq., in contact with dielec. surface, mag. susceptibility enhancement, thermodynamics 80−54460
^{3}He, liq., reinforcement of low temp. surface ferromag. instability due to ^{3}He-wall attraction 79−51373
^{3}He, liquid, surface ferromagnetic instability, attraction to solid substrate 79−46863
^{3}He, liquid-ordered ferromagnet interface magnetic Kapitza conductance, surface spin wave effects 79−99406
^{3}He, superfluid, surface magnetism 79−51361
^{3}He, surface ferromagnetism, possibility in confined geometries 77−69137
^{3}He with C particles, pulsed NMR, mag. susceptibility surface induced ferromagnetism, antiferromagnetic exchange interaction 78−79844
$HgCr_2Se_4$, ferromag. semicond., surface magnetism, magneto-optical meas. 77−20831
$HoFe_3$, effect of adsorbed H on mag. props. 77−63129
$Ho_{0.58}Tb_{0.20}Dy_{0.22}Fe_2$, magnetoelastic surface wave propagation, mag. field depend. 77−85535
Mn hyperfine particles, surface magnetisation, explanation of expt. work 78−23303
MnF_2, surface spin-flop and antiferromag. spin-flop transition 78−52257
$MnFe_2O_4$ film, bulk and surface spin waves, spin wave reson. expts. 79−73826
Mo (001) surface, electronic susceptibility and surface phase transition 79−33169
Nb, magnetic surface barrier breakdown by O diffusion, permeability meas. 79−56601
Ni (110) surface, electron spin polarisation, effect of H_2 adsorption, electron capture spectroscopy 78−14933
Ni (111), Mossbauer effect emission spectroscopy and AES 79−91329
Ni, absorption of H_2, demagnetisation of surface due to absorption 77−80990
Ni, chemisorption of H, surface magnetism 78−95510
Ni, ferromagnetic, chemisorption of H, spin-spin interactions, UPS spectra calc. 80−6630
Ni film, chemisorption induced mag. dead layers, ferromag. reson. obs. 79−91261
Ni film, ferromag., light scatt. from surface acoustic spin waves 79−33719
Ni film, magnetooptic Kerr effect meas. near crit. point 77−69811
Ni film, surface magnetisation, electric field effect 78−14991
Ni film, surface magnetoplasma waves, ATR meas. 77−69639
Ni films, evaporated, effect of CO adsorption on galvanomag. and mag. props. 79−33363
Ni films, evaporated, effect of CO adsorption on galvanomag. and mag. props. 79−33364
Ni, influence of H chemisorpt. on magnetism, ferromag. reson. spectroscopy 77−66395
Ni, mag. domains, μ^*-tensor method, temp. and surface orientation depend. 77−16098
Ni, magnetic order 78−95439
Ni, magnetic surface anisotropy of transition metals, model calc. 80−34625
Ni, spin polarisation in electron field emission, surface magnetism 78−68607
Ni, spin polarised photoemission, surface magnetism 79−52083
Ni surface, electron spin polarisation, electron capture spectroscopy 78−95645
Ni surface, spin distribution of electrons, electron capture spectroscopy 78−14932
Ni-Co, ferromagnetic resonance, surface anisotropy 78−95526
Ni-Co plate, surface anisotropy from ferromagnetic reson. 78−48049
Ni-Fe (40%), Mn coating, mag. interface effects 77−69638
Ni-Fe (40%) (111) film with C coating, surface magnetism 77−73056
Ni-Fe/Mn interface, mag. surface effects, dead layers and exchange anisotropy 77−24718
Ni-$LiNbO_3$, layered structure, mag. control of surface elastic waves 77−20666
Ni-SiO multilayer films, interface magnetisation 80−88858
NiFe, magnetic surface anisotropy of transition metals, model calc. 80−34625
NiO (001), surface layers, sublattice magnetisation temp. depend., LEED exam. 78−27018
NiO (100), antiferromag., LEED calcs. of exchange refls. 78−14949
NiO (111) surfaces, antiferromag., mag. scattering by polarised LEED, spin polarisation effect in theory 80−29529
NiO, surface sublattice magnetis., temp. depend., determ. using low energy electron exchange scatt. *(Japanese)* 77−55700
Ni(001) surface states, surface magnetisation, electron spin polarisation 80−88612
Ni(110), ferromag., surface magnetisation, polarised LEED expt. 80−97118
O single layer on Au, ferromag. props., thermomag. effect *(Russian)* 78−64256
O_2 monolayers, on graphite, mag. α-phase and α-β-phase transition 80−70530
Pb-Tl, reversible surface superconducting magnetisation 78−43531
p-$Pb_{0.82}Sn_{0.18}Te$, mag. susceptibility, inversion layers effect *(Russian)* 77−72996
Pd, film with defects, field-induced resist. min. 80−11050
Sm-Co, permanent mag., O ion impact, 5.5 keV, secondary Co ion emission, magnetisation depend. *(Russian)* 78−2967
Tb-Ho film, helimag. order, surface deform., exchange and single-ion magnetocrystalline anisotropy energy 77−66390
V fine particles, appearance of mag. moment 78−68152
V hyperfine particles, surface magnetisation, explanation of expt. work 78−23303
V, magnetic moment near surface, one-electron band model 79−82747
V surface, spin fluctuations, finite temp. mag. props. study 80−107994
YCo_3, amorphous ferromagnet, exchange dominated surface modes 78−52359
YCo_3 film, amorphous, induced and surface anisotropies, ferromag. reson. and static meas. 77−85507
YFe_2, amorphous, surface ferromag. layer, spin wave reson. Rutherford backscatt., and magnetisation meas. 79−73819
$Y_{1-x}Fe_x$, amorphous, spin resonance exam. 79−51860
$Y_3Fe_{4.6}Ga_{0.4}O_{12}$ film, surface spin wave reson. 77−85576
$YFeO_3$, thermomag. recording in surface layer of orthoferrite 79−24165
YIG, dilute, magnetoacoustic surface wave excitation by RF field on Bloch walls 80−25178
YIG ferromagnetic film, quasi surface spin wave giant oscills. *(Russian)* 80−15767
YIG, film, magnetostatic surface wave refl. at shallow groove 78−19283
YIG film, magnetostatic surface wave propag. 79−4661
YIG film, magnetostatic surface and forward volume wave oblique incident at shallow groove 80−34704
YIG, film, photoinduced mag. surface anisotropy spin wave reson. 77−4560
YIG film, shallow groove, magnetostatic surface wave reflectivity 77−73055
YIG, film, spin wave reson., complex mag. surface energies 77−4561
YIG, film, spin-wave spectra in terms of mag. boundary conditions 79−78532
YIG film, surface effects in spin wave reson. 77−16182
YIG film, surface pinning parameter, symm. props. 79−28570
YIG film, with periodic mag. struct., dispersion characts. anal. *(Japanese)* 79−42809
YIG film tangentially magnetised, magnetostatic surface wave excitation 80−29586
YIG, LPE and CVD films, boundary effects, spin wave reson. meas. 79−78447
YIG, LPE film, magnetostatic wave to exchange resonance coupling 79−82774
YIG, magnetised in raised cosine profile magnetostatic surface wave propag. 80−2567
YIG, magnetocrystalline surface anisotropy energy, one-ion mechanism 79−42756
YIG, magnetocrystalline surface anisotropy energy, one-ion mechanism 79−78362
YIG magnetostatic surface wave dispersion rel. to mag. saturation diffusion 78−2671
YIG, mulitiple mag. layer structures, magnetostatic surfacewave propag. 80−88839
YIG periodic film layer, magnetostatic surface wave propag. 80−2607
YIG, pseudo-surface magnetoelastic waves, damping *(Russian)* 78−23320
YIG slab, corrugated, magnetostatic surface-wave propagation 78−19228
YIG substrate magnetoacoustic modes, meander-line excitation 77−20670
YIG substrates, magnetoelastic surface waves, magnetostatic reson. anal. 80−20441
YIG, surface spin waves, microscopic theory, mag. field effects 78−35044
YIG thin film, metal film effect on mag. boundary conditions, spin wave reson. obs. 79−78527
YIG-dielectric layered structure, magnetostatic surface wave propag., finite width effects 77−20668
YIG-InSb system, surface magnetostatic wave interaction with drift electrons *(Russian)* 77−12185
YIG-semiconductor coupled system, magnetostatic surface wave amplification, energy anal. 77−55699
YIG-semiconductor coupled system, magnetostatic surface wave amplification, ferromag. loss 77−85434
YIG-semiconductor-dielectric-metal layered structure, amplification characts. of magnetostatic surfaces waves 78−23321
$Y_{3-x}Sm_xFe_5O_{12}$:^{57}Fe film, ion implanted, Mossbauer conversion spectra study 80−80663

magnetic susceptibility
see also molecular magnetic susceptibility; photomagnetic effect
A15 compounds, elec. struct., 3-D k.p model 78−2405
A15 compounds, high-temp. superconductors, martensitic transform., microscopic theory based on 3-dimens. band struct. 78−19752
A-15 compounds, X-point model for mag. susceptibility 78−23014
AC, depend. on magnitude meas. field 80−241
achondrite meteorites, brecciation and shock effects on mag. susceptibility and NRM 80−8603
actinide compounds, mag. and structural props. review 77−63132
actinide intermetallic cpds., cubic, var. from localised to itinerant magnetism 77−20534
actinide systems, nearly ferromag., coupled d- and f-band model 77−63211
actinide systems, spin fluctuations effect, model approach 77−28404
actinides, spin fluctuation theory, for mag. and elec. props. 78−91869

magnetic susceptibility continued
actinides, susceptibility meas. using micro-mag. susceptometer 80−13112
alaninium copper tetrahalides, exchange, mag. anisotropy, and spin diffusion contribs. to EPR linewidth 80−80597
alkali halide, ionicity trends in diamagnetism and its temp. depend. 79−19717
alkali metal azides, diamag. susceptibility, rel. to cryst. struct. 79−24127
alkali metal-transition metal double molybdates, 90-800K, paramag. behaviour *(French)* 80−39734
alkali metals, magnetic property volume depend., Knight shifts, electron spin response 80−88729
alkali metals, paramag. and electronic susceptibility calc. 78−52205
alkaline earth transition metal ternary and quaternary oxides, ATO_3, $ATi_{1-x}T_xO_3$, and $AZr_{1-x}T_xO_3$, prep., mag. props. and struct. 79−15277
alkaline earth-ReO_6, ordered or perovskite type struct., magnetic and elec. props. 79−65053
alkaline-earth-Os ternary oxide system, solid state prep. and reactions, cryst. struct., mag. and elec. props. 79−24739
alkyl β-ketoacetals, cyclic, diamag. susceptibility, O at. contribution rel. to ring closure 77−14606
alkylammonium copper chlorides, high-temp. susceptibility obs., 80-300K, ferromag. interactions 77−66274
alloy, conduction electrons mag. susceptibilty 79−87230
alloys, d-metal, magnetic susceptibility and Knight shift meas. 80−66055
aluminoborate glass, Fe and Cr ion interaction, mag. and spectral props. 80−103883
aluminosilicate glass:Co (14.3 wt.%), AC susceptibility meas. 80−88771
amorphous ferromagnet, spin wave spectrum rel. to struct. 77−66290
amorphous magnet, random anisotropy axis model in the infinite-range limit 80−88761
amorphous semiconductor, localised gap states, variable range hopping, susceptibility and EPR 77−72866
amorphous systems, mag. props. effect of random anisotropy 79−4686
Anderson impurities, interacting, pair, Fermi-liq. theory 80−44803
Anderson localised states, electron correlation effects 79−23919
Anderson model, direct interaction between impurities 80−54681
Anderson model, orbitally degenerate, exchange coupling in atomic limit, rel. to two-site Hubbard model 80−108000
Anderson model for dilute magnetic alloys, static suscept., functional integral approach 80−50050
anisotropic binary paramagnet, uniform susceptibility, critical behaviour 77−59384
anisotropic Heisenberg ferromag., inhomogeneous dynamic susceptibility tensor 80−39729
anisotropic paramagnet, statistical mechanics using second order Green's function theory 80−25074
anthracene, mag. susceptibility anisotropies, high field ^2H NMR quadrupolar effects obs. 80−25225
antiferroelectric ferrites, coupled magnetoelec. oscills. and high freq. susceptibility tensor *(Russian)* 80−93152
antiferromagnet, chain-like, parallel susceptibility 78−80137
antiferromagnet, crit. fluctuation of staggered magnetisation, AC susceptibility meas. 80−60219
antiferromagnet, cylindrical magnetic domains, statistical props. 77−40080
antiferromagnet, impurity-induced mag. susceptibility *(Russian)* 77−32172
antiferromagnet, Ising model, two-dimens., mag. susceptibility calc. 80−60225
antiferromagnet, low-dimensional susceptibility 79−28513
antiferromagnet, mag. excitations within local exchange approx. 77−69517
antiferromagnet, magnetic and thermal props. 78−14937
antiferromagnet, magnetoelectric susceptibility crit. behaviour, renormalisation group theory 78−48023
antiferromagnet, two-dimensional, approx. to susceptibilities 78−47928
antiferromagnet, two-dimensional, expansion for susceptibilities 80−70963
antiferromagnetic and ferromag. parallel susceptibilities, graphical illustration, for teaching 78−41118
antiferromagnetic chain, random, quantum spin-1/2 Heisenberg soln. 80−11148
antiferromagnetic degenerate semiconductor, thermal and mag. props. 78−19224
antiferromagnetic exchange-coupled one-dimens. anisotropic chain with S=1/2, comparison with expts. 77−20530
antiferromagnetic spherical model, eqn. of state near phase boundary 77−55681
antiferromagnetic spin Hamiltonian with four spin interactions for BCC, lattice, mean field theory 79−1652
antiferromagnetic triangular cactus tree, bond-diluted, ordered phase 80−71037
antiferromagnetism in system if itinerant electrons 80−2547
antiferromagnetism itinerant electron theory, spin susceptibilities 78−6504
antiferromagnets, disordered spin flop, bicritical behaviour, critical experiments 80−65899
antiferromagnets, magnetic susceptibilities in Heisenberg and Ising models 79−24185
antiferromagnets, random, theory of mag. excitations, antiferromag. reson. 80−97146
antiferromagnets, reln. between temp. depend. of mag. susceptibility and sp. ht. *(German)* 77−69567
antiferromagnets, uniaxial, spin dynamics near bicrit. points 77−16090
aqueous heterogeneous systems, thermal anomalies 77−32829
aromatic compounds, diamag. susceptibility 78−80123
atomic, Kirkwood relation in at. diamag., satisfaction by Thomas-Fermi model 78−9266
atomic scattering factors of first row atoms and ions, diamagnetic susceptibilities 77−68133
atoms, mag. hypersusceptibility *(Russian)* 77−14598
austenitic stainless steel, heat conductivity, low temp. mag. susceptibility meas. *(Chinese)* 79−47080
azoxybenzenes, nematic, mag. susceptibility, orientational order parameter 78−34426
α-B, rhombohedral, magnetic props. and ESR spectra 80−20452
basaltic bodies, mag. susceptibility anisotropy meas. rel. to flow and emplacement direction 79−29766
basalts, mag. grains nature and implications for palaeomag. 79−84243
magnetic susceptibility continued
basalts, mag. susceptibility anisotropy meas., torque and spinner magnetometer comparison 78−21185
basalts from deep drill holes in Iceland, susceptibility rel. to mag. layer concept 77−60365
beat effect of sp. ht. due to impurities, in external mag. field 78−10401
beryllides, Faraday method 77−47969
Bethe lattice, random ordered phase, statistical theory 77−85457
biochemical samples measurement, modification of sample holders for superconducting magnetometer 77−26367
biological systems, containing Fe, electronic and mag. struct., semiempirical MO cluster calcs. 78−62733
biphenyl, mag. susceptibility 80−25076
bis(diethylammonium) copper tetrachloride, mag. susceptibility, EPR spectra 78−68193
bis(triethylbenzylammonium)tetrachlorocuprate(II), mag. anisotropy, susceptibility, EPR of Cu^{2+} 78−52344
bis(trimethylbenzylammonium)tetrachlorocuprate(II), mag. anisotropy, susceptibility, EPR of Cu^{2+} 78−52344
bisgalvinoxyl biradical, cryst., spin-spin dipolar and exchange interactions 78−52356
Bloch electrons, nonlinear orbital magnetisation in weak mag. fields *(Russian)* 80−70931
Bloch electrons, weak magnetism, spin and spin-orbit interactions *(Russian)* 79−33443
borides, hexa- and tetra-, prep., struct., elec., mag. props., book contrib. 78−47303
borides, transition metal, rare earth, and actinide, mag. props., book contrib. 78−47978
borosilicate glass, Fe and Cr ion interaction, mag. and spectral props. 80−103883
bubble film, mag. characterisation procedures 79−78462
bubble films, characterisation by AC susceptibility meas. 78−68325
calcium copper acetate hexahydrate, mag. susceptibility behaviour at low temp. 77−24679
calcium copper acetate hexahydrate, mag. susceptibility field depend. 79−87241
calibration standard, low-field, using γ-Fe_2O_3 and glass powder mixtures 79−88989
Cambrian slates of N Wales, mag. susceptibility anisotropy and correl. with strain 79−79832
carbonyl chlorofluoride, rot. Zeeman effect, g-factors and mag. suscept. anisotropies, microwave meas. *(German)* 77−57993
chains, spin 1/2 Ising and classical Heisenberg models with alternating exhange, static props. 79−82737
chains of classical spins, weak ferromagnetism, zero-field susceptibility 79−15268
charge-density-wave metal, mag. susceptibility of cond. electrons 80−44523
charged two-dimensional isotropic Fermi liq., spin susceptibility 79−19532
Chevrel phase compounds, bonding and phys. props. rel. to struct., book contrib. 80−49209
chromium phosphinate polymer, one-dimensional antiferromagnet, spin-flop 80−50131
chromocene, mag. props., complete ligand field theory 78−31048
chromocene, mag. suscept., zero-field splitting, ligand field, 1-303K 77−89924
chrysene, mag. susceptibility anisotropies, high field ^2H NMR quadrupolar effects obs. 80−25225
classical 2-D Heisenberg model, low temp. recursion relations, high temp. series expansion 78−10639
classical Heisenberg chain with mag. impurities 77−4490
classical magnet, random one dimens., thermodynamic quantities 77−48002
classical planar spin model, two-dimens., Monte Carlo study 80−25147
classical spin glass, propagating modes in 3 dimensional planar model, dynamic struct. factors 79−99703
closed shell system, paramagnetism, harmonic oscill. model 77−58194
coal, mag. susceptibility and Mossbauer meas. 80−60464
coal, mag. susceptibility anisotropy meas., coalification process indicator 79−53340
coal banding-plane indicator, magnetic susceptibility anisotropy meas. 78−77221
cobalt formate dihydrate, mag. relax. phenomena near T_N 79−65656
cobalt formate dihydrate, ordered state, paramag. cross relax. *(Japanese)* 77−43873
cobaltocene, mag. props., complete ligand field theory 78−31048
cobaltous acetate tetrahydrate, weak ferromag. obs. below 85 mK 79−73695
composite material, inhomogeneously random, mag. susceptibility 78−19200
compressible magnet, magnetic susceptibility near critical point, trajectory integral calc. 79−99705
condensed ring systems, diamag. susceptibility, appl. to pregraphitic C 77−16039
conduction electrons magnetism at points with changing topology of isoenergetic surfaces *(Russian)* 78−52260
contactless measurements for solids using torsional resonance apparatus 79−75675
cooperative Jahn-Teller effect and paramagnetic susceptibility of S=1 systems 78−68134
copolymer model with alternating spins, kinetics 80−9768
copper (II) carboxylates, magnetic and spectroscopic props. 79−91204
copper acetates, antiferromag. exchange coupling, superexchange mech. 78−39310
copper complex $CuBr_2$ (pyrimidine)$_2$, mag. susceptibility and magnetisation curve, 1.2-4.2K 80−11177
copper formate tetrahydrate, two-dimens. spin 1/2 Heisenberg antiferromag., phase transition characts. 77−66352
copper porphyrins, mag. susceptibility and EPR, sample grinding effects 80−60420
copper quaternary thiospinels, mag. and elec. props. *(French)* 80−65771
copper tetrammine sulphate monohydrate, evidence for exchange coupled quadratic nets 77−24705
coronene, mag. susceptibility anisotropies, high field ^2H NMR quadrupolar effects obs. 80−25225
correlation length relationship to susceptibility, anomalous-dimension crossover function, renormalisation group calc. 79−42780
coupled spin $^1/_2$ phonon system, existence of sharp transition 79−69204

magnetic susceptibility continued
critical indices for systems with strong dipole interactions *(Russian)* 77−28390
critical point, complementary expressions for scaling function 80−34656
crystal growth models, zero field susceptibilities and correlations 78−34454
crystal with strong s-d exchange, mag. susceptibility and Curie-Weiss law *(Russian)* 80−25068
crystallographic two sublattice system, s=1/2, mag. susceptibilities 78−14914
cubic metal binary alloys for H energy storage 80−45787
Curie-Weiss susceptibility of local moments 78−80128
cyano-biphenyl cpds., nematic, mag. susceptibility and order parameters 79−86709
4-cyanobenzoyloxy-4′-pentylstilbene, nematic, smectic A, and orthogonal smectic B phases 80−64890
cylindrical magnetic film, calc. of impedance and susceptibility *(Russian)* 77−89992
data analysis program SUSCEPT2 78−91847
$(DBTTF)_{2.67}SnCl_6$, Peierls transition, fluctuations effect *(Russian)* 79−60809
demagnetisation eigenfunctions anal. of linear transverse magnetisation in long, thin stripes 80−34687
demagnetisation through level crossing, effect of charge fluctuations 78−52193
di(propylammonium) copper tetrachloride, mag. suscept. meas. 77−63131
dialkylammonium copper tetrachlIride, ferromag., static and dynamic mag. props. 80−50074
dialkylammonium copper tetracholorides, quasi 2-dimens., lattice- and spin-dimens. crossovers 77−59416
dialkylammonium iron tetrachloride, antiferromag., mag. susceptibility meas. 80−60220
diamagnet, measurement methods, noise anal. 77−13782
diamagnetic susceptibility, Curie law, SCF calcs. *(Russian)* 78−64183
diamagnetic susceptibility calculation using Pascal's consts., BASIC program 80−37717
diammonium layer compound, $(CH_2)_2(ND_3)_2MnCl_4$, mag. and optical props. 79−51760
diammonium layer compound, $(CH_2)_n(NH_3)_2CuCl_4$, mag. and optical props. 79−51760
diammonium layer compound, $Mn(NH_3)_2(CN)_42C_{12}H_{10}$, mag. susceptibility and sp. ht. meas. down to antiferromagnetic state 79−7999
dicarboxylic acid, solid, binary mixtures of long chain mol. systems, diamag. susceptibility 77−32154
3,3′-diethyl-2,2′-selenacyanine-$[TCNQ]_2$, elec. cond., and quasi-two-dimensional mag. props. 78−6564
diethylammonium copper chloride, Heisenberg ferromag., spin wave theory 77−89922
diethylammonium-manganese chloride, spin diffusion, quasi-two-dimensional Heisenberg paramagnet 78−88129
p,p′-diheptylazobenzene, nematic, physical props. 78−79524
5,10-dihydro-5,10-diethylphenozinium-iodide, average struct. and props. 79−90636
diisopropylammonium copper chloride, mag. interactions, susceptibility, 2-230K 80−60237
dilute Heisenberg magnet excitations near percolation threshold 79−87270
dilute magnetic alloy, sp. ht. evaluation role of fluctuations 77−69580
dilute magnetic alloys, asymmetric Anderson model, renormalisation-group approach, static props. 80−44802
dilute magnetic alloys, symm. Anderson model, renormalisation-group approach, static props. 80−44801
dilute random magnet, one-dimens., low temp. behaviour of susceptibility, sp. ht. and correl. length 79−69682
dilute simple cubic lattice, short-range quadrupolar order 79−65681
diluted Ising and Heisenberg magnets with competing interactions, phase diagrams and mag. props. 80−34672
dimerised Ising chain, free energy, mag. moment, static susceptibility 77−55651
dimethyl ammonium copper chloride, spin dynamics near crit. pt. 80−7112
dimethyl ammonium manganese trichloride, NMR for mag. ordered state at 3.6K 79−47340
dimethylamine iron tetrachloride, antiferromag., mag. susceptibility meas. 80−60220
dimethylammonium copper tetra(chlorobromide), mag. susceptibility, 1 to 30K, mag. phase transition 79−4675
dimethylammonium copper tetrabromide, quasi two-dimensional antiferromag., mag. behaviour 80−97098
dimethylammonium copper tetrachloride, crit. slowing down and anomalous relax. near Curie temp. 80−71053
dimethylammonium copper tetrachloride, ferromag., quasi two-dimensional, ordering temp., press. depend. 80−84601
dimethylammonium copper tetrachloride, two-dimens. ferromag., saturation of parallel-pumped magnons 80−97147
dimethylammonium copper tetrahalide, layer compound $(CH_3NH_3)_2Cu(Cl_xBr_{1-x})_4$, antiferro- to ferromag. transition 80−108005
dimethylammonium iron bromotrichloride, canted spin system, mag. susceptibility meas. 78−39303
dimethylammonium manganese tetrachloride-d_6, structural and mag. phase transitions, neutron scatt. and AC susceptibility meas. 80−44825
dimethylammonium manganese trichloride, antiferromag. props. 79−73694
1,5-dinitronaphthalene, diamag. cryst., mag. axis, struct. interpretation 80−50039
dipalmitoylphosphatidylcholine, changes in vol. mag. susceptibility at the phase transition 80−76770
dipolar conducting liquids, rel. to mag. transport props. at ambient temp. 79−91258
dipropylammonium manganese tetrachloride, and tetrabromide, two-dimens. antiferromagnet, spin canting and exchange 80−34620
dipropylammonium manganese tetrachloride, two-dimens. weak ferromagnet, AC susceptibility 80−65823
disordered alloy, electron correl. in Hubbard model, and spin susceptibility 77−76762
disordered anisotropic antiferromagnet. random field effects 80−2580
disordered Ising model on Cayley tree, mag. transition above percolation threshold 79−73757

magnetic susceptibility continued
disordered one-dimensional conductors, interacting electron thermodynamics *(Russian)* 80−54679
disordered one-dimensional system, Hubbard model 78−10642
disordered quasi-one-dimensional systems with electron correlation, electronic properties 78−87966
disordered spin system, commutator and anticommutator Green's functions 79−51792
disordered substitutional alloy, mag. props., Heisenberg model 79−38342
disordered system, diamag. susceptibility, variational calcs. 77−8265
disordered system, orbital mag. susceptibility of conduction electrons 78−76217
dithiocarbamate complexes of Cr, Mn, Sn and Pb IR, electronic and mass spectra, mag. susceptibility, cond. meas. 80−97270
domain lattices, parallel stripe susceptibility, uniaxial anisotropy field 80−54930
double exchange mechanism theory 77−24689
double Ising chain, model in zero external field *(Russian)* 78−84430
DPPH, solid, mag. susceptibility meas. 300 to 2.2K, pair model 77−66245
DPPH-benzene complex, ht. capacity, 0.55-20K, mag. susceptibility, 0.4-300K 78−56317
dynamic, noninvariance under change of origin, use of fourth-order tensor *(French)* 77−61890
dynamical correlated-effective-field approximation 79−24122
Dyson's hierarchical model, essential singularities of borderline Ising case 78−31077
dysprosium ethylsulphate, pure dipolar Ising ferromag., critical thermodynamics 77−16095
Earth crust, mag. susceptibility, meas. at Yerington mine, Nevada 80−51323
effective exchange interactions and magnetic ground state of strongly correlated electrons 79−61036
effective field models in magnetism, unifying theory 77−32136
electron fluid, adiabatic de Haas-van Alphen effect at low temp., Fermi fluid interaction and chem. pot. effects *(Russian)* 80−84442
electron gas, Bloch, surface mag. props. in opposing elec. and mag. fields at 0K 78−63992
electron gas, Hubbard model at low temp., mag. props. *(Russian)* 78−43550
electron gas, inhomogeneous, exchange effects and nonzero temps. 80−84444
electron gas, metallic densities, dynamical dielectric function and paramagnetic spin susceptibility 80−39514
electron gas, paramag. and diamag. susceptibilities, density depend., ring diagram contrib. 79−95571
electron gas, paramag. susceptibility, RPA calc. 78−43559
electron gas, temp. depend. of mag. susceptibility 78−23224
electron gas, thermodynamic properties, weak field expansions, in uniform mag. field at T=0K 79−85066
electron gas, two-dimensional, study in intermediate mag. field 79−60743
electron gas, two-dimensional, study in weak mag. field 79−60742
electron gas at high density, mag. susceptibility determ. 77−31965
electron gas in smooth potential, orbital mag. suscept. 78−6312
electron liquids, temp. mag. transitions 77−69563
electrons in rectangular box, orbital mag. suscept. 77−85166
ellipsoid with domain struct., magnetostatic oscills., theory 80−93102
epoxy resin, mag. susceptibility, constant mag. field effect 80−11154
equation of state in crit. region with nonasymptotic terms *(Russian)* 77−28402
ethylenediammonium metal chlorides, $(NH_3CH_2CH_2NH_3)MCl_4$, M=Ni,Pd,Cu,Cd,Mn, struct. and mag. props., vibr. spectra 79−10842
ethyleneoxide, elec. dipole moment, g-values, mag. susceptibility, moments and charge distrib. 77−58077
Eu-Ag alloy, amorphous, formation and mag. props. 79−91216
exchange coupled spins, in lattice dimens. 1 and 2, 1/n expansion 77−66237
f^n-electron system, paramag. principal susceptibilities, calcs. using ang. overlap model 77−32158
Faraday balance susceptometer, computer controlled 78−65946
Faraday magnetic balance for metalloprotein solns. in 6.5-300K range 78−70170
Faraday magnetometer, meas. methods, very accurate for small samples *(Croatian)* 79−9222
Faraday method, nylon-quartz fibre support for low temp. meas. 78−65947
$Fe_{40}Ni_{40}P_{14}B_6$, $Fe_{32}Ni_{36}Cr_{14}P_{12}B_6$, amorphous Hall effect, press. and temp. depends. 77−66155
Fermi liquid, normal state, finite temp. contribs. 78−10246
Fermi liquid, paramag., with Coulomb interactions, susceptibility temp. var. 77−40017
Fermi liquid, temp. depend. of mag. susceptibility 79−65628
Fermi liquid description for temp. variation 77−63049
Fermi liquid model in external mag. field *(Russian)* 77−47952
Fermi liquid model of magnetism, susceptibility maximum in 4d and 5d transition metals 77−4480
fermion system, nearly ferromag. absence of T^2lnT term 78−10692
ferredoxin, from Clostridium pasteurianum, Mossbauer effect, ESR, and mag. susceptibility meas. 80−40961
ferrimagnet, polaritons, mag. susceptibility 80−7095
ferrimagnetic phase in crystals with low exchange fields *(Russian)* 77−32188
ferrite F-600, suspension in caster oil, residual magnetisation *(Russian)* 79−1689
ferrites, EM wave effects on mag. and optical props., lecture 78−27031
ferrites, polycryst., dynamic mag. susceptibility rel. to ferromag. reson. *(Russian)* 77−66267
ferrites, unmagnetised polycrystalline, gyrotropic susceptibility and effective anisotropy 78−64224
ferrites type 1500 NMZ and 2000 NMI, mag. susceptibility depend. on heating *(Russian)* 80−108603
ferrobimagnetic poling, differing mag. susceptibility of domain states 77−16102
ferroelectric semiconductor, spin susceptibility near ferroelec. transition 80−2710
ferrofluids, dependence on magnetic field intensity *(Czech)* 77−16109
ferrofluids, mag., optical, and hydrodynamic props.,, expt. study, review 80−60376
ferrofluids *(Czech)* 77−26345
ferromagnet, dipolar, susceptibility crossover 77−24680

magnetic susceptibility continued
ferromagnet, dynamical props. of flat parallel domain struct. *(Russian)* 78−6499
ferromagnet, high freq. crit. dynamics above T_c *(Russian)* 78−10718
ferromagnet, high frequency, kinetic and thermodynamic props. *(Russian)* 78−19340
ferromagnet, inter-atomic interaction effect on dynamic susceptibility, RPA calcs. 79−65662
ferromagnet, Ising model, diamond lattice, phase transition, crit. props. 80−93127
ferromagnet, Ising-Heisenberg-XY crossover, bicritical point, partial differential approximants for susceptibility series 77−85466
ferromagnet, itinerant, mag. props., temp. depend., functional integral approach 80−60170
ferromagnet, itinerant electron, magnetoelastic contribs. to US vel., elastic consts., and susceptibility 80−75829
ferromagnet, itinerant electron, magnon spectrum just below T_c, theory 80−65833
ferromagnet, magnetic susceptibility, spin and charge density waves, Curie temp. *(Russian)* 80−100581
ferromagnet, spin wave nonresonant excitation by varying mag. field, nonequilibrium states *(Russian)* 80−34616
ferromagnet, spin-1, appl. of high-temp. series expansion for complicated level systems 77−51863
ferromagnet, two-dimens., spin wave theory, magnetisation, susceptibility *(Japanese)* 77−47954
ferromagnet, uniaxial, dipolar crossover effects from Ising crit. behaviour 77−89961
ferromagnet, uniaxial, quantum anomalies in susceptibility during second order phase tansitions *(Russian)* 78−19226
ferromagnet, uniaxial dipolar, crossover behaviour, theory 80−29559
ferromagnet, with weakly bound ferromag. impurity, thermodynamic and dynamic props. *(Russian)* 78−27032
ferromagnet. Bloch electrons, dynamic longit. spin susceptibility 79−19709
ferromagnet with admixture of antiferromag. bonds, thermodynamic functions *(Russian)* 79−87224
ferromagnetic, electron fluid, polar spin waves *(Russian)* 77−89938
ferromagnetic, mag. excitations within local exchange approx. 77−69517
ferromagnetic alloy, binary ordered, dynamic mag. susceptibility, spin wave stiffness constant 79−38307
ferromagnetic alloy, temp. depend. of mag. props. and sp. ht., mag. phase transition region 78−64207
ferromagnetic alloy, transition to spin glass ordering 80−34628
ferromagnetic alloys, conc., spin fluctuations, SCR theory and CPA calcs. 78−64290
ferromagnetic bodies calc., rectangular, using iterative methods *(Slovak)* 79−4656
ferromagnetic film, mag. props., rel. to struct. 79−91270
ferromagnetic film, transverse bioped susceptibility, two-dimens. micromagnetism 80−11231
ferromagnetic films, spin correl. functions, crit. indices 80−7133
ferromagnetic instability in two-band Hubbard model 79−1653
ferromagnetic materials, temp. modulation, phase sensitive detect., theory 77−12098
ferromagnetic metal, transient enhancement of AC susceptibility, domain wall pinning centre diffusion 77−20633
ferromagnetic metals, spin fluctuation theory, Curie temp., mag. susceptibility 80−65937
ferromagnetic spin system, mag. susceptibility and correl. length crossover relationship 79−78395
ferromagnetic system, singularity in susceptibility, random spherical model in nonzero mag. field 77−55677
ferromagnetism, Hubbard model, mag. susceptibility, modified Stoner criterion 79−51736
ferromagnetism, singlet state, theory 77−12073
ferromagnets and antiferromagnets, transverse dynamical susceptibility within the local exchange approx. 78−76229
finite disordered Hubbard cluster, thermodynamic and mag. props. 77−85409
first row elements, ground state, self-consistent orbitals with uniform long-range behaviour 80−9485
fluid electrophysical effect control by susceptibility variation *(Russian)* 79−95628
frozen spin state, static susceptibility, piezomag. effect 77−51914
frustrated two-dimensional planar model, spin-spin correl. 80−11212
frustrationless models, rel. to spin glasses 80−29561
full wafer magnetic bubble films, devices for characterisation 79−78461
garnet:Nd^{3+}, doped, Schottky specific heat and mag. susceptibility calcs. 79−51759
garnet epitaxial film, anisotropy consts. from reciprocal of susceptibility meas. 77−73057
glass, magnetic susceptibility measurement, torsional reson. technique 80−82796
graphite, diamagnetism with quasilinear dispersion law, orbital susceptibility, valence bands *(Russian)* 80−80475
graphite, polycryst., EPR meas. rel. to temp., crystallite orientation, paramag. suscept. 78−35023
graphite intercalation compound, $C_{8.8}K$, mag. susceptibility fluctuations near supercond. transition temp. 79−78259
graphite intercalation cpds., mag. susceptibility, tight-binding model 80−44796
graphite intercalation cpds. with alkali metal, interlayer screening and mag. susceptibility 80−44794
graphite ribbon, interlayer interaction effects on diamagnetism London theory 78−52201
graphite-alkali metal intercalation cpds., electronic props. 80−45202
graphite-alkali metal intercalation cpds., large anisotropy and stage depend. 80−44795
graphite-nitrate residue compounds, phys. props. 78−10199
graphite-UF_6 intercalation compounds, NMR exam. 78−39416
greenalite, two-dimens. mag. order 79−61188
guanidinium vanadium sulphate hexahydrate, susceptibility meas. spin-lattice relax. effects 77−66279
gyromagnetic medium with parametric pumping, LF transverse susceptibility *(Russian)* 79−1658
HBT liquid crystal, mag. susceptibility and anisotropy, smectic, nematic, isotropic phases 78−18748
HCP metals, and alloys, anisotropy of phys. props. rel. to texture 79−91700

magnetic susceptibility continued
HCP metals, mag. susceptibility near $2^1/_2$th order electron transition, non-linear magnetisation anal. *(Russian)* 80−44859
heavily doped semiconductor, n-type, disordered mag. system, hierarchy of exchange interactions 80−80235
Heisenberg, ferromagnet, classical, with dipole-dipole interaction, renormalisation group and crit. exponents 80−60351
Heisenberg, ferromagnet, nearly two-dimensional and nearly one-dimensional thermodynamic props., Green's function investigation 79−15275
Heisenberg anisotropic antiferromag., spectrum and correlation functions 79−28499
Heisenberg anisotropic ferromagnet, Bogoliubov inequalities, inhomogeneous dynamic susceptibility, single particle matrix Green's function 79−95564
Heisenberg anisotropic ferromagnet, collective Green function, longit. susceptibility *(Russian)* 79−65631
Heisenberg anisotropic ferromagnet, longit. correl. function, generating Green functions 78−6500
Heisenberg antiferromagnet, ABX_3-type, exchange interaction and zero-point spin reduction 77−12080
Heisenberg antiferromagnet, Green function theory 80−107975
Heisenberg antiferromagnet, one dimens., spin-flop transition 79−73723
Heisenberg antiferromagnet, one-dimens., impure, mag. susceptibility 80−60168
Heisenberg antiferromagnets, quadratic spin 1/2, sp. ht. and susceptibility, comparison with $Cu(C_5H_5NO)_6(BF_4)_2$ data 77−66353
Heisenberg antiferromagnetic alternating spin 1/2 chains, susceptibility calcs., spin-Peierls transition 79−78394
Heisenberg antiferromagnetic chain, random, low temp. thermodynamic props. in zero mag. field 80−34657
Heisenberg antiferromagnets, $S=\infty$ two-dimensional, approx. to susceptibility 77−80905
Heisenberg chain, ferromag., with biquadratic exchange, spin correl. length, susceptibility and spin diffusion *(Russian)* 77−69568
Heisenberg ferromagnet, anisotropic, collective Green's function, dynamical RPA 80−70925
Heisenberg ferromagnet, longitudinal dynamic susceptibility 78−64181
Heisenberg ferromagnet, longitudinal static spin susceptibility at $T<T_c$ 80−50114
Heisenberg ferromagnet, quasi-two-dimensional $S=^1/_2$, expt. susceptibilities compared with high-temp-series expansion analysis 77−4506
Heisenberg ferromagnet, structurally and chemically disordered, critical behaviour 77−43838
Heisenberg ferromagnet, two-dimens. second order phase transition 77−16094
Heisenberg ferromagnet, with single-ion anisotropy, correlation functions calc. 78−31076
Heisenberg ferromagnets, surface effect on thermodynamic props. and excitation spectra 79−11282
Heisenberg linear chain, alternating spin quantum numbers, mag. and thermodynamic props. 80−34578
Heisenberg linear chain, disordered, q-depend. mag. susceptibility 78−27010
Heisenberg linear chain, with nearest and next-nearest neighbour interactions 77−63059
Heisenberg linear chain magnets with unlike spins, exactly soluble model 77−16030
Heisenberg magnet, classical one-dimensional, with biquadratic exchange interaction, correlation functions and susceptibility calc. 77−36048
Heisenberg magnet, dil. three dimensional, static behaviour at finite temps., Monte Carlo calc. 79−73752
Heisenberg magnet, two-dimensional classical, mag. props., Monte Carlo calc. 78−23231
Heisenberg magnets, pure and pseudo-one-dimens. temp. depend. of EPR freqs. 78−6563
Heisenberg model, anisotropic, susceptibility high-temp. series expansion 78−43546
Heisenberg model, critical behaviour, high temp. susceptibility and internal energy series 78−34987
Heisenberg model, planar, classical, with biquadratic interactions, theory 77−72970
Heisenberg open finite chains, zero field, susceptibility calc. as function of reduced temp. 77−51868
Heisenberg paramagnet, site- and bond-diluted, correl. function and susceptibility 77−51869
Heisenberg spin glass, high temp. series, order parameter susceptibility 79−15312
Heisenberg-biquadratic and Blume-Emery-Griffiths interactions dipolar and quadrupolar susceptibility 78−76257
Heisenberg-biquadratic and Blume-Emery-Griffiths interactions dipolar and quadrupolar susceptibility 78−76258
Heisenberg-Dzyaloshinsky-Moriya model, high temp. expansions for zero-field susceptibility and specific heat 79−33497
Heisenberg-Ising bonds, randomly mixed three dimens. system, critical props. 78−76249
p-heptyl-p'-cyanobiphenyl, refractive index, dielec. const., mag. susceptibility, orientational ordering *(Dutch)* 80−33884
hexaferrites, $M(BaFe_{12}O_{19})$, mag. characts. correlation with substituting ions at. nos. *(Russian)* 79−91218
high field meas. using vibrating sample magnetometer *(Japanese)* 79−75559
high spin/low spin transition, model including lattice dynamics 77−63202
high-field solenoid field gradient appl. 80−31813
Hubbard Hamiltonian, two-site, half-filled band, thermodynamic props. 77−24505
Hubbard Hamiltonian, two-site extended, with arbitrary electron density 79−38297
Hubbard model, arbitrary electron density case, functional integral approach 78−76219
Hubbard model, computer renormalisation-group technique 79−19716
Hubbard model, doubly degenerate, functional integral approach 79−99711
Hubbard model, doubly degenerate, long range order 80−50029
Hubbard model, dynamic elec. and mag. susceptibilities near metal-insulator transition, functional-integral method 77−28119
Hubbard model, high temp. series expansion 78−23239
Hubbard model, local moments 78−95414
Hubbard model, one-dimens. half-filled band Holstein-Frolich modified, transport props. 78−23237

magnetic susceptibility continued
Hubbard model, single band with infinite repulsion on 2×2×2 lattice, thermodynamic props. 79−87225
Hubbard model, two-point doubly degenerate in half-filled case, thermodynamics 77−4492
Hubbard model calc., isothermal longitudinal susceptibility of strongly correlated electrons 80−25069
igneous rock bodies, in situ mag. meas. 79−84521
II-VI semiconductors, mag. susceptibility, effect of physical parameters 80−44793
III-V semiconductor effect of covalent bonding on mag. susceptibility 80−11153
III-V semiconductors, calc. using MOLCAO approx. 79−42732
ilvaites, Mossbauer spectra and mag. features 80−7248
impurity spin-unpolarised lattice nuclei interaction, dynamic susceptibility 79−69648
impurity uniaxial ferromagnet, thermodynamics below Curie point *(Russian)* 77−43801
induced moment systems, effect of spin fluctuations 80−2585
induced-moment singlet-triplet model, high-temp. series expansion 79−73653
inert gas atom, Thomas-Fermi model with Fermi-Amaldi correction 79−81156
inert gases, relation between diamag. susceptibility and electronic polarisability 77−14597
interacting free at Bloch electrons, mag. susceptibility determ. 77−16017
interacting single-domain grains, thermoremanence and ideal magnetization calc. 79−25232
intermediate valence, mag. susceptibility and mag. instabilities 80−39532
intermediate valence, phase diagram and Kondo behaviour 80−29366
intermediate valence, three-site, six-electron, even-parity model 80−20125
intermediate valence compounds, dynamic susceptibilities 80−70653
intermediate valence compounds, mag. susceptibility and sp. ht., mean-field theory of periodic Anderson model 78−47937
intermediate valence compounds, phonon produced instabilities, periodic Anderson model 78−79964
intermediate-valence systems, magnetic-nonmagnetic transitions, heuristic model 79−73718
Invar, itinerant electron character 77−66240
Invar, mag. phase transitions, linear expansion coeff. and mag. susceptibility meas. 77−69553
Invar, mag. susceptibility in technical saturation region and internal stress 77−85429
Invar, magnetic and thermal anomalies 80−34603
ion, Thomas-Fermi-Dirac model 77−67981
ionic compounds, amorphous, exhibiting Mossbauer spectra, mag. props. *(French)* 80−80490
ions, positive or negative, electron density, semi-statistical model 78−21850
iron(II)-A-zeolites, reduction, mag. and Mossbauer study 80−71115
iron (III) salicylates, Mossbauer and IR spectra, mag. susceptibility 80−50242
iron porphyrin chlorides, X-ray, EPR and mag. susceptibility obs., intermol. exchange interaction 78−10765
iron tetraphenylporphyrin chloride, electron spin pairs, low and ultralow temps. 77−77092
Ising and Heisenberg ferromagnets with biquadratic exchange, uniaxial anisotropy, susceptibility calc. 79−99670
Ising antiferromagnet, BCC, in mag. field, Monte Carlo calcs. 78−31032
Ising antiferromagnet, nonlinear response to high freq. mag. field, quantum theory *(Russian)* 80−93066
Ising antiferromagnet with next-nearest-neighbour interactions, tricritical exponents and crossover behaviour 77−16089
Ising chain, amorphous, finite, thermodynamic behaviour 79−61028
Ising chain, double, transverse susceptibility *(Russian)* 80−88727
Ising chain, in transverse field, variational treatment, static props. at zero temp. 79−4642
Ising chain, linear, three dimensional phonon field 77−73036
Ising chain, one-dimens., with generalized molecular field 79−91242
Ising chain, random one-dimensional, in transverse field, thermodynamics 77−77019
Ising chain, with next-nearest neighbour interactions, mag. responses to spin-Peierls transition 80−71054
Ising chain with random bonds, remanence and non-exponential relax. 79−73751
Ising chains, random bond, thermodynamics and correl. functions 79−15270
Ising dilute magnetic alloys, local mag. fields and fluctuations 77−40061
Ising disordered spin system on Cayley tree 79−51783
Ising double chain, compressible, mag. susceptibility and thermodynamic props. 79−15320
Ising ferromagnet, high-freq. props. quantum theory, susceptibility tensor calcs. *(Russian)* 80−11143
Ising ferromagnet, rectangular, determ. of critical indices 79−28537
Ising ferromagnet, S=1, single-ion type uniaxial anisotropy, cluster-variation method appl. in pair approx. 78−68281
Ising ferromagnet, two-dimens., order parameter and induced susceptibility 80−71036
Ising ferromagnets, correlation decay, zero-field susceptibility, mass gap 80−50116
Ising lattice, triangular, antiferromag. to ferrimag. transition 77−20522
Ising linear chain, disordered, q-depend. mag. susceptibility 78−27010
Ising mixed ferromagnetic-antiferromagnetic systems with arbitrary spin, critical temp. 79−78407
Ising model, adiabatic susceptibility and specific heat at const. magnetisation 80−7114
Ising model, amplitude universality and confluent corrections to scaling 77−80898
Ising model, bond random, ferromagnetic-antiferromag. mixture, triangular cactus tree, statistical theory 80−75702
Ising model, bond-dilute two-dimensional, crit. behaviour 79−8009
Ising model, cluster size and percolation 79−65630
Ising model, critical exponents for high temperature series expansion 79−99701
Ising model, critical temperature, modulated Pade approximant 80−84605
Ising model, free energy and susceptibility inequalities, phase transition 78−43541
magnetic susceptibility continued
Ising model, kinetic with triplet interactions, Monte Carlo anal. 80−7061
Ising model, low temp. expansions for 4-D simple hypercubic lattice 79−61025
Ising model, max. susceptibility locus crit. behaviour 80−71040
Ising model, mean size of clusters, series expansion 77−28350
Ising model, one-dimens., wavevector depend. of fluctuations in cluster approx. 80−12999
Ising model, quantal and finite-sized, dimensional crossover 78−95444
Ising model, random, in transverse field, CPA approach 77−36040
Ising model, random, susceptibility and magnetisation 77−80899
Ising model, random band, cumulant expansion to glass-like phase 77−8319
Ising model, random bond, susceptibility and specific heat of glass like phase, cumulant expansion 78−6533
Ising model, spin 1/2, susceptibility and fourth field derivative for $T>T_c$ and d=4 79−61024
Ising model, spin glass, mean field theory 79−4680
Ising model, spin glass in Bethe-Peierls-Weiss and other mean-field approximations 79−65682
Ising model, surface crit. behaviour, layer and local susceptibility 80−71058
Ising model, three-dimens. mag. susceptibility and sp. ht., high temp. series anal. 80−22295
Ising model, three-dimensional, with four-spin interaction, exact soln. 80−88711
Ising model, Toulouse frustration effect 79−24167
Ising model, transition temperature for square cactus tree with random bonds 78−41240
Ising model, valency transitions 78−60297
Ising model, with transverse field, crit. behaviour of susceptibility 77−12127
Ising model, with transverse field, ferromagnetic and antiferromagnetic susceptibilities 80−60160
Ising model on tetrahedron lattice, four spin interactions, high temp. susceptibility 77−28349
Ising model spin glass, Monte Carlo calc. of mag. suscept. 78−31079
Ising model with free surface, series anal. 80−25062
Ising models, zero field susceptibilities and correlations 78−34454
Ising O(2), O(3) and O(4) spin systems, Hamiltonian string-coupling expansions 80−20426
Ising paramagnet, impure, influence of spatial short range order 78−43542
Ising quenched bond model, statistical theory of random ordered phase 77−12075
Ising spin 1/2 model on FCC lattice, exponent γ 79−73656
Ising spin gass, glass, Edwards-Anderson order parameter instability 80−71043
Ising spin glass, calc. of wavevector depend. susceptibility 77−63223
Ising spin glass, d-dimensional, frustration effect 80−108019
Ising spin glass, d-dimensional, frustration effect and dilution problems 80−108018
Ising spin glass, remanent magnetisation, Monte Carlo exam. 79−61166
Ising spin glass, vanishing of Edwards-Anderson parameter 78−43597
Ising spin glass, with RKKY interaction, props. 79−24177
Ising spin glasses, Edwards-Anderson model, autocorrelation function logarithmic decay account 79−78406
Ising square lattice, phase transitions, next nearest neighbour interactions 80−50128
Ising susceptibility, appl. of integral approx. methods 79−71392
Ising system, cubic $S=^1/_2$ model, lattice dimensionality crossovers anal. 78−39347
Ising system, two-dimens., transverse field crit. props., renormalisation and scaling 78−21080
Ising system with quenched impurities, high temp. expansion methods 79−78422
Ising systems of different spin values, random system 80−11144
Ising transverse bond-diluted model, appl. of CPA 79−56551
Ising-like ordered phases, calcs. of bicritical crossover scaling functions 77−55678
isotropic ferromagnet, critical behaviour in random uniaxial anisotropy model 79−38349
isotropic spin system, momentum-shell recursion relations in $2+\varepsilon$ dimensions 78−6498
itinerant electron antiferromagnetism, effect of mag. field 78−27013
itinerant electron ferromagnetism, spin fluctuation theory 78−80151
itinerant electron ferromagnets, magneto-volume effects 80−60397
itinerant electron magnets, spin fluctuations and thermodynamic props. 79−65687
itinerant electron model, susceptibility, local exchange approx. calc. 80−60169
itinerant electron model for ferro- and antiferromag. systems, dynamic susceptibility 77−72988
itinerant electrons with energy dependent effective interaction 78−19209
itinerant ferromagnet, sloppy spin waves above T_c 77−72979
itinerant-electron ferromagnetism, possible coexistence with itinerant-electron antiferromagnetism 78−39286
itinerant-electron systems with narrow bands, single-site spin fluctuation theory 80−97049
IV-VI semiconductors, mag. susceptibility near ferroelec. transition pt. *(Russian)* 79−95568
kaolinite, aq. suspension, mag. and optical props., Fe_2O_3 impure particles 78−76933
Kapton, pyrolysed, cond. polymer, transport and mag. props. 80−96887
Kondo Hamiltonians diagonalisation, zero-temp. mag. susceptibility 80−93078
Kondo system, comparison of nuclear orientation and magnetisation expt. 77−63297
Kovar, effect of magnetic electrons on atomic interactions 77−43820
laccase, mag. susceptibility 79−92125
layered compounds CDW instability rel. to supercond. T_c 78−14856
layered crystal, mag. quantisation investig. *(Russian)* 78−23054
lecithin membranes, mag. susceptibility anisotropy, phase contrast microscope obs. 78−92601
linear chain of classical spins with logarithmic nearest neighbour pair potential, phase transition 77−36085
linear conductor, interchain coupling role 78−6294
linear conductor role of interchain coupling mag. susceptibility and CDW response evaluated 77−47751

magnetic susceptibility continued
liquid, dia-/paramag. solns. and ferrimag. suspensions, rel. to magneto-chem. separation 77−20628
liquid alloys, magnetic properties, review 79−51741
liquid crystals, prep. and phys. props., book 80−105444
liquid crystals, thermodynamic props. calc. 80−103464
liquid metal, electron states, esp. opt. and mag. props., review 78−2882
liquid metal, rel. to theories of electronic structure 77−1536
liquid metals, spin-orbit interactions effect on mag. susceptibility, effective pseudohamiltonian 80−29299
long wavelength spin susceptibility from particle-particle scattering, logarithmic temp. control 80−7124
low temperature depend. of elec. resist., mag. suscept., heat capacity, Hall const. *(Russian)* 78−30900
low-temperature materials props. and appl. *(German)* 80−3081
lymphocytes, living and dead, mag. props. and mag. sedimentation 80−35925
lyotropic nematic liquid crystals, mag. susceptibility, mol. aggregation meas. 80−19690
lysozyme, anomalous diamag. susceptibility and elec. cond. 79−29498
lysozyme, mag. suscept. 77−43807
magnet power supply, current-regulated, for mag. reson. and susceptibility meas. 77−22587
magnetic fluids, particle cluster configuration, Monte Carlo study 80−88827
magnetic susceptibility behaviour *(Russian)* 77−80912
magnetisation distribution in magnetostatic oscillations 78−68293
magnetite, low stress effects on susceptibility and coercive force 78−16001
magnetometer, supercond. oscillating sample, for water solns. water suscept. meas. 77−49753
manganese acetate, crit. slowing down, 180-350 MHz 77−16083
manganese acetate tetrahydrate, crit. relax. studied by HF mag. susceptibility 78−39299
manganese acetate tetrahydrate, paramag. susceptibility, spin trimer model 80−97055
manganese acetate tetrahydrate, susceptibility and magnetis. meas., crit. exponents and crossover behaviour 77−66309
manganese carboxylate, dodecanuclear mixed-valence, prep., struct., and mag. props. 80−107196
manganese formate dihydrate, Zn- and Mg-substituted, anomalous crit. phenomena 80−60316
manganese stearate, mag. two-dimensional system, mag. susceptibility 78−10669
manganese zinc formate dihydrate, two-dimens. antiferromag., anomalous crit. phenomena, neutron scatt. and PMR obs. 80−50104
many-electron system, antiparallel spin correls. 77−4307
many-fermion system, wave-number-depend. susceptibility, low temp. and long wavelength, anal. struct. 77−40016
marble, mag. susceptibility anisotropy development through cryst. preferred orientation of calcite 78−56286
marine sediments, mag. stratigraphy using susceptibility meas. 79−84520
MBBA, nematic, mag. susceptibility and order parameters 79−86709
MBBA, refractive index, dielec. const., mag. susceptibility, orientational ordering *(Dutch)* 80−33884
measurement, AC mutual inductance bridge using operational amplifiers 78−89508
measurement, appl. of microcomputer-aided data-processor *(Japanese)* 79−63283
measurement by NMR gaussmeter 79−2797
measurement by Thorpe-Senftle method, correction for ferromag. impurities 77−59378
measurement system, for student laboratory 80−4491
measurement using low-temp. mag. balance *(Russian)* 79−75556
measurement using multiple purpose 7T NbTi split coil supercond. mag. system 79−71486
Merck nematic phases, ZLI 1052 and ZLI 389, mag. susceptibility anisotropy and order parameter 79−86704
mesophase pitch, magnetically-oriented, phys. props., mol. struct. 80−64885
metal, effects of impurities and temp. *(Russian)* 78−84429
metal, electron-phonon interaction, magnetism influence 77−73040
metal, ferromagnetic, longitudinal spin susceptibility 79−61078
metal, indirect coupling between localised mag. moments by narrow band electrons 80−70942
metal, orbital magnetic and spin paramag. susceptibilities, effect of strain 77−16137
metal, paramagnetic, logarithmic terms of susceptibility 78−80126
metal, Pauli susceptibility enhancement for strong electron correl., Gutzwiller theory 77−43527
metal, quasimagnetic impurity, exact solution of Wolff's model 78−56105
metal borides, $MM_4'B_4$ (M=Y,R; M′=Os,Ir), mag. meas., Curie Weiss behaviour 80−20375
metal film, electronic density of states, sp. ht. and spin susceptibility 77−15730
metal surface, spin susceptibility, density-functional approach 77−90011
metal-insulator transition, density-functional theory 80−75507
metallic glasses, electronic structure, neutron scatt., elec. resist., Hall coeff., mag. susceptibility and XPS 78−23013
metallic glasses, prep., characterization, review struct., formation, electronic, mag. and mechanical props., review 78−3074
metallic particles, small, effect of spin-orbit interaction on spin susceptibility 77−59433
metallic substances, retention and exchange of 4f electrons *(Dutch)* 79−1587
metallomacrocytes, mixed valent, cofacial assembly, cond. polymeric material 80−70143
metals, diamag. susceptibility, determ. from average internal pot. 77−28367
metals, electric properties calc., book 79−28274
metals, exchange-correlation enhanced spin-susceptibilities calc. 77−85415
metals, HCP struct., anisotropy of paramagnetostriction 77−32231
metals, monovalent, magnetic susceptibility, impurities effect, free electron gas model 79−91206
metals, optical data determ. of individual contributions 77−12088
metals, with mag. impurities, kinetic exchange interaction, Curie-Weiss high temp. susceptibility 79−33457
metals and alloys, amorphous, exhibiting Mossbauer spectra, mean magnetic props. *(French)* 80−80489
magnetic susceptibility continued
meteorites, evidence for primordial mag. field in parent body era 78−45293
Metglas 2826-A, anomalous magnetisation, critical effects, superparamagnetism 77−8328
$MgAl_{2-x}Fe_xO_4$ solid solution system, solid state properties study 80−93094
microcanonical high-temp. expansion 78−2638
micromagnetic susceptometer with variable temp. 4.2K to 300K for small sample meas. 80−73395
mixed valence compounds, dynamic susceptibility, RPA study of Anderson lattice 80−97075
mixed valence compounds, mag. susceptibility calcs. Falicov-Kimball model 79−42745
mixed valence compounds, periodic Anderson model self-consistent treatment, specific heat, susceptibility 79−99514
mixed valence cpds., mag susceptibility and sp. ht., periodic Anderson model, CPA alloy analogue method 80−15474
mixed valence state, electronic structure, spin-orbit interaction effects, mag. susceptibility 80−54657
mixed-valence systems, mag. behaviour, model calc. 77−80901
mixture of two antiferromag. with different easy axis, mag. props. 79−4660
molecules, rigid-body, librating mag. susceptibility 80−25076
Mott insulator susceptibility 79−78302
moving magnet-stationary sample susceptibility balance 78−70169
Nambu-Goldstone modes, effect on longit. correl. functions 77−16018
narrow band gap semiconductor, ferroelec. transition, quantising mag. field effect 79−87403
nearly ferromagnetic Fermi systems, spin-conserving approx. spin susceptibility 78−47982
nearly ferromagnetic Fermi systems, temp. depend. of spin susceptibility 79−8008
negative ion, singly-charged, Thomas-Fermi-Amaldi eqn., approx. variational soln. 80−52870
nematic liquid crystal, diamagnetic susceptibility, refractive index, density and polarisability 77−15315
nematic liquid crystal, magnetic susceptibility temp. depend. *(Russian)* 79−51737
nematic liquid crystals, temp. depend. of mag. susceptibility 80−25103
neodymium ethyl sulphate, cryst. c-axis demag. from 25000G, magneto-hydrodynamic props. to 0.01K 77−20599
neodymium ethyl sulphate enneahydrate, 2-27K, appl. as mag. thermometer 79−63224
neptunium cyclopentadienyl compounds, $(C_5H_5)_3NpX$, (X=F, Cl, Br, I, $(SO_4)_{1/2}$), mag. susceptibility 80−11152
neutron matter, energy per particle, effective mass and mag. susceptibility relations 79−75885
neutron matter mag. susceptibility, lowest-order constrained variationsl calc. 79−75884
neutron scattering, polarisation depend. 79−47255
New Brunswick rocks, density and magnetic susceptibility meas. 77−44968
Ni-Pt-P, metallic glass, electronic structure, pulsed NMR study 80−75869
niobates, mixed metal, Eu oxidation state, mag. props., Mossbauer study 80−66080
NMP-TCNQ, magnetic susceptibility and chem. pot. of two-site Hubbard Hamiltonian 77−47963
noble metals, monovalent, magnetic susceptibility, impurities effect, Fermi surface effects 79−91207
non-stoichiometric phase, physico-chemical props. 80−29532
nonlinear, tensorial props. 77−24661
nonmagnetic metal, s-d exchange model exact solution, mag. susceptibility, mag. impurity interactions *(Russian)* 80−70943
nonoptically active media, susceptibilities, elec. and mag. polarisation fluctuation 77−77140
4-octyloxy-4′-heptyl-α-cyanstilbene liquid cryst., mag. props. 78−87615
one dimensional randomly dilute Ising ferromagnet, dynamics 80−70922
one-dimensional charge transfer conductors, press. effects on mag. props., review 78−6505
one-dimensional disordered spin system with isotropic antiferromag. interaction, susceptibility and Knight shift *(Russian)* 78−88202
one-dimensional disordered systems, magnetism 80−25152
one-dimensional electron system, generalised susceptibilities in mag. field, fluctuations *(Russian)* 77−80750
one-dimensional Fermi system, mag. susceptibility, and dielec. function of two-dimensional Coulomb gas 78−10387
one-dimensional fermion system, dynamic mag. susceptibility calc., bound magnon states 78−6290
one-spin ferromagnet, high temp. series expansion for mag. susceptibility and sp. ht. 80−25148
orbital, effect of cond. electron motion two-dimen. in cryst., math. anal. *(Russian)* 77−51889
orbital magnetic susceptibility, effects of impurities 77−47962
orbitally-degenerate interacting impurity thermodynamics, stress field depend. due to point defects, dislocations 79−69477
organic conductors, quasi one-dimensional, low temp. mag. susceptibility 80−93069
organic liquids, diamagnetism, mass mag. suscept. meas., temp. depend. 80−97054
oxide, polycryst., dynamic susceptibility of bulging domain wall model 78−23296
oxides with perovskite struct., neutron diffr., ferri- and ferromag. props. 78−52214
oxovanadium carboxylates, near one-dimensional antiferromagnetism, thermal and mag. props. calc. 77−20602
oxyhaemoglobin, mag. props. and structure 78−48751
oxyhaemoglobin, mag. susceptibility of frozen aq. soln., 25 to 250K 78−6507
oxyhemocyanin, mag. susceptibility 79−92125
PAA, refractive index, dielec. const., mag. susceptibility, orientational ordering *(Dutch)* 80−33884
paraffins, solid, binary mixtures of long chain mol. systems, diamag. susceptibility 77−32154
paramagnet with noninteracting mag. moments, magnetisation *(Russian)* 78−47938
paramagnetic exchange enhanced alloy, double d-band model 77−66238
paramagnetic matrix with ferromagnetic inclusions, determ. 79−97407
paramagnetic metals, temp. depend. of susceptibility, microscopic Fermi liq. theory 77−28364

magnetic susceptibility continued
paramagnetic susceptibility of axial cryst. systems 79−42730
paramagnetic vapours and condensing materials, apparatus for susceptibility meas., 300-1600K *(Russian)* 79−93178
paramagnetism, closed-shell many-electron systems 77−20539
paramagnets, itinerant electron, spin wave like modes 77−63067
paramagnon theories, three dimensional renormalisable 77−69577
paramagnons and magnons in quantum Heisenberg model 79−82739
particulate materials, meas. by levitation in paramag. solns. 77−10070
Permalloy film, mag. susceptibility meas. anal. *(German)* 77−16133
phase diagram near Lifshitz point, uniaxial magnetisation 77−80935
phase transition in X-Y and Heisenberg models, Ising free energy and susceptibility 78−43595
phenyl alkyl ammonium copper chloride, quasi-two-dimens. Heisenberg ferromag., mag. props. 77−66273
phenyl benzoate and thiobenzoate, 4,4′-disubstituted, mag. susceptibility anisotropy and order parameter 79−86704
p-phenylenebis(galvinoxyl)biradical, molar mag. susceptibility, 4-300K 78−47939
pion condensate props. in mag. field, superconductivity, mixed state *(Russian)* 80−49974
planar model, two-dimensional, crit. props. 78−10702
plane rotor model, static and dynamic crit. behaviour, Monte Carlo simulation 79−38334
poly-γ-benzyl-L-glutamate, lyotropic liq. cryst., trifluoroacetic acid effect on viscoelasticity, susceptibility 77−84644
poly-γ-benzyl-L-glutamate-dioxane liq. cryst., orientational order temp. depend., diamag. susceptibility 77−47966
polyacetylene:AsF_5, mag. susceptibility, Fermi surface density of states, semicond.-metal transition 79−95566
polyacetylene:AsF_5, soliton doping mechanism, mag. susceptibility meas. 80−107979
polyethylene mag. susceptibility, constant mag. field effect 80−11154
polymer, suscept. and neutron scatt. function 77−12099
polyparaphenylene:SbF_5, pure and doped, metallic, absence of Pauli paramagnetism, mag. susceptibility meas. and ESR obs. 80−97060
polyribonucleotide complexes, mag. field orientation of nematic liq. cryst. solns., light scatt. and birefr. meas. 79−82152
polysulphur nitride:Br mag. susceptibility, linear temp. depend. 80−25114
potassium chloranil, IR spectra, mag. and optical props., phase transition and solvation 77−43983
Potts model, four state, series studies 79−85088
Potts model, Monte Carlo simulation in three dimens. 80−163
Potts model, three-component, phase transitions *(Russian)* 77−89971
Potts s-state model on Cayley tree Bethe-Peierls critical coupling 80−103844
1,3-propanediammonium tetrachloromanganate(II) mag. props. 4.2-220K 77−20567
pseudo one-dimensional kinetic Ising model, dynamic susceptibility 80−50025
pulsed magnetic fields, measurement using Cu-Be search coils 79−63281
PVC magnetoelectrets, mag. susceptibility 80−2687
pyridenes ^{15}N NMR chem. shifts, paramag. relax. reagent effect 78−15042
pyrocarbon, diamagnetic susceptibility increase, mag. field intensity depend. *(Russian)* 79−82752
quantum oscillations, low temp., mag. instabilities in electron liq., electron liquid *(Russian)* 78−87928
quasi-one dimensional organic systems, ESR 78−52358
quinolinium manganese (II) chloride monohydrate, crystal struct. and mag. susceptibility 79−19239
p-quinquephenyl, nematic, mag. susceptibility and order parameters 79−86709
random annealed one-dimensional Ising spin system, site model, specific heat, susceptibility 77−32139
random binary Ising system with transverse field, Curie temp., paramagnetic susceptibility 80−65938
random exchange Heisenberg antiferromagnetic chain, exchange-coupled pair model 80−20423
random Hubbard alloys, paramag. susceptibility singularities, derived from Fermi liquid approach 78−43547
random Ising bond interactions, paramag. phase, thermodynamic props. 77−20523
random Ising ferromagnet, upper bounds 80−34663
random Ising model with transverse field term 79−56545
random magnet, Ginzburg-Landau model 78−10704
random magnet, LF response function 78−6493
random mixture of classical spins on infinite Cayley tree, susceptibility 77−89917
random mixture of ferro- and antiferromag. exchange interactions, high temp. expansion 78−23280
random spherical model, crit. dynamics 80−44844
random uniaxial systems with dipolar interactions, crit. dynamics 77−73034
rare earth$_{50}$Ag$_{50}$, amorphous, bulk mag. props., field, time and temp. depends. 77−89932
rare earth alloys, cryst. field effects on thermal props. 77−12072
rare earth alloys, R_2Pt (R=Gd, Tb, Dy, Ho, Er), magnetic susceptibility meas., mag. transition obs. 80−60222
rare earth alloys, R_3Pt_4, R=Nd, Gd, Tb, Dy, Ho, Er, Tm, mag. props., 4.2 to 160K 79−78343
rare earth alloys, $R_{69}Ni_{31}$, amorphous, Curie temp., mag. susceptibility and coercive force, 4.2 to 300K 80−93092
rare earth alloys, $R(Fe_xRh_{1-x})_2$, mag. props., Mossbauer spectra 80−25108
rare earth alloys, $RAuNi_4$, (R=Gd, Tb, Dy, Ho, Tm, Yb and Er), mag. props. 77−20595
rare earth alloys, RBe_{13}, XPS, resist. and susceptibility study 80−71565
rare earth alloys, RCu_x, mag. props., 4.2 to 200K 79−87233
rare earth alloys, RFe_4Al_8, cryst. struct. mag. props. and hyperfine interactions 78−87648
rare earth alloys, RFe_4Al_8, mag. props., Mossbauer spectra, ordering effects 77−63179
rare earth alloys, RZn_{12} and RCu_4Al_8, mag. struct. and interactions 80−25092
rare earth amorphous alloys, antiferromagnetism, mol. field approx. 78−80142
rare earth binary insulating compounds, exchange interactions, paramag. susceptibility expts. 80−60177
rare earth complexes, formation and props., book contrib. 80−43204
magnetic susceptibility continued
rare earth compound, $R_{1-x}Mo_6S_8$, magnetically ordering, supercond. props. 79−56373
rare earth compounds, mag. moment and valence fluctuations 78−23244
rare earth compounds, mag. susceptibility in intermediate valence state 78−14928
rare earth compounds, pseudospin model of valency transition 77−72819
rare earth compounds, R_2MoO_5, cryst. struct., IR spectra, elec. and mag. props. 80−33954
rare earth compounds, R_2MoO_5, preparation, exam. of higher oxygen pressure limit, mag. susceptibility *(French)* 78−76618
rare earth compounds, $R_2V_2O_7$, (R=Tm, Yb, Lu), physical props. 78−39320
rare earth compounds, $R_xMo_6S_8$ mag. susceptibility meas., 1.3-300K 78−14936
rare earth dodecaborides, mag. susceptibility temp. depend., 90-1200K 80−20374
rare earth dodecaborides, nature of magnetism *(Russian)* 78−31049
rare earth double nitrate, Van Vleck temp. independent suscept. 78−43555
rare earth ethyl sulphates, sp. ht., susceptibility 79−24129
rare earth heavy binary alloys, press. effect on mag. props. *(Japanese)* 77−43835
rare earth intermetallic, RCu_4Ag, mag. props. and cryst. struct. 77−20562
rare earth intermetallic cpds., mag. props., book contrib. 80−39759
rare earth intermetallics, cubic, third-order mag. susceptibility, quadrupolar effects 79−99674
rare earth intermetallics, R_2Al and R_2Au, mag. characts. 78−68183
rare earth intermetallics, RAl_2-Gd(Er)(Dy)(Nd), dil., (R=La, Yb, Lu), EPR and mag. susceptibility 80−15797
rare earth intermetallics, RGa_2, mag susceptibility, 1.5-300K and Neel temp. 78−68184
rare earth intermetallics, RGa_2, ordering and exchange interactions 80−39779
rare earth intermetallics, RM_{12}, mag. interactions, mag. meas. and neutron diffr. 77−63103
rare earth intermetallics, RMg_2, cryst. and mag. props., ordering 78−68185
rare earth intermetallics, $RNiSi_3$, 80-1200K *(Russian)* 77−66281
rare earth intermetallics, RPt, (R=Gd, Tb, Dy, Ho, Er, Tm), structs. and mag. props. 80−50069
rare earth iron silicides, $R_2Fe_4Si_9$ and $RFeSi_3$, cryst. struct. and mag. suscept., temp. depend. *(Russian)* 78−34957
rare earth metals, heavy, liq., mag. susceptibility meas. 80−75740
rare earth metals, mag. and transport props. 79−69658
rare earth metals and alloys, ferromag. props., book contrib. 80−75725
rare earth metasilicates, $R_2(SiO_3)_3$, mag. susceptibility, temp. depend., 77-800K 80−20372
rare earth molybdates, mag. susceptibility meas. 79−69650
rare earth molybdenum selenides, $R_xMo_6Se_8$, coexistence of superconductivity and long-range magnetic order 79−11264
rare earth molybdenum selenides, supercond., mag. props., 0.7 to 295K 77−32113
rare earth niobates, pyrochlore structure, synthesis and props., 79−11533
rare earth niobates, R_3NbO_7, 77-300K 79−87226
rare earth orthochromites, mag. interactions and weak ferromagnetism 78−52220
rare earth orthocobaltites, $R_{1-x}Sr_xCoO_3$ and $La_{1-x}M_xCoO_3$, itinerant electron ferromagnetism obs. 78−10660
rare earth orthotitanates, $RTiO_3$, metallic and semicond. elec. and mag. props. 79−38068
rare earth orthovanadites, phase transitions and Jahn-Teller distortions 79−28548
rare earth oxides, binary, struct. and props., book contrib. 80−45292
rare earth oxyfluorides, mag. susceptibility, 2-1000K *(Russian)* 79−82750
rare earth palladinides, R_3Pd_4, mag. props. 77−47980
rare earth selenides of yttrium subgroup, paramag. props. *(Ukrainian)* 77−32153
rare earth sesquioxides, 300 to 900K, mag. susceptibility and Curie temp. meas. 78−56288
rare earth sesquioxides, exchange interactions, paramag. susceptibility expts. 80−60177
rare earth silicides, RFe_2Si_2, mag. props. 4.2 to 950K 77−20544
rare earth spin glass alloys, low field susceptibilities 78−84446
rare earth strontium vanadates, $R_{1-x}Sr_xVO_{3-0.1x}$, elec. cond. and mag. susceptibility, temp. depend., 77-300K 77−47816
rare earth systems, Anderson model susceptibility for high mag. impurity conc. 77−63069
rare earth systems, metallic, with unstable valence, model for thermodynamic props. 77−69487
rare earth tetraborides, mag. and elec. props., metallic character 80−20386
rare earth titanium oxides, $RTiO_3$ type, bulk mag. and struct. props., ferrimag. order 80−107993
rare earth titanotantalates, temp. depend., 78-293K 77−36050
rare earth tungstates, mag. susceptibility determ. 77−4495
rare earth vanadites, mag. ordering, susceptibility meas., 60-300K 77−32190
rare earth Y alloys, Neel temps., mag. susceptibility meas. 77−73025
rare earth-copper intermetallic cpds., RCu_2, metamag., mag. props. 79−87242
rare earth-copper intermetallic cpds., RCu_2, metamag., mag. props. 79−87243
rare earth-Cu intermetallic compds. single crysts., mag. props. 80−54892
rare earth-Fe-Al alloys, RFe_4Al_8, mag. props. 78−52250
rare earth-iron, RFe_2, Laves phase intermetallics, ordered and paramagnetic phases, mean field exchange consts. 80−50084
rare earth-Pt, RPt_5, low temp. mag. susceptibility 80−93075
rare earth-transition metal alloys, amorphous, electronic and mag. props. 80−93093
rare earth-transition metal alloys, $RM_2Si_{2-x}Ge_x$ and $RM_{4+x}Al_{8-x}$, magnetism and hyperfine interactions, magnetisation and Mossbauer effect studies 80−75892
rare earth-transition metal intermetallics, struct. and props. review 78−10668
rare earth-Zn_{12}, mag. props. and structs. 78−84393
rare-earth alloy, RSb, (R=Er, Ho, Dy, Tb, Nd, Gd), mag. props., hydrostatic press. depend. 77−80918

magnetic susceptibility continued
rare-earth compounds, antiferromag., mag. props., cryst. field theory 78−27006
rare-earth compounds, antiferromag., mag. props., cryst. field theory 78−27007
rare-earth-Cu double oxides, catalytic props., mag. props., elec. conductivity 79−66350
rare-earth-Pd alloy, mag. props. 77−20547
rats, living, meas. meters 80−72391
retinal rod external segment mag. anisotropy decrease after total photolysis 77−52838
review of literature 1975-1977, instrumentation, chem. anal. applications, and bioscience 78−82006
rhombic distortion of cryst. lattice at low temp. 78−2253
rock strain from mag. susceptibility anisotropy 77−78170
rocks, susceptibility anisotropy meas. using inductive magnetometers 78−85541
rocks, uniaxial stress effect on reversal of initial susceptibility, single-domain theory 77−9401
rotating coordinate system with quadrupole splitting, paramag. susceptibility 80−11178
ruby:Cr^{3+}, ESR saturation, dynamical mag. susceptibility increase in zero mag. field 77−40122
ruthenates, $ACu_3Ru_4O_{12}$, A=Na,Ca,Sr,Cd,La,Pr,Nd, synthesis, cryst. struct., mag. and elec. props. *(French)* 80−107151
S=1, singlet ground state systems, mag. props. 80−11157
S=1 generalised Ising model, stability conditions 80−20427
s-d model, double exchange interaction, susceptibility *(Russian)* 78−56283
Schiff's bases, nematic phys. props. 79−99057
semiconductor, amorphous, diamagnetic susceptibility enhancement 79−65640
semiconductor, diamagnetic susceptibility of excitonic molecules *(Russian)* 80−7074
semiconductor, diamagnetism rel. to chem. bonds 77−59380
semiconductor, disordered, with soft Coulombic aperture, screening and absorpt. of long EM waves *(Russian)* 78−23001
semiconductor, ferromagnetic, longitudinal response function 77−72831
semiconductor, magnetic susceptibility of hot electrons 78−10648
semiconductor, narrow band gap, ferromagnetism of electrons in filled band *(Russian)* 79−78300
semiconductor, tetrahedrally coordinated, temp. depend. of diamagnetic susceptibility *(Rumanian)* 80−88717
semiconductor and semimetal powders, EPR, effect of mag. field depend. of elec. parameters 79−99749
semiconductor in quantizing mag. field, plasma surface states of electrons, paramag. susceptibility 79−11195
semiconductors, diamond-type, magnetic susceptibility of light and heavy holes 79−42734
semiconductors, magnetic, static magnetic properties, mean field approach 80−7090
simple metals, solid and liq., electronic struct., mag. susceptibilities calc. 78−52204
single-ion anisotropy, magnetic systems, high temp. series expansion 80−34576
singlet ground state system in mag. field, anisotropic exchange interaction effect on props. 79−91224
singlet-triplet system in paramag. phase, low-freq. response 80−60172
site Ising model, spin glass phase, transition temps. 79−95592
soils from archaeological sites, Mossbauer and mag. susceptibility studies of Fe oxides 77−30224
speromagnetism phase transition, random distrib. mol. field model 79−73730
spin, in two-dimens. cryst., math. anal. *(Russian)* 77−51889
spin 1/2 Kondo system, static susceptibility and relax. rate 79−65646
spin 1/2 Kondo system, thermodynamical props. 78−52209
spin glass, classical, low temp. behaviour of three-dimens. planar model 79−73725
spin glass, cluster mean field theory 77−80949
spin glass, cluster mean field theory and evidence for spin clusters 79−78382
spin glass, cluster mean-field model, static props. 79−4689
spin glass, crit. props., simple soluble model 77−12141
spin glass, dil., conc. expansions at zero temp., Ising model 80−60303
spin glass, effective field distrib., time dependent order parameters 77−43843
spin glass, EPR frequency and mag. transverse susceptibility with remanent magnetisation *(French)* 80−7145
spin glass, FCC lattice with RKKY interaction, numerical calc. 78−52275
spin glass, generalised mean field theory with spin correls. 78−2691
spin glass, Heisenberg mode, RPA approx. 80−65904
spin glass, high-temperature series for order-parameter susceptibility 79−28534
spin glass, infinite range model, stability and susceptibility in Parisi's soln. 80−88762
spin glass, infinite-ranged model, mean field theory hypothesis 80−97104
spin glass, Ising, cryst. field effects 77−85460
spin glass, Ising, two-dimensional, Monte Carlo evidence for absence of phase transition 78−19260
spin glass, molecular field approx. *(Russian)* 77−80940
spin glass, nonmagnetic defects, sp. ht., susceptibility and resist. determ. 79−19738
spin glass, one dimens. ideal, dynamical susceptibility and relax. behaviour 80−65950
spin glass, order-parameter susceptibility, series expansion 77−43839
spin glass, phenomenological theory 78−19263
spin glass, relaxation times, influence of spectral distrib. on freq. depend. of freezing temp. 80−44848
spin glass, remanent magnetisation using Monte Carlo methods 79−78421
spin glass, RKKY, low temp. susceptibility, spin-depend. curvature, Ising model MRF approx. 77−66366
spin glass, rock magnetism type behaviour 77−66361
spin glass, scaling at crit. temp. 78−10714
spin glass, self-consistent mean random field approximation, comparison with $n\to 0$ expansion 77−20622
spin glass, self-consistent theory of cusps in susceptibility 77−77066
spin glass, Sherrington-Kirkpatrick model, finite system, low temp., susceptibility, entropy 78−34993
magnetic susceptibility continued
spin glass, thermodynamics, virial expansion vs. T^{-1} expansion 77−66362
spin glass film, quench-condensed, apparatus for measurement of initial paramagnetic susceptibility 79−54160
spin glass with non-random interactions, three-dimensional X-Y model 77−55673
spin glass with nonmagnetic defects *(Russian)* 78−60298
spin glass with short range interaction in neighbourhood of percolation threshold *(Russian)* 78−68282
spin glass-ferromagnetic systems, differential susceptibility 78−88131
spin glasses, 2-dimens., computer expts. 77−80945
spin glasses, dynamical susceptiblity calc. 77−85477
spin glasses, fluctuation theory, mag. susceptibility and sp. ht. 79−24176
spin glasses, free energy, order parameter expansion, random bond model 80−84609
spin glasses, mag., transport props. *(Czech)* 78−80149
spin glasses, magnetic susceptibility, temp. depend. 79−61125
spin glasses, monoionic anisotropy, influence on transform. to paramag. state *(Russian)* 79−28529
spin glasses, phase transition, mag. susceptibility, specific heat, Ising model calcs. *(Russian)* 80−34671
spin glasses, recent progress in numerical simulation 79−69689
spin glasses, review 77−69578
spin glasses, sp. ht. and susceptibility, random series method 80−44542
spin glasses, susceptibility, time dependent, rel. to spin self-correlation, Monte Carlo model simulations 79−47290
spin glasses, susceptibility, wave-vector-depend., theory 80−11209
spin glasses, thermodynamic props., cluster mean-field theory using Ising Hamiltonian 79−33499
spin glasses, zero-field susceptibility 77−48005
spin glasses dipolar anisotropy and crit. behaviour in small AC fields 77−32199
spin glasses with short-range interaction in mag. field 79−28539
spin Hamiltonian, constant-coupling, higher-order, statics and dynamics 80−60262
spin model, random mag. bonds, phys. props. near crit. point 78−84440
spin susceptibility of a many electron system 77−69465
spin system, random thermodynamic props. using Bethe-Peierls-Weiss approx. 79−78387
spin systems, coupled itinerant localised systems, dynamic magnetic response 80−34583
spin systems, longit. paramag. suscept. inhomog. broadening conditions 78−88169
spin systems, random annealed, crit. amplitudes for susceptibility 78−43600
spin systems, randomly competing, random ordered phase, frustration, phenomenological theory 80−60349
spin wave theory of spin 1/2 X-Y model, phase transition, susceptibility 80−7068
spin-glass, one-dimens., sp. ht. and mag. susceptibility calcs. 80−7120
spin-glass, two-dimensional Ising model, low temp. dynamic props. 80−20425
spin-phonon system, transition to self-trapping 80−10606
spin-S XY-model, susceptibility series expansions 79−28540
spin-state transitions in solids, two-phonon model 79−56170
spinels, domain wall formation inhibition, effect on bulk mag. props. 80−11220
SQUID magnetometer with temp. control, spontaneous magnetisation and mag. susceptibility meas. 80−68221
SQUID system, automatic, magnetisation meas. appl. 78−57153
static properties of spin systems with truncated secular dipolar coupling 78−88130
steel, austenitic stainless, magnetic susceptibility and magnetisation, low temp. 80−25102
steel, austenitic stainless, Mn alloy, sound vel. anomalies near spin glass transition 79−82795
steel, austenitic stainless, Neel temperature and max. susceptibility calcs. 77−43833
steel, austenitic stainless type 304N, machining induced deformation transformation, mag. evaluation 79−83195
steel, Fe-Ni-Cr mag. susceptibility and magnetoresistance, temp. depend. *(Ukrainian)* 77−73004
steel, induced anisotropy influence on mag. props., thermomagnetic working *(Russian)* 80−55549
steel, stainless, VNS-2USh, α to and from γ transformation investigation by thermomagnetic structural anal. *(Russian)* 79−83197
steel, VKS-210, α to and from γ transformation investigation by thermomagnetic structural anal. *(Russian)* 79−83197
steels Kh18N(10-25), mag. susceptibility, 4.2 to 300K, and magnetoelasticity *(Russian)* 80−65812
step model, critical behaviour, high temp. susceptibility and internal energy series 78−34987
Stoner glass, disordered itinerant-electron system, spin-glass condensation 79−78424
subdominant critical indices for the ferromagnetic susceptibility of the spin-1/2 Ising model 80−100574
substitutional alloys of intermediate valence systems, static mag. susceptibility con. and temp. depend. 80−84586
superconducting composites, granular, Ginzburg-Landau theory, props. 80−88673
superconducting crystals without symm. centres, paramag. susceptibility 77−15994
superconducting magnet system, 7 T NbTi split-coil, for measurements in 2 to 300K range 79−58746
superconducting small metal particles ground state energy and orbital mag. susceptibility 80−49983
superconducting susceptometer, automatic, sensitivity calibration, biological appl. 78−57154
superconductor, magnetic, Fermi surface nesting effect on mag. instability 80−54831
superconductor, magnetic, spin fluctuation and US attenuation 80−80445
superconductor, magnetic, spin-spiral ordering 80−2517
superconductor, thermodynamics of magnetism and supercond., mol. field theory 80−34668
superconductors, magnetic ordering, susceptibility calc. 79−99656
superconductors, spin susceptibility of conductivity electrons, spatial dispersion *(Russian)* 79−51719
susceptibilities of S=1/2 XY model on the square lattice at T=0 80−88732

magnetic susceptibility continued
susceptometer, high sensitivity, based on SQUID magnetometer 78−49872
susceptometer for biomedical meas., Fe stored in human tissue, in vivo 80−101245
tantalates, mixed metal, Eu oxidation state, mag. props., Mossbauer study 80−66080
$(TCNQ)_5^{4-}(DEPA)_2^{4+}$, cryst. struct., elec. and mag. props. 77−72605
$(TCNQ)(TTF)_{1-x}$-$(TSeF)_x$, quasi 1-D metal, mag. susceptibility, temp. depend. 77−8267
TCNQ alkali salt, spin-Peierls transition 80−29395
TCNQ complexes, disordered, thermodynamics of random exchange models 80−103826
TCNQ complexes, $Qn(TCNQ)_2$, NMePh.TCNQ, and Li^+TCNQ^-, extrinsic and intrinsic mag. susceptibility 78−43556
TCNQ complexes with dipyranylidene and dithiadipyranylidene, high cond. investigs. and related props. 78−6368
TCNQ complexes with ferrocenes, charge transfer type, struct. and mag. props. 80−24439
TCNQ salt, 1,1′-diethyl-2,2′-cyanine-$[TCNQ]_2$, electric and mag. props. 79−42523
TCNQ salt, $(DEPE)^{2+}(TCNQ)_4^{2}$, elec. and mag. props. of two crystallographic form 77−28166
TCNQ salt, (N-methylphenazinium)$_x$(phenazine)$_{1-x}$, 1 band filling, carrier mogility and disorder effects 80−24904
TCNQ salt, $(NMP)_{0.5}$(phenazine)$_{0.5}$ TCNQ, transport props. 80−24891
TCNQ salt, $(TMA^+)_3(I_3^-)(TCNQ^-)_2(TCNQ^0)$, struct., phys. props. and lattice distortion evidence 78−6305
TCNQ salt, $(TSeF)_x(TTF)_{1-x}$-TCNQ, struct., elec. and mag. props., review 80−20158
TCNQ salt, DECA $(TCNQ)_2$, struct., phys. props. and irreversible phase transition 78−6273
TCNQ salt, dibenzo-TTF-$TCNQCl_2$, one-dimens. mag. semicond., mag. and elec. props. 80−88601
TCNQ salt, HMTTF-TCNQ, electron-electron interactions, mag. susceptibility and optical reflectivity 77−81104
TCNQ salt, HMTTF-TCNQ, quasi-one-dimensional organic conductor, mag. susceptibility meas. 78−6508
TCNQ salt, K-TCNQ, spin-Peierls system, paramag. susceptibility, Heisenberg chains 79−38299
TCNQ salt, MeDABCO$(TCNQ)_2$, optical, elec., and mag. props. 80−65539
TCNQ salt, MEM$(TCNQ)_2$, dielec. const. obs., DC and microwave cond. obs. 80−59963
TCNQ salt, MEM$(TCNQ)_2$, phase transition electronic struct. interpretation 80−24781
TCNQ salt, MEM$(TCNQ)_2$, phase transitions, elec. cond., ESR, mag. susceptibility study 80−24981
TCNQ salt, $Mn(TCNQ)_2$, mag. props. 77−85558
TCNQ salt, N-methyl-N-ethyl-morpholinium-$(TCNQ)_2$, spin-Peierls transition 79−82803
TCNQ salt, N-propyl-quinolinium$(TCNQ)_2$, defect conc. depend. phase transition 80−44577
TCNQ salt, $NMP_{0.63}$phenazine$_{0.37}$TCNQ, mag. susceptibility, 0.03-4.2K 80−25191
TCNQ salt, NPQn $(TCNQ)_2$, neutron irrad. induced defect concentration depend. phase transition 80−29449
TCNQ salt, pyridine $(TCNQ)_2$, phase transition at 80K investig. and interpret. 78−6530
TCNQ salt, pyridinium $(TCNQ)_2$, low temp. mag. phase transition, ESR study 80−25139
TCNQ salt, quinolinium, electron spin location, elec., mag., and thermal props. 80−25189
TCNQ salt, quinolinium $(TCNQ)_2$, mag. chain double resonance study, deuteration 80−25250
TCNQ salt, quinolinium $(TCNQ)_2$, transport props. 80−24891
TCNQ salt, tetramethylhexamethylenediammonium-TCNQ-iodine, elec. and mag. props., struct., specific heat 80−24898
TCNQ salt, TMTSF-DMTCNQ, mag. susceptibility meas. under press. 80−29521
TCNQ salt with MDCA cation, first order phase transition 79−73122
TCNQ salts, aminopyridinium $(TCNQ)_2$, elec. and mag. props., 4.2 to 300K 80−24889
TCNQ salts, complex, with symmetric and asymmetric donors, transport and mag. props. 78−6315
TCNQ salts, $Mn(TCNQ)_2$ and hydrates, mag. and elec. props. 79−82767
TCNQ salts, n-methylacridium $(TCNQ)_2$, 2,2′bipyridinium $(TCNQ)_2$ and $Qn(TCNQ)_2$, with asymmetric donors, mag. susceptibility, 0.035-4.2K 80−25190
TCNQ salts, PMR, electron-proton couplings, local susceptibilities 79−82883
TCNQ salts, Rb^+TCNQ^-, and TMB^+TCNQ^-, triplet exciton dipolar splitting tensors rel. to mag. susceptibility 77−62839
TCNQ salts with asymmetric donors 78−60264
TCNQ-ϕ_4DTP, chemisorbed O_2 effects on mag. susceptibility 80−15679
TCNQ-NMP, disordered, paramag. susceptibility 78−10645
TCNQ-NMP, transport props. 80−24891
TCNQ-NMP type crystals, density of states, rel. to low temp. paramag. susceptibility *(Russian)* 77−85127
TCNQ-TSeF, mag. suscept. meas. 78−56287
TCNQ-TTF, chemisorbed O_2 effects on mag. susceptibility 80−15679
terbium ethyl sulphate, mag. and thermal props. 79−7971
ternary chalcopyrite, diamag. susceptibility, bond orbital theories 77−55761
tetraethylammonium neptunium hexachloride, Mossbauer spectra and mag. susceptibility meas. 80−108140
tetramethylammonium copper chloride, S=1/2 Heisenberg 1-dimens. ferromag., mag. props. 79−82766
tetramethylammonium neptunium hexachloride, Mossbauer spectra and mag. susceptibility meas. 80−108140
tetranuclear cluster, eigenvalues spectrum of spin Hamiltonian calc., thermodynamics props. *(French)* 77−35902
tetrathiofulvalene-based salts, isomorphous series systematic investig. of solid-state props. 77−55517
tetrathiotetracenenickel bis(ethylene-1,2-dithiolene), one-dimens. cond., preparation and props. 77−85201
$(TETTF)(TCNQ)_2$, charge transfer complex, phys. props. and phase transition 78−64032
TMBP.HCNB and TMBTP.HCNB complexes, elec. and mag. props. 78−6512
magnetic susceptibility continued
TMMC:Cu(Ni)(Cd), mag. and non-mag. impurity effects on suscept. and Neel temp. 77−66312
TMMC:M, impurity (M) effects on Neel temp. and low temp. mag. susceptibility 78−88113
TMMC, crossover transition, effects on susceptibility and EPR shift 80−71047
TMMC, linear antiferromag., mag. phase diagram, expt. and theoretical study 80−71038
TMNB, ferromag. chains with easy-plane anisotropy, exchange const., anisotropy const. and g-value 77−80927
TMNB, linear S=1 ferromag., easy plane anisotropy, low-temp. mag. props. 78−23250
TMNC, ferromag. chains with easy-plane anisotropy, exchange const., anisotropy const. and g-value 77−80927
TMNC, linear S=1 ferromag., easy plane anisotropy, low-temp. mag. props. 78−23250
$(TMTSF)_2PF_6$, ESR g-factor, linewidth, spin susceptibility, metal-insulator transition 80−103887
$(TMTSF)_2PF_6$, quasi-dimens. cond., diamagnetic AC susceptibility 80−103781
$(TMTSF)_2X$, (X=PF_6^-, AsF_6^-, SbF_6^-, BF_4^-, NO_3^-) highly conducting salts, props. 80−59969
TMTTF salts, $(TMTTF)_2$-X, (X=BF_4^-, ClO_4^-, SCN^-, PF_6^-, Br^-), physical props. 79−47085
transition metal, 3d and 4d, local density theory, mech. and mag. props. evaluation 78−91630
transition metal, band model, mag. susceptibility of exchange-enhanced paramagnet 78−2644
transition metal, FCC, semi-infinite, susceptibilities near (001) surface 80−15701
transition metal, mag. susceptibility, spin wave spectrum for improved itinerant-localised electron model 79−1654
transition metal, magnetic ground state props., simple one-electron theory 77−63063
transition metal, symmetric clusters, susceptibility, Schrodinger exchange model 79−7955
transition metal alloy, electronic structure, mag. props. 78−95254
transition metal alloys, ferromag., high-field susceptibility 80−7083
transition metal alloys, spin glass behaviour, simple itinerant model 78−84436
transition metal alloys, static magnetic suscept. calc. *(Russian)* 77−77036
transition metal binary alloys, importance of diagonal and off-diagonal disorders 77−63085
transition metal borides, cryst. struct., prep. methods, chem., elec., mag. props., appls., book contrib. 78−47307
transition metal carbides, 3d metal, interatomic interaction 79−1569
transition metal chalcogenides, MU_8X_{17}, (X=S or Se), mag. susceptibilities 79−61073
transition metal complex, MX_3.b(hexamethylenetetramine).nH_2O, optical reflection spectra, mag. suscept. 79−56810
transition metal complexes, acetylacetonates, mag. susceptibility and optical reflection spectra 77−59381
transition metal complexes with 1,2,4-triazole, mag. susceptibility, 2-300K, struct., antiferromag. props. 77−77045
transition metal compounds and dil. alloys, mag. ordering phenomena in high mag. fields 80−50075
transition metal diborides, 3d metal, interatomic interaction 79−1569
transition metal diborides, C32-type, phys., chem. props., appls., review, book contrib. 78−47308
transition metal germanium borides, metallic resist. mag. suscept. 79−42731
transition metal glasses and amorphous films, supercond. and electronic props. 79−73612
d-transition metal hydride, mag. suscept. and quasirigid model *(Russian)* 78−26805
transition metal hydrides, magnetic props., book contrib. 79−82754
transition metal hydrides and deuterides, conc.-temp. depend. of mag. susceptibility 80−29523
transition metal intercalates of Ni and Ta dichalcogenides, magnetic susceptibility, function of temp. 80−39756
transition metal magnetic alloys, dilute, props., review of theory 79−15282
transition metal mononitrides, 3d metal, interatomic interaction 79−1569
transition metal oxides, 3d metal, interatomic interaction 79−1569
transition metal sulphides, selenides and phosphides, NaCl struct., supercond. props. 79−4613
transition metal vanadates, elec. and mag. props., stoichiometry 78−51991
transition metal vanadates, elec. and mag. props. 79−78094
transition metal-noble metal spin glass films, mag. props. 80−60306
transition metals, 3d, ferromag. props., book contrib. 80−75724
transition metals, 4d and 5d, susceptibility max. and grand Fermi-liq. effect 77−63082
transition metals, 4d and 5d, susceptibility maximum, Fermi liquid model of magnetism 77−4480
transition metals, BCC, 3d series, numerical calc. of orbital mag. susceptibility 79−82764
transition metals, double d-band model, delocalisation of electrons 77−76743
transition metals, double d-band model, dynamic susceptibilities calc. 77−1535
transition metals, paramagnetic susceptibility, phonon instability, mixed localised-collective electron states 80−103811
transition metals, role of electron correlation 77−72974
transition metals, surface- or defect-induced magnetism, nearly half-filled bands 79−1671
transition metals and alloys, noncrystalline 78−95280
3d-transition-metal dichalcogenides, mag. props. rel. to Hubbard model 79−78373
transverse dynamic susceptibility and spin waves in itinerant electron SPW states 80−97076
transverse dynamical, self consistent many-body theory, appl. to spin waves in itinerant ferromagnets 79−73702
trimethylammonium cobalt trichloride, metamagnet, AC susceptibility and exchange consts. 80−70961
trimethylammonium copper chloride dihydrate, mag. props., evidence for lattice dimensionality 77−89967
trimethylammonium copper heptachloride, one-dimens. ferromag., mag. susceptibility, 2 to 300K 79−61077

magnetic susceptibility continued
trimethylammonium manganese bromide, mag., anisotropy, biquadratic exchange 78−14952
TRM direction, mag. shape anisotropy effect, appl. to basalts 79−29758
$TSeTBr_{0.5}$, phase transition, mag. props., thermal capacity and cond. *(Russian)* 79−99537
αTTF:Br, transport and mag. props., effect of doping 80−24934
TTF(MBDT) spin-Peierls transition, mag. exchange interactions, mag. props. 80−25138
TTF salts, physical props., Fermi energy scaling of metal-insulator transition temp. 77−8081
TTF salts, PMR, electron-proton couplings, local susceptibilities 79−82883
TTF-bis-dithiolene metal complex compounds, donor-acceptor type, one-dimens. mag. variety and props. 77−66271
TTF-bisdithiolene metal complexes, spin Peierls transition 77−4523
TTF-TCNQ, 53 and 38K transitions, mag. and elec. props. meas., doping effect 77−66159
TTF-TCNQ, ^{13}C Knight shift and spin-lattice relax. meas., local susceptibility determ. 77−4571
TTF-TCNQ, CDW instability, classical vs. crit. behaviour 78−39041
TTF-TCNQ, covalon conduction 78−10427
TTF-TCNQ, deuterated, isotope effect on mag. susceptibility 80−25080
TTF-TCNQ, divergent mag. responses at $2k_F$ and structural phase transitions 80−20376
TTF-TCNQ, elec. cond. and spin susceptibility, press. and temp. depend. 80−24894
TTF-TCNQ, electronic energy level shift, mag. susceptibility, anomalous temp. var. 79−4499
TTF-TCNQ, enhancement of mag. susceptibility by Coulomb correlations 77−77023
TTF-TCNQ, implications of amplitude solitons in incommensurate Peierls systems 80−92841
TTF-TCNQ, mag. suscept. meas. 78−56287
TTF-TCNQ, phase transitions and CDW state, controlled disorder effects 80−15507
TTF-TCNQ, phase transitions and CDW state, induced defect depend., transport and mag. studies 80−24980
TTF-TCNQ, pure and irrad. crystal, nonlinear transport at low temp. activated susceptibility 79−4552
TTF-TCNQ, quasi one-dimensional low temp. mag. susceptibility 80−93069
TTF-TCNQ, single cryst., mag. susceptibility in phase transition region, two-gap model 78−6511
TTF-TCNQ and related cpds., magnetic props., press. effects 77−47981
TTF-TCNQ complex, trans-diethyl-dimethyl TTF-TCNQ, one-dimens. cond. 80−96853
TTF-TCNQ low temp. mag. susceptibility, neutron irrad. effects 80−60311
TTF-TCNQ type salt, trimethylene-TTF-TCNQ, unsymmetric cation, phys. props. 78−76059
$TTF.PtS_4C_4(CF_3)_4$, quasi-one-dimensional cpd., exchange, thermal and mag. study 78−68209
$TTT_{1.2}NiS_4C_4H_4$, quasi-one-dimensional cond., cryst., mag. and elec. props. 78−10424
$TTT_2-(I_3)_{1+x}$, physical props., elec., mag. and optical meas. 80−24908
TTT_2I_3, organic metal, mag. susceptibility meas. 78−23241
$(TTT)_2I_3$, metal-insulator phase transition, elec. cond. meas. 78−14719
$TTT-(I_3)_{0.5}$, one-dimens. metal, mag. susceptibility, elec. resist., thermopower meas. 78−87967
two-component spin system in alternating mag. field, dynamical behaviour, susceptibility 79−99715
two-dimensional crystal, mag. susceptibility, math. anal. *(Russian)* 77−51889
two-sublattice biquadratic systems, phase transitions 79−99710
type II magnetism in mixed magnets and spin glasses 78−23281
uniaxial ferromagnet, domain struct. in mag. field 80−103853
V-Fe (29-35 at%), ferromag., mag. props. near crit. conc. for ferromagnetism 78−19225
Van Vleck compounds, LF dynamics, NMR linewidth, RKKY exchange mechanism role 80−103812
Van Vleck susceptibilities, hydrostatic press. shifts, appl. of parametrisation 78−72120
vanadyl carboxylates, EPR and mag. susceptibility, near one-dimens. antiferromagn. 77−63265
VI_2, mag. structs. and props. 79−61063
vibronic ferroelectric semiconductor, mag. susceptibility calc. 80−2711
W-dichalcogenide, valence band nature, elec. and mag. props 78−39014
wall susceptibility of materials having spherical grains with statistical distribution of diameters 78−95454
water, twice distilled, effect of mag. field on rotational IR spectra 79−54849
weakly disordered uniaxial ferromagnet, phase transition *(Russian)* 78−23291
Wolff model, effective mag. interactions between impurity and conduction electrons 78−68143
Wolff model, thermodynamic props., local moments in dil. alloys, var. method 80−65781
X-Y model, rigorously solvable, numerical computations 77−1534
X-Y model, spin 1/2, high temp. longitudinal susceptibility 79−87275
X-Y model, spin Peierls transition in mag. field 79−56537
X-Y model, two-dimens., vortex formation in Monte Carlo calcs. 77−63224
X-Y model, two-dimensional, disordered, finite susceptibility phase 79−61031
X-Y model critical behaviour, high temp. susceptibility and internal energy series 78−34987
X-Y models, classical, confluent-singularity anal. of thermodynamic functions, planar-rotator model on FCC lattice 79−69686
XY model, Monte Carlo simulation, phase transition with vortices 77−43799
ytterbium ethyl sulphate, crystal field effects on mag. and hyperfine props. of Yb^{3+} 80−97101
zero field susceptibility in d=4, n=0 limit, confluent logarithmic singularities 78−54308
A-Mn, dil., mag. susceptibility and single impurity effects 78−64186
Ag Animalu transition metal model pot. invest. 80−75711
Ag-based alloys, α-phase, mag. susceptibility correl. with lattice parameter 78−68154
Ag-Dy(Er), dil., cryst. field and spin exchange parameters, susceptibility and ESR expts. 77−40129
magnetic susceptibility continued
Ag-Fe, dil., estimate of Kondo temp. from static mag. susceptibility meas. 78−19214
Ag-Fe alloy, local moment system, low. temp. susceptibility, Mossbauer effect meas. 77−43810
Ag-Fe alloy film, mag. susceptibility max. 79−24173
Ag-In(Sn), HCP ζ-phase, magnetic susceptibility 78−47946
Ag-In(Sn)(Pb)(Bi)(Sb), liquid alloy, thermoelectric powder and magnetic susceptibility 77−8076
Ag-Mn, dil., spin glass, AC susceptibility 79−33490
Ag-Mn, dil., thin-film spin glass, mag. susceptibility and T_G meas., 1.2-60K 79−38346
Ag-Mn, dilute spin glass, AC susceptibility and ESR meas. 79−7968
Ag-Mn, spin glass, mag. susceptibility hydrostatic press depend., RKKY interaction 80−44845
Ag-S(Se)(Te), liq., mag. susceptibility meas., electron localisation and chem. bonding 80−60178
$Ag_{0.6}Au_{0.4}Mn$, dil., effect of mean free path on strength of RKKY interaction 78−39291
AgNi, dil., mag. susceptibility of isolated Ni atoms 80−65777
AgPd alloys with Mn and Fe impurities mag. susceptibility 79−73677
Ag_2S, metal-nonmetal transition, crystallographic, optical, mag. and transport props. 78−6418
Ag_2Se, metal-nonmetal transition, crystallographic, optical, mag. and transport props. 78−6418
$Ag_{1-x}Sn_{1+x}Se_{2-y}$, supercond. and normal state props. 77−36008
Al alloys, non-transition metal effect on Landau diamag. susceptibility 77−63075
Al, dynamic susceptibility, model pot. theory 80−75710
Al film with Er impurity, spin-flip scatt. and supercond. order parameter dynamics 79−78267
Al-Cr (Mn), magnetic susceptibility, single impurity and interaction effects 77−63093
Al-Cu-Fe, liquid, mag. moment and transition from mag. to nonmag. state 79−24132
Al-Mn(Cr), dil. alloys, single impurity and interaction effects in susceptibility 77−8269
Al-Ni alloys, solid and liq. mag. susceptibility, 600-1650°C *(Russian)* 80−15685
Al-Si, magnetic susceptibility and elect. resistivity, 500 to 1000°C, struct. sensitive props. *(Russian)* 78−15550
Al-Zn, liq., physical props. study by electrodiffusion method *(Czech)* 77−84956
$Al_2Mn_3Si_3O_{12}$, amorphous insulating spin glass, susceptibility and magnetisation meas. 80−88765
β-Al_2O_3:Mn(Co)(Ni), absorpt. and emission spectra, mag. susceptibility 79−87471
β-Al_2O_3-Na_2O:Cr, absorpt. and emission spectra, mag. susceptibility 79−15495
β-Al_2O_3-Na_2O:Fe, coordination site, oxidation state, Mossbauer, absorpt., emission spectra, mag. susceptibility meas. 78−68431
$Al(OH)_3$, coprecipitated with $Cr(OH)_3$ gel, mag. and optical studies, calcination 79−47995
$(Al_2O_3)_{0.2}(Ho_2O_3)_{0.2}(SiO_2)_{0.6}$, amorphous low temp., AC susceptibility, freq. depend. of spin freezing temp. 79−82808
$Al_{0.35}V_2O_5$, spin glass phase, low temp. mag. susceptibility meas. 80−29565
Am metal, Faraday method, 3.5 to 13.1 kOe 77−28369
AmAs, Faraday method, 3.5 to 13.1 kOe 77−28369
AmN, Faraday method, 3.5 to 13.1 kOe 77−28369
As-Se glass, magnetic susceptibility meas. at room temp. *(Japanese)* 79−82748
As-Se glassy system, mag. susceptibility 77−55657
As-Se(Te) systems, mag. susceptibility comp. depend. 77−80908
AsF_5-intercalated graphite, mag. spin susceptibility, density of states at Fermi energy 79−7966
$As_2S_{3-x}Te_x$, opt. and mag. props., comp. influence 77−77225
$As_2S_{3-x}Te_x$, ternary chalcogenide glassy system, optical absorpt., mag. susceptibility and AC cond. meas. 80−55125
As_2Se_3:Fe, glassy, mag. susceptibility investig. of doping effect 77−77024
As_xSe_{100-x} glasses, temp. depend. of mag. susceptibility and EPR 77−63073
Au, Animalu transition metal model pot. invest. 80−75711
Au-Co, liquid alloys, ^{59}Co NMR studies, spin and orbital susceptibilities 79−95660
Au-Co solid solution, mag. susceptibility 79−61081
Au-Co solid solution, mag. props., freq. depend. suscept. maximum 79−69655
Au-Fe, mictomagnet, freq. depend. of susceptibility max. 78−95445
Au-Fe, spin glass, transition temp., freq. depend. 80−97113
Au-Fe, spin glasses, alternating susceptibility 80−65912
Au-Fe (22 at.%), ferromag. phase, AC susceptibility near T_c 78−43575
Au-Fe alloy, spin glass behaviour in low DC field 77−66373
Au-Fe alloy film, mag. susceptibility max. 79−24173
Au-Fe alloys, magnetism and atomic clustering 80−103810
Au-Fe spin glass, susceptibility cusp, influence of Fe clusters 79−61163
Au-Fe spin glasses in low DC fields, susceptibility and thermoremanence 77−77063
Au-In(Sn), HCP ζ-phase, magnetic susceptibility 78−47946
Au-Mn alloys, equiatomic region of phase diagrams crystallographic and mag. exam. 78−52755
Au-Mn-Cr(Pd) alloy, ferro- to non-mag. transform. 77−12117
Au-Ni, mag. clustering 79−7977
Au-Pd-Au sandwich, obs. of strongly enhanced mag. susceptibility 80−93076
Au-Si-Mn, amorphous spin glass film, mag. susceptibility 79−42775
Au-V Kondo alloys, mag. susceptibility and NMR Knight shift in conc. independent region 77−77027
AuFe alloy films, mag. susceptibility, Fe concentration and annealing depend. 79−61119
AuFe, spin glass freezing above ferromag. percolation limit 78−52264
$Au_{85}Fe_{15}$, and $Au_{82}Fe_{18}$, mag. props. 80−84592
$AuGa_2$ film, supercond., mag. susceptibility and Knight shift press. depend. 77−43777
$(Au_xPb_{1-x})_{1-c}Fe_c$, ferromag. and spin glass ordering 78−56335
Au_4V, effect of structural changes on phys. props. 78−31400
β-B, rhombohedral, localised states charact., review, book contrib. 78−47728
α-B, rhombohedral, temp. depend. 80−34585
BH, susceptibility and mag. screening calcs. 77−57861

magnetic susceptibility continued
B_2O_3-Na_2O-Fe glass, mag. susceptibility 79−42733
B_2O_3-PbO-GeO_2-Fe_2O_3 glasses, mag. props. and Mossbauer spectra, spero-mag. order at low temps. 80−80530
$B_2O_3.Fe_2O_3.nMO$ (M=Fe, Co, Ni, Cu, Mg), synthesis and mag. props. 80−20384
$B_2O_3.Fe_2O_3.nMO$, (n=2 or 4, M=Mg, Co, Ni, Cu), mag. props., transitions 80−75763
Ba-Sr-Pb hexaferrites, prep. by cernet procedure, mag. props. 77−32174
$Ba_5(Ba_{1-x}Al_x)Fe_2S_8[S_{1-y}(S_2)_y]$, cryst. struct., Mossbauer and mag. behaviour 77−55273
$Ba_2Bi^{3+}Bi^{5+}O_6$, structure and elec., mag., thermal props. vs. temp. X-ray and neutron powder diffr. study 79−19189
$BaCa_{1/2}Ru_{2/3}O_3$, biquadratic exchange interaction between Ru^{5+} ions in (Ru_2O_9) clusters 77−20580
$BaCo_2(AsO_4)_2$, planar X-Y model, mag. ordering 77−66256
Ba_2CoS_3, linear chain antiferromag., mag. susceptibility meas. and Mossbauer spectra 80−107992
$Ba_3Fe_{2-x}Lu_xUO_9$, crystallographic and mag. props. *(French)* 77−15380
$Ba_3Fe_2ReO_9$, siegnette magnets with hexagonal barium titanate structure 78−76397
Ba_2FeS_3, linear chain antiferromag., mag. susceptibility meas. and Mossbauer spectra 80−107992
$Ba_xLa_{1-x}CoO_3$, x=0 to 0.5, structural, elec. and mag. props., Zener double exchange and Goodenough's model 79−65663
BaLaMRuO$_6$, (M=Mg, Fe, Co, Ni, Zn), cubic ordered perovskites, Mossbauer and mag. susceptibility meas. 80−75889
Ba_2MnS_3, linear chain antiferromag., mag. susceptibility meas. and Mossbauer spectra 80−107992
$Ba_4NbRu_3O_{12}$ and $Ba_4TaRu_3O_{12}$, $(Ru_3O_{12})^{13-}$ cluster obs. in presence of orbital degeneracy and spin-orbit coupling *(French)* 80−70655
$Ba_2Ni_3F_{10}$, cryst. struct. and antiferromag. props. 80−107153
$BaNi_2M_xFe_{16-x}O_{27}$, effect of M=Sc^{3+} or In^{3+} on props. 77−47978
Ba_2NiReO_6, mag. and cryst. struct. 77−20554
BaO-Fe_2O_3 system, splat cooled phases struct., magnetisation and susceptibility 300-1100K *(French)* 77−48017
BaO-Fe_2O_3-B_2O_3 glass, splat cooled, low temp. micromagnetism 80−34660
BaO-Fe_2O_3-Na_2O glass, mag. props. 78−88123
BaO-Fe_2O_3-(Na_2O) glass, rapidly quenched, mag. and ferrimag. props. 80−75744
$Ba_3(PO_4)_2$ transition metal ion, optical and magnetic props. 78−64196
$Ba_3Re_2O_9$, cryst. struct., mag. and semicond. props. 79−10836
$BaSi_2$, semicond.-metal transition, high-press. and temp. 78−43299
$BaTiO_3$, 3d element doped, phase stability, phase transition temp., mag. susceptibility meas. 78−38835
$BaTiO_3$ and $BaTi_{1-x}Fe_xO_{3-x}F_x$, electrical, optical and mag. props., photoelectrolysis 77−47856
$BaTiO_3$, magnetochemical exam. of phase transition, mag. suscept. meas. 78−88265
$BaTiO_3$:X(X=Cr, Mn, Fe, Co, Ni, Zn, Ga), annealed in H_2 and O_2, valence change in phase stability 80−20600
$BaVS_3$, elec. resist., mag. susceptibility, structural transition amd Mossbauer effect meas. 77−84923
$BaVS_3$, exam. of ferromagnetic, antiferromagnetic behaviour, depending on stoichiometry 78−52233
$BaVS_3$, mag. and elec. props. 79−91214
$BaVS_3$, magnetisation and neutron study 80−84588
$BaVS_3$:Fe, Mossbauer and mag. studies, electronic state of Fe 80−108130
$BaVSe_3$, one-dimensional, struct. and mag. props. 80−28993
$BaX_{1/3}Ru_{2/3}O_3$ (X=Ca, Cd, Mg, Sr), crystal struct., mag. susceptibility and exchange integrals *(French)* 77−16037
Ba_2XRuO_6(X=La,Eu), ^{99}Ru Mossbauer spectra and other techniques 80−29659
$Ba_2Zn_2Fe_{12}O_{22}$, anisotropic magnetisation and susceptibility 78−84411
Be, ground state reduced first order density matrix CI calc., mag. shielding const. and diamagnetic susceptibility 79−6872
Be intermetallics, MBe_{13}, (M=Y, La, Ce, Lu, Th), lattice spacings and susceptibilities 80−65778
Be, magnetic suscept. anomalous temp. depend. *(Russian)* 79−4650
Be, orbital magnetism, effect of energy spectrum features *(Russian)* 77−85414
Be, spin susceptibility, electronic effective mass, spin density functional calcs. 78−43291
$Be_5(Fe_{1-x}Mn_x)$, mag. and calorimetric props. 77−63083
$Be_{1-x}Mn_x$, Be-rich, NMR and paramag. susceptibility 80−71206
Bi-Mn, dil. liq. alloy, static and dynamic props. of localised Mn moments 79−82755
Bi-Sb, magnetic susceptibility, 4.2 to 270K, field and band parameter depend. 77−36051
Bi-Sb(-As), band struct., effects of Sb and As, mag. susceptibility meas. *(Russian)* 80−65775
Bi-Se, fused, mag. susceptibility, temp. and conc. depend. 77−36052
Bi-Sn, maximum diamagnetism rel. to electron density 80−54865
Bi-Te, fused, mag. susceptibility, temp. and conc. depend. 77−36052
Bi-Te(Se), liq., diamag. susceptibility, semicond./metal behaviour 78−14927
Bi-Te(Se), liq. chalcogenides, elec. cond. and mag. susceptibility 79−51578
Bi_2O_3-ZnO(CdO), elec. cond., dielec. const., mag. susceptibility meas., effect of melting transition 77−7849
$Bi_3Sr_{1-x}Eu_x$, supercond. and mag. ordering 78−56252
Bi_2Te_3, chemical bonding models, correctness test using mag. susceptibility, and chemical substitution 78−67680
Bi_2Te_3, p- and n-type, free charge carrier mag. susceptibility, 90-650K 78−10643
BiTeI, influence of lamination effects on mag. suscept. *(Russian)* 78−80125
BiTeI, layered cryst., anisotropy and temp. depend. of mag. susceptibility 79−73673
β'-$Cu_xV_2O_5$, mag. and spectroscopic study, semiconductor to metal transition 80−2628
C, amorphous, anomalous low temp. mag. and thermal props. 78−10647
C, anthracene char, density fluctuations effect on physical properties 78−51420
C, char, amorphous, mag. interactions between localised spins 80−34587
C chars, thermally activated paramagnetism, mag. susceptibility meas. 80−75709
C, evaporated, paramag. and diamag. susceptibility meas., 77 to 1400K 77−28362

magnetic susceptibility continued
C fibre, as-processed, diamag. studies 77−25165
C fibre reinforced epoxy resin, diamag. susceptibility as fibre alignment characterisation method 78−84381
C fibres struct. and physical props. effects of B additions and heat treatment temp. 78−68715
C, pregraphitic, diamag. suscept. rel. to temp., energy level calcs. *(French)* 78−34951
C, pregraphitic crystallites, appl. of theory of diamag. susceptibility of condensed ring systems 77−16039
C-C σ bonds, mag. suscept., refined variational calc. 77−68136
C-fibres, from pitch mesophase, ptich and PAN, diamag, susceptibility meas. 79−69649
C-H bonds, mag. suscept., vector pot. variational calc. 77−68137
C_8AsF_5 intercalation compound, NMR and static mag. susceptibility meas. 78−88214
$C_8Br_xCl_{1-x}$ intercalate, crystallographic, elec., mag. props. 80−107184
$CD_{1-x}In_xCr_2S_4$, ferromagnetic spinel, Cr^{3+} exchange interaction mechanism, Cr^{2+} relaxation, EPR line width depend. 79−69715
$(CH_3NH_3)_2FeCl_2Br_2$, two-dimensional antiferromag., field depend. of susceptibility meas. 77−63130
C_8K, intercalation compound, superconductivity 78−91827
C_8K, intercalation cpd. with graphite, supercond. props. 80−44755
CO complex, with 1,2,4-triazole, mag. susceptibility, 2-300K, struct. 77−77045
CO, elec. and mag. props., mol. beam elec. reson. spectroscopy 77−61791
CO group, NMR chem. shift, solvent's dielectric const. effect, mag. anisotropy 79−42847
CS_2, liq., diamagnetism, mass mag. suscept. meas., temp. depend. 80−97054
CaB_6-SmB_6, mag. props., comp. depend. 80−50034
$CaCo_2(PO_4)_2$, reflection spectrum and mag. susceptibility meas. 77−59586
$CaCrF_5$, one-dimens. magnetism *(French)* 79−73670
$CaCu_3Ti_4O_{12}$, mag. struct. and props. *(French)* 77−69495
CaF_2:Tm^{3+}, 8.2 keV excited state, mag. props., Schottky ht. capacity, nucl. quadrupole splitting 78−76037
CaF_2+Yb^{3+}, Stark level Zeeman energies, mag. susceptibiltiy, Schottky specific heat, crystal field splitting 78−26831
$CaFeF_5$, one-dimens. magnetism *(French)* 79−73670
$CaFeO_3$, preparation, cryst. struct., mag. and elec. props. 78−44066
$CaIr_xTi_{1-x}O_3$, semiconductor, struct., mag. and elec. props. 79−91046
$Ca_2Mn_3O_8$, mag. props. 79−78339
$Ca_2Mn_3O_8$, mag. props. and EPR 79−91215
$Ca_2MnO_{4-x}F_x$, antiferromagnetic props. and elec. cond. *(French)* 80−29526
$Ca(OH)_2$, mag. ordering of proton spins 79−73746
$CaSO_4$:Sm phosphors, mag. susceptibility temp. depend. 300-453K 78−52196
$CaS_2O_3.6H_2O$, cryst. data and mag. susceptibility 77−76368
CaSb, resist., susceptibility and thermopower rel. to electronic struct. 78−67935
$CaV_{12}O_{30}$, phase transitions, elec. cond., susceptibility and sp. ht. meas. 78−14776
$CaWO_4$:Er^{3+}, magnetocaloric behaviour, cryst. field theory 77−4520
Ca_2XRuO_6 (X=Y,La,Eu), ^{99}Ru Mossbauer spectra and other techniques 80−29659
Cd alloys, spin and spin-orbit contribs. to mag. susceptibility *(Russian)* 79−11287
Cd, magnetic susceptibility, temp. depend., electron-phonon interaction effects 79−61046
Cd, spin-orbit interac. contrib. to mag. susceptibility of interacting electrons 77−63084
Cd-Cr, dil., estimates of s-d interaction from supercond. transition temp. and mag. susceptibility 78−43561
Cd-Cr(Mn)(Ni), dil., mag. and supercond. props. 79−38237
Cd-Hg, ω-phase, mag. susceptibility *(Russian)* 79−87231
Cd-Mg, and Cd-Mg-Hg, magnetic susceptibility behaviour *(Russian)* 77−80912
Cd-Mg, mag. susceptibility near $2^1/_2$th order electron transition, non-linear magnetisation anal. *(Russian)* 80−44859
Cd-Sn alloy, superconductivity and microstructure 80−107949
$Cd_{1-x}Ag_xCr_2Se_4$, Ag acceptor states effect on exchange interaction 80−20397
$Cd_3Cr_2Ge_3O_{12}$, antiferromagnetic ordering of Cd^{3+}, sp. ht. and mag. susceptibility meas. 77−16062
$CdCr_2S_4$, single crysts., EPR linewidth near Curie point, temp. and susceptibility depend. 77−63272
$CdCr_2S_4$:Cu, magnetic microregions caused by s-d exchange 77−77050
$CdCr_2S_{4-\gamma}$, spinel, anomalies in paramag. susceptibility, Curie pt. *(Russian)* 77−80910
$CdCr_2Se_4$, crit. behaviour near Curie point 78−31068
$CdCr_2Se_4$, reactor radiation influence on ferromagnetic phase transform. *(Russian)* 80−75760
$CdCr_2Se_4$:In(Ga)(Cu), magnetic microregions caused by s-d exchange 77−77050
$Cd_{1-x}Ga_xCr_2S_3$, spinel, anomalies in paramag. susceptibility, Curie pt. *(Russian)* 77−80910
$CdGe_{1-x}M_xAs_2$ (M=Si,Sn,Pb), amorphous struct., mag. susceptibility 78−22651
$CdGe_{1-x}Sn_xAs_2$, amorphous, radial distrib. anal. and mag. susceptibility meas. 77−43152
CdHg alloy, ω phase, mag. susceptibility anisotropy w.r.t. uniform compression *(Russian)* 80−71143
$Cd_{1-x}In_xCr_2S_{4-x}P_x$, ferromagnetic spinel, Cr^{3+} exchange interaction mechanism, Cr^{2+} relaxation, EPR line width depend. 79−69715
$CdInGaS_4$:Er^{3+}, cryst. field parameters, thermal and mag. props. calc. 77−20540
$CdIn_2S_4$:Er^{3+}, cryst. field parameters, thermal and mag. props. calc. 77−20540
$Cd_{1-x}Mg_x$, energy spectrum pseudopotential calcs., mag. props., impurity scatt. *(Russian)* 80−65430
$Cd_{1-x}Mg_x$, mag. props. and electron spectrum parameters *(Russian)* 79−33453
$Cd_{1-x}Mg_x$, magnetic susceptibility anisotropy, press. effects, electronic phase transitions *(Russian)* 80−54869
$Cd_2Mn_3O_8$, mag. props. 79−78339
$Cd_2Mn_3O_8$, mag. props. and EPR 79−91215
$Cd_{1-x}Mn_xTe$, magnetic behaviour of Mn 78−14938

magnetic susceptibility continued
$CdPS_3$, layered, organometallic intercalates, X-ray diffr., optical absorpt. and mag. props. 80−45103
CdS, amorphous antiferromag., mag. props. of dilute neutral donors 79−78367
CdS, doped, amorphous antiferromagnet model, susceptibility and spin-flip Raman scatt. meas. 80−97057
CdS, magnetic susceptibility, grinding-induced states 79−61040
CdS, model $S=^1/_2$ amorphous antiferromagnet, spin polarisation 78−52288
CdS, powder, mechanically induced localised states in energy gap 80−2354
CdSb:Ge, anisotropy of elec., mag. props. 78−34829
CdSe, magnetic susceptibility, grinding-induced states 79−61040
CdTe, mag. susceptibility at 20-1400°C 77−12085
CdTe:Fe-group metals, mag. susceptibility *(Russian)* 79−56496
CdTe:Ge, mag. props. 78−56289
CdTe:Mn^{2+}, exciton refl. spectra and mag. susceptibility 80−66253
CdTe:Mn(Fe)(Ni), exciton refl., photoluminesc., and mag. suscept. meas., influence of impurities 77−39787
$CdTm_2Se_4$, mag. susceptibility meas. 4.2 to 300K cryst. field approx. 77−66246
(Ce, La)Al_3, near stabilisation of Ce moment upon dilution 79−91209
β-Ce, 2-300K, Neel temp. 77−4320
Ce alloys, Kondo effect, mag. suscept. exam., appl. to $CeIn_3$ 77−8270
Ce alloys, Kondo system, mag. susceptibility calc. in Anderson model 77−55661
Ce binary and pseudobinary intermetallics, struct. and mag. data 80−20129
Ce compounds, Anderson model, exchange parameter, Kondo temp., mag. susceptibility 79−1656
Ce cubic intermetallics, interconfig. fluctuations 80−20130
Ce dilute alloys, cryst. field and Kondo effect 77−43809
α-Ce, exchange-enhanced, elec. resist. T^2 depend., press. effect 80−96845
γ-Ce, field induced mag. form factor 78−68151
Ce intermetallics, CeX_2Si_2 (X=Cu, Ag, Au), ^{29}Si NMR and mag. susceptibility 79−61246
Ce, liq., 4f electron susceptibility temp. depend. 80−20378
α-Ce, susceptibility, sp. ht. and magnetisation 79−28512
Ce-Co-Si system, mag. props. in 77-300K range *(Russian)* 78−56290
Ce-Fe-Si system, mag. props. in 77-300K range *(Russian)* 78−56290
Ce-La, mag. ordering, sp. ht., susceptibility and resist. 78−68238
Ce-La alloys, DHCP, low temp. mag. and elec. props. 77−62911
Ce-Ni-Si system, mag. props. in 77-300K range *(Russian)* 78−56290
Ce-Pt, paramag. suscept. 79−61047
Ce-Th, mag. suscept. and sp. ht. 79−78411
CeAl, mag. props. and mag. struct. 78−6517
$CeAl_2$, Anderson lattice system, mag. moment reduction, press. effects 80−7093
$CeAl_2$, low temp. mag. props., Kondo effect 80−20381
$CeAl_2$, magnetisation curves under high mag. field and hydrostatic press. 77−63233
$CeAl_3$, magnetic susceptibility, dense Kondo system 77−63087
$Ce_{30}Au_{20}$, amorphous, cryst. field effects and mag. interactions, magnetisation and transport props. meas. 78−68191
$Ce_{80}Au_{20}$, metallic glass, mag. ordering and cryst. field effects, speromagnetism 80−80531
CeB_6, mag. and electronic props. 80−71048
CeB_6, resist. anomaly and mag. ordering obs. 79−61110
$CeBe_{13}$, intermediate valence state, XPS, resist. and susceptibility study 80−71565
CeC_2, mag. props. 80−108008
$CeCl_3(Br_3)$, interaction parameters, high freq. meas. of adiabatic differential susceptibility 78−68211
Ce(Cu,Ni)$_2$, pseudobinary phases, struct. and mag. props. rel. to Ce valence 78−6032
$CeCu_4$ Knight shifts and mag. susceptibility 79−95656
$CeCu_5$, Knight shift and mag. susceptibilities 79−95656
$Ce_xDy_{1-x}C_2$, solid solns., mag. props. 80−108008
$Ce_xEu_{1-x}B_6$, 80-1000K 79−73674
$Ce_{1-x}Gd_xRu_2$, superconductivity and ferromagnetism coexistence, 60 mK-4.2K, spin echo NMR 78−84349
Ce(In, Sn)$_3$, mag. susceptibility, temp. depend., intermediate valence 80−65779
$CeIn_3$, Kondo effect, mag. suscept. exam. 77−8270
$CeIn_3$, Neel temp., hydrostatic press. depend. 80−29549
$CeIn_{3-x}Sn_x$, conduction electrons role in valency fluctuations 78−47741
$CeIn_{3-x}Sn_x$ mixed valence system, low-temp. susceptibility, paramagnon study 80−97077
$CeIn_{3-x}Sn_x$, scaling behaviour near valence instability, mag. susceptibility and mag. transitions 80−25111
$Ce_xLa_{1-x}Al_3$, Kondo system, mag. susceptibility, 1.5 to 20K 79−78310
$Ce_xLa_{1-x}B_6$ solid solutions, Weiss const. antiferromagnetic ordering calcs., mag. props. *(Russian)* 79−91212
$(Ce_xLa_{1-x})Be_{13}$, mag. intermediate valence behaviour 79−24131
$(Ce_xLa_{1-x})_2Mg_3(NO_3)_{12}.24H_2O$, mag. susceptibility meas., AC method meas., appl. as thermometer in mK region 77−17999
$Ce_{1-x}La_xSn_3$ (x=0 to 1), mag. susceptibility and magnetisation, lattice parameters, X-ray and neutron diffr. meas. 80−49675
$Ce_2Mg_3(NO_3)_{12}$, AC mag. susceptibility, mag. field depend., 1-4K 79−56516
$Ce_2Mg_3(NO_3)_{12}$, spin-lattice relax., dynamic susceptibility meas., liq. He contact effects 80−66011
$CeMn_2Si_2$, cryst. and mag. struct. determ. 78−52225
$CeNbO_{4+x}$, oxidation-reduction reactions 78−39930
$CeNb_3O_9$, $CeNbO_4$, $CeNbO_{7.6}$, electron config. of Ce ions, mag. sucept., L_3 absorpt. edge, resist. 79−43063
$CeNi_2$-$CePt_2$ system, structural and mag. studies on valence behaviour of Ce 80−103809
$CeNi_3$, and ternary hydride, mag. props. 80−108007
$CeNi_4Al$, mag. susceptibility, H adsorption-desorption cycle effects 80−107990
CeP(As), single crystals, low temp. thermal, electrical and mag. props. meas. 78−27051
$CePd_3$, susceptibility, sp. ht. and magnetisation 79−28512
$CePd_3$-Er, dil., low field mag. susceptibility, electro-nuclear effects 80−60189
$CePd_3$-Gd, ultralow interaction temp. and cryst. field effects for Gd impurities 79−61100

magnetic susceptibility continued
$Ce_{1-x}Pr_xAl_2$, mag. struct., comp. depend., neutron diffr. and mag. susceptibility meas. 80−50054
$Ce_{1-x}Pr_xAl_2$, mixed mag. phase at low temp. 78−68228
$CePt_3$, ^{195}Pt NMR and susceptibility meas. 77−63299
$CePt_5$, mag. susceptibility, 4.2 to 295K *(German)* 79−47233
$CeRh_{3-x}Pd_x$, electronic and cryst. struct. comparison, catalytic behaviour 78−84398
$CeRh_{3-x}Pd_x$, lattice spacing and mag. suscept., effect of prep. and hydrogenation 77−58976
$CeRh_{3-x}Pd_x$, powdered alloys, catalytic behaviour correlation with electronic struct., lattice struct. and surface comp. 79−82181
$CeRu_2$, change of valence of Ce ions, induced by H absorption, supercond. disappearance 79−47185
$CeRu_2$, H absorption induced Ce valence change, mag. and supercond. props. 80−50042
CeS, mag. props., sp. ht. and thermal expansion 78−60292
$Ce_{1-x}Sc_xPd_3$, intermediate valence of Ce, susceptibility, lattice const., ESR meas. 80−103648
CeSe, mag. props., sp. ht. and thermal expansion 78−60292
$CeSn_3$, low temp. mag. behaviour, press. induced valence change 77−63078
$CeSn_3$, mixed valence cpd., electronic struct. and mag. props. 80−70649
$CeSn_3$, polarised neutron study of induced magnetisation 80−34594
$CeTaO_{4+x}$, oxidation-reduction reactions, phase equilibrium, thermogravimetry and magnetic susceptibility meas. 78−39930
CeTe, mag. props., sp. ht. and thermal expansion 78−60292
$Ce_{0.736}Th_{0.264}$, induced mag. form factor 79−78307
$Ce_{1-x}Th_x$, mixed valence systems, spin dynamics and mag. ordering 78−68162
$CeTl_3$, mag. susceptibility, magnetisation, neutron diffr., elec. resist., and sp. ht. meas. 80−75733
$Ce_2(WO_4)_3$, mag. susceptibility, paramag. Curie temp., 300-900K 79−82753
$(Ce_xY_{1-x})Fe_2$, mag. susceptibility and Mossbauer meas., lattice parameters 80−97068
^{249}Cf metal, expanded FCC phase 77−28368
ClCN, ground and first excited bending, vibr. state, props., mol. beam elec. reson. 80−37823
Cm, antiferromag. state, paramag. suscept. meas., electronic struct. *(Czech)* 78−80133
Cm metal, Faraday method, 3.5 to 13.1 kOe 77−28369
CmAs, Faraday method, 3.5 to 13.1 kOe 77−28369
CmN, Faraday method, 3.5 to 13.1 kOe 77−28369
^{244}Cm metal 77−28368
Co, atomic layers, Pauli paramagnetism to band ferromagnetism transition thickness depend. 78−72377
Co, band model of high temp. magnetism 78−26809
Co complex, Co II high spin binuclear species, magnetic exchange and anisotropic susceptibilities 78−39308
Co complex, $CoCl_2$(indazole)$_2$, linear chain ferromagnetism 79−56519
Co complex, $CoCl_2$(pyrazole)$_2$, linear chain ferromagnetism 79−56519
Co complex, Co(III) five coordinate, paramagnetic behaviour 79−15276
Co complex, Co(II)(1,2,4-triazole)$_2$(NCS)$_2$ quasi two-dimens. canted S=1/2 antiferromag. 80−70976
Co complex, tetra-μ-benzoato-bis(4-methylquinoline)dicobalt II, triclinic cryst., antiferromag. exchange 78−39309
Co intermetallics with d-metals, temp. depend., 77-500K *(Russian)* 77−80911
Co, Stoner model, mol. field coeff., temp. and field depends. 77−72975
Co-Al, mag. struct. of Co rich intermetallic cpd., neutron scatt., cluster model 78−80130
Co-Al alloys, deformed, mag. props., positron annihilation *(Russian)* 77−85416
Co-based Heusler alloys, Co_2TAl, (T=Ti, Zr, Hf), paramag. state NMR and susceptibility meas. 79−65643
Co-Fe, double hexagonal alloys, crystalline and mag. props. *(Japanese)* 79−73132
Co-Fe-Nb alloy, mag. precipitation-hardening and Bloch wall pinning 78−80173
Co-Fe-Ti alloy, precipitation hardened, rel. between struct. and mag. props. 78−95470
Co-M alloys, M=Si, Ge, Al, Ga, band model of high temp. magnetism 78−26809
Co-Mn, FCC, mictomagnetism, magnetisation and mag. susceptibility meas. 80−60310
Co-Mn alloys, ferromagnetic, high field mag. susceptibility meas. 80−75729
Co-Mn-Sn liquid alloy, magnetic props. *(German)* 79−87235
Co-Ni (5 to 95 at.%), paramag. props., 800-1800°C *(Russian)* 77−55660
Co-P grains, mag. props. *(French)* 79−33510
Co-V, solid and liq., mag. susceptibility and electronic struct. 80−39738
$CoAl_xGa_{2-x}O_4$, mag. interactions, susceptibility obs., 4.2 to 300K 79−15294
$CoAs_3$, prep. and characterisation 77−77356
$Co_2(AsO_4)Cl$, temp. depend. of mag. susceptibility 80−70962
$Co_{100-x}B_x$, amorphous, mag. struct., mag. susceptibility meas. 80−80485
$Co_{1.8}BaFe_{0.2}^{2+}Fe_{16}^{3+}O_{27}(Co_{1.8}W)$, magnetoelastic props. under spin-reorientation conditions 79−69709
$CoBr_2.2H_2O$, metamagnetic, relax. phenomena at phase transitions 79−24164
$Co(C_5H_5NO)_6(ClO_4)_2$ [$(BF_4)_2$], X-Y antiferromagnet, Neel temp., spin correlation functions 80−60345
$CoCO_3$, mag. props., microscopic level calcs. *(Russian)* 80−97078
$CoCl_2.2NC_5H_5$, quasione dimens. Ising system, thermodynamic props. 78−27042
$Co_{1-x}Cu_xCr_2S_4$, paramag. susceptibility 80−20373
$Co_{0.7}Cu_{0.3}Cr_2S_{4-x}Se_x$, ferrimag. chalcospinel, paramag. susceptibility 80−15681
CoF_2, phase transition in transverse mag. field, magnetoelastic interactions 79−65676
CoF_2, spin excitations in longitudinal mag. field 79−69657
$Co_xFe_{1-x}Cl_2.2H_2O$ solid soln., mag. props. and phase diagram 79−78346
$(Co_{1-x}Fe_x)_2Y$, substitutional Fe atoms effect on mag. and elec. props., paramagnon scatt. 77−36054
$Co_{54}Ga_{46}$, superparamag. response to low DC fields 80−44860
Co_xGa_{1-x} alloys, cluster spin glass, host and impurity NMR and AC susceptibility 80−71194
Co_xGa_{1-x}, β-phase, spin glass behaviour 80−44837

magnetic susceptibility continued
Co_xGa_{1-x}, cluster spin glass, AC susceptibility in DC mag. fields, 77 to 500K 80−34670
$CoGa_{2-x}Fe_xO_4$, x=0.1−0.4, mag. susceptibility temp. depend. *(Russian)* 80−70957
$CoGa_2O_4$, mag. props. 78−23254
$Co_xMg_{1-x}Al_2O_4$, struct., catalytic activity, Co^{2+} ion distrib. 78−30595
$Co_{50}Mn_xGa_{50-x}$, ordering and disordering phenomena, mag. study 80−70154
$Co_3Mn_3Si_2$, Curie-Weiss law depend. of susceptibility, mag. props. *(Russian)* 79−65655
$Co^{2+}Mo^{4+}O_3$, defect spinel struct., elec. and mag. props. 80−70176
$CoMoO_4$, mag. susceptibility and electrical transport props. 79−56511
$Co(NH_4)_2(SO_4)_2.6H_2O$, LF relax. meas. 78−15012
$Co(NH_4)_2(SO_4)_2.6H_2O$ Tutton salt, low-temp. spin orientation, mag. props. 0-0.1K, differential mag. susceptibility 79−15286
$CoNb_2O_6$, Co^{2+}-Co^{2+} interaction, susceptibility and magnetisation, 3.3-300K 77−8282
$CoNb_2O_6$, magnetic struct., neutron diffr. and mag. susceptibility meas. 80−15693
$Co_{1/3}NbS_2$, intercalate, metallic cond., Hall effect and mag. props. 77−76789
$Co_{1-x}Ni_xAl$, Knight shift and mag. susceptibility study, electron struct. peculiarities *(Russian)* 80−15814
CoNiP film, amorphous, electrolytic, prep. and props. *(Slovak)* 79−51823
CoO, non-stoichiometry and temp.-depend. mag. susceptibility 79−82768
$CoO-Al_2O_3-SiO_2$, spin glass, magnetic aftereffects 79−61176
$CoO-Al_2O_3-SiO_2$ glass, mag. ordering, Mossbauer exam. 77−24764
$CoO-Al_2O_3-SiO_2$ spin glass, new state in very weak mag. field 79−78416
CoO-ZnO-MgO ternary systems, solid solns., struct. charact. 80−60629
CoP_3, prep. and characterisation 77−77356
$Co_xPd_{80-x}Si_{20}$, amorphous, low field susceptibility near transition temp. 77−66359
$Co_xPd_{80-x}Si_{20}$, amorphous, structural and mag. heterogeneities 80−80484
$CoRh_xGa_{2-x}O_4$, mag. interactions, susceptibility obs., 4.2-1000K 79−15293
Co_2RhS_4, mag. semicond., mag. and elec. props. 80−93121
CoS_2, microscopic mag. props., NMR meas. 79−91306
CoSb, at. struct. and mag. susceptibility 77−39561
$CoSb_3$, prep. and characterisation 77−77356
$CoSe_{1.95}$, NMR and susceptibility meas., absence of antiferromag. 77−16060
$CoSe_2$, bulk mag. susceptibility, anomalous temp. depend., NMR and X-ray diffr. meas 79−87229
Co_5Sm crystals, microstruct., homogeneous precip. and nucleation 80−104160
Co_3Sn, mag. polarisation and susceptibility *(German)* 80−104147
$Co_{1-x}Te$, fluctuating localised mag. moments, d band motion, Mossbauer study 80−65768
$Co_2(Ti,Mn)Sn$, Heusler alloy, mag. meas. 79−47261
$CoTi_{1-x}Al_x$, mag. and electronic props., ferromag. and paramag. state 80−65814
CoU_2S_5, mag. struct. and props. 80−11166
$Co_xZn_{1-x}Rh_2O_4$, mag. props., EPR spectra, antiferromag. order 80−75736
$Co_xZn_{1-x}Rh_2O_4$ spinel, crit. conc. for long range mag. order, expt. evidence 79−47239
$Co_{2-y}Zn_yTiO_4$, cation distrib. and mag. props. 78−14939
$Co_{2-y}Zn_yTiO_4$, spinel series, exchange integrals, mag. struct. and coercive force, magnetisation meas. 77−69507
$Co(urea)_2Cl_2.2H_2O$, two-dimens. mag. props., cryst. struct., specific heat 80−75777
Cr, and alloys, surface- or defect-induced magnetism, nearly half-filled bands 79−1671
Cr, antiferromagnetic, calc. using two band model electronic spectrum 78−10663
Cr antiferromagnetic with nonmagnetic impurities, mag. susceptibility using two band model 80−2559
Cr complex, trimeric clusters, low temp. mag. props. 78−76261
Cr complexes with glycilglycine, structure, optical, e.p.r. and mag. investig. 77−1103
Cr-Fe, dilute, localised moment cluster model, ferromagnetic exchange coupling 80−39774
Cr-Fe, low conc. alloys, coexistence of itinerant antiferromagnetism with paramagnetism 78−84386
Cr-Fe, mag. moment of Fe, mag. suscept. meas. 79−61079
Cr-Fe (14 wt.%), spin density wave and spin glass ordering coexistence at low temps. 79−61059
Cr-Fe alloys, antiferromag., elec. resistivity, Kondo effect 79−60812
$Cr-Fe_x$ (x=0.5, 1.5 and 3.5 at.%), antiferromag., Kondo anomaly 80−11163
Cr-Fe-V, dil., V effect on para- to incommensurate and commensurate transitions 78−68260
Cr-Fe-V, effects of V on mag. transition, elec. and mag. props. 77−69554
Cr-Ge system, phase anal. and physical props. 79−24160
Cr-Ge system, XPS, X-ray and neutron diffr. and mag. meas. to study chem. bonding and electronic struct. 80−60749
Cr-Mn alloys, antiferromag. and weak ferromag., elec. props. 79−56514
Cr-Mo, behaviour of mag. impurities 79−4672
Cr-Mo-Fe (2, 14 wt.%), spin density wave and spin glass ordering coexistence at low temps. 79−61059
Cr-Ni(V), dil., mag. susceptibility, 77 to 400K *(Russian)* 80−50066
Cr-Re, dil. alloy, mag. susceptibility temp. depend., thermal expansion coeff. *(Russian)* 78−76225
Cr-Re(Ru)(Os)(Ta)(V)(Nb), Invar alloys, thermal expansion, plasticity, elec. resist. and mag. suscept. *(Russian)* 79−55907
Cr-S system, mag. props. *(Japanese)* 77−43825
Cr-Si, dilute alloy, mag. susceptibility and Neel temp. meas. 80−71017
Cr-Si-Fe, mag. moment of Fe, mag. suscept. meas. 79−61079
Cr-Si-V, (2, 0.1 at.%), paramag. to commensurate spin density wave transition 80−65875
Cr-Si-V, dil., V effect on para- to incommensurate and commensurate transitions 78−68260
Cr-V-Fe, mag. moment of Fe, mag. suscept. meas. 79−61079
CrB_2, CrB, and Cr_5B_3, mag. and thermal props. at low temps. 80−20385
CrB_2, crystal growth by floating-zone method, elec. and mag. props. 77−1801

magnetic susceptibility continued
$CrBr_3$ anisotropic ferromagnet. crit. mag. relax., field and temp. depend. 79−1717
$CrBr_3$, HF spectra, susceptibility, spin waves in domain walls *(Russian)* 80−80909
CrH, electronic props., H alloying effects, book contrib. 79−82522
$Cr_xMn_{1-x}As$, antiferromag. to ferromag. transitions, superexchange-double exchange mag. coupling, susceptibility and resist. obs. 80−50070
$Cr_xMn_{1-x}As$, mag. susceptibility anomaly at displacive phase transition 80−93091
$Cr_{0.5}NbSe_2$, cryst. struct., metallic cond., mag. and phys. props. *(French)* 80−33956
CrO_n, mag. and optical obs., prep. by calcination of $CrCl_3$ 79−24736
Cr_2O_3, magnetic susceptibility, near Neel temp. 79−56509
$Cr(OH)_3$, coprecipitated with $Al(OH)_3$ gel, mag. and optical studies, calcination 79−47995
$CrPS_4$, phys. props. and Li intercalates 79−19788
$Cr_xPd_{82-x}Ge_{18}$ amorphous alloys, magnetoresist., mag. susceptibility, magnetisation 78−80148
$CrS_{1-x}Se_x$, antiferromag. props., struct., variations near Neel temp. 78−64199
$CrSe_2$, layered, phys. and elec. props. 80−44594
$Cr_{3\pm x}Se_4$, struct., elec. and mag. props. 80−107160
Cr_3Se_4, mag. susceptibility and sp. ht. meas. *(French)* 79−56507
$Cr_3Se_xS_{4-x}$, mag. susceptibility and sp. ht. meas. *(French)* 79−56507
$Cr_2Se_{3-x}Te_x$, mag. props. and lattice parameters, comp. depend. 77−66263
$Cr_3Se_{4-x}Te_x$, mag. props. and lattice parameters, comp. depend. 77−66263
Cr_3Si, mag. susceptibility, 2 to 300K, rel. to electron energy spectrum 80−60185
$(Cr_{1-x}Ti_x)_5S_6$, mag. props. 77−69548
$Cr_{1-x}V_xCo$, localised mag. moment of Co impurity 78−27014
$Cr_{1-x}V_xCo$, mag. state of Co impurity, NMR exam. 78−27100
$CrVO_4$, Neel temp., mag. susceptibility meas. 80−29550
$(Cr_{1-x}V_x)_5S_6$, mag. props. 77−69548
Cs, fluid, metal-nonmetal transition and mag. interactions 80−49602
Cs fluid, metallic and nonmetallic, mag. props. 80−44799
Cs^+ and Cs, analytic SCF HF ground state wave function, ionis. pot., mag. props. 77−18785
Cs-Ag, dil., electronic struct., density functional approach, appl. to elec. and mag. props. 80−44492
Cs-Au(Sb), liq. alloys., mag. susceptibility and electronic struct. 77−1537
Cs-Sb(Au) liq. alloys, metal-nonmetal transition and change in electronic and mag. props. 77−51790
Cs_2CoCl_4, mag. susceptibility and magnetisation curve meas. 80−11176
Cs_2CoCl_4, paramag. mag. exchange rel. to low temp. mag. characts. 77−55669
$CsCoCl_3.2H_2O$ interchain exchange low temp. susceptibility 78−19240
$CsCrCl_3$, mag. structure and excitations, neutron diffr. and susceptibility meas. 80−44806
$CsFeCl_3$, single cryst. mag. susceptibility meas. 77−20560
$Cs_2FeCl_5.H_2O$, cryst. struct., superconducting susceptometer mag. meas. 79−73717
$Cs_2FeCl_5.H_2O$, mag. phase boundaries, susceptibility, 3D Heisenberg antiferromag. behaviour 78−84420
Cs_2FeF_5, mag. struct. and one-dimens. antiferromagnetism 80−60209
$CsGa_{1-x}Fe_xS_2$, tetrahedrally coordinated Fe atoms in low spin state, mag. props. and neutron diffr. study *(German)* 80−88714
$Cs_2KTmBr_6(Cl_6)(F_6)$, Cs_2NaTmF_6 and Cs_2RbTmF_6, mag. behaviour 2.9 to 251.3K, cryst. field levels, ang. overlap model *(German)* 80−29520
Cs_2KYbF_6, mag. behaviour, 3.5-251.3K *(German)* 80−50041
$CsMHoF_6$, (M=Na, K, Rb), mag. behaviour *(German)* 80−65774
$CsMnCl_3$, antiferromagnetic resonance, parametric spin wave excitation *(Russian)* 80−93183
$CsMnCl_3.2H_2O$:Cu, parallel susceptibility, impurity effect on spin-flop field *(French)* 78−43569
$CsMnCl_3.2H_2O$:Cu(Co), quasi one-dimens. antiferromag., mag. impurity effect on Neel temp. and spin-flop field 79−61099
$CsMnF_3$, antiferromag., suscept. oscillations beyond threshold for parametric excitation of electronic magnons *(Russian)* 77−59398
$CsN_{1-x}Mn_xF_3$, hexagonal perovskites, struct. evolution and mag. props., effects of high pressure 79−41987
$Cs_2NaCe(III)Cl_6$ high symmetry complex, low temp. Raman spectrum CF splitting, paramag. susceptibility temp. depend. *(German)* 77−12380
$Cs_2NaErCl_6$, mag. susceptibility and IR and Raman spectra meas., crystal field splitting determ. 80−100652
Cs_2NaYCl_6:^{249}Cf, mag. susceptibility of Cf^{3+} in octahedral site 77−12089
$Cs_2NaYbCl_6$, electronic struct., paramag. susceptibility and electronic Raman spectrum, cryst. field parameters *(German)* 77−63072
$Cs_2NaYbF_6(Br_6)$, mag. behaviour, 3.5-251.3K *(German)* 80−50041
$CsNiBr_3$, nearly one-dimensional antiferromag., thermal and mag. props. meas. 77−77041
$CsNiCl_3$, linear chain antiferromag., mag. props., 1.1 to 7K 79−61076
$CsNiCl_3$, mag. props. 79−73736
$CsNiF_3$, linear S=1 ferromag., easy plane anisotropy, low-temp. mag. props. 78−23250
$CsNiF_3$, longit. paramag. susceptibility, reaction field approx. 80−97059
$CsNiF_3$, quasi-one-dimens. Heisenberg system, reaction field approx. and dipolar interaction 77−36088
$CsNiF_3$, quasielastic neutron scatt. around Neel-point 80−75768
$CsNiF_3$, single cryst. mag. susceptibility meas. 77−20560
Cs_2NpCl_6, Mossbauer spectra and mag. susceptibility meas. 80−108140
$CsPr(MoO_4)_2$, energy levels and mag. props. of Pr^{3+} ion *(Russian)* 79−7810
$Cs_{1-x}Rb_xMF_3$ (M=Mg, Co, Ni, Zn), hexagonal fluoride perovskite structural evolution by cationic substitution *(French)* 80−24430
Cs_2RbYbF_6, mag. behaviour, 3.5-251.3K *(German)* 80−50041
$CsTmO_2$, mag. props. of normal-temp. form, 2.9-251.3K *(German)* 79−91205
$CsVBr_3$, mag. behaviour of V^{2+} in one- and two-dimens. Heisenberg systems 77−66235
$CsVCl_3$, mag. behaviour of V^{2+} in one- and two-dimens. Heisenberg systems 77−66235
$CsVX_3$, X=Br, Cl, I, mag. props. *(French)* 77−16059
$CsYbO_2$, normal-temp. form, mag. props. *(German)* 80−54864
Cu, Animalu transition metal model pot. invest. 80−75711
Cu complex, 1,2-ethanediammonium tetrachlorocuprate, layered struct. mag. susceptibility 80−7094

magnetic susceptibility continued
Cu complex, (4,4′-bipy H_2)$CuCl_6$, with infinite linear chains of dimeric units, struct. and mag. susceptibility 80−96498
Cu complex, $[C_6H_5(CH_2)_nNH_3]_2CuCl_4$, n=1,2,3, two-dimens. ferromagnet, NMR and mag. susceptibility 77−16058
Cu complex, chloride monodimethylsulfoxide, spin $^1/_2$ ferromag. Heisenberg linear chain, cryst. struct. and mag. susceptibility 80−15706
Cu complex, chloride tetramethylsulfoxide, spin $^1/_2$ ferromag. Heisenberg linear chain, cryst. struct. and mag. susceptibility 80−15706
Cu complex, $Cu_3Cl_6(H_2O)_2$.2 tetramethylsulphone, mag. interactions, susceptibility, 2-230K 80−60237
Cu complex, dichloro(dimethylnitrosamine)copper(II), magnetic phase transition, ^{14}N NQR obs. 80−11289
Cu complex, dichloro(dimethylnitrosamine) Cu II, mag. props., ^{14}N NQR obs. 80−54988
Cu complex, halocuprates, ferromagnetic insulator, two-dimens. Heisenberg layers, mag. susceptibility 80−50068
Cu complex, strong antisymmetric exchange 78−34976
Cu complex, tetrameric Cu(II) complex, higher-order spin coupling 79−99690
Cu complex, with 1,2,4-triazole, mag. susceptibility, 2-300K struct. 77−77045
Cu complex with adenine, powder, physical properties obs. *(Japanese)* 77−43878
Cu complex with L-phenylalanine amino acid, ESR spectra and magnetic susceptibility measurement 80−34761
Cu complexes, with tridentate Schiff bases, exchange interactions, EPR, mag. susceptibility 78−23324
Cu complexes with amino acids, static mag. susceptibility and effective mag. moment 77−12082
Cu, dynamic susceptibility, model pot. theory 80−75710
Cu, magnetic susceptibility, thermal density of states, non-local exchange-correlation effects 78−14924
Cu, nuclear antiferromagnetism, NMR obs. 79−78538
Cu, nuclear susceptibility thermometer rel. to ^{199}Sn Mossbauer effect thermometer, 6 mk to 1K 79−35737
Cu, spin density wave fluctuations in nuclear spins, susceptibility, internal energy 80−50115
Cu triazole complexes, finite Heisenberg chain effects, temp. depend. 79−47230
Cu-Al-Co liquid alloys, constant Co-content of 5 wt.%, mag. props. *(German)* 80−88720
Cu-Al-Fe, dil. liq. alloy, localised mag. state interactions *(German)* 77−1539
Cu-Al-Mn, Heusler alloy, magnetic prop. investig. of struct. transitions *(German)* 77−8289
Cu-Al-Mn liq. alloys, susceptibility behaviour 80−93077
Cu-Al-Mn spin glass, field depend. suscept. 79−73739
Cu-based alloys, α-phase, mag. susceptibility correl. with lattice parameter 78−68154
Cu-Co, solid soln., mag. susceptibility near solubility boundary *(Russian)* 79−15281
Cu-Co heterobinuclear complex, cryst., mag. susceptibility of Cu-Co(fsa)$_2$ en, $3H_2O$ 80−2556
Cu-Cr alloys, dil., mag. susceptibility 77−63092
Cu-Fe, dil., internally oxidised mag. and electrical prop. 77−12100
Cu-Fe, dil., local susceptibility, Mossbauer meas. 78−19400
Cu-Fe alloy, dil. dynamic susceptibility around T_k, satellite nucl. spin-lattice relax. time meas. 77−4573
Cu-Fe alloy, local moment system, low temp. susceptibility, Mossbauer effect meas. 77−43810
Cu-Fe alloy film, mag. susceptibility max. 79−24173
Cu-Fe dilute alloys, Kondo system, static and dynamic susceptibilities, hyperfine studies 77−63090
Cu-Ga(Ge), liq., diamagnetism 78−72326
Cu-M, M=Al,Cd,In,Ga,Zn, magnetic susceptibility, comp. and temp. depend., melting effects 78−52202
Cu-Mn, mag. irreversibility and metastability 78−19279
Cu-Mn, mictomag., massive short-range antiferromagnetism 77−12139
Cu-Mn, spin glass, meas. of order parameter 80−34642
Cu-Mn, spin glass, transition temp., freq. depend. 80−97113
Cu-Mn, spin glasses, alternating susceptibility 80−65912
Cu-Mn (7 at.%), magnetic susceptibility, clustering, band model of heterogeneous magnetics 77−43823
Cu-Mn (8 at.%), spin glass, neutron scatt. and susceptibility investig. of spin dynamics 77−40076
Cu-Mn alloy, effect of ageing on mag. props. 77−28366
Cu-Mn alloy spin glass, macroscopic mag. anisotropy, transverse susceptibility and zero field NMR enhancement 80−80525
Cu-Mn-Al, Heusler alloys, ferromag. inclusions, mag. props. and struct. study *(Russian)* 80−80570
Cu-Ni, mag. ordering temp. depend. on atomic short-range order from susceptibility meas. 79−61159
Cu-Ni alloy, critical conc. for ferromagnetism 78−14969
Cu-Ni film, ferromag., mag. susceptibility meas., 30-130°C 79−95615
Cu-Ni-Co, mag. props. of system of disperse ferromag. particles, 73 to 673K *(Russian)* 80−65968
Cu-Ni-Fe (14, 7 wt.%), solid soln., decomposed, magnetostatic interaction between ferromag. particles *(Russian)* 77−80967
Cu-Ni-Fe solid solution, after precip., susceptibility of interacting superparamag. grains 79−99733
Cu-Pd, mag. susceptibility and electronic struct. of ordering *(Russian)* 80−11161
Cu-Pd alloy, singularities of physical props. and ordering *(Russian)* 78−76643
Cu-Sn, self-diffusion of Sn, correl. with other props. *(Russian)* 79−23764
Cu-transition metal alloy, internal adsorpt. and mag. susceptibility, grain size effects *(Russian)* 78−19759
$CuAl_{1-x}Fe_xS_2$ system, delocalisation of d-electrons, mag., elec. and optical obs. 78−34804
$Cu_2(AsO_4)Cl$, temp. depend. of mag. susceptibility 80−70962
CuAu, mag. susceptibility and electronic struct. of ordering *(Russian)* 80−11161
Cu_3Au, mag. susceptibility and electronic struct. of ordering *(Russian)* 80−11161
$Cu_2{}^{I}B^{II}C^{IV}X_4$, ($B^{II}$=Zn, Mn, Fe, Co; C^{IV}=Si, Ge, Sn; X=S, Se), X-ray elec. and mag. meas. 79−65660
$CuBr_2$, finite Heisenberg chain effects, temp. depend. 79−47230
$Cu(C_5H_5NO_6)(BF_4)_2$, sp. ht. and susceptibility, comparison with quadratic spin 1/2 Heisenberg antiferromag. calcs. 77−66353

magnetic susceptibility continued
CuCl, anomalous diamagnetism, high temp. Meissner effect *(Russian)* 78−34955
CuCl, high press. phases and anomalous props. 79−7689
CuCl, pressure depend. of structural, chemical, elec. and mag. props. 80−96596
$CuCl_2$, anhydrous, single cryst., mag. behaviour in low temp. ordered phase 79−7974
$CuCl_2$, anhydrous paramagnetic phase, mag. susceptibility depend. on temp. 79−7965
$CuCl_2$, finite Heisenberg chain effects, temp. depend. 79−47230
$CuCl_2$.TMSO, ferromag. spin $^1/_2$ linear chain, mag. susceptibility 78−68180
$CuCrS_2$ single cryst., spectral study and phys. props. *(French)* 80−29002
$CuCr_2S_{4-\gamma}$, spinel, anomalies in paramag. susceptibility, Curie pt. *(Russian)* 77−80910
$CuCr_2Se_4$, crit. behaviour near Curie point 78−31068
$CuCr_2Se_4$, experimental obs. 78−76227
$Cu_{1-x}Cr_2Se_4$, influence of excess Cu on physical props. 80−103836
CuFe solid solns., quenched from vap. phase, mag. props. 80−60307
$CuFe_2O_4$-$CuGa_2O_4$, physicochem. props. *(French)* 77−44233
Cu_xFeS_4, mag. ordering and vacancy clustering, mag. susceptibility and Mossbauer spectra meas. 77−85625
Cu(II)-DL-proline complex, ESR, magnetic susceptibility and optical absorption 80−93167
n-$CuInS_2$, mag. props., obs. 80−70939
$CuK_2Cl_4.2H_2O$, 3-dimens. Heisenberg ferromag., crit. behaviour 77−20594
$CuK_2Cl_4.2H_2O$, Heisenberg ferromag., press. effect on Curie temp. and susceptibility 77−28386
$CuK_2Cl_4.2H_2O$, Heisenberg ferromag., mag. props. at high press. 77−69512
$CuK_2Cl_4.2H_2O$, Heisenberg ferromag., mag. field effect on susceptibility near crit. point 80−39758
$Cu_xMg_{1-x}Al_2O_4$, spinel solid solns., solid-state and surface props. 77−66415
CuMn spin glass, AC susceptibility 80−60305
CuMn, spin glass, remanence, new approach from zero field NMR 80−34785
CuMn, spin glass low DC field mag. susceptibility using SQUID 79−69684
$Cu_{0.98}Mn_{0.02}$, spin glass, Heisenberg mode, RPA approx. 80−65904
Cu_2MnAl, dynamical mag. susceptibility, spin waves, calc. from band struct. 80−54871
Cu_2MnAl superparamagnetic particles in Cu_3Al lattice, magnetic moment ferromagnetic ordering *(Russian)* 79−78444
$Cu_xMo_6S_8$, $1.5\leq x\leq 3.55$, low temp. phase diagram, 1.2-320K 77−85371
$Cu(NH_4)_2Br_4.2H_2O$, 3-dimens. Heisenberg ferromag., crit. behaviour 77−20594
$Cu(NH_4)_2Br_4.2H_2O$, Heisenberg ferromag. press. effect on Curie temp. and susceptibility 77−28386
$Cu(NH_4)_2Br_4.2H_2O$, Heisenberg ferromag., mag. props. at high press. 77−69512
$Cu(NH_4)_2Br_4.2H_2O$ Heisenberg ferromagnet, mag. props. in mag. field 80−34637
$Cu(NH_3)_4(NO_3)_2$, single cryst., low temp. susceptibility and sp. ht., 10 behaviour 77−89929
$Cu(NH_4)_2.Br_4.2H_2O$, Heisenberg ferromagnetic, singularity shift approx. by power functions 79−7992
$Cu(NO_3)_2.2^1/_2H_2O$, high field phase transition, susceptibility and NMR meas. 77−69559
$Cu(NO_3)_2.2^1/_2H_2O$, singlet ground-state system, mag. props., short-range ordered state 78−23289
$Cu(NO_3)_2.2.5H_2O$, linear Heisenberg antiferromag., mag. and thermodynamic props. 79−61136
$Cu_4NiSi_2S_7$, X-ray cryst. struct. determ., mag. props. 80−107172
CuO-CdO-Fe_2O_3, sintered ferrite, preparation, mag. susceptibility, DC resistivity 80−34598
CuO-ZnO-Fe_2O_3, sintered ferrite, preparation, mag. susceptibility, DC resistivity 80−34598
Cu_2O-CuO-MoO_3, subsolidus phase diagram, mag. props. 80−50615
$(Cu_3Pt)_{1-c}Mn_c$, mag. suscept. and effect of atomic order and disorder 77−24669
$CuRb_2Br_1.2H_2O$, three-dimens. ferromag., crit. susceptibility exponents in Curie temp. region using relax. techniques 77−66304
$CuRb_2Br_4.2H_2O$, 3-dimens. Heisenberg, ferromag., crit. behaviour 77−20594
$Cu(Rh_{1-x}Cr_x)S_4$, spinel system, susceptibility and metallic resistivity, anomalies due to s-d interaction 80−70958
Cu_2S-Tl_2S system, phase diagram 80−20906
Cu_xS, $1\leq x\leq 2$, quantum temp. size effect and magnetism *(Russian)* 80−103764
$Cu_{2-x}Se$, electric, thermal and magnetic props. investigation in low temp. phase *(Croatian)* 79−11299
$Cu_{2-x}Se$, nonstoichiometric, diamag. and paramag. props., susceptibility meas. 80−70936
$CuSe_2O_5$, strongly antiferromag. coupled Cu linear chain, orbital props. 80−100580
$Cu_2U_6S_{13}(Se_{13})$, cryst. struct. and magnetic props. *(French)* 80−96496
α-$Cu_xV_2O_5$, EPR and mag. susceptibility meas. 80−2627
$Cu_xV_2O_5$, nonmetallic bronze, low field sp. ht. and mag. suscept. 78−72357
CuV_2S_4, preparation, cryst. struct. and physical props. *(French)* 79−55714
$Cu_{0.65}VS_2$, cryst. struct. and phys. props. *(French)* 79−60334
$Cu_{0.75}VS_2$, cryst. struct. and phys. props. *(French)* 78−14328
$Cu_{60}Zr_{40}$ glassy metal, photoemission and mag. susceptibility 79−28896
dimethylammonium manganese tetrachloride, 2D Heisenberg antiferromag., spin wave anal. 80−54879
Dy, Curie-Weiss law anisotropy, paramag. susceptibility meas. 80−15686
Dy, domain effects near order-disorder and order-order ferromagnetic transitions 80−65886
Dy, liq., mag. susceptibility, elec. resistivity 80−20377
Dy, mag. anisotropy and susceptibility 77−69539
Dy, magnetic domain structure, hysteresis, thermal modulation study 80−71082
Dy, parasusceptibility meas., 4.2-130K, spin wave anal. 79−95583
Dy-Fe-Al, pseudobinary alloys, mag. props. 77−59397
Dy-Th, single cryst., mag. susceptibility, transitions, anisotropy 80−54873

magnetic susceptibility continued
Dy-Y, paramag. susceptibility in basal plane and hexagonal axis 77−20548
$DyAG$, cubic antiferromagnet, multiaxis phase transitions 79−78377
$DyAsO_4$, phase transitions obs. 80−70412
$DyAu_6$, mag. props. temp. depend. *(French)* 77−51879
DyC_2, mag. susceptibility, temp. depend. 79−87239
$Dy_xCe_{1-x}Ru$, supercond., mag. order 79−87189
$DyCo_2Si_2$, mag. props. 80−107988
$DyCrO_4$, determ. of mag. struct. by neutron diffr. 79−51753
DyF_3, transferred hyperfine interaction, NMR study 78−68393
$Dy(Fe_xNi_{1-x})$, mag. interactions, mol. field model 77−73010
$Dy(Fe_xNi_{1-x})_2$, mag. behaviour, susceptibility and Mossbauer expts., 4.2-1300K 78−52235
$Dy_3Fe_5O_{12}$, formation mechanism from metallic oxides 77−48376
$Dy_3Ga_5O_{12}$, crystal field effect on paramag. props. of Dy^{3+} ion 80−50040
$Dy_3Ga_5O_{12}$, dipolar magnet, sp. ht. and magnetisation meas. 80−60344
DyIG, mol. field coeffs., magnetisation and mag. susceptibility anal. 78−95406
$Dy_2(MoO_4)_3$, mag. susceptibility, ferromagnetism, mol. field theory 78−34966
$Dy_{1.2}Mo_6S_8$, mag. ordering in supercond. state, resist. and AC susceptibility meas. 78−19194
$DyNi_2Si_2$, mag. props., 4.2-200K 80−84602
Dy_2O_3, 300 to 900K, mag. susceptibility and Curie temp. meas. 78−56288
$Dy_2O_2SO_4$, antiferromag., mag. props. and Zeeman effect meas. 79−33464
$Dy_2O_2SO_4$, mag. ordering, magnetisation, AC susceptibility and Zeeman effect meas. 80−60205
$DyPO_4$, susceptibility near mag. phase boundaries 78−52258
DyScFe garnets, mag. props. 77−47979
Dy_2Se_3, mag. susceptibility 77−40032
$DyVO_4$, basal plane magnetisation anisotropy under Jahn-Teller distortion 78−68222
$DyVO_4$, phase transitions obs. 80−70412
$Dy_2(WO_4)_2$, mag. props., 300 to 900K 79−28510
Dy_2ZrS_5, mag. and sp. ht. meas. on polycrystalline samples 78−23253
Er, magnetisation and susceptibility in basal plane in strong mag. field *(Russian)* 80−50145
Er, magnetisation in strong pulsed mag. field, differential susceptibility meas. *(Russian)* 79−19729
$Er_3Au_3Sb_4$, mag. suscept. meas., 4 to 300K 79−51742
$Er(C_2O_4)(C_2O_4H).3H_2O$, single cryst., mag. susceptibility, 1.5-20K, g-factors 77−77094
$Er_{65}Co_{35}$, amorphous, amg. ordering, susceptibility, magnetisation and hysteresis meas. 78−68190
$ErCo_2Si_2$, mag. props. 80−107988
$ErFe_3$, mag. anomalies at 47 and 131K 77−63134
ErGa garnet, crystal field theory calcs. 77−8259
ErH_3, cryst. fields and mag. props. 78−68181
$Er_{1-x}Ho_xRh_4B_4$, re-entrant supercond. and mag. ordering 78−60240
$(Er_{1-x}Ho_x)Rh_4B_4$, superconductive and mag. interactions, hydrostatic press. effect 80−49973
ErIG, magnetic props. of single cryst., 4.2-600K 79−78341
$Er_2(MoO_4)_3$, mag. susceptibility, ferromagnetism, mol. field theory 78−34966
$Er_{1.2}Mo_6S_8$, mag. ordering in supercond. state, resist. and AC susceptibility meas. 78−19194
$Er_xMo_6Se_8$, long-range antiferromag. order and supercond. coexistence 78−10715
$ErNi_5$, cryst. field parameters in ferromag., paramag. states, susceptibility meas. 77−63139
$ErNi_2Si_2$, mag. props., 4.2-200K 80−84602
Er_2O_3, 300 to 900K, mag. susceptibility and Curie temp. meas. 78−56288
Er_2O_3, mag. susceptibility, elec. cond. and dielectric const., hopping cond. 77−12083
$Er_2O_2SO_4$, antiferromag., mag. props. 1.6 to 40K 79−33464
$ErRh_{11}Sn_{3.6}$, synthesis, supercond. and mag. props. 80−100547
Er_2Se_3, mag. susceptibility 77−40032
Er_2Te_3, magnetic susceptibility meas., cryst. field interpretation 80−11156
$Er_2(WO_4)_3$, mag. props., 300 to 900K 79−28510
$Er_xY_{1-x}Al_2$, mag. props. meas. and neutron diffr. data 80−7126
Er_2ZrS_5, mag. and sp. ht. meas. on polycrystalline samples 78−23253
Eu-As-S, glass forming region, Raman and IR obs. *(French)* 79−99080
Eu-Cd compounds, Mossbauer effect, mag. props. and lattice consts. 77−36164
$EuAl_2S_4$, mag. susceptibility and EPR meas. 80−71173
EuB_6, correlation between mag. struct. and elec. props. 77−63192
EuB_6, ferromag., mag. props. 80−2561
EuB_6, pure single crystals, magnetic and electric props. 80−11260
$EuB_{6-x}C_x$, pure and doped, mag. and transport props. 80−54689
$Eu_2B_5O_9Cl(Br)$, synthesis and characterisation 80−39039
$EuCl_2$, $EuCl_2$-$EuCl_3$, $EuCl_2$.HCl, mag. props., 77-292K 78−52197
$EuFe_4Al_8$, mag. ordered, mixed valency of Eu, X-ray, susceptibility and Mossbauer spectra studies 79−19728
$EuGa_2S_4(Se_4)$, mag. susceptibility and EPR meas. 80−71173
$Eu_{1-x}Gd_xS$ and $Eu_xSr_{1-x}S$, spin glasses, transition temp., freq. depend. 80−97113
Eu_2IrH_5, prep., cryst. struct., mag. and elec. props. 80−88117
EuM_2Ge_2, M=Mn, Fe, Co, Ni, Cu, magnetism and hyperfine interactions 78−76228
$Eu_2Mg_3(NO_3)_{12}.24H_2O$, Zeeman effect in ahsorpt. spectrum 77−63402
$EuNi_xCu_{5-x}$, mixed valency of Eu, consistency of susceptibility and Mossbauer expts. 78−52407
$EuNi_xZn_{5-x}$, mixed valency of Eu, consistency of susceptibility and Mossbauer expts. 78−52407
EuO, magnetic susceptibility, quasiphase transition 79−65684
EuO, magnetic susceptibility critical exponent, corrections to scaling 80−103846
EuO, zero-wave vector kinetic coefficient near T_c 79−73714
EuO:Eu, doped ferromag. semicond., carrier density and mag. susceptibility rel. to M-S transition 77−72820
Eu_2O_3, large single crystals, production and props. rel. to structural anisotropy *(French)* 77−36396
$EuO_{1-x}N_x$, ferromag. semicond., elec. and mag. props. *(French)* 78−79993

magnetic susceptibility continued
EuO(S)(Se)(Te), cryst. and electronic struct., mag., elec., and optical props., book contrib. 80−39760
EuPd, mech. of H absorption, Mossbauer, mag. and X-ray diffr. meas. 78−38846
$Eu_{1-x}{}^2R_x{}^+O_{1-x}$ (R=Nd, Eu, Gd), lattice parameters, mag. and elec. props. 80−100578
$EuRh_2$, mech. of H absorption, Mossbauer, mag. and X-ray diffr. meas. 78−38846
EuS, ferromag. semicond., high field susceptibility, spin waves 80−75735
EuS film, magnetic props. using transverse Kerr and Voigt effects 77−52054
EuS, single cryst., high-field susceptibility meas., temp. range 2.5 to 16.5K 80−84589
EuS, spin relax. in crit. region 78−52270
EuS, spin relaxation crit. behaviour 78−76251
EuS, three dimens. Heisenberg ferromagnet, crit. relax. spectra mag. susceptibility 79−8000
$EuSO_4$, sp. ht. and susceptibility meas. 78−14977
$Eu_2(SO_4)_3.8H_2O$, mag. props., thermal var., cryst. field reduced matrix elements 77−51875
$EuSb_2$, cryst. struct. and antiferromag. props. 79−32973
Eu_2Sb_3, cryst. struct., elec. and mag. props. 80−33958
$EuSm_2S_4$, mag. props. 78−68237
$Eu_{1-x}Sm_xS$, ESR, exchange interaction, susceptibility, elec. cond., thermoelectric power 80−93174
$Eu_5Sn_3S_{12}$, mag. and thermodynamic props., metamagnetism 80−60273
(Eu_xSr_{1-x}) S dilute, spin-cluster freezing observation by low-freq. mag. absorpt. 79−78404
$Eu_xSr_{1-x}M_4O_{11}$, M=Nb, Ta, electrophys. and mag. props. 77−89760
$Eu_{1-x}Sr_xS$, non-metallic system, spin glass behaviour 79−24175
$Eu_xSr_{1-x}S$, blocking of pairs and spin glass freezing 79−61174
$(Eu_xSr_{1-x})S$, dilute, magnetic 'blocking' 79−78348
$Eu_xSr_{1-x}S$, dilute Heisenberg magnet, complex susceptibility of blocked spins 80−15740
$Eu_xSr_{1-x}S$, ferromagnet-spin glass transition, mag. ordering, mag. susceptibility and neutron scatt. meas. 80−50135
$Eu_xSr_{1-x}S$, insulating spin glass, mag. props. 80−2589
$Eu_xSr_{1-x}S$, non-metallic spin glass system 79−61175
$Eu_xSr_{1-x}S$, paramag. susceptibility, expt. and comparison with high temp. series expansion 80−60176
$Eu_xSr_{1-x}S$, spin glass to ferromag. transition, neutron scatt. and susceptibility meas. 80−60254
$(Eu_xSr_{1-x})S$, very dil., magnetisation dynamics 80−65915
$EuTi_{1.5}W_{0.5}O_6$, Stark sublevels in mag. suscept. and luminesc. 77−51876
Eu_2VO_4, prep. and props. 77−15379
$Eu_3V_2O_7$, prep. and props. 77−15379
$Eu_3VTa_2O_9$, prep., characterisation and mag. props. 78−26535
$Eu_2(WO_4)_3$, mag. susceptibility, elec. cond. and dielec. const. meas. 77−11916
$Eu_2(WO_4)_3$, mag. susceptibility, paramag. Curie temp., 300-900K 79−82753
$Eu_2(WO_4)_3$, molar mag. susceptibility meas., 4.2-900K 77−4507
$Eu_2(WO_4)_3$, molar mag. susceptibility, DC elec. cond., thermopower meas. 79−15172
$Eu_{1-x}Yb_xO(S)$, solid soln., ferromag. semicond., increase of exchange interaction 78−88109
F_2, mag. shielding and susceptibility, finite perturbation mol. orbitals calcs. 77−46513
Fe (III)M (II)$F_5.7H_2O$, M=Fe, Co, Ni, Zn, antiferromagnetism 77−59395
Fe, [111] oriented whisker, mag. domain struct. and approach to saturation 79−82814
Fe alloys, temperature-time instability of initial susceptibility meas., using bridge instrument with electronic demagnetiser *(Slovak)* 78−57989
Fe, atomic layers, Pauli paramagnetism to band ferromagnetism transition thickness depend. 78−72377
Fe, BCC, mag. relax. due to C and N meas., 210 to 410K 77−36102
Fe base amorphous alloys, Invar and Elinvar characts. 80−29592
Fe complex, $[Fe(S_2C_2O_2)_2X]^{2-}$, (X=Cl,Br,I), Mossbauer effect, EPR, mag. susceptibility 79−11366
Fe complex, bis[2-(2-pyridylamino)−4-(2-pyridyl)thiazole]Fe(II) complexes, high spin-low spin transitions 77−8456
Fe complex, dithiocyanato bis(4-methyl-1, 10-phenanthroline) iron, Mossbauer effect and magnetism down to 0.98K 77−28490
Fe complex, Fe (II) pseudo-tetragonal high-spin cpds., paramag. susceptibility amd Mossbauer quadrupole splitting 78−26834
Fe complex, Fe_xM_{1-x}(1,10-phenanthroline)$_2(NCS)_2$, M=Mn,Co,Ni, spin crossover, Mossbauer and magnetism study 80−44980
Fe complex, $Fe(Br)[S_2CN(C_2H_5)_2]_2$, 3-D Ising ferromag., cryst. susceptibility, 1.5-20K 80−20390
Fe complex, $Fe(Cl)[S_2CN(C_2H_5)_2]_2$, single cryst. susceptibilities 78−31057
Fe complex, $Fe(Cl)[S_2CN(C_2H_5)_2]_2$, susceptibility near critical pt. 79−24147
Fe complex, $Fe(Cl)[S_2Cn(C_2H_5)_2]_2$, 3-D Ising ferromag., cryst. susceptibility, 1.5-20K 80−20390
Fe complex, Fe(II) and Fe(III) cyanides-3d transition metal, mag. suscept., reflectivity spectra, cryst. field 79−56808
Fe complex, Fe(II) oxalato-bridged chain compounds, Mossbauer spectra 80−15890
Fe complex, Fe(1,2,4-triazole)$_2(NCS)_2$, quasi-2-dimens. S=$^1/_2$ antiferromag., mag. props., hidden canting 80−107986
Fe complex, Fe(5-methylpyrazole)$_4X_2$, X=Cl, Br, I, mag. susceptibility, mag. saturation; Mossbauer and ligand field spectra, single model interpretation 78−23064
Fe complex, Fe(papt)$_2$, high spin $^5T_2$⇌low spin $^1A_1$ transition, Debye-Waller factors and magnetism 78−80259
Fe complex, Fe(pyrazole)$_4X_2$, X=Cl, Br, I, mag. susceptibility, mag. saturation; Mossbauer and ligand field spectra, single model interpretation 78−23064
Fe complex, halobis(morpholyldithiocarbamato)Fe(III), solvation effects, mag. susceptibility and Mossbauer spectra 78−27129
Fe complex, $K_3[Fe(SCN)_6].4H_2O$, optical reflection spectrum, mag. suscept., permittivity, dehydration temp. 79−56809
Fe complex, tetraphenylporphynate iron III bromide, mag. props., zero-field splitting 80−34584
Fe complex, tris(1-pyrrolidinecarbodithioato)iron(III), and related cpds. mag. props., struct. 77−89933
Fe complex, with 1,2,4-triazole, mag. susceptibility, 2-300K, struct. 77−77045

magnetic susceptibility continued
Fe complex (2, 9-dimethylphenanthroline) sulphate, mag. props., Mossbauer spectra 80−66081
Fe complexes, cycanides, mag. susceptibility and optical reflection spectra 77−59382
Fe complexes, electronic and mag. struct., semiempiricial MO cluster calcs. 78−62733
Fe complexes, FeOCl[Co(cyclopentadienyl)$_2$]$_{0.16}$ and FeOCl[Fe(cyclopentadienyl)$_2$]$_{0.16}$, Mossbauer and mag. susceptibility meas. 80−44176
Fe complexes, mag. susceptibility, Mossbauer spectra 78−15071
Fe complexes, S-bridged binuclear, orbitally dependent exchange 77−24688
Fe complexes with dimethylformamide, dimethylthioformamide, Mossbauer and mag. props. 80−39974
α-Fe, cyclically deformed, mag. props. 77−28412
Fe, deformed, dislocation structure determ. from magnetic props. 78−55874
Fe, ferromag., dynamic susceptibility calc. 80−80488
Fe, magnetic susceptibility, lineshape and moment analysis, magnon excitations 79−99693
Fe, paramagnetic, orbital magnetic susceptibility calc. 80−7075
Fe particles in glass-like C matrix, identification and props. 80−11229
Fe, plastically deformed, dislocation arrangement exam. by ferromag. techniques 78−63774
Fe, plastically deformed, high field suscept. anisotropy and domain struct. 78−15002
Fe powder, meas. by high frequency pulse technique 78−93739
Fe, spin susceptibility, high-field, spin-density functional formalism 80−70959
Fe, Stoner model, mol. field coeff., temp. and field depends. 77−72975
Fe whiskers, AC susceptibility, critical slowing down of mag. fluctuations 77−69594
Fe-Al, ferromag.-mictomag. transition, intermediate superparamag. 77−12140
Fe-Al, paramag. props., T_c to 1500K 78−68153
Fe-Al$_2$O$_3$ granular films, superparamagnetism and relax. effects 80−71118
Fe-B, amorphous, Invar-type alloy, mag. moment and high field susceptibility 78−34965
Fe-B, amorphous, mag. aftereffect, initial susceptibility time depend. 80−88829
Fe-B, liq., mag. susceptibility meas. 80−75740
Fe-B-C alloys, amorphous, temp. depend. of magnetisation 79−73690
Fe-B(P) amorphous alloy, Invar effects, mag. props. meas. 79−56594
Fe-C melt, mag. susceptibility and short range order, 900-1800°C 78−84382
Fe-Cr (70-92 at.%), coexistence of ferro- and antiferromagnetism *(Russian)* 78−47955
Fe-Cr alloys, mixed ferro-/antiferromag. interactions *(Russian)* 77−32173
Fe-Cr-Ni, mag. state at low temps. *(Russian)* 78−56298
Fe-Cr-Ni alloy, austenitic, Neel temp. and max. susceptibility predictions comp. effects 77−43833
Fe-Mn alloys, mag. susceptibility and conc. depend. of Neel point *(Russian)* 79−47279
Fe-Mn(0 to 80 wt.%), paramagnetic susceptibility by Faraday method, band model interpretation *(Russian)* 77−20545
Fe-Nb alloys, mag. and Mossbauer meas. 77−63133
Fe-Ni, quenched irreversible alloy, zero or negative thermal dilatation, para-process mag. susceptibility 79−4419
Fe-Ni alloy, FCC, high-field susceptibility and spin wave spectrum 79−56493
Fe-Ni alloys, FCC, mag. props. calc. 79−65659
Fe-Ni based alloy, amorphous rapidly quenched, mag. props. 77−66269
Fe-Ni Invar, magnetisation and high field susceptibility 79−56518
Fe-Ni Invar, magnetovolume coupling enhancement factor, temp. depend. 80−88851
Fe-Ni Invar alloys, Arrott plots rel. to itinerant electron characts. 77−73009
Fe-Ni Invar alloys, thermodynamic props. 79−56560
Fe-Ni Invar anomalies, explanation in terms of itinerant electron magnetism 80−75705
Fe-Ni-Co-Ti, martensite cryst. lattice tetragonality, $\gamma \rightleftharpoons \alpha$ transform. *(Russian)* 79−61587
Fe-Ni-Cr, Elinvar, struct. and mag. props., singularities during tempering *(Russian)* 80−50627
Fe-Ni(Co), solid and liq., paramag. susceptibility and electron struct., 800-1800°C *(Russian)* 80−25081
Fe-Ni(Cr), Invar, exchange interactions between ferromag. and antiferromag. components 80−29545
Fe-Pd Invar alloys, elec. and mag. props. and thermal expansion 80−75732
Fe-Pt, Invar alloy, paramag. susceptibility 80−70940
Fe-Pt, Invar alloy, thermodynamic properties, effects of forced magnetostriction 79−11331
Fe-Pt alloy, ordered, anisotropy of mag. props. *(Russian)* 78−60280
Fe-Si(Ge)(Al), solid and liq. paramag. props. *(Russian)* 77−66247
Fe-Ti, magnetism and H_2 storage 80−70941
Fe-Ti:H(D), isotope effects of diatomic TiH and TiD complexes 79−47259
Fe-V-C melts, electron struct., mag. susceptibility meas. *(Russian)* 78−47729
Fe^{3+}-doped crystals, cryst. field calc. 78−76035
Fe_2 magnetism, randomised exchange field theory 80−39733
$Fe_{3-x}Al_xO_4$, cation distrib., mag. and other phys. props. 77−43818
$Fe_{100-x}B_x$, amorphous, mag. struct., mag. susceptibility meas. 80−80485
$Fe_{80}B_{20}$ amorphous ribbon, initial susceptibility time lag 80−100579
$Fe(BF_4)_2.6H_2O(6D_2O)$, phase transition, mag. susceptibility and anisotropy and permittivity meas. 79−23718
$FeBMO_4$, M=Mg, Cu, Co, Ni, mag. props. meas. 80−34607
$FeBO_3$, magnetisation near crit. temp., up to 3 kbar hydrostatic press., scaling theory 77−8316
$FeBO_3$, weak ferromag., mag. field influence on crit. behaviour of susceptibility 78−14942
$FeBO_3$-MBO_3 solid soln., (M=Mn, Cr, Al, Ga, In), synthesis, crystal chem. and mag. props. 78−31058
$FeCl_2.2H_2O$-$CoCl_2.2H_2O$ random mixture, phase diagram 79−73748
$FeCl_2$(pyrazole)$_2$, linear-chain cpd., low-temp. mag. behaviour 80−71253
$Fe_{1-x}Co_xAl$, Knight shift and mag. susceptibility study, electron struct. peculiarities *(Russian)* 80−15814
$Fe_{1-x}Co_xCl_2$, mag. phase diagram 80−11198
$Fe_{(1-x)}Co_xCl_2.2H_2O$, random mixture of anisotropic antiferromags., isotropic state obs. 78−84396
$FeCoF_5.2H_2O$, ferrimag. props., suscept. and transitions, 3-296K 79−87240
$Fe_{1-x}Co_xGe_2$ solid solns., mag. susceptibilities, multiple stages in mag. transitions, effective mag. moment 77−8286
$Fe_xCo_{1-x}Rh_2S_4$, spinel struct., X-ray, mag., elec. and Mossbauer spectra meas. 77−12278
$Fe_xCo_{1-x}Si$ alloys, disordered, hydrostatic pressure effects on mag. props. 77−32175
$Fe_xCo_{1-x}Si$, mag. props., effect of hydrostatic press. 77−12101
$Fe_xCo_{1-x}Si$, mag. props. 79−56532
$Fe_xCo_{1-x}Si$(Ti), magnetic props., sp. ht. and resist. meas. 79−61120
$Fe_xCo_{1-x}Ti$, high press. mag. props. 78−23271
$Fe_xCo_{1-x}Ti$, mag. props. 79−56532
$FeCr_2S_{4-x}Se_x$ chalcospinels, ESR spectrum and paramag. susceptibility 80−15789
$Fe_{0.5}Cu_{0.5}Cr_2S_4$, ESR spectra, elec. and mag. props., Curie temp. 80−97137
$Fe_xCu_{1-x}Cr_2Se_4$, crystallographic and image props. 80−39049
$Fe_xCu_{1-x}Rh_2S_4$, mag. tetrahedral intrasublattice interaction, X-ray, magnetisation and Mossbauer expts. 78−52241
FeF_2, mag. sp. ht. near Neel temp. mag. susceptibility meas. 80−60341
FeF_3, amorphous, mag. props. and Mossbauer spectra, speromagnetism and mictomagnetism 80−75778
FeF_3, amorphous, noncryst. magnet with antiferromag. interactions 79−91228
FeF_3, magnetic susceptibility near Neel point 77−55670
$Fe_2F_5.2H_2O$, ferrimagnetism, susceptibility obs. 5-300K, phase transition 79−4658
$Fe_5(Fe_{1-y}Co_y)$, mag. and calorimetric props. 77−63083
$FeGa_2O_4$, magnetic props. by Mossbauer effect, neutron diffr. and magnetisation meas. 77−43918
$FeGa_2Se_4$, elec. cond., phase diagram 80−88301
$FeGe_2$ canted antiferromagnet, mag. susceptibility anisotropy and temp. dependence 80−25112
Fe_xI_y cyclodextrin, quasi-one-dimens. cpd., synthesis, elec. and mag. props. 80−2380
Fe(III) compounds, $A_2FeX_5.H_2O$, (A=alkali ion, X=Cl or Br), antiferromag. props. and struct. 78−31056
Fe_5LiO_8, magneto-crystalline anisotropy, magnetoelectric effect interpretation *(French)* 79−47316
$(Fe_{1-x}M_x)_2P$, (M=Co,Ni), magnetisation, susceptibility, thermal expsn. 79−11302
$FeMgBO_4$ and $FeMg_2BO_5$, mag. props., spin glass behaviour 79−61145
$Fe_{1-x}Mn_xCl_2$, disordered, Raman scatt. from Fe^{2+} and Neel temp. 80−60579
$(Fe_{1-x}Mn_x)_{75}P_{16}B_6Al_3$, amorphous, spin-glass-ferromag. multicritical point, AC susceptibility meas. 80−50117
Fe_2MnSi, antiferro- and ferromag. props. 77−12104
$Fe_{78}Mo_2B_{20}$, amorphous ferromag., mag. props. 79−38309
$FeNb_2O_6$, magnetisation, 1.4-80K, antiferromag. ordering 78−10666
$Fe_{1/3}NbS_2$, intercalate, metallic cond., Hall effect and mag. props. 77−76789
Fe_xNbSe_2 (2H), mag. susceptibility meas., 1.3-300K 80−39740
$Fe(Nb_{1-x}W_x)O_4$, mag. and elec. props. and Mossbauer effect 79−78590
$(Fe_{0.5}Ni_{0.5})$-Co, solid and liq., paramag. susceptibility and electron struct., 800-1800°C *(Russian)* 80−25081
$Fe_{1-x}Ni_xAl$, Knight shift and mag. susceptibility study, electron struct. peculiarities *(Russian)* 80−15814
$FeNiBO_4$, $FeNi_2BO_5$, Mossbauer spectra, mag. relax. 80−15889
$FeNiBO_4$, mag. and Mossbauer studies 79−65661
$FeNi_2BO_5$, mag. and Mossbauer studies 79−65661
$Fe_{80-x}Ni_xB_{20-y}P_y$, amorphous, Rayleigh region and coercive force 80−88806
$(Fe_{0.5}Ni_{0.5})_{1-x}Co_x$, paramag. susceptibility, solid and liq. phases 1000-1800°C *(Russian)* 77−16040
$Fe_{40}Ni_{38}Mo_4B_{18}$, metallic glass, mag. and transport props. 80−39752
$(Fe_{1-x}Ni_x)_2P$, mag. props. 78−23248
$(Fe_{0.04}Ni_{0.96})_{80}P_{10}B_{10}$, amorphous magnetisation, field and temp. depend. 80−39755
$Fe_{27}Ni_{53}P_{14}B_6$, amorphous, Hall resist. and mag. props., short range order effects 80−34422
$Fe_{40}Ni_{40}P_{14}B_6$, high-field suscept. and spin wave spectrum 78−10662
$Fe_{40}Ni_{40}P_{14}B_6$, quenched amorphous, high field susceptibility and microstructure 77−69506
$Fe_xNi_{80-x}P_{14}B_6$, amorphous, sp. ht. and susceptibility meas., spin glass and mictomag. props. 78−68274
$FeNi_2S_4$, violarite, mag. and elec. props., struct. determ. 77−43633
$(Fe_{1-x}Ni_x)_{77}Si_{10}B_{13}$ amorphous alloy system, saturation mag. moment, Curie temp., mag. susceptibility 80−39753
FeO-FeS, mag. susceptibility, eutectic phase diagram *(Russian)* 80−15682
Fe_2O_3 amorphous film, Mossbauer spectra, mag. props. 80−15851
Fe_2O_3 amorphous RF sputtered thin films, Mossbauer and mag. study 80−34714
α-Fe_2O_3, haematite, mag. susceptibility meas. near Morin temp. 77−59404
α-Fe_2O_3, haematite, mag. susceptibility, near high temp. mag. phase transition 79−56510
α-Fe_2O_3, haematite, temp. mag. hysteresis near Morin temp. 79−56566
γ-Fe_2O_3, sat. moment *(French)* 77−85431
Fe_2O_3-BaO-B_2O_3, magnetic props. of Fe-rich amorphous oxide *(French)* 80−80511
Fe_2O_3-Dy_2O_3-Na_2O-B_2O_3 glass, AC mag. susceptibility, antiferromag. interactions 77−32179
α-Fe_2O_3-Li_2O, structural and thermal phase behaviour from mag., spectral and thermal studies 80−2673
Fe_2O_3-PbO-B_2O_3 glass, X-ray and electron microscope studies, mag. and Mossbauer effect meas. 80−28919
Fe_2O_3-TeO_2 system, mag. props. 78−27020
Fe_3O_4 (magnetite), mag. susceptibility under hydrostatic press. and implications for tectonomagnetism 80−26504
Fe_3O_4 ferrofluid suspension, mag. props., stability 79−87293
Fe_3O_4 ferrofluids, spin glass behaviour 80−71120
Fe_3O_4, magnetite, anhysteretic remanence and thermoremanence susceptibility, particle size depend. 77−5191
Fe_3O_4, magnetite, magnetoelec. effect at 77K and cryst. symm. 80−29593

magnetic susceptibility continued
Fe_3O_4, magnetite particles, interaction fields effect on hysteretic props. 80−54921
$xFe_2O_3(1-x)[PbO.3B_2O_3]$ glasses, mag. props. 77−73012
$20Fe_2O_3.80[3B_2O_3.(1-x)PbO.xGeO_2]$ glass, phys. props. 80−49119
FeP, mag. suscept., resistivity and thermal expansion meas. 78−2661
α-FeP_4, diamag., semicond., Mossbauer study 80−50243
Fe_2P, magnetisation, susceptibility, thermal expansion and elec. resist. meas. 77−77037
$Fe_{2-x}P$, first order ferro- to paramag. transition, 216K, susceptibility obs. 78−39322
$Fe_2(PO_4)Cl$, temp. depend. of mag. susceptibility 80−70962
$Fe(Pd_{1-x}Au_x)_3$ ordering alloys, mag. props., 4.2 to 500K *(Russian)* 79−47301
$Fe_{25}Pd_{50}Au_{25}$, atomic ordering influence on mag. props. and elec. resistance *(Russian)* 80−7551
$Fe_xPd_{80-x}Si_{20}$, amorphous, structural and mag. heterogeneities 80−80484
$Fe_xPd_{80-x}Si_{20}$, low field susceptibility near transition temp. 77−66359
$Fe_xPd_{82-x}Si_{18}$ metallic glass, mag. transitions, weak ferromagnetism 80−100583
Fe_3Pt Invar alloy, anomalous Curie const., susceptibility meas. 80−75731
$Fe_{3-x}Pt_{1+x}$, ordered and disordered, mag. props. at low temp. 79−56517
$FeRh_2S_4$, mag. semicond., mag. and elec. props. 80−93121
FeS_2 (marcasite), temp. depend. mag. susceptibility 80−20391
FeS_2, mag. susceptibility press. depend., bandstruct. calcs. 78−19212
FeS_2, natural single cryst., 4.2-620K 77−40031
FeS_2, pyrite, Van Vleck susceptibility, temp. depend. 80−34589
$Fe_{0.9}S$, ferrimag. transition, mag., thermodynamic props., kinetics 79−47280
β-$FeSO_4$, high-temp. polymorph, stability, mag. struct., mag. props. 77−43815
$Fe(SO_3F)_2$, Mossbauer and electronic spectra, cryst. field splittings, mag. hyperfine interactions 77−48096
$FeSO_4.n\,H_2O$ (n=1,4,5,7), Fe^{2+} ion mag. interaction with crystallisation water protons, proton NMR obs. 80−60447
$FeSb_2$, quasi-magnetic semicond., mag. susceptibility 80−39757
$Fe_{1+\delta}Sb$, nonstoichiometry influence on mag. props. *(Russian)* 80−65813
$Fe_{1+x}Sb$-CoSb solid soln., mag. props., Mossbauer spectra, solubility limits, and lattice consts. *(Russian)* 77−59394
$Fe_{1+x}Sb$-NiSb solid soln., mag. props., Mossbauer spectra, solubility limits, and lattice consts. *(Russian)* 77−59394
$Fe(Sb_{1-x}Te_x)_3$ system cpds., prep., cryst. struct., elec. and mag. characteris. 80−108349
Fe_3Se_4, mag. props., 4.2-600K 78−43570
Fe_3Se_4, thermal expansion, compressibility, magnetisation, susceptibility and magnetostriction 77−66318
η-Fe_5Si_3, thermal and mag. props. 77−36080
$FeSn(OH)_6$, mag. props. 78−43574
$FeSnO(OH)_5$, mag. props. and cryst. struct. 78−43574
Fe_xTaS_2, metallic, mag. susceptibility at low temp. 80−70972
$Fe_xTa_{1-x}S_2$ (1T), low-spin high-spin equilib., susceptibility and Mossbauer expts. 77−48109
$Fe_{1-x}Te$, fluctuating localised mag. moments, d band motion, Mossbauer study 80−65768
Fe_2TeO_5, mag. struct. 78−27020
$FeTh_2S_5$, mag. struct. and props., neutron diffr. and mag. meas. 80−60201
FeTi, hydrogen energy storage, surface segregation *(German)* 79−77872
FeTi, hydrogenation, effect of surface segregation on mag. props. 78−84819
FeTi, surface and mag. props., heat treatment and hydrogenation effects 80−75447
$FeTiO_3$, ilmenite, lunar and terrestrial, cell dimensions and antiferromagnetism 77−21764
Fe_2TiO_5, anisotropic spin glass behaviour 79−99707
Fe_2TiO_5, anisotropic spin glass type behaviour 80−60296
$Fe_{3-x}Ti_xO_4$, $0.5 \leq x \leq 1$, mag. props. of antiferromag. phase 80−70960
$Fe_{3-x}Ti_xO_4$, spin glass behaviour, susceptibility and hysteresis meas. 80−65917
$(Fe_{1-x}V_x)_3Ge$, magnetic and X-ray studies 80−1966
$FeVO_4$, Neel temp., mag. susceptibility meas. 80−29550
$Fe_{0.35}V_2O_5$, spin glass phase, low temp. mag. susceptibility meas. 80−29565
$Fe_xV_{1-x}O_2$, mag. props. and Mossbauer spectra meas. 78−31136
θ-$Fe_xV_2O_5$, spin glass and paramag. props., susceptibility, EPR and Mossbauer studies 80−75782
$(Fe_xV_{1-x})V_2S_4$, and $(Fe_xV_{1-x})V_4S_8$, mag. props. 78−27034
Ga, magnetic susceptibility near melting point 80−60186
Ga-Cu(Tl)(In), liq., mag. susceptibility *(Russian)* 78−6513
Ga-rare earth alloys, phase diagram determ. 78−15366
Ga-Te alloys, liq., mag. susceptibility 77−51881
Ga-Te liquid alloys, mag. susceptibility 77−59383
Ga-Zn(In)(Ta)(Sn)(Bi)(Pb), liquid binary alloys, magnetic susceptibility *(Russian)* 77−24671
GaAs, exam. of magnetic susceptibility and absorption spectra 79−1778
GaAs:Co, neutral state of Co impurities, optical absorption and mag. susceptibility 78−39578
GaAs:Co^{2+} (Ni^{3+}), mag. and optical props. 78−10763
GaAs:Ni, behaviour of Ni impurity in $3d^8$ state, mag. susceptibility meas. 78−47737
GaAs-ZnSe system, heterovalent solid solns. of substitution, prep. and investig. 77−24553
$Ga_{1-x}Co_x$, cluster spin glass system, host and impurity NMR studies 79−65745
$Ga_{0.67}Cr_2S_4$, semiconducting thiospinelide, spin glass type mag. ordering *(Russian)* 80−50123
$Ga_{1-x}In_xSe$, magnetic susceptibility anisotropy, chemical bonds, electron density distribution *(Russian)* 80−50073
$Ga_{1-x}Mn_xSb$ alloys, mag. phase transition obs. 78−52248
$Ga_{1-x}Mn_xSb$, elec. cond., mag. susceptibility, Hall const., and thermo-EMF, 80 to 1000K *(Russian)* 80−88549
GaP, exam. of magnetic susceptibility and absorption spectra 79−1778
GaP:rare earth, magnetic susceptibility, impurity states 79−61044
GaP-based III-V solid solns., bonding and energy gap, mag. meas. 78−18580
GaP_xAs_{1-x}, exam. of magnetic susceptibility and absorption spectra 79−1778

magnetic susceptibility continued
GaS, mag. susceptibility anisotropy, chem. bonding *(Russian)* 79−61045
GaS-YbS system, phase diagram, reacts., thermal, mag. and elec. meas. 79−11578
GaSe, mag. susceptibility anisotropy, chem. bonding *(Russian)* 79−61045
Ga_2Se_3-FeSe, phase diagram, elec. cond., mag. susceptibility 80−88301
$GaSe_{1-x}S_x$, magnetic susceptibility anisotropy, chemical bonds, electron density distribution *(Russian)* 80−50073
Gd, AC susceptibility, temp. modulation studies, domain property thermal relaxation 79−61072
Gd, AC susceptibility and temp. modulation near Curie point 77−4515
Gd alloys, amorphous, mag. props. and ferromag. reson. 80−54952
Gd clusters in faujasite type zeolites, mag. suscept. temp. depend. 78−14925
Gd, domain effects near order-disorder and order-order ferromagnetic transitions 80−65886
Gd, liq., mag. susceptibility, elec. resistivity 80−20377
Gd Ni_2Si_2, mag. props., 4.2-200K 80−84602
Gd, transient enhancement of AC susceptibility, domain wall pinning 77−20633
Gd-Ag, vap. quenched alloys, struct. and mag. props. 78−84461
Gd-Ag (0-16 at.%), vapour-quenched, struct. and mag. props. 78−38980
Gd-Ag(Cu) alloy film, amorphous, struct. and mag. props. 78−52318
Gd-Al sputtered amorphous films, spin glass state 77−66393
Gd-Al(C)(Cu)(Ga)(Ni)(Pd)(Rh) alloys, amorphous, mag. and elec. props. 80−80499
Gd-Co amorphous films, RF sputtered, magnetisation ripple effects 80−11232
Gd-Co-Mo film, amorphous, in-plane susceptibility near compensation point 78−64238
Gd-Co(-Mo) films, amorphous, inhomogeneities of mangetization and anisotropy 79−65698
Gd-Co(Ni)(Cu)(Rh)(Ru)(Pd)(Ga), amorphous, mag. props. and ferromag. reson. 80−75862
Gd-Cu sputtered amorphous films, ferromag. props. 77−66393
Gd^{3+}-doped crystals, cryst. field calc. 78−76035
$Gd_{56}Ag_{46}$, amorphous, susceptibility and magnetisation, 6-300K *(French)* 77−36060
$GdAl_2$-$GdCo_2$ system, EPR and mag. props. 79−33478
$Gd_{0.37}Al_{0.63}$ film, amorphous, spin-glass order parameter meas. 77−28396
$GdAlO_3$, bicrit. and tetracrit. behaviour, susceptibility obs. 77−47992
$GdAlO_3$:La, antiferromag., random-field crit. and multicritical behaviour 80−65939
GdAuSn, mag. props. 77−85439
GdB_6 single crystals, mag. behaviour and structure change at low temp. 80−71018
GdC_2, mag. susceptibility, temp. depend. 79−87239
$Gd_{1-x}Ca_xAl_2$, mag. props. and phase relations 80−107991
$Gd_xCe_{1-x}Ru_2$, coexistence of supercond. and spin glass mag. freezing 77−28283
$GdCl_3$, crystn. field parameter of Gd^{3+} 80−10930
$GdCl_3$, interaction parameters, high freq. meas. of adiabatic differential susceptibility 78−68211
Gd_2Co, amorphous ferromag. obtained by splat cooling, local and bulk mag. props. 79−1685
$Gd_{65}Co_{35}$, amorphous, amg. ordering, susceptibility, magnetisation and hysteresis meas. 78−68190
$Gd_2Co_6Al_{11}$, NMR and mag. susceptibility 79−15367
$Gd(Co_xFe_{1-x})_2$, mag. props., composition and temp. depend. 79−15289
GdCoMo film, amorphous, sputtered, ferrimag., in-plane susceptibility near compensation point 78−64240
$Gd(Co_xNi_{1-x})_2$, mag. props., composition and temp. depend. 79−15289
$GdCo_2Si_2$, mag. props. 80−107988
GdCu, electrical resistivity and length changes with temp., hysteretic behaviour 80−97600
$Gd_2Cu_6Al_{11}$, NMR and mag. susceptibility 79−15367
$Gd(Cu_{1-x}Gd_x)$, pseudobinary alloy, mag. susceptibility and elec. resist. at low temp. 80−34602
GdCuSn, mag. props. 77−85439
$Gd_xDy_{1-x}C_2$, solid soln., mag. susceptibility, temp. depend. 79−87239
$Gd_xEr_{1-x}Rh_4B_4$, mag. ordering near supercond. region 79−73696
$Gd_xEu_{1-x}B_6$, solid solns., mag. susceptibility, 80 to 1000K *(Russian)* 80−88713
$Gd(Fe_xAl_{1-x})_2$, magnetic behavior 80−108079
$GdFeB_4$, mag. susceptibility meas., paramag. Curie-Weiss behaviour 79−61041
$Gd_3Fe_5O_{12}$, formation mechanism from metallic oxides 77−48376
$Gd_3Ga_5O_{12}$, mag. phase diagram, AC susceptibility meas. 80−60265
GdH_3, magnetisation and mag. suscept. 77−43821
$Gd_xLa_{1-x}B_6$, solid solns., mag. susceptibility, 80 to 1000K *(Russian)* 80−88713
$Gd_xLa_{1-x}Zn$, magnetisation and paramag. suscept. 78−88101
GdM_2Ge_2, M=Mn, Fe, Co, Ni, Cu, magnetism and hyperfine interactions 78−76228
GdN, mag. interaction and carrier conc. 80−71005
$GdN_{1-x}O_x$, magnetic interaction and carrier conc. 80−71005
$Gd_xNd_{1-x}Zn$, ferromag., mag. susceptibility and magnetisation, temp. depend. 80−70975
$GdNi_5$, anomalous behaviour near Curie point 78−91880
$Gd_2Ni_{17-x}Al_x$, mag. behaviour in paramagnetic region 79−73675
Gd_2NiTiO_6, mag. study, paramag. behaviour *(French)* 79−46629
c-Gd_2O_3, electrical cond., dielectric const. mag. susceptibility, polymorphic transition 77−59505
$Gd_2O_2SO_4$, antiferromag., mag. props. 1.6 to 40K 79−33464
GdP-GdS systems, mag. exchange interactions, free carrier conc. 78−60278
$Gd(PO_3)_3$, 2-27K, appl. as mag. thermometer 79−63224
$Gd_xPd_{82-x}Si_{18}$ amorphous alloy, 4.2-300K 77−66248
$GdRh_4B_4$, magnetic and electrostatic props., NMR study 80−93195
GdS, low temp. phase transitions, mag. moment orientation, spin flip 79−99700
GdS, meas. of opto-magnetic interactions at low mag. fields 80−2735
$Gd_{3-x}S_4$, ferromag., elec. props. near Curie temp. 80−107788
GdScFe garnets, mag. props. 77−47979
GdSe, low temp. phase transitions, mag. moment orientation, spin flip 79−99700
Gd_2Se_3, mag. susceptibility 77−40032
$GdSn_3$, Neel temp., hydrostatic press. depend. 80−29549

magnetic susceptibility continued
$Gd_{70}Tb_{30}$, magnetisation, AC susceptibility and microwave absorption meas. 80−60221
GdTe, low temp. phase transitions, mag. moment orientation, spin flip 79−99700
$Gd_xTh_{1-x}Ru_2$, coexistence of supercond. and spin glass mag. freezing 77−28283
$GdV_{1-x}M_xO_3$ (where M=Cr or Fe), solid solns., elec. and mag. props 79−23967
$Gd_2(WO_4)_3$, mag. susceptibility, paramag. Curie temp., 300-900K 79−82753
$Gd_2(WO_4)_3$, molar mag. susceptibility, DC elec. cond., thermopower meas. 79−15172
$(Gd_xY_{1-x})Al_2$, ferromag. and spin glass like behaviour, magnetisation meas. 80−75734
$(Gd_xY_{1-x})Fe_2$, Fe mag. behaviour, FMR measurements, mag. props., Vangsness relation anal. 79−78336
$(Gd_xY_{1-x})Fe_2$, high temp. mag. behaviour 77−1538
$Gd_xY_{1-x}Zn$, ferromag., mag. susceptibility and magnetisation, temp. depend. 80−70975
Gd_2ZrS_5, mag. and sp. ht. meas. on polycrystalline samples 78−23253
$Gd_{3-x}\square_xS_4$, transport and mag. props., mag. Wigner localisation 80−97069
$(Ge,Pb)_{1-x}Mn_xTe$, mag. and elec. props. meas. 80−29534
Ge:Sb(As), experimental data anal. 77−35933
Ge-As-Te system, glasses, magnetochemical exam. 78−88092
Ge-Te alloy, liq., magnetic susceptibility 79−87232
$GeFe_2O_4$, single crysts., elec. and mag. props, optical absorpt. spectra 80−54719
$Ge_{1-x}Mn_xTe$, magnetic behaviour of Mn 78−14938
HF_2^-, mag. shielding and susceptibility, finite perturbation mol. orbitals calcs. 77−46513
$H_{1.6}MoO_3$, electronic props., mag. susceptibility and spectra 80−80266
H_2O, liquid, diamagnetism, temp. dependence, NMR chemical shift calcs., molecular interactions data 80−75707
H_2O, liquid, equation for mag. susceptibility, electric polarisability 80−75708
He, diamag. suscept., form factor, variational method 77−18813
He, singlet-triplet anticrossing, elec. field induced 77−14404
^{3}He, adsorbed film on Grafoil, NMR, intermediate and near-monolayer coverages 79−46878
^{3}He adsorbed on graphite, mag. props., 2-D gas behaviour 78−47631
^{3}He, BCC, NMR multiple echoes, soln. of eqn. of motion of magnetisation 79−86961
^{3}He, BCC solid, exptl. mag. props., four spin exchange explanation 79−69319
^{3}He, BCC solid, nucl. mag. order and paramag. susceptibility 80−59757
^{3}He, cryst., HF susceptibility, ferromag. reson. type *(Russian)* 77−59175
^{3}He film, adsorbed on graphite, nucl. mag. susceptibility below 4.2K 77−20155
^{3}He in Grafoil, ultralow temp. NMR mag. susceptibility, surface magnetisation and transition 78−79843
^{3}He, liq., exchange model 80−88387
^{3}He, liq., in contact with dielec. surface, mag. susceptibility enhancement, thermodynamics 80−54460
^{3}He, liq. confined in Al_2O_3 and Pt powders and Grafoil, NMR expts. 79−51371
^{3}He, liquid, surface ferromagnetic instability, attraction to solid substrate 79−46863
^{3}He on graphite, two dimensional quantum crystal *(Russian)* 78−60001
^{3}He, solid, low temp. mag. and thermal props. due to bound state Frenkel vacancies 79−56019
^{3}He, solid, mag. susceptibility near ordering temp., pulsed NMR meas. 78−18869
^{3}He, solid, mag. susceptibility, transition, thermodynamic study 78−60003
^{3}He, solid, mag. susceptibility meas. using double sample cell NMR technique 79−63225
^{3}He, solid, melting, formal treatment of low temp. props. 79−69315
^{3}He, solid, spin diffusion at very low temp., multiple echo amplitudes, inverse susceptibility 79−19423
^{3}He, solid, susceptibility along melting curve, 20 mK to nucl. ordering temp. 77−31837
^{3}He, solid BCC, four spin exchange, susceptibility behaviour below 10 mK 78−10253
^{3}He, solid BCC, mag. susceptibility and sp. ht. 79−69318
^{3}He, solid BCC, nucl. spin mag. ordering with spin exchange 77−89615
^{3}He superfluid, B-phase, dynamic NMR and static suscept. meas. using RF-SQUID 77−51565
^{3}He, superfluid, gauge group and p-wave phases 79−23798
^{3}He, superfluid, heat capacity, spin susceptibility, NMR and viscosity *(Danish)* 78−22921
^{3}He superfluid, phys. props. *(Danish)* 78−2325
^{3}He, superfluid, response theory calcs., corrections to mag. susceptibility, binding energies, density 78−67883
^{3}He, superfluid, spin susceptibilities, flow depend. 78−14528
^{3}He, superfluid B-phase, spin collective excitations 79−46861
^{3}He, superfluid B-phase, static spin susceptibility 78−30807
^{3}He with C particles, pulsed NMR, mag. susceptibility surface induced ferromagnetism, antiferromagnetic exchange interaction 78−79844
^{3}He-^{4}He, superfluid, osmotic and mag. props., review *(French)* 80−10733
^{3}He-^{4}He dil. mixture, mag. susceptibility 77−7939
^{3}He-^{4}He film, adsorbed on graphite, nucl. mag. susceptibility below 4.2K 77−20155
Hf-C-N-O-H, solid solns. of H, exam. of props. 80−29172
HfB_2, mag. susceptibility temp. depend. *(Russian)* 79−82749
$HfMn_2$, Curie-Weiss law depend. of susceptibility, mag. props. *(Russian)* 79−65655
$HfSe_{2-x}Te_x$ and $HfTe_{2-x}$, elec. resist. and mag. suscept. studies 80−44599
$Hf_xTa_{1-x}C_y$ solid solns., mag. susceptibility, 20-1300K *(Russian)* 78−39287
HfV_2, C15 supercond., dielec. transitions, temp. depend. of resist. and mag. susceptibility, 4.2-300K 79−38136
HfV_2, dielectric phase transition, elec. resist. temp. depend. 79−65525
HfV_2, elec. resist. and mag. suscept., anomalous temp. depend. 79−69491
HfV_2, supercond., dielec. phase transition *(Russian)* 78−64168
$Hg_{2.86}AsF_6$, linear chain, anomalous low temp. sp. ht. 78−14476
magnetic susceptibility continued
$Hg_{1-x}Cd_xTe$, props. and appls., book contrib. 77−39834
$HgCo(NCS)_4$ calibration standard, low temp. molar mag. suscepts. meas. 78−65947
$HgCr_2Se_4$, crit. behaviour near Curie point 78−31068
$Hg_{1-x}Mn_xS(Se)$ solid solution, magnetic props. 79−51758
$Hg_{1-x}Mn_xTe$, mag. props., 4.2-300K 77−4508
$Hg_{1-x}Mn_xTe$, mag. props., self-consistent two spin cluster model 80−54874
$Hg_{1-x}Mn_xTe$, mag. susceptibility, 2.3-300K 77−63074
$Hg_{1-x}Mn_xTe$, mag. susceptibility, 2.4 to 300K 80−20379
$Hg_{1-x}Mn_xTe$, magnetic behaviour of Mn 78−14938
$Hg_{1-x}Mn_xTe$, microwave helicon propag. and helicon excited EPR 77−43637
$Hg_{1-x}Mn_xTe$, zero-gap semicond., indirect-exchange interactions 80−29370
HgTe, Γ_8 symm. acceptor centre hole mag. props. *(Russian)* 80−88733
Ho, liq., mag. susceptibility, elec. resistivity 80−20377
$HoAl_xGa_{2-x}$, mag. props. and phase transitions 80−25133
$HoAlO_3$, electronic and nucl. mag. ordering, mol. field approx. 80−60157
$HoAu_3$, mag. phase diagram 80−75761
$Ho_3Au_3Sb_4$, mag. suscept. meas., 4 to 300K 79−51742
$HoCo_2$, paramag. and ordered phases, Pauli type Co susceptibility, polarised neutron diffr. obs. 77−63077
$HoCo_{5.5-x}Mn_x(Fe_x)(Ni_x)(Cu_x)$, cryst. struct. and mag. props. 80−75800
$HoCo_2Si_2$, mag. props. 80−107988
$Ho(Fe_xNi_{1-x})$, mag. interactions, mol. field model 77−73010
$Ho(Fe_xNi_{1-x})_2$, mag. behaviour, susceptibility and Mossbauer expts., 4.2-1300K 78−52235
HoIG, anomalous Faraday behaviour, mag. props. 79−82955
HoIG, mol. field coeffs., magnetisation and mag. susceptibility anal. 78−95406
$Ho(Ir_xRh_{1-x})_4B_4$ pseudoternary system, supercond. and mag. ordering 80−70876
$Ho_2(MoO_4)_3$, mag. susceptibility, ferromagnetism, mol. field theory 78−34966
$Ho_{1.2}Mo_6S_8$, re-entrant ferromag. supercond., heat capacity and AC mag. susceptibility 79−60948
$Ho_{1.2}Mo_6S_8$, supercond. destruction by mag. ordering 77−69449
$HoNi_5$, ferromag., magnetisation and paramag. susceptibility 80−25082
$HoNi_{0.7}Cu_{0.3}$, mag. behaviour 79−99688
$HoNi_2Si_2$, mag. props., 4.2-200K 80−84602
Ho_2O_3, 300 to 900K, mag. susceptibility and Curie temp. meas. 78−56288
$(Ho_2O_3)_{0.194}(Al_2O_3)_{0.227}(SiO_2)_{0.579}$, amorphous, low temp. spin glass behaviour 80−60297
$Ho_2O_2SO_4$, antiferromag., mag. props. and Zeeman effect meas. 79−33464
$Ho_2O_2SO_4$, mag. ordering, magnetisation, AC susceptibility and Zeeman effect meas. 80−60205
$Ho_2O_2SO_4$, magnetic phase diagram, magnetisation and mag. susceptibility meas. 80−15720
$HoRh_4B_4$, low temp. mag. props. 80−88728
Ho_2Se_3, mag. susceptibility 77−40032
$HoVO_3$, antiferromag., at. and mag. struct., neutron diffr. meas. 79−24142
$HoVO_4$, RF susceptibility below 1K, mag. sp. ht. 80−84585
$Ho_2(WO_4)_3$, mag. props., 300 to 900K 79−28510
$Ho_cY_{1-c}Sb$ system, magnetisation, elec. resist., and sp. ht. meas. 80−60213
$Ho_xY_{1-x}Sb$, mag. props. 80−34634
In powders, uncoated and Cu-coated, fluctuation diamag. susceptibility above T_c 79−78309
In-Sb alloys, liq., MP to 1000°C, anomalies due to electron-ion interaction 77−20546
In-Se(Te), liq., mag. susceptibility meas., electron localisation and chem. bonding 80−60178
In-Te alloys, liq., mag. susceptibility 77−51881
In-Te liquid alloys, mag. susceptibility 77−59383
In-Tl, exam. of magnetic susceptibility in solid and liquid states, and X-ray data *(Russian)* 79−28503
In-Tl alloys, supercond. transition in martensitic two phase region, AC mag. susceptibility meas. 77−72936
InAs:Mn, NMR, magnetoresist., Hall effect and mag. susceptibility meas. 78−26888
InP:Te, mag. props. of conduction electrons 78−6510
$In_{1-x}Pb_xTe$, single crystals, mag. susceptibility 79−51738
InR_2 (R-Y, Nd, Sm, Gd, Tb, Dy, Ho, Er, Tm), mag. props., 4.2 to 270K 79−56512
InSb, magnetic freeze out *(Japanese)* 78−39130
InSb:Mn, NMR, magnetoresist., Hall effect and mag. susceptibility meas. 78−26888
InSe, mag. susceptibility anisotropy, chem. bonding *(Russian)* 79−61045
p-In_6Se_7, Faraday meas. of mag. susceptibility, 110 to 400K *(Russian)* 77−35867
$IrGe_{1.5}S_{1.5}(Se_{1.5})$, new skutterudite relation compounds, prep. and charact. 78−52700
$IrMn_{1+x}Sb$ alloys, crystal struct., and mag. props. 78−34466
$IrSn_{1.5}S_{1.5}$, new skutterudite relation compounds, prep. and charact. 78−52700
K, Pauli susceptibility and Knight shift meas., electron wave functions 80−44937
K, spin susceptibility and volume dependence 79−95569
$K_2BaCu(NO_2)_6$, antiferromagnetic Heisenberg spin 1/2 simple quadratic lattice, mag. and caloric meas. 79−78397
KC_{24}, intercalated graphite cpd., anisotropic mag. susceptibility and phase transitions 79−19370
$KClO_3$-$CsClO_3$, NQR, mag. susceptibility meas. 78−35059
$KCoF_3$, antiferromag., obs. of domains by X-ray topography 78−14981
$KCoF_3$, mag. suscept. and Neel temp. determ. 77−77044
$KCoF_3$, single crystal, mag. susceptibility, ^{19}F NMR and static measurements 79−11301
$K_2Co_2(SO_4)_3$, cubic langbeinite struct., low temp. mag. susceptibility 78−56299
$KCrO_2$, two-dimensional antiferromag., mag. props. *(French)* 78−23251
$K_2CuCl_4.2H_2O$ structure compounds, 3-dimens. ferromag., exchange anisotropy by NMR 77−55714
$KCuF_3$, antiferromag., low-dimensional susceptibility 79−28513
$KCuF_3$, chain-like antiferromag., parallel susceptibility 78−80137

magnetic susceptibility continued
K_2CuF_4, spin relax., crit. behaviour, high freq. susceptibility meas. 80−65936
K_2CuF_4, two-dimens. ferromag., saturation of parallel-pumped magnons 80−97147
$K_3Fe(CN)_6$, electronic struct., electron density, elec. field gradient, mag. susceptibility and g-tensor 79−91006
$K_3Fe(CN)_6$, Mossbauer and susceptibility expts. 77−40038
$K_2FeCl_5(H_2O)$, phase diagram, antiferromag., paramag. and spin flop phases 80−44831
$KFeF_4$, amorphous, mag. props. and Mossbauer spectra, speromagnetism and mictomagnetism 80−75778
K_2FeF_5, mag. struct. and one-dimens. antiferromagnetism 80−60209
KFe_2O_3, β'' phase, mag. props., hyperfine interactions, Mossbauer study 80−20524
$KFeS_2$, cryst. struct. and mag. ordering, neutron diffr. and mag. susceptibility meas. 80−54867
KH_2PO_4, low impurity content, magnetic anisotropy *(Russian)* 78−6506
K_2IrCl_6, mag. susceptibility in ordered and paramag. phases 79−73759
$K_3Mn(CN)_6$, low-spin mag. studies 79−95582
$K_2Mn_{1-x}CoF_4$, mag. and neutron scatt. exam. 79−33466
K_2MnF_4, EPR g-shift and anisotropic mag. susceptibility 77−85546
K_2MnF_4, two-dimensional antiferromag., crit. behaviour, quasielastic neutron scatt. 77−85468
$K_3Mn_2F_7$, double layer antiferromagnet 77−16061
$K_3Mn_2F_7$, double-layer antiferromag., mag. prop. meas. and calc. 77−55666
$K_3Mn_2F_7$, double-layer antiferromag., mag. ordering, neutron scatt. meas. 79−61062
$K_3Mn_2F_7$, two magnon Raman scatt., magnon dispersion, susceptibility, Green's function methods 80−50340
$K_3Mn_3F_7$, Heisenberg double-layer antiferromag., neutron scatt. 79−61065
$K_2Mn_{1-x}Fe_xF_4$, anisotropy on two and three dimens. mag. order 77−66259
$K_2Mn_{1-x}Fe_xF_4$, mag. and neutron scatt. exam. 79−33466
$K_2Mn_2(SO_4)_3$, cubic langbeinite struct., low temp. mag. susceptibility 78−56299
$KNiF_3$, antiferromag., obs. of domains by X-ray topography 78−14981
K_2NiF_4, two-dimensional antiferromag., crit. behaviour, quasielastic neutron scatt. 77−85468
$K_2Ni_2(SO_4)_3$, cubic langbeinite struct., low temp. mag. susceptibility 78−56299
K_2O-Al_2O_3-B_2O_3:Fe_2O_3, glasses, liq.-liq. phase separation, Fe^{3+} ions rel. to mag., optical props. 77−15322
$K_2PbCu(NO_2)_6$, antiferromagnetic Heisenberg linear spin 1/2 chain, mag. and caloric meas. 79−78397
$K_2Pt(CN)_4Br_{0.3}.3H_2O$, one-dimens. cond. transition, spin suscept. and DC cond. temp. depends. 78−84198
$K_2Pt(CN)_4Br_{0.3}.xH_2O$, one-dimensional cond., effects of dehydration on mag. props. 77−85549
KUO_3, EPR and mag. susceptibility, temp. depend. 79−33451
$K_2V_8O_{16}$, Hollandite type compound, synthesis, struct. and magnetic props. 79−11543
$K[(OH)_{0.42}(O_2)_{0.50}]$, cubic solid soln., structural and mag. study *(French)* 80−107177
$(La,Ce)B_6$ dil. alloy, Kondo effect, impurity-impurity interaction, mag. susceptibility, mag. to non mag. transition 78−47948
$(La,Ce)B_6$, low temp. mag. props. 79−61043
(La, Ce)Sn_3, dil. alloys, supercond. and normal state props. 78−76184
(La,Gd)Al_2, mag. props. 78−52299
(La, Gd)Al_2 spin glass, suscept. and sp. ht., mag. field depend. 79−61173
(La,Gd)Al_2 spin glasses, reversible and irreversible mag. susceptibility 80−15738
$(La,Gd)B_6$, dil. alloy, spin glass behaviour, 4.2 to 200K AC mag. susceptibility, RKKY calcs. 78−47994
$(La,Gd)B_6$, mag. susceptibility, zero field, 0.04 to 10K 78−10696
(La,Th)-Ce, dilute alloys, mag.-nonmag. transition of impurity moments, environment effects 77−40034
(La,Y)Ce, dil., Kondo supercond., transition temp., susceptibility and resist. 80−65733
La, FCC, NMR 4.2 to 296K, mag. susceptibility and sp. ht. 80−15813
La intermetallics, LaX_2Si_2 (X=Cu, Ag, Cu), ^{29}Si NMR and mag. susceptibility 79−61246
La-Gd-Au, amorphous spin glasses, mag.-cluster description 79−42776
La-Gd-Au alloys, amorphous, high Gd content, bulk mag. props. 77−59426
La_{1-x} Eu_x B_6 solid solutions, cryst. lattice defectiveness, mag. susceptibility and elec. conductivity 80−15083
LaAg, band calcs., rel. to mag. and electronic props. and martensitic transform. 77−8014
LaAg, electronic struct., susceptibility, sp. ht. and Knight shift meas. 77−43485
$LaCO_{1-x}M_xO_3$, M=Mg, Ti, cryst. struct., elec. and mag. props. 79−86748
$(La_{0.8}Ca_{0.2})MnO_{3+y}$, mag. props., Faraday method meas. 80−103832
$La_{1-x}Ca_xVO_3$, struct., elec. and mag. props., temp. and conc. depend. *(French)* 77−4293
$La_{1-x}Ce_xB_6$, Kondo system, low-field impurity susceptibility, 0.03 to 8K 77−63095
$LaCoO_3$, Mott isolator, paramag. props., calc. 80−93071
La_2CoO_4, mag. behaviour obs. 80−70971
LaEu, mag. supercond., phase diagram, bulk susceptibility meas. 77−59353
$(La_{1-x}Gd_x)Al_2$, spin glass, susceptibility maximum freq. depend. 79−61172
$La_{80-x}Gd_xAu_{20}$, amorphous dil. alloy, RKKY interaction, magnetisation meas. 77−32207
$(La_{1-x}Gd_x)_{1.0}Mo_6Se_8$, Gd-rich, supercond. state, phase transition, sp. ht. anomaly and mag. susceptibility 78−6480
La_3In, mag. susceptibility and normal state NMR meas. 78−31118
$LaLi_{0.5}Ir_{0.5}O_3$, perovskite, prep. and mag. study 80−80486
LaMg, Pauli paramagnet, mag. susceptibility, nonlinear band behaviour 80−75706
$LaMnO_3$, monoclinic and cubic perovskite struct., mag. props., neutron diffr. meas. 78−27022
La_3NbO_7, weberite-type, elec., mag. and opt. props. 77−85212
(LaNd)Sn_3, containing Nd impurities, supercond. and normal state props. 80−49967

magnetic susceptibility continued
$LaNi_5$, crystal field investigation from inelastic slow neutron scatt. expts. 80−39538
$LaNi_5$ hydrides, 4.2K paramag. susceptibility 80−70934
$LaNi_5$, magnetism and H_2 storage 80−70941
$LaNi_5$, self restoring of active surface, photoemission, mag. susceptibility study 78−48280
$LaNi_{1-x}Co_xO_3$, mag. props. 77−85411
$LaNi_{1-x}Fe_xO_3$, mag. props., 7 to 300K 79−4648
$LaNi_{1-x}Fe_xO_3$, magnetisation meas. and ^{57}Fe Mossbauer studies 80−93217
$LaNi_{1-x}Fe_xO_3$, semicond. and metallic phases, elec. and mag. props. 79−78102
La_2NiO_4, La_2CuO_4, magnetic properties obs. 80−70937
$La_{80-x}Pr_xAu_{20}$, amorphous, mag. and supercond. props. 80−75713
$La_{1-x}Pr_xSn_3$, singlet ground-state system, mag. susceptibility 78−19215
$(La_{1-x}Pr_x)_3Tl$, comp. depend. of paramag. susceptibility, simple phenomenological model 77−16041
$LaPt_3$, ^{195}Pt NMR and susceptibility meas. 77−63299
$LaRu_2$, H absorption induced Ce valence change, mag. and supercond. props. 80−50042
$LaRu_2$, supercond. disappearance on H absorption 79−47185
$LaRu_xFe_{1-x}O_3$ perovskites, cryst. struct., elec., mag. and Mossbauer behaviour 77−55274
$La_xSm_{1-x}B_6$ solid solns., mag. susceptibility meas. *(Russian)* 79−28501
$La_{1-x}Sr_xCoO_3$ ($0.5 \leq x \leq 1.0$), mag. props. 79−24154
$La_{2-x}Sr_xCoO_4$, mag. behaviour obs. 80−70971
$La_{1-x}Sr_xCrO_3$ ($0 \leq x \leq 0.4$), localised level hopping transport 80−10974
$La_{1-y}Tb_yAg$, crystal field effects, normal and superconducting states 78−2621
La_3Tl, mag. susceptibility and normal state NMR meas. 78−31118
$LaV_{1-x}M_xO_3$ (where M=Cr or Fe), solid solns., elec. and mag. props 79−23967
Li, 3.7-294K, mass susceptibility *(German)* 78−68156
Li, Pauli susceptibility meas. by CESR method 79−42735
Li, Pauli susceptibility meas. by CESR transmission 79−61217
Li, spin susceptibility and volume dependence 79−95569
Li-Mg alloy, BCC, var. with temp. *(Russian)* 77−51878
Li-Pd, phase diagram and mag. props. 77−90321
Li-Pt, phase diagram for comp. range 0-40 at.% Pt, mag. and elec. props. *(German)* 80−84912
Li-transition metal dioxide intercalation compounds, mag. props., decomposition effects 80−25075
$LiBO_2$-In_2O_3, phase composition, mag. props, elec. cond. 80−55365
$Li_2B_2O_4$-$LiFe_5O_8$, borate glass, mag. props. of Fe^{3+} cations 80−100599
$Li_2B_2O_4$-$LiFe_5O_8$ glass, rapidly quenched, mag. and ferrimag. props. 80−75744
$LiCrO_2$, two-dimensional antiferromag., mag. props. *(French)* 78−23251
$Li_xCr_yV_{1-y}S_2$, Mossbauer and mag. studies 79−73869
$LiErF_4$, low-temp. mag. susceptibility, evidence of antiferromag. ordering 78−23249
$LiFeS_2$, magnetic hyperfine interactions, Mossbauer spectra and mag. susceptibility meas. 80−29658
$Li_xFe_yV_{1-y}S_2$, Mossbauer and mag. studies 79−73869
$Li_2Gd_4(MoO_4)_7$, ferroelec. and paramag. props. 78−39517
LiH, solid, mag. susceptibility calc. 77−85412
$LiHoF_4$, crit. behaviour of mag. suscept. 79−33465
$LiHoF_4$, uniaxial dipolar ferromag. crit. behaviour 79−61149
$LiHoF_4$, uniaxial dipolar ferromag., critical behaviour, mag. susceptibility meas. 80−80528
$(Li_2O$-Al_2O_3-$SiO_2)$:Fe_2O_3, glass, pyroceramic form., colour centres, magnetochem. investig. 77−16537
$LiRF_4$ (R=Tb,Ho,Er), cryst. field parameters, mag. susceptibility meas., 0.3 to 100K 80−60214
$LiTbF_4$, ferromag., susceptibility, sp. ht., renormalisation group theory test 77−16087
$LiTbF_4$, mag. props., crit. behaviour at marginal dimensionality 80−54906
$LiTbF_4$, uniaxial dipolar ferromag., critical behaviour, mag. susceptibility meas. 80−80528
$LiTb_{0.5}Y_{0.5}F_4$, mag. susceptibility, dilution effect on critical behaviour of dipolar uniaxial ferromagnet 80−34635
$LiTb_{0.5}Y_{0.5}F_4$, uniaxial dipolar ferromag., critical behaviour, mag. susceptibility meas., effect of Y^{3+} dilution 80−80528
$LiTmF_4$, local mag. field at ^{19}F rel. to paramag. susceptibility, NMR meas. *(Russian)* 77−81023
$LiUO_3$, EPR and mag. susceptibility, temp. depend. 79−33451
$Li_2VS_2(Se_2)$ based topochemical cells, low voltage behaviour 79−92069
$LiY_{1-x}Er_xF_4$, phase relationships and melting, mag. characterisation 77−39665
$LiYF_4$:Er^{3+}, magnetocaloric behaviour, cryst. field theory 77−4520
$LiYF_4$:Tm^{3+}, cryst. field parameters, appls. 77−20277
$Li_{0.5-z/2}Zn_xFe_{2.5-z/2}O_4$, field magnetisation and susceptibility 79−82762
Lu-rare earth, dil., cryst. fields 78−80127
LuB_{12}, 90-1200K 80−50032
$LuCo_2$, anomalous high-field magnetisation 78−47958
$(Lu_{1-x}Ho_x)Rh_4B_4$, interaction between superconductivity and magnetism 79−38248
$LuMn_2$, Lu_6Mn_{23}, H_2 absorption effect on mag. props. 77−89931
$LuRh_4B_4$, magnetic and electrostatic props., NMR study 80−93195
$LuRh_4B_4$, superconducting and normal state props. 79−73632
$LuRhO_3$, elec., mag. and photoelectrochemical props. 80−96925
$Lu_2V_2O_7$, pyrochlore struct., mag. props. 78−72335
metals, model pseudopotential calcs., elastic consts., spin susceptibility, Fermi surface distortions 78−79922
Mg, KKR calc. using potentials with exchange and correlation 79−11060
Mg, spin susceptibility, electronic effective mass, spin density functional calcs. 78−43291
Mg-Eu, dil. alloy, mag. suscept. meas. 77−89925
Mg-Mn, dil., mag. props., EPR meas. 79−73804
Mg-rare earth dilute alloy, mag. susceptibility and magnetisation 80−15689
$MgEr_2S_4$, magnetisation and susceptibility, exchange interactions obs. 78−52242
MgEu, dil. alloy, cold worked, valence transform. of Eu due to defect association, mag. suscept. and Mossbauer meas. 77−51404
$Mg_{1-x}Mn_xTe_2$, random dil. antiferromagnet, mag. props. 80−54870
Mg_2Ni, magnetism and H_2 storage 80−70941
MgO, lattice defects., calcination temp. effect 80−15091

magnetic susceptibility continued
MgO-ZnO-Fe_2O_3, sintered ferrite, preparation, mag. susceptibility, DC resistivity 80−34598
$MgSO_4.xH_2O$, mag. susceptibility, polaris. paramag., water of crystallisation effect 78−31047
MgU_8X_{17}, (X=S or Se), mag. susceptibilities 79−61073
Mn carbides and nitrides, $Mn_3MC(N)$, M=metal, perovskite type, mag. props. 78−43588
Mn complex, manganese (II)(1,2,4-triazole)$_2$$(NCS)_2$, 2-dimens. Heisenberg antiferromag., mag. props. 78−72336
Mn complex, $Mn(SCN)_2(C_2H_5OH)_2$, two-dimens. Heisenberg magnet, cryst. struct. and mag. props. 79−60337
Mn complex, with 1,2,4-triazole, mag. susceptibility, 2-300K struct. 77−77045
Mn, FCC, itinerant antiferromag., spin susceptibilities and collective excitations, many band effects 77−63140
α-Mn, NMR and susceptibility max., paramag. phase 78−56386
Mn ternary carbides, Mn_3MC, M=metal, mag. props. 77−63116
Mn ternary nitrides, Mn_3MN, M=metal, mag. props. 77−63116
Mn-Bi mictomagnetic alloy, mag., elec. and elastic props. *(Russian)* 80−108028
Mn-Ni, thermal expansion, mag. susceptibility, lattice consts. 80−100341
Mn-Ni-Ti (Zr) systems, and mech. props. thermal expansion for different heat treatments *(Japanese)* 79−29123
Mn-Ni(Pd), atomic and mag. order, neutron diffr. exam. 79−73697
Mn-Pt, Elinvar props., −150 to 500°C *(Japanese)* 77−52385
Mn-Pt, exam. of Elinvar props., from −150 to 500°C 78−76684
Mn-Zn ferrites, mag. parameters, determ. from RF susceptibility 79−82769
$MnAs_{0.97}P_{0.03}$, orthorhombic, mag. anisotropy 77−43832
$MnAs_{1-x}P_x$, mag. susceptibility anomaly at displacive phase transition 80−93091
MnB_2, polycryst., magnetoresist. and mag. props. *(Russian)* 80−92907
MnBi, mictomag. alloys, elastic props. *(Russian)* 80−7141
$Mn(Br_{1-x}Cl_x)_24H_2O$, antiferromagnetism, controllable anisotropy 80−93116
Mn_3C, Mn_5C_2, $Mn_{15}C_4$, Mn_7C_3 and $Mn_{23}C_6$, mag. susceptibility temp. depend. 79−51754
$MnCO_3$, nuclear spin waves from antiferromag. reson. line temp. depend. *(Russian)* 78−48050
$Mn_xCd_{1-x}(NH_3)_2.Ni(CN)_4.2C_6H_6$, Hofmann type mixed cryst., mag. props. 79−4659
$MnCl_2.4H_2O$, isothermal and adiabatic susceptibilities near field depend. anitferromag. phase transitions 77−69561
$Mn_{1-x}Cr_xP$, mag. susceptibility and transitions 79−47256
$Mn_{17.5}Cu_{82.5}$, mictomag. process, susceptibility and resist. meas. 78−3157
$MnEr_2S_4$, magnetisation and susceptibility, exchange interactions obs. 78−52242
MnF_2, antiferromag., magnetocryst. anisotropy, susceptibility, static torque meas. 77−69545
MnF_2, Heisenberg antiferromag., props. calc. 77−85406
MnF_2, mag. anisotropy at OK 79−33473
MnF_2, mag. susceptibility, crit. behaviour near Neel point 79−91217
MnF_2, spin-flop bicritical point, susceptibility and RF absorpt. meas. 79−87277
MnF_2, uniaxial antiferromag. anisotropy in paramag. susceptibility, cluster variation theory 78−52200
$MnFe_2O_4$, differential high field susceptibility 77−28376
$Mn_{1-x}Fe_xP$, magnetisation, susceptibility and mag. transitions 79−47256
$Mn_{5-x}Fe_xSi_3$, elec. resist. and mag. susceptibility, ferromag. to antiferromag. transition 80−80504
$MnGd_2S_4$, mag., struct. and Mossbauer effect study 78−51507
Mn_3In, antiferromag., mag. susceptibility, X-ray and neutron diffr. 79−11314
$Mn_xMg_{1-x}S$, mag. props. 77−66244
$Mn_xMg_{1-x}S$ solid solution, mag. props. 78−60269
$Mn_{1-x}Mg_xSe$, mag. and struct. phase transitions, mag. susceptibility and X-ray diffr. study 80−71022
$Mn_xMg_{1-x}Y_2S_4$, magnetisation and susceptibility, exchange interactions obs. 78−52242
$Mn^{2+}Mo^{4+}O_3$, defect spinel struct., elec. and mag. props. 80−70176
$Mn(NH_3)_2Ni(CN)_42C_{12}H_{10}$, phase transition, mag. susceptibility, sp. ht. 79−91234
$Mn(NH_3)_2.Ni(CN)_4.(benzene)_2$, antiferromag. ordering, mag. susceptibility, sp. ht. and Neel temp. meas. 77−12128
$Mn_{0.25}NbS_2$, mag. anomaly rel. to struct. disordering 78−43557
$Mn_{1/3}NbS_2$, intercalate, metallic cond., Hall effect and mag. props. 77−76789
$Mn_{73}Ni_{27}$, generalised susceptibility, spin wave contrib., inelastic mag. neutron scatt. 79−47262
$MnO:Mn_3O_4$, mag. props., susceptibility and magnetisation meas. 80−65824
$MnO-Al_2O_3-SiO_2$, amorphous, spin glass like behaviour at low temp. 79−61177
$MnO-Al_2O_3-SiO_2$, amorphous spin glass, AC susceptibility 80−80520
$MnO-B_2O_3$, polycryst. cpds., mag. susceptibility and ^{11}B NMR 79−8056
γ-MnOOH, antiferromag., prep. and mag. props., EPR meas. 79−87310
$x.MnO.(1-x)[19TeO_2.PbO]$, glass, antiferromag. behaviour, mag. props. 80−50072
MnP, Lifshitz point, transverse differential susceptibility meas. 80−84599
$Mn_xPd_{82-x}Ge_{18}$, amorphous alloys, mag. props. 78−91906
α-MnS, polycryst. and oriented single cryst., phase transition at 131K 78−6157
MnSb, interstitial cations, mag. and crystallographic study 79−55698
MnSb, resist., susceptibility and thermopower rel. to electronic struct. 78−67935
α-MnSe, mag. and struct. phase transitions, mag. susceptibility and X-ray diffr. study 80−71022
MnSe, mag. suscept., thermal expansion and elec. resist. meas. 78−34964
$MnSe_2$, pyrite struct., mag. suscept. and thermal expansion 77−32176
MnSi amorphous, conc. spin glass system, temp. effect on susceptibility 79−61142
MnSi, amorphous, sputtered, mag., elec., struct. and thermal props., spin glass behaviour 80−50124
MnSi, amorphous magnetisation meas. 80−34599
MnSi, itinerant electron system, helical spin structure 78−23234
MnSi, low field mag. studies 78−23255
MnSi, NMR and susceptibility above T_c 78−43665

magnetic susceptibility continued
MnSi(Ge), amorphous, spin glass transition, AC susceptibility meas. 80−75779
$Mn_5(Si_{1-x}Ge_x)_3$, magnetic and cryst. struct., ferromag. props. 77−59391
Mn_3SnN, perovskite type struct., mag. props., neutron and Mossbauer meas. 77−32159
$MnTe_2$, pyrite struct., susceptibility, 4.2-450K, exchange consts. 77−77040
$MnTiO_3$, quasi-two dimens. antiferromag., mag. crit. behaviour 77−32191
$Mn_{23}Y_6D_x$, D atom location, neutron diffr. study, and magnetism *(French)* 80−24426
MnY_2S_4, magnetisation and susceptibility, exchange interactions obs. 78−52242
MnZn ferrite, polydispersive spin relax. near Curie temp., mag. susceptibility meas. 77−69513
MnZn ferrite, wall topography change induced by external press. 80−34734
MnZn ferrites, mag. susceptibility freq. spectrum, effect of pressure 78−95420
Mo complexes, bis-carboxylate Mo(V), struct. and catalytic reactivity 77−77804
Mo, Knight shift and mag. susceptibility, temp. depend. *(German)* 78−10791
Mo, Knight shift and mag. suscept. temp. depend. 78−15043
Mo oxides, magnetic susceptibility meas., temp. effect 80−103822
Mo, plastically deformed single cryst., mag. susceptibility *(Russian)* 80−93074
Mo ternary chalcogenides, supercond., compared with band struct. calcs. 78−51871
Mo X-ray electron spectra, paramag. susceptibility, depend. on plastic deform. for single crystals 77−28683
Mo-Al-Ge, new compounds, structure and props. 80−39003
Mo-Co Kondo alloy, Co impurity susceptibilities, Knight shift 80−88721
Mo-dichalcogenide, valence band nature, elec. and mag. props. 78−39014
Mo-Fe, local magnetisation from Mossbauer meas. 77−20549
Mo-Fe, spin glass and mictomag. regimes, sp. ht., resist. and susceptibility meas. 77−69581
Mo-Fe alloy, local moment system, low temp. susceptibility, Mossbauer effect meas. 77−43810
Mo_2B_5 and MoB_4, thermal, elec., and mag. props. 80−20187
$MoCl_5$-MoF_5 system, magnetochem. and IR study of phase struct. 77−85710
MoFe, occurrence of spin glass and mictomagnetic regimes, props. meas. 77−16085
MoO_2, cryst., neutron diffr., mag. props. 77−16038
$Mo_{1-x}Re_xCo$, mag. state of Co impurity, NMR exam. 78−27100
$(Mo_{1-x}Ru_x)_{80}P_{20}$, amorphous, supercond. and electronic props. 78−88057
$(Mo_{1-x}Ru_x)_{80}P_{20}$, amorphous, liq. quenched, mag. susceptibility, supercond. and electronic props. 79−56376
MoS_2, prep. and mag. props. *(French)* 80−93072
$Mo_6S_8(Se_8)$, heat capacity and mag. props., 2-30K 79−42692
$Mo_{1-x}V_x$, supercond., NMR and mag. susceptibility meas. 79−56388
$(Mo_xV_{1-x})_2O_5$, mag. and spectroscopic investigation 80−25206
N_2 complex, $NiC(C_6H_5NO)_6(NO_3)_2$, singlet ground-state systems, field induced mag. long range order 80−60266
NH_4CoF_3, susceptibility and magnetisation meas. 77−85432
$(NH_4)_2CuBr_4.2H_2O$, ferromag., static and dynamic mag. props. 80−50074
NH_4FeF_4, mag. and Mossbauer obs. *(French)* 78−19389
NH_4FeF_4, two-dimens. antiferromagnetism 77−66444
$N_2H_6FeF_5$, one-dimens. magnetism, mag. suscept. and Mossbauer reson. exam. 77−51893
$N_2H_6FeF_5$, one-dimens. antiferromagnetism 77−66444
$(NH_4)_2IrCl_6$, mag. susceptibility in ordered and paramag. phases 79−73759
$(NH_4)_6MnMo_9O_{32}.8H_2O$, mag. susceptibility, rel. to EPR, zero field splitting parameter 77−36122
NH_4N_3, diamag. susceptibility, rel. to cryst. struct. 79−24127
NI_3Al, structural order and homogeneity, X-ray, mag. susceptibility and Mossbauer meas. 77−63663
Na, conduction electron spin props. 77−8036
Na, Pauli susceptibility meas. by CESR method 79−42735
Na, Pauli susceptibility meas. by CESR transmission 79−61217
Na, spin susceptibility and volume dependence 79−95569
Na-Cd, liq., diamagnetism 78−72326
Na-Fe fluorophosphate glass, Mossbauer study, mag. and optical props. 80−16065
Na-Ga alloy, solid and liq., mag. susceptibility and elec. cond. *(Russian)* 80−29522
Na-Tl, liq., diamagnetism 78−72326
NaA neolyte, Hg cluster transition to paramagnetic state due to mag. field *(Russian)* 80−60183
$Na_{1-x}Bi_x$ liq. alloys, metal-nonmetal transition, mag. susceptibility meas. 79−82525
$NaCeS_2$, mag. susceptibility, 3.7 to 297K, extended mol. field model 79−87227
$NaClO_3$-$CsClO_3$, NQR, mag. susceptibility meas. 78−35059
$Na_2Co_2Ti_6O_{14}F_2$, characterisation and mag. props., 90-800K, $Na_xTi_4O_8$ bronze isotypes *(French)* 80−39735
$NaCrO_2$, two-dimensional antiferromag., mag. props. *(French)* 78−23251
$Na_2Cr_2Ti_6O_{16}$, characterisation and mag. props., 90-800K, $Na_xTi_4O_8$ bronze isotypes *(French)* 80−39735
$NaFeF_4$, amorphous, mag. props. and Mossbauer spectra, speromagnetism and mictomagnetism 80−75778
$NaFeF_4$, two-dimens. antiferromagnetism 77−66444
α-$Na_3Fe_2(PO_4)_3$ orthophosphate, cryst. and vitreous, Mossbauer spectroscopy and mag. susceptibility *(French)* 80−80657
$Na_2FeTi_6O_{16}$, characterisation and mag. props., 90-800K, $Na_xTi_4O_8$ bronze isotypes *(French)* 80−39735
$Na_3M_2Li_3F_{12}$, M=Al, Fe, fluoride garnets, high press. form 77−76554
$NaMnCl_3$, 4.2-350K, quasi-two-dimens. antiferromagnetism 77−59399
$Na_2Ni_2Ti_6O_{14}F_2$, characterisation and mag. props., 90-800K, $Na_xTi_4O_8$ bronze isotypes *(French)* 80−39735
$Na_2O-B_2O_3$ glass, annealing and base comp. effect 79−91811
$Na_2O-Fe_2O_3-SiO_2$ glass, partially crystallised 78−23302
$Na_2O.2Al_2O_3.5SiO_2:Fe^{3+}$, Mossbauer effect and magnetometric exam. 78−6613

magnetic susceptibility continued
Na_3RuO_4, mag. props., isolated tetranuclear cluster model 79−24180
$Na_{1-x}Sb_x$, liq., mag. susceptibility 78−14926
$NaUO_3$, anomaly in mag. susceptibility-temp. curves 77−32152
$Na_{1.9}V_{12}O_{29.7}$, phase transitions, elec. cond., susceptibility and sp. ht. meas. 78−14776
β-$Na_xV_2O_5$, antiferromag. props. and weak ferromagnetism 79−78337
$Na_xV_2O_5$ β-phase single cryst., phase transitions EPR meas. 78−95514
$Na_xV_2O_5$, nonmetallic bronze, low field sp. ht. and mag. suscept. 78−72357
Na_xVS_2, intercalation cpd., mag. phase transitions 77−69558
$Na_xVS_2(Se_2)$, mag. and elec. props. rel. to struct. transitions 78−91848
Na_xVSe_2, intercalation cpd., mag. and structural phase transitions 77−69558
$Na_2V_2Ti_6O_{16}$, characterisation and mag. props., 90-800K, $Na_xTi_4O_8$ bronze isotypes *(French)* 80−39735
Na_xWO_3 enhanced T_c, interband coupling 78−91804
$Na_20.3B_2O_3.xFe_2O_3$, borate glass, Fe^{3+} spin state and distrib. meas. 80−39966
Nb carbide interstitial phases, elec. and mag. props., neutron radiation effects 79−77640
Nb, high crit. flux density gradient near surface 79−87221
Nb, NMR study up to 1700K, Knight shift and spin-lattice relax. time 80−2653
Nb, spin fluctuations effect on T_c, from sp. ht. and mag. suscept. 80−7030
Nb-C-N-O-H, solid solns. of H, exam. of props. 80−29172
Nb-Ge-Fe, effect of Fe on supercond. and mag. props. 79−56351
Nb-H, exam. of electron structure 80−29306
Nb-Hf (38 at.%) superconductor, peak effect, summation problem, mag. history flux pinning force 80−20362
Nb-Mo alloy, electronic density of states, temp. depend. of elec. resist. and mag. susceptibility 77−11891
Nb-S system, phase relations at high temp., elec. and mag. props. 80−29932
Nb_2Al, $NbAl_3$, supercond. and mag. props. 77−47922
Nb_3Al based ternary solid solns., supercond. transition temp., paramag. susceptibility and lattice parameters meas. *(Russian)* 77−43766
Nb_3Al, superconductivity, crit. temp., paramag. susceptibility comp. depend. *(Russian)* 77−66219
Nb_3Al-Ni(Cr)(Fe) mag. impurities effect on supercond. props. 77−1524
$Nb_xCr_{1-x}O_2$, cryst. prep. and struct., mag. props. 78−52198
Nb_3Ga-Nb_3Pt, temp. depend., and supercond. props. *(Russian)* 77−59347
$Nb_{78}Ga_{22-x}Mn_x$, supercond. props., influence of Mn mag. impurities 80−54825
$Nb_{80}Ga_{20-x}Mn_x$, supercond. props., influence of Mn mag. impurities 80−54825
NbH_x, proton Knight shift and mag-suscept., high resolution meas. 77−55716
$Nb_{1-x}Mo_xSe_2$, supercond. transition temp. and mag. susceptibility 77−12043
$Nb_{50}Ni_{50-x}Fe_x$, amorphous, mag. ordering and local random anisotropy 78−68273
$Nb_{50}Ni_{50-x}Fe_x$, magnetically dil. glass, 3d moments, mag. susceptibility and magnetisation meas. 79−95574
Nb_2O_5, partly reduced, mag. and elec. props. 77−43593
$NbS_2(Se_2)$ intercalation complexes with 3d transition metals, mag. and metallic transport props. 80−44814
Nb_3Sb, 4 to 294K, magnetic susceptibility meas. 79−99675
$NbSe_2$:Fe, local moment form., mag. susceptibility meas. 79−82756
$NbSe_3$, mag. anomalies at CDW transitions 80−11158
$NbSe_3$, mag. susceptibility, CDW effect 80−88716
$NbSe_3$, phase transitions, phys. props. meas. 77−8005
$NbSe_3$, superconducting transitions and diamagnetism 80−84526
Nb_3Sn, electronic props. calc. 79−7780
Nb_3Sn-Fe(Co)(Mn), mag. impurities effect on supercond. props. 77−1524
$Nb_{1-y}Ti_ySe_2$, supercond. transition temp. and mag. susceptibility 77−12043
$Nb_{1-x}V_xSe_2$, elec. and mag. anomalies at CDW transition 80−107722
$Nb_{1-x}W_xSe_2$ x=0 to 0.15, elec. resist., mag. suscept., heat capacity, structural, supercond. transition *(Russian)* 78−31006
Nd^{3+}:scheelite-type crysts,, magnetic, thermal properties, cryst. field calcs. 78−91875
Nd-La, mag. ordering, sp. ht., susceptibility and resist. 78−68238
$NdAg_x$, low temp. mag. meas. 80−107989
$Nd_{21}Ag_{79}$, and $Nd_{50}Ag_{50}$, amorphous, mag. props. 80−60182
$NdCl_3$, adiabatic susceptibility meas., interaction tensors for Nd^{3+} ions 77−69485
$Nd_{64}Co_{36}$, amorphous, amg. ordering, susceptibility, magnetisation and hysteresis meas. 78−68190
$Nd_xEu_{1-x}B_6$ solid solution, mag. susceptibility, lattice parameters, Weiss temp. 80−29535
$NdFeTiO_5$, mag. susceptibility, 4.2-77K, antiferromag. ordering obs. 78−68186
$NdFeTiO_5$, magnetic props. and crystal growth 78−92185
$Nd_2(MoO_4)_3$, mag. susceptibility, elec. cond. and thermoelec. power 78−88091
Nd_3NbO_7, weberite-type, elec., mag. and opt. props. 77−85212
Nd_2NiO_4, Nd_2CuO_4, magnetic properties obs. 80−70937
NdO, mag. props., lattice consts., and X-ray absorpt. spectra 80−44798
Nd_2O_3, A-type, optical absorpt. spectrum and paramag. susceptibility 79−56811
Nd_2O_3, magnetisation and mag. susceptibility Curie-Weiss behaviour 77−4505
$NdRh_4B_4$, possible obs. of coexistence of supercond. and long-range mag. order 79−82730
NdScFe garnets, mag. props. 77−47979
$NdSn_3$, Neel temp., hydrostatic press. depend. 80−29549
$Nd_2Ti_2O_7$, Nd_2TiO_5, paramag. props., mag. susceptibility meas. 1.6 to 70K 78−10649
$NdTlO_3$, physicochem. props. 80−25625
$NdVO_3$-$CaVO_3$ solid solns., mag. props. rel. to cryst. struct. 78−43571
$Nd_2(WO_4)_3$, elec. transport and mag. props. meas. 77−24668
$Nd_2(WO_4)_3$, mag. susceptibility, paramag. Curie temp., 300-900K 79−82753
$Nd_2(WO_4)_3$, molar mag. susceptibility, DC elec. cond., thermopower meas. 79−15172
$Nd_xY_{1-x}Zn$ system, solid soln., mag. susceptibility, 77 to 600K *(Russian)* 80−65776
magnetic susceptibility continued
Ni alloys, mag. moment distrib. 77−32178
Ni, atomic layers, Pauli paramagnetism to band ferromagnetism transition thickness depend. 78−72377
Ni, band model of high temp. magnetism 78−26809
Ni complex, $(Ni(C_2H_5NO)_6)(NO_3)_2$, field induced level crossing and cryst. struct. 79−47070
Ni complex, $[Ni(en)_2Cl]_2Cl_2$, heat capacity, X-ray diffraction and mag. meas., phase transition 78−47515
Ni complex, Ni(5-methylpyrazole)$_4X_2$, (X=Cl, Br, I), mag. props., EPR, ligand field calcs. 77−62880
Ni complex, tris(ethylenediamine)nickel(II) nitrate, mag. props. from susceptibility and sp. ht. meas., 0.3-3.0K 78−91877
Ni complex, with 1,2,4-triazole, mag. susceptibility, 2-300K, struct., antiferromag. props. 77−77045
Ni, crossover phenomena, stress induced above Curie point, neutron scatt. study 79−61113
Ni, deformed, magnetic susceptibility anisotropic changes 78−27025
Ni, dynamical spin susceptibility, noninteracting spin band model 78−31059
Ni, effective Coulomb interaction momentum depend. band model 79−78298
Ni ferrite, quenched, Neel temp. and initial susceptibility 80−75762
Ni, ferromag., dynamic susceptibility calc. 80−80488
Ni film, few atomic layers thick, transition from Pauli paramag. to band ferromag. 80−44885
Ni, film, mag. susceptibility correlation with SAW attenuation 79−47310
Ni film, transition from Pauli paramagnetism to band ferromagnetism 79−61192
Ni, Hopkinson effect, mag. field depend. *(Russian)* 79−4657
Ni, magnetic susceptibility, generalised, neutron scatt. meas. 80−34606
Ni, normal magnetisation meas. by rotating sample magnetometry 77−69514
Ni, paramag., model calc. of dynamical spin susceptibility 77−69489
Ni, paramag. region, Fe and Co impurity effects on susceptibility, Faraday obs. *(Russian)* 80−88731
Ni, paramagnetic, temp. depend. of spin susceptibility 79−4651
Ni, single-domain particles, LF mag. susceptibility, 2K up to Curie point 80−29582
Ni, Stoner model, mol. field coeff., temp. and field depends. 77−72975
Ni-Co, high-field susceptibility, spin-wave spectrum, CPA calc. 80−65818
Ni-Co, solid and liq., paramag. susceptibility and electron struct., 800-1800°C *(Russian)* 80−25081
Ni-Cr alloys, low temp. transform. mechanism, electrophys. props. obs. *(Russian)* 77−59777
Ni-Cu, ferromagnetic and spin glass transition, DC magnetisation meas. 79−78369
Ni-Cu, high-field susceptibility, spin-wave spectrum, CPA calc. 80−65818
Ni-Cu, low field magnetisation meas., mag. props. comp. depend. 78−91879
Ni-Cu-Mn alloys, mag. and galvanomag. meas. 77−89928
Ni-Fe, 79 NM alloy, gamma and neutron influence on mag. susceptibility comparative study *(Russian)* 80−39751
Ni-Fe, high-field susceptibility, spin-wave spectrum, CPA calc. 80−65818
Ni-Fe film, differential susceptibility, struct. const. and losses 79−91271
Ni-In(Sn), electrical cond. and magnetic susceptibility of B 8_2-compounds *(German)* 79−42520
Ni-M, alloys, M=Si, Ge, Al, Ga, band model of high temp. magnetism 78−26809
Ni-M, dil., high field susceptibility 78−52230
Ni-Mn alloys, ferromagnetism-to-spin glass phase transition and strong mag. field effect 80−75773
Ni-Pd alloys, mag. props., average and local density of states, CPA calc. 77−59242
Ni-Pd-P, metallic glass, electronic structure, pulsed NMR study 80−75869
Ni-Pd-Si, amorphous, low-field mag. susceptibility meas., 4.2-580K 79−61057
Ni-Pt alloy, spin susceptibility, temp. variation, band model calc. 77−28365
Ni-Pt disordered alloy, off-diagonal, T-matrix itinerant electron ferromagnetism calcs. 80−25067
Ni-rare earth intermetallics, RNi_3, amorphous alloys, mag. and transport props. 79−42513
Ni-Rh alloys, disordered, vol. paramagnetostriction calc. 77−80985
Ni-Rh alloys, thermal EMF, elec. resist., mag. susceptibility, mag. moment and Curie temps., 18-500°C *(Russian)* 77−20288
Ni-Ta, dil., crit. behaviour of local magnetization, PAC and magnetisation meas. 78−48098
Ni-V, solid and liq., mag. susceptibility and electronic struct. 80−39738
Ni-V(Nb)(Ta)(Si)(Ge), dil., mag. props. at elevated temps. 77−63089
$Ni_{0.95}$ S Fe, spin glass, spin flop in exchange field 80−34640
$Ni_3Al(Ga)$, off-stoichiometric alloy, inverse mag. susceptibility rel. to defect conc. 80−60216
$Ni_{100-x}B_x$, amorphous, mag. struct., mag. susceptibility meas. 80−80485
$Ni_3B_7O_{13}I$, phase transition, X-ray diffr. obs., 77-300K, rel. to mag. susceptibility anomaly 77−47573
$NiBr_2.6H_2O$, antiferromag. transition, susceptibility and sp. ht. meas. 77−69587
$NiBr_2.6H_2O$, antiferromag. ordering and paramag. behaviour 78−14941
$Ni(C_5H_5NO)_6(ClO_4)_2$, susceptibility and magnetisation meas., field, freq. and temp. depend. 77−66279
$Ni_xCd_{(1-x)}(NH_3)_2$. $Ni(CN)_4.2C_6H_6$, mag. susceptibility meas. 77−63126
$NiCl_2.2H_2O$, mag. phase diagram and exchange parameters 77−77054
$Ni_xCo_{3-x}O$, composition depend antiferromagnetic-ferrimagnetic ordering, mag. susceptibility meas. 80−70973
$Ni_{1-x}Cr_xS$, elec. transport, mag. susceptibility and DTA meas. 80−96954
$Ni_{0.7}Cu_{0.3-x}Si_x$, magnetic props., 4.2 to 800K 77−8290
$NiFe_2O_4$, domain wall size and mag. losses in freq. spectra 77−85481
$Ni_xFe_2O_4$ series, chem. and mag. transformation, X-ray diffr. and mag. susceptibility study 79−51774
$(Ni_{1-x}Fe_x)S$, solid solns., electronic props., X-ray, thermal and Mossbauer study 79−78376
$Ni_{1-x}Fe_xS_2$ (x=0 to 0.075), weak ferromag. exam. 79−51755
$NiI_2.6H_2O$, disordered linear chain mag., ESR, mag. susceptibility and NMR meas. 77−20688

magnetic susceptibility continued
$Ni_{1-x}Li_xO$, $0.01 \leq x \leq 0.08$, mag. susceptibility in region 80 to 800K *(Russian)* 78−2664
$Ni_pMg_{(1-p)}(OH)_2$, random magnet, AC susceptibility 79−47258
Ni_3Mn, thermoremanent magnetisation and blocking temp. 80−34601
Ni_xMn_{1-x} disordered alloy, mag. interactions exam. 77−24687
NiMnGe, crystal and spiral mag. struct., Neel temp., X-ray and neutron diffr. 77−16052
$NiMnGe_{1-x}Si_x$, mag. props., neutron diffr. and magnetometric meas., 80-600K 80−65793
$(Ni_{0.75}Mn_{0.25})_{82}Si_{10}B_8$, amorphous, exchange anisotropy, mag. susceptibility meas., 4.2K to room temp. 80−11186
$Ni_2Mn_xT_{1-x}Sn$, T=Ti(V)(Cr), ferromag., magnetisation, susceptibility 77−12102
$Ni(NH_3)_2Ni(CN)_4.2C_{12}H_{10}$, mag. susceptibility, sp. ht., spin arrangements and transition obs. 77−20590
$Ni(NO_3)_2.4H_2O$, two spin ordered states under mag. field 79−15308
$Ni(NO_3)_2.6H_2O$, susceptibility and specific heat meas., spin ordering, antiferromag. spin pair coupling 80−7084
$NiNb_2O_6$, antiferromag., principle mag. susceptibility and field induced magnetisation meas. 77−20589
$NiNb_2O_6$, magnetisation and susceptibility, antiferro-paramag. transition, expt. and theory 77−43822
$Ni_{1/3}NbS_2$, intercalate, metallic, cond., Hall effect and mag. props. 77−76789
NiO (111) platelets, magnetic anisotropy investigation by torque and mag. susceptibility meas. 80−54885
NiO, AC susceptibility, temp. depend. 78−10664
NiO fine particles, mag. props. rel. to physicochem. props. 78−52315
NiO, magnetic susceptibility, near Neel temp. 79−56509
NiO:Cr, effect of Cr additives on structure parameters *(Bulgarian)* 80−44319
$Ni_{1-x}P_x$, electrodeposited, amorphous, mag. and transport props. 78−52106
$Ni(Rh_{1-x}Cr_x)_2S_4$, ferromag. spinel system with metallic conduction 79−56513
$Ni_{1-x}Rh_xS$, nonvolume effect of Rh substitution on paramag. metal-antiferromag. nonmetal transition 79−28277
NiS_2, pyrite type, mag. struct., antiferromag. refl. of neutron diffr., susceptibility meas. 77−69497
NiS_2, weak ferromagnetic semiconductor single crystal, elec. and magnetic props. 77−85226
$NiS_2O_3.6H_2O$, cryst. data and mag. susceptibility 77−76368
NiS_yTe_{1-y}, mag. susceptibility, correl. with metal-insulator transition data 79−24145
NiSb, at. struct. and mag. susceptibility 77−39561
NiSb, resist., susceptibility and thermopower rel. to electronic struct. 78−67935
$NiSe_2$, paramag. props., NMR, mag. susceptibility 80−60175
$NiSiF_6.6H_2O$, EPR spectrum at low temp. 78−43632
$NiSiF_6.6H_2O$, ferromag. ordering, susceptibility and heat capacity obs. 79−61080
$NiSnF_6.6H_2O$, ferromag. ordering, susceptibility and heat capacity obs. 79−61080
$Ni_{1-x}Te$, fluctuating localised mag. moments, d band motion, Mossbauer study 80−65768
$Ni_2(Ti,Mn)Sn$, Heusler alloy, mag. meas. 79−47261
$NiTiF_6.6H_2O$, mag. and struct. transitions 78−68257
$Ni_3(VO_4)_2$, Neel temp., mag. susceptibility meas. 80−29550
$NiWO_4$ monoclinic antiferromagnet, orientational phase transition and intermediate state *(Russian)* 80−15725
NiZn ferrite, wall topography change induced by external press. 80−34734
NiZn ferrites, mag. susceptibility freq. spectrum, effect of pressure 78−95420
NiZn ferrites, nonstoichiometric, initial susceptibility and microstruct. 80−84591
$Ni_xZn_{1-x}Fe_2O_4$, catalytic oxidation of CO, mag. props., kinetic parameters and composition depend. 80−16723
$Ni_xZn_{1-x}Mn_2O_4$, mag. props. 78−43573
Ni_xZr_{1-x} metallic glass, crystallisation kinetics, elec. resist. and mag. susceptibility meas. 80−103659
$NiZrF_6.6H_2O$, uniaxial ferromagnetism 78−80143
$NpCo_2Si_2$ and $NpFe_2Si_2$, itinerant magnetism obs. 77−28406
NpH_x, mag. props., 4 to 700K 79−61075
$NpIr_2$, itinerant antiferromagnetism 79−61154
NpM_2Ge_2, Neel point and hyperfine interactions, Mossbauer and magnetisation meas. 77−1555
$NpRe_2$, mag. susceptibility 78−68182
$(Np_{1-x}U_x)Fe$, Mossbauer spectra, magnetism and hyperfine interactions 80−20529
O_2, adsorbed layer on graphite film, mag. susceptibility 78−43241
O_2 adsorbed layer porous Vycor glass, props. characteristic of amorphous antiferromag. obs. 78−10665
O_2 adsorbed layers, on Vycor and Grafoil substrates, mag. susceptibility as probe of restricted geometry 79−51436
O_2 solid, α-β transition, mag. susceptibility *(Russian)* 80−6592
O_2, solid, temp. depend. as function of press. and mag. field, α-β transition obs. 77−47991
Os-Re alloy, mag. suscept. of HCP transition metal alloys *(Russian)* 78−80138
P-As-Se glasses, mag. susceptibility, dielec. const., opt. props. 78−64184
P-Se system glasses, magnetochem. investig. 77−51325
P-Se-Te system glasses, mag. susceptibility and opt. props. 80−25079
$PaSb_2$ and Pa_3Sb_4, cryst. structs., mag. susceptibility *(French)* 79−65641
Pb-Te, molten mag. susceptibility, conc. and temp. depend. 78−80121
$PbCo_2(PO_4)_2$, mag. susceptibility, elec. cond. and optical refl. 79−56495
$2PbFe_{1/2}Nb_{1/2}O_3$-Pb_2FeReO_6, comp., struct., dielec. and mag. props. 80−2704
$2PbFe_{1/2}Ta_{1/2}O_3$-Ba_2FeReO_6, comp., struct., dielec. and mag. props. 80−2704
$2PbFe_{1/2}Ta_{1/2}O_3$-Pb_2FeReO_6, comp., struct., dielec. and mag. props. 80−2704
$PbMnFeF_7$ and Pb_2MnFeF_9, vitreous, insulating, evidence of spin-glass transition 80−97112
$Pb_{1-x}Mn_xTe$, single cryst., mag. susceptibility 79−73672
$PbMo_{5.1}S_6$, high supercond. T_c, soft mode behaviour 78−14855
PbS, mol. diamag. susceptibility, bonding types 78−31046
PbSe, electron gas magnetisation, energy band parameters determ., use of Faraday effect 80−45047
PbSe, Faraday effect and electron gas magnetisation, Kane two band model calcs. *(Russian)* 80−34899
$p\text{-}Pb_{0.82}Sn_{0.18}Te$, mag. susceptibility, inversion layers effect *(Russian)* 77−72996
$Pb_{0.82}Sn_{0.18}Te$, narrow gap semicond., mag. susceptibility meas. *(Russian)* 78−84397
$Pb_{1-x}Sn_xTe$, Faraday effect and electron gas magnetisation, Kane two band model calcs. *(Russian)* 80−34899
$Pb_{1-x}Sn_xTe$, mag. and kinetic props. near ferroelec. transition 80−11160
$Pb_{1-x}Sn_xTe$, narrow gap solid solns., mag. susceptibility and energy band spectrum 79−28276
$Pb_{1-x}Sn_xTe$, narrow gap semicond., theory of mag. susceptibility 80−93070
$Pb_{1-x}Sn_xTe$: Mn, Mn mag. and elec. active states, mag. impurity behaviour 80−44627
PbTe:Fe, single crystals, state and behaviour of Fe, mag. props. 80−93080
PbTe:In, mag. susceptibility, temp. depend., 4.2 to 200K 80−65773
Pd, band model, mag. susceptibility of exchange-enhanced paramagnet 78−2644
Pd, confined geometry, p-wave supercond. or itinerant ferromag. 80−11129
Pd, electronic struct., effects of press. and alloying with Ru, Rh, Ag, and Rh+Ag 78−91581
Pd, generalised susceptibilities and phonon anomalies, band struct. calcs. 79−90953
Pd, liq., mag. susceptibility 78−95415
Pd, mag. suscept. temp. depend. 78−60265
Pd, sd hybridisation, paramagnetic Curie temp. and susceptibility *(Russian)* 80−103808
Pd, spin fluctuation model interpretation of mag. susceptibility 80−80477
Pd, spin-density functional theory of temp. depend. spin susceptibility 79−56497
Pd-Ag(Mo)(Nb)(Rh)(Ru), dilute, low temp. sp. ht and mag. susceptibility 77−62650
Pd-Co-P amorphous alloy, mag. an elec. props. 77−40043
Pd-D, mag. susceptibility 6 to 150K 79−38300
Pd-Fe, very dilute, very low temp., spin glass-like behaviour 79−99708
Pd-Fe disordered alloy, Landau model for mag. props. 77−66276
Pd-Fe-Mn, differential susceptibility, spin glass and ferromag. transition 79−61169
Pd-Fe-Mn, dil. alloy, high press. study 80−34600
Pd-Fe-Mn, ferromagnetic-spin glass transition 78−39339
Pd-H, mag. susceptibility 6 to 150K 79−38300
Pd-Mn, spin freezing in spin glass phase, susceptibility meas., sp. ht. analysis 77−69582
Pd-Mn(Fe), mag. ordering phenomena, neutron scatt. obs. 80−44812
Pd-Ni, local susceptibilities, ^{61}Ni Mossbauer spectroscopy 78−95536
Pd-Ni alloy, dil., ferromagnetism, local moments, susceptibility, magnetisation and Curie temp. *(Russian)* 78−88115
Pd-Ni alloy, paramag. giant moments 78−56291
Pd-Ni disordered alloy, Landau model for mag. props. 77−66276
Pd-Pt alloys, mag. props., average and local density of states, CPA calc. 77−59242
Pd-Rh alloys, disordered, vol. paramagnetostriction calc. 77−80985
Pd-Rh-Ag, magnetic susceptibility press. depend., d-band deform. and exchange var. 77−47967
Pd-Rh-Ag alloy, pressure effect, up to 4000 atm. 77−16142
Pd-Si, liq., mag. susceptibility 78−95415
Pd-Si(−Cu), glassy, liq. and cryst., mag. and elec. props. 77−66249
Pd-Ti, hydrogenation, lattice spacings, microhardness and mag. susceptibility meas. 79−77557
Pd-W, elect. resist., mag. susceptibility, Hall coeffs., in plastically deformed state and after annealing *(Russian)* 79−66174
PdAgFe, ferromag., Curie temp. depend. on susceptibility, non-mean field theory 80−44829
PdF_2 flourite-type form, mag. props., structure studies *(French)* 80−34187
$(Pd_{0.67}Fe_{0.33})_{1-x}Au_x$, ordering effects on mag. props. *(Russian)* 78−47942
$(Pd_{0.9965}Fe_{0.0035})Mn_{0.05}$, ferromag. and spin-glass props. 80−2590
PdFeRh, ferromag., Curie temp. depend. on susceptibility, non-mean field theory 80−44829
PdH_x, electronic props., H alloying effects, book contrib. 79−82522
$Pd_{1-x}H_x$, (x=0.59, 0.65), 4.2 to 300K temp. range 78−18953
β'-PdIn, electrical resistance, mag. susceptibility and IR freq. dispersion *(Russian)* 80−107759
$(Pd_{1-y}M_y)_{100-x}Fe_x$, M=Ag, Rh, exchange-enhanced alloys, mag. ordering 79−61050
$Pd_{1-y}Mn_yH_x$ alloy, spin glass, transition temp., susceptibility and EPR meas. 80−65930
$Pd_2MnIn_{1-y}Sb_y$, Heusler alloy, mag. order obs. 80−29528
$Pd_2MnIn_{1-x}Sn_x$, mag. order exam. 77−40036
$Pd_2MnSn_{1-x}Sb_x$, mag. order exam. 77−40036
$Pd_{0.98}Pr_{0.02}$, dil. alloy, mag. susceptibility meas. 79−19583
$(Pd_{95}Rh_5)Co$, exchange enhanced system, AC susceptibility meas. 77−16096
$Pd_{35}Zr_{65}$, mag. susceptibility meas. 80−75740
Pr, elastic constants, magnetic effects 78−68355
Pr, quasielastic mode damping, dynamic susceptibility 80−15705
Pr-Ce(Tm), mag. order onset, elec. resistivity 80−20416
Pr-rare earth dilute alloy, low field magnetic props. 78−84443
$PrAg_x$, low temp. mag. meas. 80−107989
$Pr_{21}Ag_{79}$, $Pr_{50}Ag_{50}$, and $Pr_{10}Lu_{40}Ag_{50}$, amorphous, mag. props. 80−60182
PrAl, annealed, mag. props. and mag. struct. 78−6517
$PrAl_2$, cryst. field interpretations of inelastic neutron scatt. meas. and mag. props. 79−56174
$Pr_{1-x}Ca_xAl_2$, mag. props. and phase relations 80−107991
$PrCl_3$, cooperative Jahn-Teller ordering of elec. dipoles in non-Kramers doublets 78−15115
$PrCo_2$, strongly exchange-enhanced paramagnetism, susceptibility 80−60179
$PrCu_2$, Jahn-Teller transition, susceptibility, elec. resist., thermal expansion and acoustic meas. 77−20276
$PrCu_4$ and $PrCu_5$, Knight shift, mag. susceptibilities 79−95570
PrEu(Gd), magnetic interactions, Mossbauer spectra quadrupole splitting, crystal field parameters 80−39907

magnetic susceptibility continued
PrH_2, cryst. field splitting, reciprocal susceptibility, book contrib. 79−82754
$PrIr_2(Pt_2)(Rh_2)(Ru_2)$, sp. ht., differential susceptibility and elec. resist. meas., 1.4-40K 80−71063
PrN, compressibility, mag. susceptibility and NMR freq. shift meas. 77−85595
$PrNi_5$, crystal field investigation from inelastic slow neutron scatt. expts. 80−39538
$PrNi_5$, crystal-field effects, comparison of calcs. with expts. 79−87071
$PrNi_5$, LF dynamics and ^{141}Pr thermal relax., coupling parameter and RKKY exchange mechanism 80−103812
$PrNi_5$, metallic Van Vleck paramag., nucl. interactions, NMR meas. 80−44953
$PrNi_5$, powder, in contact with liq. ^3He, thermal relaxation and heat capacity 79−44909
Pr_2NiO_4, Pr_2CuO_4, magnetic properties obs. 80−70937
PrO, mag. props., lattice consts., and X-ray absorpt. spectra 80−44798
Pr_6O_{11}, mag. and transport props., multiphonon hopping conduction 78−19211
$Pr(OH)_3$, Jahn-Teller antiferroelectric ordering 78−10859
PrP, nonstoichiometric, with singlet ground state, induced van Vleck ferromag. spin glass 77−66378
$PrPt_3$, ^{195}Pt NMR and susceptibility meas. 77−63299
PrS, hydrostatic press. depend. of mag. suscept. 78−80122
$PrSn_3$, Neel temp., hydrostatic press. depend. 80−29549
$Pr_2(WO_4)_3$, mag. susceptibility, paramag. Curie temp., 300-900K 79−82753
Pt, band model, mag. susceptibility of exchange-enhanced paramagnet 78−2644
Pt, generalised susceptibilities and phonon anomalies, band struct. calcs. 79−90953
Pt, spin fluctuation model interpretation of mag. susceptibility 80−80477
Pt, spin-density functional theory of temp. depend. spin susceptibility 79−56497
Pt-Au(Al)(In)(Sn)(Zr), solid soln., magnetic props. and lattice parameters *(German)* 79−87236
Pt-Co system, low temp. susceptibility 80−65920
Pt-Cr, disordered, atomic order-disorder transform. effect on resist. min. 80−65911
Pt-Cr alloys, (13-18 at.% Cr) resistivity and AC susceptibility, temp. 1.4−300K 78−2461
Pt-Cr(Nb)(Re)(Rh)(V), dil. alloy, 0.5 at.% ^{195}Pt NMR for local mag. susceptibility 78−84484
Pt-Fe alloy, low field AC susceptibility 79−73698
Pt-Fe alloy, ordered, T-c phase diagram, antiferro- and ferromagnetism *(Russian)* 80−65871
Pt-Fe alloys, supported, mag. prop. meas. in H_2 and O_2, 77 to 700K 79−91257
Pt-Fe ordered alloy, multiply mag. phase transitions 80−60264
Pt-Mn alloy, dil., low temp. susceptibility, spin glass and Kondo behaviour 77−66372
Pt-Ni, mag. inhomogeneity, low field DC susceptibility meas. 78−56301
Pt-Ni alloys, disordered, vol. paramagnetostriction calc. 77−80985
Pt-Ni disordered alloy, Landau model for mag. props. 77−66276
Pt-transition metal, dil., mag. susceptibility and NMR meas. 78−39290
PtCr, AC susceptibility near percolation limit, ordered and disordered alloy 80−65900
Pt_3Fe, transport and mag. props. near Neel temp. 79−7976
PtMn, spin glass, nonlinear susceptibility and sp. ht. 80−60304
PtMn spin glass alloy, cooperative freezing, susceptibility meas. 79−91233
PuH_x, mag. props., 4 to 700K 79−61075
$PuRe_2$, mag. susceptibility 78−68182
pyridine, elec. dipole moment, g-values, mag. susceptibility, moments and charge distrib. 77−58077
R_2In, R_3In, R=Gd, Tb, Dy, Ho, Nd, mag. props. 80−108009
RM_4Al_8 (M=Cr, Mn, Fe, Cu), magnetism and hyperfine interactions 80−25256
$ROsB_4$, R=Y, Gd, Tb, Dy, Ho, Er, Tm, struct. and mag. props. 78−79584
$RRuB_4$, R=Y, Cd, Tb, Dy, Ho, Er, Tm, struct. and mag. props. 78−79584
$RbCoCl_3.2D_2O$, metamagnetic phase transition, crystallographic and mag. struct., neutron diffr. meas. 80−44174
$RbCoCl.2H_2O$, Dzyaloshinsky-Moriya linear chain magnet, spin counting 79−38304
$Rb_2Co_xMg_{1-x}F_4$, antiferromag., static critical phenomena, neutron diffr. obs. 79−56528
$RbCrI_3$, radiocrystallographic and mag. study *(French)* 79−46632
$Rb_2CuBr_4.2H_2O$, ferromag., static and dynamic mag. props. 80−50074
$Rb_2FeCl_5.H_2O$, cryst. struct., superconducting susceptometer mag. meas. 79−73717
Rb_2FeF_5, mag. struct. and one-dimens. antiferromagnetism 80−60209
$RbMnCl_3$, high-pressure cubic phase, mag. props. 79−47260
Rb_2MnCl_4, 2D Heisenberg antiferromag. spin wave analysis 80−54879
$RbMnF_3$, Heisenberg antiferromagnet, spin diffusion below T_N 78−34968
$Rb_3Mn_2F_7$, double-layer antiferromag., mag. prop. meas. and calc. 77−55666
$RbMn_{1-x}Mg_xCl_3$, dilute pair antiferromag., mag. susceptibility and ESR meas. 79−78338
$Rb_2Mn_{0.5}Ni_{0.5}F_4$, site-random two-dimensional antiferromag., crit. behaviour, quasielastic neutron scatt. 77−85468
$RbNiCl_3$, mag. props. 79−73736
$RbNiF_3$ spin lattice, susceptibility, Heisenberg model *(Russian)* 80−65893
$RbNi_xMn_{1-x}F_3$, powder, mag. props. 80−2560
$RbUO_3$, EPR and mag. susceptibility, temp. depend. 79−33451
$RbVCl_3$, mag. props. *(French)* 77−16059
Re-W alloy, mag. suscept. of HCP transition metal alloys *(Russian)* 78−80138
Rh based ferromag. Heusler alloys, peaks in low field AC susceptibility 80−50071
$RhGe_{1.5}S_{1.5}$, new skutterudite relation compounds, prep. and charact. 78−52700
Rh_2MnX, (X=Al, Ga, In, Tl, Sn, Pb, Sb), Heusler and Heusler-related cpds., mag. and cryst. props. 77−20568
Ru based ferromag. Heusler alloys, peaks in low field AC susceptibility 80−50071
magnetic susceptibility continued
Ru-Nb alloy, mag. suscept. of HCP transition metal alloys *(Russian)* 78−80138
RuF_5, mag. props. 80−15707
$Ru_2Ge_{3-x}Sn_x$, and $Ru_2Ge_{3-y}Si_y$, diffusionless phase transitions, elec. and mag. props. 80−96871
RuS_2 amorphous, prep. at ambient temp., magnetic structure 80−35119
S, mag. susceptibility meas. rel. to heat treatment 78−34952
S-Se-Te semicond. glasses, mag. suscept. meas., refractive index 78−34952
S-Se(Te)(Tl), liq. semicond., bonding energies and entropies, mag. susceptibility meas. 80−49082
$(SN)_x$, brominated, temp. depend. of static mag. susceptibility 79−33452
$(SN)_x$, mag. props. in supercond. state 77−51842
$(SN)_x$, Meissner effect, mag. susceptibility meas. 80−20351
$(SN)_x$, temp.-depend. of elec. resist. and mag. susceptibility, density of states determ. 77−51877
Sb-Te, fused, mag. susceptibility, temp. and conc. dependence 77−36052
Sb-Te(Se), liq., diamag. susceptibility, semicond./metal behaviour 78−14927
Sb_2S_3, elec. and mag. props., carrier transport mechanism 78−47792
Sb_2Se_3 crystals, mag. and elec. props. 80−96873
Sb_2Te_3, free charge carrier mag. susceptibility, 300-600K 78−10644
Sb_2Te_3, mag. and elec. props., carrier excitation 78−43395
Sc hydrides, mag. susceptibility, mag. props. in single-phase region explained by proton model *(Russian)* 78−47961
Sc, temp. depend., theoretical explanation 78−47944
Sc-Ag(Cu)(Pd)(Rh)(Ir)(Ru), electronic struct., susceptibility, sp. ht. and Knight shift meas. 77−43485
Sc-Gd(Tb), spin glasses, low-field susceptibility, role of single-ion anisotropy 77−48000
Sc-H, conc.-temp. depend. at room temp. of elec. resist. thermo-EMF, mag. susceptibility, and Hall coeff. 80−29382
$ScAl_2$-Er(Dy)(Nd), dil., EPR and mag. susceptibility 80−15797
$ScAl_2$-Eu, intermediate valence on Eu ions, Mossbauer isomer shift 80−84587
Sc_3In, itinerant electron ferromag., NMR and relax. 78−6586
$(Sc_xLu_{1-x})_2V_2O_7$ 80−29547
ScN_x, region of homogeneity, physicochem. props. 78−52018
ScSi, paramag. susceptibility 80−50035
$Sc_2(SiO_3)_3$, mag. susceptibility, temp. depend., 77-800K 80−20372
Se, mag. susceptibility meas. rel. to heat treatment 78−34952
Se-Te, liq., localised impurity states, mag. susceptibility of Co and Mn solutes 77−51882
Se-Te alloys, liq., electronic props., mag. susceptibility meas. 79−95567
Si, diamag. and dielec. susceptibility, temp. depend. 78−10646
Si, diamagnetism of excitons and biexcitons, recomb. spectra *(Russian)* 80−7412
n-Si inversion layer, electron mag. suscept. 78−52009
Si, liq., mag. susceptibility and diamag.-paramag. transition at melting pt. 78−95415
p-Si, n-channel inversion layers, mag. susceptibility of electrons in presence of quantising mag. field. 80−75650
Si:B, heavily doped, paramagnetic props., anomalous hole spin susceptibility *(Russian)* 80−54861
Si:Gd, magnetic props. and interaction of impurities 79−11286
Si:P, heavily doped, paramagnetic spin susceptibility 79−78306
SiTe-ATe, A=Ga, In, Tl, solid solns., mag. suscept. meas., defects 78−43552
$(SiTe)_{1-x}(ATe)_x$, A=Ge, Sn, Pb, solid soln. with small substitution *(Russian)* 80−70933
Sm, polycrystalline with ferromag. impurities, mag. props., 1.5-300K 77−69547
Sm-Fe, dil., valence impurity state, inference from mag. susceptibility 78−95270
$SmAu_6$, mag. props. temp. depend. *(French)* 77−51879
$SmCl_2$, mag. props., 77-292K 78−52197
Sm_2CuO_4, magnetic properties obs. 80−70937
$SmFeO_3$, HF susceptibility, crit. divergence in spin reorientation temp. region *(Japanese)* 77−43836
$Sm_{1-x}Gd_xS$ (x=0.15 to 0.18), magnetic susceptibility meas., phase transition 77−63071
$Sm_{1-x}Gd_xS$, metal-insulator transition, induced by temp. and press. *(Japanese)* 79−51488
$Sm_{1-x}La_xB_6$, valence transition, lattice parameter and mag. susceptibility meas. 80−59929
$Sm_{1-x}La_xS$, mag. suscept., moment, impurity effects, indirect exchange interaction 78−68147
$SmMn_3C$ noncolinear mag. struct., mag. transition *(French)* 77−69494
$Sm_6Mn_{23-x}Fe_x$, magnetic behaviour, temp. and comp. depend. 80−93090
SmN, magnetic props., neutron diffr. and mag. susceptibility meas. 80−50036
SmO, mag. props., lattice consts., and X-ray absorpt. spectra 80−44798
$SmRh_4B_4$, coexistence of supercond. and antiferromag. order 80−11140
SmS, mag. susceptibility in semicond. phase, in homogeneity region 79−28502
SmS, press. effect on lattice parameter, mag. susceptibility, and reflectivity 79−56272
Sm_3S_4, mag. susceptibility meas., valence state of Sm 80−15684
Sm_3S_4, magnetic susceptibility and valence fluctuations 77−8266
$SmS_{1-x}As_x$ solid solns., intermediate valence phase, lattice const. and mag. susceptibility meas. 79−87245
$SmS_{1-x}P_x$, intermediate valence cpd., lattice parameter and mag. susceptibility 80−7091
$SmSb_{1-x}S_x$, magnetic ordering and configuration mixing 78−68179
$SmSb_xS_{1-x}$, intermediate valence, susceptibility and lattice parameter meas. 78−51943
Sm_3Se_4, valence fluctuation, mag. susceptibility meas. 80−97056
$SmSn_3$, NMR Knight shift, extension to low temp. 77−20735
$SmTi_{1.5}W_{0.5}O_6$, Stark sublevels in mag. suscept. and luminesc. 77−51876
$Sm_2(WO_4)_3$, mag. susceptibility, paramag. Curie temp., 300-900K 79−82753
$Sm_2(WO_4)_3$, molar mag. susceptibility, DC elec. cond., thermopower meas. 79−15172
$Sm_{1-y}Yb_yB_6$, valence transition, lattice parameter and mag. susceptibility meas. 80−59929
Sm_2ZrS_5, mag. and sp. ht. meas. on polycrystalline samples 78−23253
Sn-rare earth, dil. liq., elec. resist. and mag. susceptibility 78−43350
Sn-Se(Te), liq., mag. susceptibility meas., electron localisation and chem. bonding 80−60178

magnetic susceptibility continued
Sn-Te alloy, liq., magnetic susceptibility 79−87232
SnAs, Sn_3As_2, and Sn_4As_3, mag. susceptibility components 78−43551
$SnCo_2O_4$ spinel, mag. props. 77−1543
$Sn_{1-x}Mn_xTe$, electronic struct., transport props., mag. ordering effects 80−65441
$Sn_{1-x}Mn_xTe$, magnetic behaviour of Mn 78−14938
$SnMo_3S_6$, high supercond. T_c, soft mode behaviour 78−14855
SnSe, and $SnSe_2$, mag. susceptibility components 78−43551
SnTe, ferroelec. transition, quantising mag. field effect 79−87403
SnTe, mag-props., effect of structure transition 78−6158
SnTe-PbTe solid solns., defects from susceptibility meas. 77−84737
$(SrCaR)_2(Cr_xGa_{1-x})O_4$, R=La or Sm, mag. 2-D oxide, phys. props. 78−47974
$Sr_{2x}Eu_{2-2x}NbO_4$, synthesis and props. 77−52265
$Sr_{1-x}Eu_xS$, dilute spin glass, mag. props. 79−78386
$SrF_2:Ce^{3+}$, cryst. field energies 80−59941
$SrF_2:Tb^{3+}$, mag., thermal and hyperfine props. 80−29368
$Sr_7Fe_{10}O_{22}$, mag. props. and spin order 78−52232
$SrLaCoO_4$, struct. and mag. props., electronic struct. of trivalent Co *(French)* 79−86760
$Sr_{0.5}La_{1.5}Li_{0.5}Fe_{0.5}O_4$, high spin configuration stabilisation for Fe^{4+} *(French)* 80−88519
$SrRuO_3$ single cryst., reduced ferromag. moment obs. 77−20564
$SrSm_2S_4$, mag. props. 78−68237
$Sr_{1.1}V_{12}O_{29.9}$, phase transitions, elec. cond., susceptibility and sp. ht. meas. 78−14776
$Sr_3VTa_2O_9$, prep., characterisation and mag. props. 78−26535
Sr_2YRuO_6, ^{99}Ru Mossbauer spectra and other techniques 80−29659
TCNQ salts, mag. props. 77−43869
TCNQ salts, Qn(TCNQ)$_2$ and N-propyl-Qn(TCNO)$_2$, low temp. mag. susceptibility, neutron irrad. effects 80−60311
TTF-TCNQ, pure and irrad., nonlinear transport, ESR study, 1.2-4.2K 80−20167
Ta, s-, d- and orbital contributions to mag. susceptibility, nucl. acoustic reson. determ. 79−51868
Ta-W alloy, electronic density of states, temp. depend. of elec. resist. and mag. susceptibility 77−11891
TaH_x, phase diagram, mag. susceptibility 78−84778
TaH_x, proton Knight shift and mag. suscept., high resolution meas. 77−55716
TaS_2 (2H), quantum oscillations and Fermi surface 79−37960
TaS_2 intercalation complexes, superconductivity 78−91803
TaS_2 intercalation complexes with 3d transition metals, mag. and metallic transport props. 80−44814
TaS_2:Fe, local moment form., mag. susceptibility meas. 79−82756
$TaSe_2$ (2H), anisotropy in mag. susceptibility 78−43558
$TaSe_2$:Fe, local moment form., mag. susceptibility meas. 79−82756
$TaSe_3$, superconducting transitions and diamagnetism 80−84526
Tb, critical magnetic studies 80−15745
Tb, liq., mag. susceptibility, elec. resistivity 80−20377
Tb, magnetisation, AC susceptibility and microwave absorption meas. 80−60221
Tb, magnetisation intensity in antiferromag. state and mag. field induced phase transforms. *(Russian)* 80−65811
Tb, small particles, disappearance of mag. order., mag. susceptibility and magnetisation meas. 77−16117
Tb-Sc(Y)(La)(Lu)(Yb)(Mg)(Th), mag. ordering temps., susceptibility meas. 80−25136
Tb-Y-Zn, magnetic props. conc. and temp. depend. *(Russian)* 77−47989
$Tb_{52}Ag_{48}$, amorphous, bulk magnetic props., evidence of strong local anisotropy 77−43830
$TbAg_{1-x}Zn_x$ solid solns., mag. props. *(Russian)* 77−77049
$TbAl_xGa_{2-x}$, mag. props. and phase transitions 80−25133
$TbAsO_4$, ferromag., static and AC susceptibility meas. 80−29533
$TbAu_3$, mag. phase diagram 80−75761
$TbAu_6$, mag. props. temp. depend. *(French)* 77−51879
$Tb_3Au_3Sb_4$, mag. suscept. meas., 4 to 300K 79−51742
$TbCo_2$, polarised neutron diffr. exam. of mag. struct. 79−73681
$TbCo_2Si_2$, mag. props. 80−107988
$TbCrO_4$, mag. susceptibility and magnetis. meas., 1.7-1000K, Curie pt. positron 77−66266
$Tb_{0.27}Dy_{0.73}Fe_2$, LF magnetoelastic effects 78−68348
$Tb_{0.27}Dy_{0.73}Fe_2$, perpendicular suscept., magnetomechanical coupling and shear modulus 78−91918
TbF_3, transferred hyperfine interaction, NMR study 78−68393
$TbFeO_3$, mag. susceptibility, temp. depend., effective field at Tb ion sites 80−75742
$TbFeO_3$, magnetisation exam. 77−24681
TbG_3, uniaxial ferromagnet, logarithmic corrections to crit. behaviour 78−60294
TbH_{2-x}, TbD_{2-x}, mag. susceptibility conc. depend. 80−70968
TbIG, magnetisation and mag. susceptibility meas. along (111) direction, 4.2-295K 77−80917
TbIG, mol. field coeffs., magnetisation and mag. susceptibility anal. 78−95406
$Tb_{1.2}Mo_6S_8$, mag. ordering in supercond. state, resist. and AC susceptibility meas. 78−19194
$TbNi_5$, ferromag., magnetisation and paramag. susceptibility 80−25082
$TbNi_2Si_2$, mag. props., 4.2-200K 80−84602
Tb_2O_3, 300 to 900K, mag. susceptibility and Curie temp. meas. 78−56288
$Tb(OH)_3$, powder and single crystal, mag. props. 80−2558
$Tb_2O_2SO_4$, antiferromag., mag. props. 1.6 to 40K 79−33464
TbP, singlet-groundstate magnetism, static mag. props. 80−7109
$TbPO_4$, phase transitions at low temp. 80−15237
$TbPO_4$, zircon struct., cryst. field analysis 80−80232
TbScFe garnets, mag. props. 77−47979
$Tb_2(WO_4)_3$, mag. props., 300 to 900K 79−28510
$Tb_{0.76}Y_{0.24}$, spin waves rel. to cond. electron susceptibility 78−68195
$Tb_{0.26}Y_{2.74}Fe_5O_{12}$ garnet, mag. transition, mag. props. anomaly 80−93120
Tb_2ZrS_5, mag. and sp. ht. meas. on polycrystalline samples 78−23253
Tc film, electrodeposited, supercond. transition, AC susceptibility meas. 79−95539
Tc film, supercond. transition, complex susceptibility 80−29495
Te, hole susceptibility anisotropy, spin contrib. and total 77−85413
Te, liq., temp. depend. 78−47943
Te, liquid, localized impurity states, paramag. susceptibilities 78−64185
Te, mag. susceptibility meas. rel. to heat treatment 78−34952

magnetic susceptibility continued
$TeCr_2O_6$, exchange interactions within binuclear entity $(Cr_2O_{10})^{14-}$ 80−60236
$ThC_{0.063}$ single crystal, elastic consts., Debye temp. and mag. susceptibility 77−90386
$ThCo_5$ itinerant electron metamagnetism, polarised neutron study 80−39742
Th_7Co_3, effect of absorbed H_2 on mag. behaviour 80−60184
$ThCu_3Mn_4O_{12}$, mag. struct. of new perovskite-type ferrimag. 78−52222
$ThMn_2$, Th_6Mn_{23}, H_2 absorption effect on mag. props. 77−89931
Th_7Ni_3, effect of absorbed H_2 on mag. behaviour 80−60184
$ThRe_2$, mag. susceptibility 78−68182
Ti alloys, data handbook of low temp. mech. and phys. props. 80−22153
α-Ti alloys VT1 and VT5, struct. and phys. props., H_2 effect 80−108576
α-Ti, anisotropy of susceptibility and elec. resist. *(Russian)* 77−66292
Ti, high purity, data handbook of low temp. mech. and phys. props. 80−22153
Ti-Al (30 to 57 wt.%), phase equilibria from mag. susceptibility studies 79−60483
Ti-C-N-O-H, solid solns. of H, exam. of props. 80−29172
Ti-Co-Al(Ga), Th_6Mn_{23} type struct., mag. susceptibility *(Russian)* 79−42736
Ti-Cu alloys, mag. susceptibility meas., paramagnetic susceptibility meas. Curie temp. and mag. moments calc. *(Russian)* 78−34956
Ti-Fe, magnetic susceptibility depend. on phase composition *(Russian)* 80−54875
Ti-Fe-Al(Ga), Th_6Mn_{23} type struct., mag. susceptibility *(Russian)* 79−42736
Ti-H exam. of electron structure 80−29306
Ti-Nb-Zr-Fe, supercond. and paramag. props., effect of Fe additions *(Russian)* 80−65730
Ti-Ni, electron phase transition XPS, optical spectra and mag. susceptibility meas. 80−19943
Ti-Ni-Al(Ga), Th_6Mn_{23} type struct., mag. susceptibility *(Russian)* 79−42736
Ti-Ni-Co cubic B_2 alloys, phonon enhancement of electronic sp. ht. near martensitic transform. 79−60522
Ti-U(Cr)(Mo)(W), dilute, superconducting transition temp. and mag. suscept. 78−47899
Ti-V, anomalous elec. resistivity, mag. susceptibility, soft-phonon induced structural inhomogeneities 78−60104
$(Ti_{1-x}V_x)_2O_3$ spin glass, mag. props., metallic antiferromagnetism 79−82791
$TiBe_2$, itinerant antiferromag., mag. susceptibility and elec. cond. meas. 79−19726
$TiBe_2$, itinerant antiferromagnetism, mag. susceptibility obs. 79−15288
$TiBe_{2-x}Cu_x$, high press. study of Curie temp. and mag. susceptibility 80−84600
TiC, mag. suscept. rel. to temp. in homogeneity region 78−34953
TiC, vapour deposited coatings, elec. resist., mag. susceptibility and adhesion meas. 77−44395
TiC-VC, mag. susceptibility, elec. cond. and thermoelec. props. 80−50033
TiC-ZrC, mag. susceptibility, elec. cond. and thermoelec. props. 80−50033
TiC-ZrC, solid soln., conc. and temp. dependence of props. 80−39736
TiC_xO_y are $TiC_xO_yH_m$, cubic phases, mag. susceptibility 80−15680
$TiCl_3$, layer compound, theoretical study of phase transition, paramag. susceptibility calc. 79−10945
$Ti_{1-x}Co_x$, electronic struct. and anomalies of elec. and mag. props. 80−6710
Ti(Fe, Co), off-stoichiometric alloy, inverse mag. susceptibility rel. to defect conc. 80−60216
$TiMn_2$, Curie-Weiss law depend. of susceptibility, mag. props. *(Russian)* 79−65655
TiN-CrN systems, solid solns., mag. props. 77−12086
$Ti_{0.5}NbSe_2$, cryst. struct., metallic cond., mag. and phys. props. *(French)* 80−33956
$Ti_{1-x}Ni_x$, electronic struct. and anomalies of elec. and mag. props. 80−6710
TiO_2:Ta, Ti^{3+}-Ti^{3+} exchange interaction *(French)* 77−89945
TiO_2-P_2O_5 glasses, reduced, mag. susceptibility, 1 to 400K, mag. exchange between Ti^{3+} ions 79−73691
TiO_x, interstitial alloy, electronic state, XPS, mag. susceptibility and elec. resist. 77−12486
Ti_3O_5-V; semicond.-metal transition, resist., enthalpy and mag. susceptibility changes obs. 77−62965
Ti_4O_7 and $(Ti_{1-x}V_x)_4O_7$, metal-insulator transitions, EPR, elec. and mag. props. 80−2336
Ti_5O_9, phase transitions, elec. cond., mag. susceptibility, sp. ht., EPR and struct. aspects 78−10526
TiS_2, resistivity, Hall effect and mag. suscept. 78−79991
$TiSe_2$, semimetal, electronic props., superlattice form. 77−15532
$Ti_{1+x}Se_2$, superlattice form., phase transform., mag. susceptibility meas. 77−15383
$Ti_xV_{1-x}Cy$ solid solutions, mag. susceptibility and band struct. 79−51739
$Ti_{1-y}V_yH_x$, electronic props., H alloying effects, book contrib. 79−82522
$(Ti_{0.9}V_{0.1})_2O_3$, spin glass, dynamic mag. susceptibility meas. 80−39792
$(Ti_{1-x}V_x)_2O_3$, nonlinear magnetisation at spin glass phase transition temp. 79−78403
$(Ti_{1-x}V_x)_2O_3$, single crystal, anisotropic susceptibility 79−87228
$(Ti_{1-x}V_x)_2O_3$, spin glass, nonlinear susceptibility and sp. ht. 80−60304
$(Ti_{1-x}V_x)_2O_3$, spin glass props. and anisotropy, comp. depend. 77−66368
$(Ti_{1-x}V_x)_2O_3$, spin-glass props., 0.05-300K 80−25149
$(Ti_{1-x}V_x)_2O_3$, susceptibility and ^{51}V NMR expts., spin glass behaviour 77−66369
$(Ti_{1-x}V_x)_4O_7$, mag. susceptibility calcs. 78−91850
$Ti_{1-x}V_xS_2$, resistivity, Hall effect and mag. suscept. 78−79991
$Ti_{1-x}V_xSe_2$, mag. susceptibility, 4.2-300K 80−60188
Tl-Bi(Sb) alloys, liq., MP to 1000°C, anomalies due to electron-ion interaction 77−20546
Tl-Te, liq. alloys, mag. susceptibility rel. to elec. cond. and density of states 77−51880
Tl-Te liquid alloys, mag. susceptibility 77−59383
$Tl_xAs_{2-x}S_{3-x}$ glasses, opt. and mag. props., comp. influence 77−77225
$TlAsSe_2$, diamag., thermal expansion rel. to temp. at cryst.-melt transition 78−34954
$TlCoF_3$ paramagnetic, nonmagnetic atomic nuclei spin density, NMR study 80−29633
$TlGaS_2$-$TlGaSe_2$, phase and composition-property diagrams 80−55366

magnetic susceptibility continued
$TlInS_2$-$TlInSe_2$, phase and composition-property diagrams 80−55366
$TlMnCl_3$, weak ferromag. and mag. struct., temp. depend. 78−19219
TlN_3, diamag. susceptibility, rel. to cryst. struct. 79−24127
Tl_2Se, diamag., thermal expansion rel. to temp. at cryst.-melt transition 78−34954
Tl_2Se_3, diamag., thermal expansion rel. to temp. at cryst.-melt transition 78−34954
Tl_xSe_{1-x}, liquid semiconductor, diamagnetism and paramagnetism, dangling bond paramag. centres, mag. susceptibility obs. 80−44797
Tl_xTe_{1-x}, liq. semicond. alloy, mag. susceptibility rel. to diffusive transport 77−20541
$Tl_2(Te_xSe_{1-x})$ mixtures, liq., electrical conductivity and mag. susceptibility 80−88715
$Tl_2Te(Se)(S)$, liq., mag. susceptibility 79−24128
Tm, para-, ferro- and ferrimag. and c-axis modulated phases 78−2660
$Tm_3Au_3Sb_3$, mag. suscept. meas., 4 to 300K 79−51742
TmCd quadrupolar ordering and magnetic interactions 79−73676
$TmCo_2$, paramag. and ordered phases, Pauli type, Co susceptibility, polarised neutron diffr. obs. 77−63077
$Tm_{1-x}Lu_xZn$, third-order mag. susceptibility, quadrupolar effects 79−99674
$TmNi_2Si_2$, mag. props., 4.2-200K 80−84602
Tm_2O_3, 300 to 900K, mag. susceptibility and Curie temp. meas. 78−56288
Tm_2O_3, susceptibility, 4.2-270K 77−12081
TmO_6S_8, low temp. Mossbauer study and mag. susceptibility 80−80656
$Tm_2O_2SO_4$, antiferromag., mag. props. 1.6 to 40K 79−33464
$TmRh_4B_4$, mag. and supercond. props., mag. susceptibility and sp. ht. meas. 79−78344
TmSe, intermediate valence cpd., susceptibility, single-ion approach 80−70935
TmSe, mag. props. and struct. 80−25109
TmSe, mixed valence cpd., thermal, mag., and transport props. 79−61074
TmSe, paramag. intermediate valence cpd., single ion approach to susceptibility 79−61042
TmSe, spin dynamics, neutron scatt. study 79−24178
TmSe, susceptibility, Tm^{2+} and Tm^{3+} charcts. 80−25110
Tm_2Se_3, mag. susceptibility meas. 4.2 to 300K cryst. field approx. 77−66246
Tm_3Se_4, mag. susceptibility 77−40032
Tm_xSe, $0.87<x<1.05$, mag., thermal and transport props., comp. depend. 78−68239
Tm_xSe, valence instabilities, antiferromag. order 80−20128
$TmSe_{0.83}Te_{0.17}$, spontaneous magnetisation, mag. susceptibility, magnetostriction, elec. cond. 79−24146
$TmVO_4$, enhanced nuclear cooling and spin-lattice relax. time 80−80632
$TmVO_4$, Jahn-Teller distortion, RF susceptibility and NMR meas. 80−44930
$Tm_2V_2O_7$, pyrochlore struct., mag. props. 78−72335
$Tm_2(WO_4)_3$, mag. props., 300 to 900K 79−28510
$Tm_xY_{1-x}Se$, Kondo effect, Van Vleck behaviour 80−25085
TmZn, magnetic-ion-lattice interactions, cryst. elec. field 77−4540
U complex, cyclopentadienyl-U-halides, paramag., U IV ligand interaction, mag. susceptibilities, 1-300K *(German)* 79−15279
U complex, UCl_4.3DMBA(.3MAA), mag. exchange interaction 79−78303
U complex, $U(acac)_4$, cryst. fields, mag. susceptibility, chem. shift *(French)* 78−84179
U dipnictides, elec. and mag. props. 78−84399
U monopnictides, mag. props. 78−43554
U sesquichalcogenides, mag. props. temp. depend. 77−8287
U tetragonal compounds, mag. props. 80−15704
U-Ga system cpds., elec. resist., paramag. susceptibility magnetis., temp. depend., mag. struct. 77−20559
U-Pt, paramag. suscept. 79−61047
UAl_2, dynamical susceptibility, diffuse neutron scatt. study 79−24138
UAl_2, low temp. mag. susceptibility 79−38301
UAl_2, transport props., susceptibility and sp. ht. 80−11174
UAs, anisotropic susceptibility 79−42754
UAs, anisotropic susceptibility 80−7087
U_3As_4, high-field suscept. at He temp. 77−89935
$UAs_2(Sb_2)$, heat capacities, antiferromag.-paramag. transitions 78−76253
$UC_{1-x}N_x$, NMR of ^{13}C and ^{15}N, 5f electrons nature, mag. susceptibility, spin fluctuations 77−20736
UCl_5, mag. susceptibility, ESR and g-value, crystal field model anal. 79−91292
UCo_2, elec. resist. and mag. susceptibility meas., non-stoichiometry influence 77−63088
UCo_2, mag. props., ferromag. transition *(Russian)* 78−68148
$U(Co_{1-x}Fe_x)_2$, ferromag. onset, susceptibility and resist. meas. 80−70967
$U(Co_xNi_{1-x})_2$, cryst. struct. and mag. props. at 4.2K 80−54175
UCu_5, mag. props. and NMR 77−20734
β-UD_3, electronic props., metallic character 80−6693
$UF_4(Cl_4)(Br_4)(I_4)$, paramag., U IV ligand interaction, mag. susceptibilities, 1-300K *(German)* 79−15279
UFe_2, nonstoichiometry effects on Curie temp., susceptibility obs. 80−25131
UGa_2, cryst. struct., mag. and magnetoelastic props. *(Russian)* 79−38364
UGeS(Se)(Te), mag. susceptibility, struct. in temp. range 4.2 to 300K 78−10667
UMn_2, mag. props., ferromag. transition *(Russian)* 78−68148
UMn_2-UCo_2, mag. props., ferromag. transition *(Russian)* 78−68148
UMn_2-UFe_2, mag. props., ferromag. transition *(Russian)* 78−68148
UN, antiferromag., mag. susceptibility, elec. resist. and elastic consts. meas. 77−69510
UN, mag. susceptibility under press. 80−7086
UN, single crystal, mag. props. 77−77042
$U_2N_2As(P)(S)(Se)$, 4.2-1000K, cryst. field and exchange interactions 77−20569
$U_2N_2Bi(Sb)(Te)$, mag. props. 78−72333
$UNi_{5-x}Cu_x$, NMR and press. effects 80−25230
UO_2, spin wave spectrum, mag. susceptibility, sp. ht. *(Russian)* 79−33470
$U(OH)_2SO_4$, antiprismatic crystal field, paramag. susceptibility, 4.2 to 300K 79−1655
$U(OH)_2SO_4$, cooperative Jahn-Teller effect, mag. susceptibility meas. 78−72121
magnetic susceptibility continued
$U(OH)_2SO_4$, mag. susceptibility, heat capacity anomalies at 21K 80−11151
$U_6O_4(OH)_4(SO_4)_6$, antiprismatic crystal field, paramag. susceptibility, 4.2 to 300K 79−1655
UOX_2 (X=Cl, Br, I) crystal struct., IR spectra, and mag. meas. *(French)* 79−60331
UP, anisotropic susceptibility 80−7087
UP-PrP (NdP) systems, mag. phase diagrams 78−84424
U_3P_4, Knight shift, paramag. susceptibility 77−66430
U_3P_4, single cryst., Barkhausen effect 77−28410
UPb_3, crystal field energy levels, magnetisation and susceptibility, neutron spectra obs. 80−50064
UPd_3, anomalous behaviour in low temp. props. 79−28108
URe, mag. susceptibility 78−68182
URh_3, magnetisation density 78−52203
US, ferromag., AC mag. susceptibility at high press. 80−7085
$U(SO)_2.4H_2O$, antiprismatic crystal field, paramag. susceptibility, 4.2 to 300K 79−1655
USb, anisotropic susceptibility 80−7087
$USiO_4$, cryst. field parameters, paramag. susceptibility, 2-500K 77−55658
$U_{1-x}Th_xAl_2$, mag. susceptibility, low temp. depend. 80−11173
$(U_xTh_{1-x})S$, metallic, 5f virtual bound states, elec. resist. and mag. susceptibility meas. 77−28363
$U_xTh_{1-x}Sb$, valence change of U accompanied by singlet-ground-state ferromag. 80−70965
$(U_xTh_{1-x})Se$, metallic, 5f virtual bound states, elec. resist. and mag. susceptibility meas. 77−28363
$(U_xTh_{1-x})S(Te)$ solid solns., electronic struct., mag. susceptibility and elec. resist. obs. 77−20551
V, dynamic susceptibility, model pot. theory 80−75710
V, electronic density of states, effective mass, electron-phonon interaction, Coulomb pseudopot. *(Russian)* 78−26804
V fine particles, appearance of mag. moment 78−68152
V hyperfine particles, appearance of mag. moments, mag. susceptibility meas. 77−36097
V, orbital magnetic susceptibility calc. 80−7075
V, small particles, crystal structure, magnetic and superconducting props. 80−97121
V, spin fluctuations effect on T_c, from sp. ht. and mag. suscept. 80−7030
V surface, spin fluctuations, finite temp. mag. props. study 80−107994
V-Cr alloy, electronic density of states, temp. depend. of elec. resist. and mag. susceptibility 77−11891
V-Fe, ferromagnetism to mictomagnetism at low Fe conc. 78−91878
V-Fe, mag. ordering temp. depend. on atomic short-range order from susceptibility meas. 79−61159
V-H, effect of neutron irrad. on electrical resistance, magnetic susceptibility 80−29063
V-H, exam. of electron structure 80−29306
V-Mn-Cr, disordered BCC state, mag. phase diagram, mag. and elec. props. 77−63185
V-Pt, sp. ht. and mag. meas. in ordered and disordered phases 80−70422
V-Zr-Nb alloy, rel. between density of states and martensitic and superconducting phase transition temps. 78−10594
$V_{1-x}Al_xO_{2\pm y}$, mag. and struct. props. meas. 78−2658
$(V_{1-x}Cr_x)_3Si$, mag. susceptibility, 4.2 to 320K, density of states model 80−7035
$V_{3-x}Cr_xSi$, x=0 to 3, struct., supercond. and mag. props. 80−1962
VF_2, nearly one-dimensional, paramag. susceptibility 79−15278
$V_{1-x}Fe_xO_{2-x}F_x$, $0<x<0.20$, magnetic susceptibility and electron cond. *(German)* 80−39754
$V_{1-x}Fe_xO_{2-x}F_x$, mag. susceptibility *(German)* 79−78305
V_3Ga, NMR and mag. suscept. *(Russian)* 78−39420
V_3Ga, structure effects on supercond. props. and electron spectrum *(Russian)* 77−80862
V_3Ga-V_3Pt, temp. depend. and supercond. props. *(Russian)* 77−59347
$V_{1-x}Ga_xO_2$, M1→T phase transition, X-ray and mag. meas. 77−11692
$V_{1-x}Ga_xO_2$, phase transitions, semicond. metal transition, antiferromag. props. 77−11969
V_3Ge, low temp. props., mag. suscept. and resistance 78−19213
$V_3Ge_xOs_{1-x}$, low temp. props. 79−99652
VH_x, electronic props., H alloying effects, book contrib. 79−82522
VH_x, Knight shift and spin-lattice relax. of proton NMR, local electronic environment of protons 77−16194
VH_x, proton Knight shift and mag-suscept., high resolution meas. 77−55716
V_2(Hf,Zr), NMR and mag. susceptibility, density of states determ. *(Russian)* 80−66053
V_2Hf, NMR meas., mag. susceptibility, Knight shift and elec. field gradient determ. *(Russian)* 78−23359
$V_2Hf_{1-x}Ta_x$, C15 supercond., electronic and lattice props. 78−68110
$V_2Hf_{1-x}Zr_x$, normal and supercond. state, transition temps., mag. susceptibility and specific heat determ. *(Russian)* 80−60132
$V(Ir_{1-x}Pt_x)_3$, mag. props., ferromagnetism, comp. depend. 77−77039
V_xMo_{1-x} solid soln., mag. susceptibility 79−91208
VN-CrN systems, solid solns., mag. props. 77−12086
$V_{2-x}Nb_3Hf$, NMR of ^{51}V and mag. susceptibility, 20-300K *(Russian)* 80−93192
$V_{0.5}NbSe_2$, cryst. struct., metallic cond., mag. and phys. props. *(French)* 80−33956
$V_{1-x}Nb_xSe_2$, CDW anomalies, Nb substitution effects, mag. susceptibility, 16-300K 79−38005
VO_2, magnetic susceptibility in insulating and metallic phases, electron-electron and electron-lattice interactions 80−96788
VO_2, metallic, magnetisation distribution and band structure 78−76223
VO_2:Ga, Mo, temp. dependence. with Mo content, Ga constant 78−76121
VO_x, mag. susceptibility temp. depend. 79−47229
V_2O_3, 500 to 530K, magnetic susceptibility meas., high temp. transition, interacting Hubbard bands 78−39325
V_2O_3-Al_2O_3 solid soln., interactions between V atoms, comp. and temp. depend. of mag. susceptibility 77−8056
V_2O_{3+x}, $0\leq x\leq 0.08$, mag. and elec. props. 80−49833
V_2O_5-MoO_3 solid soln., number of V^{4+} ions, magnetic and thermogravimetric exam. 78−52199
V_2O_5-V_2O_4-$BaZnO_2$ glass, V ion states, mag. and elec. props. 80−88556
V_3O_5, electrical, thermodynamic and mag. props. at metal-semicond. transition, homogeneity range 77−4413

magnetic susceptibility continued
V_3O_5, insulator-metal phase trnasition at 450K, properties 78−39023
V_3O_5, Mo,Ti, and Ga doping effects on conductivity transition 77−11971
V_3O_5-Ti_3O_5, DTA, mag. susceptibility and X-ray diffr. study 80−70970
V_3O_7, microscopic mag. props., NMR 80−7177
V_nO_{2n-1} ($3 \leq 3 \leq 9$), Magneli phases, mag. susceptibilities at low temp. 80−20389
V_nO_{2n-1}, insulating Magneli phases, mag. susceptibility and sp. ht. meas. 80−34604
VOCl, and $Li_{0.8}$VOCl intercalation cmpd., magnetic, optical and electrical props. 79−95402
$V_{1-x}Re_xO_2$ ($0 \leq x \leq 0.15$), insulator-metal transition, DTA, X-ray, mag. and elec. meas. 78−10353
$V_{1+x}S_2$, local moment formation, X-ray, mag. susceptibility and NMR meas. 77−69511
V_3S_4, antiferromag. order, ^{51}V NMR spectrum 79−56625
V_5S_8, single cryst., mag. props. 78−88098
V_5S_8:Fe, Mossbauer and mag. studies, electronic state of Fe 80−108130
$V_{2-x}Sb_xO_4$, defect struct. exam., temp. depend. 78−18635
VSe_2, CDW states, correl. mag. and transport props. 79−73494
VSe_2, CDW states, intrinsic mag. props., mag. susceptibility and NMR obs. 78−68397
VSe_2, metallic behaviour obs., anomalous elec. and mag. props., temp. effects 77−15819
V_3Se_4, antiferromag. order, ^{51}V NMR spectrum 79−56625
V_3Se_4, itinerant antiferromag., spin fluctuations, NMR study 80−75874
V_5Se_8, itinerant antiferromag., spin fluctuations, NMR study 80−75874
$VSe_{2-x}S_x$ ($0<x<2$) solid solutions, characterisation 80−88730
V_3Si, appl. of new three-dimens. k.p model for A-15 cpds. 78−23015
V_3Si based ternary solid soln., supercond. T_c and paramag. susceptibility *(Russian)* 77−59348
V_3Si, electron spectrum characts., mag. susceptibility depend. on resistivity ratio 79−95320
V_3Si, magnetic susceptibility, density of states model for lattice transformation in A-15 compounds 80−65219
V_3Si, neutron irrad., sound velocity, magnetic susceptibility and upper critical field 78−88074
V_3Si, supercond. and struct. transitions *(Russian)* 78−52118
V_3Si, temp. depend. of mag. susceptibility *(Russian)* 77−36053
V_3Si-Fe, mag. impurities effect on supercond. props. 77−1524
$V_3Si_xOs_{1-x}$, supercond. transition temp. and paramag. susceptibility 79−28436
V_2Ta, NMR meas., mag. susceptibility, Knight shift and elec. field gradient determ. *(Russian)* 78−23359
VTe, mag. and elec. transport props. 80−92897
$V_{1-x}Ti_xO_{1.75}$, synthesis and mag. susceptibility obs. 78−23243
$V_xTi_{1-x}S_2$, elec. and mag. props. 79−65504
V_2Zr, NMR meas. mag. susceptibility, Knight shift and elec. field gradient determ. *(Russian)* 78−23359
W, plastically deformed single cryst., mag. susceptibility *(Russian)* 80−93074
W-Fe, dil., spin glass props., DC mag. susceptibility meas. 78−68283
W-Fe alloys, spin glass props., DC susceptibility and remanence meas., 1.6 to 295K 80−29560
W_2B_5 and WB_4, thermal, elec., and mag. props. 80−20187
WC, sputter deposited coatings, elec. resist., mag. susceptibility and adhesion meas. 77−44395
WCr_2O_6, exchange interactions within binuclear entity $(Cr_2O_{10})^{14-}$ 80−60236
WV_2O_6, exchange interactions within binuclear entity $(V_2O_{10})^{14-}$ 80−60236
WV_2O_6, magnetic susceptibility, behaviour in terms of quasi-isolated binuclear units 80−97073
Y ferrite-garnet, porous polycrystal, law of approach to saturation *(Russian)* 78−47956
Y, magnetic and elec. props., 100 to 900K *(Russian)* 80−25077
Y-H, exam. of electron structure 80−29306
Y-Ni amorphous alloy, spontaneous magnetisation, Curie temp. and paramag. susceptibility 78−68189
Y-rare earth, dil., cryst. fields 78−80127
Y-rare earth metal, mag. susceptibility, 4.2 to 300K, Neel temps. 79−19735
YAG, Yb^{3+} crystalline field, Schottky specific heat, paramagnetic susceptibility temp. depend. 77−11882
YAG:Er^{3+}, crystal field theory calcs. 77−8259
YAl_2-Er(Dy)(Nd), dil., EPR and mag. susceptibility 80−15797
YB_{12}, 90-1200K 80−50032
YCo_2, anomalous high-field magnetisation 78−47958
$YCoO_3$, spin state of Co^{3+} ion, X-ray photoemission line broadening 79−82751
YCo_2Si_2, mag. props. 80−107988
$Y_{0.98}Dy_{0.02}$, spin glass, calorimetric exam. 78−68270
$(YEuTmCa)_3(FeGe)_5$ bubble garnet films, ion-implanted, mag. susceptibility meas. 79−47311
YFe_2 amorphous, spin-glass and mag. blocking transitions, low field DC susceptibility meas. 79−61141
YFe_2, amorphous concentrated spin glass, susceptibility, Mossbauer and neutron scatt. meas. 80−39783
$Y(Fe_{1-c}Al_c)_2$, local model for mag. behaviour 77−63135
$Y(Fe_cAl_{1-c})_2$, mag. props. 79−38308
$Y(Fe_xCO_{1-x})_2$ model, Co, mean mag. moment composition depend.; reciprocal susceptibility, thermal var. 78−47945
$YFe_{2x}Mn_{2-2x}$, mag. props. and FMR 79−95581
YFe_2O_4, low temp. phase transitions and mag. props. 80−7106
$Y_3Fe_5O_{12}$, amorphous, mag. moments, susceptibility, Mossbauer studies 79−78345
$Y_3Fe_5O_{12}$, formation mechanism from metallic oxides 77−48376
YFe_2Si_2, mag. props. 4.2 to 950K, diamag. Fe atoms 77−20544
YGa garnet, Yb^{3+} crystalline field, Schottky specific heat, paramagnetic susceptibility temp. depend. 77−11882
$Y_3Ga_5O_{12}$, rare-earth doped garnet, high temp. mag. susceptibility 79−78347
$Y_{3-x}Gd_xFe_5O_{12}$, field depend. of susceptibility *(Russian)* 78−68176
$Y_{3-x}Gd_xFe_5O_{12}$, mag. phase diagrams, mag. transitions, exchange interaction *(Russian)* 80−54896
YH_x ($x=1.92$ to 1.98), magnetic and elec. props., 100 to 900K *(Russian)* 80−25077
YIG, domain wall size and mag. losses in freq. spectra 77−85481
YIG, Faraday effect, influence of mag. field on sublattice contributions 80−88975

magnetic susceptibility continued
YIG, Hf response and thermodynamic props. *(Russian)* 78−72338
YIG, homogeneous mag. relax. near phase transition *(Russian)* 78−23351
YIG, polycryst., initial and reversible parallel susceptibilities, hydrostatic press. effects 80−75835
YIG: Si single crysts., mag. props. 80−107981
$(Y_xLu_{1-x})_2V_2O_7$ semiconducting ferromag. pyrochlore, mag. props. 80−29547
YM_4Al_8 (M=Cr, Mn, Fe, CU), magnetism and hyperfine interactions 80−25256
YMg, Pauli paramagnet, mag. susceptibility, nonlinear band behaviour 80−75706
YMn_2, lattice consts. and mag. props. before and after H_2 absorption 77−36061
YMn_2, Y_6Mn_{23}, H_2 absorption effect on mag. props. 77−89931
Y_6Mn_{23}, lattice consts. and mag. props. before and after H_2 absorption 77−36061
YNi_3, loss of ferromagnetism after H_2 absorpt., Pauli paramag. props. 80−34588
YNi_3, magnetism resurgence, neutron diffr. and mag. props. study 80−65819
YPd_3-Gd, ultralow interaction temp. and cryst. field effects for Gd impurities 79−61100
Y_5Pd_2, mag. props. 77−20547
YRh, electronic struct., susceptibility, sp. ht. and Knight shift meas. 77−43485
YS, superconductor, resonances in generalised susceptibility and phonon anomalies 79−60443
$Y_{1-x}Tb_xPd_3$, magnetisation, magnetostriction, and inelastic neutron spectra 80−65998
$YV_{1-x}M_xO_3$ (where M=Cr or Fe), solid solns., elec. and mag. props 79−23967
YVO_4:Nd^{3+}, zircon struct., cryst. field analysis 80−80232
YVO_4:Tm^{3+}, cryst. field parameters, appls. 77−20277
Yb, FCC, Fermi surface parameters, de Haas-van Alphen effect, press. depend. 77−28092
Yb intermetallic compounds, mag. susceptibility, 1.4 to 1060K, investig. of Yb valency 77−20543
YbAg, thermally excited interconfiguration crossover 77−16042
$YbAl_2$ and $YbAl_3$, intermediate valency cpds., paramag. susceptibility, 1.4 to 1060K 77−63079
$YbAl_3$, susceptibility, sp. ht. and magnetisation 79−28512
YbAu, thermally excited interconfiguration crossover 77−16042
YbB_{12}, valence state and mag. props. 80−50031
YbB_6, mag. and transport props. 80−54689
$YbCl_2$, mag. props., 77-292K 78−52197
YbCu, thermally excited interconfiguration crossover 77−16042
YbCuAl, intermediate valency cpds., paramag. susceptibility, 1.4 to 1060K 77−63079
YbCuAl, intermediate-valent, nucl. reson. and relax. 79−78550
YbCuAl, mixed valence behaviour, mag. props. 78−68150
YbCuAl, mixed valence cpd., dynamic susceptibility, neutron inelastic scatt. 80−65807
YbCuAl, mixed-valence behaviour, mag. susceptibility and sp. ht. 77−80939
YbCuAl, susceptibility, sp. ht. and magnetisation 79−28512
$YbFe_xMo_6S_8$, singularities in mag. and supercond. props. 79−51710
$YbGa_2$, intermediate valency cpd., paramag. susceptibility, 1.4 to 1060K 77−63079
YbGaG, mag. props. between 44-600 mK 80−80517
$Yb_3Ga_5O_{12}$, dipolar magnet, sp. ht. and magnetisation meas. 80−60344
$Yb_{0.99}Gd_{0.01}$CuAl, intermediate Yb valence states, mag. props. 79−51743
$YbInAu_2$, intermediate valence cpd., mag. susceptibility expts., 4.2-280K 78−39288
$YbMo_6S_8$, low temp. Mossbauer study and mag. susceptibility 80−80656
$YbNi_2Ge_2$, intermediate valence cpd., mag. susceptibility expts., 4.2-280K 78−39288
Yb_2O_3, 300 to 900K, mag. susceptibility and Curie temp. meas. 78−56288
$YbOsB_4$, mag. susceptibility meas., paramag. Curie-Weiss behaviour 79−61041
$YbRuB_4$, mag. susceptibility meas., paramag. Curie-Weiss behaviour 79−61041
$YbS_{1.387}$, magnetic and thermal props. 80−34586
$Yb_xSc_{1-x}Al_3$, valence fluctuation system, suscept. meas. 78−68149
ζ-Yb_2Se_3, mag. susceptibility and cryst. field parameters 80−65510
$YbSi_{1.8}$, valence fluctuation cpd., X-ray anal., mag. susceptibility and linear expansion coeffs. 79−77569
Yb_3Si_5, valence fluctuation cpd., X-ray anal., mag. susceptibility and linear expansion coeffs. 79−77569
Yb_xSy, synthesis and mag. props. 78−23242
$Yb_2V_2O_7$, pyrochlore struct., mag. props. 78−72335
$Yb_2(WO_4)_3$, mag. props., 300 to 900K 79−28510
$Yb_{1-x}Y_xCuAl$, disordered extended Anderson model, CPA-alloy analogue treatment 80−65506
$Yb_{1-x}Y_xCuAl$, intermediate Yb valence states, mag. props. 79−51743
YbZn, thermally excited interconfiguration crossover 77−16042
Zn, magnetic susceptibility behaviour, dislocation and elastic deform. effects *(Russian)* 77−80912
Zn, spin-orbit contrib. to mag. susceptibility of interacting electrons 77−63084
$Zn_xCn_{0.1}Fe_{2.9}O_4$, Cu, Zn substituted magnetite, domain wall resonance, mag. props. 80−15756
$ZnCr_2Se_4$, magnetoelastic coupling, mag. suscept. meas. 78−76288
$ZnFe_2O_4$, neutron damage effects, superparamag. state replacement cascades 77−16051
$ZnIn_2S_4$:Er^{3+}, cryst. field parameters, thermal and mag. props. calc. 77−20540
$Zn_cM_{1-c}Fe_2O_4$, M=Ni^{2+}, Co^{2+}, Fe^{2+}, $Zn_cMFe_{2-c}O_{4-c}F_c$, M=Ni^{2+}, Co^{2+}, calc. of saturation magnetisation by cluster components 77−43817
$Zn^{2+}Mo^{4+}O_3$, defect spinel struct., elec. and mag. props. 80−70176
$Zn_{1-x}Ni_xCr_2S_4$, spin struct., mag. props. meas. 77−85428
Zn_2PdO_4, cryst. struct. and mag. props. meas. *(French)* 77−15381
$ZnSnCuO_4$, cryst., struct., mag. susceptibility obs. 78−2085
ZnTi ferrites, electron exchange between Fe^{2+} and Fe^{3+}, paramag., Mossbauer spectra and susceptibility meas. 77−63327
Zr carbide interstitial phases, elec. and mag. props., neutron radiation effects 79−77640

magnetic susceptibility continued
Zr hydride interstitial phases, elec. and mag. props., neutron radiation effects 79−77640
Zr, mag. susceptibility, plastic deform. effect *(Russian)* 80−65984
Zr-C-N-O-H, solid solns. of H, exam. of props. 80−29172
Zr-Co-Ga alloy, mag. susceptibility in phases of structural type Th_6Mn_{23} *(Russian)* 79−24130
Zr-Cu-Ga alloy, mag. susceptibility in phases of structural type Th_6Mn_{23} *(Russian)* 79−24130
Zr-H, effect of neutron irrad. on electrical resistance, magnetic susceptibility 80−29063
Zr-H, exam. of electron structure 80−29306
Zr-Hf, mag. susceptibility, elec. cond., Hall conc. thermoEMF conc. depend. *(Russian)* 80−39551
Zr-Ni-Ga alloy, mag. susceptibility in phases of structural type Th_6Mn_{23} *(Russian)* 79−24130
Zr-Pd, metallic glasses, electronic props. and supercond. 79−73486
Zr-Ti, alloy, mag. susceptibility, elec. cond., Hall conc. thermoEMF conc. depend. *(Russian)* 80−39551
ZrC-NbN, mag. susceptibility, zone struct., conc. and temp. depends. 77−8788
ZrCu, constitutional and struct. studies, by mag. susceptibility, metallography and X-ray diffr. 80−70166
$Zr_{40}Cu_{50}Fe_{10}$, magnetically dil. glass, 3d moments, mag. susceptibility and magnetisation meas. 79−95574
$Zr_{40}Cu_{60-x}Fe_x$, electronic and mag. props. 77−8271
$Zr_{40}Cu_{60-x}Gd_x$, magnetically dil. glass, 4f moments, mag. susceptibility and magnetisation meas. 79−95575
$Zr_{40}Cu_{60-x}M_x$ (M=Fe,Mn,Gd,Tb), amorphous, mag. ordering and local random anisotropy 78−68273
$Zr_{40}Cu_{50}Mn_{10}$, magnetically dil. glass, 3d moments, mag. susceptibility and magnetisation meas. 79−95574
$Zr_{40}Cu_{60-x}Tb_x$, magnetically dil. glass, 4f moments, mag. susceptibility and magnetisation meas. 79−95575
$Zr_{0.9}Fe_{0.1}V_2$, NMR and mag. susceptibility 78−95527
$Zr_xHf_{1-x}V_2$, polycrystalline superconductor, resist. and mag. susceptibility, transition temp., temp. depend. 80−25113
$ZrMn_2$, Curie-Weiss law depend. of susceptibility, mag. props. *(Russian)* 79−65655
ZrN-NbC solid solns., mag. susceptibility and elec. resist. in 300-1300K range 77−24670
$Zr_{0.5}Nb_{0.5}C_xN_{1-x}$, mag. susceptibility, zone struct., conc. and temp. depends. 77−8788
$Zr_{0.99}Pt_{0.99}V_2$, NMR and mag. susceptibility 78−95527
$ZrRh_{3-x}Pd_x$, electronic and cryst. struct. comparison 78−84398
$ZrRh_{3-x}Pd_x$, powdered alloys, catalytic behaviour correlation with electronic struct., lattice struct. and surface comp. 79−82181
$ZrSiO_4$:Er(Yb), anisotropic mag. susceptibility meas. 77−43806
$Zr(V,Al)_2$, struct., supercond. props., elec. resist. and mag. susceptibility, 4.2 to 300K *(Russian)* 79−15246
$ZrV_{2-\delta}$, supercond., dielec. phase transition *(Russian)* 78−64168
ZrV_2, C15 supercond., dielec. transitions, temp. depend. of resist. and mag. susceptibility, 4.2-300K 79−38136
ZrV_2, dielectric phase transition, elec. resist. temp. depend. 79−65525
ZrV_2, elec. resist. and mag. suscept., anomalous temp. depend. 79−69491
ZrV_2, Knight shift vs. susceptibility plot 80−75712
ZrV_2, NMR and mag. susceptibility 78−95527
$ZrZn_2$, high press. study of Curie temp. and mag. susceptibility 80−84600
$ZrZn_2$, high purity, mag. props., pulsed fields up to 17 T 78−64198
$ZrZn_2$, phonon contrib. to Stoner enhancement factor, ferromag. and possible superconductivity 80−25070

magnetic switching
amorphous toroidal core, switching characts. and domain structs. 78−95477
electrometric circuit switching by magnetically controlled contact 77−79108
ferroics, secondary, polycryst., poling effects 77−16102
magneto-optical controlled transparencies, page composers 78−50932
orthogonal lattice, interacting hysteresis dipoles, lattice sums and switching, chain breakdown 77−51860
particles, interacting, switching behaviour, dipole and Stoner-Wohlfarth models 80−44870
temperature measurement, using magnetically controlled reed switches *(French)* 80−57291
Wiegand effect and applications *(Spanish)* 80−31735
Wiegand effect voltage pulse generation 79−81322
$(Co,Fe)_{80}B_{20}$ glass, induced anisotropy and time changes of permeability 80−75815
CrO_2 acicular particle suspensions, mag. props., optical meas. 80−44874
γ-Fe_2O_3:Cr, pure and doped, acicular particle suspensions, mag. props., optical meas. 80−44874
Ni-Fe oxidised films, easy-axis switching 79−91266
Ni-Fe-Co alloy films for logic devices, mag. switching vel., anisotropy field and coercive force *(Korean)* 77−51930
NiZnCo ferrites, switching time and coeff., hydrostatic press. effect 80−88802

magnetic tape equipment
see also magnetic tape storage
magnetic tape station interface to CAMAC for on-line data acquisition and reduction system 77−34532

magnetic tape recorders *see tape recorders*

magnetic tape storage
see also magnetic tape equipment
analogue system for fast light curve registration, lunar occultations appl. 79−53725
BWR, Hatch-1, core management data magnetic tape transfer to central office 78−21719
computerised tomographic scan data format 78−73243
NMR spectra, automatic system, for recording, processing and summation 80−27327
unsupervised data gathering, operation of receiving stations *(Italian)* 80−4692

magnetic tape stores *see magnetic tape storage*

magnetic tapes
see also magnetic tape equipment; magnetic tape storage
audio, with synchronised dual message, preparation, for dichotic listening research 78−57010

magnetic tapes continued
cinefilm sound recording, 35 mm, acoustoelectric data *(Russian)* 79−18665
demagnetisation curve, hysteresis model represent *(German)* 77−36096
dispersion factor, influence on tape props. *(Russian)* 79−52788
electroacoustic characteristics, multiple printing appl. *(Russian)* 77−38048
ferromagnetic dispersions characteristics, structural and magnetic, for cinematography appl. *(Russian)* 78−16886
Fick's diffusion coefficients, of pseudobinary gas-steam mixtures rel. to mag. tapes prod. *(German)* 79−27735
flaws, calcs. of field reflections 80−104387
gyroremanent magnetisation in anisotropic mag. material 80−50142
linear velocity meas. scanistor 79−71425
magnetic field diffr. meas. on axes of disks and apertures, Babinet principle, complex spirals 80−102599
magnetographic inspection, determ. of magnetisation regimes 80−108665
nonsteady mag. field induction meas. by prerecorded tape signal attenuation 79−67355
particle dispersion and particle orientation 80−15762
properties investigation and recording process simulation, vibration magnetometer appl. *(German)* 78−70164
recent magnetic sound recording tape *(Japanese)* 80−33406
recording head wear by magnetic tape, wear meas. using Knoop diamond indentations 77−70192
recording on particulate media, conference, Gardone Riviera, Italy (Sep. 1979) 80−41930
roughness measurement using stereoscopic SEM 79−67254
single particle material for tape and disc manufacture, prep., props., and appls. 78−52308
sound recording synchronisation with 16 mm film, time-code system appl. 78−24874
sound track, digital method of synchronisation with cinefilm *(German)* 79−35866
static and antihysteretic mag. props. 80−44868
stressed-strained state, determ. of a coil of mag. tape 79−14283
stripe applications in sound and film recordings 79−85188
wear by Permalloys and SUS 304 *(Japanese)* 78−39916
Co films layered over Cr by DC sputtering for digital mag. recording 79−83118
CrO_2 powders, print through values and mag. characts. 80−44871
CrO_2, single mag. particle, remanent coercive force and remanent loop meas. 78−95480
Fe-Co alloy particles for mag. tapes, mag. props. 78−95479
γ-Fe_2O_3 acicular particles, coercivity, magnetic recording tape appls. 78−14983
γ-Fe_2O_3 powders, influence of densification on mag. props. 78−95481
γ-Fe_2O_3 recording tapes, orientation, Mossbauer, X-ray and electron microscope meas. 77−16219
γ-Fe_2O_3, single mag. particle, remanent coercive force and remanent loop meas. 78−95480
γ-Fe_2O_3:Co, impact-induced demagnetisation, magnetostriction and coercive force, appl. in mag. recording 77−16111
Fe_3O_4:Co, impact-induced demagnetisation, magnetostriction and coercive force, appl. in mag. recording 77−16111
NiFe, rapid surface and vol. magnetisation, eddy-current-limited domain wall motion 77−12159

magnetic thin film devices
see also magnetic bubble devices
compensation-point Hall effect temperature sensor 78−93679
cross-tie shift register memory device 79−78484
ferromagnetic thin film magnetometer, development and performance 80−31808
garnet, numerical display element exploiting rag domains 78−68339
garnet film, double heteroepitaxy, magneto-optical devices for phase matching *(French)* 77−3675
magnetic soft and hard materials, garnets, magnetic properties and applications, structural props. 80−65760
magneto-optical controlled transparencies, page composers 78−50932
magneto-optical photoconductor sandwich 77−40213
measurement transducers appls. *(Polish)* 80−4700
multiple-reflection-type light modulator using Kerr effect in mag. thin film 78−79110
periodic magnetic signal detection by magnetoresistance sensor *(Japanese)* 78−57997
Permalloy electrodeposited film, for cylindrical magnetometer sensor 77−82576
Permalloy film magnetometer, mag. props. and LF noise 78−48005
Permalloy magnetoresistive mag. field and current sensor 77−10048
Permalloy thin-film head pole struct., domain configurations, SEM obs. 80−65975
SAW garnet oxides image sensor *(Japanese)* 77−27429
SQUID gradiometer, DC, design optimisation 80−98951
Ni-Fe-Co alloy films for logic devices, mag. switching vel., anisotropy field and coercive force *(Korean)* 77−51930
YIG film filter, theory of characts. 79−42808
YIG LPE film, optical waveguide in mag. strip domains *(French)* 77−83979
YIG nonreciprocal thin film acoustic device, design, appl. of cct. theory of elastic waveguides 77−85042

magnetic thin film stores *see magnetic film stores*

magnetic thin films
see also magnetic epitaxial layers
alloy film codeposition using pure metallic wire mesh 78−39688
alloys, surface magnetism props., Curie temp., Ising model 80−108039
amorphous, struct. and mag. props., review 80−93148
amorphous ferrimagnetic alloy, mag. anisotropy from dipolar interactions 79−87252
amorphous film sputtering for bubble devices, multiple target method 77−16493
amorphous films of rare earth transition metal system, preparation by co-sputtering 79−56928
anisotropic thin film strips, wall motion *(German)* 79−28573
anisotropy, magnetic, rel. to columnar microstruct., sputtered and vapour deposited films 80−39822
anisotropy, magnetostriction and micromagnetism 77−73062
anisotropy field measurement, cylindrical films 77−13783
antiferromagnetic, two dimens. spin-wave theory, spontaneous magnetisation parameter depend. 80−34714

magnetic thin films continued
Barkhausen effect, general behaviour and stationarity along hysteresis loop 78−56357
Barkhausen effect, statistical anal., instrumentation, computer interfacing 78−82008
Bloch wall structure, horizontal, mag. bubble domains in implanted films 80−71131
Bloch-line rotation instability during gradient propagation of S=0 bubble in an in-plane field 77−40095
bubble, domain wall oscillations and dynamic collapse, saturation velocity and ballistic overshoot theory 77−8372
bubble device materials, single-layer, ion-implantable small, design and development 79−82844
bubble domain existence in absence of mag. field, near phase transition 78−48012
bubble domain film, growth induced order parameter, estimation from coercive force meas. 80−39828
bubble domain interactions, dynamics, theory 80−71132
bubble domain statics and dynamics, micromag. study 80−71081
bubble domains, magnetoelastic interactions 80−103865
bubble film, domain wall mass, under large in-plane fields 79−95618
bubble film, ellipsometric meas. of thickness and refr. index 79−78463
bubble film, mag. characterisation procedures 79−78462
bubble film, magnetoelastic interactions 80−65976
bubble film, quenching of coercive force by domain wall restoring forces, theory and expt. test 79−78460
bubble film, uniaxial anisotropy energy, effect of ion implantation 79−78476
bubble films, characterisation by AC susceptibility meas. 78−68325
bubble films, spin wave and magnetoelastic resonance meas. 78−91913
bubble garnet, domain-wall dynamics in in-plane field 79−87296
bubble garnet, ion-implanted, gradientless propulsion for S=1 bubble 79−78470
bubble garnet film, non-implanted, surface mag. struct. 80−84628
bubble garnet film, saturation velocity, in-plane field effects 80−108041
bubble material, coherent precession mode of twisted wall 79−78468
bubble materials, props. and prep. methods, review *(Rumanian)* 80−93149
bubble materials, validity of one-dimens. wall theory 78−56361
bubble motion due to closure domain interaction with loop current 77−85525
bubble propagation by domain drag in amorphous films 79−42814
bubble shape, eqn. of motion of domain wall 79−78467
charged domain walls, variational method calc. 80−11235
charged domain walls in implanted layers, theory 80−71130
coating stresses in oriented transformer steel determ. by bending expts. *(German)* 79−28569
complex surface pinning parameter and quasi-localised surface spin wave modes 80−50150
curling-type magnetic domains in narrow film strips 77−48020
cylindrical, critical curve meas., sense signal and magnetisation connection *(Slovak)* 77−24717
cylindrical magnetic film, calc. of impedance and susceptibility *(Russian)* 77−89992
dialkylammonium copper tetrachloride, ferromagnetic layer compound, magnetostatic mode excitation 80−29538
dipolar magnet, surface effects on phase transitions, local spontaneous polarisation 80−2708
disc containing bubble, two-dimens. magnetostatic reson. 79−78469
domain boundaries, nonlinear oscills. *(Russian)* 78−56358
domain boundaries study using Faraday effect, structure and movement *(Dutch)* 77−63242
domain structure, honeycomb *(Russian)* 78−56360
domain wall discontinuities during pulsed mag. reversals *(Russian)* 78−48008
domain wall energy analysis 79−99721
domain wall struct. by Faraday effect 79−65702
domain walls, micromagnetic dynamics, numerical integration of Landau-Lifshitz-Gilbert eqn. 79−56580
domain walls, micromagnetic dynamics, numerical model 78−72382
domain width in in-plane field, Faraday rot. meas. 77−4534
dynamic collapse expt., in presence of inplane field 77−85479
electron states in longitudinal mag. field 78−91784
epitaxial, thickness meas., interferometric method 79−35675
epitaxial garnet films for magnetic bubble memories *(Czech)* 78−88147
exchange-coupled two-layer film switching, differential permeability *(Russian)* 78−27061
ferrimagnetic alloy, amorphous, dipolar mechanisms for mag. anisotropy 78−64233
ferrimagnetic materials with high uniaxial anisotropy 78−43581
ferrite, magnetostriction const., mag. saturation and internal stress, ferromag. reson. determ. *(Russian)* 77−16126
ferrite film, plasma sputtering, influence of heating support on struct. and props. *(Russian)* 79−78445
ferrite film, prop. by plasma jet spraying microstruct. and magnetic props. 78−6546
ferrite film, reactive RF sputtering prep., high mag. recording density 77−12528
ferrite garnet, ion-implanted, hard mag. bubble suppression mechanism 80−44890
ferrite plate, stable bubbles near compensation point 77−40099
ferrite-garnet film, local conc. of effective mass of domain boundaries *(Russian)* 77−12179
ferrite-garnet film, waveguide light propag. charact., integrated optics appl. *(Russian)* 78−1346
ferrite-semiconductor composite struct., bulk magnetostatic wave instability, theory 77−12186
ferrofluid decorated mag. domain patterns, Fraunhofer diffr., domain struct. determ. 78−6541
ferrofluid patterns, zigzag form of charged domain wall 80−44852
ferromagnet, depend. of Curie temp. and spontaneous magnetisation on film thickness 77−32222
ferromagnet, domain wall motion, effect of transverse mag. field 78−68292
ferromagnet, dynamical props. of flat parallel domain struct. *(Russian)* 78−6499
ferromagnet, heterogeneity influence on static and dynamic props. of domain walls *(Russian)* 80−65974
ferromagnet, mag. anisotropy and defect distrib. *(Russian)* 77−59434
ferromagnet, mag. props. meas. using planar magnetoresist. effect 78−21186

magnetic thin films continued
ferromagnet, on antiferromag. backing, parametric reson. *(Russian)* 77−90043
ferromagnet, uniaxial anisotropy, approx. determ. of anisotropy const. 78−2713
ferromagnet, with unidirectional anisotropy, domain struct., mag. field effect *(Russian)* 78−19289
ferromagnetic, ϕ^4 domain walls, magnetisation, occurrence of crit. point 78−95500
ferromagnetic, band model of domain struct. 77−36105
ferromagnetic, Brillouin scattering from spin waves 80−65843
ferromagnetic, bubble domain lattice, parametric excitation of oscillations 77−8374
ferromagnetic, crit. angle of external mag. field for surface spin waves 79−47309
ferromagnetic, direct determ. of mag. domain wall profiles, using split detector STEM 80−103867
ferromagnetic, dynamics near transition pt. from homogeneous to inhomogeneous magnetis. state 80−108038
ferromagnetic, electric-charge-induced magnetisation 79−69700
ferromagnetic, electron-nuclear oscillations in conditions of strong coupling between electronic and nuclear subsystems *(Russian)* 79−19782
ferromagnetic, elliptical spin precession correction factor in spin-wave reson. theory 80−20464
ferromagnetic, influence of interference field harmonics on mean magnetisation vector *(Polish)* 79−40092
ferromagnetic, mag. bubble, effect of propag. on shape 77−16134
ferromagnetic, mag. props., rel. to struct. 79−91270
ferromagnetic, magnetostriction meas. from deflection in mag. field 77−10068
ferromagnetic, magnon avalanche under NMR saturation 78−10783
ferromagnetic, n-vector model with Kac-type interactions 77−59436
ferromagnetic, nonlinear spin wave parametric resonance 80−2642
ferromagnetic, parametric oscill. with biaxial anisotropy 80−103861
ferromagnetic, phenomenology of domain walls review *(Rumanian)* 78−60324
ferromagnetic, resistivity anisotropy theory 77−59342
ferromagnetic, review of developments *(Japanese)* 77−69635
ferromagnetic, thick film, reson. transmission of EM energy via phonons 80−60382
ferromagnetic, transverse Kerr magneto-optical effect, thickness depend. 77−59559
ferromagnetic, two dimens. spin-wave theory, spontaneous magnetisation parameter depend. 80−34714
ferromagnetic, unipolar simple domain walls *(Rumanian)* 79−19752
ferromagnetic, with domain struct., magnetostatic oscills. 78−48010
ferromagnetic, with nearest neighbour and next nearest neighbour exchange interactions spin-wave excitations 79−73783
ferromagnetic (111) films, macrostripe and microstripe domain structs. *(Russian)* 79−28572
ferromagnetic bilayer compounds, spin-wave resonance, effect of random dilution 79−61236
ferromagnetic exchange coupled two-layer film, mag. reversal exchange energy const. *(Russian)* 77−59435
ferromagnetic film, cross tie domain wall struct. and energy 77−59438
ferromagnetic film, domain wall width meas. with electron microscope, astigmatism effects 79−19753
ferromagnetic film, Fourier optics, mag. struct. determ. *(Russian)* 78−39371
ferromagnetic film, ground state, effect of surface and bulk anisotropy *(Russian)* 79−11328
ferromagnetic film, magnetostatic surface wave propag. 79−4661
ferromagnetic film, of cubic symmetry, depend. of Curie temp. on thickness and boundary conditions 78−19287
ferromagnetic film, shift of ant. temp. as result of Raman scatt. 80−54909
ferromagnetic film, sinusoidal voltage prod., mag. field meas. 78−26972
ferromagnetic film, spin wave parametric reson. near phase transition 79−8053
ferromagnetic film, tangentially magnetized, spin wave instability 78−2712
ferromagnetic film, transverse bioped susceptibility, two-dimens. micromagnetism 80−11231
ferromagnetic film domain wall profile determ. by differential phase contrast electron microscopy 79−61195
ferromagnetic film in mag. field, pulsed laser beam induced EMF *(Russian)* 77−55564
ferromagnetic film thickness meas. by diffraction electron microscopy 78−86392
ferromagnetic film with domain structure, transient state, mag. field calc. 77−4536
ferromagnetic films, Bloch wall struct. and anisotropy, analytical representation 78−88151
ferromagnetic films, electrodeposition, thickness control, magnetisation meas. 78−23306
ferromagnetic films, spin correl. functions, crit. indices 80−7133
ferromagnetic films, spin wave excitation by microwave antenna field 80−44816
ferromagnetic gates for ultracold neutrons 77−46440
ferromagnetic layer in perpendicular mag. field, ground state, spin wave reson. 77−85512
ferromagnetic nonmetallic film, stand exchange mode determ. 80−2565
ferromagnetic plate, domain struct. during spin reorientation, phase diagram *(Russian)* 78−52320
ferromagnetic resonance, low freq., thin film with uniaxial-biaxial anisotropy 79−8055
ferromagnetic resonance in cylindrical mag. domains *(Russian)* 78−10780
ferromagnetic slab, retarded EM modes 78−84405
ferromagnetic surface-rearranged thin film, spinwave spectrum, derivation from generalisation of Bogoliubov canonical transform. 79−69702
ferromagnetic tangentially magnetised, parallel pump spin wave instability 77−8294
ferromagnetic thin film, mag. domain wall energy determ. 79−95620
ferromagnetic thin film edge domain structures, Bitter pattern. obs. 77−73063
ferromagnetic thin film energy absorption by magnetisation vector forced oscillation *(Polish)* 77−80970
ferromagnetic thin films, fabrication by sputtering, and mag. props. 78−91881

magnetic thin films continued
film, evaporated, galvanomag. and mag. props., thickness depend. 78−23181
film for optical image recording, banded domain structure, effect of recording field strength on energy charact. *(Russian)* 78−19297
films, induced mag. anisotropy, temp. depend. *(Russian)* 79−42757
full wafer magnetic bubble films, devices for characterisation 79−78461
garnet, gradient bubble propag., ballistic overshoot 77−12170
garnet, gradientless propulsion of bubbles 77−4535
garnet, ion-implanted, bubble collapse field, in-plane mag. field effect 77−73060
garnet, ion-implanted film, crit. curves for determining magnetisation directions 79−91263
garnet, ion-implanted film, large automotion of $S=^{1}/_{2}$ bubble 79−24203
garnet, low loss bubble material, wall struct. changes 77−89994
garnet, magnetic bubble materials, review 80−50153
garnet, minimum bubble drive field, ion implantation effect 77−24721
garnet, Permalloy-coated, bubble properties 78−2715
garnet, Permalloy-coated film, bubble vel. and stability, influence of planar domains 80−39831
garnet bubble film with induced anisotropy, domain wall energy 79−19750
garnet film, 1 μm bubble contiguous-disk device, orientation depend. of propagation margin 79−82846
garnet film, Bi substituted, LPE growth 77−1798
garnet film, bubble, anisotropy field and nonmagnetic regions in implanted layers, ferromag. reson. study 79−99774
garnet film, bubble, [111]-oriented simple method of meas. cubic anisotropy const. 78−19285
garnet film, dynamic charges in bubble domain lattice 78−60325
garnet film, ion implanted bubble circuits 79−78473
garnet film, ion implanted bubble propag., wall states 77−16128
garnet film, ion-implanted, controlled generation and discrimination of χ_+ and χ_- bubbles by single bias pulse 79−51826
garnet film, ion-implanted, discrimination of S=1 and S=0 bubbles by dynamic bubble collapse 79−51825
garnet film, mag. bubble domain, annealing by laser pulse 80−15769
garnet film, magnetic rag-domains, appl. to magneto-optical displays 78−91912
garnet film, motion of mag. bubble domains near point defect 79−28575
garnet film, physics of domain walls 79−99727
garnet film, uniaxial, cubic anisotropy effect 77−89998
garnet film, wall velocity at high drive fields 77−85518
garnet film ion implanted contiguous disk structure dynamics of 1 μm bubbles 79−78474
garnet film LPE growth, for bubble memory appl., review, book contrib. 79−70009
garnet films, (111)-oriented, cubic anisotropy meas. 80−54924
garnet films, bubble statics, dynamics *(Japanese)* 78−52326
garnet films, domain lattices, parallel stripe susceptibility, uniaxial anisotropy field 80−54930
garnet films for a fast bubble devices 80−25168
garnet thin film, bubble domain lattice collapse charact. in alternating mag. field 80−54932
garnet thin film waveguide, magneto-optical effects 77−54802
garnet-ferrite film thickness meas. with UM-2 monochromator interference attachment 78−3035
garnets, film, ion-implanted, domain wall mobility 78−95495
garnets, meas. of Faraday effect and susceptibility using magnetooptical apparatus 80−105680
garnets, skew cylindrical mag. domains, light modulator appl. anal. 79−38360
garnets films, containing Ca and Ge refr. index meas., 0.56-0.97 microns 77−52192
GdCo amorphous film, magnetic compensation walls 77−8375
heavy ion-solid surface collision cascade theory and expt. *(Japanese)* 80−11527
Heisenberg film, spin-one isotropic, with biquadratic interactions, phase transition 77−20611
Heisenberg thin films 79−38359
hollow half bubbles, static forces, bubble nucleation 77−85522
holographic recording materials and devices, book contrib. 78−25838
hypercritical films, stress-induced uniaxial anisotropy influence on domain struct. *(Russian)* 79−69703
hysteresis curve, multiple particle model *(German)* 78−80178
infinite film, bubble domains with twisted walls, calc. 78−64245
Invar, mag. props. and elec. resist. 77−32221
Invar film, superfine mag. struct. *(Russian)* 80−80572
Invar films, exchange interaction depend. on lattice parameter, spin-wave reson. and magnetisation meas. *(Russian)* 79−42751
ion-implanted bubble garnet film, vel. asymmetry during stripe head propag. 80−39834
Ising film, diluted, surface and bulk magnetic phases 79−82797
itinerant-electron ferromagnetic film on nonmagnetic metallic substrate, mag. props. 80−20371
Kac-Baker model of partially finite spin systems 77−20621
laser radiation recording method 77−54674
layer systems, mag. polaritons 78−31060
layered, directional coupling of magnetostatic surface waves 79−38358
liquid thin layer with two free boundaries, instability conditions, surface wave dispersion eqn. *(Russian)* 78−1752
Lorentz microscopy, mag. domain images resolution, computer calcs. 78−35004
Lorentz microscopy, thin film and bulk specimen, recent advances 78−35002
Lorentz microscopy using STEM for domain wall profiles determ. 78−35003
magnetic moment, coupled oscills. in elec. circuit during HF mag. reversals *(Russian)* 78−23307
magnetic properties meas. on saturated substrate 80−13108
magnetic soft and hard materials, garnets, magnetic properties and applications, structural props. 80−65760
magnetic wave interaction with drifting charges 78−95485
magnetisation changes during main stage of nonuniform rot. *(Russian)* 77−32224
magnetization amplitude and direction var. electron-microscope obs. procedure 78−6548
magneto-optical props. meas., data reading system appl. *(Russian)* 77−1572
magnetocardiogram, effect of torso geometry 77−60222
magnetooptical interference 79−28724

magnetic thin films continued
magnetostatic wave-current interaction, characterisation by coupling constant 78−84403
manganese stearate, two-dimensional mag. struct. 80−108040
manganese stearate monolayer, two-dimensional mag., prep. and characterisation 78−31097
metallic amorphous film, bubble technology *(Polish)* 77−77076
metallic amorphous films for mag. bubble memories, materials review *(Polish)* 80−34715
metallic glass, magnetostrictive film, overlay for variable SAW delay line 78−63240
metallic glasses, Brillouin-Mandelstam scattering from thermal and excited magnons 80−70980
metallic multilayers, ferromag. reson. formal treatment 77−73083
metallic multilayers, ferromag. reson. numerical example and semiquantitative model 77−73084
micromagnetic struct. of planar charged walls 79−78478
$Mn_{1-x}Cu_xSb$ films, $0 \leq X \leq 0.3$, magneto-optical props. 79−51981
multilayer gyrotropic structures, light propag. anal. *(Polish)* 79−3809
multilayer structure of semiconductor, dielectric and mag. film, constant EMF 79−69583
multilayer thin films, spin wave resonance, model 78−76316
neutron depolarisation in refl. and refraction at mag. film surface *(Russian)* 78−95493
noise, influence of external random fields *(Russian)* 78−64229
noise due to amplitude and phase fluctuations *(Russian)* 77−77075
orthoferrite cryst. films, local coercivity of domains boundaries *(Russian)* 80−80578
orthoferrites, skew cylindrical mag. domains, light modulator appl. anal. 79−38360
oxides, hydrothermal crystallisation, review, book contrib. 79−69974
Permalloy, Bloch wall motion obs. *(German)* 77−16133
Permalloy, conductor crossing effect on bubble propagation margins 80−29588
Permalloy, corrosion kinetics, mass and resist. change techniques, comparison 78−27675
Permalloy, domain wall mass and energy, wall vel. depend. calc. 80−2614
Permalloy, double layer, wall splitting effect 77−85530
Permalloy, electrodeposition, mag. props. *(French)* 78−64488
Permalloy, films, Faraday rotation effect dispersion 80−40092
Permalloy, galvanomag. rotation charact., under uniaxial stress 78−84466
Permalloy, in weak field, pulse mag. reversal mechanism *(Russian)* 77−80976
Permalloy, mag. microstruct. obs. in nonlinear ripple magnetis. case *(Russian)* 80−65971
Permalloy, magnetic leakage fields above stripe domains 77−77077
Permalloy, magnetoconductivity modulation by substrate electrostriction 79−60908
Permalloy, mobility of Bloch lines 77−28421
Permalloy, Neel wall transitions into cross-tie walls 79−95619
Permalloy, obliquely deposited, mag. anisotropy, annealing and deposition parameter effects *(Russian)* 77−80971
Permalloy, on quartz, two-layer disc, bending reson. vibrs. *(Russian)* 77−24797
Permalloy, oscillatory metallic field effect and surface magnetoelasticity 79−56282
Permalloy, oxidation, quartz cryst. microbalance, AES and XPS obs. 78−27676
Permalloy, oxidised film, magnetic noise, low temp. depression *(Russian)* 79−99734
Permalloy, quasistatic and pulsed mag. reversals of Neel domain walls *(Russian)* 78−39374
Permalloy, stray fields arising during pulse reversal 77−80980
Permalloy, streaming of domain walls *(Russian)* 78−72380
Permalloy, submicroscopical magnetisation structs. induced by fields normal to film plane 79−1697
Permalloy, two-layer, with magnetostatic coupling, creep of domain boundaries *(Russian)* 77−43857
Permalloy, velocity of motion of nonequilibrium walls of edge domains *(Russian)* 79−1694
Permalloy, with small surface anisotropy, ferromag. reson. 77−69701
Permalloy barrier film, worm-like motion of domain boundaries *(Russian)* 78−39375
Permalloy cylindrical film, magnetisation in crossed steady/alternating fields, easy axis dispersion influence 79−8024
Permalloy film, break-cross-tie domain walls, thickness depend. 78−43619
Permalloy film, coercive force associated with domain boundary displacement *(Russian)* 80−50151
Permalloy film, corrosion induced defects, scanning Auger microscopy 77−40464
Permalloy film, domain nucleation using low intensity US 80−34731
Permalloy film, domain walls, magnetisation components distrib. 79−87298
Permalloy film, domain walls streaming *(Russian)* 79−82842
Permalloy film, electrodeposition with zero magnetostriction composition, technological control 79−33955
permalloy film, Fe-overcoated, optical and magneto-optical charact., mag. preps. 79−82956
Permalloy film, hysteresis loop meas. using magnetooptical system 79−69707
Permalloy film, implanted with C ions, HCP struct. formation, electron diffr. study *(Russian)* 79−82469
Permalloy film, magnetoresistive determ. of anisotropy energy and its strain depend. 79−56575
Permalloy film, movement of circular Bloch line in cross-tie wall 78−31099
Permalloy film, multi- and single-layer, reson. curves subjected to tangential mag. reversals *(Russian)* 80−50195
Permalloy film, perpendicular anisotropy, structural and thermal stresses *(Russian)* 79−4708
Permalloy film, stripe domain struct., distrib. of magnetisation *(Russian)* 77−66396
Permalloy film, with band domain struct., pulse mag. reversals *(Russian)* 79−38361
Permalloy film corrosion characterisation by crystal oscillator microbalance and resistance meas. 78−7101
Permalloy film demagnetising field and magnetisation curve determ. 77−73059

magnetic thin films continued
Permalloy film oxidation, microbalance, AES, ESCA and sputter profiling 78−15600
Permalloy film strip, unidirectional domain wall propag. with in-plane magnetisation 80−71134
Permalloy film strip, wall curvature calc. with in-phase magnetisation 78−2717
Permalloy films, domain propelling tunnel, domain struct. displacement *(Russian)* 79−99736
Permalloy films, domain struct., nonuniform rotation of magnetisation *(Russian)* 79−47313
Permalloy films, M-H curve meas., magneto-optical instrument *(Japanese)* 77−37953
Permalloy films, oxidation effects on atmospheric corrosion, AES, XPS and ion sputtering anal. 80−11829
Permalloy films, thickness depend. of Bloch line mobility 79−24204
Permalloy films with band domain struct., thermomag. recording, resolving power *(Russian)* 80−75769
Permalloy narrow stripes, permeability 77−89987
Permalloy platelet, transmission reson. meas. 77−20710
Permalloy platelets, FMR mode positions, spin pinning 77−4562
Permalloy RF sputtered films, O effects in mag. and elec. props. 80−100603
Permalloy RF sputtered films, struct.-sensitive mag. props. 80−34705
Permalloy sputtered film, bevelling by chemical etching, for this film mag. header 78−92375
Permalloy thick film coercivity control 80−15764
Permalloy thin film cores, domain wall motion and flux patterns, Kerr magneto-optic effect obs. 80−34721
Permalloy thin films, break-cross-tie wall energy 80−88842
Permalloy-Co film, domain walls, magnetisation ripple *(Russian)* 79−47314
Permalloy-Cu(Al) two-layer films, mag. anisotropy, grain boundary diffusion *(Russian)* 80−71122
Permalloy-Mn film, diffusion aftereffect causing mag. state change *(Russian)* 80−103860
Permalloy-SiO multi-layer flat ring cond., with circular anisotropy, mag. props. *(Russian)* 77−8366
perpendicularly magnetised, surface and vol. magnetoelastic waves *(Russian)* 80−93151
phase states when easy magnetisation axis is inclined rel. to film surface *(Russian)* 80−103864
pulse magnetic reversal in high freq. field in ferromag. reson. range *(Russian)* 80−11230
pulsed magnetic reversal studies using magneto-optical stroboscope 78−4667
rare earth compounds, $RFeO_3$, amorphous films for mag. bubble memories, materials review *(Polish)* 80−34715
rare earth garnet thin films, macroscopic magn. props., magneto-optical expts. 80−46764
rare earth iron alloy, amorphous, cosputtered, struct. and mag. props. 78−60323
rare earth iron garnets, Ca-Ge substituted, mag. loss and domain wall mobility 80−65980
rare earth-Co amorphous alloys, mag. compensation temp. 77−66277
rare earth-Co systems, anomalous Hall effect and Kerr rotation obs. 77−11897
rare earth-transition metal, amorphous, microstruct., TEM obs. 78−72018
rare earth-transition metal, amorphous, microstruct. and magnetism 78−64230
rare earth-transition metal alloy amorphous film, magnetostriction, dipolar mechanism 78−95502
rare earth-transition metal alloys amorphous thin films, anisotropic mag. and microstruct. props. 78−95487
rare earth-transition metal amorphous alloy films with single mag. species 77−16121
rare earth-transition metal amorphous film, microstruct. 77−51619
rare earth-transition metal amorphous films, radiation damage 77−66398
rare earth-transition metal amorphous thin films, mag. potential distribution and wall velocity meas. 80−34725
rare earth-transition metal amorphous thin films for thermomag. recording 80−20403
rare earth-transition metal garnets, $R_3M_5O_{12}$, amorphous films for mag. bubble memories, materials review *(Polish)* 80−34715
rare-earth-transition metal amorphous films, domain structure, technique for observation 78−91914
recorders of optical images, sensitometry using glass Nd laser *(Russian)* 77−79178
resonance props. in network of cylindrical mag. domains *(Russian)* 80−50194
saturation magnetisation and uniaxial anisotropy determ. using torque meas. 79−95614
soft ferromagnetic film, theoretical wall mobility 80−34677
spin pinning and mag. surface reconstruction, effect on standing spin waves 77−1600
spin wave resonance, surface mode magnetisation, inhomogeneities effect 77−69710
spin wave resonance, surface modes, influence of inhomogeneities of magnetisation 77−12205
spin wave resonance line broadening by dislocations 78−64275
sputtering technique for high rate deposition 79−28917
standing spinwave resonance in film with nearest and next-nearest neighbour exchange 78−68390
static wall structure, in bubble films, under large in plane fields 78−76282
strip films, bulk and surface spin oscills., mag. reson. 80−97149
stripe domain struct. of film, with perpendicular anisotropy, theory *(Russian)* 80−65973
stripe domain structure, magnetostatic modes 78−68333
stripe domain structure, mechanism of mag. reversals *(Russian)* 77−80978
striped domain struct., 2D model of distrib. of magnetisation *(Russian)* 78−88149
substructural defect anal. by coherent methods *(Russian)* 79−61190
surface and interface magnetism by Mossbauer spectroscopy 80−7218
surface pinning parameter, complex angle depend. 77−63239
surface spin waves and surface anisotropy effects at finite temp. 79−78452
surface state swapping effect 77−90040
magnetic thin films continued
surface states, theory, in spin wave resonance, review 80−84654
switching, uniform rotational high speed, dynamical crit. switching curve 77−32220
thermomagnetic recording of optical data *(Russian)* 79−47286
thickness meas. of ferromagnetic films of high conductivity using magnetic reluctance thickness gauge 80−68178
time-magnifier, IR-range, construction 80−13139
torque measurement, analysis method, saturation magnetisation and anisotropy const. determ. 77−8368
transition metal surfaces, mag. props. 80−44861
twisted domain wall energy, thickness depend., simplified calc. *(Slovak)* 80−103862
two-dimensional nonscalar system, dynamics of symmetry-breaking long-ranged order 77−20613
uniaxial ferromagnet domain struct., phase transition *(Russian)* 80−108044
vacuum magnetometer for steady-state parameters meas. 77−22579
vertically suspended, torque curve meas., first-order calc. anal. 80−86354
$(YSmEuCa)_3(FeGe)_5O_{12}$, garnet film, ion implanted, bubble domain props. 78−88152
Ag-Fe alloy film, mag. susceptibility max. 79−24173
Ag-Mn, dil., thin-film spin glass, mag. susceptibility and T_G meas., 1.2-60K 79−38346
Au-Fe alloy film, mag. susceptibility max. 79−24173
Au-Fe film spin glass, low temp. resistivity, mean free path effects 78−80163
Au-Yb thin films, ESR spectra, strain effects 80−71172
$BaO-Fe_2O_3$ system, splat cooled phases struct., magnetisation and susceptibility 300-1100K *(French)* 77−48017
Bi garnet-MnBi film structure, thermomag. information recording appls. *(Russian)* 78−23305
$(BiTm)_3(FeGa)_5O_{12}$ ion implanted epitaxial garnet film, bubble domains, cryst. struct. disorder 80−93150
$CdCr_2S_4$, ferromagnetic semiconductor films, prep. and props. *(Japanese)* 79−47308
$CdCr_2Se_4$ films, mag. hysteresis, domain struct., mag. viscosity 80−25169
$CdCr_2Se_4$, mag. linear and circular dichroism and Faraday rot. 79−99966
Co, amorphous, magnetoresist., in fields up to 80 kG 77−39823
Co, amorphous ferromag. film, resist. anisotropy rel. to struct. 77−72926
Co, and alloys, ferromag. films, coercive force, ion plating prep. 77−28730
Co, atomic layers, Pauli paramagnetism to band ferromagnetism transition thickness depend. 78−72377
Co, electrodeposited coating, struct. and magnetic props. 79−46985
Co, electrodeposited film, saturation magnetisation and perpendicular anisotropy meas. 78−76277
Co, evaporated, uniaxial mag. anisotropy 77−51929
Co, even magneto-optical transmission effects, 0.4-1.25 μm 77−32354
Co ferrite film prep. by vac. evaporation and annealing 77−85939
Co, ferromag. film, ion plating prep., coercive force and magnetoresist. 77−12546
Co, ferromag. film, magnetoresistance parameter meas. *(Spanish)* 80−2485
Co film, ion beam sputtering prep., struct. and mag. props. 80−35085
Co film, low-angle grain boundary struct. *(Russian)* 79−42807
Co film, mag. anisotropy study using NMR spin echo method 80−60384
Co film, mag. domain wall obs. by electron holography 80−80582
Co film, magnetic domain wall width, shadow and interf. electron microscope exam. 79−11330
Co films layered over Cr by DC sputtering for digital mag. recording 79−83118
Co, linear mag. birefr. dispersion 77−69807
Co, on Cu, Mossbauer emission spectra 78−19387
Co, plated film, magnetisation and mag. interface anisotropy 77−85510
Co, sputtered film, high coercivity and high hysteresis loop squareness 79−91259
Co-B(-Cr) thin film glasses, mag. props. and corrosion resist. 80−80576
Co-CoO films, evaporated, exchange anisotropy 80−88841
Co-Cr films, mag. props. in range of transition from thin-film to hypercritical state *(Russian)* 79−51824
Co-Cr mag. film, crystallographic texture formation effects on props. *(Russian)* 80−108471
Co-Cr recording films, perpendicular mag. anisotropy, hysteresis loop, microstruct., TEM obs. 78−95491
Co-Fe, film, mag. and hyperfine field exam. of uniaxial anisotropy 77−66391
Co-Fe alloy films, magnetostriction and orientation of easy magnetisation axes *(Russian)* 79−19756
Co-Fe-B, amorphous, mag. annealing behaviour 79−73782
Co-Fe-B and Co-Fe-Cr-P-B sputtered amorphous films, mag. props. and corrosion resist. 79−28567
Co-Fe-P film, ferromag., coercive force meas. 78−10737
Co-Gd amorphous film, struct., mag. anisotropy consts., saturation magnetisation *(Russian)* 79−99735
Co-Gd-Mo, amorphous film, mag. props., temp. depend. 78−10734
Co-Gd-Mo films, sputtered, O effects on mag. props. during annealing 80−89374
Co-Gd-Mo-Ar film, amorphous, mag. props. 78−80182
Co-Gd-Mo(Au), amorphous, Hall effect 77−85347
Co-Gd(Ho), amorphous, stripe domains and mag. anisotropy by Lorentz microscopy 77−63243
Co-Gd(Tb)(Sm), magneto-optic coeff. and refr. index, ellipsometric determ. 80−71501
Co-Ni, electrodeposition, mag. props. *(French)* 78−64488
Co-Ni, ferromag. film, ion plating prep., coercive force and magnetoresist. 77−12546
Co-Ni-P electrolytic layers, partial anhysteretic remanent magnetisation, additivity prop. *(French)* 80−44882
Co-P, amorphous, spin wave dispersion law, spin wave reson. obs. *(Russian)* 78−88196
Co-P, amorphous electrodeposited films, domain wall motion, Kerr effect 78−60322
Co-P, cryst. and amorphous mag. films, ferromag. resonance line width *(Russian)* 78−88192
Co-P amorphous alloy, ferromagnetic reson. exam. 79−28620
Co-P amorphous alloy film, mag. domain struct. 77−69604
Co-P amorphous alloys, electrodeposited, magnetic anisotropy 79−28568

magnetic thin films continued
Co-P amorphous film, domain struct., influence of planar anisotropy 79−78472
Co-P electroless film on Al base disc substrate, microstruct. rel. to mag. props. 78−68304
Co-P films, electrodeposited, magnetic recording media *(Japanese)* 80−29587
Co-P films with various preferred orientations, mag. props. 80−100604
Co-Pt, electrodeposited, saturation mag. induction, mag. anisotropy and coercive field meas. *(French)* 80−2610
Co-Pt alloy, electrolytic deposition conditions over large comp. range *(French)* 80−45242
Co-Re, sputtered film, high coercivity and high hysteresis loop squareness 79−91259
Co-W alloy electrolytic coatings, heat treatment effects on coercivity, hysteresis and structure *(Russian)* 80−60381
Co(-Re) sputtered films, mag. props. and microstructures 79−82837
$Co_{79}Fe_{6.5}B_{14.5}$ amorphous thin films, zero magnetostriction, high magnetisation 80−34708
$(CoFeB)_{100-x}Cr_x$ thin films, magnetic props. and corrosion resist. 80−34709
$(Co_{1-x}Fe_xNi_y)_{80}(Si_{1-z}B_z)_{20}$, amorphous films, spin wave spectra 80−34777
$CoFe_2O_4$ film, Faraday rot., birefr. 77−1663
$Co_xFe_{3-x}O_4$, magnetooptic recording material, mag. and magnetooptic props. 77−20832
CoGd, H_2 and N_2 contaminated amorphous films, mag. props. 79−1690
CoNiB, corrosion-resistant amorphous mag. thin films 80−54923
CoNiP, amorphous, electrolytic, prep. and props. *(Slovak)* 79−51823
CoP-NiCoP, composite ferromag. film, exchange coupling between soft and hard layers, FMR obs. 79−78448
CoPt, on Al_2O_3, quantitative electron microprobe analysis 77−9150
$CoPt_3$, electrolytic films, saturation mag. induction, coercive fields, thickness depend. *(French)* 80−44883
Cr, size effects on spin density waves, struct. and elec. props. 77−80973
Cr-Co-Ni hard film on Mo substrate for magnetic recording 80−2608
CrO_2 amorphous thin films, Mossbauer and magnetisation data 80−34712
CrO_2, ferromag. films, epitaxial growth in air, electron diffr. and SEM obs. 79−42410
Cr_7Te_8 film, optical and magneto-optical props., appl. as storage medium 78−23545
Cu HCP film, uniaxial, mag. domain struct. 80−60385
Cu/Ni coherent modulated structures, electronic struct. and magnetism 80−103620
Cu-Fe, interface, ferromagnetic and cond. spin reson. mode coupling 79−78521
Cu-Fe alloy film, mag. susceptibility max. 79−24173
Cu-Ni, ferromagnetic, mag. susceptibility meas., 30-130°C 79−95615
Cu-Ni, film, compositionally modulated, enhanced magnetisation density 78−84460
Cu-Ni, interface, ferromagnetic and cond. spin reson. mode coupling 79−78521
Cu-Ni films, thickness depend. of Curie temp., resist. meas. 78−6545
Cu-Ni thin films, ferromag., Hall effect meas. 80−80428
Cu-Permalloy, interafce, ferromagnetic and cond. spin reson. mode coupling 79−78521
Dy, helimag. order, surface deform., exchange and single-ion magnetocrystalline anisotropy energy 77−66390
Dy, magnetoelastic waves, GHz, excitation, field depend. 78−72378
Dy-Fe, amorphous ferrimag. film, mag. props. and Curie point writing 77−12164
Dy-Fe, amorphous film, Kerr readout characts. 79−15439
Dy-Fe alloy, amorphous, contact printing 77−73061
$Dy_{0.25}Co_{0.75}$, amorphous, displacement of mag. compensation temp. by elastic stress *(Russian)* 78−19284
DyCu film, amorphous, asperomagnetic domains, Barkhausen jumps in hysteresis loop 80−75822
Dy_xCu_{1-x}, amorphous film, magnetisation meas., local anisotropy effects 78−68309
DyFe amorphous film, Mossbauer and mag. meas. 80−15844
DyIG, noncrystalline, Mossbauer and magnetisation data 80−34828
DyM_3, M=Fe, Co, Ni, amorphous, mag. struct. and moments 77−66260
Er film, magnetoelastic excitations, phonon spectroscopy and forbidden transitions 79−82853
$(ErBi)_3Fe_{5-x}Ga_xO_{12}$, ferrimag., splitting of domains into layers 77−28420
$Er_2EuFe_{5-x}Ga_xO_{12}$, rag-domain garnet film, controlled variation of props. under O_2 annealing 79−15328
$Er_3Fe_5O_{12}$, low temp. CVD epitaxial film growth and mag. props. 79−42406
$(Eu,La,Ca)_3(Fe,Ga,Al_5)O_{12}$, LPE, growth-induced orthorhombic anisotropy 77−20652
$(Eu,Lu)_3(Fe,Al)_5O_{12}$, epitaxial, increased domain wall velocities, due to orthorhombic anisotropy 77−20653
$(Eu,Y)_3Fe_5O_{12}$, low temp. CVD epitaxial film growth and mag. props. 79−42406
$(Eu,Yb)_3Fe_5O_{12}$, low temp. CVD epitaxial film growth and mag. props. 79−42406
$EuEr_2Ga_{0.7}Fe_{4.3}O_{12}$, garnet thin films, magnetisation orientation, temp. depend. 80−71125
EuGaYIG, bubble dynamics, anisotropy depend., ferromag. reson. expts. 77−63240
$Eu_{1-x}Gd_xS$ films, mag. and elec. props. 80−15766
EuIG, noncrystalline, Mossbauer and magnetisation data 80−34828
EuO film for thermomagnetic recording, anisotropy of resolving power 80−20404
EuO film threshold characteristics in holographic and bit recording *(Russian)* 80−63944
EuO, light scatt. from spin waves and magneto-optic hysteresis meas. 80−97244
EuO, nonstoichiometric film with excess EU, optical, magneto-optical and elec. props. 79−8204
EuO, thermomag. effects for reversible holographic storage 77−34851
$EuO_{1-\Delta}$, thin film, Faraday effect dispersion and transmission, 0.5-1.1 μ, 20.4 and 77K, anion vacancies 79−19945
EuS, ferromag. semicond. film, Hanle effect, optical orientation time consts. meas. 77−40214
EuS, ferromagnetic film, optically induced magnetisation amplification, Curie temp. increase *(Russian)* 77−24719
magnetic thin films continued
EuS film, influence of prep. on mag. props. 79−24201
EuS, film, intrinsic demagnetising fields 78−10735
EuS films, ferromag., optical spectra and light scatt. from spin waves 80−16116
EuS films, mag. and elec. props. rel. to stoichiometry and defects 80−97122
EuS, light scatt. from spin waves and magneto-optic hysteresis meas. 80−97244
EuS, mag. surface reconstruction, ferromag. reson. 78−10781
EuS, magnetic props. using transverse Kerr and Voigt effects 77−52054
EuS, thermoreflectance spectra below Curie temp. 77−66550
EuTe, spin alignment, high field Faraday rotation expt. 77−63401
$(EuY)_3(FeGa)_5O_{11}$, ferrite garnet film, mag. bubble motion delay 79−91269
Fe, amorphous film, Hall effect and magnetisation *(Russian)* 77−35922
Fe, and alloys, ferromag. films, coercive force, ion plating prep. 77−28730
Fe, atomic layers, Pauli paramagnetism to band ferromagnetism transition thickness depend. 78−72377
Fe, density of states, photoemission expts. above and below T_c, rel. to magnetism model 77−20536
Fe discontinuous film, Mossbauer effect exam. of magnetic state 77−24769
Fe, domain wall struct. obs. by Lorentz electron microscopy 77−85527
Fe evaporated at oblique incidence, columnar grain struct. using anisotropy field meas. 77−59231
Fe, evaporated at oblique incidence, optical and mag. anisotropies 80−7134
Fe, even magneto-optical transmission effects, 0.4-1.25 μm 77−32354
Fe, FCC, antiferromag. ordering, Mossbauer expts. 77−85508
Fe, ferromag. film, magnetoresistance parameter meas. *(Spanish)* 80−2485
Fe, ferromag. film, surface states, surface magnetisation and electron spin polarisation 80−65648
Fe film, amorphous and polycrystalline, Hall effect, resistivity and mag. moment 78−91786
Fe film, antiferromagnetic ordering, Mossbauer spectroscopy 78−14990
Fe, film, asymmetric 180° Bloch walls, Lorentz electron microscopy obs. 78−27063
Fe film, C ion implanted, HCP struct. formation, electron diffr. study *(Russian)* 79−82469
Fe film, chemisorption induced mag. dead layers, ferromag. reson. obs. 79−91261
Fe film, coated, interface magnetism by Mossbauer spectroscopy 80−75890
Fe film, effect of tensile stress on mag. domain struct. 78−68332
Fe film, enriched, NMR obs. 78−39443
Fe film, ferromag. reson., thermodynamical anal. 79−42840
Fe, film, ion beam sputtering prep., struct. and mag. props. 80−35085
Fe film, low-angle grain boundary struct. *(Russian)* 79−42807
Fe film, magnetoelastic excitations, phonon spectroscopy and forbidden transitions 79−82853
Fe film, nuclear magnetisation relax. at 77 to 500K 78−60352
Fe film, on Cu and Ag substrates, mag. props., Mossbauer spectra meas. 80−11233
Fe film, single crystal, less than 1000 Å thick, inclined 90° walls 78−72384
Fe film, vacuum deposited, resist. minimum 80−44741
Fe film coated by MgO, MgF_2 and Sb, surface mag. 80−7196
Fe film coated by MgO, Mossbauer spectra, mag. hyperfine field 80−7221
Fe films, ferromagnetic reson., photoacoustic detection 80−80613
Fe, finely dispersed, superparamagnetism, Mossbauer meas. 78−68303
Fe foil, electrodeposited, phys. and mag. props. 79−91275
Fe, Hall resist., effect of N impurity codeposition 78−64146
Fe, high rate deposition by sputtering from two facing targets 77−85938
Fe, linear mag. birefr. dispersion 77−69807
Fe, mag. structures and stresses, ferromagnetic resonance 78−72375
Fe, microwave subharmonic generation, transmission reson. expt. 77−20709
Fe multilayer films stability, Mossbauer spectra 80−29651
Fe sputtered film, amorphous, Mossbauer study and electron diffr. obs. 80−75897
Fe thin films, surface demagnetisation due to chemisorption, ferromagnetic reson. study 80−80616
Fe thin layers, vacuum coated on PMMA, mag. behaviour during mech. stress cycles *(German)* 80−80581
Fe, transverse Kerr magneto-optical effect enhancement by surface magnetoplasma waves 77−52056
Fe, ultra-thin Mossbauer spectroscopic studies of mag. props. 80−44970
Fe, ultrathin film, mag. hyperfine field, temp. and thickness depend. 78−39478
Fe-Al (30 or 45 at.%), elec. resist. and magnetoresist., atomic ordering effects *(Russian)* 77−80853
Fe-B, amorphous, mag. annealing behaviour 79−73782
Fe-B, sputtered amorphous film, strong stripe domains, Kerr effect obs. and theory 79−91265
Fe-B ferromag. film, props. 79−4709
Fe-B-Cr(Si) thin film glasses, mag. props. and corrosion resist. 80−80576
Fe-based oxide film, phase comp., thermal analysis 77−51928
Fe-c, Fe-Si-B, and Fe-Cr-P-C sputtered amorphous films, mag. props. and corrosion resist. 79−28567
Fe-Co, magnetisation induced uniaxial anisotropy, dislocations effects 78−43618
Fe-Co (46%), evaporated, uniaxial mag. anisotropy 77−51929
Fe-Co film, magnetisation induced uniaxial anisotropy 77−48016
Fe-Co films, ordered and disordered, Mossbauer study 79−24241
Fe-Co-Cr film RF sputtering for magnetic recording 80−2947
Fe-Co-Si-B sputtered amorphous thin film, coercivity, galvanomagnetic props., resistivity 80−29578
Fe-Cu metastable dil. alloy film, hyperfine interactions 78−52398
Fe-Gd, amorphous, mag. props., mean field analysis 78−64236
Fe-Gd, amorphous, O_2 contamination effects on mag. props. 78−64231
Fe-Gd amorphous film, struct. and mag. props. 80−20439
Fe-Gd amorphous films with comp. gradient, volume and surface hysteresis *(Russian)* 78−88148
Fe-Gd(Tb), magneto-optic coeff. and refr. index, ellipsometric determ. 80−71501

magnetic thin films continued
Fe-Ge amorphous films, conversion electron Mossbauer spectra, mag. moments 77−16231
Fe-La(Zr) amorphous films, mag. props., Mossbauer effect and magnetisation meas. 79−69701
Fe-Ni, amorphous, martensite form. time and struct. 80−104159
Fe-Ni, electrodeposition, mag. props. *(French)* 78−64488
Fe-Ni, electrolytic film, coercive force depend. on electroplating conditions *(French)* 77−55691
Fe-Ni, ferromagnetic films, domain boundary creep relaxation effects *(Russian)* 79−82840
Fe-Ni, mag. and struct. props., effect of O_2 partial press. during deposition 79−90903
Fe-Ni, vacuum-deposited, internal stresses, thickness and comp. effects *(Russian)* 77−80713
Fe-Ni evaporated films with perpendicular anisotropy, magnetoresistance obs. 78−2585
Fe-Ni film, $\alpha \rightarrow \gamma$ transition, Mossbauer effect *(Russian)* 77−40154
Fe-Ni film, electrodeposited, struct. and mag. props. 80−107668
Fe-Ni films, dynamic domains and pulse mag. reversals *(Russian)* 79−28571
Fe-Ni films, lattice constants rel. to mag. moments *(Russian)* 77−32218
Fe-Ni films, scatt. of homogeneous spin waves by anisomeric oriented plane, ferromag. reson. 78−19336
Fe-Ni/Fe, bimetal film, exchange const. determ. from hysteresis loops *(Russian)* 77−48015
Fe-Ni/pure Fe exchange coupled films, mag. reversals, hard layer thickness effects *(Russian)* 78−56359
Fe-Ni-Co film, electron-nucl. mag. reson. 78−35063
Fe-Ni-Co foils, mag. reversals of mag. domains in low-coercivity channels *(Russian)* 79−42813
Fe-Ni-Cr, ferromag. reson. meas. *(Russian)* 77−1601
Fe-Ni-Cr, vapour-deposited film, effect of condensation temp. on form. of metastable phases and mag. props. 79−65700
Fe-Ni-Cr vapour deposited film metastable phase formation *(German)* 78−38984
Fe-P, amorphous, ion implanted, struct. and domain struct. obs. 79−91272
Fe-P electrodeposited foil, amorphous, mag. domains 80−75821
Fe-Sb amorphous films, Mossbauer effect study 80−75896
Fe-Si, amorphous, magnetostriction, anisotropy 77−1575
Fe-Si amorphous film, crystallisation, Mossbauer studies 80−33900
Fe-Si amorphous film, struct. and crystallisation, Mossbauer study 80−11300
Fe-Si amorphous films, mag. and magnetoelastic props. 79−99746
Fe-Si ferromag. film, props. 79−4709
Fe-Si film, amorphous, conversion electron Mossbauer study 78−84507
Fe-Si-Al, Sendust, 12 μ thick film prep. by sputtering, mag. and other props. 77−55888
Fe-Si-Al Sendust alloy ribbon form, rapid quench prepared, elec. cond., coercive field, permeability 79−83151
Fe-Si-B amorphous films, mag. props. 80−34710
Fe-Si-Cr, sputtered,corrosion reduction, effect of Cr obs. 80−80573
Fe-SiO multilayer film, interface magnetisation 80−7135
Fe-Y(Lu) amorphous films, mag. props., Mossbauer effect and magnetisation meas. 79−69701
$Fe_{1-x}B_x$ film, optical and magneto-optical characts., mag. preps. 79−82956
$Fe_{80}B_{20}$, sputter deposited amorphous, low field mag. props. 78−68335
Fe_xC_{1-x} amorphous sputtered film, mag. props. 78−68311
FeCoB, corrosion-resistant amorphous mag. thin films 80−54923
$Fe_{0.5}Co_{0.5-x}Cr_x$ films, vacuum-deposited cryst. and mag. struct. *(Russian)* 80−93081
$(Fe_xCo_{1-x})_{100-y}(Si_{0.4}B_{0.6})_y$ amorphous alloy zero magnetostrictive, mag. props. 79−99743
FeGd, H_2 and N_2 contaminated amorphous films, mag. props. 79−1690
Fe_xGd_{1-x}, $0.5>x>0.65$, amorphous film, FMR, spin wave spectra 77−16181
Fe_xGe_{1-x}, amorphous, FMR meas. of mag. props., temp. and comp. depend. 77−69636
Fe_xGe_{1-x} amorphous film, low temp. conversion electron Mossbauer spectroscopy 78−48101
Fe_xGe_{1-x} amorphous film, XPS and Mossbauer exam. 79−56577
α''-$Fe_{16}N_2$ film, mag. mechanism, at. mag. moment *(Korean)* 79−7973
$Fe_{1-x}Ni_x$ ($x<29$at.%), γ-phase dispersion, Mossbauer spectra 78−52399
$(Fe_{1-x}Ni_x)_{80}B_{20}$ amorphous soft magnetic films 79−82836
$Fe_{40}Ni_{40}C_{14}P_6$ amorphous film, dislocation and mag. struct., neutron diffr. study 80−70956
Fe_2O_3 amorphous film, Mossbauer spectra, mag. props. 80−15851
Fe_2O_3 amorphous RF sputtered thin films, Mossbauer and mag. study 80−34711
Fe_2O_3 amorphous thin films, Mossbauer and magnetisation data 80−34712
β-Fe_2O_3, CVD and characterisation 77−44172
α-Fe_2O_3 film, prep. by reactive condensation and mag. props. 78−64241
β-Fe_2O_3, hyperfine interactions below and above mag. ordering temp., Mossbauer obs. 77−69745
Fe_3O_4 film, prep. by reactive condensation and mag. props. 78−64241
Fe_3O_4, film, quantitative sputter rates, AES, ellipsometry determ. 78−72661
Fe_3O_4, magnetite, coercive force and lattice const. 78−2707
Fe_3O_4, spherulitic film growth, elec. and mag. props. 78−68627
$Fe_{1-x}Pd_x$ film, UHV deposited, effects of applied stress on B-H loops 78−64239
$Fe_{1-x}Pd_x$ films, vacuum deposited, mag. and corrosion props. 79−56574
FeSb alloy films, vapour-deposited, formation of metastable phase 80−44437
$Fe_{1-x}Si_x$ film, optical and magneto-optical characts., mag. preps. 79−82956
Fe_xSi_{1-x} amorphous alloys, magnetisation meas. showing crit. conc. at $x=0.4$ 77−59429
Fe_xSi_{1-x}, amorphous film, magneto-optic Kerr effect 80−66158
$Fe_{76}(Si_{0.5}B_{0.5})_{25}$, amorphous, sputtered, thermal stability 78−76280
Fe_xSn_{1-x} amorphous alloy films, magnetisation meas. and Mossbauer spectra 78−95489
Fe_xSn_{1-x}, amorphous film, struct. and mag. props. 80−65972
FeTiB, corrosion-resistant amorphous mag. thin films 80−54923
$Fe_{0.85}V_{0.15}$, ^{51}V NMR, spin echo expts., 77 and 300K 77−69728
$(Gd,Tm,Y)_3(Ga,Fe)_5O_{12}$, bubble domain gradient propag., elliptical distortion and bias compensation 78−19292

magnetic thin films continued
Gd film, magnetoelastic excitations, phonon spectroscopy and forbidden transitions 79−82853
Gd-Ag, vap. quenched alloys, struct. and mag. props. 78−84461
Gd-Ag (0-16 at.%), vapour-quenched, struct. and mag. props. 78−38980
Gd-Ag(Cu) alloy film, amorphous, struct. and mag. props. 78−52318
Gd-Al sputtered amorphous films, spin glass state 77−66393
Gd-Al(Cu), amorphous alloy films, mag. phase diagram, spin glass and ferromag. regions 78−68234
Gd-Co, amorphous, Ar sputtered, struct. 78−63946
Gd-Co, amorphous, for bubble device appl., prep. and perpendicular anisotropy 77−69641
Gd-Co, amorphous, inverted and biased loops 77−89996
Gd-Co, amorphous, magnetisation and anisotropy meas. 77−8370
Gd-Co, amorphous, magnetisation processes near compensation point 77−40101
Gd-Co, amorphous, perpendicular uniaxial anisotropy, dominant contrib. of preferential resputtering effect 77−36103
Gd-Co, amorphous, phase separation as source of perpendicular anisotropy 78−64244
Gd-Co, amorphous, RF sputtered, prep. and props. 79−1693
Gd-Co, amorphous, selective resputtering-induced anisotropy 78−72376
Gd-Co, amorphous, sputtered very thin film struct. 77−15707
Gd-Co, amorphous, stability of small bits to temp. and mag. field changes 78−68314
Gd-Co, amorphous ferrimagnet, mag. anisotropy, effect of ion bombard. during prep. 79−1692
Gd-Co, amorphous ferrimagnet, anisotropic short range order effects on mag. props. 79−1691
Gd-Co, amorphous film, anisotropy due to resputtering effect 77−89989
Gd-Co, amorphous film, RF sputtering, DC bias role 77−16494
Gd-Co, amorphous film, with cylindrical mag. domains, sputtering prep. *(Russian)* 77−12176
Gd-Co, amorphous films, mag. props. ferromag. reson. meas., 20-520°C *(Russian)* 80−97144
Gd-Co, and Gd-Co-Mo, amorphous, mag. props., annealing effects 78−64235
Gd-Co, and Gd-Co-X (X=Mo, Cu, Au), sputter deposited amorphous alloy, substrate bias, magnetic anisotropy, annealing 78−48006
Gd-Co, bias-sputtered, dipolar mechanisms for mag. anisotropy 78−64233
Gd-Co, evap. amorphous film, mag. props. 77−24720
Gd-Co, evap. amorphous films, anisotropy, magnetisation and FMR meas. 77−66392
Gd-Co, evaporated amorphous film, perpendicular anisotropy by controlled O_2 contamination 77−89990
Gd-Co, evaporated and sputtered, struct. and mag. anistoropy, electron microscopy 79−56578
Gd-Co, LV multitarget sputtered film, substrate bias effect on anisotropy 77−16125
Gd-Co, layer structure, mag. torque and anisotropy 77−63246
Gd-Co, sputtered, inert gas incorporation effect on uniaxial anisotropy 78−64232
Gd-Co, sputtered film, growth induced anisotropy 77−16123
Gd-Co, thermally evap. amorphous film, mag. anisotropy 77−16122
Gd-Co alloy, sputtered film, mag. props. determ. *(Chinese)* 78−2714
Gd-Co amorphous film, DC or RF sputtered, mag. props., He^+-backscatt. investig. 77−20650
Gd-Co amorphous film, mag. anisotropy 77−20649
Gd-Co amorphous film, magnetisation processes near compensation point 77−69644
Gd-Co amorphous film, sputtered perpendicular mag. anisotropy 79−56576
Gd-Co amorphous film, sputtered, perpendicular anisotropy exam. 79−73707
Gd-Co amorphous film, sputtered, FMR spectra 79−73822
Gd-Co amorphous film 80−34725
Gd-Co amorphous films, annealed, short-range order and perpendicular mag. anisotropy 80−15765
Gd-Co amorphous films, correlation between struct. and mag. props. *(Chinese)* 80−54532
Gd-Co amorphous films, mag. anisotropy, static and ferromag. reson. expts. 79−33477
Gd-Co amorphous films, mag. struct., mag. bubbles, electron diffr. study *(Chinese)* 80−71126
Gd-Co amorphous films, preparation by bias sputtering, composition homogeneity 78−72379
Gd-Co amorphous films, RF sputtered, magnetisation ripple effects 80−11232
Gd-Co amorphous films, struct. and mag. anisotropy 80−20438
Gd-Co amorphous sputtered films, magnetoelastic contrib. to perpendicular anisotropy, internal stress meas. 78−95490
Gd-Co amorphous sputtered film, magnetostriction and anisotropy 80−39821
Gd-Co amorphous thin film, mag. and optical props., conc. depend 79−19748
Gd-Co amorphous thin films, crystn. process and domain struct. *(Chinese)* 80−54533
Gd-Co based amorphous sputtered films, microstruct. variability and mag. anisotropy, implanted ion effects 80−88459
Gd-Co film, sputtered from segment target, composition and mag. props. 78−27062
Gd-Co film, temp. depend. of mag. aftereffect *(Russian)* 79−8021
Gd-Co films, amorphous, mag. anisotropy from torque meas. 77−47987
Gd-Co films, anomalous magneto-optical hysteresis loops obs. 77−12174
Gd-Co rare earth-transition metal alloy, influence of gaseous phase on mag. props. *(Polish)* 80−39820
Gd-Co sputtered amorphous films, resistivity anomalies, 42 to 300K *(Chinese)* 80−7001
Gd-Co sputtered films, preparation process, props. 77−59688
Gd-Co-Au amorphous magnetic films, domain wall obs. by Lorentz electron microscopy 77−80979
Gd-Co-Cu amorphous, influence of biased magnetron deposition parameters on props. 77−43856
Gd-Co-Fe, amorphous, bias-sputtered, uniaxial perpendicular anisotropy 78−64234
Gd-Co-Mo, amorphous, Ar sputtered, struct. 78−63946
Gd-Co-Mo, amorphous, bubble and stripe domain wall vel. meas. 77−40094
Gd-Co-Mo, amorphous, in-plane susceptibility near compensation point 78−64238

magnetic thin films continued
- Gd-Co-Mo, amorphous, mag. props., ion implantation damage effects 77−89991
- Gd-Co-Mo, amorphous, sputtered very thin film struct. 77−15707
- Gd-Co-Mo, amorphous mag. bubble dynamics 77−89997
- Gd-Co(-Au) amorphous film, domain wall dynamics near compensation point 79−1696
- Gd-Co(-Au) film, ferrimag. amorphous, coated with Permalloy films, mag. props. 79−1695
- Gd-Co(-Mo), amorphous, inhomogeneities of mangetization and anisotropy 79−65698
- Gd-Co(Fe) amorphous films, microstruct. and mag. anisotropy 79−82838
- Gd-Cu sputtered amorphous films, ferromag. props. 77−66393
- Gd-Fe, amorphous, in-situ ion beam sputtered, microstruct. and Lorentz mag. struct. 78−63947
- Gd-Fe, amorphous, mag. props., annealing effects 78−64235
- Gd-Fe, amorphous film, Kerr readout characts. 79−15439
- Gd-Fe, amorphous film, stress induced anisotropy 77−89989
- Gd-Fe, amorphous film, thermomagnetic writing 78−84428
- Gd-Fe, amorphous sputtered film, magnetostriction 79−47320
- Gd-Fe, co-evap. amorphous film, anomalous hysteresis loop, domains obs. 77−89995
- Gd-Fe, DC bias RF sputtered film, mag. props. 77−16124
- Gd-Fe, LV multitarget sputtered film, substrate bias effect on anisotropy 77−16125
- Gd-Fe, sputter deposited amorphous alloy, substrate bias, magnetic anisotropy, annealing 78−48006
- Gd-Fe alloy, amorphous, contact printing 77−73061
- Gd-Fe amorphous film, atomic diffusion of deposited Co 79−73346
- Gd-Fe amorphous films, anisotropy dispersion, FMR meas. 79−73824
- Gd-Fe amorphous films, stress contrib. to perpendicular anisotropy 80−75819
- Gd-Fe amorphous films with CeO_2 coatings, Kerr magneto-optical effect enhancement 79−19866
- Gd-Fe amorphous sputtered films, magnetoelastic contrib. to perpendicular anisotropy, internal stress meas. 78−95490
- Gd-Fe rare earth-transition metal alloy, influence of gaseous phase on mag. props. *(Polish)* 80−39820
- Gd-Fe-Y, amorphous film, thermomagnetic writing 78−84428
- Gd-Fe(Co) amorphous films, O_2 adsorption, effect on perpendicular anisotropy 80−34713
- Gd-Fe(Co) film, amorphous, preferential resputtering effect induced anisotropic distrib. of atomic pairs 78−63950
- Gd-Mo-Mo amorphous film, domain drag effect obs. 78−91911
- Gd-Ti(V)(Cr)(Mg)(Nb)(Ge)(Si)(Au) amorphous films, spontaneous Hall effect and elec. resist. 80−80251
- Gd-transition metal, amorphous film, galvanomag. effects, Hall detector 77−89882
- $Gd_{0.37}Al_{0.63}$, amorphous, spin-glass order parameter meas. 77−28396
- $Gd_{0.37}Al_{0.63}$, amorphous film, anomalous resonance field shift 79−73821
- $Gd_{0.37}Al_{0.63}$ sputtered film, amorphous, conc. spin glass, microwave reson. spectrum obs. 78−15018
- GdCo, amorphous, for thermomagnetic recording *(Japanese)* 80−11562
- GdCo, amorphous, sputtered, in-plane anisotropy induced by rare gas annealing 78−84458
- GdCo, amorphous film, MCD *(Japanese)* 78−39530
- GdCo amorphous film, O_2 contaminated, TEM obs. of source of perpendicular anisotropy 78−14993
- a-GdCo film, magneto-optical Kerr effect spectra 77−12458
- GdCo film structure, dependent on substrate type *(Russian)* 80−24747
- GdCo, sputtered amorphous, incorporation of Ne, Ar and Kr 77−44163
- GdCo sputtered amorphous film, third elements effect on mag. anisotropy 79−91260
- $Gd_{1-x}Co_x$, amorphous, Curie and compensation temps., effect of O or Ar impurity 77−40093
- $Gd_{1-x}Co_x$ amorphous thin film, magnetostriction 79−91281
- $Gd_{1-x}Co_x$, film, resistivity, Hall effect, domain wall density 78−76169
- $Gd_{25}Co_{75}$, amorphous film, low field magnetoresist. and domain drag 78−68014
- Gd_xCo_{1-x} annealing amorphous film, ferromag. reson. 77−85580
- $(Gd_{1-x}Co_x)_{1-y}Ar_y$ amorphous mag. film, elec. and mag. prop. depend. on Ar 80−80410
- $(Gd_xCo_{1-x})_{1-y}Ar_y$ amorphous films, effective anisotropy field, ferromag. reson. obs. 80−71123
- GdCoAu amorphous film, bias field depend. of domain drag propagated bubble domains 79−78471
- a-GdCoAu(Mo) films, perpendicular anisotropy temp. depend., Lorentz microscopy 77−28419
- GdCoMo amorphous alloy films, susceptibility, uniaxial anisotropy field 80−54930
- GdCoMo film, amorphous, sputtered, ferrimag., in-plane susceptibility near compensation point 78−64240
- GdCoMo, sputtered amorphous, incorporation of Ne, Ar and Kr 77−44163
- $Gd_{6.9}Co_{74.0}Mo_{12.8}Ar_{6.3}$, amorphous film, spin wave reson. 79−73823
- Gd_xCu_{1-x}, amorphous film, magnetisation meas., fully aligned moment 78−68309
- GdFe amorphous film, Mossbauer and mag. meas. 80−15844
- GdFe film structure, dependent on substrate type *(Russian)* 80−24747
- GdFe homogeneous amorphous films, compensation point switching, magneto-optical Kerr signal anal. 80−15726
- $GdFe_2$ films, electron beam deposited, amorphous and cryst., mag. and struct. props. 79−4710
- Gd_xFe_{1-x} film, mm-wave ferrimag. reson. using optically pumped waveguide laser source 77−55710
- $(Gd_{1-x}Fe_x)_{1-y}Bi_y$ amorphous films, saturation magnetisation, Kerr and Faraday rotation 80−40093
- GdFe(Co), amorphous film, XPS meas. 79−87295
- $Gd_x(Fe_{1-y}Co_y)_{1-x}$, evap. amorphous film, mag. anisotropy due to pair ordering 77−32219
- $Gd_{18}Fe_{82-x}Ni_x$, amorphous film, mag. and galvanomag. props. 77−24715
- $(Gd_{1-y}Nd_y)_{1-x}Fe_x$ amorphous bubble films with good temp. characts. 79−95616
- Gd_xNi_{1-x} sputtered amorphous films, mag. props. and Hall meas. 78−95488
- $Gd_{0.9}YTm_{1.1}Ga_{0.44}Fe_{4.56}O_{12}$, ion implanted, ferromag. reson. meas. 78−68385
- Ge-Fe amorphous film, sputtered, stress induced anisotropy 79−73706
- Ge-Se-Fe films, metallic and semicond., amorphous, mag. and elec. props. 78−52319

magnetic thin films continued
- Ho, helimag. order, surface deform., exchange and single-ion magnetocrystalline anisotropy energy 77−66390
- Ho-Co, evaporated, struct. and mag. anistoropy, electron microscopy 79−56578
- Ho-Co amorphous film, anomalous Hall hysteresis loops near compensation point 78−19286
- HoCo amorphous, sputtered, in-plane anisotropy induced by rare gas annealing 78−84458
- Ho_xCo_{1-x} amorphous films, microstruct. and mag. anisotropy 79−82838
- Ho_xCu_{1-x}, amorphous film, magnetisation meas., local anisotropy effects 78−68309
- La-Fe, amorphous alloy film, spin reson. meas. 78−68389
- La-Fe alloy, amorphous, sputtered at high rate, mag. props. 80−75753
- $(LaTmCa)_3(Fe_{5-x}Ge_x)O_{12}$ film, high g, for mag. bubble applics. 77−85529
- Li ferrite film, magnetic circular and linear dichroism, temp. depend. 79−69815
- Lu-Fe, amorphous alloy film, spin reson. meas. 78−68389
- $Lu_{3-x}Ca_xFe_{5-x}Si_xO_{12}$ film on $Ca_3Ga_2Ge_3O_{12}$, mag. bubble props. 77−28418
- LuTb garnet, scratch-modified mag. domain patterns 78−48007
- MgMn ferrite, magnetostriction const., mag. saturation, and internal stresses *(Russian)* 77−16126
- α-Mn, low temp. resist., rel. to deposition conditions 79−78223
- Mn-Bi, amorphous, form. and crystn. 79−28923
- Mn-Bi, film, low field magnetoresist. and domain drag 78−68014
- Mn-Bi, magnetically uniaxial, strongly anisotropic, discontinuous mag. reversal singularities *(Russian)* 77−48010
- Mn-Bi, negative transverse magnetoresist. in c-plane, domain wall effects 77−20465
- Mn-Bi, perpendicular anisotropy film, galvanomag. props., hysteresis loops 77−20464
- Mn-Bi magneto-optic memory system 77−85511
- Mn-Cu-Bi ternary cpd. thin films for magneto-optic memory applic. *(Japanese)* 77−63238
- Mn-Cu-Ni-Bi, magneto-optic film for storage appl. 77−12165
- MnAlGe film, mag. domains and amorphous to cryst. phase transition, electron microscopy obs. 80−71129
- MnBi, ferromag., diffr. efficiency of mag. holograms, Faraday effect 77−32355
- MnBi film anisotropy field intensity meas. by Faraday rotation *(Russian)* 77−12162
- MnBi films, prep. by ionised-cluster beam deposition technique, magnetooptical props. 80−100790
- MnBi films, stability of magneto-optical props. on pulse heating *(Russian)* 78−88282
- MnBi, fine mag. domains. SEM obs. 79−24202
- MnBi, ionized-cluster beam and reactive ionized-cluster beam deposition 80−16202
- MnBi magnetic film, method for recording holograms of diffusely scattering objects 78−74862
- MnBi, magnetic hologram recording appl. *(Russian)* 77−1573
- MnBi, magnetic reversal mechanism, hysteresis loops for polycryst. and single cryst. specimens *(Russian)* 78−60318
- MnBi, on Al_2O_3, quantitative electron microprobe analysis 77−9150
- MnBi, optical, magneto-optical and struct. props. 77−1664
- MnBi, optical radiation spectral conversion 79−64344
- MnBi, struct. and mag. props. 79−47315
- MnBi-Bi garnet film struct., thermomagnetic recording 80−100588
- $Mn_{2-x}Cr_xSb$ film, prep. and mag. props. 78−48009
- MnCuBi, coated with SiO layer, Kerr readout characts. 77−85509
- MnCuBi, for mag. storage appl., prep. by RF sputtering and props. 77−8369
- $MnCu_{1-x}Dy_xBi_{0.86}$, mag. and magneto-optical props., appl. as storage medium 77−8550
- $Mn_{1-x}Cu_xSb$ film, ferromag. reson. 78−31114
- $MnFe_2O_4$, bulk and surface spin waves, spin wave reson. expts. 79−73826
- $Mn_xFe_{3-x}O_4$ ferrite film, exchange interaction depend. on conduction electrons *(Russian)* 80−34621
- $Mn_xFe_{3-x}O_4$, spin wave reson., exchange const. 77−16183
- MnGaGe film, mag. domains and amorphous to cryst. phase transition, electron microscopy obs. 80−71129
- $Mn_xPd_{82-x}Ge_{18}$, amorphous alloys, mag. props. 78−91906
- MnPt, disordered film produced by RF sputtering, ferromag. behaviour 78−68310
- $MnSb_{1-x}Sn_x$ films, Faraday rotation, optical absorpt. coeffs. 80−97242
- $Mn_{0.75}Ti_{0.25}Bi$ films as magnetooptic storage medium, mag. interferogram recording 78−19288
- NI, chemisorption of H_2, isothermal desorption near Curie temp., rate meas. 80−29268
- Nd-Co film, amorphous, exam. of domain struct. 78−68336
- $Nd_{0.35}Co_{0.65}$, vacuum evaporated, magnetisation ripple struct., TEM and defocused Lorentz microscopy 80−7136
- Nd_xCo_{1-x} film, amorphous, mag. props. meas. 78−68312
- Nd_xFe_{1-x} film, amorphous, mag. props. meas. 78−68312
- Ni, 618 MHz SAW attenuation rel. to mag. field 77−40110
- Ni (001) film, self consistent calc. of surface phenomena 79−73560
- Ni (100) films, spin density by self-consistent linear APW method 80−65710
- Ni alloys, magnetic props. at freq. up to 1 MHz *(Russian)* 77−8330
- Ni, amorphous film, getter sputtered at 25K, resistivity, Curie temp. 78−52673
- Ni, and its alloys, spin polarised tunnelling expts. 78−39372
- Ni and Ni alloys, tunnel currents, spin polarisation, simple band theory interpretation 79−78451
- Ni, atomic layers, Pauli paramagnetism to band ferromagnetism transition thickness depend. 78−72377
- Ni, density of states, photoemission expts. above and below T_c, rel. to magnetism model 77−20536
- Ni, effect of He ion implantation on domain struct., Lorentz electron microscopy 77−20654
- Ni electrodeposit, mag. domain struct., neutron depolarisation 78−2716
- Ni, electrodeposited film, saturation magnetisation and perpendicular anisotropy meas. 78−76277
- Ni, electrodeposited film, thermal anal., occlusion of gases rel. to mag. props. 80−59823
- Ni electrodeposits on (001)Cu films, growth and mag. anisotropy 79−42810

magnetic thin films continued
Ni, electroplated layers, internal friction and ΔG effect, rel. to bath comp. and annealing 78−19296
Ni, evaporated, effect of CO adsorption on galvanomag. and mag. props. 79−33363
Ni, evaporated, effect of CO adsorption on galvanomag. and mag. props. 79−33364
Ni, evaporated, for use as variable delay SAW device, magnetostrictive effects 80−71144
Ni, evaporated, galvanomag. props., oscill. due to CO adsorption 77−1496
Ni, evaporated, uniaxial mag. anisotropy 77−51929
Ni, evaporated at oblique incidence, residual stress, mag. anisotropy meas. 78−22992
Ni, even magneto-optical transmission effects, 0.4-1.25 μm 77−32354
Ni, ferromag. film, ion plating prep., coercive force and magnetoresist. 77−12546
Ni, ferromag. film, magnetoresistance parameter meas. *(Spanish)* 80−2485
Ni, ferromag. film, surface states, surface magnetisation and electron spin polarisation 80−65648
Ni, few atomic layers thick, transition from Pauli paramag. to band ferromag. 80−44885
Ni film, adsorbed $H_2(CO)$, ferromag. reson. exam. 78−15028
Ni film, C ion implanted, HCP struct. formation, electron diffr. study *(Russian)* 79−82469
Ni film, CO adsorption effect on galvanomagnetic and magnetic props. 78−43490
Ni film, chemisorption induced mag. dead layers, ferromag. reson. obs. 79−91261
Ni film, effects of finite size on crit. phenomena, resistivity anomaly 79−38192
Ni film, evaporated, galvanomag. and mag. props. 78−23180
Ni film, ferromag., light scatt. from surface acoustic spin waves 79−33719
Ni film, ferromag. reson., thermodynamical anal. 79−42840
Ni film, ferromagnetic (100) and (110), energy bands 79−1630
Ni film, ion beam sputtering prep., struct. and mag. props. 80−35085
Ni film, low-angle grain boundary struct. *(Russian)* 79−42807
Ni, film, mag. susceptibility correlation with SAW attenuation 79−47310
Ni film, magnetoelastic excitations, phonon spectroscopy and forbidden transitions 79−82853
Ni film, microstructure of charged boundary between ferromag. domains 79−69705
Ni film, multi- and single-layer, reson. curves subjected to tangential mag. reversals *(Russian)* 80−50195
Ni film, polycrystalline, resist., conduction electrons and s-d exchange interaction 78−19021
Ni film, RF sputtered on $LiNbO_3$, SAW delay variation obs. 79−56102
Ni film, single cryst., domain width from ferromag. reson. 80−39879
Ni film, spin wave resonance 79−33542
Ni film, strained and strain-free, ferromag. reson. meas. 78−95525
Ni film, surface magnetisation, electric field effect 78−14991
Ni film, thickness dependence of perpendicular mag. anisotropy 77−80974
Ni film, two-dimens. ⟨110⟩ domain wall 77−69648
Ni film (111), ferromag., energy bands and planar densities of states, LCAO calc. 79−4509
Ni films, Faraday rotation effect dispersion 80−40092
Ni films, ferromagnetic reson., photoacoustic detection 80−80613
Ni, granular, tunnelling of spin-polarised electrons and magnetoresist., exchange effects 77−12024
Ni, influence of H chemisorpt. on magnetism, ferromag. reson. spectroscopy 77−66395
Ni, linear mag. birefr. dispersion 77−69807
Ni, mag. field depend. surface acoustic wave attenuation meas. 77−20674
Ni, mag. structures and stresses, ferromag. resonance 78−72375
Ni, magnetooptic Kerr effect meas. near crit. point 77−69811
Ni, plated film, magnetisation and mag. interface anisotropy 77−85510
Ni, platelet, transmission reson. meas. 77−20710
Ni, surface magnetoplasma waves, ATR meas. 77−69639
Ni, temp. depend. of magneto-optical effects 77−81167
Ni, thin films, surface demagnetisation due to chemisorption, ferromagnetic reson. study 80−80616
Ni, transverse Kerr magneto-optical effect enhancement by surface magnetoplasma waves 77−52056
Ni, vacuum deposited on liquid-He-cooled sapphire, galvanomag. props. 79−95519
Ni-alloys, spin polarised tunnelling 78−95494
Ni-Au, amorphous, ferromagnetic, anomalous Hall resist. 77−15832
Ni-Au, amorphous, magnetoresist., in fields up to 80 kG 77−39823
Ni-B alloy film, magnetisation-temp. characts., order-disorder transform. *(Japanese)* 78−76279
Ni-B electroless-plated amorphous films, anomalous mag. temp. characts. 80−96757
Ni-B thin film glasses, mag. props. and corrosion resist. 80−80576
Ni-Co, ferromag. films, magnetoresistance effect, crystal struct. 78−68017
Ni-Co, magnetisation induced uniaxial anisotropy, dislocations effects 78−43618
Ni-Co, platelets, FMR field and linewidth, room temp. 77−4563
Ni-Co film, magnetisation induced uniaxial anisotropy 77−48016
Ni-Co film, spin wave resonance 79−33542
Ni-Co film, spin-wave reson. exam. 78−2746
Ni-Co thin films, spin-wave reson. obs., exchange stiffness const. 80−44924
Ni-Co-P, amorphous electrodeposited films, domain wall motion, Kerr effect 78−60322
Ni-Co-P, ferromag. film, amorphous to cryst. transition, diffr. and resistivity meas. 78−60587
Ni-Co(Fe) film, anal. of main component by atomic absorpt. spectrophotometry 77−70381
Ni-Cr thin film production by HF cathode sputtering *(Bulgarian)* 79−19992
Ni-Fe, Barkhausen noise spectra meas. 77−16131
Ni-Fe, differential susceptibility, struct. const. and losses 79−91271
Ni-Fe, electrodeposition, role of buffers and anions 80−25583
Ni-Fe, film, anomalous Hall and Nernst-Ettingshausen effect, contribution of phonon and impurity scatt. *(Russian)* 78−64145

magnetic thin films continued
Ni-Fe, film, domain struct., effect of biaxial stresses 78−88153
Ni-Fe, film, magnetisation induced uniaxial anisotropy, substrate temp. depend. 77−8367
Ni-Fe, Kerr magnetooptic effect, appl. to waveguide type optical modulator, theory 77−11015
Ni-Fe, low field domain wall mobility 80−25167
Ni-Fe, magnetisation reversal magnetoresistance meas. 77−16132
Ni-Fe, relax. effects in domain boundary creep *(Russian)* 77−24723
Ni-Fe (15%), evaporated, uniaxial mag. anisotropy 77−51929
Ni-Fe (20 wt.%), thin film ferromagnetic band, magnetisation under domain creep conditions *(Russian)* 79−91262
Ni-Fe alloy, extraordinary viscous magnetic wall motion 78−84465
Ni-Fe film, domain struct., uniaxial stress effects 78−10740
Ni-Fe film, effect of tensile stress on mag. domain struct. 78−68332
Ni-Fe film, ferromag. reson. under weak influence of eddy currents *(German)* 77−8412
Ni-Fe film, mag. and hyperfine field exam. of uniaxial anisotropy 77−66391
Ni-Fe film, thermally activated domain wall motion 80−88777
Ni-Fe film, unidirectional anisotropy by exchange coupling, appl. to biasing of magnetoresist. read head 78−91907
Ni-Fe films, coercivity control for single-level masking bubble devices using surface modification and intermediate layers 79−51816
Ni-Fe films, energy change of Bloch wall with angle to easy axis, calc. *(Slovak)* 80−103863
Ni-Fe films, in state of undersaturation in perpendicular fields, micromagnetic struct. *(Russian)* 79−61193
Ni-Fe films, magnetisation reversal in narrow strips, TEM study 80−34720
Ni-Fe films, US generation by ferromag. reson. 78−88155
Ni-Fe films, viscous magnetic domain wall motion anal. 79−95617
Ni-Fe multilayered films, mag. domain structures 79−82847
Ni-Fe narrow stripes, mag. props. and domain struct. 79−82843
Ni-Fe overlay, influence on bubble device performance 79−78466
Ni-Fe oxidised film, extraordinary viscous wall motion at extreme vel. 78−14997
Ni-Fe oxidised films, easy-axis switching 79−91266
Ni-Fe/Mn interface, mag. surface effects, dead layers and exchange anisotropy 77−24718
Ni-Fe-Co, domain wall energy meas., by domain tip propagation method 77−55692
Ni-Fe-Co, magnetoelastic vibr. generation during high freq. mag. reversals *(Russian)* 78−60320
Ni-Fe-Co, nonmagnetostrictive, mag. props., effect of deposition parameters of Al underlayer 77−77078
Ni-Fe-Co (17,3 wt.%), thin film ferromagnetic band, magnetisation under domain creep conditions *(Russian)* 79−91262
Ni-Fe-Co alloy, for logic devices, mag. switching vel. anisotropy field and coercive force *(Korean)* 77−51930
Ni-Fe-Co films, nonmagnetostrictive, magnetoresistance effects 78−35013
Ni-Fe-Co films, saw tooth domains investigated 78−14994
Ni-Fe-Co(Mo) films, anal. of main component by atomic absorpt. spectrophotometry 77−70381
Ni-Fe-Cr film, hysteresis loop meas. using magnetooptical system 79−69707
Ni-Fe-Cr soft magnetic film plating bath 79−43465
Ni-Fe-Ho film strips, domain struct. and new rot. processes 77−85533
Ni-Fe-Pd thin films, mag., surface and corrosion props. 80−34707
Ni-Fe-Rh, magnetic and corrosion props. 80−34702
Ni-Fe(Cr) alloy, electron spin polarisation, meas. using supercond. tunnel junction 77−69637
Ni-$LiNbO_3$, layered structure, mag. control of surface elastic waves 77−20666
Ni-Mn alloy, heat treatment influence obs. *(German)* 77−56118
Ni-P, amorphous, ion implanted, struct. and domain struct. obs. 79−91272
Ni-P, amorphous, NMR expts. and interpretation 79−8060
Ni-P, electrodeposited film, thermal anal., occlusion of gases rel. to mag. props. 80−59823
Ni-P electrodeposit, magnetisation coercivity and magnetostriction 78−68338
Ni-S, electrodeposited film, thermal anal., occlusion of gases rel. to mag. props. 80−59823
Ni-SiO multilayer film, interface magnetisation 80−7135
Ni-Ti(Mn)(Cu), tunnelling electron spin polarisation 77−73058
NiFe film, domain wall mass and relax. time from forced oscills. 80−71133
NiFe film, ferromag. reson., thermodynamical anal. 79−42840
NiFe film, sputtered, physical props. 79−77938
NiFe film, stationarity and behaviour of Barkhausen noise 79−24198
NiFe, film deposition, sputter gun system, bubble device appls. 77−12532
NiFe, pulse switching at low temp. 80−103868
NiFe, single and multilayer thin films, strip domains, inplane magnetisation 80−103866
NiFe stripes, mag. props. and domain struct. 80−44886
NiFe thin films, magnetoresistance, quasi-static characts. 80−107766
NiFe-Ho film strips, curling-type mag. domains 77−48020
$Ni_{0.83}Fe_{0.17}$ films, reson. oscills. of mag. domain walls and Bloch lines, stroboscopic electron microscopy 80−54931
$Ni_xFe_yCr_{1-x-y}$ films, struct., mag. props., and corrosion resist. 80−34706
$NiFe_2O_4$ epitaxial film on NdGG, structural and ferromagnetic reson. meas. 77−1574
NiO, thin films with spinel-type defect structure, FMR study 80−39877
NiS, electrolytically deposited, mag. props., S content influence 80−44884
Ni(100) platelet surface optical and magneto-optic consts. 78−15151
$PbFe_{12}O_{19}$ hexagonal ferrite amorphous films for mag. bubble memories, materials review *(Polish)* 80−34715
Permalloy, domain struct., influence of planar anisotropy 79−78472
$(PrGdYb)_{3-x}Bi_x(FeAl)_5O_{12}$ system, LPE growth and magnetooptical props. 79−65842
$SmCo_5$ films, struct. transformations effect on coercive force and mag. reversal *(Russian)* 80−20436
$SmCo_5$ hydride films, mag. props. 78−68306
$SmCo_5$, mag. domains structure rel. to crystal defects, electron microscopy 80−103856
$SmCo_5$ thin film, hydride form., kinetics, mag. monitoring 80−35571

magnetic thin films continued
SmGa garnet, scratch-modified mag. domain patterns 78−48007
$(SmTm)_3(FeGa)_5O_{12}$, small-bubble appl. 79−82845
$(Sr/Ba)(Fe/Al/Ga)_{12}O_{19}$ solid soln. crystal for hexaferrite layer substrate *(German)* 78−23672
$SrFe_8Al_4O_{19}$, thin film LPE growth and mag. props. 80−80992
(Tb,Dy)-Fe amorphous films prep. by cosputtering, magnetoelastic props. 80−97429
Tb, GHz magnetoelastic wave excitation, field depend. 78−52334
Tb-Fe, amorphous ferrimag. film, thermomag. writing using He-Ne laser 77−12163
Tb-Fe, amorphous ferrimag. film, mag. props. and Curie point writing 77−12164
Tb-Fe, amorphous film, Kerr readout characts. 79−15439
Tb-Fe, amorphous sputtered film, magnetostriction 79−47320
Tb-Fe, undoped and O-doped, amorphous, microstruct. and mag. props. 79−91273
Tb-Fe alloy, amorphous, contact printing 77−73061
Tb-Fe amorphous film, sputtered, stress induced anisotropy 79−73706
Tb-Fe amorphous film, thermomag. contact printing 77−89986
Tb-Fe amorphous magnetic films, domain wall obs. by Lorentz electron microscopy 77−80979
Tb-Fe amorphous thin films, magnetic after-effect, Kerr magneto-optic effect obs. 80−97123
Tb-Fe sputtered films, amorphous, mag. aftereffect due to domain well motion 79−73780
Tb-Ho, helimag. order, surface deform., exchange and single-ion magnetocrystalline anisotropy energy 77−66390
Tb_xCu_{1-x}, amorphous film, magnetisation meas., local anisotropy effects 78−68309
Tb_xFe_{1-x}, amorphous magnetostriction and magnetisation 78−68305
Ti-Permalloy films, interdiffusion, Auger anal. and X-ray diffr. obs., degradation of mag. props. 80−34251
Tm ferrogarnet film, cylindrical mag. domain motions, domain boundary oscills. *(Russian)* 80−71140
W/EuS field emitters, electron emission current depend. on annealing temp., mag. props. 80−16160
$(Y,Ca)_3(Fe)_2(FeGe)_3O_{12}$ film, exchange const., ferromag. reson. meas. 79−8023
$(Y,Eu)_3(Ga,Fe)_5O_{12}$, bubble wall state stability obs. 77−20651
$(Y,Gd,Yb)_3(Fe,Ga)_5O_{12}$ film, magnetisation processes and domain struct. near compensation temp. 78−14996
$(Y,Sm,Ca)_3(Ge,Fe)_5O_{12}$, bubble wall state stability obs. 77−20651
$(Y, Sm, Lu, Ca)_3(Fe, Ge)_5O_{12}:Ne^+$, film, $S=1$ bubbles dynamic props., temp. depend. 77−20658
$(Y,Sm,Lu,Ca)_3(Ga,Ge,Fe)_5O_{12}$, film growth and mag. props. for bubble-memory appl. 79−87297
$(Y,Sm)_3(Ga,Fe)_5O_{12}$ films, growth from melt, growth property control 78−27395
$(Y,Sm)_3(Ga,Fe)_5O_{12}/(Eu,Er)_3(Ga,Fe)_5O_{12}$ double-layer self-biasing garnet films, dynamic behaviour of domain walls 80−34722
Y-Co, amorphous alloy film, spin reson. meas., exchange stiffness 78−68389
Y-Fe, evap. amorphous alloys, thermomag. history effects 77−66389
Y-Sm ferrogarnet *(Russian)* 80−71140
$(YBi)_3Fe_{5-x}Ga_xO_{12}$, ferrimag., splitting of domains into layers 77−28420
$Y_2BiFe_{3.8}Ga_{1.2}O_{12}$, magnetooptic interference of light 77−32458
$Y_2BiFe_{3.8}Ga_{1.2}O_{12}$, film, dynamics of domain walls 78−27065
$Y_2BiFe_5O_{12}$ garnet films, magnetooptical interference 79−28724
$(YBi)_3.(FeGa)_5O_{12}$ film, interaction between Bloch walls and dislocations *(Russian)* 79−61196
$(YCdYbBi)_3(FeAl)_5O_{12}$, cylindrical domain wall vel. anisotropy *(Russian)* 77−59440
YCo_3, amorphous, DC sputtered, easy axis and easy plane magnetisation 78−64237
YCo_3, amorphous, sputtered, in-plane anisotropy induced by rare gas annealing 78−84458
YCo_3 amorphous film, domain struct., influence of planar anisotropy 79−78472
YCo_3 amorphous films, ^{59}Co spin echo study 80−80636
YCo_3 film, amorphous, induced and surface anisotropies, ferromag. reson. and static meas. 77−85507
YCo_3 film, amorphous, impurity like relaxation mechanism 79−73820
$(YErCa)_3(Fe_{5-x}Ge_x)O_{12}$ film, high g, for mag. bubble applics. 77−85529
$(YEuTmCa)_3(FeGe)_5$ bubble garnet films, ion-implanted, mag. susceptibility meas. 79−47311
$(YEuTmCa)_3(GeFe)_5O_{12}$, Bloch loop punch-through in mag. bubbles 77−59437
$(YEuTm)_3(FeGa)_5O_{12}$ film, dynamic props. of bubble domains by high speed photography 80−15771
$(YEuTm)_3(FeGa)_5O_{12}$ garnet film, bubble domain steady state motion on a circle 80−29589
YEuTmGa garnet bubble film, dynamic diffuse wall deform. 80−54927
$(YEuTm)_3(GaFe_5)O_{12}$ ferrite garnet films, mag. bubbles, translational motion, mechanism for inertial effects 80−100606
$Y_{1.57}Eu_{0.78}Tm_{0.65}Ga_{1.05}Fe_{3.95}O_{12}$ film, gradient propagation, overshoot and creep 78−19291
$(YEuYbCa)_3(FeGe)_5O_{12}$ film, mag. σ-bubbles, automation props. 78−88150
$(YEuYbCa)_3(FeGe)_5O_{12}$ film, isolated straight stripe domain dynamic props. 79−33514
$(YEuYbCa)_3(GeFe)_5O_{12}$ bubble film with ion-implanted layer, FMR study 80−2643
YFe_x, $(x\simeq 2)$, magnetoelastic excitations obs. 78−68307
Y_xFe_{1-x} amorphous films, microstruct. and mag. anisotropy 79−82838
$YFeO_3$, mag. bubble stray field distrib. meas. using micro Hall element 77−40097
$YFeO_3$, skew bubbie domains, stripe domains 77−89999
$Y_{1.4}Gd_{0.6}BiFe_{3.8}Ga_{1.2}O_{12}$ film, bistable bubble domains, static, dynamic and optical props. 79−28574
$Y_{2.55}Gd_{0.45}GaFe_4O_{12}$, garnet thin films, magnetisation orientation, temp. depend. 80−71125
$(YGdYbBi)_3(FeAl)_5O_{12}$ ferrite-garnet films, effect of in-plane field on dynamics of domain walls 80−65979
$(YGdYbBi)_3(FeAl)_5O_{12}$ epitaxial garnet film, uniaxial ferromagnet domain struct., phase transition *(Russian)* 80−108044
YIG, Bi-substituted, LPE film, optical absorpt. changes due to impurity incorporation 77−1702
YIG, CVD film, boundary effects, spin wave reson. meas. 79−78447
magnetic thin films continued
YIG, cylindrical mag. domains, translational motion 80−108043
YIG dielectric layered struct. magnetostatic bulk wave steering 80−25166
YIG, exchange interaction constant, from paramag. resonance spectra of spin waves 79−42811
YIG, ferrimag., determ. of freq. of magnetostatic modes 77−36104
YIG, ferromag. film on nonmag. substrate, magnetoelastic wave propag. 79−99744
YIG film, calc. of magnetostatic mode freq. 78−68313
YIG film, domain struct., influence of planar anisotropy 79−78472
YIG film, low field microwave excitations of mag. domain walls 79−78456
YIG, film, magnetoelastic Lamb wave velocity changes, theory 78−91923
YIG film, magnetostatic surface wave propag. 79−4661
YIG film, magnetostatic forward volume wave excitation 79−82775
YIG film, magnetostatic surface and forward volume wave oblique incident at shallow groove 80−34704
YIG film, magnetostatic surface wave propag. in nonuniform mag. field 80−80574
YIG film, oblique incidence of magnetostatic waves on metallic grating 78−19229
YIG film, periodically corrugated, insertion loss, reson. linewidth effect 80−80614
YIG, film, spin-wave spectra in terms of mag. boundary conditions 79−78532
YIG film, surface pinning parameter, symm. props. 79−28570
YIG film tangentially magnetised, magnetostatic surface wave excitation 80−29586
YIG film-dielectric layer-conductor struct., magnetostatic bulk wave propag. dispersion relations 80−54925
YIG films, deposition by DC sputtering from two facing targets 78−31341
YIG films, MCD spectrum 79−28722
YIG, magnetostatic surface wave propag. in nonuniform mag. field, anal. 80−20437
YIG, magnetostatic wave linewidth, wave no. depend., mag. relax., rods and films *(Russian)* 78−2667
YIG, metal film effect on mag. boundary conditions, spin wave reson. obs. 79−78527
YIG, microwave generation and manipulation of magnetic domains 78−39378
YIG, mulitiple mag. layer structures, magnetostatic surfacewave propag. 80−88839
YIG, on GdGaG, mag. excitations, diffusion layer effects 78−31112
YIG periodic film layer, magnetostatic surface wave propag. 80−2607
YIG sandwiched between grounded dielectric layers, magnetostatic bulk wave propagation 80−60380
YIG substrates, magnetoelastic surface waves, magnetostatic reson. anal. 80−20441
YIG, surface effects in spin wave reson. 77−16182
YIG, tangentially magnetised, magnetoelastic Lamb waves propagating 79−82856
YIG thin film gyromag. waveguide, on GGG substrate, optical propag. props. Faraday effect 80−74513
YIG, thin films, magnetostatic modes at Q-band freq. 80−65828
YIG, with periodic mag. struct., dispersion characts. anal. *(Japanese)* 79−42809
YIG:Ca film, strong mag. reson. of Fe^{4+} 78−48047
YIG:Co film, influence of stress induced anisotropy on domain struct. 80−100605
YIG:La,Ga, film, LPE-grown, Ga incorporation, depend. of magnetisation on growth rate 80−84627
YIG:La,Ga film, uniaxial anisotropy, variation along growth direction 77−28416
YIG:La film, for microwave applics., growth and ferromag. reson. meas. 78−3008
YIG:La(Ga) films, ferromagnetic resonance, ion implantation effect 80−97145
YIG-dielectric layered structure, magnetostatic surface wave propag., finite width effects 77−20668
$Y_{2.85}La_{0.15}Fe_{3.85}Ga_{1.15}O_{12}$ garnet, mag. props., ion implantation effect, Mossbauer study 80−97166
$(YLuSmCa)_3(FeGe)_5O_{12}$ garnet film, bubble domain expansion, fuzzy wall struct. 80−71128
YSmCaFeGe, mag. garnet films, segregation of Ca and Ge in LPE growth 80−29959
$Y_{3-x}Sm_xFe_5O_{12}:^{57}Fe$ film, ion implanted, Mossbauer conversion spectra study 80−80663
$Y_{2.6}Sm_{0.4}Ga_{1.2}Fe_{3.8}O_{12}$, ion-implanted, bubble domain behaviour 77−12177
$(YSmLuCa)_3(GeFe)_5O_{12}$, garnet film, refractive index dispersion 78−88273
$YSm_{0.5}Lu_{0.7}Ca_{0.8}Ge_{0.8}Fe_{4.2}O_{12}$ film, magnetic bubble propagation with 8 μm period ion implanted propagation patterns 79−78475
YSmLuCaGeIG films, epitaxial growth with 3 μm magnetic bubbles 79−61518
$(YSmLu)_3(FeGaSc)_5O_{12}$, submicron mag. bubble garnet 80−54929
$(YSmTmCa)_3(GeFe)_5O_{12}$ film, YY pattern racetrack discrimination and state stability of $S=1$ and 0 bubbles 78−91908
$(YSmTm)_3(FeGa)_5O_{12}$, small-bubble appl. 79−82845
$Y_{1.5}Tb_{1.5}Al_{0.65}Fe_{4.35}O_{12}$, garnet thin films, magnetisation orientation, temp. depend. 80−71125
Zr-Co(Fe), amorphous alloy film, spin reson. meas. 78−68389

magnetic transition temperature
see also Curie temperature; Morin temperature; Neel temperature
actinide compound, ferromag. with mag. axial symmetry, temp. depend. of magnetisation 77−40044
alloy, binary random Heisenberg ferromagnet transition temp., crit. conc. RKKY model 78−52266
alloy, quenched random, phase diagrams, multicritical points, mixed anisotropies 79−38343
anisotropic magnet, dil., crit. behaviour near percolation threshold 80−88767
antiferroelectric ferrites, coupled magnetoelec. oscills. and high freq. susceptibility tensor *(Russian)* 80−93152
Bethe lattice, random ordered phase, statistical theory 77−85457
binary magnetic alloy, transition temp. determ. using branching theory *(Russian)* 78−68235

magnetic transition temperature continued
borides, transition metal, rare earth, and actinide, mag. props., book contrib. 78−47978
critical temperature for Ising systems with regularly arranged impurities 80−44785
dilute magnetic systems, with nearest-neighbor and next-nearest neighbour interactions, crit. temp. 79−61121
effective Hamiltonian approximation, quenched and annealed random systems 80−93125
FCC Ising ferromagnet., cluster variation approx. 78−68278
Fermi liquid, mag. ordering temp. close to phase transition *(Russian)* 79−78427
ferromagnet, Ising amorphous, crit. temp. 80−11207
ferromagnet, order-disorder transition, Green function theory 77−89962
ferromagnet, with liq.-like disorder, excitations 79−61084
ferromagnetic, anisotropic, Green-function theory 77−16025
ferromagnetic classical spin systems, n-component, upper bound on transition temp. 79−61122
ferromagnetic plane rotors, crit. temp. and correl. functions 78−14974
ferromagnets, phase transformation theory, easy axis anisotropy, quadrupole interaction, renormalisation method calcs. *(Russian)* 79−65671
film, surface spin waves and surface anisotropy effects at finite temp. 79−78452
heavy rare-earth alloys, mag. ordering temps., Heisenberg exchange 79−61103
Heisenberg antiferromagnet, excitations at finite temp. using CPA 79−56554
Heisenberg antiferromagnet, Green function theory 80−107975
Heisenberg ferromagnet, intermediate quadrupolar phase existence 79−51784
Heisenberg ferromagnet, transition temp., mean field upper bound 80−97048
Heisenberg ferromagnet mixed crystal, mag. props. 80−34579
Heisenberg film, spin-one isotropic, quadratic interactions, quadrupolar-paramag. T_c 78−64210
Heisenberg model, planar, classical, with biquadratic interactions, theory 77−72970
Heisenberg random ferromag., cluster approx. 79−82807
interface free energy and transition temp. 77−73041
Ising and Heisenberg inhomogeneous mixture, quenched system, critical temp. 80−88770
Ising antiferromagnet, phase boundary, crit. temp. field depend., Monte Carlo anal. 78−34995
Ising ferromagnet, bond-diluted, with first and second neighbour interactions 78−91870
Ising ferromagnet, FCC, cluster variation approx. 78−27049
Ising ferromagnet, transition temp. in integral representation 77−77059
Ising magnet, compressible, critical temperature shift due to spin-phonon interaction 79−99712
Ising model, appl. of square lattice variational approxs. 79−56555
Ising model, critical exponents for high temperature series expansion 79−99701
Ising model, randomly diluted, on honeycomb lattice, thermodynamic props. 80−54902
Ising model transition temperature in new mean-field theory 79−51785
Ising model with random quenched broken bond disorder, bounds on crit. temp. 78−2688
Ising pair-quartet interactions, PAD approx. 80−11202
Ising spin glass, d-dimensional, frustration effect 80−108019
Ising system, Lifshitz points, phase diagram transition temp. determ. interface free energy vanishing 79−99716
itinerant magnets and superconductors, structural instabilities, phase diagrams 78−14922
itinerant-electron antiferromagnet, effect of mag. field on crit. temp. 78−60293
$La_{1-x}Gd_xRu_2$, mag. ordered superconductor, re-entrant superconductivity 78−88059
Lifshitz point, occurrence in mag. alloys, review 78−52265
long-range ordered material, anomalous spin-flip scatt. rate near ordering temp. 79−82802
metal hydrides, rare earth and intermetallic, electronic and mag. props., Mossbauer study 80−34830
metallic very small particles, mag. ordering temps., ferro- and antiferromag. spin structures 77−73027
metamagnetic Ising model, phase diagram and crit. points, const. coupling approx. 78−34991
metamagnetic trictritical point, effective exponent β 80−71045
mixed magnets, competing spin glass and mag. order, phase diagrams, crit. points 80−39802
Mossbauer effect method for ordering temp. and order parameter exponent meas. 79−51776
random binary system, mag. transition temp. and sp. ht. 77−77065
rare earth alloys, CPA calc. of mag. moments and transition temps. 78−84423
rare earth compounds, $R(Rh_{0.85}Ru_{0.15})_4B_4$, mag. ordering and supercond. 78−14861
rare earth compounds, RMo_6X_8, X=S,Se, coexistence of supercond. and antiferromag. order 79−65579
rare earth compounds, RRh_4B_4, coexistence of supercond. and ferromag. order 79−65579
rare earth intermetallic cpds., mag. props., book contrib. 80−39759
rare earth-Al_2(Zn), mag. coupling mechanism from ordering tear 79−4655
rare earth-Fe-Al alloys, RFe_4Al_8, mag. props. 78−52250
rare earth-transition metal alloys, CPA calcs., moments and transition temps. 78−52252
semiconductor, narrow band gap, ferromagnetism of electrons in filled band *(Russian)* 79−78300
site Ising model, spin glass phase, transition temps. 79−95592
spherical model, accel. of convergence of 1/d expansion for crit. temp. 78−19265
spin glass, relaxation times, influence of spectral distrib. on freq. depend. of freezing temp. 80−44848
spin glass, Sherrington-Kirkpatrick, white and weighted averages over solns. of Thouless-Anderson-Palmer eqns. 80−108012
spin glasses, freezing of EPR relaxation rates 79−99713
spin glasses, transition temperature, conc. depend. 77−85463
spin Hamiltonians, infinite-range, exact solns. 79−78281
spin-1/2 cubic lattice, with anisotropic exchange, configs. 80−65926
spin-Peierls transition in mag. field, phonon freq., Heisenberg model calcs. 80−25151

magnetic transition temperature continued
triangular Ising lattice with small second neighbour interaction crit. temps. 78−56331
TTFCuBDT, spin-Peierls transition in spin 1/2 Heisenberg chains, RPA calcs. 80−25150
X-Y model, spin Peierls transition in mag. field 79−56537
X-Y quasi-one-dimens. system anisotropic, spin-Peierls phase transition, tricritical point 80−25142
Au-Fe, spin glass, transition temp., freq. depend. 80−97113
Au-Fe (17 at.%) alloy, fission fragment irrad., simulation of neutron effects 77−80549
$B_2O_3.Fe_2O_3.nMO$, (n=2 or 4, M=Mg, Co, Ni, Cu), mag. props., transitions 80−75763
$BaO-Fe_2O_3-B_2O_3$ glass, Mossbauer study of struct. and mag. props. 79−47369
$BaO-Fe_2O_3-Na_2O$ glass, mag. props. 78−88123
$CaLaFeO_4$, two-dimens. mag. props. rel. to cryst. struct. 80−75776
$Ca_2MnO_{4-x}F_x$, antiferromagnetic props. and elec. cond. *(French)* 80−29526
$Cd_{1-x}Mn_xTe$, EPR, mag. crit. point 80−39851
$CeAl_2$, anisotropic magnetostriction near antiferromagnetic transition 78−88157
Co complex, $Co(C_5H_5NO)_6I_2$, simple cubic X-Y mag., specific heat, mag. exchange anisotropy meas. 78−39346
Cr alloyed with d-transition elements, magnetic transformations, triple point *(Russian)* 80−88747
Cr, spin-flip transition temperature, press. depend. from elastic const. meas. 80−65944
Cr_2O_3, mag. phase boundaries near bicrit. and Neel points 78−34980
$(1-x)Cr_2O_3-x\alpha Fe_2O_3$, influence of Fe^{3+} on phase transition *(Russian)* 79−28522
$(1-x)Cr_2O_3-x\alpha Fe_2O_3$, mag. phase diagram, EPR method *(Russian)* 79−28521
$CsNiF_3$, one-dimensional magnet, dynamics, mol. field theory approach 80−34614
$Cs_{1-x}Rb_xMF_3$ (M=Mg, Co, Ni, Zn), hexagonal fluoride perovskite structural evolution by cationic substitution *(French)* 80−24430
Cu-Mn, spin glass, transition temp., freq. depend. 80−97113
$CuK_2(SO_4)_2.6H_2O$-liquid ^3He interface, ferromagnetic-like transition temp. at 29.5 mK for solid 79−56001
$Dy_{0.25}Co_{0.75}$ film, amorphous, displacement of mag. compensation temp. by elastic stress *(Russian)* 78−19284
$Dy_xEr_{1-x}FeO_3$, transition to antiferromag. state, Dy^{3+} conc. effects 77−66319
$Dy_xTm_{1-x}FeO_3$, transition to antiferromag. state, Dy^{3+} conc. effects 77−66319
$(Er_{65}Fe_{35})_{100-x}B_x$ glasses, mag. props. 79−73693
$ErFeO_3$, low-temperature spin reorientation 79−65683
$ErH_2(D_2)$, mag. props., 1.5 to 10K, Mossbauer meas. 79−78578
$Er_{1-x}Ho_xRh_4B_4$, re-entrant supercond. and mag. ordering 78−60240
C-,D-$Er_2Si_2O_7$, antiferromag. transition temps. 79−52097
Eu-Cd compounds, Mossbauer effect, mag. props. and lattice consts. 77−36164
Eu^{2+}-ionic compounds, magnetic interaction potential 78−10682
EuB_6, ferromag. and antiferromag. sp. ht meas., 1.8-77K 80−65948
$Eu_{1-x}Gd_xS$ and $Eu_xSr_{1-x}S$, spin glasses, transition temp., freq. depend. 80−97113
$EuMg_5$, Mossbauer effect, effective moments, mag. ordering temp. and isomer shifts 80−34833
Eu_2Mg_{17}, Mossbauer effect, effective moments, mag. ordering temp. and isomer shifts 80−34833
$EuPt_x$ compounds, partial valence change, ^{151}Eu Mossbauer and magnetisation obs. 80−70167
EuSe, mag. struct. and transition temp., indirect exchange 78−91860
EuTe, mag. struct. and transition temp., indirect exchange 78−91860
EuX_5, X=Cu, Zn, Ag, Au, cond. electron spin polarisation effects 77−63136
Fe complex, $Fe(Br)[S_2CN(C_2H_5)_2]_2$, 3-D Ising ferromag., cryst. susceptibility, 1.5-20K 80−20390
Fe-SiO_2, granular compund, superpara- to ferromag. transition temp. meas. 77−69633
$(Fe_xMn_{1-x})_{75}P_{16}B_6Al_3$, amorphous, mag. ordering temp., hyperfine field distrib., elec. resist. 80−34633
$(Fe_xMo_{1-x})_{75}P_{16}B_6Al_3$, amorphous, effects of Mo on mag. props., Mossbauer meas. 79−73859
β-Fe_2O_3 film, hyperfine interactions below and above mag. ordering temp., Mossbauer obs. 77−69745
Fe_3O_4, magnetocrystalline anisotropy, anomolies in magnetostriction and elastic constants 80−60244
FeOCl, Mossbauer spectra, lattice dynamics, hyperfine interactions 80−44985
$GaMo_5S_6$, mag. and struct. transition temps., press. effects, 0-6 kbar *(Russian)* 77−89956
Gd_4 magnetocrystalline anisotropy, temp. and press. depend. 77−20586
Gd^{3+} Gd-ionic compounds, magnetic interaction potential 78−10682
$Gd(Al_{1-x}Mn_x)_2$, ordering on crystallographic sites, X-ray diffr. 78−38662
$GdAlO_3$, bicrit. and tetracrit. behaviour, susceptibility obs. 77−47992
$Gd_xEr_{1-x}Rh_4B_4$, effects of Gd ion on supercond. transition temp., mag. transition temp. and upper crit. field 79−56392
$(Gd_{65}Fe_{35})_{100-x}B_x$ glasses, mag. props. 79−73693
$HoAlO_3$, neutron diffr. at 0.04K, mag. ordering *(French)* 78−10653
$Ho_{12}Fe_{32}O_2$, struct. and ferrimag. props., neutron diffr. obs. 79−78319
$HoH_2(D_2)$, mag. props., 1.5 to 10K, Mossbauer meas. 79−78578
$KCrO_2$, two-dimens. mag. props. rel. to cryst. struct. 80−75776
$K_2FeCl_5(H_2O)$, phase diagram, antiferromag., paramag. and spin flop phases 80−44831
$K_2Mn_{1-x}Fe_xF_4$, vs. transition temperature, phase diagram, critical lines crossing tetracritical point, discussion 78−39326
$LiCrO_2$, two-dimens. mag. props. rel. to cryst. struct. 80−75776
Mn carbides and nitrides, $Mn_3MC(N)$, M=metal, perovskite type, mag. props. 78−43588
MnBi, mictomag. alloys, elastic props. *(Russian)* 80−7141
MnCoSi, effect of press on mag. transition temp. *(Russian)* 80−25137
$MnCr_{2-x}V_xS_4$, mag. struct., Yafet-Kittel to Neel ferrimagnet transition temp. 77−66264
$Mn_{1.77}Sn$, 170K transitions temp. in ferrimag. state, pressure and γ-irrad. effects 77−51902
$NaCrO_2$, two-dimens. mag. props. rel. to cryst. struct. 80−75776
$NbS_2(Se_2)$ intercalation complexes with 3d transition metals, mag. and metallic transport props. 80−44814

magnetic transition temperature continued
Nd, mag. struct., 18.6K mag. phase transition 80−65799
$Ni_{80-x}Fe_xP_{14}B_6$, amorphous alloy, resistivity variations near critical temp. 79−73488
$Ni(NO_3)_2.6H_2O$, susceptibility and specific heat meas., spin ordering, antiferromag. spin pair coupling 80−7084
NiS_2, high press. effect on mag. transition temps. 78−91866
$Pd_{1-y}Mn_yH_x$ alloy, spin glass, transition temp., susceptibility and EPR meas. 80−65930
$Pr_{0.9}Ca_{0.1}MnO_3$, mag. struct. neutron diffr. and magnetisation study 79−61061
$PrIr_2(Pt_2)(Rh_2)(Ru_2)$, sp. ht., differential susceptibility and elec. resist. meas., 1.4-40K 80−71063
Rh borides, RRh_3B_2 (R=rare earth), supercond. and mag. props. 80−97028
Ru borides, RRu_3B_2 (R=rare earth, Y, Th, or U), supercond. and mag. props. 80−97028
$SrLaFeO_4$, two-dimens. mag. props. rel. to cryst. struct. 80−75776
TaS_2 intercalation complexes with 3d transition metals, mag. and metallic transport props. 80−44814
$(Tb_{1-x}Gd_x)_3Co$, intermetallic cpd. mag. props., phase transform, and mag. hystersis *(Russian)* 80−93113
UAL_2, band magnetism due to f-electrons, T_{sf} 77−73039
VI_2, mag. struct., long- and short-range order and Mossbauer spectroscopy 80−65803
VO_2, doped, morphology, structure and props. *(German)* 78−59823
V_3O_7, hyperfine interactions, inelastic spin flip neutron scatt. 77−28372
$(Y_{65}Fe_{35})_{100-x}B_x$ glasses, mag. props. 79−73693
$Y(Rh_{0.85}Ru_{0.15})_4B_4$, mag. ordering and supercond. 78−14861
YbIG, mean field phase diagrams 78−23269
$Zn_{0.75}Ni_{0.25}Fe_2O_4$, mixed ferrite-spinel, helicoidal struct. 79−47242

magnetic transitions
see also critical fluctuations; ferromagnetic-antiferromagnetic transitions; ferromagnetic-paramagnetic transitions; magnetic transition temperature; paramagnetic-antiferromagnetic transitions
actinide compounds, mag. ordering and struct. transforms. 77−20596
actinide compounds, specific heat meas., review 80−6524
actinide intermetallics, mag. ordering, review 77−20598
actinide monopnictides, anomalous mag. props., planar coupling theory 80−60245
adsorption equilibrium anomalies near crit. points of substrate 78−79895
alkali hyperoxides, ionic π-electron systems, magnetogyration 80−93155
alkyl ammonium manganese chloride, birefringence, two-dimens. mag. behaviour, magneto-optical meas. 78−31175
alkylammonium copper chlorides, high-temp. susceptibility obs., 80-300K, ferromag. interactions 77−66274
alloy, binary, magnetic, interface struct., Monte Carlo simultion 80−60317
alloy, binary, simultaneous mag. and spatial long-range order 77−69491
alloy, FCC, binary, on Ising system, sublattice magnetisation, tricrit. point, simulation 79−33491
alloy, quenched random, phase diagrams, multicritical points, mixed anisotropies 79−38343
amorphous ferromagnets, possibility of low temp. phase below ferromag. phase 79−4674
amorphous insulator, phase diagram and statistical mechanics 78−52268
amorphous Ising antiferromagnetic model, frustration effects 80−103838
amorphous magnet spin glass phase possibility *(Russian)* 78−72362
amorphous materials, phase transition theory for new spin structure *(Chinese)* 79−24166
amorphous substance, ferromag. or spin glass transitions 78−2690
amorphous systems, excitations and critical phenomena within framework of phenomenological models 78−52267
amorphous systems, mag. props. effect of random anisotropy 79−4686
anisotropic antiferromagnet, phase transition, with external mag. field 79−11316
anisotropic binary paramagnet, uniform susceptibility, critical behaviour 77−59384
anisotropic exchange interactions, effect on singlet ground state system 80−65852
anisotropic Fermi liquid, mag. order and transitions, phenomenological theory *(Russian)* 77−36038
anisotropic ferromagnet with biquadratic exchange, crit. temp. 77−12124
anisotropic ferromagnet with biquadratic exchange, critical temp. 77−40075
anisotropic lattice spin systems, phase transitions 78−73930
anisotropic magnets, dil., scaling representation meas. percolation threshold 80−88766
anisotropic $S=^1/_2$ ferromagnet, reson. susceptibility, statistical mech. theory 77−8413
anisotropic spin-phonon coupling model, exact solutions *(Russian)* 80−100590
antiferromagnet, anisotropic, correction to scaling in specific heat 78−80168
antiferromagnet, crit. resist. below T_c 78−68004
antiferromagnet, disorded spin-flop, random-field effects 80−11208
antiferromagnet, dynamic scaling deviation 77−31820
antiferromagnet, effect of inelastic scatt. on resistive anomalies at mag. crit. points 77−55675
antiferromagnet, FCC, Ising model, mag. phase diagram, ordering, Monte Carlo calc. 80−103833
antiferromagnet, first order orientational transition, sound propag. anomalies 77−1580
antiferromagnet, first-order orientational phase transition, second acoustic-harmonic generation 78−27067
antiferromagnet, ground states, phase transitions and spin wave spectra 79−87246
antiferromagnet, Ising model, crit. props., calc. 80−65946
antiferromagnet, isotropic, crossover behaviour of mag. phase boundaries 79−78370
antiferromagnet, itinerant model, spin density wave transition, impurities effect 77−72986
antiferromagnet, mag. moment and sp. ht. fluctuations near critical temp. 78−91867
antiferromagnet, magnetic phases, spin configurations in external field 80−70955
antiferromagnet, magnetisation fluctuations of first-order spin-flop phase transition near crit. point 77−24708
antiferromagnet, one-magnon light scatt. from spin-flop and paramag. regions, effect of anisotropy 79−33677

magnetic transitions continued
antiferromagnet, phase transformations in strong mag. fields, mag. moments collapse, strengthened magnetoelastic links *(German)* 78−68227
antiferromagnet, phase transition crossover from first- to second-order in symmetry-breaking field 79−82805
antiferromagnet, quantum critical dynamics with mode coupling 80−108024
antiferromagnet, residual stress induced domains, specific heat meas. anal. 78−60286
antiferromagnet, rhombohedral, spin-reorientation phase transition *(Russian)* 80−93122
antiferromagnet, second-order phase transition, weakening of effect of fluctuation in order parameter near crit. point 79−15316
antiferromagnet, single-ion anisotropy, theory of metamag. phase transitions 78−39327
antiferromagnet, sound generation by EM wave near orientational phase transform. of first kind *(Russian)* 78−39329
antiferromagnet, three-dimensional, fluctuation-induced first-order phase transitions, Monte Carlo calc. 77−85465
antiferromagnet, two-sublattice Neel-type, stable spin configurations, external mag. field and single-ion orthorhombic anisotropy effects 80−60249
antiferromagnet, type I and type II, first-order phase transition 78−39332
antiferromagnet, uniaxial, influence of field direction and single-ion anisotropy on phase diagram 77−16072
antiferromagnet, uniaxial, mag. polaritons in spin-flop phase 78−23349
antiferromagnet, uniaxial, spin configuration in ferromag. phase, field and temp. depend. 79−38321
antiferromagnet with two pairs of mag. sublattices, crit. thermodynamics *(Russian)* 78−60300
antiferromagnetic dielectric, crit. behaviour of exciton relaxation consts. 78−84442
antiferromagnetic effective spin 1/2 system correlated effective field theory 79−73759
antiferromagnetic Heisenberg chain, first order spin-Peierls transition 78−34986
antiferromagnetic Ising model, triangular, with transverse field, zero temp., ground-state props. 80−7115
antiferromagnetic Ising model on triangular lattice, phase diagram, free energy 78−23283
antiferromagnetic spherical model, eqn. of state near phase boundary 77−55681
antiferromagnetic triangular cactus tree, bond-diluted, ordered phase 80−71037
antiferromagnets, Berezinski transition, effective temp. *(Russian)* 80−65889
antiferromagnets, disordered spin flop, bicritical behaviour, critical experiments 80−65899
antiferromagnets, light scatt. as probe for dynamical crit. props. 79−15314
antiferromagnets, n=4 type II, phase transitions, Landau Ginzburg Wilson Hamiltonian 80−15735
antiferromagnets, order parameter of dimens. 6 and 3 79−42762
Ashkin-Teller-Potts model, dil., crit. behaviour 80−65897
atom+diatom, rot. inelastic scatt., mag. transitions, time reversal symm. 80−48066
band-diluted random Ising model, criticality and crossover 78−56320
Baxter-Wu model, site impure modified crit. behaviour and crossover 80−60322
BCC crystal, anisotropic spin-pair correlation function, neutron mag. crit. scatt. cross-section 80−60194
BCC Ising model with competing interactions, fluction-induced first-order transition 80−20424
BCC magnetically ordered alloys, effects on at. ordering-spontaneous magnetisation reln. *(Russian)* 78−19261
Bethe lattice, random ordered phase, statistical theory 77−85457
Bethe lattice, statistical theory of random ordered phase 77−80895
(2,2′-bi-2-thiazoline) iron thiocyanate, high spin to low spin transition, X-ray diffr. and Mossbauer obs. 79−38418
biaxial antiferromagnet, spin configuration in longitudinal mag. field *(Russian)* 79−7998
biaxial Lifshitz point problem in 3-dimens., spin wave theory 80−88759
bicritical and tetracritical points, dynamic scaling and corrections to scaling 78−68247
bicritical points, eqns. of state, cubic anisotropy and tetracriticality 77−55679
bicritical points, eqns. of state, Ising-like ordered phases 77−55678
bifurcation approach to phase transitions, external field inclusion 78−14446
bimetal foil, magnetic-transforms., Mossbauer spectroscopy *(Russian)* 78−6607
binary alloy, annealed Ising ferromagnet 78−47927
binary alloys, mag. interactions effects on phase separation 78−27047
binary alloys, magnetic interface struct. 80−29564
binary paramagnetic mixtures, phase separations, tetracritical phenomena 79−65638
Bloom-Chapel model, phase transition 79−78418
Blume-Capel model, 2- and 3-dimens., renormalisation group results 77−43840
Blume-Emery-Griffiths-Potts model, 2-dimens., phase diagram and crit. props. 77−20620
bond and site percolation, renormalisation group results 79−149
bond percolation model, site-cluster distribs. and eqn. of state 77−74329
Bose glass, marginal fluctuations 80−2586
bubble domain existence in absence of mag. field, near phase transition 78−48012
Callan-Symanzik equation, perturbation analysis, crit. indices 78−52294
chain-like metamagnet, absence of first-order transitions 79−51794
chalcogenide spinels, electroconductivity and electron exchange ferromag.-ferrimag. phase transition 78−84207
chromindur, phase separation, Mossbauer obs. 78−88116
classical 2-D Heisenberg model, low temp. recursion relations, high temp. series expansion 78−10639
classical planar spin model, two-dimens., Monte Carlo study 80−25147
close packed lattices of ferro- and antiferromag. exchange integrals, glass-like phase 78−10697
commensurate phases, spatially modulated, in simple Ising model 80−79909

magnetic transitions continued
competing interaction systems, R-S model, series expansion and rigorous results 78−19201
compressible dilute Ising systems, critical behaviour 80−108017
compressible magnet, magnetic susceptibility near critical point, trajectory integral calc. 79−99705
compressible magnet with exchange anisotropy, crit. behaviour 78−39354
conduction electrons magnetism at points with changing topology of isoenergetic surfaces *(Russian)* 78−52260
Conference, Freudenstadt and Bad Nauheim, Germany (March and April 1978) 79−24121
conference on magnetism, Munster, Germany (Mar. 1977) 78−10626
continuous spin model, exactly soluble, for mag. and distortive systems 77−85470
continuous-spin Ising ferromagnets phase transitions 78−60260
cooperative Jahn-Teller effect and related problems 77−62878
coupled phonon-linear Heisenberg chain system, phase transition 78−64208
critical behaviour and crossover phenomena, renormalisation group arguments, review 77−66324
critical fluctuations obs. using Mossbauer spectroscopy 80−39955
critical indices of primary and secondary order parameters using birefringence 77−28541
critical phenomena, recent theoretical developments 77−87713
critical phenomena review 77−24699
critical scattering, static and dynamic scaling theories 79−42783
crossover, field-induced, in mag. chain, scaling theory 80−54904
crossover exponents, crit. behaviour of quadrupole ordering parameter 77−66339
cubic antiferromagnetic, first to second order transition crossover 78−10709
cubic crossover, approx. renormalisation group calc. 77−49701
cubic crystal with dipole forces and anisotropic correlation function, phase transitions *(Russian)* 79−38504
cubic lattices, fully frustrated, phase transitions, Gaussian and spherical model, free energy calcs. 80−60281
d-dimensional lattice spin model, multicritical pt. 77−36041
demagnetised cubic magnetic crystals, effect of magnetoelastic interactions on spin-orientation phase transitions 79−73761
dense neutron matter, ferromag. transition, pure hard core gas model 78−70478
di(ethyleneammonium) manganese tetrachloride, 2-dimens., EPR linewidth and spin-dimens. crossover 77−69670
dialkylammonium compounds, $(C_nH_{2n+1}NH_3)_2MX_4$, cryst. growth solubility, and props. 78−43999
dialkylammonium copper chlorides, mag. and struct. transitions, IR absorption 77−52097
dialkylammonium copper tetracholorides, quasi 2-dimens., lattice- and spin-dimens. crossovers 77−59416
diamagnetic metal, crit. point of diamag. transition of first kind, and NMR linewidth 77−59469
diammonium layer compounds $(CH_2)_n(NH_3)_2MnCl_4$, quasi-two-dimens. antiferromag., magnetis., spin-flop and crit. exponents 77−66311
diethylammonium copper chloride, Heisenberg ferromag., spin wave theory 77−89922
dil. classical, crit. props. Heisenberg ferromagnet 79−28536
dilute ferromagnet, Ising model, crit. props. in percolation limit 79−1677
dilute Heisenberg magnet excitations near percolation threshold 79−87270
dilute simple cubic lattice, short-range quadrupolar order 79−65681
diluted classical Heisenberg ferromagnet, position space treatment 79−87268
dimensionality lowering in phase transitions with random fields 77−47999
dimethylammonium copper chloride bromide, mag. props., pulsed NMR expts. 80−11292
dimethylammonium copper tetra(chlorobromide), mag. susceptibility, 1 to 30K, mag. phase transition 79−4675
dimethylammonium copper tetrabromide, quasi two-dimensional antiferromag., mag. behaviour 80−97098
dimethylammonium copper tetrachloride-tetrabromide mixed cryst., mag. transition 80−65874
dimethylammonium manganese tetrachloride-d_6, structural and mag. phase transitions, neutron scatt. and AC susceptibility meas. 80−44825
dimethylammonium manganese trichloride, antiferromag. props. 79−73694
dipolar magnet, surface effects on phase transitions, local spontaneous polarisation 80−2708
disordered anisotropic antiferromagnet. random field effects 80−2580
disordered binary alloy, mag., with mixed exchange interaction, crit. behaviour *(Russian)* 79−1675
disordered Heisenberg binary magnetic alloy with mixed exchange interaction, compensation point *(Russian)* 77−51898
disordered Ising model on Cayley tree, mag. transition above percolation threshold 79−73757
disordered spin system, crit. dynamics, shape functions for $T>T_c$ 77−77069
disordered spin systems, crit. dynamics 77−43844
disordered spin systems, dynamic crit. behaviour 77−66343
disordered spin systems, tricrit. behaviour 80−60319
disordered substitutional alloy, mag. props., Heisenberg model 79−38342
disordered system, critical phenomena 78−52269
disordered system, percolation mechanism for long range magnetic order 78−52273
distortive transition, three-dimens. one-component model, mol. dynamics 78−51646
domain wall, phase transition, three-dimensional XY model 79−51805
double spin $^1/_2$ lattice gas model, phase diagrams 77−20521
doublet-triplet mag. system, dipolar and quadrupolar ordering 79−8004
dynamic scaling near bicrit. points 78−6535
dynamical correlation functions and scattering from spin fluctuations near magnetic phase transitions 79−73747
dynamical plane rotator model, dynamical correl. functions in mol. field approx. 80−88758
dynamics of spins interacting with quenched random impurities 77−40065
Dyson's hierarchical model, critical isotherm 77−59370
Dyson's hierarchical model, essential singularities of borderline Ising case 78−31077
Dyson's hierarchical model, Heisenberg models and n-vector 78−31078

magnetic transitions continued
Edwards-Anderson spin glass model in two dimensions, numerical results 80−97100
effective potentials, Ginzburg-Landau model 78−52287
elastic properties of magnetic materials, review 80−7142
electron gas, Hubbard model at low temp., mag. props. *(Russian)* 78−43550
electron liquids, temp. mag. transitions 77−69563
electron-hole paired systems, ferromagnetic ordering phase diagram 80−97097
energy density fluctuation, at fixed wavevector, max. below T_c 79−69225
equation of state in crit. region with nonasymptotic terms *(Russian)* 77−28402
equivalent neighbour model, generalised, derivation of high temp. lattice consts 80−77721
exciton ferromagnet, inhomogeneous state *(Russian)* 78−88132
excitons, in magnetically ordered dielectric, review *(Russian)* 77−80943
extended defect system, phase transform., critical props. 80−103455
Fermi liquid, normal, mag. ordering at absolute zero 79−38344
Fermi liquid model in external mag. field *(Russian)* 77−47952
ferrimagnet, cubic, mag. phase diagram, domain struct. analysis *(Russian)* 78−19249
ferrimagnet, dil., sequence of mag. transforms. *(Russian)* 78−19252
ferrimagnet, uniaxial two-sublattice, energy spectrum, magnetisation, and crit. field, Green function method 80−25060
ferrimagnetic film, uniaxial epitaxial, induced canted mag. struct., problem of domain wall broadening 78−35016
ferrimagnetic resonance near mag. compensation temp. 77−51963
ferrite, phase transforms. near compensation pt., theory *(Russian)* 77−8312
ferrite spinels, dielec. permeability tensor and transmittance, transition to single lattice struct. *(Russian)* 79−87465
ferroelectric antiferromagnetics, spin wave fluctuations in strong mag. fields *(Russian)* 79−82773
ferroelectric antiferromagnets, phase transformations *(Russian)* 80−93114
ferrofluids, phase diagrams and eqn. of state 80−60280
ferromagnet, anisotropic, critical behaviour in external field, renormalisation group approach 77−20601
ferromagnet, anisotropic, in external mag. field, continuous phase transition existence 80−108011
ferromagnet, anisotropic, influence of spatially varying field on phase transitions 80−60339
ferromagnet, anisotropic, with external field, crit. pts. derivation 80−103837
ferromagnet, bubble lattice existence near compensation point *(Russian)* 77−80977
ferromagnet, critical behaviour at field-induced transition at mag. displacive limit 77−66335
ferromagnet, critical dynamics under quenched random magnetic fields 79−4681
ferromagnet, dipolar, susceptibility crossover 77−24680
ferromagnet, disordered, low temp. renormalisation group 78−10688
ferromagnet, effect of inelastic scatt. on resistive anomalies at mag. crit. points 77−55675
ferromagnet, elec. resist., just below crit. temp., effect of mag.-domains 80−39557
ferromagnet, excitonic, zero-sound excitations, Fermi liq. model 80−93101
ferromagnet, harmonic rotator, Coulomb plasma and related models, renormalisation group treatment 78−88135
ferromagnet, harmonic rotator, Coulomb plasma and related models, case of dimensions $D<2$ and $D>2$ 78−88136
ferromagnet, harmonic rotator, Coulomb plasma and related model, two dimens. case 78−88137
ferromagnet, Ising model, diamond lattice, phase transition, crit. props. 80−93127
ferromagnet, Ising model, nonuniform mag. field method, crit. correlation function approximations, calc. 80−20407
ferromagnet, Ising model, transition point calc. 80−20408
ferromagnet, Ising-Heisenberg-XY crossover, bicritical point, partial differential approximants for susceptibility series 77−85466
ferromagnet, mean spherical model, Langevin approach 78−72350
ferromagnet, multiaxial, domain struct., applied stress effect *(Russian)* 78−76267
ferromagnet, random quenched, crit. behaviour, effective exponents, renormalisation 80−60326
ferromagnet, random uniaxial, dipolar interactions, crossover behaviour, renormalisation group equations numerical soln. 80−50136
ferromagnet, randomly dilute, essential singularities 77−20615
ferromagnet, remanent magnetisation during thermal demagnetisation near a phase transition 78−88142
ferromagnet, soft, hysteresis rel. to irreversible phase transition 80−34693
ferromagnet, spin-one, uni- and biaxial anisotropy, Heisenberg, Ising and planar models 78−34989
ferromagnet, spin-s Ising model, crit. curve 79−4679
ferromagnet, thermodynamic stability and ctit. points, comparison with simple fluid 78−16766
ferromagnet, three-dimens., crossover in dynamic exponent, hyperfine interaction vs. neutron scatt. expts. 78−84437
ferromagnet, translationally invariant, renormalisation group struct., crit. phenomena 77−51907
ferromagnet, two-dimensional, dipole forces and phase transition *(Russian)* 79−51782
ferromagnet, unaxial, random with dipolar interactions, crit. amplitude ratio change 78−31083
ferromagnet, uniaxial, dipolar crossover effects from Ising crit. behaviour 77−89961
ferromagnet, uniaxial, domain struct. and elastic props. in orientation region of phase transitions *(Russian)* 78−19270
ferromagnet, uniaxial, quantum anomalies in susceptibility during second order phase tansitions *(Russian)* 78−19226
ferromagnet, uniaxial dipolar, crossover behaviour, theory 80−29559
ferromagnet, with long-range interactions, low temp. renormalisation group 77−63206
ferromagnet, with mag. axial symmetry, magnetisation and phase transitions 77−85487
ferromagnet with single ion anisotropy, collective modes 77−28354

magnetic transitions continued
ferromagnet-antiferromagnet alloys, phase diagrams and multicrit. points in random mixed magnets 79−73756
ferromagnetic, anisotropic, in random longitudinal field, multicrit. point, theory 80−54903
ferromagnetic, Peierls condition and no. of ground states 78−80150
ferromagnetic, uniaxial, dynamical behaviour near mag. transition point *(Russian)* 78−84431
ferromagnetic alloy, temp. depend. of mag. props. and sp. ht., mag. phase transition region 78−64207
ferromagnetic alloy, transition to spin glass ordering 80−34628
ferromagnetic chain with isotropic long range interaction 77−12137
ferromagnetic crystals, uniaxial anisotropy, first order magnetisation processes theory 80−60242
ferromagnetic dielectric, crit. behaviour of exciton relaxation consts. 78−84442
ferromagnetic dynamic structure factor in scaling region to first order in ϵ=6-d 77−63208
ferromagnetic film, ϕ^4 domain walls, magnetisation, occurrence of crit. point 78−95500
ferromagnetic film, shift of ant. temp. as result of Raman scatt. 80−54909
ferromagnetic film, spin wave parametric reson. near phase transition 79−8053
ferromagnetic films, nonlinear spin wave parametric resonance 80−2642
ferromagnetic films, spin correl. functions, crit. indices 80−7133
ferromagnetic fluid, 1D Ising and 3D Heisenberg solns. 77−85478
ferromagnetic fluid, molecule system eqn. of state, exchange interactions, spin independent forces 77−59412
ferromagnetic intermediate spherical model, critical temp. 77−63053
ferromagnetic Ising model, spin-one three dimensional, single-ion anisotropy, crit. behaviour 80−80540
ferromagnetic Lifshitz point, symmetry derived crit. modes 79−73758
ferromagnetic materials, phase transition, mathematical bifurcation process 80−29572
ferromagnetic metal, transient enhancement of AC susceptibility, domain nucleation, crit. effects 77−20633
ferromagnetic phase transitions, nucl. spin dynamics in anisotropic systems 80−11205
ferromagnetic phase transitions, nucl. spin dynamics in isotropic systems 80−11204
ferromagnetic plate, domain struct. during spin reorientation, phase diagram *(Russian)* 78−52320
ferromagnetic plate, domain struct. near first-order phase transition resembling second-order transition 80−93139
ferromagnetic plate, phase diagram in magnetic field *(Russian)* 77−48018
ferromagnetic semiconductor, energy and mobility of spin polarons 80−70982
ferromagnetic semiconductor, homogeneous state, phase transition and stability 78−6528
ferromagnetic semiconductor, phase transition and instability of homogeneous state 77−28398
ferromagnetic semiconductors, bound mag. polaron 79−90976
ferromagnetic semiconductors with doubly charged donors, quasiphase transition 79−65684
ferromagnetic spin system, mag. susceptibility and correl. length crossover relationship 79−78395
ferromagnetic spin system, under quenched random mag. field, phase transition crit. dynamics 79−82798
ferromagnetic spin systems, low temp. phase transitions 79−56538
ferromagnetic spin-one system, quadrupolar to paramagnetic phase transition 77−80934
ferromagnetic superconductor, vortex structure 80−25055
ferromagnetic system with quenched random impurities, random spherical model in nonzero mag. field 77−55677
ferromagnetic systems, crit. experiments, field theory, Borel transform. 80−80541
ferromagnetic thin films, n-vector model with Kac-type interactions 77−59436
ferromagnetism, Bethe-Peierls-Weiss model, phase transition calc. 79−2585
ferromagnetism, itinerant electron model, spin quantization direction fluctuations, short range order. 80−34582
ferromagnetism, mol. field theory, appl. of catastrophe theory, for teaching 79−35467
ferromagnetism, singlet ground state, Heisenberg Hamiltonian model 79−11283
ferromagnets, easy axis anisotropy, quadrupole interaction, renormalisation method calcs. *(Russian)* 79−65671
ferromagnets, long-range, low temp. series for magnetization, crit. exponents 79−61131
ferromagnets, quantum critical dynamics with mode coupling 80−108023
ferromagnets, uniaxial, nonuniversal props. in dipolar crit. region 77−24703
ferromagnets, uniaxial, US attenuation and kinetic coeffs. near crit. point, renormalisation group theory 79−4715
ferromagnets and antiferromagnets, EM and acoustic energy attenuation in many-domain magnets 80−7140
ferromagnets and ferroelectrics, theoretical development 78−43815
ferromangetic conductor, electric field response and electrofluctuation instability *(Russian)* 78−56083
field induced mag. transition criterion 78−88143
first kind PT1 transformations *(Russian)* 79−69670
first order instability in finite model system, computer simulation 80−65932
first-order, intrinsic volume magnetostriction concept 80−29562
first-order transition induced by cubic anisotropy 79−4688
Fisher renormalised Ising exponents in compressible spherical model 77−30113
fluctuations and mag. eqn. of state 78−64194
frustration network, phase transitions 80−2596
Gaussian-to-Heisenberg crossover, specific heat, renormalised perturbation theory 80−60356
Gd-alloy, ferromagnetic, nuclear spins as probe for mag. coupling and crystallographic order 78−10799
Gentalloy, in Fe-W system, damping capacity *(Japanese)* 79−20094
Ginzburg-Landau-Wilson model, n-component, derivation of nonlinear σ-model, in low temp. limit 80−44787
Green's function theory in quadrupolar-coupled quasi-Heisenberg system 79−38340
Green's function theory of systems with dipolar and quadrupolar pair interactions 77−63222
gyrotropy, an implicity form of ferroicity 79−73286
harmonic rotor model, interactions, spirals and phase transitions with and without long range order 80−60350
heat magnetization in the singlet-triplet model 78−64211
Heisenberg, ferromagnet, spin-one, uni- and biaxial anisotropy, RPA and mol. field approx. 78−34989
Heisenberg antiferromagnet, one dimens., spin-flop transition 79−73723
Heisenberg antiferromagnet, phase transitions in quantum spin systems 78−84434
Heisenberg antiferromagnet, randomly dilute, MFA-VCA theory 77−63219
Heisenberg antiferromagnet, randomly diluted, field-induced phase transitions 77−36089
Heisenberg antiferromagnet, uniaxial, props. by Green's function method 77−85406
Heisenberg antiferromagnetic alloy, critical behaviour *(Russian)* 78−88128
Heisenberg antiferromagnetic alternating spin 1/2 chains, susceptibility calcs., spin-Peierls transition 79−78394
Heisenberg bicritical points in antiferromagnets, universality tests 80−84604
Heisenberg chain, classical anisotropic, scaling theory 80−80515
Heisenberg classical compressible model, phase transition exam., anisotropic exchange 77−59414
Heisenberg classical spins on triangular cactus tree, random ordered phase 79−87265
Heisenberg ferromagnet, anharmonic, renormalised magnons and phonons 78−91837
Heisenberg ferromagnet, crit. dynamics in 2+ϵ dimens., low temp. phase 78−76262
Heisenberg ferromagnet, critical dynamics of impurity spin below T_c 80−71076
Heisenberg ferromagnet, dil. spin $^1/_2$, renormalisation group treatment 79−69679
Heisenberg ferromagnet, dipole-dipole interaction, quantisation axis, magnetisation and critical point effects 78−34946
Heisenberg ferromagnet, eqn. of state, using modified Gell-Mann Low renormalisation group 77−63225
Heisenberg ferromagnet, isotropic with biquadratic exchange 78−39344
Heisenberg ferromagnet, one-dimens., symm. crossover 79−87269
Heisenberg ferromagnet, spin wave excitations at finite temp., CPA calc. 77−32142
Heisenberg ferromagnet, transition temp. calc., depend. on spin and coordination no. *(Russian)* 77−47997
Heisenberg ferromagnet, with biquadratic exchange, first-order quadrupolar transition 77−69571
Heisenberg ferromagnet, with biquadratic exchange interaction 78−34999
Heisenberg ferromagnet with biquadratic exchange 79−38338
Heisenberg ferromagnet with higher-order exchange interactions, thermodynamic props. 79−42770
Heisenberg ferromagnetic alloy, critical behaviour *(Russian)* 78−88127
Heisenberg film, spin-one isotropic, with biquadratic interactions, phase transition 77−20611
Heisenberg magnet, quasi-two-dimensional phase transition at marginal dimensionality 79−38332
Heisenberg magnet, two-dimens., glasslike ordering Monte Carlo calcs. 79−82740
Heisenberg metamagnet, collinear, mag. phase diagram 80−71035
Heisenberg model, amorphisation *(Russian)* 78−80118
Heisenberg model, anisotropic, existence of phase transitions 77−32202
Heisenberg model, antiferromag., phase diagram and multicrit. behaviour 78−56337
Heisenberg model, bosonisation and crit. behaviour 77−80948
Heisenberg model, classical, compressible spin system, zero temperature phase diagram 78−6536
Heisenberg model, critical behaviour, high temp. susceptibility and internal energy series 78−34987
Heisenberg model, disordered ferromag. states, random exchange integrals 80−80550
Heisenberg model, layered magnet, phase transitions 78−76252
Heisenberg model, magnetic transitions 80−25141
Heisenberg model, random, thermodynamics, cluster approx. 77−16032
Heisenberg model, randomly dilute, renormalisation group calcs. 80−60321
Heisenberg model, singular bounds on free energy and susceptibility 78−43595
Heisenberg model, spin-S, mapped onto interacting Bose field 79−47291
Heisenberg model, three dimensional, crit. exponents and corrections to scaling 80−7117
Heisenberg model, two-dimensional spin 1/2 anisotropic, quantum renormalisation approach 77−66348
Heisenberg multi-quadratic isotropic model, LRO, phase transf., exchange interactions *(Chinese)* 80−88756
Heisenberg n-component classical model, low temp. renormalisation group and symm. breaking perturbation, first-order transition 79−15315
Heisenberg paramagnet, electronic spin dynamics, NMR 78−76266
Heisenberg spin system, one-dimensional, dynamical behaviour 80−29567
Heisenberg spin systems, absence of mag. phase transitions, Hubbard identity calcs. 78−34992
Heisenberg-biquadratic and Blume-Emery-Griffiths interactions dipolar and quadrupolar susceptibility 78−76257
Heisenberg-Ising bonds, randomly mixed three dimens. system, critical props. 78−76249
helical order and its onset at Lifshitz point 78−34996
helical order onset, renormalisation group approach 77−66344
helically ordered magnetic systems, commensurability effects on crit. behaviour 77−66334
helimagnetic-ferromagnetic transition for two-dimens. spins case 77−66349
hierarchical model, critical and tricritical behaviour 78−10712
high pressure physics and technology, conf., Moscow, Russia (May 1975) 78−51611
high spin/low spin transition, model including lattice dynamics 77−63202
high-temperature representation of anisotropic rotator, XY and Heisenberg models for dimensions D≥2 80−11146

magnetic transitions continued
Hubbard antiferromagnetic semiconductor, collective excitations, weak coupling limit 78−19210
Hubbard Hamiltonian, phase transitions 77−85462
Hubbard model, antiferromagnetic ground state 79−82742
Hubbard model, arbitrary electron density case, functional integral approach 78−76219
Hubbard model, conductivity and characteristic temp. 77−32150
Hubbard model, doubly degenerate, functional integral approach 79−99711
Hubbard model, electron struct. in mag. field *(Russian)* 78−60287
Hubbard model, equivalent spin Hamiltonian, for phase transition studies 80−80474
Hubbard model, extended, Hamiltonian free energy function 78−6531
Hubbard model, FCC lattice, mag. and elec. props. 78−56334
Hubbard model, ferromag. phase transition 77−77062
Hubbard model, magnetic instabilities, influence of short-range correlation effects 79−7963
Hubbard model, Mott metal-insulator transition, ten-fold spin-orbital degeneracy 78−52285
Hubbard model, one-dimensional, with nearest and second nearest neighbour hopping in Hartree-Fock approx. 77−32149
Hubbard model, random one-body approx., higher dimens. lattices 79−37945
Hubbard model, single band, magnetic phase diagram, cluster variational calc. 80−60340
Hubbard model, static approx. 77−1558
Hubbard model, two band, magnetic behaviour 78−80119
Hubbard model with nearest and next nearest neighbour hopping in Hartree Fock approx. 78−52189
hyperfine experiments on mag. crit. phenomena, selective review 78−43722
ilvaites, Mossbauer spectra and mag. features 80−7248
impurity effect on T=0 transition, crit. oscills. in scaling laws corrections 78−76259
incommensurate phase transition, Bethe-Peierls and mol. field approx. 80−20599
induced-moment singlet-triplet model, high-temp. series expansion 79−73653
induced-moment singlet-triplet model, rel. between ground-state moment and crit. temp. 79−78282
insulator, mag. transition sp. ht. anomaly, photoacoustic meas. 80−4773
intermediate valence compounds, phonon produced instabilities, periodic Anderson model 78−79964
Invar, mag. phase transitions, linear expansion coeff. and mag. susceptibility meas. 77−69553
Invar, single crysts., rel. to Hall effect and transverse magnetoresist., 4.2-120K *(Russian)* 77−59277
Ising, quenched dil. random-bond model, CPA difference eqn. and crit. curves 80−2584
Ising antiferromag. phase boundaries, hard-core lattice gas calcs. 80−80542
Ising antiferromagnet, BCC, crit. behaviour in mag. field, Monte Carlo calc. 78−31088
Ising antiferromagnet, FCC, nearest neighbour interactions, Monte Carlo method 80−80544
Ising antiferromagnet, finite field, second-order phase boundary series investigation 79−42777
Ising antiferromagnet, induced staggered mag. fields, g-factor mechanism 77−55676
Ising antiferromagnet, triangular, improved mol. field approach 79−73745
Ising antiferromagnet, with zero field splitting, multicritical behaviour 77−12136
Ising antiferromagnet with next-nearest-neighbour interactions, tricritical exponents and crossover behaviour 77−16089
Ising chain, in transverse field, variational treatment, static props. at zero temp. 79−4642
Ising chain, one-dimens., with generalized molecular field 79−91242
Ising chain, with next-nearest neighbour interactions, mag. responses to spin-Peierls transition 80−71054
Ising clusters, small, Monte Carlo calc. of critical temp. 77−63209
Ising disordered spin system on Cayley tree 79−51783
Ising ferro and antiferromagnet random bond mixture, on s.c. lattice, phase transition 77−12131
Ising ferro- and antiferromagnet, quenched random mixture, Bethe approx. for phase transition 77−16082
Ising ferromagnet, 2-D, with quenched bond disorder, critical temp. 78−56328
Ising ferromagnet, annealed, of binary alloys 77−59368
Ising ferromagnet, comparison with plane rotor 80−60348
Ising ferromagnet, crit. correlation-function approxs. 78−56324
Ising ferromagnet, crit. exponents in integral representation 78−56325
Ising ferromagnet, disordered, approximate treatment 78−52262
Ising ferromagnet, equivalence of different order parameters 77−36082
Ising ferromagnet, exponent inequalities at roughening transition 77−32204
Ising ferromagnet, four-dimensional logarithmic correction to mean-field order parameter 79−73754
Ising ferromagnet, phase boundary rigidity, Onsager Temperley model 77−28394
Ising ferromagnet, phase coexistence, translation invariance and stability 80−80513
Ising ferromagnet, randomly dilute, conc. expansion study 80−60315
Ising ferromagnet, randomly dilute, determ. of transition temp. by Monte Carlo simulations 77−12130
Ising ferromagnet, randomly dilute, with second neighbour expansion study 77−85452
Ising ferromagnet, renormalised crit. behaviour 78−52272
Ising ferromagnet, S=1, single-ion type uniaxial anisotropy, cluster-variation method appl. in pair approx. 78−68281
Ising ferromagnet, site diluted, crit. props. 78−72351
Ising ferromagnet, spin-operator reduction relations, representation 78−95443
Ising ferromagnet, three-dimens., transition temp. with two- and four-spin interactions 79−42769
Ising ferromagnet, two-dimens., order parameter and induced susceptibility 80−71036
Ising ferromagnet, with transverse single-ion anisotropy, phase transitions 78−19259
magnetic transitions continued
Ising ferromagnet and spin glass systems, random, crit. dynamics 80−34666
Ising ferromagnet ordering conditions 79−42719
Ising ferromagnet with two- and four-spin interaction, improved product average decomposition method 80−20406
Ising frustration pots., phase transition 80−52142
Ising kinetic model, nonlinear crit. slowing down, first moment relax. time 77−51910
Ising lattice, triangular, antiferromag. to ferrimag. transition 77−20522
Ising lattices, finite, series expansion anal. of crit. temp. shifts 79−61134
Ising magnet, metastable, in negative field, near criticality 80−84608
Ising magnet, random, with frustration, zero-temp. props. from series expansions 79−61129
Ising magnet coupled to isotropic elastic medium, first order transition, renormalisation method 80−68151
Ising metamagnet, dilute tricritical point calcs. 80−50099
Ising mixture, quenched random, on Cactus tree 77−16081
Ising model, 3-D, partition function integration, collective variables method *(Russian)* 77−37824
Ising model, 3-dimens., critical exponent γ 79−93051
Ising model, 3D, long range pot. 77−66379
Ising model, antiferromagnet, phase boundary determ. by real space renormalisation group methods 78−88134
Ising model, basis distrib. 78−16748
Ising model, bond random, ferromagnetic-antiferromag. mixture, triangular cactus tree, statistical theory 80−75702
Ising model, bond-dil. two-dimens., phase transition 80−60320
Ising model, classical, in transverse field, Monte Carlo simulation, statical props. 78−56326
Ising model, cluster size and boundary distrib. near percolation limit threshold 77−20624
Ising model, cluster size and percolation 79−65630
Ising model, compressible, crit. behaviour, applic. of renormalisation group methods 77−82464
Ising model, compressible, position space renormalisation group approach 79−56552
Ising model, compressible, transform. into continuous spin Hamiltonian, renormalisation group treatment 77−66347
Ising model, compressible random, crit. behaviour 78−80160
Ising model, constant-coupling approx., successive phase transitions 80−97108
Ising model, continuous, first and second order phase transitions 77−9965
Ising model, continuous-variable, real-space renormalisation group method 80−100589
Ising model, crit. exponents, series-expansion approach 79−61138
Ising model, critical behaviour, scaling functions for quantum crossover 78−68249
Ising model, critical dynamics, time-dependent real-space renormalisation group 80−60282
Ising model, critical exponents for high temperature series expansion 79−99701
Ising model, critical exponents universality using entangled scale transform. on lattice 77−66346
Ising model, critical indices for normal random field 77−77064
Ising model, critical temperature, modulated Pade approximant 80−84605
Ising model, cumulant approximation is crit. region 78−76255
Ising model, Devil's staircase and harmless staircase, oscillating interactions through elastic stairs or other harmonic fields 80−88296
Ising model, exact differential renormalisation at criticality 79−73755
Ising model, ferromag. coupled, semi-infinite, with free surface, renormalisation group approach 78−14975
Ising model, ferromagnet-spin glass transition 79−78421
Ising model, hyperscaling, renormalisation group theory examination 77−66337
Ising model, interface free energy and crit. line, nearest and next nearest neighbour interactions 78−39352
Ising model, Kadanoff block transformation by Monte Carlo technique 77−69574
Ising model, kinetic, nonlinear critical relaxation 78−34988
Ising model, Lee-Yang branch point and crit. behaviour 78−68253
Ising model, looped tree-like lattice, phase transition 80−7113
Ising model, n-replica method, crit. behaviour of spin glasses 79−42767
Ising model, one dimensional, with infinite radius of interaction in transverse magnetic field 80−2587
Ising model, one-dimensional, long range, metastability 80−42166
Ising model, pair and triplet interactions, mean-field eqn. of state 77−16021
Ising model, phase transition near percolation threshold 77−33956
Ising model, quantal and finite-sized, dimensional crossover 78−95444
Ising model, quantum classical crossover critical behaviour in transverse field 77−66331
Ising model, quenched bond-diluted, new approach 77−32138
Ising model, quenched-bond disorder, cluster extension of effective-interaction approximation 80−93130
Ising model, random, $\varepsilon^{1/2}$ expansion of crit. behaviour, higher order corrections 78−27050
Ising model, random band, cumulant expansion to glass-like phase 77−8319
Ising model, random bond, susceptibility and specific heat of glass like phase, cumulant expansion 78−6533
Ising model, randomly dilute, crit. and thermodynamic props. 79−8005
Ising model, renormalisation group calc. of crit. props. of free mag. surface 77−40068
Ising model, S=1/2, mol. field theory with correlations 79−82804
Ising model, spatially modulated phase, Monte Carlo study 79−95598
Ising model, spatially nonhomogeneous, correl. functions 80−60314
Ising model, spin fluctuation waves in critical point region *(Russian)* 77−33970
Ising model, spin glass, dil., low temp. phase diagram and crit. props. 78−60291
Ising model, spin-one, bilinear and biquadratic interactions 80−75772
Ising model, spin-s, corrections to scaling for spin-pair correls., series anal. 77−16027
Ising model, surface crit. behaviour, layer and local susceptibility 80−71058
Ising model, surface critical behaviour, renormalisation group theory 78−47988

magnetic transitions continued
Ising model, three dimensional, crit. exponents, scaled eqn. of state 77−8262
Ising model, three-dimens., crit. index. for correl. length 78−84444
Ising model, three-dimensional, two-spin correlation function, method for phase diagram 78−56323
Ising model, three-dimensional, with four-spin interaction, exact soln. 80−88711
Ising model, transition temperature for square cactus tree with random bonds 78−41240
Ising model, transverse, quantum crossover 78−43596
Ising model, tricritical phenomena, nearest neighbour and next nearest neighbour interactions 77−69566
Ising model, two dimens., metastability, dynamic Monte Carlo method, transfer matrix 78−72354
Ising model, two dimens. small mag. field approx. near T_c 79−42773
Ising model, two-dimens., ferromagnet-spin glass transition, Monte Carlo calc. 80−60287
Ising model, two-dimens., quantum field theory calc. of correl. function 77−32205
Ising model, two-dimens., with transverse field, phase diagram and crit. props., from real space renormalisation group 78−52295
Ising model, two-dimensional, crit. exponents, one-dimensional three-spin cell calc. 78−68280
Ising model, valency transitions 78−60297
Ising model, with regularly spaced blocks of impurities, crit. temp. and sp. ht. 77−69576
Ising model, with transverse field, crit. behaviour of susceptibility 77−12127
Ising model, with transverse field 77−77016
Ising model in transverse field, spin dynamics, mode coupling 78−56332
Ising model in transverse field in one-dimens., zero-temp., renormalisation 79−38347
Ising model lattice, impurities and probe independence of hyperfine crit. exponents 79−87267
Ising model of bond mixtures, spin glass transition, renormalisation group approach 78−43601
Ising model on Bethe lattice with competing interactions, phase diagram 78−64177
Ising model on Cayley tree 77−59421
Ising model phase boundary, line of analytic singularities 80−60283
Ising model strips, scaling theory, wall effects in crit. systems 80−80539
Ising model with bilinear and biquadratic interactions, mag. transitions 78−23275
Ising model with biquadratic interaction, phase transition, Monte Carlo method 80−60352
Ising model with clusters, transition temp., real-space renormalisation techniques 79−78420
Ising model with competing interactions, critical properties and exact results 80−93129
Ising model with competing interactions, solitons and phasons 80−34653
Ising model with nearest neighbour ferromagnetic interactions, phase transition theorems 77−22501
Ising model with random exchange bonds, phase diagram 78−43604
Ising pair correlation function Gaussian basis distrib. of density fluctuations *(Russian)* 77−33969
Ising quenched bond model, statistical theory of random ordered phase 77−12075
Ising replica magnets, phase struct. 80−39777
Ising soluble model for crit. behaviour of imperfect mag. cryst. 77−66355
Ising spin glass, d-dimensional, frustration effect and dilution problems 80−108018
Ising spin glass, dil., at zero temp., (1/2)-state Potts model 79−42768
Ising spin glass near percolation threshold 78−72352
Ising spin glasses, dual transformation into ferromagnetic models, critical temp. in frustrated models 79−73763
Ising spin system, coupled to acoustic and optic lattice modes, critical behaviour 80−71044
Ising spin systems on Cayley tree-like lattices, spontaneous magnetisation, correlation function far from boundary 78−68137
Ising spins on square lattice, theory of frustration effect 77−89959
Ising square lattice, phase transitions, next nearest neighbour interactions 80−50128
Ising susceptibility, appl. of integral approx. methods 79−71392
Ising system, finite, statistically layered, crit. phenomena 78−95446
Ising system, Lifshitz points, phase diagram transition temp. determ. interface free energy vanishing 79−99716
Ising system, local crit. behaviour at impurities 77−48001
Ising system, two-dimens., transverse field crit. props., renormalisation and scaling 78−21080
Ising system with many-spin interactions 78−6532
Ising systems, frustrated, interface entropy, phase transitions 79−19711
Ising transverse bond-diluted model, appl. of CPA 79−56551
Ising two-dimensional spin systems, decimation transforms. 77−77017
Ising type model, elastically coupled, effects of dipolar forces on crit. sound attenuation in uniaxial systems 80−50158
Ising-like model, four dimens., excitation spectrum, mol. dynamics 78−95411
isotropic antiferromagnets, crit. dynamics using renormalisation group methods 79−8006
isotropic ferromagnet, critical behaviour in random uniaxial anisotropy model 79−38349
isotropic magnet, Goldstone mode singularities eqn. of state, magnetisation curve, perturbation theory calcs. 78−43607
isotropic N-component spin system, with long- and short-range interactions, crit. behaviour 78−76256
isotropic spin system, cubic lattice, step model of phase transitions, critical behaviour 78−60290
isotropic two-dimensional magnetism, long range forces effect 78−52291
itinerant antiferromagnetism, s-band Hubbard model, zero temp. props. 77−4493
itinerant electron magnetism, thermodynamic aspects 77−72992
itinerant electron paramagnets, coupled charge and spin fields 77−72991
itinerant electron system, coexistence of antiferro- and ferromagnetism 78−2645
itinerant magnet with unmag. electron bands, phase diagram 79−91202
itinerant magnets, anomalous sound attenuation near mag. transition temp. 78−15004
Kac-Baker model of partially finite spin systems 77−20621
Kondo alloys, mag. interactions 77−59385
magnetic transitions continued
Kondo Lattice, renormalisation group approach 77−63086
Kondo lattice and Kondo effect 79−78312
Landau's second-order phase transition theory, appl. to two order parameters systems, Ising model 78−43599
Landau critical point, low temp. renormalisation group and 1/N expansion 79−35656
Landau-Lifshitz equation, new conservation law *(Russian)* 79−95559
lattice gas model, double spin 1/2, for mag. annealed binary alloy and nematic mixture 77−66342
lattice internal rearrangement modes, correlation betwen lattice structural and magnetic structural transitions 78−47987
lattice spin model with multicrit. pt., soln. in spherical model limit 77−66338
Lifshitz criterion violation 78−80167
Lifshitz point, crit. exponents calc., k-space instability on λ line 77−65014
Lifshitz point, critical behaviour, universal amplitude ratio calc. 79−33496
Lifshitz point, critical exponents, ε-expansion 78−65899
Lifshitz point, ferromag., renormalisation-group anal. of crit. modes in cryst. systems 79−82806
Lifshitz point, phase diagram, systems with easy plane of magnetisation 77−80936
Lifshitz point, phase diagram, uniaxial magnetisation 77−80935
Lifshitz point, phase diagram for tetragonal crysts. with easy plane of magnetisation 78−39321
Lifshitz point, phase diagrams and crit. behaviour 80−65928
Lifshitz points, crit. behaviour near, Monte Carlo calc. 79−24170
Lifshitz points and Landau theory in presence of mag. field 80−60338
linear chain of classical spins with logarithmic nearest neighbour pair potential 77−36085
magnetic alloys, binary, spinodal decomp., computer simulation study of interface behaviour 80−84913
magnetic crystal, with impurity centre, anomaly of width and lineshape of light absorpt. 78−76499
magnetic Debye crystal, with magnon-phonon coupling, crit. changes in vibr. modes 79−95094
magnetic disordered systems, Monte Carlo anal., review, book contrib. 79−82809
magnetic materials, transparent, optical studies of phase transitions 77−66481
magnetic order coexistence with charge density waves 80−97096
magnetic ordering due to exchange-crystal splitting 79−8010
magnetic ordering in antiferromagnets without spatial struct., phase transitions *(Russian)* 80−50134
magnetic structure symm. anal. in neutron studies periodicity changes at mag. phase transitions 79−99680
magnetic structures, symmetry anal. in neutron studies, phase transition concept 79−99679
magnetic system with cryst. field pots., Green's function theory and high temp. series expsn. 80−15673
magnetic systems and mixtures, phase diagrams, Monte Carlo studies, book contrib., review 79−82313
magnetically ordered cryst., dislocation drag, magnetoelastic waves 80−103332
magnetisation theory, of slab of finite thickness, role of positive surface energy 80−15724
magneto-optical linear and nonlinear effects, general system 77−52058
manganese acetate tetrahydrate, crit. relax. studied by HF mag. susceptibility 78−39299
manganese acetate tetrahydrate, susceptibility and magnetis. meas., crit. exponents and crossover behaviour 77−66309
manganese stearate, mag. two-dimensional system, mag. susceptibility 78−10669
manganese zinc formate dihydrate, two-dimens. antiferromag., anomalous crit. phenomena, neutron scatt. and PMR obs. 80−50104
mean field theory, Ginzburg criterion and marginal dimensionality 77−69067
metal:magnetic ion, ESR, book 77−48037
metal, electron-phonon interaction, magnetism influence 77−73040
metal, mag. susceptibility, effects of impurities and temp. *(Russian)* 78−84429
metal, thermopower near magnetic and order-disorder critical points 79−65454
metal, uncompensated, interband transition, effect on Curie temp. of ferromagnetic phase transition 79−7994
metal-insulator transition, density-functional theory 80−75507
metals, crit. transverse US attenuation, spin fluctuations 78−48022
metals, Neel temp. and crit. exponents determ. from electronic transport coeffs. 77−69556
metamagnet, compressible, renormalisation group theory of pseudocritical point 80−60337
metamagnet with temp. depend. anisotropy in classical approx. 79−33481
metamagnetic model in field of arbitrary direction 79−95593
metamagnetic phase diagram, determ. method 78−68254
metamagnetic transition in magnets with multi-sublattices *(Russian)* 78−23267
metamagnetic transitions in crystals with low exchange fields *(Russian)* 77−32188
metamagnetic trictritical point, effective exponent β 80−71045
metamagnetism, temperature induced, caused by mag. anisotropy 80−11195
Metglas 2826A, Invar related system, high press. Mossbauer spectra 79−56642
microcanonical high-temp. expansion 78−2638
Migdal transformation, renormalisation group, recursion relations 80−34647
mischmetal-Co system, thermomagnetic analysis of intermediate phases 80−93115
mixed Ising and Heisenberg coupling, crit. props. 78−19256
mixed magnets, competing spin glass and mag. order, phase diagrams, crit. points 80−39802
$Mn_{1.98-x}Cr_xFe_{0.02}Sb$, Mossbauer effect exam. 78−68432
Monte Carlo methods in statistical physics, book 79−80528
Monte Carlo simulation, in systems with competing interactions 78−14963
Monte Carlo simulation of model spin systems 80−20421
Monte Carlo simulation of quantum spin systems, two dimens. X-Y model 78−27011

magnetic transitions continued
Mossbauer isomer shift at phase transitions, book contrib. 79−87352
Mossbauer line, exchange narrowing 77−85627
multicritical (order O) magnetisation eqn. of state, renormalisation group calc. 78−31085
multicritical behaviour, two-variable approximants using series extrapolation method 77−66336
multicritical points in mag. systems, review of exptl. studies 77−66325
n-vector lattice spin model near two-dimens., crit. temp. 77−8324
narrow band gap semiconductor, antiferromag. in strong mag. field *(Russian)* 77−28387
Neel ferrimagnet, field-induced spin-orientational phase transitions 80−2576
Neel ferrimagnets, phase transitions, field-induced spin-orientational 80−75767
neutron diffraction studies of phase transitions and crit. phenomena, book contrib. 79−60229
neutron inelastic magnetic scatt., book contrib. 77−89944
neutron scattering, transitional, ambiguity in exptl. results 77−47546
neutron scattering in critical region, differential cross section 78−39294
nickel hexapyridol perchlorate, $Ni(C_5H_5NO)_6(ClO_4)_2$, sp. ht., mag. ordering transition 77−48004
$NiWO_4$, antiferromag., low symmetry exhibited during spin-flop phase transition 80−60263
NMR, resonant, near mag. transition 78−76265
NMR frequency, amplification and dynamic shift, rel. to local mag. props. *(Russian)* 77−20722
nonlinear dynamics of first order phase transitions 79−11322
nonmagnetic-paramagnetic transition in one-dimens. electron system due to spin excitations *(Russian)* 78−43606
nontranslationally invariant spherical model, exact soln., phase transition 77−37833
nonuniform ferromagnet, spontaneous magnetisation, mean field theory *(Chinese)* 78−91865
nuclear dipolar magnetic ordering, dipole-dipole interactions review 77−85475
nucleation centre formation in mag. phase transitions of first kind 78−2683
one dimensional system, Kondo lattice and weak antiferromagnetism 77−73038
one-dimensional classical and quantum chains, spin-Peierls transition theory 77−66375
one-dimensional conductor, Curie const. discontinuity explained as paramag. domain tip alignment 77−16035
one-dimensional electron system, with attractive interaction in mag. field, paramag. transition 80−7072
one-dimensional magnetic system, spin anisotropy and exchange alternation 80−34644
one-dimensional quasiclassical spin wave model in mag. field, static and dynamical props. 77−66284
one-dimensional semi-infinite chain, enhanced surface exchange interaction, mag. relax. 80−29558
ordered continuously degenerate systems, props. 79−93040
ordered magnetic cpds., selective sublattice dilution, percolation problem 80−103850
ordering temps. determ. by Bethe-Peierls-Weiss (BPW) method 80−54912
organic salts, neutral-ionic interface, energy states and mag. props., VB anal. 79−4537
orientation transitions, stabilising effect of high freq. fields *(Russian)* 77−89972
orthoferrites near spin-flip temp., magnetoelastic waves 78−19301
paramagnetic crystal, mag. ordering, spin-phonon mechanism *(Russian)* 78−60302
paramagnetic ions, spontaneous coherent state transition, susceptibility singularities 77−40119
paramagnetic to helicoidal or sinuosidal state transition *(Russian)* 77−63193
paramagnetic-helical crit. line, near Lifshitz point 78−23278
parametric excitation of sound near phase transition point in ferro-, ferri- and antiferromagnets 79−69710
partly disordered magnetic structures 77−51908
percolation clusters, one dimens., crit. exponents 78−31082
percolation models, spin representation and cluster distribs. 78−34998
Permalloy-Mn film, diffusion aftereffect causing mag. state change *(Russian)* 80−103860
phase diagram of magnets with two-sublattices *(Russian)* 78−23268
phase transformations, Ising and other models, book contrib., review 77−37825
phase transitions in strongly random systems, review 79−58647
phase transitions with two order parameters, Landau theory, mag. reorientation 80−103456
physics of transitions, introduction 78−26660
planar classical Heisenberg model, quadrupole phase transition 78−95447
planar magnets, quasi-two-dimensional, dynamics of vortices 80−71066
planar model, two-dimensional, crit. props. 78−10702
planar rotator model, one-hypercube renormalisation group transform. 78−72353
planar spin two-dimens. model, mag. correlation function, self-consistent calc. 80−29563
plane rotator model, two dimens., mag. equilib. props., Monte Carlo method 78−47990
polarised neutron scatt. meas. method 79−87257
α,ω-polymethylene diammonium metal (II) tetrahalides, cryst. growth, solubility and props. 78−43999
position space renormalisation of spin systems with long-range forces, critical exponents 78−24755
Potts model, 1st and 2nd order transitions, renormalisation group soln. 79−99706
Potts model, appl. of Legendre transformation 78−80156
Potts model, discrete, three spin thermodynamic behaviour, Kikuchi cluster variational method anal. 79−35640
Potts model, first order phase transitions, Monte Carlo renormalisation group method 80−34645
Potts model, first-order phase transform., three-state model, Monte Carlo renormalisation group method 79−99709
Potts model, Monte Carlo simulation in three dimens. 80−163
Potts model, spin anisotropy and crossover 78−56339
Potts model, three state, lower bound renormalisation transformation 77−28347

magnetic transitions continued
Potts model, three-component, phase transitions *(Russian)* 77−89971
Potts model, three-state, first order phase transitions 80−60333
Potts model on square lattice, specific heat critical exponents 77−20606
Potts s-state model, exact critical surface on triangular and honeycomb lattices 79−148
1,3-propanediammonium tetrachloromanganate(II) mag. props. 4.2-220K 77−20567
quantum compressible Ising model, critical behaviour 80−108016
quantum spin glass theory 80−103839
quantum spin model, appl. of projective renormalisation group 80−84607
quantum spin system, two-dimens., frustration, renormalisation group study 80−80535
quantum spin systems, exact boson representation and crit. behaviour 79−78423
quantum spin systems, Migdal renormalisation group approach 79−38333
quantum spin systems and classical counterparts 77−57294
quantum systems, one-dimens. isotropic X-Y model, zero temp. renormalisation group method 79−82800
quantum systems, two-dimens. Ising model, zero temp. renormalisation group method 79−82801
quasi one-dimensional system, helicoidal and sinusoidal ordering *(Russian)* 78−10717
quasi-low dimensional spin system, 3-D mag. ordering, randomness effects 78−10710
quasi-one-dimensional system, first and second order phase transitions, qualitative theory 78−31086
quasi-one-dimensional systems, spin-lattice Peierls instabilities, static and dynamic aspects 80−71052
quasi-one-dimensional systems, statistical mech., thermodynamic props., mag. transition 77−26246
quasi-one-dimensional systems, three-dimens. ordering in system of weakly coupled chains 78−6295
quasi-two-dimensional planar spin system, mag. transition 80−65951
quenched random alloy with competing anisotropies, decoupled tetracrit. point 77−12138
quenched random magnets, thermodynamic behaviour from position-space renormalisation group 78−68244
quenched random spin systems, dynamical replica methods, nonequilib. critical phenomena 78−43602
quenched random spin systems, spin glass and related orderings 78−10706
random and spatially inhomogeneous magnetic materials, exact model results 78−52271
random anisotropic magnetic alloys, multicrit. points 77−16091
random antiferromagnets, crit. and multicritical props. 80−60332
random ferromagnets, crit. exponents 78−10694
random ferromagnets, Ginzburg criterion, critical fluctuations 80−71032
random hierarchical model, crit. props. 80−71072
random Ising bond interactions, paramag. phase, thermodynamic props. 77−20523
random Ising magnet, phase diagrams 80−7065
random Ising system, critical index and temp. 79−56543
random Ising system, mag. critical index 79−56544
random mixture of Heisenberg and Ising bonds, singularity 77−59411
random $n \geq 4$ vector models, renormalisation group technique in $4-\varepsilon$ dimensions 77−16088
random n-vector model, renormalisation group analysis, crossover behaviour 77−85459
random n-vector model, smooth cut-off renormalisation group eqns. 77−85458
random ordered phase, effective field approx. 79−1676
random site Ising model near percolation threshold 78−23282
random spin models with coupling to nonfluctuating parameter, crit. behaviour 79−47292
random spin system, scaling function for two-point correlations 78−80147
random system, crit. behaviour near 2nd order phase transition lines intersection 78−68276
random uniaxial systems with dipolar interactions, phase transitions 77−72677
random-spin systems, with short range interaction, static crit. behaviour 78−39328
randomly diluted lattice, phase transitions, near percolation threshold, scaling theory 77−40066
randomly disordered alloys, ferromagnetism onset, mag. inhomogeneity 80−75774
randomly distributed interaction centres, mol. field distrib. function *(Russian)* 80−44834
rare earth alloys, $CaZn_5$ type struct., mag. symmetry 79−24143
rare earth alloys, mag. phase diagram 78−10684
rare earth alloys, phase transitions in complex mag. struct. *(Russian)* 78−72361
rare earth alloys, R_2Pt (R=Gd, Tb, Dy, Ho, Er), magnetic susceptibility meas., mag. transition obs. 80−60222
rare earth alloys, random anisotropic magnetic alloys, multicrit. points 77−16091
rare earth alloys, RCo_2, elec. resistivity, thermopower, X-ray struct. meas. 80−24874
rare earth amorphous alloys, antiferromagnetism, mol. field approx. 78−80142
rare earth amorphous alloys, random mag. anisotropy, antiferromag., Monte Carlo calcs. 79−33471
rare earth compounds, Kramers, temp. renormalised spectrum of mag. excitations, cryst. field level ordering 77−20516
rare earth compounds, $R_xMo_6S_8$ mag. susceptibility meas., 1.3-300K 78−14936
rare earth compounds, RCo_2 metamagnetic transitions in internal fields 80−60272
rare earth compounds, RMo_6X_8, (X=S, Se), supercond. and long range mag. order coexistence 80−15642
rare earth compounds, RRh_4B_4, supercond. and long range mag. order coexistence 80−15642
rare earth compounds, ternary, superconductivity and ferromagnetism 79−69617
rare earth compounds and alloys, spin-reorientation transitions, review 77−36073
rare earth dihydrides and dideuterides, electronic and mag. props. 80−25260

magnetic transitions continued
rare earth ferrite garnet single crystals, spin reorientational phase transitions *(Russian)* 78−39349
rare earth intermetallic cpds., cryst. field effects rel. to mag. props. 80−59933
rare earth intermetallics, RFe_2 and $R(Co_{0.98}\ Fe_{0.02})_2$, magnetostrictive material, changes in vibr. modes near mag. phase transition 79−90736
rare earth iron garnets, crit. field for phase transition, spectra calc. 77−8553
rare earth metal, anomalous sound attenuation near mag. transition temp. 78−15004
rare earth metal, magnetic properties, nonlinear s-f exchange interaction effect 80−15711
rare earth metal films, room temp. i.r. cond., rel. to mag. transitions 77−1745
rare earth metals, electronic sound attenuation anomalies at transition to helical phase, Fermi surface topology *(Russian)* 80−92807
rare earth metals, heavy, magnetic phase transitions *(Russian)* 79−7993
rare earth mixed valence compounds, charge dominated fluctuation props. comparison, mag. moments and ordering 80−54659
rare earth molybdenum sulphides, supercond. and magnetism coexistence *(Japanese)* 80−7025
rare earth orthoferrite, second-order reorientation transition, NMR signal relax. 77−90066
rare earth orthoferrite, stripe domain struct. near spin-reorientation points 77−24707
rare earth orthovanadites, phase transitions and Jahn-Teller distortions 79−28548
rare earth pnictides, mag. props. 78−72325
rare earth pnictides, phase diagram for cubic model in Kikuchi cluster variational method 79−35639
rare earth systems, high pressure studies, review 79−69193
rare earth trihydrides, light, low-temp. sp. ht., mag., elec., and cryst. field splitting effects 80−49379
rare earth-Co system, spin reorientation and sp. ht. anomaly *(Japanese)* 79−47287
rare earth-cobalt intermetallics, RCo_2, spontaneous vol. magnetostriction, first order phase transition obs. 77−12183
rare earth-Fe_2 Laves phase intermetallics, mag. ordering temps. by DTA 79−47283
rare earth-transition metal (4f-3d) intermetallic cpds., mag. moment and mag. anisotropy 80−25107
rare earths, heavy, mag., electronic struct., book 78−60259
renormalisation group approach for percolation, mag. indices 77−69572
renormalisation group approach to critical phenomena, ferromagnetic example 78−8497
renormalisation group approach to scaling, phys. appl. 78−49634
renormalisation group technique, review 77−20625
renormalisation group techniques 77−2633
renormalisation group transformations and critical phenomena *(Chinese)* 78−95128
renormalised mean-field approach to crit. behaviour, two- and three dimens. Ising models 79−38339
resistance critical behaviour, temp. and mag. field depends. 77−73037
rotationally inelastic scattering, mag. transitions, time reversal symm. 80−53105
scaling function near mag. critical point, complementary expressions 80−34656
scaling hypothesis with finite correl. length at phase transition point 79−73743
scaling relations, dynamic, linear and nonlinear, in renormalisation group theory 77−8321
screw spin ordered state through dipole-dipole interaction 78−39337
second order, group theoretical anal. 79−91239
second order phase transition, nonvalidity of Lifshitz condition, appl. to heavy lanthanides *(Chinese)* 78−51643
second order phase transitions, superspace group description *(Chinese)* 80−8942
second order transitions, with fluctuations, symmetry changes 77−63220
second-order transitions in metals, high-speed dilatometry 77−89951
semiconductor, exciton ferromagnetism 79−28293
semiconductor, mag. ordering in systems with low carrier densities 78−2684
semiconductor, with impurities, accompanying semicond.-metal transition 77−59257
semiconductors, electronic properties, critical behaviour, theory 80−96861
simple magnetic systems, crit. exponent β, meas. review 79−73732
singlet ground state system in mag. field, anisotropic exchange interaction effect on props. 79−91224
site-disordered spin systems, generalised CPA 77−20513
small superconductor in magnetic field, first and second order phase transitions 80−2519
solid solution, crit. phenomena of random spin systems, renormalisation group approach 78−52263
solitons in condensed matter physics, theory 80−50122
solitons near critical point, neutron scattering observation 80−34650
space environment applications for critical phenomena and condensation, second order phase transformations 79−46783
speromagnetism phase transition, random distrib. mol. field model 79−73730
spherical model, Gaussian random magnetic fields 78−19264
spherical model, isotropic Lifshitz point in $2<d<4$ dimens. 78−29062
spherical model, phase separation, symmetry breaking fields study 80−88760
spherical model, phase separation 79−44869
spin glass, cluster mean field theory and evidence for spin clusters 79−78382
spin glass, crit. props., simple soluble model 77−12141
spin glass, critical behaviour, dynamic scaling theory 77−40063
spin glass, dil., conc. expansions at zero temp., Ising model 80−60303
spin glass, dynamical instability, effect of external mag. field 79−33493
spin glass, dynamics near transition, classical soft-spin models 79−95599
spin glass, FCC lattice with RKKY interaction, numerical calc. 78−52275
spin glass, high-temperature series for order-parameter susceptibility 79−28534
spin glass, infinite range model, stability and susceptibility in Parisi's soln. 80−88762
spin glass, Ising, two-dimensional, Monte Carlo evidence for absence of phase transition 78−19260
magnetic transitions continued
spin glass, Ising model, existence of phase transition 78−56327
spin glass, low temp. renormalisation group 78−10688
spin glass, Mattis model 77−8322
spin glass, mean field theory and ϵ-expansion 78−10705
spin glass, model, exactly soluble *(Russian)* 77−80944
spin glass, nonmagnetic defects, sp. ht., susceptibility and resist. determ. 79−19738
spin glass, order-parameter susceptibility, series expansion 77−43839
spin glass, scaling at crit. temp. 78−10714
spin glass, self-consistent theory of cusps in susceptibility 77−77066
spin glass, spin freezing, exptl. obs. 77−73032
spin glass, transitions, field-induced, masking effects 80−65943
spin glass Kondo transition resist. max. 79−19584
spin glass systems, experimental props. and theories 79−65688
spin glass transition, cumulant expansion of free energy of disordered systems 80−71067
spin glass transition, lower crit. dimensionality 80−60291
spin glass transition, rel. to roughening transition in crystal growth theory 78−27045
spin glass transition, search for, using series methods 77−89960
spin glass with non-random interactions 77−55673
spin glasses, 2-dimens., computer expts. 77−80945
spin glasses, anisotropic, crossover effects 79−65692
spin glasses, dilute, at zero temperature, low concentration series expansion 80−93131
spin glasses, free energy, order parameter expansion, random bond model 80−84609
spin glasses, monoionic anisotropy, influence on transform. to paramag. state *(Russian)* 79−28529
spin glasses, order parameter for replica symmetry breaking 80−44835
spin glasses, phase transition, fluctuations of local spins, mean-field theory 80−34661
spin glasses, phase transition, mag. susceptibility, specific heat, Ising model calcs. *(Russian)* 80−34671
spin glasses, quartic operators in Ising, X-Y, and Heisenberg systems 79−33498
spin glasses, random mixture of Ising systems, phase boundaries 80−60285
spin glasses, recent progress in numerical simulation 79−69689
spin glasses, superconductivity 79−28428
spin glasses, susceptibility, wave-vector-depend., theory 80−11209
spin glasses, theory, review 78−2696
spin models planar, duality props. and phase diagrams 80−60286
spin Peierls transition, gap eqns. 80−24801
spin system, critical, in random mag. field, supersymmetry, neg. dimensions 79−97533
spin system, cubic model, Monte Carlo simulation, phase transitions 80−34646
spin system, n-component, with coupling to non-ordering parameter 77−51906
spin system, random thermodynamic props. using Bethe-Peierls-Weiss approx. 79−78387
spin system with double electron exchange order-order transitions 77−4522
spin systems, tricritical phase transition, eqn. of state, critical exponents, logarithmic corrections 78−27048
spin wave damping, magnetic materials with canted mag. struct., thermodynamic and high freq. props. 80−11184
spin wave theory of spin 1/2 X-Y model, phase transitions 80−7068
spin waves in weak antiferromagnetic exchange field system 78−43577
spin-flop multicritical points in systems with random fields and in spin glasses 79−33495
spin-glass, obs. by DC Josephson effect 80−100594
spin-glass transition temperature and order parameter 79−42771
spin-one Ising model with bilinear and biquadratic interactions 79−65677
spin-one Ising system, phase diagram 78−95441
spin-one Ising system with biquadratic interaction 79−4683
spin-Peierls phase diagrams, obs. and models 80−60330
spin-Peierls transition, dynamic struct. factor 78−14964
spin-Peierls transition, first-order, theory 77−20605
spin-Peierls transition, mag. field depend. 78−80170
spin-Peierls transition in Heisenberg Hubbard models 78−68242
spin-Peierls transition in mag. field, phonon freq., Heisenberg model calcs. 80−25151
spin-reorientation phase transitions, crit. behaviour 77−12132
spin-spin correlation function near the critical point 79−11319
spinels, diluted, percolation and mag. order 78−68165
SQUID magnetometer with temp. control, spontaneous magnetisation and mag. susceptibility meas. 80−68221
statistical mechanics 78−71830
steel, austenitic stainless, Cr-Ni, elec. resistivity and struct.-mag. transitions at low temp. 79−99527
steel, austenitic stainless type 304N, machining induced deformation transformation, mag. evaluation 79−83195
steel, magnetisation transitions, Barkhausen noise 78−91894
steel, stainless, Invar related system, high press. Mossbauer spectra 79−56642
steel, stainless, metallographic technique for detection of ferromagnetic δ-ferrite to paramagnetic σ-phase 79−61816
step model, critical behaviour, high temp. susceptibility and internal energy series 78−34987
Stoner glass, disordered itinerant-electron system, spin-glass condensation 79−78424
structural and mag. phase transforms., integral rational basis of invariants *(Russian)* 80−62602
superconductor, ferromagnetic, critical behaviour, coexistence near supercond.-ferromag. multicritical point 79−47197
superconductor, helical ordering of spins 80−88669
superconductor to ferromagnetic transition, EM effects 79−51708
superparamagnetic system in spontaneous coherent state, phase transitions 78−47991
surface, itinerant antiferromagnetism and density waves 79−82743
surface magnetisation profile, in crit. region by ϵ-expansion, Wilson perturbation theory calc. 80−50100
surface magnetisation profile singularities near critical point 80−103843
surface of magnetic systems, multicritical phenomena 77−32208
system with two parameters, Mott and ferromagnetic transitions, phase diagram of the extended Caron Pratt model 79−15083

magnetic transitions continued
systems far from thermodynamic equilib., dissipative structures, broken symm. equilib. phase transition theory 80−65827
TANOL, free radical, spin flopping transition, temp. depend., mag. anisotropy energy 80−54890
TCNQ salt, dibenzo-TTF-TCNQCl_2, one-dimens. mag. semicond., mag. and elec. props. 80−88601
TCNQ salt, K-TCNQ, spin-Peierls system, paramag. susceptibility, Heisenberg chains 79−38299
TCNQ salt, N-methyl-N-ethyl-morpholinium-$(TCNQ)_2$, spin-Peierls transition 79−82803
TCNQ salt, N-propyl-quinolinium$(TCNQ)_2$, defect conc. depend. phase transition 80−44577
TCNQ salt, pyridinium $(TCNQ)_2$, low temp. mag. phase transition, ESR study 80−25139
tensor order parameters for magnetic-structural phase transitions in strong spin-lattice coupled crysts. 80−50125
tetragonal XY-like antiferromagnet, multicritical behaviour, global phase diagrams 79−42779
thermodynamics, model 77−47998
three-state Potts model variant, phase behaviour 78−68259
TMMC, crossover transition, effects on susceptibility and EPR shift 80−71047
TMMC, linear antiferromag., mag. phase diagram, expt. and theoretical study 80−71038
TMMC, one-dimens. antiferromagnet, XY-Ising transition under mag. field 79−91244
TMMC, XY-Ising crossover transition, quasi-elastic neutron scatt. obs. 80−44826
transition metal, BCC isothermal compression to 100 kbar 78−43069
transition metal, magnetic order at surfaces 78−95439
transition metal alloy disordered host, actinide impurity localised magnetism 77−51883
transition metal alloys, magnetically ordered, effect of magnetic field on P-T diagram 78−52246
transition metal chalcogenides, Mott metal-insulator and mag. phase diagrams 78−10354
3d-transition metal complexes, low spin-high spin paramag. transition, Ising model calc. 80−93073
transition metal pnictides, displacive and mag. transitions 80−59616
transition probability, system size depend., consequences for stochastic eqns. 78−41258
3d-transition-metal dichalcogenides, mag. props. rel. to Hubbard model 79−78373
triangular Ising lattice with anisotropic interactions 78−47926
tricritical phase transition, critical exponents, classical N-component spin systems 78−4579
tricritical points in systems with random fields 79−33494
tricritical scaling in spherical model limit 78−68248
tricritical system, scaling field description of first-order transition 78−95442
tricriticality, nonuniversality 79−78392
tricriticality and the failure of scaling in the many-component limit 79−6071
triplet Ising model on triangulated dice lattice, phase transitions 77−17918
TTF(MBDT) spin-Peierls transition, mag. exchange interactions, mag. props. 80−25138
$(TTF)CuS_4C_4(CF_3)_4$, spin Peierls system, mag. field effects 80−7123
TTF-BDT(M), BDT=$S_4C_4(CF_3)_4$, M=Cu, Au, spin-Peierls transition, sp. ht. meas. 77−28401
TTF-bis-dithiolene metal complex compounds, donor-acceptor type, one-dimens. mag. variety and props. 77−66271
TTF-bisdithiolene metal complexes, spin Peierls transition 77−4523
TTF-$CuS_4C_4(CF_3)_4$, spin-Peierls system, high-field phase 80−39816
TTF.CuBDt, spin 1/2 Heisenberg chain, spin-Peierls transition 79−61135
TTFCuBDT, spin-Peierls transition in spin 1/2 Heisenberg chains, RPA calcs. 80−25150
TTT-$(I_3)_{0.5}$, one-dimens. metal, mag. susceptibility, elec. resist., thermopower meas. 78−87967
two dimensional percolation, crit. amplitudes, universality test 77−13727
two state approximation, for sp. ht. anomalies associated with phase transition 79−26013
two-dimensional anisotropic N-vector models 79−85095
two-dimensional Ising antiferromagnet, neutron scatt., review 80−50103
two-dimensional Ising model, real space renormalisation transform. 78−2687
two-dimensional Ising system, crossing over to two-dimensional Heisenberg system 80−93123
two-dimensional planar magnet, crit. slowing down in transverse autocorrel. function 78−95448
two-dimensional systems, phase transitions 78−68241
two-spin correlation function, dipolar crossover 80−80516
two-sublattice biquadratic systems, phase transitions 79−99710
two-sublattice magnetic system with fourth-order uniaxial anisotropy and strong antisymmetric exchange in transverse mag. field 79−56530
two-sublattice system, with strong antisymm. exchange and fourth order anisotropy, mag. configs. 78−68167
uniaxial antiferromagnet, crit. dynamics at bicritical points 80−15321
uniaxial antiferromagnet, effect of magnetostriction on reorientation phase transitions 79−69674
uniaxial antiferromagnetic, phase diagram, spin flop transition *(Russian)* 80−100587
uniaxial dipolar magnet, critical dynamics and statics 77−59422
uniaxial ferromagnet, domain struct. in mag. field 80−103853
uniaxial ferromagnet, in transverse mag. field, quantum theory *(Russian)* 79−15297
uniaxial ferromagnet, phase front motion 79−82792
uniaxial ferromagnet domain struct., phase transition *(Russian)* 80−108044
uniaxial Heisenberg antiferromagnet, phase diagrams 80−15730
uniaxial Lifshitz point, Monte Carlo calcs. 78−39353
universal relations among crit. amplitudes 77−66341
VI_2, mag. structs. and props. 79−61063
weak ferromagnet, paramagnons and phase transitions 77−61015
weak ferromagnetism, associated with third-order invariants *(Russian)* 78−95435
weakly disordered uniaxial ferromagnet, phase transition *(Russian)* 78−23291

magnetic transitions continued
Wilson's renormalisation group recursion eqns., critical phenomena in spin systems 78−4581
Wilson renormalisation group equation, soln. by scaling field eqn. 78−68252
X-Y(s=1/2) model, renormalisation group method, triangular lattice 77−26247
X-Y magnetically dilute ferromagnet, two dimens. lattices 77−63056
X-Y magnets, two-dimens., with annealed non-mag. impurities 79−78391
X-Y model, biquadratic, spin one, variation of Curie temp. 80−97102
X-Y model, classical, high-temperature expansion, correl. length and transition temp. 79−33447
X-Y model, crit. props., review 77−66326
X-Y model, critical behaviour, high temp. susceptibility and internal energy series 78−34987
X-Y model, critical properties near Lifshitz point, Monte Carlo study 79−28543
X-Y model, disordered, two-dimens., phase transition 79−82789
X-Y model, isotropic spin 1/2, phase transitions in quantum spin systems 78−84434
X-Y model, quantum effects and dynamics at low temps., path integral approach 80−84584
X-Y model, quantum effects in critical props., in transverse magnetic field 78−2689
X-Y model, S=1/2, phase transitions at T=0, z-field renormalisation group method 80−71051
X-Y model, self avoiding walk approx. 77−4488
X-Y model, spin 1/2, anal. of high temp. series expansions of some thermodynamic quantities in four dimensions 80−50098
X-Y model, two dimensional, Monte Carlo simulation and phenomenological theory of phase transition 78−6534
X-Y model, two-dimens., vortex formation in Monte Carlo calcs. 77−63224
X-Y model, two-dimens. spin 1/2, temp. marginality by linear renormalisation transform. 79−38341
X-Y model for linear chain, struct. transition under external mag. field and stress 77−12126
X-Y model singular bounds on free energy and susceptibility 78−43595
XY model, Monte Carlo simulation, phase transition with vortices 77−43799
$Ag_{1/2}In_{1/2}Cr_2S_4$, first order macro to microdomain transition 77−69562
Al-Fe, alloy with mixed types of order, uniform mag. phase diagram 79−78368
$Al_2La_xCe_{1-x}$, low temp. mag. props. 80−20564
$Al_2Mn_3Si_3O_{12}$, spin correlations and phase transitions, neturon diffr. exam. 78−84390
Au-Co, liquidus line determ. by mag. meas. 80−60250
Au-Fe, alloy with mixed types of order, uniform mag. phase diagram 79−78368
Au-Fe, dil., crit. dynamics 80−60325
Au-Fe, spin-glass, characteristic temps. 79−38348
Au-Mn-Cr(Pd) alloy, ferro- to non-mag. transform. 77−12117
Au-Ni, heat capacity, 1.5 to 15K 78−95452
$B_2O_3.Fe_2O_3.nMO$ (M=Fe, Co, Ni, Cu, Mg), synthesis and mag. props. 80−20384
$Ba_2Co_{1.65}Fe_{0.35}{}^{2+}Fe_{28}{}^{3+}O_{46}$, temp.-mag. field phase diagram, torque method 80−60276
$BaFe_4Ti_2O_{11}$, R-type hexaferrite, spin struct. and mag. props. 78−52216
$BaMnF_4$, low temp. dielec. props. and phase transitions 77−20790
$BaMnF_4$, magnetic neutron scatt. from structurally distorted cryst. 80−93086
$BaMnF_4$, phase transitions, review 79−78378
$BaMnF_4$, struct. and mag. transitions, magnon dispersion curves, nearest neighbour exchange consts. 79−42760
$BaVS_3$, mag. transition and hyperfine interaction, neutron spin-flip scatt. obs. 80−97093
$BaVSe_3$, one-dimensional, struct. and mag. props. 80−28993
$BaZn_{1.38}Co_{0.62}Fe_{16}O_{27}$, W-type hexaferrite cryst., first order magnetisation processes 78−95472
Bi, vapour, optical activity, Faraday effect, parity nonconservation, mag. transitions *(Russian)* 80−55070
CO, chemisorbed layer on Au(Pt), mag. phase transition obs. *(Russian)* 77−77083
$Ca_3Mn_2Ge_3O_{12}$, mag. struct. study 80−2554
$CaO-Al_2O_3-Fe_2O_3$, and resonance spectroscopy study *(Russian)* 77−55733
$Ca(OH)_2$, mag. ordering of proton spins 79−73746
$CdCr_2S_4$, Heisenberg ferromag., obs. of dynamic dipolar crossover, ESR linewidths meas. 79−24209
$CdCr_2(S_xSe_{1-x})_4$, magneto-conc. diagram *(Russian)* 77−4517
$CdCr_2Se_4$, crit. behaviour near Curie point 78−31068
$CdCr_2Se_4$, reactor radiation influence on ferromagnetic phase transform. *(Russian)* 80−75760
$Cd_{1-x}Mg_x$, magnetic susceptibility anisotropy, press. effects, electronic phase transitions *(Russian)* 80−54869
$Cd_{1-x}Zn_xCr_2Se_4$, mag. semicond., neutronographic obs. *(Russian)* 79−11297
Ce compounds, rocksalt type, low temp. thermal props. 78−84445
Ce monochalcogenides, cryst. field effects, phase transitions 80−24853
Ce monochalcogenides, mag. ordering, expt. test for ε-expansions with n=4 80−60259
Ce monopnictides, anomalous mag. props., planar coupling theory 80−60245
Ce monopnictides, cryst. field effects, phase transitions 80−24853
Ce-Pt, paramag. suscept. 79−61047
$CeAg_xIn_{1-x}$, cubic to tetragonal phase transform., conc. dependence by resist. meas. 78−2252
$CeAl_2$, Anderson lattice system, ground state props. 80−20443
$CeAl_2$, conf. Kondo system, sp. ht. meas. 78−52210
$CeAl_2$, electronic transition under pressure, resist. meas., rel. to mag. to nonmag. transition 79−33311
$CeAl_2$, magnetic ordering, 24 component Ginzburg-Landau model 80−97095
$CeAl_2$, NMR, cryst. field effects and mag. order in low temp. phase 78−68391
$CeAl_3$, singlet ground state at T=0, mag. ordering 2.5-6K 78−84388
Ce_3Al_{11}, mag. ordering at low temps. under press., relation to $CeAl_3$ props. 79−19745
CeB_6, anomalous sp. ht. intrinsic mag. phase transitions obs. 80−108027
CeBi, lattice distortion modes and mag. structural transitions 79−78325

magnetic transitions continued
CeBi, phase diagram in mag. field, hydrostatic press. effect 80−25132
CeBi(Sb), anisotropic mag. ordering and mag. structural transitions 79−78324
$Ce_{0.73}Ho_{0.27}Ru_2$, superconductors, mag. correlations and crystal-field levels 80−34547
$CeIn_{3-x}Sn_x$, scaling behaviour near valence instability, mag. susceptibility and mag. transitions 80−25111
$Ce_{1-x}La_x$ alloy, thermoelectric power 79−78080
$Ce_{1-x}La_x$, thermoelectric power, mag. transition temps. 80−20154
$Ce_x(La_{0.76}Y_{0.24})_{1-x}Sb$, mag. phase diagrams, exchange interaction variation-thermodynamic model 79−65673
$Ce_{1-x}Pr_xAl_2$, mixed mag. phase at low temp. 78−68228
CeSb, commensurate-commensurate transitions and devil's staircase 79−78317
CeSb, mag. phase diagram and mag. struct., neutron diffr. determ. 77−63182
CeSb, mag. phase transitions, zero applied mag. field 78−31070
CeSb, mag. transition, effect of applied mag. field 78−43590
CeSb, phase diagram and mag. struct. 77−85422
CeSe, mag. ordering, ε expansion predictions, neutron diffr. obs. 79−61060
CeTe, mag. ordering, ε expansion predictions, neutron diffr. obs. 79−61060
$Ce_{1-x}Th_x$, mixed valence systems, spin dynamics and mag. ordering 78−68162
Co complex, $Co(C_5H_5NO)_6(ClO_4)_2$ and $Co(C_5H_5NO)_6(BF_4)_2$, $S=^1/_2$ XY magnet, sp. ht. below 1K 77−55682
Co complex, dipyridyl chloride, metamag., mag. struct., NMR 77−85418
Co-mischmetall system, phase relations, microstruct., mag. props. 80−104118
$CoBr_2.2H_2O$, metamagnetic, relax. phenomena at phase transitions 79−24164
$CoBr_2.2H_2O$, phase transitions in ferrimag. state 77−63191
$CoBr_2.6(0.48D_2O, 0.52H_2O)$ spin-flop system, intermediate phase existence, sublattice magnetisation reorientation 80−80510
$CoBr_2.6[(1-x)H_2O.xD_2O]$, mag. intermediate phase, magnetisation and neutron scatt. meas. 80−60195
$CoCO_3$, antiferromag., Raman spectra, 2-300K 77−32380
$CoCl_2.2H_2O$, antiferromag., light scatt. from phonons and magnons 80−40104
$CoCl_2.2H_2O$, metamagnetic transition, microscopic dynamics 77−16073
$CoCl_2.2H_2O$, metamagnetic, ^{55}Mn NMR of impurity spin 77−85613
$CoCl_2.2NC_5H_5$, 1-dimens. Ising ferromag., charact. EPR modes 79−91287
CoF_2, phase transition in transverse mag. field, magnetoelastic interactions 79−65676
$Co_{2.94}Fe_{0.06}S_4$ Mossbauer ^{57}Fe spectrum, mag. transition, lattice atomic occupancy 77−48095
$CoFe_2Se_4$, low-temp. thermal expansion anomalies and isothermal compressibility, mag. ordering and magnetorestriction 79−38363
$Co_{1-c}Mn_cF_2$, antiferromagnet mag. impurities, spin excitation spectrum collective rearrangement in external mag. field 80−50199
$CoNb_2O_6$, ordered state, field induced mag. transitions 77−16074
$Co_xNi_{1-x}Cl_2.6H_2O$, solid solution, mag. props. and phase diagram, calc. 80−7104
$CoO-Al_2O_3-SiO_2$ spin glass, new state in very weak mag. field 79−78416
$Co_xPd_{80-x}Si_{20}$, amorphous, low field susceptibility near transition temp. 77−66359
$CoS_{2-x}Se$, magnetism and metamagnetic transition, neutron diffr. and NMR meas. 80−15717
$CoS_{2-x}Se_x$, conc. and temp. effects on metamagnetic transition 80−15716
$Co(S_xSe_{1-x})_2$, $(0\leq x\leq 1)$, mag. props. and elec. resist. 79−65657
$CoSe_2$, paramag. metal, sp. ht., Mossbauer effect, absence of ordering 77−16036
Cr alloyed with d-transition elements, magnetic transformations, triple point *(Russian)* 80−88747
Cr and alloys, itinerant antiferromagnetism and density waves at surface 79−82743
Cr and Cr alloys, structural changes during low-temp. phase transform. *(Russian)* 79−52202
Cr, antiferromag., nature of spin-flip transition 77−63186
Cr, antiferromag., spin density waves, mag. anisotropy, spin-flip transition 77−69540
Cr, antiferromagnetic, US attenuation and phase diagram 80−103831
Cr, electronic structure model, Invar effect, antiferromagnetic-non mag. transitions 80−20370
Cr, hyperfine interactions on ^{111}Cd-probe nuclei, TDPAC meas. 80−75904
Cr, mag. phase diagram, near, spin-flip temp., US attenuation 80−60267
Cr, magnetic phase diagram in external mag. field, spin reorientation curve, critical point coordinates *(Russian)* 80−29548
Cr, magnetic torque anal. in thermally activated domain model, near spin-flip temp. 77−63229
Cr, spin density wave, CDW and strain wave, effect of spin polarisation of reservoir and imperfect nesting 78−56284
Cr, spin density waves detected by Ta mag hyperfine field meas. 78−60364
Cr, strain and spin-flip transition, Landau theory 78−39318
Cr-Fe, alloy with mixed types of order, uniform mag. phase diagram 79−78368
Cr-Fe, antiferromag. Cr-rich, avalanche effect due to nucleation-controlled phase transition from metastable mag. state 79−73750
Cr-Fe, dil., latent heat exam. of magnetic transitions 79−61156
Cr-Fe, dil., spin correlations and neutron scatt. near crit. conc., theory 80−60327
Cr-Fe (0.8-8 at.%) alloy, mag. phase transforms, sp. ht. obs. *(Russian)* 77−80941
Cr-Fe alloy, mag. phase transition, sp. ht. meas. 77−12120
Cr-Ge, dilute alloy, phase diagram of spin density wave states 79−24158
Cr-Mn (0.5 at.%) alloy, mag. phase transforms, sp. ht. obs. *(Russian)* 77−80941
Cr-Os, magnetic transition T-P-C diagram, triple points *(Russian)* 80−54895
Cr-Pt alloys, neutron diffraction study, (100) magnetic peak, magnetic structure transitions 79−56506
Cr-Re, surface spin-density wave near T_N 79−91238
Cr-Sb alloy, dil., mag. phase diagram, elec. resist. and thermal expansion obs. 79−1669

magnetic transitions continued
Cr-Si, dil., latent heat exam. of magnetic transitions 79−61156
Cr-Si alloys, first order transition of spin density wave state, thermal expansivities meas. 77−85453
CrAs, heat capacity, enthalpy increments, thermodynamic props., 5 to 1280K 78−91450
$CrAs_{0.42}Sb_{0.58}$, mag. and struct. transitions under press., elec. resist. meas. 78−27038
$Cr_{1-x}Fe_x$, Mossbauer spectra, mag. behaviour 80−20532
$Cr_xFe_{2-x}CaO_4$ mag. phase transitions meas. *(Russian)* 79−75556
$Cr_xMn_{1-x}As$, mag. susceptibility anomaly at displacive phase transition 80−93091
CrN, mag. struct. and first-order antiferromag. transition 79−61132
Cr_2O_3, mag. phase boundaries near bicrit. and Neel points 78−34980
Cr_2O_3, magnetostriction anomalies near mag. field induced transitions 77−66315
CrS_xTe_{1-x} (x=0 to 0.2), magnetic props. study 80−11194
CrTe, effect of high pressures on magnetic properties 78−52238
CrTe, mag. ordering under high-press., ferromag. transition, ESR and neutron diffr. *(French)* 78−31053
CrTe, neutron diffr. at high press., mag. transition *(Russian)* 79−38326
Cr_5Te_6, magnetoresist. in region of mag. phase transforms. *(Russian)* 77−66299
$CsCoCl_3$, 1-D Ising antiferromag., mag. phase transitions 79−51779
$CsCoCl_3$, 10 Ising antiferromag., mag. excitations, electronic Raman and IR absorption spectra 78−2668
$CsCoCl_3$, Ising like antiferromag., mag. phase transition, ^{133}Cs NMR 80−7184
$CsCoCl_3$, mag. struct., neutron diffr. meas. 78−43563
$CsCoCl_3.2D_2O$, crit. behaviour along metamag. phase transition 77−59409
$CsCoCl_3.2D_2O$, metamag., thermodynamic props. near multicrit. pt. 77−66305
$CsCuBr_3$, quasi-1-dimens., NQR obs. 80−54987
$CsCuCl_3$, quasi-1-dimens., NQR obs. 80−54987
$Cs_2FeCl_5.H_2O$, mag. phase boundaries, susceptibility, 3D Heisenberg antiferromag. behaviour 78−84420
Cs_2IrCl_6, hyperfine spectra of mag. ordered state at very low temp., Mossbauer meas. 77−69744
$CsMi_3$, (M=V, Cr, Mn), Mossbauer spectra, struct., electronic and mag. props. 80−15908
$CsMnBr_3.2D_2O$, mag. phase diagram near bicrit. point 79−15302
$CsMnBr_3.2D_2O$, spin-flop systems, neutron scatt. expts. 79−61109
$CsMnBr_3.2D_2O$, spin-flop system, extended scaling near bicrit. pt. 79−51752
$CsMnCl_3.2H_2O$, mag. phase diagram near bicritical point 80−71021
$CsMnCl_3.2H_2O$, quasi-one-dimensional antiferromag., phase diagram *(French)* 80−20405
$CsMnCl_3.2H_2O$:Cu, parallel susceptibility, impurity effect on spin-flop field *(French)* 78−43569
$CsMnF_3$, isotropic antiferromag., crossover behaviour of mag. phase boundaries 79−78370
$CsMnF_3$, mag. phase boundaries, XY to Ising crossover, virtual bicritical point 80−50095
$CsMnF_3$, ordering temp., virtual bicritical pt. 79−61128
$CsNiBr_3$, double ordering in mag. linear chain system, sp. ht. and NMR data 79−28545
$CsNiCl_3$, double ordering in mag. linear chain system, sp. ht. and NMR data 79−28545
$CsNiCl_3$, linear chain antiferromag., mag. props., 1.1 to 7K 79−61076
$CsNiCl_3$, mag. props. 79−73736
$CsNiCl_3$, nearly one-dimensional antiferromag., spin-flop transition 78−6527
$CsNiF_3$, demagnetising effects on antiferromag. reson. 80−15803
$CsNiF_3$, field depend. mag. behaviour, mag. linear dichroism 79−73903
$CsNiF_3$, single cryst. mag. susceptibility meas. 77−20560
Cu complex, 1,2-ethanediammonium tetrachlorocuprate, layered struct. mag. susceptibility 80−7094
Cu complex, dichloro(dimethylnitrosamine)copper(II), magnetic phase transition, ^{14}N NQR obs. 80−11289
Cu complex, dichloro(dimethylnitrosamine) Cu II, mag. props., ^{14}N NQR obs. 80−54988
Cu, NMR study on nuclear ordering below 1 μK 80−93187
Cu-Mn, spin glass, meas. of order parameter 80−34642
Cu-Mn (8 at.%), spin glass, neutron scatt. and susceptibility investig. of spin dynamics 77−40076
Cu_3Au type antiferromagnet Ising lattice, finite entropy at T=0, phase transition 77−89958
$CuBr_2$, quasi-1-dimens., NQR obs. 80−54987
CuCl, disordered, diamag. transition 80−34636
$CuCl_2$, anhydrous, mag. phase transition 80−80506
$CuCl_2$, anhydrous, single cryst., mag. behaviour in low temp. ordered phase 79−7974
$CuCl_2$, quasi-1-dimens., NQR obs. 80−54987
$CuCl_2.2D_2O$, staggered magnetisation, neutron diffr. obs. 78−39296
$CuCl_2.2H_2O$, antiferromag., range of existence of intermediate state, NMR expt. 77−59410
$CuCl_2.2H_2O$, influence of high hydrostatic press. on intermediate state associated with spin flopping 78−35020
$CuCl_2.2H_2O$, NMR, high press. effect on existence domain width of intermediate state 79−87255
$CuCr_2S_4$, mechanism for phase transition from ferromag.-ferrimag. state *(Russian)* 77−36075
$CuCr_2Se_4$, crit. behaviour near Curie point 78−31068
$CuCr_2Se_4$, mechanism for phase transition from ferromag.-ferrimag. state *(Russian)* 77−36075
Cu_5FeS_4, mag. ordering and vacancy clustering, mag. susceptibility and Mossbauer spectra meas. 77−85625
$Cu_{1/2}In_{1/2}Cr_2S_4$, transition from long-range to short-range mag. ordering 77−36087
$CuK_2Cl_4.2H_2O$, 3-dimens. Heisenberg ferromag., crit. behaviour 77−20594
$CuK_2Cl_4.2H_2O$, Heisenberg ferromagnet, spontaneous magnetisation under press. *(Russian)* 77−36058
$CuK_2Cl_4.2H_2O$, Heisenberg ferromag., mag. field effect on susceptibility near crit. point 80−39758
$Cu(NH_4)_2Br_4.2H_2O$, 3-dimens. Heisenberg ferromag., crit. behaviour 77−20594
$Cu(NH_4)_2Br_4.2H_2O$, Heisenberg ferromagnet, phase transition in mag. field 79−7992

magnetic transitions continued
$Cu(NO_3)_2.2^1/_2H_2O$, high field phase transition, susceptibility and NMR meas. 77−69559
$Cu(NO_3)_2.2^1/_2H_2O$, long-range ordered state, mag. props. 78−39417
$CuRb_2Br_4.2H_2O$, 3-dimens. Heisenberg, ferromag., crit. behaviour 77−20594
$Cu_{2-x}Se$, nonstoichiometric, diamag. and paramag. props., susceptibility meas. 80−70936
$CuSeO_4.5H_2O$, $CuSO_4.5H_2O$ and $CuBeF_4.5H_2O$, linear-chain antiferromag., mag. phase transition investig. 77−55684
$Cu_{0.75}VS_2$, cryst. struct. and phys. props. *(French)* 78−14328
$D\text{-}_{12}Fe_{32}O_2$, anomalous magnetisation, compensated to uncompensated mag. arrangement transition 78−52254
Dy, field induced transitions of helical state 78−72349
Dy, helical antiferromagnetic phase, basal plane anisotropy 78−84412
Dy, helical-fan, helical-ferromagnetic and fan-ferromagnetic transitions, phase boundary determ. 79−24161
Dy, magnetocaloric effects between 84 and 280K 79−73721
Dy, US attenuation in mag. field 77−40104
Dy-Cu, amorphous, mag. phase diagram, magnetisation and sp. ht. meas. 80−80532
DyAG, crit., tricrit., and crossover phenomena, light scatt. 78−68251
DyAG, forced magnetostriction meas. 78−68349
DyAG, induced staggered mag. fields and order parameters 77−63099
$DyAl_2$, first order transition and tricrit. points, three-state Potts model 78−43589
DyAlG, tricrit. wing exam. 77−73026
$Dy_3Al_5O_{12}$, magneto-optical rotation in transverse field 79−73902
$DyAu_2$, long-duration pulsed mag. field appl. to magnetisation meas. 79−61183
$DyCo_2$-$DyAl_2$ system, mag. and structural studies 80−108006
$DyCo_5$, rotational type spin reorientation, collinear to canted spin struct. change 77−63214
$DyCo_{5.3}$ noncollinear mag. struct. appearance in mag. fields, magnetostriction meas. *(Russian)* 80−100607
$DyFe_2$, amorphous, ultrasonic exam. below T_c 79−73793
$DyFe_{0.998}Co_{0.002}O_3$, mag. transition, NMR meas. 78−27036
$DyFe_{0.998}Co_{0.002}O_3$, orthoferrite, freq. and relax. of ^{57}Fe NMR signal near Morin spin-reorientation phase transition 79−69744
$DyFeO_3$, magnetic intermediate state at antiferromag. to weakly ferromag. transition *(Russian)* 77−40059
$DyFeO_3$, phase domains, polarisation microscope obs. 77−28407
$DyFeO_3$, spin reorientation near Morin temp., magnetooptical exam. 78−68284
$Dy_{0.5}Ho_{0.5}FeO_3$ orthoferrite, domain struct., temp. depend. 80−71086
DyIG, noncrystalline, Mossbauer and magnetisation data 80−34828
$DyMo_6S_8$, superconductor, neutron scatt. exam. of mag. phase 79−73680
$DyPO_4$, mag. phase diagram and crit. exponents, MCD obs. 77−66307
$DyPO_4$, metamagnet, mag. phase transitions, elastic neutron scatt. study 79−78371
$DyPO_4$, metamagnet, phase diagram, tricritical point 79−28544
DySb, magnetisation study, intermediate metamagnetic phase transitions 79−99698
$DyVO_4$, basal plane magnetisation anisotropy under Jahn-Teller distortion 78−68222
Er, US attenuation, longitudinal, in mag. ordered region and at phase transitions 77−28422
Er, US attenuation in mag. field, temp. and field depend. 79−91279
Er US attenuation near magnetic transitions at 53.9 and 83.8K 79−55837
ErB_4, antiferromag. props. *(French)* 77−20566
ErB_4, mag. and elec. props., metallic character 80−20386
ErB_4, mag. phase diagram, neutron diffr. study 80−50091
ErB_4, theory of metamagnetic transitions *(Russian)* 78−95436
$ErCrO_3$, field-induced spin reorientation relax. 79−78402
$ErCrO_3$, phonon Raman spectra rel. to mag. ordering 77−52100
$ErFe_3$, 47K magnetic anomaly, point charge crystal field model 77−20517
$ErFe_3$, Mossbauer and magnetisation investig. of 47K mag. anomaly, atomic rearrangement 77−20766
$ErFeO_3$, second-order reorientation transition, NMR signal relax. 77−90066
$ErFeO_3$, sound velocity meas. at high press., spin-reorientation transition 78−76254
$ErFeO_3$, spin flip, Faraday effect and absorption spectrum meas. 77−43842
$ErFeO_3$, temp. depend. of neutron depolarisation factor meas. near spin reorientation transition 77−16053
$Er_{1-x}Ho_xRh_4B_4$, mag. and supercond. transitions, cryst. field effects 80−107950
$ErRh_4B_4$, reentrant supercond., mag ordering, neutron diffr. obs. 78−14879
$ErRh_4B_4$, superconductivity destruction at onset of long-range mag. order 77−76994
$ErRh_4B_4$, superconducting and mag. transitions, alpha particle irradiation damage effects 79−60954
$ErRh_4B_4$, superconductor, neutron scatt. exam. of mag. phase 79−73680
$Er_{1-x}Tm_xRh_4B_4$, mag. and supercond. transitions, cryst. field effects 80−107950
$Er_xY_{1-x}Al_2$, mag. props. meas. and neutron diffr. data 80−7126
$Er_xY_{3-x}Fe_5O_{12}$, spin reorientation transitions 78−2686
$Er_xY_{1-x}Rh_4B_4$, mag. and supercond. transitions 80−70874
$Er_xY_{1-x}Rh_4B_4$, supercond. phase transitions, recentering temp. to normal ferromag. state 80−7024
Eu chalcogenide, spin-disorder Raman scatt., mag. phase depend., theory 78−10887
Eu chalcogenides, magnetic semiconductor, light scatt. exam. 79−61372
$EuB_{6-x}C_x$, Mossbauer spectra, cond. electrons effect 80−20545
$EuFe_4Al_8$, mag. ordered, mixed valency of Eu, X-ray, susceptibility and Mossbauer spectra studies 79−19728
EuIG, noncrystalline, Mossbauer and magnetisation data 80−34828
EuO, crit. behaviour of opt. absorpt. edge 77−59418
EuO, magnetic susceptibility, quasiphase transition 79−65684
EuO, zero-field critical relax. rate, mode-coupling theory 77−69593
EuO, zero-wave vector kinetic coefficient near T_c 79−73714
EuS, spin relax. in crit. region 78−52270
$EuS_{1-x}Se_x$, mag. phase diagram, from temp. depend. of magnetisation 80−7105
EuS(Se)(Te)(O), Raman scatt. near mag. phase transitions 79−47458
EuSe, first- and second-order Raman scatt. near T_N 79−61374
magnetic transitions continued
EuSe, Hall effect, elec. cond. and magnetoresistance temp. depend. 79−33296
EuSe, mag. phase depend. Raman scatt. 78−10886
EuSe, mag. phase stability, theory 77−63183
EuSe, Raman scatt. near mag. phase transitions 79−61373
EuSe, spin config. stabilisation by lattice distortion 78−52251
EuSe, spin structs., mol. field theory 78−31054
EuSe(Te), magnetic phase transitions, thermal modulation spectroscopy study *(French)* 80−97301
EuSe(Te), spin order and fluctuations, Raman scatt. study 80−97273
$EuSm_2S_4$, mag. props. 78−68237
$Eu_xSr_{1-x}S$, ferromagnet-spin glass transition, mag. ordering, mag. susceptibility and neutron scatt. meas. 80−50135
$Eu_xSr_{1-x}S$, onset of ferromagnetism for x near 0.5 neutron diffr. obs. 79−24181
$Eu_xSr_{1-x}S$, spin glass to ferromag. transition, neutron scatt. and susceptibility meas. 80−60254
$Eu_xSr_{1-x}S$, spin-glass props. and mag. transition 80−97105
EuTe 79−61373
EuTe, high field Faraday rot., 1.7-3 eV 77−52131
Fe complex, bis[2-(2-pyridylamino)−4-(2-pyridyl)thiazole]Fe(II) complexes, high spin-low spin transitions 77−8456
Fe complex, $Fe_xM_{1-x}(1,10\text{-phenanthroline})_2(NCS)_2$, M=Mn,Co,Ni, spin crossover, Mossbauer and magnetism study 80−44980
Fe complex, $Fe(papt)_2$, high spin $^5T_2$⇌low spin $^1A_1$ transition, Debye-Waller factors and magnetism 78−80259
Fe complex, halobis(morpholyldithiocarbamato)Fe(III), solvation effects, mag. susceptibility and Mossbauer spectra 78−27129
Fe complex, halobis(morpholydithiocarbamato)Fe(III), Mossbauer HFS spectra, mag. relax. and cooperative transitions 78−27130
Fe complex, tris(1-pyrrolidinecarbodithioato)iron(III), and related cpds. mag. props., struct. 77−89933
Fe, dynamic exponent, crossover obs., TDPAC Meas. 80−108021
Fe, first order shock induced mag. transitions characts. and discrimination from TRM 78−64205
Fe garnet, Bi-substituted, film, domain boundary transform. into canted phase at compensation point 77−24724
γ-Fe precipitates in Cu, Invar related system, high press. Mossbauer spectra 79−56642
Fe whiskers, AC susceptibility, critical slowing down of mag. fluctuations 77−69594
Fe-Al, ferromag.-mictomag. transition, intermediate superparamag. 77−12140
Fe-Al, spin glass transition, Monte Carlo study 80−39801
Fe-Al (0.27 to 0.50 at.%), spin glass behaviour, microscopic model, Ising lattice, exchange and superexchange 80−39800
Fe-Al-Fe, phase diagram, microscopic model 80−34630
α-Fe-Be(P)(Mo)(W)-Co, effect of Co on solubility anomaly due to mag. transition *(Japanese)* 79−42257
α-Fe-Be(Ti)(Mo)(P)(Sb), effect of mag. transition on solubility of alloying elements *(Japanese)* 79−42256
Fe-Co alloy, order-disorder and α-γ transitions 77−25042
Fe-Mn, annealed, α-γ phase transformation obs. 78−75831
Fe-Mn, Mossbauer spectroscopy of temp. hysteresis of phase transformations *(Czech)* 80−29949
Fe-Mn-As, crystal struct. and magnetic props. of intermetallic cmpds. with Cu_2Sb type struct. *(Japanese)* 78−59785
Fe-Mn-Cr(Ni), mag. and crystallographic transformation depend. on Cr-Ni addition *(Russian)* 79−83334
Fe-Mo system, rel. to Mo diffusivity in pure Fe 77−4214
Fe-Ni, Invar, Curie point, annealing effects and time depend. 80−80508
Fe-Ni Invar anomalies, low spin to high spin transition 79−56558
Fe-Ni magnetic ordering, effect on diffusibility, penetrability and solubility of H_2 *(Russian)* 77−24435
Fe-Ni-Al, type YuN14DK25BA, thermomag. treatment 80−16512
γ-Fe-Ni-Cr, magnetic phase diagram *(Russian)* 78−39292
Fe-Ni-Pt alloy, Invar behaviour 79−56531
Fe-P-C alloys, amorphous, mag. anisotropy, Mossbauer obs., prior cooling effects *(Russian)* 77−32300
Fe-Pd Invar alloy, Young's modulus, magnetostriction, Curie temp. 80−65988
Fe-Pt, high mag. field phase transition 77−66301
Fe-Rh, mag. phase transitions, triple point 79−1672
Fe-Ru (30-60 at.%) alloy, mag. ordering, Mossbauer obs. 77−4585
$FeAl_x$, ferromag. to mictomag. transition, Mossbauer meas. 77−24692
$Fe_{0.7}Al_{0.3}$, local environment effects and magnetic clustering 78−10658
$FeBO_3$, spin-reorientation phase transition *(Russian)* 80−93122
$FeBO_3$, weak ferromag., mag. field influence on crit. behaviour of susceptibility 78−14942
$FeBO_6$, critical indices splitting of sublattice magnetisation *(Russian)* 78−60299
Fe_3BO_6, MOssbauer spectra in spin reorientation region 77−52002
Fe_3BO_6, spin-reorientation, elec. resist. and microwave absorption 78−14751
Fe_3BO_6, weak ferromag. and antiferromag. reson. modes obs. 77−69706
Fe_3BO_6, weak ferromagnetism and spin reorientation, antiferromag. reson. spectra 78−6580
$FeBr_2$, Faraday rot., optical absorption, multicrit. behaviour 77−4627
$FeBr_2$, metamagnetic, optical study of mag. phase diagram 78−56312
$FeBr_2$, optical props. around Neel temp. 79−78658
$FeCl_2$, collinear metamag., mag. phase diagram 80−71035
$FeCl_2$, light scatt., metamagnetic transition effects 77−4513
$FeCl_2$, logarithmic corrections to tricritical scaling 80−65940
$FeCl_2$, magnetic phase diagram, optical studies 78−88121
$FeCl_2$, metamagnetic, sound propag. near tricritical point 78−48024
$FeCl_2$, metamagnetic hysteresis, magnetooptical rot. meas. 77−40057
$FeCl_2$, optical props. around Neel temp. 79−78658
$FeCl_2$, tricritical dynamcis, model 77−39719
$FeCl_2.2H_2O$, antiferromag.-metastable state obs. in metamag. transition 77−66314
$FeCl_2.2H_2O$-$CoCl_2.2H_2O$ random mixture, phase diagram 79−73748
$FeCl_2.2H_2O$-$CoCl_2.2H_2O$, random mixture with competing spin anisotropies, tetracrit. transition, neutron diffr. obs. 80−2575
$Fe_{1-x}Co_xCl_2$, mag. phase diagram 80−11198
$Fe_{1-x}Co_xCl_2.2H_2O$, random mixture with competing spin anisotropies, tetracrit. behaviour 80−60324
$FeCoF_5.2H_2O$, ferrimag. props., suscept. and transitions, 3-296K 79−87240
$(Fe_{1-x}Co_x)_3P$, cryst. struct. and mag. props. 78−19222
$Fe_xCo_{1-x}Si$, mag. props. 79−56532

magnetic transitions continued
$Fe_xCo_{1-x}Ti$, mag. props. 79−56532
Fe_xCr_{1-x}, spin-wave evolution crossing from ferromag. to spin-glass regime 80−97080
FeF_2, antiferromag. spin flop boundary 78−84419
$Fe_2F_5.2H_2O$, ferrimagnetism, susceptibility obs. 5-300K, phase transition 79−4658
Fe_3Ge, mag. props. of cubic and hexagonal phases 77−8475
Fe_xGe_{1-x} amorphous film, XPS and Mossbauer exam. 79−56577
FeI, magnon energies, phase transitions of eight sublattice model 77−59463
FeI_2, magnetic phase transitions, Mossbauer spectra in high mag. fields 80−39936
Fe(II) complexes, high spin-low spin transition, phenomenological thermodynamic model 79−69675
Fe(III) compounds, $A_2FeX_5.H_2O$, (A=alkali ion, X=Cl or Br), antiferromag. props. and struct. 78−31056
$(Fe_{1-x}M_x)_3P$, cryst. struct. and mag. props. 78−19222
$Fe_xMg_{1-x}Cl_2$, metamag. percolation, Ising model calc. 79−28542
$Fe_xMg_{1-x}Cl_2$, metamagnetic transition, magnetooptic exam. of mag. phase diagram 77−63175
$Fe_{2.1-x}Mn_xAs$, $0 \leq x \leq 2.1$, mag. and crystallographic meas. 78−2679
$(Fe_{1-x}Mn_x)_3P$, cryst. struct. and mag. props. 78−19222
$(Fe_{1-x}Mn_x)_{75}P_{16}B_6Al_3$, amorphous, spin-glass-ferromag. multicritical point, AC susceptibility meas. 80−50117
$(Fe_{1-x}Mn_x)Si$, US vel. rel. to mag. struct. and phase transforms *(Russian)* 77−47976
$(Fe_{1-x}Mn_x)_3Si$, mag. phase diagram determ. 77−24697
$FeNH_4(SO_4)_2.12H_2O$, Mossbauer study mag. transition in region 0.024-0.029K 79−38417
$Fe_{1-x}Ni_x$ (x<29at.%), γ-phase dispersion, Mossbauer spectra 78−52399
$(Fe_{1-x}Ni_x)_3P$, cryst. struct. and mag. props. 78−19222
$(Fe_{0.04}Ni_{0.96})_{80}P_{10}B_{10}$, amorphous, mictomagnetic to ferromag. transition 78−34981
α-Fe_2O_3 (haematite), Morin transition effect on hydrostatic isothermal compression 78−85539
α-Fe_2O_3, haematite, birefr. under uniaxial stress in mag. field *(Russian)* 78−88285
Fe_2O_3, haematite, mag. field induced phase transition meas. by magneto-optic methods 78−10686
α-Fe_2O_3, haematite, mag. susceptibility, near high temp. mag. phase transition 79−56510
α-Fe_2O_3, haematite, magnetic field induced phase transition 78−41337
α-Fe_2O_3, hematite, interdomain phase transition 79−65675
α-Fe_2O_3, hematite, Morin transition, Mossbauer mag. diffr. spectra 80−20562
α-Fe_2O_3, magneto-optical meas. of orientation of antiferromag. vector accompanying phase transition *(Russian)* 78−14961
Fe_2O_3-BaO-B_2O_3, magnetic props. of Fe-rich amorphous oxide *(French)* 80−80511
Fe_3O_4, mag. crit. scatt., neutron spectroscopy 77−20614
Fe_3O_4, magnetite, and related Jente spinels, mag. crit. point behaviour 80−60342
Fe_3O_4, magnetite Mossbauer spectra, mag. dipolar and elec. quadrupole effects 80−20544
Fe_3O_4, monoclinic phase, saturation magnetisation near Verwey temp. 77−77038
Fe_3O_4, typical spontaneous symmetry breakdown in solid state 80−34737
$Fe_3O_{4-x}F_x$, specific heat in neighbourhood of Verwey temp. 79−33500
Fe_2P, spin wave excitations meas. 80−65831
$Fe_3(PO_4)_2(OH)_2$ synthetic barbosalite, temp. depend. quadrupolar and mag. hyperfine interactions 80−25255
$Fe(Pd_{1-x}Au_x)_3$, mag. struct. ferro-antiferromagnetism coexistence *(Russian)* 79−82759
$Fe_{34}Pd_{46}P_{20}$, amorphous, sp. ht. and resist. near ferromag. phase transition 78−56333
$Fe_xPd_{80-x}Si_{20}$, low field susceptibility near transition temp. 77−66359
$Fe_xPd_{82-x}Si_{18}$ metallic glass, mag. phase diagram, weak ferromagnet-spin glass transition 80−54893
$Fe_xPd_{82-x}Si_{18}$ metallic glass, mag. transitions, weak ferromagnetism 80−100583
FeS, zinc blende type, crystallographic and Mossbauer obs. 78−87650
$Fe_{0.9}S$, ferrimag. transition, mag., thermodynamic props., kinetics 79−47280
Fe_9S_{10}, antiferro- to ferrimag. transition, Mossbauer and mag. exam., diffusion of Fe during transition 79−73716
Fe_9S_{10}, polytypism, Fe diffusion near antiferromag. to ferrimag. transition 80−44830
$FeSb_xO_{4-y}$, defect struct. and mag. transition, elec. transport and Mossbauer expts. 78−59803
Fe_7Se_8, 3c struct., spin axis transition 78−14967
Fe_xSi_{1-x}, amorphous, struct. and mag. props., giant moment form. at mag. ordering 78−68192
Fe_xSi_{1-x} amorphous alloys, magnetisation meas. showing crit. conc. at x=0.4 77−59429
1T-$Fe_{0.1}Ta_{0.9}S_2$, mag. modulation of lattice electric field gradient 77−85628
$Fe_xTa_{1-x}S_2$ (1T), low-spin high-spin equilib., susceptibility and Mossbauer expts. 77−48109
Fe_2TiO_4, ulvospinel, mag. props. weak ferromag. in 4-200K temp. range 78−56351
θ-$Fe_xV_2O_5$, spin glass and paramag. props., susceptibility, EPR and Mossbauer studies 80−75782
$Ga_{1-x}Mn_xSb$ alloys, mag. phase transition obs. 78−52248
Gd, ferromag., transport props., crit. behaviour 80−65522
Gd-Al(Cu), amorphous alloy films, mag. phase diagram, spin glass and ferromag. regions 78−68234
$GdAg_{1-x}In_x$, magnetic transition temp., effect of hydrostatic press. 78−76244
$GdAlO_3$, crossover effects near spin-flop multicritical point 78−68245
$GdAlO_3$:La, antiferromag., random-field crit. and multicritical behaviour 80−65939
$GdAlO_3$:La, random antiferromagnets, crit. and multicritical props. 80−60332
$Gd_{80}Au_{20}$, amorphous ferromag., critical phenomena and mag. props. 77−85469
$Gd_xEr_{1-x}Rh_4B_4$, ferromag. and structural transitions, low temp. calorimetric meas. 79−55888
$Gd_xEr_{1-x}Rh_4B_4$, mag. and supercond. transitions 78−68127
$Gd_xEr_{1-x}Rh_4B_4$, mag. ordering near supercond. region 79−73696
$Gd_3Ga_5O_{12}$, mag. phase diagram, AC susceptibility meas. 80−60265

magnetic transitions continued
GdIG, spin-orientation phase transitions, magneto-optic and visual exam. 77−24675
$GdMn_2$-$GdAl_2$ intermetallics, mag. props., 80-650K 78−60282
$GdMn_2$-$GdAl_2$ system, mag. and structural studies 80−108006
GdS, low temp. phase transitions, mag. moment orientation, spin flip 79−99700
GdSe, low temp. phase transitions, mag. moment orientation, spin flip 79−99700
GdTe, low temp. phase transitions, mag. moment orientation, spin flip 79−99700
$GdV_{0.2}Fe_{0.8}O_3$, mag. transition to antiferromag. state with weak ferromagnetism at 560K and 650K respectively 79−23967
$Gd_xY_{1-x}Rh_4B_4$, mag. and supercond. transitions 78−68127
Ge, pure, magnetic phase transition between electron-hole drops and free-excitons 78−6278
H_2, solid, with low ortho-fraction, ferrorotational transition *(Russian)* 79−60597
^{3}He, BCC lattice, quadruple exchange in Heisenberg antiferromagnet 77−89616
^{3}He, BCC solid, exptl. mag. props., four spin exchange explanation 79−69319
^{3}He, HCP, and adsorbed ^{3}He with triangular lattice, exchange and mag. order 80−107606
^{3}He, in Grafoil, NMR obs. of magnetisation 79−51370
^{3}He, liquid, EPR of negative ions, antiferromagnetic transition possibility *(Russian)* 80−15322
^{3}He, solid, deform.-assisted pairing, magnetic transition interpreted 78−2334
^{3}He, solid, mag. ordering, NMR study 80−54470
^{3}He, solid, mag. phase diagram from static magnetisation meas. 80−84342
^{3}He, solid, mag. susceptibility, transition, thermodynamic study 78−60003
^{3}He, solid, mag. transition, defect-melting model 79−28172
^{3}He, solid, melting, formal treatment of low temp. props. 79−69315
^{3}He, solid, nuclear antiferromag. reson. 80−54471
^{3}He, solid, nuclear spin ordering in applied mag. fields 77−51568
^{3}He, solid locked in magnetism 79−56033
HfNi, hyperfine critical exponents, TDPAC meas. of bulk meas. 77−8465
$HgCr_2Se_4$, crit. behaviour near Curie point 78−31068
Ho, low field susceptibility and helical-ferromag. field induced phase transition 78−47975
Ho, magnetic phase diagrams, helicoid-ferromag. transform. *(Russian)* 80−50089
Ho, magnetic phase transition, second order, order parameter in mag. field, neutron diffr. 79−61104
Ho, phase transition along mag. field, X-ray obs., 77-292K *(Russian)* 77−4504
Ho-Co amorphous film, anomalous Hall hysteresis loops near compensation point 78−19286
Ho-Cu intermetallics, resist. and magnetoresist., mag. ordering obs. 80−70677
Ho-Sm, magnetic phase diagrams, helicoid-ferromag. transform. *(Russian)* 80−50089
Ho-Tb (50 wt.%) alloy, mag. phase diag. from anomalous US propag. 78−6526
$HoAl_xGa_{2-x}$, mag. props. and phase transitions 80−25133
$HoCo_2$:^{57}Fe, easy magnetisation directions, spin rotation like transitions 77−63168
$HoFe_2$, amorphous, ultrasonic exam. below T_c 79−73793
HoIG, spin reorientation from Faraday effect meas. 79−51780
$HoMo_6S_8$, superconductor, neutron scatt. exam. of mag. phase 79−73680
$Ho_{1.2}Mo_6S_8$, supercond. destruction by mag. ordering 77−69449
$Ho_2O_2SO_4$, magnetic phase diagram, magnetisation and mag. susceptibility meas. 80−15720
HoP, flopside mag. struct. to ferromag. transition, elastic neutron scatt. obs. 80−50058
$HoPO_4$, metamagnet, mag. phase transitions, elastic neutron scatt. study 79−78371
$HoRh_4B_4$, low temperature magnetic properties 80−88728
HoSb, mag. phase diagram, quadrupolar interactions 80−65820
$Ho_xTb_{1-x}Fe_2$, single cryst., spin orientations 78−84425
$HoVO_4$, enhanced nuclear cooling and antiferromagnetism 79−61070
$KCoF_3$, antiferromag., obs. of domains by X-ray topography 78−14981
K_2CuF_4, two-dimensional planar ferromagnet, giant fluctuation of spins *(Japanese)* 80−54894
K_2FeF_5, one dimens. antiferromag., zero point spin reduction 77−85456
K_2FeF_5, one-dimens. antiferromag., single cryst. Mossbauer spectra 78−23376
K_2IrF_6, hyperfine spectra of mag. ordered state at very low temp., Mossbauer meas. 77−69744
K_2MnF_4, two-dimensional antiferromag., crit. behaviour, quasielastic neutron scatt. 77−85468
$K_3Mn_3F_7$, Heisenberg double-layer antiferromag., neutron scatt. 79−61065
$K_2Mn_{0.987}Fe_{0.022}F_4$, antiferromag., mag. field induced transitions, neutron scatt. meas. 79−82782
$K_2Mn_{1-x}Fe_xF_4$, tetracrit. line in x-H-T phase diagram, neutron scatt. exam. 78−47977
$KNiF_3$, antiferromag., obs. of domains by X-ray topography 78−14981
$KNiF_3$, isotropic antiferromag., phase diagrams, US meas. 78−68350
$KNiF_3$, isotropic antiferromag., crossover behaviour of mag. phase boundaries 79−78370
$KNiF_3$, low anisotropy antiferromag., phase boundary crossover behaviour 79−38324
K_2NiF_4, two-dimensional antiferromag., crit. behaviour, quasielastic neutron scatt. 77−85468
(La,Ce)Al_2, conf. Kondo system, sp. ht. meas. 78−52210
(La,Ce)B_6 dil. alloy, Kondo effect, impurity-impurity interaction, mag. susceptibility, mag. to non mag. transition 78−47948
La-Ce alloy, press. induced spin glass to Kondo phase transition, resist. meas. 79−24174
$(La_{0.8}Ca_{0.2})MnO_{3+y}$, mag. sp. ht. and Debye temp. 79−61124
$LaCoO_3$, structural phase transition involving changes in spin and valency 78−79765
La_2CoO_4, mag. behaviour obs. 80−70971
$LaH_{2.69}$ low temp. phase transition. sp. ht. meas. 78−14665

magnetic transitions continued
$La_{0.5}Sr_{0.5}CoO_3$, ferromagnetic phase transition obs. at 230K, heat capacity meas. *(Japanese)* 80−54898
$La_{2-x}Sr_xCoO_4$, mag. behaviour obs. 80−70971
$LiErF_4$, low-temp. mag. susceptibility, evidence of antiferromag. ordering 78−23249
$Li_{0.5}Fe_{1.25}Ga_{1.25}O_4$, ferrimag. with local canted struct. thermal expansion anomalies 79−73762
$Li_{0.17}Fe_{2.17}Zn_{0.66}O_4$, ferrimag. with local canted struct. thermal expansion anomalies 79−73762
LiHLiH array, Mott transition mag. analog, Hamiltonian for paramagnetic-diamagnetic transition 79−95565
$LiHoF_4$, uniaxial dipolar ferromag. crit. behaviour 79−61149
$LiHoF_4$, uniaxial dipolar ferromag., critical behaviour, mag. susceptibility meas. 80−80528
$Li_2IrCl_6.xH_2O$, hyperfine spectra of mag. ordered state at very low temp., Mossbauer meas. 77−69744
$LiTbF_4$, magnetisation near crit. pt., temp. and field depend. 79−38337
$LiTbF_4$, uniaxial dipolar ferromag., critical behaviour, mag. susceptibility meas. 80−80528
$LiTb_{0.5}Y_{0.5}F_4$, mag. susceptibility, dilution effect on critical behaviour of dipolar uniaxial ferromagnet 80−34635
$LiTb_{0.5}Y_{0.5}F_4$, uniaxial dipolar ferromag., critical behaviour, mag. susceptibility meas., effect of Y^{3+} dilution 80−80528
$Mg_xFe_{3-}O_4$, polycryst., Verwey type transition, resist., magnetisation, Mossbauer effect and permeability obs. 80−75764
Mn complex, $Mn(SCN)_2(C_2H_5OH)_2$, two-dimens. Heisenberg magnet, cryst. struct. and mag. props. 79−60337
α-Mn, electronic structure model, Invar effect, antiferromagnetic-non mag. transitions 80−20370
Mn metallic perovskite, structural instability *(French)* 79−100123
Mn-Al-C, ferromag., transform. kinetics 80−34627
Mn-Bi mictomagnetic alloy, mag., elec. and elastic props. *(Russian)* 80−108028
γ-Mn-Cu, antiferromagnetism, martensitic transformation 79−1673
Mn-Pt (<29 at.%), eutectoid transform., antiferromag. struct. transform. *(French)* 78−92259
Mn-ZnF_2, crit. neutron scatt. 78−52249
MnAs, orthorhombic, low temp. magnetic transitions *(Russian)* 80−11193
MnAs, struct. and mag. props., temp. depend., neutron study 79−47246
Mn_2As-Mn_2Sb, structural and magnetic props. determ. 78−76248
$MnAs_{1-x}P_x$, mag. susceptibility anomaly at displacive phase transition 80−93091
Mn_3B_4, Hall effect temp. depend. mag. struct. effects *(Russian)* 77−51764
$MnCl_2$, $MnBr_2$, mag. phase diagram, optical absorption meas. 77−4514
$MnCl_2.4H_2O$, antiferromagn., nucl. orientation 78−43652
$MnCl_2.4H_2O$, biaxial antiferromag., bicritical region, sp. ht. meas. 78−68246
$MnCl_2.4H_2O$, isothermal and adiabatic susceptibilities near field depend. anitferromag. phase transitions 77−69561
$MnCl_2.4H_2O$, single cryst., mag. phases, obs. by ^{54}Mn nucl. polarisation 77−81031
$Mn_{0.27}Co_{0.73}Cl_2.6H_2O$, antiferromag., sp. ht. meas., phase transition obs. 79−78415
$Mn_3Cr_2Ge_3O_{12}$ garnet, antiferromag. ordering *(Russian)* 78−80146
$Mn_{1.88}Cr_{0.12}Sb$, antiferromag.-ferrimag. transition, neutron crit. scatt. and crossover effect 80−71023
$Mn_{1.88}Cr_{0.12}Sb$, magnetic phase transition effect on magnon renormalisation 77−59405
$Mn_{1.88}Cr_{0.12}Sb$, magnon renormalisation 77−69520
$Mn_{1.88}Cr_{0.12}Sb$, thermomagnetic props., antiferromag. to ferrimag. transition 77−63194
$Mn_{2-x}Cr_xSb$, exchange-inversion interaction and acoustical magnon soft mode 77−40049
$Mn_{1-x}Cu_xCr_2S_4$, phase relationships and mag. phase diagram 79−78374
MnF_2, antiferromagnetic phase stability limit near spin-flop boundary 78−10683
MnF_2, nuclear spin-lattice relax. and magnon lifetime near spin-flop transition 77−69721
MnF_2, spin-flop bicritical point, susceptibility and RF absorpt. meas. 79−87277
MnF_2, surface spin-flop and antiferromag. spin-flop transition 78−52257
MnF_2:Ni^{2+}, IR fluoresc., field depend., exchange energy 78−68543
$Mn_{0.97}Fe_{0.03}As$, field induced ferromag. phase *(Russian)* 77−36070
$Mn_{1-x}Fe_xAs$, high-pressure phase, magnetic properties 78−52247
$Mn_{1-x}Fe_xAs$, magnetic transition under high press., exchange striction model calcs. *(Russian)* 80−50096
$Mn_{2-x}Fe_xSb$, mag. struct. and spin flop transition, ^{57}Fe Mossbauer expts. 77−66261
$Mn_{2-x}Fe_xSb$, Mossbauer effect exam. 78−68432
$(Mn_{1-x}Fe_x)_5Si_3$, solid soln., mag. transitions sp. ht., magnetisation and thermal expansion meas. 77−16075
Mn_3Ge_2, textured, thermal expansion, 158K transformation *(Russian)* 77−32196
$Mn_{1-x}M_xAs$, M=V, Cr, Fe, Co, mag. props., phase diags. 77−66300
$Mn_{1-x}Mg_xSe$, mag. and struct. phase transitions, mag. susceptibility and X-ray diffr. study 80−71022
$Mn(NH_3)_2Ni(CN)_42C_{12}H_{10}$, phase transition, mag. susceptibility, sp. ht. 79−91234
$Mn(Nb_{0.5}Ta_{0.5})_2O_6$, non-uniaxial spin-flop magnet, crit. exponents, neutron diffr. meas. *(German)* 77−16086
$Mn(Nb_{0.5}Ta_{0.5})_2O_6$, nonuniaxial spin-flop magnet, bicrit. lines, crossover 78−14973
$Mn(Nb_{0.5}Ta_{0.5})_2O_6$, random and spin-flop magnet, neutron crit. scatt. 79−24169
$Mn(Nb_{0.5}Ta_{0.5})_2O_6$, spin flop magnet, four dimens. phase diagram and multicrit. phenomena 79−15304
MnNiGe, coupled nature of mag. and struct. transition under press. 79−8033
MnO, mag. phase transition, first-order 77−47988
MnO-Al_2O_3-SiO_2 glass, spin freezing, muon spin depolarisation 78−39491
MnP, ferro-spiral transition, neutron scatt. studies 80−65876
MnP, Lifshitz point, transverse differential susceptibility meas. 80−84599
MnP, low field magnetoresistances, mag. phase diagram purity depend. 80−107816
MnP, magnetisation and spin waves temp. depend. 79−91221

magnetic transitions continued
MnSb, hyperfine interactions at ^{57}Fe and ^{119}Sn, Mossbauer spectroscopy, spin-flop transition obs. 78−23375
Mn_2Sb, Bi-modified, mag. first order phase transition 79−51777
Mn_2Sb, hyperfine fields of ^{121}Sb in several mag. phases 79−28650
Mn_2Sb, large anisotropy in mag. hyperfine field at ^{121}Sb, Mossbauer spectra meas. 77−73101
$Mn_2Sb_{1-x}Bi_x$ ($0 \leq x \leq 0.175$), mag. transition, thermal expansion, thermomag. effects and lattice constant changes *(Japanese)* 79−78375
$Mn_{1+x}Sb_{1-x}Sn_x$, nuclear Zeeman effect, Mossbauer meas. 79−28654
$Mn_2Sb_{1-x}Sn_x$, mag. transitions, Mossbauer meas. 78−52406
α-MnSe, mag. and struct. phase transitions, mag. susceptibility and X-ray diffr. study 80−71022
MnSi amorphous, conc. spin glass system, temp. effect on susceptibility 79−61142
MnSi, mag. phase diagram, US attenuation meas. 77−63188
MnSi, US velocity anomalies near mag. transition 78−19302
$Mn_5(Si_xGe_{1-x})_3$ solid solution, mag. ordering, magnetisation and neutron scatt. meas. 78−27023
MnTe, effect of press. on Neel temp. and lattice parameter 79−95594
$Mn_{2-x}V_xSb$, $0.08 \leq x \leq 0.25$, mag. props. modification by V 77−36071
MnZn ferrite, thermal cond. of single crystals 77−36079
$Mn_{1-x}Zn_xF_2$, linear mag. birefr., crit. behaviour 77−52061
Mo_5GaS_6, specific heat temp. depend. 77−63199
$Mo_5SnGa_{0.5}S_6$, specific heat temp. depend. 77−63199
N_2 complex, $NiC(C_6H_5NO)_6(NO_3)_2$, singlet ground-state systems, field induced mag. long range order 80−60266
NH_4CoF_3, susceptibility and magnetisation meas. 77−85432
$(NH_4)_2ReCl_6(IrCl_6)$, proton relaxation near antiferromagnetic phase transitions 80−80640
$NaMnCl_3$, mag. struct. and spin-flip transition, powder neutron diffr. exam. 80−60210
β-$Na_xV_2O_5$, antiferromag. props. and weak ferromagnetism 79−78337
Nd, magnetic structure, 2D modulated 80−15697
Nd, magnetic structure and crit. behaviour 78−47951
Nd, single cryst. elastic consts., 4.2 to 300K, mag. ordering effects 77−15477
Nd, sp.ht., 1.5-10K, in applied fields 0-1.3T 79−61158
$NdCO_2$:^{57}Fe, easy magnetisation directions, spin rotation like transitions 77−63168
$(NdCu_3)(Ti_3Fe)O_{12}$, synthesis, cryst. struct. and Mossbauer exam. 78−84505
$Nd_{1-x}Dy_xCo_5$, rotational type spin reorientation, appl. to thermomagnetic generator 77−85451
$NdFeO_3$, mag. transition, NMR meas. 78−27036
$NdH_{2.70}$, low temp. phase transition, sp. ht. meas. 78−14665
$Nd_{1-x}La_x$ alloy, thermoelectric power 79−78080
$Nd_{1-x}La_x$, thermoelectric power, mag. transition temps. 80−20154
Ni complex, hexa(pyridine-N-oxide)$(ClO_4)_2$, field-induced mag. ordering in S=1 singlet ground-state 78−23288
Ni crystals, at mag. crit. temp., sp. ht. rounding 79−95595
Ni dynamic exponent, crossover obs., TDPAC meas. 80−108021
Ni, optical constants at high temp. 79−24281
Ni, stress-induced crossover phenomena above Curie point 77−4543
Ni-Cd, dil., ferromagnetic dynamic crit. exponent, hyperfine interaction vs. neutron scatt. expts. 78−84437
Ni-Cu, ferromagnetic and spin glass transition, DC magnetisation meas. 79−78369
Ni-Mn alloys, ferromagnetism-to-spin glass phase transition and strong mag. field effect 80−75773
Ni-P-B alloy, amorphous, giant moments and short-range orders 77−4499
Ni-Pt alloys, thermal expansion, mag. contribs. 77−43355
Ni-Y, amorphous, resist. and magnetoresist. meas., weak itinerant ferromagnet 78−68018
Ni_3Al, thermal expansion, mag. contribs. 77−43355
NiAs crystal lattice alloys and cpds., mag. transitions, mag. field and high press. effects 79−82780
$Ni_3B_7O_{13}I$, 10K mag. transition and accompanying struct. transition 77−69565
$Ni_3B_7O_{13}I$, phase transition, X-ray diffr. obs., 77-300K, rel. to mag. susceptibility anomaly 77−47573
$Ni_3B_7O_{13}I$, shear modulus anomalous temp. depend. 78−43061
$Ni_3B_7O_{13}I$, struct. and mag. transitions, light scatt. study 79−24308
$NiBr_2$, commensurate and incommensurate mag. struct., neutron diffr. study 80−97067
$NiBr_2.6H_2O$, antiferromag. transition, susceptibility and sp. ht. meas. 77−69587
$NiBr_2.6H_2O$, antiferromag. ordering and paramag. behaviour 78−14941
$NiCl_2.2H_2O$, mag. phase diagram and exchange parameters 77−77054
$Ni_{1-x}Co_xF_2$, Raman scatt. by mag. excitations 77−55775
$NiCr_2O_4$, ^{61}Ni Mossbauer effect studies of hyperfine interactions, mag. dipole and elec. quadrupole 78−43746
NiF_2, tetragonal to orthorhombic transition at high press., possible mag. ordering 78−18765
Ni_3Fe, compression induced magnetic anisotropy, annealing effect 80−93112
$Ni_{1-x}Fe_2O_4$ ferrites, mag. thermal expansion anomaly 77−69595
$Ni_xFe_2O_4$ series, chem. and mag. transformation, X-ray diffr. and mag. susceptibility study 79−51774
NiI_2 anhydrous, magnetic phase transition, neutron diffr. study 80−71033
NiI_2, antiferromagnetic, neutron diffr. and sp. ht. meas. 77−55663
$NiI_2.6H_2O$, disordered linear chain mag., ESR, mag. susceptibility and NMR meas. 77−20688
$Ni_xMg_{1-x}O$, EPR in magnetoconcentrated solid solution *(Russian)* 80−39856
$Ni_xMg_{1-x}(OH)_2$, random magnet, magnetisation 79−24195
Ni_3Mn, anal. of irrad. disordering data 79−1466
Ni_3Mn, mag. domains perpendicular to AC demagnetising field 77−20632
$Ni_xMn_{1-x}Cl_2$, sp. ht., 2-28K, anomalies *(Russian)* 77−89970
NiMnGe, mag. struct., and mag. phase transitions 77−63187
$Ni(NO_3)_2.4H_2O$, two spin ordered states under mag. field 79−15308
$Ni(NO_3)_2.6H_2O$, rhombic cryst. field, spin ordering in mag. field 77−77058
NiO, antiferromag. ordering, mag. transition-state approach 80−80507
NiO, mag. transition, neutron scatt. exam. 78−56313
NiO, thermal expansion, birefringence, AC susceptibility, temp. depend. 78−10664
NiS_2, antiferromag. metallic state, neutron diffr. study 79−38325

magnetic transitions continued
NiS_2, neutron diffr. anomaly at Curie temp., antiferromag. refl. 78−76260
NiS_2, pure and Co doped, ferromag. props. 79−91227
$Ni_{0.991}S$, sublattice magnetisation temp. var., neutron diffr. 77−40077
$NiS_{2-x}Se_x$ phase diagram, intermediate valence effects 80−103834
$NiTiF_6.6H_2O$, mag. and struct. transitions 78−68257
$NiWO_4$ monoclinic antiferromagnet, orientational phase transition and intermediate state *(Russian)* 80−15725
$NiWO_4$, monoclinic antiferromag., domain struct. induced by strong mag. field 80−44856
$Ni_{1-x}Zn_xFe_2O_4$, statistical model and phase transform. *(German)* 77−85473
$NpCo_2Si_2$ and $NpFe_2Si_2$, itinerant magnetism obs. 77−28406
NpH_x, mag. props., 4 to 700K 79−61075
NpO_2, mag. transition at 25K, Kramers doublet as cryst. field ground state 80−59936
O, solid, magnetic props. theory for Heisenberg system *(Russian)* 80−54900
O_2, adsorbed layer on graphite film, mag. susceptibility 78−43241
O_2 adsorbed on graphite, mag. phase transition, theory 78−38811
α-O_2, elementary excitations, effect of mag. anisotropy *(Russian)* 78−76317
Pb compounds, perovskites, polymorphic transformations possibility, mag. anal. elec. ordering effects 80−55389
$Pb_5Ge_3O_{11}$, multidomain mat., opt. anisotropy meas. at mag. crit. temps. 77−16279
$Pb_{1-x}Sn_xTe$, basic electrons energy spectrum near mag. phase transition *(Russian)* 79−90955
$PbTiO_3$-$CaFe_{2/3}W_{1/3}O_3$, solid solutions 78−43816
Pd based 3d metal alloys, mag. phase diagram calc. 78−80144
Pd, triplet pairing, spin fluctuation contrib. 78−10711
Pd-Ag-Fe, (0.5, 1.0, 2 at.% Fe), elec. resist. reduction near ferromag. and spin glass ordering 77−69299
Pd-Co, dil., breakdown of ferromag. order, magnetoresist. obs. 80−71046
Pd-Co (0.1-45.7 at.%), thermo EMF at 4.2-300K *(Russian)* 80−92881
Pd-Fe, onset of ferromagnetism 78−23270
Pd-Fe, Pd-Fe-H and Pd-Fe-D, Mossbauer effect, internal hyperfine field temp. depend. 77−12283
Pd-Fe, very dilute, very low temp., spin glass-like behaviour 79−99708
Pd-Fe (0.54-8.0 at.%), thermo EMF at 4.2-300K *(Russian)* 80−92881
Pd-Fe-Mn, differential susceptibility, spin glass and ferromag. transition 79−61169
Pd-Fe-Mn, ferromagnetic-spin glass transition 78−39339
Pd-Mn, alloy with mixed types of order, uniform mag. phase diagram 79−78368
Pd-Mn, ferromagnetism to spin glass behaviour transition 80−71062
Pd-Ni, disordered alloy, onset of ferromagnetism, effect of press. 79−61111
Pd-Ni, onset of ferromagnetism 78−23270
Pd-Ni (15-90 at.%), thermo EMF at 4.2-300K *(Russian)* 80−92881
Pd-Ni alloys, onset of ferromag. 79−56533
$Pd_{0.95}Gd_{0.05}$, transition temp. determ., magnetisation data 77−12123
$Pd_{80-x}Si_{20}Fe_x$, amorphous, low x, hyperfine interactions and mag. ordering temp. 79−15303
(1,10-phenanthroline-2-carbaldehyde phenylhydrazone) iron perchlorate, high spin to low spin transition, X-ray diffr. and Mossbauer obs. 79−38418
Pr, magnetic ordering due uniaxial stress, mag. excitons by neutron scatt. 78−84467
Pr-Ce(Tm), mag. order onset, elec. resistivity 80−20416
Pr-Nd (5%), impurity modes and mag. ordering 78−84422
$PrAg_x$, low temp. mag. meas. 80−107989
$PrCo_{5\pm x}$, high field first order transitions, role of K_3 anisotropy const. 80−65879
PrSb, mag. excitations, press. depend., inelastic neutron scatt. meas. 78−10699
Pr_3Se_4, induced ferromagnet, effect of press. on magnetisation 78−95422
$PrSn_3$, thermal expansion and transverse elastic const. near mag. phase transition 80−60394
Pr_3Tl, critical fluctuations temp. depend. 80−25160
Pr_3Tl, thermal expansion and transverse elastic const. near mag. phase transition 80−60394
Pr_3Tl, transition temp. and magnetisation 80−25161
$PrVO_3$, neutron diffr. exam. of first order mag. transition 78−2685
Pt-Co alloys, crit. neutron scatt. in crit. conc. region for onset of ferromagnetism 78−72347
Pt-Fe, dil., breakdown of ferromag. order, magnetoresist. obs. 80−71046
Pt-Fe alloy, ordered, T-c phase diagram, antiferro- and ferromagnetism *(Russian)* 80−65871
Pt-Ni alloys, onset of ferromag. 79−56533
Pt_3Fe, transport and mag. props. near Neel temp. 79−7976
PtMn, spin glass, nonlinear susceptibility and sp. ht. 80−60304
PuC_{1-x} and Pu_2C_3, sp. ht., 10 to 300K, mag. ordering 77−28403
PuH_x, mag. props., 4 to 700K 79−61075
$RbCoCl_3.2D_2O$, metamagnetic phase transition, crystallographic and mag. struct., neutron diffr. meas. 80−44174
$Rb_2Co_pMg_{1-p}F_4$, dilute antiferromag. two dimens. Ising system, phase boundary effective medium theory 80−50130
Rb_2CrCl_4, planar ferromag., spin waves 80−65835
$RbCuCl_3$, quasi-1-dimens., NQR obs. 80−54987
$RbFeCl_3.2H_2O$, 2D Ising system, crit. fluctuations, Mossbauer spectra study 80−44842
Rb_2IrCl_6, hyperfine spectra of mag. ordered state at very low temp., Mossbauer meas. 77−69744
$RbMnCl_3$, structural phase transition 78−91442
$RbMnCl_3$, twinning struct., cryst. domains, orientation mag. transition *(Russian)* 80−107275
Rb_3MnCl_4, quasi-2D-antiferromag., linear birefr. and optical absorpt. spectra 80−71385
$RbMnF_3$, isotropic antiferromagnetic, T-H phase diagram as test of theory 77−32192
$RbMnF_3$, isotropic antiferromag., phase diagrams, US meas. 78−68350
$RbMnF_3$, isotropic antiferromag., crossover behaviour of mag. phase boundary, US meas. 78−80145
$RbMnF_3$, isotropic antiferromag., crossover behaviour of mag. phase boundaries 79−78370
$Rb_2Mn_cMg_{1-c}F_4$, dil. antiferromag., mag. correlations, neutron scatt. meas. 77−66356
$Rb_2Mn_cMg_{1-c}F_4$, two-dimens. antiferromag., spin fluctuations, neutron diffr. study 80−44846
magnetic transitions continued
$Rb_2Mn_{0.5}Ni_{0.5}F_4$, site-random two-dimensional antiferromag., crit. behaviour, quasielastic neutron scatt. 77−85468
$RbNiCl_3$, mag. props. 79−73736
$RbNiCl_3$, nearly one-dimensional antiferromag., spin-flop transition 78−6527
Rh-Ni alloy, onset of ferromag. 79−56533
Si, amorphised by ion implantation, EPR obs. of mag. ordering 79−24186
Si, liq., mag. susceptibility and diamag.-paramag. transition at melting pt. 78−95415
$SmCo_5$, amorphous, supermag.-ferromag. transition and directional crystallisation 80−65891
$SmCrO_3$, spin reorientation phase transition, second order nature 77−80950
$SmFeO_3$, HF susceptibility, crit. divergence in spin reorientation temp. region *(Japanese)* 77−43836
$Sm_3Fe_5O_{12}$, spin-reorientation phase transition, NMR spectra and anisotropy consts. meas. 77−28458
$SmH_{2.84}$, sp. ht., second-order phase and cryst. field splitting effects 79−87279
SmIG, mag. phase transitions, Mossbauer spectroscopy obs. 80−80509
$SmMn_3C$ noncolinear mag. struct., mag. transition *(French)* 77−69494
$Sm_{0.05}Tb_{0.45}FeO_3$, singularities of domain struct. in spin-flip region 78−19272
$Sm_{0.55}Tb_{0.45}FeO_3$, orthoferrite cryst., domain memory effect *(Russian)* 77−55693
$Sm_xY_{3-x}Fe_5O_{12}$, spin reorientation transitons 78−2686
$Sr_2Co_2O_5$, characterisation and mag. props. *(French)* 79−90619
$SrLaCoO_4$, struct. and mag. props., electronic struct. of trivalent Co *(French)* 79−86760
$SrSm_2S_4$, mag. props. 78−68237
TaS_2 (aniline)$_{3/4}$, low-field magnetisation meas. on small cryst. in supercond. phase 79−87188
$TaSe_2$:Fe, local moment form., mag. susceptibility meas. 79−82756
Tb, critical magnetic studies 80−15745
Tb, ferromagnet, field depend. of elastic const. c_{66} 80−15181
Tb, magnetic phase diagram, US meas. of elastic const. 80−15721
Tb-Gd alloy, spin orientation transition obs. 79−99714
Tb-Y, magnetostriction, mag. and elec. props. 78−27068
$TbAl_xGa_{2-x}$, mag. props. and phase transitions 80−25133
$TbAsO_4$, ferromag., static and AC susceptibility meas. 80−29533
$TbAsO_4$, mag. ordered, neutron diffr. study 79−47238
$TbCo_2$, polarised neutron diffr. exam. of mag. struct. 79−73681
$TbCo_{5.1}$, singularities of mag. transition *(Russian)* 77−77053
TbD_2, sublattice magnetisation, cryst. elec. field effects 78−39295
$Tb_{0.27}Dy_{0.73}Fe_2$, anomalous thermal expansion and magnetostriction 77−90003
TbF_3, mag. phase diagram, crit. and tricrit. behaviour 78−14959
$Tb_3Fe_5O_{12}$, mag. phase transition exam. 79−19736
$Tb_3Fe_5O_{12}$, quasiantiferromag. state magnetised along two-fold symmetry axis, mag. phase diagram 77−69564
$Tb_3Fe_5O_{12}$, weak field mag. transition, magneto-optical and magnetisation meas. 77−69551
Tb_xGd_{1-x}, orientation phase transitions near Curie pt., magnetization and magnetocaloric effect meas. *(Russian)* 79−87261
TbIG, Faraday rotation and transition of spin config. at high mag. fields 80−39776
TbIG, neutron depolarisation near mag. compensation point 77−24709
$TbMo_6S_8$, superconductor, neutron scatt. exam. of mag. phase 79−73680
Tb_2O_2S, tunnelling effect and mag.-cryst. transition, neutron diffr. expts. 77−63180
TbP, singlet-groundstate magnetism, static mag. props. 80−7109
$TbPO_4$, linear optical birefr. meas. near bicritical point 80−15719
$TbPO_4$, specific heat from 1.2 to 6K 78−14475
$Tb_pY_{1-p}AsO_4$, crystallographic, mag. phase transition as function of temp. and Tb conc. 78−43334
$Tb_{0.2}Y_{2.8}Fe_5O_{12}$, Mossbauer investigation of spin-reorientation transition 78−88243
$Tb_{0.26}Y_{2.74}Fe_5O_{12}$, anomalous props., 200-250K 79−28527
$Tb_{0.26}Y_{2.74}Fe_5O_{12}$ garnet, mag. transition, mag. props. anomaly 80−93120
$Tb_xY_{3-x}Fe_5O_{12}$, spin-reorientation phase transitions, neutron depolarisation factor 78−27037
TbZn, elec. resist., behaviour at mag. crit. points 80−65901
TcF_6, heat capacity, entropy Gibbs energy, 2.23-350K 78−38852
$ThCo_5$, mag. transition due to Co moment change, metamagnetism of 3d-band 77−63184
$(ThCu_3)(Mn_2Fe_2)O_{12}$, synthesis, cryst. struct. and Mossbauer exam. 78−84505
$TiBe_2$, cubic Laves compound, sp. ht. rel. to intinerant antiferromag. 79−82356
$Ti(Fe_{1-x}Co_x)$, density of states estimation from magnetisation and resistivity meas. 78−84119
TiN-CrN systems, solid solns., mag. props. 77−12086
$(Ti_{1-x}V_x)_2O_3$, spin glass, nonlinear susceptibility and sp. ht. 80−60304
$(Ti_{1-x}V_x)_4O_7$, metal-insulator transition and mag. behaviour 78−51895
Tm magnetic transitions, effect of H_2 in solid solns., elec. resist. meas. 80−100585
$Tm_{2.2}Bi_{0.8}Fe_{3.5}Ga_{1.5}O_{12}$ epitaxial film, Faraday effect and domain struct. near compensation point 77−20838
TmCd(Zn), quadrupolar phase transitions, magnetoelastic and quadrupolar coupling consts. 80−15744
$TmCrO_3$, temp. and field-induced spin reorientation, magnetisation meas. 77−69588
$TmFe_2$, amorphous, neutron scatt. at transition, spin diffusion, magnetisation meas. 78−68174
$TmFeO_3$, acoustic vel. and attenuation shifts at spin reorientation phase transition 80−65986
$TmFeO_3$, domain struct. in spin reorientation region, Faraday effect obs. 77−20835
$TmFeO_3$, temp. depend. of neutron depolarisation factor meas. near spin reorientation transition 77−16053
TmSe, intermediate valence state, resistivity of magnetically ordered ground state 79−1683
TmSe, mag. props. and struct. 80−25109
TmSe, mixed valence systems, spin dynamics and mag. ordering 78−68162
TmSe, mixed valency, field-depend. mag. phase transitions 78−10657
Tm_xSe, $0.87<x<1.05$, mag., thermal and transport props., comp. depend. 78−68239

magnetic transitions continued
Tm_xSe, low temp. props., effect of composition 77−80775
$TmSe_{0.83}Te_{0.17}$, spontaneous magnetisation, mag. susceptibility, magnetostriction, elec. cond. 79−24146
TmZn, cooperative Jahn-Teller effect 78−67998
U-Pt, paramag. suscept. 79−61047
UAs, magnetisation, ferrimag. spin struct. 80−7088
UAs, magnetisation, in fields up to 40 T 79−33505
UAs, search for lattice distortions at low temps. 80−79759
UAs, sp. ht. meas., 5-300K, mag. transition obs. 80−50101
U_3As_4, ferromag., mag. field induced phase transitions 80−65887
U_3As_4, heat capacity, 5-300K, ferromag. transition obs. 80−88769
U_3As_4, high-field magnetisation, field-induced phase transition near hard (100) directions 77−28413
UAs(Sb), anisotropic mag. ordering and mag. structural transitions 79−78324
UFe_2, giant magnetoelastic deform. of cryst. struct. mag. props. *(Russian)* 80−93159
UI_3 sublattice magnetisation, mechanism 77−55671
UN-ZrN, Young's modulus antiferromagnetic anomaly 80−92583
$U_2N_2As(P)(S)(Se)$, stability diagram of mag. phases 77−20569
U_2N_2Te, and related cpds., crit. behaviour 78−43605
UNi_2, mag. phase transition, elec. resist. meas. 80−97094
UO_2, mag. ordering lattice internal rearrangement transition, theory 80−20402
UO_2, mag. struct. 77−59389
UO_2, phase transition crossover from first- to second-order in symmetry-breaking field 79−82805
UP, magnetisation, in fields up to 40 T 79−33505
UP, vol. changes at mag. transitions 80−7107
UP-PrP (NdP) systems, mag. phase diagrams 78−84424
$UP_{1-x}S_x$, sp.ht. and electronic struct. 79−91240
UPTe, and UAsTe, crit. behaviour 78−43605
UPd_3, crystalline electric field levels of U, neutron scatt. exam. 78−60267
UPd_2Si_2, magnetic phase transition, neutron diffr. meas. 79−47284
$USb_{0.9}Te_{0.1}$, multiaxial mag. ordering, magnetisation and neutron scatt. meas. 79−51750
$U_xTh_{1-x}As$, mag. phase diagram, magnetisation meas. 80−60271
V complex, $[C(NH_2)_3]V(SO_4)_2.6H_2O$, mag. sp. ht., low-temp. crit. behaviour *(Japanese)* 78−56340
V-Fe, ferromagnetism to mictomagnetism at low Fe conc. 78−91878
V-Ni alloy, onset of ferromag. 79−56533
$(V_{1-x}Cr_x)_2O_3$, Raman scatt. and phase transitions 80−71420
VO_2, discontinuous metal insulator and spin dimerisation transition, Hubbard model 78−51893
V_2O_3, 500 to 530K, magnetic susceptibility meas., high temp. transition, interacting Hubbard bands 78−39325
V_2O_3, high temp. mag. phase transition studied by US vel. meas. *(Russian)* 79−33520
V_2O_3, phase transitions, Raman scatt. expts., 20-300K 78−39538
V_3O_5, heat capacity anomaly near 425K, and enthalpy change 77−47576
V_6O_{11} single crystals, heat capacity anomaly at 172K 78−10197
V_nO_{2n-1}, Magneli phases, sp. hts. 0.4 to 50K 79−42774
V_5S_8, single cryst., mag. props. 78−88098
$Y(Co_{1-x}Ni_x)_5$, spontaneous magnetisation mag. anisotropy, spin reorientation transformation *(Russian)* 80−7082
$(YEu)_3(FeGa)_5O_{12}$ rigid magnetic bubble transition to normal behaviour 78−95501
YFe_2 amorphous, spin-glass and mag. blocking transitions, low field DC susceptibility meas. 79−61141
$YFe_{1-x}Co_xO_3$, reorientation transitions, neutron diffr., mag. behaviour *(Russian)* 77−24678
$YFe_{1-x}Mn_xO_3$ orthoferrite, spin reorientation, mag. torque meas. 78−47979
$YFeO_3$, Co^{2+} substituted, reorientational transitions 77−59419
YFe_2O_4, low temp. phase transitions and mag. props. 80−7106
$Y_{2.6}Gd_{0.4}Fe_{3.9}Ga_{1.1}O_{12}$, epitaxial uniaxial film, mag. phase diagram, optical expts. *(Russian)* 77−48022
$Y_{3-x}Gd_xFe_5O_{12}$, mag. phase diagrams, mag. transitions, exchange interaction *(Russian)* 80−54896
$(YGdYbBi)_3(FeAl)_5O_{12}$, epitaxial garnet film, with mag. compensation point, behaviour of 'compromise' phase boundary 78−60321
$(YGdYbBi)_3(FeAl)_5O_{12}$ epitaxial garnet film, uniaxial ferromagnet domain struct., phase transition *(Russian)* 80−108044
YIG, homogeneous crit. relax. in dipole region *(Russian)* 78−10782
YIG, homogeneous mag. relax. near phase transition *(Russian)* 78−23351
YIG, mag. and magneto-optic props., temp. and exchange field depend. 77−24824
$Y_{1-x}Tb_xCo_5$, spontaneous magnetisation anisotropy, spin reorientation transforms. *(Russian)* 80−7082
Yb, FCC phase, low temp. mag. props., impurity effects 80−20387
YbIG, H parallel to (100), transition between canted phases, liquid-vap.-like critical point 77−80938
YbIG, mag. transitions at low temp., soft mode existence 77−69557
YbIG, mean field phase diagrams 78−23269
$Zn_2BaFe_{12}O_{22}$, mag. phase transitions, magnetostriction temp. depend. *(Russian)* 78−34983
$ZnCr_2O_4$, mag. phase with short range order *(French)* 77−63203
$Zr(Fe_{1-x}Al_x)_x$, transition region, spin glass or long range mag. order 80−44841
$Zr(Fe_{1-x}Co_x)_2$, density of states estimation from magnetisation and resistivity meas. 78−84119
$Zr(Fe_{1-x}Co_x)_y$, transition region, spin glass or long range mag. order 80−44841

magnetic traps
see also magnetic bottles
2XIIB magnetic mirror device, neutral beam injection 80−28782
β-ratio, low pressure plasma, linked magnetic wells in Min-B 78−30468
adiabatic, cyclotron heating mechanism *(Russian)* 78−5890
adiabatic, drift cone instability suppression by electron heating *(Russian)* 80−53959
adiabatic, small axial perturbation due to displaced solenoid *(Russian)* 78−21800
adiabatic trap, charged particles motion, mag. field inhomogeneity effect, drift instability *(Japanese)* 77−43054
ambipolar, hydrodynamic plasma equilib. *(Russian)* 79−98951

magnetic traps continued
ambipolar, plasma instabilities, appl. to fusion reactors *(Russian)* 79−55535
ambipolar trap, ballooning effect in flute oscillations and plasma stability limits *(Russian)* 80−106955
ambipolar trap, transverse loss reduction method *(Russian)* 80−10417
ambipolar traps, transport processes, neo-classical theory *(Russian)* 78−71518
Astron Accelerator, 5 MeV, 400 A, 500 MHz modulation system for beam energy 77−24202
astron ion ring, stability against poloidal perturbations 78−83599
Astron ion-ring equilibria, theory 79−64894
Astron kink stability, toroidal mag. field 79−19077
Astron particle layer, precession and kink motion 79−64895
axially-symmetric ambipolar trap, flute oscills. stability limits *(Russian)* 80−103176
baseball coil, mag. field by dipole-layer model 78−59647
blocked picket fence, plasma leaks, Langmuir probe obs. 77−51220
charged particle confinement in superposed cylindrical cusp field and biconical cusp field 78−18435
charged particle motion, in axially symm. trap, stability *(Russian)* 78−71519
closed poloidal heliotron, accelerated electron focusing *(Russian)* 80−106961
closed trap with three dimens. axis, plasma confinement 77−72471
cluster interaction with longitudinal mag. field 77−27708
collisionless plasma, axially symmetric mag. trap, finite $\beta(\ll 1)$ *(Russian)* 77−3971
corpuscular diagnostic techniques appl. to investigation 77−43069
CTR, engineering and technology considerations *(Spanish)* 79−36399
current sheet generation in rarefied plasma, mag. flux plasma trap appls. 80−38698
cusp field with RF plugging, appl. thermonucl. plasma 77−76169
cusp fields, plasma confinement time investigation using Monte Carlo simulation, collision effects 80−64770
cusp-shaped mag. fields, plasma confinement, review 77−76178
dissipative trapped ion instability and anomalous transport 78−22483
divertor fluxes in stellarators and torsatrons, azimuthal distrib. 80−6216
drift-mode stability analysis for the Tandem Mirror 80−64704
EBT, toroidal MHD equilibrium 80−87871
electron beam compression in asymmetric mag. cusp 77−89288
electron beam-neutral gas interaction in mag. cusp field 77−24111
electrostatic bounce modes in mirror plasmas 80−1790
electrostatically plugged spindle cusp, density and decay time, microwave interferometry 77−58881
ELMO Bumpy Torus, microwave coupling 80−99328
ELMO Bumpy Torus, ring power balance optimisation 80−99316
ELMO Bumpy Torus Proof-of-Principle, proposed mag. system 80−99296
EM bottle, multigap, plasma losses *(Russian)* 79−90447
EM confinement system, energy distributions of plasma electrons and ions 80−79542
EM trap, KEMP II, charged particle energy and momentum calcs., Vlasov equilib. *(French)* 77−43018
EM trap, surface contamination effects on plasma density 78−9822
EM trap confinement, microwave investig. *(Russian)* 80−10416
Engineering Test Facility work on magnetic confinement 80−52787
feedback stabilisation of flute oscills. in direct traps *(Russian)* 77−47184
field reversal induced by intense rotating electron beam in initially neutral gas 78−42768
field reversed mirror reactor, parametric anal. and preliminary conceptual design 79−71973
field reversing ion rings, precessional mode stabilisation by multipole fields 77−89298
flute oscillations stability in ambipolar traps *(Russian)* 79−46452
fusion reactor, neutral beam injector mag. cusp plasma source, design and fabrication 80−99377
fusion reactor, tandem mirror confinement 79−71972
fusion reactors, open system, AC direct energy convertor 79−4197
glass-CO_2-hybrid laser system for plasma prod. and heating in mag. traps 80−24196
helical instability, effect of mag. shaping 78−42781
helical magnetic axis trap, plateau and banana diffusion regimes 80−10425
Heliotron D, RF heating, equilibrium and stability 80−28777
high beta MHD theory, stellarator equilibrium and stability, mirror traps and reverse field machines 80−28778
hollow-cathode multipole boundary ion source, IBIS, plasma prod. and containment system 78−74521
Jupiter-1 M, one slit EM open trap *(Russian)* 80−83970
laser produced plasma in cusp field, RF plugging 80−28783
laser solenoid, for fusion power appl. 77−47250
leakage velocity through low-β line cusp meas. 77−35380
line cusp plasma leaks, mass scaling 77−35374
magnet technology, conference, Bratislava (1977) 79−30499
magnetic cusp, relativistic electron beam driven inertial fusion, transport calcs. 78−75268
magnetic fusion program in US, recent exptl. results 79−85781
magneto-electrostatic reactor, power gain factor 80−48933
magneto-electrostatic traps, classical transport processes *(Russian)* 78−75403
microwave heating of plasma in EM trap *(Russian)* 80−10400
mirror configuration for heating of K plasma with hot W filament array 80−33789
mirror machine end-loss processes, review 77−55164
mirror machines, 2XIIB neutral-beam-heated, extreme UV spectroscopy 80−74002
moving plasmoid reactors using advanced fuel, modularisation 80−99312
multi-baseball magnetic trap system, plasma confinement 79−23443
multidipole, mag. confinement time of primary ionising electrons 78−55739
multidipole mag-field for surface trapping of primary electrons 80−33810
multidipole plasma density 78−94929
multiple magnet system for homogeneous steady state plasma 78−59660
multipole confinement of laser plasma, radial and axial arrangement 80−83974
negative mass instability, nonlinear development, effect on intense microwave generation 78−75285
neo-Z-pinch, mag. fusion appls. 80−103180

magnetic traps continued
non-axisymmetric open trap, longit. plasma losses *(Russian)* 80−33799
nonlinear equilibrium state of wave-beam, kinetic theory *(Russian)* 80−106888
octupole, levitated, instabilities in trapped ion regime 77−68847
open, axially symmetric, reson. particle diffusion, homogeneous model *(Russian)* 79−98952
open trap plasmas, electronic loss layer formation, low freq. oscill. anomalous electron diffusion *(Russian)* 79−90383
open traps, axially symmetric, transverse particle losses 80−28784
open traps, electron thermal flux reduction *(Russian)* 78−47153
open-ended device, internal ring end-stopper 78−47149
open-system plasma mag. confinement, effect of time-variable boundaries on end loss 79−37530
PARODIE device for construction of large size homogeneous stationary plasma *(French)* 78−14223
particle losses in ambipolar plasma trap *(Russian)* 77−84485
picket fence cusped mag. field, electrostatic self-plugging 79−27815
plasma confinement, review 78−94928
plasma confinement in multislit EM trap, model description *(Russian)* 80−96382
plasma confinement mag. field, computer simulation of finite linear multipole with closed ends 77−35382
plasma-field boundary, particle losses, skin layer structure *(Russian)* 79−4167
probkotron plasma stabilisation system, automatic, against flute oscills. *(Russian)* 80−24211
quadrupole cusp, drift surfaces 79−14599
quadrupole-coupled orbital resonances in the Cornell electron-ring experiment 79−4172
RECE-Berta device with external Ioffe fields, fast electron anomalous losses 77−84483
relativistic electron beam transport in cusp field of Angara-Koltso system 79−68945
relativistic electron beams, mag. focusing, equilib. surface ripples 79−3618
resistivity, trapped electron regime, collisional theory 77−84412
reverse loss-cone instability in ambipolar trap *(Russian)* 80−106893
reversed field pinch reactor, 600 MWe, plasma physics and reactor parameters 79−71976
RF heating of magnetized rarefied plasma 80−24195
RF intense heating, energy confinement 80−38674
ripple trapping coefficient, poloidal variation 80−87923
rippled trapped particles, depletion, in Alcator A Tokamak 80−87924
rotating plasma, in mirror trap, equilib. state *(Russian)* 78−75259
solar radiofreqs. radiation, metre-band type I-bursts, stable confinement of fast electrons 79−80296
spherical multipole magnetic trap, plasma containment 80−87937
spindle-cusp confinement, high-beta sheath form., theoretical analysis 78−59612
spindle-cusp container, laser-produced high-β plasma 78−59650
superconducting magnet system appls. *(Slovak)* 78−87474
surface magnetic cusps, error in plasma leak meas. 79−60197
surface multipole guide field for plasma injection 78−14194
tandem mirror fusion reactors, axisymmetric sloshing-ion plugs 80−73998
tearing instability in cylindrical plasma configurations *(Russian)* 80−10370
Tokamak magnetic fusion R+D, ISX and PDX programs 80−37586
Tormac, confinement system, magnetoacoustic heating studies 80−24217
Tornado trap, filling by discharge plasma in crossed electric and mag. fields *(Russian)* 77−7583
toroidal fusion reactor design based on reversed field pinch 79−71977
ultracold neutron storage 77−23344
vacuum arc plasma flow in plasma-optical system *(Russian)* 80−106992
Yupiter 2 EM trap *(Russian)* 79−90446
μ^+, nonadiabatic motion stability in mag. confinement system, numerical simulation 77−61646
π^+, nonadiabatic motion stability in mag. confinement system, numerical simulation 77−61646

magnetic variables control
electromagnet field control system 77−37950
field, in microwave EPR spectrometer, block for electronic digital sweep 77−26371
field of Tokamak, control coil optimum design, nonlinear optimisation 77−27744
field stabilisation using directly coupled IC op. amps, for EPR spectrometer *(Czech)* 79−26095
field strength, winding supply current regulator based on industrial thyristor convertors 77−37921
flute oscillation suppression by automatic EM control *(Russian)* 78−30464
high-coercivity, magnetisation characteristic linearity determ. using flux controlling technique *(Russian)* 80−100597
microwave spectrometer, RE1301, wide-range magnetic current regulator 79−21779
NMR spectrometer automatic magnetic field control, 0.1 to 2 T *(French)* 79−30450
periodic magnetic signal detection by magnetoresistance sensor *(Japanese)* 78−57997
plasma flute oscillation suppression, regulator synthesis *(Russian)* 80−24212
probkotron plasma stabilisation system, automatic, against flute oscills. *(Russian)* 80−24211
pulsed eight-solenoid system, magnetic field distrib. control 77−87793
ring shaped mass produced magnets *(Russian)* 77−26346
rocket geomagnetic aspect horizontal component sensor *(Japanese)* 78−24421
stabilised source of magnetic induction 78−94360
Fe analysing magnet, fast precise field control 79−45883

magnetic variables measurement
see also fluxmeters; magnetic field measurement; magnetic permeability measurement; magnetometers
anisotropy, meter based on permanent magnet torsion balance *(Bulgarian)* 79−30493
anisotropy, microwave freq., meas. using square resonant cavity 79−93173
anisotropy meas. at microwave freq., experimental results 80−52279
approaching saturation in polycrystalline materials, meas. apparatus and method *(Chinese)* 79−24144

magnetic variables measurement continued
automatic M-H curve recorder in high magnetic fields *(Japanese)* 79−71500
automatic NMR gaussmeter *(Polish)* 77−79133
average induction meas. in nonuniform field, generalised correction determ. 77−57369
Barkhausen effect, mag. thin films, statistical anal., instrumentation, computer interfacing 78−82008
Barkhausen noise meas. method 79−17452
bubble collapse and stripout field, microwave meas. technique using mag. reson. apparatus 77−20661
bubble film, mag. characterisation procedures 79−78462
bubble materials characterisation using spatial filtering 77−12175
capacitice instrument for magnetostriction meas. at low temps. and high magnetic fields 78−93742
circular dichroism in 200 to 850 nm region, construction of dichrograph 80−101806
circular dichroism of matrix-isolated high-temp. molecules 80−86356
coercimeter, type KIFM-1, inspection of the mechanical props. of rolled steel 78−72973
coercimeter KIFM-1 with automatic measurement of the demagnetizing current 80−68229
coercimeters with EM attachments 77−12765
coercive force, automatic meas. by remote means, for ferromag. metals and alloys 79−24690
coercive force, differential meas., appl. to ELA steel 77−71351
coercive force measurement with superimposed sensor 78−88612
coercivity, meas. on soft mag. materials 77−41659
coercivity meter attachment, with automatic current setting and recording for heat treatment monitoring 77−87795
coercivity meter magnetic heads 78−57996
coercivity of amorphous bubble-domain materials, measurement using Hall-effect hysteresigraph 79−73786
complex dielec. and mag. props., modified von Hippel least square fit determ. 78−21179
conference on precision EM meas., Braunschweig, Germany (Jun. 1980) 80−98903
constant magnetomotive force, testing and anal. using mag. potentiometer 78−62210
cryogenic construction material magnetisation meas. *(Slovak)* 78−93693
Curie temp., pressure cell with cubic-anvil press 80−13109
Curie temperature, determ. using magnetic pendulum *(Japanese)* 80−82797
Curie temperature determ. by AC ccts. 77−49749
Curie temperature of ferrites, by magnetic method *(Czech)* 79−93176
cylindrical magnetic domain material coercive force meas. 77−79130
deviation ballistic method appl., calibration procedure *(Polish)* 79−71498
diamagnetic susceptibilities, noise in meas. methods 77−13782
disaccommodation in ferromagnets, electronic device for automatic measurement *(Japanese)* 80−68227
disaccommodation measurement in Rayleigh range using semi-automatic equipment *(Polish)* 80−31812
domain patterns obs., of highly-oriented Si steel, using ferromagnetic colloid technique 80−11856
dynamic induction coeffs., direct meas., appl. to supercond. coils with ferromag. frames *(French)* 77−61096
dynamic magnetization curves, apparatus for display on CRO 79−17451
eddy currents in magnetic measurements 78−12730
electrical steel sheet, magnetostriction meas. using Hall effect transducer *(German)* 80−13111
epitaxial garnet films, technique for magnetostriction coeff. meas. 80−243
EPR signal recording method, without field modulation 77−34009
Faraday balance susceptometer, computer controlled 78−65946
Faraday effect and susceptibility of garnet films, meas. using magnetooptical apparatus 80−105680
Faraday magnetic balance for metalloprotein solns. in 6.5-300K range 78−70170
ferrofluid susceptibility meas. device and method *(Czech)* 77−26345
ferromagnetic film, mag. props. meas. using planar magnetoresist. effect 78−21186
ferromagnetic materials in strong fields, equipment using Hall transducer 80−4745
ferromagnetic pick-up for iron sheet local magnetic properties *(Russian)* 78−77946
ferromagnetic ring complex reluctivity meas. using AC bridge cct. *(Russian)* 78−54412
ferromagnetic single crystal balls, portable instrument for axes of easy magnetis. determ. 78−8424
ferromagnetic sphere in nonuniform mag. field, magnetisation meas. arrangement 80−42242
ferromagnetic wire, circular magnetisation meas. 78−70167
ferromodulation meas. transducers, with increased temp. stability 80−52281
film, vertically suspended, torque curve meas., first-order calc. anal. 80−86354
flux density, electromagnetreference measure free from hysteresis effects for checking of meters 80−77817
flux density using galvanometric 3-component mag. induction gauge 80−105682
flux standards, representation and transmission methods 77−67408
full wafer magnetic bubble films, devices for characterisation 79−78461
galvanomagnetic effects, at pressures up to 27 kbar, using low-temperature hydrostatic pressure chamber 80−47069
hard magnetic material charact. *(Russian)* 77−18054
hard material demagnetisation curve evaluation 80−90869
hot carrier oscillatory magnetoresistance phenomena studies, magnetic field modulation technique 78−4657
hydrostatic pressure cell, up to 90 kbars, appl. 79−17436
hysteresigraph with data printout 79−58760
hysteresis loop tracer for mag. phase detection 80−22393
hysteresis loops in ferromagnetic microobjects 79−69707
hysteresisgraph with discontinuous sweep mode 80−86351
induction calibration units, description 78−74035
induction in magnetic loops, small-dimension, using Hall probe method *(Hungarian)* 78−4665
induction meas., shielded field coil, standard 77−74466
induction standards, representation and transmission methods 77−67408
induction unit, 2 to 10 T, USSR special standard 77−30191

magnetic variables measurement continued
inductometer calibrator, U-738, description 78−74034
instrument design, magnetic losses Si-Fe sheets appl. *(Rumanian)* 77−79131
Kerr magneto-optic microscope and measuring system 78−58023
laboratory apparatus 78−81743
layer magnetic properties meas. on saturated substrate 80−13108
loss, form factor influence *(Rumanian)* 80−68226
low temp. mag. suscept., nylon-quartz fibre support 78−65947
M-H curves, magneto-optical instrument for *(Japanese)* 77−37953
macroscopic quadrupole field meas. with SQUID magnetometer, order determ. 79−24140
magnetic bubble materials, coercivity meas. method *(Chinese)* 79−71429
magnetic props. meas. in high mag. fields, review *(Japanese)* 78−52303
magnetic recording tapes vibration magnetometer appl. *(German)* 78−70164
magnetic susceptibility, AC mutual inductance bridge using operational amplifiers 78−89508
magnetic susceptibility, appl. of microcomputer-aided data-processor *(Japanese)* 79−63283
magnetic susceptibility, high field, meas. using vibrating sample magnetometer *(Japanese)* 79−75559
magnetic susceptibility determ., paramagnetic matrix with ferromagnetic inclusions 79−97407
magnetic susceptibility instrument, supercond., automatic, biological appl. 78−57153
magnetically-soft materials, mag. characts. determ. methods, review 79−40593
magnetisation direction angle meas. with vibr. sample magnetometer, appl. to $SmFeO_3$ 77−26366
magnetisation intensity, meas. method for ferromag. material in static mag. field 77−49751
magnetisation of small ferrite samples, extraction method 80−242
magnetisation process, measurement techniques, in pulsed ultrahigh mag. fields *(Japanese)* 78−89509
magnetistaion, low-drift meas. using SQUID system 77−82574
magneto-microwave Kerr effect in semiconductors and ferrites using K-band interferometer 80−52263
magneto-modulation sensor, even-harmonic type, performance study *(Russian)* 77−53958
magneto-optical stroboscope with pulse height analyser for rapid magnetisation variations 79−67356
magnetocrystalline anisotropy, magnetometer for meas. in superconducting solenoid from 4 to 300K 77−2673
magnetocrystalline anisotropy energy of ferromagnetic materials, capacitance torquemeter 78−93743
magnetocrystalline anisotropy torque in sheared crysts., meas. 78−24830
magnetometer for induction meas. of moving mag. body, passband selection 78−251
magnetoresistance and Hall EMF, of low-resistance materials, by AM method 80−52278
magnetoresistance of semiconductors, automatic device for temperature dependence determ. 80−52270
magnetostriction, device for meas. at high temps. 77−26365
magnetostriction, dynamic, using induction method *(Russian)* 77−56171
magnetostriction, interferometric meas. method 78−12731
magnetostriction, meas. with recording rot. field magnetostrictometer 78−12733
magnetostriction, optical interferometric method of measurement *(Japanese)* 79−65705
magnetostriction in ferromagnetic films 77−10068
magnetostrictive vibration meas., laser interferometric technique 80−37059
magnets testing, permanent, test parameters selection w.r.t. errors 80−52280
micro-magnetic susceptometer for actinides 80−13112
milli gaussmeter for weak AC magnetic field intensity measurements *(Chinese)* 79−71485
molecular dipole moment, meas. using simple apparatus for undergraduates 77−57118
moment standards, representation and transmission methods 77−67408
moving magnet-stationary sample susceptibility balance 78−70169
non-uniform magnetisation and vibrating-sample magnetometer 78−54414
nonellipsoidal sample, demagnetising factor meas., magnetoelastic Rayleigh wave convolution 77−10072
oscillographic ferrometer 77−71353
paramagnetic components, use of static magnetic flaw detector 77−90571
paramagnetic vapours and condensing materials, apparatus for susceptibility meas., 300-1600K *(Russian)* 79−93178
Permalloy, reference materials characts. obs., temperature effect 80−80563
Permalloy ferromagnetic noise eval. 79−2799
photomagnetic, SQUID magnetometer appl. 80−98950
polycrystalline and amorphous strips, magnetostriction consts. determ. method 80−86355
powders, ferromag. and ferrimag., conc. characts. of magnetic props. 77−73052
power loss meas. under sinusoidal flux conditions 80−86348
precision EM measurements conference, Boulder, Colorado (June 1976) 77−18010
pulsed magnetic analyser, IMA-5 80−104399
Rayleigh constant of ferromagnet, electronic technique 78−12732
remanence, weak, accurate meas. 80−68225
RF SQUID system, microwave biased, appl. to magnetic aftereffect 79−26089
rigid body systematic deflection by suspension vibration in mag. field *(Russian)* 79−9223
ring magnet characts., meas. rate improvement *(Russian)* 77−26346
ring specimens, computer controlled mag. meas. system 80−86346
rotating magnetometer appl. to ferromag. materials 77−49750
rotatory hysteresis meas. of ferromagnetic specimen 77−87794
saturation, Helmholtz coil and fluxmeter system 78−93738
semiautomatic portable coercimeter 79−34250
Shubnikov de Haas effect meas. system set-up, expt. *(Polish)* 77−72873
single magnetic particles, remanent loop measurement 80−17967
single strip test frame with double yokes *(Japanese)* 78−82012
soft magnetic materials, meas. methods, review 80−86345

magnetic variables measurement continued
soft magnetic materials meas., in yoke, Br and Hc parameters estimation *(Czech)* 78−65944
soft-magnetic materials during pulse remagnetisation, use of stroboscopic convertor 77−5876
spin glass film, quench-condensed, apparatus for measurement of initial paramagnetic susceptibility 79−54160
spin waves line width of ferrites, suitability for microwave appl. characterisation 77−20571
SQUID application to measurements in fundamental physics 79−26087
SQUID biomedical appl., iron overloaded liver non-invasive diagnosis 80−101244
SQUID system for low drift high sensitivity magnetisation meas. 80−86347
SQUID using Nb thin film microbridge *(Japanese)* 80−31816
steel, austenitic stainless, weld metal, delta ferrite content measurement 78−31600
steel, coercive force measurement method of quality inspection of heat and thermomechanically treated parts 79−5113
steel, cold-rolled, isotropic, specific magnetic loss meas. at high frequency 80−101808
steel, elect., mag. props. determ. with Epstein hysteresis tester 80−60364
steel, massive object inspection, coercimeter with attached electromagnetic appl. 79−70277
steel sheets, apparatus for mag. props. meas. in freq. range 50 to 10000 Hz 79−30497
steel strips, electrotechnical, mag. props. meas. using AC compensated permeameter 80−86352
superconducting cable, magnetisation anisotropy meas. in hysteresis loss using Hall sensors 80−17966
superconducting solenoid, effect of constructional features on magnetic parameters 79−21786
superconducting susceptometer, automatic, sensitivity calibration, biological appl. 78−57154
superconductivity, definition of terms for fundamental states, flux phenomena, meas. practices 78−34916
susceptibility, AC, depend. on magnitude meas. field 80−241
susceptibility, balance appl., thermal noise effect 78−65906
susceptibility, demonstration system for student laboratory 80−4491
susceptibility, Faraday magnetometer for small samples *(Croatian)* 79−9222
susceptibility, meas. by levitation in paramag. solns. 77−10070
susceptibility, review of literature 1975-1977, instrumentation, chem. anal. applications, and bioscience 78−82006
susceptibility meas. calibration standard, low-field, using γ-Fe_2O_3 and glass powder mixtures 79−88989
susceptibility measurement by Thorpe-Senftle method, correction for ferromag. impurities 77−59378
susceptibility measurement using 7T NbTi split coil supercond. mag. system 79−71486
susceptibility measurement using low-temp. mag. balance *(Russian)* 79−75556
susceptibility of Fe alloys, initial, temp.-time instability, using bridge instrument with electronic demagnetiser *(Slovak)* 78−57989
susceptometer for biomedical meas., Fe stored in human tissue, in vivo 80−101245
temperature dependences, of permanent magnets, automated apparatus for −150 to 300°C range 80−31809
tesla (T) unit acceptance in SI system for magnetic induction *(Slovenian)* 79−40526
test instruments for magnetically hard materials *(Russian)* 77−67479
three-needle magnetic induction convertor, practical problems *(Russian)* 78−70165
torque method, vertically suspended specimen, field intensity effect 80−86353
unit mag. moment primary USSR state standard 79−2753
very high field meas. of mag. materials 80−68224
weak magnetic losses, meas. method, and its appl. to MnZn ferrite 77−51926
Wiegand effect, influence on magnetic sensors *(Spanish)* 80−31735
Co-rare earth magnets testing method for mag. parameters 79−49260
Fe, coercive force measurement method of quality inspection of heat and thermomechanically treated parts 79−5113
Fe-Si sheets nondestructive testing, using ferromagnetic colloid and surface flux meas. techniques *(Slovak)* 79−5090
Si, on sapphire, Schottky magnetodiode, integrated mag. sensor 80−68223
Sm-Co alloy magnets, operational control of residual induction, maximum mag. energy 79−15324

magnetic wells *see magnetic traps*

magnetisation
see also Barkhausen effect; coercive force; demagnetisation; magnetic aftereffect; magnetic anisotropy; magnetic domains; magnetic hysteresis; magnetisation reversal; magnetostatic waves; remanence; spontaneous magnetisation
actinide compound, ferromag. with mag. axial symmetry, temp. depend. of magnetisation 77−40044
actinide compounds, mag. and structural props. review 77−63132
actinides, band structure Fermi surface, magnetisation density 78−84140
alloy, binary, with mixed ferro- and antiferromag. exchange, magnetisation, phenomenological theory *(German)* 78−56297
alloy, FCC, binary, on Ising system, sublattice magnetisation, tricrit. point, simulation 79−33491
alloys, magnetisation calc. method based on moments of density of states 80−65770
Alnico 5 and 8, spinodally decomposed magnetic alloy, magnetic flux temp. coeff. *(Japanese)* 78−35006
amorphous alloy, mag. props. and appls. 78−95475
amorphous alloys, ferromagnetic props. and appl. 80−50143
amorphous alloys, for magnetic amplifiers and thermal recording appl. *(German)* 79−19744
amorphous alloys, mag. props. rel to device appl. 80−88804
amorphous alloys 77−16054
amorphous ferromagnet, apparent spin wave stiffness, low temps. 79−82776
amorphous ferromagnet, excitations, calc. using hard sphere models 77−66289
amorphous ferromagnet with random anisotropy, temp depend. of magnetisation 79−78442

magnetisation continued
amorphous ferromagnet with random uniaxial anisotropy, hysteresis, magnetisation 77−80963
amorphous ferromagnets, book contrib. 80−75743
amorphous ferromagnets, dispersion rels. and spin-wave spectroscopy *(Russian)* 79−7983
amorphous ferromagnets, ferromag. saturation, spatially random magnetostatic, magnetocrystalline, magnetostrictive and exchange fluctuations 78−60277
amorphous ferromagnets, hidden excitations, theory 80−75748
amorphous ferromagnets, itinerant electron model, Invar anomalies, review 78−95413
amorphous ferromagnets, mag. fundamentals, props. and appl. *(German)* 79−28557
amorphous ferromagnets, spatial fluctuations of magnetisation 79−19727
amorphous Heisenberg ferromagnet, spin wave excitations and magnetization curve 79−15292
amorphous insulator, phase diagram and statistical mechanics 78−52268
amorphous magnet, magnetisation, mag. moment temp. distrib. 80−15848
amorphous magnetic materials, props. *(Japanese)* 79−28561
analytical approx., accuracy investigation *(Bulgarian)* 80−71111
anharmonic Heisenberg ferromagnet, renormalised magnons and phonons 77−59373
anisotropic ferromagnet, one-dimensional Landau-Lifshits eqn. multisoliton solutions *(Russian)* 80−71014
anisotropic magnet mixture, Heisenberg spin system by Monte Carlo simulation 79−78408
anisotropic media, simple spin systems, magnetisation modes and evolution matrices 79−4734
anisotropic solids with magnetic symm., unified dynamic theory 78−77713
anisotropy and ferromagnetic reson., linear electric field effects 80−65854
antiferromagnet, crit. fluctuation of staggered magnetisation, AC susceptibility meas. 80−60219
antiferromagnet, Heisenberg or X-Y model, one-dimens., Friedel type oscills. 78−60296
antiferromagnet, induced staggered magnetic fields, microscopic mech. 80−80527
antiferromagnet, linear chain, biquadratic exchange interaction effects 77−63062
antiferromagnet, magnetisation, crit. spin-flop angle, temp. and field depend. *(Russian)* 80−7111
antiferromagnet, magnetisation fluctuations of first-order spin-flop phase transition near crit. point 77−24708
antiferromagnet, magnetoelectric susceptibility crit. behaviour, renormalisation group theory 78−48023
antiferromagnet, nonlinear magnetisation waves *(Russian)* 79−91251
antiferromagnet, second-order phase transition, weakening of effect of fluctuation in order parameter near crit. point 79−15316
antiferromagnet, uniaxial, critical magnetic field, influence of superconductivity 79−87219
antiferromagnet, uniaxial S=1, effect of cryst. field anisotropy 77−28344
antiferromagnetic and ferromag. parallel susceptibilities, graphical illustration, for teaching 78−41118
antiferromagnetic cubic model, one-dimens., ground states and magnetization in mag. field 79−78372
antiferromagnetic degenerate semiconductor, thermal and mag. props. 78−19224
antiferromagnetic Ising lattice, degeneracy at crit. mag. field and zero temp. 79−8007
antiferromagnets, anisotropic, mixture of two, with different easy axis, oblique antiferromag. phase 77−59408
antiferromagnets, nonlinear waves 80−84612
antiferromagnets, uniaxial, spin dynamics near bicrit. points 77−16090
antiferromagnets, weakly linear magnetisation density waves 77−51888
automatic M-H curve recorder in high magnetic fields for supercond. solenoid *(Japanese)* 79−71500
ballistic instrument, errors associated with circuit magnetisation parameters 80−22391
basalt, hypervelocity cratering and impact magnetization, lunar surface simulation 77−91115
BCC magnetically ordered alloys, effects on at. ordering-spontaneous magnetisation reln. *(Russian)* 78−19261
Bi-Ni base alloys, heterogeneous, supercond., magnetisation meas. *(French)* 78−6477
binary alloys, concentration derivatives and correlation functions of intrinsic variables 77−17937
α-bis(N-methylsalicylaldiminato) copper II, dynamic behaviour of antiferro- to ferromagnetic transition 79−73715
Bloch electrons, nonlinear orbital magnetisation in weak mag. fields *(Russian)* 80−70931
Bloch equations solution in presence of varying B_1 field, selective pulse analysis 80−25222
Bloch wall bound spin waves, equations of motion 80−34612
Bloch wall of finite size, distrib. of Neel segments *(Russian)* 78−56348
bond model, statistical theory of random ordered phase, uniform magnetisation 77−85401
borides, ternary, struct. classification, props., book contrib. 78−47309
boson magnetised ideal gas, effect of confinement, anal. 80−12987
bubble memory device, magnetisation distrib. in Permalloy strip *(Russian)* 77−48021
caesium perfluoro-octanoate/D_2O system, ^2H NMR quantum orders, RF pulses 80−103892
charged wall behavior in 1-μm bubble implanted structures 78−91892
chemisorption and magnetisation, book 77−25311
chromindur, origin of coercivity, Lorentz microscopy, magnetisation and Mossbauer effect 78−64219
coal, mag. and Mossbauer characterisation 78−64903
composite multifilamentary superconductor carrying DC transport currents, transient field losses 80−84551
composite superconductor, effect on losses in variable mag. field of mag. props. 80−34549
composite superconductor, transport current, interaction with transient external field 79−33393
composite superconductors for fusion magnets, current distrib. and losses 77−28331
conference, Donetsk, USSR (Sept. 1977). 79−82733
magnetisation continued
copper benzoate, low-dimensional Heisenberg antiferromag., high field magnetisation 80−80558
copper complex $CuBr_2$ (pyrimidine)$_2$, mag. susceptibility and magnetisation curve, 1.2-4.2K 80−11177
copper formate bisurea dihydrate, magnetisation curves 78−23298
copper formate tetradeuterate, paramag., induced staggered magnetisation, NMR 77−12212
copper formate tetrahydrate, antiferromag. phase, neutron diffr. study 80−93085
copper tetraamine sulphate, two-dimensional Heisenberg antiferromag., high field magnetisation 80−80558
covariant representation of microscopic charge and current densities in terms of polarisation and magnetisation fields 79−71
cross relaxation under action of 90° pulse trains, characts. 80−60402
cryogenic construction material magnetisation meas. *(Slovak)* 78−93693
crystalline materials, magnetisation density distrib. determ. by polarised neutron beam technique 79−77456
cubic ferromagnetic single crystal, magnetisation process 77−69622
cubic Ising ferromagnet, three spin interaction effect on mag. props. 80−54910
cubic spline functions representation of magnetisation curves *(German)* 80−71112
Curie-Weiss model, random magnetisation, statistics, asymptotic behaviour 79−4639
current loops, thermodynamics, teaching 80−90633
current transformer magnetisation curve, piece-wise linear, design method *(Russian)* 80−100598
curves, computer-aided approximation *(German)* 77−8338
cylindrically symmetric bubbles, static and dynamic props. 80−39835
de Haas-van Alphen effect, demagnetising fields and magnetic interaction 78−10332
deep-sea sediments, magnetisation, particle flocculation effects 79−70781
dialkylammonium copper chloride, nearly 2-D ferromag., low temp. NMR 77−28455
dialkylammonium copper chlorides, mag. and struct. transitions, IR absorption 77−52097
diamagnetic contribution to thermal fluctuations of magnetisation of diamagnetics 78−23240
diammonium layer compound, $(CH_2)_2(ND_3)_2MnCl_4$, mag. and optical props. 79−51760
diammonium layer compound, $(CH_2)_n(NH_3)_2CuCl_4$, mag. and optical props. 79−51760
diammonium layer compounds $(CH_2)_n(NH_3)_2MnCl_4$, quasi-two-dimens. antiferromag., magnetis., spin-flop and crit. exponents 77−66311
1,8-dichlorooctane, quadrupolar relax. centres, limited spin diffusion 80−100649
dielectric magnetic media, polaris. and magnetisation fluctuations 77−81047
dielectric thin slab. magneto-exchange modes with arbitrary pinning 77−63261
dilute local moment local magnetisation, Kondo-like deviations from free spin behaviour 80−44800
diluted ferromagnetic systems, cluster theory, second-neighbour interaction 77−89965
dimethyl ammonium copper chloride, spin dynamics near crit. pt. 80−7112
dimethylammonium iron chloride, two-dimens. antiferromag., ^{57}Fe Mossbauer obs., sublattice magnetis. 77−66443
dipolar solid, multiple-pulse spin locking 77−20742
dipolar uniaxial ferromagnet, equation of motion, nonlinear response near critical point 79−99717
dipropylammonium copper chloride, nearly 2D ferromag., spin wave theory 77−85436
direction angle meas. with vibr. sample magnetometer, appl. to $SmFeO_3$ 77−26366
dirty superconductor, fluctuation diamagnetism *(Russian)* 79−51721
disordered Heisenberg spin model, magnetisation calc. 80−60167
disordered magnetic substances, statistical props. *(Russian)* 78−35000
disordered spin system, commutator and anticommutator Green's functions 79−51792
distribution in isolated transition, digital magnetic recording 80−29580
divergence free cylindrically symmetric magnetisation patterns 77−69621
domain boundary parade motion, low freq. *(Russian)* 80−103852
domain structure, theory, band model of ferromagnetism approach 77−80954
double Ising chain, model in external field *(Russian)* 79−82735
ϕ Draconis, short period Ap star, discovery of mag. field 77−33511
dynamic behaviour, macroscopic eqns. *(Russian)* 78−19274
$DyNi_{3,4}$, magnetisation data 77−32177
Dyson's hierarchical model, at critical point 77−59370
Dyson's hierarchical model, essential singularities of borderline Ising case 78−31077
easy direction, meas. with aid of phase theory 80−65963
easy plane amorphous wire, magnetisation, variational calc. 80−71098
eddy-current flaw detection of long ferromag. products, magnetizing device parameters 80−89447
electric steel, induction above magnetisation curve knee from pole density texture 77−12151
electron and magnetisation densities in molecules and crystals, Arles, France (Aug. 1978) 80−105428
electron gas, relativistic, spin-polarised, Bloch theory 80−15465
electron-hole pairing systems, current states and domains 80−54614
equations based on laws of thermodynamics 77−89982
Eu-Ag alloy, amorphous, formation and mag. props. 79−91216
exchange processes, two-dimensional NMR spectrosc. investig. 80−25218
exchange vortexes of magnetisation, micromagnetic bubble domains 80−71138
extended Hubbard model, ferromag. solns. 80−80473
FCC alloys, atomic ordering and antiferromagnetism 78−72330
$Fe_xCo_{1-x}Ti$, ferromag., high-field and high-press. mag. behaviour 78−91919
Fe-Cr-Co-Si-Mo, plastic deform. influence on structure and mag. props. *(Russian)* 79−70176
Fermi fluids, nonlinear response of strongly coupled fluids, appl. to polarisation diags. 77−7931
Fermi fluids, propagation techniques for equilibrium strongly coupled fluids 77−7932
ferredoxin synthetic analogues, $[Fe_4S_4(SR)_4]^{3-}$ clusters, Mossbauer effect, EPR, and mag. props. 80−41057

magnetisation continued
ferrimagnet, magnetisation curves, spin reorientational phase transitions 79−82785
ferrimagnet, uniaxial two-sublattice, magnetisation intensity and crit. fields *(Russian)* 78−68285
ferrimagnetic phase in crystals with low exchange fields *(Russian)* 77−32188
ferrite, light diffr. by magnetisation inhomogeneities, multiple refl. 80−2733
ferrite, magnetisation effect on RF dispersion of permeability *(Russian)* 79−4700
ferrite, regulation in expts. on self-acceleration of electron beam 80−63425
ferrite, two-sublattice, thermodynamic functions in mag. field *(Russian)* 77−32197
ferrite film, determ. by ferromag. reson. method *(Russian)* 77−16126
ferrite spheres, magnetisation, resonance oscillation freq. determ. 80−71106
ferrite spinels, normal and inverse, solid state chem. expts. for students 80−36815
ferrites, anomalous permeability in Polder-Smit region 78−19278
ferrites, hexagonal, mag. anisotropy 77−20581
ferrites, hexagonal, model, two-sublattice uniaxial systems with strong antisymmetric exchange 78−47971
ferrites, stability of nonlinear homogeneous magnetisation precession *(Russian)* 78−48001
ferrites, wave beam propagation in longitudinally magnetised gyrotropic media *(Russian)* 80−23607
ferrites of divalent metals, prep. by double decomp. reaction, mag. charcts. *(French)* 79−33463
ferrofluid, dynamic magnetisation obs. 78−72370
ferrofluid, particle size distrib. parameters 79−1687
ferrofluid, relax. in external mag. field, cubic cryst. case 80−71113
ferrofluids, magnetisation, absence of anisotropy effects 80−50146
ferroinsulators, spin waves and uniform transverse magnetization, oscillatory eigenstates *(Russian)* 80−11181
ferroliquid, magnetoelastic oscills. 79−94639
ferromagnet, amorphous, Landau-Ginzburg theory, magnetisation and Curie temp. 80−75700
ferromagnet, amorphous, law of approach to magnetic saturation, effect of precipitates 78−72334
ferromagnet, amorphous, magnetisation, temp. depend. effect of nonrandom anisotropy 80−39773
ferromagnet, Bloch walls correlation and magnetic loss 78−95456
ferromagnet, domain wall cavity interaction energy, coercive field 77−8335
ferromagnet, domain wall dynamic slowing down *(Russian)* 79−78438
ferromagnet, domain wall mobility, damping, dipole-dipole interaction 80−93140
ferromagnet, domain wall motion, pinning by lattice defects, magnetisation 80−71079
ferromagnet, dynamic magnetic field on fast charged traversing particle 79−38423
ferromagnet, dynamic slowing down of dislocations near Curie point *(Russian)* 79−8036
ferromagnet, flux density curve anal., transverse magnetisation by variable mag. field *(Russian)* 79−69696
ferromagnet, high frequency, kinetic and thermodynamic props. *(Russian)* 78−19340
ferromagnet, Ising model, diamond lattice, phase transition, crit. props. 80−93127
ferromagnet, itinerant, mag. props., temp. depend., functional integral approach 80−60170
ferromagnet, localised nonlinear oscillations, unidimensional magnetisation soliton, analytic soln. *(Russian)* 79−78437
ferromagnet, magnetisation at low temp., disorder induced behaviour 78−52234
ferromagnet, magnetisation curves, spin reorientational phase transitions 79−82785
ferromagnet, magnetisation noise and power loss 79−24197
ferromagnet, meas. using oscillographic ferrometer 77−71353
ferromagnet, nonequilibrium magnon state under nonresonance alternating mag. field 79−87248
ferromagnet, nonlinear localised magnetisation wave as bound state of large no. of magnons *(Russian)* 77−89940
ferromagnet, nonlinear localised wave of magnetisation as bound state of magnons *(Russian)* 77−63160
ferromagnet, nuclear magnetisation motion, hyperfine field microscopic inhomogeneity, NMR freq. shift *(Russian)* 80−80623
ferromagnet, photoelectric effect rel. to saturation magnetisation 80−65618
ferromagnet, planar cyclic remagnetisation under sinusoidal induction *(Russian)* 78−80177
ferromagnet, polycrystal, magnetisation law, Bloch wall motion *(French)* 79−95606
ferromagnet, random anisotropy amorphous, initial magnetisation, remanence and coercivity 77−80964
ferromagnet, remanent magnetisation during thermal demagnetisation near a phase transition 78−88142
ferromagnet, rigid boundary model, magnetisation distrib. function *(Russian)* 77−80955
ferromagnet, tight binding model, surface magnetisation 80−103807
ferromagnet, two-dimens., spin wave theory, magnetisation, susceptibility *(Japanese)* 77−47954
ferromagnet, two-dimensional magnetisation, spin wave theory *(Japanese)* 77−20578
ferromagnet, uniaxial, magneto-dipole interaction influence on one dimensional magnetisation soliton *(Russian)* 80−54880
ferromagnet, uniaxial, with flat-parallel domain struct., classical phenomenological description 78−56316
ferromagnet, uniaxial with single-ion and exchange anisotropies, magnetisation in transverse mag. field 78−56277
ferromagnet, with liq.-like disorder, excitations 79−61084
ferromagnet, with mag. axial symmetry, magnetisation 77−85487
ferromagnet in strong alternating mag. field, eqn. of motion of total mag. moment *(Russian)* 78−88097
ferromagnet magnetisation, influence of high intensity longitudinal sound waves 80−103875
ferromagnetic, anisotropic, Green-function theory 77−16025
ferromagnetic alloy, transition to spin glass ordering 80−34628
magnetisation continued
ferromagnetic array of pseudospin S=1/2, nearest neighbours anisotropic exchange mag. stability at 0K 77−1547
ferromagnetic crystal, magnetisation in high fields, influence of internal field nonuniformity 79−51819
ferromagnetic crystal with defects, expressions for dispersion and average EMF due to magnetisation discontinuities *(Russian)* 79−51800
ferromagnetic crystals, magnetoelastic interactions, linear Cosserats theory 79−28576
ferromagnetic degenerate semiconductor, magnon spectrum near instability of homogeneous state 79−28516
ferromagnetic film, ϕ^4 domain walls, magnetisation, occurrence of crit. point 78−95500
ferromagnetic film, electric-charge-induced magnetisation 79−69700
ferromagnetic film, ground state, effect of surface and bulk anisotropy *(Russian)* 79−11328
ferromagnetic film, influence of interference field harmonics on mean magnetisation vector *(Polish)* 77−40092
ferromagnetic film, mag. props., rel. to struct. 79−91270
ferromagnetic film, mag. props. meas. using planar magnetoresist. effect 78−21186
ferromagnetic film, of cubic symmetry, depend. of Curie temp. on thickness and boundary conditions 78−19287
ferromagnetic film, transverse bioped susceptibility, two-dimens. micromagnetism 80−11231
ferromagnetic films, Bloch wall struct. and anisotropy, analytical representation 78−88151
ferromagnetic films, electrodeposition, thickness control, magnetisation meas. 78−23306
ferromagnetic Heisenberg chain, weakly bound magnon states *(Russian)* 80−100591
ferromagnetic insulators at parallel pumping, nonlinear magnetisation dynamics 77−8288
ferromagnetic layer in perpendicular mag. field, ground state, spin wave reson. 77−85512
ferromagnetic material, magnetisation characts. approximation *(Russian)* 78−31094
ferromagnetic material NDT, magnetising device, stabilization of Barkhausen discontinuities 80−89457
ferromagnetic materials, coercive force determ. *(Russian)* 79−73764
ferromagnetic materials, Curie point determ. from saturation magnetisation-temp. charact. 78−60281
ferromagnetic materials, magnetisation curved optimal analytical representation, automatic choice method *(Italian)* 78−47998
ferromagnetic materials, noise charact., applicability of physical similitude 79−4705
ferromagnetic materials, temp. modulation, phase sensitive detect., theory 77−12098
ferromagnetic metal, inhomogeneously magnetised, muon (μ^+) method, mag. struct. study 79−42739
ferromagnetic metal surface, Fermi level shift by charging, mag. moment and hyperfine splitting 77−20677
ferromagnetic metals, spin fluctuation theory, Curie temp., mag. susceptibility 80−65937
ferromagnetic parts, magnetisation by use of applied electromagnets 78−72999
ferromagnetic plate, nonlinear magnetostatic waves *(Russian)* 78−35014
ferromagnetic plates, domain struct. and magnetisation curves *(Russian)* 79−19743
ferromagnetic porous material, coercive field 78−14984
ferromagnetic semiconductor, degenerate, surface magnetisation 77−8385
ferromagnetic semiconductor, nonlinear magnetoelec. effect 77−20676
ferromagnetic semiconductors, dielectric function depend. on magnetisation, light absorpt. coeff. *(Russian)* 80−15467
ferromagnetic semiconductors, s-f interaction on conduction band, red shift effect theory 80−59872
ferromagnetic shield walls, in varying mag. field, AC magnetisation effects 77−26368
ferromagnetic single crystal balls, portable instrument for axes of easy magnetis. determ. 78−8424
ferromagnetic single crystal with cubic symmetry, mag. and magnetoelastic props. 79−15332
ferromagnetic sphere in nonuniform mag. field, magnetisation meas. arrangement 80−42242
ferromagnetic superconductors, self-induced vortices, magnetisation, Gibbs free energy 80−70916
ferromagnetic thin film energy absorption by magnetisation vector forced oscillation *(Polish)* 77−80970
ferromagnetic thin film magnetometer, development and performance 80−31808
ferromagnetic wire, circular magnetisation meas. 78−70167
ferromagnetic wire, Fe alloy, torsion stress influence on magnetisation obs. *(Slovak)* 77−90468
ferromagnetics, in unidirectional field, math. model *(Russian)* 77−24660
ferromagnetics, uniaxial, domain structure, influence of rapidly oscillating mag. field *(Russian)* 77−43847
ferromagnetics in unidirectional field, magnetisation, math. model *(Russian)* 78−88140
ferromagnetism, itinerant electron model, spin quantization direction fluctuations, short range order. 80−34582
ferromagnetism, singlet ground state, Heisenberg Hamiltonian model 79−11283
ferromagnets, exchange and dipolar coupled, spin wave renormalisation, Damon-Eshbach surface spin waves 80−2564
ferromagnets, itinerant electron, lattice props. depend. on cond. electron magnetisation, elastic props. 79−61035
ferromagnets, long-range, low temp. series for magnetization, crit. exponents 79−61131
ferromagnets, magnetic vortex as topological soliton in Landau-Lifshitz eqns. *(Russian)* 80−7097
ferromagnets, magnetisation stimulation by nonresonance AC mag. field *(Russian)* 80−65962
ferromagnets, phase transformation theory, easy axis anisotropy, quadrupole interaction, renormalisation method calcs. *(Russian)* 79−65671
ferromagnets, spin wave excitation due to parallel pumping, mag. impurity interactions *(Russian)* 80−80497
ferromagnets, weakly linear magnetisation density waves 77−51888
ferromagnets with double exchange, quantum theory 78−19204

magnetisation continued
field induced mag. transition criterion 78−88143
film, cylindrical, critical curve meas. and sense signal connection *(Slovak)* 77−24717
film, determ. from analysis of torque meas. 77−8368
film, evaporated, galvanomag. and mag. props., thickness depend. 78−23181
film, ferromag., dynamics near transition pt. from homogeneous to inhomogeneous magnetis. state 80−108038
film, mag. phase states when easy magnetisation axis is inclined rel. to film surface *(Russian)* 80−103864
film, magnetization amplitude and direction var., electron-microscope obs. procedure 78−6548
film, saturation magnetisation and uniaxial anisotropy determ. using torque meas. 79−95614
film, striped domain struct., 2D model of distrib. of magnetisation *(Russian)* 78−88149
film, uniform rotational high speed switching, dynamical crit. switching curve 77−32220
fine particle recording medium, packing density rel. to chain assembly 78−10731
flaw detection method evaluation, for components with difficult shape 77−90556
fluctuations, excitations and induced moments in system with two singlet levels 79−61022
garnet, epitaxial film, mag. bubble props., permanent local modification by laser annealing 80−2612
garnet, ion-implanted film, crit. curves for determining magnetisation directions 79−91263
garnets, photoinduced phenomena 79−99718
Gd-alloy, ferromagnetic, nuclear spins as probe for mag. coupling and crystallographic order 78−10799
Goldstone mode singularities, eqn. of state of isotropic magnet 79−42803
graphite, 4.2K magnetisation meas. in mag. fields up to 150 kG, diamag. props. 77−32156
graphite, low temp. magnetisation in strong mag. fields, filled band contrib. 77−32157
greenalite, two-dimens. mag. order 79−61188
Griffiths singularity in a non-dilute Ising chain 79−78285
guanidinium vanadium sulphate hexahydrate, susceptibility meas. spin-lattice relax. effects 77−66279
gyroscope, coupled to rotating ring, Barnett effect 78−86260
Hartree-Fock calculations, magnetisation equations *(Russian)* 78−27016
HCP metals, mag. susceptibility near $2^{1}/_{2}$th order electron transition, non-linear magnetisation anal. *(Russian)* 80−44859
heavy particle beam, electron cooling, magnetisation effects *(Russian)* 78−70219
Heisenberg, ferromagnet, classical, with dipole-dipole interaction, renormalisation group and crit. exponents 80−60351
Heisenberg amorphous ferromagnet, magnetisation and Curie temp., CPA calc. 80−75703
Heisenberg anisotropic antiferromag., spectrum and correlation functions 79−28499
Heisenberg antiferromagnet, anisotropic, excitations at finite temp., CPA calcs. 79−95562
Heisenberg antiferromagnet, disordered, magnetic atom-conc. near percolation threshold, mag. props. *(Russian)* 78−80171
Heisenberg antiferromagnet, uniaxial, props. by Green's function method 77−85406
Heisenberg ferromagnet, appl. of variational method for systems with discrete energy levels 78−31074
Heisenberg ferromagnet, classical, Monte Carlo calc. 78−23229
Heisenberg ferromagnet, dipole-dipole interaction, quantisation axis, magnetisation and critical point effects 78−34946
Heisenberg ferromagnet, low temp. behaviour in spectral density method 80−50028
Heisenberg ferromagnet, mag. excitation near surface of high Miller indices 77−51871
Heisenberg ferromagnet, magnon renormalisation 80−65849
Heisenberg ferromagnet, spin waves at low temp., method of variational derivatives 79−24152
Heisenberg ferromagnet, stepped surface, spin-wave modes calc. 77−73015
Heisenberg ferromagnet, surface magnetisation profile and localised magnons 80−70985
Heisenberg ferromagnet containing nonmagnetic impurity, local mean spin deviations 77−66236
Heisenberg ferromagnet in critical region, Bloch renormalised spin wave approx. 79−82784
Heisenberg ferromagnet mixed crystal, mag. props. 80−34579
Heisenberg ferromagnet with higher-order exchange interactions, thermodynamic props. 79−42770
Heisenberg magnet, dil. three dimensional, static behaviour at finite temps., Monte Carlo calc. 79−73752
Heisenberg magnet, two-dimens., glasslike ordering Monte Carlo calcs. 79−82740
Heisenberg metamagnet, collinear, mag. phase diagram 80−71035
Heisenberg model, finite magnetisation assuming ferromag. coupling 78−43541
Heisenberg model, magnetisation upper bound, Bogoliubov's inequality 77−43803
Heisenberg model, spin glass state, magnetisation of dil. mag. impurities, molecular field approx. 77−20623
Heisenberg model with one-ion anisotropy, closing relns. for Green's functions 78−2642
hexaferrites, $M(BaFe_{12}O_{19})$, mag. characts. correlation with substituting ions at. nos. *(Russian)* 79−91218
high-energy magnetic materials, props., treatment procedures and testing *(Italian)* 80−54914
horizontally dipped LPE film, inhomogeneities, spin wave reson. meas. 79−91298
Hubbard III approximation, numerical results for arbitrary values of correlation energy and electron density 77−51874
Hubbard model, neutral, strong-coupling props. 77−24667
Hubbard model, two-point doubly degenerate in half-filled case, thermodynamics 77−4492
hypercritical films, stress-induced uniaxial anisotropy influence on domain struct. *(Russian)* 79−69703
hysteresis processes, characterisation by isomorphic transform method *(Russian)* 80−80562

magnetisation continued
impurity uniaxial ferromagnet, thermodynamics below Curie point *(Russian)* 77−43801
integral equation for magnetostatic problems with thin plates or shells 78−50675
interacting single-domain grains, thermoremanence and ideal magnetization calc. 79−25232
intermetallic compounds, containing d-transition metal, hydrogenated, magnetism 80−34609
Invar, anomalous magnetisation and magnetoresistance under high mag. fields 77−80764
Invar, effect of deform. by cold rolling 77−48556
Invar, elec. transport props. and Invar features *(Russian)* 78−14710
Invar, hysteresis loop displacement 78−52312
Invar, magnetic and thermal anomalies 80−34603
Invar, magnetocryst. anisotropy rel. to magnetisation 77−16070
Invar, thermal expansion coeff. relationship to magnetisation 80−15269
Invar film, mag. props. and elec. resist. 77−32221
Invar films, exchange interaction depend. on lattice parameter, spin-wave reson. and magnetisation meas. *(Russian)* 79−42751
inverse spinel ferrite, mol. field theory 79−61021
ionic compounds, amorphous, exhibiting Mossbauer spectra, magnetic props. *(French)* 80−80490
Ising chain, in transverse field, variational treatment, static props. at zero temp. 79−4642
Ising chain, one-dimens., with generalized molecular field 79−91242
Ising chain, random-bond, in mag. field 78−39281
Ising disordered chains, ferromag., long-time relax. 80−34652
Ising ferromagnet, disordered, approximate treatment 78−52262
Ising ferromagnet, gaussian fluctuations of mol. field, magnetisation and free energy 80−70918
Ising lattice, triangular, antiferromag. to ferrimag. transition 77−20522
Ising model, 1-D, energy conserving relax. 80−20420
Ising model, bond-dilute two-dimensional, crit. behaviour 79−8009
Ising model, cluster size and percolation 79−65630
Ising model, cubic lattice, high temp. expansion at magnetisation of ninth order *(Russian)* 80−54858
Ising model, ferromagnetic, Diophantine moment problem and analytic struct. in activity 79−61026
Ising model, kinetic with triplet interactions, Monte Carlo anal. 80−7061
Ising model, magnetisation probabilities and metastability 80−29516
Ising model, one-dimensional transverse-field, in complex longitudinal field, real-space renormalization group method, T=0 80−103806
Ising model, random, susceptibility and magnetisation 77−80899
Ising model, randomly dilute, crit. and thermodynamic props. 79−8005
Ising model, spatially modulated phase, Monte Carlo study 79−95598
Ising model, spin glass state, magnetisation of dil. mag. impurites, molecular field approx. 77−20623
Ising model, surface magnetic order, Cayley tree approx. 77−72964
Ising model, two dimens., metastability, dynamic Monte Carlo method, transfer matrix 78−72354
Ising model, two-dimensional semi-infinite, correlation functions, local magnetisation 80−71074
Ising model in 4-D, critical isotherm 79−44871
Ising model in transverse field in one-dimens., zero-temp., renormalisation 79−38347
Ising model spin glass, phase transitions 77−8327
Ising models, quenched, with random ferromag. interactions, magnetisation upper bound 77−66233
Ising quadratic two-dimensional ferromagnet with three spin interactions 80−2542
Ising spin systems on Cayley tree-like lattices, spontaneous magnetisation, correlation function far from boundary 78−68137
Ising spins, disordered linear chain, relaxation, 1-D Glauber model, effect of disorder 80−65761
Ising triangular model, in mag. field, Markov process anal. 77−13708
isopermalloy, permeability stability calc. rel. to texture *(Chinese)* 80−65959
isotropic antiferromagnets, crit. dynamics using renormalisation group methods 79−8006
isotropic ferromagnet, with two mutually orthogonal sinusoidal mag. intensities, planar cyclic remagnetisation *(Russian)* 80−80561
isotropic magnet, Goldstone mode singularities eqn. of state, magnetisation curve, perturbation theory calcs. 78−43607
isotropic model ferromagnet, longitudinal spectrum calc. 78−10627
isotropic spin system, momentum-shell recursion relations in $2+\varepsilon$ dimensions 78−6498
isotropic three-sublattice ferrimagnet, magnetisation 80−2605
itinerant electron ferromagnet, effective Lorentz force and Landau level 78−80120
itinerant electron ferromagnetism at zero temp. 78−56285
itinerant electron ferromagnets, magnetisation fluctuations, Landau-Lifshitz eqn. 79−73729
itinerant electron system, coexistence of antiferro- and ferromagnetism 78−2645
itinerant ferromagnet, effect of planar defects on electronic struct. and mag. ordering 79−99672
itinerant ferromagnet, magneto-volume ext. 77−66404
Kac-Baker model of partially finite spin systems 77−20621
Landau-Ginzberg ferromagnet, static and dynamic correl. functions near magnetization curve 79−15318
linear transverse in long thin stripes, demagnetisation eigenfunctions anal. 80−34687
lodestones, microstruct., mag. props. and magnetisation 78−16004
low-drift magnetisation measurement, SQUID system 77−82574
magnetic domain wall motion, magneto-dipole EM wave radiation generation *(Russian)* 80−80555
magnetic fluid as continuum with internal degrees of freedom 80−60377
magnetic moment waves, nonlinear, limiting vel. and types *(Russian)* 78−60276
magnetic semiconductor, conduction electron spectrum, influence of nonlinear spin waves 79−28270
magnetic semiconductor, photomagnetisation, photoinduced heterojunctions 77−63259
magnetic susceptibility instrument, supercond., automatic, biological appl. 78−57153
magnetic susceptibility quantum oscillations, low temp., mag. instabilities in electron liq. *(Russian)* 78−87928
magnetically hard materials testing instrument, pulse magnetiser design *(Russian)* 77−67481

magnetisation continued
magnetically uniaxial ferromagnetic particles, high-anisotropy many domain, magnetisation, hysteresis *(Russian)* 79−91256
magnetically-soft materials, mag. characts. determ. methods, review 79−40593
magnetisable and polarisable media with microstructure, models 80−88708
magnetisation curve analytic functions, numerical parameter calc., variational methods appl. *(Russian)* 80−14267
magnetised structure evaluation via virtual magnetic charges 80−57341
magnetization curve and Gaussian error function *(German)* 80−50137
magnetoelastic crystal, cubic, acoustic SHG, static magnetisation effects *(Russian)* 78−56362
magnetographic inspection, determ. of magnetisation regimes 80−108665
magnetostatic oscillations, magnetisation distribution 78−68293
magnetostrictive ferromagnet, conditions for stress induced bulk moments 79−78493
Magnico alloy, with Si, Nb, Ti effect of Ub on mag. props. and grindability 77−63811
manganese acetate tetrahydrate, Heisenberg ferrimag. magnetisation 79−47304
massive object with one pole of electromagnetic, magnetisation 79−50190
measurement method for ferromag. material in static mag. field 77−49751
measurement techniques, in pulsed ultrahigh mag. fields *(Japanese)* 78−89509
megagauss field, magnetisation meas. techniques 78−93739
metal, cond. electron polarisation, magnetisation densities, neutron mag. form factors 77−72981
metal, indirect coupling between localised mag. moments by narrow band electrons 80−70942
metal-insulator transition, density-functional theory 80−75507
metallic ferromagnet, antiresonance region, EM wave propag., Maxwells' eqns. soln. 80−66038
metallic glass, splat cooled, mag. props. 80−80491
metallic glasses, mag. props., struct., and prep., book contrib. 79−65665
metallic glasses, mag. props. exam. *(German)* 77−89977
metallic glasses, soft mag. props. 79−73774
metallic glasses and amorphous magnetism, review 79−82818
metals, narrow-band, magnetism and mag. excitations 77−69478
metals, neutron mag. form factors, magnetisation densities, APW wavefunction calcs. 79−47243
metals, quantum magneto-dimensional effects, open Fermi surfaces, conduction electrons *(Russian)* 80−80487
metamagnetic transition in magnets with multi-sublattices *(Russian)* 78−23267
metamagnetism, spontaneous, four-ion anisotropy as source 79−47277
Metglas 2605, and 2605 A, transport props., resist. and magnetoresist. 79−1590
Metglas 2826-A, anomalous magnetisation, critical effects, superparamagnetism 77−8328
microcomputer-aided data-processor for mag. susceptibility *(Japanese)* 79−63283
microcrystals, magnetically ordered, high temp. behaviour 78−84456
micromagnetism, numerical calcs. 80−11222
microscopic charge and current densities in terms of polarisation and magnetisation fields 78−8251
microwave ferrites, saturation magnetisation determ. *(German)* 79−67357
mixed-valence systems, mag. behaviour, model calc. 77−80901
mixture, one-dimens., random, of Ising S=1 and $^1/_2$ spins, mag. props., spin distrib. 78−95407
model magnet, for reson. spectrometer, reproducibility of fields, field heights and magnetisation props. of materials *(German)* 78−24832
molybdenum chalcogenides, multicomponent, physical props. 80−84577
multicritical (order O) magnetisation eqn. of state, renormalisation group calc. 78−31085
multifilamentary superconductor with alternating twist, losses in transverse pulsed field 78−10602
multifilamentary superconductors with alternating twist, losses in transverse pulsed fields 79−30508
nematic liquid crystals, orientation fluctuations in high mag. field, quenching, birefringence effects 80−64892
neodymium ethyl sulphate, magnetothermodynamics, absolute temp. scale, mag. moment and magnetization , below 0.5K 78−34984
neutron diffraction magnetisation density distrib. expt. determs., review 77−77034
neutron studies of magnetic densities and magnetic excitations, book contrib. 80−11170
$NiWO_4$, antiferromag., low symmetry exhibited during spin-flop phase transition 80−60263
NMR image resolution from sensitive line method, magnetisation vector 79−93182
non-uniform magnetisation and vibrating-sample magnetometer 78−54414
nonexchange surface spin waves at interface between two ferromagnets 80−29544
nonoptically active media, susceptibilities, elec. and mag. polarisation fluctuation 77−77140
nonuniform ferromagnet, spontaneous magnetisation, mean field theory *(Chinese)* 78−91865
nuclear reactor magnetic scattering expt., deviations from saturation 79−31355
obsidian, Lipari and Teotihuacan origin, Mossbauer, magnetisation, X-ray diffr. and fluoresc. study 80−46173
one dimensional randomly dilute Ising ferromagnet, dynamics 80−70922
one-dimens. alternating X-Y model time-depend. spin correl. functions and ergodic props. 78−31031
one-dimensional Heisenberg magnet, in mag. field, dynamic correlations 80−70926
one-dimensional planar magnets, low temp. NMR 80−44943
one-dimensional semi-infinite chain, enhanced surface exchange interaction, mag. relax. 80−29558
order parameter, liquid ferromagnet, model calculation 78−88088
oriented Si steel, magnetisation hysteresis loops prediction 78−64221
orthorhombic ferrimagnets, domain wall motion at near sonic velocity, magnetoelastic interactions 80−34683
paramagnet, classical, wavelength-depend. fluctuations in mag. field 80−7069

magnetisation continued
paramagnet with noninteracting mag. moments, magnetisation *(Russian)* 78−47938
paramagnetic crystal, magnetisation change by light pulse 80−70932
paramagnetic gas in radiation field, magnetisation 78−78667
paramagnetic salts, field depend. of spin-lattice relax. 78−6567
paramagnetic semiconductor, heavily doped, linear response functions and magnetoresist. 77−51770
paramagnets, strongly enhanced itinerant, theory of anomalies in field depend. of magnetisation 77−69488
particle inspection, combined magnetization of parts by rectified single half-period fields 79−52575
Peierls-Hubbard model, antiferromagnetism and lattice distortion 77−55656
Permalloy, film, magnetoconductivity modulation from changes in magnetisation direction 79−60908
Permalloy, T- and I-shaped elements with cylindrical mag. domains, magnetisation distrib. 77−77074
Permalloy cylindrical film, magnetisation in crossed steady/alternating fields, easy axis dispersion influence 79−8024
Permalloy ferromagnetic noise eval. 79−2799
Permalloy film, domain walls, magnetisation components distrib. 79−87298
Permalloy film, domain walls streaming *(Russian)* 79−82842
Permalloy film, hysteresis loop meas. using magnetooptical system 79−69707
Permalloy film, M-H curve meas., magneto-optical instrument *(Japanese)* 77−37953
Permalloy film, mag. microstruct. obs. in nonlinear ripple magnetis. case *(Russian)* 80−65971
Permalloy film, velocity of motion of nonequilibrium walls of edge domains *(Russian)* 79−1694
Permalloy I-bar elements, magnetostatic effects, unifying overview of domain and continuum results 80−44853
Permalloy overlay bars, bubble stray field effect on domain wall struct., interference contrast technique 79−78457
Permalloy thin films, Neel wall transitions into cross-tie walls 79−95619
Permalloy-Co film, domain walls, magnetisation ripple *(Russian)* 79−47314
Permalloy-Rh, film, influence of Rh on corrosion resist. and mag. props. 80−3235
Permalloy-SiO multi-layer flat ring cond., with circular anisotropy, mag. props. *(Russian)* 77−8366
permanent magnet, iterative calc. method for magnetisation 77−83777
permanent magnetic material, radial pulse magnetisation, magnetising and testing fixtures 77−8354
permanent magnets, pulse magnetisation monitoring by pulse magnetometer 77−45871
permanent magnets review 79−42801
permeable specimen, magnetisation distribution, saturation approach 80−80566
phase transition thermodynamics, theory of magnetisation, role of positive surface energy 80−15724
phase transitions in quantum X-Y and Heisenberg models 80−25141
plane Ising lattice, local magnetisation depend. on linear defects *(Russian)* 80−2595
polarisation and magnetisation of electronic matter 80−75929
polariser for magnetising liquid, in NMR devices 80−57351
polyacrylic acid:Fe^{3+}, electron state of Fe^{3+}, Mossbauer and magnetisation obs. 79−73872
polycrystal subjected to successive asymmetrical hysteresis cycles, mag. props. evolution, reptation phenomenon *(French)* 78−10730
polyethylene, linear, melt props. correl. with chain length distribs. *(Russian)* 80−37920
porous anisotropic magnets, approach to mag. saturation 80−93146
Potts model, four state, series studies 79−85088
Potts model, Monte Carlo simulation in three dimens. 80−163
proton synchrotrons, magnetisation of ferrites in tunable accelerating resonators 80−68983
pulsed magnetic field measurement using Cu-Be search coils 79−63281
quantum field theory, external field depend. anal. 77−10165
quantum systems, one-dimens. isotropic X-Y model, zero temp. renormalisation group method 79−82800
quark gas in intense mag. field 79−85061
quinolinium $(TCNQ)_2$, random exchange Neisenberg antiferromag. chain, intermediate field magnetisation meas. 80−103857
radial field polariser for magnetising a moving liquid 78−250
random exchange Heisenberg antiferromagnetic chain, exchange-coupled pair model 80−20423
random ferromagnet, with long-range interactions, dynamics 77−89942
random Glauber chain, relax. of magnetisation, numerical studies 80−60313
random ordered phase in site model, statistical theory 79−47218
random spherical model, crit. dynamics 80−44844
random-bond Ising chain, ground-state energy, magnetostriction and zero-point entropy calcs. 79−7957
rare $earth_{50}Ag_{50}$, amorphous, bulk mag. props., field, time and temp. depends. 77−89932
rare earth alloy, amorphous, ferromag. state, non-axial elec. field gradient effect 80−75728
rare earth alloys, amorphous, high field magnetisation and magnetoresistance 78−72136
rare earth alloys, amorphous, mag. props. rel. to struct., review 79−15298
rare earth alloys, amorphous, random anisotropy antiferromag. model 78−95428
rare earth alloys, amorphous random anisotropy ferromagnetism in pair approx. 79−47276
rare earth alloys, Curie temperature, high press. effects *(Japanese)* 80−20444
rare earth alloys, R_3Pt_4, R=Nd, Gd, Tb, Dy, Ho, Er, Tm, mag. props., 4.2 to 160K 79−78343
rare earth alloys, $RAuNi_4$, (R=Gd, Tb, Dy, Ho, Tm, Yb and Er), mag. props. 77−20595
rare earth alloys, RCoAl, mag. props. 78−2659
rare earth alloys, RFe_4Al_8, mag. props., Mossbauer spectra, ordering effects 77−63179
rare earth alloys, RZn_{12} and RCu_4Al_8, mag. struct. and interactions 80−25092
rare earth amorphous alloys, random anisotropy antiferromag. model 80−20399

magnetisation continued
rare earth amorphous alloys, random mag. anisotropy, antiferromag., Monte Carlo calcs. 79−33471
rare earth cobalt intermetallics, Cu or Ni-substituted, narrow Bloch walls, magnetisation, 4.2K 77−8333
rare earth ferrite-garnets, compensation temp., rare earth ion influence 79−51775
rare earth garnets, prep. and props. book contrib. 80−44193
rare earth garnets, RIG, (R=Tb, Dy, Ho, Er), spontaneous Faraday rot. rel. to sublattice magnetisation 80−66159
rare earth germanide, RFe_2Ge_2, magnetisation and Neel temp. 77−8310
rare earth germanides, RMn_2Ge_2, 4.2-1200K 77−8285
rare earth impurities in s-band metals, Kondo anomaly 78−52208
rare earth intermetallic, $R(Fe_{1-x}Mn_x)_2$, phase struct., mag. and Mossbauer meas. 77−20563
rare earth intermetallic, RCu_4Ag, mag. props. and cryst. struct. 77−20562
rare earth intermetallic cpds., mag. props., book contrib. 80−39759
rare earth intermetallics, R_2Al and R_2Au, mag. charact. 78−68183
rare earth intermetallics, RAl_2-Gd(Er)(Dy)(Nd), dil., (R=La, Yb, Lu), EPR and mag. susceptibility 80−15797
rare earth intermetallics, RCo_2, itinerant metamagnetism, Van Vleck model 79−78297
rare earth intermetallics, RGa_2, ordering and exchange interactions 80−39779
rare earth intermetallics, RGa, mag. props., 4.2-350K 77−63230
rare earth intermetallics, RMg_2, cryst. and mag. props., ordering 78−68185
rare earth intermetallics, RPt, (R=Gd, Tb, Dy, Ho, Er, Tm), structs. and mag. props. 80−50069
rare earth iron garnets, anisotropic, mag. props., high field and low temp. 80−75801
rare earth iron garnets, level intersection and instability of mag. struct. *(Russian)* 77−43816
rare earth iron intermetallics, RFe_2, (R=Sc, Lu, Y), mag. props., 80-1300K *(Russian)* 80−75750
rare earth iron intermetallics, RFe_2, magnetostrictive, book contrib. 80−75838
rare earth metal, electron interactions rel. to lattice props. *(Russian)* 77−35901
rare earth metals, mag. and transport props. 79−69658
rare earth mixed ferrite-chromites, mechanism of polarisation of rare earth ions 79−42740
rare earth molybdenum selenides, supercond., mag. props., 0.7 to 295K 77−32113
rare earth molybdenum sulphides, $R_{1.2}Mo_6S_8$, low temp. magnetisation meas., and supercond. props. 79−8018
rare earth orthochromites, mag. interactions and weak ferromagnetism 78−52220
rare earth orthoferrites, parameters of interaction between rare earth and Fe ions, theory and expt. 79−73705
rare earth orthoferrites, slow neutron elastic scattering, domain boundary observation *(Russian)* 79−82811
rare earth orthotitanites, unusual mag. props., role of mag. moments 78−84400
rare earth orthovanadites, phase transitions and Jahn-Teller distortions 79−28548
rare earth permanent magnets, physics and technology 80−20433
rare earth silicides, RFe_2Si_2, mag. props. 4.2 to 950K 77−20544
rare earth silicides, RMn_2Si_2, 4.2-1200K 77−8285
rare earth tetraborides, mag. and elec. props., metallic character 80−20386
rare earth transition metal intermetallic permanent magnets, props. and technology, book contrib. 79−65696
rare earth-Co, RCo_3 (R=Gd, Dy and Ho), effect of absorbed H_2 on mag. behaviour 79−33483
rare earth-Co alloys, R_2Co_{17}, substituted 77−89947
rare earth-Co amorphous alloys, mag. compensation temp. 77−66277
rare earth-Co permanent magnets, microstruct., TEM obs., magnetisation 78−91901
rare earth-cobalt intermetallic, RCo_2, sublattice magnetisation, powder neutron diffr. meas. 79−19725
rare earth-copper intermetallic cpds., RCu_2, metamag., mag. props. 79−87242
rare earth-copper intermetallic cpds., RCu_2, metamag., mag. props. 79−87243
rare earth-Fe alloy, amorphous, random anisotropy model, generalised mol. field calcs. 77−28345
rare earth-Fe-Al alloys, RFe_4Al_8, mag. props. 78−52250
rare earth-gold amorphous alloys, R_4Au, anisotropy versus exchange 80−34624
rare earth-iron, RFe_2, Laves phase intermetallics, ordered and paramagnetic phases, mean field exchange consts. 80−50084
rare earth-Mg, magnetisation and neutron diffr. meas. 77−63105
rare earth-nonmagnetic metal intermetallic cpds., struct. and props., review 79−95377
rare earth-transition metal alloys, amorphous, Hubbard hamiltonian, mag. props. 77−72985
rare earth-transition metal alloys, amorphous, struct. and mag. props., book contrib. 80−39818
rare earth-transition metal alloys, cryst. and amorphous, mag. props. 77−73008
rare earth-transition metal alloys, disordered, magnetisation behaviour 80−71099
rare earth-transition metal amorphous alloy films with single mag. species 77−16121
rare earth-transition metal amorphous film, Kerr and Hall effect meas. 77−24722
rare earth-transition metal hydrides, magnetic props., book contrib. 79−82754
rare earth-transition metal intermetallics, struct. and props. review 78−10668
rare earths, band structure Fermi surface, magnetisation density 78−84140
rare-earth, mag. supercond., appl. of boson theory to mixed state 80−7050
rare-earth compounds, antiferromag., mag. props., cryst. field theory 78−27006
rare-earth compounds, antiferromag., mag. props., cryst. field theory 78−27007

magnetisation continued
rare-earth-Ni alloy, RNi_2 (R=Gd, Tb, Dy, Ho or Er), Mossbauer effect of ^{57}Fe 77−69743
relaxation phenomena and thermodynamic vectorial internal degrees of freedom 77−77145
remagnetisation, hyperfine structure collapse, review of γ-reson. spectroscopy under HF excitation 77−48113
representation of internal and external fields of two dimensional magnetised bodies *(German)* 78−78849
rigid magnetic continuum, classical theory 78−34944
ring ferromagnetic samples, remagnetisation dynamics *(Russian)* 78−19275
ruby, magnetisation precessing, optically induced, near level anticrossing points in $^4A_2$ 77−36111
ruby, optically induced magnetisation 78−76292
sediment magnetisation, water content effects 79−70785
sediments from Lake Zurich, magnetisation of detrital and chemical samples 79−70787
self-channelled states of mag. moment in rotating mag. field *(Russian)* 78−88102
semi-infinite Heisenberg ferromagnet, macroscopic theory of response functions and appl. to light scatt. 80−20410
semiconductors, magnetic, static magnetic properties, mean field approach 80−7090
Sendust ribbon, mag. props. 80−15761
ship magnetism, rel. to mag. compass, history, Airy-Scoresby controversy 78−4451
short rectangular prism, field-depend. local surface magnetisation, numerical calc. 77−36110
simple ferromagnets, crit. behaviour 80−60331
single domain grain assembly, theory for magnetisation processes 80−88828
single particle material for tape and disc manufacture, prep., props., and appls. 78−52308
singlet ground state system in mag. field, anisotropic exchange interaction effect on props. 79−91224
soft ferromagnetic cylinders and spheres, micromagnetics 77−12150
soft magnetic material, analysis by means of Barkhausen noise cross spectra 79−24199
soft magnetic metals, ideal, AC response 78−64223
solid torsional oscillators, rotating frame, nucl. spin polarisation losses, torsional spectroscopy 80−31821
spin glass, dynamical theory of quenched site model 79−19742
spin glass, Ising, two-dimensional, Monte Carlo evidence for absence of phase transition 78−19260
spin glass, mean field approx. 78−52280
spin glass, relax., mean field approx. 78−52281
spin glass, self-consistent mean random field approximation, comparison with $n\to 0$ expansion 77−20622
spin glass-ferromag. alloys, high-field magnetisation 79−33488
spin glasses, magnetisation relaxation time near freezing temp., HF calc. 80−34665
spin glasses, relax. of magnetisation and order parameters 78−27043
spin Hamiltonians, infinite-range, exact solns., closed form magnetisation eqn. 79−78281
spin model, random mag. bonds, phys. props. near crit. point 78−84440
spin system, transient phenomena, soln. using eigen-coordinate system of magnetisation vector 80−25116
spin wave resonance, surface mode magnetisation, inhomogeneities effect 77−69710
spin wave resonance, surface modes, influence of inhomogeneities of magnetisation 77−12205
spin-$^1/_2$ XY model, thermodynamic quantities, high-temp. series expansions anal. 80−7067
spin-glass, two-dimensional Ising model, low temp. dynamic props. 80−20425
spin-lattice relaxation time meas. using saturation, inversion and fast inversion expts. 80−57356
spin-lattice relaxation times meas., mathematical formulation 80−62703
spin-Peierls phase diagrams, obs. and models 80−60330
spin-Peierls transition in mag. field, phonon freq., Heisenberg model calcs. 80−25151
spin-Peierls transition in magnetic field 78−84441
spinel structure ferrite, magnetisation using Neel's mol. field theory 79−87223
SQUID system for low drift high sensitivity magnetisation meas. 80−86347
steel, austenitic, magnetisation meas. of stability 77−1579
steel, austenitic, Ni-Ti, alloy N35T5, ageing, magnetisation and Curie temp. depend. on plastic deform., Mossbauer studies *(Russian)* 79−69669
steel, austenitic stainless, magnetic susceptibility and magnetisation, low temp. 80−25102
steel, C, residual stress induced by uniaxial deform., mag. meas. 77−73390
steel, Cr-Ni-Mo-V, magnetic induction, struct. dependence *(Czech)* 80−50141
steel, determ. of saturation mag., for residual austenite and props. of standard *(French)* 79−73766
steel, high speed tool, wear, effect of magnetisation on tool life 80−89361
steel, LF mag. field, oscillations in envelope of harmonic levels, struct.-mech. charact. determ. 78−60940
steel, martensitic, sp. ht. and magnetisation meas. 1.2 to 10K 80−71059
steel, mild, acoustic emission during magnetisation, stress effects 79−82854
steel, nonoriented, mag. props. texture, Cr addition effect 77−1880
steel, stainless, cold plastic deform. effect on struct. and props. 80−29113
steel, stainless, type 316, neutron irradiated, ferrite formation, study by mag. meas. and TEM 79−37742
steel, thin sheet flaw detector, magnetisation system 77−12751
steel, transformer, anisotropy of temp. depend. of mag. props. *(Russian)* 78−39362
steel, types 45 and U8, plastically deformed, magnetoelastic props. *(Russian)* 80−44893
steel bearing parts, magnetic inspection of heat treatment quality 78−73007
steel fibres, polycrystalline, Mossbauer spectroscopy 80−44959
sublattice metamagnet, temp. dependent anisotropy, magnetisation curves, mag. transitions, classical approx. 80−39795

magnetisation continued
superconducting accelerator magnets, magnetization effects on field shape 79−31253
superconducting cylinder, type II, magnetisation change induced by current near upper crit. field 80−70890
superconducting magnets, influence of magnetization in multifilamentary composites on central field 79−65599
superconducting slab, type 1, first stage magnetisation and metastable migration field 80−15655
superconducting solenoid, automatic M-H curve recorder in high magnetic fields *(Japanese)* 79−71500
superconductor, ferromagnetic, mean-field theory 79−65586
superconductor, type I, critical field for nucleation of n-domains 77−1515
superconductor, type-II, magnetisation, rel. to anisotropy of upper crit. field 80−54832
superdense stars, quantum theory of magnetism 79−92753
superparamagnet, magnetodipole broadening of reson. line *(Russian)* 79−38385
superparamagnetic particles, magnetic moment time development and discrete orientation model 80−60378
superparamagnetic particles, magnetis. vector movement, relax. freqs. *(Russian)* 79−95610
superparamagnetic particles, Mossbauer spectra, magnetisation vector precession 80−15872
superparamagnetic particles, motion of magnetisation vector 79−56494
superspin in NMR, appl. to ABX system 80−60426
surface and interface magnetism by Mossbauer spectroscopy 80−7218
surface magnetisation, size effect 78−15008
surface magnetisation profile singularities near critical point 80−103843
T bar, domain wall study employing ferrofluid, rel. to magneto-optical Kerr effect meas. 80−60360
TANOL, linear chain antiferromagnet, long-range order, magnetisation, PMR 78−23266
TCNQ, dimer gas model 78−87926
TCNQ salts, Qn(TCNQ)$_2$ and Cs(TCNQ)$_3$, surface magnetism 78−2703
TCNQ salts, surface magnetism, magnetisation field curves meas. 77−59428
thick wall elliptical bubbles, magnetisation distrib. 77−69649
thin film, with uniaxial-biaxial anisotropy, low freq. ferromag. reson. 79−8055
three-dimensional permeable solid, magnetisation distrib., computer calc. 78−72366
titanomaghemite, synthetic, cation distrib. 78−55856
transformer steel magnetic loss variation due to nonuniform normal press. *(Russian)* 79−91250
transient and steady-state characts. with hysteresis, digital simulation 77−66385
transition metal alloy, electronic structure, mag. props. 78−95254
transition metal alloys, amorphous, mag. props., chem. short-range order 80−75739
transition metal alloys, amorphous, mag. props., structure and preparation 80−75737
transition metal alloys, Curie temperature, high press. effects *(Japanese)* 80−20444
transition metal complexes with 1,2,4-triazole, mag. susceptibility, 2-300K, struct., antiferromag. props. 77−77045
transition metal compounds and dil. alloys, mag. ordering phenomena in high mag. fields 80−50075
transition metal surface, spin orientation effect of shallow electrons by magnetization 79−65881
transition metal surfaces, mag. props. 80−44861
3d-transition metal-metalloid cryst. and glassy alloys, electronic struct. from magnetisation and Mossbauer meas. 80−29363
transition metal-rare earth alloys, amorphous, mag. props., mean field anal. 79−4701
transition metal-rare earth intermetallics, two sublattice system with high competing single ion anisotropies, model 80−39767
transition metals, ferromag., dil. H electronic struct. 80−70638
transition metals and alloys, magnetisation in high mag. field, Arrott-Noakes plot 80−54919
3d-transition-metal dichalcogenides, mag. props. rel. to Hubbard model 79−78373
triaxial crystals, domain struct. and magnetisation phenomena *(Russian)* 79−47295
tridimensional numerical calc. of magnetic fields using summation method *(German)* 80−106414
trimethyl ammonium cobalt chloride, magnetisation temp. depend. 80−7128
trimethylammonium manganese heptachloride(-bromide), antiferromag. chain systems, high-field magnetisation meas. 79−61187
(TTF)$CuS_4C_4(CF_3)_4$, spin Peierls system, mag. field effects 80−7123
TTF-bis-dithiolene metal complex compounds, donor-acceptor type, one-dimens. mag. variety and props. 77−66271
TTF-$CuS_4C_4(CF_3)_4$, spin-Peierls system, high-field phase 80−39816
TTF-TCNQ, surface magnetism 78−2703
tube, magnetization with transverse field, approx. soln. 80−69321
twin crystals, magnetic reversals, role of magnetostatic interaction *(Russian)* 78−39361
twisted uniaxial polycrystals, magnetisation process, model 79−91254
two-dimensional antiferromagnets, diffusion-controlled mode coupling, EPR linewidth 79−51844
two-dimensional lattice, cluster expansion method 78−34942
two-spin system, solid without spin-lattice relax., NMR theory *(German)* 78−88197
type I superconductor, mag. dipole effect on order parameter *(French)* 77−89899
type I superconductor, magnetisation in thermodynamic and metastable phases 80−93027
type II magnetism in mixed magnets and spin glasses 78−23281
type II supercond., rot. in mag. field, flux density distrib. 78−43536
type II superconductor, bounded, intermediate state struct. form. near crit. field, role of surface 80−80465
type II superconductor, cylindrical, rotating in mag. field, dissipation determ. 77−28309
type II superconductor, giant-vortex state, temp. depend. 80−7051
type II superconductor, ideal, wire, macroscopic current in longitudinal field 78−84366
type II superconductor, magnetisation, critical state model 79−47212
magnetisation continued
type II superconductors, magnetisation curves, boson method calcs. 78−39258
uniaxial ferromagnet, arbitrary spin and single-ion anisotropy of second order, Green's function 78−84379
uniaxial ferromagnet, in transverse mag. field, quantum theory *(Russian)* 79−15297
uniaxial ferromagnet, neutron depolarisation calc. 78−64192
uniaxial ferromagnetic crystal, irreversible rotation processes 80−39768
uniaxial ferromagnets with single ion anisotropy in transverse field 77−32143
uniaxial materials with shape anisotropy, magnetisation curves 78−60313
US, large magnetic anisotropy exam. 77−20585
very high field meas. of mag. materials 80−68224
vicalloy-2, high heating rate effect on mag. props. *(Russian)* 77−81328
weak ferromagnet, domain wall dynamics, nonlinear waves, mag. solitons *(Russian)* 80−75793
weak ferromagnet, with easy plane anisotropy correl. functions and magnetisation, temp. depend. *(Russian)* 80−84581
weak magnetic field, absolute intensity meas., use of RF biased SQUID 80−82794
X-Y model, finite magnetisation assuming ferromag. coupling 78−43541
X-Y model, for ground-state magnetisation 79−65629
X-Y model, one-dimensional S=$^1/_2$, autocorrelation function for x-component of magnetisation 77−77018
X-Y model, spin 1/2, thermodynamic props., high temp. series expsn. 78−47929
Ag, resonant and nonresonant conduction-electron-spin transmission 80−75857
Ag-Fe, Kondo system, magnetisation, Mossbauer expts. 77−77028
$Ag_{0.6}Au_{0.4}Mn$, dil., effect of mean free path on strength of RKKY interaction 78−39291
Al, acoustomag. effect, temp. depend. *(Russian)* 77−72941
Al, nucl. mag. thermometry using SQUID magnetometer 77−26292
Al, supercond. film, precursor diamagnetism, magnetisation meas. 77−32115
Al-Mn, dil., magnetisation, 2-0.01K 79−4652
Al_2Ce, Al_3Ce, nucl. orientation exam. of Ce ground state at very low temp. 78−67999
AmB_2 (B=Al, Co, Fe, Rh, Ru), crystal structure, mag. props. of Laves phases 77−27851
$AmFe_2$, high temp. mag. props., 300 to 1100K 79−51757
Au, resonant and nonresonant conduction-electron-spin transmission 80−75857
Au-Co, liquidus line determ. by mag. meas. 80−60250
Au-Fe, dil., approach to saturation of magnetisation 78−56293
Au-Fe, Kondo system, magnetisation, Mossbauer expt. 77−77028
Au-Fe (3.1-10.4 at.%) spin glass alloys, high field magnetisation curves 80−11213
Au-Fe (4.2 at.%), spin glass, DC magnetisation, field depend. 80−97103
Au-Gd, dil., fine struct. splitting, magnetisation meas. 79−56498
Au-Mn alloys, reversible and irreversible DC magnetisation in spin glass regime 80−65908
Au-Mn-Cr(Pd) alloy, ferro- to non-mag. transform. 77−12117
Au-Ni, mag. clustering 79−7977
Au-Ni, magnetisation and sp. ht., ferromag., paramag. and crit.-conc. regions 79−38330
$(Au_xPb_{1-x})_{1-c}Fe_c$, ferromag. and spin glass ordering 78−56335
Au_4V, partially disordered, magnetisation distrib., polarised neutron diffr. study 79−47244
BMn, ferromag., ^{55}Mn magnon-induced pseudoquadrupole processes 79−19802
$B_2O_3.Fe_2O_3.2CoO$, mag. props. up to 1200K transitions and magnetisation curves 77−36069
$B_2O_3.Fe_2O_3.2MgO$, mag. props. up to 1200K transitions and magnetisation curves 77−36069
Ba hexaferrite, irradiated by fast neutrons, mag. props. 80−97116
$BaCo_2(AsO_4)_2$, planar X-Y model, mag. ordering 77−66256
$Ba_2Co_{2x}Zn_{2-2x}Fe_{12}O_{22}$, mechanically oriented, topotactic prod. technique, mag. props. 80−35140
$BaO-Fe_2O_3$, chemically coprecipitated, mag. props., orientation 80−15763
$BaO-Fe_2O_3$ system, splat cooled phases struct., magnetisation and susceptibility 300-1100K *(French)* 77−48017
$BaO-Mn_2O_3-B_2O_3$, amorphous mag. oxide, field-cooling effect *(Japanese)* 80−84615
$BaVS_3$, mag. and elec. props. 79−91214
$BaVS_3$, magnetisation and neutron study 80−84588
$Ba_3WFe_2O_9$ and $Ba_3WFe_2O_{8.42}$, crystallographic and mag. props., comparative study 80−103303
$BaZn_{1.38}Co_{0.62}Fe_{16}O_{27}$, W-type hexaferrite cryst., first order magnetisation processes 78−95472
$Ba_2Zn_{2-2(x+y)}Cu_{2x}Cd_{2y}Fe_{12}O_{22}$, mag. props. and Mossbauer spectrum 80−75765
$Ba_2Zn_{2-2x}Cu_{2x}Fe_{12}O_{22}$, hexagonal ferrites, prep. and mag. characterisation 79−1727
$BaZn_2Fe_{16-x}Al_xO_{27}$, saturation magnetisation, anisotropy field and Mossbauer meas. 77−69508
$BaZn_2Fe_{16-x}M_xO_{27}$ (M=Al, Ga, In, Sc), mag. props. and Mossbauer effect 80−75766
$Ba_2Zn_2Fe_{12}O_{22}$, anisotropic magnetisation and susceptibility 78−84411
BamSrmPb hexaferrites, prep. by cernet procedure, mag. props. 77−32174
Be, magnetoacoustic quantum oscills. due to mag. breakdown orbits, and derivative of magnetisation meas. 77−43479
BeCu pressure clamp cell, for low temp. specific heat and magnetisation meas. 80−17956
$Be_5(Fe_{1-x}Mn_x)$, mag. and calorimetric props. 77−63083
$Be_2Mn_{1-x}Fe_x$, mag. props., giant moment clusters 79−28508
Bi-MnBi, directionally solidified composite, processing parameter role on mag. props. 80−35352
Bi-MnBi, mag. props. singularities, electron microscope exam. *(Russian)* 78−39363
Bi-MnBi directionally solidified eutectic alloys, struct. and mag. props. 79−51815
$Bi_2Fe_4O_9$, antiferromag., mag. glass props. *(Russian)* 77−4519
$Bi_{95.6}Mn_{4.4}$, magnetisation of ferromag. precipitates, effect of ultrasonic pulses 80−2121
C, amorphous, anomalous low temp. mag. and thermal props. 78−10647
C, char, amorphous, mag. interactions between localised spins 80−34587
C powder magnetisation thermometry for very low temps. 79−63219

magnetisation continued
CO complex, with 1,2,4-triazole, mag. susceptibility, 2-300K, struct. 77−77045
$(CO_{1-x}Fe_x)$-B-Si, amorphous mag. props. *(Japanese)* 77−85433
Ca ferrite, composition and mag. props., anisotropy field, magnetisation 80−71109
Ca, Ge-substituted garnet, LPE growth atm. effects on bubble props. 77−20655
$Ca_{2x}Bi_{3-2x}V_xFe_{5-x}O_{12}$ ferrogarnet, magnetis. distrib., correl. with morphological habit 79−42802
$Ca_3Mn_2Ge_3O_{12}$, mag. field induced transition 80−50094
$(CaO.nFe_2O_3)_{100-x}(La_2O_3)_x$ ferrite, permanent mag. material, mag. props. and preparation 79−83148
Cd-Co(-Mo), amorphous films, thermal stability of mag. props. *(Japanese)* 79−47307
Cd-Mg, mag. susceptibility near $2^1/_2$th order electron transition, nonlinear magnetisation anal. *(Russian)* 80−44859
$Cd_{1-x}Ag_xCr_2Se_4$, Ag acceptor states effect on exchange interaction 80−20397
$CdCr_2Se_4$, excitation of spin waves by current carriers, magnetisation and elec. cond. reduction *(Russian)* 79−7981
$CdCr_2Se_4$, study of photoinduced changes 80−80567
$CdCr_2Se_4$:Cu(In), ferromag. semicond., mag. and elec. props. 77−20588
$CdCr_2Se_4$:Ir(Cu), mag. props. near Curie temp. *(Russian)* 77−63234
$Cd_{1-x}In_xCr_2Se_4$, electric, photoelectric and mag. props., metal-semicond. transition *(Russian)* 80−54738
$Cd_{1-x}Mn_xTe$, magneto-optical props. of free excitons rel. Mn^{2+} ions spin alignment 79−47419
CdS, amorphous antiferromag., mag. props. of dilute neutral donors 79−78367
α-Ce, susceptibility, sp. ht. and magnetisation 79−28512
$CeAl_2$, and $CeAl_3$, magnetisation and sp. ht. 80−20418
$CeAl_2$, mag. ordering and anomalous ground state, neutron diffr. obs. 79−78331
$CeAl_2$, magnetisation curves under high mag. field and hydrostatic press. 77−63233
Ce_3Al_{11}, competition between ferro- and antiferromag. interactions 80−60258
Ce_3Al_{11}, mag. ordering at low temps. under press., relation to $CeAl_3$ props. 79−19745
$Ce_{30}Au_{20}$, amorphous, cryst. field effects and mag. interactions, magnetisation and transport props. meas. 78−68191
$Ce_{80}Au_{20}$, metallic glass, mag. ordering and cryst. field effects, speromagnetism 80−80531
CeB_6, resist. anomaly and mag. ordering obs. 79−61110
CeBi, phase diagram in mag. field, hydrostatic press. effect 80−25132
$CeBi_xSb_{1-x}$, mag. props. and press. effects 80−71026
$CeCo_5$, magnetisation and coercive strength 77−55688
Ce_2Co_7, and ternary hydride, mag. props. 80−108007
$CeFe_2$, H_2 absorption effect on mag. props. and struct. 77−40045
$CeFe_2$, magnetostriction and magnetisation 80−39844
$CeIn_3$, magnetisation and sp. ht. 80−20418
$Ce_{1-x}La_xSn_3$ (x=0 to 1), mag. susceptibility and magnetisation, lattice parameters, X-ray and neutron diffr. meas. 80−49675
$CeMM_{0.8}Sm_{0.2}Co_5$, (MM=mischmetal), thermal props. *(German)* 77−8359
CeP(As), single crystals, low temp. thermal, electrical and mag. props. meas. 78−27051
$CePd_3$, susceptibility, sp. ht. and magnetisation 79−28512
$CeRu_2$, change of valence of Ce ions, induced by H absorption, supercond. disappearance 79−47185
$CeRu_2$, H absorption induced Ce valence change, mag. and supercond. props. 80−50042
CeS, mag. props., sp. ht. and thermal expansion 78−60292
CeSb, mag. phase diagram for mag. field applied along ⟨111⟩ direction 79−33458
CeSb, press. effect. on mag. props. 78−23315
$CeSb_xAs_{1-x}$, mag. props. and press. effects 80−71026
CeSe, mag. ordering, ε expansion predictions, neutron diffr. obs. 79−61060
CeSe, mag. props., sp. ht. and thermal expansion 78−60292
$CeSn_3$, field induced form factor, temp. depend. 79−78308
$CeSn_3$, polarised neutron study of induced magnetisation 80−34594
CeTe, mag. ordering, ε expansion predictions, neutron diffr. obs. 79−61060
CeTe, mag. props., sp. ht. and thermal expansion 78−60292
$Ce_{0.736}Th_{0.264}$, induced mag. form factor 79−78307
$CeTl_3$, mag. susceptibility, magnetisation, neutron diffr., elec. resist., and sp. ht. meas. 80−75733
CeX (X=P, As, Sb, Bi), neutron inelastic scatt. expts. 80−19674
$(Ce,Y_{1-x})Fe_2$, mag. susceptibility and Mossbauer meas., lattice parameters 80−97068
$(Co, Cu, Fe)_5Ce$, sintered permanent magnets, magnetic charact. 78−60608
Co alloys, amorphous, effects of metalloids on mag. props. 80−75738
Co, atomic layers, Pauli paramagnetism to band ferromagnetism transition thickness depend. 78−72377
Co based amorphous alloys, struct. and thermomag. meas. 77−16055
Co, electrodeposited film, saturation magnetisation and perpendicular anisotropy meas. 78−76277
Co ferrite film prep. by vac. evaporation and annealing 77−85939
Co, ferromag., local mag. field at positive muon 77−12295
Co fine particles in Cu, interface magnetisation 80−88858
Co, itinerant ferromag., Fermi surface and single particle excitations 80−34350
Co, Kerr equatorial effect freq. spectra anisotropy, dielectric permeability tensor *(Russian)* 80−55072
Co, Stoner model, mol. field coeff., temp. and field depends. 77−72975
Co-3d transition metal alloys, hyperfine field and mag. perturbation distrib., NMR spectra meas. 79−61263
Co-B alloys, amorphous, mag. moment and exchange stiffness constant 79−1662
Co-B alloys, amorphous, saturation magnetisation, mag. moments, X-ray diffr. obs. 79−4704
Co-B-Si, mag. props. different in amorphous and cryst. phases 77−69617
Co-B(-Cr) thin film glasses, mag. props. and corrosion resist. 80−80576
Co-C, ferromag., prep. by splat-quenching, obs. of electronic struct. of interstitial C 77−62868
Co-Fe alloy, Invar characts. 77−1550
magnetisation continued
Co-Fe alloy films, magnetostriction and orientation of easy magnetisation axes *(Russian)* 79−19756
Co-Fe-Mn, dil. ferromag. alloy, mag. moment, saturation magnetisation meas. 78−64195
Co-Fe-Nb alloy, mag. precipitation-hardening and Bloch wall pinning 78−80173
Co-Fe-Nb-Mo, semihard magnetic alloy, magnetic props. 78−95469
Co-Fe-Ni semihard magnetic alloy, directional distrib. of magnetisation changes connected with Barkhausen effect 78−14985
Co-Fe-Ni-Si-B glasses, soft mag. props. 79−73774
Co-Fe-Ti alloy, precipitation hardened, rel. between struct. and mag. props. 78−95470
Co-Gd-Mo, amorphous film, mag. props., temp. depend. 78−10734
Co-Gd-Mo-Ar film, amorphous, mag. props. 78−80182
Co-H, solid soln., magnetisation curve 78−84452
Co-Mn, FCC, mictomagnetism, magnetisation and mag. susceptibility meas. 80−60310
Co-Mn alloys, ferromagnetic, high field mag. susceptibility meas. 80−75729
Co-Mn-Ni-Fe-Si-B amorphous alloys, mag. props., low magnetostriction 80−75832
Co-Ni-Fe, semi-hard magnet, irreversible magnetisation changes, directional distrib. 79−24196
Co-Ni-Fe-Si(B), amorphous ribbon, magnetostriction meas. 80−15778
Co-Ni(Ti)(Cu)(Mn), cryst. struct. and stacking fault influence on mag. props. *(Russian)* 80−25164
Co-P, amorphous, ferromag. antireson. 24 GHz microwave transmission, mag. props. 80−34778
Co-P amorphous alloys, electrodeposited, magnetic anisotropy 79−28568
Co-Pt, atomic ordering props. and domain growth in strong pulsed mag. field *(Russian)* 80−54918
Co-Sm-Gd(Ho) magnets, prep. and characterisation 77−8351
Co-Ti (9 at.%), decomp. kinetics, elec. resist., hardness, and saturation magnetisation during ageing *(Russian)* 80−50587
$CoAl_xGa_{2-x}O_4$, mag. interactions, susceptibility obs., 4.2 to 300K 79−15294
$Co_{100-x}B_x$, amorphous alloys, saturation magnetostriction and annealing behaviour 80−34739
$Co_{100-x}B_x$, glassy alloys, mag. props. 79−73689
$Co_{1.8}BaFe_{0.2}^{2+}Fe_{16}^{3+}O_{27}(Co_{1.8}W)$, magnetoelastic props. under spin-reorientation conditions 79−69709
$CoBr_2.6(0.48D_2O, 0.52H_2O)$ spin-flop system, intermediate phase existence, sublattice magnetisation reorientation 80−80510
$CoBr_2.6[(1-x)H_2O.xD_2O]$, mag. intermediate phase, magnetisation and neutron scatt. meas. 80−60195
$CoCl_2.2H_2O$, Ising antiferromag., high field transverse magnetisation meas. 80−93143
$CoCl_2.2H_2O$, magnetisation temp. depend. 80−7128
$CoCl_2.2H_2O$, metamagnetic transition, microscopic dynamics 77−16073
$CoCl_2.2NC_5H_5$, magnetisation temp. depend. 80−7128
$Co_{79}Fe_{6.5}B_{14.5}$ amorphous thin films, zero magnetostriction, high magnetisation 80−34708
$(CoFeB)_{100-x}Cr_x$ thin films, magnetic props. and corrosion resist. 80−34709
$Co_xFe_{1-x}Cl_2.2H_2O$ solid soln., mag. props. and phase diagram 79−78346
$CoFe_2O_4$, fine particles, surface effects on saturation magnetisation 77−69630
$Co_{1-x}Fe_{2+x}O_4$, prep. by wet and ceramic methods, struct., mag. and surface props. 78−52307
$Co_xFe_{3-x}O_4$ film, magnetooptic recording material, mag. and magnetooptic meas. 77−20832
$Co_{0.54}Ga_{0.46}$, frequency depend. magnetisation, superparamagnetic behaviour 80−84624
Co_xGa_{1-x}, NMR expts. interpretation 80−75870
$Co_2Ga_{2-x}Cu_x$, mag. and struct. phases from magnetisation, neutron, X-ray diffr. techniques 78−52253
$Co_2Ga_{1.95}Fe_{0.05}$, mag. behaviour, Mossbauer effect and DC magnetisation meas. 80−50244
$Co_2Ga_{2-x}M_x$ (M=V, Cr, Mn, Fe), mag. props. and order 77−12093
$Co_2Ga_{2-x}Ni_x$, mag. and struct. phases from magnetisation, neutron, X-ray diffr. techniques 78−52253
$CoGa_2O_4$, mag. props. 78−23254
Co(GaTiV) alloys, ferromag. onset, electron conc. depend. 80−60203
$(Co_{1-x}Mn_x)_2B$, $0 \le x \le 1$, magnetisation, lattice consts., press. depend. of Curie temp. 80−7137
CoMn(Cr)(V)(Ti), dil., low temp. specific heat and magnetisation 80−65925
$Co_{50}Mn_xGa_{50-x}$, ordering and disordering phenomena, mag. study 80−70154
$CoNb_2O_6$, Co^{2+}-Co^{2+} interaction, susceptibility and magnetisation, 3.3-300K 77−8282
$CoNb_2O_6$, ordered state, field induced mag. transitions 77−16074
$Co_{2-x}(Ni,Fe)_xTiSn$, Heusler alloy, positive contribs. to hyperfine fields, magnetisation and NMR meas. 78−43654
$Co_xNi_{1-x}Cl_2.6H_2O$, solid solution, mag. props. and phase diagram, calc. 80−7104
$Co_x(Ni_{0.5}Cu_{0.5})_{1-x}Fe_2O_4$ ferrite, relation between elec. cond. and mag. anisotropy 80−75548
$Co_{2-x}Ni_xTiSn$, mag. ordering, ^{119}Sn Mossbauer spectroscopy and magnetisation meas. 78−43753
$Co_{80}P_{20}$ glass, room temp. 77−63125
$Co_xPd_{80-x}Si_{20}$, amorphous, structural and mag. heterogeneities 80−80484
$CoPt_3$, electrolytic films, saturation mag. induction, coercive fields, thickness depend. *(French)* 80−44883
$CoRh_xGa_{2-x}O_4$, mag. interactions, susceptibility obs., 4.2-1000K 79−15293
CoS_2, ferromagnet, elec. resist. and thermal expansion anomalies 80−15542
$CoS_{2-x}Se$, magnetism and metamagnetic transition, neutron diffr. and NMR meas. 80−15717
$CoS_{2-x}Se_x$, conc. and temp. effects on metamagnetic transition 80−15716
$Co(S_xSe_{1-x})_2$, high field magnetisation, metamag. 79−91253
$Co_{75}Si_{25-x}B_x$ glass, metalloid comp. depend. 77−55665
Co_5Sm sintered magnet, effect of surface conditions on mag. props. 79−28556
$Co_2(Ti,Mn)Sn$, Heusler alloy, mag. meas. 79−47261
$CoTi_{1-x}Al_x$, form. of mag. moment of Co atom, X-ray diffr., mag. meas. and NMR 77−43819

magnetisation continued
$CoTiO_3$, antiferromag., mag. anisotropy, magnetisation meas. 80−65856
Co_2TiSn, Heusler alloy, positive contribs. to hyperfine fields, magnetisation and NMR meas. 78−43654
CoU_2S_5, mag. struct., exchange energy, magnetisation and neutron diffr. expts. 78−68170
CoU_2S_5, mag. struct. and props. 80−11166
Co_2Z ferroxplana form. process peculiarities 80−89368
$Co_xZn_{1-x}Rh_2O_4$, mag. props., EPR spectra, antiferromag. order 80−75736
$Co_xZn_{1-x}Rh_2O_4$ spinel, crit. conc. for long range mag. order, expt. evidence 79−47239
Cr antiferromagnetic, magnetisation process *(Russian)* 78−15007
Cr, δ- and BCC, fine particles, mag. props. 78−52314
Cr, hyperfine interactions on ^{111}Cd-probe nuclei, TDPAC meas. 80−75904
Cr hyperfine particles, surface magnetisation, explanation of expt. work 78−23303
Cr-Fe, dil., magnetisation, Fe local moments 80−60215
Cr-Fe, spin-glass phase, magnetisation curve test for mag. ordering 80−11201
Cr-Fe-O, rutile type oxides, obtained from thermal decomp. of $Cr_{1-x}Fe_x$·OOH, Curie temp. and saturation magnetisation 79−24740
Cr-Mn alloys, magnetisation process, magnetisation in 90-300K range *(Russian)* 78−15007
Cr-Rh, dil., hyperfine fields meas. 79−47056
Cr-S system, mag. props. *(Japanese)* 77−43825
CrB_3, crit. spin-relax. in hard mag. direction 78−72390
CrO_2 amorphous thin films, Mossbauer and magnetisation data 80−34712
$Cr_xPd_{82-x}Ge_{18}$ amorphous alloys, magnetoresist., mag. susceptibility, magnetisation 78−80148
CrS-FeS, sulphorspinel, struct. and elec. props. 80−49834
CrS_xTe_{1-x} (x=0 to 0.2), magnetic props. study 80−11194
$Cr_{3\pm x}Se_4$, struct., elec. and mag. props. 80−107160
CrTe, effect of high pressures on magnetic properties 78−52238
$CrTe_{1+x}$, thermal expansion and spontaneous magnetostriction *(Russian)* 78−48017
Cr_5Te_6, high press. effects on magnetisation and mag. transitions, 77 to 360K 77−77057
Cs^-, in tetrahydrofuran soln., transient photoelectron nutation 79−3418
Cs_2CoCl_4, mag. susceptibility and magnetisation curve meas. 80−11176
$CsCoCl_3.2D_2O$, crit. behaviour along metamag. phase transition 77−59409
$CsCoCl_3.2D_2O$, metamag., thermodynamic props. near multicrit. pt. 77−66305
$CsMnCl_3.2H_2O$, spin wave anal. 77−8292
$CsMn_{1-x}Co_xCl_32H_2O$, random mag. mixture, oblique-antiferromag. phase obs. 80−93142
$CsMnF_3$, struct. with compensated magnetisation in noncollinear phase *(Russian)* 78−88095
Cs_2NaRCl_6 (R=Ce, Nd), tetragonal distortion from cubic symm., magnetisation and NMR meas. 80−34403
$CsNiF_3$, crit. exponent crossover, quasielastic neutron scatt. around Neel point 77−24693
$CsNiF_3$, NMR and relax. exam. 78−52371
$CsNiF_3$, one dimensional ferromag., magnetisation, FMR, 2.61-20K 77−20719
$CsNiF_3$, quasi-one-dimensional ferromagnet, subthreshold parallel pumping of magnons 80−75745
$Cs_3VCl_6.4H_2O$, magnetisation of ground state, field-induced level crossing 79−47068
Cu complex, with 1,2,4-triazole, mag. susceptibility, 2-300K struct. 77−77045
Cu, resonant and nonresonant conduction-electron-spin transmission 80−75857
Cu/Ni coherent modulated structures, electronic struct. and magnetism 80−103620
Cu-Al-Mn, partial decomp. of β_1 phase, effect on mag. props. and martensitic transform. *(Russian)* 80−45306
Cu-Cr, dil., spin-density magnetisation near Cr atoms, NMR study 80−80626
Cu-Fe, interface, ferromagnetic and cond. spin reson. mode coupling 79−78521
Cu-Fe, Kondo system, magnetisation, Mossbauer expts. 77−77028
Cu-Fe alloy, dil. dynamic susceptibility around T_k, satellite nucl. spin-lattice relax. time meas. 77−4573
Cu-Mn, mag. viscosity below freezing temp. 80−65910
Cu-Mn, magnetisation curves 79−24172
Cu-Mn (16.7 at.%), spin glasses, alternating magnetisation 79−91241
Cu-Mn alloy, dil., evidence for Mn clustering from high field magnetisation curves 79−78426
Cu-Mn spin glass, magnetisation curves, time depend. 80−15743
Cu-Ni, film, compositionally modulated, enhanced magnetisation density 78−84460
Cu-Ni, interface, ferromagnetic and cond. spin reson. mode coupling 79−78521
Cu-Ni alloy, critical conc. for ferromagnetism 78−14969
Cu-Ni evaporated thin film couple interdiffusion obs. 78−43187
Cu-Ni-Fe (14, 7 wt.%), solid soln., decomposed, magnetostatic interaction between ferromag. particles *(Russian)* 77−80967
Cu-Permalloy, interafce, ferromagnetic and cond. spin reson. mode coupling 79−78521
$CuCl_2$, anhydrous, single cryst., mag. behaviour in low temp. ordered phase 79−7974
$CuCl_2.2D_2O$, staggered magnetisation, neutron diffr. obs. 78−39296
$CuCl_2.2H_2O$, antiferromag. to paramag. transition, high field magnetisation meas. 78−64204
$CuCl_2.2H_2O$, magnetoelastic props. under press., antiferromagnetic resonance, lattice parameters 80−29598
$Cu_{0.67}Cr_{1.78}Se_{2.67}Br_{1.34}$, polycrystalline mag. semicond., mag. and elec. props. 79−7846
$CuCr_2Se_{4-x}Y_x$, (Y=Cl, Br), magnetisation, Curie const. 79−91225
Cu_5FeS_4, mag. ordering and vacancy clustering, mag. susceptibility and Mossbauer spectra meas. 77−85625
$Cu_{1-x}In_xCr_2S_4$, light induced magnetisation 78−76275
$CuK_2Cl_4.2H_2O$, Heisenberg ferromagnet, spontaneous magnetisation under press. *(Russian)* 77−36058
$CuK_2Cl_4.2H_2O$, Heisenberg ferromag., mag. props. at high press. 77−69512
CuMn, magnetisation processes below freezing temp. 80−15748
magnetisation continued
CuMn-like alloys, model calcs. on magnetisation processes in moderate fields below freezing temp. 79−24188
Cu_2MnAl, Heusler alloy, magnetisation mag. anisotropy, magnetostriction and elastic consts. 78−23318
Cu_2MnAl superparamagnetic particles in Cu_3Al lattice, magnetic moment ferromagnetic ordering *(Russian)* 79−78444
$Cu_2Mn(Al_{1-x}Sn_x)$, Heusler alloys, thermal effects, saturation magnetisation 77−85499
$Cu(NH_4)_2Br_4.2H_2O$, Heisenberg ferromag., mag. props. at high press. 77−69512
$Cu(NH_4)_2Br_4.2H_2O$ Heisenberg ferromagnet, mag. props. in mag. field 80−34637
$Cu(NO_3)_2.2^1/_2H_2O$, long-range ordered state, mag. props. 78−39417
$Cu(NO_3)_2.2^1/_2H_2O$, singlet ground-state system, mag. props., short-range ordered state 78−23289
$Cu(NO_3)_2.2.5H_2O$, linear Heisenberg antiferromag., mag. and thermodynamic props. 79−61136
$Cu(Rh_{1-x}Cr_x)S_4$, spinel system, susceptibility and metallic resistivity, anomalies due to s-d interaction 80−70958
$CuSeO_4.5H_2O$, $CuSO_4.5H_2O$ and $CuBeF_4.5H_2O$, linear-chain antiferromag., mag. phase transition investig. 77−55684
$Cu[Ni_{0.5}Mn_{1.5}]O_4$, magnetisation and magnetostriction, fields up to 11 kOe, 4-160K *(Russian)* 78−19304
dimethylammonium manganese tetrachloride, 2D Heisenberg antiferromag., spin wave anal. 80−54879
Dy, change in easy axis during magnetisation 77−8306
Dy, elastic constants, magnetoelastic contrib. 80−15777
Dy, mag. characts. in strong mag. field 77−89936
Dy, magnetic phase transitions, field-induced, isothermal magnetisation meas., 79−24161
Dy, US attenuation in mag. field 77−40104
Dy-Fe-Al, pseudobinary alloys, mag. props. 77−59397
Dy-Fe-O system, O-stabilised intermetallic $Dy_{12}Fe_{32}O_2$, prep. and characterisation 77−8956
Dy-Sc, magnetic relax. phenomena 79−33579
Dy-Sm(Eu), mag. props. at low temp. in high mag. fields 79−56570
Dy-Y, magnetisation and hysteresis, temp., depend. 79−69673
DyAG, adiabatic magnetisation, optical obs. 78−88283
$DyAl_2$, first order transition and tricrit. points, three-state Potts model 78−43589
$DyAl_2$, magnetisation, three-state Potts model 79−42804
$DyAsO_4$, phase transitions obs. 80−70412
$DyAu_2$, long-duration pulsed mag. field appl. to magnetisation meas. 79−61183
DyB_4, mag. behaviour, in strong mag. field *(Russian)* 78−88119
DyBi, mag. behaviour 80−71025
$Dy_xCe_{1-x}Ru$, supercond., mag. order 79−87189
$Dy_xCe_{1-x}Ru_2$, supercond., mag. props. 79−11267
$Dy(Co_xNi)_2$, intrinsic mag. aftereffect obs. 77−63237
$DyCo_2$-$DyAl_2$ system, mag. and structural studies 80−108006
$DyCo_{5.3}$ noncollinear mag. struct. appearance in mag. fields, magnetostriction meas. *(Russian)* 80−100607
Dy_xCu_{1-x}, amorphous film, magnetisation meas., local anisotropy effects 78−68309
$DyFe_2$, high field magnetostriction and magnetisation 78−84471
$DyFe_2$, magnetisation and magnetic anisotropy 78−91862
$DyFe_3$, effect of adsorbed H on mag. props. 77−63129
$DyFe_{3.4}$, magnetisation data 77−32177
$DyFe_2H_2$, mag. props., ^{57}Fe and ^{161}Dy Mossbauer spectra and magnetisation meas. 79−78579
$Dy_3Ga_5O_{12}$, crystal field effect on paramag. props. of Dy^{3+} ion 80−50040
$Dy_3Ga_5O_{12}$, dipolar magnet, sp. ht. and magnetisation meas. 80−60344
DyIG, mag. and magnetooptical props., temp. and field depends. 77−89927
DyIG, mol. field coeffs., magnetisation and mag. susceptibility anal. 78−95406
DyIG, non-cryst., Mossbauer and magnetisation studies 80−44979
DyIG, noncrystalline, Mossbauer and magnetisation data 80−34828
$DyIn_3$, magnetisation 80−25106
DyMg, mag. props., neutron diffraction and magnetisation meas. 77−16045
Dy_6Mn_{23}, magnetic moments, magnetisation 80−25094
Dy_6Mn_{23}, noncollinear mag. struct., magnetization meas. 79−78322
$DyNi_2$, single cryst. mag. props. 77−24684
$Dy_2O_2SO_4$, mag. ordering, magnetisation, AC susceptibility and Zeeman effect meas. 80−60205
$Dy_2O_2SO_4$, magnetic struct. in antiferromag. and ferrimag. states 80−15695
$DyPO_4$, mag. phase diagram and crit. exponents, MCD obs. 77−66307
$DyPO_4$, metamagnet, discontinuity in magnetisation 79−28544
DySb, biquadratic exchange interactions, magnetisation above Neel point 77−69533
DySb, magnetisation study, intermediate metamagnetic phase transitions 79−99698
DySb, quadrupole interactions above T_N 79−78304
DyScFe garnets, mag. props. 77−47979
$DyVO_4$, phase transitions obs. 80−70412
Er, elastic constants, magnetoelastic contrib. 80−15777
Er, magnetisation, quantum jump 80−60369
Er, magnetisation and susceptibility in basal plane in strong mag. field *(Russian)* 80−50145
Er, magnetisation in strong pulsed mag. field, differential susceptibility meas. *(Russian)* 79−19729
Er-Fe amorphous alloys, mag. props. 79−90557
$ErCo_2$, amorphous, mag. correlations, neutron exam. 79−73682
$ErCo_2$, amorphous, mag. correlations, neutron exam. 79−73683
Er_2Co_{17}, magnetisation, magnetocryst. anisotropy and magnetostriction 77−8303
$Er_{65}Co_{35}$, amorphous, amg. ordering, susceptibility, magnetisation and hysteresis meas. 78−68190
$(ErCo_2)_x(ErAl_2)_{1-x}$, mag. and struct. investigations of intermetallic systems 78−95440
$Er_2Co_{17-x}Fe_x(Mn_x)(Ni_x)$, saturation magnetisation, Curie temp., easy direction, and anisotropy field 77−8304
$ErCrO_3$, magnetisation, NMR freq. temps. depend. weak ferromagnetic-antiferromagnetic spin reorientation transition 80−29631
$Er_2EuFe_{5-x}Ga_xO_{12}$, rag-domain garnet film, controlled variation of props. under O_2 annealing 79−15328

magnetisation continued
$ErFe_2$-YFe_2, and $ErFe_2$-$LuFe_2$, mag. props., 80-1300K *(Russian)* 80−75750
$ErFe_3$, Mossbauer and magnetisation investig. of 47K mag. anomaly, atomic rearrangement 77−20766
$Er(Fe_{1-x}Co_x)_3$, spin reorientation, easy axis of magnetisation 80−25144
$ErFe_2H_{3.9}$, mag. props. and lattice consts., effect of hydrogen absorpt. 77−20561
$Er_3Fe_{5-x}In_xO_{12}$, lattice consts., T_c, mag. saturation, K-absorpt. and Mossbauer spectra, 80K *(Russian)* 77−20954
$Er_6(Fe_{1-x}Mn_x)_{23}$, mag. props. and mol. field coeffs. 78−39319
$ErFeO_3$, parameters of interaction between rare earth and Fe ions, theory and expt. 79−73705
ErH_3, cryst. fields and mag. props. 78−68181
$(Er_{0.6}Ho_{0.4})Rh_4B_4$, reentrant supercond., magnetisation meas. near lower crit. temp. 80−25043
ErIG, magnetic props. of single cryst., 4.2-600K 79−78341
$Er_xLa_{1-x}Cu$, and $Er_xY_{1-x}Cu$, antiferromag., mag. and resist. behaviour 80−34412
ErMg, mag. props., neutron diffraction and magnetisation meas. 77−16045
Er_6Mn_{23}, magnetic moments, magnetisation 80−25094
Er_6Mn_{23}, noncollinear mag. struct., magnetization meas. 79−78322
$ErRh_4B_4$, magnetisation and elec. resist. at low temp. 79−56374
$ErRh_4B_4$, supercond. and mag. props. 79−4631
$ErRh_4B_4$, superconducting thin films, critical mag. field 80−75693
$Er_xY_{1-x}Al_2$, mag. props. meas. and neutron diffr. data 80−7126
$Er_xY_{3-x}Fe_5O_{12}$, garnet, mag. anisotropy and magnetostriction 80−11189
$Er_xY_{1-x}Rh_4B_4$, mag. and supercond. transitions 80−70874
ErZn, magnetoelastic and quadrupolar couplings 78−52328
$(Eu,Lu)_3Fe_5O_{12}$, submicron bubble films on rare earth-Ga garnet substrates, prep. and mag. props. 78−91909
Eu, mag. anisotropy of helicoidal struct., magnetisation, 4.2-300K *(Russian)* 79−56499
EuB_6, correlation between mag. struct. and elec. props. 77−63192
EuB_6, electronic struct., transport and mag. props. 80−96782
EuB_6, ferromag., mag. props. 80−2561
EuB_6, mag., transport and thermal props. 79−73738
$EuB_{6-x}C_x$, magnetisation, effects of C 80−25163
$EuEr_2Ga_{0.7}Fe_{4.3}O_{12}$, garnet thin films, magnetisation orientation, temp. depend. 80−71125
$Eu_{1-x}Gd_xO$, mag. props., transport meas. 80−97117
EuIG, non-cryst., Mossbauer and magnetisation studies 80−44979
EuIG, noncrystalline, Mossbauer and magnetisation data 80−34828
$(EuLu)_3Fe_5O_{12}$, Ga, Al or (Ca,Ge) substituted, mag. props. and growth of 2 μm bubbles 78−91910
EuO, degenerate ferromag. semiconductor, mechanism of transition to insulating state *(Russian)* 77−8024
EuO:Gd, elec. cond. under hydrostatic press., Curie temp. 80−96881
EuO:Gd, mag. props. and instability phenomena 79−1666
EuO:Gd, pure and doped, elec., mag., and optical props. rel. to electronic conc. 80−96880
EuO:Gd, surface mag. props. 80−71566
EuPd, mech. of H absorption, Mossbauer, mag. and X-ray diffr. meas. 78−38846
$EuRh_2$, mech. of H absorption, Mossbauer, mag. and X-ray diffr. meas. 78−38846
EuS, ferromagnetic film, optically induced magnetisation amplification, Curie temp. increase *(Russian)* 77−24719
EuS, hyperfine field and magnetisation temp. depend., NMR meas. 77−8422
$EuS_{1-x}Se_x$, mag. phase diagram, from temp. depend. of magnetisation 80−7105
$Eu_{0.14}Si_{0.31}O_{0.55}$ glass, optical, magnetic, and magneto-optical props., chemical clustering 79−42951
$Eu_{0.14}Si_{0.31}O_{0.55}$, insulating amorphous mag., optical, mag., and magneto-optical props. 79−61344
$Eu_5Sn_3S_{12}$, mag. and thermodynamic props., metamagnetism 80−60273
(Eu_xSr_{1-x}) S dilute, spin-cluster freezing observation by low-freq. mag. absorpt. 79−78404
$Eu_{1-x}Sr_xS$, non-metallic system, spin glass behaviour 79−24175
$Eu_xSr_{1-x}S$, insulating spin glass, mag. props. 80−2589
$Eu_xSr_{1-x}S$, non-metallic spin glass system 79−61175
$(Eu_xSr_{1-x})S$, very dil., magnetisation dynamics 80−65915
$Eu_{1-x}Yb_xO(S)$, solid soln., ferromag. semicond., increase of exchange interaction 78−88109
Fe, [111] oriented whisker, mag. domain struct. and approach to saturation 79−82814
Fe aerosol powders, oxidised, nucl. gamma reson. study *(Russian)* 79−1725
Fe alloys, amorphous, effects of metalloids on mag. props. 80−75738
Fe alloys, amorphous, mag. saturation, spin wave stiffness, temp. depend. 80−75741
Fe alloys, amorphous, room-temp. saturation induction 78−95476
Fe alloys, amorphous, saturation magnetisation, Curie temp. and size effect 80−65815
Fe alloys, anisotropic precipitation struct. in external mag. field *(German)* 78−72785
Fe, amorphous film, Hall effect and magnetisation *(Russian)* 77−35922
Fe and Fe-Ni Metglas alloys, ohmic and Hall resist. 100-700K, mag. behaviour 80−80254
Fe, atomic layers, Pauli paramagnetism to band ferromagnetism transition thickness depend. 78−72377
Fe based amorphous alloys, struct. and thermomag. meas. 77−16055
Fe, cast, high Cr, phase composition, mech. props. rel. to heat treatment 79−29108
Fe complex, $Fe(1,2,4\text{-triazole})_2(NCS)_2$, quasi-2-dimens. $S=^1/_2$ antiferromag., mag. props., hidden canting 80−107986
Fe complex, tetraphenylporphynate iron III bromide, mag. props., zero-field splitting 80−34584
Fe complex, with 1,2,4-triazole, mag. susceptibility, 2-300K, struct. 77−77045
Fe, de Haas-van Alphen effect and exchange splitting, effect of pressure *(Russian)* 78−95252
Fe dilute alloys, itinerant 3d electron spin density oscills. around solute atoms 77−72978
Fe discontinuous film, Mossbauer effect exam. of magnetic state 77−24769
Fe, ferromag. film, surface states, surface magnetisation and electron spin polarisation 80−65648

magnetisation continued
Fe film, ultra-thin Mossbauer spectroscopic studies of mag. props. 80−44970
Fe film coated by MgO, MgF_2 and Sb, surface mag. 80−7196
Fe garnet, ferrimagnetic, sublattice magnetisation calc. 77−16063
Fe garnets, sublattice magnetisation curves, Mossbaeur study 80−75808
Fe, grade EA, plastically deformed, magnetoelastic props. *(Russian)* 80−44893
Fe, H_2 embrittlement and H_2 adsorption 80−89401
Fe, irreversible magnetisation changes, directional distrib. 79−24196
Fe, itinerant ferromag., Fermi surface and single particle excitations 80−34350
Fe, lunar and meteoritic, first order shock induced mag. transitions characts. and discrimination from TRM 78−64205
Fe, magnetisation process in high mag. fields in crit. region 77−85498
Fe meteorites, thermoremanence hypothesis rel. to origin of magnetisation 78−65564
Fe, muon$^+$, 40 MeV, traversing magnetised plates, dynamic mag. fields 79−38422
Fe, noncrystalline, mag. hyperfine data from Mossbauer spectra 78−39477
Fe, oxidised powder, soft mag. props. oxide film-Fe composite material, magnetically soft, preparation, elec., mag. props. 77−8778
Fe particles, dispersed in Hg, mag. props., aggregate form. 80−60375
Fe particles in glass-like C matrix, identification and props. 80−11229
Fe particles in Hg, ferromag. liquid, mag. props., ageing effects 77−12154
Fe powder, passivating oxide layer comp. 78−31558
Fe, residual stress induced by uniaxial deform., magnetic meas. 77−73390
Fe sheet, surface magnetisation, ferromag. nucl. reson. meas. 78−60348
Fe single crystal frames, use in transient field meas., surface magnetisation meas. 79−59324
Fe, small particles, magnetisation-pressure isotherms for H_2 and SO_2 78−39949
Fe, spin wave and Stoner contribs. 77−73017
Fe, Stoner model, mol. field coeff., temp. and field depends. 77−72975
Fe, thermal cond., elec. resist., Lorenz number and magnetisation, crit. behaviour 77−4521
Fe, var. in mag. moment of ferromags. during plastic deform. *(Russian)* 77−66401
Fe, whisker, mag. crit. phenomena, size effects 78−68258
Fe whisker, mag. memory function at crit. temp. 77−24714
Fe whisker, magnetisation curve meas. using SQUID system 80−86347
Fe whiskers, inverse Wiedemann effect, torsional strain and azimuthal mag. field influence 80−108045
Fe whiskers, magnetisation in small mag. fields, investigation using Kerr magneto-optic effect 80−2603
Fe-Al, ferromag.-mictomag. transition, intermediate superparamag. 77−12140
Fe-Al (25 at.%), anomalous magnetic behaviour *(Japanese)* 77−48011
Fe-Al_2O_3 granular films, superparamagnetism and relax. effects 80−71118
Fe-Al-Co-Ni, Alnico alloys, irreversible remagnetisation processes in rotating fields *(Russian)* 79−8015
Fe-B, amorphous, Invar-type alloy, mag. moment and high field susceptibility 78−34965
Fe-B, amorphous ferromag., Invar type, magnetisation, elec. resist. and thermal expansion meas. 78−2663
Fe-B, amorphous metallic glasses, high-temp. mag. anal. 78−91258
Fe-B (14-25 at.%), amorphous, saturation magnetisation, temp. and comp. depend. 77−85430
Fe-B alloys, rapidly quenched metastable solid solns., prop. and mag. props. 78−92218
Fe-B amorphous alloy, annealed, microstruct. and mag. domain changes 80−75790
Fe-B amorphous alloys, Mossbauer spectra, soft ferromag. props. 80−11302
Fe-B amorphous Invar alloy, elastic props., Elinvar characts. and ΔE effect 79−56595
Fe-B metallic glass, role of Fe_3B in crystn., mag. and Mossbauer expts. 78−94997
Fe-B metallic glass, struct. and crystallisation, Mossbauer spectra, calorimetry and magnetisation meas. 79−23528
Fe-B metallic glasses, short-range orders 79−65002
Fe-B metallic glasses, struct., stability and crystn. 80−75173
Fe-B-C, amorphous, effects of replacement of B by C on mag. props. 80−84621
Fe-B-C alloys, amorphous, temp. depend. of magnetisation 79−73690
Fe-B-C amorphous alloy, formation, mag. props., thermal stability and density 80−75796
Fe-B-C amorphous alloys, effect of Si addition on mag. props. 80−34694
Fe-B-Cr(Si) thin film glasses, mag. props. and corrosion resist. 80−80576
Fe-B-Si amorphous alloys, crystallisation temp., Curie temps., saturation magnetisation 79−82820
Fe-B-Si-C amorphous alloys, prep. and props. 80−88748
Fe-Co, film, magnetisation induced uniaxial anisotropy, dislocations effects 78−43618
Fe-Co film, magnetisation induced uniaxial anisotropy 77−48016
Fe-Co films, optical props. order-disorder transformation influence, absorpt. band existence *(Russian)* 79−65942
Fe-Co-Cr alloys, atomic mag. moment, magnetisation, Mossbauer spectra and NMR spin echo spectra 77−63127
Fe-Co-Mn, BCC, mag. state of Mn, NMR and saturation magnetisation meas. 78−39442
Fe-Co-Mn alloys, BCC, atomic mag. moment, magnetisation, Mossbauer spectra and NMR spin echo spectra 77−63127
Fe-Co-V(-Ni), annealing effect on microstruct. rel. to mag. and mech. props. 80−89267
Fe-Cr (10 to 70 at.%), ferromag. reson., anisotropy const., and saturation magnetisation *(Russian)* 77−81013
Fe-Cr alloy, mag. moments and Fe site hyperfine fields 78−76276
Fe-Cr alloys, crit. mag. props. near ferromag. Curie points 77−63216
Fe-Cr-Al alloys, localised mag. moment determ. and electron struct. 77−66268
Fe-Cr-Co, mag. props. of ductile permanent ductile alloys *(Chinese)* 79−19746
Fe-Cr-Co, mechanism of coercive force 80−34674

magnetisation continued
Fe-Cr-Co, spinodally decomposed magnetic alloy, magnetic flux temp. coeff. *(Japanese)* 78−35006
Fe-Cr-Co alloy, coercive force mechanism 80−71103
Fe-Cr-Co alloys, mag. props., heat treatment effects *(Russian)* 78−39365
Fe-Cr-Ni, Fe-Co-Mn, Fe-Cr-Co and Fe-Ni-Mn alloys, BCC, atomic mag. moments determ. 77−59396
Fe-Cr-b amorphous Invar alloy, elastic props., Elinvar characts. and ΔE effect 79−56595
Fe-Gd amorphous film, struct. and mag. props. 80−20439
Fe-Gd film, amorphous, mag. props., mean field analysis 78−64236
β-Fe-Ge, mag. props. from X-ray, magnetisation and Mossbauer meas. 79−42755
Fe-La(Zr) amorphous films, mag. props., Mossbauer effect and magnetisation meas. 79−69701
Fe-Mn-P-B-Al metallic glass, exchange anisotropy 77−16068
Fe-Ni, (35 wt.%), transport props. and Invar features *(Russian)* 78−51973
Fe-Ni (23 wt.%), struct., composition changes during α to γ transform., martensite plastic deformation influence *(Russian)* 80−11642
Fe-Ni alloy type YuNDK25B, anomalous magnetocaloric effect 80−60278
Fe-Ni alloys, FCC, mag. props. calc. 79−65659
Fe-Ni based alloy, amorphous rapidly quenched, mag. props. 77−66269
Fe-Ni Invar, magnetisation and high field susceptibility 79−56518
γ-Fe-Ni Invar alloy, phase mixture produced by long annealing 79−5065
Fe-Ni Invar alloys, splat quenched, mag. props. 80−75799
Fe-Ni Invar anomalies, explanation in terms of itinerant electron magnetism 80−75705
Fe-Ni-Co-Cu-Ti YuNDKT alloys, impaired mag. props. with C and S additions 80−60368
Fe-Ni-Cr, at. distrib. effect on mag. props. *(Russian)* 78−2657
Fe-Ni-Cr, vapour-deposited film, effect of condensation temp. on form. of metastable phases and mag. props. 79−65700
Fe-Ni-Cr film, depend. on magnetisation of ferromag. reson. linewidth *(Russian)* 77−1601
Fe-Ni-Mn, BCC, mag. state of Mn, NMR and saturation magnetisation meas. 78−39442
Fe-Ni-Mn-H, ferromag., magnetisation curves 78−88144
Fe-Ni-Te alloys, magnetisation 79−7975
Fe-Ni(-Al)(Mn) Invar alloys, mag. heterogeneities *(Russian)* 77−66251
Fe-Ni(Pt), Invar alloy, magnetic excitation exam. by neutron diffr. 79−56521
Fe-Ni(35.4 at.%) Invar alloys, T^2 term contribution to magnetisation 80−71096
Fe-P, amorphous, temp. depend. of saturation magnetisation 78−19223
Fe-Pt, high mag. field phase transition 77−66301
Fe-Pt, Invar type, strong ferromagnetism, mag. props. 78−64197
Fe-Pt, ordered single cryst., magnetisation in strong mag. field *(Russian)* 78−47954
Fe-Pt Invar alloy, homogeneous strong ferromagnet, thermal expansion and mag. props 79−91278
Fe-rare earth, dil., contact contribution to mag. hyperfine interaction of rare earth impurities 77−80932
Fe-Si, amorphous film, comp. depend. 77−1575
Fe-Si, Bloch wall motion, irreversible processes 79−78431
Fe-Si, domain struct., influence of insulating coating, high voltage SEM obs. 77−1565
Fe-Si, ferromag., magnetisation in high fields, influence of internal field nonuniformity 79−51819
Fe-Si, grain oriented, misorientation effects on mag. props 80−88792
Fe-Si, non-oriented sheets, production and props. 80−88797
Fe-Si, simple domain structs., magnetisation jumps 77−69624
Fe-Si, steel sheet static mag. props., elastic tensile stress effect 78−47999
Fe-Si, strips and rods, spatial extent of flux due to irreversible changes of mag. polarisation 79−33506
Fe-Si, thin cryst., domain struct. behaviour during magnetisation *(Russian)* 78−2697
Fe-Si (3 wt.%), domain wall drift due to nucleation during cyclic magnetisation 78−95461
Fe-Si (3 wt.%), grain oriented, domain wall variation throughout magnetisation cycle 78−95459
Fe-Si (3 wt.%), grain-oriented, domain wall profiles throughout magnetisation cycle 80−88781
Fe-Si (3 wt.%), Mossbauer spectra, domain magnetisation vector rotations, domain struct. 79−69761
Fe-Si (3 wt.%), nonoriented sheets, magnetisation, tensile stress effects 80−88845
Fe-Si (3 wt.%), polycrystal in mag. field, stress induced magnetisation, synchrotron Bragg refl. topography obs. 80−50139
Fe-Si (3 wt.%), rotational power losses, freq. depend. 78−91888
Fe-Si (3 wt.%), stripe domain structure, dynamic behaviour at high max. induction values *(Russian)* 80−80553
Fe-Si (3 wt.%) laminations, magnetostriction behaviour associated with closure domain spikes 80−75834
Fe-Si (3 wt.%) mag. domain motion quasi-lifetime topography using white synchrotron radiation, mag. field effects 79−42797
Fe-Si (3%wt.), dynamics of 180° domain boundaries and electromag. losses *(Russian)* 79−51801
Fe-Si (3.25 wt.%) alloy, single cryst. with (007) planes, domain struct. influence on mag. torque 80−108034
Fe-Si (3.5 wt.%), dynamic neutron depolarisation meas. of ferromag. domain struct. 79−82812
Fe-Si (3.5 wt.%) picture frame, domain wall bowing, time-depend. neutron depolarisation 78−95458
Fe-Si-B amorphous films, mag. props. 80−34710
Fe-Si-B amorphous powder, production by spark erosion, and mag. props. 77−90290
Fe-Si-B metallic glass, magnetisation meas. 78−23252
Fe-Si-B metallic glasses, mag. props., depend. on metalloid content 77−85485
Fe-SiO multilayer film, interface magnetisation, neutron Bragg refl. 78−56355
Fe-SiO multilayer film, interface magnetisation 80−7135
Fe-SiO multilayer films, interface magnetisation 80−88858
Fe-SiO_2, granular compund, superpara- to ferromag. transition temp. meas. 77−69633
Fe-W-Cr-Mo-Co (18,12,3,x wt.%) alloy, cold working effect obs. *(Japanese)* 77−40428

magnetisation continued
Fe-Y(Lu) amorphous films, mag. props., Mossbauer effect and magnetisation meas. 79−69701
$(Fe\text{-}Co\text{-}Ni)_{78}Si_8B_{14}$, amorphous, low coercivity and zero magnetostriction 78−23299
$Fe_{1-x}B_x$ metallic glasses, struct. and cryst., Mossbauer spectra, DSC, and magnetisation meas. 79−94906
$Fe_{1-x}B_x$, polycrystalline and amorphous sputtered films, Brillouin spectra 80−2775
$Fe_{100-x}B_x$, amorphous alloys, saturation magnetostriction and annealing behaviour 80−34739
$Fe_{100-x}B_x$, crystalline and glassy, low temp. magnetisation study 79−95608
$Fe_{100-x}B_x$ metallic glass, magnetisation meas. 78−80134
$Fe_{80}B_{20}$, amorphous ferromag., temp. depend. of hyperfine field distrib. 78−43756
$Fe_{80}B_{20}$, amorphous ferromag., hyperfine field distrib., Mossbauer effect 78−60371
$Fe_{80}B_{20}$, amorphous ferromag. metallic glass, stress-induced rot. of magnetisation, Mossbauer study 80−20445
$Fe_{80}B_{20}$ glass, magnetisation reorientation, Mossbauer effect 80−66092
$Fe_{80}B_{20}$, metallic glass, ferromag. props. 77−16107
$Fe_{81}B_{19}$ amorphous alloy, mag. anisotropy temp. depend. 78−14953
$Fe_{83.4}B_{16.6}$, amorphous, mag. props. and microstruct., cooling rate and melt overheating effects 80−65965
Fe_xB_{100-x}, amorphous, mag. props., ^{57}Fe Mossbauer spectra and magnetisation meas. 79−95693
$Fe_{80}B_{20-x}M_x$ (X=Al, Si, Ge, C, P) and $(FeCo)_{80}B_{20}$ glass, magnetisation, Curie and crystn. temps. 79−87289
$FeBMO_4$, M=Mg, Cu, Co, Ni, mag. props. meas. 80−34607
$FeBO_3$, crit. behaviour, Mossbauer and magnetisation meas. *(Russian)* 79−61106
$FeBO_3$, magnetisation near crit. temp., up to 3 kbar hydrostatic press., scaling theory 77−8316
$FeBO_3$-MBO_3 solid soln., (M=Mn, Cr, Al, Ga, In), synthesis, crystal chem. and mag. props. 78−31058
$FeBO_6$, critical indices splitting of sublattice magnetisation *(Russian)* 78−60299
$Fe_{82}B_{18-x}Si_x$ glasses, soft mag. props. 79−73774
Fe_xC_{1-x} amorphous sputtered film, mag. props. 78−68311
$FeCO_3$, mag. field drawn destruction of antiferromag. destruction, light depolarisation at mag. transform. *(Russian)* 78−23432
$FeCl_2$, in transverse mag. field, magnetoelastic coupling effect on mag. props. 79−28582
$FeCl_2$, logarithmic corrections to tricritical scaling 80−65940
$FeCl_2$, metamagnet, scaling props. of magnetisation and heat capacity, test of tricritical scaling 80−60336
$FeCl_2.2H_2O$-$CoCl_2.2H_2O$ random mixture, phase diagram 79−73748
$FeCoF_5.2H_2O$, ferrimag. props., suscept. and transitions, 3-296K 79−87240
$Fe_xCo_{1-x}S_2$, ferromagnetic solid soln., magnetisation depend. on Fe conc. 79−7990
$FeCo_2Si$, Heusler type materials, mag. props. 77−40042
$(Fe_{0.5}Co_{0.5})Si$, weak itinerant ferromag., polarised neutron scatt. exam. 77−4503
$Fe_{3-x}Co_xSi$, structural, mag. moment, and hyperfine field behaviour, local environment model 79−65762
$Fe_xCo_{1-x}Si$ alloys, disordered, hydrostatic pressure effects on mag. props. 77−32175
$Fe_xCo_{1-x}Si$, mag. props., effect of hydrostatic press. 77−12101
$(Fe_xCo_{1-x})_{100-y}(Si_{0.4}B_{0.6})_y$ amorphous alloy zero magnetostrictive, mag. props. 79−99743
$Fe_xCo_{1-x}Si(Ti)$, magnetic props., sp. ht. and resist. meas. 79−61120
$Fe_xCo_{1-x}Ti$, high press. mag. props. 78−23271
$(Fe_{1-x}Cr_x)$-P-C, amorphous mag. props. *(Japanese)* 77−85433
$Fe_{1-x}Cr_xBO_3$, magnetisation, 4.2-600K 78−68187
$Fe_xCu_{1-x}Rh_2S_4$, mag. tetrahedral intrasublattice interaction, X-ray, magnetisation and Mossbauer expts. 78−52241
FeF_2:Mn, Heisenberg antiferromagnet, impurity thermodynamics, NMR meas. 79−61098
FeF_3, amorphous, mag. props. and Mossbauer spectra, speromagnetism and mictomagnetism 80−75778
FeF_3, amorphous, noncryst. magnet with antiferromag. interactions 79−91228
FeF_3, canted antiferromag., spin echo spectra of ^{57}Fe and ^{19}F nuclei 80−2662
$Fe_2F_5.2H_2O$, ferrimagnetism, susceptibility obs. 5-300K, phase transition 79−4658
$Fe_5(Fe_{1-y}Co_y)$, mag. and calorimetric props. 77−63083
Fe_xGd_{1-x}, 0.5>x>0.65, amorphous film, FMR, spin wave spectra 77−16181
$FeGe_2$, antiferromag., biquadratic exchange 80−2371
Fe_3Ge, mag. props. of cubic and hexagonal phases 77−8475
Fe_xGe_{1-x} amorphous alloys, high field mag. meas. 79−82765
Fe_xGe_{1-x}, amorphous film, FMR meas. of mag. props., temp. and comp. depend. 77−69636
Fe_2Hf, ferromagnetism in hexagonal and cubic compounds 77−36074
$Fe_{3-x}In_xO_4$, ferrospinels, cation distrib., Curie point and magnetisation meas. 79−42095
Fe_5LiO_8, magnetoelectric-effect and magnetisation process 79−1688
$(Fe_{1-x}M_x)_2P$, (M=Co,Ni), magnetisation, susceptibility, thermal expsn. 79−11302
$Fe_{2(1-y)}Mg_{1+y}Ti_yO_4$ spinel, incomplete mag. ordering, static magnetisation and Mossbauer meas. 77−16056
$(Fe_{1-x}Mn_x)_3Al$ alloys, disordered, mag. moments and distrib. on lattice sites, magnetisation and spin echo meas. 77−63112
$(Fe_{1-x}Mn_x)_3Al$, mag. moments determ. from magnetisation and neutron and electron diffr. expts. 79−56520
$(FeMn)_3Si$ alloys, mag. props. rel. to Mn conc. by magnetisation meas. 77−59393
$Fe_{3-x}Mn_xSi$, struct., magnetisation, and spin echo expts., rel. to local environment model 77−20518
$Fe_{78}Mo_2B_{20}$, amorphous ferromag., mag. props. 79−38309
$Fe_{78}Mo_2B_{20}$, exam. of mag. props. between 300 and 900K 78−85010
$(Fe_{93}Mo_7)_{80}B_{10}P_{10}$, amorphous, neutron scatt. investig. of spin waves, magnetisation 77−47984
$FeNb_2O_6$, 1.4-80K, antiferromag. ordering 78−10666
$Fe_{65}{}^{60}Ni_{35}$, electron irradiated, small angle neutron scatt. 78−52218
$Fe_{70}{}^{60}Ni_{30}$, small angle neutron scatt., magnetisation inhomogeneity 78−52218
$Fe_{38}Ni_{38}B_{24}$, amorphous, magnetisation and FMR expts. 79−95607

magnetisation continued
$Fe_{40}Ni_{40}B_{20}$, amorphous ferromag., resist. and galvanomagnetic props., rel. to magnetisation 78−14712
$Fe_{80-x}Ni_xB_{20}$ and $Fe_{80-x}Ni_xP_{14}B_6$ amorphous alloys, microhardness correl. with mag. props. 80−88826
$(Fe_xNi_{1-x})_{80}B_{20}$, $(Fe_xNi_{1-x})_{80}P_{14}B_6$, new soft amorphous ferromagnetic glasses *(Croatian)* 79−11298
$(Fe_xNi_{1-x})_{80}B_{20}$, amorphous alloys, engineering mag. props. 79−51832
$Fe_{1.6}Ni_{78.4}B_{10}P_{10}$ metallic glass, superparamag. behaviour, chem. inhomogeneities role 80−84625
$Fe_{65}(Ni_{1-x}Cr_x)_{35}$, mag. viscosity and anomalies near Curie temp. 79−73781
$Fe_{65}Ni_{28}Mn_1$, disordered, mag. struct. near ferro-antiferromagnetic transition 80−60211
$Fe_{40}Ni_{38}Mo_4B_{18}$, amorphous, mag. anisotropy, Mossbauer study 80−65864
$Fe_{40}Ni_{38}Mo_4B_{18}$ ribbon, magnetic characterisation 80−34680
$(Fe_{1-x}Ni_x)_2P$, mag. props. 78−23248
$(Fe_{1-x}Ni_x)_{80}P_{20}$, amorphous, ferromagnetic alloys, mag. anomalies of Invar type *(Russian)* 80−93089
$(Fe_{0.04}Ni_{0.96})_{80}P_{10}B_{10}$, amorphous magnetisation, field and temp. depend. 80−39755
$Fe_{40}Ni_{40}P_{14}B_6$, (Metglas 2826), ferromag. Curie temp. determ. 78−64206
$Fe_{40}Ni_{40}P_{14}B_6$, amorhpous ribbon, influence of torsion on mag. props. 80−7138
$Fe_{40}Ni_{40}P_{14}B_6$, amorphous ribbon, cold rolling, annealing mag. props. 77−8958
$Fe_{40}Ni_{40}P_{14}B_6$, amorphous, mag. polarisation in approach to ferromag. saturation 80−80560
$Fe_{40}Ni_{40}P_{14}B_6$, induced anisotropy energy and saturation magnetisation temp. depend., torque magnetometer meas. 78−10680
$Fe_{40}Ni_{40}P_{14}B_6$, Metglas 2826, magnetising processes 78−10725
$(Fe_xNi_{1-x})_{80}P_{10}B_{10}$, amorphous, weak itinerant ferromag., Arrott plots 77−73007
$(Fe_{1-x}Ni_x)_{75}P_{16}B_6Al_3$, amorphous, saturation magnetisation, temp. depend., ferromag. reson. meas. 79−73818
$(Fe_xNi_{1-x})_{75}P_{16}B_6Al_3$, amorphous, spin wave excitations and low temp. magnetisation 79−33468
$(Fe_xNi_{1-x})_{75}P_{16}B_6Al_3$, magnetisation temp. depend., spin wave theory 80−44927
$Fe_{29}Ni_{49}P_{14}B_6Si_2$, Metglas 2826B, Hall, elec. resist., magnetisation and heat capacity meas. 78−68019
$Fe_{29}Ni_{49}P_{14}B_6Si_2$, Metglass 2826B, saturation magnetisation, temp. depend., ferromag. reson. meas. 79−73818
$(Fe_{1-x}Ni_x)_{77}Si_{10}B_{13}$, amorphous, Landau-Ginzburg theory, magnetisation and Curie temp. 80−75700
$Fe_{62.4}Ni_{15.6}Si_7B_{15}$ amorphous ferromagnetic alloy, anomalous magnetisation possible reasons, Mossbauer spectra *(Russian)* 79−78441
$(Fe_{0.2}Ni_{0.8})_{1-y}(SiO)_y$, Permalloy material, magnetisation, temp. and impurity atom conc. depend., band model calcs. *(Russian)* 80−93088
$(Fe_yNi_{1-y})_{1-x}(SiO)_x$, dielec. effect on magnetisation and Faraday rot. *(Russian)* 78−39298
$Fe_{1.985}Ni_{0.975-x}Zn_xCo_{0.04}O_{4+\gamma}$, elementary coupling energy of Co^{2+} to lattice 77−1549
Fe_2O_3 amorphous thin films, Mossbauer and magnetisation data 80−34712
γ-Fe_2O_3, fine particles, surface effects on saturation magnetisation 77−69630
α-Fe_2O_3, haematite, reduction by H_2, mag. field effect 77−12827
γ-Fe_2O_3, microstruct. and magnetisation 80−44875
α-Fe_2O_3, Mossbauer spectra near Neel temp., critical indices, magnetisation *(Russian)* 80−66094
γ-Fe_2O_3, prep. from thermal decomp. of $[Fe_3(HCOO)_6(OH)_2]HCOO.4H_2O$ and characterisation 78−80741
Fe_2O_3-BaO-B_2O_3, magnetic props. of Fe-rich amorphous oxide *(French)* 80−80511
Fe_2O_3-BaO-CoO system, phase comp. and mag. props., Bi_2O_3 additions effect 79−29032
Fe_3O_4 (magnetite), multidomain particles magnetisation 79−66686
Fe_3O_4 (magnetite), piezomag. response depth depend. rel. to tectonomagnetism as earthquake precursor 80−26465
Fe_3O_4 ferrofluid suspension, mag. props., stability 79−87293
Fe_3O_4, magnetite, magnetoelec. effect at 77K, elec. field depend. of mag. anisotropy 80−29594
Fe_3O_4, magnetite, reduced A-site moments, polarised neutron study 79−47253
Fe_3O_4, monoclinic phase, saturation magnetisation near Verwey temp. 77−77038
Fe_3O_4:^{119}Sn, magnetic interactions, Mossbauer spectra, A and B sublattice magnetisation 79−15301
Fe_xO_y powder coated with $NaPO_3$, anomalous coercivity increase 77−89980
α-FeOOH.nH_2O, hydrogoethites, weak ferromag. props. 77−53042
$Fe_{1-x}P_x$ dilute alloys, electronic struct., mag., elec. and struct. props. 79−37971
Fe_2P, grown in liq. Cu medium, composition and mag. props. 79−11313
Fe_2P, magnetisation, susceptibility, thermal expansion and elec. resist. meas. 77−77037
$Fe_{2-x}P$, first order ferro- to paramag. transition, 216K, susceptibility obs. 78−39322
$Fe_{80}P_{20}$ glass, room temp. 77−63125
$Fe_{79}P_{13}B_8$ amorphous alloys, splat cooled, Mn, Cr and V substituted, mag. and transport props. 80−84593
$Fe_{80}P_{16}B_1C_3$, ferromag. metallic glass, Mossbauer spectra, crystn. 77−12276
$Fe_{75}P_{15}C_{10}$ amorphous foil, ferromag. domain orientation, Mossbauer exam. 78−52402
$Fe_{75}P_{15}C_{10}$ foils, amorphous, ferromag. domain orientation, Mossbauer study 78−15000
FePd epitaxial film, vacuum-deposited, for thermomag. recording, mag. and magneto-optical props. *(Russian)* 78−60319
$Fe(Pd_{1-x}Au_x)_3$ ordering alloys, mag. props., 4.2 to 500K *(Russian)* 79−47301
$Fe_{25}Pd_{50}Au_{25}$, atomic ordering influence on mag. props. and elec. resistance *(Russian)* 80−7551
$Fe_xPd_{80-x}Si_{20}$, amorphous, structural and mag. heterogeneities 80−80484
$Fe_xPd_{82-x}Si_{18}$, amorphous, magnetisation, magnetoresist., spin glass and ferromag. phases 80−34697

magnetisation continued
$Fe_xPd_{82-x}Si_{18}$ metallic glass, long range interaction and spin wave interactions 80−65949
FePt epitaxial film, vacuum-deposited, for thermomag. recording, mag. and magneto-optical props. *(Russian)* 78−60319
Fe_3Pt Invar alloy, mag. props., martensitic transform. 79−78365
FeS_2, oxidation, Mossbauer spectroscopic and magnetokinetic studies, 400-500°C 80−44880
FeS_2, pyrite, magnetokinetics of oxidation, appl. to mag. separation from coal 77−12161
Fe_3S_4, galvanomagnetic props., resist. and Hall effect meas., 4.2-300K 80−54673
Fe_9S_{10}, antiferro- to ferrimag. transition, Mossbauer and mag. exam., diffusion of Fe during transition 79−73716
Fe_9S_{10}, polytypism, Fe diffusion near antiferromag. to ferrimag. transition 80−44830
$Fe_{1+\delta}Sb$, nonstoichiometry influence on mag. props. *(Russian)* 80−65813
$Fe_{1+x}Sb$-CoSb solid soln., mag. props., Mossbauer spectra, solubility limits, and lattice consts. *(Russian)* 77−59394
$Fe_{1+x}Sb$-NiSb solid soln., mag. props., Mossbauer spectra, solubility limits, and lattice consts. *(Russian)* 77−59394
Fe_3Se_4, thermal expansion, compressibility, magnetisation, susceptibility and magnetostriction 77−66318
Fe_7Se_8, 3c struct., spin axis transition 78−14967
Fe_2Si-transition metal alloys, Heusler type materials, mag. props. 77−40042
Fe_3Si, 3d transition metal substituted, limits of solubility, mag. props. and electron conc. 78−10670
Fe_3Si-based alloy, dil., cond. electron polarisation and moment perturbations 78−68224
Fe_xSi_{1-x}, amorphous, high field magnetisation meas. 78−39367
Fe_xSi_{1-x}, amorphous, struct. and mag. props., giant moment form. at mag. ordering 78−68192
Fe_xSi_{1-x} amorphous alloys, meas. showing crit. conc. at x=0.4 77−59429
$Fe_3Si_{1-x}Al_x$, hyperfine interactions and structural disorder, spin echo, X-ray and magnetisation meas. 77−32289
$Fe_3Si_{1-x}Al_x$, magnetisation and lattice parameter data 79−69732
$(Fe_{1-x}Si_x)_{1-y}By$, metallic glass, mag. props., crystallisation 80−65885
Fe_2SiS_4, Mossbauer effect and magnetisation meas. of mag. struct. *(French)* 77−12282
Fe_3Sn_2, mag. props., neutron diffr. and magnetisation meas. 79−11294
Fe_3Sn_2, magnetic properties, ^{119}Sn Mossbauer study 79−91323
Fe_3Sn_2, Mossbauer effect and magnetisation meas. 78−31132
Fe_xSn_{1-x}, amorphous, mag. behaviour 78−95478
Fe_xSn_{1-x} amorphous alloy films, magnetisation meas. and Mossbauer spectra 78−95489
$FeTiO_3$, ilmenite, lunar and terrestrial, cell dimensions and antiferromagnetism 77−21764
Fe_2TiO_4 magnetisation, Mossbauer spectra 79−87244
Fe_2TiO_4, ulvospinel, mag. props. weak ferromag. in 4-200K temp. range 78−56351
Fe_2TiO_5, spin glass system, cation distrib. Mossbaeur spectra 80−71248
$Fe_{2.4}Ti_{0.6}O_4$, titanomagnetite, single-crystal, mag. props. of multidomain TRM 78−56345
FeU_2S_5, mag. struct., exchange energy, magnetisation and neutron diffr. expts. 78−68170
$(Fe_{1-x}V_x)_3Ge$, magnetic and X-ray studies 80−1966
$Fe_xV_{1-x}O_2$, mag. props. and Mossbauer spectra meas. 78−31136
$Fe_{3-x}V_xSi$, struct., magnetisation, and spin echo expts., rel. to local environment model 77−20518
GaAs:Fe, static magnetis. rel. to doping method and heat treatment conditions 77−36092
(Gd, Bi)$_2$ (Fe, Ga)$_5O_{12}$ magneto-optic LPE garnet films, high-energy heavy ion irrad., props. 80−71390
$(Gd,Bi)_3(Fe,Ga)_5O_{12}$ epitaxial garnet film, nucl. tracks effect on mag. props. 80−11234
Gd, easy axis of magnetisation as function of press. and temp. 77−63231
Gd, electron irradiated, relation of defect densities to Rayleigh parameters 77−62517
Gd, magnetisation and magnetocaloric effects *(Russian)* 78−34985
Gd, meas. of easy direction of magnetisation with aid of phase theory 80−65963
Gd, nonmagnetic inclusions, effect on easy direction 77−77052
Gd-Al(Cu), amorphous alloy films, mag. phase diagram, spin glass and ferromag. regions 78−68234
Gd-Ce(Eu)(Yb), magnetocrystalline anisotropy, magnetisation and torque curve meas. 80−65859
Gd-Co, and Gd-Co-Mo films, amorphous, mag. props., annealing effects 78−64235
Gd-Co, evap. amorphous film, mag. props. 77−24720
Gd-Co, evap. amorphous films, anisotropy, magnetisation and FMR meas. 77−66392
Gd-Co amorphous film, mag. anisotropy 77−20649
Gd-Co amorphous film, magnetisation processes near compensation point 77−69644
Gd-Co amorphous ribbons, mag. props. and Invar effects 80−2574
Gd-Co amorphous thin film, mag. and optical props., conc. depend 79−19748
Gd-Co film, amorphous, magnetisation and anisotropy meas. 77−8370
Gd-Co film, amorphous, magnetisation processes near compensation point 77−40101
Gd-Co film, amorphous, perpendicular uniaxial anisotropy, dominant contrib. of preferential resputtering effect 77−36103
Gd-Co film, amorphous, RF sputtered, prep. and props. 79−1693
Gd-Co film, amorphous, selective resputtering-induced anisotropy 78−72376
Gd-Co film, amorphous ferrimagnet, anisotropic short range order effects on mag. props. 79−1691
Gd-Co film, sputtered from segment target, composition and mag. props. 78−27062
Gd-Co-Cu film, amorphous, influence of biased magnetron deposition parameters on props. 77−43856
Gd-Co-Mo alloy film, amorphous ion implantation damage effects 77−89991
Gd-Co-Ni series intermetallics, induced moments, magnetisation meas. 77−63138
Gd-Dy alloy, mag. anisotropy, magnetisation meas. 77−12115
Gd-Er alloy, mag. anisotropy, magnetisation meas. 77−12115

magnetisation continued
Gd-Fe, DC bias RF sputtered film, mag. props. 77−16124
Gd-Fe amorphous alloys, mag. props. and crystn. 79−90557
Gd-Fe film, amorphous, mag. props., annealing effects 78−64235
Gd-Ho alloy, mag. anisotropy, magnetisation meas. 77−12115
Gd-Mn alloy, mag. props. and effect of H_2 absorpt. 78−19250
Gd-Mn(-Co) alloys, amorphous, ferrimag. props. and Hall effect 79−73692
Gd-Sm(Eu), mag. props. at low temp. in high mag. fields 79−56570
Gd-Tm alloy, mag. anisotropy, from magnetisation meas. at 4.2K 78−68216
Gd-transition metal, amorphous film, galvanomag. effects, Hall detector 77−89882
$Gd_{56}Ag_{46}$, amorphous, susceptibility and magnetisation, 6-300K *(French)* 77−36060
$GdAl_2$, anomalous change of Curie temp. 78−47976
$GdAl_2$-$GdCo_2$ system, EPR and mag. props. 79−33478
$Gd_{80}Au_{20}$, amorphous ferromag., critical phenomena and mag. props. 77−85469
$Gd_{80}Au_{20}$, amorphous ferromag., mag. and transport meas. 77−89930
$Gd_{1-x}Ca_xAl_2$, mag. props. and phase relations 80−107991
GdCo amorphous film, O_2 contaminated, TEM obs. of source of perpendicular anisotropy 78−14993
$GdCo_2$, ^{59}Co hyperfine field, temp. depend. splitting 77−8447
$GdCo_2$, adsorption of H_2, effect on mag. props. 77−20185
Gd_2Co, amorphous ferromag. obtained by splat cooling, local and bulk mag. props. 79−1685
$Gd_{65}Co_{35}$, amorphous, amg. ordering, susceptibility, magnetisation and hysteresis meas. 78−68190
$Gd_{67}Co_{33}$, amorphous ferromag., mag. and transport meas. 77−89930
Gd_xCo_{1-x} annealing amorphous film, ferromag. reson. 77−85580
$(Gd_{1-x}Co_x)_{1-y}Ar_y$ amorphous mag. film, elec. and mag. prop. depend. on Ar 80−80410
$Gd(Co_xFe_{1-x})_2$, mag. props., composition and temp. depend. 79−15289
$Gd(Co_xNi_{1-x})_2$, mag. props., composition and temp. depend. 79−15289
$GdCrO_3$, magnetisation, appl. of molecular field theory 79−4637
Gd_xCu_{1-x}, amorphous film, magnetisation meas., fully aligned moment 78−68309
$GdCu_{1-x}Zn_x$, mag. struct. determ. 79−87238
$Gd_xEr_{1-x}Rh_4B_4$, mag. ordering near supercond. region 79−73696
GdFe, amorphous films, thermal stability of mag. props. *(Japanese)* 79−47307
$GdFe_2$, easy direction of magnetisation 80−20535
$GdFe_2$ films, electron beam deposited, amorphous and cryst., mag. and struct. props. 79−4710
$GdFe_3$, effect of adsorbed H on mag. props. 77−63129
$Gd(Fe_{1-x}Al_x)_2$, magnetisation, Curie temps., and mean mag. moments 79−51817
$(Gd_{1-x}Fe_x)_{1-y}Bi_y$ amorphous films, saturation magnetisation, Kerr and Faraday rotation 80−40093
$Gd(Fe_xCo_{1-x})_2$, paramag. behaviour, itineracy 78−39289
$Gd_{18}Fe_{82-x}Ni_x$, amorphous film, mag. and galvanomag. props. 77−24715
$Gd_3Fe_5O_{12}$, nucl. gamma reson., anomalous behaviour of intensity 77−12289
GdH_3, magnetisation and mag. suscept. 77−43821
GdIG, local mag. anisotropy in stress field of single dislocation 80−88744
GdIG single crystal plates for magnetooptical information storage 79−7997
$GdIn_3$, magnetisation 80−25106
$Gd_xLa_{1-x}Zn$, magnetisation and paramag. suscept. 78−88101
$Gd_{1-x}M_x$, M=Co, Ni, Fe, temp. depend. of magnetisation 77−77043
GdMg, sp. ht., magnetisation and stability of canted struct. 79−78412
$GdMn_2$-$GdAl_2$ intermetallics, mag. props., 80-650K 78−60282
$GdMn_2$-$GdAl_2$ system, mag. and structural studies 80−108006
Gd_6Mn_{23}, magnetic moments, magnetisation 80−25094
Gd_6Mn_{23}, noncollinear mag. struct., magnetization meas. 79−78322
$(GdMn_2)_x(GdAl_2)_{1-x}$, mag. and struct. investigations of intermetallic systems 78−95440
GdN, and $GdN_{1-x}O_x$, mag. interactions 80−60218
GdN, mag. interaction and carrier conc. 80−71005
$GdN_{1-x}O_x$, magnetic interaction and carrier conc. 80−71005
$Gd_xNd_{1-x}Zn$, ferromag., mag. susceptibility and magnetisation, temp. depend. 80−70975
$Gd_{68}Ni_{32}$, amorphous ferromag., mag. and transport meas. 77−89930
Gd_xNi_{1-x} sputtered amorphous films, mag. props. and Hall meas. 78−95488
$GdNi_2H_4$, effect of absorbed H_2 on struct. and mag. behaviour 78−2682
$GdNi_2H_4$, effect of H_2 absorption on struct. and mag. behaviour 78−10685
GdP-GdS systems, mag. exchange interactions, free carrier conc. 78−60278
$Gd(Rh_{1-x}Fe_x)_2$, $x \leq 0.15$, magnetisation and EPR studies 80−34767
$GdRh_2H_x$, $GdRu_2H_x$, struct. and mag. props., Mossbauer and magnetisation meas. 80−71271
$Gd_{3-x}S_4$, ferromag., elec. props. near Curie temp. 80−107788
Gd_xS_y, nonuniform ferro-antiferromag. ordering, 1.6 to 300K range obs. *(Russian)* 77−69504
GdScFe garnets, mag. props. 77−47979
GdTb, ferromag., magnetisation and microwave absorpt. 80−65816
$Gd_{70}Tb_{30}$, magnetisation, AC susceptibility and microwave absorption meas. 80−60221
$(Gd_xY_{1-x})Al_2$, ferromag. and spin glass like behaviour, magnetisation meas. 80−75734
$(Gd_xY_{1-x})Fe_2$, Fe mag. behaviour, FMR measurements, mag. props., Vangsness relation anal. 79−78336
$(Gd_xY_{1-x})Fe_2$, high temp. mag. behaviour 77−1538
$Gd_xY_{1-x}Fe_3$, saturation magnetisation, magnetostriction, Curie temp., ferrimag. ordering, exchange field *(Russian)* 78−68343
$Gd_{1.8}Y_{1.2}Fe_5O_{12}$, nucl. gamma reson., anomalous behaviour of intensity 77−12289
$Gd_xY_{1-x}Zn$, ferromag., mag. susceptibility and magnetisation, temp. depend. 80−70975
$Gd_{3-x}\square_xS_4$, transport and mag. props., mag. Wigner localisation 80−97069
H solid, spin-aligned, rapid decay mechanisms at 0K in large magnetic fields 77−72741
H, spin-polarised, density, magnetisation, compression and thermal leakage 80−44391
H, spin-polarised, mag. eqn. of state 80−100374
^{3}He, A-phase, props. near transition to A_1-phase *(Russian)* 79−7728
^{3}He, adsorbed on Vycor glass under press., nature of phases, entropy and magnetisation expts. 80−49458
^{3}He, BCC, four-spin interaction effects on ordering processes 77−39721
^{3}He, BCC, NMR multiple echoes, soln. of eqn. of motion of magnetisation 79−86961
^{3}He, FCC, vacancy induced spin polarons 80−59756
^{3}He, in Grafoil, NMR obs. of magnetisation 79−51370
^{3}He in Grafoil, ultralow temp. NMR mag. susceptibility, surface magnetisation and transition 78−79843
^{3}He, liq., highly mag. polarised, prep. and obs. 79−46870
^{3}He, liq., polarisation effect on mag. ordering, melting curve 80−80021
^{3}He, liq. and solid., spin polarised, thermodynamical nuclear orientation 79−46879
^{3}He, solid, low temp. mag. and thermal props. due to bound state Frenkel vacancies 79−56019
^{3}He, solid, mag. ordering, NMR study 80−54470
^{3}He, solid, mag. phase diagram from static magnetisation meas. 80−84342
^{3}He, solid, magnetic polarisation around vacancies, on two-dimens. lattice 79−51368
^{3}He, solid, magnetisation through nucl. ordering temp. meas. 78−18870
^{3}He, superflow, gap functions, critical currents, susceptibilities 80−103531
^{3}He superfluid, A-phase, transverse magnetisation relaxation and superfluid spin flows *(Russian)* 80−34265
^{3}He, superfluid, A-phase uniform magnetisation precision instability in mag. field *(Russian)* 79−95232
^{3}He, superfluid, expts. on magnetisation 77−31827
^{3}He, superfluid, longitudinal magnetisation, relax. meas. 79−51355
^{3}He superfluid, magnetic relaxation in hydrodynamic region *(Russian)* 79−95239
^{3}He, superfluid, meas. of A⇄B transition in mag. field near polycritical point 77−11760
^{3}He, superfluid, nonlinear motion of magnetisation, parallel ringing 80−107597
^{3}He, superfluid, order parameter, sp. ht., mag. props., sound propag., hydrodynamic props., book contrib. 79−99388
^{3}He, superfluid, p-wave spin triplet pairing Hamiltonian, 5-D spin 80−75400
^{3}He, superfluid, spin relaxation effects in nonlinear parallel ringing of magnetisation 78−6193
^{3}He, superfluid, static magnetisation 78−56008
^{3}He, superfluid, tip-angle-depend. mag. relax. 78−43203
^{3}He, superfluid A phase, obs. of magnetisation reversals during relax. meas. 78−79842
^{3}He superfluid A-phase, exptl. studies of solitons 80−88386
^{3}He, superfluid A-phase, longitudinal mag. relax. 80−59751
^{3}He, superfluid B-phase, spin relax. far below T_c, damping of magnetisation ringing 79−51353
^{3}He-A, superfluid, ferromagnetic orbital magnetisation 78−38902
^{3}He-Z near A. phase transition, collective oscill. hybridisaiton *(Russian)* 80−80020
$HfCo_6$, saturation magnetisation, Co mag. moment and electron transfer 77−73005
$Hf(Fe_{1-x}Co_x)_2$, mag. props., Mossbauer spectra and magnetisation meas. 80−39948
$HfFe_{2-x}Si_x$, Laves pseudo-binary compound, cubic C15 phase stabilisation 77−39559
Hg, liquid, ferromag., containing Fe particles, time depend. magnetisation 80−44877
$Hg_{2.86}AsF_6$, linear-chain cpd., anisotropic Meissner effect, magnetisation meas. 77−85387
$Hg_{3-\delta}AsF_6$, linear chain compound, mag. field induced residual resist., anisotropic supercond. 80−24897
$Hg_{1-x}Fe_xTe$ mixed crystals, zero gap, magneto-optical evidence of exchange interactions 80−45045
$Hg_{1-x}Mn_xTe$, mag. props., self-consistent two spin cluster model 80−54874
$Hg_{1-x}Zn_xCr_2Se_4$, magnetic struct., neutrongraphic and mag. investigation *(Russian)* 80−88726
Ho, magnetoelastic interactions 78−64252
Ho-Sm(Eu), mag. props. at low temp. in high mag. fields 79−56570
Ho-YIG, magnetic props. in strong fields at low temp., Ising approx. calcs. *(Russian)* 80−54920
$HoAl_2$, Ho moment reorientation, polarized neutron diffr. study 79−42761
$HoAl_2$, magnetisation and neutron diffr. meas., cryst. field and exchange 77−63163
$HoAl_2$, magnetisation reorientation 79−87291
HoAlGa, mag. props. and struct. 78−39302
$HoAu_3$, mag. phase diagram 80−75761
Ho_2Co_{17}, magnetisation, magnetocryst. anisotropy and magnetostriction 77−8303
$HoCo_{5.5-x}Mn_x(Fe_x)(Ni_x)(Cu_x)$, cryst. struct. and mag. props. 80−75800
$HoCo_{5-x}Ni_x(Cu_x)$, lattice parameters and mag. props. 79−82817
Ho_xCu_{1-x}, amorphous film, magnetisation meas., local anisotropy effects 78−68309
$HoFe_2$, magnetostriction and magnetisation temp. depend. 79−73795
$HoFe_3$, effect of adsorbed H on mag. props. 77−63129
$HoFe_2H_{4.5}$, mag. props. and lattice consts., effect of hydrogen absorpt. 77−20561
$HoFe_2O_4$, magnetic props., 77-300K 80−11225
HoIG, mol. field coeffs., magnetisation and mag. susceptibility anal. 78−95406
HoIG, spin reorientation from Faraday effect meas. 79−51780
$HoNi_5$, ferromag., magnetisation and paramag. susceptibility 80−25082
$Ho_2O_2SO_4$, mag. ordering, magnetisation, AC susceptibility and Zeeman effect meas. 80−60205
$Ho_2O_2SO_4$, magnetic phase diagram, magnetisation and mag. susceptibility meas. 80−15720
$Ho_2O_2SO_4$, magnetic struct. in antiferromag. and ferrimag. states 80−15695
$HoRh_4B_4$, low temperature magnetic properties 80−88728
HoSb, mag. phase diagram, quadrupolar interactions 80−65820
$(Ho_{0.58}Tb_{0.2}Dy_{0.22})Fe_2$, microwave mag. props. 80−65860
$Ho_xTb_{1-x}Fe_2$, single crystals, continuous spin orientations, magnetisation easy direction 78−84453
$Ho_xY_{1-x}(Fe_{0.1}Co_{0.9})_2$, ^{57}Fe hyperfine interaction, mag. props., Mossbauer study 80−39951

magnetisation continued
$Ho_cY_{1-c}Sb$ system, magnetisation, elec. resist., and sp. ht. meas. 80−60213
$Ho_xY_{1-x}Sb$, mag. props. 80−34634
HoZn, magnetoelastic and quadrupolar couplings 78−52328
In-Bi (22 at.%), directionally grown eutectic two phase superconductors, magnetisation behaviour 77−28293
In-Bi (2.5 at.%), supercond. foils, transport current effect on magnetisation 79−56379
In-Pb (7 at.%) alloy cylinder, magnetisation change induced by current near upper crit. field 80−70890
In_2Bi, magnetisation curve, interpretation using boson formulation of supercond. 78−2619
β-In_3Sn, crystn., decomp. and superconductivity 79−91579
Ir_3Cr, yield stress and saturisation magnetisation 80−16389
$K_3Co(CN)_6$, spin 7/2 system, quadrupolar relax. parameters 78−56392
K_2CuF_4, 2-D ferromagnet, optical and magneto-optical props. 77−52062
K_2CuF_4, nearly two-dimens. Heisenberg ferromag., renormalised spin wave theory 77−66285
$K_2FeCl_5(H_2O)$, antiferromag., press. depend. on spin-flop transition 80−80505
$K_3Fe(Cn)_6$, mag. and thermodynamic props. below 0.4K in mag. fields 79−56542
$KFeF_3$, magnetisation density of Fe^{2+} 79−78313
$KFeF_4$, amorphous, mag. props. and Mossbauer spectra, speromagnetism and mictomagnetism 80−75778
K_2FeF_4, two dimensional easy plane antiferromag., neutron scatt. expts. 80−65838
K_2MnF_4, two-dimens. antiferromag., diffusion-controlled mode coupling, EPR linewidth 79−51844
K_2MnF_4, two-dimens. Heisenberg antiferromag., field and temp. depend. of magnetic 77−66272
K_2MnF_4, two-dimensional antiferromag., NMR, magnetisation field-depend., spin-wave theory 77−63294
K_2MnF_4:Zn(Mg)(Ni), mag. effects of impurities 80−65869
K_2MnF_4:Zn(Mg)(Ni), local magnetisation, NMR and Green's function study 80−65870
$K_3Mn_2F_7$, quadratic double-layer antiferromag., NMR, spin-wave anal. of sublattice magnetisation 77−63293
$K_3Mn_2F_7$, quadratic double-layer Heisenberg antiferromagnet, sublattice magnetis., NMR obs. 77−66270
$K_3Mn_3F_7$, Heisenberg double-layer antiferromag., neutron scatt. 79−61065
$K_2Mn_{1-x}Ni_xF_4$, antiferromagnets, impurity associated and host magnetizations, NMR exam. 78−10800
$KNiF_3$, ^{19}F spin-lattice relaxation 80−93211
$(La,Ce)B_6$, low temp. mag. props. 79−61043
$(La,Gd)Al_2$, mag. props. 78−52299
$(La,Gd)Al_2$, spin glass, cluster glass and magnetisation characts. for different comps. 77−69585
La ferrite, composition and mag. props., anisotropy field, magnetisation 80−71109
La-Gd-Au, amorphous spin glasses, mag.-cluster description 79−42776
La-Sm-Lu iron garnet film grown as NdGaG substrates, mag. props. 80−44888
La_2Co_7, mag. saturation and anisotropy, density, lattice parameters 77−85426
$La_{80-x}Gd_xAu_{20}$, amorphous, supercond. and spin-glass regime, magnetisation and resist. meas. 77−36011
$LaMnO_3$, monoclinic and cubic perovskite struct., mag. props., neutron diffr. meas. 78−27022
$LaNi_5$, H_2 absorption in thin film hydriding alloys 80−65238
$LaNi_{1-x}Fe_xO_3$, mag. props., 7 to 300K 79−4648
$LaNi_{1-x}Fe_xO_3$, magnetisation meas. and ^{57}Fe Mossbauer studies 80−93217
$LaNi_{1-x}Mn_xO_3$, ^{55}Mn NMR study, magnetisation meas., ferromag. and Pauli paramag. components 80−7191
$LaRu_2$, H absorption induced Ce valence change, mag. and supercond. props. 80−50042
$LaRu_2$, supercond. disappearance on H absorption 79−47185
La_3S_4, high crit. mag. field supercond., elec. resist., sp. ht. and magnetisation 80−2532
$La_{1-x}Sr_xCoO_3$ ($0.5 \leq x \leq 1.0$), saturation magnetisation as function of composition 79−24154
$La_{1-x}Tb_xAl_2$, competing paramag. anisotropy from cryst. field and indirect quadrupolar coupling 80−60180
Li ferrites, porous, porosity effect on saturation of magnetisation 80−108036
Li-Ti ferrite, microwave props. 77−40082
Li-Zn ferrite, mag. and microstruct. props., effect of V_2O_5 addition *(Japanese)* 77−28415
$Li_2B_2O_4$-$LiFe_5O_8$, borate glass, mag. props. of Fe^{3+} cations 80−100599
$Li_{0.5}Fe_{2.5-x}Cr_xO_4$ press. depend. of anisotropy consts. 80−65865
$Li_{0.5}Fe_{2.5}O_4$ Ru substitution effect on struct. and mag. props., and max. solubility determ. 80−75364
$Li_{0.5}Ga_{0.095}Fe_{1.55}O_4$ ferrites, linear magnetostriction in weak field, 150 to 300K *(Russian)* 77−80983
$LiHoF_4$, uniaxial dipolar ferromag. crit. behaviour 79−61149
$LiMnCrF_6$, ferrimagnetic, magnetic props. *(French)* 79−1668
$Li_xMn_{1-x}Se$, anomalies obs. in mag. and elec. props. 77−69509
$Li_{0.04}Na_{0.1}Fe_{2.5}O_4$, $Li_{0.3}Na_{0.2}Fe_{2.5}O_4$, ferrites, form., X-ray, chem. and mag. anal. 77−36424
$LiTbF_4$, magnetisation near crit. pt., temp. and field depend. 79−38337
LiTi, substituted ferrite, cation distribution, Mossbauer, X-ray, neutron diffr. study 80−28975
LiTiZn ferrites, elec. resist., mag. props., effect of Bi addition 78−95474
LiZn, substituted ferrite, cation distribution, Mossbauer, X-ray, neutron diffr. study 80−28975
$Li_{0.5-z/2}Zn_xFe_{2.5-z/2}O_4$, field magnetisation and susceptibility 79−82762
$Li_{0.5(1-x)}Zn_xFe_{2.5-0.5x}O_4$, canted spin struct., neutron diffr. study 78−68175
$Li[Ni_{0.5}Mn_{1.5}]O_4$, magnetisation and magnetostriction, fields up to 11 kOe, 4-160K *(Russian)* 78−19304
Lu-Gd, dil., positive exchange Kondo system, magnetisation and resist. 78−68158
Lu-Mn alloy, mag. props. and effect of H_2 absorpt. 78−19250
Lu-rare earth, dil. alloy cryst. field determ. 78−10651
$LuCo_2$, anomalous high-field magnetisation 78−47958
$LuCo_2$, high-field magnetisation, Fermi liquid model 79−11303
$LuFe_2$, ferromag., magnetisation density, neutron diffr. study 80−60217
$Lu_2V_2O_7$, pyrochlore struct., mag. props. 78−72335

magnetisation continued
Mg-rare earth dilute alloy, mag. susceptibility and magnetisation 80−15689
$MgEr_2S_4$, magnetisation and susceptibility, exchange interactions obs. 78−52242
$Mg_{0.5}Fe_{2.5}O_4$, ferrimag. epilayer, superparamag. interface, mag. props., FMR 78−95492
$Mg_xFe_{3-x}O_4$, cation redistribution, effect of composition and thermal treatment 79−27966
$Mg_xFe_{3-x}O_4$, polycryst., Verwey type transition, resist., magnetisation, Mossbauer effect and permeability obs. 80−75764
MgMn ferrite film, determ. by ferromag. reson. method *(Russian)* 77−16126
Mh-Rh-Cr, mag. transition, effect of press. 77−16077
γ-Mn, antiferromagnetic, self-consistent bandstructure calcs. 80−88475
Mn carbides and nitrides, $Mn_3MC(N)$, M=metal, perovskite type, mag. props. 78−43588
Mn complex, manganese (II)(1,2,4-triazole)$_2$(NCS)$_2$, 2-dimens. Heisenberg antiferromag., mag. props. 78−72336
Mn complex, with 1,2,4-triazole, mag. susceptibility, 2-300K struct. 77−77045
Mn hyperfine particles, surface magnetisation, explanation of expt. work 78−23303
Mn-Al-C, permanent magnet, mag. props., machinability 77−85505
Mn-Cu, mag. and cryst. struct., neutron and X-ray diffr. meas. *(Russian)* 78−22694
Mn-Ga, Elinvar charact. *(Japanese)* 79−61638
Mn-Ga (19 to 30 at.%), phase equilib. diagrams, X-ray diffr., thermal expansion, and mag. meas. *(Japanese)* 78−39743
Mn-Ga (19.0 to 31.2 at.%), exam. of phase diagram, using X-ray diffr., thermal expansion and mag. meas. 78−76634
Mn-H, hydride formation in high press. range 80−65235
Mn-H(D), ferromag., thermal, struct. mag. props. 78−88145
Mn-Zn ferrites, single crystal, machining effect obs. *(Japanese)* 77−21295
MnAs, generalised P-T phase diagram, mag. and structural phase transition 80−39780
Mn_2As-Mn_2Sb, structural and magnetic props. determ. 78−76248
$MnAs_{1-x}P_x$, double exchange ferromag. coupling, magnetisation meas. 80−75751
$MnAs_{1-x}P_x$, high spin-low spin transition 77−20591
MnB, NMR of ^{55}Mn 77−28468
MnB_2, polycryst., magnetoresist. and mag. props. *(Russian)* 80−92907
$MnCl_2$, $MnBr_2$, mag. phase diagram, optical absorption meas. 77−4514
$Mn_{0.27}Co_{0.73}Cl_2.6H_2O$, antiferromag., sp. ht. meas., phase transition obs. 79−78415
$Mn_{1-x}Co_xSb$, press. effect on saturation magnetisation *(Russian)* 77−80919
$Mn_{1-y}Cr_yAs$, double exchange ferromag. coupling, magnetisation meas. 80−75751
$Mn_3Cr_2Ge_3O_{12}$ garnet, antiferromag. ordering *(Russian)* 78−80146
$MnCr_2S_4$, substituted, mag. struct. and transitions 80−65795
$Mn_{2-x}Cr_xSb$, exchange-inversion interaction and acoustical magnon soft mode 77−40049
$MnEr_2S_4$, magnetisation and susceptibility, exchange interactions obs. 78−52242
MnF_2, Heisenberg antiferromag., props. calc. 77−85406
MnF_2, spin-flop transition obs. by neutron diffr. 79−73734
$Mn_{1-x}Fe_xAs$, high-pressure phase, magnetic properties 78−52247
$Mn_{1-x}Fe_xAs$, magnetic transition under high press., exchange striction model calcs. *(Russian)* 80−50096
$MnFe_{2-x}In_xO_4$, magnetic props., In substitution effects *(Russian)* 78−91849
$MnFe_2O_4$:Sn, hyperfine mag. fields at ^{119}Sn and ^{57}Fe nuclei, influence of press. 79−99811
$Mn_xFe_{3-x}O_4$ ferrite film, exchange interaction depend. on conduction electrons *(Russian)* 80−34621
$Mn_{1-x}Fe_xP$, magnetisation, susceptibility and mag. transitions 79−47256
$(Mn_{1-x}Fe_x)_5Si_3$, solid soln., mag. transitions sp. ht., magnetisation and thermal expansion meas. 77−16075
Mn_3Ge, elec. and mag. props. *(Russian)* 77−76792
$Mn_xMg_{1-x}S$, mag. props. 77−66244
$Mn_xMg_{1-x}S$ solid solution, mag. props. 78−60269
$Mn_xMg_{1-x}Y_2S_4$, magnetisation and susceptibility, exchange interactions obs. 78−52242
$Mn(Nb_{0.5}Ta_{0.5})_2O_6$, nonuniaxial spin-flop magnet, bicrit. lines, crossover 78−14973
$Mn(Nb_{0.5}Ta_{0.5})_2O_6$, random and spin-flop magnet, neutron crit. scatt. 79−24169
$Mn(Nb_{0.5}Ta_{0.5})_2O_6$, spin flop magnet, four dimens. phase diagram and multicrit. phenomena 79−15304
$MnNiSi_{1-x}Ge_x$, mag. props. 77−12118
MnO, mag. phase transition, first-order 77−47988
MnO-MgO-ZnO-Fe_2O_3, grade 1.3 VT ferrite formation from hydroxides 77−90302
MnP, magnetisation and spin waves temp. depend. 79−91221
$Mn_xPd_{82-x}Ged_{18}$, amorphous alloys, mag. props. 78−91906
MnPt, disordered film produced by RF sputtering, ferromag. behaviour 78−68310
MnSb, interstitial cations, mag. and crystallographic study 79−55698
$Mn_{1+\delta}Sb$, ferromag., mag. disturbance around Mn interstitials 80−54868
Mn_2Sb, Bi-modified, mag. first order phase transition 79−51777
$Mn_2Sb_{1-x}Bi_x$, temp. depend. of magnetisation *(Japanese)* 79−78375
$Mn_{1+x}Sb_{1-x}Sn_x$, magnetisation and Curie temp., prep. and comp. depends. 78−64200
MnSi, helically ordered state, ^{55}Mn and ^{28}Si NMR 78−43655
MnSi-CoSi solid solution, mag. props. 78−56403
$Mn_5(Si_xGe_{1-x})_3$ solid solution, mag. ordering, magnetisation and neutron scatt. meas. 78−27023
Mn_3SnN, perovskite type struct., mag. props., neutron and Mossbauer meas. 77−32159
$MnTiO_3$, quasi-two dimens. antiferromag., mag. crit. behaviour 77−32191
$Mn_{2-x}V_xSb$, $0.08 \leq x \leq 0.25$, mag. props. modification by V 77−36071
$Mn_{23}Y_6D_x$, D atom location, neutron diffr. study, and magnetism *(French)* 80−24426
MnY_2S_4, magnetisation and susceptibility, exchange interactions obs. 78−52242
$(Mn_{0.7}Zn_{0.3})_xFe_yO_4$, electromag. props. rel. to Fe content 78−43613
Mo-Fe, dil., Kondo effect of RKKY interaction 78−31052

magnetisation continued
Mo-Fe, Kondo system, magnetisation, Mossbauer expts. 77−77028
Mo-Fe, local magnetisation from Mossbauer meas. 77−20549
MoFe, occurrence of spin glass and mictomagnetic regimes, props. meas. 77−16085
NH_4CoF_3, susceptibility and magnetisation meas. 77−85432
Na-Fe fluorophosphate glass, Mossbauer study, mag. and optical props. 80−16065
$NaFeF_4$, amorphous, mag. props. and Mossbauer spectra, speromagnetism and mictomagnetism 80−75778
$NaMnCl_3$, antiferromagnet, exciton self-localisation luminesc. and excitation spectra *(Russian)* 80−11456
$NaMnCl_3$, mag. props., 2-25K, antiferromag.-paramag. transition *(Russian)* 78−88125
$NaMnCrF_6$, ferrimagnetic, magnetic props. *(French)* 79−1668
Na_3RuO_4, mag. props., isolated tetranuclear cluster model 79−24180
$Na_xVS_2(Se_2)$, mag. and elec. props. rel. to struct. transitions 78−91848
Nb, cylindrical and ellipsoidal, rotational magnetisation and torque meas. in mag. field 78−43515
Nb, flow stress, depend. on magnetic fields 77−73311
Nb, lower critical field anisotropy 78−76201
Nb, supercond., magnetisation near anisotropy of generalised Ginzburg-Landau parameters 79−4630
Nb, superconducting, anisotropy of crit. field, magnetisation meas. 79−78260
Nb, superconductor, deformational twinning, mag. props. *(Russian)* 79−95543
Nb, with Nb_2N precipitates, flux pinning, magnetization, bulk flux density gradient, and neutron scatt. meas. 79−56472
Nb-Ga (16 to 28 at.%), transition temp., upper critical field and magnetisation curves 77−80866
Nb-Ge-Fe, effect of Fe on supercond. and mag. props. 79−56351
Nb-Hf (38 at.%) superconductor, peak effect, summation problem, mag. history flux pinning force 80−20362
Nb-Ti (50%), supercond., cryostat design for magnetisation study *(Spanish)* 80−75673
Nb-Ti superconducting cylinders, dynamically stabilised, differences in shielding versus trapping behaviour 77−47933
$Nb_{78}Ga_{22-x}Mn_x$, supercond. props., influence of Mn mag. impurities 80−54825
$Nb_{80}Ga_{20-x}Mn_x$, supercond. props., influence of Mn mag. impurities 80−54825
$Nb_{78}Gn_{22-x}Fe_x$, $Nb_{80}Ga_{20-x}Fe_x$, A15 phase supercond. 79−87181
$Nb_{50}Ni_{50-x}Fe_x$, amorphous, mag. ordering and local random anisotropy 78−68273
$Nb_{50}Ni_{50-x}Fe_x$, magnetically dil. glass, 3d moments, mag. susceptibility and magnetisation meas. 79−95574
Nb_3Sn multifilament superconductors, designed for high B appl., losses 79−33414
Nb_3Sn superconducting multifilamentary conductors, AC losses 79−33394
$Nb_{73}Ta_{27}$, supercond., flux density distrib. meas., differential magnetisation loop method 77−32129
NbTi, superconducting, orientation effects on magnetisation 77−28287
NbTi wire, supercond., magnetisation rel. to field orient. 78−52151
$Nb_xY_{3-x}Fe_5O_{12}$, low-temp. magnetocrystalline anisotropy study 79−95586
$Nd_{21}Ag_{79}$, and $Nd_{50}Ag_{50}$, amorphous, mag. props. 80−60182
$NdAl_2$, magnetostriction in high mag. fields 79−99745
$NdCo_5$, spin reorientation, magnetisation and torque curves, 77-925K 77−4532
$Nd_{0.35}Co_{0.65}$ film, vac. evaporated, magnetisation ripple struct., TEM and defocused Lorentz microscopy 80−7136
Nd_2Co_7, mag. saturation and anisotropy, density, lattice parameters 77−85426
$Nd_{64}Co_{36}$, amorphous, amg. ordering, susceptibility, magnetisation and hysteresis meas. 78−68190
Nd_xCo_{1-x} film, amorphous, mag. props. meas. 78−68312
NdF_3, mag. props. between 2 and 4.2K *(French)* 79−61039
$NdFe_2$, preparation and mag. props. 80−25259
Nd_xFe_{1-x} film, amorphous, mag. props. meas. 78−68312
$NdIn_3$, magnetisation 80−25106
NdO, mag. props., lattice consts., and X-ray absorpt. spectra 80−44798
Nd_2O_3, magnetisation and mag. susceptibility Curie-Weiss behaviour 77−4505
$NdRh_4B_4$, possible obs. of coexistence of supercond. and long-range mag. order 79−82730
NdScFe garnets, mag. props. 77−47979
$(Nd_xSm_{(1-x)})_2(Co_{0.7}Fe_{0.3})_{17}$, mag. anisotropy 80−34622
$Nd_2Ti_2O_7$, Nd_2TiO_5, paramag. props., mag. susceptibility meas. 1.6 to 70K 78−10649
$Nd_2Y_{1-x}Co_5$, saturation magnetisation and anisotropy, 4.2K-T_c 77−85427
Ni (110), polarised LEED study of magnetism 80−71102
Ni, acoustic emission during magnetisation, stress effects 79−82854
Ni, anisotropic magnetisation meas., 4-250K 80−65862
Ni, atomic layers, Pauli paramagnetism to band ferromagnetism transition thickness depend. 78−72377
Ni, band structure, rel. to lattice const., spin polarised APW calc., magnetisation meas. 80−20073
Ni complex, with 1,2,4-triazole, mag. susceptibility, 2-300K, struct., antiferromag. props. 77−77045
Ni, creep, effect of AC mag. field, 1.5-4.2K *(Russian)* 79−11657
Ni, critical exponent β for hyperfine fields, PAD techniques 78−19403
Ni crystals in strong mag. field, EM excitation and vel. dispersion of sound *(Russian)* 80−39837
Ni dispersions, semi-amorphous, on Al_2O_3-graphite, mag. characterisation 80−44876
Ni, electrodeposited film, saturation magnetisation and perpendicular anisotropy meas. 78−76277
Ni, ferromag. film, surface states, surface magnetisation and electron spin polarisation 80−65648
Ni, ferromagnetic antiresonance transmission at 24 GHz, temp. depend., g-factor and magnetisation 77−51959
Ni, ferromagnetic domain struct., static neutron depolarisation meas. 79−82812
Ni film, CO adsorption effect on galvanomagnetic and magnetic props. 78−43490
Ni film, evaporated, for use as variable delay SAW device, magnetostrictive effects 80−71144
Ni film, evaporated, galvanomag. and mag. props. 78−23180
magnetisation continued
Ni film, evaporated, oscill. due to CO adsorption 77−1496
Ni film, ferromag. reson., thermodynamical anal., and saturation magnetisation 79−42840
Ni film, few atomic layers thick, transition from Pauli paramag. to band ferromag. 80−44885
Ni film, influence of H chemisorpt. on magnetism, ferromag. reson. spectroscopy 77−66395
Ni film, microstructure of charged boundary between ferromag. domains 79−69705
Ni film, surface magnetisation, electric field effect 78−14991
Ni film, temp. depend. of magneto-optical effects, rel. to magnetisation 77−81167
Ni film, transition from Pauli paramagnetism to band ferromagnetism 79−61192
Ni film, two-dimens. (110) domain wall 77−69648
Ni film, vac, deposited on liquid-He-cooled sapphire, galvanomag. props. 79−95519
Ni films, evaporated, effect of CO adsorption on galvanomag. and mag. props. 79−33363
Ni films, evaporated, effect of CO adsorption on galvanomag. and mag. props. 79−33364
Ni foil, sat. magnetis. during cathodic charging with hydrogen 78−71860
Ni, hydrostatic press. effect on magnetisation Procopiu effect and hysteresis meas. 77−48023
Ni, hyperfine field and magnetisation, press. and temp. depend. 80−6795
Ni, itinerant ferromag., Fermi surface and single particle excitations 80−34350
Ni, mag. excitations variation of de Haas-van Alphen frequency 79−8019
Ni, magnetisation and relative vol. temp. depend. near Curie point *(Russian)* 78−14962
Ni, magnetisation effect on channelling and blocking of proton beam 77−69022
Ni, magnetisation in pulsed field up to 320 kOe, 283 to 693K, band theory *(Russian)* 77−80920
Ni, magnetisation process in high mag. fields in crit. region 77−85498
Ni, magnetisation temp. depend. exam. using ^{61}Ni NMR 77−73089
Ni, magnetised mono- and polycryst., activation vol. var. during low temp. deform. *(Russian)* 78−3178
Ni, magneto-volume effects calc., rel. to itinerant electron model 78−43621
Ni, magnetocryst. anisotropy consts., determ. from magnetisation perpendicular to applied field 78−68219
Ni, magnetocrystalline anisotropy energy, temp. and magnetisation depend. 78−6525
Ni, magnetoelastic effect on longitudinal compression, weak field spin rotation model 79−82851
Ni, magnetoelastic effects, ΔE-effect and macroeddy current damping, internal friction meas. 78−64253
Ni, normal magnetisation meas. by rotating sample magnetometry 77−69514
Ni, photoelectric effect in paramag. and ferromag. states, Auger spectra 78−95649
Ni, single cryst., magnetisation and US attenuation, mag. field depend. *(Russian)* 78−6559
Ni, spin wave and Stoner contribs. 77−73017
Ni, Stoner model, mol. field coeff., temp. and field depends. 77−72975
Ni, twisted tubular polycryst. sample in axial mag. field, circular magnetisation 77−32230
Ni, W-fibre reinforced, fabrication, heat treatment, and mag. and mech. props. 77−40408
Ni:B, impurity electronic struct. calc., ^{12}B NMR data anal., magnetisation decrease 79−47046
Ni:F, ion-implanted, mag. hyperfine field, anomalous temp. depend., PAC meas. 79−4754
Ni-Al-Fe(Co), electrical and mag. anomalies due to substitutional atoms 77−15839
Ni-Au, local environment effects, magnetisation decrease 79−65664
Ni-B alloy film, magnetisation-temp. charact., order-disorder transform. *(Japanese)* 78−76279
Ni-B thin film glasses, mag. props. and corrosion resist. 80−80576
Ni-C, ferromag., prep. by splat-quenching, obs. of electronic struct. of interstitial C 77−62868
Ni-Co, film, magnetisation induced uniaxial anisotropy, dislocations effects 78−43618
Ni-Co (25 wt.%), single crysts., mag. annealing effect on magnetostriction and magnetisation *(Japanese)* 80−34744
Ni-Co (25 wt.%), single crysts., mag. annealing effect on magnetostriction and magnetisation at high temps. 80−108047
Ni-Co film, magnetisation induced uniaxial anisotropy 77−48016
Ni-Cr-Mo-Mn alloy 02KhN40MB, corrosion-resist, heat-resist., phys. and mech. props. 80−35411
Ni-Cr(Mo), oxidation effect on magnetic props. *(Russian)* 78−23868
Ni-Cr(V)(Co)(Mn)(Mo)(Ru)(Fe), spin wave stiffness consts., RPA CPA band model 79−61088
Ni-Cu, local environment effects, magnetisation decrease 79−65664
Ni-Cu, low field magnetisation meas., mag. props. comp. depend. 78−91879
Ni-Cu, mag. anisotropy, temp. and conc. depend. 77−63172
Ni-Cu-H systems, Curie temp. during phase transitions under high press. H_2 80−71029
Ni-Fe (20 wt.%), thin film ferromagnetic band, magnetisation under domain creep conditions *(Russian)* 79−91262
Ni-Fe alloy, W-fibre reinforced, fabrication, heat treatment, and mag. and mech. props. 77−40408
Ni-Fe alloys, pulse permeability and loss in toroidal core pulse current transformers 78−43615
Ni-Fe conductor, EM pulse shielding, magnetisation curves 80−28143
Ni-Fe films, in state of undersaturation in perpendicular fields, micromagnetic struct. *(Russian)* 79−61193
Ni-Fe narrow stripes, mag. props. and domain struct. 79−82843
Ni-Fe-Co (17,3 wt.%), thin film ferromagnetic band, magnetisation under domain creep conditions *(Russian)* 79−91262
Ni-Fe-Co film, nonmagnetostrictive, effect of deposition parameters of Al underlayer 77−77078
Ni-Fe-Cr, extraordinary Hall effect, elec. and mag. meas. at 77 and 300K 80−34421
Ni-Fe-Cr film, hysteresis loop meas. using magnetooptical system 79−69707

magnetisation continued
Ni-Fe-Mn, ferromag. reson. linewidth and saturation magnetisation 78−72418
Ni-Mn, hydrogenation kinetics, magnetisation, interstitial H influence 80−35528
Ni-Mn, low temp. kinetic props., 4.2-77.3K, magnetization *(Russian)* 79−19568
Ni-Mn, temp.-resist. graph deflection points, mag. moment orientation rel. to magnetisation matrix *(Russian)* 79−60788
Ni-Mn (5%), magnetisation curve reduction 78−31096
Ni-Mn alloy, disordered, exchange-anisotropy field, magnetisation curves 78−72365
Ni-Mn alloy, disordered, mag. struct., high field twist deform. 78−68166
Ni-Mn alloys, equilib. ordered, high field magnetisation 77−85491
Ni-Mn alloys, ferromagnetism-to-spin glass phase transition and strong mag. field effect 80−75773
Ni-Mn-H, hydride phase form. and decomposition in hygh-press. gaseous H_2, magnetisation meas. 79−56953
Ni-Mn-H solid solutions, mag. props. 80−88753
Ni-P, amorphous alloys, low temp. mag. props., comp. depend. 77−66387
Ni-P, amorphous magnetisation, NMR and coercive force meas. 77−32187
Ni-P electrodeposit, magnetisation coercivity and magnetostriction 78−68338
Ni-P-B alloy, amorphous, giant moments and short-range orders 77−4499
Ni-Pd, FCC disordered polycryst. alloy, magnetisation, band ferromag. 78−80180
Ni-Pd-Mn ternary alloys, mag. characts., use for thermoseed 80−107995
Ni-rare earth intermetallics, RNi_3, amorphous alloys, mag. and transport props. 79−42513
Ni-Rh ferromagnetic alloy, mag. moment spatial distrib. 77−66275
Ni-Ru, environmental effects and mag. moment distrib., magnetisation and neutron scatt. meas. 79−91211
Ni-Ru (3.3 at%), magnetisation, magnetocrystalline anisotropy, magnetostriction and elastic consts., thermal variations 79−28563
Ni-Ru (≤4 at.%), influence of alloying on mag. anisotropy 80−71010
Ni-SiO multilayer film, interface magnetisation 80−7135
Ni-SiO multilayer films, interface magnetisation 80−88858
Ni-Ta, dil., crit. behaviour of local magnetization, PAC and magnetisation meas. 78−48098
Ni-Ti (9.6 wt.%), mag. study on phase decomposition *(Japanese)* 80−15758
Ni-Zn ferrite, electrical cond., Seebeck coeff. and saturation magnetisation 77−20315
Ni-Zn ferrites, hot-pressed, key props. 78−15348
$Ni_{0.95}$ S Fe, spin glass, spin flop in exchange field 80−34640
Ni_3Al, itinerant ferromag., Fermi surface and single particle excitations 80−34350
$Ni(C_5H_5NO)_6(ClO_4)_2$, susceptibility and magnetisation meas., field, freq. and temp. depend. 77−66279
$Ni_xCo_{1-x}Cl_2.6H_2O$, mixed uniaxial planar antiferromag., magnetisation process 80−88788
$(Ni_{1-c}Co_c)_{0.78}P_{0.14}B_{0.08}$, amorphous, mag. props., local environment model 77−12119
$(Ni_xCu_{1-x})_2MnSn$, mag. props. and lattice parameter, composition depend. 77−80916
NiF_2, magnetisation and antiferromagnetic resonance freq. in mag. field *(Russian)* 80−34781
$Ni_{1-3x}^{2+}Fe_{2+2x}^{3+}Vac_xO_4^{2-}$ (Vac=cation vacancy), solid solns., cryst. lattice imperfections 80−39069
Ni_3Fe, effect of alloying with Cr, Mo, W or Cu *(Russian)* 78−39095
$NiFe_2O_4$, exchange integrals from magnetisation meas. 79−47273
$NiFe_2O_4$ ferrite, mag. props., neutron irrad. 80−103858
$NiFe_2O_4$-Fe_2O_3, effects of excess Fe_2O_3 on mag. props. 77−85495
$Ni_xFe_{3-x}O_4$, spinels, fine particles, magnetic properties obs. 80−71031
$(Ni_{100-x}Fe_x)_{79}P_{13}B_8$, amorphous dil. alloys, spin glasses, magnetisation meas. 79−61178
$Ni_{1-x}Fe_xS_2$ (x=0 to 0.075), weak ferromag. exam. 79−51755
NiH_x, magnetization, elec. resist., and non-occurrence of supercond. 79−56195
NiI_2 anhydrous, magnetic phase transition, neutron diffr. study 80−71033
$Ni_xMg_{1-x}(OH)_2$, random magnet, magnetisation 79−24195
NiMn, high field magnetisation 80−2557
Ni_3Mn, neutron irradiated, disordering by replacement collision sequences, saturation magnetisation meas. 77−47492
Ni_3Mn, thermoremanent magnetisation and blocking temp. 80−34601
Ni_xMn_{1-x} disordered alloy, mag. interactions exam. 77−24687
$NiMnGe_{1-x}Si_x$, mag. props., neutron diffr. and magnetometric meas., 80-600K 80−65793
$Ni_2Mn_xT_{1-x}Sn$, (T=Ti, V or Cr), Heusler alloy, mag. moment exam. 77−24682
$Ni_2Mn_xT_{1-x}Sn$, T=Ti(V)(Cr), ferromag., magnetisation, susceptibility 77−12102
$Ni(NO_3)_2.6H_2O$, rhombic cryst. field, spin ordering in mag. field 77−77058
$NiNb_2O_6$, antiferromag., principle mag. susceptibility and field induced magnetisation meas. 77−20589
$NiNb_2O_6$, magnetisation and susceptibility, antiferro-paramag. transition, expt. and theory 77−43822
NiO (001), surface layers, sublattice magnetisation temp. depend., LEED exam. 78−27018
NiO (111) surfaces, antiferromag., mag. scattering by polarised LEED, spin polarisation effect in theory 80−29529
NiO, mag. transition, neutron scatt. exam. 78−56313
NiO, surface sublattice magnetis., temp. depend., determ. using low energy electron exchange scatt. *(Japanese)* 77−55700
NiO:Fe, exchange anisotropy of Ni-ferrite precipitates 79−28520
$Ni_{1-x}P_x$, electrodeposited, amorphous, mag. and transport props. 78−52106
$Ni_{80}P_{20}$ glass, room temp. 77−63125
$Ni(Rh_{1-x}Cr_x)_2S_4$, ferromag. spinel system with metallic conduction 79−56513
NiS film, electrolytically deposited, S content influence 80−44884
NiS_2, mag. torque curve 79−47305
NiS_2, pure and Co doped, ferromag. props. 79−91227
NiS_2, spin struct. and mag. props. 78−39300
NiS_2, weak ferro- and antiferromag., magnetisation and neutron diffr. meas. 80−65794

magnetisation continued
$Ni_{0.991}S$, sublattice magnetisation temp. var., neutron diffr. 77−40077
$Ni_2(Ti,Mn)Sn$, Heusler alloy, mag. meas. 79−47261
$NiTiO_3$, antiferromag., mag. anisotropy, magnetisation meas. 80−65856
$NiWO_4$, monoclinic antiferromag., domain struct. induced by strong mag. field 80−44856
NiZn ferrite, exchange integrals, magnetisation data and mol. field theory 78−19241
NiZn ferrite, ZrO_2 additions influence on sintering and physicochem. props. 80−108369
NiZn ferrites, comp., X-ray diffr. and saturation magnetisation obs. 78−18617
NiZnCo ferrites, voltage response under sinusoidal and pulse magnetisation effected by hydrostatic press. 80−88846
$Ni_{0.32}Zn_{0.68}Fe_2O_4$, mag. props. and neutron damage 77−47973
$Ni_{0.8}Zn_{0.2}Fe_2O_4$, twisted tubular polycryst. sample in axial mag. field, circular magnetisation 77−32230
$Ni_{1-x}Zn_xFe_2O_4$ spinel, low-temp. transitions and spin configurations, Mossbauer study 78−27144
Ni(001) surface states, surface magnetisation, electron spin polarisation 80−88612
Ni(110), ferromag., surface magnetisation, polarised LEED expt. 80−97118
Np intermetallics, NpM_2Si_2, (M=Cr, Mn, Fe, Co, Ni, Cu), Mossbauer and magnetization expts. 78−31138
$NpCo_2Si_2$ and $NpFe_2Si_2$, itinerant magnetism obs. 77−28406
$NpFe_{2-x}Co_xSi_2$, mag. and hyperfine props. 79−51887
$NpFe_{2-x}Co_xSi_2$, mag. and hyperfine props. 80−7247
NpH_x, mag. props., 4 to 700K 79−61075
NpM_2Ge_2, Neel point and hyperfine interactions, Mossbauer and magnetisation meas. 77−1555
$NpSe_3$, Np_3Se_5 and $NpTe_3$, magnetis. meas. 77−20542
$(Np_{1-x}U_x)Fe$, Mossbauer spectra, magnetism and hyperfine interactions 80−20529
Pb, penetration field and magnetisation curve, lattice defect effects 77−28292
Pb superconducting slabs, magnetisation and migration field, reversible stage 80−65737
Pb-2n, work hardening in mixed state *(Russian)* 79−42707
Pb-In-Ag, transport current distribution in longitudinal mag. field 80−25057
Pb-Tl, reversible surface superconducting magnetisation 78−43531
$PbFe_{12}O_{19}$, Mossbauer spectra, domain magnetisation vector rotations, domain struct. 79−69761
$Pb_{0.84}In_{0.16}$, barriers to flux entry and exit, magnetisation meas. 79−60963
PbNa, supercond., flux density distrib. meas., differential magnetisation loop method 77−32129
PbSe, electron gas magnetisation, energy band parameters determ., use of Faraday effect 80−45047
PbSe, Faraday effect and electron gas magnetisation, Kane two band model calcs. *(Russian)* 80−34899
$Pb_{1-x}Sn_xTe$, Faraday effect and electron gas magnetisation, Kane two band model calcs. *(Russian)* 80−34899
Pd, electronic struct., field-induced magnetisation density and mag. form factor 77−4496
Pd, magnetic properties in para-process region *(Russian)* 78−2672
Pd-Co, dilute alloy, ferromag. ordering, depend. on Co impurity at low temp. 79−61055
Pd-Co-P amorphous alloy, mag. an elec. props. 77−40043
Pd-Cr spin glass, magnetisation and magnetoresist. meas. 79−69680
Pd-Fe, magnetic anisotropy near Curie point, quasi domain struct. *(Russian)* 80−65867
Pd-Fe (25-55 at.%) ^{57}Fe effective field and mag. struct., Mossbauer and magnetisation expts. *(Russian)* 77−90085
Pd-Fe alloys, dil., anisotropy of neutron polarisation near ferromag. phase transition 77−32234
Pd-Fe alloys, disordered FCC, exchange stiffness consts., temp. depend. of magnetisation 77−69528
Pd-Fe alloys, H_2 absorption and mag. behaviour 78−35012
Pd-Fe disordered alloy, Landau model for mag. props. 77−66276
Pd-Fe-Mn, ferromag. and spin-glass props; comment 80−2591
Pd-Fe-Mn, ferromagnet-spin glass, thermal expansion forced, magnetostriction and magnetisation under high press. 80−65255
Pd-H system, type I and type II supercond. behaviour, homogeneity effects 77−28291
Pd-Mn, Curie temp. and magnetisation, vol. depend. 80−34629
Pd-Mn, dil. alloy, giant moment at very low temp. 78−88094
Pd-Mn, dil. alloy, very temp. magnetisation 80−34692
Pd-Mn, ferromagnetism to spin glass behaviour transition 80−71062
Pd-Mn, spin glass-ferromag. alloys, high-field magnetisation 79−33488
Pd-Ni, disordered alloy, onset of ferromagnetism, effect of press. 79−61111
Pd-Ni, local susceptibilities, ^{61}Ni Mossbauer spectroscopy 78−95536
Pd-Ni alloy, dil., ferromagnetism, local moments, susceptibility, magnetisation and Curie temp. *(Russian)* 78−88115
Pd-Ni alloy, paramag. giant moments 78−56291
Pd-Ni alloys, onset of ferromag. 79−56533
Pd-Ni disordered alloy, Landau model for mag. props. 77−66276
$(Pd_{0.67}Fe_{0.33})_{1-x}Au_x$, ordering effects on mag. props. *(Russian)* 78−47942
$Pd_{50}Fe_{37.5}Co_{12.5}$, elec. resist., depend. on composition, relative magnetisation and long-range order *(Russian)* 79−56189
$(Pd_{0.9965}Fe_{0.0035})Mn_{0.05}$, ferromag. and spin-glass props. 80−2590
$Pd_{0.95}Gd_{0.05}$, mag. transition temp. determ., magnetisation data 77−12123
PdH_x foils, supercond. props. 77−32114
PdMn, giant moment-spin glass high field magnetisation, exchange parameter, saturation moment estimation 79−61143
$Pd_2MnIn_{1-y}Sb_y$, Heusler alloy, mag. order obs. 80−29528
$Pd_2MnIn_{1-x}Sn$, and $Pd_2MnIn_{1-y}Sb$, Heusler alloys, mag. order, disorder effects 80−88723
$Pd_2MnIn_{1-x}Sn_1-_x$, mag. order exam. 77−40036
$Pd_{1+x}MnSb$ Heusler alloys, magnetic hyperfine fields on ^{111}Cd, TDPAC and magnetisation meas. 80−93219
$Pd_2MnSn_{1-x}Sb_x$, mag. order exam. 77−40036
Pr, magnetisation and magnetostriction in pulse fields from 3-78K 79−99747
Pr-Eu, dil., magnetisation, Mossbauer spectra 80−15928
Pr-Nd alloy, elec. resist. and magnetisation 77−66367

magnetisation continued
Pr-Tb alloy, elec. resist. and magnetisation, spin glass behaviour 77−66367
$Pr_{21}Ag_{79}$, $Pr_{50}Ag_{50}$, and $Pr_{10}Lu_{40}Ag_{50}$, amorphous, mag. props. 80−60182
PrAs, crystal field press. depend., negative point charge model representation 79−42502
PrBi, crystal field press. depend., negative point charge model representation 79−42502
$Pr_{1-x}Ca_xAl_2$, mag. props. and phase relations 80−107991
$Pr_{0.9}Ca_{0.1}MnO_3$, mag. struct. neutron diffr. and magnetisation study 79−61061
$Pr_{1-x}Ca_xMnO_3$, struct. and magnetisation study 80−65804
$PrCo_5$, uniaxial ferromag. cryst., irreversible rotation processes 80−39768
$PrCo_{5\pm x}$, high field first order transitions, role of K_3 anisotropy const. 80−65879
Pr_2Co_7, mag. saturation and anisotropy, density, lattice parameters 77−85426
$Pr(Co_{0.7}Cu_{0.3})_5$, anomalous magnetisation curves 80−15757
$Pr(Co_{1-x}Cu_x)_5$, saturation magnetisation anisotropy 78−47960
$Pr_2(Co_{1-x}Fe_x)_{17}$, hard direction magnetisation, 5-300K, and anisotropy field 77−12114
$PrCu_5$, nuclear induced ferromagnetism 79−61069
$PrFe_2$, preparation and mag. props. 80−25259
$PrIr_2(Pt_2)(Rh_2)(Ru_2)$, hyperfine sp. ht. and magnetisation meas. at 4.2K 80−75775
PrO, mag. props., lattice consts., and X-ray absorpt. spectra 80−44798
PrS, hydrostatic press. depend. of mag. suscept. 78−80122
PrSb, crystal field press. depend., negative point charge model representation 79−42502
PrSe, crystal field press. depend., negative point charge model representation 79−42502
$Pr_3Se_4(S_4)$, induced ferromagnet, mag. props. under hydrostatic press. 80−60395
$Pr_xSm_{1-x}Co_5$, magnetisation and magnetocryst. anisotropy 78−68215
PrTe, crystal field press. depend., negative point charge model representation 79−42502
Pr_3Tl, critical fluctuations temp. depend. 80−25160
Pr_3Tl, hyperfine interactions, sp. ht. and magnetisation meas. 79−28531
Pr_3Tl, transition temp. and magnetisation 80−25161
Pt, mag. field induced conduction electron , polarisation, magnetisation density, and neut neutron mag. form factor 78−18945
Pt, paramagnetic, induced magnetic form factor, 73 kOe at 78K 79−33454
Pt-Fe alloy, ordered, T-c phase diagram, antiferro- and ferromagnetism *(Russian)* 80−65871
Pt-Fe ordered alloy, multiply mag. phase transitions 80−60264
Pt-Ni alloys, onset of ferromag. 79−56533
Pt-Ni disordered alloy, Landau model for mag. props. 77−66276
Pt_3Cr, ferrimag., magnetisation density, polarised neutron diffr. meas. 80−60204
Pt_3Fe, collision cascades, neutron induced superparamagnetism *(Russian)* 78−2166
$Pt_{50}Fe_{12.5}Co_{37.5}$, elec. resist., depend. on composition, relative magnetisation and long-range order *(Russian)* 79−56189
$Pt_{37.5}Pd_{12.5}Co_{50}$, elec. resist., depend. on composition, relative magnetisation and long-range order *(Russian)* 79−56189
$Pt_{125}Pd_{37.5}Fe_{50}$, elec. resist., depend. on composition, relative magnetisation and long-range order *(Russian)* 79−56189
$PuFe_2$, ferromag. mag. cross section, form factors, saturation magnetisation values, polarized neutron study 79−47245
$PuFe_2$, high temp. mag. props., 300 to 1100K 79−51757
PuH_x, mag. props., 4 to 700K 79−61075
PuP, ferromag. mag. cross section, form factors, saturation magnetisation values, polarized neutron study 79−47245
$PuTe_3$, magnetis. meas. 77−20542
R_2In, R_3In, R=Gd, Tb, Dy, Ho, Nd, mag. props. 80−108009
RM_4Al_8 (M=Cr, Mn, Fe, Cu), magnetism and hyperfine interactions 80−25256
Rb^-, in tetrahydrofuran soln., transient photoelectron nutation 79−3418
$RbFeF_3$, magnetisation density of Fe^{2+} 79−78313
$RbMnCl_3$, twinning struct., cryst. domains, orientation mag. transition *(Russian)* 80−107275
Rb_2MnCl_4, 2D Heisenberg antiferromag. spin wave analysis 80−54879
Rb_2MnCl_4 antiferromagnet, spin flopping of sublattice mag. moments in mag. fields 79−69687
$RbMnF_3$, Heisenberg antiferromagnet, spin diffusion below T_N 78−34968
Rh-Ni alloy, onset of ferromag. 79−56533
Rh_2CoSn, metallic ferromagnet, hyperfine mag. field temp. depend. *(Russian)* 78−80265
Rh_2FeSn, metallic ferromagnet, hyperfine mag. field temp. depend. *(Russian)* 78−80265
Rh_2MnX, (X=Al, Ga, In, Tl, Sn, Pb, Sb), Heusler and Heusler-related cpds., mag. and cryst. props. 77−20568
$(SN)_x$, mag. props. in supercond. state 77−51842
$(SN)_x$, magnetization meas. in supercond. regime 79−56375
$(SN)_x$, supercond., obs. of Meissner effect 78−6478
$(SN)_x$, supercond. polymer, mag. props. meas. 80−107953
$(SNBr_{0.4})_x$, magnetization meas. in supercond. regime 79−56375
$(SNBr_{0.4})_x$, supercond. polymer, mag. props. meas. 80−107953
Sc-Dy(Er)(Tb), dil. alloy, high field magnetisation 78−56292
Sc-Gd, spin glasses, low temp. sp. ht. and magnetisation 80−65913
Sc-rare earth, dil. alloy, cryst. field determ. 78−10651
$ScAl_2$-Er(Dy)(Nd), dil., EPR and mag. susceptibility 80−15797
$ScFe_{2-2x}Al_{2x}$, mag. props., composition depend. 77−20593
$(Sc_xLu_{1-x})_2V_2O_7$ 80−29547
SiH_4, magnetisation relax., appl. of theory of spin-lattice relax. 80−50214
$((SiO_2)_{45}(CaO)_{55})_{65}$ $(Fe_2O_3)_{35}$ glass, effect of melt atmosphere on mag. props. 78−68299
$(Sm,Lu)_3Fe_5O_{12}$, submicron bubble films on rare earth-Ga garnet substrates, prep. and mag. props. 78−91909
Sm intermetallics temp. depend. of Sm^{3+} magnetisation, exchange and cryst. field effects 77−8302
Sm^{3+} in magnetically ordered Sm compounds, crystal-field effects on crossover temp. of magnetisation 79−69656
Sm^{3+} in ordered compounds magnetisation temp. depend., exchange and cryst. field effects 77−51890
magnetisation continued
Sm-Co, amorphous, plasma-sprayed, role of Ar or H_2 atm. in mag. props. and crystn., rel. to H_2 storage 80−64898
Sm-Co, permanent mag., O ion impact, 5.5 keV, secondary Co ion emission, magnetisation depend. *(Russian)* 78−2967
Sm-Hf-Co alloy, rare-earth electron transfer 77−40028
$SmCO_5$ based permanent magnets, props. and cryst. orientation *(Russian)* 80−20431
$SmCO_5$ magnets, heating effects 79−38357
$SmCO_5$ magnets, sintering time effect on props. 79−95977
$Sm_2(Co, Cu, Fe, M)_{17}$, M=Nb, V, Ta, Zr, effect of M on mag. props. 77−89978
$SmCo_5$, H_2 absorption in thin film hydriding alloys 80−65238
$SmCo_5$ hydride films, mag. props. 78−68306
$SmCo_5$, intrinsic magnetic props. 79−82779
$SmCo_5$, radial pulse magnetisation, magnetising and testing fixtures 77−8354
$SmCo_5$ single crystals subjected to shock waves, magnetisation, creation of high-coercivity state *(Russian)* 77−66384
$SmCo_5$, sintered, hard mag. material, magnetisation behaviour 80−75805
$SmCo_5$, sintered, mag. props. *(German)* 77−43852
$SmCo_5$, sintered, orientation of particle easy axes, statistical model 77−8305
$SmCo_5$ sintered magnets, struct. and magnetic charact., sintering temp. influence *(Russian)* 79−52397
$SmCo_5$, substituted alloy, low reversible temp. coeff. 78−68178
$SmCo_5$, temp. depend. of Sm^{3+} magnetisation, exchange and cryst. field effects 77−8302
$SmCo_{5+x}$, Cu and Fe modified, coercive force, demagnetization curves *(Czech)* 79−42805
Sm_xCo_y, mag. and struct. investigations of intermetallic systems 78−95440
Sm_xCo_y, mag. props. 78−43568
$SmCo_{3.5}Cu_{1.5}$, time dependent magnetisation 78−80176
$SmCo_{4.3}Cu_{0.7}$, highly anisotropic ferromag., mag. state after large Barkhausen jump *(Russian)* 79−4699
$SmCo_{5-y}Cu_y$, giant intrinsic magnetic hardness, high field meas. 78−68289
$Sm(Co_{0.86-x}Cu_{0.14}Fe_x)_7$, permanent magnet, sintering and heat treatment effects 80−39817
$Sm_2(Co_{1-x}M_x)_{17}$, bulk magnetisation and magnetocryst. anisotropy, interpretation 77−40055
$Sm_2(Co_{1-x}M_x)_{17}$, magnetocryst. anisotropy and bulk magnetisation 77−40054
$SmCo_{5-x}Ni_x$, giant intrinsic magnetic hardness, high field meas. 78−68289
$Sm_2Co_{17-x}Ni_x$, effect of Ni on mag. props. 78−68296
$Sm_xDy_{1-x}Co_5$, temp. compensated magnetic material, mag. and struct. characterisation 78−68177
$Sm_xEr_{1-x}Co_5$, temp. compensated magnetic material, mag. and struct. characterisation 78−68177
$Sm_{2-x}Gd_xCo_{17-y}Mn_y$, saturation magnetisation and anisotropy field temp. depend., suitability for microwave/millimetre wave TWT 79−82824
$Sm_{0.3}Lu_{0.2}Tm_{0.2}Y_{1.45}Ca_{0.85}Fe_{4.15}Ge_{0.85}O_{12}$, LPE growth, saturation magnetisation, collapse field, bubble diameter 78−95703
$(SmLuYCa)_3(FeGe)_5O_{12}$ film, ion implant profile 79−78477
$Sm_xNd_{1-x}Co_5$ powders, mag. props. *(Russian)* 79−51812
$SmNi_{5-x}Cu_x$, giant intrinsic mag. hardness due to randomised cryst. field interactions 78−68208
SmO, mag. props., lattice consts., and X-ray absorpt. spectra 80−44798
$Sm_{0.6}R_{0.4-x}M_xCo_5$ (R=Gd, Dy, M=Pr, Nd), temp. coeff. of magnetisation 80−34688
Sm_2S_3, mixed valence compound, mag. and thermal props. 79−78400
Sm_3S_4, mixed valence compound, mag. and thermal props. 79−78400
Sm_3Se_4, mixed valence compound, mag. and thermal props. 79−78400
$Sm_xTb_{1-x}Co_5$, temp. compensated magnetic material, mag. and struct. characterisation 78−68177
$Sm_{0.1}Y_{1.9}CaFe_4GeO_{12}$, LPE growth, saturation magnetisation, collapse field, bubble diameter 78−95703
Sn, acoustomag. effect, temp. depend. *(Russian)* 77−72941
$SnCo_5$, magnetisation and cohesive strength 77−55688
$SnCo_2O_4$ spinel, mag. props. 77−1543
$Sn_{0.5}Eu_{0.5}Mo_6S_8$, supercond., spin polarisation, NMR, Mossbauer effect and bulk magnetisation meas. 77−43782
$Sn_{1-x}Mn_xTe$, $0.02<x<0.08$, transport and magnetic properties, low magnetic field 79−99569
$Sn_{1-x}Mn_xTe$, IR reflectivity, elec. susceptibility mag. order effects 79−47433
SnTe:Mn, ferromag.-ordering, transverse magnetoresist. and Hall effect meas. 77−85240
$Sr_2(Co_{1-x}M_x)_{17}$, M=Mn, Ti, Zr, powders, influence of substitutes on mag. props. 80−100601
$SrFe_8Al_4O_{19}$, thin film LPE growth and mag. props. 80−80992
$SrFe_{12}O_{19}$ ceramic compact, sublattice magnetisation and textures 78−68426
$SrO.6Fe_2O_3$, ultrafine, microstruct. development during sintering, mag. props. 79−70022
TaS_2 (aniline)$_{3/4}$, low-field magnetisation meas. on small cryst. in supercond. phase 79−87188
$TaSe_2$:Fe, competition between charge and spin density waves, Landau-Ginzburg theory 79−95352
Tb, conduction electron polarisation and high field magnetisation 78−72332
Tb, critical magnetic studies 80−15745
Tb, elastic constants, magnetoelastic contrib. 80−15777
Tb, ferromagnet, field depend. of elastic const. c_{66} 80−15181
Tb, mag. characts. in strong mag. field 77−89936
Tb, magnetisation, AC susceptibility and microwave absorption meas. 80−60221
Tb, magnetisation in basal plane, calc. 80−70969
Tb, magnetisation intensity in antiferromag. state and mag. field induced phase transforms. *(Russian)* 80−65811
Tb, small particles, disappearance of mag. order., mag. susceptibility and magnetisation meas. 77−16117
Tb-Er alloy, magnetisation process of helical spin struct., neutron diffr. and magnetisation meas. 77−43850
Tb-Fe, amorphous magnetism in bulk samples 77−66278
Tb-Fe amorphous film, thermomag. contact printing 77−89986
Tb-Fe film, undoped and O-doped, amorphous, microstruct. and mag. props. 79−91273
Tb-Gd alloy, spin orientation transition obs. 79−99714

magnetisation continued
Tb-Y, magnetostriction, mag. and elec. props. 78−27068
$TbAg_{1-x}In_x$, mag. and transport props. 78−43572
TbAlGa, mag. props. and struct. 78−39302
$TbAu_3$, mag. phase diagram 80−75761
TbB_4, ferromag. ordering, neutron scatt. meas. 78−10655
$TbCo_{5.1}$, sublattice magnetisation, temp. depend., neutron diffr. anal. *(Russian)* 80−103815
Tb_2Co_{17}, magnetisation, magnetocryst. anisotropy and magnetostriction 77−8303
$TbCrO_4$, mag. susceptibility and magnetis. meas., 1.7-1000K, Curie pt. positron 77−66266
Tb_xCu_{1-x}, amorphous film, magnetisation meas., local anisotropy effects 78−68309
TbD_2, mag. struct., neutron diffr. study 77−85421
TbD_2, sublattice magnetisation, cryst. elec. field effects 78−39295
$Tb_{0.27}Dy_{0.73}Fe_2$, magnetisation and magnetic anisotropy 78−91862
$(Tb_{0.27}Dy_{0.73})Fe_2$, magnetisation, ferromag. domains 80−25162
TbF_3, mag. phase diagram, crit. and tricrit. behaviour 78−14959
$TbFe_2$, high field magnetostriction and magnetisation 78−84471
$TbFe_2$, magnetisation, ferromag. domains 80−25162
$TbFe_2$, magnetisation and magnetic anisotropy 78−91862
$TbFe_2$, magnetoelastic props., magnetostriction hysteresis *(Russian)* 80−29590
Tb_xFe_{1-x} film, amorphous, magnetostriction and magnetisation 78−68305
$TbFeO_3$, mag. susceptibility, temp. depend., effective field at Tb ion sites 80−75742
$Tb_3Fe_5O_{12}$, mag. phase transition exam. 79−19736
$Tb_3Fe_5O_{12}$, quasiantiferromag. state magnetised along two-fold symmetry axis, mag. phase diagram 77−69564
Tb_xGd_{1-x}, orientation phase transitions near Curie pt., magnetization and magnetocaloric effect meas. *(Russian)* 79−87261
TbIG, anisotropic garnet, mag. struct., magnetisation and Faraday rotation obs. 78−68169
TbIG, appl. of superposition model to cryst. field 78−68132
TbIG, magnetisation and mag. susceptibility meas. along (111) direction, 4.2-295K 77−80917
TbIG, mol. field coeffs., magnetisation and mag. susceptibility anal. 78−95406
$(Tb_cLa_{1-c})Be_{13}$, mag. struct., cryst. field effects, neutron diffr. study 80−65789
TbMg, mag. struct. and mag. props. 77−8275
$TbNi_5$, ferromag., magnetisation and paramag. susceptibility 80−25082
TbScFe garnets, mag. props. 77−47979
$Tb_{1-x}Y_x$ alloy, helicoidal antiferromag. to ferromag. transition 78−10687
$Tb_xY_{1-x}Co_{5+0.1x}$, exchange interactions and magnetocrystalline anisotropy 80−34618
$Tb_xY_{3-x}Fe_5O_{12}$, anomalies of magnetisation and magnetostriction obs. in strong fields, 4.2K 77−1581
Th-Mn alloy, mag. props. and effect of H_2 absorpt. 78−19250
Th-Y-Ce, supercond., magnetisation of Ce impurities, sp. ht. meas. 78−47904
$ThCo_5$, lattice consts., magnetisation, and anisotropy fields 79−78364
Th_7Co_3, effect of absorbed H_2 on mag. behaviour 80−60184
$ThCo_{5-x}Mn_x$, struct. and magnetisation exam., temp. depend. 78−2662
$ThFe_3$, H_2 absorption effect on mag. props. and struct. 77−40045
$Th_{1-x}Fe_x$ amorphous alloys, mag. props. and Mossbauer spectra 79−91326
Th_7Fe_3, H induced change from supercond. to mag. ordered state 79−28525
$ThFe_2Ge_2$, 4.2-273K 77−8310
$Th_7Fe_3H_{14.2}$, Mossbauer spectra, mag. props. 80−15852
Th_7Ni_3, effect of absorbed H_2 on mag. behaviour 80−60184
$ThNi_{5-x}Mn_x$, struct. and magnetisation exam., temp. depend. 78−2662
$Th_{65}Sc_{35}Ce$, supercond., magnetisation of Ce impurities, sp. ht. meas. 78−47904
$Th_{1-x}Y_xCo_{5-y}Fe_y$, lattice consts., magnetisation, and anisotropy fields 79−78364
$(Ti,V)_2O_3$, field and temp. depend., down to 1.6K 77−8284
Ti ferrite, magnetisation effect on channelling and blocking of proton beam 77−69022
Ti-Permalloy thin film diffusion couples, low temp. interdiffusion interdiffusion 78−71889
$TiBe_{1.8}Cu_{0.2}$, ferromag., magnetisation density 80−103817
Ti(Fe,Co)H_y, mag. and ^{57}Fe Mossbauer studies 80−71272
$Ti(Fe_{1-x}Co_x)$, density of states estimation from magnetisation and resistivity meas. 78−84119
$(Ti_{1-x}V_x)_2O_3$, nonlinear magnetisation at spin glass phase transition temp. 79−78403
$(Ti_{1-x}V_x)_2O_3$, $O<x<0.1$, magnetisation and mag. moments 80−65772
$(Ti_{1-x}V_x)_2O_3$, spin glass to antiferromag. regime 78−52276
$(Ti_{1-x}V_x)_2O_3$, spin glass and metallic antiferromagnetism 78−68268
Tm, para-, ferro- and ferrimag. and c-axis modulated phases 78−2660
TmB_4, mag. behaviour, in strong mag. field *(Russian)* 78−88119
TmCd quadrupolar ordering and magnetic interactions 79−73676
$TmCrO_3$, temp. and field-induced spin reorientation, magnetisation meas. 77−69588
$TmFe_2$, amorphous, neutron scatt. at transition, spin diffusion, magnetisation meas. 78−68174
$TmFe_2$, low temp. magnetisation and magnetostriction 78−64249
$TmFe_2$, magnetisation and magnetic anisotropy 78−91862
$TmFe_2H_{4.3}$, mag. props. and lattice consts., effect of hydrogen absorpt. 77−20561
$TmFeO_3$, parameters of interaction between rare earth and Fe ions, theory and expt. 79−73705
TmSe, mag. props. 80−97086
$Tm_2V_2O_7$, pyrochlore struct., mag. props. 78−72335
$Tm_xY_{1-x}Se$, Kondo effect, Van Vleck behaviour 80−25085
TmZn, cooperative Jahn-Teller effect 78−67998
TmZn, magnetic-ion-lattice interactions, cryst. elec. field 77−4540
α-U, induced magnetisation density 78−47952
U sesquichalcogenides, mag. props. temp. depend. 77−8287
U-Ga system cpds., elec. resist. paramag. susceptibility, magnetis., temp. depend., mag. struct. 77−20559
UAl_2, high field, high press. mag. props. 80−11172
UAs, magnetisation, ferrimag. spin struct. 80−7088
U_3As_4, ferromag., mag. field induced phase transitions 80−65887
U_3As_4, mag. anisotropy, magnetisation meas. 80−50085
U_3As_4, mag. struct. obs. 77−20559

magnetisation continued
$UCo_{5.3}$, mag. props., cryst. and domain struct. *(Russian)* 77−4529
$UCo_{5.3}$, mag. props. and cryst. struct. *(Russian)* 77−51925
UFe_2, magnetisation meas. 79−51756
UGa_2, cryst. struct., mag. and magnetoelastic props. *(Russian)* 79−38364
UGe_3, magnetisation density, neutron scatt. meas. 80−50038
UN, magnetisation, in fields up to 40 T 79−33505
UN, single crystal, electronic props. 77−77061
UN, system with two singlet levels, fluctuations, excitations and induced moments 79−61022
$U_2N_2Bi(Sb)(Te)$, mag. props. 78−72333
U_2N_2Te, powdered, high field magnetisation 78−35008
UPb_3, crystal field energy levels, magnetisation and susceptibility, neutron spectra obs. 80−50064
UPt, weak ferromag., magnon heat capacity, magnetisation and mag. entropy 77−24685
URh_3, magnetisation density 78−52203
US, low field mag. props. 77−73047
US, temp. mag. field and orientation depend. 77−63232
$USb_{0.8}Te_{0.2}$, magnetisation and polarised neutron studies 79−56515
$USb_{0.8}Te_{0.2}$, magnetisation and neutron meas., mag. moments 80−15703
$USb_{0.9}Te_{0.1}$, multiaxial mag. ordering, magnetisation and neutron scatt. meas. 79−51750
$USb_{0.9}Te_{0.1}$, multiaxial mag. structure 80−15696
UTe, crit. exponents, neutron and magnetisation meas. 80−88823
UTe, magnetisation and neutron meas., mag. moments 80−15703
$U_xTh_{1-x}As$, mag. phase diagram, magnetisation meas. 80−60271
$(U_xTh_{1-x})S$, mag. props. rel. to elec. struct., 1.5-300K 77−1557
$(U_xTh_{1-x})Sb$, magnetisation, U valence change 80−7089
V hyperfine particles, surface magnetisation, explanation of expt. work 78−23303
V, lower critical field anisotropy 78−76201
V-Ni alloy, onset of ferromag. 79−56533
V_1 single cryst., supercond., Ginzburg-Landau parameters, magnetisation meas. 78−2620
$V_xCr_{3-x}S_4$, elec. and mag. props. 79−28523
$V_{3-x}Cr_xSi$, x=0 to 3, struct., supercond. and mag. props. 80−1962
$V(Ir_{1-x}Pt_x)_3$, mag. props., ferromagnetism, comp. depend. 77−77039
VO_2, metallic, magnetisation distribution and band structure 78−76223
V_3O_7, microscopic mag. props., NMR 80−7177
V_4O_7, sublattice magnetisation temp. depend., ^{51}V NMR 79−91301
V_xO_y, metal-insulator transition, external mag. field effects 80−92819
V_5S_8, paramag. cryst., struct. factors using polarised neutron diffr. 80−15691
$VSe_{2-x}S_x$ ($0<x<2$) solid solutions, characterisation 80−88730
W (100), optical magnetisation from spin polarised photoemission 79−78830
W, resonant and nonresonant conduction-electron-spin transmission 80−75857
$(Y,Ca)_3(Fe,Ge)_5O_{12}$ LPE layer, exchange stiffness coeffs., 30-300K 79−78464
$(Y,Lu)_3(Fe,Sc)_5O_{12}$ LPE layer, exchange stiffness coeffs., 30-300K 79−78464
$(Y,Sm)_3(Ga,Fe)_5O_{12}$ epitaxial layers, annealing effect on mag. props. 79−61191
Y garnet, inhomogeneous collective magnon oscill. excited by RF field *(Russian)* 80−100582
Y-Fe, evap. amorphous alloys, thermomag. history effects 77−66389
Y-Gd, spin glasses, low temp. sp. ht. and magnetisation 80−65913
Y-Mn alloy, mag. props. and effect of H_2 absorpt. 78−19250
Y-rare earth, dil. alloy, cryst. field determ. 78−10651
YAl_2-Er(Dy)(Nd), dil., EPR and mag. susceptibility 80−15797
YCo_2, anomalous high-field magnetisation 78−47958
$Y_{1-x}Co_x$, temp. depend. of magnetisation 77−77043
$Y_{2+x}Co_{17-2x}$ single crystal, magnetocrystalline anisotropy 79−38320
$Y_2(Co_{1-x}M_x)_{17}$, bulk magnetisation and magnetocryst. anisotropy interpretation 77−40055
$Y_2(Co_{1-x}M_x)_{17}$, magnetocryst. anisotropy and bulk magnetisation 77−40054
$Y_2Co_{17-x}Ni_x$, effect of Ni or mag. props. 78−68296
$YCrO_3$, magnetisation, NMR freq. temps. depend. weak ferromagnetic-antiferromagnetic spin reorientation transition 80−29631
$Y_xEr_{1-x}Al_2$, paramag. anisotropy 80−39737
YFe_2, amorphous, surface ferromag. layer, spin wave reson. Rutherford backscatt., and magnetisation meas. 79−73819
$Y_{1-x}Fe_x$, amorphous, spin resonance exam. 79−51860
$Y(Fe_{1-c}Al_c)_2$, mag. and Mossbauer study, local environment effects 78−27033
$Y(Fe_cAl_{1-c})_2$, mag. props. 79−38308
$Y(Fe_xAl_{1-x})_2$, mag. order in pseudobinary systems down to millikelvin temps. 78−19251
$Y_6(Fe_{1-x}Al_x)_{23}$, cryst. struct. and mag. props. 79−82180
$YFe_{5-x}Al_xO_{12}$, impurity redistrib. kinetics, temp. depend., vacancy effects 80−75263
$Y_3Fe_{5-z}Al_zO_{12}$, mixed garnet, cation distrib., temp. depend., magnetisation study 80−79831
$YFe_{1-x}Ga_xO_3$, zone refined, exam. of Curie point and magnetisation 79−4673
$YFe_{5-x}Ga_xO_{12}$, impurity redistrib. kinetics, temp. depend., vacancy effects 80−75263
$Y_3Fe_{5-x}Ga_xO_{12}$, mag. domains and cryst. defects 80−75789
$Y_3Fe_{5-x}Ga_xO_{12}$, substituted garnet, floating zone grown, FMR line width, saturation magnetisation 80−29626
$Y_3Fe_{5-z}Ga_zO_{12}$, mixed garnet, cation distrib., temp. depend., magnetisation study 80−79831
$Y(Fe_{1-x}Ir_x)_2$, magnetisation, mag. hyperfine field 80−20531
$Y(Fe_{1-x}Mn_x)_2$, mag. order onset 80−25135
$Y(Fe_{1-x}Mn_x)_2$, Mossbauer spectra and mag. props. 80−39952
$Y_6(Fe_{1-x}Mn_x)_{23}$, struct. and mag. props. 80−25083
$Y_6(Fe_xMn_{1-x})_{23}$, mag. order in pseudobinary systems down to millikelvin temps. 78−19251
$Y_2(Fe_{1-x}N_x)_{17}$, magnetic properties, Mossbauer spectra *(Chinese)* 78−95433
$YFe_{3-x}Ni_x$, electronic sp. ht., saturation magnetisation and lattice parameter meas. 78−68261
YFe_2O_4, parasitic ferrimagnetism 79−4703
YFe_2Si_2, mag. props. 4.2 to 950K, diamag. Fe atoms 77−20544
$Y_{1-x}GdCo_5$, exchange interactions and magnetocrystalline anisotropy 80−34618

magnetisation continued
$Y_{3-x}Gd_xFe_{5-y}Al_yO_{12}$, solid solns., IR absorpt. spectra, physical props. 80−55082
$Y_{3-x}Gd_xFe_5O_{12}$, solid solns., IR absorpt. spectra, physical props. 80−55082
$Y_{2.55}Gd_{0.45}GaFe_4O_{12}$, garnet thin films, magnetisation orientation, temp. depend. 80−71125
YIG, cation sites distrib. and valence states 79−99167
YIG, crit. behaviour, Mossbauer and magnetisation meas. *(Russian)* 79−61106
YIG, distrib. of easy magnetisation axes near edge dislocation *(Russian)* 80−44891
YIG, Faraday rot. rel. to sublattice magnetisation 79−33675
YIG, ferromagnetic resonance and magnetostatic waves in inhomogeneous internal field *(Russian)* 80−54954
YIG film-dielectric layer-conductor struct., magnetostatic bulk wave propag. dispersion relations 80−54925
YIG, Hf response and thermodynamic props. *(Russian)* 78−72338
YIG, magnetic domain wall motion in high drive fields 80−65955
YIG, magnetisation density, polarized neutron expts. 78−52215
YIG, open die hot pressing, spin wave and FMR line width 80−89170
YIG, optical detection of scatt. of homogeneous precession of magnetisation by defects 79−69728
YIG, polariser neutron study of covalency effects 80−2552
YIG spheres, anomalously low saturation threshold of magnetostatic modes 79−69729
YIG, substituted, effect of electron bombardment on mag. and elec. props. 79−42103
YIG, thermomag. anal. by electron diffr. 80−108035
YIG: Si single crysts., mag. props. 80−107981
YIG:Co LPE films, with rectangular bubble domains, prep. and props. 79−82848
YIG:Ho(Er), magnetisation anomalies in strong mag. fields *(Russian)* 77−43854
YIG:La,Ga, film, LPE-grown, Ga incorporation, depend. of magnetisation on growth rate 80−84627
YIG-rare earth garnet solid solutions, magnetisation temp. depend. calcs. 80−20388
$Y_{2.85}La_{0.15}Fe_{3.85}Ga_{1.15}O_{12}$ garnet, mag. props., ion implantation effect, Mossbauer study 80−97166
$Y_{3-x}La_xFe_{5-y}Ga_yO_{12}$, mag. bubble film, low freq. ferrimag. reson. 78−31110
$(Y_xLu_{1-x})_2V_2O_7$ semiconducting ferromag. pyrochlore, mag. props. 80−29547
YM_4Al_8 (M=Cr, Mn, Fe, CU), magnetism and hyperfine interactions 80−25256
YMn_2, lattice consts. and mag. props. before and after H_2 absorption 77−36061
Y_6Mn_{23}, lattice consts. and mag. props. before and after H_2 absorption 77−36061
Y_6Mn_{23}, magnetic moments, magnetisation 80−25094
$Y_{1-x}Nd_xCo_5$, exchange interactions and magnetocrystalline anisotropy 80−34618
YNi_3, loss of ferromagnetism after H_2 absorpt., Pauli paramag. props. 80−34588
YNi_3, magnetism resurgence, neutron diffr. and mag. props. study 80−65819
Y_xNi_{1-x}, amorphous, high press. magnetisation and Curie temp. 80−20442
$Y_{1-x}R_xCo_5$, R=Gd,Tb,Nd, ferrimag., magnetisation, exchange interactions, mag. anisotropy 80−80565
YRh_4B_4, supercond., anomalous cond.-electron polaris. 80−25047
$Y_{2.6}Sm_{0.4}Fe_{5-x}Ga_xO_{12}$, epitaxial, domain wall crit. vel., effect of material parameters 79−99740
$(YSmLuCa)_3(FeGaGe)_5O_{12}$, reproductibility in bubble garnet LPE growth 78−92204
YSmLuCaFeGe garnets, growth and temp. characts. of small bubbles 78−80183
$(YSmLuCa)_3(FeGe)_5O_{12}$, mag. props. and growth of 2 μm bubbles 78−91910
$Y_{1.5}Tb_{1.5}Al_{0.65}Fe_{4.35}O_{12}$, garnet thin films, magnetisation orientation, temp. depend. 80−71125
$Y_{1-x}Tb_xPd_3$, magnetisation, magnetostriction, and inelastic neutron spectra 80−65998
$Y_{1-x}Th_xFe_3$, saturation magnetisation, fields up to 120 kOe, comp. depend. 77−8283
Yb, FCC, nucl. orientation of 3d impurities and magnetisation meas. 78−64280
Yb, FCC phase, low temp. mag. props., impurity effects 80−20387
Yb-Eu alloys, mag. ordering, magnetisation meas. 80−7081
$YbAl_3$, susceptibility, sp. ht. and magnetisation 79−28512
$YbBe_{13}$, mag. props. and EPR meas. 80−11175
YbCuAl, mixed valence behaviour, mag. props. 78−68150
YbCuAl, mixed-valence behaviour, mag. susceptibility and sp. ht. 77−80939
YbCuAl, mixed-valent cpd., thermal expansion and magneto-volume effects 80−66005
YbCuAl, susceptibility, sp. ht. and magnetisation 79−28512
$YbFe_2$, Laves phase compounds, synthesis, mag. props., ^{57}Fe Mossbauer effect 78−10807
$YbFe_2$, preparation and mag. props. 80−25259
YbGaG, mag. props. between 44-600 mK 80−80517
$Yb_3Ga_5O_{12}$, dipolar magnet, sp. ht. and magnetisation meas. 80−60344
$Yb_{0.99}Gd_{0.01}CuAl$, intermediate Yb valence states, mag. props. 79−51743
$Yb_2Ti_2O_7$, crystal field props., ^{170}Yb Mossbauer spectroscopy 79−4750
$Yb_2V_2O_7$, pyrochlore struct., mag. props. 78−72335
$Yb_{1-x}Y_xCuAl$, intermediate Yb valence states, mag. props. 79−51743
$Zn_2Ba_2Fe_{12}O_{22}$, phase transition, mag. props. *(Russian)* 79−51837
$ZnFe_2O_4$, neutron damage effects, superparamag. state replacement cascades 77−16051
$Zn_xFe_{3-x}O_4$ ferrite, mag. struct., Mossbauer spectra and magnetisation study, 4.2K 80−103818
$Zn_xFe_{3-x}O_4$, mag. ordering and domain wall relax. 77−8336
$Zn_cM_{1-c}Fe_2O_4$, M=Ni^{2+}, Co^{2+}, Fe^{2+}, $Zn_cMFe_{2-c}O_{4-c}F_c$, M=Ni^{2+}, Co^{2+}, calc. of saturation magnetisation by cluster components 77−43817
$Zn_{1-x}Ni_xCr_2S_4$, spin struct., mag. props. meas. 77−85428
$Zn_xNi_{1-x}Fe_2O_4$, magnetic props. rel. to localised canting model 77−32161
Zr-3d Laves phase binary and pseudobinary intermetallics, mag. props. H absorpt. effect 80−88821
magnetisation continued
Zr-Mn (up to 0.3%), high-magnetic field magnetisation and magnetoresistance 78−10652
$Zr_{40}Cu_{50}Fe_{10}$, magnetically dil. glass, 3d moments, mag. susceptibility and magnetisation meas. 79−95574
$Zr_{40}Cu_{60-x}Fe_x$, electronic and mag. props. 77−8271
$Zr_{40}Cu_{60-x}M_x$ (M=Fe,Mn,Gd,Tb), amorphous, mag. ordering and local random anisotropy 78−68273
$Zr_{40}Cu_{50}Mn_{10}$, magnetically dil. glass, 3d moments, mag. susceptibility and magnetisation meas. 79−95574
$Zr(Fe,Al)_2$, weak itinerant ferromag., mag. anisotropy effects on mag. isotherms 80−11187
$Zr(Fe_{1-x}Co_x)_2$, density of states estimation from magnetisation and resistivity meas. 78−84119
$Zr(Fe_{1-x}Co_x)_2$, press. effects on ferromag. to paramag. transition 77−66302
$Zr(Fe_xCo_{1-x})_2$, mag. order in pseudobinary systems down to millikelvin temps. 78−19251
$(Zr_{1-x}Nb_x)Fe_2$, magnetovolume effects and Invar characters 80−15773
$Zr_{1-x}Nb_xZn_2$, microscopic mag. props., NMR investigation 80−15807
$ZrZn_2$, high purity, mag. props., pulsed fields up to 17 T 78−64198

magnetisation reversal
Alnico type YuNDK25DA alloy permanent magnets, thermal mag. hysteresis 80−75818
amorphous ribbons, twisted, magnetisation process, domain theory 80−71101
anisotropic materials, magnetisation reversal, 1/H law 78−84454
banded domain structure, magnetostatically coupled with uniaxial substrate, mag. reversals *(Russian)* 78−48016
current threshold sensor, struct. and operational features 80−34689
ferromagnet, stress indication by transverse and longitudinal internal induction 77−16138
ferromagnet with narrow domain boundaries, magnetic reversal processes 79−87287
ferromagnetic film, two-layer exchange coupled, mag. reversal, exchange energy const. *(Russian)* 77−59435
ferromagnetic fine particles, stability of magnetisation curling mode and magnetisation helicoid struct. 80−11227
ferromagnetic particle system, micromagnetism and mag. reversal 79−82830
ferromagnetic thin film, mag. domain wall energy determ. 79−95620
film, domain wall discontinuities during pulsed mag. reversals *(Russian)* 78−48008
film, magnetisation changes during main stage of nonuniform rot. *(Russian)* 77−32224
film, pulse magnetic reversal in high freq. field in ferromag. reson. range *(Russian)* 80−11230
film, two-layer, exchange-coupled, switching, differential permeability *(Russian)* 78−27061
film, with stripe domain structure, mechanism of mag. reversals *(Russian)* 77−80978
garnet epitaxial film, Faraday effect and magnetometrical meas. 78−52317
Invar, magnetisation reversal, fast, forced by external RF mag. field, Mossbauer obs. 78−52311
NDT by external induction and field selective display 78−15618
nondestructive inspection of ferromagnets, using magnetic noise method 78−72997
palaeomagnetic field intensity determ. by remagnetisation in alternating field 77−9535
Permalloy, magnetisation reversal, fast, forced by external RF mag. field, Mossbauer obs. 78−52311
Permalloy film, in weak field, pulse mag. reversal mechanism *(Russian)* 77−80976
Permalloy film, stray fields arising during pulse reversal 77−80980
Permalloy film, with band domain struct., pulse mag. reversals *(Russian)* 79−38361
Permalloy film demagnetising field and magnetisation curve determ. 77−73059
Permalloy films, domain struct., nonuniform rotation of magnetisation *(Russian)* 79−47313
rare earth alloy, $R(Co,M)_5$, magnetisation reversal and high coercive force, domain boundary pinning *(Russian)* 77−8345
rare earth-$(Co_{1-x}Ni_x)_5$, single cryst., mag. props., mag. reversal 77−85489
rare earth-Co-Ni alloys, $Pr(CoNi)_5$ type, mag. props. and mag. reversal phenomena *(Russian)* 77−51924
rare earth-cobalt intermetallics, permanent magnet production and props. 78−52309
Rayleigh constant of ferromagnet, electronic technique 78−12732
rectangular hysteresis loop magnets, rel. to nuclei formation, invariance of generalised model *(Russian)* 77−32214
$Sm_{1-x}R_xCo_5$ (R=Y, La, Ce, Nd), mag. props., domain boundary pinning on statistical conc. heterogeneities *(Russian)* 79−99728
soft ferromagnetic cylinder, point singularities and magnetisation reversal 80−11223
steel, electrotech., losses on mag. after effect *(Russian)* 77−66388
superparamagnetic spheres, magnetisation curling 77−8363
thermomagnetic recording singularities at Curie point, cylindrical domain form. *(Russian)* 77−8318
titanomagnetite in basalts, mag. coupling in partial self-reversal assoc. with increased mag. viscosity 77−73717
$BaFe_{12}O_{19}$ microparticles, magnetisation reversal, hysteresis loop obs. 80−75813
$BaFe_{12}O_{19}$ powder, hysteresis of microwave absorpt. and magnetisation reversal 80−75814
$Bi_{0.96}Mn_{0.04}$, powder particles, magnetisation 77−48014
Co_5Sm, magnetic domains, nucleation and pinning, magneto-optical Kerr effect 80−39811
Cu-Mn spin glass, magnetisation reversal and macroscopic mag. domain obs. 79−61168
CuMn, spin glass, mag. hysteresis meas. 80−34691
CuMn, spin glass, remanence, new approach from zero field NMR 80−34785
Dy-Fe, amorphous ferrimag. film, mag. props. and Curie point writing 77−12164
α-Fe, cyclically deformed, mag. props. 77−28412
Fe, high purity, mag. viscosity mechanism 78−19282
Fe in circular magnetic field, self-reversal 78−14982

magnetisation reversal continued
Fe-Ci (3 wt.%), local magnetisation losses, grain orientation effect 80−88817
Fe-Co-V, Vicalloy, magnetisation reversal by stretching and twisting 80−34733
Fe-Co-X alloys, semihard wires, creeping magnetisation reversal 77−16106
Fe-Cr-Co, magnetic domain walls, Lorentz microscopy 80−103854
Fe-Fe_3O_4, sintered two-phase soft mag. material, prep. and props. 77−63813
Fe-Ni films, dynamic domains and pulse mag. reversals *(Russian)* 79−28571
Fe-Ni/Fe, bimetal film, exchange const. determ. from hysteresis loops *(Russian)* 77−48015
Fe-Ni/pure Fe exchange coupled films, mag. reversals, hard layer thickness effects *(Russian)* 78−56359
Fe-Ni-Co foils, mag. reversals of mag. domains in low-coercivity channels *(Russian)* 79−42813
Fe-Ni-Co-Mo-Ge alloy 40NKM, excess mag. noise after various thermomag. treatments *(Russian)* 80−29575
Fe-Ni-Mn, Invar, RF collapse and thermal effects, Mossbauer study 80−100624
Fe-Si (3 wt.%), eddy current and hysteresis losses, role of domain struct. *(Russian)* 77−80961
Fe-Si (3.5 wt.%), domain wall behaviour, neutron study 78−84451
$Fe_{80}B_{15}Si_5$ metallic glass, large uniaxial magnetostrictive anisotropy, magnetisation reversal 80−34736
$Fe_5Co_{75}B_{20}$, amorphous, magnetisation reversal and domain boundary configs. 80−88809
$(Fe_{1-x}Ni_x)_{80}P_{10}B_{10}$, amorphous microwires, magnetisation reversal and anisotropy 78−91885
$Fe_{40}Ni_{40}P_{14}B_6$, Metglas 2826, amorphous ribbon under tension, mag. domain walls and pulsed magnetisation reversal 80−88825
$(Fe_xNi_{1-x})_{80}P_{10}B_{10}$, amorphous, magnetisation reversal and domain boundary configs. 80−88809
FeSi, domain struct. and magnetisation reversal, time depend. neutron depolarisation 80−50138
FeSi picture frame single cryst., domain wall motion and magnetisation reversal, time-depend. neutron depolarisation study 80−88782
Fo-Fe-Nb, cold-worked and aged, mag. props. and microstruct. 80−34690
$HoCo_2$, magnetisation reorientation 78−23300
Mn-Bi, magnetically uniaxial, strongly anisotropic, discontinuous mag. reversal singularities *(Russian)* 77−48010
MnBi, domain boundaries shift, mag. reversal processes 79−87286
MnBi, domain boundary inertia during mag. reversals *(Russian)* 80−88776
MnBi film, magnetic reversal mechanism, hysteresis loops for polycryst. and single cryst. specimens *(Russian)* 78−60318
MnBi particles, demagnetised, coercivity, remanence and magnetisation reversal 78−19281
MnBi, two-phase coercive force for domain wall motion, mag. reversal nucleation mechanism *(Russian)* 77−48009
$Mn_{3-x}Ni_xB_4$, with onset of spontaneous magnetisation below T_N, singularities of mag. props. *(Russian)* 77−59427
Ni fibres, reversal by curling, coercivity meas. 77−69625
Ni, magnetic permeability, reversible, deform. and ion implantation effects 77−48013
Ni, US induced mag. reversals, stroboscopic electron microscope obs. 77−48026
Ni wire in Ag matrix, coercivity meas. 77−20642
Ni-Fe, film, magnetoresist. meas. 77−16132
Ni-Fe films, magnetisation reversal in narrow strips, TEM study 80−34720
Ni-Fe-Co film, magnetoelastic vibr. generation during high freq. mag. reversals *(Russian)* 78−60320
Ni-Mn alloys, remanent magnetisation reversal, local environment model 79−33507
NiFe tape, rapid surface and vol. magnetisation, eddy-current-limited domain wall motion 77−12159
NiFe, US induced mag. reversals, stroboscopic electron microscope obs. 77−48026
Ni_3Mn, partially ordered, remanence reversal 77−69619
$SmCo_5$ based permanent magnets with low reversible temp. coeff. 79−51814
$SmCo_5$ based ternary and quaternary permanent mag. materials with low reversible temp. coeffs. 79−82822
$SmCo_5$, Cu-modified, magnetisation reversal mechanism 77−8350
$SmCo_5$, domain wall nucleation sites and magnetization reversal 79−56563
$SmCo_5$ films, struct. transformations effect on coercive force and mag. reversal *(Russian)* 80−20436
$SmCo_5$, sintered, hard mag. material, magnetisation behaviour 80−75805
$SmCo_5$, sintered, magnetic reversal processes *(German)* 77−32216
$Sm(Co_{0.84}Cu_{0.16})_{6.9}$, microstruct. and domain struct., mag. reversal *(Russian)* 80−20429
$SmCo_{3.5}Cu_{1.5}$, mag. aftereffects, coercive mechanism, magnetisation reversal 77−69634
$SmCo_4Cu$, domain boundaries shift, mag. reversal processes 79−87286
$SmCo_4Cu$, nonuniform comp., domain struct. and mag. reversals process *(Russian)* 79−1681
$Sm_2Cu_{1.6}Zr_{0.16}Fe_{3.3}Co_{12}$, enhancement of mag. props. 79−82825
$Sm_{1-x}Pr_xCo_5$ single crystals, magnetocryst. anisotropy and stepwise mag. reversals *(Russian)* 77−66291
Tb-Fe, amorphous ferrimag. film, mag. props. and Curie point writing 77−12164
WC-Co alloys, microstresses in two phases, mag. investig. 77−59879
WC-TiC-Co alloys, microstresses in two- and three-phases, mag. investig. 77−63758
$YFeO_3$, domain boundary inertia during mag. reversals *(Russian)* 80−88776

magnetism
see also antiferrimagnetism; antiferromagnetism; band model of magnetism; diamagnetism; electromagnetism; ferrimagnetism; ferromagnetism; geomagnetism; Heisenberg model; Ising model; magnetic moments; magnetic monopoles; metamagnetism; paramagnetism; rock magnetism; stellar magnetism; superparamagnetism; weak ferromagnetism; X-Y model
bibliography of William Fuller Brown, Jr 80−8751
book, magnetism and metallurgy of soft magnetic materials 78−31029

magnetism continued
Bose operator expansions of tensor operators in theory of magnetism 77−63061
chiral order in helimagnets 79−42715
conference, 2nd joint INTERMAG-MMM, New York, USA (July 1979) 80−27031
conference, Amsterdam, Netherlands (Sept. 1976) 77−63047
conference, Bad Nauheim, Germany (Mar. 1976) 77−8255
conference, Cleveland, USA (Nov. 1978) 79−73651
Conference, Freudenstadt and Bad Nauheim, Germany (March and April 1978) 79−24121
conference, Krusevac, Yugoslavia, Sept. 1978 79−56104
conference, Minneapolis, USA (Nov. 1977) 78−64176
conference, Munich, Germany (Sep. 1979) 80−56997
conference, Munster, Germany (March 1979) 80−12843
conference, Pittsburgh, USA (June 1976) 77−12071
conference on magnetic alloys and oxides, Haifa, Israel (Aug. 1977) 78−52183
David Ausubel learning theory as reference system for content organisation in physics 80−22172
developments during past 25 years, personal reminiscences 80−36829
Dyson's hierarchical model, critical isotherm 77−59370
education, magnetic charge quasiclassical quantisation 77−87595
elementary particle magnetic layered theory, including gravity 77−30353
experimental magnetism, book 80−8747
Fermi liquid model, susceptibility maximum in 4d and 5d transition metals 77−4480
force field inside magnet, for teaching 78−54123
free energy, random magnetic system 78−2634
Ginzburg-Landau theory of two antagonistic order parameters, magnetism and superconductivity 79−38242
gravi-magnetic hypothesis reconsidered 79−44362
gravitational analogue 78−65851
Green's function theory of systems with dipolar and quadrupolar pair interactions 77−63222
history from Maxwell to discovery of electron spin *(German)* 79−25816
layered crystal, mag. quantisation investig. *(Russian)* 78−23054
magnet symmetry, and quasiparticle spectra at low momenta 79−42726
magnetic multipoles in time dependent fields 80−99597
magnetostatic multipole expansion, using scalar pot., for teachers 78−61995
magnetostatic problems, soln. by MAGGY2 problem package 80−28134
mixed-valence systems, mag. behaviour, model calc. 77−80901
neutron scattering and magnetism, conference, Julich, Germany (Aug. 79) 80−41934
one dimensional model systems, theoretical survey 78−68129
one-dimensional classical spin chain with random interactions, exact calcs. 79−4687
one-dimensional magnets, thermodynamic behaviour, lattice compressibility effects 79−56482
percolation models, spin representation and cluster distribs. 78−34998
percolation problem, Hausdorff dimension of largest cluster and backbone, numerical estimates 79−97316
periodic lattice, theory of coexistence of supercond. and magnetism, supercond. transition temp. 80−34543
point-multipole expansion, current distrib., for teachers 78−61992
Potts model, three state, lower bound renormalisation transformation 77−28347
Potts model, three-component, phase transitions *(Russian)* 77−89971
quantum crystal, magnetically ordered, phenomenological theory 77−7944
quantum mechanics, key to understanding magnetism 79−24125
quantum mechanics, quantitative understanding of magnetism *(Polish)* 79−51733
quantum theory appl. *(Czech)* 79−44765
quenched system, statistical thermodynamics 77−66363
random one dimensional classical magnet, thermodynamic quantities 77−48002
random spherical model, sp. ht., Griffiths singularity 77−8325
renormalisation group anal. 80−17838
review, specific heats of magnetically-ordered materials 79−42763
review of superconductivity and magnetism *(Hungarian)* 79−47226
rigid magnetic continuum, classical theory 78−34944
SI units 79−2743
solid state, book 77−72962
SUPERCHARGE game for student visualis. of equipot. surfaces 79−30179
superconductor, thermodynamics of magnetism and supercond., mol. field theory 80−34668
teaching w.r.t. chemistry, guide to units 80−12871
theoretical developments from 1949-1974, personal memories 80−31438

magneto-optical devices
beam shifter and polarization converter using wedge etalons 79−32054
bounce-cavity modulator, direct AM 80−5769
bubble spatial light modulators, appl. in optical processing systems 78−79139
chalcogenide spinels, Faraday effect optical isolators for CO_2 laser system 78−50816
circulator, polarisation independ., for optical fibre transmission systems 80−23779
circulator, polarization-independent, configuration method 80−38095
controlled transparencies, page composers 78−50932
cylindrical magnetic domain material coercive force meas. 77−79130
diffraction gratings with alterable magnetic domains for optoelectronics 78−63197
electric current measurement, AC, using magneto-optical methods, principles and advantages *(Polish)* 80−105676
Faraday cell polarimeter magnetic potential difference calc. 77−82587
Faraday effect in lightguide, weak microwave field meas. 80−73463
Faraday element fabrication for intracavity laser appls. 78−66852
Faraday filter, freq. locking of CW dye laser to Na D-lines 78−5487
Faraday filter, freq. locking of CW dye laser to Ne absorpt. lines 79−22989
Faraday rotation isolator, fibre-optic communication applications 80−48408
Faraday rotator and Glan-Taylor prisms, circulator for optical fibre transmission 80−23769
Faraday rotator isolator for laser systems, solid state switching 77−88734
Faraday rotator using low Verdet constant material 80−69520

magneto-optical devices continued
Faraday rotators in fibre Raman lasers 80−58775
filter, for solar vel. fields meas. 79−25507
garnet double layer prod. for magneto-optical devices, LPE 77−21043
garnet film, double heteroepitaxy, magneto-optical devices for phase matching *(French)* 77−3675
garnet film, magnetic rag-domains, appl. to magneto-optical displays 78−91912
garnet film, numerical display element exploiting rag domains 78−68339
garnet films, for magneto-optic appls., substituted rare earth garnet substrate crystals 78−31351
garnet LPE film, laser beam deflector 77−54803
garnets, skew cylindrical mag. domains, light modulator appl. anal. 79−38360
gyrotropic waveguide switching elements at optical wavelengths 79−37049
Hanle effect quantum one-component magnetometer stability and operating range 78−82011
holographic platform, optical path stabilisation with magnetooptic periodic grating 80−99678
integrated isolator using Faraday and Cotton-Mouton effects 77−79966
integrated optics and thin-film technology 77−54815
isolator, based on Faraday rotator, for diode laser, struct. simplification 80−1209
isolator for integrated optics using Faraday and Cotton-Mouton effects 77−88964
Kerr magneto-optic microscope and measuring system 78−58023
Kerr magneto-optic probe, small region meas. of Permalloy I-bars 78−68328
laser beam steering device, stripe domain approach 78−13816
laser sensing system for elec. and mag. fields in power transmission 77−45870
M-H curve measurement of mag. films *(Japanese)* 77−37953
magneto-optical photoconductor sandwich 77−40213
meas. of Kerr and Faraday effects, with accuracy up to 0.001° 80−47087
memories, state of the art 77−42494
memory system principles and descriptions *(German)* 78−29910
metal cryostat, optical meas. at 0.4K 80−73369
modulator, lecture on optoelectronic devices 78−25990
modulators, switches and deflectors, physical principles and Czechoslovak developments *(Czech)* 80−19090
multifunction integrated optic device with mag. alterable phase grating 77−11048
multilayer gyrotropic structures, light propag. anal. *(Polish)* 79−3809
multiple-reflection-type light modulator using Kerr effect in mag. thin film 78−79110
near IR Faraday rotation isolators 78−18042
optical shutter for fusion laser, Faraday cell highly uniform mag. field production 78−13719
optically pumped ruby far IR quantum counter 77−38001
orthoferrites, skew cylindrical mag. domains, light modulator appl. anal. 79−38360
photo-optical polarising optical system as elec. signal generator 79−1000
Raytheon laser gyroscope using MnBi magnetic mirror 78−79064
ring laser gyroscope, Raytheon four freq., mag. mirror, Faraday and Zeeman biassing 80−1269
ring laser gyroscope for missile guidance using magneto-optic bias mirror 78−79061
spectral conversion of optical radiation in mag. film 79−64344
storage, laser beam deflecting system appl. 77−7103
stroboscope, for mag. thin film pulsed mag. reversal studies 78−4667
stroboscope with pulse height analyser for rapid magnetisation variations 79−67356
TE-TM mode convertor coupling and phase matching coeffs. 77−54816
waveguide, semileaky thin film, for modulator appl. 77−62055
CaVG IR Faraday rotator and modulator 78−10900
$CdCr_2S_4$ Faraday effect isolator, laser damage tests 77−46750
$CdCr_2S_4$, hot-pressed, optical isolation appl. at 10.6 μm, intrinsic absorpt. props. 78−42368
CdS, fast modulator for CO_2 laser, using two-photon magnetoabsorpt. 77−88805
CdS, fast optically controlled modulator using two-photon magnetoabsorpt., for CO_2 laser 78−13736
CdTe AC Faraday rotation devices for far IR laser intracavity polarisation modulation 80−58613
$(Co,Cr,Fe)_3O_4$, $(Co,Rh,Fe)_3O_4$ film magnetooptical switches, for laser beam synchronisation 80−58615
$(ErEu)_3(FeGa)_5O_{12}$ film, for mag. writing and magneto-optical displays 78−6549
Hg cell, enhanced Faraday effect for reversible depolarisation, communication scrambling appl. 77−42596
I switch, active modulation of transmission based on Zeeman effect 79−22994
InSb, 100 W average power 10.6 μm isolator based on interband Faraday effect 79−59706
Mn-Bi memory systems 77−85511
Mn-Cu-Bi ternary cpd. thin films for magneto-optic memory applic. *(Japanese)* 77−63238
$Mn_{0.75}Ti_{0.25}Bi$ films as magnetooptic storage medium, mag. interferogram recording 78−19288
Ne discharge Faraday filter, dye laser freq. locking to absorpt. lines 77−79870
Rb cell, enhanced Faraday effect for reversible depolarisation, communication scrambling appl. 77−42596
$YFeO_3$ platelets, domain wall mobility, dynamic coercivity 78−91884
$Y_3Ga_xFe_{5-x}O_{12}$, HF Faraday light modulator, optical characts. crystal struct. depend. 77−39052
YIG, computer optical isolator for near IR region 78−83104
YIG Faraday rotation optical isolator, intensity fluctuation suppression in $LiNdP_4O_{12}$ laser 79−81437
YIG LPE film, optical waveguide in mag. strip domains *(French)* 77−83979
YIG substituted film waveguides, TE→TM mode conversions 78−66904
YIG, YGaIG, Faraday effect and IR radiation modulation 79−10403
ZnSe, Faraday effect visible optical isolator 77−75657

magneto-optical effects
see also Faraday effect; Kerr magneto-optical effect; magnetic circular dichroism; magnetoabsorption; magnetoreflectance; optical constants; Zeeman effect
alkali halide:Tl^+, magneto-optical rot. dispersion anomaly near absorpt. bands 77−63400
alkoxy-cyanobiphenyls, isotropic phase, Cotton-Mouton effect 80−16013
alkyl ammonium manganese chloride, birefringence, two-dimens. mag. behaviour, magneto-optical meas. 78−31175
alkyl-cyanobiphenyls, isotropic phase, Cotton-Mouton effect 80−16013
anisotropic ferromagnet, one-magnon light scatt., temp. depend. 77−52063
anisotropic magnetic crystals with natural optical activity optical props. 78−60415
anthracene: tetracene, singlet exciton trapping mechanism, fluoresc. mag. field modulation obs. 77−77267
anthracene:rhodamine, triplet exciton density, isotope substitution effect, in weak mag. field 77−90184
anthracene:tetracene, singlet exciton fission, fluoresc. in mag. field 79−69877
anthracene:tetracene crysts., mag. field modulation of scintillation under α-irrad. 77−48256
anthracene, electron irrad., creation and evolution of excited states, scintillation obs. 78−92128
anthracene, singlet exciton fission, fluoresc. in mag. field 79−69877
anthracene, singlet exciton fission, prompt and delayed fluoresc. mag. field depend., temp. effects 78−52540
antiferromagnet, IR absorption on impurity excitations near upper edge of spin-wave band 80−80829
antiferromagnet, one-magnon light scatt., effect of anisotropy 79−33676
antiferromagnet, two-magnon Raman scatt., temp. effects 77−48178
antiferromagnet, two-magnon Raman scatt., temp. effects 77−48179
antiferromagnetic crystal, birefringence, optical class lowering induced by longitudinal mag. field *(Russian)* 79−8127
antiferromagnetic garnet, absorpt. and luminesc. spectra, cryst. field and exchange interactions 77−73154
antiferromagnetic polaritons, inelastic light scatt., theory 77−73144
antiferromagnetic semiconductor, magnon-plasmon interaction and its effect on Raman scatt., theory 78−56302
antiferromagnetics, with displaced 3d-ions, mech. of electric dipole absorption of light *(Russian)* 77−32406
aromatic hydrocarbons, liq. solns., delayed fluoresc., mag. field induced polarisation inversion 77−88485
aromatic hydrocarbons in soln., mag. field effects on delayed fluoresc., perturbation theory applic. 77−30913
atomic forward reson. scatt. spectrometry using magneto-optical effect *(Japanese)* 78−76956
atomic parameters, mag. scanning method obs., accuracy 79−27116
atomic spectra, Rydberg states, simultaneous strong elec. and mag. fields 78−78663
atomic spectra in intense mag. fields, theory and appl. to dense stars atmospheres 80−105160
atomic system, hydrogenlike, polarised monochromatic laser radiation absorption in electronic transitions, DC mag. field effects 80−9563
atomic vapours, effects of magnetic fields on four-wave mixing processes 79−23024
atoms interacting with polarised light, resonant Voigt effect, analysis 79−76390
1,2-benzanthracene, monomer and excimer fluoresc. in soln., triplet-triplet annihilation and mag. field depend. 78−78738
benzene, magneto-optic rotatory dispersion curves 80−45040
benzene, orientational correlation parameter for liquid 79−73090
3,4-benzpyrene, monomer and excimer fluoresc. in soln., triplet-triplet annihilation and mag. field depend. 78−78738
Brillouin-Mandelstam scattering from thermal and excited magnons 80−70980
canted magnetic structure media, effect of light absorpt. on quadratic magneto-optic effects 77−24826
canted magnetic structured materials, exciton spectra, optical props. 80−70622
CBOOA, nematic, mag. field depend. of laser light scatt., interf. rings 78−26434
CBOOA, nematic phase laser light scatt., mag. field depend., crit. deform. *(Japanese)* 78−2826
chemical spectroscopy and dynamics, higher-order susceptibility effects, laser appls. 79−40625
cholesteric liquid crystal, incident angle dependence calc. 78−43834
cholesteric liquid crystals, planar texture, field-induced square grid perturbation 79−90531
cholesteric prism, light refr. under applied mag. field *(French)* 78−80319
circular polarisation of emission, magnetically induced, appl. to inorganic complexes 78−78005
circular polariser for refl. in far IR 78−79114
circularly polarised light, right- and left-handedness, sign conventions for magneto-optical effects *(Japanese)* 78−23433
colloidal dispersion, linear birefr. and dispersion 78−8431
colloidal graphite, in mag. field, optical transmission meas., polarisation depend. 78−31712
compact optical circulator for near-infrared region 79−23063
concentration of light, by regular domain structures *(Russian)* 79−24297
conference, Zurich, Switzerland (Sept. 1976) 77−52047
continuous flow cryostat, for measurement in pulsed magnetic fields 78−37017
copper acetate monohydrate, ESR in resonant cavity, meas. of Cotton-Mouton-Voigt effect *(French)* 78−89514
Cotton-Mouton effect in Jupiter ionosphere and magnetosphere, rel. to decametre radio emission modulation 80−67643
cryostat for magneto-optical measurements, with balanced thermal dilations, 1.7 to 300K 79−63203
crystal point groups, electric and magnetic field-induced Raman tensors, effective charges 78−43848
cubic ferr-te garnet, diffracted light polarisation characts., spin and magnetoelastic waves 80−20614
cyano-biphenyls, nematic liq. crysts., director fluctuation quenching by mag. field *(French)* 78−87613
cylindrical magnetic domains, light diffr. 79−73908
diammonium layer compound, $(CH_2)_2(ND_3)_2MnCl_4$, mag. and optical props. 79−51760

magneto-optical effects continued
diammonium layer compound, $(CH_2)_n(NH_3)_2CuCl_4$, mag. and optical props. 79−51760
diammonium layer compound, ND_3-$(CH_2)_2$-ND_3CuCl_4, antiferromag., magneto-optical meas. birefringence 78−68483
diatomic molecules, optical orientation under circularly polarised laser excitation 77−65443
1,4-dibromonaphthalene, triplet-triplet exciton annihilation in quasi-1-dimens. cryst. 78−27297
9,10-dichloroanthracene, mag. field effect on exciton processes and photodetrapping 77−4668
diethylammonium manganese tetrachloride, quasi two-dimensional antiferromag., magnon sideband in absorption spectra 78−43895
dipole absorption, due to electron-electron interaction of electrons occupying Landau levels 78−27195
disordered ferromagnetic alloys, even magneto-optical effects, light cond. tensor 79−4792
disordered system in mag. field, frequency dependence of conductivity tensor, theoretical investigation 80−70725
domain boundary parade motion, low freq. *(Russian)* 80−103852
domain lattice of transparent crystal regular birefr. regions, optical wave diffr. divergence 80−102616
doped semiconductor plasma, inelastic light scatt., spin diffusion 77−36241
EM wave, stimulated Brillouin scatt., transverse static mag. field effect 80−50355
EM wave propag. in strip transmission line in magnetic field 77−28552
EM waves polarisation, in magnetically ordered crystals 80−108189
EPR Cotton-Mouton-Voigt effect in reson. cavity *(French)* 79−47324
ethylammoniumtetrachlorochromate, optical absorption intensity, short-range spin correlation 80−108185
exchange and dipoles coupled ferromags., light scatt. from mag. surfaces, response theory 79−42820
F-centres, relaxed excited state, spin polarisation, saturated optical pumping 79−15522
Fabry-Perot spectrometer instrumental function determ., Voigt function assignation *(Spanish)* 80−52322
Faraday rotation, and mag. field dependence of exciton absorption lines in semiconductors, high mag. fields 80−27321
ferrimagnet, one-magnon light scatt. effect of quadratic magneto-optical coupling 79−11407
ferrimagnetic single crystal layer, light diffr. by mag. bubbles *(German)* 79−56769
ferrite, light diffr. by magnetisation inhomogeneities, multiple refl. 80−2733
ferrite garnet, optic axes determ. using two sublattice model mag. birefr. 77−8555
ferrite rod, magnetised, propap., interference and relax. of magnetostatic waves, magneto-optical obs. 79−73704
ferrite spinels, dielec. permeability tensor and transmittance, transition to single lattice struct. *(Russian)* 79−87465
ferrite-garnet film, waveguide light propag. charact., integrated optics appl. *(Russian)* 78−1346
ferrocytochrome c, mag. reson. Raman opt. activity at different laser wavelengths 77−38681
ferrofluid, magnetically induced polarisation, particle size determ. 77−73130
ferrofluid birefringence, construction of mag. fields *(Russian)* 77−65553
ferromagnet, anisotropic, theroy of light scatt. 77−90161
ferromagnet, light scatt. by spin waves 80−45086
ferromagnet, linear mag. birefr. *(Russian)* 80−93284
ferromagnet, magneto-optical effects and current operator form *(Russian)* 77−81084
ferromagnet, optical excitation of spin complexes, bound-magnon states 77−28554
ferromagnet, refractive index, magnetic contribution 79−28727
ferromagnet, surface, Brillouin light scatt. by spin waves 80−93359
ferromagnetic alloy, disordered, theory 77−12366
ferromagnetic film, Fourier optics, mag. struct. determ. *(Russian)* 78−39371
ferromagnetic fluid, magneto-optical activity in polarised reflected light *(Russian)* 78−76438
ferromagnetic helical structures, magnetooptic light interaction 79−65843
ferromagnetic medium, magnetised, unattenuated refracted wave propag., optical modulation appl. *(Russian)* 78−25774
ferromagnetic metals, magneto-optical effects, electron scatt. 77−90133
ferromagnetic plate, EM wave diffr. by domain walls 79−99724
ferromagnetic semiconductor, HF magnon generation by pumping *(Russian)* 77−24686
ferromagnetic semiconductor, magnon damping under intense radiation 77−63150
ferromagnetic semiconductor, Raman scatt. due to magnon-spin flip of cond. electrons 77−20839
ferromagnetic semiconductor, refr. index variation in strong alternating mag. field 80−23741
ferromagnetic semiconductor, spectrum of quantum spin waves in field of strong EM wave 78−91857
ferromagnetic slab, light scattering from bulk and surface spin waves, theory 80−71389
ferromagnetic surface, spin fluctuations and light scatt. 80−84727
ferromagnetic suspension, birefringence in mag. field *(Russian)* 77−43979
ferromagnetic thin films, Brillouin scattering from spin waves 80−65843
film, magnetic depolarisation curve, influence of multiple re-emission *(Russian)* 77−28550
film, magnetic depolarisation curve, influence of multiple re-emission *(Russian)* 77−28551
fluids, polarisation state of light scatt. in elec. and mag. fields, symmetry indications 80−29751
fluorophate glasses, containing rare earth ions, magneto-opt. characts. 80−64126
formaldehyde, mag. rot. spectrum, singlet-triplet perturbations 78−25580
formaldehyde-d_2, $\tilde{A}^1A_2$-$\tilde{X}^1A_1$ system, mag. rot. spectra 79−98127
frequency dependent cond. tensor for polaron in mag. field 77−52057
frequency dependent dielectric function of gapless semiconductors in a magnetic field 78−63994
gapless semiconductor, magnetic field resonance states *(Polish)* 80−88508

magneto-optical effects continued
garnet, doped magnetic, ang. variation of induced anisotropy, symm. of centres 78−2676
garnet, uniaxial, phase diagram, domain wall struct., near compensation point *(Russian)* 77−12149
garnet film waveguide, Cotton-Mouton effect 77−3650
garnet films, (111)-oriented, cubic anisotropy meas. 80−54924
garnet films, susceptibility of parallel stripe domain lattices, magneto-optical study 80−54930
garnet thin film waveguide, magneto-optical effects 77−54802
garnets, IR refl., ATR, Voigt and Faraday expts. 80−66180
garnets, review 79−99859
gas, inhomogeneous layer, transmission calc. for spectral line with Voigt profile 80−59164
gas, photon echo in a magnetic field at small areas of the exciting pulses 80−95961
gas annular laser, with anisotropic resonator, longit. mag. field effects 79−27293
gas laser, linearly polarized waves, interaction with longitudinal mag. field 80−95936
gas laser, single mode, mode polarisation in transverse mag. fields 78−22107
gas laser, theory of polarisation effects 80−23660
gas lasers, mode interactions in longit. mag. field, active medium dispersion effects 80−63967
gases, optical SHG, quadrupole moment pot. by mag. field 77−46760
gases, spectral line form. depth in mag. field *(Chinese)* 80−105159
geminate recombination of radical ions in polar solvent, mag. field modulation, fluoresc. quenching 77−4912
glass, magneto-optical properties of US light diffr. 78−76437
glyoxal, gas phase emission spectra, mag. quenching 77−18968
graphite, suspensions, particle shape influence on light absorpt. in mag. field 80−60549
graphite-Br_2, intercalation process 78−63965
ground state Zeeman splittings, reson. Raman spectra and mag.-optical activity 80−5579
Heisenberg paramagnet, two-spin Raman scatt. at high temp. 77−40225
4'-n-heptyl-4-cyanobiphenyl, nematic, mag. field depend. of birefringence and order parameter 77−76534
4'-n-heptyloxy-4-cyanobiphenyl, 70CB, anomalous mag. field induced birefr. in isotropic phase 78−56461
high magnetic field behaviour of solids and plasmas, conference, Cambridge, MA, USA (Sept. 1978) 79−60667
HOBHA, smectic A to C transition, crit. biaxiality *(French)* 77−4039
homogeneous wave energy flux under conical refraction and induced gyrotropy 78−17861
III-V semiconductor, acceptor levels, anisotropy of Zeeman splitting and polarization of luminesc. in mag. field 79−24365
III-V semiconductors, magneto-optical spectra of free excitons, manifestation of electron-hole exchange effects 77−59561
imaging of domain struct. in thick cryst., multiple diffr. effects 77−8552
instrumentation appls. *(Japanese)* 79−14099
IR cooling calcs., simple strategies for inclusion of Voigt effects 79−94768
Jahn-Teller impurity centres, piezo-optics and magneto-optics 78−39579
ketyl radical+benzophenone, triplet-doublet energy transfer, viscosity and mag. field effects 77−71850
large-molecule system, field-induced birefringence theory 78−76421
laser radiation frequency spectrum control, phase polarisation method 77−75583
laser spectroscopy, appls., conf., Graz, Austria, (Jun. 1978) 79−26137
layered and chain crystals, electron energy spectrum in mag. field *(Russian)* 77−20220
light diffraction, by cylindrical and elliptical domains *(Russian)* 79−1753
light diffraction by domain gratings, and appl. 80−88970
light diffraction in mag. bubble fields 79−73904
light diffraction in thick layers with regular domain structure 80−108188
light scattering, space-time symmetry rel. to light scatt. in elec. and mag. fields 80−29750
linear and nonlinear effects in system with dispersion and mag. ordering 77−52058
liquid, new optical effects, elec. analogue of Faraday effect 77−81085
liquid, of chiral mols., magnetorefractive effect, linear 80−25343
liquid crystals, domain instabilities in elec. and mag. fields 79−94875
liquid crystals close to nematic-isotropic transition, Cotton-Mouton effect meas. 79−99302
liquid short chain molecules, optical investig. of mol. motions 80−40123
liquids, Cotton-Mouton effect 79−47417
liquids, transparent isotropic, electro-optical and magneto-optical effects, review 78−84553
longitudinal static spin wave struct., magnetotropic interaction of light *(Russian)* 80−93285
low-temperature investigations using flowthrough opt. cryostat with superconducting solenoid 80−105651
macromolecules, scatt. methods, conf., Prague, Czechoslovakia, (July 1976) 79−1764
magnetic bubble dynamics by rotating gradient meas. 79−51827
magnetic colloids, birefringence and dichroism, magnetically-induced, sign inversion 80−60548
magnetic crystal, with impurity centre, anomaly of width and lineshape of light absorpt. 78−76499
magnetic crystals, intrinsic magneto-optical effects, phenomenological anal. 79−33679
magnetic fluids, light scattering and polarisation 80−60616
magnetic fluids, mag., optical, and hydrodynamic props.,, expt. study, review 80−60376
magnetic fluids, optical birefr. and dichroism in mag. field 80−60547
magnetic semiconductor, light scatt. by magnons, appl. to $CdCr_2Se_4$ and EuTe 77−69805
magnetic semiconductors, critical behaviour of electronic properties, theory 80−96861
magnetic stray fields, optical detection 78−31602
magnetic system appl. of synchrotron radiation 77−24730
magnetic thin films, props., data reading system appl. *(Russian)* 77−1572
magneto-microwave effects, rel. to EPR 77−55853
magneto-nonlocal fluids, optical properties 77−58840
magnetoelectric susceptibilities, phenomenological rules for computation 80−55068

magneto-optical effects continued
magnon light diffr., parametrically stimulated magnons *(Russian)* 77−12368
matrix isolated species, mag. circ. dichroism and mag. circularly polarised luminesc. 78−46379
matrix theory fundamentals of active electrooptic and magnetooptic media *(Russian)* 78−63005
MBBA, optical transparency VS mag. field 79−46570
megagauss magnetic field production and appl. to solid-state magneto-optical spectroscopy 79−71491
megawatt sub-mm pulse production by stimulated magneto-Raman scatt. 77−50719
methylammoniumtetrachlorochromate, optical absorption intensity, short-range spin correlation 80−108185
methylene phenanthrene cryst., delayed fluoresc., mag. field effect, sense depend. 77−73160
methylglyoxal, fluoresc. mag. field effect 80−102535
microscopic theory, hybrid excitations 79−24298
microwave, rel. to ESR, review 77−69667
molecular anisotropy from molar Cotton-Mouton and Kerr constants 77−46652
molecular crystals, diffusion mediated exciton processes, mag. field depend. of fission and fusion 79−37998
molecular gas, radiationless transitions in mag. field 78−66580
molecular second-order mag. props. by London field-dependent orbitals calcs. 77−42225
molecules, electronic transitions, g-factor determ. by polarisation plane mag. reson. rot. *(Russian)* 78−70954
multi-level atomic systems, reson. lineshapes and shifts in rot. mag. field 77−68010
naphthalene, triplet exciton annihilation and triplet spin relax. 80−29792
naphthalene (-d_8), gamma irradiated soln., fluoresc. mag. field depend., spin correls. 77−44492
narrow band gap semiconductors, conference, Warsaw, Poland (Sept. 1977) 79−82582
narrow band gap semiconductors, conference, Warsaw, Poland (Sept. 1977) 80−49703
nematic cell, twisted, Leslie threshold field verification 77−84638
nematic layers, optical phase difference and capacitance, elec. and mag. field depend. 80−28911
nematic liquid cryst., Freedericksz transition in mag. field, domain struct. 80−33880
nematic liquid crystal, pretransitional effects, mol. statistical calc. 77−27990
nematic product dynamic scatt. characteristics in mag. field 77−77177
nematic-isotropic transition, correlation functions, Cotton-Mouton coeffs. 80−15228
nondipolar liquids, axially-symm., diamag. mols., Kerr effect and Cotton-Mouton effect meas. 78−39524
nonmutual optical effects, in an external mag. field 80−40097
trans-p-n-octyloxy-α-methyl-p′-cyanophenyl cinnamate, mag. and elec. birefr. in isotropic phase 80−80744
optical fibres, single mode, polarisation and magnetooptic props., expt. meas. 78−33830
optical recording media, review 78−71172
ordered material, light propag. along domain boundary 77−8554
oriented spheroids, magnetically oriented, expression for scattering and absorption cross sections 78−29899
paramagnetic ions in cubic crysts. in const. mag. field and variable EM field, adiabatic basis 80−88972
paramagnetic liquid, depolarized light scatt. in mag. field 80−80759
paramagnetic molecules in rigid isotropic medium, mag. linearly polarised emission 78−68545
parametric transformation of light polarisation in crystals 78−1153
partial atomic vapour pressure, meas. by forward light scatt., transverse mag. field 79−16087
perfluorobenzene, orientational correlation parameter for liquid 79−73090
perfluorocarbons, γ-irrad. solns., mag. field effect on fluoresc. 80−55677
periodic magnetic structure, light propag., paramagnetic interaction 77−55774
Permalloy film, hysteresis loop meas. using magnetooptical system 79−69707
phase transitions, birefringence changes 77−28541
phase-polarisation nonlinear high-resolution spectroscopy in longit. mag. field 79−41423
phenanthrene:anthracene, delayed fluores. of cryst. in mag. field 79−52023
photodissociation pulsed laser with mag. field gain modulation 77−58343
photoexciton dispersion in mag. field *(Russian)* 78−48152
polar semicond., secondary radiation intensity oscills., effect of high mag. field 79−19880
polar semiconductors, resonant magneto-Raman scatt. 79−51958
polarisation of EM waves in transparent magnetically-ordered cryst. 77−4629
polarised light in materials research, birefr., electro-, magneto-, elasto- and acousto-optics 77−48143
polarized emission, mol. theory by quantum field theory 77−83633
polymer, amorphous, bulk, structure models and exptl. methods, review 78−22671
polymer glasses and melts, struct., review of expt. results 79−37636
PVC, magneto-electrets, refr. index, temp. and mag. field effects 78−6655
pyrene, monomer and excimer fluoresc. in soln., triplet-triplet annihilation and mag. field depend. 78−78738
pyrene cryst., delayed fluoresc., mag. field effect, sense depend. 77−73160
quasi-homogeneous magneto-optically active media, Muller and Jones matrices 79−8126
Raman scattering of Raman-inactive phonon polaritons 80−91843
Raman spectroscopy of chiral molecules in mag. fields 80−102532
rare earth chlorides, doubly degenerate E-phonons, mag. field splitting 77−43297
rare earth compounds, magneto-optical effects rel. to 4f electron excitation energies, XPS 77−52222
rare earth compounds, paramagnetic, Faraday and Cotton-Mouton effects for acoustic phonons 78−52476
rare earth garnets, prep. and props. book contrib. 80−44193
rare earth impurities in crystals, magneto-Raman effect 78−43864
rare earth iron garnets, spectra calc. using exact microscopic Hamiltonian 77−8553

magneto-optical effects continued
rare earth metals, ferromagnetic theory of low-temp. and freq. depend. of extraordinary kinetic effects *(Russian)* 79−91408
rare earth metals, optical props., review 77−40259
rare earth orthoferrites, Raman scatt. from magnons, anisotropy consts. determ. 80−66178
rare earth systems, crystal field effects 78−67987
rare earth systems, mag. field depend. of polaritons 79−33246
rare earth trichlorides, magnetic phonon splitting, Raman spectra 77−52099
reabsorption method at high optical densities for two identical tubes 80−38528
regular domain structs., magneto-optical characts., optoelectronics appls. 80−40098
resonance Raman scattering, first and second order, in mag. field, theory 77−36242
resonant light scattering from magnetic excitations, review 80−97290
rhodopseudomonas sphaeroides, reaction centre triplet state fluoresc. mag. field depend. 78−53358
ring laser, emission spectrum control by mag. field induced phase anisotropy of active medium 79−94264
ring laser, nonreciprocal effects on appl. of transverse mag. field to active medium 80−53341
ring laser placed in longit. mag. field, nonlinear nonreciprocity effects 80−43377
ring laser with nonreciprocal-element, nonlinear phenomena due to mag. field inhomogeneity 78−50824
RNA solns., oriented in DC mag. field light scatt. 79−2004
rotatory dispersion, meas. at absorpt. freq., pulsed field technique 77−59557
ruby:Cr^{3+}, high mag. field spin-lattice relax. rates in ground state of ion 79−61407
ruby, echo intensity depend on mag. field, Cr^{3+} and ^{27}Al nuclei super-hyperfine interaction 79−68419
ruby, luminescence, absorption of R and N lines, effect of mag. field 80−60550
ruby, luminescence, red emission intensity at various temps., mag. field depend. 77−32423
ruby, spin dependency of optical feeding into $\bar{E}(^2E)$ metastable doublet 79−28812
ruby cryst. R-line absorpt. and dispersion spectra, mag. field effects *(Russian)* 78−92056
scattering of light by crysts., in book 80−2774
semiconductor, appl. of two-ray methods of modulation spectroscopy *(Russian)* 78−54469
semiconductor, donor-acceptor pair luminesc. polarisation with optical orientation 77−24895
semiconductor, ferromag., electronic props., effect of electron-ion spin coupling 77−28359
semiconductor, ferromagnet, light scatt. from magnons under strong fields, appl. to $CdCr_2Se_4$ 78−84554
semiconductor, intervalley cyclotron-phonon reson., IR absorption in mag. field 78−60448
semiconductor, magneto-optic effects due to optical alignment of electrons and nuclei 78−6654
semiconductor, many-photon absorption by intraband transitions in mag. field 78−27261
semiconductor, optical absorption of diamagnetic excitons in crossed mag. and elec. fields 78−10874
semiconductor, overheating magneto-optic instability 77−1661
semiconductor, photoionisation of deep impurity centres in quantising mag. field 78−6330
semiconductor, recombination radiation mag. depolaris., spin level quadrupole splitting of lattice nuclei *(Russian)* 79−38666
semiconductor, spin injection, carrier polarisation, luminesc. polarisation 77−15957
semiconductor, submillimetric magneto-optical props., strip line technique 80−60554
semiconductor, variable band, recomb. radiation polarisation oscills. in mag. field *(Russian)* 77−77283
semiconductor in quantising mag. field, Stark effect *(Russian)* 77−73126
semiconductor in quantized mag. field, multiphoton Stark effect *(Russian)* 78−72541
semiconductor laser, magn. birefr. influence on stimulated emission spectrum 78−17941
semiconductor physics, conf., Edinburgh, Scotland (Sept. 1978) 79−95303
semiconductor plasma, magnetised, stimulated Brillouin scatt. 80−33085
semiconductor with non-spherical bands, many-photon magneto-optical absorption 78−19451
semiconductor with nonparabolic bands, diamag. excitons, optical absorpt. in mag. field 77−55487
semiconductor with nonparabolic bands, in mag. field, many photon Frenz Keldysh effect 78−92055
semiconductors, free electron scattering and dynamical cond. 78−2476
semiconductors, p-type, mag. oscills. of momentum distribution of hot photoexcited electrons *(Russian)* 80−2854
semiconductors, relax. and reson. struct. in magneto-optical spectra 80−29723
single-mode fibre birefringence and optical activity obs. 78−1394
sodium octyl benzene sulphonate, micellar aq. soln., Cotton-Mouton effect in mag. field 79−16047
spectra of hybrid excitations from transverse photons, excitons, magnons interactions, magneto-optical media 78−80320
spectroscopy, mag. field modulation apparatus 77−34032
spectrum profiles in the presence of Stark, Lorentz and Doppler broadenings 78−86820
spinless particle moving in harmonic pot., magneto-optical props. 78−42106
steel, austenitic, thermonuclear reactor walls, ferromagnetic layer form. magneto-optical testing method 80−35465
stress apparatus for magneto-transport and far-infrared magneto-optical experiments 79−35708
submicron magnetic objects, mag. struct. study using magnetooptic micromagnetometer 80−57349
symmetric-top molecules, dilute gas, non-reson. microwave absorpt., kinetic theory 79−68901
tensor operators, symm. props. 77−52033
p-terphenyl, cryst., highly excited states decay, mag. field effects 78−10962

magneto-optical effects continued
p-terphenyl, single cryst., delayed fluoresc., mag. field depend., 130-300K 79−69879
p-terphenyl, triplet exciton annihilation and triplet spin relax. 80−29792
p-terphenyl solns., mag. field effects on scintillation pulse shape, ion pair recomb. 77−16835
tetracene:pentacene, pressure-induced phase transition, mag. field effect on guest fluoresc. 79−33083
tetracene:pentacene, thermally activated heterofission, fluoresc. 77−85787
tetracene, cryst., prompt fluoresc., mag. field depend. 77−85788
tetracene, cryst., solid-state transitions, Raman spectra, prompt fluoresc. in mag. field 79−99865
tetracene, press.-induced phase transition, fluoresc. mag. field depend. 77−1728
tetracene, singlet exciton fission, kinematic theory 78−87913
tetracene, singlet exciton fission and fluorescence, mag. field depend. 78−39026
transition metal fluorides, magneto-optical effect in longitudinal mag. field *(Russian)* 77−85694
transition metal surface, spin orientation effect of shallow electrons by magnetization 79−65881
transparent magnetic material, wave props. of domain wall 78−48011
TTF-TCNQ film, mag. field effects on IR spectra *(French)* 77−48260
TTF-TCNQ film on KBr, IR spectra in mag. field 77−16310
two-photon magnetooptic effects, theory 77−83629
ultrahigh magnetic field magneto-optical meas. using image convertor camera *(Japanese)* 77−67505
vibrational magneto-optical effect in cryst. 80−45043
Voigt contour of spectral line, nomogram for parameters determ. 80−52321
Voigt curve anal. *(Russian)* 77−36207
Voigt effect, superconvergent sum rules, for isotropic non-mag. materials 77−16285
Voigt geometry cubic crystals, odd magnetooptical effects 78−19450
Voigt parameters, determination using nonideal interferometer *(Russian)* 79−9240
Voigt profile, analytical approximation for spectral profile analysis *(Spanish)* 79−76384
Voigt profile measured over finite frequency range, parameters determ. 80−106870
water, twice distilled, effect of mag. field on rotational IR spectra 79−54849
wurtzite-type crystals, magnetopolaritons 79−78019
YIG, optical absorption and magneto-optic spectra 79−99860
zero gap semiconductor, magnetooptical and impurity effects 80−6721
AgBr, magneto-optics, two-phonon pinning interaction 79−91411
AgBr, new shoulder in luminesc. spectra, triplet excitons 80−20706
AgBr, shoulder in luminesc. spectra due to triplet excitons 79−15525
AgBr, triplet exciton luminesc. in external mag. field, calc. 77−81148
Ag_2O, exciton luminesc. spectra, mag. field influence 80−80860
$Al_xGa_{1-x}As$, optically magnetised, luminescence polarisation anisotropy, hysteresis effect symmetry props. 80−34982
Ar, continuous optical discharge, mag. field effect 78−18479
Ar laser resonator, effect of axial mag. field on loss increase 79−76716
Ar, positive column, moving striations in longitudinal homogeneous mag. field 78−67523
Ba, diamag. quasi-Landau spectrum near ionis. threshold, two-photon ionis. spectra obs. 78−58642
$BaF_2:Tm^{2+}$, EPR, optical recording in weak mag. field 78−68376
Bi, EM wave dispersion and damping, Voigt configuration, non-local calcs. 80−100475
Bi film, optical, magneto-optical and struct. props. 77−1664
Bi film, transparency meas. in mag. field, electronic isoenergetic surface cross section *(Russian)* 79−47532
Bi, HF EM wave propagation in Voigt configuration 78−68045
BiIG, transparent, domain struct. realignment in external mag. field 78−10739
CS_2, orientational correlation parameter for liquid 79−73090
Ca, vap., optical SHG, quadrupole moment rot. by mag. field 77−46760
Ca-H_2, single freq. laser, 5.54 μm emission, mag. field tuning 78−46634
$CaF_2:D^{2+}$ submm. magnetospectroscopy, tunable far IR laser potential 78−52481
$CaF_2:Eu^{2+}$, circular polarisation in luminesc. and optical orientation 78−6740
$CaF_2:Eu^{2+}$, photoluminesc. mag. circ. polaris. 80−89056
$CaF_2:Tm^{2+}$, EPR, optical recording in weak mag. field 78−68376
$Cd_{1-x}Mn_xTe$, exchange interaction, magneto-optical spectra 80−25348
Cd_x-$Hg_{1-x}Te$, cyclotron magneto-optical resons., photoconductivity meas. *(Russian)* 78−23133
Cd_3As_2, highly doped, Shubnikov-de Haas type oscills. in optical transmission 79−61352
$CdBr_2$:Co, spectroscopic studies of interactions 80−29769
$CdCl_2$:Co, spectroscopic studies of interactions 80−29769
$CdCr_2S_4$ ferromag. semicond. film, props. 78−76175
$CdCr_2S_4$, polycrystalline films, mag. semicond., spinel-type, magneto-optical effects *(Japanese)* 79−47415
$CdCr_2S_4$, spin dependent phonon Raman scatt., resonance effects 77−73145
$CdCr_2S_4(Se_4)$, ferromagnetic semiconductors, spinel-type, resonance Raman scattering and electronic structure *(Japanese)* 79−47421
$CdCr_2S_4(Se_4)$, thermoreflectance, photoconductance, Raman scatt. near mag. phase transition 80−97298
$CdCr_2Se_4$, energy structure, magnetooptic effects 80−71394
$CdCr_2Se_4$, ferromag. semiconductor, light scatt. from magnons under strong fields 78−84554
$CdCr_2Se_4$ film, mag. linear and circular dichroism and Faraday rot. 79−99966
$CdCr_2Se_4$, magnetic red shift origin, specular reflectivity, band struct. 80−40127
$CdCr_2Se_4$, photoferromag. effect quenching, photocond. 78−68488
$CdCr_2Se_4$, refr. index variation in strong alternating mag. field 80−23741
$CdCr_2Se_4$, single crysts., mag. semicond., spinel-type, magneto-optical effects *(Japanese)* 79−47415
$CdCr_2Se_4$, spin dependent phonon Raman scat., resonance effects 77−73145
$Cd_{1-x}Fe_xCr_2S_4$ series of magnetic semiconductors, expt. *(Japanese)* 77−40212
$Cd_{1-x}Fe_xCr_2S_4$, single cryst., mag. semicond., spinel-type, magneto-optical effects *(Japanese)* 79−47415

magneto-optical effects continued
$Cd_{1-x}Hg_xCr_2Se_4$, ferromag. semicond. surface magnetism, magneto-optical meas. 77−20831
CdMnTe, semimagnetic semiconductor, band structure, optical properties 79−95331
$Cd_{1-x}Mn_xTe$, exchange induced ionization of bound excitons, luminesc. meas. 80−97328
$Cd_{1-x}Mn_xTe$, magneto-optical props. of free excitons rel. Mn^{2+} ions spin alignment 79−47419
CdS, doped, amorphous antiferromagnet model, susceptibility and spin-flip Raman scatt. meas. 80−97057
CdS electronic two- and one-photon Raman scatt. via biexcitons, stimulated config. obs. mag. field shift 80−103963
CdS, magnetoreflectance and magnetoluminesc. of A exciton 78−39597
n-CdS, new type photoconduction due to magneto-phonon reson. 77−55565
CdS, spatial diffusion of excitons under intense excitation 77−44061
CdS(Se), magnetooptic study of P line at high excitations, biexciton binding energy values 78−48220
CdS(Se), magnetopolaritons in wurtzite-type crystals 79−78019
CdSe, magnetoreflectance and magnetoluminesc. of A exciton 78−39597
$CdTe:Mn^{2+}$, luminesc. and magnetooptic reson., mag. field effect 80−93390
$Cd_{1-x}Zn_xCr_2Se_4$, ferromag. semicond., surface magnetism, magneto-optical meas. 77−20831
$CeCl_3$, mag. field depend. of polaritons 79−33246
$Ce_xLa_{1-x}F_3$, paramag. mixed crystal, scattering of optical phonons by rare earth ions 78−68518
Cl_2, matrix isolated, Zeeman effect and magnetically polarised luminesc. 78−46379
Co, epitaxial films, even magneto-optical effects 80−76007
Co film, even magneto-optical transmission effects, 0.4-1.25 μm 77−32354
Co film, linear mag. birefr. dispersion 77−69807
Co, thin films, optical and magneto-optical permittivities 80−66163
Co-Fe-Si-B, ferromag., magneto-optical spectra in amorphous and cryst. states *(Russian)* 80−84749
Co-Gd(Tb)(Sm) film, magneto-optic coeff. and refr. index, ellipsometric determ. 80−71501
$CoCO_3$, Brillouin-Mandelstam light scatt. obs. of spin wave spectra 80−93358
$CoCO_3$, exciton and magnon excitation spectra *(Russian)* 78−23467
$CoCO_3$, LF exciton and Raman spectra, one-magnon and two-magnon scatt. 80−93333
$CoCO_3$, light interaction with spin system at antiferromag. reson. 77−69707
$CoCO_3$, light scatt. by thermal magnons and magnons excited by antiferromag. reson. 79−82965
$CoCO_3$, light scatt. from magnons and phonons excited by microwave pumping 80−66213
$CoCO_3$, linear magneto-optical effect, birefr. 80−66155
$CoCO_3$, weakly ferromag., light scatt. on spin waves *(Russian)* 78−72419
CoF_2, 180-degree antiferromag. domain obs. by new magnetooptical effect 80−44855
CoF_2, linear and quadratic mag. birefr. 80−16005
CoF_2, linear magneto-optical effect, birefr. 80−66155
CoF_2, spin excitations in longitudinal mag. field 79−69657
CoF_2, visual obs. of 180° antiferromag. domains, mag.-optical effect *(Russian)* 79−61349
$Co_xFe_{3-x}O_4$ film, magnetooptic recording material, mag. and magnetooptic props. 77−20832
$Co_xFe_{3-x}O_4$, single cryst. mag. films, holograms recording and thermomagnetic writing 78−55324
CrO_2 acicular particle suspensions, mag. props., optical meas. 80−44874
Cr_7Te_8 film, optical and magneto-optical props., appl. as storage medium 78−23545
Cs, $6S_{1/2}$-$7P_{1/2}$ transition, photon echo polarisation rotation in mag. field 78−22180
Cs halides, electronic struct. of self-trapped excitons magneto-optic props. 79−33805
CsBr, luminesc., mag. circ. polaris., self-trapped excitons, EPR 79−33805
CsBr, self-trapped excitons, magneto-optical props., 1.3-50K 80−49606
$CsFeCl_3$, linear chain ferromag., optical absorpt. and dichroism in mag. field 77−77237
CsI, luminesc., mag. circ. polaris., self-trapped excitons 79−33805
CsI, self-trapped exciton electronic struct., semi-empirical mol. orbital method 80−49605
CsI, self-trapped excitons, magneto-optical props., 1.3-50K 80−49606
$CsMnCl_3.2H_2O$, quasi-one-dimensional antiferromag., luminesc. enhancement in mag. field *(Russian)* 79−91487
$CsMnF_3$, mag. field- and temp.-depend. of light absorption spectra 78−52528
$CsMnF_3$, optical investig. of spontaneous tilt of mag. sublattices *(Russian)* 77−40215
$CsNiF_3$, 1D ferromag., optical absorption and spin dynamics 80−71417
$CsNiF_3$, double-excitonic optical transition intensity, exchange and dimensionality effects 77−69591
$CsNiF_3$, field depend. mag. behaviour, mag. linear dichroism 79−73903
$CsPbCl_3$, exciton states, magneto-optical investigation 80−29328
$Cs_2ZrCl_6:Re^{4+}$, cryst., mag. circularly polarised emission 77−28613
Cu, crossing effect in 3249Å emission line, mag. field strength depend. 78−25491
Cu, fine interaction of surface electrons, IR spectra 80−16041
CuBr, 1S exciton triplet state, magneto-optical props. 80−25345
$CuBr_4^{2-}$, ground state Zeeman splittings, reson. Raman spectra and mag.-optical activity 80−5579
CuCl double-pulse laser, weak axial mag. field effects on energy output 78−42327
$CuCl_2.2H_2O$, X-band ESR magneto-microwave effects 77−28434
$CuF_2.2H_2O$, powder, Cotton-Mouton-Voigt effect and EPR in Q-band *(French)* 79−8045
$CuF_2.2H_2O$, X-band ESR powder spectrum and related magneto-microwave effects 79−24214
$Cu(NH_4SO_4)_2.6H_2O$, X-band ESR magneto-microwave effects 77−28434
Cu_2O, exciton luminesc. spectra, mag. field influence 80−80860
DyAG, adiabatic magnetisation, optical obs. 78−88283
DyAG, light scatt. from metamag. domains, crit. exponent determ. 77−66482

magneto-optical effects continued
$Dy_3Al_5O_{12}$, antiferromag., optical birefringence in fields along [111] meas. 77−28540
$Dy_3Al_5O_{12}$, magneto-optical rotation in transverse field 79−73902
$DyFeO_3$, mag. field induced intermediate state, magneto-optical effect meas. 77−55672
$DyFeO_3$, orthoferrite, hysteresis props. obs. 77−77071
$DyVO_4$, cooperative Jahn-Teller phase transition, linear birefr. meas. 80−88960
$Er_2EuFe_{5-x}Ga_xO_{12}$, rag-domain garnet film, controlled variation of props. under O_2 annealing 79−15328
Eu chalcogenides, paramagnetic, optical orientation of 4f electrons 77−69799
Eu chalcogenides, resonant Raman scattering model via magnetic exciton in ferromagnetic phase 80−93326
Eu-chalcogenides, magnetic exciton states optical props. 77−31948
Eu-Fe garnet, light mag. linear birefringence and dichroism near absorption band *(Russian)* 80−55063
EuO, ferromagnetic, mag. field effect on optical absorpt. edge, piezotransmission spectra 78−95578
EuO, ferromagnetic piezotransmission behaviour in magnetic field 80−97272
EuO, light scatt. by spin waves 80−45086
EuO, light scatt. from bulk and surface spin waves 78−19497
EuO, light scatt. from spin waves and magneto-optic hysteresis meas. 80−97244
EuO, optical orientation of f-electrons, Curie temp. variation due to exchange interactions *(Russian)* 79−15431
EuO, reflectivity spectra near absorpt. edge 79−47471
$Eu_{1-x}O$, optical absorpt. spectra at metal insulator transition 78−10928
EuO(S), ferromagnetic electronic structure, absorption, thermoreflection and thermotransmission spectra *(French)* 80−97300
EuO(S)(Se), spin assisted Raman scatt. theory 78−43866
EuO(S)(Se)(Te), cryst. and electronic struct., mag., elec., and optical props., book contrib. 80−39760
EuO(S)(Se)(Te), spin order and fluctuations, Raman scatt. study 80−97273
EuS, absorpt. spectrum, change near mag. saturation using quasi-particle multi-band theory 79−61342
EuS, ferromag. semicond. film, Hanle effect, optical orientation time consts. meas. 77−40214
EuS, film, intrinsic demagnetising fields 78−10735
EuS film, magnetic props. using transverse Kerr and Voigt effects 77−52054
EuS films, ferromag., optical spectra and light scatt. from spin waves 80−16116
EuS, light scatt. from spin waves and magneto-optic hysteresis meas. 80−97244
EuS(Se), mag. phase depend. Raman scatt. 78−10886
EuSe(Te), magnetic phase transitions, thermal modulation spectroscopy study *(French)* 80−97301
$Eu_xSr_{1-x}S$, magneto-optical redshift in absorpt. and photoluminesc., mag. short-range order 80−71388
EuTe, antiferromagnet, phonon Raman scatt. from spin superstructures 80−16030
EuTe, mag. 'Bragg' scatt. obs. through Raman scatt. 80−66179
EuX, X=chalcogen, antiStokes luminesc. 77−63455
Fe, epitaxial films, even magneto-optical effects 80−76007
Fe, ferromag., spectral thermal emission, partial circular polarisation 78−18806
Fe, ferromag., spectral thermal emission, partial circular polarization, rel. to magneto-optic Kerr effect 79−23751
Fe, ferromagnetic, partial circular polarisation of thermal emission in mag. field 80−71387
Fe film, even magneto-optical transmission effects, 0.4-1.25 μm 77−32354
Fe film, linear mag. birefr. dispersion 77−69807
Fe garnet, optical radiation interaction with magnetostatic waves 80−76009
Fe, light scatt. by spin waves 80−45086
Fe, light scatt. from surface and bulk thermal magnons 80−45087
Fe, monocryst. and polycryst., thermal emission, magneto-optic circular polarisation obs. 80−70435
Fe, thermal acoustic magnons, Brillouin scatt. meas. 78−95424
Fe-Gd(Tb) film, magneto-optic coeff. and refr. index, ellipsometric determ. 80−71501
Fe-Ni-B(-P), ferromag., magneto-optical spectra in amorphous and cryst. states *(Russian)* 80−84749
$Fe_{80}B_{20}$, amorphous, Brillouin scatt. from magnons, ferromag. reson. 80−65844
$FeBO_3$, antiferromag., optical absorpt. spectra, role of local mag. mode 79−28785
$FeBO_3$, $FeBO_6$, magneto-optical materials, single cryst. growth *(Japanese)* 79−47612
$FeBO_3$, mag. linear dichroism and absorpt. spectra, exciton-magnon absorpt. mechanism 80−66160
$FeBO_3$, magnon dispersion by light scatt. and ferromag. reson. 77−55668
$FeBr_2$, metamagnetic, optical study of mag. phase diagram 78−56312
$FeBr_2$, optical props. around Neel temp. 79−78658
α-Fe_2C_3, anisotropic linear mag. birefr., light modulation 77−8548
$FeCl_2$, magnetic phase diagram, optical studies 78−88121
$FeCl_2$, metamagnet, optical determ. of thermodynamic phase diagram 78−60285
$FeCl_2$, metamagnetic hysteresis, magnetooptical rot. meas. 77−40057
$FeCl_2$, mixed antiferromag.-paramag. state, light scatt. in mag. field 77−40069
$FeCl_2$, optical props. around Neel temp. 79−78658
$FeCl_2.2H_2O$, metamagnetic, resonant magnon-optical phonon coupling 79−28773
$Fe_xCo_{1-x}Cl_2$, metamagnet, mag. phase diagram by mag. induced light scatt. 80−65883
FeF_2 antiferromag., anomalous anti-Stokes/Stokes Raman scatt. intensity ratio 80−66177
FeF_2, one-magnon Raman scatt., anomalous behaviour of anti-Stokes-Stokes intensity ratio 80−40115
FeI_2, spin waves and two magnon bound states, mag. field IR absorption meas. 80−65840
$Fe_xMg_{1-x}Cl_2$, metamagnetic transition, magnetooptic exam. of mag. phase diagram 77−63175
magneto-optical effects continued
$Fe_xMg_{1-x}Cl_2$, metamagnet, mag. phase diagram by mag. induced light scatt. 80−65883
$Fe_{1-x}Mn_xCl_2$, disordered, Raman scatt. from Fe^{2+} and Neel temp. 80−60579
$Fe_{46}Ni_{40}P_{16}B_6$, ferromagnetic amorphous alloy, even magneto-optic effects 77−55776
α-Fe_2O_3 and α-Fe_2O_3:Mn, linear mag. birefringence near Morin transition 77−52052
α-Fe_2O_3, haematite, birefr. under uniaxial stress in mag. field *(Russian)* 78−88285
α-Fe_2O_3, haematite, linear mag. birefr., Morin transition 77−8309
Fe_2O_3, haematite, mag. field induced phase transition meas. by magneto-optic methods 78−10686
Fe_2O_3, haematite, optical indicatrix deform. and rot. during field induced phase transition 78−68482
α-Fe_2O_3, hematite, surface magnetism, magneto-optical meas. 77−20831
α-Fe_2O_3, magneto-optical meas. of orientation of antiferromag. vector accompanying phase transition *(Russian)* 78−14961
α-Fe_2O_3, pure and Mn doped, characts. of Morin phase transition, linear mag. birefringence meas. 77−69560
γ-Fe_2O_3:Cr, pure and doped, acicular particle suspensions, mag. props., optical meas. 80−44874
Fe_3O_4 ferrofluid suspension, mag. props., stability 79−87293
Fe_3O_4, IR refl., ATR, Voigt and Faraday expts. 80−66180
Fe_3O_4 in suspension, ferromagnetic colloid, optical meas. 78−10906
Fe_3O_6, O_2 annealed, optical absorpt., spin struct., polaronic absorpt., cryst. field transitions 78−68493
$Fe_{1-x}Zn_xF_2$, dil. antiferromag., Raman scatt. expts. 79−78666
$Fe_xZn_{1-x}F_2$, Neel point and short range order, dilution effects, mag. birefr. obs. 80−71019
GaAs, donor van der Waals interactions, spectral lineshapes 80−11450
GaAs, donor-acceptor type complex, mag. field splitting of photolum. line 79−15512
p-GaAs epitaxial layers, electron-hole plasma, quantum effects in magnetoluminesc. 78−72591
GaAs, excitons in arbitrary mag. fields 80−96798
GaAs, hot photoluminescence depolarisation in mag. field, 0.4 eV energy state electron lifetime *(Russian)* 80−16086
n-GaAs, interband transition times, luminesc. depolarisation obs. *(Russian)* 79−33831
n-GaAs, laser beam self-focusing in mag. field, carrier mechanism 78−33788
p-GaAs, magnetoluminesc. of cond. band to acceptor transition 77−1716
p-GaAs:Zn, diffusional doping, photoluminesc. in mag. field 77−16384
GaAs-$Al_xGa_{1-x}As$ superlattice, mag. field induced dimensionality change 78−64381
GaAs-AlGaAs DH injection laser, emission energy, wavelength depend. in strong mag. fields 80−48248
GaAs-$Ga_xAl_{1-x}As$ laser, magn. birefr. influence on stimulated emission spectrum 78−17941
p-GaP:Zn,S, spin polarisation of donors and acceptors in mag. field, optical and microwave study 80−93393
GaSe, exciton magneto-optical spectra 80−25347
GaSe, lamellar crystal, exciton translational mass from magneto-Stark effect *(Russian)* 78−48153
GaSe, magnetoluminesc. at 4.2K 79−61345
GaSe, optical orientation and alignment of free excitons, on resonant excitation *(Russian)* 77−90196
$(Gd,Bi)_3(Fe,Ga)_5O_{12}$ magneto-optic film, ion irrad. effect on storage props. 78−52324
Gd, ferromag., magneto-optical reson., optical consts. determ. 78−6657
Gd-La, magneto-optic reson. *(Russian)* 79−47426
$GdAlO_3:Cr^{3+}$, mag. field effects on fluoresc. 80−2850
GdCoMo amorphous films, susceptibility of parallel stripe domain lattice, magneto-optical study 80−54930
$Gd_3Ga_5O_{12}$, IR refl., ATR, Voigt and Faraday expts. 80−66180
GdIG, IR refl., ATR, Voigt and Faraday expts. 80−66180
$(GdPrBi)_3(FeGaIn)_5O_{12}$, pure and In^{3+} doped, near IR absorpt. and Faraday rot. 78−95580
GdS, meas. of opto-magnetic interactions at low mag. fields 80−2735
n-Ge, Brillouin scatt. by phonon zero sound, in quantising mag. field 77−69847
Ge, diamagnetic excitons, fundamental absorption edge, Faraday config. 79−8144
Ge, electron-hole drop and exciton atmosphere 80−6748
Ge, electron-hole drop luminesc., phonon wind induced anomalous depend. at low mag. fields 80−34980
Ge, electron-hole drop magnetoplasma resonance 79−60722
Ge, electron-hole drops, IR magnetoplasma absorptions 80−6728
Ge, electron-hole drops at high mag. fields 79−60721
Ge, electron-hole liq. thermalisation between mag. field split valleys 80−25444
Ge, exciton contrib. to oscillatory magnetophotocond. 79−15180
Ge, exciton luminesc. polarisation in mag. field *(Russian)* 77−12436
Ge, luminescence circular polarisation in mag. field, Landau levels paramag. splitting 77−32435
Ge, magnetoluminescence of electron-hole liq. 80−29790
Ge, pure, magnetic phase transition between electron-hole drops and free-excitons 78−6278
Ge:Al(B)(P), impurity ground state levels from photo-thermal cond. in mag. field 77−51699
H, in strong magnetic field, so(4,2) algebra use in perturbation theory 80−47845
H, strongly bound states in intense mag. field 80−37721
He I, excited states decay, lifetime meas., lab. mag. field effects 77−10640
He, level crossing signals in inhomogeneous mag. field *(German)* 77−27037
He, liq., surface with trapped electron, parallel mag. field effect on interband transition 78−87835
He, positive column, moving striations in longitudinal homogeneous mag. field 78−67523
He, Voigt profile, absorpt. line calcs. for the 396.5, 361.4, 318.7, 492.2, 587.6 and 447.1 nm lines 80−99471
He, Voigt profile, line absorpt. calcs. of 388.9 nm triplet, 501.6 nm singlet lines 78−90123
He-Cd hollow cathode laser, axial mag. field effect on oscills. 79−59681
He-Cd laser energy characts., with longit. mag. field *(Russian)* 77−50661
$He-Cd^+$ laser output, effects of transverse mag. field 79−86169

magneto-optical effects continued
He-Ne, single mode laser, mode polarisation in transverse mag. fields 78−22107
He-Ne double mode laser in axial mag. field. *(Russian)* 79−86160
He-Ne laser, mag. polarised performance 77−14750
He-Ne laser, simultaneous oscillation at 0.63 and 3.39 μm, output power depend. on loss in mag. fields *(Japanese)* 80−32959
He-Ne laser, spatial anisotropy induced by cascade laser transitions 78−29931
He-Ne laser frequency stabilisation using mag. field tuning dip 79−55153
He-Ne laser saturation resonance in static magnetic field 77−54693
He-Ne ring laser, nonreciprocal effects with transverse mag. field applied to active medium 80−91820
He-Ne ring laser placed in longit. mag. field, nonlinear nonreciprocity effects 80−43377
Hg, atoms, detection by forward scatt. of reson. radiation in mag. field and Voigt effect *(Japanese)* 77−60155
HgCdTe, recomb. effects, mag. quantum oscills. in Auger transition rate 79−82610
$Hg_{0.77}Cd_{0.23}Te$ nonlinear optical IR generation 80−58642
$Hg_{1-x}Cd_xTe$, magnetooptical and impurity effects 80−6721
$Hg_{1-x}Cd_xTe$ mixed crysts., magneto-opt. obs., semicond. config., semimetal-semicond. transition 77−73131
$Hg_{1-x}Cd_xTe$, semimetallic state, magneto-optical investig. of Landau levels and band parameters 77−63410
$HgCr_2Se_4$, ferromag. semicond., surface magnetism, magneto-optical meas. 77−20831
n-$HgCr_2Se_4$, ferromagnetic semiconductor, plasmon refl., 86 to 320K 80−50346
$HgCr_2Se_4$, thermoreflectance, photoconductance, Raman scatt. near mag. phase transition 80−97298
$Hg_{1-x}Mn_xTe$, magnetooptical and impurity effects 80−6721
$Hg_{1-x}Mn_xTe$, semimetallic, giant spin splitting induced by exchange interactions 77−28150
HgSe,, Fermi surface anisotropy parameters, magneto-optical effect 80−25350
HgSe, magnetooptical and impurity effects 80−6721
HgTe, magnetooptical study of Γ_8 bands anisotropy 79−82984
HgTe, temp. depend. of energy gap, oscillatory magnetotransmission meas. 79−15441
HgTe type semiconductors, spin-flip transitions in magneto-optics and magneto-transport 80−50306
I, photodissociation laser, active medium gain in mag. field 77−79816
I_2 laser, with programmed mag. field 78−33750
I_2, use as test mol. in modern spectroscopy, review 78−90317
IBr, magnetic rot. spectrum, rot. and vibr. anal. 78−70861
$In_{1-x}Ga_xAs_yP_{1-y}$, oscillatory magneto-transmission, band parameters 79−60707
$In_{0.58}Ga_{0.42}Sb$, interband magneto-optical transitions, arbitrary field orientation 79−42948
$In_{1-x}Ga_xSb$ alloy system, interband magnetooptical study using Schottky barrier 79−8124
$In_{1-x}Ga_xSb$, band parameter variations 80−20084
InP injection laser, strong mag. field effect on emission 77−58329
InSb, absorpt. saturation by nonequilib. electron-hole plasma weak mag. field effect 78−9418
n- InSb, hot electron energy relax. in quantizing mag. fields 78−31259
InSb, impurity polarons at two LO-phonon region, magneto-optical anomalies 79−61227
n-InSb, in MIS struct., accumulation layer submillimetric cyclotron resonance obs. 77−39912
InSb, interband magneto-optical transitions, arbitrary field orientation 79−42948
InSb, intraband photocond. in mag. fields 79−47123
InSb, laser beam self-focusing, effect of quantising mag. field 77−42578
n-InSb, laser induced magneto-photoconductivity, conduction band transitions 77−55566
InSb, magneto-optical anomalies of impurity electrons, two-LO-phonon region 78−72415
n-InSb, magneto-optical transitions from deep levels, photocond. obs. 80−55069
InSb, one- and two-photon magneto-optical transitions 77−16284
n-InSb, optical phonon emission in intraband magneto-optical transitions, photocond. meas. 80−34481
p-InSb, photoexcited exciton spin-flip scatt. 80−74434
n-InSb, photoluminesc. in crossed EM fields *(Russian)* 77−24892
InSb, polar semicond., resonant magneto-Raman scatt. 79−51958
n-InSb, spin flip Raman scatt. from electrons in localised donor states 77−3630
p-InSb, stimulated magneto-Raman scatt. obs. 77−83924
n-InSb, surface polaritons, excited by microwave magnetoplasma 79−19530
InSb type semiconductor, spin-flip transitions in magneto-optics and magneto-transport 80−50306
InSb-Au Schottky barrier, photovoltaic spectra and magneto-optical transitions, Landau levels and excitons 77−47858
InSb-NiSb, eutectic, intraband magneto-optical studies, far IR transmission spectra 79−61371
InSb-type semiconductors, shallow donor states in magneto-optical props. 80−6785
InSe, direct gap exciton exam. by magneto-optics and photoconductivity 79−19527
$IrCl_6^{2-}$, ground state Zeeman splittings, reson. Raman spectra and mag.-optical activity 80−5579
K, stimulated electronic Raman light scatt. by mag. sublevels 78−50492
K vapour, mag. sublevels, stimulated electron Raman scatt. *(Russian)* 78−50861
KBr:Ag, mag. field effect on luminesc. of paired Ag^- ions 78−27313
KBr:Tl, Jahn-Teller system, negative mag. circular polarisation in emission spectrum 80−20694
KCl, perturbed M-centre triplet state, M-F centre exchange mechanisms 79−69884
KCl:Au^-, fluorescence, stress and mag. field depend., Jahn-Teller effect and relax. processes 77−48220
KCl:Ca(Yb), Z_2 and Z_2^+ centres, excited state, magnetooptical spectra 80−108233
KCl-Tl, Jahn-Teller system, negative mag. circular polarisation in emission spectrum 80−20694
KCl(Br), F-centre emission, mag. circular polarisation 80−108251
KCl(Br), triplet state lifetime of F_2 centre, mag. field effect 78−35177

magneto-optical effects continued
K_2CoF_4, 2-dimens. Ising antiferromag., mag. excitons, Raman scatt. obs. 80−66181
K_2CoF_4, two-dimens. Ising antiferromag., nearest neighbour correl. function, birefr. expts. 80−71386
$KCuF_2$, linear chain Heisenberg antiferromag., nearest neighbour correl. function, birefr. expts. 80−71386
KF(Cl)(Br), mag. props. of relaxed excited state of F-centre, vibronic theory 78−60502
$KFeCl_3$, linear chain ferromag., optical absorpt. and dichroism in mag. field 77−77237
KI doped with F-centres, mag. vibr. Raman scatt. 77−4636
KI:In^+, luminesc. decay, excited state symm. and g-value 79−99922
KI:Sn^{2+}, red emission, mag. field effect on radiative decay time 79−33818
KI:Sn^{2+} luminesc. decay, excited state symm. and g-value 79−99922
KI:Tl^+, A_T emission, mag. circular polarisation, WKB approx. for nonradiative transition rate 80−55180
KI:Tl, Jahn-Teller system, negative mag. circular polarisation in emission spectrum 80−20694
$KMgF_3$:Ni, Ni-Ni pair optical spectra 80−45042
$KMn_{1-x}Co_xF_3$, Raman scatt. by mag. excitations 77−55775
$KMnF_3$, antiferromag. cryst., luminesc. enhancement in mag. field, exciton model *(Russian)* 77−48214
K_2MnF_4 and K_2NiF_4, two-dimens. antiferromag., two-magnon Raman scatt. linewidth, finite temp. 77−66508
K_2MnF_4, quadratic layer antiferromag., intrinsic emission obs. 77−20906
$KNiF_3$, and K_2NiF_4, double-excitonic optical transition intensity, exchange and dimensionality effects 77−69591
$KNiF_3$, refr. index, isotropic exchange contrib. 77−69808
KTb_3F_{10}, mag., optical, magneto-optical behaviour 78−68484
LC-440, optical transparency VS mag. field 79−46570
$LaF_3:Pr^{3+}$, ultrahigh resolution photon echo spectroscopy 80−28285
Li, atomic absorpt. spectra, high mag. field, quasi-Landau reson. 78−90109
Li ferrite film, magnetic circular and linear dichroism, temp. depend. 79−69815
Li, motional Stark effect in high mag. field 79−63958
$LiIO_3$, irreversible double refraction in mag. field *(Russian)* 77−59560
$LiTbF_4$, ferromag., spontaneous magnetisation at marginal dimensionality, magneto-optical effect meas. 77−24683
$LiTbF_4$, mag., optical, magneto-optical behaviour 78−68484
$MgCl_2$:Co, spectroscopic studies of interactions 80−29769
MgO:Cr, high resolution far IR spectroscopy of lower energy levels of Cr^{2+} 80−80822
MgO:Cr^{2+}(V^{2+}), coupling of T_{1u} and T_{2u} vibr. to $^2E_g \rightarrow {}^4A_{2g}$ transition 77−63453
Mn film, optical, magneto-optical and struct. props. 77−1664
MnAs in suspension, ferromagnetic colloid, optical meas. 78−10906
MnBi film, magnetic hologram recording appl. *(Russian)* 77−1573
MnBi film, optical, magneto-optical and struct. props. 77−1664
MnBi films, prep. by ionised-cluster beam deposition technique, magnetooptical props. 80−100790
MnBi films, stability of magneto-optical props. on pulse heating *(Russian)* 78−88282
$Mn_{1-x}Co_xF_2$, Raman scatt. by mag. excitations 77−55775
MnCuBi film, optical and magneto-optical props. 77−4695
$MnCu_{1-x}Dy_xBi_{0.86}$ film, mag. and magneto-optic props., appl. as storage medium 77−8550
MnF_2, inelastic light scatt. from antiferromag. polaritons, theory 77−73144
MnF_2, magnetic, thermal, elastic refraction of light, mag. order influence on refractive index *(Russian)* 80−34880
MnF_2, two-magnon Raman scatt., temp. effects 77−48179
MnF_2:Ni^{2+}, IR fluoresc., field depend., exchange energy 78−68543
MnO, linear optical anisotropy meas. at antiferromag. transition 77−36205
$Mn_{1-x}Zn_xF_2$, linear mag. birefr., crit. behaviour 77−52061
$Mn_xZn_{1-x}F_2$, Neel point and short range order, dilution effects, mag. birefr. obs. 80−71019
$2HMoS_2$, far IR optical and magneto-optical absorpt. 77−52078
$MoSe_2$, exciton spectra 80−97296
NO_2, fluoresc. quenching mechanism in mag. field 78−74696
Na atomic vapour, optical sum-freq.-generation interference 77−42569
Na, mag. field quantum beats in two-photon free-induction decay 79−13692
Na, mag. perturbed gas, distortionless optical pulse propag. 78−22179
Na, vap., optical SHG, quadrupole moment rot. by mag. field 77−46760
Na_2, optical orientation under circularly polarised laser excitation 77−65443
NaBr(I), optically activated F→F′ centre conversion in mag. field 80−108253
$Na_3Pr(C_4H_4O_5)_3.2NaClO_4.6H_2O$, single cryst., forbidden $A_1 \rightarrow A_1$ transition, mag. field induced intensification 80−50302
Ne discharge positive column in longitudinal mag. field, metastable atom radial density distrib. obs. 78−67496
Ne, positive column, moving striations in longitudinal homogeneous mag. field 78−67523
Ni complexes, $Ni(PX_3)_4$ (X=F, OCH_3, Cl, CH_3, H), CNDO/2 calc. of magneto-optical props. and electronic content of metal-ligand bonds 77−23430
Ni, epitaxial films, even magneto-optical effects 80−76007
Ni film, even magneto-optical transmission effects, 0.4-1.25 μm 77−32354
Ni film, linear mag. birefr. dispersion 77−69807
Ni, light scatt. from surface and bulk thermal magnons 80−45087
Ni, polycryst., thermal emission, magneto-optic circular polarisation obs. 80−70435
Ni, surface polariton modes, correlation with attenuated total reflection minima, computational study 78−31265
Ni, thermal acoustic magnons, Brillouin scatt. meas. 78−95424
Ni-Fe-Cr film, hysteresis loop meas. using magnetooptical system 79−69707
$Ni_{1-x}Co_xF_2$, Raman scatt. by mag. excitations 77−55775
NiFe tape, rapid surface and vol. magnetisation, eddy-current-limited domain wall motion 77−12159
$Ni_xFe_yCr_{1-x-y}$ films, struct., mag. props., and corrosion resist. 80−34706
α-O_2, antiferromagnetic polycrystal, splitting of exciton absorpt. lines in mag. field *(Russian)* 80−103943
PAA, optical transparency VS mag. field 79−46570

magneto-optical effects continued
Pb film, current-induced flux motion, studied at 100 ns time resolution 79−47208
Pb film, supercond., flux dynamics during current-induced breakdown, magneto-optical flux detection 77−24646
$Pb_{1-x}Ge_xTe$, n- and p-type, effective masses 80−44481
PbI_2 (2H), layer cpd., band parameter determ. 79−95332
PbI_2, exciton magneto-optical spectra 80−25347
$Pb_{0.9}Sn_{0.1}Te$, situated in quantizing magnetic field, photolum. spectra 79−71461
$Pb_{1-x}Sn_xTe$, epitaxial layers, photolum. in mag. field 79−83033
$Pb_{1-x}Sn_xTe$, inter- and intraband magneto-optical transitions 80−25346
p-PbTe, far IR obs. of shallow bound states in high mag. fields 78−23444
PbTe, far IR spin flip reson. 79−82979
p-PbTe film, for IR magneto-optics, 8-30K 78−23543
PbTe, ion implanted, magneto-optical expts. *(German)* 79−28848
p-PbTe, lattice dielectric const. in far IR region, magnetotransmission meas. 79−78605
PbTe, magneto-optical pinning phenomena 79−82962
PbTe, magneto-optical transitions and band parameters 79−82961
p-PbTe, magneto-optics of free and bound carriers 79−82985
$(PrGdYb)_{3-x}Bi_x(FeAl)_5O_{12}$ system, LPE growth and magnetooptical props. 79−65842
Rb, circ. polarised reson. fluoresc. excited with π polarised D_2 line, 0-170 G 79−41133
Rb, optical pumping of vap. in mag. field, at. alignment 79−31476
Rb Rydberg levels in intense mag. field, diamag. struct. 79−26958
RbBr-Ag, mag. field effect on luminesc. of paired Ag^- ions 78−27313
RbCl(Br), F-centre emission, mag. circular polarisation 80−108251
$RbCoF_4$, 2-dimens. Ising antiferromag., mag. excitons, Raman scatt. obs. 80−66181
Rb_2CrCl_4, optical absorption intensity, short-range spin correlation 80−108185
$RbFeCl_3$, linear chain ferromag., optical absorpt. and dichroism in mag. field 77−77237
$RbFeCl_3$, singlet ground state one-dimens. ferromag., 2-magnon excitation, far IR spectra obs. 77−69831
$RbMnCl_4$, changes in birefr. due to spin flopping 79−73910
$RbMnCl_4$, quadratic layer antiferromag., intrinsic emission obs. 77−20906
Rb_3MnCl_4, quasi-2D-antiferromag., linear birefr. and optical absorpt. spectra 80−71385
$RbMn_{1-x}Co_xF_3$, Raman scatt. by mag. excitations 77−55775
$RbMnF_3$, two-spin Raman scatt. at high temp. 77−40225
$RbMnF_3$:Ni, antiferromag., exchange splitting of $^3T_{2g}E$ state, fluorescence meas. 77−12419
Ru complex in PMMA matrix, mag. induced circular polarisation of emission meas. 78−58058
Si (100) surface accumulation layer, subband struct. and inter-subband absorption in strong mag. field 78−39177
Si, amorphous, mag. field depend. of luminesc. 79−43034
Si exciton luminescence in mag. field or under uniaxial stress 78−27322
Si inversion layers, far IR reson. magnetotransmission, temp. and band gap light depend. 78−64363
Si, non-equilib. orientation of electrons in electron-hole droplets in mag. field *(Russian)* 77−36294
Si:Al, bound exciton and bound multiexciton complexes, electronic structure, luminesc. obs. 79−56139
Si:B recombination emission polarisation of bonded multiple-exciton complexes in mag. field *(Russian)* 78−2905
SiC, laser Raman spin-flip scatt. from excitons, luminesc. 80−80786
Sr, diamag. quasi-Landau spectrum near ionis. threshold, two-photon ionis. spectra obs. 78−58642
Sr, vapour, effects of magnetic fields on four-wave mixing processes 79−23024
$SrF_2:Eu^{2+}$, circular polarisation in luminesc. and optical orientation 78−6740
$SrF_2:Tm^{2+}$, EPR, optical recording in weak mag. field 78−68376
$SrF_2:Tm^{2+}$, modulation magnetooptic spectroscopy of cross-relaxation resonances 79−15381
$Tb_3Fe_5O_{12}$, weak field mag. transition, magneto-optical and magnetisation meas. 77−69551
TbIG, [111] magnetoelastic props., rel. to Cotton-Mouton birefringence, 90-500K 80−103876
TbIG, anisotropic linear mag. birefr., light modulation 77−8548
TbIG, mag. birefringence rel. to sublattices 79−28723
TbIG, mag. linear double refr., two-sublattice model *(Russian)* 79−28728
TbIG, refr. index, higher-order anisotropic mag. contrib. 77−69808
$TbPO_4$, linear optical birefr. meas. near bicritical point 80−15719
Te, photo-excited carriers, far IR magneto-spectroscopy 80−50343
TlBr, resonant polaron coupling and excitons under mag. field 80−71383
VI_2, antiferromagnet, phonon Raman scatt. from spin superstructures 80−16030
VI_2, mag. 'Bragg' scatt. obs. through Raman scatt. 80−66179
V_2O_3, Raman scatt. and phase transitions 80−71420
Xe, laser light irrad. in mag. field, light modulation theory 78−82698
Xe, laser light irrad. in mag. field, light modulation expt. 78−82699
$YAlO_3:Pr^{3+}$, ultrahigh resolution photon echo spectroscopy 80−28285
$Y_{3-x}Bi_xFe_{5-y}Ga_yO_{12}$, epitaxial film, domain wall dynamics *(Russian)* 78−2718
$Y_2BiFe_5O_{12}$ garnet films, magnetooptical interference 79−28724
$YFeO_3$, domain walls vel. *(Russian)* 79−28553
$YFeO_3$ plate, anisotropy of domain wall velocity, magneto-optical obs. 79−99725
$Y_{1.4}Gd_{0.6}BiFe_{3.8}Ga_{1.2}O_{12}$ film, bistable bubble domains, static, dynamic and optical props. 79−28574
YIG, and Ga-substituted YIG, mag. birefringence rel. to sublattices 79−28723
YIG, anisotropic linear mag. birefr., light modulation 77−8548
YIG bubble films, light scatt. from spin waves, hysteresis meas. by Voigt effect 80−15770
YIG, diffr. of laser radiation by parametrically excited elastic and magnetoelastic waves 78−19338
YIG, forced magneto-optical rot. 79−61347
YIG, light scatt. by parametric spin waves with longit. pumping *(Russian)* 78−43648
YIG, mag. linear double refr., two-sublattice model *(Russian)* 79−28728
magneto-optical effects continued
YIG, magneto-optical coeffs. induced by elec. and mag. dipole transitons 77−52060
YIG, magnetostatic precession modes, optical investigation 78−19337
YIG, optical detection of scatt. of homogeneous precession of magnetisation by defects 79−69728
YIG, optical spectroscopic exam. of ferromag. reson. *(Russian)* 77−48057
YIG, parametrically excited wave discrete structure obs., light diffr. and modulation *(Russian)* 79−95650
YIG, perpendicular pumping, spin wave instabilities, laser probing 77−43889
YIG, refr. index, isotropic exchange and higher-order anisotropic mag. contribs. 77−69808
YIG, spin and magnetoelastic waves on longit. mag. pumping, optical obs. *(Russian)* 80−29727
YIG, transparent, domain struct. realignment in external mag. field 78−10739
YIG:Gd, Ga, optical probing of magnetoelastic Rayleigh waves 79−78495
YIG:Si, thermomagnetic processing and illum. effects on mag. props. *(Russian)* 77−8410
$(YLaBi)_3(FeGa)_5O_{12}$, pure and In^{3+} doped, near IR absorpt. and Faraday rot. 78−95580
YScIG, expitaxial film, magneto-spatial interaction, conversion coeffs. 77−55774
$Zn_{1-x}Co_xF_2$, Raman scatt. by mag. excitations 77−55775
ZnS:Mn^{2+}, $^4T_1$ state, magneto-optical meas. 77−20833
p-ZnTe 79−43028
ZnTe, luminesc., I_2 bound exciton 77−12432
ZnTe, spin flip scatt. of laser light 77−43976
ZnTe, spin flip scatt. of laser light 77−43977
ZnTe, spin-flip plus phonon scatt., line shape and shift in peak position 79−73907

magnetoabsorption
antiferromagnet, 1-dimens., two-spin IR absorpt., Green's function and classical moments theories 77−40025
antiferromagnet, biaxial low-dimensional, two-magnon absorpt. in collinear phase *(Russian)* 77−69803
antiferromagnet, hexagonal, light interaction *(Russian)* 77−36257
antiferromagnet, radiation problem of parallel pumping, magnon-photon interaction 79−51934
antiferromagnetic, light absorption in freq. region of exciton and exciton-magnon transitions 77−48149
dimethylammonium copper chloride, magneto-optical props., 0.03-13.5 eV 77−52132
disordered-semiconductors, optical magnetoabsorption coeff. calc. in strong mag. field 80−16011
ferromagnetic disordered binary alloy, CPA theory of magnetoabsorption, electron scatt. mechanisms *(Russian)* 77−8549
ferromagnetic semiconductor, absorpt. edge and cond. band width, temp. and mag. field depend. 77−36267
ferromagnetic semiconductors, dielectric function depend. on magnetisation, light absorpt. coeff. *(Russian)* 80−15467
magnetic impurity ion in mag. ordered cryst., optical absorpt., exchange interaction effects 77−16355
magnetic ordered cryst., with degenerate orbital impurities, one- and two-magnon light absorption 77−63444
magnetically ordered crystals with orbital degenerated impurities, single- and two-magnon absorpt. by localised excitations *(Russian)* 77−69858
magnetooptical parameter sums, sum rule analogue 79−89697
metal-insulator-mseiconductor structure, magnetooptic absorpt. with participation of optical phonons 79−99858
metal-insulator-semiconductor struct., magnetooptic interband absorption by semicond. surface layer 80−93288
MIS, magnetooptic absorption by electron gas, optical phonon effects 80−97248
mixed semiconductor with comp. fluctuation, kinetics of intraband absorpt. and magnetoabsorption coeff. 79−19865
molecular systems, photoselection, orient. relax. rel. to emission mag. induced circular polarisation 78−70860
nonlinear absorption of EM waves by band charge carriers in laser field 77−14767
oxide semiconductor crystals, with forbidden energy gap, review of spectroscopic props. 78−2876
polar semiconductor, free carrier magnetoabsorpt. by photon-ionised impurity magnetoplasmon processes 79−38117
ruby, Cr^{3+} ion doped, R-line region, absorpt. spectrum, dispersion rel. to mag. field 80−2732
semiconductor, ferromagnetic, localised states on imperfections and red shift of absorpt. edge 77−66527
semiconductor, impurity absorption in mag. field and resonant laser radiation 77−52145
semiconductor, interband absorpt. in strong parallel mag. and elec. fields 80−6799
semiconductor, multiphoton absorption by charge carriers in mag. field 77−28553
semiconductor, optically anisotropic, effect of modulation of mag. field on absorption 80−34898
semiconductor, optically anisotropic, magnetoabsorpt., light freq. modulation effect 80−66162
semiconductor, optically anisotropic, modulation of direction of mag. field 79−73911
semiconductor, saturated state, interaction with weak EM wave in quantising mag. field 77−16288
semiconductor with nonspherical bands, absorpt. in crossed elec. and mag. fields 77−40264
semiconductor with nonspherical bands, diamag. excitons and Franz-Keldysh effect 78−72554
semiconductors, impurity electro- and magnetoabsorpt. coeffs., deep levels 79−24340
semiconductors, impurity-induced free-carrier magnetoabsorption 79−42950
semiconductors, mixed with composition fluctuations and imperfect, interband magnetoabsorption 78−15152
semiconductors, nondegenerate, free carrier absorpt. in quantising mag. fields 80−45044
semiconductors, two-photon absorption in crossed elec. and mag. fields 77−85693

magnetoabsorption continued
semiconductors, weakly polar, intraband magnetoabsorption theory 79−42949
semiconductors with degenerate valence band, diamg. excitons, and oscillatory magnetoabsorpt. of GaSb 77−76754
semiconductors with narrow band gap, multiphoton magneto-absorption and electro-absorpt. *(Russian)* 79−19867
two-phonon transitions, phonon assisted, in mag. field, four-band model 77−36260
Voigt effect, reson. absorpt. description 80−30302
zinc chlorophyll b, triplet state population at 4.2K, magnetic field effects 77−30915
AgBr, optical absorpt. of indirect exciton in high mag. field 78−60486
AgCl, optical absorpt. of indirect exciton in high mag. field 78−60486
Bi hole pocket, far-IR magnetospectroscopy, electron-electron interaction effects 77−77211
Bi, microwave magneto-absorption, NENP Cohen model 77−39766
$Bi_{1-x}Sb_x$, far IR magnetoabsorption, band struct. study 80−50351
CaF_2:Dy crystal with M centre, antiresonance line, mag. field effect 80−55138
$CaF_2:Sm^{2+}$, optical absorption and magneto-optic. props. 77−59595
$CdCl_2:Fe^{2+}$, magneto optical study, ferromagnetically coupled Fe(II) pairs 78−6711
CdMnTe crystals, exciton binding energy, magnetoabsorption and magnetoreflectivity 79−38523
$Cd_{1-x}Mn_xTe$ mixed crystals, excitonic magnetoabsorption 80−40095
CdS, creation of 2P excitons by two photon magneto-absorption 78−2432
CdS, fast modulator for CO_2 laser, using two-photon magnetoabsorpt. 77−88805
CdS, fast optically controlled modulator using two-photon magnetoabsorpt., for CO_2 laser 78−13736
CdTe, oscillatory magnetoabsorpt. spectra 80−40096
$CoCO_3$, two-sublattice noncollinear antiferromag., exciton-magnon light absorpt. mechanisms *(Russian)* 80−89017
$CoCO_3$, weakly ferromag., light absorpt. dichroism and mag. config. 80−66223
$CsFeCl_3$, linear chain ferromag., optical absorpt. and dichroism in mag. field 77−77237
$CsMnF_3$, hexagonal antiferromagnet, light interaction *(Russian)* 77−36257
$CsMnF_3$, light absorpt. spectrum in mag. fields up to 300 kOe *(Russian)* 77−52115
CuCl, excitons bound to neutral donor impurities, magneto absorption spectra 79−56816
Cu(II)-DL-proline complex, ESR, magnetic susceptibility and optical absorption 80−93167
Cu_2O, optical absorpt. due to paraexciton in strong mag. field 77−28596
Cu_2O, relationship between interband transitions and spectrum of diagmagnetic excitons in moderate mag. fields 79−91412
$DyCrO_3$, Cr^{3+} exciton-Dy^{3+} spinflip absorpt. 77−73153
DyIG, magneto-optical absorption, near IR 80−40094
$ErCrO_3$, dynamic spin reorientation process, magneto-optical meas. 77−69590
$Eu_2Mg_3(NO_3)_{12}.24H_2O$, Zeeman effect in ahsorpt. spectrum 77−63402
EuO, Eu-rich, IR absorpt. spectra, 4.2 to 300K, transitions assoc. with O vacancies 77−52142
EuTe, optical absorpt. in high mag. field 79−28726
Fe_3BO_6, polarised absorpt. spectra in range of $^6A_1 \rightarrow {}^4T_1$, $^4T_2$ transitions 77−52092
$FeBr_2$:$MnBr_2$, magnon modes and impurity spin reson. 79−15501
FeI_2, far IR magnetoabsorption, excitation of two spin deviations 78−80339
FePd epitaxial film, vacuum-deposited, for thermomag. recording, mag. and magneto-optical props. *(Russian)* 78−60319
FePt epitaxial film, vacuum-deposited, for thermomag. recording, mag. and magneto-optical props. *(Russian)* 78−60319
GaAs, heavily-doped, band gap, magnetoabsorpt. oscills. obs. 78−18960
GaAs, photoabsorption and magnetoabsorption effects 77−16332
GaSb, degenerate valence band, diamag. excitons and oscillatory magnetoabsorpt. 77−76754
GaSb, oscillatory magnetoabsorption and excitons 77−55777
$Gd_2(MoO_4)_3$, low temp. optical absorpt., external mag. field influence 78−43896
Ge, electron-hole droplets, conc. in mag. field, magnetoplasma absorpt. spectra meas. *(Russian)* 77−24854
Ge, electron-hole drops, far IR magneto-optical effects 78−84565
Ge exciton and electron-hole drop decay, far IR magnetoabsorption obs. 77−40252
Ge, far IR magneto-absorption of donor-bound excitons, pseudo-acceptor model 77−63418
Ge, far IR magnetoabsorption, excitons, electron-hole drops and impurities 78−6664
Ge, far IR magnetoabsorption of free and bound excitons 78−52474
Ge, internal Stark effect on impurity states, low-temp. magnet. absorption meas. 80−60636
Ge, optical absorption from indirect transitions at high mag. fields 79−47441
Ge:In, magneto-optical transitions between discrete levels of In acceptor, far-IR obs., 4.2K 78−2890
$Hg_{0.985}Cd_{0.015}Se$, interband $\Gamma_6 \rightarrow \Gamma_8$ magnetoabsorption and band parameters 79−82960
HgCdTe, interband magnetoabsorption and band struct. 79−82959
$Hg_{1-x}Cd_xTe$ mixed crysts., magneto-opt. obs., semicond. config., semimetal-semicond. transition 77−73131
$Hg_{1-x}Cd_xTe$, n-surface inversion layers study 80−25017
$Hg_{1-x}Fe_xTe$ mixed crystals, zero gap, magneto-optical evidence of exchange interactions 80−45045
HgMnTe, interband magnetoabsorption and band struct. 79−82959
$Hg_{1-k}Mn_kTe$, impurity magnetoabsorpt. 79−91473
$Hg_{1-x}Mn_xTe$, exchange interaction effect on $\Gamma_8 \rightarrow \Gamma_8$ magnetoabsorption 79−61351
$Hg_{1-x}Mn_xTe$ mixed crystals, zero gap, effect of exchange on interband magneto-absorption 78−23443
HgSe, interband $\Gamma_6 \rightarrow \Gamma_8$ magnetoabsorption and band parameters 79−82960
HgSe, interband $\Gamma_6 \rightarrow \Gamma_8$ magnetoabsorption, temp. study 80−76032
n-HgTe, far IR magnetoabsorption involving resonant acceptor states 79−69813
HgTe, long-wavelength magneto-absorptions 80−11397
HgTe, photocond. and magnetoabsorption, 1.4-20K 78−34859
magnetoabsorption continued
HgTe, uniaxial stress effect on magneto-optical props. 77−59558
HgTe, zero-gap semicond., absorpt. spectrum in mag. field 80−11370
InAs, fine struct. of diamag. excitons, oscillatory magnetoabsorpt. obs. 78−18971
InP, excitons bound to neutral donors in VPE layers, luminesc. and absorpt. obs. 79−42460
InP, oscillatory interband magnetoabsorption meas. 79−73909
n-InSb, Landau-level-electron lifetimes, saturation meas. of magnetoabsorption 78−48150
n-InSb, magneto-photoconductivity, phonon assisted combined reson. magneto-optical absorpt. reson. 78−47831
InSb, magnetoacoustic wave excitation by acoustic wave propagation 80−88597
p-InSb, shift of fundamental absorpt. edge in crossed elec. and mag. fields 80−76034
InSe, high field magnetoabsorpt. of hydrogenic excitons at second direct gap 80−6729
KBr(F), orbital g-factor and spin-orbit splitting of F-centre excited state, magnetoabsorpt. and MCD 78−2886
KCl(Br), triplet state lifetime of F_2 centre, mag. field effect 78−35177
K_2CuF_4, two-dimens. ferromag., magneto-optical props., absorpt., MCD and MLD 79−87419
$KFeCl_3$, linear chain ferromag., optical absorpt. and dichroism in mag. field 77−77237
$KMgF_3:Fe^{2+}$, Jahn-Teller quenched spin-orbit, splitting of $^5T_{2g}$ state 77−63442
$LaF_3:Dy^{3+}$, magnetospectroscopy with optically pumped far IR laser 79−33737
MgO:Ni, optical absorpt. spectrum in mag. field, and 2p-3d charge transfer 77−52141
$MnCl_2.2H_2O$, magnetically ordered phase, $^6A_{1g}$ to $^4T_{2g}$ transition absorpt. lines, Zeeman effects 78−6699
$MnCl_2.2H_2O$, ordered, paramag. phases, optical absorpt. spectra, V-lines, Zeeman effects 78−6698
$MnCl_2.2H_2O$, paramag. phase, external mag. field depend. of $^4T_{2g}$(II) Kramer doublets of Mn^{2+} 78−6700
MnF_2, spin-flop bicritical point, susceptibility and RF absorpt. meas. 79−87277
MnO, absorption line shape, magnon sidebands 77−52128
MoS_2, 2H phase, far IR magnetoabsorption and refr. index meas. 77−24847
NaCl(Br), orbital g-factor and spin-orbit splitting of F-centre excited state, magnetoabsorpt. and MCD 78−2886
$NiBr_2$, ^{1}Eg spin-forbidden transition, temp. depend. and magnetoabsorpt. 78−48151
PbI_2, exciton states, high field magnetoabsorption 77−52130
PbTe, two photon magnetoabsorption *(Russian)* 80−60553
$RbFeCl_3$, linear chain ferromag., optical absorpt. and dichroism in mag. field 77−77237
Rb_3MnCl_4, quasi-2D-antiferromag., linear birefr. and optical absorpt. spectra 80−71385
Si inversion layer, IR spectrum, 10^5G effect on linewidth 78−946
Si inversion layer, inter-subband optical absorpt. in mag. field 77−32375
Si inversion layers, low density, far IR resonant magnetoabsorption 77−55789
Si, inversion layers, submillimeter cyclotron reson. at low electron density 79−60925
Te conduction band parameters, interband magnetoabsorption meas. in Faraday configuration 77−89695
TlI with CsCl struct., exciton magnetoabsorption 77−28593
$TmAsO_4$, optical side bands, absorpt. spectra in mag. fields 77−52123
$YCrO_3$, antiferromag., exciton absorption lines obs. during field induced spin-reorientation 77−63397
ZnS, two-photon absorption in crossed elec. and mag. fields 77−85693

magnetoacoustic effects
see also magnetoacoustic resonance
amorphous ferromagnetic ribbon, HF mag. characts., magnetostriction role 77−66408
antiferromagnet, easy-plane, acoustic wave damping, effective phonon-phonon interactions 79−73797
antiferromagnet, first order orientational transition, sound propag. anomalies 77−1580
antiferromagnet, first-order orientational phase transition, second acoustic-harmonic generation 78−27067
antiferromagnet, low temp., absorption of sound 79−69711
antiferromagnet, parametric excitation of sound near phase transition point 79−69710
antiferromagnet, rel. to theory of relax. 77−24750
antiferromagnet, relax. processes, spin-sound wave coupling 78−60340
antiferromagnet, sound damping by phonon-magnon interaction, high Neel temp. *(Russian)* 78−43626
antiferromagnet, sound generation by EM wave near orientational phase transform. of first kind *(Russian)* 78−39329
antiferromagnet, with easy plane anisotropy, nonlinear self-interaction of acoustic waves *(Russian)* 78−80187
antiferromagnetic semiconductor, sound propagation 78−72211
Barkhausen noise, appl. to residual stresses evaluation in welding 80−76436
cholesteric liquid crystal, mag. aligned, anisotropic US propag. 78−42895
conservation laws for media with freq. dispersion 78−5597
cubic ferromagnet, second magnetoacoustic harmonic generation *(Russian)* 79−42816
cubic magnetoelastic crystal, acoustic SHG, static magnetisation effects *(Russian)* 78−56362
defects in magnetized samples, magnetostrictive conversion of US waves into EM fields 80−66008
domain wall velocity, acoustic wave effect 77−12171
elastic properties of magnetic materials, review 80−7142
electron ferromagnet, longit. US attenuation due to spin fluctuations 79−56588
exciton ferromagnet, spin-lattice relax., light and US absorption *(Russian)* 79−7960
Fermi surface, local flattening effect of acoustic wave absorpt. and dispersion *(Russian)* 79−51471
ferrimagnet, parametric excitation of sound near phase transition point 79−69710
ferrites, effects of magnetoelastic interactions on sound propag. 77−27413

magnetoacoustic effects continued
ferrodielectric, sound absorption due to interaction with magnons *(Russian)* 77−69663
ferrodielectric, sound wave damping, due to phonon-magnon interactions 77−36107
ferrofluid, US attenuation anomaly in mag. field 78−68345
ferrofluid, US response time, mag. field depend. 79−1702
ferrofluid, US vel. anisotropy in mag. field 78−68344
ferromagnet, acoustic wave scatt. and reemission by moving domain walls 77−24713
ferromagnet, continuous EM-acoustic conversion, normal skin effect case, expt. *(Russian)* 77−59304
ferromagnet, domain walls, hypersound effect *(Russian)* 79−51810
ferromagnet, magnetostriction is magnetic field, sound-spin wave coupling 79−15334
ferromagnet, multidomain, with 180° Bloch walls, sound generation by RF field *(Russian)* 77−32235
ferromagnet, parametric excitation of sound near phase transition point 79−69710
ferromagnet, planar, US attenuation, spin-phonon coupling, magnons and magnetostriction contrib., calc. 80−34611
ferromagnet, polydomain magnetic struct., excitation of sound 78−88162
ferromagnet, pure and random uniaxial with dipolar interaction, US attenuation 80−11239
ferromagnet, with periodic domain struct., magnetoacoustic singularities of sound propag. *(Russian)* 77−24727
ferromagnet magnetisation, influence of high intensity longitudinal sound waves 80−103875
ferromagnetic, thick film, reson. transmission of EM energy via phonons 80−60382
ferromagnetic and nonferromagnetic conductor, scattering by associated helical-sonic and spin-helical-sonic waves *(Russian)* 79−24136
ferromagnetic conductor magnetoelastic surface wave attenuation 77−20667
ferromagnetic liquid, US vibr., reson. excitation by mag. field *(Russian)* 78−48020
ferromagnetic metal, itinerant electron model, for US propagation and structural instabilities 78−95508
ferromagnetic metals, itinerant electron, theory of crit. US propag. 77−69655
ferromagnetic metals, ultrasound attenuation, EM generation 80−108046
ferromagnetic single cryst., US attenuation anomalies *(German)* 77−8381
ferromagnets, uniaxial, US attenuation and kinetic coeffs. near crit. point, renormalisation group theory 79−4715
garnet epitaxial film, elastic surface wave propag., magnetoelastic effect 77−20669
graphite, giant quantum attenuation of sound waves 80−54741
heating of semiinfinite body under periodic loading *(Russian)* 77−50855
Ising type model, elastically coupled, effects of dipolar forces on crit. sound attenuation in uniaxial systems 80−50158
itinerant electron ferromagnets, elastic props. and electronic struct. 80−66001
itinerant ferromagnet with helical spin struct., US attenuation 79−78497
itinerant magnets, anomalous sound attenuation near mag. transition temp. 78−15004
itinerant-electron ferromagnet, US propag. and struct. instabilities, screening effects 77−69653
liquid-solid interface, plane sound wave reflection and refraction in mag. field 80−38150
magnetic crystal, sound velocity temp. depend. anomaly 77−72891
magnetic fluids, US attenuation, MHD approach 80−60389
magnetoelastic SAW velocity on magnetised ferrite substrate, nonreciprocity 80−80587
magnetostrictive SAW generation efficiency meas. of residual stress 77−28972
many-domain magnetics, phenomenological theory of EM and sound energy attenuation 80−7140
metal, acoustic breakdown, electron energy spectrum *(Russian)* 78−18948
metal, acoustic wave drag, acousto-elec.-mag. effects *(Russian)* 79−19638
metal, cyclotron reson. and geometric oscills. of sound velocity 77−20230
metal, electron-phonon interaction, magnetism influence 77−73040
metal, EM sound generation in cyclotron reson. regime *(Russian)* 77−69381
metal, in mag. field phonon spectrum, nonadiabatic effects *(Russian)* 78−19106
metal, Pippard sound-attenuation oscillating angular depend. *(Russian)* 80−103613
metal, Raman scatt. of sound in quantising mag. field 78−60171
metal, SAW absorption with and without external mag. field *(Russian)* 77−31936
metal, theory of electronic transport of sound packets in parallel mag. field *(Russian)* 78−84261
metal film, ion sound velocity in mag. field *(Russian)* 78−18982
metal with paramagnetic centres, sound absorption temp. and freq. depend. *(Russian)* 78−34827
metal with several carrier groups, acoustic attenuation in strong mag. field *(Russian)* 77−47868
metallic film, conduction electron surface scatt. process, magnetoacoustic oscillations *(Russian)* 80−15575
metallic films, ultrasound attenuation, size magnetoacoustic effect *(Russian)* 80−107869
metals, anomalous sound propag. by cond. electrons 80−11048
metals, ferromag., max. in acoustic attenuation at low mag. fields 80−93158
metals and semimetals, two-phonon sound absorption in quantising mag. field 79−28382
multidimensional wave radiation from source with Gaussian time variation and Gaussian approx. distrib. about spherical sheet 78−45487
one-dimensional magnetic systems, sound attenuation at finite temp. 77−63247
orthoferrites near spin-flip temp., magnetoelastic waves 78−19301
oscillation excitation in strongly inhomogeneous plasma 80−38641
PAA, nematic liq. cryst., effect of magnetic field on US vel. and absorpt. 78−18707
paramagnetic crystal, mixed spin-phonon waves *(French)* 77−66400
Permalloy film, domain nucleation using low intensity US 80−34731
magnetoacoustic effects continued
piezoelectric nondegenerate semicond., magnetoacoustic effects of nonparabolic band struct. 80−96948
piezoelectric semiconductor, inhomogeneous, amplification of acoustic wave 79−69561
piezoelectric semiconductor-plasma, parametric excitation of helicon and acoustic waves 80−107837
piezomagnetic rod, demagnetizing field effect, longitudinal-effect extensional vibration 78−95504
plasma, cold, bounded and cylindrical, viscous damping of magnetoacoustic oscillations 80−24151
plasma, weakly inhomogeneous, nonlinear magnetoacoustic waves 80−48867
powder, torsional vibr. and stimulated echo with long memory, two and three pulse echo *(Russian)* 77−63258
rare earth metal, anomalous sound attenuation near mag. transition temp. 78−15004
rare earth metals, electronic sound attenuation anomalies at transition to helical phase, Fermi surface topology *(Russian)* 80−92807
rare earth-Fe alloys, highly magnetostrictive, isotropy breaking magnetoelastic behaviour 78−72386
rare earth-Fe alloys, magnetostrictive, elastic props. 78−84469
rare-earth metals, US attenuation, exchange striction, and spin-phonon interaction 79−33518
rare-earth metals, US attenuation in applied fields 77−51933
rod position monitoring transducer system for nuclear power plant, magneto-sonic type 78−33262
semiconductor, planar acoustomagnetoelec. effect, theory 80−60052
semiconductor, sound absorption at very low temps. 79−95089
semiconductor, zincblende struct., phonon attenuation in presence of internal strains and mag. field 78−76118
semiconductor subjected to mag. and US fields, EM radiation gain 80−48201
semiconductors, diamond-type, doped, US attenuation and electron-phonon scatt. in mag. field 79−46771
semiconductors, ferromagnetic, parametric amplification of coupled spin, helical and acoustic waves *(Russian)* 80−2621
semiconductors, heat pulse absorpt. in nonquantising mag. fields 80−60054
semiconductors, intervalley acoustoimpurity resonance 80−107868
semimetal, phonon spectrum, influence of mag. field induced quasi-local levels 78−18946
semimetal, Raman scatt. of sound in quantising mag. field 78−60171
semimetals, giant quantum attenuation of sound, fluctuation effect of gas-liq. type transition 78−39168
semimetals, US attenuation in strong mag. field, theory 77−11844
solar atmosphere magnetoacoustic gravity waves 77−29752
solar chromosphere, magnetoacoustic wave propag., resonance phenomena 77−13306
solid, dipole-dipole ordering in nuclear spin system by acoustic pulse 79−11333
sound attenuation in magnetic field at the $2^1/_2$-order phase transition *(Russian)* 80−100487
sound transmission by electrons in conditions of resonant interaction *(Russian)* 79−7774
steel, austenitic stainless, Mn alloy, sound vel. anomalies near spin glass transition 79−82795
steel, Cr, EM excitation and recording of US 80−34748
stellar atmospheres, transverse mag. field effects on linear waves in radiating scatt. medium 77−56911
superconductor, intermediate state, magnetoacoustic size effect *(Russian)* 80−7047
surface wave excitation by meander lines 78−19298
thermal fluctuations during amplification of magnetoacoustic surface waves 78−88158
turbulence, nonlinear interaction of magneto-sound waves 78−45134
underwater explosions and implosion, generation of sonomagnetic pulses 80−43510
US excitation and detection in mag. polarised nonferromag. metals, elastic displacements 78−53091
US excitation and detection in mag. polarised nonferromagnetic metals., dispersion relations 78−56856
US spectrum, RF field in multidomain struct. 78−68056
US waves in magnetically polarised media, determ. of polarisation plane rotation and ellipticity *(Russian)* 79−1699
Wigner crystal, long-wavelength excitations in strong mag. fields 79−82533
Al, acoustomag. effect, temp. depend. *(Russian)* 77−72941
Al, EM generation of ultrasound, obs. of anomalies 78−84131
Al, US quantum oscillation exam of third-zone Fermi surface 78−47695
Be, magnetoacoustic quantum oscills. due to mag. breakdown orbits, and derivative of magnetisation meas. 77−43479
Bi, acoustic waves, giant quantum attenuation at high mag. fields, angular depend. *(Japanese)* 79−4585
Bi, attenuation coefficient of sound, effect of impurity on gas-liq. type phase transition 78−39167
Bi, electron band models, simultaneous meas. of giant quantum oscills. and diamag. reson. 78−14653
Bi, gas-liquid type transform. and sound attenuation in strong mag. fields, electron-hole correl. effects 80−88598
Bi, giant quantum attenuation of sound, anomalous temp. depend. 77−76728
Bi, giant quantum attenuation of sound due to electronic phase transitions 79−60718
Bi, giant quantum attenuation anomalies of sound waves at high mag. field, temp. and freq. depend. 80−70587
Bi, giant quantum attenuation anomalies of sound waves at high mag. field, extra attenuation peaks 80−70588
Bi, Landau level spin splitting factor, US exam. 77−20281
Bi, longitudinal magnetoacoustic effects on energy bands 77−28095
Bi, magnetoacoustic attenuation peak at low temp. 79−91105
Bi, magnetoacoustic attenuation, tilt effect 79−91106
Bi, magnetoacoustic attenuation, line shape anal. 80−2429
Bi, nonequilibrium phonons, negative differential cond., life time oscills. *(Russian)* 78−76117
Bi, spin splitting factors of electrons for heavy mass directions 77−31935
Bi, US attenuation in strong mag. fields, electron-hole correlation effects 80−11049
Bi, US velocity, renormalisation in mag. field 77−59246
Bi-Sb alloys, magnetoacoustic attenuation, tilt effect 79−91106

magnetoacoustic effects continued
BiMn, with ferromag. inclusions, magnetisation changes by US pulses 80−34732
$Bi_{1-x}Sb_x$, magnetoacoustic attenuation 80−2428
$Bi_{1-x}Sb_x$, magnetoacoustic attenuation, line shape anal. 80−2429
$CeAl_2$, magnetoelasticity, rot. invariance and magnetoacoustic birefringence 79−87304
$CeAl_2$ sound vel. in high mag. fields 79−78500
CeB_6, magnetostriction, US absorpt. and thermal expansion 80−66004
Co, US damping temp. and mag. field depend. *(Russian)* 78−23313
Co-Pt ferromagnetic alloy, 6 T ultrasonic study of magnetoelastic coupling 80−93154
Cr, antiferromagnetic, polarisation domain effects on US velocity 78−52329
Cr, antiferromagnetic, US attenuation and phase diagram 80−103831
Cr, mag. phase diagram, near, spin-flip temp., US attenuation 80−60267
Cr, US velocity and damping in Neel temp. range, thermocyclic treatment effect *(Russian)* 79−91282
Cr_2O_3, elastic consts., distance depend. of mag. interactions, US vel. meas. 77−4539
Cr_2O_3, US wave vel. near mag. transition 78−84263
$CsNiCl_3$, one-dimens. antiferromag., US attenuation, crit. behaviour 77−66308
$CsNiCl_3$, one-dimens. antiferromag., US attenuation 78−88156
$CsNiF_3$, planar ferromagnet, US attenuation, spin-phonon coupling, magnons and magnetostriction contrib., calc. 80−34611
Cu, carrier scattering rate, temp. dependence, magnetoacoustic experiments 80−44671
Cu, US attenuation by open-orbit electrons, role of deformation potential 79−73428
Cu, ultrasonic velocity meas., mag. field depend. 78−19104
Cu-Mn alloy, spin-glass, US exam. 78−68351
CuCoNi ferrite magnetoacoustic oscills. rel. to microstruct. 77−85536
Dy, antiferromagnetic, thermal expansion, US attenuation anomalies 79−47319
Dy, magnetic phases, US study 78−31101
Dy, US attenuation in mag. field 77−40104
Dy, US attenuation maxima in mag. field 77−16140
$DyFe_2$, amorphous, mag. struct., US meas. 79−99683
Er, US attenuation, longitudinal, in mag. ordered region and at phase transitions 77−28422
Er, US attenuation in mag. field, temp. and field depend. 79−91279
$ErFeO_3$, sound velocity meas. at high press., spin-reorientation transition 78−76254
Fe-Ni-C, Invar, coated, Mossbauer spectra, effect of applied RF mag. field 80−80645
Fe-rare earth alloys, amorphous, magnetoelasticity and moment rot., US vel. calc. and neutron scatt. meas. 80−65992
$FeCl_2$, metamagnetic, sound propag. near tricritical point 78−48024
$(Fe_{1-x}Mn_x)Si$, US vel. rel. to mag. struct. and phase transforms *(Russian)* 77−47976
$(Fe_{1-x}Mn_x)_3Si$, mag. phase diagram determ. 77−24697
Fe_2O_3, haematite, SHG, acoustic detect. of modulated sound wave *(Russian)* 78−43623
Ga, anomalous US penetration at low temp., effect of trajectorial electron transfer *(Russian)* 77−43670
Ga, electronic struct. under pressure, Fermi surface meas. using magnetoacoustic technique *(Russian)* 77−47716
GaYIG, magnetoelastic surface wave attenuation 77−20667
Gd-Y (40 wt.%) alloy, magnetic phase transitions, elastic consts. meas. 78−14957
$GdVO_4$, antiferromag., US attenuation at 9 GHz 77−24728
Ge, electron-hole drop drag, interaction with thermal pulses 80−103631
Ge magnetoacoustic effects in the drag of electron-hole drops by phonons 78−68057
Ge, phonon drag of electron-hole drops in longit. quantizing mag. field *(Russian)* 78−64070
In, helicon resonance acoustic satellites, flexural acoustic wave spectrum *(Russian)* 80−2415
In, US absorption and dispersion, lineshape studies of quantum oscills., anomalous behaviour 78−63966
In, US velocity dispersion in external mag. field 80−20446
In, US wave polarisation plane and ellipticity rot. in mag. field, doppleron interactions *(Russian)* 79−15335
n-InSb, degenerate, acoustomagnetoelec. effect obs. 78−72207
n-InSb, magnetoacoustic effects using two-band model 78−60170
InSb, magnetoacoustic wave excitation by acoustic wave propagation 80−88597
n-InSb, non-degenerate, linear longitudinal elec. cond., US wave effects in DC mag. field 80−88599
n-InSb, non-degenerate semicond., magnetoacoustic effect 80−20257
n-InSb, Wigner cryst., long-wavelength excitations in strong mag. fields 79−82533
$KMgF_3:Ni^{2+}$, acoustic Faraday and Cotton-Mouton effects, theory 80−65987
$KNiF_3$, isotropic antiferromag., phase diagrams, US meas. 78−68350
K_2NiF_4, 2D antiferromag., volume depend. of superexchange, US velocity meas. of T_N 78−19237
MnO, multidomain single cryst. and monodomain cryst., crit. and elastic behaviour, T_N to 300K 77−66407
MnP, US vel. and crit. attenuation, longit. waves, external mag. field 78−27035
MnSi, crit. transverse US attenuation, spin fluctuations 78−48022
MnSi, mag. phase diagram, crit. US attenuation 77−12122
MnSi, mag. phase diagram, US attenuation meas. 77−63188
MnSi, US velocity anomalies near mag. transition 78−19302
$Mn_{0.53}Zn_{0.35}Fe_{2.12}O_4$, and Ti substituted, acoustic losses 79−24207
Mo, Fermi surface ang. shear deform., US vel. quantum oscill. meas. 79−77985
Mo, Fermi surface press. depend., surface impedance and US attenuation oscills. in mag. field 77−43476
Mo hole ellipsoid scatt. rate temp. dependence, magnetoacoustic obs. 79−51472
Mo magnetoacoustic effect shear wave selectivity 79−47131
Mo, scatt. rate temp. depend. from magnetoacoustic expts. 79−65522
Mo, to 500 MHz, crystal lattice distortion 78−91604
Nb hole ellipsoid scatt. rate temp. dependence, magnetoacoustic obs. 79−51472
Nb, scatt. rate temp. depend. from magnetoacoustic expts. 79−65522
Nb-Hf(26 at.%), mixed state, magnetoacoustic attenuation 77−4473

magnetoacoustic effects continued
Nb_3Sn, acoustic soft modes in high mag. fields, soft sound vel. meas. 77−43482
Ni crystals in strong mag. field, EM excitation and vel. dispersion of sound *(Russian)* 80−39837
Ni film, 618 MHz SAW attenuation rel. to mag. field 77−40110
Ni film, mag. field depend. surface acoustic wave attenuation meas. 77−20674
Ni film, oriented, hypersound excitation at 8.9 GHz by exploiting mag. anisotropy 77−85541
Ni, single cryst., magnetisation and US attenuation, mag. field depend. *(Russian)* 78−6559
Ni, US attenuation, mag. field and temp. depend. 77−90008
Ni, US induced mag. reversals, stroboscopic electron microscope obs. 77−48026
Ni-Fe films, US generation by ferromag. reson. 78−88155
Ni-$LiNbO_3$, layered structure, mag. control of surface elastic waves 77−20666
NiFe, US induced mag. reversals, stroboscopic electron microscope obs. 77−48026
NiZn ferrite, magnetic field effect on Rayleigh wave attenuation 78−6557
$RbMnF_3$, isotropic antiferromag., phase diagrams, US meas. 78−68350
$RbMnF_3$, isotropic antiferromag., crossover behaviour of mag. phase boundary, US meas. 78−80145
Sb, quantum oscillations of vel. of sound meas. in mag. field 78−39004
Sn, acoustomag. effect, temp. depend. *(Russian)* 77−72941
Sn, sound absorption giant resonance, produced by coherent mag. breakthrough *(Russian)* 80−6700
Sn, sound attenuation and velocity depend. on mag. field *(Russian)* 80−29446
Sn, white, US quantum oscillations exam. at 0.1K 78−47694
Tb, elastic modulus in mag. field, US meas. using CdS transducer 77−11151
Tb-Ho (50%), antiferromagnetic, thermal expansion, US attenuation anomalies 79−47319
$Tb_{0.3}Dy_{0.7}Fe_2$, sound velocity mag. field and temp. depend. elastic moduli calcs. 80−39839
$Tb_{0.3}Dy_{0.7}Fe_2$, US velocity and attenuation obs. 77−28423
$TbFe_2$, amorphous, mag. struct., US meas. 79−99683
Te, acoustoelectric instability of current, mag. field influence 79−73547
Te, magnetoacoustic effect 77−62963
$(Ti_{1-x}V_x)_2O_3$, US velocities in high mag. field 78−84262
$TmFeO_3$, acoustic vel. and attenuation shifts at spin reorientation phase transition 80−65986
TmSb, cryst. field effects on elasticity, rot. and higher order interactions 77−63251
UN, sound velocity temp. depend. anomaly 77−72891
UN, sound velocity temp. depend. anomaly in elastic consts. determ. 77−72892
V, US waves interaction with cond. electrons, double-pulse comparison spectrometer appl. 78−1526
V, ultrasonic velocity meas., mag. field depend. 78−19104
V_2O_3, high temp. mag. phase transition studied by US vel. meas. *(Russian)* 79−33520
V_3Si, appl. of new three-dimens. k.p model for A-15 cpds. 78−23015
V_3Si, soft mode sound vel. in mag. field rel. to density of states 78−14647
V_3Si, US anomaly when cooled below martensitic and supercond. transition temps. 80−20354
W, Fermi surface press. depend., surface impedance and US attenuation oscills. in mag. field 77−43476
W hole ellipsoid scatt. rate temp. dependence, magnetoacoustic obs. 79−51472
W magnetoacoustic effect shear wave selectivity 79−47131
W, scatt. rate temp. depend. from magnetoacoustic expts. 79−65522
W, to 500 MHz, crystal lattice distortion 78−91604
$Y_3Fe_{5-x}Ga_xO_{12}$, inhomogeneous stress effect on ferromagnetic resonance, elastic consts. from sound vel. meas. 79−24219
$YFeO_3$, transit time meas. of domain-wall mobilities, magnetostatic and magnetoacoustic effects 79−42794
YIG, dilute, magnetoacoustic surface wave excitation by RF field on Bloch walls 80−25178
YIG substrate magnetoacoustic modes, meander-line excitation 77−20670
YIG substrates, magnetoelastic surface waves, magnetostatic reson. anal. 80−20441
YIG, thermal attenuation of US waves, 500-1000 MHz 77−84854

magnetoacoustic resonance
see also ferroacoustic resonance
antiferromagnets, magnetoacoustic resonance of domain boundaries *(Russian)* 80−65636
canted magnetic struct. crysts., magnetoacoustic resonance, elastic vibrations 80−29599
collective-acoustic resonance in system for parametric spin waves 79−69727
electron gas, resonance absorption in quantising mag. field 78−10522
ferrite, magnetoacoustic reson. in strong mag. field 80−11309
ion-ion hybrid damping in D_2-H_2 plasma 79−77361
magnetic bubble domain lattice 78−88161
metals, ultrasonic wave propagation by open-orbit electrons at reson. condition 78−51877
metals and alloys, EM acoustic reson. for elastic moduli meas. 80−15573
Ag, magnetoacoustic spin-orbit antireson. 78−26808
n-$Cd_{0.245}Hg_{0.755}Te$, magnetophonon reson. and quantum oscillations 77−39902
Ge, acceptor ground-state, US attenuation meas. *(Japanese)* 78−19105
Ge:Ga, magnetoacoustic resonance attenuation, Zeeman splitting of acceptor ground state 77−47869
He plasma, strongly inhomogeneous, magnetoacoustic reson. 80−69994
n-InSb, magnetophonon effect exam. using field modulation technique 78−26918
n-InSb, transverse magnetophonon reson., oscillatory amplitude and damping 78−47813
Mo, Doppler shifted cyclotron reson., doppleron-phonon reson. *(Russian)* 77−32262
YIG spheres, anomalously low saturation threshold of magnetostatic modes 79−69729

magnetoacoustics *see magnetoacoustic effects*

magnetocaloric effects
see also magnetic cooling; thermomagnetic recording; thermomagnetic treatment
antiferrimagnet, two-sublattice, spin waves, magnetocaloric effect 78−31073
antiferromagnets, reln. between temp. depend. of mag. susceptibility and sp. ht. *(German)* 77−69567
B-phase at equilib., formalism 80−88384
cylindrical magnetic domains, possibility of thermomagnetic generation *(Russian)* 78−6539
$Eu_{1-x}Gd_xO$, mag. semicond., specific heat 79−69688
ferrimagnet, mag. field direction effect 79−78379
ferrite pyromagnetic detector for IR Nd laser pulses 77−82606
ferromagnets, uniaxial, negative magnetocaloric effect 79−82783
guanidinium vanadium sulphate hexahydrate, mag. behaviour in applied fields below 1K 77−66376
Invar, ferromagnetism and antiferromagnetism coexistance at low temp. 77−66320
mischmetal-Co system, thermomagnetic analysis of intermediate phases 80−93115
neodymium ethyl sulphate, magnetothermodynamics, absolute temp. scale, mag. moment and magnetization , below 0.5K 78−34984
pyromagnetic detector for wideband laser radiation *(Russian)* 79−93220
$Al_2O_3:V^{3+}$, magnetocaloric effect in high magnetic fields 80−25140
$BaCo_{1.65}Fe_{16.35}O_{27}$, spin reorientation obs. using magneticaloric effect *(Russian)* 77−32195
Be, single crystal, magnetothermal switch for electrocaloric refrigeration, 4 to 15K 79−80624
Br-graphite, intercalation cpd., magnetothermal oscill. and charge-density waves 80−11199
C, amorphous, anomalous low temp. mag. and thermal props. 78−10647
$CaWO_4:Er^{3+}$, magnetocaloric behaviour, cryst. field theory 77−4520
CrB_2, CrB, and Cr_5B_3, mag. and thermal props. at low temps. 80−20385
$CuSeO_4.5H_2O$, $CuSO_4.5H_2O$ and $CuBeF_4.5H_2O$, linear-chain antiferromag., mag. phase transition investig. 77−55684
Dy, mag. characts. in strong mag. field 77−89936
Dy, magnetocaloric effect and mag. phase transitions, 80 to 300K 80−60279
Dy, magnetocaloric effects between 84 and 280K 79−73721
EuO, magnetocaloric effect in high magnetic fields 80−25140
Fe-Ni alloy type YuNDK25B, anomalous magnetocaloric effect 80−60278
Fe-Ni(Cr), Invar, exchange interactions between ferromag. and antiferromag. components 80−29545
Gd, magnetisation and magnetocaloric effects *(Russian)* 78−34985
β-$Gd_2(MoO_4)_3$, antiferromag., polarised ferroelec., ferroelastic, magnetothermodynamics 79−7996
$HoFe_2O_4$, magnetic props., 77-300K 80−11225
$LiYF_4:Er^{3+}$, magnetocaloric behaviour, cryst. field theory 77−4520
$Mn_{1.88}Cr_{0.12}Sb$, thermomagnetic props., antiferromag. to ferrimag. transition 77−63194
$Mn_{1-x}M_xAs$, M=V, Cr, Fe, Co, mag. props., phase diags. 77−66300
MnZn ferrite, weak mag. losses, microcalorimetric meas. 77−51926
$Nd_{1-x}Dy_xCo_5$, rotational type spin reorientation, appl. to thermomagnetic generator 77−85451
Ni complex, $Ni(C_5H_5NO)_6(ClO_4)_2$, field induced antiferromag., magnetocaloric effect 80−29551
Ni-Pd-Mn, ternary FCC solid soln., saturation magnetisation and Curie temp., medical appl. *(Japanese)* 79−61114
$Sm_{0.7}Er_{0.3}FeO_3$ spin reorientation photomagnetic motor 78−2695
Tb, mag. characts. in strong mag. field 77−89936
Tb, magnetocaloric effect in high magnetic fields 80−25140
Tb-Gd alloy, spin orientation transition obs. 79−99714
Tb-Y, helicoid antiferromag. ferromag. transition, magnetostriction and magnetocaloric effect *(Russian)* 77−80937
Tb_xGd_{1-x}, orientation phase transitions near Curie pt., magnetization and magnetocaloric effect meas. *(Russian)* 79−87261

magnetocrystalline anisotropy *see magnetic anisotropy*

magnetoelastic effects
alkali hyperoxides, ionic π-electron systems, magnetogyration 80−93155
amorphous ferromagnetic alloys, micromagnetic eqns. for case of dipolar and magnetocryst. fluctuations 80−11171
amorphous ribbons, magnetostrictive, theory of giant ΔE effect 77−85537
anisotropic solids with magnetic symm., unified dynamic theory 78−77713
antiferromagnet, magnetoelastic coupling in nonlinear acoustic phenomena, exchange interaction effects *(Russian)* 77−90010
antiferromagnet, magnetoelastic soliton propag. 80−66003
antiferromagnet, magnetoelasticity, exchange enhancement 79−87299
antiferromagnet, magnon damping, influence of magnetoelastic interaction 79−28517
antiferromagnet, parametric excitation of sound near phase transition point 79−69710
antiferromagnet, phase transformations in strong mag. fields, mag. moments collapse, strengthened magnetoelastic links *(German)* 78−68227
antiferromagnetic, uniaxial, magnetoelastic interaction investigation 79−69674
antiferromagnets, easy-plane, nucl. spin wave relax. 80−65850
antiferromagnets, magnetoacoustic resonance of domain boundaries *(Russian)* 80−65636
azoxybenzene, nematic liq. crystal, elastic consts., varying mag. field and temp. 78−18540
banded domain structure, magnetostatically coupled with uniaxial substrate, mag. reversals *(Russian)* 78−48016
boundary value problems in magneto-elastodynamics 79−49046
boundary value problems in two-dimens. 77−19525
bubble films, spin wave and magnetoelastic resonance meas. 78−91913
bubble materials, magnetoelastic interactions 80−65976
buckling of rectangular plates, edge effect influence 77−80988
buckling plate in uniform transverse mag. field 79−24208
compressible magnet with exchange anisotropy, crit. behaviour 78−39354
conducting film in mag. field, dynamics 77−85539
cubic crystal, magnetoelastic interaction effect on antiferromag. reson. freq. *(Russian)* 77−69711
cubic magnetoelastic crystal, acoustic SHG, static magnetisation effects *(Russian)* 78−56362
cylindrical shell with strain depend. permeability, torsional response in radial and axial mag. fields 79−19754
demagnetised cubic magnetic crystals, effect of magnetoelastic interactions on spin-orientation phase transitions 79−73761
diethylammonium manganese chloride, antiferromag., low temp. luminesc. spectra, magnetoelastic effect 80−2810
dimethylammonium manganese chloride, antiferromag., low temp. luminesc. spectra, magnetoelastic effect 80−2810
dynamics, mixed boundary value problems, vibr. circular plate in mag. field 78−67034
Earth deformation, mag. field effects 80−109085
elastic properties of magnetic materials, review 80−7142
elastic system incremental inductance, magnetoelastic instability of structures carrying electric current 79−73789
elastic wave reflection from mag. materials with conical spiral struct. *(Russian)* 78−88154
electrically conducting elastic plate, vibrs. in transverse mag. field, shear deformation *(Russian)* 79−81756
ferrimagnet, parametric excitation of sound near phase transition point 79−69710
ferrite window cores, magnetoelastic props., compressive stresses influence measurements using photo stress method *(Polish)* 80−93134
ferroelectric ferro- and antiferromagnet, energy gap in spin wave spectrum 78−91858
ferroliquid, magnetoelastic oscills. 79−94639
ferroliquids, phenomenological theory 79−16042
ferromagnet, cubic, elastic props., group theoretical approach 80−29600
ferromagnet, cubic, magnetoelastic interaction energy, arbitrary coordinate system 78−52335
ferromagnet, dislocation effects on phys. props. at $T \neq 0K$ *(Russian)* 77−8378
ferromagnet, itinerant electron, magnetoelastic contribs. to US vel., elastic consts., and susceptibility 80−75829
ferromagnet, magnetoelastic gap in spin wave spectrum *(Russian)* 77−59400
ferromagnet, nonlinear magnetoelastic effects and phase transforms. *(Russian)* 78−48015
ferromagnet, stress meas. by internal induction 77−62222
ferromagnet, with screw dislocation, density of magnon states 78−84402
ferromagnet in low mag. field, simplified model 77−90004
ferromagnetic beams, prismatic elastic, deformation by external mag. field 80−34749
ferromagnetic cantilevered beam plate, magnetoelastic buckling 79−18761
ferromagnetic circular ring, elastic buckling in radial mag. field 78−23314
ferromagnetic conductor, cylindrical, acoustic wave propag., EM field behaviour 80−88857
ferromagnetic crystals, magnetoelastic interactions, linear Cosserats theory 79−28576
ferromagnetic elastic solid, two coplanar Griffith cracks, singular stresses 80−65985
ferromagnetic materials, magnetoelastic effect/stress and strain in plane stressed state 77−77718
ferromagnetic materials, SHG 77−36109
ferromagnetic metal, band struct. contribs. to shear consts., deform. pot. formalism and Stoner model 79−91280
ferromagnetic metals, ultrasound attenuation, EM generation 80−108046
ferromagnetic resonance, phonon propagation 78−88194
ferromagnetoelastic poling, differing piezomag. coeffs. of domain states 77−16102
ferromagnets, easy plane, containing dislocations, static props. 79−95626
ferromagnets, hard, elastic, relaxation effects, vectorial internal variables, rational thermodynamics 80−75828
ferromagnets, higher order surface couplings 78−79212
film, magnetocryst. anisotropy and magnetoelastic consts., micromag. theory 77−73062
fusion reactor superconducting magnet magentoelastic energy calcs., finite element anal. 78−55002
fusion reactor vacuum vessel, magnetic stress induced by plasma motion, 3-dimens. anal. 78−66370
garnet epitaxial film, elastic surface wave propag., magnetoelastic effect 77−20669
garnets growth-induced lowering of magnetoelastic symmetry 78−64255
hexagonal material, Δs effect, anisotropic contrib. 77−90005
homogeneous isotropic magnetoelastic bodies with couple stresses, spherical inclusions, boundary value problems 77−46917
hydroelastic instability of ferromagnetic plate in magnetic field 77−68483
internal friction calc. *(Russian)* 77−35633
Invar, influence of magnetoelastic effects on lattice vibrs., neutron scatt. meas. 78−2722
Invar alloys elastic and magnetoelastic effects 79−56589
itinerant electron ferromagnets, elastic props. and electronic struct. 80−66001
itinerant electron magnetism, thermodynamic aspects 77−72992
itinerant ferromagnets, magnetoelastic props., thermodynamic aspects 80−66002
magnetocrystalline anisotropy constants, phonon-induced temp. depend. 80−65858
magnetodielectrics, magnetoelastic coupling 79−87300
magnetoelastic effects in mag. ordered regime 78−15003
magnetoelastic/piezoelectric composite media, SH-type guided elastic waves, transmission line model 78−27069
magnetostriction in terms of hexagonal and cubic harmonics up to degree 6 80−88856
magnetothermoelastic interactions in cylindrical conductor, mechanocaloric effect 80−7139
magnetoviscoelastic initially-stressed conducting medium, plane Lamb's problem 79−37183
magnetoviscoelastic solids under initial stress, surface waves 79−84140
many-domain magnetics, phenomenological theory of EM and sound energy attenuation 80−7140
medium loaded at points, motion anal. *(Russian)* 77−59442
metal, ferromag., antiferromag., magnetoelastic coupling effect on magnetoelec. reson. 80−75837
metal rods, stress state and fracture in pulsed mag. field 80−81201

magnetoelastic effects continued
metallic glass, isotropic and anisotropic magnetoelastic effects, review 78−68352
metallic systems with rare earth impurities, US attenuation in mag. field, absorpt. mechanisms 79−15336
micromagnetic perturbation theory 78−14912
nonlinear, equation of motion *(Russian)* 77−80981
nonlinear, equations of motion *(Russian)* 79−19755
nonlinear acoustic effects, in magnetoelastic media 77−36109
nonlinear model, propagation of weak discontinuities *(Italian)* 79−65703
one domain ferromagnetic insulators, spin wave and elastic wave interactions 79−73700
orthorhombic ferrimagnets, domain wall motion at near sonic velocity, magnetoelastic interactions 80−34683
paramagnetic metal, band struct. contribs. to shear consts., deform. pot. formalism and Stoner model 79−91280
parametric excitation on spin waves in the induced magnetoelastic crystals *(Russian)* 78−60272
Permalloy, thin film, oscillatory metallic field effect and surface magnetoelasticity 79−56282
plate, magnetoelastic energy and temp. depend. of mag. domain width *(Russian)* 79−47317
porous anisotropic magnets, approach to mag. saturation 80−93146
press. or stress induced, neutron scatt. obs. 80−65880
pressure gauges with monolithic cores *(Polish)* 78−24810
probe with controlled magnetic reluctance under poles 78−40011
railway rail steel NDT, residual stresses meas. using magnetoelastic effect 77−81379
random magnet, LF response function 78−6493
random uniaxial systems with dipolar interactions, phase transitions 77−72677
rare earth alloys, RFe_2, magnetostriction studies, book contrib. 80−39846
rare earth alloys and intermetallic cpds., US attenuation, temp. and mag. field depend. 80−15195
rare earth chlorides, doubly degenerate E-phonons, mag. field splitting 77−43297
rare earth Co Laves phase cmpds., elastic props. rel. to temp., mag. field 79−51834
rare earth cobalt intermetallics, RCo_2, elastic moduli, 4.2-300K 78−52332
rare earth compounds, hexagonal, cryst. field effect in thermal expansion 80−49390
rare earth compounds, multipolar interactions, evidence and origins 80−59935
rare earth intermetallic compounds, quadrupolar interactions, parastriction 80−60400
rare earth intermetallic cpds., cryst. field effects rel. to mag. props. 80−59933
rare earth intermetallics, parastriction, magnetoelastic and quadrupolar exchange coeffs. 79−19758
rare earth intermetallics, quadrupole interactions, magnetoelasticity 80−15489
rare earth intermetallics, RFe_2, spontaneous magnetoelastic distortion, X-ray diffr. expts. 77−63253
rare earth intermetallics, structural instabilities 80−24587
rare earth iron garnets, contribution of Fe ions in noncubic magnetostriction from crystal field model 78−43622
rare earth metals, paramag., c_{11}, c_{33}, mag. field depend. 77−16143
rare earth orthoferrites, mag. dipole anisotropy and magnetostriction 79−73710
rare earth zinc intermetallics, RZn, magnetoelastic consts. 78−15005
rare earth-Al, RAl_2, spontaneous cell distortion due to cryst. field, magnetoelastic consts. 77−63255
rare earth-Co alloy, Curie temp. determ. 79−65672
rare earth-Co alloys, ferromag., first and second order transitions 80−34631
rare earth-Fe_2 Laves phase compounds, magnetostriction anisotropy 77−63250
rare earth-Fe alloys, highly magnetostrictive, isotropy breaking magnetoelastic behaviour 78−72386
rare earth-Fe alloys, magnetoelastic props. *(Japanese)* 78−23316
rare earth-Fe alloys, magnetostrictive, elastic props. 78−84469
rare earth-iron alloys, elastic vs. magnetoelastic anisotropy 78−68347
rare earth-transition metal alloy amorphous film, magnetostriction, dipolar mechanism 78−95502
rare earth-Zn alloys, ferromag., parastriction and magnetoelastic coeffs. 80−65996
relativistic magnetoelasticity, infinitesimal discontinuities *(French)* 79−25853
relativistic theories of materials, book 78−81907
semiconductors, antiferromagnetic resonance rel. to surface impedance, magnetoelastic contrib. 80−50200
semiconductors, magnetic, spin wave electron amplification theory 80−97083
sheared crystal, magnetocrystalline anisotropy torque meas. 78−24830
soft ferromag. elastic solid with finite crack, linear theory 77−66410
soft ferromagnetic elastic solid, magnetoelastic interaction with penny shaped crack in const. mag. field 79−18829
sound propagation, nonlinear effects of magnetoelastic interactions 77−27413
spin glass, parametric amplification of spin waves by elastic pumping *(Russian)* 80−65895
spin-Peierls phase diagrams, obs. and models 80−60330
spontaneous symmetry breaking and magnon-phonon spectra 80−65991
steel, magnetoelastic consts. from magnetostriction consts. *(Russian)* 79−51831
steel, magnetoelastic effect, differential and susceptibility consts. *(Russian)* 79−42817
steel, types 45 and U8, plastically deformed, magnetoelastic props. *(Russian)* 80−44893
steels Kh18N(10-25), mag. susceptibility, 4.2 to 300K, and magnetoelasticity *(Russian)* 80−65812
superconducting ring, buckling in toroidal mag. field 79−64550
superconducting torus, magnetoelastic buckling experiments 79−64549
transducer, force measuring, EM, design and appl. *(Russian)* 78−16784
transducer impedance calc., use of energy balance equation of dynamic magnetoelastic coupling 78−35019
transition metals, 3d, ferromag. props., book contrib. 80−75724

magnetoelastic effects continued
triaxial crystals, domain struct. and magnetisation phenomena *(Russian)* 79−47295
viscoelastic medium, disturbances under transient tangential force and mag. field 80−92070
weak discontinuity propagation in magnetoelastic system with discontinuous coefficients 79−51835
Al, fluxural oscillations in longitudinal mag. field, sound attenuation, magnetoelasticity *(Russian)* 80−54844
$Al_2O_3:V^{3+}(Fe^{2+})$, hyperfine splitting and magnetoelastic consts., freq. crossing spectroscopy 80−107392
$Ca_3Fe_2Ge_3O_{12}$, antiferromagnetic reson., anisotropy and magnetoelastic interaction effects *(Russian)* 77−69712
$Cd_3Cr_2Ge_4O_{12}$, antiferromagnetic reson., anisotropy and magnetoelastic interaction effects *(Russian)* 77−69712
$CeAl_2$, magnetoelasticity, rot. invariance and magnetoacoustic birefringence 79−87304
$CeAl_2$, mode softening due to magnetoelastic interaction, elastic consts. meas. 1.5 to 280K 77−32233
CeBi, magnetoelastic effects, anisotropic mag. behaviour 80−25176
CeBi(Sb), enhanced lattice-displacement effects on cryst. field and anomalous mag. anisotropy 79−73477
CeSb, crystal field effect in thermal expansion 78−19305
CeSb, magnetoelastic effects, anisotropic mag. behaviour 80−25176
CeSb, press. effect. on mag. props. 78−23315
Co, magnetocrystalline anisotropy consts. meas., 77-700K 78−43582
Co-Ni, magnetocrystalline anisotropy consts. meas., 77-700K 78−43582
Co-Pt ferromagnetic alloy, 6 T ultrasonic study of magnetoelastic coupling 80−93154
$Co_{80}B_{20}$, amorphous metal ribbon, stresses, magnetoelastic anisotropy and zero-field mag. domain struct. 80−44896
$Co_{1.8}BaFe_{0.2}Fe_{16}O_{27}$, influence of spin-reorientation on magnetoelastic props. *(Russian)* 79−8028
$Co_{1.8}BaFe_{0.2}{}^{2+}Fe_{16}{}^{3+}O_{27}(Co_{1.8}W)$, magnetoelastic props. under spin-reorientation conditions 79−69709
CoF_2, deformed, magnetoelastic interactions and single-domain antiferromag. state 77−43849
CoF_2, phase transition in transverse mag. field, magnetoelastic interactions 79−65676
$CoFe_2Se_4$, low-temp. thermal expansion anomalies and isothermal compressibility, mag. ordering and magnetorestriction 79−38363
$Co_{0.25}Mn_{0.75}Fe_2O_4$, ferromag. reson. in frozen lattice model, anisotropy consts. 79−51859
CoP, and CoNiP, cylindrical amorphous electrodeposited layers, mag. props., torsion influence 80−88848
$Co_xZn_{1-x}Fe_2O_4$, elastic behaviour, mag. field and temp. depend. 79−87301
Dy, elastic consts. in paramag. temp. range, magnetoelastic contrib. 77−4538
$Dy_{0.25}Co_{0.75}$ film, amorphous, displacement of mag. compensation temp. by elastic stress *(Russian)* 78−19284
$DyFe_{1-x}Co_xO_3$, magnetostriction, thermal expansion and elastic moduli near Morin point 77−8383
$DyPO_4$, metamagnet, phase diagram, influence of internal strains 79−28544
$Dy_{0.7}Tb_{0.3}Fe_2$, magnetostrictive material, liq. phase sintering 78−64493
Er, elastic constants, magnetoelastic contrib. 80−15777
Er film, magnetoelastic excitations, phonon spectroscopy and forbidden transitions 79−82853
ErCu, magnetic excitations 80−25115
$ErFeO_3$, SAW meas. of magnetoelastic effects 80−75839
$ErFeO_3$, sound velocity meas. at high press., spin-reorientation transition 78−76254
ErSb, crystal field effect in thermal expansion 78−19305
ErZn, magnetoelastic and quadrupolar couplings 78−52328
Fe base amorphous alloys, magnetoelastic props. *(Japanese)* 78−23316
Fe, domain wall-dislocation interaction, magnetoelastic damping 78−14980
Fe film, magnetoelastic excitations, phonon spectroscopy and forbidden transitions 79−82853
Fe, grade EA, plastically deformed, magnetoelastic props. *(Russian)* 80−44893
Fe, magnetoelastic excitations and ferromagnetic resonance 79−82879
Fe, plastically deformed, high field suscept. anisotropy and domain struct. 78−15002
Fe, pure, magnetoelastic damping at low shear stress amplitudes *(French)* 77−59441
Fe single crystals (111), elasticity modulus variation, depend. on external mag. field *(Russian)* 79−82849
Fe, static and dynamic magnetoelastic coupling 77−20665
Fe-B(P) amorphous alloys, anomalous thermal expansion, ΔE effect, Invar and Elinvar charact., delay time 80−80589
Fe-Cr-B, amorphous, Elinvar and Invar charact. *(Japanese)* 80−11832
Fe-Mn alloys, elasticity modulus anomaly and magnetoelastic effect *(Russian)* 79−28578
Fe-Mn(Si)(Cr)(Ni), effect of alloying additions on magnetoelastic effects 78−43624
Fe-Ni (35 to 100%), magnetoelastic attenuation of torsional vibr. and shear modulus defect *(Russian)* 77−80982
Fe-Ni based metallic glasses, search for Invar-like magnetoelastic behaviour 79−56596
Fe-Ni(Pt) Invars, elastic and mag. props., magnetoelastic interaction effects *(Russian)* 80−84631
Fe-R alloys, mag. elastic properties 78−52331
Fe-rare earth alloys, amorphous, magnetoelasticity and moment rot., US vel. calc. and neutron scatt. meas. 80−65992
Fe-Si, steel sheet static mag. props., elastic tensile stress effect 78−47999
Fe-Si (3 wt.%), oriented, losses and domains, mech. stress effects 80−88852
Fe-Si (up to 8 wt.%), magnetostriction temp. and comp. depend. 77−66405
Fe-Si amorphous films, mag. and magnetoelastic props. 79−99746
Fe-Tb, magnetoelastic hysteresis, elastic stress and mag. field depend. *(Russian)* 80−65982
$FeBO_3$, magnetically tunable ultrasonic transducers for shear waves 80−74682
$FeBO_3$, magnetoelastic coupling, antiferromag. reson. deform. depend. meas. 77−73069
$FeBO_3$, magnon dispersion by light scatt. and ferromag. reson. 77−55668

magnetoelastic effects continued
$FeBO_3$, parametric echo, magnetoelastic NMR excitation *(Russian)* 80−66072
$FeBO_3$, spin wave dispersion at small wavevectors, Brillouin scatt. and ferromag. reson. 78−47962
$Fe_{81.5}B_{14.5}Si_4$, amorphous metal ribbon, stresses, magnetoelastic anisotropy and zero-field mag. domain struct. 80−44896
$FeCl_2$, in transverse mag. field, magnetoelastic coupling effect on mag. props. 79−28582
$(Fe_{1-x}Ni_x)_{83}B_{17}$, amorphous alloys ferromagnetic resonance 80−108080
$Fe_{40}Ni_{40}B_{20}$, amorphous, high-field magnetisation curve, spin wave spectrum and microstructural inhomogeneities 80−15702
$Fe_{40}Ni_{38}Mo_4B_{18}$ and $Fe_{78}Mo_2B_{20}$ amorphous ribbons, magnetoelastic effects in as-quenched and stress-relieved states 80−80588
$Fe_{40}Ni_{40}P_{14}B_6$, amorhpous ribbon, influence of torsion on mag. props. 80−7138
$Fe_{40}Ni_{40}P_{14}B_6$, amorphous, ΔE effect, pole effect 77−16136
$Fe_{40}Ni_{40}P_{14}B_6$, amorphous, mag. polarisation in approach to ferromag. saturation 80−80560
Fe_3O_4, magnetoelastic props. *(Japanese)* 78−23316
Fe_2P, magnetisation, susceptibility, thermal expansion and elec. resist. meas. 77−77037
$Fe_{75}P_{15}C_{10}$, amorphous, ΔE effect, pole effect 77−16136
$Fe_2(Tb_{0.2}Dy_{0.22}Ho_{0.58})$, highly magnetostrictive alloy, vibrating-reed meas. of ΔE effect and internal friction 79−42819
Gd film, magnetoelastic excitations, phonon spectroscopy and forbidden transitions 79−82853
Gd, magnetoelastic anomaly at 240K, spin reorientation region 77−40105
Gd, magnetoelastic excitations and ferromagnetic resonance 79−82879
Gd, static and dynamic magnetoelastic coupling 77−20665
Gd-Co amorphous sputtered films, magnetoelastic contrib. to perpendicular anisotropy, internal stress meas. 78−95490
Gd-Fe, amorphous sputtered film, magnetostriction 79−47320
Gd-Fe amorphous sputtered films, magnetoelastic contrib. to perpendicular anisotropy, internal stress meas. 78−95490
GdIG, local mag. anisotropy in stress field of single dislocation 80−88744
Ho, elastic consts. in paramag. temp. range, magnetoelastic contrib. 77−4538
Ho, magnetoelastic coupling in paramag. region 77−80984
Ho, magnetoelastic interactions 78−64252
$HoAl_2$, magnetoelastic effects on elastic consts., 4.2-280K 78−72385
$Ho_xTb_{1-x}Co_2$ lave phase compounds, elastic props., temp. and magnetic field dependence 80−60393
HoZn, mag. excitations near spin rot. temp., neutron scatt. study 79−19731
HoZn, magnetic excitations 80−25115
HoZn, magnetoelastic and quadrupolar couplings 78−52328
$KCoF_3$, antiferromag. domain wall motion under external stress 80−80583
$KMgF_3:Fe^{2+}$, anomalous acoustic relax. absorpt. and APR 80−88864
$La_{1-x}Tb_xAg(Sn_3)(Al_2)$, paramag. anisotropy of Tb^{3+} in cubic cryst. field 80−15687
Mn-Ni, single cryst. or polycryst., elastic anomalies at antiferromag. transition 78−14972
Mn-Ni alloys, γ-phase antiferromag., lattice distortion and elastic props., ΔE effect interpret. 77−20671
MnBi, mictomag. alloys, elastic props. *(Russian)* 80−7141
$Mn_{0.82}Fe_{2.18}O_4$, anelasticity, 280 to 730K, 125 kHz vibr. study 78−87740
MnO, antiferromag. reson., low freq. branch gap due to magnetoelastic interaction 77−40134
MnO, first order mag. phase transition, elastic consts. meas. 77−66316
MnO, magneto-elastic coupling by dipolar interactions and spin orientation 79−78494
MnO, multidomain single cryst. and monodomain cryst., crit. and elastic behaviour, T_N to 300K 77−66407
Nd, elastic constants, low-temp., mag. field depend. 78−76290
Nd, mag. ordered, single cryst. elastic consts. meas., 4-50K 77−63249
$NdAl_2$, elastic constants, 4.2K to 280K, crystal field effects 77−11615
$NdAl_2$, magnetostriction in high mag. fields 79−99745
$NdVO_4$, magnetoelastic interactions, finite strain and rot. effects, elastic consts. 79−87303
Ni crystals in strong mag. field, EM excitation and vel. dispersion of sound *(Russian)* 80−39837
Ni, effective mag. anisotropy const., magnetoelastic contrib. 78−14951
Ni, electroplated layers, internal friction and ΔG effect, rel. to bath comp. and annealing 78−19296
Ni film, magnetoelastic excitations, phonon spectroscopy and forbidden transitions 79−82853
Ni, magnetoelastic and magnetostrictive sensitivities, reversible and irreversible components *(Russian)* 80−25172
Ni, magnetoelastic effects, ΔE-effect and macroeddy current damping, internal friction meas. 78−64253
Ni, magnetoelastic excitations and ferromagnetic resonance 79−82879
Ni, phonon assisted magnon transmission at 24 GHz 79−82878
Ni, phonon generation and attenuation at FMR 80−39875
Ni, static and dynamic magnetoelastic coupling 77−20665
Ni, under longitudinal compression, magnetisation anomaly explanation by weak field spin rotation model 79−82851
Ni wire, polycryst., magnetoelastic hysteresis with torsion, inverse Wiedemann effect *(Spanish)* 77−73064
Ni-Fe-Co film, magnetoelastic vibr. generation during high freq. mag. reversals *(Russian)* 78−60320
Ni-Pd alloy, magnetostriction and mag. anisotropy meas. 79−4713
Ni_3Al, elastic moduli changes at Curie point 77−66406
Ni_3Fe, domain struct. after tensile deform., dislocation effects 80−71083
NiZn ferrites, Villari effect 80−88847
$NpFe_2$, lattice distortions in ferromag. phase, X-ray obs. 80−15774
$NpNi_2$, lattice distortions in ferromag. phase, X-ray obs. 80−15774
Pb, fluxural oscillations in longitudinal mag. field, sound attenuation, magnetoelasticity *(Russian)* 80−54844
Pd-Fe, magnetic anisotropy near Curie point, quasi domain struct. *(Russian)* 80−65867
Pd-Fe alloys, dil., anisotropy of neutron polarisation near ferromag. phase transition 77−32234
Pr, antiferromagnetic ordering 80−15709
Pr, magnetic excitations, exchange, crystal field and magnetoelastic interactions 80−2563

magnetoelastic effects continued
Pr, magnetoelastic effects, zero field single cryst. elastic consts. meas. 77−66403
Pr, soft mode excitation behaviour under press., long range order 80−39838
$PrAl_2$, elastic constants, 4.2K to 280K, crystal field effects 77−11615
PrSb, crystal field effect in thermal expansion 78−19305
PrSb, magnetic to nonmagnetic transition, press. or stress induced, neutron scatt. obs. 80−65880
$PrSn_3$, thermal expansion and transverse elastic const. near mag. phase transition 80−60394
Pr_3Te_4, paramagnet, rotational invariance and magnetoelastic phenomena 77−48027
Pr_3Tl, thermal expansion and transverse elastic const. near mag. phase transition 80−60394
PuP, lattice distortions in ferromag. phase, X-ray obs. 80−15774
$RbMnF_3$, antiferromag., mag. props. 79−8032
$SmCo_5$, single-cryst. and liq. phase sintered, elastic stiffness consts., US velocity obs. 77−73066
$SmCrO_3$, spin reorientation phase transition, second order nature 77−80950
SmSb, crystal field effect in thermal expansion 78−19305
Tb compounds with garnet and zircon structure, anisotropic magnetoelastic props. 77−69660
Tb, elastic constants, magnetoelastic contrib. 80−15777
Tb, elastic consts. in paramag. temp. range, magnetoelastic contrib. 77−4538
Tb, magnetic phase diagram, US meas. of elastic const. 80−15721
Tb-Fe, amorphous sputtered film, magnetostriction 79−47320
Tb-Gd alloy, single cryst., mag., magnetoelastic and elec. props. *(Russian)* 78−2677
$TbCo_2$, spontaneous distortion, mag. props. due to cryst. field, exchange field, magnetoelastic energy 79−61096
$Tb_{0.27}Dy_{0.73}Fe_2$, LF magnetoelastic effects 78−68348
$Tb_{0.3}Dy_{0.7}Fe_2$, elastic vs. magnetoelastic anisotropy 78−68347
$Tb_{0.3}Dy_{0.7}Fe_2$, magnetoelastic coupling meas. by US method 77−69652
$Tb_{0.3}Dy_{0.7}Fe_2$, magnetostrictive, resonant coupling of shear waves 79−33517
$Tb_{0.3}Dy_{0.7}Fe_2$, sound velocity mag. field and temp. depend. elastic moduli calcs. 80−39839
$TbFe_2$, magnetoelastic props., magnetostriction hysteresis *(Russian)* 80−29590
$TiFe_xCo_{1-x}$, thermal expansion and magnetoelastic effects 80−80585
$(Ti_{1-x}V_x)_2O_3$, spin-glass props., 0.05-300K 80−25149
TmCd, parastriction, magnetoelastic and quadrupolar exchange coeffs. 79−19758
TmCd quadrupolar ordering and magnetic interactions 79−73676
TmCd(Zn), quadrupolar phase transitions, magnetoelastic and quadrupolar coupling consts. 80−15744
$TmFeO_3$, magnetoelastic props. at spin reorientation region 77−8382
TmSb, crystal field effect in thermal expansion 78−19305
TmSb, paramagnet, rotational invariance and magnetoelastic phenomena 77−48027
TmTe, crystal field effect in thermal expansion 78−19305
TmZn, magnetic-ion-lattice interactions, cryst. elec. field 77−4540
TmZn, parastriction, magnetoelastic and quadrupolar exchange coeffs. 79−19758
UAl_2, elastic consts., temp. and mag. field depend. 80−55450
UFe_2, giant magnetoelastic deform. of cryst. struct. mag. props. *(Russian)* 80−93159
V, fluxural oscillations in longitudinal mag. field, sound attenuation, magnetoelasticity *(Russian)* 80−54844
Y-Co, Curie temp. determ. 79−65672
Y-Co, ferromagnet, first and second order transitions 80−34631
YFe_x film, ($x \simeq 2$), magnetoelastic excitations obs. 78−68307
$Y_3Fe_{5-x}Ga_xO_{12}$, inhomogeneous stress effect on ferromagnetic resonance 79−24219
$YFeO_3$, domain wall motion, magnetoelastic coupling 79−78435
$(YGd)(GaFe)_5O_{12}$ epitaxial film, nonlinear magnetoelastic effects *(French)* 80−34745
YIG, distrib. of easy magnetisation axes near edge dislocation *(Russian)* 80−44891
YIG, nonreciprocal attenuation of magnetoelastic Rayleigh waves 80−60399
YIG, SAW transducers, approximate theory 79−68533
YIG:Yb, magnetoelastic coupling of Yb ions, ferromag. reson. meas. 77−69698

magnetoelastic waves
amplification of magnetoelastic Love waves by interaction with carrier waves in layered composite 79−28577
antiferromagnet, nuclear spin oscillations, interaction with lattice vibrs. 80−70996
antiferromagnet, parametrically excited, possible maser effect 78−48051
antiferromagnet, sound damping by phonon-magnon interaction, high Neel temp. *(Russian)* 78−43626
antiferromagnet with dislocation, phonon relaxation 79−69216
asymmetric elastic medium, electrically conducting, magneto-thermo-elastic waves anal. 80−15772
bar under initial stress, magneto-elastic torsional waves 79−23260
canted magnetic struct. crysts., magnetoacoustic resonance, elastic vibrations 80−29599
compression wave diffraction by penny-shaped crack in presence of mag. field 79−47318
cone helix structured magnet, elastic wave spectrum *(Russian)* 78−68342
convolution with magnetoelastic Rayleigh waves on bulk YIG 79−64404
cubic crystal, highly magnetostrictive, magnetoelastic surface waves on (110) plane 78−52327
cubic ferr-te garnet, diffracted light polarisation characts., spin and magnetoelastic waves 80−20614
elastic properties of magnetic materials, review 80−7142
electrically conducting elastic layers, anal. *(Russian)* 78−48021
ferrite-semiconductor hybrid struct., magnetoelastic wave interaction with drifting carriers 80−54934
ferrite/semiconductor composite struct., SH type wave propag. 78−23319
ferroelectric antiferromagnet, coupled ferroelec.-magnetoelastic waves 77−51935
ferromagnet, cubic, magnetoelastic interaction energy, arbitrary coordinate system 78−52335

magnetoelastic waves continued
ferromagnet, surface magnetoelastic waves in the presence of exchange interactions and pinning of surface spins 78−80186
ferromagnetic conductor magnetoelastic surface wave attenuation 77−20667
ferromagnetic crystals, magnetoelastic interactions, linear Cosserats theory 79−28576
ferromagnetic insulator, magnetoelastic wave dispersion rels. and normal modes 77−55694
ferromagnetic plate, infinitely long, hydroelastic instability exposed to non-conducting fluid flow 77−84173
ferromagnetic polycrystalline materials, mag. impulse produced magnetoelastic waves *(Italian)* 78−2720
ferromagnetic substrates, propag. of surface magnetoelastic waves 77−55698
films, ferromagnetic, perpendicularly magnetised, surface and vol. magnetoelastic waves *(Russian)* 80−93151
Love magnetoelastic surface wave propagation in laminates 80−38322
Love waves, in stratified magnetoelastic solid with material boundary 78−32015
magnetic film, bubble domains, magnetoelastic interactions 80−103865
magnetically ordered cryst., dislocation drag, magnetoelastic waves 80−103332
magneto-viscoelastic wave propag. in Voigt type material 78−31100
magnetoelastodynamics problem with mixed boundary conditions 80−1466
magnetothermoelastic plane Lamb's problem in initially stressed conducting medium 78−67077
magnetothermoelastic Rayleigh waves with thermal relaxation in uniform magnetostatic field 80−2617
magnetothermoviscoelastic waves reflection at semi-infinite solid boundary 80−48633
magnon-phonon coupling, continuum approach, general eqns., background soln. 79−95622
magnon-phonon coupling, continuum approach, hexagonal symmetry, wave propagation 79−95623
metallic glass ribbon, magnetostrictive stress depend. of longitudinal wave vel. 80−75825
neutron star crust, correl. between speeds of fast and slow magnetoelastic modes 79−8942
nonellipsoidal sample, demagnetising factor meas., magnetoelastic Rayleigh wave convolution 77−10072
orthoferrites near spin-flip temp. 78−19301
orthorhombic ferrimagnets, domain wall motion at near sonic velocity, magnetoelastic interactions 80−34683
periodic coupling of piezoelec. and magnetoelastic surface waves 78−10269
piezoelectric-magnetic-semiconductor composite, Love wave propagation characs. 79−1704
plane waves in electrically conducting and magnetizable viscoelastic isotropic solids subjected to a uniform magnetic field 79−28580
propagation in initially deformed conductors *(Russian)* 77−80987
random media, coupled EM and elastic waves 79−28579
rare earth intermetallics, magnetoelastic waves, LF, theory 78−64250
Rayleigh wave convolver internal efficiency calc. 77−23817
Rayleigh wave propagation in strongly magnetostrictive materials 77−40111
Rayleigh waves in magneto-thermoelastic solids with thermal relaxation 79−28581
review *(Japanese)* 78−23317
ribbon position sensor 79−80603
SAW velocity on magnetised ferrite substrate, non-reciprocity 80−80587
shear, horizontal, integral representation 77−90009
shell, orthotropic, axisymmetric vibrs. in mag. field, asymptotic solns. 80−2620
shock loading, linear and nonlinear problems *(Russian)* 77−39246
surface wave convolution, approx. theory 78−68354
surface-wave excitation, comparison of grating and meander-line transducers 79−50557
torsional wave diffraction by penny shaped crack, in axial mag. field 79−24206
ultrasonics symposium, Cherry Hill (1978) 79−50472
US bulk wave electromagnetoacoustic excitation 79−57195
wave propagation in deformed conductors *(Russian)* 79−19761
Co rod, spontaneous vibr. modes excited by reversible magnetostriction 79−56587
$CoCl_2.2H_2O$, magnon-phonon interactions and two-magnon Raman scatt., magnetoelastic waves and selection rules 80−34917
Dy film, magnetoelastic waves, GHz, excitation, field depend. 78−72378
Fe rod, spontaneous vibr. modes excited by reversible magnetostriction 79−56587
$FeBO_3$, parametric echo, magnetoelastic NMR excitation *(Russian)* 80−66072
$FeCl_2.2H_2O$, magnon-phonon interactions and two-magnon Raman scatt., magnetoelastic waves and selection rules 80−34917
$Fe_{40}Ni_{40}P_{14}B_6$ Metglass, spontaneous vibr. modes excited by reversible magnetostriction 79−56587
GaYIG, magnetoelastic surface wave attenuation 77−20667
$Ho_{0.58}Tb_{0.20}Dy_{0.22}Fe_2$, magnetoelastic surface wave propagation, mag. field depend. 77−85535
$Ho_{0.58}Tb_{0.2}Dy_{0.22}Fe_2$ magnetoelastic surface wave dispersion obs. 79−47321
Ni rod, spontaneous vibr. modes excited by reversible magnetostriction 79−56587
Ni, spin-elastic wave three freq. interactions, parameters, excited wave amplitudes *(Russian)* 79−91276
Ni-$LiNbO_3$, layered structure, mag. control of surface elastic waves 77−20666
NiZn ferrite, magnetic field effect on Rayleigh wave attenuation 78−6557
$(Ni_xZn_{1-x})_{0.5}Fe_2O_4$, spontaneous vibr. modes excited by reversible magnetostriction 79−56587
Tb film, GHz magnetoelastic wave excitation, field depend. 78−52334
Y garnet, propagation characts. obs. 77−40107
YGaIG, magnetoelastic wave propagation time dispersion reduction 80−75836
YIG, diffr. of laser radiation by parametrically excited elastic and magnetoelastic waves 78−19338
YIG, ferromag. film on nonmag. substrate, magnetoelastic wave propag. 79−99744
YIG, film, magnetoelastic Lamb wave velocity changes, theory 78−91923
YIG film, tangentially magnetised, magnetoelastic Lamb wave propag. 79−82856
YIG, magnetoelastic wave dispersion rels. and normal modes 77−55694
YIG, magnetoelastic wave propagation time dispersion reduction 80−75836
YIG, magnetostatic precession modes, optical investigation 78−19337
YIG monocrystals, echo of magnetoelastic waves 77−55697
YIG, nonreciprocal attenuation of elastic surface waves 77−55696
YIG, nonreciprocal attenuation of magnetoelastic Rayleigh waves 80−60399
YIG nonreciprocal thin film acoustic device, design, appl. of cct. theory of elastic waveguides 77−85042
YIG, parametrically excited reson. magnetostatic modes of spin, elastic and magnetoelastic waves 79−56523
YIG, parametrically excited wave discrete structure obs., light diffr. and modulation *(Russian)* 79−95650
YIG, pseudo-surface magnetoelastic waves, damping *(Russian)* 78−23320
YIG rod, inhomogeneously magnetised, prog. characts. 78−15006
YIG, spin and magnetoelastic waves on longit. mag. pumping, optical obs. *(Russian)* 80−29727
YIG substrate magnetoacoustic modes, meander-line excitation 77−20670
YIG substrates, magnetoelastic surface waves, magnetostatic reson. anal. 80−20441
YIG:Gd, Ga, optical probing of magnetoelastic Rayleigh waves 79−78495
YIGaG, magnetoelastic wave propag. time and total loss, freq. depend. *(Russian)* 77−43859
$Y_{3-x}La_xFe_{5-y}Ga_yO_{12}$, mag. bubble film, low freq. ferrimag. reson. 78−31110

magnetoelectric effects
advances in basic magnetism during past twenty-five years 80−36791
anisotropic media, piezomagnetoelectric effects 80−25174
anisotropic solids with magnetic symm., unified dynamic theory 78−77713
antiferroelectric ferrites, coupled magnetoelec. oscills. and high freq. susceptibility tensor *(Russian)* 80−93152
antiferromagnet, magnetoelectric susceptibility crit. behaviour, renormalisation group theory 78−48023
atomic systems, nonlinear magnetoelec. susceptibility, Faraday effect, laser intensity depend. 78−59076
carnauba wax magneto-electret, Struve function 78−76287
ceresin wax magnetoelectret, X-ray diffr. pattern 78−6014
electric current density, induced by external mag. field, gauge invariant method calcs. 78−82665
EM wave propagation, standing wave pattern form. when magnetoelec. constant is nondiagonal tensor 79−27135
ferroelectric and antiferroelectric phase transitions, magnetoelec. effect 80−100637
ferroelectric antiferromagnet, coupled ferroelec.-magnetoelastic waves 77−51935
ferroelectric antiferromagnet, damping of spin waves and 'hard' excitation effect 79−28518
ferroelectric antiferromagnetics, spin wave fluctuations in strong mag. fields *(Russian)* 79−82773
ferroelectric antiferromagnets, exchange enhancement of the magnetoelectric coupling 78−88159
ferroelectric ferro- and antiferromagnet, energy gap in spin wave spectrum 78−91858
ferroelectrics, P- and T-nonconserving interactions, macroscopic effects 78−84532
ferroelectroantiferromagnetics, spin wave spectrum and exchange amplification of magnetoelectric correlation 79−38311
ferrofluid, dielec. behaviour in uniform mag. field 80−60390
ferromagnetic semiconductor, nonlinear magnetoelec. effect 77−20676
ferromagnetoelectric poling, differing magnetoelec. coeffs. of domain states 77−16102
magnetic materials, review *(Japanese)* 80−50159
magnetic semiconductor, classical and quantum theory, magnon drag effect 80−34746
magnetoelectrets, possible mech. of mag. field effects 80−93157
naphthalene, mag. polarised electret, X-ray diffr. obs. 78−43775
noncentrosymmetryic crystal with cooperative Jahn-Teller effect, ferroelectric transition 77−8532
nonlinear susceptibility, three-dimens. model 80−39845
phenomenological rules for computation, magnetoelectric susceptibilities 80−55068
piezoelectrics, magnetoelec. reson. *(Russian)* 79−42904
PMMA, tubular magnetoelectrets, TSC obs. 78−88250
polarisability constants, by composition series technique 79−56586
polyethylene, tubular magneto-electret, surface charge characts., forming temp./mag. field depend. 77−32318
polyvinylidene fluoride magnetoelectret, AF and RF charge and dielectric characts. 80−40038
PVC, magneto-electrets, refr. index, temp. and mag. field effects 78−6655
PVC, magnetoelectret form., RF thermomagnetic treatment, dielectric aftereffects 78−6625
PVC magnetoelectrets, mag. susceptibility 80−2687
quartz, magnetoelec. reson. *(Russian)* 79−42904
semiconductors, antiferromagnetic, magnetoelec. effect, magnetization and ferroelec. props. 80−25180
shellac and bee's wax, orientation solidification in mag. field, magneto-electrets, X-ray diffr. 77−12299
silastic, magneto-electret of tubular shape, surface charge 78−56419
toxic air ion effects due to tachyon magnetoelectric dipoles and beta rays 80−35999
$BaMn_{0.99}Co_{0.01}F_4$, magnetoelec. phenomena, dielec. behaviour near Neel temp. 80−71151
$BaMnF_4$, dielec. anomaly, mechanism, spin canting 78−10744
$BaMnF_4$, phase transitions review 79−78378
$BaMnF_4$, spectroscopy, ferroelectric/ferromagnetic coupling 79−19845
$BaMnO_4$, ferroelectrically induced ferromagnetism 77−73067
$BaTiO_2$, Fe-Co-Ti-Ba-O, composites ferroelectric, idealised analysis *(Russian)* 80−20440

magnetoelectric effects continued
$BaTiO_3$-Ni ferrite, piezoelectric-piezomagnetic sintered two-phase composite, magnetoelec. conversion 77−12181
Bi-Sb, solid solns., thermoEMF in transverse mag. field 77−47841
Bi-Sb alloy, magnetothermoelec. quality factor of single crystals 77−51771
$Bi_2Bi_4Fe_2Ti_3O_8$, dielec. and magnetoelec. props. 78−95562
$BiFeO_3$, pyroelectric-antiferromag., magnetoelectric effect *(Russian)* 78−43625
$BiFeO_3$-$Pb(Fe_{0.5}Nb_{0.5})O_3$, ferroelec., magnetoelec. obs. temp. and conc. depend. 80−50156
CdTe, nonlinear magnetoelec. susceptibility, three-dimens. model 80−39845
$Co_3B_7O_{13}Cl$, polydomain ferroelec., magnetoelec. effect below Neel temp. 78−10745
Cr_2BeO_4, magnetoferroelectricity, weak pyroelectric effect 79−42914
Cr_2O_3, antiferromag. reson. and mech. of parallel magnetoelectric effect 79−47337
Cr_2O_3, dielec. const. in mag. field, nonlinear magnetoelec. effect in Neel pt. region 80−66006
Cr_2O_3, magnetoelec. effect, SQUID magnetometer meas. 79−87302
Cr_2O_3, magnetoelectric effect mechanism, magnetoelec. susceptibility and antiferromag. reson. elec. shift meas. 80−44894
Cr_2O_3, magnetoelectric susceptibility meas. by SQUID, 1.6-4.2K 77−20664
$Fe_3B_7O_{13}Br$, $Fe_3B_7O_{13}Cl$, polydomain ferroelec., magnetoelec. effect below Neel temp. 78−10745
Fe_5LiO_8, magneto-crystalline anisotropy, magnetoelectric effect interpretation *(French)* 79−47316
Fe_5LiO_8, magnetoelec. effect interpretation by magneto-cryst. anisotropy *(French)* 79−33515
Fe_5LiO_8, magnetoelectric-effect and magnetisation process 79−1688
Fe_3O_4, lattice parameters, NMR freqs., and magnetoelec. pots. near 12K 80−71146
Fe_3O_4, magnetically biased, linear and bilinear magnetoelec. susceptibility, 4.2K 77−40106
Fe_3O_4, magnetite, magnetoelec. effect at 77K and cryst. symm. 80−29593
Fe_3O_4, magnetite, magnetoelec. effect at 77K, elec. field depend. of mag. anisotropy 80−29594
Fe_3O_4, magnetite, magnetoelec. effect temp. depend. obs. by mag. field rot. in a-c plane at 10K 80−71145
Fe_3O_4, magneto-electric effect temp. depend. at 10K 79−78498
Fe_3O_4, magnetoelectric effects from electric field depend. macroscopic mag. anisotropy energy 77−69656
Fe_3O_4, typical spontaneous symmetry breakdown in solid state 80−34737
GaAs, magnetoelectric susceptibility, nonlinear, three-dimens. model 80−39845
$GdAlO_3$, magnetoelec. susceptibility, mag. struct., mag. phase diagram and crit. coeffs. 77−66303
$GdAlO_3$, magnetoelectric susceptibility, crit. behaviour 78−10743
He positive column ionisation waves, influence of longitudinal mag. field 78−67522
^{3}He-A superfluid slab, magnetoelectric textures, capacitive meas. 78−22924
$LiFe_5O_8$, second order magnetoelectric effect 77−66409
$Li_{0.5}Fe_{2.5}O_4$, uniaxial anisotropy energy, elec. field depend. 78−68346
$MgCr_2O_4$, magneto-electric splitting of crystal field Γ_2-level of Cr^{3+} ion, neutron spectroscopic obs. 79−19562
$Ni_3B_7O_{13}I$, magnetoelectric tensor component detection 79−95625
$Ni_3B_7O_{13}I$, nonlinear magnetoelec. and dielec. props. 79−65704
PVC, tubular magneto-electret, surface charge characts., forming temp./mag. field depend. 77−32318
S magnetoelectret, thermally stimulated discharge current 79−91341
$ZnCr_2Se_4$, screw spin structure, magnetoelectric effect 80−75827
ZnTe, nonlinear magnetoelec. susceptibility, three-dimens. model 80−39845

magnetofluidynamics *see magnetohydrodynamics*

magnetogasdynamics *see magnetohydrodynamics*

magnetohydrodynamic conversion
1 MW generator, cold wall type, expt. investigation *(Japanese)* 78−59688
40 MWe pilot plant 79−52945
aerospace propulsion, by laser radiation absorption 77−3998
air heater, directly fired, materials and design concepts testing 79−52949
air heater operability and materials testing 80−35703
baseload power plant for intermediate and peaking duty 80−35702
closed cycle MHD power generation, history of development and physics research need 80−45717
coal-fired MHD flow facility, development and operation 80−66982
coal-fired MHD power generation, plant development in United States, present status 80−16818
coal-fired MHD system, retrofitting to existing non-coal power stations 80−66983
coal-fired plant, thermal modelling of components 79−52946
coal-fired process, NO_x control, expt. results 79−52947
coal-fired steam power plant, economic optimisation 79−52942
combustion products, O_2 effects 78−18388
commercial viability of MHD/steam power generation systems 80−35701
commercialisation in United States, 1978 potential 79−52944
conduction channel, optimal operating characts. calcs. *(Russian)* 78−47190
conversion channel plasma flow computation by finite difference methods 78−22470
cylindrical plasma filament under axisymmetric perturbation, numerical anal. 80−106853
desalinator appl., using solar energy, prototype design and operation 79−74508
Doublet III fusion research device, United States, construction 77−46404
end effects with a slowly varying magnetic field in a MHD channel with segmented electrodes 80−45716
environmental assessment of a coal-fired open-cycle MHD power plant 80−35795
fundamental physical principles 78−75440
fusion reactor, Tokamak, divertor mag. piston action, elec. AC power direct generation 80−102324

magnetohydrodynamic conversion continued
future energy concepts, Conf. London, England (Jan.-Feb. 1979) 79−43709
heat recovery, chemical, in system using natural gas *(Russian)* 77−68702
India's research of MHD power generation potential 79−48141
induction MHD pump channel, EM field and longit. boundary effect, 2-dimens. theory *(Russian)* 78−47188
magnetospheric plasma as energy source for space instrumentation 77−64605
MHD power generation, future prospects 80−35700
microwave induced plasma 77−80224
one-dimensional flow of real gas in diverging channel, thermoelectric current effects 79−32692
open-cycle, 1978 reappraisal in United Kingdom 79−48140
open-cycle coal-fired liquid-metal MHD 80−40875
petroleum-acetylene-O_2 combustion products, seeded, elec. cond., for MHD power plant 78−34256
phase equilibria data, need for in development of magnetohydrodynamics 79−11551
pollutants, emissions and controls 80−30613
power generation cycles 80−16817
principle, research and 1979 development trends *(German)* 80−7949
principle and effectiveness, development trends *(Czech)* 79−87996
prospects in Soviet Union 77−67868
steam combined-cycle power plant, combustion air temperature variations reduction, computer simulation appl. 79−52943
steel smelting using MHD generator 79−70453
superconducting dipole magnet system design, with integrated control system 79−52948
superconducting magnet/MHD power generator system, design and trade-off analyses 79−52950
superconducting materials, appl. *(Japanese)* 78−47925
thermonuclear fusion research, economic factors 80−73991
weakened fusion plasma in MHD channel, generation aspects 79−43778
Cs applicability, owing to low ionisation potentials *(Hungarian)* 80−3526
H_2-O_2 seeded system for MHD generator, elec. cond. 80−76642
NO_x emissions from coal-fired MHD power plants, simplified correlations for prediction 80−97842
Rb applicability, owing to low ionisation potentials *(Hungarian)* 80−3526

magnetohydrodynamic convertors
1 MW class generator, cold wall type generating channel expt. *(Japanese)* 78−55756
acceleration nozzle, with supersonic flow deformation 78−26181
accelerator, thermodynamic props., mag. field strength, Hall currents in arc region 77−65917
acoustic instability of flow in MHD channel 79−64842
air-core magnetic system, induced fields in conducting medium 80−43796
alkali metal-inert gas, inhomogeneous mixture, nonequilib. processes under conditions of T-layer form. 78−91079
arc switching near electrodes, elec. current oscills. 79−55569
blow-down experiment, Eindhoven *(Dutch)* 80−33827
boundary layer effect on transport phenomena in MHD generators 79−23463
boundary layer voltage loss determ., simplified technique 77−72507
cathode spot erosion, thermal conduction-diffusion model 78−5955
ceramic materials appl., fireproof *(Czech)* 79−70455
channel, near electrode-free wall, plasma instability, flow inhomogeneity effect 78−26338
channel and regions, eddy current losses due to magnetic field variations 80−40874
channel design, two-dimensional, w.r.t. velocity, Mach number and pressure profiles 79−83604
channel electrical characts., equivalent ccts. 80−75106
channel electrode surface temp. selection, effect of working body props. 79−55573
channel subsonic flow, gas dynamic, elec. parameters 79−55567
channel with Hall and ion slip currents, forced convective heat transfer 80−33823
channel with sectioned electrodes, integrated characts. *(Russian)* 78−26343
characteristics improvement, using current parallel to magnetic field 80−1751
closed cycle, N_2 addition to plasma, stability 79−19014
closed cycle generator, with fully ionized seed, power density, electrical efficiency 79−10721
closed cycle MHD power generation, history of development and physics research need 80−45717
closed-cycle topping generator system, nonequilib. ionisation 77−72508
coal-fired cored brick regenerative heat exchangers 79−1353
coal-fixed, high-temp. plasma, mol. beam mass spectrometric sampling system 80−52358
coaxial induction machine, travelling mag. field, laminar flow *(Russian)* 78−5815
cold wall Faraday type generating channel, design and performance 78−22574
combustion chamber, conical-type, aerodynamic effects on working process 78−42835
combustion driven MHD generator, boundary-layer profile meas. 77−24194
combustion product plasma, near-electrode contraction conditions 78−94946
combustion products, O_2 effects 78−18388
combustion products, turbulence in channel 79−64866
combustion products plasma characterisation, generator channel flow, diagnostic techniques 80−43993
combustion products plasma with mixed alkali impurities, elec. cond. calc. 79−86621
combustion stability 79−32827
conduction MHD pump with current leakage, equivalent circuit *(Russian)* 78−26346
conduction type with reciprocal motion of composite working element 80−84009
conductivity and power output ionization stability, and boundary layer effects 80−1752
constant velocity Faraday-type generator, transient characteristics 80−10440

magnetohydrodynamic convertors continued
contactless MHD pump with EM asymmetry, max. press. calc. *(Russian)* 78−26340
cumulative magnetic generator with flux diffusion, current and energy amplification 77−89327
current concentration due to Hall effect, elimination by variable resistive electrodes 77−80378
current density and elec. field dependence on plasma thermodynamic pulsation *(Polish)* 77−80268
current distribution in MHD channel with one pair of electrodes 77−39475
design of MHD inductors *(Russian)* 78−26347
diagonal channel, conversion efficiency optimisation by sliding descent method, turbulence *(Russian)* 78−75226
diagonal channel equivalent energy circuit 79−55571
diagonal conducting wall generators, performance theory 77−31529
diagonal electrode config., nonuniform conductivity in boundary layer, effect on local characts. 77−39471
diagonal type generator end effects anal. by means of equivalent cct. *(Japanese)* 78−87505
diagonal type nonequilibrium plasma generator, and effects anal. *(Japanese)* 77−80377
diagonal-type, nonequilib. plasma, optimisation, steam plant appl. 78−67443
diagonal-type nonequilibrium plasma MHD generator, electrode internal and external connection effects 78−91165
diagonal-type nonequilibrium plasma MHD generator, resistive electrode and mag. flux distrib. effects 79−41884
diagonal-wall MHD generator design optimisation by nonlinear programming *(Polish)* 78−79477
diffusers, subsonic, design and performance 79−83607
diffusers performance obs., supersonic and subsonic 79−83608
disc generators, anal. of collisional plasma rotating inside cylindrical annulus 78−22466
discharge struct. in noble gas generator 78−91166
disk-type, fluid-mechanical scaling laws 79−83606
duct length in nonequilib. generators 77−7601
duct potential and current distribution, two- and three-dimensional analysis, finite element method appl. 80−24259
duct wall, semi-hot, thermal stress design study *(Japanese)* 78−13890
duct with compensating bars, EM field distrib. *(Russian)* 78−26344
dynamo, approx. design, equivalent circuit diagram 80−84008
electric power fluctuations due to Hall and ion slip currents 77−68879
electric power generation, physical principle and research progress *(Chinese)* 79−82104
electrode switching in end zone of series generator 79−1347
electrode units in MHD channel, temp. distrib. 78−59258
electrode-free wall, flow instability 77−35330
electrodes, current distribution 77−43084
electrodes in arc regime of operation, math. model 79−86620
electron heating in nonequilib. channel 79−1345
electron temperature difference in flow core of MHD accelerator channel 79−10722
electrothermal instability in Hall disc generator, ion fly wheel effect 79−4191
EM field equations averaging, at finite mag. Reynolds nos. *(Russian)* 79−1351
end effects in a MHD channel with diverging electrode walls 80−89657
energy characteristics, mag. field and channel geometry effects calcs. *(Russian)* 77−47172
energy characts. during cooling by gas injection through channel *(Russian)* 78−38557
energy emitted by working medium of MHD generator, meas. 80−103078
equivalent networks, for convectors with non-uniform gas *(Italian)* 80−3525
exploding wire pulse generator characts. 77−55196
explosive coaxial MHD generator, model *(Russian)* 77−51245
explosive electrical generator with resistive load, design and performance 77−55195
external electromagnetic fields, dipolar approx. accuracy *(Russian)* 78−47192
Faraday generator, current profile optimisation, electrode cond. profile 78−94939
Faraday generators, longitudinal baffling 80−64790
Faraday MHD generator in scheme with thermonuclear reactor, efficiency 79−1349
Faraday MHD generator with thermonuclear reactor, efficiency 78−75432
Faraday MHD generator-operating region 80−103132
Faraday MHD generators, electrical performance, nonideal conditions effects 79−32830
Faraday type linear diverging combustion gas generator, non-equilibrium ionisation effects *(Japanese)* 77−47277
Faraday type MHD duct, lead wire position along resistive electrode, effect on current distrib. 77−76214
Faraday-type MHD generator optimisation, using a computer method *(Polish)* 78−79476
flow due to current between parallel electrodes *(Russian)* 78−26345
fluids engineering, Conf. San Francisco, CA, USA (Dec. 1978) 79−83550
fossil fuels for use in MHD power stations 80−72074
frame type MHD channel, optimal selection of frame and transverse cross section form 78−91164
framed MHD channels, two-dimens. inhomogeneities effect on characts. 78−9853
fusion reactor, mirror type, MHD gas turbine energy conversion 79−41885
fusion reactors, MHD decelerators for removal of fuel pellet microexplosion energy 80−13801
fusion-MHD power plant, exhaust plasma pulsed accel. 78−62644
gaseous electrode effect on MHD channel performance 77−84543
generator channel, turbulent MHD boundary layer 77−43085
generator performance, plasma effective Ohm's law due to anisotropic inhomogeneities 78−67316
generators, coaxial, magnetic field distrib. *(French)* 78−55758
heat exchange in channel, ion slippage 78−75431
heat transfer problems, overview 78−87503
high-temperature MHD generator, shock tube plasma source 77−35372
hydrocarbon fuels combustion prod. plasma with alkali impurity, elec. cond. 79−55466

magnetohydrodynamic convertors continued
induction channel, liquid metal flow *(Russian)* 78−26341
induction machine, duct local flow charact. at large EM interaction parameter *(Russian)* 78−5818
induction MHD accelerator *(French)* 77−62410
induction MHD generator using alternating magnetic field 79−87997
induction MHD machine, integrated characts. *(Russian)* 78−26342
insulation wall deterioration *(Japanese)* 77−24200
interelectrode arcs and electrode pots. fluctuations 79−1348
interelectrode gap, increasing its electrical strength by gas blowing 78−9854
ionisation of additive, conductivity of combustion products 77−39472
isothermal expansion of a two-phase fluid in a magnetohydrodynamic generator duct 80−1695
laminar flow, longitudinal dynamic effects determination for Na, Al, Sn, and Hg *(Rumanian)* 80−64792
linear induction MHD machine, elec. cond. body motion in mag. field *(Russian)* 77−7468
linear induction MHD machine, ferromag. yoke effects calcs. *(Russian)* 78−75434
linear induction MHD machines, effectiveness of side bars *(Russian)* 78−47189
linear induction MHD pump, liq. metal flow, energetic characts. *(Russian)* 77−3882
liquid metal MHD generator, thermodynamics *(German)* 77−948
liquid metal MHD generator, wall-jet gas injection 80−28830
liquid metal MHD loop dynamic analysis 77−39479
liquid metal piston dynamics, math. model *(Russian)* 80−74996
liquid metal-gas two-phase MHD generator, pot. loss mechanisms, rel. to fluid dynamic processes 77−39359
liquid-metal, two-phase, power generation cycle, interfacial heat and mechanical energy transfers 80−1409
local characts., transverse current inhomogeneity in MHD channel 80−24146
long duration experiments, using flat plate metal electrodes and metal feed electrodes *(Japanese)* 77−89325
magnet, transverse-field water-cooled for MHD research 77−84528
metal electrodes erosion 80−24260
MHD channel, frame-type, two-dimens. elec. effects, numerical parametric soln. 78−42834
MHD generator, electrothermal instability in the seeded combustion gas boundary layer near cold electrodes 78−71547
MHD generator, simplest physical model 78−71548
MHD power generation, future prospects 80−35700
near-cathode region of metallic electrodes, arc discharge 79−1346
non-equilibrium, ionisation instability, finite boundary layer effect calc. 79−19098
non-equilibrium MHD generators, ionisation instability 77−72506
nonequilibrium channel, thermal diffusion of charge carriers, effect on electron density, obs. 79−68959
nonequilibrium MHD duct with resistive electrodes, computer simulation, performance characts. calc. 77−72509
nonequilibrium MHD power generation using nonseeded Ar plasma 77−24196
nonequilibrium plasma generator, diagonal type, 2-D numerical anal. 78−30491
open cycle generator channels, interelectrode strength *(Ukrainian)* 80−49016
open cycle MHD generator, channel metal surfaces, elec. characts. of boundary layer 77−39473
open cycle MHD generator, theory of nonuniform electrical conduction 80−28831
open-cycle, cathode spots on electrode slag films 77−89326
open-cycle, losses effect on characts. 77−68876
open-cycle, supersonic flow of combustion products, nonequilib. physico-chem. processes 80−103196
open-cycle MHD generator, electrode fabrication by plasma deposition 77−39474
oxy-acetylene combustion products, seeded, elec. cond. rel. to MHD power generation 77−3922
performance optimization of an MHD generator with physical constraints 80−40876
phase transition in condenser *(Russian)* 79−1350
plasma generator, diagonal nonequilibrium type, end effects 79−7492
plasma interelectrode breakdown, model 79−55572
plasma of combustion products at 2200 to 2600K, electron conc. rel. to MHD conversion 78−1889
plasma turbulence in combustion channel 80−75057
power take-off design for diagonal-conducting-wall MHD channels 80−89656
principle, research and 1979 development trends *(German)* 80−7949
pulsed, limiting energy generated, load characts. depend. 78−42833
pulsed fusion reactor energy conversion modelling 77−3165
pulsed generator for deep EM sounding of Earths crust 79−48589
pulsed induction discharge, Hall effect 79−64833
pulsed isothermal plasma generator plant for study of MHD flows 78−1907
pulsed MHD convertor, threshold energy characts. for elec. power production with resistive load 78−1908
rare earth chromite based electrode material development for MHD generators 80−84893
refractory channel walls, ceramic elements, thermal stresses calc. 77−70075
refractory materials in generator channel, thermophysical props. 77−28054
review of physical phenomena in MHD plasma generators 78−83623
screened duct, conducting liq. layer mag. field interaction, screening effects *(Russian)* 78−5819
segmented electrode wall, compressible laminar boundary layer separation 77−27598
series channels characteristics with diminishing electrode commutation angle 80−48818
series generator, transition region geometry 80−84010
series MHD generators, performance characteristics, loading factor influence 80−43790
shock tunnel MHD generator, high power density experiments 77−24195
simulated MHD combustion chamber working on natural gas and O^2 enriched air, NO formation investigation 80−106984
single-load, in combined steam power stations, performance and efficiency obs. *(Italian)* 80−26148

magnetohydrodynamic convertors continued
spirally-wound pump, EM processes in secondary medium, model *(Russian)* 77−3881
steam, production of short bursts of power 80−64789
structural analysis of power losses in liquid-metal slip contacts 80−43795
subsonic flow in MHD channel, acoustic stability 78−9764
subsonic MHD channel, acoustic props., calc. for longitudinal oscills. 77−35405
superconducting mag. system, saddle-shaped, construction 78−22579
superconducting magnet, structural analysis 77−27739
superconducting magnet system for U-25 MHD facility (Argonne) 77−27740
superconducting magnet systems for generators 78−55759
superconducting magnets for MHD test facility and base load power plant 77−27741
supersonic flow, in MHD generator, with inclined input stream *(Russian)* 78−94837
supersonic flow in generator channel, with slanted entrance stream 79−77429
supersonic MHD generator, working body thermodynamic props., chem. kinetics effect 78−91163
test facility safety analysis methodology and documentation system 80−61388
thermal plasma energy, direct conversion to electrical energy *(Russian)* 78−87502
thermodynamic and electric param. determ. *(Polish)* 77−7602
transverse edge effect attenuation 79−41883
U-25, diagnostics system data processing 78−26339
U-25, flow in channel 80−24261
U-25B MHD unit, channel construction 79−32829
U-25B MHD unit for expts. in strong electric and mag. fields 79−32828
uncompensated DC conduction pump MHD channel, pumping and generating characts. *(Russian)* 79−1352
variable operation, Faraday machine appl. 80−35699
velocity and current distributions inlet region, performance and efficiency anal. 79−92085
Window-Frame, with nonuniform velocity and conductivity in transverse plane, electric effects, anal. 79−68960
working fluid elec. cond. temp. depend. 79−4194
Ar magnetic helical arc electrode, for MHD generator, visible, RF and probe diagnostics 78−9867
Cu cathode spot, MHD generator channel conditions, temp. calc. 78−26359
H_2-O_2, duct flow calc., two-dimensional, velocity, temperature and electrical conductivity profiles determ. 79−83605
He requirements for superconducting power network 79−50897
He unit requirements, for superconductive energy appl. in USA 78−89999
K addition atoms, automatic system for conc. meas. 79−50892
K-seeded combustion layer near cold electrode 78−26335
K_2SO_4, seed, vaporisation thermodynamics, MHD generation appls. 77−9112
$LaCrO_3$-MgO, LC20M electrode material in open cycle MHD systems, thermionic emission characts. 80−97394
Na MHD generators, optimisation for maximum electrical efficiency, output and power factor *(Rumanian)* 80−64793
ZrO_2 stabilised with lime, possible electrode material *(Rumanian)* 80−65575
ZrO_2-Y_2O_3-Nd_2O_3, high-temp. thermophys. props., MHD generator electrode mat. 78−26663

magnetohydrodynamic generators *see magnetohydrodynamic convertors*

magnetohydrodynamic waves
Alfren waves, propag. in Earth liq. core, mag. field variations 77−81794
Alfven, parametric excitation by pump mag. field on high temp. plasma 77−65859
Alfven, Tokamak reactor toroidal effects, direct mag. field approx. *(Russian)* 77−51166
Alfven and magnetoacoustic wave mode coupling in solar corona, cold plasma approx. 78−12178
Alfven drift wave, from lower hybrid wave parametric decay 77−68791
Alfven kinetic wave parametric excitation by whistler waves 77−27668
Alfven nonlinear gravit. drift waves and β limitations in Tokamaks 80−92369
Alfven parametric excitation by pump mag. field 77−31448
Alfven perturbations in nonuniform plasma *(Russian)* 78−26259
Alfven pulse-excited instability in neutral sheet, mag. field lines reconnection dynamics *(Russian)* 80−1768
Alfven wave, compressional, in laser heating of plasmas, filamentation instability 77−35342
Alfven wave, obliquely propagating, nonlinear behaviour 78−75288
Alfven wave, shear, low freq., heating in Heliotron-D, diagnostics 78−1858
Alfven wave absorpt., MHD and guiding centre plasma models comparison 77−42969
Alfven wave at ATS 6, soln. with finite ionospheric conductivity 79−12346
Alfven wave damping in nonuniform plasma, continuous spectrum phase mixing 78−47112
Alfven wave decay instability in hot plasma, two liq. hydrodynamic approx. *(Russian)* 79−7452
Alfven wave energy spectrum temporal evolution, nonlinear Landau damping rel. to solar wind 78−53813
Alfven wave energy transformation and heating by acoustic waves for stimulated Mandelstam-Brillouin scatt. *(Russian)* 77−11328
Alfven wave excitation by fast ion beam in two-component Tokamak, Coulomb collisions 79−37509
Alfven wave excitation by fast ions, finite-β plasma 78−51299
Alfven wave heating, plasma resistive effects 78−1857
Alfven wave heating in Proto-Cleo stellarator 77−7565
Alfven wave heating in Proto-Cleo stellarator 78−83587
Alfven wave heating in toroidal plasma 80−28740
Alfven wave heating of a theta pinch 78−75379
Alfven wave heating of high beta plasma 77−39436
Alfven wave in stochastic mag. field Markovian approx. 77−51168
Alfven wave instability excitation by trapped α-particles 77−65855
Alfven wave plasma heating, helical launching struct., Proto-Cleo stellarator 77−72456
Alfven wave prod. in ion-acoustic parametric decay 77−975
Alfven wave propag. in solar atmosphere 78−53909

magnetohydrodynamic waves continued
Alfven wave propagation in density gradient in sunspots 77−33437
Alfven wave reflection at density transition region 77−29754
Alfven wave resonant mode conversion, kinetic processes in plasma heating 77−19730
Alfven wave scattering, integral eqns. 80−83848
Alfven wave system, eqn. of state, thermodynamic props., Bose-Einstein statistics 78−87397
Alfven wave turbulence, interaction with whistler wave turbulence 80−64728
Alfven waves, accelerated particles distrib. function, self-similar solns. 79−32757
Alfven waves, accelerated particles distrib. function, self-similar soln. 80−56702
Alfven waves, appls. to plasma heating in linear and toroidal geometries 79−10676
Alfven waves, charged particle diffusion and perpendicular flux 77−84406
Alfven waves, circular polarisation, propagation in mag. field, spiky soliton 80−28662
Alfven waves, circularly polarised, spiky soliton soln. to nonlinear evolution eqn. 80−38590
Alfven waves, collapse, energy transfer mechanisms *(Russian)* 77−76075
Alfven waves, exact, nonlinear, existence of solitons 80−24159
Alfven waves, excitation in clusters of galaxies intracluster space rel. to gas heating 79−25735
Alfven waves, excitation of convective cells in plasma *(Russian)* 78−47097
Alfven waves, finite amplitude circularly polarised, instability 78−28502
Alfven waves, finite amplitude solitary 78−83551
Alfven waves, finite-amplitude circularly polarised, instability 79−4122
Alfven waves, in stochastic mag. field, Khasminskii's theorem 80−59198
Alfven waves, interaction with trapped electrons in Tokamak *(Russian)* 77−11338
Alfven waves, interplanetary, evidence from mag. field large scale struct. 79−29962
Alfven waves, ion beam effect on stability *(Russian)* 78−38468
Alfven waves, Landau damping in solar wind 80−21885
Alfven waves, liq., metal gigajoule energy storage device, secondary flow 77−39353
Alfven waves, monochromatic non-WKB, normals evolution in solar wind 80−101521
Alfven waves, parametric amplification in plasma 77−27667
Alfven waves, parametric excitation and amplification in wall stabilised DC arcs 77−35340
Alfven waves, parametric excitation in cylindrical plasma 80−24157
Alfven waves, satellite, interaction with α-particles in Tokamak, quasi-linear theory 77−42995
Alfven waves, torsional, axisymmetric, discrete/continuous spectra, appl. to waveguide 78−59587
Alfven waves, turbulent, particle accel. and plasma heating in radiogalaxy 77−13227
Alfven waves collisionless damping in inhomogeneous plasma, initial value problem soln. 79−64864
Alfven waves generated by an inverted plasma energy distribution 78−85775
Alfven waves in α-effect turbulent dynamo 79−72954
Alfven waves in finite-β current carrying plasma, monoenergetic fusion product effects 78−91101
Alfven waves in ionosphere, boundary condition 79−53611
Alfven waves in ionosphere/magnetosphere, rel. to coherent anomalous resist. assoc. with electrostatic shocks 80−4189
Alfven waves in Jupiter magnetosphere, rel. to Io interaction with plasma torus 80−98604
Alfven waves in near-Earth plasma stimulated excitation by pulsed radio emission 79−58192
Alfven waves in solar atmosphere above coronal holes, rel. to energy balance and solar wind accel. 79−92746
Alfven waves in solar photosphere, refl. rel. to sunspots cooling 79−5799
Alfven waves in solar transition zone and corona, refl. and disorder 79−12453
Alfven waves in solar wind, models 79−16789
Alfven waves in sunspots, prod. by convective overstability in mag. field in downdraft 80−21960
Alfven waves modulational instability, solitons 78−59576
Alfven waves self-modulation by cyclotron instability in magnetosphere *(Russian)* 78−40765
Alfven waves shear driven instability 77−72433
Alfven waves transmission through Earth's bow shock, theory and obs. 78−45157
Alfven-acoustic-gravity wave propag. and reflection, compressible, inviscid, perfectly conducting isothermal fluid 77−51124
Alfven-drift wave coupling, destabilisation 77−19694
Alfven-type drift oscills., microinstabilities 78−22496
Alfvenic surface waves in solar corona, reson. absorpt. and coronal loops heating 79−16905
anisotropic surface wave system, common wave phenomena appl. 77−24029
asymptotic shock wave propagation in EM field 77−75982
atmosphere, MHD wave propag. in presence of rot. and variable mag. field 79−40024
blast wave in gravitational field 78−83496
Cassiopeia A, Alfven waves generation rel. to radio spectrum secular flattening 80−101637
cold plasma, Alfven shock waves in presence of effective electron-ion collisions 78−26286
collisionless shocks, extended Rankine-Hugoniot relations 78−75209
complex demodulation for nonstationary data anal. *(French)* 79−70922
convectively neutral fluids, perturbation spectra of pure MHD oscills. 77−41292
Coriolis force influence on LF waves in rotating plasmas 78−75309
cosmic rays interplanetary accel., one-dimens. model with moving MHD shock wave 79−80119
current-driven collisional drift and Alfven instabilities 79−46445
cylindrical MHD shock wave propag. 79−98815
damping, effective conductivity in weakly ionized plasma 77−51160
dispersion of small amplitude waves in relativistic magnetohydrodynamics 79−4176
drift Alfven waves, convective cells form. by modulational instability 79−77364

magnetohydrodynamic waves continued
drift-Alfven mode stability, local theory 79−19012
drift-Alfven waves in a sheared magnetic field, numerical anal. 79−94788
electron heating due to kinetic shear Alfven wave 79−90425
electron interaction at bounce resonance, magneto-acoustic wave excitation *(Russian)* 78−22473
electrostatic lower hybrid wave, nonlinear decay to whistler and Alfven wave pair 78−26275
explosion interactions in magnetisable ideally cond. media *(Russian)* 77−55037
F_2-layer, MHD waves ducted propag. 77−2299
fast ion excitation of monochromatic Alfven waves *(Russian)* 77−19718
ferrofluid, relativistic conducting, wave propagation, velocities *(French)* 77−15138
finite amplitude solitary Alfven waves 80−53973
finite element calculation of MHD spectrum of straight plasma column with arbitrary cross section 77−11327
finite-β collisional plasma, temp. fluctuations and wave induced losses with draft-Alfven instability 77−3934
Galaxy, waves propag. from galactic centre rel. to origin of 3 kpc arm and North Polar Spur 77−87547
gas flows in inclined mag. field, simple stationary waves *(Russian)* 77−27603
geomagnetic Pc 4 pulsation event, satellite meas. of Poynting vector of standing MHD waves 78−45162
geomagnetic Pc 5 quiet-time pulsation events (Spacequakes), origin in outer magnetosphere 79−40025
geomagnetic pearl-type pulsations, nonlinear evolution, role of proton injection processes 79−35065
geomagnetic Pg pulsations, obs. 79−29940
geomagnetic Pi 2 pulsations, polarisation characts. and phase differences at conjugate stations 79−21107
geomagnetic pulsations, high latit., time of flight calcs. 79−62688
geomagnetic pulsations, long-period, synchronous obs. on ATS-6 satellite and at Earth surface 79−12345
geomagnetic ULF pulsations obs. at large longit. separations, rel. to interplanetary mag. field directions 77−87201
geometrical wave coupling in solar wind 78−77450
helical MHD oscillations, dynamic props. obtained from amplitude-phase freqs. *(Russian)* 77−89258
helical system, MHD instabilities 80−1829
helical waves in tail of Comet Morehouse (1908 III), WKB approximation theory 80−4305
HF heating by MHD waves of finite press. plasma *(Russian)* 80−83950
hydromagnetic stability of compressible fluid 79−32689
hydromagnetic-inertial-gravity waves, propag. in magnetic-velocity shear 79−55422
interplanetary Alfven waves, Fokker-Planck theory for cosmic ray diffusion 77−29606
interplanetary Alfven waves, influence of shock waves rel. to solar particle propag. 77−49250
interplanetary medium, Alfven and magnetosonic waves from mag. field power spectra 77−29617
interplanetary medium, Alfven Mach number rel. to collisionless shock waves thickness 80−90314
interplanetary medium, Alfven waves rel. to mean free path of low-rigidity cosmic rays 80−98524
interplanetary medium, slow MHD shock waves 78−12068
interplanetary MHD waves, nonlinear steepening and Landau damping 78−28477
interplanetary shock waves in turbulent medium, energetic particles interaction 80−4210
interplanetary waves due to solar surface oscillations, geophysical effects 79−8777
interstellar Alfven waves, rel. to cosmic rays from dense mol. clouds 77−13190
interstellar cloud, effect of nonlinear torsional Alfven waves on cloud rot. mag. braking during star form. 80−90493
interstellar dense clouds, differential rotation producing MHD waves causing heating 78−8096
interstellar medium, cosmic ray generated anisotropic MHD turbulence 77−45532
interstellar medium, inertial range of weak MHD turbulence 77−45528
ion ring, precessional mode stabilisation using general mag. multipole field 77−24174
ionising MHD shock wave propag., in nonuniform medium 78−5874
ionized medium, technique for rot. freq. meas. 80−41730
ionosphere, elec. field oscills. meas. near auroral arc, assoc. with MHD wave 78−65457
ionosphere, geomag. pulsations damping 78−49218
ionosphere, lower total cond. vars. effect on long-period MHD pulsations propag. 78−40730
ionosphere, MHD wave propag. characts. 77−2298
ionosphere, MHD waves as cause of simultaneous F-region and geomag. oscills. 77−9615
ionosphere, obs. of concurrent 0.005 to 0.5 Hz precip. pulsations and mag. field pulsations 77−53307
ionosphere, slow MHD waves theory 78−45093
ionospheric disturbances, effect on guided MHD waves 78−73568
jet, two-dimensional, effect of density and cond. discontinuities on MHD stability 77−31396
Jupiter as source of MHD waves, solar activity effects 78−57526
Jupiter magnetosphere, MHD waves rel. to particle accel. 79−12428
Kapitza MHD gravity-capillary waves in liq. film falling by permeable bed 78−67277
kink instability and energy principle in toroidal plasma 79−10650
laminar boundary layer flow along flat plate with transverse mag. field, MHD stability 79−27709
Lorentz covariant eikonal method, dispersion relation, for cold one-component plasma 77−27663
magnetic flux tubes in solar atmosphere, wave modes 79−29984
magnetic-velocity shears, linear wave motions 77−58799
magnetisable fluid, conductive, nonlinear magnetosonic waves 80−59121
magnetoacoustic turbulence, collision free mechanism *(Russian)* 78−22502
magnetoelastic oscillations of electrically conducting elastic layers, anal. *(Russian)* 78−48021
magnetogasdynamic spherical shock waves, propag. in exponential medium 79−84664

magnetohydrodynamic waves continued
magnetogravity waves, propag. in isothermal conductive atmosphere 79−92670
magnetohydroelectric waves in fluid dielectric 79−27703
magnetopause, MHD waves interaction 77−91372
magnetopause Kelvin-Helmholtz instability, effect of finite ion Larmor radius 79−80096
magnetosheath, dayside, MHD waves rel. to plasma press. anisotropy and mirror instability 77−37483
magnetosheath and magnetosphere, mag. fluctuations anal. rel. to Pc pulsations reson. theory 79−80092
magnetosphere, Alfven and compressional waves coupling 78−89001
magnetosphere, Alfven wave stimulation by trapped electrons, geomag. pulsation generation *(Russian)* 77−22003
magnetosphere, Alfven waves, axisymmetric, dipole field model with finite ionospheric cond. 79−29941
magnetosphere, Alfven waves and elec. currents over auroral arc 77−33296
magnetosphere, Alfven waves and trapped particles nonlinear bounce resonant interaction 79−48624
magnetosphere, Alfven waves excitation by bouncing electron beams rel. to nightside mag. pulsations 80−4203
magnetosphere, assoc. elec. field, mag. field and electron precip. fluctuations 78−81507
magnetosphere, characteristics rel. to plasma density gradients near L=4 77−25878
magnetosphere, effect of bounce resons. on Alfven waves generation outside plasmasphere 79−12344
magnetosphere, first adiabatic invariant for charged particle interacting with linearly polarised plane wave 77−78580
magnetosphere, hydromagnetic pulsations generation by Kelvin-Helmholtz instability 78−73584
magnetosphere, increasing freq. wave generation in evening sector during substorms 79−62680
magnetosphere, kinetic Alfven wave turbulence producing anomalous transport phenomena 78−57402
magnetosphere, latit. dependent waves and impulse-produced waves 77−49245
magnetosphere, localised compressional MHD waves, in ring current 77−64543
magnetosphere, long-period geomag. oscills. rel. to energetic particle fluxes modulation 79−25407
magnetosphere, magnetoacoustic waves generation by high-freq. turbulence 77−13187
magnetosphere, MHD rarefaction wave rel. to plasma sheet thinning model 77−78579
magnetosphere, MHD wave energy, effect of geomag. latitude 77−25889
magnetosphere, MHD waves orientation 79−8783
magnetosphere, particle flux instability and geomag. pulsations generation 77−49232
magnetosphere, particle flux modulations by Pc 5 waves, Ogo 5 obs. 77−87190
magnetosphere, Pc 4 compressional pulsation obs. from geostationary orbit near local midnight 79−80094
magnetosphere, plasma sheet modes rel. to Pi 2 pulsations 79−66875
magnetosphere, relativistic electrons interaction with Alfven waves *(Russian)* 78−49229
magnetosphere, statistical study of Pc3 magnetic pulsations at synchronous orbit 77−45256
magnetosphere, toroidal line resons. rel. to continuous (Pc 3,4) pulsations in European sector 80−21877
magnetosphere, ULF waves obs. with mag. and elec. sensors on GEOS-1 79−25410
magnetosphere hydromagnetic oscills., VLF noise intensity modulation 78−45139
magnetosphere plasma, MHD wave coupling region, rapid changes 79−75050
magnetosphere substorm-associated long-period hydromagnetic waves, longit. extent 78−40772
magnetosphere surface waves, particle accel. and auroral arcs form. 77−9621
magnetosphere ULF waves, cold plasma densities meas. comparison with VLF whistlers 78−28436
magnetotail, Alfven wave generation via proton accelerator 78−73582
Maxwell stress tensor in turbulent medium, calc. *(Russian)* 78−71483
MHD gravity waves, dispersion on running stream of inviscid elec. cond. liq. 78−59502
MHD modes in Tokamaks, X-ray techniques 78−47175
MHD-gravity waves, over-reflection in stratified flow 77−11207
micropulsations reson. struct. in magnetosphere, multiple satellite obs. 77−33289
near-Alfvenic upper-hybrid envelope solitons 79−98898
neutral current layer dissociation, external plasma effect *(Russian)* 78−18409
nonlinear Alfven wave in an ultra-relativistic electron-positron plasma 80−106905
nonlinear Alfven waves, in hot plasma, struct. and stability *(Russian)* 79−37473
nonlinear behaviour of axisymmetric waves in plasma 78−59573
nonlinear effects in propag. of torsional waves in plasma 78−59574
nonlinear magnetostatic modes and twisting modes with magnetic islands 80−106900
nonlinear monochromatic wave, source of particles effect *(Russian)* 78−9779
nonlinear plasma waves, limit shock waves 79−77382
nonlinear sonic wave, excitation by quasi-monochromatic Alfven pumping 80−106649
nonlinear theory of propag. in turbulent plasma *(Russian)* 78−14165
oblique shock waves calc. 79−77263
optically thin medium, weak MHD discontinuity propag. 79−46438
paramagnetism of plasma in RF field 79−46490
parametric interaction between two Alfven waves 78−67336
Pc1 ducted propagation in upper ionosphere 77−17292
Pc 5 micropulsations, examination of ionospheric reson. region by dual auroral radar system 78−65454
Pc 5 waves, OGO-5 obs., ground-magnetosphere correl. 77−9623
perturbations due to localised flows, eddy theorem 79−41822
physiological aqueous solution, possibility of wave excitation 80−94246
plane isotropic magnetogasdynamic waves, Burgers's eqn. 78−51247
planetary waves propag. on beta plane through mag. and vel. shear 77−60457

magnetohydrodynamic waves continued
plasma, Alfven and magnetoacoustic vortices *(Russian)* 77−80302
plasma, Alfven wave heating 77−68817
plasma, Alfven wave nonlinear self-precession and wavenumber shift 80−10389
plasma, compressible magnetic-field reconnexion 80−6226
plasma, current discharge, mag. reconnection temporal evolution near mag. neutral line 79−32756
plasma, drift Alfven waves in Tokamaks, instability 78−79431
plasma, fast magnetoacoustic-Alfven waves interaction, instability phenomena 77−62351
plasma, hydrodynamic wave description including electron spin 80−38643
plasma, in Tokamak thermonuclear reactor, MHD modes drift phenomena, kinetic method *(Russian)* 80−1827
plasma, inhomogeneous, Alfven and ion-Bernstein waves, mode conversion and tunnelling 78−34300
plasma, ionising MHD shock wave struct. *(Russian)* 77−7541
plasma, magnetoacoustic disturbance, hydrodynamic instability in nonuniform plasma flow *(Russian)* 80−1766
plasma, magnetoplasma wave, quasistatic density perturbation, universal formula 79−60131
plasma, MHD waves parallel to mag. field, modulational instability 77−15181
plasma, MHD waves segregation in ideal medium 78−87440
plasma, modulation instability *(Russian)* 77−89259
plasma, non-Hermitian radial mode eqns. 77−89244
plasma, nonlinear MHD mode struct. in pinch 77−974
plasma, nonuniform, kinetic theory of MHD instability 77−15190
plasma, obliquely propagating nonlinear Alfven wave, perturbation method approach 77−15176
plasma, sheared Alfven waves, transient growth 79−41824
plasma, two-electron temp., nonlinear hydromag. waves 79−98884
plasma flow, steady, shock and soliton solutions 77−15172
plasma heating by Alfven waves in Proto-Cleo stellarator 78−9802
plasma ion heating, by nonlinear ion-sound waves, excited by whistlers and Alfven waves *(Russian)* 79−27783
plasma LF wave excitation by AM microwaves 77−62366
plasma supersonic flow around conducting bodies, inductive interaction *(Russian)* 79−27789
plasmas, non-uniform, finite pressure, hydromagnetic oscills. coupling modes, two-fluids model 79−21108
plasmasphere, lower ionosphere effect on MHD modes 79−35055
plasmo-hydrodynamical modes, model eqn. for study 77−42976
propagation and interaction of m=0 torsional waves 77−65850
propagation in anisotropic media, electrical dissipation effects *(Japanese)* 78−87445
propagation in inhomogeneous mag. fields 79−60121
propagation in mag. flux sheath in presence of vel. field 79−62735
propagation in rotating cylindrical annulus, model for Earth mantle-core interface 78−28194
relativistic MHD growth and decay discontinuities 80−92280
relativistic self-inductive radiative fluid 79−41772
relativistic shock waves, plasma and condensed medium 77−24035
resistive drift Alfven waves in sheared mag. fields 80−64718
shear Alfven waves, quasi-linear theory 80−64714
shear flow stability and Alfven waves in magnetised plasma 80−96360
shock wave, plane, magnetogasdynamic, variable strength 79−98813
shock wave propagation at conducting gas boundary 78−79383
shock wave propagation in inhomogeneous atmosphere 79−55426
shock wave refl. from conducting wall *(Russian)* 77−80223
shock waves, particle refl., energy spectrum and pitch angle distrib. 79−35126
shock waves in thermally-conducting medium 78−59581
shock waves with heat addition 79−55427
simple waves and strong discontinuities in a magnetizable medium 80−69935
solar atmosphere, hydromagnetic wave particle interactions rel. to moving type IV radio bursts 79−40174
solar atmosphere, MHD-gravity wave critical levels 78−77531
solar atmosphere, propag. of MHD shockwaves 78−24503
solar atmosphere, sound generation by Alfven waves with random phases 78−7979
solar atmosphere and solar wind, momentum and energy transport by waves 78−4162
solar atmosphere upper layers, convective noise waves dissipation in mag. struct. 78−65600
solar chromosphere, magnetoacoustic wave propag., resonance phenomena 77−13306
solar corona, Alfven waves above sunspots from forbidden line obs. 77−78732
solar corona, fast mode waves evanescence 78−89147
solar corona, heating, dissipation of elec. currents or MHD surface waves 79−75180
solar corona, heating and wave generation by prominence turbulence 80−72907
solar corona, loop heating by fast mode waves 80−41801
solar corona, MHD wave mode coupling, stratified media 78−20775
solar corona, MHD waves, mode coupling, reduction of coupled eqns. 78−20776
solar coronal heating and solar wind accel. by Alfven waves 77−71098
solar coronal heating by Alfven waves 77−29785
solar flare, 1973 September 5, radio data and theoretical model for fast-mode MHD shock wave 79−92734
solar magnetic flux elements vibr. modes in stratified atm. 79−16902
solar magnetoatmospheric waves, inhomogeneous wave eqn. 77−82189
solar magnetoatmospheric waves conical propag. and spicule motions 77−49351
solar quiescent prominences, Alfven waves rel. to vertical struct. of vel. fields 77−53522
solar transition zone, Si IV line profile vars., rel. to MHD disturbances 78−28626
solar type II radio bursts, radiation from MHD shock front *(Russian)* 77−87259
solar wind, accel. by Alfven wave flux from Sun 80−85923
solar wind, Alfven waves local instabilities in high speed streams 78−77546
solar wind, deposition of momentum and energy by MHD waves 77−37493
solar wind, dynamic mag. struct. of large amplitude Alfvenic vars. 80−72734
solar wind, first adiabatic invariant for charged particle interacting with linearly polarised plane wave 77−78580
solar wind, MHD shock waves numerical simulation 78−77449
solar wind, MHD solitons theory 80−4217
solar wind, microscale fluctuations obs. rel. to Alfven waves 77−87224
solar wind extended heating by fast MHD waves 77−53504
solar wind high-speed streams, accel. by Alfven waves 78−45298
solar wind high-speed streams, nonlinear Alfven waves 77−33315
solar wind large amplitude Alfven waves propag. direction rel. to average interplanetary mag. field 80−26709
solar wind physical processes 79−75071
solar wind wave spectrum, consequences of microinstability onset 77−87222
spectrum of elliptic plasma column 77−31451
stationary periodic waves with Hall dispersion, magnetohydrodynamic approx. *(Russian)* 77−27661
stellar atmospheres, MHD waves propag. in mag. flux tube 78−69789
stratified compressible atmosphere with shear MHD wave-energy flux 78−93053
subauroral red arc event caused by kinetic Alfven waves 78−93026
substorm associated long period MHD waves 77−87195
Sun, coronal thermal stability during fast mode wave heating 80−90397
Sun, use of MHD pulses as diagnostic technique 80−109405
sunspots, Alfven waves rel. to thermal struct. 77−5517
sunspots, MHD wave damping 77−5514
sunspots cooling mechanism, overstability and Alfven wave prod. 77−78733
supernova remnant simulation by MHD wave fronts *(Italian)* 79−53885
supernova remnants, MHD wave fronts, filamentary struct. form. 78−81668
supernova remnants, waves effects on cosmic rays escape and adiabatic energy losses 79−16771
supra-thermal trapped electron quasi-linear diffusion, mag. drift reson. and Alfven wave excitation *(Russian)* 79−27748
surface hydromagnetic waves, dissipation 80−21904
surface hydromagnetic waves, props. and astrophysical appls. 79−25462
surface MHD waves in arc discharge, low freq. spectrum, instabilities *(Russian)* 77−68762
surface wave excitation by charged particle beams 77−55157
surface waves on cylindrical fluxtubes rel. to Sun 79−75098
switch-on shocks, ionis., heating 77−80320
symmetric wave modes in magnetic flux sheath 78−49304
synchrotron radiation from MHD shock wave front of magnetic field discontinuity, astrophysical appls. 77−25939
thermonuclear Alfven instability stabilisation in high press. tokamak, mag. surface distortion *(Russian)* 79−27758
Tokamak, noncircular cross section, fast neutral atom injection, collective processes, Alfven waves *(Russian)* 77−47221
toroidal relativistic beams, kink instability, shear Alfven modes 77−76122
turbulent dynamo problem *(Russian)* 78−63501
turbulent plasma, electron distribution function, correlation anal. 79−14547
turbulent plasma, kinetic Alfven waves, coherent, anomalous damping 77−31469
turbulent plasma, plasmon gas oscillations *(Russian)* 78−47120
ULF magnetospheric waves, identification using cross-spectral matrix *(French)* 79−70929
ultra-relativistic electron-positron plasma, macroscopic wave behaviour 80−106904
unstable continuous spectrum, noncircular rotating θ pinch 79−94779
upper atmosphere, MHD waves absorpt. as heating source 79−53588
vertically propagating, in isothermal atm. with horizontal mag. field 80−6162
Vlasov stability, particle reson. effects in axisymm. field reversal config. 78−83553
weak discontinuities, growth and decay 79−86519
whistler waves, modulated by kinetic Alfven and ion quasimodes 77−80293
whistler-Alfven turbulence interaction 80−75058
Woods' MHD waveguide, guided modes, locally excited MHD waves, wave eqn. 77−51199
Bi, EM wave dispersion and damping, Voigt configuration, non-local calcs. 80−100475
H_2 plasma, MHD and transverse ionising shock waves, jump conditions, ionis. effects 79−32775

magnetohydrodynamics
see also magnetohydrodynamic conversion; magnetohydrodynamic convertors; magnetohydrodynamic waves; plasma magnetohydrodynamics
α^2-dynamos, finite amplitude, with large scale in compressible circulation, theory 78−81534
α-effect dynamo, determ. for slow and fast rot. 79−40069
α-effect turbulent dynamo, consistency 79−72954
$\varepsilon \mathrm{grad}^2 u = \delta u/\delta y$, $0<\varepsilon\ll 1$, over rectangle, asymptotic soln., MHD appl. 77−9863
acoustic pulse propag. dispersion effects calc. *(Russian)* 78−5809
air-Hg flow, stratified, co-current, in rectangular channel, interfacial wave structure 80−74955
Alfven shock evolution is classical MHD *(French)* 78−18352
alternating flow in circular pipes of finite conductivity *(Japanese)* 79−7414
anisotropic explosion of magnetized spheroids 80−67532
annular channel with radial mag. field, Poiseuille flow, Hall effect 78−67276
anti-dynamo theories, compressible flow effect 80−56361
arc welding electrode metal drop free surface calc., MHD anal. *(Russian)* 78−5822
astronomical MHD, monograph 78−40816
astrophysical nonlinear dynamos, multiple period dynamo wave oscills. and solar cycle modulations 79−16813
astrophysical plasma charged particle accel. by MHD shock waves 80−101532
asymptotic stability of nonisothermal MHD, invariance principle appl. 79−97197
atmosphere hydromagnetic dynamo 78−96335
atmospheric whistler source location and generating proton spectra 77−64542
axial flow in triangular pipe, transverse mag. field effects 80−53870

magnetohydrodynamics continued
axial MHD flow in triangular pipe with transverse mag. field 78−59498
axisymmetric body in viscous conducting rotating fluid in mag. field, slow motion 79−50805
axisymmetric convection in prescence of mag. field, solar granulation and sunspots appl. 80−12724
axisymmetric jet of magnetisable fluid, stability 80−14835
axisymmetric MHD flow due to current spreading *(Russian)* 77−65810
axisymmetric steady flow, slightly conducting gas in mag. field 77−15128
Benard problem, uniform mag. field, local pot. method 77−84333
Bernoulli flow, singular point 78−4099
Bernoulli integral and circulation rate conservation in magnetisable liq. *(Russian)* 78−87400
Bianchi type-I MHD cosmologies 77−67150
Bianchi universes, magnetic fields and fluids with conductivity 80−83864
binary stars, MHD oscills. and particle acceleration 79−58382
black hole fields, MHD relativistic processes 78−12280
black hole MHD 78−12281
blast wave problem in conducting gas 79−37414
blast waves, cylindrical, nonsimilarity solns. 77−39357
blast waves, magneto-gasdynamic radiative, cylindrical, similarity soln. 79−37338
blunt obstacles in channels, MHD with inertia 77−84330
BN-600 reactor first loop, MHD phenomena 80−37421
boundary layer, unsteady, similarity problems 78−1633
boundary layer flow, on flat plate, effects of varying velocity 78−67275
boundary layer flow between two oscillating discs 77−39355
boundary layer flow on flat plate, effect of transpiration 77−24028
boundary layer flow past vertical plate similarity solns. 77−65803
boundary layer function, MHD flow over flat plate 79−27696
boundary layer function in MHD flow over flat plate, asymptotic behaviour 79−46393
boundary layer growth in 3-dimens. with aligned mag. field 79−64790
boundary layer on porous plate with suction and blowing 78−34201
boundary layer similarity eqns. of mHD flow past a semi-infinite flat plate with heat transfer, exact numerical solns. 80−83861
boundary layer transition and turbulence, mag. field as investig. tool 80−1696
boundary layers, laminar, control problem *(German)* 78−91024
boundary layers, unsteady MHD, on porous plate in rot. system 77−24027
Brinkley-Kirkwood method, appl. to shock waves in stellar atm. *(Russian)* 78−93102
bubble growth in magnetic field 77−7462
bubble motion in liquid Hg 78−91021
capillary discharge, high-current, magnetogasdynamic regime 79−86628
Cassiopeiae A, supernova remnant, mag. field origin 80−85989
Cauchy problem for general relativistic perfect magnetofluid 78−70024
cavitation bubble, in magnetisable fluid, mag. field and press. effects on shape *(Russian)* 77−27608
cavitation in nonuniform mag. fields 80−19518
cell, capillary-Hg electrolyte, elec. characts. rel. to mag. field, gravity 77−1937
channel, annular, finite length *(Chinese)* 80−43781
channel, curved, of rectangular cross section, 3-dimens. MHD, numerical investigation 79−94734
channel, effect of force field nonuniformity on flow *(Russian)* 78−47044
channel, elec. cond. fluid in mag. field with incident EM wave, mag. press. 80−33698
channel, EM field eqns. averaging at finite mag. Reynolds no. 79−77282
channel, rectangular, inhomogeneously cond. flow calc. 79−94732
channel, vertical, round, in nonuniform mag. field, steady-state MHD convection 80−33696
channel entry MHD flow in axial mag. field 77−47097
channel flow, complex shapes, elec. field theory *(Russian)* 77−3879
channel flow, effects of couple stresses 78−18353
channel flow, fluid with variable viscosity, free convection effects 78−14090
channel flow, minimax principle 77−15133
channel flow, under transverse magnetic field 78−47043
channel flow effect of force field nonuniformity 79−86520
channel flow eqns. between electrode walls, fast parabolic module 77−72423
channel flow heat transfer, Hall effect and ion slip 77−80220
channel flow heat transfer, third-kind temp. boundary conditions 77−47095
channel with uniform wall heat flux, heat transfer, Hall and ion-slip current effects 80−92230
charge particle electric double layer, large distortion by shear flow 79−68818
charged gas flow, multicomponent eqns. *(Russian)* 79−14488
charged homogeneous cosmologies, theory 79−25767
charged particle transport in turbulent magnetic fields, perpendicular diffusion coeff. 77−42920
chemically reactive channel flow, effect of external circuit on dispersion of soluble matter 79−1267
chemically reactive flow near slender wing with supersonic leading edge *(Italian)* 79−14495
chemically reactive flow parameter distrib. near weak shock wave *(Italian)* 79−14494
circle theorems for inviscid steady flows 80−59043
circulatory assist device using blood pumping by mag. field 77−56518
coal slag particles deposition rate on channel wall, theoretical and expt. studies review *(Japanese)* 78−38413
coaxial cylinders, curved channel MHD, difference eqn. soln., Dean's problem 79−94731
cold cathode low press. arc retrograde motion in strong mag. field, theory 79−27858
collineation and motion in an electromagnetic field with induction 79−50804
combustion fronts in relativistic MHD *(French)* 77−47115
combustor and channel temp. meas., microprocessor based Na reversal instrument 80−73364
comet tails, hydromagnetic models 80−56773
cometary plasma acceleration, role of mag. structs. 80−46486
cometary plasma tails fine structure 79−12432
comets, MHD model 79−2522
comets plasma tails, disconnection rel. to mag. field line reconnection at interplanetary sector boundaries 78−93155
magnetohydrodynamics continued
compensated, two channel conduction MHD pump with leakage current, obs. *(Russian)* 78−75228
composite mixture, flow through porous medium, Rayleigh-Taylor instability 80−69912
compressible, subsonic flow meas., use of Pitot tube probe 77−84347
compressible finitely conducting rotating fluid in mag. field, Rayleigh-Taylor instability 80−10228
compressible fluids, thermal instability in presence of mag. field and rotation 77−89204
compressible laminar boundary layer separation from segmented electrode wall of MHD generator 77−27598
conducting dusty fluid, unsteady flow through rectangular channel with time depend. press. gradient 79−14486
conducting flow over oscillating plate with suction or intermediate layer 77−47098
conducting fluid, flow and heat transfer in channel in mag. field *(Russian)* 78−75218
conducting fluid, heated below, stability in parallel mag. and gravit. fields 77−7472
conducting fluid, laminar rot. in cylindrical vessel, elec. and mag. field effects *(Russian)* 78−75222
conducting fluid, nonstationary flow in tube in mag. field *(Russian)* 78−75219
conducting fluid, two dimens. motion, mag. field evolution, anti-dynamo theorem extension *(Russian)* 80−59127
conducting fluid film drainage over permeable wall in transverse mag. field 79−41761
conducting fluid in annulus, MHD laminar flow 77−42922
conducting fluid in crossed fields MHD rot., appl. nuclear rocket motor *(Russian)* 78−47059
conducting fluid in cylindrical MHD induction pump, laminar flow 80−43788
conducting fluid in porous box, thermohydromag. stability and onset of convection 77−62308
conducting fluid with spherical particle suspension oscillating flow in mag. field 80−79408
conducting fluids, dynamics under rotational mag. forces 80−48820
conducting liq., heated layer in mag. field, convection stability numerical calc. *(Russian)* 78−47053
conducting liq. in half-space and plane channel, nonuniform mag. field, nonstationary flow *(Russian)* 78−47057
conducting liq. in mag. field, convective flow stability *(Russian)* 78−47052
conducting liq. layer, surface tension effects, MHD convection stability and thermocapillarity *(Russian)* 78−47054
conducting liquid, eddy current induced pumping, longit. current in corrugated tube *(Russian)* 78−75216
conducting liquid, in cylindrical induction furnace, velocity and EM field distrib. calcs. *(Russian)* 77−47106
conducting liquid, plane-parallel shear flow, elec. current and mag. field effects *(Russian)* 78−75221
conducting liquid flow on moving porous plate with Hall effect 79−18964
conducting liquid in crossed electric and mag. fields, instability *(Russian)* 78−26211
conducting media, flow dynamics, complex geometry, in strong mag. fields *(Russian)* 77−47103
conducting medium, high temp. plane flow turbulence, mag. field effect *(Russian)* 77−65811
conducting non-Newtonian liq., shear disturbance propag., mag. field effect *(Russian)* 77−65809
conduction flowmeter, weighting function, mag. field distrib. effects *(Russian)* 77−47121
conduction MHD systems, feedback and self-excitation threshold calcs. *(Russian)* 77−47108
conduction pump for filling casting mold 80−43798
conductive fluids local induced voltage velometry *(German)* 79−86517
conductor, MHD kink instability 80−6307
conic MHD channel, in single phase inductor field *(Russian)* 78−94842
constrained minimum energy problem in relativistic MHD 80−92238
convection, forced horizontal flow between moving porous walls 77−68695
convection, free, near plane and axisymmetric bodies 79−94728
convection, free, viscous flow past porous plate with suction, mass transfer effects 78−87398
convection, mag. field effect *(Russian)* 78−26201
convection, magnetic, mean field approx., boundary layer method 80−69930
convection, natural, in presence of transverse mag. field similarity soln. 78−67197
convection, nonstationary, in plane vertical channel *(Russian)* 77−27615
convection along plate, MHD boundary layer eqns. soln. 77−11276
convection in boundary layer, overplane and axisymm. bodies, theory 79−77270
convection in horiz. layer *(Russian)* 78−26202
convection in infinite channel 77−72361
convection in rapidly rot. fluid layer, stability, rel. to geomagnetism 79−50808
convection in vertical annular pipe, rad. mag. field 79−60068
convection in vertical cylinder, unsteady 79−77271
convection with rot. spatial heat source, stability 79−4085
convective collapse of flux tubes 79−66989
convective flow through channel with conducting walls, Hall effects 78−5802
convective flow through porous channel with Hall and wall conductance effects 80−74993
convective heat transfer in feebly ionised air 79−23370
convective instability of thin mag. flux tubes, solar convection zone model 79−75183
convective instability-MHD instability analogy, AC and DC fields *(Russian)* 77−65807
convective stability depend. on mag. field in magnetizable liq. *(Russian)* 78−47051
convectively driven MHD dynamo, models, solar dynamo appl. 78−42668
converging cylindrical detonation waves in magnetogasdynamics 79−77265
cosmic ray confinement, effect of interstellar MHD turbulence 77−49246

magnetohydrodynamics continued
cosmological models, perfect fluid, plane symmetry 80−82556
cosmology, anisotropic MHD model 79−35437
Couette flow, effects of couple stresses for electrically conducting fluid, skin effect 78−91020
Couette flow, Hall and ion-slip effects, heat transfer 79−94726
Couette flow, Hall effect in rot. system 80−74991
Couette flow, unsteady, between two plates when one subjected to random pulses 80−69938
Couette flow, with variable wall temp., heat transfer 79−27640
Couette flow and heat transfer in rotating system 77−35246
Couette flow stability, transformation of perturbation eqns. 77−7474
Couette flow stability in presence of mag. field 79−23373
Couette flow with Hall currents, stability, numerical soln. 77−72360
Couette flow with porous boundary 80−53876
Couette MHD flow instability, cond. liq., finite disturbances effect *(Russian)* 77−65808
Crab and Vela pulsars, pulsed emission prod. by synchrotron mechanism 79−35283
current carrying non-Newtonian fluid past a nonconducting sphere at low Reynolds number 79−64784
current-carrying conductor, MHD instability suppression, skin effect in strong electric field 77−951
V1057 Cygni, hydromag. model of peculiar activity *(Russian)* 78−49442
cylinder in conducting fluid, radial mag. field effects *(Russian)* 77−3874
cylinder in inviscid conducting fluid flow, non-aligned mag. field distortion 77−27597
cylindrical inductive MHD pump, external mag. field, dipole calcs. *(Russian)* 77−3884
dense ionised gas, MHD flow with viscous stress relax., similarity anal. 78−22427
detonation wave propag. with allowance for radn. and mag. field 79−64796
detonation waves, radiative MHD flow *(Russian)* 77−89207
dielectric fluid, hydromagnetic interaction 79−75097
diffuser, self-similar MHD flows with induced mag. fields 78−34205
diffuser flow across homogeneous magnetic field 79−1262
diffusion in porous system in crossed electric and mag. fields 78−34202
diffusive instability of steady MHD flow, rel. to geomagnetism 79−50807
dilatant media, shear perturbation propag., nonlinear effects in mag. field *(Russian)* 77−27612
disc in electrically conducting fluid, hydromagnetic flow due to torsional oscillations about non-zero mean 80−74992
discontinuities, single-point identification method *(Russian, English)* 79−75092
discontinuity, normal vector determ. using magnetic meas. data *(Russian. English)* 79−75091
discontinuity propagation along bi-characteristics 80−59125
discontinuity surface stabilisation in magnetisable media by mag. field 80−48806
discrete mathematical model construction from principle of least action 80−38502
disperse system in EM field, hydrodynamics *(Russian)* 77−80222
dispersive magnetisable media, hydrodynamics including Brownian motion 80−59120
dispersive surface wave generation 77−47111
disturbances in conducting shallow liquid 79−27705
div B, nonzero, effect on numerical soln. 80−69939
double boundary layers on an electrically conducting plane surface in a rotating environment 79−46397
double radiosources, magnetogasdynamics 80−26999
droplet motion in electrically conducting fluid, EM field effects *(Russian)* 77−3878
duct, circ., laminar convective MHD heat transfer for 3rd kind temp. boundary conditions 78−87342
duct, nonconducting walls, MHD volumetric flow rate under uniform mag. field 80−1691
duct, rectangular, MHD flow under uniform transverse mag. field at high Hartmann no. 77−55094
duct flow, appl. of iterative finite element Kantorovich meth. 77−74205
duct flow, boundary value problem, dual extremum principles, operators and bounding functionals 79−64791
duct flow studies, fusion reactor technology 78−29651
dusty viscous conducting liquid, unsteady flow in annulus in mag. field 78−38412
dye dispersion with harmonically varying concentration in MHD channel flow 78−38414
dynamo action in conducting sphere and Backus' condition 78−28195
dynamo in differential rotation 77−53582
dynamo theory, astronomical mag. fields modifications, review 77−73946
dynamo theory *(Russian)* 77−47110
dynamo theory of planetary and stellar magnetic fields *(French)* 79−35161
Earth, hydromagnetic dynamo, axially symmetric model 79−62430
Earth's dynamo, MHD, book contrib. 78−61331
Earth core, dynamics of fluid core with inward growing boundaries 80−76934
Earth core, example of nonlinear geomag. dynamo action 77−73637
Earth core, geomag. field 60 year vars. models and mantle elec. cond. 79−8596
Earth core, mag. Reynolds number for three spherical eddies kinematic dynamo 79−8597
Earth core, mean-field electrodynamics and dynamo theory of geomag. field 77−73636
Earth core fluid vel. and mag. field bounds imposed by MHD $\alpha\omega$-dynamo 78−36101
Earth core torsional oscillations, induced by Sun 78−44793
Earth core-mantle interface, MHD rel. to geomag. and gravit. fields correl. 77−2085
Earth global dynamics, Canadian contribs., 1971-79 period 80−8262
Eckart flow in conducting liq. or gas, acoustoelectric current prod. 79−27707
effective magnetic viscosity due to hydrodynamic turbulence in weak large scale mag. field 77−33340
Ekman and Hartman layers on plate with variable suction or blowing 78−38416
Ekman layer, near accelerated porous media, flow anal. 77−75987
Ekman layer on free convection past infinite porous flat plate 80−14830
magnetohydrodynamics continued
Ekman layer on porous flat plate, heat transfer, steady asymptotic soln. 78−79385
elastico-viscous fluid rot. in mag. field, unsteady flow induced by oscill. plate 78−67273
elastico-viscous MHD fluctuating flow past porous plate, heat transfer 79−90342
electrical potentials, uniqueness of solns. to extended class of elliptic boundary value problems 80−69937
electrically conducting fluid, MHD, Lagrangian invariants and first integrals *(French)* 77−58796
electrically conducting fluid, MHD natural convection flows, buoyancy effects 78−18351
electrically conducting medium, rotation at exit of coaxial MHD channel 80−83853
electrically conducting rarefied gas near accelerated porous plate, MHD flow 80−14836
electrically-conducting fluid, mag. flux linkage, planetary dynamo theory 80−8536
electrically-conducting fluid, mag. flux linkage, relativistic case, planetary dynamo theory 80−12655
electrodynamically coupled streams, MHD flow in tubes *(Russian)* 77−27609
electrolyte MHD effects as model for turbulent hydrodynamic processes *(Russian)* 78−40610
electrolyte nonlinear wave processes, in dispersive media, MHD stimulation 77−7473
electrolytes, chemically reacting, heterogeneous processes kinetics control *(Russian)* 78−27768
electromagnetic field anal., computer methods, MHD and finite elements method 80−32879
electromechanical simulation averaging of EM fields in channel flow 79−77277
elliptic column instability, mag. surface separatrix, 2-D MHD eqns. *(Russian)* 77−51212
elliptic equations and systems, free-boundary problem solution method 80−69941
EM flowmeter, with nonuniform mag. field, for liq. metals *(Russian)* 77−47122
EM induction pumps, fluids, laminar flow, charact. anal. 79−32699
EM pump and plant with liq.-metal working fluid, review *(Russian)* 77−19639
EM wave generated by compression shock, in weak mag. field 79−77292
energy decay, kinetic and magnetic 78−42672
energy emitted by working medium of MHD generator, meas. 80−103078
entrance flow, vertical channel, thermal convection, linear anal. 78−38410
equilibria, by secondary bifurcation, rectangular boundary conditions 78−42673
equilibria numerical analysis *(Japanese)* 79−41760
equilibrium equations, convergence of iterative schemes 80−59115
equilibrium figures with magnetic field 77−45303
exact soln., generalised procedures 80−14838
exploding or collapsing magnetized rotating spheroid, mag. dipole radiation 79−35106
fast magnetic field line reconnection in elec. cond. incompressible fluid 77−55097
Fermi-accelerated cosmic rays mediation of shock front 80−85829
Ferraro's law of isorotation, relativistic analogues 78−21035
ferrofluid, convective stability of horizontal layer in mag. field *(Russian)* 77−3885
ferrofluid, helical flow with heat cond. between coaxial porous tubes 79−23371
ferrofluid, permeability in alternating mag. field 80−48808
ferrofluid behaviour in the presence of a rotating nonhomogeneous mag. field *(French)* 80−96313
ferrofluid constitution examination by rotating test tube method 80−33693
ferrofluid droplet, interphase boundary hydrostatic charact. in uniform mag. field 80−33692
ferrofluid flow in circular pipe, uniform mag. field effects 80−43782
ferrofluid flow under influence of rotating mag. fields 80−59118
ferrofluid motion, rot. mag. field effects 77−950
ferrofluids, dissipative process in non-homogeneous mag. field 80−59119
ferrofluids, Landau and Lifshitz hydrostatic press., thought expts. 80−59111
ferrohydrodynamics, mag. relax. models 79−94706
ferroliquid, deviation of free flow by inhomogeneous mag. field 77−65800
ferroliquid in annular channel, hydromag. stability, thermomagnetic effect 79−94593
ferromagnetic colloid, natural convection, mag. field effects *(Russian)* 77−62307
ferromagnetic colloids, helical flow in mag. field *(Russian)* 78−75213
ferromaghetic convection in crossflow over a cylinder, heat transfer rate 80−1558
ferromagnetic cylinder in MHD liquid, drag coeff. *(French)* 79−72952
ferromagnetic fluid, in appl. mag. field equilib. surface patterns 77−84332
ferromagnetic fluid, stability in vertical magnetic field, variational approach *(German)* 80−96316
ferromagnetic fluid in inhomogeneous mag. field, thermal convection 80−1559
ferromagnetic fluid rotating about vertical axis, convective instability of layer 79−27698
ferromagnetic fluids, convective heat transfer 79−98725
ferromagnetic layer boiling, mag. characteristics meas. 78−59499
ferromagnetic liquid, particle anisotropy, asymmetric model *(Russian)* 77−27607
ferromagnetic suspension, mag. field effect on heat transfer, thermal cond. 78−59500
ferromagnetic suspension, magnetorheological charact. meas., errors 80−33550
ferromagnetic suspension serving as a liquid magnet 80−84622
ferromagnetic suspensions, convective heat transfer and thermophysical props., mag. field effects 79−77264
ferrosuspension, magnetorheologic charact. *(Russian)* 77−65786
ferrosuspension, MHD flow, heat transfer *(Russian)* 78−26203
ferrosuspension, motion in rot. homogeneous mag. field *(Russian)* 77−27604

magnetohydrodynamics continued
ferrosuspension, motion induced by travelling mag. field *(Russian)* 77−27606
ferrosuspensions, internal rotations and the other transport phenomena 80−28573
ferrosuspensions, mag. field effects on mech. props. 78−87321
film between porous circular discs with velocity slip 80−74997
finite element method applic., time-independ. coupling analysis between mag. and vel. fields *(Japanese)* 78−30362
finite-amplitude thermal convection and geostrophic flow in a rotating magnetic system 80−87813
flat plate, MHD unsteady flow of Maxwell fluid, relaxation parameter 80−24101
flow, impulsively started plate, Hall effect 78−1747
flow and heat transfer, porous disc eccentric rotations at infinity 79−18965
flow andheat transfer over semi-infinite plate under transverse mag. field 77−80225
flow between critical states, induced by rot. mag. field, struct. *(Russian)* 78−75211
flow between rotating parallel porous walls 79−64779
flow due to an electric discharge from a finite size electrode 78−79388
flow field computations in distributing collectors, MHD heat exchanger *(Russian)* 78−75227
flow in annular and linear channels, boundary layer conditions *(Chinese)* 79−37404
flow in channel of complex cross section *(Russian)* 79−32698
flow in presence of transverse magnetic field, boundary layer soln. 79−55425
flow near a time-varying accelerated porous plate 79−23372
flow near oscillating porous flat plate under body force action 80−24102
flow over porous plate, Hall effect 78−51246
flow over stretching sheet 79−72956
flow parameter determ. by holographic interferometry *(Hungarian)* 78−22433
flow past porous flat plate, Hall effects 78−14093
flow past solid spherical drop at low Reynolds and Hartmann numbers 80−6158
flow rate convertor, EM, optimal mag. system design 79−77313
flow rate regulators for liq. metal systems, MHD or mechanical *(Russian)* 78−75229
flow stability, energy theory 77−55095
flowmeter, EM, vel. profile invariance, sensitivity, error *(Russian)* 77−24042
flowmeter, with circ. cross section, inhomogeneous mag. field effect on signal 80−33709
flowmeter, with circ. cross section, symmetry conditions effect on signal, arbitrary vel. profile 80−33708
flows, shunt coeffs. *(Russian)* 78−47060
flows and turbulence, second Bat-Sheva seminar, Beer-Sheva, Israel, (March 1978) 79−60070
fluctuating flow of viscous cond. fluid on porous plate in rot. medium with transverse mag. field 79−90340
fluctuating free convection flow on horizontally magnetised plate 80−33683
fluid film, press. distrib. between axially oscillating parallel circular plates in magnetic field 78−19904
fluid layer, stability in rot. frame of reference with temp. and conc. gradients 77−27600
fluidised bed hydrodynamic structure effects of DC mag. field *(Russian)* 77−65801
fluidised beds, heat exchange rate control, using magnetic field *(Russian)* 77−55083
Fokker-Planck equatn. numerical solutn. 80−18622
force-free magnetic fields, variational approach and appl. to solar active regions mag. field 80−62011
forced convection, with transverse mag. field, surface curvature effect 77−35245
forced convection in channel bounded by plate and permeable bed, Hall effects 80−69934
forced convection in HF EM fields 77−39354
forced convection in presence of external mag. field, similarity soln. group theoretic approach 79−77266
forced flow through horizontal channel, Hall effect, buoyancy force effects 80−53871
forced oscillations of an enclosed rotating fluid under a uniform magnetic field 79−32688
free and forced convective flow between porous plates with Hall effect 79−41763
free boundary capillary MHD flows 80−43794
free conducting shear layers, stability in transverse mag. field *(German)* 77−15132
free convection about semi-infinite plate in strong cross field, skin friction, heat transfer 77−15134
free convection effects on MHD accel. flow past vertical porous limiting surface 80−23996
free convection effects on oscill. flow of viscous incompressible fluid past porous limiting surface 79−81985
free convection heat transfer on a magnetic cylinder in a uniform magnetic field 80−83852
free convection in finite vertical channel, magnetic field effects 78−67270
free MHD convection, near plane and axisymmetric bodies, approx. soln. *(Russian)* 78−94832
free shift stationary flow, in strong field, of viscous fluid 80−28576
free-stream vel. and press. gradients, effects on MHD boundary-layer control 79−55423
frozen-in and resistive force-free magnetic fields *(Chinese)* 79−80210
frozen-in magnetic phenomena in collisionless plasma 79−82052
function averaging in two-dimens. problems *(Russian)* 78−26209
fundamental problems in general fluid dynamics and hydromag. dynamo theory, book contrib. 77−84213
fusion reactor blankets, MHD coolant flows, 3-D model 80−23119
galactic dynamo, numerical models 79−40262
galactic spiral structures, origin 79−25714
galaxies, new MHD theory rel. to Hubble sequence 77−71142
Galilean satellites, dynamo mag. fields possible strengths 79−16873
gas, boundary layer swirling nozzle and diffuser flows with mag. field 80−1693
gas, conducting, stream flow in orthogonal mag. and mass forces fields *(Russian)* 77−27618

magnetohydrodynamics continued
gas, magnetised conducting, 1-dimens. stationary adiabatic motion in tube *(Russian)* 77−84336
gas and dust electrocond. flow in elec. and mag. fields *(Russian)* 77−39358
gas clouds, stability of self-gravitating magnetized system 79−21170
gas dynamics, equatorial propagation of axisymmetric magneto-radiative shocks 80−79349
gas flow, applicability of MHD eq. exact soln. *(Russian)* 77−24032
gas outflows and inflows with viscous, ohmic and thermal dissipation between inclined walls 77−11278
gasdynamic flow in orthogonal magnetic field, arbitrary gas law 77−15125
gaseous rotating masses with mag. fields, stability and existence of bifurcation point 78−53924
gases, mass transfer, mag. field effects 78−63535
general relativistic anal. of self-gravitating perfect magnetofluid 78−36905
general relativistic magnetofluids 77−49655
general relativistic MHD, asymptotic waves and critical time 79−41771
general relativity conference, Trieste, Italy, 1975, July 78−8285
general relativity conformal groups, appl. *(French)* 80−101
generalised polar diagrams of plane-parallel stationary simularity flows, waves 80−96314
generalised state equation in MHD, conditions of exceptionality and struct. *(Italian)* 77−80221
generalized equation of state, charact.-shock and struct. exceptionality 79−10614
glass industry, magneto-hydrodynamic phenomena, of mixing *(Polish)* 80−64647
gravitating plasma polytropes in magnetostatic equilib., analytical solns. 80−94701
gravitational collapse, anisotropic, mag. field strength var., MHD approx. calcs. 77−11283
gravitational instability of composite plasma, effect of gyroviscosity and ion viscosity 77−87255
gyrator effects on magneto-fluid dynamic turbulence in strong mag. field 78−42670
Hall and ion slip currents effect on heat transfer in MHD fluid in channel 79−27702
Hall effect on MHD flow induced by oscill. disc in rot. fluid 79−18968
Hall effect on unsteady flow due to rotating infinite disc 78−18354
Hall effects in unsteady Couette flow 77−15127
Hamiltonian formulation, using generalised EM antipotentials 77−68694
Hartmann boundary layer control of spin-up of stratified, conducting fluid 77−42923
Hartmann flow, nonlinear stability, monoharmonic analysis 80−83850
Hartmann flow between nonconducting walls, commencement 79−18962
Hartmann flow in heated channel, thermal instability 77−7461
Hartmann flows, resonant perturbations *(Russian)* 79−32685
Hartmann layers, current content 77−72366
Hartmann MHD flow, radiative transfer 80−6161
heat front in weak mag. field, EM field perturbation *(Russian)* 78−94835
heat transfer, effects of pressure gradient, suction, injection 80−53872
heat transfer between porous discs, one rotating one at rest 80−28561
heat transfer bibliography, Japanese works 79−23317
heat transfer bibliography 78−63425
heat transfer in MHD channel flow of rarefied gas, external circuit effects 80−83860
heat transfer in rarefied MHD laminar channel flow 80−48687
heat transfer in two-dimens., parallel plane channel flow 80−14833
heavy liquid, free surface equilibrium and stability between charged and bent vertical surfaces 80−48812
helical flow, linear and nonlinear stability 79−37408
helical turbulence, diffusion of passive-scalar and mag. fields, computer simulation 77−11272
helical turbulence, nonlinear dynamo effect 77−3873
helical turbulence, numerical simulation 78−38415
helical velocity and magnetic fields, stability 78−73624
helicity effects in hydromagnetic dynamo process 77−42924
hemisphere in MHD rotating stratified fluid 80−100039
hemispherical container, flow induced by distributed current source and mag. field 80−92234
high conductivity in mean field electrodynamics 77−949
high gradient magnetic separation at moderate Reynolds number 80−38500
homogeneous mixtures, motion in EM field 79−94725
homopolar with incomplete electrodes, on dimens. MHD flow *(Chinese)* 79−64777
hot layer, hydromagnetic stability, effect of non-uniform elec. cond. 79−14485
Howard's semi-circle theorem 79−90344
hydrodynamic suspensions, physical property variations *(Russian)* 78−47022
hydromagnetic capillary instability of a liquid jet with an axial flow 80−74990
hydromagnetic convection post marginal state, amplitude determ., Landau's conjecture 79−77286
hydromagnetic flow over a conducting thick porous plate with Hall effects 79−64789
hydromagnetic free convection flow, similarity solutions 79−27639
hydromagnetic free convection past infinite porous flat plate in rot. system, slip effects 79−81989
hydromagnetic free jet boundary layer equations, similar soln. 79−50811
hydromagnetic free shear layers in rotating flows 79−14493
hydromagnetic generalised Benard problem, mag. field character, stratified layer stability 79−77267
hydromagnetic penetration in a rotating fluid 80−14839
hydromagnetic Stokes flow past rotating sphere 79−32694
hydromagnetic thermal instability of rotating fluid layer, Hall current effects 79−27699
hydromagnetic thermal shear flow stability 79−32690
hypersonic stagnation point boundary layers with massive blowing in presence of mag. field 79−94649
hypersonic streams in mag. field, secondary shock waves *(Russian)* 78−87401
ideal gas, polarisable or magnetisable, one-dimensional flow *(Russian)* 77−47102
ideal gas self-similar rotation *(Russian)* 79−72955

magnetohydrodynamics continued
incompressible fluid MHD flow over flat plate, press. gradient, fluid injection effects 77−68698
incompressible MHD flow with heat transfer between inclined walls 79−68819
induced in container by rapidly alternating or rot. mag. field 79−64785
induction flow-meas. theory for poorly conducting fluids 78−38429
induction flowmeter, large cross-section pipe, calc. method 79−7422
induction machines in DC breaking mode, operating anal. 80−48816
induction MHD pump, active zones, effective forces, EHDA integrator study 80−43797
induction MHD pumps, with transverse mag. flux, active element optimisation *(Russian)* 78−94840
induction pump, flow through helical channel, pressure field effect 80−87815
induction pump, linear, cylindrical EM field distrib. *(Russian)* 78−5820
induction pump, transverse and longitudinal fringe effects in channel 80−83854
induction pump channel press. loss, laminar liq. metal flow friction losses *(Russian)* 78−75224
induction pump with side bars, thrust-flow characts. at large Re_m *(Russian)* 78−75231
induction stirring of semicontinuously cast ingots *(Russian)* 78−6915
ingot formed in EM crystalliser, control of metal melt circulation *(Russian)* 78−84790
ingot forming from melt, liq. containment by EM field 80−35120
instability, helical symmetry, linear theory 79−94729
instability by magnetic buoyancy, solar interior appl. 79−75100
interface between conducting liq. and insulating atm., destabilising effect of alternating mag. field *(French)* 77−62306
interpenetrating EM structural continua, constitutive eqns. *(Russian)* 77−65805
interplanetary disturbances generated by simulated solar wind vel. perturbations, MHD soln. 77−29615
interplanetary medium, discontinuities, identification method 80−109322
interplanetary medium and near-Earth space, MHD discontinuities with Hall effect 77−25899
interplanetary plasma field characteristics of directional discontinuities 77−29722
interplanetary plasma flow from strong flare, 1972, August 4 to 5, struct. rel. to mag. storm 79−53653
interplanetary plasma flow hydromagnetic struct. rel. to geomag. Pc 1 pulsations 78−45142
interplanetary plasma stream of August 4, 1972, hydromagnetic struct. 78−28475
interplanetary shock waves interaction with bow shock-magnetopause system 80−26712
interplanetary shock waves interaction with cometary atmospheres 77−22032
interstellar cloud rotation, mag. braking of aligned rotator during star form., exact time-depend. soln. 80−90493
interstellar clouds, ambipolar diffusion, rel. to star form. 79−40237
interstellar clouds, mag. fields influence on OB associations subgroups sequential form 80−4408
interstellar clouds angular momentum problem and mag. braking, time independent soln. 79−62884
interstellar gas hydrostatic equilib. in solar neighbourhood 79−30098
interstellar magnetic field amplification in collisionless shock waves 77−49459
interstellar magnetised gaseous discs, gravitational instability 80−4424
interstellar matter, Parker instability in 2-dimens., using MHD energy principle *(French)* 77−64831
interstellar medium, equilib. configs. stability, hydromagnetic energy principle 80−82448
interstellar MHD shocks, grain disruption 78−4317
interstellar nonrotating magnetic gas clouds collapse, numerical calcs. 80−105299
intrinsic equations for the magnetofluid flows 79−37409
invariants, complex vectors in MHD 79−37415
ionised gas in applied mag. field, acoustic instabilities 78−9719
isentropic flow in magnetohydrodynamics *(French)* 79−32682
isothermal expansion of a two-phase fluid in a magnetohydrodynamic generator duct 80−1695
jet, magnetisable liquid, stability 80−83831
jets, electrically conducting plane and annular, in axial mag. field, instability 77−35247
jets, laminar and turbulent, elec. cond. fluid with transverse mag. field 79−77261
jets, quasi-parallel, MHD instability 78−83495
journal bearing in rotating MHD flow, system characts. *(French)* 79−1263
Jupiter, lower atmosphere MHD rel. to atmosphere differential rot. 80−46467
Jupiter magnetodisc, MHD turbulence rel. to plasma transport into outer magnetosphere 79−58297
Jupiter-Io electrodynamic interaction, theory 78−81583
Kelvin-Helmholtz hydromagnetic instability, of streaming layer in unbounded self-gravitational field 80−53878
Kelvin-Helmholtz instability in supersonic and super-Alvenic fluids 80−87816
kinematic dynamo action, helical symm. in unbounded fluid conductor 80−10315
kinematic dynamo action, helical symm. in unbounded fluid conductor 80−10316
kinematic dynamo of three spherical eddies, model 78−69286
Knudsen molecular gas in mag. field, transport phenomena 80−33684
laminar boundary layer, on permeable surface, in crossed elec. and mag. fields *(Russian)* 78−75118
laminar boundary layer flow along flat plate with transverse mag. field, MHD stability 79−27709
laminar boundary layer with variable elec. cond., nonstationary flow *(French)* 77−39356
laminar boundary layers, nonsimilar incompressible flow, finite-difference scheme 78−79386
laminar compressible MHD boundary layer flow, effect on heat transfer 79−14489
laminar flow, dynamic characteristics, in rot. mag. field, symm. effects *(Russian)* 78−47063
laminar flow, suspended particle motion stability *(Russian)* 78−5808
laminar flow down vertical wall 77−11270
laminar flow in entrance region of flat duct 78−30367
magnetohydrodynamics continued
laminar flow in parallel-plate channel with unequal wall temperature, thermal entry heat transfer 77−42927
laminar flow in rot. mag. field *(French)* 78−51248
laminar flow of electrically conducting fluid in axial mag. field *(French)* 78−42667
laminar MHD flow with chem. reactions, solute dispersion 79−23378
laminar MHD pipe flow with heat transfer 79−14482
laminar motion incircular duct in the presence of a transverse mag. field with several dipoles *(French)* 79−90345
laminar plane-wall jet flow 79−55424
laminar plume above a line heat source in a transverse magnetic field 78−67269
laminar source flow between parallel porous discs with equal suction and injection, in mag. field 77−84331
Landau-Squire jet, radially diverging elec. current, exact soln. *(Russian)* 78−5816
linear induction machine, MHD processes in channel 80−83859
linear induction machines, performance characteristics from longitudinal edge effect 80−48817
linear induction MHD machines, instability *(Russian)* 78−94841
linear induction MHD pump, cylindrical, electrodynamic forces *(Russian)* 78−94843
linear induction MHD pump, DC, mag. field obs. *(Russian)* 77−7469
linear induction motor, fluid flow induced in liquid metals, investigation 80−43800
linear induction pump, cylindrical with inclined coils, electrodynamic force calc. 79−77281
linear induction pump, instabilities at low flow rates 79−77279
linear induction pumps, cylindrical, for liq. Na *(Russian)* 78−94839
liquid, undergoing inhomogeneous Poiseuille flow, spin echo signal shape *(Russian)* 80−50225
liquid axisymmetric flow in rot. mag. field, stationary instability *(Russian)* 78−5813
liquid film on vertical surface, viscous lifting and drainage 78−18348
liquid in rot. system, Hall effects on MHD Couette flow and heat transfer 79−41681
liquid in travelling mag. field, perturbation development *(Russian)* 78−5811
liquid jets, behaviour in electric and mag. fields 80−43783
liquid metal, flow and energetic characts. in linear induction MHD pump *(Russian)* 77−3882
liquid metal, jets, breakup in mag. field *(Russian)* 78−47062
liquid metal, temp. pulsation cross correlation coeffs., in longitudinal mag. field *(Russian)* 77−65815
liquid metal, unsteady channel flow with transversely applied mag. field 77−84328
liquid metal flow, in open channel, MHD regulation, armature reaction calc. *(Russian)* 77−47107
liquid metal flow at high Hartmann no. in variable area ducts, nonuniform mag. field effect 78−30363
liquid metal flow in curved channels, transversely applied mag. field 80−14829
liquid metal flow in duct at high Hartmann number, wall cond. effects 79−94720
liquid metal flow rate meas. method 80−43793
liquid metal gas inclusions, bubble release dynamics, mag. field effects *(Russian)* 77−3865
liquid metal high Hartmann number flows in ducts with conducting walls 80−33689
liquid metal in periodic EM field, mean MHD flow, turbulent stresses calc. *(Russian)* 78−47056
liquid metal MHD, review of flow problems and cellular motion 78−83498
liquid metal MHD induction pump, transversely closing mag. flux, optimisation of parts 79−77278
liquid metal MHD pump, performance indices channel geometry *(Russian)* 78−5821
liquid metal motion, with azimuthal and axial forces, in EM trough *(Russian)* 79−1259
liquid metal plane layer, elec. current induced MHD flow, industrial furnace appl. *(Russian)* 78−5817
liquid metal pump, conical MHD channel of single-phase inductor 79−77280
liquid metal pump, linear induction, research and development studies 79−77276
liquid metal rectangular duct flow with opposite walls conducting and insulating 80−33688
liquid metal transient flow at electrode in linear cond. motor 80−43792
liquid metal two phase flow, gaseous phase redistrib. in strong mag. field 79−37410
liquid metal vapour, laminar film condensation under effect of electromotive force 79−1258
liquid metal-gas two-phase MHD generator, pot. loss mechanisms, rel. to fluid dynamic processes 77−39359
liquid metals, flow, and energy characts., in linear induction MHD pump *(Russian)* 77−47104
liquid metals, flow in tube in mag. field, turbulent transfer coeff. *(Russian)* 78−75220
liquid metals, flow velocity structure, in nonuniform const. mag. field *(Russian)* 78−75215
liquid metals, MHD rot., vel. meas. by vane type sensor *(Russian)* 77−47123
liquid metals in cylindrical ducts with transverse mag. fields 79−27708
liquid metals laminar flow in curved channels, transversely applied mag. field, flow anal. 80−59116
liquid nonstationary two-dimens. flow, rot. mag. field, differential eqns. *(Russian)* 78−5814
liquid to vapour transformations, mechanics of two phase flows 77−89532
lubricant in gap in journal bearing 80−10319
RR Lyrae stars, hydromagnetic processes as cause of period changes 80−105261
magnetic buoyancy in rotating gas, effect of fine electrical and thermal conductivities 78−57436
magnetic circuit, field calcs. *(Russian)* 77−3883
magnetic field, flow stability of thin layer *(Russian)* 78−9721
magnetic field generation at high mag. Reynolds number, finite resistivity effect 78−36448
magnetic field growth in helical turbulence 79−18967

magnetohydrodynamics continued
magnetic fields and convection dynamic interaction, solar photosphere appl. 78−24458
magnetic flow of viscous gas between rotating surfaces of revolution 79−46395
magnetic fluid, cylindrical column, motion in rot. mag. field *(Russian)* 78−75212
magnetic fluid, in current-carrying plate field, free vertical convection *(Russian)* 77−65806
magnetic fluid, in homogeneous rot. mag. field, torques, hydrodynamics 79−94632
magnetic fluid, motion in external mag. field, Couette and Poiseuille flow 79−14491
magnetic fluid, Newtonian eqns. and exact unidimensional nonstationary solns. *(Russian)* 78−47048
magnetic fluid, penetration through porous medium with uniform mag. field oblique to interface 80−59107
magnetic fluid, spherical drop, motion in rot. mag. field *(Russian)* 78−75212
magnetic fluid, surface wave excitation, by travelling mag. field *(Russian)* 77−47099
magnetic fluid, thermoconvective instability, with mag. field perturbations 78−94847
magnetic fluid (cable coolant), natural convection heat transfer 78−94846
magnetic fluid as continuum with internal degrees of freedom 80−60377
magnetic fluid boundary layer, flow stability 79−64782
magnetic fluid in rotating vessel, flow in homogeneous mag. field 80−33691
magnetic fluid layer in mag. field, instability *(Russian)* 78−26210
magnetic fluid with intrinsic ang. momentum, one-dimensional nonstationary waves 80−33690
magnetic fluids, conducting, low intensity jump struct. *(Russian)* 78−75214
magnetic fluids, conference, Orlando, USA (Mar. 1980) 80−56995
magnetic fluids, heat and mass transfer 80−59123
magnetic fluids, mag., optical, and hydrodynamic props.,, expt. study, review 80−60376
magnetic fluids, response to mech., mag. and thermal forces 80−59122
magnetic fluids, US attenuation, MHD approach 80−60389
magnetic flux ropes and convection 78−71399
magnetic flux tubes, vibration modes, general dispersion relation 80−94706
magnetic gyrotropy in a medium with inhomogeneous density 79−94730
magnetic instabilities of rot. gas in presence of radial gravit. force and azimuthal mag. field 78−47046
magnetic liq. birefringence and dichroism kinetics, Brownian diffusion *(Russian)* 78−5806
magnetic liquid film flow in mag. field, laminar regime 78−34203
magnetic liquid surface equilibrium forms *(Russian)* 77−27605
magnetic liquid thin layer with two free boundaries, instability conditions, surface wave dispersion eqn. *(Russian)* 78−1752
magnetic sphere, self-gravitating, exact soln. for differential rotation 79−84665
magnetic-velocity shear, hydromag.-intertial-gravity waves propag. 79−55422
magnetically saturated fluid, continuum mechanics, global balance law approach 80−60388
magnetisable fluid, motion in rotating homogeneous mag. field 80−28572
magnetisable liquid, thermomagnetic convection between coaxial cylinders with distributed heat source 79−94622
magnetisable liquid, thin layer instability 79−41762
magnetisable suspensions, hydrodynamic in travelling mag. field 80−48807
magnetised fluids, surface instability in nonisothermal layer *(Russian)* 78−94834
magnetised liquids, separated by thin elastic film, surface stability 79−94727
magnetised relativistic continuum, shock invariants *(French)* 79−25944
magneto-acoustic wave stability in thermally conducting compressible fluid 80−48803
magneto-acoustic waves, generation and radn. in compressible fluid 77−68699
magneto-gravitational instability and suspended particles 77−45302
magnetoaerodynamic forces on oscill. circular cylindrical shell, simple harmonic motion 79−1257
magnetoatmospheric instabilities, Hilbert space approach to max. growth rate 80−31172
magnetocumulative generator, megampere pulse shaping, explosively compressed plasma column *(Russian)* 78−1912
magnetoelectrolysis in steady Hartmann flow cells, hydrodynamics, mass transport 77−36759
magnetoelectrolytic convection, accuracy of estimation method 80−14691
magnetofluid, self-gravitating, local behaviour of congruences 78−89384
magnetogasdynamic parallel flows, inviscid stability 80−69933
magnetogasdynamics, axially symmetric explosion 80−62007
magnetogasdynamics, reciprocal type transformations 80−48804
magnetogasdynamics, singular surfaces of order one, ideal non-conducting gases 79−18971
magnetohydroelectric interaction, realisability 80−53874
magnetorheological systems, heat transfer 79−81988
magnetosheath, shock wave form. due to SSC 78−45147
magnetosphere, field line MHD torsional oscill. rel. to mini-substorm and long-period Pi 2 event *(Japanese)* 80−94653
magnetosphere, hydromag. energy spectra depend. on solar wind vel. and interplanetary mag. field direction 80−67476
magnetosphere, MHD torsional oscills. in orthogonal curvilinear coordinates rel. to micropulsations 79−80097
magnetosphere convection, one-dimensional gasdynamical model 78−81508
magnetosphere frontside boundary layer, reconnection problem 78−89010
magnetotail reconnection, expected signatures 78−96361
materials, review 80−40240
Maxwell equations, in Minkowski space-time and Poincare group 79−30301
Maxwell fluids, immiscible, hydrodynamic flow through non-conducting rectangular channel 80−100038
MBBA/CC mixtures, cholesteric phase, torsional shear flow in elec. and mag. fields 79−86697

magnetohydrodynamics continued
metal, liq. flow redistribution using const. mag. fields *(Russian)* 79−1261
metals, liquid, duct flow, hot-film probe vel. meas. 80−75009
metals in metallic containers, thermoelectric MHD 79−64787
MGD flow, radiation-conditioned Gaussian induced cone field 78−67283
MHD flow past accelerated plate, Hall effects 80−92275
MHD shear flow, struct. turbulence, anomalous impulse transfer *(Russian)* 77−27610
micropolar fluids, channel flow, Hartmann problem 79−18963
micropolar fluids, model for asymmetric MHD *(Russian)* 77−35251
mixtures, flowing, motion in EM field *(Russian)* 79−32686
moving conducting fluid inductive interaction with external main windings, config. effects *(Russian)* 78−75225
moving ribbon conductor, interaction with field of ferromag. inductor 80−48815
multidimensional magnetogasdynamic flows, shock wave propagation and breaking 79−98818
multipole MHD throttle with annular duct 80−43789
nematic liquid cryst., Freedericksz transition in mag. field, domain struct. 80−33880
nematic liquid crystal, incompressible, two dimens. coupled eqns. flow in mag. field *(French)* 77−84329
nematic liquid crystals, coherent neutron scatt. studies, review 79−41956
nematic liquid crystals, homogeneous instabilities 78−63674
nematic liquid crystals, MHD effect, high resolution NMR *(Russian)* 78−15040
nematic liquid crystals, MHD instabilities 77−27828
nematic liquid crystals, shear flow, effect of mag. fields and boundary conditions, PAA example 77−7668
nematic liquid crysts., 3D model, theory of magnetohydrodynamic effect 79−41955
neutral sheet two-dimens. equilib. in gravit. field 79−66919
neutron star interiors, MHD eqns. 79−35288
neutron star magnetosphere, plasma dynamics and accretion, fate of sinking filaments 80−51798
neutron stars, accreting, normal mode anal. of interchange instability at magnetopause 77−13376
neutron stars, potential drops above pulsar polar caps, nonneutral beam accel. 78−4267
neutron stars, rotating, magnetic, accretion torques rel. to pulsating X-ray sources period changes 80−31320
non-Newtonian fluid, Hartmann flow, hydrodynamic stability, viscous core effects *(Russian)* 77−27611
non-Newtonian incompressible fluid with pressure gradient and fluid injection, MHD flow 80−33686
noncanonical Hamiltonian density formulation of perfect fluid 80−103010
nonequilibrium magneto gasdynamic flow, geometrical parameters of streamline trajectories 78−38409
nonisothermal magnetisable fluid, thermal convective stability, modulated mag. field effects 80−64646
nonlinear astrophysical dynamos, bifurcation of steady dynamos from oscillating dynamos 78−49306
nonlinear stability, perturbations resonant interaction *(Russian)* 78−26204
nonlinear wave propagation in relativistic continuum mechanics, limiting cases of relativistic magnetohydrodynamics 80−22203
nonstationary MHD convection, in vertical circular channel *(Russian)* 78−94833
nonsteady MHD thermal boundary layer, in incompressible laminar flow with variable elec. cond., approx. soln. 78−91022
nonsteady turbulent MHD flows in plane channels and circular tubes 80−48810
nonuniform const. mag. field, flow vel. struct., numerical calc. *(Russian)* 78−47058
nonuniform medium, canonical variables in MHD 77−15131
nonviscous flow equations, steady plane, plane radial, and vortex flow 79−32697
nonviscous perfectly conducting gas, vorticity adiabatic flow, theoretical study 78−91023
nozzle flow, secondary flow, axisymmetric elec. current 78−79381
oblique flat plate, MHD flow patterns, at high Reynolds number *(Japanese)* 79−64786
one-dimensional flow of conducting medium isomag. shock waves 77−89205
one-dimensional flow of real gas in diverging channel, thermoelectric current effects 79−32692
one-dimensional isentropic flow, of ideal perfectly conducting fluid *(French)* 80−69936
ordinary differential eqns., suppression of inherent instabilities in initial value methods 79−9090
oscillating porous flat plate, MHD flow with variable suction 77−65802
oscillating porous flat plate boundary layer, hydromagnetic flow 78−51250
oscillating porous plate, Hall current and rot. effects on MHD flow 78−5803
oscillating source flow of ducting fluid between parallel discs 80−99986
oscillatory flow, free convection effects 80−53865
oscillatory flow of electrically conducting fluid past porous plate, free convection currents 79−55428
oscillatory flow past flat plate, Hall current effects 79−98816
oscillatory flow past impulsively started porous limiting surface, variable suction 79−86518
oscillatory flow past semi-infinite plate 78−14091
oscillatory hydromagnetic free convection flow past an infinite vertical flat plate with suction 79−32687
oscillatory MHD boundary layer flow, free convection effects 78−91018
p-azoxyanisole, nematic phase Couette flow mag. field and boundary condition effects 77−3887
parallel flow, interaction of bounded subsonic and unbounded supersonic MHD streams 79−37419
parallel flows, stability anal. by finite element anal. 79−81843
parallel plate porous slider, magnetohydrodynamic, optimum profile 79−47781
paramagnetic fluid flow through an annulus with porous walls 79−41748
paramagnetic particle trajectories in a lattice of parallel magnetized fibers 80−53204
partially ionised fluid, thermal instability, compressibility and collisional effects 78−55693
particle acceleration by MHD shock turbulence 80−87894

magnetohydrodynamics continued
particle EM ejection coefficient in two-phase MHD flow 79−77273
particles accelerated by Alfven waves, distrib. function self-similar solns. 79−32757
perfect magnetofluid, Lie invariance of stress-energy tensor 78−42671
periodic MHD oscillations, stability, perturbation theory 80−83858
permanent magnet immersed in mag. liq., buoyancy forces obs. *(Russian)* 78−47050
perturbations and completeness of solns. 78−1810
perturbations for finite magnetic Reynolds number 80−1757
Phase V, nematic, transient response to redirected mag. field, EPR study 80−33879
pipe flow, single and two phase 80−53869
piston, magnetic field effect, self-similar magnetogasdynamic problem with radiative heat transfer 80−64578
plane compressible MHD flows 79−50809
plane constantly inclined MHD flow with isomeric geom. 77−51125
plane interface between two viscoelastic superposed cond. fluids, instability in mag. field 80−1694
plane stagnation point flow in the presence of transverse magnetic field 80−14834
plane wave-plane shock interaction in magnetofluiddynamics 80−69931
planetary dynamo theories *(German)* 78−40852
plasma sheet oscillations, magnetospheric substorms effect 77−17296
plasmasphere, mag. field effects on plasma density distrib. 77−17288
point force in a stratified fluid in a cylinder under a magnetic field 80−14776
point source in rotating fluid in cylindrical tube in mag. field 79−14490
Poiseuille flow with flexible boundaries, MHD stability 77−11277
Poiseuille perturbed pipe flow in nonuniform axisymmetric mag. field, anal. 80−24104
polarisable and magnetisable medium, internal momentum, MHD and state eqns. *(Russian)* 77−65804
polyatomic gas, viscous flow in mag. field, vector polarisation 77−42438
polytropic stars with toroidal magnetic fields, hydromagnetic instabilities 79−8905
porous channel flow, exact soln. 77−31393
porous plate, with time-varying motion, surrounded by viscous cond. liq. 78−51251
porous solid layer form. on viscose fibre, EM field effect *(Russian)* 77−66595
porous straight channel, MHD flow 80−69932
porous-walled squeeze film, transverse mag. field and effect of slip 79−77262
power-law non-Newtonian conducting fluid, laminar boundary layer in transverse mag. field 80−33694
Poynting's theorem for moving media, Lerche's relativistic theory 79−48660
Prandtl-Meyer MHD flow, nonstationary numerical calcs. *(Russian)* 77−27614
pressure surface in magneto-gas dynamics *(German)* 80−14841
projective relativity and MHD, MHD tensor struct. 79−85030
protostars, magnetic, quasistatic contraction due to mag. flux leekage 80−98662
protostellar cloud ang. momentum problem, mag. breaking 80−82342
pulsar, plasma coupling, boundary conditions 80−94823
pulsar magnetosphere, relativistic particle curvature radiation 80−77434
pulsar magnetosphere models, interior and exterior struct., pair prod. 80−46594
pulsar magnetospheres, relativistic MHD wind or plasma wave 80−31317
pulsar magnetospheres, vacuum gaps 79−30082
pulsar polar cap, inhomogeneous struct. and radiation processes 79−25623
pulsar polar caps, pair prod. discharges 77−53618
pulsar polar caps, pot. drops and ultrarelativistic particle accel. along curved mag. field 78−53970
pulsars, electrostatic shear flow instability of relativistic nonneutral beams 79−53847
pulsars, finite force face cold plasma atm. models, plasma differential rot. 80−77378
pulsating viscous flow superposed on steady laminar motion 80−92228
pump, AC conduction type, for ferrous metal 80−33701
pump, direct-current uncompensated conduction-type, exptl. characts. 79−77283
pump, uncompensated DC cond. type, pumping and generating characts. *(Russian)* 79−1352
pumps for Hg transfer in chlorine and caustic soda production 80−43787
quasar emission line clouds, radiation pressure-driven Rayleigh-Taylor instability 79−35419
radial flow between planes, mag. field orientation effects calcs. *(Russian)* 77−7465
radiative, diffusive MHD eqns., ALFVEN two-dimens. code based on SHASTA 79−32684
radiative acoustics eqn., effect of non-transverse magnetic field 77−87252
radiative heat transfer in horizontal magnetohydrodynamic channel flow with buoyancy effects and an axial temperature gradient 79−60069
radiative magnetogasdynamic Couette flow with variable parameters 80−14840
radiative magnetogasdynamics, propagation of weak MHD discontinuities 78−63505
radiative MHD, with planar symmetry, invariant solns. 80−24099
radio sources, extended, extragalactic, MHD instabilities and electron accel. 80−27000
radio sources, extragalactic, relativistic electron clouds rel. to variable radio emission temporal characts. *(Russian)* 80−62307
radio sources, formation of knots in relativistic flows as model for compact synchrotron sources variability 80−105369
radio sources, superluminal, mag. dipole model 80−56959
rarefied gas channel flow, effects of external cct. 80−33630
rarefied gas flow near time-varying accelerated plate 77−11271
Rayleigh-Benard convection, flux ropes, dynamic effects 79−46166
Rayleigh-Taylor instability, general oblique mag. field effect 79−94591
Rayleigh-Taylor instability, two superposed cond. fluids, with suspended particles 78−87399
Rayleigh-Taylor instability of a conducting viscous fluid in a magnetic field 80−43785
rectangular duct flow with opposite walls conducting and insulating 80−33688
magnetohydrodynamics continued
rectangular MHD channels, nonuniform conducting flow calcs. *(Russian)* 77−27613
redistribution of liquid metal flows using const. inhomogeneous mag. fields 79−77285
relativistic, definite material scheme 79−25943
relativistic, evolution system study of generalised scheme *(French)* 77−65799
relativistic Boltzmann eqn. and MHD eqns. with radiative reaction 80−36956
relativistic electromagnetic fluid flows, geometrical aspects 79−72950
relativistic electromagnetic fluids and Ricci collineations 79−35605
relativistic EM fluid flows 80−52094
relativistic EM fluids, constitutive theory 78−57843
relativistic ferromagnetohydrodynamics, mag. field effect on struct., waves *(French)* 79−27716
relativistic fluid, infinite thermal conductivity, Cauchy problem solutions, existence and uniqueness *(Italian)* 80−48821
relativistic infinite electrically conducting fluids, strong shock waves 77−39365
relativistic invariant, magnetofluid dynamics, eqns. of motion for charged particle and charged fluid 80−87821
relativistic magnetofluid and space-like conformal mappings 80−75001
relativistic magnetofluid flows, geometry 80−46895
relativistic magnetofluids and symmetry mappings 79−27700
relativistic magnetofluids and symmetry mappings 79−23379
relativistic magnetofluids and symmetry mappings. II 79−27701
relativistic self-inductive radiative fluid, wave propag. 79−41772
relativistic shock wave, propag. in presence of transverse mag. field 78−75207
resistive diffusion of strong mag. field in tenuous conducting gas 77−78625
resistive magnetic tearing, energetics 79−96904
reversed field pinch, MHD turbulence model 77−24144
reversed field pinch, resistive and MHD instability, unstable central region 77−27704
reversed field pinch, tearing mode MHD eqns., linear and non-linear calc. 77−27705
review, of MHD channel and boundary layer flow, rel. to energy sources 79−37403
rigid ellipsoidal particles in external field, dil. suspension, rheological eqns. *(Ukrainian)* 80−48661
root mean square magnetic field, in turbulent diffusion 78−36449
rotating channel, heat transfer, wall conductances effect 78−51245
rotating channel of parallel plates, Hall effects on hydromagnetic flow and heat transfer 77−42926
rotating conducting fluid in horizontal mag. field, Rayleigh instability 77−15126
rotating fluid with stratification, Boussinesq. approx. of linearised eqns. 78−79387
rotating gas, perfectly conducting compressible in mag field under gravity, wave dipersion relations *(Chinese)* 80−77276
rotating gaseous masses, adiabatic stability 77−91516
rotating Hall plasma, self gravitational instability, MHD stability 80−14890
rotating inviscid flow, in cylinder, axial field and point force 78−18349
rotating relativistic neutron star, interior MHD struct. 79−71062
rotating self-gravitating fluid sphere with uniform distrib. of heat sources, MHD convective instability 77−29264
rotating stratified flow, in horizontal mag. field, stability 78−67246
rotating stratified fluid, hydromagnetic stability 78−55692
rotating superposed fluids, MHD instability, flow through porous medium 78−14089
rotating viscoelastic fluid layer heated from below, MHD convective instability 77−58800
rotational flow, homogeneous fluid in cylindrical tube past circular disc 79−46398
rotational flow, stability in axial and toroidal mag. fields 77−31394
rotational stability sufficiency conditions 79−10616
Saturn, lower atmosphere MHD rel. to atmosphere differential rot. 80−46467
sausage instability growth time, current-carrying liq. cond. 78−67279
screw pinch, sharp boundary Vlasov fluid stability anal. 77−24071
secondary stationary flow between cylinders *(Russian)* 78−26206
self-gravitating gas masses containing axisymmetric mag. fields, equilib. structs. 80−94708
self-gravitating gas-particle suspension, magneto-gravitational instability, with conduction 79−29989
self-gravitating magnetofluids collineations and motions 77−51135
separation of high energy plasma in mag. and gravitational fields 80−67547
separatory motions of dia-/paramag. solns. and ferrimag. suspensions in mag. field 77−20628
shear flow, energy transfer from turbulent to mean motion 77−35252
shear flow stability 78−51244
shear inviscid flow, vortex sheet stability 80−28571
shear turbulence with transverse mag. field 79−32695
shock, axisymmetric, equatorial propag. 77−19640
shock and detonation wave propagation in channel in nonuniform EM field *(Russian)* 77−58798
shock wave collisions, anal. theory, vel., incidence angle and mag. field effects 77−7415
shock wave ionisation in transverse magnetic field, finite-difference methods 78−51249
shock wave propag. and growth in inhomogenous fluid 78−67272
shock wave propag. in non-homogeneous media 77−7459
shock wave refraction 78−1749
shock wave smoothing with artificial heat conduction 78−67271
shock waves, oblique propag. *(Russian)* 79−14483
shock waves, overtaking interaction 78−71369
shocked solar wind viscous flow behaviour at Venus ionopause 79−75068
shocks, axisymmetric, equatorial propag. 77−75985
shocks in magneto-radiative gas 79−37423
singular hypersurfaces, asymptotic regularisation as alternative to distrib. 80−36923
singular lines of one-dimensional force-free magnetic field 79−66920
sink flow with transverse mag. field, boundary layer thickness 80−69940
slip flow, MHD, over porous plate, with variable suction, heat transfer 78−79337
slip flow regime over porous plate, skin friction and heat transfer 77−31392

magnetohydrodynamics continued
slow flow in channel, porous walls, periodic mag. field effects 77−27599
slow flow of cond. fluid in curved channel with rectangular cross-section 77−7463
slow viscous flow in rectangular cavity 80−19517
slowly spreading jets, MHD instability 80−87818
small scale magnetic fields in turbulence, Saffman's approx. 80−106851
smectic A liquid cryst., propag. undulation mode 79−14672
solar active regions, mutual hydrodynamic attraction of mag. knots 78−53898
solar active regions, nonlinear stage of instability due to local Joule overheating 78−61839
solar activity, current theories *(French)* 79−84760
solar atmosphere, acoustic waves interaction with mag. flux tubes 80−85911
solar atmosphere, magnetic energy build-up 77−45391
solar atmosphere, MHD fluctuations due to magnetosonic wave propag. in warm plasma 80−77275
solar atmosphere, rope structure of rising mag. field *(Russian)* 78−40898
solar atmosphere, thin magnetic tube instability rel. to network struct. 80−12725
solar chromosphere, hydromagnetic struct. near supergranule boundary 77−13298
solar chromosphere-corona transition region, mass motions in impulsive flarelike brightenings, OSO-8 obs. 79−35217
solar convection zone, buoyant mag. flux tubes rel. to $\alpha\omega$-dynamo 77−45385
solar convection zone, solar cycle driven by dynamo action of global convection 77−56903
solar cool corona pressure and energy balance over sunspots 77−13291
solar corona, plasma heating by anomalous current dissipation 78−53895
solar corona, turbulent heating role 80−12715
solar corona streamer, drift pair radio burst theory 79−25558
solar coronal, transients, MHD models, 1973 August 21 event simulation 79−35215
solar coronal arcades mag. instability, two ribbon flares origin 80−72911
solar coronal hole in northern polar region, simulation, MHD eqns. 78−4168
solar coronal holes, models of flows 79−58313
solar coronal loop, plasma physics model and dynamic MHD behaviour 77−45371
solar coronal loops, thermal instabilities in magnetically confined plasmas 80−36600
solar coronal magnetic loops, struct., MHD stability theory 78−28632
solar coronal magnetic loops, structure, equilib. theory 78−12192
solar coronal transients, MHD models in meridional plane, mag. field effect 79−5798
solar coronal transients, two-dimens. numerical solns. for model corona 78−20774
solar coronal transients, two-dimens. plane anal. 78−20773
solar cosmic ray particles, accel. in expanding coronal mag. bottle 80−77244
solar cycle, as nonlinear oscill. of general mag. field driven by nonlinear dynamo 78−40889
solar cycle, MHD dynamo model 77−17536
solar dynamo, mag. buoyancy effects 77−78734
solar dynamo, nonlinear MHD model 78−53918
solar eruptive processes, onset theory 78−61840
solar evolving force-free magnetic fields, variational formulation 78−93182
solar flare, models, current interruption and impulsive flux transfer 79−12438
solar flares, emerging flux model 78−4165
solar flares, flash phase and current sheets thermal evolution 77−17485
solar flares, force-free mag. fields evolution, nonequilib. states and preflare stage 80−105213
solar flares, mag. structs. models and predictions of flux rope theory 80−21955
solar flares, phenomenological model 78−49407
solar flares, role of plasma turbulence 77−17476
solar flares, trigger mechanism for emerging flux model 78−89162
solar fundamental flux tubes, generation, periodic field reversal 79−53792
solar fundamental flux tubes, rising and durability 79−53791
solar hard X-ray bursts, thermal models 80−94766
solar intense magnetic fields and umbral dots 77−29783
solar loop prominences form. mechanism, MHD approx. *(Russian)* 77−87363
solar loop prominences formation, kinematic model 78−7965
solar magnetic field, turbulent diffusion, Eulerian formalism 79−16901
solar magnetic fields, floating-up time rel. to solar activity 11-year cycle 80−101580
solar magnetic fields, flux-rope-fibre theory 78−77525
solar magnetoatmospheric wave eqn., critical levels 77−78747
solar photosphere, hydrodynamic mag. pumping rel. to mag. fields fine struct. 80−98646
solar photosphere, mag. fields hydraulic concentration, dynamical effects in stratified atmosphere 77−13294
solar photosphere, small-scale mag. fields and convection 78−53906
solar photosphere magnetic fields, hydraulic concentration near equipartition 77−13293
solar surges, local mag. field strength rel. to dynamics of descending stage *(Chinese)* 80−105221
solar twisted flux tube theory, stability 77−60737
solar type III radio bursts, electron exciters obs. near 1 AU 80−46513
solar wind, Alfven waves, non-linear interaction with compressive fast magnetosonic waves 80−105142
solar wind, coronal-interplanetary expansion, sheet-current approach 78−20807
solar wind, dynamic mag. struct. of large amplitude Alfvenic vars. 80−72734
solar wind, flow around magnetosphere rel. to magnetopause position 78−49236
solar wind, high speed interactions, MHD model of interplanetary disturbances 79−40051
solar wind, MHD turbulence props. 80−61977
solar wind, multispacecraft obs. of microscale fluctuations 77−87224
solar wind, plasmadynamical processes review *(German)* 80−109323
solar wind, stream-assoc. fluctuations rel. to radial var. of average wind parameters 77−45278

magnetohydrodynamics continued
solar wind corotating stream interaction regions obs. by Pioneer 10 and 11, dynamic MHD modelling 79−2461
solar wind disturbances during 1972 August solar flares, MHD modelling 78−45174
solar wind low-frequency wave packet, passage across stand-off shock front 78−45138
solar wind magnetic dips 79−75072
solar wind radial expansion, appl. of MHD moment eqns. 77−64584
solar wind turbulence 80−85834
solar wind-magnetosphere interaction, model, MHD eqns. 79−53663
solar wind-magnetosphere interaction, time-dependent global simulation 78−88991
solitary fluid transient compression wave in rectangular duct in transverse mag. field 78−59503
solitary fluid transients in rectangular ducts with transverse mag. fields 79−77288
solitons, upper hybrid, formation from MHD perturbations 79−90348
solute dispersion in porous medium in MHD flow between parallel plates, homo- and heterogeneous reaction effects 78−55697
sonomagnetic pseudoradiation from submerged acoustic sources 78−18093
space time permeated by compressible, thermally conducting self-gravitating field, props. 79−71315
space-times, family of contracted Ricci collineations symmetry mappings 80−51650
sphere, nonconducting, slowly rotating in steady MHD flow, exact soln. 80−33695
sphere, spinning, motion in conducting fluids, drag forces, Magnus transverse forces and dragging torque *(Russian)* 80−87817
sphere motion in infinite conductive fluid, variable mag. dipole located within sphere case 80−19519
spherical conducting fluid system, press. distrib. in crossed elec. and mag. fields *(Russian)* 77−47109
spherical mass. MHD stationary equilibrium in uniform rotation *(Italian)* 77−55093
spiral galaxies, magnetogasdynamic mechanism of rotation *(Russian)* 77−87536
stability of aligned, stratified, compressible magnetoatmospheric shear flow 78−26197
stability of flow in temp. and conc. field 78−30360
stability of hydromagnetic flows in a temperature field 80−92231
stability of thermally radiative magnetofluiddynamic channel flow 77−15129
stable 3 dimens. MHD equilib., numerical model anal. 77−27665
stagnation-point boundary layer with hot wall, mag. field effect 77−72359
star, magnetic flux tube, buoyancy and equilib. 80−109420
stars., exact MHD solns. for rotating magnetic objects. 78−69800
stars, F- and G-type, mag. accel. of winds and ang. momentum loss 77−13334
stationary flow between porous rotating cylinders in a radial magnetic field 80−83857
stationary waves at the surface of a magnetizable liquid in a stream impinging on a point barrier 80−83805
steady and nondissipative flows, geometric results 80−48819
steady flow between a rotating and a porous stationary disc in the presence of transverse magnetic field 78−79382
steady flow past circular cylinder 77−51126
steady plane magnetohydrodynamic flows with orthogonal magnetic and velocity fields 79−27697
steady state flow in coaxial channel, with scanning mag. field, approx. model *(Russian)* 77−3877
steady state turbulent flow, flow near wall, heat mission, theory *(Russian)* 78−5810
steady-state MHD convection in a vertical annular duct in a radial magnetic field 80−48809
steel, MHD industrial smelting, techniques, economics *(Russian)* 77−24980
stellar atmosphere, thermal-convective instability, radiative transfer effects 78−53929
stellar atmospheres, hydromagnetic flow near oscillating porous limiting surface 78−12200
stellar convection in rot. magnetic star, toroidal field effect 80−41816
stellar magnetism, MHD processes near compact superdense objects 79−40206
stellar relativistic centrifugal winds, appl. to pulsars 78−96473
stellar wind flow, axisymm. ideal MHD eqns. 78−89174
stimulated linear acceleration bremsstrahlung 79−92658
stochastic particle accel. by MHD turbulence 80−31203
stochastic stability of MHD equilibria 79−77414
Stokes' problem, mass transfer effects of MHD free convective flow 80−62003
Stokes approx., eqns. with homogeneous operators *(Russian)* 79−60071
Stokes approximation for two-dimens. flow in strong mag. fields 80−83849
Stokes problem, boundary layers and skin friction 80−14837
Stokes problem, hydromagnetic free convection flow for porous vertical limiting surface with const. suction 80−90328
Stokes problem for infinite vert. plate, hydromagnetic free convection effects 80−10318
Stokes problem for vertical plate, free convection 79−18970
Stokes problem for vertical plate, mass transfer and free convection current effects 79−90347
stratified flow between oscillating disks, boundary layers 80−28570
streamline flow round an array of profiles in a magnetic field perpendicular to the plane of the flow 80−83856
strong internal mag. field diffusion through radiative envelope of 2.25 $M_\odot$ star 78−85931
subsonic MHD channel, acoustic props., calc. for longitudinal oscills. 77−35405
suction effect near accelerated plate 80−92232
Sun, convection zone, mean-field MHD 77−56900
Sun, dynamo action of mean flow from latitude depend. heat transport 80−90378
Sun, dynamo theory and mean-field MHD 77−56901
Sun, dynamo theory and solar cycle 77−53564
Sun, eruptive prominences and coronal transients 80−56809
Sun, mag. buoyancy theory 79−21256
Sun expanding mag. arch, MHD oscill. rel. to moving type IV radio bursts modulation 80−26833

magnetohydrodynamics continued
sunspot cycle morphology, theory *(Chinese)* 80−12722
sunspot magnetic field and vel. quasiperiodic oscills. *(Russian)* 78−12186
sunspots, heat flux in subphotospheric layers, rel. to umbral granulation 78−73692
sunspots and magnetic flux tubes physics, umbral dots and longitudinal overstability 80−26825
sunspots and physics of mag. flux tubes, aerodynamic drag 79−71012
sunspots and physics of mag. flux tubes, aerodynamic lift on thin cylinder in convective flows 79−101126
sunspots and physics of mag. flux tubes, general nature of sunspots 79−75168
sunspots and physics of mag. flux tubes 79−101127
sunspotsand physics of mag. flux tubes, aerodynamic lift 79−101125
supercritical Taylor-Couette flow 80−33702
supernovae, magnetorotational explosion in cylindrical model 80−101605
supernovae, MHD model 80−46588
superposed conducting fluids, hydrodynamic and hydromagnetic stability 79−18969
surface instability of nonisothermal layers 79−77272
suspensions moving in mag. field, continuity eqns. *(Russian)* 77−55098
swirling viscous flow with applied mag. field, differential eqns. for boundary layer 78−22428
switch on shocks, hydromagnetic 77−84337
T Tauri type stars, hydromag. model of peculiar activity *(Russian)* 78−49442
Taylor column irregularity in rapidly rotating MHD fluid, mag. field effects 80−43786
temp. distrib. for flow between coaxial cylinders with wall temp. discontinuity 80−1690
temperature sheaths, probes and electrodes in MHD plasma 78−55726
thermal boundary layer flow near oscill. limiting surface, stellar atm. appl. 78−94831
thermal convection instability in hydromagnetics, effect of suspended particles 79−53709
thermal convection onset under const. flux boundary conditions, mag. field effect 78−69676
thermal convection suppression by distributed automatic regulator *(Russian)* 78−30364
thermal instability of an internally heated fluid layer in a magnetic field 80−53875
thermal instability of layer of micropolar fluid, in transverse field 80−87812
thermal unsteady boundary layer flow 77−7460
thermally radiative channel flow, stability 78−55695
thermodiffusive mixture flows, Hall and ion-slip effects, uniqueness theorem 78−87415
thermoelectric MHD, appl. to fission and fusion reactors and metallurgy 79−50806
thermoelectric MHD, pipe end problem, boundary layers and rotation 80−69942
three-dimensional incompressible flow, with mag. neutral points 79−64788
Titan, dynamo mag. fields possible strengths 79−16873
Tokamak, experimental power reactor, plasma studies 78−66418
tokamak, internal resistive modes, (m=1, n=1) and (m=2, n=1) MHD eqns. linear anal., toroidal coupling 77−43048
Tokamak, noncircular, reactor size plasma MHD equilib. calc. 77−24121
Tokamak hybrid breeder blanket, liq. metal coolant, MHD effects 78−74481
Tokamak MHD processes, Kadomtsev-Pogutse eqns. numerical simulation, kink modes and internal disruption 77−43047
Tokamak-driven hybrid breeder reactor, liquid metal coolant, MHD effects 79−17974
toroid, pseudostatic resistive hydromagnetic equilibria 79−98819
transient phenomena, simultaneous solns. to coupled gasdynamic-EM equations of motion 80−6157
transport processes, relativistic generalisation in continuum *(Hungarian)* 78−89383
transverse magnetic field, streamline orthogonal-net anal. 79−37417
tube flow, law of resistance to motion *(Russian)* 78−26207
turbulence, 2-D, hydrodynamic and plasma applications, dynamical eqns., diffusion, MHD, superfluidity, review 80−69769
turbulence, development and generation *(French)* 80−79407
turbulence, homogeneous, incompressible fluid, functional charact. 78−18355
turbulence, hydromagnetic, appl. of Karman's energy transfer process 79−81991
turbulence, low mag. Reynolds number 78−94845
turbulence, numerical simulation and closure techniques 79−90343
turbulence, one dimens. model, conditions for global regularity and onset of singularities *(French)* 79−50803
turbulence, statistical theory distrib. functions 79−37412
turbulent boundary layer, at permeable surface, in crossed elec. and mag. fields *(Russian)* 78−94836
turbulent boundary layer, effect of weak MHD forces 77−24026
turbulent boundary layer flow at porous surface, in crossed inhomogeneous fields 79−77274
turbulent boundary layers in rot. circ. vessel, drag 80−33697
turbulent channel flow, conducting fluid in external elec. and mag. field *(Russian)* 77−3875
turbulent channel flows, asymptotic theory 78−30368
turbulent duct flow, turbulence suppression in liq. 78−94844
turbulent flow relaxation theory test, MHD expt. 79−98814
turbulent fluids, mag. energy transfer in weak mag. fields 78−18350
turbulent free convection in mag. field, statistical charact., vortices 80−79310
turbulent heat and momentum transfer in 2-dimens. channel with transverse mag. field 78−94848
turbulent medium with density gradient, MHD effects, appl. solar convection *(Russian)* 78−47055
turbulent MHD flows, residual disturbances after laminarisation, entry effects 80−6160
turbulent stream with 2-dimens. struct. perturbation, shear region momentum transfer *(Russian)* 78−5812
turbulent thermal convection in presence of rot. and mag. field, stellar and planetary dynamos appl. 80−6042
twisted magnetic fields, stability 78−45217
two channel DC EM pump, expt. study 80−43791

magnetohydrodynamics continued
two-dimens. MHD turbulence, second order closure 79−32693
two-dimensional Hartmann flows, for fluid with cross-stream dependent elec. cond. 79−64771
two-dimensional MHD parallel plane channel flow, heat transfer 79−32701
two-dimensional MHD turbulence, small-scale struct., singularities form. 79−46396
two-dimensional turbulence, in plane channel, in azimuthal mag. field *(Russian)* 77−47101
two-dimensional turbulence transition, dynamics in mag. field *(Russian)* 77−3886
two-phase flow, separation by solenoid *(Russian)* 77−7466
two-phase flow through cracked porous media in mag. field, imbibition 78−34200
two-phase liquid metal flow in strong mag. field, MHD pressure drop 79−23368
unsteady Couette flow through porous wall in presence of mag. field 80−53856
unsteady flow between two coaxial cylinders 77−68701
unsteady flow due to unsteady plate 79−14481
unsteady flow of an electrically conducting dusty viscous liquid through a channel 79−14484
unsteady flow of elec. cond., incompressible, viscous fluid, MHD 78−59496
unsteady free convection flow, past hot vertical plate, calcs. 77−75986
unsteady free convection flow past a vertical porous plate with variable suction and transverse magnetic field 79−32691
unsteady free convection flow past vertical porous plate 78−30361
unsteady free convection past a hot vertical plate 78−87396
unsteady free convective flow past infinite plate with time depend. suction 79−27704
unsteady hydromagnetic thermal boundary layer problem, numerical treatment 80−92227
unsteady laminar flow of elastic viscous fluid through porous channel, applied mag. field effects 80−38499
unsteady magnetoaerodynamic forces on finite length oscillating circular cylindrical shell, dynamic response problem 79−64776
unsteady magnetohydrodynamic flow through a channel 79−37413
unsteady MDH convective diffusion, exact anal. 79−72953
unsteady MHD eqn. solns., for explosion in non-homogeneous media, num. anal. 79−64778
unsteady MHD flow in rotating system, Hall current effects 80−33704
unsteady MHD forces on oscillating shell, transient soln. 79−64775
unsteady rotating boundary layer flows between porous plates 77−47112
unsteady thermal boundary layer flow with zero heat transfer, astrophys. appl. 77−87250
unsteady viscous MHD flow, through porous channel with constant suction 79−72951
Uranus magnetic dynamo, implications for mantle struct. and comp. 80−4298
variational principle using Lagrangian approach for infinitely conducting fluid 79−32683
velocity meter for cond. flow, charact., freq. depend. calibration *(Russian)* 77−65819
viscoelastic conducting fluid, MHD flow 80−92229
viscoelastic conducting fluid on oscill. plate in mag. field 77−72365
viscoelastic fluid, MHD flow past porous plate in slip flow 79−4084
viscoelastic free convection boundary layer flow past porous plate 80−10317
viscoelastic Maxwell fluid, unsteady flow between parallel planes, in transverse mag. field 78−38411
viscoelastic Rivlin-Ericksen fluids, unsteady flow through circular and coaxial ducts in radial mag. fields 78−42632
viscomagnetic heat flux, in a Burnett regime, gas kinetic theory 78−71400
viscoplastic conducting liq., finite perturbations, Hartman flow instability *(Russian)* 78−47049
viscous conducting fluid, laminar flow, boundary effect in helical induction machine *(Russian)* 77−47105
viscous electrically cond. fluid, laminar free shear flow, transverse mag. field effect 80−48811
viscous flow, stability in curved channel 78−9720
viscous flow between two rotating porous cylinders, in axial mag. field 77−72364
viscous flow past moving plate with suction 77−11268
viscous fluid, electrically conducting, flow between rotating and stationary porous coaxial discs 80−43799
viscous fluid, incompressible, hydromagnetic free convective flow past vertical porous wall, mass transfer 80−64645
viscous fluid between rotating surfaces of revolution *(Polish)* 77−55096
viscous fluid flow over infinite rotating disc with suction, existence of soln. 78−30366
viscous fluid layer with heat source, stability in presence of inclined mag. field 77−89206
viscous fluid magnetic throughflow in slot, inertia effect 79−37418
viscous incompressible conducting fluid flow between parallel plates 79−14487
viscous incompressible conducting fluid past infinite flat plate suction 77−68697
viscous incompressible electrically conducting fluid flow between parallel plates, const. mag. field 77−68700
viscous incompressible fluid, MHD flow between a rotating and a stationary disc 78−63502
viscous laminar unsteady flow over infinite flat plate 79−37406
viscous MHD fluid flow 77−27620
voltage losses near electrodes 80−103079
vortex flow generation, viscous fluid with spherical boundary, by AC EM field 78−5804
vortex sheet stability in compressible perfectly conducting fluids 80−14831
vortical flow, electrically-induced, from hemispherical electrode 79−94733
vorticity suppression of cond. fluid by applied mag. field 77−35249
wall conductance effects on convective horizontal channel flow 79−23374
wall friction in channel flow, MHD flow in channel, wall friction 78−14092
water, ion drag meas. by microfluxmeter 78−79384
water, MHD free convection flow past infinite porous plate 80−33703

magnetohydrodynamics continued
waves in stratified heavy incompressible fluid, mag. field presence 78−59495
weak discontinuities, growth and decay 79−86519
weak discontinuities in a conducting magnetizable medium 80−48805
weak MHD discontinuities, growth and decay 77−84327
weakly conducting dielectric liquid, plane jet in strong nonuniform mag. field *(Russian)* 78−94838
weat discontinuities in magneto-gasdynamics with finite electrical conductivity 79−18966
white dwarf degenerate cores, thermomagnetic instability conditions 80−77395
with time-depend. suction, between parallel walls 79−37279
ZT-1 reversed field pinch, derated mode MHD stability and diffusion 77−27701
Fe_2O_4, suspension in oil, motion in rotating mag. field *(German)* 77−75983
Fe_3O_4, suspensions, ferrofluid motion, rot. mag. field effects 77−950
Ge, electron-hole drop magnetostruction 78−87912
Ge, electron-hole liquid, MHD effects 80−80190
Hg, acoustic streaming meas. 79−64380
Hg, flow and energetic charact. in linear induction MHD pump *(Russian)* 77−3882
Hg layer with rot. and mag. field, cell sizes at thermal convection onset 77−54991
Hg, liq., flow in transverse mag. field, laminar and transition, channel wall effects 78−63500
Hg, liq., flow transition, in mag. field, 2-dimens. to 3-dimens. turbulence *(Russian)* 77−7471
Hg, liq., turbulent channel flow, in mag. field, spatial correl. and vorticity *(Russian)* 77−3876
Hg, natural convection in mag. field parallel to the gravity vector 79−81990
Hg, transition and turbulent flow in curved channels under transverse mag. field 80−79396
Hg-Ar, two phase flow in vertical tube, transverse mag. field, bubbles and slug flow 77−84303
K heat pipe, heat transport characteristics, transverse mag. field effects 79−37127
K, stagnant, mag. field infuence on boiling 77−47096
Li:NH_3, soln., free MHD convection near horizontal cylinder *(Russian)* 77−7467
$MnCl_2$, aq. soln., thermomagnetic convection, in transverse flow round cylinder *(Russian)* 77−47100
Na, incipient boiling in the presence of a mag. field 79−37411
O_2 gas, magnetically enhanced thermal convection 79−50802
O_2, magnetothermal convection in nonuniform mag. field 78−1746
O_2-N_2, gas mixtures, mass transfer, mag. field effects 78−63535

magnetomechanical effects
see also gyromagnetic effect; magnetoelastic effects; magnetoelastic waves; magnetostriction
adhesive wear, in presence of magnetic field, model 77−28913
amorphous ferromagnetic alloys, domain struct. and mag. microstruct., review 80−15751
cantilever fastened plate, structural sensitivity of magnetoelastic effect 79−39095
coating stresses in oriented transformer steel determ. by bending expts. *(German)* 79−28569
conducting mag. top, fast rot. in inhomogeneous alternating mag. field 79−41264
cubic antiferromagnetic, first to second order transition crossover 78−10709
cutting tools, diffusive wear, mag. field effect 80−60985
dimethylammonium copper tetrachloride, ferromag., quasi two-dimensional, ordering temp., press. depend. 80−84601
elastic compliance, cooperative mag. contrib., exchange striction mechanism 77−40108
$Fe_xCo_{1-x}Ti$, ferromag., high-field and high-press. mag. behaviour 78−91919
ferromagnet, conditions for stress induced bulk moments 79−78493
ferromagnet, dislocation effects on piezomag. coeff. tensor *(Russian)* 77−8378
ferromagnet, dynamic slowing down of dislocations near Curie point *(Russian)* 79−8036
ferromagnet, flow stress, effect of magnon mechanism of dislocation drag 77−69662
ferromagnet, local variation in mag. anisotropy due to linear defects *(Russian)* 78−68214
ferromagnet, mech. behaviour in microplastic strain region *(Russian)* 78−39838
ferromagnet, multiaxial, domain struct., applied stress effect *(Russian)* 78−76267
ferromagnet, pinned domain wall motion, magnetic damping studies 80−65956
ferromagnet, single domain, isolated pores and brittle cracks *(Russian)* 78−39381
ferromagnet, stress indication by transverse and longitudinal internal induction 77−16138
ferromagnetic crystal, magnetic damping due to pinned domain wall motion 79−56598
ferromagnetic materials, fracture-induced magnetic effect 77−80986
ferromagnetic metals, magneto-volume effect, Invar phenomena 80−66007
ferromagnetic ordered structures, domain structure, effect of defects, electron microscopy 78−64214
ferromagnetic plate, homogeneous, natural oscills., subject to delay 79−28624
ferromagnetic wire, Fe alloy, torsion stress influence on magnetisation obs. *(Slovak)* 77−90468
ferrosuspensions, mag. field effects on mech. props. 78−87321
frozen spin state, static susceptibility, piezomag. effect 77−51914
fusion reactor, Tokamak constant tension D-shaped coils, lateral support struct. 78−55013
fusion reactor coil, multilayer structs., laminated beam theory anal. 78−55011
fusion reactor design, dynamic analysis of electromagnetomechanical field by finite element method *(Japanese)* 78−8967
fusion reactor solenoid, orthotropic, finite element stress anal. 78−55010
garnet epitaxial film, stress induced magnetocrystalline anisotropy 80−71013

magnetomechanical effects continued
Invar, mag. phase transitions, linear expansion coeff. and mag. susceptibility meas. 77−69553
Invar, Mossbauer effect at high press. 80−15858
Invar alloys, bulk modulus anomaly, rel. to itinerant electron model of ferromag. 77−48025
Invar-type alloys, review of magnetomechanical effects and state of art of materials 78−52330
ionic crystals, fracture in mag. field 78−59855
liquid crystal, smectic-C, elastic deform. 77−35477
magnetic alloys, dil., press. effects 79−99676
magnetic sound determ. of H_2 absorpt. in metals *(Russian)* 77−60009
magnetically saturated fluid, continuum mechanics, global balance law approach 80−60388
magnetite, low stress effects on susceptibility and coercive force 78−16001
magnetite stressed to failure, mag. behaviour rel. to earthquake prediction 78−32068
magneto-elasticity, stresses in plate with holes 77−866
magnetostrictive ferrites, magnetising field influence on amplitude depend. of mechanical props. 78−2723
metal, ferromagnetic, mechanically stressed, magnetic-inductive method of discontinuous vibration detection, theory *(German)* 79−20315
metallic glass, Fe Mossbauer effect at high press. 80−15858
microspecimens in strong mag. fields, device for tensile and creep tests 79−15903
non-magnetic material wear in presence of magnetic field 80−60982
Permalloy film, galvanomag. rotation charact., under uniaxial stress 78−84466
Permalloy film, magnetoresistive determ. of anisotropy energy and its strain depend. 79−56575
piezomagnetic effects, theory of optical and acoustic prop. interactions 77−4621
pole effect, theory 80−25175
quartz, isentropic compression by ultrastrong mag. field *(Russian)* 78−47468
quartz, mag. field effect on fundamental and overtone modes 77−12182
rare earth alloys, Curie temp. *(Japanese)* 80−20444
rare earth intermetallics, neutron scatt., induced moment magnetism, high press. 80−15699
rare earth-Fe_2, magnetomech. coupling and Young's modulus 78−84472
rare earth-transition metal alloys, cryst. and amorphous, mag. props. 77−73008
rigid body systematic deflection by suspension vibration *(Russian)* 79 9223
rocks, effect of stress cycling and inelastic volumetric strain on remanent magnetisation 78−88820
rocks, piezomagnetic effect due to lake ground loading 80−8346
rocks remanent magnetisation, uniaxial stress effects, stress cycling and domain state depend. 80−26505
rocks stressed to failure, mag. behaviour rel. to earthquake prediction 78−32068
shock compression of solids, review 80−24534
steel, 11YuA, cold worked, heat treated, electromagnetomech. props. NDT 79−4980
steel, austenitic, magnetisation meas. of stability 77−1579
steel, C, magnetomechanical acoustic emission for residual stress NDT 80−71149
steel, ferritic, magnetomechanical acoustic emission for residual stress NDT 80−71149
steel, mild, acoustic emission during magnetisation, stress effects 79−82854
steel, mild, fatigue softening and hardening detected from Barkhausen noise 80−76428
steel, Si, permeability change due to stress variation after demagnetization in Rayleigh region 80−88854
steel, stainless, Mossbauer effect at high press. 80−15858
steel VNS-2, damping capacity, magnetomechanical, phase transform. effects 78−31445
stiffness of conducting bodies config. in time-varying mag. field 80−43230
stimulated Raman effect, electromagnetic-mechanical model experiment *(German)* 78−86077
superconducting five coil partial torus, buckling and vibrs. 77−79128
superconducting magnets, pulsed, hysteretic and mechanical loss calcs. 79−80649
superconducting transversely isotropic solenoid, electromech. stress anal. 77−79127
TCNQ salt, TMTSF-DMTCNQ, mag. susceptibility meas. under press. 80−29521
toroidal field coils, bending-free, for Tokamak reactor 78−55012
transformer steel magnetic loss variation due to nonuniform normal press. *(Russian)* 79−91250
transition metal, 3d, giant internal mag. press. and compressibility anomalies, itinerant model 77−16034
transition metal, bulk modulus, effect of correlations and ferromag. order 78−34564
transition metal, dislocation magnetism *(Russian)* 78−39379
transition metal alloys, Curie temp. *(Japanese)* 80−20444
transition metal alloys, magnetically ordered, effect of magnetic field on P-T diagram 78−52246
transition metal alloys, magnetovolume effects near crit. conc. for ferromag. 79−56591
vibrating reed, influence of magnetomechanical pole-effect 79−73791
volcanic rocks from Mt. Etna, stress effects on magnetic props. 77−37192
Ag-Mn, spin glass, mag. susceptibility hydrostatic press depend., RKKY interaction 80−44845
Al, magnetoplasic effect and eddy current heating *(Russian)* 77−43858
Al plastic deformation depend. on mag. field at 4.2K *(Russian)* 79−91754
Al, plastically deformed by pulsed mag. field, mobility of Fe atoms, radiotracer profiles 79−28584
Al-Ag(10 at.%), supercond., flux pinning, torque meas., decomp. effect 77−1525
$BaTiO_3$-Ni ferrite, piezoelectric-piezomagnetic sintered two-phase composite, magnetoelec. conversion 77−12181
CdHg, ω phase, mag. susceptibility anisotropy w.r.t. uniform compression *(Russian)* 80−71143
CeAg, mag. and structural phase transition at hydrostatic press., elec. resist. meas. 79−61102

magnetomechanical effects continued
$CeAl_2$, electronic transition under pressure, resist. meas. 79−33311
$CeAl_2$, magnetisation curves under high mag. field and hydrostatic press. 77−63233
$CeAl_2$, multiple-q structure or coexistence of different mag. phases, neutron diffr. study 80−107985
CeBi, phase diagram in mag. field, hydrostatic press. effect 80−25132
$CeIn_3$, Neel temp., hydrostatic press. depend. 80−29549
Co, flow stress, effect of mag. field 77−20673
Co-Pt, amplitude depend. of internal friction *(Polish)* 79−95627
CoF_2, domain formation in staggered field induced by uniaxial stress, neutron diffr. exam. 78−76289
$(Co_{1-x}Mn_x)_2B$, $0 \leq x \leq 1$, magnetisation, lattice consts., press. depend. of Curie temp. 80−7137
Cr, magnetic torque anal. in thermally activated domain model, near spin-flip temp. 77−63229
Cr, Q-vector locking, press. induced hardening 80−103870
Cr, specific heat of strained and annealed samples 79−38331
Cr, spin density wave phases, domains 80−103871
Cr, spin density wave Q-vector, temp. and press. depend. 80−11167
Cr-Al, effect of Al concentration and hydrostatic press. on Neel temp. 79−33482
Cr-Co (4.0 at.%) alloy, antiferromag., disappearance of resist. min. under press., and press. coeff. of T_N 80−10960
$CrSb_{1-x}As_x$ press. effect on Neel point 80−71147
CrTe, effect of high pressures on magnetic properties 78−52238
CrTe, neutron diffr. at high press., mag. transition *(Russian)* 79−38326
Cu, electron-dislocation interaction, influence of mag. fields on flow stress meas. 77−31672
Cu-Ni-Fe, magnetic properties, heat treatment and compressive stress effects 80−60367
$CuCl_2.2H_2O$, flop of sublattice moments and Neel temp., press. effects, NMR obs. 77−40058
$CuCl_2.2H_2O$, influence of high hydrostatic press. on intermediate state associated with spin flopping 78−35020
$CuK_2Cl_4.2H_2O$, Heisenberg ferromagnet, spontaneous magnetisation under press. *(Russian)* 77−36058
$CuK_2Cl_4.2H_2O$, Heisenberg ferromag., mag. props. at high press. 77−69512
$Cu(NH_4)_2Br_4.2H_2O$, Heisenberg ferromag., mag. props. at high press. 77−69512
$Cu(NH_4)_2Br_4.2H_2O$, uniaxial ferromag. insulator, influence of press. on magnetisation 77−69661
Dy, magnetoplastic deform., 70-90 kOe, 4.2K 77−8376
$DyFe_2$, amorphous, ultrasonic exam. below T_c 79−73793
$Er_{1-x}Gd_xRh_4B_4$, supercond. and mag. transitions at press. up to 19 kbar 79−38236
$(Er_{1-x}Ho_x)Rh_4B_4$, superconductive and mag. interactions, hydrostatic press. effect 80−49973
EuB_6, Hall effect and resistivity data, ferromagnetic ordering temp., pressure depend. 80−60010
EuGaYIG:Cr, epitaxial garnet film, interaction pot. of domain walls with localised stress fields 80−44889
Fe, compression deformed single cryst., induced uniaxial anisotropy 78−52336
α-Fe, cyclically deformed, mag. props. 77−28412
Fe film, effect of tensile stress on mag. domain struct. 78−68332
Fe, flow stress, effect of mag. field 77−20673
Fe, high purity, dislocation-magnetic domain wall interaction, magnetomechanical damping expts. 78−39360
Fe, high purity, magnetic field variations 80−93156
Fe, high purity, magnetomechanical sampling, magnetic field variations 80−93156
Fe, high-purity, magnetic 90° domain wall-dislocation tangle interaction, magnetomechanical damping expts. 79−78496
Fe, internal friction near Curie point 79−24567
Fe, magnetic disaccommodation, low temp. in neutron-irrad. sample, Bordoni relax. 77−4542
Fe, magnetisation self-reversal, tensile stress effect 78−14982
Fe, magnetomechanical acoustic emission for residual stress NDT 80−71149
Fe, Mossbauer effect at high press. in α-, ε- and γ-phases 80−15858
Fe, plastically deformed by pulsed mag. field, mobility of Fe atoms, radiotracer profiles 79−28584
Fe polycrystalline, two ferromag. methods for eval. of fatigue limit 80−89438
Fe, pure, tensile deform., sources of acoustic emission 78−19814
Fe, stress fields and strains energies associated with closure domains 77−1563
Fe thin layers, vacuum coated on PMMA, mag. behaviour during mech. stress cycles *(German)* 80−80581
Fe, US velocity anomalies at elevated temp. 78−75830
Fe, var. in mag. moment of ferromags. during plastic deform. *(Russian)* 77−66401
Fe whiskers, elastically and plastically deformed, mag. domain structs. 80−15752
Fe, zig-zag 90° Bloch wall, magnetoelastic problem 77−4526
Fe:C(N), small concs. determ., mag. and mech. relax. methods 80−7879
Fe-Al (12 wt.%) alloy 23 kHz US transducer piezomagnetic props. 78−59240
Fe-Al (25 at.%), long-range ordered, compression induced mag. anisotropy 77−69546
Fe-Al(25 at.%), mag. anisotropy induced by plastic deform., dislocations, long-range order 77−4544
Fe-B, amorphous, induced anisotropy, development by mag. annealing and under applied mech. stress 80−65868
Fe-B, amorphous, induced anisotropy by heat treatment in mag. field and under applied mech. stress 80−75758
Fe-B phase ferromag. amorphous alloys, stiffening below Curie temp., pole effect *(Japanese)* 80−84632
Fe-B-Si amorphous ribbons, effect of annealing conditions on magnetomechanical props. 80−34740
Fe-Co (35 wt.% and 52 wt.%), heat treated, decrease in sensitivity of mag. props. to mech. stresses *(Russian)* 78−56363
Fe-Co based alloys (52KF, 35KKh, 35KFN), effect of heat treatment and mech. working, on sensitivity of mag. props. to mech. stresses *(Russian)* 79−34161
Fe-Co-V, Vicalloy, magnetisation reversal by stretching and twisting 80−34733
Fe-Mo, damping capacity *(Japanese)* 78−11259
Fe-Ni, FCC alloy, magnetovolume instability 79−8031

magnetomechanical effects continued
Fe-Pt, plastic deform. effect on struct. singularities and mag. props. *(Russian)* 80−44892
Fe-Si, grain oriented, effect of tensile stress on domain struct. 78−95462
Fe-Si, grain oriented, misorientation effects on mag. props 80−88792
Fe-Si, grain oriented sheet, AC hysteresis, surface struct. and elastic stress effects 80−88791
Fe-Si, grain oriented transformer sheets, permeability and magnetostriction, tensile stress effects 80−88843
Fe-Si, mag. losses, depend. on stress and orientation 77−1882
Fe-Si, mag. props., stress and reannealing effects 80−88844
Fe-Si, maze domains upon appl. of horizontal mag. field or mech. tension 80−11218
Fe-Si (3 wt.%), elec. field gradient by trigonal and tetragonal distortions 77−8474
Fe-Si (3 wt.%), internal friction, instantaneous, depend. on phase of torsional oscills. *(Russian)* 80−71142
Fe-Si (3 wt.%), mag. domain wall contrast in synchrotron X-ray topographs 80−75792
Fe-Si (3 wt.%), magnetisation variation during bending oscills., rel. to ΔE effect *(Russian)* 80−65983
Fe-Si (3 wt.%), nonoriented sheets, magnetisation, tensile stress effects 80−88845
Fe-Si (3 wt.%), oriented, losses and domains, mech. stress effects 80−88852
Fe-Si (3 wt.%) alloy, mag. domain movements prod. by mech. stress 79−87284
Fe-Si (3 wt.%) domain struct., tensile load effects *(Russian)* 78−47995
Fe-Si (3 wt.%) laminations, grain oriented, plastically deformed, anomalous losses 80−88853
Fe-Si (3.5 wt.%), Barkhausen noise, strain depend., interaction of dislocations and domain walls 77−12155
Fe-W (5%), internal friction, mag. and nonmag. components *(Russian)* 78−48018
Fe-Zn alloys, coercive force anisotropy after cold plastic deform. *(Bulgarian)* 80−75809
$Fe_{80}B_{20}$, amorphous, transverse magnetoresist., stress effect 80−15501
$Fe_{80}B_{20}$, amorphous ferromag. metallic glass, stress-induced rot. of magnetisation, Mossbauer study 80−20445
$Fe_{80}B_{20}$ amorphous ribbons, magnetomechanical coupling constant and Young's modulus, mag. annealing 79−15333
$FeBO_3$, Curie temp. displacement under press. up to 3 kbar 77−20603
$Fe_{40}B_{40}P_{14}B_6$ and $Fe_{80}B_{20}$, Metglas 2826 and 2605, amorphous ribbon, power loss variation with freq. and applied stress 80−88849
$FeCl_2$, reorientation of mag. moments under mech. stresses at 0K 80−93153
$Fe_{71}Co_6B_{20}$, glassy ribbon, magnetostatic effects 79−73790
$(Fe_{0.9}Co_{0.1})_xSi_yB_z$, $(Fe_{1-x}Co_x)_{78}Si_8B_{14}$ amorphous ribbons, magnetomech. coupling and saturation magnetostriction 78−68353
$Fe_{78}Mo_2B_{20}$, amorphous, transverse magnetoresist., stress effect 80−15501
$Fe_{40}Ni_{40}B_{20}$, amorphous ribbon, power loss variation with freq. and applied stress 80−88849
$Fe_{40}Ni_{40}P_{14}B_6$, amorphous, thermal stress effect on mag. easy axis 77−80928
$Fe_{40}Ni_{40}P_{14}B_6$, amorphous, stress-induced mag. easy axis 79−33516
$Fe_{40}Ni_{40}P_{14}B_6$, amorphous, transverse magnetoresist., stress effect 80−15501
$Fe_{40}Ni_{40}P_{14}B_6$, Metglas 2826, amorphous ribbon core, appl. in force transducer 78−93669
$Fe_{40}Ni_{40}P_{14}B_6$, Metglas 2826, amorphous ribbon under tension, mag. domain walls and pulsed magnetisation reversal 80−88825
α-Fe_2O_3, magneto-optical meas. of orientation of antiferromag. vector accompanying phase transition *(Russian)* 78−14961
Fe_3O_4 (magnetite), mag. susceptibility under hydrostatic press. and implications for tectonomagnetism 80−26504
Fe_3O_4 (magnetite), piezomag. response depth depend. rel. to tectonomagnetism as earthquake precursor 80−26465
$Fe_{80}P_{13}C_7$, amorphous ribbon, giant ΔE effect, magnetomech. coupling factor 77−8379
$Fe_{78}Si_{10}B_{12}$ amorphous ribbons, magnetomechanical coupling constant and Young's modulus, mag. annealing 79−15333
$GaMo_5S_6$, mag. and struct. transition temps., press. effects, 0-6 kbar *(Russian)* 77−89956
Gd-Co film, with layer struct., mag. torque and anisotropy 77−63246
$GdCo_5$, large Barkhausen discontinuities, effect of dynamic elastic stresses *(Russian)* 78−39364
$GdSn_3$, Neel temp., hydrostatic press. depend. 80−29549
Ge-Fe amorphous film, sputtered, stress induced anisotropy 79−73706
$HoFe_2$, amorphous, ultrasonic exam. below T_c 79−73793
$K_2FeCl_5(H_2O)$, antiferromag., press. depend. on spin-flop transition 80−80505
La-Ce alloy, press. induced spin glass to Kondo phase transition, resist. meas. 79−24174
$Li_{0.5}Al_xFe_{2.5-x}O_4$, polycrystalline, ferromag. reson. absorpt. curves, stress effects *(Russian)* 77−20713
$Li_{0.5}Fe_{2.5-x}Cr_xO_4$ press. depend. of anisotropy consts. 80−65865
α-Mn, electronic structure model, Invar effect, antiferromagnetic-non mag. transitions 80−20370
Mn-Cu alloy, plastic deform. mechanism and shape-memory effect, mag. struct. obs. *(Russian)* 78−60705
Mn-Cu alloys, stressed, diffuse neutron scatt. exam. 78−47950
MnAs, orthorhombic, low temp. magnetic transitions *(Russian)* 80−11193
MnCoSi, effect of press on mag. transition temp. *(Russian)* 80−25137
γ-MnCu, antiferromag., stressed, mag. defects meas. by neutron polarisation anal. 80−50076
MnF_2, antiferromag. and piezomag. domain struct., neutron topography study 80−71088
$Mn_{1-x}Fe_xAs$, high-pressure phase, magnetic properties 78−52247
MnNiGe, coupled nature of mag. and struct. transition under press. 79−8033
MnTe, effect of press. on Neel temp. and lattice parameter 79−95594
$Mn_{1-x}Ti_xAs$, ferro- to paramag. transition, press. effect up to 7 kbar 77−89954
MnZn ferrite, mag.-mechanical-microstruct. interaction 77−1578
MnZn ferrite, wall topography change induced by external press. 80−34734
MnZn ferrites, internal friction and ΔE effect depend. on demagnetisation method 80−80584
MnZn ferrous ferrites, mag. permeability stress depend. 80−88822

magnetomechanical effects continued
Mo, mag. field effect on mech. props. and dislocation struct. *(Russian)* 79−42818
Mo, mechanical props. and dislocation struct., mag. field effect 80−54935
Nb, flow stress, depend. on magnetic fields 77−73311
Nb, mag. field effect on mech. props. and dislocation struct. *(Russian)* 79−42818
Nb, mechanical props. and dislocation struct., mag. field effect 80−54935
$NdSn_3$, Neel temp., hydrostatic press. depend. 80−29549
Ni, (110) film, strain effects on mag. anisotropy 77−80972
Ni, acoustic emission during magnetisation, stress effects 79−82854
Ni, creep, effect of AC mag. field, 1.5-4.2K *(Russian)* 79−11657
Ni, creep, mag. field effects, 30-250 Oe 77−16141
Ni, crossover phenomena, stress induced above Curie point, neutron scatt. study 79−61113
Ni Curie temp., press. depend., using press. cell developed for meas. with cubic-anvil press 80−13109
Ni, deformation in const. mag. field, 4.2K *(Russian)* 80−29591
Ni film, microstructure of charged boundary between ferromag. domains 79−69705
Ni, hydrostatic press. effect on magnetisation Procopiu effect and hysteresis meas. 77−48023
Ni, internal friction, instantaneous, depend. on phase of torsional oscills. *(Russian)* 80−71142
Ni, mag. field effect on creep, 4.2K *(Russian)* 77−90000
Ni, magnetic aftereffect reactivation of single crystal by plastic deform. 79−65697
Ni, magnetic internal friction peak bifurcation in rot. mag. field *(Russian)* 78−39380
Ni, magnetically ordered state, softening with varying mag. field *(Russian)* 78−35017
Ni, magnetised mono- and polycryst., activation vol. var. during low temp. deform. *(Russian)* 78−3178
Ni, magnetoplastic effect and eddy current heating *(Russian)* 77−43858
Ni, neutron depolarisation near Curie point *(German)* 78−14934
Ni, pure and doped, mech., mag. relax. meas. dumb-bell self-interstitital reorientation *(German)* 78−52879
Ni, simultaneous obs. of Barkhausen and magnetoplastic effect 79−28583
Ni, stress induced cross-over effect near Curie point *(German)* 80−103873
Ni, stress induced crossover effect near Curie point *(German)* 80−103874
Ni, stress-induced crossover phenomena above Curie point 77−4543
Ni-Cu(Pd)(Pt)(Rh), ferromag., press. effect on Curie temp. 79−51781
Ni-Fe film, effect of tensile stress on mag. domain struct. 78−68332
Ni-Mn, ordered and disordered, press. effect on Curie temp. 80−71148
Ni-Mn (up to 32 at.%), Curie temp., press. depend., using press. cell developed for meas. with cubic-anvil press 80−13109
$NiFe_{2-x}Al_xO_4$, stress-induced anisotropy in LPE grown single cryst. films, domain struct. 79−28238
$Ni_{1-x}Fe_2O_4$ ferrites, mag. thermal expansion anomaly 77−69595
$(Ni_xFe_{1-x})_{80}P_{10}B_{10}$, amorphous, Curie temp., press. effect 80−75833
NiS_2, antiferromag. metallic state, neutron diffr. study 79−38325
NiS_2, high press. effect on mag. transition temps. 78−91866
NiZn ferrite, mag.-mechanical-microstruct. interactions 77−1578
NiZn ferrite, wall topography change induced by external press. 80−34734
NiZn ferrites, internal friction and ΔE effect depend. on demagnetisation method 80−80584
NiZnCo ferrites, switching time and coeff., hydrostatic press. effect 80−88802
NiZnCo ferrites, voltage response under sinusoidal and pulse magnetisation effected by hydrostatic press. 80−88846
Pd-Rh-Ag, mag. susceptibility, pressure effect up to 4000 atms. 77−16142
Pr, elastic constants, magnetic effects 78−68355
Pr, magnetic ordering, stress induced 80−15776
Pr, magnetic ordering due uniaxial stress, mag. excitons by neutron scatt. 78−84467
PrSb, neutron scatt., press. induced antiferromag. 80−15699
$Pr_3Se_4(S_4)$, induced ferromagnet, mag. props. under hydrostatic press. 80−60395
$PrSn_3$, Neel temp., hydrostatic press. depend. 80−29549
Pr_3Tl, critical fluctuations temp. depend. 80−25160
Pr_3Tl, induced ferromag., mag. props. under hydrostatic press. 78−56315
Tb-Fe amorphous film, sputtered, stress induced anisotropy 79−73706
Tb-Ho, US attenuation and elastic consts. in 3 mag. phases, 4.2 to 300K 77−72645
Tb-Ho alloy, influence of internal strain on Neel temp., thermal expansion and elastic const. meas. 77−63176
$Tb_{0.26}Dy_{0.74}Fe_2$, temp. depend. of magnetomechanical coupling factor 77−90002
$Tb_{0.27}Dy_{0.73}Fe_2$, perpendicular suscept., magnetomechanical coupling and shear modulus 78−91918
$Tb_{0.27}Dy_{0.73}Fe_2$, vertically zoned, magnetomechanical coupling and magnetostriction 80−65999
$Tb_xDy_yHo_zFe_2$, temp. depend. of magnetomechanical coupling factor 77−90002
$TbFe_2$ monocrystalline (111), under elastic compressive stresses, domain structure *(Russian)* 79−91247
$TiBe_{2-x}Cu_x$, high press. study of Curie temp. and mag. susceptibility 80−84600
$Ti(Fe_{1-x}Co_x)$, ferro- to paramag. transition, press. depend. 77−73028
TmSe, mag. ordering under press., neutron diffr. obs. 80−70947
UAl_2, high field, high press. mag. props. 80−11172
UN, mag. susceptibility under press. 80−7086
U_3P_4, press. effects on elec. resist. and Curie temp. 80−75559
US, ferromag., AC mag. susceptibility at high press. 80−7085
$Y_6(Fe_{1-x}Mn_x)_{23}$, ferro- to paramag. transition, press. depend. 77−73028
$Y_{2.01}Gd_{0.99}Fe_{4.925-x}Mn_xO_{12}$, comp. depend. of mag. props., and stress sensitivity control 78−27057
YIG, polycryst., initial and reversible parallel susceptibilities, hydrostatic press. effects 80−75835
Y_xNi_{1-x}, amorphous, high press. magnetisation and Curie temp. 80−20442
$ZnCr_2Se_4$, magnetoelastic coupling, mag. suscept. meas. 78−76288

magnetomechanical effects continued
Zr, mag. susceptibility, plastic deform. effect *(Russian)* 80−65984
$ZrZn_2$, high press. study of Curie temp. and mag. susceptibility 80−84600

magnetometers
see also magnetic field measurement
absolute vector magnetometer for meas. absolute direction of geomagnetic field 79−16703
aerial prospecting magnetometer cable length optimisation *(Russian)* 77−73881
Akulov torque magnetometer, extensometric measuring head, exam. 78−54411
alkali metal-He quantum magnetometer 80−17965
automatic NMR gaussmeter *(Polish)* 77−79133
automatic proton magnetometer with autodyne spin detector 79−71503
automatic rotating-head torque magnetometer 78−21183
automatic spinner magnetometer for rock specimens 80−101455
carrier-domain magnetometer, novel Si mag. field sensor 79−9224
cryogenic, for palaeomag. intensity determ. by continuous thermal cycling technique 77−37425
cryogenic free-precession ^3He magnetometer using a SQUID 79−6153
cylindrical flux-gate sensor, using electrodeposited Permalloy film 77−82576
depth measuring apparatus for borehole logging 79−5643
detector types, study and comparison *(Spanish)* 78−4008
development trends *(Italian)* 79−80650
digital pulse magnetometer for monitoring pulse mag. of permanent magnets 77−45871
EPR spectroscopy data handling and processing method *(German)* 77−53968
Explorer 35 spacecraft magnetometers sensitivity rel. to lunar mag. permeability study 77−56846
Faraday, elimination of mag. contrib. of sample holder 79−21788
Faraday, susceptibility, meas. methods, very accurate for small samples *(Croatian)* 79−9222
Faraday magnetometer using Bitter coils 80−62695
Faraday-type, with controlled field gradient, construction 77−57367
ferromagnetic probe, MF-21F 78−93744
ferromagnetic probe magnetometer with synchronous detector, operational analysis *(Russian)* 79−44921
ferromagnetic thin film magnetometer, development and performance 80−31808
ferromodulation meas. transducers, with increased temp. stability 80−52281
flux-gate magnetometer flight performance in Bhaskara satellite 80−72746
fluxgate, interference of signal *(Japanese)* 80−37060
fluxgate, remote geophysical operations appl. 77−53246
fluxgate magnetometer, orientation error in inclination meas. *(Chinese)* 79−88477
fluxgate magnetometer on Pioneer Venus Orbiter, design and operation 80−67496
fluxgate magnetometer using sensor with direct time-coded output signal 78−89510
fluxgate magnetometer with time coded output signal of sensor 79−21785
fluxgate magnetometers, on International Sun-Earth Explorers 1 and 2 78−85804
fluxgate magnetometry, review 79−35800
fluxgate system for Pioneer Venus Orbiter spacecraft 77−87229
geomagnetic anal. appl. *(Russian)* 77−26283
geomagnetic field meas. with quartz H magnetometer, calc. of horiz. component 80−105062
geomagnetic fluctuations meas. on sea-floor, ULF-ELF 80−77152
geomagnetic monitoring system for International Magnetospheric Study 79−29882
gradient magnetometers, appl. to induced elec. currents meas. in Alaska oil pipeline 80−98231
gradiometer, thin film DC SQUID 77−30187
Hall, system of calibration and checking in 0.3 to 6.0 T range 80−17964
Hall effect sensors for mag. fields to 23 T, comparison of InAs, InSb and GaAs probes 77−10066
Hall-effect magnetometers for rocket attitude meas. 79−21148
Hanle effect magnetometer freq. optimisation, computer anal. and expt. 77−18057
Hanle effect quantum one-component magnetometer stability and operating range 78−82011
high field (up to 23 T), low temp. (1.5-300K) methods and instrumentation 77−30171
horizontal magnetic variometer with feedback field *(French)* 78−12001
hysteresis loops, oscillography using ferroprobe transducers 79−87785
induced torque magnetometer 77−13784
induction magnetometer, high permeability metal core solenoid sensor absolute sensitivity 80−31133
induction meas. of moving mag. body, passband selection 78−251
induction type, for biomag. fields *(German)* 79−88207
induction-coil magnetometers, Fe cored, optimisation theory at audio and higher freqs. 79−85156
isochronous cyclotron mag. field automatic meas. system 78−82547
Josephson effect applications 77−20503
Josephson effects applications, review 77−8243
laser sensing system for elec. and mag. fields in power transmission 77−45870
leakage flux sensors for improved Burrows permeameter 77−10067
low temperature, for meas. for mag. props. of whiskers 79−63284
low temperature, for meas. of mag. moment of metallic whisker single crystals 79−88986
lunar magnetometers, data errors and EM induction studies 79−96932
magnetic field gradient production for magnetometers using current carrying strips 77−45872
magnetised ferromagnetic object induced signal charact. *(Japanese)* 77−53963
magnetocardiogram meas. first order gradiometer and DC-thin film SQUID 80−89877
magnetoencephalography, sensitivity distrib. 80−101246
magnetopneumography, analytic methods 80−104713
magnetostatic variometers, selection of separation distance 77−13129
marine proton magnetometer, optimum towing conditions 79−2393

magnetometers continued
marine proton magnetometers, calc. method of EMF for sensors precession signal *(Russian)* 78−65428
marine sounding, absolute magnetometer appls. 79−62600
microcomputer-aided data-processor for mag. susceptibility *(Japanese)* 79−63283
MIS-3M magnetic measuring system (USSR), testing small permanent magnets 80−62699
MPP-1 stationary precision proton magnetometer, errors and calibration 79−53535
multichannel, using galvanomagneto-recombination convertors 80−31810
narrow line ^{87}Rb magnetometers, sensitivity to local geomag. field chnages, and noise reduction 80−26636
NMR, automatic field-tracking, 0.1 to 3.2 T, for use with ESR/NMR spectrometers 79−63279
NMR, display using freq. to magnetic field convertor 79−71490
NMR, large-scale automation 80−57343
NMR, phase detector comparison *(Polish)* 78−70171
NMR magnetic induction meter for solenoid calibration 78−21187
NMR magnetometer, mag. field meas. and stabilisation of CERN muon storage ring 77−57779
NMR magnetometer, precision field averaging, for low and high fields, using flowing water 79−67359
NMR magnetometer, type 9298, homogeneous mag. field meas. 78−32839
NMR magnetometer type 9298, for 1 to 68 kGr 78−77950
NMR magnetometers for CERN muon storage ring, calib. 77−57780
optically pumped, design, characts. and development 79−93177
PAG-5 air and marine proton magnetometer *(Russian)* 77−60489
Permalloy film magnetometer, mag. props. and LF noise 78−48005
Permalloy magnetoresistive mag. field and current sensor 77−10048
portable T-MP field proton magnetometer for high accuracy geomag. field meas. 77−29467
precision using COS/MOS circuit 77−26344
proton magnetometer, synchronous polarisation method advantages *(Russian)* 77−60482
proton magnetometers, toroidal sensor directivity characts. *(Russian)* 77−60483
pulse magnetometer output amp., improving accuracy of pulse magnetometer meas. 79−2793
quantum, effect of external sinusoidal magnetic fields on sensitivity *(Russian)* 80−90870
quantum, He, impurities influence on signal parameters *(Russian)* 78−82010
quantum, optical pumping, alternating polarity modulating pulses, meas. errors *(Russian)* 80−90871
quantum, threshold sensitivity and short-term fluctuations determ. 80−22394
quantum magnetometer spin oscillator, phase error detection 77−74468
quantum magnetometer using optical pumping, broadband freq. multiplier 77−37951
quantum magnetometer with Hanle effect, three layer superconducting shield 77−53962
quantum magnetometry, polarised spin system relax. meas. *(Russian)* 78−12737
real-time magnetometer data transmission via telephone lines 77−13126
RF SQUID, construction, geomag. microfluctuation meas. appl. *(Japanese)* 79−5641
RF SQUID, hysteretic behaviour, spiral model *(German)* 78−49868
RF SQUID magnetometer, effect of noise on performance 79−54159
RF SQUID magnetometer, synchronous demodulation, amplitude- and phase-sensitive detection 80−105679
RF-SQUID magnetometer, biased by harmonic magnetic flux meas. stability 79−93175
ring-core magnetometer, for mag. meas. in interplanetary space during Halley-Venus mission *(Japanese)* 80−94672
ring-core magnetometer, high sensitivity, for balloons, high-altitude mag meas. *(Japanese)* 80−94608
ring-core magnetometer sensor for articulatory meas. of jaw movements 80−101243
ring-core type magnetometer, for space vehicles, geomag. fluctuations high-sensitivity obs. *(Japanese)* 80−94671
ripple field magnetometer, for magnetocrystalline anisotropy meas. in superconducting solenoid 77−2673
rotating, appl. to mag. props. determ. for ferromag. materials 77−49750
rotating sample, role of eddy currents in studies of magnetic anisotropy 79−63278
rotating sample magnetometer, for magnetocrystalline anisotropy meas. in superconducting solenoid 77−2673
rotating sample magnetometer for contactless conductivity meas. 80−73391
sea floor temporal mag. variation measurement, fluxgate system 80−51581
search-coil, for LF mag. stray field meas. *(German)* 77−41657
search-coil, testing and calibration, mag. field simulation system, noise meas. *(German)* 77−49754
self-oscillating quantooptical magnetometer for diffusion coeff. meas. 77−76018
sensor measuring articulatory characteristics of tongue and jaw point movements in connected sounds of Japanese 80−26243
Shimadzu magnetic detectors, MB series, for location of feromag. substances *(Japanese)* 77−53964
Skylark rocket attitude control using magnetometers and Moon sensor 79−25436
solar magnetometer at Kodaikanal Observatory, design and performance 78−61743
space applications of LF supercond. sensors inc. SQUID devices 80−56691
spinning magnetometer, absolute calibration method 78−54413
spinning-plate magnetometer, for meas. 10^{-8}-10^{-2} T fields 78−37039
SQUID, 430 MHz, AC-biased, quantum limited 80−101809
SQUID, AC, low inductance, low crit. current, analysis 77−10071
SQUID, AC-biased, classical to macroscopic quantum transition 80−98953
SQUID, AC-biased, noise, slew rate and stability 80−98948
SQUID, appl. to human brain mag. response monitoring 77−29231
SQUID, appl. to magnetic ion concentration, in maser crystals 78−82007
SQUID, biomagnetic instrumentation and meas. 80−36181
SQUID, DC, circuits, optimisation 80−13056
SQUID, DC, noise limitations 79−21784

magnetometers continued
SQUID, enhanced sensitivity using resonant input circuit 79−35799
SQUID, fabrication and LF and HF appls. 77−22583
SQUID, for dilute magnetic alloy studies, calibration 79−67358
SQUID, geophysical, dewar systems design 80−101462
SQUID, low-inductance, with two microwave junctions 77−82579
SQUID, magnetoretinographic meas. of retina injuries in eye 80−104702
SQUID, meas. of magnetocardiogram and cardiac output 80−104709
SQUID, microwave, high sensitivity, characts. meas. 79−35798
SQUID, optomagnetic meas. appl. 80−98950
SQUID, RF-driven, rock magnetism and palaeomag. appls. 77−45201
SQUID, thin film, for mag. field meas. 77−74463
SQUID, thin film type, mag. field sensitivity, galvanic coupling to supercond. antennae *(German)* 79−85154
SQUID, with independent pumping 80−105685
SQUID 3-axis magnetometer, for magnetotelluric meas. with remote reference 79−29866
SQUID appl. to high sensitivity mag. susceptometer 78−49872
SQUID appl. to nuclear gyros and magnetometers, high stability and sensitivity 80−98949
SQUID detection of high sensitivity mag. reson. 79−75560
SQUID differential magnetometers, design criteria 79−26088
SQUID fabrication and applic. to magnetometer *(Japanese)* 77−65048
SQUID fluxgate magnetometers, magnetopneumographic meas. 80−104711
SQUID gradiometer, DC, thin-film, design optimisation 80−98951
SQUID gradiometric magnetometers, balancing system 79−63285
SQUID instruments and shielding for low level mag. meas. 77−40840
SQUID magnetometer, archaeomagnetic intensity meas. 78−352
SQUID magnetometer, broadband and higher-power, for small signal A-D convertor 78−62211
SQUID magnetometer appl. to nucl. mag. thermometry 77−26292
SQUID magnetometer for meas. of macroscopic quadrupole field for antiferromagnetic order determ. 79−24140
SQUID magnetometer in conjunction with superconducting magnets as susceptometers 79−26086
SQUID magnetometer with selective pickup loop to biomagnetic meas. 79−63286
SQUID magnetometer with temp. control, spontaneous magnetisation and mag. susceptibility meas. 80−68221
SQUID magnetometers, AC-biased, macroscopically quantised, higher harmonics in Josephson effect 80−98952
SQUID magnetometers, signal detection of 1/f noise 79−26091
SQUID sensor, offset temp. coeff. 77−26359
strong magnetic field induction metrology 78−37040
submicron magnetic objects, mag. struct. study using magnetooptic micromagnetometer 80−57349
superconducting, appl. to vector magnetocardiogram meas. 77−29213
superconducting, modification of sample holders 77−26367
superconducting, oscillating sample, for water solns. vol. suscept. meas. 77−49753
superconducting, use in strain transducer 77−37877
superconducting gyroscope, development of London moment readout 79−26090
superconducting gyroscope, high accuracy all angle readout using quantised flux 77−26223
superconducting magnetic gradiometer, LF noise spectra 77−33203
superconducting magnetometer for ocean bottom magnetic field meas. 77−87102
superconducting magnetometers for very weak fields 79−30510
superconducting quantum magnetometer cct. and characteristics 79−40594
superconducting quantum magnetometer with two-contact sensor, asymptotic characteristics 79−6155
superconductive electronics, conf., Charlottesville, USA (Mar. 1978) 79−28447
superconductive gradiometers, for measuring magnetic effects of geophysical origin 80−101463
susceptometer for biomedical meas., Fe stored in human tissue, in vivo 80−101245
Switzerland geomagnetic survey instrumentation and results *(French)* 78−15966
Tesla-ammeter (F4354/1) with digital display, investigation of const. mag. fields 77−26364
thermomagnetometers, for rocks remanent mag. meas. 78−85719
thin-film DC SQUID gradiometer 79−9228
torque and spinner systems, comparison for basalts mag. susceptibility anisotropy 78−21185
torque magnetometer for vacuum-to-high-pressure H_2 environments 80−4746
two-dimensional magnetometer array, for ground-based obs. of auroral zone elec. currents. 80−90245
UHF SQUID magnetometer using coded (4.2K) GaAs FET preamplifier, biased at 430 MHz 80−52282
UHF SQUID magnetometer using varactor-tuned 4.2K GaAs FET amplifier 80−31814
undersea, for meas. transient mag. field horizontal components *(French)* 78−40670
vacuum magnetometer for thin film steady-state parameters 77−22579
variable temp. multimode magnetometer 78−74037
vector, stabilisation using independent servo system 78−77355
vector aeromagnetometer instrument set, accuracy in bench tests 78−45016
vector aeromagnetometer instrument system, design principles 78−28335
vector He magnetometer on International Sun-Earth Explorer C spacecraft 78−85795
vector magnetometer sensor orientation, accurate calibration 78−53741
vibrating pickup-loop magnetometer for local depend. of mag. fields 79−26092
vibrating reed magnetometer of high sensitivity for small ferromagnetic particles meas. 80−73397
vibrating sample, for direction angle of magnetisation meas., appl. to $SmFeO_3$ 77−26366
vibrating sample, operation and appls. *(German)* 79−93172
vibrating sample magnetometer, using vacuum-tight bellows, design and construction *(Japanese)* 79−75559
vibrating-coil magnetometer, appl. to coercivity meas. on soft mag. materials 77−41659
vibrating-sample, and non-uniform magnetisation 78−54414
vibration, magnetic recording tapes props. investigation and recording process simulation *(German)* 78−70164

magnetometers continued
vibratory, for high temp. anal. of low stability carbon steel 77−28946
Voyager magnetic field experiment 78−24431
weak field absolute induction meas. HFS magnetometer 78−77949
Cs Hanle effect magnetometer characteristics and evaluation results 77−79586
Cs quantum magnetometer with superconducting shield 77−18055
He Mz magnetometer, improving accuracy by reducing intensity of optical pumping 80−62700
^{4}He magnetometer, pulsed optical pumping to reduce mag. reson. freq. error 79−67360
^{4}He, optically pumped *(Japanese)* 80−8434
Rb, optical pumped magnetometer *(Japanese)* 79−21790

magnetooptics *see magneto-optical effects*

magnetoplasma *see plasma*

magnetoplasmadynamics *see plasma magnetohydrodynamics*

magnetoreflectance
cholesteric liquid crystal, incident angle dependence calc. 78−43834
dimethylammonium copper chloride, magneto-optical props., 0.03-13.5 eV 77−52132
ferrimagnetic dielectric, near UV reflection-spectra, meridional and polar intensity effects *(Russian)* 78−39572
ferromagnetic metals, near UV reflection-spectra, meridional and polar intensity effects *(Russian)* 78−39572
graphite, far IR magnetospectroscopy of Landau level structure 79−73906
graphite, magnetoreflection under press., Landau level transitions 80−50303
graphite, minority carriers and H-point magnetorefl. spectra 77−63398
graphite and graphite-Br intercalation compounds, magnetoreflectivity in high fields under press., energy band parameters 79−61346
graphite intercalated with Br_2, Fermi level, far IR magnetorefl. expts. 77−40228
graphite intercalation compounds, interband Landau level transitions 77−52095
graphite intercalation cpds., K-point effective masses and Fermi level shifts, magnetorefl. study 80−50305
II-VI compounds, magnetoreflectance of exciton-polaritons 79−91410
inverse 1st moment, normal refl.-weighted magnetorefl., dispersion theoretic derivation 78−76436
reflectivity, normal, superconvergent sum rules 77−85678
relaxation, magneto-optical, reflected rad. polarisation plane, monopolar mag. field pulses on solid surface 77−81086
semiconductor, Wannier-Mott polaritons in mag. fields, review 78−2437
TTF-TCNQ film on KBr, IR spectra in mag. field 77−16310
zero-gap semiconductors, dynamic dielec. function in mag. field, appl. to magnetoreflection spectra 79−15108
zincblende structure semiconductor in intermediate mag. field, exciton spectra 78−18969
As, interband, magnetorefl. for circularly polarised radiation 78−2840
As, magnetoreflection of circularly polarised IR radiation, band struct. 77−52094
Bi, magnetoreflectance, L-pt. band parameters 80−25344
Bi, magnetoreflection of circularly polarised IR radiation, band struct. 77−52094
Bi, magnetoreflectivity in high fields under press., energy band parameters 79−61346
Bi, reson. Landau level transitions 77−52096
$Bi_{1-x}Sb_x$, reson. Landau level transitions 77−52096
$Cd_{1-x}Mn_xTe$, exchange interaction, magneto-optical spectra 80−25348
$Cd_xHg_{1-x}Te$ epitaxial graded gap layers, plasma reflection and magnetoreflection 80−71391
CdMnTe crystals, exciton binding energy, magnetoabsorption and magnetoreflectivity 79−38523
$Cd_{1-x}Mn_xTe$, effect of Mn $3d^5$ states on band struct., exciton refl. struct. in mag. field 79−11094
$Cd_{1-x}Mn_xTe$, semimagnetic, exchange interactions between localised and delocalised electrons 80−97245
CdS, magnetoreflectance and magnetoluminesc. of A exciton 78−39597
CdS(Se), magnetoreflectance spectra of anisotropic II-VI semiconds. by mag. field modulation 77−66519
CdSe, magnetoreflectance and magnetoluminesc. of A exciton 78−39597
CdTe, exciton magnetoreflectance spectra, multicomponent polaritons, Zeeman splitting 80−88974
Cr, ferromagnetic surface layer on antiferromag. bulk, determ. by surface magnetoplasma wave detect. 78−68356
EuO(S)(Se)(Te), phase transition spectroscopy 77−63426
EuS, thermo- and magnetorefl. spectra, dynamical spin fluctuation effect on exciton state 77−52126
GaAs, epitaxial layer, magneto-plasma-reflectivity effects, difference method meas., IR region *(German)* 77−12363
GaAs, exchange interaction, analytical and nonanalytical parts, from polariton spectra in mag. fields 80−50367
n-GaAs:Sn epitaxial layer, free carrier relax. time, transverse magneto-plasma refl. 77−90212
GaN epitaxial layer, magneto-plasma-reflectivity effects, difference method meas., IR region *(German)* 77−12363
GaP/Te(S), IR lattice band profile, electron spin reversion in mag. field, Nf-R curve 79−28771
$Hg_{1-x}Cd_xTe$, interband magnetoreflectance 78−19448
$Hg_{1-x}Cd_xTe$, magnetoreflection studies 79−82963
$Hg_{1-x}Cd_xTe$, props. and appls., book contrib. 77−39834
HgI_2, phonon struct. in wavelength modulated refl. spectra and mag. circular dichroism 79−8125
$Hg_{1-x}Mn_xTe$, semimagnetic, exchange interactions between localised and delocalised electrons 80−97245
InP, exchange interaction, analytical and nonanalytical parts, from polariton spectra in mag. fields 80−50367
InP, free excitons in high mag. fields, band struct. 77−52129
InSb, conduction and valence band effective mass parameters 79−60689
InSb, Landau level struct., magneto-electroreflectance 80−25349
$Pb_{1-x}Sn_xTe$, far IR magneto-optical meas. 79−61343
$Pb_{1-x}Sn_xTe$, inter- and intraband magneto-optical transitions 80−25346
PbTe epitaxial film, many valley semicond., band population effects, intraband magneto-optical props. 79−78007
PbTe, far IR magnetorefl., band struct. 80−76010
n-PbTe, far IR magnetotransmission and refl., dielec. function 77−52091
p-PbTe, MIS struct. inversion layer sub-bands, IR magnetoreflectance obs. 80−44731
PbTe, magnetoreflectance of surface space charge layers 78−52475

magnetoreflectance continued
PbTe surface space charge layers, far IR magnetoreflectance meas. 78−64349
Sb, magnetoreflection of circularly polarised IR radiation, band struct. 77−52094
TlCl, magnetoreflectance of $X_6^+ \times X_6^-$ exciton meas. 79−38525
$Y_3Fe_{5-x}Sc_xO_{12}$, garnets, magnetooptical spectra, 15000-21000 cm^{-1} 77−90131
ZnSe, cubic, magnetoreflectance of Γ_6-Γ_8 exciton ground state 78−23495
ZnSe, cubic, magnetoreflection of s-excitons 78−60426
ZnSe, cubic, valence band parameters, magnetoreflectance of Γ_6-Γ_8 exciton 78−60056
ZnSe, magnetoreflectance of exciton-polaritons, semiclassical treatment 79−99857
ZnSe, valence-band parameters and g-factors from free-exciton magnets reflectance 79−73905
ZnTe, magnetoreflectance meas. on Γ_6-Γ_8 exciton 78−6656
ZnTe, valence band parameters and free exciton reduced mass, free exciton magnetoreflectance 80−45046

magnetoresistance
see also Corbino effect
actinides, low temp. magnetoresist. calc. 77−59278
alkali metals, elec. and thermal cond. in weak mag. fields 80−65535
alloy, amorphous, magnetic, transport props. 79−73485
alloys, dil., mag. field and impurity interaction effects on resist., Anderson model 79−51554
amorphous alloy, temp. and mag. field dependences of resist. 78−2459
amorphous ferromagnets, resist. and magnetoresist. 77−66148
amorphous metallic alloys, resistivity 79−69486
amorphous semiconductors, DC and AC cond., high field effects, magnetoresist., EPR, carrier transport, review *(Japanese)* 77−35943
Anderson localised states, electron correlations effect 79−65499
Anderson localised states, negative magnetoresistance 79−28357
Anderson model, ground state, var. trial function approach 80−59913
anisotropic solid with macroscopic inclusions, elec. consts. *(Russian)* 78−68002
anisotropy of hopping conduction, percolation theory 78−72156
antiferromagnetic metals, two-band model 78−79979
asymmetric Anderson Hamiltonian, ground state, magnetoresist. calc. 80−65503
asymmetric Anderson model, ground state fundamental nature 79−90932
band modification caused by impurities and magnetophonon effect 79−42562
bronze, spherical powder, negative magnetic resistance changes 77−1410
carrier relaxation process in quantising mag. field, elastic scatt. mechanisms, relax. matrix, longit. magnetoconductivity 79−15166
charge carrier with anisotropic energy spectrum, cond. oscills. in quantised mag. field *(Russian)* 80−6886
charged two-dimensional isotropic Fermi liq., static and dynamical props. 79−19532
chemisorption on metal films, use of external mag. field, review 78−72003
clean metal magnetoresistance in solid and liquid phases *(Russian)* 80−107767
$CoCr_2S_4$ films, galvanomagnetic and thermoelec. props. 80−54717
cokes, graphitised, Raman spectra, effective Debye parameter, magnetoresist. 78−44231
conducting media, EPR line shape, magnetoresist. effect 80−84638
critical behaviour, temp. and mag. field depends. 77−73037
critical behaviour in magnetic systems 78−87955
crystal symmetry, cubic and non-cubic, distinguished by weak field galvanomagnetic meas. 80−60009
cubic crystals, weak field magnetoresistance skewness imposed by mag. field 80−34416
cubic semiconductor with ellipsoidal valleys, magnetoresist. 80−80300
degenerate semiconductor, electron g-factor determ., Shubnikov-de Haas type oscills. 80−20070
degenerate semiconductor, film, with unlike surfaces, theory of kinetic effects *(Russian)* 79−51694
degenerate semiconductors, hot electron transport in parabolic energy bands, kinetic theory, transport coeffs. 80−29412
degenerate semiconductors, transverse magnetoresistance in strong mag. fields 79−99565
diamond, irradiated, Hall current meas. by split electrode method 77−1435
dilute magnetic alloy, cond. electron scatt. asymm. 77−62916
dilute magnetic alloys, calc. 77−62918
dilute nearly magnetic alloys, magnetoresist. calc. LSF approx. of Anderson model 77−62901
dirty superconductors, anisotropic, fluctuation magnetoconductivity 79−56393
double injection p-i-n structures in magnetic field 80−107899
education, Shubnikov-de Haas oscills., InSb degenerate semiconductor, third-year undergraduate expt. 79−9051
epitaxial films, cubic and noncubic (001)- and (111)-oriented, and surface layers, unified weak-field magnetoresist. 79−47110
extrinsic semiconductors, negative magnetoresist., Hubbard model *(Russian)* 78−47816
ferrimagnetic semiconductors, magnetomagnon reson. 79−69663
ferromagnet, itinerant electron, magnetoresist. and anomalous Hall effect due to electron-phonon interactions 80−70680
ferromagnet, low-field magnetortesistance and domain drag 78−68014
ferromagnet, metallic, thermopower near crit. point, inelastic scatt. processes 77−15836
ferromagnetic film, mag. props. meas. using planar magnetoresist. effect 78−21186
ferromagnetic film, sinusoidal voltage prod., mag. field meas. 78−26972
ferromagnetic metal, with domain struct., resistivity 78−95285
ferromagnetic nondegenerate semiconductor, magnetoresistance 80−11019
film, evaporated, galvanomag. and mag. props., thickness depend. 78−23181
film, galvano- and thermomag. phenomena, theory *(Russian)* 78−14743
film, metallic, electron transport phenomena *(Czech)* 77−51827
film with unlike surfaces, magnetomorphic oscills., generalised Sondheimer model 78−56243
films, (111) oriented, and surface layers, unified weak field magnetoresistance 79−95514

magnetoresistance continued
finite fibre, fluctuation magnetocond. 80−24956
galvanomagnetic phenomena, difficulties in nonlinear theory 79−11151
gapless semiconductor, transport coeffs. in quantum limit 80−80302
graphite, anisotropic elec. cond. rel. to stacking disorder 80−34437
graphite, artificial, electrophys. props. 77−51745
graphite, carrier mobility, temp. depend. determ. from magnetoresist. expts. 80−11009
graphite, galvanomagnetic and thermomagnetic effects at low temp. 80−44618
graphite, galvanomagnetic effects, temp. and field dependencies 78−64050
graphite, high-field galvanomagnetic props. 77−62941
graphite, neutron irradiated, effect on quantum limit Shubnikov-de Haas oscills. 78−95304
graphite, neutron irradiation, electron transport, annealing study 80−39165
graphite, pyrolytic, galvanomag. effects, effect of fast neutron irradiation 80−34465
graphite, resistivity and magnetoresistance, 4.2 to 293K 80−100459
graphite, with small-sized blocks, negative magnetoresist. *(Russian)* 80−49779
graphite intercalated with AsF_5, quantum oscillatory phenomena 80−107823
graphite intercalated with nitrate, galvanomagnetic props. 78−76092
graphite intercalation cpds., Fermi surface and transport props., LCAO model 80−80159
graphite intercalation cpds. with K, Rb, or Cs, phase transitions, resistive anomalies, electronic props. 79−95405
graphite nitrates, elec. props. perpendicular to layers, resistance, magnetoresistance, charge transport mechanisms 80−80268
graphite-AsF_5 intercalation compounds, resist. and magnetoresist. 79−99590
graphite-Br_2, intercalation process 78−63965
graphite-K intercalation compounds, electronic props., resistivity, Hall effect and magnetoresistance 80−75585
head Barkhausen noise voltage meas. 79−82821
heavily doped semiconductor, electron density dependent ordering parameter and role in elec. prop. anomalies *(Russian)* 77−43582
heavily doped semiconductor, magnetoconductivity, effect of resonant phonon-plasmon coupling 80−24954
HMTSF-TCNQ, metallic state at He temps., elec. props. and band struct. 79−65462
HMTSF-TCNQ, obs. of the de Haas-Shubnikov oscills. 78−84201
hot electron magnetophonon effect, mag. field modulation tech. *(Japanese)* 79−15171
III-V compounds, n-type, new meas. method for compensation and spatial fluctuations of impurities 78−6404
III-V semiconductors transport parameters, review 79−19587
inflowing structure, Anderson localisation, elec. cond. temp. depend. *(Russian)* 80−103639
n-InP, magneto-impurity resonances, obs. of central cell struct. 78−95303
Invar, anomalous magnetisation and magnetoresistance under high mag. fields 77−80764
Invar, elec. transport props. and Invar features *(Russian)* 78−14710
Invar, magnetovolume contrib. to temp. variation of magnetoresist. 77−31999
Invar, single crysts., Hall effect and transverse magnetoresist., 4.2-120K *(Russian)* 77−59277
inversion layers, carrier effective mass, contribs. of electron-electron and electron-phonon interactions 78−64087
longitudinal, in weak mag. fields, theory *(Russian)* 78−87965
low-temp. resistivity in mag. field 78−91667
magnetic field dependent phase shifts present in the measurement of quantum oscillatory effects 79−77983
magnetic field prod. and meas. 78−8425
magnetic measurements, eddy currents 78−12730
magnetophonon effect, modulating freq. influence on oscillatory struct. *(Japanese)* 79−15170
magnetophonon resonance effects, effect of additional laser illumination 78−72417
magnetoresistance anisotropy, planar Hall effect 79−23947
many-valley semicond., current-voltage characts., intrinsic magnetoresistance 79−38108
many-valley semiconductors, ellipsoidal energy surface, high field magnetoresist. and magnetothermal EMF 77−43621
measurement, influence of supercond. contacts 78−21184
metal, anisotropy effects on US cyclotron resonance 79−73816
metal, closed Fermi surface, galvanomagnetic phenomena, in intermediate magnetic fields *(Russian)* 78−34822
metal, closed-orbit, uncompensated, elec. and thermal magnetoresist., quadratic field depend. 79−95388
metal, compensated, high field magnetoresist. 77−8074
metal, ferromagnetic, dynamic scatt. effects on crit. transport props. 78−84239
metal, irrad., containing self-interstitials and vacancies, electronic transport props. 78−60105
metal, magnetic surface states induced linear magnetoresistance 79−60798
metal, Shubnikov-de Haas oscillations in strong elec. fields *(Russian)* 77−47794
metal, with closed orbits, high-field magnetoresistance of point defects 79−7819
metal film, cond. electron focusing by inhomogeneous mag. field *(Russian)* 80−70850
metal film, polycryst., longit. magnetoresist. 79−78224
metal films, resistance and magnetoresistance 79−61225
metal thin wires, size effect correlation to longitudinal magnetoresistance 78−34824
metal with open Fermi surface, intrinsic magnetoresist. 77−11899
metal-insulator-semiconductor structure, DC cond. and Shubnikov-de Haas effect 80−11012
metallic film, oscill. kinetic effects, boundary electron scatt. *(Russian)* 78−52104
metallic rare earths, conference, St. Pierre-de-Chartreuse, France (Sept. 1978) 80−12844
metals, compensated and uncompensated, effect of spherical voids on electrical magnetoresistivity 80−65531
metals, electron theory and cond. props., contrib. of Sir Rudolf Peierls, 1928-1935 80−57054
magnetoresistance continued
metals, inhomogeneous, magnetoresist. and Hall coeff. 79−95387
metals, magnetoresistance of localized impurities, multiple scatt. theory 78−43360
metals, quantum oscillation effects in weak mag. field *(Russian)* 79−11105
Metglas 2605, and 2605 A, transport props., resist. and magnetoresist. 79−1590
monocarbides of subgroups IVa and Va, kinetic props., review 78−47613
MOS structure, magnetoresistance in range of low temps. and high mag. fields *(Russian)* 77−66203
MOS structures, hot electron transport, expt. review 78−30994
MOSFET, ionic scatt. effect on Shubnikov-de Haas amplitudes in Si inversion layers 79−42653
negative magnetoresistance, appl. to heavily doped superconductors 80−107818
noble metal-rare earth alloy, dil., magnetotransport props., theory 78−39097
noble metals containing rare earth impurities, magneto-transport props. 78−68015
nonhomogeneous semiconductor, galvanomagnetic effects 79−91077
normal-superconducting composites, magnetoresistance and Hall coeff., classical theory 80−84547
paramagnetic semiconductor, heavily doped, linear response functions and magnetoresist. 77−51770
periodic magnetic signal detection by magnetoresistance sensor *(Japanese)* 78−57997
Permalloy, film, magnetoconductivity modulation by substrate electrostriction 79−60908
Permalloy, thin film, oscillatory metallic field effect and surface magnetoelasticity 79−56282
Permalloy film preparation by RF sputtering 78−3044
Permalloy magnetoresistive mag. field and current sensor 77−10048
Permalloy magnetoresistive mag. field sensor, performance calc. 80−57342
Permalloy proximity transducer based on magnetoresistance effect 78−57929
Permalloy-Rh, film, influence of Rh on corrosion resist. and mag. props. 80−3235
piezoelectric semiconductor, scatt. anisotropy in longit. quantizing mag. fields 78−26890
plasma, magnetoresistance, due to density or concentration inhomogeneities 78−47099
polyacetylene:AsF_5, heavily doped, transport props., evidence for metallic state 79−87121
polyacetylene film, doped, transport props. 80−24913
polycrystalline metals with open Fermi surface linear magnetoresist. calcs. 78−56129
pyrolytic graphite, magnetoresistance positive-negative transition *(Russian)* 80−96923
pyrolytic graphite c-axis longitudinal magnetoresistance in quantum limit 78−47814
quasi-two dimensional conductor, galvanomagnetic props., optical analogy *(Russian)* 80−60108
random system, 2-D, spin-orbit interaction and magnetoresistance 80−70728
rare earth alloys, amorphous, high field magnetisation and magnetoresistance 78−72136
rare earth alloys, amorphous, magnetoresistivity, exchange scatt. model 78−95287
rare earth amorphous alloys, random anisotropy antiferromag. model 80−20399
rare earth amorphous alloys, random anisotropy magnetism 80−65853
rare earth amorphous alloys, transport props. 80−20152
rare earth metal, conduction electron interactions, anisotropic 80−15492
rare earth metals, mag. and transport props. 79−69658
read head for magnetic tape recorders using magneto-resistance principle 80−87688
residual pseudo-macrostress, X-ray meas. errors due to plastic deform. 77−68544
resistance thermometer, Speer C, low-temp. magnetoresistance props. 78−49835
semicond. alloy, spin splitting and effective g-factor of T-holes *(Russian)* 77−51643
semiconductor, anisotropic electron scatt. on magneto-resistance coeff. 77−76844
semiconductor, antiferromagnetic, spin-magnetomagnon resonance 80−2566
semiconductor, cubic, Seitz coefficients calc. for resistivity 80−6880
semiconductor, defect interactions, radiation physics *(Russian)* 79−46702
semiconductor, effect of pot. fluctuations induced by cryst. inhomogeneities 80−49780
semiconductor, free carrier mobility and density, four-probe magnetoresist. meas. 77−43626
semiconductor, galvanomagnetic-effects in strong elec. field 78−56163
semiconductor, gapless, magnetophonon reson. for hot electrons and holes *(Russian)* 79−4565
semiconductor, high field longitudinal magnetoresist and bound states 78−23113
semiconductor, in strong UHF electric fields 77−1437
semiconductor, intrinsic, quantum theory of transverse galvanomag. phenomena, model of two standard bands *(Russian)* 77−62945
semiconductor, magnetic field modulation meas. technique *(Japanese)* 79−51614
semiconductor, magnetic field modulation technique for hot carrier oscillatory magnetoresistance phenomena studies 78−4657
semiconductor, magnetophonon oscillation separation techniques, advanced methods 78−2499
semiconductor, magnetophonon resonance due to two-phonon scatt. by acoustic phonons 77−69356
semiconductor, magnetophonon resonance oscills., peak shape, theory 80−107824
semiconductor, magnetoresist. of strongly correlated electrons in narrow energy bands, Hubbard model 77−32029
semiconductor, magnetoresistance, due to density or concentration inhomogeneities 78−47099
semiconductor, magnetoresistance quantum limit for impurity scatt. 79−91083
semiconductor, model, transport phenomena in presence of medium range disorder *(French)* 78−56162

magnetoresistance continued
semiconductor, n-type, nonequilibrium photoelectron distribs. and absolute negative cond. in quantising mag. fields 80−65622
semiconductor, narrow gap, mag. quantum oscills. of Auger transition rate 77−69340
semiconductor, near intrinsic magnetoresist. effect determ. of carrier density and mobility 78−2501
semiconductor, non-parabolic, magnetoresistance, quantum limit behaviour 79−28359
semiconductor, nondegenerate nonpolar, quantum theory of magnetophonon reson. 77−28200
semiconductor, nonparabolic, inelastic acoustic phonon scatt., in longit. quantising mag. field 77−28196
semiconductor, odd magnetophotoresist. effect 77−15908
semiconductor, odd magnetoresist. in Hf elec. field 77−28198
semiconductor, photostimulated odd magnetoresist. 77−15910
semiconductor, piezoelec., degenerate, transverse magnetoresist. in strong field, quantum effect 80−80299
semiconductor, quantum limit magnetoresist. for acoustic phonon scatt. 77−76847
semiconductor, surface space charge layer spectroscopy 77−20386
semiconductor, transverse magnetoresist. effects on Hall voltage meas., theory 77−72870
semiconductor, zero-gap, magnetophonon oscills. of transverse magnetoresist. in strong elec. fields 80−96916
semiconductor film, cell for measuring electrophys. parameters over wide temp. range 77−51830
semiconductor film, inhomogeneous, transverse magnetoresist., size effects 78−72293
semiconductor longitudinal magnetoresist. in quantising mag. field, var. calc. 77−43630
semiconductor magnetoconductivity, practical approx. to integrals 77−15870
semiconductor materials temperature dependence meas., using automatic device 80−52270
semiconductor thin films, Hall effect and magnetoresist. determ. in weak and strong mag. fields by four-probe method 79−60853
semiconductor with charged defects, elec. cond. and magnetoresist. 80−20225
semiconductor-insulator boundary, space charge layers, HF magnetoconductivity 78−60231
semiconductors, degenerate, energy band structure effect on transverse magnetoresistance 80−88580
semiconductors, free electron scattering and dynamical cond. 78−2476
semiconductors, nondegenerate, effect of nonparabolicity on transverse magnetoresist. 77−51763
semiconductors, photomagnetoelectric effect, expt. parameters rel. to material props. 79−99584
semiconductors, quantum magnetoresist. results, using pulsed fields up to 35 T 79−73528
semiconductors, superoperator theory 80−49776
semiconductors temperature dependences meas., automated installation 80−31792
semimetal, degenerate, quantum theory of transverse galvanomag. phenomena, model of two standard bands *(Russian)* 77−62945
semimetals, Hall coefficient and magnetoresist. of interacting two carrier system 79−69530
Shubnikov de Haas effect meas. system set-up, expt. *(Polish)* 77−72873
Shubnikov-de Haas quasi-periodic oscill. curves, harmonic analysis, computer method *(Russian)* 78−39132
simple metals, mech. for transverse linear magnetoresist. 79−23949
solid with parabolic electron band, relaxation time oscillations in strong mag. field 79−60855
spatially inhomogeneous system, galvanomagnetic effects *(Russian)* 78−72129
Speer C resistance thermometer, magnetoresist. effect 78−4624
Speer C resistors, low-temp. magnetoresist. meas. by NaF:OH and KCl:OH capacitance thermometers 78−4623
spin-glass alloys, magnetoresistance, Boltzmann formalism calcs. 80−88540
static conductivity change under quantum cyclotron reson. 78−39143
steel, Fe-Ni-Cr mag. susceptibility and magnetoresistance, temp. depend. *(Ukrainian)* 77−73004
stripe head vel. meas. using magnetoresist. signal 78−68316
superconducting fluctuation induced magnetoconductivity in anisotropic bulk and fibrous samples 79−95545
superconductor, type II inhomogeneous, impedance in Shubnikov phase *(Russian)* 78−23212
superlattice semiconductor, odd photomagnetoresistance effect 79−95425
TCNQ salt, HMTSeF;TCNQ, temp. and press. depend. 77−35929
TCNQ salt, TMTSF-DMTCNQ, metallic state at low temp. under pressure 79−91033
TCNQ-HMTSF, de Haas-Shubnikov oscills. 80−10956
tetrathiotetracene iodine high-conductivity complex, TTT_2I_3, magnetoresist. *(Russian)* 77−39886
thin film, magnetoresistance, specular reflectivity angular depend. *(Russian)* 80−100453
thin films, (001)-oriented, and surface layers, weak-field magnetoresist. anal. 79−56329
thin films, superconducting fluctuation influence on magnetoresistance *(Russian)* 80−54815
thin layer magnetic recording heads *(German)* 78−68013
thin surface layer, interactions between nondegenerate electrons, effect on cyclotron resonance, mag. cond. *(Russian)* 80−15802
thin wire, negative longit. magnetoresist., kinetic theory 78−34821
three-dimensional systems, negative magnetoresist. 80−75591
TMTSF-DMTCNQ, metallic state, transport props. 80−24974
TMTSF-DMTCNQ, metallic state at low temp. under press. *(French)* 79−82579
transducers for strong mag. field meas. at 4.2-300K temp. range 78−45660
transition metal alloys, nearly mag., low temp. magnetoresist. calc. 77−59278
transition metal based alloys and actinides, nearly mag., low-temp. magnetoresist. 78−39091
transverse, quantum limit behaviour with short and long range impurity scatt. 77−4366
transverse dynamic magnetoresistance and cyclotron reson. damping 79−4576
$TTT_2(I_3)_{1+x}$, physical props., elec., mag. and optical meas. 80−24908
magnetoresistance continued
$(TTT)_2I_3$, optical, spin-reson., magnetoresist. study, nature of ground state 78−68023
two dimensional electron-impurity system, theory of transverse dynamic magneto-conductivity 79−38105
two-dimensional CDWs, pinning and cond. in mag. fields 79−42610
unipolar crystals, intrinsic magnetoresist. in heating elec. field 78−72180
very high field meas. of mag. materials 80−68224
whisker blades, RF size effect, expt. technique and line shapes 79−65511
wurtzite structure semiconductor, transport in longit. quantizing mag. field 78−26891
n-InSb, strong electric fields *(Russian)* 78−19056
A, magnetoresistance, field strength function, electrodeless methods 79−91026
Ag-Cr dilute alloys, negative magnetoresist. in pulsed fields up to 35T 77−62899
Ag-Dy(Ho)(Tm), dil., high field magnetoresist. 80−15503
Ag-Dy(Tb) alloy, dil., magnetoresistance meas., contrib. from quadrupole and exchange scatt. 79−78078
Ag-Mn, dil. alloy, transverse magnetoresist. in spin glass regime 80−34417
Ag-Mn dilute, magnetoresist. and Hall effect, field-depend. electron scatt. 77−43581
$AgTe_2I$, Fermi surface meas. by Shubnikov-de Haas effect 77−39767
Al alloy, dilute, Matthiessen's rule deviations in strong mag. field 80−44571
Al alloys, low temp. standard resist., appl. in resistors and strain gauges 77−17997
Al and dilute alloys with Ge and Zn, magnetoresist. depend. on temp., 4.2-70K 80−70682
Al, anomalous behaviour of low temp. magnetoresistivity *(Russian)* 77−31998
Al, cryst. and polycryst., inhomogeneity effects on galvanomagnetic props. 78−60109
Al, elec. resist. and magnetoresist., anisotropic temp. depend. *(Russian)* 79−11103
Al, electrical resist. and magnetoresist., 2 to 40K, Matthiessen rule deviations *(Russian)* 77−31996
Al film, transversal magnetoresist. meas. 77−72925
Al, granular, hopping cond., supercond., magnetoresist., Zeeman splitting 78−60243
Al, granular supercond., normal state cond. 80−88529
Al, high purity, elec. field distrib. in strong mag. fields *(Russian)* 79−11104
Al, high purity single cryst., longit. magnetoresist. anisotropy 77−76793
Al, impurity low-field galvanomag. coeffs., 4 OPW calcs. 77−69304
Al, low-field galvanomag. props., Fermi surface and defect struct. effects 77−4323
Al, mag. breakdown, open trajectories, temp. depend. *(Russian)* 77−35921
Al, magnetomorphic oscillations, magnetoresist. and Hall coeff. meas. 77−28159
Al, magnetoresist., linear growth in strong. mag. fields *(Russian)* 78−51972
Al, magnetoresistance, path integral method calc. 80−65537
Al, magnetoresistance oscillations near [001] axis 79−56197
Al, magnetoresistance size effect, effect of cyclotron orbit nature 78−47767
Al, nuclear acoustic resonance, influence of longitudinal and transverse magnetoresistivity 79−24222
Al, single crystals, high purity, anisotropy of apparent resist. in longit. mag. fields 80−75550
Al, Sondheimer size effect, phonon-limited mean path, 1.8-12K 80−49698
Al, stabiliser for fusion reactor supercond. mag., neutron irrad. effects on magnetoresistance 80−34062
Al, thermoelectric power and Nernst-Ettingshausen effect 78−56134
Al, transverse magnetoresist. meas., magnetic breakdown 77−47795
Al, with dilute pt. defects, thermopower, Hall effect and magnetoresist. 79−65458
Al, with linear lattice defects, temp. depend. of magnetoresist. and Matthiessen's rule departure *(Russian)* 80−84456
Al-Ag alloys, dilute, electrical magnetoresist., temp. depend., mag. breakdown 79−99532
Al-Cu, dil., anisotropic scattering of conduction electrons on dilute Cu impurities 79−47082
Al-Ga(Mg)(Zn), electrical resist. and magnetoresist., 2 to 40K, Matthiessen rule deviations *(Russian)* 77−31996
Al-Ge, galvanomag. transport coeffs., Hall effect 79−91029
Al-Mn, dil., magnetoresist. meas. 77−28160
Al-Mn (0.55-5 at.%), magnetoresist. depend. on mag. field and impurity conc. 77−62896
Al-Mn alloys, dil., magnetoresist. meas. 77−62900
n-$Al_xGa_{1-x}As$, variable-gap crystal, magnetoresistance 78−34850
Au, magnetoresist of quenched and annealed metal, defect scatt. 79−4981
Au polycrystalline wire, internal oxidation of impurities, rel. to elec. resist. and magnetoresist. 78−83842
Au-Co, electron scatt., spin-orbit effects 80−65533
Au-Cu-Fe spin glass alloys, impurity mag. resist. meas. 80−59972
Au-Fe, dil. alloy, transverse magnetoresist. in spin glass regime 80−34417
Au-Fe (Mn)(Co), spin glass transition and anomalous Hall effect 79−61162
Au-Fe (4.4 and 4.8 at.%), isotropic spin glass behaviour and transverse magnetoresist. 77−15830
Au-rare earth alloy, dil., magnetoresist., quadrupole scatt. effects 78−39096
AuFe, spin glass, anomalous magnetoresistance 79−78077
AuMn, mictomagnetic, Hall and magnetoresist. effects 78−43361
$Au_{50-x}Pd_xZn_{50}$, ($0 \leq x \leq 15.02$), β'-phase, Hall effect and elec. cond. 80−107768
$AuTe_2I$, Fermi surface determ. by Shubnikov de Haas effect 77−51639
$Au_{100-x}Zn_x$, ($47 \leq x \leq 52$), β-phase, Hall effect and elec. cond. 80−107768
Be, magnetoresistence at low angles between current and mag. field *(Russian)* 78−68012
Bi, charge carrier interaction with twinning planes in strong transverse mag. fields *(Russian)* 80−88577

magnetoresistance continued
Bi, cylindrical thin crystal, size effect oscills. in longit. magnetoresist. *(Russian)* 77−69357
Bi, deformation calculations, band struct. variation, electron phase transitions due to deform. *(Russian)* 80−65137
Bi, deformation theory of the charge carrier spectrum from Shubnikov-de-Haas data *(German)* 78−84235
Bi, electron isoenergetic surface, variation of connectivity under press. *(Russian)* 78−60050
Bi, energy spectrum changes under strong uniaxial compression, Shubnikov-de Haas effect 77−28098
Bi, energy spectrum variation under strong uniaxial tension 79−73432
Bi, epitaxial film, EM meas. in mag. fields up to 85 kG 77−32095
Bi, Fermi surface, change in connectivity under press. 79−73431
Bi filament, size-quantized, magnetoresist. oscills. 78−19062
Bi film, carrier conc., mobility and 1/f noise 80−44748
Bi film, carrier conc. and mobility, resist., galvanomag. and thermoelec. meas. 78−52111
Bi film, high-mobility, quantum size effects, struct. and kinetic charact. improvement 79−91174
Bi film, in situ meas., MFP and specular scatt. parameter determ. 78−2589
Bi film, kinetic props. of electrons 77−63011
Bi, in high mag. fields *(Japanese)* 80−54720
Bi, longit. thermomag. amplifier 77−47838
Bi, magnetoresist. under phonon generation conditions 77−11940
Bi, magnetoresistance, high temp. oscills., props. *(Russian)* 80−65606
Bi, magnetotransport props. in quantising mag. fields 77−20340
Bi, nonlinear properties under sound generation conditions 79−60845
Bi, phonon generation rate, nonreciprocity of current-voltage curve *(Russian)* 77−89776
Bi, Shubnikov de Haas effect 79−28361
Bi, Shubnikov-de Haas effect and Fermi surface under strong uniaxial deform. 77−43474
Bi, Shubnikov-de Haas effect *(Russian)* 79−7840
Bi, Shubnikov-de Haas effect in high mag. fields 80−2404
Bi, static skin effect 78−56177
Bi, thin cylindrical monocryst., dimens. oscills. of longitudinal magnetoresist. *(Russian)* 77−8124
Bi thin wire, resist. anomaly, possibility of one-dimensional quantum size effect 80−54809
Bi, transverse magnetoresist. high-temp. oscills., rel. to Fermi surface *(Russian)* 77−24570
Bi, transverse magnetoresistance, field depend., static skin effect 79−11149
Bi whiskers, electron transition on simple extension, elec. resist. and magnetoresist. meas. *(Russian)* 80−29422
Bi, whiskers, hardness, elec. props. *(Russian)* 78−51874
Bi wire, field effect and magnetoresist., surface scatt. 77−43570
Bi:Sn(Pb), carrier dispersion law, Shubnikov-de Haas meas. 77−20345
Bi-Sb, semiconductor-semimetal transition under pressure 78−34870
Bi-Sb, Shubnikov-de Haas effect and semimetal-semicond. transition in high mag. fields 80−44674
Bi-Sb alloy film, elec. resist., magnetoresist., Hall coeff., 4.2K, conc. depend., anomalous size effect *(Russian)* 77−89884
Bi-Te, combination freq. in Shubnikov-de Haas and surface impedance oscillations *(Russian)* 78−10476
Bi-Te, electron isoenergetic surface, variation of connectivity under press. *(Russian)* 78−60050
p-$Bi_{0.9}Sb_{0.1}$, Fermi surface anisotropy var. on press. induced transition to gapless state *(Russian)* 77−43483
$Bi_{0.9}Sb_{0.1}$, magnetophonon effect on hot electrons *(Russian)* 80−107814
$Bi_{0.91}Sb_{0.09}$, magnetoresistance anisotropy in strong magnetic field 79−82613
n-$Bi_{0.924}Sb_{0.076}$, energy spectrum variation under strong uniaxial tension 79−73432
$Bi_{0.925}Sb_{0.075}$, semiconductor-semimetal transition under tensile strain, Shubnikov-de Haas oscills. obs. 80−44678
$Bi_{1-x}Sb_x$, band inversion under press., Fermi surface anisotropy, galvanomag. meas. 77−51637
$Bi_{1-x}Sb_x$, combination freq. in Shubnikov-de Haas and surface impedance oscillations *(Russian)* 78−10476
$Bi_{1-x}Sb_x$, deformation calculations, band struct. variation, electron phase transitions due to deform. *(Russian)* 80−65137
n-$Bi_{1-x}Sb_x$, determ. carrier dispersion relation parameters 79−38107
$Bi_{1-x}Sb_x$ epitaxial layers, effect of film thickness on elec. props. *(Russian)* 79−11244
$Bi_{1-x}Sb_x$ epitaxial thin films, galvanomag. props. in semimetal and semicond. regions 79−11254
$Bi_{1-x}Sb_x$ film, low temp. anomalies of elec. props. and quantum size oscillations 79−65571
$Bi_{1-x}Sb_x$, mag. field and ang. depend. 78−19063
$Bi_{1-x}Sb_x$, semicond. alloy, mag. freeze-out effect, superlow temps. *(Russian)* 77−89775
$Bi_{1-x}Sb_x$, semicond.-semimetal transition, temp. and press. depend. of transport props. 78−76120
$Bi_{1-x}Sb_x$ semiconducting alloy, band struct. study, Shubnikov-de Haas effect *(Russian)* 80−80181
$Bi_{1-x}Sb_x$, Shubnikov-de Haas effect, Abrikosov-Falkovskii treatment of Fermi surface anisotropy *(Russian)* 78−43285
$Bi_{1-x}Sb_x$, solid soln., temp. depend. of weak-field galvanomag. coeffs. *(Russian)* 80−70724
$Bi_{1-x}Sb_x$, thin film, elec. props., composition variations *(Russian)* 79−7841
$Bi_{1-x}Sb_x$ thin films, elec. props., 4.2-300K, magnetoresistivity meas. *(Russian)* 79−24087
$Bi_{1-x}Sb_x$:Te(Sn), dispersion law of charge carriers *(Russian)* 79−87114
n-$(Bi_{1-x}Sb_x)_2Te_3$, magneto-Seebeck and Shubnikov-de Haas effect 79−42568
$(Bi_{1-x}Sb_x)_2Te_3$, highest valence band struct., Shubnikov-de Haas effect 78−14661
$Bi_{2-x}Sb_xTe_{3-y}Se_y$ solid solution, density-of-states effective mass, carrier mobility temp. depend. 80−24931
n-$Bi_2(Se_xTe_{1-x})_3$, Shubnikov-de Haas oscills., 1.7-4.2K 77−15874
n-Bi_2Te_3, magnetoresist. under uniaxial stress 77−35956
Bi_2Te_3, Shubnikov-de Haas effect, high press. effect on band struct. 77−51767
Bi_2Te_3-Sb_2Te_3 film, cond., galvanomag. Seebeck and Nernst-Ettingshausen effects under press., band model 77−47907
$Bi_2(Te_{1-x}S_x)_3$, low field magnetocond. meas. 79−87117
$Bi_2(Te_{1-x}S_x)_3$, quasi 2-D cryst., I-V and magnetocond. meas. 77−85360
magnetoresistance continued
$Bi_2Te_{2.7}Se_{0.3}$, magnetoresistance and Hall EMF meas., using AM method 80−52278
$Bi_2Te_{3-x}Se_x$ solid solution, Hall effect anisotropy parameter, thermoelectric power, depend. on carrier density 79−69536
$Br_{1-x}Sb_x$, alloy wire, magnetoresistance in high longitudinal fields *(Russian)* 79−87113
C disordered, variable-range hopping cond. and negative magnetoresist. 80−34436
C fibres, from mesophase pitch, resist. magnetoresist., EPR and mech. props. rel to struct. 79−78116
C, glassy, negative magnetoresist. 78−23118
C, glassy and fibrous, density of states, magnetoresistance theory appl. 80−44620
C pregraphitic, negative magnetoresist. 80−34466
C resistance thermometers, determination of magnetoresistance in liquid He temp. range 80−31752
Cd, compensated metal, linear magnetoresist., semiclassical transport theory 77−35925
Cd, size oscillations in magnetocond. 77−4324
Cd, thermo EMF oscills. on mag. breakdown *(Russian)* 79−60801
$Cd_{1-x}Ag_xCr_2Se_4$, ferromag., magneto-resistance exam. *(Russian)* 78−84238
Cd_3As_2, anisotropy of electronic g*-factor 80−44483
Cd_3As_2, band struct. and g-factor, Shubnikov-de Haas oscills. meas. 80−49598
Cd_3As_2, band struct. from Shubnikov-de Haas and de Haas-van Alphen effects 80−49597
Cd_3As_2, Shubnikov-de Haas effect 80−11020
n-Cd_3As_2, vacuum evaporated, Shubnikov-de Haas effect 79−99644
$CdCr_2S_4$ crystal growth, structural defects, physical properties 80−60759
p-$CdCr_2S_4$, single cryst., elec. cond. 79−15148
$CdCr_2S_4$:In, single cryst. prep. and elec. props. 79−38727
$CdCr_2S_4$:In(Ga), resist. and magnetoresist. meas., effect of donor impurities 79−19608
$CdCr_2Se_4$, ferromag. semicond., conc. anomalies rel. to red shift of absorpt. edge 80−70732
$CdCr_2Se_4$, temp. depend. of resist. and magnetoresist., influence of Se vacancies 78−60130
$CdCr_2Se_4$:Ag, magneto-electrical props. temp. behaviour depend. on dopant conc. *(Russian)* 80−11006
p-$CdCr_2Se_4$:Ag, oscillatory magnetoresist., temp. and mag. field depend. 78−52011
$CdCr_2Se_4$:Cu(In), ferromag. semicond., mag. and elec. props. 77−20588
$CdCr_2Se_4$:Ga, sp. elec. resist., temp. and mag. field depends. *(Russian)* 78−26893
$CdCr_2Se_4$:Ga(Ag), and pure, photocond. and photomagnetoresist. spectra 77−80809
$CdCr_2Se_4$:Ga(In), photoconductivity, photomagnetoresistance near Curie point *(Russian)* 80−100485
$CdCr_2Se_4$:In, influence of Se-deficiency on props. 78−30921
$CdCr_2Se_4$:In, nondegenerate ferromagnetic semiconductor, positive magnetoresistance 78−2505
$CdCr_2Se_4$:In , impurity band, photocond. spectral depend. 78−19088
$CdCr_2Se_4$:In(Ga), elec. resist. and magnetoresist., 2 to 200K 80−96876
$CdCr_2Si_4$:Ga, negative magnetoresist. effects near Curie temp. 79−11152
$Cd_{1-x}Fe_xCr_2S_4$:Cu, effect of doping on elec. props. and Curie temp. 78−84214
n-$Cd_{0.245}Hg_{0.755}Te$, magnetophonon reson. and quantum oscillations 77−39902
$Cd_xHg_{1-x}Te$, influence of nonparabolicity on transverse magnetoresist. near transition to zero gap 80−20228
n-$Cd_xHg_{1-x}Te$, magnetophonon oscills. of transverse magnetoresist. 78−72177
$Cd_xHg_{1-x}Te$, magnetoresist. near gapless state, 77-370K 78−2503
$Cd_xHg_{1-x}Te$ magnetoresistor prep. and props. 79−7844
$Cd_xHg_{1-x}Te$, magnetoresistance in range 4.2 to 300K 79−11156
$Cd_xHg_{1-x}Te$, photomagnetic and galvanomagnetic effects in quantising mag. fields 80−20223
$Cd_xHg_{1-x}Te$, resistivity, Hall effect and magnetoresist. in strong elec. field 77−28199
$Cd_xHg_{1-x}Te$, strong elec. field effect on galvanomagnetic effects 79−11159
n-$Cd_{1-x}In_xCr_2Se_4$, effect of doping on elec. cond. and magnetoresist. 78−72174
$Cd_{1-x}In_xCr_2Se_4$, electric, photoelectric and mag. props., metal-semicond. transition *(Russian)* 80−54738
CdO, magnetoresistance, temp. depend. of degenerate, narrow and broad samples 78−95306
Cd_3P_2, energy band struct. and electron mobility at low temp. 79−37984
n-CdS, reson. obs. in far IR transverse magnetophotoconductivity 78−30949
CdSe, electrical cond. near metal-insulator transition 79−73550
p-$CdSnAs_2$, Hall effect, thermo EMF, thermomagnetic effects 80−107822
p-$CdSnAs_2$, heavily doped, elec. transport props. under elastic deformation 80−96915
$Cd_{3-x}Zn_xAs_2$, cryst., two-band and impurity conduction, 1.8 to 370K 78−19057
Ce-alloys, dil., elec. resist. in presence of external mag. field 78−19022
$Ce_{30}Au_{20}$, amorphous, cryst. field effects and mag. interactions, magnetisation and transport props. meas. 78−68191
CeB_6, mag. and electronic props. 80−71048
$CeCoSi_2$ film, Hall effect and magnetoresist. *(Russian)* 80−11109
Co based alloys, resistivity magnetoresistance, s,p impurities in ferromag. host 78−68008
Co, ferromag. film, ion plating prep., coercive force and magnetoresist. 77−12546
Co, ferromag. film, magnetoresistance parameter meas. *(Spanish)* 80−2485
Co film, amorphous, in fields up to 80 kG 77−39823
Co-Mn alloys, FCC, mag. moments of Mn atoms 78−76226
Co-Ni, ferromag. film, ion plating prep., coercive force and magnetoresist. 77−12546
$Co_{1-x}Fe_xCr_2S_4$, ferrimag. spinel semicond., Curie temp. variation with composition and elec. props. 77−15849
$Co_2Ga_{2-x}Fe_x$, elec. resist., temp. and mag. field depend., mag. contrib. 80−96846
$Co_2Ga_{2-x}Fe_x$, mag. field depend. of resist., 5.80K 80−70676
$(Co_{1-x}Ni_x)_{75}(PBAl)_{25}$, amorphous, high-field magnetoresist. meas. 80−34423

magnetoresistance continued
CoS_2, ferromagnet, elec. resist. and thermal expansion anomalies 80−15542
CoS_2, galvanomagnetic effect of single cryst. 80−96912
$Co(S_xSe_{1-x})_2$, galvanomag. effects, obs. and interpretation 80−70726
Cr, antiferromag., electron interference oscills. and spin-density-wave energy gaps at Fermi surface 80−49574
Cr, antiferromag., transverse magnetoresist., electron interference oscills. 80−65534
Cr, transverse magnetoresist. meas. in antiferro- and paramag. states, 15 to 80°C 77−85197
$Cr_xPd_{82-x}Ge_{18}$, amorphous, RF sputtered, elec. resist. and magnetoresist., Kondo type behaviour 78−76066
$Cr_xPd_{82-x}Ge_{18}$ amorphous alloys, magnetoresist., mag. susceptibility, magnetisation 78−80148
Cr_5Te_6, magnetoresist. in region of mag. phase transforms. *(Russian)* 77−66299
Cu and ilute Cu-Au alloy, magnetoresist. depend. on temp., 4.2-70K 80−70682
Cu, electronic relax. time in Sondheimer size effect, temp. depend. 79−87086
Cu normal metal in composite superconductor, neutron irradiation effects 79−38049
Cu, polycryst., transverse magnetoresistance, effective medium approx. 79−87083
Cu, polycryst. magnetoresist. due to crystal defects 78−56128
Cu polycrystalline plate, electric current distortion effects 77−72853
Cu, quenched, Hall coefficient, relaxation times, Fermi surface 80−84460
Cu, stabiliser for fusion reactor supercond. mag., neutron irrad. effects on magnetoresistance 80−34062
Cu wire, negative longitudinal magnetoresist. size effect 80−80252
Cu-Cr dilute alloys, negative magnetoresist. in pulsed fields up to 35T 77−62899
Cu-Mn, dilute, magnetoresist. and Hall effect, field-depend. electron scatt. 77−43581
Cu-Ni, comp. modulated alloy films, transport props., 10 to 300K 79−95515
Cu-P wire, phosphor bronze, magnetoresist. upper limit 77−43567
Cu-Si-Zn wire, silicon bronze, magnetoresist. upper limit 77−43567
$CuCr_2Se_{4-x}Br_x$, elec. resistance, Hall const., magnetoresistance singularities *(Russian)* 79−91078
$Cu_{0.67}Cr_{1.78}Se_{2.67}Br_{1.34}$, polycrystalline mag. semicond., mag. and elec. props. 79−7846
$Cu_yCr_2Se_{4-x}Br_x$, ferromag. magneto-resistance exam. *(Russian)* 78−84238
$CuCr_2Se_4(S_4)(Te_4)$, binary and ternary solid solns., mag. and elec. props. 80−2407
CuH dilute alloy, Hall coefficient, relaxation times, Fermi surface 80−84460
$Cu_xMo_6S_8$, Hall effect and magnetoresistivity 78−95400
$Cu_xMo_6S_8$, normal-state electronic props., Fermi surface and supercond. parameter derivations 79−60850
Dy, ferromag. fields up to 75 kOe, 1-70K 77−20297
$Dy_{1-x}Sm_x$, magnetoresist. of polycryst. specimens in fields up to 44 kOe *(Russian)* 80−92880
Eu, antiferromag., thermal cond., elec. and thermal magnetoresist., at low temps. 77−69301
Eu, elec. resist., effect of mag. field near Neel point 77−8073
Eu, irreversible component rel. to antiferromag. struct. *(Russian)* 77−35920
Eu, longit. magnetoresist. at low temps. and up to 80 kG 77−55515
EuB_6, electronic struct., transport and mag. props. 80−96782
EuB_6, resist., Hall effect, and magnetoresist. under hydrostatic press., 4.2 to 300K 80−96879
EuIG:Si, magnetoresistance meas. 79−78120
$Eu_{2.9}Lu_{0.1}Fe_5O_{12}$:Si, magnetoresistance meas. 79−78120
EuO, photoelectron anomalous transport phenomena 78−23114
EuSe, bound mag. polaron, temp. and field depend. of resist. 79−90976
EuSe, dynamical conductivity in high mag. fields 79−78118
EuSe, giant negative magnetoresistance, anomalous carrier density mag. field depend. 80−49774
EuSe, Hall effect, elec. cond. and magnetoresistance temp. depend. 79−33296
EuTe, magnetic impurity states, mag. and transport props. 80−96913
Fe alloys, magnetic resist. anisotropy, two-current model 77−20295
Fe based alloys, resistivity magnetoresistance, s,p impurities in ferromag. host 78−68008
Fe, ferromag. film, magnetoresistance parameter meas. *(Spanish)* 80−2485
Fe, irradiated with electrons then annealed, magnetoresistance at 20K *(French)* 80−103677
Fe, mag. breakdown and Hall resist., theory and model calcs. 80−75552
Fe, magnetoresistance, grain-oriented mag. steel sheet *(German)* 78−68020
Fe thin layers, vacuum coated on PMMA, mag. behaviour during mech. stress cycles *(German)* 80−80581
Fe, whisker, deviations from Kohler's rule 80−70673
Fe whiskers, galvanomag. size effects 78−14709
Fe-Al (30 or 45 at.%) film, atomic ordering effects *(Russian)* 77−80853
Fe-Al_2O_3 granular films, superparamagnetism and relax. effects 80−71118
Fe-Co-Si-B sputtered amorphous thin film, coercivity, galvanomagnetic props., resistivity 80−29578
Fe-N alloy, dil., galvanomag. effects, 4.2-250K 78−87964
Fe-N, (35 wt.%), transport props. and Invar features *(Russian)* 78−51973
Fe-Ni, $Fe_{65}(Ni_{1-x}Cr_x)_{35}$, low-temp. elec. and galvanomag. props. rel. to mag. boundaries *(Russian)* 77−35910
Fe-Ni evaporated films with perpendicular anisotropy, obs. 78−2585
Fe-Sb(Sn), dil., spontaneous magnetoresistance anisotropy and deviations from Mattheissen's rule 79−51553
Fe-Si amorphous film, Hall const. and magnetoresistive effect 78−52105
Fe-V(Cr)(Mo)(W)(Ti)(Nb) alloys, split bands evidence from sp. ht. and elec. transport data 77−24515
Fe-Y, amorphous, resist. and magnetoresist. meas., local moment system 78−68018
Fe_3Al, magnetoresistance tensor depend. on degree of ordering, −196 to 650°C *(Russian)* 77−31997
$Fe_{80}B_{20}$, amorphous, transverse magnetoresist., stress effect 80−15501

magnetoresistance continued
$(Fe_{1-x}Co_x)_{78}Si_{10}B_{12}$, amorphous, Hall effect and magnetoresist. *(Japanese)* 77−85199
$Fe_{1-x}Cu_xCr_2S_4$, Hall effect and magnetoresist. 79−78119
$Fe_{1-x}Cu_xCr_2S_4$, mag. semicond., mag. props. and elec. cond. *(Japanese)* 79−47111
$(FeMn)_3Si$ alloys, mag. and crystallographic props. 77−59393
$Fe_{78}Mo_2B_{20}$, amorphous, transverse magnetoresist., stress effect 80−15501
$Fe_{40}Ni_{40}B_{20}$, amorphous ferromag., resist. and galvanomagnetic props., rel. to magnetisation 78−14712
$Fe_xNi_{80-x}B_{20}$ and $Fe_xNi_{80-x}P_{14}B_6$ metallic glasses, low temp. resist. and galvanomag. effects, mag. state influence 80−84461
$Fe_xNi_{80-x}B_{20}$, $Fe_xNi_{80-x}P_{14}B_6$, amorphous ferromag., galvanomag. props. 79−56196
$Fe_xNi_{80-x}B_{20}$ glass, resist., magnetoresist., and thermoelec. power 80−70681
$Fe_{40}Ni_{38}Mo_4B_{18}$, metallic glass, mag. and transport props. 80−39752
$Fe_{40}Ni_{40}P_{14}B_6$, amorphous, transverse magnetoresist., stress effect 80−15501
$Fe_xNi_{1-x}P_{14}B_6$, amorphous, spin-glass regime, magnetoresist. meas. 80−34418
$Fe_xNi_{80-x}P_{14}B_6$ glass, resist., magnetoresist., and thermoelec. power 80−70681
$(Fe_{1-x}Ni_x)_{75}(PBAl)_{25}$, amorphous, high-field magnetoresist. meas. 80−34423
$(Fe_{1-x}Ni_x)_{78}Si_{10}B_{12}$, amorphous, Hall effect and magnetoresist. *(Japanese)* 77−85199
Fe_2O_3, natural haematite, weakly ferromag., magnetoresist. *(Russian)* 78−23110
Fe_3O_4, magnetite, change in state due to applied mag. fields obs. in magnetoresistance meas. 77−43623
Fe_3O_4, magnetite, magnetoresist., applied mag. field effects 80−80301
$Fe_xPd_{82-x}Si_{18}$, amorphous, magnetisation, magnetoresist., spin glass and ferromag. phases 80−34697
1T-$Fe_xTa_{1-x}S_2$, Anderson localisation, elec. resist. and magnetoresist. meas. 80−44596
Ga, oscillatory magnetoresist. meas., Fermi surface model 77−62898
$Ga_{1-x}Al_xAs$, Shubnikov-de Haas oscillation, in semiconductor superlattice 77−62947
n-$Ga_{1-x}Al_xSb$, transport phenomena in low and high mag. fields 78−80007
GaAs, compensated, influence of electron gas heating on negative magnetoresist. 77−89778
GaAs, compensated, magnetoresist. and magnetothermoelec. power meas. 77−43627
GaAs, compensated, magnetoresist. and Hall effect 77−66176
GaAs, compensated, Shubnikov-de Haas oscills. 77−11941
GaAs, electrical and optical props. at low temps. 80−39636
GaAs, electron mobility temp. depend. 79−91084
n-GaAs epitaxial film, magnetoresist. at low temp., geometric effect 80−93015
GaAs epitaxial films on strongly doped substrate, basic parameter meas. utilising magnetoresist. and SEM techniques under cathodoluminesc. conditions 80−65728
GaAs, epitaxial layer, effective doping density, comparison of Hall and magnetoresistance meas. 77−11938
GaAs, epitaxial layers on conductive substrate, elec. characterisation 78−91790
GaAs, Gunn oscillator, magnetoresist. meas. of mobility and noise 77−62948
GaAs, heavily doped, electron effective mass, Kane equation calcs. 79−77989
n-GaAs, heavily doped, impurity-band cond., DC cond., Hall mobility, and magnetoresist. meas. 80−49733
n-GaAs, hot electron magnetophonon resonance, Fourier anal. 80−54718
GaAs, influence of strong transverse mag. field on Gunn effect 80−6854
n-GaAs, longitudinal magnetophonon reson. and Fourier anal. 79−4569
n-GaAs, magneto-impurity effect, review 79−91081
n-GaAs, magnetophonon resonance, Fourier anal. 79−91080
GaAs n^+2n^+ epitaxial multilayers, carrier conc. from Fourier transform anal. of magnetoresist. signal 79−38205
GaAs, negative differential mobility and geometrical magnetoresist. calc. 77−43624
GaAs semiconducting resistance thermometer for low temp. measurement 0.3 to 350K range 79−58687
GaAs, shallow donors, screening, energy spectrum of electrons and cond. mech. 79−7831
GaAs, Shubnikov-de Haas oscillations in semiconductor superlattice 77−62947
GaAs, valence band struct. obtained by magnetophonon effect 77−76748
GaAs:Cr, parameters determ. using cond., Hall-effect and magnetoresist. meas. *(Slovak)* 78−47802
p-GaAs:Cr, semi-insulating, illumination effect on mobilities 77−32043
p-GaAs:Cr, semi-insulating, mobilities and carrier concentrations, temp. depend. 80−70702
GaAs:Mn(Ni), negative magnetoresist. meas. 77−51768
GaAs-$Al_xGa_{1-x}As$, heterojunction and superlattice, magnetophonon reson., polaron mass 80−44715
GaAs-$Al_xGa_{1-x}As$ heterojunctions, LPE grown, 2D electron gas obs. 79−99606
GaAs-$Al_xGa_{1-x}As$ heterojunction interface, two-dimensional hole gas obs., Shubnikov-de Haas meas. 80−80357
GaAs-$Al_xGa_{1-x}As$ multilayers, two-dimens. transport at high mag. fields 80−65724
GaAs-$Al_xGa_{1-x}As$ superlattice, electronic props. 80−11080
GaAs-AlGaAs:Si heterojunction interface, two-dimens. electron gas, Hall effect and cyclotron reson. meas. 79−65530
GaAs-$Ga_{1-x}Al_xA$ heterostruct. superlattice, props. in high mag. fields 79−73570
GaAs-$Ga_{1-x}Al_xAs$ superlattice, sub-band dimensionality 78−63981
GaAs-GaAlAs, superlattice, subband related anisotropy in negative magnetoresistivity 80−11082
$Ga_xIn_{1-x}As_yP_{1-y}$, conduction band and phonons, Shubnikov-de Haas effect, magnetophonon resonance, Raman scattering 80−24795
$Ga_xIn_{1-x}As_yP_{1-x}$, epitaxial layers on InP, expt. determ. of effective masses 79−65370
$Ga_xIn_{1-x}As_yP_{1-y}$, electron effective mass, cyclotron reson. and magnetophonon effect meas. 80−103618
$Ga_{0.3}In_{0.7}Sb$, negative differential mobility and geometrical magnetoresist. calc. 77−43624

magnetoresistance continued
GaP, electrical and optical props. at low temps. 80−39636
n-GaP epitaxial layers, transverse magnetoresist. *(Russian)* 77−76964
n-GaSb, Shubnikov-de Haas effect, effective mass, Dingle temp., and g-factor 79−51602
n-GaSb:Te, elec. transport mechanism in cond. band from Hall mobility and transverse mangetoresist. meas. 79−73531
p-GaSb:Zn, hole transport props. from 77 to 300K 79−73530
Gd, 4.2-220K, temp. depend. anisotropy 77−62903
Gd, magnetoresistance anisotropy, Fermi surface model 79−91025
Gd-Au(Ni)(Co), amorphous ferromag., mag. and transport meas. 77−89930
Gd-rare earth metal, dil. resist. anisotropy due to impurities 77−62902
Gd-transition metal, amorphous film, galvanomag. effects, Hall detector 77−89882
$Gd_{67}Co_{33}$, amorphous, elec. resist. and magnetoresist. 80−49693
Gd_2S_3 with excess Gd, magnetoresist. meas. 80−49777
Ge, amorphous, anomalous magnetoresistance 80−6877
Ge, amorphous anomalous magnetoresist., hopping model 78−23117
Ge amorphous films, high elec. field cond. and magnetoresist. at 4.2K 80−49748
Ge bicrystal, cond., Hall effect and Shubnikov-de Haas oscills. 80−10984
Ge, bicrystal, two-dimensional electronic phenomena at He temp. *(Russian)* 79−56273
Ge bicrystal cleavage plane, Shubnikov-de Haas oscills. *(Russian)* 78−64094
Ge, degenerate, doped with nonmag. impurities, Kondo effect 78−14746
Ge, electrical and optical props. at low temps. 80−39636
Ge, electron-hole droplet magnetoresistance 78−14744
Ge, electron-hole droplets, reson. scatt. of free carriers 78−2500
p-Ge film, fragmented struct., elec. cond., Hall coeff. and magnetoresist. meas. 77−15979
p-Ge film, tranverse magnetoresist. meas. 78−72293
p-Ge film on GaAs, cond., Hall effect and transverse magnetoresist., anisotropy 79−51697
p-Ge, heaviliy doped, anomalous magnetoresist. under uniaxial compression *(Russian)* 79−33302
n-Ge, heavily doped, negative magnetoresistance model, spin-up spin-down electron effective mass variations 79−95423
P-Ge, heteroepitaxial film, galvanomagnetic effects, influence of mechanical stresses 79−91171
n-Ge, hopping magnetoresistance percolation analysis 79−38106
p-Ge, hopping transport at high mag. field at uniaxial stress 79−95412
p-Ge, linear magnetoresist. in strong elec. fields 77−43632
n-Ge, magnetoresist. anisotropy, in quantizing mag. fields, under conditions of mixed scatt;. 77−15877
Ge, magnetoresistance meas., transverse diffusion currents on source of error 79−7843
Ge, magnetoresistance of electron-hole liq., percolation model 80−96920
Ge, many-valley semicond., current-voltage charact., intrinsic magnetoresistance 79−38108
Ge, n- and p-type, magneto-impurity effect, review 79−91081
p-Ge, negative magnetoresist. and Hall effect, press. and field depend. 80−70733
Ge, neutron irrad., Hall effect and magnetoresist. meas. 80−6883
p-Ge, odd magnetoresist., ionised impurity scatt., theory 78−72178
p-Ge, odd magnetoresist. in strong elec. and mag. fields 79−51612
p-Ge, odd magnetoresist. of warm holes 77−43628
p-Ge, odd magnetoresist. under weak carrier heating conditions 80−96917
Ge, photocurrent magneto-oscillations 80−6911
n-Ge, plastically deformed, elec. cond., magnetoresistance, Hall effect study *(Russian)* 79−99568
Ge, relax. time energy depend. and surface galvanomag. props. 78−43459
n-Ge thin plate, transverse magnetoresist. meas., size effect 78−72179
Ge, transmutation doped, high field magnetoresist. of hopping transport 78−10474
n-Ge, transverse magnetoresist. effects on Hall voltage meas., theory 77−72870
n-Ge, uniaxially deformed, longitudinal magnetoresist. in quantising mag. field 79−15168
Ge, valence band struct. obtained by magnetophonon effect 77−76748
n-Ge:O, impurity-saturated, dislocation-free, anomalously high magnetoresist., vacancy effects 77−43629
Ge:Sb, heavily doped, anomalous magnetoresist., metallic impurity cond., down to 5 mK 79−65502
Ge:Sb, low temp. anomaly of impurity cond. 79−95428
GeSe, antiferromagnetic behaviour, res. to negative magnetoresistance effect 79−73719
Hg, solid, resistivity ratio, 1.65 to 234K 80−59952
$Hg_{3-\delta}AsF_6$, linear chain compound, mag. field induced residual resist., anisotropic supercond. 80−24897
$Hg_{3-\delta}AsF_6$, quasi one-dimensional, anomalous magnetoresistance 80−24884
$Hg_{3-\delta}AsF_6$, quasi-one-dimens., mag. field induced residual resistivity 79−1596
$Hg_{1-x}Cd_xGe$, quantum oscillations of magnetoresistivity *(Russian)* 80−11007
$Hg_{1-x}Cd_xSe$, (x=0 to 0.15), Shubnikov-de Haas oscillations, influence of level broadening 79−11155
HgCdTe, Magneto transport anomalies at low carrier densities, Wigner crystallisation 80−20222
n-$Hg_{0.8}Cd_{0.2}Te$, microwave bolometer heterodyne receiver based on magnetic field induced phase transition 80−13135
$Hg_{0.82}Cd_{0.18}Te$, electronic anomalous mass near reson. acceptor level, Shubnikov-de Haas meas. 80−80163
$Hg_{0.86}Cd_{0.14}Te$, spin-flip electron scatt., longit. magnetoresist. obs. 77−43622
$Hg_{1-x}Cd_xTe$, props. and appls., book contrib. 77−39834
$Hg_{1-x}Cd_xTe$, semiconducting phase, acceptor states and galvanomagnetic effects 80−11017
$Hg_{1-x}Cd_xTe$, transverse magnetoresist. in extreme quantum limit 77−39885
$Hg_{1-x}Cd_xTe$, zero-bandgap state induced by press., galvanomag. props. 77−47725
$Hg_{a-x}Cd_xTe$, (x<0.16), semimetallic phase, acceptor states and galvanomagnetic effects 80−6882
$HgCr_2Se_4$, ferromag. semicond., transport props. 78−68039

magnetoresistance continued
$HgCr_2Se_4$, n-type ferromag. semicond., galvanomagnetic props. 80−70727
HgI_2, photoexcited, Hall effect, magnetocond., and cyclotron reson., carrier mobility and effective mass 77−59294
$Hg_{1-x}Mn_xSe$, band struct. from anomalous Shubnikov-de Haas effect 80−20080
HgMnTe, semimagnetic semiconductor, band structure, transport phenomena 79−95331
$Hg_{1-x}Mn_xTe$, acceptor reson., states in high mag. field 80−49668
$Hg_{1-x}Mn_xTe$, energy levels at Γ-point in intense mag. fields, Shubnikov-de Haas effect meas. 80−24951
n-$Hg_{1-x}Mn_xTe$, quantum transport phenomena, exchange interaction influence 78−76093
$Hg_{1-x}Mn_xTe$, Shubnikov de Haas effect and quantum oscills. of thermoelec. power 80−49781
$Hg_{1-x}Mn_xTe$, thermo-oscills. of magnetoresist. 79−56249
$Hg_{1-x}Mn_xTe$, transverse magnetoresistance in quantised mag. fields 80−96922
HgSe, band struct. and spin splitting Shubnikov de Haas study 80−65445
HgSe, Shubnikov-de Haas oscills. in pulsed mag. field, Fermi energy var. 77−15873
HgSe, Shubnikov-de Haas oscills., electron conc., g-factor and Dingle temp. 77−69354
HgSe, Shubnikov-de Haas effect 78−6402
HgSe, Shubnikov-de Haas determ. of electron g factors 80−6704
HgTe, acceptor reson., states in high mag. field 80−49668
HgTe, gapless semicond., magnetophonon conc. oscills. *(Russian)* 77−11943
HgTe, magnetophonon oscills. of thermoelec. power 80−49789
HgTe type semiconductors, spin-flip transitions in magneto-optics and magneto-transport 80−50306
HgTe, uniaxially compressed, anomalous magnetoresist. and band crossing 79−65501
Ho, single cryst., transverse magnetoresist. 77−66154
Ho-Cu intermetallics, resist. and magnetoresist., mag. ordering obs. 80−70677
$HoCu_2$, mag. struct. and elec. resist., neutron diffr. obs. 80−60206
$Ho_{1.2}Mo_6S_8$, supercond. destruction by mag. ordering 77−69449
In, conducting flat plate, electrostatic pot. distrib. transverse magnetoresistance, electrode effects 78−60108
In film, transversal magnetoresist. meas. 77−72925
In, linear magnetoresistance increase by artificial voids 79−60799
In, mag. breakdown exam., magnetoresist. meas. 78−6351
In wire, linear magnetoresist., effect of voids 78−51974
n-InAs, EPR, oscillations of transverse magnetoresistance in weak mag. field 79−91086
InAs, longitudinal magnetoresistance in extreme quantum limit *(Russian)* 80−11008
n-InAs, magnetophonon resonance under hydrostatic press. 77−47832
n-InAs, negative magnetoresist. in extreme quantum limit 78−64051
n-InAs, Shubnikov-de Haas oscills., conduction electron density, phonon scatt. 77−15768
n-InAs, Shubnikov-de Haas effect, effective mass, Dingle temp., and g-factor 79−51602
n-InAs, Shubnikov-de Haas transverse kinetic coeffs., quantum oscills. 80−49778
InAs:Mn, NMR, magnetoresist., Hall effect and mag. susceptibility meas. 78−26888
InAs-GaSb heterostruct. superlattice, props. in high mag. fields 79−73570
InAs-GaSb superlattices, two-dim. electronic structure, Shubnikov-de Haas oscill. obs. 78−75995
InAs-GaSb superlattice, semiconductor-semimetal transition obs. 80−44710
InAs-GaSb superlattices, semicond.-semimental transition obs. 80−49882
InAs-GaSb superlattices, mag. field induced semimetal-semicond. transition 80−65656
$InAs_{1-x}P_x$, magnetophonon effect 79−65500
$InAs_{1-x}P_x$, electron effective mass cyclotron reson. and magnetophonon effect 80−24786
$In_{0.9}Ga_{0.1}As_{0.22}P_{0.78}$, effective mass meas. by Shubnikov-de Haas oscills. 78−34754
$In_{1-x}Ga_xAs_yP_{1-y}$, electron effective mass from Shubnikov-de Haas meas. 80−80298
$In_{1-x}Ga_xP_{1-y}As_y$ LPE films, hot electron and magnetotransport props. 78−26977
$In_xGa_{1-x}P_yAs_{1-y}$, electron effective mass and Dingle temp., Shubnikov-de Haas oscills. 80−59859
n-InP, compensated, elec. props., space-charge effects 80−65569
n-InP, compensated impurity conduction and negative magnetoresist. 79−28360
InP, electrical and optical props. at low temps. 80−39636
InP, electron transport props., mag. field and temp. depend. 80−92888
InP epitaxial films, grown on heavily doped substrates, carrier mobility study, magnetoresist. meas. 80−60116
InP, epitaxial layer, effective doping density, comparison of Hall and magnetoresistance meas. 77−11938
InP, Gunn oscillator magnetoresist. meas. of mobility and noise, contact effects 77−62948
n-InP, magneto-impurity effect, review 79−91081
InP, negative differential mobility and geometrical magnetoresist. calc. 77−43624
InSb, charact. and phys. props., review *(Japanese)* 80−39576
p-InSb, deformed, giant negative magnetoresistance 78−87990
n-InSb, EPR, oscillations of transverse magnetoresistance in weak mag. field 79−91086
InSb, electrical effects of dislocation, galvanomag. props. 78−23119
n-InSb, electron gas degeneration in strong mag. field 77−66173
InSb, extrinsic and intrinsic, interaction of transverse magnetoresist. effects 80−65596
n-InSb, freq. depend. cond. tensor in quantising mag. fields *(German)* 80−29419
n-InSb, galvanomag. props. at low temp., carrier localisation, metallic impurity cond. 77−28195
n-InSb, galvanomagnetic props. at low temp., mag. field induced metal-nonmetal transition 77−76845
n-InSb, Hall coeff. and magnetocond. in mag. freeze-out regime 79−60849

magnetoresistance continued
n−InSb, Hall effect and magnetoresist. in mag. freeze-out region 79−15165
n-InSb, Hall effect and magnetoresist. in extreme quantum limit, stress depend. 80−11021
n-InSb, heavily compensated, hopping cond. in mag. field 79−7842
InSb, high field quantum magnetotransport theory 78−30941
InSb, high-purity specimen irradiated at 80K, transport prop. and defect annealing 78−95307
n-InSb highly doped semicond., transverse magnetoresistance in strong mag. field 79−56246
n-InSb, hot electron magnetophonon effect, 77K, mag. field modulation method 78−60140
InSb, intrinsic magnetoresistance 79−69534
InSb, inversion asymm. splitting of cond. band, Shubnikov-de Haas meas. 78−10348
p-InSb inversion layer, magnetotransport 78−64138
n-InSb, longitudinal magnetoresistance in extreme quantum limit *(Russian)* 80−11008
InSb, low temp. electron mobility, theory and expt. 77−89759
n-InSb, low temp. resonance excitation of negative magnetoresistance *(Russian)* 78−56159
InSb, magneto-surface transport props. 77−43693
InSb, magnetoconcentration effect, nonlinear current carrier recomb. 79−33298
p-InSb, magnetoconductivity and cyclotron reson. in inversion layers 80−49946
InSb, magnetophonon effect temp. depend., 80 to 190K 77−59293
n-InSb, magnetophonon effect exam. using field modulation technique 78−26918
n-InSb, magnetophonon effect, temp. depend. below 90K 79−56247
n-InSb, magnetophonon reson. under hot electron conditions 77−24568
p-InSb, magnetophonon reson. of holes 79−95424
N-InSb, magnetophonon resonance, damping factor by mag. field modulation technique 80−6878
p-InSb, magnetophonon resonance due to non-equilib. electron injection 80−6881
n-InSb, magnetophonon struct. obs. in transverse magnetoresist. 78−23120
InSb magnetoresistive elements, fundamental effects *(Japanese)* 80−11013
n-InSb, magnetotransport experiments, surface treatment induced effects 80−34468
n- InSb, mangetophonon structure in magnetoresist., elec. field depend. 78−30943
n-InSb, narrow gap, appl. of effect of pot. fluctuations induced by cryst. inhomogeneities 80−49780
n-InSb, negative longit. magnetoresist., carrier conc. and mobility depend., 77K 80−60007
p-InSb, negative magnetoresist. under press. 80−20224
p-InSb, negative piezomagnetoresist. and Hall effect meas., antiferromag. order form. 78−19061
n-InSb, photo-induced magnetophonon reson., 4.2K, peak shifts 78−84250
n-InSb, quantum magnetophonon oscills. of piezoresist. 77−15880
n- InSb, Shubnikov-de Haas effect, CO_2 laser induced hot electron effects 78−30957
n-InSb, Shubnikov-de Haas effect expts. on optically heated electrons 79−73529
n-InSb, Shubnikov-de Haas effect 80−11015
n-InSb, Shubnikov-de Haas transverse kinetic coeffs., quantum oscills. 80−49778
n-InSb, spin-magnetophonon resonance 80−96918
InSb, thin film, magnetoresistivity, depend. on mag. field strength at room temp. 79−65568
InSb, thin films, electrophysical props. obs. 80−103765
n-InSb, transverse magnetoresist. in strong mag. fields 79−4571
InSb type semiconductor, spin-flip transitions in magneto-optics and magneto-transport 80−50306
p-InSb, uniaxially deformed, mag. field induced semicond.-metal transition 79−95457
InSb, valence band struct. obtained by magnetophonon effect 77−76748
InSb:Ge, uniaxially compressed, anisotropy of elec. props. 78−19035
p-InSb:In, two-phase polycryst. films, negative magnetoresist. 80−11011
InSb:Mn, NMR, magnetoresist., Hall effect and mag. susceptibility meas. 78−26888
InSb:NiSb, size reson. scatt. from hard cylindrical pot. obs. in magnetoresist. 79−95421
InSb:Te, anomalous anisotropy of magnetoresist. and g-factor 77−47831
InSb-NiSb, eutectic alloy, Te-doped, electrophys. props. 77−35955
InSb-NiSb, longit. thermomag. amplifier 77−47838
In_3Sn, pulsed high field magnetoresist., 77K 79−73493
K, longitudinal elec. and thermal magnetoresistivities obs. 80−88541
K, magnetoresistance anomalies due to inhomogeneities, examination 78−56130
K, magnetoresistance in terms of inhomogeneity models of current jetting and channelling 78−56131
n-$KTaO_3$, Shubnikov-de Haas oscills. 79−73426
$KTaO_3$, Shubnikov-de Haas effect, cond. band struct. 80−10875
$(La,Gd)Al_2$, dil. alloy, magnetoresistivity determ. 79−73495
La-Gd-Au, amorphous, mag. field depend. of resist. minima 77−59275
$LaAl_2$, magnetoresist. and de Haas-van Alphen effect, Fermi surface model 79−15069
LaB_6, transverse magnetoresistance meas. 80−107764
LaB_6:Ce, Kondo system, magnetoresist. down to 0.04K, anisotropy 77−11904
$(La_{1-x}Gd_x)Al_2$, dil., reverse resistance anomaly 78−76054
$La_{0.65}Pb_{0.35}MnO_3$, transport props. near Curie points 78−88100
$La_{0.71}Pb_{0.29}MnO_3$, metal-semicond. transition at Curie point, transport props. obs. 79−73554
Li ferrite, carrier transport phenomena 78−19039
$Li_xMn_{1-x}Se$, anomalies obs. in mag. and elec. props. 77−69509
Li_2O-Fe_2O_3-Pr_6O_{11}(Er_2O_3)(CeO_2)(Eu_2O_3), Hall effect and magnetoresist. 78−34849
Lu-Gd, dil., positive exchange Kondo system, magnetisation and resist. 78−68158
Mg, quantum interference effect in transverse magnetoresistance 77−35854
Mg, quantum interference effect in transverse magnetoresistance 77−35855
Mg, quantum interference effect in transverse magnetoresistance 77−35856
Mg-Gd(Ho), dil., magnetoresist., anomalous Hall effect 80−15502
Mg-rare earth metal dil. alloys, anisotropic magnetoresist. 77−62905
MgMn ferrite, carrier transport phenomena 78−19039
α-Mn, antiferromag., temp. and field depend. 78−2464
Mn-Bi film, negative transverse magnetoresist. in c-plane, domain wall effects 77−20465
Mn-Bi film, with perpendicular anisotropy, galvanomag. props., hysteresis loops 77−20464
$MnAs_{1-x}P_x$, low temp. resistivity minimum 77−8122
MnB_2, polycryst., magnetoresist. and mag. props. *(Russian)* 80−92907
Mn_3Ge, elec. and mag. props. *(Russian)* 77−76792
MnP, high field magnetoresistance 80−107817
MnP, low field magnetoresistances, mag. phase diagram purity depend. 80−107816
$Mn_xPd_{82-x}Ge_{18}$ amorphous alloys, elec. resistivity and magnetoresistivity 79−51543
$Mn_xPd_{82-x}Ge_{18}$, amorphous alloys, mag. props. 78−91906
$Mn_{1.18}Zn_{0.06}Co_{0.01}Fe_{1.75}O_4$, transport props. near Curie points 78−88100
Mo, transverse galvanomag. and thermomag. coeffs. 77−20298
Mo-Permalloy, galvanomag. props. 77−39822
Mo_2B_5 and MoB_4, thermal, elec., and mag. props. 80−20187
n-Si, (111) inversion layers, valley splitting, Shubnikov de Haas oscills. 80−65698
Na, size oscillations in magnetocond. 77−4324
Nb, supercond., magnetoresist. and mag. breakdown in field up to 175 kOe *(Russian)* 77−20492
$NbSe_2$:Fe (2H), pure and doped, magnetoresist. and elec. resist. temp. depend. rel. to CDW form. 80−44574
$NbSe_2$-Fe, dil. alloy, magnetotransport and superconductivity 77−55516
$NbSe_3$, CDW form., supercond. and Fermi surface determ., press. study 80−70891
$NbSe_3$, CDW linear chain metal, two band model in ohmic region 79−38056
$NbSe_3$, conductivity anisotropy and transverse magnetoresistance 79−38055
$NbSe_3$, Fermi surface, press. effects, Shubnikov-de Haas effect meas. at 1.5K 80−20068
$NbSe_3$, oscillatory magnetotransport, Fermi surface anisotropy, Hall effect, g-factor, Dingle temp. 78−51975
$NbSe_3$, quantum oscillation, Fermi surface exam. 78−60049
$NbSe_3$, Shubnikov-de Haas oscills. 78−2502
$NbSe_3$, two band model and galvanomagnetic study 80−20176
$NbSe_2$(2H), layered metallic magnetoresist. and Fermi surface above and below CDW onset temp. 79−19578
$NbSe_2$(2H), low field magnetoresist. and anomalous transport props. 80−65602
NbTi, RF magnetoresistance, flux flow resistivity 79−61002
NbTi/In granular composite, resistivity mag. field depend. 80−15654
Nd, antiferromag., thermal cond., elec. and thermal magnetoresist., at low temps. 77−69301
Nd, longit. magnetoresist. at low temps. and up to 80 kG 77−55515
Nd, magnetoresistance, mag. struct., elec. resistance at low temps. *(Russian)* 80−54936
Nd, transport props., low temp., effect of mag. field 80−70679
$NdSn_3$, magnetoresistance 80−24877
Ni alloys, magnetic resist. anisotropy, two-current model 77−20295
Ni alloys, spontaneous resistivity anisotropy 77−39821
Ni based alloys, resistivity magnetoresistance, s,p impurities in ferromag. host 78−68008
Ni, ferromag. film, ion plating prep., coercive force and magnetoresist. 77−12546
Ni, ferromag. film, magnetoresistance parameter meas. *(Spanish)* 80−2485
Ni film, CO adsorption effect on galvanomagnetic and magnetic props. 78−43490
Ni film, evaporated, galvanomag. and mag. props. 78−23180
Ni film, evaporated, oscill. due to CO adsorption 77−1496
Ni film, granular, tunnelling of spin-polarised electrons and magnetoresist., exchange effects 77−12024
Ni films, evaporated, effect of CO adsorption on galvanomag. and mag. props. 79−33364
Ni films, evaporated, effect of CO adsorption on galvanomag. and mag. props. 79−33363
Ni, powder, magnetic resistance changes 77−1411
Ni-Au film, amorphous, in fields up to 80 kG 77−39823
Ni-Co, ferromag. films, magnetoresistance effect, crystal struct. 78−68017
Ni-Co films, electron-beam evaporated, magnetoresist. anisotropy, deposition temp. effect 80−34528
Ni-Cu, magnetoresistivity anisotropy, spin mixing 80−88538
Ni-Cu alloy, magnetoresistance anisotropy, planar Hall effect 79−23947
Ni-Cu alloys, spontaneous resist. anisotropy 77−89752
Ni-Cu-Mn alloys, mag. and galvanomag. meas. 77−89928
Ni-Fe, film, magnetisation reversal, magnetoresistance meas. 77−16132
Ni-Fe-Co films, nonmagnetostrictive, magnetoresistance effects 78−35013
Ni-Fe-Pd thin films, mag., surface and corrosion props. 80−34707
Ni-P, amorphous alloys, low temp. mag. props., comp. depend. 77−66387
Ni-rare earth intermetallics, RNi_3, amorphous alloys, mag. and transport props. 79−42513
Ni-Si, magnetoresistivity anisotropy, spin mixing 80−88538
Ni-SiO_2, granular film, hopping cond., magnetoresist. 78−56240
Ni-Sn(Sb), dilute ferromagnetic alloy, resistivity and magnetoresist. anisotropy 79−11106
Ni-Y, amorphous, resist. and magnetoresist. meas., weak itinerant ferromagnet 78−68018
$(NiAl)_{1-x}M_x$, M=3d transition metal, elec. resist. and magnetoresist. 77−43580
NiFe thin films, magnetoresistance, quasi-static characts. 80−107766
Ni_3Fe single crystals, longitudinal magnetoresist. meas. 80−70675
$Ni_{1-x}P_x$, electrodeposited, amorphous, mag. and transport props. 78−52106
NiS_2, anomalous magnetoresist. 79−78121
NiS_2, weak ferromagnet, galvanomagnetic effect 79−11148
Pb, compensated metal, linear magnetoresist., semiclassical transport theory 77−35925
$Pb_{1-x}Ge_xTe$, n- and p-type, effective masses 80−44481

magnetoresistance continued
PbI_2 (2H), electronic transport and cyclotron reson. 79−28369
$PbMo_6S_8$, Hall effect and magnetoresistivity 78−95400
$PbMo_6S_8$, normal-state electronic props., Fermi surface and supercond. parameter derivations 79−60850
PbO_2 compressed powder magnetoresistance and apparent carrier mobility 80−35669
PbO_2 pressed powder, Hall voltage and change of cond. in transverse mag. fields 79−4567
PbS, anomalous magnetoresist. 80−107813
PbSe, carrier density depend. of cyclotron mass, Shubnikov-de Haas effect 79−73533
PbSe, film with pot. barrier, magnetoresistance anisotropy 79−91172
n-PbSe, pressure induced transition to gapless state 78−2533
$Pb_{1-x}Sn_xGe$:In, press.-induced transition to gapless state, galvanomag. effects 78−19108
$Pb_{1-x}Sn_xSe$, band struct. and transport props., hydrostatic press. effects 80−15452
$Pb_{1-x}Sn_xSe$, carrier density depend. of cyclotron mass, Shubnikov-de Haas effect 79−73533
$Pb_{1-x}Sn_xSe$, determ. of anisotropy coeff. of Fermi surface, magnetoresist. meas. 78−51878
$Pb_{1-x}Sn_xSe$, energy band parameter determ. from Shubnikov-de Haas effect 77−69227
PbSnTe, Magneto transport anomalies at low carrier densities, Wigner crystallisation 80−20222
n-$Pb_{0.8}Sn_{0.2}Te$ film, magnetophonon reson., 55-90K 79−7913
p-$Pb_{0.8}Sn_{0.2}Te$, magnetophonon effect obs. 78−23115
$Pb_{0.8}Sn_{0.2}Te$:Cd, influence of Cd doping on high field magnetoresist. and Hall effect 80−75590
n-$Pb_{0.82}Sn_{0.18}Te$, conduction band struct., determ. by Shubnikov-de Haas meas. 78−2504
$Pb_{0.82}Sn_{0.18}Te$, narrow band gap, relax. time for Shubnikov-de Haas effect 78−80006
$Pb_{1-x}Sn_xTe$, energy spectrum under hydrostatic pressure 79−65381
n-$Pb_{1-x}Sn_xTe$, galvanomag. effects, alloy scatt., 4.2K 77−39880
$Pb_{1-x}Sn_xTe$, heteroepitaxial film, fundamental absorpt. edge and Shubnikov-de Haas effect 79−24381
$Pb_{1-x}Sn_xTe$ narrow gap solid alloys, hole Fermi surface, galvanomag. and oscill. effect obs. *(Russian)* 77−69345
p-$Pb_{1-x}Sn_xTe$, Shubnikov-de Haas effect under press. 79−69413
$Pb_{1-x}Sn_xTe$:In, carrier spectroscopic g-factors, magnetoresistance, temp. depend. 80−6705
$Pb_{1-x}Sn_xTe$:In, energy spectra modifications due to comp. changes and press. appl. 80−10915
$Pb_{1-x}Sn_xTe$:In film, anomalous elec. props. 78−10477
n-PbTe, epitaxial, time dependent negative weak field magnetoresist. 78−64151
n-PbTe epitaxial film, magnetophonon and Shubnikov-de Haas oscills. 78−60234
p-PbTe, Fermi surface parameters depend. on carrier density, Shubnikov-de Haas oscills. 79−42435
p-PbTe film, magnetophonon effect obs. 78−23115
n-PbTe film, transverse magnetoresistance oscillations, depend. on film thickness 79−65567
PbTe, Magneto transport anomalies at low carrier densities, Wigner crystallisation 80−20222
n-PbTe, noncubic (111) oriented epitaxial films, weak field magnetoresistance 80−75584
p-PbTe, quantum oscillations in inversion layer 77−85245
p-PbTe, relax.-time anisotropy 77−35954
PbTe, resonant scattering, photocond. 80−6910
PbTe, struct. of second valence band cond. of warm carriers and magnetoresist. 77−89697
PbTe:In, Shubnikov-de Haas oscillatory effects, quasilocal impurity level 80−92912
Pd-Co, dil., breakdown of ferromag. order, magnetoresist. obs. 80−71046
Pd-Co-P amorphous alloy, mag. an elec. props. 77−40043
Pd-Co(Ni), dil. local orbital moment evidence 77−20299
Pd-Cr spin glass, magnetisation and magnetoresist. meas. 79−69680
Pd-Fe, magnetoresist., rel. to dil. ferromag. model 78−30907
Pd-Fe(Co)(Ni) dilute alloys, ferromag., magnetoresist. 78−91665
Pd-Mn (1-10 wt.%), mag. ordering, influence on resistivity 80−75557
Pd-Ni alloys, kinetic props., transverse magnetoresistance *(Russian)* 77−76790
Pd-Pt, low temp. magnetoresistance up to 60 kG 78−91668
PdFe alloy, magnetoresistance meas. below 295K 79−78070
$Pd_{80}Si_{20}$, amorphous, elec. resist. and magnetoresist. 80−49693
Pr, longit. magnetoresist. at low temps. and up to 80 kG 77−55515
Pr, mag. scatt., effect of cryst. field levels 77−62904
Pr, transport props., low temp., effect of mag. field 80−70679
$PrSn_3$, magnetoresistance 80−24877
Pt-Co, dil, magnetopower, magnetoresistivity 78−68016
Pt-Fe, dil., breakdown of ferromag. order, magnetoresist. obs. 80−71046
Pt-Fe(Co)(Mn), dil., skew scatt. Hall effect, magnetoresist. and mag. anisotropy, orbital magnetism of impurity 80−70678
Ru, electronic structure and mag. breakdown, galvanomag. props. obs., 1.3-20.4K 78−91600
Ru, giant thermopower oscillations due to magnetic breakdown trajectories 79−60688
Ru, magnetoresistance and Hall effect under mag. breakdown conditions *(Russian)* 79−95389
Ru, thermopower and magnetoresistance meas., mag. breakdown 78−47766
$(SN)_x$ crystal, galvanomagnetic effects meas. 77−85246
$(SN)_x$, elec. cond., galvanomag. effects 79−91091
$(SN)_x$ film, Hall effect, elec. cond. and magnetoresist. meas. 78−84314
$(SN)_x$ halogenated derivatives, cond. and magnetoresist., 4.2-300K 80−24915
$(SN)_x$, intrinsic cond. anisotropy from galvanomag. effect obs. 78−6369
$(SN)_x$, negative magnetoresistance below 4.2K 79−51611
$(SN)_x$ single crystal, transverse magnetoresistance 78−72140
$(SN)_x$ single crystals, galvanomag. effects 79−19582
$(SN)_x$, superconducting fluctuation induced magnetoconductivity in anisotropic bulk and fibrous samples 79−95545
$(SNBr_{0.4})_x$, $(SNI_{0.02})_x$, $(SN[ICl]_{0.01})_x$, influence of halogen on DC conductivity and magnetoresist. 78−91682
Sb, carrier density at press. up to 80 kbar, magnetoresist. and Hall effect obs. 79−73534
Sb, carrier energy spectrum, effect of hydrostatic pressure 78−87903
magnetoresistance continued
Sb, carrier transport, magnetoresistivity, field-dependent tensor study 80−39609
Sb, effect of surface layer current, on transport coeffs., and meas. of Kapitza resist. 77−69348
Sb, energy spectrum variation under strong uniaxial tension 79−73432
Sb, mutual drag effect, temp. effect 78−52012
Sb, superficial cond. effects 77−28235
Sb whisker crystals, magnetoresist., size effects *(Russian)* 79−7821
Sb whiskers, quantum oscills. of magnetoresist. *(Russian)* 78−60145
Sb-Ge (1.2 to 2.2 at.%), carrier transport, magnetoresistivity, field-dependent tensor study 80−39609
Sb-Sn (0.5 to 1.0 at.%), carrier transport, magnetoresistivity, field-dependent tensor study 80−39609
$Sb_{1-x}Bi_x$ alloys, Shubnikov-de Haas *(Russian)* 78−23007
Sb_2S_3, galvanomag. props. and elec. resist., temp. depend. 78−43419
Sc-Gd, dil., reverse resist. anomaly and negative magnetoresist. 80−84459
Sc_3In, itinerant electron ferromagnet, spin fluctuations 77−73096
Se, Se:Te, amorphous, negative magnetoresist., doping depend. 78−56161
Se, trigonal, transverse magnetoresistance meas., influence of illumination 80−65607
$Se_{60}Te_{30}Ge_{10}$, amorphous, neg. magnetoresist. 79−51603
n-Si (001) on sapphire, galvanomag. effect for holes, valence band 79−91166
Si (100) inversion layers, effective masses, Shubnikov-de Haas oscills. under mechanical stress 77−43625
Si (100) MOST, comparison of Shubnikov-de Haas effect and cyclotron reson. under uniaxial stress 80−20320
Si, (100) surface, effective mass and collision time 78−64081
Si, amorphous, anomalous magnetoresist., hopping model 78−23117
Si, amorphous, anomalous magnetoresistance 80−6877
Si amorphous, negative magnetoresist., localised mag. states 80−70731
Si, electron transport and ionisation at high fields 78−30933
n-Si, γ-irrad., galvanomagnetic effect anisotropy rel. to layer inhomogeneity 79−33299
n-Si, heavily doped, negative magnetoresistance model, spin-up spin-down electron effective mass variations 79−95423
n-Si, impurity-assoc. magnetophonon reson. 80−20221
Si, influence of one-dimensional superlattice on two-dimensional electron gas 77−43683
Si inversion layer, in strong mag. fields, electron localisation 78−60219
Si inversion layer, photoconductivity meas. 78−10498
n-Si inversion layer, resist. minima in surface quantum oscills. 78−60215
Si inversion layer, surface quantum oscillation under pressure 78−60228
n-Si inversion layer, thermal activation of two-dimens. Shubnikov de Haas cond. extrema 78−60218
Si inversion layers, high field magnetocond. 77−32020
p-Si inversion layers, hot carrier effects in high mag. field, 1.25-20K 78−34908
n-Si inversion layers, in strong mag. field, quantum galvanomag. expts. 78−60214
Si inversion layers, magnetocond. in ground Landau level, defect diffusion in Wigner cryst. 77−39914
Si, inversion layers, magnetic localisation of electrons 78−43481
n-Si, inversion layers, many-valley electron-phonon interactions, piezoresistance, anisotropic cond., Shubnikov-de Haas oscillations 78−52096
Si inversion layers, random pair attractive interaction model of carrier correl., compared with expt. 78−60212
Si, inversion layers, resolution of Shubnikov-de Haas paradoxes 80−39648
Si inversion layers, stress and intersubband correlation 78−60227
n-Si, layer impurity distrib., γ-ray and neutron irradiated, transverse magnetoresist and Hall effect meas. 78−19058
Si MOS (111) inversion layers, angular dependent negative magnetoresist. 78−80062
Si MOS devices, Anderson localisation in Landau level tails, anal. of Shubnikov-de Haas cond. minima 77−76947
Si MOS inversion layers, negative magnetoresist. 80−49922
Si MOSFET, n-type inverted, surface, mag. field depend. of valley splitting 79−19650
Si MOSFET, n-type inverted surface channel, reproducibility of electronic props. 79−99628
Si, MOSFETs, Shubnikov-de Haas oscills. from electron irrad. induced two-dimens. leakage channel 79−19671
n-Si, magnetoresistance, growth layer influence, effect of randomly distributed inhomogeneities 80−20229
Si, many-valley semicond., current-voltage characts., intrinsic magnetoresistance 79−38108
Si n-channel (100) inversion layer, valley splittings, enhancement by many-body effects 77−85331
Si n-channel (100) MOSFETS, Shubnikov-de Haas oscills. on mag. fields up to 35 T 79−91154
Si, n-type inverted MOSFET (100) surfaces, quantitative determ. of valley splitting 79−51678
Si, negative differential mobility and geometrical magnetoresist. calc. 77−43624
Si, neutron irrad., Hall effect and magnetoresist. meas. 80−6883
n-Si, neutron or γ-irrad., elec. props., in strong elec. fields 79−95416
p-Si, odd magnetoresist. under weak carrier heating conditions 80−96917
Si, on sapphire, MOS inversion layer, magnetoconductance oscillations 80−20325
Si on sapphire, residual strain effect on elec. props. *(Japanese)* 80−84522
n-Si on sapphire magnetoresistance anisotropies and electronic struct. obs. 77−20471
Si on sapphire thin film, Hall effect, magnetoresistance *(French)* 80−65601
Si, recomb. centre study by spin-depend. photocond. 80−49805
a-Si, resonant and non-resonant photoconductivity changes 80−49814
a-Si, resonant and non-resonant luminesc. changes theory 80−50410
n-Si, size-induced magnetoresist. in strong elec. fields 80−65582
Si, superlattice and 2-D electron gas 78−64080
Si surface, MOS struct. band structure, minigaps, magnetoresistance, cond., space charge layers 80−92980
n-Si, surface quantum oscills. in inversion layers under uniaxial press. 78−88041
n-Si, warm-electron magnetoresist. 79−65503
Si:In amorphous films, EPR, elec. cond., and magnetoresist. 80−50160

magnetoresistance continued
Si:P, amorphous, CVD, substitutional doping, electronic props. 79−23923
Si:P, amorphous, substitutionally doped CVD, electrical props. 79−99566
Si:P, ion implanted, resist. changes induced by ESR 78−68377
Si:P, polycryst. films, elec. props., EPR, defect states, doping effects 80−75660
Si-Al_2O_3, inversion layer subbands, magnetocond. oscills. 78−64124
Si-SiO_2 (111) interfaces, sixfold valley degeneracy in electron inversion layers 80−49936
Si-SiO_2 boundary, surface charge transport in valence band of Si 80−70789
Si-SiO_2 inversion layer, n-channel, anomalous magnetoresist., model 80−96996
SiC, cubic, magnetoresistance and Hall mobility, field and orient. depend. *(Russian)* 77−69346
β-SiC, deform. potential and effective mass anisotropy, Hall constant 79−90949
Si(100) inversion and accumulation layers, effective mass and collision time of electrons, oscillatory magnetoconductance 78−34909
Si(100) inversion layers, magnetoelec. and piezoresist. evidence for mobility domains 77−4447
n-Si(100) inversion layers on sapphire, surface quantum oscills. 78−19158
p-Si(111) surface inversion layer, Cs covered, negative magnetoresist. in 2D impurity band 78−64135
Sm, longit. magnetoresist. at low temps. and up to 80 kG 77−55515
Sm, magnetoresistivity and elec. resist., 4.2 to 300K *(Russian)* 80−88539
Sm, transport props., low temp., effect of mag. field 80−70679
$Sm_{1-x}La_xS$, magnetoresist. in semicond. and metallic phases 80−96914
SmS, semicond., anomalously high magnetoresist., Hall coeff. and elec. resist. meas. 78−10479
$SmS_{1-x}As_x$, magnetoresist. in semicond. and metallic phases 80−96914
$Sm_{1-x}Y_xS$, magnetoresist. in semicond. and metallic phases 80−96914
Sn, galvanomagnetic props., temp. depend. meas. in single cryst. 80−96850
Sn, polycrystalline high-purity wires, anomalous magnetoresist. meas. 78−47765
β-Sn, transverse magnetoresist., temp. depend. in mag. field *(Russian)* 80−107765
p-SnTe, film and bulk, weak-field magnetoresistance 78−84236
SnTe:Mn, ferromag.-ordering, transverse magnetoresist. and Hall effect meas. 77−85240
n-$SrTiO_3$, magnetoresist. meas., band struct. exam. 77−85242
$(TSeT)_2Cl$ complex, metal-semimetal transition, magnetoresist. and cond. *(Russian)* 79−38138
$(TSeT)_2Cl$, one-dimens. conductor, metallic phases 80−20159
TaS_2, 1T, anomalous magnetoresist., CDW state 78−72173
TaS_2 (2H), quantum oscillations and Fermi surface 79−37960
TaS_2 (4Hb) layer cpd., oscillatory magnetotransport obs. 77−85241
1T-TaS_2, and 1T-$TaS_{2-x}Se_x$, Anderson localisation, elec. resist. and magnetoresist. meas. 80−44596
TaS_2-Fe, dil. alloy, magnetotransport and superconductivity 77−55516
TaS_2(1T), anomalously large negative magnetoresist. at ultra low temps. 79−60852
$TaSe_2$ (2H), magnetoresistance in commensurate CDW state, Fermi surface topology 77−43576
$TaSe_2$:Fe, competition between charge and spin density waves, Landau-Ginzburg theory 79−95352
$TaSe_2$/(2H) layer cpd., oscillatory magnetotransport obs. 77−85241
$TaSe_2$-Fe, dil. alloy, magnetotransport and superconductivity 77−55516
$TaSe_3$, oscillatory magnetotransport, Fermi surface anisotropy, Hall effect, g-factor, Dingle temp. 78−51975
$Ta_{1-x}Ti_xS_2$ (1T), magnetoresistance in the Anderson localized states near the metal-nonmetal transition 80−88479
$Ta_{1-x}Ti_xS_2$ (1T), magnetoresist. near metal-nonmetal transition at ultra low temps. 80−88600
Tb, anisotropic electron spin wave scatt. 77−15831
Tb, single cryst., transverse magnetoresist. 77−66154
$TbAg_{1-x}In_x$, mag. and transport props. 78−43572
TbIG:Si magnetoresistance meas. 79−78120
Te, galvano- and thermomagnetic effects 78−30939
Te, impurity spectroscopy 80−65499
Te, inversion layer, surface quantum levels, calc. from Shubnikov de Haas meas. and triangular surface pot. well 79−15207
Te inversion layers, surface quantum oscillations 77−89777
Te inversion layers, surface quantum transport 78−64088
Te inversion layers in mag. fields 80−44690
Te, lightly doped, galvanomagnetic props. in fields up to 140 kOe 78−91707
p-Te, magneto-impurity effect, review 79−91081
Te, rel. to mag. inversion of Hall effect *(Russian)* 77−4376
Te, two types of carriers 80−60013
Te, undoped, elec. cond., magnetoresist. and Hall meas., hydrostatic press. effect 77−47830
Te, weakly doped, impurity spectroscopy, magnetoresist. meas. under nonohmic conditions 78−30942
Ti-Cr disordered alloy, gap nature of electron spectrum in region of struct. instability *(Russian)* 78−18947
Ti-Permalloy thin film diffusion couples, low temp. interdiffusion interdiffusion 78−71889
$Ti_{1-x}Co_x$, electronic struct. and anomalies of elec. and mag. props. 80−6710
TiN-CrN system solid solns., electrophys. and galvanomag. props., energy spectra 77−15847
$Ti_{1-x}Ni_x$, electronic struct. and anomalies of elec. and mag. props. 80−6710
$Ti_{0.99}V_{0.01}Se_2$, negative mgnetoresist. and nonlinear cond. 79−87105
$Ti_{0.99}V_{0.01}Se_2$, negative magnetoresist. and nonlinear cond. 80−44617
TlTe single crystal, resistivity, Hall coeff., magnetoresistance, thermoelec. power 78−43418
TmSe, mixed valence cpd., thermal, mag., and transport props. 79−61074
Tm_xSe, $0.87<x<1.05$, mag., thermal and transport props., comp. depend. 78−68239
Tm_xSe, magnetoresist. and Hall effect, stoichiometry effects 80−65597
U_3As_4, elec. resist. in vicinity of Curie point, influence of mag. field 77−69314
UAsSe, strongly anisotropic ferromag., negative magnetoresist. meas., 77-135K 77−89774

magnetoresistance continued
UGe_3, compensated metal, topological props. of Fermi surface, magnetoresist. meas. 78−6350
UIr_3, uncompensated metal, topological props. of Fermi surface, magnetoresist. meas. 78−6350
V, Fermi surface and magnetic breakdown, magnetoresistance and thermopower behaviour 79−33222
VN-CrN system solid solns., electrophys. and galvanomag. props., 77 to 1300K 77−24567
V_5S_8, metallic evidence of spin flopping by magnetoresist. meas. 78−6352
W, compensated metal, linear magnetoresist., semiclassical transport theory 77−35925
W, magnetoresistance of size influenced samples, temp. depend. 79−28338
W plates, multiple Sondheimer oscills. *(Russian)* 79−60796
W, RF size effect, surface electron scatt. influence *(Russian)* 80−2414
W, single cryst. plates, magnetoresistance, temp. depend. *(Russian)* 79−7820
W, thin wire, negative longit. magnetoresist., kinetic theory 78−34821
W-Re, amorphous wire, elec. resist., 2-20K, dimens. and mag. field depend., quantum localisation 80−39547
W_2B_5 and WB_4, thermal, elec., and mag. props. 80−20187
Y-Gd, dil., reverse resist. anomaly and negative magnetoresist. 80−84459
YIG, magnetoresistance of bulk and epitaxial films 78−91706
Yb, film, amorphous and cryst., transport props. rel. to band struct. *(Russian)* 77−12026
Zn, $2^1/_2$ order phase transition, magnetoresist. anisotropy change under stress *(Russian)* 77−62907
Zn, monocryst., electron motion, Hall effect and Fermi surface 77−47793
$ZnCr_2Se_4$:In, magnetoresist. and elec. resist. above and below Neel temp. *(Russian)* 80−88576
$Zn_xHg_{1-x}Se$, galvanomagnetic effects, Shubnikov-de Haas oscill. determ. of band struct. 80−6884
$Zn_xHg_{1-x}Te$, impurity influence on thermomagnetic effects and elec. cond. 79−60856
ZnMn, dil., magnetoresist. meas., temp. depend. anisotropy 80−65532
ZnO, strong accumulation layers, negative magnetoresistance 78−6428
ZnO surface, quantised accumulation layer magnetoresistance, spin scattering model 79−69529
n-ZnSe, impurity band, Hall effect, elec. cond., mobility and magnetoresist. expts. 77−35888
ZnSe:In, heavily compensated, negative magnetoresistance 79−91079
$ZnY_{0.95}R_{0.05}$ resist. anisotropy due to impurities 77−62902
Zr-Mn (up to 0.3%), high-magnetic field magnetisation and magnetoresistance 78−10652
ZrC-C composite system, negative magnetoresist. 80−60008
$ZrZn_2$, weak itinerant electron ferromagnet, resistivity 77−72850

magnetoresistance, thermal *see thermal magnetoresistance*

magnetoresistivity *see magnetoresistance*

magnetosphere
see also magnetospheric electromagnetic wave propagation; radiation belts
100 to 500 kHz noise, rel. to auroral arcs and field aligned currents and auroral electrons accel. 79−66859
A_p-index, 1964-1976, rel. to geomag. field and interplanetary field states 80−104866
albedo particles accumulation in geomag. field in equatorial regions 77−60546
Alfven and compressional waves, coupling theory 78−89001
Alfven wave at ATS 6, soln. with finite ionospheric conductivity 79−12346
Alfven wave stimulation by trapped electrons, geomag. pulsation generation *(Russian)* 77−22003
Alfven waves, axisymmetric, dipole field model with finite ionospheric cond. 79−29941
Alfven waves, generation in magnetotail via proton accelerator 78−73582
Alfven waves, interaction with trapped electrons *(Russian)* 77−11338
Alfven waves and trapped particles nonlinear bounce resonant interaction 79−48624
Alfven waves generated by an inverted plasma energy distribution 78−85775
Alfven waves generation outside plasmasphere, effect of bounce resons. 79−12344
Alfven waves in near-Earth plasma stimulated excitation by pulsed radio emission 79−58192
Alfven waves self-modulation by cyclotron instability *(Russian)* 78−40765
Alfven-acoustic-gravity wave propag. and reflection, compressible, inviscid, perfectly conducting isothermal fluid 77−51124
alpha-particles acceleration near magnetosphere 79−62675
anti-loss-cone plasma, electrostatic instabilities 78−34286
antiloss cone instability 77−25867
ARAKS and electron beam injection expts. 78−36405
ARAKS experiment, picture tube with curved microchannel plates, appl. *(French)* 78−40671
ARAKS expt., spectrometers for artificially injected particles 79−21143
ARAKS Project 79−21021
artificial Ba clouds, laser scatt. by metallic particles in two-phase nozzle flow into vacuum 77−35194
asymmetric ring current coupling with eastward electrojet 78−7823
S.Atlantic anomaly region, aeronomic and geophysical indicators anal. 79−58187
atmospherics, coherence function appl. to GEOS-observed chorus and hiss automatic recognition 79−44307
ATS-6 radio beacon studies, review 80−56677
AUOS-MAGIK satellite, instruments and measurements, magnetospheric research *(German)* 79−88562
aurora, review of current knowledge 79−84564
aurora primary ions, above diffuse midnight aurora 80−41595
aurora quiet-time patterns rel. to magnetospheric convection 80−17433
auroral absorption substorm, onset obs. 78−96362
auroral acceleration region, altitudinal double-layer criterion 80−94656
auroral arcs formation and V-potential double layers 80−103185
auroral arcs global formation, numerical simulation in three-dimensionally coupled ionosphere magnetosphere 80−67446
auroral arcs location near substorm onsets 78−88968

magnetosphere continued
auroral Birkeland current systems, anomalous resistivity effects 77−9591
auroral convection over $60° \leq \Lambda \leq 75°$: Millstone Hill incoherent scatter obs. 80−67454
auroral electric field, description based on plasma interaction with geomag. field 80−46342
auroral electric field, model 79−53608
auroral electron diffuse surge zone, equatorial boundary model 78−69610
auroral electron discontinuity in magnetosphere morning sector, location meas. by Molniya-1 satellite 79−8778
auroral electrons, accel. in array of auroral arcs 78−36357
auroral electrons, bounce periods rel. to latitude effect in pulsating patches periodicity 80−31155
auroral electrons, origin of large-scale longit. intrusions 77−64510
auroral field lines, region of intense plasma wave turbulence 77−45228
auroral km radiation ang. distrib., satellite obs. 77−60530
auroral oval and polar cap mag. field perturbs., rel. to charged particles and interplanetary mag. field 78−45160
auroral oval equiv. current flow near dusk, inversion techniques 79−58164
auroral particle dumping into ionosphere and magnetotail structure 80−109313
auroral particles, adiabatic movement in magnetosphere neutral sheet field 78−28421
auroral particles adiabatic motion, dipole field corrections 77−91373
auroral particles adiabatic motion in presence of dipole mag. field 77−60547
auroral phenomena, role of mag. mirroring in magnetosphere-ionosphere current system 78−20572
auroral processes, IAGA/IAMAP symposium (Seattle, August 1977) 79−88521
auroral proton bursts struct. during mag. quiet times and substorms 77−29531
auroral proton source in magnetosheath 77−33240
auroral radiation, theory of generation 79−75051
auroral region, self-consistent particle and parallel electrostatic field distrib. 78−45120
auroral substorm absorption events, at low auroral latits., apparent equatorward propag. 79−8769
auroral zone, Kosmos 721 obs. of relativistic electrons 80−8492
auroral zone, postmidnight electron precipitation time structure and stable trapping limit 79−101013
auroral zone current system, fluctuations rel. to geomag. pulsations 77−87188
auroral zone electric fields at 1 R_E altitude 78−57397
auroral zone electric fields rel. to interplanetary magnetic field vars. 78−77431
auroral zone magnetic field lines, electrostatic wave measurements 79−88555
auroral zone physics, review 77−17268
axisymmetric toroidal Alfven wave resonances effect of finite ionosphere conds. 79−75035
balloon and rocket programs, conf. Bournemouth, England (1980, Aug.) 80−105433
beam-plasma interaction experiment, using electron beam from JIKIKEN satellite *(Japanese)* 80−94655
Bernstein wave convective props. 80−90292
Birkeland current sheets in dayside polar region, rel. to interplanetary field 80−90289
Birkeland currents, high altitude obs. 78−36397
Birkeland currents, primary sources 80−31176
Birkeland currents, TRIAD satellite obs. 79−16755
Birkeland currents at high-latitude, suprathermal electron contrib. 80−90290
black holes, magnetosphere, charge particle trapping 78−57573
boundary layer, hydromagnetic waves driven by vel. shear 80−105133
boundary layer, plasma, energy and momentum transfer from magnetosheath to magnetosphere 77−22008
boundary layer and magnetopause layer characts., Imp 6 obs. 79−80084
boundary layer at low-latitude, fluid mech. model 80−85808
boundary layers, geometrically explicit model 78−12055
boundary observations along Imp 7 orbit, locations and wave level vars. 78−28442
bow shock, Alfven waves transmission, theory and obs. 78−45157
bow shock, backstreaming ions interaction with solar wind 80−101499
bow shock, collisionless shocks simulation and laboratory expts. 80−87893
bow shock, conference, Strasbourg, France (1978 August 31 to September 1) 80−82573
bow shock, current-driven instabilities in laminar perpendicular shock 78−77430
bow shock, DC mag. field obs. 80−90306
bow shock, electron/ion energy distrib., comparison with laboratory turbulent plasma 78−5945
bow shock, first evidence and early studies, historical introduction 80−85816
bow shock, initial ISEE mag. field obs. 80−90307
bow shock, ion acoustic stability anal. 78−81506
bow shock, ion and electron heating two stream instability 77−53320
bow shock, ion populations in upstream solar wind rel. to magnetosheath energetic ions 79−21124
bow shock, ISEE magnetic field profiles 79−58196
bow shock, kinetic models of shocks in collisionless plasmas 80−90330
bow shock, magnetopause and plasmapause, interplanetary shock waves interaction, noncoherent response method 77−64587
bow shock, model for ion thermalisation 77−25876
bow shock, modified two-stream instability, EM effects 77−70946
bow shock, nonlinear plasma processes in upstream solar wind 80−85833
bow shock, obs. of backstreaming protons in upstream solar wind 80−90309
bow shock, orientation and shape in three dimensions 79−101030
bow shock, origin of 30-100 keV protons in upstream region 79−48622
bow shock, quasi-parallel struct. correl. with Pc 3, 4 micropulsations activity 77−25870
bow shock, review of upstream energetic-particle meas. 80−90308
bow shock, satellite obs. of macroscopic struct. 80−85815
bow shock, solar wind interaction with backstreaming ions 80−90287
bow shock, solar wind upstream deceleration rel. to diffuse upstream ions origin 80−98528
bow shock, theory of magnetic shocks in collisionless plasma 80−85854

magnetosphere continued
bow shock, three-dimensional shape 80−85832
bow shock, upstream particle events obs. close to shock and 200 R_E upstream 80−77247
bow shock, upstream sheets of energetic electrons 79−75042
bow shock, upstream wave boundary determ. method *(Italian)* 78−24409
bow shock and magnetopause study by noncoherent response method 77−49230
bow shock and Pc 3-4 micropulsations, effects of interplanetary mag. field orientation and solar wind vel. 79−53672
bow shock interaction, backstreaming ions and interplanetary mag. field 80−101500
bow shock ion acceleration, upstream region obs., review 80−31168
bow shock plasma, possible generation mechanisms of low-freq. waves ($\lesssim$50 Hz) 80−90312
bow shock vicinity, low-freq. waves obs. 80−90311
bow shock-magnetopause system, interplanetary shock waves interaction 80−26712
bremsttrahlung X-rays from relativistic electron precipitation 79−75014
charged particle beam movement 78−69616
charged particle fluxes, obs. by JIKIKEN scientific satellite *(Japanese)* 80−94654
charged particle fluxes meas. on geostationary orbit 79−80082
charged particle interaction with linearly polarised MHD plane wave, first adiabatic invariant approximations 77−78580
charged particle precip. through cleft, correl. with thermospheric density 77−87146
charged particle trapping by vertices of lines of force and lateral trapping 77−91377
charged particle-beam interactions, space and laboratory plasma workshop 78−7821
charged particles, HEOS-2 meas. 78−61671
charged particles motion in one-dimens. mag. current sheets 78−65464
charged particles near bow shock, ISEE-1 ULECA obs. 79−58198
charged particles trajectory traces 79−16761
Choe-Beard model using perturbation method 77−64539
chorus, occurrence patterns and normalised freq. 77−9625
chorus generation, critical electron pitch angle anisotropy 77−2308
chorus generation by energetic electrons during substorms, theory 78−96356
chorus VLF and ELF emission, plasmapause origin model 80−41608
cleft in local summer, perturbation of upper ionosphere *(French)* 78−4022
cleft region dynamics 80−101483
closed model revived and extended 79−53668
coherent anomalous resistivity, in region of electrostatic shocks 80−4189
cold plasma densities, comparison of ULF and VLF meas. 78−28436
cold plasma diagnostics using satellite meas. of VLF signals from ground transmitters 77−49183
collisionless electrostatic drift waves, linear theory, space plasma appls. 79−1305
collisionless plasma fluid model and cosmic plasmas elec. current systems 79−84658
conf. Tokyo, Japan, 1978, AEROS and TAIYO satellite results 80−46340
conference, June 1979, Alpbach, Austria 80−36776
configuration, evidence from thermal plasma enhancements in topside ionosphere 77−9617
configuration long-term changes, implications of auroral changes during 18th and 19th centuries 80−98498
conjugate electron precipitation, high time resolution riometer and X-ray meas. 80−41666
continuous (Pc 3,4) pulsations, complex demodulation rel. to magnetosphere toroidal line resons. 80−21877
convection, influence on laser ionosphere current and wind systems 77−5386
convection, rel. to upper atmosphere dynamics 77−29525
convection, role in global scale electrodynamic coupling of ionosphere high and low latit. regions 80−77194
convection, role of hot plasma 78−32297
convection, role of particle precip. 79−25400
convection and wave-particle interactions 78−61679
convection driving force 79−8782
convection elec. field assoc. with ionospheric anomalous equatorial elec. field and interplanetary mag. field northward turning 79−70914
convection electric field, divergence rel. to auroral currents and elec. pots. and precip. generation 80−67453
convection electric field, model 78−89004
convection electric field, rel. to global distrib. of electron density in F_2-layer 77−64514
convection electric field model based on Explorer 45 obs. 79−12350
convection in polar cap, after interplanetary mag. field becomes northward 80−94658
convection intensification, effect on mid-latitude ionosphere 80−105122
convection of magnetosphere plasma affecting ionosphere electron density disturbance spatial struct. 80−41606
convection rel. fields, dynamics and interrelations with polar ionosphere struct. 80−4176
convective electric field during isolated substorm, F-region electron density and ion vel. meas. 78−65452
cosmic plasma properties from magnetospheric research, use in astrophys. 78−93051
cosmic ray intensity variations of magnetospheric origin, Sayan spectrograph data 79−84606
cosmic ray propagation, asymm. periodic oscills. in Stormer problem 77−78586
cosmic rays distrib. above 400 km altitude beneath radiation belts 78−49227
cosmic rays south-north asymmetry in high latit. magnetosphere, 1969-77 period 79−84600
coupling with ionosphere and atmosphere rel. to nighttime E-region electric fields 79−35034
current densities, evaluation from results of scalar geomag. field meas. 77−13186
current distribution quantitative modelling 78−88988
current instability on short wave drift oscills., nonlinear theory *(Russian)* 80−53981
current interruption in collisionless plasma, by non-linear electrostatic waves 79−75052
current interruption mechanism in collisionless plasma 78−42721

magnetosphere continued
current sheet, one-dimens. problem, adiabatic solns. 79−40028
current sheet in compressible plasma, self-similar resistive decay 80−1755
current system, steady state, for high-latit. mag. activity, comprehensive model 79−92636
current systems, N.polar cap mag. variations associated with interplanetary field 80−41645
current systems during magnetic storms 79−12349
cusp region, precipitation and ion convection rel. to interplanetary mag. field 80−90288
cusp region on dayside, field line topography, precipitation implications 80−85822
cusp-magnetosphere interface, EM and electrostatic emissions during substorms 79−66880
cusplike electron precipitation regions during 1977, September 19 to 21 event, DMSP-F2 obs. 79−35056
cyclotron soliton theory of Earth's kilometric radiation 80−94657
D_{st} variation asymmetry, as function of local time 80−41643
daily mag. variations meas. in Alaska, atmos. current system 80−85590
dawn magnetosheath, ISEE-1 electron spectrometer results 79−58200
day cusp dynamics, tracking via long-period geomag. pulsations obs. 79−53656
dayside, particle meas. and mag. perturb. rel. to interplanetary mag. field 79−75044
dayside cleft, mag. field perturbations rel. to interplanetary mag. field 79−40023
dayside cleft aurora, N_2^+ 3914 Å, O I 5577 and 6300 Å emissions obs. 77−2294
dayside cleft emission, Dec. 1976 obs., 6300 Å photometry 80−46332
dayside cleft plasma, Torde rocket expts. 77−60549
dayside cleft precipitating electron energy spectra from rocket flight 78−20578
dayside cleft region, photometric obs. at 6300 Å 80−41586
dayside cusp, diurnal latitude variation 78−20586
dayside cusp, field-aligned currents obs. 77−29591
dayside cusp, solar wind plasma injection 77−33288
dayside cusp proton acceleration by mag. merging at magnetopause 78−12054
dayside cusp region, plasma props. 79−12352
dayside cusp region, thermal electron densities and temps. 77−78574
dayside magnetopause, electric field topology 78−57398
dayside magnetopause, ISEE obs. of flux transfer events 79−44306
dayside magnetopause, mechanism of plasma penetration and electron escape 78−61672
dayside magnetosphere, expansions and contractions rel. to mag. flux transfer 78−96355
dayside plasmapause position, Pc 3 and 4 spectral analysis 80−56681
dayside polar cusp, ionospheric and field-aligned currents relationship 79−35058
dayside south polar cusp, field-aligned currents rel. to interplanetary mag. field 79−35059
DC electric field and ion temp. meas. using ion analyzers 79−21147
detached plasma formations, investigation by noncoherent response method *(Russian)* 77−29584
detached plasma region detect. 78−7836
detached plasma regions, wave propagation characts., instability phenomena 77−25880
discrete VLF line radiation within transmitter-induced amplification bands, satellite obs. 78−96360
distant geomagnetic tail, Pioneer 7 and 8 obs. 77−64548
distant magnetotail, lower-hybrid-drift wave turbulence 79−25399
distant plasma mantle, evidence from Pioneer 7 obs. 77−22017
disturbance, link with outer radiation belt electron intensity increase 80−77225
disturbances, rel. to troposphere. pot. gradient slow vars. and short-period pulsations 79−12188
double layers and electrostatic shocks in space, review 80−36460
downward flowing ions and ionospheric ions injection into plasma sheet 80−26694
drift boundary approximations in simple magnetospheric convection models 80−26693
drift instabilities, assoc. with particles in ring current and plasma sheet inner edge 79−12351
drift-mirror instability 77−49229
drift-mirror instability in curved mag. field 78−45145
drifting energetic protons at synchronous orbit, pitch angle dispersion meas. 78−77428
duroral zone ionospheric modification, incoherent scatter radar obs. 77−82083
dusk to dawn transient elec. field in nightside magnetosphere, possible origin 79−96863
dusk-dawn asymmetry, in magnetosphere response to interplanetary mag. field B_z component 77−2310
dynamics during auroral electrojet events, from energetic electron intensity changes at synchronous orbit 79−66882
dynamics rel. to equatorial ionosphere, effects of polar-equatorial elec. coupling 78−93029
dynamo, small scale, multiple layer model 79−53612
effect of interplanetary mag. field on geomag. activity *(Hungarian)* 79−25544
electric and mag. fields at high latits. 78−12057
electric and mag. fields rel. to magnetosphere-ionosphere coupling 79−66870
electric current fields at magnetopause and in radiation zone 79−53658
electric currents and magnetic var. induced on the ground 77−70594
electric currents in cosmic plasmas 78−12094
electric currents in hot adiabatic plasma, theory 78−89002
electric currents over auroral arc, theory 77−33296
electric double layer, electron velocity distrib. on high pot. side 80−70010
electric double layers, plasma physics 78−69898
electric field, around rot. mag. dipole 78−45141
electric field, boundary condition for Alfven waves at ionosphere 79−53611
electric field, influence on thermosphere N.Polar Cap winds 80−67445
electric field, large-scale, from VLF chorus dynamic spectrum 79−8775
electric field, mag. field and electron precip. fluctuations 78−81507
electric field, plasma density and temp., field-aligned currents, S3-3 satellite obs. 80−26699
electric field effect on charged particle drift in Mead and Mead-Williams geomag. field 79−84592
electric field from VLF burst freq. drift rate 79−92639
electric field in VLF to HF range, EXOS-B obs. 80−67478
electric field induced instability 77−70942
electric field measurements in the solar wind, bow shock, magnetosheath, magnetopause, and magnetosphere 79−40053
electric field model used to predict ionosphere plasma convection at high latitude 80−41612
electric field of a time-dependent Alfven-type neutral sheet 79−25403
electric field on disturbed days, at mid-latitude 80−77230
electric field power spectra, double probe meas., Doppler shift effects 80−26634
electric field sources and streams *(German)* 78−28453
electric field strength vector meas. problems 78−16245
electric fields, and currents, related geomag. vars., review 80−105121
electric fields, high-latit., empirical models 77−45255
electric fields, large-scale, obs. and theory 77−87208
electric fields, potential and inductive during auroras 80−21878
electric fields, quasistatic, meas. between 3-7 R_E 79−29942
electric fields, role in form. of high-latit. ionosphere 78−28370
electric fields, transmission in polar ionosphere and Equator 78−65456
electric fields absence rel. to particle entry 80−41669
electric fields and currents, origin and structure *(German)* 78−32196
electric fields and currents influence on thermospheric circulation and comp. 80−17446
electric fields effect on O_2 and O distrib. in mesosphere and thermosphere 79−66850
electric fields from phase and group path meas. of VLF whistlers 78−49234
electric fields generated by fast charged particle drift, cold plasma polarization drift effect 77−17298
electric fields in quiet plasmasphere, dynamo origin, whistler data 78−77426
electric fields of magnetospheric origin in ionosphere, simulation 80−4177
electric fields parallel to mag. field, remote sensing expt. 78−40776
electric fields parallel to mag. lines, studied by electron injection expts. 80−72702
electric fields penetration along geomag. force lines, electrostatic approach applicability 80−4178
electrical characteristics, rel. to field-aligned current sources in high-latit. ionosphere 80−72674
electrical coupling to lower atmos., quasi-static model 80−61865
electron beam injection, beam-plasma discharge at low press. and mag. field strengths 78−42769
electron beam interactions in high-latit. magnetosphere, artificial auroral streaks obs. 78−89036
electron beams, counter-streaming in stationary background, longitudinal mode instability 78−26273
electron beams, counterstreaming, at altitudes of 1 R_E over auroral zone 80−67474
electron bursts source region, distance determ. from auroral-zone X-ray microbursts power spectra 77−78556
electron cyclotron harmonic instabilities 78−77424
electron cyclotron harmonic wave instability during temp anisotropy relaxation 79−53671
electron cyclotron instabilities, multi-harmonic, theory 78−87442
electron cyclotron plasma instability, multiharmonic, numerical calc. 80−41659
electron densities and temperatures, results from Intercosmos-10 Langmuir probe expts. *(German)* 79−2469
electron densities determinatoin, whistler inversion via spectral expansion 80−8495
electron density, small scale struct. from plasma resons. on-line tracking 79−35073
electron density expt. results from ISEE 79−58210
electron density rel. to whistler dispersion 78−93050
electron distribution function, assoc. with electrostatic emissions, dayside 80−17445
electron drift echoes at geostationary orbit 78−61678
electron echoes, from conjugate regions of magnetosphere, distrib., Araks expt. *(Russian)* 79−40019
electron flux intensity rel. to form of auroral absorpt. bays 78−69619
electron flux modulations rel. to geomagnetic pulsations 78−16247
electron flux variations, in inner radiation belt 80−67470
electron fluxes at outer trapping boundary, Kosmos 426 satellite obs. 77−64530
electron intensity fluctuations meas. from Cosmos 484 satellite 80−72698
electron irregularities, field aligned, rel. to partly ducted whistlers propag. 78−65463
electron leakage, artificially stimulated, optical and VLF emission obs. 77−64549
electron plasma oscillation bursts correl. with whistlers 80−72703
electron population regions, from magnetopause to ionosphere 80−77235
electron precipitation, flux modulation rel. to pulsating aurora 78−73562
electron precipitation, inverted-V event characteristics 79−75019
electron precipitation during substorm, modulation by hydromagnetic waves 80−105113
electron precipitation equatorward boundary, Isis 1 and 2 obs. rel. to instantaneous nightside auroral oval 78−32289
electron precipitation in slot region, time persistence of features 78−28395
electron pulsations, spectral characts., Intercosmos 5 data 77−70938
electron temperature, estimation via VLF waves propagating in directions near reson. cone 77−82086
electrons, epithermal dumbbell distrib. Prognoz 7 obs. following-shock wave 80−109321
electrons, evidence for trapped flux limit from pulsating aurorae 80−72666
electrons, intense keV fluxes obs. over polar cap during poststorm quieting 77−25835
electrons, low energy, enhancements assoc. with VLF emissions 77−33285
electrons of energy 0.3-3.0 MeV, satellite obs. 80−51632
electrons pitch angle diffusion, instabilities rel. to pulsating aurora 3 Hz modulation 79−25391
electrostatic charge buildup on ATS 6 and 1976-059A 80−72744
electrostatic cyclotron harmonic instability, theory and expt. 79−29945

magnetosphere continued
electrostatic double layers, lab. expt. 79−60177
electrostatic double layers, review 78−67368
electrostatic emissions and cold plasma densities 80−26696
electrostatic field, struct. in wake of body in rarefied plasma flow 77−91402
electrostatic field due to Earth rotation 78−44771
electrostatic H^+ cyclotron waves near one Earth radius altitude in polar magnetosphere 78−45154
electrostatic ion cyclotron waves, nonlinear steepening 80−31175
electrostatic ion loss-cone waves nonlinear generation by plasma turbulence 77−41269
electrostatic ion-cyclotron instability during quiet times and auroral proton precip. 77−33256
electrostatic noise at solar wind plasma freq. beyond Earth's bow shock, mag. field-shock connection 79−70939
electrostatic shocks, as source of discrete auroral arcs 78−45153
electrostatic shocks, double layers and anomalous resistivity, definitions 78−45152
electrostatic wave excited by current pulse in warm magnetoplasma, theory 80−77240
electrostatic wave trapping at frequencies below proton plasma frequency, anal. *(Russian)* 77−78573
electrostatic waves, GEOS-1 obs., rel. to plasma parameters 79−29944
electrostatic waves capture in equatorial region 77−49235
electrostatic waves interaction with warm electrons of geomag. equator 79−70934
electrostatic waves near upper hybrid reson., free energy source 80−85805
electrostatic waves near upper hybrid reson. freq., comparison with linear instability theory 79−84590
electrostatic waves near upper hybrid resonance freq. 80−12616
ELF, VLF and LF waves obs. during large mag. storms 77−29594
ELF and VLF noise, diurnal var. observed on low-altitude satellite at latit. of Sanae 77−87181
ELF chorus, OGO 5 search coil magnetometer data anal. 77−25887
ELF chorus, substorm dependences of two types 78−28437
ELF-VLF emissions, quasi-periodic, assoc. with Pc 3.4 mag. pulsations, geomag. conjugacy 80−67475
EM cyclotron instability, effect of plasma drift 79−60150
EM instabilities in anisotropic loss-cone plasma 77−87185
EM instability in substorm mode saturation by mag. trapping 78−24412
EM ion cyclotron instability, enhancement by cold plasma, numerical-experimental investigation 77−33287
EM wave propagation, rel. to magnetosphere instabilities 77−87186
energetic electron belt form. and decay during 1974 July 4-6 mag. storm 78−69617
energetic electron environment model revision 78−61681
energetic electrons, distrib. in geomag. field 77−22006
energetic electrons, dynamics of high latit. trapping boundary during substorm 77−91374
energetic electrons, nonlinear pitch angle scatt. by coherent VLF waves 78−89011
energetic electrons characts. in boundary layer vicinity 78−89000
energetic electrons energy dispersion with progressive precip. 77−53293
energetic electrons in polar cusp and high latit. plasma sheet, source regions 80−41667
energetic electrons undisturbed trapping boundary at low altitudes 79−2441
energetic heavy ions from Jupiter, possible detect. at Skylab orbit 80−26684
energetic ions, substorm assoc. injections obs. by GEOS-1 and ATS-6 around synchronous altitude 79−35075
energetic ions expected charge states 79−80105
energetic ions of ionospheric origin in magnetosphere 79−66874
energetic particle acceleration, lab. and space expts. 77−5400
energetic particle flux meas. by International Sun-Earth Explorer A and B spacecraft 78−85799
energetic particle fluxes, modulation due to long-period geomag. oscills. 79−25407
energetic particle meas. at 6.6 R_E, electron micropulsations 79−16764
energetic particle meas. at 6.6 R_E, high-energy proton drift echoes 79−16765
energetic particle meas. at 6.6 R_E, low-energy electron anisotropies and short-term substorm predictions 79−16766
energetic particle penetration into inner magnetosphere during storms 80−72716
energetic particle precipitation, Kosmos 484 polar meas. 80−8491
energetic particle streams injection, evolution of energy spectra and pitch angle distrib. 78−45148
energetic particles investigation using Sambo programme of balloon expts. 79−80081
energetic proton bursts, simultaneous multispacecraft obs. 79−2440
energetic protons and electrons in distant magnetosheath, magnetotail and solar wind, simultaneous meas. 79−16760
energetic protons near Earth's bow shock, pitch angle distribs. 80−26683
energetics, comparison with Jovian magnetosphere 79−58201
energy flow and current systems closure, rel. to upstream solar wind parameters 78−57400
energy flow at magnetopause rel. to geomagnetic activity 78−28428
entry layer, Explorer 33 obs. 77−33290
entry layer, plasma obs. by HEOS 2 satellite 78−61669
equatorial elec. field during storm, obs. of whistlers 80−85817
equatorial electric field at L=2.3, power density 80−82146
equatorial pitch angle anisotropy in outer radiation belt, adiabatic modulation 78−89003
equatorial plasmasphere, gyroharmonic emissions induced by energetic ions 79−101009
equatorial region bays, interplanetary mag. field sector polarity influence 80−8489
equatorward auroral boundary characts. near midnight from DMSP images 79−16733
equilibrium magnetic flux distrib. in moving force tube 78−69618
ether drag theory and the reference frames of relativistic physics 80−12905
evening diffuse aurora and conjugate electron fluxes near magnetospheric equator, electron precipitation 79−101008
evening sector, proton cyclotron instability during substorms *(Russian)* 77−91378
EXOS-B, magnetospheric research satellite, instrumentation 79−48649
external transverse elec. field effects on whistlers polarization 78−28427

magnetosphere continued
fast electron intensity rel. to that in interplanetary space 77−33282
field aligned current above auroral arc, e^- and H^+ precipitation obs. 80−77215
field aligned current distribution, from S_q^P obs. in Alaska 80−85813
field-aligned auroral currents, effect on ionosphere currents and elec. fields 78−96339
field-aligned current flow during moderate geomag. activity periods 77−70943
field-aligned currents, effect on ionosphere, TRIAD obs. 79−40013
field-aligned currents, OGO 5 and Triad satellite obs. 77−33279
field-aligned currents in morning sector, rel. to auroral electrojet 77−29573
field-aligned electric currents, global distrib. of induced ionospheric fields and currents 80−109303
field-aligned selfconsistent elec. field 78−69615
field-line reconnection, static-state model 78−61677
foreshock, energies of backstreaming protons 77−5398
from spectral characts. of geomag. field vars. 77−87179
frontside boundary layer, reconnection problem 78−89010
galactic cosmic rays, inside magnetosphere, local energy spectra calc. *(Russian)* 78−16258
general study of upper atm. *(Chinese)* 79−75039
geomagnetic activity, correl. with solar wind speed long-term averages 78−32301
geomagnetic activity, cyclical nature due to interplanetary field 80−81813
geomagnetic activity, K-index 3-hr range, geophys. meaning 80−82143
geomagnetic activity indexes rel. to interplanetary magnetic field *(Russian)* 78−16249
geomagnetic activity indices, magnetospheric modulation, harmonic anal. of Km, Kn and Ks 78−40468
geomagnetic bays, rel. to auroral and geomag. activity and interplanetary mag. field in (1968) 79−53654
geomagnetic bays rel. to geomagnetic activity and 1972 interplanetary magnetic field 80−105124
geomagnetic coordinate system, high latitude station location, error determination 80−4202
geomagnetic daily variations influenced by interplanetary field 80−85591
geomagnetic diagnosis, book 78−89015
geomagnetic field disturbances produced by interplanetary mag. field B_z-component pulses 78−73583
geomagnetic field elements annual line, magnetosphere source component 79−20752
geomagnetic field fluctuations at synchronous orbit, power spectra 78−96358
geomagnetic field fluctuations at synchronous orbit, rel. to particles radial diffusion 78−96359
geomagnetic field line forced oscills. due to ionospheric cond. change 79−48623
geomagnetic field meas. from near-Earth orbit, review of obs. 80−56347
geomagnetic field reconnection with interplanetary mag. field, untenability of models 77−22007
geomagnetic field vars., correl. with solar oscills. re-examined 78−89013
geomagnetic fluctuations, high sensitivity obs. by new space-borne ring-core type magnetometer *(Japanese)* 80−94671
geomagnetic H-component regular daily var. at Alibag, solar cycle depend. 79−8593
geomagnetic indices, equivalent linear amplitude, evidence for strong artificial components 78−89008
geomagnetic indices impulse response to interplanetary mag. field 80−51622
geomagnetic induction sources, variability rel. to induction vectors local time vars. 78−85477
geomagnetic micropulsations 80−41638
geomagnetic monitoring system for International Magnetospheric Study 79−29882
geomagnetic pulsations, connections with interplantary mag. field 78−85773
geomagnetic pulsations, long-period, synchronous obs. on ATS-6 satellite and at Earth surface 79−12345
geomagnetic regular daily var., magnetospheric contrib. 77−9627
geomagnetic S_q variations field, magnetically conjugate structs. variability 79−58191
geomagnetic storm sudden commencement, uniform ionosphere transient response rel. to preliminary reverse impulse 80−8477
geomagnetic tail, distrib. of B_z 79−80091
geomagnetic tail, topology 77−53331
geomagnetic tail region, anomalous resist. 79−12353
geomagnetic transfer functions at pulsation periods 80−72417
geomagnetic variation field modeling during substorms, current system anal. 80−105130
geomagnetic variations correl. with interplanetary mag. fields 80−41642
geomagnetic variations in N. polar cap region, rel. to interplanetary field 80−41644
GEOS, dynamics response study mission 78−4072
Geos 1 and 2 satellites, keV plasma expt., magnetospheric electrons and ions distrib. 80−41695
GEOS electron beam experiment S 329 78−93075
Geos satellite, first six months' obs. 78−61705
GEOS-1 meas. of electric and magnetic wave fields and cold plasma parameters 79−48620
GEOS-1 mission, review 79−29971
GEOS-1 wave experiment 79−25444
geostationary orbit, strong electron pitch angle diffusion obs. 79−58194
geosynchronous orbit during eclipse, satellite charging 79−16792
geosynchronous plasma, analytical simulation 79−84594
geosynchronous satellite environment, ion contaminant cloud 80−72701
global morphology of light ions from ESRO-4 satellite 77−25844
gyroharmonic emissions due to energetic electrons in plasmas 79−80086
handbook, of upper atmosphere, ionosphere and magnetosphere 78−73557
Harang discontinuity and substorm injection boundary relation 78−20576
heat energy equations, time-depend., numerical soln. 80−21875
heavy ion circulation, theory 77−64533
heavy ions, origin 79−80104
hectometric and kilometric emission in August 1972, effect on solar emission obs. 77−25994
high latitude expts., conf. (Ajaccio, Corsica, 24-29 April 1978) 79−35019

magnetosphere continued
high latitude geophysical phenomena, fluctuations in temporal and spatial covariation 77−70950
high latitude proton obs. by NOAA 2 77−87198
high-energy electron drift echoes obs. by ATS 5 satellite 78−28447
high-energy particle flows in dayside magnetosphere, correl. with daytime absorpt. surges 78−73575
high-energy particle prod. and nonstationary convection 77−53312
high-energy protons produced by substorms, interplanetary conditions 80−51615
high-latit. magnetosphere, average parallel elec. field from perpendicular elec. field vars. below 8000 km 80−72706
high-latitude convection field inhomogeneities, parallel elec. fields and inverted-V precip. events 77−33297
high-latitude electrostatic turbulence, polarisation, freq. and wavelengths 78−88981
high-latitude geomagnetic variations and substorms, review 77−91381
hiss, auroral and ELF, source regions of fine struct. 77−87203
hiss emissions, VLF transmitter-induced quiet bands quantitative interpretation 79−66878
hot collisionless plasma, fluid description and limits to double-adiabatic approximation 78−75262
hot ion component of magnetospheric plasma, rel. to electron component, obs. and implications 79−80106
hydromagnetic energy spectra, depend. on solar wind vel. and interplanetary mag. field direction 80−67476
hydromagnetic oscillations coupling modes in non-uniform finite press. plasmas, rel. to geomag. pulsations 79−21108
hydromagnetic phenomena described by elec. currents 80−36495
hydromagnetic pulsations, generation by Kelvin-Helmholtz instability 78−73584
hydromagnetic wave rotation between magnetosphere and ground 80−61969
induced elec. fields in ionosphere-magnetosphere system, review 80−94647
inductive electric fields, self consistent calcs. 79−80093
inert gas precipitation, gases of solar and terrestrial origin, Skylab foil obs. 80−41653
inner radiation belt electron precipitation, meas. 80−67452
inner radiation belt proton spectra from Kosmos 721 satellite 80−72699
interaction with interplanetary shock, computer simulation 78−16243
interaction with plasma flow, review of magnetospheric studies 78−65496
International Magnetosphere Research programme, review *(Russian)* 80−17467
International Magnetospheric Study, 1976 to 1979, objectives and areas of study 79−2374
International Magnetospheric Study, data management 80−4206
International Magnetospheric Study, progress report 78−20587
International Magnetospheric Study, Satellite Situation Center 77−53197
International Magnetospheric Study (IMS) and Antarctic and Southern Hemisphere Aeronomy Year (ASHAY) 77−87210
International Magnetospheric Study and International Sun-Earth Explorer mission 78−12069
International Sun Earth Explorer 1, electron spectrometer expt. 78−85809
International Sun-Earth Explorer, three-spacecraft programme 78−28485
International Sun-Earth Explorer 1 and 2, fast plasma expt. 78−85800
International Sun-Earth Explorer (ISEE) mission, review 80−90320
International Sun-Earth Explorer A, DC and low-freq. elec. field meas. instrumentation 78−85807
International Sun-Earth Explorer A, plasma comp. expt. 78−85810
International Sun-Earth Explorer B, EGD positive ion expt. 78−85805
International Sun-Earth Explorer mission 78−61701
International Sun-Earth Explorer-1, quasi-static and low-freq. elec. fields meas. 78−85808
International Sun-Earth Explorers 1 and 2, fluxgate magnetometers 78−85804
International Sun-Earth Explorers 1 and 2, medium energy particles expt. 78−85811
interplanetary elec. field penetration, balloon meas. 78−57408
interplanetary magnetic field B_y-component interaction, magnetosphere response dusk-dawn asymmetry 78−89006
interplanetary magnetic field effects on auroral oval and plasmapause 79−80186
interplanetary magnetic field interaction, diurnal and seasonal vars. of Y-component effect on low-latit. geomag. field 80−56354
interplanetary magnetic field interaction, geomag. activity rel. to Hale sector boundary 79−75055
interplanetary magnetic fields influencing atmos. elec. currents 80−105126
interplanetary particles pitch distrib. distortion by bow shock 79−35088
interplanetary shock, negative impulse at equatorial stations in sudden storm commencement 79−16768
inverse loss cone electrons, temp. anisotropy quasi-linear relaxation due to interaction with electrostatic waves *(Russian)* 80−109314
inverted V event, scale of elec. field along mag. field, satellite obs. 80−41662
inverted V events, energetic ion obs. from ESRO 1A satellite 78−81502
ion beam experimental on Spacelab, source design 80−85840
ion beam injection from engines of proposed solar power satellites 80−82149
ion composition and origin, of high-altitude region during mag. storm 80−82144
ion composition dynamics, GEOS mass spectrometer obs. 79−35069
ion counterstreaming of O^+ and H^+ in plasmasphere 80−72700
ion cyclotron wave turbulence, nonlinear effects, lab. expt., magnetosphere appl. 80−24170
ion cyclotron waves and high-energy protons, nonlinear interaction in Earth's magnetosphere *(Russian)* 80−17444
ion exchange with solar wind 79−40050
ion flux oscillations of ultralow frequency, particle obs. 80−41657
ion heating in auroral zone, by electrostatic ion cyclotron waves 80−72686
ion mass spectrometer, satellite-borne, 0-16 keV energy range, magnetosphere appl. 77−13207
ion-cyclotron instability driven by oppositely directed proton streams 79−62690
magnetosphere continued
ion-cyclotron wave amplification for typical radial profiles of magnetospheric parameters 77−25886
ionisation ducts, detect. via JIKIKEN (EXOS-B) satellite VLF Doppler shift meas. *(Japanese)* 80−94651
ionosphere electric fields induced by ion drag and substorms 80−77199
ionosphere field-aligned currents caused by magnetosphere convection 80−90278
ionosphere-magnetosphere current system, generating Pi ULF waves 80−85819
ionosphere-magnetosphere electrodynamic interaction, during 1960, April 1, disturbance 78−28372
ionosphere-protonosphere interaction, dynamic model 77−45220
ions, ionospheric source with transverse acceleration 80−12604
IPDP pulsations, assoc. source movements 79−25404
IPDP source regions and resonant proton energies 79−53673
irregularities, formation and evolution by mag. flux tubes interchange 80−21876
ISEE-1 electric field meas. results 79−40037
JIKIKEN (EXOS-B) scientific satellite, magnetosphere obs. *(Japanese)* 80−94674
Kelvin-Helmholtz instability in magnetoplasma 79−23407
keV plasma, obs. by (GEOS-1) 79−35068
kilometric harmonic radiation generation 77−45353
kilometric radiation, spatial struct. studies 77−25873
kilometric radiation charact., initial results from JIKIKEN (EXOS-B) satellite obs. *(Japanese)* 80−94648
kilometric radiation from auroral zone, coherent nonlinear theory 80−101495
kilometric radiation from auroral zone, propagation direction 80−101497
kilometric radiation generation, inner magnetosphere auroral zone 80−105128
kinetic Alfven wave turbulence producing anomalous transport phenomena 78−57402
km radiation, satellite obs. of spectral props. 77−82084
km radiation emission from polar cusp and dayside magnetosheath 77−29597
km wavelength radn. generation by cyclotron solitary waves *(Russian)* 78−40764
laboratory and space plasmas, conference, Nagoya, Japan (1977 December 8 to 9) 80−4470
Langmuir envelope solitons in turbulent plasma 78−67334
Langmuir probe expts. on Intercosmos 10, results, rel. to VLF emissions *(German)* 77−70939
large transient electric fields, obs. 78−28440
large-scale electric field, rel. to geomag. activity and terrestrial kilometric radiation 77−87159
latitude-dependent waves and impulse-produced waves 77−49245
LF ion acoustic perturbation emission in presence of stationary whistler turbulence 77−49242
LF radiation source located at 2.5 R_E, satellite elec. field data 80−41656
lobe plasma at lunar distance 79−53666
long-period hydromagnetic waves, substorm-associated, longit. extent meas. 78−40772
longitudinal currents, dynamic processes in turbulence development 80−67469
loss cone distributions of radiation belt electrons 77−29593
low energy electrons and protons, HEOS-2 obs. 78−36407
low latitude whistler characteristics, correlation with geomagnetic activity *(Japanese)* 79−16769
low shock electron heating, high temporal resolution obs. 79−58197
low-energy plasma, obs. at synchronous orbit 78−77435
lower cleft boundary, latit. rel. to sudden commencement absorpt. events at S. pole 78−77437
macroscopic electric fields, review 78−49238
macroscopic electric fields 78−69609
magnetic curl in front of magnetosphere boundary, laboratory expts. 80−85804
magnetic current sheets, effect of press. anisotropy on equilib. struct. 79−12354
magnetic disturbances, effects on high-latit. ionospheric absorpt., riometer meas. 80−8488
magnetic field, closed lines and auroral forms 78−36356
magnetic field, quantitative models evaluation 77−9629
magnetic field aligned electric fields, mechanisms 77−9618
magnetic field line reconnection in magnetotail 79−80102
magnetic field line reconnection mechanisms in collisionless plasma 79−77352
magnetic field lines reconnection, clouds-in-cells plasma model 77−84490
magnetic field models 80−41640
magnetic field on magnetospheric boundary, determ. from laboratory simulation data 78−57396
magnetic field reconnection, current instability in reconnecting current sheets 77−37486
magnetic field variations by axisymmetrical magnetospheric current systems *(German)* 80−51609
magnetic field-aligned potential drops, prod. by electrostatic ion cyclotron turbulence 78−45155
magnetic fluctuations in magnetosheath and magnetosphere, anal. rel. to Pc pulsations reson. theory 79−80092
magnetic flux transfer, correlative study 79−101024
magnetic merging during substorms and solar flares, role of O-type neutral lines 79−53665
magnetic mirroring and auroral phenomena 77−73901
magnetic mirroring of charged particles, cause of parallel elec. fields 77−25868
magnetic noise of low-freq., generated on auroral field lines 80−101494
magnetic pulsations, 5 to 50 mHz, correl. with interplanetary mag. field rel. to generation region 77−29590
magnetic reconnection, plasma accel., heating and shock form. 78−40773
magnetic storm, 1972, August 4 to 5, rel. to flare interplanetary plasma flow hydromagnetic struct. 79−53653
magnetic storm sudden commencements, global struct. 77−56795
magnetic storms, D_{st} contrib. to aurora equatorward shift 79−75013
magnetic storms, magnetosphere rel. to positive ionospheric storms worldwide distrib. 79−44290
magnetic tail, plasma flow pulsations obs. 78−77436
magnetic-field-aligned elec. currents in cold collisionless plasma 79−1298
magnetic-field-aligned elec. fields generation mechanisms 80−77233

magnetosphere continued
magnetised, high-cond. mag. tearing 77−7527
magnetoacoustic waves, generation by high-freq. turbulence 77−13187
magnetoatmospheric instabilities, Hilbert space approach to max. growth rate 80−31172
magnetoatmospheric instabilities, max. growth rates 77−53573
magnetopause, compressible reconnection model 77−37485
magnetopause, dayside mag. merging and polar cusp geometry 79−66884
magnetopause, duskside, low-energy electrons and ions dynamics, Helios 1 and 2 obs. 79−75045
magnetopause, dynamic equilib. plasma configurations 77−5397
magnetopause, energetic electron layer, obs. along distant magnetotail 79−2443
magnetopause, energetic electron spectrum meas. from Prognoz 3 80−72697
magnetopause, energetic particle obs. and boundary motion 80−41650
magnetopause, history of understanding 78−61667
magnetopause, MHD flow, elec. field generation 78−40760
magnetopause, microstructure and plasma interactions 78−61673
magnetopause, plasma acceleration evidence for reconnection 80−26701
magnetopause, plasma wave turbulence obs. 80−51610
magnetopause, rot. simple and shock waves in anisotropic plasma 77−91369
magnetopause, symposium (Amsterdam, 7-10 September 1976) 78−57405
magnetopause, tangential component obs. 79−70930
magnetopause, tangential electric field, three-dimens. energetic ion obs. 79−40038
magnetopause, theory based on rotational shock wave 80−41641
magnetopause, three-dimensional shape 79−101029
magnetopause altitude during geomag. reversals, solar wind stagnation point calc. 77−22019
magnetopause and bow shock, ISEE obs. of energetic particles 79−40036
magnetopause and low shock, standoff distances rel. to solar sector changes 77−5134
magnetopause and magnetotail particle burst obs. 80−85820
magnetopause at dawn, plasma flow obs. by Voyager 1 80−41655
magnetopause behaviour depend. on interplanetary magnetic field, magnetosphere erosion *(Hungarian)* 77−74010
magnetopause characts. from three-dimens. energetic particle distribs. 79−53669
magnetopause configuration in two dimens. *(German)* 80−31167
magnetopause crossings at 6.6 R_E by ATS-1 77−9620
magnetopause energetic electron layer along distant magnetotail 77−53317
magnetopause form and electric field in continuum medium model 79−75041
magnetopause Kelvin-Helmholtz instability, effect of finite ion Larmor radius 79−80096
magnetopause motion during 1972 August, satellite obs. at 5.2 R_E 77−53326
magnetopause nose, structure of tangential discontinuities 78−61674
magnetopause obs., ISEE magnetometer results 79−40033
magnetopause obs., techniques and results 78−61668
magnetopause position rel. to Pc 2-4 pulsations period 77−91375
magnetopause shape and structure during 1972 August, satellite obs. at 5.2 R_E 77−53327
magnetopause shapes, general solns. 78−28443
magnetopause structure, model 77−91371
magnetopause structure, obs. and implications for mag. reconnection 79−80103
magnetopause structure from Ogo 5 obs., classical reconnection model 79−58195
magnetopause surface fluctuations, Voyager 1 obs. 80−51613
magnetopause wave-particle viscous effects, role of electrostatic flow shear instability 80−96359
magnetosheath, antisolar energy flow, Imp 7 obs. 79−80088
magnetosheath, dawnside, H^+ and He^{++} mass and energy anals. 80−4204
magnetosheath, dayside, plasma press. anisotropy and mirror instability 77−37483
magnetosheath, electrostatic turbulence meas. 79−66881
magnetosheath, energetic plasma ions obs. 79−21106
magnetosheath, form. time of isotropic particle vel. distrib. in medium with MHD turbulence 78−28420
magnetosheath, microscale mag. fluctuations during quiet conditions, probability distrib. functions 78−4053
magnetosheath, obs. of energetic electrons of magnetospheric origin and correl. with geomag. activity 79−80095
magnetosheath, obs. of energetic electrons of magnetospheric origin 80−90310
magnetosheath, plasma depletion obs. at dayside magnetopause 79−66876
magnetosheath, Prognoz 4 obs. of ≲2 MeV electrons and cold plasma 80−90296
magnetosheath, turbulence rel. to solar wind ion injections in morning auroral oval 80−98502
magnetosheath and kilometric radiation scattering at very high altitudes 79−101025
magnetosheath burst of medium nuclei, obs. from Imp 8 (1974, Feb. 16) 80−101501
magnetosheath bursts of predominantly medium nuclei, Imp 8 obs. (1974 February 16) 79−29937
magnetosheath distortion of pitch angle distribs. of solar protons 78−40768
magnetosheath plasma, props. during August 1972 77−25904
magnetosheath protons accel., generation of solar wind LF oscills 77−33310
magnetosphere, characts. at 0840-1040 hours local time, satellite obs. 80−101498
magnetosphere boundary layer, field-aligned currents theory 80−67473
magnetosphere-ionosphere electrical coupling, two-dimens. model 80−61938
magnetospheric and space plasma physics (1966-76) *(Japanese)* 78−24410
magnetotail, adiabatic particle motion in nearly drift-free mag. field 78−57399
magnetotail, av. config., Imp 6 magnetic field data 79−75048
magnetosphere continued
magnetotail, energetic electron anisotropies and magnetic field topology 77−5399
magnetotail, energetic particle activity rel. to auroral activity 80−51614
magnetotail, high-latitude proton pitch angle distrib. during 1970 April 16 solar proton event 79−53670
magnetotail, hot tenuous plasmas, fireballs and boundary layers 78−57404
magnetotail, hot tenuous plasmas, fireballs and boundary layers, comments 78−89012
magnetotail, localised induced elec. field 77−53329
magnetotail, lower-hybrid-drift instability and mag. field line reconnection 77−45254
magnetotail, mag. field rel. to solar wind rel. vars. 77−22005
magnetotail, mag. merging obs. and form. of plasma sheet 77−87189
magnetotail, mag. reconnection causing shock wave plasma accel. 80−51618
magnetotail, magnetic merging obs., appl. to solar flares 77−17301
magnetotail, neutral sheet, particle accelerations 80−72696
magnetotail, O^+ obs. 77−33284
magnetotail, obs. of hot tenuous plasmas, fireballs and boundary layers 77−29588
magnetotail, particle accel. by induced substorm electric field 77−73909
magnetotail, plasma flow during substorm 80−51616
magnetotail, plasma sheet thinning and presubstorm field changes 78−96352
magnetotail, self-consistent theory, general soln. for quiet tail with vanishing field-aligned currents 80−26689
magnetotail, substorm assoc. current changes 79−12347
magnetotail, substorm electric field effects on charged particles 78−77425
magnetotail, substorm magnetic fields, 3-dimens. analysis 78−61666
magnetotail, transient elec. field evidence from energetic proton and electron anisotropies 77−53318
magnetotail and plasma sheet, energetic electron obs. 77−53324
magnetotail assoc. phenomena at 3100 Earth radii 79−96861
magnetotail boundary large amplitude substorm motion 79−62684
magnetotail boundary processes, hot tenuous plasmas, fireballs and boundary layers 78−77438
magnetotail configuration near midnight during quiet and weakly disturbed periods, mag. field modelling 78−96354
magnetotail dynamic structure simulation by powered double probe *(Japanese)* 79−25406
magnetotail dynamics 79−80100
magnetotail fireball microstructure 77−70941
magnetotail lobe and plasma sheet, solar proton entry in 1971 April 22 event 79−101026
magnetotail lobe plasma, double-peaked ion spectra as evidence for massive ions 78−32299
magnetotail magnetic field 79−80089
magnetotail near midnight during quiet and weakly disturbed periods 78−96353
magnetotail neutral sheet southward mag. field rel. to energetic electrons distrib. and substorms 80−26695
magnetotail neutral sheet wavy profile, Imp 5 meas. 78−61665
magnetotail observing satellite GEOS-3, proposed mission 80−82163
magnetotail particle acceleration, satellite obs. 80−31170
magnetotail phenomena and auroral acceleration 80−85818
magnetotail plasma at lunar distance response to changes in interplanetary mag. field, solar wind and substorms 79−70932
magnetotail plasma flow during plasma sheet expansions, Vela 5, 6 and Imp 6 obs. 77−49240
magnetotail plasma layer structure and auroral particle dumping into ionosphere 80−109313
magnetotail plasmas, magnetic fields and magnetic reconnection 79−75049
magnetotail reconnection, expected signatures 78−96361
magnetotail stretched configuration, dynamic evolution theory 80−72719
magnetotail structure, effect of interplanetary mag. field orientation 80−105131
magnetotail structure, theories 79−80099
magnetotail substorm processes, hot tenuous plasmas, fireballs and boundary layers 78−32300
magnetotail time-depend. config. changes and plasma sheet thinning 79−35063
magnetotail transient phenomena rel. to substorms 79−80101
material charging in space environment 80−109327
measuring technique using in situ excitation of plasma resonances *(French)* 78−20529
merging with interplanetary field, half-wave rectifier response 80−72710
MF duct formation and bubble initiation 80−72712
MHD discontinuities with Hall effect 77−25899
MHD surface waves, particle accel. and auroral arcs form. 77−9621
MHD wave coupling region in plasma, rapid changes 79−75050
MHD wave energy in magnetospheric cavity, effect of geomag. latitude 77−25889
MHD wave propagation, in presence of rot. and variable mag. field 79−40024
MHD waves, as cause of simultaneous ionospheric and geomag. oscills. 77−9615
MHD waves, characteristics rel. to plasma density gradients near L=4 77−25878
MHD waves interaction with magnetopause 77−91372
MHD waves orientation 79−8783
micropulsations at magnetospheric equator, Pc 3, 4, 5 observed by geosynchronous satellite 80−41647
micropulsations near plasmapause, elec. field obs. 80−85814
micropulsations resonance structure, multiple satellite obs. 77−33289
micropulsations with long period, global electric circuit model 80−41646
microscopic plasma processes rel. to reconnection 78−61676
midlatitude convection electric fields, occurrence rel. to ring current development 78−57395
midlatitude electric fields at ionospheric heights, magnetospheric effect 79−2433
midlatitude plasmasphere, trapped photoelectrons and secondary electrons 78−69565
midnight sector, coexistence of two substorms 77−53330
midnight trapping boundary, energetic particles pitch angle distribs. 78−28445
mini-substorm and long-period Pi 2 event, 1978 December 11, Jikiken satellite obs. *(Japanese)* 80−94653

magnetosphere continued
mirroring particles, charge exchange lifetime depend. on mirror latit. 77−22009
model, based on phenomenological mag. field 80−12619
model, two-dimens., eigenvalues, magnetotail currents 79−53662
modulation of geomag. activity, harmonic anal. of am, an and as indices 79−66605
Molniya 1 satellite, radiation doses meas. 79−8774
Moon-magnetosphere interaction and possible lunar core size 79−25525
morning sector, eastward movement of auroral radio absorption events 77−56792
morphological scheme of post-storm event 79−88523
natural radio emissions, Geos I identification 78−53774
near-Earth plasma, 0 to 100 keV, quantitative models review 80−36459
near-Earth plasma sheet, mag. neutral line search, obs. at lunar distance 78−16250
near-Earth plasma sheet, search for mag. neutral line 77−25872
near-Earth radiation environment, review 79−12359
neutral current layer, cosmic ray spectrum *(Russian)* 80−4211
neutral points position in two-dimens. model 77−25865
neutral sheet, shape and posn., statistical determ. 80−72717
neutral sheet current layer, unsteady magnetic merging in one dimension 79−80090
neutral sheet effect on magnetospheric plasma 77−49243
neutral wind in upper atmosphere, rel. to magnetospheric disturbances in aurora borealis zone *(Norwegian)* 78−24399
nightside auroral km radiation origin and polarization 78−45161
nonstationary processes study via incoherent response method, phase fluctuations effects 78−45184
northern cleft, ionosonde obs. 77−29595
oblique rotator production of EM field, lowest order solns. 79−21176
open and closed models, expt. evidence 79−8771
open and closed models, exptl. proof 79−62674
open magnetic field lines near subsolar region, particle obs. 80−85810
OPEN program for investigation of origins of plasma in Earth's neighborhood 80−109318
outer, electrostatic emissions between electron gyroharmonics 79−16763
outer plasmasphere hot zone, Prognoz ion temp. meas. 77−25845
outer radiation zone struct. in simple model of convecting magnetosphere 77−25877
outer zone electrons, evidence for very weak pitch angle diffusion 78−28399
paired electrostatic shocks in polar regions, satellite obs. 77−29601
palaeomagnetosphere, third type of planetary magnetosphere during polarity reversals and geomag. excursions 78−61683
parallel electric field, signature in ion and electron distribs. in vel. space 78−89005
parallel electric fields in collisionless plasma, particle signature 78−77439
parallel electric fields signature in collisionless plasma 77−53323
particle (electric current) model 80−17442
particle acceleration in auroral magnetosphere 80−31171
particle drift absence in translationally symmetric mag. fields 79−37454
particle dynamics in low freq. EM waves, magnetosphere particle flux in inhomogeneous plasma 80−1804
particle flux instability and geomag. pulsations generation 77−49232
particle flux mapping and conjugate points calc., magnetospheric field models 79−29950
particle fluxes, modulation by Pc 5 waves, Ogo 5 obs. 77−87190
particle injection during 1974 August 18 substorms 78−28444
particle precipitation caused by monochromatic VLF signals 77−49238
particle precipitation caused by single injected whistler-mode wave 77−56797
particle radial diffusion, estimate from elec. & mag. field fluctuations 80−90293
particle trajectories at mag. neutral point 79−66886
particles pitch angle diffusion by bounce reson., theory 78−36408
Pc3 magnetic pulsations at synchronous orbit, statistical study of ATS 6 obs. 77−45256
Pc3 micropulsations, depend. of occurrence on AE index of mag. activity *(Russian)* 77−44914
Pc3 pulsations, propag. obs. 77−22004
Pc5 pulsations, model of magnetosphere and ionosphere elec. and mag. fields 80−77234
Pc 1 magnetic pulsations, statistical study at synchronous orbit 77−25875
Pc 1 pulsation signal causing horizontal propag. 80−51604
Pc 1 pulsations, relation to interplanetary plasma flow struct. 78−45142
Pc 1 pulsations generation region location, hot and cold plasma parameters estimation 79−35064
Pc 1-2 wave obs. in outer magnetosphere 80−12618
Pc 3 micropulsations, theory with orthogonal curvilinear coordinates 79−80097
Pc 3 pulsations, obs. in congugate areas around L=4 77−45260
Pc 3 to 5 nightside pulsations origin, Alfven waves excitation by bouncing electron beams 80−4203
Pc 4,5 geomagnetic pulsations generation, influence of bounce effects 80−4197
Pc 4 compressional pulsation, obs. by three satellites in geostationary orbit near local midnight 79−80094
Pc 4 pulsation event, satellite meas. of Poynting vector of standing MHD waves 78−45162
Pc 4 pulsation event in plasmasphere, meridional characts. 79−5716
Pc 5 generation mechanism in morning sector, comments 79−84595
Pc 5 giant pulsations in outer magnetosphere, HEOS-1 data survey 77−2307
Pc 5 micropulsations, examination of ionospheric reson. region by dual auroral radar system 78−65454
Pc 5 micropulsations in morning sector, generation mechanism 78−61686
Pc 5 pulsation power depend. on cond. vars. in morning sector 79−62687
Pc 5 pulsations, features during solar cycle 78−36406
Pc 5 pulsations recorded in auroral regions, Earth induction effects on vertical polarisation 79−12355
Pc 5 waves, OGO-5 obs., ground-magnetosphere correl. 77−9623
Pc micropulsations, polarization states, detection 79−74966
pearl-type pulsations, nonlinear evolution, role of proton injection processes 79−35065
periodic motions totality in meridian plane of mag. dipole 78−12052
perturbation magnetic fields and current systems associated with eastward drifting auroral structures 79−75009
magnetosphere continued
perturbations caused by mag. storms, review of obs. 80−98495
perturbed Stormer problem, long periodic solns. families 80−17440
photoelectron distrib. with interhemispheric coupling, two-stream methods 79−62669
photoelectron flux var. effects on geosynchronous spacecraft potential 79−80087
photoelectron fluxes in ionosphere and plasmasphere, solar activity effects 78−16374
physical processes and magnetospheric research, review of selected topics 78−65466
physics, advances with GEOS-1 (conference, Innsbruck, Austria, 1978) 79−35066
physics, review 79−12356
physics *(Chinese)* 80−82153
Pi3, long-period irregular mag. pulsations, reviews 78−45164
Pi 2 micropulsations, harmonics in power spectra assoc. with plasmapause 77−25885
Pi 2 pulsations, equatorial, fine struct., rel. to magnetosphere cavity reson. 80−72721
Pi 2 pulsations, initial movements arrival at conjugate stations 80−31173
Pi 2 pulsations, polarisation characts. and phase differences at conjugate stations 79−21107
Pi pulsation at high latitude, rel. to plasma convection 80−77226
pitch angle diffusion eqn. of trapped particles in presence of loss. cone, finite difference integration 79−70931
planar magnetic binaries problem, areas of motion 78−96386
planetary, magnetic field determ., by solar coronal plasma and solar wind interactions *(Dutch)* 77−67054
plasma, collisionless, stability of contact discontinuity, solar wind and magnetosphere boundary appls. 80−62002
plasma, fast proton injection, nonlinear evolution of ion cyclotron waves *(Russian)* 79−55490
plasma, interaction of knowledge from astrophysical and lab. plasmas 80−59166
plasma, lower hybrid turbulence, nonlinear LF spectrum cutoff 78−4041
plasma, MHD vortices *(Russian)* 77−80302
plasma, three-dimens. meas. by ISEE spacecraft 79−40035
plasma acceleration caused by shocks resulting from mag. reconnection 80−51618
plasma and energetic particles counterstreaming in magnetotail, satellite obs. 79−35060
plasma as energy source for space instrumentation 77−64605
plasma beam-magnetic dipole interactions, simulation expts. 77−7585
plasma condensation, diagnostics from mag. field records on geostationary satellite 79−58189
plasma convection, (U,B,K) coord. system 79−2442
plasma convection, high-latit., and ionospheric depletion, effect of displaced geomag. and geographic poles 80−26680
plasma convection, numerical simulation 79−62679
plasma convection and auroral particles energy spectra 77−49234
plasma convection behind plasmapause rel. to polar ionosphere struct. 78−40731
plasma convection in polar regions, model calcs. 80−82151
plasma convection system 80−41651
plasma density, GEOS-1 relaxation sounder meas. 79−35072
plasma density and temperature, GEOS-1 multi-expt. determ. 79−35074
plasma density sensitive instabilities 77−25879
plasma diagnostics, use of trigger VLF emission 78−45149
plasma discontinuity obs. using geostationary differential phase method during storms 78−20584
plasma drift in radial direction at nighttime, and coupling to ionosphere 80−77239
plasma dynamics, vertical displacement during substorms 80−4184
plasma dynamics problems 79−8772
plasma entry into magnetosphere, role of irregularities 80−56680
plasma experiments, magnetospheric physics simulation 79−88549
plasma flow, collisionless hydrodynamics rel. to Larmor freq. 78−69637
plasma flow, rel. to poleward-directed elec. fields near ionospheric projection of plasmapause 78−20574
plasma flux from strong flare rel. to magnetospheric disturbances 78−73600
plasma injection and diamagnetism 79−80085
plasma injection and time depend. convection electric fields 80−8494
plasma instabilities due to antiloss cone *(Russian)* 79−21105
plasma instability, reunification of mag. field in plane layer *(Russian)* 77−58860
plasma instability theory for anisotropic vel. distribs. *(Russian)* 78−12053
plasma mantle, magnetotail boundary layer obs. 78−61670
plasma mantle and ionospheric plasmas, field aligned distrib. 78−57406
plasma meas. by Prognoz-4, ions and electrons in disturbance 77−41271
plasma measurements, by International Sun-Earth Explorers 1 and 2 quadrispherical LEPEDEAS 78−85801
plasma oscills. interaction with EM waves propagating along magnetic field lines *(Russian)* 78−4036
plasma parameters, adiabatic motion in dipole mag. field in presence of longit. electrostatic fields 79−77349
plasma parameters along satellite trajectories 80−8490
plasma phsyics, book 79−84696
plasma physics, appl. to interstellar clouds and star form. 78−73744
plasma physics, book 79−84625
plasma physics, global problems and soln. 78−20588
plasma populations, in simple open model 80−90295
plasma sheet, adiabatic accel. of ions induced by convection 78−88997
plasma sheet, cause of thinning during magnetospheric substorms 80−72705
plasma sheet, electrostatic shock waves model rel. to auroral electron precip. 77−9616
plasma sheet, form. resulting from plasma mantle dynamics 79−40022
plasma sheet, interactions with lunar surface at Apollo 14 site 77−2354
plasma sheet, magnetised plasma slow convection theory 80−109312
plasma sheet, near-Earth, search for mag. neutral line from Imp 6 mag. field obs. 78−89007
plasma sheet, particle dynamics 79−66879
plasma sheet, plasma flows rel. to discrete auroras occurrence and lifetimes 80−67447
plasma sheet, press. anisotropies meas. 78−89009
plasma sheet, quiet time, precip. rel. to steady state aurora 79−40000
plasma sheet and daytime polar cusp dynamics rel. to solar flare proton intensity north-south asymm. 77−17297

magnetosphere continued
plasma sheet boundary, energetic protons 79−35062
plasma sheet dynamics, satellite obs. 80−26687
plasma sheet dynamics, variability assoc. with substorms 80−98518
plasma sheet dynamics and mag. storms, conceptual model 80−77236
plasma sheet mag. neutral line, IMP 6 obs. 77−53325
plasma sheet modes rel. to Pi 2 pulsations 79−66875
plasma sheet origin of electrons precipitating in assoc. with diffuse aurora 80−41614
plasma sheet outer boundary, particle struct. obs. 80−41654
plasma sheet outer boundary, satellite meas. and field-line mapping during substorms 78−88990
plasma sheet thinning, one-dimensional model 77−78579
plasma sheet thinnings, plasma flow 78−28432
plasma simulation expts., similarity laws 80−46347
plasma stability during storm conditions, Alfven waves and drift modes 80−82150
plasma trough, stable pancake distribs. of low energy electrons 79−70933
plasma trough of dayside, warm plasma obs. at geosynchronous orbit 80−51611
plasma turbulence information from ground-based data 79−62676
plasma two-dimensional inertial turbulence evidence from elec. field spectra 78−36399
plasma vortices, satellite meas. 79−40021
plasma waves, in distant magnetotail 77−29592
plasma waves, investigation by International Sun-Earth Explorer 1 and 2 78−85802
plasma waves, ISEE-1 and -2 results 79−58199
plasma waves, obs. during JIKIKEN (EXOS-B) satellite initial phase *(Japanese)* 80−94675
plasma waves, review 78−28451
plasma waves, stimulated, in magnetosphere, JIKIKEN (EXOS-B) satellite expts. *(Japanese)* 80−94649
plasmapause, 1-30 Hz waves generation by reson. electron instability 78−49235
plasmapause, correlated electron precipitation and magnetic IPDP events 78−28388
plasmapause, drift wave analysis 78−61650
plasmapause, drift waves 78−40748
plasmapause, electron density profile meas. stimulated plasma wave results *(Japanese)* 80−94650
plasmapause, energetic particle precip. causing auroral patches 77−33241
plasmapause, generation of Pc 1 pulsations 77−87200
plasmapause, ion comp. from VLF hiss obs. *(Japanese)* 77−21999
plasmapause, ion cyclotron waves rel. to proton precip. and stable auroral red arc form. 78−49197
plasmapause, low-altitude proton distrib. 79−21092
plasmapause, position obs. by (Explorer 45) 77−53285
plasmapause, radio sounding by geostationary satellite *(Japanese)* 78−85770
plasmapause, rel. to Pc 3 pulsations spatial distrib. at Earth surface 79−53659
plasmapause, shocks and solitons 77−25840
plasmapause, spectra peculiarities of VLF emission 77−25852
plasmapause, spontaneous polarization of a turbulent magnetized plasma 80−19580
plasmapause, surface waves rel. to topside ionosphere ELF emission pulsations and geomag. SPP 79−58157
plasmapause, transport eqns. for low speed thermal proton flows 79−44304
plasmapause, VLF ground based obs. 77−25851
plasmapause, whistlers and VLF noise propag. 78−40749
plasmapause afternoon sector, simultaneous ULF and strong riometer absorption events 77−25849
plasmapause and BDI positions during magnetic storm of 1972, Feb. 13-17th 80−56666
plasmapause as plasma sheath, min. thickness 77−25842
plasmapause crossing by JIKIKEN (EXOS-B) satellite, detect. by VLF Doppler shift crossing *(Japanese)* 80−94651
plasmapause electric field variation from pulsation-pearl method, effect of substorm phases 77−25848
plasmapause location and H^+ density decreases, correl. 78−81500
plasmapause location from Oreol 2 data 80−8473
plasmapause location rel. to HF backscatter curtains 79−58165
plasmapause location rel. to Pc 1 propagation paths and whistler obs. 77−9604
plasmapause physics, conf., Grenoble, 1975, Aug. 77−25838
plasmapause props. and struct. rel. to micropulsations 77−25846
plasmapause region, Pc 3 pulsations space-time distrib. 77−49237
plasmapause signatures in ionosphere and magnetosphere 78−57391
plasmapause sounding from geostationary satellite, feasibility 78−93043
plasmapause steady state positions from McIlwain's electric field models 77−25839
plasmas, new concept for EM and electrostatic waves detect. 77−9549
plasmas, thermal and suprathermal, obs. by GEOS-1 S-302 expt. 79−35070
plasmasphere, 500-3500 km attitude region, electron density and temp., dawn and dusk sectors 78−32293
plasmasphere, as source of PC 1 pearl pulsations in equatorial India 79−25405
plasmasphere, characteristic size determ. from solar wind meas. 77−49224
plasmasphere, cold plasma density 79−101010
plasmasphere, columnar electron content 77−60533
plasmasphere, corotation electric field 77−25841
plasmasphere, cyclotron instability, mag. field longit. inhomogeneity effect *(Russian)* 77−3929
plasmasphere, diffusion of monoenergetic photoelectron fluxes 79−75018
plasmasphere, dynamo electric field aligned currents theory 78−81499
plasmasphere, electron content and scintillations, deduced from study of ATS-6 radio beacon signals *(French)* 79−58184
plasmasphere, electron density and temp. latit. vars. 78−28383
plasmasphere, electron precip. and LF noise emissions during mag. storm. 79−80069
plasmasphere, electron temp. and conc. at 3000 km altitude, ISIS-1 meas. 79−101004
plasmasphere, fluxes and spectra of Auger electrons and photoelectrons 78−45094
plasmasphere, gyroresonance interactions 77−25850
magnetosphere continued
plasmasphere, horiz. inhomogeneities, whistler obs. 80−4168
plasmasphere, ion cyclotron waves, Hawkeye 1 obs. 77−70928
plasmasphere, lower ionosphere effect on MHD modes 79−35055
plasmasphere, mag. field effects on plasma density distrib. 77−17288
plasmasphere, magnetospheric and ionospheric elec. field simultaneous obs. 80−105110
plasmasphere, material motion rel. to generation of ionospheric current and wind systems 77−13161
plasmasphere, mid-latit., He ions behaviour 80−41630
plasmasphere, mid-latitude, nighttime electron content, geophysical disturbance effects, 1974 August to November 80−94642
plasmasphere, midlatit., plasma energy balance eqns., analytical soln. 77−17287
plasmasphere, midlatitude, mathematical model of photoelectron fluxes 77−67009
plasmasphere, midlatitude thermal plasma affected by quiet time EM drifts 80−85807
plasmasphere, nightside, substorm elec. fields detect. by whistler obs. 79−40009
plasmasphere, nonlinear attenuation of geomagnetic pulsations on bounce resonances 79−62681
plasmasphere, outlying struct. from whistler obs. 77−2304
plasmasphere, parameter determ. from geomagnetic pulsation amplitudes 77−25847
plasmasphere, parameters of energetic electron distrib. function 78−4035
plasmasphere, photoelectron flux buildup 78−40745
plasmasphere, slant total electron content temporal vars. rel. to ring current intensity and plasmapause 78−28404
plasmasphere, total electron content, ATS-6 radio beacon expt. meas. 77−2303
plasmasphere, unducted VLF energy from tropical lightning and effects 77−21980
plasmasphere, wave-particle interactions, ELF-HF obs. from EXOS-B 80−67467
plasmasphere asymmetry in noon-midnight direction from Prognoz satellites 77−25843
plasmasphere composition and density, equilib. model 79−66860
plasmasphere convection patterns observed simultaneously from two ground stations, from whistler data 79−62673
plasmasphere deformations, dynamical interpretation of OGO-5 obs. 78−81501
plasmasphere effects of localised sources on quiet time electron precip. 77−87157
plasmasphere electron content, magnetic storm effect 78−36403
plasmasphere electron content, solar wind influences during magnetic storms 79−16767
plasmasphere electron density, whistler data on solar cycle, annual and diurnal vars. 78−88985
plasmasphere of Earth, review 79−12329
plasmasphere origin, dimensions and particle precip. 78−69584
plasmasphere response to quiet mag. conditions onset, plasma convection patterns 77−45244
plasmasphere struct. from geomagnetic pulsation data 77−45257
plasmasphere structure from whistler records at Belsk, Poland 78−20581
plasmasphere-ionosphere total electron content meas. by SHF differential phase shift method 78−36304
polar, magnetotail lobe and interplanetary low energy electrons, satellite obs. 78−73587
polar cap, discrete EM emissions obs. in 0.1 to 1 Hz range 77−25862
polar cap, mag. field perturbations compared to solar electron profile 80−72718
polar cap, variable period micropulsations, props. and generation mechanism 77−25863
polar cap and DP11-variations 79−62677
polar cap current system rel. to B_y component of IMF 79−101023
polar cap electric field structures with a northward interplanetary magnetic field 79−44305
polar cap electron acceleration regions rel. to interplanetary mag. field direction 80−26698
polar cap electron fluxes, electron trapping and energization on open field lines 78−28441
polar cap plasma flow entry region, longit. position 80−67472
polar cleft, position and motion rel. to F-lacunae distrib. and occurrence freq. 80−4193
polar cusp, field-aligned currents, convection elec. fields and ULF-ELF waves 79−75043
polar cusp, Hawkeye 1 plasma wave obs. 78−77422
polar cusp, low altitude, correlated elec. field and low-energy electron meas. 78−40770
polar cusp, low-freq. pulsations possible generation mechanism 79−53657
polar cusp, movements from dayside aurora rel. to substorm currents and dayside merging 79−96852
polar cusp, plasma waves and instabilities 78−12058
polar cusp dynamics from data on electrons with energy >40 keV and protons with energy <65 keV 77−17295
polar cusp electrons at noon meridian, energisation 78−77434
polar cusp plasma, feedback stabilisation of drift-cyclotron instability 78−7838
polar field-aligned currents, ionosphere elec. fields prod. 78−65455
polar magnetic substorm development, two-dimensional magnetometer array study 77−91368
polar magnetopause, energetic and relativistic electrons obs. 77−70945
polar region, VLF noise generation by electron beams 78−4039
polar regions, adiabatic potential transitions properties 79−5713
polar regions, small-scale transverse magnetic disturbances 78−77423
polar substorms, equatorial-auroral ionosphere coupling 78−32291
polar wind morphology in mag. quiet conditions 80−72713
probing via impulsive plasma accelerators, tests under cosmic conditions 77−53399
proportional counter, with thin mica windows, for low-energy particles 80−109260
proton fluxes during 1978 February, Geostationary Meteorological Satellite (GMS) obs. 79−75056
proton ring current, precip. rel. to auroral E-region form. 78−45088
proton-cyclotron harmonics, instability due to anti-loss cone proton distribs. 80−56678
proton-cyclotron instabilities, in non-uniform loss-cone magnetospheric plasma 80−90286
protonosphere, electron content meas. from American and European sectors 78−45151

magnetosphere continued
protonosphere, induced proton flow into collapsing post-sunset ionosphere 78−49222
protonosphere plasma densities and fluxes rel. to quiet night ionosphere decay rates 78−81493
protonosphere-F-region nighttime proton fluxes 78−93034
protonosphere-ionosphere, plasma fluxes, ATS-6 obs. 78−28409
protonosphere-ionosphere coupling, postsunset obs. with Arecibo radar 79−70915
protonosphere-ionosphere thermal plasma flow, convection elec. field effects 79−62672
protonospheric replenishment after geomagnetic storm 78−28452
protons trapped in geomagnetic field, dynamics 79−16756
pulsar magnetosphere model, cylindircal, with particle inertia but no dissipative forces 80−51796
pulsar magnetosphere numerical modelling 77−29871
quadrupole shape 80−101492
quasi-parallel, quasi-laminar bow shock, field and particle data 77−37484
quiet auroral arcs, feedback instability in ionosphere-magnetosphere system 78−57379
quiet dayside cusp, AE-C and -D low-energy particle obs. 78−28390
quiet magnetotail, self-consistent theory in three dimensions 77−33286
quiet-time Pc 5 pulsation events (Spacequakes), origin in outer magnetosphere 79−40025
quiet-time plasma irregularities at 1400 km in cleft region 78−88995
radar observation method, meas. of auroral zone elec. field 80−51573
outer radiation belt, maximum fluxes of electrons with E>1 MeV (1958-1971) 80−61968
radiation belt electrons, struct. of loss cone 78−40774
radiation belts, effects of man-made VLF waves 78−45150
radiation belts, high-energy electrons behaviour during reson. interaction with geomag. pulsations 78−28422
radiation dose meas. by Molniya satellites, 1965-71 period 78−96350
radiation environment of space vehicles electronic components, laboratory simulation 80−94689
radio waves, obs. during JIKIKEN (EXOS-B) satellite initial phase *(Japanese)* 80−94675
random EM wave field in magnetoplasma, anal. of six component meas. 79−27782
rapidly rotating magnetosphere, interchange stability 77−17423
reconnection, substorms and energetic particle acceleration 80−31169
reconnection models, criticism 78−49233
relativistic electron precip. spikes at midlatits. 77−29599
relativistic electron precipitation and resonance with ion cyclotron waves 79−8758
relativistic electrons interaction with Alfven waves *(Russian)* 78−49229
resonance electrons beam, cyclotron interaction with VLF wave packet 79−53652
response to interplanetary mag. field changes, substorms 78−4038
reverse polarity field-aligned currents at high latit. 77−53322
RF emission, in electron beam-plasma and beam-beam interactions 78−45137
ring current, asymmetric, vars. rel. to elec. currents prod. in high-latit. ionosphere 77−21971
ring current, energetic particles as source of low-latit. E-region ionisation 78−77415
ring current, growth rel. to interplanetary quantity ε 79−75057
ring current, localised compressional MHD waves 77−64543
ring current, particle injections and pulsations of decreasing period rel. to D_{st} vars. field 79−53655
ring current, protons precip. rel. to auroral E-layer seasonal vars. 79−8746
ring current, quiet-time, obs. concerning relationship to ionosphere electron temps. at trough latits. 79−101015
ring current, rel. to D_{st} index annual and daily vars. 78−96351
ring current, rel. to geomag. field aperiodic var. during sporadic mag. storm 77−67012
ring current, search for He ions during mag. storm recovery phase 77−70947
ring current and antiloss cone drift instability 77−22016
ring current comp. and dynamics during 1977 December 11 mag. storm, ISEE-1 obs. 79−84589
ring current composition change from equatorial aurora obs. 78−36401
ring current consisting of He ions during mag. storm recovery phase 77−22014
ring current decay inconsistencies with proton charge exchange, evidence for He ions 77−22015
ring current during quiet field variability, mid-latitude 80−72714
ring current electron trajectories associated with VLF emissions 79−2444
ring current growth, axially symmetric model 79−40030
ring current growth during mag. storm main phase, time-dependent soln. 77−60545
ring current ion composition at L>4, Prognoz-7 obs. 80−98517
ring current ions, charge exchange lifetimes 79−25409
ring current ions, low and high altitude obs. during mag. storm recovery phase 77−70948
ring current ions, pitch angle depend. of charge exchange lifetime 77−56796
ring current ions and 1 to 30 Hz waves simultaneous equatorial obs. 77−22012
ring current magnetic field at magnetically quiet geomagnetic equator 80−105123
ring current magnetic field characts., spherical harmonic analysis 80−101493
ring current of magnetic storm, origin by inward displacement of trapped particles 80−72708
ring current particles, Injun 5 obs. during major mag. storm 78−88987
ring current particles ionic identification 77−22013
ring current plasma injection, correl. with solar wind parameters 78−96363
ring current proton interaction with electron cyclotron emissions 77−25853
ring current proton precipitation, energy depend. 77−78565
ring current proton ULF waves propag. direction, ATS 6 obs. at 6.6 R_E 77−64536
ring current protons asymmetric injection during 1974 July 6 mag. storm 78−45144
ring current protons dynamics during 1974 January 25 mag. storm 79−80083
magnetosphere continued
ring current radii determ. from cosmic ray data during mag. storm 79−62685
ring current region, Post-Rosenbluth quasilinear diffusion coeff. 78−36404
ring current rel. to VLF noise storms 77−91376
ring current unstable waves, role of charge exchange 77−49225
S_q variation, magnetosphere or ionosphere dynamo? 80−109090
S polar cusp, low energy electrons obs. by AE-C during 1977, September 21 geomag. storm 79−35076
satellite measurements, results from ISEE-1 and ISEE-2 79−29935
satellite plasma sheaths, streaming instabilities, elec. equilib., one-dimens. particle simulation 77−22036
search for interplanetary quantity controlling development of magnetospheric storms, review 80−17447
SEPAC for ionosphere and magnetosphere studies from Space Shuttle/Spacelab 77−73925
shear instability: auroral arc deformation and anomalous momentum transport 78−77433
shielding of atmosphere and evolution of life 80−104883
shock wave formation in magnetosheath due to SSC 78−45147
simulation studies of space 79−58217
slot electron precipitation, induced by VLF transmissions 78−32296
solar cosmic-ray fluxes in high-latit. magnetosphere, isotropic diffusion model calc. 77−64531
solar energetic protons, auroral zone precip. assoc. with storm sudden commencements 77−82081
solar proton albedo neutron flux north-south asymm. meas. 79−75061
solar proton event, 1970, April 16, features in interplanetary space and magnetosheath 77−87215
solar proton penetration, influence of magnetosheath 78−20583
solar protons, 1970, April 16, pitch angle distribs. transform. from solar wind into magnetosheath 77−87216
solar protons, flare-time asymmetry and anisotropy 77−33280
solar protons, struct. of fluxes in high-latit. magnetosphere in April (1972) 77−64532
solar protons in polar regions (August 1970) 78−16256
solar pulsation with 2^h40^m period, possible magnetospheric origin 78−7961
solar terrestrial physics, symposium, Innsbruck, (May to June 1978) 79−58278
solar wind, impulsive penetration of filamentary plasma elements 77−78581
solar wind compression, rel. to solar cycle var. in geomag. external spherical harmonic coeffs. 80−85592
solar wind dynamo, energy coupling function 79−96860
solar wind energy absorption, rel. to upper atmosphere heating 77−37471
solar wind flow around magnetosphere, peculiarities rel. to magnetopause position 78−49236
solar wind interaction, Chapman-Ferraro image method graphs correction 80−12620
solar wind interaction, effects of solar wind EM field 78−28419
solar wind interaction, model, MHD eqns. 79−53663
solar wind interaction, passage of low-freq. wave packet across stand-off shock front 78−45138
solar wind interaction, time-dependent global simulation 78−88991
solar wind interaction instabilities 78−5888
solar wind irregularities impulsive penetration into magnetosphere by interplanetary mag. field direction 79−29939
solar wind penetration, nonstationary model *(French)* 78−88989
solar wind plasma injection at dayside magnetospheric cusp 78−40775
solar wind plasma penetration of magnetopause 78−61675
solar wind variations during August 1972, magnetosphere response 77−25888
solar wind-magnetosphere dynamo, energy coupling function and substorms 80−105134
solar wind-magnetosphere dynamo affected by IMF vector 80−85824
solar wind-magnetosphere energy coupling, geomag. disturbances 80−85821
solar-terrestrial energy orders of magnitude *(German)* 77−70940
South Atlantic Anomaly spatial shift 78−28449
Space Experiments with Particle Accelerators (SEPAC), program for first Spacelab mission 79−48650
space simulation plasma chamber, elec. field meas. with double probes, atm. appl. 79−64909
spacecraft, charge neutralisation via electron emitter *(Japanese)* 80−94673
spacecraft charging by magnetospheric plasmas, effects, counter measures 77−22035
stationary frozen-in coordinate system 78−40761
stationary turbulence regions and anomalous resist. in magnetosphere plasma 80−38649
storm-time magnetic field changes, ionospheric-magnetospheric contribs. 80−12612
Stormer problem, effect of perturbation on periodic solns. 78−20582
Stormer problem, numerical determ. of asymmetric periodic solns. 77−49270
Stormer problem, periodic motions in mag. dipole meridian plane 78−85841
Stormer problem, periodic motions in mag. dipole meridian plane 78−89053
stormtime Pc 5 pulsations, obs. at synchronous orbit, correl. with partial ring current 78−45163
stratified compressible atmosphere with shear MHD wave-energy flux 78−93053
stratosphere-ionosphere-magnetosphere coupling at midlatitudes, 1969-74, southern hemisphere 77−9471
strong Langmuir turbulence as source of km-wide RF radiation *(Russian)* 77−9630
structure and stability properties 78−77440
structure from space obs., review 77−45253
subsatellites launched from Spacelab, for atm., magnetospheric and plasma physics research 77−21944
subsolar magnetopause, ISEE plasma obs. 79−40034
substorm, definition of phenomena 80−82145
substorm, DP_{11} and DP_{12} current systems at midlatit. conjugate points 77−29582
substorm, energy transfer 79−12343
substorm, ionospheric disturbance, location and development study 80−4185

magnetosphere continued
substorm, onset model 79−29938
substorm activity and assoc. VLF emissions near plasmapause 77−45258
substorm and auroral activity, development after southward turning of interplanetary mag. field 78−28435
substorm associated electrons, satellites simultaneous obs., dawn-dusk elec. field calc. 77−33292
substorm associated field-aligned currents large-scale characts. 78−45156
substorm associated particle fluxes, vars. at L=6 to 8 obs. by (GEOS-1) 79−35067
substorm development and Pi 2 pulsations parameters var. 77−25864
substorm electric fields in plasmasphere, model based on whistler data 80−41661
substorm inhomogeneities affected by ionosphere, experimental verification proposed 80−4199
substorm physics, book 77−33298
substorm related electron and proton bursts over polar cap 77−91380
substorm sequences, unified phenomenological model 78−77432
substorms, 1970, March 6, plasma sheet thinning and interplanetary mag. field polarity 77−25874
substorms, Akasofu parameter interpretation 79−75053
substorms, assoc. three-dimens. current system modelling 77−56793
substorms, assoc. with relativistic electron precip. events 77−25827
substorms, comprehensive model current system for high-latit. mag. activity 79−92640
substorms, dayside aurora response 77−87148
substorms, ground magnetogram timing of onset 79−88553
substorms, Imp 6 meas. of particle entry in distant polar cusp 79−2439
substorms, impulsive flux transfer events, theory 77−17495
substorms, ionosphere elec. fields determ. from Doppler sounding 80−4169
substorms, magnetic energy conversion 80−56682
substorms, magnetosphere global fine structural forms. development 79−58190
substorms, multiple satellite studies of plasma sheet radial dynamics 77−25871
substorms, multiple-satellite studies of polar mag. substorms and convection bays 78−45159
substorms, onset and intensification, Pi 2 micropulsations as indicators 79−88552
substorms, onset identification via Pi 2 mag. pulsation 77−9626
substorms, onset in magnetotail 79−88554
substorms, plasma sheet recovery and auroral zone poleward leaps 79−25401
substorms, radiation belt energetic electron precip., natural depletion mechanism for stratospheric O_3 77−41134
substorms, relation to interplanetary mag. field, model 77−29587
substorms, role of ionosphere, field-aligned currents generation 78−88998
substorms, similarities and differences with solar flares 77−17477
substorms, statistical mag. signature 78−49237
substorms, trapped particle outer boundary motion, obs. at synchronous orbit 77−29586
substorms, ULF mag. vars. assoc. with ionospheric cond. changes 78−88994
substorms 78−69613
substorms and Pi 2 pulsations assoc. mechanism 77−22018
substorms and solar flares, similar plasma processes 80−41671
substorms assoc. with interplanetary energy flux 79−48636
substorms at night, ionospheric effects 79−62656
substorms correl. with terrestrial kilometric radiation 78−28450
substorms effect on plasma sheet oscills 77−17296
substorms rel. to interplanetary magnetic field orientation changes 78−28478
substorms rel. to solar plasma clouds and streams 77−87207
substorms triggering by solar wind discontinuities 77−29596
synchronous orbit low energy ion flux, pitch angle distrib. 80−85812
synchronous orbit magnetosphere behaviour during nighttime substorm 80−85811
tail, explosive tearing mode reconnection 78−88992
tail, intense oscills., modulation instability at lower hybrid reson., strongly turbulent plasma *(Russian)* 78−59563
tail, interplanetary mag. field interaction, Alfven pulse-excited instability *(Russian)* 80−1768
tail dynamics and viscous drag/magnetic merging combination 79−84593
tail plasma sheet, adiabatic plasma convection 79−25408
tail region mag. field configuration, obs. 80−41649
tangential magnetopause structure, unified kinetic model 80−41652
tearing structures in equilib. current sheet 79−48621
test particle in mag. field, pot. 80−106872
thermosphere, dynamics at high latits., magnetospheric convection effects 79−8733
three-parameter, two-dimensional model 77−49228
three-parameter two-dimensional model, configurations with least energy 77−91370
tidal effects of Sun and Moon 77−87184
topology during 1971 December 14 to 21 solar-terrestrial event, rel. to polar cap 6300 Å emission 79−75012
transport of dissipating photoelectrons 78−69611
transverse electric fields rel. to field aligned currents, model 78−77397
transverse electrical conductivity 77−49227
trapped electroncs dynamics in auroral zone during substorm 78−40767
trapped energetic particle spectra, effect of injection location 80−72711
trapped particles, self-consistent diffusion on bounce-drift reson. with geomag. pulsations 79−58188
trapped photoelectrons and secondary electrons in mid-latitude plasmasphere 78−16244
trapping boundary at midnight, sharply defined L depend. energy threshold for anisotropy 80−41649
trapping of particles at 90° pitch angle for very long times 80−72709
turbulence characts. from Pi 2 pulsations attenuation along meridional profile 78−28426
turbulent diffusion regimes along the pitch angle in a geomagnetic trap *(Russian)* 79−55534
turbulent plasma, conductivity anisotropy and effects 77−13182
turbulent regions, rel. to ULF elec. field fluctuations in dayside auroral oval 80−98505
two-sheet configuration model, reconnection of lines of force 78−45140
ULF activity in Pc 3-4 range, correl. with interplanetary mag. field radial orientation 78−28434
magnetosphere continued
ULF oscillation of ion flux during Pc 4, 5, ATS 6 obs. 80−72707
ULF plasma waves, high latit. ground based obs. 78−49228
ULF wave growth rates, effects of trapped particle bounce resonances 77−64544
ULF waves analysis, techniques using spectral matrix 77−13137
ULF waves obs. with mag. and elec. sensors on GEOS-1 79−25410
upstreaming energetic ions and electrostatic H^+ cyclotron waves 80−51620
upward flowing energetic ions of ionospheric origin, latit., diurnal and altitudinal distribs. 78−49199
V-shock, electron accel. mechanism for discrete aurora 79−8737
vertical electric currents, rel. to polar ionosphere current systems computation 78−45090
VLF and magnetosphere structure, magnetic storms 80−72724
VLF chorus, evidence for excitation by electrical power transmission lines 77−78572
VLF coherent waves stimulated growth 77−33291
VLF echoes excited by Isis 2 HF transmitter, theory of electrostatic wave excitation 80−77240
VLF emissions rel. to auroral X-ray bremmstrahlung 78−45106
VLF hiss emissions, simultaneous obs. at Brorfelde, Chambon-la-Foret and Moshiri 78−81509
VLF hiss generated by suprathermal electrons 77−22010
VLF injected wave obs. by Explorer 45 and Imp 6 77−53321
VLF noise event observed at Sakushima (1978 September 29) 79−101031
VLF noise intensity, modulation by hydromagnetic oscills. 78−45139
VLF plasma waves, obs. and comparison with high energy electron flux by EXOS-B satellite *(Japanese)* 80−94652
VLF saucer source region 80−41664
VLF wave activity, Sunday decreases 79−66883
VLF wave events at L=4 correl. to optical emission 80−101468
VLF wave measurement at ground station, antenna pickup for vertical elec. field 80−105063
VLF waves, nonlinear effects on magnetosphere/ionosphere plasma *(Russian)* 78−32287
VLF waves triggered by natural whistlers 80−98521
wave coupling across contact discontinuity in collisionless plasma 79−8780
wave-particle interactions satellite research review, Ariel 3, 4, Geos, ISEE satellites appl. 80−90317
weak global magnetic disturbances, characts. and origin 79−53660
whistler duct obs. by ISIS satellites 77−22020
whistler ducts in outer plasmasphere, form. 78−57407
whistler extrapolation, comparison of systematic errors in different methods 77−53334
whistler extrapolation via linear-Q anal. and extrapolation factor, systematic errors 77−53333
whistler instability in anti-loss-cone plasma 77−64545
whistler sonograms, anal. of quasiperiodic struct. 77−53316
whistler stationary turbulence stability and evolution 77−45259
whistler wave-electron beam nonlinear interaction, computer simulation 77−3938
whistlers, meas. via remote unmanned ELF/VLF goniometer receiver in Antarctica 80−21854
whistlers, source regions of fine struct. 77−87203
X-ray K-shell emission at satellite altitude from proton precipitation 78−61641
X-rays from magnetospheric electrons, rocket-borne, astronomy affected 78−61640
Ba plasma injection, via front-end electroreactive accelerators 77−53400
H^+, O^+, conc. meas., Aureole 2 satellite mass spectrometer obs. 78−53766
He^+, He^{2+}, nonadiabatic behaviour during quiet time conditions, theory and obs. 78−45158
He^{2+} and O^{2+} ions of terrestrial origin, discovery in outer magnetosphere 78−32295
O ions, energetic, in radiation belts, charge states theory 78−77427
O^+ energetic ions precip. during mag. storms and magnetosphere-thermosphere coupling 80−26665

magnetospheric electromagnetic wave propagation
6.6 kHz transmission, linear and nonlinear amplification in magnetosphere 78−40771
atmospherics, sweepers modulation struct. in HF and VHF bands 79−5707
atmospherics propagation, simultaneous obs. made in Japan and Thailand 80−98520
ATS-6 radio beacon data, rel. to geophysical disturbance effects on mid-latit. plasmasphere nighttime electron content 80−94642
auroral absorption substorm, onset obs. 78−96362
auroral electron beam, assoc. EM radiation bursts during substorms 79−88557
auroral kilometric radiation coherent generation by nonlinear beatings between electrostatic waves 80−26691
auroral kilometric radiation correl. with inverted-V electron precip. 80−26692
auto and cross-correlation analysis techniques on-board spacecraft *(French)* 79−70925
chorus and power line harmonics 79−101028
circumterrestrial plasma faraday inverse effect *(Russian)* 80−4190
coherent VLF signal injection into magnetosphere, threshold power for growth 80−101496
coherent VLF waves, nonlinear pitch angle scatt. of energetic electrons 78−89011
cosmic noise absorption during substorms 80−72727
CW whistler, influence on magnetospheric noise 77−82087
discrete EM emissions obs. in 0.1 to 1 Hz range in polar cap 77−25862
ducted whistler mode signals, Pc 4-5 pulsation effects on Doppler shift 78−4040
echo induced suppression of coherent VLF transmitter signals 77−87191
electron-coherent whistler wave interaction, rel. to precipitation 80−46349
ELF, VLF and LF waves obs. during large mag. storms 77−29594
ELF emissions, geographic control search 80−12615
ELF emissions, obs. at Moshiri, Japan 78−24413
ELF emissions during substorm activity periods, local time var. 77−53328
ELF-VLF emissions, quasi-periodic, interaction with Pc 3-4 mag. pulsations 80−67475

magnetospheric electromagnetic wave propagation continued
ELF/VLF ground-based obs. at high latits. during GEOS-1 and ISEE-1 and -2 passes 79−29949
equatorial plasmasphere, gyroharmonic emissions induced by energetic ions 79−101009
examination of VLF whistler pulse analysis 80−17441
excitation in magnetosphere rel. to plasma instabilities *(Russian)* 78−12053
frequency-time filtering of ULF signals and magnetospheric channel characterisation *(French)* 79−70920
generation, comparative obs. 80−26685
growth rate of LH and RH modes rel. to magnetosphere energetic particle instabilities 77−87186
gyroharmonic emissions due to energetic electrons in plasmas 79−80086
HF and VLF propag., expt. results 77−25861
HF peculiar lunar echoes, guided wave propag. in ionosphere and magnetosphere 78−93032
HF radio noise study during auroral substorms, freq. range 8 to 25.5 MHz 80−41670
HF radioemission during ARAKS expt., ground-based obs. 79−21078
HF signals, magnetospheric propag. mechanism 80−4196
HF signals magnetospheric propag. on Earth-Earth path, exptl. investigations 80−4195
hiss, generation beyond plasmapause by magnetosonic waves 77−82085
kilometric radiation, theory 79−70900
kilometric radiation from auroral zone, propagation direction 80−101497
kilometric radiation scattering at very high altitudes 79−101025
layered plasma, use of Fuchsian differential eqns. 80−75060
magnetic equator observations, amplitude and differential propagation delay data 78−7839
magneto-active plasma, group-vel. direction 80−59201
magnetoactive collisional plasma, dielectric tensor, refl. index and attenuation 80−59202
magnetoplasma, refr. index profiles in layered media, extraordinary mode 80−77223
magnetosphere cold plasma diagnostics using satellite meas. of VLF signals from ground transmitters 77−49183
magnetospheric physics, review of selected topics 78−65466
magnetospheric waves, digital techniques for ULF wave polarisation analysis *(French)* 79−70923
man-made VLF waves, effects on radiation belts struct. 78−45150
MF duct formation and bubble initiation 80−72712
modulational instability of whistler-mode signals 78−85774
morning sector, eastward movement of auroral radio absorption events 77−56792
multicomponent time-varying signals, unambiguous determ. of fine structures *(French)* 79−70921
navigation systems, ionospheric and plasmaspheric effects 77−82100
near-space radio noise environment characteristics and sources 78−89034
noncoherent response method for bow shock and magnetopause study 77−49230
northern cleft, ionosonde obs. 77−29595
parametric decay of non-ducted whistler-mode signal 80−6239
Pi propagation at nighttime, obs. on E-W axis 80−98519
plasma temperature anisotropy instability affecting propagation 80−46350
plasma wave emissions from auroral field lines 79−88556
plasmapause, LF radio sounding by geostationary satellite 78−69648
plasmapause, radio sounding by geostationary satellite *(Japanese)* 78−85770
plasmapause, sounder design using ray tracing studies from geostationary satellite 80−4191
plasmapause, whistlers and VLF noise propag. 78−40749
plasmapause as a VLF waveguide 77−87193
plasmasphere, horiz. inhomogeneities, whistler obs. 80−4168
plasmasphere, VLF ducts modelling 79−58202
plasmasphere, whistler duct positions 77−53301
plasmasphere convection patterns observed simultaneously from two ground stations, from whistler data 79−62673
plasmaspheric ELF hiss, origin, importance of wave propag. and plasmapause 80−26672
polar cusp, field-aligned currents, convection elec. fields and ULF-ELF waves 79−75043
polar cusp, wave scatt. of particles rel. to low-freq. pulsations generation 79−53657
power line radiation effects, transmitter simulation 79−12348
power-line harmonic radiation effects on Earth's radiation belts 79−80098
prolongitudinal mode whistlers, raytracing in transition level gradient model 78−4042
protonosphere, electron conc. inhomogeneities meas. by whistler method 77−67011
QT mode whistlers, LHR effect 77−70923
radio beacon signals, ATS-6, plasmaspheric electron content and scintillations *(French)* 79−58184
radio signal transmission, long-delay echoes generation, models 80−26670
radio waves, obs. during JIKIKEN (EXOS-B) satellite initial phase *(Japanese)* 80−94675
radio waves, propag. mode determ. using stimulated plasma wave results *(Japanese)* 80−94650
radio waves, pulsed, stimulated excitation of Alfven waves in near Earth plasma 79−58192
radio window theory, transmission coeff. 80−61953
radiowave propagation, HF and VLF propag. between mag. conjugate pts. on Earth surface 80−41639
radiowave propagation rel. to plasma density, GEOS-1 relaxation sounder meas. 79−35072
resonant particle effects in Langmuir and whistler waves, long-time-scale plasma simulation 78−42796
riometer obs. during Pc 4-5, concurrent obs. in phase with magnetic data 80−82147
satellite signals, phase shifts due to plasma shock waves and solitons 77−45273
side-band mutual interaction of whistler-mode waves 80−82148
slow nonpotential modes propag. 77−64535
space plasma front parameter determ. by noncoherent response 77−45274
super whistler, theory and anal. 80−26688
sweeper activity in the HF and VHF bands, relation to magnetospheric phenomena 77−56689
magnetospheric electromagnetic wave propagation continued
time delay effects, on radionavigation, observations 78−7831
transverse EM waves, drift instabilities assoc. with ring current and plasma sheet 79−12351
trigger VLF emission, appl. to magnetosphere plasma diagnostics 78−45149
trigger VLF emission theory 77−17294
triggered VLF emissions and detrapped electrons 78−77421
ULF, identification using cross-spectral matrix *(French)* 79−70929
ULF MHD wave azimuthal characts. near L=4 77−87197
ULF or VLF emissions, apparent and real fine struct. 80−26697
ULF wave propag., axisymmetric guided mode sources in magnetosphere model 80−77231
ULF wave-particle interactions, dynamic cross correlation studies *(French)* 79−70926
ULF waves, conjugated ground-satellite relationships 79−29947
ULF waves detected on GEOS-1 satellite, amplitude and polarisation anal. *(French)* 79−70924
v.h.f. and u.h.f. ATS-6 radio beacon meas. of total electron content 77 2303
VLF and magnetosphere structure, magnetic storms 80−72724
VLF and ULF waves, comparison of magnetosphere cold plasma densities meas. 78−28436
VLF burst freq. drift rate rel. to large-scale electric field 79−92639
VLF cross meridian refraction at 500-600 km height, electron density 80−46339
VLF Doppler signatures theory rel. to magnetospheric density struct. 77−87202
VLF ducts, protonospheric-ionospheric modelling 78−28446
VLF echoes excited by Isis 2 HF transmitter, theory of electrostatic wave excitation 80−77240
VLF emission and radiation belt electron lifetime 79−62682
VLF emission modulation freq. shift relative to geomagnetic pulsation freq. 80−77229
VLF emissions, mid-latitude obs. at Yakutsk 79−62683
VLF emissions and electron precip., modulation temporal-spectral anal. from Interkosmos 5 data 77−64511
VLF emissions assoc. with low energy electron enhancements 77−33285
VLF emissions during mag. storms, Ariel 3 and ground-based obs. 77−56794
VLF emissions near plasmapause assoc. with substorm activity 77−45258
VLF hiss, convective beam amplification 79−40029
VLF injected wave obs. by Explorer 45 and Imp 6 77−53321
VLF monochromatic signals causing particle precipitation 77−49238
VLF noise storms rel. to magnetospheric ring current 77−91376
VLF phase reversal experiment 77−25866
VLF power line radiation effects on trapped electrons 79−12357
VLF propagation, theory of rays and foci in magneto-ionic medium 80−105135
VLF pulse propagation and distortion, fast Fourier transform investig. 80−56679
VLF quasiperiodic emissions interaction with micropulsations, model 78−61682
VLF saucer source region 80−41664
VLF signal echoes after double transverse through magnetosphere *(Russian)* 77−29585
VLF signal interruption causing emission triggering 80−51617
VLF signals, Doppler shift meas. by JIKIKEN (EXOS-B) satellite *(Japanese)* 80−94651
VLF signals, time-varying, determination of wave normal directions *(French)* 79−70927
VLF transmission induced slot electron precip. 78−32296
VLF transmissions causing induced precip. of inner zone electrons 78−88996
VLF transmitter, ground-based, obs. on GEOS-1 of 10.2-13.6 kHz signals 79−25411
VLF transmitter, ground-based, reception of signals on GEOS-1 79−29948
VLF transmitter induced quiet bands in hiss emissions, quantitative interpretation 79−66878
VLF transmitter signals, prod. of quiet bands in mid-latit. hiss 77−64534
VLF triggered emissions, beam-plasma instability appl. 79−14564
VLF wave activity during mag. storm, stimulated by power line radiation 77−87199
VLF wave injection experiment, receiver on International Sun-Earth Explorer A 78−85806
VLF wave injection expt., discrete line radiation obs. within transmitter-induced amplification bands 78−96360
VLF wave packet, cyclotron interaction with reson. electrons beam 79−53652
VLF wave propag. and bouncing period, plasma inhomogeneity effect 77−53319
VLF waves, conjugated ground-satellite relationships 79−29946
VLF waves obs. by GEOS-1 79−29943
VLF waves propagating in directions near reson. cone, appl. to electron temp. estimation 77−82086
VLF whistler obs. of radial plasma drift and coupling to ionosphere 80−77239
VLF whistler-mode transmissions, Pc 3 micropulsation obs. 79−8781
whistler, occurrence rate variation with geomagnetic latitude 79−40010
whistler amplification at freq. > upper cut-off freq. 78−40763
whistler analyser, semiautomated, using spectrum analyser and programmable tracking filter 79−74975
whistler analysis methods, ground-based obs. *(French)* 78−36398
whistler analysis methods, theoretical whistlers *(French)* 78−40762
whistler damping near electron gyrofreq. due to cold-plasma injection, rel. to magnetosphere 80−28659
whistler dispersion, automatic meas. by phase locked loop discriminator *(Japanese)* 77−91312
whistler dispersion, group delay automatic meas., ionosphere and magnetosphere electron density 78−93050
whistler ducting in plasmasphere, ray-trace study 80−72704
whistler ducts formation and lifetime 78−61684
whistler ducts in outer plasmasphere, form. 78−57407
whistler low-latitude coordinate observation system using direction finder and real-time analyser 80−67479
whistler mode, instabilities 79−88551
whistler mode, interpretation of 6-component measurements 80−83921
whistler mode instability, parallel elec. field effect 80−26700

magnetospheric electromagnetic wave propagation continued
whistler mode key-down signals amplitude pulsations 77−29598
whistler mode signals, initial results from tracking receiver direction finder 78−77429
whistler modes, obliquely propagating 77−80288
whistler parametric instability, pitch-angular electron scatt. *(Russian)* 78−77420
whistler precursor emissions and whistlers, ducted propagation 80−85809
whistler precursors, catalytic role of power line radiation 78−12056
whistler propag. theory 77−45261
whistler propagation at low latits., review 78−73586
whistler propagation in magnetospheric plasma 80−90294
whistler propagation in thermal plasma, elec. field parallel to geomag. field 80−41663
whistler propagation times eqn., inversion via spectral expansion 80−8495
whistler pulse, self-distortion in plasma 79−46456
whistler range, wave radiation in plasma *(Russian)* 78−36400
whistler wave, in nonuniform mag. field, test particle correlation, simulation 79−37486
whistler wave modulation, nonlinear theory 80−26686
whistler wave trapping phenomena 77−15195
whistler waves, modulated by kinetic Alfven and ion quasimodes 77−80293
whistler waves modulation instability 77−72450
whistler-mode signals, man-made, spacecraft obs. near electron gyrofrequency 78−28418
whistler-mode waves focusing and interference in spatially varying mag. field 78−65465
whistler-mode waves guidance through plasmasphere 78−93054
whistlers, coherent nonlinear interaction dependent on wave amplitude 80−72715
whistlers, Dowden-Allcock approximation generalisation and comparison with Bernard approximation 80−51607
whistlers, duct struct. and formation 80−94659
whistlers, low-latitude, conditions of duct trapping 79−84586
whistlers, meas. of occurrence rate during geomagnetic magnetosphere storms 80−12621
whistlers, nature, types and observations, review 80−36458
whistlers, non-ducted propag. 78−36402
whistlers, partly ducted, over Europe, propag. theory 78−65463
whistlers, possible mechanism for precursors 77−25869
whistlers, two-dimens. nonlinear self-modulation 77−80295
whistlers and pearl type waves, stability 78−12051
whistlers observed at Sofia during decreasing solar activity period, dispersion characts. 79−8779
whistlers resonance interaction with electrons, bunching effect 78−45146

magnetostatic wave devices
bulk wave propagation in multilayered structure 80−60380
ferrite-semiconductor structure with volume magnetostatic waves, effect of convolution 80−54761
semiconductor-dielectric-YIG-metal system, amplification of surface and bulk waves 77−1582
status report of SAW and magnetostatic wave devices, transversal filters appl. 80−28394
transducers, magnetostatic forward volume wave excitation 79−82775
n-GaAs-YIG layered structure, magnetostatic surface wave amplification 78−88107
YIG film waveguide, with periodic mag. struct., dispersion characts. anal. *(Japanese)* 79−42809
YIG-semiconductor coupled system, magnetostatic surface wave amplification, ferromag. loss 77−85434

magnetostatic waves
banded domain structure, magnetostatically coupled with uniaxial substrate, mag. reversals *(Russian)* 78−48016
bound by DC mag. field gradients 77−89941
composite semiconductor-ferrite struct., surface magnetostatic spin wave interactions *(Russian)* 80−88739
current-wave interaction, characterisation by coupling constant 78−84403
dialkylammonium copper tetrachloride, ferromagnetic layer compound, magnetostatic mode excitation 80−29538
dielectric thin slab. magneto-exchange modes with arbitrary pinning 77−63261
diethylammonium copper chloride, non-Lorentzian EPR lineshape and magnetostatic modes 77−43862
dipole-exchange spin waves in cylindrical ferromag. *(Chinese)* 78−6521
ellipsoid with domain struct., magnetostatic oscills., theory 80−93102
epitaxial film device appl. 77−32223
ferrimagnetic materials 80−39878
ferrimagnetic spheroids 77−73013
ferrite, single crystal with domain struct. *(Russian)* 77−32236
ferrite rod, magnetised, propap., interference and relax. of magnetostatic waves, magneto-optical obs. 79−73704
ferrite rod with domain structure, magnetostatic waves and internal field *(Russian)* 78−76236
ferrite rods, magnetised longitudinally, surface mode propag. 80−54878
ferrite sheet, magnetised, excitation of surface EM waves 78−10747
ferrite slab, transversely magnetised, adjacent to semicond., mag. surface wave amplification 78−72339
ferrite-semiconductor composite struct., bulk magnetostatic wave instability, theory 77−12186
ferrite-semiconductor structure, surface magnetostatic wave instability 78−76235
ferrite-semiconductor structure with volume magnetostatic waves, effect of convolution 80−54761
ferrodielectrics, ferromag. reson., press. influence 78−88193
ferromagnet, uniaxial, quantum anomalies in susceptibility during second order phase tansitions *(Russian)* 78−19226
ferromagnet-semiconductor structure, periodic, surface magnetostatic waves 78−27070
ferromagnet-semiconductor structure, surface wave gain, ang. depend. 77−51938
ferromagnetic bar and gyrotropic cylinder, magnetostatic modes 77−77048
ferromagnetic film, magnetostatic surface wave propag. 79−4661
ferromagnetic film, with domain struct., magnetostatic oscills. 78−48010
ferromagnetic plate, nonlinear magnetostatic waves *(Russian)* 78−35014
ferromagnetic plate, surface magnetostatic wave excitation 80−25119

magnetostatic waves continued
ferromagnetic semiconductor, LF magnetostatic waves with discrete spectrum 77−89792
ferromagnetic slab, finite thickness, magnetostatic theory of response functions, appl. to Brillouin scatt. 79−61083
ferromagnetic slab, magnetostatic volume wave dispersion relations, metal effects 78−47963
ferromagnetic-semiconductor-dielectric multilayer struct., convective surface wave instability 77−24732
field of defect in plane parallel plate, calc. 78−72986
film disc containing bubble, two-dimens. magnetostatic reson. 79−78469
films, ferromagnetic, perpendicularly magnetised, surface and vol. magnetoelastic waves *(Russian)* 80−93151
garnet film, magnetoelastic energy of stripe domain patterns 78−68334
gyromagnetic slab magnetised in arbitrary direction, magnetostatic mode characteristics 78−2670
hexagonal planar ferrite slab, magnetostatic modes 77−24731
IEEE International Microwave Symposium, Orlando (1979) 79−68356
layered magnetic thin film, directional coupling of surface waves 79−38358
long rectangular bars, with domain struct. *(Russian)* 77−66383
magnetically uniaxial ferromagnetic particles, high-anisotropy many domain, magnetisation, hysteresis *(Russian)* 79−91256
magnetisation distribution in magnetostatic oscillations 78−68293
multilayer planar structure, magnetostatic propag. 77−16120
normally magnetised disc, reson. modes 77−81015
parametric mode coupling in amplification, magnetostatic echo 77−4545
Permalloy film, double layer, wall splitting effect 77−85530
Permalloy film magnetometer, mag. props. and LF noise 78−48005
Permalloy I-bar elements, magnetostatic effects, unifying overview of domain and continuum results 80−44853
Permalloy platelets, FMR mode positions, spin pinning 77−4562
semiconductor-dielectric-YIG-metal system, amplification of surface and bulk waves 77−1582
semiconductor-ferrite-semiconductor structure, absolute instability of magnetostatic surface waves interacting with drifting carriers 78−95486
stripe domain structure, magnetostatic modes 78−68333
surface, dispersion relation, effect of metal 78−19232
surface, EM field meas., using loop-shaped and linear probes 77−41658
surface magnetostatic wave, travelling-wave amplification anal. using Maxwell equations *(Japanese)* 78−6560
YIG, reson. magnetostatic modes, spectrum in inhomogeneous mag. field 79−28621
Fe garnet, optical radiation interaction with magnetostatic waves 80−76009
Fe-Si, strips and rods, spatial extent of flux due to irreversible changes of mag. polarisation 79−33506
n-GaAs-YIG layered structure, magnetostatic surface wave amplification 78−88107
MnF_2 spheres, magnetostatic modes in antiferromag. reson. 77−1599
$PbFe_{12}O_{19}$ platelets, ferromag. reson. absorpt. of close-packed bubble lattice 77−69709
YIG, anomalous subsidiary absorpt. butterfly curves at 9.16 GHz and 300K 79−82875
YIG, corrugated slab, surface wave propagation 78−27072
YIG, dielectric layered struct., magnetocrystalline anisotropy effects, group delay time 79−78355
YIG dielectric layered struct. magnetostatic bulk wave steering 80−25166
YIG epitaxial film, magnetostatic volume wave propag. 78−10736
YIG epitaxial film and cryst., bound magnetostatic waves controlled by field gradients 78−95425
YIG, ferromagnetic resonance and magnetostatic waves in inhomogeneous internal field *(Russian)* 80−54954
YIG film, calc. of magnetostatic mode freq. 78−68313
YIG film, dielec. layered struct., magnetostatic volume wave propag. 78−95426
YIG film, dielec. layered struct., magnetostatic bulk wave power flow and energy distrib. 80−34610
YIG film, ferrimag., determ. of freq. of magnetostatic modes 77−36104
YIG, film, magnetostatic surface wave refl. at shallow groove 78−19283
YIG film, magnetostatic surface wave propag. 79−4661
YIG film, magnetostatic forward volume wave excitation 79−82775
YIG film, magnetostatic surface and forward volume wave oblique incident at shallow groove 80−34704
YIG film, magnetostatic surface wave propag. in nonuniform mag. field 80−80574
YIG film, oblique incidence of magnetostatic waves on metallic grating 78−19229
YIG film, shallow groove, magnetostatic surface wave reflectivity 77−73055
YIG film, shallow groove effect on magnetostatic forward volume wave reflection 78−84473
YIG film, surface wave propag. in nonuniform mag. field, anal. 80−20437
YIG film, with periodic mag. struct., dispersion characts. anal. *(Japanese)* 79−42809
YIG film tangentially magnetised, magnetostatic surface wave excitation 80−29586
YIG film-dielectric layer-conductor struct., magnetostatic bulk wave propag. dispersion relations 80−54925
YIG, LPE film, magnetostatic wave to exchange resonance coupling 79−82774
YIG, magnetised in raised cosine profile magnetostatic surface wave propag. 80−2567
YIG magnetostatic surface wave dispersion rel. to mag. saturation diffusion 78−2671
YIG, magnetostatic wave echo, 9440 MHz, room temp. 77−43887
YIG, magnetostatic wave linewidth, wave no. depend., mag. relax., rods and films *(Russian)* 78−2667
YIG, mulitiple mag. layer structures, magnetostatic surfacewave propag. 80−88839
YIG multilayered film, magnetostatic spectrum 78−23350
YIG, normally magnetised disc, reson. modes 77−81015
YIG, parametrically excited reson. magnetostatic modes of spin, elastic and magnetoelastic waves 79−56523
YIG, parametrically excited wave discrete structure obs., light diffr. and modulation *(Russian)* 79−95650
YIG periodic film layer, magnetostatic surface wave propag. 80−2607
YIG, pseudo-surface magnetoelastic waves, damping *(Russian)* 78−23320

magnetostatic waves continued
YIG sandwiched between grounded dielectric layers, magnetostatic bulk wave propagation 80−60380
YIG, single cryst. film, pinning effects on magnetostatic modes 78−31111
YIG slab, corrugated, magnetostatic surface-wave propagation 78−19228
YIG slab, magnetostatic forward vol. waves delay characts. 79−99691
YIG slab, partially magnetised, expt. obs. of group delay 80−7100
YIG spheres, anomalously low saturation threshold of magnetostatic modes 79−69729
YIG, spin-wave and magnetostatic mode attenuation, double-pulse echo method 79−82874
YIG, subsidiary absorpt. spin-wave instability threshold, anomalous struct. 80−34776
YIG substrates, magnetoelastic surface waves, magnetostatic reson. anal. 80−20441
YIG, thick epilayer, unpinned magnetostatic modes 77−63290
YIG, thin films, magnetostatic modes at Q-band freq. 80−65828
YIG-dielectric layered structure, magnetostatic surface wave propag., finite width effects 77−20668
YIG-Ge layer structure, amplification of bulk magnetostatic waves 78−34972
YIG-InSb system, surface magnetostatic wave interaction with drift electrons *(Russian)* 77−12185
YIG-semiconductor coupled systems, energy anal., magnetostatic surface wave amplification 77−55699
YIG-semiconductor-dielectric-metal layered structure, amplification characts. 78−23321
Zn_2Y, dielectric layered struct., magnetocrystalline anisotropy effects, group delay time 79−78355

magnetostriction
acoustic noise source in magnetic core of power transformers, prediction, control 79−18648
additive pulses from internally stressed magnetostrictive wire bundle 79−99742
alkali hyperoxides, ionic π-electron systems, magnetogyration 80−93155
amorphous alloys, mag. props. and appls. 79−8016
amorphous ferromagnet, micromagnetic theory 78−10661
amorphous ferromagnetic ribbon, HF mag. characts., magnetostriction role 77−66408
amorphous ferromagnets, ferromag. saturation, spatially random magnetostatic, magnetocrystalline, magnetostrictive and exchange fluctuations 78−60277
amorphous magnetic layers, SAW device appl. 80−28389
amorphous ribbon, saturation magnetostriction, and electronically controllable delay line 79−1700
amorphous ribbons, magnetostrictive, theory of giant ΔE effect 77−85537
antiferromagnet, appl. stress effects on equilib. config. 78−56365
antiferromagnet, relax. processes, spin-sound wave coupling 78−60340
antiferromagnet, weakly anisotropic, effective anharmonicity of elastic subsystem 77−69658
antiferromagnets, magnetoacoustic resonance of domain boundaries *(Russian)* 80−65636
application and practical significance *(German)* 78−23311
capacitice instrument for magnetostriction meas. at low temps. and high magnetic fields 78−93742
cavitational corrosion of materials in molten metals on const. mag. field appl. *(Russian)* 80−60987
composite garnet ferrite epitaxial film ferromag. resonance obs. 77−85578
cubic crystal, highly magnetostrictive, magnetoelastic surface waves on (110) plane 78−52327
defects in magnetized samples, magnetostrictive conversion of US waves into EM fields 80−66008
demonstration experiment for teachers, using Kerr magneto-optical effect 78−69949
dislocated ferromagnet, inhomogeneous magnetisation near dislocation effect on FMR linewidth 80−25213
domain wall junctions, magnetostrictive displacements at surface 78−48014
dynamic, measurement using induction method, hysteresis loops *(Russian)* 77−56171
elastic properties of magnetic materials, review 80−7142
elastic wave with struct. of EM wave in magnetostrictive media *(Russian)* 77−16251
electrical steel sheet, magnetostriction meas. using Hall effect transducer *(German)* 80−13111
EM field induction in vacuum by US wave in magnetostrictive conductive half space, anal. 77−73415
epitaxial garnet films, technique for magnetostriction coeff. meas. 80−243
ferrimagnetic spinel, magnetostriction effects from Mn^{3+}, Co^{2+} and Fe^{2+} ions 79−91277
ferrite, epilayers for bubble appl. 80−39829
ferrite, magnetoacoustic reson. in strong mag. field 80−11309
ferrite, US testing 78−53084
ferrite film, determ. by ferromag. reson. method *(Russian)* 77−16126
ferrites, effects of compression on magnetostriction 77−40109
ferrites, magnetising field influence on amplitude depend. of mechanical props. 78−2723
ferrites, magnetostriction due to Co^{2+} ions, effect of excited states 80−65990
ferrites, magnetostrictive, relationship between static parameters and piezoactivity 78−95507
ferromagnet, cubic, elastic props., group theoretical approach 80−29600
ferromagnet, effect on domain neighbourhood *(Russian)* 78−39356
ferromagnet, inhomogeneous, Landau's theory of second-order phase transition 80−50092
ferromagnet, itinerant electron, magnetoelastic contribs. to US vel., elastic consts., and susceptibility 80−75829
ferromagnet, magnetostriction is magnetic field, sound-spin wave coupling 79−15334
ferromagnet, modulus defect due to internal strain 78−76286
ferromagnet, planar, US attenuation, spin-phonon coupling, magnons and magnetostriction contrib., calc. 80−34611
ferromagnet, rectilinear screw dislocation, magnetisation distrib. 80−44897
ferromagnet, soft, non-zero magnetostriction, hysteresis rel. to irreversible phase transition 80−34693

magnetostriction continued
ferromagnetic alloys, amorphous, sputter-deposited, soft mag. props., magnetostriction 80−34696
ferromagnetic amorphous alloys, thermal expansion anomaly near Curie temp. *(Japanese)* 77−85542
ferromagnetic bar, stressed, reverse magnetostrictive effect *(Rumanian)* 80−84630
ferromagnetic crystal with dislocations, mag. anisotropy *(Russian)* 77−8377
ferromagnetic domain theory, quasi-dislocation theory appl. *(Japanese)* 80−60358
ferromagnetic film, magnetostriction meas. from deflection in mag. field 77−10068
ferromagnetic materials, magnetostrictive sensitivity, experimental study *(Bulgarian)* 77−55695
ferromagnetic metal polycrystals, model for magnetostrictive EM generation of US guided waves 78−22236
ferromagnetic polycrystalline materials, mag. impulse produced magnetoelastic waves *(Italian)* 78−2720
ferromagnetic polycrystals, cubic, domain structure under torsion *(Spanish)* 79−91246
ferromagnetic single crystal with cubic symmetry, mag. and magnetoelastic props. 79−15332
ferromagnetic solids, magnetomechanical effects, magnetostriction, hysteresis, stress, yielding, fatigue damage, crack growth *(Polish)* 80−71150
ferromagnets, horizontally polarised shear wave generation using magnetostrictively coupled meander-coil EM transducers 79−46144
ferromagnets, US vibrs., review of γ-reson. spectroscopy under HF excitation 77−48113
ferrous formate dihydrate, mag. sp. ht. 79−91235
film, magnetocryst. anisotropy, magnetostriction and micromagnetism 77−73062
garnet, magnetostriction effects from Mn^{3+}, Co^{2+} and Fe^{2+} ions 79 91277
garnet film bubble material, orthorhombic anisotropy and positive magnetostriction 77−85513
garnet films, LEP growth-induced anisotropy, magnetostriction theory 79−95624
garnets, growth-induced lowering of magnetoelastic symmetry 78−64255
garnets, magnetic anisotropy and magnetostriction 79−99748
Heisenberg ferromagnets, BCC, with $K_2CuCL_4.2H_2O$ struct., ^{17}O transferred hyperfine interactions 78−39439
hexagonal and cubic harmonics up to degree 6 80−88856
hexagonal material, Δs effect, anisotropic contrib. 77−90005
hypercritical films, stress-induced uniaxial anisotropy influence on domain struct. *(Russian)* 79−69703
interferometric meas. method for small effects 78−12731
Invar, dislocation motion anomaly 80−10554
Invar, mag. susceptibility in technical saturation region and internal stress 77−85429
Invar, magnetovolume contrib. to temp. variation of magnetoresist. 77−31999
Invar, stainless, thermal expansion, elastic props. and Mossbauer effect 79−56502
Invar, volume magnetostriction 79−56590
itinerant electron ferromagnetism, press. effects on mag. props. 77−66241
itinerant electron ferromagnets, magneto-volume effects 80−60397
itinerant ferromagnet, magneto-volume ext. 77−66404
itinerant ferromagnets, magnetoelastic props., thermodynamic aspects 80−66002
laminated magnetostrictive plates, bending vibrs., reson. excitation 78−10746
long rods, radial motion under axial mag. field 78−68456
magnetic Debye crystal, with magnon-phonon coupling, crit. changes in vibr. modes 79−95094
magnetic material, fluctuational breakdown of metastable states at phase transitions *(Russian)* 78−52245
magnetic materials, magnetostriction and its significance *(German)* 79−4712
magnetic transitions, first-order intrinsic volume magnetostriction concept 80−29562
magnetoelastic media, nonlinear acoustic effects 77−36109
magnetostrictive ferrites, energy dissipation in high-freq. cyclic loading 80−15779
martensitic transformation point shift, in strong mag. field, magnetostriction effect *(Russian)* 80−108440
materials and devices, review *(Japanese)* 78−23316
mathematical models for direct and reverse magnetostriction *(Rumanian)* 80−25171
measurement device for high temperature expt. 77−26365
measurement of magnetostrictive vibr., laser interferometric technique 80−37059
metal, orbital magnetic and spin paramag. susceptibilities, effect of strain 77−16137
metal under Shoenberg effect conditions, Young modulus anomalies *(Russian)* 78−35018
metallic glasses, characts. and appls. *(French)* 80−39815
metallic glasses, mag. props., effect of mech. deform. 80−39840
metallic glasses, mag. props., struct., and prep., book contrib. 79−65665
metallic glasses, mats. props. review 77−4043
metallic structures, magnetostriction method of measuring elastic stresses 78−72985
metallic-glass ribbon, stress dependences of longitudinal wave velocity 80−75825
metals, HCP struct., anisotropy of paramagnetostriction 77−32231
Metglas 2605 ribbon, saturation magnetostriction meas. by small-angle magnetisation rot. 80−60391
Metglas 2826 ribbon, saturation magnetostriction meas. by small-angle magnetisation rot. 80−60391
microdeformation transducer calibration for geodesy and instrumental geophysics *(French)* 78−12004
nucleation centre formation in mag. phase transitions of first kind 78−2683
optical fibre magnetic field sensors 80−69510
optical fibre magnetostrictive perturbation for possible mag. field detect. 80−53450
optical interferometric method of measurement *(Japanese)* 79−65705
Permalloy, corrosion resist. and mag. props., effect of Cr addition 77−86219

magnetostriction continued
Permalloy film, electrodeposition with zero magnetostriction composition, technological control 79−33955
Permalloy film, temp. depend. of mag. anisotropy anal. *(Russian)* 77−51901
permalloy films, thermoelastic stresses and magnetostriction effects during light recording *(Russian)* 79−97465
Permalloy films with band domain struct., thermomag. recording, resolving power *(Russian)* 80−75769
Permendur, 50-KF, effects of compression on magnetostriction 77−40109
phase diagrams of magnets with two sublattices *(Russian)* 78−23268
phase transitions with two order parameters, Landau theory, mag. reorientation 80−103456
piezomagnetic rod, demagnetizing field effect, longitudinal-effect extensional vibration 78−95504
polycrystalline and amorphous strips, magnetostriction consts. determ. method 80−86355
powder material US pulse echoes and suppression 77−28520
pulse-producing wire plating 80−2618
quadratic, exactly soluble model 79−8030
rare earth alloys, highly magnetostrictive props. 77−12180
rare earth alloys, RCo_2 and R_2Fe_{17}, Invar props. 79−56593
rare earth alloys, RFe_2, magnetostriction studies, book contrib. 80−39846
rare earth alloys, vol. magnetisation, point charge cryst. field model 77−63254
rare earth alloys for magnetostrictive underwater sound transducers 80−19204
rare earth aluminium Laves phase cpds., RAl_2, anisotropic magnetostriction, temp. depend. 80−39841
rare earth garnets, prep. and props. book contrib. 80−44193
rare earth intermetallics, magnetostriction and struct. distortion 77−63248
rare earth intermetallics, quadrupole interactions, magnetoelasticity 80−15489
rare earth intermetallics, RAl_2, cryst. field volume magnetostriction calc. 79−8029
rare earth intermetallics, RFe_2, spontaneous magnetoelastic distortion, X-ray diffr. expts. 77−63253
rare earth intermetallics, RFe_2 and $R(Co_{0.98}\ Fe_{0.02})_2$, magnetostrictive material, changes in vibr. modes near mag. phase transition 79−90736
rare earth iron garnets, contribution of Fe ions in noncubic magnetostriction from crystal field model 78−43622
rare earth iron garnets, site ordering and magnetostriction 77−90007
rare earth iron intermetallics, RFe_2 type, magnetostriction in polycryst. samples 77−73065
rare earth Laves phase compounds, $R_xR_{1-x}Fe_2$, magnetostriction, anisotropy energy 80−25177
rare earth metals, mag. and transport props. 79−69658
rare earth metals and some alloys, X-ray diffraction obs. of magnetostriction and phase transitions 77−73068
rare earth orthoferrites, mag. dipole anisotropy and magnetostriction 79−73710
rare earth-Al Laves phase intermetallics, RAl_2, R=Gd, Ho, Dy, Tb, cubic Laves phase compounds, exchange striction determ. 80−44895
rare earth-cobalt intermetallics, RCo_2, spontaneous vol. magnetostriction and thermal expansion meas. 77−12183
rare earth-Fe_2 compounds, magnetoelast. props., book contrib. 80−75838
rare earth-Fe_2 Laves phase compounds, magnetostriction anisotropy 77−63250
rare earth-Fe alloys, highly magnetostrictive, isotropy breaking magnetoelastic behaviour 78−72386
rare earth-Fe alloys, magnetostrictive, elastic props. 78−84469
rare earth-Fe alloys, RFe_2, temp. depend of coercivity 79−61185
rare earth-Fe Laves phase alloys, sintering, magnetostrictive props. 77−16139
rare earth-Fe rod, US resonance with large eddy currents 80−54933
rare earth-Tb-Fe alloys, $R_xTb_{1-x}Fe_2$, Laves phase type, magnetostriction *(Russian)* 77−51932
rare earth-transition metal alloy amorphous film, magnetostriction, dipolar mechanism 78−95502
rare earth-transition metal amorphous alloy film, magneto-elastic tensors, pair model calcs. 78−80185
rare earth-transition metal intermetallics, struct. and props. review 78−10668
rare earth-Zn alloys, ferromag., parastriction and magnetoelastic coeffs. 80−65996
rare-earth metals, US attenuation, exchange striction, and spin-phonon interaction 79−33518
Rayleigh wave propagation in strongly magnetostrictive materials 77−40111
review *(Rumanian)* 80−34747
rock, reversible effect of small uniaxial stress on remanent mag., single-domain theory 78−20393
SAW generation efficiency meas. of residual stress 77−28972
semiconductor, metamagnetic, magnetostriction ferrons 78−88160
SH wave magnetostrictive generation model for ferromag. materials 79−55836
spin Hamiltonians, infinite-range, exact solns. 79−78281
spontaneous symmetry breaking and magnon-phonon spectra 80−65991
steel, C, residual stress induced by uniaxial deform., mag. meas. 77−73390
steel, dynamic magnetostriction meas. using induction method *(Russian)* 77−56171
steel, ferromagnetic, transduction efficiency using magnetostrictively coupled meander-coil EM transducers 79−46144
steel, induced anisotropy influence on mag. props., thermomagnetic working *(Russian)* 80−55549
steel, magnetostriction effect, depend. on magnetising field intensity *(Russian)* 79−51831
steel, stainless, Cr-Ni, low temp. plastic deformation, in mag. field 79−83256
steel, structural, 34KhN3M, heat treatment effect on magnetostriction 80−104306
steel, transformer, cold-rolled effect of uniaxial elastic stress on dynamic magnetostriction *(Russian)* 77−69651
steel 40Kh2N20, paraprocess magnetostriction near martensitic point in mag. field *(Russian)* 79−82850
strain modulated ferromagnetic resonance obs. 78−76285
tape cores carrying current, torsional stress effects 80−34742
magnetostriction continued
theory, rel. to X-ray topography data 78−64254
theory and measurement techniques, book contrib. 80−11241
transition metal, ferromag., band theory of linear magnetostriction 80−71141
transition metal alloys, AFe_2 and ACo_2, Invar effect, magnetovolume meas. 79−56592
transition metal amorphous alloys, mag. props. 80−29576
transition metals, 3d, ferromag. props., book contrib. 80−75724
uniaxial antiferromagnet, effect of magnetostriction on reorientation phase transitions 79−69674
wheatstone bridge technique for magnetostriction measurements 80−57348
Ag-Tb(Ho)(Dy)(Er)(Tm) dil., single and polycrystals, low temp. magnetostriction meas. 79−78501
Al_3Ce, thermal expsn. below 1K, and magnetostriction meas. 79−90803
$Ca_3Fe_2Ge_3O_{12}$, antiferromag. single crystal garnet *(Russian)* 79−8027
$CdCr_2Se_4$, influence of Co ions on anisotropy and magnetostriction, ferromag. reson. meas. 77−69659
$CeAl_2$, Anderson lattice system, thermal expansion meas. 1.5 to 10K 79−37860
$CeAl_2$, Anderson lattice system, ground state props. 80−20443
$CeAl_2$, anisotropic magnetostriction near antiferromagnetic transition 78−88157
CeB_6, magnetostriction, US absorpt. and thermal expansion 80−66004
$CeFe_2$, magnetostriction and magnetisation 80−39844
$(Co,Fe,M)_{78}Si_8B_{14}$ amorphous alloys (M=V,Nb,Ta,Cr,Mo,W,Mn or Ni), zero magnetostriction and low field mag. props. 80−34741
Co, electrodeposited film, saturation magnetisation and perpendicular anisotropy meas. 78−76277
Co film, evaporated, uniaxial mag. anisotropy 77−51929
Co, magnetic anisotropy induced by magnetic and stress annealing 78−35010
Co, magneto-volume effects calc., rel. to itinerant electron model 78−43621
Co, modulus defect due to internal strain 78−76286
Co rod, spontaneous vibr. modes excited by reversible magnetostriction 79−56587
Co-B(-Cr) thin film glasses, mag. props. and corrosion resist. 80−80576
Co-Fe, soft mag. props. rel. to metallurgical aspects 80−88810
Co-Fe alloy, HCP and DHCP, magnetostriction consts. determ. 78−80184
Co-Fe alloy, Invar characts. 77−1550
Co-Fe alloys, effect of annealing on magnetostrictive vibrs. 78−6558
Co-Fe amorphous alloys, high permeability props. *(Japanese)* 77−51927
Co-Fe amorphous alloys, worked, perminvar type mag. hysteresis loop, longit. Kerr effect obs. 80−65958
Co-Fe-B and Co-Fe-Cr-P-B sputtered amorphous films, mag. props. and corrosion resist. 79−28567
Co-Fe(Ni), magnetic anisotropy induced by magnetic and stress annealing 78−35010
Co-Mn-Ni-Fe-Si-B amorphous alloys, mag. props., low magnetostriction 80−75832
Co-Ni-Fe-Si(B), amorphous ribbon, magnetostriction meas. 80−15778
Co-Si-B, amorphous ribbon, saturation magnetostriction meas. by small-angle magnetisation rot. 80−60391
$Co_{100-x}B_x$, amorphous alloys, saturation magnetostriction and annealing behaviour 80−34739
$Co_{80}B_{20}$, amorphous metal ribbon, stresses, magnetoelastic anisotropy and zero-field mag. domain struct. 80−44896
$Co_{1.8}BaFe_{0.2}Fe_{16}O_{27}$, influence of spin-reorientation on magnetoelastic props. *(Russian)* 79−8028
$Co_{1.8}BaFe_{0.2}{}^{2+}Fe_{16}{}^{3+}O_{27}(Co_{1.8}W)$, magnetoelastic props. under spin-reorientation conditions 79−69709
$Co_{74}Fe_6B_{20}$, metallic glass, zero magnetostriction, magnetisation charact. 77−12158
$Co_{79}Fe_{6.5}B_{14.5}$ amorphous thin films, zero magnetostriction, high magnetisation 80−34708
$Co_{57}Fe_5Ni_{10}(Si,B)_{28}$, amorphous, soft mag. props., switched-mode power supply appls. 80−88850
$CoFe_2Se_4$, low-temp. thermal expansion anomalies and isothermal compressibility, mag. ordering and magnetorestriction 79−38363
$Co_{40}Ni_{40}B_{20}$, magnetostriction, temp. depend. 78−91921
$Co_{35}P_{15}$, amorphous, strip domains, anisotropy const. effects 80−29571
$Co_{1-x}Ti_x$, ferromag. props., Ti conc. effect 80−54872
Cr, antiferromag., magnetostriction and torque meas. below spin-flip transition 77−63186
Cr, antiferromag., stress depend. of Fermi surface, oscillatory magnetostriction meas. 77−11846
Cr, antiferromag., stress depend. of spin density wave state, magnetostriction meas. 77−63257
Cr, antiferromagnetic, mixed state, mag. torque and magnetostriction meas. 77−89909
Cr, strain and spin-flip transition, Landau theory 78−39318
Cr-Co, phase transformations and magnetostriction *(Russian)* 80−103869
Cr-Fe, magnetically insensitive Invar-type alloys *(Japanese)* 79−8034
Cr-Fe alloys, itinerant antiferromag. effect of mag. impurities 77−32186
Cr-Fe alloys, polycrystalline, antiferromag., elastic moduli and thermal expansion meas. 77−43860
Cr-Fe-Co dilute alloys, Neel temp., thermal expansion rel. to Co content 79−47281
Cr-Mn alloys, magnetisation process, magnetisation in 90-300K range *(Russian)* 78−15007
Cr-Ni-Mo 40KhN2MA, magnetostriction used in inspection after heat treatment 80−108673
Cr-Re, phase transformations and magnetostriction *(Russian)* 80−103869
CrAs, mag. transition under press., volume striction mechanism 77−24696
Cr_3C_2-(WC)-Ni, sintered, cavitation erosion resistance *(Japanese)* 77−52500
Cr_2O_3, magnetostriction anomalies near mag. field induced transitions 77−66315
$CrSb_{1-x}As_x$, exchange striction and press. effect on Neel temp. 77−63189
$CuCl_2.2H_2O$, magnetoelastic props. under press., antiferromagnetic resonance, lattice parameters 80−29598
CuCoNi ferrite magnetoacoustic oscills. rel. to microstruct. 77−85536
$CuCr_2Se_4$, crystal growth from melt, exam. of props. 80−55283

magnetostriction continued
Cu_2MnAl, Heusler alloy, magnetisation mag. anisotropy, magnetostriction and elastic consts. 78−23318
$Cu[Ni_{0.5}Mn_{1.5}]O_4$, magnetisation and magnetostriction, fields up to 11 kOe, 4-160K *(Russian)* 78−19304
Dy, meas. re-analysis, domain effects corrected by phase theory 78−6555
Dy, single crystal, plastic and magnetoplastic deform. 77−63713
DyAG, forced magnetostriction meas. 78−68349
$Dy_3Al_5O_{12}$, magnetostriction, role of order parameter 79−73796
$DyCo_2$, field induced vol. magnetostriction 78−91920
$DyCo_{5.3}$ noncollinear mag. struct. appearance in mag. fields, magnetostriction meas. *(Russian)* 80−100607
$Dy(Fe,Al)_2$, saturation and remanent magnetostriction meas. 77−63256
$DyFe_2$, high field magnetostriction and magnetisation 78−84471
$DyFe_2$, magnetisation and magnetic anisotropy 78−91862
$DyFe_2$, phonon softening below Curie temp., Mossbauer effect 77−4589
$DyFe_3$ and Dy_6Fe_{23}, magnetostriction, room temp. to 80K 80−65993
$DyFe_{1-x}Co_xO_3$, magnetostriction, thermal expansion and elastic moduli near Morin point 77−8383
$DyFeO_3$, spontaneous magnetostriction 79−56599
$Dy_{0.7}Tb_{0.3}Fe_2$, magnetostrictive material, liq. phase sintering 78−64493
$Dy_xTb_{1-x}Fe_2$, and $Ho_xTb_yDy_{1-x-y}Fe_2$, high magnetostriction cpd., mag. anisotropy origins 78−68217
$ErCo_2$, field induced vol. magnetostriction 78−91920
Er_2Co_{17}, magnetisation, magnetocryst. anisotropy and magnetostriction 77−8303
Er_2Co_{17}, single cryst., magnetostriction const. temp. depend., 78 to 300K 79−51836
$ErFe_3$ and Er_6Fe_{23}, magnetostriction, room temp. to 80K 80−65993
Er_6Fe_{23}, magnetostriction, temp. depend., 20 to 350K 80−65994
$ErRh_4B_4$, supercond. and mag. props. 79−4631
$ErRh_4B_4$, thermal expansion and magnetostriction meas. at low temp. 79−56374
$Er_xY_{3-x}Fe_5O_{12}$, garnet, mag. anisotropy and magnetostriction 80−11189
ErZn, preferred mag. domain orientation, and microstructural defects, magnetostriction meas. 79−73769
EuO, spin-spin correl. function, above T_c 77−4541
EuS, exchange magnetostriction in paramagnetic phase 79−78492
(Fe,Co,Ni)-Si(B), amorphous mag. alloy, magnetostriction rel. to soft mag. props. 80−84633
$(Fe,X)O_4$, (X=Ti, Co, Mg, Mn, Ni), magnetostriction calcs. *(Dutch)* 80−2619
Fe base amorphous alloys, Invar and Elinvar charcts. 80−29592
Fe, bulk modulus and thermal expansion coefficient, mag. contributions 79−8039
Fe film, ferromag. reson., thermodynamical anal., effect of mech. stress 79−42840
Fe group ions in singlet ground state, magnetocryst. anisotropy and magnetostriction 77−73021
Fe, high purity, mag. viscosity mechanism 78−19282
Fe, magneto-volume effects calc., rel. to itinerant electron model 78−43621
Fe, magnetoelastic excitations and ferromagnetic resonance 79−82879
Fe, plastically deformed, dislocation arrangement exam. by ferromag. techniques 78−63774
Fe, polycryst., magnetostriction sign change under compressive stress 80−29596
Fe, residual stress induced by uniaxial deform., magnetic meas. 77−73390
Fe rod, spontaneous vibr. modes excited by reversible magnetostriction 79−56587
Fe, spontaneous volume magnetostriction 80−65989
Fe, zig-zag 90° Bloch wall, magnetoelastic problem 77−4526
Fe-Al, domain struct. and magnetostriction, heat treatment effect 80−60398
Fe-Al alloys, rapidly quenched, mag. props. 80−29579
Fe-B, amorphous ferromag., Invar type, magnetisation, elec. resist. and thermal expansion meas. 78−2663
Fe-B, binary alloys, giant ΔE effect and Elinvar charcts. 78−76291
Fe-B ferromag. film, props. 79−4709
Fe-B metastable alloys, Mossbauer spectroscopy and electron microscopy 79−28653
Fe-B-Cr(Si) thin film glasses, mag. props. and corrosion resist. 80−80576
Fe-B(P) amorphous alloy, Invar effects, mag. props. meas. 79−56594
Fe-B(P) amorphous alloys, anomalous thermal expansion, ΔE effect, Invar and Elinvar charcts., delay time 80−80589
Fe-c, Fe-Si-B, and Fe-Cr-P-C sputtered amorphous films, mag. props. and corrosion resist. 79−28567
Fe-Ci, high permeability, mag. props., applied stress effects 80−34726
Fe-Co, amorphous alloy, stress effect on mag. domain struct. 79−33502
Fe-Co (46%) film, evaporated, uniaxial mag. anisotropy 77−51929
Fe-Co amorphous ribbon, mag. props. in low fields 79−73777
Fe-Co-Ni-Si-B amorphous alloy, magnetostriction and permeability, effect of annealing 79−1701
Fe-Co-V, anelastic phenomena, related to atomic order, exam. of magnetostriction *(French)* 78−80579
Fe-Cr-B, amorphous, Elinvar and Invar charact. *(Japanese)* 80−11832
Fe-Cr-B amorphous alloys, corrosion resistance, Invar and Elinvar charcts. *(Japanese)* 79−96213
Fe-Cr-Co, heat treatment effect on strain gauge factor *(Japanese)* 78−6954
Fe-Mn alloy, magnetovolumetric anomaly *(Russian)* 78−64248
Fe-Ni, coercive force depend. on grain struct. and inclusions 77−20635
Fe-Ni, mechanisms of EM generation and detection of US Lamb waves 78−39382
Fe-Ni alloy, low-noise, for cores of ferromag. probes and mag. modulators 79−8017
Fe-Ni alloy toroidal core, magnetic noise *(Russian)* 78−60308
Fe-Ni alloys, Invar effect explanation in localised moment model *(Russian)* 77−76580
Fe-Ni based metallic glasses, hydrostatic press. effect on mag. props. 78−19300
Fe-Ni FCC alloys, invar effect by local moment model 77−90006
Fe-Ni Invar, magnetovolume coupling enhancement factor, temp. depend. 80−88851
Fe-Ni Invar alloys, forced and spontaneous magnetostriction 78−48019
Fe-Ni Invar alloys, thermodynamic props. 79−56560
Fe-P-B-Al, amorphous, magnetostriction as function of glass formers 78−19299

magnetostriction continued
Fe-Pd crystalline alloy, positive large linear magnetostriction 80−25173
Fe-Pd Invar alloy, Young's modulus, magnetostriction, Curie temp. 80−65988
Fe-Pt, Invar alloy, strong ferromagnetism, magnetostriction and thermal expansion 79−8037
Fe-Pt, Invar alloy, thermodynamic properties, effects of forced magnetostriction 79−11331
Fe-Pt, Invar type, charact. magnetovolume effects 79−82855
Fe-Pt Invar, magnetovolume effects 79−56597
Fe-Pt Invar alloy, homogeneous strong ferromagnet, thermal expansion and mag. props 79−91278
Fe-R alloys, mag. elastic properties 78−52331
Fe-Si, (110) [001] oriented, mag. props., compressive stress effects 80−60392
Fe-Si, amorphous film, comp. depend. 77−1575
Fe-Si, grain oriented transformer sheets, permeability and magnetostriction, tensile stress effects 80−88843
Fe-Si, grain-oriented, AC magnetostriction at high temp., mag. annealing effects 77−20672
Fe-Si, grain-oriented, magnetostriction, and domain struct. 79−1703
Fe-Si, grain-oriented, surface coating effect on transverse magnetostriction 77−66402
Fe-Si, internal friction anisotropy, dynamic magnetostriction *(Russian)* 78−2194
Fe-Si (110)[001} sheet, normal stress effect on magnetostriction 77−40102
Fe-Si (3 wt.%), domain wall spacing and losses, orientation depend. 78−56343
Fe-Si (3 wt.%), Goss oriented, stress effects 78−91916
Fe-Si (3 wt.%), grain orientated, negative magnetostriction, theory 78−91917
Fe-Si (3 wt.%), mag. loss and magnetostriction, DC flux alternation effects 80−88794
Fe-Si (3 wt.%), mag. props., stress coating effects 80−34728
Fe-Si (3 wt.%) grain-oriented transformer sheet, effect of phosphate coating containing Cr_2O_3 and CaO 77−16135
Fe-Si (3 wt.%) laminations, isotropic and cube-on-face, magnetostriction behaviour 80−39843
Fe-Si (3 wt.%) laminations, magnetostriction behaviour associated with closure domain spikes 80−75834
Fe-Si (3 wt.%) steel, high permeability, magnetostriction, stress inducing coating effects 80−34730
Fe-Si (3.25 wt.%), mag. props., influence of struct. and chemical composition of surface oxide layer 78−2700
Fe-Si (6.5 wt.%), effect of ordering on mag. props. 79−51833
Fe-Si (up to 8 wt.%), magnetostriction temp. and comp. depend. 77−66405
Fe-Si amorphous films, mag. and magnetoelastic props. 79−99746
Fe-Si ferromag. film, props. 79−4709
Fe-Si single crysts., interaction of {110} 90° walls with lattice imperfections 80−39807
Fe-Si-Al (6,4 wt.%), Sendust alloy, effect of Ni content on mag. props. 78−72897
Fe-Si-Al-Ni alloy, Super Sendust, Ni content and thermomag. treatment effects 77−4861
Fe-Si-B amorphous films, mag. props. 80−34710
$(Fe\text{-}Co\text{-}Ni)_{78}Si_8B_{14}$, amorphous, low coercivity and zero magnetostriction 78−23299
Fe_3Al, ordered, magnetostriction and thermal expansion 80−39842
$Fe_{3-x}Al_xO_4$, cation distrib., mag. and other phys. props. 77−43818
$Fe_{1-x}B_x$ amorphous films, mag. props. and thermal stability 79−78446
$Fe_{100-x}B_x$ ($11.5 \leq x \leq 22$), magneto-volume effect 78−91922
$Fe_{100-x}B_x$ amorphous alloys, magnetostriction meas. 79−19760
$Fe_{100-x}B_x$, amorphous alloys, saturation magnetostriction and annealing behaviour 80−34739
$Fe_{100-x}B_x$ glass, magnetostriction meas., temp. depend. 79−73792
$Fe_{100-x}B_x$ ribbon, magnetostriction exam. 79−73794
$Fe_{80}B_{20}$, binary amorphous ferromagnet, magnetostriction constant 79−4749
$Fe_{80}B_{20}$ glass, low-field mag. props. 77−8380
$Fe_{80}B_{20}$ glass, temp. depend. of magnetostriction 77−59443
$Fe_{80}B_{20}$, magnetostriction, temp. depend. 78−91921
$Fe_{80}B_{20}$, metallic glass, ferromag. props. 77−16107
$Fe_{80}B_{20}$ metallic glass, crystn. and struct. relax., Mossbauer effect study 80−75182
$Fe_{80}(B_yC_{1-y})_{20}$, amorphous, saturation magnetostriction, comp. effects 80−34735
$Fe_{80}B_{15}Si_5$ metallic glass, large uniaxial magnetostrictive anisotropy, magnetisation reversal 80−34736
$Fe_{80}(B_ySi_{1-y})_{20}$, amorphous, saturation magnetostriction, comp. effects 80−34735
$Fe_{81.5}B_{14.5}Si_4$, amorphous metal ribbon, stresses, magnetoelastic anisotropy and zero-field mag. domain struct. 80−44896
$Fe_{100-x}Be_x$, amorphous ribbon, saturation magnetostriction, and electronically controllable delay line 79−1700
Fe_xC_{1-x} amorphous sputtered film, mag. props. 78−68311
$Fe_{80-x}Co_xB_{20}$, ferromag. metallic glass saturation magnetostriction meas. 77−36108
$Fe_{35}Co_{32}B_{20}Si_{10}Al_3$, stress-induced variation in magnetisation and dynamic magnetostrictive charact. 80−88855
$(FeCoNi)_8B_{20}$, glass, evidence supporting split-band model from magnetostriction 78−95509
$(Fe_xCo_yNi_{1-x-y})_{78}Si_8Bi_{14}$ amorphous ribbons, saturation magnetostriction and vol. magnetostriction 77−85538
$(Fe_{1-x}Co_x)_{80}P_{13}C_7$ amorphous alloy, soft mag. material, props. 77−4533
$(Fe_{0.9}Co_{0.1})_xSi_yB_2$, $(Fe_{1-x}Co_x)_{78}Si_8B_{14}$ amorphous ribbons, magnetomech. coupling and saturation magnetostriction 78−68353
$(Fe_{1-x}Co_x)_{75}Si_{15}B_{10}$ amorphous alloy, soft mag. material, props. 77−4533
$(Fe_{1-x}Co_x)_{78}Si_8B_{14}$ ribbon, magnetostriction exam. 79−73794
$Fe_5Co_{70}Si_{15}B_{10}$, amorphous ribbon, zero magnetostriction, low residual mag. loss 77−12157
$(Fe_xCo_{1-x})_{100-y}(Si_{0.4}B_{0.6})_y$ amorphous alloy zero magnetostrictive, mag. props. 79−99743
$(Fe_xCo_{1-x})_{78}Si_8B_{14}$, amorphous, saturation magnetostriction, strain modulated FMR obs. 80−75863
$FeGe_2$, antiferromag., Fermi surface, stress effects, oscillatory magnetostriction and torque meas. 80−103616
$Fe_{80-x}Ni_xB_{20}$, ferromag. metallic glass, saturation magnetostriction meas. 77−36108

magnetostriction continued
$(Fe_{1-x}Ni_x)_{80}B_{20}$ amorphous soft magnetic films 79−82836
$(Fe_xNi_{1-x})_{80}B_{20}$, $(Fe_xNi_{1-x})_{80}P_{14}B_6$, new soft amorphous ferromagnetic glasses *(Croatian)* 79−11298
$(Fe_xNi_{1-x})_{80}B_{20}$, amorphous alloys, engineering mag. props. 79−51832
$Fe_{80-x}Ni_xB_{20-y}P_y$, amorphous, Rayleigh region and coercive force 80−88806
$(FeNi)_{80}Bi_{17.5}Al_2Si_{0.5}$, stress-induced variation in magnetisation and dynamic magnetostrictive charact. 80−88855
$Fe_{40}Ni_{40}(Mo,Si,B)_{20}$, amorphous, soft mag. props., switched-mode power supply appls. 80−88850
$Fe_{40}Ni_{38}Mo_4B_{18}$ glassy alloy, high permeability, low field mag. charact. 78−68301
$(Fe_{1-x}Ni_x)_{80}P_{10}B_{10}$, amorphous, magnetostriction meas. by ferromag. reson., induced anisotropy 77−32232
$Fe_{40}Ni_{40}P_{14}B_{06}$, amorphous, strip domains, anisotropy const. effects 80−29571
$Fe_{40}Ni_{40}P_{14}B_6$ Metglass, spontaneous vibr. modes excited by reversible magnetostriction 79−56587
α-Fe_2O_3, haematite, birefr. under uniaxial stress in mag. field *(Russian)* 78−88285
γ-Fe_2O_3:Co, impact-induced demagnetisation, magnetostriction and coercive force, appl. in mag. recording 77−16111
Fe_3O_4, magnetocrystalline anisotropy, anomolies in magnetostriction and elastic constants 80−60244
Fe_3O_4, magnetoelastic coupling effect on anisotropy below transition temp. 77−69657
Fe_3O_4:Co, impact-induced demagnetisation, magnetostriction and coercive force, appl. in mag. recording 77−16111
$Fe_{75}P_{15}C_{10}$, temp. depend. of the ΔE-effect 78−80188
$Fe_{1-x}Pd_x$ film, UHV deposited, effects of applied stress on B-H loops 78−64239
Fe_3Pd, quenched, or annealed exam. of magnetostriction, galvano- and thermomagnetic props. *(Russian)* 79−19757
Fe_3Pt Invar alloy, mag. props., martensitic transform. 79−78365
Fe_3Pt, Invar alloy, theory of elastic-anomalies 78−95505
FeS, zinc blende type, crystallographic and Mossbauer obs. 78−87650
Fe_3Se_4, thermal expansion, compressibility, magnetisation, susceptibility and magnetostriction 77−66318
$Fe_{100-x}Si_x$ ribbon, magnetostriction exam. 79−73794
$Fe_xSi_yAl_z$ ribbon, magnetostriction exam. 79−73794
$Fe_2(Tb_{0.2}Dy_{0.22}Ho_{0.58})$, highly magnetostrictive alloy, vibrating-reed meas. of ΔE effect and internal friction 79−42819
$Fe_{1-x}Ti_x$, ferromag. props., Ti conc. effect 80−54872
Fe_2TiO_4, cooperative Jahn-Teller effect, neutron scatt. study 80−49678
$GDCo_2$, forced vol. magnetostriction and induced moment 77−36106
$(Gd,Lu)_3(Fe,Mn,Al)_5O_{12}$ epilayer with orthorhombic anisotropy, domain wall vel. 78−52322
Gd compounds, NaCl type, exchange striction 78−84409
Gd, magnetoelastic excitations and ferromagnetic resonance 79−82879
Gd-Co amorphous sputtered film, magnetostriction and anisotropy 80−39821
Gd-Dy, thermal expansion meas., exchange and magnetocryst. interactions *(Russian)* 77−12184
Gd-Fe, amorphous sputtered film, magnetoelastic coupling energy const. 79−47320
Gd-Fe amorphous films, stress contrib. to perpendicular anisotropy 80−75819
$GdAl_2$, anisotropy and magnetostriction 78−10741
$GdCo_2$, magnetovolume effects in itinerant electron ferromagnets 79−8038
$Gd_{1-x}Co_x$ amorphous thin film, magnetostriction 79−91281
$Gd(Co_{1-x}Ni_x)_2$ compounds, NMR and thermal expansion 80−66070
$GdVO_4$, antiferromag., US attenuation at 9 GHz 77−24728
$Gd_xY_{1-x}Fe_3$, saturation magnetisation, magnetostriction, Curie temp., ferrimag. ordering, exchange field *(Russian)* 78−68343
Ge, electron-hole drop magnetostruction 78−87912
Ge, field induced distortion of electron-hole drop 77−85540
$HgCr_2Se_4$, influence of Co ions on anisotropy and magnetostriction, ferromag. reson. meas. 77−69659
Ho, low field susceptibility and helical-ferromag. field induced phase transition 78−47975
$HoCo_2$, field induced vol. magnetostriction 78−91920
$HoCo_2$, vol. magnetostriction, point charge cryst. field model 77−63254
Ho_2Co_{17}, magnetisation, magnetocryst. anisotropy and magnetostriction 77−8303
Ho_2Co_{17}, single cryst., magnetostriction const. temp. depend., 78 to 300K 79−51836
$Ho_xDy_yTb_{1-x-y}Fe_2$, Laves phase cpds., anisotropy and magnetostriction 77−63167
$HoFe_2$, magnetostriction and magnetisation temp. depend. 79−73795
$HoFe_3$ and Ho_6Fe_{23}, magnetostriction, room temp. to 80K 80−65993
Ho_6Fe_{23}, magnetostriction, temp. depend., 20 to 350K 80−65994
$HoRh_4B_4$, low temperature magnetic properties 80−88728
$Ho_{0.58}Tb_{0.2}Dy_{0.22}Fe_2$ magnetoelastic surface wave dispersion obs. 79−47321
$Ho_xTb_{1-x}Fe_2$, and $Ho_xTb_yDy_{1-x-y}Fe_2$, high magnetostriction cpd., mag. anisotropy origins 78−68217
$K_2CuCl_4.2H_2O$ structures, BCC Heisenberg ferromags., transferred hyperfine interactions of ^{17}O, magnetostriction effects 77−69725
$KNiF_3$, low anisotropy antiferromag., phase boundary crossover behaviour 79−38324
$KNiF_3$, magnetostriction, X-ray diffractometry and strain gauge meas. 80−65997
Li-Co ferrite, mag. anisotropy induced by thermomag. treatment, ionic order effect, magnetostriction meas. 80−103830
$Li_{0.5}Fe_{2.5}O_4$, microwave material, mag. props., review 79−33504
$Li_{0.5}Ga_{0.095}Fe_{1.55}O_4$ ferrites, linear magnetostriction in weak field, 150 to 300K *(Russian)* 77−80983
$LiTmF_4$, van-Vleck paramagnet, giant magnetostriction *(Russian)* 80−103872
$Li[Ni_{0.5}Mn_{1.5}]O_4$, magnetisation and magnetostriction, fields up to 11 kOe, 4-160K *(Russian)* 78−19304
Lu_2Co_{17}, single cryst., magnetostriction const. temp. depend., 78 to 300K 79−51836
Mg-Tb(Dy)(Ho)(Tm), dil., macroscopic shape effect due to quadrupole orientation, magnetostriction and thermal expansion meas. 80−60396
$Mg_xFe_{3-x}O_4$, magnetostriction consts., 80 to 320K 78−95503
MgMn ferrite film, determ. by ferromag. reson. method *(Russian)* 77−16126
Mn-Ni, thermal expansion, mag. susceptibility, lattice consts. 80−100341
magnetostriction continued
Mn-Ni alloys, antiferromag., Invar-like thermal expansion and spontaneous volume magnetostriction 77−69654
Mn-Ni alloys, Mn-rich, structural changes associated with antiferromag. ordering 77−69085
MnAs pseudocrystals, ferromag. and ferro-paramag. transition region 77−4537
$(Mn_{1-x}Cr_x(Fe_x))B$, Invar charact. 77−15602
MnFe ferrite, mechanically induced anisotropy, effect on mag. permeability 78−47970
$Mn_{1+x}Fe_{2-x}O_4$, magnetostriction meas., inversion degree influence 77−73070
MnO, antiferromag. reson., press. depend., and magnetostriction consts. 78−19339
MnO, linear optical anisotropy meas. at antiferromag. transition 77−36205
MnSi, US velocity anomalies near mag. transition 78−19302
MnZn ferrite, mechanically induced anisotropy, effect on mag. permeability 78−47970
MnZn ferrite disc, excitation of radial mode vibration due to AC 79−69708
MnZn polished ferrite, electron diffraction meas. method appl. *(Japanese)* 78−10742
$Mn_{0.4}Zn_{0.42}Fe_{2.16}O_{4+x}$, permeability, rel. to intrinsic mag. props. 79−4702
Mo, Fermi surface, homogeneous strain response 78−34753
Mo-permalloy, magnetic permeability and order form. kinetics under annealing, conc. depend. 77−8356
NH_3 halides, acoustic anomalies above critical temps., volume magnetostriction type terms 80−2123
$NaFeF_2$, Mossbauer and low-temp. dilatometry study *(French)* 80−80662
$NdAl_2$, magnetostriction in high mag. fields 79−99745
Ni, alloying effect of magnetostriction and rolling texture *(Russian)* 77−32229
Ni, and Ni alloys, texture and magnetostriction 77−36671
Ni, effective mag. anisotropy const., magnetoelastic contrib. 78−14951
Ni, electrodeposited film, saturation magnetisation and perpendicular anisotropy meas. 78−76277
Ni electrodeposits on (001)Cu films, growth and mag. anisotropy 79−42810
Ni film, effect of He ion implantation on domain struct., Lorentz electron microscopy 77−20654
Ni film, evaporated, for use as variable delay SAW device, magnetostrictive effects 80−71144
Ni film, evaporated, uniaxial mag. anisotropy 77−51929
Ni film, ferromag. reson., thermodynamical anal., effect of mech. stress 79−42840
Ni film, strained and strain-free, ferromag. reson. meas. 78−95525
Ni, forced magnetostriction at 4.2K 80−50155
Ni, magnetoelastic and magnetostrictive sensitivities, reversible and irreversible components *(Russian)* 80−25172
Ni, magnetoelastic excitations and ferromagnetic resonance 79−82879
Ni, magnetostriction, lattice parameter changes, direct X-ray obs. 78−15001
Ni, magnetostrictive vibr. obs. by laser interferometric technique 80−66000
Ni, Matteucci effect for tubular samples 78−43620
Ni, modulus defect due to internal strain 78−76286
Ni, NP-2T, effects of compression on magnetostriction 77−40109
Ni, rectilinear screw dislocation, magnetisation distrib., mag. moment anal. 80−44897
Ni rod, spontaneous vibr. modes excited by reversible magnetostriction 79−56587
Ni, spontaneous magnetostriction determ. method, molecular field theory study *(Russian)* 80−50157
Ni, thermal softening, influence of alternating mag. field *(Russian)* 78−23312
Ni, transduction efficiency using magnetostrictively coupled meander-coil EM transducers 79−46144
Ni, twisted tubular polycryst. sample in axial mag. field, circular magnetisation 77−32230
Ni wire, polycryst., inverse Wiedemann effect for low torsional stress 79−11332
Ni-B thin film glasses, mag. props. and corrosion resist. 80−80576
Ni-Co (25 wt.%), single crysts., mag. annealing effect on magnetostriction and magnetisation *(Japanese)* 80−34744
Ni-Co (25 wt.%), single crysts., mag. annealing effect on magnetostriction and magnetisation at high temps. 80−108047
Ni-Co amorphous alloys, magnetostriction 80−34738
Ni-Fe, film, domain struct., effect of biaxial stresses 78−88153
Ni-Fe, soft mag. props. rel. to metallurgical aspects 80−88810
Ni-Fe, split bands rel. to sp. ht., g-factor and magnetostriction data 77−72977
Ni-Fe (15%) film, evaporated, uniaxial mag. anisotropy 77−51929
Ni-Fe film, domain struct., uniaxial stress effects 78−10740
Ni-Fe-Cr, extraordinary Hall effect, elec. and mag. meas. at 77 and 300K 80−34421
Ni-Fe-Nb, Hardperm, origin of high magnetic permeability 77−8362
Ni-Fe-Nb-Mo (11.42, 6.92, 1.54 wt.%), Hardperm, high magnetic permeability alloys 77−8361
Ni-P electrodeposit, magnetisation coercivity and magnetostriction 78−68338
Ni-Pd alloy, magnetostriction and mag. anisotropy meas. 79−4713
Ni-Pt alloys, mag. props. under hydrostatic press. 78−6556
Ni-Rh alloys, disordered, vol. paramagnetostriction calc. 77−80985
Ni-Ru (3.3 at%), magnetisation, magnetocrystalline anisotropy, magnetostriction and elastic consts., thermal variations 79−28563
NiF_2, thermal expansion and magnetostriction, 55K to room temp. 80−80586
NiFe film, ferromag. reson., thermodynamical anal., effect of mech. stress 79−42840
NiFe, magnetising energy, anisotropic effects 80−88743
NiFe soft magnetic alloys, magnetic props., effect of annealing and fabrication *(German)* 78−53004
$Ni_{50}Fe_{30}B_{20}$, magnetostriction, temp. depend. 78−91921
$Ni_xFe_{3-x}O_4$, magnetostriction, 80 to 300K, depend. on comp. and electron ordering on octahedral sites 80−65995
NiO, exchange striction 78−56309
$Ni_{1-x}Ti_x$, ferromag. props., Ti conc. effect 80−54872

magnetostriction continued
NiZnCo ferrite, excess Fe type, saturation magnetostriction meas., oxidation effects 79−82852
$Ni_{0.8}Zn_{0.2}Fe_2O_4$, twisted tubular polycryst. sample in axial mag. field, circular magnetisation 77−32230
$(Ni_xZn_{1-x})_{0.5}Fe_2O_4$, spontaneous vibr. modes excited by reversible magnetostriction 79−56587
O_2 monolayers, on graphite, mag. α-phase and α-β-phase transition 80−70530
Pb, Fermi surface, uniaxial stress depend. 79−65362
Pd-Fe alloys, dil., anisotropy of neutron polarisation near ferromag. phase transition 77−32234
Pd-Fe-Mn, ferromagnet-spin glass, thermal expansion forced, magnetostriction and magnetisation under high press. 80−65255
Pd-Ni, thermal expansion and magnetostriction meas. near crit. conc. for ferromagnetism 80−65881
Pd-Rh alloys, disordered, vol. paramagnetostriction calc. 77−80985
Pr, magnetisation and magnetostriction in pulse fields from 3-78K 79−99747
Pt-Ni alloys, disordered, vol. paramagnetostriction calc. 77−80985
rare earth-Tb-Fe alloys, $R_xTb_{1-x}Fe_2$, (R=Gd, Sm, Dy, He, Zr), props. of near magnetostrictive materials 77−51934
$RbMnF_3$, antiferromag., mag. props. 79−8032
Re, Fermi surface, Landau quantum oscill. meas. in magnetostriction, stress and strain derivatives 80−107691
Si-Fe, ferromagnetic domains and their junctions, simulation of X-ray topographs 79−78434
$SmCo_5$, intrinsic magnetic props. 79−82779
$SmCo_5$, single cryst. and liq. phase sintered, field depend. 77−63245
$SmFe_3$ and Sm_6Fe_{23}, magnetostriction, room temp. to 80K 80−65993
$SmFeO_3$, magnetostriction meas. in spin reorientation region 78−2721
SmIG, correlation between magnetostriction effect and transition hysteresis 79−73761
$Sm_xY_{3-x}Fe_5O_{12}$, magnetostriction comp. depend., 78 to 300K 77−77082
$(SrCaR)_2(Cr_xGa_{1-x})O_4$, R=La or Sm, mag. 2-D oxide, phys. props. 78−47974
(Tb,Dy)-Fe amorphous films prep. by cosputtering, magnetoelastic props. 80−97429
(Tb,Dy)Fe_2 alloys, giant magnetostriction *(Chinese)* 79−51830
Tb compounds with garnet and zircon structure, anisotropic magnetoelastic props. 77−69660
Tb, high-pressure phase, mag. field effects *(Russian)* 77−66021
Tb-Fe, amorphous sputtered film, magnetoelastic coupling energy const. 79−47320
Tb-Gd, spontaneous striction and phonon contributions to thermal expansion *(Russian)* 79−90800
Tb-Gd alloy, spin orientation transition obs. 79−99714
Tb-Y, Fermi surface topology var., mag. and elec. props. *(Russian)* 77−80723
Tb-Y, helicoid antiferromag. ferromag. transition, magnetostriction and magnetocaloric effect *(Russian)* 77−80937
Tb-Y, magnetostriction, mag. and elec. props. 78−27068
$TbAl_2$, origin of magnetostriction 79−78499
$TbCo_2$, magnetocrystalline anisotropy and spontaneous magnetostriction 80−75831
$TbCo_2$, origin of magnetostriction 79−78499
$TbCo_2$, rhombohedral distortion at low temp. 80−34743
$TbCo_2$, X-ray obs. of low temp. modifications of crystal struct. *(Russian)* 78−75632
Tb_2Co_{17}, magnetisation, magnetocryst. anisotropy and magnetostriction 77−8303
$Tb_{0.27}Dy_{0.13}Fe_{1.98}$, grain-oriented, permeability, magnetomechanical coupling and magnetostriction 79−78491
$Tb_{0.27}Dy_{0.73}Fe_2$, anomalous thermal expansion and magnetostriction 77−90003
$Tb_{0.27}Dy_{0.73}Fe_2$, magnetisation and magnetic anisotropy 78−91862
$Tb_{0.27}Dy_{0.73}Fe_2$, vertically zoned, magnetomechanical coupling and magnetostriction 80−65999
$Tb_{0.3}Dy_{0.7}Fe_2$, magnetostrictive, resonant coupling of shear waves 79−33517
$Tb_{0.3}Dy_{0.7}Fe_2$, prep. by powder metallurgy, magnetostrictive props. 80−75826
$Tb_{0.3}Dy_{0.7}Fe_2$, US velocity and attenuation obs. 77−28423
$Tb_xDy_{1-x}Fe_2$, Laves phase alloy, magnetostriction depend. on powder orientation before sintering 78−76284
$Tb_{0.20}Dy_{0.22}Ho_{0.58}Fe_{1.95}$, grain-oriented, permeability, magnetomechanical coupling and magnetostriction 79−78491
$TbFe_2$, high field magnetostriction and magnetisation 78−84471
$TbFe_2$, magnetisation and magnetic anisotropy 78−91862
$TbFe_2$, magnetoelastic props., magnetostriction hysteresis *(Russian)* 80−29590
$TbFe_2$, X-ray obs. of low temp. modifications of crystal struct. *(Russian)* 78−75632
$TbFe_3$ and Tb_6Fe_{23}, magnetostriction, room temp. to 80K 80−65993
Tb_xFe_{1-x} film, amorphous, magnetostriction and magnetisation 78−68305
$TbFeO_3$, metamag. phase transitions, mag. struct. instability *(Russian)* 79−61107
$Tb_xGd_{1-x}Al_2$, magnetic anisotropy, magnetostriction 78−56364
TbIG, [111] magnetoelastic props., rel. to Cotton-Mouton birefringence, 90-500K 80−103876
TbIG, anisotropic forced magnetostriction meas. 78−64251
$Tb_2Lu_1Fe_5O_{12}$ film, magnetostriction meas. using double cryst. X-ray diffractometry 78−84468
$TbPO_4$, anomalous magnetostriction at low temp. 78−84470
$Tb_{1-x}Y_x$ alloy, helicoidal antiferromag. to ferromag. transition 78−10687
$Tb_xY_{3-x}Fe_5O_{12}$, correlation between magnetostriction effect and transition hysteresis 79−73761
$Tb_xY_{3-x}Fe_5O_{12}$, anomalies of magnetisation and magnetostriction obs. in strong fields, 4.2K 77−1581
Tm_2Co_{17}, single cryst., magnetostriction const. temp. depend., 78 to 300K 79−51836
$TmFe_2$, low temp. magnetisation and magnetostriction 78−64249
$TmFe_2$, magnetisation and magnetic anisotropy 78−91862
$TmFe_3$ and Tm_6Fe_{23}, magnetostriction, room temp. to 80K 80−65993
TmSe, mixed valence cpd., thermal, mag., and transport props. 79−61074
Tm_xSe, $0.87<x<1.05$, mag., thermal and transport props., comp. depend. 78−68239
magnetostriction continued
$TmSe_{0.83}Te_{0.17}$, spontaneous magnetisation, mag. susceptibility, magnetostriction, elec. cond. 79−24146
TmZn, cooperative Jahn-Teller effect 78−67998
UAs_xSe_{1-x}, lattice distortion below Curie temp. 77−63252
UGa_2, cryst. struct., mag. and magnetoelastic props. *(Russian)* 79−38364
UGa_2, mag. and magnetoelastic props. 80−15775
US, elastic consts. temp. depend. in para- and ferromag. regions 79−77666
V_3Si, US anomaly when cooled below martensitic and supercond. transition temps. 80−20354
W, Fermi surface, uniaxial strain depend., quantum oscills. in magnetostriction, US vel., with torque 77−28094
Y_6Fe_{23}, magnetostriction, temp. depend., 20 to 350K 80−65994
$Y_3Fe_{5-x}Al_xO_{12}$, $Y_{3-x}Gd_xFe_5O_{12}$, linear expansion 77−48024
$Y_3Fe_{5-x-y}Co_xGe_yO_{12}$, anisotropy and magnetostriction, ferromag. reson. expts., 4.2-500K 78−27030
$YFe_{1-x}Co_{x/2}Ti_{x/2}O_3$, magnetostriction meas. in spin reorientation region 78−2721
$YFe_{0.62}Cr_{0.38}O_3$, compensation of weakly ferrimag. moment 79−8035
YIG, magnetostriction meas. with recording rot. field magnetostrictometer 78−12733
YIG, porous and fine grain polycrystalline, temp. depend. of effective linewidth 77−85574
YIG:Fe^{2+}, magnetostriction const. temp. depend., ferromag. reson. meas. 77−40103
YIG:V, mag. anisotropy and magnetostriction, effect of V 78−27029
$Y_{2.85}La_{0.15}Fe_{3.75}Ga_{1.25}O_{12}$ epitaxial film, magnetostriction consts., microwave reson. meas. 77−24716
YPd_3, rare earth impurities, magnetostriction 79−4714
$Y_{1.62}Sm_{0.21}$ $Lu_{0.27}Cu_{0.9}Ge_{0.9}Fe_{4.1}O_{12}$, implanted bubble garnet, anisotropy profile, FMR study 80−7103
$Y_{1-x}Tb_xPd_3$, magnetisation, magnetostriction, and inelastic neutron spectra 80−65998
YbB_4, mag. props. *(French)* 77−20566
YbCuAl, mixed-valent cpd., thermal expansion and magneto-volume effects 80−66005
$YbFe_2$, cryst. elec. field and exchange interac., ^{170}Yb Mossbauer obs., magnetostriction contrib. 80−108124
$YbFe_2$, Mossbauer spectra, cryst. elec. field and exchange interaction 79−47368
$Zn_2BaFe_{12}O_{22}$, mag. phase transitions, magnetostriction temp. depend. *(Russian)* 78−34983
$Zn_2Ba_2Fe_{12}O_{22}$, phase transition, mag. props. *(Russian)* 79−51837
$Zr(Fe_{1-x}Co_x)_2$, ferromag. and mictomag., thermal expansion and forced volume magnetostriction 80−75830
$Zr(Fe_{1-x}Co_x)_2$, magnetovolume effects, thermal expansion and forced vol. magnetostriction meas. 80−29595
$(Zr_{1-x}Nb_x)Fe_2$, magnetovolume effects and Invar characters 80−15773
$Zr_xTb_{1-x}Fe_2$, Laves phase alloys, magnetostriction *(Russian)* 77−51932

magnetostrictive devices
amplifier-discriminator for magnetostriction spark chambers 78−868
diffraction grating residual ruling errors, magnetostrictive correction method 79−50454
force transducer, digital, using multi-aperture ferrite core *(Japanese)* 79−93133
force transducer 79−2757
magnetic bubble lattice propagation control by standing acoustic waves 79−82841
magnetostrictive core dimens., influence on internal friction and shear modulus 'defect' 78−95506
mobility analogy equivalent cct. of magnetostrictive transducer in presence of eddy currents 80−48540
parallel recording system for magnetostrictive spark chambers 78−867
radiating magnetostrictive transducers, impedance determ. 79−32173
radiation reactance of magnetostrictive transducer, spherical scatterer effect 80−48531
rare earth iron magnetostrictive underwater sound transducer 78−13881
reactor diagnosis by acoustic meas. methods, magnetostrictive and piezoelec. high-temp.-resistant sensors 80−32411
review of materials and devices *(Japanese)* 78−23316
SAW delay line, variable, using magnetostrictive metallic glass film overlays 78−63240
transducer, accuracy study *(Bulgarian)* 77−53878
transducer, electrical matching technique 77−35008
transducer, Fe-cored, choke-type, compressive force meas. *(Polish)* 78−12684
transducer, wideband electrical matching 78−5626
transducer sonar, hollow spherical scatterer effects on radiation resistance at air-water surface 77−39125
transducer terminated in arbitrary elec. impedance, elec. cct. anal. 78−5627
transducers, magnetostrictively coupled meander-coil EM, horizontally polarised shear wave generation in ferromagnets 79−46144
transducers, matching with cavitating water 78−94503
US magnetostriction vibrator efficiency meas. *(Japanese)* 78−9523
US probes using extensional, torsional and flexural waves 79−50562
wire readout system for spark chamber, transducer S/N ratio improvement 77−79518
Fe-Al (12 wt.%) alloy 23 kHz US transducer piezomagnetic props. 78−59240
(Tb,Dy)-Fe amorphous films prep. by cosputtering, delay line characts. 80−97429

magnetostrictive microphones *see microphones*

magnetostrictive transducers *see magnetostrictive devices; transducers*

magnetothermal effects *see magnetocaloric effects*

magnetrons
anode sheath, crossed field low press. discharge in magnetron and Penning cell 77−11432
cavity plane magnetron, averaging method, electron tongues *(Russian)* 78−37037
circular magnetrons, high rate sputter deposition 78−72665
cold cathode ion gun for sputter etching apparatus 79−34170
cylindrical magnetron, prod. of annular electron bunches 77−10136
diode, cathode heating and back bombardment, calcs. 77−8713
discharge, DC, Ar filled diode, spectroscopic obs. 80−44010
gas discharge, magnetron geometry, mag. field and press. effects 77−43090

magnetrons continued
helical electron beam shaping using synthesis of axially symmetrical systems 80−309
injection guns used in screw electron beams in cyclotron resonance masers, synthesis *(Russian)* 78−17889
ion magnetron, with split electrodes, radial ion (electron) cluster rot., fusion appl. 78−17415
ion magnetron scaling law 79−27855
ion source of inert gas ions, highly effective 78−66003
ion sputtering, thin film layers deposition uniformity investigation *(Russian)* 80−20787
ion-sputtering system operating principles and appls. 79−100050
lens magnetron tetrode, 8 mm, oscillation control *(Russian)* 79−26070
magnetic discharge cells with nonuniform periodic magnetic field 80−101799
manometer, magnetic-discharge open-type, with inhomogeneous mag. field 80−31730
mass spectrometer appl. using inverse magnetron and ion source on outside 80−57416
microspherical substrates, magnetron sputter coating, appl. to laser fusion targets 79−78883
microtron booster resonator in HF path 78−830
microwave power source for electrodeless discharge lamps 79−36969
moving deposition mode of magnetron sputtering *(German)* 78−39690
negative ion high current beams, source plasma parameters determ. 77−83376
oscillations spectra, average freq. depend. on anode voltage 77−49747
planar magnetron sputtering 78−72725
planar-magnetron sputtering source, modified 78−95693
plasma production modified magnetron discharge facility 78−75380
reactive DC sputtering, magnetron-plasmatron processing and instrumentation, review 80−35090
relativistic, diffracted output 600 kV anode voltage, 500 MW peak power, 3.3 cm, 20 ns *(Russian)* 78−24823
relativistic, intense microwave emission 79−12822
sputtering equipment and application status 79−83124
sputtering source, design of production sputtering system 79−66006
sputtering source with coaxial cylindrical electrode config. *(Japanese)* 78−23617
sputtering target/substrate configuration 78−39687
sputtering with magnetron cathode *(Czech)* 79−52114
stability, amplitude and freq. fluctuation reduction by cathode emission control 77−49746
H^- ion source 77−38528

magnets
see also electromagnets; permanent magnets; superconducting magnets
airgap, EM field uniformity correction by coil correct design *(Russian)* 77−53959
bar magnets, torque theory 77−13527
force on magnet immersed in ferrofluid, surface integral calc. 78−94350
high magnetic field behaviour of solids and plasmas, conference, Cambridge, MA, USA (Sept. 1978) 79−60667
hybrid magnets for high mag. field generation, polyhelix coils, optimization calcs. 80−240
interaction force calc. between permanent and ferromagnetic material *(Russian)* 77−26347
ion optical system, magnet design for high current implantation or small isotope separators 80−68222
low field magnet, computer controlled, for optical and magnetic resonance studies 80−95113
non-superconducting magnet structures for near-term, large fusion experimental devices 80−86973
ring shaped, mass produced, magnetic characts. meas. rate improvement *(Russian)* 77−26346
strong rare earth cobalt quadrupoles, general props. and configurations for particle accel. 79−68083
structural design features for commercial fusion power reactor magnet systems 80−86975
technology, conference, Bratislava (1977) 79−30499
Tokamak fusion reactor toroidal magnet system, technology-constrained scaling 79−76138
wiggler magnets, standard, effects on synchrotron radiation spectrum and storage ring operation 78−62670
Sm-Co ring magnets for BWO, 110 to 170 GHz, design and appl. *(German)* 80−105684
$SrO.nFe_2O_3$ isotropic ferrite magnets, manuf. process and mag. props. *(Japanese)* 80−29915

magnitude convertors
see also transducers
12 kHz IC resistance-frequency convertor *(Russian)* 78−81963
electrodynamic convertor, ring-shaped, operation and appls. *(Polish)* 78−12685
ferromagnetic DC convertor for process monitoring 77−57359
magnetic angle convertor accuracy test method 78−77948
marine seismic survey, modified integrating A/D convertor *(Russian)* 78−49142
miniature pressure-frequency convertor with pulse output 78−57926
stroboscopic, digital soft-magnetic materials properties meas. appl., during pulse remagnetisation 77−5876
thermoelectric convertor error due to crystallographic misorientation anisotropy 78−77904
thousandfold pulse duration convertor for automatic pen recorders 77−56521
time-amplitude convertor for 20 to 100 ns 77−50334

magnons
see also phonon-magnon interactions; spin waves
actinide systems, nearly magnetic, thermoelectric power determ. 78−56133
alkali hyperoxides, ionic π-electron systems, magnetogyration 80−93155
alloy, pseudobinary, ferromag., magnon energy derivation 80−107996
amorphous solids, low-energy excitations of phonons, magnons, electrons rel. to struct. factor 80−44488
anfiferromagnet, superexchange, charge transfer light absorpt. 78−34975
anharmonic, one dimensional ferromagnet, magnon and lattice deformation, bound state 79−78357
anharmonic Heisenberg ferromagnet, renormalised magnons and phonons 77−59373
anisotropic ferromagnet, one-magnon light scatt., temp. depend. 77−52063

magnons continued
anisotropic linear spin chain, two-magnon problem with arbitrary interaction radius 78−72320
antiferromagnet, biaxial low-dimensional, two-magnon absorpt. in collinear phase *(Russian)* 77−69803
antiferromagnet, cubic, flopped nuclear magnon relax. rates 77−63149
antiferromagnet, dislocation slowing down due to spin waves *(Russian)* 79−95584
antiferromagnet, easy plane, specific props. 79−1665
antiferromagnet, easy-plane, antiferromag. reson. linewidth and relax., theory 80−71189
antiferromagnet, FCC lattice of second kind, surface magnons and mag. structs. 78−23261
antiferromagnet, high frequency properties, spin wave spectra corrections magnon interactions *(Russian)* 80−54876
antiferromagnet, impure, Heisenberg model, impurity banding and mag. reson., theory 80−93181
antiferromagnet, magnon and phonon damping, effect of intermediate state lifetime 79−24151
antiferromagnet, magnon damping, influence of magnetoelastic interaction 79−28517
antiferromagnet, magnon-photon interaction for EM wave vector perpendicular to sublattice magnetisation 79−69662
antiferromagnet, neutron scatt. by magnons, modulated spin amplitudes 80−75722
antiferromagnet, NMR under magnon bottleneck conditions, eqns. of motion 77−66429
antiferromagnet, nucl. spin-lattice relax., possible magnon bottleneck 77−32283
antiferromagnet, one-magnon light scatt., effect of anisotropy 79−33676
antiferromagnet, one-magnon light scatt. from metamagnetic phase effect of anisotropy 79−33678
antiferromagnet, one-magnon light scatt. from spin-flop and paramag. regions, effect of anisotropy 79−33677
antiferromagnet, quasi-two-dimens., nonreson. HF field absorpt. *(Russian)* 77−63287
antiferromagnet, radiation problem of parallel pumping, magnon-photon interaction 79−51934
antiferromagnet, spin wave parametric instability *(Russian)* 78−34971
antiferromagnet, two-dimensional, with easy-plane anisotropy, mag. excitations and two-magnon Raman scatt. 80−65839
antiferromagnet, two-magnon Raman scatt., temp. effects 77−48178
antiferromagnet, two-magnon Raman scatt., temp. effects 77−48179
antiferromagnet, uniaxial, mag. polaritons in spin-flop phase 78−23349
antiferromagnet nucl. spin lattice relax., field depend. of dipolar-induced two-magnon process 78−6593
antiferromagnetic, light absorption in freq. region of exciton and exciton-magnon transitions 77−48149
antiferromagnetic, noncollinear, exciton-magnon light absorpt. at $T \neq O$ *(Russian)* 78−23482
antiferromagnetic insulator, light scatt. in strong mag. field 78−72523
antiferromagnetic insulator, strongly anisotropic, spin config. and magnon spectrum 77−8279
antiferromagnetic polaritons, dispersion relation and light scatt. 77−35871
antiferromagnetic polaritons, inelastic light scatt., theory 77−73144
antiferromagnetic resonance, relaxation mechanism 77−12204
antiferromagnetic resonance linewidth theory, multimagnon processes contrib. 77−69708
antiferromagnetic resonance relaxation, multimagnon processes 77−4564
antiferromagnetic semiconductor, heavily-doped, stability of canted order 77−12095
antiferromagnetic semiconductor, magnon-plasmon interaction and its effect on Raman scatt., theory 78−56302
antiferromagnetic semiconductor, magnon-spin flip excitations in Raman scatt., g-factors 77−66494
antiferromagnetic semiconductor, theory of Raman scatt. due to magnon-spin flip excitation 77−36209
antiferromagnetics, with displaced 3d-ions, mech. of electric dipole absorption of light *(Russian)* 77−32406
antiferromagnets, exciton motion 80−70617
antiferromagnets, magnon damping due to impurity scatt. 78−68206
antiferromagnets, magnon damping in zero external mag. fields, magnon-magnon interactions 80−70988
antiferromagnets, magnon parametric generation with impulses at Brillouin zone boundary *(Russian)* 80−29540
antiferromagnets, spin waves, microwave and optical expts., review 80−50081
binary ferromagnetic alloys, with itinerant electrons, magnon lifetime, theory 78−34949
biquadratic exchange systems, low temp. spectrum and elementary excitation damping 77−72969
biquadratic systems, spin 3/2, elementary excitations in antiquadrupolar, ferrimag. and ferromag. phases 79−51763
α-bis (N-methylsalicylaldiminato) copper II, one-dimens. spin-$^1/_2$ Heisenberg antiferromag., high-field spin dynamics 80−71224
Bloch wall, narrow, magnetic excitations, pole field effect 78−91853
Bose expansion for general spin, exact 80−31662
Bose gas of Heisenberg ferromag., transport eqn. 77−12112
Brillouin-Mandelstam scattering from thermal and excited magnons 80−70980
coherent generation by optical technique using mag. Raman nonlinearity 78−68201
collective excitations, brief review of expt. and theory 77−1381
cubic ferromagnet, localised magnon modes in narrow domain walls 77−69523
damping, numerical integration to fourth order of perturbation theory *(Russian)* 79−56522
damping at low temps. *(Russian)* 77−36062
DC resistivity as functional of generalised dynamical susceptibilities, solid state model 79−28330
di(alkyl ammonium)copper tetrachloride, two-dimens. magnon and phonon thermal cond. in high mag. fields 77−69123
dialkylammonium copper chloride, two-dimens. ferromag., energy transport by paramag. magnons 77−80909
dialkylammonium manganese tetrachloride, quasi two-dimensional antiferromag., temp. depend. of absorption spectra 78−43894
diethylammonium manganese chloride, antiferromag., magnon sideband exam. by absorpt. spectra 77−12108
diethylammonium manganese tetrachloride, quasi two-dimensional antiferromag., magnon sideband in absorption spectra 78−43895

magnons continued
dilute alloy, localised magnon mode in extended Wolff-Clogston 79−61097
dilute ferromagnet, slow neutron inelastic scatt. by spin excitations, cluster approx. 80−11168
dimethylammonium copper tetrachloride, two-dimens. ferromag., saturation of parallel-pumped magnons 80−97147
dislocated ferromagnet, inhomogeneous magnetisation near dislocation effect on FMR linewidth 80−25213
disordered media, spin wave propagation, nonlinear magnon interactions *(Russian)* 80−80496
dispersion relations for energy eigenvalues of two magnon bound state 78−47964
edge modes localised at apex of semi-infinite right-angle wedge 77−63148
electron-magnon interaction effects on Ward-Takahashi identities in itinerant electron ferromag. 80−39730
elementary excitations damping *(Russian)* 79−28515
ethylammoniumtetrachlorochromate, optical absorption intensity, short-range spin correlation 80−108185
FCC lattice, second-neighbour surface magnons 77−28378
ferrimagnet, one-magnon light scatt. effect of quadratic magneto-optical coupling 79−11407
ferrimagnet, polaritons, mag. susceptibility 80−7095
ferrimagnet, two sublattice, mag. polaritons 80−65845
ferrimagnetic semiconductor, cyclotron-magnon reson. 79−69725
ferrimagnetic semiconductors, magnetomagnon reson. 79−69663
ferrimagnets, one-magnon light scatt., temp. dependence, two-sublattice systems 78−31061
ferrites, frequency tripling of spin waves due to longitudinal pumping excitation *(Russian)* 80−88740
ferromagnet, anisotropic, magnon spectrum, FMR line intensity, Curie pt. behaviour *(Russian)* 77−69694
ferromagnet, anisotropic, theroy of light scatt. 77−90161
ferromagnet, chain type, with uniaxial exchange, localised one-magnon states in presence of impurity *(Russian)* 77−63143
ferromagnet, dislocation effects on phys. props. at $T \neq 0K$ *(Russian)* 77−8378
ferromagnet, dispersion relations for energy eigenvalues of two magnon bound state 78−47964
ferromagnet, domain wall dynamic slowing down *(Russian)* 79−78438
ferromagnet, flow stress, effect of magnon mechanism of dislocation drag 77−69662
ferromagnet, Heisenberg, spin wave relaxation due to dipole interactions, damping temp. depend. 79−69664
ferromagnet, Heisenberg model, two-magnon reson. in absence of bound states, calc. 80−60423
ferromagnet, itinerant electron, magnon spectrum just below T_c, theory 80−65833
ferromagnet, light scatt. by spin waves 80−45086
ferromagnet, magnon bound state formation *(Russian)* 77−63162
ferromagnet, magnon drops and mag. solitons 79−61093
ferromagnet, many-domain, indirect interaction of electrons via spin waves 77−85382
ferromagnet, multidomain with 180° Bloch walls, nonlinear magnons 78−34967
ferromagnet, NMR, under magnon bottleneck conditions, eqns. of motion 77−66429
ferromagnet, nonequilibrium magnon state under nonresonance alternating mag. field 79−87248
ferromagnet, nonlinear localised magnetisation wave as bound state of large no. of magnons *(Russian)* 77−89940
ferromagnet, nonlinear localised wave of magnetisation as bound state of magnons *(Russian)* 77−63160
ferromagnet, nucl. spin-lattice relax., possible magnon bottleneck 77−32283
ferromagnet, one dimensional, effect of biquadratic exchange on solitary waves 80−65836
ferromagnet, one-dimensional localised nuclear magnon modes 80−93098
ferromagnet, optical excitation of spin complexes, bound-magnon states 77−28554
ferromagnet, parallel pumping, in microwave field, magnon-photon interaction 79−51861
ferromagnet, photon-photon bond state via magnons 79−61458
ferromagnet, planar, US attenuation, spin-phonon coupling, magnons and magnetostriction contrib., calc. 80−34611
ferromagnet, spin wave nonresonant excitation by varying mag. field, nonequilibrium states *(Russian)* 80−34616
ferromagnet, spin wave system, kinetic eqn. on parametric excitation *(Russian)* 79−87249
ferromagnet, three dimens., N-magnon coupled states *(Russian)* 77−12111
ferromagnet, with screw dislocation, density of magnon states 78−84402
ferromagnet magnetisation, influence of high intensity longitudinal sound waves 80−103875
ferromagnet with easy-plane anisotropy, HF magnon energies, kinematic consistency 80−93097
ferromagnetic, amorphous, magnetic and phonon rotons 79−61087
ferromagnetic, electron fluid, polar spin waves *(Russian)* 77−89938
ferromagnetic, surface-rearranged thin film, magnon spectrum using generalised Bogoliubov canonical transform. 79−69702
ferromagnetic alloy, local density of one-magnon states, cluster-Bethe-lattice approximation 77−32181
ferromagnetic alloys, itinerant electron model, spin wave stiffness const. calc. 80−34613
ferromagnetic alloys, itinerant electrons, magnon stiffness const. 77−63155
ferromagnetic chain, anisotropic, kink excitations, nonlinear model 80−54881
ferromagnetic chain, characts. of soliton-like mag. excitations 80−39762
ferromagnetic crystal bar, square cross section, magnon excitations 77−77047
ferromagnetic degenerate semiconductor, magnon spectrum near instability of homogeneous state 79−28516
ferromagnetic degenerate semiconductors, Curie temp. 78−6529
ferromagnetic film, magnon avalanche under NMR saturation 78−10783
ferromagnetic Heisenberg chain, weakly bound magnon states *(Russian)* 80−100591
ferromagnetic linear chain, Heisenberg Hamiltonian, existence of isolated magnon 79−4666

magnons continued
ferromagnetic linear chains of spin 1/2 particles, one-magnon states 78−14946
ferromagnetic metal, electron-magnon mass enhancement 77−15748
ferromagnetic metal, magnon and cond. electron relax. processes *(Russian)* 80−7102
ferromagnetic metallic glasses, Brillouin scattering 78−92085
ferromagnetic metals, s-d exchange interactions, effect on attenuation of spin waves *(Russian)* 79−19730
ferromagnetic metals, with domain struct., low-temp. resist. 77−47791
ferromagnetic metals, zero temp. magnon exchange effects 77−51897
ferromagnetic nondegenerate semiconductors, magnon drag thermoelec. power calcs. 78−80012
ferromagnetic one-dimensional chain, solitary magnon propag. 77−63146
ferromagnetic polariton linewidths, theory 78−87918
ferromagnetic resonance, line width, inhomogeneous broadening, magnon scatt. 78−35043
ferromagnetic resonance, phonon propagation 78−88194
ferromagnetic resonance in anisotropic Heisenberg model, magnon-magnon, phonon-magnon interactions *(Russian)* 80−11274
ferromagnetic semiconductor, CESR line width, two-magnon exchange splitting 80−29621
ferromagnetic semiconductor, free carrier absorption below Curie temp. 79−47440
ferromagnetic semiconductor, HF magnon generation by pumping *(Russian)* 77−24686
ferromagnetic semiconductor, magnon coupling to plasmons and LA phonons, s-d model 80−29536
ferromagnetic semiconductor, magnon damping under intense radiation 77−63150
ferromagnetic semiconductor, magnon instability, under intense EM field 77−40048
ferromagnetic semiconductor, magnon-plasmon system 79−69659
ferromagnetic semiconductor, multispin indirect exchange, localised magnons *(Russian)* 78−56311
ferromagnetic semiconductor, optical transparency, photoferromag. effect, Curie temp. shift *(Russian)* 78−72387
ferromagnetic semiconductor, Raman scatt. due to magnon-spin flip of cond. electrons 77−20839
ferromagnetic semiconductor, refr. index variation in strong alternating mag. field 80−23741
ferromagnetic semiconductor, surface localised low energy electron-magnon states *(Russian)* 80−88734
ferromagnetic semiconductor, thermoelec. amplification of magnons 78−14748
ferromagnetic semiconductor absorpt. edge and cond. band width, electron-magnon scatt. 77−36267
ferromagnetic semiconductors, carrier mobility, electron-two magnon scatt. Hall effect 78−51992
ferromagnetic semiconductors, dielectric function depend. on magnetisation, light absorpt. coeff. *(Russian)* 80−15467
ferromagnetic semiconductors, free carrier absorpt. of radiation 80−97227
ferromagnetic semiconductors, Raman scattering of light on plasmon excitations 80−2738
ferromagnetic semiconductors, self-consistent electron-magnon oscillations 80−7098
ferromagnetic slab, asymmetrical guided mag. polaritons 80−88738
ferromagnetic slab, light scattering from bulk and surface spin waves, theory 80−71389
ferromagnetic systems, solitary bound states of magnons and lattice deformations, Dyson-Maleev representation 78−91838
ferromagnetism, in narrow S-band with inclusion of intersite correlations 77−63066
ferromagnetism, itinerant, local band theory, nonlinear Landau Lifshitz eqns. 78−31042
ferromagnetism, itinerant, local band theory, spin waves 78−31041
ferromagnets, anisotropic, HF magnon energy renormalisation, kinematic consistency 80−29539
ferromagnets, conducting, magnon spectra and magnetoacoustic reson. singularities *(Russian)* 80−50154
ferromagnets, homogeneous, magnon bottle neck and magnon avalanche effects, microscopic theory 79−51877
ferromagnets, magnetic vortex as topological soliton in Landau-Lifshitz eqns. *(Russian)* 80−7097
ferromagnets, magnetisation stimulation by nonresonance AC mag. field *(Russian)* 80−65962
ferromagnets, magnon relaxation, spin-orbit interaction, itinerant electron ferromagnets 80−11179
ferromagnets, metallic, spin wave damping, magnetisation relax. 78−88106
ferromagnets, spin wave excitation due to parallel pumping, mag. impurity interactions *(Russian)* 80−80497
ferromagnets crystal, $S \geq 1$, ground state of mag. polaron *(Russian)* 77−63142
garnet, substituted polycryst., low FMR linewidth, relax. processes 77−20718
Heisenberg, ferromagnet, three-dimens. solitons 79−82741
Heisenberg amorphous ferromagnet, magnetisation and Curie temp., CPA calc. 80−75703
Heisenberg anisotropic antiferromag., spectrum and correlation functions 79−28499
Heisenberg antiferromagnet, anisotropic, spectrum and correl. functions in spin-flop phase in generalized HF approx. 78−39283
Heisenberg antiferromagnet, light scatt. off surface 78−23475
Heisenberg antiferromagnet, magnon renormalisation, two-magnon Raman scatt., kinematic interaction 78−23228
Heisenberg antiferromagnet, magnon renormalisation 78−23259
Heisenberg antiferromagnet, second order self-energy 78−56279
Heisenberg chain, classical, solitons and magnons 80−60161
Heisenberg chain, classical continuous, magnon-soliton phase shift 80−107998
Heisenberg chain, ferromagnetically coupled and in mag. field, second magnons 79−65666
Heisenberg chain, in external field, magnon relaxation *(Russian)* 78−91854
Heisenberg chain of spins, nonuniform, two-magnon excitation spectrum *(Russian)* 78−23256
Heisenberg continuous chain, quantum solitons as magnon bound states 80−60162

magnons continued
Heisenberg ferromag. localised magnons around surface impurity *(Russian)* 78−84376
Heisenberg ferromagnet, amorphisation, anisotropically distrib. exchange forces *(Russian)* 77−85408
Heisenberg ferromagnet, anharmonic, renormalised magnons and phonons 78−91837
Heisenberg ferromagnet, critical points and two-magnon spectrum 79−87274
Heisenberg ferromagnet, cubic, with next nearest neighbour interactions, two-magnon bound states 80−70977
Heisenberg ferromagnet, disordered, pair effects in bond model 79−78290
Heisenberg ferromagnet, Faddeev eqns. for three-magnon T-matrix 77−36045
Heisenberg ferromagnet, FCC, two-magnon bound state 77−20575
Heisenberg ferromagnet, linear, with applied mag. field, second-magnon like excitations 80−65837
Heisenberg ferromagnet, localised magnons around impurity 78−39305
Heisenberg ferromagnet, localized magnons in a spin chain with two 'surface' impurities 79−38310
Heisenberg ferromagnet, longitudinal dynamic susceptibility 78−64181
Heisenberg ferromagnet, mag. excitation near surface of high Miller indices 77−51871
Heisenberg ferromagnet, magnon renormalisation, higher approx. 78−14945
Heisenberg ferromagnet, magnon renormalisation 80−65849
Heisenberg ferromagnet, quasiclassical description, soliton solutions 78−39282
Heisenberg ferromagnet, S=1/2, two magnon bound states, redefinition 79−42725
Heisenberg ferromagnet, spin waves at low temp., method of variational derivatives 79−24152
Heisenberg ferromagnet, strongly anisotropic with impurities, in transverse field, one-magnon states 77−69476
Heisenberg ferromagnet, surface magnetisation profile and localised magnons 80−70985
Heisenberg ferromagnet, three-dimens., two magnon states, effect of next nearest neighbour interactions 78−64178
Heisenberg ferromagnetic one-dimens. chain, solitary magnon solution 77−69473
Heisenberg Hamiltonian generalisation for case of atomic system with variable atomic spin value 78−14669
Heisenberg magnet, impurity band resonance at 0K, theory 80−66041
Heisenberg magnets, with two kinds of exchange interactions, surface magnons and surface spin arrangements 77−36043
Heisenberg model, with anisotropic biquadratic exchange interaction, two-magnon bound states 77−28356
HF magnons, generated by nonequilib. electrons, instability of system 78−27096
impurity relaxation in nonresonance field, phonon amplification *(Russian)* 80−100310
indirect exchange between local moments, cyclotron reson. effect 77−40051
Ising ferromagnet, one-dimens., with mag. impurity, one-magnon states 77−36042
Ising model, one dimensional, with infinite radius of interaction in transverse magnetic field 80−2587
itinerant electron ferromag., Ward-Takahashi identities, zero temp. case 79−73669
itinerant electron ferromagnet, two magnon bound states 77−20537
itinerant electron ferromagnetic alloys, magnon energy, effect of ordering 79−7986
itinerant electron ferromagnetism at zero temp. 78−56285
itinerant ferromagnet, electron-magnon interactions 79−99673
itinerant ferromagnet, thermodynamics 79−4645
itinerant strong ferromagnetism, effect of electron correlations 79−7962
kinetic eqns. in parametric ultrasonically excited ferromagnets 80−44820
kinetic equation for spin waves in a weak alternating magnetic field 79−42750
layer systems, mag. polaritons 78−31060
lecture 78−27026
light diffraction on parametric magnons *(Russian)* 77−12368
local paramagnon model, second-order phase transition, impurity effects calcs. 77−77067
localisation in condensed matter, electrons, phonons and magnons 80−10905
mag. excitations, atomically rough surfaces, isolated cluster of overlayer spin 78−31102
magnetic model with spin-phonon interaction 77−80896
magnetic ordered cryst., with degenerate orbital impurities, one- and two-magnon light absorption 77−63444
magnetic semiconductor, light scatt. by magnons, appl. to $CdCr_2Se_4$ and EuTe 77−69805
magnetic semiconductors, magnetoelectric effect, classical and quantum theory, magnon drag effect 80−34746
magnetically ordered cryst., indirect nuclear spin interactions 80−103847
magnetically ordered crystals with orbital degenerated impurities, single- and two-magnon absorpt. by localised excitations *(Russian)* 77−69858
magneto-optical crystals, spectra of hybrid excitations from transverse photons, excitons, magnons interactions 78−80320
magnon-magnon interaction in square lattice 78−2669
magnon-photon interaction in ferromagnets, construct. and radiation effects 80−71188
manganese aluminosilicate glass, insulating spin glass, exchange dipole optical transition 80−40136
metal, ferromagnetic, excitations in mag. field, theory *(Russian)* 77−8291
metallic ferromagnetics, two-magnon scatt. on dislocations, resonance linewidth broadening 77−20708
metals, ferromagnetic, point contact spectroscopy, electron-magnon interactions *(Russian)* 80−54766
metals, spin fluctuations, mag. field effect, electronic sp. ht. and elec. resist. 80−108026
methylammoniumtetrachlorochromate, optical absorption intensity, short-range spin correlation 80−108185
α-bis(N-methylsalicylaldiminato)-copper (II), ^1H NMR spin-lattice relax. time, spin dynamics 79−99786
molecular crystals, spectroscopy, bibliography for 1976 78−72585
multimagnon bound states, unphysical solns. to Faddeev eqns. 77−18440
magnons continued
nearly ferromagnetic Fermi systems, temp. depend. of spin susceptibility 79−8008
neutron inelastic magnetic scatt., book contrib. 77−89944
nonequilibrium electrons polarised opposite to magnetisation, HF magnon prod. *(Russian)* 78−23262
nonlinear, nonlinear Schrodinger equation and solitons 78−6523
nontransition metals, spin excitations 79−82770
one dimensional magnet with easy plane, solitons and magnons 78−23260
one-dimensional ferromagnet, quasiclassical approach to many-magnon bound states *(Russian)* 78−23222
one-dimensional ferromagnet with biquadratic exchange, solitary bound states of magnons and lattice deform. 79−19732
one-dimensional planar magnets, low temp. NMR 80−44943
one-magnon states in BCC Heisenberg antiferromag., spectral density near stepped surfaces 80−20396
orbiton-magnon bound states in spin-like materials at zero temp. 78−39306
paramagnet and ferromagnet, multibeam spin wave representation 79−4664
paramagnetic metal with nonmag. impurities, spin-flip scatt. 77−4497
paramagnon theories below three dimensions for itinerant strongly interacting fermion system 79−38298
paramagnons and magnons in quantum Heisenberg model 79−82739
parametric excitation on spin waves in the induced magnetoelastic crystals *(Russian)* 78−60272
periodic lattice, theory of coexistence of supercond. and magnetism, supercond. transition temp. 80−34543
photon effects on magnon splitting 78−64276
photon magnon bound states in ferromag. 78−47711
plane Heisenberg spin lattice, two-magnon excitations 79−42749
quantum field theory of solids, book 77−31922
quantum spin systems, exact boson representation and crit. behaviour 79−78423
rare earth metals, magnon dispersions in ferromag. and screw structs., nonlinear s-f exchange interaction effect 80−75746
rare earth metals and alloys, ferromag. props., book contrib. 80−75725
rare earth orthoferrites, Raman scatt. from magnons, anisotropy consts. determ. 80−66178
rare earth systems, mag. excitations, review of neutron scatt. data 80−60227
resonant light scattering from magnetic excitations, review 80−97290
scattering, effect of ellipticity on direction of spinwave rays 79−1659
semiconductor, antiferromagnetic, spin-magnetomagnon resonance 80−2566
semiconductor, ferromag., electronic props., effect of electron-ion spin coupling 77−28359
semiconductor, ferromag., localised magnon mode relax. theory 80−70986
semiconductor, ferromag., short wavelength magnon generation 80−70987
semiconductor, ferromagnet, light scatt. from magnons under strong fields, appl. to $CdCr_2Se_4$ 78−84554
sine-Gordon chain, classical, low freq. dynamics 80−108020
solid-state theory, introduction, book 79−33215
spin chain, two magnon problem 78−6502
spin chain with easy plane type anisotropy, coupled magnon states *(Russian)* 79−33469
spin system, mag. excitations, polarised neutron inelastic and quasi-elastic scattering 80−50045
spin wave excitation by uniform precession of magnetisation due to two magnon scatt. 78−68207
spin waves, space disordered media phenomenological Lagrangian, exchange, relativistic interactions *(Russian)* 80−29537
spontaneous symm. breaking and loop expansions 78−2640
statistical props. at high concentrations, parastatistics description 77−51674
superconductivity-ferromagnetism coexistence, transition temp., magnon freq., indirect exchange 80−44757
thin ferromagnetic resonators, intermodulation distortion, spin waves 78−48048
three magnon bound state eqn., physical eigenstate 79−4663
TMMC, one dimens. antiferromag., neutron scatt. exam. of impurity effects 78−43598
TMMC, one-dimens. magnet, local magnon modes 80−65829
TMMC, one-dimensional, EPR at HF and low temp. 78−80205
TMMC linear chain antiferromag., optical absorption, magnon sideband intensities calc. 77−59569
transition metal alloys, ferromag. local ordering effect on spin wave stiffness const. 77−66282
transition metal alloys, ferromagnetic, low temp. resist. calc. 80−24919
trimethylammonium cobalt chloride, low-dimensional Ising-like system, nucl. spin-lattice relax. of protons meas. 77−85609
trimethylammonium cobalt trichloride dihydrate, Ising-like system, nucl. spin-lattice relax. of ^1H and ^{35}Cl 80−29638
type I superconductor, paramagnon effect on nucl. spin-lattice relax. rate 77−32119
weak ferromagnet, paramagnons and phase transitions 77−61015
weak ferromagnet, single-ion anisotropy, one-magnon Raman processes 78−27234
AuMn, mag. struct., phase transition, and magnon spectrum, random anisotropy effects 80−88722
BMn, ferromag., ^{55}Mn magnon-induced pseudoquadrupole processes 79−19802
$BaCoF_4$, low temp. magnon effects on polarisation 79−42905
$BaMnF_4$, struct. and mag. transitions, magnon dispersion curves, nearest neighbour exchange consts. 79−42760
$BaNiF_4$, low temp. magnon effects on polarisation 79−42905
$(CH_3)_3NHCoCl_3.2H_2O$, chain ferromag. two magnon bound state, nuclear spin-lattice relax. 78−88206
$CdCr_2Se$, ferromag. semicond., high field effects, magnon carrier scatt. 78−87981
$CdCr_2Se_4$, ferromag. semiconductor, light scatt. from magnons under strong fields 78−84554
$CdCr_2Se_4$, refr. index variation in strong alternating mag. field 80−23741
n-$CdCr_2Se_4$, single crystal, transport props. near Curie temp. *(Japanese)* 78−6406
$CdCr_2Se_4$:Ag, ferromag. linewidth and eddy current losses 79−33541

magnons continued
$CdCr_2Se_4$:In, ferromag. semicond., carrier mobility, electron-two magnon scatt. Hall effect 78−51992
Ce compounds with group V elements, antiferromag., temp.-renormalised longit. mag. excitations 77−51862
$CeAl_2$, mag. behaviour 2.5 to 300K, neutron scatt. meas. 77−63110
CeSb, ferromag., mag. excitation spectrum, inelastic neutron scatt. obs. 79−78352
$Co_{1-x}B_x$, polycrystalline and amorphous sputtered films, Brillouin spectra 80−2775
$CoBr_2$, lamellar, field depend. of uniform magnon. energies, antiferromag. reson. meas. 77−73086
$CoBr_2$, magnon Raman scatt. 79−15462
$CoBr_2(Cl_2).2H_2O$, linear chain metamag. system, phonon and magnon widths 77−36065
$CoCO_3$, antiferromag., Raman spectra, 2-300K 77−32380
$CoCO_3$, Brillouin-Mandelstam light scatt. obs. of spin wave spectra 80−93358
$CoCO_3$, exciton and magnon excitation spectra *(Russian)* 78−23467
$CoCO_3$ far IR spectrum, HF antiferromag. resonance and two-magnon absorption 77−40136
$CoCO_3$, LF exciton and Raman spectra, one-magnon and two-magnon scatt. 80−93333
$CoCO_3$, light interaction with spin system at antiferromag. reson. 77−69707
$CoCO_3$, light scatt. by thermal magnons and magnons excited by antiferromag. reson. 79−82965
$CoCO_3$ light scatt. from parametric magnons and phonons *(Russian)* 80−34937
$CoCO_3$, light scatt. from magnons and phonons excited by microwave pumping 80−66213
$CoCO_3$, long wave IR spectrum, high freq. antiferromag. reson. *(Russian)* 78−31115
$CoCO_3$, spin excitation energies, quantum theory *(Russian)* 80−88735
$CoCO_3$, spin wave excitation by uniform precession of magnetisation due to two magnon scatt. 78−68207
$CoCO_3$, spin wave spectra light scatt. expts., review 80−50081
$CoCO_3$, two-sublattice noncollinear antiferromag., exciton-magnon light absorpt. mechanisms *(Russian)* 80−89017
$CoCO_3$, weak ferromagnet, optic study of spin wave spectrum *(Russian)* 79−47263
$CoCO_3$, weak ferromagnet, antiferromag. reson. and two-magnon absorpt. *(Russian)* 80−29627
$CoCO_3$, weakly ferromagnetic, light scatt. accompanying spin system excitation by high microwave power *(Russian)* 78−2745
$CoCO_3$, weakly ferromag., light scatt. on spin waves *(Russian)* 78−72419
$CoCl_2$, antiferromag., elementary excitations 77−69519
$CoCl_2$, antiferromag. elementary-excitations, electronic Raman scatt. meas. 77−80922
$CoCl_2$, lamellar, field depend. of uniform magnon. energies, antiferromag. reson. meas. 77−73086
$CoCl_2$, one-magnon Raman scatt. 78−43877
$Co_{75-x}Fe_xSi_{15}B_{10}$, quenched ferromag. ribbon, Brillouin spectra 80−2776
$(Co_{1-x}Fe_x)_2Y$, substitutional Fe atoms effect on mag. and elec. props., paramagnon scatt. 77−36054
Cr, mag. struct., phase transition, and magnon spectrum, random anisotropy effects 80−88722
Cr_2O_3, magnon energy temp. renormalisation calc. 77−1531
$CsCoBr_3$, ID Ising antiferromagnet, spin dependent Raman scattering from phonons and electronic excitations 80−103948
$CsCoBr_3$, quasi ID Ising antiferromag., polarised Raman scatt. from mag. excitations 80−66182
$CsCoBr_3$, quasi one dimensional antiferromag., magnon Raman scatt. 80−11395
$CsCoCl_3$, 1-D Ising antiferromag., mag. phase transitions 79−51779
$CsCoCl_3$, 10 Ising antiferromag., mag. excitations, electronic Raman and IR absorption spectra 78−2668
$CsCoCl_3$ spin dynamics, neutron scatt. study 80−80493
$CsMnBr_3$, quasi-one-dimens. antiferromagnet, inelastic neutron scatt. 78−14929
$CsMnCl_3.2H_2O$, antiferromag. resonance and two-magnon absorpt. *(Russian)* 77−81014
$CsMnCl_3.2H_2O$, antiferromag. reson. and two-magnon absorpt. 79−61234
$CsMnCl_3.2H_2O$, nonequilibrium magnon population obtained by optical pumping *(Russian)* 80−11457
$CsMnCl_3.2H_2O$, quasi-onedimens., antiferromag. reson. and assoc. two-magnon excit. *(Russian)* 77−51962
$CsMnCl_3.2H_2O$, subthreshold two-magnon absorpt., depend. on freq., temp. and mag. field, exchange coupling const. *(Russian)* 80−71184
$CsMnF_3$, antiferromag., suscept. oscillations beyond threshold for parametric excitation of electronic magnons *(Russian)* 77−59398
$CsMnF_3$, antiferromag., variation of spin wave spectrum in interaction between magnons 80−65841
$CsMnF_3$, exciton-magnon interactions in optical transition, absorpt. and emission spectra meas. 80−70981
$CsMnF_3$, mag. field- and temp.-depend. of light absorption spectra 78−52528
$CsMnF_3$, mag. struct., phase transition, and magnon spectrum, random anisotropy effects 80−88722
$CsMnF_3$, magnon absorption and luminesc. 80−7400
$CsMnF_3$, parametric excitation of magnons, effect of RF modulation of mag. field 80−65842
$CsMnF_3$, parametric magnon excitation, relaxation *(Russian)* 78−23352
$CsMnF_3$, parametric nuclear magnon excitation, mag. field modulation *(Russian)* 80−107999
$CsMnF_3$, RF modulation effect on parallel microwave pumping threshold *(Russian)* 80−29628
$CsMnF_3$, spin wave spectrum obs , review 80−50081
$CsNiF_3$, low frequency dynamics in external mag. field 80−108020
$CsNiF_3$, one dimensional planar model with symm. breaking fields, thermodynamics, static props. 80−97111
$CsNiF_3$, one-dimens. magnet, local magnon modes 80−65829
$CsNiF_3$, quasi-one-dimensional ferromagnet, subthreshold parallel pumping of magnons 80−75745
$CsNiF_3$, stochastic motion of Sine-Gordon-solitons, spin-correlation function 80−93105
$CsNiF_3$, subthreshold parallel pumping of magnons and antiferromag. reson. 80−71185
Cu_2MnAl Heusler alloy, inelastic magnon scatt. of neutrons 77−4509

magnons continued
dimethylammonium manganese tetrachloride, 2D Heisenberg antiferromag., spin wave anal. 80−54879
Dy, ferromag., rel. to magnetoresist., fields up to 75 kOe, 1-70K 77−20297
Dy-Y alloy, rel. to scatt. of cond. electrons by spin disorder 78−47778
$ErCo_2$, mag. excitation spectrum, neutron inelastic scatt. obs. 79−78351
$ErFe_2$, spin excitations, neutron scatt. obs. 77−63153
$ErFeO_3$, temp. depend. of neutron depolarisation factor meas. near spin reorientation transition 77−16053
EuO, anti-Stokes luminesc., magnon assisted 78−31252
EuO, light scatt. by spin waves 80−45086
EuO, transport properties at ferromag. reson. 78−68387
EuO:Gd, electron mobility below Curie temp. 78−91696
EuO(S)(Se), surface magnons and surface mag. struct. 77−36066
$Eu_xSr_{1-x}S$, Heisenberg spin glass system, excitations 80−84610
EuTe, antiferromag. FCC lattice of second kind, surface magnons and mag. structs. 78−23261
EuX, X=chalcogen, antiStokes luminesc. 77−63455
$Eu_{1-y}X_yS$ (X=Sr,Gd), spin-disorder-induced Raman scatt. from phonons, expt. investigation 80−20635
EuX(X=O,S,Se) 80−20635
Fe, elastic and magnon-inelastic spin polarised low energy electron scatt. 78−34970
Fe, elec. resist. between 2 and 30K, deviations from Matthiessen's rule 80−10944
Fe, light scatt. by spin waves 80−45086
Fe, light scatt. from surface and bulk thermal magnons 80−45087
Fe, magnetic susceptibility, lineshape and moment analysis, magnon excitations 79−99693
Fe, plastically deformed, high field suscept. anisotropy and domain struct. 78−15002
Fe, point contacts between ferromag. metals, singularities depend. in d^2V/dI^2, phonon spectra 79−60457
Fe, thermal acoustic magnons, Brillouin scatt. meas. 78−95424
Fe-Al, low energy Stoner excitations, spin wave obs. in neutron scatt. study 79−51770
Fe-Mn-Ni antiferromag. alloy, neutron scatt. exam. of antiferromagnons 77−66283
Fe-Ni(Pt), Invar alloy, magnetic excitation exam. by neutron diffr. 79−56521
Fe_3Pt, ordered ferromagnetic alloy, magnetic excitation obs. 80−70978
Fe_3Al, order-disorder transition effect on low energy spin waves 79−47271
$Fe_{1-x}B_x$, polycrystalline and amorphous sputtered films, Brillouin spectra 80−2775
$Fe_{100-x}B_x$, quenched ferromag. ribbon, Brillouin spectra 80−2776
$Fe_{80}B_{20}$, amorphous, Brillouin scatt. from magnons, ferromag. reson. 80−65844
$Fe_{80}B_{20}$, ferromagnetic metallic glasses, Brillouin scattering 78−92085
$FeBO_3$, antiferromag., two magnon reson. Raman scatt. 79−33703
$FeBO_3$, mag. linear dichroism and absorpt. spectra, exciton-magnon absorpt. mechanism 80−66160
$FeBO_3$, magnon dispersion by light scatt. and ferromag. reson. 77−55668
$FeBO_3$, weak ferromagnet, spin wave band struct. and microwave props. 79−1661
Fe_3BO_6, polarised absorpt. spectra in range of $^6A_1 \rightarrow {}^4T_1$, $^4T_2$ transitions 77−52092
$FeBr_2$, metamagnetic, optical study of mag. phase diagram 78−56312
$FeBr_2$, optical props. around Neel temp. 79−78658
$FeBr_2$:Mn^{2+}, layered antiferromag., infinity mode NMR study 79−38390
$FeCl_2$, magnetic materials, transparent, optical studies of phase transitions 77−66481
$FeCl_2$, one-magnon Raman scatt. 78−43877
$FeCl_2$, optical props. around Neel temp. 79−78658
$FeCl_2.2H_2O$, linear chain metamag. system, phonon and magnon widths 77−36065
$Fe_{68}Co_{32}$, ferromagnet, magnon heat cond. and lifetimes, 1-2 to 4.5K 77−16066
FeF_2 antiferromag., anomalous anti-Stokes/Stokes Raman scatt. intensity ratio 80−66177
FeF_2, one-magnon Raman scatt., anomalous behaviour of anti-Stokes-Stokes intensity ratio 80−40115
FeF_2:Co^{2+}, impurity-induced magnon, influence of localisation 80−11182
FeF_2:Mn, antiferromag. reson. and local magnon mode, FIR laser study 80−66042
FeF_2:Mn, Heisenberg antiferromagnet, impurity thermodynamics, NMR meas. 79−61098
FeF_2:Mn, Heisenberg model, impurity band resonance at 0K, theory 80−66041
FeI, magnon energies, phase transitions of eight sublattice model 77−59463
FeI_2, far IR magnetoabsorption, excitation of two spin deviations 78−80339
FeI_2, neutron inelastic scatt. from mag. excitations 80−50078
FeI_2, spin waves and two magnon bound states, mag. field IR absorption meas. 80−65840
$Fe_{1-p}Mg_pCl_2$, magnetic excitations 78−91852
$Fe_{1-x}Mn_xCl_2$, disordered, Raman scatt. from Fe^{2+} and Neel temp. 80−60579
$Fe_{1-x}Mn_xCl_2$, low-lying electronic excitations in antiferromag. and paramag. phases Raman scatt. study 80−71414
$Fe_{76}Mo_4B_{20}$, quenched ferromag. ribbon, Brillouin spectra 80−2776
$Fe_xNi_{80-x}B_{20}$, quenched ferromag. ribbon, Brillouin spectra 80−2776
$Fe_{40}Ni_{40}P_{14}B_6$, ferromagnetic metallic glasses, Brillouin scattering 78−92085
$Fe_{1-x}O$, low-energy mag. excitation dispersion curves 79−4665
$Fe_{1-x}O$, wustite, cryst. dynamics, mag. excitations, neutron scatt. study *(French)* 79−51740
$Fe_{1-x}O$, wustite, phonon and magnon props., inelastic neutron scatt. 78−52236
α-Fe_2O_3, antiferromag., reson. two magnon Raman scatt. obs. 77−63417
α-Fe_2O_3, antiferromag., two magnon reson. Raman scatt. 79−33703
$FePt_3$, neutron scattering study of spin waves 78−91856
$Fe_{1-x}Zn_xF_2$, dil. antiferromag., Raman scatt. expts. 79−78666
$Fe_{1-x}Zn_xF_2$, dil. antiferromag., electronic and mag. props., Raman scatt. and optical absorpt. study 80−108207

magnons continued
Gd, microcontact magnon spectra, electron-magnon interaction *(Russian)* 80−54768
Gd-Dy alloy, magnon contribution to electrical resist. *(Russian)* 78−39087
$GdCu_2Si_2$/Mo, point contact spectroscopy of magnons 79−38312
GdIG, one-magnon light scatt. with and without compensation temps. 78−31062
GdIG, spin wave intrinsic relaxation, magnon damping at low temps. 80−29543
GeTe:Mn, thermoelec. power, 2.5-25K, magnon drag effect 78−56169
H solid, spin-aligned, rapid decay mechanisms at 0K in large magnetic fields 77−72741
^{3}He, normal liquid, elementary excitations, density and spin density, zero sound mode, press. depend. RPA model calcs. 80−59749
^{3}He, superfluid, A-phase, viscosity tensor, generalised paramagnon model 80−39379
Ho, microcontact magnon spectra, electron-magnon interaction *(Russian)* 80−54768
$HoCo_2$, mag.excitations, neutron inelastic scatt. meas. 80−60231
K_2CoF_4, pseudo Ising antiferromag., inelastic light scatt. by mag. excitons 80−11377
K_2CoF_4, two dimensional Ising antiferromag., magnon band width estimated 77−12389
K_2CoF_4, two-dimensional antiferromag., one- and two-magnon Raman scatt. 79−51945
$K_2CoF_4:Mn^{2+}$, impurity induced mag. excitations, magnon gap mode, far IR spectra obs. 80−44821
K_2CrCl_4, ionic ferromag., temp. depend. intensity in optical absorption 77−12399
K_2CuF_4, magnon condensation 79−91220
K_2CuF_4, magnon condensation obs. in quasi-2D planar ferromag. phase 80−60232
K_2CuF_4, microwave excitation, optical detection of ferromagnetic reson. 80−50197
K_2CuF_4, obs. of magnon density of states by subthreshold steady-state absorption 77−12107
K_2CuF_4, spin-wave relaxation, parallel pumping expt. 79−4729
K_2CuF_4, two-dimens. ferromag., saturation of parallel-pumped magnons 80−97147
K_2FeF_4, antiferromagnet, two-dimensional, mag. excitations 80−80492
K_2FeF_4, Raman scatt. in two dimens. antiferromagnet 78−19488
K_2FeF_4, two dimensional planar antiferromag., mag. excitations, Raman and far IR spectra obs. 78−72343
K_2FeF_4, two-dimensional antiferromag., with easy-plane anisotropy, mag. excitations and two-magnon Raman scatt. 80−65839
$KMn_{1-x}Co_xF_3$, Raman scatt. by mag. excitations 77−55775
$KMnF_3$, antiferromag., multi-magnon luminesc. sidebands 78−76525
$KMnF_3$, exciton and exciton-magnon emission 79−33779
$KMnF_3$, exciton line and magnon satellite in UV spectrum at high press. *(Russian)* 79−4517
$KMnF_3$, stress-induced phase transition, optical props. meas. 77−20067
K_2MnF_4 and K_2NiF_4, two-dimens. antiferromag., two-magnon Raman scatt. linewidth, finite temp. 77−66508
K_2MnF_4, Heisenberg antiferromag., magnon renormalisation 78−23259
K_2MnF_4, nucl. spin-magnon relax. time, temp. depend., NMR study 80−25117
K_2MnF_4, ordered quadratic-layer Heisenberg antiferromag., nucl. spin-magnon relax. 80−71217
K_2MnF_4, quadratic layer antiferromag., intrinsic emission obs. 77−20906
K_2MnF_4, quadratic layer antiferromag., field induced two magnon nuclear spin-lattice relax. 79−61258
$K_2MnF_4:Ni^{2+}$, and undoped, magnon spectra, Raman and far IR spectra meas. 77−20573
$K_3Mn_2F_7$, antiferromagnet, two magnon Raman scatt. 78−15164
$K_3Mn_2F_7$, quadratic double layer antiferromag., two-magnon Raman scatt. 80−66183
$K_3Mn_2F_7$, two magnon Raman scatt., magnon dispersion, susceptibility, Green's function methods 80−50340
$KNiF_3$, ^{19}F spin-lattice relaxation 80−93211
K_2NiF_4, nucl. spin-magnon relax. time, temp. depend., NMR study 80−25117
K_2NiF_4, ordered quadratic-layer Heisenberg antiferromag., nucl. spin-magnon relax. 80−71217
K_2NiF_4, quadratic layer antiferromag., field induced two magnon nuclear spin-lattice relax. 79−61258
$K_3Ni_2F_7$, quadratic double layer antiferromag., two-magnon Raman scatt. 80−66183
$KNi_xMn_{1-x}F_3$, mixed antiferromagnet, light scatt. meas. 80−16025
$KNi_xMn_{1-x}F_3$, two-magnon Raman scatt. 77−66509
Li ferrite, $Fe(Li_{0.55}Fe_{0.45})O_4$, one-magnon light scatt. with and without compensation temps. 78−31062
Li-Cr ferrite, $Fe(Li_{0.5}Fe_{0.25}Cr_{1.25})O_4$, one-magnon light scatt. with and without compensation temps. 78−31062
$MnCO_3$, parametric excitation of magnons, effect of RF modulation of mag. field 80−65842
$MnCO_3$, RF modulation effect on parallel microwave pumping threshold *(Russian)* 80−29628
$MnCO_3$, spin wave spectrum obs., review 80−50081
$MnCO_3$, parametric nuclear magnon excitation, mag. field modulation *(Russian)* 80−107999
$Mn_{1-x}Co_xF_2$, Raman scatt. by mag. excitations 77−55775
$Mn_{1.88}Cr_{0.12}Sb$, antiferromag.-ferrimag. transition, neutron crit. scatt. and crossover effect 80−71023
$Mn_{1.88}Cr_{0.12}Sb$, magnetic phase transition effect on magnon renormalisation 77−59405
$Mn_{1.88}Cr_{0.12}Sb$, magnon renormalisation 77−69520
$Mn_{2-x}Cr_xSb$, exchange-inversion interaction and acoustical magnon soft mode 77−40049
MnF_2, antiferromag., multi-magnon luminesc. sidebands 78−76525
MnF_2, antiferromagnetic phase stability limit near spin-flop boundary 78−10683
MnF_2, inelastic light scatt. from antiferromag. polaritons, theory 77−73144
MnF_2, mag. anisotropy at OK 79−33473
MnF_2, magnon-photon interaction for EM wave vector perpendicular to sublattice magnetisation 79−69662
MnF_2, nuclear spin-lattice relax. and magnon lifetime near spin-flop transition 77−69721
MnF_2, one-magnon luminesc. sidebands of excitonic transition 78−60517
MnF_2, parallel pumping studies of magnon damping 80−70990
magnons continued
MnF_2, thermal cond., mag. field effects, magnon contrib. 78−38890
MnF_2, thermal cond., possibility of magnon contrib. 78−38889
MnF_2, two-magnon Raman scatt., temp. effects 77−48179
$MnF_2:Fe^{2+}$, temp. depend. of magnon pair-mode energies, Raman scatt. meas. 77−20577
MnF_2:Zn, shift and broadening of optical transitions 79−38579
MnO, absorption line shape, magnon sidebands 77−52128
MnO, antiferromag., magnon lifetime and its effect on magnon sideband 77−12106
MnO, Jahn-Teller effect on optical absorption spectra 78−52484
MnO, magnon lifetime 77−69518
MnO, magnon-sideband lineshape, exciton-phonon interaction effects 80−65846
MnP, sp. ht., 1.5-8.0K 79−91236
MnS, thermal cond., temp. depend., paramag.-antiferromag. transition effects 80−65321
Nb, spin fluctuations effect on T_c, from sp. ht. and mag. suscept. 80−7030
Nd, thermal cond. at low temps. *(Russian)* 79−11100
Ni, elastic and magnon-inelastic spin polarised low energy electron scatt. 78−34970
Ni, ferromagnetic, electron-magnon interactions 78−68205
Ni, forbidden magnon scatt., polarized neutron meas. 79−78350
Ni, light scatt. from surface and bulk thermal magnons 80−45087
Ni, magnetically ordered state, softening with varying mag. field *(Russian)* 78−35017
Ni, magnetocrystalline anisotropy energy, temp. and magnetisation depend. 78−6525
Ni, point contacts between ferromag. metals, singularities depend. in d^2V/dI^2, phonon spectra 79−60457
Ni, thermal acoustic magnons, Brillouin scatt. meas. 78−95424
Ni-Fe, elementary excitations, exchange stiffness const., inelastic neutron scatt. study 79−47294
Ni-Mn, spin wave stiffness const., low temp. neutron scatt. meas. 79−51768
Ni-transition metal alloys, electron-magnon scatt., deviation from Matthiesen's rule in elec. resist. 77−4319
$NiCl_2$, Raman spectrum at and below antiferromagnetic ordering temp. 79−99871
$Ni_{1-x}Co_xF_2$, Raman scatt. by mag. excitations 77−55775
$Ni_{1-x}Co_xO$, LF magnons, inelastic neutron scatt. exam. 77−66288
NiO, antiferromag., two magnon reson. Raman scatt. 79−33703
O, solid, magnetic props. theory for Heisenberg system *(Russian)* 80−54900
α-O_2, cryst., exciton, exciton-magnon, and biexciton absorpt. at 1.5K 80−84750
α-O_2, cryst., exciton effects, spectra *(Russian)* 79−47481
α-O_2 crysts., absorption band at 1.3K, $^1\Sigma_u^- \leftarrow {}^3\Sigma_g$ transition *(Russian)* 77−48186
α-O_2, elementary excitations, effect of mag. anisotropy *(Russian)* 78−76317
O_2 isotopically mixed crystals, IR absorption spectra (7000-15000 cm^{-1}) at 1.5K *(Russian)* 77−32362
α-O_2, solid, quasi 2D antiferromag., magnon and libron excitation spectra *(Russian)* 77−36067
O_2, solid, struct. elementary excitation spectrum and thermodynamic props. *(Russian)* 79−55696
Pd_cAg_{1-c}, possibility of superconductivity 80−10862
$Pt_{0.75}(Cr_{1-x}Mn_x)_{0.25}$, pseudobinary, magnon energy derivation 80−107996
Pt_3Mn, obs. of magnon sp. ht. 77−63217
$RbCoF_3$, antiferromag., anisotropic exchange, dispersion relations of mag. excitations 77−69532
Rb_2CoF_4, pseudo Ising antiferromag., inelastic light scatt. by mag. excitons 80−11377
Rb_2CrCl_4, optical absorption intensity, short-range spin correlation 80−108185
Rb_2CrCl_4, zone centre magnon gap determ., exciton-magnon combination band meas. 79−61082
$RbFeCl_3$, singlet ground state one-dimens. ferromag., 2-magnon excitation, far IR spectra obs. 77−69831
$RbFeCl_3.2H_2O$, pseudo one-dimens. Ising cpd., multiple magnon bound states 79−42723
$RbFeCl_3.2H_2O$, pseudo-one-dimens. canted Ising antiferromag., spin-cluster reson. 79−61233
$RbFeCl_3.2H_2O$, pseudo-one-dimensional canted Ising antiferromag., spin-cluster excitations 80−70989
Rb_2FeF_4, antiferromagnet, two-dimensional, mag. excitations 80−80492
Rb_2FeF_4, two dimensional planar antiferromag., mag. excitations, Raman and far IR spectra obs. 78−72343
Rb_2FeF_4, two-dimensional antiferromag., with easy plane anisotropy, mag. excitations and two-magnon Raman scatt. 80−65839
$RbMnCl_4$, quadratic layer antiferromag., intrinsic emission obs. 77−20906
Rb_2MnCl_4, 2D Heisenberg antiferromag. spin wave analysis 80−54879
Rb_3MnCl_4, quasi-2D-antiferromag., linear birefr. and optical absorpt. spectra 80−71385
$RbMn_{1-x}Co_xF_3$, Raman scatt. by mag. excitations 77−55775
$RbMnF_3$, antiferromag., multi-magnon luminesc. sidebands 78−76525
$RbMnF_3$, antiferromagnetic resonance, optical detection, luminescence 80−7174
$RbMnF_3$, exciton and exciton-magnon emission 79−33779
$RbMnF_3$, zone-boundary magnon energy and damping, Raman scatt. meas. 78−31202
Rb_2NiF_4, planar antiferromagnet, cluster-Bethe-lattice method 80−22306
Tb, ferromag., electron-magnon interaction and elec. resist., 1.5 to 50K 79−60790
Tb, magnon lifetimes at 4.2K 80−15710
Tb, microcontact magnon spectra, electron-magnon interaction *(Russian)* 80−54768
Tb/Mo, point contact spectroscopy of magnons 79−38312
Tb-Y, single cryst., magnon component of elec. resist. 77−15827
$TmFeO_3$, temp. depend. of neutron depolarisation factor meas. near spin reorientation transition 77−16053
UAl_2, spin fluctuations, mag. field effect, electronic sp. ht. and elec. resist. 80−108026
UPt, weak ferromag., magnon heat capacity, magnetisation and mag. entropy 77−24685
V, spin fluctuations effect on T_c, from sp. ht. and mag. suscept. 80−7030

magnons continued
$(V_{1-x}Cr_x)_2O_3$, Raman scatt. and phase transitions 80−71420
Y garnet, inhomogeneous collective magnon oscill. excited by RF field *(Russian)* 80−100582
$YCrO_3$, mag. circular dichroism and Faraday rotation in R-lines region 79−28725
$YFeO_3$, spin-wave damping of domain walls 79−42795
YIG, domain wall mobility and mass meas. method *(Russian)* 80−108033
YIG, FMR line broadening, two-magnon scatt. contribs. 77−20711
YIG, high amplitude collective oscills., double parametric reson. *(Russian)* 77−28451
YIG, intrinsic microwave emission, coupling to waveguide system, magnon system cooling 77−24912
YIG, one-magnon light scatt. with and without compensation temps. 78−31062
YIG, one-magnon Raman scatt., Faraday rot. 80−66156
YIG, optical detection of scatt. of homogeneous precession of magnetisation by defects 79−69728
YIG, optical spectroscopic exam. of ferromag. reson. *(Russian)* 77−48057
YIG, parametric excitation of spin waves in single-domain and polydomain states 77−12206
YIG, spin and magnetoelastic waves on longit. mag. pumping, optical obs. *(Russian)* 80−29727
$Y_{0.22}Ni_{0.78}$ amorphous alloy, low temp. sp. ht. 79−65680
$Zn_{1-x}Co_xF_2$, Raman scatt. by mag. excitations 77−55775

Magnus effect *see fluid dynamics*

mail *see postal services*

maintenance *see maintenance engineering*

maintenance engineering
see also computer maintenance
accident at Three Mile Island, lessons learned 80−57929
aluminium plants electrolytic baths, power consumption limitation method *(Russian)* 80−3366
analysers, instrumentation and operation 78−69237
biomedical electronic equipment, training programmes 79−96681
biomedical electronic equipment in forward army hosptials 79−96683
biomedical electronic equipment in hospitals 79−96682
biomedical electronic equipment maintenance, inspection, hospitals appl. 79−96684
biomedical electronic thermometers, review 78−69235
blood gas analysers, review 78−69238
blood pressure instruments, direct systolic/diastolic meas., review 78−69234
blood pressure instruments, noninvasive arterial meas. using US Doppler effect 78−69167
BWR control rod drive hydraulic return nozzle repair 80−23043
BWR operating experience and outage services 77−46397
BWR power plant, routine checks and radiation protection 78−74462
CANDU-PHW, valve maintainability, design, application, layout, administrative factors 78−25318
cardiac output analysers, equipment, maintenance and ccts., review 78−69239
cardiac pacemaker principles, specifications and testing, review 78−69258
commercial Tokamak fusion power reactor remote systems requirements 79−13525
concentrator/photovoltaic system design for electricity and heat generation 79−61997
defibrillators, review of instruments and maintenance 78−69251
ECG, servicing techniques 79−96677
ECG amplifiers, instruments and maintenance, review 78−69232
electrical instruments in photometric laboratory 80−86283
electrical measuring instruments, portable, repair and test rooms *(German)* 77−2665
electro-medical servicing, quality maintenance 78−77126
FFTF Interim Examination & Maintenance cell equipment mock-up testing 79−9816
fibre-optic communication systems for electric power companies 78−1422
fossil fuel utilisation, appls. 80−61234
fusion reactor, Culham Conceptual Tokamak Reactor Mk II, reactor costs and maintenance 77−74978
fusion reactor, STARFIRE project, maintenance considerations 80−102346
fusion reactor, Tandem Mirror Reactor power plant, maintenance and handling economics 80−102311
fusion reactor, UWMAK-III, non-circular, Tokamak, power reactor design 77−74979
fusion reactors, cassette blanket and vacuum building concepts 78−66386
fusion reactors, shielding and maintainability in an experimental Tokamak 80−99287
fusion reactors, Tokamaks, maintenance design requirements and economics 80−99285
hospital critical care unit instrumentation care and servicing, book 78−69231
hospital test instruments, scientific and medical instrumentation capability 78−69242
hot cell manipulator remote decontamination facility and repair station 79−9911
hot fuel examination facility/north, equipment repair room modifications 79−9723
Ignition Test Reactor remote maintenance system requirements 79−9885
Indian nuclear power station effluent monitoring system requirements and experience 79−13552
Indian Point Unit No.2 reactor vessel, detection and identification of loose object 80−18553
inertial confinement fusion generating remote systems, laser driver sources 79−9886
intensive care unit/coronary care unit safety 78−69252
Japanese reactor fuel reprocessing plant remote maintenance 79−9840
LMFBR experimental reactor JOYO, construction and function tests *(Japanese)* 78−33266
master-slave manipulators and remote maintenance in nuclear research 77−71682
medical CRT displays, review 78−69240
medical devices, evaluation and preventative maintenance 77−44777
medical electronic maintenance, hospital appl. 79−100771

maintenance engineering continued
medical electronics equipment, maintenance and repair organisation 77−40814
medical equipment standardisation and maintenance, role of Indian Central Scientific Instruments Organisation 79−74778
medical equipment technical servicing, determ. of range of preventive maintenance 78−85421
Millstone power plant, Unit 3 design 80−22922
near-future Tokamak power reactor remote servicing considerations 79−9887
nuclear medicine instruments maintenance, IAEA programme in Southeast Asia 80−46082
nuclear power conf., Chicago, United States, July 1979 80−794
nuclear power plants, diagnostic system using noise anal. 78−50279
nuclear reactor containments, in-service leakage tests 79−67895
nuclear safety systems, periodic testing, time dependent unavailability anal., FRANTIC computer code 78−29588
nuclear stations, maintenance optimization through trend monitoring 80−18552
online sensor cleaning 78−77883
pH meters, online, problems and solutions 78−53282
pollution control equipment operation and maintenance 78−61615
power line elec. field effect on communication line maintenance personnel 78−40353
power plant machinery monitoring and online diagnostic systems 79−9810
power station, heat treatment, post weld, during construction and maintenance 80−93574
PWR steam generator repair options 80−22923
radioactive waste calcining facility, remote maintenance development facility installation 77−54342
radiographic equipment servicing by hospital-based group 78−69247
radiography equipment safety and preventative maintenance in rural community hospitals 77−40758
reactor fluid systems, program for initial cleaning 80−23047
recorders, direct-writing analogue type, biomedical appls., techniques and maintenance, review 78−69241
reliability and maintainability symposium, Los Angeles (1978) 78−50250
remote maintenance to comply with new legislation limiting occupational radiation exposure, in United States 80−106210
respiratory monitors, instrumentation and maintenance, review 78−69236
shafts of power plant machinery, US metal fatigue crack detect. 77−77716
solar hotwater and heating systems, availability aspects 80−61314
sound and vibration monitoring, signal processing developments 78−83181
thermodynamic aspects of wear and tear, entropy and negentropy *(German)* 79−3907
Tokamak Experimental Power Reactor remote maintenance considerations 79−9883
Tokamak fusion reactor, design modifications to simplify remote maintenance 80−18613
Tokamak fusion reactor maintainability considerations 79−9882
Tokamak fusion test reactor, in-vessel maintenance remote manipulator system 80−18611
Tokamak Fusion Test Reactor remote handling and maintenance 79−9884
tube inspection, new acoustic device characteristics 77−68343
turbogenerators, high capacity, heating reduction measures for enhanced reliability and interval between maintenance *(Russian)* 80−96175
X-ray apparatus electrical circuit fault classification 77−21604
Pb accumulators developments *(Czech)* 79−70446
Zr, PWR fuel dissolution process remote maintenance cell 79−9838

Majorana forces *see nuclear forces*

majority algebra *see algebra*

Malter effect *see secondary electron emission*

man-machine systems
see also ergonomics
cardiac pacemaker function control, value of patient participation 77−81716
human factor studies, conf., San Francisco, USA (Oct. 1977) 78−48742
industrial temperature measurement techniques, man/machine interface enhancement 77−22545
manual control operator performance, gain and vibration effects interaction 78−44756
myoelectric processor and human operator dynamic error performance 79−96714
nervous system disease diagnosis using control characts. in manual control system 79−83990
nuclear accident phenomena, human elements *(French)* 78−57084
nuclear power stations, control rooms, human factors design approaches, improvement of man-machine interface, error reduction 80−63327
nuclear power stations, human operator errors, analytical model 80−63329
pulsilogium of Sanctorius, cardiac pulse rate meas. 79−71215
reliability, NATO Advanced Study Institute, Liverpool, England (Jul. 1973) 77−38396
robots and manipulators, symposium, Warsaw (Sept., 1976) 78−53574
sensory information processing, parallel and sequential *(French)* 77−12873
stereo image processing, control system 78−4728
stereoscopic imaging synthesis allowing for real positioning of operator's head *(Russian)* 79−64391
voice communication, speech production mechanisms and models *(Spanish)* 80−87665
weather forecaster console for satellite data handling system 80−90205

management
see also management science; research and development management
centralized management systems for Kagawa Prefecture irrigation-water system *(Japanese)* 80−89684
democratic control of science and technology 79−75316
energy and air pollution consequences of traffic systems management 79−52990
energy systems, logistic substitution model 80−89600
environmental assessment, management system for local development project in Japan 79−57503
environmental control, ORAKEL experimental conferencing for citizen participation 79−57499
floods in United States, management and economic aspects 77−41073

management continued
groundwater, computer assisted management *(German)* 79−57989
groundwater, finite element discrete kernel generator 78−92873
groundwater and surface water management by decomposition 77−64345
groundwater flow model using finite element method 78−92874
groundwater management, system response function hierarchy 77−64346
high-level radioactive waste management 80−37470
human factor studies, conf., San Francisco, USA (Oct. 1977) 78−48742
human resources, quality assurance, reliability in nuclear power plant construction 79−97776
Indian scientists' role in policy making process, critical assessment 80−90653
Lake George ecosystem management model development 78−36217
lake runoff management, ecosystem model WINGRA III 78−36216
LWR fuel cycle, high level waste, management 77−359
Meteosat programme organisation and management 78−36422
natural resources, training problems 77−82011
nuclear fuel, financing and accounting, effects of Pu uncertainty 78−13243
nuclear fuel accounting system, nuclear inventory and management system program 78−13245
nuclear fuel cycle management, interdisciplinary approach in education and research activities 77−38433
nuclear power in developing countries, regulatory capability transfer 80−13634
nuclear power station, radioactive waste management 77−74974
nuclear power stations, quality and safety criteria *(French)* 77−3154
nuclear power system, quality assurance 77−61632
peat resource management policy formulation, systems approach 80−30324
radioactive waste, report on 1977 IAEA conference *(Dutch)* 77−79446
radioactive waste, reprocessing philosophy, German waste management *(German)* 79−54565
radioactive waste management, closed nuclear fuel cycle, W.Germany 79−619
radioactive waste management alternatives 77−46367
radioactive waste management practices in selected European countries 80−37471
regional nuclear fuel cycle centres, IAEA study project 78−37429
regional wastewater management systems, chance constrained approach 79−57513
regional water quality management, goal programming approach 79−57514
regional water quality management, pilot study 79−57515
remote sensing technology transfer to operational data system 77−78513
reservoir design and management, SESLP model 79−2314
reservoir management for irrigation, chance-constrained linear programming 79−2317
water quality management alternatives, equity measures 77−25715
water quality management planning in coastal zone, stratified water circulation forecasting 79−5543
water resource management, gaming-simulation appl. in Hunter River Valley, New South Wales 79−57517
water-resource development project design, optimal apportionment scheme appl. *(French)* 80−77019

management information systems
see also database management systems; management science
King Faisal Specialist Hospital (Saudi Arabia) information system 78−57105
microprocessor, in industry *(French)* 80−17729
nuclear material management, at BWR fuel fabrication plant 79−85750
nuclear safety requirements assessment, Integrated Safeguards Information System establishment 79−85681
physics in Europe, bibliography 79−40341
river management operational system development using weather radar 78−40718
steelworks computerised spectrometric analysis and management information system 80−89574
USA Energy R&D Administration effluent date collection and reporting system 79−13545
weather maps, structural description of contour maps 80−101419

management science
see also critical path analysis; PERT
fusion reactor, plasma divertor expt., management techniques and procedure 78−54891
groundwater salinity and river basin salt balance management 77−78276
nuclear power plants, startup, staffing program, scope, tasks, resources, constraints, anal., implementation 80−63341
optics industry, business side, conf., San Diego, USA (Aug. 1978) 79−81354
photographic department, appls. and organization at large hospital 79−17514
physics in Europe, bibliography 79−40341

management techniques *see management science*

Mandelstam representation
average multiplicity, transverse momentum and total cross section, new upper bound 79−35970
cross section rise in high energy strong interactions, multipomeron exchange, Mandelstam diagrams 78−41516
crossing symmetric amplitude with Regge poles 78−54621
cut extrapolation method for data anal., crossed channel Mandelstam cuts, symm. $\pi\pi$ scatt. 77−49867
deep inelastic asymptotics 79−85244
double scattering struct. in old-fashioned perturbation theory 79−9310
dual model, automodel asymptotics *(Russian)* 79−93388
elastic scattering amplitude, absorptive part, lower bounds on slope parameter 77−34114
extended unitarity in hadronic multichannel scatt. with attractive Coulomb interactions *(German)* 77−82692
hadron elastic scattering and inclusive k_T^2 distrib. s-channel unitarity correl. 79−26258
hadron-hadron high energy scatt., Jost-Lehmann-Dyson representation, light cone singularities 78−17049
hadronic targets, spin-$^1/_2$, Compton scatt., optimal sum-rule inequalities 80−105815
helicity amplitude two particle unitarity for arbitrary spin 77−54058
Legendre Pade approximants to scatt. amplitudes, convergent sequences 79−85014
meson-meson Regge theory with crossing symmetry and unitarity, strong coupling 77−65177

Mandelstam representation continued
meson-meson Regge theory with crossing symmetry and unitarity, weak coupling 77−67676
nuclear fission, Mandelstam-Sommerfeld-Watson transformation *(Rumanian)* 80−47463
quantisation of Yang-Mills field and Mandelstam's theory in gauge-independent path-dependent formalism 77−30249
S-matrix theory, inverse scatt. problem 77−45981
Slavnov-'t Hooft identities in Mandelstam's formalism 78−45776
two-body scatt. amplitude, upper bound on inclusive cross section 78−45815
two-variable analyticity, phase-shift anal. 80−77987
N form factors 78−74256
π-π interaction, lectures, theory and expt. results, analyticity, unitarity, phase-shifts, current algebra 77−50008
π^0-π^0 partial wave amplitudes, crossing symmetric dispersion relations 78−50048
$\pi^0\pi^0$ amplitude bounds 77−34107

manganese
see also nuclei with .....
adsorption on silicon gel, Mn^{2+} adsorption rel. to H_2O adsorpt., EPR study 79−5180
AES meas. 77−36323
alkali chloride:Mn^{2+}, spin Hamiltonian parameters, binding energies for cation vacancy complexes 80−96461
alkali chloride:Mn^{2+} luminesc. spectra and decay *(German)* 77−48234
alkali halide: Mn^{2+}, powder EPR *(Spanish)* 77−48036
alkali trihydrogen selenite: Mn^{2+} single crystal, EPR 78−72396
alloy systematics, rel. to the long periodic table, allotropy of Fe and Mn 79−37649
aluminate:Eu^{2+}, Mn^{2+}, luminescence, efficiency of $Eu^{2+}\rightarrow Mn^{2+}$ energy transfer, struct. effects 77−8629
aluminates:Mn, Eu, red Mn^{2+}-luminesc. 79−61420
aluminophosphate glass:Mn:Mg(Sr), optical props. H_2O effects 77−28600
ammonium oxalate monohydrate: Mn^{2+}, ESR, 77-345K 79−19768
ammonium oxalate monohydrate:Mn^{2+}, model for defect formation, EPR 80−103880
amorphous, elec. cond. calc., t-matrix approach 77−55510
anodic oxidation of Mn in solns. of Mn salts *(French)* 78−11520
antiferromagnetic, NMR exam. 77−16193
antiferromagnetic, spin wave mode, wave function calcs. 80−20098
antiferromagnetism itinerant electron theory, spin susceptibilities 78−6504
Arabian Sea, DSDP Site 220, Fe, Mn and Ti distrib. 77−73708
atom, collisional and radiative excited, lifetime meas. 80−91501
atom, doublet struct. of Kα-hypersatellite 78−5167
atom, elastic and inelastic electron scatt. 10 to 100 eV 78−70934
atom, electronic spectra of 3s and 3p levels and X-ray K spectra, many-config approx. 80−32615
atom, fine struct. levels fitting, config. interaction effect, spin-orbit and electrostatic interaction parameters 80−69248
atom, giant-resonance autoionisation 79−89649
atom, HFS, many-body and relativistic effects 78−37565
atom, ionisation potential, term value, correlation energy by vertical anal. 78−41964
atom, Kα^h hypersatellite spectra and K-shell double photoionisation cross-section 78−21874
atom, K-shell ionisation cross sections, proton induced 77−23556
atom, laboratory hyperfine struct. for astrophysical interest 78−17818
atom, $M_{2,3}$ absorpt. spectra in UV, single-config. Hartree-Fock multiplet theory 78−78656
atom, nucl. quadrupole moments from laser-RF double reson. spectroscopy 80−57682
atom, $O^{2+,3+,4+,5+}$ induced K-shell X-ray production cross section, 7 to 24 MeV 77−61850
atom, orbital energies, ab initio rel. to pseudopot. calcs. 78−82613
atom, spin magnetic moment densities, spin density functional method calcs. 77−67969
atom, UV absorpt. spectra, 3p-excitation, super Coster-Kronig decay 79−13659
atom, UV absorption spectra, 3d and 4s excitation spectra, spectator electron model validity 79−85926
atom, X-ray fluorescence Kα hypersatellites 77−18830
atom, X-ray production by protons by 0.5 to 2.0 MeV energy 78−66646
atom, X-ray spectra, chemical bonding and multiple ionis. effects 78−50630
atomic electron collision cross sections 77−42410
atomic transition probabilities, oscill. strengths 78−74601
Baltic Sea ferromanganese concretions, trace metal distrib. rel. to accretion rates 77−81864
BCC and FCC struct., X-ray absorption spectra, Mossbauer spectra, comparison *(Russian)* 78−64299
borate glass:Mn^{2+}, EPR spectra 77−8394
borate laser glasses, Cl^- coordinated, Tl^+, Mn^{2+} and Nd^{3+} impurities, absorpt. and X-ray obs. 79−38575
cathodoluminophor, Mn-activated, nature of ageing 78−10994
CdS:N, Mn, ion implanted, anomalous enhancement of EPR signal of Mn^{2+} 78−27080
chalcogenide glasses:Cu(Mn), elec. cond. increase on impurity addition 77−11920
charged particle prod. cross sections for 14 MeV neutrons, Ti, V, Cr, Mn 80−42648
Chesapeake Bay, impact on anoxia on Mn fluxes 79−92099
chloroplast, EPR signal II and Mn-water splitting, factors influencing stability 78−24038
coating on BN powder particles, thermal stresses generated in vac. deposition 77−40455
coating on Ni-Fe (40%), mag. interface effects 77−69638
collinear spin structure of γ-phase, stability 80−107984
concentration determ. in atm. and rainwater in Vizcaya, Spain *(Spanish)* 78−57264
concentrations in NE.Pacific water 80−101384
corrosion, at high temp. in pure SO_4 80−50774
corrosion, model for cond. mechanism in oxide, rel. to basic atomic processes of metal corrosion 77−25198
cyclic deposition of desert varnish on rocks 79−16469
deep sea nodules deposits, telemetering methods *(German)* 80−26623
deep-sea Mn nodules, quant. distrib. and metal content *(Japanese)* 80−8292

manganese continued
deep-sea nodules, diffusion-controlled growth model 79−2212
determ., in seawater, graphite furnace atomic absorption spectroscopy 80−40768
determ. in water and organic materials, flameless atomic absorpt. spectrometry with wire loop atomiser 80−45586
determination, in atmosphere, flameless atomic absorpt. in particle size fractionated aerosols 78−69434
determination, in cement, by direct atomisation AAS *(Japanese)* 79−70413
determination, in Fe-, Ni-alloys by neutron activation anal., nondestructive, destructive methods 77−63987
determination, in salt, spectrochem. method *(Russian)* 79−29440
determination, in steels, by spectrographic method using combined discharge 79−57327
determination by AAS, interference effects, rel. to atomisation methods 79−83521
determination by plasma jet emission spectroscopy, using desolvation system with US nebuliser 78−68960
determination in environmental waters by neutron activation anal. 79−74584
determination in gasoline, by AAS using N_2O-H_2 flame, calibration methods 78−15729
diamond, synthetic, γ-Mn cluster existence, neutron diffr. obs. 77−89464
diffusion characteristics in Ag, 1051 to 1220K 80−15308
diffusion in Co, 860-1246°C, and Co-Mn alloys, mag. transform effects 77−24427
diffusion in Cu 77−62674
diffusion in Ni, radiation-enhanced, effect of point defect fluxes 77−89588
diffusion of Mn^{2+} in MgO, EPR 78−91477
distribution in alloy steel welds, laser emission microanal. method 78−61110
in early type peculiar stars, abundances 77−78803
electronic structure model, Invar effect, antiferromagnetic-non mag. transitions and α-phase 80−20370
energy levels, Mn I to Mn XXV, review 78−21841
enthalpy of solution at 1320K, enthalpy of form. of Mn_5C_2 78−59945
estuarine Mn distributions, effect of rapid precip. of river water dissolved Mn 79−62516
estuarine river water, particulate heavy metal content, Cochin backwater, India 80−7964
extended X-ray finestructure observation 80−25482
extraction equilirbium, with versatic acid 911 79−43620
FCC, itinerant antiferromag., spin susceptibilities and collective excitations, many band effects 77−63140
film, anomalous low temp. resistivity 78−91789
film, anomalous low-temp. resist. 78−2583
film, elec. resist., deposition rate effect 80−97010
film, heat treated, lattice distortion energy, resist. meas. 79−19492
film, low temp. resist., rel. to deposition conditions, for α-Mn 79−78223
film, optical, magneto-optical and struct. props. 77−1664
film, refractive index determ. using Rayleigh-Lowe refractometer 80−7427
film, resistivity-temperature variation 79−24085
film, vacuum-evaporated, H(D) uptake kinetics and energetics 80−88430
film, variation of elec. resist. with deposition conditions 77−43746
film, variation of resist. with deposition rate 77−43747
galactic cosmic rays, isotopic composition, balloon meas. 78−89024
garnet:Mn^{2+}, spin Hamiltonian parameters, g-factors, temp. depend. EPR obs. 77−48038
gas phase, He I photoelectron spectra, photoionisation cross section meas. 79−98051
glass:Mn^{2+}, EPR, low-field hyperfine struct. 78−95513
guanidinium aluminium sulphate hexahydrate:Mn^{2+}, NMR 78−91939
HD 94028, subdwarf, Mn abundance and Mn/Fe ratio 78−45328
hydrothermal circulation in deep sea and Mn distrib. in Galapagos Rift 77−86939
hydrothermal Mn in deep sea, scavenging residence time and Mn/^{3}He relationships 78−32121
hyperfine particles, surface magnetisation, explanation of expt. work 78−23303
intercalation compound with TaS_2, NbS_2, microstructure 77−84729
internal magnetic pressure and compressibility anomalies, itinerant model 77−16034
interstellar Mn, depletion derived from S 59 obs. of 67 stars 79−2563
ion implantation system for ZnS electroluminescent films 78−30658
isothermal diffusion in pure NaCl and KCl 77−47625
isotopic composition of primary cosmic rays 79−70937
K-shell ionisation cross sections, slow electron impact 80−83498
K-shell X-ray prod. by $^{14}N^+$ bombardment 80−91482
laser, atomic, finely dispersed metal particle active medium 80−91777
laser, cataphoretic at. distrib. in chloride-He discharge 77−31092
laser, high pulse rate, self heating with He buffer gas 77−23664
laser, stimulated emission mechanism, energy characts. 77−3571
lead acetate trihydrate:Mn^{2+}, ESR, elec. cond. 80−93165
liquid, multiple scatt. calcs. of resist. 78−76039
liquid, solubility of N_2, exam. 78−51685
lithium potassium tartrate monohydrate: Mn^{2+}, isomorphism with lithium ammonium tartrate monohydrate, EPR obs. 80−29607
localised moments, detection by electron energy loss spectra 77−69949
magnetic moment calcs., band struct. for paramag., antiferromag. and ferrogam. states 80−60223
magnetoresistance in antiferromag. α-Mn, temp. and field depend. 78−2464
marine Mn concretion growth rates, nonradiometric considerations 78−61393
micas and amphiboles, Mn rich, Mossbauer spectra 79−38412
micronodules from NW Atlantic, SEM determination of morphology and chemistry 80−81869
molten, contact reaction with graphite 80−15342
muscle membrane, insect, permeation of Mn, Cd, Zn and Be through Ca channels 77−56357
n=2-2 transitions in XUV spectra, anal. 80−102472
$(NH_4)_2SO_4$:Mn^{2+}, ferroelec. phonon driven phase transform., reduction of spin Hamiltonian consts. 78−92033
nickel acetate tetrahydrate:Mn^{2+}, EPR spectra, angular var. calc. 80−54940
nodule, sediment-water interface and submergence dynamics 78−28217
nodule growth in Jervis Inlet, British Columbia, effect of sediment-water exchange on Mn deposition 78−96187
manganese continued
nodule growth rate form ^{10}Be meas. using tandem Van de Graaff accelerator 79−74967
nodule growth rate meas. using radioactive ^{10}Be and ^{26}Al 78−40537
nodule mining and processing with nuclear meas. 77−4975
nodules, deep sea, from Pacific Ocean, Pt conc. determ. *(German)* 79−44169
nodules, deep-sea, diagenetic features, X-ray spectral and SEM anal. 79−16099
nodules, distrib. of transition metals by X-ray absorption microanal. 78−68957
nodules, from sea-bed, isotopic and elemental composition, U, Pa, Th, radiochem. anal. 78−77215
nodules, mineralogy and comp. changes from long-term seafloor mineral exposure expts. 79−5471
nodules, on deep ocean floor struct., composition, economic pot. 79−29747
nodules and Deep Ocean Mining Environment Study phase I and II, prospect 78−16164
nodules from Pacific Ocean, growth rates from U series and hydration-rind decay 77−29280
Pacific Ocean, Mn distrib. 80−56494
paramagnetic α-Mn, NMR and susceptibility max. 78−56386
particulate Mn over Galapagos Spreading Centre, hydrothermal source 79−39699
phosphate glass Mn^{2+}, luminesc. colour change 80−7392
plagioclase:Mn^{2+}, ligand field bands of impurity luminesc. centres and their site occupancy 78−88350
positronium form. in two-photon positron annihilation 79−61462
potassium oxalate, Mn^{2+} EPR spectra 80−39858
quartz:Mn, X-ray and thermally stimulated luminesc. *(Russian)* 78−84626
radioactivation analysis, of biological and geological materials, separation methods *(French)* 77−90700
radionuclide accumulation by oysters in reactor effluent, math. model 77−81589
river water solution with Fe and organic material, estuarine mixing implications 80−17296
sea-floor nodules, geological history 77−25674
seafloor around Vulcano Island, Mn mineralisation in volcanic and hydrothermal sediments *(French)* 79−62482
seawater Mn conc. and balance, surface samples 78−3815
Si:Mn, surface characterised by negative electrochemical pot., electronic props. 80−44695
skin lesion Mn, Cu and Zn conc. meas. by neutron activation 80−17063
solubility of N_2, 650-1030°C, 13-25 at.% N range 79−90783
solutes in liquid Se-Te, mag. susceptibility meas. 77−51882
spallogenic isotopes in Fe meteorites, radial distrib. 80−67488
spectrochemical analysis of biological solns. using wall stabilised arc source 80−41343
spin fluctuations effect on sp. ht. of β-phase 79−82788
spin fluctuations in α-phase, temp. depend. of elec. resist. 77−62913
sputtering in inert atm., with uncooled cathode, oxidation of metallic coatings, X-ray diffr. obs. 78−3041
steel, alloyed with Cr, Mo, Co, Mn, martensitic point position depend. on cooling rate *(Russian)* 79−70063
steel, Cr-Mn-W(Mo), W and Mo addition effect on carbide form. in type 30 KhG *(Russian)* 79−87638
stopping power of 0.5-2.0 MeV ^4He ions, elastic backscatt. meas. 78−87730
strontium acetate hemihydrate:Mn^{2+}(Cu^{2+}), EPR, spin Hamiltonian anal. and unit cell symmetry 80−29603
strontium formate:Mn^{2+}, cryst., e.p.r., spin Hamiltonians 77−4552
suspended Mn-rich particulate matter in coastal marine waters 78−11911
tetramethylammonium cadmium trichloride:Mn^{2+}, EPR spectrum temp. depend. 78−19314
thin film, DC resist., activation energy, thickness depend. 80−84518
thin films, vacuum deposited, in elec. field, resist., struct. 80−103761
tris-sarcosine calcium bromide and chloride solid solns., Mn^{2+} doped, EPR linewidths and ferroelec. behaviour 79−24213
tris-sarcosine calcium chloride:Mn^{2+} ferroelec. dynamics, EPR and ENDOR study 80−75972
trissarcosine calcium chloride:Mn^{2+}, ferroelec., electron spin-lattice relax. 78−80208
TSCC:Mn^{2+}, microscopic, mechanism of ferroelectric transition, EPR fine struct. tensor calc. 78−35104
Tutton salt:Mn^{2+}, EPR, 298K, spin-Hamiltonian parameters, cryst. fields 78−27086
Tutton salts:Mn^{2+}, EPR, 300K 79−51848
vaporization, thermodynamic study by Knudsen-cell mass spectrometry 79−10937
vapour, use in laser projection microscope with image-brightness amplifier 80−106541
vapour impulsive production after discharge current pulses through halide vapours *(Russian)* 79−90491
vapour laser, self-terminating, max. pulse repetition freq. 80−23677
X-ray absorpt. discontinuity, shape and extended fine struct. 80−66324
X-ray crystal struct. refinement, for β-Mn 79−14735
X-ray emission spectra, $K\beta_{1,3}$, low energy plasmon $K\beta'$ satellite 79−74020
X-ray emission spectra, L_l and L_η 78−39631
X-ray emissive short-wave satellite lines in K-series, mech. of formation *(Russian)* 79−91538
X-ray $K_{\alpha 1,2}$ and $K_{\beta 1}$ lines, photon excitation of Mn and K-capture in ^{55}Fe *(Russian)* 77−77321
X-ray K_β emission spectrum, unpaired electron and plasmon effect 77−12468
X-ray K-emission satellites, quasi-stationary states and origin 80−80903
X-ray resonant Raman scatt. and fluoresc. near K-absorpt. edge 79−52042
XPS, valence bands 78−35249
ZnS:Mn,Cu, thin-film phosphors, LV DC electroluminescence 79−11472
Ag-Pd-Mn mag. susceptibility, effect of Mn impurities 79−73677
AgCl:Mn^{2+}, recombination processes, radioluminescence 78−2915
$Al_xGa_{1-x}As$:Mn epitaxial layers, Mn-O association, EPR meas. 77−69677
AlN:Mn, luminescence at high excitation levels 77−1721
AlN:Mn, vol. and surface excited luminesc. 79−38630
Al_2O_3:Cr^{3+}, Mn^{3+} spin lattice relax. time meas. of Cr^{3+} 79−99755

manganese continued
β-Al_2O_3:Mn, absorpt. and emission spectra, mag. susceptibility 79−87471
Al_2O_3:Mn, appl. of differential method for low temp. thermal cond. meas. 79−63227
Al_2O_3:Mn^{2+}, EPR meas., comparison with theory of EPR of S-state ions 77−1587
α-Al_2O_3:Mn^{2+}, intensity of forbidden $\Delta m=2$ EPR lines of S-state ions with axial cryst. environments 77−77090
Al_2O_3:Mn^{3+}, electronic and vibronic Raman scatt. 78−2839
Al_2O_3:Mn^{3+}, Jahn-Teller Mn^{3+} ions, phonon spectroscopy and thermal cond. meas. 80−88282
Al_2O_3:Mn^{3+} under uniaxial stress, Jahn-Teller model 80−88521
β-Al_2O_3-Na_2O:Mn^{2+}, EPR of Mn^{2+} 78−6569
β-Al_2O_3-Na_2O:Mn^{2+}, ESR exam. 78−19313
As_2Se_3, effect of Cu and I, investigated by Mn^{2+} EPR spectra 77−73075
As_2Se_3:Mn^{2+} film, reversible photostructural change, ESR obs. 77−32411
As_xSe_{100-x}:Mn^{2+}, $0\leq x\leq 70$, EPR, composition depend. and struct. 77−24736
$BaAl_{12}O_{19}$:Mn, phosphor, vac. UV excitation spectra, appl. to gas discharge display 80−2816
$BaMgF_4$:Mn^{2+} ferroelec., EPR and ENDOR study, cryst. field tensor 80−71162
$BaMo_4$, M=Mo,W, EPR spectrum, temp. depend. of zero field splitting 79−15346
BaO:Mn^{2+}, impurity pot. well shape calcs. 78−87950
BaO-B_2O_3 glass, $Mn^{2+}\rightarrow Nd^{3+}$ energy transfer, fluoresc. obs. 77−8621
BaT:O_3:Mn, ferroelec. domain stabilisation by bulk ordering of defects 79−42925
$BaTiO_3$ ceramic dielectric capacitor, processing prop. relations, hysteresis, permittivity 80−80730
$BaTiO_3$:Mn, annealed in H_2 and O_2, valence change in phase stability 80−20600
$BaTiO_3$:Mn, polycrystn., annealing effect on transition temps. 80−3100
$BaTiO_3$:Mn^{2+}, electrooptical effect, charge transfer mechanism, defect. pair form. 79−38519
Ba_2ZnS_3:Mn, luminescent props. 77−77292
$Bi_{12}GeO_{20}$:Mn, Cr, reversible photochromic effects, absorpt. spectra before and after illum. 79−91471
BiI_3:Mn^{2+}, ESR, spin-lattice relax., temp. depend. 78−88178
$Bi_{12}SiO_{20}$:Mn, Cr, reversible photochromic effects, absorpt. spectra before and after illum. 79−91471
$CaCO_3$:Mn, calcite, EPR and ENDOR absorpt. spectra of divalent Mn in single cryst. 79−47328
$CaCO_3$:Mn^{2+}, calcite, on axis half-field forbidden lines, numerical prediction 77−16161
CaF_2:Ce,Mn, heavily-doped phosphor, cathode-ray irrad., energy transfer 79−87509
CaF_2:Gd^{3+}, Mn^{2+}, photo- and radioluminesc. investig. of intracentric energy transfer 77−16378
CaF_2:Mn, CaF_2:Eu,Mn, single crystal predisintegration phenomena, SEM cathodolum. obs. 80−59502
CaF_2:Mn, EPR and optical absorpt. spectra 80−93171
CaF_2:Mn, low temp. X-irrad., Mn centres, optical absorpt. and emission props. 80−60635
CaF_2:Mn, thermolum. induced by monoenergetic parallal beam 81 MeV diffr. neutrons 77−52883
CaF_2:Mn, X-irrad., impurity effects on defect prod. 80−92525
CaF_2:Mn, X-irrad., thermolum. 80−60686
CaF_2:Mn^{2+},Yb^{3+}, efficient luminesc. energy transfer from Mn^{2+} to Yb^{3+} 78−19536
CaF_2:Mn^{2+},Yb^{3+}, luminescent energy transfer efficiency obs. 78−6777
CaF_2:Mn^{3+}, fluorite, radiation and thermal redox processes 80−55678
CaI_2:Mn, recomb. processes, luminesc. characts. *(Russian)* 80−25450
$CaMO_4$:Mn^{2+}, M=Mo,W, EPR spectrum, temp. depend. of zero field splitting 79−15346
CaO:Mn phosphor, surface radical recomb. and cathodoluminesc. *(Russian)* 78−6787
CaO:Mn^{2+}, impurity pot. well shape calcs. 78−87950
$Ca_2P_2O_7$:Sb, (Sb,Mn), luminesc., activation, colour centres *(Russian)* 78−92123
$Ca_2P_2O_7$:Sb, Mn, luminesc., colouration 80−2828
β-$Ca_3(PO_4)_2$:Sb, Mn, luminesc., colouration 80−2828
$Ca_3(PO_4)_2$:Sb,(Sb,Mn), luminesc., activation, colour centres *(Russian)* 78−92123
$Ca_{10}(PO_4)_6(OH)_2$:Mn, thermoluminesc. 77-500K, X-irrad. at 77K *(French)* 78−15234
$Ca_5(PO_4)_3OH$:Mn, synthesized by hydrothermal method in CaO-P_2O_5-H_2O, thermoluminescence study rel. to starting mixture 78−95612
$Ca_5(PO_4)_3OH$:Mn^{2+}, thermolum. props. 80−2877
CaS:Mn,Ce, phosphor, fluoresc. spectrum, fine struct., $^4T_{1g}(^4G)\rightarrow{}^6A_1(^6S)$ transition 80−45130
CaS-Bi, Mn, phosphors, thermoluminesc., phosphoresc. 78−2928
CaS-Pb,Mn, phosphors, thermoluminesc. and fluoresc. spectra 78−64396
$CaSO_4$:Mn, phosphor, thermoluminesc., low energy ion excitation 77−55838
$CaSo_4$:Mn trap depth, thermolum. meas. 77−36301
$CaWO_4$:Mn^{2+}, polycryst., EPR spectra calc. using Bir's method, compared with expt. 79−1707
$CaWO_4$:Mn^{5+}, new EPR center *(Russian)* 79−1709
$CdBr_2$:Mn, electron-phonon interaction, lattice vibr. effective energies *(Russian)* 78−59911
$CdBr_2$:Mn^{2+}, layered, pressure effect of ESR on axial field const. of spin Hamiltonian *(Russian)* 77−32254
$CdCl_2$:Mn^{2+}, e.s.r. spectra meas. 77−4554
$CdCl_2$:Mn^{2+}, null points in zero-field splitting of mag. impurity levels 79−87066
$Cd(ClO_4)_2.6H_2O$:Mn^{2+}, phase transition, EPR of Mn^{2+} meas. 79−56604
CdF_2:Mn, thermolum., recomb. processes 78−15237
CdF_2:Mn, Y, deconversion due to vacuum heat treatment, elec. resist. and electron probe meas. 79−24025
CdF_2:Mn,Y, in MIS struct., blue-green electrolum. 79−52025
CdF_2:Mn films, electroluminesc. meas. *(French)* 79−11471
CdF_2:Mn^{2+},Y^{3+}, thermal stability under vacuum, effect of heat treatment on resist. 79−23969
CdI_2:Mn, electron-phonon interaction, lattice vibr. effective energies *(Russian)* 78−59911
CdI_2:Mn^{2+}, EPR 78−68362
manganese continued
$CdMoO_4$:Mn^{2+}, EPR spectrum, temp. depend. of zero field splitting 79−15346
$Cd(NH_4)_2(SeO_4)_2.6H_2O$:$Mn^{2+}$, EPR of Mn^{2+}, spin-Hamiltonian parameters 79−33528
$Cd(NO_3)_2.4H_2O$:Mn^{2+} single cryst., low symm. effects in EPR 77−90020
CdS:Mn, vacuum deposited film, Mn migration, EPR and X-ray study 80−65411
CdS:Mn gamma-irradiated ESR meas. 79−11342
CdS:Mn^{2+}, cryst., X-band ESR 78−2730
CdS:Mn^{2+}, doped, spin-lattice relax. exam. 77−40120
CdS:Mn^{2+}, spin-lattice relax. ang. depend. 79−73807
CdS:Mn^{2+}, temp. depend. of rate of spin-lattice relax. 79−42832
CdS:Mn(Co), intensity and spectral distrib. of luminescence *(Russian)* 77−16392
CdTe:Mn, exciton refl., photoluminesc. and mag. suscept. meas., influence of impurities 77−39787
CdTe:Mn, introduction of elec. active defects 80−103647
CdTe:Mn, photoionisation absorption spectrum 78−23502
CdTe:Mn, spin-lattice coeffs. of Mn^{2+} 80−84646
CdTe:Mn^{2+}, exciton refl. spectra and mag. susceptibility 80−66253
CdTe:Mn^{2+}, luminesc. and magnetooptic reson., mag. field effect 80−93390
CdTe:Mn^{2+}, magneto-optical and microwave-optical double reson. meas. of exciton band *(Russian)* 77−81087
CdY_2S_4: Mn, superhyperfine interaction of Mn, ESR spectra 77−63271
Co salts: Mn^{2+}, EPR, spin-lattice relax. time meas., 180-380K 78−64268
CoF_2:$MnSu^{2+}$, anisotropic antiferromagnet, spin impurity approx. *(Russian)* 79−87253
$CoK_2(SO_4)_2.6H_2O$:Mn^{2+}, EPR spectra, spin-Hamiltonian anal. 77−77088
$CoSO_4.7H_2O$:Mn^{2+}, host spin-lattice relax. narrowing in single cryst. 78−27079
$CsCaCl_3$:Mn, EPR, 4.2 to 450K, ferroelec. transition 80−60414
Cs_2GeF_6:Mn^{4+}, magnetically circularly polarised emission and MCD of vibronic lines 77−16377
Cs_2HfCl_6:Mn^{2+}, ESR of mol. jumps, zero-field splitting tensor 77−51944
CsI(Br):Mn phosphors, luminesc. spectra 77−59610
$CsMF_3$:Mn^{2+}, (M=Ca,Cd), zero-field splitting of Mn^{2+}, superposition model *(French)* 79−15267
$CsMgCl_3$:Mn^{2+}, EPR spectrum temp. depend. 78−19314
$CsSiF_6$:Mn^{4+}, splitting of vibronic levels 78−60496
Cs_2SiF_6:Mn^{4+}, IR absorpt. band, electron-vibr. effect 80−108238
Cs_2SiF_6:Mn^{4+}, Jahn-Teller effect in $^4T_{2g}$ state, Zeeman meas. 80−29367
$CsSrCl_3$:Mn^{2+}, structural transitions, EPR meas. 78−34619
Cs_2TiF_6:MnF_6^{2-}, $^4A_2\rightleftarrows{}^2E_g$ transition of Mn^{4+}, absorpt., emission, linear and MCD, MCE 78−10929
Cs_2ZrCl_6:Mn^{2+}, ESR of mol. jumps, zero-field splitting tensor 77−51944
Cu:Mn, NMR satellite data rel. to impurity struct. 78−35052
Cu_2O:Mn, photomemory mobility components, charged centre conc. 80−103725
Fe-Mn deposits on abyssal sea floor, geochem. 79−12107
Fe-Mn diffusion pair, mutual diffusion coeffs. calc. by computer 79−69299
Fe-Mn interdiffusion in almandine garnet, expt. meas., rel. to compositional zoning 79−77812
Fe-Mn powders, reactions with NH_4Cl and $(NH_4)_2CO_3$ 80−11597
$FeBr_2$:Mn^{2+}, antiferromag., impurity spin reson. 77−43876
$FeBr_2$:Mn^{2+}, layered antiferromag., infinity mode NMR study 79−38390
$FeCO_3$:Mn^{2+}, far IR host and impurity excitations, antiferromag. and paramag. temp. ranges 77−52140
FeF_2:Mn, antiferromag., NMR relax., impurity bonding 80−66061
FeF_2:Mn, antiferromag. reson. and local magnon mode, FIR laser study 80−66042
FeF_2:Mn, Heisenberg antiferromagnet, impurity thermodynamics, NMR meas. 79−61098
FeF_2:Mn, Heisenberg antiferromag., impurity banding and mag. reson., theory 80−93181
FeF_2:Mn, Heisenberg model, impurity band resonance at 0K, theory 80−66041
FeF_2:Mn, mag. polariton, impurity mode enhancement and superradiance effects 79−28622
$FeK_2(SO_4)_2.6H_2O$:Mn^{2+}, EPR spectra, spin-Hamiltonian anal. 77−77088
α-Fe_2O_3:Mn, characts. of Morin phase transition, linear mag. birefringence meas. 77−69560
α-Fe_2O_3:Mn, linear mag. birefringence near Morin transition 77−52052
Fe_2O_3:Mn, surface props. 79−65302
$Fe(OH)_3$, coprecipitation with Cu, Ag, Au; Ge, Sn, Pb; Mn and Ca 79−70415
$FeSiF_6.6H_2O$:Mn^{2+}, EPR line positions and intensities, spin Hamiltonian 79−65714
GaAs:Mn, implanted, ion channelling meas. for lattice location of impurities 79−4332
GaAs:Mn, LPE layer, near band edge photoluminescence, 2K, low excitation intensities 78−48218
GaAs:Mn, Mn-O association, EPR meas. 77−69677
GaAs:Mn, negative magnetoresist. meas. 77−51768
GaAs:Mn, p-type semiconductors, internal strain on bound hole-phonon interaction 78−91492
GaAs:Mn, photoluminesc., emission props. and radiative mechanism 79−56842
GaAs:Mn epitaxial layers, fabrication and electrical props. 77−80859
p-GaAs:Zn, Mn, degenerate, tunnel p-n junction and semicond.-metal struct., I-V characts. 78−72252
$Ga_{1-x}In_xAs$:Mn grown by LPE, elect. props. 80−100541
$Ga_xIn_{1-x}P$:Mn, ESR of Mn 79−11341
GaP:Mn, ENDOR of cubic $^{55}Mn^{2+}$ 79−69749
GaSb:Mn struct., thermo EMF, galvanomag. props. rel. to dopants, eutectic $Mn_{0.6}Ga_{0.4}Sb$ form. 77−15869
GaSb:Te,Zn(Te,Mn), prep. and electrophys. props. 79−87116
GaSe:Mn, ESR spectra, influence of temp. and antiferromag. inclusions 79−99763
Ge:Mn, amorphous, cond. increase by Mn doping 78−72155
Ge:Mn, amorphous, EPR meas. 77−85559

manganese continued
Ge:Mn, impedance characts., near threshold of excitation of recomb. waves 77−69342
Ge:Mn, Sb, recombination waves, convective instability development 80−70721
Ge:Mn, Sb 80−96906
GeO_2:Mn^{2+}, EPR, struct. of vitreous and crystn. states 77−48039
$Ge_{25}S_{75}$:Mn, bond struct. and character in Ge-S system, EPR obs. 80−66014
$Ge_{40}S_{60}$, $Ge_{25}S_{75}$ glasses, Mn^{2+} EPR spectra investigation 79−11340
$Ge_{40}S_{60}$:Mn, bond struct. and character in Ge-S system, EPR obs. 80−66014
GeTe:Mn, degenerate semicond., EPR of Mn^{2+} 79−11339
GeTe:Mn, thermoelec. power, 2.5-25K, magnon drag effect 78−56169
HIO_3:Mn, growth and struct. perfection, effect of impurity ions 77−12514
HgSe:Mn^{2+}, temp. depend. of EPR of ^6S state ions 80−80593
HgTe:Mn, impurity scatt. contrib. to electron mobility and thermoelec. power 77−15852
I_2:Mn, doping effect on elec. cond., semicond. props. 80−49732
In-Mn, Lu-Mn relative activity ratios, in natural UO_2 reactor fuel 78−58347
InAs:Mn, NMR, magnetoresist., Hall effect and mag. susceptibility meas. 78−26888
InAs:Mn powder, quadrupole interactions in NMR spectra 79−51880
InAs:Mn^{3+}, Jahn-Teller effect for ion impurities 80−107753
$InMn_3$, crystallographic anal., new form of γ-brass struct. with a P cell 79−99116
InP:Mn, planar reactive deposition on CdS, heterostruct. formation and elec. evaluation 78−72738
InSb:Mn, heat treatment effects on elec. props. 78−43411
InSb:Mn, NMR, magnetoresist., Hall effect and mag. susceptibility meas. 78−26888
InSb:Mn, powder, quadrupole interactions in NMR spectra 79−51880
InSb:Mn^{2+} nondegenerate semicond., mag. impurity indirect interaction *(Russian)* 80−34591
$In_{2-x}Sn_xO_{3-y}$-ZnS:Mn thin film structure, surface morphology and electro-optical props. *(Russian)* 80−49554
$KCdF_3$:Mn^{2+}, evidence for F distortion, ligand ^{19}F ENDOR meas. 78−23369
KCl-KBr:Mn mixed cryst. system for thermoluminescence dosimetry, glow curves, dose response 78−24150
K_2CoF_4:Mn^{2+}, impurity induced mag. excitations, magnon gap mode, far IR spectra obs. 80−44821
KI:Mn^{2+}, elec. field effect on mech. of recomb. 78−80397
KMF_3:Mn^{2+}, (M=Mg,Zn,Mn,Cd), zero-field splitting of Mn^{2+}, superposition model *(French)* 79−15267
K_2MF_4:Mn^{2+}, (M=Mg,Zn,Mn), zero-field splitting of Mn^{2+}, superposition model *(French)* 79−15267
$KMgF_3$:Mn^{2+}, crystl. field theory, superposition model 77−28149
$KMgF_3$:Mn^{2+}, exchange and spin-orbit interactions, optical spectra study 79−95817
$KMgF_3$:Mn^{2+}, MCD and linear dichroism, 3d→4s transitions 79−56768
$KMgF_3$:Mn^{2+} high energy absorption spectra interpretation 78−6716
$KNiF_3$:Mn^{2+}, isotropic Heisenberg ferromagnet, localised spin-wave modes, biquadratic exchange effects 77−51896
K_2O-B_2O_3:Mn^{2+} glass, fine struct. parameter distribs., EPR meas. 80−11256
$KZnF_3$, Cu^{2+} and Mn^{2+} exchange interactions, luminesc. line temp. depend. 79−69480
$KZnF_3$:Mn^{2+}, Cu^{2+}, exchange coupled, luminesc. props. 79−33781
$KZnF_3$:Mn^{2+}, exchange and spin-orbit interactions, optical spectra study 79−95817
$KZnF_3$:Ni^{2+}, Mn^{2+}, interference transition electric dipole mechanism 80−34896
$La_2Mg_3(NO_3)_{12}.24H_2O$:$Mn^{2+}$, linear electric field effect on ground state splitting, EPR 78−80198
La_2O_3:Mn^{2+}, position and intensity of forbidden hyperfine lines, ESR spectra 79−19775
$(La_2O_3)_{1-x}$-$(CeO_2)_x$:Mn, valence state of Mn, effect of annealing in H_2 atm., ESR obs. *(French)* 80−71164
$(La_2O_3)_{0.95}(CeO_2)_{0.05}$:$Mn^{2+}$, X-band EPR study 80−60409
$La_2Zn_3(NO_3)_{12}.24H_2O$:$Mn^{2+}$, pair spectra and mag. props. of Mn^{2+} 77−8396
$La_2Zn_3(NO_3)_{12}.24H_2O$:$CO^{2+}$, Mn^{2+}, Ni^{2+}, mag. exchange interactions, EPR 77−36118
$Li_2B_4O_7$:Mn, thermolum. response to pions 80−101270
$LiBaF_3$:Mn^{2+}, EPR, spin Hamiltonian parameters 79−65718
$LiBaF_3$:Mn^{2+}, having inverse periodic struct., ENDOR study 80−97162
LiCl:Mn, electron transfer absorption bands 79−95810
LiCl(Br):Mn^{2+}, optical absorpt., charge transfer spectra 80−2797
LiF:U, Mn, EPR of Mn^{4+} centre, g-values and hyperfine struct. 77−12192
α-$LiIO_3$:Mn^{2+}, EPR of impurity ion and radn. induced defects *(German)* 78−84480
α-$LiIO_3$:Mn^{3+}, absorption spectra, impurity environments 78−27275
$LiNbO_3$:Mn, photorefractive sensitivity, holographic and photocurrent investig. 77−24581
Li_2O-B_2O_3:Mn^{2+} glass, fine struct. parameter distribs., EPR meas. 80−11256
$Mg(ClO_4)_2.6H_2O$:Mn^{2+}, cryst., EPR 78−91935
$MgCs_2(SeO_4)_2.6H_2O$:Mn^{2+}, EPR spectrum 78−64261
MgF_2:Mn, X-ray luminesc. yield temp. depend. 77−4680
MgF_2:Mn, X-ray luminesc., activator flash 79−65958
MgF_2:Mn^{2+}, Coulomb and exchange interaction consts. optical spectra line assignment, new technique 80−45124
MgF_2:Mn^{2+}, MCD and linear dichroism, 3d→4s transitions 79−56768
MgF_2:Mn(Co), photoluminesc. due to X-rays, colour centre thermal breakdown 79−24359
MgF_2:Mn(Co), thermoluminesc. and TSC in activator band 79−24359
$Mg(H_2O)_6SiF_6$:Mn^{2+}, phase transition effects in EPR spectrum 79−42831
$MgK_2(SO_4)_2.6H_2O$:Mn^{2+}, EPR spectra spin-Hamiltonian anal. 77−77088
$Mg(NH_4)_2(SeO_4)_2.6H_2O$:$Mn^{2+}$, EPR spectra 80−100608
MgO:Fe^{3+}, Mn^{2+}, X-irrad. induced anion Frenkel defects, stabilisation by Fe^{3+}, optical and ESR obs. 77−68969
MgO:Mn, X-ray stimulated luminesc. 79−28802
MgO:Mn^{2+}, clustering of mag. ions, study method 80−11155
MgO:Mn^{2+}, EPR, 94-600K, temp. depend. of cubic spin Hamiltonian parameter 78−60332
manganese continued
MgO:Mn^{2+}, EPR of polycrysts. with varying impurity concentration *(Russian)* 77−28438
MgO:Mn^{2+}, phonon spectroscopy using supercond. tunnel junctions 79−65157
MgO:Mn^{2+}, redox behaviour, ESR and X-ray diffr. 78−52341
MgO:Mn^{2+}, spin Hamiltonian parameters, lattice expansion and vibr. effects 80−24851
MgO:Mn^{2+}, spin-lattice relax. time, meas. 80−66020
MgO:Mn^{2+} EPR, X-band freq., powder pattern for cubic symm. anal. *(Spanish)* 78−43636
MgO:Mn^{3+}, ground state exam., thermal conductivity meas. 79−42497
MgO:Mn^{3+}, HF phonon spectroscopy using supercond. tunnel junctions 80−65178
MgO:Mn^{4+}, diffuse interstellar absorpt. bands origin 79−30101
MgO-Mn^{2+}, Q band ESR spectrum, spin Hamiltonian calcs. *(French)* 78−64262
MgO-NH_4F-GeO_2:Mn phosphor, luminance. spectra due to UV irrad., 26-294°C 79−83005
$Mg(OH_2)_6(NO_3)_2$:Mn^{2+}, EPR spectra, crystal field symm. and strength 77−69674
$Mg(PO_3)_2$:Mn^{2+}, EPR, computer simulation compared with expt. *(French)* 79−95635
$MgRb_2(SeO_4)_2.6H_2O$:Mn^{2+}, EPR spectra 80−100608
$MgSeO_4.6H_2O$:Mn^{2+}, EPR obs., rel. to Mn crystallographic sites 78−79628
Mg_2SiO_4:Mn^{2+}, elec. field gradients, asymmetry parameters 80−54660
$MgTe_2$:Mn, pyrite phase, strong axial cryst. field of Mn^{2+}, EPR meas. 78 27081
$MgTiO_3$:Mn^{3+}, EPR spectra 79−91285
^{54}Mg, removal from waste water by oxine-impregnated activated charcoal 80−9344
Mn (II), (III), determ. in industrial wastes 78−61105
γ-Mn, antiferromagnetic, self-consistent bandstructure calcs. 80−88475
γ-Mn electrodeposition influence of Cu, Ag, and Be impurities *(Russian)* 79−47938
γ-Mn, enthalpy of fusion at 1386K 80−6490
Mn I, absorpt. spectrum, 1305-2040 Å, ionis. energy 79−26921
Mn I, inner shell absorpt. spectrum, 3d wavefunction collapse 77−23455
Mn II-lecithin lipid-water system, NMR and EPR obs. 80−61168
Mn III, revision and extension of spectrum, fundamental configs. *(Spanish)* 79−22637
Mn III-VI, struct. and transition probabilities, ab initio calc. using Thomas-Fermi central pot. 79−3360
β-Mn, struct., polyhedron model 78−79563
Mn V, $3d^24s$-$3d^24p$ transition 79−63943
Mn V, $3d^3$-$3d^24p$ transition obs. energy level assignments 78−55134
Mn V, forbidden transitions laboratory wavelengths 78−50496
Mn V, semiempirical calc. of energy spectra 77−46499
Mn VI, classification of absorption lines, 800-1550 Å 78−9103
Mn VI, colorimetric determ., appl. to Egyptian Mn ores 78−53285
Mn XIV, level struct. and predicted intercombination lines 80−14098
Mn XV, wavelengths and energy levels, spectral obs. 77−428
Mn XVI, ionisation pot. in Ne isoelectric sequence 78−5363
Mn XVII to Mn XXII ions spectrum emitted by Tokamak produced plasma 80−10437
Mn^-, in soln., EPR relax. probe 78−31104
Mn^-, oscillator strengths, from level lifetimes and branching ratios 78−17619
Mn^+, Sternheimer valence shielding antishielding factor including exchange 77−85182
$Mn^{2+,3+}$ effect on sodium polyelectrolyte impedance parameters in electrochem. cell 80−21296
Mn^{2+} and $P700^+$, light-dependent reactions in pulsed illuminated chloroplasts 79−53062
Mn^{2+}, crystalline spherical pot., effect on Fermi-contact term 80−20140
Mn^{2+}, cubic spin-Hamiltonian parameters in inorganic compounds, superposition model anal. 80−20367
Mn^{2+} dopant in CaF_2, CdF_2, BaF_2 78−27265
Mn^{2+} doped in calcium cadmium acetate hexahydrate, EPR 79−65715
Mn^{2+}, doped ion in divalent metal cpds., Szigeti charge and correl. with hyperfine coupling const. 80−96831
Mn^{2+}, EPR in polycrysts. of low symmetry, computer simulation *(French)* 79−95635
Mn^{2+}, EPR in Tutton salts, crystal field and hexahydrate distortion 78−91938
Mn^{2+} EPR of doped powder samples, hyperfine line intensities and axial cryst. field 79−78511
Mn^{2+}, EPR powder pattern analysis in cubic crystalline fields 79−47327
Mn^{2+} EPR spectra in glasses with g_{ef}=4.29 computer simulation 80−34764
Mn^{2+} EPR study of struct. changes in chalcogenide glasses 78−79534
Mn^{2+} effect on DNA helix-ball transition 79−70514
Mn^{2+}, effects on prolonged depolarising afterpot. in barnacle photoreceptor 80−8051
Mn^{2+}, Fermi contact interaction, spin density distrib., X_α calc. 77−54514
Mn^{2+}, fluoresc. quenching of organic excited singlet states, rate meas., mechanism 77−38685
Mn^{2+}, Hartree-Fock calcs., exchange pot. simplification 77−75054
Mn^{2+}, hyperfine forbidden ESR lines in cadmium acetate trihydrate, spin Hamiltonian calc. *(French)* 77−28431
Mn^{2+}, impurities in $CaCO_3$, magonite EPR, orthorhombic spin-Hamiltonian parameters 80−2631
Mn^{2+}, impurity ion in frozen aq. solns., effect on Fe^{3+} spin-spin relax., Mossbauer obs. 79−33573
Mn^{2+} in crystals with different site symmetries, luminesc. spectra 78−80400
Mn^{2+} in ionic crystals, exchange-coupled, optical spectra *(Rumanian)* 79−87474
Mn^{2+}, in nearly tetrahedral clusters, ^4E levels, orbit-lattice interaction and Jahn-Teller effect, spectra obs. 80−24860
Mn^{2+}, in polycrysts., EPR spectra calc. using Bir's method 79−1707
Mn^{2+}, in soln., non-radiative transitions as Forster's energy transfer to solvent vibrations 80−1014
Mn^{2+} in tetramethylammonium cadmium chloride, EPR meas. 77−59452
Mn^{2+} ions in Scheelites, zero-field splittings 80−75531
Mn^{2+}, paramagnetic changes in mammary tumours during development in rat 79−39425
Mn^{2+} partitioning in olivine and silicate melts 79−66683

manganese continued
Mn^{2+} salt soln., ESR expt. using balanced resonator 77−53966
Mn^{2+}, spin-Hamiltonian parameters, superposition model analysis 77−15798
Mn^{2+}, Zeeman interaction, relativistic corrections and very small g-shifts, contrib. to EPR 78−72393
Mn^{2+}, zero-field splittings, correl. with axial site distortions, superposition model 80−93168
Mn^{3+}, magnetostrictive effects in garnets and ferrimagnetic spinels 79−91277
$Mn^{6+,7+}$, in (MnO_4) type ions, metal X-ray K absorption spectra, low energy maxima interpretation 79−74019
Mn/MnO, relative chemical potential of oxygen *(German)* 78−31642
Mn-barium stearate-Mn structs., internal voltage work function meas. 79−82684
Mn-Cu_2O Schottky-barrier solar cells, surface anal. using AES 79−43759
Mn-Ge multilayer neutron monochromator, neutron diffr. expts. 77−84589
Mn-Ge planar interface, first phase to nucleate 77−62764
Mn-MgF, cermet film, evaporated, variation of elec. resist. with prep. conditions 77−43746
Mn-MgF, cermet film, variation of resist. with deposition rate 77−43747
Mn-MgF_2 cermet, heat treated, lattice distortion, resist. meas. 79−19492
Mn-MgF_2 cermet film, resistivity-temperature variation 79−24085
Mn-Sb two layer film, cpd. formation kinetics, ion backscatt., X-ray diffr. and mag. meas. 77−72801
Mn-SiO, annealed cermet films, elec. resist., composition depend. 80−97007
Mn-SiO cermet film, silicide form. during deposition 77−12535
Mn-SiO cermet films, DC and AC resist. 80−54804
Mn-SiO cermet films, elec. resist., annealing behaviour 80−54803
Mn-SiO cermet thin film, DC resist., activation energy, thickness depend. 80−84518
Mn-substituted garnet film, growth charact. and mag. props. 80−39826
Mn^{2+}-Cu^{2+} coupled pair, ESR spectrum, strong isotropic exchange model 80−29606
Mn^{2+}-F , overlap and covalency contrib. to zero field splitting, LCAO-MO calc. 80−24850
Mn^{2+}-$KBrO_3$-H_2SO_4-KBr system, chem. automat with three steady states 80−7769
Mn^{2+}-O^{2-} , overlap and covalency contrib. to zero field splitting, LCAO-MO calc. 80−24850
Mn^{2+}-oxalacetic acid-H_2SO_4-$KBrO_3$, chaos type reactions anal. 80−85165
Mn+H^+, K X-ray production, 0.2-0.5 MeV, ionis. cross-section 79−31459
Mn+N^+, X-ray production cross section, $K\beta/K\alpha$ ratio, 0.5-2.5 MeV/amu 77−54526
MnI, transition probability and solar abundance, beam foil TOF meas. 79−40154
MnII-ATP system, exchange mechanism, FT NMR and EPR obs. 79−22733
$MnNa_6(So_4)_4$, vanthoffite cryst. struct. lattice parameters and thermal behaviour 77−19929
MnO, K X-ray absorpt. discontinuity, shape and extended fine struct. 80−66324
MnO_2, K X-ray absorpt. discontinuity, shape and extended fine struct. 80−66324
Mn_2O_3, K X-ray absorpt. discontinuity, shape and extended fine struct. 80−66324
Mn_3O_4, K X-ray absorpt. discontinuity, shape and extended fine struct. 80−66324
^{51}Mn, chondrite exposure ages study using longlived spallogenic isotope 79−53776
^{53}Mn, cosmic-ray produced, in meteorites, neutron activation anal. 79−30018
^{53}Mn, in stony meteorites, determ. by activation anal. for cosmic ray effects investig. 78−12018
^{53}Mn, preparation in cyclotron by target bombard., extraction, anal. 77−61441
^{54}Mn radioactive tracer diffusion in Pt *(French)* 79−51306
^{54}Mn radioactive tracer diffusion in Mn-Pt alloys *(French)* 79−86915
^{54}Mn radionuclide adsorption charact. in waste water on oxine-impregnated activated charcoal 79−89394
^{54}Mn, sediment-bound, absorpt. through digestive tract of marine demersal fish 79−92400
^{54}Mn, thermotransport in KCl, Soret effect meas. 77−47624
^{54}Mn, uptake of gamma-emitting activation products in plants 80−30614
^{55}Mn, metastable states, hyperfine struct., laser RF double reson. study 79−72260
^{55}Mn, variation of hyperfine splitting consts. with interatomic distance for $3d^5$ ions 80−97133
^{52m}Mn, new short-lived, generator-produced radionuclide, positron tomography appl. 80−109006
$(NH_4)_2Cd_2(SO_4)_3$:Mn^{2+}, UO_2^{2+}, luminesc., vibr. modes 79−38629
$(NH_4)_2Co(SeO_4)_2.6H_2O$:$Mn^{2+}$, EPR 77−90017
$NH_4H_2PO_4$, Mn^{2+}, Mn^{3+} and MnO_4 ions effect on cryst. habit 77−58992
$NH_4H_2PO_4$, Mn^{3+} doping effect on Curie temp. and dielec. permittivity 77−59532
$(NH_4)_2Ni(SeO_4)_2.6H_2O$:$Mn^{2+}$, EPR spectra, spin quenching 78−2732
$(NH_4)_2SeO_4$:Mn^{2+}, single cryst., EPR and phase transition 79−73805
NaCl, Mn^{2+}-□ reorientation, ESR elec. field effect meas. 79−8050
NaCl:Ca^{2+},Mn^{2+}, EPR of Mn^{2+}, effect of Ca^{2+} on Mn^{2+} vacancy dipole decay 78−56371
NaCl:Mn, impurity-vacancy dipole aggregation, role of dimers and trimers, reanal. of dielec. and cond. data 79−1458
NaCl:Mn, nucleation of Au, surface imperfection effects 77−15699
NaCl:Mn^{++}, Mg^{++}, doubly doped, ionic thermocurrent study of linear dimer 80−79977
NaCl:Mn^{2+}, CN , EPR spectrum rel. to Mn^{2+}-vacancy-CN^- complex 80−54942
NaCl:Mn^{2+}, dimer detection, EPR and ITC expts. 78−59833
NaCl:Mn^{2+}, ESR and elec. field effects 77−28441
NaCl:Mn^{2+}, elastic wave damping, 300-1800 MHz, acousto-optical obs. 79−69198
NaCl:Mn^{2+}, electrolytically coloured, CESR 77−16174
NaCl:Mn^{2+}, influence of elec. field on flow stress 79−51193
NaCl:Mn^{2+}, ionic thermocurrents, comparison between microscopic and phenomenological anal. 79−51302
manganese continued
NaCl:Mn^{2+}, radiation-induced colouring, room temp. kinetics 79−55736
NaCl:Mn^{2+}, thermolum. spectra, mechanisms 80−80873
NaCl:Mn^{2+}, X-irrad., thermoluminesc. and EPR 79−61444
NaCl:Mn^{2+}, X-irrad. effects on divalent metal aggregates, EPR meas. 79−82263
NaCl:Mn^{2+}, X-ray irradiated, thermolum. and EPR 77−81161
NaCl:Mn^{2+}, Z_4-like centre, absorpt. spectra obs. 78−76498
NaCl:Mn^{2+} crysts., electrolysis, dendrite form., mechanism 77−1934
NaCl-NaF:Mn^{2+}, point defects, ionic thermal current and optical meas. 80−6403
NaF: Mn^{2+}, VUV absorpt. spectrum and EPR 80−55142
NaF:Mn, role of Mn^{2+} in thermolum. 80−97353
NaF:Mn^{2+}, two-step photoionisation, laser-active F_2^+ centre form. 79−963
$NaHSO_4$:Mn^{2+}, EPR 79−24215
$NaNO_2$:Mn^{2+}, ferroelectric phase metastable struct., EPR obs. 78−60328
$NaNO_2$:Mn^{2+}, zero-field splitting, ferroelec. soft-mode contrib., phase transition, EPR obs. 79−15344
$NaNbO_3$:Mn^{2+}, ESR, temp. depend., −269-750°C, fine splitting 77 51948
$NaNbO_3$:Mn^{2+}, ferroelec., memory effect, ESR meas. 79−28696
$NaNbO_3$:Mn^{2+}, T_2 phase, EPR spectra 78−88179
Na_2O-B_2O_3:Cu^{2+}, Mn^{2+} glasses, Cu^{2+}-Mn^{2+} interaction studied by ESR 80−93166
Na_2O-B_2O_3:Mn^{2+} glass, fine struct. parameter distribs., EPR meas. 80−11256
Na_2S:Mn^{2+}, polycrystalline, EPR and luminesc. of Mn^{2+} 78−27082
Na_2S:Mn^{2+} single crystal, EPR expts. and interpretation 79−1708
$NaZnGeO_4$:Mn, electrolum., ionisation domains 80−84787
$NbSe_2$:Mn, Kondo effect, mag. ordering and superconductivity 77−62915
$NbSe_2$:Mn, supercond., anomalous flux flow and matching 77−12069
$Nd_3Mg_3(NO_3)_{12}.24H_2O$:$Mn^{2+}$, EPR spectra, spin Hamiltonian anal. 79−33527
$Nd_2Zn_3(NO_3)_{12}.24H_2O$, EPR of Mn^{2+}, Gd^{3+} doped single crystal 79−24212
Ni-Fe/Mn interface, mag. surface effects, dead layers and exchange anisotropy 77−24718
Ni-Mn multilayer for monochromators and supermirrors, neutron reflectivities 80−22880
Ni+Mn, inner shell vacancy prod., impact parameter depend. 77−6906
Ni_2MnSn, ferromag. Heusler alloy, electronic struct., spin polarisations, theory 80−54598
$Ni(NH_4)_2(SO_4)_2.6H_2O$, Mn^{2+} doped, EPR study 80−34763
NiO:Mn, microhardness, plasticity, ageing effects 79−43291
$Ni(OH_2)_6(NO_3)_2$:Mn^{2+}, EPR spectra, crystal field symm. and strength 77−69674
$NiSO_4.7H_2O$, Mn^{2+} doped, EPR study 80−34763
$_{28}^{58}Ni^{n+}$+$_{25}$Mn($_{50}$Sn)($_{82}$Pb), 45, 94, and 138 MeV Ni inner shell vacancy production, impact parameter depend. 79−41130
$Nz(ClO_4)_2.6H_2O$:Mn^{2+}, EPR obs. of high temp. phase transition 79−28598
PbF_2:Mn^{2+}, NMR linewidth with mag. tagging for superionic cond. parameters determ. 77−81021
PbF_2:Mn^{2+}, superionic, cryst. field fluctuation dynamics, EPR 78−23328
PbI_2:Mn^{2+}, EPR 78−68362
$PbMo_4$, M=Mo,W, EPR spectrum, temp. depend. of zero field splitting 79−15346
PbO-SiO_2:Mn^{2+} glass, EPR 78−39392
$Pb_3(PO_4)_2$:Mn^{2+}, EPR study around ferroelastic transition point of $Pb_3(PO_4)_2$ 78−76303
$Pb_{1-x}Sn_xTe$: Mn, Mn mag. and elec. active states, mag. impurity behaviour 80−44627
Pb(Zr,Ti)O_3:Mn ceramics, anomalous dielec. losses 79−42892
$Pr_2Mg_3(NO_3)_{12}.24H_2O$:$Mn^{2+}$, X-band EPR 77−66418
$Pr_2Zn_3(NO_3)_{12}.24H_2O$:$Mn^{2+}$, EPR 78−64270
$RbCaF_3$:Mn^{2+}, overlap and covalency contrib. to zero field splitting, LCAO-MO calc. 80−24850
RbCl:Mn^{2+}, spin-Hamiltonian parameters anal., superposition model applicability 79−28592
$RbMF_3$:Mn^{2+}, (M=Mn,Cd,Ca), zero-field splitting of Mn^{2+}, superposition model *(French)* 79−15267
$RbMgF_3$:Mn, low-temp. radiation damage, optical absorption meas. 78−22761
$RbMgF_3$:Mn^{2+}, EPR obs. and struct. interpret. *(French)* 80−50167
Rh_2MnSn, Heusler alloy, Sn hyperfine field, Mossbauer exam. 77−43920
Si:Mn, amorphous, cond. increase by Mn doping 78−72155
Si:Mn, amorphous, EPR meas. 77−85559
Si:Mn, charcts. of residual cond. 79−15188
p-Si:Mn, defect levels, transient capacitance spectroscopy 78−6322
p-Si:Mn, giant residual cond. 80−20250
Si:Mn, γ-irrad., interaction of deep-level impurity atoms with radiation defects 77−76457
Si:Mn, impurity states, localised orbital approach 80−92851
Si:Mn, influence of neutron irradiation on elec. props. 78−55895
Si:Mn, negative photoconductivity 79−38132
Si:Mn, photosensitivity, residual cond. effects 78−19099
p-Si:Mn, temp.-elec. instability, photocond. meas. 77−1448
Si:Mn,Bi, standard, doubly implanted, Rutherford backscattering meas. at MeV energies, screening corrections 80−88204
Si:Mn amorphous films, ESR and elec. cond. 80−50171
Si:Mn^0, spin-lattice relax. of Jahn-Teller centres, coexistence of minima with different symmetries 80−80602
p-Si-Mn contact, barrier height 80−34510
$Sm_2Mg_3(NO_3)_{12}.24H_2O$:$Mn^{2+}$, EPR spectra, 77-298K 79−15342
SnO_2-Cu_xS-ZnS:Mn,Cu-Al_2O_3-Al, light-emitting struct., cond. and electrolum., heat treatment 80−97345
SnO_2-ZnS:Mn thin film structure, surface morphology and electro-optical props. *(Russian)* 80−49554
SnTe:Mn, EPR as probe of phase transitions 80−15790
SnTe:Mn, ferromag.-ordering, transverse magnetoresist. and Hall effect meas. 77−85240
SnTe:Mn, NMR shift meas. 80−97154
SnTe:Mn, NMR study 4.2 to 300K *(French)* 80−54960
$Sr_{0.5}Ba_{0.5}Nb_2O_6$:Mn, ceramic additive effect on ferroelec. and pyroelec. props. 77−16256
SrCl:Mn^{2+}, shape of potential well, calc. 78−87951

manganese continued
$SrCl_2$:Mn^{2+}(Co^{2+}), cubic impurity EPR spectra, elec. field effect, mechanism 78−68361
$SrMo_4$, M=Mo,W, EPR spectrum, temp. depend. of zero field splitting 79−15346
SrO:Mn^{2+}, EPR expts. 77−20691
SrO:Mn^{2+}, impurity pot. well shape calcs. 78−87950
SrS:Mn, Zr phosphor, photodielectric effect 80−107848
SrS:Zr,Mn, yellow and red fluoresc. mechanism 77−32419
$SrTiO_3$:Mn^{n+}, reduced, EPR of Mn centres 78−35029
TiO_2:Mn, ESR spectrum anal. *(French)* 78−19309
TiO_2:Mn, impurity levels, photocurrent and ESR meas. 80−29346
TiO_2:Mn^{2+}(Mn^{4+}), anatase single cryst., ESR spectra at 77K, 300K 78−10764
TiO_2:Mn^{4+}, rutile, temp. depend. of EPR 78−76299
TiO_2:Si(Fe)(Ni)(Mn)(Cr), anodes, performance in photoelectrolysis of water 79−74407
$TlCdF_3$:Mn^{2+}, zero-field splitting of Mn^{2+}, superposition model *(French)* 79−15267
YAG:Mn, impurity-induced O^- colour centres, absorpt. and fluoresc. spectra 77−1709
$(Zn,Mg)_2GeO_4$:Mn^{2+} phosphor, for low press. fluoresc. lamps, luminesc. characts. 78−10960
$(Zn,Mg)_3(PO_4)_2$:Mn^{2+}, cathodoluminescence obs. 80−71492
Zn silicates:Mn, sintered, photocond. *(German)* 79−51627
$ZnAl_2S_4$:Mn, superhyperfine interaction of Mn, ESR spectra 77−63271
$ZnCr_2Se_4$:Mn, paramagnetic, giant cubic anisotropy 80−7073
ZnF_2:Mn, thin films, electroluminescence, brightness voltage characts. hysteresis 80−20709
ZnF_2:Mn^{2+}, zero-field splitting, appl. of complete d-electron calc. 77−15799
$ZnGa_2O_4$:Mn^{2+}, EPR, spin Hamiltonian parameters 80−25195
$ZnGeF_6.6H_2O$:Mn (II), phase transition, ESR meas. 77−62636
$ZnK_2(SO_4)_2.6H_2O$:Mn^{2+}, EPR spectra, spin-Hamiltonian anal. 77−77088
$Zn(NH_3)_4(ClO_4)_2$:Mn, EPR study of Mn^{2+} detection of structural transition 79−87308
$Zn(NH_4)_2(SeO_4)_2.6H_2O$:$Mn^{2+}$, EPR spectra 80−100608
ZnO:Mn^{2+}, phosphors, emission spectra, impurity effects 77−32420
$ZnRb_2(SeO_4)_2.6H_2O$:Mn^{2+}, EPR spectra 80−100608
ZnS:Cu, Cl, Mn film, AC electrolum. 80−60680
ZnS:Cu, Mn DC electroluminescent powder panels, bulk and junction effects 80−89068
ZnS:Mn, AC thin film electroluminesc., filamentary emission and memory effect 79−38672
ZnS:Mn, AC thin-film electrolum. devices, electrolum. efficiency profiles 79−65931
ZnS:Mn, Cu, Cl films, AC electrolum. 80−60679
ZnS:Mn, Cu powder devices, DC electroluminesc. 79−38674
ZnS:Mn, dopant conc. effect on stacking fault energy 80−2041
ZnS:Mn, electrolum. film, direct impact excitation of Mn centres 77−24900
ZnS:Mn, electrolum. films, activating impurity diffusion coeff. *(Russian)* 77−84995
ZnS:Mn, electroluminescent film, stimulated emission *(Russian)* 77−19255
ZnS:Mn, impurity-induced Raman scatt., central force const. reduction 77−32379
ZnS:Mn, luminesc., exciton struct. 79−33801
ZnS:Mn, phosphor, surface changes following interaction with H *(Russian)* 78−72602
ZnS:Mn, Raman spectra, impurity induced first order transitions 78−88310
ZnS:Mn, self-activated and Mn^{2+} emission, high press. action 80−16093
ZnS:Mn, vibr. modes of transition element impurities 78−76472
ZnS:Mn AC thin film devices, domain electrolum. 80−66303
ZnS:Mn AC thin film electrolum. device, filament behaviour 80−20712
ZnS:Mn co-deposited electrolum. thin film device, phys. and elec. characterisation 80−20713
ZnS:Mn electroluminescent films, amplification factor during electric field excitation, population inversion *(Russian)* 79−78757
ZnS:Mn film, AC electrolum., memory effect 78−15228
ZnS:Mn film, AC electrolum., memory effects 79−38673
ZnS:Mn film, current conduction and light emission, physical mechanism 78−14840
ZnS:Mn film, electroluminescence theory 79−11470
ZnS:Mn film, emission centres of DC electrolum. 78−68564
ZnS:Mn film, luminesc. of highly efficient DC diodes 77−8630
ZnS:Mn film, spectral and electro-optical props. 77−1736
ZnS:Mn film device, laser modulation of electrolum. 78−52576
ZnS:Mn film in SnO_2-ZnS-Cu_xS-ZnS:Mn-Al_2O_3-Al struct., electrolum. 79−33837
ZnS:Mn films, photoluminesc. and electroluminesc., excitation mechanism of luminesc. centres 79−11459
ZnS:Mn films, surface struct., microrelief rel. to morphology of SnO_2 transparent cond. support 79−56092
ZnS:Mn Schottky diodes, reverse-biased, electroluminescence, hot electron impact excitations 80−25005
ZnS:Mn-H atom systems, surface physiochem. changes, radical recombination luminesc. investig. 79−56863
ZnS:Mn^{2+}, $^4T_1$ excited state, absorpt., MCD, Jahn-Teller model 78−43907
ZnS:Mn^{2+}, $^4T_1$ state, magneto-optical meas. 77−20833
ZnS:Mn^{2+}, $^4T_2$ level, Zeeman splittings, Jahn-Teller effect 80−40141
ZnS:Mn^{2+}, heavily doped, anomalies in reflectivity 77−20891
ZnS:Mn^{2+}, Jahn-Teller effect in fluorescent level 78−52566
ZnS:Mn^{2+}, spin-lattice coupling coeffs. of Mn^{2+} ions in stacking faults 77−20690
ZnS:Mn^{2+}, spin-lattice relax. time, continuous saturation expts., spin diffusion 77−36120
ZnS:Mn^{2+}, spin-lattice relaxation, EPR, optical phonons 80−39852
ZnS:Mn^{2+} phosphor, exciton struct. in luminesc. excitation spectra 77−52176
ZnS:Mn^{2+} phosphors, luminesc. excitation spectra and exciton struct. 80−55164
ZnS:Pb^{2+}(Mn^{2+}), high press. luminesc., localised excitations 78−19534
ZnS-Mn crystal, polarisation meas., luminesc. and Raman spectra 79−8138
$ZnSO_4.7H_2O$:Mn^{2+}, EPR 77−16165
ZnS_xSe_{1-x}:Mn(Cu), luminesc. obs. 78−60519
ZnSe:Al(Mn), elec. and luminesc. props. 77−39844
manganese continued
ZnSe:Mn, deep centres, photolum., photocapacitance and photocurrent expts. 78−39053
ZnSe:Mn, Schottky diode, direct impact excitation of luminescent centres 79−7900
ZnSe:Mn, single crysts., associated pt. defects, EPR method 77−48040
ZnSe:Mn thin film, AC electrolum. 79−47519
ZnSe:Mn/n-GaAs low threshold thin film DC electrolum. cell, pulse-excited characts. 80−76081
ZnSe:Mn-Ge epitaxial heterostructs., growth, struct. 78−43257
ZnSe:Mn^{2+}, ligand HFS calcs., EHT-SCCC, scattered-wave, LCAO methods, comparison with expt. 77−55501
ZnSe:Mn^{2+}, refined spin Hamiltonian parameters *(French)* 77−63268
ZnSe:Mn^{2+} Schottky barrier diodes, spin depend. cond. and photovoltage 79−91141
ZnSe:Mn^{2+}-n-Ge thin film electrolum. cell with low-threshold voltage 80−84786
ZnSe:Mn^{3+}, Jahn-Teller effect in fluorescent level 78−52566
ZnSe:Mn-n-GaAs, single cryst. substrate low threshold DC electrolum. 77−63465
ZnSe+Mn^{2+}, LCAO calc. of d-orbital splitting 77−28148
$ZnSiF_6 6H_2O$:Mn^{2+}, ESR spectrum, effect of uniaxial compression 80−29609
Zn_2SiO_4:As,Mn, enhanced luminesc. stimulation, 20-320K *(German)* 77−20900
Zn_2SiO_4:Mn, cathodoluminesc. yield, calorimetric method determ. *(Russian)* 77−20938
Zn_2SiO_4:Mn, energy storage effect and retrieval 80−100684
Zn_2SiO_4:Mn, phosphoresc. decay into second-order components 77−20907
Zn_2SiO_4:Mn film, electron beam depth-dose functions, cathodoluminesc. 80−2867
Zn_2SiO_4:Mn phosphor, luminesc. saturation under intense vac. UV irrad. 79−56841
Zn_2SiO_4:Mn phosphor, efficiency enhancement by $AlPO_4$ substitution 80−11452
Zn_2SiO_4:Mn^{2+}, quantum yield in candoluminescence process by low energy H^+ ion bombard. 79−65930
Zn_2SiO_4:Mn^{2+} phosphor, for low press. fluoresc. lamp, luminesc. characts. 78−10960
ZnTe:Mn, exciton refl. band, giant mag. splitting *(Russian)* 78−56079
ZnTe:Mn, exciton refl. spectra 80−2806
ZnTe:Mn, mag. field splitting α n=2 exciton state *(Russian)* 78−79940
ZnTe:Mn, ordering mechanism 80−2572
ZnTe:Mn, spin-lattice coeffs. of Mn^{2+} 80−84646
ZnTe:Mn^{2+}, forbidden transitions of Mn^{2+} induced by hyperfine interactions 80−60458
ZrO_2-CaO:Mn^{2+}, EPR spectra, impurity substitution behaviour in various phases 77−16160
$(ZrO_2)_{0.9}(Y_2O_3)_{0.1}$:Cr, Mn, stabilised single crystal, EPR of Mn^{2+} and Cr^{3+} obs. 80−66024

manganese alloys
see also Elinvar; Invar; manganese compounds
alumel, B versus H measurement from 25 to 180°C 78−23297
Alumel, thermocouple alloy, heat treatment effects on thermoEMF and mag. flux 77−63235
Cu-Mn alloys, thermodynamics, suitability as electrodes 79−66339
D16 extruded rod, substruct, anisotropy and decomp. at subboundaries *(Russian)* 77−25095
dilute alloys, amorphous, exhibiting Mossbauer effect, mean mag. props. *(French)* 80−80489
ferromagnetic ordered structures, domain structure, effect of defects, electron microscopy 78−64214
Heusler alloy, Mn-containing hyperfine field and magnetic behaviour 79−78360
Heusler alloy, Mn-containing theory of spin waves 79−78354
Heusler alloys, ferromag. alignment rel. to conduction electron polarisation 80−60235
Heusler alloys, hyperfine fields and mag. interactions, NMR spectra 78−88222
hyperfine fields in weakly antiferromag. β-Mn alloys, NMR meas. 78−39441
Inconel 800, simulated, steam oxidation 80−76405
intermetallic compounds, containing d-transition metal, hydrogenated, magnetism 80−34609
intermetallic compounds, energy of veriform struct. 78−91882
Kovar, effect of magnetic electrons on atomic interactions 77−43820
manganin foil like gauge calibration in planar shock wave expts. 80−95091
manganin resistance gauge for high pressure meas. 77−10036
manganin stress gauges, low-impedance, for precision measurement in severe shock-wave environments 80−38367
manganin thin film microtransducers for elastohydrodynamic lubrication studies 80−37048
$Mn_{1.98-x}Cr_xFe_{0.02}Sb$, Mossbauer effect exam. 78−68432
$Mn_{1-x}Cu_xSb$ films, $0 \leq X \leq 0.3$, magneto-optical props. 79−51981
Monel, Ni-Cu-Fe-Mn, resistance spot weld quality evaluation, using stress wave emission technique 78−53066
Monel 400, corrosion susceptibilities in synthetic geothermal brines 77−86223
Monel 400, stress corrosion cracking in high temp. caustic soln. 77−59964
mutual alloying behaviour of the elements straddling the line Li-Mg-Cu-Au in the long periodic table 78−84769
$(Ni_{1-x}Co_x)_{0.98}Mn_{0.02}$, average mag. moment of Mn atoms 79−28509
Nichrome, volatilisation of oxides during oxidation at 1200°C 78−23873
Nimonic alloy, effect of annealing on hardness, carbide phase strengthening *(Russian)* 79−34137
NK, thermocouple alloy, heat treatment effects on thermoEMF and mag. flux 77−63235
Permalloy-Mn film, diffusion aftereffect causing mag. state change *(Russian)* 80−103860
pnictides, energy bands, electron correl. effects 78−14688
rare earth germanides, RMn_2Ge_2, magnetisation, 4.2-1200K 77−8285
rare earth intermetallic, $R(Fe_{1-x}Mn_x)_2$, phase struct., mag. and Mossbauer meas. 77−20563
rare earth intermetallics, RMn_2Si_2 and RMn_2Ge_2, cryst. struct. 78−59782
rare earth silicides, RMn_2Si_2, magnetisation, 4.2-1200K 77−8285

manganese alloys continued
rare earth ternary alloys, RT_6Al_6, T=Cr, Mn, Fe, Cu, cryst. struct. 80−107110
SA, thermocouple alloy, heat treatment effects on thermoEMF and mag. flux 77−63235
Silumin, AlSi10Mn, struct. and mech. props., Na modification effects 77−63786
steel, 35G16, plastic deformation, shape recovery during γ to and from ε, ε' transformations *(Russian)* 79−83196
steel, alloy, cluster formation susceptibility in 40 KhN, influence of isothermal working in H_2 *(Russian)* 78−56643
steel, alloy, Cr-Cu-Mn-C, HT80, effect of grain size on sensitivity to reheat cracking *(German)* 78−72856
steel, alloy, Fe-Ni-Mn-Si-Cr-Ni-Mo, effect of metallurgy on stress corrosion cracking, and hydrogen embrittlement 78−60885
steel, alloy, Mn (1 to 10 wt.%), Mossbauer, X-ray and electron microscope studies of martensite 78−56621
steel, alloy, Mn-Si-C, exam. of fracture toughness for sheets, using linear elastic fracture mechanics 78−56762
steel, alloy, Ni-Cr-Mn, type 4340 intergranular brittle fracture, exam. by impact testing and Auger spectroscopy 78−52978
steel, alloy, Si-Mn(Mn-Cr), heat treated, exam. of microfractographic aspects of fatigue cracks *(Japanese)* 78−52959
steel, alloy, softening process in deformed type 15GYuT, metallographs *(Russian)* 78−52840
steel, alloy cyclic strength after strain hardening and tempering, precip. hardened 40FT, and 40 78−52988
steel, austenitic, Cr-Mn, Kh4G18F, microstruct. and mech. props. during tensile deform. *(Russian)* 79−20114
steel, austenitic, Cr-Mn, martensitic transform. effect on hardening kinetics and fracture resist. of friction surface *(Russian)* 80−50727
steel, austenitic, Cr-Mn, metastable, plasticity, contrib. of martensitic transform. during deform. *(Russian)* 80−30018
steel, austenitic, existence of carbide M_5C_2 phase, electron microdiffr. analysis *(Russian)* 78−23727
steel, austenitic, Mn-Al, low temp. appl. explosion test of fracture mode *(Chinese)* 78−31496
steel, austenitic, Mn-Ni-Cr, Mn effects on cracking *(German)* 77−59889
steel, austenitic, Mn-V-C, discontinuous precipitation, grain boundary struct. effect 79−29068
steel, austenitic, type 110G13, martensitic transform. effect on hardening kinetics and fracture resist. of friction surface *(Russian)* 80−50727
steel, austenitic Cr-Mn, $M_{23}C_6$ carbide precipitates comp., heat and thermomech. treatment influence *(Russian)* 80−40361
steel, austenitic stainless, biphase, ferritic, ageing and thermomech. treatment effects on struct. and props. 80−35226
steel, austenitic stainless, Cr-Ni-Mo-Mn, Mo, Mn and ageing effects 78−35413
steel, austenitic stainless, Mn alloy, sound vel. anomalies near spin glass transition 79−82795
steel, austenitic stainless, Ni free, corrosion obs. 79−24652
steel, C, diffusion of H_2, SCC via martensite form. cooling rate changes on Mn and Ni addition *(Russian)* 78−56813
steel, C-Mn and C-Mn-Nb, weldable, high temp. thermomechanical treatment 79−15709
steel, C-Mn-Cr-Mo (0.4, 0.8, 1.1, 0.25 wt.%) C, Ni, Mo, Cr addition effects on toughness of bainite 78−11327
steel, C-Mn-Nb, Nb microalloying, weldable, structural, recrystallization and precipitation induced by high temp. deform. *(French)* 79−61632
steel, Co-Cr-Ni-Mo-Mn (39.65, 20.25, 15.33, 7.08, 1.9 wt.%) carbide formation during tempering after plastic deformation 80−16330
steel, Cr, carbide form. depend. on Mn, Cr, V additions, cementite stabilisation, microstruct. *(Russian)* 80−55399
steel, Cr-C-Mn, struct. prop. rel., design of struct. steels for high strength and toughness 80−97491
steel, Cr-Cu-Mn, fatigue crack propag. rate eval. by J integral method *(Japanese)* 79−8346
steel, Cr-Mn, annealing effect on mech. props. for cryogenic appl. *(Russian)* 78−19788
steel, Cr-Mn, metastable constitution diagram and phase transforms. *(Russian)* 80−50590
steel, Cr-Mn, powder forged, fracture processes and fracture toughness 78−72870
steel, Cr-Mn (13, 19 wt.%), elastic const. behaviour, anomalous, low temp. 80−97521
steel, Cr-Mn-C-Si (20, 14, 0.2, 0 to 3 wt.%), high-temp. oxidation *(Russian)* 80−25904
steel, Cr-Mo, Mn and Si effect on temper embrittlement, comp. and carbide precip. effects 80−85037
steel, Cr-Mo-V, combined Cr-Mn addition effects on hardenability 78−7046
steel, Cr-Mu-W, carbide form., W effect 80−76259
steel, Cr-Ni-Mo-Mn, wetting of TiC, expt. planning investigation 80−60822
steel, creep-resistant pipe steel, influence of chemical comp. on formability *(German)* 78−84900
steel, Cu-Mn-Zn, Zn addition effects in powder forgings produced by liquid solid alloying 78−11157
steel, emission spectrochemical analysis of Nb, effect of Mn, interference for Nb II 3194.977 Å 77−21457
steel, Fe-Mn-(Cr)-C, intermediate phase form. during martensite form. 77−12626
steel, fine grained C-Mn-V-Al-N, relationship between ferrite and austenite grain size 80−3001
steel, high Mn, austenite grain size, effect of rolling and V, Ti and Zr additions *(Korean)* 77−12632
steel, high Mn, heat resistant, alloying additions, effect on mech. props. *(Korean)* 77−12631
steel, high Mn mandrels, wear resist., surface layer chem. comp. influence *(Russian)* 79−52444
steel, high-strength, fatigue crack growth rate and crack tip shapes, cyclic bending *(Russian)* 80−71740
steel, low alloy, reactor pressure vessel, effect of Mn and C content on irrad. response 79−20196
steel, low alloy, S and Mn influence on high temp. strength and ductility after solidification from melt *(German)* 80−81106
steel, low C, containing P, Mg effect on annealing texture, mech. props. and plastic anisotropy 78−27536
steel, low C, Mb-Nb, reheated, quenched, tempered, microstruct. 77−36550

manganese alloys continued
steel, low C, Mn, laws of banding structure form. *(Slovenian)* 78−83776
steel, low C, Mn effect on recrystallisation and texture *(French)* 80−3110
steel, low C Mn-V, VC effects on strength and brittleness 77−70055
steel, low-alloy, case carburised, retained austenite effect on contact fatigue strength 80−30096
steel, low-alloy, V effect on mech. props. 80−35312
steel, low-Mn low-C, susceptibility to brittle fracture 80−76340
steel, maraging, heating of thin samples with brief ageing, N6G4M, ON18K9M5T 78−52866
steel, maraging, investigation with lower Ni and Co contents *(Chinese)* 78−84812
steel, Mn, H_2 embrittlement mechanism *(Korean)* 78−68774
steel, Mn, solutioning of castings in salt baths 78−23871
steel, Mn, stacking fault energy rel. to mech. props. *(French)* 79−43339
steel, Mn, tempered, sementite crystals, carbide phase segregation, X-ray study *(Russian)* 78−35391
steel, Mn, tempering, initial stages of carbide form., electron diffr. *(Russian)* 78−19760
steel, Mn, type 35SGM, magnetic, electrical, and mech. props. after tempering and hardening 79−66086
steel, Mn (13.5 wt.%) hardening mechanism during friction 79−96152
steel, Mn and Mn-Ti, cryogenic mech. props. and intergranular brittleness *(Korean)* 79−70164
steel, Mn-C (1, 0.1 wt.%) strip, hot rolled, P effect on mech. props. 78−27532
steel, Mn-C-O, phase equilibrium, Mn effects at liquidus temp. *(Russian)* 77−66625
steel, Mn-Cr, blank hardened, shot peening effect on bending fatigue strength *(German)* 78−35402
steel, Mn-Cr, normalised, shot peening effect on bending fatigue strength *(German)* 78−35401
steel, Mn-Cr, tempered, case hardened, shot peening effect on bending fatigue strength *(German)* 79−24645
steel, Mn-Cr-Ni-N, N effect on relaxation behaviour, internal friction temp. depend. *(Russian)* 78−52872
steel, Mn-Cr-V, crack propag. resist. at hardness indentation, and fracture toughness *(German)* 79−29220
steel, Mn-Cr-V, structural changes during solution annealing *(Czech)* 78−84864
steel, Mn-Mo, castings, mech. props., Cu and Sn trace elements effect 80−66596
steel, Mn-Mo (3, 0.4 wt.%), specimen fracturing device for ion microprobe analyser, appl. to grain boundary segregation 77−21341
steel, Mn-Mo-Nb, high strength, ductile, acicular ferrite struct. 77−21191
steel, Mn-Mo-Ni, embrittling effects of residual elements 80−66655
steel, Mn-Nb-Al-C, crack progag. and hot ductility during straightening concast strand 80−66646
steel, Mn-Ni-Al, nonmagnetic, carbide-intermetallic strengthening 79−83208
steel, Mn-Ni-Cr, diffusion of Fe, Mn, Si, V and W *(Czech)* 77−59148
steel, Mn-Ni-Mo low alloy steels for nuclear appl., toughness and heat treatment 80−5239
steel, Mn-Si, St 52-3, cleavage fracture toughness, temperature and notch sharpness influence *(German)* 80−35291
steel, Mn-Si, St 52-3, fracture toughness determ. from yield strength and cleavage fracture strength *(German)* 80−35292
steel, Mn-V reinforcing type, strain ageing characts. rel. to mech. props. 80−84969
steel, MnCr (16, 5 wt.%), bending fatigue behaviour improvement by surface treatment *(German)* 78−84957
steel, MnMoNi(Cr), pressure vessel, stress relief cracking 79−43404
steel, Ni-Mn (16, 2 wt.%), 40N16G2, single crystal, stabilisation and destabilisation mechanisms *(Russian)* 78−23732
steel, Ni-Mn-C, austenitic, proof stress change meas. by internal friction with martensitic transform. 78−56638
steel, quench ageing effect of Mn content on C and N precipitation and mech. props. *(German)* 78−31409
steel, Si (6.5 wt.%) Mn, Ni and Al additions influence obs., on mech. and magnetic props. *(Slovak)* 79−5064
steel, Si-Mn, 27SG, heat treated sheets, underwater explosive forming *(Polish)* 79−34052
steel, Si-Mn, ferrite-pearlite structs., fatigue crack propagation *(Russian)* 79−34126
steel, Si-Mn, non-magnetic, minimum electroresistivity, −268 to 0°C *(Russian)* 79−91021
steel, Si-Mn-C (1.6-2.0, 0.4-0.6, 1.1-1.4 wt.%), cast graphitised, heat treatment effects on mech. props. and wear resist. 79−96050
steel, Si-Mn-Ni-Cr-Mo, acoustic emission during stress corrosion cracking appl. to materials testing 78−53042
steel, stainless, austenitic, Cr-Ni-Mn-Si-Mo-C alloy, 13Khi8N10G3S2M2, elastic moduli exam. after thermomechanical treatment *(Russian)* 79−24558
steel, stainless, austenitic high Mn, thermally induced segregation 79−4971
steel, stainless, Cr-Ni-Mn, N strengthened, low-temp. elastic props. 79−70109
steel, stainless, type Kh17N13M2T, strengthening by plastic deformation and cold working *(Russian)* 78−52839
steel, wear resistant, review of abrasive adhesive and rolling wear *(Korean)* 79−24624
steel austenitic, Mn and Mn-Cr, thermal expansion *(German)* 77−59127
steel Cr-Mn (13, 19 wt.%), for liquefied natural gas appls., material and weld props. 79−61736
steel Cr-Mn (13, 19 wt.%), liquefied natural gas appls., materials and weld props. 79−61735
steel low C, Mn surface segregation during annealing, kinetic studies 78−27528
Supermalloy, 24 GHz ferromagnetic antiresonance transmission 77−51957
Supermalloy, 9, 24 and 38 GHz ferromagnetic reson. absorpt., line shapes 77−51958
supermalloy, foil, microwave transmission, parallel RF and mag. fields 77−59462
A-Mn, dil., mag. susceptibility and single impurity effects 78−64186
Ag-Cu-Zn-Mn, solder, UTS, room temp. to 4.2K 79−57064
Ag-Mn, annealing twins rel. to stacking fault energy 79−33006

manganese alloys continued
Ag-Mn, conc. spin glasses, thermopower 80−65538
Ag-Mn, dil., anomalous thermal expansion below 50K 78−51710
Ag-Mn, dil., nuclear orientation expts. 78−43713
Ag-Mn, dil., spin glass, AC susceptibility 79−33490
Ag-Mn, dil., thin-film spin glass, mag. susceptibility and T_G meas., 1.2-60K 79−38346
Ag-Mn, dil., valence and core level spectra, XPS study 80−84838
Ag-Mn, dil. alloy, transverse magnetoresist. in spin glass regime 80−34417
Ag-Mn, dilute spin glass, AC susceptibility and ESR meas. 79−7968
Ag-Mn, spin glass, anomalous Hall effect 78−30908
Ag-Mn, spin glass, mag. susceptibility hydrostatic press depend., RKKY interaction 80−44845
Ag-Mn, spin glass alloy, elec. resist. 77−8067
Ag-Mn, spin-flip scatt. time, superconductive tunnelling 79−8003
Ag-Mn (20 at.%), mag. virtual bound state alloys, XPS of core states 79−47588
Ag-Mn alloys, dilute, low temp. elec. resist. *(Russian)* 78−68024
Ag-Mn dilute, magnetoresist. and Hall effect, field-depend. electron scatt. 77−43581
Ag-Mn film, supercond. proximity effect and pair breaking, normal state mag. interactions 77−63035
$Ag_{0.6}Au_{0.4}Mn$, dil., effect of mean free path on strength of RKKY interaction 78−39291
Al-(Mn), effects of Mn on electrode or free corrosion potentials 80−100942
Al-Cu-Mg-Mn, shot peened, positron annihilation meas. 77−63833
Al-Cu-Mg-Mn (4.5, 1.5, 0.6 wt.%), alloy 2024-T3, exam. of residual strength of plate containing crack, fracture anal. 78−90792
Al-Cu-Mg-Mn (4.5, 1.5, 0.6 wt.%), thin sheet, exam. of fracture toughness, and fatigue crack growth 78−92353
Al-Cu-Mg-Mn-Fe-Si, alloy D16, effect of mechanisothermal treatment on mech. props. 78−56674
Al-Cu-Mg-Mn-Si-Fe, endurance with cyclic bending, effect of loading conditions 80−50724
Al-Cu-Mg-Mn-Si-Fe, subcritical crack growth under static plane stress 80−55528
Al-Cu-Mg-Mn-Si-Fe, torsional vibrations decrement, deformed vol. effect 80−76326
Al-Cu-Mg-Mn(-Zn-Cr), low temp. deformed, ageing and mech. props. 79−1881
Al-Cu-Mg-Si-Fe-Mn-Ti, Si, Fe, Mn and Ti effect on precipitation in solid soln. *(Korean)* 79−66064
Al-Cu-Mg-Si-Mn (2.5, 0.7, 0.7, 0.5 wt.%), alloy AK6, US inspection of heat treatment quality 78−76681
Al-Cu-Mg-Si-Mn alloy AK8, fatigue strength, effect of residual stresses and cold working 77−56101
Al-Cu-Mn, long term strength and creep 80−60925
Al-Cu-Mn, type 2219, synchrotron radiation microradiography 80−85121
Al-Cu-Mn (1-5.2, 0-0.6 wt.%), N alloying and comp. effect on mech. props. *(Bulgarian)* 80−71719
Al-Cu-Mn (6.3, 0.3 wt.%), Al 2219-T851, fatigue crack initiation and early propag. 77−32684
Al-Cu-Mn (6.3, 0.3 wt.%), alloy Al 2219-T851, crack closure load meas. during fatigue 77−63870
Al-Cu-Mn (6.3,0.3 wt.%), alloy Al 2219-T851, crack closure load development for surface microcracks 77−86226
Al-Cu-Mn-Mg alloy D16, sheet, corrosion fatigue strength, with anodised and painted surfaces *(Russian)* 78−35575
Al-Cu-Mn-Mg-Fe-Si, corrosive environment effect on fatigue crack growth rate 80−55584
Al-Cu-Mn-Mg-Fe-Si (4.48, 0.66, 1.55, 0.43, o.23 wt.%), alloy D16, relationship between intercrystallite corrosion depth, and elec. cond. 79−20220
Al-Cu-Mn-Mg-Fe-Si-Zn alloy D16, surface layers chem. composition rel. to fatigue resist., corrosion-fatigue resist. 79−29275
Al-Cu-Mn-Zr, type 2219, particle, coarsening of disk shaped Θ′ particles 80−45315
Al-Cu-Mn-Zr-Fe-Si (6,0.3,0.18,0.3,0.1 wt.%) experimental evidence of Mn enrichment in Al_2Cu precipitates by EDS in TEM 78−15415
Al-Cu-Si-Mn, type 2017S-T4, crack initiation at root of circumferential notch of round bar specimens *(Japanese)* 80−60947
Al-Li-Mn (2.8, 0.3 wt.%), recrystallised sheet, fracture behaviour, SEM and TEM study 80−97566
Al-Mg-Mn, with high Al content, resist., 1.5 to 4.2K 78−26841
Al-Mg-Mn alloy, disperse β-phase, kinetic laws of coagulation *(Russian)* 78−27519
Al-Mg-Mn alloy AMG-6M, endurance determ. by dimensionless damageability curves 79−96141
Al-Mg-Mn-Cr (4, 0.45, 0.15 wt.%), laser shock hardening of weld zones, exam. 78−39800
Al-Mg-Si alloy, Mn additions, effect on deform. 77−8876
Al-Mg-Si-Mn, Mn addition effects on fracture 78−60791
Al-Mg-Si-Mn foil, planar defect spacing meas. by TEM 78−2135
Al-Mn, Al-Cr-Mn, dil. alloys, Hall coeff. and elec. resist. 77−11898
Al-Mn, anisotropic electron scattering, Hall coefficient, path integral calc. 79−91027
Al-Mn, anodisation, intensity of luminesc. and film thickness 78−80413
Al-Mn, cold-worked and homogenised, precip. kinetics, impurity resist. and TEM meas. 77−16596
Al-Mn, cooling after recrystallisation, phase transform., X-ray and thermal anal. *(Russian)* 77−66663
Al-Mn, couple phase diagrams and thermochemical data 79−66037
Al-Mn, dil., ^{54}Mn Knight shift meas. using nucl. orientation 78−68396
Al-Mn, dil., coherent propag. and strain-induced localisation of muons 78−95537
Al-Mn, dil., core and valence band spectra, XPS study 80−84837
Al-Mn, dil., electronic states, XPS meas. 77−44117
Al-Mn, dil., magnetisation, 2-0.01K 79−4652
Al-Mn, dil., magnetoresist. meas. 77−28160
Al-Mn, dil., magnetoresist. meas. 77−62900
Al-Mn, dil., supercond., nucl. spin relax. and quasiparticle excitations 80−88680
Al-Mn, dil., superconducting and normal state, ^{27}Al spin-lattice relax. rates 79−60977
Al-Mn, dil. alloys, single impurity and interaction effects in susceptibility 77−8269
Al-Mn, dilute, NMR investig. of spin density oscills. around Mn impurities 77−4570
manganese alloys continued
Al-Mn, direct chill-cast, struct. changes during heat treating *(German)* 80−40408
Al-Mn, Kondo alloys, spin and phonon resistivity independ. 78−47777
Al-Mn, liq., dissoln. and diffusion of alloying components, 700-1000°C *(Russian)* 80−15275
Al-Mn, liquid alloys, thermodynamic charact. calc. *(Russian)* 78−27475
Al-Mn, magnetic susceptibility, single impurity and interaction effects 77−63093
Al-Mn, metastable Ll_0 phase, transformations, mag. struct., TEM study 80−3029
Al-Mn, Mn impurity displacement during He irradiation, computer simulation 77−80563
Al-Mn, μ^+ localisation temp. depend. 80−44993
Al-Mn, quenched, thermal stability *(Russian)* 80−20976
Al-Mn, solute atom displacement in mixed dumbbell interstitials for FCC lattice 78−79631
Al-Mn, splat cooling and heat treatment effect on struct. and props. *(Russian)* 77−48456
Al-Mn, struct. form. and phase transform. kinetics *(Russian)* 78−15359
Al-Mn (0.35 wt.%), quenched exam. of Mn-vacancy interaction 78−76676
Al-Mn (0.55-5 at.%), magnetoresist. depend. on mag. field and impurity conc. 77−62896
Al-Mn (1 wt.%), anodisation, yellow electrolum. from Al-Al_2O_3:Mn-electrolyte system 77−63464
Al-Mn (1 wt.%), commercial, recrystallisation 79−47710
Al-Mn (1 wt.%), single crysts., rolled to (123)[41$\bar{2}$], recrystn. textures 80−104183
Al-Mn (1 wt.%), subgrain growth during annealing after cold work 78−56656
Al-Mn (1 wt.%) corrosion in uninhibited ethylene glycol-water solutions 79−70222
Al-Mn (1.3 wt.%), corrosion inhibition in trichloroacetic acid using chloroanilines 79−83389
Al-Mn (1.8 wt.%), cold-rolled, precipitation and recrystallisation 78−27540
Al-Mn alloys, anomalous sp. ht. and nuclear spin-lattice relax. 79−46814
Al-Mn alloys, study of solidification by rapid cooling *(Japanese)* 78−88459
Al-Mn profiled alloy components pulled from melt, physicomech. props. 78−3175
Al-Mn sheet, artificial stress raiser effect on strength and local plasticity of weld joint 80−81130
τ-Al-Mn-C, permanent magnetism and microstruct. 80−75811
Al-Mn-Fe(Co)(Ni)(Cu), permanent magnetic materials, grain struct. effect *(Rumanian)* 79−73773
Al-Mn-Mg laminated composite, fatigue fracture, fatigue strength enhancement 79−87725
Al-Mn-Si, recrystallisation and precipitation 78−52824
Al-Mn-Zn, fatigue cracks, in NaCl, oil and water vapour *(Japanese)* 78−11414
Al-Mn-Zr, particle stabilized structures, hot deform. 79−47733
Al-Mn-Zr (0.9, 0.4%), strain induced continuous recrystn., rel. to superplastic behaviour 78−84915
Al-Si-Cu-Mg-Ni cast alloy, fractography *(German, English)* 79−87809
Al-Zn-Mg (4.8, 1.1 wt.%), second phase dissolution, calorimetry study 79−100193
Al-Zn-Mg-Mn, correlation of microscopic features, with macroscopic crack propagation 78−60800
Al-Zn-Mn, mech. props., Ti or Mn addition effect *(Korean)* 80−93613
$AlMg_2Mn$, H impurity detection by $^1H(^{15}N,\alpha\gamma)$ reaction 80−55767
$AlMn_x$, muon diffusion, μSR 79−56696
$Al_{45}Mn_{55}$, pure and C doped, phase transforms. 79−96022
Al_8Mn_5, rhombohedral γ-brass, direct imaging of struct. and structural defects 80−15115
Au-3d transition metal alloys, UPS study, localised states 80−93449
Au-Mn, band profile, density of states, quantum defect-Green's function calcs. 80−54599
Au-Mn, conc. spin glasses, thermopower 80−65538
Au-Mn, dil., ^{52}Mn γ-ray anisotropy down to 3 mK, Kondo and relax. effects 77−81034
Au-Mn, dil., nuclear orientation of recoil implanted ^{52}Mn 78−43716
Au-Mn, dil. spin glass, thermopower, rel. to spin glass freezing temp. 78−79983
Au-Mn, orthorhombic struct., electron diffra. and electron microscopy obs. 80−15052
Au-Mn, spin glass, anomalous Hall effect 78−30908
Au-Mn, spin glass, residual resistivity conc. depend. 80−2382
Au-Mn, spin glass alloy, elec. resist. 77−8067
Au-Mn, spin glass transition and anomalous Hall effect 79−61162
Au-Mn, spin-orbit coupling and electron scatt. 80−2370
Au-Mn, UPS study, localised states 80−93449
Au-Mn alloys, equiatomic region of phase diagrams crystallographic and mag. exam. 78−52755
Au-Mn alloys, reversible and irreversible DC magnetisation in spin glass regime 80−65908
Au-Mn dil. spin glass alloy, impurity-impurity interaction press. depend., resistivity meas. 77−20308
Au-Mn system, AABB struct., experimental evidence for occurrence 78−63698
Au-Si-Mn, amorphous spin glass film, mag. susceptibility 79−42775
$Au_2(Mn,Z)_2$, Heusler alloy, (Z=Al, Cu, Ga, In or Zn), magnetic order and coupling 79−38303
AuMn, mag. struct., phase transition, and magnon spectrum, random anisotropy effects 80−88722
AuMn, mictomagnetic, Hall and magnetoresist. effects 78−43361
AuMn, ordered, vacuum deposited epitaxial films, orientation control by external stress 80−100426
$Au_{11}Mn_4$, electron diffraction and microscopy obs. 78−75512
$Au_{11}Mn_4$ ordered phase formation, electron diffr. and microscopy study 80−107418
$Au_{11}Mn_4$, ordering, electron diffr. and high resolution TEM obs. 78−71707
Au_3Mn thin films, electron diffr. study 80−92793
Au_4Mn, atomic short range order and pair interaction, neutron diffr. exam. 78−22695
Au_4Mn, electron irrad. in electron microscope, radn. ordering 79−86818

manganese alloys continued
Au_4Mn, fully ordered, microstruct., high resolution electron microscopy 79−1439
Au_4Mn, heat treated, short-range order, diffuse X-ray diffr. study *(German)* 80−88092
Au_4Mn, high resolution dark field electron microscopy exam. of ordering 79−7615
Au_4Mn, magnetic anisotropy const., anomalous field depend. 77−12113
Au_4Mn, magnetocrystalline anisotropy temp. depend. 77−51900
Au_4Mn ordered alloy, coincidence sites in domain boundaries, high resolution TEM obs. 78−71708
Au_5Mn, ordered, coincidence sites in domain boundaries, high resolution TEM obs. 78−71708
Au_5Mn_2, electron microscope exam. of ordering 78−63697
Au_5Mn_2, monoclinic, ordering, high resolution electron microscopy 79−43290
Au_5Mn_2, phase transformations and domain structures *(French)* 78−27509
Au_5Mn_2, variants in domain struct. 77−43224
Au_2MnAl, Heusler alloy, Mossbauer, determ. of Au hyperfine field 77−4586
Au_2MnAl, Heusler alloy, ferromag., NMR meas. 78−76320
Au_2MnIn, Heusler alloy, ferromag., NMR meas. 78−76320
AuMnSb, ferromag. Heusler alloy, mag. hyperfine fields at Au and Sb sites, Mossbauer spectra 77−32303
B fibre reinforced Al-Mn, calc. of thermodynamic interaction potential between B fibre and matrix 80−11627
BMn, ferromag., ^{55}Mn magnon-induced pseudoquadrupole processes 79−19802
$Be_5(Fe_{1-x}Mn_x)$, mag. and calorimetric props. 77−63083
$Be_{1-x}Mn_x$, Be-rich, NMR and paramag. susceptibility 80−71206
$Be_2Mn_{1-x}Fe_x$, mag. props., giant moment clusters 79−28508
Bi-Mn, dil. liq. alloy, static and dynamic props. of localised Mn moments 79−82755
Bi-MnBi, directionally solidified composite, processing parameter role on mag. props. 80−35352
Bi-MnBi, mag. props. singularities, electron microscope exam. *(Russian)* 78−39363
Bi-MnBi directionally solidified eutectic alloys, struct. and mag. props. 79−51815
Bi-MnBi eutectic, directional crystallisation and microstruct. *(Russian)* 77−55915
Bi-MnBi eutectic composites, microstructure and mag. props., annealing effect 79−82827
Bi-MnBi eutectic region, of Bi-Mn phase diagram 80−81034
BiMn, ferromag., nucl. orientation of Bi isotopes 78−13010
BiMn, with ferromag. inclusions, magnetisation changes by US pulses 80−34732
$Bi_{0.96}Mn_{0.04}$, powder particles, magnetisation 77−48014
$Bi_{95.6}Mn_{4.4}$, magnetisation of ferromag. precipitates, effect of ultrasonic pulses 80−2121
C-Mn-V power station component, fracture toughness and fatigue characts. 79−20192
Cd-Mg, dil., elec. resistivity, phonon local mode effect 78−6347
Cd-Mg, dil. alloy, single cryst., electrical resistivity and deviations from Matthiessen's rule 79−23943
Cd-Mn, dil., energy splittings of Mn ions 78−67989
Cd-Mn, dil., lattice state effects on pair breaking 77−8219
Cd-Mn, dil., mag. and supercond. props. 79−38237
Cd-Mn, dil., single cryst., low temp. mag. anisotropy 77−59386
$CdGeAsMn_x$ glass, recrystallisation 80−44133
Ce-Mn-Co, temp. conc. limits of homogeneous compounds *(Russian)* 78−23666
Ce-Mn-Co(Fe)(Ni), cryst. struct. determ. 77−11508
Ce-Mn-Cu systems, phase equilibria at 600 and 400°C *(Ukrainian)* 80−11625
Ce-Mn-Ni system, phase diag. 77−52283
$CeMn_2Si_2$, cryst. and mag. struct. determ. 78−52225
$CeMn_2(Si_xGe_{1-x})_2$, $Ce(Mn_{1-x}B_x)_2Si_2$, (B=Fe, Cu) mag. props. 80−25134
Co-Cr-Mo-Ni-Fe-Si-Mn-C, protective coatings by B diffusion, microstruct. and mech. props. 78−11427
Co-Fe-Mn, dil. ferromag. alloy, mag. moment, saturation magnetisation meas. 78−64195
Co-Ga-Mn, small-angle mag. neutron scatt., states of mag. order study rel. to Mn and Fe substitution 79−11292
Co-Mn, cryst. struct. and stacking fault influence on mag. props. *(Russian)* 80−25164
Co-Mn, dil., hexagonal hyperfine field at ^{54}Mn, nucl. orientation meas. 79−8057
Co-Mn, dil., NMR-ON meas., mag. hyperfine splitting const. of ^{52}Mn 78−43651
Co-Mn, FCC, mictomagnetism, magnetisation and mag. susceptibility meas. 80−60310
Co-Mn, interdiffusion 77−89595
Co-Mn (0 to 45 wt.%), high temp. oxidation 80−35371
Co-Mn (10.24 at.%), Mn diffusion, 903-1148°C 77−24427
Co-Mn (5.22 at.%), Mn diffusion, 868-1200°C, mag. transform. effects 77−24427
Co-Mn alloys, FCC, mag. moments of Mn atoms 78−76226
Co-Mn alloys, ferromagnetic, high field mag. susceptibility meas. 80−75729
Co-Mn alloys, Nernst-Ettinghausen effect and electrical resistivity *(Russian)* 78−14714
Co-Mn-Ni-Fe-Si-B amorphous alloys, mag. props., low magnetostriction 80−75832
β-Co-Mn-Sn Heusler alloy, constitution and magnetic props. *(German)* 79−34009
Co-Mn-Sn liquid alloy, magnetic props. *(German)* 79−87235
$Co_2Ga_{2-x}Mn_x$, elec. resist. anomalies 79−38044
$Co_2Ga_{2-x}Mn_x$, mag. props. and order 77−12093
CoMn, dil., low temp. specific heat and magnetisation 80−65925
$CoMn_3$, mag. susceptibility, 77-500K *(Russian)* 77−80911
$(Co_{1-x}Mn_x)B$, ferromag., internal fields meas. by NMR spin echo 80−29646
$(Co_{1-x}Mn_x)B$, paramag., spin echo NMR spectra, ferromag. transition, spin-lattice relax. 80−29645
$(Co_{1-x}Mn_x)_2B$, magnetocrystalline anisotropy meas., 4.2-300K 80−71006
$Co_2Mn_xFe_{1-x}M$, (M=Ga,Ge,Si,Sn), hyperfine fields of Fe impurities, Mossbauer effect meas. 78−31130

manganese alloys continued
$Co_{50}Mn_xGa_{50-x}$, cryst. struct. transform. of B2 type *(German)* 79−91642
$Co_{50}Mn_xGa_{50-x}$, ordering and disordering phenomena, mag. study 80−70154
CoMnP, cryst. mag. struct., neutron diffr. study *(French)* 80−59439
CoMnP, ferromagnetism and metamagnetism, polarized neutron diffr. study 80−44809
CoMnSi, $CoMnSi_{0.85}Ge_{0.15}$, mag. props. 79−42758
Co_2MnSi, ferromag. Heusler alloy, spin echo NMR meas. 77−63319
$Co_3Mn_3Si_2$, Curie-Weiss law depend. of susceptibility, mag. props. *(Russian)* 79−65655
$CoMnSi_{1-x}Ge_x$, amg. props. 80−60270
$Co_2(Ti,Mn)Sn$, Heusler alloy, mag. meas. 79−47261
$(Cr, Mn)_2As$, mag. props. and struct. 78−64190
Cr-Fe(Co)-Mn, dil., antiferromag., elec. resist. min., press. and impurity effects 80−59970
Cr-Mn, order of mag. transitions in antiferromag. alloys 79−4677
Cr-Mn, strain wave and spin density wave intensities, neutron diffr. 78−60266
Cr-Mn (0.5 at.%), mag. phase transforms, sp. ht. obs. *(Russian)* 77−80941
Cr-Mn alloys, antiferromag. and weak ferromag., elec. props. 79−56514
Cr-Mn alloys, elec. resist. near T_N 77−69313
Cr-Mn alloys, magnetisation process, magnetisation in 90-300K range *(Russian)* 78−15007
$Cr_{0.6}Mn_{0.4}$, mag. moment, neutron diffr. study 79−33459
$Cr_{0.98}Mn_{0.02}$, spin dynamics and spin wave form factor, neutron scatt. expt. 77−40047
$Cr_{995}Mn_{005}$, spin density wave Q vector, vel. depend. 79−4669
CrN-MnN, synthesis and props. 77−40405
Cu-Al-Fe-Mn, phase transform. during continuous cooling *(German, English)* 79−70044
Cu-Al-Fe-Mn (10,3,2 wt.%), phase comp. struct., continuous cooling from β-phase effect 79−24499
Cu-Al-Mn, duplex shape memory effect after nonuniform plastic deform. *(Russian)* 80−25759
Cu-Al-Mn, Heusler alloy, magnetic prop. investig. of struct. transitions *(German)* 77−8289
Cu-Al-Mn, hypereutectic, martensitic transform., effect of β_1-phase decomposition *(Russian)* 78−23705
Cu-Al-Mn, partial decomp. of β_1 phase, effect on mag. props. and martensitic transform. *(Russian)* 80−45306
Cu-Al-Mn liq. alloys, susceptibility behaviour 80−93077
Cu-Al-Mn spin glass, field depend. suscept. 79−73739
Cu-Al-Ni-Fe-Mn, cast Ni-Al bronze, fracture metallography 78−27597
Cu-Ga-Mn, liq., Mn impurities, elec. resist. 79−51545
Cu-Mg, high temp. oxidation 79−43485
Cu-Mn, classical RKKY model, thermodynamic props. 78−39333
Cu-Mn, de-alloying props. 80−104332
Cu-Mn, diffusive redistrib. during friction *(Russian)* 78−52999
Cu-Mn, dil., anomalous thermal expansion below 50K 78−51710
Cu-Mn, dil., in supercond. proximity, localised bands 78−10613
Cu-Mn, dil., interaction between local mag. moments 77−1540
Cu-Mn, dil., Kondo deviations of Mn electron spin relax. and g-factor, NMR meas. 79−51747
Cu-Mn, dil., Kondo system, host NMR exam. 78−80246
Cu-Mn, dil., local mag. moments, neutron scatt. study 79−61058
Cu-Mn, dil., local mag. moments and Kondo effect, theoretical model 79−69651
Cu-Mn, dil., local moment fluctuations, NMR meas. 77−63091
Cu-Mn, dil., mag. heat capacity, conc. and temp. depend. 79−61164
Cu-Mn, dil., NMR data, ionic model and Kondo temp. 78−68399
Cu-Mn, dil., NMR satellite data, rel. to electronic struct. 78−68398
Cu-Mn, dil., oxide film form. in ammoniacal Cu(II) solns., AES obs. 80−45415
Cu-Mn, dil., spin density magnetisation near magnetic atoms 79−33545
Cu-Mn, dil., spin glass, thermopower, rel. to spin glass freezing temp. 78−79983
Cu-Mn, dil., spin-glass dynamics, NMR meas. 78−31120
Cu-Mn, dil. alloy, spin glass, host NMR, spin freezing 77−40138
Cu-Mn, dil. alloy, spin glass, host NMR, spin freezing 77−40139
Cu-Mn, dil. alloys, conc. depend. of resist. maximum 77−62893
Cu-Mn, dilute, magnetoresist. and Hall effect, field-depend. electron scatt. 77−43581
Cu-Mn, dilute solid soln., exam. of recrystallisation and stored energy 78−52836
Cu-Mn, effect of ageing on mag. props. 77−28366
Cu-Mn, exchange-coupled localised moments, Korringa relaxation rate 80−75851
Cu-Mn, γ-phase interdiffusion obs., chem. comp. depend. *(Japanese)* 78−2307
Cu-Mn, impurity spin dynamics in magnetic glasses at low frequencies *(French)* 78−88126
Cu-Mn, interdiffusion *(Japanese)* 77−51554
Cu-Mn, interdiffusion 78−18848
Cu-Mn, itinerant to local moment magnetism transition with comp. 77−72984
Cu-Mn, mag. irreversibility and metastability 78−19279
Cu-Mn, mag. viscosity below freezing temp. 80−65910
Cu-Mn, magnetisation curves 79−24172
Cu-Mn, microconductors, cast, struct. and physical props. exam 78−44232
Cu-Mn, mictomag., massive short-range antiferromagnetism 77−12139
Cu-Mn, Mn effect on stainless steel embrittlement during soldering 79−47773
Cu-Mn, Mn K X-ray emission and XPS lines, width and asymm. 78−19605
Cu-Mn, molecular field distribution function in disordered Ising model *(Russian)* 80−54859
Cu-Mn, positrons as probe of phase transforms. 78−31401
Cu-Mn, spin glass, ^{63}Cu NMR linewidth and relax. meas. 77−69583
Cu-Mn, spin glass, anomalous Hall effect 78−30908
Cu-Mn, spin glass, meas. of order parameter 80−34642
Cu-Mn, spin glass, transition temp., freq. depend. 80−97113
Cu-Mn, spin glass, US meas. of crit. exponent α′ 79−78384
Cu-Mn, spin glass alloy, elec. resist. 77−8067
Cu-Mn, spin glass alloy, magnetic excitations, neutron scatt. 78−10695
Cu-Mn, spin glass materials, mag. field dependence of susceptibility peak 80−103840
Cu-Mn, spin glasses, alternating susceptibility 80−65912

manganese alloys continued
Cu-Mn, zero field ESR in spin glass state 80−66017
Cu-Mn (10 at.%), meas. of mag. viscosity below freezing temp. 79−24171
Cu-Mn (15 at.%), mictomagnetic, short-range ordering, neutron scatt. polarisation anal. 80−50110
Cu-Mn (16.7 at.%), spin glasses, alternating magnetisation 79−91241
Cu-Mn (3, 5, 10 at.%), surface segregation of Mn and oxide film form., AES study *(French)* 79−66065
Cu-Mn (3 to 20 at.%), high temp. steady state tensile deform. *(Japanese)* 78−52917
Cu-Mn (38 to 58 wt.%), age hardened, exam. of precipitation and strengthing 78−72782
Cu-Mn (3.%), specific heat below 3K 79−61165
Cu-Mn (4.7 at.%), spin glass, spin correlations, neutron scatt. cross section meas. 79−51790
Cu-Mn (7 at.%), magnetic susceptibility, clustering, band model of heterogeneous magnetics 77−43823
Cu-Mn (8 at.%), spin glass, neutron scatt. and susceptibility investig. of spin dynamics 77−40076
Cu-Mn (8 to 75 at.%), spin correl., neutron polarisation anal. study 80−65905
Cu-Mn alloy, classical RKKY model, zero temp. dynamic struct. factor 78−68271
Cu-Mn alloy, manganin, hysteresis-corrected calibration under shock loading 80−74818
Cu-Mn alloy, spin glass, neutron scatt. 78−68265
Cu-Mn alloy, spin-glass, US exam. 78−68351
Cu-Mn alloys, Cu-rich, heat treated, segregation obs. *(Russian)* 78−27517
Cu-Mn alloys, vacuum deposited, electrophys. props. 77−63006
Cu-Mn dil., evidence for Mn clustering from high field magnetisation curves 79−78426
Cu-Mn dil. spin glass alloy, impurity-impurity interaction press. depend., resistivity meas. 77−20308
Cu-Mn Kondo system, ^{54}Mn nucl. orientation 78−68421
Cu-Mn mictomagnet, effect of ageing on mag. moment 77−43841
Cu-Mn spin glass, hysteresis loops, temp. and field depend. 80−15742
Cu-Mn spin glass, magnetisation reversal and macroscopic mag. domain obs. 79−61168
Cu-Mn spin glass, magnetisation curves, time depend. 80−15743
Cu-Mn spin glass, saturated thermoremanent magnetisation, time and temp. evolution 79−61167
Cu-Mn spin glass, specific heat below 3K, spin glass freezing temp. 79−95600
Cu-Mn spin glass, spin freezing and exchange narrowing of mag. reson. 80−60411
Cu-Mn spin glass alloy, neutron scatt. meas. of Edwards-Anderson order parameters 79−11323
Cu-Mn spin glass alloy, spin correl. function, combined neutron spin echo and polarisation anal. 80−50107
Cu-Mn spin glass neutron diffr. expts. *(French)* 78−43593
Cu-Mn spin glasses, spin dynamics, neutron scatt. meas. 79−8002
Cu-Mn-Al, constricted hysteresis loop rel. to microstruct. 78−19273
Cu-Mn-Al, Heusler alloy, single cryst. and polycryst., martensitic transform. *(Russian)* 78−48398
Cu-Mn-Al, Heusler alloys, ferromag. inclusions, mag. props. and struct. study *(Russian)* 80−80570
Cu-Mn-Al, mag. props. and atomic ordering 79−24139
Cu-Mn-Al alloys, displaced hysteresis loop and microstructure obs. 80−84613
Cu-Mn-Au(Pt) spin glasses, anisotropic exchange interactions, effect of nonmag. impurities 80−80534
Cu-Mn-Ni, thin film, vacuum deposited, struct., elec. cond. *(Russian)* 78−19668
Cu-Mn-Ni alloy, Manganin, elec. resist. under static pressures up to 110 kbar, pressure gauge appl. 79−1594
Cu-Mn-P alloys, phase diagram *(Russian)* 80−20891
Cu-Mn-S, Mn surface segregation and Mn/S cosegregation 80−40367
Cu-Mn-Ti film, physical and electrical props. *(Russian)* 77−66208
Cu-Mn(1%) spin glass, remanent mag., zero-field NMR obs. 79−33492
Cu-Ni alloys, alloying additions effect on thermal conductivity, 20-400°C *(Russian)* 77−59159
Cu-Ni-Mn, cast, strength and hot ductility, Mn, effect 80−66595
Cu-Ni-Mn (20,20wt.%), structural transform., X-ray and hardness study *(French)* 78−39760
Cu-Ni-Zn-Mn fine grained precipitation-hardenable alloy, high strength and ductility 80−100805
Cu-Zn-Mn, de-alloying props. 80−104332
Cu-Zn-Mn, steady-state diffusion of Zn and Mn 80−70445
β-Cu-Zn-Mn (43.4, 3.8 wt.%), order-disorder transformation temperature effect on quench hardening 78−95745
Cu_2Mg, electronic struct. volume depend. 79−65366
CuMn, acceleration of coarsening by temp. changes, study by resistivity meas. 79−47718
r-CuMn, annealing ordered phase study by neutron diffr. 80−89265
CuMn, dil., anisotropic hyperfine coupling, NMR study 80−65784
CuMn, hysteresis, spin orbit scattering effect on anisotropy in spin glass state 80−71095
CuMn, magnetisation processes below freezing temp. 80−15748
CuMn spin glass, AC susceptibility 80−60305
CuMn, spin glass, mag. correls., neutron scatt. study 80−50105
CuMn, spin glass, mag. hysteresis meas. 80−34691
CuMn spin glass, μ^+ zero-field spin relax. probe for spin dynamics 80−97177
CuMn, spin glass, random moments time correl., zero field muon spin relax. meas. 80−60335
CuMn, spin glass, remanence, new approach from zero field NMR 80−34785
CuMn spin glass, specific heat and entropy 80−60354
CuMn, spin glass low DC field mag. susceptibility using SQUID 79−69684
CuMn-like alloys, model calcs. on magnetisation processes in moderate fields below freezing temp. 79−24188
$Cu_{0.86}Mn_{0.14}$, hysteresis loop development 80−65922
$Cu_{0.95}Mn_{0.05}$, spin glass, inelastic neutron scatt., time-of-flight and three-axis techniques 80−50108
$Cu_{0.95}Mn_{0.05}$, spin glass, low temp. mag. excitation spectrum, inelastic neutron scatt. obs. 80−50109
$Cu_{0.98}Mn_{0.02}$, spin glass, Heisenberg mode, RPA approx. 80−65904
γ-$Cu_{15}Mn_{85}$, antiferromag., neutron diffr. 80−2550

manganese alloys continued
Cu_3Mn, atomic short-range order, TOF neutron diffraction 79−10831
Cu_3Mn, interaction between local mag. moments 77−1540
$Cu_{75}Mn_{25}$, concentrated spin glass, elec. resist., depend. on hydrostatic press. 79−69685
$Cu_{75}Mn_{25}$, spin glass, EPR line breadth, exchange-narrowed 79−15345
Cu_2MnAl, alloy, energy band calc. by nonrelativistic SAPW method 79−4507
Cu_2MnAl, dislocation structure, antiphase boundary energies, deformation behaviour prediction *(Russian)* 79−65085
Cu_2MnAl, dynamical mag. susceptibility, spin waves, calc. from band struct. 80−54871
Cu_2MnAl, ferromag. Heusler alloy, polarised neutron study of mag. moment density 78−84391
Cu_2MnAl Heusler alloy, inelastic magnon scatt. of neutrons 77−4509
Cu_2MnAl, Heusler alloy, single crystal, plastic deform. 77−44308
Cu_2MnAl, Heusler alloy, spin waves, neutron inelastic scatt. meas. 77−80921
Cu_2MnAl, Heusler alloy, magnetisation mag. anisotropy, magnetostriction and elastic consts. 78−23318
Cu_2MnAl Heusler alloy, elec. resistivity 79−91020
Cu_2MnAl, Heusler alloy, decomposition at 360°C 80−7536
Cu_2MnAl, plastically deformed, domain struct., X-ray diffr. and electron microscope obs. *(Russian)* 79−20110
Cu_2MnAl superparamagnetic particles in Cu_3Al lattice, magnetic moment ferromagnetic ordering *(Russian)* 79−78444
Cu_2MnAl-Pd_2 MnAl mixed Heusler alloys, mag. props. 80−60269
$Cu_2Mn_{0.863}Al_{1.057}$, Heusler alloy, mag. moment distrib., polarised neutron study 79−47247
$Cu_2Mn_{0.98}Al_{1.02}$, Heusler alloy, hyperfine fields at sp elements, spin echo NMR meas. 78−84496
$Cu_{2+x}Mn_{1-x}Al$, omega phase, roles of electron microscopy and electron diffraction *(French)* 78−27524
$Cu_{3-x}Mn_xAl$, and $Cu_2Mn_{2-y}Al_y$, Heusler alloys, order-disorder transitions 80−59619
$Cu_2Mn(Al_{1-x}Sn_x)$, Heusler alloys, thermal effects, saturation magnetisation 77−85499
$Cu_2MnAl_{1-x}Sn_x$, Mossbauer effect study 80−60473
$Cu_{2.0}Mn_{0.94}In_{1.0}$, In-Heusler single crystal, elec. resist. 78−60107
$Cu_2MnIn_{1-x}Sn_x$ alloy, compositional SRO, hyperfine interactions 80−71065
Cu_2MnSn(In), Heusler alloy, hyperfine field at ^{111}Cd, TDPAC meas. 78−43705
$Cu_{1-x}Pd_xMnSb$, mag. phase transition 80−60268
$(Cu_3Pt)_{1-c}Mn_c$, mag. suscept. and effect of atomic order and disorder 77−24669
β-Cu(ZnMn), slip geometry, anomalous strengthening 78−10056
$DyMn_2$, H_2 absorpt., Mossbauer study 80−44987
Dy_6Mn_{23}, magnetic moments, magnetisation 80−25094
Dy_6Mn_{23}, noncollinear mag. struct., magnetization meas. 79−78322
$DyMn_2Si_2$, Mossbauer spectra 80−20558
Er-Fe-Mn, cryst. struct. and H_2 capacity 77−89543
$Er_2Co_{17-x}Mn_x$, magnetisation, Curie temp., anisotropy 77−89947
$Er_2Co_{17-x}Mn_x$, saturation magnetisation, Curie temp., easy direction, and anisotropy field 77−8304
$Er(Fe_{1-x}Mn_x)_2$, struct. determ. by X-ray diffr. *(Russian)* 77−76358
$Er_6(Fe_{1-x}Mn_x)_{23}$, mag. props. and mol. field coeffs. 78−39319
Er_6Mn_{23}, magnetic moments, magnetisation 80−25094
Er_6Mn_{23}, noncollinear mag. struct., magnetization meas. 79−78322
Fe, cast, Mn, wear resist. and hardening, struct. effect 79−87734
Fe-As-Mn, Mn additions to Fe-As melts, influence on surface tension and density *(Russian)* 80−15337
Fe-As-Sn-Mn, melts, As and Sn distrib., Si, Cr, and Mn influence *(Russian)* 80−16274
Fe-C-Mn (0.5, 0.6 wt.%), powder forged, mech. props. 80−21096
Fe-C-Mn-Si (4, 2, 1.5 wt.%), cast wire, influence of B addition on struct. and elec. cond. *(Russian)* 80−55391
Fe-C-Si-Mn, cast, high C, K_1 phase formation due to peritectoid transitions *(Russian)* 79−11548
Fe-Co-Mn, BCC, atomic mag. moment, magnetisation, Mossbauer spectra and NMR spin echo spectra 77−63127
Fe-Co-Mn, BCC, mag. state of Mn, NMR and saturation magnetisation meas. 78−39442
Fe-Co-Mn, dil. alloys, NMR freq. temp. depend., spin echo meas. 78−64296
Fe-Co-Mn, mag. moment of Mn atoms, polarised neutron scattering 79−11290
Fe-Co-Mn and Fe-Ni-Mn, BCC, atomic mag. moments determ. 77−59396
Fe-Cr-Mn, Cr and Mn effect on N_2 solubility above 1000°C *(Bulgarian)* 79−65203
Fe-Cr-Mn, influence of alloying with Ni, Mo, N on defect conc. energy *(Russian)* 80−54241
Fe-Cr-Mn alloys, Mn content effect on Cr distrib. in suboxide layers *(Russian)* 77−12732
Fe-Cr-Mn-C, high temp. oxidation, X-ray and weight gain meas. *(Russian)* 78−15571
Fe-Cr-Mn(Ni-Mn)-C, carbide-austenite equilibria, 1173 to 1373K, microscopic and X-ray obs. 78−44085
Fe-Cr-Ni-Mn-Mo, liquid, N_2 solubility 78−44087
Fe-Cu-Mn, analysis and synthesis of phase diagrams 79−11563
Fe-Mn, additive effect on eutectoid transformation of Fe 78−52799
Fe-Mn, annealed, α-γ phase transformation obs. 78−75831
γ-Fe-Mn, antiferromag., mag. and crystallographic transformations 77−55964
Fe-Mn, as cast, pseudo-composite struct. resulting from interdendritic segregation, cryogenic materials appl. *(French)* 80−93556
Fe-Mn, atomisation of melt, powder charact. 78−19688
Fe-Mn, BCC, ferromag., spin wave stiffness constant 78−91851
Fe-Mn, dil., local mag. moments, polarised neutron elastic diffuse scatt. 80−50088
Fe-Mn, dil. alloy, mag. moment distrib., temp. depend., diffuse polarised neutron scatt. study 79−47250
Fe-Mn, dilute, short-range ordering and segregation ascending diffusion *(Russian)* 77−24406
Fe-Mn, dislocation mobility and internal friction, effect by alloying in α-Fe *(Russian)* 77−31671
Fe-Mn, dissolution rate into molten Al, convection mass transfer *(Japanese)* 78−71858
Fe-Mn, effect of alloying additions on magnetoelastic effects 78−43624

manganese alloys continued
Fe-Mn, effect of N on cryst. lattice parameter of austenite *(Russian)* 78−67683
Fe-Mn, electron redistrib. and BCC struct. stability, Mossbauer meas. *(Russian)* 79−42873
Fe-Mn, electron state density and elec. resist. 80−39558
Fe-Mn, ε-martensite, preferred orientation and constitution, reverse pole figures *(Russian)* 80−104178
Fe-Mn, FCC to HDP transform. 79−61581
Fe-Mn, fracture mechanism in various temperature and stress intervals *(Russian)* 79−24600
Fe-Mn, γ to α transition on cooling, struct. and microhardness investig. *(Russian)* 77−44246
Fe-Mn, γ to ε phase transform. induced by high press. and plastic deform. 78−68686
Fe-Mn, high-temp. sulphidation, scale struct., corrosion kinetics 80−50777
Fe-Mn, jump stress relaxation obs. during cooling before martensitic transform. *(Russian)* 79−38884
Fe-Mn, layers formed by reaction with molten Al, X-ray, EPMA and hardness meas. *(Japanese)* 78−72926
Fe-Mn, liquid, diffusion of H_2 *(German)* 78−14487
Fe-Mn, mag. susceptibility and conc. depend. of Neel point *(Russian)* 79−47279
Fe-Mn, martensitic FCC→BCC transform., orientation relation, diffractometric determ. *(Russian)* 77−44240
Fe-Mn, mechanical twinning of close-packed hexagonal ε-phase during plastic deform. *(Russian)* 80−60909
Fe-Mn, Mossbauer spectroscopy of temp. hysteresis of phase transformations *(Czech)* 80−29949
Fe-Mn, Mossbauer study near martensitic transform. temp. 78−3128
Fe-Mn, plastic deformation mechanism, meas. of microplasticity 78−60720
Fe-Mn, shape memory effect *(Russian)* 78−38771
α-Fe-Mn, singularities of martensite struct. *(Russian)* 80−28948
Fe-Mn, splat-quenched, martensite formation obs. 77−44247
Fe-Mn, stacking fault energy, Mn conc. depend. *(Russian)* 77−1836
Fe-Mn, struct. and props., effect of Nb, C and Si alloying *(Russian)* 77−90360
Fe-Mn, struct. defects effect on interdiffusion 80−15314
Fe-Mn, thermodynamic props. *(Czech)* 77−85990
Fe-Mn, unlimited component solubility, intercrystallite internal adsorption *(Russian)* 80−39294
Fe-Mn, warm rolled, rel. contribs. of texture and grain shape to props. 79−91705
Fe-Mn, X-ray exam. of dynamic characts. *(Russian)* 77−62608
Fe-Mn 8%, type K1525 thermal cycling, effect on impact toughness 80−7608
Fe-Mn (-C), Mn influence on martensitic transform in presence of strain *(Russian)* 80−20934
Fe-Mn (0.5 wt.%), Burgers vector of dislocation determ. by weak-beam image in HVEM 80−103351
Fe-Mn (1 at.%), strain age hardening 80−108472
Fe-Mn (10 to 14 at.%), martensitic transforms., dilatometric effects and X-ray diffr. meas. *(Russian)* 78−6922
Fe-Mn (12% Mn), decomposition during plastic deform., Mossbauer parameters *(Russian)* 77−36166
Fe-Mn (14.1 wt.%), G14, α-martensite formation in mag. field 79−91648
Fe-Mn (15(24)(30)wt.%), high hydrostatic pressure influence on stress-strain curve 80−25805
Fe-Mn (18.6 wt.%), HCP-FCC martensitic transform., Mossbauer effect meas. 78−44121
Fe-Mn (2 to 8 wt.%) alloys, phase transformations, tempering influence *(Russian)* 80−25735
Fe-Mn (22 wt.%), ε→γ transformation, effect of H_2 pressure up to 23 kbar on transition temp. *(Russian)* 79−24517
Fe-Mn (32.5 and 38.3 wt.%), steel sheet, exam. of form limit diagrams and damage 78−48461
Fe-Mn (8 wt.%), quenched, exam. of intergranular embrittlement 78−76745
Fe-Mn (8.25 wt.%), irreversible temper embrittlement, Mossbauer spectra, impact strength depend. on interstitials *(German)* 79−74235
Fe-Mn (9 to 20 wt.%), ^{57}Fe Mossbauer spectroscopy in phase transformations 80−29948
Fe-Mn (up to 8 wt.%), microstructure, mech. props. and fracture *(Japanese)* 80−35304
Fe-Mn alloy, magnetovolumetric anomaly *(Russian)* 78−64248
Fe-Mn alloys, α, ε and γ, brittleness 80−35314
Fe-Mn alloys, elasticity modulus anomaly and magnetoelastic effect *(Russian)* 79−28578
Fe-Mn alloys, high-purity, martensitic transform., heat treatment effect 79−56979
Fe-Mn alloys, quantitative phase anal., correction factor for texture 79−52528
Fe-Mn base alloy, mag. preferred directions 78−39370
Fe-Mn cast alloys, homogenisation annealing and chemical diffusion *(Czech)* 80−66551
Fe-Mn mag. contributions to γ→ε phase transformations 80−25694
Fe-Mn-Al-C, form. of ductile Ni_3Al by split quenching, mech. props. 79−100197
Fe-Mn-Al-C, hardening during ageing, 450-750°C *(Russian)* 78−3135
Fe-Mn-As, crystal struct. and magnetic props. of intermetallic cmpds. with Cu_2Sb type struct. *(Japanese)* 78−59785
Fe-Mn-B, B effect on intergranular embrittlement 80−108555
Fe-Mn-C, anomalous changes in austenite and martensite lattice parameters 80−50636
Fe-Mn-C, atomic interaction structure in carbides 78−42955
Fe-Mn-C, austenitic, strain-induced γ to ε transform., active slip systems 77−48427
Fe-Mn-C, cast iron and steel, Mn effects on struct. 78−23696
Fe-Mn-C, γ→ε→α′ martensitic transform. 79−24523
Fe-Mn-C, lattice parameters of cementite, annealing effect 80−29007
Fe-Mn-C, martensitic transform., Mossbauer obs. *(Russian)* 78−6927
Fe-Mn-C, struct. superplasticity 80−76317
Fe-Mn-C, structural var. during warm deform. in γ→ε transform. region *(Russian)* 77−81293
Fe-Mn-C, thermodynamic analysis 77−32563
Fe-Mn-C, variation of martensite morphology with Mn and C composition 80−50635
Fe-Mn-C (0.7, 0.9 wt.%), pearlitic, deform. 77−86095
Fe-Mn-C (11.5, 0.2 to 1.6 wt.%), water quenched, effect of C on phase composition, abrasion, plasticity *(Russian)* 78−35445
Fe-Mn-C system, Gibbs energy, high temp. phase relations 78−80779
Fe-Mn-C system, isothermal sections, 873 to 1373K, computer plotting 78−6893
Fe-Mn-C-Si alloy, G20 type, vol. effects during γ→ε transform., lattice parameters of γ-and ε-phases, Si and Mn effects *(Russian)* 78−6918
Fe-Mn-C-Si alloy G20, effect of Si and Mn additions on phase composition in multiple γ⇄ε transitions *(Russian)* 78−95743
Fe-Mn-Co-Ni-Cr, antiferromag. props., Neel temp. determ. 78−88124
Fe-Mn-Cr-C, twinning and strain induced FCC to HCP transform. 77−44248
Fe-Mn-Cr(Ni), mag. and crystallographic transformation depend. on Cr-Ni addition *(Russian)* 79−83334
Fe-Mn-Cu-C, Cu effect on ε′-martensite, X-ray obs. of heating effects *(Russian)* 79−87667
Fe-Mn-Mi, martensitic, morphology and substruct. study 77−70059
Fe-Mn-Nb-V, high Mn, dispersion strengthening 77−16602
Fe-Mn-Ni, age hardenable, struct. and strength 77−52339
Fe-Mn-Ni, fracture toughness, thermomechanical treatment effects 78−60794
Fe-Mn-Ni antiferromag. alloy, neutron scatt. exam. of antiferromagnons 77−66283
Fe-Mn-Ni base maraging alloys, age hardening 79−74170
Fe-Mn-Ni-C, age hardenable, struct. and strength 77−8844
Fe-Mn-O, phase equilibrium diagram *(German)* 78−15355
Fe-Mn-O melts, formation of oxide inclusions, cryst. pulling, Bridgeman tests *(German)* 80−35074
Fe-Mn-P-B-Al metallic glass, exchange anisotropy 77−16068
Fe-Mn-PBAl, amorphous mixed mag. system, resist. minima 79−60784
Fe-Mn-S, thermodynamics, activity of FeS-MnS solid soln., 1100 to 1400°C 78−6902
Fe-Mn-S, thermodynamics, solid/liquid phase equilibria, 1100 to 1300°C 79−47663
Fe-Mn-S, thermodynamics, solubility of S and Mn in γ-Fe, 1100 to 1300°C 79−47662
Fe-Mn-S melt, S evaporation *(Russian)* 78−19716
Fe-Mn-Sb, phase comp. 80−16267
Fe-Mn-Si-C, cast, Mn effect on struct. during solidification 79−83191
Fe-Mn-Si-C, minimum of elec. resist. near LNT *(Russian)* 77−66707
Fe-Mn-Ti alloys, austenitic, precipitation strengthened 80−25714
Fe-Mn-Ti-Al, magnetic texture rel. to annealing temp., Mossbauer investig. 77−28499
Fe-Mn-V-C austenitic steel, discontinuous precipitation, morphological changes 80−3078
Fe-Mn-Zn, high-temperature phase diagram *(German)* 80−108390
Fe-Mn(0 to 80 wt.%), paramagnetic susceptibility by Faraday method, band model interpretation *(Russian)* 77−20545
Fe-Mo-Mn-C, carbide-austenite equilibria, 1173 to 1373K, microscopic and X-ray obs. 78−44085
Fe-MuS eutectics, unidirectional solidification *(German)* 80−100827
Fe-Ni-C-Mn (3.56, 3.25, 0.6 wt.%), solid soln., quenched, changes during annealing to crystal structure, mech. props. *(Russian)* 79−34076
Fe-Ni-Cr-Mn-Al-Ti Incoloy 800, exam. of scale morphology, alloying element distrib. after oxidation 78−80677
Fe-Ni-Cr-Ti-Mn-Mo, (25.8, 14.04, 2.17, 1.27, 1.30 wt.%), superalloy A-286, precipitation hardening, exam. of fracture toughness and mech. props. 78−92355
Fe-Ni-Mn, BCC, mag. state of Mn, NMR and saturation magnetisation meas. 78−39442
Fe-Ni-Mn, concentration ferromag. antiferromag. phase transition and mag. state diagram. *(Russian)* 80−20401
Fe-Ni-Mn, dil. alloys, NMR freq. temp. depend., spin echo meas. 78−64296
Fe-Ni-Mn, martensite, aged, grain boundary embrittlement 79−96144
Fe-Ni-Mn, martensitic transforms., expt. investigation *(French)* 78−84803
Fe-Ni-Mn, temp. coeff. of linear expansion *(Russian)* 77−80634
Fe-Ni-Mn, two-stage martensitie transformation kinetics, depend. on austenite initial state *(Russian)* 79−74151
Fe-Ni-Mn (20, 5 wt.%), rel. orientation between adjacent martensite laths 80−76254
Fe-Ni-Mn (20, 5 wt.%), surface martensite, crystallography and morphology 80−40354
Fe-Ni-Mn alloy, habit plane and morphology of lath martensites 77−8823
Fe-Ni-Mn alloy, martensitic transform. kinetics *(Russian)* 77−81262
γ-Fe-Ni-Mn alloys, spin glass state, short and long range order investigation 80−65808
Fe-Ni-Mn martensitic alloy, precipitation 77−12630
Fe-Ni-Mn melt, thermodynamic dissolution of O_2 *(Russian)* 78−27473
Fe-Ni-Mn-C (5.9, 4.4, 0.48 wt.%) alloy, elastic moduli near martensitic transform.* 80−7619
Fe-Ni-Mn-H, ferromag., magnetisation curves 78−88144
Fe-Ni-Si-Mn-Cr(Co-Mo), effect of prolonged aging on mag. props. 80−16513
Fe-Sb-Mn, dil., interactions and precip., Mossbauer study 80−39997
Fe-Sb-Mn, interactions and segregations, Mossbauer and X-ray diffr. study 80−70415
Fe-Si-Mn, ductility and mag. props., Mn addition effects 78−76704
Fe-Si-Mn, effect of Mn addition on mag. props. and elec. resist. 78−91890
Fe-Si-Mn (3, 0.004 to 0.1 wt.%), Mn effect on oxidation in H_2O-H_2 atmos. 78−31560
Fe-Si-Mn (6.5 wt.%, up to 0.12 wt.%), elongation, cold workability and mag. permeability meas. 77−12667
Fe-Ti-Mn, exam. of interrelations between phase diagrams and hydriding props. 79−8277
Fe_2-Mn-Al alloys, Fe-rich, disordered, local moments on Fe and Mn 77−43811
Fe_3Al-Mn, ternary ordered solid soln., formation by substitution 77−43177
FeMn, dil., diffuse scatt. cross sections, polarized neutrons 78−43567
γ-FeMn, itinerant antiferromag., spin dynamics, neutron scatt. meas. 77−12105
$Fe_{1-x}Mn_x$, elec. resist., anomalies in temp. depend. 79−23942
Fe_3Mn-Fe_3Si, slow neutron polariser, by single cryst. (111) refl. 80−49052
$(Fe_{1-x}Mn_x)_3Al$ alloys, disordered, mag. moments and distrib. on lattice sites 77−63112

manganese alloys continued
$(Fe_{1-x}Mn_x)_3Al$, local Mn moment distrib., neutron scatt., nucl. spin echo *(Russian)* 77−12091
$(Fe_{1-x}Mn_x)_3Al$, mag. moments determ. from magnetisation and neutron and electron diffr. expts. 79−56520
Fe_2MnAl, dislocation structure, antiphase boundary energies, deformation behaviour prediction *(Russian)* 79−65085
Fe_2MnAl, plastically deformed, domain struct., X-ray diffr. and electron microscope obs. *(Russian)* 79−20110
$Fe_{3-x}Mn_xAl$, ordering of Fe atoms, X-ray diffr. meas. and mid gamma reson. anal. *(Russian)* 80−96469
$Fe_{2.1-x}Mn_xAs$, $0 \leq x \leq 2.1$, mag. phase transitions 78−2679
$(Fe_{100-x}Mn_x)_{79}P_{13}B_8$ amorphous alloys, splat cooled, mag. and transport props. 80−84593
$(Fe_{1-x}Mn_x)_{75}P_{16}B_6Al_3$, amorphous, spin-glass-ferromag. multicritical point, AC susceptibility meas. 80−50117
$(Fe_xMn_{1-x})_{75}P_{16}B_6Al_3$, amorphous, mag. ordering temp., hyperfine field distrib., elec. resist. 80−34633
$(Fe_{1-x}Mn_x)_{75}P_{15}C_{10}$, amorphous, mag. ordering, Mossbauer study 80−39747
$(Fe_{1-x}Mn_x)_{75}P_{15}C_{10}$, amorphous pair radial distrib. functions, neutron scatt. study 80−49128
$Fe_xMn_{1-x}Pt_3$, ferro-antiferromag. transform. at 4.2K *(Russian)* 78−88117
$(FeMn)_3Si$ alloys, mag. and crystallographic props. by diffr., resist. and magnetisation meas. 77−59393
$(Fe_{1-x}Mn_x)Si$, US vel. rel. to mag. struct. and phase transforms *(Russian)* 77−47976
$(Fe_{1-x}Mn_x)_3Si$, $(Fe_{1-x}Co_x)_3Si$, order distrib., hardening effect *(Russian)* 77−89410
$(Fe_{1-x}Mn_x)_3Si$, mag. phase diagram determ. 77−24697
$(Fe_{1-x}Mn_x)_3Si$, sp. ht. at low temps., mag. transitions *(Russian)* 77−32189
Fe_2MnSi, antiferro- and ferromag. props. 77−12104
Fe_2MnSi, Heusler type material, mag. props. 77−40042
$Fe_{3-x}Mn_xSi$, evidence for the ang. depend. of the hyperfine interactions 78−76241
$Fe_{3-x}Mn_xSi$, limits of solubility, mag. props. and electron conc. 78−10670
$Fe_{3-x}Mn_xSi$, Mossbauer and NMR exam. of site substitution and mag. struct. 77−12092
$Fe_{3-x}Mn_xSi$, struct., magnetisation, and spin echo expts., rel. to local environment model 77−20518
$Fe_{1-x}Mn_xSn$, spin reorientation, Mossbauer study, 77 to 400K 80−97172
$Fe_{1-x}Mn_xSn$, transferred hyperfine fields at ^{119}Sn, Mossbauer spectroscopy 79−33582
$Fe_{0.49}Mn_{0.01}Ti_{0.5}H_x$, localised vibrs., sp. ht. obs., room temp. 80−65248
$(Fe_{1-x}Mn_x)_2Y(B)$, Mn effect on Fe mag. moments, Mossbauer and mag. meas. 80−71016
$Fe_{0.5}(Ni_xMn_{1-x})_{0.5}$, elec. resist., anomalies in temp. depend. 79−23942
$Fe_{0.5}(Ni_xMn_{1-x})_{0.5}$, FCC, anomalies in sp. ht. and thermal expansion in paramag. temp. range 79−19739
$Fe_{0.65}(Ni_{1-x}Mn_x)_{0.35}$, Mossbauer spectra, ^{57}Fe hyperfine field distrib. 80−20533
$Fe_{65}(Ni_{1-x}Mn_x)_{35}$, anomaly of subcrit. neutron scatt. and depolarisation effects at antiferro- to ferromag. transition *(Russian)* 77−47996
$Fe_{65}(Ni_{1-x}Mn_x)_{35}$, H solid solutions magnetisation behaviour in pulsed mag. fields 79−65674
$Fe_{65}(Ni_{1-x}Mn_x)_{35}$, magnetic struct. and inhomogeneities by neutron scatt. and Mossbauer effect *(Russian)* 77−63122
$Fe_{65}Ni_{28}Mn_7$, disordered, mag. struct. near ferro-antiferromagnetic transition 80−60211
Fe_3Si-Mn, dil., cond. electron polarisation and moment perturbations 78−68224
$Fe_{1.2}Te$-MnTe phase relations in presence of excess Fe 77−52292
Gd-Mn, amorphous film, galvanomag. effects, Hall detector 77−89882
Gd-Mn alloy, mag. props. and effect of H_2 absorpt. 78−19250
Gd-Mn(-Co), amorphous, ferrimag. props. and Hall effect 79−73692
$Gd(Al_{1-x}Mn_x)_2$, alloys soft X-ray emission spectra investigation 79−91537
$Gd(Al_{1-x}Mn_x)_2$, ordering on crystallographic sites, X-ray diffr. 78−38662
$GdMn_2$, H_2 sorption props. 79−86980
$GdMn_2$-$GdAl_2$ intermetallics, mag. props., 80-650K 78−60282
$GdMn_2$-$GdAl_2$ system, mag. and structural studies 80−108006
Gd_6Mn_{23}, magnetic moments, magnetisation 80−25094
Gd_6Mn_{23}, noncollinear mag. struct., magnetization meas. 79−78322
$(GdMn_2)_x(GdAl_2)_{1-x}$, mag. and struct. investigations of intermetallic systems 78−95440
Ge-Mn, liq., calorimetric investigation of heats of mixing, and entropies of mixing 79−95165
$HfMn_2$, Curie-Weiss law depend. of susceptibility, mag. props. *(Russian)* 79−65655
$HoCo_{5.5-x}Mn_x$, cryst. struct. and mag. props. 80−75800
HoFeMn, Laves phase, mag. moment on Ho, neutron diffr. obs. 77−63107
$HoMn_2$, Laves phase, mag. moment on Ho, neutron diffr. obs. 77−63107
In-Mn, dil., film, ion implanted, supercond, and mag. props. 77−15987
In-Mn, dil., supercond. film, H_{c2} meas., mag. impurity effects, pair breaking theory 79−42708
In-Mn, dilute alloy, local excited states, electron tunnelling observation 80−34565
In-Mn, discontinuity in sp. ht. at supercond. transition 79−60971
In-Mn films, supercond., sp. ht. discontinuity and transition temp. meas. 79−60969
InMn, ion implanted, influence of O and lattice disorder on Kondo resist. 79−38061
$IrMn_{1+x}Sb$ alloys, crystal struct., and mag. props. 78−34466
$Ir_{1.07}Mn_{1.07}Sn_{0.88}$, ferromag. Heusler alloy, ^{193}Ir and ^{119}Sn hyperfine fields 79−78581
$La_{0.9}Eu_{0.1}Ni_{4.6}Mn_{0.4}$, absorption-desorption props. of H_2, degradation mechanism, Mossbauer study 80−88431
Li-Mn liquid alloys, form factor effects, pseudopotentials, resist. calc. 80−103608
Lu-Mn alloy, mag. props. and effect of H_2 absorpt. 78−19250
$LuMn_2$, Lu_6Mn_{23}, H_2 absorption effect on mag. props. 77−89931
Ma-Cu (10 at.%), antiferromag. defect scatt., neutron polarisation anal. 78−2652
manganese alloys continued
Mg cast iron, effect of heat treatment on phase comp., microstruct., wear resistance 77−56006
Mg-Al-Zn-Mn (8, 0.5, 0.3 wt.%) casting alloy, penetration resistance 80−100901
Mg-Mn, dil., cryst. field and spin parameters, transmission ESR obs. 77−40130
Mg-Mn, dil., energy splittings of Mn ions 78−67989
Mg-Mn, dil., mag. props., EPR meas. 79−73804
Mg-Mn, dil. alloy, de Haas-van Alphen effect, exchange interaction, Kondo effect 78−88093
Mg-Mn, dil. alloy, single impurity Kondo behaviour in elec. resist. *(French)* 79−60815
Mg-Mn-Ce, MA8, dislocations at grain boundaries and grain-boundary glide 78−64605
Mg-Mn-Ce, structural changes and deformation during superplastic flow 78−15472
Mg-Mn-Ce (1.5, 0.3 wt%), superplasticity role of diffusional creep *(Russian)* 80−97528
Mg-Mn-Ce (1.5%, 0.3%), dislocation slip during superplastic deform. *(Russian)* 77−21214
Mg-Mn-Ce alloy, superplastic deform., role of grain boundaries 78−19843
Mg-Ni-S, electroforming, mech. props. rel. to heat treatment 80−35133
Mh-Rh-Cr, mag. transition, effect of press. 77−16077
Mn cast Fe, W effect on transform. in thin surface layers during dry sliding friction 77−21289
β-Mn-^{57}Fe-^{119}Sn alloy mag. props. from Mossbauer effect obs. *(Japanese)* 80−15933
Mn-(Fe)-Si-C, activity determ. by vapour press. meas. *(Japanese)* 77−63631
Mn-Ag, XPS meas., Fermi level to 1000 eV below it 80−66389
Mn-Al, vacuum codeposited, disorder of $MnAl_6$ phase in recovery process 78−51854
Mn-Al alloy, domain struct., cryst. defect effects 77−69609
Mn-Al alloys, permanent magnet material development 78−91895
Mn-Al permanent magnets, defect structure, mag. props. TEM obs. 78−91902
Mn-Al-C, ferromag., transform. kinetics 80−34627
Mn-Al-C, ferromag. alloy, transform. kinetics 80−76229
Mn-Al-C, fine-grained cast struct., remanence and coercive force 80−60365
Mn-Al-C, metallic magnets investigations, present state *(Polish)* 80−107987
Mn-Al-C, permanent magnet, mag. props., machinability 77−85505
Mn-Al-C (70, 29.5 wt.%) alloy magnet, Almax, anisotropic, mag. props. *(Japanese)* 80−60371
Mn-Al-C alloy, anisotropic, permanent magnet appl., properties and production *(German)* 79−8309
Mn-Al-C anisotropic permanent mag., cryst. orientation and form., X-ray diffr. anal. 79−82778
γ- Mn-Au, magnetic struct. for compositions near onset of antiferromag. ordering 77−63111
Mn-bearing binary substitutional alloy systems, props., applicability of statistical thermodynamic approach 80−88336
Mn-Bi, film, low field magnetoresist. and domain drag 78−68014
Mn-Bi, magnetically uniaxial, strongly anisotropic, discontinuous mag. reversal singularities *(Russian)* 77−48010
Mn-Bi alloy, melting and solidification under microgravity, mag. props. *(German)* 80−45296
Mn-Bi alloys, mag. props. improvement study *(Japanese)* 78−43617
Mn-Bi eutectic alloy, mag. anisotropy 78−68220
Mn-Bi film, amorphous, form. and crystn. 79−28923
Mn-Bi film, negative transverse magnetoresist. in c-plane, domain wall effects 77−20465
Mn-Bi film, with perpendicular anisotropy, galvanomag. props., hysteresis loops 77−20464
Mn-Bi magneto-optic memory system 77−85511
Mn-Bi mictomagnetic alloy, mag., elec. and elastic props. *(Russian)* 80−108028
Mn-C, coupled phase diagrams and thermochemical data 79−66036
Mn-Cr-Mo-C, master alloys, development for low alloyed PM steel 80−50576
Mn-Cr-Ti layers on low C steel, composite, residual stresses rel. to arc-spraying parameters *(German)* 80−104077
Mn-Cu, acoustic shock pulse characts., stress amplitude and temp. depend. 79−19323
Mn-Cu, alloying addition and heat treatment effects on damping capacity 78−3165
Mn-Cu, alloying behaviour and high damping capacity 80−35160
γ-Mn-Cu, antiferromag. defect neutron scatt. study 79−47252
γ-Mn-Cu, antiferromagnetism, martensitic transformation 79−1673
γ-Mn-Cu, changes in cell dimensions at martensitic transform. 78−19750
Mn-Cu, high-damping, acoustic shock pulse attenuation and vel., stress amplitude and temp. depend. 77−15503
Mn-Cu, mag. and cryst. struct., neutron and X-ray diffr. meas. *(Russian)* 78−22694
γ-Mn-Cu, metastable, structural aspects of decomposition 79−1871
Mn-Cu, mictomagnetic props., neutron diffr. obs. 80−65906
Mn-Cu, plastic deform. mechanism and shape-memory effect, mag. struct. obs. *(Russian)* 78−60705
Mn-Cu, shape-memory effect at martensitic transform., cryst. and mag. struct. 77−36610
γ-Mn-Cu (10 at.%), spin wave studies using neutron diffraction 80−70991
Mn-Cu (25, 62 wt.%), elast. consts., temp. depend., 170-300K *(Russian)* 80−81095
Mn-Cu (25 wt.%) alloy, critical shear stresses of twinning and glide 79−87693
Mn-Cu (25 wt.%) rod, transverse vibrations, energy dissipation, static longitudinal load effect 80−81099
Mn-Cu (75, 25 wt.%), rod, coupled flexural and torsional vibrs., energy dissipation 80−89281
Mn-Cu (9.3 wt.%), cryst. struct. at FCC to FCT transform. *(Russian)* 80−11643
Mn-Cu alloy, local premartensitic instability in FCC phase 80−40355
Mn-Cu alloy, volume effect, paramagnetic-antiferromagnetic and structural transition, lattice consts. 80−39007
Mn-Cu alloys, mechanical damping at 40 kHz 78−23755

manganese alloys continued
Mn-Cu alloys, spinodal decomp. at 380°C, neutron diffr. anal. *(Russian)* 79−20023
Mn-Cu alloys, stressed, diffuse neutron scatt. exam. 78−47950
Mn-Cu structural alloys, physicomechanical props. 77−12652
Mn-Cu-Al alloy under torsion, anomalous elasticity and transformation plasticity obs. *(Russian)* 78−75834
Mn-Cu-Bi ternary cpd. thin films for magneto-optic memory applic. *(Japanese)* 77−63238
Mn-Cu-Ni-Bi, magneto-optic film for storage appl. 77−12165
Mn-Cu-Zn system, optimum heat-treatment routine for max. damping 79−87670
Mn-Cu(Ni), melt solubility and activity of S *(Russian)* 77−25012
Mn-Cu(Sn), liquid alloys, thermochemistry 79−56962
γ-Mn-Fe, FCC→FCT transform. temp. and Neel temp., X-ray and neutron diffr. expts. *(Russian)* 78−84797
γ-Mn-Fe, Mn rich, damping capacity 79−83252
Mn-Fe-C, melts, activities of Mn at 1673K 80−50597
Mn-Fe-C, phase instability 80−11628
Mn-Fe-Si-C, melts, activities of Mn at 1673K 80−50597
β-Mn-Fe-Sn, weak itinerant electron antiferromagnetism, Mossbauer spectra meas. 77−36158
α-Mn-Fe(Cr), influence of Fe and CR on Neel point *(Russian)* 77−1554
Mn-GA system, cryst. struct. and degree of order *(Chinese)* 79−51048
Mn-Ga, DO_{22} type alloys, magnetic props., crystal struct. *(Japanese)* 78−59784
Mn-Ga, Elinvar charact. *(Japanese)* 79−61638
Mn-Ga, mag. and cryst. struct. in conc. region of gamma phase, temp. depend. *(Russian)* 79−65649
Mn-Ga (19 to 30 at.%), phase equilib. diagrams, X-ray diffr., thermal expansion, and mag. meas. *(Japanese)* 78−39743
Mn-Ga (19.0 to 31.2 at.%), exam. of phase diagram, using X-ray diffr., thermal expansion and mag. meas. 78−76634
Mn-Ga (24.1 wt.%), reversible memory of form, X-ray diffr. expts. *(Russian)* 79−5006
Mn-Ga system, X-ray struct. investigation, solubility *(Chinese)* 80−88084
Mn-Ge, antiferromagnetic, NMR exam. 77−16193
Mn-Ge (10.3 to 15.5 wt.%), reversible memory of form, X-ray diffr. expts. *(Russian)* 79−5006
Mn-Ge (5 to 90 at.%) liquid alloy, electrical resistivity *(Russian)* 77−55509
Mn-Ge amorphous films, short-range order, electron diffr. obs. 80−39473
Mn-H(D), ferromag., thermal, struct. mag. props. 78−88145
Mn-N, liquid, N soln. 79−99321
Mn-N system, γ-Mn and hexagonal ζ-phase equilibrium calcs. 79−61565
Mn-Nd, mag. props. for bulk amorphous deposits *(Japanese)* 79−95971
Mn-Ni, γ-phase antiferromag., lattice distortion and elastic props., ΔE effect interpret. 77−20671
Mn-Ni, shape memory effect 78−35386
Mn-Ni, single cryst. or polycryst., elastic anomalies at antiferromag. transition 78−14972
Mn-Ni, thermal expansion, mag. susceptibility, lattice consts. 80−100341
γ-Mn-Ni (15 at.%), antiferromag. defect scatt., neutron polarisation anal. 80−50056
Mn-Ni alloys, Mn-rich, structural changes associated with antiferromag. ordering 77−69085
Mn-Ni antiferromag., Invar-like thermal expansion and spontaneous volume magnetostriction 77−69654
γ-Mn-Ni-C, elastic anomalies, martensitic transformation in Mn rich alloys 78−84807
Mn-Ni-C system, pressure effect on melting diagram *(Russian)* 77−55943
Mn-Ni-Ti (Zr) systems, and mech. props. thermal expansion for different heat treatments *(Japanese)* 79−29123
Mn-Ni-Ti(Zr), non-ferromagnetic Elinvar-type alloys 79−24566
Mn-Ni-V(Nb)(Ta), nonferromagnetic Elivar type, mech. props. meas. 77−48473
Mn-Ni(Pd), atomic and mag. order, neutron diffr. exam. 79−73697
Mn-Ni(V)(Fe)(Ti)-Al, phase stability 77−48397
γ-Mn-Pd, antiferromag. defect neutron scatt. study 79−47252
γ- Mn-Pd, magnetic struct. for compositions near onset of antiferromag. ordering 77−63111
Mn-Pd (10 at.%), antiferromag. defect scatt., neutron polarisation anal. 78−2652
Mn-Pt, diffusion of ^{54}Mn, radioactive tracer study *(French)* 79−86915
Mn-Pt, Elinvar props., −150 to 500°C *(Japanese)* 77−52385
Mn-Pt, exam. of Elinvar props., from −150 to 500°C 78−76684
Mn-Pt, mag. struct., neutron diffr. study 79−91210
Mn-Pt (<29 at.%), eutectoid transform., antiferromag. struct. transform. *(French)* 78−92259
Mn-Sb(Sn)(In), liq., elec. resist. meas. 77−51721
Mn-Si, activity determ. by vapour press. meas. *(Japanese)* 77−63631
Mn-Si, liq. alloys, equilibria between MnO-SiO_2-CaO-MgO slags 80−10639
Mn-Si, liq. thermodynamic props., rel. to alloy form. 77−7875
Mn-Si (62.5 to 63.8 wt.%), phase anal. and cryst. struct. *(Japanese)* 80−15049
Mn-Si liquid alloy, vapour-pressure meas. using torsion effusion method 79−42215
Mn-Si-C, melts, activities of Mn at 1673K 80−50597
Mn-Si(C), melt, activation determ. by vapour press. meas. 80−16279
β-Mn-Sn, Mossbauer and neutron diffr. exam. 77−66253
Mn-steel, cryst. geometry in formation of ε′-, ε-, ϰ′- and α-martensitic phases *(Russian)* 78−76648
Mn-Tb, dil., hyperfine interactions, nuclear orientation 80−15929
Mn-Ti surface treatment on Al_2O_3 insulators 79−24261
Mn-Ti-Fe, ternary phase diagram, computer calculations 80−45274
Mn-V-Al, magnetic props., heat treatment effects 79−29233
Mn-V-Mo-C master alloys, development for low alloyed PM steel 80−50576
Mn-V(Cr)(Fe)(Co)(Ni), spin fluctuations effect on sp. ht. 79−82788
Mn-Y-Zn-Cd alloy,phase equilibria, plastic deformation, microhardness *(Russian)* 80−40334
Mn-Zn ferrite single crystals, mech. polishing effect on mag. props. *(Japanese)* 80−16569
Mn-Zr-S, phase equilibrium *(German)* 78−72764
MnAg alloys, XPS meas. 80−60751
τ-MnAl, estimated theoretical limit of mag. moment 80−97072

manganese alloys continued
$Mn_{1.11}Al_{0.89}$, crit. behaviour, neutron diffr. meas. 78−34982
$Mn_{1.11}Al_{0.89}$, neutron diffr. investig. of mag. struct., degree of order 77−55662
$Mn_{1.11}Al_{0.89}$, unit cell parameters, temp. depend. 79−55697
Mn_4Al_{11}, X-ray cryst. struct. 80−38999
$Mn_{55}Al_{45}$ alloy, permanent mag. props., depend. on particle size 78−91899
MnAlGe film, mag. domains and amorphous to cryst. phase transition, electron microscopy obs. 80−71129
MnAs, high spin state electron config. *(Japanese)* 77−43812
$MnAs_{0.925}P_{0.075}$, low spin state electron config. *(Japanese)* 77−43813
$MnAs_{0.97}P_{0.03}$, orthorhombic, mag. anisotropy 77−43832
γ-MnAu, antiferromag., phase diagram, X-ray diffr. and Young's modulus meas. 80−71024
$MnAu_2$, helical antiferromagnetic compound, optical props. and electronic struct., visible and IR obs. *(French)* 80−45101
$MnAu_2$, helical antiferromag., optical absorpt., density of states 80−66224
$MnAu_2$, optical consts., 0.5-3.5 eV, intra-and interband absorpt. *(French)* 78−10916
$MnAu_4$, domain struct. exam. by powder method *(German)* 78−91883
MnBi, domain boundaries shift, mag. reversal processes 79−87286
MnBi, domain boundary inertia during mag. reversals *(Russian)* 80−88776
MnBi film, electrical props., in situ annealing effect 80−65708
MnBi film, ferromag., diffr. efficiency of mag. holograms, Faraday effect 77−32355
MnBi film, hologram form. at 2.76 μm, using $CaF_2:Er^{3+}$ crystal laser 79−10270
MnBi film, magnetic hologram recording appl. *(Russian)* 77−1573
MnBi film, magnetic reversal mechanism, hysteresis loops for polycryst. and single cryst. specimens *(Russian)* 78−60318
MnBi film, on Al_2O_3, quantitative electron microprobe analysis 77−9150
MnBi film, optical, magneto-optical and struct. props. 77−1664
MnBi film, optical radiation spectral conversion 79−64344
MnBi film anisotropy field intensity meas. by Faraday rotation *(Russian)* 77−12162
MnBi film for recording optical information, analogue charact. *(Russian)* 78−50716
MnBi films, stability of magneto-optical props. on pulse heating *(Russian)* 78−88282
MnBi, ionized-cluster beam and reactive ionized-cluster beam deposition 80−16202
MnBi, Kerr effect and TEM obs. of mag. domains 77−89974
MnBi, mictomag. alloys, elastic props. *(Russian)* 80−7141
MnBi particles, demagnetised, coercivity, remanence and magnetisation reversal 78−19281
MnBi particles, effect of grinding on coercivity 77−36098
MnBi, thin film, fine mag. domains, SEM obs. 79−24202
MnBi, thin film, struct. and mag. props. 79−47315
MnBi, two-phase coercive force for domain wall motion, mag. reversal nucleation mechanism *(Russian)* 77−48009
MnBi-Bi garnet film structure, thermomag. information recording appls. *(Russian)* 78−23305
MnBi-Bi garnet film struct., thermomagnetic recording 80−100588
$Mn_{46}Co_{54}$, amorphous alloy prep. by high-rate sputtering, struct. and prop. characteris. 79−24462
$Mn_{1-x}Co_xSb$, press. effect on saturation magnetisation *(Russian)* 77−80919
MnCoSi, effect of press on mag. transition temp. *(Russian)* 80−25137
MnCoSi, mag. struct. *(French)* 78−39323
$Mn_{1.88}Cr_{0.12}Sb$, antiferromag.-ferrimag. transition, neutron crit. scatt. and crossover effect 80−71023
$Mn_{1.88}Cr_{0.12}Sb$, magnon renormalisation 77−69520
$Mn_{1.88}Cr_{0.12}Sb$, thermomagnetic props., antiferromag. to ferrimag. transition 77−63194
$Mn_{2-x}Cr_xSb$, exchange-inversion interaction and acoustical magnon soft mode 77−40049
$Mn_{2-x}Cr_xSb$ film, prep. and mag. props. 78−48009
$(Mn_{0.95}Cr_{0.05})_3Si$, sp. ht. at low temps., mag. transitions *(Russian)* 77−32189
γ-MnCu, antiferromag., stressed, mag. defects meas. by neutron polarisation anal. 80−50076
γ-MnCu crystals, antiferromag. Czochralski growth 80−97420
γ-MnCu, Mn-rich, inclined spin axis, neutron diffr. study 80−75723
MnCu, neutron scatt. near crit. comp., effects of stress and ageing 79−19722
$Mn_{17.5}Cu_{82.5}$, mictomag. process, susceptibility and resist. meas. 78−3157
MnCuBi film, coated with SiO layer Kerr readout charact. 77−85509
MnCuBi film, for mag. storage appl., prep. by RF sputtering, and props. 77−8369
MnCuBi film, optical and magneto-optical props. 77−4695
$MnCu_{1-x}Dy_xBi_{0.86}$ film, mag. and magneto-optic props., appl. as storage medium 77−8550
$Mn_{1-x}Cu_xSb$, ferromag., NMR exam. 77−12207
$Mn_{1-x}Cu_xSb$ film, ferromag. reson. 78−31114
$Mn_{0.97}Fe_{0.03}As$, field induced ferromag. phase *(Russian)* 77−36070
$Mn_{1-x}Fe_xAs$, high-pressure phase, magnetic properties 78−52247
$Mn_{1-x}Fe_xAs$, mag. props. in ground state *(Russian)* 78−56294
$Mn_{1-x}Fe_xAs$, magnetic transition under high press., exchange striction model calcs. *(Russian)* 80−50096
$Mn_{1-c}Fe_cPt_3$, noncollinear mag. structs., neutron diffr. anal. *(Russian)* 80−25087
$Mn_{2-x}Fe_xSb$, mag. struct. and spin flop transition, ^{57}Fe Mossbauer expts. 77−66261
$Mn_{2-x}Fe_xSb$, Mossbauer effect exam. 78−68432
$Mn_{1-x}Fe_xSi_{1.7}$, solid soln. system, temp. depend of conductivity and thermo-EMF, conc. depend of Hall const. 77−11913
$Mn_{5-x}Fe_xSi_3$, elec. resist. and mag. susceptibility, ferromag. to antiferromag. transition 80−80504
$Mn_{77}Fe_4Si_{19}$, cryst. struct. and superstruct. 77−35511
Mn_3Ga, formation of DO_{22} superstruct. and para-antiferromag. transition 79−19737
Mn_3GaC, mag. symmetry of ordered phases 78−71698
MnGaGe film, mag. domains and amorphous to cryst. phase transition, electron microscopy obs. 80−71129
Mn_3GaN, sp. ht., 6 to 350K, mag. and crystallographic phase transitions 80−71060

manganese alloys continued
MnGe, amorphous, spin glass transition, AC susceptibility meas. 80−75779
Mn_2Ge_7, high-temp. phase, X-ray powder cryst. struct. *(German)* 80−39005
Mn_3Ge, elec. and mag. props. *(Russian)* 77−76792
Mn_3Ge, triangular spin ordering, weak ferromagnetism 79−47237
Mn_3Ge_2, $Mn_{11}Ge_8$, amorphous thin films, quasieutectic model, electron diffr. investigation of short range order 79−69013
Mn_3Ge_2, textured, thermal expansion, 158K transformation *(Russian)* 77−32196
Mn_3In, antiferromag., mag. susceptibility, X-ray and neutron diffr. 79−11314
$Mn_{1-x}M_xAs$, M=V, Cr, Fe, Co, mag. props., phase diags. 77−66300
$Mn_{0.6}Ni_{0.4}$, liq., soln. enthalpies of C and Mn, enthalpy determ. for graphite-diamond transform. and Mn_5C_2 form. 78−59945
$Mn_{73}Ni_{27}$, generalised susceptibility, spin wave contrib., inelastic mag. neutron scatt. 79−47262
$Mn_{0.6}Ni_{0.4}B_{0.02}$, liqs., enthalpy of formation of B_4C at 1320K 79−11814
MnNiGe, coupled nature of mag. and struct. transition under press. 79−8033
$Mn_xNi_{1-x}Sb$, spin glass state and synthesis in high temp. and press. atmospheres 78−23277
β-$Mn_{66}Ni_{20}Si_{14}$, X-ray crystal struct. refinement 79−14735
$MnNiSi_{1-x}Ge_x$, mag. props. 77−12118
$Mn_xPd_{82-x}Ge_{18}$ amorphous alloys, elec. resistivity and magnetoresistivity 79−51543
$Mn_xPd_{82-x}Ged_{18}$, amorphous alloys, mag. props. 78−91906
MnPt, disordered film produced by RF sputtering, ferromag. behaviour 78−68310
MnSb, electronic state, neutron diffr. study 78−87906
MnSb, hyperfine interactions, ^{119}Sn Mossbauer obs. 77−40160
MnSb, interstitial cations, mag. and crystallographic study 79−55698
MnSb, magnetic losses, ferromagnetic resonance and antiresonance 80−100618
MnSb, resist., susceptibility and thermopower rel. to electronic struct. 78−67935
MnSb-Mn_2Sn alloy system, continuous series of solid solns., homogeneity and ferromagnetic props. 79−52159
$Mn_{1.15}Sb$, Kerr effect and TEM obs. of mag. domains 77−89974
Mn_2Sb, Bi-modified, mag. first order phase transition 79−51777
Mn_2Sb, domain and domain wall resons. in ^{55}Mn NMR spectrum 80−25219
Mn_2Sb, large anisotropy in mag. hyperfine field at ^{121}Sb, Mossbauer spectra meas. 77−73101
Mn_2Sb, spin-wave dispersion relations, exchange interactions, neutron inelastic scatt. 80−65832
$Mn_2Sb_{1-x}Bi_x$ ($0 \le x \le 0.175$), mag. transition, thermal expansion, thermomag. effects and lattice constant changes *(Japanese)* 79−78375
$MnSb_{1-x}Sn_x$ films, Faraday rotation, optical absorpt. coeffs. 80−97242
$MnSb_{1-x}Sn_x$, zero-field NMR investig. of domains and domain walls 77−32271
$Mn_{1+x}Sb_{1-x}Sn_x$, magnetisation and Curie temp., prep. and comp. depends. 78−64200
$Mn_{1+x}Sb_{1-x}Sn_x$, nuclear Zeeman effect, Mossbauer meas. 79−28654
$Mn_2Sb_{1-x}Sn_x$, mag. transitions, Mossbauer meas. 78−52406
MnSi, amorphous, spin glass transition, AC susceptibility meas. 80−75779
MnSi, amorphous, sputtered, mag., elec., struct. and thermal props., spin glass behaviour 80−50124
MnSi, amorphous magnetisation meas. 80−34599
MnSi, crit. transverse US attenuation, spin fluctuations 78−48022
MnSi, electronic energy band struct., self-consistent APW calc. 80−65433
MnSi, helically ordered state, ^{55}Mn and ^{28}Si NMR 78−43655
MnSi, itinerant electron system, helical spin structure 78−23234
MnSi, itinerant electron system, neutron scatt. 78−68194
MnSi, itinerant ferromag. spin dynamics field depend. 79−38315
MnSi, low field mag. studies 78−23255
MnSi, mag. anisotropy exam., ferromag. to antiferromag. transition 79−73708
MnSi, mag. phase diagram, crit. US attenuation 77−12122
MnSi, mag. phase diagram, US attenuation meas. 77−63188
MnSi, μ^+ Knight shift, temp. depend. 78−80270
MnSi, μ^+ probe, itinerant electrons spin fluctuations 79−56671
MnSi, μ^+ spin relax. 79−56670
MnSi, NMR and μSR, microscopic mag. props. *(Japanese)* 78−52368
MnSi, NMR and susceptibility above T_c 78−43665
MnSi, weak itinerant ferromag., mag. excitations, neutron scatt. obs. 78−34969
MnSi, weak itinerant ferromagnet, mag. excitations 79−7985
MnSi-CoSi solid solution, mag. props. 78−56403
MnSi-Si system, striations and cryst. struct. of matrix 80−103292
$MnSi_{\sim 1.73}$ crystal growth and characterisation 80−93474
Mn_3Si, electronic structure, X-ray spectra comparison with band struct. calcs. 80−97383
Mn_5Si_3, interface struct. and growth mechanism from melt 79−14715
Mn_5Si_3, polycrst., mag. struct., 66-100K *(Russian)* 78−68161
Mn_5Si_3-Mn_5Ge_3, electrical resistivity meas., order-disorder transition 80−10945
$Mn_{85.5}Si_{14.5}$, R-phase, cryst. struct. 78−42953
$Mn_5(Si_{1-x}Ge_x)_3$, magnetic and cryst. struct., ferromag. props. 77−59391
$Mn_5(Si_xGe_{1-x})_3$ solid solution, mag. ordering, magnetisation and neutron scatt. meas. 78−27023
$Mn_{1.77}Sn$, 170K transitions temp. in ferrimag. state, pressure and γ-irrad. effects 77−51902
Mn_3Sn, triangular spin ordering, weak ferromagnetism 79−47237
Mn_3SnN, perovskite type struct., mag. props., neutron and Mossbauer meas. 77−32159
$Mn_{0.75}Ti_{0.25}Bi$ films as magnetooptic storage medium, mag. interferogram recording 78−19288
$Mn_{2-x}V_xSb$, $0.08 \le x \le 0.25$, mag. props. modification by V 77−36071
$Mn_{23}Y_6D_x$, D atom location, neutron diffr. study *(French)* 80−24426
β_1-MnZn, ferromag., spin wave contrib. to nucl. spin-lattice relax. time meas. 77−36147
Mn_3ZnN, sp. ht., 6 to 350K, mag. and crystallographic phase transitions 80−71060
Mo-Mn alloy, plasticity, fracture, strength depend. on C content *(Russian)* 80−35257
Mo-Mn metalloceramic alloy, brittle fracture investigation, segregation, morphology, struct. *(Russian)* 80−55503
manganese alloys continued
Mo-Mn powder mixture, X-ray diffr. exam. of reaction between Mo and Mn, during sintering 80−16242
Mo-Mn-Fe-Si/Al_2O_3 ceramic seal, interfacial phases 78−72011
Monel, Norton-Bailey parameters, from creep rupture data 80−30098
Nb-Mn, internal impurity adsorption effect on bond type of intercrystallite zones 77−16684
$Nb_{78}Ga_{22-x}Mn_x$, supercond. props., influence of Mn mag. impurities 80−54825
$Nb_{80}Ga_{20-x}Mn_x$, supercond. props., influence of Mn mag. impurities 80−54825
$NbMn_2Si_2$, Mossbauer and magnetisation expts. 78−31138
Nb_3Sn-Mn, mag. impurities effect on supercond. props. 77−1524
Ni-Al bronze, fracture toughness 77−81312
Ni-Al-Mn alloy system, oxidation resist. 79−24661
Ni-Co-Mn, dil. alloys, NMR freq. temp. depend., spin echo meas. 78−64296
Ni-Co-Mn, dil. ferromag. alloy, mag. moment, saturation magnetisation meas. 78−64195
Ni-Cr-Mn alloy solidification, effects of Si, Mo and Co alloying 79−83193
Ni-Cr-Mn-Fe-Nb (20,3,3,2.5 wt.%), short-range order effects on tensile behaviour 80−25793
Ni-Cr-Mo-Fe-Mn, Kh12M23, intermetallic phases exam. *(Russian)* 78−39740
Ni-Cr-Mo-Mn alloy 02KhN40MB, corrosion-resist, heat-resist., phys. and mech. props. 80−35411
Ni-Cu-Mn, dil. alloys, NMR freq. temp. depend., spin echo meas. 78−64296
Ni-Cu-Mn, mag. and galvanomag. meas. 77−89928
Ni-Fe-Mn, ferromag. reson. linewidth and saturation magnetisation 78−72418
Ni-Fe-Mn alloy, NMR signals due to Mn atoms with antiparallel moments 78−27113
Ni-Fe-Mn ferromagnetic alloy, magnetic state of Mn atom, local environment effect 77−66298
Ni-Mn, dil., mag. moment distribs. and environmental effects, neutron scatt. obs. 80−60247
Ni-Mn, disordered, disordered, exchange-anisotropy field, magnetisation curves 78−72365
Ni-Mn, disordered, mag. struct., high field twist deform. 78−68166
Ni-Mn, disordered FCC, stiffness const., single cryst. neutron inelastic scatt. meas. 77−20558
Ni-Mn, equilib. ordered, high field magnetisation 77−85491
Ni-Mn, hydrogenation kinetics, magnetisation, interstitial H influence 80−35528
Ni-Mn, low temp. anomalies of elec. resist. *(Russian)* 79−60788
Ni-Mn, low temp. kinetic props., 4.2-77.3K *(Russian)* 79−19568
Ni-Mn, mag. moment and asphericity of spin density distrib., polarised neutron scatt. obs. 80−44813
Ni-Mn, ordered and disordered, press. effect on Curie temp. 80−71148
Ni-Mn, ordering by nucleation and growth and by spinodal decomposition *(French)* 78−27471
Ni-Mn, permeability, diffusion and solubility of H 80−107573
Ni-Mn, remanent magnetisation reversal, local environment model 79−33507
Ni-Mn, spin polarised tunnelling expts. 78−39372
Ni-Mn, spin wave stiffness const., low temp. neutron scatt. meas. 79−51768
Ni-Mn, spin wave stiffness consts., RPA CPA band model 79−61088
Ni-Mn, tunnelling electron spin polarisation 77−73058
Ni-Mn (10~40 wt.%), γ solid soln., interdiffusion 80−100366
Ni-Mn (17-27 at.%), low-angle neutron diffr., anomalous crit. scatt. *(Russian)* 80−60193
Ni-Mn (5%), magnetisation curve reduction 78−31096
Ni-Mn (up to 32 at.%), Curie temp., press. depend., using press. cell developed for meas. with cubic-anvil press 80−13109
Ni-Mn alloy, NMR signals due to Mn atoms with antiparallel moments 78−27113
Ni-Mn alloys, ferromagnetism-to-spin glass phase transition and strong mag. field effect 80−75773
Ni-Mn base polynary alloys, magnetic and elect. props. *(Japanese)* 78−15551
Ni-Mn base polynary alloys, magnetic, and elec. props., composition and heat treatment effects 79−11710
Ni-Mn disordered alloys, mag. moment and Curie point 78−76243
Ni-Mn ferromagnetic alloy, magnetic state of Mn atom, local environment effect 77−66298
Ni-Mn film, magnetic properties obs., heat treatment influence *(German)* 77−56118
γ-Ni-Mn solid soln., interdiffusion 1073 to 1323K *(Japanese)* 79−99374
Ni-Mn-Al-Si-Co, Alumel, Ettingshausen-Nernst coeff. and transport props. from 200 to 473K 80−44573
Ni-Mn-Co(Fe), low temp. anomalies of elec. resist. *(Russian)* 79−60788
Ni-Mn-Cu, interdiffusion at 1173K *(Japanese)* 79−99375
Ni-Mn-H, hydride phase form. and decomposition in hygh-press. gaseous H_2, magnetisation meas. 79−56953
Ni-Mn-H solid solutions, mag. props. 80−88753
Ni-Pd-Mn, ternary FCC solid soln., saturation magnetisation and Curie temp., medical appl. *(Japanese)* 79−61114
Ni-Pd-Mn ternary alloys, mag. characts., use for thermoseed 80−107995
Ni-Si-Al alloy system, oxidation resist. 79−24661
Ni-Zn-Mn-Fe spinel, crystn. from soln. in melt 80−2945
$(Ni_xCu_{1-x})_2MnSn$, mag. props. and lattice parameter, composition depend. 77−80916
$(Ni_{1-x}Fe_x)_{99}Mn$, ferromagnetic, NMR study of local environment effect, relaxation mechanism 80−7193
Ni_3(Mn, Al), ordering process mechanism by neutron diffr. *(Russian)* 77−55961
Ni_3(Mn,Cu), ordering kinetics, neutron diffr. and elec. resist. meas. *(Russian)* 77−47379
NiMn, high field magnetisation 80−2557
$Ni_{1-x}Mn_x$, ferromagnetic, NMR study of local environment effect, relaxation mechanism 80−7193
$Ni_{1+x}Mn_{1-x}$, martensite nucleation 77−59787
Ni_3Mn, antiphase domain struct. *(Russian)* 78−39814
Ni_3Mn, at. ordering during annealing, mag. field effect 78−15394
Ni_3Mn, atomic rearrangements during fast and thermal neutron irradiation 79−42114

manganese alloys continued
Ni_3Mn, change of H_2 diffusivity with order-disorder transformation 80−59729
Ni_3Mn, dislocation struct. after heat treatments, TEM *(Russian)* 77−8848
Ni_3Mn, dissociation of superdislocations and plastic deform. mech. *(Russian)* 78−52909
Ni_3Mn, elec. resist., relax. time near order-disorder transition 78−87788
Ni_3Mn, ferromagnetic reson. field and line width temp. depend. 3-300K 79−95651
Ni_3Mn film, anomalous behaviour of Hall effect *(Russian)* 77−28262
Ni_3Mn, fission neutron disordering at 5K, exam. 78−47434
Ni_3Mn, mag. domains perpendicular to AC demagnetising field 77−20632
Ni_3Mn, magnetic phase exam. 77−20631
Ni_3Mn, neutron irradiated, disordering by replacement collision sequences, saturation magnetisation meas. 77−47492
Ni_3Mn, nonstoichiometric, order-disorder transition, A1 to $L1_2$ *(French)* 79−1861
Ni_3Mn, order-disorder transform. *(Russian)* 77−59776
Ni_3Mn, ordered at below Kurnakov temp. then deform., a/2⟨110⟩ dislocations and deform. antiphase boundaries *(French)* 77−51384
Ni_3Mn, partially ordered, field induced uniaxial anisotropy at low temp. 77−40053
Ni_3Mn, partially ordered, remanence reversal 77−69619
Ni_3Mn, partially ordered, spin-wave dispersion relation, inelastic neutron scatt. meas. 80−20394
Ni_3Mn, thermoremanent magnetisation and blocking temp. 80−34601
Ni_3Mn thin films, transmission spectra, structural order depend. 80−66318
Ni_xMn_{1-x} disordered alloy, mag. interactions exam. 77−24687
$Ni_2Mn_{0.9}Fe_{0.1}Sn$, Fe site hyperfine field and mag. moment, Mossbauer effect meas. 78−76365
NiMnGe, crystal and spiral mag. struct., Neel temp., X-ray and neutron diffr. 77−16052
NiMnGe, mag. struct., and mag. phase transitions 77−63187
$NiMnGe_{1-x}Si_x$, mag. props., neutron diffr. and magnetometric meas., 80-600K 80−65793
Ni_2MnIn, Heusler alloy, order-disorder phase transitions, X-ray diffr. meas. 77−66640
$Ni_2Mn_xM_{1-x}Sn$ (M=Ti,V) mag. hyperfine fields, ^{119}Sn Mossbauer spectra study 80−55003
$Ni_2Mn(Mn_xSn_{1-x})$, Heusler alloy, antiferromagnetic order, X-ray and neutron diff. 78−64189
NiMnSb, hyperfine mag. field at Cd impurity, TDPAC study 80−39906
$Ni_{1+x}MnSb$, mag. hyperfine field on ^{111}Cd, TDPAC obs. 78−43709
$(Ni_{0.75}Mn_{0.25})_{82}Si_{10}B_8$, amorphous, exchange anisotropy, mag. susceptibility meas., 4.2K to room temp. 80−11186
NiMnSn, Heusler alloy, hyperfine field at ^{111}Cd, TDPAC meas. 78−43705
Ni_2MnSn alloy, ionic spin distribution and RKKY interactions 78−27028
Ni_2MnSn, Heusler alloy, mag. interactions and cond. electron polarisation, spin echo NMR meas. 77−77125
Ni_2MnSn, itinerant ferromagnet, neutron inelastic scatt. 79−7970
$Ni_2MnSn(In)(Sb)$, Heusler alloy, hyperfine field at ^{111}Cd, TDPAC meas. 78−43705
$Ni_2Mn_xTi_{1-x}Sn$, Mossbauer spectra, mag. hyperfine field 80−15857
$(Ni_{1-x}Rh_x)_{99}Mn$, ferromagnetic, NMR study of local environment effect 80−7192
$(Ni_{1-x}Rh_x)_{99}Mn$, ferromagnetic, NMR study of local environment effect, relaxation mechanism 80−7193
$(Ni_{1-x}Ru_x)_{99}Mn$, ferromagnetic, NMR study of local environment effect 80−7192
$Ni_2(Ti,Mn)Sn$, Heusler alloy, mag. meas. 79−47261
$Pb\text{-}Cu_{99.8}Mn_{0.2}\text{-}Pb$ superconducting junction, crit. currents 79−69633
Pb-Mn, dil., supercond. film, H_{c2} meas., mag. impurity effects, pair breaking theory 79−42708
$Pb_2MnSb_{0.99}Sn_{0.01}$, ^{119}Sn Mossbauer study, compositional and heat treatment effects 79−42875
Pd-Fe-Mn, differential susceptibility, spin glass and ferromag. transition 79−61169
Pd-Fe-Mn, dil. alloy, high press. study 80−34600
Pd-Fe-Mn, ferromag. and spin-glass props; comment 80−2591
Pd-Fe-Mn, ferromagnet-spin glass, thermal expansion forced, magnetostriction and magnetisation under high press. 80−65255
Pd-Fe-Mn, ferromagnetic-spin glass transition 78−39339
Pd-Fe-Mn, spin glass-ferromag. alloys, high-field magnetisation 79−33488
Pd-Fe-Mn alloy, spin glass-ferromagnetic systems, differential susceptibility 78−88131
Pd-Mn, alloy with mixed types of order, uniform mag. phase diagram 79−78368
Pd-Mn, Curie temp. and magnetisation, vol. depend. 80−34629
Pd-Mn, dil., depend. of neutron small-angle scatt. intensities on appl. mag. field and temp. 79−11291
Pd-Mn, dil., mag. moment distrib., polarised neutron diffuse scatt. meas. 77−80914
Pd-Mn, dil., mag. ordering, sp. ht. calc. by Monte Carlo method 77−77030
Pd-Mn, dil. alloy, giant moment at very low temp. 78−88094
Pd-Mn, dil. alloy, very temp. magnetisation 80−34692
Pd-Mn, dilute, nuclear orientation expt., Mn impurity giant moment 77−63296
Pd-Mn, dilute, paramag. diffuse neutron scatt. 77−63094
Pd-Mn, ESR meas., evidences of bottlenecked relax. for Mn^{2+} ion 78−72401
Pd-Mn, ferromagnetism to spin glass behaviour transition 80−71062
Pd-Mn, mag. ordering phenomena, neutron scatt. obs. 80−44812
Pd-Mn, NMR of ^{27}Al meas. 77−12215
Pd-Mn, spin freezing in spin glass phase, susceptibility meas., sp. ht. analysis 77−69582
Pd-Mn, spin glass, low temp. spin dynamics, numerical studies 79−78385
Pd-Mn, spin glass-ferromag. alloys, high-field magnetisation 79−33488
Pd-Mn (1-10 wt.%), mag. ordering, influence on resistivity 80−75557
Pd-Mn (10 at.%), spin glass, inelastic neutron scatt. exam. 79−61170
Pd-Mn alloy, spin glass, neutron scatt. 78−68265
Pd-Mn system, superstructure, electron diffr. and X-ray powder diffr. study 79−94958

manganese alloys continued
$(Pd_{0.996}Co_{0.004})_{1-x}Mn_x$ alloys, ferromag. and spin glass transition, NMR 79−65761
$(Pd_{0.9965}Fe_{0.0035})Mn_{0.05}$, ferromag. and spin-glass props. 80−2590
$(Pd_{0.9965}Fe_{0.0035})_{1-x}Mn_x$, mag. behaviour at Fe sites, Mossbauer effect meas. 80−66085
Pd_xH-^{54}Mn, dil., nucl. orientation of ^{54}Mn 77−12257
$Pd(M_nCo)$, giant moments, Mossbauer study of ^{57}Fe 80−44969
PdMn, giant moment-spin glass high field magnetisation, exchange parameter, saturation moment estimation 79−61143
Pd_3Mn, disordered, mag. correls., neutron scatt. study 80−50105
$Pd_{1-y}Mn_yH_x$ alloy, spin glass, transition temp., susceptibility and EPR meas. 80−65930
$Pd_2MnIn_{1-y}Sb_y$, Heusler alloy, mag. order obs. 80−29528
$Pd_2MnIn_{1-x}Sb_x(Sn_x)$, Heusler alloy, Mossbauer effect exam., mag. coupling 79−69755
$Pd_2MnIn_{1-x}Sb_x(Sn_x)$, Heusler alloy, Mossbauer effect exam., hyperfine interactions in ferromag. phase 79−69756
$Pd_2MnIn_{1-x}Sn$, and $Pd_2MnIn_{1-y}Sb$, Heusler alloys, mag. order, disorder effects 80−88723
$Pd_2MnIn_{1-x}Sn_x$-Cd; dil., Heusler alloy, hyperfine mag. field on Cd, TDPAC obs. 79−8075
$Pd_2MnIn(Sn)(Sb)$, Cd impurities, hyperfine field meas. 78−15074
$Pd_2MnIn_{1-x}Sn_{1-x}$, mag. order exam. 77−40036
$Pd_2Mn_{1-x}Nb_xSn$, Heusler alloy, NMR and mag. coupling 78−43676
PdMnSb, Heusler alloy, hyperfine fields of 5sp shell impurities substituting Sb, Mossbauer spectra 78−80261
PdMnSb, hyperfine field at ^{125}Te, Mossbauer expts., compared with Jena-Geldart model 78−43707
PdMnSb, Pd_2MnSb, Heusler alloys, ^{129}I mag. hyperfine struct., Mossbauer meas. 79−83580
$Pd_{1+x}MnSb$ Heusler alloys, magnetic hyperfine fields on ^{111}Cd, TDPAC and magnetisation meas. 80−93219
Pd_2MnSb and PdMnSb, Heusler alloy, hyperfine field at ^{111}Cd, TDPAC meas. 78−43705
Pd_2MnSb, ferromag. Heusler alloy, mechanical and heat treatment effects 79−78582
Pd_2MnSb, Heusler alloy, hyperfine fields of 5sp shell impurities substituting Sb, Mossbauer spectra 78−80261
Pd_2MnSb, mag. hyperfine field of ^{129}I, Mossbauer spectra 78−43706
Pd_2MnSb:^{119}Sn, ferromag., mag. hyperfine structure, Mossbauer obs. 77−32309
$Pd_{2-x}MnSb$, struct., appl. as improved neutron polariser 80−60199
$Pd_2MnSb_{1-x}Sn_x$, Mossbauer meas. of ^{119}Sn mag. hyperfine struct. 77−12258
Pd_2MnSn alloy, ionic spin distribution and RKKY interactions 78−27028
Pd_2MnSn, ferromag. Heusler alloy, electronic struct., spin polarisations, theory 80−54598
Pd_2MnSn, Heusler alloy, interaction between local mag. moments 77−1540
Pd_2MnSn, Heusler alloy, mag. interactions and cond. electron polarisation, spin echo NMR meas. 77−77125
Pd_2MnSn, Heusler alloy, NMR and mag. coupling 78−43676
$Pd_2Mn_{0.95}Sn_{1.05}$, hyperfine mag. fields, Mossbauer spectra 80−15870
$Pd_2Mn_{0.98}Sn_1In_{0.02}$, Heusler alloy, hyperfine fields at sp elements, spin echo NMR meas. 78−84496
$Pd_2MnSn_{1-x}Sb_x$, Heusler alloy, Mossbauer effect exam., hyperfine interactions in ferromag. phase 79−69756
$Pd_2MnSn_{1-x}Sb_x$, mag. order exam. 77−40036
$Pd_2MnSn_{1-x}Sb_x$, Mossbauer spectra, mag. hyperfine field 80−15868
$Pd_2Mn_xV_{1-x}Sn$, Heusler alloy, structural disorder, Mossbauer study 80−80650
Pt-Mn, dil., low temp. susceptibility, spin glass and Kondo behaviour 77−66372
Pt-Mn, dil., nuclear orientation exam. 79−61171
Pt-Mn, dil., skew scatt. Hall effect, magnetoresist. and mag. anisotropy, orbital magnetism of impurity 80−70678
Pt-Mn, dil. alloy spin glass, mag. sp. ht. 78−14966
Pt-Mn dilute alloy, cubic foil, Mn spin behaviour, nuclear orientation technique 78−27044
Pt-Mn dilute alloys, spin glass, low temp. resist. meas., cluster model explanation 78−26851
Pt-Mn-Sn alloy, mag. hyperfine fields 79−1737
$Pt_{0.75}(Cr_{1-x}Mn_x)_{0.25}$, pseudobinary, magnon energy derivation 80−107996
PtMn, spin glass, nonlinear susceptibility and sp. ht. 80−60304
PtMn spin glass alloy, cooperative freezing, susceptibility meas. 79−91233
Pt_3Mn, cryst. dynamics at 80K 79−23688
Pt_3Mn, mag. excitation dispersion relation 80−25090
Pt_3Mn, obs. of magnon sp. ht. 77−63217
$Pt_3Mn_xCr_{1-x}$ alloys, mag. props. 80−2562
$Pt_3Mn_xCr_{1-x}$, electronic specific heat meas. comparison with band model calcs. 80−54400
PtMnSb, hyperfine mag. field at Cd impurity, TDPAC study 80−39906
PtMnSn, ^{197}Au and ^{119}Sn hyperfine fields, Mossbauer expt. 78−72439
PtMnSn(Sb), Cd impurities, hyperfine field meas. 78−15074
Rh-Pd-Mn, dil. alloy, mag. moment 78−95416
Rh_2MnGe, ferromag. Heusler alloy, hyperfine mag. field meas. by TDPAC technique 79−78580
$Rh_2MnGe(Pb)$, hyperfine mag. field at Cd impurity, TDPAC study 80−39905
Rh_2MnPb, hyperfine fields, ferromag., NMR and Mossbauer effect studies 80−71259
Rh_2MnSb, hyperfine fields, ferromag., NMR and Mossbauer effect studies 80−71259
Rh_2MnSn, and related cpds., with Heusler and Heusler-related struct., mag. props. 77−8311
Rh_2MnSn, ferromag., mag. hyperfine fields, time differential PAC meas. 77−81040
Rh_2MnSn, ferromag. Heusler alloy, hyperfine fields, spin echo meas. 77−63314
Rh_2MnSn, ferromag. Heusler alloy, hyperfine mag. field meas. by TDPAC technique 79−78580
Rh_2MnSn, Heusler alloys, hyperfine mag. field at Sn 78−39482
Rh_2MnSn, mag. hyperfine fields at Rh and Sn sites, and their temp. depend. 78−43708
Rh_2MnX, (X=Al, Ga, In, Tl, Sn, Pb, Sb), Heusler and Heusler-related cpds., mag. and cryst. props. 77−20568
Sc-Fe-Ga, isothermal sections of phase diagram *(Ukrainian)* 78−92235

manganese alloys continued
Sc-Mn-Ga, isothermal sections of phase diagram *(Ukrainian)* 78−92235
Si-Mn, liquid alloys, thermodynamic charact. calc. *(Russian)* 78−27475
$Sm_2(Co,Mn)_{17}$, exchange and crystal field parameters, anisotropy meas. 77−69535
$Sm(CoFeCuMn)_7$, coercive force and anisotropy temp. depend. 78−68297
$Sm_2(Co_{0.8}Fe_{0.14}Mn_{0.04}Cr_{0.02})_{17}$, sintered, hard mag. props. 77−8340
$Sm_2(Co_{1-x}Mn_x)_{17}$, bulk magnetisation and magnetocryst. anisotropy, interpretation 77−40055
$Sm_2(Co_{1-x}Mn_x)_{17}$, magnetocryst. anisotropy 77−40054
$Sm_{2-x}Gd_xCo_{17-y}Mn_y$, saturation magnetisation and anisotropy field temp. depend., suitability for microwave/millimetre wave TWT 79−82824
$Sm_6Mn_{23-x}Fe_x$, magnetic behaviour, temp. and comp. depend. 80−93090
$Sr_2(Co_{1-x}Mn_x)_{17}$, powders, influence of substitutes on mag. props. 80−100601
Th-Mn alloy, mag. props. and effect of H_2 absorpt. 78−19250
$ThCo_{5-x}Mn_x$, struct. and magnetisation exam., temp. depend. 78−2662
$ThMn_{12}$ type structure, role of elongated rhombic dodecahedron in alloy structures 79−32946
$ThMn_2$, Th_6Mn_{23}, H_2 absorption effect on mag. props. 77−89931
$ThMn_{5-x}Al_x$, homogeneity regions, X-ray powder diffr. study 79−77554
$Th_6Mn_{23}H_x$, H induced mag. ordering obs. 77−85423
$ThNi_{5-x}Mn_x$, struct. and magnetisation exam., temp. depend. 78−2662
Ti alloy fatigue, stability of energy dissipative charact. 77−21209
Ti-Al-Mn, endurance with cyclic bending, effect of loading conditions 80−50724
Ti-Mn, eutectoid decomposition 79−24491
β-Ti-Mn, exam. of reloading yield points 78−72822
Ti-Mn, fine cryst. struct. by diffuse X-ray and electron scatt. *(Russian)* 79−99329
Ti-Mn, hydride form. *(Japanese)* 77−52629
Ti-Mn, superplastic, microduplex grain struct. stabilisation 78−44058
Ti-Mn (0.4 and 12 wt.%), bonding between α-β interfaces, subsequent deform. 78−14517
Ti-Mn (15 wt.%), Baushchinger effect, grain boundary contrib. 79−47759
α-βTi-Mn (4.3 wt.%), interface phase struct. 77−44212
α-β Ti-Mn (8 wt.%), calc. of stress-strain curves by finite element method, comparison with expt. curve 78−84924
α-β Ti-Mn (8 wt.%), calcs. of stress-strain curve, stress and strain distribs., discussion 80−7637
α-β Ti-Mn (8 wt.%), stress-strain curve and stress and strain distrib. calcs., reply to discussion 80−7638
α, α+β, β-Ti-Mn alloys, Bauschinger effect during cyclic straining 79−43310
Ti-Mn alloys, elec. and thermal props. *(Russian)* 78−19020
α-β Ti-Mn alloys, etching and electropolishing to reveal α and β-grain size 78−3254
Ti-Mn base beta alloys, H effect on stability solid soln., hardness *(Japanese)* 77−81261
β-Ti-Mn slip band spacing, correlation with α-Ti-Al 79−99211
Ti-Zr-Cr-Mn/$LaNi_5$ hydriding alloy mixtures for H energy storage 80−45788
$Ti(Al_xMn_{1-x})_2$, $0<x<0.4$, influence of Al on H sorption props. X-ray cryst. struct. determ. 79−28198
TiC-(Mo-Cr-Ni-Mn) steel alloy, optimum comp. and manufacture conditions, Mn effect 80−84896
$TiCo_{1-x}Mn_x$, H absorption-desorption characteristics 80−96735
TiMn, faceted parent martensite interface 80−6417
$TiMn_{1.5}$, hydrogen storage appl. *(Japanese)* 80−61443
$Ti_{1-x}Zr_xCr_{2-y}Mn_y$, C14 type alloy, hydride form. *(Japanese)* 78−19944
$Ti_{1-x}Zr_xM1_{2-y-z}Cr_yV_2$, hydrogen storage appl. *(Japanese)* 80−61443
$Ti_{1-x}Zr_xMn_2$, hydride formation, hydriding charact. of reversible uptake 78−44402
U-Mn metallic glasses, glass form. and thermal stability 80−75183
UMn_2, mag. props., ferromag. transition *(Russian)* 78−68148
UMn_2, structural transition from cubic to monoclinic, neutron and X-ray obs. 78−75833
UMn_2, transport props., influence of lattice distortion 80−100452
UMn_2-UCo_2, mag. props., ferromag. transition *(Russian)* 78−68148
UMn_2-UFe_2, mag. props., ferromag. transition *(Russian)* 78−68148
V-Mn, equiatomic, ordering kinetics and antiphase domain coarsening 80−7559
V-Mn-Cr, disordered BCC state, mag. phase diagram, mag. and elec. props. 77−63185
δ-VMn, ordering and disordering behaviours 77−48428
$V_{3-x}Mn_xGa$, cryst. struct. and microhardness meas. 79−86740
$V_{75-x}Mn_xGa_{25}$, supercond. transition temp. and electron-phonon coupling parameter 79−60952
Y-Mn alloy, mag. props. and effect of H_2 absorpt. 78−19250
Y-Mn(-Co), amorphous, paramag. props. and Hall effect 79−73692
$Y_2(Co_{1-x}Mn_x)_{17}$, bulk magnetisation and magnetocryst. anisotropy interpretation 77−40055
$Y_2(Co_{1-x}Mn_x)_{17}$, magnetocryst. anisotropy 77−40054
$Y_6(Fe, Mn)_{23}$, itinerant ferromagnet, magneto-volume, expts. 77−66404
$Y(Fe_{1-x}Mn_x)_2$, mag. order onset 80−25135
$Y(Fe_{1-x}Mn_x)_2$, Mossbauer spectra and mag. props. 80−39952
$YFe_{2x}Mn_{2-2x}$, mag. props. and FMR 79−95581
$Y_6(Fe_{1-x}Mn_x)_{23}$, ferro- to paramag. transition, press. depend. 77−73028
$Y_6(Fe_{1-x}Mn_x)_{23}$, Mn-rich compounds, Mossbauer effect study 80−71276
$Y_6(Fe_{1-x}Mn_x)_{23}$, struct. and mag. props. 80−25083
$Y_6(Fe_xMn_{1-x})_{23}$, mag. order in pseudobinary systems down to millikelvin temps. 78−19251
YMn_2, lattice consts. and mag. props. before and after H_2 absorption 77−36061
YMn_2, Y_6Mn_{23}, H_2 absorption effect on mag. props. 77−89931
Y_6Mn_{23}, ferrimag., mag. interactions, polarized neutron diffr. meas. 79−78322
Y_6Mn_{23}, lattice consts. and mag. props. before and after H_2 absorption 77−36061
Y_6Mn_{23}, low temp. specific heat determ. 80−65896
Y_6Mn_{23}, magnetic moments, magnetisation 80−25094
$YMn_{2-x}Co_x$, mag. order in pseudobinary region 79−99689
$Y_6(Mn_{0.75}Fe_{0.25})_{23}$, mag. scatter state, hysteresis loops 78−56350
$Y_6(Mn_{1-x}Fe_x)_{23}$, hydriding charact. and mag. props. 77−69527
$YMn_{2-x}Fe_xH_z$, mag. props., ordering temps. 80−71028
$Y_6Mn_{23}H_x$, influence of absorbed H on mag. behaviour 77−85423
Zn-^{54}Mn, nuclear orientation meas. 79−65644
Zn-Mn, dil, mag. anisotropy, Hartree-Fock calcs. 80−11162
manganese alloys continued
Zn-Mn, dil., energy splittings of Mn ions 78−67989
Zn-Mn, dil., Kondo effect and impurity interactions in resist., 0.05-14K 78−14721
Zn-Mn, dil., mag. anisotropy below 1K, low field magnetisation meas. 80−20382
Zn-Mn, Kondo alloys, spin and phonon resistivity independ. 78−47777
Zn-Mn, Kondo-system, ion implantation as method for study 80−70241
Zn-Mn, supercond., thermal cond. compared with Shiba's theory 77−8228
Zn-Mn dilute alloy, Kondo effect anisotropy 77−43578
ZnMn, dil., magnetoresist. meas., temp. depend. anisotropy 80−65532
Zr-Mn (up to 0.3%), high-magnetic field magnetisation and magnetoresistance 78−10652
Zr-Mn alloys, impurity and self-diffusion 79−60540
Zr-Mn-H, synthesis at high H pressure exam. of props. 80−29924
$Zr(Co_xCr_{1-x})_2$, H absorption and desorption props. 77−55448
$Zr_3Co_{1-x}Mn_x$, phase stability and supercond. T_c 78−80519
$Zr_{40}Cu_{50}Mn_{10}$, magnetically dil. glass, 3d moments, mag. susceptibility and magnetisation meas. 79−95574
$Zr_{40}Cu_{60-x}Mn_x$, amorphous, mag. ordering and local random anisotropy 78−68273
$Zr_{40}Cu_{60-x}Mn_x$, amorphous alloy, mag. interactions 78−95432
$Zr(Fe_xM_{1-x})_2$, H absorption and desorption props. 77−55448
$ZrMn_2$, Curie-Weiss law depend. of susceptibility, mag. props. *(Russian)* 79−65655
$ZrMn_2$, mag. props. H absorpt. effect 80−88821
$Zr(Mn_xCo_{1-x})_2$, Laves phase, phenomenological model for H_2 absorption capacity 77−84935
$ZrMn_2D_3$, deuterated hexagonal Laves-phase, D atoms interstices and diffusion paths, positional disorder 79−73334
$Zr(Mn_xFe_{1-x})_2$, Laves phase, phenomenological model for H_2 absortion capacity 77−84935
$ZrMn_2H_x$, proton NMR relax. time and Knight shifts, diffusional activation energies meas., sorption props. 80−75871
$Zr(Mn_xM_{1-x})_2$ (M=Fe, Co), H_2 absorpt. capacity 80−88433

manganese compounds
see also manganese alloys
acetate, crit. slowing down, 180-350 MHz 77−16083
acetate tetrahydrate, crit. relax. studied by HF mag. susceptibility 78−39299
acetate tetrahydrate, Heisenberg ferrimag. magnetisation 79−47304
acetate tetrahydrate, neutron diffr., cryst. struct. 77−47436
acetate tetrahydrate, paramag. susceptibility, spin trimer model 80−97055
acetate tetrahydrate, single cryst., ESR spectra, temp. depend. 77−43877
acetate tetrahydrate, susceptibility and magnetis. meas., crit. exponents and crossover behaviour 77−66309
additives to MnZn ferrites, effect on X-ray spectra *(Ukrainian)* 79−52046
adipate dihydrate, cryst. struct., H-bonding and O atom coordination 80−96506
alkali halide:MnO_4^{2-}, frozen solns., absorpt. spectra, 4.2 to 300K 79−87467
alkyl ammonium manganese chloride, birefringence, two-dimens. mag. behaviour, magneto-optical meas. 78−31175
aluminosilicate, ganophyllite, cryst. struct. 78−75633
aluminosilicate glass, insulating spin glass, exchange dipole optical transition 80−40136
antiferromagnetic, crysts. with spin-forbidden transitions, two-photon light absorption *(Russian)* 77−48185
carbides and nitrides, $Mn_3MC(N)$, M=metal, perovskite type, mag. props. 78−43588
chalcogenide-II-VI compound solid solutions, cryst. growth and physico-chem. props. 79−14711
Cl Mn II complex with protein, EPR spectra and zero field splitting interaction 78−35793
complex, $Mn(C_5H_5NO)_6(BF_4)_2$, mag sp. hit below 1K 77−89968
di(ethyleneammonium) manganese tetrachloride, 2-dimens., EPR linewidth and spin-dimens. crossover 77−69670
di(methylammonium) manganese tetrachloride, LF Raman spectra and phase transitions 77−63414
dialkyl ammonium manganese chloride, phases and structural phase transitions, DSC and X-ray diffr. meas. 77−47574
dialkylammonium manganese chloride, order-disorder transition mechanism 78−79772
dialkylammonium manganese chloride, soft modes, phase transitions 78−79723
dialkylammonium manganese tetrachloride, lattice consts. and phase transition temps. 79−86779
diammonium layer compound, $Mn(NH_3)_2(CN)_4 2C_{12}H_{10}$, mag. susceptibility and sp. ht. meas. down to antiferromagnetic state 79−7999
dichlorophosphate complexes, cryst. struct. ^{35}Cl NQR obs. 80−108108
diethylammonium manganese chloride, antiferromag., magnon sideband exam. by absorpt. spectra 77−12108
diethylammonium manganese chloride, Heisenberg magnet, spin diffusion, EPR study 80−66019
diethylammonium manganese chloride, planar Heisenberg magnet, spin diffusion, EPR study 80−15793
diethylammonium manganese chloride, T_1 and T_2 meas. by LODESR 78−15064
diethylammonium manganese tetrachloride, IR active modes, interlayer and intralayer forces 77−59575
dimethyl ammonium manganese chloride, sp. ht., quasi-one dimens. behaviour 78−52293
dimethyl ammonium manganese trichloride, NMR for mag. ordered state at 3.6K 79−47340
dimethylammonium copper manganese chloride, two-dimens. mixed magnet, EPR 80−66030
dimethylammonium manganese chloride, neutron diffr., 188K, cryst. struct. 77−47434
dimethylammonium manganese chloride, neutron diffr., 404K, cryst. struct. 77−47435
dimethylammonium manganese tetrachloride, antiferromag. and spin-flop resonance obs., 70 to 100 GHz 80−71190
dimethylammonium manganese tetrachloride, elastic props. 79−60418
dimethylammonium manganese tetrachloride, IR active modes, interlayer and intralayer forces 77−59575

manganese compounds continued
dimethylammonium manganese tetrachloride, phonon density of states, expt. and calc. 80−54323
dimethylammonium manganese tetrachloride-d_6, structural and mag. phase transitions, neutron scatt. and AC susceptibility meas. 80−44825
dimethylammonium manganese trichloride:Cd(Cu), impurities in quasi-one-dimens. Heisenberg systems, anisotropy effect 80−80502
dimethylammonium manganese trichloride, antiferromag. props. 79−73694
dimethylammonium manganese trichloride, pseudo one-dimens. Heisenberg antiferromag., phase diagrams 79−61148
dipropylammonium manganese tetrachloride, and tetrabromide, two-dimens. antiferromagnet, spin canting and exchange 80−34620
dipropylammonium manganese tetrachloride, two-dimens. weak ferromagnet, AC susceptibility 80−65823
ditetraethylammonium manganese bromide $^4T_1$ excited state, absorpt., MCD, Jahn-Teller model 78−43907
ethylammonium tetrachloromanganate, dielec. props. in phase transition region 80−55011
ethylenediammonium manganese chloride, struct. and mag. props., vibr. spectra 79−10842
ferrite, magnetic permeability, photoinduced reduction *(Rumanian)* 80−75794
ferrite, monocrystalline epitaxial layers, surface spin-wave modes in ferromag. reson. 78−2743
ferrite, spinel type catalytic oxidation of CO, role of mag. exchange interactions 78−56916
ferrite bubble film struct., EM and RHEED, Mn and Mn-Cu ferrites 77−11801
ferrites, Fe^{2+} ion contrib. to induced anisotropy and mag. after-effect 77−36101
ferrites, Fe-excess, charge carriers, optical props. 80−34874
ferrites, photogalvanomagnetic effects 80−34483
formate dihydrate, 2-D Heisenberg antiferromag., sp. ht. 78−14965
formate dihydrate, Zn- and Mg-substituted, anomalous crit. phenomena 80−60316
halogenides, optical spectra, metal-ligand bonds *(Russian)* 79−51986
hollandite type structures, rel. between β-gallia, rutile psilomelane, ramsdellite and $Ga_4Ti_{x-4}O_{2x-2}$ type structs. 79−37664
K-absorption edge energy shift 79−4870
manganese(II) propionate dihydrate, cryst. struct. determ. 77−80495
manganese (II) D-gluconate hydrate, X-ray cryst. struct. determ. 79−77587
manganese carboxylate, dodecanuclear mixed-valence, prep., struct., and mag. props. 80−107196
manganese copper formate dihydrate, conc. depend. of EPR linewidth 79−38376
manganese formate dihydrate, IR absorption spectra 79−19893
manganese zinc formate dihydrate, two-dimens. antiferromag., anomalous crit. phenomena, neutron scatt. and PMR obs. 80−50104
materials processing in Spacelab 78−35295
metallic perovskite, structural instability *(French)* 79−100123
methylene manganese, electronic struct., equilib. geometry, ab initio SCF calcs. 77−71747
α-MnS, elec. props. meas. 78−87971
oleate, in benzene soln., liq. and solid, positron annihilation 77−1152
oxalate, crystal growth in silicate gel, X-ray diffr. and i.r. spectrum 77−4724
oxalate hydrates, prep. and cryst. props. 77−76377
oxide, catalysis of graphitisable C graphitisation 80−89166
oxides, AES meas. 77−36323
oxides, effective atomic charge rel. to chemical shifts in transition metal compound XAS 79−78788
oxides, hydrothermal crystallisation, review, book contrib. 79−69974
oxides, radionuclide adsorption rel. to radioactive waste disposal 78−69349
oxides, XPS study, electron binding energies, spin orbit splittings, exchange splittings 79−78839
oxides in soils and sediments, Co and actinide adsorption 79−66422
press. or stress induced, neutron scatt. obs. 80−65880
1,3-propanediammonium $MnCl_4$, 2-dimens. antiferromagnet, with dipolar broadening, spin diffusion, EPR obs. 79−38371
1,3-propanediammonium tetrachloromanganate(II) mag. props. 4.2-220K 77−20567
pyridinium manganese (II) chloride monohydrate, crystal struct. and mag. susceptibility 79−19239
pyridinium manganese trichloride, pseudo one-dimens. Heisenberg antiferromag., phase diagrams 79−61148
pyrophosphates, physicochem. charact. 77−39562
quinolinium manganese (II) chloride monohydrate, crystal struct. and mag. susceptibility 79−19239
stearate, Langmuir-Blodgett layers, high resolution X-ray diffr. 80−80126
stearate, Langmuir-Blodgett layers on Ag, IR surface EM wave prism spectroscopy 78−52587
stearate, literally two-dimensional magnet, mag. ordering, EPR 79−28597
stearate, mag. two-dimensional system, mag. susceptibility 78−10669
stearate, quasi two-dimensional, dil., ESR line width 80−71155
stearate, two-dimensional mag. struct. 80−108040
stearate film, Langmuir-Blodgett type, multilayers, periodic and near-periodic, small-angle interference of reflected X-rays 79−94846
stearate monolayer, two-dimensional mag., prep. and characterisation 78−31097
TCNQ salt, $Mn(TCNQ)_2$, mag. props. 77−85558
TCNQ salts, $Mn(TCNQ)_2$ and hydrates, mag. and elec. props. 79−82767
ternary cabides and nitrides, Mn_3MN and Mn_3MC, M=metal, mag. props. 77−63116
di-(tetraethylammonium)tetrahalomanganate, mag. circular and linear dichroism obs. 80−29725
tetramethylammonium manganese(II) tribromide, cryst. struct. at 235 and 115K 78−63745
tetramethylammonium manganese trichloride, ESR meas., evidence for two paramag. species 79−61208
tienshanite, cryst. struct. determ. 78−83800
TMMC:Cu, EPR lines, dynamic effect of low-symmetric spin distrib. 80−39854
TMMC:Cu, EPR linewidth freq. depend., spin dynamics 80−15794
TMMC, classical Heisenberg antiferromagnet, one-dimens., dynamic props., review 80−15737

manganese compounds continued
TMMC, crossover transition, effects on susceptibility and EPR shift 80−71047
TMMC, Cu-substituted, spin dynamics, neutron scatt. cross section 80−60312
TMMC, effect of impurity spins on three-dimensional ordering 79−24159
TMMC, EPR lines in one-dimensional mag. systems, dynamic effect of low-symmetric spin distrib. 80−39853
TMMC, half-field EPR transitions in 1-D Heisenberg paramagnet 79−51843
TMMC, Heisenberg antiferromagnet, magnetism in one dimension, mag. behaviour 79−28495
TMMC, linear antiferromag., mag. field effect on nucl. spin-lattice relax. time, 2 to 4.2K 79−61255
TMMC, linear Heisenberg antiferromagnet, EPR half-field transitions 80−15792
TMMC, low-symmetry spin distrib. effect on EPR line 80−66018
TMMC, mag. heat capacity and Neel temp. in mag. field 79−61147
TMMC, one dimens. Heisenberg system, shift of half-field EPR line 78−23325
TMMC, one dimensional antiferromagnet, EPR expts. 80−20454
TMMC, one-dimens. antiferromag., nonlinear dynamics 80−80521
TMMC, one-dimens. antiferromag., spin wave line widths, neutron scatt. study 79−51767
TMMC, one-dimens. magnet, local magnon modes 80−65829
TMMC, one-dimensional paramag., half-field EPR transition 77−80995
TMMC, paramagnetic relax. rates, anisotropic diffusion model 77−69668
TMMC, quasi-1D antiferromag., mag. phase diagram 80−2573
TMMC, spin dynamic exam., effect of mag. field at low temp. 79−73733
TMMC, symmetry crossover in spin dynamics, proton spin lattice relax. calc. 77−40147
TMMC, XY-Ising crossover transition, quasi-elastic neutron scatt. obs. 80−44826
TMMC linear chain antiferromag., optical absorption, magnon sideband intensities calc. 77−59569
trimethylammonium manganese chloride dihydrate, optical absorpt. spectrum, 300K, 90K, cryst. field parameters 78−27253
trimethylammonium manganese heptachloride(-bromide), antiferromag. chain systems, high-field magnetisation meas. 79−61187
trimethylammonium manganese trichloride, Heisenberg antiferromag. chain, specific heat and EPR 80−65931
vanadates, elec. and mag. props., stoichiometry 78−51991
X-ray absorption near edge structures in simple and complex tin compounds 80−104013
$Al_2Mn_3Si_3O_{12}$, amorphous spin glass, spin relax. 79−65685
$Al_2Mn_3Si_3O_{12}$ amorphous spin glass, spin dynamics, neutron scatt. meas. 80−15741
$Al_2Mn_3Si_3O_{12}$, amorphous insulating spin glass, susceptibility and magnetisation meas. 80−88765
Al_2O_3-SiO_2-MnO-Cr_2O_3-B_2O_3 system, additive in sintering of high-alumina ceramic 79−61544
BaF_2-MnF_2-FeF_3 system, X-ray investigation, struct. relations, liquid-solid equilibria diagram, study by DTA *(French)* 79−34017
BaF_2-MnF_2-$M'F_3$ (M'=V,Cr), comparative study of barium fluorides rel. to 1st transition series elements *(French)* 79−69090
$BaMnF_4$, dielec. anomaly, mechanism, spin canting 78−10744
$BaMnF_4$, luminesc., emission from localised traps 79−33777
$BaMnF_4$, mag. and structural phase transitions, neutron scatt. obs. 79−87259
Ba_2MnReO_6, new seignettomagnets and ferroelectrics 78−19425
BaO-Mn_2O_3-B_2O_3, amorphous mag. oxide, field-cooling effect *(Japanese)* 80−84615
$(CH_4)NMnCl_3$, nearly-one-dimensional cpd., energy migration rel. to impurity trap behaviour 77−55811
Ca-Mn-S-Se system, multicomponent solubilities 80−108416
$(Ca_{0.15}Mn_{0.8}Fe_{0.05})SiO_3$, rhodonite lattice imaging of struct. defects 80−49240
$Ca_3Mn_2Ge_3O_{12}$ garnet, metamagnetic transition, high anisotropy peculiarities *(Russian)* 80−60274
$Ca_2Mn_3O_8$, mag. props. 79−78339
$CaMn_4(Si_5O_{15})$, rhodonite cryst. struct., compared with synthetic germanates 78−30600
$CaMn[B_2O_5]$, synthetic Mn-kurchatovite, cryst. struct. 79−14777
$Ca_2Mn_7[Si_{10}O_{28}](OH)_2.5H_2O$, inesite, cryst. struct., X-ray determ. 79−19227
CaO-MnO system, solid soln. form. and analysis 80−28996
CaO-MnO-SiO_2 system glasses, vitrification and crystallisability 77−7853
CaO-SiO_2-MnO molten mixtures, struct. and phys. props. *(French)* 80−24635
CaO-SiO_2-MnO system, melts, densities, molar vols., thermal expansivity *(French)* 79−51183
CaO-SiO_2-MnO systems, melts, elec. cond., struct. *(French)* 79−51287
Ca_2PO_4Cl:MnO_4^{3-}, polarised electronic spectrum 77−52137
CaX-MnX, X=S, Se, Te, solubility limits 80−44320
$Cd_{1-x}Mn_xTe$, exchange interaction, magneto-optical spectra 80−25348
CdF_2+MnF_2, elec. cond. and electroluminesc. 79−87508
$Cd_xMn_{1-x}Fe_2O_4$, substitution effect on mag. struct. and exchange interaction *(Russian)* 78−47949
$Cd_2Mn_3O_8$, mag. props. 79−78339
$Cd_{1-x}Mn_xSe$, fundamental optical props. 80−84751
CdMnTe crystals, exciton binding energy, magnetoabsorption and magnetoreflectivity 79−38523
CdMnTe, exciton ground state, magnetic field influence 80−54616
CdMnTe, semimagnetic semiconductor, band structure, optical properties 79−95331
$Cd_{0.6}Mn_{0.6}Te$ crystals, $Mn(3d^5)$ band, photoemission evidence 80−11535
$Cd_{1-x}Mn_xTe$, acceptor photoionisation and light-to-heavy hole absorpt. 79−65908
$Cd_{1-x}Mn_xTe$, EPR, mag. crit. point 80−39851
$Cd_{1-x}Mn_xTe$, effect of Mn $3d^5$ states on band struct., exciton refl. struct. in mag. field 79−11094
$Cd_{1-x}Mn_xTe$, exchange induced ionization of bound excitons, luminesc. meas. 80−97328
$Cd_{1-x}Mn_xTe$, Faraday rot. meas. up to 150 T 80−29722
$Cd_{1-x}Mn_xTe$, indirect exchange interaction 80−97087
$Cd_{1-x}Mn_xTe$, interband Faraday rot., appl. of mixed semicond. calcs. 79−61348

manganese compounds continued
$Cd_{1-x}Mn_xTe$, magnetic behaviour of Mn 78−14938
$Cd_{1-x}Mn_xTe$, magneto-optical props. of free excitons rel. Mn^{2+} ions spin alignment 79−47419
$Cd_{1-x}Mn_xTe$ mixed crystal, fundamental absorption edge 78−10919
$Cd_{1-x}Mn_xTe$ mixed cryst., giant exciton Faraday rotation 78−27260
$Cd_{1-x}Mn_xTe$ mixed crystals, excitonic magnetoabsorption 80−40095
$Cd_{1-x}Mn_xTe$ mixed crystals, Raman spectra 80−103961
$Cd_{1-x}Mn_xTe$, semimagnetic, exchange interactions between localised and delocalised electrons 80−97245
$Cd_{1-x}Mn_xTe$, spin-orbit coupled bands, indirect exchange interaction via electrons 80−34407
CdTe-Mn system, reaction of components, DTA, microstruct. and microhardness obs. 79−38804
$ClMn(CO)_5$, Mn-C-O deformation modes, group theoretical anal., for teaching 78−11
$(Co,Mn)SiF_6.6H_2O$, phase transition at low temp., IR spectra 79−24302
$(Co_{1-x}Mn_x)_2B$, $0 \leq x \leq 1$, magnetisation, lattice consts., press. depend. of Curie temp. 80−7137
$Co_{1-c}Mn_cF_2$, antiferromagnet mag. impurities, spin excitation spectrum collective rearrangement in external mag. field 80−50199
$Co_{0.25}Mn_{0.75}Fe_2O_4$, ferromag. reson. in frozen lattice model, anisotropy consts. 79−51859
$^{57}CoMn_2O_4$, after effects of orbital electron capture 79−73870
$Co_{3-x}Mn_xO_4$, solid soln., synthesis, effect of Bi_2O_3 admixture upon props., thermistor appl. 78−15325
$Co_{3-x}Mo_xO_4$ films, prep., struct. and elec. characteris. 80−108353
CoS-MnS, phase study by X-ray obs., lattice const. 79−1854
$Cr_xMn_{1-x}As$, antiferromagnetic-ferromagnetic transition, mag. moment and elec. resist. meas. 80−15718
$Cr_xMn_{1-x}As$, antiferromag. to ferromag. transitions, superexchange-double exchange mag. coupling, susceptibility and resist. obs. 80−50070
$Cr_xMn_{1-x}As$, mag. susceptibility anomaly at displacive phase transition 80−93091
$Cr_{1-x}Mn_xO_2$, hyperfine mag. fields at ^{119}Sn, Mossbauer study 80−71260
$Cr_{1-x}Mn_xSi_2$, semicond. props. 78−79992
CrN-MnN, rhombic distortion of cryst. lattice at low temp. 78−2253
CrN-MnN, synthesis and props. 77−40405
$(Cr(NH_3)_6)[MnCl_5(H_2O)]$, X-ray cryst. struct. anal. 79−4285
$CsBr:MnO_4^{2-}$, optical and vibronic spectra 79−65909
$CsI:MnO_4^{2-}$, multiple-order Raman scatt., and absorpt. spectra 77−40229
$CsMnBr_3$, triang. antiferromagnet, spin wave theory 79−7978
$CsMnBr_3:Nd^{3+}$, nearly 1-dimens. cryst., emission spectrum, extensive energy transfer 79−15516
$CsMnBr_3.2D_2O$, extended scaling in spin flop system 79−73737
$CsMnBr_3.2D_2O$, mag. phase diagram near bicrit. point 79−15302
$CsMnBr_3.2D_2O$, spin-flop systems, neutron scatt. expts. 79−61109
$CsMnBr_3.2D_20$, spin-flop system, extended scaling near bicrit. pt. 79−51752
$CsMnCl_3$, antiferromagnetic resonance, parametric spin wave excitation *(Russian)* 80−93183
$CsMnCl_3$, mag. anisotropy measurement 79−11310
$CsMnCl_3(Br_3)$, rare earth doped, energy transfer, emission spectra obs. 80−20684
$CsMnCl_3.2H_2O$, antiferromag. resonance and two-magnon absorpt. *(Russian)* 77−81014
$CsMnCl_3.2H_2O$, antiferromag. reson. and two-magnon absorpt. 79−61234
$CsMnCl_3.2H_2O$, diagonal elastic const., thermal expansion coeffs., ultrasonic velocity meas. 80−79853
$CsMnCl_3.2H_2O$, quasi-one-dimensional antiferromag., luminesc. enhancement in mag. field *(Russian)* 79−91487
$CsMnCl_3.2H_2O$, quasi-one-dimensional antiferromag., phase diagram *(French)* 80−20405
$CsMnCl_3.2H_2O$, subthreshold two-magnon absorpt., depend. on freq., temp. and mag. field, exchange coupling const. *(Russian)* 80−71184
$CsMnCl_3.2H_2O:Cu(Co)$, quasi one-dimens. antiferromag., mag. impurity effect on Neel temp. and spin-flop field 79−61099
$CsMn_{1-x}Co_xCl_2H_2O$, random mag. mixture, oblique-antiferromag. phase obs. 80−93142
$CsMn_{1-x}Co_xCl_3.2H_2O$, impure Heisenberg linear chain, EPR meas. 78−43634
$CsMnF_3$, antiferromagnet, struct. with compensated magnetisation in non-collinear phase *(Russian)* 78−88095
$CsMnF_3$, exciton migration, excitation and luminesc. study *(Russian)* 80−66264
$CsMnF_3$, mag. phase boundaries, XY to Ising crossover, virtual bicritical point 80−50095
$CsMnF_3$, NMR saturation, nuclear spin wave excitation, large freq. shifts *(Russian)* 80−50207
$CsMnF_3$, parametric nuclear magnon excitation, mag. field modulation *(Russian)* 80−107999
$CsMnF_3$, specific heat, crossover from Heisenberg to XY like behaviour 77−85461
$CsMnF_3$, spin echo form., parametric mechanism, spin dynamics *(Russian)* 78−23367
$CsMnI_3$, Mossbauer spectra, struct., electronic and mag. props. 79−91320
$CsMnI_3$, Mossbauer spectra, struct., electronic and mag. props. 80−15908
$CsMnX_3.2H_2O$ (X=Cl,Br), pseudo one-dimens. Heisenberg antiferromag., phase diagrams 79−61148
$Cs_2SiF_6:MnF_6^{2-}$, vibronic optical spectra from lattice dynamic study of Cs_2SiF_6 79−60449
Cu-Mn ferrite films, LPE growth 80−96752
Cu-Mn ferrites, heat treatment effect on props. 77−28838
CuFeCrMn spinel oxides, struct. determ., mag. states of Mn^{3+} ions *(Russian)* 78−19227
$Cu_2Mn_3O_8$, cryst. struct. *(French)* 77−58987
$Cu(OH)_2$-α-$Mn(OH)_2$, phase transition during ht. treatment 78−23659
(Fe, Mn)-V spinels, complex, oxidation, effect of Cr_2O_3, TiO_2, MgO additions 79−43453
(Fe, Mn)B and $(Fe, Mn)_2B$, lattice constants of solid solns. *(Italian)* 77−48402
$(Fe,Mn)_3C$, crystallochemical struct. *(Russian)* 77−55271
$(Fe,Mn)_5C_2$, crystallochemical struct. *(Russian)* 77−55271
$(Fe,Mn)_7C_3$, crystallochemical struct. *(Russian)* 77−55271
$(Fe,Mn)O_4$, magnetostriction calcs. *(Dutch)* 80−2619
$(Fe, Mn)O_x$, thermodynamic characts. deduced from Wustite reaction *(Italian)* 77−48401

manganese compounds continued
$(Fe,Mn)WO_4$, mixed cryst., magnetically disordered system, Mossbauer and neutron diffr. meas. 77−16225
$FeBr_2:MnBr_2$, magnon modes and impurity spin reson. 79−15501
$Fe_{1-x}M_xCl_2$, disordered, Mn spin excitations by microwave absorption at high freqs. 80−34759
$(Fe_{0.19}^{2+}Mg_{0.56}^{2+}Mn_{0.25}^{2+})[Fe_{1.87}^{3+}Al_{0.13}^{3+}]O_4^{2-}$, influence of Fe^{2+} ion substitution on electron hopping, Mossbauer study 80−71247
$(Fe_{0.55}^{2+}Mg_{0.32}^{2+}Mn_{0.03}^{2+}Cu_{0.10}^{2+})[Fe_{1.74}^{3+}Al_{0.26}^{3+}]O_4^{2-}$, influence of Fe^{2+} ion substitution on electron hopping, Mossbauer study 80−71247
FeMn hydrated oxides, ferromanganese freshwater nodules, antiferro- to speromag. order 77−70649
$Fe_{1-x}Mn_xBO_3$, synthesis, cryst. chem. and mag. props. 78−31058
$(Fe_xMn_{1-x})_3C$ in steel, X-ray K-absorpt. spectra *(Russian)* 78−6813
$Fe_{1-x}Mn_xCl_2$, disordered, Raman scatt. from Fe^{2+} and Neel temp. 80−60579
$Fe_{1-x}Mn_xCl_2$, low-lying electronic excitations in antiferromag. and paramag. phases Raman scatt. study 80−71414
$(Fe_{1-x}Mn_x)_3P$, cryst. struct. and mag. props. 78−19222
$Fe_{2-x}Mn_xP_{1-y}As_y$, band model of mag. props. 77−40029
$Fe_{2-x}Mn_xP_{1-y}As_y$, mag. props., Mossbauer obs. 77−40156
$Fe_xMn_{1-x}(1,10\text{-phenantholine})_2(NCS)_2$, spin crossover, Mossbauer and magnetism study 80−44980
FeO-MnO-SiO_2 system, melts, viscosity rel. to temp., composition *(Czech)* 79−19387
$2FeO.SiO_2$-$2MnO.SiO_2$ melt, free energy of mixing 79−61572
$2.33FeO.TiO_2$-$2.33MnO$-TiO_2 melt, free energy of mixing 79−61572
FeS-MnO melt, exam. of viscosity and self-diffusion 79−95198
FeS-MnS melt, exam. of viscosity and self-diffusion 79−95198
FeS-MnS phase relationships in presence of excess Fe 77−4768
$GaMn_3(C_{1-x}N_x)$, mag. struct., phase transition, rel. to valence instabilities in rare earth compounds *(French)* 80−34596
$Ga_{1-x}Mn_xSb$, elec. cond., mag. susceptibility, Hall const., and thermo-EMF, 80 to 1000K *(Russian)* 80−88549
Ga_2Se_3-MnSe system, crystallographic study, phase diagram, DTA and X-ray diffr. determ. *(French)* 79−24506
$(Ge,Pb)_{1-x}Mn_xTe$, mag. and elec. props. meas. 80−29534
$Ge_{1-x}Mn_xTe$, magnetic behaviour of Mn 78−14938
GeTe-MnTe, heat treatment effect on struct., elec. props. 80−54725
GeTe-MnTe-SnTe system, compds., GeTe phase transition temp., elec. props., thermal cond. 79−43220
GeTe-MuTe, temp. characts. of phase transition, MnTe influence 80−20926
$HMn(CO)_5$, mol. struct., gas phase electron diffr. expt. 78−13623
$Hg_{1-x}Mn_xS$, EPR, order-disorder transition temp. 80−50176
$Hg_{1-x}Mn_xS$, phase studies and hydrothermal synthesis 77−48333
$Hg_{1-x}Mn_xS(Se)$ solid solution, magnetic props. 79−51758
$Hg_{1-x}Mn_xSe$, band struct. from anomalous Shubnikov-de Haas effect 80−20080
$Hg_{1-x}Mn_xSe$, EPR, order-disorder transition temp. 80−50176
$Hg_{1-x}Mn_xSe$, spin-orbit coupled bands, indirect exchange interaction via electrons 80−34407
HgMnTe, interband magnetoabsorption and band struct. 79−82959
HgMnTe, semimagnetic semiconductor, band structure, transport phenomena 79−95331
$Hg_{1-x}Mn_xTe$, impurity magnetoabsorpt. 79−91473
$Hg_{1-x}Mn_xTe$, 1.7 to 3.5 eV, reflectivity spectra 78−43899
$Hg_{1-x}Mn_xTe$, acceptor reson., states in high mag. field 80−49668
$Hg_{1-x}Mn_xTe$, EPR, order-disorder transition temp. 80−50176
$Hg_{1-x}Mn_xTe$, EPR investigation of ordering effects 79−47330
$Hg_{1-x}Mn_xTe$, energy levels at Γ-point in intense mag. fields, Shubnikov-de Haas effect meas. 80−24951
$Hg_{1-x}Mn_xTe$, exchange interaction effect on $\Gamma_8 \rightarrow \Gamma_8$ magnetoabsorption 79−61351
$Hg_{1-x}Mn_xTe$, far IR interband absorption obs. 79−33696
$Hg_{1-x}Mn_xTe$, far IR studies of lattice and free carrier effects 78−39544
$Hg_{1-x}Mn_xTe$, helicon-excited ESR 79−95437
$Hg_{1-x}Mn_xTe$, indirect exchange interaction 79−61094
$Hg_{1-x}Mn_xTe$, indirect exchange interaction 80−97087
$Hg_{1-x}Mn_xTe$, mag. field induced microwave transparency 80−49797
$Hg_{1-x}Mn_xTe$, mag. props., 4.2-300K 77−4508
$Hg_{1-x}Mn_xTe$, mag. props., self-consistent two spin cluster model 80−54874
$Hg_{1-x}Mn_xTe$, mag. susceptibility, 2.3-300K 77−63074
$Hg_{1-x}Mn_xTe$, mag. susceptibility, 2.4 to 300K 80−20379
$Hg_{1-x}Mn_xTe$, magnetic behaviour of Mn 78−14938
$Hg_{1-x}Mn_xTe$, magnetooptical and impurity effects 80−6721
$Hg_{1-x}Mn_xTe$, microwave helicon propag. and helicon excited EPR 77−43637
$Hg_{1-x}Mn_xTe$ mixed crystals, zero gap, effect of exchange on interband magneto-absorption 78−23443
$Hg_{1-x}Mn_xTe$, non-parabolic zero-gap semicond., indirect exchange interaction 80−80498
n-$Hg_{1-x}Mn_xTe$, quantum transport phenomena, exchange interaction influence 78−76093
$Hg_{1-x}Mn_xTe$, semimagnetic, exchange interactions between localised and delocalised electrons 80−97245
$Hg_{1-x}Mn_xTe$, semimetallic, giant spin splitting induced by exchange interactions 77−28150
$Hg_{1-x}Mn_xTe$, Shubnikov de Haas effect and quantum oscills. of thermoelec. power 80−49781
$Hg_{1-x}Mn_xTe$, spin-orbit coupled bands, indirect exchange interaction via electrons 80−34407
$Hg_{1-x}Mn_xTe$, thermo-oscills. of magnetoresist. 79−56249
$Hg_{1-x}Mn_xTe$, transverse magnetoresistance in quantised mag. fields 80−96922
$Hg_{1-x}Mn_xTe$, zero-gap semicond., indirect-exchange interactions 80−29370
HgSe-MnSe system, phase exam., solubility limit 77−36488
HgTe-MnTe, growth from two-phase melts, crystallisation characts. 77−36393
InSb-MnSb eutectic alloy, temp. depend. of conductivity and Hall effect, field depend. of Hall coeff. 77−24566
$KBr:MnO_4^-$, many-phonon impurity reson. Raman scatt. 80−60603
$KBr:MnO_4^-$, model system, reson. Raman spectra, general behaviour obs. 80−60592
$KBr:MnO_4^-$, optical and IR absorpt. spectra, internal vibr. of MnO_4^-, freq. and type of symm. 79−15466
$KBr:MnO_4^-$, vibronic spectra interpretation 79−37770
$KCl:MnO_4^-$, Raman scatt. spectra, bands due to ν_1, vibr. of MnO_4^{2-} 79−15466

manganese compounds continued
$KCl(Br):MnO_4^-$, vibronic absorption spectra 78−10924
$KClO_4:MnO_4^-$, reson. Raman excitation profiles for totally symmetric mode, vibronic struct. 80−50309
$K_3Mn(CN)_6$, low-spin mag. studies 79−95582
$KMnCl_3$, rare earth doped, energy transfer, emission spectra obs. 80−20684
$KMn_{1-x}Co_xF_3$, Raman scatt. by mag. excitations 77−55775
$K_2Mn_{1-x}CoF_4$, mag. and neutron scatt. exam. 79−33466
$KMnF_3$, antiferromagnetic resonance in strong mag. field *(Russian)* 79−8054
$KMnF_3$, exciton and exciton-magnon emission 79−33779
$KMnF_3$, exciton line and magnon satellite in UV spectrum at high press. *(Russian)* 79−4517
$KMnF_3$ lattice parameters, temp. depend., 21°C to MP 77−76583
$KMnF_3$, luminesc., emission from localised traps 79−33777
$KMnF_3$, specific heat near Neel temp. *(Russian)* 80−100340
K_2MnF_4, 2-dimens. antiferromagnet, with dipolar broadening, spin diffusion, EPR obs. 79−38371
K_2MnF_4, quadratic layer antiferromag., field induced two magnon nuclear spin-lattice relax. 79−61258
K_2MnF_4, two-dimens. antiferromag., diffusion-controlled mode coupling, EPR linewidth 79−51844
$K_3Mn_2F_7$, two magnon Raman scatt., magnon dispersion, susceptibility, Green's function methods 80−50340
$K_3Mn_3F_7$, Heisenberg double-layer antiferromag., neutron scatt. 79−61065
$K_2Mn_{1-x}Fe_xF_4$, layered antiferromag., anisotropy effects on mag. ordering, neutron diffr. study 79−47254
$K_2Mn_{1-x}Fe_xF_4$, mag. and neutron scatt. exam. 79−33466
$K_2Mn_{1-x}Fe_xF_4$, tetracrit. line in x-H-T phase diagram, neutron scatt. exam. 78−47977
$K_2Mn_xM_{1-x}F_4$, (M=Mg,Zn,Cd), 2-dimens. antiferromag., sidebands on EPR lines 78−56370
$K_2Mn_cMg_{1-c}F_4$, EPR spectra 78−76298
$K_2Mn_cMg_{1-c}F_4$, impurities effect on EPR spectra 79−91283
K_xMnO_2, layer struct. elec. cond. props. *(French)* 78−26542
$K_2MnP_2O_7.3H_2O$, physicochem. characts. 77−39562
$K_2Mn_2(SO_4)_3$, cubic langbeinite struct., low temp. mag. susceptibility 78−56299
$K_2Mn_2(SO_4)_3$, optical and dielectric props. 79−11403
$K_2Mn_2(SO_4)_3$, phase transition, X-ray diffr. study of high and low temp. phases 78−38832
$K_2Mn_2(SO_4)_3$, phase transition press. effect, dielectric const. meas. 79−37834
$KMn_{0.18}Zn_{0.82}F_3$, excitation of Mn^+ clusters, neutron scatt. 78−68200
$K_2Mn_5[Si_{12}O_{30}].H_2O$, synthetic Mn milarite, cryst. struct. 78−18618
$K_3SO_4:MnO_4^{2-}$, electronic struct. by ESR 80−44906
$K(Zn,Mn,Co)F_3$, crysts., Mn, Co distrib., as function of cryst. region *(German)* 78−14375
$LaNi_5H_6$ sponges, Mn substitution, neutron diffr. 80−24427
$LaNi_{1-x}Mn_xO_3$, ^{55}Mn NMR study, magnetisation meas., ferromag. and Pauli paramag. components 80−7191
La_2O_3-Mn_2O_3-Cr_2O_3, synthesis and properties of solid solutions 78−44038
$Li_{0.5}Fe_{2.5}O_4$-$CuFe_2O_4$-$MnFe_2O_4$, structural characteristics and mag. props. of solid solutions 77−35696
$LiMnCrF_6$, ferrimagnetic, magnetic props. *(French)* 79−1668
LiMnSc ferrites, role of intergranular microstresses in control of coercive force 77−20640
$Li_xMn_{1-x}Se$, anomalies obs. in mag. and elec. props. 77−69509
LiMnZn ferrites, elementary coupling energy to lattice of Mn^{3+} ions, depend. on T_c 77−69534
Mg-Cu-Mn-Ni-Fe-O, UHF ferrites, synthesis, physicochem. state, mag. and dielec. parameters 79−11536
Mg-Mn ferrite, finely divided, synthesis 77−28773
Mg-MnO_2, short-circuited cell, use as portable heater 79−61964
$MgF_2:Co^{2+}$, MCD and linear dichroism, 3d→4s transitions 79−56768
$(MgFe_2O_4)_{1-y}(Mn_3O_4)_y$, polycrystalline, coercive forces 78−39366
$(MgFe_2O_4)_{x-1}(Mn_3O_4)_x$, soft ferrite, squareness ratio and max. induction 79−99730
MgMn ferrite, electrical cond., thermoelectricity, magnetoresistance meas. 78−19039
MgMn ferrite, mag. noise features at low temps. *(Russian)* 78−27060
MgMn ferrite, reaction during ferrite form. X-ray phase and mag. anal., contact volt. amperometry 77−21068
MgMn ferrite CVD epitaxial layers, bubble domains in remanence and demagnetised states 77−85516
MgMn ferrite film, magnetostriction const., mag. saturation, and internal stresses, ferromag. reson. determ. *(Russian)* 77−16126
$Mg_{0.8}Mn_{0.2}Fe_{1.8}Al_{0.2}O_4$, grade 6SChl ferrite, milling conditions effect on fine cryst. struct. and activity 79−24483
$MgMn_2O_4$, formation in phase transition during ht. treatment of $Mg(OH)_2$-α-$Mn(OH)_2$ 78−23659
Mg_6MnO_8, EPR in magnesium-manganese spinel *(Russian)* 78−91936
$Mg_{1-x}Mn_xTe_2$, random dil. antiferromagnet, mag. props. 80−54870
MgMnZn ferrite, ultrafine powder, prod. by cryochemical, freeze drying, spray drying or soln. techniques 80−55336
MgO ceramics fireproof, direct energy conversion appl. *(Czech)* 79−70455
MgO, dipolar magnetostatic energy calc. 79−18323
$Mg(OH)_2$-α-$Mn(OH)_2$, phase transition during ht. treatment 78−23659
(Mn,Cd)Cr_2S_4 and (Mn,Cd)S solid soln., equilib. composition *(German)* 77−36486
(Mn,Co)Cr_2S_4 and (Mn,Co)S solid soln., equilib. composition *(German)* 77−36486
(Mn,Co)O⇌(Mn,Co)Al_2O_4, and (Mn,Co)O⇌(Mn,Co)Cr_2O_4, ion exchange equilib., 1100°C 77−32566
(Mn,Mg)$Mg(OH)_2[ZnSiO_4]$, herstmannite, comparison with $Ca[ZnSiO_4].H_2O$, clinohedrite 79−19228
(Mn,Ni,Zn) ferrite single cryst., flame fusion cryst. growth, conc. change 77−77369
(Mn,Zn)Cr_2S_4 and (Mn,Zn)S solid soln., equilib. composition *(German)* 77−36486
(Mn,Zn)Fe_2O_4:Si, Ca, Ti, second phase effect on elec. and mag. props. 80−60986
Mn bi-univalent cpds., soln., activity and osmotic coeffs., H_2O activity, Gibbs energy, molality depend. 80−51964
Mn complex, $[Mn(urea)_6](UO_4)_2$, thermal expansion coeff., crystal field parameters, phosphoresc., absorv., excitation spectra 78−43932
manganese compounds continued
Mn complex, manganese (II)(1,2,4-triazole)$_2(NCS)_2$, 2-dimens. Heisenberg antiferromag., mag. props. 78−72336
Mn complex, Mn amine, luminesc. spectra *(French)* 79−51997
Mn complex, $MnCl_2$ with 3,5-lutidine hydrochloride, cryst., luminesc. 77−52153
Mn complex, $MnCl_2$.3,5-lutidene hydrochloride complex, photoluminesc. and photoexcitation 78−92106
Mn complex, $Mn(SCN)_2(C_2H_5OH)_2$, two-dimens. Heisenberg magnet, cryst. struct. and mag. props. 79−60337
Mn complex, papaverine hydrochloride with $MnCl_2$, cryst., luminesc. 77−55812
Mn complex, with 1,2,4-triazole, mag. susceptibility, 2-300K struct. 77−77045
Mn complex, with 4-benzylpyridine hydrochloride, photoluminesc. props. 80−89044
Mn complexes, verification of laws of luminesc. of solids 78−60506
Mn complexes, with pyridine, excitation luminesc., ligand field effect 77−48213
Mn complexes in solution, hyperfine linewidth in EPR spectra 78−91937
Mn II complex with amino acids and peptides in D_2O, NMR line widening 77−56328
Mn III chloro complexes, IR and Raman vibr. spectra 77−68038
Mn minerals, photoluminesc. 79−95829
Mn salt, ion solvation enthalpies in various solvents *(French)* 79−69264
Mn $TiRO_5$, R=Pr,Nd,Sm,Eu,Gd,covalency contribs. to Mossbauer spectra 78−10808
Mn/MnO, relative chemical potential of oxygen *(German)* 78−31642
Mn-B system, microhardness and phase analytical studies 79−24502
Mn-C, activity determ. by vapour press. meas. *(Japanese)* 77−63631
Mn-C_2H_2 and Mn-C_2H_4, π-bonded, pot. energy curves, SCF calc. 78−75136
Mn-Fe-O ferrite system, thermodynamic stability, dissociation and phase relations *(Japanese)* 80−55378
Mn-Ge, thermophysical props., at elevated temp. 80−103493
Mn-H, hydride formation in high press. range 80−65235
Mn-MnS-FeS-Fe reciprocal system, interaction between three liq. miscibility gaps 77−7865
Mn-S-O system, sulphate and sulphide reaction equilibria 77−52640
Mn-S-O system, sulphide-sulphate equil., solid state EMF obs. 79−83492
Mn-Si, liq. alloys, equilibria between MnO-SiO_2-CaO-MgO slags 80−10639
Mn-Si intermetallides, melt struct. rel. to growth mechanism 77−84681
Mn-Si-O, phase equilibrium *(Russian)* 77−66630
Mn-W-O system, phase relations in dioxide-trioxide region, 1373K 78−11212
Mn-Zn ferrite, domain struct. and initial permeability, effect of O nonstoichiometry 78−35001
Mn-Zn ferrite, extraordinary Hall effect 79−51615
Mn-Zn ferrite, oxidation-reduction equilib. and struct. defects 77−20189
Mn-Zn ferrite powder, spray dried calcination 77−12558
Mn-Zn ferrites, grain boundary exam. using TEM and AES 80−107268
Mn-Zn ferrites, mag. parameters, determ. from RF susceptibility 79−82769
Mn-Zn ferrites, permittivity anal. and meas. *(Russian)* 79−15391
Mn-Zn ferrites, single-crystal, machining effect obs., on magnetisation curves *(Japanese)* 77−21295
Mn-Zn ferrospinels, carrier transfer phenomena 80−54727
Mn-ZnF_2, crit. neutron scatt. 78−52249
$Mn_3Al_2Ge_3O_{12}$, garnet, mag. ordering, neutron diffr. patterns 78−19220
$Mn_3Al_2(SiO_4)_3$, Mossbauer spectra and absorpt. bands 80−55144
$Mn_3Al_2Si_3O_{12}$, amorphous, spin-glass, insulating, Mn^{2+} mag. reson. 80−65918
MnAs, estimation of ionic states through neutron form factor meas. 77−63115
MnAs, formation of nuclei in ferromag. paramag. transition, thermal hysteresis 79−73720
MnAs, generalised P-T phase diagram, mag. and structural phase transition 80−39780
MnAs in suspension, ferromagnetic colloid, optical meas. 78−10906
MnAs, optical props., 0.3-14 eV 77−52122
MnAs, orthorhombic, low temp. magnetic transitions *(Russian)* 80−11193
MnAs, PTH phase diagram of mag. transitions, Curie point 80−44832
MnAs pseudocrystals, magnetostriction, anisotropy 77−4537
MnAs, second-order phase transition, elastic anomalies 79−10908
MnAs, single cryst. whiskers, morphology and cryst. orientation, SEM and X-ray diffr. study 79−60664
MnAs, struct. and mag. props., temp. depend., neutron study 79−47246
Mn_2As-Mn_2Sb, structural and magnetic props. determ. 78−76248
$MnAs_{0.85}P_{0.15}$, optical props., 0.3-14 eV 77−52122
$MnAs_{0.88}P_{0.12}$, excitonic absorpt., derivative refl. spectra 80−25406
$MnAs_{0.925}P_{0.075}$, estimation of ionic states through neutron form factor meas. 77−63115
$MnAs_{0.95}P_{0.05}$, anisotropy of elec. cond. and Hall effect 80−92908
$MnAs_{0.96}P_{0.04}$, latent ferromagnetism 80−11197
$MnAs_{1-x}P_x$, double exchange ferromag. coupling, magnetisation meas. 80−75751
$MnAs_{1-x}P_x$, high spin-low spin transition 77−20591
$MnAs_{1-x}P_x$, low temp. resistivity minimum 77−8122
$MnAs_{1-x}P_x$, mag. and crystallographic anal. 79−47257
$MnAs_{1-x}P_x$, mag. susceptibility anomaly at displacive phase transition 80−93091
$MnAs_{1-x}P_x$ mixed crystals, metallic magnetically ordered, Hall effect 80−65536
$MnAs_{1-x}P_x$ whiskers, thermoelectric power, 5 to 350K, phonon drag effects and mag. transitions 79−28363
$MnAs_{1-x}Sb_x$, mag. and crystallographic anal. 79−47257
MnB, NMR of ^{55}Mn 77−28468
MnB_{12}, growth from melt and phys. props. 80−20782
MnB_2, polycryst., magnetoresist. and mag. props. *(Russian)* 80−92907
Mn_3B_4, Hall effect temp. depend. mag. struct. effects *(Russian)* 77−51764
$Mn_3(BO_3)_2$, synthetic jimboite, X-ray cryst. struct. determ. 79−42035
$Mn_3B_7O_{13}Cl$ improper ferroelec., orthorhombic phase, Raman spectrum, lattice vibrs. 78−43849
MnBi holographic film, reduction of thermomag. recording energy threshold *(Russian)* 80−43302
MnBi magnetic film, method for recording holograms of diffusely scattering objects 78−74862

manganese compounds continued
MnBi, problems for holographic recording *(Russian)* 80−91761
$MnBr_2$, mag. phase diagram, optical absorption meas. 77−4514
$MnBr_2$, vibr. struct. in cryst. field electronic transitions 78−59895
$MnBr_2$, XPS, satellite of Br 4s line 78−56556
$MnBr_2$-pyridine(piperidine)-HBr complexes, excitation spectra, ligand field theory 77−27103
$Mn(Br_{1-x}Cl_x)_2 4H_2O$, antiferromagnetism, controllable anisotropy 80−93116
$MnBr_2.4H_2O$, high-resolution sp. ht. meas. near Neel temp. 77−28393
$Mn_{23}C_6$, solid-state ^{13}C NMR spectra 79−24220
Mn_3C, Mn_5C_2, $Mn_{15}C_4$, Mn_7C_3 and $Mn_{23}C_6$, mag. susceptibility temp. depend. 79−51754
Mn_5C_2, enthalpy of formation at 1320K, from enthalpy of soln. expts. 78−59945
$Mn(CN)_3.(H_2O)_{0.57}$, mag. interactions, theory 80−97085
$MnCO_3$, antiferromag., relax. of nuclear spin waves, temp. and wave vector depend. *(Russian)* 77−90042
$MnCO_3$, antiferromag. reson. linewidth due to relax. processes 77−24750
$Mn(CO)_3$, bond angles, hybrid bond orbital calcs. 78−94188
$MnCO_3$ crystals, gel. grown, Ca^{2+}, Ni^{2+} impurity influence, SEM study 80−20778
$MnCO_3$, NMR saturation, nuclear spin wave excitation, large freq. shifts *(Russian)* 80−50207
$MnCO_3$, new types of nuclear spin echo, single pulse and parametric echo 77−69726
$MnCO_3$, nuclear spin waves from antiferromag. reson. line temp. depend. *(Russian)* 78−48050
$MnCO_3$, parametric excitation of magnons, effect of RF modulation of mag. field 80−65842
$MnCO_3$, parametrically excited antiferromagnetic, possible maser effect 78−48051
$MnCO_3$, point-dipole theory and optical birefringence 79−73896
$MnCO_3$, RF modulation effect on parallel microwave pumping threshold *(Russian)* 80−29628
$MnCO_3$, single-pulse nuclear spin echo shaping of ^{55}Mn 77−32290
$MnCO_3$, spin echo form., parametric mechanism, spin dynamics *(Russian)* 78−23367
$MnCO_3$, spin wave spectrum obs., review 80−50081
$MnCO_3$, spin waves excitation 79−82772
$MnCO_3$, weak ferromag., antiferromag. reson., phenomenological theory 78−60339
$Mn_2(CO)_{10}$, extended CNDO calc. 80−918
$Mn(CO)_5Br$, ν(CO) region, IR and Raman spectra in organic solvents 79−41169
$Mn(^{12}CO)_{5-y}(^{13}CO)_yX$(X=Cl, Br), $0<y<5$, vibr. spectra in the 2000 cm^{-1} region of mixed and isotopic crystals 78−84585
$Mn(CO)_5Cl(Br)(I)$, thermodynamic props. tabulation 79−24808
$Mn(CO)_4(NO)$, appl. of HF and CI calcs. 80−9513
$(Mn_2(CO)_8\{GeMn(CO)_5I\}_2)$, X-ray cryst. struct. determ. 80−54190
$Mn(C0)_5$ Br-Re$(C0)_5$Br, polycryst., ν(C0) vibr. intermol. Raman intensity transfer 80−60564
$Mn_xCd_{1-x}(NH_3)_2.Ni(CN)_4.2C_6H_6$, Hofmann type mixed cryst., mag. props. 79−4659
$Mn_xCd_{1-x}Se$ single crysts., photoluminesc., composition depend. 80−80854
$Mn_xCd_{1-x}Te$, far IR refl. spectra, phonon spectra 78−52497
$Mn_xCd_{1-x}Te$, lattice vibrs., Raman and IR spectra meas. 80−93311
$Mn_xCd_{1-x}Te$, phonons, Raman scatt. and IR absorpt. meas. *(French)* 80−97275
$MnCl_2$, aq. soln., thermomagnetic convection, in transverse flow round cylinder *(Russian)* 77−47100
$MnCl_2$, cryst., self-consistent band struct., intersecting spheres model 80−75505
$MnCl_2$, EPR and NMR, solid and liq. states, 300-1450K 77−73077
$MnCl_2$, EXAFS amplitudes, many-body effects 80−97379
$MnCl_2$, energy spectrum of valence electrons, X-ray emission spectra 77−16430
$MnCl_2$, enthalpy calc. for solid and liq. phases 77−43349
$MnCl_2$ in soln., luminesc., strong vibronic coupling 79−65922
$MnCl_2$, lattice dynamics, density of states and sp. ht. calc. 80−92624
$MnCl_2$, mag. phase diagram, optical absorption meas. 77−4514
$MnCl_2$, molten, struct. anal. by X-ray diffr. 78−63661
$MnCl_2$ vapour laser, output spectrum as function of excitation conditions 79−68387
$MnCl_2$, vibr. struct. in cryst. field electronic transitions 78−59895
$MnCl_2$:Co^{2+} polarised IR absorpt. spectra 77−40269
$MnCl_2$-He discharge, cataphoretic Mn discharge 77−31092
$MnCl_2$-inert gas laser, energy charact. *(Russian)* 77−665
$MnCl_2$-KCl system, molten, EPR spectra, linewidth study 78−88173
$MnCl_2$-lutidine HCl complex, photoexcitation, photoluminesc. 78−27301
$MnCl_2$-tetra-n-butylammonium halide melts, density, elec. cond., and viscosity 80−24631
$MnCl_4$, fine struct. of Mn^{2+} lines 79−33780
$MnCl_4^{2-}$, electronic energy levels calc. by conventional and X alpha Hartree-Fock methods 78−66470
$MnCl_4^{2-}$ is approx. trigonal symmetry in organic cpds., EPR of Mn^{2+}, zero-field splittings and site distortions 79−56607
$MnCl_2(Br_2)(I_2)$, prep. using chem. transport via gas complexes *(German)* 79−15599
$Mn(ClO_4)_2/NaClO_4$ in aq. soln., interaction between Mn^{2+} and ClO_4^-, NMR studies 80−71212
$Mn(ClO_4)_2.6H_2O$-polyacrylonitrile, complex permitt. meas. by time-domain spectroscopy 77−49741
$MnCl_2.2ACl$, (A=Li, Na, K, Rb, Cs), melts, Raman spectra of $MnCl_4^{2-}$ ion 79−24310
$MnCl_2.2H_2O$, magnetically ordered phase, $^6A_{1g}$ to $^4T_{2g}$ transition absorpt. lines, Zeeman effects 78−6699
$MnCl_2.2H_2O$, magnetisation and mag. resonance 79−11349
$MnCl_2.2H_2O$, ordered, paramag. phases, optical absorpt. spectra, V-lines, Zeeman effects 78−6698
$MnCl_2.2H_2O$, paramag. phase, external mag. field depend. of $^4T_{2g}$(II) Kramer doublets of Mn^{2+} 78−6700
$MnCl_2.2H_2O$, phonons and electronic transitions, Raman spectra 79−28761
$MnCl_2.2H_2O$, Raman spectra and lattice dynamics 79−28742
$MnCl_2.2H_2O$, wagging and rocking band intensities of water 78−27200
$MnCl_2.4H_2O$, antiferromagnet, symm. of field-induced phases, mag. space groups 77−32166
$MnCl_2.4H_2O$, antiferromag., magnetic and thermal props. 78−14937
$MnCl_2.4H_2O$, antiferromagn., nucl. orientation 78−43652

manganese compounds continued
$MnCl_2.4H_2O$, antiferromag., low temp. thermal cond. 80−65320
$MnCl_2.4H_2O$, biaxial antiferromag., bicritical region, sp. ht. meas. 78−68246
α-$MnCl_2.4H_2O$, crossover from divergent to non-divergent nature of paramag. transition 79−73735
$MnCl_2.4H_2O$, isothermal and adiabatic susceptibilities near field depend. anitferromag. phase transitions 77−69561
$MnCl_2.4H_2O$, single cryst., mag. phases, obs. by ^{54}Mn nucl. polarisation 77−81031
$MnCl_2.6NH_3.MnCl_2.2NH_3$, solar energy storage system heating and cooling 80−81484
$MnCo_3$, parametric nuclear magnon excitation, mag. field modulation *(Russian)* 80−107999
$Mn_3(Co(CN)_6)_2.xH_2O$, mol. vibr. in cryst., normal mode anal., Raman and IR obs. 77−76494
$Mn_{0.27}Co_{0.73}Cl_2.6H_2O$, antiferromag., sp. ht. meas., phase transition obs. 79−78415
$Mn_{1-x}Co_xF_2$, Raman scatt. by mag. excitations 77−55775
$Mn_xCo_yNi_zO_4$, spinel ceramic, current noise in thermistor bolometer 77−51793
$MnCo_2O_4$ DC sputtered films, struct. and elec. props. 80−54812
$MnCo_2O_4$ spinel, synthesis, effect of Bi_2O_3 admixture upon props., thermistor appl. 78−15325
$Mn_{1-x}Co_xSb$, ferromagnetic, NMR exam. 79−24228
$Mn_{1-y}Cr_yAs$, double exchange ferromag. coupling, magnetisation meas. 80−75751
$MnCrF_5$, antiferromag., mag. struct. *(French)* 78−52211
$MnCrF_5$, cryst. struct. *(French)* 77−47403
$Mn_3Cr_2Ge_3O_{12}$ garnet, antiferromag. ordering *(Russian)* 78−80146
$Mn_3Cr_2Ge_3O_{12}$, magnetically ordered Mn^{2+} and Cr^{3+} ions *(Russian)* 77−8281
$Mn_{1+x}Cr_{2-x}O_4$, noncollinear ferrimagnets, induced anisotropy 77−73022
$Mn_{2.5}Cr_{0.5}O_4$, mag. struct., neutron diffr. obs. 79−33460
$Mn_xCr_{3-x}O_4$, cubic and tetragonal structs., neutron diffr. obs. 79−19369
$Mn_xCr_{3-x}O_4$, dilute Jahn-Teller system, simple model 80−44547
$Mn_xCr_{3-x}O_4$, mag. struct. determ. by neutron diffr. 77−40035
$Mn_xCr_{3-x}O_4$ spinels, miscibility gap boundaries, annealing expts. 77−86012
$Mn_{1-x}Cr_xP$, mag. susceptibility and transitions 79−47256
$MnCr_2S_4$, mag. struct. under applied mag. field 80−97065
$MnCr_2S_4$, substituted, mag. struct. and transitions 80−65795
$MnCr_2S_4$, thermal stability, thermochemical, thermodynamic and crystallochemical props. of chalcogenide spinels 77−51519
$Mn_{1.88}Cr_{0.12}Sb$, magnetic phase transition effect on magnon renormalisation 77−59405
$Mn_{2-x}Cr_xSb$, sintered, intrinsic coercivity 77−89983
$MnCr_2Te_4$, elec. props., 100 to 650K *(Russian)* 79−11115
$MnCr_{2-x}V_xS_4$, mag. struct., Yafet-Kittel to Neel ferrimagnet transition temp. 77−66264
$Mn_{1-x}Cu_xCr_2S_4$, phase relationships and mag. phase diagram 79−78374
MnD_x, synthesized at high pressures, neutron diff. anal. of struct. 80−28977
$MnEr_2S_4$, magnetisation and susceptibility, exchange interactions obs. 78−52242
MnF, MnF_2, EPR, in inert gas matrices, high spin mag. parameters, level diagrams 78−66565
$Mn^{2+}F^-$ and $Mn^{2+}F^-Mn^{2+}$ systems, transferred hyperfine interaction at F^- site 80−70657
MnF_2, ATR spectra and surface EM wave dispersion anisotropic case 77−77215
MnF_2, absolute first order Raman polarisabilities 78−64369
MnF_2, antiferromag., magnetocryst. anisotropy, susceptibility, static torque meas. 77−69545
MnF_2 antiferromag., mag. space groups, Clebsch-Gordan coeff. calcs. 80−79731
MnF_2, antiferromag., multi-magnon luminesc. sidebands 78−76525
MnF_2, antiferromag. and piezomag. domain struct., neutron topography study 80−71088
MnF_2, antiferromag. domains, obs. using neutron technique 78−64213
MnF_2, antiferromag. polaritons, dispersion relation and light scatt. calcs. 77−35871
MnF_2, antiferromag. reson. relax., multimagnon processes 77−4564
MnF_2, antiferromagnetic phase stability limit near spin-flop boundary 78−10683
MnF_2, biexciton decay, time resolved laser spectra 78−75999
MnF_2, Cotton-Mouton Voigt effect using microwave polarimeter *(French)* 78−74040
MnF_2, d-orbital directed photoemission using AlK_α radiation 79−95901
MnF_2, EM and acoustic energy attenuation in domain magnets 80−7140
MnF_2, EPR and NMR, solid and liq. states, 300-1450K 77−73077
MnF_2, elastic constant determ. by US pulse echo overlap 79−14874
MnF_2, fluorescence props. 79−73994
MnF_2, heat capacity and entropy, 10 to 300K, mag. ordering contrib. 77−16080
MnF_2, heat transport by magnons, effect of magnon-phonon thermal relax., calc. 77−39705
MnF_2, Heisenberg antiferromag., props. calc. 77−85406
MnF_2, Heisenberg system, ordered phase, reaction field approx., anisotropy presence 79−61030
MnF_2, high temp. polymorphism and thermal props. 80−75199
MnF_2 in Ar matr-x, X-band ESR spectra, extra line assignment 79−81218
MnF_2, inelastic light scatt. from antiferromag. polaritons, theory 77−73144
MnF_2 lattice parameters, temp. depend., 21°C to MP 77−76583
MnF_2, local mag. ordering above Neel point, EPR *(German)* 77−36125
MnF_2, MCD spectrum, Zeeman splitting of purely excitonic lines 77−40262
MnF_2, macroscopic quadrupole field meas. with SQUID magnetometer, order determ. 79−24140
MnF_2, mag. anisotropy at OK 79−33473
MnF_2, mag. susceptibility, crit. behaviour near Neel point 79−91217
MnF_2, magnetic, thermal, elastic refraction of light, mag. order influence on refractive index *(Russian)* 80−34880
MnF_2, magnon-photon interaction for EM wave vector perpendicular to sublattice magnetisation 79−69662
MnF_2, molten, superexchange, EPR linewidth 79−19774
MnF_2, nuclear spin lattice relax. exam. 78−76331
MnF_2, nuclear spin-lattice relax. and magnon lifetime near spin-flop transition 77−69721

manganese compounds continued
MnF_2, one-magnon luminesc. sidebands of excitonic transition 78−60517
MnF_2, parallel pumping studies of magnon damping 80−70990
MnF_2, piezo-optical effect, birefringence variation on uniaxial compression *(Russian)* 80−34887
MnF_2, radiation damage, energy transfer, radiolysis, effect of defect centres 78−2161
MnF_2, Raman spectra, cross section determ. 78−56471
MnF_2, reson. NMR near phase transition 78−76265
MnF_2, resonant phonon-magnon scatt., phonon spectroscopy obs. 79−65150
MnF_2, rutile type, polymorphism at high press., distorted fluorite phase 79−69050
MnF_2, SCF-Xα MO calcs. of core photoelectron shake-up satellites 77−20991
MnF_2, solid and molten paramag., high-temp. EPR linewidth meas. 77−4548
MnF_2, specific heat, Heisenberg to Ising crossover near Neel temp. 78−47980
MnF_2 spheres, magnetostatic modes in antiferromag. reson. 77−1599
MnF_2 spin wave lifetime, theory compared with expt. 80−60228
MnF_2, spin waves, light scatt. lineshape 78−23476
MnF_2, spin-flop bicritical point, susceptibility and RF absorpt. meas. 79−87277
MnF_2, spin-flop transition obs. by neutron diffr. 79−73734
MnF_2, surface spin-flop and antiferromag. spin-flop transition 78−52257
MnF_2, thermal cond., mag. field effects, magnon contrib. 78−38890
MnF_2, thermal cond., temp. depend., role of reson. scatt. of phonons by OH^- defects 78−38889
MnF_2, two-exciton light absorption, with four-photon excitation *(Russian)* 78−35186
MnF_2, two-exciton many photon absorption, effect of statistical props. of light on intensity *(Russian)* 78−95589
MnF_2, two-magnon Raman scatt., temp. effects 77−48179
MnF_2, two-spin light scattering, disordered phase rutile antiferromags. 78−80336
MnF_2, uniaxial antiferromag. anisotropy in paramag. susceptibility, cluster variation theory 78−52200
MnF_2, valence-electron density of states, XPS meas. 77−69963
MnF_2, X-ray diffr. investig. of high-press. polymorphism 77−43324
MnF_2, zero-field splitting of Mn^{2+}, appl. of complete d-electron calc. 77−15799
MnF_2:^{111}Cd, hyperfine fields, PAC meas. 77−48104
MnF_2:Eu^{3+}(Er^{3+}), fluorescence props. 79−73994
MnF_2:Fe^{2+}, temp. depend. of magnon pair-mode energies, Raman scatt. meas. 77−20577
MnF_2:LiF, anelastic relax. of Li^+-Li^+ split interstitial defect 79−77678
MnF_2:Ni^{2+}, IR fluoresc., field depend., exchange energy 78−68543
MnF_2:Zn, shift and broadening of optical transitions 79−38579
MnF_6^{2-}, $A_2^{I}M^{IV}F_6$ hosts, luminesc., IR and Raman spectra, 5K, assignments 77−20904
Mn_4F, non-collinear component in mag. struct. 80−25089
MnFe ferrite, mechanically induced anisotropy, effect on mag. permeability 78−47970
MnFe ferrites, reson., effect of EM propagation 78−64277
$Mn_{1-x}Fe_xCr_2S_4$, Fe II electronic struct., Mossbauer spectra 80−15876
$MnFe_{2-x}In_xO_4$, magnetic props., In substitution effects *(Russian)* 78−91849
$MnFeO_2$:^{55}Mn, NMR freq. dynamical shift for nuclei in domain walls *(Russian)* 77−40148
$MnFeO_4$:^{57}Co, Mossbauer spectrum, 4s covalent bonding 80−20540
$MnFe_2O_3$, superexchange interactions, three-sublattice anal. 79−61095
$MnFe_2O_4$, additional spin echo of ^{55}Mn nuclei 80−60455
$MnFe_2O_4$, discontinuous growth, effect of equilib. segreg. at boundaries 77−51336
$MnFe_2O_4$, exchange splitting of ionic S-state, neutron spectra 78−52240
$MnFe_2O_4$, ferrite, dynamic shift of NMR freq. of nuclei located in domain walls 80−15823
$MnFe_2O_4$ film, bulk and surface spin waves, spin wave reson. expts. 79−73826
$MnFe_2O_4$ magnetic moments and high field susceptibilities, spin model 77−28376
$MnFe_2O_4$, nuclear reson. and relax. from domains and domain walls 77−8448
$MnFe_2O_4$, prep. by double decomp. reaction, mag. charact. *(French)* 79−33463
$MnFe_2O_4$, valence states, NMR investig. *(Czech)* 78−72420
$MnFe_2O_4$, valency states, NMR 77−51987
$MnFe_2O_4$:Sn, hyperfine mag. fields at ^{119}Sn and ^{57}Fe nuclei, influence of press. 79−99811
$Mn_{0.82}Fe_{2.18}O_4$, anelasticity, 280 to 730K, 125 kHz vibr. study 78−87740
$Mn_{0.9}Fe_{2.1}O_4$, low resistivity ferrite cylinder, FMR absorp. 79−1718
$Mn_{1-x}Fe_{2+x}O_{4+\delta}$, ferrites, homogeneity region, cluster component model 78−35367
$Mn_{1+x}Fe_{2-x}O_4$, magnetostriction meas., inversion degree influence 77−73070
$Mn_xFe_{3-x}O_4$, dielec. function and polar Kerr rotation, 0.5-3.6 eV 80−66221
$Mn_xFe_{3-x}O_4$ epitaxial films, mag. and reson. props. 80−50149
$Mn_xFe_{3-x}O_4$ ferrite film, exchange interaction depend. on conduction electrons *(Russian)* 80−34621
$Mn_xFe_{3-x}O_4$ film, spin wave reson., exchange const. 77−16183
$Mn_xFe_{3-x}O_4$ NMR of Mn^{3+} in B-sites 78−35061
$Mn_xFe_{3-x}O_4$, optical props. 80−20606
$y(Mn_xFe_{3-x}O_4)$-(1-y)B_2O_3 glasses, elec. and struct. props., 400-1000K 79−51575
$Mn_xFe_{3-x}O_{4+\gamma}$, average directional order, cation valency and repartition on A- and B-sites *(French)* 78−39369
$Mn_xFe_{3-x}O_{4+y}$, prep., resist., hysteresis loop and mag. disaccommodation *(Spanish)* 77−73045
$Mn_{1-x}Fe_xP$, magnetisation, susceptibility and mag. transitions 79−47256
$MnFe_2(PO_4)_2(OH)_2.6H_2O$, strunzite, cryst. chem., Mossbauer study 80−39975
$(Mn_{1-x}Fe_x)_5Si_3$, solid soln., mag. transitions sp. ht., magnetisation and thermal expansion meas. 77−16075
$(Mn_{1-x}Fe_x)_5SiC$, magnitude of quadrupole splittings, Mossbauer study 78−43747
$Mn_3Ga_{1-x}Mn_xN$, perovskite struct., phase transformations *(French)* 80−81048
manganese compounds continued
$Mn_3GaN_{1-x}C_x$, perovskite struct., phase transformations *(French)* 80−81048
$MnGa_2S_4$, synthesis electrophys. props. 77−51747
$Mn_{0.75}Ga_{2.17}S_4$, twinning and cryst. struct. determ. *(French)* 78−83798
$Mn_{0.6}Ga_{0.4}Sb$, eutectics, galvanomag. props., thermo EMF 77−15869
$MnGd_2S_4$, mag., struct. and Mossbauer effect study 78−51507
$MnGeO_3$, HP phase transform. 80−19941
MnH_2 in Ar matr-x, X-band ESR spectra, extra line assignment 79−81218
MnH_4, electronic structure, ab initio calcs. 79−89601
MnH(MnD), $^7\Sigma$-state, mol. parameters, ESR and optical spectrosc. 78−94264
$MnH_2(MnD_2)$, $^6A_1$ state, mol. parameters, ESR and optical spectrosc. 78−94264
$Mn(H_2PO_2)_2.2H_2O$, X-ray cryst. struct. determ. and refinement, heavy-atom method 79−19194
$Mn^{II}(H_2PO_4)_2.2H_2O$, cryst. and powder diffr. data *(French)* 80−24419
$MnHPO_4.3H_2O$ and $MnDPO_4.3D_2O$, IR absorpt. and Raman spectra, vibr. assignments 80−97257
$Mn_xHg_{1-x}Te$, long-wavelength optical phonons, IR refl. obs., 50-300 cm^{-1}, 90 and 295K 77−36243
MnI_2, adsorbed ^{36}Ar film on cleavage faces, layer-like charact., neutron diffr. obs. 79−86994
MnI_2, Mossbauer spectrum, electronic and mag. props. 77−32302
MnI_2, polymorphic phase changes of adsorbed NO 77−31900
MnI_2, SCF-Xα MO calcs. of core photoelectron shake-up satellites 77−20991
MnMg ferrite, products if reaction of ferrogel with $MnCl_2$ solution 77−12582
$Mn_xMg_{1-x}O$, solid solution EPR, mag. interactions *(Russian)* 80−44908
$Mn_xMg_{1-x}S$, mag. props. 77−66244
$Mn_xMg_{1-x}S$ solid solution, mag. props. 78−60269
$Mn_{1-x}Mg_xSe$, mag. and struct. phase transitions, mag. susceptibility and X-ray diffr. study 80−71022
$Mn_xMg_{1-x}Y_2S_4$, magnetisation and susceptibility, exchange interactions obs. 78−52242
$Mn^{2+}Mo^{4+}O_3$, defect spinel struct., elec. and mag. props. 80−70176
$Mn_{8-y}Mo_{3+y}Si_8$, cryst. struct. *(French)* 78−38675
$Mn_2N_{0.86}$, cryst. and mag. struct. at low temps. *(French)* 77−73003
$Mn_2N_{0.86}$, crystal struct. determ. by neutron and X-ray diffr. *(French)* 77−80461
Mn_4N, mag. struct. non-collinearity, neutron diffr. obs. 80−65796
$Mn_4N_{0.8-1}$, NMR of ^{55}Mn, reson. curve fine splitting, spin echo meas. 78−2768
Mn_4N_x, non-stoichiometric, ^{14}N NMR 79−91302
Mn_6N_5 film, cryst. struct. and phase transform. exam. by electron diffr. 78−10189
Mn_xN, metallographic exam. *(Bulgarian)* 79−100319
Mn_xN_y, prep., rate of formation, chem. stability 78−11185
$Mn(NH_3)_2Ni(CN)_4C_{12}H_{10}$, phase transition, mag. susceptibility, sp. ht. 79−91234
$Mn(NH_3)_2.Ni(CN)_4.(benzene)_2$, antiferromag. ordering, mag. susceptibility, sp. ht. and Neel temp. meas. 77−12128
MnNO, appl. of HF and CI calcs. 80−9513
$Mn(NO_3)_2$, aq. electrolyte, apparent molar heat capacity and volume, of 298.15K 79−65208
$Mn(NO_3)_2.H_2O$, cryst. struct. 77−58980
$Mn_2NaSi_3O_8(OH)$, serandite, synthesis, struct., physicochem. props. 79−43187
$Mn_{11-z}Nb_zGe_8$, cryst. struct. *(French)* 78−38675
$MnNb_2O_6$, bonding characterisation 78−38680
$MnNb_2O_6$, flux growth 77−21015
$MnNb_2O_6$, force fields rel. to cryst. struct. *(French)* 80−107104
$Mn_{0.25}NbS_2$, mag. anomaly rel. to struct. disordering 78−43557
$Mn_{0.26}NbS_2$, intercalation compound, struct. and photoemission meas. 77−16453
$Mn_{1/3}NbS_2$, intercalate, metallic cond., Hall effect and mag. props. 77−76789
$Mn(Nb_{0.5}Ta_{0.5})_2O_6$, non-uniaxial spin-flop magnet, crit. exponents, neutron diffr. meas. *(German)* 77−16086
$Mn(Nb_{0.5}Ta_{0.5})_2O_6$, nonuniaxial spin-flop magnet, bicrit. lines, crossover 78−14973
$Mn(Nb_{0.5}Ta_{0.5})_2O_6$, random and spin-flop magnet, neutron crit. scatt. 79−24169
$Mn(Nb_{0.5}Ta_{0.5})_2O_6$, spin flop magnet, four dimens. phase diagram and multicrit. phenomena 79−15304
$Mn_{3-x}Ni_xB_4$, mag. props. *(Russian)* 77−51923
$Mn_{3-x}Ni_xB_4$, with onset of spontaneous magnetisation below T_N, singularities of mag. props. *(Russian)* 77−59427
$Mn_xNi_{1-x}Cl_2.nH_2O$, antiferromag., sp. ht. meas. 79−91226
MnO, ^{19}F isomer shift, time differential PAD 77−12280
MnO (100), surface struct., LEED study 80−39396
MnO, $A^6\Sigma^+$-$X^6\Sigma^+$ electronic transition, rot. and hyperfine struct. 80−74134
MnO, absorption line shape, magnon sidebands 77−52128
MnO, alpha-particle irrad., Mossbauer study of nucl. reaction aftereffects 80−40015
MnO, antiferromag., magnon lifetime and its effect on magnon sideband 77−12106
MnO, antiferromag., temp. depend. of elastic consts., US study 80−79854
MnO, antiferromag. reson. linewidth below and above T_N 77−40133
MnO, antiferromag. reson., low freq. branch gap due to magnetoelastic interaction 77−40134
MnO, antiferromag. reson., press. depend., and magnetostriction consts. 78−19339
MnO, antiferromagnetic-paramagnetic phase transiton at high press. 80−39778
MnO based pigments, willemite struct., synthesis 80−20855
MnO, cryst., Debye characteristic temp. calcs. 79−37796
MnO, cubic antiferromag., magnon-phonon sideband in fine-struct. of optical absorption 77−59590
MnO, cubic NaCl-type cryst., Debye temp. 80−54333
MnO, dielec. behaviour, Dick and Overhauser shell model calcs. 80−45001
MnO, EPR and NMR, solid and liq. states, 300-1450K 77−73077
MnO, EPR spectra of ceramic and epitaxial monocrystalline thin film samples *(Russian)* 80−11252
MnO, ESR spectra, matrix isolated at 4K 78−33531

manganese compounds continued
MnO, elastic props. singularities near phase transition 77−16093
MnO, electron energy loss spectra exam. 78−72652
MnO, electronic cond., rel. to basic processes of Mn corrosion 77−25198
MnO, electronic struct. calc. 78−43297
MnO, ferrobimagnetic poling 77−16102
MnO, first order mag. phase transition, elastic consts. meas. 77−66316
MnO, H_2 ortho⇌para conversion on mag. surfaces 79−47969
MnO, Hall mobility of photoelectrons 77−69352
MnO, hydrated, adsorpt. of Cs and Sr radioisotopes 78−3822
MnO impurity in silicate melt, effect on elec. cond. *(Ukrainian)* 77−69104
MnO, Jahn-Teller effect on optical absorption spectra 78−52484
MnO, $K_{\beta 5}$ X-ray emission spectrum, low energy plasmon satellite A 78−2945
MnO, $K\beta_{1,3}$ X-ray emission spectra, low energy plasmon $K\beta'$ satellite 79−74020
MnO, L_l and L_η X-ray emission spectra 78−39631
MnO, lattice dynamics, coherent inelastic neutron scatt. 78−59899
MnO, lattice dynamics calc. 79−46769
MnO, lattice dynamics using three body force shell model 77−76506
MnO, lattice vibrs., phonon dispersion curves, neutron scatt. study 79−42177
MnO, linear optical anisotropy meas. at antiferromag. transition 77−36205
MnO, mag. phase transition, first-order 77−47988
MnO, magnon lifetime 77−69518
MnO, magnon-sideband lineshape, exciton-phonon interaction effects 80−65846
MnO, multidomain single cryst. and monodomain cryst., crit. and elastic behaviour, T_N to 300K 77−66407
MnO, muon probe expts. 77−63351
MnO, negative muon spin rot., paramag. shift 79−56706
MnO, neutron diffr. meas., 100 to 700K, spin correls, above and below T_N 77−59390
MnO, optical absorpt. spectra fine struct. 77−32393
MnO, paramag., μ^- spin rotation at O site 77−20785
MnO, paramag., neutron scatt., spin-wave-like excitations, obs. 78−68146
MnO, paramagnetic, positive muon longit. spin relax., temp. depend. 78−80268
MnO, positive muon spin relax. 79−56669
MnO, reduction by C, surface reactions, CO regeneration *(Russian)* 80−66772
MnO, SCF CI calcs., ground and first excited states, bonding mechanism 77−14347
MnO, two phonon density of states 77−7808
MnO, X-ray determ. of electron density distribs., atomic scatt. factors 80−15078
MnO, X-ray $K\beta$ emission spectra, unpaired electron and plasmon effects 78−19603
MnO:Mn_3O_4, mag. props., susceptibility and magnetisation meas. 80−65824
MnO:Mn^{2+}, EPR, antiparallel spin coupling above Neel point, antiferromagnetic clusters *(German)* 77−16168
MnO-Al_2O_3-SiO_2, amorphous, spin glass like behaviour at low temp. 79−61177
MnO-Al_2O_3-SiO_2, amorphous, remanent magnetisation short time depend. 80−65919
MnO-Al_2O_3-SiO_2, amorphous spin glass, AC susceptibility 80−80520
MnO-Al_2O_3-SiO_2, spin glasses, low-field susceptibility, freq. depend. 78−47981
MnO-Al_2O_3-SiO_2 glass, spin freezing, muon spin depolarisation 78−39491
MnO-Al_2O_3-SiO_2 glass, spin freezing, muon spin depolarisation, superparamag. domain model 78−68272
MnO-Al_2O_3-SiO_2 glass, optical spectra 78−68528
MnO-B_2O_3, polycryst. cpds., mag. susceptibility and ^{11}B NMR 79−8056
MnO-CdO(ZnO), solid solns. prep., struct. 78−95157
MnO-CoO-O_2, semicond. solid solns., ageing effects on elec. cond. 78−23085
MnO-H_2, interaction with surface, quantum chemical study 80−45549
MnO-MgO, EPR concentration dependence in magnetically diluted crystals with strong spin-spin interaction 79−42826
MnO-P_2O_6 system, formation of manganese phosphates 77−90331
MnO-SiO_2 melt, viscosity and polymerisation *(Russian)* 78−26712
MnO-SiO_2 slag, SiO_2 solubility and MnO activity 79−52184
MnO-SiO_2-TiO_2 melt, electrical cond. meas. and electrolytic anal. *(Japanese)* 78−38861
MnO-SiO_2-ZrO_2 molten slag system-molten steel interface, wetting angles, surface tension *(Czech)* 79−19432
MnO-ZnO-MgO-Fe_2O_3 ferrites, effect of Fe^{2+} ion on initial permeability 77−8357
MnO_2 (pyrolusite), UV irradiated, simulation of Viking gas exchange reaction on Mars 80−72831
MnO_2, activity in CaO-SiO_2-MnO ternary system, Gibbs-Schumann calc. *(Italian)* 79−20461
MnO_2, additive for activated sintering of SnO_2 77−36415
MnO_2 additive for $Pb(Zn_{1/3}Nb_{2/3})O_3$-$PbTiO_3$-$PbZrO_3$ and $Pb(Mg_{1/3}Nb_{2/3})O_3$-$PbTiO_3$-$PbZrO_3$ ceramics, HF filters appl. *(Japanese)* 80−60507
MnO_2 batteries, type LR9, cathode composition, quality effects *(Polish)* 79−52920
MnO_2 battery-grade, resistivity rel. to water content *(German)* 79−96431
MnO_2, β and γ conductivity meas. by new method 80−45517
MnO_2, catalytic graphitization of nongraphitizable C 80−97440
MnO_2, DC cond., water content depend. 77−80774
MnO_2 dispersion mode on Al_2O_3 and SiO_2 powder supports, N adsorption obs. 80−81363
MnO_2, doped, dry cell depolariser, hydrazine reduction kinetics 80−89603
MnO_2, ESR spectra, matrix isolated at 4K 78−33531
γ-MnO_2 electrode, impedance in alkaline solns. 79−70350
MnO_2, electrodeposited from hot acidic solutions, preferred crystal growth 77−81232
MnO_2, $K\beta_{1,3}$ X-ray emission spectra, low energy plasmon $K\beta'$ satellite 79−74020
MnO_2 porous powders, Al_2O_3 and SiO_2 coated, changes in surface free energy for N adsorption 80−84363
manganese compounds continued
MnO_2 powder electrical charact. obs. battery grade, highly hydrated 79−100501
β-MnO_2 powders, Hall carrier mobility mixing rule *(German)* 78−52008
MnO_2, preparation and characterisation of doped samples for appl. as dry-battery depolarisers 80−89602
MnO_2 submicron particle collection, by H_2 bubbles 78−11560
MnO_2, X-ray emission spectra, plasmon satellites 79−99985
MnO_2, X-ray $K\beta$ emission spectra, unpaired electron and plasmon effects 78−19603
MnO_2:Li(Mo)(V), Zn^{2+} ion specific adsorpt. kinetics, ^{65}Zn γ-ray scintillation investig. 80−70529
MnO_3, ESR spectra, matrix isolated at 4K 78−33531
MnO_4, aqueous soln., ^{55}Mn nuclear mag. shielding, NMR obs., O isotope exchange 77−10691
MnO_4, ESR spectra, matrix isolated at 4K 78−33531
MnO_4^-, aq. soln., O isotope substitution, ^{55}Mn NMR 77−30890
MnO_4^-, bond lengths and coordination numbers, EXAFS meas. 79−51043
MnO_4^-, electronic struct. determ. from X-ray spectra 78−86885
MnO_4^- ion, ^{18}O enriched, matrix isolated IR spectra, force consts. 80−52985
MnO_4^-, reson. Raman lines, Stokes-antiStokes intensity ratio meas. 77−6786
$(MnO_4)^-$ type ions, metal X-ray K absorption spectra, low energy maxima interpretation 79−74019
MnO_4^-, valence mol. orbital energy, nonempirical pseudopot. 79−22592
MnO_4^-, valence-shell MO calc. with pseudopot. 78−907
MnO_4^{m-} chromophore, tetrahedral, electronic spectra 77−58032
MnO_x-valve metal oxide interface, electron injection and reactions 77−76936
$Mn_{1-x}O$, single cryst. growth by skull melting 80−84844
Mn_2O_3 in Fe-containing glass-ceramics, strength 77−48380
Mn_2O_3, thermal decomposition, exam. by thermogravimetric methods 78−80743
Mn_3O_4, cryst. growth using $K_2S_2O_7$ as flux material 80−71582
Mn_3O_4 film, form. on glass surface from Mn^{2+} ions in water *(Japanese)* 80−45411
Mn_3O_4, hausmannite, tetragonal-cubic transform., X-ray anal. 80−103288
Mn_3O_4, reduction by C and CO, exam. by thermogravimetric methods 78−80743
Mn_3O_4:^{119}Sn, hyperfine field exam., Mossbauer meas. 77−69753
Mn_3O_4:Li(Cr)(Al)(S), and pure Mn_3O_4, elec. cond. and thermo-EMF 80−20231
Mn_3O_4:S, defect struct. and elec. props., electron, hole conc. 80−44601
Mn_3O_4-Co_3O_4 spinels, phase diagram anal., thermodynamic props. 80−3009
MnO_3Cl, matrix isolated species, MCD spectrosc. appls. 78−46378
$Mn_8O_{10}Cl_3$, cryst. struct., X-ray diffr. meas. *(French)* 77−47381
$Mn_8O_{10}Cl_3$, preparation and props. *(French)* 77−4086
$MnO_3F(Cl)$, He (I) photoelectron spectra, metal-ligand bonding, EHMO calc. 78−9193
$Mn(OH)SO_4.2H_2O$, cryst. struct. determ. from X-ray data, least squares refinement 79−37675
$Mn(OH_2)_6(SiF_6)$, phase transitions, spectrometric exam. *(French)* 78−88291
$(Mn_3O_4)_{1-x}(MgAl_2O_4)_x$, $0<x<1$, mixed oxide spinels, chemical shifts of Mn K-absorpt. edge 80−29828
γ-MnOOH, antiferromag., prep. and mag. props., EPR meas. 79−87310
MnOOH, α- and γ-phase, thermal decomp., 20 to 670°C 80−35521
MnOOH, mag. ordering, fine struct. and crit. behaviour, neutron diffr. meas. 80−65800
$(MnO)_nV_2O_5$, (n=1, 2, 3), elec. and mag. props. 79−78094
MnO.Al_2O_3.SiO_2, spin glass materials, mag. field dependence of susceptibility peak 80−103840
x.MnO.(1−x)[19TeO_2.PbO], glass, antiferromag. behaviour, mag. props. 80−50072
xMnO.(100−x)[19TeO_2.PbO], EPR studies of Mn^{2+} ion distribution 80−71167
MnP, and Mn_2P, enthalpy and heat capacity at high temp. 77−11704
MnP, anisotropic, ferromagnetic microwave resonance relations 80−15805
MnP, elec. resist. of different mag. phases, temp. depend. 80−54691
MnP, ferro-spiral transition, neutron scatt. studies 80−65876
MnP, high field magnetoresistance 80−107817
MnP, Lifshitz point, transverse differential susceptibility meas. 80−84599
MnP, low field magnetoresistances, mag. phase diagram purity depend. 80−107816
MnP, magnetisation and spin waves temp. depend. 79−91221
MnP, metallic, band struct., X-ray spectral obs. 78−11019
MnP, method for determ. of successive mag. struct. *(Russian)* 80−39741
MnP, noncubic ferromag., relax. times for domain and wall resonances 77−77119
MnP, sp. ht., 1.5-8.0K 79−91236
MnP, spin polarised energy band struct., electronic specific heat, APW calcs. 80−65431
MnP, US vel. and crit. attenuation, longit. waves, external mag. field 78−27035
MnP, valence electron energy spectrum, deduced from X-ray spectra and XPS 79−99984
MnP_2, nonequilibrium luminesc. and relaxation processes, 25 to 300K *(Russian)* 78−80415
Mn_2P, heat capacity, mag. entropy and thermodynamic functions 77−80630
$Mn(PO_3)_3$, cryst. struct. determ. *(French)* 78−55843
$Mn_3(PO_4)_2$ coating on steel, wear resistant appl. 80−16609
$Mn_2P_2O_7.5H_2O$, physicochem. charact. 77−39562
$MnPS_3$ and $MnPSe_3$, antiferromag., mag. props., NMR meas. 79−24223
$(Mn_xRe_{1-x})_2(CO)_{10}$, Raman spectra, intramol. vibr. coupling, ^{13}C substitution 79−47431
$Mn_xRe_{1-x}(CO)_5X$(X=Cl, Br), $0<x<5$, vibr. spectra in the 2000 cm^{-1} region of mixed and isotopic crystals 78−84585
MnS, CVD crystal growth, role of Mn-Al-Cl complexes 80−84840
MnS, core level binding energies and valence band spectra, XPS meas. 78−80455
MnS, crit. behaviour, neutron diffr. exam. 78−80169
MnS, cryst., Debye characteristic temp. calcs. 79−37796

manganese compounds continued
MnS, cubic NaCl-type cryst., Debye temp. 80−54333
α-MnS, defect energetics and range of homogeneity 78−47317
MnS, exchange perturbation theory 77−69529
MnS, γ and α phases, hydrothermal syntheses 77−48333
MnS, phase transform. at 200°C, diffusive and deformational mechanisms 80−65216
α-MnS, polycryst. and oriented single cryst., phase transition at 131K 78−6157
MnS, precipitate distribution, in grain oriented Fe-Si, electron microscope observation *(Chinese)* 78−95751
MnS solubility in Kh18N11 stainless steel, determ. method 80−84910
MnS, thermal cond., temp. depend., paramag.-antiferromag. transition effects 80−65321
MnS, X-ray determ., Debye-Waller factors, Debye temp. and vibration amplitudes 78−55928
MnS, X-ray L-emission spectra of S *(Japanese)* 78−15254
MnS-$CuInS_2$, phase relations, 400 to 1300°C, X-ray and microscopic exam. 79−1853
MnS-Y_2S_3, chem. twinning, electron microscopic study 79−46678
MnS_2, antiferromagnetic ordering, effective electron model 77−47975
MnS_2, core-level and valence-band XPS 80−93450
MnS_2, first order antiferromag. phase transition 77−8317
MnS_2, mag. ordering, indirect exchange interactions *(French)* 78−43566
MnS_2, mag. ordering at low temps., exchange perturbation theory 77−69529
$MnSO_4$, aq. solns., viscosity meas., viscous flow activation energy, entropy *(Japanese)* 77−43363
$MnSO_4$ bath technique for neutron source emission rate meas. 79−9980
$MnSO_4$, effect of press. on ion pair dissoc., cond. of aq. solns. 78−53218
α-$MnSO_4$, mag. interactions 79−78361
$MnSO_4$, mag. struct. and phase transitions, neutron diff. study 80−60208
$MnSO_4$, propan-1,3-dioic acid, H_2O_2, KIO_3, $HClO_4$, I_2, periodic chem. reactions, bi- and tristability, rel. to biological mech. *(French)* 78−80726
$MnSO_4+H_2O$ solutions, relaxation freq. and activation energy depend. on conc. 78−55913
$MnSO_4.H_2O$, hydrate librational modes in IR spectra 78−48161
$MnSO_4.H_2O$, IR spectra, H_2O external modes temp. depend. 78−58683
$MnSO_4.4H_2O$, p-p vector orient., PMR obs. 78−52361
MnSb, cryst. growth from nonstoichiometric melt, and cryst. chem 78−35286
MnSb, cryst. pulling with seed from nonstoichiometric melt 77−16488
MnSb, electronic struct., XPS meas. 78−2990
MnSb, hyperfine interactions at ^{57}Fe and ^{119}Sn, Mossbauer spectroscopy 78−23375
MnSb, optical props., 0.05 to 5 eV 77−48194
MnSb-CrSb, NiAs-type system, single crystals, neutron diffr. studies 80−60200
$Mn_{1+\delta}Sb$, ferromag., mag. disturbance around Mn interstitials 80−54868
$Mn_{1+\delta}Sb$, Mn electronic state, neutron diffr. study 80−65806
Mn_2Sb, hyperfine fields of ^{121}Sb in several mag. phases 79−28650
$MnSb_2S_4$, synthesis, electrophys. props. 77−51747
MnSe, and $MnSe_2$, thermodynamic props. 80−19958
MnSe, CVD crystal growth, role of Mn-Al-Cl complexes 80−84840
MnSe, core level binding energies and valence band spectra, XPS meas. 78−80455
α-MnSe, mag. and struct. phase transitions, mag. susceptibility and X-ray diffr. study 80−71022
MnSe, mag. suscept., thermal expansion and elec. resist. meas. 78−34964
MnSe, thermal hysteresis, ESR spectra 79−99758
MnSe, vaporization, thermodynamic study by Knudsen-cell mass spectrometry 79−10937
$MnSe_2$, antiferromagnetic ordering, effective electron model 77−47975
$MnSe_2$, core-level and valence-band XPS 80−93450
$MnSe_2$, IR lattice vibrs., dielectric dispersion 79−28735
$MnSe_2$, mag. ordering, indirect exchange interactions *(French)* 78−43566
$MnSe_2$, mag. ordering at low temps., exchange perturbation theory 77−69529
$MnSe_2$, pyrite struct., mag. suscept. and thermal expansion 77−32176
β-$MnSeO_4$, mag. interactions 79−78361
α-$MnSeO_4$, magnetic interactions, neutron inelastic scatt. study 80−107980
MnSi amorphous, conc. spin glass system, temp. effect on susceptibility 79−61142
MnSi, itinerant electron helical mag., ESR 77−59446
MnSi, Mn_5Si_3, valence shell XPES 79−43105
MnSi, μ^+ spin-lattice relax rate, paramag. phase, near T_c, temp. depend. 79−19825
MnSi, US velocity anomalies near mag. transition 78−19302
MnSi, weak itinerant magnetic compound, paramagnetic response function, polarised neutron scattering 80−107982
$MnSi_x$, X=1.72 to 1.75, IR absorpt., transmission, refl., spectra 80−60600
$Mn_{15}Si_{26}$, growth by Bridgman method and chemical transport, X-ray structural analysis 79−100043
Mn_5Si_3, elastic moduli, phase transitions, ultrasonic velocity 80−92589
Mn_nSi_{2n-m}, thermoelectric and optical props. 78−91714
Mn_5SiB_2, cell dimensions 79−24502
$MnSiF_6$, phase transform. and relax., EFG and quadrupole spectra 77−51995
$MnSiF_6.6H_2O$, optical absorption spectra, 77-300K, assignments 77−36259
$MnSiF_6.6H_2O$, specific heat, thermal cond., simultaneous meas., method, 90-300K, near phase transition 77−37892
$MnSiF_6.6H_2O(.6D_2O)$, near IR spectrum, 80K, assignments 78−48164
$MnSiN_2$, 180°C Neel temp., mag. struct. and atomic coords., neutron diffr. meas. *(French)* 77−32168
Mn_2SiO_3, effect of vibration during sintering, on electrical resistivity 80−16258
Mn_2SiO_4, tephroite, thermal expsn., 25-850°C 79−60527
Mn_2SiO_4-MnO eutectic composite, EFG die-top geom. effect on solidification interface shape 77−48420
$(Mn_xSn_{1-x})Fe_2O_4$ thin film LPE on Bridgman grown Zn_2TiO_4 substrate 79−100065
$MnSnO_3$, ordered ilmenite phase, cryst. struct. 78−47288

manganese compounds continued
Mn_2SnO_4-Mn_3O_4 system, spinel solid soln. form., atm. effects 77−43332
Mn_2SnS_4, cryst. struct. refinement and mag. struct. determ. *(French)* 80−107131
$MnTa_2O_6$, columbite struct., X-ray diffr., IR and Raman spectra *(French)* 78−63727
$MnTa_2O_6$, force fields rel. to cryst. struct. *(French)* 80−107104
$Mn_{1/3}TaS_2$, Hall coefficient and resistivity 80−39610
$Mn_{1/3}TaS_2$, magnetic susceptibility, function of temp. 80−39756
$Mn_{1/4}TaS_2$, Hall coefficient and resistivity 80−39610
$Mn_{1/4}TaS_2$, magnetic susceptibility, function of temp. 80−39756
MnTe, CVD crystal growth, role of Mn-Al-Cl complexes 80−84840
MnTe, core level binding energies and valence band spectra, XPS meas. 78−80455
MnTe, effect of press. on Neel temp. and lattice parameter 79−95594
MnTe film, elec. props. 78−43498
MnTe, film, vapour deposition 78−47677
MnTe, magnetic resonance at high hydrostatic pressure 78−76247
MnTe, optical props. and electronic struct. 78−6682
MnTe, resistivity anomalies at mag. transitions, sp.ht. 80−39785
$(MnTe)_{1-x}$-$(As_2Te_3)_x$ solid solns., thermoelec. props. 79−42567
$MnTe_2$, antiferromagnetic ordering, effective electron model 77−47975
$MnTe_2$, mag. ordering, indirect exchange interactions *(French)* 78−43566
$MnTe_2$, mag. ordering at low temps., exchange perturbation theory 77−69529
$MnTe_2$, Mossbauer spectra, hyperfine field 80−15866
$MnTe_2$, pyrite struct., susceptibility, 4.2-450K, exchange consts. 77−77040
$(MnTe)_{1-x}(Bi_2Te_3)_x$ ($x \leq 0.05$) solid solution, electrophys. props. 80−24925
Mn_2TeO_6, magnetic structure, stability of mag. modes, neutron diffraction study *(French)* 80−39744
$MnThSe_3$, synthesis, cryst. characts. *(French)* 78−51517
$Mn_{1-x}Ti_xAs$, ferro- to paramag. transition, press. effect up to 7 kbar 77−89954
$MnTiNdO_5$, distrib. of Mn^{3+} and Ti^{4+} ions, Mossbauer spectrum 77−69747
$MnTiO_3$, HP phase transform. 80−19941
$MnTiO_3$, quasi-two dimens. antiferromag., mag. crit. behaviour 77−32191
$Mn_3(VO_4)_2$, X-ray powder diffr. and IR spectra 78−10016
$Mn_{12-x}W_xP_7$, solid solns., prep., cryst. struct. *(French)* 78−63723
MnX_2 solns., (X=Cl, Br, I), heavy at. effect on rate consts. of radiative and non-radiative transitions 79−78736
MnX_2(X=F, Cl, Br), discrete variational Xα cluster calcs. 80−15444
$Mn_{23}Y_6D_x$, D atom location, neutron diffr. study *(French)* 80−24426
MnY_2S_4, magnetisation and susceptibility, exchange interactions obs. 78−52242
MnZn ferrite, appreciable SiO_2 content, origin of core losses, microstructure and mag. props. 78−64225
MnZn ferrite, combined Sn-Ti substitutions, improved props. *(German)* 77−20644
MnZn ferrite, combined Bridgeman-zone levelling cryst. growth technique 80−35076
MnZn ferrite, gas phase fluorination for improved props. 78−52306
MnZn ferrite, high cond., magneto-microwave Kerr effect 77−43888
MnZn ferrite, initial mag. permeability rel. to mag. anisotropy 80−80557
MnZn ferrite, laser drilling and cutting, anal. of results using computer model 79−70180
MnZn ferrite, mag. anisotropy, effect on recording head characts. 80−39765
MnZn ferrite, mag. loss accommodation depend. on freq. and amplitude of mag. field *(Russian)* 80−34686
MnZn ferrite, mag. permeability spectra, 0.001-100 MHz range *(Russian)* 77−8355
MnZn ferrite, mag. permeability accommodation depend. on mag. field *(Russian)* 80−34685
MnZn ferrite, mag. relax., permeability and loss tangent determ. at 4.2 to 300K 77−32263
MnZn ferrite, mag.-mechanical-microstruct. interaction 77−1578
MnZn ferrite, mechanically induced anisotropy, effect on mag. permeability 78−47970
MnZn ferrite, microstructure and initial permeability, presintering process effect 80−89367
MnZn ferrite, MoO_3 addition effect on grain growth kinetics and densification 79−61550
MnZn ferrite, natural, intrasite cation ordering and clustering 77−12259
MnZn ferrite, nonstoichiometric, neutronographic determ. of cation distrib. *(Bulgarian)* 78−83656
MnZn ferrite, O_2 stoichiometry effect on fracture 80−25826
MnZn ferrite, optical refl. and electroreflection spectra obs. 78−27262
MnZn ferrite, polycrystalline, doped, DC resist. 78−47788
MnZn ferrite, polydispersive spin relax. near Curie temp., mag. susceptibility meas. 77−69513
MnZn ferrite, post sintering cooling rate effects on props. 77−63604
MnZn ferrite, prep. and magnetic props. 78−19254
MnZn ferrite, props. rel. to raw materials *(German)* 77−21074
MnZn ferrite, quantitative anal., using X-ray fluorescence 78−40090
MnZn ferrite, spray dried agglomerates, compaction response, fracture, deform. 79−43172
MnZn ferrite, surface damaged layer, mag. domain obs. by taper section SEM 77−59423
MnZn ferrite, temperature dependence of Hall mobility 78−30944
MnZn ferrite, thermal cond. of single crystals 77−36079
MnZn ferrite, Ti substituted, vacancy contents and phase equilibria 80−29012
MnZn ferrite, wall topography change induced by external press. 80−34734
MnZn ferrite, weak mag. losses, microcalorimetric meas. 77−51926
MnZn ferrite disc, excitation of radial mode vibration due to AC 79−69708
MnZn ferrite fabricated by hot isostatic pressing, recording head appl. 80−35139
MnZn ferrite fillers for elastic mag. materials, prep. and props. 79−52143
MnZn ferrite particles, mag. filtration from air streams 77−4945
MnZn ferrite powder prep., wet method 80−89180
MnZn ferrite powders, reactive, mag. materials obtained by compaction 80−89182

manganese compounds continued
MnZn ferrite single cryst., high temp. phase transform. characts., growth techniques *(Chinese)* 79−33927
MnZn ferrite single cryst., Bridgman growth and appl. *(Chinese)* 79−33928
MnZn ferrite single crystals, growth by Bridgman technique, book contrib. 79−69977
MnZn ferrites, cationic distrib. and Curie temp. *(Russian)* 79−91232
MnZn ferrites, doped; determ. of grain boundary composition, using Auger spectroscopy *(German)* 79−23618
MnZn ferrites, elec. cond. mechanism in paramag. and ferrimag. phases 80−15524
MnZn ferrites, field depend. of mag. permeability accommodation *(Russian)* 79−69694
MnZn ferrites, form. of comp. heterogeneity during high-temp. sintering 80−60818
MnZn ferrites, hot pressed, mechanism of protective action of ZnO coating *(Russian)* 79−15822
MnZn ferrites, impurity induced exaggerated grain growth 78−92222
MnZn ferrites, initial mag. permeabilities under low temp. reactor irrad. 77−36093
MnZn ferrites, internal friction and ΔE effect depend. on demagnetisation method 80−80584
MnZn ferrites, low loss, highly stable, study *(Slovene)* 78−27055
MnZn ferrites, mag. domains on worked surfaces 79−99722
MnZn ferrites, mag. susceptibility freq. spectrum, effect of pressure 78−95420
MnZn ferrites, neutron diffr. exam. of influence of technology on mag. and cryst. parameters 79−42741
MnZn ferrites, post sinter-cooling rates effects 80−89369
MnZn ferrites, spinel use of phase equilibria in manufacture 79−11596
MnZn ferrites, thin struct. of $K\beta_5$ and $L\alpha_{1,2}$ emission bands of Fe *(Ukrainian)* 79−78790
MnZn ferrites, Ti substituted, mag. permeab. meas., grain boundary comp. AES obs. 78−95473
MnZn ferrous ferrite, initial mag. permeability second-order magnetocrystalline anisotropy influence 80−88820
MnZn ferrous ferrites, mag. permeability stress depend. 80−88822
MnZn polished ferrite worked layer magnetic characts. changes meas. *(Japanese)* 78−10742
MnZn, pressing powders, spray dried, pressing behavjour and props. 80−11617
MnZn soft ferrites, commercial grade, microstruct. rel. to mag. props. 80−34009
MnZn-ferroferrites, sintered, microstruct., TEM study *(Dutch)* 80−2036
$Mn_{1.18}Zn_{0.06}Co_{0.01}Fe_{1.75}O_4$, transport props. near Curie points 78−88100
$Mn_{1-c}Zn_cF_2$, antiferromag. reson., far IR spectrum, CPA calc. 77−20716
$Mn_{1-c}Zn_cF_2$, Heisenberg antiferromag., linear mag. birefringence meas. 77−16277
$Mn_{1-x}Zn_xF_2$, antiferromagnetic reson. freq. from far IR transmittance spectra 77−69695
$Mn_{1-x}Zn_xF_2$, linear mag. birefr., crit. behaviour 77−52061
$Mn_{1-x}Zn_xF_2$, randomly diluted uniaxial antiferromagnet, CPA theory 79−78388
$Mn_cZn_{1-c}F_2$, crit. neutron scatt. near percolation threshold 78−2693
$Mn_xZn_{1-x}F_2$, antiferromag. spin flop crit. field 79−24218
$Mn_xZn_{1-x}F_2$, CPA estimate for Neel temp. 78−76245
$Mn_xZn_{1-x}F_2$, Neel point and short range order, dilution effects, mag. birefr. obs. 80−71019
$Mn_xZn_{1-x}F_2$, three dimens. Heisenberg-Ising antiferromag., fluctuations near percolation threshold 79−78390
$MnZnFe_4O_8$, duplex struct. formation during sintering, grain growth study 79−11541
$Mn_{0.4}Zn_{0.42}Fe_{2.16}O_{4+x}$, permeability, rel. to intrinsic mag. props. 79−4702
$Mn_{0.510}Zn_{0.417}Fe_{2.073}O_{4+\delta}$ relationship between magnetic permeability and stoichiometry 79−42799
$Mn_{0.53}Zn_{0.35}Fe_{2.12}O_4$, and Ti substituted, acoustic losses 79−24207
$Mn_{0.7}Zn_{0.3}Fe_2O_4$, temp. depend. of microwave resistivity 79−69540
$(Mn_{0.7}Zn_{0.3})_xFe_yO_4$, electromag. props. rel. to Fe content 78−43613
$Mn_{1-x}Zn_xFe_2O_4$, noncollinear mag. structure, Mossbauer spectrum 77−69501
$Mn_{1-x}Zn_xFe_2O_4$, prepared by wet method, neutron diffr. and high field Mossbauer expts. 80−75719
MnO, electronic polarisability of ions 77−40175
MnO_2 powders with admixed fine materials, density and conductivity under pressure 80−54682
$Mn_4[AsSi_3O_{12}(OH)]$, cryst. struct. determ. and refinement 80−1970
$Mn_2[Fe(CN)_4]$, and $Mn_3[Fe(CN)_6]_2$, mag. susceptibility, reflectivity spectra and cryst. field 79−56808
Mo-Mn-SiO_2 mixture, premetallizing of high alumina ceramics 79−47792
$MuCl_2.nH_2O$, cryst. struct. *(German)* 80−1987
$(NH_3\text{-}(CH_2)_2\text{-}NH_3)Cd_{1-x}Mn_xCl_4$, Mn^{2+} single ions, clusters and layers, ESR study 79−78507
$(NH_4)_6MnMo_9O_{32}.8H_2O$, mag. susceptibility, rel. to EPR, zero field splitting parameter 77−36122
$NH_4MnP_2O_7.H_2O$, physicochem. characts. 77−39562
$(NH_4)_2SO_4:MnO_4^-$, X-ray irrad. damage, optical absorpt. spectra study 80−66246
$NaCa_2Mn_2V_3O_{12}$, antiferromag., spin wave contrib. to sp. ht., λ-anomaly at 25.05K T_N 77−77068
NaCl:$MnCl_2$, Suzuki phase precip. obs. by TEM, misfit dislocations 77−31776
NaCl-CsCl-$MnCl_2$, molten salt system, molar volume and elec. cond. meas. 80−34217
NaCl-CsCl-$MnCl_2$, molten salt system, molar volume and elec. cond. meas. 80−34218
$NaMnCl_3$, antiferromagnet, exciton self-localisation luminesc. and excitation spectra *(Russian)* 80−11456
$NaMnCrF_4$, cryst. struct. *(French)* 77−47402
$NaMnCrF_6$, ferrimagnetic, magnetic props. *(French)* 79−1668
Na_xMnO_2, layer struct. elec. cond. props. *(French)* 78−26542
$Na_2MnP_2O_7.4H_2O$, physicochem. characts. 77−39562
$Na_6Mn(Ti[Si_6O_{18}])$, Kazakovite, cryst. struct. determ. 80−19782
$Na_2O\text{-}Mn_2O_3\text{-}TiO_2$ ternary systems, X-ray investigation 79−51067
$NaPO_3\text{-}Mn(PO_3)_2$, cpd. formation 77−52307
$Nd(Mn_{1-x}Cr_x)_2Si_2$, mag. and structural props. 79−78342
$Ni_xMn_{1-x}Cl_2$, sp. ht., 2-28K, anomalies *(Russian)* 77−89970
manganese compounds continued
$Ni(OH_2)\text{-}\alpha\text{-}Mn(OH_2)$ system, precip. and ht. treatment 77−85916
$Pb_{1-x}Mn_xTe$ (x=0.005, 0.001, 0.05), solid solns., exam. of electrical and thermal props. 79−1599
$Pb_{1-x}Mn_xTe$, photovoltaic effect, p-n junction, energy gap determ. 80−92931
$Pb_{1-x}Mn_xTe$, single cryst., mag. susceptibility 79−73672
Pt-Mn(III)-porphyrin electrode for possible wet solar cell 79−100529
ramsdellite type structures, rel. between β-gallia, rutile, psilomelane, hollandite and $Ga_4Ti_{x-4}O_{2x-2}$ type structs. 79−37664
$RbMnCl_3$, specific heat near Neel temp. *(Russian)* 80−100340
$RbMnCl_3$, structural phase transition 78−91442
$RbMnCl_3$, twinning struct., cryst. domains, orientation mag. transition *(Russian)* 80−107275
$RbMnCl_4$, changes in birefr. due to spin flopping 79−73910
Rb_2MnCl_4, Heisenberg antiferromag., spin wave anal. 79−61237
Rb_2MnCl_4, rare earth doped, energy transfer, emission spectra obs. 80−20684
$RbMn_{1-x}Co_xF_3$, Raman scatt. by mag. excitations 77−55775
$RbMnF_3$, antiferromagnetic resonance, optical detection, luminescence 80−7174
$RbMnF_3$, exciton and exciton-magnon emission 79−33779
$RbMnF_3$, isotropic antiferromag., crossover behaviour of mag. phase boundary, US meas. 78−80145
$RbMnF_3$, NMR, modes interaction *(Russian)* 77−59468
$RbMnF_3$, nucl. spin waves *(Russian)* 78−34973
$RbMnF_3$, nuclear spin waves spectra, relaxation, parametric excitation, NMR dynamic shift *(Russian)* 80−11180
$RbMnF_3$, spin wave widths 80−97081
$RbMn_{1-x}Mg_xCl_3$, dilute pair antiferromag., mag. susceptibility and ESR meas. 79−78338
$Rb_2Mn_xMg_{1-x}F_4$, spin dynamics near percolation threshold, EPR study 80−39859
$RbMnP_2O_7.3H_2O$, physicochem. characts. 77−39562
$RbPO_3\text{-}Mn(PO_3)_2$ system, $Rb_2Mn(PO_3)_4$ and $RbMnP_3O_9$ form. 79−78943
$ScMn_{0.25}Si_{1.75}$, X-ray determ. of struct., new representative of struct. type $ZrSi_2$ 78−79595
$SiO_2\text{-}CaO\text{-}Na_2O\text{-}MnO_2$ system, water, alkali, acid resist., chem. durability 79−34162
$SmMn_3C$ noncolinear mag. struct., mag. transition *(French)* 77−69494
$Sn_{1-x}Mn_xTe$, $0.02<x<0.08$, transport and magnetic properties, low magnetic field 79−99569
$Sn_{1-x}Mn_xTe$, degenerate mag. semicond., thermoelec. power meas. 80−29392
$Sn_{1-x}Mn_xTe$, electronic struct., transport props., mag. ordering effects 80−65441
$Sn_{1-x}Mn_xTe$, IR reflectivity, elec. susceptibility mag. order effects 79−47433
$Sn_{1-x}Mn_xTe$, magnetic behaviour of Mn 78−14938
SnTe-MnTe, degenerate semicond., anomalous Hall effect 80−29420
$(SnTe)_{1-x}(MnTe)_x$, ESR, effect of Mn ion conc. on line width and area 78−35026
Sr_2MnReO_6, new seignettomagnets and ferroelectrics 78−19425
$Ti/RuO_2/MnO_2$ electrode, anode characts. 78−68897
Ti-MnO_2, porous anode for matrix-type electrochemical cell 77−81414
TiN-MnN, solid solns., electrophys. props. 77−35914
TiO-MnO solid soln., lattice thermal cond. 79−23791
$TlMnCl_3$, refr. index and birefr., struct. transition effects 77−90126
$TlMnCl_3$, specific heat near Neel temp. *(Russian)* 80−100340
V-Mn-O system, phase comp. during oxide prep. 78−27447
VN-Mn, solid solns., electrophys. props. 77−35914
$V_xO\text{-}Mn_yO$, solid solutions, exam. of thermal conductivity 78−79827
$WO_3\text{-}MnO\text{-}P_2O_5$ system, glass form. and memory effects 77−76888
$Y_2O_3\text{-}Mn_2O_3$, solid-phase reactions 77−48405
$Zn_xFe_yMn_zFe_2O_4$, ferrite, production from Fe_2O_3, effect of impurities on props. *(German)* 79−4925
ZnMn ferrites, prepared by wet chemical and ceramic methods, comparison of struct. and mag. props. *(German)* 79−24470
$ZnMn_{1-x}Cr_xFeO_4$, Mossbauer effect, quadrupole splitting 80−29664
$Zn_{0.8}Mn_{0.2}Fe_2O_4$, spin interaction, neutron diffr. and Mossbauer effect meas. 77−4501
$Zn_xMn_{1-x}Fe_2O_4$, Mossbauer spectra exam. 77−40155
$Zn_xMn_{1-x}Fe_2O_4$, substitution effect on mag. struct. and exchange interaction *(Russian)* 78−47949
$Zn_{0.3}^{2+}Mn_{0.7}^{2+}Mn_y^{3+}Fe_{2-y}^{3+}O_4$, Mossbauer hyperfine field meas. 77−81033
$Zn_xMn_{2-x}Sb$, anti-PbFCl type, cryst. struct. and ferromag. ordering 77−84723
$ZnO\text{-}Bi_2O_3\text{-}CoO\text{-}MnO\text{-}Sb_2O_3$ (97.5, 0.5, 0.5, 1.0 mole%), exam. of elec. props. at different annealing temps. 80−3099
$ZnO\text{-}Bi_2O_3\text{-}Sb_2O_3\text{-}Co_2O_3\text{-}MnO_2\text{-}Cr_2O_3$, nonohmic ceramic, microstruct. exam. 78−47292
$ZnO\text{-}GeO_2\text{-}MnO\text{-}B_2O_3$ wideband cathodoluminescent phosphor 80−55196
ZnS:MnF_2 films, effect of Mn conc., XPS obs. 79−33886
ZnS-MnS, phase relations, 400 to 1300°C, X-ray and microscopic exam. 79−1853
ZnS-MnS-$CuInS_2$, sobsolidus equilib., phase diagrams 80−3016

manometers
see also pressure measurement
absolute thermodynamic manometer for ultralow pressure control 79−35766
airtightness meas., interference resistance of manometer type equipment 79−52598
automated electromanometer, appl. for nuclear materials safeguarding 80−99211
automatic pressure recording method, 5 to 10^{-2} torr 79−85148
balance appl., thermal noise effect 78−65906
biological pressure meter, up to 40 kPa and 4 kPa, temperature and time stability 79−84059
blood pressure Hg manometer contactless readout and recording cct. 77−81603
calibration method in high- and ultrahigh-vacuum regions 78−16807
calibration pressure generation, fundamental methods *(French)* 79−58670
capacitance diaphragm manometer, linearity check between 10^{-4} and 10^{-1} Torr 77−2663
capacitance manometer with stainless steel bellows-sealed membrane 78−54383

manometers continued
cerebrospinal fluid pressure meas. and controlled withdrawal 79−39538
constant pressure manometer with frequency read out, electrocapillary element appl. 80−73380
corrosive gas laser systems, capacitance manometer design and perform. 79−36909
dial pressure gauges, reliability tests and failure mechanisms *(Rumanian)* 79−40557
diaphragm pressure-sensitive charact. plotting by tabular analytical method *(Russian)* 78−8397
differential capacitance manometer for fast volume determ. 77−87734
differential pressure meas., optical interference system 78−86323
electromanometric system frequency response visualisation device 77−48890
electromanometry, Medicor equipment for meas. of blood and body fluid press. 77−90943
electronic sphygmomanometer, direct and indirect methods for blood pressure meas. 79−25125
endoscopic manometry in gastroenterology 78−92730
excess pure pressure measurement with liq. manometers 77−52566
free-piston, effective area calculation for systems with gas lubrication 78−93714
free-piston manometer comparison, weight relocation method 80−90831
glass membrane manometer for high-temperature measurement 80−86329
interchangeable differential manometer test technique and equipment 77−57320
interferometric, method of operation 78−24808
interferometric, using He-Ne laser 77−110
interferometric oil micromanometer 79−63263
interferometric oil micromanometer as primary vacuum standard 79−88970
ionisation manometric transducer, PMI-2, cathode protection 77−74416
Knudsen, modified, for meas. of low gas press. and thermal accommodation coeffs. 77−26320
linearly varying pressure rate meas., instrument design 78−8395
liquid, sensitivity, wetting hysteresis effect 80−98926
liquid filled, advantages 78−49792
liquid level control of stored above or below ground, selection 78−21093
low-pressure calibration method using vacuum technique 78−74015
magnetron-type, with inhomogeneous mag. field 80−31730
membrane, differential, for low pressures meas. 80−31777
membranes nonlinear charact. calc. *(Czech)* 79−26021
micromanometer, conversion to large range digital readout 77−2716
micromanometer for electrical readout 79−6136
micromanometer test scheme and standard instruments 77−79049
mimatron, magnetic-discharge, with two coaxial anodes 79−17433
nonlinear liq. column oscills. in manometer, theory and expt. 78−90922
oscillatory flow in U-tube manometers, effect of drag reducing polymer additives 80−64584
pneumatic facilities for linear dimension meas., parameter selection 78−73964
pressure reducer, piston type, for continuous pressure meas. up to 1 MPa 78−4602
recording, simplified design, student laboratory apparatus appl. 79−58502
recording mercury manometer, student apparatus 77−26119
reference air/water multitube, for testing precision transducers with pneumatic output signals 78−93717
reference free-piston, oxidation process for trimming mass of weights 78−93715
reference manometer free-piston rotation with changes in tilt angle 77−57316
results processing technique, simplified, for testing type-MMN micromanometers 79−35692
rhino-manometer, nose aerodynamics meas. 79−83956
rhino-rheo-manometer for dynamic and static nasal pressure meas. with capacitance probes 79−83961
rhinomanometer, new-type, and relating test experiences 79−100768
sphygmomanometry, automatic indirect methods, equipment, for blood press. meas. 77−81616
spring-piston differential manometer 77−67456
strain gauge manometer for pressures up to 14 kbar *(German)* 77−26322
tensometric, clamped disc diaphragm flexure nonlinearity anal. *(Russian)* 79−211
thermostat for, accurate to 1500°C 79−49225
tubular spring type for subatmospheric and small excess fluid pressure, performance improvement 78−81940
U-shaped, Hg for 1300 to 2300 torr range 80−31784
U-tube, fluid free oscillation, Navier-Stokes equations solution and expt. verification *(Japanese)* 80−6142
U-tube water manometer, for water injection dew point hygrometer *(Japanese)* 80−8998
US interferometric manometers for low and medium vacua 77−67455
vacuum press. meas. considerations *(French)* 78−49846
vacuum valve construction, mounted on pressure pickup 80−47066
variable pressure manometer, electrocapillary element appls. and properties 80−73379
Hg, automatic press. recording by capacitive sensor 77−37871

manufacture
see also electron device manufacture; electronic equipment manufacture; steel manufacture
1200 MWe FBR steam generators, Creys-Malville in France, manufacture 80−27797
cermet elec. heating element contacts, plasma deposition 78−11364
curved glass mirror manufacture for linear solar concentrators 79−62124
fission reactor pressure vessel and circuit development, conf. report 80−47541
fission reactors, VVER 440, design and engineering props., production and assembly 80−91207
fusion reactor, Heliotron E, vacuum chamber construction using electron beam welding 80−106180
fusion reactor, Large Coil Program, General Dynamics Convair/IGC manufacturing engineering 80−106169
fusion reactor, neutral beam ion source, core snubber network design, fabrication and testing 80−102378
fusion reactor, TEXT, toroidal field coil fabrication 80−91267
fusion reactor, TFTR, neutral beam injector prototype, construction and performance 80−99390
manufacture continued
fusion reactor vacuum vessel, large, ultra high vacuum, design and manufacturing problems 80−99276
gas cooled fast breeder reactor core element fabrication technology 77−18682
heavy water moderated, experience 77−83070
homopolar generator, fast discharge machine, design, fabrication, testing, for fusion reactor 78−54952
LWR pressure vessels, Sweden 77−71688
magnetic core production method, ferromag. probe appl. 78−44334
medical electronic equipment in India, noninvasive diagnostic techniques appl. 79−96698
microelectrode tip fabrication method 77−81758
neutral beam, continuously operating, convectively cooled ion accelerator, mech. design and fabrication 80−102374
neutral beam source, cryopumping and mag. shielding, fabrication and operating cost 80−106229
neutral beam source manufacturing at Lawrence Livermore Laboratory 80−102377
nuclear medical instrumentation, India appl. 79−96653
optical fibre, low-loss 77−65632
optical fibre fabrication and drawing processes 78−90532
optical fibre ribbons and cables manufacture, mech. props. 78−90533
piston-type flowmeter prover specifications *(Japanese)* 77−62320
Plante cell formation using NO_3^- process 79−96437
pollution problems from fertilizer manufacture 79−34450
prosthetic equipment manufacturing and selling problems *(Japanese)* 78−44702
SAW device manufacturing methods and technology progress report 77−39173
solar energy paraboloid concentrator fabrication, simplified method 80−16837
solar water heaters, aluminium alloy rolled-welded heating panels production and use 79−96421
space manufacture, mining Apollo and Amor asteroids for raw materials 77−91467
superconducting coils, for low current DC beam line magnets 77−82575
surveying instruments 77−82027
technology transfer, medical electronics manufacture appl. 79−96680
terrestrial solar generators, design, fabrication, testing and economic power generation 80−45672
toroidal field coil construction and appl. *(German)* 78−54877
transparent conducting layers, tunnel furnace *(Hungarian)* 78−35303
vertical axis wind turbines 80−66929
Ag-Zn batteries, miniature, fabrication and charact. *(Polish)* 80−93866
Al microdisc targets for single beam laser expts., prod. method 78−1865
C fibres, production from coal tar pitch, heat treatment *(German)* 78−44033
Nb-Ti, multifilamentary, Mirror Fusion Test Facility, superconductor core manufacturing and quality 80−93521
Nb_3Sn high field superconductors, filamentary, manuf. and appl. limits *(German)* 77−55647
Si photovoltaic industry, environmental control, economic and ecological requirements 80−94026

manufacturing ADP *see manufacturing data processing*

manufacturing computer control
see also computerised numerical control; manufacturing data processing; process computer control
galvanising process, digital control system for Zn coating distrib. 78−19960
HTGR fuel rod length meas. and control microcomputer system 79−71942
optical component fabrication by diamond turning 79−76899
optical fibre fabrication, computer-aided MCVD system *(Japanese)* 79−59852
optical fibres, MCVD fibre fabrication system design 79−55255
optical systems, aspherical, manufacturing and testing techniques development *(Italian)* 80−48467
polisher, computer controlled, efficiency 80−91938

manufacturing data processing
see also manufacturing computer control
NDT, data processing and acquisition for product quality control 80−11862
noise control, costs and legal requirements 78−33957
nuclear fuel fabrication plant, U safeguarding, management information system 79−85750
pharmaceutical quality control system 79−52798
solar cell arrays, economics modelling of photovoltaic module manufacturing, SAMICS methodology developments 80−55860
steelworks computerised spectrometric analysis and management information system 80−89574

manufacturing industries
data logging status and prospects 79−93114
high-temperature power-technological industrial processes use of nuclear power, reviews 79−26729
optical instrument manufacturing, cyclical growth characteristics and prediction 79−76862
powder metallurgical parts, development, and manufacture of semifinished products 80−50578

manufacturing processes
see also cold working; cutting; drawing (mechanical); extrusion; forging; forming processes; hot pressing; hot working; joining processes; machining; manufacture; rolling; sintering
abrasive particle shape control and quantitative eval. apparatus 78−4586
automated, thermal equipment power temperature regulation using AC power Veritron controllers *(German)* 79−80598
capillaries, ultrafine, with diameters between 0.5 and 60 μm, fabrication and calibration 77−30135
cermet elec. heating elements, sintering in elec. furnance, optimum conditions 77−90287
dimensional gauging using scanning laser beam 78−57898
explosive compaction of metal powders 78−64501
fusion reactor, TFTR poloidal field coils, tooling and manufacture 80−91262
impact noise from industrial machinery, effect on hearing loss 79−18599
inductive stirring of metal melts, surface velocity meas. on 30000 lb charge 78−11139
industrial visual testing, photographic methods as technical aid *(German)* 80−31923

manufacturing processes continued
noise abatement methods in foundry operations 77−72115
noise reduction techniques applied during design stage 79−18596
non-Gaussian distribution laws for statistical error theory generalisation *(German)* 80−22315
optical fibre drawing process control, optimisation theory appl. 79−90039
high cis-,1,4-polybutadiene, orientation effects induced by shear rate in capillary extrusion 77−48389
polycarbonate styrene-acrylonitrile copolymer mixture, determ. of phase structure, electron microscopy 80−103272
polyethylene, direct ram extrusion, correl. between chain folding and tensile modulus 77−44209
polyurethane artificial ventricle construction with seamless interior *(German)* 79−8581
porous material deformation anal. using upper bound theory, appl. to extrusion *(Japanese)* 77−46937
powder metallurgical parts, development, and manufacture of semifinished products 80−50578
punch pressing, air ejector noise abatement 78−90600
PVC, plasticised, processing-morphology-mech. props. relation 79−8264
PVC, technological obs. and methods 79−7349
rubber, C-black loaded SBR, elec. cond., effect of milling and thermal-oxidative ageing 77−55529
single crystal permanent magnet, industrial technology and equipment for manufacturing process 80−35075
steel, 20Kh, warm extrusion effects on struct. and mech. props. 77−44311
steel, TRIP, hydrostatic extrusion shock treatment rel. to strength and plasticity 77−44281
Cu, contact, texture, rel. to manufacturing procedure 77−16611
Ni-Nb(-Cu)-C, NbC dispersed supercond. tapes, fabrication and charcts. 78−19773
n-PbTe, cold hydroextrusion, plastic deform. rel. to thermoelec. props., struct. 77−11945
Si solar cells, crystal growth, heat exchanger method, fixed abrasive slicing technique 80−35082
ZnSe cold pressing 77−52258

many-body problems
see also BCS theory; quantum statistical mechanics; renormalisation
3π dynamics, two-body unitarity and analyticity 77−18205
3-body problem with one infinite mass particle, integral and Schrodinger eqn. equivalence 80−18255
3-body problem with one infinite mass particle, Schrodinger and integral eqn. soln. equivalence 80−77636
π electron Hamiltonian, ab initio derivation by nonperturbative open shell formalism 78−21846
π-electron system, self-consistent many-body theory, self-energy effect 79−63901
σ model relativistic, finite temp., renormalisation, many body problem, interacting nucleons 77−18178
A=15-18, effective interaction from coupled cluster many-body method extension 80−22701
abnormal nuclear matter, many body forces, σ-model Lagrangian field theory 77−6277
alkali atoms, hyperfine interactions of excited states, Brueckner and natural orbitals 77−3283
angular momentum projection in nuclear physics 77−50066
antisymmetrisation effects in nuclear collisions, projection operator techniques 78−46036
applications, review of development 80−46968
applied inverse problems, book 79−49017
astronomy, dynamical, Hill's stability concept generalisation 79−92656
atom, calc. of induced elec. and mag. moments 77−57884
atom, heavy, parity non-conserving E1 matrix elements, many body calcs. 80−47924
atom, HFS, many-body and relativistic effects 78−37565
atom, nucl. quadrupole coupling const., relativistic many-body perturbation theory 78−37566
atom and mol. excitation, many-body perturbation theory, eqns. of motion formulation 77−88373
atom surface scatt., reflection and sticking coeffs., short range forces, low energy limit 80−40208
atom-polyatom collisions, quantal many-body approach 77−30943
atomic collisions, classical many-body collision model incorporating Heisenberg and Pauli principles 80−63511
atomic electron scattering, in laser field, Green's function 79−31679
atomic electron scattering, second-order many-body theory 80−32832
atomic four-body problems, Faddeev eqns., appl. to ^{6}Li 79−59569
atomic four-body problems, Faddeev eqns. in momentum representation 79−59524
atomic many-body perturbation theory with radially restricted basis functions 80−78526
atomic photoionisation, many-body perturb. calcs. 79−59406
atomic physics, few-body problems 77−27137
atomic systems, collisions and interactions calc. method 80−46726
atomic systems, many-electron autoionisation states, transition probability and autoionisation rate, perturbation theory Z-expansion 80−52863
atomic theory, few-charged particle problem 77−26977
atomic three-body systems, channel coupling array theory 77−19005
atoms, collective dynamics, hydrodynamic approach and many body approach based on RPA calcs. 80−47855
atoms, correl. problem for open and closed shell system, coupled cluster approach 80−47842
atoms, heavy, parity non-conservation, relativistic many-body perturbation theory 78−923
atoms, MBPT appl., comparison with problem for nuclei 80−47406
atoms, nucl. vol. isotope shift theory, many electron effects 80−47851
atoms, photoionisation cross sections, electron correl. reson. struct., relax. effects many body perturbation calcs. 80−47852
atoms, Schrodinger eqn. standard solns. 80−47863
atoms, Z=46-54, $L_{\gamma 2,3}$ emission spectra, breadth, dynamical effects 80−32645
Baer-Kouri-Levin-Tobocman many body scatt. theory, Feshbach projection operator method 80−508
baryon system, strong interacting, finite temp. many body theory, phase transition 77−65210
BBG theory developments, hole and particle lines, dispersion effects and healings 80−22719

many-body problems continued
BBGKY hierarchy for hard spheres in one dimens., uniqueness 78−29041
Bencze-Redish-Sloan connected kernel eqns., new derivation method 78−78330
benzene, π electron system, excitation energy, appl. of MBPT 80−52876
Bethe-Faddeev wave function generalisation to N-body clusters 77−57639
Bethe-Salpeter equation, reduction to equiv. Schrodinger eqn., appl. to muonium and positronium 79−2933
binary dense gaseous mixtures, struct. and thermodynamic props., molecular dynamics study 80−64866
binary liquid solutions, struct. and thermodynamic props., molecular dynamics study 80−64866
Bogolyubov method, equilibrium system many body correlation function contracted description *(Russian)* 80−38888
book, scatt. theory in quantum mechanics 78−49573
Bose gas, hard-disc, low density, two-dimens. many-body problem 78−95195
boson, nonrelativistic, potentials, attractive discreteness of ground state 80−46957
boson condensate, dynamic eqn. functional formulation, many body theory 80−84334
boson expansions, convergence of various methods 79−93037
boson system, 1-D, with δ-function interactions, time-depend. Hartree approx. 79−9184
boson system, condensed, canonical ensemble approach 78−89400
boson system, one-dimens., many-body scatt. processes nonrelativistic $|\phi|^4$ theory 77−30093
boson system bound state, pulsating soliton solns. *(Russian)* 77−74267
bound states and resons. from separable pots., T matrix 77−30036
bound states of 2N, 3N and 4N systems, nuclear forces 79−71800
bound three and four particle systems, two particle resonance poles and energy spectra 78−41204
boundary conditions, spherical, for computer experiment 80−105597
breakup three-body collisions, exact and approx. calcs. 77−88088
Brownian motion theory developments 79−25990
Brueckner approach to Sutherland one-dimens. many body problem 77−87660
Brueckner condition for MO selection in correlated orbitals 77−23436
Brueckner-Bethe calculations of nuclear matter 80−22718
Chakravarty-Woo eqn., extension and appl. to liq. ^{4}He, liq. ^{3}He, and nucl. matter 80−68124
channel coupling nuclear scatt. scheme, N-particle transition operators 78−569
charged three body problems with Coulomb pots. 80−18256
chemical dynamics, generalised Langevin theory, formulation and equiv. harmonic chain representation 80−35504
circular restricted three body problem , three-dim. stability of plane periodic orbits 77−17333
classical content of many-body quantum mechanics 79−53998
classical Liouville operators, eigenvalue problems 77−26228
classical systems, minimal specific energy 79−90364
cluster models, Faddeev-Yakubovskii coupling 80−105816
coarse grained variables, dynamics, exact results 79−80500
collective excitations, brief review of expt. and theory 77−1381
collective Hamiltonian subdynamics and collective states, geometric approach 80−8904
collective momenta existence Tomonaga's method extension 79−54011
collective motion in many boson system, collective coords. theory 77−57277
collective quantum fields for many body systems, appl. to BCS, ^{3}He and type II superconductors *(German)* 79−35917
collective subspace of many-body Hilbert space, generator coord. approach, kinematics 78−70055
collective vibrs., generator coord. description, double perturbative theory 77−79031
commutation symmetry for system of identical particles *(Russian)* 80−12944
comparison with binary collision cascade models up to 1 keV 78−29051
composite particle scatt., integral eqns. taking Pauli principle into account 78−86496
composite particles, nonrelativistic many-body theory, foundations and statistical mechanics 80−82947
computational atomic and molecular physics, conf., Nottingham, England, (Sept. 1978) 79−59567
computer experiments and their applications *(Polish)* 78−89420
conference on few body systems and nuclear forces, Graz, Austria (Aug. 1978) 79−67567
conference on few body systems and nuclear forces, Graz, Austria (Aug. 1978) 79−80880
conference on many-body theories, Trieste, Italy (Oct. 1978) 80−22135
configuration interaction and coupled cluster solns., analytic continuation 78−62147
configuration space basis state generation, U(n) matrix elements 80−86120
constrained systems, quantisation, path-integral nonlinear effects 79−21574
contracted orbital formulation of many-body perturbation theory 80−87026
core-hole processes, electronic Hamiltonian, many-body theory 80−91443
Coulomb effects in three body reactions with two charged particles 78−78331
Coulomb Green's function Sturmian expansion, Goldstone diagrams and reduction theorems 78−898
Coulomb off shell two body amplitudes, numerical computation 80−46858
Coulomb scattering, N-particle, cluster props. 80−73192
Coulomb systems, thermodynamic functions, phase transitions 79−85108
Coulomb systems HF eqn. solns. 77−46479
Coulomb two-centre problem, phaseshifts 79−63069
coupled electron pair models and many-body perturb. calcs. 79−59363
coupled eqns. many body scatt. formalism, test on three-body model 78−50139
coupled second order differential equations, soln. 79−40398
coupling master equation for N-subsystems *(Chinese)* 79−93038
covalent semiconductor, valence band calc. using many-electron theory 80−15434
crossing symmetry of many-particle amplitudes 79−40694
crystal defects, functional eqn., Tamm Dancoff procedure, canonical transformation *(German)* 80−84448

many-body problems continued
cyclopropane, ionis. pot., many-body Green's function method 77−67972
(d,d) scatt., discretized three-body problem 78−33194
decompositions into three- and four-body wave function channels 78−78333
dense stellar matter in asymptotically free gauge theories, high density limit 77−53421
density matrix , harmonic oscill. approx. 80−13391
density spatial distrib. of free particles in triangular pot. well 77−17905
deuteron breakup and stripping, three-body model 79−515
deuteron scattering from N-body scatt. theory, approx. three body model 79−75934
diagrammatic many-body perturbation expansion, computer program 78−50454
diagrammatic many-body perturbation expansion, ladder energies, computer program 78−50455
diagrammatic many-body perturbation expansion, ring energies, computer program 78−50456
diagrammatic many-body perturbation theory applicable to arbitrary model spaces 80−47844
diatomic molecules, excitation energies, oscillator strengths, many body approach, eqns. of motion method 80−47969
dielectric behaviour of materials undergoing dipole alignment transitions 80−88922
p-difluorobenzene, electronic struct., many-body calc., photoelectron spectrum assignment 77−23421
dilated three-body Schrodinger operators, scatt. theory 79−17256
Dirac particle+two Klein-Gordon particles, relativistic three-body wave equation, preon model 80−73574
direct energy minimisation methods in self-consistent nuclear fields, ground state props. 80−22702
direct interactions, relativistic addition in point form of dynamics 79−58907
dominant partition method 80−47455
dynamical instability of nonrelativistic many-body systems 77−49619
dynamics of molecules in contact with an external medium at equilibrium 79 9179
Eckart Hamiltonian, transformation approach 80−101726
education, one-dimens. many body model with two- and three-body forces, exact Hartree soln. 79−9065
efimov effect in an analytically solvable model 79−63083
elastic two-fragment collisions, multiple scatt., optical pot. and N-body approaches 79−93573
electron correlation problem, graphical unitary group approach, appl. to ketene 79−76324
electron gas, classical and quantal treatment involving integral eqns. 78−41228
electron gas, interacting, elec. cond. 78−95276
electron gas, interacting, local-field correction to dielectric constant, review 80−107731
electron gas, two-dimensional, study in weak mag. field 79−60742
electron gas, uniform, electronic props. of H and He impurities 80−96807
electron shell, types of collective motion 79−63886
Epstein-Nesbet partitioning of full Hamiltonian, second-quantisation representation 77−3254
equations of motion-Green's function methods, wave function approach 77−65416
equations of state in many body theory 80−42183
equilibrium configuration for one-dimens. problem, pair pots. 78−4513
ethylene, self-consistent many-body theory, self-energy effect 79−63901
ethylene imine, ionis. pot., many-body Green's function method 77−67972
ethylene oxide, ionis. pot., many-body Green's function method 77−67972
EXAFS amplitudes, many-body effects 80−97379
exchange effects in direct reactions, antisymmetrisation and three body models 80−13446
exponential operator approximants, many-body appl. 77−9896
extended Fermi systems, hypernetted-chain calcs., convergence props. 78−24733
factorisation of classical and quantum S-matrix, rel. to conservation laws 77−30277
factorization properties and spurious solutions in N-body scattering theories 79−12987
Faddeev eqn., reduction to 1 dimension by Galerkin method using cubic splines 77−26189
Faddeev eqns. approx. solns., possibility of complex eigenvalues 77−9909
Faddeev equations, two-potential formula, three-body scattering 80−4893
Faddeev integral eqns. for three charged particles *(Russian)* 80−8830
Faddeev-Yakubovsky equations for two distinct pairs of identical particles 77−82832
Fadeev's eqns., close coupling method for three-particle scatt. *(Russian)* 77−61222
Fadeev integral eqns. for 3 particles in boundary condition model, wave function determ. 78−54248
Fermi model fluid eqn. of state, nuclear matter appl. 77−18443
Fermi systems, review of methods in quantum field theory 78−8338
Fermi-hypernetted-chain method, upper bound on variational energy 77−291
fermion energy lower bound models 77−37809
fermion hypernetted chain approx., optimal correlation functions for liquid ^{3}He, electron gas 80−24822
fermion many body systems, Tamm-Dancoff method based on SO(2N+1) regular representation 79−35629
fermion system with higher symmetries, energy spectrum 77−5698
fermion theory based on SO(2N+1) Lie algebra of fermion operators 77−67374
fermion two- and three dimens. density oscills., Tomonaga boson operators 78−41232
few body dynamics, conf. 77−18368
few body dynamics analytical continuation, nuclear shell model, resonances and bound states *(Russian)* 79−40860
few nucleon systems, resonating group model 78−29431
few-body methods, stat. mechanics, atomic and molecular physics, nuclear N-body problem 79−85379
few-body problem, deuteron, EM effects, three body bound state, break-up reactions 79−85384
few-body quantum system stochastic variational method for all conventional N-N pots. 77−53799
few-body scatt. in quantum mechanics, soln. methods 79−85010

many-body problems continued
few-nucleon systems, analytical continuation of the core constants 79−71803
few-nucleon systems, bound states, bridge concept 77−22927
few-nucleon systems, computational methods, Faddeev eqn. 77−22907
FHNC equations, derivation 79−54048
field theory model of NNπ system, three-body problem, disconnectedness problem 78−29276
finite Fermi systems, symmetrized correl. functions, renormalisation procedure 78−4555
finite nuclei, pairing correls. including virtual mesons 77−41899
finite volume statistical mechanics for highly singular two body pots., many particle interactions 77−5752
five-body equation, wave function treatment for binary partitions 78−16686
fluid semiclassical statistical mech., quantum effects nonperturbative incorporation 79−64819
form factor approach 79−79
four body equation 77−17857
four body system, decoupled Yakubovski eqn. optical pot. and physical implications 78−78334
four charged particle system, two-body Coulomb singularities *(Russian)* 79−30291
four nucleon system, nonrelativistic soluble field theoretic formalism 77−2918
four nucleon wave functions, Taylor series method 78−66223
four particle problem in resonating group approx., integral eqns. 77−2960
four particle systems, eigenfunction/eigenvalue problem, effective Hamiltonians in paired channels 78−13037
four-body, K-matrix formalism, bound state scatt. theory 77−17858
four-body final states, nonrelativistic anal. 77−37779
four-body model of four-nucleon system, spin and isospin effects 79−71802
four-body problem, ang. momentum reduction anal. 77−37767
four-body problem, appl. of hyperspherical functions 79−21981
four-body problem, wave function soln. 78−86190
four-body problems, unitary pole approx., few-nucleon system appls. 78−516
four-body scatt., transition amplitudes determ. 78−24983
four-body system, energy dependent pole approx. 79−71801
four-hadron isobar model 79−26263
four-nucleon integral eqn. solns. using effective UPA 79−71794
four-nucleon problem, integral eqn. approach, pair-wise interactions *(Russian)* 77−88052
four-nucleon problem, microscopic K-matrix continuous spectrum *(Russian)* 77−61352
Friedrichs model unitary regularisation for many particle system 80−32039
fully symmetric nonlinear theories, Green's function methods, SCF theory 77−61180
gas, high density, resonant dielec. susceptibility 77−76023
gas, high density, resonant dielectric susceptibility, collective excitation transfer effect 77−76024
geminal expansions, symmetrised, N-completeness 79−63068
general algebraic treatment of identical particles in scattering processes 78−81891
generalised optical potentials, four-body problems 80−22781
generalized Boltzmann equation for many-body distributions 79−30351
Ginzburg-Landau model, dynamic renormalisation group anal. in large n limit 79−9193
Glauber approx. corrections, nucleon-nucleus scatt., nuclear density distrib. 78−50166
gravitational gas, one-dimens., Schrodinger eqn. for N-body problem 77−33943
Green's function method for many-body problem for relativistic meson field theory, book contrib. 80−357
Green's functions determ. using ab initio calcs. 79−80506
Green's functions in quantum theory, book 79−65147
Green diagrams, group theory anal. 78−28992
half off-shell phase eqns. for non-local interactions 78−70019
half shell t-matrix parametrisation for delineated two-body bound state 77−18407
half-phase shell shift in terms of on-shell phase function 78−29279
Hamiltonian, zero-order, for many-body perturbation theory 80−9483
Hamiltonian formulation of N-body theories, effective interactions and many-body corrections 79−75938
Hamiltonian model for N, π and Δ in many body problems 79−85417
hard rods, in finite 1-D mixture, time displaced correlation functions 78−54287
harmonic forces, translationally invariant wave function of many-body system 77−61018
Hartree approx., time dependent, 1-D system of bosons with attractive δ-function interactions 78−16728
heavy ion collisions, eqns. of motion in Ehrenfest's theorem 79−17916
Helmholtz equation, 1-D three-body problem, Sommerfeld Maluzhinetz transformation 80−62524
Hermite polynomials, zeros 78−20938
high density matter, relativisitc quantum many-body problem 78−4909
Hunziker's theorem, proof 77−26190
hyperspherical expansion of many-particle wave functions, singularities at partial wave origin 77−74264
identical particle scatt., general algebraic theory 78−86185
impulse approx., neglect of binding 79−112
inclusive cross section density matrix and scaling props., quantum field theory 77−41872
infinite gradient systems, asymptotic behaviour 79−40386
infinite nuclear matter ambiguities, harmonic oscillator and infinite well solns. 80−22742
inhomogeneous many-body system integral equations for quantum liquids and solids 80−22732
integral equation and resonating group methods relation 77−18493
integral equations, spurious solns., in N-particle quantum scatt. theory 78−65812
integral equations for three- and four-nucleon problem, resonating group approx. 77−18432
intermolecular mechanics, three-body Coulomb interaction, adiabatic representation 79−31640
inverse scattering transforms, Zakharov-Shabat and Schrodinger-type, connection 78−21006

many-body problems continued
involute set of integrals for completely integrable problems with pair interaction 77−22448
ion, singly-charged, sufficient conditions for finite no. of bound states 79−10047
ionic solid, many body effects on fourth order elastic coefficients 77−72647
ionisation potentials, sum rule, Manne Åberg theorem connection, many body Green's function formalism 80−27930
isobar degrees of freedom, binding energy from BHF approx. 80−22734
isobar degrees of freedom in nuclear matter, binding, NN interactions and 2π exchange 80−22735
isospectral matrices, finite transforms 80−105529
Jahn-Teller system, T×t strongly coupled 77−28147
Jastow and exact many fermion theories, comparison 77−17908
Jordan-Wigner representation of CAR algebra, boson expansions 78−36850
K-harmonic solution for three bound unequal particles 80−12940
K-harmonics in one dimension 79−2584
K-harmonics method, higher approx. 78−78287
K-harmonics method for nuclear many body problem with two-body interaction 78−33125
kinetic equation for a weakly-coupled test-particle 79−54039
kinetic few-body propagator by exact inversion 80−86123
kinetic theory, formal struct. 77−13683
Klein paradox as many-particle problem 77−2717
Klein-Gordon particles+Dirac particle, relativistic three-body wave equation, preon model 80−73574
linear response and Hartree-Fock, coordinate space representation and gradient iteration 80−18216
linear response theory, many-body van Hove limit 78−62156
linear response theory and area preserving mappings, review 78−62174
Lipkin model, quasi-spin pairing and struct. 79−485
Lipkin model special case for Hartree-Fock and many-body problem solns. 79−13229
Lippman-Schwinger eqn., soln. by Galerkin method using cubic splines 77−26189
Lippmann Schwinger eqns. for three charged particles 80−4580
Lippmann-Schwinger eqn., trinucleon bound-state problem 78−33156
liquid metal, electron momentum density, perturbed Green's function method 78−60052
localised site cluster expansion, interacting paramagnetic sites, spin symmetry projection 79−7951
low lying excited states, extension of ground state variational methods 79−36177
magnon elementary excitations damping *(Russian)* 79−28515
many body perturbation expansion, fourth order linked diagrams for quadruply-excited states 79−59364
many-body resonances, analytical continuation of bound states examination 79−75955
many-body scatt. theory, orthogonalised distorted waves and optical potentials 79−75940
many-boson absorption, nonreson. maximum 78−8343
many-electron interaction in crystals, symmetry group basis 77−51682
many-fermion system, Monte Carlo simulation 78−12644
many-fermion theory, expS or coupled cluster form 78−29048
many-particle Hamiltonian with two-particle singular pots., self-adjointness 77−67311
many-particle Hamiltonians in symmetry spaces, finiteness of discrete spectrum 79−2719
mass centre separation in homogeneous mag. fields 79−80
mass distrib. of disrupting three-body systems 77−49277
massless Yang-Mills field and many-body pot. 78−29258
Maxwell-Boltzmann statistical distrib. function of ideal gaseous assembly 80−17858
Mayer cluster function and quantum two-body t matrix 80−17859
metal, 3d, X-ray emission and XPS broadening, many-body effects and intra-atomic exchange 77−44090
metal, with stored H, electronic struct., many electron theory 80−49667
minimal relativistic dynamics of the 3π and $\pi\pi$N systems 79−75702
model three-body problem in the molecular mass limit 79−49068
molecular dynamics method in statistical physics, review 80−18895
molecular polarisability, scaling and Pade approximants, many-body perturbation theory 80−42952
molecular structure, many-body scatt. calcs., channel coupling array method 79−31362
molecule, calc. of induced elec. and mag. moments 77−57884
molecule, mag. susceptibility, calcs. using completely minimising gauge functions 77−6702
molecules, Fokker-Planck eqns., stochastic modeling 80−43128
molecules, ground state props., coupled cluster and MBPT methods appl. 80−47881
molecules, valence and core photoionisation, spectral lines, many body effects 80−47853
Molien function of a symmetric group 80−8857
Monte Carlo computations of multidimens. integrals 77−57164
Monte Carlo methods in quantum many-body problems, nuclear physics 80−22727
Monte Carlo methods in statistical physics, book 79−80528
multichannel nuclear reactions, connected kernel formalism 78−46038
multichannel quantum mechanical scatt., time independent theory 77−17859
multichannel quantum scatt., two-Hilbert space formulation 78−28986
multichannel scatt. theory in two spaces 79−88839
multichannel scattering, exact and Glauber amplitudes 80−13421
multichannel T-matrix, separable form, relevance to few-body problem 77−57471
multielectron configuration, evaluation of matrix elements of energy operator 79−63895
multilocal theory, relativistic mechanics of interacting particles 78−16638
multimagnon bound states, unphysical solns. to Faddeev eqns. 77−18440
multiparticle cores in nuclei, matter fluctuations, binding energy, repulsion correlations 79−75864
multiparticle scatt., time depend., arrangement-channel quantum mech. 77−41503
multiparticle scattering, weighted Hilbert space 79−75380
multiple scattering approximations in 3-body problems, comparison 79−84
Muskhelishvili-Omnes equation and final state interactions 80−17821

many-body problems continued
$(N\pm1)$ particle system resonances dilated Green's function approach 79−71295
$N\geq4$-particle systems, approximation methods 77−22906
$N\geq4$-particle systems, nonrelativistic dynamical eqns. 77−22906
N identical particles, Rayleigh-Ritz principle complement for energy spectrum 80−5074
N interacting particle canonical distrib. from kinetic theory 80−105569
N-body integral eqns. and orthogonality scatt. 77−17861
n-body quantum system, time depend. scatt. theory for infinite delta function pots. 78−49704
N-body scatt., filter operators in linked-cluster formalism 79−45040
N-body scatt. in two-cluster region 78−28975
N-body scatt. systems, explicit bounds for total scatt. cross section 79−80462
N-body scattering, general formalism, relationships between formulations 79−75412
N-body scattering theory, unified connected theory of few-body reaction mechanisms 79−71822
N-body Schrodinger operators, eigenfunctions, wave packets, pointwise bounds 79−12634
N-boson problem, nonlocal interactions 79−71296
N-completeness problem, soln. for many electron systems 77−23405
N-dimensional systems, exact time-depend. invariants 80−8824
n-fermion problem, new boson expansion, appl. to ^{4}He 78−511
n-particle relativistic phase space integral, invariant variables, Monte Carlo calc. algorithm 79−9312
N-particle scatt., dynamical eqns., for transit operators 77−18428
N-particle scatt. ionisation T matrix 79−44777
n-particle scatt. theory, asymptotic completeness 79−75413
N-particle Schrodinger eqn., macroscopic behaviour, superconductor and fermion systems 78−60242
N-particle system, many body correl. and scatt. amplitudes 79−30683
N-particle system with separated collective motion, Hamiltonian *(Russian)* 77−5701
narrow resonances in the continuum 79−85435
narrow-band solids, Hubbard Hamiltonian, derivation from many-body Hamiltonian 79−56112
neutron, alpha and nuclear matter, ground vacuum states 80−22738
neutron and nuclear matter, variational calc. models 80−22724
neutron distribution in nuclei, elastic and inelastic proton scattering, review 80−22649
neutron gas, crystallisation, zero-order, Bethe-Fermi homework potential 80−63117
neutron matter, spin and tensor correlations, cluster expansion hypernetted chain eqns. 80−22728
neutron or nuclear matter, spin depend. correlations, variational method 80−22726
neutron star matter, abnormal phase 78−20849
non-Hermitian bound state formalisms based on N-body scatt. theory, quantal rules 79−75939
non-hermitian potls., completeness relns. in scatt. theory 77−17854
nonlocal continuous potentials, theory of integral operators and eigenvalue anal. 78−8274
nonrelativistic supersymmetry, relevance to many-body problems 80−22537
nonsingular integral eqn. for three body scatt. problem 78−62106
nonstationary systems, invariants and radiation 78−36929
normal ordering, identities 78−86059
nuclear, variational calculations in harmonic oscillator basis 77−6263
nuclear 4-body problem, configuration space approach 78−46012
nuclear break up process as three body problem, Faddeev eqns. 78−89842
nuclear coherent recoil dominance, basis for quasi two-body scaling 78−50140
nuclear collisions, relativistic, classical many-body calc. 79−17918
nuclear many body problem, boson-fermion descript. *(Chinese)* 78−82297
nuclear many body scattering, channel coupling array theory, wave function formalisms 80−78235
nuclear many-body problem as relativistic field theory 77−10336
nuclear many-body problems, finite density Hartree-Fock anal. 77−18457
nuclear matter, Brueckner Bethe and variational calcs. review, nuclear saturation problem 80−22745
nuclear matter, constrained variational calcs., three body and N* (1234) contribs., cluster energy 80−22743
nuclear matter, dispersion relations, HF method for hard core interactions *(German)* 78−54713
nuclear matter, exp(S) formalism, n-body Schrodinger eqn. 77−22918
nuclear matter, fermion hypernetted chain variational calc. 80−22725
nuclear matter, many-body correl. simulation by pair excit. amplitudes 77−2923
nuclear matter, three-body problem, variational and Bethe-Faddeev methods 80−27586
nuclear matter, variational techniques, review 80−22748
nuclear matter BBG theory, auxiliary single particle field for binding energy 80−22723
nuclear matter binding energy from low density expansions, Brueckner-Hartree-Fock approx. 80−22720
nuclear matter props., charge dependent N-N potential, HF calcs. 78−50115
nuclear medium, solid like aspect with alternating layer spin and π condensation 80−22733
nuclear meson dynamics in many-body problem, HF approx. 77−22917
nuclear n-body reaction calcs., integral transform applicability 78−4920
nuclear physics, many-body forces, review, book contrib. 79−97670
nuclear reactions, connected kernel formalism 78−4921
nuclear scatt., variational principles for true three- and four-particle scatterings 80−78233
nuclear scattering, coupled channel eqns. and off shell transforms. 78−402
nuclear structure, algebraic variational approach 77−18451
nuclear surface phenomena, Yakubovski eqn. appl. to N-body systems 79−75931
nuclear system, total energy, static Hartree-Fock calcs. 80−47414
nuclei, spherical, quasi-particle theory, modification of BCS basis 80−63109
number operators for composite particles in nonrelativistic many-body theory 80−94982

many-body problems continued
off-shell continuation of scattering amplitude in quantum mech., inverse method 79−49423
off-shell transformations and wave function formalisms in many-body scattering theories 79−75937
one-dimensional many-body problems, exact results, review *(Russian)* 79−80460
one-dimensional three body system, δ-interaction, exact bound-state soln. 77−5694
open shell RPA unitary group formulation, Hartree Fock stability eqns. 80−52860
open shell systems, wave operator hierarchy eqns. 79−41087
open-shell systems, many-body perturbation theory, coupled cluster approach 79−31360
operator formulation of statistical mechanics 78−24734
orbit-orbit interaction, new tensor expansion, matrix and graphical forms 80−14064
orthogonal polynomials, asymptotic density of zeros 79−30286
P scatering, 0.8 to 1.5 GeV, neutron distrib. anal. 79−26429
Pade approximant of T-matrix elements, convergence in few-nucleon systems 79−21975
pair potentials, equilib. configuration of one-dimens. many-body problems 78−49692
pairing Hamiltonian, general, approximate solns., by variational method 78−36931
pairing rotations and quadrupole modes, many-quasiparticle excitations 80−18165
paramagnet, electron state density for narrow-band model with Coulomb interaction 80−10852
particle number increase effects *(French)* 78−37539
n-particle quantum system, energy operator discrete spectrum 79−85006
particle-hole propagator, order analysis 77−38602
path integral approach to many-nucleon systems and time-dependent Hartree-Fock 80−78180
path integrals and time-dependent mean-field theories, many-body problem, Hartree-Fock eqns., Slater determinants 80−37342
path-integral in collective fields and its application to nuclear and hadron physics *(Russian)* 79−93277
perturbation theory, many-body, arbitrary point group symmetry, wave operator matrix elements 80−23311
phase equiv. potls., invariant physical props. 77−17855
photoemission, external, many-body aspects, Green's functions 78−72703
photoemission, many electron and final state effects, book contrib. 79−61498
photon emission by N-independent excited atoms, wave functions 77−57895
physical transition operators, off-shell continuations 77−22980
pion condensation, field theoretic many-body system 80−22703
plasma, one-component, virial pressure 80−38536
polar emission in fission, nuclear orbiting, three-body trajectory classical calc. 79−3131
pole expansions of nonlinear partial differential eqns., corresponding many body problems 77−82372
polyatomic molecule+atom, many body approach 79−31645
polyatomic molecules, excitation energies, oscillator strengths, many body approach, eqns. of motion method 80−47969
polymer expansion for quantum many-body problem 80−57181
position operators for relativistic non-interacting n-particle system 78−41182
potential scattering, boundary condition model, two and three nucleon problems *(Russian)* 78−86491
power series soln. of coupled eqns. and three-body problem 80−86145
probability amplitudes of transitions between not necessarily stationary states, coupling const. 80−36902
product represenation in effective range theory 78−78273
programmable procedure for generating many-particle states 80−27169
QED, S-matrix anal. as three-body interaction Klauder phenomenon interpretation 79−80777
qualitative methods in problem solving, graduate text book 77−71239
quantised many-body problem, dissipative system wave eqn. 80−86104
quantum chemistry, many body perturbation theory fourth order calc. of correl. energy 80−14087
quantum chemistry, spin-free, alternacy, quantum no. assignment 79−9988
quantum chemistry, spin-free, particle-hole and pairing symmetries 79−6812
quantum field theory, multilocal, Fock-space technique, particle creation effects 80−77945
quantum isolated system, scatt. theory reformulation 78−49718
quantum many-particle systems in curved spacetime 80−98751
quantum mechanical systems, evolution of structure and order 77−41528
quantum systems, interacting particles, ground state energy per particle 80−68064
quantum systems, mutual bonding of particles 80−101724
quantum three particle system, action-angle variables 80−95708
quantum three-body problem, distorted Faddeev eqns. with coupled channel approach 80−52635
quantum-mechanical kinetic energy as measure of information in distribution 80−101725
quasiparticle pairing at arbitrary densities, soluble model 77−6252
quasiparticle picture, at. and mol. systems, breakdown for inner valence electrons 78−5112
R-matrix method for nuclear reactions, errors in Tobocman's formulation 79−63642
real time Green's function 78−57855
realistic NN pot. construction for three body systems and nuclear matter 80−22699
recoil effect, light particle scatt. by two heavy particles *(Russian)* 78−82129
reduced matrix eqn. for many-body scatt., symm. solns. 78−29433
reduction procedure, on-shell integral eqns. for scatt. amplitude 77−67594
relativistic, Hamiltonian n-particle systems, advanced retarded polarisation 78−29017
relativistic, three-particle bound states, wave function calcs. 78−8558
relativistic composite particle scatt., quasipotl. approach 78−404
relativistic Hamiltonian mechs., position variables 80−27123
relativistic Lagrangian for multilocal model 77−87690
relativistic many body theory, finite temp. and density., elementary particle symmetries 79−49403
many-body problems continued
relativistic many-body theory, quantum chromodynamics and neutron stars/supernova 79−40752
relativistic particle systems, remarks on 1961 paper 77−67326
relativistic RPA determ. of oscill. strengths and excitation energies 80−47925
relativistic theory, spectral-function sum rules 77−67591
relativistic theory of many-electron atoms, H_+ and h_+ and related HF eqns. derivation 80−99458
relativistic three-body problem, unitarity and analyticity 77−18495
relativistic two-body forces in many-body systems, Weinberg and Yukawa interactions 80−32203
relaxational dynamics, renormalisation group anal., scaling fields and variables 80−105602
renormalisation group approach to scaling, phys. appl. 78−49634
resonance theory in indefinite metric spaces 80−101730
resonances, extended virial theorem, complex acaling, Schrodinger operators 79−21575
resonating-group method for nuclear many-body problems, review 79 9497
response function and effective potential, self consistent theory 79−35628
restricted three body problem, asymptotic solns. near collinear libration points 77−91414
restricted three body problem, critical generating orbits for second species, periodic solns. 78−4089
ring diagrams in nuclear matter, many-body forces contrib., ρ and π exchange 80−22740
rotated Hamiltonian resolvent, approx. in scatt. region 77−71233
rotational motion, in many paritcle systems, description using collective variables 79−40830
RPA and pairing vibration approximations, multiple basis set calcs. 77 5755
rubbers, swollen, low-freq. dynamics, optical and mech. props. 80−43626
scalar meson field and many-body forces, book contrib. 80−359
scattering, struct. of many-body wavefunctions 78−62119
scattering operator of few-body quantum mechanical system, sum of two-body potential operators 80−62516
scattering subspace defn. in nonrelativistic quantum theory 77−33889
scattering theory of ≥4 particles, on the unique soln. 78−21005
Schrodinger eqn., complete exact solution to the translation-invariant N-body harmonic oscillator problem 80−31558
Schrodinger equation, exact solns. for translation-invariant harmonic atoms 78−32725
Schrodinger equation, three-body problem with hard cores, 1-D, reduction to 2-D Helmholtz eqn. 80−62523
Schrodinger equation, three-body problem with hard cores, 1-D, eigenvalue lower bounds 80−68069
Schrodinger equation, wave functions, generalised wave operators for system of three charged nonrelativistic particles 79−75398
Schrodinger equations, three-body problem, bound state eigenvalues lower bounds, upper bounds by Rayleigh-Ritz method 80−68068
Schrodinger many-body operator decomposition 77−22434
Schwinger variational principle for bound states and scatt. problems 78−16932
self consistent RPA for three body forces in Fermi systems 78−89810
semiclassical canonical density matrix, approx. semigroup props. 78−16723
semiconductor, Raman scatt., one-phonon final states and many-body effects 80−34913
semirestricted three body problem 77−25932
separable approx. to local interactions, exponential pot. 79−508
separable interaction of composite particles with inclusion of the Pauli principle 79−85389
separable many-particle interactions, free energy calcs. 77−9954
separable many-particle interactions, free energy per particle, convex-envelope formulation 78−32781
separable quasipotential formulation of the relativistic dynamics for three point particles 79−12989
separable short range interaction system, free energy per particle 77−26238
short-range asymptotic wave function method, appls. 78−24727
simple fluid, one-component, liquid-vapour phase coexistance, surface tension determ. from many body pot. 80−49465
simple quantum liquids, Jastrow variational wave functions, for nuclear matter, liquid ^{3}He and ^{4}He 80−22729
singularities in four-body final-state amplitudes 79−26264
singularity analysis of N-body scattering wave functions 79−71286
Skyrme-type interactions, spectroscopy of light nuclei, density dependent Hartree-Fock 80−22717
solid dielectric loss peak, many-body interpretation 80−15953
solid universal dielectric response law, many-body interpretation 80−15952
solids, large thermal fluctuations, kinetic eqns. for many-body treatment 79−54037
solvable many-body problems, special solns. of partial differential eqns., poles and zeros motions 78−41226
space time inhomogeneous Gibbs ensembles, dynamics of macro-observables 79−9182
spatial correlations and elementary excitations in many-body systems 80−22730
spectral distribution methods in effective interaction theory 78−86489
sphere-wall attraction, many-body formula, approximation 78−21000
spinless particle many-body problem, multiconfigurational approx. 78−4518
spurious solutions in few-body equations 79−75402
stationary nonlinear Hartree eqn., asymptotic soln. 78−49723
statistical crystal model, small amplitude acoustic perturbations and Debye-Waller factors 78−55930
Stockmayer-type polarisable mols., N-particle dynamics 77−68089
sum rules for coeffs. of fractional parentage 77−50067
Sun-Jupiter-asteroid circular and elliptic problem comparison at commensurabilities 77−56819
superconductivity and elementary particles theory, review 80−4911
symmetrical basis in the three-body problem *(Russian)* 79−40861
symmetries and statistics in many-particle systems, group theory aspects 77−18452
systems with weak coupling between remote particles, novel first integrals 77−65003
Tabakin rank-one potl. in orthogonality condition model, 3-body energy 77−18423

many-body problems continued
TDHF eqns. for quantum mechanical many body systems 78−78296
ten-electron systems, correl. energy, fourth order diagrammatic, many body Rayleigh Schrodinger perturbation theory 80−63556
thermodynamic characteristics with separation of nearest-neighbour interaction 77−41559
third cluster coefficient for square well discs 79−85072
Thomas-Fermi theory, many-body atomic theory 78−21849
three body calculation of ^{6}Li energy levels and d-α elastic scatt. 77−54158
three body nonrelativistic problem, symmetric elimination of c.m. motion 78−69974
three body phase space distribs., Monte Carlo calcs. 80−37393
three body problem, Green function hierarchy 79−75941
three body problem, Lippmann-Schwinger eqns. 79−44785
three body problem for general even power potential with applications 79−25900
three body problem for hyperbolic and Coulomb potentials 80−22223
three body problem in quantum mechs., singularities, Lavine's method appl. *(French)* 77−67310
three body problem near triple collision 77−17336
three body problem with energy dependent potentials 77−18413
three body problem with three body forces, special solns. to integral eqns. 79−75869
three body scatt., spline function moment methods 80−505
three body Schrodinger operators, scatt. theory, using abstract stationary theory 79−17265
three body separable expansion amplitude 77−18430
three body systems, spectral and scatt. theory of Schrodinger eqn. 77−45715
three body systems in nuclear physics, review 78−517
three body zero covariant equations 77−17856
three fermion system with exchange potential, asymptotic soln. of Schrodinger eqn. 77−38229
three fixed centres problem 77−25933
three nucleon clusters in nuclear matter, intermediate Δ-states, exchange diagrams calc. 78−17112
three particle Coulomb problem for two electron systems, hyperspherical coords. framework 80−52875
three particle reactions, S-matrix theory kinematic props. 78−54578
three particle scatt. rates, double scatt., T-matrix singularities 78−32727
three particle systems, diffractive prod. and relativistic rescatt. 79−12988
three particle systems, reaction mechanism and approx. models 79−80904
three particle systems with Coulomb interaction, scatt. and breakup eqns. exact solns. 80−504
three particles with Coulomb interaction, binding energy and scatt. states *(Russian)* 80−5051
three resonantly interacting particles, level spectrum 77−17860
three resonantly interacting particles, scatt. processes and bound states *(Russian)* 79−54017
three spinless particles, eigenvalues of Faddeev eqn. kernel determ. 77−2565
three- and four-body eqns. with half-off-shell input 77−18429
three- and four-body interaction props., hyperspherical expansion convergence *(Russian)* 78−518
three- and four-nucleon systems, dynamical eqns. and approx. methods 77−22905
three-body, basis expansion for hyperspherical approach to triton model 78−54693
three-body, two-pion exchange forces, ^{4}He calc. 77−41895
three-body Amado-Lovelace eqn. at positive energies, anal. soln. 78−16938
three-body Bethe-Faddeev equations and single-particle potentials in nuclei 79−97684
three-body breakup reacts., dynamics 78−13040
three-body eigen wave function of a continuous spectrum, asymptotic form 79−5994
three-body Faddeev eqns., analytical soln. 77−38104
three-body forces in 3- and 4-nucleon systems 78−29400
three-body K-operators and unitary approx., appl. to (d,p) and (d,d) 77−18499
three-body one-dimens. three-force problem, path integration 77−49624
three-body problem, bound state and scatt. problems 78−16684
three-body problem, coupled channel method calcs., Faddeev approach 78−86929
three-body problem, decoupled integral eqns. 78−24982
three-body problem, number of discrete levels 77−49636
three-body problem, partial wave amplitude singularities for multiple scatt. series diagrams 79−71664
three-body problem, relativistic description, deuteron breakup appl. 77−46156
three-body problem, variational method appl. to He atom *(German)* 77−33881
three-body problem in one dimension 80−82655
three-body problem of two electron atoms 80−83286
three-body problem with Bargmann potentials 78−82274
three-body problems, Schrodinger perturbation theory in adiabatic rep. *(Russian)* 77−60976
three-body problems with local potls. in coord. space 77−26594
three-body quantum system, negative point spectrum 77−5683
three-body reactions with charged particles 79−75968
three-body scatt. amplitudes, appl. of contour rot. 78−567
three-body scatt. problem, cluster expansions, effective intercluster pots. 80−5082
three-body scattering equations, nonsingular representation, partial-wave anal. 80−91021
three-body system, computation method for eigenvalues and eigenvectors 78−24681
three-body system, conditions for absence of bound states 77−45725
three-body system in mesoatomic physics, adiabatic two level approx. *(Russian)* 79−22870
three-body system S energy levels, functional integration 77−67323
three-body systems, number of bound states and Efimov's effect 80−31536
three-body vertices with two-body techniques 77−18435
three-hadron physics, book 77−45980
three-nucleon bound state, soln., perturbational approach to Faddeev eqn. 79−30793
three-nucleon elastic scatt., hyperspherical harmonics 77−57636
three-nucleon system, coherence effect, N-particle generalisation, final state interactions 78−89833
three-nucleon system, fractional-parentage construction of wave function 77−14041
three-particle relativistic kinematics 80−27602
three-particle scatt., finite cross section 79−85011
three-particle scatt., on-shell prescription 78−8559
three-particle scatt. operator, correl. pattern representation 77−13684
three-particle scatt. rates, disconnected T matrix singularity 78−32726
three-particle scattering, subtraction techniques 78−24694
three-particle scattering, unitary regularization *(Russian)* 78−28999
three-particle system, orthogonal projection 78−90
three-particle system (two charged particles), scatt. theory *(Russian)* 79−12991
time delay in N-body scattering 79−75695
time dependent-correlations in many body systems, theory 77−82460
time inversion and mobility 80−101722
Toda lattice, poles, soliton solns. 79−75368
topologically distinct diagrams, tensor notation 77−57274
transition metals, 3d, electron impact excited soft X-ray spectra, resonances and many body effects 80−50468
transition operators, CCA class, under particle interchange, unexpected behaviour 79−75694
translation invariant N-body problem, exact solns. to Schrodinger eqn. 78−65801
translation-invariant atomlike identical particles systems, lower energy bounds, nonrelativistic quantum mechs. 78−86187
trinucleon system bound by one-boson-exchange force 77−18414
trinucleon wave functions, anal. of shape 77−18434
Trojan asteroids, long-periodic solution in restricted three body problems 77−17337
Trojan asteroids, restricted three body problem 77−74003
two charged clusters collision, scatt. amplitudes and integral eqns. 80−68614
two cluster scattering amplitudes, dilation anal. reson. rel. to scatt. reson. 79−40389
two or three electrons, interacting with localised mag. moment, wave function determ. *(French)* 79−12636
two- and three-particle scatt. for relativistic systems in light front dynamics *(Russian)* 80−62892
two-body bound state and half off-shell t-matrix parametrisation 77−18424
two-body scatt. T matrix in real-time formalism 78−41230
two-body scattering in force field 79−85012
two-body transition matrix and UPA model, convergence props. of generalised separable expansion 78−16939
two-cluster scattering of N-charged particles 79−40387
two-particle fractional parentage coeffs. in unitary scheme 77−41905
two-particle resonance+particle interactions, scatt. amplitude, arbitrary spins *(Russian)* 77−74621
two-space scattering theory, with applications to many-body problems 79−17264
unitarily equivalent multiparticle Hamiltonian systems yielding equal scattering for corresponding states 78−77756
unitary group approach to molecular electronic structure 80−5467
unitary group formulation of many-electron theory and quantum organic chemistry 80−106270
unitary pole expansion, physical basis 77−18406
Universe, high density matter, many body treatment, pulsars 80−26738
variational calculation for model nuclear matter using a new integral equation method 78−82301
variational localised site cluster expansion, wave function ansatze, many body theory 79−6827
variational localised site cluster expansion, wave function higher ansatze, linear Heisenberg model 79−7959
variational principles for true three- and four-particle scatterings 80−18254
VB theory, many-body, variational localised-site cluster expansions 79−60669
vertex function and crossing symmetry 80−62515
vortices, quantised, ang. momentum, creation and significance 78−24675
Ward identities for charged and neutral Fermi liquids 77−41530
wave equation of particle density operator 77−53830
weakly coupled mixtures of charged particles at zero temperature 80−140
Wigner's (2n+1) rule in MBPT 80−42095
(αnp) three-body elastic scatt. calc. using hyperspherical harmonics 79−63640
(d,p), 1.7-15 MeV, rearrangement collisions three body model, bound state approx., DWBA calcs. 79−93595
d(d^*)N coupling constants via spectator functions 78−46011
$e^+e^-e^-$, two-electron at., three-body problem, binding energy 79−3372
(γ,π), few body pion photoprod. in Δ-resonance, region 80−42636
Nd S-wave scatt., dispersion relation approach to three-body systems, unitarity approx. 79−506
NN hard core as relativistic effect 77−87994
NN potentials, based on meson exchange, discussion and appl. to nuclear matter 79−80815
NNπ system, effective 3-body with unusual disconnected struct. 79−75861
NNπ system relativistic anal. appl. to ^{3}H(π,π) elastic scatt. 77−61457
N$\pi\pi$ dynamics, medium energy, dispersion relations, isobar expansion for πN 80−4917
(π,π), many-body response problem, reaction channel m-croscopic treatment 79−85547
(π, π') many body QFT framework anal., final state particle-hole correlations 80−13508
πd field theoretical model, effective semi-relativistic three-body problem 78−86454
πN scatt., separable interactions for three-body problems 78−78113
$\pi\pi$ scatt., separable interactions for three-body problems 78−78113
qq interactions and nonrelativistic quark model 80−73682
Al, liquid, electron momentum density, correlations and ionic potentials 78−60052
Al, positron annihilation studies using high-density proportional chambers 80−25478
Ar, double photoionisation, many-body perturbation approach 78−17634
Ar, isoelectronic sequence, many-body photoionization calcs. 78−17631
Ar, M-shell photoionis., many-body interactions 79−10081

many-body problems continued
$Ar+Ar_2$, exchange and dissoc. interactions, three-body effects calcs. 77−9069
BF, $X^1\Sigma^+$ state, many-body effects, HF STO calcs., diagrammatic perturbation theory 77−50355
Be, Auger transitions, fluoresc. yield calcs., correl. effects 77−18869
Be-like system, numerical many-body perturbation calcs. using multiconfig. model space 80−47907
$^8Be(\alpha,\alpha)^8Be$ elastic scatt. generalised optical potentials, three-body approximation *(Russian)* 79−13313
$^8Be(n,n)^8Be$ elastic scatt. generalised optical potentials, three-body approximation *(Russian)* 79−13313
$^8Be(t,t)^8Be$ elastic scatt. generalised optical potentials, three-body approximation *(Russian)* 79−13313
CH^-, electron correl. energies, Pade approximants and many-body perturbation theory 79−59366
CO, ground state, third-order many-body perturbation theory 79−10015
CO, $X^1\Sigma^+$ state, diagrammatic many-body perturbation theory, pot. curves 79−10014
CO_2, lattice energies, non-additive three body contributions, triple-dipole term 80−54168
CS, $X^1\Sigma^+$ ground state, diagrammatic perturbation theory calcs. 78−29737
Ca+Ca, classical many-body model for heavy ion collisions 80−536
Cd, photoionisation cross section, many-body perturbation theory, dipole length and vel. calc. 78−78674
Cu, positron annihilation studies using high-density proportional chambers 80−25478
Eu, HFS, many-body and relativistic effects 78−37565
Eu, hyperfine interaction calc., relativistic many-body approach 77−46504
Fe, Auger transitions, two-electron-one-photon radiative rate calc. 77−18869
Gd^{3+}, hyperfine interactions, relativistic CI using many-body calcs. 78−78638
Ge, ion bombarded, radiation defect formation, atom-atom collision cascades modelling 80−10582
H atom gas with unsaturated electron shells, third virial coeff. calcs. 79−90752
H^-, many-body perturbation theory with radially restricted basis functions 80−78526
$H+H_2 \rightarrow H_2+H$, classical three-body problem. calcs., effective reaction cross section *(Russian)* 79−39144
H_2, electric dipole polarisability, many-body perturbation theory calcs. 78−21839
H_2, four-body system, adiabatic representation 80−91530
H_2^+ three lower states, three body problems, separations of variables 80−36903
H_2CS, ionis. pot., many-body Green's function method 77−67965
HF, $X^1\Sigma^+$ state, many-body effects, HF STO calcs., diagrammatic perturbation theory 77−50355
H_2O, ground state, energy, bond parameters, diagrammatic perturbation theory calcs. 78−25414
H_2O, ground state correlation energy, diagrammatic perturbation theory 80−18774
H_2O, linewidths and press. shifts, in N_2 and air, Anderson theory and quantum many-body theory 78−74708
H_2O, many body perturbation theory fourth order calc. of correl. energy 80−14087
H_2O, many electron Green's function calcs. optical pot. 80−58126
H_2S, ionis. pot., many-body Green's function method 77−67965
$^2H(\alpha,\alpha)^2H$, three body calcs., Pade technique 78−46074
$^2H(\alpha,\alpha p)n$, 15-42 MeV, ^6Li 1^+ resonance and breakup amplitude, three body model 79−75954
$^2H(d,p)^3H$, four-body calc. solns. 79−71855
$^2H(n,n)$, ghost states and Pauli principle for many-body scatt. 79−76001
$^2H(n,n)$, local soft core NN pots., quasiparticle formalism 79−6529
$^2H(\pi,\pi)^2H$, 142 MeV, elastic cross section and polarisation observables 79−75791
^3H binding energy, 3N bound state with separable interactions, Faddeev theory corrections 80−13388
^3H, three-particle system for nonlocal interactions with continuum bound states 79−75870
$^3H(e,e')nd$, three-body calc. 78−33170
$^3H(\mu,\nu)3n$, transitions from bound to continuum three nucleon states 80−5128
$^3H(p,p)$, 4-12 MeV, Amado model quasi-three body calc. 78−25191
He, electron scatt., ionisation, elastic and inelastic collisions, many body theory appl. 80−48093
He, ground state radial limit, piecewise polynomial basis functions 78−37560
He, many electron system, photoionisation and photoexcitation, at. transition strong config. interaction effect 80−47909
He-like two electron atoms, three-body problem 79−3372
^3He, A-phase, collective modes of gap parameter for axial state 77−7937
^3He charge form factor, 3N bound state with separable interactions, Faddeev theory corrections 80−13388
^3He, liq., binding energy, variational calcs. by Pandharipande's method 80−101752
^3He liquid, binding energy calcs., Pandharipande method 79−65269
^3He-^4He film, many body approaches to liquid-vapour transition 78−51783
$^3He(e,e')pd$, three-body calc. 78−33170
$^3He(p,p)$, polarised p, below 6 MeV, anal. power meas. for four nucleon system levels 79−71837
$^3He(p,p)^3He$, four-body calc. solns. 79−71855
^4He, liq., binding energy, variational calcs. by Pandharipande's method 80−101752
^4He, liq., ground and low excited state struct., pair-pair correlation function 80−24694
^4He, liq., ground state from HNC and BBGKY eqns., elementary diagram effects 80−24693
^4He liquid, binding energy calcs., Pandharipande method 79−65269
^4He photodisintegration, 9-dimens. space hyperspherical harmonics 79−75975
^4He, superfluid, hard-sphere model, crit. anal. 78−51769
$^4He(d,d)$, 4.8-6.8 MeV, ^6Li resonances, phase shift analysis 79−75953
^5He, effective 3- and 4-body forces in 5 nucleon system 79−477
$_\Lambda{}^4He$-$_\Lambda{}^4H$ bound states using 4-body eqns. and separable pots. 79−75893

many-body problems continued
La, electron impact excited soft X-ray spectra, resonances and many body effects 80−50468
Li cluster, density functional calcs. 77−8031
Li halides, F-band energies press. effect 78−60086
Li I, $2s^2sp$ and $1s2s^2$ decay rates many-body perturbation theory calc. 79−59376
Li, two-photon ionis., many-body perturbation theory 79−22679
$Li^+ + CO_2$, rot. vibr. energy transfer, 1 to 10 eV, many body theory 80−28093
LiF, $X^1\Sigma^+$ state, many-body effects, HF STO calcs., diagrammatic perturbation theory 77−50355
LiH, many body perturbation theory fourth order calc. of correl. energy 80−14087
LiH, many electron Green's function calcs. optical pot. 80−58126
^5Li, effective 3- and 4-body forces in 5 nucleon system 79−477
^6Li, α-d relative wave functions using three different models 79−75872
^6Li, $\alpha+p+n$ model, numerical soln. of coupled Faddeev eqns. 79−17831
^6Li, αnp elastic scatt., 0.2-5.0 keV, three body model, phase shift, total cross section 79−75875
^6Li, three-body model using hyperspherical harmonics 78−29411
$^6Li(^3He,^3He)$, 27 MeV, cross sections, three body and optical model calcs. 79−76009
$^7Li(\alpha,\alpha)^7Li$ elastic scatt. generalised optical potentials, three-body approximation *(Russian)* 79−13313
Mg_2, pot. energy curve for $X^1\Sigma_g^+$ state, many-body perturbation calcs. 78−55216
Mn, HFS, many-body and relativistic effects 78−37565
N, nucl. quadrupole coupling const., relativistic many-body perturbation theory 78−37566
N_2, electronic ground state correl. energy, many-body diagrammatic perturbation theory calc. 78−917
N_2, excitation energies, eqn. of motion-Green's function calcs., 3rd order contribs. 77−65417
α-N_2, lattice energies, non-additive three body contributions, triple-dipole term 80−54168
N_2, shake-up peak positions and intensities calcs. using eqns. of motion Green's function method 78−86910
N_2F_2, trans- and cis-isomers, photoelectron spectra, Green's function calc. 77−83650
Na cluster, density functional calcs. 77−8031
Na, photoionisation cross-section, electron correls. Brueckner-Goldstone calcs. 77−6742
Ne, Auger energies, intensities, for initial K vacancy, many body calc. 77−18869
Ne, double photoionisation, many-body perturbation approach 78−17634
Ne, isoelectronic sequence, many-body photoionization calcs. 78−17631
Ne+Ne, classical many-body model for heavy ion collisions 80−536
Ni, chemisorbed H_2 photoemission spectrum, Anderson model parameterisation 77−40334
$^{58}Ni(d,d)$, three-body model with adiabatic approx. 79−40934
^{16}O and Sd shell nuclei, binding energy from realistic Hamiltonians and spectral distrib. theory 80−22678
^{16}O, energy calcs., Jastrow variational method extension, FAHT cluster expansion 80−22677
^{16}O, RPA calc., many-body oscills. problem 78−82298
^{208}Pb and neighbouring nuclei, shell model calcs. with correlated pairs basis 80−22712
^{208}Pb region, finite Fermi systems, review 78−537
Pr^{3+}, correlation contributions to nuclear antiscreening factor, many-body calc. 79−56153
Rb, HFS, many-body and relativistic effects 78−37565
Si, ion bombarded, radiation defect formation, atom-atom collision cascades modelling 80−10582
Si MOSFET, surface quantum states, two-dimensionality of many-body effects 80−103740

many-particle systems *see statistical mechanics*

many-valley semiconductor materials *see many-valley semiconductors*

many-valley semiconductors
amplifying Gunn diodes, nonlinear effects 79−51622
anisotropic, kinetic theory of impact ionisation 78−14740
anisotropic size effects, review 77−32032
antiferromagnetic or atomic ordering effects on conduction electrons 80−2329
biexcitons in multivalley semicond. 77−66120
bipolar diffusion, intervalley overpopulation *(Russian)* 78−23092
bound multi-exciton complexes, density-matrix functional approach 80−96794
cascade capture of charge carriers in quantised mag. field, appl. to many-valley semicond. *(Russian)* 79−4572
conductivity, electron-electron scatt., memory function 80−10967
conductivity in heating electromag. wave 80−84483
conductivity in RF heating field *(Russian)* 78−76085
cubic, anisotropic acoustoelectric effect, thermo-EMF anisotropy fluctuation depend. on ultrasound freq. 79−69562
cubic, cond. in warm electron region, phenomenological theory 77−43586
cubic, elec. conductivity tensor, warm electron range 78−39123
cubic, with ellipsoidal valleys, magnetoresist. 80−80300
current-voltage characteristics, with multivalued depend. of current on elec. field 78−26876
current-voltage characts., intrinsic magnetoresistance 79−38108
deformation potential screening by free electrons in multivalley cond. band 77−76756
degenerate semiconds., supercond. transition temp. *(Russian)* 78−56254
degenerate semiconductor, intervalley phonon scatt., energy loss rate and momentum relax. time 79−15139
dispersive screening and Bloch function interference, large binding 79−51525
domain instability, two-beam model 79−47116
donor binding energies, variational calc. 78−23041
donor impurity levels and excitons, shallow-deep instabilities 80−75520
effective mass theory of intervalley mixing 77−47763
electric breakdown criteria 78−19046
electron distrib. function in alternating fields, single particle Monte Carlo method 77−89791
electron-impurity system *(Russian)* 79−69464
electronic structure of D^- ion 79−95369
energy bands, D_1 and D_2', relative displacement radar influence of shear deform. 79−15080

many-valley semiconductors continued
energy states calc. of negative donor ion, high stress and stress free cases 78−2444
ferromagnetic multivalley anisotropic, electron autolocalisation *(Russian)* 80−92848
film, electric field absorpt. coeff., self-consistent film pot. 79−69612
film, light absorpt. 79−83043
film, size-quantised with tilted valleys, two-photon absorpt. 79−95869
films, photogalvanic effect calcs., electron mean free path, size effect 80−34487
free-electron screening of short-range scatt. pot. 80−49704
galvanomagnetic effect for hot electrons 77−32028
galvanomagnetic effects 79−11157
n-Ge, noise and hot carrier diffusion in mag. fields 79−11193
heavily doped, pressure volume characts. nonlinearity, intervalley electron redistrib. 77−8012
heavily doped scattering mechanisms resist. and Hall maxima 80−75586
high field magnetoresistance and magnetothermal EMF, ellipsoidal energy surface 77−43621
high field transport, inter-valley scatt., intra-collisional field effect 80−34455
hot electron distrib. function, response to step changes in elec. field 80−24937
III-V semiconductor n-channel inversion layers, subband struct. and gate-controlled Gunn effect 77−76929
III-V semiconductors, negative resistance and peak velocity in central (000) valley 79−73522
impurity band for screened impurities 79−47053
impurity electron states, localised, with low binding energy 80−24835
indirect gap semiconductor, valley-orbit interaction and effective-mass theory 78−23043
inelastic light scattering, single particle excitation 80−29749
intervalley cyclotron-phonon reson., IR absorption in mag. field 78−60448
intervalley junction in homogeneously doped semicond., phenomenological model 77−4433
intervalley transfer of population by ambipolar diffusion 79−11128
intravalley carrier transfer, transverse photo-EMF for various absorpt. coeffs. 79−69551
inversion layer, transient response of hot electrons, calc. 80−49747
inversion layers, electronic ground state 77−43731
inversion layers, optical props. of CDW ground states 77−43732
lattice scattering mechanism in quantised inversion layers 79−78187
light absorption by free carriers at surface 78−48200
longitudinal bulk EMF due to inhomogeneities 78−19045
magnetic, electron fluctuon states spin direct interactions 80−29364
metal-insulator transition at finite temp., calc. 80−49603
MOS, n-type inversion layers, two-valley model low temp. phase study, CDW coupling consts. 78−72275
MOS charge layer n-channel (001) surface induced valley splitting 79−28414
Mott transition, critical carrier conc. 77−47747
photoionisation of neutral deep impurity centres, photon drag of carriers 78−26828
quantised inversion layers hot electron microwave cond. calc. 77−43734
quasi-two-dimensional, transient response under hot electron conditions 78−60223
screened donor impurities, binding energy calc., anisotropic mass effect 78−10399
n-Si, elec. cond. in weakly heating alternating elec. field 79−23977
size effect, influence of space-charge regions on boundary conditions 77−89790
size-induced changes in valley populations in strong elec. fields 80−6855
space charge, contrib. of different charge carriers *(French)* 80−34458
superconductivity, energy gap and crit. temp. 79−1638
thermoelectric power, depend. of longitudinal mag. field 80−39618
two-photon transitions from deep neutral impurity centres, light absorpt. and drag effect 79−91478
two-valley semiconductor, domain instability *(Russian)* 77−62934
two-valley semiconductor, hot electron instability, intervalley scatt. *(Russian)* 80−92921
two-valley semiconductors, carrier vel.-field characts. under high elec. field 80−70713
US propagation, nonlinear effects 77−59305
valley-splitting without effective-mass approx. 80−15586
AgBr, exciton relaxation by intervalley scattering 80−20644
AgBr:AgCl, mixed crystals, first order reson. Raman scatt., momentum conservation relax. 79−56790
n-AlSb, acoustoelectric effect due to piezoelectrically active wave 80−80331
Bi, intervalley scatt. influence on mobilities, thermopower calc. 78−26866
$Bi_{0.89}Sb_{0.11}$, effect of band structure on the dispersion of magnetoplasma waves 77−47845
$Bi_{1-x}Sb_x$, solid soln., temp. depend. of weak-field galvanomag. coeffs. *(Russian)* 80−70724
$Ga_{1-x}Al_xAs$, intervalley energy gaps, temp. junction, exptl. determ. 80−80179
n-GaAs, conductivity relax. times in warm electron range, intervalley transitions 77−55537
n-GaAs, diffusion coeff., Monte Carlo calc., rel. to trapped domain behaviour 78−56152
GaAs, diffusion coeff. of hot electrons 79−15156
GaAs, dynamical response of electron distrib. to high elec. field fluctuations 77−51758
n-GaAs, high temp. mobility anal. in three-valley (Γ_6^c-L_6^c-X_6^c) model 79−99544
GaAs, impurity centres ionis. by Auger electrons, carrier relax. *(Russian)* 79−51594
GaAs, influence of strong transverse mag. field on Gunn effect 80−6854
GaAs, temp. depend. of intervalley gap from Schottky diodes meas., thermionic emission theory generalization 79−73586
GaAs, three level cond. band struct., uniaxial stress effects, resist. and Gunn effect threshold meas. 77−85137
n-GaAs, three valley band struct., high temp. Hall mobility 80−29318
n-GaAs, two stream instability 78−2509
n-GaAs, two-valley semicond., helicon wave instability 77−47842
n-GaAs, two-valleyed semicond., hot electron diffusion coeff., random walk calc. 78−68033
GaAs-GaAlAs (100) abrupt interface, carrier transmission and refl. coeffs. 79−69588
many-valley semiconductors continued
GaAs-metal contacts, intervalley scatt. effect on current-voltage characts. 77−89845
$GaAs_{1-x}Sb_x$ electron intervalley transfer and drift velocity calc. 77−80778
$Ga_{1-x}In_xP_{1-y}As_y$, electron transient drift vel., influence of effective mass and alloy scatt. 80−2384
$Ga_xIn_{1-x}Sb$, electron transport props. calc. by Monte Carlo method 77−76834
n-GaP, acoustoelectric effect due to piezoelectrically active wave 80−80331
GaP, excited 1s-level of S-bound excitons 79−82996
n-GaP, inversion layers, broken-symmetry ground states 77−47873
n-GaP, many-valley semiconductor, relative displacement of D_1 and D_2', bands under shear deform. influence 79−15080
GaP, multiband and multivalley effective mass theory for impurities 79−65409
GaP, scatt. mech., mobility tensor 80−6826
n-GaP:Te, doping parameters calc., by means of Hall data analysis 78−51925
GaSb, E_1 and $E_1+\Delta_1$ edges using electroreflectance, Franz-Keldysh oscills., high mag. fields 77−66518
n-GaSb, galvanomagnetic effects 78−72172
GaSb, space charge, contrib. of different charge carriers *(French)* 80−34458
n-Ge, Brillouin scatt. by phonon zero sound, in quantising mag. field 77−69847
Ge, current-voltage characts., intrinsic magnetoresistance 79−38108
Ge, cyclotron reson. in strong elec. fields, classical theory 80−7172
Ge, deep donor character of muons and protons 80−10911
Ge, donor polarizability, multivalley effective mass calc. 80−96817
n-Ge, effect of non-parabolicity in quantum mechanical treatment of cyclotron reson. 77−31937
n-Ge, elastically deformed, anisotropy of thermoelec. effect 78−19066
n-Ge, elec. breakdown criteria 78−19046
Ge, elec. conductivity tensor, warm electron range 78−39123
Ge, electron mobility in Δ_{1c} minima, temp. depend. 79−65473
Ge, electron-hole liq. thermalisation between mag. field split valleys 80−25444
Ge, electron-hole liquid, ground state props. under ⟨111⟩ uniaxial stress 79−69428
Ge, electron-hole plasma, helical instability excitation in strong. mag. field *(Russian)* 77−69368
n-Ge, H-linear planar Hall effects of hot electrons 78−76082
n-Ge, Hall effect, uniaxial deform. effects 80−65605
Ge, hot-electron diffusion coefficient 78−87982
n-Ge, IR absorption by hot carrier 80−40087
Ge, intervalley diffusion of hot electrons 78−84227
n-Ge inversion layers, broken-symmetry ground states 77−47873
Ge, localised states due to isocoric donor impurities 77−76768
Ge, multivalley struct., helical instability *(Russian)* 79−47101
Ge, oscillistor effect in strong mag. fields, ambipolar drift and breakdown 78−2511
N-Ge, phenomenological cond. relax. time, uniaxial stress and electron-electron scatt. effects 77−15862
Ge, piezoresistance, energy and momentum relax. of charge carriers 78−47786
n-Ge, piezoresistance with deform. axis symm. rel. to all const. energy ellipsoids 77−55533
Ge, piezospectroscopic determ. of electron-phonon to hole-phonon interaction 79−95783
Ge plate, anisotropic cond. thickness depend., intervalley scatt. *(Russian)* 77−85352
Ge, solid-state plasma, ultrafast transient response, theory and expt. 77−80748
n-Ge, uniaxially stretched along [111] axis, negative differential conductance 77−51759
Ge:As, uniaxially stressed, electronic Raman scatt. from valley-orbit transitions 78−15166
Ge:As donor binding energies variational calc. 78−23041
Ge:As(P)(Sb), impurity photocond. spectra under uniaxial compression 80−44656
Ge:As(Sb) many valley effects obs. on D^- state energy 78−6323
n-Ge:Au piezoresistance in presence of deep levels, stress anisotropy 80−10979
Ge:Li, thermal cond., 0.4-20K, Li valley-orbit splitting 79−15111
Ge:Sb, heavily doped, scatt. of electrons 77−59283
γ-GeTe, investigation by elec. resist., latent heat of phase transform. and plasma refl. of light 79−99317
$InAs_{1-x}P_x$ epitaxial layers, sub-threshold velocity-field characts., intervalley separation 77−63010
n-InSb, characts. of Gunn effect 77−55538
InSb, current-voltage characteristics at room temperature and high hydrostatic pressure 80−88560
n-Si, (111) inversion layers, valley splitting, Shubnikov de Haas oscills. 80−65698
Pb chalcogenides, elec. cond. anisotropy in strong electric fields *(Russian)* 79−38082
$Pb_{1-x}Ge_xTe$, n- and p-type, effective masses 80−44481
PbS, dispersion relation for magnetoplasma waves 79−51506
PbSe, dispersion relation for magnetoplasma waves 79−51506
$Pb_{1-x}Sn_xTe$ films, size quantisation, optical orientation of free carriers 80−20725
$Pb_{1-x}Sn_xY$ (Y=Te, Se, S), interband absorption under linearly polarised light excitation 78−92089
$Pb_{1-x}Sn_xY$, Y=Te, Se, S, photocond. anisotropy rel. to lifetimes 78−52032
PbTe, dispersion relation for magnetoplasma waves 79−51506
PbTe epitaxial film, band population effects, intraband magneto-optical props. 79−78007
n-PbTe epitaxial film, magnetophonon and Shubnikov-de Haas oscills. 78−60234
PbTe film, light absorpt. 79−83043
n-PbTe, Hall effect of hot electrons 77−55547
PbTe, recombination radiation polarisation direction, two-photon selective energy valley occupation *(Russian)* 77−20924
n-Si, 77K hot electron repopulation and anisotropy *(Japanese)* 79−82600
Si (001)-SiO_2, n-inversion layer, valley splitting without effect mass approx. 80−15586

many-valley semiconductors continued
Si (100) inversion layers, effective masses, Shubnikov-de Haas oscills. under mechanical stress 77−43625
Si (111) inversion layers, CDWs, effect of four valley interaction terms 79−33324
n-Si (111) MOS charge layer, optical spectrum of inter-subband transition 78−64133
Si, Auger recombination 78−26883
Si, current-voltage characts., intrinsic magnetoresistance 79−38108
Si, deep donor character of muons and protons 80−10911
Si, donor ground state wave functions 78−87937
Si, donor polarizability, multivalley effective mass calc. 80−96817
Si, donors, dispersive screening and Bloch function interference, large binding 79−51525
Si, doped, basis functions for studying intervalley effects 79−69442
n-Si, elec. cond. control by hot electron intervalley transfer 80−59993
Si, high-index surface, valley-valley splitting in inversion layers 78−39219
Si, hot electron diffusivity, theory 77−62940
n-Si intervalley electron-phonon deform. pot. consts. from high-field transport props. 77−62938
Si, intrinsic, two-phonon assisted free exciton recomb. radiation 78−2922
Si inversion layer, elec. break-through, exactly solvable model 78−56234
Si inversion layer, influence of natural superlattice on 2-dimens. electron gas spectrum *(Russian)* 78−68064
Si inversion layer, transient response of hot electrons, calc. 80−49747
n-Si inversion layers, broken symmetry states 79−15229
Si, inversion layers, intervalley transitions and subband splitting 77−20455
n-Si, inversion layers, many-valley electron-phonon interactions, piezoresistance, anisotropic cond., Shubnikov-de Haas oscillations 78−52096
Si inversion layers, resolution of Shubnikov-de Haas paradoxes 80−39648
Si inversion layers, stress effects on electronic props. 78−43476
n-Si, inverted MOSFET surfaces, quantum oscills. in mag. fields up to 10 T 79−56318
n-Si, ionisation of low donor levels and recomb. of hot electrons at low temp. 79−51596
Si, localised states due to isocoric donor impurities 77−76768
Si MOSFET, n-type inverted, surface, mag. field depend. of valley splitting 79−19650
n-Si, many-valley semicond., relative displacement of D_1 and D_2' bands under shear deform. influence 79−15080
Si, many-valley semiconductor, linear galvanomag. effects of hot electrons 79−11154
Si, multiband and multivalley effective mass theory for impurities 79−65409
Si, multivalley struct., helical instability *(Russian)* 79−47101
n-Si, multivalued Sasaki effect 80−107795
Si n-channel (100) inversion layer, valley splitting, formulation by extended zone effective mass theory 77−85329
Si n-channel (100) inversion layer, theory of valley splitting, electric break through 77−85330
Si n-channel (100) inversion layer, valley splittings, enhancement by many-body effects 77−85331
Si, n-channel inversion layers, multivalley effective mass theory 79−47136
Si, n-type inverted MOSFET (100) surfaces, quantitative determ. of valley splitting 79−51678
n-Si, noise, small signal conductivity and diffusion in strong elec. fields 79−11192
n-Si, nonlinear birefr. and dichroism at microwave freqs. and intervalley scatt. 79−19602
Si, phonon-mediated intervalley electron-electron interaction 78−95125
Si, photovoltaic and photomagnetic effects, rel. to intervalley electron transfer 80−60034
Si, piezo−spectroscopic study of ratio of electron−TO phonon to hole−TO phonon interaction 79−24289
Si, piezoresistance, energy and momentum relax. of charge carriers 78−47786
Si, piezospectroscopic determ. of electron-phonon to hole-phonon interaction 79−95783
Si, screening of donor ions by delocalised electrons 79−69466
n-Si, shear deformed, Smith-Herring and mobility change piezoresistance 80−6842
n-Si, surface conductivity anisotropy in accumulation layers 78−10536
Si, transport phenomena in strong elec. fields, intervalley electron scatt. 79−56240
Si, two-dimensional inversion layer on surface, minigap and conductivities 80−20267
n-Si, uniaxially deformed, intervalley scatt., 78-300K 77−20330
Si, uniaxially stressed, excitonic molecule emission spectra, electron valley degeneracy effects 80−60669
n-Si, warm-electron magnetoresist. 79−65503
Si:Al, bound exciton and bound multiexciton complexes, electronic structure, luminesc. obs. 79−56139
Si:Al, valley-orbit splitting of bound exciton states 79−28290
n- Si:O, charge carrier scattering on neutral centres 80−49762
n-Si:P, low-compensated, Hall factor, electron-phonon interactions 79−4570
Si:P donor binding energies, variational calc. 78−23041
Si-SiO_2 inversion layers, applied stresses, cyclotron masses and CDWs 77−55596
n-SiC, 6H polytype, expitaxially grown, electronic props. meas. 77−39975
SiC (15 R), polytype, many valleyed polar semicond., electron-hole-liquid, obs. from excitation and time delayed spectra 79−28289
SiC (6H), epitaxial film, electronic props. 79−60942
Si(100), inversion layer, interaction induced transition at low density 80−15581
Si(100) inversion layers, two-dimensional electron fluid, spin density, valley density waves 77−69400
TlBr, piezoreflectance of first exciton band obs. 78−64347
TlCl, piezoreflectance of first exciton band obs. 78−64347

manybody problems *see many-body problems*

map drawing *see cartography*

marine systems
see also ships
air temp. sensor error analysis 77−78437
buoy for oceanographic and atmos. data acquisition, using Meteosat data transmission *(German)* 80−90224
California harbours, vessel-related contamination by Cu and other metals 79−88010
cosmic ray detector located in deep ocean 80−98522
cylindrical shell modal velocities, numerical fluid loading coeffs. 77−5669
lift bag, salvage device for deep ocean 80−82107
magnetometer for sea floor temporal mag. variation meas. 80−51581
magnetometer for sea-floor mag. fluctuations, ULF-ELF 80−77152
marine reactor systems, Monte Carlo reliability anal. of power and heat removal systems *(Japanese)* 78−58396
Mobile Initial Condition Indicator, submersible, dynamic approach to marine exploration 79−5687
NAVSTAR Global Positioning System, sea trials results 80−12645
ocean mining, position location system 78−45046
ocean thermal energy conversion (OTEC), emerging programme of significance to marine community 78−44875
Oceans 1976 conference, Washington (Sept 1976) 77−5241
oceans '77, conference, Los Angeles, CA, (17-19 October, 1977) 78−45040
oceans '78, ocean challenge, conference (Washington, DC, USA, 1978, September 6 to 8) 79−5658
offshore surveys, accurate positioning at distances to 400 km 80−12328
photometer for deep-sea work, using acoustic telemetering 80−98460
radio teletype communication system, satellite based, INMARSAT 80−26614
radiocommunication buoy, antennas and operating freqs. *(Russian)* 80−109253
radiofacsimile weather chart receiver and recorder 80−46297
resources and meas. techniques, conference, San Diego (1979) 80−41943
seismic exploration data acquisition systems 77−29445
seismic survey, modified integrating A/D convertor *(Russian)* 78−49142
seismology hydrophone system for ocean bottom deployment 80−51582
semisubmersible stable platform 'Kaimalino', design 77−5350
ship speed determ., new acoustical method 79−14178
sonar for smaller ships, clutter spatial correlation signal processor 79−3833
submersibles for research work, remotely operated vehicles 80−82105
survey instrumentation, requirements and appls. 79−84508
thermal energy conversion plant design, oceanographic data interpretation 78−44874
thermal imaging system material and design considerations 80−42259
tow system with depth control, hydrographic and current meas. 80−17403
two stroke compression ignition engines, heat exchange modelling 80−30529
undersea power supplies, radioisotope thermoelectric generators appl. 79−48150
wave power generation buoy, Japanese *(German, English)* 79−83558
windmills in North Sea, for 20% of UK's electricity demand 80−97759
$LiSOCl_2$ battery undersea applications 80−45658

mark scanning equipment
magnetic tape linear velocity meas. scanistor 79−71425
resonant cantilevered fibre-optic scanner 80−53428
square-field scanned image construction time optimisation *(Russian)* 80−63933

marketing
see also commerce
camera market, status and growth prospects, USSR 80−27367
fibre optics, 1977-8 USA trends 79−18513
fibre optics technology and connector systems, marketing 80−69522
fibre-optic technical innovations and market development 80−10008
fission reactor fuel, for PWR, French status *(French)* 80−627
fission reactor fuel preparation and reprocessing, aspects 77−88267
French nuclear industry competitiveness *(French, English)* 79−89489
nuclear policy, United States 77−61634
ocean thermal energy conversion, US OTEC development programme overview 79−83613
retail equity, NBS Standard Reference Materials 80−86249
solar energy consumer profile and application incentives 79−57391

Markov chains *see Markov processes*

Markov processes
acoustic noise, fluctuating, effects of standard deviation and fluctuation freq. of sound level on annoyance *(Japanese)* 79−18583
air pollutants vertical dispersion in neutral surface layer, Markov Chain simulations 79−88399
Alfven wave in stochastic mag. field Markovian approx. 77−51168
alkali halide cryst., V_k-centres, thermal motion theory *(Russian)* 77−47451
asymptotic phase enlargement of weak inhomogeneous Markov processes *(Ukrainian)* 80−46973
atmospheric precip.-time struct., daily precip. amounts modelling with Markov-I chain 80−101401
atmospheric precipitation as chain-dependent process 78−7712
atom, two-level fluoresc. Markovian and non-Markovian behaviour 77−6718
atom in strong EM field, characts. calc. using quantum theory of Markovian processes 80−32943
autoparametrically coupled systems, stochastic stability of stationary response 78−20961
beam on nonlinear spring support, random vibr. 78−55585
beam on nonlinear spring support, random vibr. 80−33515
Bernard convection, and linear fluctuation theory, Markovian processes and irreversibility 80−87766
biological multistate systems, freq. of cyclic processes 80−108834
biological system modelling via optimisation operators 79−1994
bivariate point process connected with electronic counters 77−67406
Block equation, standard form, Markovian relaxation 79−58621
boson field, damping superoperator eigenvalue problem, direct soln. 80−57180
branching diffusion and Markov processes *(Russian)* 79−26009
branching processes, general, minimal moment conditions in limit theory 78−89404
Brownian motion, generalised Einstein theory for nonequilibrium fluctuations 80−31672
Brownian motion, generalised scalar case, computer simulation 80−77704

Markov processes continued
Brownian motion, velocity field, generalised Langevin equation 80−147
cardiac rhythm disturbances, Markov process model *(German)* 79−2019
causal nonrandom vectorial functionals of random processes with independent increments *(French)* 77−26144
cavity, single-mode photon emission/radiation, Gibbs vs. information theoretic entropies 78−16765
cell classification multistage systems, stochastic models 78−77143
cell motility and adhesion measures, model 77−66804
chain reversibility *(Chinese)* 80−46971
characteristic function eqn. of Markov process, Langevin process applications 80−57192
chemical reactions, complex, kinetics, Markov chain appl., teaching 80−27085
chemical reactor simulation *(French)* 79−32706
chemical system dynamics, simulation method 77−60035
class construction for processes invariant under a time change *(French)* 80−17869
classical filtering model, optimal impulse control, separation theorem *(French)* 80−90659
classical processes, nonequivalence to quantum mechanics 80−62583
classification problems of discrete and stationary stochastic signals 79−63002
coagulating droplets, statistical distrib. 79−74425
collision operators as generators of Markov processes and their spectra 79−63150
comets, short-period orbital evolution 80−46484
communication between two self-organizing systems modelled by controlled Markov chains 79−39335
condensed phases, molecular rototranslation, single particle theory 80−64932
continuous stochastic measures and Markov operators 79−97303
continuous stochastic semi-group resolvent, Laurent series appl. 77−53759
continuous-time linear system, varying environment, state estimation methods 79−12581
copolymer cooperative reactions sequential anal., Markov chain structure 77−36753
corrosion under random exposure conditions 80−40579
coupled-core nuclear reactors, irreversible circulation of fluctuation 80−27700
critical dynamics, real-space renormalisation group approach 80−31699
crystallisation theory, master equations for two-component system *(Russian)* 78−47258
current algebras, Markov representations, T-positivity 77−18199
decision process monotone optimal policies 77−53757
decision processes, infinite-horizon, denumerable-state, finite-state approx. 80−68130
denumerable state infinite horizon contracted Markov decision processes, finite state approx. 80−46974
derivation of equations for characteristic functional 80−57197
deterministic dynamics, relationship to probabilistic description 80−4646
deterministic dynamics to probabilistic descriptions 80−68029
dielectrics, electron multiplication, phonon scatt., ionisation rate calcs., Markov processes 80−50267
diffusion, dynamical theory 79−80515
diffusion processes, extremal paths 78−73944
diffusion processes, general, path integral formulation 77−33844
diffusion processes in Riemannian spaces, path integrals 79−17370
diffusion product *(French)* 80−8909
diffusion theory, Markov and non-Markov forms of diffusion eqns. 77−13715
diffusive and non-diffusive processes, escape and splitting probabilities 79−75459
dilute solutions, Monte Carlo algorithm for preferential sampling near solutes 77−51287
dipolar solids, nuclear spin-lattice relax. from hindered rot. 78−52373
direct solar energy, Markov chain simulation with one minute binning *(French)* 80−61293
Dirichlet forms, construction of stochastic processes 80−8921
Dirichlet forms and Markov processes, book 80−73119
Dirichlet stochastic problem *(French)* 78−89406
discrete multiplicative processes in Markovian environments, long run growth rates 79−75453
discrete nonstationary system, profit accumulation process *(Ukrainian)* 78−89308
disequilibrium theory applied to two-spin Glauber model 80−31669
disordered chains, electronic props. 80−2363
dry and wet days occurrences, Markov chain model 78−7698
earthquake recurrence, semi-Markov model 80−98247
ECG monitoring, R-R interval prediction models compared 78−35996
elastic stochastic medium, dynamics *(Russian)* 78−41163
embedding problem for Markov chain with three states, Bang-Bang representation 80−31673
entropy and macroscopic disequilibrium, Markovian relax. 77−14539
entropy prod. in discrete Markov system 79−17340
EPR spectra of stable radicals, slow molecular motion study, review 80−25212
ergodic distrib. of Markov chain *(Ukrainian)* 79−49164
ergodic state with least mean recurrence time in Markovian kinetics 77−49668
Euclidean fields, uniqueness, global Markov property in trigonometric interaction case 79−89053
euclidean image of soliton coherent state 78−32989
Euclidean Markov massive fields of higher integer spin 77−201
exact transport eqn. for randomly perturbed focusing medium 79−81344
exciton transport in mol. cryst., generalised master eqns. under delocalised initial conditions 79−26003
exciton transport in strong intersite coupling limit, long-range transfer states 79−37995
exponential growth of Markovian products of random matrices *(French)* 80−90656
extended hadrons, functional eqns. soln. by stochastic methods 78−21376
external dichotomous Markovian noise, coloured noise induced transitions 79−58638
fast fission reactor system, stochastic method for calc. of Rossi-α parameter 77−61502
Fenyes-Nelson stochastic model of quantum mechanics 80−86
Fermi golden rule and Markov master eqns. 78−36935
finite Markov chains, book 77−2520
Markov processes continued
fission reactor, coupled cores, neutron transit time determ. by noise anal. method 78−37413
fission reactor neutron gas, nonequilibrium thermodynamics *(Japanese)* 78−62595
fission reactors, coupled core system, noise sources in coupling medium, stochastic study 80−22962
fission reactors, CRBR shutdown system, Markovian reliability anal. 80−27761
fission reactors, supervised protective systems, proability level of readiness anal., four-state Markov process 80−27762
fluctuation-dissipation theorem for contracted descriptions of Markov processes 79−54054
fluctuations of macrovariables in nonlinear systems, Langevin eqn. approach 77−33946
fluid, Monte Carlo calculations, optimisation of sampling algorithms 80−54099
fluid, randomly-stirred, vel. correlations, variational principle for path-integral functionals 78−81846
Fokker-Planck eqn., information theoretical derivation, drift and diffusion characterised relax. 77−49699
Fokker-Planck equation derivation for system interacting weakly with heat bath 80−17900
Fokker-Planck-Kolmogorov type equations *(Russian)* 80−145
Friedrichs model, soln. through exact Markovian master eqn. 78−81913
functional integral representation, for general continuous processes 79 9086
Gaussian generalised stochastic fields, Markov property 80−22287
Gaussian Markov random fields, discrete parameter, generalised potential theory 80−57185
Gaussian stochastic Euclidean covariant fields, Markov property 78−21322
general master eqn. soln. asymptotic behaviour, stochastic process symmetry properties 78−62152
general state space, uniform and ratio limit theorems for Markov renewal and semi-regenerative processes 79−21661
generalised collision integral *(Russian)* 79−48
generalised Fenyes-Nelson model for free scalar field theory 80−105769
genetic systems, dynamics of neutral mutation 78−86220
geophysical data acquisition *(Italian)* 80−109254
global Markov property for Euclidean and Lattice fields 79−67469
halfhour solar radiation values from hourly values for Kuwait, Markovian insolation model appl. 79−44236
heat and mass transfer experimental data acquisition system operational analysis models *(Russian)* 79−80588
heat conduction, stochastic theory of atomic chain coupled to two reservoirs 78−54319
heavy ion reactions, 10-200 MeV/N, Markovian and non-Markovian effects in transition probabilities 80−102175
Hilbert space formalism for probability theory 77−60955
hourly global radiation sequences, stochastic simulation 80−36382
hydrodynamic equations, stress tensor and local eqn. 80−82720
hydrodynamic equations from constitutive equations 80−82721
hyperfinite spin system, Markov semigroup, phase transition, nonstandard anal. 79−97302
ice-water-steam system, two-dimens. triangular lattice model, matrix calc., props. 77−27975
importance concept in Markov processes, generalised neutron physics method 78−4471
inclinable pipe, suspension in turbulent flow, Markovian model, eddies 80−48790
infinite particle system with additive interactions 79−80509
infinite particle systems, Markov processes existence *(French)* 78−16733
inhomogeneous Poisson flow with conductor function controlled by Markov chain, asymptotic behaviour 80−95032
intramolecular dynamics, random coupling model, multiphoton excitation, kinetic eqns. 80−63700
inverse super operator construction for Markovian master equation 78−57864
irreversibility, Onsager Casimer symmetry 80−62580
irreversibility of thermodynamic processes, derivation from microscopic reversibility 79−71393
irreversible stationary chain, decomposition into detailed balance part and circulative part *(Chinese)* 79−88876
Ising lattice gas model, 2-d, Markovian behaviour 79−88885
Ising triangular model, in mag. field, Markov process anal. 77−13708
kinetic Markovian equations, derivation, generating functional technique 77−9946
kinetic systems, steady state conc. calc., Markov matrix method 77−52613
kinetic theory of gases, stochastic approach and functional models 79−60091
Kuwait hourly stochastic insolation model 79−58068
laminated composites, mechanics of homogenisation and random evolutions 80−28423
Langevin equation, modified, functional integral and operator formalisms 79−63152
Langevin equations, WKB-type expansion 80−86212
lattice systems, attractive, global Markov property for + and − states 80−82725
lattice walks grown with Markov chain sampling, variance reduction 79−27121
lattice-valued random walks with Markov chain dependent steps 79−71377
leaf optical system modelled as stochastic process 77−44877
leaf radiation stochastic model 77−32880
Lie group, central limit theorem *(French)* 80−52127
linear Boltzmann system, stochastic model of spatially heterogeneous fluctuations *(Russian)* 77−22497
linear operators conditional averaging 79−71233
linear oscillator, nonstationary narrow band response and first passage probability, stochastic process 80−62465
linear relaxation equations in the nonequilibrium statistical operator method 79−30362
linear system with nondelta-correlated parameter fluctuations, statistical anal. 80−95036
LMFBR cooling systems, reliability modelling appls. 80−57838
localization of eigenstates in one-dimensional infinite disordered systems with off-diagonal randomness 80−17876

Markov processes continued
low-density gas, motion and absorption in porous medium, stochastic calcs. 77−7449
LWR, risk-sensitive Markovian policies for detection and maintenance of fatigue cracks in pressure vessels 79−54534
macromolecular replication processes, with selection, stochastic theory 77−68145
macroscopic open systems, hard mode stationary states generated by fluctuations 79−12721
magnetisation jumps assoc. with irreversible displacement of domain boundaries, statistical theory *(Russian)* 77−8346
Markov fields in noncommutative probability theory on W* algebras 79−97260
Markov properties in the Hida sense and Goursat representations for index process in R or R^2 *(French)* 79−71230
Markovian σ-algebras, resolvents and quasi-continuity *(French)* 79−71229
Markovian nature of the two-dimensional self-avoiding random walk problem 80−4648
Markovian sources and Zipf's laws *(French)* 77−26145
mass transport kinetics in sheared particulate beds, Markov chains appl. 79−60057
master equation, path integral solns., stationary Markov process 78−86233
master equation, two expansions in terms of jump size 77−82472
master equation and asymptotic representation, derivation and solution 78−57881
master equation exact solutions for energy transfer from molecule in heat bath 79−88875
master equation for time evolution, network theory 77−5642
master equation treatment of single reservoir limit 78−29050
master equations, Langevin description 80−31676
master equations for unstable particles, weak coupling limit 77−45794
matrix diagonalisation methods applic. *(Dutch)* 77−41451
meson trajectories, Reggeon field theory 79−45037
meteorological data, Markov theory used for spacecraft launch planning 77−45091
minimal Markov process generated by second order differential operator, reversibility *(Chinese)* 80−68127
molecular crystals, phononless exciton band lineshape, excitation transfer, stochastic models 80−107711
molecular dissociation, RRKM formula correction by non Boltzmann character factors, Markov eqns. 80−71891
molecular rotation and translation interaction 80−69262
molecules, Fokker-Planck eqns., stochastic modeling 80−43128
multiple Markov sequences of interpoint intervals, inverse density modulation, rel. to removal spike trains 79−20529
multiplicative decision chains, dynamic programming recursions 77−53758
multistep compound cross section from Markovian processes 80−83090
Nelson's stochastic field, tensor field quantisation 80−105574
nematic liq. crystal spin-relaxation, composite Markov process, rot. reorientation and director fluctuations 77−62471
neural automaton model I/O characteristic for semi-Markov impulse sequences *(Japanese)* 80−16917
neural transformations of random signals, Wiener and of functionals of Markov chain 80−76727
neuronal spike trains, dependency as estimation measure 77−25357
neuronal spike trains, simulation, multiple Markov sequences 77−25413
neutron density fluctuations in on-off controlled reactor, exact stochastic anal. 79−36308
NMR relaxation measurements, formalism for systems with multiple degrees of freedom 78−46368
noise theory, linear and nonlinear, use of general equation for Markov processes 79−21533
non-Gaussian stochastic processes, operators method of anal. *(Russian)* 78−16627
non-Hamiltonian systems, detailed balance condition 77−30096
non-Markoffian effect due to hidden state variables 79−17350
non-Markov processes, memory effects, elimination by transform. 80−42146
non-Markovian quantum stochastic processes and their entropy 79−49163
nonequilibrium processes in open systems, fluctuation dissipation relations, p-n junction appl. *(Russian)* 79−58668
nonequilibrium quantum statistical mechanics 77−82456
nonlinear diffusion process, path integral evaluation, by Fourier series 78−70075
nonlinear kinetic eqns. soln. by Monte Carlo method *(Russian)* 77−5735
nonlinear Langevin eqn. for Markov processes with white Gaussian and generalised Poisson noise, Kramers-Moyal form of master eqn. 79−21653
nonlinear Markov processes, curved phase spaces, path integral soln. Lagrangian, appl. to general relativity 77−26216
nonlinear Markovian system, fluctuations 79−75460
nonlinear oscillator, randomly excited, energy envelope approx. 79−14319
nonpolar semiconductor, normalised theory of impact ionisation and vel. saturation using Markov chain 79−91067
nonrelativistic Markoff field, stochastic quantisation 79−67181
nuclear fuel drum storage capacity computation via inventory model 79−9776
nuclear reactor multiplex systems, reliability, reliability with repair and availability 79−41012
nucleation, early stage, nonlinear relax. process, Markov process framework 78−70060
on-line reactivity meter, comparison between direct and polarity correlation techniques for projected Gauss Markovian process 79−54528
one-dimensional Markov processes, transition probability densities calc. using Fokker-Planck eqn. 80−42047
one-mass vibroshock system, forced random oscills., treatment by Markov process methods 79−14335
Onsager relations from Markov system master eqn., symmetry props. 77−22482
Onsager-Machlup Lagrangian, for continuous Markov processes 79−80522
open BSC model, dynamics in weak coupling limit 79−2738
open dynamical systems, macroscopic description, Markovisation method 78−62146
open systems theory, appl. to unstable particles 79−17281
Markov processes continued
optic tract fibers, cat, Markov properties of nonstationary spike trains 80−51077
organic compounds, complex, nuclear relaxation influence on stimulated emission 80−48019
oscillator systems, nonlinear stochastic models 79−80525
oscillators, with nonlinear damping, first passage failure time anal. 79−6053
oscillators with nonlinear restoring forces, first passage failure probability calc. 78−42562
particle motion in stochastic force fields 78−73928
particle motion through matter, fluctuations in cascade processes 80−5456
particulate material deformation mechanism as Markov process *(Japanese)* 80−14562
path integral representation of conditional probability 77−5741
patient safety design, probabilistic approach by appl. of Markov chains to n-element environments 77−37106
phase transitions, kinetic theory, master equations *(Russian)* 78−47498
polymeric networks, macromol. chain conforms., computer simulation, network form. process *(Russian)* 78−70994
polymers, linear, viscoelasticity theory, unimolecular approx. 79−50613
polymers, self-consistent field approximation, BBGY and Kirkwood calcs. *(Russian)* 79−64981
powder particle motion and segregation by density difference in V-type mixer 80−45250
power and temp. fluctuations for reactor with temp. feedback, exact statistical anal. 79−36309
power reactor, neutron density fluctuations, stochastic nonlinear model, Fokker-Planck eqn. 78−58316
precipitation daily occurrence process, Markov chain modelling 78−61464
probabilistic methods for stationary problems of linear transport theory 80−167
PWR nuclear reactor, Markov model for quantitative systems interactions anal. of system unavailability 80−22898
QCD jets, Markov branching processes 80−27463
QED, indefinite metric axioms, Markov property failure 78−41444
quantum dynamical semigroups and spin multipole relaxation in isotropic surroundings 78−86813
quantum field construction from Markov fields 78−8504
quantum field theory, Markovian homogeneous multicomponent Gaussian fields 80−77933
quantum field theory, probabilistic techniques 78−49952
quantum harmonic oscillator, driven and stochastically modulated, reduced eq. of motion 78−77764
quantum lattice systems 79−40476
quantum Markovian master eqns. 79−144
quantum Markovian processes 78−29049
quantum mechanics stochastic model, equivalence to Markov processes 78−86188
quantum nonequilib. statistical mech., classical Markov stochastic process 77−33938
quantum statistical mech., subdynamics 77−2604
quantum system coupled to thermal reservoir, generator in weak coupling limit 79−88883
quantum tunnelling, time dependent stochastic quantisation theory 78−41197
quantum two-level system, damped and stochastically modulated, reduced eq. of motion 78−77764
quenched-in vacancies, stochastic theory for clustering, general mathematical props. 79−65073
queueing system central limit theorem 78−32658
radiative transfer, adding algorithm for Markov chain formalism 80−21902
radiative transfer in diatomic gas, vibr. nonequil., probabilistic modelling 80−33434
radiative transfer in planetary atmosphere 78−36447
random field model for grain interaction effects in photographic emulsion 77−54002
random medium with finite inhomogeneity correl. range, EM wave fluctuations *(Russian)* 78−78870
random nonGaussian backgrounds, simulation, calc. spatial correl. function 78−79089
random walks with Markovian steps *(French)* 80−17868
rate processes in condensed media, master eqns. 80−77687
reactor noise theory as a Markov process 78−74420
regenerative decision models, iterative methods appl. 77−53756
Reggeon field theory and Markov processes 78−77774
Reggeon field theory on a lattice, critical behaviour, Monte Carlo calc. 80−18126
regularisation by Dirichlet forms 80−86208
relativistic Markov processes in quantum mechanics, Feynman path integrals 79−21576
relativistic semigroup, Lorentz group and tachyons *(Russian)* 77−82801
relaxation process as contraction of Markovian type multidimensional one 80−31671
reservoir storage, distrib. of max. deficit of partial sums of variables 80−4651
reservoirs with Markovian inflows, modelling 78−16080
resonance fluorescence in Markovian stochastic fields 80−83573
response and fluctuation theorems for stationary Markov systems 78−62153
River Nile, Kalman forecasting model 80−31081
second order optical processes, stochastic theory 79−94201
sedimentation, three-parameter Markov model 78−34183
sedimentation Markov model for very slow settling of dilute suspension 78−22406
sedimentation of monodisperse suspension of solid particles in viscous fluid, Markov model 80−28551
semiconductors, electron multiplication, phonon scatt., ionisation rate calcs., Markov processes 80−50267
semicontinuous random walk with discrete time, generalisation *(Ukrainian)* 78−54302
semigroup, Markov, invariant measure and ergodic property *(Chinese)* 80−62578
sink method with absorbing barriers 78−73834
solar energy space and water heating systems, Markov model 79−74501
solar energy storage tank, Markovian model of behaviour *(French)* 79−24912
solar space heating system analysis, with aid of computer 79−61950

Markov processes continued
solid, H-bonded, bond failure theory 79−73246
spectral properties of physical processes of Markov-correlated events, theory 79−21664
spectral props. of physical processes of Markov-correlated events, applications 79−21665
speech anal., reflection coefficient estimates based on Markov chain model 80−83710
static conductivity of 1-D disordered systems 77−49697
stationary turbulence, path integral functional description, variation principle 79−77083
stochastic linear system with non-white fluctuations of parameters, differential description *(Russian)* 79−145
stochastic processes introduction for physicists 79−25988
stochastic quantisation processes, review, Markov processes, Martingales, quantum dynamics 80−94969
strong Markov process time change *(French)* 78−62151
subsystem interacting with thermal bath. kinetic eqn., Markov approx. 80−47006
symmetry basis and generalised thermodynamic pots. 79−97304
systems of imprimitivity 78−8347
teaching approach to linear birth-and-death and similar processes 79−80400
time correlation functions, in discrete chaotic process 79−25985
time evolving system, markovian density operator, generalised H-theorem 79−49184
total positivity and the embedding problem for Markov chains 79−93041
trajectory instabilities in dissipative systems, numerical expts. 78−41235
transition matrices for Markov chain sampling, model systems, convergence rate comparisons 77−57165
transition operator for Markov and non-Markov processes, interpolation model 80−8910
tuning fork oscillator internal random disturbances *(Russian)* 80−62459
turbulence fully developed, quasi-normal Markovian approx. 80−53756
turbulent dynamo, dynamic eqn. of magnetic field 80−32880
two-dimensional Gauss-Markov field, pinned Karhunen-Loeve transform 77−83827
two-parameter process, Markov property *(French)* 80−68129
two-state random walk 77−5742
two-valued symmetrical processes indexed by circle *(French)* 78−89407
velocity of light Markov process, Klein-Gordan quantum statistic, quantum mechanics 80−98808
vertical gyroscope theory, nonlinear problem *(Russian)* 78−51053
vibration systems simultaneous continuous and discrete stochastic processes, compact eqn. *(German)* 79−55337
visual activity lateral impedance theory, Markov processes appl. 79−2046
visual system of fly, giant neuron performance, spike generation 80−108886
wear of bearing surfaces *(Russian)* 77−59943
weather data, Markov chain modelling 77−49124
Weiner-Einstein processes, Markov, maxima and first-passage-time statistics 80−68134
white noise, Gaussian and Poisson, Markov fields and local operators 80−57186
zero sound, in classical liq., excitation, damping, memory function approach 78−67771
zero-two laws, recurrent process characterisation *(French)* 80−27217
pp high-energy collision multiplicity distribution, Markov and log-normal models 78−89753
$^{209}Bi+^{136}Xe$, stochastic model for strongly damped collisions with liquid drop driving forces 78−89834
Fe XV, line intensity and linewidths at high electron density, generalised population ratio 80−99481
H II regions density fluctuatons, statistical approach 80−77468

Mars
1971 dust storm, diurnal thermal tide, topography effects 77−45341
active seismic exploration and liquid water in crust 80−67607
aeolian environment, differential redistrib.*rates 79−44399
aeolian features, bright and dark crater streaks 78−32381
aeolian sedimentation on Earth and Mars, comparisons 80−31042
angular momentum of seasonally condensing atmospheres, appl. to Mars 80−26735
Arsia Mons, Pavonis Mons, Ascreus Mons, Tharsis region volcanoes, structural evolution 78−65531
astrolabe obs., 1975-76 winter period *(French)* 78−32378
astrolabes obs. from Paris Observatory (winter 1977-78) *(French)* 79−70982
astrometry, position and ephemerides (1975-1976) *(French)* 78−45252
astrometry, positions determ. with Odessa meridian circle, (1974 to 1975) *(Russian)* 79−44394
astrometry with Danjon astrolabe at San Fernando Observatory (Jan. to Feb. 1978) *(French)* 80−94736
atmospeere, O_3 layer and two aerosol layers detect. by Mars 5 spacecraft UV obs. 78−49357
atmosphere, ^{15}N enrichment rel. to cosmic ray interactions in early solar system 78−73669
atmosphere, ^{40}Ar origin 77−64687
atmosphere, air mass along ray in spherical model 77−29688
atmosphere, chemical composition deduced from twilight glow obs. 80−56739
atmosphere, cloud microphysics anal. 79−16853
atmosphere, CO 115 GHz microwave line detect. 77−74000
atmosphere, comp. of surface layer 78−20706
atmosphere, composition and structure, Viking 1 results 77−13265
atmosphere, composition at surface, Viking 1 lander preliminary analysis 77−13268
atmosphere, diurnal composition var. model 79−84702
atmosphere, effect of regolith adsorption on rare gases relative concs. 78−49358
atmosphere, electron cooling by electron impact excitation of CO_2 78−57481
atmosphere, electron energy deposition in CO_2, excitation, ionization and heating 79−45857
atmosphere, energetic electrons absorpt. by Ar gas 77−31420
atmosphere, evidence for tides from occultation of ε Geminorum 77−37550
atmosphere, frontal systems during N polar hood passage over lander site before dust storm 79−84718
Mars continued
atmosphere, general circulation model, including dust and topography 80−90354
atmosphere, grain saltation estimation 77−17398
atmosphere, H_2O vapour, comparison of spacecraft meas. 79−8871
atmosphere, H_2O vapour high-altitude profile 79−8869
atmosphere, impact ejecta trajectories, drag and gravity effects, analytic solns. 78−40854
atmosphere, isotopic N composition rel. to past history 77−17406
atmosphere, large-scale dynamics, heat transfer by baroclinic eddies and topographically forced long waves 78−45255
atmosphere, low latitude circulation 77−41343
atmosphere, lower, O_3 distrib. and photochemistry 79−35169
atmosphere, multidimensional radiative transfer 77−64638
atmosphere, N_2 dayglow prediction 77−53452
atmosphere, N atom loss rate, calc. 80−46452
atmosphere, numerical circulation model with topography for S.Hemisphere 77−5480
atmosphere, O_3 vertical distrib., Mariner 9 UV spectral obs. 79−66952
atmosphere, O I dayglow red emission at 630 nm 80−62063
atmosphere, O isotopes, implications for evolution of volatiles 77−17400
atmosphere, O spectral line shape following mol. dissociative excitation 80−105097
atmosphere, optical props. during 1971 dust storm 77−13274
atmosphere, optical props. during 1971 dust storm *(Russian)* 78−93138
atmosphere, photochemistry 77−91458
atmosphere, photochemistry and evolution, Viking obs. 78−20692
atmosphere, photoelectrons caused by solar photons of less than 80 Å 80−56744
atmosphere, phys. parameters calc. *(French)* 78−7901
atmosphere, probe flight charact., scale model expts. 78−7854
atmosphere, radiation-induced cooling 78−85885
atmosphere, radiative equilibrium temp. affected by O_3 80−72827
atmosphere, response to heat sources and perturbations *(Chinese)* 80−85748
atmosphere, review 77−13273
atmosphere, role in shaping of planetary surface 78−7905
atmosphere, seasonal press. variations *(French)* 77−29687
atmosphere, seasonal var. of O_3 density 79−70984
atmosphere, solar wind sputtering rel. to mass loss 78−53855
atmosphere, struct. and extinction from ε Geminorum occultation obs. 78−7898
atmosphere, structure from Viking 2 entry meas. 77−56858
atmosphere, thermal radiative transfer, numerical modelling 80−8574
atmosphere, travelling thermal wave effect on circulation 80−8388
atmosphere, turbulent mixing coeff. and homopause height 78−49354
atmosphere, upper, ion and electron temps. 79−16862
atmosphere, upper, temp. struct. from ε Geminorum occultation obs. 79−53749
atmosphere, Viking 1 preliminary meteorological results 77−13266
atmosphere, water vapour global seasonal var. and implications for permafrost 79−84714
atmosphere, water vapour mapping expt., Viking preliminary results 77−13263
atmosphere, water vapour vertical distrib. 79−84713
atmosphere, waves or turbulence evidence from occultation of ε Geminorum 79−53748
atmosphere, W.W. Campbell's spectroscopic study 77−71047
atmosphere and climate, early evolutionary stages 79−8696
atmosphere boundary layer, momentum and heat turbulent flux, Viking 1 obs. 80−72810
atmosphere circulation, estimated characts. 77−17393
atmosphere composition model 78−69721
atmosphere descent trajectories using parachute-rocket system for soft landing 78−69640
atmosphere descent vehicle, aerodynamic braking arc control algorithm 79−84629
atmosphere diurnal tide, influence of Martian polar caps 79−96943
atmosphere dust affecting surface and atmos. heating 80−67625
atmosphere model and water vapour distrib. 79−40113
atmosphere modelling, multilayer radiative transfer 80−46451
atmosphere opacity, 1977 obs. from Viking 80−41753
atmosphere opacity during July-November 1976, Viking orbiter obs. 78−20676
atmosphere phenomena during major dust storms, meas. at surface 79−84708
atmosphere pressure, annual cycle meas. by Viking landers 1 and 2 80−72812
atmosphere pressure, seasonal var. as affected by S polar cap 79−84716
atmosphere relative humidity 80−72826
atmosphere structure expt. on Viking spacecraft, techniques, instruments and accuracy 77−13205
atmosphere suspended dust particles, props. and effects 79−84717
atmosphere thermal IR properties, 15 μm band meas. 79−84710
atmosphere thermal IR properties, dust and ice clouds detect. from Viking IRTM spectral meas. 79−84712
atmosphere thermal IR properties, global behaviour at 7, 9, 11 and 20 μm 79−84709
atmosphere thermal IR properties, local dust clouds effects 79−84711
atmosphere thermal tides and dust storms, direct evidence for coupling 79−84719
atmosphere-regolith exchange of CO_2, rel. to atm. press. and response to insolation changes 78−73668
atmospheric aerosol props. from Viking lander imaging data 78−20698
atmospheric Kr and Xe, Viking obs. 77−56856
atmospheric meas., Viking Meteorology Experiment 77−33384
atmospheric oblateness from ε Geminorum occultation obs. 77−5483
atmospheric parameters from Mars 6 descent module radio data 77−33386
atmospheric struct. Viking obs. 78−20691
atmospheric thermal regime, long wavelength radiation fluxes 77−33385
atmospheric volatiles, comparison with Earth, rel. to meteoritic source 78−36482
basalts, redox state 78−77217
bow shock location compared with Mercury, Venus and Earth 78−28560
braided channels rel. to fluvial features on Earth 79−2507
bright spots in 1971 dust storm, multiple light scatt. in craters 77−60705
brightness distribution over planetary disc, determ. from light refl. meas. 80−17512
brightness temp. predictions, 1975 December to 1978 October 77−9683

Mars continued
canals requiem 78−16326
canyon origins 78−89098
canyons, structure rel. to E.African rift system 79−40111
carbonate formation in Marslike environments 78−61778
channels, classification and form. time based on Viking data 78−20669
chemical composition of interior, cosmochemical model 80−72813
chemical weathering, thermodynamic stability of minerals and alteration products from mafic igneous rocks 78−45257
Chryse Planitia, geology 78−20673
Chryse Planitia region, search for organic and volatile inorganic compounds 77−17407
Chryse Planitia sample, Viking X-ray fluorescence expt. 77−17410
clay minerals, prod. by alteration of glass 78−89097
climate, past, present and future 78−7900
climate oscills., latitude depend. and oscill. spectra 80−90355
climatic change on terrestrial planets, review 79−53742
climatology from Viking 1 after 20 sols 77−17409
closest approaches to Earth 79−16866
cloud formations, reflectivity time var., visible photometry obs. 80−72840
cloud obs. by Masr 3 in 0.36 to 1.38 μ range 77−53450
cloud positions during 1907-73 period, topographic control 78−36479
clouds over Tharsis volcanoes, diurnal props. 80−94738
colour photographs from space probe *(German)* 77−53445
conference, Second International Colloquium on Mars, Pasadena (Jan. 1979) 80−62370
conjunctions with ε Cancri in Praesepe (1950-2000 period) 77−91460
control net, 1977 May, using Mariner 9 pictures 78−73667
core, formation, history and energetics 79−84694
cosmic-ray interactions with rocks and atmosphere, gamma-ray spectra 77−53448
crater count ages, ice and sand impact crater implications 80−67614
crater depth study, evidence for subsurface volatiles 80−85878
crater doublets expected frequency 78−61777
crater ejecta emplacement, atmos. effects 80−56747
crater ejecta-emplacement in Coprates quadrangle 80−56745
crater saturation and equilibrium, Monte Carlo simulation 77−71038
crater streaks in Chryse Planitia region, early Viking results 78−65534
crater-associated streaks, diffusion-deposition patterns 79−16863
crater-associated streaks, nature and visibility 79−16864
crater-associated wind streaks in north equatorial zone, statistical study 78−45256
cratering, empirical chronology and implications 78−77512
cratering, standard curve rel. to Moon, possible new time scale 77−33391
craters, 4 to 10 km diameter, distrib. and relations to global geologic units 78−65528
craters, evolutionary tracks 77−91134
craters, production rates and retention ages rel. to geological history 77−60699
craters, size-frequency distrib. law 78−36480
craters and plains, comparative studies of Moon, Mars and Mercury 77−53439
crust, possible fossil H_2O liquid-ice interfaces 78−65539
crustal evolution in silicate planets, review 78−61774
cusp of magnetosphere, to explain Mars 5 mag. and plasma obs. 80−51685
Cydonia region, geological obs. from Viking 78−20674
deflections of the vertical rel. to triaxial ellipsoid 77−73997
Deimos, evidence for strong interaction with solar wind 79−8787
Deimos, loose material downslope movement obs. 80−94737
Deimos, photometry from Viking orbiter images 80−72838
Deimos, spacecraft imaging 78−89102
Deimos, spectral evidence for carbonaceous chondrite surface comp. 80−41754
Deimos, surface features map and props. 80−31224
Deimos, surface morphology, comp. and props. 78−89103
Deimos, surface photometry 77−29696
Deimos, Viking Orbiter imaging results 79−35170
descent spacecraft, ballistics 77−33319
desert features created by wind, Western Desert of Egypt compared with Mars 80−72815
development and structure, Earth and Moon comparison *(German)* 77−67055
Dirac's Large Numbers hypothesis testing using precision ranging to Mars 77−45616
disc IR spectrum, comparison with terrestrial analogues optical props. 78−85879
doublet craters, expected freq., replies and criticisms 79−2509
dune morphology and distrib., compared to Earth 80−72814
dust, scattering by nonspherical particles and optical props. 79−25535
dust and ice hazes, Mariner 9 TV limb obs. 79−5772
dust clouds and frictional generation of glow discharges 77−78708
dust clouds and prebiotic molecules 77−64688
dust clouds during 1971 dust storm, physical characts. 79−84704
dust clouds physical props., surface layer particles mean radius 78−45258
dust complex refractive index, wavelength depend. and comp. 77−29695
dust deposits in Martian north polar region, evolution 80−31225
dust in Martian atmosphere, Viking orbiter imaging obs. 79−84707
dust storm, 1973, maps from hourly photographs 77−5477
dust storm, IR opacity of atmos. 80−72822
dust storm 1971-2, Mariner 9 IR spectra, composition and particle size distribs. 77−41345
dust storm obs., 1978, Jan. 78−24482
dust storm of 1971, cloud form., multicolour TV photometry obs. 80−101546
dust storms, global, exploration methods *(Czech)* 78−32374
dust storms, monitoring using atm. transparency meas. *(Russian)* 78−36481
dust storms, opacity from Viking IR thermal mapping 80−82253
dust storms 77−49324
dust storms and polar cap recession rate correl. *(Italian)* 77−91461
dusty atmosphere, solar heating rates 78−85878
dynamics, atmospheric and surface props. from Viking radio tracking data 77−56865
dynamics obs. from Viking lander tracking data anal. 80−77314
eccentricity origin in secular resonances 80−46449
ephemerides and position, 1975 to 1976, additional information *(French)* 79−44392
Mars continued
equatorial flattening 80−4282
equatorial thermosphere, struct. and dynamics 77−53451
erosional processes and channelized water flows 80−67611
evolution of interior, atm., ocean, Viking mission Mars information, appl. to Earth 77−78709
exospheric density and escape fluxes of atomic isotopes 79−5771
expansion and gravit. constant changes, limits 78−28155
extratropical cyclones, Viking Orbiter 1 obs. during summer season 79−44398
far IR obs., temp. determ. 79−12431
far IR spectrum, 45-115 μm obs. 77−29681
feroxyhyte (δ-FeOOH), possible occurrence on surface of Mars 80−85879
fine particles in drifts, Viking 1 obs. 77−17412
flood features formation by water release from confined aquifers 79−84722
fluidized crater morphology 80−67613
fresh cratering characts. as function of discuss., comments 77−73998
fretted terrain, erosional debris flow 78−65537
gamma ray quantum flux var. calc. as function of surface relief and distance 79−80249
ε Geminorum occultation, obs. from C.E. Kenneth Mees Observatory 78−53853
ε Geminorum occultation (1976 April 8), obs. at Princeton 78−57482
ε Geminorum occultation by Mars, McDonald Observatory obs. 77−60702
generalised figure, size and orientation *(Russian)* 78−40857
geodetic control using natural satellite imaging 79−70959
geologic evolution of terrestrial planets 77−53442
geological evolution data from Viking probes *(French)* 80−8578
global colour variations on Martian surface, Viking II results 78−65527
global topography, harmonics and geophysical implications 78−85880
gravitational field, stationary points coordinates 78−53805
gravitational figure, global and regional props. 79−62784
gravitational spectrum, determ. from Mars Mariner 9 orbiter tracking 80−41744
gravity, twelfth degree and order spherical harmonic model 80−67608
gravity anomalies and tectonics, review 80−98593
gravity anomalies due to topography, comparison with Earth 80−21939
gravity field, combined Viking and Mariner 9 results 78−20688
gravity field, comparison of results obtained from Viking 1 and 2 and Mariner 9 80−8577
gravity field spherical harmonic representation using short-arc technique 77−73999
gravity map, Viking Orbiter 2 results 79−58291
heavy ions in solar wind plasma flow 80−8576
Hellas basin, Viking bistatic radar observations 79−84723
Hellespontus dunes, terrestrial analogues 77−29697
highland and lowland units relative ages, Viking contribs. to Mariner studies 78−65529
hypsometric curve construction and crust evolution model 80−77315
ice-covered rivers 80−17526
igneous processes, impact crater and basin control 80−67615
impact craters, emplacement of ejecta by surface flow 78−20671
inert gases in atmosphere, accretion from protoplanetary nebula 80−109385
insolation, latitudinal, seasonal and atmospheric effects 77−60704
integral photometry, (August 1975 to January 1976) 78−61780
interior, solid-state convection, obs. evidence 79−84692
internal struct. and props. 77−82141
internal structure, theoretical models and seismic props. 78−40856
internal structure evolution, calc. 77−82137
ionosphere, $(CO_2)_2^+$ photodissoc., lab. mass spectra 77−6867
ionosphere, ionic reactions in lab. and planetary atmospheres, probe data 80−59168
ionosphere, normal horizontal gradient effects on radio signals phase meas. 77−29691
ionosphere, photoelectron fluxes 79−53751
ionosphere, post-Viking model 79−25532
ionosphere, proton affinities and cluster ion stabilities in CO_2 and CS_2 77−77760
ionosphere, theoretical model in light of Viking obs. 78−96419
ionosphere, Viking retarding potential analyzer obs. 78−20690
IR photometric function and bolometric albedo 77−29698
isophotes, as clue to aerosol characts. 77−29699
isotope abundances in atmosphere 79−58284
isotopic ratios and minor constituents from Mariner 9 77−82142
lander, effectiveness of min. final vel. criterion in spacecraft descent trajectories synthesis 77−64590
landform degradation evidence from crater depth/diameter relations 77−37536
landscape and rock type, comparison with Earth 77−9688
late heavy bombardment in inner solar system 77−71019
lightning in atmosphere, chemical impact 79−96940
liquid water saturated regolith in early Martian history, pedogenic and mineralogical consequences 78−65538
lithosphere, possible S overabundance 80−72832
lithosphere global TRM in presence of central dipole field, theory 80−31223
lithosphere thickness estimation from elastic flexure theory 79−16860
lobate debris aprons and similar flows, distrib. 80−67619
Lunae Planum−Chryse Planitia region, plains and channels 80−67612
magnetic field, dimensional anal., simple model 79−58286
magnetic field, Mars 2 and 3 evidence 78−49361
magnetic field, Mars 3 evidence re-examined 78−49359
magnetic field, Mars 5 evidence 78−49362
magnetic field, Mars 5 evidence re-examined 78−49360
magnetic field, measurementss of Mars 2, 3 and 5 spacecraft 80−36538
magnetic field, spacecraft meas. 79−2503
magnetic field 79−80261
magnetic fields in early solar system, recorded in lunar rocks, meteorites and planets 79−5765
magnetic minerals, obs. by Viking extended mission 80−72830
magnetic particle detect. in dust by Viking lander 77−17411
magnetosphere, effect of Deimos 80−41752
Maja and Kasei Valles, channel morphology 80−67610
mantle, geological implications of high density 78−65532
meteoric material distrib. near terrestrial planets, methematical modelling 79−96976

Mars continued
meteorite impact ejecta, depend. of mass and energy lost on planetary escape vel. 78−45295
meteorological parameters, Viking Lander sites 79−88615
meteorological results from Viking 2 77−53455
meteorology, dynamical phenomena during June-November 1976, Viking orbiter imaging results 78−20675
meteorology, obs. during three seasons at surface 78−89096
microwave absorption in atmosphere 77−71045
mirages, possibility of Viking lander obs. 77−29693
mm wavelength spectral lines detectability 79−5769
moment of inertia 79−58290
moment of inertia and isostasy 77−33390
moment of inertia rel. to existence of core 78−7902
moons, dynamical evolution and origin 78−89104
near surface atmosphere, isotope ratios and noble gas upper limits 77−17408
neutral upper atmosphere composition, Viking obs. 77−56857
Noctis Labyrinthus-Valles Marineris regions, structure pattern anal. 77−29694
north polar cap, 1975-1978 photographic obs. 80−72823
north polar cap, 1977-1978 regression obs. 80−72825
north polar region, Viking 2 orbiter imaging 77−56864
north pole summer temps., dirty water ice 77−56866
northern summer ice cap, Viking 2 water vapour obs. 77−53454
obliquity oscills., fourth-order accuracy in orbital eccentricity and inclination 79−48724
obliquity oscills., Tharsis uplift effect 79−48725
occultation of ε Geminorum, 1976, April 8, theory of light curve 77−53567
occultation of ε Geminorum, 1976 April 8, atm. temp. var. *(French)* 77−53449
occultation of ε Geminorum, photometric obs. 77−91527
occultation of ε Geminorum, planetary atm. temp. struct. determ. 77−87306
occultation of ε Geminorum, planetary atmosphere temp. profiles 79−2508
occultation of ε Geminorum (1976 April 8), preliminary results 77−37545
occultations by eclipsed Moon, 100 BC to 3000 AD period 77−49319
Olympus Mons, subglacial origin and aureole deposits 80−67617
Olympus Mons aureole, characts. and origin 77−87308
Olympus Mons aureole and perimeter scarp, origin 80−77317
Olympus Mons Escarpment, origin by erosion of pre-volcano substrate 77−5481
opposition effect, Viking Orbiter 1 obs. of Chryse-Acidalia region 79−44397
opposition effect, Viking Orbiter obs. 79−25536
orbit determination on basis of radar and visible observations 80−90323
orbital analysis by Kepler, construction and rejection of first oval orbit 78−62027
organic compound search by Viking, final conclusions 80−67627
outflow channels, hydraulics of water flows, terrestrial equivs. 79−40112
outflow channels erosion, implications of sediment transport modes in channelised water flows 80−98363
oxidation of surface, constraints due to atmospheric chemical processes 77−5475
palaeoclimate and enhanced atmospheric CO_2 80−46450
palaeoglaciation due to solar radiation reduction *(French)* 79−34857
Paris Observatory astrolabe obs. *(French)* 77−49322
permafrost, thermodynamics 80−67621
permafrost features 78−20670
permafrost in subsoil *(Italian)* 79−21217
phase function, July to November 1976, Viking orbiter photometric obs. 78−20677
Phobos, composition, evidence for carbonaceous chondrite surface from spectral anal. 78−49365
Phobos, equilibrium figures 77−33388
Phobos, evidence for carbonaceous chondritic composition from multicolour obs. with Viking lander cameras 78−49366
Phobos, first encounter by Viking Orbiter-1, mass and density determ. 78−49364
Phobos, grooves distrib., morphology and possible origin 80−72837
Phobos, Marsshine and shape/size determ. 79−44396
Phobos, mass from Viking Orbiter radio tracking data, density estimate 78−32380
Phobos, mass from Viking Orbiter radio tracking data 78−32379
Phobos, modelling and mapping 79−40115
Phobos, of grooves, cratering hypothesis supported 78−57484
Phobos, orbital inclination evolution 80−67628
Phobos, origin of grooves, seismic effects of large meteoroid impact *(Russian)* 78−69754
Phobos, photometry and origin of dark markings on crater floors 79−16861
Phobos, photometry from Viking orbiter images 80−72838
Phobos, props., comp. and origin *(Norwegian)* 78−36478
Phobos, scale model using Mariner 9 obs. and solar simulation technique 78−28566
Phobos, spacecraft imaging 78−89102
Phobos, striations as evidence for tidal stress 77−78707
Phobos, surface density of impact craters 77−37547
Phobos, surface features map and props. 80−31224
Phobos, surface morphology, comp. and props. 78−89103
Phobos, surface photometry 77−33389
Phobos, Viking 1 Orbiter, encounter, trajectory analysis 80−12641
Phobos and Deimos, Mariner and Viking pictures 77−41347
Phobos and Deimos, preliminary results from Viking obs. 78−20681
Phobos and Deimos, Viking imaging, primary mission overview 78−20680
Phobos and Deimos, Viking photographs, surface features 79−21218
Phobos and Deimos 77−49323
Phobos and Deimos orbital evolution 80−26770
Phobos surface grooves, hybrid origin 80−31229
Phobos transit of Mars viewed by Viking cameras 78−69723
Phoenicis Lacus and Coprates regions, tectonic trends inventory 80−77316
photocatalytic oxidation of organic compounds 78−85883
photochemistry of CO_2-H_2O-N_2 atmosphere 77−29692
photodesorption from mineral surfaces and effects on atmospheric stability 78−7903
photographic position meas. *(Russian)* 78−93137
photographic positions in 1973 and 1974, Pulkovo normal astrograph obs. *(Russian)* 78−28567
photographic zenith tube obs. during 1975 and 1978 oppositions 79−40109
photometric imaging in 0.35-1.10 μ range 1973 opposition 77−71044
photosynthetic microorganism response to atmosphere, model 79−40114
physics of atmosphere, surface and interior, book 79−101104
pitted and fluted rock, compared with wind eroded Egyptian rock 80−72816
polar areas, volatiles behaviour, model 78−49363
S polar cap, seasonal recession as seen by Viking 79−84715
polar cap winds, numerical model 79−96942
polar landscapes evolution, interplay of perennial ice cover and dust storm intensity vars. 79−84721
polar regions, Mariner 9 and Viking obs. of layered deposits 78−7899
polar regions, stepped topography origin 78−65536
polygonal troughs on Mars northern plains, origin 80−98590
position determ. in 1978 using Double Zeiss Astrograph, Belgian obs. *(French)* 80−72809
positional photographic obs. with Pulkovo double short-focus astrograph, (1973 to 1974) *(Russian)* 79−96944
positions, obs. with Algiers astrolabe (winter 1973) *(French)* 78−61775
positions, obs. with Danjon astrolabe of San Fernando Observatory *(French)* 78−57483
positions, obs. with Paris astrolabe (1975 to 1976) *(French)* 78−61776
positions (1975-6), Paris Astrolabe obs., corrections *(French)* 79−44393
positions and ephemeris corrections from Paris astrolabe obs. *(French)* 79−101103
prime meridian, and longitudes of Viking landers 78−16327
primitive atmosphere and implications for channel form. 78−65543
primitive atmosphere temp. history with reducing greenhouse effect 77−87031
probe atmospheric entry, optimal trajectories with two-dimensional control 77−91400
pseudocraters in Cydonia region 80−67618
radio brightness, longit. depend. confirmation 80−21937
radio brightness, rot. vars. 77−45340
radio emission in H_2O 1.35 cm line 78−20664
radio emission meas. by Mars 5 spacecraft 77−29689
radiowave propag. for atmosphere composition anal. 79−21204
rampart craters, areal distrib. 79−84706
rampart craters, form. by impact in viscous-liq. targets, exploratory expts. 78−65530
rampart craters, morphology 78−53854
regolith, as reservoir of volatiles 80−17524
regolith, implications of abundant hygroscopic minerals 78−65541
regolith, water vapour adsorption and ice form. 78−65540
review 77−74002
ring, production by destruction of Phobos 79−66951
ring structures, rock mechanics theory 77−64675
rotation model, including precession and nutation 80−21938
rotation period, determ. from transits of albedo stations across central meridian (1659 to 1971) 80−98588
rotation theory in Euler angles 80−51684
rough planar suffaces, radar, visual and thermal characts. 80−98589
saltation threshold, interparticle force, surface roughness and low atm. density effects 77−5478
sand blown by wind, threshold windspeed laboratory expts. 80−72811
sand sea (erg) in north polar region, wind patterns 80−67624
satellite mass estimation from multiple Viking Orbiter encounter 77−56831
satellites, 100 years since discovery, review of studies 78−73670
satellites, crater density interpretation 80−82252
satellites, effect of proximity to Roche limit on dynamical behaviour of ejecta 80−98592
satellites, history of discovery 78−89099
satellites, history of discovery and positional obob. (1877 to 1977) 78−89101
satellites, orbits rel. to Mars mass, oblateness and polar axis position 78−89100
satellites, origin by impact rupture of single body 77−64704
satellites, positional photographic obs. during 1973 October at Pulkovo *(Russian)* 78−28568
seismic obs. by Viking 2 lander 78−20700
seismicity, Viking Lander II seismometer, no recorded events 79−80262
soft landing guidance algorithms based on terminal control principles 78−73602
soil, fine-grained component model based on Viking lander data 78−85882
soil, particle gathering mechanisms *(Russian)* 77−91462
soil analysis, proportional counters in X-ray fluoresc. spectrometer aboard Viking Lander 78−40792
soil and surface temps. at Viking sites 77−56867
soil density and dielectric permittivity, Mars probe radio obs. 78−69722
soil density from 3 cm meas. 79−88614
soil density map rel. to surface albedo, topography and geology 80−109388
soil magnetic particles, Viking lander 2 obs. 77−56859
soil physical props. at Viking 1 site 77−17413
soil transport by winds 80−31228
soils, planetary chemical-biological search possibilities 79−40176
solar wind interaction, role of planetary ionosphere and magnetosphere 80−72835
solar wind interaction, satellite meas. with charged particle traps 77−13200
solar wind interaction region, ion flux meas. interpretation 80−8575
solar wind interaction with ionosphere, electrodynamic model 79−84624
solar wind near Mars, Mars 2 plasma and magnetic meas. 77−53384
south polar cap, residual CO_2 frost in spring and summer 80−72820
south polar region, eolian features rel. to polar vortex, seasonal var. 80−31227
Soviet lunar and planetary exploration, handbook 80−62398
spacecraft final descent vel. control in atm., autonomous navigation algorithm 77−29620
spacecraft orbital transfer from Earth, minimal flight time calc. 78−4090
spacecraft placement in orbit using atmospheric braking 78−69639
spectral reflectance, near IR, surface comp. determ. 79−21216
spectral reflectance during 1973 opposition, 0.33-1.10 μ photoelectric photometry 77−60703

Mars continued
spectrophotometric and colour estimates of Viking lander sites 78−20693
spin axis orientation and Viking 1 lander posn. from radio tracking data 77−13269
spiral clouds, Viking Orbiter images during 1978 northern summer 79−75133
supernova and solar wind rel. to atmospheric evolution, implications of Viking data 77−87307
surface, data from Viking spacecraft 78−61779
surface, search for organic substances and inorganic volatile compounds, Viking expt. 78−20707
surface, structure, atmosphere, magnetic field, development *(Hungarian)* 77−73987
surface, wave tilt sounding of multilayered structures 80−61926
surface and atmosphere, IR thermal mapping by Viking 77−13264
surface and atmosphere, review *(Russian)* 78−20667
surface and atmosphere temps., Viking obs. 77−56868
surface atmospheric pressure, Viking 1 lander verification of radio occultation meas. 77−22129
surface brine presence, Cl and sulphate abundance detect. 80−82254
surface characts. in N. hemisphere, Arecibo obs. at 2380 MHz 79−25533
surface chemistry, mineralogic and petrologic implication, Viking lander sites 77−56855
surface chemistry, Viking gas exchange expt. 77−17399
surface colour change at Viking landing site 80−72829
surface composition from reflectance spectroscopy, summary 80−72834
surface electrical props., Viking lander bistatic radar meas. 78−20686
surface feature, Viking 2 lander obs. 77−56853
surface features, Viking 1 lander photographs 77−13267
surface features nomenclature, Latin and Russian versions 79−8870
surface heights, correl. with latits. of polar hood boundaries 77−5482
surface layer structure prediction *(Russian)* 77−41342
surface markings, change in opinion on nature, 1877 to 1914 period 79−80406
surface materials, chemistry, anal. of Viking X-ray fluoresc. spectrometer data *(German)* 78−85884
surface meteorological results, Viking 1 and 2 landers 78−20702
surface morphology, review 80−56748
surface particle motion inferred from Viking lander cameras 78−20694
surface physical props., Viking 1 lander preliminary results 77−17402
surface properties, obs. by Earth-based radar at 70, 12.5, and 3.8 cm wavelengths 77−91457
surface properties at Viking 2 site 77−56860
surface roughness from Arecibo radar obs. 78−28565
surface sample inorganic chemistry, Viking lander sites 77−56854
surface shape determ. from limb photographs by spacecraft 79−8845
surface slopes, roughness and reflectivity, radar obs. during 1975 opposition 78−45254
surface soil thermal model 78−49356
surface structure forecast, based on thermal conditions 78−77502
surface structure from optical and IE refl. spectrum and thermal props. 77−29690
surface thermal properties, effect of nonideal surface 80−72819
surface topography, photometric study method 79−25537
tectonic evolution 80−67606
tectonics and volcanism, review *(Russian)* 79−48726
Tempe area, detection of abnormally light area 78−28569
tephigram of CO_2 atmosphere 78−73671
S.Tharsis, radar altimetry 80−98591
Tharsis province, geologic sequence, geometry, deform. mechanism 79−75134
Tharsis province, isostatic model 80−12701
Tharsis region, volcanic shield dating from impact crater obs. 77−5476
thaumasia crustal dome, fossilized early forming Tharsis uplift 79−70983
thermal evolution, calc. 79−2501
thermal history and evolution, theoretical model 78−65533
thermal inertia, longit. var. rel. to var. of 2.8 cm brightness temp. 80−105191
thermal map of northern equatorial and temperate latitudes 80−72818
thermal maps of Chryse basin channel terrain 80−72817
thermosphere, depend. of struct. on solar activity 77−64686
thermosphere, effects of energetically produced O_2^+ on ion temps. 79−96945
thermosphere, heat sources prod. by solar UV radiation absorpt. 77−25965
Tiu Vallis, longit. grooving origin, responsible fluid types 80−26769
topographic synthetic contour mapping 78−45253
topography, photogrammetric portrayal 80−67609
topography, role of CO_2 permafrost 78−65535
troposphere, radio beam curvature effect on phase meas. 78−49118
upper atmosphere, composition and struct., Viking obs. 77−53453
upper atmosphere, H Lyman α radiation meas. with absorpt. cell spectrophotometer 78−28519
upper atmosphere absorption of solar UV, interaction model 80−56746
upper atmosphere composition and struct. from Viking neutral meas. spectrometers 78−20689
upper atmosphere isotopic composition, Viking 1 obs. 77−17405
upper atmosphere structure and dynamics, review 77−33382
upper atmosphere structure from Viking spacecraft expts. 79−25534
UV observations by TD1A and OAO-2 satellites 77−91459
Valles Marineris, landslides 80−67620
Valles Marineris geology, anal. of imaging from Viking 1 orbiter primary mission 78−20672
variable surface features, Viking primary mission study 78−20678
Viking, extended mission 80−67514
Viking, first mission 77−13262
Viking, initial exp. analysis 77−41341
Viking 1975 Mars lander interactive computerized video stereophotogrammetry 78−20650
Viking 1 and 2, surface photography 77−2361
Viking 1 and 2 expeditions, scientific results *(Hungarian)* 78−73666
Viking 1 and 2 lander results *(Swedish)* 77−71043
Viking 1 lander, location on surface of Mars 78−65479
Viking 1 landing and early expt. results 77−2362
Viking 1 landing sites, radar obs. rel. to site choice 77−13272
Viking 1 landing sites selection 77−13271
Viking 1 orbiter photographic obs. 77−2363
Viking 2 landing and first photographs of Mars' surface 77−9689
Viking 2 landing site, photographs 77−17396

Mars continued
Viking 2 landing site search 77−17404
Viking and search for life, gas exchange expt. indicators 77−37549
Viking biological experiments 78−20711
Viking biological expts., essential findings 78−65542
Viking biological investigation, preliminary results 77−17415
Viking biological investigations, review and status 79−80263
Viking biology experiments simulation, possible surface reactions 78−7904
Viking C assimilation expts. 78−20708
Viking experiment, computer image processing, basic techniques 77−91403
Viking experiments, superoxides theory *(French)* 77−71046
Viking gas exchange expt., Chryse and Utopia surface samples, results 78−20710
Viking gas exchange reaction, simulation on UV irradiated MnO_2 substrate 80−72831
Viking I and II photography anal. of Martian surface *(Croatian)* 78−12132
Viking inorganic chemistry results, chem. and mineralogical interpretation 78−20705
Viking IR thermal mapper, design 78−57440
Viking labelled release biology expt. 77−56863
Viking labelled release expt., radiorespirometry 77−37548
Viking labelled release expt., results 78−20709
Viking lander, preliminary obs. 77−91463
Viking Lander 1 life detection expt., chemical interpretation 78−32382
Viking lander 1 site, geology 78−20695
Viking lander 2 site, geology 78−20696
Viking lander biology expts., review 77−91407
Viking lander biology instrument 78−49347
Viking Lander camera, optical system and design 78−53794
Viking lander camera data, image processing 78−20649
Viking lander camera search for life 78−20697
Viking Lander I project 77−33321
Viking lander photographs 77−2360
Viking lander preliminary findings *(German)* 77−78711
Viking lander sample field obs., current status 80−67626
Viking Lander seismometer 78−16274
Viking lander sites, spectrophotometric and colour estimates 78−85881
Viking lander sites, surface materials 78−20699
Viking lander sterilisation and biological expt. containment 77−17327
Viking Lander tracking contributions to Mars mapping 80−12702
Viking landers, imaging obs. during one Mars year 79−80265
Viking landers, locations and Mars physical ephemeris from radio tracking data 78−20685
Viking Landers 1 and 2, 1977 winter survival prospects 77−74001
Viking Landers and unsuccessful search for life 78−49367
Viking magnetic properties expt., results 78−20701
Viking Mars lander, hydrazine terminal descent engine, thermal design 77−87234
Viking mission, biological implications 79−8872
Viking mission, optical equipment 77−29627
Viking mission, radio science investigations 78−20684
Viking mission, review 77−73933
Viking mission, review of planetary data 80−72839
Viking mission, review of surface sampling and landing of second vehicle 77−17403
Viking mission and search for life 77−25969
Viking mission operations strategy 77−17325
Viking mission results 80−82255
Viking missions, example of planetary exploration 78−12076
Viking missions, scientific results review 77−56852
Viking orbital colorimetric images 77−17414
Viking orbiter and lander photographs 77−17397
Viking Orbiter and Lander stereo image processing 78−81554
Viking orbiter images, IPL processing 78−20679
Viking orbiter imaging expt., preliminary results 77−17401
Viking Orbiter rectified photography, planimetric Martian triangulation 77−87276
viking Orbiter stereophotogrammetry 78−77493
Viking Orbiter visual imaging system, surface photographing using slow-scan TV cameras 77−45282
Viking orbiters, radio occultation meas. of Mars atmosphere and topography and atmosphere 80−72836
Viking orbiters, scientific missions 78−20612
Viking orbiting and landing mission *(German)* 78−93139
Viking primary mission, thermal and albedo mapping 78−20683
Viking programme, biological expts. *(Hungarian)* 79−44329
Viking project, imaging expts. on orbiters and landers 77−56851
Viking project, instrumentation, scientific experiments and results 79−16865
Viking project, summary 78−20611
Viking project and search for organic life *(Swedish)* 77−22128
Viking pyrolytic release expt., assimilation meas. 77−41346
Viking radio occultation meas. of atmosphere and topography 78−20687
Viking results−life or active soil chemistry 77−37546
Viking results from early meas. on surface 77−33383
Viking seismic expt., prelim. results 77−56861
Viking surface sampler subsystem, acquisition assembly 79−12380
Viking X-ray fluorescence expt., anal. methods and results 78−20703
Viking X-ray fluorescence expt., sampling strategy, lab. simulation 78−20704
Viking-1 meteorological meas. 77−29686
Viking-2 site, discrete wind events during northern summer 79−16859
Vikings 1 and 2, results before 1976, November superior conjunction 77−29701
volatile outgassing vel. to Viking rare gas abundances 77−45342
volcanic features, obs. from Viking orbiters 78−20668
volcanic modification of impact craters, intrusions 78−77513
volcanic sulphate aerosol, formation and deposition 80−72828
volcanism and thermal tectonics on one-plate planets 78−77507
volcanism in cratered terrain hemisphere 78−81576
volcano-ice interactions, landforms 80−67616
volcanoes evidence for explosive volcanic density currents 79−84705
volcanology and tectonics rel. to Earth 79−30002
water coverage, polar ice discovery 77−22130
water vapour, obs. from Viking orbiters 78−20682
watery past of Mars, implications of Mariner and Viking obs. 80−17527
wind, crater generated lee waves 80−72824
wind activity detect. by seismometer at Viking Lander 2 site 79−84703

Mars continued
wind blown deposits, silt-clay electrostatic aggregates 80−21940
wind speed requirements for particle motion 77−5479
wind streaks, seasonal and secular var., Mariner 9 and Viking obs. 80−67622
windblown dust, threshold speeds and particle sizes 77−45083
windblown particle abrasion, erosion of quartz and basaltic sand 80−17525
yardangs and wind erosion 80−67623
Ar content of atmosphere, Viking 1 X-ray fluorescence spectroscopy 77−13270
Ar degassing models 77−29700
C assimilation expts., Viking 77−56862
CO abundance calc. 77−33387
CO_2 adsorption and capillary condensation on clays, significance for volatile storage and atmospheric history 80−72833
CO_2 atmosphere, erosion by solar wind energetic atomic particles 80−72736
CO_2 frost streaks in south polar cap 80−31226
CO_2 IR heterodyne spectroscopy in atmosphere 77−41344
CO_2 ice clouds, brightness temp. and radiative props. 80−105192
CO_2 photoionisation and photoelectron energy distrib. in thermosphere 79−2506
CO_2 solid, optical properties in IR region 80−72821
Fe-FeS, core formation, radioactive element diffusion, thermal history 79−84724
H I Lyman α emission meas. at solar minimum 79−12417
H thermal escape from atmosphere, assoc. non-Maxwellian effects 79−80264
O_2 dayglow and O_3 abundance latit. var. 79−53750
O_3, global distrib. 77−78710

martensitic steel
$\alpha \rightarrow \gamma$ transformation during rapid heating of N18K9M5T and N25 77−59788
abrasive wear resistance, effect of tempering strain martensite 77−56116
age hardening with Cu, Nb additions, exam. of hardness 80−7681
ageing, effect of H_2 on stresses in process of $\gamma \rightarrow \alpha$ transformation *(Russian)* 80−76252
ageing, influence of neutron irradiation *(Czech)* 78−84859
ageing of 05kh3N2MD2, hardness depend. on temperifig temp. *(Russian)* 79−24544
alloying element effect on coarsening behaviour of cementite particles in ferrite 80−66518
austempering effects on H_2 yield *(Russian)* 77−55996
ball bearing, fatigue damage, influence of dispersed phases in martensitic matrix 80−108549
Bauschinger effect, structural sensitivity *(Russian)* 79−52303
BCC α-martensite form. from FCC γ-phase during quenching orientation relationship *(German)* 77−25050
brittle fracture resistance, struct. after quenching effects, tempering effects 79−57104
brittle fracture susceptibility, heat treatment effects 77−21190
carbide formation during tempering on martensite decomp. and ductility 78−23733
cavitation failure in liq. O_2 77−44405
cold rolling, effect of transformations during quench hardening and tempering 77−55989
composite vessels, welded, glass fibre reinforced plastic wound, struct. strength 80−97552
corrosion cracking in chloride and alkaline solutions, 07Kh16N4B 80−55576
corrosion cracking mechanism in Cl^- and sulphide containing environment *(Russian)* 77−59969
corrosion resistance and mechanical performance in medical instruments 79−39537
corrosion resistant, review of heat treatment, mech. and corrosion resist. characts. *(Korean)* 79−24653
corrosion resistant type 07Kh16N4B, long time strength and ductility, 340 to 450°C 79−100233
corrosion under boiled conditions, Mossbauer spectroscopy study 79−47800
cracks formation mechanism obs., grinding, impingement cracks and strain influence *(Japanese)* 78−56747
critical temp. of transformation determ. 77−90349
cryogenic, 03Kh12N10MT, fracture toughness and structural strength 77−59927
crystal structure, X-ray diffr. study 78−79565
crystal structure variation during heating, role of Mn and Al *(Russian)* 79−46600
cutlery, pitting corrosion 80−100962
dendritic structure assessment with Elypovist electropolisher 77−52565
dislocation structure, amplitude independ. internal friction obs. *(Bulgarian)* 77−19966
duplex ferrite, microstructure resistance optimisation to fracture 80−40482
elastic interaction of H_2 with precipitates 78−3129
emulsion, mag. and dielec., prep. by abrasion of austenitic steel with Fe_2O_3 or Al_2O_3 suspension 78−27826
etching technique, for revealing struct. inhomogeneities 80−61035
even elongation and relative hardening, effects of struct., comp. and testing temp. 78−52926
fatigue, scale effect, structural parameter effect in rotary bending *(French)* 78−23822
fatigue crack growth rates, stress ratio dependence 79−70148
fatigue crack nucleation from inclusions, rotating beam determ. of true min. stress *(French)* 77−25122
fatigue crack propag., effect of intercrystalline fracture associated with temper brittleness *(French)* 80−16463
fatigue damage, development rate by exoelectron meas. 80−25835
fatigue life, low-cycle, temp. and strain rate effects 80−85056
ferritic martensitic, effect of ductility of second phase on ductile fracture 78−19847
ferritic-martensitic steels, fatigue crack tip plastic zone *(Japanese)* 80−71738
formation of α-martensite in crossing region of ε-martensite platelets *(German)* 78−3126
fractography, facets classification *(Slovak)* 79−20173
fusion reactor first wall/blanket material 80−32451
grain size effects in H_2 assisted cracking, austenitising 77−28901

martensitic steel continued
hardened, martensite struct. characts., Cu and Al additions effect *(Russian)* 78−19709
heat-resistant, martensitic, Kh12NMFB weldability 80−20987
high C, Co addition effect on strength *(Korean)* 78−68736
high C, struct. transform. during low temp. tempering *(Russian)* 77−59737
high C, tempering, nuclear gamma reson. meas. *(Russian)* 79−1883
high strength, hypereutectoid, low alloy, microcrack frequency and fracture toughness rel. to martensitic struct. *(Czech)* 77−70163
high-C, formed from hot-worked austenite, struct. *(Russian)* 78−6950
high-tempered bainite and mass martensite, shock toughness, −196°C *(Russian)* 77−16663
impact bending failure resistance, initial crack length and tempering effects 78−31530
interface model of $(3, 15, 10)_F$ martensite 78−31408
Kh15N5AM3, combined heat treatment and mech. working *(Russian)* 77−55997
lattice anomalies, relationship with thermodynamic props. of C in austenite *(Russian)* 78−59781
lattice structure obtained by deform. of austenite 70Kh5G4 *(Russian)* 78−88464
LNG storage and transportation system material, tensile and yield strength 79−70133
low C, 10Kh2G3M, development of plastic deform., slip and dislocation struct. *(Russian)* 79−15722
low C, development and props. *(Russian)* 80−20933
low C, martensitic, fracture toughness variations during tempering 78−60812
low C, nitriding, exam. of case props. 78−85045
low C, packet martensite struct. and localisation of residual austenite, electron microscope obs. *(Russian)* 80−25695
low C, tempered, lath martensite, Ni (5 wt.%), microstruct./yield strength relationship 77−21234
low C wire, strain tempering by rapid heating *(Japanese)* 78−31428
low C without Ni, for deep-well sucker rods, corrosion fatigue 80−55588
low Si, martensite struct. and mech. props. *(Korean)* 80−93614
low tempered, high strength, fatigue crack, propag. rate *(Czech)* 78−64770
low-alloy steel, abrasive wear resistance, effect of C content, annealing quenching 77−56115
magnetic field effect on retained austenite transformation 77−16580
maraging steel, ageing kinetics and struct. of N12K7M5TYu, effect of high temp. deform. of austenite *(Russian)* 80−84960
maraging steel, VKS-210, α to and from γ transformation investigation by thermomagnetic structural anal. *(Russian)* 79−83197
martensitic-ferritic steels, microdefect accumulation during creep, effects of heat treatment, hardening 79−24550
medium alloy, quenched state, deform. hardened, ageing effects *(Russian)* 77−21179
microcrack growth, in ferrite grain in two-phase martensitic-ferritic steel 80−21070
mild, semi-killed, tempering, effect of microstruct. and hardness 77−21184
modulated struct. form. by tempering, high resolution electron microscopy obs. 79−96042
neutron radiation effects, delayed fractures suppression *(Czech)* 78−67743
Ni-Cr-Mo, electroslag refined, fracture toughness and fatigue behaviour 80−81171
nitriding in metastable condition 80−30167
plastic deformation, struct. transforms. *(Russian)* 77−16606
plastic deformation influence in type N17K12M5T steel on mech. props. *(Russian)* 80−76305
quenched, strength variation rel. to H behaviour 77−59924
quenched, tensile and compressive deform. resist. *(Russian)* 78−19819
quenching, effect on structure and wear resist. 77−21175
quenching to form martensite, morphology and struct., electron microscope and electron diffr. study *(French)* 77−73291
retained austenite study by X-ray diffr. *(Korean)* 78−44143
specific heat and magnetisation, 1.2 to 10K 80−71059
stainless, CrMoV, stress effect on pitting susceptibility 80−16542
stainless, high alloy, fatigue cracks, effect of chem. comp. and heat treatment *(Russian)* 77−25144
stainless, in SO_4 solns., activation pH and susceptibility to H_2 assisted stress corrosion cracking 80−97619
stainless, metallic second phases, effect on steel behaviour, review 78−31503
stainless maraging steel, VNS-2USh, α to and from γ transformation investigation by thermomagnetic structural anal. *(Russian)* 79−83197
stainless types 403 and 616, temp. depend. of low cycle fatigue behaviour 80−7667
steel, austenitic-martensitic 0Kh15N5M, ductile fracture 78−3226
steel, low C, type AISI 1018, microstruct. effects on fatigue crack growth 79−61718
steels, ferritic and martensitic, C and N migration at low temps., monograph 80−22149
strain hardened martensite, resist. to tempering, exam. 80−16348
strain hardening at high temps. in type 28Kh3SNMVFA *(Russian)* 79−74174
strength and embrittlement, early stages of martensite decomp. effect 80−35227
strengthening involving austenite fine grain processing *(Russian)* 77−52358
structural, corrosion resist. under stress effect of strain ageing with hydroextrusion *(Russian)* 79−38853
structural and mechanical props. of type Kh13N9D2MT martensitic aged steel *(Russian)* 80−93600
structure, ^{57}Fe Mossbauer spectra 80−15051
structure of Fe-C martensite, quenched, and heated to 293K, Mossbauer obs. *(Russian)* 77−59784
submicrostructure alterations in ageing and plastic deform. *(Ukrainian)* 79−79032
tEM examination of microcracking in plate martensite *(German, English)* 79−91887
temper embrittlement 79−87722
tempered, C and low alloy, hardness, effect of alloying additions 78−27629
tempered martensite embrittlement of type SAE 4340 80−30084
thermal expansion, of heavily doped steels and alloys 80−103501

martensitic steel continued
thermally and thermomechanically treated, struct. and decomposition of martensite 78−19784
thermomechanical treatment, high temp., effect of austenite deform. on martensite stability during low temp. tempering 80Kh5 79−57018
twinned martensite, crystallog. singularities in reverse martensitic transform. *(Russian)* 77−32571
void swelling response after fast reactor irradiation 80−6437
X-ray analysis of partially disintegrated martensite, appl. of method of moments 79−52223
Al steel, κ'-martensite struct. and $\kappa' \rightarrow \alpha_m$ transform., X-ray diffr. *(Russian)* 77−59786
Al, steel, relax. twins in martensite, electron diffr. and electron microscopy *(Russian)* 78−47391
Al-C redistribution of C during tempering *(Russian)* 77−90371
C, electron irrad., reversible C at. redistrib. 77−65991
C, tempering induced decomposition and segregation, atom probe study 80−3112
Cr (12%), temper embrittlement 80−66650
Cr-C(12, 0.15 wt.%) type AISI 410, role of C in embrittlement phenomena 80−93652
Cr-Co-Ni-Mo, notch toughness, rel. to sensitivity to stress conc. 78−31532
Cr-Mn(Ni), Mn and Ni additions, effect on corrosion resistance and hardness 80−104342
Cr-Mo, effect of Mo on high-temp. props. 80−85005
Cr-Ni, deform., effect of phase composition and struct. *(Russian)* 77−25102
Cr-Ni, grain refining and phase transforms. effect on plasticity *(Russian)* 78−39837
Cr-Ni, martensite defect identification by positron annihilation 78−39867
Cr-Ni-Co-Mo-Ti, Kh12N8K5M3TYu, ageing of C free martensite *(Russian)* 79−1884
Cr-Ni-Mo-Cu, ε phase particle precipitation from martensite, local internal stress relaxation *(Russian)* 79−78969
Cr-Si-Mn-Ni-Mo-C, resist. to deform. and fracture, C effect 80−71757
Fe-C-Al, law of variation of cryst. lattice parameters, X-ray diffr. analysis *(Russian)* 77−52322
Fe-Ni-C, martensitic, mech. and fracture charact., effect of starting austenite heterogeneity *(Slovak)* 78−19792
Fe-Ni-C, martensitic, modulation of local C atom cumulation during ageing *(Slovak)* 78−19790
Fe-Ni-C, mech. charact., effect of ageing and tempering *(Slovak)* 78−19791
Fe-Ni-C martensite morphology, butterfly-lenticular transition temp., Cr addition effect *(Japanese)* 80−81053
low-C martensitic, Ni addition influence on toughness and ductile-brittle transition 80−30099
Mn (1 to 10 wt.%), Mossbauer, X-ray and electron microscope studies of martensite 78−56621
Ni (1 to 9 wt.%), Mossbauer, X-ray and electron microscope studies of martensite 78−56621
Ni (26.4 wt.%), partially twinned, slip lines obs. 78−84913
Ni, martensite decomposition *(Russian)* 79−1841
Ni-C, microstructural distrib. of cathodic H_2, autoradiography *(French)* 79−99234
Ni-Co-Mo(W), ageing, thermal recovery 77−56011

martensitic transformations
see also shape memory effects
A15 compounds, comparison of Landau theories 78−67824
A15 compounds, high-temp. superconductors, martensitic transform., microscopic theory based on 3-dimens. band struct. 78−19752
A15 compounds, supercond. rel. to struct. transform. 78−14873
A-15 compounds, struct. transformations and soft phonon modes, microscopic theory *(Chinese)* 79−37803
A-15 type compounds, relation between martensitic and supercond. phase transition 80−29497
acoustic emission anal., signal recovery technique for martensitic transformation study 78−60965
ageing, effect of H_2 on stresses in process of $\gamma \rightarrow \alpha$ transformation *(Russian)* 80−76252
alloy, austenitic, mechanical changes after electrolytic quenching *(Russian)* 80−50653
alloy, formation of laminated martensitic structures *(Russian)* 78−39771
alloy steels, ferrite and alloy carbide interrelation 80−3040
alloys, phase transition premonitory phenomena, exam. by electron diffr. and microscopy *(French)* 80−59651
alloys with twinned martensite, crystallog. singularities in reverse martensitic transform. *(Russian)* 77−32571
austenitic stainless steel, recrystallisation transformation energies, α' to γ, effect of Si content and deformation by rolling *(French)* 77−48433
austenitic steel, ageing after deform. in pre-martensitic state, internal friction meas. *(Russian)* 77−77477
austenitic steel, hardened by thermomechanical treatment with ageing, influence of stabilisation on mech. props. *(Russian)* 77−52356
austenitic steel transformation temp. and crack prevention in weld cooling 79−83200
brass, Cu-Zn (39(40) wt.%), shape memory effect and martensitic transform. depend. on heating-cooling cycles *(Russian)* 80−97482
brass, martensite form. in cyclic transform., reproducibilities 77−16582
brass, martensite stability 79−91650
β-brass, martensitic, transform hardening and energy dissipation 77−21141
brass, martensitic transform., short range order effect 79−61586
brass, nonradial diffuse streaks and complex diffuse scatt. patterns of electrons 79−7527
β_1 brass containing α-precipitates, reversible shape memory effect *(Japanese)* 78−60711
brass single crystal, martensite form. and shape memory effect mech. 78−19744
Carnot cycles, transform. temp. and latent heat under applied stress, rel. to shape memory effect 77−28874
ceramics, transformation toughening, martensitic transforms. in crack-tip stress fields 80−104154
computer coupling of phase diagrams and thermochemistry 77−77460
conference, phase transformations in metallurgy, York, England (Apr. 1979) 80−2994

martensitic transformations continued
crystal geometry, of martensitic transformations, electron microscopy study *(Russian)* 80−108441
crystallographic reversibility 78−6925
crystallography of BCC to 9R transform., generalised mathematical model 79−34037
dislocation inheritance, crystallography, describable by nonuniform lattice strain *(Russian)* 80−81056
dislocation inheritance during martensitic transforms. *(Russian)* 79−52211
dislocation motion, effect of anisotropic elastic medium 77−28811
dislocations and lattice transformations, book contrib. 80−107242
double martensitic transformation, distribution of austenitic orientation *(Russian)* 78−64540
elastic wave generation comparable to Bain deform., role of multiphonon processes *(Russian)* 80−84246
electron-phonon interaction effect on martensitic transform mechanism *(Russian)* 78−3127
electronic system with two-fold degenerate band, free energy change due to electron-phonon coupling, martensitic transition temp. 79−42500
ellipsoidal inclusion elastic field, appl. to martensite formation 77−48436
external stress effects on equilibrium morphology, thermodynamic model *(Russian)* 78−52804
ferroelectrics, domain structure as outcome state for poling procedure 80−80728
ferromagnet, nonlinear magnetoelastic effects and phase transforms. *(Russian)* 78−48015
ferrous martensites, trace analysis of (112) transform. twins 77−86030
habit plane of martensite 78−18572
intermetallic compounds, press. depend. of martensitic and supercond. transition temp. 79−19681
internal stress relax. effect on microstruct. and kinetic features 77−44250
isopropyl ammonium chloroplatinate and chlorostannate, ferroelastic transition, thermal, optical, and elastic meas. 79−28096
itinerant magnets and superconductors, structural instabilities, phase diagrams 78−14922
Kurjumov-Sachs, Bogers-Burgers, Nishiyama and Zener models, rel. to crystallographic theory 77−63672
lenticular martensite growth by transformation wave propag. 80−81055
lonsdalite→graphite phase transform. mechanism, electron diffr. expts. 79−28099
magnetostriction effect, on martensite transformation point shift in strong mag. field *(Russian)* 80−108440
marmem engines, martensitic transform. and shape memory effect 78−6920
martensite crystal, dislocation representations of development kinetics 80−39086
martensite crystal lattice, transform. mech. and C atom behaviour 77−25051
martensite energy due to order inherited from austenite 77−28813
martensitic memory alloy composite, for prefabricated constructions *(Russian)* 77−21059
martensitic transformations, electron microscopy and diffr. studies 79−68989
materials interactions, stability, phase transformations, thermodynamics and corrosion 78−88444
mechanical model, nonlinear 78−87789
mechanism, position of C atoms in martensite lattice *(Russian)* 77−8820
mechanism 77−4780
memory alloy engine, efficiency 80−71648
metal, martensitic memory mechanism *(Russian)* 77−21217
metals and alloys, martensitic transitions accompanied by interactions between phases *(Russian)* 80−7568
metals and alloys, nonlinear anelasticity and the martensitic transformation 79−61634
metals and alloys, shock wave effect on martensitic transform. *(Russian)* 80−96595
minimization of elastic energy and phenomenological crystallographic theory 78−31407
molecular crystal, p-dichlorobenzene, crystallographic aspects 77−19891
Nb_3Sn, lattice anharmonicity 79−8300
β_1-Ni-Al, premartensitic transformation 78−76645
Nitinol memory material for solid-state engine 78−59288
nucleation, lattice instabilities near planar defects, localised soft mode theory for martensitic transforms. 78−10159
nucleation affected by metallurgical treatment 78−80547
nucleation and streaming 78−39774
nucleation general concept, general concepts, FCC to HCP transform. 77−36502
nucleation mechanism, FCC→BCC and other martensitic transforms. 77−36503
nucleation mechanism, kinetics 77−36504
nucleation of martensite at dislocations, elasticity model 80−55393
nucleation site, variation in number 77−12621
nucleation site, variation in number 77−12622
nucleation time, estimate in martensitic; transformation 80−29954
ordered cubic alloys, reversible martensitic transformations 78−27516
orientation relationship definition, anal. method 78−60670
β-phase alloys, Landau theory 80−108444
phase hardening effects on M_s 78−23708
phthalocyanine, metal-free, molecular imaging and phase transformations using electric microscopy 79−33198
polyethylene, cross-linked crysts., rel. to deform. mechanism 78−15469
polyethylene, high-density, oriented, rel. to deform. mechanisms 78−44171
polyethylene, high-density, semicryst., fold-surface morphology effect on deform. processes 78−34447
premartensitic phenomena, nucleation, shape memory effect, review 80−3041
pseudoelastic single crystal fatigue 79−52364
quenching in const. magnetic field, struct. peculiarities *(Russian)* 79−52204
rare earths, light, stacking faults and magnetism, transform. effects 80−75840
review 80−3037
shape memory alloy, martensite boundaries, lattice imaging study 80−107359
shape memory alloy, recovery stress determ. 79−15665
shape-memory alloys, props. and appl. 80−30049

martensitic transformations continued
shape-memory alloys, shape recovery cycle thermal efficiency 80−108445
single crystals under large loads, theoretical elastic behaviour, review and appl. 80−71681
stainless steel, austenitic Cr-Ni, stability, tensile and compressive strain depend., 4-373K 77−25052
steel, 15Kh15N5AMZ, martensitic transform., inverse, plastic deform. effect, 200 to 550°C *(Russian)* 77−73274
steel, 30Kh3SNMBF, α-phase nucleation and growth, influence of supercooled austenite state *(Russian)* 77−48435
steel, 35NiCr18, bainite transformation, study with aid of hot stage microscope 80−76253
steel, 50N29 type, self-consistent junctions and spatial relative organisation 80−19750
steel, $\alpha \rightarrow \gamma$ transformation during rapid heating of N18K9M5T and N25 77−59788
steel, α-martensite formation in crossing range of ε-martensite platelets *(German)* 78−3126
steel, alloy, martensitic transforms. during deform. of types N28, N29, N30 and N31 78−56639
steel, alloy, transform. kinetics of supercooled austenite in 12Kh1MF, structural method 78−52801
steel, alloy, type 60 ND 11, martensitic transform. effect on stress development during quenching *(French)* 79−91712
steel, alloy, type AISI 4340, martensitic transformation, TEM study 80−3043
steel, alloy 40Kh, sulphide cracking resistance, strengthening method influence 80−55577
steel, alloy type N24M5, martensitic transform. microkinetics 78−56637
steel, alloyed with Cr, Mo, Co, Mn, martensitic point position depend. on cooling rate *(Russian)* 79−70063
steel, austenite stabilisation during $\alpha \rightleftarrows \alpha$ transition *(Russian)* 78−44117
steel, austenitic, 0Kh14AG12M, temp. depend. of mech. props. and kinetics of phase transforms. *(Russian)* 78−92297
steel, austenitic, 33N25Yu3F, hardening, effect of quenching and ageing temps. *(Russian)* 77−81267
steel, austenitic, 70Kh5G4, martensite lattice struct. obtained by deform. *(Russian)* 78−88464
steel, austenitic, aged, stress induced martensitic transform., mech. props. *(Russian)* 79−87632
steel, austenitic, Cr-Mn, Kh4G18F, microstruct. and mech. props. during tensile deform. *(Russian)* 79−20114
steel, austenitic, Cr-Mn, metastable, plasticity, contrib. of martensitic transform. during deform. *(Russian)* 80−30018
steel, austenitic, deform., struct., transform. kinetics hot working effects *(Russian)* 77−52361
steel, austenitic, hydrogenation effect, different stability characts. 78−35383
steel, austenitic, martensitic transform., alternating elastic stressing effects 77−86029
steel, austenitic, martensitic transform., mechanism and kinetics, TEM, X-ray and optical obs. *(Rumanian)* 78−19746
steel, austenitic, martensitic transform. at crack tip 77−70051
steel, austenitic, martensitic transform. at propagating fatigue crack 78−19745
steel, austenitic, martensitic transform. during low temp. alternating torsion *(Russian)* 78−23706
steel, austenitic, martensitic transform. effect on hardening kinetics and fracture resist. of friction surface of 45Kh12G8 and 110G13 *(Russian)* 80−50727
steel, austenitic, martensitic transform. temp., singularities in 50Kh2N22 *(Russian)* 78−68689
steel, austenitic, metastable, alloy 000Kh18N10 creep at low temps. 77−1861
steel, austenitic, metastable, hardening by cycling of martesitic transform. during rapid heating, in 30N24M4 and 50N21M3 *(Russian)* 79−20074
steel, austenitic, phase transform to pearlite and martensite, kinetics, stresses due to quenching, anal. *(Japanese)* 78−27508
steel, austenitic, quenched state, influence of austenite stability on impact strength *(Russian)* 80−81146
steel, austenitic, type En58B, martensite formation and reversion, effect on void swelling 80−11641
steel, austenitic, type M316, martensite formation and reversion, effect on void swelling 80−11641
steel, austenitic, undergoing martensitic transform. during deform., temp. depend. of yield point *(Russian)* 77−66677
steel, austenitic, wire rod, austenite transform. kinetics accompanying interrupted cyclic cooling *(Russian)* 79−70064
steel, austenitic 03KhAG19, fatigue crack development at normal and low temps., struct. effects *(Russian)* 78−35480
steel, austenitic metastable, fatigue, effect of deformation-induced martensitic transformation *(Japanese)* 78−15514
steel, austenitic metastable, formation of martensite under load, effect on mech. props. *(Russian)* 77−86026
steel, austenitic N31, mechanical instability in premartensitic state *(Russian)* 77−73273
steel, austenitic stainless, 18-8, effect of H on martensitic transformation *(Chinese)* 80−55394
steel, austenitic stainless, cavitation erosion resistance, martensitic transform. effect *(Russian)* 78−35524
steel, austenitic stainless, Cr-Mn, austenite stability during deform. 77−70050
steel, austenitic stainless, electron beam welding effect, on mech. props. of steels 310L, 316, 21-6-9 78−48498
steel, austenitic stainless, fatigue and cyclic stress-strain characts. austenite-martensite transform. effect 80−21109
steel, austenitic stainless, hydride study by X-ray diffr., rel. to martensitic transform. *(Japanese)* 77−81263
steel, austenitic stainless, martensitic transform. effect during static and fatigue loading 77−52325
steel, austenitic stainless, metastable, transform. depend. ductility, temp. and deform. effects 78−3185
steel, austenitic stainless, Mn-Cr, austenite decomposition by deform., rel. to mech. props. *(Russian)* 78−27515
steel, austenitic stainless, Neel temperature and max. susceptibility calcs. 77−43833
steel, austenitic stainless, neutron-irradiated, gamma-alpha transformation 79−96027
martensitic transformations continued
steel, austenitic stainless, stacking fault effect on martensitic transform. during plastic deform. *(Russian)* 80−25696
steel, austenitic stainless, stress corrosion cracking in H_2SO_4-NaCl soln., Ni and N_2 effects *(Japanese)* 79−100289
steel, austenitic stainless, type 304, intergranular H_2 assisted fracture, exam. of mechanism 78−80644
steel, austenitic stainless, unlubricated, friction, wear and microstruct. of types 304, 316 and Nitronic 60 80−108589
steel, austenitic stainless, welded explosively, induced martensites morphology 80−104153
steel, austenitic stainless type 304N, machining induced deformation transformation, mag. evaluation 79−83195
steel, austenitic-ferritic Ni-Cr, 12Kh21N5T, phase and struct. transform. *(Russian)* 78−95748
steel, austenitic-martensitic, phase comp., struct. and mech. props. 80−29974
steel, BCC α-martensite, form. from FCC γ-phase during quenching, orientation relationship *(German)* 77−25050
steel, C, diffusion of H_2, SCC via martensite form. cooling rate changes on Mn and Ni addition *(Russian)* 78−56813
steel, C, martensitic by quenching 80−3038
steel, C, martensitic points, effect of cooling rate *(Russian)* 79−43247
steel, C, massive martensitic transformation kinetics 80−81060
steel, C, transform. kinetics, heat cond. and elastic-plastic stresses during quenching *(Japanese)* 80−25688
steel, carburised, transform. of residual austenite, mag. field effects *(Russian)* 80−29952
steel, carburized and quenched, residual stresses *(Japanese)* 80−89262
steel, cold rolling, effect of transformations during quench hardening and tempering 77−55989
steel, complex alloy, Cr (12-18 wt.%), transformation behaviour *(German)* 80−40349
steel, Cr, stress relaxation, superplasticity and thermal cycling *(Russian)* 80−21019
steel, Cr (3 wt.%), $\gamma \rightarrow \alpha$ transformation singularities in intermediate transformation temp. interval *(Russian)* 79−91644
steel, Cr-C (18, 0.9 wt.%), cavitation, abrasion resistance, effect of unstable austenitic struct. *(Russian)* 77−16695
steel, Cr-Mn, effect of composition, plastic deformation, and heat treatment on martensitic transformation 79−100141
steel, Cr-Mn, unstable austenite, martensitic transform., effect of alloying, heat treatment, and deform. 78−19751
steel, Cr-Mn, X-ray diffr. exam. of fine struct. during deform. *(Russian)* 78−38661
steel, Cr-Mn type, optimum rate of martensite transform. during loading *(Russian)* 77−16579
steel, Cr-Mo-V pressure vessel, microstruct. parameters and yielding rel. to plastic deform. 80−89318
steel, Cr-Ni (18%, 12(8)%), martensite formation and reversion, effect on void swelling 80−11641
steel, determ. of critical temp. using change in ultimate strength above yield point 77−90349
steel, duplex ferritic/ martensitic, design for improved mech. props., heat treatment, TEM obs. 77−63697
steel, En8, surface hardening by 2 kW CW CO_2 laser 79−83396
steel, eutectoid notch toughness, tempering at moderate temps., effect of quenching temp. 77−21193
steel, Fe-Cr-Ni (17.20, 7.34 wt.%), transform.-induced plasticity 78−23774
steel, Fe-Mn-(Cr)-C, intermediate phase form. during martensite form. 77−12626
steel, ferromagnetic, U8, magnetic method of martensite transform. study *(Russian)* 79−87631
steel, high C, 80Kh5G5 and 120N12, austenite hot deform. effect on martensitic transform. *(Russian)* 77−48434
steel, high Mn, mech. props., strain induced martensitic transform., effect of austenite predeformation 77−16649
steel, high Ni, orientational variations of martensite transform. during deform of metastable austenite 78−84805
steel, high Ni (19 wt.%), thermal stabilisation of austenite 78−15397
steel, high-speed, low temp. mag. cycling effects on ferromag. struct. 80−100928
steel, hypoeutectoid, C22, recrystn., influence of carbides distrib., X-ray exam. *(German)* 79−38850
steel, interface model of $(3, 15, 10)_F$ martensite 78−31408
steel, Kh18N9T, strengthening by vibrational stirring effect 80−40405
steel, low alloy, isothermal studies 77−36497
steel, low C, $\gamma \rightarrow \alpha$ transform., martensitic mechanism *(Russian)* 79−47682
steel, low C, packet martensite struct. and localisation of residual austenite, electron microscope obs. *(Russian)* 80−25695
steel, low or medium alloy, work hardening effect on martensitic transform. cond. *(French)* 80−16329
steel, mag. field effects 79−87630
steel, magnetic field effect on retained austenite transformation 77−16580
steel, marageing, austenite formation, stability, transformation to martensite *(Russian)* 79−91646
steel, maraging, $\alpha \rightarrow \gamma$ transform. rate *(Russian)* 77−8821
steel, maraging, α to γ transform. and austenite stabilisation *(Russian)* 79−52212
steel, maraging, effect of thermal cycling (γ to and from α) on props. 80−20986
steel, maraging influence of H content on γ-α transform. during welding *(Russian)* 79−78962
steel, maraging low-Ni, isothermal martensitic transformations *(Russian)* 78−88465
steel, martensitic growth 80−108439
steel, martensitic low C, development and props. *(Russian)* 80−20933
steel, martensitic transformation, lattice deform. 78−27511
steel, martensitic-bainitic, lath morphology effect on yield stress, martensitic and ductile-brittle transition temps. 79−100215
steel, medium-C, singularities in low temp. α-martensite decomp. *(Russian)* 77−8814
steel, metastable alloys, singularities of $\alpha \rightarrow \gamma$ transform. and hardening *(Russian)* 79−52210
steel, metastable austenitic stainless, fatigue damage, static and dynamic simultaneous obs. *(French)* 78−88516
steel, Mn, form. of twinned struct. *(Russian)* 78−64542

martensitic transformations continued
steel, Mn, Mn influence on martensitic transform in presence of strain *(Russian)* 80−20934
steel, Mn, plastic deformation, shape recovery during γ to and from ε, ε' transformations *(Russian)* 79−83196
steel, Mn-C, formation of filamentary V(C,N) precipitates during diffusional $\gamma \rightarrow \alpha$ transform *(Russian)* 79−1865
steel, Mn-Mo-Nb-C, transform. charact. and struct. during continuous cooling 79−29057
steel, Ni (17 wt.%), martensitic deform. temp., cryst. struct. effect *(Russian)* 80−66576
steel, Ni (19 and 24 wt.%), austenite thermal stabilisation at sub-zero temps. 77−52324
steel, Ni (9 wt.%), tempered, mech. stability of retained austenite 79−24521
steel, Ni-Co-C (9, 4, 0.2 wt.%) enthalpy, sp. ht. to 2000K 79−10960
steel, Ni-Cr, enthalpy of martensitic transform. 77−63670
steel, Ni-Mn directional martensitic transform expt. 79−11613
steel, Ni-Mn-C, austenitic, proof stress change meas. by internal friction with martensitic transform. 78−56638
steel, Ni-Mo, sintered, martensitic transformation due to cold working, metallographic study 78−44127
steel, Ni-rich, tetragonality anomalies of martensite 77−77478
steel, Ni-Ti, high-alloy, precipitation hardening, fatigue strength 79−79103
steel, quenching to form martensite, morphology and struct., electron microscope and electron diffr. study *(French)* 77−73291
steel, stainless, 12Kh13 and 15Kh11MF, austenite transform. kinetics 79−87612
steel, stainless, 18-8, stress corrosion cracking in H_2SO_4-NaCl soln., strain induced martensite effects *(Japanese)* e77−56152
steel, stainless, $\alpha+\gamma$ phase, tensile deform. induced α' martensite, morphology 78−44122
steel, stainless, ε-martensite, direct obs. of reverse transform. 77−55967
steel, stainless, austenite stabilisation by H cathodic impregnation *(German)* 79−47680
steel, stainless, austenite stability, deform. rel. to $\gamma \rightarrow \alpha$ transform. kinetics 79−24522
steel, stainless, austenitic, explosively welded, orientation relationship in martensitic transform. 80−104158
steel, stainless, austenitic type 304, acoustic emission identification, opt. microscopy obs. 80−81062
steel, stainless, Cr-Ni (18, 9 wt.%), cold rolled, struct. 79−83214
steel, stainless, ferritic, Ni-free, effect of V, Ti addition on ductility 79−79048
steel, stainless, H_2 induced ε-HCP martensite, TEM obs. 79−34033
steel, stainless, highly deformed zone and cyclic strain history near fatigue crack tip *(Japanese)* 79−34145
steel, stainless, hydrogenation different stability charact. 78−35383
steel, stainless, Kh18N10T, low cycle loading effect on martensitic phase transforms, substruct. development *(Russian)* 79−15664
steel, stainless, Kh18N10T, struct. and mechanical props., effect of previous deform. in rolling *(Russian)* 79−29099
steel, stainless, martensite formation, in situ obs. 80−25692
steel, stainless, martensite nucleation, in situ electron microscope obs. 80−7572
steel, stainless, martensite nucleation and growth, expt. study 78−3125
steel, stainless, martensite nucleation mechanisms, HVEM obs. 80−104157
steel, stainless, martensite nuclei obs., role of defects in nucleation 80−25693
steel, stainless, martensite to austenite transform. at various heating rates *(Russian)* 78−76649
steel, stainless, metastable, determ. of strain-deform. martensite content 78−3282
steel, stainless, reversibility of plastic strain during fatigue with martensitic transform. 78−31526
steel, stainless, shock loaded, residual martensite obs. 80−104414
steel, stainless, strain induced martensitic transform. effect on low cycle fatigue 77−55965
steel, stainless, two-phase ($\alpha+\gamma$), twin-related lath occurrence rel. to fracture elongation 77−90443
steel, stainless, type 304, hydrogen assisted cracking, martensite formation on deformation effects 79−52362
steel, stainless, VNS-2USh, α to and from γ transformation investigation by thermomagnetic structural anal. *(Russian)* 79−83197
steel, stainless, wire, axial texture after electroplastic drawing, X-ray struct. investigation *(Russian)* 80−104177
steel, stainless 18-8, stress corrosion cracking in H_2SO_4-NaCl soln., martensite form. *(Japanese)* 78−92396
steel, stainless 304, shock loading response, grain size effect 77−36601
steel, stainless Kh15N9Yu, elastic limit, effect of microstruct. and heat treatment 79−83251
steel, stainless type 03Kh13AG19, deformation temp. influence on dislocation struct *(Russian)* 80−11698
steel, stress calcs, using statistical model *(Russian)* 80−93557
steel, thermomechanical treatment effect on mech. props. and microstruct. *(French, German)* 79−66090
steel, tool, martensite plate size, austenitization 79−24549
steel, TRIP, fatigue strength 80−108552
steel, TRIP, strengthened by hydrostatic extrusion, struct. and mechanical props. *(Russian)* 78−76647
steel, type 12X18H10T, strengthening based on intensifying heat exchange processes in martensitic transformation region *(Russian)* 79−70065
steel, type 1Kh17N2, alloying element redistrib. during friction *(Russian)* 77−81326
steel, type 304, twinning and martensitic phases on hydrogen-charging, TEM 77−21222
steel, types 10G2 and 18G2F, formation of transform. microtwins in ferrite *(Russian)* 79−1866
steel, with 4% Al, κ'-martensite struct. and $\kappa' \rightarrow \alpha_m$ transform., X-ray diffr. *(Russian)* 77−59786
steel 1095, quenched, Mossbauer study of surface martensite 77−32578
steel 120Kh3G3, lattice defects during $\gamma \rightarrow \alpha \rightarrow \gamma$ transform., electron microscopy obs. *(Russian)* 79−47681
steel 12Kh18N10T, struct. and mech. props. after prolonged working at −183°C 77−55988
steel 40Kh2N20, paraprocess magnetostriction near martensitic point in mag. field *(Russian)* 79−82850
steel 52100, compressive strain induced austenite transform. 77−86027

martensitic transformations continued
steel austenite to martensite transformation, orientation relationships 79−78964
steel bearing, surface-ground, residual stress fatigue property comparison 80−60975
steel Ni, N22, X-ray diffr. study of austenite lattice near martensitic transform. *(Russian)* 79−1868
steel Ni, type 52X2H23, martensitic transform. induced by pulsed mag. field 79−15667
steel OKh18N10T, subjected to low temp. thermal cycling, rel. to. temp. depend. of yield point *(Russian)* 78−48489
steel parts, martensite form., hardening cracks, acoustic emission investig. possibility 79−29177
steel tool, martensitic plate arrangement following austenisation 77 40420
steel VKS-210, α to and from γ transformation investigation by thermomagnetic structural anal. *(Russian)* 79−83197
steel VNS-2, damping capacity, magnetomechanical, phase transform. effects 78−31445
steels, 110G13 and 40Kh10G10, hardening and structural transformations during friction *(Russian)* 77−52527
steels, high strength stainless, types 1Kh15N5AM3 and 1Kh16N4AB, phase transformations 80−20931
steels, KW12M and 40G5, X-ray diffr. study of austenite lattice near martensitic transform. *(Russian)* 79−1868
steels 2Kh13 and 20Kh1M1FTR, sulphide cracking resistance, strengthening method influence 80−55577
strain energy controlled shape of cryst. forming due to martensite transform. or decomposition 78−38648
strain energy near a free surface 79−61558
strain induced FCC to HCP transform. kinetics 77−44249
stress induced, STEM study 80−47155
stress induced in single crystal, thermodynamic anal. 79−43249
superconducting A15 compounds, martensitic and supercond. transition models, anisotropy of vortices and US anomaly, review *(Japanese)* 78−23216
superconductivity in A15 compounds, microscopic model 77−8226
superconductors, type II, review of mechanical behaviour and stress effects 77−86083
symmetry changes 77−62635
theoretical analysis and physical transformation model for a self-accommodating group of 9R martensitic variants 79−33088
thermodynamic anal. of work performance under stress, theory 79−74153
thermodynamic stability of structural states *(Russian)* 79−43246
thermodynamics and morphology, under influence of external stresses *(Russian)* 78−23701
thermoelastic, equilibrium temp. 77−63671
thermoelastic, equilibrium. temp. 77−66644
thermoelastic, exam. of equilibrium transition temp. 78−56635
thermoelastic, factors affecting internal friction peak 77−28812
thermoelastic, hysteresis, exothermic and endothermic effects *(Russian)* 78−19749
$\alpha+\beta$-Ti alloy, singularities of decomposition of β solid solutions, low temp. range *(Russian)* 79−1867
Tishomingo Fe meteorite, microstructural study rel. to martensitic transform. 79−16898
Twin City (Georgia) meteorite, lack of martensite rel. to place of origin 78−65567
twin thickness, elastic energy 78−95750
twinning, mech. result of deform. or martensitic transform. hypothesis 77−62550
Zircaloy-2, martensitic transform. contrib. to strength and work hardening, and martensite flow props. 78−84842
β'-NiAl, Ni rich, electron diffr. pattern anomalies, rel. to martensitic transform. and short range ordering 78−6926
Ag-Cd (45 at.%), morphology and crystal struct. of stress-induced martensites 78−68693
Ag-Cd (45 at.%), morphology and struct. of bainite plates in β' phase 79−52213
Ag-Cd (47 at.%), crystal struct. and internal defects of thermoelastic martensite 77−48438
Ag-Zn (38 at.%), thermoelastic martensite form., morphology and struct. 77−63669
Al steel, austenite, martensite cryst. struct. changes on γ irrad. 79−90699
Al-Ni, thermoelastic phase transform., acoustic emission 80−3039
Al-Ni (63.6 at.%), elastic softening and electron diffr. anomalies prior to martensitic transform. 77−86078
Al_4Ca, phase transformation, struct. and orientation relationships 79−78963
Al_2O_3 phase transformations, γ to α, produced by shock wave working 80−16305
Au-Ag-Cd, martensitic transformation, preceding struct. anomaly 78−68692
Au-Ag-Cd alloys, martensitic phase transition, elastic anomalies and mode softening 79−91647
Au-Ag-Cd pseudobinary alloys, thermodynamic study of order-disorder and martensitic transform. 78−48399
Au-Cd (47.5 at.%), single cryst., temp. and press. derivatives of elastic consts. near transform. 77−63667
Au-Cu-Ga, solid soln., phase systems, valence electron density effects *(French)* 78−19724
β-Au-Cu-Zn, martensitic transformation temps. ageing and quenching effect 79−47687
$Au_{52.5}Ag_xCd_{47.5}$, pseudoelastic behaviour associated with thermoelastic martensitic transform. 80−16304
AuCd.r, cryst. struct. determ. 77−84699
AuCu II plates, growth mechanism 79−56976
$AuCuZn_2$, shear elastic const. meas. 77−28810
Au(Pd)-2n, Hall coeff., specific elec. resistivity and X-ray powder diffraction 78−72774
BN, martensitic character of transition from wurtzite-type to graphitelike modification 79−43248
$BaTiO_3$, ferroelectric-paraelectric transform., basic struct. and charact. 79−95717
$BaTiO_3$, phase transition exam. 78−64326
Bi-Pb alloy, rel. to press. effects on supercond. crit. temp. *(Russian)* 77−20484
$Cd(OH)_2$ decomposition, martensitic character of struct. transition, CdO crystallite shape determ. *(French)* 78−10194

martensitic transformations continued
Ce, critical isomorphic $\gamma \rightleftarrows \alpha$ transition, phase equilibrium curve *(Russian)* 80−55397
$CeAg_xIn_{1-x}$, cubic to tetragonal, conc. dependence by resist. meas. 78−2252
Co, anomalous plasticity near martensitic transform. temp. *(Russian)* 78−6971
Co, HCP films, chem. reduced, electrodeposition on Cu, Ni FCC crysts., struct. 79−11527
Co, HCP-FCC transition, mag. domain behaviour, Lorentz electron microscopy 77−80958
Co, influence of FCC phase retained at room temp. on mech. props. 79−47677
Co, magnetic anisotropy induced by magnetic and stress annealing 78−35010
Co, martensitic HCP-FCC transition, neutron scatt. obs. 79−51252
Co, martensitically transforming, state of surface 78−43223
Co, surface structure in HCP and FCC bulk phases 78−51807
Co-Al alloy, multilayer martensite phases, illustration of polytype structures 80−84932
Co-Cu (8 wt.%), X-ray anal. of 126-layer rhombohedral martensite α'-phase 77−44251
Co-Cu alloy, multilayer α'-phase form. during martensitic transform. *(Russian)* 77−59785
Co-Fe, morphology and certain props. of α-and η-phase martensite *(Russian)* 77−1838
Co-Fe(Ni), magnetic anisotropy induced by magnetic and stress annealing 78−35010
Co-Ni alloy, slip charact., and fatigue, FCC twinning and FCC to HCP martensite transform. effect 80−35182
Co-Ni-Cr-Mo, mech. props., effect of twinning and FCC to HCP transform. 77−4779
Co-Ti, multilayer and imperfect martensitic phases form. 78−19754
Co-Ti alloys, transformation depend. on ageing, cryst. struct. 79−91649
Cr-Ni steel, carburised, effect of atm. during heating to quenching temp. on austenite decomp. 77−56157
Cu, wire, axial texture after electroplastic drawing, X-ray struct. investigation *(Russian)* 80−104177
Cu-Al (10 wt.%), deformed and tempered transform. during heat treatment of β' martensite *(Rumanian)* 79−34031
Cu-Al (12 wt.%), acoustic emission related to props. 79−34032
Cu-Al-Mn, partial decomp. of β_1 phase, effect on mag. props. and martensitic transform. *(Russian)* 80−45306
Cu-Al-Mn(Ni)(Fe)(Co), hypereutectic, martensitic transform., effect of β_1-phase decomposition *(Russian)* 78−23705
Cu-Al-Ni, 2H to 6R lattice restructurization during deform., anomalous elasticity 78−19753
Cu-Al-Ni, elastic const. behaviour near Ms 77−12623
Cu-Al-Ni, formation of martensitic phases during deform. by extension 79−20048
Cu-Al-Ni, habit plane for SIM $\gamma' \rightleftarrows \beta_1'$ transform. 78−56640
Cu-Al-Ni, heredity of martensitic transformations 79−47688
Cu-Al-Ni, long period martensite phases, X-ray diffr obs. 80−7571
Cu-Al-Ni, phase diagram associated with stress induced martensitic transform. 79−8272
Cu-Al-Ni, positron annihilation study of vacancies before and after martensitic transform. 79−99971
Cu-Al-Ni, quenched, complex martensite form. 79−56977
Cu-Al-Ni, stress induced martensite 77−36500
Cu-Al-Ni (14, 2.5 wt.%). thermodynamics of thermoelastic martensitic transform. 79−61585
β-Cu-Al-Ni (14, 3 wt.%), single cryst., thermal effect due to stress induced martensite formation 80−81059
Cu-Al-Ni (14, 4.5 wt.%), premartensitic alterations 77−12655
Cu-Al-Ni (14.0 4.2 wt.%), two stage superelasticity, successive martensite to martensite transform. 77−8826
β_1-Cu-Al-Ni (14.2, 4.3 wt.%), quenched, rel. of 2H type phase with martensitic transformations 79−74149
Cu-Al-Ni (14.5, 3 wt.%), fatigued, polycrystn., pseudoelastic, dislocation and martensite substructs. 79−82223
Cu-Al-Ni alloy, thermoelastic transformation hysteresis loop width strain rate depend. *(Russian)* 79−100138
Cu-Al-Ni alloy single crystals, anomalous elasticity orientation depend., martensitic phase struct. during strain 79−87634
Cu-Al-Ni alloys, deformed, fine struct. of martensite *(Russian)* 78−6923
Cu-Al-Ni alloys, successive stress-induced martensitic transformations and associated transformation pseudoelasticity 79−43245
Cu-Al-Ni Marmen alloys, rapid solidification and ageing 80−76245
Cu-Al-Zn, structural phenomena preceding martensitic transform. 77−12624
Cu-Al(23.5 at.% and 25.3 at.%), martensitic transform., positron annihilation meas. 77−16578
Cu-Fe (1 wt.%), stress induced martensitic transformation of spherical Fe particles, exam. 78−52803
Cu-Fe(2.5 wt.%), isothermally reacted austenite stability in very small particles 77−48432
Cu-Ge (10-12 wt.%), intermediate ξ'-phase form. during deform. *(Russian)* 78−19747
Cu-Mn-Al, Heusler alloy, single cryst. and polycryst. *(Russian)* 78−48398
Cu-N, quenched, complex martensite form. 79−56977
Cu-Si, mech. of formation of martensitic struct. *(Russian)* 78−23702
Cu-Si, phase transform, exam. *(Russian)* 77−8822
Cu-Si alloy, FCC→HCP transition mechanism 77−77479
Cu-Sn, deformed, martensitic transformation *(Russian)* 79−15668
Cu-Sn (16.5 wt.%) alloy, stress induced martensite from γ phase 79−70066
Cu-Sn (25 wt.%), struct. after ultrahigh-speed quenching *(Russian)* 78−80563
Cu-Sn (25 wt.%), struct. changes with ageing *(Russian)* 77−40421
β'Cu-Zn, martensite to martensite transformations 79−11615
Cu-Zn single crystal, pseudoelastic effects 79−47739
Cu-Zn-Al, internally faulted martensite, TEM obs. 78−3124
Cu-Zn-Al, martensitic phase transformation effect on low cycle fatigue behaviour 80−7666
Cu-Zn-Al, martensitic transform., short range order effect 79−61586
β-Cu-Zn-Al, ordering, TEM obs. 78−39768
Cu-Zn-Al, single cryst., stress induced martensitic transformation 80−45308
martensitic transformations continued
β-Cu-Zn-Al, US elastic const. meas. near martensitic transform. temp. 78−39827
Cu-Zn-Al (26, 4 wt.%), martensitic transform. temp. variation after low temp. ageing 79−15666
Cu-Zn-Al (35.45, 1.72 wt.%), memory effect and martensitic transform. *(Russian)* 79−43320
Cu-Zn-Al alloy, lattice dynamical study of premartensitic state, phonon meas. 79−77696
Cu-Zn-Al alloys, dendritic struct. obs. 77−8810
Cu-Zn-Al cubic alloy, phonon sp. ht. near martensitic transform. 79−60521
Cu-Zn-Al Marmem alloy, β_1 phase superstruct. obs., rel. to transform. mode 78−39776
Cu-Zn-Al martensite, β-phase, single cryst., elastic waves behaviour as function of temp. 79−55807
Cu-Zn-Al martensite, lattice dynamics, neutron scatt. meas. 80−88286
Cu-Zn-Al martensite, the rubber effect 79−47684
Cu-Zn-Al martensites, model for rubber like behaviour 79−47685
Cu-Zn-Al wire, rapidly solidified, X-ray diffr. and therm. anal. comparison of martensites before and after solidification 79−43227
Cu-Zn-Ga alloy, configs. of martensite variants, shape deform. matrices 77−12620
Cu-Zn-Si, deform. close to martensitic transform. temp. 77−63714
β-Cu-Zn-Si, premartensitic instability 77−12625
β-CuZn, acoustic emission rel. to stress induced martensitic transformation 80−81061
CuZnAl single crystal, thermodynamic anal. of martensitic transform. under stress 79−87635
Fe alloy, design, fundamental aspects, phase transformation utilization *(Korean)* 79−66058
Fe alloy, martensitic transform., critical driving force, effect of alloying elements 77−48437
Fe alloy type G18, martensitic $\gamma \rightleftharpoons \varepsilon$ transformation, dislocation pile-ups, ε phase nucleation *(Russian)* 80−55396
Fe, Armco and carbonyl, kinetic singularities of plastic deform. during $\gamma \rightarrow \alpha$ transform. *(Russian)* 78−92262
Fe, α-, γ-, crysts., twinning, martensitic transforms., correspondence matrices *(German)* 78−31406
Fe, cast, increase in yield strength, after phase transformations 78−44125
Fe, cast, Mn, wear resist. and hardening, struct. effect 79−87734
Fe, cast, Ni resist alloy, austenitic type ChN15D7Kh2, struct. stability 79−87633
Fe, cast white Cr 78−44124
Fe, effect of plastic deform. and martensite transformation on Fe atom mobility *(Ukrainian)* 78−55974
α-Fe, growth rate of γ-phase 79−20049
Fe, H martensite production *(Ukrainian)* 77−52321
Fe, martensitic transform., induced by H_2 *(Russian)* 77−66643
Fe, martensitic transformation at high temp., transform. temp., growth rate, stress relaxation 78−56636
Fe, morphology and transition temp. 80−3042
Fe, polycryst., influence of α-γ transform. on creep *(Russian)* 80−89289
Fe, splat-quenched, microhardness and martensite 80−76359
α-Fe, struct. after polymorphic transform. under press. *(Russian)* 80−29946
Fe-Al-C steel, singularities of struct., electron microscope and electron diffr. analysis *(Russian)* 77−77476
α-Fe-Al(Zn), ⟨111⟩ fibre texture development through diffusion process without α-γ transform 79−100170
Fe-As (0.22 to 1.68 wt.%), martensitic transform., struct. features 77−36499
β-Fe-Be, pseudotwinning and pseudoelasticity 79−96056
Fe-C, martensitic transformation, thermodynamical study *(Chinese)* 80−55395
Fe-C-Al steels, law of variation of cryst. lattice parameters, X-ray diffr. analysis *(Russian)* 77−52322
Fe-C-Cr-Mo(Ni)(V), white cast, effect of abrasion on carbide microstructure *(German)* 78−88540
Fe-C-Ni-Cr, athermal alloy, exam. of martensite transformation kinetics 78−80545
Fe-Co, Mossbauer investig. of order-disorder and α-γ transitions 77−48110
Fe-Co alloys, M_s calcs. 77−8824
Fe-Co-Mo ternary system, phase diagram *(Russian)* 80−16269
Fe-Co-V, Vicalloy, $\alpha \rightarrow \gamma$ transform. under plastic deform., morphological singularities *(Russian)* 77−32576
Fe-Cr alloys, M_s calcs. 77−8824
Fe-Cr-C, crystallography of austenite-ferrite/carbide transformation 80−16303
Fe-Cr-C, isothermal transformations 80−16302
Fe-Cr-C solid solns., ordering and γ to α transforms, effect of heat treatment *(Russian)* 79−24520
Fe-Cr-Ni, single crystal anomalies in curve of critical shear stress versus temp. at low temps. 77−16656
Fe-Cr-Ni, stable and metastable, thermal expansion, 4.2-290K *(Russian)* 78−47537
Fe-Cr-Ni, textured ($\alpha+\gamma$) alloy, α' lath martensite formation 78−95749
Fe-Cr-Ni, two phase ($\alpha+\gamma$) alloys, transformation-induced plasticity 77−63721
Fe-Cr-Ni (12, 15 wt.%) austenitic alloy, Ni^{6+} irradiated, void swelling and phase stability, Si and Ti effects 80−65055
Fe-Cr-Ni (18,14 wt.%), γ to ε to α martensitic transform., external stress effect, double tensile deform. exam. 80−108438
$\alpha+\beta$-Fe-Cr-Ni (23.19, 4.91 wt.%), orientation relationship between austenite and lath martensite 78−39775
Fe-Cr-Ni alloy, austenitic, Neel temp. and max. susceptibility predictions comp. effects 77−43833
Fe-Cr-Ni alloy, deforming stresses anomalous temp. depend. *(Russian)* 77−81296
$\alpha+\gamma$Fe-Cr-Ni alloy, stress-induced α'-martensite occurrence 78−23704
Fe-Cr-Ni alloys, linear expansion, 4.2-300K rel. to antiferromag. rearrangement 78−43146
Fe-Mn, as cast, pseudo-composite struct. resulting from interdendritic segregation, cryogenic materials appl. *(French)* 80−93556
Fe-Mn, γ to α transition on cooling, struct. and microhardness investig. *(Russian)* 77−44246
Fe-Mn, jump stress relaxation obs. during cooling before martensitic transform. *(Russian)* 79−38884

martensitic transformations continued
Fe-Mn, martensitic FCC→BCC transform., orientation relation, diffractometric determ. *(Russian)* 77−44240
Fe-Mn, Mossbauer study near martensitic transform. temp. 78−3128
Fe-Mn (-C), Mn influence on martensitic transform in presence of strain *(Russian)* 80−20934
Fe-Mn (10 to 14 at.%), martensitic transforms., dilatometric effects and X-ray diffr. meas. *(Russian)* 78−6922
Fe-Mn (14.1 wt.%), G14, α-martensite formation in mag. field 79−91648
Fe-Mn (18.6 wt.%), HCP-FCC martensitic transform., Mossbauer effect meas. 78−44121
Fe-Mn alloy, splat-quenched, martensite formation obs. 77−44247
Fe-Mn alloys, high-purity, martensitic transform., heat treatment effect 79−56979
Fe-Mn mag. contributions to γ→ε phase transformations 80−25694
Fe-Mn-C, anomalous changes in austenite and martensite lattice parameters 80−50636
Fe-Mn-C, γ→ε→α′ martensitic transform. 79−24523
Fe-Mn-C, structural var. during warm deform. in γ→ε transform. region *(Russian)* 77−81293
Fe-Mn-C alloy, Mossbauer obs. *(Russian)* 78−6927
Fe-Mn-Cr-C, twinning and strain induced FCC to HCP transform. 77−44248
Fe-Mn-Nb-V, high Mn, dispersion strengthening 77−16602
Fe-Mn-Si-C, minimum of elec. resist. near LNT *(Russian)* 77−66707
Fe-N (10 at.%), structural transforms., expt. investig. *(Russian)* 77−12613
Fe-Ni, α→γ conversion, electron microscope and X-ray spectral microanal. 79−78966
Fe-Ni, elect. phenomena rel. to martensitic avalanche *(French)* 78−68691
Fe-Ni, enthalpy of transform. of γ to α′ and α′ to γ transforms. *(French)* 79−47683
Fe-Ni, FCC, elastic props. and stability near martensitic transform. temp. *(Russian)* 78−6921
Fe-Ni, FCC alloy, magnetovolume instability 79−8031
Fe-Ni, influence of hydrogen press. on temp. of martensitic transform. *(Russian)* 78−27514
Fe-Ni, martensite burst transformation, supercooling 78−84806
Fe-Ni, martensitic transform. dynamic, quasi-static atomic displacements, NGR, X-ray and electron scatt. meas. *(Russian)* 78−68688
Fe-Ni, martensitic transformation, microscopic mechanism *(Russian)* 79−34036
Fe-Ni, reverse martensitic transform., prior deform. effect 77−63668
Fe-Ni, strain energy controlled shape of cryst. forming due to martensite transform. or decomposition 78−38648
α-Fe-Ni, struct. after polymorphic transform. under press. *(Russian)* 80−29946
Fe-Ni, thermal diffusivity during martensitic and austenitic transform. *(French)* 77−59781
Fe-Ni (18 wt.%), martensitic transform., external stress effect *(French)* 78−23707
Fe-Ni (20 to 31 wt.%), exam. of martensitic transform. and reverse transform. using differential and thermomagnetic resistance analysis *(French)* 79−52214
Fe-Ni (28 wt.%), martensitic reversion, effect of internal stresses *(French)* 77−21142
Fe-Ni (29 wt.%), martensite nucleation at dislocations, elasticity model 80−55393
Fe-Ni (29.3%), N29, kinetics and morphology, ordering role 77−63673
Fe-Ni (29.58 wt.%), acoustic absorpt. and emission associated with martensitic transform. 79−34035
Fe-Ni (31 wt.%), thermoelastic martensite obs. 80−3052
Fe-Ni (32 wt.%), martensitic transform., study by fast electronic amplification *(French)* 77−86028
Fe-Ni (33.7 wt.%), γ-phase stability near martensitic transform., shear modulus obs. *(Russian)* 79−4966
Fe-Ni alloy, diffusivity, heat capacity and thermokinetic behaviour, simultaneous meas. *(French)* 77−1235
Fe-Ni alloy, effect of electron irradiation and deform. on martensitic transform. 77−16581
Fe-Ni alloy, effect of plastic deform. and martensite transformation on Fe atom mobility *(Ukrainian)* 78−55974
Fe-Ni alloy, martensitic transform., influence of thermal and electron irrad. treatment of austenite *(Russian)* 80−66509
Fe-Ni alloy, solid solution, vibr. analogue of Bain deform. and morphology of martensite in 78−2224
Fe-Ni alloys, γ- and α-phase struct. in supercooled austenite *(Russian)* 77−66642
Fe-Ni alloys, influence of hydrostatic press. on γ to α′ transform. during plastic deform. *(Russian)* 79−15663
Fe-Ni alloys, mag. state of austenite and γ→α transform. *(Russian)* 80−40350
Fe-Ni alloys, reverse martensite start temp., heating rate effects *(Russian)* 78−6924
Fe-Ni alloys, shape memory effect, martensite fine struct. effect *(Russian)* 79−52215
Fe-Ni alloys, struct. of γ and α-phases near martensitic transform. point *(Russian)* 78−64541
Fe-Ni austenite, α→γ transform and stabilisation, Mossbauer and electron microscopy obs. *(Russian)* 78−23703
Fe-Ni austenite, precipitation hardened, transform. strengthening 79−24531
Fe-Ni binary alloy, specific heat temp. depend., α to γ transformation *(Russian)* 79−83198
Fe-Ni film, amorphous, martensite form. time and struct. 80−104159
Fe-Ni Invar, magnetovolume coupling enhancement factor, temp. depend. 80−88851
Fe-Ni martensites, deform. twinning for crystals with transform. twin microstruct. 77−31677
Fe-Ni single crystals, stress induced martensite 77−8827
Fe-Ni system, ferro-antiferromag. transition, γ phase mag. struct. 79−91231
Fe-Ni-Al-Ti alloy, N27Yu2T2, aged austenite, diffuse electron scatt. distrib. during martensitic deform. *(Russian)* 78−60669
Fe-Ni-C, austenite cryst. volume effect on martensitic transformation temp. 80−40352
Fe-Ni-C, HVEM study of strain induced martensite 79−20047
Fe-Ni-C, martensite nucleation, tensile prestraining effect 77−8828
Fe-Ni-C, martensitic, H_2 effect on fracture charact. *(Czech)* 78−60746

martensitic transformations continued
Fe-Ni-C, martensitic, internal friction 77−16633
Fe-Ni-C, martensitic transform., new investigation method *(French)* 79−91881
Fe-Ni-C, mech. and structural props. under cathodic H_2 at elevated temps. *(French)* 77−59920
Fe-Ni-C, N31, martensitic point lowering by microplastic deform. and room temp. ageing *(Russian)* 77−25049
Fe-Ni-C, role of strain in deform. induced martensitic transform. *(Japanese)* 78−92263
Fe-Ni-C, thin foil, high voltage TEM exam. of martensitic form. 78−92264
Fe-Ni-C (10, 0.6 wt.%), effect of austenite yield strength on martensitic transformation 78−39772
Fe-Ni-C (19 to 30, 0.04 to 0.8 wt.%) alloys, transformation of martensite in austenite, optical and electron microscopic exam. *(Russian)* 78−35382
Fe-Ni-C (21, 0.6 wt.%), stress assited and strain induced martensite morphologies 78−3187
Fe-Ni-C (24, 0.45 wt.%), martensites, TEM observation of double twinning 78−76651
Fe-Ni-C (24, 0.45 wt.%), single crystal, plastic deform. effect on martensitic burst transform. 79−15695
Fe-Ni-C (24, 0.5 wt.%), struct. of burst and isothermal martensites 79−38825
Fe-Ni-C (25, 0.02 wt.%), thermal stabilisation role in martensitic transformations 80−25697
Fe-Ni-C (25, 0.2 wt.%), strain-induced martensite *(Korean)* 80−71646
Fe-Ni-C (26.4, 0.24 wt.%), austenitic single crysts., effect of prior deformation on martensite burst transformation, SEM obs. 79−38823
Fe-Ni-C (27, 0.23 wt.%), work hardening and martensitic transform. at 263K 79−100143
Fe-Ni-C (30, 0.5 wt.%) single cryst., stress induced martensitic transform. 80−60860
Fe-Ni-C (30.59, 0.02 wt.%), effect of loading on transformation of retained austenite to martensite 79−47686
Fe-Ni-C (31, 0.1 wt.%), kinetics of deform. induced martensite, shock loading and grain refinement effects 78−15395
Fe-Ni-C (31, 0.1 wt.%), metastable austenite, fractography 77−59919
Fe-Ni-C (31, 0.1 wt.%), pre-deformation and temp. effect on transformation-deformation behaviour 80−3127
Fe-Ni-C (31.1, 0.02 wt.%), coarse grained, microstructural aspects of martensitic transform. 79−56978
Fe-Ni-C (31.1, 0.02 wt.%), kinetics analysis of temp. rate of nucleation of a thermal martensitic transformation 79−78965
Fe-Ni-C (31.24, 0.21 wt.%) effect of deformation and ageing after deformation, on martensitic transformation temp. 78−76650
Fe-Ni-C (31.9, 0.02 wt.%), metallographic study of austenite grain size effect on martensite kinetics 79−1863
Fe-Ni-C (31.9,0.02 wt.%), determ. of number and size distrib. of martensitic plates 80−76255
Fe-Ni-C (32.7, 0.01 wt.%), athermal marrtensitic transition investigation by acoustic emission *(Russian)* 79−91645
Fe-Ni-C (9, 0.1 wt.%), effect of intercritical tempering on impact energy, exam. of mech. props. 78−52861
Fe-Ni-C alloy, austenitic, pre-deform. effects on TRIP *(Japanese)* 77−8890
Fe-Ni-C alloy, external stress effects on equilibrium morphology, thermodynamic model *(Russian)* 78−52804
Fe-Ni-C alloy, Mossbauer obs. *(Russian)* 78−6927
Fe-Ni-C alloy, N31, austenite state in premartensitic temp. interval *(Russian)* 78−56634
Fe-Ni-C alloy, splat-quenched, martensite formation obs. 77−44247
Fe-Ni-C austenite, metastable, influence of prior deform. on yield stress 78−15461
Fe-Ni-C austenitic single crysts., deform. props., martensitic transformation, SEM study 79−29143
Fe-Ni-Co-C (29.6, 10.7, 0.009 wt.%), thermal stabilisation role in martensitic transformations 80−25697
Fe-Ni-Co-Mo alloys, struct. transform. produced during tempering 77−86058
Fe-Ni-Co-Mo phase diagram and structure *(Russian)* 80−20899
Fe-Ni-Co-Ti, coherent particles effect inherited by martensite on α→γ transformation *(Russian)* 80−108443
Fe-Ni-Co-Ti, martensite cryst. lattice tetragonality, γ⇌α transform. *(Russian)* 79−61587
Fe-Ni-Cr (23, 5 wt.%), martensite orientation formed under uniaxial stress alloy [001] 77−77475
Fe-Ni-Cr austenitic steel, martensitic transform. kinetics, metastability criterion *(French)* 78−68690
Fe-Ni-Cr-C, effect of austenite yield strength, stacking fault energy, on martensite morphology 78−80546
Fe-Ni-Cr-C, martensitic transform. effect of austenite prestrain above M_d temp. 78−15398
Fe-Ni-Mn, γ→α, γ→ε transforms., expt. investigation *(French)* 78−84803
Fe-Ni-Mn (20, 5 wt.%), rel. orientation between adjacent martensite laths 80−76254
Fe-Ni-Mn (20, 5 wt.%), surface martensite, crystallography and morphology 80−40354
Fe-Ni-Mn alloy, martensitic transform. kinetics *(Russian)* 77−81262
Fe-Ni-Mn-C (5.9, 4.4, 0.48 wt.%) alloy, elastic moduli near martensitic transform. 80−7619
Fe-Ni-Mn(Mo) alloys, two-stage martensitic transformation kinetics, depend. on austenite initial state *(Russian)* 79−74151
Fe-Ni-Mo, annealing, influence on struct. of austenite *(Russian)* 80−81057
Fe-Ni-Ti, martensite, tetragonality, X-ray obs. 77−63665
Fe-Ni-Ti (25.9, 2.15 wt.%), exam. of effect of inhomogeneous solid soln., on martensitic transformation *(Russian)* 79−34034
Fe-Ni-Ti (27.4, 2 to 3 wt.%), aged, stress induced martensitic transform., mech. props. *(Russian)* 79−87632
Fe-Ni-Ti (31.2, 5.3 wt.%), γ-phase ageing effect on martensitic transform. *(Russian)* 77−28814
Fe-Ni-Ti alloys, high pressure effect on martensite crystal nucleation and growth *(Russian)* 78−39769
Fe-Ni-V, austenite, martensite elec. cond. depend. on heating *(Russian)* 79−70177
Fe-Ni-V alloy, ageing of martensite *(Russian)* 78−39808
Fe-Ni-V-C alloy, reverse α to γ transformation, previous deformation influence on struct. and props. *(Russian)* 79−100139

martensitic transformations continued
Fe-Ni-WC hard alloy, struct. and props. 79−79007
Fe-Ni-(C), substruct. of ausformed martensite 77−36548
Fe-Ni(-Mn)(Cr)(V), concentration ferromag. antiferromag. phase transition and mag. state diagram. *(Russian)* 80−20401
Fe-Ni(Mn) alloy, shape memory effect *(Russian)* 78−38771
Fe-Ni(28 at.%), Mossbauer scattering, martensitic transformation, evidence of soft modes 80−93223
Fe-Ni(29.5at%) alloy, martensitic transform., position lifetime spectra meas. 77−36498
Fe-Pd (31.2 wt.%), thermoelastic FCC-FCT martensitic transformation 80−104156
Fe-Pt, crystallography and morphology studies, lenticular thin plate transition, thin plate morphology 79−1862
Fe-Pt, nearly thermoelastic, irreversible lattice defects formed by martensitic transform. cycles 78−60671
Fe-Pt (22-24 at.%) austenite, long range order parameter, temp. depend. 80−40353
Fe-Pt (23,24,25 at.%), effect of austenite ordering on some thermoelastic transform. factors 78−88466
Fe-Pt (24 at.%), colour metallographic technique, for studying microstructural reproducibility, in martensitic transformations 78−72954
Fe-Si-N alloy, BCC→FCC transform., martensitic character obs. *(Russian)* 78−48397
Fe_3Pb, reversible shape memory effect, rel. to microstruct. memory and residual stresses 77−90419
Fe_3Pt, atomic thermal vibr. anisotropy, martensitic transform. model *(French)* 80−70355
Fe_3Pt austenites, ordering kinetics 80−104155
Fe_3Pt austenitising conditions on M_s temp. 80−81088
Fe_3Pt, interface struct. of martensite 78−48400
Fe_3Pt Invar alloy, mag. props., martensitic transform. 79−78365
Fe_3Pt, martensite austenite interface, twin thickness in martensite 77−32579
Fe_3Pt, martensitic transform., change from nonthermoelastic to thermoelastic type 78−19755
Fe_3Pt, off stoichiometric, austenite ordering and martensite tetragonality 77−36501
Fe_3Pt, premartensitic phenomena *(French)* 79−8297
Fe_3Pt, stoichiometric composition, internal friction, microdeform. and memory effect, rel. to martensitic transform. *(French)* 77−52323
^4He, HCP→FCC transition, temp. hysteresis 78−56021
HfV_2, supercond. compound, thermal expansion at low temp. 78−76189
In-Cd alloy crystal, phenomenological study of FCC⇄FCT transform. *(Japanese)* 79−100140
In-Tl, crystallographic reversibility of martensitic transform. 78−6925
In-Tl alloy, FCC→FCT martensitic transformation, on cooling, enthalpy meas. and X-ray exam. 78−39773
In-Tl alloys, supercond. transition in martensitic two phase region, AC mag. susceptibility meas. 77−72936
In-Tl single crystal, phase transform. X-ray topographic study *(Japanese)* 78−31405
LaAg, band calcs., rel. to mag. and electronic props. and martensitic transform. 77−8014
Li, martensitic phase transitions, and phase diagrams at moderate press. 78−72775
Li single cryst., US attenuation and vel. measurements in vicinity of martensitic phase transformation 80−75358
Mn-Al-C, ferromag. alloy, transform. kinetics 80−76229
γ-Mn-Cu, antiferromagnetism, martensitic transformation 79−1673
γ-Mn-Cu, changes in cell dimensions at martensitic transform. 78−19750
Mn-Cu, mag. and cryst. struct., neutron and X-ray diffr. meas. *(Russian)* 78−22694
Mn-Cu, shape-memory effect at martensitic transform., cryst. and mag. struct. 77−36610
Mn-Cu (9.3 wt.%), cryst. struct. at FCC to FCT transform. *(Russian)* 80−11643
Mn-Cu alloy, local premartensitic instability in FCC phase 80−40355
Mn-Cu alloy, volume effect, paramagnetic-antiferromagnetic and structural transition, lattice consts. 80−39007
Mn-Ni, shape memory effect 78−35386
γ-Mn-Ni-C, elastic anomalies in Mn rich alloys 78−84807
Mn-steel, cryst. geometry in formation of ε′-, ε-, ϰ′- and α-martensitic phases *(Russian)* 78−76648
ND_4Br, phase states and transition, from ESR of Cu^{2+} 79−99762
NH_4Br, supercooled, polymorphic transform., struct. correspondences and mechanisms 80−107097
NH_4CNS, kinetic-morphological types of polymorphic transform., relax. theory 78−9993
Na, conduction electron spin props. 77−8036
Na, martensitic phase transitions, and phase diagrams at moderate press. 78−72775
Na, martensitic phase transition energetics 79−99314
Na, martensitic transform. obs. neutron scatt. meas. 77−15581
Na wires, size effect and temp. depend. of resist., martensitic transform. effect 79−51691
Na-NaO-Na struct., inelastic tunnel effect, spectra, potential barrier parameters 79−95511
Nb-Ti, metallurgical treatment, effects on props. 79−38846
Nb-Ti(Zr), type II superconductor, mech. behaviour and stress effects 77−86083
$Nb_{1-x}Sn_x$, sp. ht., supercond. T_c and martensitic transform. *(French)* 78−43508
Nb_3Sn, [111] transverse acoustic phonon softening near martensitic transform. 79−73283
Nb_3Sn, A-15 supercond. cpd., martensitic transform. 79−60499
Nb_3Sn, coupling with supercond. transition 78−44126
Nb_3Sn, lattice microstrain induced metastable phase, low temp. struct. and props. 77−8482
Nb_3Sn, phonon softening in [ζζζ] transverse modes, neutron scatt. obs. 79−33062
Nb_3Sn, Young's modulus, 4.2-300K, behaviour near martensitic transition 80−66564
Ni, effect of plastic deform. and martensite transformation on Fe atom mobility *(Ukrainian)* 78−55974
$β_1$-Ni-Al, elastic softening and electron diffr. anomalies prior to martensitic transform. 77−8825
Ni-Al solid solutions, Ni-rich, phase transforms. during quenching 77−32577

martensitic transformations continued
Ni-Al system, ordering and instability of β phase near martensitic transform. *(Russian)* 80−45304
β-Ni-Co-Al, metallographic, X-ray diffr., and elec. resist. obs. *(Russian)* 78−19748
β-Ni-Cu-Zn, electron microscopy of premartensitic state 79−66059
Ni-Ti, martensitic phase transformation effect on low cycle fatigue behaviour 80−7666
Ni-Ti, near equiatomic alloy, TEM exam. of austenite-martensite interface 78−51401
Ni-Ti, structural instability, deform. effects on electron energy spectrum 80−39284
Ni-Ti, working medium in heat engine, rel. to engine efficiency *(Russian)* 78−48449
Ni-Ti (49.7 at.%) alloy, deform. behaviour and shape memory effect 77−32638
Ni-Ti (51.5 at.% Ni) metallide, thermal cond., elec. resistivity, 90-450K 78−68009
Ni-Ti alloy, near equiatomic, pretransform. lattice instability, TEM and electron diffr. 79−11616
Ni-Ti alloy, struct. and props., self-propagating high temp. synthesis *(Russian)* 78−26492
Ni-Ti mech. memory alloys, tensile props. *(Korean)* 77−63724
Ni-Ti shape memory alloy processing and medical applications *(German)* 80−17203
Ni-Ti-Co, Co effect on martensitic transform. temp. and low temp. props. *(Korean)* 78−11224
$α'_2$-Ni-Zn-Cu martensite, thermoelastic, microscope obs., TEM 77−55966
β-NiAl alloy, elastic soft modes preceding martensitic phase transition 79−4388
$β_2$-NiAl alloys, Young's modulus, −196 to 800°C, effect of martensitic transforms. 79−83253
$Ni_{1+x}Mn_{1-x}$, martensite nucleation 77−59787
NiTi equiatomic alloy, single cryst. elastic consts. near martensitic transform. 80−75283
NiTi, martensitic transform. rel. to low frequency internal friction peaks 79−96024
NiTi, premartensitic transformation of B2 phase, shape memory 80−84931
NiTi, reversible martensitic transformations 78−27516
NiTi, shape memory effect, struct. characts., TEM $2^1/_2$ D imaging obs. 80−108446
NiTi, stacking faults prod. by martensite transition, lattice imaging electron microscopy obs. 79−96026
NiTi, thermoelastic martensites, effect of martensitic transformation on fatigue crack growth rates 79−29166
NiTiCu, shape memory alloys, electron microscope and X-ray diffr. study of struct. 79−82179
$PbTiO_3$, phase transform., different kinetic types 80−71347
Pu-Ga alloys, δ→α transform. kinetics 77−25047
$(SN)_x$, polymeric, shear transformation to orthorhombic phase 77−55257
$(SN)_x$, stress-induced phase change geometry 78−23776
steels, Cr-C-Mn(Ni), struct. prop. rel., design of struct. steels for high strength and toughness 80−97491
Th-C-N system, existence of new β'ThCN' phase, struct. and thermodynamic study *(French)* 80−92499
Ti alloy VT20, phase composition and structure effect on mech. props. 79−38958
Ti alloys, reversibility of martensitic transformations *(Russian)* 80−108442
Ti alloys, types VTZ-1 and VT8, two phase, mechanism and kinetics of metastable β and α″ phases dissociation *(Russian)* 79−74152
Ti, martensitic transformation, strain energy minimisation 77−21140
Ti-Ag(Au)(Si), existence of β to $α_m$ phase transformation 78−44123
Ti-Al-Mo-Cr alloy weldment containing orthorhombic martensite, autotempering behaviour and alpha precip. strengthening 80−84976
Ti-Al-Mo-Sn-Si (2.25, 4, 11, 0.25 wt.%), type IMI 680, internal friction study of martensitic transformations 80−7573
Ti-Al-Mo-Sn-Si (2.25, 4, 11, 0.25 wt.%), type IMI 680, stability of martensitic phases 80−7574
Ti-Al-Mo-Sn-Si (4, 4, 4, 1/2 wt.%), type IMI 551, internal friction study of martensitic transformations 80−7573
Ti-Al-Mo-Sn-Si (4, 4, 4, 1/2 wt.%), type IMI 551, stability of martensitic phases 80−7574
Ti-Al-V (6, 4 wt.%), type IMI 318, internal friction study of martensitic transformations 80−7573
Ti-Al-V (6, 4 wt.%), type IMI 318, stability of martensitic phases 80−7574
Ti-alloy, VTZ-1 and VT8, decomposition of metastable phases, effect of plastic deform. *(Russian)* 78−39770
Ti-coated C steel, effect of heat treatment on struct. and props. 77−56159
Ti-Cr-Zr, martensite formation, chemical composition effect 80−50634
Ti-Fe-Ni (67, 30, 3 wt.%), reversible shape alteration *(Russian)* 80−71647
Ti-Mo, martensitic transform., water quenched from β-region 79−38826
Ti-Mo-Fe (3, 0.13 at.%), metastable phases, Mossbauer study 80−7243
Ti-Nb alloys, Fe, Mo, V, Ta alloying additions on microstruct. after combined treatment *(Russian)* 77−59826
Ti-Ni, effect of alloying on crit. points and martensitic transform. hysteresis 80−20935
Ti-Ni, electron phase transition XPS, optical spectra and mag. susceptibility meas. 80−19943
Ti-Ni, hysteresis-free 'memory' effects 78−35385
Ti-Ni, martensite transform. B2-B19′, optical props. and electron struct. *(Russian)* 80−34878
Ti-Ni, monoclinic to triclinic phase *(Russian)* 80−81058
Ti-Ni, multiplicity of structural transitions, phase diagrams, elec. cond. meas. 80−71649
Ti-Ni, reversible shape changes during martensitic transform., dislocation struct. stability *(Russian)* 77−63666
Ti-Ni, thermoelastic phase transform., acoustic emission 80−3039
Ti-Ni (50.4 wt.%), thermal conversion efficiency of ideal thermoelastic marmem cycle 79−66057
Ti-Ni (51 at.%), plastic deform., two reversible form change effects *(Russian)* 77−8881
Ti-Ni (51 at.%), thermoelastic transform., hysteresis, exothermic and endothermic effects *(Russian)* 78−19749
Ti-Ni alloys, absorpt. of H_2, press.-composition-temp. relationships, enthalpy, entropy 80−2267

martensitic transformations continued
Ti-Ni-Co cubic B_2 alloys, phonon enhancement of electronic sp. ht. near martensitic transform. 79−60522
Ti-Ni-Co(Fe) alloys, shape memory temp., alloying effect 79−38912
Ti-Ni-Cu (44.5, 10 wt%), opposing stress effect on shape memory and martensitic reversion 78−44185
Ti-Ni-Fe, multiplicity of structural transitions, phase diagrams, elec. cond. meas. 80−71649
Ti-Ni-Fe, plasticity associated with cryst. lattice stability loss *(Russian)* 79−61652
Ti-V-Ru alloy system, metastable phases form. *(Russian)* 77−21098
TiC hard coating on Co, effect of martensitic transform. in substrate causing cracks 79−29060
TiH_2, band model of martensitic phase transition 80−29953
TiMn, faceted parent martensite interface 80−6417
TiNi, imperfect elasticity, elastic after-effect on basis of martensitic transformation theory *(Russian)* 79−100198
TiNi, strain recovery, memory effect, in martensite phase *(Russian)* 77−4806
$Ti_{50}Ni_{47}Fe_3$, premartensitic phases, neutron scatt., sp. ht. and electron microscopy obs. 79−96025
U, anomalous thermal prop. behaviour at low temp. interpret. 77−28018
α-U, martensitic behaviour 79−29059
α-U, martensitic behaviour 79−29058
α-U, variable low temp. martensitic behaviour 78−41818
U-Mo-Nb-Zr-Ti (0.75, 0.75, 0.75, 0.5 wt.%), heat treatment effect on microstruct. and mech. props. 78−23729
U-Mo(Nb) and U-Mo(Nb)-Zr alloys, shear martensitic transform. during quenching, plastic deform. and annealing 77−28815
U-Nb (14 at.%), martensitic and polymorphic transformations 80−60861
U_3Si, reversible twinning, in-situ obs. 80−104241
V-H system, crystallography of βVH precipitation 77−52326
V-Zr-Nb alloy, rel. between density of states and martensitic and superconducting phase transition temps. 78−10594
V_2(Hf, Zr) Laves phase compounds, electrical resistivity, temp. dependence 78−76047
VO_2, film, semiconductor-metal phase transition, fast laser kinetic studies 79−69419
V_3Si, A-15 supercond. cpd., martensitic transform. 79−60499
V_3Si, A15 compound, microscopic model of supercond. and martensitic transform. 77−8226
V_3Si, coupling with supercond. transition 78−44126
V_3Si, d-spacing fluctuations above Martensitic phase transition 80−7570
V_3Si, EFG and band struct. 77−35861
V_3Si, electron charge distrib., martensitically transforming single cryst., X-ray diffr. meas. 78−75631
V_3Si, martensitic transform., thermal expansion meas. in normal and supercond. states 79−56381
V_3Si, mixed state, ultrasonic anomaly 77−55644
V_3Si, mixed state A15 struct., Gibbs free energy and lower crit. field temp. depend. 77−55643
V_3Si, neutron irrad., neutron diffraction studies 78−88076
V_3Si, soft mode sound vel. in mag. field rel. to density of states 78−14647
V_3Si, supercond. and struct. transitions *(Russian)* 78−52118
V_3Si, thermal expansion meas., 4.2 to 293K 79−56382
Zr base alloys, formation of phases precipitated from β solid solutions *(Russian)* 79−1869
Zr-Cr (1.9 wt.%), β-quenched and tempered, struct. changes in martensite struct. 79−66061
Zr-Cr (1.9 wt.%), β-quenched and tempered, $ZrCr_2$ precipitation, TEM study 79−66062
Zr-H formation, of $\delta \rightarrow \gamma$ transformation 80−84929
Zr-H formation, the $\delta \rightarrow \varepsilon$ transformation 80−84930
Zr-Ir hardened alloys, metastable phases *(Ukrainian)* 79−34000
Zr-Mo-Nb-V-Sn (1,2,2,2 wt.%), heat treatment, transform. reactions and mech. props. 79−24545
Zr-Mo-Sn (3,2 wt.%), heat treatment, transform. reactions and mech. props. 79−24545
β-Zr-Mo-(Al)(Ti)(La), metastable, deform. induced transform. 78−52805
Zr-Os quenched alloys, metastable phases *(Ukrainian)* 78−84804
Zr-Sn (1.5 wt.%), martensitic transform. contrib. to strength and work hardening, and martensite flow props. 78−84842
Zr-Ta (5 wt.%), martensitic transform. by rapid cooling, non-equilib. precipitation 79−34075
$Zr_{50}Co_{50-x}Ni_x$, transform. and deform. studies 79−1864
ZrCu, constitutional and struct. studies, by mag. susceptibility, metallography and X-ray diffr. 80−70166
ZrO_2, metastable, tetragonal, erosive damage depth, martensitic transform. effect 79−61738
ZrO_2, tetragonal polycryst., sintering and props. 79−29008
ZrV_2, anomalous softening at martensitic transform. 80−93630

maser clocks *see atomic clocks*

masers
active rod with varying paramagnetic ion concentration, microwave amplification *(Russian)* 77−88686
alkali metal, Rydberg states and microwaves, spectroscopy, masers and superradiance study 80−53248
alkali Rydberg atom system, transient maser action 79−86153
antiferromagnet, parametrically excited, possible maser effect 78−48051
atomic freq. standards, transfer of freq. stability to quartz-crystal resonator 80−17927
atomic H source, H_2 dissoc. in discharge 79−86637
beam maser spectroscopy, appl. to Zeeman effect determ. in H_2O_2 78−90152
bright IR star monitoring at 2.7 μm 78−16433
VY Canis Majoris, OH and H_2O microwave maser emission obs. 78−53949
VY Canis Majoris, OH masers very long baseline interferometric obs. 78−36712
VY Canis Majoris, OH/IR star, 1612 MHz OH maser multibaseline VLBI obs. 80−12766
R Cassiopeiae, Mira variable, vel. struct. in SiO maser spectrum 78−12248
celestial masers physics, review 79−21455
circulating resonance, parallel magnetic and electric fields, theory of operation *(Russian)* 77−75464
circulating resonance maser monotron, starting conditions in presence of electron vel. scatt. *(Russian)* 77−71966

masers continued
circulating resonance monotron, synchronisation *(Russian)* 77−38842
circumstellar masers, assoc. with IR objects and compact dust-bounded H II regions 77−26032
circumstellar shells of long-period variables, weak maser emission pedestal assoc. with SiO maser 78−93256
coherent radiation novel sources, book 79−27231
compact H II regions, review of radio obs. 78−16507
cool stars, H_2O maser emission, catalogue of 82 objects 79−8909
cosmic, emission by nebular regions and stellar atmospheres 78−89242
cosmic H_2O maser sources, W 49N and W 51 global radiotelescope obs. *(Russian)* 77−22072
cosmic masers, collision-collisional pumping model *(Russian)* 80−90560
cosmic masers, role of dust in pumping 78−36716
cosmic masers and star formation *(German)* 79−58410
cosmic OH molecules, detection of monopoles by nonlinear effects in interstellar masers 77−91609
cosmic OH/IR sources, microwave spectra, galactic distrib., radial velocity 78−16432
CRM-monotron, low-frequency fluctuations calc. *(Russian)* 77−88684
CRM-twistron, maximum amplification band *(Russian)* 77−88685
cyclotron maser, high-current and plasma filled, theory 78−17890
cyclotron maser, relativistic, high-current, exptl. characts. 80−9844
cyclotron maser, theory of solid-state device 79−41361
cyclotron maser instability, linear and self-consistent nonlinear theory 77−38847
cyclotron maser instability, quasi-linear theory, calc. of microwave generation efficiency 80−1783
cyclotron maser instability in intense hollow electron beams, effect of energy and axial momentum spreads 80−1782
cyclotron resonance, collective and single-electron interactions of electron beams with EM waves 78−55330
cyclotron resonance, multimode regimes *(Russian)* 77−31083
cyclotron resonance maser, high power MM wave source−gyrotron *(Japanese)* 80−23654
cyclotron resonance maser tube with transverse current, theory of oscillation 79−89877
cyclotron resonance maser with high current relativistic electron beam 79−13942
cyclotron-resonance maser amplifier with freq. conversion 78−55329
cyclotrons resonance maser, Vlasov-Maxwell eqns., guided wave field theory 80−14309
V1057 Cygni, OH obs. 80−36629
NML=V1489 Cygni, OH/IR star, 1612 MHz OH maser multibaseline VLBI obs. 80−12766
development, recollection by Townes 79−21517
Dicke maser Hamiltonian, A^2 term relevance 80−83577
Dicke maser model, equilibrium states for mean field models 80−46961
Dicke maser model, radiation damping, phase transition, presence of phonons 77−19224
Dicke maser model-van der Waals spin system thermodynamic equivalence 80−83572
Dicke model, dynamical struct. 80−37985
Dicke model, phase transition, counter rot. and $(A)^2$ terms in Hamiltonian 77−23641
diffraction radiation pulses, spectral characts. 80−32946
electron beam cyclotron maser config., meas. of EM wave energy generated 77−38786
electron cyclotron maser, fundamental mode, linear theory 80−58496
electron cyclotron maser, gyrotron, efficiency enhancement, nonlinear theory 80−91768
electron cyclotron maser, historical review 77−38843
electron cyclotron maser, instability, linear and self-consistent nonlinear theory 77−38844
electron cyclotron maser, mm-wave source appls., review 77−88683
electron cyclotron maser as high power travelling wave amp. of MM waves 80−1176
electron cyclotron maser device theory 80−58494
electron cyclotron maser history 77−38845
electron cyclotron maser in overmoded cavity, nonlinear multimode formulation 80−58495
EM electron cyclotron instability, axial and azimuthal bunching mechanisms 78−51295
fluctuating intensity regimes in lasers and masers 80−19015
formaldehyde maser in IRS 1 in NGC 7358, SHF band obs. 80−67822
free electron devices for light prod., history, book contrib. 79−27147
free-electron masers with quasicircular undulators 79−55102
frequency standard, thermal noise effect meas. on amplitude of oscillation 80−98898
galactic H_2O vapour sources, maser phase duration galactic distrib. 79−35343
galactic masers, role of plasma effects in generating high-vel. and symmetric spectral features 80−31378
giant stars, search for water vapour absorpt. lines 77−78804
gyromonotron, operating characteristics at 35 GHz 80−58497
gyromonotron design, 240 GHz, using supercond. magnet system 80−58498
gyrotron, stimulated emission of cyclotron radiation, review 77−34865
gyrotron efficiency, CW and pulsed power achievements 79−31849
gyrotrons and dopplertrons, coherent radiation from magneto-resonant relativistic electron beams, book contrib. 79−27227
with helical electron beams, extended and intense with space-charge forces, trajectory anal. *(Russian)* 79−918
HF current generation by photochemical reaction products *(Russian)* 78−78985
high-power microwave generation by relativistic electron beams 78−5444
historical aspects *(Japanese)* 79−81403
W Hydrae, long-period variable, suspected Zeeman splitting in OH masers 80−36632
inhomogeneous cosmic masers, numerical calcs. of saturation behaviour 78−20898
injection priming of pulsed molecular-beam maser oscillator 79−27226
interferometric multiple beam, construction and exptl. results *(French)* 79−45919
interstellar, IR spectrum of OH 26.5+0.6, polysaccharide grain model 78−12342
interstellar, wide spectrum H_2O source detect. at 22 GHz 77−74120
interstellar H_2 vibrational excitation in intense UV fluxes 78−36647
interstellar H_2O maser, in shock-induced star form. region in (NGC 281) 79−25688
interstellar H_2O maser emission, new sources detect. 80−62298

masers continued
interstellar H_2O maser in H II region complex (RCW 48-49) 77−57102
interstellar H_2O maser sources, near IR pumping 77−78862
interstellar H_2O masers in H II regions, time vars. obs. 79−88725
interstellar H_2O masers near type I OH masers, obs. 79−25671
interstellar H II/OH maser regions, heating by ion streams 80−56912
interstellar maser lines intensity vars. due to induced Compton scatt. 78−4319
interstellar masers, Λ-doublet population inversion in OH, OD, CH, CD and NH^+ collisions 80−22065
interstellar masers, assoc. with isentropic instabilities 77−17644
interstellar masers membership in star form. regions rel. to population categories 80−17645
interstellar OH, ground state Λ doublet maser emission as result of overlapping far IR transitions 77−45533
interstellar OH and H_2O, radial vel. struct. 77−33617
interstellar OH and H_2O masers, form. by thermal instability of radiative shock 80−67821
interstellar OH maser clouds, saturation effects 77−91657
interstellar OH maser source, OH 205.1-14.1, 1667 MHz emission monitoring 77−64819
interstellar OH maser sources, accurate position meas. 80−46646
interstellar OH masers, 18 cm lines pumping by H+OH collisions 79−48892
interstellar OH masers in direction of H_2O masers, new discoveries 78−12393
interstellar type I OH masers, positions, polarisation, nearby H_2O masers, radio and IR props. 79−25671
IRC+10374, IRC+10523, IR stars, H_2O maser emission detect. 80−62298
IRC+10420, stellar OH maser VLBI obs. rel. to mag. field 79−25742
IRC+10420, supergiant star, new OH maser feature spatial struct. 79−48946
late-type stars with OH, H_2O or SiO maser emission, catalogue 79−70965
long-period variable stars, maser activity rel. to Hδ emission, obs. 79−88685
M33, galaxy, detect, of H_2O maser emission 77−29926
magnetic ion concentration, in maser crystals 78−82007
MCR monotron synchronization by external harmonic signal applied to resonator 80−43312
megawatt sub-mm pulse production by stimulated magneto-Raman scatt. 77−50719
methanol, interstellar, search for microwave emission 78−32543
microwave emission, by plasma produced electrons orbiting a positively charged wire 80−92272
millimetric generation, stimulated scatt., relativistic electron beam, zero freq. pump field 77−88687
Mira variables, H_2O emission characts. 77−45447
multimegawatt gyrotron design for controlled thermonuclear reactor heating 80−59256
nuclear Zeeman, stability of generation of asymmetrical inhomogeneously broadened line 78−82939
OH 205.1−14.1, unusual OH maser, new flare report and 1667 MHz line obs. 80−98734
OH maser luminosity and expansion velocity gradient in Mira envelopes 79−71043
OH masers, interstellar, obs. near Orion population stars 80−67716
Orion A, 22 GHz water line giant outburst 80−8703
Orion A, SiO and H_2O maser obs. 78−8085
Orion H_2O masers, matter outflow in star formation last stages 78−8091
Orion methanol masers, interferometric and multitransitional study 80−67891
U Orionis, Mira variable, relation between 1612 MHz flare and light curve 80−56844
U Orionis, stellar OH maser VLBI obs. rel. to mag. field 79−25742
paramagnetic crystal, quantum amplification and absorpt. of EM wave in moderating structure 80−87361
parametric instability in a stream of phased oscillators, nonlinear theory 80−5719
S Persei, M-type supergiant, circumstellar OH maser emission obs. 77−22218
phase amplitude characteristics with paramag. cryst. saturation effect 78−46555
phase and frequency instabilities in precision frequency sources, characterisation and mathematical models 79−2750
pheromone:beeswax far IR maser, possible cabbage looper moth control 77−77870
pheromone, cabbage looper moth sex scent, 17 μm emission rel. to moth control 77−73507
protostellar H_2O maser sources, disc struct. 79−48784
pulsars radio emission, curvature radiation absorpt. theory and possible maser effect 79−75090
pumping of interstellar masers and absorption of trapped line photons by dust 79−25460
quantum amplifiers and their application in space research, review 80−36503
quantum frequency standard with pulsed optical pumping of Rb^{87} vapours, performance factor 80−78823
quantum mechanical model 78−50745
quasi-optical open resonators, phase struct. of field, meas. method *(Russian)* 78−29925
quasi-stellar objects, gravitationally pumped masers model 78−54071
radiative stability and time vars. of interstellar masers 79−35340
radio astronomy receivers, low-noise 4-stage K-band maser system, 18.3 to 26.5 GHz 79−2481
reference frequency stability transfer to quartz crystal oscillator 79−54108
relativistic cyclotron, intense relativistic electron dynamics 77−68158
relativistic electron beam, submillimetric pulse production by stimulated magnetoresonant Raman scatt. 77−38846
relativistic electron beam Raman laser 78−74877
relativistic electron beam sources of microwave radiation 78−46556
relativistic gyratron, coherent microwave mag. bremsstrahlung, general theory of masers *(Russian)* 78−1141
RF maser, chemical pumping of nuclear Zeeman energy levels 77−79793
ring-type state selector and space focuser for mols. with positive induced dipole moment, appl. to mol. beam maser 78−54503

masers continued
Roberts 22, bipolar nebula with OH emission, visual, radio and IR obs. 80−94859
ruby, research and development 80−27094
ruby maser, K-band, 500 MHz bandwidth 80−63966
ruby maser with wide tuning band 80−53247
ruby reflected-wave maser, with K-band tuning range and large instantaneous bandwidth 79−50275
ruby rod TW amplifier with variable Cr^{3+} conc. *(Russian)* 79−94202
rutile, travelling-wave type, for radio astronomy in 20-40 GHz freq. range 77−3562
Rydberg atom maser emission, heterodyne detection 80−78822
AH Scorpii, M-type supergiant, circumstellar OH maser emission obs. 77−22218
screw electron beams, systems form. synthesis *(Russian)* 78−17889
semiconductor subjected to mag. and US fields, EM radiation gain 80−48201
solar corona, gyro-synchrotron maser possibilities 79−48756
spectral line broadening mechanism of maser with beam of inflying atoms 80−106503
spherical open resonator, approx. theory *(French)* 80−48301
spherical top molecules, possible microwave interstellar maser lines 78−41020
stars, late supergiants and long period variables, radial vel. determ. 80−77410
stellar H_2O maser emission, circumstellar shell model 77−60765
stellar OH masers, struct. 77−53583
stellar SiO masers, $J=1\rightarrow0$ $v=1$ and 2 masers relative intensity and vel. 80−4339
stellar water vapour maser sources, microwave and IR obs. 79−67037
stimulated linear acceleration bremsstrahlung 79−92658
strophotronic source, radiation induction 77−46710
submillimetric magnetoresonant scatt. from relativistic electron beams 77−38792
successive oscillatory fields, molecular beam resonance method 80−91706
supergiant OH maser sources, optical radial vels. 77−49378
supergiant stars, radial vel. meas., expanding dust cloud effects on maser source 79−5816
symbiotic stars, radio mol. maser line obs. 80−72960
three-level, collisional relax. rates between rot. states 78−22106
three-level, collisional relax. times 78−13675
time and freq. standards, design principles and characteristics 77−22533
travelling-wave, for 85-90 GHz, using slot-fed guide slow wave cct. 77−5429
two-level, population inversion, information approach, Maxwell demon 80−86241
two-resonator CRM oscillator with external feedback 80−87362
Type I OH maser sources, obs. of nearby compact H II regions 78−8094
vinyl bromide, CO_2 laser pumped, stimulated emission at 45 freqs. 77−645
W33 A, OH maser, 3.4 to 33 microns emission obs. 77−22287
W3(OH), interstellar OH maser, struct. from VLBI synthesis obs. 80−105368
W3 (OH), 8 to 13 micron spectrophotometry of compact maser source 77−57070
W49, stimulated Raman scatt. and high vel. H_2O maser features 77−49463
W51 Main, H_2O maser emission 80−8701
W75 maser sources, 1667 MHz line profile features 79−5914
water, interstellar, in W3(OH), rapid time vars., models 79−17058
waveguide reflection maser with broad tunability 78−5443
zero point energy noise effect 79−72546
$Al_2O_3:Cr^{3+}$, solid-state nuclear spin-flip maser pumped by dynamic nuclear polarisation 77−31084
C stars, search for HCN and CH maser emissions 80−51856
CH, interstellar, maser emission obs. towards W49 region 77−87511
CH, interstellar, maser emission obs. towards various galactic objects 77−87512
CH, interstellar, radio obs. 78−28751
CO maser emission in evolved stars expanding envelopes, line profiles 80−82334
$Cr^{3+}:Be_3Al_2(Si_6O_{18})$, synthetic emerald crystal, quantum paramag. amplifier with resonator 79−89878
Cs beam frequency standard, frequency stability *(Japanese)* 77−108
Cs freq. standard, stability determ. method 77−83842
Cs, optically pumped, cavity, buffer gas, press., temp., freq., characts. 77−10880
^{133}Cs, freq. standard, optimum conditions for population inversion for 0-0 transition 80−78824
$Fe^{3+}:Al_2SiO_5$, andalusite travelling wave maser in 40 to 46 GHz freq. range *(Ukrainian)* 80−53246
$Fe^{3+}:TiO_2$, low noise travelling wave maser, noise temp. 80−32945
$Fe^{3+}:TiO_2$ 86-88 GHz low-noise TW maser 80−69354
H atomic frequency standard and maser development by NASA 77−37861
H atomic passive frequency standard 77−37860
H, atomic resonance effects on long-term freq. stability 77−75465
H, autotuning systems, theoretical anal. based on freq. or phase method 80−83575
H beam production in maser dissociator, performance characts. 78−87034
H, frequency changes due to nonuniform magnetic field 80−99687
H, hyperfine transition, affected by coherently excited Zeeman transitions 79−72544
H maser, field-operable design improvements 79−55099
H maser autotuning system analysis 79−55101
H maser cavity, tuning using variable capacitance diode 79−72545
H maser design for NAVSTAR Global Positioning System satellite clock 78−58969
H maser failure mode identification 77−37862
H maser improvements at Smithsonian Astrophysical Observatory 78−58971
H maser microwave resonator, miniature design 79−55097
H maser response to coherent Zeeman perturbations 78−58972
H maser with double configuration bulb for wall shift meas. 78−58970
H passive maser frequency standard 79−55100
H spacecraft maser, operating development model 79−54105
H, Teflon TFE 42, FEP 120 coatings, wall shift comparison 78−78984
H, temp. dependence of wall and spin exchange effects, expt. 77−79792

masers continued
H, time-dependent freq. shift obs. 78−89457
H VLG-11 maser, performance evaluation 79−55098
H, with automatically tuned resonators 80−95859
H-maser clocks, synchronization using very-long-baseline interferometry 79−88920
H_2 dissociator envelope degradation, AES characterisation rel. to appl. in atomic clock 77−61876
H_2, frequency standard appl. stability improvements and cavity tuning 78−21099
H_2 maser freq. standard using dual modulation 80−98900
H_2 maser wall shift and unperturbated hyperfine freq. of ground state of H_2 atom 80−98901
H_2, multitube collimator, used to stabilise maser frequency standard 80−91769
H_2, temp. dependence of wall shift, 295 to 395K 80−83576
H_2, time-dependent freq. shifts obs. 79−21713
H_2, tuning, amplifiers and limiters with level independ. phase shifts 77−19223
H_2O, collisional pumping in circumstellar shock wave 77−53675
H_2O cosmic masers, influence of dust on collisional pumping 78−54030
H_2O emission in W49N, W51 and Sagittarius B2, high vel. features 77−9779
H_2O, emission search from globular star clusters 79−30094
H_2O, in dense interstellar mol. clouds, high sensitivity survey 78−85988
H_2O, interstellar, 22 GHz obs. with resurfaced Parkes radiotelescope 77−33347
H_2O, interstellar, accurate interferometric positions at 1.35 cm 78−45374
H_2O, interstellar, emission features, VLBI obs. in W49 N 77−26038
H_2O, interstellar, Herbig-Haro objects and interstellar bullets 79−35329
H_2O, interstellar, in mol. clouds assoc. with small Hα emission regions 79−17042
H_2O, interstellar, lines very-high-velocity satellite features generation by stimulated Raman scatt. 78−73746
H_2O, interstellar, maser emission increase in W3(OH) 77−53672
H_2O, interstellar, survey in southern hemisphere 77−91599
H_2O interstellar masers, high vel. structures, origin *(Russian)* 79−25697
H_2O maser emission from external galaxies, detects. 78−45417
H_2O maser emission from supergiant star S Persei, 22 GHz variability 78−49461
H_2O maser features, high-velocity, in W3(OH), obs. 80−31339
H_2O maser in H II region NGC 289, obs. 78−28740
H_2O maser line evidence for circumstellar ring systems in supergiant stars 78−89195
H_2O maser near RT Serpentis, obs. 79−8932
H_2O maser source in Orion A, obs. of outburst *(Russian)* 80−105320
H_2O maser source near NGC 2071, discovery 78−73768
H_2O maser sources, spectra and autocorrel. anal. 78−65713
H_2O maser sources in different stages of evolution, new VLBI maps 80−26954
H_2O maser sources in galactic plane, southern hemisphere survey 80−73054
H_2O maser sources in W3, accurate positions 78−4332
H_2O masers, 22 GHz galactic plane survey, 14 new sources 80−77464
H_2O masers, interstellar obs. with resolution of 0.0008 arcsec 77−74154
H_2O masers assoc. with late-type variable stars, structure 79−71037
H_2O masers assoc. with mol. clouds, VLBI aperture synthesis obs. 79−21368
H_2O masers associated with compact H II regions in Sagittarius B2 77−13486
H_2O masers in NGC 6334, positions and spectra rel. to star form. 80−73025
H_2O masers located near Herbig-Haro objects, discoveries 79−21369
H_2O masers near OB associations, 22 GHz obs. 79−25649
H_2O sources in Galaxy, sites of newly formed OB stars 78−12390
H_2O sources near Herbig-Haro objects 7-11, 22 GHz obs. 80−73019
H_2O, stellar, detect. of new sources 78−32466
H_2O, stellar, time vars., 22 GHz obs. 79−30077
H_2O, vapour, turn-on in H II region W3(OH) 78−36677
H_2O maser in S252 (NGC 2175) star forming complex, discovery 80−4411
^{3}He, opt. pumped maser, saturation polaris. intensity depend. *(Russian)* 77−7046
^{3}He, optically oriented nuclei, maser excitation and characts., appls. 78−17891
^{3}He, optically oriented nuclei, in two-chamber cell, spin maser appls. 78−17892
n-InAs, nucl. maser effect 78−19345
InSb film cyclotron-frequency submillimetric oscillation generation model 77−80801
NH_3 beam maser, behaviour study using Fabry-Perot resonator *(French)* 78−42315
NH_3, interstellar, nonmetastable levels obs. 79−25665
NH_3 J=K=1 line mol. beam maser emission, ring-type focusing 80−28119
NH_3 molecular beam maser with semi-confocal cavity, output power spectral distrib. 80−43311
OH 1612 MHz masers, unsuccessful search in symbiotic stars 80−12774
OH and H_2O masers assoc. with compact H II regions, model 78−81666
OH astronomical maser sources OH 231.8+4.2, CY Canis Majoris, M1−92, UHF obs. 80−90550
OH emission from late-type stars, time var., correl. with visual magnitude 77−60764
OH emission from Mira variables, high-sensitivity search 78−89203
OH, interstellar, class I, IR obs. of nearby compact H II regions 77−45525
OH, interstellar, new main line maser obs. with probable Zeeman pattern 80−56908
OH interstellar, temporal var. 78−53817
OH main line emission from globular clusters, high sensitivity search 80−62207
OH main line maser in interstellar cloud, pumping mechanism 80−67824
OH maser emission, rot. states, hyperfine states, microwave spectra, interstellar appl. 80−32694
OH maser emission, rot. excitation by H_2 at interstellar temps. 80−62232
OH maser emission from W3 (OH), Zeeman effect 78−93377

masers continued
OH maser in pulsating Mira type variables atm., IR line overlap pumping mechanism 80−72764
OH maser lines from long-period variable stars, struct. and saturation 78−93264
OH maser pumping efficiency of Mira variable stars 80−82379
OH maser source OH 351.78−0.54, UHF obs. (1980 August) 80−101644
OH maser sources, interstellar, radiative transport effects on inversion 80−17681
OH maser sources near galactic centre, systematic search at 1612 MHz 79−35415
OH masers assoc. with IR stars, very long baseline interferometric obs. 77−53699
OH masers in Orion Nebula, obs. 78−16493
OH masers near newly formed OB stars, assoc. with H_2O masers 78−12390
OH type I source G 109.7+2.2 near Herbig-Haro object *(Russian)* 80−17684
OH, weak interstellar masers detect. in H_2O masers direction 77−33618
OH/IR stars, OH main lines masers inversion 78−28664
OH/IR unidentified Type II stars, galactic distrib. and kinematics from 1612 MHz survey 78−49450
OH-CH rotationally inelastic collisions, maser action 79−94068
OH+ion anisotropy, OH removal by magnetic heating 79−98328
OH($^2\Pi$)+H, rel. to interstellar OH maser action 79−101186
Rb atomic frequency standard, optical pumping phenomenon and techniques, review 77−65022
Rb, magnetometric devices appl., threshold sensitivity and short-term fluctuations determ. 80−22394
Rb maser oscillator, freq. domain meas. of freq. stability 80−83574
Rb maser response to coherent Zeeman perturbations 78−58972
Rb optically pumped at. beam clock, theory 77−34866
^{85}Rb unperturbed hyperfine transition frequency determ. 77−7047
^{87}Rb, long term freq. stability, rel. to at. hyperfine transition 79−98029
^{87}Rb maser and related oscillators, time- and frequency-domain stability 78−58968
^{87}Rb optically pumped freq. standard, buffer mixtures for gas cell 78−82938
SiO 86.2 GHz maser, astronomical sources polarisation props. 80−4449
SiO circumstellar maser 78−16511
SiO, detect. at 7 mm wavelength in M- and S-type stars 78−4215
SiO, emission from Mira variable stars, new sources 78−32467
SiO, emission obs. in long-period variable stars 78−4225
SiO, luminosity in Mira variable stars correl. with spectral type 77−33512
SiO maser emission in OH/IR stars, new transition detect. 78−53954
SiO maser in Orion-KL nebula VLBI obs. at 43 GHz 79−92836
SiO maser line evidence for circumstellar ring systems in supergiant stars 78−89195
SiO maser obs. in late-type stars at 43 GHz 77−74067
SiO maser variability at 86 GHz of R Leonis, *o* Ceti and Orion A 80−41839
SiO masers in IR stars 79−71036
SiO masers in late-type stars, VLBI obs. at 43 GHz 79−92779
SiO pump mechanism and luminosity of long-period variable stars 79−92772
SiO stellar sources, 43 GHz obs. 79−16942
TiO_2:Cr^{3+}, maser, 8 mm, 15 MHz bandwidth, 15-18 dB gain at 4.2K *(Russian)* 78−25844

masking (acoustic) *see hearing; speech intelligibility*

masks
see also semiconductor device manufacture
aspectrogram filtering, multiplying mask prod., photographic method 79−27196
coherent optical pattern recognition using normalized invariant moments 80−99653
diffraction grating form. on optical waveguide surface, ion-beam etching through photoresist mask 80−14492
edge detection and coding using directional masks 77−79774
evaporated interdigital electrodes, masks fabrication 78−24775
fibre-optic planar multimode coupling structure fabrication by ion exchange 80−64233
films, deposition profile with shadow effect, theoretical model 79−82473
Gaussian beams, divergence reduction using phase masks *(Russian)* 79−27308
high-resolution holographic aplanatic objective *(French)* 77−83837
holographic data recording phase-random mask production by multichannel acousto-optical modulator *(Russian)* 79−94179
IC photomask and wafer linewidth meas. using optical spatial coherence 80−77850
III-V semiconductors, MBE developments in device fabrication, masking procedures 79−78902
image dissector tube with minicomputer control suitable for IC mask inspection 79−55065
incoherent optical correlator using projected fringes patterns, for object shape and contour control 79−97357
information storage and processing phase mask fabrication and testing 79−27195
interleaved glass layer prism for semiconductor mask testing 80−43425
ion implantation, semiconductor device processing 80−34031
ion milling, string segment motion algorithm 80−71779
ion-beam etching on ion-etched structs., sample inclination and rotation effects 79−15831
laser beam metal-coated apodising apertures 77−19439
linewidth meas. by diffraction pattern analysis 77−37960
linewidth meas. effects of optical microscope operating parameters 77−37977
linewidth meas. with coherent optical microscope 77−37978
linewidth measurement using optical microscope 77−79147
magnetic bubble memory chip fabrication, single level masking approach 79−78486
MIS solar cells, etched slotted mask for direct deposition of metal contact pattern 80−97786
multicolour image storage on black and white film, using crossed grating 79−31813
multiple exposure hologram generation from controlled transparencies *(Russian)* 79−94177
multiplex holography with chirp-modulated binary phase-coded reference-beam masks 79−27202

3 8198 307 019 719
THE UNIVERSITY OF ILLINOIS AT CHICAGO

THIS BOOK IS FOR USE
ONLY IN THE LIBRARY
IT DOES NOT CIRCULATE